Terpyridines Functionalised with Ferrocenyl Groups of Different Redox Potential

Ulrich Siemeling,*[a][1] Udo Vorfeld,[a] Beate Neumann,[a] Hans-Georg Stammler,[a] Piero Zanello,[b] and Fabrizia Fabrizi de Biani[b]

Keywords: Terpyridine ligands / Ferrocenes / Iron / Ruthenium / Cyclic voltammetry

2,2′:6′,2′′-Terpyridines bearing a substituent X in the 4′-position [**3a**: X = Fc–C≡C–*p*-C_6H_4; **3b**: X = $Fc^{\#}$–C≡C–*p*-C_6H_4; Fc = $(C_5H_5)Fe(C_5H_4)$, $Fc^{\#}$ = $(C_5Me_4H)Fe(C_5Me_4)$] were prepared by Pd^0-catalysed cross-coupling reactions. **3b** was characterised by X-ray structure analysis. [(**3a**)$RuCl_2$(DMSO)] (**4a**) and [(**3b**)$RuCl_2$(DMSO)] (**4b**) were obtained by reaction of [$RuCl_2(DMSO)_4$] with 1 equivalent of **3a** and **3b**, respectively, while the analogous reaction with 2 equivalents afforded [(**3a**)$_2$Ru][PF_6]$_2$ (**5a**) and [(**3b**)$_2$Ru][PF_6]$_2$ (**5b**), respectively, after precipitation with aqueous [NH_4][PF_6]. Similarly, [(**3a**)Ru(tpy)][PF_6]$_2$ (**6**) was isolated from the reaction of **4a** with 2,2′:6′,2′′-terpyridine (tpy). Compounds **3** and **5** were investigated by cyclic voltammetry, which revealed that the introduction of eight methyl groups leads to the expected cathodic shift of the $E^{0\prime}$ values of ca. 0.44 V for the ferrocenyl-centered redox processes.

(Oligopyridine)Ru^{II} complexes exhibit unique photophysical as well as photo- and redox-chemical properties.[2] They have frequently been found to be excellent photosensitisers. Among the oligopyridine ligands 2,2′:6′,2′′-terpyridines bearing redox-active groups in the 4′-position are currently attracting much attention, since they can be used for the construction of geometrically well-defined metal complexes, which show fascinating properties based on intramolecular electron- and energy-transfer processes. For example, Ru^{II} complexes of such terpyridines have been utilised for the construction of donor/sensitiser dyads and donor/sensitiser/acceptor triads.[2a–g] These and related assemblies allow the investigation of photoinduced vectorial charge separation over large distances, which is, inter alia, of fundamental importance for solar light energy conversion.[3]

Owing to their well-behaved redox chemistry[4] as well as their chemical robustness and synthetic versatility, ferrocenyl units are very attractive donor groups in such assemblies, and several ferrocenyl-functionalised terpyridines have been synthesised for this reason.[5] However, it has turned out that ferrocenes, their (redox-)chemical advantages notwithstanding, show a serious disadvantage. [$(C_5H_5)_2$Fe] quenches photoexcited (oligopyridine)Ru^{II} complexes not only reductively, but also by triplet energy transfer.[6] The triplet energy of ferrocene has been estimated to be ca. 1.8 eV,[7] which is below the typical excited-state energy of (oligopyridine)ruthenium complexes.[2h–j] Consequently, both energy transfer and reductive quenching are thermodynamically favourable in this system. This finding has caused strong reservations as to whether ferrocenyl units can be used as donor groups in relevant assemblies, since for photoinduced charge-separation processes energy transfer is undesirable.[2g]

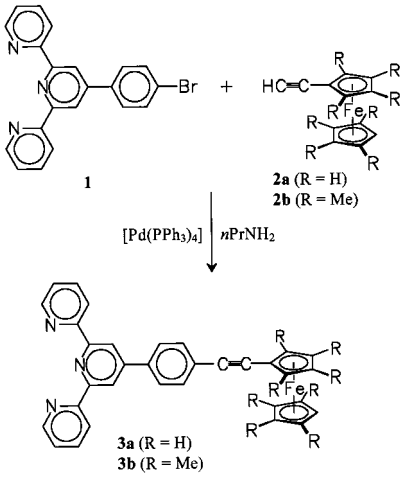
Undoubtedly, ferrocenyl groups could very well be utilised advantageously in this context, if it proved possible to shift the competition between energy transfer and reductive quenching in favour of the latter by judicious choice of molecular parameters. Comparative studies using ferrocene and various oligomethylferrocenes as quenchers indicate that reductive quenching can be favoured by increasing its thermodynamic driving force (i.e. by increasing the reducing power of the donor).[6][8] There is a linear relationship between the number of methyl groups and the redox potential of a ferrocene, each methyl group causing a cathodic shift of ca. 55 mV,[4][9] while leaving the triplet energy essentially unaffected.[6] However, systematic investigations of the general factors influencing the competition between energy transfer and reductive quenching in oligonuclear complexes, although of fundamental interest, have not been performed so far.[10] For such an investigation two points are of vital importance. Firstly, it is necessary to study geometrically well-defined compounds, since otherwise meaningful results, which can be compared with the predictions of current theories of electron and energy transfer,[11] cannot be obtained. Secondly, in order to obtain unequivocal results it is essential to be able to single out the effect of the variation of a single molecular parameter.

For this reason we have prepared derivatives of 2,2′:6′,2′′-terpyridine (tpy) with ferrocenyl (Fc) and octamethylferrocenyl ($Fc^{\#}$) groups attached to the 4′-position by means of a *para*-phenylene and an acetylene spacer unit.[12] In this communication we report on the synthesis of these compounds and present first results from their coordination chemistry as well as preliminary electrochemical investigations.

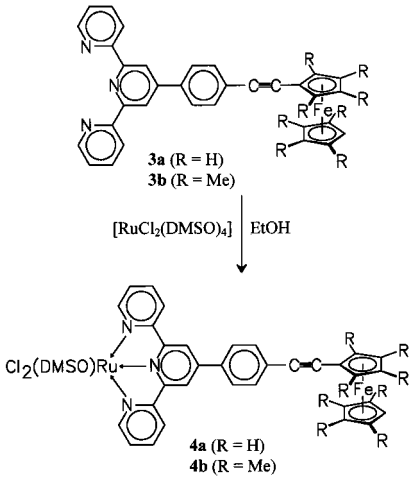
Sonogashira-type cross-coupling[13] of 4′-(4-bromophenyl)-2,2′:6′,2′′-terpyridine (**1**)[14] with FcC≡CH (**2a**)[15] and

[a] Fakultät für Chemie der Universität Bielefeld, Universitätsstraße 25, D-33615 Bielefeld, Germany
[b] Dipartimento di Chimica, Università di Siena, Pian dei Mantellini 44, I-53100 Siena, Italy

 © WILEY-VCH Verlag GmbH, D-69451 Weinheim, 1999 1434–1948/99/0101–0001 $ 17.50+.50/0



Scheme 1



Scheme 2

$Fc^{\#}C{\equiv}CH$ (**2b**)[16] in *n*-propylamine in the presence of $[Pd(PPh_3)_4]$[17] as catalyst[18] afforded the redox-functionalised terpyridines **3a** and **3b**, respectively (Scheme 1).

A single-crystal X-ray structure analysis was performed for **3b**. A view of the molecule is shown in Figure 1.

The cyclopentadienyl rings are arranged in an eclipsed orientation and exhibit an average Fe−C bond length of 206 pm, which is nearly identical to the value observed for decamethylferrocene (205 pm).[19] The acetylene group is almost linear [C(14)−C(19)−C(20) 177.5(3)°, C(19)−C(20)−C(21) 176.6(3)°] and has a C−C distance of 119.3(4) pm; the distance between each acetylene carbon atom and the sp^2-hybridised carbon atom attached to it is 143.1(4) [C(14)−C(19)] and 144.0(4) pm [C(20)−C(21)]. These values are unexceptional and compare well with those of other structurally characterised (phenylethynyl)ferrocenes.[20] The dihedral angle between the best planes of the C_6 ring and the central C_5N ring of the terpyridyl unit is 26.9° and that between the cyclopentadienyl ring containing the atoms C(10)−C(14) and the C_6 ring has a value of 29.1°. The three C_5N rings are almost coplanar (dihedral angles 3.3 and 7.0°) and exhibit transoid configurations about the interannular C−C bonds as is commonly observed for such compounds.[21]

We have started to develop the coordination chemistry of the new redox-functionalised terpyridines by using established methods.[18b] For example, the mono(terpyridine)ruthenium(II) complexes [(**3a**)$RuCl_2$(DMSO)] (**4a**) and [(**3b**)$RuCl_2$(DMSO)] (**4b**) were prepared by treating one equivalent of **3a** and **3b**, respectively, with $[RuCl_2(DMSO)_4]$[22] in refluxing ethanol (Scheme 2).

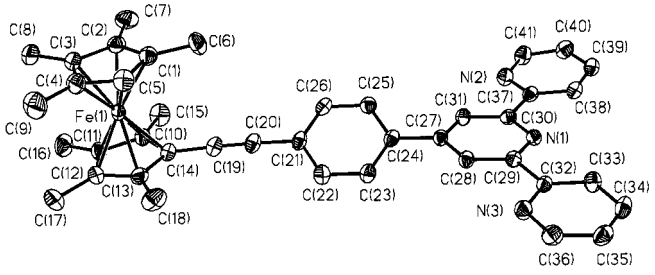
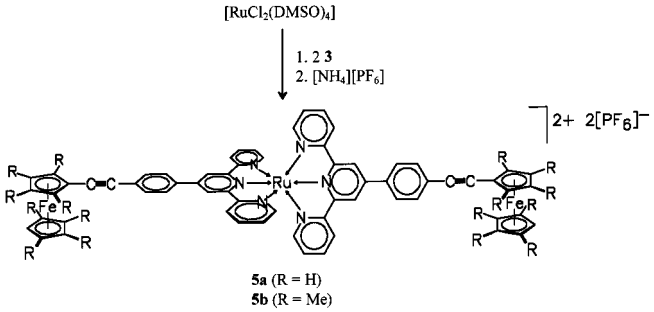


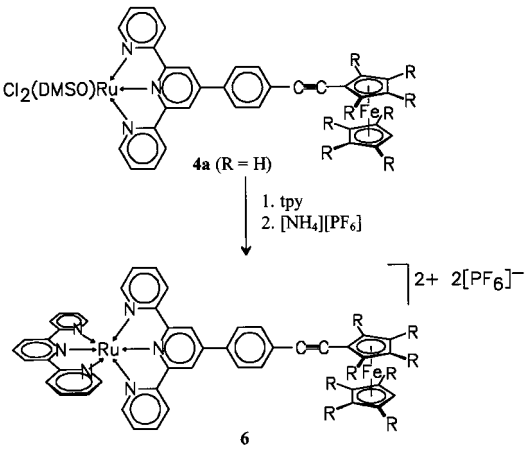
Figure 1. Molecular structure of **3b** in the crystal; selected bond lengths [pm] not discussed in the text: C(24)−C(27) 148.7(4), C(29)−C(32) 149.5(4), C(30)−C(37) 149.4(4).

Reaction of two equivalents of **3a** and **3b** with $[RuCl_2(DMSO)_4]$ in refluxing ethanol afforded the homoleptic Ru^{II} complexes $[(\mathbf{3a})_2Ru][PF_6]_2$ (**5a**) and $[(\mathbf{3b})_2Ru][PF_6]_2$ (**5b**), respectively, after precipitation with aqueous ammonium hexafluorophosphate (Scheme 3).



Scheme 3

It has also proved possible to synthesise a heteroleptic bis(terpyridine)ruthenium(II) complex, namely [(**3a**)Ru(tpy)]$[PF_6]_2$ (**6**), which was obtained by treating **4a** with one



Scheme 4

equivalent of tpy in refluxing ethanol and subsequent precipitation with aqueous ammonium hexafluorophosphate (Scheme 4).[23]

Preliminary electrochemical investigations of the terpyridine ligands **3a** and **3b** and their Ru^{II} complexes **5a** and **5b** by cyclic voltammetry demonstrate that the redox potential of the ferrocenyl moieties present in the terpyridines is not affected by complexation (Table 1). Furthermore, it is evident that the introduction of eight methyl groups in the novel redox-functionalised terpyridines and their Ru^{II} complexes leads to a cathodic shift of the $E^{0\prime}$ values of ca. 0.44 V for the ferrocenyl-centered redox processes. This is exactly the value expected for the influence of eight methyl groups (i.e. 8 × 55 mV, vide supra) and shows that in the present system oligomethylferrocenyl groups behave as reliable donors with predictable and precisely adjustable redox potentials.

Table 1. Formal electrode potentials (in V, vs. SCE) for the ferrocenyl-centered oxidation process of compounds **3** and **5** in dichloromethane solution[a]

Compound	**3a**	**3b**	**5a**[b]	**5b**[b]
$E^{0\prime}{}_{0/+}$	0.50	0.06	0.49	0.06

[a] Conditions: 298 K; $[NBu_4][PF_6]$ supporting electrolyte (0.2 M); scan rate 0.10 V; confidence limit 0.01 V. − [b] $E^{0\prime}$ values [V] for the oxidation/reductions of the central Ru complex moiety: 1.23/ −1.22, −1.52.

In summary, we have prepared novel terpyridines functionalised with ferrocenyl and octamethylferrocenyl groups. First results indicate that both symmetrical and unsymmetrical bis(terpyridine)ruthenium complexes are accessible by established routes, which augurs well for the development of a rich coordination chemistry of these redox-functionalised ligands. Cyclic voltammetry has revealed that the ferrocenyl moieties in the new ligands and their complexes are redox-chemically well behaved. We are currently extending our studies to analogous terpyridines containing only $(C{\equiv}C)_n$ (n = 1, 2) spacer groups.[24] These and related oligomethylferrocenyl-functionalised ligands should be excellently suited for the preparation of libraries of donor/sensitiser assemblies, which for the first time will allow the detailed investigation of the competition between energy transfer and reductive quenching in a geometrically well-defined system by systematic variation of a single molecular parameter, namely the redox potential of the donor. We will report on such studies in due course.

Experimental Section

General: All manipulations were performed in an inert atmosphere (purified argon or dinitrogen) by using standard Schlenk and cannula techniques or a conventional glovebox. − Solvents and reagents were appropriately dried and purified by using standard procedures. − NMR spectra were recorded at 300 K with a Bruker DRX 500 spectrometer operating at 500.13 MHz for ^1H; TMS was used as external reference. − UV/Vis spectra were recorded with a Uvikon 860 spectrophotometer (Kontron Instruments). − Fast atom bombardment (FAB) mass spectra were obtained by the LSIMS ionisation technique (3-nitrobenzyl alcohol matrix) with a VG Autospec instrument. − Materials and apparatus used for the electrochemical investigations have been described elsewhere.[25] − Elemental analyses were performed by the Microanalytical Laboratory of the Universität Bielefeld.

Terpyridine 3a: A solution of 4′-(4-bromophenyl)-2,2′:6′,2′′-terpyridine (**1**) (1.25 g, 3.22 mmol), ethynylferrocene (**2a**) (680 mg, 3.24 mmol), and $[Pd(PPh_3)_4]$ (230 mg, 0.199 mmol) in *n*-propylamine (50 mL) placed in a thick-walled Rotaflo ampoule was stirred for 14 h at 55°C. The solution was allowed to cool to room temp. The product was filtered off, washed with diethyl ether, and dried in vacuo. A second crop was obtained by reducing the volume of the filtrate. Brownish-orange microcrystalline solid, m.p. 231°C; yield 1.40 g (84%). − ^1H NMR ($CDCl_3$): δ = 4.25 (s, 2 H, C_5H_4), 4.26 (s, 5 H, C_5H_5), 4.52 (s, 2 H, C_5H_4), 7.33 (m, 2 H, 5,5′′-H), 7.60 ("d", apparent J = 8.1 Hz, 2 H, C_6H_4), 7.84−7.87 (m, 4 H, C_6H_4 and 4,4′′-H), 8.65 (d, J = 7.9 Hz, 3,3′′-H), 8.71−8.73 (m, 4 H, 6,3′,5′,6′′-H). − $^{13}C\{^1H\}$ NMR ($CDCl_3$): δ = 65.0, 68.9, 70.0, 71.5 (Fc); 85.5, 90.1 (C≡C); 118.6, 121.4, 123.9, 124.8, 127.2, 131.9, 136.9, 137.4, 149.1, 149.5, 156.0, 156.2 (aryl rings). − FAB MS; *m*/*z*: 518 $[M + H]^+$, 517 $[M^+]$. − $C_{33}H_{23}FeN_3$ (517.41): C 76.61, H 4.48, N 8.12; found C 76.43, H 4.81, N 8.57.

Terpyridine 3b: By a procedure analogous to that described for **3a** 1.26 g (76%) of **3b** was obtained from **1** (1.03 g, 2.64 mmol), ethynyloctamethylferrocene (**2b**) (850 mg, 2.64 mmol), and $[Pd(PPh_3)_4]$ (183 mg, 0.158 mmol) in *n*-propylamine (40 mL) as orange platelets, m.p. 221°C. − ^1H NMR ($CDCl_3$): δ = 1.69, 1.74, 1.78, 1.91 (4 s, 4 × 6 H, Me); 3.37 (s, 1 H, C_5Me_4H); 7.34 (m, 2 H, 5,5′′-H); 7.60 ("d", apparent J = 8.1 Hz, 2 H, C_6H_4); 7.86−7.88 (m, 4 H, C_6H_4 and 4,4′′-H); 8.66 (d, J = 7.9 Hz, 3,3′′-H), 8.73 (d, J = 5.2 Hz, 2 H, 6,6′′-H); 8.74 (s, 2 H, 3′,5′-H). − $^{13}C\{^1H\}$ NMR ($CDCl_3$): δ = 8.9, 10.0, 10.6, 10.8 (Me); 71.8, 81.2, 81.3, 81.4, 82.4 (C_5-Fc[#]); 89.0, 90.5 (C≡C); 118.6, 121.4, 123.8, 125.8, 127.2, 131.5, 136.9, 149.1, 149.7, 156.0, 156.2 (aryl rings). − FAB MS; *m*/*z*: 630 $[M + H]^+$, 629 $[M^+]$. − $C_{41}H_{39}FeN_3$ (629.63): C 78.21, H 6.24, N 6.67; found C 77.88, H 6.49, N 6.76.

Complex 4a: A stirred mixture of **3a** (125 mg, 0.242 mmol) and $[RuCl_2(DMSO)_4]$ (117 mg, 0.240 mmol) in ethanol (10 mL) was refluxed for 15 h and subsequently allowed to cool to room temp. The product was filtered off, washed with ethanol, and dried in vacuo. Light-violet platelets; yield 132 mg (71%). − ^1H NMR ($[D_6]$DMSO): δ = 3.61 (s, 6 H, Me_2SO); 4.31 (s, 5 H, C_5H_5); 4.39, 4.67 (2 s, 2 × 2 H, C_5H_4); 7.53 (m, 2 H, 5,5′′-H); 7.73 ("d", apparent J = 7.9 Hz, 2 H, C_6H_4); 7.99 (m, 2 H, 4,4′′-H); 8.28 ("d", apparent J = 7.9 Hz, 2 H, C_6H_4); 8.80 (d, J = 7.5 Hz, 2 H, 3,3′′-H); 8.99 (s, 2 H, 3′,5′-H); 9.36 (d, J = 4.8 Hz, 2 H 6,6′′-H). − $^{13}C\{^1H\}$ NMR ($[D_6]$DMSO): δ = 40.4 (Me_2SO); 64.0, 67.6, 69.2, 69.8, 71.2, 85.0 (Fc and C≡C); 118.5, 123.5, 126.4, 127.8, 131.7, 132.1, 133.3, 136.7, 155.6, 157.3, 158.8 (aryl rings). − FAB MS; *m*/*z*: 767 $[M]^+$, 732 $[M - Cl]^+$, 689 $[M - Me_2SO]^+$. − $C_{35}H_{29}Cl_2FeN_3ORuS$ (767.52): C 54.77, H 3.81, N 5.47; found C 53.98, H 4.30, N 5.38.

Complex 4b: By a procedure analogous to that described for **4a** 135 mg (78%) of **4b** was obtained from **3b** (124 mg, 0.197 mmol) and $[RuCl_2(DMSO)_4]$ (95 mg, 0.196 mmol) in ethanol (10 mL) as a light-violet microcrystalline solid. − ^1H NMR ($CDCl_3$): δ = 1.70, 1.75, 1.82, 1.97 (4 s, 4 × 6 H, Me); 2.71 (s, 6 H, Me_2SO); 3.39 (s, 1 H, C_5Me_4H); 7.35 ("d", apparent J = 8.2 Hz, 2 H, C_6H_4); 7.49 (m, 2 H, 5,5′′-H); 7.67 ("d", apparent J = 8.2 Hz, 2 H, C_6H_4); 7.72 (m, 2 H, 4,4′′-H); 8.05 (d, J = 8.9 Hz, 2 H, 3,3′′-H); 8.06 (s, 2 H, 3′,5′-H); 9.33 (d, J = 5.2 Hz, 2 H, 6,6′′-H). − $^{13}C\{^1H\}$ NMR

Table 2. X-ray structure analysis data of **3b**

Empirical formula	$C_{41}H_{39}FeN_3$	μ [mm^{-1}]	0.498
Formula weight	626.60	$F(000)$	2656
Space group	monoclinic, $C2/c$	Index ranges	$0 \le h \le 60$, $0 \le k \le 10$, $-21 \le l \le 21$
a [Å]	46.87(2)	θ range [°]	1.74−27.51
b [Å]	8.372(5)	Reflections collected	7522
c [Å]	16.600(8)	Independent reflections	7432 [R(int.) = 0.0588]
β [°]	93.35(4)	Data/restraints/parameters	7432/0/414
V [$Å^3$]	6503(6)	Goodness-of-fit on F^2	1.023
Z	8	Final $R1$[a] [$I > 2\sigma(I)$]/$wR2$[b]	0.0560 (5164 reflections)/0.1500
ρ(calcd.) [g/cm^3]	1.286	Larg. diff. peak/hole [$e/Å^3$]	0.4/−0.5

[a] $R1 = \Sigma||F_o| - |F_c||/\Sigma|F_o|$. − [b] $wR2 = \{\Sigma[w(F_o^2 - F_c^2)^2]/\Sigma[w(F_o^2)^2]\}^{0.5}$.

($CDCl_3$): δ = 8.7, 9.7, 10.4, 10.6 (Me-Fc#); 42.9 (Me_2SO); 82.0−85.0 (br.), 88.1, 92.8 (C_5-Fc# and C≡C); 119.1, 123.6, 126.8, 127.1, 131.4, 133.5, 136.6, 153.7, 159.1, 159.3 (aryl rings). − FAB MS; *m/z*: 879 $[M]^+$, 844 $[M - Cl]^+$, 801 $[M - Me_2SO]^+$. − $C_{43}H_{45}Cl_2FeN_3ORuS$ (879.74): C 58.71, H 5.16, N 4.78; found C 58.52, H 5.13, N 4.64.

Complex 5a: A stirred mixture of **3a** (250 mg, 0.483 mmol) and [$RuCl_2(DMSO)_4$] (117 mg, 0.241 mmol) in ethanol (30 mL) was refluxed for 15 h and subsequently allowed to cool to room temp. and filtered. 1.0 mL of a saturated aqueous solution of ammonium hexafluorophosphate was added dropwise to the red filtrate. The precipitate was filtered off, washed with ethanol and water, and dried in vacuo. Dark red microcrystalline solid; yield 130 mg (38%).− ^{1}H NMR ([D_6]DMSO): δ = 4.35 (s, 10 H, C_5H_5); 4.43, 4.67 (2 s, 2 × 4 H, C_5H_4); 7.29 (m, 4 H, 5,5′′-H); 7.56 (d, J = 5.1 Hz, 4 H, 6,6′′-H); 7.87 ("d", apparent J = 7.2 Hz, 4 H, C_6H_4); 8.07 (m, 4 H, 4,4′′-H); 8.51 ("d", apparent J = 7.1 Hz, 4 H, C_6H_4); 9.14 (d, J = 7.2 Hz, 4 H, 3,3′′-H); 9.53 (s, 4 H, 3′,5′-H). − $^{13}C\{^1H\}$ NMR ([D_6]DMSO): δ = 64.0, 69.3, 69.9, 71.3 (Fc); 85.3, 91.6 (C≡C); 120.8, 124.9, 125.1, 127.8, 128.0, 131.9, 135.2, 138.0, 152.2, 155.1, 158.0 (aryl rings). − UV/Vis (acetonitrile): λ (lg ε) = 230 nm (4.78), 272 (4.84, sh), 284 (4.86), 312 (4.97), 326 (4.94, sh), 495 (4.62). − FAB MS; *m/z*: 1281 $[\mathbf{5a} - PF_6]^+$, 1136 $[\mathbf{5a} - 2\ PF_6]^+$. − $C_{66}H_{46}F_{12}Fe_2N_6P_2Ru$ (1425.84): C 55.60, H 3.25, N 5.89; found C 56.00, H 3.56, N 6.21.

Complex 5b: By a procedure analogous to that described for **5a** 41 mg (59%) of **5b** was obtained from **3b** (53 mg, 0.084 mmol) and [$RuCl_2(DMSO)_4$] (20 mg, 0.041 mmol) in ethanol (8 mL) as a brown microcrystalline solid. − ^{1}H NMR ([D_6]DMSO): δ = 1.68−1.92 (br. m, 48 H, Me), 3.44 (s, 2 H, C_5Me_4H), 7.28 (m, 4 H, 5,5′′-H), 7.55 (d, J = 5.3 Hz, 4 H, 6,6′′-H), 7.82 ("d", apparent J = 7.4 Hz, 4 H, C_6H_4), 8.07 (m, 4 H, 4,4′′-H), 8.45 ("d", apparent J = 7.7 Hz, 4 H, C_6H_4), 9.01 (d, J = 8.0 Hz, 4 H, 3,3′′-H), 9.50 (s, 4 H, 3′,5′-H). − $^{13}C\{^1H\}$ NMR ([D_6]DMSO): δ = 8.6, 9.7, 10.4, 10.5 (Me-Fc#); 71.6, 80.4, 80.5, 81.6, 81.8 (C_5-Fc#); 88.6, 92.1 (C≡C); 120.9, 124.8, 126.0, 127.7, 128.1, 131.4, 134.8, 138.0, 152.2, 155.1, 158.0 (aryl rings). − UV/Vis (acetonitrile): λ (lg ε) = 226 nm (5.01), 272 (4.93, sh), 284 (4.94), 309 (5.01), 328 (4.93, sh), 356 (4.77), 494 (4.71). − FAB MS; *m/z*: 1505 $[\mathbf{5b} - PF_6]^+$, 1360 $[\mathbf{5b} - 2\ PF_6]^+$. − $C_{82}H_{78}F_{12}Fe_2N_6P_2Ru \times 2\ H_2O$ (1686.31): C 58.41, H 4.90, N 4.98; found C 58.57, H 5.06, N 5.12.

Complex 6: A stirred mixture of **4a** (96 mg, 0.125 mmol) and 2,2′:6′,2′′-terpyridine (29 mg, 0.124 mmol) in ethanol (25 mL) was refluxed for 15 h and subsequently allowed to cool to room temp. and filtered. 1.0 mL of a saturated aqueous solution of ammonium hexafluorophosphate was added dropwise to the red filtrate. The precipitate was filtered off, washed with ethanol and water, and dried in vacuo. Brown microcrystalline solid; yield 70 mg (49%). − ^{1}H NMR ([D_6]DMSO): δ = 4.34 (s, 5 H, C_5H_5); 4.42, 4.65 (2 s, 2 × 2 H, C_5H_4); 7.24−7.28 (m, 4 H, **3a**-5,5′′-H and tpy-5,5′′-H); 7.43 (d, J = 5.5 Hz, 2 H, **3a**-6,6′′-H); 7.54 (d, J = 5.5 Hz, 2 H, tpy-6,6′′-H); 7.86 ("d", apparent J = 8.1 Hz, 2 H, C_6H_4), 8.02−8.06 (m, 4 H, **3a**-4,4′′-H and tpy-4,4′′-H); 8.50 ("d", apparent J = 8.1 Hz, 2 H, C_6H_4); 8.54 (m, 1 H, tpy-4′-H); 8.83 (d, J = 8.0 Hz, tpy-3,3′′-H); 9.09−9.13 (m, 4 H, **3a**-3,3′′-H and tpy-3′,5′-H); 9.51 (s, 2 H, **3a**-3′,5′-H). − $^{13}C\{^1H\}$ NMR ([D_6]DMSO): δ = 64.0, 69.3, 69.9, 71.3 (Fc); 120.9, 121.0, 123.9, 124.0, 123.7, 124.8, 124.9, 127.7, 131.9, 133.5, 135.0, 135.8, 138.0, 145.8, 152.1, 154.7, 155.1, 157.7, 157.8 (aryl rings). − UV/Vis (acetonitrile): λ (lg ε) = 218 nm (4.78), 272 (4.74), 284 (4.70, sh), 308 (4.93), 326 (4.81, sh), 486 (4.48). − FAB MS; *m/z*: 852 $[\mathbf{6} - 2\ PF_6]^+$. − $C_{48}H_{34}F_{12}FeN_6P_2Ru \times H_2O$ (1159.72): C 49.71, H 3.13, N 7.25; found C 49.47, H 3.18, N 7.44.

Crystal Structure Determination of 3b[26]: An orange crystal with dimensions 1.00 × 0.60 × 0.10 mm was used for data collection at 183(2) K with a Siemens $P2_1$ four-circle diffractometer with graphite-monochromated Mo-K_α radiation (λ = 0.71073 Å). The structure was solved by direct methods. Programs used were Siemens SHELXTL PLUS[27] and SHELXL 97[28]. Full-matrix least-squares refinement on F^2 was carried out anisotropically for the non-hydrogen atoms. Hydrogen atoms were included at calculated positions using a riding model. Further X-ray structure analysis data are given in Table 2.

Acknowledgments

This work was financially supported by the Deutsche Forschungsgemeinschaft, the Volkswagen-Stiftung and the Fonds der Chemischen Industrie. A generous gift of ruthenium trichloride from the Degussa AG is greatfully acknowledged. U. S. thanks Prof. Dr. Johann W. Buchler and Prof. Dr. Max Herberhold for helpful discussions. U. S. and U. V. thank Prof. Dr. Peter Jutzi and Dipl.-Chem. Birgit Kleinebekel for a generous gift of ethynyloctamethylferrocene.

[1] Presented in part at the Chemiedozententagung, Essen, Germany, March **1998**, abstract B29.

[2] Reviews: [2a] V. Balzani, S. Campagna, G. Denti, A. Juris, S. Serroni, M. Venturi, *Acc. Chem. Res.* **1998**, *31*, 26−34. − [2b] J.-P. Collin, P. Gaviña, V. Heitz, J.-P. Sauvage, *Eur. J. Inorg. Chem.* **1998**, 1−14. − [2c] F. R. Keene, *Coord. Chem. Rev.* **1997**, *166*, 121−159. − [2d] F. Barigelletti, L. Flamigni, J.-P. Collin, J.-P. Sauvage, *J. Chem. Soc., Chem. Commun.* **1997**, 333−338. − [2e] A. Harriman, R. Ziessel, *J. Chem. Soc., Chem. Commun.* **1996**, 1707−1716. − [2f] V. Balzani, A. Juris, M. Venturi, S. Campagna, S. Serroni, *Chem. Rev.* **1996**, *96*, 759−833. − [2g] J.-P. Sauvage, J.-P. Collin, J.-C. Chambron, S. Guillerez, C. Coudret, V. Balzani, F. Barigelletti, L. De Cola, L. Flamigni, *Chem. Rev.* **1994**, *94*, 993−1019. − [2h] K. Kalyanasundaram, *Photochemistry of Polypyridine and Porphyrin Complexes*, Academic

Press, London, **1992**. – [2i] V. Balzani, F. Barigelletti, L. De Cola, *Top. Curr. Chem.* **1990**, *158*, 31–71. – [2j] A. Juris, V. Balzani, F. Barigelletti, S. Campagna, P. Belser, A. von Zelewsky, *Coord. Chem. Rev.* **1988**, *84*, 85–277.

[3] Recent reviews concerning natural photosynthesis: [3a] K. Brettel, *Biochim. Biophys. Acta* **1997**, *1318*, 322–373. – [3b] R. C. Jennings, R. Bassi, G. Zucchelli, *Top. Curr. Chem.* **1996**, *177*, 147–181. – [3c] R. van Grondelle, J. P. Dekker, T. Gillbro, V. Sundstrom, *Biochim. Biophys. Acta* **1994**, *1187*, 1–65. – Recent reviews concerning artificial photosynthesis: [3d] Contributions in *Prog. Inorg. Chem.* **1997**, *44*. – [3e] W. Rüttinger, G. C. Dismukes, *Chem. Rev.* **1997**, *97*, 1–24. – [3f] H. Kurreck, M. Huber, *Angew. Chem.* **1995**, *107*, 929–947; *Angew. Chem. Int. Ed. Engl.* **1995**, *34*, 849–866. – [3g] E. Amouyal, *Sol. Energy Mater. Sol. Cells* **1995**, *38*, 249–276. – [3h] D. Gust, T. A. Moore, A. L. Moore, *Acc. Chem. Res.* **1993**, *26*, 198–205. – [3i] M. R. Wasielewski, *Chem. Rev.* **1992**, *92*, 435–461. – [3j] *Photochemical Conversion and Storage of Solar Energy* (Eds.: F. Pelizzetti, M. Schiavello), Kluwer, Dordrecht, **1991**.

[4] [4a] P. Zanello in *Ferrocenes* (Eds.: A. Togni, T. Hayashi), VCH, Weinheim, **1995**, chapter 7. – [4b] W. E. Geiger in *Organometallic Radical Processes* (Ed.: W. C. Trogler), Elsevier, Amsterdam, **1990**, chapter 5.

[5] [5a] I. R. Butler, S. J. McDonald, M. B. Hursthouse, K. M. A. Malik, *Polyhedron* **1995**, *14*, 529–539. – [5b] E. C. Constable, A. J. Edwards, R. Martínez-Máñez, P. R. Raithby, A. M. W. Cargill Thompson, *J. Chem. Soc., Dalton Trans.* **1994**, 645–650. – [5c] B. Farlow, T. A. Nile, J. L. Walsh, A. T. McPhail, *Polyhedron* **1993**, *12*, 2891–2894. – [5d] C. Chambron, C. Coudret, J.-P. Sauvage, *New. J. Chem.* **1992**, *16*, 361–367.

[6] E. J. Lee, M. S. Wrighton, *J. Am. Chem. Soc.* **1991**, *113*, 8562–8564.

[7] A. Maciejewski, A. Jaworska-Augustyniak, Z. Szeluga, J. Woytrzak, J. Karolczak, *Chem. Phys. Lett.* **1988**, *153*, 227–232 and references therein.

[8] [8a] K. L. Cunningham, C. R. Hecker, D. R. McMillin, *Inorg. Chim. Acta* **1996**, *242*, 143–147. – [8b] R. Giasson, E. J. Lee, X. Zhao, M. S. Wrighton, *J. Phys. Chem.* **1993**, *97*, 2596–2601. – [8c] F. R. Lemke, R. M. Granger, D. A. Morgenstern, C. P. Kubiak, *J. Am. Chem. Soc.* **1990**, *112*, 4052–4054.

[9] [9a] P. G. Gassmann, D. W. Macomber, J. W. Hershberger, *Organometallics* **1983**, *2*, 1470–1472. – [9b] A. J. Deeming in *Comprehensive Organometallic Chemistry*, vol. 4 (Eds.: G. Wilkinson, F. G. A. Stone, E. W. Able), Pergamon Press, Oxford, **1982**, chapter 31.3.

[10] F. Scandola, M. T. Indelli, C. Chiorboli, C. A. Bignozzi, *Top. Curr. Chem.* **1990**, *158*, 73–149.

[11] Reviews: [11a] R. A. Marcus, N. Sutin, *Biochim. Biophys. Acta* **1985**, *811*, 265–322. – [11b] N. Sutin, *Acc. Chem. Res.* **1982**, *15*, 275–282.

[12] These spacers are known to influence the photophysical properties of relevant Ru^{II} complexes very favourably. See: [12a] R. Ziessel, *Angew. Chem.* **1998**, *110*, 1804–1807; *Angew. Chem. Int. Ed.* **1998**, *37*, 1717–1720. – [12b] A. Benniston, A. Harriman, V. Grosshenny, R. Ziessel, *New J. Chem.* **1997**, *21*, 405–408. – [12c] V. Grosshenny, A. Harriman, R. Ziessel, *Angew. Chem.* **1995**, *107*, 2921–2925; *Angew. Chem. Int. Ed. Engl.* **1995**, *34*, 2705–2708. – [12d] A. C. Benniston, V. Grosshenny, A. Harriman, R. Ziessel, *Angew. Chem.* **1994**, *106*, 1956–1958; *Angew. Chem. Int. Ed. Engl.* **1994**, *33*, 1884–1885. – [12e] C. R. Hecker, A. K. I. Gushurst, D. R. McMillin, *Inorg. Chem.* **1991**, *30*, 538–541.

[13] K. Sonogashira in *Metal-catalyzed Cross-coupling Reactions* (Eds.: F. Diederich, P. J. Stang), Wiley-VCH, Weinheim, **1998**, chapter 5.

[14] For a two-step synthesis giving 64% yield, see: [14a] U. Vorfeld, Doctoral Thesis, Univ. of Bielefeld, **1998**. – [14b] P. Korall, A. Börje, P.-O. Norrby, B. Akermark, *Acta Chem. Scand.* **1997**, *51*, 760–766. –
For a one-pot method giving 20% yield, see: [14c] W. Spahni, G. Calzaferri, *Helv. Chim. Acta* **1984**, *67*, 450–454.

[15] H. Schottenberger, B. Anderson, S. F. Martin, *Org. Synth.* **1996**, *73*, 262–269.

[16] P. Jutzi, B. Kleinebekel, *J. Organomet. Chem.* **1997**, *545–546*, 573–576.

[17] D. R. Coulson, L. C. Satek, S. O. Grim, *Inorg. Synth.* **1972**, *13*, 121–124.

[18] [18a] V. Grosshenny, F. M. Romero, R. Ziessel, *J. Org. Chem.* **1997**, *62*, 1491–1500. – [18b] V. Grosshenny, R. Ziessel, *J. Organomet. Chem.* **1993**, *453*, C19–C22.

[19] D. P. Freyberg, J. L. Robbins, K. N. Raymond, J. C. Smart, *J. Am. Chem. Soc.* **1979**, *101*, 892–897.

[20] See, for example: [20a] H. Fink, N. J. Long, A. J. Martin, G. Opromolla, A. J. P. White, D. J. Williams, P. Zanello, *Organometallics* **1997**, *16*, 2646–2650. – [20b] J. T. Lin, J. J. Wu, C.-S. Li, Y. S. Wen, K.-J. Lin, *Organometallics* **1996**, *15*, 5028–5034. – [20c] R. P. Hsung, C. E.Chidsey, L. R. Sita, *Organometallics* **1995**, *14*, 4808–4815.

[21] See, for example: E. C. Constable, A. M. W. Cargill Thompson, D. A. Tocher, M. A. M. Daniels, *New J. Chem.* **1992**, *16*, 855–867 and references therein.

[22] I. P. Evans, A. Spencer, G. Wilkinson, *J. Chem. Soc., Dalton Trans.* **1973**, 204–209.

[23] Complexes **5b** and **6** were obtained as hydrates (see Experimental Section). Although hexafluorophosphate salts of bis(terpyridine)ruthenium(II) complexes are usually isolated in unsolvated form, exceptions may occur in the case of ferrocenyl-substituted systems (see ref.[5b]).

[24] U. Siemeling, U. Vorfeld, F. Fabrizi de Biani, F. Laschi, P. Zanello, report presented at the Post-ICCC meeting on *Electrochemistry of Coordination and Organometallic Compounds*, Certosa di Pontignano, Siena, Italy, September **1998**.

[25] A. Togni, M. Hobi, G. Rihs, G. Rist, A. Albinati, P. Zanello, D. Zech, H. Keller, *Organometallics* **1994**, *13*, 1224–1234.

[26] Crystallographic data (excluding structure factors) for the structure reported in this paper have been deposited with the Cambridge Crystallographic Data Centre as supplementary publication no. CCDC-103120. Copies of the data can be obtained free of charge on application to CCDC, 12 Union Road, Cambridge CB2 1EZ, UK (Fax (internat.): + 44-1223/336-033; E-mail: deposit@ccdc.cam.ac.uk).

[27] G. M. Sheldrick, *SHELXTL PLUS*, Siemens Analytical Instruments, Madison, WI, USA, **1990**.

[28] G. M. Sheldrick, *SHELXL 97*, University of Göttingen, Germany, **1997**.

Received September 24, 1998
[I98328]

Cyclic Ketiminoboranes

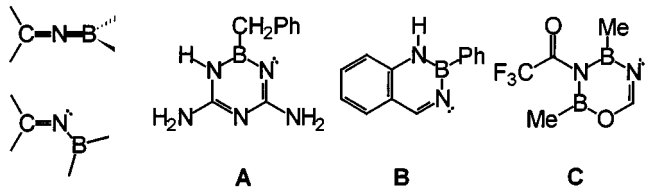
Norbert Weis,*[a] Hans Pritzkow,[a] and Walter Siebert[a]

Dedicated to Prof. M. F. Hawthorne on the occasion of his 70th birthday

Keywords: Boranes / Diazaboroles / Heterocycles / Ketiminoboranes / Crystal Structures

The cyclocondensation reaction of benzil-bis(trimethylsilylimin) (**3**) and Cl_2B–N*i*Pr_2 via silicon-boron exchange results in the solvent-dependent formation of the 1,3,2-diazaborole **1a** or the 1,3,6,8,2,7-tetraazadiborecin **2a**. Using the more rigid 9,10-bis(trimethylsilylimino)phenanthrene instead of **3** only the five-membered heterocycle 4,5-biphenylene-2-diisopropylamino-1,3,2-diazaborole (**1b**) is formed. The cyclic ketiminoboranes are characterized by NMR and X-ray diffraction data. The 1,3,2-diazaborole ring is almost planar, while the conformation of the 1,3,6,8,2,7-tetraazadiborecin has the shape of a figure-eight loop.

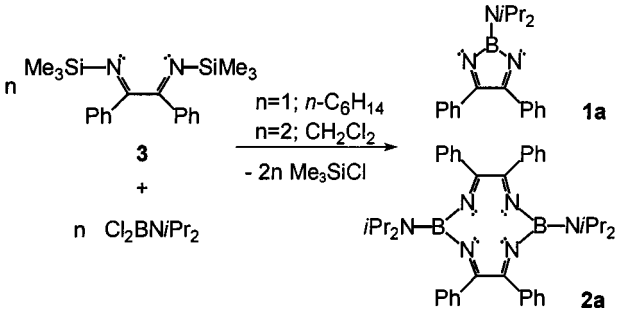
More than 35 years ago Hawthorne[1] synthesized the first examples of alkylideneaminoboranes. Information about their geometry and BNC bond order were obtained from IR data and X-ray structure analyses[2]. The results were complemented by theoretical studies[3], which postulate a cumulene-like arrangement for the >C=N=B< group. Geometry-optimized calculations on 6-31G niveau resulted for $HB(N{=}CH_2)_2$[4] and $B(N{=}CH_2)_3$[5] energetic differences of 74 and 12 KJ/mol, respectively, between the linear and bent CNB structure.



Scheme 1

A cumulene-like arrangement is difficult to verify in small cyclic molecules, in which the C=N−B unit may be compared with an allyl cation. To our knowledge only a few six-membered heterocycles such as **A**−**C**[6,7,8] with an incorporated C=N−B unit have been described. A dithiatetraazadiborocin[9] is an example of an eight-membered ring with B−N=S units.

Here we present the five- and ten-membered boron-nitrogen heterocycles 4,5-diphenyl-2-diisopropylamino-1,3,2-diazaborole (**1a**), 4,5-biphenylene-2-diisopropylamino-1,3,2-diazaborole (**1b**) and 2,7-bis(diisopropylamino)-4,5,9,10-tetraphenyl-1,3,6,8,2,7-tetraazadiborecin (**2a**), obtained via silicon-boron exchange reactions and characterized by X-ray structure analyses.



Scheme 2

The reaction of benzil-bis(trimethylsilylimin) (**3**)[10] with (diisopropylamino)dichloroborane in *n*-hexane leads to the formation of **1a** in 71% yield. Its composition follows from NMR and MS data. The ^{11}B-NMR signal is shifted 7 ppm to lower field (δ = 37) relative to comparable non-cyclic ketiminoboranes $R_2N{-}B(N{=}CPh_2)_2$ (R = Me, Et)[11][12]. This shift is a consequence of the orbital symmetry, which does not allow an interaction of the free electron-pair of the ketiminonitrogen atom and the p_z orbital of the boron atom in the five-membered heterocycle. With four π electrons the diazaborole **1a** should posses strong acceptor properties, however, its chemical reduction to the corresponding 6 π aromatic [**1a**]$^{2-}$ has not been succesful. The cyclovoltammogram of **1a** exhibits an irreversible reduction at $E_{1/2}$= −1.28 eV. Because single crystals of **1a** could not be obtained, crystalline **1b** was synthesized by reacting 9,10-bis(trimethylsilylimino)-phenanthrene with $Cl_2B{-}Ni Pr_2$. A dimerization of **1b** to a ten-membered ring does not take place, prevented by the syn-conformation of the fixed 1,4-diazadiene. In the ^{1}H-NMR spectrum the expected doublet and septet for the isopropyl group and four signals of the aromatic hydrogen atoms are observed in correspondence

[a] Anorganisch-Chemisches Institut der Universität Heidelberg, Im Neuenheimer Feld 270, D-69120 Heidelberg, Germany
Fax: (internat.) +49 (0)6221/54-5609
E-mail: ci5@ix.urz.uni-heidelberg.de

 © WILEY-VCH Verlag GmbH, D-69451 Weinheim, 1999 1434−1948/99/0101−0007 $ 17.50+.50/0

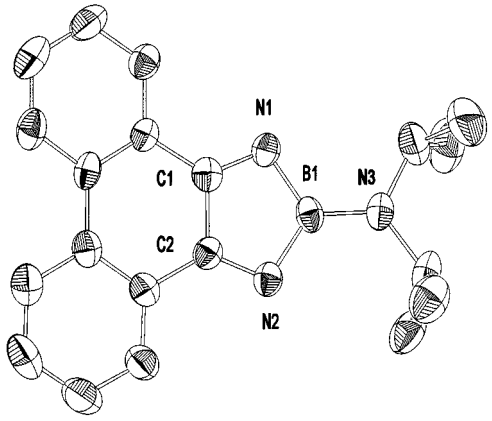


Figure 1. Molecular structure of **1b** in the crystal. Selected bond lengths [Å] and angles [°] for molecule A: B1−N3 1.383(7), B1−N1 1.505(7), B1−N2 1.506(7), C1−N1 1.296(6), C2−N2 1.295(6), C1−C2 1.513(7), N1−B1−N3 121.7(5), C1−N1−B1 101.5(4), N1−B1−N2 111.8(4), C15−N3−B1−N2 2.5.

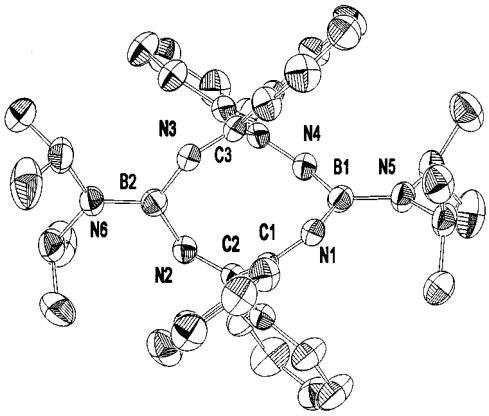


Figure 2. Molecular structure of **2a** in the crystal. Selected bond lengths [Å] and angles [°]: N5−B1 1.407(3), N6−B2 1.400(3), N1−B1 1.458(3), N4−B1 1.470(3), C1−N1 1.277(2), C2−N2 1.273(3), C3−N3 1.277(2), C4−N4 1.276(2), C1−C2 1.525(3), C3−C4 1.513(3), C1−N1−B1 128.6(2), C4−N4−B1 127.3(2), C3−N3−B2 127.9(2), C2−N2−B2 128.6(2), N1−B1−N4 121.5(2), N2−B2−N3 119.7(2), N1−B1−N5 119.9(2), N4−B1−N5 118.7(2), N2−B2−N6 120.6(2), N3−B2−N6 120.6(2), N1−C1−C2−N2 104.9, N3−C3−C4−N4 105.2.

with the symmetry of the molecule. The ^{11}B-NMR signal of **1b** is observed at the same shift (δ = 37) as for **1a**.

In methylenchloride as solvent the silicon−boron exchange reaction leads to the ten-membered 2,7-bis(diisopropylamino)-4,5,9,10-tetraphenyl-1,3,6,8,2,7-tetraazadiborecin (**2a**) in 62% yield. Its ^{11}B-NMR signal at δ = 28 appears at higher field than that of **1a**, **b**. Two signals for the methyl group of the isopropylamino substituents in the ^{1}H- and ^{13}C-NMR spectra point to a hindered rotation around the B−N(*i*Pr)$_2$ bonds.

By slow diffusion of *n*-hexane into the CH_2Cl_2 solution of **1b** single crystals suitable for an X-ray structure analysis were obtained. The two independent molecules in the cell show no significant difference.

The molecule is almost planar. The five-membered diazaborole has two short C=N double bonds [1.295(6)−1.304(6) Å] and two longer B−N bonds [1.495(7)−1.515(7) Å]. The exocyclic B−N bond lengths [1.383(7), 1.386(7) Å] are in the region of B=N double bonds. The C−C bond length [1.508(7), 1.513(7) Å] is quite short. From this point of view **1a**, **b** may be described as triazaborafulvene derivatives.

2a crystallizes in cubes; its X-ray structure analysis shows that the heterocycle deviates considerably from planarity. The arrangement of the ring can be described as a figure-eight loop, being built from two 1,4-diazadiene units in anti conformation with a torsion angle of 105°, which are bridged by two B−N*i*Pr$_2$ units. As indicated by the distances [N5−B1: 1.407(3) Å], the exocyclic B−N bonds have double-bond character. The bond lengths in the C=N−B units [C=N: 1.277(2) Å, =N−B: 1.458(3) Å] correspond to the values reported for a B(N=CH$_2$)$_3$[5]. One has to consider that the R$_2$C=N planes are turned out of the plane around the boron atoms. This geometry allows a partial interaction between the electron pair of the nitrogen atom and the p$_z$-orbital of the boron atom, as indicated by the high-field shift in the ^{11}B-NMR spectrum.

Experimental Section

General: Reactions were carried out under dry argon, using standard Schlenk techniques. Solvents were dried, distilled, and saturated with nitrogen. Glassware was dried with a heat-gun in high vaccum. − ^{1}H-, ^{13}C-, ^{11}B NMR: BRUKER AC 200 spectrometer, NMR references are $(CH_3)_4Si$ and $BF_3 \cdot Et_2O$. − Mass spectra were obtained with a Finnigan MAT 8200 plus spectrometer using EI technique. Cyclic voltammetry data (EG&G PARC 175 potentiostat): Pt disc (1mm) working electrode, CH_2Cl_2 solution, 0.1 M Bu_4NPF_6 as supporting electrolyte, Pt-wire as auxiliar electrode, SCE as reference electrode.

1a: 362 mg (2 mmol) of Cl$_2$BN(*i*Pr)$_2$ dissolved in 10 mL of *n*-hexane was added dropwise within 50 min to a solution of 704 mg (2 mmol) **3** in 20 mL of *n*-hexane at room temp. After stirring for 14 h the yellow precipitate was filtered and washed with a small amount of cold *n*-pentane (0°C), yield: 447 mg (1.4 mmol, 71%) of **1a**. − ^{1}H NMR (δ in $CDCl_3$): 7.52−7.47 (m, 4 H, C_6H_5), 7.40−7.24 (m, 6 H, C_6H_5), 4.37 [sept, *J* = 6.8 *Hz*, 2 H, C*H*(CH$_3$)$_2$], 1.47 [d, *J* = 6.8 *Hz*, 12 H, CH(C*H*$_3$)$_2$]. − ^{13}C NMR (δ in $CDCl_3$): 178.5 (C=N), 136.3 (*i*-C, C_6H_5), 130.2, 129.1, 127.8 (CH, C_6H_5), 47.9 [*C*H(CH$_3$)$_2$], 24.5 [CH(*C*H$_3$)$_2$]. − ^{11}B NMR (δ in $CDCl_3$): 36.6. − MS (70 eV,EI): m/z (%): 317 (16) [M$^+$], 214 (27) [M − C_6H_5CN]$^+$, 171 (64) [M − C_6H_5CN, −*i*Pr]$^+$, 103 (24) [$C_6H_5CN^+$], 44 (100) [*i*PrH$^+$]. − m.p. 185−187°C.

1b: 362 mg (2 mmol) of Cl$_2$BN(*i*Pr)$_2$ dissolved in 10 mL of CH_2Cl_2 was added dropwise within 30 min to a solution of 700 mg (2 mmol) 9,10-bis(trimethylsilylimino)phenanthrene in 20 mL of CH_2Cl_2 at 0°C. After stirring for 14 h at room temp. the solvent and $ClSiMe_3$ were removed in vaccuo. The residue was dissolved in 2 mL of CH_2Cl_2 and *n*-hexane was allowed to diffuse into the solution at room temp. After 15 days crystalline **1b** was filtered, yield: 197 mg (0.6 mmol, 31%). − ^{1}H NMR (δ in $CDCl_3$): 8.37−8.33 (m, 2 H, C_6H_5), 7.95−7.92 (m, 2 H, C_6H_5), 7.53−7.44 (m, 2 H, C_6H_5), 7.36−7.28 (m, 2 H, C_6H_5), 4.38 [sept, *J* = 6.7 *Hz*, 2 H, C*H*(CH$_3$)$_2$], 1.48 [d, *J* = 6.7 *Hz*, 12 H, CH(C*H*$_3$)$_2$]. − ^{13}C NMR (δ in $CDCl_3$): 172.8 (C=N), 135.6 (*i*-C, C_6H_5), 132.7, 128.4, 124.1 (CH, C_6H_5), 48.4 [*C*H(CH$_3$)$_2$], 24.9 [CH(*C*H$_3$)$_2$]. − ^{11}B NMR (δ in $CDCl_3$): 37.1. − m.p. 202−206°C (decomp.).

2a: 905 mg (0.5 mmol) of $Cl_2BN(iPr)_2$ dissolved in 20 mL of CH_2Cl_2 was added within 1 h dropwise to a solution of 1.76 g (5 mmol) **3** in 50 mL of CH_2Cl_2 at room temp. After stirring for 14 h the solvent and $ClSiMe_3$ were removed in vaccuo. The residue was dissolved in 10 mL of CH_2Cl_2 and 5 mL of *n*-hexane was added. After 50 h at 6°C 1.91 g (3.0 mmol, 62%) **2a** was filtered. − ^{1}H NMR (δ in $CDCl_3$): 7.72−7.67 (m, 8 H, C_6H_5), 7.40−7.28 (m, 12 H, C_6H_5), 3.46 [sept, J = 6.7 *Hz*, 4 H, C*H*$(CH_3)_2$], 0.96 [d, J = 6.7 *Hz*, 6 H, CH(C*H*$_3)_2$], 0.91 [d, J = 6.7 *Hz*, 6 H, CH(C*H*$_3)_2$]. − ^{13}C NMR (δ in $CDCl_3$): 164.3 (C=N), 137.4 (*i*-C, C_6H_5), 130.4, 128.8, 127.8 (CH, C_6H_5), 45.3 [*C*H$(CH_3)_2$], 21.8 [CH(*C*H$_3)_2$]. − ^{11}B NMR (δ in $CDCl_3$): 28.2. − MS (70 eV, EI): *m/z* (%): 634 (1) [M^+], 428 (56) [M − $(C_6H_5CN)_2]^+$, 328 (100) [M − $(C_6H_5CN)_2$, − N*i*$Pr_2]^+$. − m.p. 150−152°C.

Crystal Structure Determination: Unique intensity data sets were collected at −70°C with a four-circle diffractometer (Mo-K_α radiation λ = 0.71073 Å, graphite monochromator, ω-scan). Empirical absorption corrections (ψ-scans) were applied. The structures were solved by direct methods [SHELXS86][13] and refined by least squares methods based on F^2 with all mesured reflections [SHELXL97][14]. All non-hydrogen atoms were refined anisotropically. − Crystallographic data (excluding structure factors) for the structures reported in this paper have been deposited with the Cambridge Crystallographic Data Center **1b**: CCDC-102512, **2a**: CCDC-102512. Copies of the data can be obtained free of charge by application to CCDC, 12 Union Road, Cambridge CB2 1EZ, UK; fax: int. code +44 (0)1223/ 336-001; e-mail: deposit@ccdc.cam.ac.uk.

1b: Crystal Data: Orthorhombic, $P2_1cn$, a = 8.524(5), b = 16.080(9), c = 25.950(14) Å, Z = 8; 2084 reflections, $R1$ = 0.059.

2a: *Crystal Data:* Monoclinic, $P2_1/c$, a = 10.948(6), b = 10.433(5), c = 32.990(17) Å, β = 95.12(2), Z = 4; 4599 reflections, $R1$ = 0.047.

Acknowledgments

This work was supported by the Graduiertenkolleg "Selektivität und Reaktivität in der organischen und metallorganischen Synthese und Katalyse" and the Deutsche Forschungsgemeinschaft (SFB 247).

[1] M. F. Hawthorne, *Tetrahedron* **1962**, *17*, 117−122.
[2] J. R. Jennings, I. Pattison, C. Summerford, K. Wade, B. K. Wyatt, *Chem.Comm*. **1968**, 250; C. Summerford, K. Wade, *J. Chem. Soc. (A)* **1969**, 1487−1491.
[3] V. G. Dorokov, M. F. Lappert, *J. Chem. Soc. (A)* **1969**, 433.
[4] T. K. Ha; *J. Mol. Struct*. **1986**, *136*, 165−176.
[5] D. R. Armstrong, G.T. Walker, *J. Mol. Struct*. **1986**, *139*, 47−62.
[6] Süddeutsche Kalkstickstoffwerke; DE 1243202 (**1965**); CA; EN; 68,69053r; (**1968**).
[7] H. L. Yale, F. H. Bergeim, F.A. Sowinska, J. Bernstein, J. Fried, *J. Am. Chem. Soc.* **1962**, *84*, 688−690.
[8] W. Maringgele, A. Meller, *Chem. Ber.* **1979**, *112*, 1595−1605.
[9] H. W. Roesky, S. K. Mehrotra und S. Pohl, *Chem. Ber.* **1980**, *113*, 2063−2068.
[10] G. Tuchenhagen, K. Rühlmann, *Liebigs Ann. Chem*. **1968**, *711*, 174−183
[11] B. M. Mikhailov, G. S. Ter-Sarkisyan, N. A. Nikolaeva, V. G. Kiselev, *Izvest. Akad. Nauk, SSSR Ser. Khim*. **1972**, 2320
[12] B. M. Mikhailov, K. L. Cherkasova, *Zh. Obshch. Khim*. **1973**, *43*, 857
[13] G. M. Sheldrick, *SHELXS86*, Univ. Göttingen, **1986**
[14] G. M. Sheldrick, *SHELXS97*, Univ. Göttingen, **1997**

Received August 6, 1998
[I98270]

Formation and Structures of [1,2–Bis(*N*-*tert*-butylcarbamoyl)-cyclopentadienyl]zirconium Complexes – Coordination Chemistry of a "Fulvenologous" Malonic Amide Anion Ligand System

Katrin Klaß,[a] Lothar Duda,[a] Nina Kleigrewe,[a] Gerhard Erker,*[a] Roland Fröhlich,[a] and Elina Wegelius[a]

Dedicated to Professor Bernt Krebs on the occasion of his 60th birthday

Keywords: Functionalized Cp ligand / κ^2O,O′-Chelate / Carboxamido-substituted cyclopentadienides / Zirconium complexes

Treatment of sodium cyclopentadienide with two molar equivalents of *tert*-butyl isocyanate yields sodium 1,2-bis(*N*-*tert*-butylcarbamoyl)cyclopentadienide (**6**). The $[C_5H_3(1,2\text{-}CONHCMe_3)_2]Na$ reagent **6** adds to $Cp_2Zr(CH_3)Cl$ (**8**) to yield $Cp_2Zr(CH_3)[C_5H_3(CONHCMe_3)_2]$ (**9**). In **9** the $C_5H_3(CONHCMe_3)_2$ ligand is bonded to zirconium through one of its carboxamido-oxygen atoms (κ*O*-coordination). Treatment of **6** with $CpZrCl_3(THF)_2$ yields $CpZrCl_2[C_5H_3\text{-}(CONHCMe_3)_2](THF)$ **11**. In **11** the 1,2-bis(*N*-*tert*-butylcarbamoyl)cyclopentadienide moiety serves as a C_s-symmetric chelate ligand, binding to zirconium through both carbamoyl oxygens (κ^2*O,O′*-coordination). The same seven-membered metallacyclic structural type is found in the reaction products of **6** with $ZrCl_4(THF)_2$ in 1:1 and 2:1 molar ratios. The former yields the distorted octahedral complex $ZrCl_3[C_5H_3(CONHCMe_3)_2](THF)$ (**12**), the latter gives the chiral octahedral system $ZrCl_2[C_5H_3(CONHCMe_3)_2]_2$ (**13**). In solution, complex **13** undergoes a thermally induced enantiomerization process (Λ ⇌ Δ interconversion), for which a Gibbs activation energy of $\Delta G^{\ddagger}_{enant} = 14.0 \pm 0.3$ kcal mol^{-1} was determined by dynamic ^{1}H-NMR spectroscopy. The κ^2*O,O′*-coordination of the $[C_5H_3(1,2\text{-}CONHCMe_3]^-$ ligand in the complexes **11**, **12**, and **13** was secured by X-ray crystal structure analyses.

Introduction

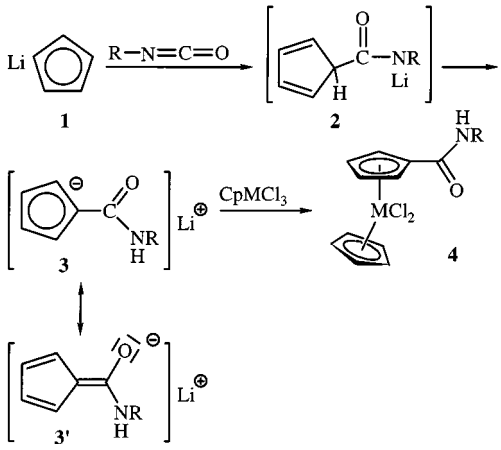
Compounds derived from mono- and especially from bis(η-cyclopentadienyl) group 4 metal complexes have become of enormous importance in organometallic chemistry and catalysis.[1] Numerous variations at the Cp-ring systems have been devised and carried out, many of those in the development of improved homogeneous metallocene Ziegler catalysts and related systems. Most of the variations involved the attachment or anellation of hydrocarbyl moieties.[2] Functional groups have much less frequently been used for derivatising the Cp-rings, although there has been a variety of group 4 metallocene examples bearing Cp-side chains that contain amino-, phosphanyl-, or borane (and borate) substituents.[3] However, the more reactive carbonyl-derived functional groups are still very rarely found attached to Cp-type ring systems in group 4 metallocene and related chemistry. Following the pioneering work by M. D. Rausch et al.[4] we have searched for new ways of introducing reactive carbonyl substituents, especially carboxamide-derived groups at Cp-ligands, and then to attach them to the electropositive, oxophilic early transition metals.

We had previously shown that the cyclopentadienyl anion rapidly adds to a variety of alkyl- and arylisocyanates.[5][6] Subsequent to the carbon-carbon coupling step a rapid proton transfer takes place and the respective *N*-aryl- or *N*-alkylcarboxamido-substituted cyclopentadienides were obtained with moderate to good yields and selectivities. Formally these systems constitute carbamoyl-substituted cyclopentadienyl anion systems, but their fulvenoid mesomeric resonance structures must probably be taken into account for their ample structural and electronic description.[7] Nevertheless, transmetallation of the $[C_5H_4\text{–}CONHR^-]$anion equivalents to e.g. titanium straightforwardly led to the selective formation of (η^5-C_5H_4–CONHR)[Ti] complexes, such as e.g. **4**. Only coordination of the ligand system through the five cyclopentadienyl ring carbon atoms was observed. The carboxamide functional group did not participate in the bonding of this ligand type to the central group 4 metal center. This was unequivocally shown by an X-ray crystal structure analysis of a representative example.[5]

This raises the question about the structural consequences that arise from attaching more than one electron-withdrawing carboxamido-substituent at the anionic Cp ligand. Especially in the case of two "*ortho*"-positioned carbonyl substituents,[8] that can cooperatively remove cyclopentadienide electron density, a situation might arise where the remaining Cp-nucleophilicity is not sufficient to warrant binding of the carbocyclic ring system to an early transition

[a] Organisch-Chemisches Institut der Universität Münster, Corrensstr. 40, D-48149 Münster, Germany
Fax: (internat.) +49 (0)251/ 83 36503
E-mail: erker@uni-muenster.de

 © WILEY-VCH Verlag GmbH, D-69451 Weinheim, 1999 1434–1948/99/0101–0011 $ 17.50+.50/0

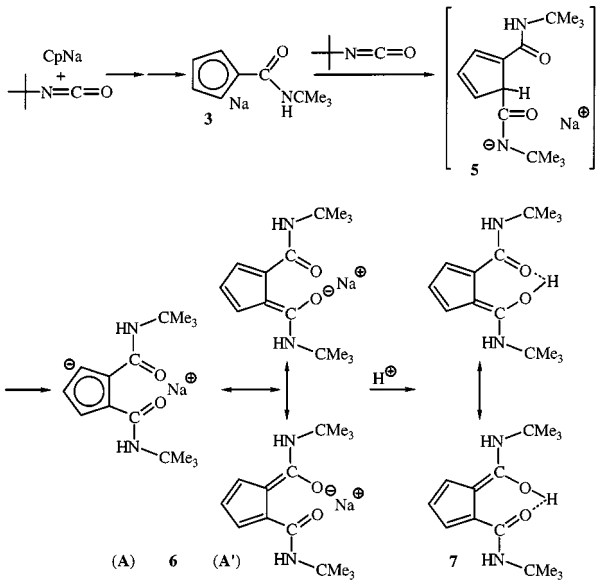


Scheme 1. Formation and metal coordination of the $[C_5H_4CONHR]^-$ ligand

metal center. Then a situation is conceivable where a switching of the preferred coordination mode from η^5-CpX_2 to potentially favored chelate bonding through the substituent nitrogen or, more likely, oxygen atoms might occur. We have prepared such a ligand system and attached it to a series of organometallic zirconium containing frameworks of decreasing overall electronic unsaturation to see which of the possible coordination modes, η^5-cyclopentadienyl or bis(carboxamide) substituent κ^2O,O'-chelate is favored.

Results and Discussion

The 1,2-biscarbamoyl-Cp ligand system employed in this study was selectively prepared by treatment of sodium cyclopentadienide with two molar equivalents of *tert*-butyl isocyanate in tetrahydrofuran. The twofold addition took place readily at temperatures between 0°C and room temperature. In view of our earlier work[5] it must be assumed that the reaction sequence proceeds through the monofunctionalized intermediates **2** and **3** (see Scheme 1, but in this case with the Na^+ counterion). Apparently, the anion **3** still contains a sufficiently nucleophilic substituted cyclopentadienide ring system to allow for a rapid subsequent attack at the strongly electrophilic sp-hybridized carbon atom of the *tert*-butyl isocyanate reagent present in the solution. Again, proton transfer seems to be rapid at the stage of the intermediate resulting from the addition reaction (compound **5** in Scheme 2) to give the doubly carbamoyl substituted anionic ligand system **6**. The twofold *tert*-butyl isocyanate addition reaction sequence is strictly 1,2-selective. This is probably due to a pronounced anion-stabilization in **6**, as it is illustrated by the fulvenoid resonance forms **6A/6A′** (see Scheme 2).[8] Indeed, the NMR spectra of **6** indicate a delocalized C_{2v}-symmetric structure in solution. There is only one set of $^1H/^{13}C$ NMR signals for the pair of symmetry-equivalent $-CONHCMe_3$ substituents (for details see the Experimental Section). Also, complex **6** exhibits an apparent AX_2 ^1H-NMR spin pattern of the central C_5H_3 unit (δ 6.73, d, 2 H; 6.25, t, 1 H; ^3J = 3.6 Hz; corresponding ^{13}C NMR ***C***H signals at δ 115.1 and 108.8). Hydrolysis of **6** gives the neutral system **7**. The spectroscopic features (e.g. ^1H NMR $-O$*H* signal at δ 19.7 in $CDCl_3$) indicate the presence of a fully enolized tautomer with $C{=}O\cdots H{-}O-$ bridging hydrogen. Again, the obtained product **7** exhibits NMR spectra that are consistent with a fully delocalized C_{2v}-symmetric species in solution. It thus seems justified to consider the compound **7** (and the anion **6** derived from it) as fulvene-expanded analogues of the respective malonic amides. One might, therefore, term such systems "fulvenologous" β-dicarbonyl compounds. The compounds **7** and **6** may then be regarded as a fulvenologous malonic amide or malonic amide anion, respectively.



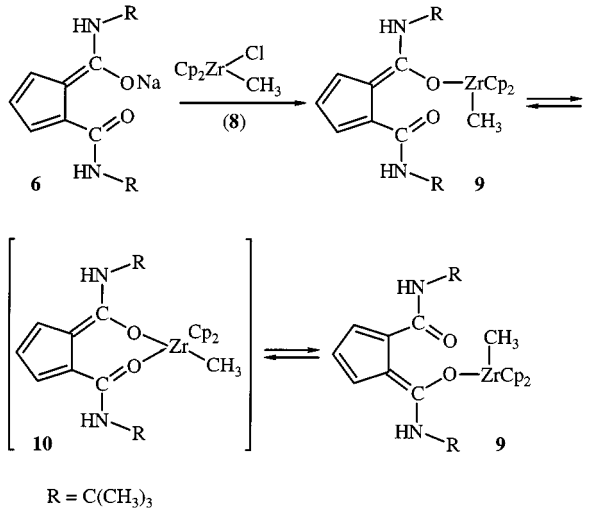
Scheme 2. Preparation of a $[C_5H_3(CONHR)_2]^-$ ligand

The anion **6** was then reacted with a variety of zirconium complexes with a varying degree of coordinative unsaturation and electrophilicity. We first treated the reagent **6** with $Cp_2Zr(CH_3)Cl$ (**8**).[9]

Complex **8** reacts rapidly with **6** in a 1:1 molar ratio in toluene solution. The product **9** of the composition $Cp_2Zr(CH_3)[C_5H_3(CONHCMe_3)_2]$ was isolated in ca. 60% yield. The NMR spectra of **9** are in accord with a C_s-symmetric structure in solution. The complex contains a pair of symmetry-equivalent η^5-cyclopentadienyl ligands ($^1H/^{13}C$ NMR signals observed at δ 6.22/112.1) and a single metal-bound CH_3 group (δ 0.38/29.7 in CD_2Cl_2 solution). The $C_5H_3(CONHCMe_3)_2$ ligand is unsymmetrically coordinated to zirconium. It exhibits two sets of ^1H- and ^{13}C-NMR resonances of the $-CONHCMe_3$ groups, five separated ^{13}C-NMR resonances of the carbon atoms of the C_5H_3 ring and an ABC-type ^1H-NMR pattern for the C_5H_3 hydrogen resonances (at 213 K, 150/600 MHz). This spectroscopic behavior is incompatible with the formation of a complex containing an η^5-$C_5H_3X_2$ ligand in addition to a pair of η^5-C_5H_5 moieties. We must assume that the $C_5H_3(CONHCMe_3)_2$ ligand in **9** is bonded to zirconium through oxygen. We assume that complex **9** contains one uncomplexed $-CONHCMe_3$ substituent, i.e. that the $C_5H_3(CONHCMe_3)_2$ ligand is only attached to the

Cp_2ZrCH_3 unit through one of the carbonyl oxygen atoms (i.e. κ^1*O*-coordination). This structural interpretation seems to be called for in view of the observation of two very different ^{1}H-NMR chemical shifts of the respective NH amido hydrogen atoms (at 213 K and 600 MHz in CD_2Cl_2 observed at δ 12.91 and 6.00, respectively). The IR spectrum is in accord with this interpretation: in this series of $[C_5H_3(CONHCMe_3)_2]$zirconium complexes (see below) only complex **9** exhibits a band (at 1643 cm^{-1}) that can be attributed to a free uncoordinated carboxamido functional group.

Complex **9** shows dynamic NMR spectra. Raising the temperature from 213 K rapidly leads to coalescence of the pairs of diastereotopic groups at the $C_5H_3(CONHCMe_3)_3$ ligand. From the ^{1}H NMR coalescence of the $C(CH_3)_2$ resonances (200 MHz, T_c = 289 K, Δν = 22 Hz) a Gibbs activation energy of $\Delta G^{\neq}_{\text{exchange}}$ = 14.9 ± 0.3 kcal mol^{-1} was determined.[10] We assume that a pentacoordinate $Cp_2Zr(CH_3)[C_5H_3(CONHCMe_3)_2]$ structure (**10**) is likely to be formed as an intermediate which has both carbonyl oxygen atoms coordinated at the available coordination sites at the front of the bent metallocene wedge.[11] Opening and closing these bonds similarly as it has been shown to proceed in $\eta^2 \rightleftarrows \eta^1 \rightleftarrows \eta^2$-acyl group 4 metallocene isomerizations and related processes[12] probably provides an ample mechanistic scheme for describing the automerization process observed to take place in complex **9** (see Scheme 3).

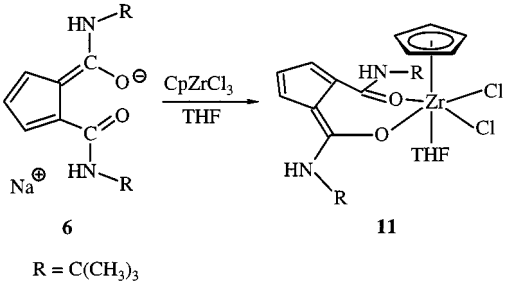


Scheme 3. Formation and dynamic behavior of **9**

We next reacted (η-cyclopentadienyl)zirconium trichloride[13] (as the bis-THF adduct) with the ligand system **6**. The chloride substitution reaction proceeds cleanly in a 1:1 stoichiometry, and we have isolated the product **11** in >70% yield as a solid from the reaction mixture. Single crystals of **11** suited for an X-ray crystal structure analysis were obtained by letting pentane diffuse through the gas phase into a toluene/dichloromethane solution of **11**. Complex **11** can be regarded as chemically C_s-symmetric, but not strictly so crystallographically. The unsubstituted cyclopentadienyl ligand is η^5-coordinated to zirconium with Zr−C(Cp) bond lengths ranging from 2.490(5) to 2.555(4) Å. The $[C_5H_3(CONHCMe_3)_2]$ ligand is bonded to the early transition metal center only through its carboxamido-oxygen atoms (Zr−O1: 2.093(3), Zr−O2: 2.081(2)Å). The ligand is part of a seven-membered metallacycle, that contains large bonding angles at the oxygen atoms[14] [C1−O1−Zr: 145.3(2)°, C2−O2−Zr: 145.0(2)°] and a rather small σ-ligand angle at zirconium (O1−Zr−O2: 82.7(1)°]. The anellated C_5H_3-ring system has no close contact to zirconium. It is in principle oriented in the C_4O_2Zr seven-membered ring plane, but bent slightly in the direction toward the adjacent η^5-cyclopentadienyl ring because of a boat-like distortion of the seven-membered metallacycle from planarity.[14a] Because of this distortion the $(\eta^5$-Cp$)[\kappa^2O,O'$-$C_5H_3(CONHCMe_3)_2]Cl_2Zr$ moiety may be regarded as a square-pyramidal subunit inside the overall octahedral coordination polyhedron around the central zirconium atom (see Figure 1). A weakly bound tetrahydrofuran ligand [Zr−O31 2.365(3)Å] trans to the η^5-Cp group completes the ligand sphere around Zr in **11**. Both the Zr−O1/O2 and the Zr−Cl1/Cl2 bonds are bent toward this THF ligand [angles O1−Zr−O31: 75.0(1)°, O2−Zr−O31: 75.2(1)°, Cl1−Zr−Cp(centroid): 104.1°, Cl2−Zr−Cp(centroid): 102.8°].

Inside the σ-bonded $C_5H_3(CONHCMe_3)_2$ ligand the double bonds are fully delocalized. There seems to be a pronounced difference in C−C bond lengths with shorter values being favored at the distal end away from zirconium, but this effect is equal for both ligand sides [e.g. C6−C5/C6−C7: 1.385(6), 1.387(3) Å; C5−C4/C7−C3: 1.398(5)/1.401(5) Å; C3−C1/C4−C2: 1.445(3)/1.436(5) Å; the length of the central conjugated C3−C4 bond is 1.440(5) Å].

The C−C(=O)−N(H)−C carboxamido groups are trans-configurated. Therefore, the bulky *tert*-butyl substituents at the carbamoyl-nitrogen atoms are oriented toward the chlorine atoms in the central O_2Cl_2Zr containing plane of the complex **11**. The corresponding bond angles at nitrogen are 128.8(4)° (C2−N2−C21) and 127.8(3)° (C1−N1−C11), respectively.



The structure of **11** in solution seems to be similar. Complex **11** shows static NMR spectra. The $C_5H_3(CONHCMe_3)_2$ ligand is C_s-symmetrically bonded to zirconium. In CD_2Cl_2 solution the single ^{1}H-NMR N*H* resonance occurs at δ 6.41 (br s, 2 H), and the C_5H_3 unit is characterized by ^{1}H-NMR resonances at δ 6.70 (d, 2 H) and 6.10 (t, 1 H, ^3J = 3.8 Hz). The observed carboxamide IR features [$\tilde{\nu}$ = 3412 and 3322 cm^{-1} (NH), 1570 and 1529 cm^{-1} (CONH)] also indicate *O*-coordination of the delocalized $C_5H_3(CONHCMe_3)_2$ ligand system to zirconium.

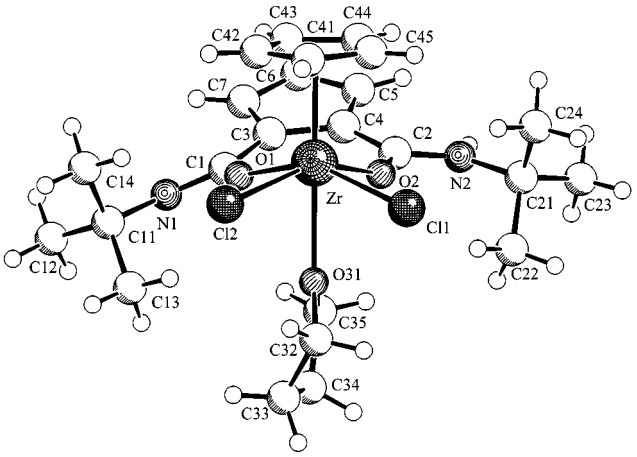
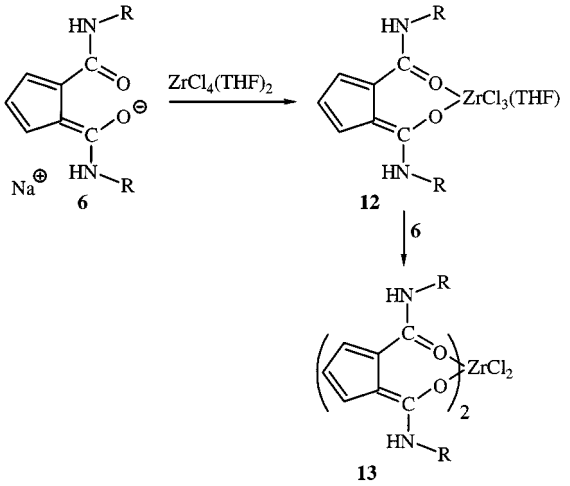


Figure 1. A view of the molecular structure of **11**; selected bond lengths and angles: Zr−O1 2.092(3), Zr−O2 2.081(2), O1−C1 1.280(4), O2−C2 1.291(4), C1−N1 1.322(5), C2−N2 1.325(5), N1−C11 1.489(5), N2−C21 1.492(5), C1−C3 1.445(5), C2−C4 1.436(5), C3−C4 1.440(5), C3−C7 1.401(5), C4−C5 1.398(5), C5−C6 1.385(6), C6−C7 1.387(5), Zr−Cl1 2.4892(11), Zr−Cl2 2.5067(10), Zr−Cp(centroid) 2.230, Zr−O31 2.365(3); O1−Zr−O2 82.73(10), O1−Zr−O31 74.96(10), O2−Zr−O31 75.18(9), O1−Zr−Cl1 152.02(8), O1−Zr−Cl2 86.07(7), O1−Zr−Cp(centroid) 103.8, O2−Zr−Cl1 91.86(6), O2−Zr−Cl2 168.54(6), O2−Zr−Cp(centroid) 102.7, O31−Zr−Cl1 77.08(7), O31−Zr−Cl2 79.18(7), O31−Zr−Cp(centroid) 177.6, Cl1−Zr−Cl2 89.93(4), Cl1−Zr−Cp(centroid) 104.1, Cl2−Zr−Cp(centroid) 102.8, Zr−O1−C1 145.3(2), Zr−O2−C2 145.0(2), O1−C1−N1 118.1(3), O2−C2−N2 117.2(3), O1−C1−C3 123.1(3), O2−C2−C4 122.6(3), N1−C1−C3 118.8(3), N2−C2−C4 120.2(3), C1−N1−C11 127.8(3), C2−N2−C21 128.8(4), C1−C3−C4 132.0(3), C2−C4−C3 129.3(3), C1−C3−C7 121.3(3), C2−C4−C5 124.1(3), C4−C3−C7 106.6(3), C3−C4−C5 106.5(3), C3−C7−C6 109.4(3), C4−C5−C6 109.7(4), C5−C6−C7 107.7(3)

We have then reacted **6** with zirconium tetrachloride. The group 4 metal halide was introduced as its tetrahydrofuran adduct (i.e. $ZrCl_4 \cdot 2$ THF), and the reaction was performed in toluene. The outcome was dependent on the chosen ratio of the reagents and it relied somewhat on the reaction conditions. Employing the reagents **6** and $ZrCl_4 \cdot 2$ THF in a 1:1 molar ratio and heating the mixture for ca. 1 d at 60°C gave a precipitate (after cooling) from which the mono-substitution product **12** was obtained by extraction with dichloromethane (35% isolated). There was a small amount of the di-substitution product **13** recovered from the toluene filtrate of this reaction. However, the complex **13** is easier prepared by treatment of **6** with $ZrCl_4 \cdot 2$ THF directly in a 2:1 molar ratio in toluene at 60°C. In this case, the product **13** was obtained in >60% yield.

Complex **12** contains a coordinated THF molecule. According to the NMR and IR spectra is exhibits very similar bonding features of the $[C_5H_3(CONHCMe_3)_2]$ ligand as found in **11**. The ligand is probably symmetrically coordinated through both oxygen atoms. The characteristic ^{1}H-NMR N*H* resonance of **12** is observed at δ 6.55 (br s, 2 H), and the IR features typical for this ligand arrangement are again observed ($\tilde{\nu}$ = 3419, 3347, 1577, 1535 cm^{-1}).

The κ^2*O,O′*-coordination of the $[C_5H_3(CONHCMe_3)_2]$ ligand of **12** was secured by the X-ray crystal structure analysis (see Figure 2). The (1,2-biscarbamoyl-Cp)Zr unit again forms a slightly boat-shaped seven-membered metallacycle.



Coordination of this ligand takes place solely through the −CONHCMe$_3$ oxygen atoms. The carbon framework is again fully delocalized and exhibits very similar bonding features as already observed for the analogously structured $[C_5H_3(CONHCMe_3)_2]$Zr unit in **11**. The in-plane oriented −CONHR groups again exhibit a trans-configurated C−C(=O)−N(H)−C(Me$_3$) framework and consequently have their bulky *tert*-butyl residues oriented towards the in-plane $ZrCl_2$ section. The coordination geometry around zirconium is almost ideally octahedral. The deviations of the O_3Cl_3Zr octahedral core from the ideal expected geometry are much smaller than e.g. observed for the $O_3Cl_2(Cp)Zr$ core in **11** (see above).

In **12** the Zr−O1 and Zr−O2 bond lengths are 2.063(2) and 2.036(2) Å, respectively.[15a] The Zr−Cl1/−Cl2 bonds are 2.426(1) and 2.448(1) Å in length, whereas the perpendicularly oriented Zr−Cl3 is shorter at 2.397(1) Å.[16] The coordinated THF molecule is located trans to it. The corresponding Zr−O31 bond length is 2.232(2) Å.[15b] This is considerably shorter than observed for the THF coordination in **11** as it is expected for a complex derived from the more electrophilic $LZrCl_3$ building block in comparison to the $LZrCl_2(Cp)$ moiety. The very close to octahedral arrangement of the core atoms of **12** around zirconium is illustrated by the close to linear arrangement of the O31−Zr−Cl3 moiety [178.62(5)°]. Also the O1−Zr−Cl1 [170.03(6)°] and O2−Zr−Cl2 [168.54(6)°] units are only slightly bent, and the deviation of the respective vectors from orthogonality is also very small [e.g.: O1−Zr−Cl2: 89.00(6)°, O2−Zr−Cl1: 91.86(6)°, O2−Zr−Cl3: 94.54(6), O1−Zr−Cl3: 95.58(6)°]. The anellated C_5H_3 ring at the C_4O_2Zr boat-shaped metallacyclic core of **12** is oriented toward the coordinated THF molecule. This is opposite of what is observed in the structurally and otherwise also conformationally related complex **11**.

Crystals of **13** were obtained by letting pentane diffuse through the gasphase into a benzene/dichloromethane solution of the 2:1 reaction product. The X-ray crystal structure analysis of **13** shows that both $[C_5H_3(CONHCMe_3)_2]$ ligands in this complex are exclusively bonded to zirconium through their carbamoyl-oxygen atoms. Again the adjacent

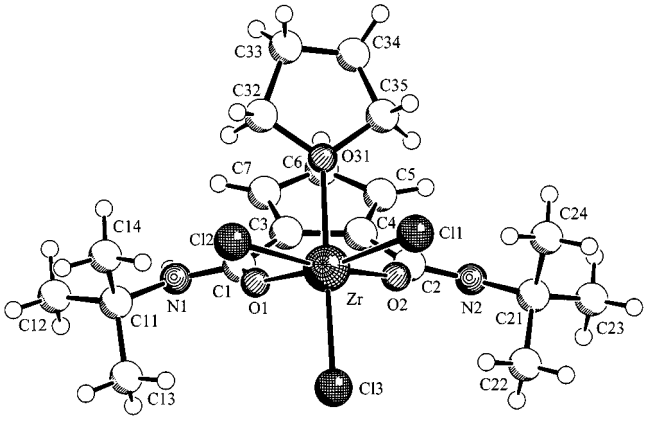


Figure 2. Molecular structure of **12**; selected bond lengths and angles: Zr−O1 2.063(2), Zr−O2 2.036(2), O1−C1 1.297(3), O2−C2 1.303(3), C1−N1 1.329(4), C2−N2 1.317(4), N1−C11 1.481(4), N2−C21 1.485(3), C1−C3 1.429(4), C2−C4 1.424(4), C3−C4 1.446(4), C3−C7 1.410(4), C4−C5 1.403(4), C5−C6 1.393(4), C6−C7 1.383(4), Zr−Cl1 2.4257(9), Zr−Cl2 2.4475(8), Zr−Cl3 2.3969(9), Zr−O31 2.232(2); O1−Zr−O2 83.73(8), O1−Zr−O31 84.70(8), O2−Zr−O31 84.15(8), O1−Zr−Cl1 170.03(6), O1−Zr−Cl2 89.00(6), O1−Zr−Cl3 95.58(6), O2−Zr−Cl1 91.86(6), O2−Zr−Cl2 168.54(6), O2−Zr−Cl3 94.54(6), O31−Zr−Cl1 85.96(6), O31−Zr−Cl2 86.37(6), O31−Zr−Cl3 178.62(5), Cl1−Zr−Cl2 93.89(3), Cl1−Zr−Cl3 93.68(4), Cl2−Zr−Cl3 94.98(3), Zr−O1−C1 144.1(2), Zr−O2−C2 146.7(2), O1−C1−N1 117.4(3), O2−C2−N2 117.5(2), O1−C1−C3 123.2(3), O2−C2−C4 122.4(3), N1−C1−C3 119.4(2), N2−C2−C4 120.0(2), C1−N1−C11 129.3(2), C2−N2−C21 128.2(2), C1−C3−C4 130.2(3), C2−C4−C3 131.0(3), C1−C3−C7 122.9(3), C2−C4−C5 122.5(3), C4−C3−C7 105.8(3) C3−C4−C5 106.5(2), C3−C7−C6 109.0(3), C4−C5−C6 109.3(3), C5−C6−C7 108.4(3).

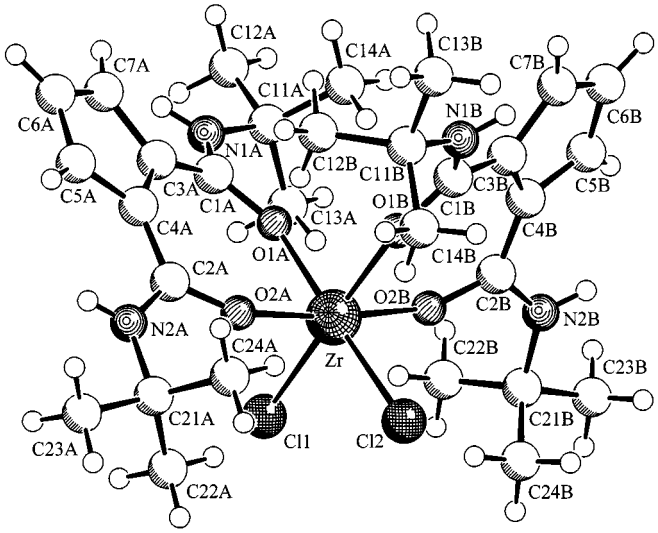


Figure 3. A view of the molecular structure of complex **13**; selected bond lengths [Å] and angles [°]: Zr−O1A 2.037(2), Zr−O1B 2.045(2), Zr−O2A 2.044(2), Zr−O2B 2.050(2), O1A−C1A 1.284(3), O1B−C1B 1.277(3), O2A−C2A 1.291(3), O2B−C2B 1.284(3), C1A−N1A 1.322(4), C1B−N1B 1.325(4), C2A−N2A 1.326(4), C2B−N2B 1.336(3), N1A−C11A 1.480(4), N1B−C11B 1.488(4), N2A−C21A 1.483(4), N2B−C21B 1.478(4), C1A−C3A 1.432(4), C1B−C3B 1.429(4), C2A−C4A 1.426(4), C2B−C4B 1.430(4), C3A−C4A 1.449(4), C3B−C4B 1.454(4), C3A−C7A 1.406(4), C3B−C7B 1.398(4), C4A−C5A 1.411(4), C4B−C5B 1.402(4), C5A−C6A 1.380(5), C5B−C6B 1.382(4), C6A−C7A 1.385(5), C6B−C7B 1.386(5), Zr−Cl1 2.4489(9), Zr−Cl2 2.4435(8); O1A−Zr−O2A 84.09(8), O1A−Zr−O1B 86.79(9), O1A−Zr−O2B 91.18(8), O1A−Zr−Cl1 90.99(7), O1A−Zr−Cl2 173.41(6), O1B−Zr−O2B 83.93(7), O1B−Zr−O2A 91.75(8), O1B−Zr−Cl1 174.66(6), O1B−Zr−Cl2 88.06(7), O2A−Zr−O2B 173.77(8), O2A−Zr−Cl1 92.85(6), O2A−Zr−Cl2 91.97(6), O2B−Zr−Cl1 91.27(6), O2B−Zr−Cl2 92.36(6), Cl1−Zr−Cl2 94.49(4), Zr−O1A−C1A 152.08(2), Zr−O1B−C1B 152.4(2), Zr−O2A−C2A 150.9(2), Zr−O2B−C2B 149.2(2), O1A−C1A−N1A 117.1(3), O1B−C1B−N1B 117.4(3), O2A−C2A−N2A 117.0(3), O2B−C2B−N2B 116.8(3), O1A−C1A−C3A 122.6(3), O1B−C1B−C3B 123.5(2), O2A−C2A−C4A 123.6(3), O2B−C2B−C4B 124.8(2), N1A−C1A−C3A 120.3(3), N1B−C1B−C3B 119.1(23), N2A−C2A−C4A 119.4(3), N2B−C2B−C4B 118.3(3), C1A−N1A−C11A 128.1(32), C1B−N1B−C11B 128.4(3), C2A−N2A−C21A 129.5(3), C2B−N2B−C21B 129.3(3), C1A−C3A−C4A 131.6(3), C1B−C3B−C4B 130.2(3), C2A−C4A−C3A 131.1(3), C2B−C4B−C3B 131.0(3), C1A−C3A−C7A 121.9(3), C1B−C3B−C7B 123.7(3), C2A−C4A−C5A 122.6(3), C2B−C4B−C5B 122.7(3), C4A−C3A−C7A 106.5(3), C4B−C3B−C7B 106.9(3), C3A−C4A−C5A 106.3(3), C3B−C4B−C5B 106.3(2), C3A−C7A−C6A 109.3(3), C3B−C7B−C6B 110.2(3), C4A−C5A−C6A 109.4(3), C4B−C5B−C6B 109.9(3), C5A−C6A−C7A 108.5(3), C5B−C6B−C7B 107.6(3).

cyclopentadienide moiety is not involved in the bonding. Chelate coordination of both ligands leads to the occurrence of two organometallic seven-membered ring systems. Their overall bonding characteristics are very similar as has already been observed for **11** and **12** (see above). The observed bond lengths (for details see the legend of Figure 3) indicate a complete π-delocalization at both the $C_5H_3CO(N)$ frameworks with individual characteristics of bond lengths and angles that have been already discussed for the related complexes **11** and **12**.

The coordination polyhedron in **13** around the central zirconium atom is close to ideally octahedral. The respective O−Zr−O, O−Zr−Cl, and Cl−Zr−Cl angles do not deviate much from the expected values of 90° or 180°, respectively (see Figure 3). In the solid state the *cis*-chelate ligands are arranged close to C_2-symmetric to give a chiral octahedral geometry of **13** (i.e. a racemate of the respective Λ and Δ enantiomers).

Complex **13** shows the expected characteristic IR features in KBr ($\tilde{\nu}$ = 3412, 3361 (NH), 1585, 1529 (delocalized amide)). The latter bands are almost unchanged when the IR spectrum is monitored in $CDCl_3$ solution (1585, 1531 cm^{-1}). This indicates that the solution structure of **13** is very similar to that observed in the solid state.

The NMR spectra indicate that the complex $[C_5H_3(CONHCMe_3)_2]_2ZrCl_2$ **13** also attains a chiral C_2-symmetric octahedral structure in solution. The ^{1}H-NMR spectrum at 213 K in CD_2Cl_2 exhibits the signals of a pair of symmetry-equivalent $[C_5H_3(CONHCMe_3)_2]$ ligands whose "right and left sides" are diastereotopic due to the chiral octahedral molecular geometry.[17] This leads to an observation of an AMX-type ^{1}H-NMR spin pattern of the C_5H_3 protons (signals at δ 6.64, 6.59, and 5.98 with coupling constants ^3J = 4.2 Hz and ^4J = 1.8 Hz). There are two N*H* resonances at δ 6.61 and 6.42 and two separate signals of the *tert*-butyl CH_3 groups (δ 1.52 and 1.18). The ^{13}C-NMR spectrum shows the analogous diastereotopic splitting of the −CONH, C_5H_3−, and $C(CH_3)_3$ resonances (for details see the Experimental Section).

With increasing temperature the NMR signals of the respective pairs of diastereotopic groups broaden and eventu-

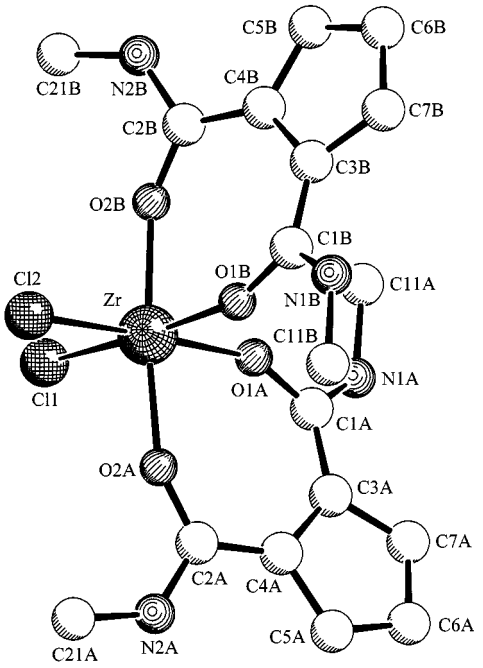
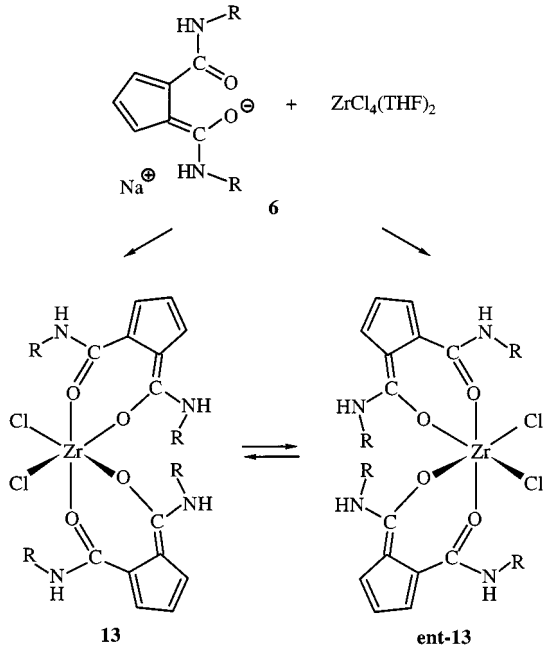


Figure 4. A projection of the octahedral core of complex **13**



Scheme 4. Formation and enantiomerization of **13**

ally undergo coalescence to give a much simplified appearance of the limiting NMR spectra at high temperature. This observation indicates a rather rapid racemization of **13**, i.e. the thermally induced interconversion of the octahedral Λ ⇄ Δ configurated enantiomers of **13** in solution. From the ^{1}H-NMR coalescence of the NH resonances of **13** an enantiomerization barrier of ΔG^{+}_{enant} (298 K) = 14.0 ± 0.3 kcal mol^{-1} was determined at the coalescence temperature. Similar enantiomerization processes have previously been observed for a variety of chiral octahedral bis-chelate ligand zirconium complexes of the general types $(A-B)_2ZrX_2$ or $(A-A)_2ZrX_2$.[18] In view of the coordination properties observed in this study of the complex $[C_5H_3(CONHCMe_3)_2]$-Cp_2ZrCH_3 (**9**, see above), and of the properties of the literature systems,[18] it is likely that the Λ ⇄ Δ-isomerization of **13** is initiated by cleavage of one of the Zr−O linkages to generate a coordinatively unsaturated intermediate of a higher molecular symmetry.

Conclusions

The reaction of cyclopentadienide with two molar equivalents of the alkylisocyanate very selectively leads to the formation of the 1,2-biscarbamoyl substituted cyclopentadienide ligand system. Attachment of this ligand to a variety of zirconium centered frameworks has in most cases investigated in this study led to the formation of κ^2*O,O′*-bonded chelate zirconium complexes. In no case was the attached C_5H_3-cyclopentadienide residue involved directly in the bonding of the $[C_5H_3(CONHCMe_3)_2]$ ligand system to the oxophilic early transition metal. In contrast, we and others had previously observed that the attachment of one −COX substituent at a Cp ring does not inhibit its η^5-C_5H_4−COX attachment to a group 4 metal.[4][5] It may be that we here have crossed a borderline, being encountered when a second electron-withdrawing −COX substituent, suitably located at the Cp framework, removes too much additional electron density from the ligand core, beyond which the coordinative ability of the chelate system exceeds that of the normal η^5-Cp arrangement. It appears that 1,2-COX− (or similarly) substituted cyclopentadienides may be regarded as π-anellated cyclic vinylogues of the ubiquitous β-diketonates and systems derived thereof. Related bis(imino)C_5H_3 ligands have just recently been found to show a complexation behavior[19] analogous to our bis(carbamoyl)C_5H_3 systems **6**, forming seven-membered chelate complex systems. Also, a variety of troponolato chelate complexes have recently been described.[20] Their ligand systems may be regarded as structural isomers of the $C_5H_3(COX)_2^-$ or $C_5H_3[CR(=NR')]_2^-$ frameworks. Opening viable synthetic pathways to novel chelate systems such as those described here and in the related recent studies could be of interest in view of the actual development and the search for new homogeneous non-metallocene group 4 metal derived Ziegler systems.[21] The catalytic properties of complexes derived from $[C_5H_3(CONHR)_2]^-$ ligand systems are currently investigated in our laboratory.

Experimental Section

General Information: All reactions with organometallic reagents or substrates were carried out under argon using Schlenk-type glassware or in a glove-box. Solvents (including the deuterated solvents used for NMR spectroscopy) were dried and distilled under argon prior to use. − The following instruments were used for spectroscopic and physical characterization of the compounds: Bruker AC 200P (^{1}H: 200.13, ^{13}C: 50.3 MHz), Bruker ARX 300, and Varian Unity Plus (^{1}H: 599.2, ^{13}C: 150.8 MHz) NMR spectrometers (spectral assignments were usually secured by GCOSY, GHSQC, and

GHMBC experiments[22]); Nicolet 5 DXC FT-IR spectrometer; melting points: DSC 2010 (Texas Instruments); elemental analyses: Foss Heraeus CHN-Rapid; X-ray crystal structure analyses: Data sets were collected with Enraf Nonius CAD4 and MACH3 diffractometers, connected to sealed tube or rotating anode generators. Programs used: data reduction MolEN, structure solution SHELXS-86, structure refinement SHELXL-93 and SHELXL-97, graphics SCHAKAL-92. Crystallographic data (excluding structure factors) for the structures reported in this paper have been deposited with the Cambridge Crystallographic Data Centre as supplementary publication no. CCDC-102777−102779. Copies of the data can be obtained free of charge on application to The Director, CCDC, 12 Union Road, CambridgeCB2 1EZ, UK [Fax: int. code +44 (1223) 336-033, E-mail: deposit@ccdc.cam.ac.uk].

The reagents $CpZrCl_3(THF)_2$[13,15a] and $Cp_2Zr(CH_3)Cl$[9] were prepared according to literature procedures.

[1,2-Bis(*N*-*tert*-butylcarbamoyl)cyclopentadienyl]sodium (6): A solution of 12.8 g (129.0 mmol, 15.2 mL) of *tert*-butyl isocyanate in 30 mL of tetrahydrofuran was added dropwise at 0°C to a solution of 5.1 g (58.0 mmol) of CpNa in 80 mL of tetrahydrofuran. The dark yellow colored reaction mixture was allowed to warm to room temperature overnight. Solvent was then removed in vacuo, and the solid residue was washed once with pentane to give the product **6** as a pale yellow solid, m. p. 178°C (DSC). − IR (KBr): $\tilde{\nu}$ = 3442 cm^{-1}, 3380 (NH), 1603, 1505 (CONH). − ^1H NMR ([D_6]benzene/[D_8]THF, 10:1.5): δ = 7.90 (br s, 2 H, NH), 6.73 (d, ^3J = 3.6 Hz, 2 H), 6.25 (t, ^3J = 3.6 Hz, 1 H, C_5H_3), 1.44 (s , 18 H, CMe_3). − ^{13}C NMR ([D_6]benzene/[D_8]THF, 10:1.5): δ = 170.7 (CONH), 116.4 (*ipso*-C, Cp), 115.1, 108.8 (CH of Cp), 50.3 and 29.6 (CMe_3). − $C_{15}H_{23}N_2NaO_2$ (286.4): calcd. C 62.92, H 8.10, N 9.78; found: C 62.53, H 8.42, N 9.12.

1,2-Bis(*N*-*tert*-butylcarbamoyl)cyclopentadiene (7): Water (50 mL) and acetic acid (1 mL) was added to an ethereal solution (50 mL) of 304 mg (1.06 mmol) of **6** at ambient temperature. The mixture was vigorously stirred and then the organic phase was separated. The aqueous phase was extracted with ether (2× 20 mL). The combined organic solutions were dried, solvent was removed in vacuo and the residue chromatographed at silicagel to give 95 mg (34%) of **7**, which was only spectroscopically characterized. − ^1H NMR (200 MHz, $CDCl_3$): δ = 19.66 (br s, 1 H, OH), 6.53 (d, ^3J = 3.9 Hz, 2 H, C_5H_3), 6.11 (t, ^3J = 3.9 Hz, 1 H, C_5H_3), 6.09 (br s, 2 H, NH), 1.46 (s, 18 H, CMe_3). − ^{13}C NMR (50 MHz, $CDCl_3$): δ = 168.2 (C=O), 117.0, 113.6 (CH of C_5H_3), 112.3 (*ipso*-C of C_5H_3), 52.4 and 29.1 (*tert*-butyl).

[1,2-Bis(*N*-*tert*-butylcarbamoyl)cyclopentadienyl]bis(η^5-cyclopentadienyl)methylzirconium (9): Chlorobis(η^5-cyclopentadienyl)methylzirconium (**8**) (500 mg, 1.8 mmol) was treated with [1,2-bis(*N*-*tert*-butylcarbamoyl)cyclopentadienyl]sodium (**6**) (530 mg, 1.8 mmol) at −78°C in 40 mL of toluene. The yellow colored mixture was stirred overnight and allowed to warm to room temperature. Filtration and solvent removal gives the yellow solid **9** in 60% yield (530 mg), m.p. 98°C (DSC). − IR (KBr): $\tilde{\nu}$ = 3443 cm^{-1}, 3091 (NH), 1643, 1586 (CONH) (in $CDCl_3$ solution: 1648, 1580). − ^1H NMR (599.9 MHz, CD_2Cl_2, 213 K): δ = 12.91 (br s, 1 H, NH), 6.44 (dd, ^3J = 3.6 Hz, ^4J = 1.8 Hz, 1 H), 6.22 (s, 10 H, Cp), 6.03 (dd, ^3J = 3.6 Hz, ^4J = 1.8 Hz, 1 H), 6.00 (br s, 1 H, NH), 5.93 (t, ^3J = 3.6 Hz, 1 H, C_5H_3), 1.33 (s, 9 H, CMe_3), 1.23 (s, 9 H, CMe_3), 0.38 (s, 3 H, Me). − ^{13}C NMR (150.8 MHz, CD_2Cl_2, 213 K): δ = 168.6 (CONH), 168.4 (CONH), 119.1, 117.5 (CH of C_5H_3), 112.1 (CH of C_5H_5), 110.6, 110.7 (*ipso*-C of C_5H_3), 109.7 (CH of C_5H_3), 51.1, 50.4 (CMe_3), 29.7 (Me), 28.5, 28.3 (CMe_3). − $C_{26}H_{36}N_2O_2Zr$ (499.8): calcd. C 62.48, H 7.26; found: C 62.38, H 7.29.

[1,2-Bis(*N*-*tert*-butylcarbamoyl)cyclopentadienyl](η^5-cyclopentadienyl)dichlorozirconium (11): $CpZrCl_3 \cdot 2$ THF (5.77 g, 14.0 mmol) was treated with [1,2-bis(*N*-*tert*-butylcarbamoyl)cyclopentadienyl]-sodium (**6**) (4.06 g, 14.0 mmol) in 50 mL of tetrahydrofuran at −78°C. The reaction mixture was stirred and allowed to warm to room temperature overnight. It was filtered and the solvent was removed in vacuo to give the product **11** as a pale yellow powder in 74% yield (5.80 g), m.p. 180°C (DSC). − IR (KBr): $\tilde{\nu}$ = 3412 cm^{-1}, 3322 (NH), 1570, 1529 (CONH) (in $CDCl_3$ solution: 1576, 1525). − ^1H NMR (CD_2Cl_2): δ = 6.70 (d, ^3J = 3.8 Hz, 2 H, C_5H_3), 6.41 (br s, 2 H, NH), 6.38 (s, 5 H, C_5H_5), 6.10 (t, ^3J = 3.8 Hz, 1 H, C_5H_3), 4.00, 1.80 (m, each 4 H, THF), 1.46 (s, 18 H, CMe_3). − ^{13}C NMR (CD_2Cl_2): δ = 169.7 (CONH), 121.4, 114.3 (CH of C_5H_3), 117.7 (CH of C_5H_5), 113.9 (*ipso*-C of C_5H_3), 71.1 (CH_2 of THF), 53.3, 29.3 (CMe_3), 25.5 (CH_2 of THF). − $C_{24}H_{36}Cl_2N_2O_3Zr$ (562.7): calcd. C 51.23, H 6.45, N 4.98; found: C 51.06, H 6.61, N 5.09.

X-ray crystal structure analysis of 11: Formula $C_{24}H_{36}Cl_2N_2O_3Zr$, M = 562.7, colorless crystal, 0.40 × 0.25 × 0.10 mm, a = 10.725(1), b = 17.410(2), c = 14.699(2) Å, β = 100.25(1)°, V = 2700.8(5) Å^3, ρ_{calc} = 1.384 g cm^{-3}, F(000) = 1168 e, μ = 6.31 cm^{-1}, empirical absorption correction via φ scan data (0.937 ≤ C ≤ 0.999), Z = 4, monoclinic, space group $P2_1/n$ (No. 14), λ = 0.71073 Å, T = 223 K, ω/2θ scans, 5789 reflections collected (-h, +k, ±l), [(sinθ)/λ] = 0.62 $Å^{-1}$, 5493 independent and 3744 observed reflections [$I \geq 2\ \sigma(I)$], 301 refined parameters, R = 0.047, wR^2 = 0.108, max. residual electron density 0.69 (-0.74) e $Å^{-3}$, hydrogens calculated and refined as riding atoms.

[1,2-Bis(*N*-*tert*-butylcarbamoyl)cyclopentadienyl]trichlorozirconium (12): [1,2-Bis(*N*-*tert*-butylcarbamoyl)cyclopentadienyl]sodium (**6**) (2.80 g, 9.8 mmol) was treated with $ZrCl_4 \cdot 2$ THF (3.70 g, 9.8 mmol) in 100 mL of toluene for 20 h at 60°C. The reaction mixture was filtered and the residue was extracted with dichloromethane to give 1.8 g (35%) of **12** as a pale yellow solid (from the toluene layer the disubstituted compound **13** was obtained as a side product). **12**: m.p. 243°C (DSC). − IR (KBr): $\tilde{\nu}$ = 3419 cm^{-1}, 3347 (NH), 1577, 1535 (CONH) (in $CDCl_3$ solution: 1575, 1530). − ^1H NMR (CD_2Cl_2): δ = 6.69 (d, ^3J = 3.9 Hz, 2 H, C_5H_3), 6.55 (br s, 2 H, NH), 6.07 (t, ^3J = 3.9 Hz, 1 H, C_5H_3), 4.16, 1.76 (m, each 4 H, THF), 1.54 (s, 18 H, CMe_3). − ^{13}C NMR (CD_2Cl_2): δ = 168.7 (CONH), 123.0, 115.3 (CH of C_5H_3), 113.1 (*ipso*-C of C_5H_3), 75.5 (CH_2 of THF), 54.3, 29.4 (CMe_3) 25.7 (CH_2 of THF). − $C_{19}H_{31}N_2O_3Cl_3Zr$ (533.0): calcd. C 42.81, H 5.86, N 5.26; found: C 42.70, H 6.50, N 5.42.

X-ray Crystal Structure Analysis of 12: Formula $C_{19}H_{31}N_2O_3Cl_3Zr$, M = 533.0, yellow crystal, 0.25 × 0.15 × 0.10 mm, a = 9.805(2), b = 15.932(4), c = 16.082(3) Å, β = 105.37(2)°, V = 2422.4(9) Å^3, ρ_{calc} = 1.462 g cm^{-3}, F(000) = 1096 e, μ = 8.06 cm^{-1}, empirical absorption correction via φ scan data (0.955 ≤ C ≤ 0.999), Z = 4, monoclinic, space group $P2_1$/n (No. 14), λ = 0.71073 Å, T = 223 K, ω/2θ scans, 5214 reflections collected (+h, +k, ±l), [(sinθ)/λ] = 0.62 $Å^{-1}$, 4923 independent and 3550 observed reflections [$I \geq 2\ \sigma(I)$], 265 refined parameters, R = 0.032, wR^2 = 0.072, max. residual electron density 0.51 (−0.57) e $Å^{-3}$, hydrogens calculated and refined as riding atoms.

Bis[1,2-bis(*N*-*tert*-butylcarbamoyl)cyclopentadienyl]dichlorozirconium (13): A reaction mixture of [1,2-bis(*N*-*tert*-butylcarbamoyl)-cyclopentadienyl]sodium (**6**, 758 mg, 2.7 mmol) and $ZrCl_4 \cdot 2$ THF (500 mg, 1.3 mmol) in 50 mL of toluene was stirred for 14 h at 60°C and then filtered. Solvent was removed in vacuo to yield 600 mg (65%) of **13** as a yellow solid, m.p. 269°C (DSC). − IR (KBr): $\tilde{\nu}$ = 3412 cm^{-1}, 3361 (NH), 1585, 1529 (CONH) (in $CDCl_3$ solu-

tion: 1585, 1531). – ^{1}H NMR ([D$_6$]benzene): δ = 6.43 (d, ^3J = 3.8 Hz, 4 H, C_5H_3), 6.36 (t, ^3J = 3.8 Hz, 2 H, C_5H_3), 6.00 (br s, 4 H, NH), 1.25 (br, 36 H, CMe_3). – ^{13}C NMR ([D$_6$]benzene): δ = 168.9 (CONH), 122.7 (CH of C_5H_3), 114.4 (*ipso*-C of C_5H_3), 114.0 (CH of C_5H_3), 53.1, 29.1 (CMe_3). – $C_{30}H_{46}N_4O_4Cl_2Zr \cdot 1/3\ C_7H_8$ (715.9): calcd. C 53.69, H 6.90, N 7.83; found: C 53.60, H 7.28, N 7.43.

X-ray Crystal Structure Analysis of 13: Formula $C_{30}H_{46}N_4O_4Cl_2Zr \cdot C_6H_6$, M = 766.9, yellow crystal, 0.25 × 0.20 × 0.10 mm, a = 13.058(2), b = 12.735(3), c = 24.172(3) Å, β = 96.43(1)°, V = 3994.4(12) Å^3, ρ_{calc} = 1.275 g cm^{-3}, $F(000)$ = 1608 e, μ = 4.49 cm^{-1}, empirical absorption correction via φ scan data (0.981 ≤ C ≤ 0.999), Z = 4, monoclinic, space group $P2_1/n$ (No. 14), λ = 0.71073 Å, T = 223 K, ω/2 θ scans, 8282 reflections collected (±h, −k, −l), [(sinθ)/λ] = 0.62 Å^{-1}, 8090 independent and 5503 observed reflections [$I \geq 2\ \sigma(I)$], 448 refined parameters, R = 0.037, wR^2 = 0.085, max. residual electron density 0.40 (−0.32) e Å^{-3}, hydrogens calculated and refined as riding atoms.

Acknowledgments

Financial support from the Fonds der Chemischen Industrie, the Deutsche Forschungsgemeinschaft, and the Ministerium für Schule und Weiterbildung, Wissenschaft und Forschung des Landes Nordrhein-Westfalen is gratefully acknowledged. E. W. thanks the Academy of Finland for financial support.

[1] G. Erker, *Angew. Chem.* **1989**, *101*, 411, *Angew. Chem. Int. Ed. Engl.* **1989**, *28*, 397; H.-H. Brintzinger, D. Fischer, R. Mülhaupt, B. Rieger, R. Waymouth, *Angew. Chem.* **1995**, *107*, 1255; *Angew. Chem. Int. Ed. Engl.* **1995**, *34*, 1143; C. A. Willoughby, S. L. Buchwald, *J. Am. Chem. Soc.* **1994**, *116*, 8952, 11703; A. H. Hoveyda, J. P. Morken, *Angew. Chem.* **1996**, *108*, 1378; *Angew. Chem. Int. Ed. Engl.* **1996**, *35*, 1262; D. Y. Kondakov, E. Negishi, *J. Am. Chem. Soc.* **1996**, *118*, 1577; J. Christoffers, R. G. Bergman, *J. Am. Chem. Soc.* **1996**, *118*, 4715; S. Thiele, G. Erker, *Chem. Ber.* **1997**, *130*, 201; D. Röttger, G. Erker, *Angew. Chem.* **1997**, *109*, 840; *Angew. Chem. Int. Ed. Engl.* **1997**, *36*, 812.

[2] W. Kaminsky, K. Külper, H.-H. Brintzinger, F. R. W. P. Wild, *Angew. Chem.* **1985**, *97*, 507; *Angew. Chem. Int. Ed. Engl.* **1985**, *24*, 507; J. A. Ewen, L. A. Jones, A. Razavi, J. D. Ferrara, *J. Am. Chem. Soc.* **1988**, *110*, 6255; W. Spaleck, M. Antberg, J. Rohrmann, A. Winter, B. Bachmann, P. Kiprof, J. Behm, W. A. Herrmann, *Angew. Chem.* **1992**, *104*, 1373; *Angew. Chem. Int. Ed. Engl.* **1992**, *31*, 1347; G. Erker, M. Aulbach, M. Knickmeier, D. Wingbermühle, C. Krüger, M. Nolte, S. Werner, *J. Am. Chem. Soc.* **1993**, *115*, 4590; M. Aulbach, F. Küber, *Chemie Unserer Zeit* **1994**, *28*, 197; M. Knickmeier, G. Erker, T. Fox, *J. Am. Chem. Soc.* **1996**, *118*, 9623; M. Könemann, G. Erker, R. Fröhlich, S. Kotila, *Organometallics* **1997**, *16*, 2900.

[3] [3a] K. P. Stahl, G. Boche, W. Massa, *J. Organomet. Chem.* **1984**, *277*, 113; H. J. G. Luttikhedde, R. P. Leino, C.-E. Wilén, J. H. Näsman, M. J. Ahlgreen, T. A. Pakkanen, *Organometallics* **1996**, *15*, 3092; H. Plenio, D. Burth, *J. Organomet. Chem.* **1996**, *519*, 269; E. Barsties, S. Schaible, M.-H. Prosenc, U. Rief, W. Röll, O. Weygand, B. Dorer, H.-H. Brintzinger, *J. Organomet. Chem.* **1996**, *520*, 63; H. Plenio, A. Warnecke, *J. Organomet. Chem.* **1997**, *544*, 133. For related systems see e.g.: A. Bertuleit, C. Fritze, G. Erker, R. Fröhlich, *Organometallics* **1997**, *16*, 2891, and references cited therein. See also (reviews): P. Jutzi, J. Dahlhaus, *Phosphorus, Sulfur Silicon Relat. Elem.* **1994**, *87*, 73; P. Jutzi, J. Dahlhaus, *Coord. Chem. Rev.* **1994**, *137*, 179; J. Okuda, *Comm. Inorg. Chem.* **1994**, *16*, 185; P. Jutzi, U. Siemeling, *J. Organomet. Chem.* **1995**, *500*, 175. – [3b] C. P. Casey, F. Nief, *Organometallics* **1985**, *4*, 1218; D. Morcos, W. Tikkanen, *J. Organomet. Chem.* **1989**, *371*, 15; W. A. Schenk, C. Labunde, *Chem. Ber.* **1989**, *122*, 1489; J. Szymoniak, M. M. Kubicki, J. Besançon, C. Moise, *Inorg. Chim. Acta* **1991**, *180*, 153; W. A. Schenk, C. Neuland-Labunde, *Z. Naturforsch.* **1991**, *46b*, 573; W. Tikkanen, J. W. Ziller, *Organometallics* **1991**, *10*, 2266; M. Ogasa, M. D. Rausch, R. D. Rogers, *J. Organomet. Chem.* **1991**, *405*, 279; W. Tikkanen, A. L. Kim, K. B. Lam, K. Ruekert, *Organometallics* **1995**, *14*, 1525. See also: B. E. Bosch, G. Erker, R. Fröhlich, O. Meyer, *Organometallics* **1997**, *16*, 5449; B. Bosch, G. Erker, R. Fröhlich, *Inorg. Chim. Acta* **1998**, *270*, 446. – [3c] M. T. Reetz, H. Brümmer, M. Kessler, J. Kuhnigk, *Chimia* **1995**, *49*, 501; S. A. Larkin, J. T. Golden, P. J. Shapiro, G. P. A. Yap, D. M. J. Foo, A. L. Rheingold, *Organometallics* **1996**, *15*, 2393; D. S. Stelck, P. J. Shapiro, N. Basickes, A. L. Rheingold, *Organometallics* **1997**, *16*, 4546; R. Duchateau, S. J. Lancaster, M. Thornton-Pett, M. Bochmann, *Organometallics* **1997**, *16*, 4995; R. E. v. H. Spence, W. E. Piers, *Organometallics* **1995**, *14*, 4617; Y. Sun, R. E. v. H. Spence, W. E. Piers, M. Parvez, G. P. A. Yap, *J. Am. Chem. Soc.* **1997**, *119*, 5132; W. E. Piers, *Chem. Eur. J.* **1998**, *4*, 13. – [3d] J. Ruwwe, G. Erker, R. Fröhlich, *Angew. Chem.* **1996**, *108*, 108, *Angew. Chem. Int. Ed. Engl.* **1996**, *35*, 80; M. Bochmann, S. J. Lancaster, O. B. Robinson, *J. Chem. Soc., Chem. Commun.* **1995**, 2081; F. A. Shafig, K. A. Abboud, D. E. Richardson, J. M. Boncella, *Organometallics* **1998**, *17*, 982; H. van der Heijden, B. Hessen, A. G. Orpen, *J. Am. Chem. Soc.* **1998**, *120*, 1112; X. Song, M. Bochmann, *J. Organomet. Chem.* **1997**, *545/546*, 597.

[4] [4a] D. W. Macomber, W. P. Hart, M. D. Rausch, *Adv. Organomet. Chem.* **1982**, *21*, 1; N. J. Coville, W. Pickl, *Coord. Chem. Rev.* **1992**, *116*, 1, and references cited in these articles. – [4b] W. P. Hart, D. W. Macomber, M. D. Rausch, *J. Am. Chem. Soc.* **1980**, *102*, 1196; W. P. Hart, D. Shihua, M. D. Rausch, *J. Organomet. Chem.* **1985**, *282*, 111; M. D. Rausch, J. F. Lewison, W. P. Hart, *J. Organomet. Chem.* **1988**, *358*, 161; S. S. Jones, M. D. Rausch, T. E. Bitterwolf, *J. Organomet. Chem.* **1990**, *396*, 279; M. Ogasa, D. T. Mallin, D. W. Macomber, M. D. Rausch, R. D. Rogers, A. N. Rollins, *J. Organomet. Chem.* **1991**, *405*, 41; S. S. Jones, M. D. Rausch, T. E. Bitterwolf, *J. Organomet. Chem.* **1993**, *450*, 27.

[5] M. Oberhoff, L. Duda, J. Karl, R. Mohr, G. Erker, R. Fröhlich, M. Grehl, *Organometallics* **1996**, *15*, 4005.

[6] F. Effenberger, R. Gleiter, L. Heider, R. Niess, *Chem. Ber.* **1968**, *101*, 502.

[7] 6-Aminofulvenes can be regarded electronically as carboxamide analogues: K. Hafner, K. H. Vöpel, G. Ploss, C. König, *Org. Synth.* **1967**, *47*, 52, and references cited therein.

[8] See for a comparison: W. J. Linn, W. H. Sharkey, *J. Am. Chem. Soc.* **1957**, *79*, 4970. D. Peters, *J. Chem Soc.* **1959**, 1757; L. M. Jackman, J. C. Trewella, R. C. Haddon, *J. Am. Chem. Soc.* **1980**, *102*, 2519; K. Hartke, A. Kohl, T. Kämpchen, *Chem. Ber.* **1983**, *116*, 2653; M. I. Bruce, J. K. Walton, M. L. Williams, S. R. Hall, B. W. Skelton, A. H. White, *J. Chem. Soc. Dalton Trans.* **1982**, 2209; **1983**, 2183; M. I. Bruce, P. A. Humphrey, J. M. Patrick, B. W. Skelton, A. H. White, M. L. Williams, *Aust. J. Chem.* **1985**, *38*, 1441; M. I. Bruce, P. A. Humphrey, B. W. Skelton, A. H. White, *J. Organomet. Chem.* **1989**, *361*, 369; L. B. Kool, G. J. Kotora, *Macromolecules*, **1992**, *25*, 2582, and references cited in these articles.

[9] J. R. Surtress, *J. Chem. Soc., Chem. Commun.***1965**, 567.

[10] M. L. H. Green, L.-L. Wong, A. Seela, A. *Organometallics* **1992**, *11*, 2660, and references cited therein.

[11] H.-H. Brintzinger, L. S. Bartell, *J. Am. Chem. Soc.* **1970**, *92*, 1105; W. Lauher, R. Hoffmann, *J. Am. Chem. Soc.* **1976**, *98*, 1729.

[12] G. Erker, *Acc. Chem. Res.* **1984**, *17*, 103, and references cited therein; K. Tatsumi, A. Nakamura, P. Hofmann, P. Stauffert, R. Hoffmann, *J. Am. Chem. Soc.* **1985**, *107*, 4440.

[13] G. Erker, K. Berg, L. Treschanke, K. Engel, *Inorg. Chem.* **1982**, *21*, 1277.

[14] [14a] G. Erker, K. Engel, J. L. Atwood, W. E. Hunter, *Angew. Chem.* **1983**, *95*, 506, *Angew. Chem. Int. Ed. Engl.* **1983**, *22*, 494; G. Erker, U. Dorf, *Angew. Chem.* **1983**, *95*, 800, *Angew. Chem. Int. Ed. Engl.* **1983**, *22*, 777. – [14b] For electronically related examples see e.g.: G. Erker, W. Frömberg, J. L. Atwood, W. E. Hunter, *Angew. Chem.* **1984**, *96*, 72, *Angew. Chem. Int. Ed. Engl.* **1984**, *23*, 68; W. Frömberg, G. Erker, *J. Organomet. Chem.* **1985**, *280*, 343; G. Erker, U. Dorf, C. Krüger, Y.-H. Tsay, *Organometallics* **1987**, *6*, 680; G. Erker, W. Frömberg, C. Krüger, E. Raabe, *J. Am. Chem. Soc.* **1988**, *110*, 2400.

[15] [15a] G. Erker, C. Sarter, S. Werner, C. Krüger, *J. Organomet. Chem.* **1989**, *377*, C55; G. Erker, C. Sarter, M. Albrecht, S. Dehnicke, C. Krüger, E. Raabe, R. Schlund, R. Benn, A. Rufiñska, R. Mynott, *J. Organomet. Chem.* **1990**, *382*, 89. – [15b] R.

F. Jordan, *Adv. Organomet. Chem.* **1991**, *32*, 325, and references cited therein.

[16] For a compilation of reference values see e.g.: A. G. Orpen, L. Brammer, F. H. Allen, O. Kennard, D. G. Watson, R. Taylor, *J. Chem. Soc., Chem. Commun.* **1989**, S1.

[17] For structurally related zirconium complexes see e.g.: E. B. Tjaden, D. C. Swenson, R. F. Jordan, J. L. Petersen, *Organometallics* **1995**, *14*, 371; D. G. Black, D. C. Swenson, R. F. Jordan, R. D. Rogers, *Organometallics* **1995**, *14*, 3539; J. R. Hagadorn, J. Arnold, *Organometallics* **1994**, *13*, 4670; **1998**, *17*, 1355; R. Kempe, S. Brenner, P. Arndt, *Organometallics* **1996**, *15*, 1071; L. Matilainen, M. Klinga, M. Leskelä, *J. Chem. Soc., Dalton Trans.* **1996**, 219; P. Woodman, P. B. Hitchcock, P. Scott, *J. Chem. Soc., Chem. Commun.* **1996**, 2735; D. Walther, R. Fischer, M. Friedrich, P. Gebhardt, H. Görls, *Chem. Ber.* **1996**, *129*, 1389; S. Pritchett, P. Gantzel, P. J. Walsh, *Organometallics* **1997**, *16*, 5130; E. Solari, C. Maltese, F. Franceschi, C. Floriani, A. Chiesi-Villa, C. Rizzoli, *J. Chem. Soc. Dalton Trans.* **1997**, 2903; A. Littke, N. Sleiman, C. Bensimon, D. S. Richeson, G. A. P. Yap, S. J. Brown, *Organometallics* **1998**, *17*, 446.

[18] [18a] X. Bei, D. C. Swenson, R. F. Jordan, *Organometallics* **1997**, *16*, 3282; T. Tsukahara, D. C. Swenson, R. F. Jordan, *Organometallics* **1997**, *16*, 3303; I. Kim, Y. Nishihara, R. F. Jordan, R. D. Rogers, A. L. Rheingold, G. P. A. Yap, *Organometallics* **1997**, *16*, 3314. − [18b] P. B. Hitchcock, M. F. Lappert, D.-S. Liu, *J. Chem. Soc., Chem. Commun.* **1994**, 2637; M. F. Lappert, D.-S. Liu, *J. Organomet. Chem.* **1995**, *500*, 203; B.-J. Deelman, P. B. Hitchcock, M. F. Lappert, H.-K. Lee, W.-P. Leung, *J. Organomet. Chem.* **1996**, *513*, 281; M. Rahim, N. J. Taylor, S. Xin, S. Collins, *Organometallics* **1998**, *17*, 1315.

[19] Closely related 1,2-cyclopentadienyl diimine anions and their zirconium complexes were quite recently prepared and described independent of our work: N. Etkin, C. M. Ong, D. W. Stephan, *Organometallics* **1998**, *17*, 3656. We thank Professor Stephan for kindly informing us about this work prior to publication.

[20] H. V. R. Dias, W. Jin, Z. Wang, *Inorg. Chem.* **1996**, *35*, 6074; P. W. Roesky, *Chem. Ber.* **1997**, *130*, 859; *Eur. J. Inorg. Chem.* **1998**, 593; M. Kira, L. C. Zhang, C. Kabuto, H. Sakurai, *Organometallics* **1998**, *17*, 887; M. J. Scott, S. J. Lippard, *Organometallics* **1998**, *17*, 1769.

[21] J. D. Scollard, D. H. McConville, *J. Am. Chem. Soc.* **1996**, *118*, 10008; J. D. Scollard, D. H. McConville, S. J. Rettig, *Organometallics* **1997**, *16*, 1810; T. H. Warren, R. R. Schrock, W. M. Davis, *Organometallics* **1998**, *17*, 308; R. R. Schrock, F. Schattenmann, M. Aizenberg, W. M. Davis, *J. Chem. Soc., Chem. Commun.* **1998**, 199; V. C. Gibson, B. S. Kimberley, A. J. P. White, D. J. Williams, P. Howard, *J. Chem. Soc., Chem. Commun.* **1998**, 313; L. K. Johnson, C. M. Killian, M. S. Brookart, *J. Am. Chem. Soc.* **1995**, *117*, 6414; C. M. Killian, D. J. Tempel, L. K. Johnson, M. S. Brookhart, *J. Am. Chem. Soc.* **1996**, *118*, 11664; B. L. Small, M. Brookhart, A. M. A. Bennett, *J. Am. Chem. Soc.* **1998**, *120*, 4049; B. L. Small, M. Brookhart, *J. Am. Chem. Soc.* **1998**, *120*, 7143.

[22] S. Braun, H. Kalinowski, S. Berger,. *100 and More Basic NMR Experiments*, VCH, Weinheim **1996**, and references cited therein.

Received August 27, 1998
[I98293]

Geminal Bis(hypersilyl) Compounds – The Reaction of Tris(trimethylsilyl)silyllithium with Dialkyl(chloromethylene)ammonium Chlorides

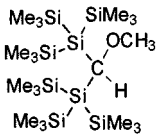
Thoralf Gross,[a] Rhett Kempe,[b] and Hartmut Oehme*[a]

Keywords: Silicon / Silanes, sterically congested / Tris(trimethylsilyl)silanes / (Chloromethylene)ammonium chlorides

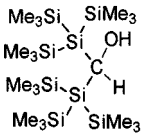
Tris(trimethylsilyl)silyllithium (**1**) reacts with dialkyl(chloromethylene)ammonium chlorides (molar ratio 2:1) to give the (dialkylamino)bis(hypersilyl)methanes $[(Me_3Si)_3Si]_2CHNR_2$ (**5a–c**; **a**: R = Me, **b**: R = Et, **c**: $R_2 = [CH_2]_5$). Due to the extreme bulkiness of the hemispherical $(Me_3Si)_3Si$ substituents, the structures of these geminal bis(hypersilyl) derivatives are characterized by tremendous distortions of their molecular skeletons. This was confirmed by X-ray structural analyses of **5a** and **5c**, which revealed considerable elongations of the central Si–C bonds (**5a**: 2.01 and 1.95 Å; **5c**: 1.99 and 1.97 Å) and an extreme widening of the Si–C–Si angles at the central sp^3-carbon atoms (**5a**: 132.6°; **5c**: 128.7°). By concentrated sulfuric acid, **5a** is converted to give, after hydrolysis, the silanol $(Me_3Si)_2Si(OH)CH_2Si(SiMe_3)_3$ (**13**). The formation of **13** is discussed as proceeding through the transient silene $(Me_3Si)_2Si{=}CHSi(SiMe_3)_3$ (**11**), generated by a formal (dimethylamino)trimethylsilane elimination from **5a** according to an acid-induced sila Peterson mechanism.

Contrary to our original expectations, the fixation of two spherically extended tris(trimethylsilyl)silyl (hypersilyl) groups at one comparatively small carbon atom proved to be surprisingly facile. Actually, geminal bis(hypersilyl) compounds are easily available by the reaction of tris(trimethylsilyl)silyllithium (**1**) with suitable C1 units. However, the experience gained from the synthesis of these compounds led to the conclusion that the approach of a second lithium silanide **1** to the α-carbon atom of a hypersilyl-substituted intermediate under conditions of a bimolecular process, i.e. with inversion of the reaction center, is hardly conceivable due to the extreme shielding of the $(Me_3Si)_3Si$ substituent in the substrate and the bulkiness of the Si nucleophile **1**. Thus, we succeeded in synthesizing methoxy–bis[tris(trimethylsilyl)silyl]methane (**2**) by consecutive replacement of the chlorine atoms of dichloromethyl methyl ether by **1**, the reaction very likely proceeding through a carbenium ion transition state.[1] Similarly, we obtained bis[tris(trimethylsilyl)silyl]methanol (**3**) from **1** and *tert*-butyl formate (2:1), as the result of the addition of **1** to the carbonyl group of the intermediate formyltris(trimethylsilyl)silane.[2] In both cases the final bis(hypersilyl) derivative is formed after attack of the lithium silanide **1** at an electrophilic planar sp^2-carbon center, thus making the steric problems, which are caused by the already fixed substituents, less significant.

A comparable stereochemical situation was expected for the reaction of **1** with dialkyl(chloromethylene)ammonium chlorides leading, as expected, to (dialkylamino)bis[tris(trimethylsilyl)silyl]methanes **5**. In this paper we describe the syntheses, the structures and the reactivity of these extremely congested functionalized geminal bis(hypersilyl) compounds. In addition, with the H_2SO_4-initiated degradation of (dimethylamino)bis[tris(trimethylsilyl)silyl]methane (**5a**) we present the first case of an acid-catalyzed sila Peterson reaction.



2



3

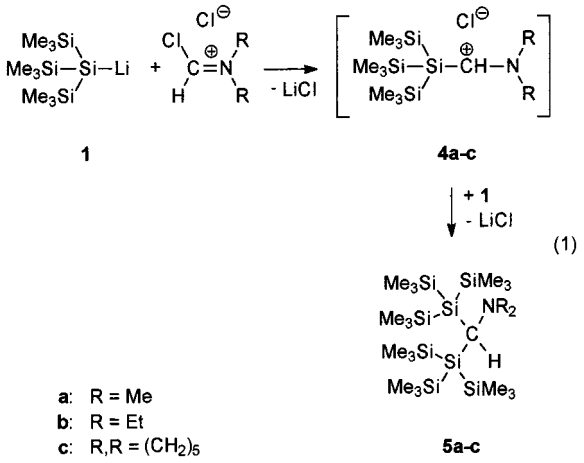
The Synthesis and Structure of (Dialkylamino)bis[tris(trimethylsilyl)silyl]methanes $R_2N–CH[Si(SiMe_3)_2]$ (5a–c)

The reaction of **1** with (chloromethylene)dimethylammonium chloride, (chloromethylene)diethylammonium chloride or (chloromethylene)piperidinium chloride (molar ratio always 2:1) led to the corrersponding (dialkylamino)-bis[tris(trimethylsilyl)silyl]methanes **5a–c** (Equation 1). We suppose the reaction to proceed through the intermediates **4a–c**, which are formed by nucleophilic substitution of one chlorine atom of the (chloromethylene)ammonium chlorides. Addition of a second equivalent of the silicon nucleophile **1** to the planar carbenium–immonium systems **4a–c** under elimination of lithium chloride affords the bis(hypersilyl) derivatives **5a–c**.

Actually, the gap formed by the two $(Me_3Si)_3Si$ hemispheres and the central carbon atom offers very limited space, obviously sufficient only for a small dialkylamino group. With increasing spatial demand of the amino sub-

[a] Fachbereich Chemie der Universität Rostock,
D-18051 Rostock, Germany
Fax: (internat.) + 49(0)381/498-1763
E-mail: hartmut.oehme@chemie.uni-rostock.de
[b] Institut für Organische Katalyseforschung an der Universität Rostock e.V.,
D-18055 Rostock, Germany

 © WILEY-VCH Verlag GmbH, D-69451 Weinheim, 1999 1434–1948/99/0101–0021 $ 17.50+.50/0



stituent the thermal stability of the compounds decreases. Thus, **5a** is moderately stable, but recrystallization from ethanol leads to partial decomposition, producing mainly hexakis(trimethylsilyl)disilane, small quantities of tris(trimethylsilyl)silane and some unidentified material. In the case of **5c** this tendency is increased, and the diethylamino derivative **5b** could not be obtained in a really pure form and was therefore characterized only by its ^{1}H-NMR spectrum where the signals of hexakis(trimethylsilyl)disilane and tris(trimethylsilyl)silane were always also identified. Single crystals of **5a** and **5c** were obtained by recrystallization from heptane at low temperature. The reaction of **1** with (chloromethylene)diisopropylammonium chloride, performed under the same conditions, failed. Besides large quantities of unidentified material only some tetrakis(trimethylsilyl)silane was isolated. Obviously, the considerable spatial demand of the diisopropylamino group prevents the fixation of two hypersilyl substituents at the central sp^3-carbon atom.

The sterically congested tertiary amines **5a–c** are colorless solids, and are stable at low temperature towards air and moisture. The structures of the compounds **5a** and **5c** were elucidated by ^{1}H-, ^{13}C-, and ^{29}Si-NMR and MS studies; for both compounds X-ray structural analyses were also performed. As found already for **2** and **3**, the solution-NMR spectra of **5a**, **c** are very straightforward. In the ^{1}H-NMR spectra, as well as in the ^{13}C-NMR spectra, only one signal was found for the $SiMe_3$ groups. The ^{29}Si-NMR spectra also show only one signal for the $SiMe_3$ silicon atoms, indicating considerable mobility of the trimethylsilyl substituents in the extremely congested molecules of **5a**, **c**. On the other hand, at room temperature separate signals were found for the two *N*-alkyl groups, which coalesce at elevated temperature. These results were interpreted as being due to a completely hindered rotation around the Si_2C-NR_2 bond (**5a**: T_c = 329 K, $\Delta\nu$ = 30.4 Hz, calcd. rotation barrier $\Delta G^{\neq}$ = 69 kJ/mol).

The results of the X-ray structural analyses of **5a** and **5c**, demonstrated in the Figures 1 and 2, confirm the expected steric congestion of the molecules. The $(Me_3Si)_3Si$ groups form two extended hemispherical shells, separated by one sp^3-carbon atom, thus opening a narrow slit, where the di-

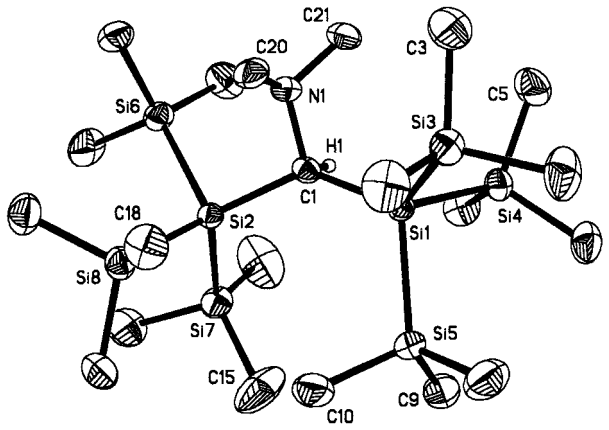


Figure 1. Molecular structure of **5a** in the crystal (ORTEP, 30% probability level, H atoms omitted except for C1H); selected bond lengths [Å] and angles [°]: C1–Si12.009(7), C1–Si2 1.947(6), C1–N1 1.493(7); Si1–C1–Si2 132.6(3), C1–Si1–Si3 120.1(2), C1–Si1–Si4 106.6(2), C1–Si1–Si5 116.9(2), C1–Si2–Si6 98.7(2), C1–Si2–Si7 114.8(2), C1–Si2–Si8 122.3(2), Si1–C1–N1 114.2(4), Si2–C1–N1 102.9(4), C1–N1–C21 115.0(5), C1–N1–C20 113.4(5), C20–N1–C21 112.5(6)

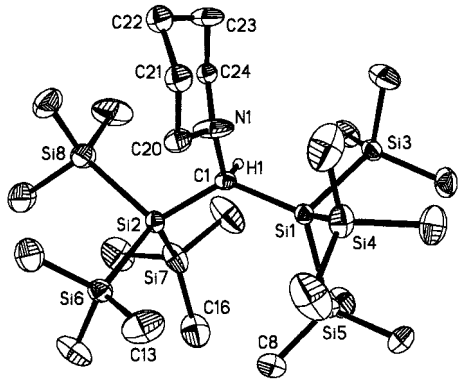
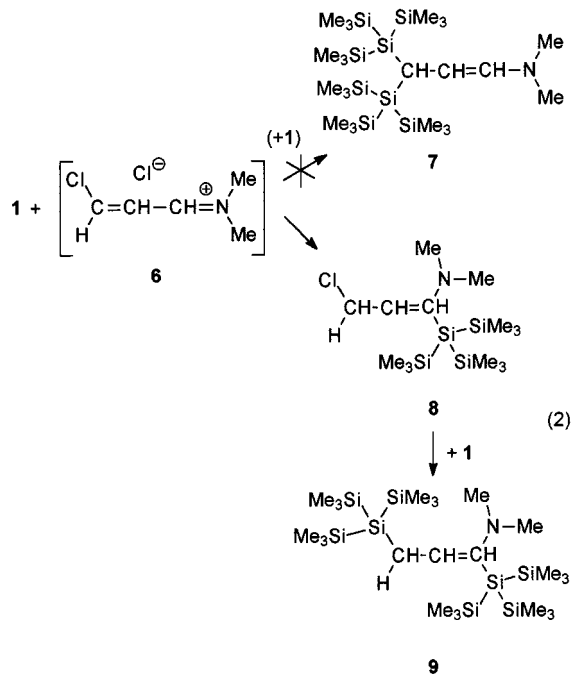


Figure 2. Molecular structure of **5c** in the crystal (ORTEP, 30% probability level, H atoms omitted except for C1 H, disordered atoms omitted for clarity); selected bond lengths [Å] and angles [°]: C1–Si1 1.992(3), C1–Si2 1.967(3), C1–N1 1.472(4); Si1–C1–Si2 128.7(2), C1–Si1–Si3 104.57(11), C1–Si1–Si4 120.96(11), C1–Si1–Si5 118.44(11), C1–Si2–Si6 120.76(12), C1–Si2–Si8 110.94(11), C1–Si2–Si7 109.29(11), N1–C1–Si1 107.1(2), N1–C1–Si2 114.0(2)

alkylamino groups are placed. The amino group is hidden by the two hypersilyl groups and it is quite obvious that the rotation about the Si_2C-NR_2 bond is frozen. The steric strain leads to a considerable elongation of the central C–Si bonds and, additionally, the pyramidal structure of the amino groups causes significant differences in these bond lengths (**5a**: C1–Si1 2.01 Å, C1–Si2 1.95 Å; **5c**: C1–Si1 1.99 Å, C1–Si2 1.97 Å). The central Si–C–Si angles widen to values of 132.6° for **5a** and 128.7° for **5c**. These results are in good agreement with the structural data obtained for **2** and **3**.[1][2] The spatial demand of the OCH_3 group in **2** is slightly smaller than that of the dialkylamino groups in **5a** or **5c** (**2**: Si–C 1.94 Å both, Si–C–Si 132.7°). An OH group is considerably smaller. Thus, the relevant Si–C bonds in **3** are shorter (1.91 and 1.93 Å), and the bond angle at the central sp^3-carbon atom is even wider (135.5°). The dialkylamino groups push the hypersilyl hemi-

spheres aside causing a deformation of the $CSiSi_3$ tetrahedra in **5a** and **5c**. The average C1−Si−Si bond angles in **5a** are 111.8 and 114.5°, and for **5c** 114.7 and 113.7°, but the individual angles are markedly different. At positions where the two hemispheres touch each other, the angles are widened (**5a**: C1−Si1−Si5 116.9°, C1−Si2−Si8 122.3°; **5c**: C1−Si1−Si5 118.4°, C1−Si2−Si6 120.8°). On the other hand, the small hydrogen atoms at the central sp^3-carbon atoms of **5a** and **5c** allow the trimethylsilyl groups in their neighborhood to evade the steric strain leading to comparatively small C−Si−Si angles (**5a**: C1−Si1−Si4 106.6°, C1−Si2−Si6 98.7°; **5c**: C1−Si1−Si3 104.6°, C1−Si2−Si7 109.3°). Due to the steric stress in the molecule, the trimethylsilyl groups approach at exceptionally short distances (**5a**: C9−C15 3.64 Å, C10−C18 3.82 Å; **5c**: C8−C13 3.66, C8−C16 3.51 Å). Also the distances of the *N*-methyl groups in **5a** to the neighboring *Si*-methyl groups (C3−C20 3.62 Å, C3−C21 3.56 Å, C5−C21 3.57 Å) are significantly shorter than the sum of the van der Waals radii of two methyl groups which amounts to about 4.00 Å.[3]

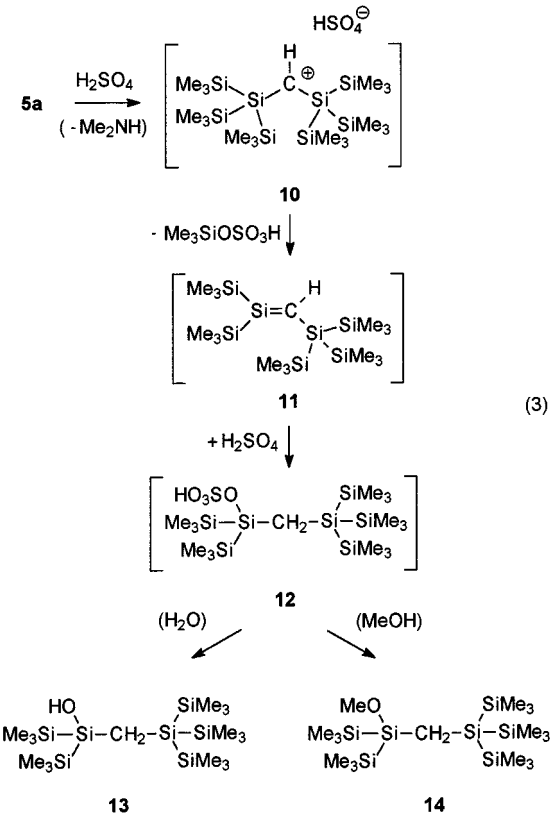
Extensive variation of the reaction outlined in Equation 1 is limited by the spatial demand of the dialkylamino substituent. However, an attractive aim was the synthesis of [2-(dimethylamino)ethenyl]bis[tris(trimethylsilyl)silyl]methane (**7**), which was intended to be achieved by the reaction of two equivalents of **1** with the vinylogous (3-chloro-2-propenylidene)dimethylammonium salt **6**. We hoped that both tris(trimethylsilyl)silyl groups may be drawn to the γ-position of the dimethyliminium salt. Two products, identified as 3-chloro-1-(dimethylamino)-1-[tris(trimethylsilyl)silyl]-1-propene (**8**) (50%) and 1-(dimethylamino)-1,3-bis[tris(trimethylsilyl)silyl]-1-propene (**9**) (13%) were, however, obtained as the result of the reaction of these components (Equation 2).



This result indicates that the first attack of the silicon nucleophile **1** occured at the α-carbon atom of the dimethyliminium chloride **6** affording **8**, and in a second reaction step the γ-chlorine atom of **8** was replaced by a further hypersilyl substituent giving **9**. A geminal bis(hypersilyl) compound could not be obtained this way.

The Conversion of 5a into the Transient 1,1-Bis(trimethylsilyl)-2-tris(trimethylsilyl)silylsilene (11) According to an Acid-Induced Sila Peterson Mechanism

Apart from their thermal instability due to the perfect shielding of the functional group, the geminal (dialkylamino)bis(hypersilyl)methanes **5a−c** were expected to be chemically rather inert. However, we noticed that **5a**, which was chosen for some studies on the reactivity of these compounds, undergoes a clean reaction with concentrated sulfuric acid. Actually, the conversion of **5a** by excess H_2SO_4 needed three days at room temperature to come to completeness, but aqueous workup afforded the silanol **13** in a yield of 60%. Workup of the same reaction mixture with methanol gave the methoxysilane **14** (30%) besides 40% of **13** (Equation 3).



The structures of **13** and **14** were proved by comprehensive spectroscopic analyses (see Experimental Section). For methoxybis(trimethylsilyl)[tris(trimethylsilyl)silylmethyl]silane (**14**) an X-ray crystal structure analysis was also performed (Figure 3), which again revealed considerable steric conges-

tion of the molecule. The central Si−C bonds are elongated (C1−Si1 1.91 Å, C1−Si2 1.87 Å) and the angle at the methylene carbon atom is widened to a value of 123.9°.

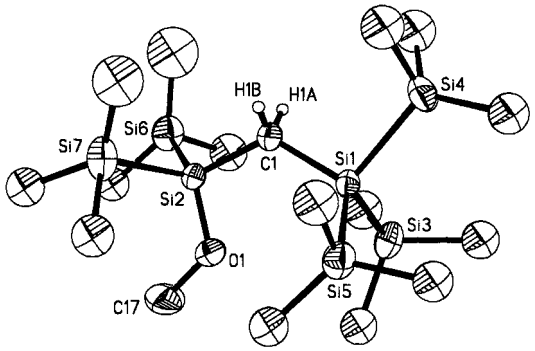


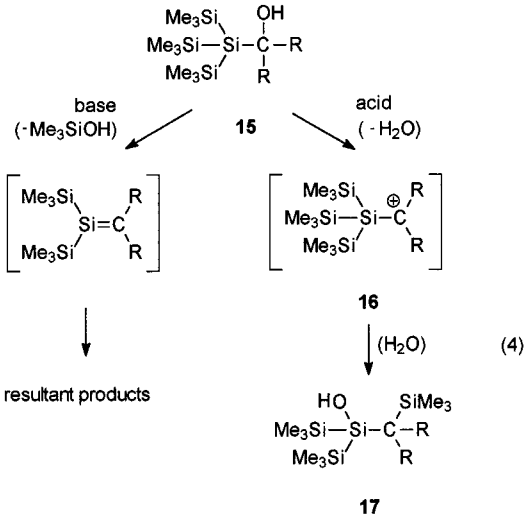
Figure 3. Molecular structure of **14** in the crystal (ORTEP, 30% probability, H atoms omitted except for C1 H_2, disordered atoms omitted for clarity); selected bond lengths [Å] and angles [°]: C1−Si1 1.914(5), C1−Si2 1.865(5), Si2−O1 1.644(4), O1−C17 1.432(7); Si1−C1−Si2 123.9(3), C1−Si1−Si3 113.2(2), C1−Si1−Si4 101.1(2), C1−Si1−Si5 115.1(2), C1−Si2−O1 106.2(2), C1−Si2−Si6 108.8(2), C1−Si2−Si7 111.5(2), Si2−O1−C17 124.1(4).

The formation of **13** and **14** is understood in terms of an acid-induced elimination of dimethylamine from **5a** under generation of the carbenium ion transition state **10**. Nucleophilic attack of the hydrogen sulfate ion at one trimethylsilyl group under cleavage of an Si−Si bond affords the silene **11**, which in the presence of excess sulfuric acid is trapped to give the silyl hydrogen sulfate **12**. Hydrolysis of **12** during the aqueous workup leads to the silanol **13**; methanolysis of **12** affords the methoxysilane **14**.

The conversion of **5a** into the silene **11** has to be interpreted as a direct Si analogue of the acid-catalyzed Peterson reaction. The original Peterson reaction, i.e. the elimination of trimethylsilanol from (2-hydroxyalkyl)trimethylsilanes with simultaneous formation of olefins, can be performed under basic as well as under acidic conditions.[4] The reaction priciple was modified in such a way, that the α-carbon atom in the (2-hydroxyalkyl)trimethylsilanes was replaced by a silicon atom. Thus, (1-hydroxyalkyl)tris(trimethylsilyl)-silanes **15**, easily available by the reaction of tris(trimethylsilyl)silylmagnesium bromide with carbonyl compounds, were subjected to the conditions of the Peterson reaction and proved to be suitable starting materials for the generation of transient silaethenes according to the base-induced sila Peterson mechanism (Equation 4).[5]

On the other hand, treatment of **15** with strong acids gives no trimethylsilanol elimination and silene generation, but the (1-hydroxyalkyl)polysilanes **15** undergo a rapid isomerisation, involving a 1,2-OH/Me_3Si exchange, under formation of the silanols **17**.[6] Similar to the reaction **5a** → **13**, this rearrangement is also supposed to proceed through a polysilanylcarbenium ion transition state **16**, but here the 1,2-trimethylsilyl migration is favored over the Me_3SiX elimination (Equation 4).

The migration of one group from a tetracoordinated silicon atom to a nascent α-carbenium ion under generation of a thermodynamically more stable transient silylium ion



appears to be a general process.[7] We suppose that this fast rearrangement generally prevents a trimethylsilanol elimination from polysilanylcarbenium ion transition states such as **16** and a silene formation along the acid-catalyzed modified Peterson mechanism. In case of the conversion **5a** → **13**, due to the extreme steric congestion of the carbenium ion **10** a shift of a trimethylsilyl group from the silicon atom to the central carbon atom is prevented or at least retarded for steric reasons, favoring in this particular case the nucleophilic attack of the hydrogen sulfate ion and the silene generation.

Experimental Section

General: All reactions involving organometallic reagents were carried out under purified argon. − NMR: Bruker AC 250 or Bruker ARX 300, tetramethylsilane as internal standard. − IR: Nicolet 205 FT-IR. − MS: Intectra AMD 402, chemical ionization with isobutane as the reactant gas. − The dialkyl(chloromethylene)ammonium chlorides were prepared using the procedure of Simchen et al.[8] applying bis(trichloromethyl) carbonate instead of phosgene as the chlorinating agent. $(Me_3Si)_3SiLi \cdot 3$ THF was prepared as reported in the literature.[9] − All yields given refer to amounts obtained after chromatographic separation and purification. − The synthesis and structure of **5a** were described in a preliminary publication.[10]

(Diethylamino)bis[tris(trimethylsilyl)silyl]methane (5b): Under stirring, 0.82 g (1.7 mmol) of **1**, dissolved in 20 mL of ether, was added dropwise into a solution of 0.14 g (0.9 mmol) of (chloromethylene)-diethylammonium chloride in 20 mL of ether at −78 °C. Stirring was continued for another hour at the same temperature and for 2 h at room temperature. After addition of water, the ethereal phase was separated, dried, and concentrated. The residue was purified by chromatography (triethylamine-treated silica gel, heptane) to obtain 0.35 g of impure **5b** containing hexakis(trimethylsilyl)disilane and tris(trimethylsilyl)silane. − ^{1}H NMR ([D_6]benzene): δ = 0.38 (s, $SiCH_3$, 54 H), 1.04 and 1.09 (2 t, ^3J = 7.3 Hz, CCH_3, 2 × 3 H), 2.48 and 2.67 (2 q, ^3J = 7.3 Hz, CH_2, 2 × 2 H), 3.82 (s, CH, 1 H).

Bis[tris(trimethylsilyl)silyl]piperidylmethane (5c): Similarly, 1.3 g (2.8 mmol) of **1** and 0.23 g (1.4 mmol) (chloromethylene)piperidinium chloride gave, after chromatographic separation (silica gel, heptane), 0.35 g (43%) of **5c**, m.p. 112−113 °C. − ^{1}H NMR

([D$_6$]benzene): δ = 0.39 (s, SiCH$_3$, 54 H), 1.41 (m, CH$_2$, 2H), 1.56 (m, CH$_2$, 4 H), 2.53 (t, ^3J = 5.2 Hz, NCH$_2$, 4 H), 3.43 (s, Si$_2$CHN, 1 H). − ^{13}C NMR ([D$_6$]benzene): δ = 4.7 (SiCH$_3$), 22.2, 25.6 and 32.2 (CH$_2$), 46.2 (CH). − ^{29}Si NMR ([D$_6$]benzene): δ = −74.6 (*Si*SiMe$_3$), −12.1 (SiMe$_3$). − MS; *m/z* (%): 590 (1) [M$^+$ − H], 344 (56) [M$^+$ − Si(SiMe$_3$)$_3$], 247 (100) [Si(SiMe$_3$)$_3^+$], 73 (64) [SiMe$_3^+$]. − $C_{24}H_{65}NSi_8$ (592.47): calcd. C 48.65, H 11.06, N 2.36; found C 46.54 (incomplete combustion), H 10.88, N 2.40.

Reaction of the Vinylogous (3-Chloro-2-propenylidene)dimethylammonium Salt 6 with 1. − Synthesis of (*E*)-3-Chloro-1-(dimethylamino)-1-[tris(trimethylsilyl)silyl]-1-propene (8) and (*E*)-1-(Dimethylamino)-1,3-bis[tris(trimethylsilyl)silyl]-1-propene (9): To a solution of 0.08 g (0.5 mmol) of **6** in 20 mL of ether, was added dropwise at −78°C, 0.49 g (1.0 mmol) of **1**, dissolved in 20 mL of ether. After warming up to room temperature, stirring was continued for 3 h. Water was added, the ethereal layer separated, dried, and concentrated. Chromatographic separation (silica gel, heptane/ethyl acetate, 20:1) gave 0.09 g (49%) of **8** (m.p. 124−126°C) and 0.04 g (13%) of **9** (m.p. 74−76°C).

8: ^{1}H NMR ([D$_6$]benzene): δ = 0.25 (s, SiCH$_3$, 27 H), 2.10 (s, NCH$_3$, 6 H), 3.14 (d, ^3J = 11.58 Hz, SiCHN, 1 H), 5.71 (d, ^3J = 13.13 Hz, CHCl, 1 H), 6.09 (dd, ^3J = 11.58 Hz, ^3J = 13.13, ClCCH, 1 H). − ^{13}C NMR ([D$_6$]benzene): δ = 1.9 (SiCH$_3$), 43.7 (NCH$_3$), 58.0 (CHN), 116.9 (ClC=*C*H), 131.8 (Cl*C*=CH). − ^{29}Si NMR ([D$_6$]benzene): δ = −73.8 (*Si*SiMe$_3$), −12.8 (SiMe$_3$). − MS; *m/z* (%): 366 (10) [M$^+$ − H], 350 (9) [M$^+$ − CH$_3$], 247 (8) [Si(SiMe$_3$)$_3^+$], 118 (100) [M$^+$ − Si(SiMe$_3$)$_3$], 73 (33) [SiMe$_3^+$]. − $C_{14}H_{36}ClNSi_4$ (366.24): calcd. C 45.91, H 9.91, Cl 9.68, N 3.82; found C 46.23, H 9.81, Cl 8.97, N 3.88.

9: ^{1}H NMR ([D$_6$]benzene): δ = 0.32 and 0.33 (2s, SiCH$_3$, 2 × 27 H), 2.30 (s, NCH$_3$, 6 H), 3.25 (d, ^3J = 10.38 Hz, SiCHN, 1 H), 5.67 (d, ^3J = 17.70 Hz, SiCH, 1 H), 6.27 (dd, ^3J = 10.38 Hz, ^3J = 17.90 Hz, NCCH, 1 H). − ^{13}C NMR ([D$_6$]benzene): δ = 1.4 and 2.2 (SiCH$_3$), 43.6 (NCH$_3$), 65.4 (CHN), 125.3 (SiC=*C*H), 145.4 (Si*C*=CH). − ^{29}Si NMR ([D$_6$]benzene): δ = −86.3 and −77.0 (*Si*SiMe$_3$), −13.1 and −12.8 (SiMe$_3$). − MS; *m/z* (%): 576 (2) [M$^+$ − H], 562 (8) [M$^+$ − CH$_3$], 533 (4) [M$^+$ − NMe$_2$], 330 (100) [M$^+$ − Si(SiMe$_3$)$_3$], 247 (9) [Si(SiMe$_3$)$_3^+$], 73 (14) [SiMe$_3^+$]. − $C_{23}H_{63}NSi_8$ (578.44): calcd. C 47.76, H 10.98, N 2.42; found C 47.91, H 10.86, N 2.66.

Bis(trimethylsilyl)[tris(trimethylsilyl)silylmethyl]silanol (13): To a solution of 0.1 g (0.18 mmol) of **5a** in 20 mL of THF, 2 mL of conc. H_2SO_4 was added gradually and the mixture was stirred for 3 d at room temperature. Then water was added, the mixture was extracted with ether and the combined extracts were neutralized with solid K_2CO_3 dried, and concentrated. Chromatographic separation (silica gel, heptane) of the residue gave 0.05 g (60%) of **13**, m.p. 65−67°C. − IR (nujol): $\tilde{\nu}$ = 3672 cm^{-1} (OH$_{free}$), 3360−3580 cm^{-1} (OH$_{ass.}$). − ^{1}H NMR ([D$_6$]benzene): δ = 0.18 (s, SiCH$_3$, 18 H), 0.31 (s, SiCH$_3$, 27 H), 0.46 (s, CH$_2$, 2 H). − ^{13}C NMR ([D$_6$]benzene): δ = −10.1 (SiCH$_2$Si), −0.93 {Si[Si(CH$_3$)$_3$]$_2$}, 1.46 {Si[Si(CH$_3$)$_3$]$_3$}. − ^{29}Si NMR ([D$_6$]benzene): δ = −83.1 [*Si*(SiMe$_3$)$_3$], −19.6 [Si(*Si*Me$_3$)$_2$], −12.6 [Si(*Si*Me$_3$)$_3$], 8.9 (SiOH). − MS; *m/z* (%): 451 (3) [M$^+$ − H], 437 (17) [M$^+$ − CH$_3$], 435 (10) [M$^+$ − OH], 379 (100) [M$^+$ − SiMe$_3$], 343 (51) [M$^+$ − HOSiMe$_3$], 247 (4) [Si(SiMe$_3$)$_3^+$]. − $C_{16}H_{48}OSi_7$ (453.16): calcd. C 42.41, H 10.68; found C 41.67 (incomplete combustion), H 10.40.

Methoxybis(trimethylsilyl)[tris(trimethylsilyl)silylmethyl]silane (14): A solution of 0.16 g (0.29 mmol) of **5a** and 2.0 mL of H_2SO_4 in 20 mL THF was stirred for 3 d at room temperature. After addition of 5 mL of dry methanol, stirring was continued for 1 h. Then water was added and the mixture was immediately extracted with ether. The ethereal extracts were dried and concentrated. Chromatographic separation of the residue (silica gel, heptane) gave 0.04 g (30%) of **14** besides 0.05 g (40%) of **13**.

14: ^{1}H NMR ([D$_6$]benzene): δ = 0.22 (s, SiCH$_3$, 18 H), 0.32 (s, SiCH$_3$, 27 H), 0.43 (s, CH$_2$, 2 H), 3.25 (s, SiOCH$_3$). − ^{13}C NMR ([D$_6$]benzene): δ = −11.7 (CH$_2$), −0.3 {Si[Si(CH$_3$)$_3$]$_2$}, 1.14 {Si[Si(CH$_3$)$_3$]$_3$}, 52.1 (SiOCH$_3$). − ^{29}Si NMR ([D$_6$]benzene): δ = −81.4 [*Si*(SiMe$_3$)$_3$], −19.9 [Si(*Si*Me$_3$)$_2$], −12.2 [Si(*Si*Me$_3$)$_3$], 13.9 (SiOMe). − MS; *m/z* (%): 465 (0.1) [M$^+$ − H], 451 (9) [M$^+$ − CH$_3$], 393 (100) [M$^+$ − SiMe$_3$], 247 (5) [Si(SiMe$_3$)$_3^+$], 73 (47) [SiMe$_3^+$]. − $C_{17}H_{50}OSi_7$ (466.22): calcd. C 43.76, H 10.81; found C 43.19, H 11.00.

Crystal-Structure Determination of 5c and 14: The crystal-structure determinations were performed with a STOE IPDS diffractometer using graphite-monochromated Mo-K_α radiation. The structures were solved by direct methods (SHELXS-86)[11] and refined by full-matrix least-squares techniques against F^2 (SHELXL-93).[12] XP (Siemens Analytical X-ray Instruments) was used for structure representations. The X-ray analysis of **5c** revealed disorder for the piperidyl ring. For **14** complete disorder for all methyl groups of the trimethylsilyl substituents was found. Further details are compiled in Table 1. Crystallographic data (excluding structure factors) for the structures reported in this paper have been deposited with the Cambridge Crystallographic Data Centre as supplementary publication nos. CCDC-101350 (**5a**),[10] -102955 (**5c**), and -102956 (**14**). Copies of the data can be obtained free of charge on application to CCDC, 12 Union Road, Cambridge CB2 1EZ, UK [Fax: (internat.) + 44(1223)336-033; E-mail: deposit@ccdc.cam.ac.uk].

Table 1. Crystal structure data of **5c** and **14**

	5c	**14**
Formula	$C_{24}H_{65}NSi_8$	$C_{17}H_{50}OSi_7$
M [g mol^{-1}]	592.49	467.20
a [Å]	29.838(6)	9.101(2)
b [Å]	12.288(3)	11.745(2)
c [Å]	21.092(4)	16.690(3)
α [°]	90	98.05(3)
β [°]	90	101.17(3)
γ [°]	90	108.74(3)
V [Å^3]	7733.4(27)	1643.8(5)
ρ [g cm^{-3}]	1.018	0.944
Z	8	2
Crystal system	orthorhombic	triclinic
Space group	*Pccn*	*P*−1
μ (Mo-K_α) [mm^{-1}]	0.291	0.296
Crystal size [mm]	0.3 × 0.3 × 0.4	0.4 × 0.4 × 0.6
Temperature [°C]	293(2)	293(2)
Scan range (θ) [°]	1.79−21.03	1.88−24.17
hkl range	0/29, −12/12, −21/21	−10/10, −13/13, 0/19
Measured refl.	14676	4872
Unique refl.	4120	4872
Observed refl.	2880	2462
Refined param.	299	213
$R1$ [$I > 2\sigma(I)$]	0.0397	0.0665
$R1$ for all	0.0624	0.1227
GoF	0.962/1.108	0.887/1.138

Acknowledgments

We gratefully acknowledge the support of our research by the Deutsche Forschungsgemeinschaft and the Fonds der Chemischen Industrie. We thank Dr. M. Michalik, Dr. W. Baumann, and Prof. N. Stoll for recording the NMR and mass spectra.

[1] E. Jeschke, T. Gross, H. Reinke, H. Oehme, *Chem. Ber.* **1996**, *129*, 841−844.
[2] T. Gross, R. Kempe, H. Oehme, *Chem. Ber.* **1997**, *130*, 1709−1714.
[3] H. Bock, K. Ruppert, C. Näther, Z. Havlas, H.-F. Herrmann, C. Arad, I. Göbel, John, J. Meuret, S. Nick, A. Rauschenbach, W. Seitz, T. Vaupel, B. Solouki, *Angew. Chem.* **1992**, *104*, 564; *Angew. Chem. Int. Ed. Engl.* **1992**, *31*, 550.
[4] I. Fleming in *Comprehensive Organic Chemistry* (Eds.: D. Barton, W. D. Ollis), Pergamon, Oxford, **1979**, vol. 3, p. 640; W. P. Weber, *Silicon Reagents for Organic Synthesis*, Springer-Verlag, Heidelberg, **1983**, p. 58.
[5] C. Krempner, D. Hoffmann, R. Kempe, H. Oehme, *Organometallics* **1997**, *16*, 1828−1832 and literature cited therein.
[6] K. Sternberg, H. Oehme, *Eur. J. Inorg. Chem.* **1998**, 177−181.
[7] Y. Apeloig, A. Stanger, *J. Am. Chem. Soc.* **1985**, *107*, 2806−2807; Y. Apeloig, A. Stanger, *J. Am. Chem. Soc.* **1987**, *109*, 272−273; R. Bakhtiar, C. M. Holznagel, D. B. Jacobson, *J. Am. Chem. Soc.* **1992**, *114*, 3227−3235 and literature cited therein.
[8] G. Wieland, G. Simchen, *Liebigs Ann. Chem.* **1985**, 2178−2193.
[9] G. Gutekunst, A. G. Brook, *J. Organomet. Chem.* **1982**, *225*, 1−3.
[10] T. Gross, R. Kempe, H. Oehme, *Inorg. Chem. Commun.* **1998**, *1*, 128−130.
[11] G. M. Sheldrick, *SHELXS-86*, University of Göttingen, Germany, **1986**.
[12] G. M. Sheldrick, *SHELXL-93*, University of Göttingen, Germany, **1993**.

Received September 17, 1998
[I98315]

Steric and Electronic Effects on the ^{103}Rh NMR Chemical Shifts of Rh^{I}(cyclooctadiene) Compounds Bearing N-Donor Ligands

Johannes G. Donkervoort,[a] Michael Bühl,*[b] Jan Meine Ernsting,[a] and Cornelis J. Elsevier*[a]

Keywords: ^{103}Rh NMR / Rhodium complexes / Nitrogen ligands / Chemical-shift computation

In order to study electronic and steric effects on δ(^{103}Rh), the ^{103}Rh-NMR spectra of a series of [Rh(cod)L_2] complexes (with L = nitrogen, oxygen, or chloride) have been measured by gradient-enhanced HMQC (^{1}H,^{103}Rh) NMR spectroscopy. Density functional computations of representative examples have been performed at the GIAO-B3LYP level of theory. The obtained experimental values of ^{103}Rh shifts fit the generally observed trend of coordinating ligands in the first coordination sphere of the metal: P < N < O. Calculated ^{103}Rh shifts agreed to within 8 % with experimental values. The computational results indicate that the Rh–N bond distance has a larger influence on the chemical shift than the N–Rh–N angle.

Introduction

Since the development of modern inverse 2D NMR techniques, a rapid growth of available NMR data concerning insensitive metal nuclei can be discerned.[1] For example, inverse 2D X{^{103}Rh} NMR leads to a theoretical sensitivity enhancement of 360 for X = ^{31}P and 5630 for X = ^{1}H, respectively. Despite the larger amount of NMR data there is still a lack of understanding of the factors which determine the chemical shift of transition metal nuclei. From the published data it has, for instance, been concluded that changes in the first coordination sphere of the Rh nucleus result in deshielding of the metal center in the order: O > Cl ≈ N > Br > I > S ≈ Se > Te > P ≈ As ≈ Sb ≈ H ≈ C* ≈ C (C* = sp^2-carbon).[2]

It is generally accepted that the chemical shift variation of a transition metal nucleus in its coordination compound is mainly determined by the paramagnetic shielding term given by the Ramsey equation[3] which was later developed by Griffith and Orgel (Eq. 1)[4]. In this equation r_d is the expectation value of the d-orbital radius, ΣQ_N is the angular imbalance of charge and ΔE is the average excitation energy between the filled and empty d-orbitals.

$$\sigma_p = \text{const.}\ (\Delta E)^{-1} \langle r_d^{-3} \rangle \Sigma Q_N \qquad (1)$$

Changes in ΣQ_N generally bear a large influence on σ_p. Therefore this study is focused on four-coordinate, square planar Rh^I complexes of the general type [Rh(cod)L_2]. In these complexes the d-electron configuration and the symmetry at the metal are kept constant and a discussion of the observed Rh shifts can be focused on ΔE and r_d alone.[5] As earlier results indicated a dependence of the Rh shift on the applied diene,[6] only cod complexes were used in this investigation.

We have previously studied the complexes [Rh(cod)$(P)_2$][6c] and observed that variations in the first coordination sphere of the Rh nucleus indeed influenced the ^{103}Rh chemical shift according to the general order given above.[2] However, changes in the second coordination sphere, for example bite angle variations, contradicted expectations based on simple MO considerations and the Ramsey equation. This study is focussed on a series of [Rh(cod)$(N)_2$] complexes in order to evaluate changes of the ^{103}Rh shift upon a systematic variation of the nitrogen ligands. These results will be discussed in the light of theoretical calculations of δ(^{103}Rh) for several of the prepared complexes, which have recently become feasible.[7][8] Together, these efforts may result in a better insight in the factors determining variations of the δ(^{103}Rh).

Results and Discussion

Synthesis

The complexes were prepared according to literature procedures except for the new four-coordinate [Rh(cod)(*i*PrDAB)]ClO_4 (*i*PrDAB = *i*PrN=CH−CH=N−*i*Pr), **7**. Compound **7** was obtained as a dark-green solid by adding a solution of the free ligand in acetone to a solution of in situ prepared [Rh(cod)$(acetone)_x$]ClO_4 in acetone (see Experimental Section). This complex is an air-stable solid with a melting or decompostion point which lies above 300 °C. Complex **7** is readily soluble in chlorinated solvents whereas it is only slightly soluble in EtOH and MeOH.

The ^{1}H- and ^{13}C-NMR spectra of samples of **7** in $CDCl_3$ or CD_3OD at ambient temperature are consistent with a

[a] Institute of Molecular Chemistry, Universiteit van Amsterdam, Nieuwe Achtergracht 166, 1018 WV Amsterdam, The Netherlands
Fax: (internat.) +31 (0)20/ 5256456
E-mail: else4@anorg.chem.uva.nl
[b] Organisch-chemisches Institut, Universität Zürich, Winterthurerstraße 192, CH-8057 Zürich, Switzerland
Fax: (internat.) +41 (0)16356836
E-mail: buehl@oci.unizh.ch

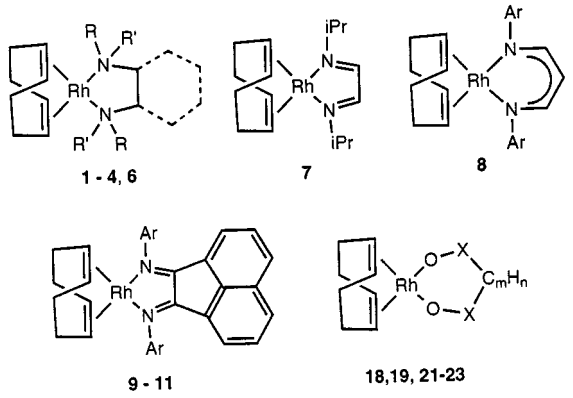
 © WILEY-VCH Verlag GmbH, D-69451 Weinheim, 1999 1434−1948/99/0101−0027 $ 17.50+.50/0

time-average C_{2v}-symmetric molecule. No dependence on the temperature has been observed by VT-NMR spectroscopy.

GE^{103}Rh-NMR Spectroscopy

The use of gradient selection is nowadays used for most 2D $^1H\{^{13}C\}$ and $^1H\{^{15}N\}$ experiments. Here we present the use of gradient selection to reduce the measuring time of $^1H\{^{103}Rh\}$ experiment and to reduce the ^1H signals not coupled to the rhodium more effectively. In the gradient-enhanced HMQC sequence: ^1H-^{103}Rh D1 − 90°(^1H) − 1/2J − 90°(^{103}Rh) − t_1/2 − GP1 − D16 − 180°(^1H) − GP2 − D16 − t_1/2 − 90°(^{103}Rh) − GP3 − 1/2J − ACQ, the equation GP1 ($\gamma H + \gamma Rh$) + GP2 ($-\gamma H + \gamma Rh$) + GP3 ($-\gamma H$) = 0 must be fulfilled. For GP1:GP2:GP3 = 90 : 44 : 50 this is true. We have tested these gradient values and compared the results with the normal HMQC pulse sequence. It was found that the number of scans per increment can be reduced from 8 or 16 to 1 or 2 without loss of information.

The ^{103}Rh NMR spectra were measured by gradient-enhanced HMQC (^1H,^{103}Rh) as described above and in the experimental section. The compound types studied have been summarized in the drawing below and can be divided into nitrogen donor complexes (**1**−**15**), chloride compounds (**16**, **17**) and oxygen donor complexes (**18**−**23**).



In order to study steric and electronic effects on the ^{103}Rh chemical shifts, density functional computations have been performed at the GIAO-B3LYP level of theory. This level has been shown to afford transition-metal chemical-shift values in good agreement with experiment for a number of organometallic compounds.[7] In addition, it has been used to study similar steric and electronic effects on $\delta(^{103}Rh)$ in related rhodium−phosphane and −cyclopentadienyl complexes.[8] Calculations have been performed for a number of complexes of this study, comprising **1**, **2**, **5**, **6**, **7**, **13**, **14**, and **18**. The experimental ^{103}Rh chemical shifts have been collected in Table 1, together with calculated values of representative examples. The theoretical ^{103}Rh chemical shifts agree well with the corresponding experimental data, with a mean absolute deviation of 44 ppm (over a range of ca. 540 ppm). When the single large deviation in the case of **7** is excluded (see below for a more detailed dicussion), the mean absolute deviation is improved to 30 ppm.

Table 1. Observed[a] and calculated[b] ^{103}Rh NMR data for complexes **1**−**23**

no.	compound	$\delta^{103}Rh$[c] observed	calculated
1	[Rh(cod)(1,2-en)]ClO_4	751	725
2a	[Rh(cod)(dmeda)]ClO_4 (trans)	784	781
2b	[Rh(cod)(dmeda)]ClO_4 (cis)	822	801
3	[Rh(cod)(1,2-$(NH_2)C_6H_4$)]ClO_4	801	
4	[Rh(cod)(1,8-$(NH_2)_2$-naphthalene)]ClO_4	804	
5	[Rh(cod)(1,3-pn)]ClO_4	849	800
6a	[Rh(cod)(tmeda)]ClO_4	978	942
6b	[Rh(cod)(tmeda)][Rh(cod)Cl_2]	949 and 1065[d]	
7	[Rh(cod)(*i*Pr-DAB)]ClO_4	914	1088
8	[Rh(cod)(ABK)]	998[e]	
9	[Rh(cod)(BIAN-R)]ClO_4 (R = C_6H_5)	1025[e]	
10	[Rh(cod)(BIAN-R)]ClO_4 (R = 2,6-(*i*Pr)$_2C_6H_3$)	1057[e]	
11	[Rh(cod)(BIAN-R)]ClO_4 (R = 4-$OMeC_6H_4$)	1059[e]	
12	[Rh(cod)(4,4′-Me_2-bipy)]ClO_4	795	
13	[Rh(cod)(bipy)]ClO_4	816	810
14	[Rh(cod)$(py)_2$]ClO_4	1009	953
15	[Rh(cod)(C_5H_4N-NH-C_5H_4N)]ClO_4	1035	
16	[Rh(cod)Cl]$_2$	1093[e]	
17	[Rh(cod)Cl_2]Et_4N	1107[e]	1168
18	[Rh(cod)(acac)]	1287[e]	1298[f]
19	[Rh(cod)(1,2-$(HO)_2$-naphthalene)]ClO_4	1301	
20	[Rh(cod)$(Me_2CO)_x$]ClO_4	1350	
21	[Rh(cod)(dppmO_2)]ClO_4	1362	
22	[Rh(cod)(bipyO_2)]ClO_4	1362	
23	[Rh(cod)(dppeO_2)]ClO_4	1373	

1,2-en = 1,2-ethylenediamine; dmeda = 1,2-*N,N′*-dimethylethylenediamine; 1,3-pn = 1,3-propylenediamine; tmeda = *N,N,N′,N′*-tetramethylethylenediamine; DAB = glyoxalbis(isopropylimine); ABK = acetylacetonato-bis(2,6-dimethylphenyl)ketimine anion; BIAN = bis(imino)acenaphthene; bipy = 2,2′-dipyridine; py = pyridine; acac = acetylacetonato anion; dppmO_2 = 1,1-bis(diphenylphosphane oxide)methane; dppeO_2 = 1,2-bis(diphenylphosphane oxide)ethane; bipyO_2 = *N,N′*-2,2′-dipyridine dioxide. − [a] All complexes in CD_3OD at T = 298 K unless otherwise stated. −[b] GIAO-B3LYP/II′ level (**17**, **18**: basis II), see Computational Details in the Experimental Section; no counterions have been included in the calculations. − [c] Relative to Ξ = 3.16 MHz; ± 1.0 ppm. − [d] T = 230K. − [e] In $CDCl_3$. − [f] See also ref.[8a]

Table 2. Observed ^{103}Rh NMR data for phosphane rhodium complexes **24**−**30**

no.	compound	$\delta^{103}Rh$[c]
24	[Rh(cod)($Ph_2P(CH_2)_2PPh_2$)]ClO_4	−505[a]
25	[Rh(cod)$(PPh_3)_2$]BPh_4	−145[b]
26	[Rh(cod)$(PEt_3)_2$]BPh_4	−132[b]
27	[Rh(cod)$(P^nBu_3)_2$]BPh_4	−94[b]
28	[Rh(cod)(PPh_3)(py)]PF_6	415[b]
29	[Rh(cod)(PPh_3)(p-Me-py)]PF_6	419[b]
30	[Rh(cod)(PPh_3)(p-Me_2N-py)]PF_6	436[b]

[a] Ref.[11] − [b] Ref.[6c]

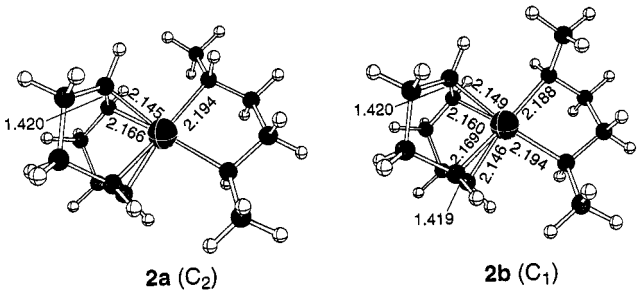
The range of observed chemical shifts extends from δ = 751 to 1035 for the complexes containing nitrogen ligands and from δ = 1287 to 1372 for those containing oxygen ligands, with an intermediate value for the chloro com-

pounds **16** and **17**. Variations in the first coordination sphere of the Rh center follow the above mentioned series given by Mann. As expected, oxygen ligands (**18**−**23**) cause the Rh center to be more deshielded when compared to nitrogen ligands, while phosphorous ligands (Table 2, **24**−**30**) result in a strongly shielded Rh center. In case of P-donors, the relative energies of occupied and vacant MOs at the ligand and the metal fragments allow for a more effective overlap in terms of σ-donation and π-backdonation. These interactions result in a larger ΔE splitting, which accounts for the strong low-frequency shift of the bis(phosphane) complexes.

In earlier studies problems were reported for [Rh(cod)X(N)] (X = halogen, N = nitrogen ligand)[6a] involving exchange processes. However, for all complexes mentioned in Table 1, except for [Rh(cod)(tmeda)]-[Rh(cod)Cl_2], **6b**, the ^{103}Rh spectra recorded at 298 K were clearly resolved. For **6b** no signal is observed at 298 K, whereas upon cooling to 230 K two signals were observed at δ = 949.0 and 1065.3. These observations can be explained by assuming the presence of two species, i.e. cationic $[Rh(cod)(tmeda)]^+$ and anionic $[Rh(cod)Cl_2]^-$. Both the cationic and anionic species were also separately prepared as their perchlorate, **6a**, and tetraethylammonium, **17**, salt, respectively. Comparing the ^{103}Rh chemical shifts of **6a** and **17** with both observed signals of **6b** indicates that the signals at δ = 949.0 and 1065.3 indeed correspond to the $[Rh(cod)(tmeda)]^+$ and $[Rh(cod)Cl_2]^-$ species, respectively. The temperature dependence of the δ(^{103}Rh) of 0.42 ppm K^{-1} and 0.52 ppm K^{-1} for $[Rh(cod)(tmeda)]^+$ and $[Rh(cod)Cl_2]^-$, respectively, is consistent with values observed for related complexes.[6a,9] Although different observations have indicated the presence of two species in solution for **6b**,[10] this is the first real evidence for the presence of this cation-anion pair in solution.

For the complex $[Rh(cod)(dmeda)]ClO_4$, **2**, two resolved signals in a 5:1 ratio are observed in the ^{103}Rh spectra pointing to the presence of two rhodium species, **2a** and **2b**. This conclusion is corroborated by the observation of two not completely resolved sets of signals for the dmeda protons in the ^{1}H-NMR spectrum. Most probably these two signals arise from the presence of two stereoisomers with the methyl groups in trans (**2a**) or in cis positions (**2b**) (Figure 1). This conclusion is corroborated by results from density functional computations (vide infra), which would predict a 10:1 molar ratio for **2a** and **2b**, respectively, based on the relative energies (**2a** lower than **2b** by 5.4 kJ/mol at the B3LYP/II′ level). In addition, the calculated chemical shifts for **2a** and **2b** are in good agreement with both observed values (see Table 1).

It has been proposed that the metal shift parallels the variation of the bulk and basicity of the ligand. In a systematic study of Rh−phosphane complexes,[6c] it was shown that an increase in basicity of the phosphane ligands results in a more shielded Rh nucleus and hence a δ(^{103}Rh) shift towards higher frequencies. In addition, a larger cone-angle of the phosphane ligand also results in a shift towards higher frequencies.



2a (C_2) **2b** (C_1)

Figure 1. Optimized structures of **2a** and **2b**

For the nitrogen−rhodium complexes of this study, similar trends in the δ(^{103}Rh) can be observed when looking at one class of comparable nitrogen ligands. For example, within the class of bidentate amine-ligands a high-frequency shift is observed upon increasing the Brønsted basicity of the ligand (cf. **1**, **2**, and **6**). This trend is in contrast with expectations based on simple MO considerations combined with the above mentioned Ramsey equation. A more basic ligand is expected to result in an increased ΔE which, according to the Ramsey equation, should result in a more shielded nucleus and hence a low-frequency chemical shift. The observation that simple MO considerations do not fit the Ramsey equation were also found for phosphane-rhodium complexes.[6c]

In the series of the pyridine complexes (**12**−**15**), a strong chelate effect is observed. Replacing both pyridine ligands in **14** for the bidentate bipy ligand, resulting in a five-membered metallacycle (**13**), causes a significant low-frequency shift of 197 ppm. Variations in this ring-size affect δ(^{103}Rh) significantly, as is evident from the high-frequency shift upon increasing the ring-size by one (cf. **13** and **15**). This same trend is also observed for the amine (cf. **1** and **5**) and diimine complexes (cf. [Rh(cod)(*i*PrDAB)], **7**, [Rh(cod)-(ABK)], **8**, and [Rh(cod)(BIAN-R)], **9**−**11**). The BIAN ligand systems are known to have a relatively large bite-angle due to the rigidity of the ligand back-bone, analogous to the rigidity of the 1,2-diaminobenzene ligand. Hence, the corresponding complex **3** shows a high frequency shift as compared to **1**. A similar observation has been made for some series of phosphane rhodium complexes, e.g. $[Rh(nbd)(Ph_2P(CH_2)_nPPh_2)]^+$,[11] where the experimental shift ranged from δ = −390 for n = 2 to δ = −210 for n = 4. Hence, the chelate-ring size appears to be one of the most important factors determining the δ(^{103}Rh) value. This size effect is believed to be mediated by changes in the bite angle at the metal. Therefore, studies were performed on the model compound $[Rh(cod)(NH_3)_2]^+$ by explicitly calculating its δ(^{103}Rh) value as a function of the bite angle.

As apparent from the results displayed in Figure 2a, there is in fact a dependence on the bite angle of the computed δ(^{103}Rh) values with a minimum near ca. 90°. Variations in the bite-angle around this 90° angle result in a more deshielded metal center and hence high-frequency shifts. Similar observations were made for rhodium(phosphane) complexes, i.e. a strong deviation from the ideal geometry of square-planar d^8-complexes leads to a high-frequency

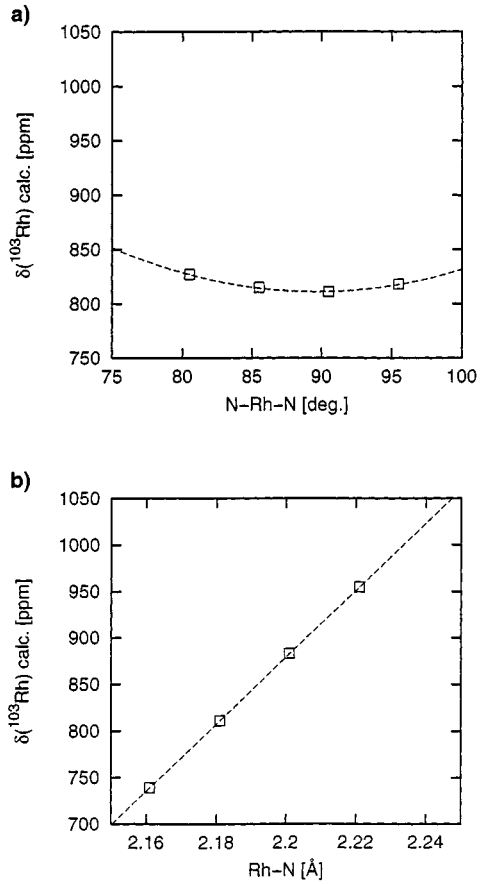


Figure 2. Calculated rhodium chemical shift of $[Rh(cod)(NH_3)_2]^+$ as a function of N−Rh−N angle and Rh−N distance

shift.[6c][11] However, for the model complex $[Rh(cod)(NH_3)_2]^+$ there seems to be only a minor variation in δ(^{103}Rh) of ca. 40 ppm in the bite-angle range between 75 and 100 typically covered in bidentate chelates. A similar result has recently been obtained in the case of rhodium(diphosphane) complexes.[8b]

According to the latter study, the ^{103}Rh chemical shifts were found to be particularly sensitive to changes in the Rh−P bond lengths, with a computed bond-length shift derivative of more than 10,000 ppm Å^{-1}. The analogous study for model compound $[Rh(cod)(NH_3)_2]^+$ now also revealed a large sensitivity of the computed δ(^{103}Rh) value to the Rh−N bond distance (see Figure 2b), albeit with a somewhat smaller slope of 3600 ppm·Å^{-1}. These results indicate that, although the bite-angle influences the δ(^{103}Rh), mainly variations in the Rh−N bond distance dominate the δ(^{103}Rh). Apparently, in rhodium−phosphane and −nitrogen complexes, variations in the chelate ring-size affect both the bite-angle and the Rh−ligand bond distance, where the latter has the larger influence on the variations in the observed δ(^{103}Rh) shift.

Using these results, we tried to separate the steric and electronic effects in the series of substituted ethylenediamine complexes **1**, **2**, and **6**, the observed ^{103}Rh chemical shifts of which cover a range of 227 ppm. Contrary to expectations based on the relative Brønsted basicity of the ligands (vide supra), a more basic ligand in this series induces a stronger deshielding of the ^{103}Rh nucleus. However, in the same series, the optimized Rh−N bond lengths increase significantly, whereas the bite angle remains essentially constant (see Table 3).[12] According to the above-mentioned results for model compound $[Rh(cod)(NH_3)_2]^+$, it is the bond-length elongation that could be responsible for the observed deshielding.

Table 3. Selected geometrical parameters of Rh(cod) complexes containing ethylenediamine derivatives and the computed d(^{103}Rh) chemical shifts

no.	ligand	Rh-N [Å]	N-Rh-N [°]	δ(with Me)[a]	δ(without Me)[b]
1	(1,2)-en	2.167	80.6	725	725
2a	dmeda (trans)	2.194	81.1	781	821
2b	dmeda (cis)	2.188/ 2.194	81.5	801	834
6	tmeda	2.239	82.2	942	974

[a] δ(^{103}Rh) computed for the fully optimized structure. [b] δ(^{103}Rh) computed for optimized structures of the respective complexes, with Me groups substituted by H atoms.

In order to assess also the effects of the added Me groups, model calculations have been performed for the parent **1** employing the geometrical parameters optimized for the derivatves **2** and **6** (i.e. by simply replacing the Me groups with H atoms). The chemical shifts computed accordingly (last column in Table 3) are thus solely the result of the structural distortions induced by the Me groups which reflect their "pure geometrical effects". Apparently, these distortions cause a strong deshielding, which is partly reduced by the "pure electronic effects" of the Me groups. The latter amounts to only ca. 30 ppm, as assessed by the difference between the entries of the last two columns in Table 3[13], compared to the overall effect of up to 227 ppm observed in going from **1** to **6**. The main origin of this deshielding is therefore a geometrical, rather than an electronic effect. A comparable shielding effect (21 ppm) is observed upon substituting bipy for 4,4′-Me_2bipy, cf. the δ(^{103}Rh) of **13** and **12**, respectively.

For more quantitative estimates of these geometrical effects, the bond-length shift derivative calculated for model compound $[Rh(cod)(NH_3)_2]^+$, 3600 ppm·Å^{-1}, was applied to **1**, **2**, and **6**. In going from **1** to **2** and from **1** to **6**, the optimized bond-length elongations are 0.026 and 0.072 Å, respectively. This corresponds to deshieldings of 94 and 259 ppm, respectively, which are in excellent accord with the calculated "pure geometrical effects" of 103 and 249 ppm, respectively.

For an interpretation of the steric and electronic influences, the above-mentioned influences have been discussed in terms of the parameters ΔE and r_d in the Ramsey equation. In general, it is possible to relate large differences in the first coordination sphere to the Ramsey equation by using a simplified MO theory, i.e. hard donor atoms result in more deshielded metal centers and hence in high-frequency shifts as compared to soft donor atoms (cf. rhodium complexes containg either oxygen (av. δ = 1300) or phos-

phorus (av. $\delta = -100$) ligating atoms, respectively). However, trends in $\delta(^{103}Rh)$ induced by second sphere variations of the applied ligands can not be related to such simplified model theories (vide supra).[6c] A more thorough investigation into the orbital symmetry and energies of the Rh complexes seems necessary. Therefore the calculated (B3LYP) molecular orbitals of complexes **1**, **2**, **6**, **13**, **14**, and model complex $[Rh(cod)(NH_3)_2]^+$ were analyzed in detail, in order to see if simple relations between appropiate ΔE values and chemical shifts could be found.

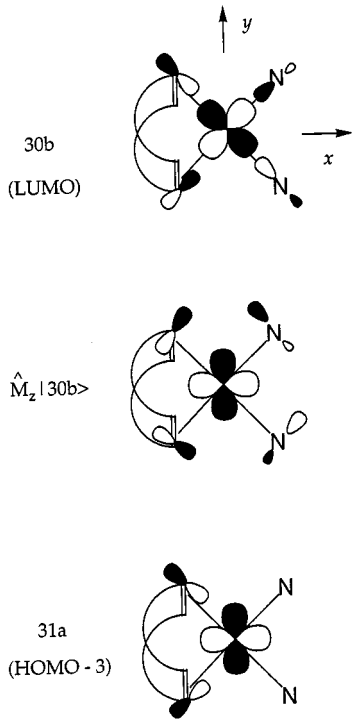


Figure 3. Highest occupied and lowest unoccupied molecular orbitals of $[Rh(cod)(NH_3)_2]^+$ fragments

The four highest occupied MOs of model complex $[Rh(cod)(NH_3)_2]^+$ are of predominant d(Rh) character, as expected, with some minor additional ligand contributions. At least one of the lowest unoccupied MOs also has large d(Rh) character [usually the LUMO, except when p-ligands are present such as in **13** and **14**; in these cases the LUMO is usually of π^*(ligand) character]. Magnetically induced coupling between suitable occupied and virtual MOs can account for paramagnetic contributions in a pictorial fashion. For example, in model compound $[Rh(cod)(NH_3)_2]^+$ the large deshielding perpendicular to the coordination plane (z direction in Figure 3) is consistent with the coupling of the LUMO (after action of the magnetic operator $\hat{M}_z$ on it, viz. the resulting orbital $\hat{M}_z|30b>$) with an occupied MO of suitable symmetry (orbital 31a, see Figure 3).[14] Unfortunately, it was not possible for the set of compounds under scrutiny, to simply relate the energy differences between the corresponding orbitals with the trends in $\delta(^{103}Rh)$. Apparently, the particular magnetic shieldings are determined by several such interactions and it is difficult to identify a single factor, such as one particular ΔE value, as the main source for the observed trends.

The same holds for complex **7** with the *i*Pr-DAB ligand where an additional deshielding is apparent in the coordination plane (corresponding to the y axis in Figure 3), consistent with paramagnetic contributions due to the coupling of the LUMO [44b, π^*(DAB) with some d_{xz}(Rh) character][15] and the HOMO [48a, d_{z2}(Rh)]. This is even more pronounced in the parent model compound, [Rh(cod)(H-DAB)]$^+$ (H-DAB = HN=CH−CH=NH), resulting in a huge predicted deshielding for the metal ($\delta_{iso} = 1505$). There is thus a huge shielding effect on $\delta(^{103}Rh)$ upon changing the substituents at the DAB nitrogen atom from H to *i*Pr ($\Delta\delta_{calc.} = -417$ ppm). Part of this effect is due to geometrical differences, but here it is the "pure electronic effect" of the *i*Pr groups which is dominating, $\Delta\delta = -262$ ppm (assessed similarly as described above for the 1,2-en derivatives). In the DAB complexes, the ^{103}Rh chemical shift is quite sensitive to subtle changes in the electronic structure, which may be one of the reasons for the unusually large deviation (more than 170 ppm) between the theoretical and experimental $\delta(^{103}Rh)$ data for **7** (see Table 1).

Conclusion

It has been found that the experimental values of the ^{103}Rh-NMR shifts of $[Rh(cod)(N)_2]^+$ complexes fit the expected trend according to the position within the spectrochemical series for substituents in the first coodination sphere of rhodium. Except for a diazabutadiene complex which turned out to be a problem case for theory, density-functional calculations have resulted in excellent numerical reproduction of the experimental shifts within 30 ppm, where the gross variation of shifts amounts to 540 ppm.

According to model calculations, it is the Rh−N distance that has a decisive influence upon the Rh chemical shift, rather than the N−Rh−N angle hitherto believed to be of prime importance for chelating ligands. These findings are consistent with recent results obtained for Rh−bis(phosphane) complexes. Effects of substituents in the second coordination sphere (e.g. alkyl vs. H substituents at the coordinating nitrogen atoms) can be partitioned computationally into geometrical and electronic contributions, the relative importance of which is depending on the ligand. Further interpretation of the origin of these secondary substituent effects on the metal shielding, e.g. in terms of the Ramsey equation, is difficult because it is hard to identify single, dominant parameters.

Experimental Section

NMR Techniques: Routine ^{1}H-NMR spectra to check purity were recorded on a Bruker AMX 300 spectrometer (300.13 MHz). All ^{103}Rh NMR measurements were carried out on a 300-MHz Bruker DRX Advance spectrometer under temperature control at 298 K using a 5-mm triple-resonance inverse probehead (^{1}H, ^{31}P{BB}) with a z gradient coil (90° ^{1}H = 7.2 ms, 90° ^{103}Rh = 19.5 ms) using the following sequence: ^{1}H-^{103}Rh GS−HMQC:[16−18] D1 − 90°(^{1}H) − 1/2J − 90°(^{103}Rh) − t_1/2 − GP1 − D16 − 180°(^{1}H) − GP2 − D16 − t_1/2 − 90°(^{103}Rh) − GP3 − 1/2J − ACQ; acqui-

sition parameters: D1 = 1 s, 1/*J*2 = 0.2−0.5 s, D16 = 50 ms, *GP* = 1 ms, 1 to 4 scans were acquired per t_1 increment, block size 2048 × 128 points for the first experiment and 2048 × 256 points for the final experiment, gradient amplitudes GP1:GP2:GP3 = 90:44:50 $G \cdot cm^{-1}$. Acquisition time 10−30 minutes for the final experiment.

The spectral width was 3000 Hz for ^1H. In the first measurement, the spectral width for ^{103}Rh was 9000 ppm which was covered by 128 t_1 increments, 16 dummy scans were used. To exclude folding and improve resolution, a second and sometimes third measurement with modified n_0(Rh) values and smaller spectral widths (at most 1900 Hz in F_1 using 256 increments) were carried out. The digital resolution of $\delta(^{103}Rh)$ was at least 3.7 Hz pt^{-1}. After zero-filling in F_1, the 512 × 512 matrix was transformed applying a sine-bell weighing function. The ^{103}Rh spectrum is obtained in F_1, and the ^1H spectrum in F_2. The absolute ^{103}Rh frequency was determined by relating it to the reference frequency Ξ = 3.16 MHz, scaled for the operating field (^1H 9 483 491 Hz) to ν_{ref} = 3.16415 MHz. Signals at higher frequencies are taken as positive.

Synthesis: All complexes, except for **7** were prepared according to published procedures: **1**−**3**, **5**−**6a**, **7**, **12**−**14**, **20**,[19] **4**,[20] **6b**,[10] **8**,[21] **9**−**11**,[22] **15**,[23] **16**,[24] **17**,[10b] **18**,[25] **19**,[20] **21**−**23**.[26]

Preparation of [Rh(cod)(*i*Pr-DAB)]ClO_4 (7): To a solution of 35.6 mg (0.1444 mmol) of $[Rh(cod)Cl]_2$ in 25 mL of acetone was added 32.5 mg (0.1444 mmol) of $AgClO_4$. The resulting mixture was stirred for 15 minutes after which the formed precipitate was filtered off. To the filtrate was added a solution of 20.2 mg (0.1444 mmol) of *i*Pr-DAB in 5 mL of acetone. The reaction mixture was stirred for 10 minutes after which the solvent was removed in vacuo. The resulting green solid was washed with pentane (2 × 10 mL) and Et_2O (2 × 10 mL), respectively, and dried in vacuo. Yield 60.9 mg (0.1350 mmol) 93%. Elem. anal. for $C_{16}H_{28}N_2O_4Rh$ found (calc.): C 42.01 (42.63), H 6.28 (6.26), N 6.14 (6.21). − ^1H NMR ($CDCl_3$, d): 8.34 (d, ^3J = 2.37 Hz, 2 H, N=C*H*), 4.40 (s br, 4 H, *H*C=C*H*), 3.32 [s, ^3J = 6.60 Hz, 2 H, C*H*$(CH_3)_2$], 2.54 (m, 4 H, CH_2), 2.02 (m, 4 H, CH_2), 1.34 [d, ^3J = 6.60 Hz, 12 H, CH(C$H_3)_2$]. $^{13}C\{^1H\}$ ($CDCl_3$, d): 87.47 and 87.31 (cod-*C*H and N=*C*H), 54.80 [*C*H$(CH_3)_2$], 30.42 (cod-*C*H_2), 22.74 [CH(*C*$H_3)_2$].

Computational Details: The same methods and basis sets as in the former theoretical studies of ^{103}Rh chemical shifts have been employed:[7b,8] Geometries have been fully optimized in the given symmetry at the BP86/ECP1 level, i.e. employing the gradient-corrected exchange-correlation functionals of Becke (1988)[27]and Perdew (1986),[28] together with a quasi-relativistic effective core potential and the corresponding [6s5p3d] valence basis set for Rh,[29]and standard 6−31G* basis[30] on the ligands (designated BP86/ECP1). Magnetic shielding tensors have been computed for the BP86/ECP1 geometries with the GIAO (gauge-including atomic orbitals)-DFT method,[31] employing a fine integration grid (75 radial shells with 302 angular points per shell), Becke′s three-parameter exchange DFT/Hartree-Fock hybrid functional[32] together with the correlation functional of Lee, Yang, and Parr[33] (denoted B3LYP), and the following basis set (denoted basis II): Rh: well-tempered [16s10p9d] basis, contracted from the 22s14p12d set[34] and augmented with two d-shells of the well-tempered series; ligands: IGLO-basis II recommended for chemical-shift calculations,[35] i.e. C,N,O: (9s5p)/[5s4p] augmented with one set of d-polarization functions; Cl: (11s7p)/[7s6p] augmented with two sets of d-polarization functions; H: (5s)/[3s] polarized with one set of p-functions. For the complexes with the N-donor ligands, the chemical shift computations employed basis II′, i.e. the same as basis II, but with a smaller DZ (double zeta) basis[35] on the hydrogen atoms. For cation **1**, the GIAO-B3LYP ^{103}Rh shieldings differed by less than 4 ppm between basis II and basis II′. Chemical shifts $\delta(^{103}Rh)$ are reported relative to σ(standard) = −878 ppm, as previously evaluated from σ(calc) vs. δ(expt) linear regressions.[7b] All calculations were performed with the Gaussian 94 program.[36]

Acknowledgments

We kindly thank Dr. P. H. M. Budzelaar, University Nijmegen, for providing us with a sample of **8**. Financial support by the Netherlands Organization for Pure Research CW-NWO under the Young Scientists Program, is gratefully acknowledged. M. B. wishes to thank Prof. W. Thiel for continuous support. Calculations were performed on a Silicon Graphics PowerChallenge (Organisch-chemisches Institut, Universität Zürich) and on IBM RS6000 workstations (C4 cluster, ETH Zürich), as well as on a NEC-SX4 (CSCS, Manno, Switzerland).

[1] R. Benn in: P. S. Pregosin (Ed.), *Transition Metal Nuclear Magnetic resonance,* Elsevier; Amsterdam, **1991**; p.103.
[2] B. E. Mann in: P. S. Pregosin (Ed.), *Transition Metal Nuclear Magnetic resonance*, Elsevier; Amsterdam, **1991**; p.177.
[3] [3a] N. F. Ramsey, *Phys. Rev.* **1950**, *77*, 567. − [3b] N. F. Ramsey, *Phys. Rev.* **1950**, *78*, 699. − [3c] N. F. Ramsey, *Phys. Rev.* **1951**, *83*, 540. − [3c] N. F. Ramsey, *Phys. Rev.* **1952**, *86*, 243.
[4] J. S. Griffith, L. E. Orgel, *Trans. Faraday Soc*. **1957**, *53*, 601.
[5] J. Mason, *Chem. Rev.* **1987**, *87*, 1299.
[6] [6a] R. Bonnaire, D. Davoust, N. Platzer, *Org. Magn. Reson.* **1984**, *22*, 80. − [6b] J. M. Ernsting, C. J. Elsevier, W. G. de Lange, *J. Chem. Soc., Chem. Commun.* **1989**, 585. − [6c] C. J. Elsevier, B. Kowall, H. Kragten, *Inorg. Chem*. **1995**, *34*, 4836.
[7] [7a] G. Schreckenbach, T. Ziegler, *J. Chem. Phys.* **1995**, *99*, 606. − [7b] M. Bühl, *Chem. Phys. Lett*. **1997**, *267*, 251. − [7c] Review: M. Bühl, M. Kaupp, V. G. Malkin, O. L. Malkina, *J. Comput. Chem*., in press.
[8] [8a] M. Bühl, *Organometallics* **1997**, *16*, 261. − [8b] W. Leitner, M. Bühl, R. Fornika, C. Six, W. Baumann, E. Dinjus, M. Kessler, C. Krüger, A. Rufinska, submitted for publication.
[9] K. D. Gruninger, A. Schwenk, B. E. Mann, *J. Magn. Reson.* **1980**, *41*, 354.
[10] [10a] M. A. Garralda, L. Ibarlucea, *J. Organometal. Chem*. **1986**, *311*, 225. − [10b] M. A. Garcia, M. A. Garralda, L. Ibarlucea, *Polyhedron* **1988**, *7*, 1067.
[11] J. M. Ernsting, C. J. Elsevier, W. G. J. de Lange, K. Timmer, *Magn. Res. Chem*. **1991**, *29*, S118.
[12] No solid-state structures for the series **1**, **2**, and **6** are published; steric effects similar to those discussed here, however, can be noted in a cationic Rh(COD) complex with *N*-(2-aminoethyl)-piperidine as ligand (E. Anzuela, M. A. Garralda, R. Hernandez, L. Ibarlucea, E. Pinilla, M. A. Monge, *Inorg. Chim. Acta*, **1991**, *185*, 211): the Rh−N bond lengths to the primary and tertiary amine N atoms, 2.107(6) and 2.176(7) A, respectively, are shorter than the corresponding DFT data in Table 3 (cf. entries for **1** and **6**), but the difference between these distances is very similar in both cases, ca. 7 pm elongation from primary to tertiary amine.
[13] Somewhat counterintuitively, roughly the same effect is seen for **2** and **6** upon substituting two and four Me groups, respectively.
[14] For similar arguments see for instance:[14a] Y. Ruiz-Morales, G. Schreckenbach, T. Ziegler, *J. Phys. Chem*. **1996**, *100*, 3359. − [14b] Y. Ruiz-Morales, G. Schreckenbach, T. Ziegler, *Organometallics* **1996**, *15*, 3920.
[15] Similar characteristics (i.e. ligand-π* character and contributions from the metal) have been computed for the LUMO of other DAB complexes, which is important for their UV/vis spectra, see for instance M. P. Aarnts, M. P. Wilms, K. Peelen, J. Fraanje, K. Goubitz, F. Hartl, D. J. Stufkens, E. J. Baerends, A. Vlcek, *Inorg. Chem*. **1996**, *35*, 5468.
[16] S. Braun, H.-O. Kalinowski, S. Berger, in *100 and More Basic NMR Experiments.* **1994**, 360−363.
[17] [17a] R. E. Hurd, B. K. John, *J. Magn. Reson.* **1991**, *91*, 648−653. − [17b] J. Ruiz-Cabello, G. W. Vuister, C. T. Moonen,

P. van Gelderen, J. S. Cohen, P. C. M. van Zijl, *J. Magn. Reson.* **1992**, *100*, 281−303.
[18] W. Wilker, D. Leibfritz, R. Kerssebaum, W. Bermel, *Magn. Reson. Chem.* **1993**, *31*, 287−292.
[19] [19a] C. Cocevar, G. Mestroni, A. Camus, *J. Organometal. Chem.* **1972**, *35*, 389. − [19b] R. Uson, L. A. Oro, C. Claver, M. A. Garralda, *J. Organometal. Chem.* **1976**, *105*, 365.
[20] L. A. Oro, M. J. Fernandez, J. Modrego, J. M. Lopez, *J. Organometal. Chem.* **1985**, *287*, 409.
[21] P. H. M. Budzelaar, R. de Gelder, A. W. Gal, *Organometallics* **1998**, *17*, 4121.
[22] Ch. Mahabiersing, J. G. Donkervoort, C. J. Elsevier, in preparation.
[23] L. A. Oro, M. A. Ciriano, F. Viguri, C. Foces-Foces, F. H. Cano, *Inorg. Chim. Acta* **1986**, *115*, 65.
[24] A. van der Ent, A. L. Onderdelinden, *Inorg. Synth.* **1990**, *28*, 90.
[25] R. Cramer, *J. Am. Chem. Soc.* **1964**, *86*, 217.
[26] R. Uson, L. A. Oro, M. A. Ciriano, F. J. Lahoz, *J. Organometal. Chem.* **1982**, *240*, 429.
[27] A. D. Becke, *Phys. Rev. A* **1988**, *38*, 3098.
[28] [28a] J. P. Perdew, *Phys. Rev. B* **1986**, *33*, 8822. − [28b] J. P. Perdew, *Phys. Rev. B* **1986**, *34*, 7406.
[29] D. Andrae, U. Häußermann, M. Dolg, H. Stoll, H. Preuß, *Theor. Chim. Acta* **1990**, *77*, 123.
[30] WJ. Hehre, L. Radom, P. v. R. Schleyer, J. A. Pople, *Ab initio Molecular Orbital Theory*, Wiley, New York, 1986.
[31] As implemented in Gaussian 94: J. R. Cheeseman, G. W. Trucks, T. A. Keith and M. J. Frisch, *J. Chem. Phys.* **1996**, *104*, 5497.
[32] A. D. Becke, *J. Chem. Phys.* **1993**, *98*, 5648.
[33] C. Lee, W. Yang, R. G. Parr, *Phys. Rev. B* **1988**, *37*, 785.
[34] S. Huzinaga, M. Klobukowski, *J. Mol. Struct.* **1988**, *167*, 1.
[35] W. Kutzelnigg, U. Fleischer, M. Schundler, in *NMR Basic Principles and Progress* Vol. 23, Springer-Verlag, Berlin, 1990, 165.
[36] M. J. Frisch, G. W. Trucks, H. B. Schlegel, P. M. W. Gill, B. G. Johnson, M. A. Robb, J. R. Cheeseman, T. Keith, G. A. Petersson, J. A. Montgomery, K. Raghavachari, M. A. Al-Laham, V. G. Zakrzewski, J. V. Ortiz, J. B. Foresman, C. Y. Peng, P. Y. Ayala, W. Chen, M. W. Wong, J. L. Andres, E. S. Replogle, R. Gomperts, R. L. Martin, D. J. Fox, J. S. Binkley, D. J. De Frees, J. Baker, J. J. P. Stewart, M. Head-Gordon, C. Gonzales, J. A. Pople, Gaussian 94, Pittsburgh PA, 1995.

Received June 30, 1998
[I98207]

A Versatile Fluorescent System for Sensing of H^+, Transition Metals, and Aromatic Carboxylates

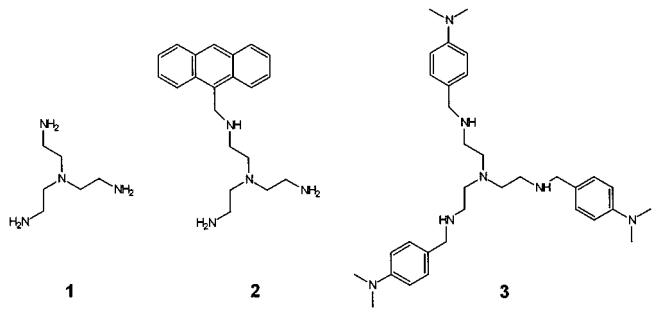
Luigi Fabbrizzi,*[a] Maurizio Licchelli,[a] Luisa Parodi,[a] Antonio Poggi[a], and Angelo Taglietti[a]

Keywords: Fluorescent sensors / Molecular recognition / Charge transfer excited states / Metal complexes / pH Sensors

The fluorescent emission of the *N,N*-dimethylaniline fragment of the tetramine system **3** varies with pH, displaying a maximum of the fluorescent intensity, I_F, at pH = 5. Binding of transition metals (Cu^{II}, Ni^{II}) induces fluorescence quenching and modifies the I_F vs. pH profile, giving rise to an OFF-ON-OFF type of sensor. The $[Zn^{II}(\mathbf{3})]^{2+}$ complex recognises carboxylate anions, both aliphatic and aromatic. Recognition is signalled via fluorescence quenching only for aromatic carboxylates.

In principle, a molecular fluorescent sensor for any kind of analyte can be built by following the fluorophore-spacer-receptor approach, i.e. by covalently linking a light-emitting fragment to a ligating subunit capable of recognising the desired substrate. Most importantly, an intra-molecular mechanism must exist that associates substrate binding and emitting activity of the fluorophore.[1−4] Thus, the recognition process can be signalled through either fluorescence enhancement or quenching. In this sense, a molecular fluorescent sensor can be well illustrated with the switch-light bulb metaphor, as an external input (a variation of analyte concentration, corresponding to a finger) operates the switch (the receptor subunit), thus turning on/off the light emission by the fluorescent fragment (the light bulb).[5]

We describe here a versatile fluorosensor for ionic analytes of varying kind, based on the tripodal tetramine tren, **1**.



1 **2** **3**

Tren is a quite good ligand for transition metal ions, imposing in most cases a trigonal bipyramidal coordination geometry.[6] Whereas four coordination sites are occupied by the amine groups of tren, the axial position, opposite to the tertiary nitrogen atom, is vacant and available for an anion. As a consequence, a metallo-tren subunit may behave as a receptor for ionic analytes. In this regard, we have recently reported on a Zn^{II}-tren system with a covalently appended anthracene fragment, $[Zn^{II}(\mathbf{2})]^{2+}$, which is able to recognise the $-COO^-$ residue.[7] However, recognition is signalled only for those anions displaying electron donor/acceptor tendencies, which quench the nearby fluorophore via an electron transfer mechanism.

We have now appended at each terminal amine nitrogen atom of tren an *N,N*-dimethylaniline subunit (DMA): *N*2-(4-dimethylaminobenzyl)-*N*1,*N*1-bis[2-(4-dimethylaminobenzylamino)ethyl]ethane-1,2-diamine, trenDMA$_3$, **3**. The DMA fragment, when irradiated at 300 nm, gives rise to a charge transfer (CT) excited state, which emits light at 360 nm. The interaction of the DMA-photoexcited fragment with analytes hosted by the tetramine receptor may induce drastic variations of the emission intensity, opening the way to fluorosensing of protons, transition metals and anions. Moreover, the protonation of the dimethylamine group of DMA, in strongly acidic solutions, destroys the CT-photoexcited state and quenches the fluorescence. This unique feature opens a further opportunity for selective signalling of ionic analyte recognition in aqueous solution.

Interaction with Protons

The emitting behaviour of **3** over the pH range 2−10 was investigated through a spectrofluorimetric titration experiment. In particular, a solution of **3** (10^{-4} mol L^{-1}) containing excess acid was titrated with a standard NaOH solution. The profile of the fluorescence intensity, I_F (%), vs. pH is displayed in Figure 1.

At very low pH (<2), the solution is very poorly emitting: in these acidic conditions, the dimethylamine group of each DMA fragment of **3** is protonated and the CT excited state cannot be achieved. On increasing pH, the intensity (I_F) of the emission band centered at 370 nm steeply increases, due to the stepwise deprotonation of the dimethylammonium groups and concurrent formation of the corresponding photoexcited state. At pH = 5.3, I_F reaches its maximum

[a] Dipartimento di Chimica Generale, Università di Pavia, Viale Taramelli 12, I-27100 Pavia Italy
Fax: (internat.) +39-382/528544
E-mail: fabbrizz@ipv36.unipv.it

 © WILEY-VCH Verlag GmbH, D-69451 Weinheim, 1999 1434−1948/99/0101−0035 $ 17.50+.50/0

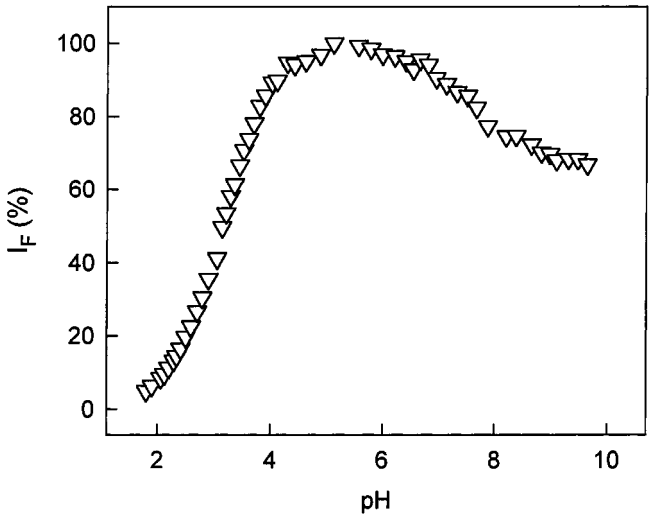


Figure 1. pH dependence of the fluorescence (λ_{exc} = 300 nm; λ_{em} = 370 nm) intensity for a solution of **3** in water

value then decreases smoothly. An emission spectrum of **3** measured at pH 8.5 is reported in Figure 2.

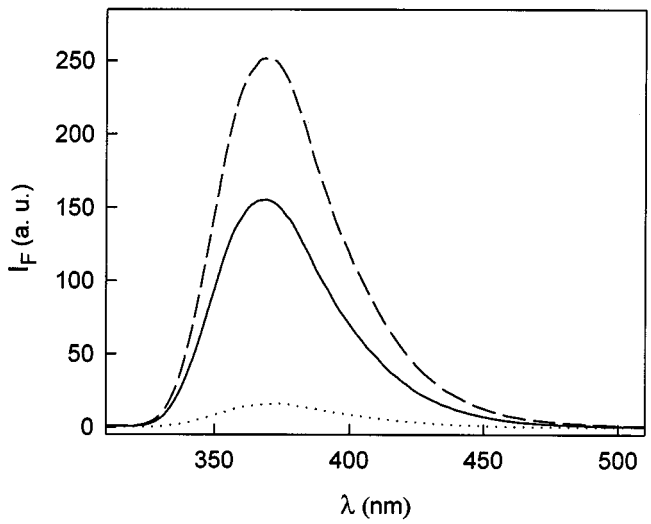


Figure 2. Emission spectra (λ_{exc} = 300 nm) in aqueous solution at pH 8.5 of: (___) free ligand **3**, (····) copper complex, (– – –) zinc complex

Progressive quenching of fluorescence after pH = 5.3 is to be ascribed to the stepwise deprotonation of the ammonium groups of the tren subunit adjacent to the DMA fragments. In fact, the amine group possesses reducing tendencies and can transfer an electron to a nearby photoexcited fluorophore, inducing fluorescence quenching.[8][9] It is possible that not only the adjacent secondary amine groups, but also the tertiary one, probably the first to deprotonate, is involved in the electron transfer process to the DMA fragment. The rather low solubility of **3** prevented a whole investigation of the stepwise protonation equilibria through potentiometric titration and determination of the pertinent pK_A values.

It should be noted that **3** belongs to the class of OFF-ON-OFF fluorosensors.[10] Sensors of this type are especially valuable, as, in contrast to usual indicators, they signal, via the fluorescent emission, the pH of the solution, within a given window. The narrower the window, the most precise and useful the sensor. In this sense, **3** is a rather poor sensor, as its peaks is poorly defined, and the window is spread over a too large pH interval.

Sensing of 3d Metal Ions

A solution of **3** containing 1 equiv. of Cu^{II} and excess acid was titrated with standard NaOH and the emission of the solution was spectrofluorimetrically monitored. In the acidic region, the I_F vs. pH profile superimposes well on the profile observed for the metal free solution. However, after reaching its maximum value at pH = 3.8, I_F decreases abruptly and full quenching is observed at pH = 5.5. The addition of Cu^{II} did not induce any changes in the shape and energy of the emission band (see Figure 3).

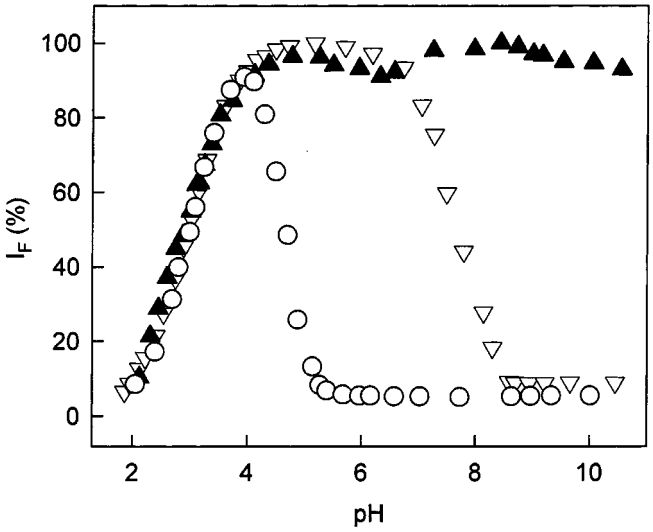


Figure 3. pH dependence of the fluorescence intensity (λ_{exc} = 300 nm; λ_{em} = 370 nm) for solutions containing equimolecular amounts of **3** in water and Cu^{II} (○); Ni^{II} (▽); Zn^{II} (▲)

Quenching is to be associated to the metal binding by the tren subunit of **3**, a process occurring in the pH = 4–5.5 interval. Transition metals typically quench proximate fluorophores via either electron transfer (eT) or energy transfer (ET) processes.[11,12] The two mechanisms can be discriminated by carrying out spectrofluorimetric studies on solutions frozen at the liquid nitrogen temperature. In fact, the occurrence of an eT process induces charge separation within the two-component system, to which a substantial rearrangement of solvent molecules is associated. Freezing prevents this rearrangement and interrupts the eT process: as a consequence, fluorescence is restored. On the other hand, an ET process induces a circular exchange of electrons, with no charge separation and no solvational rearrangement: as a consequence, the fluorophore remains quenched even when the solution is frozen at liquid nitrogen temperature and the solvent molecules are immobilised.[13] In particular, we observed that freezing at 77 K of

an equimolar solution of **3** and Cu^{II} in EtOH, did not induce any fluorescence revival, thus indicating that an ET mechanism operates. In this connection, it should be considered that Cu^{II} possesses a half-filled level of low energy (d_{z^2}, in a trigonal bipyramidal geometry), suitable for the occurrence of a double electron exchange process with a neighboring excited singlet. However other deactivation pathways (e.g. internal conversion) may be competitive in the presence of the metal ion. An intersystem crossing process could be accelerated by the proximate transition metal ion to generate a triplet state which is often non-emissive even at low temperatures.

Quite interestingly, the **3**-Cu^{II} equimolar system behaves as an extremely efficient OFF-ON-OFF pH sensor, giving rise to a well defined peak and to a narrow pH-window (2/5.5). The observed behaviour is very similar to that displayed by previously reported systems,[10] consisting of covalently linked amine, pyridine, and anthracene fragments. In those pH sensors, the quenching mechanism before and after the I_F peak (both located at pH = 6) were both of eT nature: (i) from the photoexcited anthracene subunit, An*, to the pyridinium moiety, and (ii) from the amine group to An*. In the presently investigated **3**-Cu^{II} system, the protonation of the amine group of DMA, and an ET mechanism (involving Cu^{II} and DMA*) operate.

Also when titrating **3** in presence of 1 equiv. of Ni^{II}, a peak is observed in the I_F vs. pH profile, fluorescence decrease and quenching being observed at a higher pH than in the case of Cu^{II} (see Figure 3). This is due to the intrinsically lower affinity of the tetramine subunit towards Ni^{II}, compared to Cu^{II} (constants for the M^{II} + tren = $[M^{II}(tren)]^{2+}$ equilibrium, in aqueous solution are $10^{14.95}$ and $10^{19.58}$, respectively).[14] Thus, also the **3**-Ni^{II} system gives rise to an OFF-ON-OFF behaviour even if with a rather large peak width.

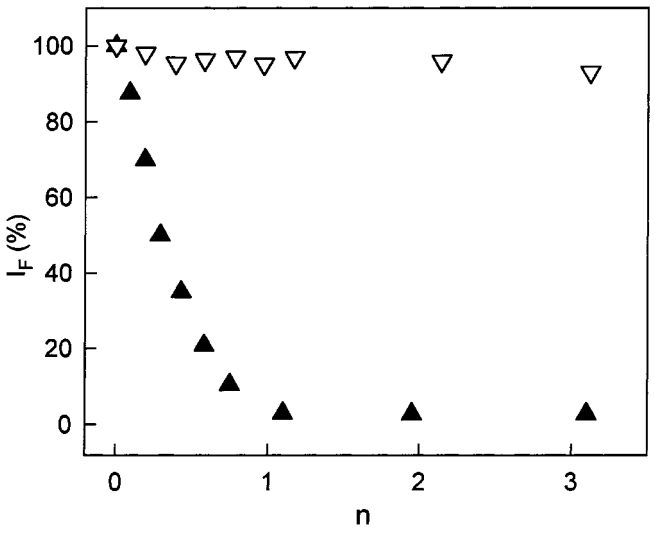


Figure 4. Discrimination of Cu^{II} and Ni^{II} by fluorescent sensor **3** in water solution buffered at pH 6 with MES buffer. Titration with Ni^{II} does not alter fluorescence (▽). On addition of Cu, I_F (λ_{exc} = 300 nm; λ_{em} = 370 nm) decreases linearly (▲); full quenching is observed with the addition of 1 equiv. *n* = number of added equivalents

On the other hand, the remarkably different affinity of the tren subunit towards Cu^{II} and Ni^{II} allows an efficient discrimination of the two metal ions to be carried out. In this connection, an aqueous solution 10^{-4} M in **3** was buffered to pH = 6 and titrated with a Ni^{II} standard solution: no alteration of the emission spectrum of the DMA fragment was observed, even after the addition of several equiv. of Ni^{II} (see Figure 4). Failure of I_F modification was due to the fact that at pH = 6 the Ni^{II} ion is not complexed by the tetramine receptor subunit. Then, the same solution was titrated with Cu^{II}. A linear decrease of I_F was observed and complete fluorescence quenching was achieved after the addition of 1 equiv. of Cu^{II}.

The Zn^{II} ion behaves quite differently with respect to Cu^{II} and Ni^{II}. In fact, on titration with standard base of an acidified solution of **3**, containing 1 equiv. of Zn^{II}, the typical increase of I_F with increasing pH was observed, which reached its maximum value at pH = 5 (see Figure 3). At this pH, the dimethylammonium group of each DMA fragment is deprotonated, which restores DMA emission. However, at pH $\geq$ 6, I_F does not begin to decrease, as observed in a metal-free solution (due to the occurrence of an eT process from the proximate amine groups) or in presence of either Cu^{II} or Ni^{II} (due to an ET mechanism involving the tetramine complexed transition metal), but maintains its maximum value until definitely basic conditions. This behaviour must be ascribed to the complexation of Zn^{II} by the tren subunit, which should occur at pH $\geq$ 6.5. In fact, metal coordination prevents the occurrence of the amine-to-DMA* eT process. On the other hand, the Zn^{II} centre, which has a d^{10} electronic configuration and does not exhibit any redox activity, cannot be involved in any ET or eT process with the nearby photo-excited fragments. The photophysical innocence of Zn^{II} as well as the coordinative unsaturation of its tren complex open the way to the design of fluorosensors for anions, whose recognition processes are based on the metal-ligand interaction (vide infra).

Sensing of Aromatic Carboxylates

The tren subunit typically imposes a trigonal bipyramidal stereochemistry to the complexed metal centre. The axial position opposite to the tertiary amine group is vacant and available for the coordination by a solvent molecule or by an anion. Thus, a metal−tren moiety can behave as a receptor for anionic substrates displaying coordinating tendencies. In this connection, the Zn^{II} derivative of a tren subunit equipped with an anthracenyl substituent (trenan, **2**) was observed to recognise aromatic carboxylates (in view of the special affinity of the $-COO^-$ group for the Zn^{II} centre), but to sense, via the anthracene fluorescence quenching, only those benzoates bearing either a donor, e.g. $-N(CH_3)_2$, or an acceptor substituent, e.g. $-NO_2$, on the 4-position of the ring.[7] Quenching was ascribed to an intra-complex eT process involving the benzoate substituent and the facing photo-excited anthracene fragment. Plain benzoate binds the Zn^{II} centre in **2**, but its recognition is not signalled by any modification of the anthracene emission.

We have tested the recognising and sensing tendencies of the Zn^{II}-**3** system towards carboxylates by carrying out spectrofluorimetric titration experiments in MeOH solution. In particular, a solution of the $[Zn^{II}(\mathbf{3})]^{2+}$ complex was titrated with a solution containing the sodium salt of the envisaged carboxylate anion. It was observed that addition of aromatic carboxylates induces quenching of the emission of the DMA fluorophore, I_F being reduced to less than 20% of the original value. I_F vs. equiv. of anion profiles for benzoate, 9-antracenoate, 4-nitrobenzoate, are reported in Figure 5.

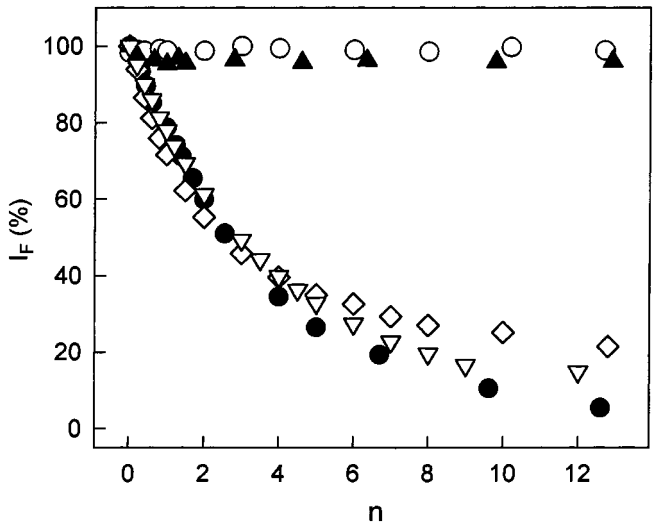


Figure 5. Spectrofluorimetric titrations (λ_{exc} = 300 nm; λ_{em} = 370 nm) of the receptor $[Zn^{II}(\mathbf{3})]^{2+}$ in methanolic solution (10^{-4} mol L^{-1}) with standard methanolic solutions of benzoate (◇); 9-anthracenoate (▽); 4-nitrobenzoate (●); acetate (▲); cyclohexylcarboxylate (○); n = number of added equivalents

Non-linear least-squares analysis of titration profiles reported in Figure 5 indicated the formation of 1:1 adducts.[15] The log$K$ values associated to the equilibrium:

$$[Zn^{II}(\mathbf{3})]^{2+} + X^- \rightleftharpoons [Zn^{II}(\mathbf{3})(X)]^+ \quad (1)$$

are reported in Table 1.

Table 1. log$K$ values for the $[Zn^{II}(\mathbf{3})(anion)]^+$ adduct formation

Anion	logK	quenching[a]
benzoate	4.69±0.04	yes
4-nitrobenzoate	4.43±0.06	yes
9-anthracenoate	4.47±0.04	yes
acetate	4.35±0.08	no
cyclohexylcarboxylate	4.08±0.08	no
chloride	3.69±0.08	no
nitrate	not bound[b]	=
perchlorate	not bound[b]	=

[a] Anion binding induces partial quenching of the emission of the DMA fragment of **3**. – [b] No alteration of titration profiles of benzoate were detected during competition experiments (see text).

Titration with aliphatic carboxylates (acetate and cyclohexylcarboxylate) did not induce any modification of the DMA emission intensity, as seen in Figure 5. However, the binding of the aliphatic carboxylates is demonstrated by competitive titration experiments involving aromatic carboxylates. As an example, titration of a solution of $[Zn^{II}(\mathbf{3})]^{2+}$ containing 10 equiv. of acetate with benzoate produces a less steep profile than that obtained in absence of acetate, indicating competition of the two substrates for the Zn^{II} site. The log$K$ values associated to the adducts of aliphatic carboxylates and other inorganic anions were calculated from the I_F vs equiv. of benzoate profiles, obtained for spectrofluorimetric titrations of solutions containing varying amounts of the investigated anion: their values are reported in Table 1. It can be seen that the values for aliphatic carboxylates are comparable with those observed for aromatic carboxylates.

It derives that the $[Zn^{II}(\mathbf{3})]^{2+}$ system is a discriminating sensor, which recognises the $-COO^-$ group, but communicates recognition only if the $-COO^-$ group is appended to an aromatic backbone. The explanation of this behaviour is not straightforward.[16] It is suggested that aromatic carboxylates interact with the DMA substituents via π stacking. This modifies the energy of the π orbitals of the DMA subunits. It should happen that the the energy of the DMA HOMO level is reduced to such an extent that its combination with the donating DMA orbital is minimized and, as a consequence, the generation of the charge transfer excited state prevented.

Experimental Section

General Considerations: All the reagents (Aldrich) were used without further purifications. – NMR data were obtained on a Bruker AMX 400 MHz. – All fluorescence measurements were carried out on a Perkin Elmer LS-50 luminescence spectrometer equipped with a 1.0 cm quartz cells. – Emission spectra at 77 K were measured in dry ethanol by using quartz sample tubes and the same luminescence accessory (Perkin-Elmer, Norwalk, CT, USA). – All pH measurements were made with an Orion 420A (Cambridge, MA, USA) digital pH meter using a combined glass-calomel electrode.

Synthesis of *N*2-(4-Dimethylaminobenzyl)-*N*1,*N*1-bis[2-(4-dimethylaminobenzylamino)ethyl]ethane-1,2-diamine (TrenDMA$_3$, **3**): 1.53 g (10.27 mmol) of 4-dimethylaminobenzaldehyde were dissolved in toluene (30 mL) and slowly added to a solution of tren (3.42 mmol) in toluene (100 mL). The reaction mixture was heated at 40°C for 24 hours. Solvent was removed under reduced pressure, and the yellow-orange oil (the imine intermediate) was dissolved in MeOH. $NaBH_4$ was carefully added in small portions, and then the reaction mixture was heated at 50°C overnight. The solvent was removed under reduced pressure and the sticky solid obtained was dissolved in 50 mL of water. The aqueous phase was extracted with CH_2Cl_2 (3× 50 mL). The organic phase was dried with $MgSO_4$ and then the solvent was distilled off, obtaining **3** as a yellow-brown oil. Yield: 70%. – MS (70 eV); *m/z* (%): 545 (6) [M^+] – ^{1}H NMR (400 MHz, $CDCl_3$): δ = 7.1 (d, J = 9 Hz, 6 H aromatic), 6.6 (d, J = 9 Hz, 6 H aromatic), 3.55 (s, 6 H) 2.8 (s, 18 H), 2.55 (t, J = 6 Hz, 6 H), 2.45 (t, J = 6 Hz, 6 H).

Spectrofluorimetric Titrations: pH titrations were performed on 10^{-4} mol L^{-1} water solutions of **3** adjusted at pH < 2 by adding small amounts of a standard solution of $HClO_4$ (1 or 0.1 mol L^{-1}). Then additions of standard solutions of NaOH (1 or 0.1 mol L^{-1}) were made until a basic pH (> 10) was obtained. Emission spectra

(excitation wavelength 300 nm) were taken after each addition of base. Titrations at buffered pH were carried out in water solutions (40 mL, 10^{-4} mol L^{-1}) . Buffered solutions were obtained with MES (pH 6). $M^{II}(ClO_4)_2$ standard (M = Zn, Cu, Ni) solutions were used and spectra recorded after every addition. Anion titrations were carried out in methanol solutions (40 mL, 10^{-4} mol L^{-1}) of an equimolecular mixture of **3** and $Zn(ClO_4)_2$. Standard solutions in methanol of sodium carboxylate salts were added, and spectra recorded after each addition.

Acknowledgments

This work was supported by C.N.R. (Progetto Finalizzato "Biotecnologie") and the Ministry of University and Research (MURST).

[1] A. W. Czarnik, *Chemistry and Biology*, **1995**, *2*, 423
[2] A. P. de Silva, H. Q. N. Gunaratne, T. Gunnlaugsson, A. J. M. Huxley, C. P. McCoy, J. T. Rademacher, T. E. Rice, *Chem. Rev.* **1997**, 97, 1515.
[3] F. Fages, *Chemosensors of Ion and Molecule Recognition*, (Eds.: J.-P. Desvergne, A. W. Czarnik), Kluwer Academic Publishers, Dordrecht **1997**, pp. 221−240.
[4] L. Fabbrizzi, M. Licchelli, P. Pallavicini, D. Sacchi, A. Taglietti, *Analyst* **1996**, *121*, 1763.
[5] L. Fabbrizzi, A. Poggi, *Chem. Soc. Rev.* **1995**, 197.
[6] M. Ciampolini, *Structure and Bonding*, **1969**, *6*, 52
[7] G. De Santis, L. Fabbrizzi, M. Licchelli, A. Poggi, A. Taglietti, *Angew. Chem., Int. Ed. Engl.* **1996**, *35*, 202.
[8] A. P. de Silva, R. A. D. D. Rupasinghe, *J. Chem. Soc. Chem. Comm.* **1985**, 1669.
[9] M. E. Huston, K. W. Haider, A. W. Czarnik, *J. Am. Chem. Soc.* **1988**, *110*, 4460.
[10] [10a] A. P. de Silva, H. Q. N. Gunaratne, C. P. McCoy, *Chem. Commun.* **1996**, 2399. − [10b] S. A. de Silva, A. Zavaleta, D. E. Baron, O. Allam, E. V. Isidor, N. Kashimura, J. M. Percarpio, *Tetrahedron Lett.*, **1997**, *13*, 2237.
[11] V. Balzani, F. Scandola, *Supramolecular Photochemistry*, Ellis Horwood, London, **1991**.
[12] L. Fabbrizzi, M. Licchelli, P. Pallavicini, A. Perotti, A. Taglietti, D. Sacchi, *Chem. Eur. J.* **1996**, *2*, 167.
[13] M. R. Wasielewski, G. L. Gaines III, M. P. O′Neil, M. P. Niemczyk, W. A. Svec in *Supramolecular Chemistry* (Eds.: V. Balzani, L. De Cola), Kluwer Academic Publishers, Dordrecht, **1992**, p. 202.
[14] C. Anderegg, V. Gramlich, *Helv. Chim. Acta*, **1994**, *77*, 685
[15] HYPERQUAD program was used: A. Sabatini, A. Vacca, P. Gans, *Coord. Chem. Rev.* **1992**, *120*, 389−405.
[16] One of the Referees suggested an alternative explanation: in particular, a non-emissive exciplex between the aromatic carboxylate and the excited aminobenzene fragment could form. Such an exciplex would be expected to undergo a fast intersystem crossing due to the carbonyl oxygen lone pairs. This would not be the case for the non-aromatic carboxylates.

Received May 8, 1998
[I98146]

Synthesis and Reactivity of Subvalent Compounds, 8[+] Aromatic Phosphenium Cations[§]

Michael K. Denk,*[a] Shilpi Gupta,[a] and Alan J. Lough[a]

Dedicated to Professor Heinrich Nöth on the occasion of his 70th birthday

Keywords: Phosphorus heterocycles / Aromaticity / Phosphenium cations / Ab initio calculations

The aromatic stabilization of cyclic phosphenium cations (general type $C_2N_2P^+$) was studied by experimental methods (synthesis, multinuclear NMR, single crystal X-ray crystallography) and quantum chemical calculations (ab initio methods). The structures of the 1,3,2-diazaphosphole derivatives [(*t*BuN–CH=CH–N*t*Bu)P$^+$]Cl$^-$ (**1**), (*t*BuN–CH_2–CH_2–N*t*Bu)P–Cl (**2**), [(*t*BuN–CH=CH–N*t*Bu)P]$^+$ PF_6^- (**3**) and [(*t*BuN–CH_2–CH_2-N*t*Bu)]P$^+$ PF_6^- (**4**) were examined by single crystal X-ray diffraction. The chloro phosphane [(*t*BuN–CH=CH–N*t*Bu)P]$^+$Cl$^-$ (**1**) has an ionic P–Cl bond and contains an aromatically stabilized phosphenium cation [shortest distance P···Cl = 275.9(2) pm], while the CC-saturated compound (*t*BuN–CH_2–CH_2–N*t*Bu)P–Cl (**2**) is covalent. The two chloro-phosphanes **1** and **2** differ sharply in their volatility and solubility in organic solvents. Compound **2** is soluble in hydrocarbons and sublimes readily at 90 °C/0.1 Torr but **1** is insoluble in hexanes and not volatile below 180 °C/0.1 Torr. The degree of aromatic stabilization in the phosphenium cation **1** was investigated by ab initio methods. For the model cations [RN–CH_2–CH_2–NR]P$^+$ and [(RN–CH=CH–NR)P]$^+$, thermochemical stabilization energies of 25.8 kcal · mol^{-1} (R = H) and 28.1 kcal · mol^{-1} (R = Me) were obtained from isodesmic hydrogenation reactions at the RHF/MP2/6–31G*//RHF/6–31G* level.

Introduction

The aromatic stabilization of inorganic ring systems has seen renewed interest both by synthetic chemists and theoreticians.[1] We are currently involved in a comparative study of aromatically stabilized 1,3-diazole derivatives **A** and their non-aromatic counterparts **B**. The 1,3-diazoles **A** and 1,3-diazolidines **B** seem to have an unsurpassed capability to stabilize the heteroelement E in the coordination number 2.

The first stable carbenes[2] and silylenes[3] were indeed of type **A** and it is likely that other elements will likewise be stabilized in unusually low coordination numbers in systems of type **A** and **B**. Likely candidates for a successful isolation would be heterocycles that are isoelectronic with the stable carbenes and silylenes such as anionic diazoles featuring dicoordinate boron, aluminum, and gallium and cationic diazoles with dicoordinate nitrogen, phosphorus, and arsenic. Apart from the appeal to stabilize elements in unusual valence states, these species would make useful, presumably highly reactive building blocks of carbenoid reactivity.

The comparison of the respective unsaturated species **A** with the saturated counterparts **B** allows the systematic and independent variation for aromaticity and the heteroelement. For some elements, the experimental comparison of **A** and **B** is already possible as these species have been described in the literature. Both stable aromatic (**A**) and non-aromatic representatives (**B**) have been described for E = C,[2] Si,[3] Ge,[4] N^+[5] and P^+[6] and, most recently, As^+.[7a,11b] For the elements of the boron group, the anionic diazoles **A** and **B** would be isoelectronic to the stable carbenes and silylenes but have not been reported to our knowledge.[8]

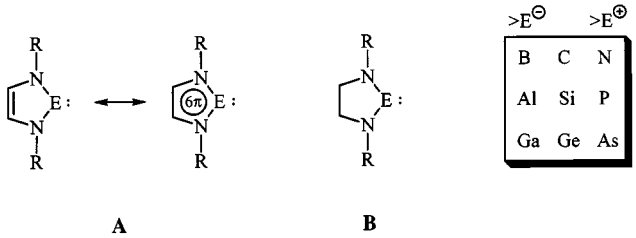


Figure 1. Aromatic 1,3-diazoles (**A**) and non-aromatic 1,3-diazolidines (**B**)

Heterocycles **A** described so far possess properties typically associated with aromatically delocalized compounds. They display unusually deshielded ring protons,[2–5] show decreased alternation in bond lengths[2–5] and exhibit reduced reactivity of **A** vs. **B**.[2–5]

For E = C,[2] Si,[3] Ge,[4] and N^+ [5] the electronic structures of **A** and **B** were investigated by ab initio methods and photoelectron spectroscopy. These studies have demonstrated substantial delocalization of the occupied π-orbitals for **A** and a stabilization of **A** vs. **B** ranging from 13 kcal·mol^{-1} for E = Ge[1] to as high as 38 kcal·mol^{-1} for E = N^+.[5] A summary of the different criteria used to

[+] Part 7: Michael K. Denk, Ken Hatano, Alan J. Lough, *Eur. J. Inorg. Chem.* **1998**, 1067–1070.

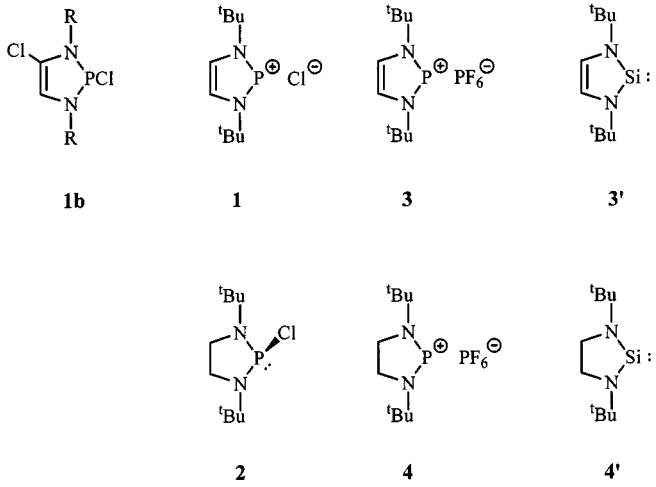
[§] The synthesis and structure of **1**–**4** were presented at the *29th Organosilicon Symposium*, Northwestern University, Evanston, Illinois, March 22–24, 1996.

[a] Department of Chemistry, University of Toronto, Mississauga, Ontario L5L 1C6, Canada
Fax: (internat.) +1-905/828-5335
E-mail: mdenk@credit.erin.utoronto.ca
Internet: http://mdenk.erin.utoronto.ca

 © WILEY-VCH Verlag GmbH, D-69451 Weinheim, 1999 1434–1948/99/0101–0041v $ 17.50+.50/0

evaluate delocalization and aromaticity is available for the carbenes and silylenes.[9] Most recently, a core electron spectroscopy study by Hitchcock's group has demonstrated that the π*-orbitals of the aromatic silylenes are delocalized as well.[3e]

We have previously studied the synthesis, structure, and bonding of a series of isostructural stable carbenes,[2c] silylenes[3] and germylenes,[4] and now report on the synthesis, structure, and aromatic stabilization of the isostructural phosphenium cations **A** and **B** (R = *t*Bu in all cases).[10]



1b **1** **3** **3'**

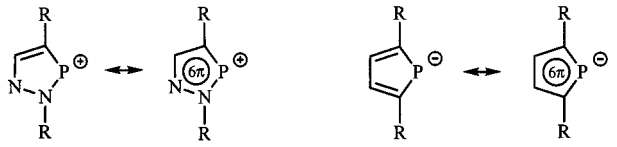
2 **4** **4'**

Figure 2. Aromatic and non aromatic phosphenium cations and chlorophosphanes and isoelectronic stable silylenes

The compounds investigated were the chlorophosphanes $[L'P]^+Cl^-$ (**1**), LP−Cl (**2**), and the stable phosphenium salts $[L'P]^+PF_6^-$ (**3**), $[LP]^+PF_6^-$ (**4**), $[L'P]^+GaCl_4^-$ (**5**), and $[LP]^+GaCl_4^-$ (**6**). Our study was triggered by the remarkably different physical properties of **1** and **2**: the chlorophosphane **2** is soluble in benzene and hexanes but **1** is insoluble in hexanes and only sparingly soluble in benzene.[11] Compound **2** is quite volatile and sublimes readily at 80°C/0.1 Torr while **1** is not volatile under these conditions. This different behavior led us to conclude that **1** is an ionic compound composed of a phosphenium cation and a chloride counterion while **2** is a covalent compound (Figure 2).[11] The crucial role of aromatic delocalization for the stabilization of **1** in its ionic form is obvious.

The related compound **1b** had previously been obtained by a special method namely in a one step synthesis from PCl_3 and the corresponding diazadiene R−N=CH−CH=N−R (R = *cyclo*-hexyl).[6b] While the authors noticed the long P−Cl bond length of 241.6(2) pm, they fell short of describing the compound as ionic or of relating the elongated P−Cl bond to the aromatic stabilization of the corresponding phosphenium cation. Instead, the elongation was attributed to electron donation from the two nitrogen lone pairs into the P−Cl σ*-orbital. No attempt was made to compare **1b** with the corresponding CC-saturated derivative.

As our comparison of **1** and **2** shows, the postulated donation of electron density from the nitrogen lone pairs to the P−Cl σ*-orbital alone is insufficient to induce the ionicity of **2**.



C **D**

Figure 3. Aromatic 1,3 and 1,2-diazaphospholes

Remarkably, the isomeric 2,3-diaza-*P*-chlorophospholes **C** were recognized as ionic on the basis of their physical and spectral properties by Schmidpeter et al.[12] and the ionicity of the P−Cl bond was attributed to the formation of an aromatic phosphenium cation 6π system.[12] The anionic phospholes **D** that were recently obtained by the Mathey's group were also described as delocalized, aromatic 6π systems.[13]

Synthesis and Stability

The chlorophosphane **2** was first described by Wrackmeyer et al. who also investigated the formation of the corresponding tetrachloroaluminate from **2** and $AlCl_3$ by spectroscopic methods.[6] Compound **1** has been obtained by us via metathesis of the corresponding diazasilole with PCl_3[11a] and had not been reported prior to our studies. The structures of **1** and **2** were reported by Carmalt et al. while this study was in progress.[11b]

The goal of this study was a detailed comparison of the chlorophosphanes **1** and **2** with the corresponding phosphenium cations. Our attempts to use $AlCl_3$ as chloride abstractor for **1** led to side reactions and were not pursued further. The use of $GaCl_3$ as chloride abstractor often gives cleaner reactions;[14] the tetrachlorogallates $[(tBuN-CH=CH-NtBu)P]^+GaCl_4^-$ (**5**)[11a] and $[(tBuN-CH_2-CH_2-NtBu)]P^+GaCl_4^-$ (**6**)[11a] were obtained from **1** and **2** without further complications. However, extensive disordering in the cation and anion sublattices precluded the determination of accurate structural data by single crystal X-ray diffraction and led us to search for new counterions. Accurate structural data were finally obtained for the hexafluorophosphates **3** and **4**. The hexafluorophosphates are easily obtained from **1** and **2** by metathesis with $AgPF_6$ in CH_2Cl_2 as colorless crystalline solids in quantitative yield.

The PF_6 and $GaCl_4$ salts **3**−**6** are quite soluble in dichloromethane and are easily purified by precipitation (layering) of the crude reaction solutions with hexanes. The salts **3**−**6** can be stored indefinitely under exclusion of air and moisture but the stability of the salts in solution depends critically on the nature of the counterion and the solvent. The PF_6 anion in the salts **3** and **4** slowly reacts with glass to form $PO_2F_2^-$ (and SiF_4) unless moisture is rigorously excluded. The reaction is easily detected by the presence of the characteristic triplet of $PO_2F_2^-$ ($\delta^{31}P = -14.7$, $^1J(P,F) = 976$ Hz).[15] Remarkably, the phosphenium cation is unaffected by this decomposition process. The reaction of PF_6^- with glass is catalyzed by water as was

recently shown by Manzano and Otero.[15] In $CDCl_3$ solution, **3** is stable indefinitely but **4** decomposes rapidly. This difference nicely illustrates the higher reactivity (lack of aromatic stabilization) of **4**. Both phosphenium cations are significantly stabilized by the counterion $GaCl_4^-$: **5** and **6** are stable indefinitely in CD_2Cl_2 and $CDCl_3$.

Structure and Bonding

The assumption that **1** is a purely ionic compound implies a nonbonding P−Cl distance and the presence of a phosphenium cation $[(t\text{BuN}-\text{CH}=\text{CH}-\text{N}t\text{Bu})\text{P}]^+$ in the crystal lattice. To justify this assumption, a detailed comparison of the chlorophosphanes **1** and **2** with each other and also with the corresponding phosphenium cations was necessary. The structure of **1** and, for comparison, the structures of **2**−**4** were determined by single crystal X-ray crystallography.[16]

While this study was in progress, the structures of **1** and **2** were reported by Carmalt et al.[11b] For **2**, our metrical parameters differ significantly form the values reported by Carmalt et al. (see below). This is especially obvious for the P−Cl bond distance: 231.36(7) pm in this study vs. Carmalt's value of 242.5(4) pm.[11b] The value of 143(1) pm reported by Carmalt for the C−C single bond in **2** is likewise too short and results probably from an unrecognized disorder of the (nonplanar) C_2N_2P ring. The superposition of two envelope structures can present itself as structure with planar C_2N_2E geometry and artificially shortened C−C bond length resulting from projections of the true bond distances. This type of disorder is easily recognized by unusually large thermal ellipsoids for the two carbon atoms and has been described previously by us for the isoelectronic germylene.[4] The value of 150.8(3) pm that we find for the C−C distance in **2** includes a modeling of disorder of the C_2-bridge and is also in much better agreement with the ab initio structures (Table 4). Accordingly, the values of our single crystal X-ray diffraction study will be used for the remainder of this study. The P−Cl distance in **1** [275.9(2) pm] is substantially longer than in **2** [231.36(7) pm]. Both P−Cl distances are shorter than the sum of the van-der-Waals radii[18] of phosphorus (190 pm) and chlorine (181 pm). With P−Cl bond lengths of ≈ 210 pm being typical for the fragment N_2P-Cl[19], even the P−Cl bond in **2** [231.36(7) pm] must be considered as unusually elongated. A comparison of the structures of **1** and **2** with the respective genuine phosphenium (type **A** and **B**) was clearly desirable and the structures of the PF_6 salts **3** and **4** were studied to this end.

In the hexafluorophosphates **3** and **4**, the closest distance between the phosphorus in the phosphenium cation and the fluorine atom of the counterion is nonbonding (322 pm for **3**, 323 pm for **4**). The values are nearly identical to the sum of van-der-Waals radii for phosphorus (190 pm)[18] and fluorine (135 pm)[18] and confirm that **3** and **4** are ionic compounds. Further proof that **3** and **4** do indeed contain phosphenium cations that are unperturbed by the counterion is

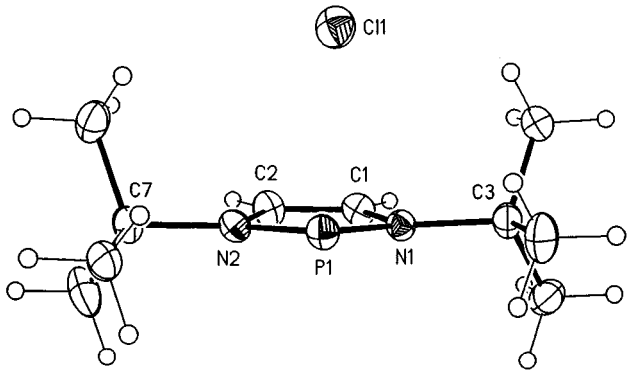


Figure 4. Molecular structure of $(t\text{BuN}-\text{CH}=\text{CH}-\text{N}t\text{Bu})\text{P}^+\text{Cl}^-$ **1** (0.5 C_6H_6), ORTEP view thermal ellipsoids are at the 50% probability level; selected bond lengths [pm] and bond angles [°] as follows: P(1)−N(1) 166.2(2), P(1)−N(2) 166.0(2), N(1)−C(1) 137.9(3), C(1)−C(2) 134.7(3), N(1)−C(3) 150.8(3), N(1)−P(1)−N(2) 90.41(10), P(1)−N(1)−C(1) 113.3(2), P(1)−N(1)−C(3) 123.8(2), N(1)−C(1)−C(2) 111.4(2), C(1)−N(1)−C(3) 123.8(2). Planar C_2N_2P-ring, closest P···Cl distance 275.9(2) pm.

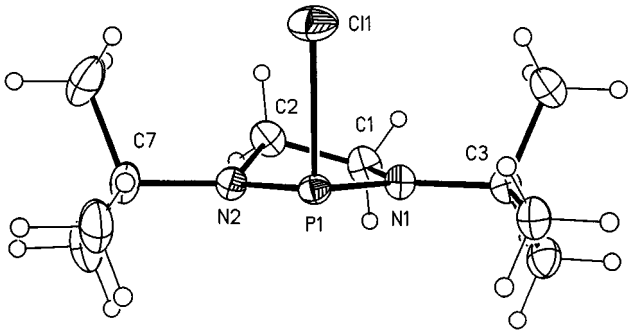


Figure 5. Molecular structure of $(t\text{BuN}-\text{CH}_2-\text{CH}_2-\text{N}t\text{Bu})\text{P}-\text{Cl}$ (**2**), ORTEP view, thermal ellipsoids are at the 50% probability level; selected bond lengths [pm] and bond angles [°] as follows: P(1)−Cl 231.36(7), P(1)−N(1) 165.2(2), P(1)−N(2) 165.6(2), N(1)−C(1) 147.1(3), C(1)−C(2) 150.8(3), N(1)−C(3) 148.8(3), N(1)−P(1)−N(2) 92.41(8), P(1)−N(1)−C(1) 114.77(13), P(1)−N(1)−C(3) 125.20(13), C(3)−N(1)−C(1) 119.9(2), C(2)−C(1)−N(1) 105.9(2). Puckered C_2N_2P-ring.

the excellent agreement between their molecular structures and those calculated (6−31G* level) for the free phosphenium cations (compare Tables 4 and 5).

The experimental structures of **3** and **4** can now be used as a yardstick to measure the phosphenium cation character of **1** and **2**. The structures of the diazaphosphole rings in **1** and **3** are practically identical. This confirm that **1** is indeed a phosphenium chloride.

The structures of **2** and **4** on the other hand show distinct differences: The P−N bond lengths are significantly shorter in **4** [161.3(2) and 161.9(2) pm] than in **2** [165.2(2) pm and 165.6(2) pm] and the N−P−N angle in **4** [96.29(11)°] is larger than in **2** [92.41(8)°]. A more detailed comparison of other structural parameters reveals that the P−N bond distance is the most sensitive structural probe to measure the phosphenium cation character in **4**.

The P−N bond length in the aromatic **3** [166.1(2) pm] is significantly longer than in **4** [161.9(2) pm]. This somewhat counterintuitive result supports the description of **3** as delocalized system: the isolated allylic N_2P fragment (in **4**)

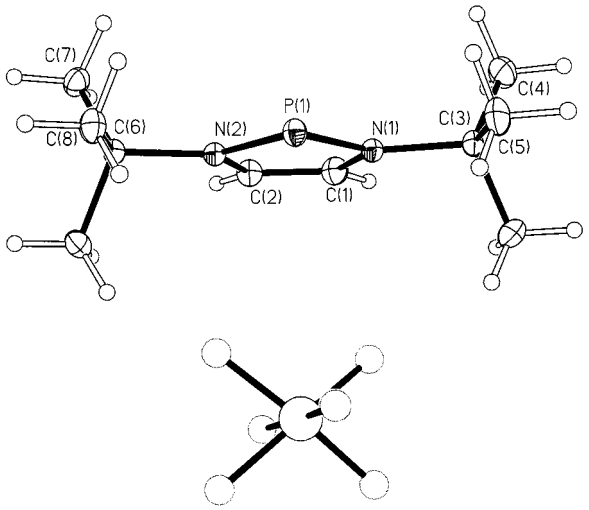


Figure 6. Molecular structure of $[(t\text{BuN}-\text{CH}=\text{CH}-\text{N}t\text{Bu})\text{P}]^{+}\text{PF}_6^{-}$ (**3**), ORTEP view, thermal ellipsoids are at the 50% probability level; selected bond lengths [pm] and bond angles [°] as follows: P(1)−N(1) 166.1(2), P(1)−N(2) 166.2(3), N(1)−C(1) 137.6(3), C(1)−C(2) 134.1(4), N(1)−C(3) 141.2(3), N(1)−P(1)−N(2) 90.71(11), C(1)−N(1)−P(1) 112.7(2), C(2)−C(1)−N(1) 111.6(2). Planar C_2N_2P-ring, closest distance P(1)···F = 322 pm.

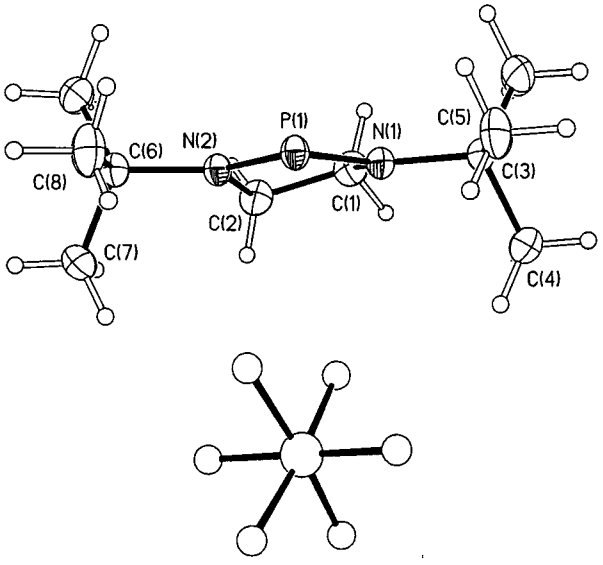


Figure 7. Molecular structure of $[(t\text{BuN}-\text{CH}_2-\text{CH}_2-\text{N}t\text{Bu})\text{P}]^{+}\text{PF}_6^{-}$ (**4**), ORTEP view, thermal ellipsoids are at the 50% probability level; selected bond lengths [pm] and bond angles [°] as follows: P(1)−N(1) 161.3(2), P(1)−N(2) 161.9(2), N(1)−C(1) 148.2(5), C(1)−C(2) 154.4(7), N(1)−C(3) 150.0(3), N(1)−P(1)−N(2) 96.29(11), C(1)−N(1)−P(1) 113.7(2), C(2)−C(1)−N(1) 105.1(4). Puckered C_2N_2P-ring, closest distance P(1)···F = 323 pm.

should experience increased delocalization and accordingly elongation of the P−N bond upon delocalization (in **3**). The nature of the phenomenon is perhaps best understood in an analogy pointed out by Sauers.[20] The C−C bond length in the cyclopentadienyl anion (141 pm) is longer than in the allyl anion (139 pm). The presence and magnitude of the effect is further evidence for a strong π-delocalization in **3**.

Silylenes R_2Si: are isoelectronic to phosphenium cations R_2P^+ and a comparison of **3** and **4** with the isostructural

Table 1. Experimental bond lengths [pm] and bond angles [°] of 1,3-diazaphospholes **1**−**4** (R = *t*Bu)

	$[L'P]^+Cl^-$ (**1**)	$[L'P]^+PF_6^-$ (**3**)	LP−Cl (**2**)	$[LP]^+PF_6^-$ (**4**)
N−P	166.0(2)	166.1(2)	165.2(2)	161.3(2)
N−P	166.2(2)	166.2(3)	165.6(2)	161.9(2)
N−C	137.9(3)	137.6(3)	147.1(3)	148.2(5)
N−C	138.9(3)	137.7(3)	147.8(2)	148.1(5)
C−C	134.7(3)	134.1(4)	150.8(3)	154.4(7)
N−P−N	90.41(10)	90.71(11)	92.41(8)	96.29(11)
N−C−C	111.4(2)	111.6(2)	105.9(2)	105.1(4)
R−N−C	122.1(2)	123.3(2)	119.9(2)	120.6(2)
P−N−C	113.3(2)	112.7(2)	114.77(13)	113.7(2)
P−N−R	123.8(2)	124.0(2)	125.20(13)	125.2(2)
Σ(N)[a]	359.2	360.0	359.9	359.5

[a] Sum of nitrogen bond angles.

stable silylenes should reveal the relative extent of aromatic stabilization in the silylenes and phosphenium cations. Table 2 compares bond distances and bond angles of the phosphenium hexafluorophosphates **3** and **4** with those of the isostructural silylenes **3′** and **4′**. The P−N distances in the phosphenium cations are ca. 4 pm shorter than one would extrapolate from the Si−N distances of the silylenes and the covalent radii of Silicon and Phosphorus.[18] This is in agreement with stronger π-bonding in the N_2P^+−allyl system compared with the N_2Si−allyl system. With the exception of the element-nitrogen bond distance, the geometries of **4** and **4′** are nearly identical.

Table 2. Experimental bond lengths [pm] and bond angles [°] of isoelectronic silylenes and phosphenium cations

	$[L'P]^+$ (**3**)	L′Si: (**3′**)	$[L'P]^+ PF_6^-$ (**4**)	LSi: (**4′**)
N−E	166.1(2)	175.3(5)	161.3(2)	171.9(3)
N−C	137.6(3)	140.0(9)	148.2(5)	148.9(6)
C−C	134.1(4)	134.7(21)	154.4(7)	152.1(14)
N−E−N	90.71(11)	90.5(10)	96.29(11)	92.0(2)
N−C−C	111.6(2)	114.1(5)	105.1(4)	106.2(7)
R−N−C	123.3(2)	120.4(22)	120.6(2)	116.4(3)
E−N−C	112.7(2)	110.5(11)	113.7(2)	113.2(2)
E−N−R	124.0(2)	128.8(13)	125.2(2)	129.7(2)
Σ(N)[a]	360.0	359.7	359.5	359.3

[a] Sum of nitrogen bond angles.

The relative extent of aromatic delocalization in the two aromatic species **3** and **3′** should be reflected by the difference between formal single bonds (C−N) and formal double bonds (C=C). The C−C double bond length of the silylene **3′** [134.7(21) pm] and the phosphenium cation **3** [134.1(4) pm] are nearly identical. The C−N bond length in **3** is shortened (−2.4 pm) vs. **3′**. This shortening of a formal C−N single bond, although not dramatic, is consistent with the conclusion that phosphenium cations of type **A** possess stronger aromatic delocalization than the isoelectronic silylenes. This is also in agreement with the chemical shifts of the respective ring protons and the results of ab initio calculations (see below).

Spectroscopy

NMR investigations of **1**−**6** were concerned with ring current effects[22] and the question to what extent the phosphenium cation character of **1** and **2** is reflected by the respective ^{31}P-NMR shifts. The hexafluorophosphates **3** and **4** with a fully developed phosphenium cation were used as ionic reference compounds. The phosphenium salts **1**, **3**, and **4** show the deshielded ^{31}P-NMR resonances of phosphenium cations but appear electron rich if compared with other phosphenium cations.[21] This documents the excellent dative stabilization of **1**, **3**, and **4**. The chemical shifts vary strongly with the solvent and to a lesser degree with concentration. All measurements were therefore standardized by measuring 1 M solutions at room temperature. This standardization is essential to reveal how the solvent and the counterion influence the ^{31}P-chemical shifts.

For **1**, polar solvents lead to strong deshielding of the ^{31}P signal. In CD_2Cl_2 and $CDCl_3$, the chemical shift of the phosphorus atom approaches the value found for the fully developed phosphenium cation in **3**. We interpret this solvatochromic behavior as a result of a solvent dependent polarization of the P···Cl contact in **1**. In the case of **1**, this polarization leads to a gradual increase of aromatic delocalization that can be monitored by ^{1}H NMR (deshielding of the ring protons by the ring current).[22] The extent of aromatic delocalization in **1** can thus be fine-tuned by using solvent mixtures. For example, the chemical shift δ^1H of the ring protons in **1** can be varied freely between 6.38 and 7.32 by using different mixtures of C_6D_6 and $CDCl_3$.

In $CDCl_3$, the chemical shift of the ring protons in **1** (δ = 7.32) approaches the value of the phosphenium salt **3** (δ = 7.66). This is good evidence that the P−Cl bond of **1** is dissociated in $CDCl_3$. Fully as expected, the most polar solvent used in this study ($CDCl_3$) leads to the most deshielded ^{31}P-NMR shifts for **1**−**6**. However, the salt $[L'P]^+PF_6^-$ (**3**) does not follow this trend. We tentatively attribute this deviation to the onset of a covalent interaction between the chlorine lone pair of chloroform and the phosphorus atom in **3**.

The chemical shifts ^{31}P and ^{1}H also depend on the nature of the counterion. This suggests that even the electronically highly stabilized phosphenium cations investigated in this study interact with the "non coordinating"[23] counterions $GaCl_4^-$ and PF_6^-.

The non-aromatic series of compounds (**2**, **4**, and **6**) displays the same type of solvatochromic behavior as the aromatic series **1**, **3**, and **5**, but the solvent induced shift variation is smaller.

The outlined solvatochromic behavior is presumably indicative for the tendency of a chlorophosphane to ionize to the corresponding phosphenium cation. Compounds like PCl_3 that do not give rise to well stabilized phosphenium cations do not display the same solvatochromic behavior. It seems likely, that the observed solvatochromic behavior extends to other chlorophosphanes $(Do)_2P-Cl$ with π-donor substituents Do. Further studies on the subject are in progress.

A comparison of NMR data for $[L'P]^+$ and the isostructural silylene and germylene is limited by the difficulties to find a common solvent. The PF_6 salts **3** and **4** are insoluble in C_6D_6 while the silylenes and germylenes are decomposed instantaneously by CD_2Cl_2 and $CDCl_3$.[24] If the partially developed phosphenium cation present in **1** is used instead of the fully developed phosphenium cation present in **3**, the chemical shifts of the ring protons follow the trend of thermochemical aromaticity obtained from ab initio calculations (see below):

$$L'Si < L'Ge < L'P^+$$

The solution NMR data of compound **2** do not match the symmetry of **2** in the solid state. In the crystal, the phosphorus atom in **2** is coordinated in a pseudo-tetrahedral environment. The protons of the ethylene bridge should fall into two distinct classes (*syn* and *anti* relative to the P−Cl bond) and a AA′BB′ spin system[25] should result. In $CDCl_3$ and CD_2Cl_2, the ^{1}H-NMR spectrum of **2** shows equivalent ring protons split into a well resolved doublet by ^3J coupling to the phosphorus atom. In the less polar C_6D_6, the signal of the ring protons is broadened and the ^3J coupling to the phosphorus atoms is lost. The apparent equivalence of the ring protons results from a dynamic process that is sensitive to the polarity of the solvent. A reversible dissociation of the chlorophosphane LP−Cl (**2**) into the (planar) $[LP]^+$ and Cl^- would allow the reattachment of the chloride from either sides of the planar N_2P^+ fragment. The result of this process is equivalent to an inversion at the phosphorus atom. Inversion of the phosphorus lone pair is hard to reconcile with the observed solvent effects.

Table 3. Solvatochromic behavior (δ^{31}P, δ^1H) of chloro phosphanes (**1**, **2**) and phosphenium cations (**3**− **6**). All shifts in ppm vs. TMS (^{1}H) or 85% H_3PO_4 (^{31}P).

Solvent	Comp.	δ^{31}P	δ^1H(=CH)	Compound	δ^{31}P	δ^1H(CH_2)
C_6D_6	[L′P]Cl (**1**)	146.7	6.38	LP−Cl	156.0	3.00
CD_2Cl_2	[L′P]Cl (**1**)	168.6	6.97	LP−Cl	166.8	3.37
$CDCl_3$	[L′P]Cl (**1**)	177.9	7.32	LP−Cl	166.5	3.39
CD_2Cl_2	[L′P]PF_6 (**3**)	203.3	8.08	[LP]PF_6 (**4**)	262.3	4.10
$CDCl_3$	[L′P]PF_6 (**3**)	189.6	7.66	[LP]PF_6 (**4**)	decomp.	decomp.
CD_2Cl_2	[L′P]$GaCl_4$ (**5**)	191.8	7.96	[LP]$GaCl_4$ (**6**)	274.7	4.10
$CDCl_3$	[L′P]$GaCl_4$ (**5**)	195.6	7.97	[LP]$GaCl_4$ (**6**)	279.2	4.18

Computational Studies

The relative degree of aromatic delocalization can be quantified by thermochemical cycles. As experimental values are not easily available for novel aromatic systems, computational approaches play an important role.

We have previously used *isodesmic* hydrogenation reactions to establish the relative stability of silylenes[3a] and germylenes[4] and now extend this approach to the isoelectronic phosphenium cations **3** and **4**.[29] Equations **a**−**d** involve the hydrogenation of the CC double bond and were chosen to investigate the degree of aromatic delocalization by testing the thermodynamic stabilities of the model compounds **7**−**10**. The *t*Bu substituent in **3** and **4** was replaced with R = H (model compounds **7H**−**10H**) or R = Me (**7Me**−**10Me**). The phosphonium cations $R_2PH_2^+$ (**9 H, 10 H, 9Me** and **10Me**) were chosen as non-aromatic reference compounds (disrupted π-delocalization). The specific combination of basis set, correlation method and isodesmic reactions used in this study is identical to the one we used to evaluate the aromatic stabilization of germylenes and silylenes. This allows a direct comparison of the calculated aromatic stabilization energies. Compounds **A** and **B** usually require bulky alkyl- or aryl substituents to be stable enough for isolation. To save computation time, these substituents are usually replaced with hydrogen in ab initio studies. We were interested to see how legitimate the replacement of alkyl substituents with hydrogen really is and thus have included the methyl compounds **7Me**−**10Me** in this study. While this study was in progress, the model compounds **7H** and **8H** were investigated by Sauers with a different basis set and a different set of isodesmic reactions.[20]

Aromatic stabilization energies (ASEs) for **7H** and **7Me** were obtained from the difference of the hydrogenation reactions **a** and **b** (|**a** − **b**| = ASE of **7H**) and **c** and **d** (|**c** − **d**| = ASE of **7Me**). It should be pointed out that an alternative system of isodesmic hydrogenation reactions (**e**−**h**) can be constructed from the oxidative addition of hydrogen to the phosphorus atom of the phosphenium cations **7** and **8** to give **9** and **10** respectively (Figure 8). Although the reaction energies for the equations **e**−**f** are different from those of the equations **a**−**d**, the aromatic stabilization energies obtained from both sets of equations are mathematically equivalent.[29b]

The results show a significant electronic stabilization of the unsaturated phosphenium cations **7H** and **7Me**. The methyl substituted phosphenium cation **7Me** possesses a slightly higher ASE (26.40 kcal·mol^{-1}) than the hydrogen derivative **7H** (25.73 kcal·mol^{-1}), a difference that is not only small but also well within the limits of the method. The use of the hydrogen substituted model compounds is thus fully adequate for the calculation of aromatic stabili-

Table 4. Experimental (**2**, **4**) and calculated (**8**, **10**) ring geometries (C_2N_2P) [pm] and [°] for CC-saturated 1,3-diazaphospholidines. R = exocyclic substituent at nitrogen

	LP−Cl (2)	**[LP]$^+$ PF_6^- (4)**	**8Me**	**8H**	**10H**	**10Me**
N−P	165.2(2)	161.3(2)	160.1	160.2	160.4	162.2
N−C	147.1(3)	148.2(5)	147.3	147.8	148.0	147.5
C−C	150.8(3)	154.4(7)	154.2	154.4	153.2	153.1
P−H	–	–	–	–	138.2	138.5
N−P−N	92.41(8)	96.29(11)	96.1	93.9	94.0	98.2
H−P−H	–	–	–	–	104.5	103.6
N−C−C	105.9(2)	105.1(4)	106.5	105.4	104.7	105.5
R−N−C	119.9(2)	120.6(2)	118.6	119.8	120.1	119.9
P−N−C	114.77(1)	113.7(2)	115.4	117.1	112.2	110.4
P−N−R	125.20(13)	125.22	126.0	122.9	124.4	126.0
Σ(N)[a]	359.9	359.5	360.0	360.0	356.7	356.3
Point-group	C_1	C_1	C_{2v}	C_2	C_2	C_2

[a] Sum of nitrogen bond angles.

Table 5. Experimental (**1**, **3**) and calculated (**7**, **9**) ring geometries [pm] and [°] for CC-unsaturated 1,3-diazaphospholes. R = exocyclic substituent at nitrogen

	[L′P]$^+$Cl$^-$ (1)	**[L′P]$^+$ PF_6^- (3)**	**7Me**	**7H**	**9H**	**9Me**
N−P	166.0(2)	166.1(2)	164.7	164.4	163.2	162.9
N−C	137.9(3)	137.6(3)	136.5	137.0	143.0	142.7
C−C	134.7(3)	134.1(4)	134.9	134.6	131.4	131.6
P−H	–	–	–	–	138.4	138.7
N−P−N	90.41(10)	90.71(11)	90.7	88.7	94.28	96.26
H−P−H	–	–	–	–	104.28	103.1
N−C−C	111.4(2)	112.0(2)	111.4	110.4	112.1	112.9
R−N−C	122.1(2)	123.3(2)	121.9	121.3	122.4	122.7
P−N−C	113.3(2)	112.7(2)	113.3	115.3	110.7	109.9
P−N−R	123.8(2)	124.0(2)	124.8	123.4	126.8	128.3
Σ(N)[a]	359.2	360.0	360.0	360.0	360.0	360.0
Point-group	C_1	C_1	C_{2v}	C_{2v}	C_{2v}	C_2

[a] Sum of bond angles around nitrogen.

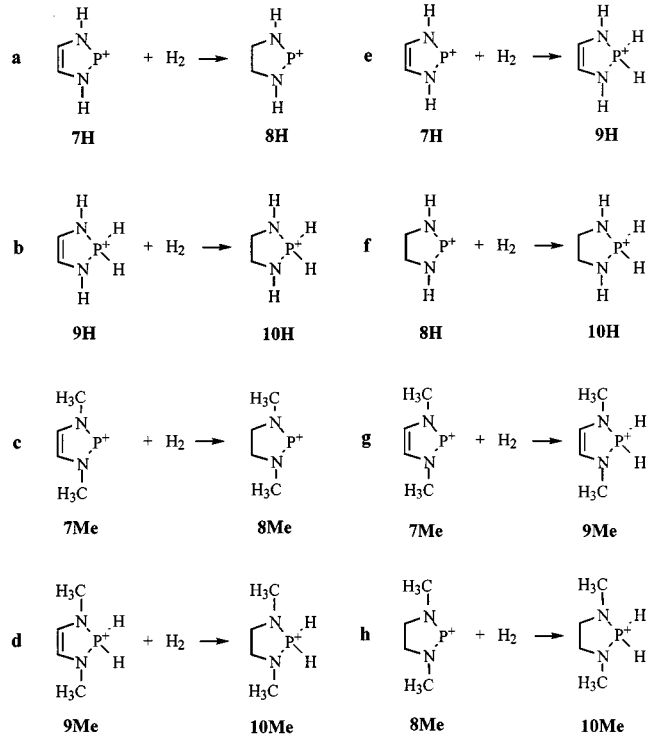


Figure 8. Isodesmic hydrogenation reactions of model compounds **7H, 9H, 7Me** and **9Me**

zation energies for the phosphenium cations and presumably for other related compounds as well.

Electron correlation at the MP2 level increases the calculated ASE values by ca. 40%. This is a good indication that the calculated ASE values represent strong differences in the degree of delocalization. Calculations at the MP4 level were restricted to the hydrogen substituted model compounds. At the MP4/6−31G*//HF/6−31G* level, a slight decrease in the ASE is observed (22.97 kcal·mol^{-1} instead of 25.73).

Table 6. Calculated reaction energies (at 0 K) for the isodesmic equations **a**−**h** and aromatic stabilization energies (ASE, **a**−**b** and **c**−**d**) in kcal·mol^{-1}

	6−31G*	MP2 / 6−31G*	MP4 / 6−31G*
a	−16.90	−2.57	−4.11
b	−34.92	−28.30	−27.08
c	−14.22	−0.05	−
d	−34.33	−26.49	−
e	+11.57	+32.59	+33.18
f	−6.45	+6.85	+10.21
g	+16.92	+38.05	−
h	−3.19	+11.61	−
|**a** − **b**|	18.02	25.73	22.97
|**c** − **d**|	20.11	26.44	−

The aromatic stabilization energies obtained from isodesmic equations like **a**−**d** and **e**−**h** require the construction of non-aromatic model compounds. Sauers has chosen the phosphines R_2P-H instead of the cationic species $R_2PH_2^+$ used in this study and obtained aromatic stabilization energies that are slightly smaller (24.0 kcal mol^{-1})[20] than the ones obtained from our approach.

The single crystal X-ray data obtained for **3** and **4** are in excellent agreement with the computational 6−31G* structures of the model compounds **7 H, 7Me**, **8 H,** and **8Me**. Not surprisingly, the structural agreement is slightly better (especially for the N−P−N bond angles) if methyl groups are placed on the nitrogen atoms (model compounds **7Me** and **8Me**).

Conclusion

In a series of isostructural, aromatic diamino-silylenes, -germylenes, and phosphenium cations, the phosphenium cations display the highest degree of aromatic delocalization on the basis of three independent criteria: alternation of bond lengths (least), deshielding of ring protons (most), and aromatic delocalization energy (most). The experimental structures of the phosphenium cations are reproduced with excellent agreement by ab initio calculations at the 6−31G* level. The NMR shifts of the investigated phosphenium salts are strongly dependent on the polarity of the solvent.

Experimental Section

All operations were carried out with usual Schlenk techniques under Argon (99.996) or in a nitrogen filled glove box (Braun, O_2 < 2 ppm H_2O < 2 ppm). Solvents were purified by distillation from purple benzophenone/potassium solutions (hexanes, benzene) or by 30 minutes of sonication with CaH_2 followed by deoxygenation with three freeze-pump-thaw cycles (deuterated solvents, CH_2Cl_2). $AgPF_6$ (Aldrich) and $GaCl_3$ (Alfa) were used as received and handled in an inert gas glovebox. All NMR measurements were performed with ca. 1 M solutions in flame-sealed sample tubes at room temperature. The chemical shifts δ are reported in ppm vs. 85% H_3PO_4 (^{31}P, external) or TMS (^1H, ^{13}C, internal). Capillaries of 85% H_3PO_4 in D_2O were used as internal reference for the ^{31}P-NMR measurements. Positive shift values represent deshielding relative to the standard. The NMR samples were observed over a period of 4 months for signs of decomposition. Satisfactory elemental analysis (C,H,N) were obtained for **1**−**4**. Single crystals were grown by slow sublimation (**1**, **2**) or by layering of half-saturated CH_2Cl_2 solutions with hexanes (**3**, **4**). Compounds **1** and **2** were obtained as described previously.[11]

Synthesis of 3/4: To a stirred solution of 1 mmol of the chlorophosphane (234 mg, **1** or 236 mg, **2**) dissolved in 20 mL of dichloromethane was added a solution of 1 mmol of $AgPF_6$ (253 mg) dissolved in 20 mL of dichloromethane dropwise and under exclusion of light. The mixture was stirred for 1 h, decanted from the precipitate (AgCl) with a syringe, the total volume reduced to 20 mL and the remaining solution layered with 20 mL of hexanes. The hexafluorophosphates **3/4** crystallized as analytically pure, colorless crystals and were isolated by filtration through a medium size frit and washing with 10 mL of hexanes. Yields: 95−100%. The analytically pure tetrachlorogallates **5/6** were obtained in analogous fashion from **1/2** (10 mmol) by treating with $GaCl_3$ (10 mmol 10% in benzene). The solvent was evaporated, the residue dissolved in 20 mL of CH_2Cl_2 and the resulting solution layered with 20 mL of hexanes, yields 90−95%.

The salts **3**−**6** can be stored indefinitely under exclusion of air and moisture. Single crystals for X-ray crystallography were grown by

recrystallization from boiling benzene (**1**), slow sublimation (**2**) or by layering of CH_2Cl_2 solutions with hexanes (**3**−**6**).

Spectroscopic Data

1: ^{1}H NMR (CD_2Cl_2): δ = 1.63 [d, ^4J(P,H) = 1.8 Hz, 18 H, CH_3], 6.97 [d, ^3J(P,H) = 1.5 Hz, 2 H, C*H*]. − ^{13}C NMR: δ = 30.41 [d, ^3J(C,P) = 10.3 Hz, *C*H$_3$], 57.83 [d, ^2J(C,P) = 7.4 Hz, *C*Me$_3$], 121.34 [d, ^2J(C,P) = 8.8 Hz, =*C*H]. − ^{31}P NMR (CD_2Cl_2): δ = 168.6 (s, br). − IR (Nujol, CsI, cm^{-1}): $\tilde{\nu}$ = 1201 s, 1079 s, 1020 m, 842 m, 790 m, 723 vs, 535 m. − **2**: ^{1}H NMR (CD_2Cl_2): δ = 1.39 [d, ^4J(P,H) = 1.8 Hz, 18 H, CH_3], 3.37 [d, ^3J(P,H) = 6.6 Hz, 4 H, CH_2]. − ^{13}C NMR (CD_2Cl_2): δ = 28.97 [d, ^3J(C,P) = 11.7 Hz, *C*H$_3$], 45.78 [^2J(C,P) = 10.2 Hz, *C*H$_2$*C*H$_2$], 54.10 [^2J(C,P) = 11 Hz, *C*Me$_3$]. − ^{31}P NMR (CD_2Cl_2): δ = 166.8 (s, br). − IR (Nujol, CsI, cm^{-1}): $\tilde{\nu}$ = 1222 s, 1209 s, 1125 m, 1089 w, 1041 s, 983 m, 863 m, 802 m, 723 w, 677 s, 666 s. − **3**: ^{1}H NMR (CD_2Cl_2): δ = 1.78 [d, ^4J(P,H) = 1.9 Hz, 18 H, CH_3], 8.08 (s, 2 H, =C*H*). − ^{13}C NMR (CD_2Cl_2): δ = 31.48 [d, ^3J(C,P) = 8.8 Hz, *C*H$_3$], 53.59 [d, ^2J(C,P) = 27.1 Hz, *C*Me$_3$], 132.96 [d, ^2J(C,P) = 2.9 Hz, =*C*H]. − ^{31}P NMR (CD_2Cl_2): δ = 202.3 (s, br, N_2P^+), −144.6 [hept, ^1J(P,F) = 711.1 Hz, PF_6^-]. The phosphorus chemical shift for PF_6^- is in good agreement with published values (δ = 142.1, ^1J = 717 Hz).[15] − IR (Nujol, CsI, cm^{-1}): $\tilde{\nu}$ = 1304 m, 1261 m, 1205 w, 1192 w, 1148 m, 1075 m, 1020 m, 830 vs, 803 m, 738 w, 723 m, 558 s, 476 w. − **4**: ^{1}H NMR (CD_2Cl_2): δ = 1.58 [d, ^4J(P,H) = 2.2 Hz, 18 H, CH_3], 4.10 [d, ^3J(P,H) = 4.5 Hz, 4 H, CH_2]. − ^{13}C NMR (CD_2Cl_2): δ = 29.68 [d,^3J(P,C) = 9.5 Hz, *C*H$_3$], 48.61 [d, ^2J(P,C) = 8.8 Hz, *C*H$_2$], 53.60 [d, ^2J(P,C) = 27.0 Hz, *C*Me$_3$]. − ^{31}P NMR (CD_2Cl_2): δ = +262.3 (s, br, N_2P^+), −144.6 [hept, ^1J(P,F) = 711.1 Hz, PF_6^-]. The phosphorus chemical shift for PF_6^- is in agreement with published values (δ = 142.1, ^1J = 717 Hz).[15] − IR (Nujol, CsI, cm^{-1}): $\tilde{\nu}$ = 1299 w, 1282 w, 1261 m, 1194 s, 1158 m, 1144 m, 1121 m, 1093 w, 1037 s, 1012 m, 986 w, 934 w, 876 m, 835 vs, 740 m, 723 s, 670 w, 558 vs.

Acknowledgments

We thank the National Science Engineering and Research Council of Canada (NSERC) for support of this work through an operating grant and Spaceoptix Inc. (Toronto) and the Connaught Foundation of the University of Toronto for additional support. The thoughtful comments of Dr. Ian Still and Dr. Juris Strautmanis during the preparation of this manuscript and Dr. Alfred Schmidpeter while this work was still in progress are gratefully acknowledged. We thank Prof. R. West and Dr. S. Powell for the crystallographic investigation of **1** and **2** in the University of Wisconsin Crystallography Laboratory (supported by the National Science Foundation (NSF) through grant CHE-9105497).

[1] F. Bernardi, A. Bottoni, A. Venturini, *J. Mol. Struct. (Theochem)* **1988**, *163*, 173−189. − K. K. Baldridge, M. S. Gordon, *J. Am. Chem. Soc.* **1988**, *110*, 4204−4208. − A. R. Katritzy, P. Barczynski, G. Musumarra, D. Pisano, M. Szafran, *J. Am. Chem. Soc.* **1989**, *111*, 7−15. − M. N. Glukhovtsev, B. Ya. Simkin, *Organometal. Chem. USSR* **1990**, *3*, 545−554. − V. I. Minkin, M. N. Glukhovtsev, B. Ya. Simkin, *Aromaticity and Antiaromaticity*, Chapter 2, Wiley, New York **1994**. − P. v. R. Schleyer, P. K. Freeman, H. Jiao, B. Goldfuss, *Angew. Chem. Int. Ed. Engl.* **1995**, *34*, 337−340; *Angew. Chem.* **1995**, *107*, 332−326. − L. Nyulászi, P. Várnai, T. Veszprémi, *J. Mol. Struct. (Theochem)* **1995**, *358*, 55−61. − P. v. R. Schleyer, H. Jiao, *Pure Appl. Chem.* **1996**, *68*, 209−218. − J. Su, X. −W. Li, R. C. Crittendon, G. H. Robinson, *J. Am. Chem. Soc.* **1997**, *119*, 5471−5472. − A. Sekiguchi, M. Tsukamoto, M. Ichinohe, *Science* **1997**, *275*, 60−61.

[2] [2a] A. J. Arduengo, R. L. Harlow, M. Kline, *J. Am. Chem. Soc.* **1991**, *113*, 361−363. − [2b] G. Boche, C. Hilf, K. Harms, M. Marsch, J. C. W. Lorenz, *Angew. Chem. Int. Ed. Engl.* **1995**, *34*, 487−489; *Angew. Chem.* **1995**, *107*, 509−513. − [2c] M. K. Denk, A. Thadani, K. Hatano, A. J. Lough, *Angew. Chem. Int. Ed. Engl.* **1997**, *36*, 2607−2609; *Angew. Chem.* **1997**, *109*, 2719−2721.

[3] [3a] M. Denk, R. Lennon, R. Hayashi, R. West, A. V. Belyakov, H. P. Verne, A. Haaland, M. Wagner, N. Metzler, *J. Am. Chem. Soc.* **1994**, *116*, 2691−2692. − [3b] M. Denk, R. K. Hayashi, R. West, *J. Chem. Soc., Chem. Commun.* **1994**, 33−34. − [3c] M. Denk, J. Green, N. Metzler, M. Wagner, *J. Chem. Soc., Dalton Trans.* **1994**, 2405−2410. − [3d] N. Metzler, M. Denk, *J. Chem. Soc., Chem. Commun.* **1996**, 2657−2658. − [3e] S. Urquhart, A. P. Hitchcock, J. Lehman, M. K. Denk, *Organometallics* **1998**, *17*, 2352− 2360.

[4] W. A. Herrmann, M. Denk, J. Behm, W. Scherer, F.-R. Klingan, H. Bock, B. Solouki, M. Wagner, *Angew. Chem.* **1992**, *104*, 1489−1492; *Angew. Chem. Int. Ed. Engl.* **1992**, *31*, 1485−1488. *For a detailed discussion of the C_2N_2E disorder see:* J. Behm, Ph. D. Dissertation, Technische Universität München, **1992**.

[5] G. Boche, P. Andrews, K. Harms, M. Marsch, K. S. Rangappa, M. Schimeczek, C. Willeke, *J. Am. Chem. Soc.* **1996**, *118*, 4925−4930.

[6] [6a] B. Wrackmeyer, J. Schiller, *Z. Naturforsch.* **1992**, *47b*, 662−667. − [6b] R. B. King, P. M. Sundaram, *J. Org. Chem.* **1984**, *49*, 1784. − [6c] A. M. Kibardin, I. A. Litvinov, V. A. Naumov, Yu. T. Struchkov, T. V. Gryaznova, Yu. B. Mikhailov, A. N. Pudovnik, *Dokl. Akad. Nauk SSSR* **1994**, *312*, 623−625. − [6d] A. M. Kibardin, I. A. Litvinov, V. A. Naumov, Yu. T. Struchkov, T. V. Griaznova, J. B. Michailov, *Dokl. Akad. Nauk. SSSR* **1988**, *298*, 369−373.

[7] N. Burford, J. A. C. Clyburn, P. Losier, T. M. Parks, T. S. Cameron, J. F. Richardson, *Phosphorus, Sulfur and Silicon* **1994**, *93/94*, 301−304. − N. Burford, T. M. Parks, G. Wu, *Phosphorus, Sulfur and Silicon* **1994**, *93/94*, 397−398. − N. Burford, C. L. B. Macdonald, T. M. Parks, G. Wu, B. Borecka, W. Kwiatkowski, T. S. Cameron, *Can. J. Chem.* **1996**, *74*, 2209−2216.

[8] *The dicoordinate anion Ph_2B^- has been suggested as a possible intermediate in the photolytic decomposition of the tetraphenylborate anion:* J. J. Eisch, K. Tamao, R. J. Wilcsek, *J. Am. Chem. Soc.* **1975**, *97*, 895−897. − J. J. Eisch, B. Shafi, M. P. Boleslawski, *Pure & Appl. Chem.* **1991**, *63*, 365−368. − *Note added in proof*: The anionic group(III) diazoles of type **A** and **B** have been investigated by ab initio methods, A. Sundermann, M. Reiher, W. W. Schoeller, *Eur. J. Inorg. Chem.* **1998**, 305−310. − For efforts directed towards the synthesis of stable dicoordinate gallium derivatives see: A. H. Cowley, D. S. Brown, A. Decken, S. Kamepalli, *J. Chem. Soc., Chem. Commun.* **1996**, 2425−2426.

[9] C. Heinemann, T. Müller, Y. Apeloig, H. Schwarz, *J. Am. Chem. Soc.* **1996**, *118*, 2023−2038. − L. Nyulászi, T. Karpati, T. Veszprémi, *J. Am. Chem. Soc.* **1994**, *116*, 7239−7242. − C. Boehme, G. Frenking, *J. Am. Chem. Soc.* **1996**, *118*, 2039−2046.

[10] *For general publications on phosphenium cations see:* I. Kawada, R. Allmann, *Angew. Chem. Int. Ed. Engl.* **1968**, *7*, 69−70; *Angew. Chem.* **1968**, *80*, 40−41. − S. Fleming, M. K. Lupton, K. Jekot, *Inorg. Chem.* **1972**, *11*, 2534−2540. − M. G. Thomas, C. W. Schultz, R. W. Parry, *Inorg. Chem.* **1977**, *16*, 994−1001. − A. H. Cowley, M. C. Cushner, J. S. Szobota, *J. Am. Chem. Soc.* **1978**, *100*, 7784−7786. − L. D. Hutchinson, E. N. Duesler, R. T. Paine, *Organometallics* **1982**, *1*, 1254−1256. − A. Cowley, R. A. Kemp, *Chem. Rev.* **1985**, *85*, 367−382. − M. Sanchez, M. −R. Mazieres, R. Bartsch, R. Wolf, J. −P. Majoral, *Phosphorus and Sulfur* **1987**, *30*, 487−490. − R. Bartsch, M. Sanchez, R. Wolf, *Phosphorus and Sulfur* **1988**, *35*, 89−92. − A. Schmidpeter, M. Thiele, *Angew. Chem.* **1991**, *103*, 333−335. − N. Burford, J. A. C. Clyburne, P. K. Bakshi, T. S. Cameron, *J. Am. Chem. Soc.* **1993**, *115*, 8829−8830. − N. Burford, P. Losier, K. Bakshi, T. S. Cameron, *J. Chem. Soc., Dalton Trans.* **1993**, 201−202. − N. Burford, P. Losier, C. Macdonald, V. Kyrimis, P. K. Bakshi, T. S. Cameron, *Inorg. Chem.* **1994**, *33*, 1434−1439. − N. Burford, P. Losier, S. V. Sereda, T. S. Cameron, G. Wu, *J. Am. Chem. Soc.* **1994**, *116*, 6474−6475. − R. W. Reed, Z. W. Xie, J. Manning, R. Mathur, R. Bau, C. A. Reed, *Phosphorus, Sulfur and Silicon and related Elements* **1994**, *93*, 485−485. −

N. Burford, J. A. C. Clyburne, P. Losier, T. M. Parks, T. S. Cameron, *Phosphorus, Sulfur and Silicon and related Elements* **1994**, *93*, 301−304. − T. Kaukorat, I. Neda, R. Schmutzler, *Coord. Chem. Rev.* **1994**, *137*, 53−107. − R. W. Reed, Z. W. Xie, C. A. Reed *Organometallics* **1995**, *14*, 5002−5004. − A. Schmidpeter in: *Comprehensive Heterocyclic Chemistry* (eds. A. Katritzky, C. Rees, E. Scriven), Vol. 4, Pergamon, **1996**, 711−818.

[11] [11a]M. K. Denk, S. Gupta, R. Ramachandran, *Tetrahedron Lett.* **1996**, *37*, 9025−9028. − [11b] C. J. Carmalt, V. Lomeli, B. G. McBurnett, A. H. Cowley, *J. Chem. Soc., Chem. Commun.* **1997**, 2095−2096. − [11c] D. Gudat, *Eur. J. Inorg. Chem.* **1998**, 1087−1094.

[12] J. Luber, A. Schmidpeter, *Angew. Chem Int. Ed. Engl.* **1976**, *15*, 111−112; *Angew. Chem.* **1976**, *88*, 91−92. − P. Friedrich, G. Huttner, J. Luber, A. Schmidpeter, *Chem. Ber.* **1978**, *111*, 1558−1563. − J. H. Weinmaier, J. Luber, A. Schmidpeter, S. Pohl, *Angew. Chem.* **1979**, *91*, 442−443; *Angew. Chem. Int. Ed.* **1979**, *18*, 412−413. − J. H. Weinmaier, G. Brunnhuber, A. Schmidpeter, *Chem. Ber.* **1980**, *113*, 2278−2290. − K. Karaghiosoff, J.-P. Majoral, A. Meriem, J. Navech, A. Schmidpeter, *Tetrahedron Lett.* **1983**, *24*, 2137−2140. − K. Karaghiosoff, W. S. Sheldrick, A. Schmidpeter, *Chem. Ber.* **1986**, *119*, 3213−3226.

[13] D. Carmichael, L. Ricard, F. Mathey, *J. Chem. Soc., Chem. Commun.* **1994**, 1167−1168. − F. Mathey, *Phosphorus Sulfur and Silicon and the related elements* **1994**, *87*, 139−148. − F. Mathey, *J. Organomet. Chem.* **1994**, 25−30. − H. J. Gosink, F. Nief, L. Ricard, F. Mathey, *Inorg. Chem.* **1995**, *34*, 1306−1307.

[14] N. Burford, J. Clyburn, personal communication, **1995**.

[15] R. Fernández-Galan, B. R. Manzano, A. Otero, M. Lanfranchi, M. A. Pelinghelli, *Inorg. Chem.* **1994**, *33*, 2309−2312.

[16] Crystal data for $[L'P]^+Cl^-$ (**1**): The compound crystallizes with 0.5 equivalents of benzene, $C_{10}H_{20}ClN_2P \bullet 0.5\ C_6H_6$, M = 273.75, crystal size = 0.5 × 0.4 × 0.2 monoclinic, space group $P2_1/n$, a = 11.056(2), b = 11.244(2), c = 13.512(2) Å, ß = 113.872(13)°, V = 1536.0(5) Å^3, Z = 4, $d_{calc.}$ = 1.184 g·cm^{-3}, λ(Mo-K_α) = 0.71073 Å, μ(Mo-K_α) = 0.336 mm^{-1}, F(000) = 588, scan type 2θ−θ, T = 113(2) K, 2.02 < 2θ < 22.50°, total unique data 2000 (R_i = 0.039), no. of observations [(F) > 4σ(F)] 4223, R = 0.034, R_w = 0.071, maximum peak in final Fourier difference synthesis 0.232 eÅ^{-3}. − Crystal data for LPCl (**2**): $C_{10}H_{22}ClN_2P$, M = 236.72, crystal size = 0.5 × 0.4 × 0.2 orthorhombic, space group $Pbca$, a = 11.8843(8), b = 11.118(2), c = 19.899(2) Å, V = 2629.2(6) Å^3, Z = 8, $d_{calc.}$ = 1.196 g·cm^{-3}, λ(Mo-K_α) = 0.71073 Å, μ(Mo-K_α) = 0.382 mm^{-1}, F(000) = 1024, scan type 2θ−θ, T = 113(2) K, 2.02 < 2θ < 22.49 °, total unique data 1719 (R_i = 0.026), no. of observations [(F) > 4σ(F)] 3434, R = 0.027, R_w = 0.065, maximum peak in final Fourier difference synthesis −0.184 eÅ^{-3}. − Crystal data for $[L'P]^+[PF_6]^-$ (**3**): $C_{10}H_{20}F_6N_2P_2$, M = 344.22, crystal size = 0.35 × 0.45 × 0.35 orthorhombic, space group $Pnma$, a = 12.149(2), b = 8.3440(9), c = 15.431(3) Å, V = 1564.2(4) Å^3, Z = 4, $d_{calc.}$ = 1.462 g·cm^{-3}, λ(Mo-K_α) = 0.71073 Å, μ(Mo-K_α) = 0.331 mm^{-1}, F(000) = 712, scan type 2θ-θ, T = 168(2) K, 5.28 < 2θ < 59.98°, total unique data 2422 (R_i = 0.0000%), no. of observations [(F) > 4σ(F)] 1618, R = 0.045, R_w = 0.071, maximum peak in final Fourier difference synthesis 0.535 eÅ^{-3}. − Crystal data for $[LP]^+[PF_6]^-$ (**4**): $C_{10}H_{22}F_6N_2P_2$, M = 346.24, crystal size = 0.32 × 0.27 × 0.19 orthorhombic, space group $Pnma$, a = 11.6987(11), b = 8.349(2), c = 16.1957(12) Å, V = 1581.8(4) Å^3, Z = 4, $d_{calc.}$ = 1.454 g·cm^{-3}, λ(Mo-K_α) = 0.71073 Å, μ(Mo-K_α) = 0.328 mm^{-1}, F(000) = 720, scan type 2θ−θ, T = 173(2) K, 5.04 < 2θ < 60.00°, total unique data 2454 (R_i = 0.0000), no. of observations [(F) > 4σ(F)] 1656, R = 0.0495, R_w = 0.1325, maximum peak in final Fourier difference synthesis 0.513 eÅ^{-3}. Data were collected on a *Siemens P4* diffractometer. No absorption correction was applied. Lorentz and polarization corrections were applied. Systematically absent reflexions were rejected and equivalent reflexions were merged. The heavy-atom positions were determined by direct methods. Subsequent difference Fourier synthesis revealed the positions of all other non-hydrogen atoms, organic hydrogen atoms were put into idealized position. The non-hydrogen atoms were refined by the full-matrix least-squares method with the hydrogen atoms "riding" on their supporting carbon atoms. A weighting scheme ($w^{-1} = \sigma^2(F) + 0.001 \cdot F^2$) was applied and the data were corrected for the effects of anomalous dispersion and secondary extinction. Crystallographic calculations were carried out using the *Siemens SHELXS-86* program[17a] on a *Silicon Graphics Indigo2* system in the *Chemical Crystallography Laboratory, University of Wisconsin, Madison*, USA (compounds **1** and **2**) or with the SHELXTL/PC[17b] program, version 5.1, on a Pentium 133 PC in the *Chemical Crystallography Laboratory, University of Toronto*, Canada (compounds **3**−**6**).

[17] [17a] G. M. Sheldrick, *Acta Crystallogr.* **1990**, *A46*, 467−473. − [17b] *Bruker Analytial X-ray Systems*, Madison, Wisconsin, USA, **1998**.

[18] J. Emsley, *The Elements*, 2nd edition, Clarendon Press, Oxford, **1991**.

[19] e.g. 210.5(9) pm in the *trans*-1,3-(Di-*tert*-butyl)-2,4-dichlorodiazadiphosphetidine, *cyclo*-(*t*BuN)$_2$(PCl)$_2$, K. W. Muir, J. F. Nixon, *J. Chem. Soc., Chem. Commun.* **1971**, 1405−1406.

[20] R. R. Sauers, *Tetrahedron* **1997**, *53*, 2357−2364.

[21] A. Schmidpeter, K. Karaghiosoff, in: *CRC Handbook of Phosphorus-31 Nuclear Magnetic Resonance Data* (John C. Tebby, ed.), CRC Press, Boca Raton, **1991**.

[22] *For ring current theories in Nuclear Magnetic Resonance see:* C. W. Haigh, R. B. Mallion, *Prog. NMR Spectroscopy*, **1980**, *13*, 103−344.

[23] *For reviews on weakly coordinating anions see:* W. Beck, K. Sünkel, *Chem. Rev.* **1988**, *88*, 1405−1416. − T. J. Marks, *Acc. Chem. Res.* **1992**, *25*, 57. − S. H. Strauss, *Chem. Rev.* **1993**, *93*, 927−942. − D. M. van Seggen, P. K. Hurlburt, O. P. Anderson, S. H. Strauss, *Inorg. Chem.* **1995**, *34*, 3453.

[24] M. K. Denk, unpublished results.

[25] E. Lustig, E. P. Ragelis, N. Duy, J. A. Ferretti, *J. Am. Chem. Soc.* **1967**, *89*, 3953−3959, R. A. Hoffmann, S. Forsén, in: *NMR, Basic Principles and Progress* **1971**, *5*, 1−165 (Eds.: P. Diehl, E. Fluck, R. Kosfeld).

[26] Cerius2™ 2.0 was developed by *Molecular Simulations Inc.* (see also http://www.msi.com).

[27] *Gaussian 94*, *Revision D.4*, M. J. Frisch, G. W. Trucks, H. B. Schlegel, P. M. W. Gill, B. G. Johnson, M. A. Robb, J. R. Cheeseman, T. Keith, G. A. Petersson, J. A. Montgomery, K. Raghavachari, M. A. Al-Laham, V. G. Zakrzewski, J. V. Ortiz, J. B. Foresman, J. Cioslowski, B. B. Stefanov, A. Nanayakkara, M. Challacombe, C. Y. Peng, P. Y. Ayala, W. Chen, M. W. J. Wong, L. Andres, E. S. Replogle, R. Gomperts, R. L. Martin, D. J. Fox, J. S. Binkley, D. J. Defrees, J. Baker, J. P. Stewart, M. Head-Gordon, C. Gonzalez, J. A. Pople, *Gaussian, Inc.*, Pittsburgh, PA, **1995**. Website: http://www.gaussian.com.

[28] W. J. Hehre, C. Radom, P. v. R. Schleyer, J. A. Pople, *Ab Initio Molecular Orbital Theory*, Wiley, New York, **1986**.

[29] [29a] Equilibrium geometries were calculated with *Cerius*$^{2™}$[26] using *Gaussian 94*.[27] Calculations were performed without symmetry restrictions. The structures were calculated at the 6−31G* level[28] and the absence of virtual frequencies for the optimized geometries was confirmed by frequency analysis at this level. Zero-point energies were calculated at the 6−31G* level and multiplied by 0.89 to correct for anharmonicity.[28] Relative energies at 0 K were obtained by adding the corrected zero-point vibrational energies to the electronic energies. Final electronic energies were obtained by single-point calculations including electron correlation at the MP2 level in the 6−31G* basis set with the optimized RHF/6−31-G* geometries (RHF/MP2/6−31G*//RHF/6−31G*). The energies were converted to kcal·mol^{-1} using the factor 1 Hartree = 627.59 kcal·mol^{-1}. − [29b] e.g.: **a** − **b** = (**7H** + H_2 − **8H**) − (**9H** + H_2 − **10H**) = (**7H** + H_2 − **9H**) − (**8H** + H_2 − **10H**) = **e** − **f**.

[30] Crystallographic data (excluding structure factors) for the structures of **1**−**4** have been deposited with the *Cambridge Crystallographic Data Centre* as supplementary publication no. CCDC−101272. Copies of the data can be obtained free of charge on applications to the Director, CCDC, 12 Union Road, Cambridge CB2 1EZ, UK [fax: Int. Code +44 (1223) 336−033. E-mail: deposit@chemcrys.cam.ac.uk].

Received May 15, 1998
[I98155]

Asymmetric Catalysis, 125[+]

Synthesis of the Stereoisomers of Methohexital by Palladium-Catalyzed Allylation

Henri Brunner,*[a] Irmgard Deml,[a] Wolfgang Dirnberger,[a] Karl-Peter Ittner,[b] Walter Reißer,[a] and Markus Zimmermann[b]

Dedicated to Professor Bernt Krebs on the occasion of his 60th birthday

Keywords: Asymmetric catalysis / Allylic alkylation / 1-Methyl-5-(1′-methylpent-2′-ynyl)barbituric acid / Palladium catalysts / Chiral phosphane imine ligands / Methohexital / Anesthetic dose

Allylation of 1-methyl-5-(1′-methylpent-2′-ynyl)barbituric acid (MBS) with allyl acetate using in situ catalysts of palladium(II) acetylacetonate and chiral phosphane imine ligands resulted in the enantioselective formation of 5-allyl-1-methyl-5-(1′-methylpent-2′-ynyl)barbituric acid (Methohexital), an important anesthetic drug. Both, MBS and Methohexital contain two stereogenic carbon atoms. In MBS, the asymmetric centre in the barbiturate system is labile due to enolization. The asymmetric centre in the hexyne side chain is stable and racemic. The two asymmetric centres of Methohexital are stable and give rise to four stereoisomers, two diastereomeric racemates. An analysis of the isomers of MBS and Methohexital was established on the basis of ^{1}H NMR and, in particular, GC including a base-line separation of the four stereoisomers of Methohexital. The stereoselectivity of the allylation is difficult to control, because the new quaternary asymmetric centre in the barbiturate ring of Methohexital is formed within the nucleophile, attacking the η^3-allyl ligand of the catalyst from the side opposite to the palladium atom. Classical optically active ligands, such as diop or norphos, give only 2–6 % ee. Chiral phosphane imine ligands are a successful class of compounds, synthesized by Schiff base condensation of (2-formylphenyl)diphenylphosphane with optically active primary amines. The most efficient ligands have a hydroxymethyl and a bulky alkyl substituent at the asymmetric centre in the imine part, e.g. the L-*iso*-leucinol and the L-*tert*-leucinol derivatives **5** and **7**. In the Pd-catalyzed allylation of MBS a kinetic resolution and the effect of the enantioselective catalyst interplay, the contributions of which are separated. For MBS the best stereoselectivity factor of the kinetic resolution $s = k_R/k_S$ was 2.6 and 83 % "ee" were achieved. The corresponding values for Methohexital were $s = 3.5$ and 80 % ee in the α-*dl* pair. For 10 mixtures of Methohexital stereoisomers the anesthetic doses for rats were determined. With 9.1 mg/kg body weight of the animal the sample obtained from the catalysis with the D-α-phenylglycinol derivative **8** gave a much lower anesthetic dose than the widely used narcotic Brevimytal®Natrium, the sodium salt of the α-*dl* racemate of Methohexital, with 13.0 mg/kg body weight.

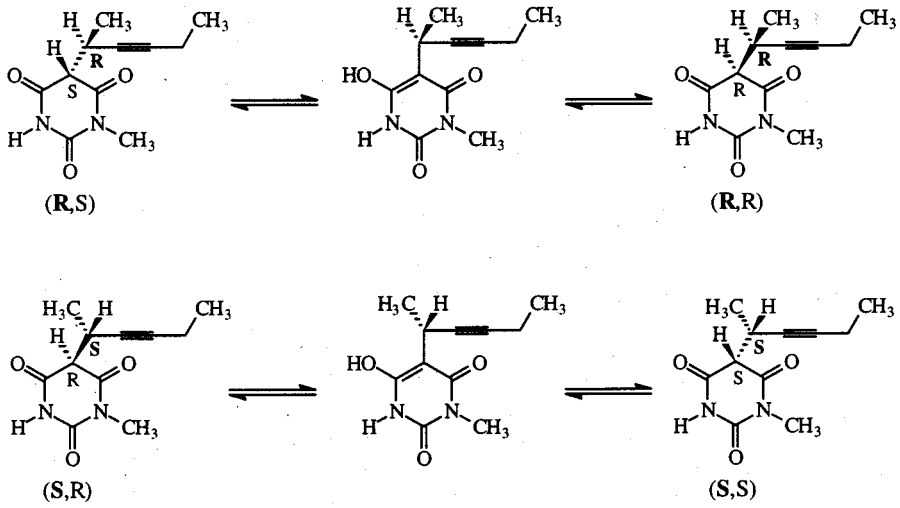
Introduction

Recently, we reported on the application of the enantioselective palladium-catalyzed allylic alkylation in the chemistry of barbituric acid derivatives.[2] The starting material 1,5-dimethylbarbituric acid could be converted into the product 5-allyl-1,5-dimethylbarbituric acid in an enantiomeric excess of up to 34% ee by variation of the bases and the optically active ligands.[2–4] In the present paper we transferred the experiences gained in the enantioselective allylation of the model system 1,5-dimethylbarbituric acid to the synthesis of 5-allyl-1-methyl-5-(1′-methylpent-2′-ynyl)-barbituric acid (Methohexital). Methohexital is a pharmaceutically important short-time anesthetic (Eli Lilly).[5–7] For a narcosis on an average 150 mg of substance are needed per person.[8,9] The sodium salt of the α-*dl* racemate of Methohexital is commercially available (trade name Brevimytal®Natrium).[5–11] Besides the allylic group there is a 1′-methylpent-2′-ynyl substituent in 5-position of the barbituric acid skeleton. Therefore, two asymmetric centres result, one in 5-position of the barbiturate system and one in 2′-position of the hexyne side chain. Consequently, there are four stereoisomers, two diastereomeric racemates (*R*,*R*)/(*S*,*S*) and (*R*,*S*)/(*S*,*R*). Gibson and Doran found different narcotic effects for the four stereoisomers.[12,13] The individual enantiomers can be obtained by regiospecific condensation of the enantiomers with respect to the 1′-methylpent-2′-ynyl side chain and subsequent diastereomer separation.[13] The advantage of a synthesis of Methohexital by Pd-catalyzed allylic alkylation is the accessibility of differ-

[+] Part 124: Ref.[1]

[a] Institut für Anorganische Chemie der Universität, D-93040 Regensburg, Germany
Fax: (internat.) + 49(0)941/9434439
E-mail: henri.brunner@chemie.uni-regensburg.de
[b] Institut für Pharmakologie der Universität, D-93040 Regensburg, Germany
Fax: (internat.) + 49(0)941/9434771
E-mail: karl-peter.ittner@klinik.uni-regensburg.de

 © WILEY-VCH Verlag GmbH, D-69451 Weinheim, 1999 1434–1948/99/0101–0051 $ 17.50+.50/0



Scheme 1. Keto-enol tautomerism of the labile asymmetric centre of MBS in the barbiturate system

ently enriched diastereomeric and enantiomeric mixtures in one reaction step.

We describe the preparation of the starting material 1-methyl-5-(1′-methylpent-2′-ynyl)barbituric acid (MBS), the analysis of its stereoisomers and its Pd-catalyzed allylation as well as the analysis of the diastereomers and enantiomers of the product Methohexital and the results of the catalytic runs (variation of base and optically active ligand). Then we report on the separation of the contributions of the kinetic resolution and the optically active catalyst, which superpose in the enantioselective Pd-catalyzed allylation of MBS. Finally, the Methohexital mixtures synthesized are tested with regard to their narcotic effect in rats.[3,4]

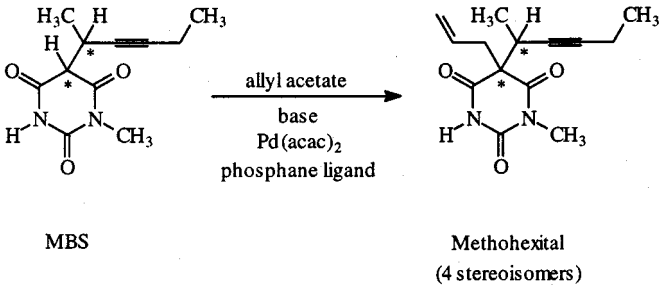
1-Methyl-5-(1′-methylpent-2′-ynyl)barbituric Acid (MBS) and Analysis of Its Stereoisomers

1-Methyl-5-(1′-methylpent-2′-ynyl)barbituric acid (MBS) is synthesized in five steps.[3,4,10−15] MBS contains two asymmetric centres. Therefore, it forms two diastereomeric pairs of enantiomers. The signals of the four stereoisomers of MBS appear in approximately equal intensities in the ^{1}H-NMR spectrum (*N*-methyl groups) after addition of the shift reagent (*S*)-(+)-1-(9′-anthryl)-2,2,2-trifluoroethanol. To follow the accumulation of the stereoisomers of MBS during the catalytic process a GC separation of the stereoisomers on a chiral CP-Chirasil-Dex-CB column (length 25 m), coated with permethylated β-cyclodextrin, was developed. Two peaks of equal areas were obtained, each of which contains the two stereoisomers of MBS, which interconvert by the keto-enol tautomerism of the labile asymmetric centre of the barbiturate system (Scheme 1).

This keto-enol tautomerism is only possible for these two stereoisomers, which have the same configuration in the hexyne side chain (bold configuration symbol), because only the asymmetric centre in the barbiturate system is involved in the tautomerism. Thus, the first peak arises either from the combination (***R***,*S*)/(***R***,*R*) and the second peak from the combination (***S***,*R*)/(***S***,*S*) or vice versa. The absolute configuration is not known. The difference in area between the two peaks is called "combined enantiomeric excess" and abbreviated by "ee". For a racemic MBS sample a "combined enantiomeric excess" of 0% "ee" was measured on the CP-Chirasil-DEX-CB column used for the analysis.

5-Allyl-1-methyl-5-(1′-methylpent-2′-ynyl)barbituric Acid (Methohexital) and Its Stereoisomer Analysis

In the Pd-catalyzed allylation of MBS a configurationally stable second asymmetric centre in 5-position of the barbiturate system of the product Methohexital is formed (Scheme 2).



Scheme 2. Synthesis of Methohexital by Pd-catalyzed allylation of MBS

The four stereoisomers of Methohexital were separated with a GC system consisting of an achiral and a chiral column (Figure 1a). The achiral column was a polar Durabond-DB-225 column (length 30 m) and the chiral column was a Chiraldex-B-DA column (length 30 m). The two enantiomeric pairs are designated α and β and the configuration in the hexyne side chain 1 and 2. Thus, the four stereoisomers of Methohexital are: α1, α2, β1, β2 (Figure 1a). The two α-peaks belong to one pair of enantiomers (α1 and α2) with the literature name α-*dl*[12][13] and the two β-peaks to the other pair of enantiomers (β1 and β2) with the literature name β-*dl*. These two pairs of enantiomers are either

(***R***,*R*)/(***S***,*S*) and (***R***,*S*)/(***S***,*R*) or vice versa. The indices 1 and 2 are choosen such, that stereoisomers with the same index have the same configuration in the hexyne side chain. Thus α1 and β1 have either the configuration (***R***,*R*)/(***R***,*S*) or (***S***,*S*)/(***S***,*R*) (analogously for α2 and β2).

Which of the stereoisomers of Methohexital have the same configuration in the hexyne side chain, was established from a chromatogram of a catalysis with a yield of 94%. As the starting material MBS was racemic with respect to the configuration in the hexyne side chain, the product stereoisomers can be combined to the diastereomeric pairs (***R***,*R*)/(***R***,*S*) or (***S***,*S*)/(***S***,*R*) only in this way, that the pairs do not have more than yields of 50%. Thus, the first and the fourth as well as the second and the third peak must have the same configuration in the hexyne side chain (Figure 1a).

The four stereoisomers of Methohexital could also be separated with a permethylated β-cyclodextrin column Chiraldex-B-PM (length 30 m). In this analysis the second and the fourth peak belong to the α-*dl* pair of Methohexital and the first and the third to the β-*dl* pair (Figure 1b). A Methohexital sample resulting from an achiral catalysis with the ligand triphenylphosphane (Table 1, entry 1) gave an enantiomeric excess, as expected, of 0% ee in the α and β series. The diastereomeric excess of α pair versus β pair was measured to be 8% de with the B-PM column compared to 7% de with the two-column system DB-225 + B-DA (Figure 1a). In the GC investigations of Methohexital samples care had to be taken to separate the starting material MBS completely from the product Methohexital, because both with the DB-225 + B-DA column system as well as with the B-PM column there was overlap[3,4].

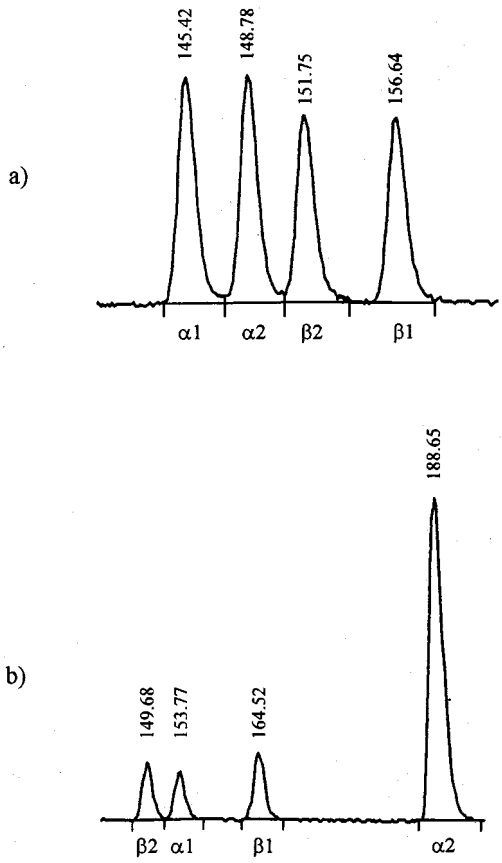


Figure 1. Separation of the four Methohexital isomers: a) on a DB-225 + B-DA column system (catalysis with ligand triphenylphosphane; Table 1, entry 1; 7% de of α pair); b) on a B-PM column (catalysis with ligand **7**; Table 2, entry 3; sample heavily enriched in α2)

Standard Catalytic Allylation of MBS to Methohexital

In the Pd-catalyzed allylation (Scheme 2) MBS is dissolved in dichloromethane/toluene (1:1). To the clear solution a base (NEt_3 or DBU) is added in 5% excess. Then 1 mol-% of palladium(II) acetylacetonate and 4 mol-% of a monodentate or 2 mol-% of a bidentate optically active phosphane are dissolved in the reaction mixture. The reaction is started by addition of allyl acetate in 11% excess. The homogeneous solution containing the "in situ" Pd/ligand complex is stirred for 72 h at 38°C. If the ligands are not soluble in dichloromethane/toluene (1:1), the dichloromethane content is increased.

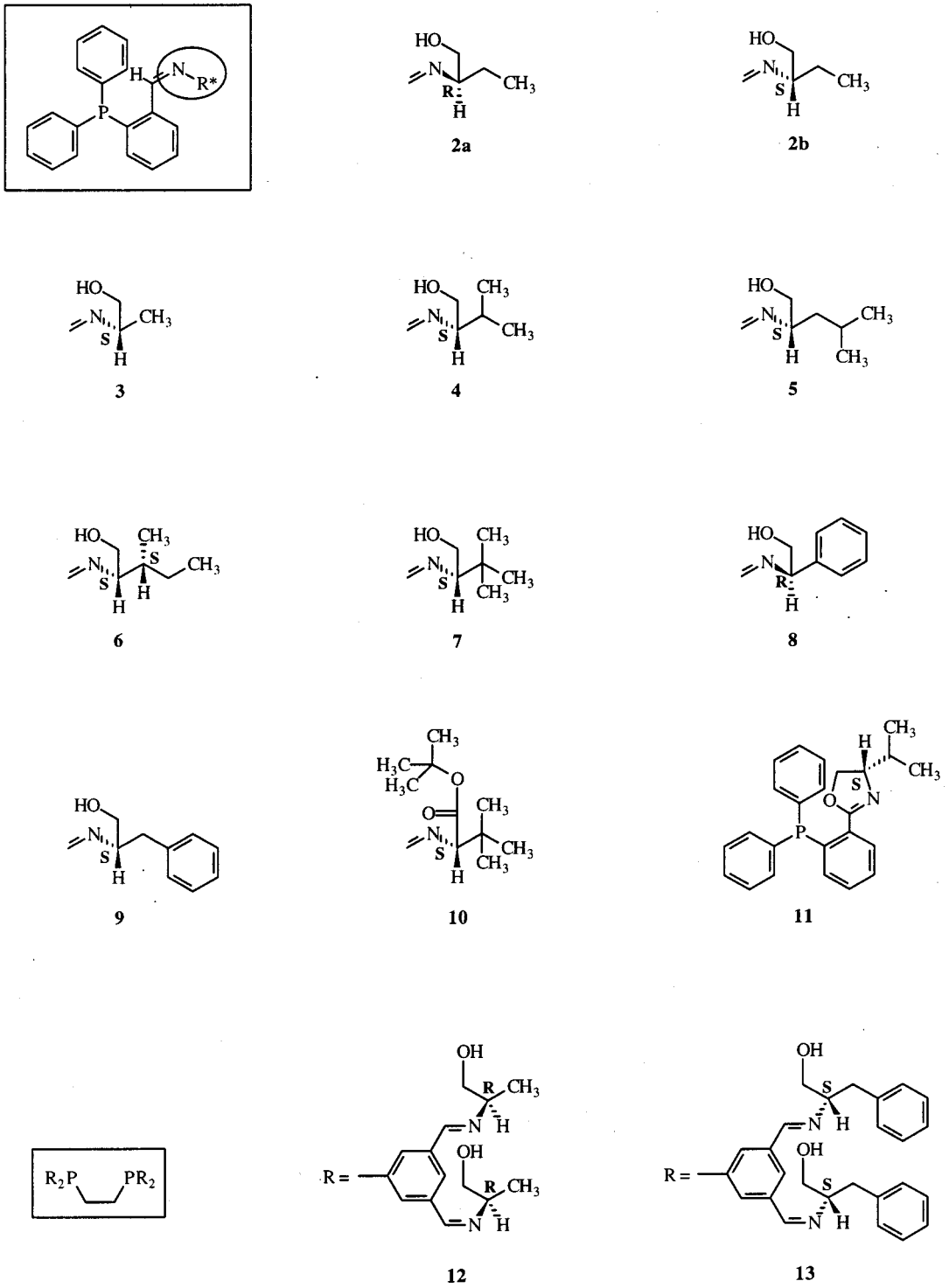
The reaction is stopped by addition of 0.2 M hydrochloric acid. From the organic layer an oily product is obtained, which is chromatographated on silica gel with dichloromethane/acetonitrile (25:1). First, the yellow (2-formylphenyl)diphenylphosphane, the hydrolysis product of the phosphane imine ligands, is eluted, then the excess of allyl acetate and small amounts of the doubly allylated by-product 3,5-diallyl-1-methyl-5-(1′-methylpent-2′-ynyl)barbituric acid (AAMBS), formed in a second allylation (*N*-allylation[2][4]). Then the product Methohexital is eluted. With a qualitative TLC test it is possible to monitor the progress of the chromatography (allyl acetate, AAMBS, Methohexital, and MBS show different yellow spots after dipping into a dilute $KMnO_4$ solution). By changing the eluent to dichloromethane/acetonitrile (3:1) the unreacted starting material MBS can be eluted. After removal of the solvent Methohexital forms a colourless oil, which crystallizes subsequently. The yield is determined by weighing. The analysis of the Methohexital stereoisomers is achieved by GC.

Chiral Ligands in the Palladium-Catalyzed Allylation of MBS

In the Pd-catalyzed allylation of MBS the achiral ligand triphenylphosphane as well as a series of chiral ligands[2] were used. The phosphane imine ligands **2a**, **2b**, **3**−**10** were obtained by Schiff base condensation of (2-formylphenyl)-diphenylphosphane with the following primary amines[2]: (*R*)-(−)-2-amino-1-butanol, (*S*)-(+)-2-amino-1-butanol, L-alaninol, L-valinol, L-leucinol, L-isoleucinol, L-*tert*-leucinol, D-α-phenylglycinol, L-phenylalaninol, L-*tert*-butyl *tert*-leucinate. Further chiral ligands were (−)-(4*S*)-2-[2′-(diphenylphosphanyl)phenyl]-4-isopropyl-1,3-oxazoline (**11**),[16,17]

(+)-1,2-bis{bis[3′,5′-bis(*N*-methyliden-(*R*)-alaninol)phenyl]phosphanyl}ethane (**12**)[2,18] and (−)-1,2-bis{bis[3′,5′-bis(*N*-methylidene-(*S*)-phenylalaninol)phenyl]phosphanyl}-ethane (**13**)[18] (Scheme 3). For a comparison the standard ligands (−)-norphos[19,20] and (−)-diop[21,22] were included. The results of the catalyses are summarized in Table 1.

mate of 7% de was obtained (Table 1, entry 1). Phosphane imine ligands induce a high diastereomeric and enantiomeric excess, if there is a hydroxymethyl substituent at the asymmetric centre near the imine group, which acts as an anchor for the incoming barbiturate anion.[2] The variation of the other side chain at the asymmetric centre leads to



Scheme 3. The phosphane imines **2**−**10**, the phosphane oxazoline **11** and the phosphane octaimines **12** an **13**

With the achiral triphenylphosphane in the Pd-catalyzed allylation of MBS a diastereomeric excess of the α-*dl* racedistinct differences in the diastereomeric and enantiomeric excess. With the (*R*) ligand **2a** an enantiomeric excess in the

Table 1. Synthesis of Methohexital by palladium-catalyzed allylation of MBS with allyl acetate; procatalyst 1 mol-% [$Pd(acac)_2$], Pd/ligand ratio 1:4, solvent 25 mL of CH_2Cl_2 + 25 mL of toluene, 38°C, 72 h; GC analysis with the DB-225 + B-DA two-column system

Entry	Ligand	Base	Yield [%][c]	ee (α1, α2) [%]	ee (β1, β2) [%]	"ee"[a] (α1+β1, α2+β2) [%]	de (α1, β1) [%]	de (α2, β2) [%]	de (α1+α2, β1+β2) [%]	s[b]
1	**1**	DBU	82	0	0	0	7 (α1)	7 (α2)	7 (α1+α2)	1.0
2	**2a**	NEt_3	52	47 (α1)	21 (β2)	27 (α1+β1)	62 (α1)	1 (α2)	40 (α1+α2)	2.3
3	**2b**	NEt_3	52	50 (α2)	14 (β1)	30 (α2+β2)	3 (β1)	60 (α2)	37 (α1+α2)	2.5
4	**3**	NEt_3	66	24 (α2)	8 (β1)	11 (α2+β2)	6 (α1)	36 (α2)	23 (α1+α2)	1.5
5	**3**	DBU	62	15 (α2)	16 (β1)	4 (α2+β2)	8 (α1)	38 (α2)	24 (α1+α2)	1.1
6	**4**	NEt_3	26	62 (α2)	3 (β1)	43 (α2+β2)	3 (β1)	61 (α2)	42 (α1+α2)	2.9
7	**5**	NEt_3	94	33 (α2)	55 (β1)	2 (α2+β2)	12 (β1)	68 (α2)	29 (α1+α2)	1.3
8, 9	**6**	NEt_3	33	62[d] (α2)	8[d] (β1)	42[d] (α2+β2)	6[d] (β1)	64[d] (α2)	44[d] (α1+α2)	3.0
			43	62 (α2)	12 (β1)	42 (α2+β2)	7 (β1)	65 (α2)	44 (α1+α2)	3.3
10	**6**	DBU	63	51 (α2)	38 (β1)	24 (α2+β2)	11 (β1)	69 (α2)	39 (α1+α2)	2.3
11, 12	**7**	NEt_3	89	40 (α2)	59 (β1)	2 (α2+β2)	23 (β1)	71 (α2)	26 (α1+α2)	1.2
			91	40 (α2)	61 (β1)	3 (α2+β2)	22 (β1)	71 (α2)	25 (α1+α2)	1.3
13	**8**	NEt_3	91	26[d] (α1)	32[d] (β2)	5[d] (α2+β2)	55[d] (α1)	3[d] (α2)	30[d] (α1+α2)	1.6
14	**8**	DBU	63	28[d] (α1)	28[d] (β2)	8[d] (α1+β1)	52[d] (α1)	0[d]	28[d] (α1+α2)	1.3
15	**9**	DBU	64	19 (α2)	6 (β1)	8 (α2+β2)	1 (β1)	23 (α2)	12 (α1+α2)	1.3
16	**10**	NEt_3	12	1 (α2)	5 (β1)	2 (α1+β1)	0	5 (α2)	3 (α1+α2)	1.0
17	**10**	DBU	10	1 (α2)	2 (β1)	0	1 (α1)	4 (α2)	3 (α1+α2)	1.0
18	**11**	NEt_3	59	3 (α1)	4 (β1)	3 (α1+β1)	4 (α1)	6 (α2)	5 (α1+α2)	1.1
19	**12**[e,f]	NEt_3	62	8 (α1)	13 (β2)	3 (α2+β2)	5 (α1)	15 (β2)	6 (β1+β2)	1.1
20	**13**[e]	NEt_3	74	12 (α1)	19 (β2)	3 (α2+β2)	18 (α1)	13 (β2)	0	1.1
21	(−)-norphos[e]	NEt_3	93	5[d] (α1)	6[d] (β2)	0[d]	15[d] (α1)	4[d] (α2)	10[d] (α1+α2)	1.0
22	(−)-diop[e]	NEt_3	93	2[d] (α1)	2[d] (β2)	0[d]	11[d] (α1)	7[d] (α2)	9[d] (α1+α2)	1.0

[a] "ee" = "combined enantiomeric excess" (see text). − [b] s = stereoselectivity factor. − [c] After chromatography. − [d] GC analysis with the B-PM column. − [e] Pd/ligand ratio 1:2. − [f] 150 mL of CH_2Cl_2 + 25 mL of toluene was used to dissolve ligand **12**.

α-*dl* pair of 47% ee (α1) and in the β-*dl* pair of 21% ee (β1) is achieved, the diastereomeric excess for the α-*dl* pair being 40% de (entry 2). The isomers added in parentheses after the ee and de values are the favoured isomers. The analogous (*S*) ligand **2b** gives a similar enantiomeric excess of the opposite stereoisomers, a similar diastereomeric excess for the α-*dl* pair and the same chemical yield (entry 3). A shortening of the ethyl group at the asymmetric centre in the ligands **2a** and **2b** to a methyl group in the ligand **3** diminishes the diastereomeric and enantiomeric excess considerably, although the chemical yield increases (entries 4, 5).

Branching of the alkyl group as in the ligands **4**−**7** leads to the highest stereoselectivities in the Pd-catalyzed allylation of MBS observed so far similar to the Pd-catalyzed allylation of 1,5-dimethylbarbituric acid[2]. With the ligands **4** and **6**, which contain an isopropyl group and a *sec*-butyl group, respectively, a high enantiomeric excess in the α-*dl* pair of 62% ee (α2) was attained, associated with a low enantiomeric excess of 3−12% ee (β1) in the β-*dl* pair, the diastereomeric excess for the α-*dl* pair being 42 and 43% de. With NEt_3 as a base, the yields are only 26−43% (entries 6, 8, 9). Using DBU leads to an increased yield of 63%. The enantiomeric excess in the α-*dl* pair decreases to 51% ee (α2), whereas the enantiomeric excesses in the β-*dl* pair rises to 38% ee (β1) (entry 10).

The ligands **5** and **7**, which carry an isobutyl group and a *tert*-butyl group at the asymmetric centre, respectively, lead to a lower enantiomeric excess in the α-*dl* pair [33 and 40% ee (α2)] but to a higher enantioselectivity in the β-*dl* pair [55, 59, and 61% ee (β1)] with yields of up to 94% using NEt_3 as a base. The diastereoselectivities are between 25 and 29% de for the α-*dl* pair (entries 7, 11, 12). If the side chain at the asymmetric centre contains a phenyl group (ligands **8** and **9**), the induced enantiomeric excess is higher for ligand **8** than for ligand **3** and distinctly lower for ligand **9** than for ligand **2b** (entries 13−15). A substitution of the hydroxymethyl group at the asymmetric centre by a *tert*-butyl ester group in the ligand **10** reduces the enantiomeric excess appreciably independent of the base used (entry 16).

The phosphane oxazoline ligand **11** gives only a low enantiomeric excess in the product Methohexital similar to the standard ligands (−)-norphos and (−)-diop (entries 17, 20, 21). The ligands **12** and **13** belong to a different group of phosphane imine ligands with two phosphorus atoms. They afford an enantiomeric excess in the various stereoisomers of 8−19% ee using the base NEt_3 (entries 18, 19). Up to now ligand **12** is the only one, which induces a diastereomeric excess in favour of the β-*dl* pair (6% de).

The Interplay of Kinetic Resolution and Catalyst Contribution

In the allylation of 1,5-dimethylbarbituric acid the 1,5-dimethylbarbiturate anion is formed, which no longer contains an asymmetric centre. Thus, there is no kinetic resolution in this reaction and the enantiomeric excess of the product 5-allyl-1,5-dimethylbarbituric acid is only dependent on the enantioselectivity of the chiral catalyst.[2] On the contrary, the starting material 1-methyl-5-(1′-methylpent-2′-ynyl)barbituric acid (MBS) for the synthesis of Me-

Table 2. The interplay of kinetic resolution and catalyst contribution in the Pd-catalyzed allylation of MBS with ligand **7**; procatalyst 1 mol-% of $[Pd(acac)_2]$, Pd/ligand ratio 1:4, solvent CH_2Cl_2/toluene (1:1), 38°C, base DBU; GC analysis of MBS with a CP-Chirasil-Dex-CB column and of Methohexital with a B-PM column

		A	B	C	D	E	F	G	H	I	J	K
					Methohexital						MBS	
Entry	Time	Yield	ee	ee	"ee"[a]	de	de	de	S[b]	unreacted	"ee"[a]	s[b]
	[h]	[%][c]	(α1, α2) [%]	(β1, β2) [%]	(α1+β1, α2+β2) [%]	(α1, β1) [%]	(α2, β2) [%]	(α1+α2, β1+β2) [%]	(from A, D calcd.)	MBS [%][c]	(1., 2.) [%]	(from A, J calcd.)
1	3	17	77 (α2)	7 (β1)	60 (α2+β2)	11 (β1)	76 (α2)	59 (α1+α2)	4.5	79	5 (1.)	1.7
2	4.5	20	80 (α2)	6 (β1)	62 (α2+β2)	18 (β1)	76 (α2)	58 (α1+α2)	5.0	77	9 (1.)	2.3
3	9	26	80 (α2)	13 (β1)	60 (α2+β2)	20 (β1)	77 (α2)	58 (α1+α2)	4.9	70	14 (1.)	2.7
4	12	32	78 (α2)	17 (β1)	57 (α2+β2)	19 (β1)	77 (α2)	57 (α1+α2)	4.7	65	19 (1.)	2.8
5	72	49	61 (α2)	30 (β1)	36 (α2+β2)	12 (β1)	71 (α2)	45 (α1+α2)	2.9	48	40 (1.)	3.5
6	72	65	42 (α2)	67 (β1)	0	27 (β1)	75 (α2)	24 (α1+α2)	1.0	–	–	–
7	72	91	46 (α2)	72 (β1)	6 (α2+β2)	24 (β1)	82 (α2)	32 (α1+α2)	1.7	7	83 (1.)	2.3

[a] "ee" = "combined enantiomeric excess". – [b] s = stereoselectivity factor. – [c] After chromatography.

thohexital contains two asymmetric centres. On addition of base the asymmetric centre in the barbiturate system is removed, but the asymmetric centre in the hexyne side chain is preserved. In the present study the asymmetric centre in the hexyne side chain of the MBS used was racemic. Therefore, two different effects can influence the distribution of the stereoisomers in the Pd-catalyzed allylation of MBS, the kinetic resolution and the enantioselective catalysis, which are both concentration-dependent. The contributions of these two effects can be calculated provided the yields of Methohexital and MBS as well as the diastereomeric and enantiomeric excess of Methohexital and MBS are known. These data were obtained from a standard catalysis with ligand **7** by taking aliquots after 3, 4.5, 9, 12, and 72 h. The yields of Methohexital and MBS were determined and their stereoisomer composition was analysed by GC as described above. In Table 2 the results and calculations are summarized together with those of two other catalytic runs.

The Kinetic Resolution in the Pd-Catalyzed Allylation of MBS with Ligand 7

Due to the kinetic resolution in the reaction with the optically active catalyst there is a chiral discrimination of the MBS anions, which have opposite configurations in the hexyne side chain. One is consumed faster to give the product Methohexital, whereas the other is enriched in the unreacted starting material. This difference in reactivity shows up in the intensity ratio of the first and the second MBS GC peak (Table 2, column J). The "combined enantiomeric excess", calculated as $[(|peak1 - peak2|)/(peak1 + peak2)] \times 100\%$ reflects the reactivity difference of the MBS stereoisomers, which have opposite configurations in the hexyne side chain.

Addition of the yield of Methohexital (column A) and the amount of unreacted MBS (column I) leads to retrieval rates of 96–98%. The missing 2–4% are lost by the treatment with 0.2 M hydrochloric acid, by the chromatographic purification or by the formation of the doubly allylated byproduct AAMBS. In a reasonable approximation the yield of Methohexital can be used to represent the overall conversion.

After 3 h, the first sample taken gave a yield of 17% of Methohexital and 79% of starting material MBS (Table 2, entry 1). The yield of Methohexital increased from 20% after 4.5 h (77% MBS) via 26% after 9 h (70% MBS) and 32% after 12 h (65% MBS) to 49% after 72 h (48% MBS), as shown in columns A and I of Table 2 (entries 2–5). In comparable reactions Methohexital yields of 65% (MBS not determined) and 91% (7% MBS) were isolated after 72 h (entries 6, 7).

Figure 2 shows the correlation between the yield of Methohexital (column A) and the increase of the "combined enantiomeric excess" of MBS (column J). With the decrease of the amount of unreacted MBS down to 7% after 72 h (entry 7) the enantioselectivities of the remaining MBS rises to an enrichment of 83% "ee" (1.). The designation (1.) means an excess of the first peak of MBS in the GC chromatogram.

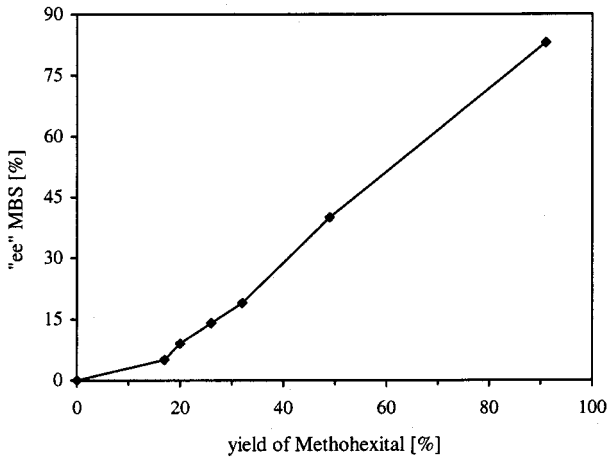


Figure 2. Correlation between the "combined enantiomeric excess" of MBS and the yield of Methohexital

With the rate constants k_R and k_S for the reaction of the two MBS anion enantiomers, the stereoselektivity factor $s = k_R/k_S$ is a measure for the kinetic resolution.[23,24] It can be calculated from the amount and the enantiomeric

excess of the unreacted starting material with Equation 1.[23,24] The values of the stereoselectivity factor *s* of MBS

$$s = \frac{\ln[(1-C)(1-ee)]}{\ln[(1-C)(1+ee)]}$$

C = conversion: 0 < C < 1 (column A); assumption: retrieval rate of 100%; ee = "ee" = "combined enantiomeric excess" in the unreacted starting material MBS: 0 < "ee" < 1 (column J)

are between 1.7 and 3.5 with an average of 2.6 (column K).

The effect of the kinetic resolution with respect to the product Methohexital can be calculated with the help of the "combined enantiomeric excess" α1 + β1 vs. α2 + β2 (vs. = versus) in column D, obtained from the four GC peaks of the Methohexital stereoisomers. The two components of each sum have the same configuration in the hexyne side chain. It decreases from 60−62% "ee" for a Methohexital yield of 17−26% via 36% "ee" for a yield of 49% to 6% "ee" for a yield of 91% (columns A and D) with increasing conversion (entries 1−5, 7). The value of 0% "ee" for a Methohexital yield of 65% does not fit into this series (entry 6). The stereoselectivity factor *s* (values between 1.7 and 5.0, column H) is calculated with Equation 2.[23,24]

$$s = \frac{\ln[1-C(1+ee)]}{\ln[1-C(1-ee)]}$$

C = conversion: 0 < C < 1 (column A); assumption: retrieval rate of 100%; ee = "ee" = "combined enantiomeric excess" in the product Methohexital: 0 < "ee" < 1 (column D)

Although the absolute configurations are not known, the starting material MBS and the product Methohexital can be correlated with respect to the configuration in the hexyne side chain. During the reaction the isomers of MBS appearing in the first GC peak are enriched. Thus, they react more slowly to the product Methohexital. The faster reacting MBS isomers lead to a growth of the GC peaks of the Methohexital stereoisomers α2 and β2. Therefore, they must have the same configuration in the hexyne side chain as the isomers of the second MBS peak.

The Contribution of the Optically Active Catalyst in the Pd-Catalyzed Allylation of MBS with Ligand 7

In addition to the kinetic resolution the optically active catalyst contributes to the stereoselectivity of the Pd-catalyzed allylation of MBS. This is reflected in the enantiomeric excess in the α series which decreases from 80% ee (α2) to 42% ee (α2) (Table 2, column B), whereas in the β series it rises from 6% ee (β1) to 72% ee (β1) (column C). Figure 1b shows the highest enantiomeric excess of 80% ee (α2) in the α-*dl* pair of Methohexital obtained up to now (entry 3).

The contribution of the optically active catalyst is concentration-dependent, because the composition of the MBS stereoisomers changes during the reaction due to the kinetic resolution. At the beginning of the reaction MBS is racemic. Thus, the influence of the optically active catalyst can be read off directly from the enantiomeric excess of Methohexital in the beginning of the MBS allylation.

Columns E and F show the diastereomeric excess α1 vs. β1 and α2 vs. β2, which involves the influence of the asymmetric centre in the hexyne side chain and the optically active catalyst on the formation of the new asymmetric centre in the barbiturate ring. For the diastereomeric excess α1 vs. β1 values between 11 and 27% de (β1) were achieved (column E) and for α2 vs. β2 values between 71 and 82% de (α2) (column F). The diastereomeric excess α1 vs. β1 and α2 vs. β2 is relatively independent of the turnover (columns A, E, F). The overall diastereomeric excess α pair vs. β pair decreases from 59 to 24% de (α pair) (column G) depending on the yield of Methohexital (column A).

Kinetic Resolution and Catalyst Contribution for the Other Ligands

The influence of the kinetic resolution in the Pd-catalyzed allylation of MBS is calculated for all the optically active ligands with Equation 2 using enantiomeric excesses α1 vs. α2 and β1 vs. β2 for Methohexital. The results are summarized in Table 1. As expected *s* is 1.0 for the achiral catalysis with triphenylphosphane, as both enantiomeric excesses α1 vs. α2 and β1 vs. β2 are 0% ee. The influence of the kinetic resolution is small for most of the ligands investigated (values for *s* between 1.0 and 1.6) except for the catalyses with the ligands **2a**, **2b**, **4**, and **6** (values for *s* from 2.3 to 3.3).

The contribution of the optically active catalyst in the Pd-catalyzed allylation of MBS for all the ligands is obvious from the enantiomeric excess in the α and β series, although most of the reactions were stopped at higher conversions. It was small for the standard ligands (−)-norphos, (−)-diop, the phosphane oxazoline ligand **11** and the phosphane imine ligand **10** containing a *tert*-butyl ester substituent with an enantiomeric excess between 1 and 6% ee. For the remaining phosphane imine ligands, which carry a hydroxymethyl substituent at the asymmetric centre, the catalyst contribution was much higher with up to 62% ee (Table 1).

Determination of the Anesthetic Doses of Methohexital Stereoisomer Mixtures in Rats

Methohexital is a common anesthetic widely used to initiate narcoses.[5−11] The four stereoisomers of Methohexital exhibit different anesthetic effects in rats, dogs and monkies.[12,13] Injected as a solution of the sodium salt into rats, the β-*l* isomer of Methohexital is the most effective of the stereoisomers with an anesthetic dose of 7 mg/kg body weight of the animal. The α-*d* stereoisomer with 11 mg/kg and the β-*d* stereoisomer with 17 mg/kg follow. For a narcosis with the α-*l* stereoisomer 35 mg/kg are necessary. With 10 mg/kg the β-*dl* racemate is more effective than the α-*dl* racemate with 15 mg/kg. However, because of undesirable stimulating post-anesthetic effects of the β-*dl* racemate caused by the β-*l* stereoisomer the extensively used narcotic is the α-*dl* racemate (Eli Lilly).

Table 3. 10 Methohexital samples and their isomer composition, the reference Brevimytal®Natrium and the anesthetic doses (AD) in Sprague Dawley rats of body weight between 560 and 720 g[25][26]

Sample	Ligand	α1 [%]	α2 [%]	β1 [%]	β2 [%]	AD [mg/kg]	Average AD [mg/kg]
1	**1**	27	27	23	23	10.8, 9.3, 11.1	10.4
2	**2a**	51.5	18.5	12	18	14.6, 13.5, 11.1	13.0
3	**2b**	17	51.5	18	13.5	15.7, 17.7, 14.8	16.1
4	**4**	13.5	58.5	14.5	13.5	17.4, 16.3, 16.4	16.7
5	**5**	22	43	27	8	16.1, 15.3, 15.7	15.7
6	**8**	41	23	13	23	8.9, 9.4, 8.9	9.1
7	**8**	41	24	12	23	17.9, 14.5, 15.6	16.0
8	**3**	26	36	22	16	14.7, 13.7, 14.3	14.2
9	**6**	13.5	58.5	15	13	14.1, 8.9, 9.5	10.9
10	**7**	19	44	29.5	7.5	22.0, 21.0, 20.1	21.0
11	reference[a]	50	50	–	–	16.3, 12.4, 10.3	13.0

[a] Protonated Brevimytal®Natrium (see Experimental Section).

For 10 mixtures of Methohexital stereoisomers, obtained by Pd-catalyzed enantioselective allylation of MBS, the anesthetic dose (AD) in rats was determined using the corneal stimulus technique[25] as described elsewhere.[26] The results were compared with those of a sample of protonated Brevimytal®Natrium (sample 11).

Table 3 summarizes the anesthetic doses obtained by standardising to 1 kg body weight of the rat. The average anesthetic dose of the samples **1**, **6**, and **9** was lower than that of Brevimytal®Natrium with 13.0 mg/kg (Table 3). In particular, sample **6** with 9.1 mg/kg had a distinctly reduced anesthetic dose. Deviations from the average value were small with this sample. However, it is conspicuous, that samples **6** and **7**, which showed marked differences in the anesthetic doses, had a closely related stereoisomer composition (Table 3).[26]

Experimental Section

The instruments used were the same as described in the preceding paper.[2] – All the syntheses and catalytic reactions were carried out with dried solvents under nitrogen. – Palladium(II) acetylacetonate and allyl acetate (Merck) were used without further purification. DBU (Fluka) was dried with $CaCl_2$, NEt_3 (Merck) with CaH_2, and distilled.

1-Methyl-5-(1′-methylpent-2′-ynyl)barbituric Acid (MBS):[3,4,13] 10.9 g (0.474 mol) of sodium was dissolved in 200 mL of refluxing absolute ethanol. After addition of 17.6 g (0.237 mol) of *N*-methylurea and stirring for 15 min, 38.0 g (0.158 mol) of diethyl (1-methylpent-2-ynyl)malonate[4,13,14] was added to the clear boiling solution within 10 min. A solid precipitated after 30 min. After 1.5 h of reflux, the solvent was removed and the product dissolved in about 750 mL of water. With vigorous stirring 80 mL of conc. hydrochloric acid was added to give an oil, which solidified. After 30 min of stirring, the product was filtered off and washed with cold water. Recrystallization from 2-propanol/water (2:1) provided colourless crystals. Yield 20.8 g (59%), m. p. 90–91.5°C. – IR (KBr): $\tilde{\nu}$ = 1754 (m), 1719 (s), 1695 (s) cm^{-1} (C=O). – ^1H NMR ($CDCl_3$, 400 MHz): δ = 8.14/8.09 (2 s, 1 H, N*H*), 3.39–3.31 (m, 2 H, OC–C*H*–C*H*), 3.303/3.298 (2s, 3 H, N–CH_3), 2.102/2.100 (2 dq, 2 H, ^5J = 2.2 Hz, ^3J = 7.5 Hz, C≡C–CH_2–CH_3), 1.444/1.440 (2d, 3 H, ^3J = 7.0 Hz, CH–CH_3), 1.040/1.038 (2 t, 3 H, ^3J = 7.5 Hz, C≡C–CH$_2$–CH_3). – $^{13}C\{^1H\}$ NMR ($CDCl_3$, 62.9 MHz): δ = 169.3/168.7 (HN–*C*O–CC$_3$), 167.5/166.8 (H$_3$C–N–*C*O–CC$_3$), 151.2/151.1 (HN–*C*O–N–CH$_3$), 86.6/86.5 (HC–*C*≡C), 76.8 (C≡*C*–CH$_2$), 54.3 (OC–*C*–CO), 31.8/31.6 (H*C*–C≡C), 27.7/27.4 (N–*C*H$_3$), 20.0/19.7 (H$_3$*C*–CH), 13.8 (CH$_2$–*C*H$_3$), 12.1 (C≡C–*C*H$_2$). – The signals appear doubled because of the two MBS diastereomers. Addition of (*S*)-(+)-1-(9′-anthryl)-2,2,2-trifluoroethanol (Super-Pirkle) to MBS in the molar rate 1:12 results also in a separationof of the enantiomers: δ = 3.059/3.054/3.043/3.035 (4s, N–CH_3), 0.940/0.938/ 0.933/ 0.927 (4 t, ^3J = 7.5 Hz, C≡C–CH$_2$–CH_3). – MS (EI, 70 eV); *m/z* (%): 222.1 (7) [M^+], 207.1 (45) [M^+ – CH_3], 193.1 (46) [M^+ – C_2H_5], 81.1 (35) [$C_6H_9^+$], 79.1 (100). – $C_{11}H_{14}N_2O_3$ (222.24): calcd. C 59.45, H 6.35, N 12.60; found C 59.52, H 6.34, N 12.63. – GC analysis of MBS: 25-m CP-Chirasil-Dex-CB column (chemically connected with permethylated β-cyclodextrin; 0.25 mm inner diameter, 0.25 µm film thickness; from Chrompack), column temp. 165°C, He pressure 1.2 bar, injector temp. 250°C, detector temp. 230°C (flame ionisation). Retention times: (1.) 23.29 min, (2.) 24.97 min; dead time t_0 (CH_2Cl_2) = 1.21 min. Separation factor: α = 1.07, resolution *R* = 3.52.

Synthesis of Methohexital by Enantioselective Palladium-Catalyzed Allylation of MBS with Allyl Acetate: 1.07 g (4.81 mmol) of MBS was dissolved in 25 mL of dichloromethane/toluene (1:1) at 38°C under nitrogen. To the clear solution 5.05 mmol of the base was added [DBU (752 µL, 769 mg) or NEt_3 (700 µL, 511 mg), respectively]. After 5 min of stirring, 14.6 mg ($4.81 \cdot 10^{-2}$ mmol) of Pd(acac)$_2$ and $19.2 \cdot 10^{-2}$ mmol of a monodentate or $9.61 \cdot 10^{-2}$ mmol of a bidentate ligand were rinsed into the reaction vessel with another 25 mL of dichloromethane/toluene (1:1). After 2.0 min, 576 µL (5.35 mmol, 536 mg) of allyl acetate was added to the clear yellow solution. Usually, the solution was stirred for 72 h at 38°C. For work-up the solution was diluted with 50 mL of dichloromethane and the reaction was stopped with 50 mL of 0.2 M hydrochloric acid. The organic layer was dried with Na_2SO_4, the Na_2SO_4 was filtered off and washed with 50 mL of dichloromethane. The solvent was removed. The remaining oily product was chromatographed on silica gel with dichlormethane/acetonitrile (25:1). If phosphane imine ligands were used in the catalysis, first the yellow (2-formylphenyl)diphenylphosphane was eluted, followed by the excess of allyl acetate and small amounts of doubly allylated MBS (AAMBS). Then the product Methohexital was eluted. The separation of the products was monitored by a qualitative TLC test (silica 60, Merck; dichloromethane/acetonitrile, 25:1), which showed how much allyl acetate, AAMBS, Methohexital and MBS were present in a specific fraction (yellow spots after dipping into a dilute $KMnO_4$ solution). All the fractions, which contained Methohexital, were combined to prevent an enrichment of the dia-

stereomers during the chromatography. After complete elution of Methohexital, the unreacted starting material MBS was eluted with dichloromethane/acetonitrile (3:1). The yield of Methohexital and unreacted MBS was determined by weighing. After about 1−2 d the colourless oil of Methohexital crystallized to a colourless solid.

Methohexital: Maximum yield 1.19 g (94%, Table 1, entry 7), m. p. 61−65°C. − IR (KBr): $\tilde{\nu}$ = 1717 (s), 1690 (s) cm^{-1} (C=O). − ^1H NMR ($CDCl_3$, 400 MHz): δ = 8.04/8.02 (2 s, 1 H, N*H*), 5.553/5.547 (2 tdd, ^3J = 7.3 Hz, $^3J_{cis}$ = 10.1 Hz, $^3J_{trans}$ = 17.0 Hz, 1 H, $H_2C{=}CH{-}CH_2$), 5.149 (md, ^3J = 17.0 Hz, 1 H, CH=CHH_{trans}), 5.084 (md, ^3J = 10.1 Hz, 1 H, CH=CHH_{cis}H), 3.293/3.286 (2 s, 3 H, N−CH_3), 3.087/3.081 (2 tq, ^5J = 2.3 Hz, ^3J = 7.0 Hz, 1 H, $H_3C{-}CH{-}C{\equiv}C{-}CH_2$), 2.864/2.852 (2 dd, ^3J = 7.3 Hz, ^2J = 13.0 Hz, 1 H, $H_2C{=}CH{-}CHH$), 2.657/2.648 (2 dd, ^3J = 7.3 Hz, ^2J = 13.0 Hz, 1 H, $H_2C{=}CH{-}CHH$), 2.102/2.099 (2 dq, ^5J = 2.3 Hz, ^3J = 7.5 Hz, 2 H, $HC{-}C{\equiv}C{-}CH_2{-}CH_3$), 1.301/1.291 (2 d, ^3J = 7.0 Hz, 3 H, $HC{-}CH_3$), 1.038/1.034 (2 t, ^3J = 7.5 Hz, 3 H, $C{\equiv}C{-}CH_2{-}CH_3$). − $^{13}C\{^1H\}$ NMR ($CDCl_3$, 62.9 MHz): δ = 171.6/170.8 (HN−*C*O−CC$_3$), 169.9/169.1 ($H_3C{-}N{-}CO{-}CC_3$), 150.4 (HN−*C*O−N−CH$_3$), 131.2 ($H_2C{=}CH$), 120.6 ($H_2C{=}CH$), 86.4 (HC−*C*≡C), 77.6 (C≡*C*−CH$_2$), 59.8 (OC−*C*−CO), 38.0 ($H_2C{=}CH{-}CH_2$), 36.0/35.6 (H*C*−C≡C), 27.6/27.5 (N−*C*H$_3$), 16.0 ($H_3C{-}CH$), 13.8 ($CH_2{-}CH_3$), 12.1 (C≡C−*C*H$_2$). All the signals appear doubled because of the two Methohexital diastereomers. − MS (EI, 70 eV); *m/z* (%): 262.1 (22) [M^+], 247.1 (30) [$M^+ - CH_3$], 233.1 (32) [$M^+ - C_2H_5$], 221.0 (81) [$M^+ - C_3H_5$], 181.0 (31) [$M^+ - C_6H_9$], 81.0 (100) [$C_6H_9^+$], 79.0 (60), 41.2 (80) [$C_3H_5^+$]. − $C_{14}H_{18}N_2O_3$ (262.31): calcd. C 64.11, H 6.92, N 10.68; found C 63.91, H 6.78, N 10.63.

GC Analysis of Methohexital: 20 mg of Methohexital was dissolved in 1 mL of dichloromethane. − Method a: 30-m Durabond-DB-225 column (25% cyanopropyl-, 25% phenyl-, 50% methylpolysiloxane; 0.25 mm inner diameter, 0.25 μm film thickness; from J & W) linked with an SiO_2 glass connector of Restek to a 30-m Chiraldex B-DA column (dipentylated β-cyclodextrin; 0.25 mm inner diameter, 0.125 μm film thickness; from astec), column temp. 145°C, H_2 pressure 2.07 bar, injector temp. 250°C, detector temp. 250°C (flame ionisation). Retention times: α1 = 145.42 min, α2 = 148.78 min, β1 = 151.75 min, β2 = 156.64 min; dead time t_0 (CH_2Cl_2) = 1.76 min. Separation factors: $\alpha_{\alpha2/\alpha1}$ = 1.02, $\alpha_{\beta2/\alpha2}$ = 1.02, $\alpha_{\beta1/\beta2}$ = 1.03. Resolutions: $R_{\alpha2/\alpha1}$ = 1.66, $R_{\beta2/\alpha2}$ = 1.53, $R_{\beta1/\beta2}$ = 2.52. − Method b: A 30-m Chiraldex B-PM column (coated with permethylated β-cyclodextrin; 0.25 mm inner diameter; from astec), column temp. 125°C, H_2 pressure 1.75 bar, injector temp. 260°C, detector temp. 260°C (flame ionisation). Retention times: β2 = 149.62 min, α1 = 153.62 min, β1 = 164.30 min, α2 = 188.38 min; dead time t_0 (CH_2Cl_2) = 0.64 min. Separation factors: $\alpha_{\alpha1/\beta2}$ = 1.03, $\alpha_{\beta1/\alpha1}$ = 1.07, $\alpha_{\alpha2/\beta1}$ = 1.15, $\alpha_{\alpha2/\alpha1}$ = 1.23, $\alpha_{\beta1/\beta2}$ = 1.10. Resolutions: $R_{\alpha1/\beta2}$ = 1.46, $R_{\beta1/\alpha1}$ = 3.81, $R_{\alpha2/\beta1}$ = 6.88, $R_{\alpha2/\alpha1}$ = 9.93, $R_{\beta1/\beta2}$ = 5.36.

3,5-Diallyl-1-methyl-5-(1′-methylpent-2′-ynyl)barbituric Acid (AAMBS): By-product of the catalysis under standard reaction conditions. AAMBS was separated by chromatography as described above. Yield 0−3%, light yellow liquid. − MS (EI, 70 eV); *m/z* (%): 302.2 (41) [M^+], 287.2 (31) [$M^+ - CH_3$], 273.1 (19) [$M^+ - C_2H_5$], 261.1 (100) [$M^+ - C_3H_5$], 221.0 (41) [$M^+ - C_6H_9$], 81.0 (66) [$C_6H_9^+$], 79.0 (41), 40.9 (84) [$C_3H_5^+$].

[1] H. Brunner, C. Krumey, *J. Mol. Catal.*, in press.
[2] H. Brunner, I. Deml, W. Dirnberger, B. Nuber, W. Reißer, *Eur. J. Inorg. Chem.* **1998**, 43.
[3] I. Deml, Dissertation, Universität Regensburg, **1998**.
[4] W. Reißer, Dissertation, Universität Regensburg, **1997**.
[5] H. Auterhoff, J. Knabe, H.-D. Höltje, *Lehrbuch der pharmazeutischen Chemie*, Wissenschaftliche Verlagsgesellschaft, Stuttgart, **1994**.
[6] W. Forth, D. Henschler, W. Rummel, *Pharmakologie und Toxikologie*, Bibliographisches Institut & F. A. Brockhaus, Mannheim, **1987**, p. 484.
[7] S. Ebel, *Synthetische Arzneimittel*, VCH, Weinheim, **1979**, p. 101.
[8] C. Lehmann, *Das Ultrakurznarkotikum Methohexital*, Springer-Verlag, Berlin, **1972**.
[9] Bundesverband der Pharmazeutischen Industrie, *Rote Liste 1996*, Editio Cantor Verlag, Aulendorf, **1996**, Nr. 65010.
[10] A. Kleemann, J. Engel, *Pharmazeutische Wirkstoffe*, Thieme Verlag, Stuttgart, **1982**, p. 578.
[11] S. Ebel, H. J. Roth, *Lexikon der Pharmazie*, Thieme Verlag, Stuttgart, **1987**, p. 430.
[12] W. R. Gibson, W. J. Doran, W. C. Wood, E. E. Swanson, *J. Pharmacol. Exp. Ther.* **1959**, *125*, 23.
[13] W. J. Doran, *J. Org. Chem.* **1960**, *25*, 1737.
[14] Eli Lilly, United States Patent, 2872448, 03.02.**1959**, prior. 04.04.**1956**; *Chem. Abstr.* **1959**, *53*, 13185D.
[15] L. Brandsma, *Preparative Acetylenic Chemistry*, Elsevier, Amsterdam, **1988**, p. 165.
[16] J. V. Allen, G. J. Dawson, C. G. Frost, J. M. J. Williams, S. J. Coote, *Tetrahedron* **1994**, *50*, 799.
[17] M. Peer, J. C. de Jong, M. Kiefer, T. Langer, H. Rieck, H. Schell, P. Sennhenn, J. Sprinz, H. Steinhagen, B. Wiese, G. Helmchen, *Tetrahedron* **1996**, *52*, 7547.
[18] M. Janura, Dissertation, Universität Regensburg, **1997**.
[19] H. Brunner, W. Pieronczyk, *Angew. Chem.* **1979**, *91*, 655; *Angew. Chem. Int. Ed. Engl.* **1979**, *18*, 620.
[20] H. Brunner, W. Pieronczyk, B. Schönhammer, K. Streng, I. Bernal, J. Korp, *Chem. Ber.* **1981**, *114*, 1137.
[21] T. P. Dang, H. B. Kagan, *Chem. Commun.* **1971**, 481.
[22] H. B. Kagan, T. P. Dang, *J. Am. Chem. Soc.* **1972**, *94*, 6429.
[23] E. L. Eliel, S. H. Wilen, L. N. Mander, *Stereochemistry of Organic Compounds*, John Wiley & Sons, Inc., New York, **1994**, p. 395.
[24] H. B. Kagan, J.-C. Fiaud, *Top. Stereochem.* **1988**, *18*, 249.
[25] T. Tervo, F. Joo, K. T. Huikuri, I. Toth, A. Palkama, *Pain* **1979**, *6*, 57.
[26] Publication in preparation.

Received May 28, 1998
[I98166]

Crystal Structure and Intercalation Properties of γ-$Zr(AsO_4)(H_2AsO_4) \times 2\ H_2O$

Julio Rodríguez,*[a] Marta Suárez,[a] M. Luz Rodríguez,[a] Ricardo Llavona,[a] M. José Arce,[a] Miguel A. Salvadó,[b] Pilar Pertierra,[b] and Santiago García-Granda[b][§]

Keywords: Zirconium arsenate / Crystal structure / Amine intercalation

The crystalline structure of γ-$Zr(AsO_4)(H_2AsO_4) \times 2\ H_2O$ (γ-ZrAs) has been refined by the Rietveld method. It has a monoclinic $P2_1$ layered structure built up from AsO_4 tetrahedra and ZrO_6 octahedra stacked along the 001 direction. The cell parameters are: a = 5.5752(6) Å, b = 6.8290(7) Å, c = 12.110(1) Å, and β = 103.03(1)°. The layered nature of γ-ZrAs is confirmed by the intercalation of *n*-alkylamines ($CH_3[CH_2]_nNH_2$; n = 0–5) as well as of cyclic amines (benzylamine, cyclohexylamine, piperidine, and pyridine). Among the linear amines, only with methyl-, ethyl-, and hexylamine is the maximum incorporation attained. With the cyclic amines, except in the case of pyridine, pure new phases are obtained, with the highest degree of intercalation being one mol of amine per mol of γ-ZrAs.

Introduction

Some insoluble acid salts of the general formula $M^{IV}(HXO_4)_2 \times n\ H_2O$ (M = Ti, Zr, Ce, Sn, Hf; X = P or As) have a layered structure, each layer consisting of a plane of tetravalent atoms sandwiched between tetrahedral phosphate or arsenate groups. Thus, these salts possess the typical characteristics of an intercalating agent and can be considered as hosts for the design and preparation of supramolecular solids with various functions.[1]

There are two major types of layered structures, usually denoted as α- and γ-layered forms.[1−4] The γ-compounds, presently formulated as $M(PO_4)(H_2PO_4) \times 2\ H_2O$, differ from the α-type in that half of the phosphate groups have all 4 oxygen atoms bonded to the metal atoms, while the other half are present as dihydrogen phosphate groups, bearing exchangeable protons.[4][5]

There is now an extensive body of literature dealing with the ion-exchange and intercalation chemistry of metal(IV) phosphates with α- and γ-type structures, the most studied compounds being α-$Zr(HPO_4)_2 \times H_2O$ (α-ZrP) and γ-$Zr(PO_4)(H_2PO_4) \times 2\ H_2O$ (γ-ZrP).[6−10] In contrast, the corresponding arsenates have been scarcely investigated. Only three layered α-type polyvalent metal arsenates are known: $Zr(HAsO_4)_2 \times H_2O$ (α-ZrAs), $Ti(HAsO_4)_2 \times H_2O$ (α-TiAs), and $Sn(HAsO_4)_2 \times H_2O$ (α-SnAs).

α-ZrAs was prepared by refluxing amorphous zirconium arsenate in arsenic acid[11][12] and the titration curves with hydroxides of alkali metal ions, Tl^+, Ba^{2+}, and NH_4^+ have been determined.[13] Although the windows connecting the cavities in α-ZrAs are about the same size as those in α-ZrP,[14] it seems that steric hindrance to the diffusion of large cations is less in α-ZrAs than in α-ZrP. Thus, the ion-exchange properties of the two compounds lead to differences in their abilities to function as sieves. α-TiAs has been scarcely studied to date; it is less stable than α-TiP and is strongly hydrolyzed, even in neutral media. Thus, ion-exchange experiments in aqueous solutions are restricted to acidic media, where only one proton is replaced by Li^+, Na^+, or K^+ ions.[15] α-SnAs has been prepared and the ion-exchange properties towards alkali metal ions have also been investigated.[16] This material is strongly hydrolyzed in alkaline media, hence it is a poor exchanger of limited utility, unless specific applications in acidic solution or in non-aqueous media are required.

To date, no γ-arsenates have been reported in the literature, although it is probable that the structure of Ce-$(HAsO_4)_2 \times 2\ H_2O$ is of the γ-type.[17][18] Some properties of metal(IV) arsenates are compiled in Table 1.

Table 1. Some properties of metal(IV) arsenates

	d [Å][a]	Free area [Å][b]	IEC [meq/g][c]	Ref.
α-$Zr(HAsO_4)_2 \times H_2O$	7.78	24.68	5.14	[14]
α-$Ti(HAsO_4)_2 \times H_2O$	7.77	22.20	5.78	[15]
α-$Sn(HAsO_4)_2 \times H_2O$	7.87	22.60	4.80	[16]

[a] Interlayer spacing. − [b] Area associated with each OH group on the plane. − [c] Ion-exchange capacity.

In a previous paper[19] we reported the hydrothermal synthesis of γ-ZrAs via its half-exchanged ammonium phase, and some preliminary data towards its characterization. In this paper, we describe the refinement of the crystal structure of γ-ZrAs by the Rietveld procedure. Furthermore, the layered nature of the compound is confirmed by the intercalation of *n*-alkylamines ($CH_3[CH_2]_nNH_2$; n = 0−5) and

[a] Departamento de Química Orgánica e Inorgánica, Facultad de Química, Universidad de Oviedo,
E-33071 Oviedo, Spain
Fax: (internat.) + 34-9/5103446
E-mail: rllg@sauron.quimica.uniovi.es
[b] Departamento de Química Física y Analítica, Facultad de Química, Universidad de Oviedo,
E-33006 Oviedo, Spain
[§] X-ray crystal structure analysis.

 © WILEY-VCH Verlag GmbH, D-69451 Weinheim, 1999 1434−1948/99/0101−0061 $ 17.50+.50/0

cyclic amines (benzylamine, cyclohexylamine, piperidine, and pyridine).

Results and Discussion

The γ-$Zr(AsO_4)(H_2AsO_4) \times 2\ H_2O$ formula for the synthesized compound was determined by means of the analytical procedures indicated in the Experimental Section.

A summary of the crystallographic data is given in Table 2, and final positional parameters are listed in Table 3. The final Rietveld refinement plot is shown in Figure 1.

Table 2. Crystallographic data for $Zr(AsO_4)(H_2AsO_4) \times 2\ H_2O$

Empirical formula	$ZrAs_2O_{10}H_6$
Molecular mass	407.1
Crystal system	monoclinic
$\rho_{calcd.}$ [g cm^{-3}]	3.01
Z	2
space group	$P2_1$
No. of contributing reflections	620 (K_α doublets)
No. of distance constraints	31
As−O distance constraint [Å]	1.67(1)
Zr−O distance constraint [Å]	2.07(1)
O···O distance constraint for PO_4 [Å]	2.72(1)
O···O distance constraint for ZrO_6 (*cis*) [Å]	2.93(1)
No. of parameters	54
R_{wp}	0.21
R_F	0.068
χ^2	37.3

$$R_{wp} = \left\{\frac{\sum_i w_i(y_{i,obs}-y_{i,calc})^2}{\sum_i w_i(y_{i,obs})^2}\right\}^{1/2},\ R_F = \frac{\sum_K |(I_{K',obs'})^{1/2}-(I_{K,calc})^{1/2}|}{\sum_K (I_{K',obs'})^{1/2}},$$

$$\chi^2 = \sum_i \frac{w_i(y_{i,obs}-y_{i,calc})^2}{(N_{obs}-N_{var})}$$

where N_{obs}, N_{var} = number of observations and variables.

Table 3. Atomic positional parameters for $Zr(AsO_4)(H_2AsO_4) \times 2\ H_2O$

Atom	*x*	*y*	*z*
Zr	0.816(1)	0.25	0.1384(3)
As1	0.220(1)	0.2429(9)	0.9381(4)
As2	0.405(1)	0.1393(9)	0.3181(4)
O1	0.027(2)	0.275(2)	0.0211(7)
O2	0.168(2)	0.0457(9)	0.8657(8)
O3	0.181(5)	0.445(1)	0.856(1)
O4	0.506(1)	0.244(1)	0.009(1)
O5	0.110(1)	0.181(2)	0.2634(6)
O6	0.588(1)	0.259(1)	0.2508(9)
O7	0.458(2)	0.8964(9)	0.312(1)
O8	0.472(2)	0.207(2)	0.4549(6)
OW1	0.036(2)	0.377(2)	0.6768(8)
OW2	0.01(1)	0.541(3)	0.479(2)

Compared with the unit cell of γ-ZrP, that of γ-ZrAs is extended in the *a* and *b* directions and compressed in the *c* direction. Accordingly, γ-ZrAs has a larger cell volume but a smaller interlayer distance (11.80 Å) than γ-ZrP (12.27 Å).

The powder pattern of γ-ZrAs reveals a certain degree of structural disorder. This is manifested by the appearance of two principal zones of extra-Bragg scattering, around 2θ = 18° and 29°. A similar effect is observed in the pattern of

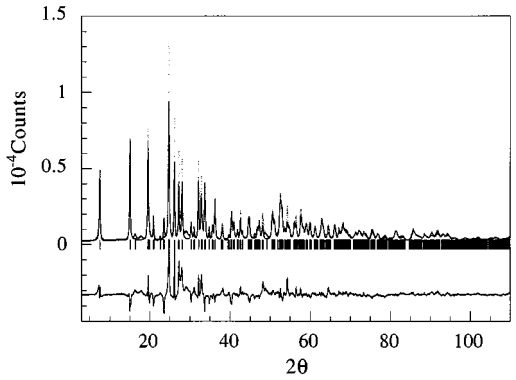


Figure 1. Rietveld refinement pattern of γ-ZrAs; points correspond to observed data; the solid line represents the calculated profile; tick marks show the positions of allowed reflections; a difference curve, on the same scale, is plotted at the bottom of the pattern

γ-TiP[20]. In the case of γ-TiP these zones appear as broad humps, whereas for γ-ZrAs sharper, better defined peaks are seen. These observations clearly indicate that both samples have a characteristic partially disordered structure.

Although the Rietveld refinement is not completely satisfactory due to the aforementioned disorder, it can clearly be stated that γ-ZrAs has a mean crystal structure akin to other known γ-phases, namely a monoclinic $P2_1$ layered structure built up from AsO_4 tetrahedra and ZrO_6 octahedra stacked along the [001] direction. A polyhedral plot of the structure is shown in Figure 2. Six-sided cavities are present between the layers. The water molecules reside inside the cavities, where they are held by hydrogen bonds.

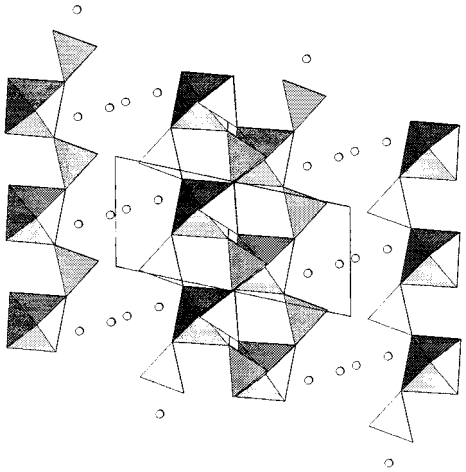


Figure 2. Polyhedral plot of the crystal structure viewed down the *b* axis; the *c* axis is vertical and the *a* axis is horizontal

Intercalation reactions of γ-ZrAs with amines were carried out in order to confirm the layered nature of the structure. The amines were chosen so as to represent the following classes: (a) primary linear amines (*n*-alkylamines), (b) primary cyclic amines (cyclohexylamine), (c) secondary cyclic amines (piperidine), (d) primary aromatic amines (benzylamine), and (e) heterocyclic amines (pyridine).

X-ray patterns of the intercalates showed the formation of new phases with basal spacings larger than in the case of γ-ZrAs (Table 4) and the total disappearance of the re-

flection at 11.80 Å, which is characteristic of the initial compound, except in the case of pyridine where this reflection persisted with a noticeable intensity. The intercalates maintain the lamellar structure, but a decrease in the order of the crystalline structure is observed.

several steps. Below 150°C, loss of water of crystallization takes place, and then between 150 and 450°C amine elimination occurs. At temperatures in excess of 500°C, ZrAs decomposition with As_2O_5 release and elimination of water due to condensation of the hydrogen arsenate groups take

Table 4. D-spacings, microanalytical data (C, N), experimental weight loss at 800°C, and tentative formulae of the intercalates

Amine	*d* [Å]	% C	% N	% weight loss	Formula
Methylamine	12.4	5.29	6.24	72.62	$Zr(AsO_4)(H_2AsO_4) \times 2\ CH_5N \times H_2O$
Ethylamine	14.7	10.08	4.55	74.25	$Zr(AsO_4)(H_2AsO_4) \times 2\ C_2H_7N \times H_2O$
n-Propylamine	18.0	10.41	4.09	72.50	$Zr(AsO_4)(H_2AsO_4) \times 1.3\ C_3H_9N$
n-Butylamine	20.1	13.35	3.92	73.52	$Zr(AsO_4)(H_2AsO_4) \times 1.3\ C_4H_{11}N$
n-Pentylamine	22.2	16.08	3.79	74.55	$Zr(AsO_4)(H_2AsO_4) \times 1.3\ C_5H_{13}N$
n-Hexylamine	24.9	23.68	4.57	79.79	$Zr(AsO_4)(H_2AsO_4) \times 2\ C_6H_{15}N \times 2\ H_2O$
Benzylamine	23.5	67.15	11.19	95.42	–
Cyclohexylamine	21.0	58.21	11.32	93.68	–
Piperidine	18.4	12.19	2.83	74.96	$Zr(AsO_4)(H_2AsO_4) \times C_5H_{11}N \times 2\ H_2O$
Pyridine	12.3	4.58	1.06	68.81	$Zr(AsO_4)(H_2AsO_4) \times 0.3\ C_5H_5N$

Figure 3 shows the X-ray patterns of some of the intercalates. It can be seen that in the case of *n*-alkylamines, the interlayer distances increase linearly with increasing number of carbon atoms in the alkyl chain (Figure 4). The resulting straight-line plot fits the equation $d_{002} = 10.0 + 2.48\ n_c$, with the slope corresponding to 2.48 Å per carbon atom. Since the increment in the alkyl chain length in a *trans-trans* conformation is generally estimated to be 1.27 Å per each additional carbon atom, the observed slope indicates, in agreement with the compositional data, that the *n*-alkylamines are arranged between the layers as a bimolecular film. The average angle α of inclination of the molecules with respect to the sheet amounts to $\sin^{-1}$ (2.48/2.54) = 77.5°. Similar behaviour has been observed for α-MP compounds (M = Zr, Ti, Hf).[21]

Tentative formulae for the intercalates were determined from elemental analysis and TG data, assuming that in all cases the final product of thermal transformations is ZrO_2 and that the change in weight is only due to amine and water losses and to γ-ZrAs decomposition with As_2O_5 release. Carbon and nitrogen contents, the total weight losses at 800°C, and the tentative formulae of the intercalates are compiled in Table 4. Analysis of these data shows that among the *n*-alkylamines, maximum uptake was only attained with methyl-, ethyl-, and hexylamine, whereas the others were only incorporated to an extent of ca. 4/3 mol of amine per mol of γ-ZrAs.

In the case of cyclic amines, the uptake does not reach the saturation level of the compound, only 1 (piperidine) and 0.3 (pyridine) mol of amine per mol of γ-ZrAs being incorporated. It was not possible to assign formulae in the case of cyclohexylamine or benzylamine since the C and N analysis values, the total weight loss at 800°C, and the apparent solidification of the amine, seemed to suggest that some amine polymerization had occurred.

Some typical TG curves for γ-ZrAs amine intercalates are reproduced in Figure 5. As can be seen, thermal decomposition on going from room temperature to 800°C occurs in

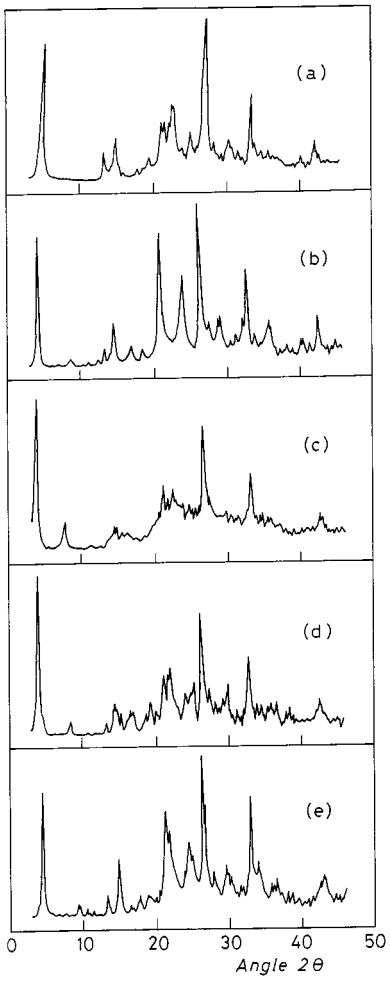


Figure 3. X-ray patterns of selected intercalates: (a) *n*-propylamine, (b) *n*-butylamine, (c) *n*-hexylamine, (d) cyclohexylamine, and (e) piperidine

place. The As_2O_5 release takes place at lower temperatures than in the case of unintercalated γ-ZrAs,[19] probably due

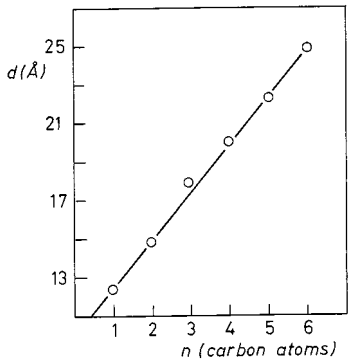


Figure 4. Interlayer distances in *n*-alkylamine intercalate compounds of γ-ZrAs as a function of the number of carbon atoms in the alkyl chain

to the loss of stability of the crystalline structure as a consequence of the presence of the amine in the interlayer space. From Figure 5, it is apparent that propylamine and butylamine intercalates do not contain water of crystallization, in contrast to the phases containing hexylamine and piperidine. For cyclohexylamine (total weight loss 93.68%) two well-differentiated losses can be observed, the first between 75 and 150°C (80.77%) corresponding to about 15.8 mol of amine per mol of γ-ZrAs, and the second at temperatures above 450°C (12.91%) corresponding to the release of As_2O_5 from γ-ZrAs and to the elimination of water upon condensation of the hydrogen arsenate groups.

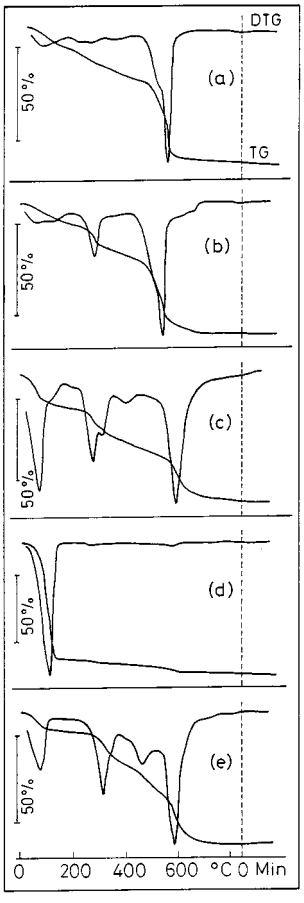


Figure 5. TG curves for selected γ-ZrAs intercalates: (a) *n*-propylamine, (b) *n*-butylamine, (c) *n*-hexylamine, (d) cyclohexylamine, and (e) piperidine

Conclusion

The crystal structure of γ-zirconium arsenate has been refined from X-ray powder diffraction data by the Rietveld method. It has a monoclinic $P2_1$ layered structure built up from AsO_4 tetrahedra and ZrO_6 octahedra stacked along the [001] direction. The final agreement factors are: R_{wp} = 0.21 and R_F = 0.068. The average As−O bond length is 1.66(1) Å.

It can be concluded that γ-ZrAs reacts readily with *n*-alkylamines, giving rise to new phases with expanded interlayer distances, which confirms its layered nature. In the case of cyclic amines, the intercalation becomes more difficult and cyclohexylamine and benzylamine form as yet uncharacterized, probably polymeric solids, the nature and composition of which will be the subject of future investigations.

Experimental Section

Synthesis: Crystalline γ-ZrAs, $Zr(AsO_4)(H_2AsO_4) \times 2\ H_2O$, was prepared by treatment of the half-exchanged ammonium phase γ-$Zr(AsO_4)[(NH_4)HAsO_4]$ with an excess of 2 M HCl, washed with deionized water, and dried in air. The half-exchanged ammonium phase was synthesized by adding a solution of $As_2O_5 \times 3\ H_2O$ and urea in an approximate mass ratio of 4:1 to zirconium propoxide (70% solution in *n*-propanol). The mixture was hydrothermally treated at 180°C for 6 d without stirring.[19] The solid obtained was characterized by X-ray diffraction, IR spectroscopy, and chemical and thermal analysis.

Structure Refinement: A sample of $Zr(AsO_4)(H_2AsO_4) \times 2\ H_2O$ (γ-ZrAs) was finely ground using an agate mortar and side-loaded onto a flat sample holder in order to minimize any preferred orientation effects. Step-scanned X-ray powder data were collected by means of a Philips PW 1050 computer-controlled automated diffractometer operating at 40 kV and 30 mA with a copper target and graphite-monochromated radiation. Data were collected in the range $3° < 2\theta < 110°$ with increments of 0.02° and a count time of 10 s per step. 22 low-angle unambiguously characterized reflections were extracted from the data and indexed by trial-and-error methods implemented in the program TREOR[22] with a monoclinic cell, giving figures of merit of M_{20} = 28[23] and F_{20} = 42(0.00837, 57).[24] Crystal data of γ-ZrAs are compared with those of γ-$M(PO_4)(H_2PO_4) \times 2\ H_2O$ (M = Ti, Zr, Hf) in Table 5.

Table 5. Crystal data for γ-phases

	γ-ZrAs	γ-HfP[25]	γ-ZrP[26]	γ-TiP[20]
Space group	$P2_1$	$P2_1$	$P2_1$	$P2_1$
a [Å]	5.5752(6)	5.3499(3)	5.3825(2)	5.186(1)
b [Å]	6.8290(7)	6.5949(4)	6.6337(1)	6.3505(8)
c [Å]	12.110(1)	12.3939(8)	12.4102(4)	11.865(3)
β [°]	103.03(1)	98.594(5)	98.687(2)	102.52(3)
V [Å^3]	449.21	432.37	438.03	381.47

In view of the similarities in the crystal data, the structural parameters of γ-ZrP[26] were used as the initial values for the Rietveld refinement using the program FULLPROF.[27] A pseudo-Voigt profile function was selected. After initial refinement of the scale, background, profile, and cell parameters, the atomic positions were refined using soft constraints for the AsO_4 tetrahedra and ZrO_6 octahedra. Additional distance constraints were needed for water molecules. All atoms were refined isotropically with a common temperature factor, $B = 1.23(8)$. No corrections were made for anomalous dispersion or absorption. Crystallographic data (excluding structure factors) for the structure reported in this paper have been deposited with the Fachinformationszentrum Karlsruhe (FIZ), D-76344 Eggenstein-Leopoldshafen, Germany, as supplementary publication No. FIZ-408717.

Intercalation Procedure: γ-ZrAs was equilibrated over a period of 7 d with the pure *n*-alkylamines or cyclic amines at 25°C according to the batch method. The solid was present in the solution in an approximate ratio of 1 g per 100 mL. The solids were subsequently separated by centrifugation, dried at 50°C for 24 h, and characterized by X-ray diffraction and thermal and chemical analysis.

Analytical Procedures: Zr and As contents of the solid samples were determined by elemental analysis using a SpectraSpec DCP-AEC spectrometer, following the dissolution of weighed amounts in HF. X-ray powder diffraction patterns were recorded with a Philips PW 1729/1720 computer-controlled diffractometer using Cu-K_α radiation ($\lambda = 1.542$ Å). Microanalytical data (C, N) were obtained with a Perkin-Elmer model 2400 elemental analyzer. The TG curves were obtained under nitrogen with a Mettler TA 4000 (TG 50) thermoanalyzer, employing a heating rate of 10°C min^{-1}.

Acknowledgments

We gratefully acknowledge the financial support of DGICYT (Spain), Research Project No. PB93−0330; CICYT (Spain), Research Project No. MAT94−0428; II P.R.I Asturias (Spain), Research Proyect No. PB-MAT97−05, and the Universidad de Oviedo, Research Project No. NP-98−522−1.

[1] [1a]G. Alberti, *Comprehensive Supramolecular Chemistry* (Eds.: G. Alberti, T. Bein), Pergamon, New York, **1996**, vol. 7, pp. 151−188. − [1b] A. Clearfield, *Progress in Inorganic Chemistry* (Ed.: K. D. Karlin), Pergamon, New York, **1998**, vol. 47, pp. 373−509.
[2] A. Clearfield, J. A. Stynes, *J. Inorg. Nucl. Chem*. **1964**, *26*, 117.
[3] A. Clearfield, R. H. Blessing, J. A. Stynes, *J. Inorg. Nucl. Chem*. **1968**, *30*, 2249.
[4] A. Clearfield, U. Costantino, *Comprehensive Supramolecular Chemistry* (Eds.: G. Alberti, T. Bein), Pergamon, New York, **1996**, vol. 7, pp. 107−150.
[5] [5a] N. J. Clayden, *J. Chem. Soc., Dalton Trans.* **1987**, 1877. − [5b] A. N. Christensen, E. K. Andersen, I. G. K. Andersen, G. Alberti, M. Nielsen, M. S. Lehmann, *Acta Chem. Scand*. **1990**, *44*, 865. − [5c] D. M. Poojary, B. Zhang, Y. Dong, G. Z. Peng, A. Clearfield, *J. Phys. Chem*. **1994**, *98*, 13616.
[6] G. Alberti, U. Costantino, *Intercalation Chemistry* (Eds.: M. S. Whittingham, A. J. Jacobson), Academic Press, New York, **1982**, pp. 147−180.
[7] F. Levy, *Intercalated Materials*, D. Reidel Publ. Co., Dordrecht, **1979**.
[8] J. R. García, R. Llavona, M. Suárez, J. Rodríguez, *Trends. Inorg. Chem*. **1993**, *3*, 204.
[9] A. Clearfield, *Progress in Intercalation Research* (Eds.: W. Muller-Warmuty, R. Schollhorn), Kluwer, Dordrecht, **1994**, pp. 223−271.
[10] A. Clearfield, U. Costantino, *Comprehensive Supramolecular Chemistry* (Eds.: G. Alberti, T. Bein), Pergamon, New York, **1996**, vol. 7, p. 127.
[11] E. Torracca, U. Costantino, M. A. Massucci, *J. Chromatogr*. **1967**, *30*, 584.
[12] A. Clearfield, G. D. Smith, B. Hammomd, *J. Inorg. Nucl. Chem*. **1968**, *30*, 277.
[13] J. P. Gupta, D. V. Nowell, M. F. Reilly, *J. Inorg. Nucl. Chem*. **1979**, *41*, 749.
[14] A. Clearfield, W. L. Duax, *Acta Crystallogr*. **1970**, *51*, 289.
[15] G. Alberti, E. Torracca, *J. Inorg. Nucl. Chem*. **1968**, *30*, 3075.
[16] U. Costantino, A. Gasperoni, *J. Chromatogr*. **1970**, *51*, 289.
[17] G. Alberti, U. Costantino, F. Di Gregorio, E. Torracca, *J. Inorg. Nucl. Chem*. **1965**, *31*, 3195.
[18] L. Zsinka, L. Szirtes, J. Mink, A. Kalman, *J. Chromatogr*. **1974**, *102*, 109.
[19] A. I. Bortun, A. Clearfield, M. Suárez, R. Llavona, J. Rodríguez, *Mat. Chem. Phys.*, in press.
[20] M. A. Salvadó, S. García-Granda, J. Rodríguez, *Mater. Sci. Forum* **1994**, *166*, 619.
[21] F. Menéndez, A. Espina, C. Trobajo, J. Rodríguez, *Mat. Res. Bull*. **1990**, *5*, 1531.
[22] P. E. Werner, L. Eriksson, M. Westdahl, *J. Appl. Crystallogr*. **1985**, *18*, 367.
[23] P. M. De Wolff, *J. Appl. Crystallogr*. **1968**, *1*, 108.
[24] G. S. Smith, R. L. Snyder, *J. Appl. Crystallogr*. **1979**, *12*, 60.
[25] L. M. Barcina, M. Suárez, R. Llavona, J. Rodríguez, M. A. Salvadó, P. Pertierra, S. García-Granda, *J. Chem. Soc., Dalton Trans.* **1998**, 99.
[26] D. M. Poojary, B. Speizer, A. Clearfield, *J. Chem. Soc., Dalton Trans.* **1995**, 111.
[27] J. Rodríguez-Carvajal, FULLPROF: *A Program for Rietveld Refinement and Pattern Matching Analysis*; Abstracts of the Satellite Meeting on Powder Diffraction of the XV Congress of the IUCr, Toulouse, **1990**, p. 127.

Received July 1, 1998
[I98209]

Cobalt-Catalyzed Hydroformylation of Olefins in the Presence of Xenon: New Experimental Evidence for Metal–Xenon Adducts

Luca Rosi,*[a] Franco Piacenti,[a] Mario Bianchi,[a] Piero Frediani,[a] and Antonella Salvini[a]

Keywords: Hydroformylations / Rare gas / Homogeneous catalysis / Carbonylcobalt compounds

The rate of cobalt-catalyzed hydroformylation of cyclohexene to cyclohexanecarboxaldehyde is significantly reduced when xenon is added to the reaction mixture at a concentration similar to that of the olefin. No significant effect is produced by helium or neon under similar conditions. These experiments suggest competitive coordination of xenon to the catalytically active cobalt species.

We have recently reported that appropriate concentrations of gases such as dinitrogen or argon produce a significant retarding effect on aldehyde formation in the cobalt-catalyzed hydroformylation of olefins.[1] This behavior has been ascribed to the ability of these additional substances to compete with dihydrogen and/or the olefin for the vacant coordination site on the catalytically active carbonylcobalt intermediate. If this interpretation is correct, the effect should depend on the availability of the outer-shell electrons of the donor, as measured by its first ionization potential (IP). As the first IP decreases on going from helium to xenon,[2][3] we would expect xenon to exhibit a higher coordination ability than the lighter rare gases, although its larger size could partly counteract this tendency.[4][5][6][7][8][9][10]

As a matter of fact, available literature data on adducts of rare gases with transition metals indicate a slightly higher coordinating ability of xenon compared to both argon and krypton.[11][12] A further relevant observation is that the bond dissociation energies (BDEs) for xenon with the pentacarbonylmetal(0) fragments of Group 6 do not show any marked dependence on the nature of the metal.[12]

With this background, we reckoned that, in extension of previous studies,[1] additional evidence for xenon coordination to a transition metal could be obtained by studying its effect on the cobalt-catalyzed hydroformylation reaction. Rate retardation would be expected if the presumably coordinatively unsaturated cobalt intermediate were to be intercepted by xenon rather than by dihydrogen and/or the olefin, thereby decreasing the steady-state concentration of the catalytically active species. The magnitude of any such effect would be difficult to predict, but some insight into this matter may be gained by considering the available thermodynamic data concerning metal−dihydrogen and metal−olefin bonds.

The tungsten−dihydrogen BDE has been estimated[13] to be 83 kJ mol^{-1} in $W(CO)_3(PR_3)_2(H_2)$, which is about 50 kJ mol^{-1} higher than that reported for the W−Xe bond in $W(CO)_5Xe$ (35.1 ± 0.8 kJ mol^{-1}[11]). If a similar difference in stability between dihydrogen and xenon is maintained under hydroformylation conditions, we may expect to see an effect on the product conversion. The manganese(I)−ligand (L) bond in $Mn(\eta^5\text{-}C_5H_5)(CO)_2L$ (L = *cis*-cyclooctene) has been estimated to require 102.4 ± 10 kJ mol^{-1} for dissociation.[14]

We report here the results of our investigation into the cobalt-catalyzed hydroformylation of cyclohexene in the presence of added xenon. Toluene was chosen as the reaction medium since competitive coordination of the catalytically active species by this solvent was anticipated to be minimized by both its self-aggregation (the relatively high enthalpy of vaporization[13g] is ΔH_v = 33.2 kJ mol^{-1} at T_{bp} = 383.6 K) and owing to the disruption of resonance energy that would occur upon coordination through only part of the π electron density.

$$RCo(CO)_4 + L \rightleftharpoons RCo(CO)_3L + CO$$

for	R = H, $Co(CO)_4$	L = H_2, olefin, Ar, Xe
for	R = alkyl, acyl	L = H_2, Ar, Xe

Our results are collected in Table 1, together with those from similar experiments (see Experimental Section) carried out in the presence of helium or neon. Helium and neon have no significant effect on the rate of the hydroformylation reaction; the slight decrease in conversion observed may be attributed to the dilution effect caused by the volume increase of the liquid medium due to the gas dissolution under the reaction conditions.

The presence of xenon has a negative effect on the rate of hydroformylation of the olefin. Taking into consideration that the experimentally determined amount of argon present in the liquid phase at 1000 bar and 373 K (0.086 mol) is, on a molar basis, approximately six times as large (see Experimental Section) as the amount of xenon (0.014 mol), the 30% drop in the conversion obtained in the presence of the latter suggests a stronger coordinating ability of xenon compared to argon, as anticipated in the introductory remarks and in agreement with the literature results.

[a] Dipartimento di Chimica Organica, Università di Firenze, Via Gino Capponi 9, I-50121 Firenze, Italy
Fax: (internat.) + 39-55/2757660
E-mail: frediani@chimorg.unifi.it

 © WILEY-VCH Verlag GmbH, D-69451 Weinheim, 1999 1434−1948/99/0101−0067 $ 17.50+.50/0

Table 1. Conversion (%) to cyclohexanecarboxyaldehyde in the hydroformylation of cyclohexene in the presence of rare gases (RG)[a]

RG	RG pressure				Ref.
	0 bar	500 bar	800 bar	1000 bar	
Helium[b]	30	29	27	–	[c]
Neon[b]	30	29	–	–	[c]
Argon[b]	30	19	10	9	[1]
	RG weight[b]				
	0 g	2.5 g	–	3.8 g	
Xenon[d]	30	25	–	21	[c]

[a] Reaction conditions: dry toluene, 7 mL; $Co_2(CO)_8$, 51 mg (0.149 mmol); cyclohexene, > 99.9% purity by GC, 504 mg (6.15 mmol); $p(CO) = 70 \pm 1$ bar (373 K); $p(H_2) = 85 \pm 2$ bar (373 K); autoclave volume, 25.4 mL; temperature, 373 K; reaction time, 3 h. – [b] Gases introduced in the following order: CO, dihydrogen, RG. – [c] This work. – [d] Gases introduced in the following order: CO (1 bar), xenon, CO (54 ± 2 bar at room temperature, 68 ± 2 bar at 373 K), H_2 (85 ± 3 bar at 373 K). Pressures are equilibrium readings after physical absorption (about 20 min).

Furthermore, in the presence of 270 bar of argon (19 mmol in the liquid phase) the conversion is not influenced, whereas in the presence the same molar amount of xenon in the liquid phase (18.5 bar, 19 mmol in the liquid phase) a reduction in the degree of conversion (16%) is observed.

In view of the BDE data mentioned above, a dihydrogen–xenon competition appears to be most likely. Catalytic hydrogenations represent another important class of reactions where indirect evidence concerning the coordinating ability of rare gases can be anticipated. Experiments along these lines, in both homogeneous and heterogeneous systems, will be undertaken in due course.

Experimental Section

The experiments in the presence of uncondensable gases (He or Ne) were carried out as follows: the catalyst, solvent, olefin, and carbon monoxide were introduced sequentially into the autoclave and the contents were heated at 373 K. Dihydrogen, followed by the additional rare gas, were then rapidly added. The reaction conditions were maintained for 3 h. In the case of xenon, which has a higher b.p. (162 K) than either helium or neon and is thus more easily condensed, the operations were carried out in the following sequence: introduction of the catalyst, solvent, olefin, xenon, and carbon monoxide at room temperature; heating to 373 K; pressurization with dihydrogen. The amount of xenon introduced was determined by the weight difference of the cylinder. At 373 K, the following equilibrium pressures (bar) were measured after introduction of xenon (weight of xenon in parentheses): 18.5 (2.5 g), 23.5 (3.8 g).

The amount of argon dissolved in the solution at 1015 bar and 373 K was experimentally determined to be about 0.086 mol; the amount of xenon (total 3.8 g) dissolved at the same temperature was estimated to be about 0.014 mol.

Acknowledgments

The authors wish to thank Prof. Fausto Calderazzo for very fruitful discussions and suggestions. This work has been partially supported by the Ministero della Università e della Ricerca Scientifica e Tecnologica (MURST).

[1] F. Piacenti, F. Calderazzo, M. Bianchi, L. Rosi, P. Frediani, *Organometallics* **1997**, *16*, 4235.
[2] IP values (eV)[3]: He (24.587), Ne (21.564), Ar (15.760), Kr (14.000), Xe (12.130).
[3] *CRC Handbook of Chemistry and Physics* (Eds.: D. R. Lide, H. P. R. Frederikse), 77th ed., Boca Raton, New York, London, Tokyo, **1994–1995**, p. 10–205.
[4] The following van der Waals radii [Å] of rare gases have been reported[5][6][7]: He (1.40, 1.49, 1.79); Ne (1.54, 1.55, 1.6); Ar (1.88, 1.88, 1.92); Kr (2.02, 2.00, 1.98); Xe (2.16, 2.18, 2.18). Attempts have been made to calculate "covalent" bond lengths [Å] for rare gases and some typical values[8] are: He (0.4–0.6); Ne (0.6–0.7); Ar (0.94–0.95); Kr (1.00–1.18); Xe (1.30). An experimental determination of the covalent radius of xenon [1.543(1) Å] in Xe_2^+ (bond order 0.5) has recently been reported,[9] which is qualitatively in agreement with the covalent radius of iodine (1.357 Å) in solid I_2,[10] considering that the increase in effective nuclear charge and the decrease in bond order on going from iodine to xenon have opposing effects of unknown relative magnitudes.
[5] A. Bondi, *J. Phys. Chem.* **1964**, *68*, 441.
[6] R. Chauvin, *J. Phys. Chem.* **1992**, *96*, 9194.
[7] G. A. Cook, in *Argon, Helium and the Rare Gases* (Ed.: G. A. Cook), vol. 1, J. Wiley, New York, **1961**.
[8] J. E. Huheey, *J. Chem. Educ.* **1968**, *45*, 791, and references therein.
[9] T. Drews, K. Seppelt, *Angew. Chem. Int. Ed. Engl.* **1997**, *36*, 273; *Angew. Chem.* **1997**, *109*, 264.
[10] F. van Bolhuis, P. B. Koster, T. Migchelsen, *Acta Crystallogr.* **1967**, *23*, 90.
[11] B. H. Weiller, *J. Am. Chem. Soc.* **1992**, *114*, 10910.
[12] J. R. Wells, E. Weitz, *J. Am. Chem. Soc.* **1992**, *114*, 2783.
[13] [13a] G. J. Kubas, *Acc. Chem. Res.* **1988**, *21*, 120. – [13b] R. H. Crabtree, *Acc. Chem. Res.* **1990**, *23*, 95. – [13c] D. M. Heinekey, W. J. Oldham, *Chem. Rev.* **1993**, *93*, 913. – [13d] D. M. Heinekey, T. A. Luther, *Inorg. Chem.* **1996**, *35*, 4396. – [13e] A. A. Gonzales, K. Zhang, S. P. Nolan, R. Lopez de la Vega, S. L. Mukerjee, C. D. Hoff, G. J. Kubas, *Organometallics* **1988**, *7*, 2429. – [13f] H. J. Wasserman, G. J. Kubas, R. R. Ryan, *J. Am. Chem. Soc.* **1986**, *108*, 2294. – [13g] See ref.[3], p. 6–110.
[14] J.-K. Klassen, M. Selke, A. A. Sorensen, G. K. Yang, *J. Am. Chem. Soc.* **1990**, *112*, 1267.

Received July 10, 1998
[I98231]

Synthesis and Structure of the First [1]Boratitanocenophanes

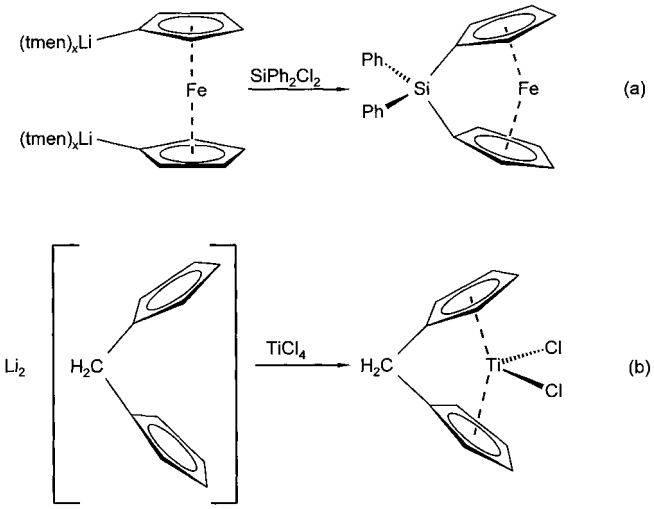
Holger Braunschweig,*[a] Carsten von Koblinski,[a] and Ruimin Wang[a]

Keywords: Boron / Titanium / Metallocenophanes / [1]Boratitanocenophanes

This paper presents two methods for the synthesis of the first [1]boratitanocenophanes. The novel biscyclopentadienylborane $[(Me_3Si)_2NB(C_5H_5)_2]$, the dilithio salt $Li_2[(Me_3Si)_2NB(C_5H_4)_2]$ (**1**) of which was characterized by multinuclear NMR methods, was prepared in situ, and served as starting material for several [1]boratitanocenophanes. $[Cl_2Ti\{(C_5H_4)_2BN(SiMe_3)_2\}]$ (**2**) was obtained in high yield by a convenient one-pot synthesis starting from **1** and $[TiCl_3(thf)_3]$, followed by oxidation with $PbCl_2$. The highly reactive $[(Me_2N)_2Ti\{(C_5H_4)_2BN(SiMe_3)_2\}]$ (**3**) was obtained by the reaction of $[(Me_3Si)_2NB(C_5H_5)_2]$, prepared in situ, with $Ti(NMe_2)_4$ and converted into the chloro derivatives $[(Me_2N)ClTi\{(C_5H_4)_2BN(SiMe_3)_2\}]$ (**4**) and $[Cl_2Ti\{(C_5H_4)_2BN(SiMe_3)_2\}]$ (**2**) by treatment with one or two equivalents of a suitable diaminochloroborane. All [1]boratitanocenophanes were characterized in solution by multinuclear NMR spectroscopy, and in addition the structure of **2** in the crystalline state was determined by a single-crystal X-ray study.

Introduction

[1]Metallocenophanes have been known for almost 30 years, and since then these compounds have attracted considerable interest due to their versatile chemistry. The first example of a [1]ferrocenophane was obtained by the reaction of dilithioferrocene·tmen (tmen = tetramethylethylenediamine) with $(C_6H_5)_2SiCl_2$ (Equation 1a).[1] Due to the high ring strain of such complexes, which depends on the covalent radius of the bridging atom, [1]ferrocenophanes undergo thermal or radiation-induced ring-opening polymerization[2a,b] yielding high molecular weight polyferrocenes.[3a–d] Corresponding [1]metallocenophanes of early transition-metal complexes were obtained, for example, by the reaction of $Li_2[H_2C(C_5H_4)_2]$ with $TiCl_4$ (Equation 1b).[4] Such metallocenophanes especially of titanium and zirconium have already proven to be highly active Ziegler–Natta-type catalysts for the olefin polymerization.[5]



We have started to investigate the synthesis and properties of [1]borametallocenophanes, since we expect a particularly interesting reactivity of such compounds. On one hand, the incorporation of the small boron atom into the bridge of a [1]ferrocenophane leads to highly strained, and thus very reactive molecules. That was already demonstrated in the case of $[Fe\{(\eta^5\text{-}C_5H_4)_2BN(SiMe_3)_2\}]$, which exhibits the highest tilt angle of 32.4(2)° recorded for a [1]ferrocenophane to date.[6] On the other hand catalytic processes with metallocenophanes of early transition metals could be accelerated by a Lewis acidic atom such as boron in the bridge. Very recently, the first [1]borazirconocenophane was synthesized and structurally characterized.[7] This compound, however, exhibits SMe_2 as a boron-coordinated base, thus cancelling the Lewis acidity of the bridging boron atom. A [1]borazirconocenophane with a three-fold coordinated boron atom was reported in 1996,[8] the structure of this product in the crystal, however, is not known.

Dilithiometallocenes, which serve as starting materials for the synthesis of [1]metallocenophanes according to Equation 1a, are only available in the case of iron and ruthenium. In order to achieve a method for the preparation of various [1]borametallocenophanes we aimed at the synthesis of bis(cyclopentadienyl)boranes as versatile ligands. In contrast to the well-developed chemistry of cyclopentadienylboranes[9a–f] the knowledge of bis(cyclopentadienyl)boranes is restricted to a few examples of the type $(C_5H_4R)_2BPh$ (R = $SiMe_3$, $SnMe_3$).[8][10] Due to decomposition during distillation these products could not be isolated in pure form. Related compounds, however, with four-coordinate boron atoms include the lithium borate $Li(OEt_2)_4[(C_5H_5)_2B(C_6F_5)_2]$[11] and the borane–pyridine adduct $(C_5H_5)_2PhBNC_5H_5$.[12]

In the present paper we report the high-yield synthesis and spectroscopic characterization of the dilithiated biscyclopentadienylborane $Li_2[(Me_3Si)_2NB(C_5H_4)_2]$ and its re-

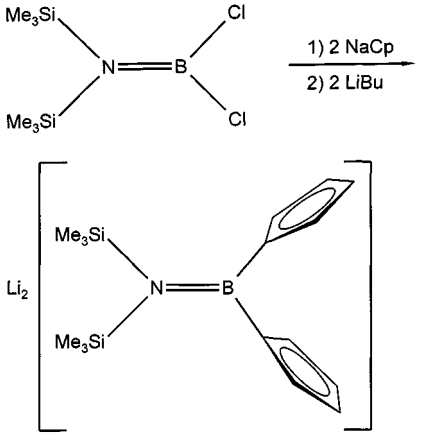
[a] Institut für Anorganische Chemie der Technischen Hochschule, Templergraben 55, D-52056 Aachen, Germany
E-mail: holger.braunschweig@ac.rwth-aachen.de

 © WILEY-VCH Verlag GmbH, D-69451 Weinheim, 1999 1434–1948/99/0101–0069 $ 17.50+.50/0

action with $[TiCl_3(thf)_3]$ giving the first [1]boratitanocenophane. An alternative route for the synthesis of such compounds starting from $[(Me_3Si)_2NB(C_5H_5)_2]$ is also described.

Results and Discussion

The reaction of $(Me_3Si)_2NBCl_2$ with a slight excess of NaC_5H_5 in hexane followed by filtration and treatment of the hexane filtrate with 2 equivalents of LiBu afforded $Li_2[(Me_3Si)_2NB(C_5H_4)_2]$ (**1**) in almost quantitative yield as a white pyrophoric solid (Equation 2).



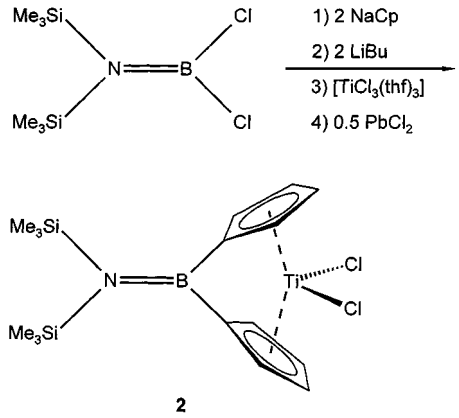
1

The structure of **1** in solution derives from the NMR spectra showing the expected signal patterns for the monosubstituted cyclopentadienyl rings and an ^{11}B-NMR signal at $\delta = 46.6$, characteristic for an aminodiarylborane. This compound proved to be highly reactive and shows considerable signs of decomposition in thf solution, and even in the solid state at ambient temperature. Hence, for subsequent syntheses we found it convenient not to store the ligand, but rather to prepare it in situ.

According to Equation 3, the [1]boratitanocenophane $[Cl_2Ti\{(C_5H_4)_2BN(SiMe_3)_2\}]$ (**2**) was obtained in a four-step one-pot synthesis. The dilithio salt **1**, which was obtained as a hexane slurry by the method described above, was treated with an equimolar amount of $[TiCl_3(thf)_3]$ at $-100\,^{\circ}C$ and the intermediate Ti^{III} species was subsequently oxidized with $PbCl_2$ according to a known procedure.[13]

Complex **2** was obtained as dark red crystals from CH_2Cl_2 in 80% yield. The compound was found to be very soluble in halogenated solvents, such as $CHCl_3$ or CH_2Cl_2, and less soluble in aromatic solvents such as benzene or mesitylene. Solutions of **2** are very sensitive to air and moisture, and an instant colour change from dark red to light green indicates decomposition.

The constitution of **2** in solution is deduced from NMR spectra. The ^{1}H-NMR spectra show the expected two pseudo triplets at $\delta = 5.53$, and 7.05 for the cyclopentadienyl protons forming an AA′BB′ spin system, and the



2

80 % yield

^{11}B-NMR signal at $\delta = 46.6$ matches that of the uncoordinated ligand.

Suitable single crystals for an X-ray structure analysis were obtained by recrystallization from benzene at 7°C (Figure 1). In the solid state the molecule exhibits a slight deviation from the ideal C_{2v} symmetry, which is assumed for its structure in solution. This is demonstrated, for example, by the twisting of the Si1−N−Si2 plane with respect to the $Cp_c1-Ti-Cp_c2$ (Cp_c = ring centroid) plane; the corresponding dihedral angle was determined to be 11.5°. The comparison of the present structure with that of $[Cp_2TiCl_2]$ shows some characteristic differences, due to the albeit small strain of **2**.[14] The tilt angle between the two cyclopentadienyl rings as well as the Cl1−Ti−Cl2 angle is larger by about 3°, while the $Cp_c1-Ti-Cp_c2$ angle decreases by almost 13° with respect to the corresponding values found for $[Cp_2TiCl_2]$. While the cyclopentadienyl rings are staggered in the latter molecule, they adopt an eclipsed conformation in the present case. The boron−nitrogen distance was found to be 138(1) pm, thus being in the expected range for a B−N double bond.

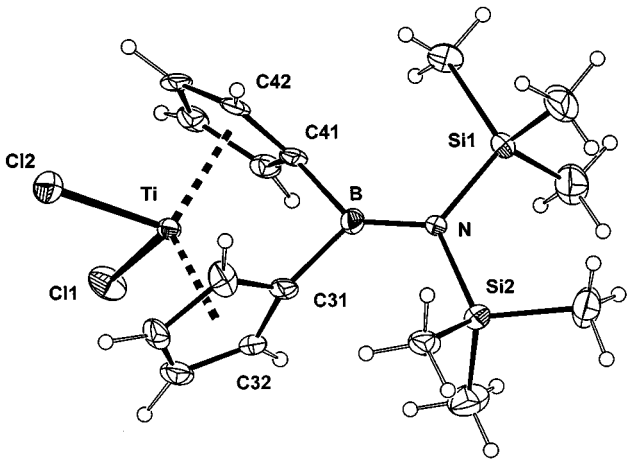
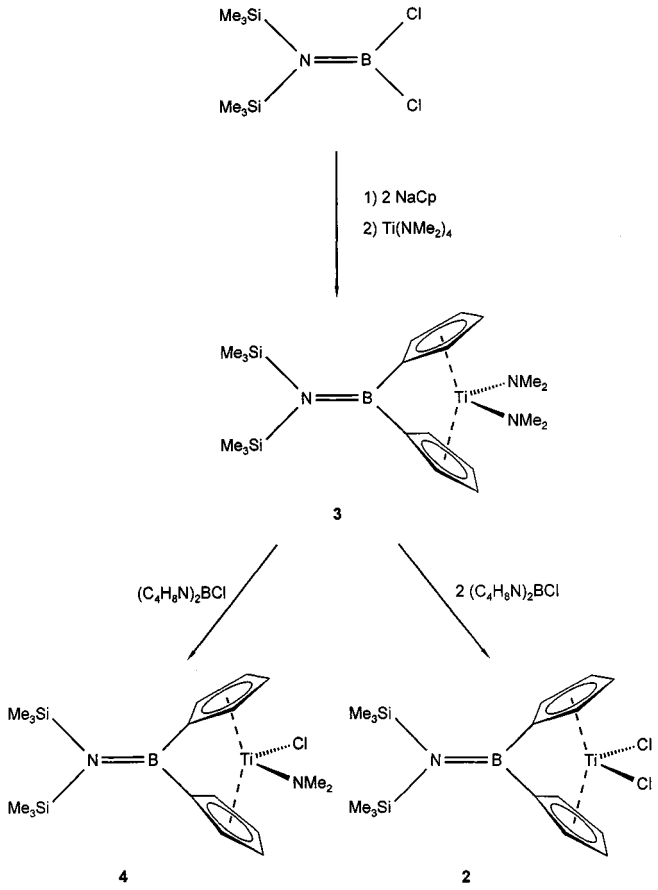


Figure 1. Structure of **2** in the crystal (ellipsoids at 30% probability); selected distances [pm] and angles [°]: Ti−Cl1 233.1(2), Ti−Cl2 233.9(2), B−N 138(1); Cl1−Ti−Cl2 97.45(9), C31−B−C41 98.3(6), C41−B−N 132.8(6), C31−B−N 128.6(6)

All attempts to obtain **2** directly from $Li_2[(Me_3Si)_2NB(C_5H_4)_2]$ (**1**) and $TiCl_4$ or $[TiCl_4(thf)_2]$ resulted in mixtures of several products, which could not be separated.

The reaction of $[(Me_3Si)_2NB(C_5H_5)_2]$ prepared in situ with $Ti(NMe_2)_4$, however, proved to be a suitable method for the direct preparation of a corresponding Ti^{IV} species. $[(Me_2N)_2Ti\{(C_5H_4)_2BN(SiMe_3)_2\}]$ (**3**) was obtained as a dark red solid in yields of about 30% with formation of two equivalents of $HNMe_2$ (Equation 4). Due to the labile NMe_2 ligands **3** shows an even greater tendency to decompose compared to $[Cl_2Ti\{(C_5H_4)_2BN(SiMe_3)_2\}]$ (**2**), and hence, cannot be stored at ambient temperature even in the solid state.

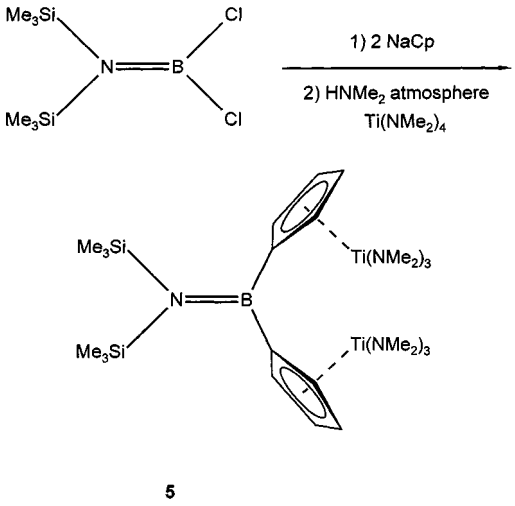


By treating this compound in situ with one or two equivalents of a chloroborane of moderate reactivity such as $(C_4H_8N)_2BCl$, however, it may be converted into the more stable chloro derivatives $[(Me_2N)ClTi\{(C_5H_4)_2BN(SiMe_3)_2\}]$ (**4**) and $[Cl_2Ti\{(C_5H_4)_2BN(SiMe_3)_2\}]$ (**2**), respectively (Equation 3), which were isolated in yields of about 40% and 15%.

These reactions occurred with substitution of the titanium-bound NMe_2 groups and formation of the corresponding triaminoborane $(C_4H_8N)_2BNMe_2$, which was characterized by ^{11}B-NMR spectroscopy from the reaction mixture ($\delta = 26.0$). The use of diaminochloroboranes proved to be crucial for this synthesis, since the more reactive aminodichloroboranes always led to decomposition of **3**.

Due to its lower symmetry, $[(Me_2N)ClTi\{(C_5H_4)_2BN(SiMe_3)_2\}]$ (**4**) shows four signals for the cyclopentadienyl groups in the ^1H-NMR spectra at $\delta = 5.08$, 5.29, 6.62, and 6.83. Furthermore, the spectroscopic findings for **3** and **4**, such as the ^{11}B-NMR signals at $\delta = 46.9$, and 46.4, are comparable to those of **2**, thus proving their structure in solution.

The instability of **3** is obviously due to the cleavage of the NMe_2 ligands, and hence we attempted to synthesize this compound under an atmosphere of $HNMe_2$. The reaction of $Ti(NMe_2)_4$ with one equivalent of $[(Me_3Si)_2NB(C_5H_5)_2]$ under a constant flow of dimethylamine, however, resulted in the formation of the dinuclear half sandwich complex **5** (Equation 5), which was isolated in yields of about 45% as a red brown solid. The structure of **5** in solution was deduced from the NMR spectra, resembling those of the related chloro derivative $[(Cl_3Ti)_2\{(C_5H_4)_2BPh\}]$, which was also characterized in the crystalline state.[10]



Conclusion

The synthesis and characterization of the first [1]boratitanocenophanes was achieved by two different methods starting from the novel bis(cyclopentadienyl)borane $[(Me_3Si)_2NB(C_5H_5)_2]$.

The highly reactive bis(dimethylamido) complex $[(Me_2N)_2Ti\{(C_5H_4)_2BN(SiMe_3)_2\}]$ (**3**) was achieved directly from the reaction of this ligand with $Ti(NMe_2)_4$, whereas the corresponding dichloro derivative $[Cl_2Ti\{(C_5H_4)_2BN(SiMe_3)_2\}]$ (**2**) was obtained by a convenient one-pot synthesis in high yield starting from the dilithiated ligand $Li_2[(Me_3Si)_2NB(C_5H_4)_2]$ (**1**), and $[TiCl_3(thf)_3]$ followed by oxidation of the intermediate Ti^{III} species with $PbCl_2$. The latter complex was chosen as a representative example for X-ray structure analysis. Compound **3** served as starting material for the preparation of $[(Me_2N)ClTi\{(C_5H_4)_2BN(SiMe_3)_2\}]$ (**4**) and $[Cl_2Ti\{(C_5H_4)_2BN(SiMe_3)_2\}]$ (**2**) by substitution of the NMe_2 group with a suitable diaminochloroborane.

[1]Metallocenophanes of group-4 elements containing a Lewis acidic atom such as boron in the bridge should serve

as effective catalysts for Ziegler−Natta-type olefin polymerizations. Our further work will focus on the utilization of the convenient synthetic method being described in this paper and especially on the investigation of the catalytic properties of such compounds. Preliminary experiments already proved **2** and **4** to be suitable catalysts for the polymerization of ethene.

Experimental Section

All manipulations were carried out under dry nitrogen with common Schlenk techniques. Solvents and reagents were dried by standard procedures, distilled, and stored under nitrogen over molecular sieves. $(Me_3Si)_2NBCl_2$,[15] NaC_5H_5,[16] $Ti(NMe_2)_4$,[17] $[TiCl_3(thf)_3]$,[18] and $(C_4H_8N)_2BCl$[19] were synthesized according to literature procedures. NMR: Varian Unity 500 at 499.843 MHz (^1H, internal standard TMS), 150.364 MHz (^{11}B, $BF_3\cdot OEt_2$ in C_6D_6 as external standard), 125.639 MHz ($^{13}C\{^1H\}$, APT, internal standard TMS); all NMR spectra were recorded in CD_2Cl_2 as solvent unless otherwise stated. Mass spectra were recorded with a Finnigan MAT 95 (70 eV) and elemental analyses (C, H, N) were obtained from a Carlo-Erba elemental analyzer, model 1106.

$Li_2[(Me_3Si)_2NB(C_5H_4)_2]$ (1): 8.23 g (93.54 mmol) NaC_5H_5 was suspended in 100 mL of hexane and a solution of 11.13 g (46.05 mmol) of $(Me_3Si)_2NBCl_2$ in 20 mL of hexane was added dropwise at ambient temperature. After stirring for 2 h, the reaction mixture was cooled to 0°C and 57.6 mL (92.10 mmol) of a 1.6 M BuLi solution was added dropwise. A white precipitate formed immediately. The reaction mixture was allowed to warm up to ambient temperature and after stirring for 1 h, all volatiles were removed in high vacuum, and the solid residue was extracted with 150 mL of hexane overnight. The mixture was filtered and the solid dried in vacuo to give **1** as a white, pyrophoric solid in yields of 98% (14.13 g). − ^1H NMR ([D$_8$]THF): δ = 0.01 [s, 18 H, $Si(CH_3)_3$], 5.83 (m, 4 H, C_5H_4), 6.45 (m, 4 H, C_5H_4). − ^{11}B NMR: δ = 46.6 (s). − ^{13}C NMR: δ = 4.31 [s, $Si(CH_3)_3$], 103.16, 106.63, 116.63 (C_5H_4).

$[Cl_2Ti\{(C_5H_4)_2BN(SiMe_3)_2\}]$ (2) (Method A): As described for **1** 3.20 g (13.24 mmol) of $(Me_3Si)_2NBCl_2$ was treated with 2.39 g (27.17 mmol) of NaC_5H_5 and to the obtained filtrate was added 16.6 mL (26.48 mmol) of 1.6 M BuLi in hexane. The light yellow suspension was stirred at ambient temperature for 2 h, cooled to −100°C, and 4.90 g (13.24 mmol) of $[TiCl_3(thf)_3]$ and 20 mL of thf were added. The mixture was allowed to come to ambient temperature, and the colour changed from light brown to dark violet. The suspension was stirred for 3 h and then treated with 1.84 g (6.62 mmol) of $PbCl_2$. After stirring for 16 h, all volatile materials were removed in high vacuum. The remaining solid was extracted with 50 mL of CH_2Cl_2 and filtered. **2** was recovered from the filtrate at −30°C as a dark red solid (4.43 g, 80%). − ^1H NMR: δ = 0.08 [s, 18 H, $Si(CH_3)_3$], 5.53 (m, 4 H, C_5H_4), 7.05 (m, 4 H, C_5H_4). − ^{11}B NMR: δ = 46.6 (s). − ^{13}C NMR: δ = 4.89 [$Si(CH_3)_3$], 114.85, 133.44 (C_5H_4). − MS; *m/z* (%): 417 (35) [M^+], 402 (15) [M^+ − Me], 382 (25) [M^+ − Cl]. − $C_{16}H_{26}BCl_2NSi_2Ti$ (418.18): calcd. C 45.96, H 6.27, N 3.35; found C 46.56, H 7.05, N 2.87.

$[(Me_2N)_2Ti\{(C_5H_4)_2BN(SiMe_3)_2\}]$ (3): As described for **1** 2.08 g (8.60 mmol) of $(Me_3Si)_2NBCl_2$ was treated with 1.51 g (17.20 mmol) of NaC_5H_5. The obtained filtrate was cooled to −30°C, and a solution of 1.93 g (8.60 mmol) of $Ti(NMe_2)_4$ in 5 mL of hexane was added dropwise. The mixture was allowed to warm up to ambient temperature, and the colour changed from yellow to dark red. After stirring for 1 h, all volatiles were removed in high vacuum, and the remaining solid was suspended in 10 mL of hexane. After filtration and removal of all volatiles under high vacuum, compound **3** was obtained as a dark red solid (1.05 g, 28%). − ^1H NMR: δ = 0.09 (s, 18 H, $Si(CH_3)_3$), 3.14 (s, 12 H, $N(CH_3)_2$), 5.42 (m, 4 H, C_5H_4), 6.73 (m, 4 H, C_5H_4). − ^{11}B NMR: δ = 46.9 (s). − ^{13}C NMR: δ = 4.89 [$Si(CH_3)_3$], 51.11 [$N(CH_3)_2$], 112.73, 131.66 (C_5H_4). − $C_{20}H_{38}BN_3Si_2Ti$ (435.43): calcd. C 55.17, H 8.80, N 9.65; found C 55.62, H 8.22, N 9.59.

$[(Me_2N)ClTi\{(C_5H_4)_2BN(SiMe_3)_2\}]$ (4): As describes for **1** 1.09 g (4.50 mmol) of $(Me_3Si)_2NBCl_2$ was treated with 0.88 g (10.00 mmol) of NaC_5H_5. The obtained filtrate was cooled to −30°C, and a solution of 1.01 g (4.50 mmol) of $Ti(NMe_2)_4$ in 5 mL of hexane was added dropwise. The mixture was allowed to warm up to ambient temperature, and treated with 0.84 g (4.50 mmol) of $(C_4H_8N)_2BCl$. After stirring for 1 h, all volatiles were removed in high vacuum, and the remaining solid was suspended in 20 mL of hexane, filtered and stored at −30°C to yield 0.79 g (41%) of compound **4** as a dark red crystalline solid. − ^1H NMR ($CDCl_3$): δ = 0.28 (s, 18 H, $Si(CH_3)_3$), 3.26 (s, 6 H, $N(CH_3)_2$), 5.08 (m, 2 H, C_5H_4), 5.29 (m, 2 H, C_5H_4), 6.62 (m, 2 H, C_5H_4), 6.83 (m, 2 H, C_5H_4). − ^{11}B NMR: δ = 46.4 (s). − ^{13}C NMR: δ = 7.53 [$Si(CH_3)_3$], 57.54 [$N(CH_3)_2$], 115.73, 117.57, 126.93, 128.54 (C_5H_4). − $C_{18}H_{32}BClN_2Si_2Ti$ (426.80): calcd. C 50.66, H 7.56, N 6.56; found C 50.23, H 7.59, N 6.39.

$[Cl_2Ti\{(C_5H_4)_2BN(SiMe_3)_2\}]$ (2) (Method B): As described for **4** 1.45 g (6.00 mmol) of $(Me_3Si)_2NBCl_2$ was treated with 1.08 g (12.30 mmol) of NaC_5H_5, and to the obtained filtrate was added a solution of 1.34 g (6.00 mmol) of $Ti(NMe_2)_4$ in 5 mL of hexane. The resulting mixture was subsequently treated with 2.24 g (12.00 mmol) of $(C_4H_8N)_2BCl$ to yield 0.38 g (15%) of **2** as a dark red crystalline solid.

$[((Me_2N)_3Ti)_2\{(C_5H_4)_2BN(SiMe_3)_2\}]$ (5): As described for **1** 1.31 g (5.40 mmol) of $(Me_3Si)_2NBCl_2$ was treated with 0.97 g (11.00 mmol) of NaC_5H_5. The obtained filtrate was cooled to −30°C, and a solution of 1.21 g (5.40 mmol) of $Ti(NMe_2)_4$ in 5 mL of hexane was added dropwise under a constant stream of $HNMe_2$. After warming up to ambient temperature, the dark red solution was stirred for 1 h and then stored under an atmosphere of $HNMe_2$ at −30° C. After 3 d, compound **5** was isolated as a red brown solid (1.60 g, 45%). − ^1H NMR (C_6D_6): δ = 0.28 [s, 18 H, $Si(CH_3)_3$], 3.18 [s, 36 H, $N(CH_3)_2$], 6.14 (m, 4 H, C_5H_4), 6.78 (m, 4 H, C_5H_4). − ^{11}B NMR: δ = 46.9 (s). − ^{13}C NMR: δ = 5.79 [$Si(CH_3)_3$], 50.35 [$N(CH_3)_2$], 113.03, 121.65 (C_5H_4). − MS: *m/z* (%) = 615 (5) [M^+ − $N(CH_3)_2$], 571 (50) [M^+ − 2 $N(CH_3)_2$], 527 (50) [M^+ − 3 $N(CH_3)_2$], 347 (100) {[$(CH_3)_3Si]_2NBCp_2Ti$}. − $C_{28}H_{62}BN_7Si_2Ti_2$ (659.64): calcd. C 50.98, H 9.47, N 14.86; found C 50.56, H 9.36, N 14.77.

X-ray Structure Determination of 2: $C_{16}H_{26}BCl_2NSi_2Ti$, ENRAF-Nonius CAD4; Mo-K_α radiation (λ = 0.71073 Å, graphite monochromator); data collection with ω scan at 203 K. Dark red platelet, 0.06 × 0.24 × 0.65 mm, monoclinic space group *C*2/*c* (No. 15), M = 418.18 g mol^{-1}, unit cell dimensions a = 28.493(8) Å, b = 10.540(4) Å, c = 15.103(5) Å, β = 112.71(3)°, V = 4184(5) Å^3, Z = 8, $\rho_{calcd.}$ = 1.33 g cm^{-3}, μ(Mo-K_α) = 7.73 cm^{-1}; 5040 reflections were collected in the scan range 2° < Θ < 25°; after Lorentz and polarization corrections, an empirical absorption correction based on azimuthal scans[20] (min. transm. 0.766, max. transm. 1.000) was applied before averaging symmetry-related intensity data. Since the crystal was not stable, intensity data were corrected for the resulting decay on the basis of three regularly measured check reflections. 2510 independent observations with $I > \sigma(I)$ in structure solution by direct methods[21] and refinement with the

SDP program system[22] for 208 variables; all non-hydrogen atoms were refined with anisotropic displacement parameters, hydrogen atoms were included in riding geometry with fixed isotropic displacement parameters [C−H = 0.98 Å, U_{iso}(H) = 1.30 U_{eq}(C)]. Convergence at R = 0.092, R_w = 0.076, $w^{-1} = \sigma^2(F_o)$, GOF = 1.324. Max. residual electron density 0.722 eÅ^{-3}. Further details on the crystal structure determination can be obtained from the Cambridge Crystallographic Data Centre (CCDC, 12 Union Road, Cambridge CB2 1EZ, UK; Fax: (internat.) + 44-1223/336-033; E-mail: deposit@ccdc.cam.ac.uk) on quoting the depository number CCDC-102132.

Acknowledgments

We thank the Deutsche Forschungsgemeinschaft and the Fonds der Chemischen Industrie for financial support.

[1] A. G. Osborne, R. H. Whiteley, *J. Organomet. Chem.* **1975**, *101*, C27−C28.
[2] [2a] D. Foucher, R. Ziembinski, R. Petersen, J. Pudelski, M. Edwards, Y. Ni, J. Massey, C. R. Jaeger, G. J. Vancso, I. Manners, *Macromolecules* **1994**, *27*, 3992−3999. − [2b] J. Rasburn, D. A. Foucher, W. F. Reynolds, I. Manners, G. J. Vancso, *J. Chem. Soc., Chem. Commun.* **1998**, 843−844.
[3] [3a] W. Finckh, B.-Z. Tang, D. A. Foucher, D. B. Zamble, R. Ziembinski, A. Lough, I. Manners, *Organometallics* **1993**, *12*, 823−829. − [3b] P. Gomez-Elipe, P. M. MacDonald, I. Manners, *Angew. Chem. Int. Ed. Engl.* **1997**, *36*, 762−764. − [3c] K. H. Pannell, H. K. Sharma, *Organometallics* **1997**, *16*, 3077−3079. − [3d] T. J. Peckham, J. A. Massey, M. Edwards, I. Manners, D. Foucher, *Macromolecules* **1996**, *29*, 2396−2403.
[4] T. J. Katz, N. Acton, *Tetrahedron* **1970**, *28*, 2497−2499.
[5] W. Kaminski, *J. Chem. Soc., Dalton Trans.* **1998**, 1413−1418 and references herein.
[6] H. Braunschweig, R. Dirk, M. Müller, P. Nguyen, R. Resendes, D. P. Gates, I. Manners, *Angew. Chem. Int. Ed. Engl.* **1997**, *36*, 2338−2340.
[7] D. S. Stelck, P. J. Shapiro, N. Basickes, *Organometallics*, **1997**, *16*, 4546−4550.
[8] K. Rufanov, E. Avtomonov, N. Kazennova, V. Kotov, A. Khvorost, D. Lemenovskii, J. Lorberth, *J. Organomet. Chem.* **1997**, *536−537*, 361−373.
[9] [9a] G. E. Herberich, A. Fischer, *Organometallics* **1996**, *15*, 58−67. − [9b] H. Grundke, P. I. Paetzold, *Chem. Ber.* **1971**, *104*, 1136−1146. − [9c] H. D. Johnson, T. W. Hartford, C. W. Spangler, *J. Chem. Soc., Chem. Commun.* **1978**, 242. − [9d] B. Boeke, Doctoral Dissertation, Technische Hochschule Aachen, Germany, **1975**. − [9e] B. M. Mikhailov, T. K. Baryshnikova, V. S. Bogdanov, *Dokl. Akad. Nauk SSSR* **1972**, *202*, 358; *Chem. Abstr.* **1972**, *76*, 140940. [9f] P. Jutzi, A. Seufert, *J. Organomet. Chem.* **1979**, *169*, 327.
[10] S. A. Larkin, J. T. Golden, P. J. Shapiro, G. P. A. Yap, D. M. J. Foo, A. L. Rheingold, *Organometallics* **1996**, *15*, 2393−2398.
[11] M. Bochmann, S. J. Lancaster, O. B. Robinson, *J. Chem. Soc., Chem. Commun.* **1995**, 2081.
[12] K. A. Rufanov, V. V. Kotov, N. B. Kazennova, D. A. Lemenovskii, E. V. Avtomonov, J. Lorberth, *J. Organomet. Chem.* 1996, *525*, 287−289.
[13] J. Okuda, T. Eberle, T. P. Spaniol, *Chem. Ber.* **1997**, *130*, 209−215.
[14] A. Clearfield, D. K. Warner, C. H. Saldarriaga-Molina, R. Ropal, *Can. J. Chem.* **1975**, *53*, 1622−1629.
[15] P. Geymayer, E. G. Rochow, U. Wannegat, *Angew. Chem. Int. Ed. Engl.* **1964**, *3*, 633.
[16] K. Ziegler, H. Froitzheim-Kühlhorn, K. Hafner, *Chem. Ber.* **1956**, *89*, 434.
[17] D. C. Bradley, I. M. Thomas, *J. Chem. Soc.* **1960**, 3857−3861.
[18] L. E. Manzer, *Inorg. Synth.* **1982**, *21*, 135.
[19] D. Loderer, H. Nöth, H. Pommerening, W. Rattay, H. Schick, *Chem. Ber.* **1994**, *127*, 1605−1611.
[20] A. C. T. North, D. C. Phillips, F. S. Mathews, *Acta Crystallogr.* **1968**, *A24*, 351.
[21] G. M. Sheldrick, *SHELXS86, Program for Structure Solution*, University of Göttingen, Germany, **1986**.
[22] ENRAF-Nonius, *SDP Version 5.0*, Delft, The Netherlands, **1989**.

Received July 10, 1998
[I98227]

Molecular Precursors to Ceramics II[+]

[(Trichlorosilyl)dichloroboryl]ethane: Synthesis and Characterisation by Means of Experiment and Theory

Marcus Gastreich,*[a] Christel M. Marian,[b] Hardy Jüngermann,[c] and Martin Jansen[d]

Dedicated to the memory of Marco Häser

Keywords: TSDE / Ceramics / Theoretical IR-spectroscopy / RI-MP2

A new compound for the molecular synthesis route to high-demand Si/B/N/C ceramics has been found and is described in this work. We report on an elegant "one-pot" synthesis of [(trichlorosilyl)dichloroboryl]ethane (TSDE, $Cl_3Si–CH-[(CH_3)(BCl_2)]$) and its structural characterisation by means of nuclear magnetic resonance and (theoretical and experimental) infra-red spectroscopy. Density functional and Hartree-Fock calculations combined with a perturbational treatment of the electron correlation have been performed. Both methods yield good agreement of theoretical and experimental spectra, with the perturbational approach being slightly superior. In a similar way to the amino compound [(trichlorosilyl)amino]dichloroborane (TADB), TSDE exhibits a planar coordination of the dichloroboryl terminus but tetrahedral neighbourhoods for both carbon and silicon. The electronic structure has been investigated and a $\sigma - n$ order of the frontier orbitals shall be discussed.

Introduction

This paper represents the second part of a series reporting on the synthesis and characterisation of molecular precursors for covalent amorphous Si/B/N/(C) ceramics. As has been shown previously,[2] the so-called *precursor route*, i.e. the way of forming covalent networks from molecular precursors with prebuilt structural units, often leads to most useful high-demand ceramics with outstanding features such as exceptional temperature resistance, corrosion stability and hardness. As examples, we have listed three novel ceramic syntheses and the resulting thermal stabilities of the compounds obtained when using the precursor route shown in Figure 1. The interested reader may find more information on this approach to high-performance ceramics in the literature.[3–5]

In order to understand the structural principles behind these syntheses we have, in this publication, combined experimental and *ab initio* techniques to study the structural properties of [(trichlorosilyl)dichloroboryl]ethane (TSDE) for which a patent has been acquired.[6]

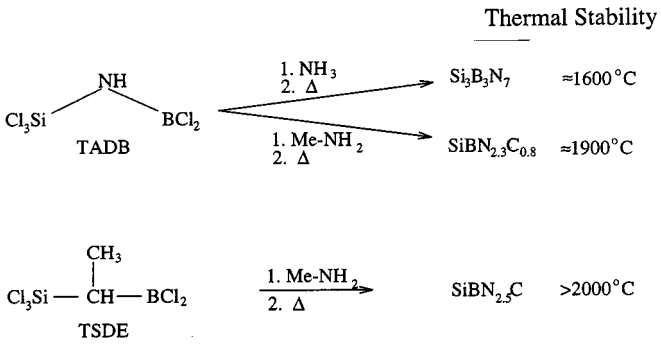


Figure 1. Novel Si/B/N/C-ceramics and their thermal stabilities

Synthesis

0.1 mol of boron trichloride was condensed at −65 °C in a round-bottomed-flask equipped with a dropping funnel and a pressure compensation valve. 0.1 mol of trichlorovinylsilane and 0.1 mol of triethylsilane were mixed and added to the boron trichloride during 15 min. The mixture was stirred for 1h and allowed to warm up to room temperature. The reaction mixture, consisting of the product and triethylchlorosilane, was distilled over a 30 cm Vigreux column. A 64.1% yield of 1-(trichlorosilyl)-1-(dichloroboryl)ethane (TSDE) was obtained at 35–40 °C/12mbar. At room temperature, the product is a colourless liquid which is extremely sensitive to moisture and air.[7]

[+] Part I: Ref.[1]

[a] Institut für Physikalische und Theoretische Chemie Universität Bonn,
Wegelerstr. 12, D-53115 Bonn, Germany
[b] GMD-Forschungszentrum für Informationstechnik GmbH, Schloß Birlinghoven,
D-53754 Sankt Augustin, Germany
[c] Bayer AG, Zentrale Forschung,
D-51368 Leverkusen, Germany
[d] Max-Planck-Institut für Festkörperforschung,
Heisenbergstr. 1, D-70569 Stuttgart, Germany

 © WILEY-VCH Verlag GmbH, D-69451 Weinheim, 1999 1434–1948/99/0101–0075 $ 17.50+.50/0

Characterisation

Experimental Setup

Infra-Red Spectrum: The IR-spectroscopic measurements were conducted using a Fourier transform infrared (FT-IR) spectrometer (model IFS 113v, Bruker Co., Karlsruhe, Germany). The equipment has a modified interferometer by Genzel. Compared to a machine with a Michelson arrangement and the same optical unit dimensions, we obtain double resolution. A globar was used as the light source in the MIR range, and a mercury-cadmium telluride photodetector registered the transmission. No smoothing operators were applied, but a baseline correction was carried out. A liquid sample of neat TSDE was deposited in a cuvette with KBr windows and the spectrum was measured in the absence of water vapor and air at 20 °C.

NMR Spectra: The liquid NMR spectra were recorded on a Bruker AMX 300 spectrometer (Karlsruhe, Germany). The samples had been prepared by mixing neat TSDE with $CDCl_3$ for ^1H as well as for ^{13}C spectroscopy.

Theoretical Methods

Energies and Geometries: Geometry optimisations were carried out with TURBOMOLE v.4.6[8,9] and Gaussian 94.[10] We employed standard relaxation routines based on the Rational-Function or the Quasi-Newton-Raphson models; the initial Hessian matrix was updated by the BFGS algorithm throughout the calculations.[11] At points of vanishing gradient, we determined the matrix of second derivatives of the energy with respect to the nuclear coordinates (Hessian matrix) and computed its eigenvalues to check for imaginary frequencies. Our former investigations were based on molecular hypersurfaces determined on the local density functional level of theory[12] with the Slater exchange- and Vosko-Wilk-Nusair-correlation functionals.[1] These data were reasonable with the exception of hydrogen bond lengths, whose vaues were a bit too long. In the present case, we therefore used the B3LYP[13−15] density functional that employs a three-parameter hybrid functional for the exchange part of the molecular energy and a gradient-corrected functional for the electronic correlation energy. As an alternate correlation treatment to the density functional formalism, we employed the efficient RI-MP2 procedure by Feyereisen, Fitzgerald and Komornicki[16] and implemented by Weigend and Häser[17] to determine both the equilibrium structure and the vibrational spectrum of [trichlorosilyl-(dichloroboryl)]ethane. For the search of the global minimum of the potential energy surface (PES) of TSDE, we have chosen molecular conformers that differed in terms of the relative torsional positions of the BCl_2, $SiCl_3$, and CH_3 groups.

In order to validate the theoretical models with respect to further analysis of the electronic structure, we first calculated the root mean square (rms) deviations of the (scaled) vibrational frequencies for the two different levels of theory. The perturbational correlation treatment was found to be slightly inferior: For B3LYP we determined an rms value of 29 wavenumbers, the perturbational formalism yielded 36 wavenumbers). In any case, we consider the RI-MP2 model advantageous on the basis that one false ordering of frequencies was obtained with the DFT formalism (see below). Thus, subsequent examinations of bonding characteristics etc. will be based on the RI-MP2 geometries, energies and Roothaan-Self Consistent Field (SCF) molecular orbitals for those very geometries.

Basis Sets: The optimisation procedures and energy determinations involved a triple zeta split valence basis set (TZVP) for all methods. It has been taken from the TURBOMOLE v.4.6[8,9] basis set library. This basis set comprises polarisation functions on all atoms including hydrogen. For very small molecules, an RI-MP2 procedure is error-prone due to an insufficient auxiliary basis; we have, however, tested the applicability of the scheme by means of single-point energy calculations on the (full) MP2-level for ammonia, pyruvic acid, CClF(CO), and TSDE itself. Logged errors lie below one millihartree (≈ 0.03 eV); the single-point energy difference (RI- and non-RI-procedures) for the same (RI-MP2-optimised) structure of TSDE only differs by 0.3 millihartrees (≈ 0.008 eV).

Vibrational Spectra: The vibrational spectra have been determined at the corresponding equilibrium geometries by calculating the second derivatives of the electronic energy with respect to the nuclear coordinates; the same basis sets have been employed here. DFT intensities were calculated analytically from the squared derivative of the dipole moment at equilibrium geometry.[18] To calculate RI-MP2 vibrational frequencies, we employed a second derivative numeric procedure that has, amongst others, been linked to the TURBOMOLE-modules. RI-MP2 infra-red intensities have also been numerically determined by calculating the squared dipole moment derivatives with the same grid as for the frequency determination (0.02 bohr ≈ 0.0106 Å). The reliability of the resulting frequencies has, besides the plausible comparison of them with the density functional vibrational values, been tested for compounds that are still easily accessible with the standard MP2-scheme and the software available to us. For these compounds, and with our grid, deviations occur in the regime of only 1−3 wavenumbers compared to analogous analytical calculations. For the intensities, we find deviations of less than one percent. These findings shall be subject to a separate publication.

Results and Discussion

Equilibrium Structure and Stability, Bonding- and Electronic Parameters

Relaxation of the geometrical degrees of freedom of either the staggered or the eclipsed conformations leads to the equilibrium structure represented in Figure 2. We determined slightly different geometric parameters by the different methods. All values and corresponding energies obtained are listed in Table 1.

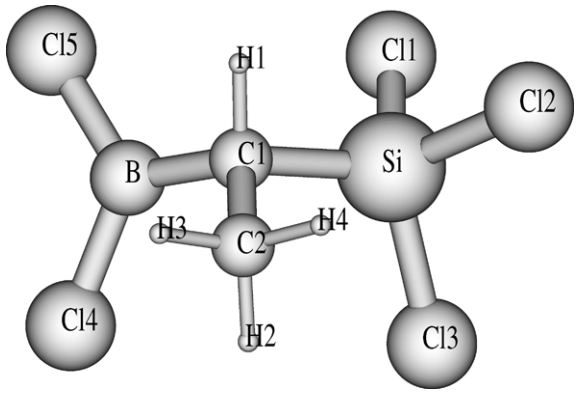


Figure 2. Equilibrium conformation of TSDE

Table 1. Equilibrium geometry data for TSDE for different theoretical models

Coordinate		Theoretical Model RI-MP2//TZVP	B3LYP//TZVP
R [Å]	Cl1−Si	2.046	2.068
	Cl2−Si	2.053	2.075
	Cl3−Si	2.048	2.069
	Si−C1	1.869	1.893
	C1−H1	1.096	1.096
	C1−C2	1.560	1.551
	C2−H2	1.089	1.089
	C2−H4	1.089	1.090
	C2−H3	1.090	1.091
	C1−B	1.560	1.567
	B−Cl4	1.748	1.763
	B−Cl5	1.748	1.764
∠ [°]	Cl1−Si−Cl2	108.39	107.80
	Cl1−Si−Cl3	109.14	108.42
	Cl2−Si−Cl3	108.52	107.97
	Cl1−Si−C1	111.71	111.94
	Cl2−Si−C1	108.73	108.90
	Cl3−Si−C1	110.28	111.66
	Si−C1−H1	103.04	101.99
	Si−C1−C2	109.83	110.34
	Si−C1−B	111.24	112.61
	H1−C1−C2	110.52	109.45
	C1−B−Cl4	120.52	121.48
	C1−B−Cl5	120.59	120.76
	C1−C2−H2	111.28	111.62
	C1−C2−H3	110.25	110.09
	C1−C2−H4	111.16	111.21
	H2−C2−H3	107.52	107.22
	H2−C2−H4	108.44	108.40
	H4−C2−H3	108.05	107.65
	Cl4−B−Cl5	118.89	117.76

The central carbon atom is almost perfectly tetrahedrally connected to a planar BCl_2 group and an $SiCl_3$ group that itself is tetrahedrally coordinated. A C−C distance of 1.560 Å corresponds to a typical single bond length. In addition, the Si−C and B−C bonds lie in the region of typical bond lengths for singly-bonded molecules. The single bond character of all bonds in TSDE is in contrast to the findings in TADB, which exhibits a partially doubly-bonded central pattern with its B−N bond having a length of 1.42 Å.[1]

We found a HOMO-LUMO gap for the closed-shell compound TSDE that amounts to 0.5161 hartrees, i.e. ≈ 13.9 eV. This value remains basically unaltered upon rotating the trichlorosilyl-, methyl-, or dichloroboryl groups as described below.

Graphical representations of the two SCF frontier orbitals are given in Figures 3 and 4.[19] Treating methyl and hydrogen as topologically equivalent, we may consider the plane defined by B−C−Si a mirror plane. The HOMO in this case corresponds to an *a'* molecular orbital with plain σ-type bonding interactions between (a) the central carbon and the boron atom and (b) between C and Si. A nodal plane on C separates these bonding components. This analysis already gives a clue to the low torsional barrier of $SiCl_3$ around the Si−C bond as shall be discussed in the

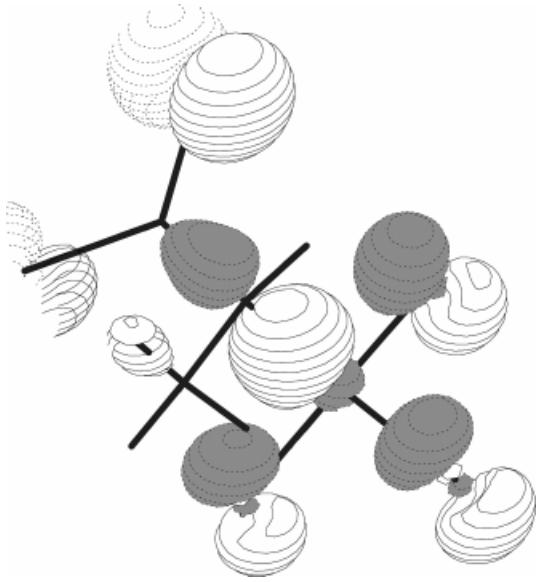


Figure 3. Highest occupied SCF-molecular orbital (HOMO) of TSDE: The BCl_2 group is in the upper left, the $SiCl_3$ group in the lower right corner

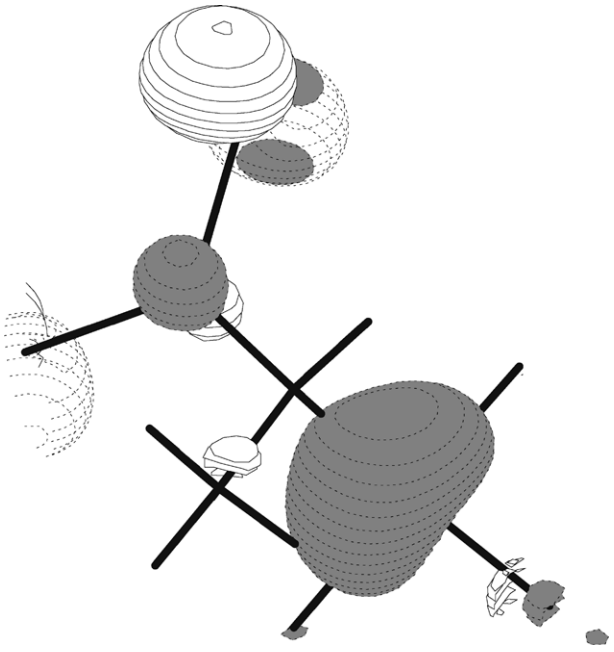


Figure 4. Lowest unoccupied SCF-molecular orbital (LUMO) of TSDE; orientation of the molcule as in Figure 3

section describing the IR spectrum. In addition, the torsion of BCl_2 around the B−C bond should be significantly easier compared to TADB. The HOMO describes the chlorine lone electron pairs as large *p atomic* orbitals that lie almost parallel to the mirror plane, resulting in non-bonded interactions with their neighbouring elements Si and B.

The LUMO, on the other hand, mainly consists of the boron and chlorine *p* atomic orbitals that are perpendicular to the BCl_2 plane. There are three nodal planes with respect to these orbitals: one within the BCl_2 plane, and the two others between B and each Cl. Thus, both B−Cl interactions are anti-bonding, which is, in fact, a very similar situation to that in TADB. The second characteristic constituent of the LUMO is a diffuse silicon atomic orbital with mostly *s* and little *p*-character, the latter being invisible in Figure 4 because of the overlying spacious *s* parts. As we did not include Rydberg or negative ion basis functions[20] in our basis set, we may not judge from this point whether this molecular orbital corresponds to a Rydberg state or not. When exciting electrons into this LUMO, one does not expect this to have a significant influence on the $SiCl_3$ and BCl_2 torsional barriers, as the corresponding interactions are nonbonding. Moreover, we have calculated that a BCl_2 torsion around B−C leaves the characteristics of the frontier orbitals mostly unaltered so that the bond distances will also remain basically the same for such a motion. In summary we can say that the electronic structure of TSDE allows a much higher flexibility when compared to TADB, and the lone pair electrons on all chlorine atoms significantly occupy the HOMO. This may well be a reason for its enhanced functionality as a network-creating agent. The fragment B−C−Si reveals a $\sigma - n$ pattern with respect to HOMO and LUMO.

Infra-Red Spectrum

Figure 5 and the enlarged detail in Figure 6 display the vibrational spectrum obtained experimentally. Embedded within each of these Figures, we have added the line spectrum from theory, and finally Table 2 lists all the data obtained in listed form.

Frequencies have been calculated without anharmonic corrections. Moreover, we have tried to minimise the effects of systematic errors during the calculation of *ab initio* frequencies by scaling the results.[21] The procedure we have applied in this context is widely known as *uniform scaling*[22] and procedes by taking a significant vibrational frequency from the theoretical spectrum and setting this to be equal to the corresponding experimental one. The resulting ratio of frequencies is then used to scale over the entire theoretical spectrum. Thus, we obtain method-specific scaling factors that are given in the header of Table 2. The reference mode was chosen to be the fifth highest in frequency at an experimental value of 1464 wavenumbers: The corresponding signal is in the mid-field region of the spectrum, it can easily be distinguished from the ones at higher wavenumbers, it is sharp, does not show any shoulders, and all theoretical models reproduce the neighbouring signal lower in energy at the experimentally observed distance of approximately ten wavenumbers. The peak chosen in this way appears to be suited best for determining a reasonable scaling factor.

In Figure 5 we have overlayed the full (scaled) RI-MP2 theoretical infra-red line spectrum with the experimental one. For the line spectrum, a ratio of $^{11}B/^{10}B \approx 80{:}20$ has been employed. Assignments from low to high frequencies are easily set up; all calculated values from theory find their

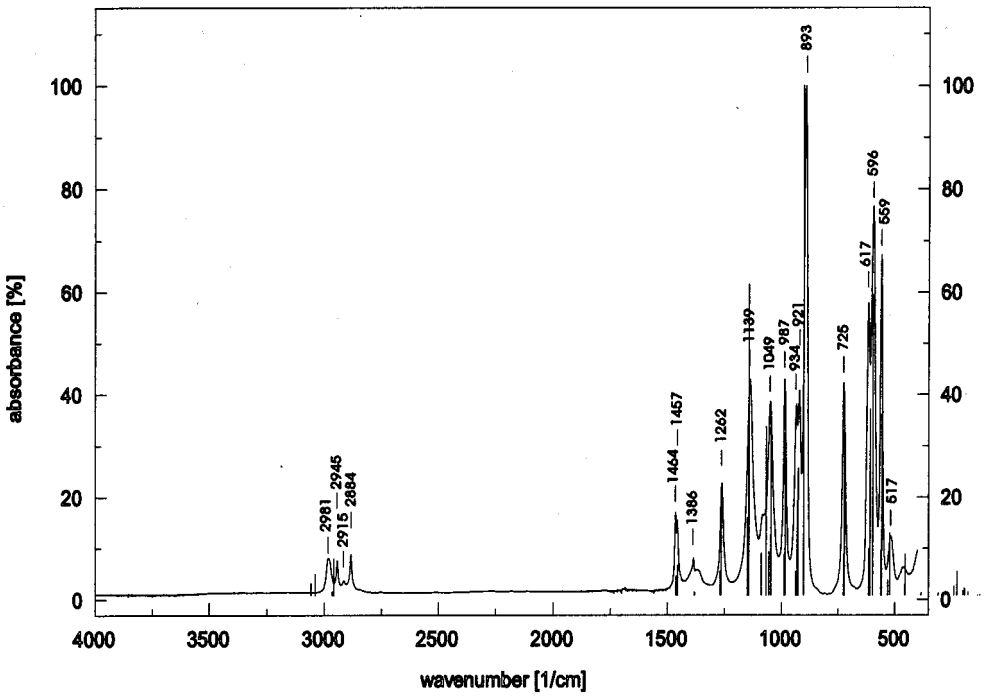


Figure 5. TSDE: Theoretical and experimental IR spectra (Overlay), theory refers to the RI-MP2 level and assumes a $^{11}B/^{10}B$ ratio of 80:20; for reasons of clarity, not all resonances are labelled

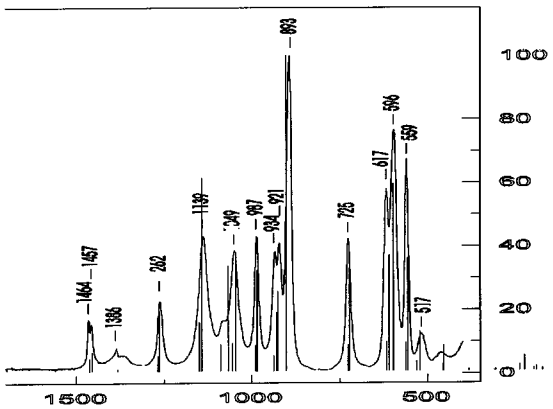


Figure 6. Infra-red spectrum as from Figure 5 − enlargement showing detail of the fingerprint region

experimental counterpart and agreement is particularly good.

Modes 1−12 are basically rocking, bending and wagging motions of the trichlorosilyl- and dichloroboryl-functions, respectively. Mode 13, which we calculate at 383 wavenumbers (scaled RI-MP2), is a combination of a breathing motion of the nuclear frame, accompanied by a slight umbrella-like motion of the methyl group. The experimental spectrum starts with its observation window at around 500 wavenumbers, so the lowest peak in energy at 467 cm^{-1} can clearly be identified with our theoretical value of 454 cm^{-1}, corresponding to mode 14, an umbrella motion of the central carbon atom, combined with symmetric Si−Cl stretching motions and a slight B−Cl stretch vibration. Mode 15 represents the strong pyramidalisation mode of boron, antiphase with Si−C stretches and the $SiCl_3$ umbrella. A theoretical value of 521 cm^{-1} nicely matches an experimental one of 517 cm^{-1}. Still, mode 16 shows a slight out-of-plane (o.o.p.) motion of a boron atom combined with a B−Cl symmetric stretch. Most characteristic for this mode though, are antisymmetric Si−Cl stretch motions and, in this case, theory and experiment agree perfectly (558 vs. 560 cm^{-1}). Mode 17 represents the strong antisymmetric Cl_2Si stretch along with a C−C−Si bending, and a calculated value of 597 wavenumbers finds its experimental counterpart at 596 cm^{-1}. Mode 18, a B−C−Si bending motion, together with an anti-symmetric stretching of the $SiCl_2$ group, shows the same agreement as before: 616 cm^{-1} from the experiment as opposed to 610 cm^{-1} from theory. Mode 19 is a Si−C stretching vibration, exhibiting frequencies of 723 cm^{-1} for the calculated model, and 725 cm^{-1} for the experimental value. This motion is certainly accompanied by a strong in-phase umbrella motion of $SiCl_3$. Mode 20

Table 2. Experimental and theoretical (unscaled and scaled) vibrational frequencies and their relative intensities

Mode	Theory						Experiment		Mode
	DFT Correlation Treatment B3LYP			Perturbation Theoretical Treatment of Correlation RI-MP2					
	ν	ν·0.9676	I[a]	ν	ν·0.9582	I[b]	ν	I	
1	18	17	0	23	22	0			1
2	44	42	0	56	53	0			2
3	80	77	0	86	82	0			3
4	114	111	0	125	120	0			4
5	131	127	0	138	132	0			5
6	169	164	1	181	173	1			6
7	186	180	1	197	189	1			7
8	194	188	0	207	198	1			8
9	205	198	0	232	222	3			9
10	223	215	4	239	229	3			10
11	240	232	1	258	247	1			11
12	307	297	0	320	307	1			12
13	377	365	1	400	383	1			13
14	453	439	9	474	454	8	467	w	14
15	523	506	14	544	521	12	517	m	15
16	549	531	42	583	558	36	559	s	16
17	584	565	54	623	597	61	596	vs	17
18	610	590	21	636	610	38	617	vs	18
19	712	689	29	755	723	33	725	s	19
20	892	863	100	941	902/923	100	893/921	vs/m	20[c]
21	937	906	24	970	930	19	934	s	21
22	1016	983	27	1028	985	33	987	s	22
23	1054	1020	39	1093	1047	35	1049	s	23
24	1106	1070	23	1116	1069	35	1083	s	24
25	1175	1137	41	1192	1143	64	1139	vs	25
26	1304	1262	12	1321	1265	19	1262	s	26
27	1427	1380	1	1444	1384	1	1386	m	27
28	1506	1457	5	1520	1456	6	1457	m	28
29	1513	1464	4	1528	1464	4	1464	m	29
30	3030	2932	1	3091	2962	7	2884	w	30
31	3047	2949	7	3098	2969	1	2915	vw	31
32	3108	3007	4	3176	3043	4	2945	w	32
33	3129	3028	3	3195	3062	2	2981	w	33

[a] 100% = 266 km/mol. − [b] 100% = 244 km/mol. − [c] Refer to text for details.

represents an antisymmetric stretching of BCl_2. We determined an experimental frequency of 893 cm^{-1} which is in accordance with theory (902 cm^{-1}) to within nine wavenumbers. As one can easily tell from looking at a model of atoms moving along this eigenvector, this should be one of the strongest modes in the infra-red spectrum, due to the fact that the dipole moment changes strongly. Indeed, both the density functional and the perturbational calculations determine this vibration as the most intense. Because of its strength we have calculated the corresponding ^{10}B isotopic shift for this mode and found a scaled RI-MP2 value of 923 cm^{-1}. Thus, we conclude that the experimental value of 921 wavenumbers corresponds to a vibration along mode 20 with a ^{10}B nucleus.

Mode 21 basically corresponds to a symmetric stretching vibration of the B−C−Si-fragment that is antisymmetric to a weak BCl_2-vibration of TSDE. A scaled theoretical value of 930 cm^{-1} is nicely reproduced by the experimentally obtained frequency at 934 cm^{-1}. Mode 22 shows the symmetric BCl_2 stretch and some C-B stretching that is antiphase with a wagging motion of the entire methyl group toward the silicon atom. Theory (985 cm^{-1}) and experiment (987 cm^{-1}) match almost perfectly. Mode 23, to which we assign an experimental value of 1049 wavenumbers (theory: 1047 cm^{-1}), shows a B−C−C antisymmetric stretching motion along with a Cl(5)−B stretch. The experimentally recorded shoulder at 1083 wavenumbers correlates with a theoretical resonance at 1069 cm^{-1}, corresponding to mode 24, a strong B−Cl stretch along with a methine-H-C−B bending. Mode 25, which we calculate at 1143 wavenumbers (in satisfactory accordance with the experimental value of 1139) appears as a strong mode in theory and experiment; the corresponding motions are (a) (SiCB) framework stretchings, mainly antisymmetric with respect to B−C and C−Si and (b) an in-plane BCl_2 bending. Mode 26 is mainly an antisymmetric C−C−B stretch. Its vibrational frequency falls into the usual region: 1262 cm^{-1} (experimental), theoretically determined at a scaled value of 1265 cm^{-1}. Mode 27 represents the pure methyl-umbrella motion. We have calculated the corresponding frequency at 1384 cm^{-1}, whereas experiment records it at 1386 cm^{-1}. Modes 28 and 29, at 1457 and 1464 (experimental) or 1456 and 1464 cm^{-1} (theory) respectively, are almost uncoupled scissoring vibrations of the methyl group. The remaining four frequencies in the region of 3000 cm^{-1} certainly belong to C−H stretches. The lowest in frequency (experimental: 2884 vs. theory: 2962) is the symmetric C−H stretch of the methyl group, and mode 31 (experimental: 2915, theory: 2969 cm^{-1}) the methine-H stretch. The density functional calculations reverse the assignment of these frequencies and only by means of a comparison of the calculated intensities (RI-MP2 vs. experiment) can these assignments safely be found. Finally, modes 32 and 33, recorded at 2945 and 2981 cm^{-1} experimentally, are the remaining antisymmetric counterparts of mode 30, the methyl stretches. We calculate these to be at 3043 and 3062 cm^{-1}. As found in most calculations, the agreement slightly deteriorates with higher energies, but the relative positions of the resonances leave assignments unambiguous. Upon turning the trichlorosilyl group through 180° around Si−C and optimising all remaining internal coordinates at the RI-MP2 level, we find a barrier with respect to the minimum of only 9 kJ/mol. Moreover, we have recalculated the vibrational spectrum after this distortion and found deviations of up to 16 wavenumbers (modes 14 and 19). Both these considerations lead us to believe that a thermal excitation should not have influenced characteristics of the experimental infra-red spectrum and that this motion is easily excited at room temperature. Similar considerations apply for the methyl group: A torsion and subsequent relaxation of the remaining internal coordinates yields an energy difference of only 12 kJ/mol above the minimum. The vibrational frequencies deviate at most by 24 cm^{-1} (mode 26) from the equilibrium values. Supported by our considerations for the bond characteristics and the frontier orbitals (see above), one should expect that, finally, a torsion of the dichloroboryl group requires less energy than in TADB (68 kJ/mol), as we had found a partially doubly bonded boron atom there. Indeed, the RI-MP2 energy difference to the minimum amounts to 38 kJ/mol, so this substituent should only be turning freely at slightly elevated temperatures.

NMR Spectrum

The ^1H-NMR spectrum (Figure 7) reveals two signals belonging to the methyl and methine groups of the precursor. The protons of the methyl group are chemically equivalent but the signal at $\delta = 1.48$ is split into a doublet because of the presence of the adjacent methine proton. Analogously, the signal of the methine proton is split into a quartet and is shifted to $\delta = 2.22$.

The signals in the ^{13}C-NMR spectrum (Figure 8) can easily be assigned to the relevant groups: The multiplet in the region of $\delta \approx 78$ belongs to solvent resonances. The methyl group produces a sharp peak at $\delta = 11.93$ whereas the resonance of the methine group is broad and flat and is shifted

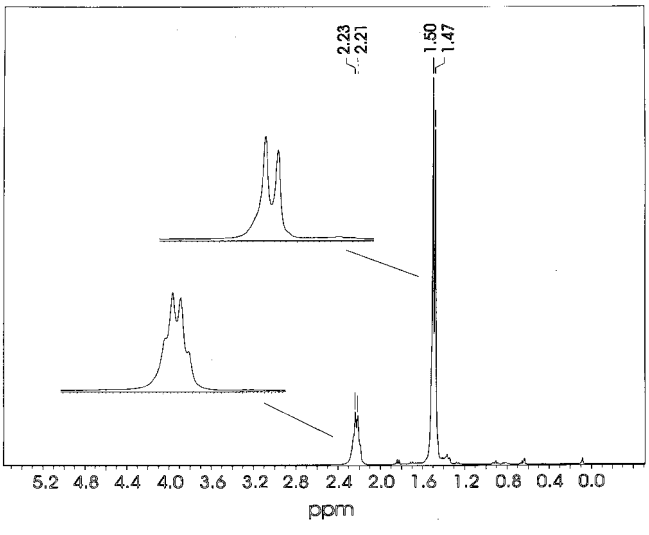


Figure 7. ^1H-NMR spectrum of TSDE

to approximately δ = 34.6. The shape of the latter signal is caused by the interaction of the ^{13}C nuclear spin (I = 1/2) with the quadrupole of the neighbouring ^{11}B (spin 3/2). Table 3 displays results of all NMR experiments conducted (^{1}H, ^{13}C, ^{29}Si, and ^{11}B).

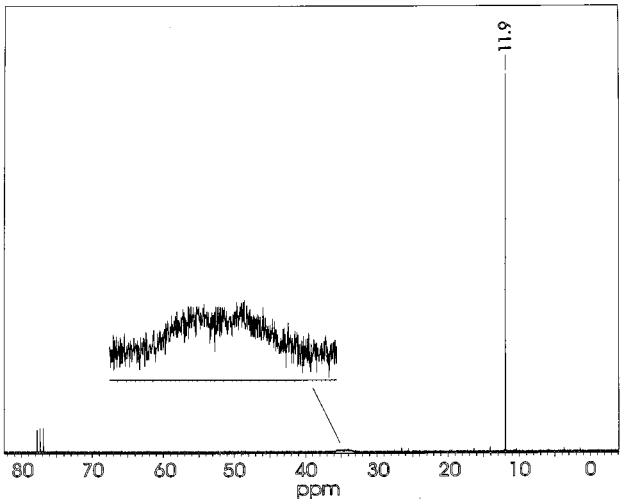


Figure 8. ^{13}C-NMR spectrum of TSDE

Table 3. NMR chemical shifts recorded for TSDE

Nucleus	Chemical shift [δ]	Assignment
^{1}H	1.48	CH_3
	2.22	CH
^{13}C	11.9	CH_3
	34.6	CH
^{29}Si	13.2	$SiCl_3$
^{11}B	67.2	BCl_2

Summary

[(Trichlorosilyl)dichloroboryl]ethane, another member of a group of molecular precursors for Si/B/N/(C) ceramics, is easily accessible through a one-pot synthesis employing boron trichloride and a mixture of trichlorovinylsilane and triethylsilane. As is the case for [(trichlorosilyl)-amino]-dichloroborane, its reasonably flexible equilibrium structure consists of a planar BCl_2 group on one side and a tetrahedral $SiCl_3$ group on the other side of the ethyl backbone. All bonds should be treated as ordinary single bonds, and the HOMO-LUMO sσquence is of $o - n$ character when focusing on the B−C−Si fragment. As far as spectroscopy is concerned, the carbon, hydrogen, boron and silicon NMR signals have been listed and are consistent with the structural analysis. Finally, we have found that second-order perturbation theory reproduces the experimental infrared spectrum with high accuracy and have made the assignments accordingly. By numerically deriving analytical RI-MP2 gradients, we are now able to determine Møller-Plesset second-order perturbational infra-red frequencies. The latter values were obtained with high accuracy for compounds that were barely accessible, or even inaccessible, to such treatment before.

Acknowledgments

This work is dedicated to the memory of Marco Häser, a very able young quantum chemist who died on August 23, 1997 − through his major contributions to the TURBOMOLE package, he substantially diminished the computational efforts we have made within this publication. We are indebted to the HLRZ Supercomputing Center in Jülich and the Cologne University Computing Center. One of us (M.G.) would like to thank Dr Stefan Grimme, Bonn, for helpful discussions. Financial support from the German Research Council (DFG) through SFB408 is gratefully acknowledged.

[1] M. Mühlhäuser, M. Gastreich, C. M. Marian, H. Jüngermann, M. Jansen, *J. Phys. Chem.* **1996**, *100*, 16551.
[2] H.-P. Baldus, O. Wagner, M. Jansen, *Mat. Res. Soc. Symp. Proc.* **1992**, *271*, 821.
[3] H.-P. Baldus, M. Jansen, *Angew. Chem. Int. Ed. Engl.* **1997**, *36*, 328.
[4] M. Peuckert, T. Vaahs, M. Brück. *Adv. Mater* **1990**, *2*, 398.
[5] R. Riedel, *Naturwissenschaften* **1995**, *82*, 12.
[6] H. Jüngermann, M. Jansen, Patent DE 19713766, **1997**.
[7] H. Jüngermann, Doctoral thesis, Bonn University, **1997**.
[8] R. Ahlrichs, M. Bär, M. Häser, H. Horn, C. Kölmel, *Chem. Phys. Lett.* **1989**, *162*, 165.
[9] M. Häser, R. Ahlrichs, *J. Comput. Chem.* **1989**, *10*, 104.
[10] M. J. Frisch, G. W. Trucks, H. B. Schlegel, P. M. W. Gill, B. G. Johnson, M. A. Robb, J. R. Cheeseman, T. Keith, G. A. Petersson, J. A. Montgomery, K. Raghavachari, M. A. Al-Laham, V. G. Zakrzewski, J. V. Ortiz, J. B. Foresman, J. Cioslowski, B. B. Stefanov, A. Nanayakkara, M. Challacombe, C. Y. Peng, P. Y. Ayala, W. Chen, M. W. Wong, J. L. Andres, E. S. Replogle, R. Gomperts, R. L. Martin, D. J. Fox, J. S. Binkley, D. J. Defrees, J. Baker, J. P. Stewart, M. Head-Gordon, C. Gonzales, J. A. Pople, *Gaussian 94, Revision B.1.*, Gaussian Inc., Pittsburgh, **1994**.
[11] H. B. Schlegel, in *Modern Electronic Structure Theory* (Ed.: D. R. Yarkony), World Scientific, **1995**, vol 2, p. 459−500.
[12] R. G. Parr, W. Yang, *Density Functional Theory of Atoms and Molecules*, Oxford University Press, Oxford, **1994**.
[13] A. D. Becke, *J. Chem. Phys.* **1993**, *98*, 5648.
[14] C. Lee, W. Yang, R. G. Parr, *Phys. Rev. B.* **1988**, *37*, 785.
[15] B. Miehlich, A. Savin, H. Stoll, H. Preuss, *Chem. Phys. Lett.* **1989**, *157*, 200.
[16] M. Feyereisen, G. Fitzgerald, A. Komornicki, *Chem. Phys. Lett.* **1993**, *208*, 359.
[17] F. Weigend, M. Häser, *Theor. Chem. Acc.* **1997**, *97(1−4)*, 331.
[18] A. Komornicki, R. L. Jaffe, *J. Chem. Phys.* **1979**, *71(5)*, 2150.
[19] G. Schaftenaar, *Molden 3.2.*, CAOS/CAMM Center, **1996**.
[20] T. H. Dunning, Jr., P. J. Hay, in *Modern Theoretical Chemistry*, vd. 3 (Ed.: H. F. Schaefer III), Plenum Press, **1977**, p. 1−27.
[21] P. Pulay, in *Modern Electronic Structure Theory* (Ed.: D. R. Yarkony), vol. 2, World Scientific, **1995**, p. 1191−1240, and references therein.
[22] W. J. Hehre, L. Radom, P. v. R. Schleyer, J. A. Pople, *Ab Initio Molecular Orbital Theory*, John Wiley, **1986**.

Received July 13, 1998
[I98229]

2,4,6-Tri-*tert*-butyl-1,3,5-triphosphabenzene as an η^6-Ligand in Transition Metal Complexes

Paul Binger,*[a] Stefanie Stutzmann,[a] Jörg Stannek,[a] Barbara Gabor,[a] and Richard Mynott[a]

Keywords: 2,4,6-Tri-*tert*-butyl-1,3,5-triphosphabenzene / η^6-Triphosphabenzene transition metal complexes / Displacement reactions / Phosphorus heterocycles / Arene complexes

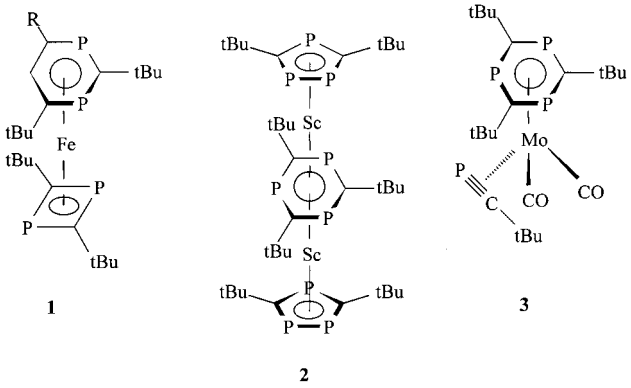
The η^6-1,3,5-triphosphabenzene transition metal complexes **12a**,**b**, **14**, and **16** have been synthesized for the first time by the displacement of η^6-arene ligands (toluene, benzene and naphthalene) with 2,4,6-tri-*tert*-butyl-1,3,5-triphosphabenzene (**9**). The new complexes have been fully characterized by a combination of elemental analysis, mass spectrometry, and ^{1}H-, ^{13}C- and ^{31} P-NMR spectroscopy.

The discovery of transition metal complexes bearing η^6-benzene ligands has been one of the landmarks in the development of modern organometallic chemistry.[1] Numerous π-arene complexes have since been synthesized,[2] not only containing purely carbon-aromatic systems, but arenes incorporating one or more heteroatoms such as N,[3] P,[4] As or Sb[5] as well. With these heteroarenes, a complication that often arises is that η^1-coordination of the lone pair of the heteroatom is more stable than η^6-coordination to a transition metal.[3−5] With phosphorus as the heteroatom, the preferred bonding mode is η^1-coordination; e.g. at room temperature $M(CO_5)THF$ complexes (M = Cr, Mo, W) react with phosphabenzenes (phosphinines) bearing practically any substituents to give the corresponding pentacarbonyl(η^1-phosphinine)metal complexes.[4][6] Only bulky substituents such as *tert*-butyl groups in the 2,6-positions prevent such an interaction.

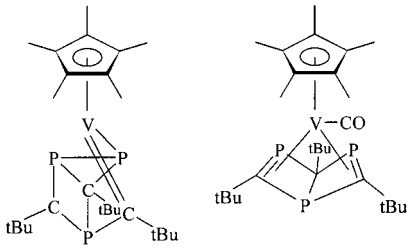
η^6-Phosphinine complexes of these metals [(η^6-C_5R_5P)$M(CO)_3$] can be prepared either from the η^1-complexes by heating above 130°C or directly from phosphinine and $M(CO)_6$ at 130−150°C.[4,7a,7b] Displacement of a benzene derivative by a phosphinine represents a further possible synthetic path for preparing e.g. [(η^6-$C_5Ph_3H_2P$)Mo-$(CO)_3$].[7c]

In contrast to phosphinine complexes, only two examples are known in which 1,3-diphosphabenzene[8] and 1,3,5-triphosphabenzene[9] are η^6-bonded to a transition metal atom. In both cases the complexes are prepared by cyclotrimerization of *tert*-butylphosphaacetylene (**8**) or by cotrimerization of two equivalents of **8** with an acetylene within the coordination sphere of a metal. An earlier report in which the synthesis of the [η^6-triphosphabenzene]molybdenum complex **3** was claimed[10] is dubious for some reason (see below).[11][12]

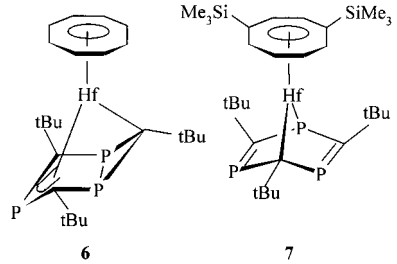
The binding mode of a cyclic $(PC-tBu)_3$ unit to a transition metal atom appears to be very flexible, depending on the transition metal and on the other ligands connected to the metal atom. This observation is illustrated by the two vanadium complexes **4** and **5**[13] and the two hafnium complexes **6**[14b,16] and **7**.[14a]



1 **2** **3**



4 **5**



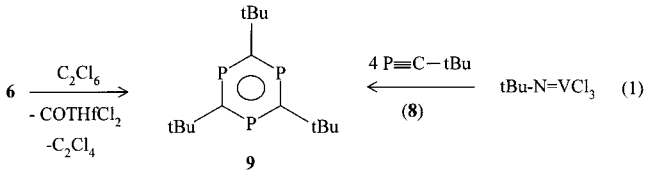
6 **7**

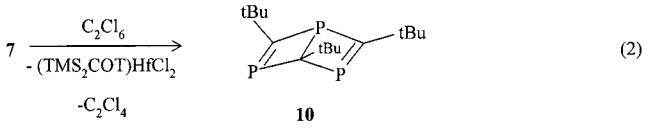
Complexes **6** and **7**, which are synthesized from *tert*-butylphosphaacetylene (**8**) and (η^4-butadiene)(η^8-cyclooctatetraene)hafnium or the corresponding [1,4-bis(trimethylsi-

[a] Max-Planck-Institut für Kohlenforschung, Kaiser-Wilhelm-Platz 1, D-45470 Mülheim a. d. Ruhr, Germany

 © WILEY-VCH Verlag GmbH, D-69451 Weinheim, 1999 1434−1948/99/0101−0083 $ 17.50+.50/0

lyl)cyclooctatetraene]hafnium complex, are the starting materials for the preparation of 2,4,6-tri-*tert*-butyl-1,3,5-triphosphabenzene (**9**) and 2,4,6-tri-*tert*-butyl-1,3,5-triphospha Dewar benzene (**10**), respectively, by reaction with hexachloroethane.[14a] For the synthesis of the triphosphabenzene **9**, a direct route has recently been developed, starting from **8** and trichlorovanadium *tert*-butylimide.[15]





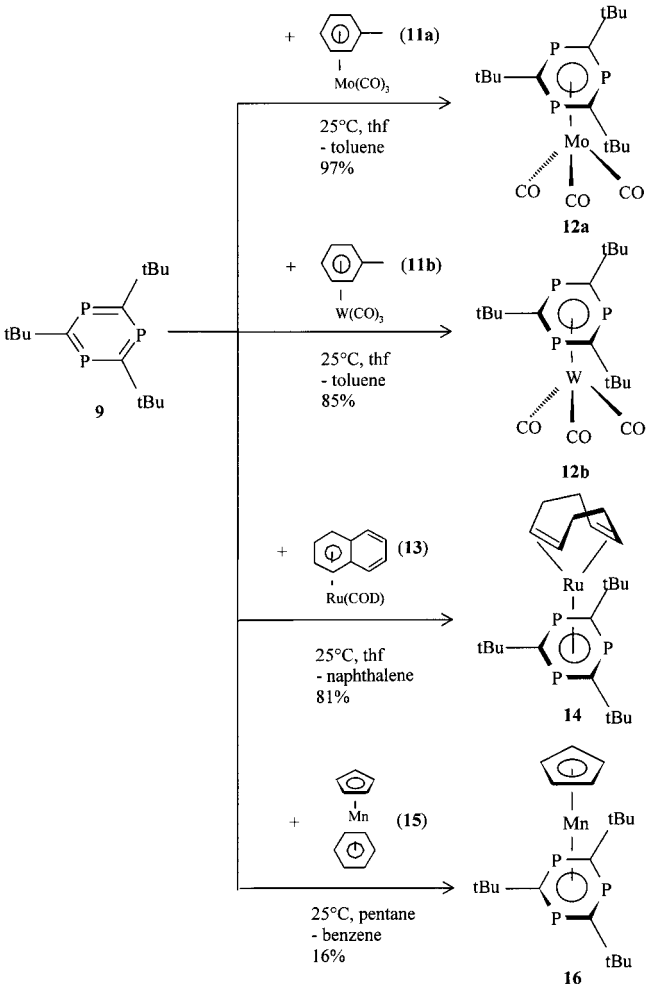
With these procedures at hand, we were able to study the reactivity of the two new heterocycles **9**[16] and **10**.[17][18] Herein we describe the synthesis of some η^6-triphosphabenzene transition metal complexes (M = Mo, W, Ru, Mn) by the displacement of η^6-bonded aromatic ligands (benzene, toluene, naphthalene).

Reactions of tricarbonyl(η^6-toluene)molybdenum (**11a**) and tricarbonyl(η^6-toluene)tungsten (**11b**) with triphosphabenzene **9** in equimolar amounts at ambient temperature result in the displacement of toluene, yielding the molybdenum and tungsten complexes **12a** and **12b** almost quantitatively. This indicates that triphosphabenzene **9** bonds more strongly to the $Mo(CO)_3$ and $W(CO)_3$ fragments than toluene. A primary interaction between one of the lone pairs of the phosphorus atoms in **9** and the metal atom is not observed. Such coordination may be prevented by the bulkiness of the two *tert*-butyl groups in the neighbourhood of the phosphorus atoms. This may also account for the fact that it is not possible to displace nitrile or carbon monoxide from $(RCN)_3M(CO)_3$, $M(CO)_6$, or $(CO)_5M(THF)$ (M = Cr, Mo, W) by **9**. It is known that 2,6-di-*tert*-butylphosphinine does not interact with transition metals via the lone pair either.[19]

The product complexes were isolated as small orange needles (**12a**) and as an orange powder (**12b**). We have so far been unable to obtain crystals suitable for an X-ray analysis. Both complexes decompose above 100°C before reaching their melting point. It is interesting to note that it was not possible to prepare tricarbonyl(η^6-triphosphabenzene)chromium in the same manner from tricarbonyl(η^6-toluene)chromium and **9**.

For the preparation of a (η^6-triphosphabenzene)ruthenium complex, (η^4-1,5-cyclooctadiene)(η^6-naphthalene)ruthenium (**13**) is an ideal starting material. Thus, reaction with the triphosphabenzene **9** leads to substitution of the naphthalene and the new (η^4-1,5-cyclooctadiene)(η^6-triphosphabenzene)ruthenium complex **14** is formed in 81% yield as an orange powder. The product was found to decompose at 105°C.

The displacement of benzene from (η^6-benzene)(η^5-cyclopentadiene)manganese (**15**) by **9** does not reach completion. The reaction proceeds at ambient temperature in pentane only until a conversion of ca. 20% is attained. After separation of the displaced benzene, the reaction does not recommence, thus excluding the possibility of an equilibrium situation. On chromatographic work-up of the reaction mixture, ca. 80% of the starting material **15** can be recovered. Remaining **9** was detected in the distillate and the resulting complex **16** was isolated as green oil in 16% yield.



Scheme 1. Synthesis of some (η^6-triphosphabenzene)metal complexes

All of the new η^6-triphosphabenzene complexes **12a**,**b**, **14**, and **16** have been characterized by elemental analysis, mass spectrometry, and NMR spectroscopy. Elemental analytical data confirm the correct compositions, which are further corroborated by the mass spectra. The molecular ion peak is seen in the mass spectrum of each complex. The $(C_3P_3tBu_3)M$ ions give rise to characteristic fragment ion peaks in the spectra of complexes **12a**, **12b**, and **14**, while in the mass spectrum of the manganese complex **16** the ion

of triphosphabenzene **9** and fragmentation ions therefrom are prominent.

The NMR spectra provide the most diagnostic information as to the constitutions of **12a**,**b**, **14**, and **16**. All spectra exhibit the characteristic feature indicative to the free triphosphabenzene ligand **9**, i.e. the three phosphorus atoms, the three ring carbon atoms, and the hydrogen atoms of the *tert*-butyl groups each appear as single signals, indicating a delocalized 6-π-electron system. The η^6-coordination is indicated by upfield shifts, which do not vary much for the ^{13}C-NMR signals ($\Delta\delta$ = 84.8−77.8, see Table 1), whereas the ^{31}P-NMR shifts are more sensitive to the metal and to the other ligands linked to the metal atom. The coupling pattern of the carbon atoms in free triphosphabenzene **9** ($A_2A'X$) is maintained when **9** is η^6-coordinated to a metal atom. In addition, W−C coupling is observed in the spectrum of **12b**. The carbon atoms of the CO groups in **12a** and **12b** also show coupling with the metal atom and with the three phosphorus atoms of **9**.

Table 1. ^{31}P- and ^{13}C-NMR data of triphosphabenzene as an η^6-ligand in metal complexes in comparison with free triphosphabenzene **9** (δ in ppm)

Compound	**9**	**12a**	**12b**	**14**	**16**
M	−	Mo	W	Ru	Mn
P[a]	232.6	57.6	38.6	59.0	−4.7
C[b]	211.8	131.8	127.0	132.6	134.0

[a] Singlet. − [b] $A^2A'X$ system.

The electronically and coordinatively saturated η^6-triphosphabenzene complexes **12a**,**b**, **14**, and **16** are thermally stable up to ca. 100°C and are rather unreactive. Thus, it was found that the ruthenium complex **14** may be used as a catalyst for the hydrogenation of 1-hexene (THF, 20°C, 20 bar H_2, 0.5 mol-%, 90 h), although the hydrogenation rate is nine times slower than that observed using (η^6-benzene)(1,5-cyclooctadiene)ruthenium as catalyst under comparable conditions.[20][21] Complex **12a** does not react with **9** under the conditions under which Cowley et al.[9] claimed to have synthesized the first η^6-triphosphabenzene complex **3** (THF, 65°C, 10 h). This result, together with the observation of Scheer et al.,[12] led us to the conclusion that Cowley et al. did not in fact synthesize complex **3**. Therefore, the complexes **12a**,**b**, **14**, and **16** can be regarded as the first unambiguously characterized mononuclear metal complexes bearing a triphosphabenzene as an η^6-coordinated ligand.

Experimental Section

All experiments were carried out under argon in anhydrous solvents. − MS: Finnigan MAT 311 ADF, 70 eV. − ^{1}H and ^{13}C NMR: Bruker AM 200 and AMX 400; chemical shifts measured relative to solvent, numerically relative to TMS. − ^{31}P NMR: Bruker AM 200 and AMX 400; external standard H_3PO_4. − Elemental analyses: Dornis and Kolbe, Mülheim a. d. Ruhr. − 2,4,6-Tri-*tert*-butyl-1,3,5-triphosphabenzene (**9**),[14a,15] tricarbonyl(η^6-toluene)molybdenum (**11a**) and tricarbonyl(η^6-toluene)tungsten (**11b**),[22] (η^4-cyclooctadiene)(η^6-naphthalene)ruthenium (**13**),[23] and (η^6-benzene)(η^4-cyclooctadiene)manganese (**15**)[24] were prepared according to published procedures.

Tricarbonyl(η^6-2,4,6-tri-*tert*-butyl-1,3,5-triphosphabenzene)-molybdenum (12a): To a solution of tricarbonyl(η^6-toluene)molybdenum (**11a**, 0.5 g, 1.8 mmol) in THF (10 mL), **9** (0.54 g, 1.8 mmol) was added at room temperature. After stirring for 4 h, the solution was concentrated to a volume of 3 mL and then cooled to −78°C. Complex **12a** precipitated as small orange needles, which were collected by filtration and dried in vacuo. Yield: 0.84 g (97%); decomp. at 103°C. − ^{1}H NMR ([D$_8$]THF, 400.1 MHz, 30°C): δ = 1.45 (s, *t*Bu). − ^{13}C NMR ([D$_8$]THF, 100.6 MHz, 30°C): δ = 215.3 ($|J_{P,P}|$ = 4.7, $J_{C,P}$ = 1.3, $J_{L,Mo}$ = 86.4 Hz, CO), 131.8 ($A_2A'X$ system, $|J_{P,P}|$ = 4.7, $^1J_{C,P}$ = 89.9, $^3J_{C,P}$ = 4.8 Hz, ring-C), 41.6 [$|J_{P,P}|$ = 4.7, $^2J_{C,P}$ = 21.7, $^4J_{C,P}$ = 0.3 Hz, ***C***$(CH_3)_3$], 36.12 [$|J_{P,P}|$ = 4.7, $^3J_{C,P}$ = 12.8, $^1J_{C,H}$ = 128 Hz, C(***C***$H_3)_3$]; all coupling constants were established by simulations. − ^{31}P NMR ([D$_8$]THF, 162 MHz, 30°C): δ = 57.6 (s). − MS (70 eV); *m/z* (%): 482 (29) [M^+], 454 (26) [M − CO^+], 398 (100) [M^+ − 3 CO], 312 (32). − $C_{18}H_{27}O_3P_3Mo$ (480.2): calcd. C 45.02, H 5.65; found C 45.04, H 5.61.

Tricarbonyl(η^6-2,4,6-tri-*tert*-butyl-1,3,5-triphosphabenzene)-tungsten (12b): To a solution of **9** (200 mg, 0.67 mmol) in THF (3 mL), a solution of tricarbonyl(η^6-toluene)tungsten (**11b**, 285 mg, 0.8 mmol) in THF (2 mL) was added at room temperature. After stirring overnight, the THF was distilled off under reduced pressure (0.5 mbar) and the residue was redissolved in pentane (1 mL). At −78°C, **12b** precipitated as an orange powder, which was collected by filtration and dried in vacuo. Yield: 322 mg (85%); decomp. at 175°C. − ^{1}H NMR ([D$_8$]THF, 200 MHz, 30°C): δ = 1.64 (t, $^4J_{P,H}$ = 1.5 Hz, *t*Bu). − ^{13}C NMR ([D$_8$]THF, 50.3 MHz, 30°C): δ = 205.1 ($J_{P,C}$ = 2.0, $J_{W,C}$ = 84.4 Hz, CO), 127.0 ($^1J_{C,P}$ = 89.8, $^3J_{C,P}$ = 4.0, $J_{W,C}$ = 13.5 Hz, ring-C), 41.9 [$^2J_{P,C}$ = 21.4 Hz, ***C***$(CH_3)_3$], 36.0 [$^3J_{P,C}$ = 12.7 Hz, C(***C***$H_3)_3$]. − ^{31}P NMR ([D$_8$]THF, 81.1 MHz, 30°C): δ = 38.6 (s). − MS (70 eV); *m/z* (%): 568 (34) [M^+], 540 (100) [M − CO^+], 510 (7) [M − 210^+], 482 (46) [M − 3 CO^+]. − $C_{18}H_{27}O_3P_3W$ (568.1): calcd. C 38.06, H 4.78; found C 38.08, H 4.74.

(η^4-1,5-Cyclooctadiene)(η^6-2,4,6-tri-*tert*-butyl-1,3,5-triphosphabenzene)ruthenium (14): To a solution of **9** (200 mg, 0.67 mmol) in THF (3 mL), a solution of the ruthenium complex **13** (270 mg, 0.8 mmol) in THF (2 mL) was added at room temperature. After stirring for 4 h, the THF was distilled off at 40°C/0.5 mbar, the residue was redissolved in pentane, and purified by column chromatography (glass column, diameter 2 cm, length 15 cm, silica gel 60, 70−230 mesh, Merck AG). The orange fraction was found to contain complex **14** contaminated by traces of naphthalene. The latter could be removed by sublimation at 60°C/0.5 mbar. The remaining orange powder consisted of pure complex **14**; yield: 275 mg (81%); decomp. at 105°C. − ^{1}H NMR ([D$_8$]THF, 200 MHz, 30°C): δ = 3.67 (br. s, 4 H, COD), 2.03 (br. s, 8 H, COD), 1.52 (s, *t*Bu). − ^{13}C{^{1}H} NMR ([D$_8$]THF, 50.3 MHz, 30°C): δ = 132.6 ($^1J_{P,C}$ = 87.2, $^3J_{P,C}$ = 5.4 Hz, ring C), 65.1 ($^2J_{P,C}$ = 1.5 Hz, COD), 42.7 [^2J = 22.6 Hz*, ***C***$(CH_3)_3$], 36.0 [$^3J_{P,C}$ = 13.2 Hz*, C(***C***$H_3)_3$], 33.9 (s, COD); * denotes *J* by comparison with simulated spectrum of complex **12a**. − ^{31}P NMR ([D$_8$]THF, 81.1 MHz, 30°C): δ = 59.0 (s). − MS (70 eV); *m/z* (%): 510 (25) [M^+], 453 (6) [M − *t*Bu^+], 402 (100) [M − COD^+], 169 (7) [$PC_2tBu_2^+$], 57 (10) [*t*Bu]. − $C_{23}H_{39}P_3Ru$ (509.6): calcd. C 54.21, H 7.71; found C 54.26, H 7.69.

(η^5-Cyclopentadienyl)(η^6-2,4,6-tri-*tert*-butyl-1,3,5-triphosphabenzene)manganese (16): To a solution of (η^6-benzene)(η^5-cyclopentadienyl)manganese (**15**, 170 mg, 0.86 mmol) in pentane (3 mL), a solution of **9** (200 mg, 0.67 mmol) in pentane (2 mL) was added at room temperature. From the resulting reaction mixture, complex **16** was separated by column chromatography (eluent: pentane; glass column, diameter 2 cm, length 15 cm, Al_2O_3, Merck AG). The green fraction was found to contain complex **16**, which was obtained as a green oil upon removal of the pentane by distillation. Yield: 40 mg (16%). – ^{1}H NMR ([D$_8$]THF, 200 MHz, 30°C): δ = 4.10 (s, 5 H, Cp), 1.66 (s, 27 H, *t*Bu). – ^{13}C{^{1}H} NMR ([D$_8$]THF, 50.3 MHz, 30°C): δ = 134 (ring C), 70.3 (Cp), 42.3 and 36.0 (*t*Bu). – ^{31}P NMR ([D$_8$]THF, 81.0 MHz, 30°C): δ = −4.6 (s). – MS (70 eV); *m/z* (%): 420 (42) [M$^+$], 282 (65) [M − $C_2tBu_2^+$], 258 (43) [M − P_2tBuH^+], 220 (21) [M − $P_2C_2tBu_2$], 169 (38), 120 (100) [CpMn], 57 (17), 55 (36). – $C_{20}H_{32}P_3Mn$ (420.3): calcd. C 57.15, H 7.64; found C 57.07, H 7.69.

Acknowledgments

This work was supported by the Deutsche Forschungsgemeinschaft (Graduiertenkolleg "Phosphor als Bindeglied verschiedener chemischer Disziplinen").

[1] First publication: E. O. Fischer, W. Hafner, *Z. Naturforsch., B* **1955**, *10B*, 665−668.
[2] Reviews: [2a] W. A. Silberthorn, *Adv. Organomet. Chem.* **1975**, *13*, 48−137. – [2b] M. L. H. Green, *J. Organomet. Chem.* **1980**, *200*, 119−132. – [2c] E. L. Muetterties, J. R. Bleeke, E. J. Wuchener, T. A. Albright, *Chem. Rev.* **1982**, *82*, 499−525.
[3] Reviews: [3a] K. H. Pannell, B. L. Kalotra, C. Parkanyi, *J. Heterocycl. Chem.* **1978**, *15*, 1057−1081. – [3b] P. Tomasik, Z. Ratajewicz, G. R. Newkome, L. Strekowski, *Chem. Heterocycl. Compd.*, Vol. 14, part A−C, John Wiley & Sons, New York, N. Y., **1985**.
[4] Review: G. Märkl in *Multiple Bonds and Low Coordination in Phosphorus Chemistry* (Eds.: M. Regitz, O. J. Scherer), Thieme Verlag, Stuttgart, **1990**, p. 220−257.
[5] Review: A. J. Ashe III, *Top. Curr. Chem.* **1982**, *105*, 125−155.
[6] [6a] J. Deberitz, H. Nöth, *J. Organomet. Chem.* **1973**, *49*, 453−468. – [6b] H. Vahrenkamp, H. Nöth, *Chem. Ber.* **1973**, *106*, 2227−2235. – [6c] K. C. Naiman, C. T. Sears, *J. Organomet. Chem.* **1978**, *148*, C31−C34.
[7] [7a] J. Deberitz, H. Nöth, *Chem. Ber.* **1970**, *103*, 2541−2547. – [7b] H. Vahrenkamp, H. Nöth, *Chem. Ber.* **1972**, *105*, 1148−1157. – [7c] J. Deberitz, H. Nöth, *Chem. Ber.* **1973**, *106*, 2222−2226.
[8] D. Böhm, F. Knoch, S. Kummer, U. Schmidt, U. Zenneck, *Angew. Chem.* **1995**, *107*, 251−253; *Angew. Chem. Int. Ed. Engl.* **1995**, *34*, 198−201.
[9] P. L. Arnold, F. G. N. Cloke, P. B. Hitchcock, J. F. Nixon, *J. Am. Chem. Soc.* **1996**, *118*, 7630−7631.
[10] A. R. Barron, A. H. Cowley, *Angew. Chem.* **1987**, *99*, 956; *Angew. Chem. Int. Ed. Engl.* **1987**, *26*, 907.
[11] J. Haas, Diplomarbeit, Universität Bonn, **1988**.
[12] M. Scheer, J. Krug, *Z. Anorg. Allg. Chem.* **1998**, *624*, 399−405.
[13] R. Milczarek, W. Rüsseler, P. Binger, K. Jonas, K. Angermund, C. Krüger, M. Regitz, *Angew. Chem.* **1987**, *99*, 957−958; *Angew. Chem. Int. Ed. Engl.* **1987**, *26*, 908−909.
[14] [14a] P. Binger, S. Leininger, J. Stannek, B. Gabor, M. Mynott, J. Bruckmann, C. Krüger, *Angew. Chem.* **1995**, *107*, 2411−2414; *Angew. Chem. Int. Ed. Engl.* **1995**, *34*, 2227−2230. – [14b] P. Binger, S. Stutzmann, J. Stannek, P. Phillips, R. Mynott, J. Bruckmann, C. Krüger, *Eur. J. Inorg. Chem.*, submitted.
[15] F. Tabellion, A. Nachbauer, S. Leininger, C. Peters, M. Regitz, F. Preuss, *Angew. Chem.* **1998**, *110*, 1318−1321; *Angew. Chem. Int. Ed. Engl.* **1998**, *37*, 1233−1235.
[16] [16a] J. Stannek, Dissertation, Universität Kaiserslautern, **1996**. – [16b] S. Stutzmann, Dissertation, Universität Kaiserslautern, **1997**.
[17] P. Binger, S. Leininger, M. Regitz, U. Bergsträßer, J. Bruckmann, C. Krüger, *J. Organomet. Chem.* **1987**, *529*, 215−221.
[18] P. Binger, S. Leininger, K. Günther, U. Bergsträßer, *Chem. Ber.* **1997**, *130*, 1491−1494.
[19] H. Lehmkuhl, R. Paul, R. Mynott, *Liebigs Ann. Chem.* **1981**, 1139−1146.
[20] P. Pertici, G. Vitulli, C. Bigelli, R. Lazzaroni, *J. Organomet. Chem.* **1984**, *275*, 113−117.
[21] F. Heinemann, J. Klodwig, F. Knoch, M. Wündisch, U. Zenneck, *Chem. Ber.* **1997**, *130*, 123−130.
[22] R. B. King, A. Fronzaglia, *Inorg. Chem.* **1966**, *5*, 1837−1846.
[23] M. A. Bennett, H. Neumann, M. Thomas, X. Wang, *Organometallics* **1991**, *10*, 3237−3245.
[24] E. O. Fischer, S. Breitschaft, *Chem. Ber.* **1966**, *99*, 2213−2236.

Received July 16, 1998
[I98235]

$Ta_{11}Si_2Se_8$ – Condensed Tetrakaidecahedral Ta_9Si Clusters Arranged to an Open Network Structure

Antje Mrotzek and Bernd Harbrecht*[a]

Dedicated to Professor Edgar Niecke on the occasion of his 60th birthday

Keywords: Selenium / Silicon / Silicides / Tantalum / Condensed cluster compounds

$Ta_{11}Si_2Se_8$ was synthesized from a pre-reacted mixture of the elements in a sealed tantalum tube at 1570 K. Mo-doped crystals were obtained in a welded molybdenum crucible by a chemical transport reaction using TeI_4 as a transport agent. The structure of $Mo_{0.11}Ta_{10.89(2)}Si_2Se_8$ has been determined by single crystal X-ray means [*Pnnm*, $Z = 2$, $a = 1184.4(1)$ pm, $b = 1939.4(1)$ pm, $c = 346.48(2)$ pm, $wR_2 = 0.069$]. The structure of the ternary phase was verified by means of a Rietveld profile fit of a powder X-ray diffractogram. The silicide is isotypic with $Ta_{11}Ni_2Se_8$. The structure is composed of Si-centred, tricapped trigonal prismatic Ta_9Si clusters. The tetrakaidecahedral Ta_9Si clusters are fused into twin chains by sharing the Ta^{pr} atoms of facing triangulated prism faces and one out of three capping atoms Ta^c. Intercluster linkage of the remaining Ta^c atoms generates a microporous $^3_\infty[SiTa_2^c\ Ta_{1/2}^c\ Ta_{6/2}^{pr}]$ substructure. The channels of the metal network are sheathed by three-, four-, five-, and sixfold coordinated Se atoms. Four-probe dc resistivity measurements revealed the Mo-doped phase to be a moderate metallic conductor. The bonding interactions contributing to the stability of $Ta_{11}Si_2Se_8$ and distinctions in bonding for $Ta_{11}Si_2Se_8$ and $Ta_{11}Ni_2Se_8$ are analysed on the basis of semi-empirical extended Hückel calculations.

Introduction

Tantalum is known to form numerous metal-rich chalcogenides with very distinctive and partly exotic structural and/or physical properties. By using the versatile metal partial structure as a guideline, four groups of tantalum subchalcogenides can be distinguished:

(1) Interpenetrating metal-centred icosahedral structures: Much of the motivation for exploring low-valent tantalum chalcogenides goes back to the findings of Franzen and Smeggil[1] that tantalum can form frameworks based on interpenetrating metal-centred icosahedra. The structures of the sulfides Ta_6S_n ($n = 1$,[1][2] 3,[1] and 4[3]), $M_xTa_{6-x}S$ (M = V, Cr),[4] $AuTa_5S$,[5] $M_xTa_{15-x}S_2$ (M = Au, Al, Ga, Ge, Sn, Sb, Pd, Pt, Rh, Ir)[6] are examples of such clusters. The small-band-gap semiconductor Ta_6Te_5[7] with a unique one-dimensional pentagonal antiprismatic chain structure, the layer-type chalcogenides $Ta_3(S,Se)_2$,[8] $Ta_5(Se,Te)_3$,[9] and $Ta_3(S,Te)_2$,[10] as well as $Ta_5(S,Te)_2$[11] exhibiting a perforated Ta partial structure and the unprecedented quasicrystalline chalcogenide $Ta_{2\sqrt{3}+3}Te_4$,[7b][12] marked by a Fourier spectrum with twelvefold rotational symmetry, belong to this group of structures. They all are composed of interpenetrating, condensed, or metal−metal-bonded M_{13} icosahedra and/or fragments thereof.

(2) Body-centred cubic fragment-structures: The structures of several other low-valent tantalum chalcogenides have in common that parts of the body-centred cubic (*bcc*) arrangement of tantalum are preserved. In contrast to sulphur, tellurium, vanadium, and chromium, homologous elements like selenium, niobium, molybdenum, and tungsten promote the formation of *bcc* fragment structures. Representatives of this group are the metal-rich layer-type structures Ta_2Se, $Ta_2(S,Se)$ [n(S)/n(Se) < 4], $Ta_5(S,Se)_2$, $Ta_9(S,Se)_4$, $M_xTa_{5-x}S_2$ (M = Mo, W), $(Nb,Ta)_2S$, and $(Nb,Ta)_5S_2$[13] and the network structures of $(Nb,Ta)_{11}S_4$ and $(Nb,Ta)_9(S,Te)_5$.[14]

(3) Quasi-one-dimensional metal-rich chalcogenides: The structures of some rare examples of this third group consist of columnar metal cores completely covered with chalcogen atoms; van der Waals interactions provide the cohesion of the strings. The tellurides M_4ETe_4 (M = Nb, Ta; E = Si, Cr, Fe, Co, Ni),[15] e.g., are composed of chains of confacial square antiprismatic clusters, $^1_\infty[SiTa_{8/2}Te_{8/2}]$. Deintercalated $LiMo_3Q_3$ (Q = Se, Te)[16] and Ta_6Te_5[7] show similar structural features.

(4) Condesed tetrakaidecahedral cluster compounds: The compounds of the fourth group contain, in addition to sulphur or selenium, an iron-group metal as a second minor component. As a consequence of a substantial difference between the Ta−Q and M−Q affinities, the partial structures of the 3d-metal and chalcogen components are spatially separated by the intermediate partial structure of the major component. At low contents of the 3d metal, the M atoms are encapsulated in tricapped trigonal prismatic Ta_9 clusters confined by 14 triangular faces. All structures of this type known so far contain columns of condensed tetrakaidecahedral clusters. The columns, however, can be linked in different ways giving rise to a variety of compositionally distinct compounds: $Ta_9M_2S_6$, $Ta_{11}M_2Se_8$ (M = Fe, Co, Ni)

[a] Fachbereich Chemie, Philipps-Universität Marburg,
Hans-Meerwein-Straße 1, D-35032 Marburg, Germany
Fax: (internat.) + 49(0)6421/288917
E-mail: fkc@mail.chemie.uni-marburg.de

 © WILEY-VCH Verlag GmbH, D-69451 Weinheim, 1999 1434−1948/99/0101−0087 $ 17.50+.50/0

and Ta_8MSe_8 (M = Co, Ni),[17] $M_{1-x}Nb_6S_{2+x}$ (M = Fe, Co, Ni, Cu), $M_{2-x}Nb_9S_{3+x}$ and $M_{2-x}Nb_8S_{4+x}$ (M = Co, Ni),[18] Hf_8MTe_6 (M = Mn, Fe), Hf_5MTe_3 (M = Fe, Co), and Zr_6MTe_2 (M = Mn, Fe, Co, Ni, Ru, Pt).[19]

In an attempt to expand the structural chemistry of tantalum-rich chalcogenides by including another main-group element we explored selected ternary tantalum-selenium systems containing a group-14 element as a minor component.[20] Here we report the synthesis and structure of a tantalum-rich silicide selenide $Ta_{11}Si_2Se_8$ which is isotypic with the compounds of the $Ta_{11}M_2Se_8$ (M = Fe, Co, Ni)[17c,d] series.

Results and Discussion

Synthesis, Analyses, Electrical Properties

Microcrystalline, single-phase $Ta_{11}Si_2Se_8$ was obtained by a gas-solid reaction from a pre-reacted stoichiometric mixture of the elements in welded tantalum tubes at 1570 K within 2 days. The results of a Rietveld refinement are shown in Figure 1. Data on the profile fit are given in Table 1. Fibrous crystals up to 3 mm in length and 20 μm in diameter (Figure 2) were obtained by a chemical vapour transport reaction in welded molybdenum crucibles using TeI_4 as a transport agent. Energy-dispersive X-ray spectroscopy (EDX) and X-ray single crystal structure analyses revealed the presence of some molybdenum in the samples. No indication of an enrichment of tellurium was obtained. The results of a structure refinement of $Mo_{0.11}Ta_{10.89(2)}Si_2Se_8$ are listed in Tables 2, 3, and 4. As expected for a metal-rich compound with extended metal−metal bonding, $Ta_{11}Si_2Se_8$ is a moderate metallic conductor. The resistivity increases steadily with increasing temperature. The values for two different samples were found to be about 1 mΩcm and 1.5 mΩcm at 10 K and 1.6 mΩcm and 2.1 mΩcm at 320 K, respectively.

Table 1. Selected parameters of the Rietveld analysis of $Ta_{11}Si_2Se_8$

Measuring parameters		
Scan-range, stepwidth (2θ) [°]		5.00−95.00 / 0.03
Total measuring time [h]		50
Radiation		Cu-K_α
Global parameters		
Number of phases		1
Number of variables		45
Profile fit		pseudo-Voigt
Background		refined
Structure and profile data		
Formula mass [g mol^{-1}]		2678.28
Space group (No.)		*Pnnm* (58)
Lattice parameters: *a* [pm]		1181.44(4)
b [pm]		1937.24(6)
c [pm]		346.33(1)
V [10^{6}pm^3]		792.66(7)
Formula units per cell		2
Coefficients for peak FWHM	*U*	0.095(7)
	V	−0.063(4)
	W	0.022787)
Preferred orientation		[0 0 1]
Perferred orientation parameter		1.189(4)
Asymmetry parameter		0.32(2)
Peak shape parameter η		0.83(2)
R_P		0.0457
R_{WP}		0.0643
R_B		0.0182

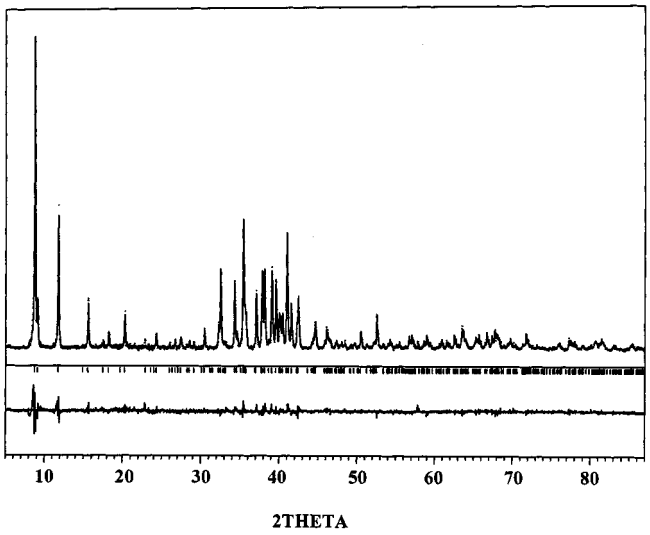


Figure 1. Rietveld profile fit of a powder X-ray diffractogram (Cu-K_α) of $Ta_{11}Si_2Se_8$, measured (points) and calculated (line) diffractogram (top), Bragg positions (middle), and difference plot (bottom)

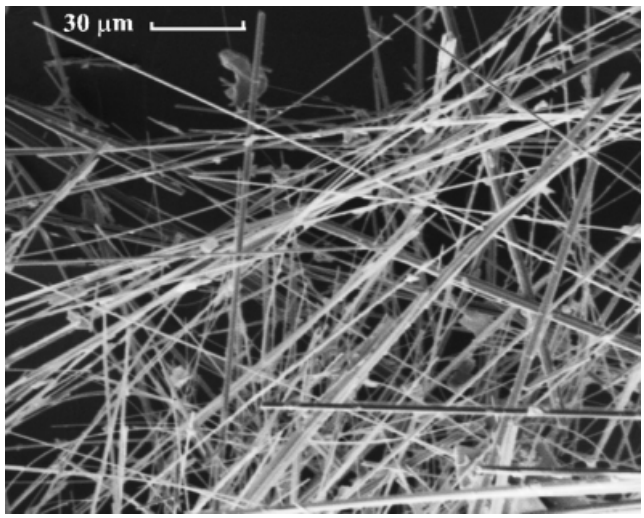


Figure 2. Scanning electron micrograph of needle-shaped crystals of $Mo_xTa_{11-x}Si_2Se_8$ transported to the lid of the molybdenum crucible

Description of the Crystal Structure

The structure is composed of eleven crystallographically inequivalent atoms: Ta1−Ta6, Si1, and Se1−Se4. They all are located in mirror planes perpendicular to the short *c* axis at *z* = 0 and 1/2 modulo 1. Figure 3 shows the structure in a projection along the short *c* axis. The basic unit of the structure is an Si-centred tricapped trigonal prism, i.e. a tetrakaidecahedral Ta_9Si cluster that is confined by fourteen triangular faces. Strong interactions between the

Table 2. Data collection and refinement parameters of $Mo_{0.11}Ta_{10.89(2)}Si_2Se_8$[a]

Crystal data	
Chemical formula	$Mo_{0.11}Ta_{10.89(2)}Si_2Se_8$
Formula mass [g mol^{-1}]	2668.37
Space group (No.)	*Pnnm* (58)
a [pm]	1184.4(1)
b [pm]	1939.4(1)
c [pm]	346.48(2)
V [10^6 pm^3]	795.9(1)
Z	2
ρ_X [g cm^{-3}]	11.137
μ [cm^{-1}]	92.99
Data collection	
Crystal size [mm]	0.02 × 0.02 × 0.31
Diffractometer	IPDS
Radiation	Mo-K_α
Monochromator	Graphite
Detector distance [mm]	50
Rotation range ϕ [°], $\phi_{incr.}$ [°]	0–200, 1
Bragg angle $2\theta_{max}$ [°]	60.9
Reflections measured	$h \leq \pm 16$, $k \leq \pm 27$, $l \leq \pm 4$
Number of reflections	9296
Completeness of data set	99.3%
Data reduction	
Program	XPREP[25b]
Absorption correction	semi-empirical
min./max. transmission	0.360/0.483
Number of unique reflections	1353
R_{int} (*F*)	0.0761
Refinement	
Program	SHELXL-96[25c]
Number of parameters	66
Number of reflections $F_o > 4\sigma(F_o)$	997
R_1 [$F_o > 4\sigma(F_o)$]/R_1 (all)	0.0289 / 0.0427
wR_2	0.0691
Goof	0.902
$\Delta\rho_{max}/\Delta\rho_{min}$ [10^{-6} e pm^{-3}]	4.06/−3.56

[a] Further details of the crystal structure determination may be obtained from the Fachinformationszentrum Karlsruhe, D-76344 Eggenstein-Leopoldshafen (Germany), on quoting the depository number CDS-408960.

Table 3. Positional parameters and displacement parameters U_{eq} [pm^2] of $Mo_{0.11}Ta_{10.89(2)}Si_2Se_8$; $z = 0$

	Wyckoff	*x*	*y*	U_{eq}
Ta1/Mo1[a]	*2a*	0	0	23(4)
Ta2	*4g*	0.33926(5)	0.28621(3)	24(1)
Ta3	*4g*	0.32286(5)	0.85596(3)	21(1)
Ta4	*4g*	0.43448(5)	0.61311(3)	23(1)
Ta5	*4g*	0.04949(5)	0.24242(3)	27(1)
Ta6	*4g*	0.32096(5)	0.45315(3)	23(1)
Se1	*4g*	0.1070(1)	0.44655(9)	40(3)
Se2	*4g*	0.4585(1)	0.17258(9)	35(3)
Se3	*4g*	0.2137(1)	0.05741(9)	32(3)
Se4	*4g*	0.2845(1)	0.71315(9)	24(3)
Si1	*4g*	0.0921(4)	0.8715(2)	22(7)

[a] Occupation factors: $b_{Ta1} = 0.89(2)$, $b_{Mo1} = 0.11$.

central Si and the peripheral Ta^{pr} atoms of the prism are indicated by a mean distance of 255.2 pm. The three capping Ta^c atoms are somewhat more distant (274.8 pm). Ta–Ta bonds contribute significantly to the stability of the cluster: The mean d_{Ta1-Ta} between Ta^{pr} and Ta^c atoms is 289.3 pm in contrast to 338.1 pm between Ta atoms of adjacent prisms. The shortest Si–Si distance corresponds to the parameter *c* (346.48 pm). In contrast to the less metal-rich phase Ta_4SiTe_4[15a,b] (d_{Si-Si} = 235.3, 244.8 pm), there are no homonuclear Si–Si bonds in $Ta_{11}Si_2Se_8$.

The clusters are condensed via common trigonal prism faces into columns, according to $^1_\infty[SiTa_{6/2}{}^{pr}Ta_3{}^c]$. Furthermore, two columns share the Ta1 atom of one out of the three capping positions, $^1_\infty[(SiTa_{6/2}{}^{pr}Ta_2{}^cTa_{1/2}{}^c)_2] = Ta_{11}Si_2$. A part of such a twin column is shown in Figure 4. Adjoining twin columns are shifted relative to each other by *c*/2. Intercluster bonding contacts between Ta3 and Ta5 (318.4 pm) link the columns to an open three-dimensional network. The resulting elongated channels are sheathed by four crystallographically inequivalent Se atoms which cover and bridge the clusters in different ways: Se2 with coordination number CN 4, $<d_{Ta-Se1}> = 262.8$ pm, and Se4 (CN 6, <269.2 pm>) connect adjacent twin columns, while Se1 (CN 3, <258.2 pm>) and Se3 (CN 5, <270.8 pm>) bridge the clusters which share capping Ta atoms. As one can clearly see from Figure 5, the coordination polyhedra of the Se atoms represent distinct fragments of a Ta_9Se cluster related to the Ta_9Si cage. The one-sided coordination of all Se atoms points to a very characteristic structural functionality of the most electronegative component of the compound: the Se atoms saturate the remaining valences of the open $Ta_{11}Si_2$ network structure by completely covering its internal surfaces.

Features of the Electronic Structure

The electronic band structures of $Ta_{11}Si_2Se_8$ and $Ta_{11}Ni_2Se_8$ were calculated with the extended Hückel method.[21] Parameters were taken from the literature,[22] and are listed in Table 5. The valence-state ionization energies H_{ii} and the coefficients of the Slater-type orbitals, c_1 and c_2, for tantalum are based on charge-iterative calculations.[20] Band structure calculations were carried out using a 30 *k* point mesh lying in the representation domain of the corresponding space group. The total density of states (DOS) and the contributions of each component of the compounds are shown in Figure 6. The total DOS of the silicide can be subdivided into four blocks:

(i) The primarily Se 4s based peak around −22 eV is not shown.

(ii) The levels between −18 and −13.5 eV are dominantly of Ta 5d and Se 4p character. Mixing of these orbitals gives rise to strong heteronuclear Ta–Se interactions.

(iii) Above a deep local minimum in the DOS around −13.5 eV a third range of Si p and Ta d based states extends up to the Fermi level. A smaller portion of these states at low energy reflects strong heteronuclear Ta–Si bonds whereas the upper levels correspond basically to extended Ta–Ta bonds. Obviously, the heteronuclear bonding interactions Ta–Se and Ta–Si are segregated energetically and spatially. There are no significant Si–Se interactions ($d_{Se-Si} \geq 382.5$ pm) contributing to the stability of this compound.

Table 4. Characteristic interatomic distances [pm] of $Mo_{0.11}Ta_{10.89(2)}Si_2Se_8$

Ta1, Mo	− 2 × Si1	272.0(5)	Ta2	− 2 × Si1	253.0(4)	Ta3	− 2 × Se1	260.4(1)
	− 2 × Se3	276.6(2)		− 1 × Se2	261.8(2)		− 1 × Se2	264.8(2)
	− 4 × Ta6	288.50(5)		− 2 × Se4	267.6(1)		− 1 × Si1	275.0(4)
	− 4 × Ta4	290.09(5)		− 2 × Ta3	291.85(7)		− 1 × Se4	280.7(2)
				− 2 × Ta5	308.38(8)		− 2 × Ta2	291.85(7)
				− 1 × Ta6	324.5(1)		− 2 × Ta6	307.49(7)
				− 1 × Ta4	331.57(9)		− 2 × Ta5	318.36(8)
				− 1 × Ta5	353.55(9)			
Ta4	− 2 × Si1	256.4(4)	Ta5	− 2 × Se2	262.3(1)	Ta6	− 1 × Se1	253.8(2)
	− 1 × Se4	263.0(2)		− 2 × Se4	268.1(1)		− 2 × Si1	256.3(4)
	− 2 × Se3	269.3(1)		− 1 × Si1	277.4(5)		− 2 × Se3	269.4(1)
	− 2 × Ta1, Mo	290.09(5)		− 2 × Ta4	305.40(8)		− 2 × Ta1, Mo	288.50(5)
	− 2 × Ta5	305.40(8)		− 2 × Ta2	308.38(8)		− 2 × Ta3	307.49(7)
	− 1 × Ta6	316.87(9)		− 2 × Ta3	318.36(8)		− 1 × Ta4	316.87(9)
	− 1 × Ta2	331.57(9)		− 1 × Ta2	353.55(9)		− 1 × Ta2	324.5(1)
	− 1 × Ta6	338.1(1)					− 1 × Ta4	338.1(1)
Se1	− 1 × Ta6	253.8(2)	Se2	− 1 × Ta2	261.8(2)	Se3	− 2 × Ta4	269.3(1)
	− 2 × Ta3	260.4(1)		− 2 × Ta5	262.3(1)		− 2 × Ta6	269.4(1)
	− 1 × Se1	327.4(3)		− 1 × Ta3	264.8(2)		− 1 × Ta1, Mo	276.6(2)
				− 2 × Se1	338.1(2)			
Se4	− 1 × Ta4	263.0(2)				Si1	− 2 × Ta2	253.0(4)
	− 2 × Ta2	267.6(1)					− 2 × Ta6	256.3(3)
	− 2 × Ta5	268.1(1)					− 2 × Ta4	256.4(3)
	− 1 × Ta3	280.7(2)					− 1 × Ta1, Mo	272.0(5)
	− 2 × Se2	345.1(2)					− 1 × Ta3	275.0(4)
							− 1 × Ta5	277.4(5)

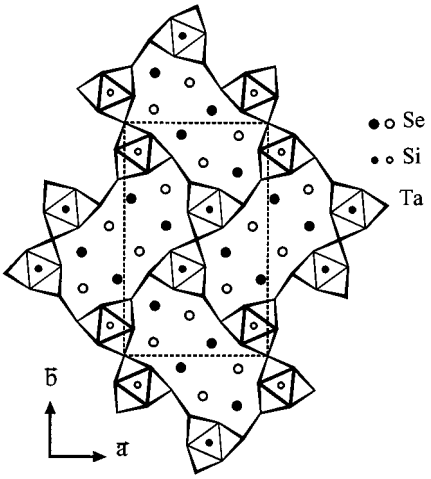


Figure 3. The structure of $Ta_{11}Si_2Se_8$ projected onto the *a,b* plane

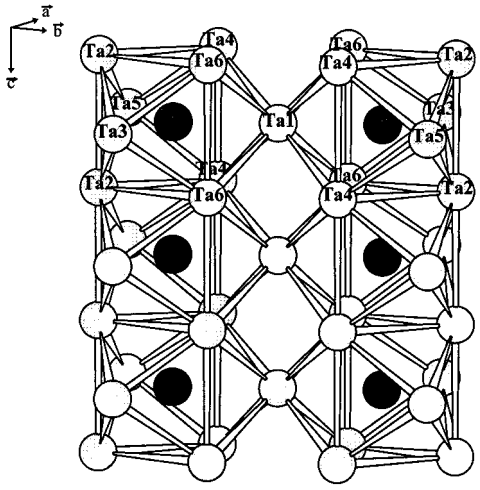


Figure 4. Part of a twin column of condensed Ta_9Si tetrakaidecahedra as present in the structure of $Mo_{0.11}Ta_{10.89(2)}Si_2Se_8$; the columns extend parallel to the short *c* axis

(iv) The states in the 6 eV wide energy window above the Fermi level (−9.8 eV) have mainly Ta d and very little Si p and Se p character. The relatively low electron concentration at the Fermi level may account for the moderate electrical conductivity of $Ta_{11}Si_2Se_8$.

Below the Fermi level the shown DOS of $Ta_{11}Ni_2Se_8$ and $Ta_{11}Si_2Se_8$ can be roughly divided into two blocks separated by a local DOS minimum at about −13.5 eV. Noticeable differences are associated with the position and influence of the states originating from the minor components, Ni and Si. Whereas the states with Ni d character are concentrated in the block at low energy, namely around −14 eV, the states with Si p character are mainly situated somewhat above the local DOS minimum at −13.5 eV in the upper block. Thus, the interactions of the low-lying Se p and Ni d with the Ta d levels give rise to a larger dispersion of the Ta d levels for $Ta_{11}Ni_2Se_8$ than for $Ta_{11}Si_2Se_8$. This difference in the dispersion is also reflected in the position of the Fermi level which resides in a local DOS minimum for the silicide but intersects a local maximum for $Ta_{11}Ni_2Se_8$.

COOP curves (crystal orbital overlap populations) of Ta−Ta, Ta−Se, and Ta−Si are shown in Figure 7. Obviously, the structure of $Ta_{11}Si_2Se_8$ affords an optimal adjustment of homonuclear Ta−Ta and heteronuclear Ta−Si interactions: these bonding states are completely populated; anti-bonding states are empty. Figure 8 illuminates the major structural distinctions of $Ta_{11}Si_2Se_8$ and $Ta_{11}Ni_2Se_8$.

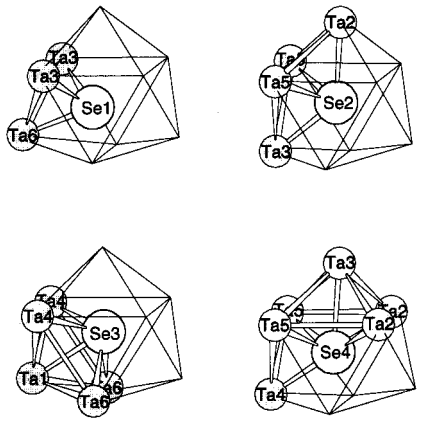


Figure 5. Single-sided Ta coordinations of the four inequivalent Se atoms schematically depicted as fragments of a fictitious Ta_9Se tetrakaidecahedron

Table 5. Parameters for the extended Hückel calculations

Element	Orbital	H_{ii} [eV]	ζ_1	ζ_2	c_1	c_2
Ta	6s	−8.88	2.28	–	–	–
	6p	−5.83	2.24	–	–	–
	5d	−10.39	4.76	1.94	0.6815	0.6815
Se[22a]	4s	−20.50	2.44	–	–	–
	4p	−14.40	2.07	–	–	–
Si[15b]	3s	−17.30	1.38	–	–	–
	3p	−9.20	1.38	–	–	–
Ni[22b]	4s	−9.17	1.83	–	–	–
	4p	−5.15	1.13	–	–	–
	3d	−13.49	5.75	2.00	0.5683	0.6292

Distinctions in Bonding for $Ta_{11}Si_2Se_8$ and $Ta_{11}Ni_2Se_8$

The isotypic compounds $Ta_{11}Si_2Se_8$ and, e.g., $Ta_{11}Ni_2Se_8$[17d] differ markedly in bonding, although the distances between the interstitial atoms Si and Ni and the nine Ta atoms of the cluster average 262.7 pm in each case. The *c* parameters, however, differ by 7 pm and the *a* and *b* parameter by about 10 pm. The Ta_9Si cluster is stretched along the pseudo-threefold axis and the capping atoms are closer to the centre (274.8 pm) than in the Ta_9Ni cluster (279.6 pm). A similar spectrum of Ta–Si distances for tetrakaidecahedrally coordinated Si is found in binary silicides like Ta_5Si_3 (Mn_5Si_3-type),[23] d_{Si-Ta}: 255.8–281.5 pm. As seen from Figure 8, a shortening of the Ta^c-Ta^{pr} distances in $Ta_{11}Si_2Se_8$ is associated with a shortening of the interprism contacts Ta4–Ta6 by 11.3 pm, and an extension of the intercluster Ta^c-Ta^c contacts by 6.3 pm. The changes in bond length, however, do not perfectly correlate with the changes of the respective MOP values. The distinctive "breathing modes" in the chains –(Ta2–Ta6–Ta1–Ta4–Ta2–Ta3–Ta5–)Ta2 of the two compounds can be traced back to a significant difference between the strength of the $Si-Ta^c$ (<0.27>) and $Ni-Ta^c$ (<0.13>) interactions: Evaluated according to the mean MOP values given in brackets, the bond strengths differ by a factor of two. There are obviously more valence electrons available for heteronuclear bonding in the Ta_9Si than in the Ta_9Ni cluster. Concomitantly, the average Ta–Se and Ta–Ta distances are both 1.1 pm longer for the silicide ($<d_{Ta-Se}>$ = 265.9 pm, $<d_{Ta-Ta}>$ = 316.7 pm) than for $Ta_{11}Ni_2Se_8$.

Substitution of Molybdenum for Tantalum

The major component of $Ta_{11}Si_2Se_8$ can be partly replaced by molybdenum. The partial substitution occurs at the Ta1 position where metal atoms are coordinated similarly to those in *bcc* tantalum itself. This position represents, so to speak, the most reduced centre of the Ta partial structure. It is partly occupied by about 10% molybdenum. The difference between the affinities Mo–Se and Ta–Se, which – according to our observations – is lower in the case of Mo–Se, may serve as a rationale for the enrichment of the minority component Mo at this particular position of the intermetallic framework. At this position, metal atoms have only two Se neighbours; the other crystallographically inequivalent Ta atoms are bound to three or four Se atoms, see Table 4.

Conclusion

(i) Air-sensitive $Ta_{11}Si_2Se_8$ is accessible by application of high-temperature synthesis techniques. Fibrous crystals can be grown by a chemical transport reaction.

(ii) The crystal structure is isotypic with those of

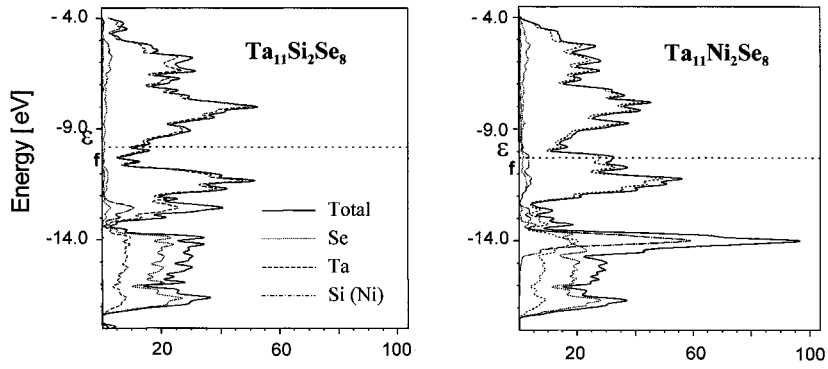


Figure 6. Total DOS and DOS projections of the constituents of (a) $Ta_{11}Si_2Se_8$ and (b) $Ta_{11}Ni_2Se_8$ in the energy window −4 to −18 eV

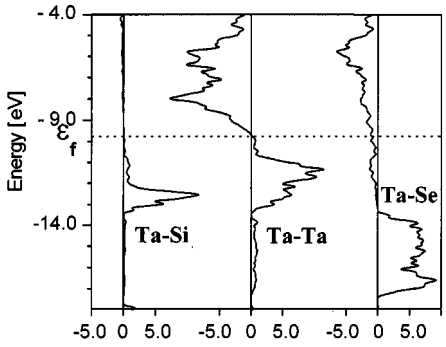


Figure 7. COOP curves of Ta−Ta, Ta−Se, and Ta−Si for $Ta_{11}Si_2Se_8$

$Ta_{11}M_2Se_8$ (M = Fe, Co, Ni). It consists of an open network of condensed tetrakaidecahedral Ta_9Si clusters. The Se atoms have a single-sided Ta coordination; they cover the internal surface of the porous $Ta_{11}Si_2$ partial structure.

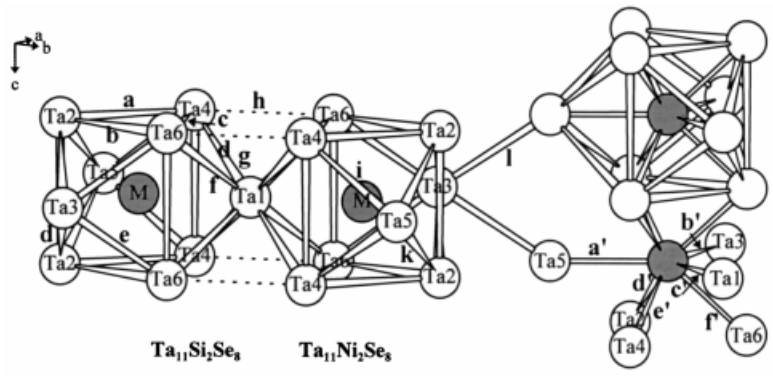
(iii) One out of six crystallographically inequivalent Ta atoms, namely Ta1 with the highest valence electron concentration for Ta−Ta bonding, can be partly replaced by molybdenum. The Mo-doped phase is a moderate metallic conductor.

(iv) Semi-empirical band structure calculations reveal striking differences in bonding for the two isotypic phases $Ta_{11}E_2Se_8$ (E = Si, Ni). The heteronuclear bonding interactions between the encapsulated atom and the Ta atoms of the Ta_9E cluster are substantially stronger for the silicide than for the Ni phase. The maximum of the projected DOS of Si is about 1.5 eV above the projected DOS of Ni. As a consequence, only the projected DOS of Si is − at least to a very large extent − energetically separated from the projected DOS of Se through a local minimum in the DOS at about −13.5 eV.

Experimental Section

Synthesis: $Ta_{11}Si_2Se_8$ was prepared in form of a grey, microcrystalline powder from a pre-reacted mixture of the elements in a sealed tantalum tube at 1570 K within 2 d. The pre-reacted mixtures were produced from the elements (Ta: Starck, 99.8%; Si: Heliotronic, 99.99%; Se: Chempur, 99.999%; total: 500−600 mg) in previously outgassed, evacuated quartz glass ampoules at 1170 K within 1 d. Up to 3 mm long and 20 μm thick, silver-shiny, needle-shaped crystals of Mo-doped $Mo_xTa_{11-x}Si_2Se_8$ were produced by a chemical vapour transport reaction in a welded molybdenum crucible starting from a compacted, stoichiometric mixture of $TaSe_2$, Ta, and Si (600 mg) and TeI_4 (8 mg) as a transport agent. The crucible was quickly heated up in an induction furnace, kept at 1870 K for 1 h and cooled down to 1450 K within 8 h. The furnace was then switched off. $TaSe_2$ and TeI_4 were prepared from stoichiometric mixtures of the elements in previously outgassed, evacuated quartz glass ampoules at 1270 K, 3 d ($TaSe_2$) and at 670 K, 3 d (TeI_4, I_2: Merck, 99.99%), respectively.

Phase Analyses: The phases of starting material and product were identified by powder X-ray diffraction measurements employing the Guinier technique (Guinier System 600, Huber; Cu-$K\alpha_1$ radiation). Silicon (a = 543.09 pm) was used as an internal standard. Powder diffractograms (PW1050/25, Philips; Ni-filtered Cu-K_α radiation) were recorded in the range 5° < 2θ < 95°; scan width: 0.03°; scan time per step: 90 s. Rietveld refinements were performed with the program LHPM.[24] The atomic positions as determined by the crystal structure refinement were used as starting parameters. Selected samples were analysed by energy-dispersive X-ray spectrometry (EDX, CS 4DV, CamScan; detector: Noran Instruments). The composition of the Mo-doped crystals was determined to be $Mo_{0.35(9)}Ta_{11.3(5)}Si_{1.2(5)}Se_{8.0(1)}$ by merging five independent analyses. A similar low Si content was also found for the ternary



	$Ta_{11}Si_2Se_8$	$Ta_{11}Ni_2Se_8$
a	331.6(0.16)	329.3(0.19)
b	324.5(0.18)	322.3(0.22)
c	316.9(0.21)	320.4(0.20)
d	291.9(0.36)	296.7(0.34)
e	307.5(0.22)	306.7(0.24)
f	288.5(0.32)	291.8(0.33)
g	290.1(0.31)	291.2(0.34)
h	338.1(0.07)	349.4(0.04)
i	305.4(0.27)	304.1(0.30)
k	308.4(0.24)	306.3(0.27)
l	318.4(0.17)	312.1(0.19)

	$Ta_{11}Si_2Se_8$	$Ta_{11}Ni_2Se_8$
a'	277.4(0.29)	281.9(0.13)
b'	275.0(0.28)	282.0(0.13)
c'	272.0(0.25)	275.0(0.12)
d'	253.0(0.37)	248.8(0.26)
e'	256.4(0.35)	255.3(0.24)
f'	256.3(0.35)	252.7(0.25)

Figure 8. Distinct structural features of $Ta_{11}Si_2Se_8$ and $Ta_{11}Ni_2Se_8$ reflected by selected distances and MOP values

phase probably due to the superposition of the Ta-*M* and the Si-*K* emission line.

Electrical Resistivity Measurements: Four-probe dc electrical resistivities of two needle-shaped crystals ($5 \times 10 \times 1000$ μm and $10 \times 20 \times 750$ μm) were measured as a function of temperature in the range 10–325 K. The four copper leads were attached along the needle axis with silver epoxy glue. Details concerning the measurements and the equipment are given elsewhere.[13c]

Crystal Structure Determination: Weissenberg and Buerger precession photographs of a crystal mounted along the needle axis yielded an orthorhombic unit cell. The lattice parameters, intensity modulations and the extinctions pointed unambigously to a phase that is isotypic with $Ta_{11}Ni_2Se_8$, space group symmetry *Pnnm*. Intensity data of two crystals ($0.02 \times 0.02 \times 0.31$ mm and $0.01 \times 0.01 \times 0.16$ mm) were collected employing an imaging plate diffraction system IPDS (Stoe) using Mo-K_α radiation and a graphite monochromator. Direct methods (SHELXS-96[25]) led to the anticipated structure. Application of a semi-empirical absorption correction based on symmetrically equivalent reflections (XPREP, SHELXTL[25]) improved the residual value R_{int} from 0.1047 to 0.0761 for the intensities in the case of the larger crystal. The calculations of the two data sets converged at $wR2 = 0.0631$ and 0.0691. The isotropic displacement parameter of one metal position, namely Ta1 situated in the centre of a Ta_9 cuboid was strikingly large. Nonrestricted refinements of the displacement parameter and a mixed occupation by Ta and Mo yielded in qualitative agreement with EDX analyses 89% (86%) Ta and 11% (14%) Mo and unobstrusive *U* values. Further information concerning the structure determination of the larger crystal is given in Table 2. Structural parameters are listed in Tables 3 and 4.

Acknowledgments

This research was generously supported by the Deutsche Forschungsgemeinschaft, the Fonds der Chemischen Industrie and by H. C. Starck. We thank Dr. Holger Kleinke for aid with the use of the extended Hückel program.

[1] [1a] H. F. Franzen, J. G. Smeggil, *Acta Crystallogr.* **1969**, *B25*, 1736–1741. – [1b] H. F. Franzen, J. G. Smeggil, *Acta Crystallogr.* **1970**, *B26*, 125–129.
[2] B. Harbrecht, *J. Less-Common. Met.* **1988**, *138*, 225–234.
[3] [3a] H. Wada, M. Onoda, *Mater. Res. Bull.* **1989**, *24*, 191–196. – [3b] S. J. Kim, K. S. Nanjundaswamy, T. Hughbanks, *Inorg. Chem.* **1991**, *30*, 159–164.
[4] B. Harbrecht, H. F. Franzen, *Z. Anorg. Allg. Chem.* **1987**, *551*, 74–84.
[5] B. Harbrecht, V. Wagner, C. Pietzonka, *J. Solid State Chem.* **1998**, *139*, 45–51.
[6] [6a] . Harbrecht, V. Wagner, *Z. Anorg. Allg. Chem.* **1994**, *620*, 969–976. – [6b] V. Wagner, Dissertation, University of Dortmund, **1994**.
[7] [7a] M. Conrad, B. Harbrecht, *IVth Eur. Conf. Solid State Chem.*, Dresden **1992**, p. 324. – [7b] M. Conrad, Dissertation, University of Dortmund, **1997**.
[8] T. Degen, B. Harbrecht, *Acta Crystallogr.* **1995**, *C51*, 2218–2220.
[9] M. Conrad, B. Harbrecht, *Z. Anorg. Allg. Chem.* **1997**, *623*, 742–748.
[10] B. Harbrecht, S. Debus, in preparation.
[11] T. Degen, B. Harbrecht, *Angew. Chem.* **1995**, *107*, 2888–2890; *Angew. Chem. Int.Ed. Engl.* **1995**, *34*, 2703–2705.
[12] [12a] M. Conrad, F. Krumeich, B. Harbrecht, *Angew. Chem.* **1998**, *110*, 1554–1557; *Angew. Chem. Int. Ed.* **1998**, *37*, 1383–1386. – [12b] M. Conrad, B. Harbrecht, *Aperiodic '97* (Eds.: M. de Boissieu, R. Currat, J.-L. Verger-Gaugry), World Scientific, Singapore, in press. – [12c] F. Krumeich, M. Conrad, H.-U. Nissen, B. Harbrecht, *Phil. Mag. Lett.* **1998**, *78*, 357–367.
[13] [13a] B. Harbrecht, *Angew. Chem.* **1989**, *101*, 1696–1698; *Angew. Chem. Int. Ed.Engl.* **1989**, *28*, 1660–1662. – [13b] K. S. Nanjundaswamy, T. Hughbanks, *J. Solid State Chem.* **1992**, *98*, 278–290. – [13c] B. Harbrecht, T. Degen, M. Conrad, *J. Alloys Comp.* **1997**, *246*, 37–50. – [13d] X. Yao, G. J. Miller, H. F. Franzen, *J. Alloys Comp.* **1992**, *183*, 7–17. – [13e] X. Yao, H. F. Franzen, *J. Am. Chem. Soc.* **1991**, 1426–1427.
[14] [14a] X. Yao, H. F. Franzen, *J. Alloys Comp.* **1992**, *182*, 299–312. – [14b] T. Degen, B. Harbrecht, *Angew. Chem.* **1995**, *107*, 1226–1228; *Angew. Chem. Int. Ed. Engl.* **1995**, *34*, 1089–1091.
[15] [15a] M. E. Badding, F. J. DiSalvo, *Inorg. Chem.* **1990**, *29*, 3952–3954. – [15b] J. Li, R. Hoffmann, M. E. Badding, F. J. DiSalvo, *Inorg. Chem.* **1990**, *29*, 3943–3952. – [15c] K. Ahn, T. Hughbanks, D. D. Rathnayaka, D. G. Naugle, *Chem. Mater.* **1994**, *6*, 418–423. – [15d] M- E. Badding, R. L. Gitzendanner, R. P. Ziebarth, F. J. DiSalvo, *Mater. Res. Bull.* **1994**, *29*, 327–336. – [15e] J. Neuhausen, E. W. Finck, W. Tremel, *Chem. Ber.* **1995**, *128*, 569–573.
[16] J. M. Tarascon, F. J. DiSalvo, C. H. Chen, J. Carroll, M. Walsh, L. Rupp, *J. Solid State Chem.* **1985**, *58*, 290–300.
[17] [17a] B. Harbrecht, H. F. Franzen, *J. Less-Common Met.* **1986**, *113*, 349–360. – [17b] B. Harbrecht, *J. Less-Common Met.* **1986**, *124*, 125–134. – [17c] B. Harbrecht, *J. Less-Common Met.* **1988**, *141*, 59–71. – [17d] M. Conrad, B. Harbrecht, *J. Alloys Comp.* **1993**, *197*, 57–64. – [17e] M. Conrad, B. Harbrecht, *Z. Kristallogr.*, submitted.
[18] [18a] B. Harbrecht, *J. Less-Common Met.* **1986**, *115*, 177–189. – [18b] X. Yao, H. F. Franzen, *J. Less-Common Met.* **1990**, *161*, L37-L40.
[19] [19a] R. L. Abdon, T. Hughbanks, *Chem. Mater.* **1994**, *6*, 424–428. – [19b] R. L. Abdon, T. Hughbanks, *J. Am. Chem. Soc.* **1995**, *117*, 10035–10040. – [19c] C. Wang, T. Hughbanks, *Inorg. Chem.* **1996**, *35*, 6987–6994.
[20] A. Mrotzek, Dissertation, Philipps University of Marburg, **1998**.
[21] [21a] R. Hoffmann, *J. Chem. Phys.* **1963**, *39*, 1397–1398. – [21b] M.-H. Whangbo, R. J. Hoffmann, *J. Am. Chem. Soc.* **1978**, *100*, 6093–6098.
[22] [22a] T. Hughbanks, R. Hoffmann, *J. Am. Chem. Soc.* **1983**, *105*, 1150–1162. – [22b] M. J. Calhorda, R. Hoffmann, *Inorg. Chem.* **1988**, *27*, 4679–4686.
[23] H. Nowotny, H. Schachner, R. Kieffer, F. Benesovsky, *Monatsh. Chem.* **1953**, *84*, 1–12.
[24] D. B. Wiles, R. A. Young, *J. Appl. Crystallogr.* **1981**, *14*, 149–151.
[25] [25a] G. M. Sheldrick, *SHELXS-96*, University of Göttingen, **1996**. – [25b] G. Sheldrick, *SHELXTL, SHELXTL-Plus*, Release 5.0 for R3 Crystallographic Research Systems, Siemens Analytical X-Ray Instruments Inc., Madison, WI, USA, **1991**. – [25c] G. M. Sheldrick, *SHELXL-96*, University of Göttingen,-Germany, **1996**.

Received July 20, 1998
[I98240]

Substituted Tungsten Fluorides

Anton Dimitrov,[a] Stefan Seidel,[a] and Konrad Seppelt*[a]

Dedicated to Professor Bernt Krebs on the occasion of his 60th birthday

Keywords: Tungsten / Fluorine / 2,2,2-Trifluoroethoxy / Bis(2,2,2-trifluoroethyl)amino / Aza-tungsta-cyclopropane

WF_6 reacts with $HOCH_2CF_3$ to form $F_5W–OCH_2CF_3$ and *cis*-$WF_4(OCH_2CF_3)_2$. CsF is added to $F_5WOCH_2CF_3$, yielding the heptacoordinated anion $[F_6WOCH_2CF_3]^-$, which has a capped octahedral structure with the oxygen ligand in an equatorial position. The first step of the reaction of WF_6 with $HN(CH_2CF_3)_2$ results in $F_5WN(CH_2CF_3)_2$. Excess $HN(CH_2CF_3)_2$ causes deprotonation, yielding the heptacoordinated $[F_5W(\eta^2CF_3–CHN–CH_2CF_3)]^-$ anion. This can be described as a tungstaazacyclopropane derivative or a π complex between F_5W^- and $CF_3–CHN–CH_2CF_3$. The only case in which MoF_6 reacts similarly is the formation of $F_5Mo–OCH_2CF_3$.

Of the 15 known hexafluorides (SF_6, SeF_6, TeF_6, MoF_6, WF_6, TcF_6, ReF_6, RuF_6, OsF_6, RhF_6, IrF_6, PtF_6, UF_6. NpF_6, PuF_6), only a few − TeF_6, WF_6, and to some extent also UF_6 − have been considered as starting material for other hexacoordinated molecular compounds prepared by means of nucleophilic substitution. There are many reasons for the failure of such simple reactions, in particular the inertness of SF_6 and SeF_6 towards nucleophilic attack, and the oxidation strengths of most other hexafluorides, which prevents a controlled nucleophilic substitution.

In the case of TeF_6, the step-by-step replacement by OR or NR_2 ligands is well known.[1−10] For UF_6 the only thoroughly investigated case[11] seems to be the replacement of the fluorine ligand by the $OTeF_5$ group. WF_6 can be transformed step by step into WF_5OR and finally to $W(OR)_6$, although the latter is usually made from WCl_6.[12−14] CF_3CH_2OH has been treated with WF_6 to give the whole series $Cl_xW(OCH_2CF_3)_{6-x}$.[15] $F_5W−NR_2$ has been prepared in a similar manner; this is the starting point of another series that ends with the known $W(NR_2)_6$.[16−18] The ligand $−N=C(CF_3)_2$ replaces five fluorine atoms of WF_6 in $FW[NC(CF_3)]_2$.[19]

In the present study, we have chosen systems with R = CH_2-CF_3, in order to obtain some stabilization by the CF_3 group, and to avoid the inertness of fully fluorinated groups such as -C_2F_5.

$F_5WO−CH_2CF_3$, *cis*-$F_4WOCH_2CF_3]_2$, and $[F_6WOCH_2CF_3]^-$

The reaction of WF_6 and CF_3CH_2OH proceeds smoothly in two steps to F_5W-OCH_2CF_3 and *cis*-$F_4W(OCH_2CF_3)_2$. The first compound is a liquid, and is structurally characterized by the ^{1}H-, ^{19}F-, and ^{13}C-NMR spectra. The ^{19}F-NMR AB_4-type spectra for the F_5W group is, of course, typical. The same method clearly indicates the *cis* position of the two alkoxy groups in $F_4W(OCH_2CF_3)_2$ by means of the ^{19}F-NMR A_2B_2-type spectra. The latter compound can also be obtained in crystalline form, and the single-crystal structure determination gives a full account of the molecular structure (see Figure 1 and Table 1).

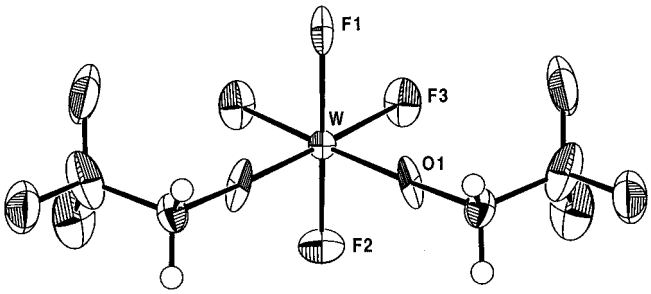


Figure 1. Structure of *cis*-$F_4W(OCH_2CF_3)_2$ in the crystal, ORTEP plot with 50% ellipsoids

Although the existence and structure of these two species is unsurprising, $F_5W−OCH_2CF_3$ is the starting material for a simple but theoretically interesting compound. It is easy to add CsF to obtain $Cs^+[WF_6OCH_2CF_3]^-$. This compound obviously has, according to a single-crystal structure determination, seven-coordinate tungsten atoms and one ligand that differs from the rest (see Figure 2 and Table 1).

WF_6 is known to add F^- to form WF_7^- and WF_8^{2-}; both anions are structurally fully characterized and turn out to be capped octahedral and square antiprismatic.[20−24] The latter structure seems to be the principle structure of the coordination number 8. For the coordination number 7 we know there are three different geometric orientations that have a very similar ligand repulsion, namely the capped octahedron, the capped trigonal prism, and the pentagonal bipyramid, listed in order of increasing ligand repulsion.[25] In the main-group series, the pentagonal bipyramid is always obtained, e.g. in IF_7 [26−29]; this is also the case for species with different ligands, such as IOF_6^-, $TeF_6OCH_3^-$

[a] Institut für Anorganische und Analytische Chemie der Freien Universität,
Fabeckstr. 34−36, D-14195 Berlin, Germany
Fax: (internat.) +49(0)30/838-3310
E-mail: seppelt@chemie.fu.berlin.de

 © WILEY-VCH Verlag GmbH, D-69451 Weinheim, 1999 1434−1948/99/0101−0095 $ 17.50+.50/0

Table 1. Selected bond lengths [pm] and angles [°]

cis-$F_4W(OCH_2CF_3)_2$	
W−F1	186(2)
W−F2	182(2)
W−F3	186(2)
W−O	181(1)
F1−W−F2	168.3(7)
F3−W−F3′	86.5(7)
etc.	
O−W−O′	93.2(9)
$Cs^+[WF_6OCH_2CF_3]^-\cdot CH_3CN$	
W−F1	189.9(7)
W−F2	192.0(6)
W−F3	190.0(7)
W−F4	191.4(7)
W−F5	186.7(8)
W−F6	188.4(7)
W−O	183.4(9)
F1−W−F2	135.4(3)
F1−W−F3	124.7(3)
F1−W−F4	136.1(3)
F1−W−F5	74.6(3)
F1−W−F6	73.0(3)
F1−W−O	79.1(4)
etc.	
FW−$N(CH_2CF_3)_2$ first modification, values for the second modification in brackets	
W−F1−5	181.9(4)−187.5(4) [182.9(7)−187.1(7)]
W−N	194.6(4) [197.1(8)]
W−N−C2	123.4(3) [122.8(5)]
W−N−C3	125.0(3) [123.7(6)]
C2−N−C3	111.6(4) [113.4(7)]
$[(CF_3CH_2)_2NH_2]^+[F_5W(\eta^2CF_3-CHN-CH_2CF_3)]^-$, first modification, values for the second modification in brackets	
W−F1−5	185.0(4)−197.9(4) [184.1(5)−196.2(5)]
W−N1	188.0(5) [187.0(8)]
W−C3	215.0(9) [212.8(9)]
N1−C3	142.6(10) [134.9(12)]
F−W−F	81.3(2)−95.2(2), 159.4(2), 166.4(2) [79.4(2)−93.3(2), 157.6(2), 169.8(3)]
N1−W−F5	161.8(2) [121.2(3)]
C3−W−F5	156.2(3) [160.4(3)]
N1−W−C3	40.8(3) [38.8(4)]
C3−N1-W	79.8(5) [81.0(5)]
N1−C3−W	59.4(4) [60.2(5)]

and $TeF_5(OCH_3)_2^-$.[30−33] The oxygen ligands always occupy axial positions in the pentagonal bipyramid. The pentagonal structures of XeF_5^- and $XeOF_5^-$ can be similarly explained.[34−36] Thus, in main-group compounds the overall structure (pentagonal bipyramid) is not the one with minimum interligand repulsion. However, the finer details such as the occupation of different sites by different ligands follow this ligand repulsion model. This finding calls for a theoretical explanation that is beyond the scope of this article.

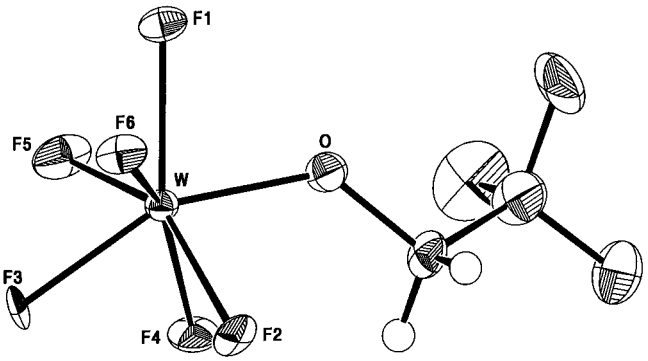


Figure 2. Structure of the $[F_6WOCH_2CF_3]^-$ anion in $Cs^+[F_6WOCH_2CF_3]^-$, ORTEP plot with 50% ellipsoid

The situation of the transition-metal compounds is also not straightforward. WF_7^- and MoF_7^- display the capped octahedral structure that the simple ligand-repulsion picture leads us to expect.[20] However, the structure of isoelectronic ReF_7 might best be described as pentagonal bipyramidal, although it is distorted into the direction of a capped octahedron.[37] ReF_7^-, with just one d electron more than WF_7^- and ReF_7, has a regular pentagonal bipyramidal structure,[38] as has $ReOF_6^-$[38], surprising results that also require a theoretical explanation beyond the interligand-repulsion model.

The reaction of $F_5W-OCH_2CF_3$ with CsF allows a test on a seven-coordinate structure, in which one ligand differs from the other six. It should be kept in mind that the analogous reaction between F_5W-OCH_3 and F^- yields only WF_5O^- and CH_3F[39] The structure of the anion $[F_6WOCH_2CF_3]^-$ is shown in Figure 2. If viewed from the direction of W−F1, the (pseudo) threefold symmetry of the anion becomes visible.

This symmetry clearly shows that the capped octahedral structure of WF_7^- is retained in $[WF_6OCH_2CF_3]^-$. A capped octahedron has three different positional sites: the capping position, three equatorial positions, and three basal positions. The $-OCH_2CF_3$ ligand occupies an equatorial position, which is obviously the site towards which the larger ligands are directed, since the W−F bond lengths of the equatorial bonds in WF_7^- are shorter than those of the basal and capping fluorine atoms.

The difference in W−F bond lengths are nearly the same as those in WF_7^-, allowing for certain small deviations induced by the one different ligand. This is also the case for the bond angles within the anion (see Table 1).

It should be kept in mind that these structures are fluxional in solution. As in WF_7^-, the different fluorine atoms in $[F_6WOCH_2CF_3]^-$ show only one signal without $^{183}W-^{19}F$ coupling, indicating rapid intermolecular fluorine exchange.

In order to check the above described structural model, we attempted to treat *cis*-$F_4W(OCH_2CF_3)_2$ with CsF. Unfortunately, however, the resulting product could not be obtained in single-crystal form.

$F_5W-N(CH_2CF_3)_2$ and $[F_5W(\eta^2CF_3-CHN-CH_2CF_3)]^-$

Like with $F_5W-N(CH_2CH_3)_2$[16], the compound $F_5W-N(CH_2CF_3)_2$ can readily be obtained from WF_6 and $HN(CH_2CF_3)_2$. It is a crystalline solid and stable at room temperature. Crystal structure investigations resulted in two different crystallizations from pentane or isopentane, a red needle-shaped modification at low temperature, and a brown one at room temperature. However, the two modifications of the $WF_5-N(CH_2CF_3)_2$ molecules are very similar (see Figure 3 and Table 1). In both cases, the nitrogen environment is completely planar, while $N(CH_2CF_3)_3$ has a pyramidally surrounded nitrogen atom. In contrast to the (alkoxy)tungsten fluorides, the different fluorine atoms on the tungsten atom are not resolved in $F_5W-N(CH_2CF_3)_2$ in the temperature range of −90 to +25°C and in different solvents.

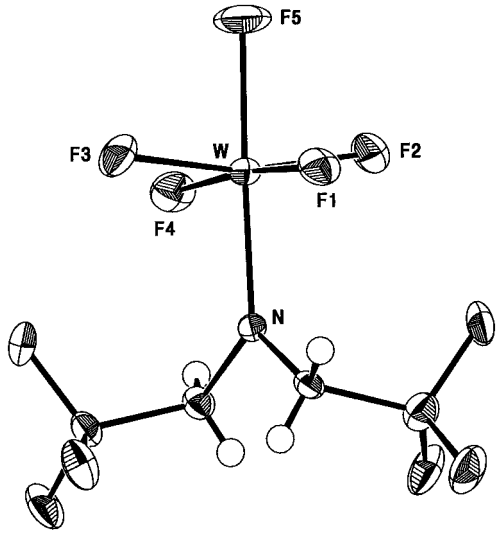


Figure 3. Structure of $F_5W-N(CH_2CF_3)_2$ in the crystal modification (1); ORTEP plot with 50% ellipsoids; overall structure and atomic numbering of modification (2) is the same

Attempts to treat $F_5W-N(CH_2CF_3)_2$ with a second equivalent of $HN(CH_2CF_3)_2$, and the reaction of WF_6 with two equivalents $HN(CH_2CF_3)_2$, do not yield the expected *cis*-$F_4W[N(CH_2CF_3)_2]_2$. Instead we obtained a red-brown compound in the form of needles or platelets; these contain an anion formed by deprotonation according to the single-crystal structure determinations, done as before on two modifications. The structure is in agreement with the complete set of ^1H-, ^{19}F-, and ^{13}C-NMR data. One remarkable feature is its tetragonal pyramidal WF_5 group, attached to a CN linkage, which forms a three-membered WNC ring (Figure 4 and Table 1). Thus, it also has a seven-coordinate tungsten atom. The counterion is $[H_2N(CH_2CF_3)_2]^+$. The anion could also be regarded as a π complex between WF_5^- and $CF_3-CHN-CH_2-CF_3$. In addition to its peculiar structure the spontaneous formation of a W−C bond with help of the weak base $HN(CH_2CF_3)_2$ is another remarkable finding.

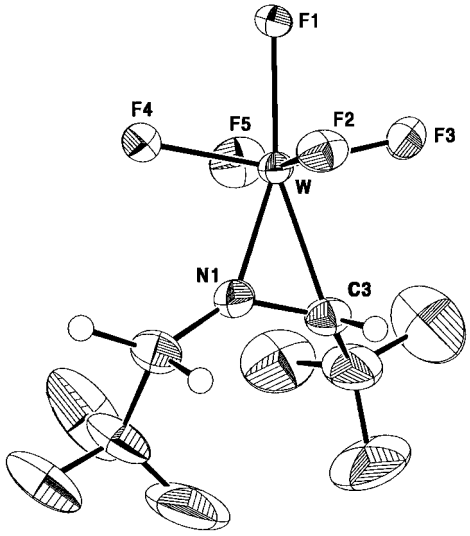


Figure 4. Structure of the anion of $[(CF_3CH_2)_2NH_2]^+[F_5W\eta_2-(CF_3-CHN-CH_2CF_3]^-$, ORTEP plot with 50% ellipsoids; overall structure and atomic numbering of modification (2) is the same

The existence of highly oxidized organometallic compounds with certain heavy transition-metal elements as central atoms, especially from Re {$(CH_3)ReO_3$, Cp^*ReO_3 [Cp* = cyclo-$(CH_3)_5C_5$]} is, of course, well known.[40] In the tungsten series recently the compounds Cp^*WF_4 and Cp^*WF_5 have been reported[41]; these may most closely resemble the tungstaazacyclopropane compound presented in this paper.

Experimental Section

General: All materials were handled in a drybox or in glass or metal vacuum systems in order to avoid hydrolysis. Reaction vessels made of FEP tubing (Perfluoro ether/propene copolymer) were often used. WF_6 and CsF were purchased from Aldrich Co.; MoF_6 and CF_3CH_2OH were purchased from Merck GmbH. $HN(CH_2CF_3)_2$ was prepared from $H_2N-CH_2CF_3$ and $C_4F_9-SO_2-O-CH_2CF_3$. Solvents were carefully dried and degassed before use.

Physical Measurements: The IR spectra were recorded with a Perkin Elmer 883 instrument, the Raman spectra with a Type 1403 of Spex Industries, 1064 nm, 300 mW; and the NMR spectra with a JEOL JNM-LA 400 instrument for ^1H, ^{19}F, and ^{13}C. Chemical shifts are given for $CFCl_3$ and tetramethylsilane as standards. Dryboxes for the use of water-sensitive compounds were obtained from Brown GmbH, Munich, Germany. Elemental analyses were performed by the Beller Co., Göttingen, Germany.

X-ray Crystallographic Procedures: When necessary, suitable single crystals were obtained as described in the experimental procedures. A suitable single crystal was cut, then mounted on an Enraf-Nonius CAD 4 four-cycle diffractometer with help of a special device (a simplified version of the one previously described).[41] Mo-K_α radiation with a graphite monochromator was used. Lattice constants were obtained by fine adjustment of 25 reflections with θ values between 20 and 25°. X-ray intensities were measured with the ω-scan method, with maximal 60 s/reflection, allowing 25% of this time for background measurements. A Lorentz polarization

and ψ absorption corrections were applied. The structures were solved and refined with the SHELX procedures.[42] All atoms were refined anisotropically, and hydrogen atoms were refined isotropically with a single vibrational parameter for all hydrogen atoms. Most hydrogen atoms could be located in difference Fourier analyses, missing hydrogen atoms were refined using a riding model. Table 2 lists further crystallographic details, while Table 1 lists selected bond lengths and angles. Crystallographic data (excluding structure factors) for the structures reported in this paper have been deposited with the Cambridge Crystallographic Data Centre as supplementary publication no. CCDC-102175. Copies of the data can be obtained free of charge on application to CCDC, 12 Union Road, Cambridge CB2 1EZ, UK [Fax: int. code + 44(1223)336-033; E-mail: deposit@ccdc.cam.ac.uk].

$F_5W-OCH_2CF_3$: 1.44 g (14.5 mmol) of CF_3CH_2OH and 5.34 g (17.9 mmol) of WF_6 are condensed at −196°C with the help of a metal vacuum line into an FEP tube equipped with a metal valve. The mixture is warmed to room temperature, and a slightly pink solution is formed. HF and excess WF_6 are removed by pumping all volatile material through an NaOH/CaO containing FEP tube, and pure $F_5W-OCH_2CF_5$ is trapped in a −40°C cold FEP trap. The result is 4.2 g (76% yield) of $F_5W-OCH_2CF_3$ as a colorless liquid. − IR (liquid): $\tilde{\nu}$ = 3024 w, 2967 w (C-H), 1438 m, 1395 s, 1285 vs, 1173 vs, 1113 s, 1043 s, 995 m, 951 s, 912 w, 846 w, 840 s, 712 s, 633 vs, 531 w, 486 w, 434 w cm^{-1}. − Raman (liquid): $\tilde{\nu}$ = 3020 (8), 2969 (12), 1438 (9), 1395 (5), 1279 (12), 1143 (35), 1043 (1), 951 (6), 841 (40), 771 (5), 734 (100), 638 (10), 618 (35), 529 (30), 364 (30), 306 (60), 247 (5), 185 (4), 122 (20) cm^{-1}. − ^1H NMR (400 MHz, CD_3CN): δ = 6.29 (q, $^3J_{FH}$ = 8 Hz). − ^{13}C NMR (100.4 MHz, CD_3CN): δ = 123.82 (q, $^1J_{CF}$ = 279 Hz). 80.40 (q, $^2J_{CF}$ = 39 Hz). − ^{19}F NMR: (376.0 MHz, CD_3CN): δ = 128.36 (d, $^2J_{FF}$ = 65 Hz), 102.69 (qt, $^2J_{FF}$ = 63 Hz), −72.15 (t, $^3J_{HF}$ = 8 Hz). − MS (70 eV, EI), for ^{186}W); *m/z* (%): 361 (35) [M^+ − F], 341 (20) [M^+ − H − 2 F], 311 (40) [$F_5W-OCH_2^+$], 281 (100) [F_5W^+], and smaller fragments. − $C_2H_2F_8OW$ (377.9): calcd. C 6.36, H 0.71, F 39.3; found C 7.01, H 0.71, F 40.2.

$F_5Mo-OCH_2CF_3$: 210 mg (2.1 mmol) of CF_3CH_2OH and 530 mg (2.5 mmol) of MoF_6 are treated and purified as described above. Obtained is a yellow liquid. − ^{19}F NMR: δ = 239.10 (d, $^2J_{FF}$ = 82 Hz). 223.99 (qt, $^2J_{FF}$ = 86 Hz), -69.96 (t, $^3J_{HF}$ = 8 Hz).

***cis*-$F_4W(OCH_2CF_3)_2$:** 378 mg (1.0 mmol) $F_5W-OCH_2CF_3$ is weighed into an FEP tube, equipped with a metal valve. With help of a glass vacuum line 250 mg (2.5 mmol) CF_3CH_2OH is condensed on it at −196°C. Warming to room temperature gives a light brown solution. Volatile HF is pumped off at room temperature. Obtained is 320 mg of *cis*-$F_4W(OCH_2CF_3)_2$ as a colorless liquid at room temperature, mp −5°C. − IR (liquid, KBr, νCH): $\tilde{\nu}$ = 1441 s, 1397 s, 1373 m, 1284 vs, 1167 vs, 1105 vs, 1050 m, 952 vs, 839 s, 3024 w, 2967 w, 712 s, 681 vs, 632 vs, 533 m cm^{-1}. − Raman (liquid): $\tilde{\nu}$ = 3010 (12), 2962 (30), 2869 (4), 2777 (4), 1440 (25), 1398 (12), 1280 (20), 1156 (50), 1031 (2), 962 (10), 839 (100), 732 (75), 667 (55), 649 (10), 619 (50), 531 (65), 360 (55), 307 (80), 250 (20), 183 (15) cm^{-1}. − ^1H NMR (CD_3CN): δ = 5.94 (q, $^3J_{HF}$ = 8 Hz). − ^{19}F NMR (CD_3CN): δ = 91.37 (t, $^2J_{FF}$ = 66 Hz), 76,68 (t, $^2J_{FF}$ = 66 Hz), −73.19 (t, $^3J_{HF}$ = 9 Hz). − MS (70 eV, EI for ^{186}W); *m/z* (%): 441 (15) [M^+ − F], 421 (8) [M^+ − H − 2 F], 391 (55) [M^+ − CF_3], 361 (100) [$F_4W - OCH_2CF_3^+$], and smaller fragments.

$C_4H_4F_{10}O_2W$ (457.9): calcd. C 10.49, H 0.88, F 41.49, W 40.1; found C 10.51, H 0.95, F 41.00, W 39.3. Single crystals are obtained by recrystallization at −30°C without solvent.

$Cs^+[F_6WOCH_2CF_3]^-$: In a dry-box 152 mg (1 mmol) of CsF and 275 mg (0.7 mmol) of $F_5W-OCH_2CF_3$ are weighed into an FEP tube. The tube is sealed and heated for 24 h to 60°C. The liquid phase disappears, and a light brown solid is formed. Recrystallisation from CH_3CN at -30°C affords $Cs^+F_6W(OCH_2CF_3)^-$ as colorless crystals. Under the microscope these appear as thin platelets. − IR (Nujol): $\tilde{\nu}$ = 1282 s, 1168 s, 1084 m, 1035 m, 983 s, 946 m, 916 w, 888 w, 830 w, 683 m, 598 vs, 502 s, 435 w cm^{-1}. − Raman (solid): $\tilde{\nu}$ = 1296 (10), 1112 (20), 983 (100, br), 841 (30), 733 (80), 711 (75), 663 (100) cm^{-1}. − ^1H NMR (CD_3CN): δ = 5.56 (q, $^3J_{HF}$ = 9 Hz). − ^{13}C NMR (CD_3CN): δ = 126.44 (q, $^1J_{CF}$ = 278 Hz), 73.91 (q, $^2J_{CF}$ = 36 Hz). − ^{19}F NMR (CD_3 CN): δ = 106.40 (s), −73.71 (t, J_{HF} = 8 Hz).

Table 2. Crystal data and structure refinements

	cis-$F_4W(OCH_2CF_3)_2$	$Cs^+[F_6WOCH_2CF_3]^-$	$F_5W-N(CH_2CF_3)_2$ (1)	$F_5W-N(CH_2CF_3)_2$ (2)	$[(CF_3CH_2)NH_2]^+$ $[F_5W\eta^2(CF_3-CHN-CH_2CF_3)]^-$ (1)	$[(CF_3CH_2)NH_2]^+$ $[F_5W\eta^2(CF_3-CHN-CH_2CF_3)]^-$ (2)
formula weight [g mol^{-1}]	457.92	570.85	458.93	458.93	640.15	640.15
temperature [°C]	−143	−143	−143	−143	−143	−143
space group	*Pbnm*	$P\bar{1}$	$P2_1/n$	$P2_12_12_1$	$P4/n$	$P2_1/c$
a [pm]	494.4(1)	530.6(1)	804.4(1)	546.4(1)	1822.5(1)	1007.5(4)
b [pm]	961.6(1)	727.1(1)	910.6(2)	1292.5(1)	1822.5(1)	1347.4(4)
c [pm]	2100.0(2)	1518.7(2)	1367.5(2)	1346.7(2)	1033.8(1)	1227.6(4)
α [°]	90	93.69(1)	90	90	90	90
β [°]	90	94.95(1)	95.13(1)	90	90	91.69(3)
γ [°]	90	94.46(1)	90	90	90	90
V [$10^6 pm^3$]	998.4(2)	580.5(1)	997.7(2)	951.0(2)	3433.6(4)	1665.7(10)
Z	4	2	4	4	8	4
$\rho_{calcd.}$ [Mgm^{-3}]	3.046	3.266	3.055	3.205	2.476	2.552
μ [mm^{-1}]	11.71	13.14	11.72	12.29	6.89	7.11
Transmission, max/min	0.95/0.84	0.85/0.62	0.98	0.99/0.89	0.98/0.82	
reflections collected	660	3613	35.30	1627	2618	3053
unique	600	3293	3443	1622	2477	2874
θ_{max} [°]	25	30	35	30	25	25
parameters	82	141	171	149	281	276
R_1 [$I > 2\sigma(I)$]	0.053	0.068	0.038	0.044	0.031	0.039
wR_2 (all data)	0.113	0.206	0.107	0.109	0.073	0.103

F_5W-N(CH_2CF_3)$_2$: 970 mg (5.3 mmol) of HN(CH_2CF_3)$_2$ is weighed into an FEP tube equipped with a metal valve. 1.7 g (5.7 mol) of WF_6 is condensed into the tube with help of a glass vacuum line at −196°C. After warming to room temperature a yellow solution and a colorless solid is formed. Excess WF_6 is pumped off, and the solution turns red. Addition of 12 mL of isopentane, centrifugation and cooling to −40°C affords red, needle-shaped crystals, yield 1.2 g (49%). − Raman (solid): $\tilde{\nu}$ = 3052 (5), 3003 (11), 1377 (12), 1022 (60), 827 m, 720 (100), 689 (35), 292 (70) cm^{-1}. − ^{19}F NMR ($CDCl_3$, r.t.): δ = −66.8 (CF_3), 143 (br., F_5W).

$H_2N(CH_2CF_3)_2^+[F_5W\text{-}\eta^2(CF_3CH_2-NCH-CF_3)]^-$: 325 mg (1.8 mol) of HN(CH_2CF_3)$_2$ is weighed into a 10-mm (inner diameter) glass tube, equipped with a teflon valve. With help of a glass vacuum line 1 mL of $CHCl_3$ as solvent and 175 mg (0.6 mmol) of WF_6 are condensed into the glass tube at −196°C. The tube is sealed and warmed to room temperature. The solution turns yellow, then orange and red due to formation of $F_5W-N(CH_2CF_3)_2$, and colorless powder precipitates. After shaking for 8 h at room temperature the color changes to yellow orange. The entire reaction mixture is kept at room temperature for 2 weeks. Brown crystals of $H_2N(CH_2CF_3)_2^+[F_5W(\eta^2CF_3CH_2-NCH-CF_3)]^-$ are formed. − Raman (solid, only peaks with at least medium intensity): $\tilde{\nu}$ = 2997 (12), 2948 (8), 1432 (10), 1413 (7), 1044 (20), 978 (10), 934 (7), 874 (30), 834 (30), 679 (28), 665 (80), 635 (10), 618 (25), 502 (35), 460 (15), 378 (15), 363 (20), 329 (25), 293 (75), 281 (75), 255 (100), 119(40) cm^{-1}. − ^{1}H NMR (CD_3CN, r.t.): δ = 5.24 (m, J_{HF} = 9 HZ, 1 H, $-CH_ACF_3$), 5.64 (m, J_{HF} = 9 Hz, 1 H, CH_BCF_3, J_{HH} = 14.7 Hz), 3.55 (s, $-CHCF_3$), 8.5 (s, $-NH_2$), 4.00 (q, $-CH_2$). − ^{13}C NMR (CD_3CN): δ = 128.9 (q, $^1J_{CF}$ = 279.5 Hz, $^2J_{CH}$ = 7 Hz, $-CH_AH_BCF_3$), 128,6 (q, $^1J_{CF}$ = 275.8 Hz, $^2J_{CH}$ = 7 Hz, $-CHCF_3$), 58.7 (q, $^2J_{CF}$ = 33.9 Hz, $^1J_{CH}$ = 146 Hz, $-CH_AH_BCF_3$), 81.7 (q, $^2J_{CF}$ = 40,5 Hz, $-CHCF_3$), 50.1 (q, $^2J_{CF}$ = 36 Hz, $^1J_{CH}$ = 149 Hz, $-CH_2CF_3$, cation), 124.1 (q, $^1J_{CF}$ = 277.8 Hz, $^2J_{CH}$ = 7 Hz, $-CH\,CF_3$ cation). − ^{19}F NMR (CF_3CN): δ = 57.5 (d, J_{FF} = 80.6 Hz, $-WF_4$), 1,2 (qt, J_{FF} = 80.6 Hz, −WF), −68.3 (t, J_{FH} = 8 Hz, $-CH_AH_BCF_3$), −62.8 (s, $-CHCF_3$), −67.8 (t, J_{FH} = 9 Hz, $-CH_2CF_3$, cation).

Acknowledgments

We thank the Fonds der Chemischen Industrie for financial support of this work.

[1] G. W. Fraser, R. D. Peacock, P. M. Watleins; *J. Chem. Soc. A* **1971**, 1125−1128.
[2] G. W. Fraser, G. D. Meikle, *J. Chem. Soc., Chem. Commun.* **1974**, 624−625.
[3] A. Clouston, R. D. Peacock, G. W. Fraser, *J. Chem. Soc., Chem. Commun.* **1970**, 1197.
[4] F. Sladky, H. Kropshofer, *Inorg. Nucl. Chem. Lett.* **1972**, *8*, 195.
[5] I. Agranat, M. Rabinowitz, H. Selig, *Inorg. Nucl. Chem. Lett.* **1975**, *11*, 185.
[6] J. W. Fraser, G. D. Meikle, *J. Chem. Soc., Dalton Trans.* **1977**, 1985.
[7] A. Engelbrecht, F. Sladky, *Monatsh. Chem.* **1965**, *96*, 159.
[8] L. Kolditz, I. Fitz, *Z. Anorg. Allg. Chem.* **1967**, *349*, 175; U. Elgad, H. Selig, *Inorg. Chem.* **1975**, *14*, 140.
[9] K. Seppelt, *Inorg. Chem.* **1973**, *12*, 2537−2839.
[10] H. Hartl, P. Huppmann, D. Lentz, K. Seppelt, *Inorg. Chem.* **1983**, *22*, 2183.
[11] K. Seppelt, *Chem. Ber.* **1976**, *109*, 1046−1052.
[12] W. McFarlane, A. M. Noble, J. M. Winfield, *J. Chem. Soc. A* **1971**, 948−953.
[13] A. M. Noble; J. M. Winfield; *J. Chem. Soc. A* **1970**, 501−506.
[14] A. M. Noble, J. M. Winfield, *J. Chem. Soc. A* **1970**, 2574−2578.
[15] H. Plenio, E. Egert, M. Nieger, H. W. Roesky, H.-G. Schmidt, G. M. Sheldrick, *J. Fluorine Chem.* **1988**, *38*, 187−204
[16] A. Majid, R. R. McLean, D. W. A. Sharp, J. M. Winfield, *Z. Anorg. Allg. Chem.* **1971**, *385*, 85-91.
[17] A. Majid, D. W. A. Sharp, J. M. Winfield, I. Hanley, *J. Chem. Soc., Dalton Trans.* **1973**, 1876−1878.
[18] D. C. Bradley, M. H. Chisholm, C. E. Heath, M. B. Hursthouse, *Chem. Commun.* **1969**, 1261.
[19] H. W. Roesky, F. Schrumpf, F. Edelmann, *Z. Naturforsch.* **1987**, *42b*, 874−876.
[20] S. Giese, K. Seppelt, *Angew. Chem.* **1994**, *106*, 473−475, *Angew. Chem. Int. Ed. Engl.* **1994**, *33*, 461−463.
[21] S. Adam, A. Ellern, K. Seppelt, *Chem. Eur. J.* **1996**, *2*, 398−401.
[22] G. W. Fraser, G. D. Meikle, *J. Chem. Soc., Chem. Commun.* **1974**, 624−625.
[23] W. A. Sunder, A. L. Wayda, D. Distefano, W. E. Falconer, J. E. Griffiths, *J. Fluorine Chem.* **1979**, *14*, 299−325.
[24] A. Beuter, W. Kuhlmann, W. Sawodny, *J. Fluorine Chem.* **1975**, *6*, 367−378.
[25] D. L. Kepert, *Inorganic Stereochemistry in Inorganic Chemistry Concepts*, vol. 6, Springer, Berlin, **1982**.
[26] K. O. Christe, E. C. Curtis, D. A. Dixon, *J. Amer. Chem. Soc.* **1995**, *115*, 1520−1526.
[27] T. Vogt, A. N. Fitch, J. K. Cockroft, *J. Solid State Chem.* **1993**, *103*, 275−279.
[28] R. Marx, A. R. Mahjoub, K. Seppelt, R. M. Ibberson, *J. Chem. Phys.* **1994**, *101*, 585−593.
[29] X. Zhang, K. Seppelt, *Z. Anorg. Allg. Chem.* **1997**, 623, 491−500.
[30] A. R. Mahjoub, T. Drews, K. Seppelt, *Angew. Chem.* **1992**, *104*, 1047−1050; *Angew. Chem. Int. Ed. Engl.* **1992**, *31*, 1036−1039.
[31] K. O. Christe, J. C. P. Sanders, G. J. Schrobilgen, W. W. Wilson, *J. Chem. Soc., Chem. Commun.* **1991**, 837−840.
[32] A.−R. Mahjoub, K. Seppelt, *J. Chem. Soc., Chem. Commun.* **1991**, 840−841.
[33] K. O. Christe, D. A. Dixon, A.-R. Mahjoub, H. P. Mercier, J. C. P. Sanders, K. Seppelt, G. J. Schrobilgen, W. W. Wilson, *J. Amer. Chem. Soc.* **1993**, *115*, 2696−2706
[34] K. O. Christe, E. C. Curtis, D. A. Dixon, H. P. Mercier, J. C. P. Sanders, G. J. Schrobilgen, *J. Amer. Chem. Soc.* **1991**, *113*, 3351.
[35] K. O. Christe, D. A. Dixon, J. C. P. Sanders, G. J. Schrobilgen, S. S. Tsai, W. W. Wilson, *Inorg. Chem.* **1995**, *34*, 1868−1874.
[36] A. Ellern, K. Seppelt, *Angew. Chem.* **1995**, *107*, 1772−1773; *Angew. Chem. Int. Ed. Engl.* **1995**, *34*, 1586−1587.
[37] T. Vogt, A. N. Fitch, J. K. Cockcroft, *Science* **1994**, *263*, 1265−1267.
[38] S. Adam, Ph. D. Dissertation, Freie Universität Berlin, Germany, **1995**, p. 58.
[39] S. Adam, Ph. D. Dissertation, Freie Universität Berlin, Germany, **1995**, p. 104.
[40] W. A. Herrmann, *Angew. Chem.* **1988**, *101*, 1269−1286; *Angew. Chem. Int. Ed. Engl.* **1988**, *27*, 1297−1313.
[41] K. Köhler, A. Herzog, A. Steiner, H. W. Roesky, *Angew. Chem.* **1996**, *108*, 331−333; *Angew. Chem. Int. Ed. Engl.* **1996**, *35*, 295−297.
[42] K. O. Christe, W. W. Wildon, R. D. Wilson, R. Bau, J. Feng, *J. Amer. Chem. Soc.* **1990**, *112*, 7619−7625.
[43] H. Schumann, W. Genthe, E. Hahn, M. B. Hossein, D. v. d. Helm, *J. Organomet. Chem.* **1986**, *299*, 67−84
[44] G. M. Sheldrick, *Program for Crystal Structure Solution*, Göttingen, **1986**; G. M. Sheldrick, *Program for Crystal Structure Refinement*, Göttingen, **1997**.

Received July 22, 1998
[I98245]

Selective Formation of *cis*(X)- and *trans*(X)-Ru(dmbpy)$(CO)_2X_2$ Complexes (X = Cl, Br, I, SCN) from Monomeric and Dimeric Ru−mono(dmbpy) Carbonyl Complexes (Dmbpy = 4,4′-Dimethyl-2,2′-bipyridine)

Pertti Homanen,[a] Matti Haukka,[a] Saija Luukkanen,[a] Markku Ahlgrén,[a] and Tapani A. Pakkanen*[a]

Keywords: Ruthenium / Halogens / Carbonyl complexes / Structure elucidation

Aqueous hydrogen halides HX (X = Cl, Br, I) are shown to be excellent halogen sources for the synthesis of a series of halogen-containing ruthenium mono(2,2′-bipyridine) carbonyl complexes Ru(dmbpy)$(CO)_2X_2$ (dmbpy = 4,4′-dimethyl-2,2′-bipyridine), as well as effective reagents for the attack of the Ru–Ru bond in the dimer [Ru(dmbpy)-$(CO)_2Cl]_2$. Selective syntheses were established for both *cis*- and *trans*-halogen complexes in the case of Cl- and of Br-containing derivatives, but the only stable isomer containing iodine was *trans*(I)-Ru(dmbpy)$(CO)_2I_2$. The failure to obtain the *cis* isomer was probably due to sterical effects. Furthermore, a novel *S*-bound *trans*(SCN) analogue was synthesized and structurally characterized. In all experiments, the reaction conditions selected led to complete halogen exchange; no mixed halogen or pseudohalogen complexes were detected.

Introduction

Mononuclear ruthenium 2,2′-bipyridine complexes exhibit excellent catalytic properties in the water-gas shift reaction[1−4] and the reduction of carbon dioxide.[5−9] These catalyst-precursor complexes have been chemically modified through the use of different halogen and pseudohalogen ligands and substituted bipyridine reagents.[9−15] Most recently, the various isomeric forms of these compounds[9][16] were studied as a means of clarifying the structure of the actual catalyst, which is believed to be polymeric. Electropolymerization experiments[16] have indicated that only *trans*-halogen complexes are able to form such polymeric species, which underlines the need for isomerically pure complexes.

This paper reports isomerically selective syntheses for chemically altered monomeric ruthenium−mono(2,2′-bipyridine) complexes. On the basis of results obtained earlier,[15] we chose to use only dimethyl-substituted bpy ligands, as this was believed likely to introduce some interesting new features to complexes with direct Ru−Ru bonds. A structural study of a dimeric complex containing the 4,4′-dimethyl-2,2′-bipyridine ligand has shown that methylated bpy ligands can be used to lock the rotation of both the carbonyl and the polypyridine ligands around the ruthenium backbone in corresponding structures, which may allow structural characterization of an ordered polymeric species. In addition, the methyl groups can be converted to carboxy or trichlorosilylethyl groups to achieve chemical anchoring of Ru−bpy complexes into oxide supports.[14,17−19]

The various halogen-containing derivatives of Ru−bpy carbonyl complexes form a useful series of compounds for investigating the Ru−Ru chain-forming properties of the oligomeric complexes, since the Ru−Ru chain-forming step will also be affected by the chemical nature of the *trans* leaving group (i.e. Cl, Br, I, SCN). Furthermore, the thiocyanate ligand, as well as various halogens, have been widely used for tuning the photo- and electrochemical properties of transition metal complexes,[20][21] most recently in modern solar-cell designs.[17][18] By far, the photochemical behavior of mono(2,2′-bipyridine) complexes has remained a relatively unexplored field of ruthenium bipyridine chemistry, and the chemically altered halogen and pseudohalogen derivatives presented in this paper thus also offer an intriguing series of compounds for future photochemical investigations.

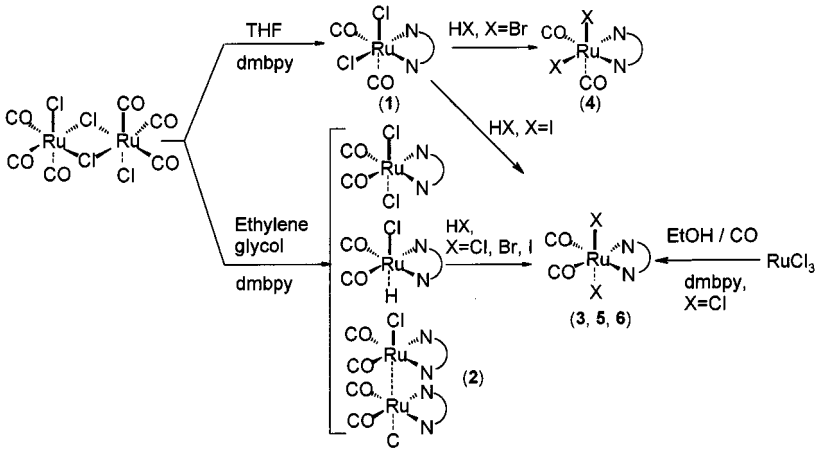
Results and Discussion

The formation of monomeric ruthenium bipyridine carbonyl complexes, such as Ru(bpy)$(CO)_2Cl_2$,[10] is complicated by the various orientations of the carbonyl and halogen ligands, which allows the coexistence of both *cis*- and *trans*-halogen isomers (third isomer with axial carbonyl groups is energetically far less favored). The choices of solvent and ruthenium reagent have been shown to determine the reaction route: synthesis with $RuCl_3$/CO/bpy[24][31] may give pure *trans*(Cl)-Ru(bpy)$(CO)_2Cl_2$, whereas syntheses based on acid-controlled $[Ru(CO)_2Cl_2]_n$/MeOH/bpy and $[Ru(CO)_3Cl_2]_2$/THF/bpy[9][10] yield both isomers. In the latter case, use of ethylene glycol instead of THF as solvent gives either hydride Ru(bpy)$(CO)_2$ClH or dimeric complex $[Ru(bpy)(CO)_2Cl]_2$. As was learned in our earlier studies,[15] methylation of the 2,2′-bipyridine ligand tends to shift the balance between *cis*- and *trans*-halogen products toward the *cis*-halogen species.

In this paper we describe the syntheses of halogen- and pseudohalogen-containing (Cl, Br, I, SCN) monomeric

[a] Department of Chemistry, University of Joensuu, P. O. Box 111, FIN-80101 Joensuu, Finland
Fax: (internat.) + 358-13/2513344

 © WILEY-VCH Verlag GmbH, D-69451 Weinheim, 1999 1434−1948/99/0101−0101 $ 17.50+.50/0



Scheme 1

Ru−dmbpy (dmbpy = 4,4′-dimethyl-2,2′-bipyridine) complexes with controlled *cis*-*trans* isomerism. *trans*-Halogen complexes are achieved by treating the *trans*-chloro complex (synthesis based on "ruthenium red carbonyl solution" as starting material) or dimer **2** with the corresponding hydrogen halide. The syntheses are summarized in Scheme 1.

Ligand-Exchange Reactions Cl → Br, I based on *cis*(Cl)-Ru(dmbpy)$(CO)_2Cl_2$ (1)

Ligand-substitution reactions with aqueous hydrogen halides have previously been studied for the monomeric parent complex *trans*(Cl)-Ru(bpy)$(CO)_2Cl_2$.[12] As in the present study, the reactions were limited to halide exchange, even though decarbonylated complexes such as $[Ru(bpy)Cl_4]^-$, $[Ru(bpy)Cl_3]^-$, and $[Ru(bpy)Cl_2]^{2-}$[12] are known. The reaction conditions selected led to complete halogen exchange, i.e. no mixed-halogen complexes were detected.

Heating of complex **1** in aqueous HBr resulted in the formation of greenish yellow precipitate. The product was analyzed by spectroscopic and X-ray diffraction measurements and identified as *cis*(Br)-Ru(dmbpy)$(CO)_2Br_2$ (**4**, Figure 1). The NMR spectra of complex **4** (in $CDCl_3$) support an unchanged *cis*-halogen arrangement, the main proof being the double CO, Me, and aromatic carbon resonances detected in the ^{1}H- and ^{13}C-NMR spectra.

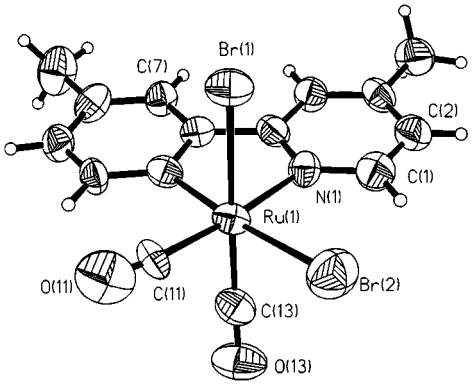


Figure 1. Structure of *cis*(Br)-Ru(dmbpy)$(CO)_2Br_2$ (**4**); the solvent molecule has been omitted for clarity

When aqueous HI was used as halogen source, the reaction changed markedly; despite several attempts, no traces of *cis*-halogen species were detected. Instead, the only product characterized (both spectroscopically and crystallographically) was *trans*(I)-Ru(dmbpy)$(CO)_2I_2$ (**6**, Figure 2). Usually, both *cis*- and *trans*-halogen forms of mono(bipyridine) complexes are highly stable, and rearrangements of coordination spheres invariably include ligand-substitution reactions. In this case, the larger size of the iodine ligand with respect to Cl and Br (ionic radii for Cl, Br, and I: 1.81, 1.95, and 2.16 Å, respectively) apparently prevents the *cis*-halogen arrangement, and strongly favors the *trans*(I) conformation.

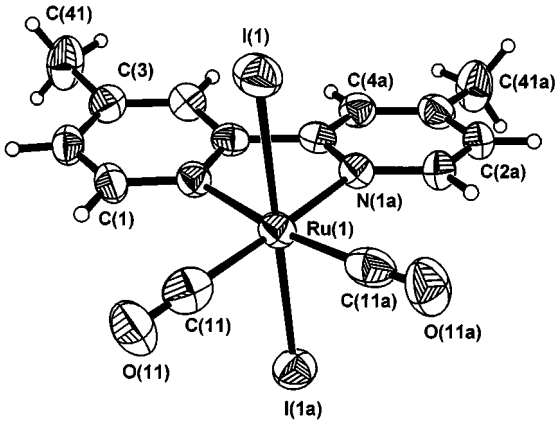


Figure 2. Structure of *trans*(I)-Ru(dmbpy)$(CO)_2I_2$ (**6**)

The structure of complex **4** does not exhibit any severe distortions compared with the chlorine-containing parent complex.[15] The bipyridine ring system is almost planar (angle between pyridine ring planes only 0.7°), although slightly bent away from the axial carbonyl group. The Ru−Br bond lengths of 2.565(1) (axial) and 2.502(2) Å (equatorial) are well within the range of bond lengths for related compounds reported earlier,[12] though, the axial halogen atom suffers slightly from the *trans* effect of the opposite carbonyl ligand. The bipyridine bite angle N(1)−Ru(1)−N(2) of 77.8(3)° is more or less typical for other Ru−bpy carbonyl complexes;[10−15] the slight distor-

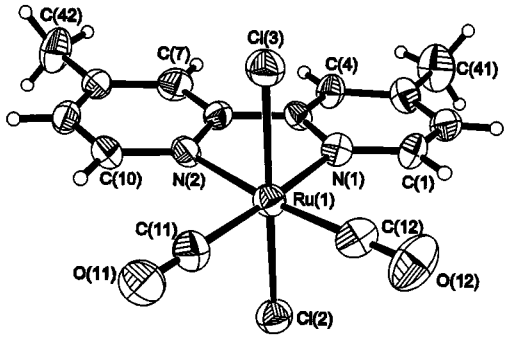


Figure 3. Structure of *trans*(Cl)-Ru(dmbpy)$(CO)_2Cl_2$ (**3**); the solvent molecule has been omitted for clarity

tion is due to the other carbonyl ligand positioned *trans* to N(1) [bond lengths Ru(1)−N(1) 2.126(8), Ru(1)−N(2) 2.076(8) Å].

Formation of Monomeric *trans*(X)-Ru(dmbpy)$(CO)_2X_2$ (X = Cl, Br, I, SCN) Complexes

Aqueous hydrogen halides proved to be excellent halogen sources in the above-described ligand-exchange reactions. In this study, we also investigated the attack of Cl^-, Br^-, and I^- on Ru−Ru bonds using dimeric [Ru(dmbpy)-$(CO)_2Cl]_2$ (**2**) as starting material. In all experiments, reactions led to breaking of the metal−metal bond and complete halogen exchange. Not surprisingly, all monomeric Ru−dmbpy compounds formed (complexes **3**, **5**, **6**) adopted *trans*-halogen configuration. This was also the case for complex **3** (Figure 3), which was synthesized by treating monomeric co-products[15] from the synthesis of complex **2**, and possibly some dimeric residues, with HCl (see Scheme 1). This experiment indicates that ethylene glycol, which was originally used to direct the complexation reaction between $[Ru(CO)_3Cl_2]_2$ and dmbpy toward dimeric species, also favors the formation of monomeric *trans*-chloride or *trans*-chloride−hydride complexes.

Since the axial positions of octahedral mono(bipyridine) complexes are sterically not hindered, they allow the *trans* coordination of relatively large ligands, such as I or *S*-bound bent SCN. Changing the halogen or pseudohalogen groups in these positions has little structural effect on the overall Ru−bpy arrangements (see Tables 2 and 3). Nevertheless, all attempts to crystallize complex **5** failed, and the identification of this complex was carried out instead by elemental analysis and interpretation of spectroscopic data. Once again, the most valuable proof came from ^{13}C-NMR data; single resonances for CO, Me, and aromatic carbon atoms supporting the *trans*-halogen arrangement were detected for all three complexes **5**, **6**, and **7**. Probably the main reason for the difficulty in obtaining single crystals from complex **5** was the tendency to form solvated crystalline species. As in the case of complex **3**, the solvent molecules eventually escape from the solid structure, destroying the crystals. Consequently, a decent X-ray diffraction analysis requires very fast data collection.

Table 1. Crystallographic data for *trans*(Cl)-Ru(dmbpy)$(CO)_2Cl_2 \cdot CH_2Cl_2$ (**3**), *cis*(Br)-Ru(dmbpy)$(CO)_2Br_2 \cdot CDCl_3$ (**4**), *trans*(I)-Ru(dmbpy)$(CO)_2I_2$ (**6**), and *trans*(SCN)-Ru(dmbpy)$(CO)_2(SCN)_2$ (**7**); dmbpy = 4,4′-dimethyl-2,2′-bipyridine

complex	**3**·CH_2Cl_2	**4**·$CDCl_3$	**6**	**7**
formula	$C_{14}H_{12}Cl_2N_2O_2Ru$	$C_{14}H_{12}Br_2N_2O_2Ru$	$C_{14}H_{12}I_2N_2O_2Ru$	$C_{16}H_{12}N_4O_2S_2Ru$
formula weight	412.24	501.14	595.13	457.49
crystal system	monoclinic	monoclinic	monoclinic	monoclinic
space group	$P2_1/c$	$P2_1/c$	$C2/c$	$P2_1/c$
a [Å]	6.516(1)	12.053(3)	6.835(1)	7.928(2)
b [Å]	22.034(4)	12.949(3)	19.009(4)	17.128(3)
c [Å]	13.263(3)	14.416(3)	13.650(3)	13.498(3)
β [°]	96.66(3)	113.14(2)	102.76(3)	93.87(3)
V [Å^3]	1891.4(6)	2069.0(8)	1729.7(6)	1828.7(7)
Z	4	4	4	4
$D_{calcd.}$ [g/cm^3]	1.746	1.992	2.285	1.662
crystal source	CH_2Cl_2	$CDCl_3/CH_2Cl_2$	CH_2Cl_2	H_2O
crystal size [mm]	0.05 × 0.1 × 0.1	0.2 × 0.3 × 0.4	0.1 × 0.2 × 0.4	0.05 × 0.1 × 0.2
color	yellow	yellow	reddish yellow	yellow
radiation	Mo-K_α	Mo-K_α	Mo-K_α	Mo-K_α
μ [mm^{-1}]	1.404	5.02	4.48	1.10
θ limits [°]	4−26	3−25	2−30	4−26
h range	0−8	0−15	−9 to 0	0−9
k range	0−27	0−16	0−26	0−21
l range	−16 to 16	−18 to 17	−18 to 19	−16 to 16
no. of unique rflns	3455	3518	2526	3616
no. of obsd data[a]	1761	1948	1483	2047
no. of params	218	229	96	227
$R1(F_o)$	0.0680	0.0546	0.0341	0.0282
$wR2(F_o^2)$[b]	0.1784	0.1554	0.0860	0.0555
x	0.0872	0.0838	0.0468	0.0104
y	0.00	0.00	0.00	0.00
goodness of fit	0.947	0.897	0.828	0.749

[a] $I \geq 2\ \sigma(I)$. − [b] $w = 1/[\sigma^2(F_o^2) + (xP)^2 + yP]$; $P = (F_o^2 + 2\ F_c^2)/3$.

Table 2. Selected bond lengths [Å] for *trans*(Cl)-Ru(dmbpy)$(CO)_2Cl_2 \cdot CH_2Cl_2$ (**3**), *cis*(Br)-Ru(dmbpy)$(CO)_2Br_2 \cdot CDCl_3$ (**4**), *trans*(I)-Ru(dmbpy)$(CO)_2I_2$ (**6**), and *trans*(SCN)-$[Ru(dmbpy)(CO)_2(SCN)_2]_2$ (**7**); dmbpy = 4,4′-dimethyl-2,2′-bipyridine

	3	**4**	**6**	**7**
Ru(1)−X(1)[a]	2.405(2)	2.565(1)	2.705(1)	2.429(1)
Ru(1)−X(2)[b]	2.390(2)	2.502(2)		2.432(1)
Ru(1)−N(1)	2.118(7)	2.126(8)	2.131(4)	2.102(2)
Ru(1)−N(2)	2.129(7)	2.076(8)		2.118(2)
Ru(1)−C(11)	1.879(10)	1.967(11)	1.911(6)	1.891(3)
Ru(1)−C(12)[c]	1.866(12)	1.849(13)		1.874(4)
C(11)−O(11)	1.117(11)	1.000(11)	1.062(6)	1.134(3)
C(12)−O(12)[c]	1.129(11)	1.154(13)		1.127(4)
C(3)−C(41)	1.514(12)	1.488(13)	1.517(7)	1.510(4)
C(8)−C(42)	1.484(13)	1.523(15)		1.508(4)
S(13)−C(13)				1.666(4)
C(13)−N(13)				1.145(4)
S(14)−C(14)				1.657(4)
C(14)−N(14)				1.153(4)

[a] X(1) = Cl(3) for **3,** S(13) for **7**. − [b] X(2) = Cl(2) for **3**, S(14) for **7**. − [c] C(12) = C(13), O(12) = O(13) for **4**.

Table 3. Selected bond angles [°] for *trans*(Cl)-Ru(dmbpy)$(CO)_2Cl_2 \cdot CH_2Cl_2$ (**3**), *cis*(Br)-Ru(dmbpy)$(CO)_2Br_2 \cdot CDCl_3$ (**4**), *trans*(I)-Ru(dmbpy)$(CO)_2I_2$ (**6**), and *trans*(SCN)-$[Ru(dmbpy)(CO)_2(SCN)_2]_2$ (**7**); dmbpy = 4,4′-dimethyl-2,2′-bipyridine

	3	**4**	**6**	**7**
X(1)−Ru(1)−C(12)[a,c]	92.3(3)	177.4(3)		90.7(1)
X(1)−Ru(1)−N(1)[a]	86.2(2)	86.1(2)		92.5(1)
X(1)−Ru(1)−N(2)	90.6(2)	86.9(2)	88.3(1)	87.7(1)
X(1)−Ru(1)−C(11)	91.3(3)	88.9(3)	91.2(2)	91.0(1)
X(1)−Ru(1)−X(2)	175.3(1)	91.4(1)	179.3(0)	174.6(0)
N(1)−Ru(1)−N(2)	76.7(3)	77.8(3)	76.9(2)	77.3(1)
N(1)−Ru(1)−X(2)[b]	89.7(2)	86.1(2)	88.3(1)	82.4(1)
N(2)−Ru(1)−C(11)	96.9(4)	100.1(4)	172.4(2)	97.4(1)
C(11)−Ru(1)−X(2)	92.6(3)	85.4(3)	88.4(2)	94.0(1)
N(1)−Ru(1)−C(11)	173.0(4)	174.6(4)	96.5(2)	173.1(1)
N(2)−Ru(1)−X(2)	86.2(2)	174.2(2)	88.3(1)	89.6(1)
C(2)−C(3)−C(41)	119.8(9)	121.3(10)	121.6(5)	121.8(3)
C(7)−C(8)−C(42)	121.0(9)	119.9(10)		121.6(3)
S(13)−C(13)−N(13)				178.6(4)
Ru(1)−S(13)−C(13)				102.2(1)
Ru(1)−S(14)−C(14)				104.8(1)
S(14)−C(14)−N(14)				178.3(3)

[a] X(1) = Cl(3) for **3,** S(13) for **7**. − [b] X(2) = Cl(2) for **3**, S(14) for **7**. − [c] C(12) = C(13) for **4**.

The coordination of thiocyanate ligands in complex **7** results in a strong ν_{SC-N} single band at 2116 cm^{-1} (in CH_2Cl_2), a value close to that found for both the *S*- and the *N*-bound Ru^{II} mono(2,2′-bipyridine) thiocyanate complexes reported earlier[13] (ν_{SC-N} values: 2116 for *S*-bound and 2109 cm^{-1} for *N*-bound, showing an unexpectedly weak tendency of the *N*-bound thiocyanate ligand to shift the SC−N stretching bands toward lower frequencies). A weak resonance at δ_{SCN} = 120 found in the ^{13}C-NMR spectrum of complex **7** matched that of the *S*-bound thiocyanate analogue [δ_{SCN} = 118 for *trans*(SCN)-Ru(bpy)-$(CO)_2(SCN)_2$], and other *S*-bound Ru−SCN complexes[21] assigned spectroscopically. The coordination mode of the SCN ligands in complex **7** was verified by X-ray crystallography (Figure 4). Since there is no severe steric hindrance, both terminal thiocyanates are bent [angles Ru−S(13)−C(13) 102.2(1)°, Ru−S(14)−C(14) 104.8(1)°]; in crystalline form the rotation of the groups is locked roughly between the two carbonyl ligands and the opposite bipyridine ring halves. The bond lengths of 2.429(1) and 2.432(1) Å for Ru(1)−S(13) and Ru(1)−S(14) are almost identical with those of the above-mentioned Ru−bpy analogue, but long relative to the range reported for other Ru^{II}−S bond lengths [2.262(1)−2.393(3) Å[32]]. The longer distances most probably are due to the competition of the carbonyl ligands for the π-electron density of the central metal atom.

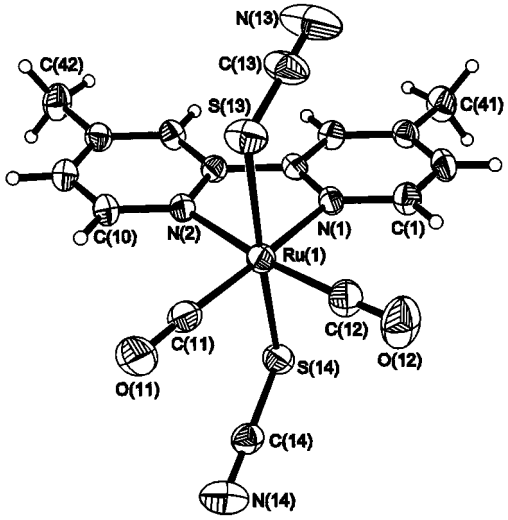


Figure 4. Structure of *trans*(SCN)-Ru(dmbpy)$(CO)_2(SCN)_2$ (**7**)

The ligand-exchange reaction Cl → SCN was also checked for complex **1** with reaction conditions similar to those used in the synthesis of complex **7**. Elemental analysis and heavily shifted ν_{CO} frequencies in the IR spectrum of the brownish-yellow product indicated the coordination of thiocyanate ligands in the complex (ν_{CO} in CH_2Cl_2: 2074 and 2020 cm^{-1}). The appearance of a strong ν_{SC-N} band at 2103 cm^{-1} with shoulder at 2117 cm^{-1} suggested the restored *cis*(CO)-*cis*(X) arrangement in this compound, where, owing to steric hindrance, the equatorial coordination position most probably was occupied by a linear NCS ligand. The poor X-ray-crystallographic data collected for the brownish-yellow disordered crystal supported the *N*-bound (linear) coordination mode for the equatorial, and *S*-bound (bent) arrangement for the axial thiocyanate. Unfortunately, poor solubility of this complex prevented detailed NMR study.

The ν_{CO} bands in the IR spectrum of a transition metal complex may be taken as a measure of backdonation from the metal atom to the ligand, where the higher the electron density of the central metal, the lower the ν_{CO} frequency. The ν_{CO} values recorded for the complexes studied here showed a slightly increasing trend for σ-bonding ligands in the order Cl ≥ Br > I, while a considerably higher value was recorded for the π-accepting SCN group. Similarly, change in the monodentate ligand affected the CO resonances in the ^{13}C-NMR spectra. A slight upfield shift was

detected in the order Cl > Br > I, which strictly follows the increasing electron affinities and decreasing ionic radii of these halogens. Interestingly, the thiocyanate ligands high-shifted the δ(CO) value of complex **7** relative to the halogen-containing derivatives, evidently due to effective shielding of the equatorial carbonyl groups by rotating SCN groups.

Conclusions

In this paper we have described synthetic procedures for obtaining chemically altered Ru(dmbpy) species and presented the basic crystallographic and spectroscopic data for identification. The complexes were modified by fundamentally simple ligand-exchange reactions and with use of substituted polypyridine ligands. Aqueous hydrogen halides were shown to serve as effective halogen sources and as suitable reagents attacking Ru−Ru bonds in dimeric [Ru(bpy)$(CO)_2Cl]_2$, which consequently led to selective formation of monomeric *trans*-halogen species. The particular combination of ruthenium reagent and solvent used in the synthesis, as well as the sterical properties of the chromophore and non-chromophore ligands, were suggested to direct the complexation reaction toward mononuclear *cis*- or *trans*-halogen species.

Experimental Section

Materials: $[Ru(CO)_3Cl_2]_2$ was purchased from Johnson and Matthey and 4,4′-dimethyl 2,2′-bipyridine (dmbpy) from Aldrich Chemicals. All solvents were of analytical grade and used as received. The parent complexes *cis*(Cl)-Ru(dmbpy)$(CO)_2Cl_2$, and $[Ru(dmbpy)(CO)_2Cl]_2$[15] were synthesized under exclusion of air with use of traditional N_2/vacuum-line techniques. The ligand-exchange reactions with aqueous hydrogen halide solutions (HCl, 37%; HBr, 48%; HI, 67%, all from Merck) were carried out in a 60-mL Berghof digestive pressure vessel[22] with PTFE liner. All product manipulations were performed in air.

Spectroscopic Studies: Infrared spectra were measured in CH_2Cl_2 solutions with a Nicolet Magna 750 FTIR spectrometer. ^{1}H- and ^{13}C-NMR spectra were recorded with a Bruker AMX 400 spectrometer with $CDCl_3$ as solvent.

Syntheses: Parent complexes *cis*(Cl)-Ru(dmbpy)$(CO)_2Cl_2$ (**1**) and $[Ru(dmbpy)(CO)_2Cl]_2$ (**2**) were synthesized from $[Ru(CO)_3Cl_2]_2$ and 4,4′-dimethyl 2,2′-bipyridine with THF or ethylene glycol used as solvent in 72% and 68% yield[15], respectively.

***trans*(Cl)-Ru(dmbpy)$(CO)_2Cl_2$ (3):** Complex **3** was synthesized by using "ruthenium red" carbonyl solution[23][24] as starting material. $RuCl_3 \cdot 3\ H_2O$ (1 g, 3.82 mmol) and 70 mL of dry ethanol were placed in a reaction vessel under nitrogen. The reaction mixture was refluxed for 8 h under CO flow, and cooled to room temperature, after which 4,4′-dimethyl-2,2′-bipyridine (0.63g, 3.82 mmol) was added. The solution was refluxed under nitrogen for an additional 2 h, and cooled to room temperature. The yellow precipitate was filtered, washed with small amounts of ethanol, and dried in vacuo (yield 83%). Additionally, a sample of complex **3** (300 mg, 0.73 mmol) was prepared as follows: A brownish-yellow mixture of monomeric by-products (ca. 500 mg) from the synthesis of complex **2**[15] was added to 15 mL of 37% hydrochloric acid and the mixture was allowed to stand at room temperature for several days. A yellow precipitate was formed during the concentration of the aqueous solution. This was washed with water and small amounts of methanol, dried in air, and analyzed by IR and NMR spectroscopy, X-ray diffraction [single crystals obtained from CH_2Cl_2 as solvated Ru(dmbpy)$(CO)_2Cl_2 \cdot CH_2Cl_2$], and elemental analysis. − $C_{14}H_{12}Cl_2N_2O_2Ru$ (412.24): calcd. C 40.8, H 2.9, N 6.8; found C 40.9, H 2.9, N 6.6. − IR (CH_2Cl_2): $\tilde{\nu}$ = 2063 (vs), 2001 cm^{-1} (vs) (both CO). − $^{13}C\{^1H\}$ NMR ($CDCl_3$): δ = 155.5−124.6 (five peaks, aromatic rings in dmbpy), 196.8 (CO), 22.0 (Me). − ^{1}H NMR ($CDCl_3$): δ = 8.99 (d, 6-H), 8.02 (s, 3-H), 7.44 (d, 5-H) (all aromatic H); 2.58 (s, Me).

Halogen-Ligand Exchange Reactions: The halogen-ligand exchange reactions were carried out in a Berghof pressure vessel using aqueous HBr (2 mL of 48% HBr/2 mL of H_2O) or HI (1.25 mL of 67% HI/3.25 mL of H_2O) and complexes **1** and **2** as starting materials.

***cis*(Br)-Ru(dmbpy)$(CO)_2Br_2$ (4):** Complex **4** was synthesized by weighing 80 mg (0.19 mmol) of complex **1** into the pressure vessel, adding 4 mL of aqueous HBr, and heating the mixture to 200°C. The temperature was maintained at 200°C for 6 h, after which the reaction vessel was cooled to room temperature. A light green precipitate was separated from the greenish solution, washed several times with water, and air-dried (yield ca. 70%). Complex **4** was analyzed by spectroscopic methods, elemental analysis, and X-ray diffraction analysis [single crystals obtained from CH_2Cl_2/$CDCl_3$ mixture as solvated Ru(dmbpy)$(CO)_2Br_2 \cdot CDCl_3$]. − $C_{14}H_{12}Br_2N_2O_2Ru$ (501.14): calcd. C 33.6, H 2.4, N 5.6; found C 33.9, H 2.4, N 5.6. − IR (CH_2Cl_2): $\tilde{\nu}$ = 2063 (vs), 2000 cm^{-1} (vs) (both CO). − $^{13}C\{^1H\}$ NMR ($CDCl_3$): δ = 156.5−124.2 (ten peaks, aromatic rings in dmbpy); 197.4, 191.2 (both CO); 22.0 (Me). − ^{1}H NMR ($CDCl_3$): δ = 8.97 (d, 6-H), 8.68 (d, 6′-H), 8.01 (s, 3-H), 7.99 (s, 3′-H), 7.49 (d, 5-H), 7.43(d, 5′-H) (all aromatic H); 2.63 (s), 2.59 (s) (both Me).

***trans*-Br−Ru(dmbpy)$(CO)_2Br_2$ (5):** Dimer **2** (60 mg, 0.08 mmol) was dissolved in 4 mL of aqueous HBr, and the mixture was heated at 200°C for 10 h. A greenish yellow precipitate was filtered off from the yellow solution, washed with water, and dried in air (yield 49%). Complex **5** was analyzed by spectroscopic methods and elemental analysis. − $C_{14}H_{12}Br_2N_2O_2Ru$ (501.14): calcd. C 33.6, H 2.4, N 5.6; found C 33.7, H 2.4, N 5.8. − IR (CH_2Cl_2): $\tilde{\nu}$ = 2062 (vs), 2000 cm^{-1} (vs) (both CO). − $^{13}C\{^1H\}$ NMR ($CDCl_3$): δ = 155.4−124.6 (five peaks, aromatic rings in dmbpy); 197.4 (CO); 22.0 (Me). − ^{1}H NMR ($CDCl_3$): δ = 8.97 (d, 6-H), 8.01 (s, 3-H), 7.43 (d, 5-H) (all aromatic H); 2.60 (s, Me).

***trans*(I)-Ru(dmbpy)$(CO)_2I_2$ (6):** Complex **6** was synthesized similarly to the Br-containing derivatives of complexes **1** and **2**, except that 4.5 mL of an aqueous HI solution was used as halogen source in each synthesis and the reaction temperature was maintained at 200°C for 20 h. The bright yellow precipitate, yields ca. 65% (from complex **1**) and 72% (from complex **2**), was analyzed by spectroscopic methods and elemental analysis, and identified as pure complex **6** in both syntheses. Crystals suitable for X-ray diffraction analysis were obtained from CH_2Cl_2 solution. − $C_{14}H_{12}I_2N_2O_2Ru$ (595.13): calcd. C 28.3, H 2.0, N 4.7; found C 28.7, H 2.0, N 4.9. − IR (CH_2Cl_2): $\tilde{\nu}$ = 2056 (vs), 1999 cm^{-1} (vs) (both CO). − $^{13}C\{^1H\}$ NMR ($CDCl_3$): δ = 155.3−124.6 (five peaks, aromatic rings in dmbpy); 198.7 (CO); 22.1 (Me). − ^{1}H NMR ($CDCl_3$): δ = 8.94 (d, 6-H), 8.00 (s, 3-H), 7.38 (d, 5-H) (all aromatic H); 2.60 (s, Me).

***trans*(SCN)-Ru(dmbpy)$(CO)_2(SCN)_2$ (7):** 70 mg (0.17 mmol) of complex **3**, 200 mg (2.0 mmol) of KSCN, and 3 mL of water were placed in an autoclave, and the mixture was heated at 140°C for 8

h. The reaction mixture was cooled slowly to room temperature, and the bright yellow precipitate was separated by filtration and washed thoroughly with water [yield 42 mg (0.09 mmol), 54%]. The product was dried under vacuum, and analyzed by spectroscopic measurements and X-ray diffraction analysis (single crystals obtained directly from the reaction vessel without recrystallization). – $C_{16}H_{12}N_4O_2S_2Ru$ (457.49): calcd. C 42.0, H 2.6, N 12.3; found C 41.7, H 2.7, N, 11.9. – IR (CH_2Cl_2): $\tilde{\nu}$ = 2069 (vs), 2016 (vs) (both CO); 2116 cm^{-1} (SCN). – $^{13}C\{^1H\}$ NMR ($CDCl_3$): δ = 155.5–125.4 (five peaks, aromatic rings in dmbpy); 195.0 (CO); 22.3 (Me); 119.6 (SCN). – ^1H NMR ($CDCl_3$): δ = 8.76 (d, 6-H), 8.11 (s, 3-H), 7.51 (d, 5-H) (all aromatic H); 2.63 (s, Me).

X-ray Data Collection and Structure Solutions: X-ray diffraction data were collected at 20°C with a Nicolet R3m (complexes **4** and **6**) or an Enraf–Nonius Kappa CCD (complexes **3** and **7**) diffractometers using graphite Mo-K_α radiation (λ = 0.71073 Å). Crystals suitable for X-ray diffraction studies were carefully chosen by microscopic examination and mounted on glass fibers. For **4** and **6**, cell parameters were obtained from 25 automatically centered reflections. Intensities were corrected for background, polarization, and Lorentz factors. Data collection, data reduction and cell refinement were carried out with the P3/P4 diffractometer program V 4.27.[25] The structures were solved by direct methods. The structure solution was carried out with the SHELXS 86 program[26] and structure refinement with the SHELXL 93 program.[27] For compounds **3** and **7**, data were collected using ϕ or combined ϕ-ω scan mode with a kcd program (Enraf–Nonius). Denzo and Scalepack programs[28] were used for cell refinements and data reductions. The structure solutions (direct methods) were carried out with the SHELXS 97 program,[29] and structure refinements with the SHELXL 97.[30] For complexes **3**, **4**, **6,** and **7**, all non-hydrogen atoms were refined anisotropically. Aromatic hydrogen atoms and methyl group hydrogen atoms were placed in idealized positions (aromatic C–H = 0.93 Å, methyl C–H = 0.96 Å). Decomposition of the solvated crystalline complex **3** was relatively rapid, requiring fast data collection with the X-ray diffractometer. The crystallographic data are collected in Table 1, the selected bond lengths and angles in Tables 2–3. Crystallographic data (excluding structure factors) for the structures reported in this paper have been deposited with the Cambridge Crystallographic Data Centre as supplementary publication no. CCDC-102482 (**3**), -102483 (**4**), -102484 (**6**), -102485 (**7**). Copies of the data can be obtained free of charge on application to CCDC, 12 Union Road, Cambridge CB2 1EZ, UK [Fax: int. code + 44(1223)336-033; E-mail: deposit@ccdc.cam.ac.uk].

[1] J. G. Haasnoot, W. Hinrichs, O. Weir, J. Voss, *Inorg. Chem*. **1986**, *25*, 4140.
[2] H. Ishida, K. Tanaka, M. Morimoto, T. Tanaka, *Organometallics* **1986**, *5*, 724.
[3] M. G. Richmond, *J. Organomet. Chem*. **1993**, *457*, 121.
[4] M. Haukka, T. Venäläinen, M. Kallinen, T. A. Pakkanen *J. Mol. Catal*., in press.
[5] J.-M. Lehn, R. Ziesel, *J. Organomet. Chem*. **1990 382**, 157.
[6] M. Ishida, K. Fujiki, T. Omba, K. Ohkubo, K. Tanaka, T. Terarda, T. Tanaka, *J. Chem. Soc., Dalton Trans.* **1990**, 2155.
[7] M.-N. Collomb-Dunnand-Sauthier, A. Deronzier, R. Ziessel, *J. Chem. Soc., Chem. Commun.* **1994**, 189.
[8] M.-N. Collomb-Dunnand-Sauthier, A. Deronzier, R. Ziessel, *Inorg. Chem*. **1994**, *33*, 2961.
[9] S. Chardon-Noblat, A. Deronzier, R. Ziessel, D. Zsoldos, *Inorg. Chem.*, in press.
[10] M. Haukka, J. Kiviaho, M. Ahlgrén, T. A. Pakkanen, *Organometallics* **1995**, *14*, 825.
[11] M. Haukka, T. Venäläinen, M. Ahlgrén, T. A. Pakkanen, *Inorg. Chem*. **1995**, *34*, 2931.
[12] M. Haukka, M. Ahlgrén, T. A. Pakkanen, *J. Chem. Soc., Dalton Trans.* **1996**, 1927, and references therein.
[13] P. Homanen, M. Haukka, T. A. Pakkanen, J. Pursiainen, R. H. Laitinen, *Organometallics*, **1996**, *15*, 4081.
[14] P. Homanen, M. Haukka, M. Ahlgrén, T. A. Pakkanen, *Inorg. Chem*. **1997**, *36*, 3794.
[15] P. Homanen, M. Haukka, M. Ahlgrén, T. A. Pakkanen, P. N. W. Baxter, R. E. Benfield J. A. Connor, *J. Organomet. Chem*. 552, **1998**, 205.
[16] S. Chardon-Noblat, A. Deronzier, Zsoldos, D;R. Ziessel, M. Haukka, T. A. Pakkanen, T. Venäläinen, *J. Chem. Soc., Dalton Trans.* **1996**, 2581.
[17] M. K. Nazeeruddin, A. Kay, I. Rodicio, R. Humphry-Baker, E. Muller, P. Liska, N. Vlachopoulos, M. Grätzel, *J. Am. Chem. Soc*. **1993**, *115*, 6382.
[18] K. Murakoshi, G. Kano, Y. Wada, S. Yanagida, H. Miyazaki, M. Matsumoto, S. Murasawa, *J. Electroanal. Chem*. **1995**, *396*, 27.
[19] P. K. Ghosh, T. G. Spiro, *J. Am. Chem. Soc*. **1980**, *102*, 5543.
[20] R. Ziessel, *Photosensitization and Photocatalysis Using Inorganic And Organometallic Compounds* (Eds.: K. Kalyanasundaram, M. Grätzel), Kluwer, Academic Publishers, Dordrecht, **1993**.
[21] O. Kohle, S. Ruile, M. Gräzel, *Inorg. Chem*. **1996**, *35*, 4779.
[22] http://www. berghofusa.com
[23] J. Chatt, B. L. Shaw, A. E. Field, *J. Chem. Soc*. **1964**, 3466.
[24] J. M. Kelly, C. M. O'Connell, J. G. Vos, *Inorg. Chim. Acta* **1982**, *64*, L75.
[25] *P3/P4 Diffractometer Program V4.27*, Siemens Analytical X-ray Instruments, **1989–1991**.
[26] G. M. Sheldrick, *SHELXS 86, Program for Crystal Structure Determination*, University of Göttingen, **1986**.
[27] G. M. Sheldrick, *SHELXL 93, Program for Crystal Structure Refinement*, University of Göttingen, **1993**.
[28] Z. Otwinowski, W. Minor, "Processing of X-ray Diffraction Data Collected in Oscillation Mode" in *Methods in Enzymology*, vol. 276 ("Macromolecular Crystallography"), part A (Eds.: C. W. Carter Jr., R. M. Sweet), Academic Press, **1997**, p. 307–326.
[29] G. M. Sheldrick, *SHELXS 97*, Program for Crystal Structure Determination, University of Göttingen, **1997**.
[30] G. M. Sheldrick, *SHELXL 97*, Program for Crystal Structure Refinement, University of Göttingen, **1997**.
[31] M.-N. Collomb-Dunand-Sauthier, A. Deronzier, *J. Electroanal. Chem. Interfacial Electrochem*. **1991**, *319*, 347.
[32] S. C. Rawle, S. R. Cooper, *J. Chem. Soc., Chem. Commun*. **1987**, 308.

Received July 31, 1998
[I98248]

Phosphinidene Transition Metal Complexes: A Combined Ab Initio MO-DFT Study of $Cr(CO)_5$–PR

Steven Creve,[a] Kristine Pierloot,[a] Minh Tho Nguyen,*[a] and Luc G. Vanquickenborne[a]

Keywords: Ab initio calculations / Density functional calculations / Phosphinidene / Carbonyl complexes

Ab initio MO and DFT calculations have been performed on phosphinidene complexes of the type $Cr(CO)_5$–PR, with R = H, CH_3, SiH_3, NH_2, PH_2, OH, and SH. The formation of the Cr–P bond essentially arises from a ligand-to-metal charge transfer. While a significant π backdonation is also observed for the $Cr(CO)_5$–PH, $Cr(CO)_5$–PCH_3, and $Cr(CO)_5$–$PSiH_3$ complexes, this is less the case for $Cr(CO)_5$–POH, $Cr(CO)_5$–PSH, and $Cr(CO)_5$–PNH_2, and the backbonding almost disappears for $Cr(CO)_5$–PPH_2. In both the lowest lying singlet and triplet states, all complexes exhibit a staggered conformation. CASSCF/CASPT2 calculations performed with the ANO basis sets indicate a closed-shell singlet ground state along the whole series. The binding energy between $Cr(CO)_5$ and PR ranges from 216 kJ/mol for $Cr(CO)_5$–PNH_2 to 127 kJ/mol for $Cr(CO)_5$–$PSiH_3$ (B3LYP values). In general, the B3LYP-DFT scheme yields reasonable qualitative and quantitative results when compared with CASPT2(12/12).

1 Introduction

Phosphinidenes (R−P) are known as important transient species in phosphorus chemistry that can be stabilized through complexation with transition metal fragments. In contrast to analogous transient intermediates such as carbenes, nitrenes, and silylenes, spectroscopic information on free phosphinidenes is rather scarce. In fact, the ESR spectrum of an aryl derivative (Mes−P) has only recently been recorded.[1] In most cases, these short-lived and highly reactive species have been trapped in transition metal complexes and can be used in this way as starting materials in organophosphorus syntheses.[2]

Recently, we[3−6] and others[7][8] have shown by high-level ab initio calculations, that phosphinidenes exhibit an inherent triplet electronic ground state but that the singlet counterparts can be stabilized strongly by substituents through both electronic and steric effects. For example, amino (R_2N−P) and phosphino (R_2P−P) derivatives containing large alkyl groups are likely to possess a closed-shell singlet ground state.[3]

Mathey[9][10] and Lammertsma[11] suggested from numerous experimental observations of the complexed species that the phosphinidene ligand within the coordination sphere of a metal fragment behaves as a typical singlet monovalent intermediate giving a higher and cleaner reactivity. Nevertheless, the identity of the ground state of complexed phosphinidenes still remains an open question.

To our knowledge, only three theoretical studies of terminal phosphinidene complexes have yet been reported. The first one dealt with an Extended Hückel study of a number of substituted phosphinidene ligands (PCH_3, PNH_2, PPH_2, ...).[12] Idealized geometries were used throughout, based on parameters chosen from experimental data on parent species. Although very useful, this study only yields a qualitative picture of the considered complexes. In two other studies, partial geometry optimizations of the $Cr(CO)_5$−PH complex were performed.[13][14] However, the P−Cr bond length turned out to be 1.9 Å at the Extended Hückel level[13] while it was found to be 2.33 Å by ROHF calculations.[14] Disagreement concerning the singlet or triplet nature of the ground state of $Cr(CO)_5$−PH also arose. In our previous study on $Cr(CO)_5$−PH,[15] high-level ab-initio calculations have been applied, removing these discrepancies. We showed that $Cr(CO)_5$−PH has a singlet ground state with a P−Cr distance of 2.268 Å. The lowest lying triplet was 35 kJ/mol higher in energy. In this work, an extension is made to $Cr(CO)_5$ complexes of different phosphinidenes PR, yielding a deeper understanding of the singlet-triplet energy problem in these species. Furthermore, the backbonding phenomenon usually observed in metal complexes will be addressed, since it is not well characterized yet for phosphinidene complexes.[16]

The theoretical study presented here, includes full geometry optimizations and high-level energy calculations on a series of simple carbonylchromium complexes, $Cr(CO)_5$−PR, in which R = H, CH_3, SiH_3, NH_2, PH_2, OH, and SH.

2 Details of the Calculations

2.1 Computational Methods

All geometries were fully optimized with density functional theory, using the B3LYP functional[17][18] in combination with 6-31G(d,p) basis sets for all atoms, except for Cr. For the latter element we used a (14*s*,9*p*,5*d*)/[8*s*,5*p*,3*d*] basis set,[19] augmented by two *p*-functions[20] with exponents 0.120675 and 0.038610, one *d*-function[21] with exponent 0.09720, and one *f*-function with exponent 1.0,

[a] Department of Chemistry, University of Leuven, Celestijnenlaan 200F, B-3001 Leuven, Belgium.

Supporting information for this article is available on the WWW under http://www.wiley-vch.de/home/eurjic or from the author.

 © WILEY-VCH Verlag GmbH, D-69451 Weinheim, 1999 1434−1948/99/0101−0107 $ 17.50+.50/0

respectively. This [8*s*,7*p*,4*d*,1*f*] basis set for Cr will be denoted hereafter as "TZ+2PDF".

In our preliminary study on the $Cr(CO)_5-PH$ complex,[15] it was found that the (U)HF, (U)MP2 or CASSCF/PT2(2/2) methods are not reliable in treating this kind of systems. Therefore, we now only consider the higher level CASSCF(12/12) and CASPT2(12/12) calculations, using the B3LYP optimized geometries. ANO basis sets were used[22] for these calculations, following the contraction scheme shown below.

	primitive	contracted
H	*7s3p*	*2s1p*
C	*10s6p3d*	*3s2p1d*
N	*10s6p3d*	*3s2p1d*
O	*10s6p3d*	*3s2p1d*
Si	*13s10p4d*	*4s3p2d*
P	*13s10p4d*	*4s3p2d*
S	*13s10p4d*	*4s3p2d*
Cr	*17s12p9d4f*	*6s4p3d1f*

Our previous study[15] pointed out that a more flexible contraction with the same primitive set does not significantly alter the results.

All B3LYP optimizations were performed using the Mulliken software,[23] while the CASSCF/CASPT2 calculations were done with the MOLCAS-4.0 code.[24]

2.2 Notations

Figure 1 gives a schematic overview of the geometries for the different complexes and their proposed shorthand notations. For the $Cr(CO)_5-PH$, $Cr(CO)_5-POH$, and $Cr(CO)_5-PSH$ complexes, two forms were considered, an "eclipsed" conformation, indicating that the P−R bond is eclipsed with one of the $Cr-C_{eq}$ bonds, and a staggered form which has its P−R bond in between two $Cr-C_{eq}$ bonds. For the $Cr(CO)_5-PCH_3/Cr(CO)_5-PSiH_3$ and $Cr(CO)_5-PNH_2/Cr(CO)_5-PPH_2$ cases, additional specifications are needed to indicate the rotational orientation of the CH_3/SiH_3 and NH_2/PH_2 groups, respectively. They are referred to as **A** and **B**, following the convention of Figure 1. As a shorthand notation for use in tables, we will, for instance, designate an eclipsed structure of the **A** type as **ec-A** and a staggered structure as **st-A**. Note from Figure 1 that the **B**-types of $Cr(CO)_5-PNH_2$ and $Cr(CO)_5-PPH_2$ have a pyramidal NH_2 or PH_2 unit, in contrast to their corresponding **A**-types.

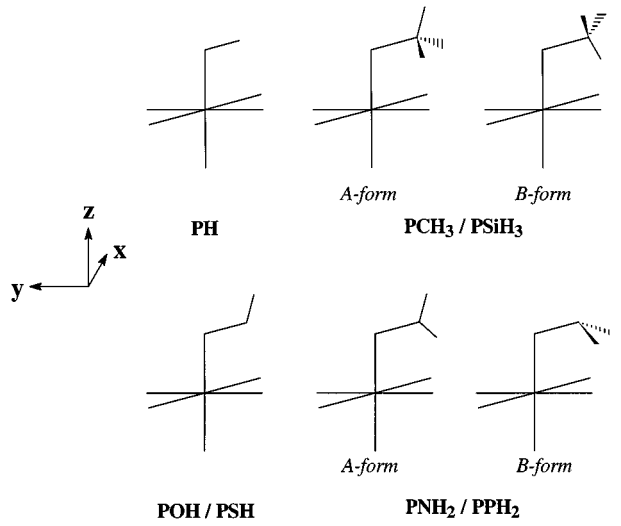


Figure 1. Schematic representation of the different $Cr(CO)_5-PR$ complexes considered, along with the naming convention; only eclipsed forms are shown in this figure

2.3 Choice of the Active Space

The quality of a CASSCF calculation on a transition metal system critically depends on the choice of the active space. This space needs to include all valence orbitals necessary for an adequate description of the metal−ligand bonding. In a previous study,[25] it was demonstrated that the ground state electronic structure of $Cr(CO)_6$ is well described by a (10/10) space, built up from the metal 3*d* orbitals and their bonding and antibonding counterparts. For $Cr(CO)_6$ this amounts to an occupied e_g (CO σ) and t_{2g} (Cr *3d*) shell, and a virtual e_g (Cr *3d*) and t_{2g} (CO π*) shell. By replacing one CO ligand by a phosphinidene unit, however, an additional difficulty arises. The PR ligand has a triplet ground state with two singly occupied $p(\pi)$ orbitals. As a consequence, both π orbitals have to be added to the original (10/10) space. This means that the active space needed for an adequate description of $Cr(CO)_5-PR$ consists of at least 12 electrons in 12 orbitals.

In the CASPT2 calculations, all valence electrons as well as the Cr semi-core 3*s*, 3*p* electrons were correlated, whereas the rest of the core (C, N, O 1*s*; Si, P, S 1*s*, 2*s*, 2*p*; Cr 1*s*, 2*s*, 2*p*) was kept frozen. Finally, first-order relativistic corrections (mass-velocity and Darwin term) have been added to the CASPT2 energies.

A remark has to be made for triplet **st-A** $Cr(CO)_5-PPH_2$. In this case, it has not been possible to perform the CASSCF/PT2(12/12) calculation with the active space specified above. It turns out that one of the active orbitals (representing the Cr−P σ bond) spontaneously leaves the active space, in favor of the entering $3p_z$(Cr) orbital. Therefore, two additional calculations have been performed on the triplet **st-A** $Cr(CO)_5-PPH_2$ species. The first was to force the calculation to keep the Cr−P σ bond in its active space, by freezing the orbitals during the CASSCF run up to 3*p*(Cr). In another calculation, a reduced (10/11) space was used, containing neither the Cr−P σ bonding orbital, nor the $3p_z$(Cr) orbital. The relative energies obtained from both approaches differed by only 1.2 kJ/mol.

3 Results and Discussion

3.1 Electronic Structure

As quite a number of geometrical effects and properties of the relative energies cannot be fully understood without

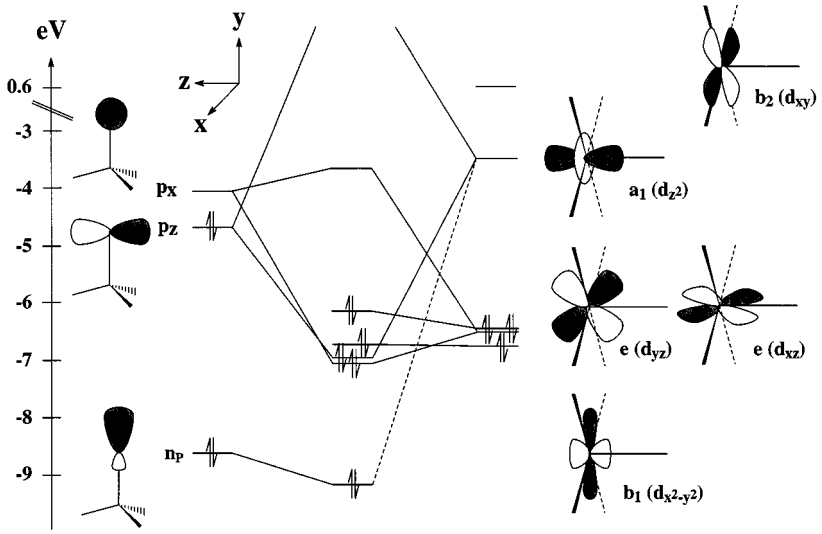


Figure 2. Schematic drawing of the orbital interactions in singlet **st-A** $Cr(CO)_5-PCH_3$

having the electronic structure of the considered complexes in mind, the latter will be discussed first.

A careful analysis of the bonding situation in $Cr(CO)_5-PH$ has already been reported.[15] Therefore, we will recall briefly here the most important features. As a guideline, the orbital correlation diagram for the singlet **st−A** $Cr(CO)_5-PCH_3$ complex shown in Figure 2, together with contour plots of the most important orbitals shown in Figure 3 are used in what follows. The highest occupied orbitals of the d^6 $Cr(CO)_5$ fragment are the *e* orbitals (d_{xz}, d_{yz}) and a b_1 ($d_{x^2-y^2}$) orbital, which are stabilised through π backbonding with the empty CO π* orbitals. The lowest unoccupied orbital is of a_1 symmetry (d_{z^2}), followed by a b_2 (d_{xy}) orbital. Both point directly towards the CO ligands and constitute the antibonding combinations arising from a σ-interaction with the CO 5σ orbitals. The PR molecule has a σ orbital directed along the P−R bond containing the phosphorus lone pair, n_P. Two phosphorus *p* orbitals, perpendicular to the P−R bond, contain another pair of electrons, usually in a triplet ground state configuration. However, the bonding is best understood by considering a singlet PR. In this case, one *p* orbital, perpendicular to the P−R bond and doubly occupied, is used to form a σ bond with the empty a_1 orbital of the $Cr(CO)_5$ fragment. The remaining empty p_x orbital of PR is in an orientation suited to π backbonding with the doubly occupied d_{xz}(Cr) orbital. The antibonding combination arising from this interaction constitutes the LUMO of the resulting complex. For clarity, the phosphinidene complex in Figure 2 is represented with a Cr−P−R angle of 90°. Optimized structures, on the other hand, have an Cr−P−R angle of 105−130°. This can be understood by considering the secondary stabilizing interaction between the phosphorus n_P lone pair and the d_{z^2}(Cr) orbital (HOMO-4 of Figure 3) which increases if the Cr−P−R angle gets larger than 90°.

It is interesting to look at the evolution of the π backbonding through the series of complexes. Figure 4 shows contour plots of the bonding orbital [with predominant d_{xz}(Cr) character] involved in the π backdonation. Immediately perceptible is the decrease of the p_x(P) orbital contribution in the series $Cr(CO)_5-PCH_3 \rightarrow Cr(CO)_5-POH \rightarrow Cr(CO)_5-PNH_2$. The same trend is seen for the analogous series of second-row R groups. There, the decrease of the *p* orbital contribution is even more pronounced (an extreme case is shown as HOMO-1 of $Cr(CO)_5-PPH_2$ in Figure 6. In order to have a more physical picture of the π backbond strength, density difference plots have also been made and are shown in Figure 5. This difference corresponds to the deformation density upon bond formation and is obtained as follows.

$$\Delta\rho = \rho_{tot}(\text{complex}) - [\rho_{tot}(\text{singlet PR}) + \rho_{tot}(Cr(CO)_5)]$$

To compute Δρ, the geometries of the fragments are frozen to their corresponding geometries in the complex. Full lines in Figure 5 correspond to an increase in total density, dotted lines to a decrease. As expected, one can see that charge is transferred from the d_{xz}(Cr) orbital to the p_x(P) orbital. Again, the extent of this charge transfer decreases as R varies in the order $CH_3 \rightarrow OH \rightarrow NH_2$. The same is also seen for the second-row series, but to a slightly higher extent. How can we understand such a weakening of the π back transfer? Table 1 shows the energy difference (Δ*E*) between the LUMO of the different PR fragments − the orbital which is involved in π backbonding − and the d_{xz}(Cr) orbital of $Cr(CO)_5$. The larger the energy difference between both partners involved in the π bond, the weaker this bond. In more chemical terms, one could say that in PNH_2, PPH_2, POH, and PSH the empty phosphorus p_x orbital is already used by the neighboring heteroatom to delocalize its lone pair, making this orbital less available for backbonding with the d_{xz}(Cr) orbital. O and S, which have a larger electronegativity than N and P, respectively, delocalize their lone pair to a lesser extent, such that the phos-

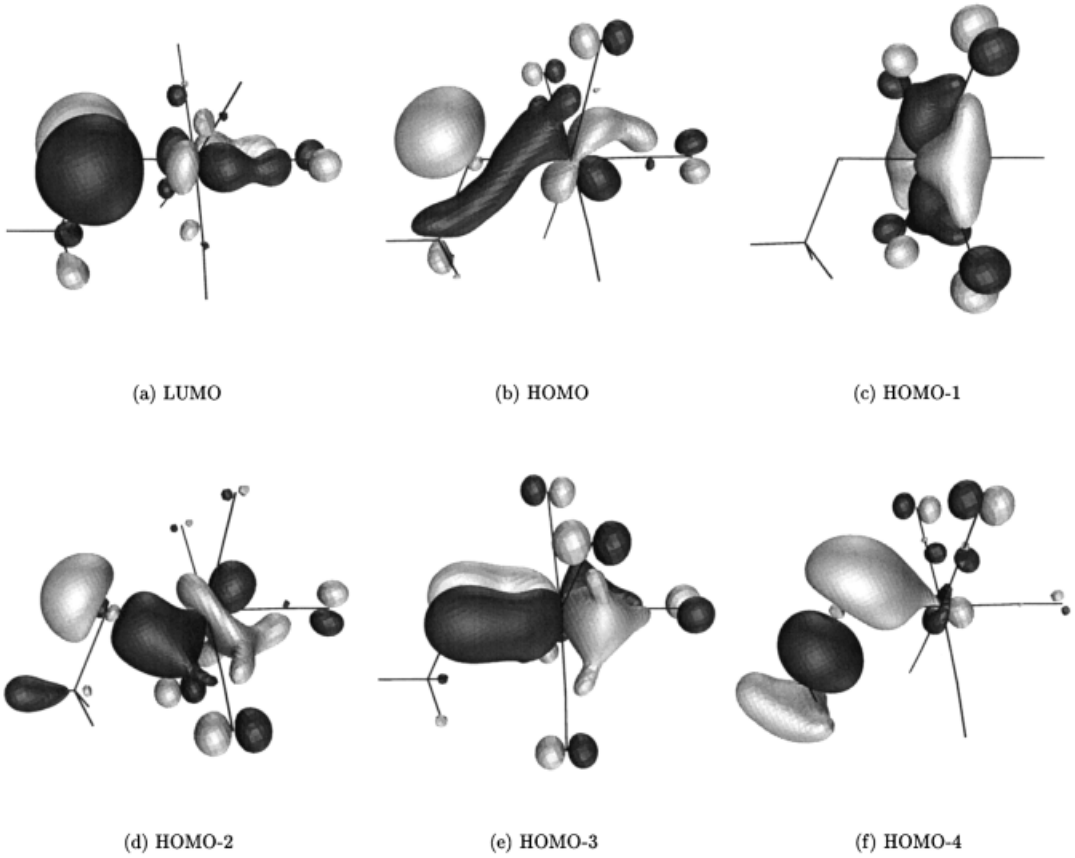


Figure 3. Molecular orbitals of the **st-A** $Cr(CO)_5-PCH_3$ molecule; the isosurfaces are plotted at a value of 0.05 a.u.

phorus p_x orbital remains more suited to backbonding with Cr in the $Cr(CO)_5-POH$ and $Cr(CO)_5-PSH$ complexes. This explains the fact that the π bond strength of $Cr(CO)_5-POH$ lies in between that of $Cr(CO)_5-PCH_3$ and $Cr(CO)_5-PNH_2$. The same applies to $Cr(CO)_5-PSH$.

For all complexes considered, the LUMO is the antibonding orbital involved in the π backbond discussed above. For R = PH, PCH_3, $PSiH_3$, this orbital is a simple antibonding combination of the p_x(P) orbital and the d_{xz}(Cr) orbital. However, for the internally conjugated PR fragments, this orbital is also antibonding between P and R. As an example, Figure 6 shows the LUMO of **st-A** $Cr(CO)_5-PPH_2$.

Calculated Mulliken charges show that the most electrophilic phosphinidene centers are found for $Cr(CO)_5-POH$ (q_P = 0.57 e^-) and $Cr(CO)_5-PNH_2$ (q_P = 0.48 e^-), whereas $Cr(CO)_5-PSiH_3$ has the least electrophilic P (q_P = 0.14 e^-). In general, the charge at the P center is considerably reduced upon excitation to the triplet state, due to an occupation of the LUMO, which is an orbital mainly localized on the PR unit. The charges at the Cr center are nearly constant throughout the series (−1.5 e^- for singlets and −1.3 e^- for triplet species). The total PR fragment charge (sum of the Mulliken charges) gives an estimate of the total charge transfer from PR to $Cr(CO)_5$. It is seen that this charge transfer is largest for $Cr(CO)_5-PNH_2$ (0.45 e^-) and smallest for $Cr(CO)_5-PSiH_3$ (0.20 e^-). As shown in a further section, these compounds also have the largest and smallest binding energy, respectively. For the triplet species, calculations show that the spin density is mainly locacted on both the Cr and P centers [ρ^S(Cr) varies from 0.61 to

Table 1. Various properties of complexed and free phosphinidenes

	$\Delta(T-S)$[a] B3LYP	$\Delta(T-S)$[a] QCISD(T)[b]	ΔE[c] [eV]
PH	−139.2	−117.2	1.86
PCH_3	−125.9	−108.8	2.56
POH	−76.5	−70.7	3.20
PNH_2	−5.0	−5.0	4.14
$PSiH_3$	−123.8	−107.1	1.82
PSH	−37.2	−25.5	2.90
PPH_2	−10.5	−5.0	3.71
	$\Delta(T-S)$[a] B3LYP	$\Delta(T-S)$[a] CASPT2[d]	B.E. [kJ/mol]
$Cr(CO)_5-PH$	24.6	36.6	137.5
$Cr(CO)_5-PCH_3$	24.4	35.8	134.9
$Cr(CO)_5-POH$	86.0	95.3	186.4
$Cr(CO)_5-PNH_2$	102.5	108.7	216.0
$Cr(CO)_5-PSiH_3$	3.8	11.2	126.9
$Cr(CO)_5-PSH$	75.2	84.4	173.4
$Cr(CO)_5-PPH_2$	30.1	23.7	137.5

[a] E(lowest lying triplet) − E(lowest lying singlet) [kJ/mol]. − [b] Using the 6−311++G(3df,2p) basis and based on (U)MP2/6−31G(d,p) geometries given in ref.[3]. A negative value corresponds to a triplet ground state. − [c] Energy difference between the LUMO of singlet PR and the d_{xz} orbital of $Cr(CO)_5$. − [d] Including relativistic corrections.

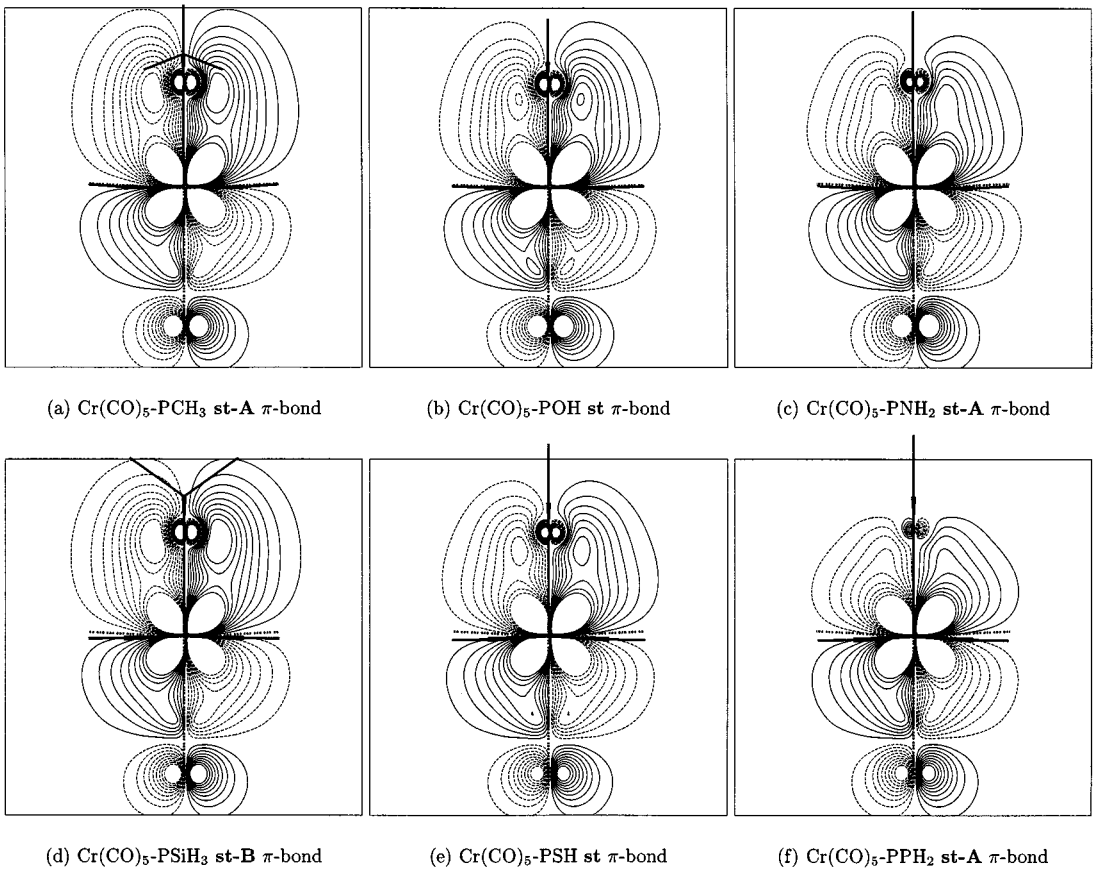


Figure 4. Contour plots of the $p_x(P)-d_{xz}(Cr)$ bonding orbital involved in π backdonation of the different complexes

Table 2. Selected geometrical parameters as obtained using B3LYP optimizations

		r(P−Cr)		r(P−R)			
		$^1A'$	$^3A''$	$^1A'$	$^3A''$		free PR
$Cr(CO)_5-PH$	**ec**	2.273	2.365	1.438	1.424	$^1\Sigma^+$	1.434
	st	2.268	2.368	1.438	1.425	$^1\Sigma^-$	1.435
$Cr(CO)_5-PCH_3$	**ec-A**	2.281	2.376	1.867	1.859	$^1A'$	1.822
	ec-B	2.282	2.378	1.861	1.861	$^3A_2$	1.861
	st-A	2.279	2.375	1.868	1.859		
	st-B	2.274	2.375	1.865	1.863		
$Cr(CO)_5-PNH_2$	**ec-A**	2.312	2.444	1.664	1.700	$^1A_1$	1.649
	ec-B	2.269	2.405	1.768	1.696	$^3A''$	1.716
	st-A	2.303	2.432	1.666	1.703		
	st-B	2.267	2.402	1.768	1.696		
$Cr(CO)_5-POH$	**ec**	2.242	2.394	1.660	1.668	$^1A'$	1.643
	st	2.239	2.392	1.662	1.670	$^3A''$	1.663
$Cr(CO)_5-PSiH_3$	**ec-A**	2.293	2.343	2.291	2.253	$^1A'$	2.236
	ec-B	2.293	2.343	2.281	2.253	$^3A_2$	2.270
	st-A	2.292	2.344	2.290	2.253		
	st-B	2.288	2.344	2.283	2.256		
$Cr(CO)_5-PPH_2$	**ec-A**	2.359	2.447	2.034	2.104	$^1A_1$	1.963
	ec-B	2.273	2.360	2.298	2.208	$^3A''$	2.210
	st-A	2.355	2.532	2.036	2.125		
	st-B	2.273	2.357	2.297	2.209		
$Cr(CO)_5-PSH$	**ec**	2.282	2.396	2.093	2.126	$^1A'$	2.002
	st	2.279	2.400	2.095	2.127	$^3A''$	2.119

0.99 e^-, while $\rho^S(P)$ lies between 1.23 and 1.45 e^-]. An extremely low $\rho^S(P)$ value is found in $Cr(CO)_5-PPH_2$, probably caused by the fact that in this molecule, a considerable amount of spin density is also found on the phosphanyl P. A full table containing the calculated mulliken charges and spin densities is supplied as supporting information (available on the WWW under http://www.wiley-vch.de/home/eurjic or from the author).

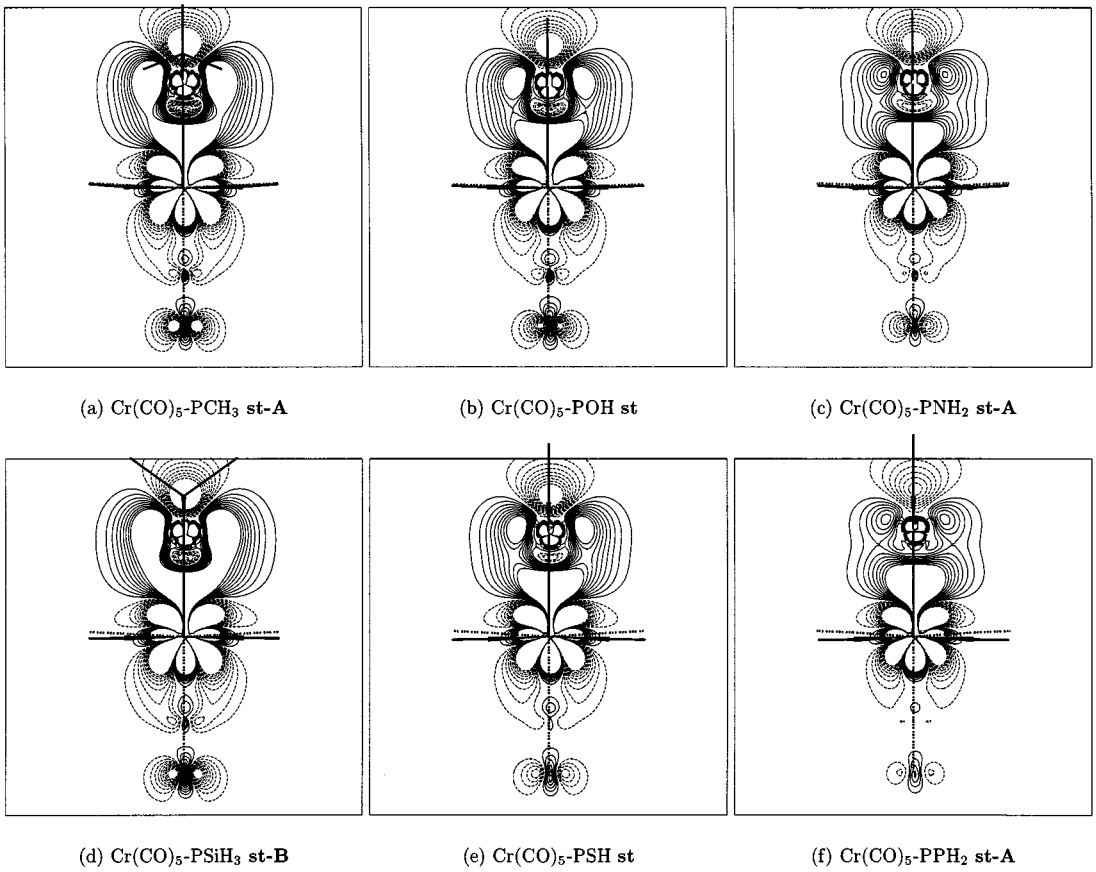


Figure 5. Density difference plots $\Delta\rho = \rho_{tot}(\text{complex}) - \{\rho_{tot}(\text{singlet PR}) + \rho_{tot}[Cr(CO)_5]\}$ of the various complexes, made in the plane containing the π backbond; full lines correspond to an increase in electron density upon bond formation, dotted lines to a decrease; the maximum and minimum contour levels are 0.009 and −0.009 a.u., respectively, with intervals of 0.001 a.u.

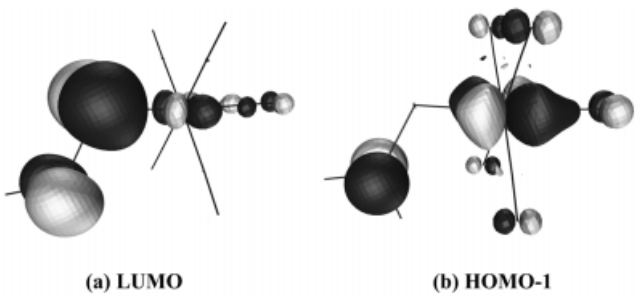


Figure 6. Some selected orbitals of the singlet **st-A** $Cr(CO)_5-PPH_2$ complex

3.2 Geometries

Optimized P−R bond lengths of free phosphinidenes are listed in Table 2. The B3LYP values are consistently slightly larger than UMP2 values obtained in previous work.[3] However, on the average, the difference in the calculated P−R distances is only about 0.01 Å, which is too small to be significant. This, together with previous work on phosphorus-containing species,[5][26] shows that B3LYP is a reliable tool to obtain geometries of phosphinidenes.

Selected geometrical parameters of the complexes of interest are shown in Table 2. Included are the P−Cr and P−R distances. For singlet $Cr(CO)_5$−PH, a P−Cr bond length of 2.27 Å was found, as compared to previously reported values of 1.9 Å (Extended Hückel)[13] and 2.33 Å (ROHF).[14] For triplet $Cr(CO)_5$−PH, a P−Cr distance of about 2.37 Å was found, significantly shorter than the 2.67 Å of the ROHF result reported earlier.[14] Hence, the need for a careful geometry optimization before obtaining accurate electronic energies of these complexes is evident. In view of the successes of DFT in the last decade[27−32] we felt that a full geometry optimization using B3LYP and the basis set specified above is a very reasonable choice.

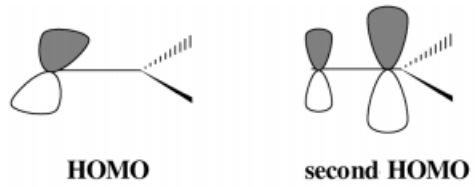
As can be seen from Table 2, in all singlet complexes the P−Cr distance is close to 2.3 Å. For the phosphane complexe $Cr(CO)_5-PH_3$, an experimental P−Cr distance of 2.35 Å was found.[33] Our calculated P−Cr distances thus suggest that the P−Cr bond in the presently studied phosphinidene complexes has nearly single bond character.

The P−Cr bond lengths of the various molecules also seem to correlate with the observed π bond strengths discussed in the previous section and shown in Figures 4 and 5. As expected, the P−Cr bond becomes shorter as the π bond strength increases. Only $Cr(CO)_5$−POH and $Cr(CO)_5$−PSH do not follow this trend. However, in view of the small differences in these bond lengths, such an apparent correlation might be questionable.

Immediately apparent from Table 2 is the lengthening of the P−Cr distances following electronic transition from the $^1A'$ to the $^3A''$ state. This effect is mainly due to the exci-

tation of an electron into the LUMO, which is strongly anti-bonding between Cr and P.

Upon closer inspection of Table 2, a number of points deserve some comment. While for $Cr(CO)_5-PCH_3$ and $Cr(CO)_5-PSiH_3$ no significant geometry differences are found between the **A** and **B** forms, the **B** forms of $Cr(CO)_5-PNH_2$ and $Cr(CO)_5-PPH_2$ exhibit considerably shorter P−Cr bonds than the corresponding **A** conformations. This effect is related to the electronic structure of singlet PNH_2 and PPH_2. In these molecules, the amino or phosphanyl π lone pair is conjugated with the empty *p* orbital on the phosphinidene P, resulting in a planar structure with sp^2 hybridization of the tricoordinated N and P atoms (see for instance ref.[3]). As a consequence, the second phosphinidene lone pair is found in a *p* orbital in the plane of the molecule. A schematic drawing of the two highest occupied molecular orbitals of both singlet PNH_2 and PPH_2 is shown in Scheme 1.



Scheme 1

The most important difference between the **A** and **B** forms of the PNH_2 or PPH_2 complexes, as can be seen from Figure 1, is not the rotation of the amino or phosphanyl group, but the fact that these groups are pyramidal in the **B** conformation, in contrast to their **A** counterparts. As such, the **B**-coordinated PNH_2 or PPH_2 phosphinidenes are no longer internally conjugated. As a consequence, the empty *p*-orbital on the ligating P-atom becomes more available for accepting a π backdonation of the metal, which results in a shorter P−Cr bond as compared to the **A** conformations.

One additional point has to be noted about the structures of $Cr(CO)_5-PNH_2$ and $Cr(CO)_5-PPH_2$. It is well known[3] that triplet PNH_2 and PPH_2 are characterized by a pyramidal structure. The triplet **A** conformations, however, were optimized within C_s symmetry where the phosphinidene unit is prevented from becoming pyramidal. It was found that, when re-optimizing the triplet **ec-A** form in C_1 symmetry, the molecule converged to the triplet **st-B** form. As such, the triplet **A** forms of $Cr(CO)_5-PNH_2$ and $Cr(CO)_5-PPH_2$ might be transition states for inversion at the pyramidal phosphinidene center or rotation around the P−R bond. Since we are not able to perform vibrational analyses of these structures, the identity of the triplet **A** $Cr(CO)_5-PNH_2$ and $Cr(CO)_5-PPH_2$ (minimum or transition structure) remains an open question.

While for $Cr(CO)_5-PCH_3$ and $Cr(CO)_5-PSiH_3$ the P−R distances are systematically shorter in the triplet structures − in contrast to the situation in free phosphinidenes (Table 2) − a reverse trend is seen for $Cr(CO)_5-POH$ and $Cr(CO)_5-PSH$ as well as for the **A** forms of $Cr(CO)_5-PNH_2$ and $Cr(CO)_5-PPH_2$. Since in these molecules the LUMO is also anti-bonding between P and R (see, for example, the LUMO in Figure 6), excitation of one electron to the LUMO causes the P−R bond to become longer with respect to the corresponding singlet form.

3.3 Relative Energies

In our previous study[15] on $Cr(CO)_5-PH$ a detailed analysis of the relative energy of the **A** and **B** forms using different methods and basis sets was performed. Here, we present only results obtained at the B3LYP and CASPT2(12/12) (including relativistic corrections) levels. The obtained relative energies are shown in Table 3. At each optimized singlet or triplet geometry, both lowest lying singlet and triplet states were calculated.

3.3.1 Conformational Behavior

We will focus on a few general characteristics of the relative energies. In every case, both B3LYP and CASPT2 methods predict a singlet staggered conformation for the ground state, except for $Cr(CO)_5-PNH_2$, where CASPT2 gives a singlet **st-A** ground state, lying 1.6 kJ/mol below the **ec-A** structure, in contrast to B3LYP, which gives a singlet **ec-A** ground state, 1.2 kJ/mol below the **st-A** form. For a given conformation, the energy difference between eclipsed and staggered is rather small; the largest value amounts to 10.7 kJ/mol [$Cr(CO)_5-PSiH_3$, **ec-B** − **st-B**, CASPT2]. Since frequency analyses were beyond the scope of this work, it is impossible to say whether the eclipsed forms are true minima on the potential energy surface. They might as well be transition structures for rotation of one staggered form to another. For the **A** and **B** forms of $Cr(CO)_5-PCH_3$ and $Cr(CO)_5-PSiH_3$ no large deviations are seen. This is, however, not true for $Cr(CO)_5-PNH_2$ and $Cr(CO)_5-PPH_2$. The important difference in coordination mode of PR for these complexes (**A** or **B**) has already been highlighted in the previous section on geometries. As expected, it is now confirmed that, for singlet complexes, the most favorable conformation is **A** while it turns out to be **B** for triplet forms.

3.3.2 Singlet-Triplet Energy Difference

Table 1 contains the singlet-triplet energy differences [$\Delta(T - S)$] for both free and complexed phosphinidenes. The $\Delta(T - S)$ values shown refer to E(lowest lying triplet) − E(lowest lying singlet). For free PR species, QCISD(T) values are also given.[3] It is seen that, on the average, B3LYP results are about 10−20 kJ/mol higher than the QCISD(T) values. Since a detailed discussion of the variation of $\Delta E(T-S)$ throughout the PR series has already been given elsewhere,[3] it will not be discussed any further in this work. While all free phosphinidenes considered have a triplet ground state, all their complexed counterparts have a singlet

Table 3. Relative energies of the complexed species considered

		B3LYP		CASPT2[a]			B3LYP		CASPT2[a]	
		$^1A'$	$^3A''$	$^1A'$	$^3A''$		$^1A'$	$^3A''$	$^1A'$	$^3A''$
$Cr(CO)_5-PH$						$Cr(CO)_5-POH$				
ec	$^1A'$	1.0	56.4	1.9	65.6	**ec**	1.4	118.9	2.4	113.4
	$^3A''$	35.0	26.3	40.7	38.9		33.8	89.6	47.8	98.3
st	$^1A'$	0.0	52.6	0.0	60.6	**st**	0.0	113.6	0.0	109.0
	$^3A''$	30.9	24.6	36.7	36.6		30.3	86.0	43.3	95.3
						$Cr(CO)_5-PSH$				
						ec $^1A'$	1.9	104.0	4.0	101.8
						$^3A''$	31.1	77.5	47.4	87.4
						st $^1A'$	0.0	99.9	0.0	96.5
						$^3A''$	27.6	75.2	42.3	84.4
$Cr(CO)_5-PCH_3$						$Cr(CO)_5-PNH_2$				
ec-A	$^1A'$	3.6	56.1	5.1	59.6	**ec-A** $^1A'$	−1.2	148.6	1.6	142.3
	$^3A''$	34.7	26.9	46.5	39.0	$^3A''$	31.0	119.6	51.7	130.4
ec-B	$^1A'$	2.9	61.1	8.	68.2	**ec-B** $^1A'$	116.1	144.1	97.0	136.9
	$^3A''$	38.0	28.2	52.9	42.6	$^3A''$	156.3	102.2	148.5	111.2
st-A	$^1A'$	0.0	51.1	0.0	53.5	**st-A** $^1A'$	0.0	146.3	0.0	140.1
	$^3A''$	28.2	24.4	39.0	35.8	$^3A''$	29.3	119.5	46.3	129.3
st-B	$^1A'$	0.0	59.5	0.9	63.1	**st-B** $^1A'$	113.3	140.9	91.9	131.9
	$^3A''$	33.4	28.3	45.6	40.4	$^3A''$	153.5	101.3	144.3	108.7
$Cr(CO)_5-PSiH_3$						$Cr(CO)_5-PPH_2$				
ec-A	$^1A'$	6.0	29.5	5.8	30.0	**ec-A** $^1A'$	0.1	148.4	2.9	142.9
	$^3A''$	35.3	4.2	45.3	13.3	$^3A''$	28.3	123.7	50.3	130.1
ec-B	$^1A'$	6.0	33.5	10.7	38.2	**ec-B** $^1A'$	33.3	65.2	18.0	53.8
	$^3A''$	38.5	6.0	50.2	15.9	$^3A''$	70.1	31.9	61.1	27.3
st-A	$^1A'$	2.9	27.3	0.5	25.3	**st-A** $^1A'$	0.0	145.5	0.0	137.8
	$^3A''$	30.3	3.8	38.7	11.2	$^3A''$	32.9	128.4	52.7	162.7[b]
st-B	$^1A'$	0.0	30.6	0.0	30.6	**st-B** $^1A'$	28.8	60.5	11.1	47.1
	$^3A''$	31.0	5.0	41.0	13.7	$^3A''$	63.6	30.1	53.0	23.7

[a] Including relativistic corrections. − [b] CASSCF frozen up to *3p*(Cr).

ground state. For the complexed forms, B3LYP apparently underestimates the CASPT2 values. It is seen that the larger the absolute value of the singlet-triplet splitting of the free PR, the smaller this quantity for $Cr(CO)_5-PR$. One exception to this rough tendency, is $Cr(CO)_5-PPH_2$. Based upon the analysis of the π bond strength of the previous section, we can tentatively say that in this case, the singlet form is less stable (ralative to other complexes) due to its very weak π backbonding. Note, however, that a direct comparison between $\Delta(T - S)$ values for free and complexed phosphinidenes might not be legitimate, since in free phosphinidenes it concerns an excitation within PR orbitals, while in complexed phosphinidenes, the excitation is from the HOMO, which is an orbital with mainly d_{yz}(Cr) character, to the LUMO, having mainly p_x(P) character.

At this point, the high relative energy of triplet **st-A** $Cr(CO)_5-PPH_2$ should be noted. As explained in the section on the choice of the active space, problems were encountered for this molecule. The most probable reason is the relatively long P−Cr bond length obtained by B3LYP for this molecule.

In summary, in order to obtain $Cr(CO)_5-PR$ complexes with singlet ground states well below the triplet state, the phosphinidene ligand should have an internally stabilized singlet state through π donation of the R group. However, if this internal π donation becomes too strong, the P-center is no longer sufficiently able to accept π donation from the $Cr(CO)_5$ fragment. As such, two opposing effects are present, yielding − for the series presently studied − an optimum for $Cr(CO)_5-PNH_2$. The latter complex has a $\Delta(T - S)$ value of 108.7 kJ/mol at the CASPT2 level.

3.3.3 Overall Stability

The main parameter to judge the overall stability of a complex is the binding energy listed in Table 1, which is defined as B.E. = E[$Cr(CO)_5-PR$] − {E(triplet PR) + E[$Cr(CO)_5$]}. As discussed in our previous study[15] on $Cr(CO)_5-PH$, CASPT2(12/12) turns out to be somewhat problematic for the B.E. of this type of compounds. Upon dissociation of the phosphinidene ligand, the (12/12) space reduces to a (10/10) space on the $Cr(CO)_5$ fragment and a (2/2) space on the PR unit. A (2/2) space on triplet PH, in fact, is a simple ROHF calculation. Considerably different CASPT2 energies were obtained when instead a (6/10) space on PH was used, including all valence orbitals and the *3d*(P) orbitals (about 34 kJ/mol). After correcting the CASPT2(12/12) binding energy for the shortcomings of the (2/2) active space and for basis set superposition errors (BSSE), values very close to the B3LYP results were obtained. Therefore, we present here only the B.E. obtained using B3LYP. The $Cr(CO)_5-PNH_2$ complex has a B.E. of 216 kJ/mol, followed by $Cr(CO)_5-POH$ (186 kJ/mol) and $Cr(CO)_5-PSH$ (173 kJ/mol). Then the B.E. drops by about 36 kJ/mol for the remaining complexes, with $Cr(CO)_5-PSiH_3$ having the lowest B.E. of 127 kJ/mol. It is thus seen that the complex having the highest $\Delta(T - S)$ also has the highest B.E.

4 Concluding Remarks

$Cr(CO)_5$ complexes of differently substituted phosphinidenes (PR, R = H, CH_3, SiH_3, NH_2, PH_2, OH, and SH) have been studied by high level ab initio (CASPT2 + relatvistic corrections) and density functional (B3LYP) methods. It is shown that the P−Cr bond is essentially formed by a ligand-to-metal σ charge transfer; π backbonding is also manifested in the complexes of PH, PCH_3, and $PSiH_3$, but its importance systematically decreases in $Cr(CO)_5-POH$, $Cr(CO)_5-PSH$, and $Cr(CO)_5-PNH_2$, and is almost absent in $Cr(CO)_5-PPH_2$. Both B3LYP and CASPT2 methods show that all complexes have a singlet, staggered ground state conformation. There is only one case [$Cr(CO)_5-PNH_2$] where B3LYP predicts a different ground state conformation from CASPT2, but the energy difference is rather small − the eclipsed-staggered energy differences are small in general. One of the most intriguing parameters, both from an experimental and theoretical point of view, is the singlet-triplet energy difference [$\Delta(T - S)$] in these complexes. While the largest gap is found for $Cr(CO)_5-PNH_2$ amounting to 103 kJ/mol at the B3LYP level and 109 kJ/mol at the CASPT2 level, $Cr(CO)_5-PSiH_3$ exhibits the smallest gap of only 4 kJ/mol at B3LYP and 11 kJ/mol at CASPT2. The binding energies (B.E.) for P−Cr bond cleavage, as computed by the B3LYP method, show a similar behavior; the largest value is 216 kJ/mol for $Cr(CO)_5-PNH_2$, while $Cr(CO)_5-PSiH_3$ has the smallest B.E. of 127 kJ/mol. The trends in $\Delta(T-S)$ and B.E. can be understood in terms of electronic structure.

The qualitative trends emphasized by CASPT2 calculations are well reproduced by the B3LYP method and, in most cases, a quantitative agreement between the two methods is found as well.

Acknowledgments

We are indebted to the Fund for Scientific Research (FWO Vlaanderen) and "Geconcerteerde Onderzoeksacties" (GOA) for continuing support and the K. U. Leuven Computing Centre for generous allocation of computer time.

[1] X. Li, S. I. Weisman, T.-S. Lin, P. P. Gaspar, A. H. Cowley, A. I. Smirnov, *J. Am. Chem. Soc.* **1994**, *116*, 7899.
[2] F. Mathey, *Multiple bonds and low coordination in phosphorus chemistry*, Georg Thieme Verlag, New York, **1990.**
[3] M. T. Nguyen, A. Van Keer, L. G. Vanquickenborne, *J. Org. Chem.* **1996**, *61*, 7077.
[4] M. T. Nguyen, A. Van Keer, L. A. Eriksson, L. G. Vanquickenborne, *Chem. Phys. Lett.* **1996**, *254*, 307.
[5] M. T. Nguyen, S. Creve, L. G. Vanquickenborne, *J. Chem. Phys.* **1996**, *105*, 1922.
[6] M. T. Nguyen, A. Van Keer, L. G. Vanquickenborne, *J. Organomet. Chem.* **1997**, *529*, 3.
[7] T. P. Hamilton, A. G. Willis, S. D. Williams, *Chem. Phys. Lett.* **1995**, *246*, 59.
[8] V. Parasuk, C. J. Cramer, *Chem. Phys. Lett.* **1996**, *260*, 7.
[9] F. Mercier, B. Deschamps, F. Mathey, *J. Am. Chem. Soc.* **1989**, *111*, 9098.
[10] A. Marinetti, F. Mathey, *Organometallics* **1984**, *3*, 456.
[11] B. Wang, K. Lammerstma, *J. Am. Chem. Soc.* **1994**, *116*, 10486.
[12] G. Trinquier, G. Bertrand, *Inorg. Chem.* **1985**, *24*, 3842.
[13] D. Gonbeau, G. Pfister-Guillouzo, A. Marinetti, F. Mathey, *Inorg. Chem.* **1985**, *24*, 4133.
[14] J. −G. Lee, J. E. Boggs, A. H. Cowley, *Polyhedron* **1986**, *5*, 1027.
[15] S. Creve, K. Pierloot, M. T. Nguyen, *Chem. Phys. Lett.* **1998**, *285*, 429.
[16] K. B. Dillon, F. Mathey, J. F. Nixon, *Phosphorus: the carbon copy. From organophosphorus to phospha-organic chemistry*, Wiley, Chichester, **1998**.
[17] A. D. Becke, *J. Chem. Phys.* **1993**, *89*, 5648.
[18] C. Lee, W. Yang, R. G. Parr, *Phys. Rev. B* **1988**, *37*, 785.
[19] A. Schäfer, H. Horn, R. Ahlrichs, *J. Chem. Phys.* **1992**, *97*, 2571.
[20] A. J. H. Wachters, *J. Chem. Phys.* **1970**, *52*, 1033.
[21] P. J. Hay, *J. Chem. Phys.* **1977**, *66*, 4377.
[22] K. Pierloot, B. Dumez, P.-O. Widmark, B. O. Roos, *Theor. Chim. Acta* **1995**, *90*, 87.
[23] IBM Corporation, *Mulliken, version 1.1.0*, **1994**.
[24] K. Anderson, M. R. A. Blomberg, M. P. F. Fulsher, V. Kell, R. Lindh, P.-A. Malmqvist, J. Noga, J. Olsen, B. O. Roos, A. J. Sadlej, P. E. M. Siegbahn, M. Urban, *MOLCAS-4.0*, University of Lund, Sweden, **1996**.
[25] B. J. Persson, B. O. Roos, K. Pierloot, *J. Chem. Phys.* **1994**, *101*, 6810.
[26] M. T. Nguyen, S. Creve, L. G. Vanquickenborne, *J. Phys. Chem. A* **1997**, *101*, 3174.
[27] T. Ziegler, *Chem. Rev.* **1991**, *91*, 651.
[28] G. Rauhut, P. Pulay, *J. Phys. Chem.* **1995**, *99*, 3093.
[29] P. J. Hay, *J. Phys. Chem.* **1996**, *100*, 5.
[30] J. Andzelm, J. Baker, A. Scheier, M. Wrinn, *Int. J. Quant. Chem.* **1995**, *56*, 733.
[31] V. G. Malkin, O. L. Malkina, L. A. Eriksson, D. R. Salahub, *Modern Density Functional Theory: A Tool for Chemistry*, vol. 2, Elsevier, Amsterdam, **1995**.
[32] M. Kaupp, V. G. Malkin, O. L. Malkina, D. R. Salahub, *Chem. Eur. J.* **1996**, *2*, 24.
[33] G. Huttner, S. Schelle, *J. Organomet. Chem.* **1973**, *47*, 383.

Received July 29, 1998
[I98254]

Zinc Complexes of Aldehydes and Ketones, 2[+] Zinc-Aldehyde Complexes with Weakly Coordinating Anions

Bodo Müller[a] and Heinrich Vahrenkamp*[a]

Keywords: Zinc / Aldehyde ligands / Weakly coordinating anions / Structural chemistry

Zinc salts of low or zero water content were obtained from the hexahydrates of zinc nitrate, zinc perchlorate, and zinc tetrafluoroborate by dehydration with triethoxymethane or by solvation with acetonitrile or nitromethane. The compounds incorporated aldehydes as ligands when treated with an excess of the aromatic aldehydes benzaldehyde, mesitylaldehyde, 2-chlorobenzaldehyde, and 4-fluorobenzaldehyde. Eighteen zinc-aldehyde complexes were isolated and identified by crystal structure determinations. All contain octahedral zinc to which 2, 3, 4, 5, or 6 aldehyde ligands are bound. Water, ethanol, and acetonitrile molecules act as coligands. Of the anions employed, BF_4^- and $SbCl_6^-$ were found to be only noncoordinating and NO_3^- only coordinating, whereas complexes with one or two perchlorate ligands were obtained in addition to perchlorate salts.

It is widely known that countless reactions of organic carbonyl compounds (esters, amides, aldehydes, ketones, etc.) can be catalyzed by metal salts or complexes. Zinc species play a dominant role in this context for preparative organic chemistry[2] as well as for enzyme-catalyzed transformations[3]. The basic function of the metal ion in these reactions is its attachment to the carbonyl oxygen to induce Lewis-acidic activation. However, since carbonyl compounds are only weak donors and since the important reactions are catalytic, metal complexes of organic carbonyl compounds are rarely isolated. Therefore, in sharp contrast to the many mechanistic proposals involving metal activation of the carbonyl function, the coordination chemistry of this function is rather underdeveloped[4].

We became interested in zinc coordination of CO-containing species during our model studies and mechanistic interpretations of zinc enzyme-catalyzed hydrolyses of esters, amides, and CO_2 by Zn−OH complexes[5]. Our attention focused on aldehydes and alkoxides as ligands when trying to reproduce the biological function of zinc-containing alcohol dehydrogenase[6] by stepwise reactions with zinc complexes[7]. We therefore set out to undertake a comprehensive study of zinc complexation by aldehydes, which led to the results presented in this and the two succeeding[8][9] papers.

The literature on metal complexation of plain aldehydes contains a few papers describing zinc complexes, i.e. hexaaldehyde solvates of zinc salts[10][11], the benzaldehyde adduct of zinc chloride[12], mono- and bis-aldehyde adducts of zinc chalcogenolates[13], chelate complexes of pyridine-2-carbaldehyde[14−16], and two zinc porphyrin complexes with η^1-coordinated benzaldehyde[17][18]. Of these examples only the latter two[17][18] and the $Zn(SeR)_2$(anisaldehyde) dimer[13] were characterized by structure determinations. Likewise, for all other metals the number of well-characterized aldehyde complexes is small, and the level of information is noteworthy only for complexes of salicylic aldehyde and its derivatives as well as for organometallic complexes of η^2 (side-on)-coordinated simple aldehydes[4]. A search of the Cambridge Crystallographic Data File has yielded just six further structures of classical metal complexes with monodentate O-coordinated aldehyde ligands.

Our systematic approach to the chemistry of zinc aldehyde complexes followed four lines: (a) monodentate plain aldehydes and zinc salts of weakly coordinating anions; (b) monodentate plain aldehydes and zinc halides; (c) chelating aldehydes derived from nitrogen heterocycles; (d) aldehyde complexes of zinc thiolates. The aims of this study were: (a) to obtain as many different compound types as possible; (b) to confirm their composition and constitution by structure determinations; (c) to elucidate the donor qualities of the aldehydes as compared to those of competing ligands like water and anions; (d) to find relationships between the complex properties and catalytic phenomena; (e) to model the structure and function of the active site of horse liver alcohol dehydrogenase. We have published a short communication describing the initial stages of this work[1]. This manuscript is the first in a series of full papers describing zinc complexes with predominant or exclusive aldehyde coordination.

Preparations and Structures

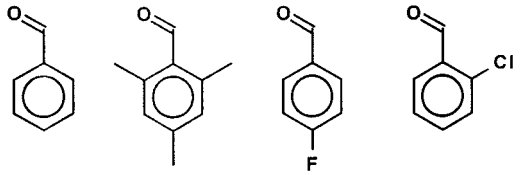
It was clear after our preliminary studies[1] that water, donor solvents, and anions with donor properties, like halides, are better ligands for the zinc ion than aldehydes. Furthermore, aliphatic aldehydes were preferentially condensed, polymerized, or underwent disproportionation to carboxylic esters rather than being incorporated into stable

[+] Part 1: Ref.[1]

[a] Institut für Anorganische und Analytische Chemie der Universität Freiburg,
Albertstr. 21, D-79104 Freiburg, Germany

 © WILEY-VCH Verlag GmbH, D-69451 Weinheim, 1999 1434−1948/99/0101−0117 $ 17.50+.50/0

complexes. This fact dictated the working procedures and the choice of aldehydes. All reactions were carried out in water-free nonpolar solvents containing high concentrations of the aldehydes or using the neat aldehydes as solvents. The water content of the zinc salts was controlled by using triethoxymethane as a dehydrating agent[19] or by starting from water-free zinc hexachloroantimonate solvates[20][21]. Thus the starting zinc compounds were $[Zn(H_2O)_6]X_2$ (X = ClO_4, BF_4, NO_3), $[Zn(CH_3CN)_6](SbCl_6)_2$, and $[Zn(CH_3NO_2)_6](SbCl_6)_2$. These compounds were treated with various aromatic aldehydes of which the following allowed the isolation of pure complexes:



benz-aldehyde **BA** | mesityl-aldehyde **MA** | 4-fluoro-benzaldehyde **FA** | 2-chloro-benzaldehyde **CA**

The hydrated zinc salt was always first dissolved in triethoxymethane before the reaction was started. For each water molecule to be removed, one equivalent of triethoxymethane was applied, plus one additional equivalent for completion of the dehydration. After drying the (partially) dehydrated zinc salt in vacuo it was treated with a large excess of the aldehyde. The resulting clear solutions were diluted with petroleum ether, which caused the aldehyde-containing zinc salts to precipitate. This process worked in all cases. However, the precipitates were never crystalline (e.g. oily) or pure when the precipitation was performed by adding petroleum ether. It was therefore essential to prepare the products by slow crystallization. This was achieved by layering the neat or dichloromethane-diluted aldehyde solutions with petroleum ether and keeping the mixture in a vibration-free place at or slightly below room temperature. In this way all products that could be obtained pure were crystalline and immediately suitable for X-ray crystallography. Due to their extremely hygroscopic nature, all handling of the compounds required the rigorous exclusion of water.

Tetraaqua-bisaldehyde complexes were obtained from zinc perchlorate and tetrafluoroborate with mesitylaldehyde. Compounds **1** and **2** were originally believed to be tetraaldehyde complexes, and only the structure determinations revealed that they contain, in the solid state, two non-coordinating aldehyde molecules that are linked by hydrogen bridges to water ligands.

$[Zn(MA)_2(H_2O)_4]X_2 \bullet 2\ MA$
1: X = ClO_4, **2**: X = BF_4

Figure 1 shows the coordination pattern of **1** and **2**. In both cases the two aldehyde ligands are in *trans* positions, and the Zn−O(aldehyde) bonds are longer than the Zn−O(water) bonds.

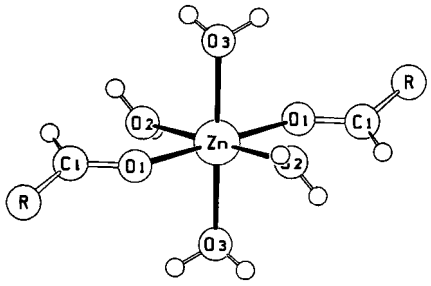


Figure 1. Zinc coordination in **1** and **2**. Bond lengths [Å] and angles [°] for **1/2**: Zn−O1 2.125(1)/2.129(2), Zn−O2 2.069(1)/2.052(2), Zn−O3 2.053(1)/2.075(2), O1−C1 1.227(2)/1.227(3), Zn−O1−C1 135.2(1)/135.5(2), O−C−C 126.0(1)/125.4(2).

Diaqua-tetraaldehyde complexes were again obtained only from $Zn(ClO_4)_2$, $Zn(BF_4)_2$ and mesitylaldehyde. Of these complexes, compound **3** again contains two aldehyde molecules in the second coordination sphere, while **4** has only zinc-coordinated aldehyde. The structure determinations showed that zinc is again *trans*-configured in both compounds (Figure 2). In these cases the Zn−O(aldehyde) and Zn−O(water) bond lengths are spread irregularly over their range from 2.04 to 2.13 Å.

$[Zn(MA)_4(H_2O)_2](ClO_4)_2 \bullet 2\ MA$ **3** $[Zn(MA)_4(H_2O)_2](BF_4)_2$ **4**

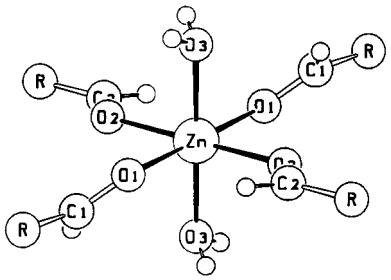


Figure 2. Zinc coordination in $[Zn(MA)_4(H_2O)_2](ClO_4)_2 \bullet 2$ MA (**3**) and $[Zn(MA)_4(H_2O)_2](BF_4)_2$ (**4**). Bond lengths [Å] and angles [°] for **3/4**: Zn−O1 2.061(3)/2.128(1), Zn−O2 2.086(2)/2.102(1), Zn−O3 2.109(2)/2.036(1), O1−C1 1.225(3)/1.233(2), O2−C2 1.226(4)/1.225(2), Zn−O1−C1 130.7(2)/122.6(1), Zn−O2−C2 132.7(2)/129.3(1), O1−C−C 125.9(3)/126.5(2), O2−C−C 125.1(3)/125.1(2).

In order to make these partially solvated zinc salts available for a wider range of aldehydes, two equivalents of ethanol were added to solutions of the bis-hydrates in various aldehydes. However, in only two cases did this lead to pure compounds, and these products were **5** and **6**. In all other cases the precipitates were non-crystalline and non-uniform. The structure determinations (Figure 3) showed that the two aldehyde, alcohol, and water ligands are each bound to zinc in an all-*trans* fashion. There is no noteworthy distinction between the Zn−O bond lengths for the aldehyde, alcohol, or water ligands.

$[Zn(A)_2(EtOH)_2(H_2O)_2]\ (ClO_4)_2$
5: A = MA; **6**: A = CA

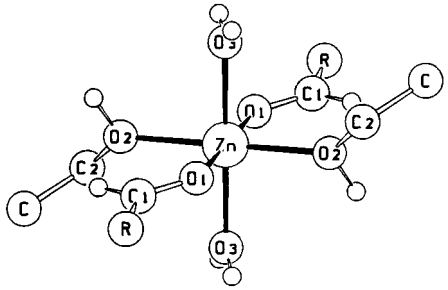


Figure 3. Zinc coordination in $[Zn(A)_2(EtOH)_2(H_2O)_2](ClO_4)_2$ (**5**: A = MA, **6**: A = CA). Bond lengths [Å] and angles [°] for **5**/**6**: Zn−O1 2.083(5)/2.098(3), Zn−O2 2.080(5)/2.057(4), Zn−O3 2.079(5)/2.011(4), O1−C1 1.230(8)/1.225(5), O2−C2 1.440(9)/1.496(9), Zn−O1−C1 130.1(5)/135.1(3), Zn−O2−C2 128.0(4)/127.0(4), O1−C−C 125.4(7)/122.1(4).

Further removal of water allowed the isolation of monoaqua complexes. In the case of 2-chlorobenzaldehyde, four aldehyde molecules and one perchlorate ion were the other ligands in complex **7**. **7** has the water and perchlorate ligands *trans* to each other (Figure 4). Although the Zn−O(aldehyde) bonds are of average length, there is a *trans* effect for the two other Zn−O bonds: the weak (long) Zn−perchlorate interaction has a strong (short) Zn−water interaction *trans* to it.

$[Zn(CA)_4(H_2O)(ClO_4)]ClO_4$
7

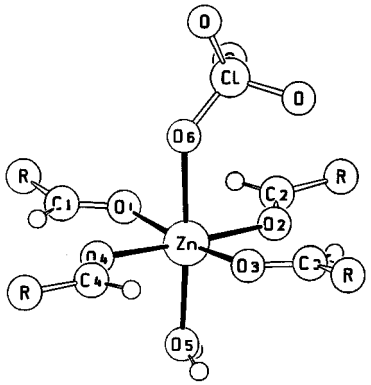


Figure 4. Zinc coordination in $[Zn(CA)_4(H_2O)(ClO_4)]ClO_4$ (**7**). Bond lengths [Å] and angles [°]: Zn−O1 2.078(4), Zn−O2 2.093(5), Zn−O3 2.068(4), Zn−O4 2.095(4), Zn−O5 2.032(6), Zn−O6 2.188(5), O1−C1 1.203(7), O2−C2 1.218(7), O3−C3 1.201(7), O4−C4 1.214(7), Zn−O1−C1 127.8(4), Zn−O2−C2 127.8(4), Zn−O3−C3 127.2(4), Zn−O4−C4 130.0(4), O1−C−C 123.8(6), O2−C−C 123.2(6),O3−C−C 123.4(6), O4−C−C 123.1(6), Zn−O6−Cl 132.4(3).

Five benzaldehyde ligands are present in complex **8**. This time there is no *trans* effect associated with the water ligand, but the average Zn−O(aldehyde) bond length of 2.09 Å is significantly longer than the average Zn−O(water) bond length of 2.02 Å (Figure 5).

$[Zn(BA)_5(H_2O)](BF_4)_2$
8

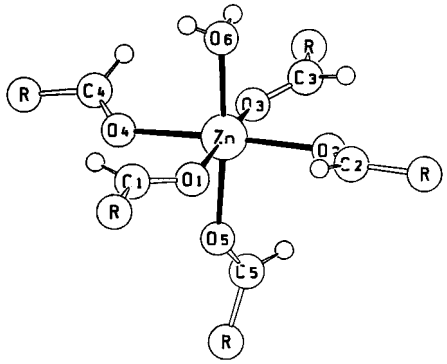


Figure 5. Zinc coordination in $[Zn(BA)_5(H_2O)](BF_4)_2$ (**8**). Bond lengths [Å] and angles [°] in the two independent molecules: Zn−O1 2.091(3)/2.118(3), Zn−O2 2.080(3)/2.079(3), Zn−O3 2.105(3)/2.078(3), Zn−O4 2.096(3)/2.086(3), Zn−O5 2.070(4)/2.080(3), Zn−O6 2.017(4)/2.031(4), O1−C1 1.215(6)/1.217(6), O2−C2 1.215(6)/1.213(6), O3−C3 1.211(6) /1.224(6), O4−C4 1.212(6)/1.213(5), O5−C5 1.216(6)/1.231(6), Zn−O1−C1 127.0(3)/129.6(3), Zn−O2−C2 127.4(3)/126.4(3), Zn−O3−C3 132.3(3)/130.3(3), Zn−O4−C4 126.6(3)/128.7(3), Zn−O5−C5 135.1(4)/127.9(3), O1−C−C 123.5(4)/124.3(4), O2−C−C 123.0(5)/123.6(4), O3−C−C 122.6(5)/122.5(5), O4−C−C 124.5(4)/124.5(4), O5−C−C 122.1(5)/123.5(4).

While no hydrated aldehyde complex of zinc nitrate could be obtained in a pure state, this was the case for the water-free complexes. In the reaction with mesitylaldehyde, complex **9** was isolated. The composition of **9** indicated that three coordination positions would be used for the zinc−nitrate interactions, i.e. one nitrate ligand would be monodentate and the other bidentate, a situation observed many times in octahedral zinc complexes. This was borne out by the structure determination (Figure 6). The three

$[Zn(MA)_3(NO_3)_2]$
9

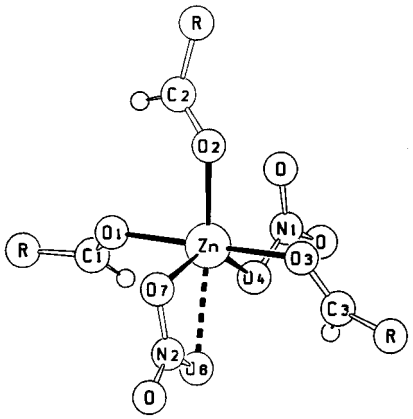


Figure 6. Zinc coordination in $[Zn(MA)_3(NO_3)_2]$ (**9**). Bond lengths [Å] and angles [°]: Zn−O1 2.075(2), Zn−O2 2.032(2), Zn−O3 2.120(2), Zn−O4 2.017(2), Zn−O5 2.098(2), Zn−O6 2.400(2), O1−C1 1.231(3), O2−C2 1.218(2), O3−C3 1.228(3), O1−C−C 125.2(2), O2−C−C 124.7(2), O3−C−C 126.7(2), Zn−O1−C1 127.7(2), Zn−O2−C2 130.7(1), Zn−O3−C3 119.2(1), O2−Zn−O4 125.1(1), O2−Zn−O5 96.3(7), O2−Zn−O6 150.9(1).

aldehyde and the three nitrate oxygen atoms are all arranged meridionally. The unsymmetrically bidentate nature of one nitrate ligand causes a severe distortion of the octahedral ligand arangement (cf. angles involving O2), and the lack of a direct *trans*-ligand makes Zn−O2 an unusually short Zn−O(aldehyde) bond.

Attempts to prepare hexa-aldehyde complexes by way of quantitative dehydration of the zinc salts did not lead to the desired products. Instead tetraaldehyde-bisperchlorate complexes were obtained from $Zn(ClO_4)_2 \bullet 6\ H_2O$. These compounds were isolated in a crystalline form by reaction with benzaldehyde, 4-fluorobenzaldehyde and mesitylaldehyde as **10**, **11**, and **12**. **12** represents another example that contained two equivalents of co-crystallized aldehyde. All three complexes have the four aldehyde ligands in a planar arrangement and the two perchlorate ligands in a *trans*-axial orientation (Figure 7). The presence of two additional aldehyde molecules per formula unit in the crystals of **12** has no influence on bond lengths or angles around zinc. By comparison the Zn−O(aldehyde) bonds are relatively short and the Zn−O(perchlorate) bonds typically long.

$[Zn(A)_4(ClO_4)_2]$
10: A = BA; **11**: A = FA; **12**: A = MA

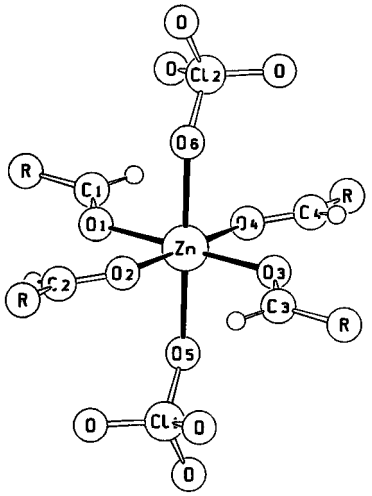


Figure 7. Zinc coordination in **10**, **11**, and **12** (**10** and **11** have zinc on an inversion center). Bond lengths [Å] and angles [°] for **10**/**11**/**12**: Zn−O1 2.063(1)/2.068(1)/2.072(3), Zn−O2 2.057(1)/2.044(1)/2.052(2), Zn−O3 −/−/2.084(3), Zn−O4 −/−/2.043(2), Zn−O5 2.143(1)/2.159(1)/2.134(3), Zn−O6 −/−/2.230(3), O1−C1 1.229(2)/1.227(2)/1.235(4), O2−C2 1.234(2)/1.231(2)/1.233(4), O3−C3 −/−/1.229(4), O4−C4 −/−/1.233(4), Zn−O1−C1 129.0(1)/128.3(1)/121.2(2), Zn−O2−C2 127.0(1)/128.9(1)/123.8(2), Zn−O3−C3 −/−/125.1(2), Zn−O4−C4 −/−/125.2(2), O1−C−C 123.3(2)/123.1(2)/126.9(3), O2−C−C 122.9(2)/122.2(2)/125.4(3), O3−C−C −/−/125.9(3), O4−C−C −/−/125.3(2), Zn−O5−Cl 132.8(3)/133.6(1)/135.0(2), Zn−O6−Cl −/− 142.4(2).

In complexes like **10**−**12** the perchlorate ligands seem to be more difficult to replace than the aldehyde ligands. This became evident when two equivalents of ethanol were added to solutions of the fully dehydrated zinc salts in the neat aldehydes. Complex **13** could be crystallized from its solution in mesitylaldehyde. Figure 8 shows the all-*trans* arrangement of its pairs of aldehyde, alcohol, and perchlorate ligands. The Zn−O(aldehyde) and Zn−O(alcohol) bond lengths are not significantly different in **13**, and all of its Zn−O bond lengths are quite similar to those in **10**−**12**.

$[Zn(MA)_2(EtOH)_2(ClO_4)_2]$
13

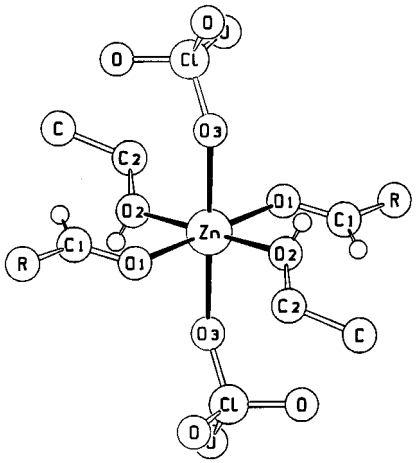


Figure 8. Zinc coordination in **13**. Bond lengths [Å] and angles [°]: Zn−O1 2.069(2), Zn−O2 2.045(3), Zn−O3 2.151(3), O1−C1 1.225(4), O2−C2 1.447(4), Zn−O1−C1 125.6(2), Zn−O2−C2 130.5(2), Zn−O3−Cl 143.1(2), O1−C−C 126.4(3).

It was thus obvious that the aldehydes are not strong enough as donors to occupy all six coordination positions at the zinc ion in the presence of the weakly coordinating anions NO_3^-, BF_4^-, or ClO_4^-. We therefore resorted to solvated zinc hexachloroantimonate as a starting material. By dissolving $[Zn(CH_3CN)_6](SbCl_6)_2$[20] in the aldehydes we found that not more than two of the acetonitrile ligands could be replaced. Complexes **14**−**16** were isolated.

trans-$[Zn(A)_2(MeCN)_4]\ (SbCl_6)_2$
14: A = BA; **15**: A = MA

cis-$[Zn(CA)_2(MeCN)_4]\ (SbCl_6)_2$
16

The structure determinations revealed that **14** and **15** are *trans*-configured (Figure 9). The mediocre quality of the data set for **14** prohibits a detailed comparison, but it is obvious that the Zn−O and Zn−N bond lengths in both complexes are practically identical and that the equatorially arranged acetonitrile ligands show a variable deviation from linearity (157−177°) at their nitrile carbon atoms.

In contrast, complex **16** is *cis*-configured (Figure 10). This time there is a distinction between the Zn−O and Zn−N bond lengths, the latter being shorter, and the acetonitrile ligands are closer to being linear. The structural features do not offer an indication as to why **14** and **15** should be *trans*- and **16** *cis*-configured.

A complete replacement of solvate by aldehyde ligands could be achieved by starting with $[Zn(CH_3NO_2)_6](SbCl_6)_2$[21], as previously reported by Driessen et al.[10][11]. The problem of fast decomposition of the products could

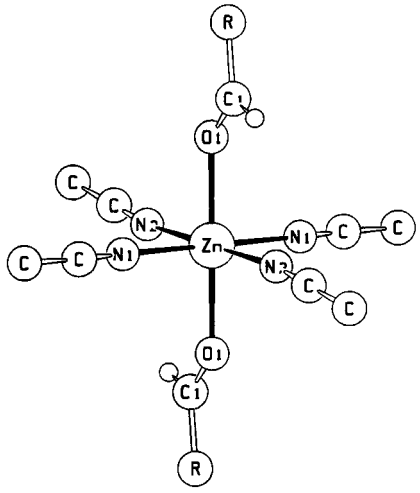


Figure 9. Zinc coordination in **14** and **15**. Bond lengths [Å] and angles [°] in **14/15**: Zn−O1 2.116(9)/2.103(3), Zn−N1 2.113(11)/2.137(4), Zn−N2 2.117(12)/2.106(5), O1−C1 1.20(1)/1.23(1), Zn−O1−C1 136(1)/129.2(3), O1−C−C 123(1)/126.4(4), Zn−N1−C 174(1)/157.3(4), Zn−N2−C 172(1)/165.1(4).

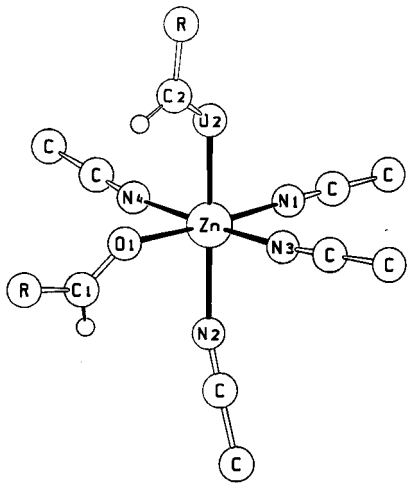


Figure 10. Zinc coordination in **16**. Bond lengths [Å] and angles [°]: Zn−O1 2.168(2), Zn−O2 2.149(2), Zn−N1 2.087(3), Zn−N2 2.165(3), Zn−N3 2.087(3), Zn−N4 2.082(3), O1−C1 1.215(4), O2−C2 1.216(4), Zn−O1−C1 131.0(2), Zn−O2−C2 128.0(2), O1−C−C 123.1(4), O2−C−C 123.8(3), Zn−N1−C 177.4(3), Zn−N2−C 164.3(3), Zn−N3−C 168.4(3), Zn−N4−C 171.5(3).

be overcome for fluoro- and chlorobenzaldehyde, making compounds **17** and **18** accessible in a pure and crystalline form.

$[Zn(FA)_6](SbCl_6)_2$ $[Zn(CA)_6](SbCl_6)_2 \bullet 4\ CA$
17 **18**

Structurally **17** and **18** are symmetrical octahedral complexes (Figure 11). Specifically, **18** shows very uniform bond lengths and angles for the aldehyde ligands and a very narrow spread of 88−92° for the angles at zinc. The lower data quality for **17** seems to have caused a wider spread of bond lengths and angles, the averages of which, however, agree well with those for **18**. The two complexes define the structural standards for homoleptic zinc-aldehyde complexes with bond lengths of ca. 2.08 Å for Zn−O and ca. 1.23 Å for C−O.

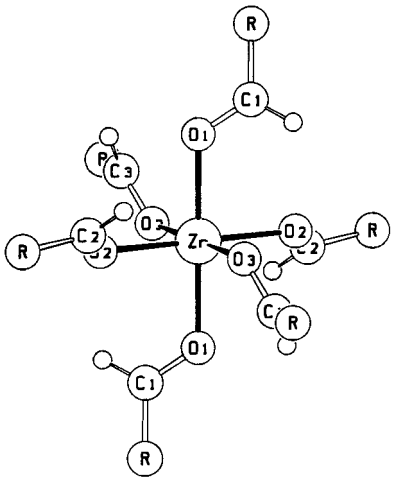


Figure 11. Zinc coordination in **17** and **18** (**18** has zinc on an inversion center). Bond lengths [Å] and angles [°] for **17/18**: Zn−O1 2.07(1)/2.073(2), Zn−O2 2.05(1)/2.078(2), Zn−O3 2.15(1)/2.075(2), Zn−O4 2.11(1)/−, Zn−O5 2.09(1)/−, Zn−O6 2.08(1)/−, O1−C1 1.26(2)/1.219(4), O2−C2 1.24(2)/1.219(4), O3−C3 1.21(2)/1.222(4), O4−C4 1.25(2)/−, O5−C5 1.19(2)/−, O6−C6 1.28(2)/−, Zn−O1−C1 122(1)/124.6(2), Zn−O2−C2 130(1)/124.5(2), Zn−O3−C3 119(1)/127.3(2), Zn−O4−C4 125(1)/−, Zn−O5−C5 130(1)/−, Zn−O6−C6 130 (1)/−.

Discussion of the Structures

All these aldehyde complexes are octahedral to a very good approximation. In most cases the valence angles at zinc deviate by not more than ±3° from 90° or ±5° from 180°, with the extremes being ±6° and ±8°, respectively. The aldehyde ligands are attached to zinc in a strict anti fashion, as expressed by the dihedral angles Zn−O−C−R, which range from 158° to 180° with an average over all structures of 174°. Furthermore, and despite some steric hindrance, the aromatic rings of the aldehydes are always coplanar with the RCHO functions, again expressed by dihedral angles ranging from 166° to 179° with an average of 176°.

Details of the Zn−O bond lengths and some internal comparisons were mentioned above for the complex types. Table 1 gives the data for a general comparison. The most interesting question is whether the bonding strength of the aldehydes can be deduced from their Zn−O distances. An inspection of Table 1 reveals that for a given complex type there is no distinction between Zn−O bond lengths according to the type of aldehyde. Instead the coligands seem to have the major influence on the strength of the zinc-aldehyde interaction. When two or more water (**1**−**6**) or acetonitrile ligands (**14**−**16**) are present the Zn−O(aldehyde) bonds are long. In turn, when only aldehyde ligands are present (**17**, **18**) or when only perchlorate is the coligand (**10**−**12**), the Zn−O(aldehyde) bonds are short. This is another demonstration of the fact that the aldehydes are very weak ligands.

Table 1. Bonding features (average values of bond lengths [Å] and angles [°]) for the zinc−aldehyde interactions

	aldehyde			coligands	
	Zn−O	O−C	Zn−O−C	X	Zn−X
1	2.13	1.23	135	$O(H_2O)$	2.06
2	2.13	1.23	136	$O(H_2O)$	2.06
3	2.10	1.23	132	$O(H_2O)$	2.06
4	2.12	1.23	126	$O(H_2O)$	2.04
5	2.08	1.23	130	$O(H_2O)$	2.08
				O(EtOH)	2.08
6	2.10	1.23	135	$O(H_2O)$	2.01
				O(EtOH)	2.06
7	2.08	1.21	128	$O(H_2O)$	2.03
				$O(ClO_4)$	2.19
8	2.09	1.22	129	$O(H_2O)$	2.02
9	2.08	1.23	126	$O(NO_3)$	2.02
				$O(NO_3)$	2.10, 2.40
10	2.06	1.23	128	$O(ClO_4)$	2.14
11	2.06	1.23	129	$O(ClO_4)$	2.16
12	2.06	1.23	124	$O(ClO_4)$	2.18
13	2.07	1.23	126	O(EtOH)	2.05
				$O(ClO_4)$	2.15
14	2.12	1.20	136	N(MeCN)	2.12
15	2.10	1.23	129	N(MeCN)	2.12
16	2.16	1.22	130	N(MeCN)	2.11
17	2.09	1.24	126	−	−
18	2.08	1.22	126	−	−

The spread of the Zn−O distances finds no reflection in the other structural features of the aldehydes. The details of the aldehyde orientation (cf. dihedral angles, see above) show no systematic relation with the Zn−O(aldehyde) bond lengths. The range of the aldehyde C=O bond lengths is too small to warrant a discussion. There is just a barely noticeable proportionality between the Zn−O−C angles and the Zn−O(aldehyde) bond lengths. When compared to the three other reported structures of zinc-aldehyde complexes[13][17][18] the structural features listed in Table 1 span the range observed there.

The coligands in complexes **1**−**16** bind to zinc in a fashion that is known to occur in such complexes[22]. Specifically the bonding alternatives for the nitrate ligand between strictly monodentate and symmetrically bidentate and the weak and variable zinc−perchlorate interactions are well known. Similarly the Zn−N(acetonitrile) bond lengths in **14**−**16** are in the reported range, as are the deviations of the Zn−N−C units from linearity found here (157−177°) in comparison to the reported range (156−178°)[22].

Complexes **17** and **18** are of general significance as they define the standard of ZnO_6 coordination by aldehydes. Their Zn−O distances of 2.08−2.09 Å compare very well with the average values for Zn−O in $Zn(H_2O)_6^{2+}$ (2.09 Å)[23] and in $Zn(alcohol)_6^{2+}$ (2.08 Å)[24]. Other reported complexes with a homoleptic ZnO_6 coordination belong to the types $Zn(pyridine\ oxide)_6^{2+}$[25], $Zn(urea)_6^{2+}$[26], and $Zn(DMSO)_6^{2+}$[27] with average Zn−O bond lengths of 2.10, 2.10, and 2.11 Å, respectively. The Zn−O bond length for the aldehyde complexes is at the lower end of all these ZnO_6 species, indicating again that donor strength and bond distances are not clearly correlated for such compounds. Instead the very narrow spread of all these Zn−O bond lengths (2.08−2.11 Å) indicates that the packing of six oxygen atoms around one zinc ion does not allow shorter contacts irrespective of the variation of the attractive forces.

Spectroscopy

The most important indication for the formation of the aldehyde complexes was the observation of the aldehyde ν(CO) IR bands at their typical locations. As shown in Table 2, the bands for coordinated aldehydes are shifted by ca. 50−80 cm^{-1} to lower wavenumbers, which is in agreement with previous observations on zinc-hexaaldehyde complexes[10][11]. In contrast, those complexes that contain cocrystallized uncoordinated aldehyde display additional ν(CO) bands that are practically unshifted.

Contrary to expectation, the ν(CO) band shifts are neither proportional to the donor strength (i.e. electron richness of the aromatic system) of the aldehydes nor inversely proportional to the donor power of the coligands (i.e. water stronger than perchlorate). Indeed complex **10**, containing benzaldehyde as one of the better aldehyde donors together with only the very weak donor perchlorate, shows the smallest Δν, and complex **6**, containing electron-poor 2-chlorobenzaldehyde together with two water and two ethanol ligands, shows the largest Δν. There seem to be, however, rather uniform Δν values for each aldehyde, e.g. −50 cm^{-1} for BA, −55 cm^{-1} for MA, −65 cm^{-1} for FA, and −80 cm^{-1} for CA. This trend should be of diagnostic value.

The IR data of the coligands and anions also yield some information (Table 2). While the water and ethanol ligands

Table 2. IR data (KBr, cm^{-1}) of the complexes

	aldehyde	$-\Delta\bar{\nu}$	coligand	anion
1	1685 s, 1635 s	5, 55	3517 m, br	1149 s, 1110 s, 1088 s, 940 m
2	1684 s, 1634 s	6, 56	3565 m, br	1148 s, 1034 s
3	1685 s, 1636 s	5, 54	3456 m	1148 s, 1110 s, 1089 s, 940 m
4	1638 s	52	3448 m	1043 s, br
5	1635 s	55	3442 m, br	1149 s, 1108 s, 1085 s, 940 w
6	1616 s	50	3526 m	1146 s, 1107 s, 1087 s, 940 w
7	1619 s	79	3446 m, br	1109 s, 1088 s
8	1651 s	50	3450 m, br	1034 s, br
9	1640 s	50	−	1465 s, br, 1390 s, 1290 s, br
10	1654 s	47	−	1149 s, 1108 s, 1086 s
11	1638 s	62	−	1150 s, 1095 s, br
12	1689 s, 1635 s	1, 55	−	1149 s, 1104, 1088 s
13	1634 s	56	3415 m	1150 s, 1091 s
14	1650 s	51	2316 m, 2290 m	−
15	1639 s	51	2317 m, 2287 m	−
16	1643 s	55	2316 m, 2296 m	−
17	1635 s	65	−	−
18	1698 s, 1627 s	0, 71	−	−

display a broad and unspecific absorption between 3400 and 3550 cm^{-1}, the ν(CN) bands of the acetonitrile ligands are characteristically shifted by 25−40 cm^{-1} to higher wavenumers[28] as compared to those of free CH_3CN. The ν(NO) bands of the nitrate ligands, as is usual[29], give no clear indication of their bonding mode (uni- or bidentate). The BF_4^- and ClO_4^- ions show their strong absorptions near 1100 cm^{-1}. For perchlorate, a medium-intensity band near 940 cm^{-1}, assignable to a fully symmetrical stretch[19], is observed only in complexes **1**, **3**, **5**, and **6**, in accord with the structural data showing that these complexes contain uncoordinated ClO_4^-.

The suitability of NMR spectroscopy for bonding discussions of the aldehyde complexes is hampered by the fact that, other than in the neat aldehydes, they dissolve only in polar organic solvents that may be stronger donors for zinc than the aldehydes. Accordingly, only small shift effects were observed when recording the spectra in [D_6]acetone. Table 3 lists the data.

Table 3. ^{1}H- and ^{13}C-NMR data for the aldehyde CHO functions (in [D_6]acetone, δ)

	δ(H)	Δδ	δ(C)	Δδ
1	10.49	+0.01	193.9	+1.3
2	10.46	−0.02	194.1	+1.5
3	10.50	+0.02	193.8	+1.2
4	10.49	+0.01	193.8	+1.2
5	10.48	±0	194.4	+1.8
6	10.31	−0.05	190.2	+0.8
7	10.39	+0.03	190.0	+0.6
8	10.12	+0.06	193.4	+0.7
9	10.45	−0.03	195.3	+2.7
10	9.96	−0.10	194.6	+1.9
11	10.00	+0.05	191.7	+0.9
12	10.46	−0.02	194.8	+2.2
13	10.48	±0	194.6	+2.0
14	10.01	−0.05	193.0	+0.3
15	10.50	+0.02	193.5	+0.9
16	10.39	+0.03	189.8	+0.4
17	9.96	+0.01	191.3	+0.5
18	10.39	+0.03	189.7	+0.3

Metal coordination of the aldehyde function should lead to deshielding of both the H and C of RCHO. Such a deshielding is actually observed with Δδ values of 1−2 ppm for the ^{13}C resonances while the ^{1}H resonances are so close to those of the free aldehydes that they cannot be discussed. The extent of deshielding decreases in the order MA > BA > FA > CA, which can be correlated with the donor strengths. The NMR spectra, however, do not show a distinction between coordinated and uncoordinated aldehydes in complexes **1**−**3**, **12**, and **18**.

The coligands ethanol and acetonitrile seem to stay coordinated to zinc in acetone solutions. Their ^{1}H-NMR resonances are shifted by 0.5−1 ppm to lower field in comparison to those of the free ligands. Likewise the ^{13}C-NMR signals are shifted downfield by up to 2.5 ppm for ethanol-CH_2, but show almost no shift for the acetonitrile resonances.

Conclusions

This work has shown that two to six aldehyde molecules can be coordinated to zinc under carefully controlled conditions. The complexes described here are those that were isolated in an analytically pure form. Many more have been prepared in a less pure form, and it is to be assumed that the various structural types can be realized by most of the aldehydes. The aldehydes are completely expelled from the ligand sphere of zinc when excess water is present. In the presence of strongly coordinating anions like the halides, completely different structural types are observed[8].

All isolated complexes were found to be octahedral. Normally they contain one to four coligands together with the aldehyde ligands. In addition to water, ethanol and acetonitrile can also not be completely replaced by the aldehydes. Under anhydrous conditions the nitrate and perchlorate anions are preferred over the aldehydes as ligands. Hexaaldehyde complexes could only be obtained by replacement of the very weak donor nitromethane and by applying an anion ($SbCl_6^-$) of extremely low donor strength.

X-ray structure determination was found to be the only method of unambiguous product identification. It has provided the structural features of zinc−aldehyde bonding. It has delivered examples of the basic ZnL_6 structure for L = aldehyde, which need to be complemented for other L, e.g. alcohol, acetone, ethers, nitromethane, acetonitrile, etc. It has been shown that slight variations in the reaction conditions can lead to quite different compositions of the complexes. Together with the low donor strength of the aldehydes this means that there exists a high degree of uncertainty when mechanistic conclusions are drawn from such structures or even from the composition of reaction solutions.

With respect to modelling the zinc enzyme alcohol dehydrogenase, this work has provided some elementary information. On the one hand it was shown that aldehydes can be bound to zinc in the presence of water, i.e. zinc can be involved in the process of aldehyde reduction. On the other hand it has become very clear that excess water replaces zinc-bound aldehydes very easily, e.g. the last step of alcohol oxidation is facile. Furthermore, the possible coexistence of alcohol and aldehyde ligands in the same complex was demonstrated. With respect to the chemical reactions happening in the enzyme, the findings of this work are of little relevance as neither the low coordination number of zinc nor the presence of a redox reagent were reproduced. It was partly for this reason that we extended our studies of zinc−aldehyde coordination to further types of ligands and coligands[8][9].

Experimental Section

The general working and measuring techniques were as described previously[30]. All experiments were carried out using carefully dried atmospheres (nitrogen or argon) and solvents. As some of the products were too moisture-sensitive for ordinary C/H/N analyses, all compounds were also characterized by zinc and anion analyses

Table 4. Reaction details

Compl.	zinc salt			$HC(OEt)_3$			aldehyde/EtOH			yield		m.p.
		g	mmol	mL	g	mmol		mL	g	mmol	g	%	°C
1	$Zn(H_2O)_6(ClO_4)_2$	1.58	4.25	2.12	1.89	12.75	MA	10	10.05	67.81	3.71	94	91
2	$Zn(H_2O)_6(BF_4)_2$	1.09	3.14	1.57	1.40	9.42	MA	7	7.04	47.50	2.64	93	99
3	$Zn(H_2O)_6(ClO_4)_2$	0.92	2.47	2.05	1.83	12.35	MA	5	5.03	33.94	2.08	71	87
4	$Zn(H_2O)_6(BF_4)_2$	0.56	1.61	1.35	1.20	8.07	MA	5	5.03	33.94	0.59	42	93
5	$Zn(H_2O)_6(ClO_4)_2$	1.03	2.77	2.30	2.05	13.83	MA	5	5.03	33.94	0.95	50	70
							EtOH	0.323	0.25	5.43			
6	$Zn(H_2O)_6(ClO_4)_2$	1.03	2.77	2.29	2.04	13.79	CA	5	6.24	44.39	1.25	67	80
							EtOH	0.323	0.25	5.43			
7	$Zn(H_2O)_6(ClO_4)_2$	1.01	2.71	2.71	2.41	16.27	CA	5	6.24	44.39	0.52	23	131
8	$Zn(H_2O)_6(BF_4)_2$	0.81	2.33	2.34	2.08	14.00	BA	5	5.22	49.19	1.06	58	87
9	$Zn(H_2O)_6(NO_3)_2$	0.48	1.61	2.14	1.91	12.91	MA	10	10.05	67.81	0.72	70	79
10	$Zn(H_2O)_6(ClO_4)_2$	1.19	3.20	4.25	3.79	25.57	BA	9	9.40	88.54	1.60	73	122
11	$Zn(H_2O)_6(ClO_4)_2$	1.10	2.95	3.93	3.50	23.63	FA	5	5.79	46.65	0.52	23	135 (dec.)
12	$Zn(H_2O)_6(ClO_4)_2$	0.87	2.34	3.11	2.77	18.69	MA	5	5.03	33.94	1.88	70	81
13	$Zn(H_2O)_6(ClO_4)_2$	1.04	2.79	3.72	3.31	22.34	MA	5	5.03	33.94	0.51	28	117
							EtOH	0.325	0.26	5.64			
14	$Zn(MeCN)_6(SbCl_6)_2$	1.09	1.11	–	–	–	BA	5	5.22	49.19	1.07	87	117 (dec.)
15	$Zn(MeCN)_6(SbCl_6)_2$	1.45	1.48	–	–	–	MA	5	5.03	33.94	1.28	72	93 (dec.)
16	$Zn(MeCN)_6(SbCl_6)_2$	1.23	1.25	–	–	–	CA	5	6.24	44.39	1.27	86	86
17	$Zn(MeNO_2)_6(SbCl_6)_2$	1.65	1.50	–	–	–	FA	5	5.79	46.65	2.10	95	105
18	$Zn(MeNO_2)_6(SbCl_6)_2$	1.51	1.37	–	–	–	CA	5	6.24	44.39	2.66	91	80

(Table 5). All starting compounds were obtained commercially, recrystallized or distilled prior to use, and stored under anhydrous conditions. The acetonitrile[20] and nitromethane[21] complexes of zinc were prepared as described. Although none of the perchlorate-containing materials were found to be explosive, all of them were handled in small quantities and with the appropriate safety precautions. The new complexes were prepared following two procedures that are outlined below and the details for which are given in Table 4. Table 5 gives data of the analytical characterizations.

Preparation of Complexes 1−13: The hydrated zinc salt was dissolved in the appropriate amount of triethoxymethane (n + 1 equivalents for removal of n equivalents of water). The solution was heated to reflux using a hot air blower for a few seconds. After cooling to room temperature, all volatiles were removed in vacuo and the residue dried in vacuo at 40−50°C for 2 h. An approximately 10-fold excess of the aldehyde was then added and the mixture stirred with warming until all reactants had dissolved. After cooling the solution to room temperature the aldehyde solution was layered carefully with 30 mL of petroleum ether (b.p. 60−70°C). Within one to two days the colourless product complex had precipitated. In those cases where the product was crystalline it was also found to be pure. The complex was filtered off, washed with a small amount of petroleum ether (b.p. 60−70°C) and dried in vacuo.

Preparation of Complexes 14−18: The solvated zinc salt was suspended in 5 mL of dichloromethane. 5 mL of the aldehyde was added with stirring upon which a clear solution was formed. This solution was layered carefully with 40 mL of petroleum ether (b.p. 60−70°C). Within a few days the product complex had precipitated as colourless crystals, which were filterd off, washed with a few mL of petroleum ether (b.p. 60−70°C) and dried for a short time in vacuo.

Structure Determinations[31]: Crystals were obtained from the reaction solutions. The crystals were then immersed in perfluorinated polyether oil for protection and attachment to the goniometer head and immediately subjected to the nitrogen flow from the diffractometer's cooling system. Diffraction data were recorded at low temperatures with the ω/2θ technique on a Nonius CAD4 dif-

Table 5. Analytical characterization

	formula mol. wt.	Analyses calcd./found C	H	Zn	X	
1	$C_{20}H_{32}Cl_2O_{14}Zn \bullet$ $2\ C_{10}H_{12}O$ 632.8 + 296.4	51.71/ 52.05	6.08/ 6.07	7.04/ 7.01	ClO_4	21.41/ 21.50
2	$C_{20}H_{32}B_2F_8O_6Zn \bullet$ $2\ C_{10}H_{12}O$ 607.5 + 296.4	– –	– –	7.23/ 7.17	BF_4	25.45/ 25.34
3	$C_{40}H_{52}Cl_2O_{14}Zn \bullet$ $2\ C_{10}H_{12}O$ 893.2 + 296.4	– –	– –	5.50/ 5.56	ClO_4	16.72/ 16.84
4	$C_{40}H_{52}B_2F_8O_6Zn$ 867.9	55.36/ 56.86	6.04/ 6.11	7.54/ 7.62	BF_4	20.01/ 19.96
5	$C_{24}H_{40}Cl_2O_{14}Zn$ 688.9	41.85/ 41.64	5.85/ 5.82	9.49/ 9.62	ClO_4	28.87/ 28.95
6	$C_{18}H_{26}Cl_4O_{14}Zn$ 673.6	32.10/ 32.56	3.89/ 3.38	9.71/ 9.84	ClO_4	29.53/ 29.76
7	$C_{28}H_{22}Cl_6O_{13}Zn$ 844.6	39.82/ 39.46	2.63/ 2.76	7.74/ 7.80	ClO_4	23.55/ 23.41
8	$C_{35}H_{32}B_2F_8O_6Zn$ 787.6	53.37/ 54.78	4.10/ 3.33	8.30/ 8.36	BF_4	22.04/ 21.83
9	$C_{30}H_{36}N_2O_9Zn$ 634.0	– –	– –	10.31/ 10.24	NO_3	19.56/ 19.62
10	$C_{28}H_{24}Cl_2O_{12}Zn$ 688.8	– –	– –	9.49/ 9.61	ClO_4	28.88/ 28.64
11	$C_{28}H_{20}Cl_2F_4O_{12}Zn$ 760.8	44.21/ 44.10	2.65/ 2.57	8.60/ 8.58	ClO_4	26.15/ 26.23
12	$C_{40}H_{48}Cl_2O_{12}Zn \bullet$ $2\ C_{10}H_{12}O$ 857.1 + 296.4	– –	– –	5.67/ 5.69	ClO_4	17.24/ 17.21
13	$C_{24}H_{36}Cl_2O_{12}Zn$ 652.8	– –	– –	10.02/ 9.98	ClO_4	30.47/ 30.38
14	$C_{22}H_{24}Cl_{12}N_4O_2Sb_2Zn$ 1110.8	– –	– –	5.89/ 5.74	Cl	38.30/ 38.42
15	$C_{28}H_{36}Cl_{12}N_4O_2Sb_2Zn$ 1194.9	– –	– –	5.47/ 5.52	Cl	35.60/ 35.68
16	$C_{22}H_{22}Cl_{14}N_4O_2Sb_2Zn$ 1179.7	22.40/ 22.37	1.88/ 1.67	5.54/ 5.50	Cl	42.07/ 42.18
17	$C_{42}H_{30}Cl_{12}F_6O_6Sb_2Zn$ 1479.0	34.11/ 34.31	2.05/ 2.26	4.42/ 4.39	Cl	28.77/ 28.86
18	$C_{42}H_{30}Cl_{18}O_6Sb_2Zn \bullet$ $4\ C_7H_5ClO$ 1577.7 + 562.3	39.29/ 38.72	2.36/ 2.62	3.06/ 3.14	Cl	36.45/ 36.73

fractometer fitted with a molybdenum tube (K_α, λ = 0.7107 Å) and a graphite monochromator. No absorption corrections were applied. The structures were solved by direct methods and refined anisotropically with the SHELX program suite[32]. The aldehyde C−H and water and alcohol O−H hydrogen atoms were located and refined freely. All other hydrogen atoms were included with fixed distances and isotropic temperature factors 1.2 times those of their attached atoms. Parameters were refined against F^2. The R

Table 6, part 1. Crystallographic details

	1	**2**	**3**	**4**	**5**	**6**
formula	$C_{20}H_{32}Cl_2O_{14}Zn$ • 2 $C_{10}H_{12}O$	$C_{20}H_{32}B_2F_8O_6Zn$ • 2 $C_{10}H_{12}O$	$C_{40}H_{52}Cl_2O_{14}Zn$ • 2 $C_{10}H_{12}O$	$C_{40}H_{52}B_2F_8O_6Zn$	$C_{24}H_{40}Cl_2O_{14}Zn$	$C_{18}H_{26}Cl_4O_{14}Zn$
mol. mass	929.12	903.84	1189.48	867.81	688.83	673.56
crystal size [mm]	0.9 × 0.6 × 0.5	0.9 × 0.7 × 0.5	1.2 × 0.8 × 0.7	0.8 × 0.7 × 0.6	0.6 × 0.5 × 0.4	0.6 × 0.5 × 0.5
space group	$P\bar{1}$	$P\bar{1}$	$P\bar{1}$	$P2_1/c$	$P\bar{1}$	$P\bar{1}$
Z	1	1	1	2	1	1
a [Å]	8.560(2)	8.500(6)	8.008(2)	8.172(2)	7.734(1)	7.604(1)
b [Å]	11.565(2)	11.505(3)	14.046(7)	15.484(2)	8.828(1)	7.616(1)
c [Å]	11.587(4)	11.547(3)	14.721(3)	17.248(3)	12.507(2)	12.640(1)
α [°]	71.94(2)	72.48(2)	109.89(4)	90	79.14(1)	86.68(1)
β [°]	87.29(2)	87.16(4)	91.30(2)	101.980(15)	89.46(1)	75.69(1)
γ [°]	84.56(2)	85.20(4)	98.50(3)	90	65.60(1)	71.54(1)
V [Å^3]	1085.5(5)	1072.7(9)	1535.2(9)	2134.9(6)	761.5(2)	672.6(2)
d(calc.) [g•cm^{-3}]	1.42	1.340	1.29	1.35	1.502	1.66
d(obs.) [g•cm^{-3}]	1.41	1.39	1.27	1.33	–	1.61
temp. [K]	183(2)	183(2)	293(2)	183(2)	183(2)	183(2)
μ(Mo-$K\alpha$) [mm^{-1}]	0.76	0.66	0.55	0.65	1.05	1.38
hkl range	h: −10 to 10 k: −14 to 13 l: −14 to 0	h: −10 to 0 k: −14 to 14 l: −14 to 14	h: −9 to 9 k: −17 to 0 l: −17 to 18	h: −10 to 9 k: 0 to 19 l: 0 to 21	h: −9 to 9 k: −10 to 10 l: −14 to 0	h: 0 to 9 k: −8 to 9 l: −15 to 15
refl. measd.	4498	4508	6256	4318	2662	2849
indep. refl.	4276	4208	6000	4176	2531	2641
obs. refl. [I>2σ(I)]	4116	4068	5047	3777	1752	2502
parameters	284	285	366	267	191	175
refl. refined	4276	4208	6000	4176	2531	2641
R_1 (obs. refl.)	0.026	0.062	0.055	0.031	0.058	0.055
wR_2 (all refl.)	0.076	0.204	0.183	0.087	0.175	0.132
residual el. density [e/Å^{-3}]	+0.3 −0.5	+1.3 −2.1	+0.9 −0.5	+0.4 −0.4	+0.6 −1.0	+1.4 −1.0

Table 6, part 2. Crystallographic details

	7	**8**	**9**	**10**	**11**	**12**
formula	$C_{28}H_{22}Cl_6O_{13}Zn$	$C_{35}H_{32}B_2F_8O_6Zn$	$C_{30}H_{36}N_2O_9Zn$	$C_{28}H_{24}Cl_2O_{12}Zn$	$C_{28}H_{20}Cl_2F_4O_{12}Zn$	$C_{40}H_{48}Cl_2O_{12}Zn$ • 2 $C_{10}H_{12}O$
mol. mass	844.53	787.60	633.98	688.74	760.71	1153.45
crystal size [mm]	1.2 × 1.0 × 0.5	1.1 × 1.0 × 1.0	1.2 × 1.0 × 0.9	0.6 × 0.5 × 0.4	1.2 × 1.2 × 0.3	0.8 × 0.7 × 0.6
space group	$C2/c$	$P2_1$	$Pbca$	$P\bar{1}$	$P\bar{1}$	$P2_1$
Z	8	4	8	1	1	2
a [Å]	34.263(6)	10.250(1)	15.65(4)	8.637(3)	8.366(1)	13.967(1)
b [Å]	14.709(3)	20.549(3)	17.40(3)	9.472(1)	9.776(1)	14.059(2)
c [Å]	13.677(3)	17.602(3)	22.24(4)	10.350(3)	10.533(1)	14.493(1)
α [°]	90	90	90	68.55(2)	68.62(1)	90
β [°]	94.640(16)	90.220(12)	90	68.88(2)	68.71(1)	90.820(9)
γ [°]	90	90	90	69.99(2)	70.56(1)	90
V [Å^3]	6870(2)	3707.4(9)	6058(2)	713.2(3)	727.2(1)	2845.6(5)
d(calc.) [g•cm^{-3}]	1.633	1.411	1.390	1.60	1.74	1.346
d(obs.) [g•cm^{-3}]	1.610	1.384	1.384	1.59	–	1.322
temp. [K]	293(2)	183(2)	183(2)	183(2)	183(2)	183(2)
μ(Mo-$K\alpha$) [mm^{-1}]	1.24	0.75	0.87	1.11	1.12	0.59
hkl range	h: −41 to 41 k: 0 to 18 l: 0 to 16	h: −12 to 12 k: −25 to 0 l: 0 to 22	h: −18 to 0 k: 0 to 20 l: 0 to 26	h: −10 to 9 k: −11 to 10 l: −12 to 0	h: −10 to 9 k: −12 to 0 l: −12 to 12	h: −17 to 17 k: 0 to 17 l: −18 to 0
refl. measd.	4376	7940	5259	2960	3016	6456
indep. refl.	4376	7692	5258	2798	2840	6210
obs. refl. [I>2σ(I)]	4376	7213	4553	2701	2765	5576
parameters	441	945	379	196	214	694
refl. refined	4376	7692	5258	2798	2840	6210
R_1 (obs. refl.)	0.057	0.041	0.032	0.027	0.034	0.037
wR_2 (all refl.)	0.171	0.124	0.093	0.079	0.094	0.108
residual el. density [e/Å^{-3}]	+1.0 −0.6	+0.5 −0.4	+0.5 −0.6	+0.4 −0.5	+0.7 −0.9	+0.5 −0.5

Table 6, part 3. Crystallographic details

	13	**14**	**15**	**16**	**17**	**18**
formula	$C_{24}H_{36}Cl_2O_{12}Zn$	$C_{22}H_{24}Cl_{12}N_4O_2Sb_2Zn$	$C_{28}H_{36}Cl_{12}N_4O_2Sb_2Zn$	$C_{22}H_{22}Cl_{14}N_4O_2Sb_2Zn$	$C_{42}H_{30}Cl_{12}F_6O_6Sb_2Zn \cdot C_7H_5FO$	$C_{42}H_{30}Cl_{18}O_6Sb_2Zn \cdot 4\,C_7H_5ClO$
mol. mass	652.80	1110.72	1194.88	1179.61	1603.04	2139.87
crystal size [mm]	0.6 × 0.2 × 0.1	0.2 × 0.2 × 0.1	0.4 × 0.4 × 0.3	0.5 × 0.4 × 0.3	0.7 × 0.5 × 0.4	0.7 × 0.5 × 0.5
space group	$P2_1/c$	*Pbca*	$P2_1/n$	*C*2/*c*	*P*1	$P\bar{1}$
Z	2	4	2	8	1	1
a [Å]	12.077(2)	19.63(2)	13.237(5)	28.648(3)	11.450(1)	12.386(1)
b [Å]	15.989(2)	10.12(2)	12.906(7)	11.432(1)	11.851(1)	13.803(1)
c [Å]	7.390(2)	20.25(2)	13.637(7)	25.909(2)	14.604(2)	15.211(2)
α [°]	90	90	90	90	66.25(1)	114.05(1)
β [°]	96.31(2)	90	102.26(4)	100.64(1)	67.06(1)	93.58(1)
γ [°]	90	90	90	90	74.78(1)	112.57(1)
V [Å^3]	1418.4(5)	4023(8)	2276.6(2)	8339.4(1)	1657.4(3)	2117.8(3)
d(calc.) [g•cm^{-3}]	1.53	1.83	1.74	1.88	1.61	1.68
d(obs.) [g•cm^{-3}]	1.50	–	–	–	–	–
temp. [K]	183(2)	183(2)	183(2)	183(2)	183(2)	183(2)
μ(Mo-*Kα*) [mm^{-1}]	1.12	2.749	2.436	2.78	1.71	1.66
hkl range	*h*: −14 to 14 *k*: 0 to 19 *l*: −9 to 0	*h*: 0 to 23 *k*: −11 to 0 *l*: 0 to 23	*h*: −15 to 15 *k*: 0 to 14 *l*: 0 to 15	*h*: −39 to 13 *k*: −14 to 13 *l*: −31 to 31	*h*: −13 to 13 *k*: 0 to 14 *l*: −16 to 17	*h*: −15 to 15 *k*: −15 to 17 *l*: −18 to 0
refl. measd.	3007	3419	3204	14166	6220	8629
indep. refl.	2782	3416	3204	8594	6216	8295
obs. refl. [$I>2\sigma(I)$]	2027	2298	3204	6723	5716	7371
parameters	182	191	223	408	703	503
refl. refined	2782	3416	3204	8594	6216	8295
R_1 (obs. refl.)	0.039	0.081	0.028	0.028	0.056	0.034
wR_2 (all refl.)	0.104	0.233	0.090	0.077	0.192	0.098
residual el. density [e/Å^{-3}]	+0.6 −0.4	+2.4 −1.9	+0.5 −0.6	+1.3 −0.9	+3.0 −0.8	+1.1 −1.0

values are defined as $R_1 = \Sigma F_o - F_c / \Sigma F_o$ and $wR_2 = \{\Sigma[w(F_o^2 - F_c^2)^2]/\Sigma[w(F_o^2)^2]\}^{1/2}$. Drawings were produced with SCHAKAL[33]. Table 6 lists the crystallographic data.

Acknowledgments

This work was supported by the Deutsche Forschungsgemeinschaft.

[1] B. Müller, M. Ruf, H. Vahrenkamp, *Angew. Chem.* **1994**, *106*, 2164−2165; *Angew. Chem. Int. Ed. Engl.* **1994**, *33*, 2089−2090.
[2] *Comprehensive Organic Synthesis* (Eds.: B. M. Trost, I. Fleming, S. L. Schreiber), Pergamon Press, Oxford, **1991**. C. Elschenbroich, A. Salzer, *Organometallic Chemistry*, Teubner, Stuttgart, **1994**.
[3] J. J. R. Frausto da Silva, R. J. P. Williams, *The Biological Chemistry of the Elements*, Clarendon Press, Oxford, **1994**. − W. Kaim, B. Schwederski, *Bioanorganische Chemie*, Teubner Studienbücher, Stuttgart, **1995**.
[4] *Comprehensive Coordination Chemistry* (Eds.: G. Wilkinson, R. D. Gillard, J. A. McCleverty), Pergamon Press, Oxford, **1988**. − Y.-H. Huang, J. A. Gladysz, *J. Chem. Ed.* **1988**, *65*, 298−303. − S. Shambayati, W. E. Crowe, S. L. Schreiber, *Angew. Chem.* **1990**, *102*, 273−290; *Angew. Chem. Int. Ed. Engl.* **1990**, *29*, 256−273.
[5] H. Vahrenkamp, *Acc. Chem. Res.* in the press.
[6] H. Eklund, B. Nordström, E. Zeppezauer, G. Söderlund, I. Ohlsson, T. Boiwe, B. O. Söderberg, O. Tapia, C. I. Bränden, A. Åkeson, *J. Mol. Biol.* **1976**, *102*, 27−59.
[7] H. Vahrenkamp, Lecture at the XXXIII International Conference on Coordination Chemistry, Firenze, **1998**, Book of Abstracts, p. 131.
[8] B. Müller, H. Vahrenkamp, *Eur. J. Inorg. Chem.* **1999**, 129−135, succeeding paper.
[9] B. Müller, H. Vahrenkamp, *Eur. J. Inorg. Chem.* **1999**, 137−144, next-succeeding paper.
[10] W. L. Driessen, W. L. Groeneveld, *Rec. Trav. Chim. Pays Bas* **1971**, *90*, 87−96.
[11] P. L. Verheijdt, P. H. van der Voort, W. L. Groeneveld, W. L. Driessen, *Rec. Trav. Chim. Pays Bas* **1972**, *91*, 1201−1204.
[12] F. Filippini, B. P. Susz, *Helv. Chim. Acta* **1971**, *54*, 835−845.
[13] M. Bochmann, K. J. Webb, M. B. Hursthouse, M. Mazid, *J. Chem. Soc., Chem. Commun.* **1991**, 1735−1737.
[14] R. H. Prince, P. Wyeth, *J. Inorg. Nucl. Chem.* **1981**, *43*, 839−843.
[15] R. H. Prince, P. Wyeth, *J. Inorg. Nucl. Chem.* **1981**, *43*, 845−848.
[16] M. Bochmann, G. Bwembya, R. Grinter, A. K. Powell, K. J. Webb, M. B. Hursthouse, M. Mazid, K. M. Abdul Malik, *Inorg. Chem.* **1994**, *33*, 2290−2296.
[17] M. P. Byrn, C. J. Curtis, Y. Hsiou, S. I. Khan, P. A. Sawin, S. K. Tendick, A. Terzis, C. E. Strouse, *J. Am. Chem. Soc.* **1993**, *115*, 9480−9497.
[18] I. Goldberg, H. Kruptsky, Z. Stein, Y. Hsiou, C. E. Strouse, *Supramol. Chem.* **1994**, *4*, 203−221.
[19] P. W. N. M. van Leeuwen, *Rec. Trav. Chim. Pays Bas* **1967**, *86*, 247−253.
[20] A. P. Zuur, W. L. Groeneveld, *Rec. Trav. Chim. Pays Bas* **1967**, *86*, 1089−1102.
[21] W. L. Driessen, W. L. Groeneveld, *Rec. Trav. Chim. Pays Bas* **1969**, *88*, 491−498.
[22] The Cambridge Crystallographic Data File contains about 20 references each for Zn−alcohol, Zn−nitrate, and Zn−acetonitrile and 12 references for Zn−perchlorate complexes.
[23] The Inorganic Crystal Structure Database lists $Zn(H_2O)_6$ salts with Zn−O distances between 2.045 and 2.138 Å.
[24] C. Sudbrake, B. Müller, H. Vahrenkamp, unpublished.
[25] C. J. O′Connor, E. Sinn, R. L. Carlin, *Inorg. Chem.* **1977**, *16*, 3314−3320.
[26] W. van de Giesen, C. H. Stam, *Cryst. Struct. Commun.* **1972**, *1*, 257−260.
[27] I. Persson, *Acta Chem. Scand. Ser. A*, **1982**, *36*, 7−12.
[28] J. Reedijk, A. P. Zuur, W. L. Groeneveld, *Rec. Trav. Chim. Pays Bas* **1967**, *86*, 1127−1137.
[29] R. Gregorzik, J. Wirbser, H. Vahrenkamp, *Chem. Ber.* **1992**,

125, 1575−1581. − C. Titze, J. Hermann, H. Vahrenkamp, *Chem. Ber.* **1995**, *128*, 1095−1103.
[30] M. Förster, R. Burth, A. K. Powell, T. Eiche, H. Vahrenkamp, *Chem. Ber.* **1993**, *126*, 2643−2648.
[31] The crystallographic data of the structures described in this paper were deposited with the Cambridge Crystallographic Data Centre as supplementary publications no. CCDC-102427 (for **1**), 102428 (for **2**), 102429 (for **3**), 102430 (for **4**), 102431 (for **5**), 102432 (for **6**), 102433 (for **7**), 102434 (for **8**), 102435 (for **9**), 102436 (for **12**), 102437 (for **10**), 102438 (for **11**), 102439 (for **13**), 102440 (for **15**), 102441 (for **14**), 102442 (for **16**), 102443 (for **17**), 102444 (for **18**). Copies of these data are available free of charge from the following address: The Director, CCDC, 12 Union Road, GB-Cambridge CB2 1EZ (Telefax: Int. +44 (0)1223/ 336 033; E-mail: deposit@chemcrys.cam.ac.uk). For a limited time they are also available on the Internet Web Site www.chemie.uni-freiburg.de/aoanchem/hv/data.html.
[32] G. M. Sheldrick, *SHELX-86 and SHELXL-93*, Programs for Crystal Structure Determination, Universität Göttingen, **1986** and **1993**.
[33] E. Keller, Program *SCHAKAL*, Universität Freiburg, **1997**.

Received August 3, 1998
[I98256]

Zinc Complexes of Aldehydes and Ketones, 3[+]
Aldehyde Complexes of Zinc Halides

Bodo Müller[a] amd Heinrich Vahrenkamp*[a]

Keywords: Zinc / Aldehyde ligands / Halide ligands / Structural chemistry

Aldehyde complexes of the zinc halides were obtained by treating $ZnCl_2$, $ZnBr_2$, and ZnI_2 under anhydrous conditions with large excesses of benzaldehyde and various substituted benzaldehydes. Their constitutions were determined by a total of 12 X-ray structure analyses. Three product types were found: $ZnHal_2(aldehyde)_2$ (**A**), $[ZnHal_2(aldehyde)]_\infty$ (**B**), and $[Zn(aldehyde)_6]$ $[Zn_2Hal_6]$ (**C**). All three dissolve readily in the corresponding aldehyde or in polar nonprotic solvents indicating the presence of solvated zinc species in solution.

In the preceding paper[1] we outlined the motivation for our studies of zinc complexation by aldehydes and ketones. The sharp discrepancy between the importance of metal ion catalysis for reactions of carbonyl-containing compounds and the scant knowledge on the chemical interactions between metal ions and carbonyl functions calls for the gathering of basic information upon which mechanistic insight is to be built. The fact that so little is known about metal complexes (other than organometallic species) of simple carbonyl compounds is a reflection of the low donor strength of these compounds. Thus for their exploration not only are anhydrous reaction conditions essential but also are all reaction media of moderate donor strength to be avoided.

While catalytic zinc in biochemical systems is never bound to halides and in fact halide ions are known to be inhibitors of some zinc enzymes[2], zinc halides are typical activators for reactions of organic carbonyl compounds. Examples in which zinc chloride is employed in higher than stoichiometric amounts are sugar acetylations, the Fischer indole synthesis, Friedel–Crafts acetylations, and various condensations[3]. After studying the coordination of carbonyl compounds to halide-free zinc species[1] we therefore turned to the corresponding studies of the pure zinc halides.

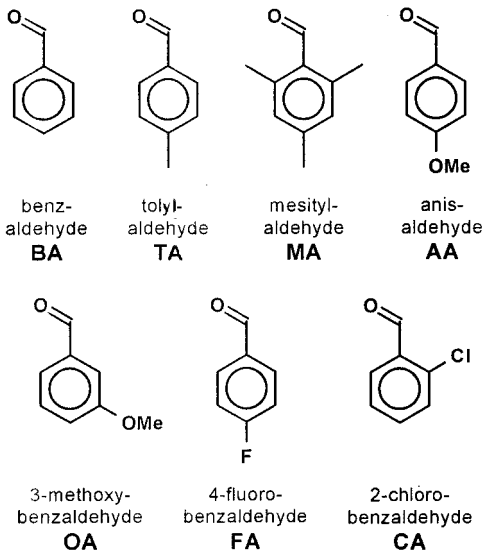
This paper, like the preceding one[1], describes aldehyde complexes. We are aware of only one related publication, i.e. one containing some data on $ZnCl_2$•benzaldehyde[4]. We scanned the coordination abilities of a broad range of aldehydes towards the zinc halides $ZnCl_2$, $ZnBr_2$, and ZnI_2. Again we observed that aliphatic aldehydes undergo condensation or polymerization reactions after addition of the zinc halide. Benzaldehyde and various substituted benzaldehydes, however, were found to be suitable as ligands. A preliminary account of our findings was published in 1994[5].

[+] Part 2: Ref.[1]

[a] Institut für Anorganische und Analytische Chemie der Universität Freiburg,
Albertstr. 21, D-79104 Freiburg, Germany

Preparations

In order to obtain the aldehyde complexes as pure, solid materials the aldehyde had to be present in a large excess and in a high concentration. In practice this meant using the aldehyde as the reaction medium which restricted the reaction to only those aldehydes that are low-melting or liquid. Pure and crystalline products were obtained with the following aldehydes:



The water-free zinc halides $ZnCl_2$, $ZnBr_2$, and ZnI_2 were prepared in diethyl ether from zinc and HCl, Br_2, and HI prior to use. They were dissolved in the aldehydes. After complete dissolution an equal volume of dichloromethane was added. The products precipitated on addition of petroleum ether. Crystalline complexes were obtained in lower yields after careful layering with petroleum ether. The resulting zinc complexes belong to one of the three classes **A**, **B**, and **C**.

 © WILEY-VCH Verlag GmbH, D-69451 Weinheim, 1999 1434–1948/99/0101–0129 $ 17.50+.50/0

$[ZnHal_2(aldehyde)_2]$ **A** $[-Hal-ZnHal(aldehyde)-]_\infty$ **B**

$[Zn(aldehyde)_6][Zn_2Hal_6]$ **C**

Class **A** type complexes, i.e. monomolecular tetrahedral $ZnHal_2(aldehyde)_2$ species, were obtained from the five aldehydes BA, TA, MA, AA, and OA. Compounds **1b** to **5c** respesent the total of 12 complexes that were isolated analytically pure. They are all extremely hygroscopic, and they should be stored at low temperatures as some of them decompose within a few days at room temperature. Eight of the complexes were subjected to crystal structure determinations; the high structural similarity between them is discussed below.

$[ZnHal_2(aldehyde)_2]$

	1b	**1c**	**2b**	**2c**	**3a**	**3b**	**3c**	**4a**	**4b**	**4c**	**5b**	**5c**
Hal	Br	I	Br	I	Cl	Br	I	Cl	Br	I	Br	I
aldehyde	BA	BA	TA	TA	MA	MA	MA	AA	AA	AA	OA	OA

The alternative class **B** type complexes, i.e. mono-aldehyde−$ZnHal_2$ species, were obtained for almost all cases in which class **A** type complexes did not result. Compounds **6a**−**9c** were isolated. Structure determinations of three of them showed them to be halide-bridged polymers in the solid state (see below). These compounds do not differ in their behaviour (solubility, hygroscopicity, thermal stability) from the monomolecular complexes, which indicates inter alia that they are molecular bis-aldehyde complexes in aldehyde solution. So far we have found no indication for the alternative constitution of the mono-aldehyde complexes as halide-bridged dimeric units.

$[ZnHal_2(aldehyde)]_\infty$

	6a	**7a**	**8a**	**9a**	**9b**	**9c**
Hal	Cl	Cl	Cl	Cl	Br	I
aldehyde	BA	MA	FA	CA	CA	CA

Quite unexpectedly, two compounds of composition $ZnHal_2 \cdot 2$ aldehyde (**10b**, **c**) were found to belong to class **C** rather than class **A**. This was proved for **10b** by structure determination and assumed for **10c** by analogy of composition and spectra. **10b** and **c** share the property of all zinc halide complexes reported here, namely, they contain only covalently bound halide. There is no obvious reason, however, why in this case dismutation into a fully aldehyde-coordinated cation and a fully halide-coordinated anion has occurred. Just like in the cases of benzaldehyde and tolylaldehyde, also in the case of fluorobenzaldehyde reaction with $ZnCl_2$ yields a 1:1 complex (**8a**) whereas reaction with $ZnBr_2$ and ZnI_2 yield 2:1 (aldehyde/zinc) complexes (**10b**, **c**).

$[Zn(FA)_6]\ [Zn_2Hal_6]$
10b: Hal = Br; **10c**: Hal = I

Structures

Eight complexes of class **A** were subjected to structure determinations. Their molecular shapes are remarkably uniform, including the fact that with the exception of **3a** they all have a crystallographic twofold axis. Figure 1 and Table 1 summarize the bonding features. All complexes are distorted tetrahedral with the O−Zn−O angle typically small (94−106°), the Hal−Zn−Hal angle typically large (122−131°), and the O−Zn−Hal angles close to the tetrahedral value (105−111°). The aldehydes are attached to zinc in a strictly anti fashion (dihedral angle Zn−O−C−C average 178°), and the aromatic rings and the CHO groups are coplanar (dihedral angle O−C−C−C average 175°).

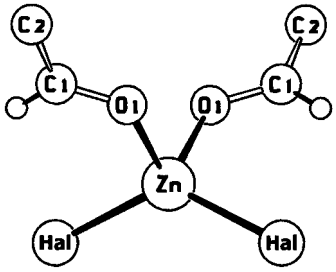


Figure 1. Zinc coordination of class **A** complexes

The zinc halide bond distances are typical and uniform for Zn−Cl, Zn−Br, and Zn−I, cf. Table 1. The Zn−O bond lengths vary only 0.03 Å about their average value of 2.035 Å. Compared to the average value of 2.09 Å for octahedral zinc-aldehyde complexes they are typically shorter. There is only one reference value in the literature for Zn−O(aldehyde) in tetrahedral complexes: in Bochmann's $[Zn(SeR)_2(AA)]_2$ it measures 2.06 Å[6]. The spread of the aldehyde C=O bond lengths is negligible. Relative to the standard value for aromatic aldehydes of 1.22 Å[7] they are only very slightly elongated due to the coordination to the metal.

Three structures of class **B** type complexes were determined. They were found to belong to two different structural types. Compound **6a** has a screw type arrangement of the polymeric backbone made up of Zn and Cl (Figure 2). Compounds **7a** and **9b** crystallize with a linear zig-zag array of zinc and halide (Figure 3). Table 2 compares the structural details of the three complexes.

Like the complexes of class **A**, those of class **B** are distorted tetrahedral, yet with a different kind of distortion. Their O−Zn−Hal angles are near the tetrahedral value, their Hal1−Zn−Hal2 angles are near 118−120°, and the Hal2−Zn−Hal2′ angles (i.e. those involving both bridging halides) are near 102°. The anti orientation of the zinc-bound aldehydes (dihedral angles 171−179°) and the coplanarity of the arene and CHO groups (dihedral angles 171−176°) are as before. In Table 2 comparison of **6a** and **7a** shows that the backbone structure of the polymers (screw-like or zigzag) is not reflected in the basic bond lengths and angles. The Zn−Hal distances have typical values for the terminal halides, cf. Table 1, but are characteristically elongated for the bridging halides. The Zn−O(al-

Table 1. Structural data [Å, °] of complexes $ZnHal_2$•2 aldehyde

	Hal	Zn−Hal	Zn−O1	O1−C1	Zn−O1−C1	O1−C1−C2
1b	Br	2.334(2)	2.043(3)	1.235(5)	125.5(3)	118.5(3)
1c	I	2.529(1)	2.046(3)	1.229(5)	126.3(3)	123.2(4)
2c	I	2.532(1)	2.046(5)	1.226(7)	127.7(4)	123.3(6)
3a[a]	Cl	2.202(7)	2.046(2)	1.222(8)	123.7(5)	124.9(6)
4a	Cl	2.199(2)	2.016(4)	1.235(7)	127.1(4)	122.0(5)
4b	Br	2.327(1)	2.014(3)	1.228(4)	126.3(3)	124.0(3)
4c	I	2.525(1)	2.024(2)	1.230(3)	126.2(2)	124.0(3)
5c	I	2.524(1)	2.041(2)	1.226(3)	124.8(2)	123.5(2)

[a] Average of two values each.

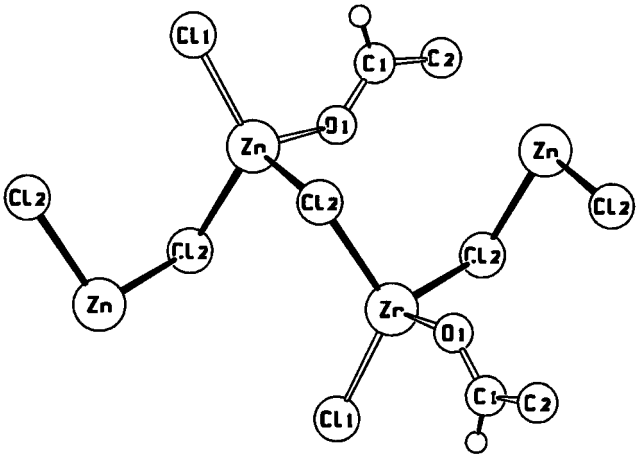


Figure 2. Polymer backbone and zinc coordination of complex **6a**

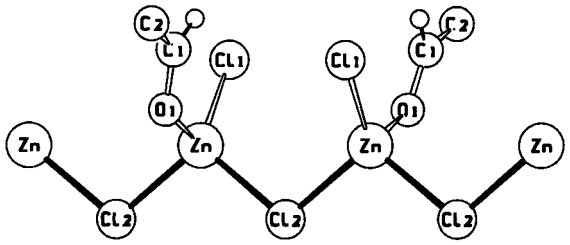


Figure 3. Polymer backbone and zinc coordination of complexes **7a** and **9b**

dehyde) bonds are still a bit shorter than those for class **A**. This must be related to the fact that only one aldehyde ligand per zinc ion is present and that the donor capacity of two of the three halide ligands is reduced because of their bridging nature.

The unexpected class **C** constitution of complexes **10b** and **c** became obvious only after the structure determination of **10b**, cf. Figure 4. The hexaaldehyde−zinc cation of **10b** corresponds to the ones structurally characterized by us for 4-fluorobenzaldehyde and 2-chlorobenzaldehyde with $SbCl_6^-$ counterions[1]. Its structural features, typically its Zn−O bond length of 2.08 Å (av.), are as observed before[1]. The $Zn_2Br_6^{2-}$ anion of **10b** belongs to the well-established class of $Zn_2Hal_6^{2-}$ complexes. While quite a number of these with Hal = Cl have been structurally characterized[8], there is just one structure each for X = Br[9] and X = I[10] in the literature. The structural details of the $Zn_2Br_6^{2-}$ ion in **10b** compare well with the reported ones. Typically both the terminal and bridging Zn−Br bonds are longer than in the neutral complexes like **9b**, and the Zn_2Br_2 rectangle is characterized by rather acute angles both at zinc and bromine.

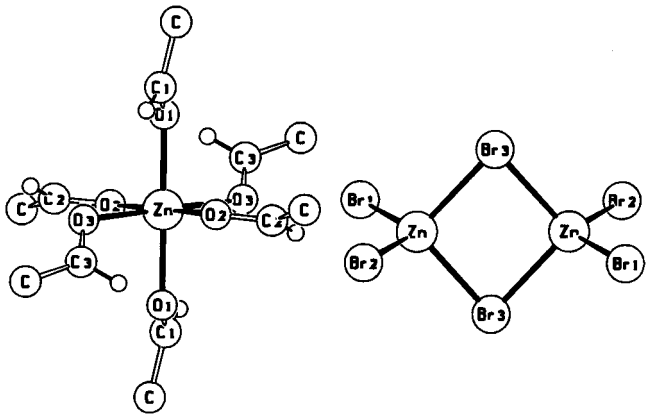


Figure 4. Coordination of zinc in the cation and anion of complex **10b**
Bond lengths [Å] and angles [°] for the cation: Zn−O1 2.073(4), Zn−O2 2.081(4), Zn−O3 2.080(4), O1−C1 1.224(8), O2−C2 1.222(7), O3−C3 1.229(7), Zn−O1−C1 124.1(4), Zn−O2−C2 129.5(4), Zn−O3−C3 119.4(4), O1−C1−C 123.6(6), O2−C2−C 124.0(6), O3−C3−C 125.3(6); for the anion: Zn−Br1 2.335(1), Zn−Br2 2.336(1), Zn−Br3 2.474(1), Zn−Br3′ 2.497(1), Br3−Zn−Br3′ 97.33(4), Zn−Br3−Zn′ 82.67(4).

Table 2. Structural data [Å, °] for complexes $[ZnHal_2$•aldehyde$]_\infty$

	Hal	Zn−Hal1	Zn−Hal2	Zn′−Hal2	Zn−O1	O1−C1	Zn−O1−C1	O1−C1−C2	Zn−Hal−Zn
6a	Cl	2.172(2)	2.293(2)	2.300(2)	2.009(5)	1.225(8)	127.8(5)	122.8(6)	107.92(7)
7a	Cl	2.177(1)	2.304(2)	2.275(2)	2.015(2)	1.230(4)	122.0(2)	122.7(3)	102.77(3)
9b	Br	2.305(2)	2.409(2)	2.408(2)	2.021(6)	1.223(9)	125.8(6)	120.5(8)	99.51(5)

Spectra

The characteristic IR bands of the complexes, i.e. the aldehyde ν(CO) bands, are listed in Table 3. A significant shift to lower wavenumbers occurs upon coordination to zinc. There is no correlation between this shift and the bonding type (i.e. classes **A**, **B**, and **C**). Instead it seems to be correlated with the electron density of the aldehydes: for electron-rich aldehydes (BA, AA), the shift is small, and for electron-poor aldehydes (FA, CA) it is large. The same observations were made for zinc-aldehyde complexes with weakly coordinating anions[1].

Table 3. ν(CO) IR bands (KBr, cm^{-1}) and their relative shifts

	ν(CO)	Δν		ν(CO)	Δν
1b	1651	−50	**5b**	1645	−57
1c	1638	−63	**5c**	1645	−57
2b	1646	−58	**6a**	1638	−63
2c	1643	−61	**7a**	1645	−59
3a	1637	−53	**8a**	1638	−62
3b	1632	−58	**9a**	1628	−70
3c	1629	−61	**9b**	1627	−71
4a	1638	−52	**9c**	1624	−74
4b	1640	−50	**10b**	1635	−65
4c	1638	−52	**10c**	1636	−64

The characteristic ^{1}H- and ^{13}C-NMR resonances result from the aldehyde CHO functions. In the complexes these resonances are shifted by small, yet significant, amounts. The ^{1}H signals are moved upfield and downfield in an irregular fashion, the ^{13}C signals are all shifted downfield, as expected due to deshielding resulting from coordination. While for the zinc−aldehyde complexes with noncoordinating anions[1] the ^{1}H-NMR shifts were so small that the possibility of aldehyde substitution by [D_6]acetone upon dissolution could not be ruled out, this is not the case here. Obviously the molecular nature and the lower coordination number of the zinc-halide complexes reported here result in a tighter binding between the cation and the aldehyde ligands.

Table 4. ^{1}H- and ^{13}C-NMR data for the aldehyde CHO functions (in [D_6]acetone, δ)

	δ(H)	Δδ	δ(C)	Δδ
1b	9.96	−0.10	192.8	+0.1
1c	9.96	−0.10	192.6	−0.1
2b	9.94	−0.04	192.3	+0.2
2c	9.95	−0.03	192.3	+0.2
3a	10.45	−0.03	193.8	+1.2
3b	10.49	+0.01	193.5	+0.9
3c	10.49	+0.01	193.6	+1.0
4a	9.83	−0.06	191.7	+0.7
4b	9.79	−0.10	192.3	+1.3
4c	9.83	−0.06	191.9	+0.9
5b	9.97	+0.01	192.6	+0.2
5c	9.99	+0.03	192.6	+0.2
6a	9.90	−0.16	193.0	+0.3
7a	9.94	−0.04	192.5	+0.4
8a	10.00	+0.05	191.5	+0.5
9a	10.37	+0.01	189.7	+0.3
9b	10.31	−0.05	189.4	±0
9c	10.23	−0.13	188.9	−0.5
10b	9.94	−0.01	191.2	+0.4
10c	9.96	+0.01	191.1	+0.3

Discussion

The strict maintenance of anhydrous conditions has made it possible to isolate zinc halide complexes of seven different aromatic aldehydes. In all compounds obtained the halides are attached covalently to zinc. Two compositions have been observed, represented by the formulae $ZnHal_2$•aldehyde and $ZnHal_2$•2 aldehyde. They appear in three structural types, monomolecular $ZnHal_2$•2 aldehyde (**A**), polymeric and halide-bridged $ZnHal_2$•aldehyde (**B**), and ionic $[Zn(aldehyde)_6][Zn_2Hal_6]$ (**C**). Notably the dimeric halide-bridged structural type $[ZnHal_2$•aldehyde$]_2$ is missing.

The NMR spectra prove the compositions of the products, and the solid-state IR data prove the aldehyde coordination by large Δν values for the aldehyde CO bands. They give no indication of the complex structures which could only be obtained by crystal structure determinations. Typically complex **10b** of type **C** does not differ spectroscopically from other $ZnBr_2$ complexes like **3b** or **5b**. Altogether the uniformity within groups of spectra or structures does not allow conclusions on structure and bonding to be drawn.

There seems to be a relation between the composition of the complexes and the electron-donor properties of the ligands. Both electron-rich aldehydes (MA, AA) and low-electronegativity halides (Br, I) favour the $ZnHal_2$•2 aldehyde composition. Conversely zinc chloride yields only polymeric 1:1 complexes with the "normal" aldehydes BA and TA, and the most electron-poor aldehyde CA appears only in the polymeric 1:1 complexes. The formation of the 1:1 complexes even in the neat aldehydes is a demonstration of the low donor strength of the aldehydes, which cannot compete with bridging halide for the coordination to zinc. The formation of complexes **10** is an unusual result of this competition in that both aldehyde and halide get their own zinc ions.

With the exception of the cation of **10** all complexes described here are tetrahedral. This can be related to the soft character of the halide ligands, while the homoleptic aldehyde complexes in **10** and the other complexes with hard coligands (water, alcohol, oxoanion) are octahedral[1]. The tetrahedral complexes are of relevance for zinc-catalyzed reactions of organic carbonyl compounds, as in organic synthesis the catalyst is most often $ZnCl_2$[3] and in the enzyme alcohol dehydrogenase the catalytic zinc has a tetrahedral $ZnNS_2O$ environment[2].

The challenge to improve this relevance faces two problems. One of them is the mostly unpredictable composition and structure of the zinc halide/aldehyde complexes. This means that reaction intermediates and catalytic pathways of zinc halide catalyzed carbonyl reactions are equally unpredictable as yet. The other is the weak attachment of the

Table 5. Reaction details

Compl.		$ZnHal_2$				aldehyde		yield		m.p.
		g	mmol		mL	g	mmol	g	%	°C
1b	$ZnBr_2$	1.11	4.93	BA	5	5.22	49.19	2.01	93	115
1c	ZnI_2	1.01	3.16	BA	5	5.22	49.19	1.57	93	94
2b	$ZnBr_2$	1.69	7.50	TA	10	10.19	84.81	3.28	94	124
2c	ZnI_2	1.02	3.20	TA	5	5.10	42.41	1.72	96	122
3a	$ZnCl_2$	0.48	3.52	MA	10	10.05	67.81	1.13	74	120
3b	$ZnBr_2$	1.57	6.97	MA	10	10.05	67.81	3.40	94	92
3c	ZnI_2	0.74	2.32	MA	5	5.03	33.91	1.28	90	136
4a	$ZnCl_2$	0.72	5.28	AA	10	11.19	82.19	2.08	96	91
4b	$ZnBr_2$	1.13	5.02	AA	6	6.71	49.31	2.23	89	117
4c	ZnI_2	0.92	2.88	AA	5	5.60	41.09	1.66	97	116
5b	$ZnBr_2$	1.11	4.93	OA	8	8.95	65.75	1.67	68	92
5c	ZnI_2	0.79	2.48	OA	5	5.60	41.09	1.24	85	86
6a	$ZnCl_2$	0.71	5.21	BA	10.5	10.96	103.30	0.96	76	117
7a	$ZnCl_2$	0.46	3.38	TA	5	5.10	42.41	0.76	88	116
8a	$ZnCl_2$	0.44	3.23	FA	5	5.79	46.61	0.81	96	125
9a	$ZnCl_2$	0.77	5.65	CA	5	6.24	44.39	1.16	74	132
9b	$ZnBr_2$	1.51	6.71	CA	7.5	9.36	66.59	2.10	86	153
9c	ZnI_2	0.93	2.91	CA	5	6.24	44.39	1.21	90	132
10b	$ZnBr_2$	1.41	6.26	FA	7.5	8.68	69.91	2.86	97	65
10c	ZnI_2	1.06	3.32	FA	5	5.79	46.61	1.70	90	71

aldehydes, which should render $ZnNX_2O$ complexes (i.e. structural models of alcohol dehydrogenase) unstable when N represents a good nitrogen donor. We have been working to overcome the latter problem, and the succeeding paper presents one possible solution[11].

Experimental Section

All preparations required strictly anhydrous conditions. The general working and measuring conditions were as in ref.[12], and the specific ones as in ref.[1]. The aldehydes were obtained commercially and distilled prior to use. The anhydrous zinc halides were prepared from zinc and HHal or Hal_2 in diethyl ether[13][14]. The new complexes were prepared following the general procedure below, details for which are given in Table 5. When they were too hygroscopic for ordinary C/H/N analysis, they were also characterized by zinc and halide analyses. Table 6 gives the analytical characterizations.

Preparation of the Complexes: The zinc halide was dissolved in a 10−20 fold excess of the aldehyde with stirring and heating. After cooling to room temp. 10 mL of dichloromethane was added. By adding 50 mL of petroleum ether (b.p. 60−70°C) a colourless precipitate was obtained, which was filtered off, washed with the petroleum ether, and dried in vacuo.

Structure Determinations[15]: Crystals were obtained by careful layering of the reaction solutions with petroleum ether (b.p. 70−90°C). They were immersed in perfluorinated polyether oil for protection and attachment to the goniometer head and immediately subjected to the nitrogen flow of the diffractometer's cooling system. Diffraction data were recorded at low temperatures with the ω/2θ technique on a Nonius CAD4 diffractometer fitted with a molybdenum tube (K_α, λ = 0.7107 Å) and a graphite monochromator. No absorption corrections were applied. The structures were solved with direct methods and refined anisotropically with the SHELX program suite[16]. The aldehyde C-H hydrogen atoms were located and refined freely. All other hydrogen atoms were in-

Table 6. Analytical characterization

	formula mol. wt.	Analyses calcd./found C	H	Zn	Hal
1b	$C_{14}H_{12}Br_2O_2Zn$	−	−	14.95/	36.53/
	437.5	−	−	14.82	36.61
1c	$C_{14}H_{12}I_2O_2Zn$	−	−	12.30/	47.76/
	531.5	−	−	12.27	47.85
2b	$C_{16}H_{16}Br_2O_2Zn$	41.28/	3.47/	14.05/	34.33/
	465.5	42.00	3.11	14.01	34.21
2c	$C_{16}H_{16}I_2O_2Zn$	34.35/	2.88/	11.69/	45.36/
	559.5	33.52	2.77	11.75	45.20
3a	$C_{20}H_{24}Cl_2O_2Zn$	−	−	15.11/	16.39/
	432.7	−	−	15.17	16.44
3b	$C_{20}H_{24}Br_2O_2Zn$	46.05/	4.64/	12.54/	30.64/
	521.6	45.90	4.56	12.60	30.52
3c	$C_{20}H_{24}I_2O_2Zn$	39.02/	3.93/	10.62/	41.23/
	615.6	38.30	3.83	10.67	41.33
4a	$C_{16}H_{16}Cl_2O_4Zn$	47.03/	3.95/	16.00/	17.35/
	408.6	46.86	3.91	15.81	17.45
4b	$C_{16}H_{16}Br_2O_4Zn$	38.63/	3.24/	13.14/	32.12/
	497.5	37.89	3.17	13.21	32.00
4c	$C_{16}H_{16}I_2O_4Zn$	32.49/	2.73/	11.06/	42.91/
	591.5	32.20	2.62	11.14	42.88
5b	$C_{16}H_{16}Br_2O_4Zn$	38.63/	3.24/	13.14/	32.12/
	497.5	36.76	3.17	13.23	31.98
5c	$C_{16}H_{16}I_2O_4Zn$	32.49/	2.73/	11.06/	42.91/
	591.5	33.14	2.67	11.18	43.03
6a	$C_7H_6Cl_2OZn$	34.68/	2.50/	26.97/	29.25/
	652.8	34.88	2.55	27.02	29.05
7a	$C_8H_8Cl_2OZn$	37.47/	3.14/	25.50/	27.65/
	256.5	37.74	3.29	25.38	27.51
8a	$C_7H_5Cl_2FOZn$	−	−	25.11/	27.23/
	260.4	−	−	25.22	27.10
9a	$C_7H_5Cl_3OZn$	30.37/	1.82/	23.62/	38.42/
	276.9	29.89	2.24	23.84	38.30
9b	$C_7H_5Br_2ClOZn$	22.99/	1.38/	17.88/	−
	365.8	22.03	1.49	17.76	−
9c	$C_7H_5ClI_2OZn$	18.29/	1.10/	14.22/	−
	459.8	16.04	1.17	14.34	−
10b	$C_{42}H_{30}Br_6F_6O_6Zn_3$	35.52/	2.13/	13.81/	33.76/
	1420.3	35.03	2.09	13.91	33.83
10c	$C_{42}H_{30}F_6I_6O_6Zn_3$	29.63/	1.78/	11.52/	44.73/
	1702.3	29.59	2.10	11.61	44.64

Table 7, part 1. Crystallographic details

	1b	**1c**	**2c**	**3a**	**4a**	**4b**
formula	$C_{14}H_{12}Br_2O_2Zn$	$C_{14}H_{12}I_2O_2Zn$	$C_{16}H_{16}I_2O_2Zn$	$C_{20}H_{24}Cl_2O_2Zn$	$C_{16}H_{16}Cl_2O_4Zn$	$C_{16}H_{16}Br_2O_4Zn$
mol. mass	437.43	531.41	559.46	432.66	408.56	497.48
crystal size [mm]	0.6 × 0.2 × 0.1	1.0 × 0.6 × 0.5	0.4 × 0.05 × 0.03	0.8 × 0.1 × 0.1	0.5 × 0.5 × 0.5	1.2 × 0.5 × 0.3
space group	*C*2/*c*	*C*2/*c*	*Fdd*2	*Pca*2$_1$	*P*2$_1$2$_1$2	*C*2/*c*
Z	4	4	8	4	2	4
a [Å]	18.816(2)	19.407(2)	19.883(2)	24.848(2)	8.964(4)	20.361(3)
b [Å]	4.832(1)	5.0240(4)	35.747(5)	4.712(2)	19.918(1)	5.634(2)
c [Å]	17.030(3)	16.878(1)	5.0360(5)	17.279(2)	4.776(3)	16.859(4)
α [°]	90	90	90	90	90	90
β [°]	104.51(11)	105.20(1)	90	90	90	110.79(2)
γ [°]	90	90	90	90	90	90
V [Å^3]	1499.0(5)	1588.0(2)	3579.4(7)	2023.1(1)	852.7(8)	1808.0(7)
d(calc.) [g·cm^{-3}]	1.94	2.22	2.08	1.42	1.59	1.83
d(obs.) [g·cm^{-3}]	–	–	–	–	1.53	1.81
temp. [K]	183(2)	183(2)	183(2)	183(2)	183(2)	183(2)
μ(Mo*K*a) [mm^{-1}]	6.96	5.43	4.82	1.49	1.77	5.79
hkl range	*h*: 0 to 23	*h*: 0 to 26	*h*: −24 to 0	*h*: 0 to 30	*h*: −11 to 0	*h*: −23 to 25
	k: −6 to 0	*k*: 0 to 7	*k*: −44 to 0	*k*: −5 to 0	*k*: −1 to 25	*k*: 0 to 7
	l: −21 to 20	*l*: −23 to 22	*l*: 0 to 6	*l*: 0 to 21	*l*: −6 to 6	*l*: −20 to 0
refl. measd.	1550	2359	983	2051	2007	1889
indep. refl.	1504	2298	983	2049	1846	1821
obs. refl. [$I>2\sigma(I)$]	1261	2190	905	1633	1688	1575
parameters	87	88	97	226	105	105
refl. refined	1504	2298	983	2048	1846	1821
R_1 (obs. refl.)	0.031	0.032	0.021	0.036	0.053	0.036
wR_2 (all refl.)	0.083	0.099	0.053	0.104	0.163	0.098
residual el. density [e/Å^{-3}]	+0.7 −0.8	+1.6 −1.1	+0.6 −0.5	+1.0 −0.5	+1.1 −0.7	+1.1 −0.8

Table 7, part 2. Crystallographic details

	4c	**5c**	**6a**	**7a**	**9b**	**10b**
formula	$C_{16}H_{16}I_2O_4Zn$	$C_{16}H_{16}I_2O_4Zn$	$C_7H_6Cl_2OZn$	$C_8H_8Cl_2OZn$	$C_7H_5Br_2ClOZn$	$C_{42}H_{30}Br_6F_6O_6Zn_3 \cdot 2\ C_7H_5FO$
mol. mass	591.46	591.46	242.39	256.41	365.75	1668.45
crystal size [mm]	0.6 × 0.4 × 0.2	0.6 × 0.2 × 0.1	0.7 × 0.03 × 0.03	0.7 × 0.3 × 0.3	0.4 × 0.2 × 0.1	0.9 × 0.8 × 0.3
space group	*C*2/*c*	*C*2/*c*	P2$_1$/*n*	*Pca*2$_1$	*Pbca*	*Pbca*
Z	4	4	4	4	8	4
a [Å]	21.303(5)	22.975(1)	12.060(3)	22.047(2)	7.352(1)	18.490(4)
b [Å]	5.673(1)	5.345(3)	4.914(1)	6.256(1)	14.026(5)	15.788(7)
c [Å]	17.182(5)	19.026(6)	14.560(5)	7.155(1)	20.262(7)	20.707(5)
α [°]	90	90	90	90	90	90
β [°]	111.25(2)	126.54(3)	94.96(3)	90	90	90
γ [°]	90	90	90	90	90	90
V [Å^3]	1935.4(8)	1877.2(2)	859.6(4)	986.9(2)	2089.4(11)	6045(3)
d(calc.) [g·cm^{-3}]	2.03	2.09	1.87	1.73	2.33	1.83
d(obs.) [g·cm^{-3}]	1.98	–	–	–	2.29	1.82
temp. [K]	183(2)	183(2)	183(2)	183(2)	183(2)	183(2)
μ(Mo*K*a) [mm^{-1}]	4.47	4.61	3.41	2.98	10.21	5.22
hkl range	*h*: −28 to 0	*h*: −28 to 22	*h*: −14 to 14	*h*: −27 to 0	*h*: −9 to 9	*h*: −22 to 9
	k: 0 to 7	*k*: 0 to 6	*k*: −5 to 0	*k*: −7 to 0	*k*: −17 to 0	*k*: −7 to 19
	l: −21 to 22	*l*: 0 to 23	*l*: −17 to 0	*l*: −8 to 0	*l*: −24 to 24	*l*: 0 to 25
refl. measd.	2396	1911	1678	1051	7706	5914
indep. refl.	2336	1849	1615	1051	2045	5905
obs. refl. [$I>2\sigma(I)$]	2231	1751	1096	993	1093	3991
parameters	105	105	100	109	109	367
refl. refined	2336	1849	1615	1051	2045	5905
R_1 (obs. refl.)	0.023	0.019	0.049	0.023	0.050	0.044
wR_2 (all refl.)	0.071	0.054	0.151	0.075	0.145	0.130
residual el. density [e/Å^{-3}]	+0.5 −1.1	+0.8 −0.6	+1.1 −1.0	+0.4 −0.5	+1.3 −1.6	+0.7 −1.2

cluded with fixed distances and isotropic temperature factors 1.2 times those of their attached atoms. Parameters were refined against F^2. The R values are defined as $R_1 = \Sigma F_o - F_c / \Sigma F_o$ and w$R_2 = \{\Sigma[w(F_o^2 - F_c^2)^2]/\Sigma[w(F_o^2)^2]\}^{1/2}$. Drawings were produced with SCHAKAL[17]. Table 7 lists the crystallographic data.

Acknowledgments

This work was supported by the Deutsche Forschungsgemeinschaft.

[1] B. Müller, H. Vahrenkamp, *Eur. J. Inorg. Chem.* **1999**, 117−127, preceding paper.
[2] *Zinc Enzymes* (Ed.: T. G. Spiro) Wiley, New York, **1983**.
[3] [3a] *Comprehensive Organc Chemistry*, Vol. 1 (Eds.: D.Barton, W. D. Ollis, J. F. Stoddart) Pergamon Press, Oxford, **1979**. – [3b] R. Brettle in ref.[3a], pp. 943−1016. – [3c] T. Laird in ref.[3a], pp. 1105−1160.
[4] F. Filippini, B. P. Susz, *Helv. Chim. Acta* **1971**, *54*, 835−845.
[5] B. Müller, M. Ruf, H. Vahrenkamp, *Angew. Chem.* **1994**, *106*, 2164−2165; *Angew. Chem., Int. Ed. Engl.* **1994**, *33*, 2089−2090.
[6] M. Bochmann, K. J. Webb, M. B. Hursthouse, M. Mazid, *J. Chem. Soc. Chem. Commun.* **1991**, 1735−1737.
[7] Taken as the average from 198 structures in the Cambridge Crystallographic Data File.
[8] for a comparative discussion cf. K. M. Doxsee, J. R. Hagadorn, T. J. R. Weakley, *Inorg. Chem.* **1994**, *33*, 2600−2606.
[9] A. Bino, D. Gibson, *Inorg. Chim. Acta* **1982**, *65*, L37−L38.
[10] P. G. Cozzi, T. Carofiglio, C. Floriani, A. Chiesi-Villa, C. Rizzoli, *Organometallics* **1993**, *12*, 2845−2848.
[11] B. Müller, H. Vahrenkamp, *Eur. J. Inorg. Chem.* **1999**, 137−144, succeeding paper.
[12] M. Förster, R. Burth, A. K. Powell, T. Eiche, H. Vahrenkamp, *Chem. Ber.* **1993**, *126*, 2643−2648.
[13] R. T. Hamilton, J. A. V. Butler, *J. Chem. Soc.* **1932**, 2283−2284.
[14] G. Brauer, *Handbuch der Präparativen Anorganischen Chemie*, Ferdinand Enke Verlag, Stuttgart, **1978**, Band 2, p. 1023−1026.
[15] The crystallographic data of the structures described in this paper were deposited with the Cambridge Crystallographic Data Centre as supplementary publication no. CCDC-102445 (for **3a**), 102446 (for **4a**), 102447 (for **4b**), 102448 (for **4c**), 102449 (for **5c**), 102450 (for **2c**), 102451 (for **1b**), 102452 (for **1c**), 102453 (for **10b**), 102454 (for **7a**), 102455 (for **6a**), 102456 (for **9b**). Copies of these data are available free of charge from the following address: The Director, CCDC, 12 Union Road, GB-Cambridge CB2 1EZ (Telefax: Int. +44 (0)1223/ 336 033; E-mail: deposit@chemcrys.cam.ac.uk). For a limited time they are also available on the Internet Web Site www.chemie.uni-freiburg.de/aoanchem/hv/data.html.
[16] G. M. Sheldrick, *SHELX-86* and *SHELXL-93*, Programs for Crystal Structure Determination, Universität Göttingen, **1986** and **1993**.
[17] E. Keller, Program *SCHAKAL*, Universität Freiburg, **1997**.

Received August 3, 1998
[I98257]

Zinc Complexes of Aldehydes and Ketones, 4[+]
Zinc Complexes of Chelating Aldehydes

Bodo Müller[a] and Heinrich Vahrenkamp*[a]

Keywords: Zinc / Aldehyde ligands / N,O Chelate ligands / Structural chemistry / Chelates

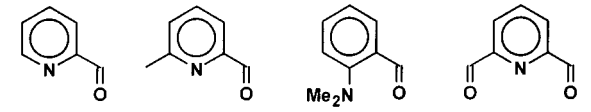
The reactions of various zinc salts with the chelating aromatic aldehydes pyridine-2-carbaldehyde, 6-methylpyridine-2-carbaldehyde, pyridine-2,6-dicarbaldehyde, and 2-dimethylaminobenzaldehyde were studied. The monoaldehydes and zinc halides yielded the tetrahedral chelate complexes $ZnHal_2$·aldehyde. Pyridine-2-carbaldehyde also formed the octahedral bis-chelate complexes $ZnHal_2$·2 aldehyde. The octahedral tris-chelate complexes $[Zn(aldehyde)_3]^{2+}$ were obtained from $[Zn(CH_3CN)_6](SbCl_6)_2$. Pyridine-2,6-dicarbaldehyde was found to be tridentate in the trigonal-bipyramidal complexes $ZnHal_2$·aldehyde. The structural variability in this system was underlined by the identification of the two unusual complexes [(pyridine-2-carbaldehyde)$_2$(H_2O)Zn–Cl–$ZnCl_3$] and [ZnI(pyridine-2-carbaldehyde)$_2$]$_2$[ZnI_4].

The importance of metal catalysis for reactions of organic carbonyl compounds in chemistry and biology, specifically by zinc compounds, has motivated us to undertake a systematic study of the interactions between the zinc ion and carbonyl-containing species. We started this study with an investigation of zinc−aldehyde complexes. The justification and scope of our work, as well as the relevant information from the literature, are summarized in our first full paper on this subject[2]. It can be stated that, to date, surprisingly little is known about the composition, structure, and bonding of metal-aldehyde adducts, be it in solution or in the solid state.

Our investigations with various zinc salts and plain aldehydes[1][2] gave rise to the conclusion that many complexes can be isolated and that they have a very rich structural chemistry, but that they are of low stability, very labile, and do not persist in solution in the presence of water or solvents of even low donor ability. We therefore sought to improve the situation by ligand design in terms of the aldehydes as well as of the coligands. Complex stabilization by chelation could be predicted to be advantageous for this purpose. We therefore used aldehydes bearing an additional nitrogen donor function, suitable for N,O chelation. A second motivation for this choice came from our attempts to model the structure and function of the enzyme alcohol dehydrogenase, in which the reacting aldehyde or alkoxide are attached to zinc as part of a ZnS_2NO donor set[3].

A search of the literature revealed that, just as for the plain aldehydes, there is very little information on the metal complexation of N,O chelating aldehydes. The only reported structural study showed that pyridine-2-carbaldehyde coordinates to CuCl only through the nitrogen atom[4]. For zinc the complex types $ZnBr_2$•2 aldehyde[5] and $Zn(SR)_2$•aldehyde[6] were described for pyridine-2-carbaldehyde, but these compounds were not structurally characterized. Structural information exists only for the somewhat related zinc halide complexes of pyridine-2-carboxylic acid esters, which contain N,O chelate rings[7]. Some work from a mechanistic point of view was reported for the zinc salt-catalyzed reduction of acyl-substituted pyridines and isoquinolines by hydride donors of the NADH type[8−10].

In order to provide a basis of isolated and structurally characterized complexes we investigated the coordinating abilities of the four typical chelating aldehydes PA, MPA, ABA, and PDA towards zinc salts. We found all four of these compounds to be suitable ligands for zinc, making ZnL, ZnL_2, and ZnL_3 complexes accessible. A small number of these results have already been described briefly[11].



2-pyridine-carbaldehyde **PA** | 6-methylpyridine-2-carbaldehyde **MPA** | 2-dimethylamino benzaldehyde **ABA** | 2,6-pyridine-dicarbaldehyde **PDA**

Preparations

The zinc halides formed 1:1 as well as 1:2 complexes with the chelating aldehydes. When a solution of the zinc halide in diethyl ether was treated dropwise with an ethereal solution of one equivalent of the aldehyde, the 1:1 complexes **1**−**3** precipitated. With pyridine-2-carbaldehyde it could be shown that the accessibility of the 1:1 complexes depends on the presence of sub-stoichiometric amounts of the aldehyde in solution and on its removal by precipitation. However, when the zinc halide and the aldehyde were dissolved simultaneously in the better solvent acetonitrile, the sub-

[+] Part 3: Ref.[1]

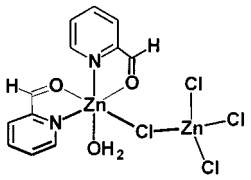
[a] Institut für Anorganische und Analytische Chemie der Universität Freiburg,
Albertstr. 21, D-79104 Freiburg, Germany

 © WILEY-VCH Verlag GmbH, D-69451 Weinheim, 1999 1434−1948/99/0101−0137 $ 17.50+.50/0

sequent crystallization yielded the 1:2 complexes **4a**−**c** regardless of the stoichiometric ratio of the reagents. Near quantitative conversion to **4a**−**c** occurred when the required 1:2 ratio was employed. Complexes **1**−**4** are stable enough to be recrystallized from organic donor solvents. Complex **4b** is the only zinc complex of a chelating aldehyde that has been described before[5].

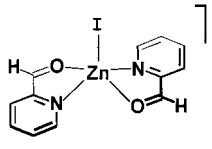
	$ZnHal_2$•A			$ZnHal_2$•2 PA
	Hal	A		Hal
1a	Cl	PA	**4a**	Cl
1b	Br	PA	**4b**	Br
2a	Cl	MPA	**4c**	I
2b	Br	MPA		
2c	I	MPA		
3a	Cl	ABA		
3b	Br	ABA		
3c	I	ABA		

Two unexpected results pointed to the subtleties inherent in these reaction systems, despite the higher stabilities of the chelating aldehyde complexes in comparison to those of the plain aldehydes. When water was accidentally present in the reaction solution for the preparation of **1a**, complex **5** was isolated instead. **5** was subsequently prepared from $ZnCl_2$, PA, and H_2O in the ratio 2:2:1. Just like complexes **4** in comparison to complex **1**, complex **5** shows a preference for higher coordination numbers in the presence of oxygen-containing ligands. In a similar fashion complex **6**, which was isolated instead of the expected yet elusive ZnI_2•PA, shows the PA ligands to be part of the five-coordinate $[ZnL_2I]^+$ cation. In both **5** and **6** the bonding preferences of the hard and soft ligands are realized by dismutation into an N,O-coordinated zinc cation and a halide-coordinated zincate anion, albeit in quite different ways and yet different from the way chosen by the compound of composition $ZnBr_2$(4-fluorobenzaldehyde)$_2$[1].



$(PA)_2(ZnCl_2)_2{\cdot}H_2O$

5



$[(PA)_2ZnI]_2\ (ZnI_4)$

6

Exclusive coordination of zinc by the chelating aldehydes could be achieved when starting with zinc compounds with weakly coordinating anions. After some futile attempts with fully dehydrated zinc nitrate, tetrafluoroborate, or perchlorate[2] or the hexaethanol zinc complex, it was found that hexa(acetonitrile)−zinc−bis(hexachloroantimonate)[12] is a suitable starting material. Treatment of this compound with the aldehydes PA and MPA resulted in the formation of the 1:3 complexes **7** and **8**. Although **7** and **8** could not be obtained as X-ray quality crystals, their constitution is confirmed by the spectra (see below), which indicate coordination of all N and O donors to zinc, thus implying octahedral ZnL_3 cations.

$[Zn(A)_3][SbCl_6]_2$

7: A = PA; **8**: A = MPA

As expected, the doubly chelating bis-aldehyde ligand PDA formed 1:1 complexes with the zinc halides. Complexes **9a**−**c** resulted from adding a solution of the ligand to a solution of the halide in ether. While we are aware of no other metal complex of PDA, the corresponding Schiff bases are popular ligands, and some zinc halide complexes are known from them[13]. As could be predicted, such complexes, like **9a**−**c**, are trigonal-bipyramidal with the halide ligands in equatorial positions.

$ZnHal_2$•PDA

9a: Hal = Cl; **9b**: Hal = Br; **9c**: Hal = I

Structures

The simplest complex type, $ZnHal_2$•aldehyde, was characterized by the structure determinations of **2b** and **2c**. Figure 1 shows that the aldehyde acts as a symmetrically chelating ligand with similar Zn−N and Zn−O bond lengths. The chelate ring is planar and is also coplanar with the aromatic ring. The $ZnHal_2$ plane is perpendicular to the ZnNO plane, i.e. tetrahedral coordination is realized to a good approximation. However, as is usual due to the geometrical restraints of the chelate ring, the N−Zn−O angle has a typically small value, which is compensated by a rather large Hal−Zn−Hal angle.

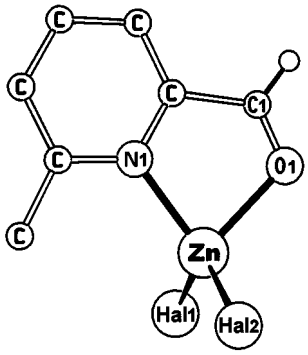


Figure 1. Molecular structure of complexes **2b** and **2c**
Relevant bond lengths [Å] and angles [°] (**2c** has two independent molecules in the asymmetric unit for which average values are given): Z−N1 2.05(2)/2.06(1), Zn−O1 2.10(1)/2.11(1), Zn−Hal1 2.334(4)/2.530(2), Zn−Hal2 2.314(3)/2.513(1), O1−C1 1.18(3)/1.21(1), N1−Zn−O1 80.3(6)/80.2(6), Hal1−Zn−Hal2 119.1(1)/122.8(3.0).

Complex **3c** shares the basic structural features of **2b** and **2c**, i.e. similar Zn−N and Zn−O bond lengths and the symmetrically distorted tetrahedral coordination of zinc (Figure 2). The six-membered chelate ring allows a larger N−Zn−O angle that is still considerably smaller than the tetrahedral angle. The six-membered chelate ring is characteristically folded along the N−O line, allowing the aromatic ring and the aldehyde function to be coplanar. This situation, however, means that unlike in all other aldehyde complexes characterized by us in this study[1][2], the zinc ion is displaced from this plane by the considerable distance

of 1.1 Å. Compared to the tetrahedral zinc halide complexes of plain aldehydes[1] the Zn−Hal distances in **2b**, **2c**, and **3c** are in the normal range, but the Zn−O distances are elongated by roughly 0.05 Å. This must be related to the presence of N donors in the molecules, which serve to better satisfy the electron-acceptor properties of the zinc ions.

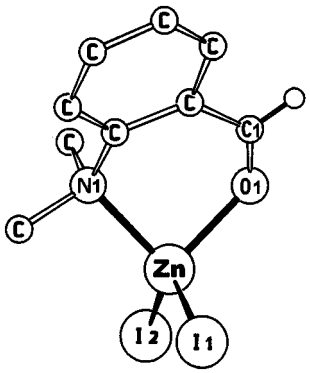


Figure 2. Molecular structure of complex **3c**
Relevant bond lengths [A] and angles [°]: Zn−N1 2.099(4), Zn−O1 2.051(3), Zn−I1 2.518(1), Zn−I2 2.518(1), O1−C1 1.222(6), N1−Zn−O1 89.3(1), I1−Zn−I2 122.07(2).

The $ZnHal_2$•2 aldehyde complexes **4a−c** crystallize with unusual molecular shapes (Figure 3). These compounds are not octahedral, as can be seen from the severe angular distortions, but their oxygen atoms are visibly oriented towards the zinc ions despite their extremely long Zn−O distances. In addition, the oxygen atoms are positioned cleanly in *trans*-positions opposite to the halide ligands such that they cannot be excluded from the ligand sphere, a situation that would render the complexes tetrahedral. Tetrahedral ZnN_2Hal_2 complexes are commonplace and, just like the tetrahedral ZnN_2S_2 complexes, define a highly preferred coordination mode. Thus it must again be concluded that the good donor qualities of the pyridine nitrogens saturate the electronic demands of the zinc ions and render further coordination by the aldehyde oxygens almost unnecessary. A similar situation was observed for zinc halide complexes of pyridine-2-carboxylic esters[7] with Zn−O distances ranging from 2.38 to 2.50 Å as compared to 2.48−2.54 Å seen here. In the pyridine-ester complexes, just as in our pyridine-aldehyde complexes, the zinc−halide distances are characteristically longer than in the tetrahedral zinc halide complexes, e.g. of the plain aldehydes[1], in accord with the higher coordination number of zinc.

The weak N−O coordination characteristic of **4a−c** is not observed in the unique complexes **5** and **6**, see Figures 4 and 5. Both **5** and **6** contain cationic units bearing two chelating aldehyde ligands attached to zinc of coordination number 5 or 6 together with anionic $ZnHal_4$ units. In **5** cation and anion are halide bridged, in **6** the ZnI_4 anions are isolated. The Zn−O distances in **5** and **6**, with an average length of 2.25 Å, are longer than those in the tetrahedral complexes **2** and **3** (see above) and also those in octahedral complexes of the plain aldehydes[2], but they are not significantly outside the range for octahedral zinc. Thus,

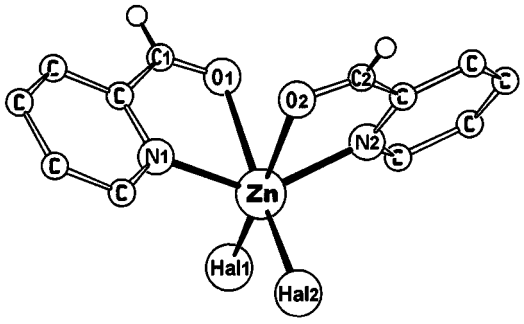


Figure 3. Molecular structures of complexes **4a−c**
Relevant bond lengths [A] and angles [°] for **4a/4b/4c**: Zn−N1 2.108(7)/2.102(15)/2.102(5), Zn−N2 2.108(7)/2.111(14)/2.117(4), Zn−O1 2.481(6)/2.498(14)/2.483(4), Zn−O2 2.544(7)/2.525(14)/2.532(4), Zn−Hal1 2.301(3)/2.450(3)/2.661(1), Zn−Hal2 2.300(3)/2.441(3)/2.665(1), O1−C1 1.20(1)/1.19(3)/1.21(1), O2−C2 1.22(1)/1.20(2)/1.21(1), N1−Zn−N2 137.7(3)/135.9(6)/136.8(2), O1−Zn−O2 80.8(2)/83.3(5)/85.8(2), Hal1−Zn−Hal2 130.7(1)/102.9(1)/101.92(3), N1−Zn−O1 72.2(2)/71.7(5)/72.1(2), N2−Zn−O2 71.0(2)/70.9(5)/71.6(2).

although the weakening of the Zn−O bonds due to the presence of the Zn−N bonds is observed, it is less pronounced because the zinc ions, due to the cationic nature of the complexes, are better electron acceptors than those in complexes **2**, **3**, or **4**. Although complexes **5** and **6** are both the first examples of their kind, their structural patterns are not singular. Both halide bridging between octahedral and tetrahedral zinc[14] and bis(chelate)-mono(halide)-zinc cations of square-pyramidal geometry[15] have been observed before.

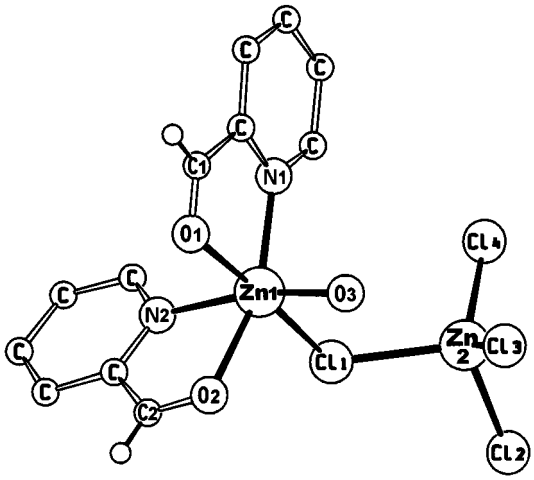


Figure 4. Molecular structures of complex **5**
Relevant bond lengths [Å] and angles [°]: Zn1−N1 2.087(3), Zn1−N2 2.108(3), Zn1−O1 2.244(3), Zn1−O2 2.267(3), Zn1−O3 2.024(3), Zn1−Cl1 2.394(1), Zn2−Cl1 2.366(1), Zn2−Cl2 2.258(1), Zn2−Cl3 2.259(1), Zn2−Cl4 2.202(1), O1−C1 1.201(5), O2−C2 1.209(5), N1−Zn1−O1 77.1(1), N2−Zn1−O2 75.3(1), N1−Zn1−O2 156.7(1), N2−Zn1−O3 163.8(1), O1−Zn1−Cl1 176.0(1).

Complexes **9a** and **9b** belong to the group of trigonal-bipyramidal $LZnX_2$ complexes in which L represents a doubly chelating tridentate ligand. Close relatives of **9a** are $LZnCl_2$ with L = terpyridyl[16] and L = 2,6-diacetylpyridinedioxime[17]. These complexes share the coplanar nature of the whole ligand L and the severe deviation of the axial

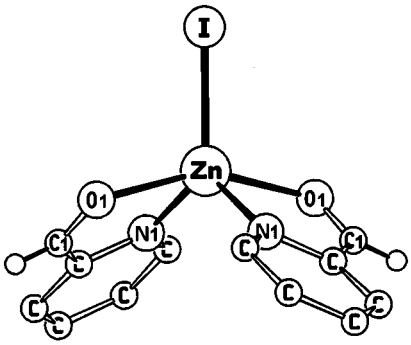


Figure 5. Structure of the cations of compound **6**
Relevant bond lengths [Å] and angles [°]: Zn−N1 2.06(1), Zn−O1 2.25(1), Zn−I 2.515(4), O1−C1 1.19(2), N1−Zn−O1 76.8(5), N1−Zn−N1′ 116.5(8), O1−Zn−O1′ 154.6(8), N1−Zn−O1′ 89.8(5), N1−Zn−I 121.8(4), O1−Zn−I 102.7(4).

ligand arrangement from linearity. However, while in the latter two complexes the axial zinc-ligand bonds (in both cases Zn−N) are not significantly longer than the equatorial Zn−N bond, the opposite is the case for **9a** and **b** (Figure 6). The Zn−O bonds are, on average, 2.34 Å long and are therefore halfway between those in tetrahedral **2** or **3** and octahedral **4**. As in complex **2** or **3** only a single nitrogen donor is present, but as is the case in **4** two aldehyde oxygen donors compete for the remaining acceptor strength of the zinc ion. Like in all other complexes described in this paper, the aldehyde C=O bond lengths do not reflect the variable strength of the Zn−O interactions. They all have lengths of around 1.21 Å with very little variation.

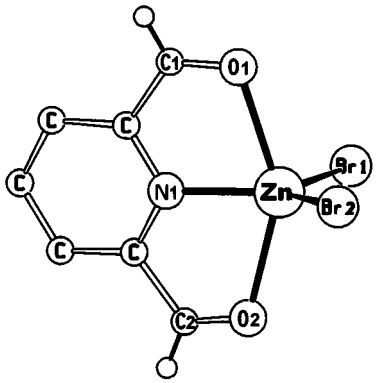


Figure 6. Molecular structure of complexes **9a** and **9b**
Relevant bond lengths [Å] and angles [°] for **9a/9b**: Zn−N1 2.046(4)/2.043(4), Zn−O1 2.336(4)/2.348(4), Zn−O2 2.322(4)/2.327(4), Zn−Hal1 2.198(2)/2.337(1), Zn−Hal2 2.189(2)/2.322(1), O1−C1 1.213(7)/1.210(6), O2−C2 1.214(7)/1.218(6), O1−Zn−O2 148.0(2)/148.2(1), N1−Zn−O1 74.0(2)/74.2(1), N1−Zn−O2 74.3(2)/74.3(1), Hal1−Zn−Hal2 121.33(6)/120.91(3).

Spectroscopy

Upon coordination to transition metals, the intense IR ν(CN) band of pyridine-derived ligands is shifted by about 10 to 50 cm^{-1} to higher wavenumbers[18][19]. This shift is observed in the +20 cm^{-1} category here, proving the expected Zn−N coordination of the pyridine-derived aldehydes (Table 1). Conversely, the aldehyde-ν(CO) band is shifted by about 50 cm^{-1} to lower wavenumbers in zinc complexes of the plain aldehydes[1][2]. Shifts to lower wavenumbers are also observed here. They are in the 40−50 cm^{-1} range for those complexes (**1**−**3**, **5**, **6**) in which, according to the structure determinations, the Zn−O interactions are strong or medium. The shifts are typically smaller when the Zn−O interactions are known to be weak (complexes **4**, **9**). For the presumably octahedral ZnN_3O_3 complexes **7** and **8** there seem to be good interactions according to the IR data. Some spectra are further complicated as far as this interpretation is concerned by showing ν(CO) bands that are split into two maxima. As this occurs irregularly and the intensity of the second band varies significantly we refrain from interpreting this observation in terms of structural details or crystal packing phenomena.

Table 1. Relevant IR data (KBr, cm^{-1}) of the complexes

	ν(CN)	Δν	ν(CO)	Δν
1a	1603	+18	1669	−44
1b	1600	+15	1679	−34
2a	1606	+13	1666	−46
2b	1604	+11	1652	−60
2c	1603	+10	1652/1675	−60/−37
3a	1208	+20	1638	−47
3b	1207	+19	1633	−52
3c	1205	+17	1630	−55
4a	1600	+15	1682/1702	−32/−11
4b	1600	+15	1679/1697	−34/−16
4c	1599	+14	1674	−39
5	1615	+30	1663/1680	−50/−33
6	1601	+16	1658	−55
7	1605	+20	1666	−47
8	1607	+22	1666	−47
9a	1597	+18	1687	−31
9b	1596	+17	1684	−34
9c	1594	+15	1680	−38

The NMR data of the complexes (see Tables 2 and 3) are characteristically different from those of the zinc complexes of plain aldehydes[1][2]. Whereas the latter show NMR spec-

Table 2. Typical ^{1}H-NMR data (in [D_6]acetone, δ) of the complexes

	δ(CHO)	Δδ	δ(H6)	Δδ
1a	10.25	+0.24	9.15	+0.39
1b	10.35	+0.34	9.24	+0.48
2a	10.25	+0.31	2.85[a]	+0.27
2b	10.33	+0.39	2.92[a]	+0.34
2c	10.31	+0.37	2.91[a]	+0.33
3a	10.15	−0.08	2.96[b]	+0.11
3b	10.14	−0.09	2.95[b]	+0.10
3c	10.10	−0.13	2.96[b]	+0.11
4a	10.17	+0.16	9.03	+0.27
4b	10.22	+0.21	9.09	+0.33
4c	10.26	+0.25	9.09	+0.33
5	10.27	+0.26	9.19	+0.43
6	10.40	+0.39	9.22	+0.46
7	10.29	+0.28	9.25	+0.49
8	10.27	+0.34	3.11[a]	+0.53
9a	10.22	+0.11	–	–
9b	10.30	+0.19	–	–
9c	10.34	+0.23	–	–

[a] Methyl group on C6. – [b] NMe_2 signal.

Table 3. Typical ^{13}C-NMR data (in [D$_6$]acetone, δ) of the complexes

	δ(CHO)	Δδ	δ(C2/C6)	Δδ
1a	193.2	−0.7	150.6/151.3	−2.9/+0.5
1b	193.5	−0.4	149.0/151.4	−4.5/+1.1
2a	196.9	+2.8	148.0/161.1	−5.2/+1.1
2b	197.2	+3.1	146.5/161.1	−6.7/+1.1
2c	197.5	+3.4	146.4/161.1	−6.8/+1.1
3a	193.8	+3.2	46.1[a]	+0.5
3b	194.4	+3.8	46.2[a]	+0.6
3c	196.7	+6.1	46.7[a]	+1.1
4a	193.5	−0.4	152.5/151.3	−1.0/+0.5
4b	193.7	−0.2	150.3/151.3	−3.2/+0.5
4c	194.1	+0.2	150.3/151.2	−3.2/+0.4
5	193.1	−0.9	150.2/151.4	−3.3/+0.6
6	194.1	+0.2	148.9/151.2	−4.6/+0.4
7	193.4	−0.50	150.8/148.6	−2.7/−2.2
8	194.2	+0.07	151.6/160.6	−1.6/+0.6
9a	192.5	−0.6	151.5	−2.5
9b	192.0	−1.1	149.7	−4.3
9c	191.6	−1.5	148.7	−5.3

[a] NMe_2 signal.

tra that are almost identical to those of the free aldehydes, thereby supporting the suspicion that the complexes dissociate in solution, all pyridine-aldehyde complexes display significant coordination shifts for the signals of the groups in the vicinity of the donor atoms N and O. In particular, the proton resonances of the aldehyde CHO groups and the ^{13}C resonances of the pyridine-C_α carbon atoms provide important evidence that the aldehyde function is coordinated to zinc in all cases, even in solution.

Discussion

The results of this work have verified the assumption that the chelate effect will lead to more stable and more inert zinc−aldehyde complexes. Unlike the complexes of the plain aldehydes, compounds **1**−**9** do not require a large excess of the aldehyde to be isolable, they result from stoichiometric amounts of the reagents in solution, they can be recrystallized from donor solvents (e.g. THF), and their NMR spectra indicate the persistence of the zinc-aldehyde binding in solution. With the exception of **5** and **6** their structures can be deduced from their compositions by assuming coordination of all donor groups. Accordingly, the structure proposed for **4b**, the only previously reported zinc complex of a pyridine aldehyde[5], was confirmed.

While the Zn−N coordination is essential for the existence of the complexes, it is also the reason for weaker Zn−aldehyde interactions. Only in the 1:1 complexes **1**−**3** are the Zn−O bonds as strong (i.e. short) as in the Zn-aldehyde complexes without N-donor ligands[1][2]. These complexes can, however, only be isolated by precipitation from solutions with low pyridine aldehyde concentrations, and when dissolved complexes **1** undergo dismutation with formation of complexes **4**. Similarly, compound **6**, having a 1:2 (zinc/aldehyde) composition in its complex cation, was the only isolable product in attempts to prepare the elusive ZnI_2•PA. This preference for the 1:2 over the 1:1 composition is a reflection of the high stability of ZnN_2X_2 species, where N represents a heteroaromatic nitrogen donor and X e.g. a halide, in zinc complex chemistry.

By adjusting the reaction conditions and the nature of the coligands, zinc complexes with one, two, or three chelating aldehydes were accessible, e.g. **1a**, **4a**, and **7** for pyridine-2-carbaldehyde. Tetrahedral, square-pyramidal, and octahedral coordination of zinc has been observed. Most typical for the chelating aldehydes are the distorted coordination geometries between tetrahedral and octahedral, as exemplified by complexes **4**, and this phenomenon is caused by the strong Zn−N and weak Zn−O interactions. The distortion is most pronounced for complexes **4** because without Zn−O interactions these complexes would be very stable tetrahedral complexes of the ZnN_2Hal_2 type. On the other hand, the absence of a second nitrogen donor makes Zn−O binding stronger and hence complexes **1**−**3** are less distorted, and likewise complexes like **5** or **7**, bearing the chelating aldehyde bound to a cationic ZnL_6 species, have stronger Zn−O interactions and hence more symmetrical coordinations due to the higher electron acceptor strength of the zinc ion. Similar observations have been made for zinc halide complexes of pyridine-2-carboxylic esters[7].

The structural variability of the complexes reported here is much greater than that of the complexes of the plain aldehydes[1][2]. The latter invariably form octahedral complexes in the absence of halide and tetrahedral complexes with halides as coligands. In the compounds reported here, halide can be coligand in tetrahedral (**1**−**3**), five-coordinate (**6**), and octahedral (**5**) complexes. As discussed above, the composition of the compounds as well as the reaction conditions influence the specific geometry. The subtleties governing this are demonstrated by the formation of **6** instead of the elusive ZnI_2•PA as well as the fact that 2-dimethylaminobenzaldehyde forms only the 1:1 complexes **3** but not 1:2 complexes like **4**. A variation of this theme concerns the dismutation reactions of some of the zinc halide complexes into cationic zinc-aldehyde and anionic zinc halide constituents, of which the latter again show structural variability by existing as isolated $ZnHal_4^{2-}$ (**6**), halide bridged $ZnHal_4^{2-}$ (**5**) or even isolated $Zn_2Hal_6^{2-}$ [together with a $Zn(aldehyde)_6^{2+}$ cation][1].

In terms of activation of the carbonyl function for catalytic reactions, the complexes described here offer important information by their variable Zn−O (aldehyde) interactions. In the complexes of the plain aldehydes, octahedral coordination agrees with Zn−O distances close to the average of 2.09 Å[2] and tetrahedral coordination with Zn−O distances averaging 2.04 Å[1]. In contrast, in the compounds reported here Zn−O bond lengths ranging from 2.05 to 2.54 Å are observed with no systematic correlation between distance and coordination number. There is, however, a correlation between Zn−O bond length and the donor/acceptor situation at the zinc ion. In complexes **1**−**3** a single nitrogen donor provides the zinc ion with insufficient electron density and hence the Zn−O bonds are short (ca. 0.05 Å above the tetrahedral reference value). On the other hand

complexes **4** would be able to exist as four-coordinated ZnN_2Hal_2 species, i.e. Zn−O coordination is not required and hence is weak (Zn−O distances ca. 0.40 Å above the octahedral reference value). Complexes **5** and **6**, as discussed above, are intermediate cases (with Zn−O distances ca. 0.15 Å above average). Complexes **9** can be referenced against complexes **1**−**3**. In the latter compounds one nitrogen and one oxygen donor both experience good Zn−O(N) interactions, while in **9** two oxygen donors have to share the remaining bonding capacity, resulting in clearly weaker Zn−O interactions (bond lengths ca. 0.25 Å above average). These variations in the Zn−O interactions are in part reflected by the IR data, which demonstrate a congruous variation of the C=O bond strengths. Thus the electronic situation of the "catalytic" zinc ion visibly influences the electronic modification of the aldehydic C=O functions, which should become effective in terms of reaction rates or reaction pathways.

In terms of modelling the enzyme alcohol dehydrogenase, complexes **1**−**3** represent an advancement as they contain Zn−O(aldehyde) together with Zn−N(heteroaromatic) coordination in the tetrahedral $ZnHal_2NO$ pattern. The realization of the enzyme-like ZnS_2NO pattern with the pyridine-aldehyde ligands calls for a replacement of the halide ligands by thiolate ligands. This has already been reported by Bochmann[6], yet without the support of a structure determination. Our own work using the chelating aldehydes and $Zn(SC_6F_5)_2$, including X-ray structural studies, will be published shortly[20].

Experimental Section

The general working and measuring conditions were as in ref.[21], the specific conditions as in ref.[2]. The aldehydes were obtained commercially and distilled or recrystallized prior to use. The anhydrous zinc halides were prepared from zinc and HHal or Hal_2, respectively, in diethyl ether[22][23], $[Zn(CH_3CN)_6]$ $[SbCl_6]_2$ was prepared according to the published procedure[12]. The new complexes were prepared following the general procedure below, details for which are given in Table 4. Table 5 gives details of the analytical characterizations.

Table 5. Analytical characterization

	formula mol. wt.	Analyses calcd./found C	H	N	Zn	Hal
1a	$C_6H_5Cl_2NOZn$	29.61	2.07	5.76	26.86	29.13
	243.4	29.59	2.16	5.66	26.89	29.02
1b	$C_6H_5Br_2NOZn$	21.69	1.52	4.22	19.68	48.09
	332.3	21.72	1.59	4.17	19.81	48.16
2a	$C_7H_7Cl_2NOZn$	32.66	2.74	5.44	25.40	27.54
	257.4	32.54	2.75	5.37	25.33	27.61
2b	$C_7H_7Br_2NOZn$	24.28	2.04	4.04	18.88	46.14
	346.3	24.42	2.10	3.97	18.95	46.22
2c	$C_7H_7I_2NOZn$	19.09	1.60	3.18	14.85	57.64
	440.3	19.30	1.64	3.15	14.77	57.78
3a	$C_9H_{11}Cl_2NOZn$	37.87	3.88	4.91	22.91	24.84
	285.5	35.78	3.72	4.58	22.99	24.96
3b	$C_9H_{11}Br_2NOZn$	28.87	2.96	3.74	17.47	42.69
	374.4	28.18	2.94	3.59	17.58	42.38
3c	$C_9H_{11}I_2NOZn$	23.08	2.37	2.99	13.96	54.19
	468.4	23.83	2.90	2.92	14.03	54.08
4a	$C_{12}H_{10}Cl_2N_2O_2Zn$	41.12	2.88	7.99	18.66	20.23
	350.5	40.89	2.86	8.08	18.71	20.16
4b	$C_{12}H_{10}Br_2N_2O_2Zn$	32.80	2.29	6.38	14.88	36.37
	439.4	32.77	2.28	6.48	14.92	36.41
4c	$C_{12}H_{10}I_2N_2O_2Zn$	27.02	1.89	5.25	12.26	47.58
	533.4	27.11	1.92	5.30	12.18	47.63
5	$C_{12}H_{12}Cl_4N_2O_3Zn_2$	28.55	2.40	5.55	25.91	28.09
	504.8	28.29	2.22	5.41	25.90	28.02
6	$C_{24}H_{20}I_6N_4O_4Zn_3$	20.80	1.45	4.04	14.15	54.94
	1386.0	20.22	1.38	3.96	14.30	54.81
7	$C_{18}H_{15}Cl_{12}N_3O_3Sb_2Zn$	20.48	1.43	3.98	6.19	40.30
	1055.7	19.93	1.35	3.85	6.32	40.08
8	$C_{21}H_{21}Cl_{12}N_3O_3Sb_2Zn$	22.98	1.93	3.83	5.96	38.76
	1097.7	21.76	1.97	3.44	6.03	38.84
9a	$C_7H_5Cl_2NO_2Zn$	30.98	1.86	5.16	24.09	26.12
	271.4	29.71	1.81	4.84	24.24	25.83
9b	$C_7H_5Br_2NO_2Zn$	23.33	1.40	3.89	18.15	44.35
	360.3	21.19	1.37	3.36	18.28	44.09
9c	$C_7H_5I_2NO_2Zn$	18.51	1.11	3.08	14.39	55.87
	454.3	18.57	1.13	3.12	14.22	55.98

Preparation of the Complexes: The zinc salt was dissolved in the organic solvent. The chelating aldehyde was added as a solution in diethyl ether with stirring. The resulting complex either precipitated immediately or after cooling the hot solutions to room temperature. After filtration the product was washed with petroleum ether (b.p. 60−70°C) and dried in vacuo.

Structure Determinations[24]: Crystals of **3a**−**c** were obtained by dissolution in CH_2Cl_2, all others by dissolution in THF/CH_2Cl_2

Table 4. Reaction details

Compl.	Solvent[a]	zinc salt				aldehyde				yield		m.p.
			g	mmol	mL solv.		mL	g	mmol	mL solv.	g	%	°C
1a	E	$ZnCl_2$	1.03	7.56	40	PA	0.72	0.81	7.56	10	1.76	96	211
1b	E	$ZnBr_2$	0.83	3.69	40	PA	0.355	0.40	3.73	10	1.07	87	162 (dec.)
2a	E	$ZnCl_2$	0.64	4.70	60	MPA	–	0.57	4.70	15	1.09	90	192 (dec.)
2b	E	$ZnBr_2$	0.71	3.15	100	MPA	–	0.38	3.14	20	0.90	82	182 (dec.)
2c	E	ZnI_2	1.08	3.38	150	MPA	–	0.41	3.39	20	1.17	79	158
3a	E	$ZnCl_2$	2.12	15.60	100	ABA	–	2.32	15.60	100	3.66	82	154 (dec.)
3b	E	$ZnBr_2$	1.12	4.97	40	ABA	–	0.74	4.96	10	1.73	93	160 (dec.)
3c	E	ZnI_2	0.76	2.38	100	ABA	–	0.35	2.35	10	0.89	81	170 (dec.)
4a	A	$ZnCl_2$	1.36	9.98	40	PA	1.90	2.14	19.98	10	2.88	82	164 (dec.)
4b	A	$ZnBr_2$	0.80	3.55	40	PA	0.675	0.76	7.10	10	1.18	76	173 (dec.)
4c	A	ZnI_2	2.84	8.90	40	PA	1.70	1.91	17.83	10	4.50	95	172 (dec.)
5	E	$ZnCl_2$	3.50	25.68	50[b]	PA	2.44	2.75	25.68	50	5.94	92	200 (dec.)
6	E	ZnI_2	1.58	4.95	100	PA	0.471	0.53	4.95	10	1.71	99	178 (dec.)
7	E/D	$Zn(MeCN)_6(SbCl_6)_2$	1.74	1.77	40[c]	PA	0.506	0.57	5.32	10	1.76	94	82 (dec.)
8	E/D	$Zn(MeCN)_6(SbCl_6)_2$	1.73	1.76	40[c]	MPA	–	0.64	5.28	10	1.66	86	105 (dec.)
9a	E	$ZnCl_2$	1.13	8.29	80	PDA	–	1.12	8.29	20	2.08	93	202
9b	E	$ZnBr_2$	1.27	5.64	80	PDA	–	0.76	5.63	20	1.83	90	182 (dec.)
9c	E	ZnI_2	0.80	2.51	80	PDA	–	0.34	2.52	20	0.96	84	198 (dec.)

[a] A = acetonitrile; D = dichloromethane; E = diethyl ether. – [b] + 0.23 mL (0.23 g, 12.80 mmol) H_2O. – [c] + 2 mL tetrahydrofuran.

Table 6, part 1. Crystallographic details

	2b	**2c**	**3c**	**4a**	**4b**
formula	$C_7H_7Br_2NOZn$	$C_7H_7I_2NOZn$	$C_9H_{11}I_2NOZn$	$C_{12}H_{10}Cl_2N_2O_2Zn$	$C_{12}H_{10}Br_2N_2O_2Zn$
mol. mass	346.33	440.31	468.36	350.49	439.41
crystal size [mm]	0.4 × 0.03 × 0.03	0.5 × 0.5 × 0.2	0.3 × 0.1 × 0.1	0.1 × 0.1 × 0.1	0.4 × 0.2 × 0.2
space group	*Fdd2*	$P2_1/n$	$P2_1/n$	$P2_1/n$	$P\bar{1}$
Z	16	8	4	4	2
a [Å]	23.075(9)	16.043(1)	7.788(1)	7.716(1)	7.687(5)
b [Å]	23.351(6)	9.140(1)	9.555(1)	13.801(3)	7.726(2)
c [Å]	7.785(7)	16.610(1)	17.805(3)	12.809(2)	12.513(4)
α [°]	90	90	90	90	97.17(2)
β [°]	90	109.03(1)	92.25(1)	100.99(1)	101.26(4)
γ [°]	90	90	90	90	94.65(4)
V [Å^3]	4195(4)	2302.5(3)	1323.9(3)	1339.0(3)	718.8(6)
d(calc.) [g·cm^{-3}]	2.19	2.54	2.35	1.74	2.03
d(obs.) [g·cm^{-3}]	–	2.50	2.26	1.71	1.97
temp. [K]	183(2)	183(2)	183(2)	293(2)	293(2)
μ(Mo-$K\alpha$) [mm^{-1}]	9.92	7.46	6.49	2.23	7.26
hkl range	h: −27 to 0	h: −19 to 0	h: −9 to 9	h: 0 to 8	h: −9 to 8
	k: −27 to 27	k: 0 to 11	k: −11 to 0	k: 0 to 16	k: −9 to 9
	l: 0 to 9	l: −19 to 20	l: −21 to 0	l: −14 to 14	l: 0 to 15
refl. measd.	1969	4665	2676	2398	1678
indep. refl.	1000	4497	2591	2221	1678
obs. refl. [$I>2\sigma(I)$]	561	3965	2406	1279	1678
parameters	103	217	127	172	172
refl. refined	1000	4497	2591	2221	1678
R_1 (obs. refl.)	0.048	0.056	0.026	0.059	0.087
wR_2 (all refl.)	0.122	0.159	0.080	0.183	0.266
residual el. density [e/Å^{-3}]	+1.0 −1.1	+2.8 −1.5	+0.8 −0.8	+3.3 −0.7	+3.3 −1.1

Table 6, part 2. Crystallographic details

	4c	**5**	**6**	**9a**	**9b**
formula	$C_{12}H_{10}I_2N_2O_2Zn$	$C_{12}H_{12}Cl_4N_2O_3Zn_2$	$C_{24}H_{20}I_6N_4O_4Zn_3$	$C_7H_5Cl_2NO_2Zn$	$C_7H_5Br_2NO_2Zn$
mol. mass	533.39	504.78	1385.95	271.39	360.31
crystal size [mm]	0.3 × 0.2 × 0.03	0.6 × 0.5 × 0.5	0.2 × 0.1 × 0.1	0.2 × 0.2 × 0.2	0.2 × 0.2 × 0.2
space group	$P\bar{1}$	$P\bar{1}$	$I\bar{4}2d$	$P2_1/n$	$P2_1/c$
Z	2	2	4	4	4
a [Å]	7.739(1)	7.997(1)	11.746(1)	7.236(2)	7.395(2)
b [Å]	7.879(1)	7.875(1)	11.746(1)	9.398(2)	9.965(2)
c [Å]	13.031(1)	15.573(1)	28.259(2)	14.382(4)	14.436(4)
α [°]	100.79(1)	100.69(1)	90	90	90
β [°]	93.79(1)	101.73(1)	90	103.37(2)	104.67(2)
γ [°]	95.08(1)	101.40(1)	90	90	90
V [Å^3]	774.7(1)	914.9(1)	3898.9(4)	951.5(4)	1029.1(4)
d(calc.) [g·cm^{-3}]	2.29	1.83	2.36	1.89	2.326
d(obs.) [g·cm^{-3}]	2.17	1.82	2.23	1.88	2.287
temp. [K]	293(2)	293(2)	293(2)	183(2)	183(2)
μ(Mo-$K\alpha$) [mm^{-1}]	5.57	3.22	6.61	3.10	10.12
hkl range	h: 0 to 9	h: −9 to 0	h: −15 to 0	h: −7 to 7	h: −9 to 0
	k: −9 to 9	k: −9 to 9	k: −15 to 0	k: 0 to 10	k: 0 to 12
	l: −16 to 16	l: −19 to 19	l: −36 to 0	l: 0 to 14	l: −17 to 17
refl. measd.	3283	3978	2282	1097	2168
indep. refl.	3045	3701	1197	1097	2007
obs. refl. [$I>2\sigma(I)$]	2411	3056	642	1096	1558
parameters	172	216	94	118	118
refl. refined	3045	3701	1197	1097	2007
R_1 (obs. refl.)	0.032	0.034	0.043	0.038	0.028
wR_2 (all refl.)	0.086	0.099	0.150	0.101	0.078
residual el. density [e/Å^{-3}]	+0.8 −0.6	+0.8 −0.4	+1.6 −0.9	+0.6 −0.5	+0.5 −0.7

(1:1). Careful layering with petroleum ether (b.p. 70−90°C) and storage of the sample in a vibration-free place yielded well-shaped crystals. These crystals were immersed in perfluorinated polyether oil for protection and attachment to the goniometer head and immediately subjected to the nitrogen flow of the diffractometer's cooling system. Diffraction data were recorded at low temperatures with the ω/2θ technique on a Nonius CAD4 diffractometer fitted with a molybdenum tube (K_α, λ = 0.7107 Å) and a graphite monochromator. No absorption corrections were applied. The structures were solved by direct methods and refined anisotropically with the SHELX program suite[25]. The aldehyde C−H hydrogen atoms were located and refined freely. All other hydrogen atoms were in-

cluded with fixed distances and isotropic temperature factors 1.2 times those of their attached atoms. Parameters were refined against F^2. The R values are defined as $R_1 = \Sigma F_o - F_c / \Sigma F_o$ and $wR_2 = \{\Sigma[w(F_o^2 - F_c^2)^2]\Sigma[w(F_o^2)^2]\}^{1/2}$. Drawings were produced with SCHAKAL[26]. Table 6 lists the crystallographic data.

Acknowledgments

This work was supported by the Deutsche Forschungsgemeinschaft.

[1] B. Müller, H. Vahrenkamp, *Eur. J. Inorg. Chem.* **1999**, 129−135, preceding paper.
[2] B. Müller, H. Vahrenkamp. *Eur. J. Inorg. Chem.* **1999**, 117−127, paper before preceding paper.
[3] H. Eklund, B. Nordström, E. Zeppezauer, G. Söderlund, I. Ohlsson, T. Boiwe, B. O. Söderberg, O. Tapia, C. I. Bränden, A. Åkeson, *J. Mol. Biol.* **1976**, *102*, 27−59. − H. Cho, S. Ramaswamy, B. V. Plapp, *Biochemistry* **1997**, *36*, 382−389.
[4] P. C. Healy, J. D. Kildea, B. W. Skelton, A. H. White, *Aust. J. Chem.* **1989**, *42*, 93−105.
[5] R. H. Prince, P. Wyeth, *J. Inorg. Nucl. Chem.* **1981**, *43*, 839−843 and 845−848.
[6] M. Bochmann, G. Bwembya, R. Grinter, A. K. Powell, K. J. Webb, M. B. Hursthouse, M. Mazid, K. M. Abdul Malik, *Inorg. Chem.* **1994**, *33*, 2290−2296.
[7] P. Gonzalez-Duarte, R. March, J. Pons, W. Clegg, L. Cucurull-Sanchez, A. Alvarez-Larena, J. F. Piniella, *Polyhedron* **1996**, *15*, 2747−2754.
[8] D. J. Creighton, J. Hajdu, D. S. Sigman, *J. Am. Chem. Soc.* **1976**, *98*, 4619−4625.
[9] A. Ohno, S. Yasui, S. Oka, *Bull. Chem. Soc. Jpn.* **1980**, *53*, 2651−2654.
[10] M. Hughes, R. H. Prince, *J. Inorg. Nucl. Chem.* **1978**, *40*, 703−712.
[11] B. Müller, M. Ruf, H. Vahrenkamp, *Angew. Chem.* **1994**, *106*, 2164−2165; *Angew. Chem. Int. Ed. Engl.* **1994**, *33*, 2089−2090.
[12] A. P. Zuur, W. L. Groeneveld, *Rev. Trav. Chim. Pays Bas* **1967**, *86*, 1089−1102.
[13] For some examples and related compounds see R. H. Prince, in *Comprehensive Coordination Chemistry*, (Eds.: G. Wilkinson, R. D. Gillard, J. A. McCleverty), Pergamon Press, Oxford, 1987, Vol. 5, pp 926−1045.
[14] H. Follner, *Z. Anorg. Allg. Chem.* **1972**, *387*, 43−51.
[15] The Cambridge Crystallographic Data File lists 20 square-pyramidal $ZnHalL_4$ structures where L_4 represents two bidentate or one tetradentate ligands. The closest relative of the cation of **6** is chloro-bispicolinato−zinc: M. A. S. Goher, M. A. M. Abu-Youssef, F. A. Mautner, *Polyhedron* **1996**, *15*, 453−457.
[16] M. Vlasse, D. Beltran-Porter, *Acta Crystallogr., Part C* **1983**, *C39*, 560−563.
[17] G. A. Nicholson, J. L. Petersen, B. J. McCormick, *Inorg. Chem.* **1982**, *21*, 3274−3280.
[18] M. M. da Mota, J. Rodgers, S. M. Nelson, *J. Chem. Soc. A* **1969**, 2036−2044.
[19] G. Anderegg, E. Hubmann, F. Wenk, *Helv. Chim. Acta* **1977**, *60*, 123−140.
[20] B. Müller, H. Vahrenkamp, unpublished. − H. Vahrenkamp, Lecture at the XXXIII International Conference on Coordination Chemistry, Firenze, **1998**, Book of Abstracts, p. 131.
[21] M. Förster, R. Burth, A. K. Powell, T. Eiche, H. Vahrenkamp, *Chem. Ber.* **1993**, *126*, 2643−2648.
[22] R. T. Hamilton, J. A. V. Butler, *J. Chem. Soc.* **1932**, 2283−2284.
[23] G. Brauer, *Handbuch der Präparativen Anorganischen Chemie*, Ferdinand Enke Verlag, Stuttgart, **1978**, Band 2, p. 1023−1026.
[24] The crystallographic data of the structures described in this paper were deposited with the Cambridge Crystallographic Data Centre as supplementary publication no. CCDC−102494 (for **4a**), 102495 (for **4b**), 102496 (for **4c**), 102497 (for **5**), 102498 (for **9a**), 102499 (for **9b**), 102500 (for **6**), 102501 (for **2b**), 102502 (for **2c**), 102503 (for **3c**). Copies of these data are available free of charge from the following address: The Director, CCDC, 12 Union Road, Cambridge CB2 1EZ, United Kingdom (Telefax: Internat. +44 (0)1223/ 336 033; E-mail: deposit@chemcrys.cam.ac.uk). For a limited time they are also available on the Internet Web Site www.chemie.uni-freiburg.de/aoanchem/hv/data.html.
[25] G. M. Sheldrick, *SHELX-86* and *SHELXL-93*, Programs for Crystal Structure Determination, Universität Göttingen, **1986** and **1993**.
[26] E. Keller, Program *SCHAKAL*, Universität Freiburg, **1997**.

Received August 3, 1998
[I98258]

1,1′-Bis(stannyl)- and 1,1′-Bis(chlorostannyl)ferrocenes Studied by Multinuclear Magnetic Resonance, Temperature-Dependent ^{57}Fe- and ^{119}Sn-Mössbauer Spectroscopy, and Electrochemistry

Max Herberhold,*[a] Wolfgang Milius,[a] Udo Steffl,[a] Klaus Vitzithum,[a] Bernd Wrackmeyer,*[a] Rolfe H. Herber,[b] Marco Fontani,[c] and Piero Zanello[c]

Keywords: Sandwich complexes / Iron / Tin / NMR spectroscopy / Mössbauer spectroscopy / Electrochemistry

The 1,1′-bis(chlorostannyl)-substituted ferrocenes $Fe(C_5H_4–SnMe_2Cl)_2$ (**2**), $Fe(C_5H_4–SnMeCl_2)_2$ (**3**) and $Fe(C_5H_4–SnCl_3)_2$ (**4**) were prepared, starting from 1,1′-bis(trimethylstannyl)ferrocene (**1**). Treatment of the chlorides with $Li[AlH_4]$ afforded the 1,1′-bis(hydridostannyl)-subsituted ferrocenes $Fe(C_5H_4–SnMe_2H)_2$ (**5**), $Fe(C_5H_4–SnMeH_2)_2$ (**6**) and $Fe(C_5H_4-SnH_3)_2$ (**7**), respectively. All complexes **1**–**7** were studied by ^{1}H-, ^{13}C-, and ^{119}Sn-NMR spectroscopy with 1D and 2D techniques. The compounds **1**–**4** were investigated by temperature-dependent ^{119}Sn- and ^{57}Fe-Mössbauer spectroscopy. The electrochemistry of **1**–**5** gave evidence of reversible one-electron oxidation processes. The molecular structure of 1,1′-bis(trichlorostannyl)ferrocene (**4**) was determined by X-ray structural analysis, and there was no indication of intra- or intermolecular Sn···Cl···Sn interactions. This direct structural information proved to be consistent with both the Mössbauer and the solution NMR spectroscopic data.

1. Introduction

In spite of the multifaceted chemistry of organotin compounds,[1] ferrocene derivatives bearing stannyl substituents at the cyclopentadienyl rings have received only scant attention.[1−4] Recent interest has focused on ferrocenophanes with one,[5] two,[6] and three[6,7] diorganostannylene moieties in the bridge. Other [3]ferrocenophanes with tin atoms in 1,3-positions and chalcogen,[7,8] nitrogen,[9] phosphorus,[9] or arsenic[9] in 2-position have been reported. The 1-stanna-[1]ferrocenophane undergoes ring-opening polymerization,[5,10] and transition-metal fragments can be inserted into the Sn−C(1) bond by oxidative addition.[11] The reaction of 1,2-distanna-[2]ferrocenophane with $Pt(C_2H_4)(PPh_3)_2$ provides access to 1,3-distanna-2-platina-[3]ferrocenophanes,[12,13] which are examples of the active intermediates in the Pt^0-catalyzed distannation of alkynes.[6,14,15]

In the present work we report on the synthesis and properties of potential precursors of ferrocenophanes containing two tin atoms, the 1,1′-disubstituted ferrocenes **1** bearing trimethylstannyl groups ($SnMe_3$), **2**−**4** bearing chlorostannyl groups ($SnMe_2Cl$, $SnMeCl_2$, and $SnCl_3$), and **5**−**7** bearing hydridostannyl groups ($SnMe_2H$, $SnMeH_2$, SnH_3) (Scheme 1). Obviously, all these ferrocene derivatives can serve as starting materials for novel organotin compounds. Their structures are of interest with respect to intra- and intermolecular interactions through chloro or hydrido bridges between tin atoms. Therefore, we have studied the compounds **1**−**7** by NMR spectroscopy in solution, by temperature-dependent ^{57}Fe- and ^{119}Sn-Mössbauer spectroscopy (**1**−**4**), by X-ray crystallography (**4**) and by electrochemical techniques (**1**−**5**).

[a] Laboratorium für Anorganische Chemie, Universität Bayreuth, D-95440 Bayreuth, Germany
[b] Racah Institute of Physics, The Hebrew University of Jerusalem, Givat Ram Campus, 91904 Jerusalem, Israel
[c] Dipartimento di Chimica dell′Università di Siena, Pian dei Mantellini 44, I-53100 Siena, Italy

2. Results and Discussion

2.1. Syntheses

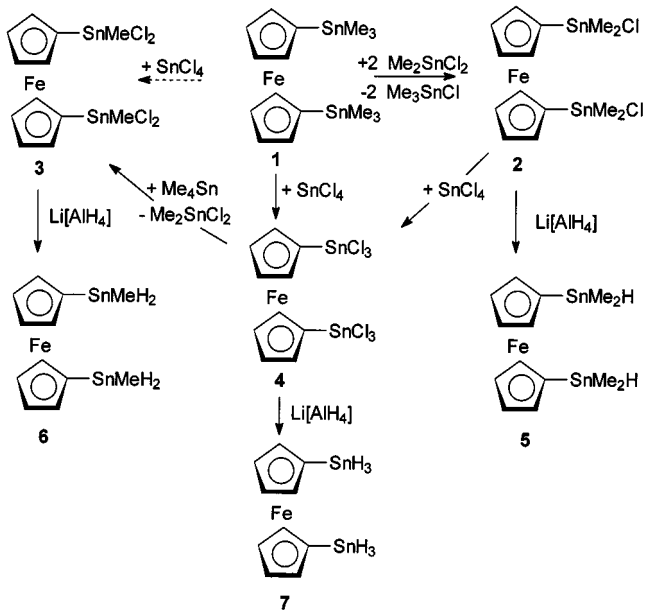
1,1′-Bis(trimethylstannyl)ferrocene (**1**) served as starting material for all preparative work. It reacts with tin tetrachloride to give the complexes **2**−**4** as stable products which can be isolated and purified by recrystallization from hexane or pentane. However, as shown in Scheme 1, the compounds **2**−**4** are obtained in higher yield and purity by using a slightly different approach. Thus, the reaction of **1** with dimethyltin dichloride affords **2** in ca. 90% yield; the properties of **2** are in agreement with those reported previously.[3f] Both **1** or **2** react with an excess of tin tetrachloride to give **4**, whereas **3** is best accessible in the pure state by the reaction of **4** with tetramethyltin in a 1:1 ratio.

Treatment of the chlorides **2**−**4** with $Li[AlH_4]$ in ether at 0°C (**5**) or −30°C (**6**, **7**) affords the tin hydrides **5**−**7**. These are more labile than the parent chlorides and were isolated as orange-yellow oils. Although they were pure according to the NMR spectra, they could not yet be crystallized.

2.2. NMR-Spectroscopic Studies

All NMR spectra (Table 1) support the proposed structures of **1**−**7**. No indication of intermolecular association can be found in C_6D_6 or $CDCl_3$ solutions. Chemical shifts and coupling constants vary in such a regular way that intramolecular interactions between the stannyl groups also

 © WILEY-VCH Verlag GmbH, D-69451 Weinheim, 1999 1434−1948/99/0101−0145 $ 17.50+.50/0



Scheme 1. Synthesis of complexes **2**−**7**

appear to be unlikely. Thus, intramolecular hydride exchange between the two tin atoms in **5**−**7** must be slow on the NMR time scale, since the magnitude of the coupling constants $|^1J(^{119}Sn,^1H)|$ is observed in the usual range [e.g. $PhSnH_3$: $^1J(^{119}Sn,^1H)$ = 1920 Hz[16]]. $^1H/^1H$-NOE difference spectra[17] show the proximity of the methyltin groups to the hydrogen atoms in 2,5- and 2′,5′-positions of the cyclopentadienyl rings, as expected, but also to the hydrogen atoms in 3′,4′- and 3,4-positions. This indicates that the stannyl groups on average avoid close mutual contacts.

^1H- and ^{13}C-resonance signals of the ferrocene unit were assigned on the basis of 2D heteronuclear $^{13}C/^1H$ shift correlations, of ^{13}C-^{13}C coupling constants (e.g. in **4**, as has been described for **1**[4]), and of the consistent trend in the ^{119}Sn-^{13}C coupling constants. The signal-to-noise ratio of the ferrocene-$^{13}C(1,1')$ resonances was much improved by using the refocused INEPT pulse sequence[18] based on $^{2,3}J(^{13}C,^1H)$, as has been suggested previously.[19] The observation of relevant cross peaks for ^{119}Sn satellites in the 2D experiments[20] revealed that the signs of the coupling constants $^3J[^{119}Sn,^1H(2,5)]$, $^4J[^{119}Sn,^1H(3,4)]$, $^2J[^{119}Sn,^{13}C(2,5)]$, and $^3J[^{119}Sn,^{13}C(3,4)]$ are alike. A typical example is shown in Figure 1. Taking into account the negative sign of $\gamma(^{119}Sn)$ and the presumably negative sign of $^3J(^{119}Sn,^1H)$ or $^3J(^{119}Sn,^{13}C)$ (reduced coupling constants $^3K > 0$), all these coupling constants should be < 0.

The changes in the coupling constants $^1J(^{119}Sn,^{13}C)$ in **1**−**4** are best explained by the concept of rehybridization[21] as a consequence of replacing the methyl groups in **1** by the more electronegative chloro substituents. The "s character" of the remaining Sn−C hybrid orbitals increases with increasing number of Sn−Cl bonds. The analogous trend, although less pronounced, is found in the case of the hydrides. An increasing number of Sn−H bonds leads to larger coupling constants $^1J(^{119}Sn,^{13}C)$. At the same time, the magnitude of $^1J(^{119}Sn,^1H)$ increases from **5**−**7**.

The tin chemical shifts $\delta^{119}Sn$ are known to be extremely sensitive even to weak associative interaction.[16] In the case of compounds **1**−**7**, only small changes in the $\delta^{119}Sn$ values result from solvent effects, dilution, or changes in temperature. The similarity between phenyl and ferrocenyl groups is reflected by the $\delta^{119}Sn$ data, e.g. of **1** (−4.2) and $PhSnMe_3$ (−28.6[16]), **4** (−23.2) and $PhSnCl_3$ (−63[16]), and **7** (−330.7) and $PhSnH_3$ (−320[16]). Spin-spin coupling between ^{119}Sn and ^{117}Sn nuclei was not observed in the complexes **1**−**7**. Altogether, the $\delta^{119}Sn$-NMR data indicate negligible inter- or intramolecular interactions in **1**−**7**.

2.3. X-ray Structural Analysis of 1,1′-Bis(trichlorostannyl)ferrocene 4

In addition to the ferrocenophanes mentioned in the introduction, there is only one report of an X-ray analysis of a 1,1′-bis(stannyl)ferrocene, namely 1,1′-bis(triphenylstan-

Table 1. ^1H-, ^{13}C-, and ^{119}Sn-NMR parameters[a] of the 1,1′-bis(stannyl)ferrocenes **1**−**7**

		δ^1H			$\delta^{13}C$				$\delta^{119}Sn$
	Stannyl	2/5-H	3/4-H	H_{Me}	C-1	C-2/5	C-3/4	C_{Me}	
1	$SnMe_3$	4.07	4.28	0.29	69.2	74.4	71.2	−8.68	−4.2
		[10.5]	[5.6]	[56.0]	[492.5]	[51.8]	[40.3]	[357.8]	
2	$SnMe_2Cl$	4.08	4.25	0.55]	70.7	74.5	72.0	−1.1	125.5
		[9.6]	[6.3]	[60.9]	[590.0]	[66.9]	[51.2]	[415.6]	
3	$SnMeCl_2$	4.25	4.28	0.65	73.2	74.7	73.1	5.77	100.4
		[10.6]	[13.0]	[74.7]	[776.4]	[96.9]	[75.4]	[508.9]	
4	$SnCl_3$	3.89	4.18		73.0	74.2	74.0		−23.2
		[14.5]	[20.8]		[1191.7]	[134.6]	[113.5]		
5	$SnMe_2H$[b]	3.99	4.23	0.26	65.8	75.0	71.4	−7.5	−102.4
		[9.4]	[n.r.]	[57.9]	[514.4]	[53.8]	[42.8]	[371.8]	
6	$SnMeH_2$[c]	3.93	4.17	0.25	62.6]	75.9	71.8	−13.0	−210.5
		[n.r.]	[n.r.]	[61.0]	[546.6]	[56.5]	[44.9]	[387.0]	
7	SnH_3[d]	3.89	4.12		59.2	76.8	72.3		−330.7
		[n.r.]	[n.r.]		[583.2]	[59.6]	[46.5]		

[a] In C_6D_6 at 25°C (ca. 5−15%), coupling constants $J(^{119}Sn,^1H)$ and $J(^{119}Sn,^{13}C)$ are given in brackets [±0.3 and ±1 Hz, respectively]; n.r.: not resolved. − [b] $\delta^1H(SnH)$ = 5.45 [1824]; $^3J(^1H,Sn,C,^1H)$ = 2.2 Hz. − [c] $\delta^1H(SnH)$ = 5.24 [1876]; $^3J(^1H,Sn,C,^1H)$ = 2.5 Hz. − [d] $\delta^1H(SnH)$ = 4.97 [1947].

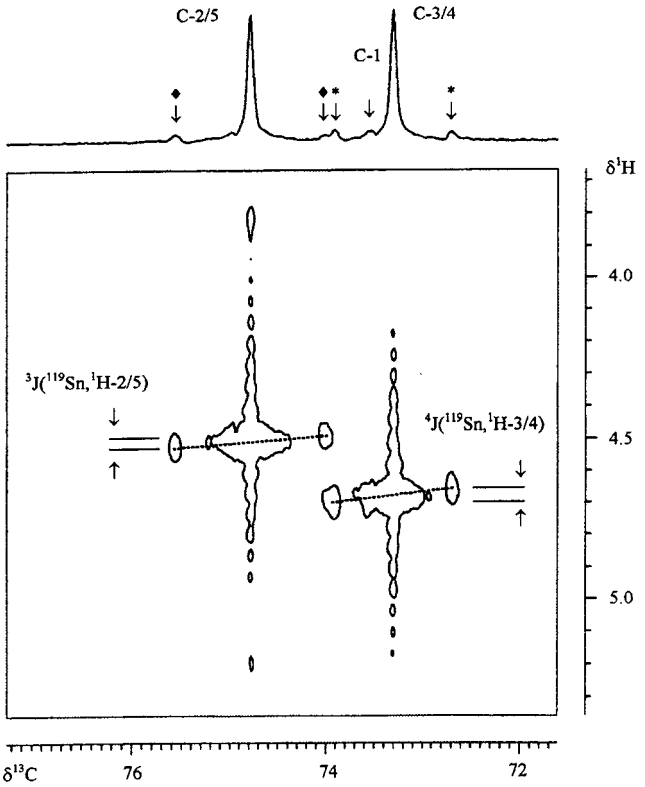


Figure 1. Contour plot of the 62.9-MHz 2D $^{13}C/^{1}H$ HETCOR experiment for $Fe(C_5H_4SnMeCl_2)_2$ (**3**) in $CDCl_3$ {$\delta^1H(2,5) = 4.51$ [12.6 Hz] and $\delta^1H(3,4) = 4.68$ [13.2]}, based on $^1J(^{13}C,^1H)$, showing the region of $^{13}C(2,5)$ and $^{13}C(3,4)$ resonances together with the $^{117/119}Sn$ satellites; the positive tilt of the cross peaks for these satellites indicates like signs of $^nJ(Sn,^{13}C)$ and $^{n+1}J(Sn,^1H)$ ($n = 2, 3$)

nyl)ferrocene.[22] In this complex, the stannyl groups are in *trans* positions, and the torsional angle τ between the cyclopentadienyl rings is 163.4(4)° (with respect to the positions of the substituted cyclopentadienyl carbon atoms). To the best of our knowledge, there is also just one example of a molecular structure of an organotin trichloride, namely methyltin trichloride, in which the surroundings of the tin atoms correspond to compressed tetrahedrons [CSnCl 120.3(3), 113.5(1)°; ClSnCl 103.58(6)°], and weak intermolecular Sn···Cl···Sn interactions [d_{Sn-Cl} = 371.4(2) pm] are proposed in order to account for the arrangement of the $MeSnCl_3$ molecules in infinite chains.[23] The molecular structure of **4** is depicted in Figure 2 together with selected bond lengths and angles.[24] The $SnCl_3$ groups are not in *trans* positions; the torsional angle τ between the cyclopentadienyl rings is 85.3°. All intramolecular Sn···Cl···Sn contacts must be extremely weak [shortest distance d_{Sn-Cl} = 526 pm], and the same is true for intermolecular contacts [shortest distance d_{Sn-Cl} = 395 pm] in spite of the infinite chains built by molecules of **4**, as shown in Figure 3. Figure 3 also shows the separation of the $SnCl_3$ from the ferrocene parts in the crystal structure. The distortion from tetrahedral symmetry around the tin atoms in **4** is even less than in $MeSnCl_3$. The complete absence of intramolecular Sn···Cl···Sn bridging in **4** is surprising, since this type of

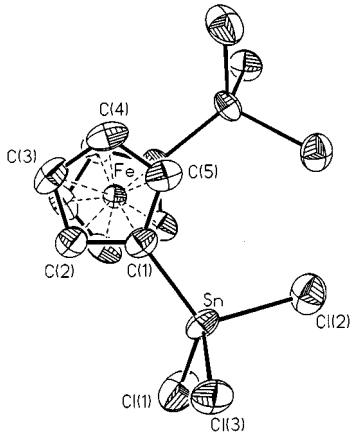


Figure 2. ORTEP plot (thermal ellipsoids represent a 50% probability; hydrogen atoms are not shown) of the molecular structure of 1,1′-bis(trichlorostannyl)ferrocene **4**; selected bond lengths [pm] and angles [°]: Sn−Cl(1) 229.2(1), Sn−Cl(2) 230.4(1), Sn−Cl(3) 230.4(1), Sn−C(1) 207.1(4), Fe−C 204.1−205.3, C−C 140.0−143.9; Cl(1)−Sn−Cl(2) 104.4(1), Cl(1)−Sn−Cl(3) 104.7(1), Cl(2)−Sn−Cl(3) 111.6(1), Cl(1)−Sn−C(1) 115.6(1), Cl(2)−Sn−C(1) 111.6(1), Cl(3)−Sn−C(1) 116.6(1)

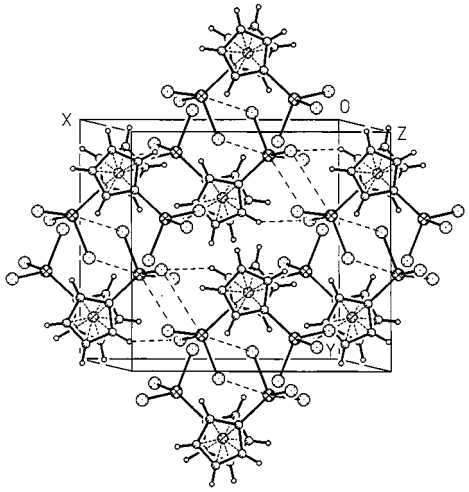


Figure 3. Packing of 1,1′-bis(trichlorostannyl)ferrocene **4** in the crystal lattice (perspective view on the *xy* plane [001])

bonding is well established in other organotin halides, e.g. in tris(dialkylhalostannyl)amines.[25]

2.4. ^{57}Fe- and ^{119}Sn-Mössbauer Spectroscopy

The Mössbauer parameters at 90 K as well as their temperature dependencies are summarized in Table 2. All of the ^{57}Fe-resonance spectra consist of well-resolved doublets having isomer shifts (I.S.) of about 0.52−0.53 mm s^{-1} at 90 K and quadrupole splittings (Q.S.) of 2.3 mm s^{-1}. These values are characteristic[26] of ferrocenyl moieties in which each cyclopentadienyl ring is ligated by a single σ bond to a main-group atom, including Sn, and are otherwise not remarkable. A typical spectrum (of **4** at 90 K) is shown in the upper part of Figure 4. The M_{eff} values, calculated[27] from the temperature dependence of the I.S. parameter fall in the range of 112−142 Da, consistent with the predomi-

Table 2. Mössbauer data (^{57}Fe and ^{119}Sn) for the compounds **1**−**4**

	I.S. (90 K) [mm s^{-1}]	Q.S. (90 K) [mm s^{-1}]	$-d\ln A/dT \times 10^{3}$[c]	$-dI.S./dT \times 10^{4}$[c]
Fe[a] resonances				
1	0.536(2)	2.336(4)	12.07	3.07(18)
2	0.536(1)	2.343(3)	8.56	3.59(15)
3	0.521(2)	2.327(5)	5.29	2.93(18)
4	0.523(1)	2.270(3)	5.55	3.71(11)
Sn[b] resonances				
1	1.235(3)	0.30(2)	31.67	3.12(57)
2	1.368(4)	3.006(6)	21.85	1.61(47)
3	1.131(6)	1.781(7)	22.08	2.22(63)
4	1.414(26)	3.137(4)	17.11	2.91(24)

[a] Relative to metallic iron at room temperature. − [b] Relative to $BaSnO_3$ at room temperature. − [c] Assuming linear regression fits.

nantly covalent character of the ferrocenyl ligand bond. As noted previously,[28] the Q.S. is temperature-insensitive and reflects primarily the thermal expansion coefficients of the covalent lattice.

With the exception of the results for **1**, the ^{119m}Sn-Mössbauer spectra also consist of well-resolved doublets, and these data (at 90 K) are again summarized in Table 2. A representative spectrum (of **4** at 90 K) is shown in the lower half of Figure 4. In contrast, the ^{119m}Sn-Mössbauer spectrum of **1** appears to consist of a single resonance maximum, despite the obvious lack of cubic symmetry around the metal atom. This lack of a resolvable quadrupole splitting in the case where the Sn^{IV} atom is ligated to nearest-neighbor atoms lacking nonbonding lone pairs has been extensively discussed in the literature.[29−33] When lone-pair electrons are present on the atom(s) σ-bonded to the Sn, a π-electron back donation into empty 6p orbitals of the tin atom is assumed to give rise to a large electric field gradient at the metal center. In the present case, the three $Sn-CH_3$ and the single $Sn-C_{Cp}$ bonds, although clearly not of T_d symmetry, give rise to four sp^3-hybrid orbitals on the tin atom which are sufficiently similar to produce a very small field gradient at the Mössbauer-active atom site. Using a Lorentzian line shape minimization procedure, the quadrupole splitting at 90 K is calculated to be ca. 0.30(2) mm s^{-1}; that is less than the natural line width.

The other three compounds **2**−**4** represent an interesting series of bonding interactions, especially with respect to the field gradients generated by the σ and π bonds around the metal center. In previous studies of organotin chlorides, the question of the effect of coordination around the Sn atom has always posed a complication in the interpretation of the relevant Mössbauer data. Thus, Me_3SnCl, which is monomeric in the vapor phase,[34] is polymeric in the solid[35] with a distorted trigonal-bipyramidal environment around the Sn atom. Similarly, the X-ray diffraction data for Me_2SnCl_2[36] reflect a sixfold coordination around the Sn atom, in which two chlorine atoms bridge adjacent Sn atoms and the two methyl groups occupying axial positions around the quasi-octahedral metal atom. Recent X-ray diffraction data[23] for $MeSnCl_3$ have been referred to above and indicate weak intermolecular Sn−Cl−Sn bonding to

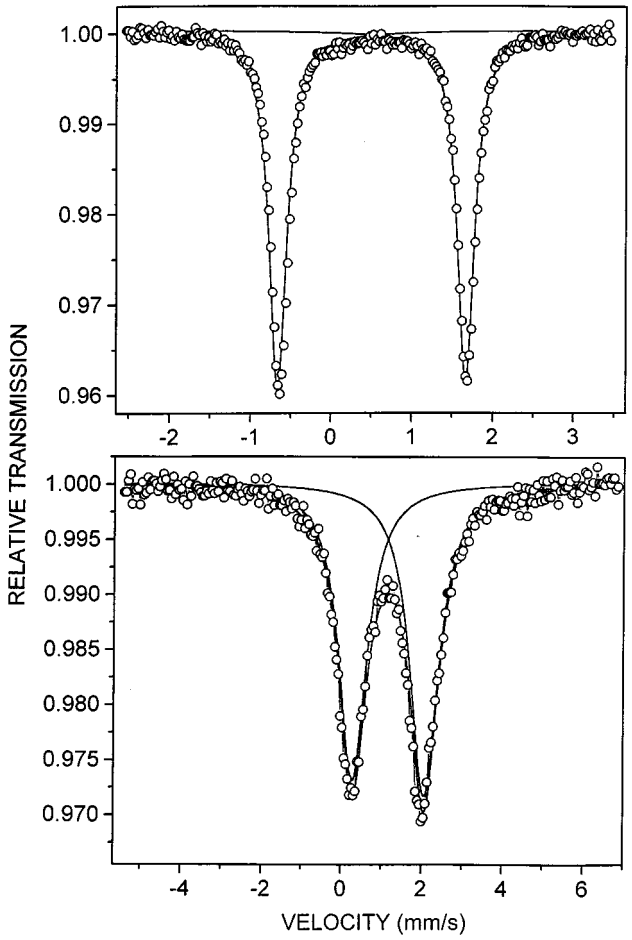


Figure 4. Representative Mössbauer spectra for **4** at 90 K; the upper trace is that of the ^{57}Fe-resonance effect, while the lower trace is that for the ^{119}Sn resonance; the full lines are the fitted data to the experimental points with each component of the doublet fitted separately; the velocity scales are relative to the centroid of a metallic iron absorbance (upper trace) and a $BaSnO_3$ absorber spectrum absorbance (lower trace) at room temperature

account for the infinite chain formation suggested by the NQR data of Petrosyan et al.,[37] but the theoretical calculations of Manning and Grodzicki[38a] and Grodzicki et al.[38b] have assumed four-coordinate metal centers in their discussion of the Q.S. and I.S. parameters of this molecule. Clearly, these variable coordinations around Sn complicate the interpretation of the Mössbauer parameters of the methyl Sn halides. In the present series of compounds, in which the bulky nature of the ferrocenyl ligand(s) clearly precludes coordination numbers larger than 4, this complication is obviated. The absence of a resolvable Q.S. in the Sn spectra of **1** has already been noted (above). The readily observed non-zero Q.S. parameter for **2**, **3**, and **4** is readily accounted for by the π back-donation effect, and the relative similarity of the Q.S. parameters for **2** and **4**, and its much smaller value for **3**, is consistent with this rationalization. Thus, **2** has one Sn−Cl and three Sn−C and **4** has three Sn−Cl and one Sn−C bond. The distortion from tetrahedral symmetry arising from one and three π bonds to the metal atom should have similar influences but with opposite sign on the field gradient at the metal center. The

effect of the bonding in **3** (i.e. two Sn−Cl bonds and one $Sn-C_{CH3}$ and one $Sn-C_{Cp}$ bond) is reflected in the ca. 40% reduction in the Q.S.

Finally, with respect to both the ^{57}Fe- and the ^{119}Sn-Mössbauer data, it is appropriate to observe that the temperature dependencies of the I.S., Q.S. and resonance effect (as reflected in the area under the resonance curve for optically "thin" absorbers) are all smooth, continuous functions in the temperature range from 90 to ca. 300 K. Thus, there is no evidence of either structural or crystallographic phase transitions in this interval for any of the compounds examined in this study. As can be noted in Table 2, the $-d\ln A/dT$ parameter of the ^{57}Fe resonance for **1** is significantly larger than for **2**, which in turn is larger than the value of this parameter for **3** and **4**, indicating a larger mean-square amplitude of vibration of the iron atom in **1** than in **4** under comparable conditions. Similarly (but less pronounced) is the decrease of the $-d\ln A/dT$ parameter extracted from the ^{119}Sn spectra, again reflective of a larger mean-square amplitude of vibration of the Sn atom in **1** than in **4**. This observation is clearly consistent with the fact that **1** is a liquid at room temperature, **2** is a low-melting solid, and **3** and **4** are crystalline materials, and thus the lattice temperature (as reflected in the lattice phonon spectrum) increases with the ratio of the number of chlorine to methyl group ligands in this series. However, there is persuasive evidence from the Mössbauer hyperfine parameters and their temperature dependencies that there are no significant intermolecular interactions in these complexes in the solid state, in agreement with the solution (C_6D_6 or $CDCl_3$) NMR data cited above.

2.5. Electrochemistry of 1−5

The typical redox behavior of the stannylferrocenes **1**−**5** is shown in Figure 5 for the example of $Fe(C_5H_4-SnMe_3)_2$ (**1**).

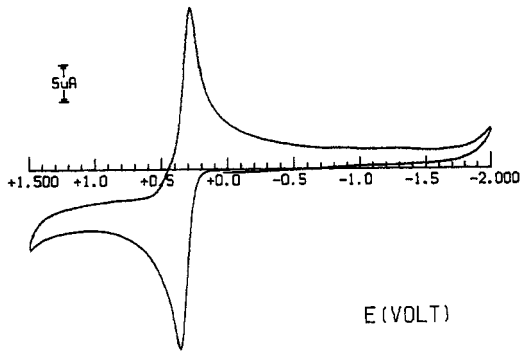


Figure 5. Cyclic voltammetric response recorded at a platinum electrode in a CH_2Cl_2 solution containing **1** ($1.1\ 10^{-3}$ mol dm^{-3}) and $[NBu_4][PF_6]$ (0.2 mol dm^{-3}); scan rate 0.2 Vs^{-1}

As expected, it is only the oxidation of the ferrocene unit which can be observed, and it is a chemically reversible process. As a matter of fact, controlled potential coulometric tests ($E_W = +0.7$ V) show the consumption of one electron per molecule. The originally yellow solution turns blue and exhibits an absorption band at $\lambda_{max} = 636$ nm which confirms the iron-centered oxidation to the ferricenium cation. The chemical reversibility of the one-electron removal is proven by the fact that the exhaustively oxidized solution of **1** displays a cyclic voltammetric profile quite complementary to that shown in Figure 5.

Analysis of the cyclic voltammetric responses with scan rates varying from 0.02 to 1.00 Vs^{-1} is diagnostic for an essentially electrochemically reversible anodic step: The current ratio i_{pe}/i_{pa} is constantly equal to unity; the current function $i_{pa}v^{-1/2}$ remains constant; the peak-to-peak separation ΔE_p slightly departs from the theoretical value of 60 mV.[41]

The same behavior is exhibited by the complexes **2**, **3**, and **5**. In contrast, although the oxidation process of **4** also appears uncomplicated on the cyclic voltammetric time scale ($E^{0\prime} = +0.73$ V), its monocation $\mathbf{4}^+$ proved to be unstable on the longer time scale of macroelectrolysis, and the electrogenerated blue solution gives rise to a reversible reduction process at $E^{0\prime} = +0.37$ V (ferrocene).

Table 3 compiles the electrochemical parameters for the oxidation process of the complexes **1**−**5**, together with some related parameters. It is easy to conclude that the formal electrode processes are exclusively governed by the inductive effects of the methyl and chloro substituents of the stannyl groups. As a matter of fact, a plot of $E^{0\prime}$ values vs. the inductive (Hammett) parameters F[42] of these substituents affords a linear correlation coefficient of 0.99, according to the equation

$$E^{0\prime}\ [V] = 0.16\ \Sigma F + 0.33$$

Table 3. Electrochemical and spectroscopic characteristics for the oxidation process of the complexes **1**−**5** in dichloromethane solution; ΣF represents the inductive effects of the substituents present in the stannyl groups

$Fe(C_5H_4-X)_2$ X =	$E^{0\prime}(0/+)$ [V]	ΔE_p[a]	λ_{max}[b] [nm]	ΣF
$SnMe_3$ (**1**)	+0.32	76	636	0.06
$SnMe_2Cl$ (**2**)	+0.46	73	634	0.88
$SnMeCl_2$ (**3**)	+0.65	92	−	1.70
$SnCl_3$ (**4**)	+0.73	70	[c]	2.52
$SnMe_2H$ (**5**)	+0.36	80	635	0.04
H	+0.37	78	620	−

[a] Measured at 0.1 Vs^{-1}. − [b] Referred to the oxidized species. − [c] See text.

3. Conclusions

Synthetic routes to 1,1′-bis(stannyl)ferrocenes are straightforward, both for chlorostannyl and hydridostannyl groups. These functionally substituted compounds should be useful starting materials for ferrocenophanes and other 1,1′-bis(stannyl)ferrocenes. There are no indications for intra- or intermolecular interactions between the stannyl groups, neither by Sn···Cl···Sn nor Sn···H···Sn bridging. This is obvious from investigations in the solid state by temperature-dependent ^{119}Sn- and ^{57}Fe-Mössbauer spec-

troscopy (**1**−**4**) and X-ray crystallography (**4**), and also in solution by multinuclear magnetic-resonance spectroscopy (**1**−**7**). The electrochemistry of **1**−**5** revealed the expected result by reversible one-electron oxidation processes involving the respective ferricenium cations.

Experimental Section

General: All compounds were handled in dry argon, and carefully dried solvents were used for syntheses and preparation of the samples for NMR measurements. Starting materials were either used as commercial products without further purification (ferrocene, Me_3SnCl, Me_2SnCl_2, $SnCl_4$, *n*-butyllithium 1.6 M in hexane) or prepared as described [$Fe(C_5H_4SnMe_3)_2$ (**1**)[4]].In general, all reactions were monitored by ^{119}Sn-NMR spectroscopy. − Electron impact (EI) mass spectra: Finnigan MAT 8500 with direct inlet. − NMR measurements: Bruker ARX 250 or DRX 500 {^{1}H, ^{13}C, ^{119}Sn NMR [inverse gated ^{1}H-decoupled or refocused INEPT spectra,[19] based on $^2J(^{119}Sn,^1H)$ = 55−75 Hz]}. Chemical shifts are given relative to Me_4Si [$\delta^1H(CHCl_3/CDCl_3)$ = 7.24, $\delta^1H(C_6D_5H)$ = 7.14, $\delta^{13}C(CDCl_3)$ = 77.0, $\delta^{13}C(C_6D_6)$ = 128.0, $\delta^{13}C(C_6D_5CD_3)$ = 20.4], and Me_4Sn [(δ^{119}Sn = 0 for $\Xi(^{119}Sn)$ = 37.290665 MHz].

X-ray Structural Analysis of 4: $C_{10}H_8Cl_6FeSn_2$; M = 634.1; orange crystal of irregular shape; size [mm] 0.35 × 0.20 × 0.18, monoclinic; space group *C*2/c, a = 12.859(2), b = 11.867(2), c = 12.212(2) Å, β = 109.21(2)°, V = 1759.6(5) Å^3, Z = 4, ρ(calcd.) = 2.394 Mg/m^3; absorption coefficient μ = 4.523 mm^{-1}, F(000) = 1184. − Data collection: Siemens *P*4 diffractometer, Mo-K_α radiation, λ = 0.71073 Å, graphite monochromator, 296 K; the single crystal was mounted in a Lindemann capillary; 2θ range 3.0−55.0°; scan type ω; reflections collected 4406, independent reflections 2026, observed reflections 1982 [$F > 2.0\ \sigma(F)$]; semi-empirical absorption correction; min./max. transmission 0.5335/1.000. − Structure solution: direct methods [SHELXTL PLUS (VMS)]; extinction correction χ = 0.00059(3), all atoms except the hydrogen atoms are described with anisotropic temperature factors, all hydrogen positions were refined by using the riding model and fixed U; weighting scheme $w^{-1} = \sigma^2(F)$; number of parameters refined 88; R = 3.29%, wR = 3.30% (observed data); largest difference peak/hole 1.74/−0.53 e/Å^3.

Mössbauer Spectra: The experimental details relating to the acquisition of both ^{57}Fe- and ^{119}Sn-Mössbauer data have been described previously.[39][40] All samples were prepared as optically thin absorbers, and mixed with BN to minimize preferential crystallite orientation with respect to the γ-ray axis of the spectrometer. The isomer shift standards used in this study are the centroids of metallic iron and $BaSnO_3$ spectra at room temperature. Spectrometer calibration was effected by the use of a 1.85 mg m cm^{-2} metallic iron absorber at room temperature. Temperature control over the period of data acquisition (generally 4−24 h, depending on temperature) was stable to better than ±0.5 K. To minimize statistical errors, more than 10^6 counts per channel were accumulated at each temperature point.

Electrochemistry: Materials and apparatus for electrochemistry have been described elsewhere.[43] All potential values are referred to the Saturated Calomel Electrode (SCE).

1,1′-Bis(chlorodimethylstannyl)ferrocene (2): A Schlenk tube was filled with $Fe(C_5H_4SnMe_3)_2$ (**1**) (1.41 g; 2.8 mmol) and Me_2SnCl_2 (1.23 g; 5.6 mmol) was added at 0°C. The mixture was heated at 140°C for 3 h while Me_3SnCl sublimed and was collected at a cooling finger (15°C). Then the mixture was cooled to room temperature and remaining traces of Me_3SnCl und Me_2SnCl_2 were removed in vacuo. A viscous dark orange oil was left which crystallized upon cooling in hexane to give an orange solid (1.4 g; 90%; m.p. 85°C). − EI MS; *m*/*z* (%): 554 (100) [M$^+$].

1,1′-Bis(dichloromethylstannyl)ferrocene (3): A two-necked flask containing $Fe(C_5H_4SnCl_3)_2$ (**4**) (1.79 g; 2.82 mmol) was cooled to 0°C and tetramethyltin (0.429 ml; 3.10 mmol, slight excess) was added. After warming slowly to 60°C, the mixture was stirred at this temperature for 4 h. After cooling, Me_2SnCl_2 and Me_3SnCl were removed in vacuo. Extraction with toluene (15 ml), filtration, removal of toluene, and washing with hexane afforded 0.79 g (65%) of a yellow solid (m.p. 126°C, dec.). − EI MS; *m*/*z* (%): 594 (100) [M$^+$].

1,1′-Bis(trichlorostannyl)ferrocene (4): Tin tetrachloride (0.9 ml; 7.54 mmol) was added to a solution of $Fe(C_5H_4SnMe_2Cl)_2$ (**2**) (1.60 g; 2.90 mmol) in CH_2Cl_2 (5 ml) and hexane (15 ml) at 0°C. The color of the reaction mixture changed rapidly from yellow to green; the mixture was stirred for 2 h at 30°C. Then all volatile material was removed in vacuo and CH_2Cl_2/hexane (1:10, v/v; 20 ml) was used to extract the product. After filtration of the yellow solution and removal of the solvents, the product **4** (1.56 g; 85%; m.p. 122°C dec.) was obtained as a yellow solid. Recrystallization from hexane afforded single crystals suitable for X-ray analysis. − EI MS; *m*/*z* (%): 634 (100) [M$^+$].

1,1′-Bis(dimethylstannyl)ferrocene (5): A solution of $Fe(C_5H_4SnMe_2Cl)_2$ (0.73 g; 1.3 mmol) in ether (20 ml) was added to a suspension of $LiAlH_4$ in ether (30 ml) at −30°C. The mixture was stirred for 5 h at room temperature. After filtration and removal of ether, a yellow oil was left (6.07g; 96%). − EI MS; *m*/*z* (%): 486 (100) [M$^+$].

1,1′-Bis(methylstannyl)ferrocene (6): A solution of $Fe(C_5H_4SnMeCl_2)_2$ (490 mg; 0.83 mmol) in ether (20 ml) was added dropwise to a suspension of $LiAlH_4$ (120 mg; 3.16 mmol) in ether (30 ml) at −30°C. The mixture was stirred for 2 h at room temperature. After removal of the solvent in vacuo, the residue was extracted with hexane, insoluble material was filtered off and hexane was removed in vacuo from the yellow-orange solution. A yellow-orange oil was left (0.37 g; 98%). − EI MS; *m*/*z* (%): 456 (30) [M$^+$].

1,1′-Bis(stannyl)ferrocene (7): The same procedure with **4** as starting material, as described for **6**, afforded **7** in almost quantitative yield as a yellow-orange oil. − EI-MS; *m*/*z* (%): 429 (30) [M$^+$].

Acknowledgments

Support of this work by the Deutsche Forschungsgemeinschaft and the Fonds der Chemischen Industrie is gratefully acknowledged. M. F. and P. Z. gratefully acknowledge the financial support of the University of Siena (ex quota 60%) and the technical assistance of Mrs. Giuseppina Montomoli.

[1] [1a] M. Pereyre, J.-P. Quintard, A. Rahm, *Tin in Organic Synthesis*, Butterworths, London, **1987**. − [1b] A. G. Davies, *Organotin Chemistry*, VCH, Weinheim, **1997**.
[2] M. Herberhold, in *Ferrocenes, Homogeneous Catalysis, Organic Synthesis, Materials Science* (Eds.: A. Togni, T. Hayashi), VCH, Weinheim, **1995**, chapter 5.
[3] [3a] T. Todo, H. Suzuki, T. Takiguchi, *Bull. Chem. Soc. Jpn.* **1970**, *43*, 288−290. − [3b] T. E. Bitterwolf, A. Campell-Ling, *Syn. React. Inorg. Metal-org. Chem.* **1977**, *7*, 367−372. − [3c] A. N. Nesmeyanov, T. P. Tolstaya, V. V. Korol′kov, *Dokl. Akad Nauk SSSR* **1973**, *209*, 1113−1116; *Chem. Abstr.* **1973**, *79*,

42650y. – [3d] R. M. G. Roberts, J. Silver, J. Azizian, *J. Organomet. Chem.* **1986**, *303*, 387–395. – [3e] D. Steinborn, M. Buthge, R. Taube, R. Radeglia, K. Schlothauer, K. Nowak, *J. Organomet. Chem.* **1982**, *234*, 277–285. – [3f] Z. Kabouche, N. H. Dinh, *J. Organomet. Chem.* **1989**, *375*, 191–195.

[4] F. H. Köhler, W. A. Geike, N. Hertkorn, *J. Organomet. Chem.* **1987**, *334*, 359–367.

[5] R. Rulkens, A. J. Lough, I. Manners, *Angew. Chem.* **1996**, *108*, 1929–1931; *Angew. Chem. Int. Ed. Engl.* **1996**, *35*, 1805–1807.

[6] M. Herberhold, U. Steffl, W. Milius, B. Wrackmeyer, *Angew. Chem.* **1996**, *108*, 1927–1928; *Angew. Chem. Int. Ed. Engl.* **1996**, *35*, 1803–1804.

[7] M. Herberhold, U. Steffl, W. Milius, B. Wrackmeyer, *Z. Anorg. Allg. Chem.* **1998**, *624*, 386–392.

[8] M. Herberhold, U. Steffl, W. Milius, B. Wrackmeyer, *J. Organomet. Chem.* **1997**, *533*, 109–115.

[9] M. Herberhold, U. Steffl, B. Wrackmeyer, manuscript in preparation.

[10] I. Manners, *Adv. Organomet. Chem.* **1995**, *37*, 131–168.

[11] I. Manners, personal communication.

[12] M. Herberhold, U. Steffl, W. Milius, B. Wrackmeyer, *Angew. Chem.* **1997**, *107*, 1545–1547; *Angew. Chem. Int. Ed. Engl.* **1997**, *36*, 1510–1512.

[13] M. Herberhold, U. Steffl, W. Milius, B. Wrackmeyer, *Chem. Eur. J.* **1998**, *4*, 1027–1032.

[14] M. Herberhold, U. Steffl, B. Wrackmeyer, manuscript in preparation.

[15] Y. Obora, Y. Tsuji, K. Nishiyama, M. Ebihara, T. Kawamura, *J. Am. Chem. Soc.* **1996**, *118*, 10922–10923.

[16] B. Wrackmeyer, *Annu. Rep. NMR Spectrosc.* **1985**, *16*, 73–186

[17] [17a] J. K. M. Sanders, J. D. Mersh, *Progr. NMR Spectrosc.* **1982**, *15*, 353–400. – [17b] G. Wider, S. Macura, P. Kumar. R. R. Ernst, K. Wüthrich, *J. Magn. Reson.* **1984**, *56*, 207–234.

[18] [18a] G. A. Morris, R. Freeman, *J. Am. Chem. Soc.* **1979**, *101*, 760–762. – [18b] G. A. Morris, *J. Am. Chem. Soc.* **1980**, *102*, 428–429. – [18c] P. Burum, R. R. Ernst, *J. Magn. Reson.* **1980**, *39*, 163–167.

[19] B. Wrackmeyer, M. Biersack, H.-D. Brendel, M. Herberhold, *Z. Naturforsch., B* **1992**, *47*, 1397–1402.

[20] [20a] A. Bax, R. Freeman, *J. Magn. Reson.* **1981**, *45*, 177–181. – [20b] B. Wrackmeyer, K. Horchler, *Magn. Reson. Chem.* **1990**, *28*, 56–61.

[21] H. A. Bent, *Chem. Rev.* **1961**, *61*, 275–311.

[22] B. M. Yamin, H.-K. Fun, B-C. Yip, O. B. Shawkataly, S. G. Teoh, *Acta Crystallogr., Ser. C* **1994**, *50*, 1551–1555.

[23] W. Frank, G. J. Reiss, D. Kuhn, *Acta Crystallogr., Ser. C* **1994**, *50*, 1904–1906.

[24] Crystallographic data (excluding structure factors) for the structure reported in this paper have been deposited with the Cambridge Crystallographic Data Centre as supplementary publication no. CCDC-102514. Copies of these data can be obtained free of charge on application to CCDC, 12 Union Road, Cambridge, CB21EZ, UK (Fax: int. code + 44-1223/336-033; E-mail: deposit@ccdc.ac.uk).

[25] A. Appel, C. Kober, C. Neumann, H. Nöth, M. Schmidt, W. Storch, *Chem. Ber.* **1995**, *129*, 175–189.

[26] R. H. Herber, B. Bildstein, P. Denifl, H. Schottenberger, *Inorg. Chem.* **1997**, *36*, 3586–3594.

[27] R. H. Herber in *Chemical Mössbauer Spectroscopy* (Ed.: R. H. Herber), Plenum Press, New York, **1984**, pp. 199–216.

[28] R. H. Herber, T. P. Hanusa, *Hyperfine Interact.* **1997**, *108*, 563–575, and references therein; see also ref.[29]

[29] N. N. Greenwood, T. C. Gibb, *Mössbauer Spectroscopy*, Chapman and Hall, London, **1971**, pp. 399–402; N. N. Greenwood, T. C. Gibb, *J. Chem. Soc.* **1966**, 43–54, and references therein.

[30] R. H. Herber, *Ann. Rev. Phys. Chem.* **1966**, *17*, 261–294.

[31] R. H. Herber, *Mössbauer Spectroscopy and its Applications*, International Atomic Energy Agency, Vienna, **1972**, pp. 257–280, and references therein.

[32] R. H. Herber, H. A. Stöckler, and W. T. Reichle, *J. Chem. Phys.* **1965**, *42*, 2447–2452.

[33] J. J. Zuckerman, "Organotin ^{119m}Sn Mössbauer Spectroscopy: The First Quarter Century", in ref.[27], pp. 267–293, and references therein.

[34] H. A. Skinner, L. E. Sutton, *Trans. Farad. Soc.***1944**, *40*, 164–185.

[35] J. L. Lefferts, K. C. Molloy, M. B. Hossain, D. Van der Helm, J. J. Zuckerman, *J. Organomet. Chem.* **1982**, *240*, 349–361.

[36] A. G. Davies, H. J. Milledge, D. C. Puxley, P. J. Smith, *J. Chem. Soc. A* **1970**, 2862–2866; see also the extensive review: P. J. Smith, *Organomet. Chem. Rev.* **1970**, *A5*, 373–402.

[37] V. S. Petrosyan, N. S. Yashina, O. A. Reutov, E. V. Bryuchova, G. K. Semin, *J. Organomet. Chem.* **1973**, *52*, 321–331.

[38] [38a] V. Männing, M. Grodzicki, *Theor. Chim. Acta* **1986**, *70*, 189–202. – [38b] M. Grodzicki, V. Männing, A. X. Trautwein, J. M. Friedt, *Jour. Phys. B* **1987**, *20*, 5595–5625.

[39] R. H. Herber, E. Bauminger, I. Felner, *J. Chem. Phys.* **1996**, *104*, 7–10.

[40] R. H. Herber, I. Manners, K. Temple, manuscript in preparation.

[41] E. R. Brown, J. R. Sandifer, in *Physical Methods of Chemistry, Electrochemical Methods* (Eds.: B. W. Rossiter, J. F. Hamilton), Wiley, New York, **1986**, vol. 2, chapter 4.

[42] C. Hansch, R. W. Taft, *Chem. Rev.* **1991**, *91*, 165–195.

[43] A. Togni, M. Hobi, G. Rihs, A. Albinati, P. Zanello, D. Zech, H. Keller, *Organometallics* **1994**, *13*, 1224–1234.

Received August 5, 1998
[I98269]

Organometallic Compounds of Group 13, 55[+]

Novel Organoaluminum Lewis Acids via Selective Aluminum-Tin Exchange Processes – Electrophilic Initiation by the Aluminum Halide and Ensuing Complexation by the Resulting Tin Halide

John J. Eisch,*[a] Katrin Mackenzie,[a] Harald Windisch,[a] and Carl Krüger[b]

Dedicated to the memory of our most esteemed colleague, the late Professor Wilhelm P. Neumann, master of organotin chemistry[c]

Keywords: Organometallics / Aluminum / Tin / Metal-metal exchange / Electrophilic reagents / Lewis acid-base complexes

With the goals of preparing novel carbaluminating reagents and mono- and bidentate organoaluminum Lewis acids, the scope and limitations of synthesizing the requisite organoalanes by the aluminum-tin exchange between an aluminum halide and the appropriate organostannane have been examined in detail. The interactions of such tin precursors as 1,2-bis(trimethylstannyl)ethyne, allyltri-*n*-butyltin, benzyltrimethyltin, and 1,2-bis(trimethylstannyl)benzene and various aluminum chlorides of the type, R_nAlCl_{3-n} (R = Me, Et), gave selective aluminum-tin exchange at the sp- or sp^2-hybridized carbon–tin bond and produced such organoalanes as allyl(methyl)aluminum chloride, benzylaluminum dichloride, 1,2-bis(diethylalumino)ethyne, 1,2-bis(dimethylalumino)benzene, 1,2-bis[chloro(methyl)alumino]benzene, and 1,2-bis(dichloroalumino)benzene in high yield. A complicating factor was the tendency of the R_3SnCl by-product to complex with the resulting organoalane. In some cases, exemplified by allyl(methyl)aluminum chloride, such complexation did not interfere with the carbaluminating action of the reagent; in other cases, exemplified by 1,2-bis[chloro(methyl)alumino]benzene, the R_3SnCl could be removed by means of π-bases and reduced pressures; and in still other structures, as with 1,2-bis(dichloroalumino)benzene, the tin chloride could not be dislodged at moderate temperatures. The structure and bonding in such tin halide–aluminum halide complexes in solution were investigated with the 1:1 adducts of $AlCl_3$ with Me_3SnCl and with nBu_3SnCl, respectively, by means of multinuclear NMR spectroscopy. Furthermore, an XRD of the solid complex, $Me_3SnCl \cdot AlCl_3$, was carried out. Such complexes were shown to consist of 1:1 ion pairs of the type $[R_3Sn^+][AlCl_4^-]$ in dilute solution and of a chiral polymeric helix in the solid state wherein planar Me_3Sn^+ units are linked to each other via bridging tetrachloroaluminate anions, $Cl–(AlCl_2)–Cl^-$. Treatment of such complexes with either benzyltriethylammonium chloride (one or two equivalents) or tetramethylphosphonium chloride leads to the displacement of Me_3SnCl and the formation of the expected ionic complexes. Finally, the importance of such novel reagents and chelating Lewis acids to organic synthesis and olefin polymerization is discussed and elucidated.

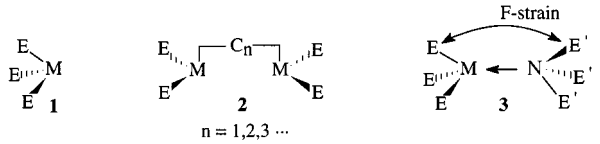
[+] Part 54: J. J. Eisch, B. W. Kotowicz, *Eur. J. Inorg. Chem.* **1998**, 761.

[a] Department of Chemistry, The State University of New York at Binghamton,
Binghamton, New York 13902−6016, USA
[b] Max-Planck-Institut für Kohlenforschung,
D-45470 Mülheim (Ruhr), Germany

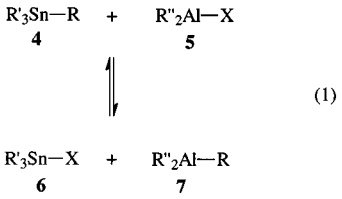
[c] Professor W. P. Neumann was born in Würzburg, Germany, on October 29, 1926. Upon the completion of studies on pyrimidopyrimidines with Professor F. G. Fischer at the University of Würzburg in 1952, he was awarded the degree Dr. rer. nat. Thereafter, he was postdoctoral research associate with Nobel Laureate Karl Ziegler with whom he embarked on his lifelong study of organotin chemistry. After habilitation on this theme at the University of Gießen in 1960, he served on the same faculty as Außerplanmäßiger Professor until 1968. He joined the faculty of the University of Dortmund in 1969 as Ordinary Professor of Organic Chemistry and until his formal retirement in 1992 he was chiefly responsible for developing the Organic Chemistry Institute of this new university. His research and scholarly work on the organometallic chemistry of tin and germanium and on organic intermediates, such as free radicals and carbenes, were reported in over 250 articles and reviews. At the time of his death on August 3, 1993 he was still at the forefront of the organic chemistry of tin, a research area on which he had composed a monograph as a young scientist (1970, Wiley) and whose high relevance to the whole field of organic chemistry his career in research has made manifest. We, his colleagues, will always fondly remember his great scientific zest and his extraordinary human warmth.

In continuing investigations directed toward the synthesis of novel Group 13 Lewis acids suitable as cocatalysts with cyclopentadienyl transition metal derivatives for Ziegler−Natta olefin polymerization catalysis, we have sought ways of preparing unsymmetrical organometallics of Group 13 whose Lewis acidity might be enhanced either by the electron-withdrawing nature of the substituent E in **1** or by the chelating effect of two proximally arrayed Lewis acid metal centers M in **2**. In the previous article of this series the possible effect of such Lewis acidity enhancing factors in selected organoboranes was examined.[1] This present study has explored the Lewis acidity of analogous unsymmetrical organoaluminum compounds in the well-established expectation that such organoaluminum analogs would exhibit greater Lewis acidities than their boron counterparts for steric and electronic reasons:[2] the smaller covalent radius of boron versus aluminum (B, 81 pm versus Al, 125 pm) increasing the steric hindrance or F-strain upon complexation (**3**) and any $p_\pi-p_\pi$ back-bonding from ligands (E) on the boron center, such as unshared electron pairs (E = X, RO, or R_2N), decreasing the boron center's Lewis acidity.

 © WILEY-VCH Verlag GmbH, D-69451 Weinheim, 1999 1434−1948/99/0101−0153 $ 17.50+.50/0

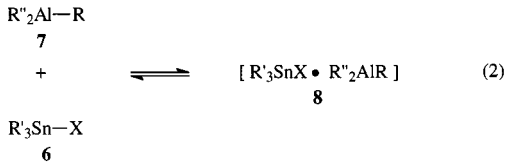


As a preparative route to such unsymmetrical organoaluminum reagents, we have availed ourselves of the selective exchange occurring between organotin compounds and aluminum halides (Equation 1).[3] Such exchanges are potentially reversible depending on the nature of the organyl substituents and on experimental conditions. Where R, R′, and R′′ are alkyl, the reaction proceeds to the left and produces tetraalkyltin compounds.[4] In the present case of interest, the reaction has been found to lead selectively to the right, producing **7**, when R in **4** is an organyl group more electronegative than alkyl, such as allyl, benzyl, aryl, or 1-alkynyl. Furthermore, the extent of tin-aluminum exchange can in some instances be feasibly controlled by removing one of the components of the equilibrium in Equation 1 from the reaction zone by volatization or complexation, in accord with LeChatelier′s principle.[5]



(1)

Because of the greater Lewis acidity of such organoaluminum derivatives, compared with their organoboron analogs, a serious complication occurs when utilizing such tin-aluminum exchanges for preparing unsymmetrical organoalanes (**7**, Equation 1): namely the organoalane **7** usually complexes more or less firmly with the organotin halide byproduct **6** (Equation 2). Such complexation (**8**) generally does not interfere in preparative tin-boron exchanges,[1] most likely because of destabilizing F-strain in such complexation (cf. **3**). This complexation in tin-aluminum exchanges (**8**) has been of dual interest to us: not only did we seek mild experimental conditions to disrupt such complexation and to isolate **7** in satisfactory yield, but also we wished to elucidate the structure and bonding in complex **8**.



(2)

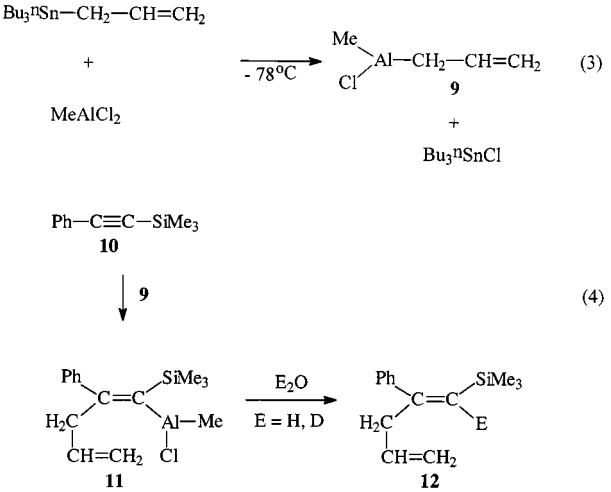
Results

Preparation of Organoalanes by Aluminum−Tin Exchange Reactions

Previous studies on generating organoboranes by boron-tin exchange processes had revealed that selective exchange of groups is achievable when the C−Sn bond is attached to an sp- or sp^2-hybridized group.[1] In addition, by combining what has been established by Neumann in his pioneering work on aluminum-tin exchanges[6] with what is known about lithium-metal exchanges,[7] it was considered likely that aluminum-tin exchanges would proceed selectively at C−Sn bonds to allylic and benzylic groups as well. The driving force for such exchanges appears to lead to the more electropositive metal atom (Li, Al) being bonded to the more electronegative carbon atom (sp-, sp^2-, or allylic-bonded organyl group) in the favored product.

Allyl(methyl)aluminum Chloride (9)

This reagent could be readily generated from the interaction of allyltri-*n*-butyltin with methylaluminum dichloride at −78°C but the high autoreactivity of such allylic alanes precluded its isolation at room temperature (Equation 3). Hence, reagent **9** was generated at −78°C in the presence of trimethyl(phenylethynyl)silane (**10**); subsequent hydrolytic work-up led to a high yield of (*Z*)-2-phenyl-1-trimethylsilyl-1,4-pentadiene (**12**). Work-up with D_2O yielded **12** deuteriated at C-2. The exclusive formation of **12** establishes that **9** had carboaluminated **10** with regio- and stereo-selectivity to form precursor **11** (Equation 4).[8]

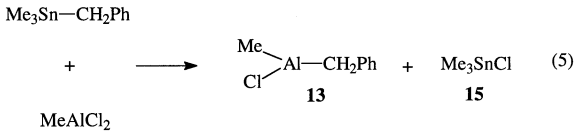


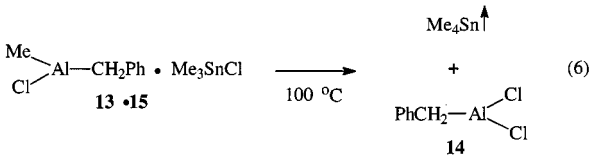
(3)

(4)

Benzylaluminum Dichloride (14)

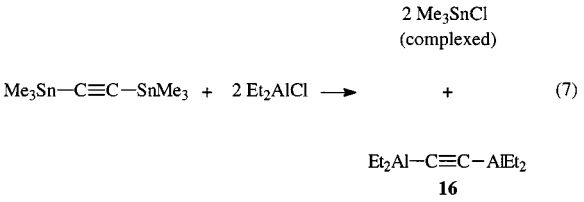
The attempted exchange between benzyltrimethyltin and methylaluminum dichloride to produce benzyl(methyl)aluminum chloride (**13**, Equation 5) took an unexpected course when the separation of **13** from its complex with **15** was undertaken. Under the conditions expected to lead to the dissociation of the complex, **13** · **15**, and the selective volatilization of **15** (100°C in mesitylene), further tin-aluminum exchange occurred with the formation of pure **14** and the volatilization of tetramethyltin (Equation 6).[9]





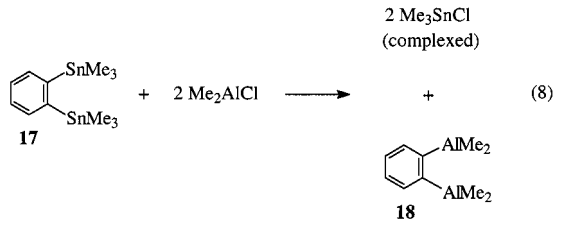
1,2-Bis(diethylalumino)ethyne (16)

The interaction of 2 equivalents of diethylaluminum chloride with one equivalent of bis(trimethylstannyl)ethyne in pentane at −30°C led to the deposition of 95% of the pale yellow **16**, which was highly pyrophoric and insoluble in benzene or chloroform. The ^{1}H-NMR spectrum of **16** from the reaction mixture from Equation 7 in THF is consistent with complexation of **16** with the ether solvent and the liberation of free Me_3SnCl: The triplet and quadruplet ethyl signals of **16** are shifted downfield from those of unsolvated Et_3Al and the singlet due to free Me_3SnCl is visible at δ = 1.2.



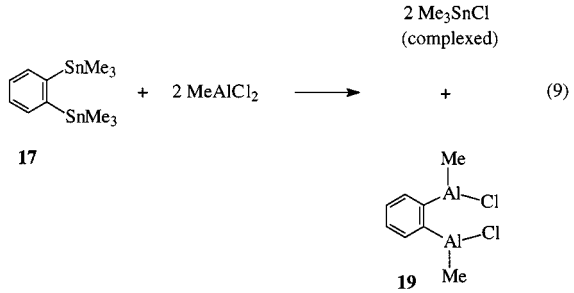
1,2-Bis(dimethylalumino)benzene (18)

The interaction of 1,2-bis(trimethylstannyl)benzene (**17**) with 2 equivalents of dimethylaluminum chloride in hexane at 25°C produced the *ortho*-dimethylalumino derivative **18** as its 1:1 and 1:2 complexes with Me_3SnCl (Equation 8), as evidenced by Me_3Sn group singlets in the δ = 0.02 to −0.02 region in the ^{1}H NMR, as well as by extra aromatic doublets in the δ = 7.0−8.0 region. Such Me_3SnCl was largely removed by warming under reduced pressure and by the distillative removal of added heptane at ordinary pressure to yield essentially free **18**.



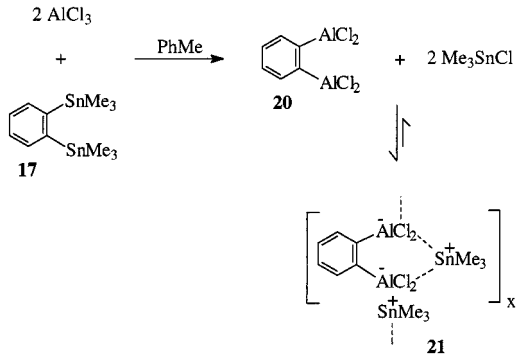
1,2-Bis[chloro(methyl)alumino]benzene (19)

Similarly, the interaction of **17** with 2 equivalents of methylaluminum dichloride in toluene at 25°C yielded the analogous *ortho*-dichloro(methyl)alumino derivative **19**, which was even more strongly complexed with the Me_3SnCl by-product than was **18**. Here the use of the π-base, toluene, for the reaction aided the dissociation and removal of Me_3SnCl from **19**. Evaporation of the toluene solvent and repeated evaporation of several added portions of toluene under vacuum served to chase off almost all of the remaining Me_3SnCl (Equation 9).[8]



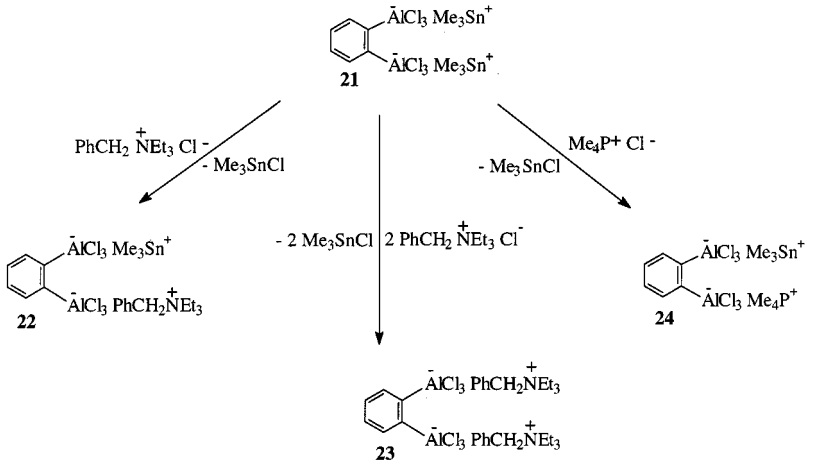
1,2-Bis(dichloroalumino)benzene (20)

Finally, the interaction of **17** with 2 equivalents of aluminum trichloride in toluene suspension led to the aluminum-tin exchange product, **20**, but in this situation the Me_3SnCl by-product remained firmly complexed with **20** to form a polymeric ion pair **21** (Scheme 1).



Scheme 1

The presence of the trichloroaluminate anion is consistent with a ^{27}Al-NMR resonance signal at δ = 105, as is the presence of a planar trimethylstannyl cation supported by the low-field ^{119}Sn-NMR peak at δ = 357.5. (More structural information on such ion-pairs follows below). Thermal dissociation of **21** under high vacuum or by use of π-basic solvents under 100°C has thus far proved to be ineffectual in removing the complexed Me_3SnCl.[8]



Scheme 2

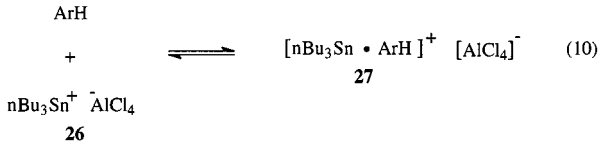
Complexation of Organotin Halides with Aluminum Halides

Trimethyltin Chloride with 1,2-Bis(dichloroalumino)benzene in a 2:1 Ratio (21)

Although Me_3SnCl is difficult to remove from complex **21**, the trimethylstannyl cation can readily be displaced either singly or dually by the benzyltriethylammonium ion (**22** and **23**, Scheme 2) or by the tetramethylphosphonium ion (**24**). In all cases, the ^{27}Al-NMR spectra display a resonance peak in the $\delta = 103$ region; in **22** and **24** the ^{119}Sn-NMR spectra have a peak in the $\delta = 317-320$ region; and in each complex the appropriate ^{1}H- and ^{13}C-NMR peaks corroborate the ionic structures and compositions.

Complexes of Trimethyltin Chloride with Aluminum Chloride (Complex 25) and of Tri-*n*-butyltin Chloride with Aluminum Chloride (Complex 26)

These 1:1 complexes were first described by Neumann, Schick, and Köster almost 35 years ago and upon the basis of the relatively high electrical conductivity of such complexes and their formula weight in dilute solution, they were depicted as ion pairs. Above 1 mol/L concentrations higher degrees of association (2−6) became significant.[9] To add to our insight into the structure of complexes **25** and **26**, a multinuclear NMR study was undertaken in solution. Noteworthy are the following observations: 1) the ^{27}Al-NMR signals occur at $\delta = 104-105$, almost identical with the reported peak for $AlCl_4^-$;[10] 2) the ^{119}Sn-NMR peaks are displayed at $\delta = 358$ and 380, respectively, consistent with the presence of a planar R_3Sn^+ cation;[11][12] and 3) the ^{119}Sn-NMR signal of complex **26** shows a significant upfield shift with increasing π-basicity of the medium: $\delta = 380$ ([D_6]benzene), 375 (toluene), 356 (mesitylene), and 338 (saturated solution of hexamethylbenzene in pentane). This last observation is consistent with such increasing π-basicity enhancing the coordination and hence the shielding of the nBu$_3$Sn$^+$ cation (**27** in Equation 10).



X-ray Crystallographic Structure of [$Me_3SnCl \cdot AlCl_3$]$_n$, Complex 25, and Its Formulation as Polymeric Trimethyltin Cationic-Tetrachloroaluminate Anionic Pairs

As shown in Figure 1 [$Me_3SnCl \cdot AlCl_3$]$_n$ (**25**) consists in the solid state of trigonal bipyramidal trimethyltin fragments and tetrahedral coordinated tetrachloroaluminate fragments forming a chiral polymeric helix.[13] The three equatorial methyl groups bonded to the tin atoms are completely planar, the Sn−C bond lengths (average, 2.109 Å, compare Tables 1−3) are within the usual range for Sn−CH_3 bonds.[14−22] The two axial positions are occupied by chlorine atoms of the tetrachloroaluminate fragments. The Sn−Cl distances are much longer than usual,[16,17,20,21] especially more than 0.30 Å longer than the Sn−Cl bond in Me_3SnCl (2.430 Å).[16][17] These values show that **25** can best be understood as a contact ion pair of trimethyltin cations and tetrachloroaluminate anions, as was already indicated by the results of the NMR-spectroscopic measurements. Therefore it would be more accurate to write an ionic formula like [Me_3Sn^+][$AlCl_4^-$] for compound **25**. Furthermore it is worth mentioning that the Sn−Cl distances alternate, each tin atom [except Sn5 with equal distances of 2.790(4) Å] has a short (average, 2.772 Å) and a long bond length (average, 2.832 Å) to a chlorine atom. The Cl−Sn−Cl angles are on an average 172.9° instead of 180°

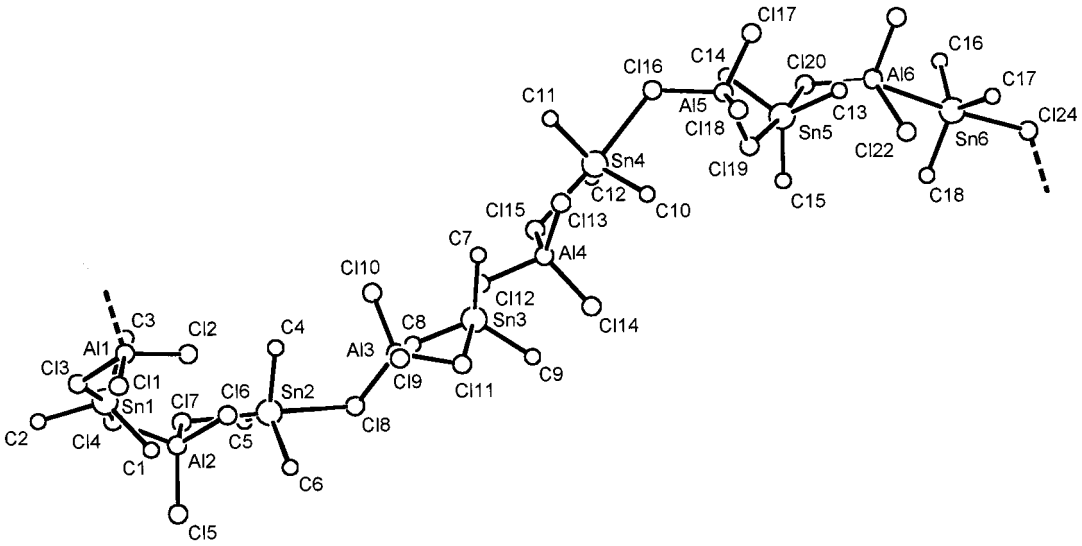


Figure 1. Structure of the polymeric chiral helix of $[Me_3SnCl \cdot AlCl_3]$ (**25**)

Table 1. Selected bond lengths and angles of $[Me_3SnCl \cdot AlCl_3]$ (**25**)

	Minimum value	Maximum value	Average value
Bond lengths [Å]			
Sn−C	2.02(2)	2.15(2)	2.109
Sn−Cl (short)	2.738(4)	2.792(5)	2.772
Sn−Cl (long)	2.800(4)	2.887(4)	2.832
Sn−Cl terminal	2.065(8)	2.109(6)	2.090
Sn−Cl bridging	2.143(7)	2.205(6)	2.171
Bond angles [°]			
C−Sn−C	116.4(7)	123.6(7)	120.0
Cl−Sn−Cl	168.1(1)	175.7(1)	172.9
Cl(terminal)−Al−Cl(terminal)	114.0(3)	116.8(3)	114.9
Cl(bridging)−Al−Cl(bridging)	103.4(2)	106.6(2)	104.8
Sn−Cl−Al	111.1(2)	122.1(2)	115.8

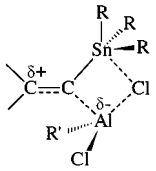
as one would expect for an ideal trigonal bipyramidal configuration.

The tetrachloroaluminate fragments show different distances from the aluminum atoms to its chlorine atoms (average, 2.090 Å) and to the bridging chlorine atoms (average, 2.171 Å), but both bonds are only 0.04 Å shorter or longer than those found for $NaAlCl_4$ (2.13 Å).[23] Also the Cl−Al−Cl angles are slightly different. The angles including the terminal chlorine atoms are on average 114.9°, whereas the Cl−Al−Cl angles for the bridging chlorine atoms are on average 104.8° compared to 109.5° for an ideal tetrahedral configuration. These structural differences at the tetrachloroaluminate fragments in this particular complex can be explained by the interactions of the bridging chlorine atoms with the trimethyltin fragments.

Discussion

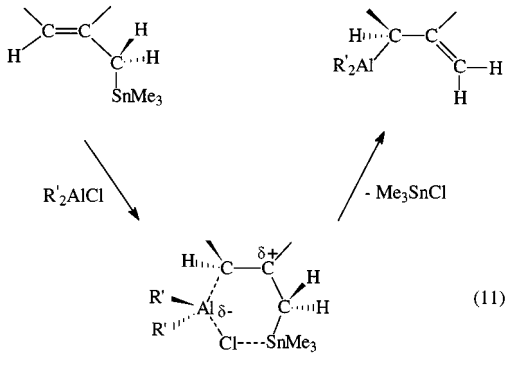
Selectivity of Aluminum-Tin Exchange

With organotin derivatives having both sp- or sp^2-hybridized and sp^3-hybridized carbon−tin bonds, such as 1,2-bis(trimethylstannyl)ethyne (**28**) and 1,2-bis(trimethylstannyl)benzene (**17**), attack by the aluminum chloride, R'_nAlCl_{3-n} (**29**), occurs cleanly and exclusively at the carbon−tin bond of higher *s*-character (Equations 7−9 and Scheme 1). This preference for aluminum-tin exchange at such sites accords with a fostered electrophilic attack of **29** at such sites through transition states similar to **30**. Attack of **29** at the α-carbon atom of the C−Sn bond is favored by the σ-bond hyperconjugation stabilizing the positive charge at the β-carbon atom.[25]



30

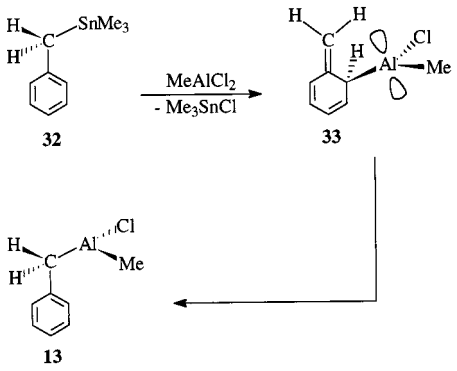
The preferential reactivity of allylic or benzylic C−Sn bonds over alkyl C−Sn bonds can be explained by similar electrophilic attack by R'_nAlCl_{3-n} (**29**) (Equations 4 and 5) except that such attack occurs at the γ-carbon atom with rearrangement (**31**, Equation 11). Here again, the favored transition state **31** is dually stabilized by σ-bond hyperconjugation of the β-carbon atom′s positive charge.



(11)

31

Applicability of this mechanism to the reaction of benzyltrimethyltin (**3**) with $MeAlCl_2$ (Equation 5) would require that the initial reaction product **33** would have to undergo facile rearrangement to **13** (Scheme 3). Transformation of **33** to **13** would involve a 1,3-suprafacial sigmatropic rearrangement which should be thermally allowed via the available p-orbital on the sp^2-hybridized aluminum atom in **33**.[25]



Scheme 3

Lewis Acidity of Aluminum Halides towards Trialkyltin Chlorides and the Structure of the Resulting Lewis Complexes

From the evidence on the spectral properties of complexes **25** and **26**, $R_3SnCl \cdot AlCl_3$, in solution (R = Me, Bu), it is clear that $AlCl_3$ can heterolyze the tin−chlorine bond completely to form the ion pair, $[R_3Sn]^+[AlCl_4]^-$. In dilute solutions of π-basic hydrocarbons such as arenes, the trialkyltin cation is probably solvated by arenes and exists as a simple solvated ion pair with the tetrachloroaluminate anion, as corroborated by ^{119}Sn- and ^{27}Al-NMR spectroscopy. The decreasing chemical shift of the ^{119}Sn signal of **26** as the π-basicity of the arene solvent increases, from δ = 380 in [D_6]benzene to 375 in toluene to 356 in mesitylene to 338 in hexamethylbenzene dissolved in pentane, is consistent with an increasing complexation of the Bu_3Sn^+ with the arene π-electron cloud and thus an increasing diamagnetic shielding of the tin cation by the π-electrons. In more concentrated solutions (> 0.01 mol/L) and especially in the solid state, planar R_3Sn cations are linked to each other by $AlCl_4$ anions through Cl−($AlCl_2$)−Cl bridges (Figure 1), whereby the bridging Sn−Cl separations are some 30 pm longer (12%) than the Sn−Cl bond in the original Me_3SnCl (at δ = 243). Such relatively weak coordination by the two chlorine atoms means that the planar R_3Sn unit is essentially still cationic.

The stability of the complex **21** between 1,2-bis(dichloroalumino)benzene (**20**) and 2 equivalents of Me_3SnCl demonstrates that an arylaluminum dichloride is still a strong enough Lewis acid to heterolyze Me_3SnCl completely. Presumably the structure of viscous **21** consists of intramolecular and intermolecular bridging of Me_3Sn^+ units between arene $AlCl_3^-$ sites (Scheme 1). The 1,2-bis(dimethylalumino)benzene (**18**) and 1,2-bis[chloro(methyl)alumino]benzene (**19**) are clearly weaker Lewis acids than **20** because the complexed Me_3SnCl can be removed by use of high vacuum and the addition of π-basic arenes (Equations 8 and 9).

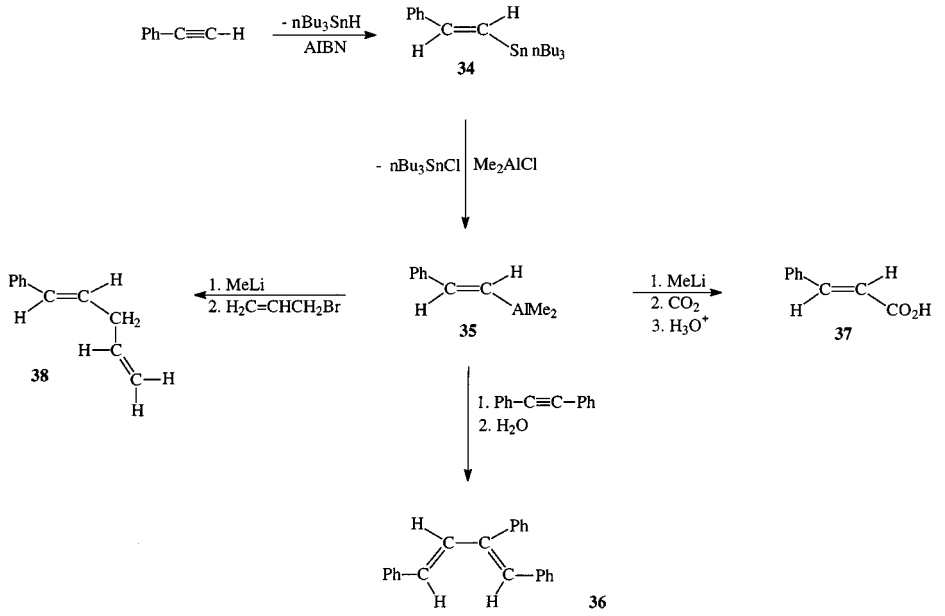
However, there is one structural feature of compounds **18**, **19**, and **20** that make them especially appealing as novel Lewis acids, and this is their potential as structurally rigid, chelating Lewis acids in Ziegler−Natta olefin polymerization. This attractive prospect motivates our continuing efforts to prepare **19** and **20** free of any complexation with Lewis bases. In the final section our recent progress in this research is outlined.

Novel Applications of Unsymmetrical Organoalanes in Organic Synthesis and Polymerization

Such aluminum-tin exchange processes constitute a most useful selective route to vinylic, allylic, acetylenic, aryl, and benzylic organoalanes in their unsolvated form. Illustrative are the preparations depicted in Equations 3, 5, 7, 18, and 19. Since the requisite organotin precursor reacts readily with $RAlCl_2$ or R_2AlCl in alkanes, toluene or dichloromethane, the organoalane can be generated free of any coordinated ether solvent and despite its auto-association, in its more electrophilic form. The weakly coordinated R_3SnX by-product can often be removed by a combination of π-basic hydrocarbons and high vacuum. In some cases, as with allyl(methyl)aluminum chloride (**9** in Equation 3), the presence of the R_3SnX does not interfere with the carbaluminating action of the organoalane.

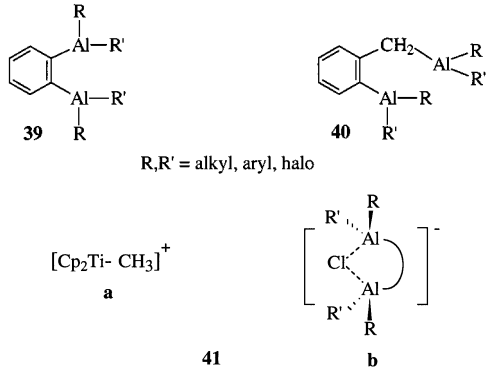
Since many organotin derivatives can be prepared by Grignard and organolithium reactions or by hydrostannations, subsequent aluminum-tin exchanges permit access to the more reactive organoalanes (Scheme 4).[26] Typical is the stereoselective generation of organoalane **35** from organotin precursor **34**. Reagent **35** can carbaluminate alkynes with selective *syn* addition (**36**),[27] undergoes carboxylation via an ate complexation with retention of configuration (**37**)[28][29] and yields the corresponding allyl derivative (**38**) by ate-complex-assisted allylation.[30] These selective reactions at the vinylic C−Al bonds, rather than at the methyl C−Al bonds, highlight the great utility of such vinylalanes in organic synthesis.

Finally, the first successful synthesis of the structurally rigid, chelating Lewis acids of types **39** and **40** from the corresponding organotin precursors has led to their evaluation as potential cocatalysts with transition metal metallocenes for the polymerization of olefins. Indeed, such cocatalysts, when employed with titanocene methyl chloride, $Cp_2Ti(Me)Cl$, in a 1:8 Ti/Al ratio, have been found decidedly superior to other aluminum cocatalysts such as $MeAlCl_2$ and even MAO, in polyethylene productivity numbers at comparable Ti/Al ratios. Productivity numbers (PN) of 2000−3000 g of polyethylene per g Ti × per h × per atm are attained with **39** and **40**, compared with PN values of 800 for MAO and 200 for $MeAlCl_2$.[31] The greater cocata-



Scheme 4

lytic efficacy of **39** and **40** may well stem from the greater binding of the chloride ion through their chelating ability (**41b**) and thus the cleaner generation and separation of the solvent-separated cation **41a**, which has been established as the active site in the metallocene polymerization of olefins.[32–34]



Experimental Section

General Techniques: All preparations and purification procedures involving manipulations with oxygen- and moisture-sensitive reagents were carried out under anhydrous, oxygen-free argon or nitrogen employing Schlenk techniques.[35] Those procedures which did not require a protective atmosphere but involved working with toxic chemicals (such as boron and tin compounds) were carried out in an exhaust hood evacuating air at 100 cubic ft/min. For the operations under reduced pressure the required vacuum was provided either by a rotary vacuum oil pump (down to 0.1 Torr) or by a water pump (down to 10 Torr) and toxic volatiles were condensed in cold traps. Commercially available solvents of reagent grade were purified according to the recommended methods.[35] Solvents used in reactions were always freshly distilled under argon or nitrogen from the appropriate drying agents: aliphatic hydrocarbons from $LiAlH_4$; toluene from sodium; dichloromethane from CaH_2; and ethers from sodium/benzophenone combinations. Deuteriated solvents (Cambridge Scientific) for NMR measurements of oxygen- and moisture-sensitive substances were vacuum-transferred to the Schlenk glass vessels and stored over Molecular Sieves (4 Å) under argon. Gas chromatographic analysis (GC) was performed with a Hewlett-Packard Chromatograph, model 5880A, with helium as the carrier gas. The ^1H- (360.1 MHz) and ^{13}C- (90.6 MHz) NMR spectra were recorded with a Bruker AM 360 spectrometer and the ^{27}Al- (78.2 MHz) and ^{119}Sn- (111.9 MHz) NMR spectra with a Bruker AC 300 spectrometer. Solid-state NMR spectra were recorded with a Bruker AC 300 spectrometer at 75.4 (^{13}C), 78.2 (^{27}Al) and 111.9 MHz (^{119}Sn). The ^1H- and ^{13}C-NMR chemical shifts are referred to resonances of the solvent [D_6]benzene. For ^{27}Al-NMR spectra aqueous $AlCl_3$ ($\delta = 0$) and for ^{119}Sn-NMR spectra Me_3SnCl (16.4% in C_6D_6: $\delta = 159.7$[28]) were used as external reference standards.

Preparation of Aluminum-Tin Complexes with Trialkyltin Chlorides

Complex 25 of Trimethyltin Chloride and Aluminum Trichloride in a 1:1 Ratio: To a suspension of 1.94 g (14.5 mmol) of aluminum trichloride in 20 mL of toluene was added 7.95 mL (7.95 mmol) of a 1.0 M solution of trimethyltin chloride in toluene via a syringe at room temperature. The resulting suspension was stirred for 3 d, filtered, and the solvent removed under reduced pressure. The remaining yellow crystals were washed with 10 mL of pentane, the pentane layer was decanted and the product dried in vacuo. In this way 2.55 g (7.7 mmol) of the crude product was obtained (97%). For further purification the crystals of **25** were again dissolved in 10 mL of toluene, the solution was filtered and cooled to −78°C. After standing overnight the solvent was decanted at a temperature of −78°C and the crystalline product was washed at room temperature with a mixture of 8 mL of pentane and 4 mL of toluene and finally dried in vacuo. − ^1H NMR (C_6D_6): $\delta = 0.88$ (s, $SnCH_3$, $^2J_{Sn-H} = 56.2/58.5$ Hz). − ^{13}C NMR (C_6D_6): $\delta = 5.7$ ($SnCH_3$, $^1J_{Sn-C} = 334.4/350.1$ Hz). − ^{27}Al NMR (C_6D_6): $\delta = 104.6$ ($W_{1/2} = 960$ Hz). − ^{119}Sn NMR (C_6D_6): $\delta = 342.0$.

Complex 26 of Tri-*n*-butyltin Chloride and Aluminum Trichloride in a 1:1 Ratio: To a suspension of 1.94 g (14.5 mmol) of aluminum trichloride in 20 mL of pentane was added 1.5 mL (5.5 mmol) of

tributyltin chloride via a syringe at room temperature. The resulting suspension was stirred for 2 d, filtered, and the solid was extracted three times with 10 mL of pentane. The solvent of the combined extracts and filtrate was removed in vacuo to leave 2.38 g of a yellow oil which was identified as the pure complex **26** by NMR spectroscopy (94%). – ^{1}H NMR (C_6D_6): δ = 0.86 (t, CH_3, 3 H), 1.29 (sext, CH_2, 2 H), 1.72 (m, CH_2, 4 H). – ^{13}C NMR (C_6D_6): δ = 13.6 (CH_3), 25.7 (CH_2, $^1J_{Sn-C}$ = 266.0/278.3 Hz), 27.0 (CH_2, $^2J_{Sn-C}$ = 75.9 Hz), 28.0 (CH_2, $^3J_{Sn-C}$ = 27.7 Hz). – ^{27}Al NMR (C_6D_6): δ = 103.7 ($W_{1/2}$ = 3000 Hz). – ^{119}Sn NMR (C_6D_6): δ = 380.4.

Complex 21 of Trimethyltin Chloride and 1,2-Bis(dichloroalumino)-benzene (20) in a 2:1 Ratio: To a suspension of 4.43 g (33.2 mmol) of aluminum trichloride in 25 mL of toluene was added 2.03 g (5.0 mmol) of 1,2-bis(trimethylstannyl)benzene[1] via a syringe at room temperature. The resulting yellow reaction mixture was stirred for 3 d and then filtered. The solvent was evaporated from the filtrate. In order to remove all volatile material the residue was heated in vacuum up to 50°C. The resulting yellow oil was washed with 10 mL of pentane, the pentane layer was decanted and the residual oil dried in vacuum. In this way 3.25 g (4.8 mmol) of the pale yellow oil of **21** was obtained in 97% yield. – ^{1}H NMR (360.1 MHz, C_6D_6, 25°C): δ = 0.86 (s, 6 H, $SnCH_3$, $^2J_{Sn-H}$ = 58.1 Hz), 6.98 (d, 2 H, C_6H_4, J_{H-H} = 7.8 Hz), 7.08 (d, 2 H, C_6H_4, J_{H-H} = 7.8 Hz). – ^{13}C NMR (90.6 MHz, C_6D_6, 25°C): δ = 5.9 ($SnCH_3$, $^1J_{Sn-C}$ = 346.3/331.7 Hz), 125.6 (C_6H_4), 128.6 (C_6H_4), 129.4 (C_6H_4). – ^{27}Al NMR (78.2 MHz, C_6D_6, 25°C): δ = 105 ($W_{1/2}$ = 20000 Hz). – ^{119}Sn NMR (111.9 MHz, C_6D_6, 25°C): δ = 357.5.

Displacement of Trimethyltin Chloride from Complex 21

Displacement of One Equivalent of Me_3SnCl by Benzyltriethylammonium Chloride. – Complex 22: To 211 mg (0.93 mmol) of benzyltriethylammonium chloride was added 3.1 mL of a 0.3 M of solution of the 2:1 complex of Me_3SnCl and 1,2-bis(dichloroalumino)benzene (**21**) (0.93 mmol) at room temperature. Stirring of the reaction mixture overnight resulted in the formation of two layers. While the upper layer was a clear yellow solution, the lower layer was a brown oil. After removal of solvent, the residue was heated in vacuum up to 40°C in order to remove all volatile material. Addition of C_6D_6 resulted again in the formation of the two layers which were separately investigated by NMR spectroscopy. The spectra of the upper layer showed no signals corresponding to starting materials or to an adduct of bis(dichloroalumino)benzene with benzyltriethylammonium chloride, but did exhibit signals for Me_3SnCl. In the spectra of the lower layer signals corresponding to the presence of the benzyltriethylammonium cation and consistent with the formation of the complex **22** were observed. – ^{1}H NMR (360.1 MHz, C_6D_6, 25°C): δ = 0.65 (t, CH_3CH_2N), 1.08 (s, $SnCH_3$), 2.13 (q, CH_3CH_2N), 3.27 (s, $C_6H_5CH_2N$), 6.80–6.90 (m, C_6H_4), 7.14–7.25 (m, C_6H_4). – ^{13}C NMR (90.6 MHz, C_6D_6, 25°C): δ = 5.9 ($SnCH_3$), 7.5 (CH_3CH_2N), 52.4 (CH_3CH_2N), 60.5 ($C_6H_5CH_2N$), 125.6 (C_6H_5), 128.5 (C_6H_4), 129.3 (C_6H_4), 129.8 (C_6H_5), 131.3 (C_6H_5), 132.0 (C_6H_5).

Displacement of Two Equivalents of Me_3SnCl by Benzyltriethylammonium Chloride. – Complex 23: To a suspension of 340 mg (1.50 mmol) of benzyltriethylammonium chloride in 2 mL of toluene was added 2.5 mL of a 0.3 M solution (0.75 mmol) of the 2:1 complex of Me_3SnCl and 1,2-bis(dichloroalumino)benzene (**21**) in toluene at room temperature. Stirring of the reaction mixture overnight resulted in the formation of two layers. While the upper layer was a pale yellow solution, the lower layer was a bright yellow oil. The separated upper layer was shown by NMR spectroscopy to contain only Me_3SnCl. The separated lower layer was washed with pentane and the residue was then heated in vacuum up to 40°C in order to remove all volatile materials. The remaining yellow residue was treated with C_6D_6 which caused again the formation of two layers, which were individually investigated by NMR spectroscopy. The spectra of the lower layer showed all signals corresponding to the reaction product, namely bis(benzyltriethylammonium) 1,2-phenylenebis(trichloroaluminate) (**23**). – ^{1}H NMR (360.1 MHz, C_6D_6, 25°C): δ = 0.75 (t, CH_3CH_2N), 2.28 (q, CH_3CH_2N), 3.46 (s, $C_6H_5CH_2N$), 6.92–6.95 (m, C_6H_5), 6.98–7.10 (m, C_6H_4), 7.22–7.26 (m, C_6H_5). – ^{13}C NMR (90.6 MHz, C_6D_6, 25°C): δ = 7.6 (CH_3CH_2N), 52.5 (CH_3CH_2N), 60.5 ($C_6H_5CH_2N$), 125.5 (C_6H_4), 125.9 (C_6H_5), 128.5 (C_6H_4), 129.2 (C_6H_4), 129.7 (C_6H_5), 131.0 (C_6H_5), 132.2 (C_6H_5). – ^{27}Al NMR (78.2 MHz, C_6D_6, 25°C): δ = 103.5 ($W_{1/2}$ = 14 Hz).

Displacement of One Equivalent of Me_3SnCl by Tetramethylphosphonium Chloride. –Complex 24: To 152 mg (1.2 mmol) of tetramethylphosphonium chloride was added 4 mL of a 0.3 M solution of complex **21** (1.2 mmol) at room temperature. Stirring the reaction mixture overnight resulted in the formation of two layers: the upper layer was a clear yellow solution and the lower layer was a golden-colored oil. After evaporating the solvent, the residue was heated in vacuum up to 40°C in order to remove all volatile materials. Addition of C_6D_6 resulted in the formation of the two layers which were individually investigated by NMR spectroscopy. The spectra of the upper layer showed only signals corresponding to Me_3SnCl, while in the spectra of the lower layer the signals of the reaction product were found, namely the 1:1 complex of tetramethylphosphonium trichloro(2-dichloroaluminophenyl)aluminate with Me_3SnCl (**24**). – ^{1}H NMR (360.1 MHz, C_6D_6, 25°C): δ = 0.82 (d, CH_3P, $^2J_{P-H}$ = 14.1 Hz), 1.04 (s, CH_3Sn, $^2J_{Sn-H}$ = 58.8 Hz), 6.96–7.22 (m, C_6H_4). – ^{13}C NMR (90.6 MHz, C_6D_6, 25°C): δ = 5.9 (CH_3Sn, $^1J_{Sn-C}$ = 345.0/358.2 Hz), 9.3 (CH_3P, $^1J_{P-C}$ = 56.0 Hz), 130.1 (C_6H_4), 134.3 (C_6H_4), 139.6 (C_6H_4). – ^{27}Al NMR (78.2 MHz, C_6D_6, 25°C): δ = 103 ($W_{1/2}$ = 1500 Hz). – ^{13}P NMR (121.4 MHz, C_6D_6, 25°C): δ = 21.4. – ^{119}Sn NMR (111.9 MHz, C_6D_6, 25°C): δ = 317.0 ($W_{1/2}$ = 30 Hz).

Aluminum-Tin Exchange Reactions

1,2-Bis(diethylalumino)ethyne (16): To a stirred solution of 0.80 g (2.3 mmol) of 1,2-bis(trimethylstannyl)ethyne (**28**), dissolved in 20 mL of dry pentane and cooled to –30°C, was added 5.0 mmol of diethylaluminum chloride in 30 mL of hexane. A pale yellow precipitate appeared almost immediately. The reaction suspension was stirred and brought to room temperature over 60 min. After removal of the volatiles in vacuo, the residue was found to be insoluble in alkanes, benzene or $CDCl_3$ but readily dissolved in THF or ether. The ^{1}H-NMR spectrum in THF showed the absence of **28** and the presence of free Me_3SnCl. Furthermore, in [D_8]THF the broaded triplet and quadruplet of the ethyl groups of **16** appeared at δ = 1.3 and 0.8, consistent with coordination of THF, rather than Me_3SnCl, at aluminum.

1,2-Bis(dimethylalumino)benzene (18): To a solution of 6.0 g (14.9 mmol) of 1,2-bis(trimethylstannyl)benzene (**17**)[1] in 20 mL of heptane was added 2.76 g (29.8 mmol) of pure dimethylaluminum chloride by syringe. The resulting solution was stirred at room temperature for 72 h and thereupon the solvent and the Me_3SnCl by-product were evaporated in vacuo without heating. The residue was redissolved in heptane and volatiles again removed under reduced pressure; this addition and evaporation of heptane was repeated to remove all traces of residual Me_3SnCl. The residual viscous pale yellow oil was essentially pure 1,2-bis(dimethylalumino)benzene (**18**) in 89% yield, as evidenced by spectral data. – ^{1}H NMR (360.1 MHz, C_6D_6, 25°C): δ = –0.41 (br., 6 H, $AlCH_3$), –0.32 (br., 6 H,

$AlCH_3$), 6.96 (dd, 2 H, C_6H_4), 7.96 (2 H, dd, C_6H_4). – ^{13}C NMR (90.6 MHz, C_6D_6, 25°C): δ = −7.7 ($AlCH_3$), 6.4 (br., $AlCH_3$), 129.7 (C_6H_4), 144.9 (C_6H_4), 160.3 (C_6H_4). – ^{27}Al NMR (78.2 MHz, C_6D_6, 15°C): δ = 174 ($W_{1/2}$ = 3200 Hz); (−8°C): δ = 179 ($W_{1/2}$ = 5200 Hz).

1,2-Bis[chloro(methyl)alumino]benzene (19): To a solution of 6.0 g (14.9 mmol) of 1,2-bis(trimethylstannyl)benzene in 20 mL of toluene were added 29.8 mmol of a solution of methylaluminum dichloride in hexane at room temperature. After stirring for 72 h, the solvents were evaporated in vacuo. In order to remove the more tightly complexed Me_3SnCl, the procedure of adding 20 mL of toluene to the reaction residue and evaporating all volatiles at 25°C in high vacuum had to be performed four times. The residue thus obtained was a pale yellow waxy substance (85% yield) whose NMR spectra corroborate that it is rather pure **19**, existing as a bridging isomeric mixture. – ^1H NMR (360.1 MHz, C_6D_6, 25°C): δ = 0.25 (br., $AlCH_3$, 2 H), 0.8 (br., $AlCH_3$, 4 H), 6.8−7.3 (m, br., C_6H_4, 2 H), 7.4−7.9 (m, br., C_6H_4, 2 H). – ^{13}C NMR (90.6 MHz, C_6D_6, 25°C): δ = −6.6 ($AlCH_3$), 4.3 (br., $AlCH_3$), 129.5 (br., C_6H_4), 137.0 (C_6H_4), 150.4 (C_6H_4). – ^{27}Al NMR (78.2 MHz, C_6D_6, 25°C): δ = 101 ($W_{1/2}$ = 5000 Hz).

Benzylaluminum Dichloride (14):[36] A solution of 7.6 g (30.0 mmol) of benzyl(trimethyl)tin in 200 mL of mesitylene was treated with 30 mL of a 1.0 M solution of methylaluminum dichloride in hexane and the resulting clear solution was stirred at 20°C for 15 h and then heated at 100−110°C for 3 h. The mesitylene was slowly evaporated at 100°C under a low pressure and caught in a cold trap. By ^1H- and ^{13}C-NMR spectroscopy the mesitylene was shown to contain tetramethyltin but not trimethyltin chloride. Spectral analysis of the residual viscous oil showed it to be pure benzylaluminum dichloride (**14**), free of any organotin by-product. – ^1H NMR (C_6D_6): δ = 2.15 (s, 2 H), 6.71 (br. s, 2 H), 6.95 (t, 1 H), 7.10 (t, 2 H). – ^{13}C NMR (C_6D_6): δ = 29 (CH_2 by DEPT), 123.6, 127.8, 127.86, 127.93.

Allyl(methyl)aluminum Chloride (9):[37] To a solution of 1.87 mL (6.0 mmol) of allyltri-*n*-butyltin and 1.13 mL (5.8 mmol) of trimethyl(phenylethynyl)silane (**10**) in 6.0 mL of toluene, cooled to −78°C, was added dropwise 6.1 mL of a 1.0 M solution of $MeAlCl_2$ in hexane. The reaction mixture was slowly brought to 0°C over 4 h. Hydrolytic work-up with aqueous NaOH and ether extraction of the organic product allowed the isolation of a mixture of tri-*n*-butyltin chloride and (*Z*)-2-phenyl-1-trimethylsilyl-1,4-pentadiene; no starting tin compound or **10** remained. The adduct **12** was cleanly separated from the nBu_3SnCl by column chromatography on silica gel with hexane eluent (90% yield). – ^1H NMR ($CDCl_3$): δ = −0.15 (s, 9 H), 3.15 (d, 2 H), 5.00 (m, H), 5.59 (s, H), 5.84 (m, H), 7.15−7.35 (m, 5 H).[7] – ^{13}C NMR ($CDCl_3$): δ = 0.0, 46.76, 116.41, 126.97, 127.75, 127.98, 135.91, 144.06, 157.43. – When a similar reaction mixture was worked up with NaOD in D_2O, the ^1H singlet at δ = 5.59 was absent in the spectrum of **12**.

X-ray Crystallographic Study of Trimethylstannyl Tetrachloroaluminate, $Me_3SnAlCl_4$ (25). – Crystal Mounting and Data Collection: A pale yellow-brown crystal of **25**, 0.25 × 0.53 × 0.42 mm in size, was mounted with a perfluorinated polyether oil on the tip of a glass fiber on the goniometer head and cooled immediately by an argon current to −173°C. Intensity data were collected with an Enraf-Nonius CAD4 diffractometer by a coupled ω-2θ scan technique with speeds varying from 1.0 to 10.0°/min depending on the standard deviation to intensity ratio of a preliminary 10°/min scan. The radiation employed was Mo-K_α with a graphite monochromator. The crystals of molecular weight 332.6 g mol^{-1} have 6 molecules per unit cell and have a calculated density of 1.97 g cm^{-3}; they belong to the triclinic crystal system and the space group of *P*l, No. 1. The absorption corrections were made by the ψ-scan method. Observed reflections were defined as those reflections with $I \geq 2\sigma(I)$. Only these were used in the solution and refinement of the structure (*F* refinement). For refinement based on F^2 all reflections were used. Refinement was done by least-squares; the quantity minimized was $\Sigma\, w(|Yo| - |Yc|)^2$, with $Y = F$ or F^2. Computations were done using VAX, Sun4, and Silicon Graphics computers. In addition to several locally written programs, the following software was used: S. L. Lawton, R. A. Jacobson, *TRACER* (cell reduction), United States Energy Commission, Report IS-1141, Iowa State University, USA, **1965**. P. Coppens, L. Leiserowitz, D. Rabinovich, *DATAP* (data reduction), *Acta Crystallogr.* **1965**, *18*, 1035. G. M. Sheldrick, *SHELXS-86* (crystal structure determination), *Crystallographic Computing 3* (Eds:. G. M. Sheldrick, C. Krüger, R. Goddard), Clarendon Press, Oxford, **1985**, dp. 175. G. M. Sheldrick, *SHELXL-93* (least-squares refinement), University of Göttingen, **1993**. E. Egert, G. M. Sheldrick, *PATSEE* (structure solution), *Acta Crystallogr.* **1985**, *A41*, 262. P. Main, S. J. Fiske, S. E. Hull, L. Lessinger, G. Germain, J.-P. Declercq, M. M. Woolfson, *MULTAN80* (structure solution), University of York, England and Louvain, Belgium, **1980**. W. R. Busing, K. O. Martin, H. A. Levy, *GFMLX, a highly modified version of ORFLS* (full-matrix least-squares refinement), Report ORNL-TM-305, Oak Ridge National Laboratory, Tennessee, USA, **1962**; H. D. Flack, (enantiomorph-polarity estimation), *Acta Crystallogr.* **1983**, *A39*, 876. P. Roberts, G. M. Sheldrick, *XANADU* (calculation of best planes, torsion angles and idealized hydrogen atom positions), University of Cambridge, England, **1976**. R. E. Davis, D. R. Harris, *DAESD* (calculation of distances and angles), Roswell Park Mem. Inst., USA, **1970**. V. Schomaker, K. N. Trueblood, *RIGID* (rigid-body analysis) *Acta Crystallogr.* **1968**, *B24*, 63. C. K. Johnson, *ORTEP* (thermal ellipsoid plot program), Report ORNL-5138, Oak Ridge National Lab., Tennessee, USA, **1976**. E. Keller, *SCHAKAL* (molecular drawing), *Chem. Unserer Zeit* **1986**, *20*, 178. B. W. van der Waal, *FSYN* (slant plane Fourier syntheses), Technical University of Enschede, Netherlands, **1975**. *SYBYL* (molecular calculations), Tripos Associates, Inc., St. Louis. *INSIGHT/DISCOVER*, Biosym Technologies, San Diego, USA. Crystallographic data (excluding structure factors) for the structure reported in this paper have been deposited with the Cambridge Crystallographic Data Centre as supplementary publication no. CCDC-103346. Copies of the data can be obtained free of charge on application to CCDC, 12 Union Road, Cambridge CB2 1EZ, UK [Fax: int. code + 44(1223)336-033; E-mail: deposit@ccdc.cam.ac.uk]

Acknowledgments

This research has received its principal financial support from the former Schering AG of Bergkamen, Germany and its successor, Witco GmbH. We wish to thank the respective directors of research, Dr. Peter Borner and Dr. Wolfram Uzick, for moral support and helpful technical discussions. The final research efforts were supported by funding from the National Science Foundation and a Senior Scientist Award to the principal investigator from the Alexander von Humboldt Foundation. Valuable technical assistance was provided by Dr. Boguslaw Kotowicz and Dr. Jürgen Weber, as well as by Ms. Leza Luchetta.

[1] J. J. Eisch, B. W. Kotowicz, *Eur. J. Inorg. Chem.* **1998**, 761. In this article the authors availed themselves of the pioneering research insights of the Nöth group into the course of boron-tin

exchange processes: H. Nöth, H. Vahrenkamp, *J. Organomet. Chem.* **1968**, *11*, 399.
[2] G. E. Coates, K. Wade, *Organometallic Compounds*, 3rd ed., vol. 2, Methuen, London, **1967**, pp. 304−319.
[3] H. Lehmkuhl, K. Ziegler, *Methoden Org. Chem. (Houben-Weyl)*, vol. XIII/4, **1970**, pp. 264−266.
[4] W. P. Neumann, *The Organic Chemistry of Tin*, Wiley-Interscience, **1970**, pp. 20−32.
[5] The chemical consequences of the principle of Le Chatelier on chemical reactions at equilibrium, when subjected to changes in temperature, pressure and/or concentration of a reaction partner, are clearly and succinctly analyzed in the textbook: N. Wiberg, *Holleman-Wiberg: Lehrbuch der Anorganischen Chemie*, 91−100th ed., de Gruyter, Berlin, **1985**, pp. 202−215.
[6] W. P. Neumann, R. Schick, R. Köster, *Angew. Chem. Int. Ed.* **1964**, *3*, 385.
[7] U. Schöllkopf, *Methoden Org. Chem. (Houben-Weyl)*, vol. XIII/1, **1970**, pp. 127−133.
[8] Product **12** has also been the exclusive adduct obtained when **10** is allowed to react with η^3-allylbis(cyclopentadienyl)titanium and then treated with H_2O or D_2O: J. J. Eisch, M. P. Boleslawski, *J. Organomet. Chem.* **1987**, *334*, C1.
[9] This method of removing the most volatile component, here Me_4Sn, from such aluminum-tin exchange equilibria has great promise for the synthesis of a variety of uncomplexed $RAlCl_2$ reagents from $RSnMe_3$ and $MeAlCl_2$, such as **20**.
[10] H. Nöth, R. Rürlander, P. Wolfgardt, *Z. Naturforsch.* **1982**, *37B*, 29.
[11] T. Birchall, V. Manivannan, *J. Chem. Soc., Dalton Trans.* **1985**, 2671.
[12] J. B. Lambert, B. Kuhlmann, *J. Chem. Soc., Chem. Commun.* **1992**, 931.
[13] The helical sinuosity in the structure of solid **25** has prompted one of us (C. K.) to view such a structure as a "DNA strand for tin soldiers".
[14] I. Lange, J. Krahl, P. G. Jones, A. Blaschette, *J. Organomet. Chem.* **1994**, *474*, 97.
[15] I. Lange, D. Henschel, A. Wirth, J. Krahl, A. Blaschette, *J. Organomet. Chem.* **1995**, *503*, 155.
[16] M. B. Hossain, J. L. Lefferts, K. C. Molloy, D. van der Helm, J. J. Zuckerman, *Inorg. Chim. Acta* **1979**, *36*, 1409.
[17] J. L. Lefferts, K. C. Molloy, M. B. Hossain, D. van der Helm, J. J. Zuckermann, *J. Organomet. Chem.***1982**, *240*, 349.
[18] E. O. Schlemper, D. Britton, *Inorg. Chem.* **1966**, *5*, 507.
[19] R. A. Forder, G. M. Sheldrick, *J. Organomet. Chem.* **1970**, *21*, 115.
[20] B. Beagley, K. McAloon, J. M. Freeman, *Acta Crystallogr.* **1974**, *B30*, 444.
[21] A. G. Davies, H. J. Milledge, D. C. Puxley, P. J. Smith, *J. Chem. Soc. A* **1970**, 2862.
[22] R. A. Forder, G. M. Sheldrick, *J. Organomet. Chem.* **1970**, *22*, 611.
[23] N. C. Baenziger, *Acta Crystallogr.* **1951**, *4*, 216.
[24] W. Hanstein, H. J. Berwin, T. G. Traylor, *J. Am. Chem. Soc.* **1970**, *92*, 829.
[25] R. B. Woodward, R. Hoffmann, *The Conservation of Orbital Symmetry*, Verlag Chemie, Weinheim, **1970**, pp. 114−140.
[26] J. J. Eisch, J. E. Galle, unpublished studies.
[27] J. J. Eisch, C. K. Hordis, *J. Am. Chem. Soc.* **1971**, *93*, 2974.
[28] J. J. Eisch, M. W. Foxton, *J. Organomet. Chem.* **1968**, *11*, P7.
[29] G. Zweifel, R. B. Steele, *J. Am. Chem. Soc.* **1967**, *89*, 2754.
[30] J. J. Eisch, G. A. Damasevitz, *J. Org. Chem.* **1976**, *41*, 2214.
[31] J. J. Eisch, W. Uzick, K. Mackenzie, S. Gürtzgen, R. Rieger, U. S. Patent 5,726,332, Mar. 10, **1988** (*Chem. Abstr.* **1998**, *128*, 192778r).
[32] J. J. Eisch, A. M. Piotrowski, S. K. Brownstein, E. J. Gabe, F. L. Lee, *J. Am. Chem. Soc.* **1985**, *107*, 7219.
[33] J. J. Eisch, K. R. Caldwell, S. Werner, C. Krüger, *Organometallics* **1991**, *10*, 3417.
[34] J. J. Eisch, S. I. Pombrik, G. X. Zheng, *Organometallics* **1993**, *12*, 3856.
[35] J. J. Eisch, *Organometallic Syntheses*, vol. 2, Academic Press, New York, **1981**, pp. 1−84.
[36] Dr. Jürgen Weber conducted this experiment and established the unexpected aluminum-tin exchange depicted in Equation 6.
[37] An undergraduate research assistant in our research group, Leza Luchetta, was first in realizing this novel generation of the allylating agent **9**.

Received August 31, 1998
[I98296]

Stabilization of Copper(III) Ions with Deprotonated Hydroxyiminoamide Ligands: Syntheses, Structures, and Electronic Properties of Copper(II) and Copper(III) Complexes

Jan Hanss,[a] Alexander Beckmann,[a] and Hans-Jörg Krüger*[a]

Keywords: Copper / Deprotonated amide ligands / Oxime ligands / Redox chemistry / High valent metal ions

Copper(II) and copper(III) complexes were prepared with two novel ligands, *N*,*N*′-bis(2-(1-hydroxyimino-2-methyl-1-phenyl)propyl)dimethylmalondiamide (H_4mal55) and *N*,*N*′-bis(2-(1-hydroxyiminoethyl)phenyl)dimethylmalondiamide (H_4mal66), both of which contain two amide and two oxime functionalities as potential ligand donor groups. The two copper(II) complexes (NEt_4)[Cu(Hmal55)] (**1**) and (NEt_4)[Cu(Hmal66)] (**2**) can be reversibly oxidized in acetonitrile at a redox potential of –0.120 and –0.075 V vs. the Fc/Fc^+ redox couple, respectively. While the quantitative electrolysis of **1** results in the preparation of the oxidized complex [Cu(Hmal55)] (**3**), which is sufficiently stable to be isolated, isolation of the oxidation product of **2** was not attempted because of its long-term instability. The properties of the complexes were investigated by means of various spectroscopic methods (UV-vis, ESR, NMR, and IR spectroscopy) and by X-ray structure analysis. The structure determinations and the spectroscopic investigations of the complexes reveal a square-planar CuN_4 coordination environment for each complex in the solid state and in acetonitrile solution. In both the oxidized and reduced oxidation states of the complexes, the coordinated ligands remain triply deprotonated with a hydrogen atom bridging both oxime oxygen atoms. The ligands can therefore be regarded as pseudo-macrocyclic. The characterization of the oxidation products clearly identifies the electron-transfer reaction as being metal-centered. For the first time, the structure of a copper(III) complex with a ligand containing oximes as donor groups was determined. The redox potentials of the copper complexes are compared to related Cu^{III}/Cu^{II} redox couples.

Introduction

The stability of highly oxidized metal ions in complexes is determined for the most part by the type of donor functions provided by the ligand. In general, anionic and highly polarizable donor groups are needed to achieve high oxidation states at the metal sites. For example, deprotonated amides as part of a multidentate ligand are well known to stabilize the trivalent oxidation state of the central ion in mononuclear copper and nickel complexes.[1] Thus, copper(III) complexes have been synthesized *and* successfully isolated with ligands which contain carboxylate,[2] amine,[2] thiolate,[3] alcoholate, and phenolate[4] or further amide groups[5] in addition to the deprotonated amide functions.

Another type of ligand donor function that has been demonstrated to generate high-valent metal ions is the deprotonated oxime group.[6] While ligand systems with oximato groups produce stable nickel(III) and even nickel(IV) complexes,[7] this ligand donor group seems to be considerably less well-established in the coordination chemistry of copper(III) ions. To our knowledge, the Cu^{III}/Cu^{II} redox chemistry has only been reported for two mononuclear copper complexes containing such ligand donor functions.[8] In these complexes the metal ion is coordinated to two imine and two oxime nitrogen atoms in a square-planar geometry.

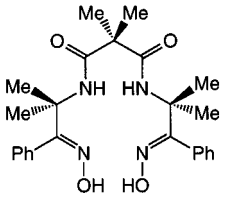
Further, since metal ions can be bound by the deprotonated oximate group via the nitrogen as well as via the oxygen atom, this type of ligand donor group has an advantage: multinuclear complexes which display interesting magnetic properties[9] can be prepared and may, therefore, be potentially useful for the development of new materials in the field of molecular magnetism.[10]

In light of the low Ni^{III}/Ni^{II} redox potentials obtained for nickel complexes with either amidate or oximate groups in the ligand environment,[11] some years ago we initiated an investigation of the complexation properties of tetradentate ligands comprised of two deprotonated amide and two oxime groups. The ligands used in this study, H_4mal55 and H_4mal66, are depicted below. They contain two amide and two oxime functions for the complexation of metal ions. Until recently[12] complexes with such a combination of donor groups in a ligand were unknown. In a recent complexation study of copper(II) ions,[12a] Kozlowski et al. employed the tetradentate amide-oxime ligand H_4pap, in which the oxime function is adjacent to the carboxylate portion of the amide group. In contrast, in both the acyclic amide-oxime ligands used in our investigation, the oximate groups lie on the side of the amine residues of the amide functions. In addition, the ligands H_4mal55 and H_4mal66 are designed to contain no hydrogen atom attached to a carbon atom in the α position to any donor atom; this feature has been shown to be very helpful in abolishing or at least in retarding possible decomposition reaction pathways of amidato complexes after the metal ion is oxidized.[2][13][14] The two ligands H_4mal55 and H_4mal66 dis-

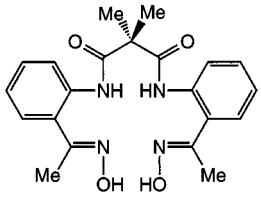
[a] Institut für Anorganische und Angewandte Chemie der Universität Hamburg,
Martin-Luther-King-Platz 6, D-20146 Hamburg, Germany
Fax: (internat.) +49(0)40/4123-2893
E-mail: krueger@xray.chemie.uni-hamburg.de

 © WILEY-VCH Verlag GmbH, D-69451 Weinheim, 1999 1434–1948/99/0101–0163 $ 17.50+.50/0

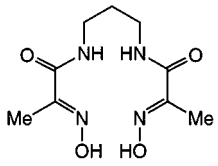
tinguish themselves by the different carbon chain lengths of the two hydroxyliminoamine components. Therefore, while ligand H_4mal55 is expected to form two five- and one six-membered chelate rings with the metal ion upon complexation, ligand H_4mal66 will render only six-membered chelate ring sizes.



H_4mal55



H_4mal66



H_4pap

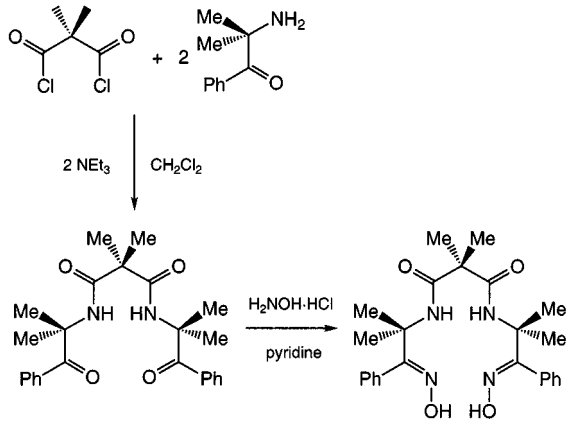
Here we introduce the results of the complexation reactions of the two novel amide-oxime ligands, H_4mal55 and H_4mal66, with copper ions, emphasizing the effects of the distinctive structural features of the ligands on the properties of the resulting complexes. The syntheses, as well as the structural and electronic properties of the copper(II) complexes, are described. The results of an electrochemical investigation, from which the isolation and first structural characterization of a copper(III) complex with oxime donor groups in the ligand environment ensued, are presented.

Results and Discussion

Preparation of the Ligands and the Copper(II) Complexes

Scheme 1 illustrates the synthesis of the ligand H_4mal55 $\times$ 0.5 H_2O, which was obtained from dimethylmalonyl dichloride and α-amino-isobutyrophenone in two reaction steps with an overall yield of 54%. Using a similar procedure, the ligand H_4mal66 $\times$ H_2O was synthesized from dimethylmalonyl dichloride and 2-amino-acetophenone in a 62% overall yield.

The red copper(II) complexes (Et_4N)[Cu(Hmal55)] (**1**) and (Et_4N)[Cu(Hmal66)] (**2**) were prepared by refluxing the corresponding ligand with one equivalent of $Cu(OAc)_2$ $\times$ H_2O in the presence of two equivalents of Et_4NOAc $\times$ 4 H_2O in absolute ethanol. The elemental analyses of both compounds suggest that the coordinated ligand is triply deprotonated. The absence of N−H stretching vibrations between 3310 and 3370 cm^{-1} in the IR spectra of the complexes indicates that both amide nitrogen atoms are deprotonated upon complexation.



Scheme 1. Synthesis of the ligand H_4mal55

Structures of the Copper(II) Complexes

Perspective views of the copper(II) complex anions are displayed in Figures 1 and 2. A comparison of selected bond lengths and angles is listed in Table 1. In the crystal lattice of **1** · 0.5 Et_2O, two crystallographically distinct, but otherwise chemically equivalent complexes are found. In both complexes **1** and **2**, the copper(II) ions are bound to two deprotonated amide and two oxime nitrogen atoms in essentially square-planar arrangements. The copper ions of the two symmetry-unrelated complex anions in the crystal lattice of **1** · 0.5 Et_2O deviate by 0.052 and 0.075 Å, respectively, from the calculated least-squares-plane of the four nitrogen donors. A similar deviation of the copper ion from the least-squares N_4-plane (0.052 Å) is observed in **2**. In both complexes, the dihedral angle between opposing CuN_2 planes does not exceed 6.5°. The structure analysis of both copper(II) complexes provides further evidence that the two oximate oxygen atoms are bridged by a proton; this is in agreement with the previously mentioned elemental analyses and IR spectra. Similar to the crystal structure of the related complex anion $[Cu(Hpap)]^-$,[12a] the hydrogen-bridging is found to be asymmetric. This feature of a hydrogen atom bridging both oximate oxygen atoms gives the ligands a pseudo-macrocyclic appearance with only six-membered chelate rings occurring in **2**, while in **1** the chelate ring sizes alternate between five and six. The interatomic O−O distance between the oxime oxygen atoms measures 2.427 ±0.005 Å and 2.417 Å for **1** and **2**, respectively.

The different fused chelate-ring sizes have a profound effect on the degree of ruffling of the pseudo-macrocyclic ring as well as on the Cu−N bond lengths. Thus, while most of the atoms of the ligands backbone in **1** (except those of the methyl and the phenyl groups) lie approximately in the same plane as the CuN_4 unit, the ligand backbone in **2** exhibits a more saddle-like appearance in order to still be capable of accommodating the copper ion. The two phenylene rings in **2** are positioned under the CuN_4 plane, forming interplanar angles of 45.0−49.2° with the CuN_4 plane, while the two oxime oxygen atoms and the atoms of the malonyl bridge are located above the CuN_4 plane. Values of 36.5° and 31.7° are calculated for the interplanar angle

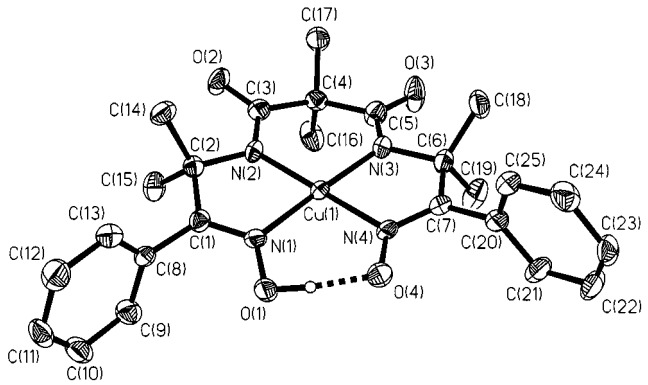


Figure 1. Perspective view of the structure of one of the two crystallographically independent $[Cu(Hmal55)]^-$ anions in **1** · 0.5 Et_2O showing thermal ellipsoids at 50% probability and the atom-numbering scheme

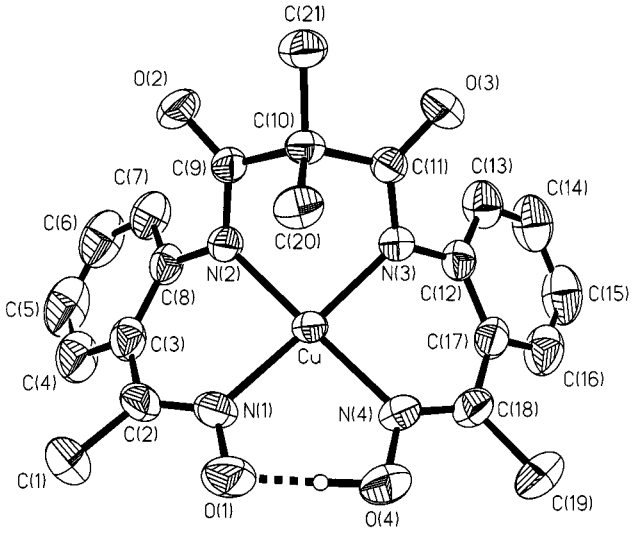


Figure 2. Perspective view of the structure of the $[Cu(Hmal66)]^-$ anion in **2** showing thermal ellipsoids at 50% probability and the atom-numbering scheme. The location of the hydrogen atom which asymmetrically bridges both oxime oxygen atoms is disordered over two positions; the present view shows only one of these positions

enclosed by the CuN_4-plane and the least-squares planes passing through the atoms N(2), C(9), C(11), and N(3) and through the atoms O(1), N(1), N(4), and O(4), respectively. In addition, the average $Cu-N_{amide}$ and $Cu-N_{oxime}$ distances in **1** of 1.906 ±0.005 Å and 1.950 ±0.011 Å, respectively, increase to 1.946 ±0.006 Å and 2.000 ±0011 Å in **2**.

The $Cu-N_{amide}$ bond lengths compare well with those found in other square-planar amidato copper(II) complexes.[3][12a][15] Reference values for $Cu-N_{oxime}$ distances in square-planar copper(II) complexes containing *vic* dioximate ligand donor groups are rare; the copper(II) ion is five-coordinate in most complexes with this type of donor function.[16] The $Cu-N_{oxime}$ bond lengths (1.954 and 1.962 Å) in the square-planar complex anion $[Cu(Hpap)]^-$, which possesses the same sequence of fused chelate ring sizes as **1**, resemble those observed in **1**.[12a]

Electronic Properties of the Copper(II) Complexes

The magnetic moments of **1** and **2** were determined to be 1.81 and 1.85 μ_B, respectively, which is consistent with the $S = 1/2$ state of the mononuclear copper(II) complexes. The ESR spectra of the complexes dissolved in an acetonitrile/toluene mixture (*v*/*v* = 1:4) and in pure ethanol were recorded at room temperature and at 100 K, respectively. The spectra are shown in Figure 3 and the ESR parameters obtained by simulation of the spectra are listed in Table 2. Thus, the solution of **1** at room temperature renders an isotropic ESR signal at $g_{iso} = 2.075$, which is split into four lines by the hyperfine coupling to the $I = 3/2$ spin of the copper nucleus. Further, superhyperfine splitting is observed due to the coupling to the nuclear spins $I = 1$ of the four nitrogen donor atoms of the ligand. The values for g_{iso} and $A^{Cu}_{iso} = 94.0 \cdot 10^{-4}$ cm^{-1} are typical for square planar or for tetragonally elongated octahedral compounds of copper(II) ions with an equatorial N_4-ligand donor environment. Through the interpretation of the powder spectrum of a frozen ethanolic solution of **1**, one arrives at the same conclusion. Thus $g_z = 2.170$ and $A^{Cu}_z = 210 \cdot 10^{-4}$ cm^{-1} have values that are predicted by a scatter plot of g_z vs. A^{Cu}_z for a monoanionic complex with a square planar or tetragonally distorted octahedral CuN_4-coordination core.[17] The *g*-values and the hyperfine coupling constants

Table 1. Selected bond lengths [Å] and angles [deg] in $(NEt_4)[Cu(Hmal55)]$ (**1**), $(NEt_4)[Cu(Hmal66)]$ (**2**), and $[Cu(Hmal55)]$ (**3**)

	$(NEt_4)[Cu(Hmal55)]$[a]		$(NEt_4)[Cu(Hmal66)]$	$[Cu(Hmal55)]$[b]
Cu−N(1)	1.940(4)	[1.951(4)]	2.010(2)	1.903(2)
Cu−N(2)	1.908(4)	[1.910(4)]	1.940(2)	1.860(2)
Cu−N(3)	1.901(4)	[1.906(4)]	1.951(2)	1.860(2)[b]
Cu−N(4)	1.961(4)	[1.949(4)]	1.989(2)	1.903(2)[b]
N(1)−Cu−N(2)	82.5(2)	[82.5(2)]	87.0(1)	83.1(1)
N(1)−Cu−N(3)	177.1(2)	[175.3(2)]	173.4(1)	175.4(1)[b]
N(1)−Cu−N(4)	93.9(2)	[94.5(2)]	94.1(1)	95.5(1)[b]
N(2)−Cu−N(3)	100.3(2)	[99.6(2)]	91.5(1)	98.0(1)[b]
N(2)−Cu−N(4)	173.3(2)	[174.4(2)]	178.8(1)	175.4(1)[b]
N(3)−Cu−N(4)	83.3(2)	[83.0(2)]	87.5(1)	83.1(1)[b]

[a] The corresponding bond lengths and angles in the crystallographically distinct second complex anion in **1** are listed in square brackets. – [b] The atom numbering scheme of $[Cu(Hmal55)]$ (**3**) (cf. Figure 6) is adapted to that of $(NEt_4)[Cu(Hmal55)]$ (**1**). Thus, the atoms N(1′) and N(2′) in Figure 6 correspond to the atoms N(4) and N(3) in Table 1, respectively.

indicate further that the unpaired electron resides in the d_{xy}-orbital of the copper(II) ion if the coordinate system is arranged in such a way that the z axis lies perpendicular to the CuN_4 plane and the x axis bisects the $N_{amide}-Cu-N_{amide}$ angle. The ESR spectra of **2** have rather similar appearances except that the g_z value is slightly larger and the $A^{Cu}{}_z$ value is smaller than that of **1**. A smaller g_z value and a larger $A^{Cu}{}_z$ value is correlated to the greater ligand field strength that the ligand $Hmal55^{3-}$ exerts on the copper ion. Thus, the ESR data confirm the presence of weaker Cu−N bonds in **2** as compared to those in **1**, a fact which has already been established by the structure determinations.

The electronic absorption spectra of the copper(II) complexes **1** and **2** are shown in Figure 4. The visible region of the spectrum corresponding to **1** comprises two absorption bands at 405 and 509 nm. Based on their positions and intensities, the bands are attributed to d−d transitions. The energy range of the absorption bands indicates either that the coordination geometry observed in the solid state is preserved in solution or that any possible axial coordination by solvent molecules must be rather weak.[18] Electrochemical evidence[19] supports the notion that, in acetonitrile, solvent molecules are, if at all, extremely weakly coordinated to the axial coordination sites. Similar d−d transitions appear as shoulders with slightly higher intensities in the spectrum of **2**; the lower energies of the absorption bands agree with the previously stated proposition that a smaller ligand field strength is exerted by the ligand $Hmal66^{3-}$ as compared to $Hmal55^{3-}$. The intense absorption around 280 nm is attributed to an amidato-to-copper(II) charge transfer transition.[20]

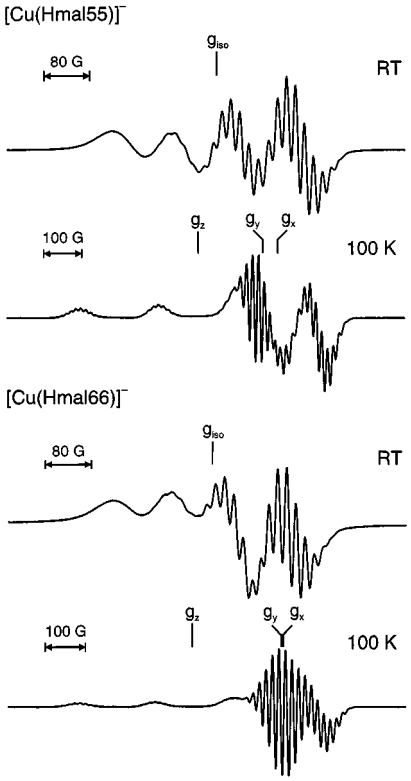


Figure 3. X-Band ESR spectra of $(Et_4N)[Cu(Hmal55)]$ (**1**) (top) and $(Et_4N)[Cu(Hmal66)]$ (**2**) (bottom) in acetonitrile/toluene (v/v = 1:4) at room temperature and as frozen glass in ethanol at 100 K (g-values are indicated)

Table 2. ESR properties of complexes **1** and **2** in acetonitrile/toluene mixture at room temperature and in frozen ethanol at 100 K

data	$(NEt_4)[Cu(Hmal55)]$	$(NEt_4)[Cu(Hmal66)]$
solution spectra at room temperature:		
g_{iso}	2.075	2.080
$A^{Cu}{}_{iso}$ (10^{-4} cm^{-1})	94.0	90.7
$A^{N}{}_{iso}$ (10^{-4} cm^{-1})	14.9	14.3
powder spectra at 100 K:		
g_x, g_y, g_z	2.037, 2.056, 2.170	2.046, 2.050, 2.200
$A^{Cu}{}_x$, $A^{Cu}{}_y$, $A^{Cu}{}_z$ (10^{-4} cm^{-1})	35.1, 33.9, 210	34.0, 28.9, 193
$A^{N}{}_x$, $A^{N}{}_y$, $A^{N}{}_z$ (10^{-4} cm^{-1})	16.1, 14.4, 13.6	15.9, 15.6, 14.0

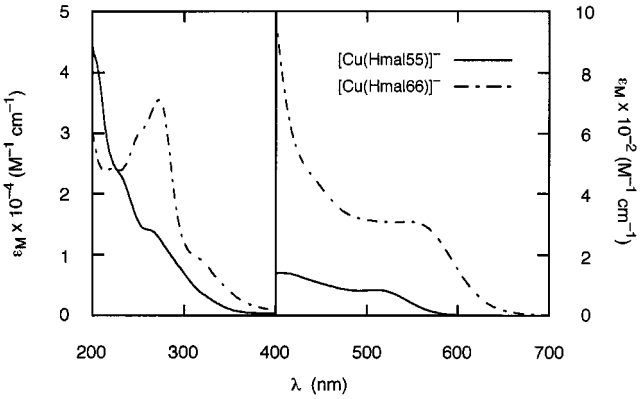


Figure 4. Electronic absorption spectra of the copper(II) complexes **1** and **2** in acetonitrile

Electrochemical Properties

The electrochemical properties of the copper(II) complexes were investigated by cyclic voltammetry and by coulometry in acetonitrile solution. The cyclic voltammograms of **1** and **2** are depicted in Figure 5. Both complexes reveal electrochemically reversible oxidation reactions (the current ratio $|i_{p,a}/i_{p,c}| \approx 1$; $i_p/v^{1/2}$ and the separation of the peak-potentials ΔE_p are independent of the scan rate v) at −120 and −75 mV vs. the ferrocene/ferrocenium (Fc/Fc^+) redox couple in acetonitrile, respectively. No reversible reductions are observed. Coulometric oxidations of the complexes at an applied potential of 80 mV for **1** and 125 mV for **2** produce dark brown-red solutions. Quantitative electrolysis demonstrates that the complexes are oxidized by one electron; immediate re-reduction results in the recovery of 98 and 95% of the reduced complexes **1** and **2**. The long-term stability of the oxidized species was examined spectrophotometrically. Thus, 95% of the oxidation product of **1** are still present after 3 d and 91% after six days, indicating that isolation of the oxidized compound should be feasible. In contrast, only 67% and 51% of the oxidized species of **2** can be detected after 3 and 6 d, respectively.[21] Due to this

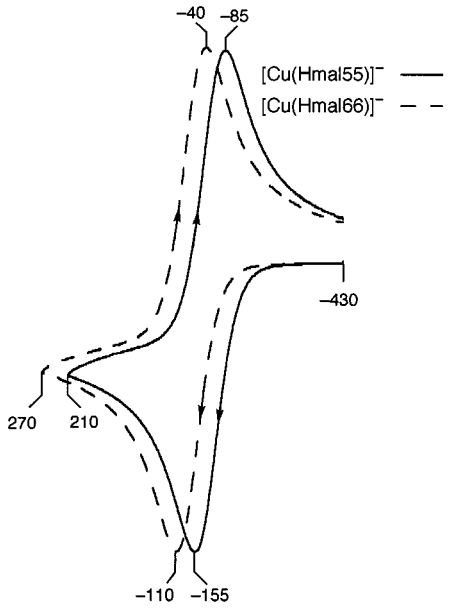


Figure 5. Cyclic voltammograms (50 mV/s) of **1** (solid line) and **2** (dashed line) at a Pt-foil electrode in acetonitrile at room temperature; peak potentials in mV vs. Fc/Fc^+ redox couple are indicated

apparent instability, no isolation of the oxidation product of **2** was attempted.

In water containing 0.05 M $NEt_4(ClO_4)$ as supporting electrolyte, the oxidation potentials for **1** and **2** were determined to be 750 and 770 mV vs. NHE, respectively. The electrochemical behavior of the complexes in water is, however, less ideal than that in acetonitrile, as demonstrated by the peak current ratio and by the incipient appearance of adsorption phenomena for the oxidation product of **1**. Addition of NEt_4OH effectuates a shift of the potential of **2** by 60 mV to a more negative value, indicating that the coordinated ligand looses its bridging proton in a more basic medium. However, the shape of the electrochemical response demonstrates decomposition of the oxidized species; for **1** oxidation was no longer observed upon addition of base; this means that the stability of the fully deprotonated copper(II) complex $[Cu(mal55)]^{2-}$ is very limited in water.

Preparation of Copper(III) Complexes

Indeed, consecutive coulometric oxidation of complex **1** in acetonitrile, evaporation of the acetonitrile, and recrystallization of the obtained residue from toluene/hexane affords analytically pure product. The elemental analysis of the compound is consistent with its formulation as [Cu(Hmal55)] (**3**). The IR spectrum of **3** is very similar to that of **1** except that the features corresponding to the counter cation NEt_4^+ are now absent. For the purpose of comparing spectroscopic data, solutions of the oxidation product of **2** were electrochemically generated in situ and, in light of the apparent instability of the oxidized species, immediately used for the respective measurements.

Structure of the Copper(III) Complex [Cu(Hmal55)]

A crystal structure determination was carried out on a single crystal of **3**. A perspective view of the complex is presented in Figure 6. In Table 1 some selected bond lengths and angles of compound **3** are compared to those of the reduced complex. Overall, the ligand environment, as well as the coordination geometry at the center ion, is preserved upon oxidation of **1**. The copper ion in **3** deviates by approximately the same amount (0.073 Å) from the least-squares N_4-plane as in **1** and also the dihedral angles between opposing CuN_2-planes are still under 6.5°. The structure analysis provides evidence that the H-bridging between the oxime oxygen atoms still persists in complex **3**. Compared to complex **1**, the Cu−N distances are reduced by 0.05 Å, indicating metal-centered oxidation. The decrease of the copper-donor atom bond lengths upon oxidation of the metal ion is, however, considerably smaller than that observed in other square-planar copper(II)/copper(III) couples with acyclic ligands.[2,3,5] In our opinion, the modest reduction of Cu−N bond lengths, despite the loss of a strongly σ-antibonding electron, can be attributed to the pseudo-macrocyclic nature of the coordinated ligand, which does not allow a tighter enclosure of the metal ion by the ligand without introduction of steric strain on the ligand backbone. A closer inspection of the structural parameters of the ligand reveals no major differences between complex **1** and **3** except that the ruffling of macrocyclic ring seems to be a little bit more pronounced in the oxidized complex. This observation is also manifested by the rather small decrease of the interatomic O−O distance between the oxime oxygen atoms from 2.427 ±0.005 Å in **1** to 2.400 Å in **3**. The $Cu^{III}-N_{amide}$ bond length of 1.860 Å is at the high end of the range of values observed for a bond length between a copper(III) ion and a deprotonated amide nitrogen donor atom.[2−5]

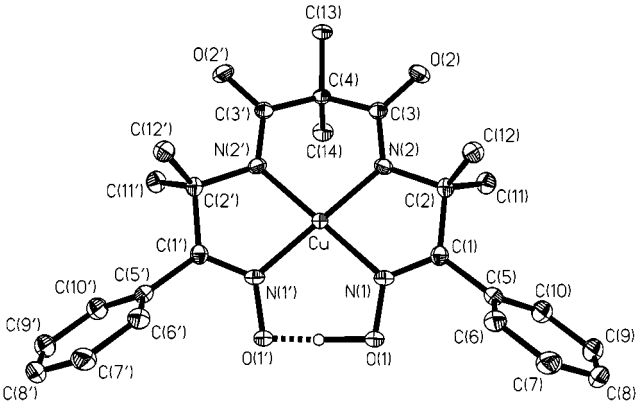


Figure 6. Perspective view of the structure of [Cu(Hmal55)] (**3**) showing thermal ellipsoids at 50% probability and the atom-numbering scheme. The location of the hydrogen atom which asymmetrically bridges both oxime oxygen atoms is disordered over two positions; the present view shows only one of these positions

As previously noticed for other amidato copper(III) complexes,[2−5] in response to the higher positive charge on the copper ion upon oxidation, the partial double bond charac-

ter of the C−N bond in the deprotonated amide function is reduced in order to provide the amide nitrogen atom with a higher negative charge. Thus, the average C−N and C−O bond lengths change from 1.325 and 1.240 Å in **1** to 1.358 and 1.233 Å in **3**, respectively. The strengthening of the C−O bond upon oxidation of the metal ion is accompanied by an increase of the C=O stretching frequency by 28 cm^{-1} in the IR spectra.

Spectroscopic Properties of the Copper(III) Complex

The diamagnetism of complex **3** which would be expected for a complex with a copper(III) ion is confirmed by NMR spectroscopy. The NMR spectrum of **3** in CD_2Cl_2 clearly establishes that the ligand is still bound to the metal ion in its triply deprotonated form, i.e. the oxime oxygen atoms are still bridged by a proton. A similar result is obtained when the oxidation product of **2** is examined by NMR spectroscopy immediately after its electrochemical generation.

Addition of a base like triethylamine to a solution of complex **3** in deuterated acetonitrile or dichloromethane seems to cause deprotonation of the oxime group, which is, however, accompanied by decomposition reaction(s) of the complex.

Intense absorption bands with extinction coefficients between 1000 and 8000 M^{-1} cm^{-1} are present in the visible regions of the electronic absorption spectra of both oxidized complexes (Figure 7). These bands are tentatively attributed to LMCT transitions. In general, two strong absorption bands are observed in the spectra of copper(III) peptide complexes at 260−280 nm and at 380−400 nm attributed to the σ and π N(peptide)-to-copper(III) charge transfer transitions, respectively.[1,22] Copper(III) imine-oximate complexes yield a LMCT band between 515 and 581 nm. The absorption bands in the electronic absorption spectra of the complexes [Cu(Hmal55)] and [Cu(Hmal66)] occur at rather similar energies. Except for the intense band around 773 nm for [Cu(Hmal66)], the visible regions in the spectra of both oxidized complexes resemble each other. The reason for the additional appearance of an intense band around 773 nm for [Cu(Hmal66)] is attributed to a LMCT transition involving the phenylene moieties of the ligand. Such LMCT transition are likely to occur with the oxidized copper ion in [Cu(Hmal66)], since here the sp^2-hybridized donor atoms are part of π-molecular orbital systems extending over the phenylene units.

Comparison of Redox Potentials

In Figure 8a, the redox potentials of compounds **1** and **2** are compared with those of some selected copper complexes in aqueous solutions. With the exception of complex **12**,[8a] all complexes contain at least two deprotonated amide functions as ligand donor groups, while complexes **1**, **2**, and **12** possess two vicinal dioximate ligand donor groups as a common feature.

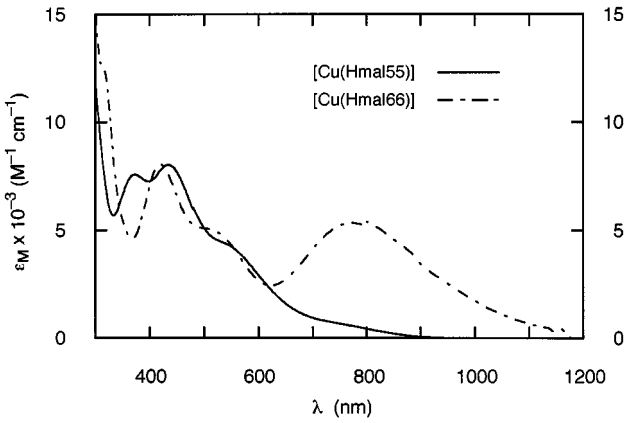


Figure 7. Electronic absorption spectra of a solution of [Cu(Hmal55)] (**3**) and an electrochemically generated solution of [Cu(Hmal66)] in acetonitrile

Complexes **4**−**12**[8a,19b,23−26] have the same square-planar CuN_4 coordination environment as complexes **1** and **2**. In addition, complexes **1**−**10** all contain a malondiamide bridge in the ligand.[19b,23,24] The type of nitrogen donor group of the two other coordination sites causes the potential to vary by approximately 0.7 V. Thus, a relatively high redox potential (1.34 V) is achieved with π-acceptor ligand donor functions such as pyridine units (**4**),[23] while the introduction of further negatively charged donor groups in addition to the two already provided by the malondiamide unit affords low potentials (e.g. complex **10**).[19b] In accordance to this general trend, the redox potentials of **1** and **2** lie between those complexes containing amine donor groups[19b,23,24] in addition to the malondiamide moiety and that of complex **10**.

The effect of the ring size of the macrocycle on the redox potential is illustrated by the complexes **6**, **8**, and **9**, which contain fifteen-, fourteen-, and thirteen-membered rings, respectively.[19b,24] Thus, the copper(III) ion is best accommodated by a small ring size, as demonstrated by the low redox potential. A similar trend is also observed in complexes with acyclic ligands where the lowest redox potentials are found with 5-5-5 fused ring systems.[23] In general agreement with this tendency, the redox potential of **2**, containing a sixteen-membered pseudo-macrocyclic ring, is 20 to 45 mV (depending on the employed solvent) higher than that of **1**, in which the pseudo-macrocyclic ring is fourteen-membered. Thus, the difference in the redox potential of 45 mV observed in acetonitrile corresponds to a 4.3 kJ mol^{-1} stabilization of the trivalent oxidation state relative to the divalent oxidation state upon changing the ring size of the pseudo-macrocycle from sixteen in **2** to fourteen in **1**. The long-term instability of the oxidation product of **2** is very likely also related to the facts that the cavity in the sixteen-membered macrocyclic ring is too large to accommodate the rather small copper(III) ion and that the already substantially ruffled ligand in copper(II) complex **2** cannot sustain any further ruffling in order to reduce the cavity size after the oxidation of the metal ion.

With respect to the dioximato complex **12**,[8b] the redox potential of complex **1**, which possesses the same pseudo-

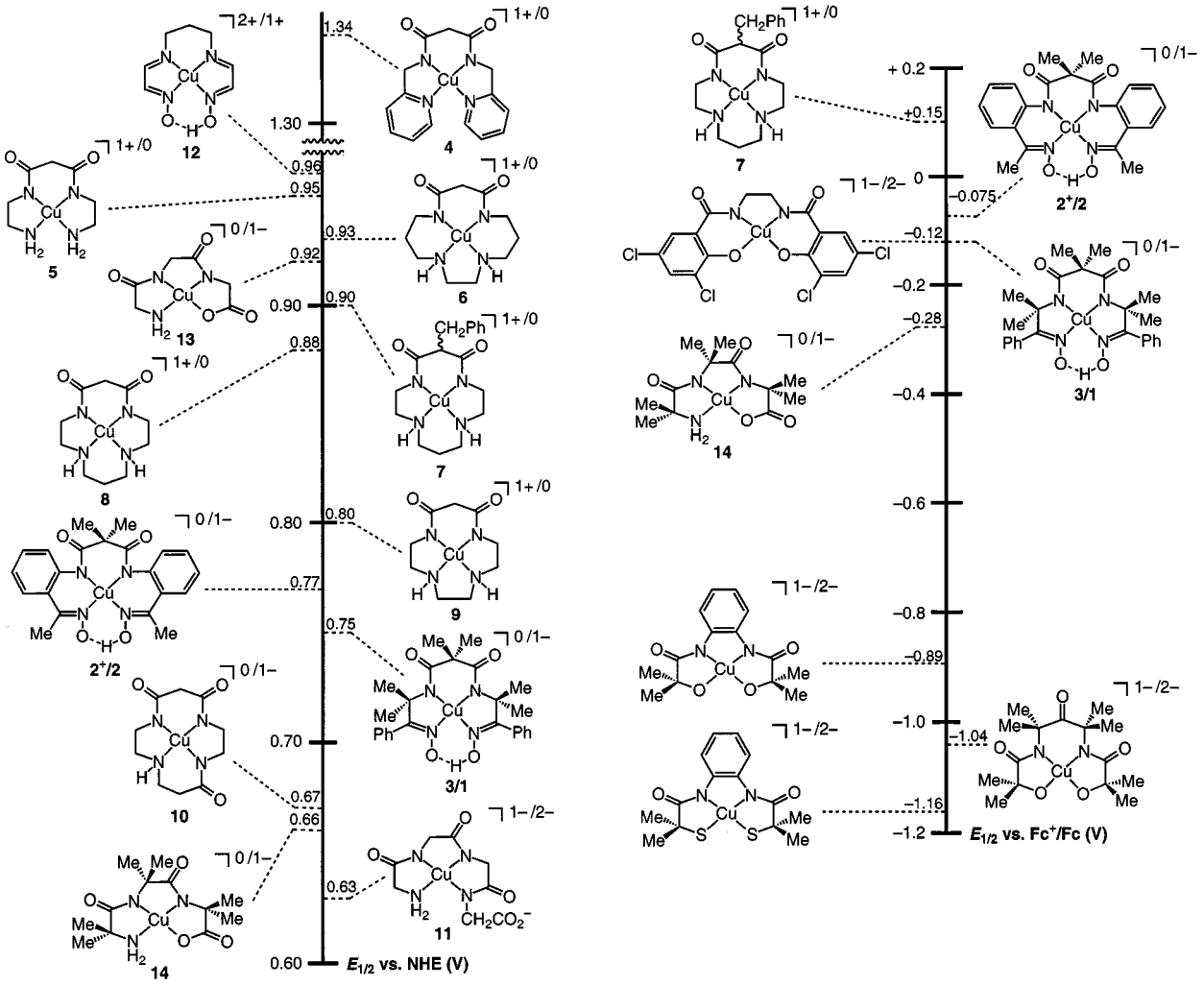


Figure 8. Schematic presentation of the redox potentials of **1** and **2** compared to those of related Cu^{III}/Cu^{II} redox couples in a) water (left) and b) acetonitrile (right). Data are taken from this work and other investigations[3,4,8a,19b,23−26]

macrocyclic ring size, is lowered by more than 200 mV. This substantial decrease is a testimony of the considerable stabilizing influence that two deprotonated amide functions exert on the high oxidation state of copper ions.

The redox properties of copper(II) peptide complexes were extensively surveyed by Margerum and coworkers.[25][26] The copper(II) complex of the triply deprotonated triglycine ligand (**13**) with a CuN_3O coordination environment is oxidized at 0.92 V.[25] Substitution of all hydrogen atoms by methyl groups (cf. **14**) causes a substantial decrease of the Cu^{III}/Cu^{II} redox potential.[26] The presence of methyl groups in α-position to ligand donor atoms may therefore be regarded as another contributing factor to the stabilization of the oxidized complex **3**.

In Figure 8b, the influence on the Cu^{III}/Cu^{II} redox potential of various donor types in combinations with two deprotonated amide donor functions is examined for square planar copper complexes dissolved in acetonitrile. Granting that chelate ring sizes are not always comparable for these complexes, a general trend, however, can still be discerned. Thus, the stabilizing influence of donor groups on the trivalent oxidation state increases in the order amine[24] < oximate ≈ phenolate[4] < deprotonated amide[26] < alcoholate[4] < alkylthiolate.[3]

Conclusion

Two novel ligands containing two amide and two oxime donor groups were synthesized and their coordination properties were investigated with copper ions. The structure analyses reveal a square-planar coordination geometry around the copper(II) ion in the solid state; this geometry is preserved upon dissolving the complexes in acetonitrile, as indicated by spectroscopic and electrochemical methods. While both amide nitrogen atoms are deprotonated, only one oxime donor group is deprotonated upon coordination of the ligand. The residual oxime hydrogen atom bridges the two *vicinal* oxime oxygen atoms, thereby furnishing the ligand with a pseudo-macrocyclic appearance.

Special emphasis was given to the investigation of the redox properties of the complexes. Thus, both copper(II) compounds can be oxidized to their corresponding copper(III) oxidation states. However, only the oxidation prod-

uct of complex **1** displays sufficient stability to be isolated, resulting in the first structural characterization of a copper(III) complex containing oximes donor functions in its ligand sphere. The coordination geometry around the copper(III) ion is essentially the same as in the reduced complex.

Experimental Section

Methods: ^{1}H-NMR: Varian Gemini 200 and Bruker AM 360, TMS as internal standard. − UV-vis: Varian Cary 5 E. − IR: Perkin-Elmer 1720 FT-IR. − ESR: Bruker ESP 300E. The ESR spectra were analyzed with the programs ESR V1.0 of Frank Neese (Diploma, University of Konstanz, June 1993) and SimFonia 1.2 of Bruker. − Electrochemistry: PAR Model 270 Research Electrochemistry Software controlled Potentiostat/Galvanostat Model 273A with the electrochemical cell placed in a glovebox. Electrochemical experiments were performed on 1−2 mM acetonitrile solutions containing 0.2 M $(Bu_4N)ClO_4$ as supporting electrolyte unless otherwise mentioned; a higher than normal electrolyte concentration was applied to minimize solution resistance. All potentials were measured vs. a SCE reference electrode at 25°C. The potentials were not corrected for junction potentials. A Pt-foil electrode was employed as the working electrode. Under these conditions the potential for the ferrocene/ferrocenium ion couple was 0.43 V. Coulometric experiments were performed using a Pt-gauze electrode. − Magnetic susceptibilities: Johnson Matthey Magnetic Susceptibility Balance at room temperature. The values for the diamagnetic susceptibilities of the ligands and the other components of the complexes were taken from the literature.[27] − Chemical analyses: Chemical analyses were carried out by the analytical laboratory of the authors′ institute and by H. Kolbe, Mülheim.

Preparation of Ligands and Complexes. − Materials: 2-Aminoacetophenone (Aldrich), dimethylmalonic acid (Merck), copper(II)-acetate monohydrate (Riedel), and tetraethylammonium acetate tetrahydrate (Fluka) were purchased from the indicated sources and used without further purification. Dimethylmalonyl dichloride[28] and 2-amino-2-methylpropiophenone hydrochloride[29] were prepared according to previously published procedures.

***N,N′*-Bis[2-(1-hydroxyimino-2-methyl-1-phenyl)propyl]dimethylmalondiamide Hemihydrate (H_4mal55 × 0.5 H_2O). − (a) *N,N′*-Bis[2-(2-methyl-1-oxo-1-phenyl)propyl]dimethylmalondiamide Monohydrate:** At room temperature, dimethylmalonyl dichloride (2.5 g, 15 mmol) was added dropwise to a stirred solution containing 2-amino-2-methylpropiophenone hydrochloride (7.2 g, 36 mmol) and triethylamine (10.4 mL, 75 mmol) in dichloromethane (150 mL). Stirring of the reaction mixture was continued for 12 h. After the addition of water (30 mL), dichloromethane was added until a clear solution was produced. The organic phase was separated and subsequently washed with 2 N HCl (200 mL), saturated sodium carbonate solution, and water before it was dried over $MgSO_4$. Removal of the solvent in vacuo yielded the product as a white solid (4.8 g, 73% yield) which was further recrystallized in EtOH in order to obtain an analytically pure sample. − $C_{25}H_{32}N_2O_5$ (440.54): calcd. C 68.16, H 7.32, N 6.36; found C 68.21, H 7.38, N 6.58. − ^{1}H NMR (200 MHz, $[D_6]Me_2SO$): δ = 0.92 (s, CH_3, 6 H), 1.43 (s, CH_3, 12 H), 7.32−7.56 (m, Ph−H, 6 H), 7.89 (d, Ph−H, 4 H), 8.00 (s, N−H, 2 H). − IR (KBr): $\tilde{\nu}$ = 3344, 1684, 1644, 1514, 1466, 1447, 1385, 1258, 1217, 1174, 1160, and 718 cm^{-1} (strong bands only). −

b) *N,N′*-Bis[2-(1-hydroxyimino-2-methyl-1-phenyl)propyl]dimethylmalondiamide Hemihydrate: A suspension consisting of *N,N′*-Bis[2-(2-methyl-1-oxo-1-phenyl)propyl]dimethylmalondiamide monohydrate (2.2 g, 5.0 mmol) and hydroxylammonium chloride (14 g, 201 mmol) in pyridine (150 mL) was stirred for 12 h at 60°C. After removal of the solvent in vacuo, the resulting solid was redissolved in chloroform (200 mL). The chloroform solution was first washed with water (200 mL), then three times with 2 N HCl (100 mL) and finally with water (100 mL). After drying the solution over $MgSO_4$, the solvent was evaporated in vacuo to yield the product (1.7 g, 74% yield) as a white solid. − $C_{25}H_{33}N_4O_{4.5}$ (461.56): calcd. C 65.06, H 7.21, N 12.14; found C 65.02, H 7.00, N 11.83. − ^{1}H NMR (200 MHz, $[D_6]Me_2SO$): δ = 1.03 (s, CH_3, 6 H), 1.42 (s, CH_3, 12 H), 7.02−7.07 (m, Ph−H, 4 H), 7.25−7.37 (m, Ph−H, 6 H), 7.95 (s, 2 H), 10.57 (s, 2 H). − IR (KBr): $\tilde{\nu}$ = 3456, 3312, 2983, 2933, 1663, 1644, 1539, 1512, 1455, 1444, 1420, 1387, 1358, 1216, 1014, 959, 771, 723, and 705 cm^{-1} (strong bands only).

***N,N′*-Bis[2-(1-hydroxyiminoethyl)phenyl]dimethylmalondiamide Monohydrate (H_4mal66 · H_2O). − (a) *N,N′*-Bis[2-(1-oxoethyl)phenyl]dimethylmalondiamide:** Dimethylmalonyl dichloride (2.02 g, 12 mmol) was slowly dropped into a solution of 2-aminoacetophenone (6.48 g, 48 mmol) in absolute toluene (50 mL) at 0°C. The reaction mixture was warmed to room temperature and stirred for 3 h. The resulting solid was collected by filtration and washed twice with toluene (30 mL). Afterwards, the solid was resuspended under intense stirring for 20 min in an aqueous solution (400 mL) saturated with sodium hydrogen carbonate. After filtration, the solid was washed with copious amounts of water and dried in vacuo at room temperature. Recrystallization of the raw product (3.02 g, 69% yield) from glacial acetic acid yields analytically pure product as a white solid. − $C_{21}H_{22}N_2O_4$ (366.42): calcd. C 68.84, H 6.05, N 7.65; found C 68.54, H 6.25, N 7.62. − ^{1}H NMR (200 MHz, $[D_6]Me_2SO$): δ = 1.62 (s, CH_3, 6 H), 2.65 (s, CH_3, 6 H), 7.23 (ddd, Ph−H_c, 2 H, J_{ac} = 1.0 Hz, J_{bc} = 7.2 Hz, J_{cd} = 8.1 Hz), 7.63 (ddd, Ph−H_b, 2 H, J_{ab} = 8.6 Hz, J_{bc} = 7.2 Hz, J_{bd} = 1.4 Hz), 8.08 (dd, Ph−H_d, 2 H, J_{bd} = 1.4 Hz, J_{cd} = 8.1 Hz), 8.55 (dd, Ph−H_a, 2 H, J_{ab} = 8.6 Hz, J_{ac} = 1.0 Hz), 11.92 (s, N−H, 2 H). − IR (KBr): $\tilde{\nu}$ = 3215, 1668, 1655, 1607, 1584, 1517, 1479, 1452, 1441, 1384, 1364, 1355, 1314, 1298, 1251, 1226, 1167, 1150, 1122, 961, 910, 762, and 605 cm^{-1} (strong bands only).

(b) *N,N′*-Bis[2-(1-hydroxyiminoethyl)phenyl]dimethylmalondiamide Monohydrate: Using a similar procedure as in the synthesis of *N,N′*-Bis[2-(1-hydroxyimino-2-methyl-1-phenyl)propyl]dimethylmalondiamide hemihydrate, *N,N′*-Bis[2-(1-hydroxyiminoethyl)-phenyl]dimethylmalondiamide monohydrate was prepared in a 90% yield (3.11 g) in the form of a white solid from *N,N′*-bis[2-(1-oxoethyl)phenyl]dimethylmalondiamide (3.02 g, 8.3 mmol) and hydroxylammonium chloride (21 g, 302 mmol) in pyridine (180 mL). An analytically pure sample was obtained by recrystallization from ethanol. − $C_{21}H_{26}N_4O_5$ (414.46): calcd. C 60.86, H 6.32, N 13.52; found C 60.53, H 6.53, N 13.67. − ^{1}H NMR (200 MHz, $[D_6]Me_2SO$): δ = 1.55 (s, CH_3, 6 H), 2.20 (s, CH_3, 6 H), 7.16 (ddd, Ph−H_c, 2 H, J_{ac} = 1.1 Hz, J_{bc} = 7.6 Hz, J_{cd} = 7.7 Hz), 7.34 (ddd, Ph−H_b, 2 H, J_{ab} = 8.1 Hz, J_{bc} = 7.6 Hz, J_{bd} = 1.4 Hz), 7.54 (dd, Ph−H_d, 2 H, J_{bd} = 1.4 Hz, J_{cd} = 7.7 Hz), 8.27 (dd, Ph−H_a, 2 H, J_{ab} = 8.1 Hz, J_{ac} = 1.1 Hz), 11.01 (s, 2 H), 11.52 (s, 2 H). − IR (KBr): $\tilde{\nu}$ = 3368, 2925, 1664, 1624, 1580, 1526, 1447, 1394, 1369, 1310, 1295, 1270, 1246, 1124, 1009, 922, and 756 cm^{-1} (strong bands only).

(NEt_4)[Cu(Hmal55)] (1): A solution was prepared from H_4mal55 × 0.5 H_2O (231 mg, 0.5 mmol), tetraethylammonium acetate tetrahydrate (261 mg, 1.0 mmol), and copper(II) acetate monohydrate (100 mg, 0.5 mmol) in absolute ethanol (50 mL). After the reaction mixture was heated at reflux for a short time, the solvent was com-

Table 3. Summary of Crystal Data, Intensity Collection and Refinement Parameters for (NEt_4)[Cu(Hmal55)]·0.5 Et_2O (**1**), (NEt_4)[Cu(Hmal66)] (**2**), and [Cu(Hmal55)] (**3**)

Data	**1**	**2**	**3**
formula	$C_{35}H_{54}CuN_5O_{4.5}$	$C_{29}H_{41}CuN_5O_4$	$C_{25}H_{29}CuN_4O_4$
M_r [g mol^{-1}]	680.37	587.21	513.06
crystal dimensions [mm]	0.5 × 0.3 × 0.2	0.6 × 0.5 × 0.5	0.7 × 0.7 × 0.03
crystal system	triclinic	monoclinic	orthorhombic
space group	$P\bar{1}$ (No.2)	$P2_1/c$ (No.14)	*Pnma* (No.62)
Z	4	4	4
a [Å]	13.317(4)	10.893(3)	9.886(2)
b [Å]	16.311(6)	9.745(2)	25.613(8)
c [Å]	19.162(7)	28.194(8)	9.081(3)
α [deg]	100.42(3)	90	90
β [deg]	102.78(3)	96.86(2)	90
γ [deg]	112.79(2)	90	90
V [Å^3]	3574(2)	2971(1)	2299(1)
ρ_{calc} [g cm^{-3}]	1.264	1.313	1.482
diffractometer	Hilger & Watts	Syntex $P2_1$	Enraf-Nonius-CAD4
temperature [K]	153	293	153
λ [Å]	0.71073(Mo-K_α)	0.71073(Mo-K_α)	1.54178(Cu-K_α)
μ [cm^{-1}]	6.56	7.76	16.78
F(000)	1456	1244	1072
scan method	ω-2Θ	ω-2Θ	ω-2Θ
2Θ limits	2.3° ≤ 2Θ ≤ 50.1°	5.1° ≤ 2Θ ≤ 55.1°	6.9° ≤ 2Θ ≤ 152.8°
unique reflections	12444	6851	2481
reflections with $F_o > 4\,\sigma(F_o)$	8259	4518	2134
number of variables (restraints)	810(5)	438(0)	166(0)
GooF on F^2 [a]	1.089	1.120	1.100
R (wR^2),% [a,b,c]	7.05 (17.21)	4.92 (12.56)	5.32 (14.63)

[a] For all reflections with $F_o > 4\,\sigma(F_o)$. − [b] $R = \Sigma||F_o| - |F_c|| / \Sigma |F_o|$. − [c] $wR^2 = \{\Sigma [w (F_o^2 - F_c^2)^2] / \Sigma [w (F_o^2)^2] \}^{1/2}$.

pletely removed in vacuo. The residue was treated with acetonitrile (40 mL) and the resulting red solution was filtered. Slow diffusion of ether into the acetonitrile solution afforded analytically pure product in the form of orange-red needles, which, upon standing, easily lost the ether molecules incorporated in the crystal lattice (234 mg, 73% yield). − $C_{33}H_{49}CuN_5O_4$ (643.33): calcd. C 61.61, H 7.68, N 10.89; found C 61.31, H 7.68, N 10.81. − Absorption spectrum (acetonitrile): λ_{max} (ε_M) 509 (84,4), 405 (141), 260 (sh, 14100), 225 (sh, 25700), and 203 (42500) nm. − IR (KBr): $\tilde{\nu}$ = 2968, 1589, 1493, 1451, 1393, 1362, 1341, 1320, 1199, 1173, 1151, 1089, 1036, 1018, 1010, 923, 886, 825, 785, 737, 699, 656, and 537 cm^{-1} (strong bands only).

(NEt_4)[Cu(Hmal66)] (2): In a procedure similar to that described for the synthesis of complex **1**, complex **2** was prepared from H_4mal66 × H_2O (207 mg, 0.5 mmol), tetraethylammonium acetate tetrahydrate (261 mg, 1.0 mmol), and copper(II) acetate monohydrate (100 mg, 0.5 mmol) as dark red blocks (202 mg, 69% yield). − $C_{29}H_{41}CuN_5O_4$ (587.22): calcd. C 59.32, H 7.04, N, 11.93; found C 59.30, H 7.06, N 11.93. − Absorption spectrum (acetonitrile): λ_{max} (ε_M) 547 (307), 430 (sh, 501), 310 (sh, 9790), 272 (35500), 251 (sh, 30000), and 223 (24200) nm. − IR (KBr): $\tilde{\nu}$ = 2985, 2950, 1617, 1597, 1586, 1573, 1481, 1439, 1394, 1350, 1304, 1262, 1245, 1174, 1083, 1000, 957, 942, 867, 841, 772, 765, 744, and 530 cm^{-1} (strong bands only).

[Cu(Hmal55)] (3): A solution of (NEt_4)[Cu(Hmal55)] (163 mg, 0.25 mmol) in acetonitrile (20 mL) containing 0.1 M $NaClO_4$ as supporting electrolyte was oxidized at +0.08 V vs Fc/Fc^+ in an electrochemical cell placed in a glove box. The electrolysis was carried out at a platinum net electrode with a PAR Model 273A Potentiostat/Galvanostat controlled by the PAR Model 270 Research Electrochemistry Software. After the oxidation was completed, the solvent was completely removed in vacuo. The solid was treated with toluene (30 mL) and the resulting dark red-brown solution was filtered. Hexane (120 mL) was layered upon the solution. Slow mixing of the two layers by diffusion afforded analytically pure product in the form of dark red blocks (64.5 mg, 51% yield). − $C_{25}H_{29}CuN_4O_4$ (513.08): calcd. C 58.52, H 5.70, N 10.92; found C 58.38, H 5.76, N 10.88. − ^{1}H NMR (360 MHz, CD_2Cl_2): δ = 1.36 (s, CH_3, 6 H), 1.64 (s, CH_3, 12 H), 7.27 (m, Ph−H, 6 H), 7.48 (m, Ph−H, 4 H), 16.68 (s, N=OH, 1 H). − Absorption spectrum (acetonitrile): λ_{max} (ε_M) 700 (sh, 944), 533 (sh, 4460), 436 (8030), 373 (7590), 279 (17700), and 242 (15900) nm. − IR (KBr): $\tilde{\nu}$ = 2986, 2937, 1617, 1593, 1560, 1452, 1394, 1371, 1362, 1351, 1224, 1200, 1124, 879, 747, and 700 cm^{-1} (strong bands only).

Solutions of [Cu(Hmal66)]: For the purpose of comparing spectroscopic data, solutions of the oxidation product of **2** in acetonitrile were electrochemically generated in situ at an applied potential of 0.125 V vs Fc/Fc^+ and, in light of the apparent instability of the oxidized species, immediately used for the respective measurements. Absorption spectrum (acetonitrile): λ_{max} (ε_M) 773 (5350), 500 (sh, 5100), 420 (8040), 313 (sh, 12600), 269 (35200), and 243 (35400) nm.

Crystal Structure Analyses of the Copper Complexes: Table 3 contains the cell parameters of the crystals and experimental details on the data collections and structure refinements. The positions of the non-hydrogen atoms were determined by SHELXS 86[30] and by Fourier difference maps using the program SHELXL-93 (**1** and **2**) or SHELXL-97 (**3**).[30] The structural parameters were refined with the program SHELXL-93 or SHELXL-97, using F^2 of all symmetry-independent reflections except those with very negative F^2-values. Empirical absorption correction on the data set of **3** was applied by using the program DIFABS. All non-hydrogen atoms were refined anisotropically unless stated otherwise. The ether molecule in **1**·0.5 Et_2O is disordered and the atoms of this crystal solvent are therefore ill defined, resulting in large temperature factors and somewhat distorted bond lengths. The non-hydrogen atoms of this molecule were therefore refined isotropically. The tetraethylammonium cation in **2** is disordered and was modeled by two separate

molecules. Half of the complex **3** is related to the other half by a symmetry plane passing through the copper atom and the atoms of the dimethylmethylene group of the dimethylmalondiamide unit. Hydrogen atoms were assigned idealized locations and their isotropic temperature factors were refined, except for those bound to the oxime oxygen atoms in **1**, in which complex the positions and the isotropic temperature factors were refined. The locations of the hydrogen atoms which asymmetrically bridge both oxime oxygen atoms in **2** and **3** are disordered over two positions.

The largest peaks (holes) in the final difference Fourier maps correspond to 1.13 (−1.12) e $Å^{-3}$, 0.56 (−0.45) e $Å^{-3}$, and 0.68 (−0.67) e $Å^{-3}$ for structures analyses of **1**, **2**, and **3**, respectively.

Crystallographic data (excluding structure factors) for the structures reported in this paper have been deposited with the Cambridge Crystallographic Data Center as supplementary publication no. CCDC-101423. Copies of the data can be obtained free of charge on application to The Director, CCDC, 12 Union Road, Cambridge CB2 1EZ, UK (Fax: Int. code +44 (1223) 336-033; E-mail: deposit@chemcrys.cam.ac.uk).

Acknowledgments

We thank the Deutsche Forschungsgemeinschaft for financial support.

[1] [1a] D. W. Margerum, *Pure Appl. Chem.* **1983**, *55*, 23−34. − [1b] D. W. Margerum, G. D. Owens, *Met. Ions Biol. Syst.* **1981**, *12*, 75−132.
[2] L. L. Diaddario, W. R. Robinson, D. W. Margerum, *Inorg. Chem.* **1983**, *22*. 1021−1025.
[3] J. Hanss, H.-J. Krüger, *Angew. Chem.* **1996**, *108*, 2989−2991; *Angew. Chem. Int. Ed. Engl.* **1996**, *35*, 2827−2830.
[4] F. C. Anson, T. J. Collins, T. G. Richmond, B. D. Santarsiero, J. E. Toth, B. G. R. T. Treco, *J. Am. Chem. Soc.* **1987**, *109*, 2974−2979.
[5] P. J. M. W. L. Birker, *Inorg. Chem.* **1977**, *16*, 2478−2482.
[6] A. Chakravorty, *Coord. Chem. Rev.* **1974**, *13*, 1−46.
[7] [7a] R. S. Drago, E. I. Baucom, *Inorg. Chem.* **1972**, *11*, 2064−2069. − [7b] A. Chakravorty, *Isr. J. Chem.* **1985**, *25*, 99−105. − [7c] G. Sproul, G. D. Stucky, *Inorg. Chem.* **1973**, *12*, 2898−2902. − [7d] J.-M. Bemtgen, H.-R. Gimpert, A. von Zelewski, *Inorg. Chem.* **1983**, *22*, 3576−3580.
[8] [8a] Y. Sulfab, N. I. Al-Shatti, *Inorg. Chim. Acta* **1984**, *87*, L23−L24. − [8b] Y. Suflab, M. A. Hussein, N. I. Al-Shatti, *Inorg. Chim. Acta* **1982**, *67*, L33−L34.
[9] [9a] D. Luneau, H. Oshio, H. Okawa, S. Kida, *Chem. Lett.* **1989**, 443−444. − [9b] H. Okawa, M. Koikawa, S. Kida, D. Luneau, H. Oshio, *J. Chem. Soc., Dalton Trans.* **1990**, 469−475. − [9c] D. Luneau, H. Oshio, H. Okawa, S. Kida, *J. Chem. Soc., Dalton Trans.* **1990**, 2283−2286. − [9d] D. Luneau, H. Oshio, H. Okawa, M. Koikawa, S. Kida, *Bull. Chem. Soc. Jpn.* **1990**, *63*, 2212−2217. − [9e] P. Chaudhuri, M. Winter, B. P. C. Della Védova, E. Bill, A. Trautwein, S. Gehring, P. Fleischhauer, B. Nuber, J. Weiss, *Inorg. Chem.* **1991**, *30*, 2148−2157. − [9f] R. Ruiz, J. Sanz, B. Cervera, F. Lloret, M. Julve, C. Bois, J. Faus, M. C. Muñoz, *J. Chem. Soc., Dalton Trans.* **1993**, 1623−1628. − [9g] F. Birkelbach, M. Winter, U. Flörke, H.-J. Haupt, C. Butzlaff, M. Lengen, E. Bill, A. X. Trautwein, K. Wieghardt, P. Chaudhuri, *Inorg. Chem.* **1994**, *33*, 3990−4001. − [9h] R. Ruiz, F. Lloret, M. Julve, M. C. Muñoz, C. Bois, *Inorg. Chim. Acta* **1994**, *219*, 179−186. − [9i] P. Chaudhuri, M. Winter, U. Flörke, H.-J. Haupt, *Inorg. Chim. Acta* **1995**, *232*, 125−130.
[10] O. Kahn, *Struct. Bonding (Berlin)* **1987**, *68*, 89−167.
[11] H.-J. Krüger, G. Peng, R. H. Holm, *Inorg. Chem.* **1991**, *30*, 734−742.
[12] [12a] A. M. Duda, A. Karaczyn, H. Kozlowski, I. O. Fritsky, T. Glowiak, E. V. Prisyazhnaya, T. Y. Sliva, J. Swiatek-Kozlowska, *J. Chem. Soc., Dalton Trans.* **1997**, 3853−3859. − [12b] C. O. Onindo, T. Y. Sliva, T. Kowalik-Jankowska, I. O. Fritsky, P. Buglyo, L. D. Pettit, H. Kozlowski, T. Kiss, *J. Chem. Soc., Dalton Trans.* **1995**, 3911−3915.
[13] J. Hanss, H.-J. Krüger, *Angew. Chem.* **1998**, *110*, 366−369; *Angew. Chem. Int. Ed. Engl.* **1998**, *37*, 360−363.
[14] T. J. Collins, *Acc. Chem. Res.* **1994**, *27*, 279−285.
[15] [15a] H. C. Freeman, M. R. Taylor, *Acta Crystallogr., Sect. B* **1965**, *18*, 939−952. − [15b] T. Toki, M. Mikuriya, H. Okawa, I. Murase, S. Kida, *Bull. Chem. Soc. Jpn.* **1984**, *57*, 2098−2105.
[16] [16a] J. A. Bertrand, J. H. Smith, D. G. VanDerveer, *Inorg. Chem.* **1977**, *6*, 1484−1488. − [16b] E. Frasson, R. Bardi, S. Bezzi, *Acta. Crystallogr.* **1959**, *12*, 201−205. − [16c] O. P. Anderson, C. M. Perkins, K. K. Brito, *Inorg. Chem.* **1983**, *22*, 1267−1273.
[17] J. Peisach, W. E. Blumberg, *Arch. Biochem. Biophys.* **1974**, *165*, 691−708.
[18] A. B. P. Lever, *Inorganic Electronic Spectroscopy*, 2nd ed., Elsevier, Amsterdam, **1984**, 554−572.
[19] Using a nonisothermal cell, the Cu^{III}/Cu^{II} redox potential shifts by maximally +10 mV upon changing the temperature from −30 to +30°C. If preferential axial coordination of solvent molecules to the copper(II) ion occurs, shifts of −30 to −50 mV are expected: [19a] M. P. Youngblood, D. W. Margerum, *Inorg. Chem.* **1980**, *19*, 3068−3072. − [19b] E. Kimura, T. Koike, R. Machida, R. Nagai, M. Kodama, *Inorg. Chem.* **1984**, *23*, 4181−4188.
[20] E. L. Solomon, K. W. Penfield, D. E. Wilcox, *Struct. Bond. (Berlin)* **1983**, *53*, 1−57.
[21] The absorption bands in the spectra of the copper(III) complexes vanish over time without new characteristic absorption bands appearing. The resulting spectra do not resemble those of the respective original copper(II) complexes indicating, that decomposition of the complexes has occurred.
[22] A. W. Hamburg, D. W. Margerum, *Inorg. Chem.* **1983**, *22*, 3884−3893.
[23] T. Sakurai, J.-I. Hongo, A. Nakahara, Y. Nakao, *Inorg. Chim. Acta* **1980**, *46*, 205−210.
[24] L. Fabbrizzi, A. Perotti, A. Poggi, *Inorg. Chem.* **1983**, *22*, 1411−1412.
[25] F. P. Bossu, K. L. Chellappa, D. W. Margerum, *J. Am. Chem. Soc.* **1977**, *99*, 2195−2203.
[26] S. T. Kirksey, Jr., T. A. Neubecker, D. W. Margerum, *J. Am. Chem. Soc.* **1979**, *101*, 1631−1633.
[27] [27a] *Landolt-Börnstein Vol II/10* (6th edition) (Eds.: K.-H. Hellwege, A. M. Hellwege), Springer Verlag, Berlin, **1967**. − [27b] *Landolt-Börnstein New Series Vol II/8 Supplement 1* (Eds.: K.-H. Hellwege, A. M. Hellwege), Springer Verlag, Berlin, **1976**.
[28] I. Smedley, *J. Chem. Soc.* **1910**, *97*, 1475−1494.
[29] S. Gabriel, *Chem. Ber.* **1911**, *44*, 57−69.
[30] *SHELXS-86*: Crystal Structure Solution Program, G. M. Sheldrick, Göttingen, **1986**. G. M. Sheldrick, in *Crystallographic Computing 3*; G. M. Sheldrick, C. Krüger, R. Goddard, Eds.; Oxford University Press, **1985**; pp. 175. − *SHELXL-93*: Crystal Structure Refinement Program, G. M. Sheldrick, Göttingen, **1993**. − *SHELXL-97*: Crystal Structure Refinement Program, G. M. Sheldrick, Göttingen, **1997**.

Received May 8, 1998
[I98144]

The Deprotonated Iminophosphorane *o*-$C_6H_4PPh_2P{=}NSiMe_3$ as a Novel Chelating Ligand in Organocopper(I) and -zinc(II) Chemistry

Stefan Wingerter,[a] Heinz Gornitzka,[b] Guy Bertrand,[b] and Dietmar Stalke*[a]

Dedicated to Professor Edgar Niecke on the occasion of his 60th birthday

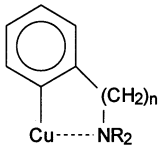
Keywords: P Ligands / N Ligands / Copper / Zinc / Structure elucidation

Lithiation of triphenyl(trimethylsilylimino)phosphorane $Ph_3P{=}NSiMe_3$ with MeLi gives the *ortho*-metallated species $[Li(o\text{-}C_6H_4PPh_2NSiMe_3)]_2{\cdot}Et_2O$ (**1**), which exhibits all the requirements of an organometallic ligand capable of side-arm donation. The deprotonated *ortho*-phenyl carbon atom gives access to metal–carbon σ bonds in transmetallation reactions, while the $Ph_2P{=}NSiMe_3$ moiety can donate to the same metal center through the imine nitrogen atom. In transmetallation reactions with CuBr, the dimeric organocopper complex $[Cu(o\text{-}C_6H_4PPh_2NSiMe_3)]_2$ (**2**) is obtained, while application of $ZnCl_2$ yields the monomeric zinc complex $[Zn(o\text{-}C_6H_4PPh_2NSiMe_3)_2]$ (**3**). Reaction with $CuCl_2$ gives access to the new diiminophosphorane $(o\text{-}C_6H_4PPh_2NSiMe_3)_2$ (**4**) through oxidative coupling at the *ortho* positions. In all the metal complexes, the $Ph_2P{=}NSiMe_3$ residue acts as a side-arm donating group through the nitrogen atom. The intermolecular N→Cu donor bond in **2** is as short as copper–amide bonds, while the N→Zn bond lengths in **3** are in the region normally found for donor bonds. Compound **4** is a molecule, possessing two $Ph_2P{=}NSiMe_3$ moieties bridged by a biphenylene group.

Introduction

Since the landmark synthesis of $LiCuMe_2$ in 1952,[1] the application of organocopper reagents in organic synthesis has continued to increase exponentially.[2] Among the d-block metals, Cu^I species play the most prominent role in regio- and stereoselective synthesis.[3] The growing number of cuprates and organocopper compounds characterized by X-ray structure analysis is clearly evident.[4] Organocopper(I) compounds CuR are generally encountered as polynuclear species, which exist either as discrete aggregates or as polymers. Transformation of these aggregates and polymers into units of lower nuclearity can either be achieved by employing very bulky groups R, or by the action of suitable Lewis bases.[5] N, P, O, or S donor centers, as well as alkynes, have been reported to stabilize copper(I) species in low aggregation states.[6] The combination of both approaches leads to the side-arm donation concept pioneered by van Koten.[7] α-Metallated aryl ligands are substituted with $R_2N(CH_2)_n$ amido groups, permitting intramolecular complexation (Scheme 1).

In the compounds discussed in this paper, the $R_2N[CH_2]_n$ amido group is formally replaced by an $Me_3SiN{=}PPh_2$ imido group within the deprotonated triphenyl(trimethylsilylimino)phosphorane $Ph_3P{=}NSiMe_3$.



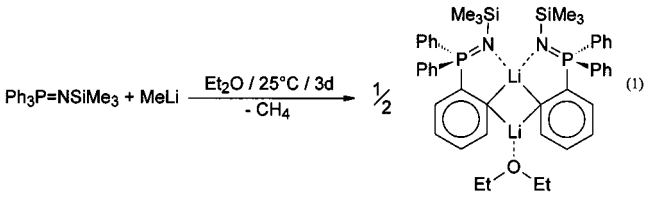
Scheme 1

The lithiation and reactivity of the trimethyl(trimethylsilylimino)phosphorane $Me_3P{=}NSiMe_3$ has been studied previously by Schmidbaur et al.[8] and the structure of the $[LiCH_2(Me_2)P{=}NSiMe_3]_4$ tetramer was recently determined by Dehnicke et al.[9] In analogy to this lithiation, the reaction of triphenyl(trimethylsilylimino)phosphorane $Ph_3P{=}NSiMe_3$ with MeLi gives $[Li(o\text{-}C_6H_4PPh_2\text{-}NSiMe_3)]_2{\cdot}Et_2O$ (**1**) according to Equation 1.[10] The C_2-symmetric dimer contains a tetrahedrally coordinated and a trigonal-planarly coordinated lithium atom. The tripyridyl(trimethylsilylimino)phosphorane $Py_3P{=}NSiMe_3$ reacts completely differently. In a reductive coupling reaction of the substituents, the phosphorus(V) center is reduced to phosphorus(III), substituted by one pyridyl, one methyl, and an Me_3SiN group. The P−N double bond in the starting material is thus converted into a single bond (Equation 2).[10]

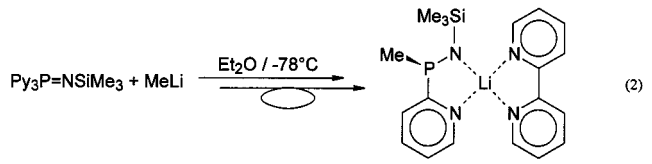
We embarked on the synthesis of organometallic compounds using lithiated triphenyl(trimethylsilylimino)phosphorane, $[Li(o\text{-}C_6H_4PPh_2NSiMe_3)]_2{\cdot}Et_2O$ (**1**), as a starting material, as this species exhibits all the requirements of a ligand capable of side-arm donation. The deprotonated *ortho*-phenyl carbon atom should give access to metal−carbon σ bonds in transmetallation reactions, while the $Ph_2P{=}NSiMe_3$ moiety should be capable of donation to the same metal center through the imine nitrogen atom.

[a] Institut für Anorganische Chemie der Universität Würzburg, Am Hubland, D-97074 Würzburg, Germany
Fax: (internat.) + 49(0)931/888-4619
E-mail: dstalke@chemie.uni-wuerzburg.de
[b] CNRS Laboratoire de Chimie de Coordination, Université Paul Sabatier de Toulouse,
205, route de Narbonne, F-31077 Toulouse Cedex, France

 © WILEY-VCH Verlag GmbH, D-69451 Weinheim, 1999 1434−1948/99/0101−0173 $ 17.50+.50/0



1



2

Results and Discussion

Preparation of 2−4

As synthetically important metals, we decided to employ monovalent Cu^{I} and divalent Zn^{II} and Cu^{II}. In a transmetallation reaction of $[Li(o\text{-}C_6H_4PPh_2NSiMe_3)]_2{\cdot}Et_2O$ (**1**) with CuBr, the dimeric organocopper complex $[Cu(o\text{-}C_6H_4PPh_2NSiMe_3)]_2$ (**2**) was obtained (Equation 3). Transmetallation using $ZnCl_2$ yielded the monomeric zinc complex $[Zn(o\text{-}C_6H_4PPh_2NSiMe_3)_2]$ (**3**) (Equation 4), while reaction with $CuCl_2$ led to the new diiminophosphorane $(o\text{-}C_6H_4PPh_2NSiMe_3)_2$ (**4**) as a result of oxidative coupling at the *ortho* positions (Equation 5).

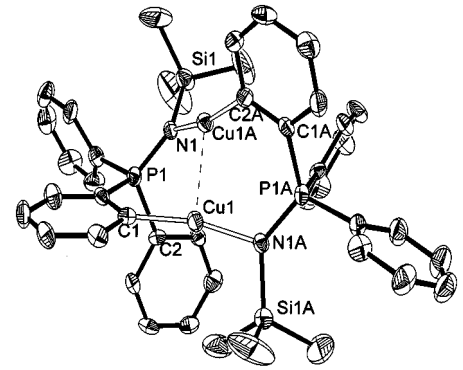
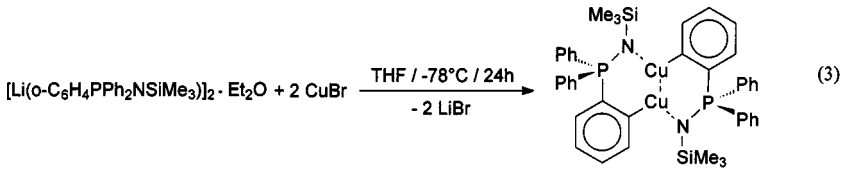


Figure 1. Solid-state structure of $[Cu(o\text{-}C_6H_4PPh_2NSiMe_3)]_2$ (**2**); anisotropic displacement parameters are depicted at the 50% probability level

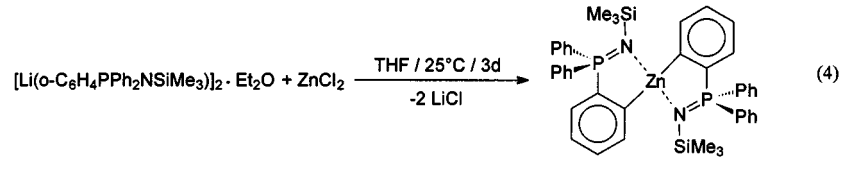
Crystal Structure of $[Cu(o\text{-}C_6H_4PPh_2NSiMe_3)]_2$ (2)

In the organocopper complex $[Cu(o\text{-}C_6H_4PPh_2NSiMe_3)]_2$ (**2**), both lithium atoms of the C_2-symmetric starting material are replaced by copper atoms to give a C_i-symmetric dimer (Figure 1).

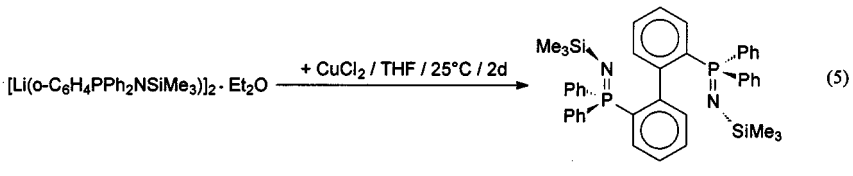
Each copper atom is coordinated to an *ortho*-carbon atom and the nitrogen atom of the $Ph_2P{=}NSiMe_3$ side-arm of a second ligand. Hence, this moiety acts as an intermolecular rather than as an intramolecular donor function. The Cu−C distance in **2** is 190.5(5) pm (Table 1), which is comparable with the Cu−C(aryl) bond length determined in monomeric $Me_2SCuC_6H_3$-2,6-bis(2,4,6-triisopropylphenyl) [Cu−C: 189.4(6) pm].[11] Both distances fall at the short end of the range observed in organocopper com-



2



3



4

pounds (mean Cu−C: 205.5 pm).[12] On average, the Cu−C(alkyl) distances appear to be slightly longer, because an sp^2 carbon atom is about 4 pm smaller than an sp^3 carbon atom.[13] The dinuclear organylcopper complex $[CuC(SiMe_3)_2C_5H_4N]_2$ shows almost the same structural motif as complex **2**. However, the Cu−C(alkyl) bond length in the former complex is 195.0(4) and 195.4(2) pm[14] in $[CuLi\{CH(Me)P(Et)_2NSiMe_3\}_2]$.[15] The Cu−N distances in both complexes are very similar; 191.1(4) pm in **2** and 191.0(3) pm in $[CuC(SiMe_3)_2C_5H_4N]_2$. Both values correspond very closely to the value of Cu−N distances in secondary copper amides $[CuNR_2]_4$, which is generally close to 191 pm.[12][16] Hence, the Cu−imide donor bond in **2** is as short as a Cu−amide bond. The latter is probably extended by the higher coordination number at the copper centers (coordination number 4−6) compared to the coordination number 2 at the copper center in **2**. Although the P=N bond [159.1(4) pm] in **2** is 2.9 pm longer than that in the starting material **1** [156.2(3) pm][10] and 4.9 pm longer than that in the parent iminophosphorane $Ph_3P{=}NSiMe_3$ [154.2(2) pm],[17] the distance falls within the range normally observed in iminophosphoranes (147−162 pm).[18]

The Cu···Cu distance of 248.79(14) pm in complex **2** is rather short, both as a consequence of the bite of the bridging chelating ligand,[19] which forces the metal centers into close proximity, as well as metal d^{10}-d^{10} closed-shell attraction.[20] Although this distance is not remarkably short (in comparison with 240.3(2) pm in $[Li(thf)_4][Cu_5Cl_4\{Si(SiMe_3)_3\}_2]$[21] and 236.9(1) pm in $[Cu_2\{Si(SiMe_3)_3\}_2BrLi(thf)_3]$[22]), the non-linear C···Cu−N angle of 167.8(2)° clearly indicates metal−metal interaction. This angle is caused by a close metal−metal contact. One would expect the metals to be pushed further out of the center (i.e. further away from the center of inversion located in the middle of the Cu···Cu vector) and a bend of the C−Cu−N unit in the opposite direction if there was no "sticky" interaction. This could easily be achieved by rotation of the metallated phenyl rings about the P−C(*ipso*) bonds. Steric requirements do not constrain the tilt of the two monomeric units and the observed lean would be maximized if the two metal cations were to favour separation.

Organozinc Compounds

The chemistry of organozinc compounds has a long history. They are used as intermediates in organic synthesis, specifically as mild alkylation or arylation agents in organometallic reactions. Organozinc reagents are generally less reactive than Grignard reagents, a property that is a distinct advantage when more gentle reaction conditions are required.[23] Furthermore, they do not tend to associate via μ_2-bridging alkyl or aryl groups like organocopper compounds. All known diarylzinc compounds are colourless solids made up of monomeric units, and are of good to moderate solubility in apolar organic solvents. Diorganozinc compounds bearing functional groups can be divided into two categories, i.e. compounds bearing substituents that do not interact directly with the central zinc atom, and compounds in which coordination of the heteroatoms of the substituents is observed.

Crystal Structure of $[Zn(o\text{-}C_6H_4PPh_2NSiMe_3)_2]$ (3)

The complex $[Zn(o\text{-}C_6H_4PPh_2NSiMe_3)_2]$ (**3**) belongs to the second group, because the two nitrogen atoms of the two $Ph_2P{=}NSiMe_3$ side-arms coordinate to the zinc atom. Hence, the o-$C_6H_4PPh_2NSiMe_3$ substituent in **3** is closely related to other bidentate monoanionic C,N-chelating ligands.[24]

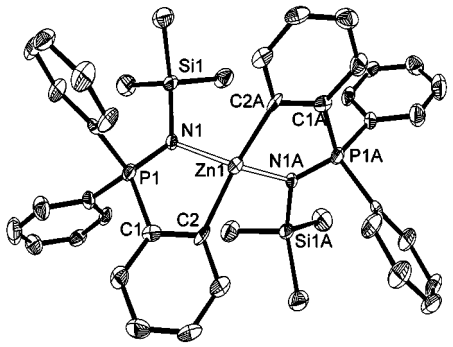


Figure 2. Solid-state structure of $[Zn(o\text{-}C_6H_4PPh_2NSiMe_3)_2]$ (**3**); anisotropic displacement parameters are depicted at the 50% probability level

The zinc atom in **3** is tetrahedrally coordinated by both carbon and nitrogen atoms of the two ligands. The metal atom resides at a center of inversion. The Zn−C distance in **3** [200.8(5) pm, Table 1] is comparable with the Zn−C distances in other diarylzinc species (194.9−201.2 pm).[25] Zn−N distances span a wide range from 182 to 232 pm.[13][26] The Zn−N dative bond in **3** measures 215.8(4) pm and is thus considerably longer than Zn−N bonds in zinc amides (182 pm for $[Zn\{N(SiMe_3)_2\}_2]$ in the gas phase[27]). In the structure of $[HZnN(Me)C_2H_4NMe_2]_2$,[28] the two zinc−amide bonds within the central Zn_2N_2 four-membered ring are 206.1 pm in length, while the two Zn←$N(Me_2)$R donor bonds measure 218.6 pm. The P=N bond in **3** [157.4(4) pm] is 1.7 pm shorter than that in **2** [159.1(4) pm].

The Coupling Product $[(o\text{-}C_6H_4PPh_2NSiMe_3)_2]$ (4)

The application of oxidative coupling to generate C−C bonds via organocopper compounds has a venerable history.[7] A large number of CuR and $CuLiR_2$ species bearing alkyl or functionalized alkyl, alkenyl, alkynyl, aryl or heteroaryl groups have been oxidatively dimerized to the symmetrical coupling products RR.[29] These oxidations have been accomplished by using $CuCl_2$, O_2 or nitrobenzene. In general, the best yields have been obtained employing $CuCl_2$ as the oxidizing reagent. Numerous reactions have been reported in which copper(II) salts have been treated with organometallic compounds [MR] to give organocopper(I) compounds [CuR] and reductive coupling products

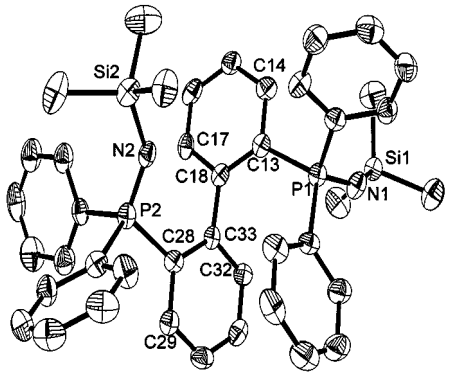


Figure 3. Solid-state structure of (o-$C_6H_4PPh_2NSiMe_3)_2$ (**4**); anisotropic displacement parameters are depicted at the 50% probability level

RR (reactions in which the CuX_2:MR molar ratio is 1:2). Reactions of species containing several M−C bonds in close proximity, such as $[Li_nR_n]$ or MgR_2 with CuX_2 afford exclusively the reductive elimination product RR. Thus, it was not surprising that we obtained the coupling product (o-$C_6H_4PPh_2NSiMe_3)_2$ (**4**) from the reaction of [Li(o-$C_6H_4PPh_2NSiMe_3$)]$_2$·Et_2O (**1**) with $CuCl_2$.

In **4**, the distances are almost identical to the corresponding distances in the iminophosphorane $Ph_3P{=}NSiMe_3$.[9] It is worthy of note that the two symmetry-independent P−N−Si angles in the iminodiphosphorane **4** are significantly different [P1−N1−Si1: 145.1(3)° and P2−N2−Si2: 138.7(3)°, see Figure 3, Table 1], as a result of the steric demand of the bulky groups.

In 1,1′-phosphorus-substituted biphenylenes, the central C2−C2′ distances range from 146.8 to 153.3 pm.[12] The $P-C_{biphenylene}$ distances are found between 182.0 and 187.5 pm, the angles P−C1−C2 vary from 114.5 to 124.2°, and the P−C1−C6 angles from 115.7 to 125.1°. The corresponding distances in **4** are 149.3(7) pm for the C2−C2′ distance of the biphenylene (C18−C33 in Figure 3), and 181.9(6) and 184.6(5) pm for the $P-C_{biphenylene}$ distances (P2−C28 and P1−C13), while the angles amount to 122.9(4) and 127.5(4)° (P−C1−C2) (P2−C28−C33 and P1−C13−C18), and 117.9(4) and 112.2(4)° (P−C1−C6) (P2−C28−C29 and P1−C13−C14). It seems worthy of note that the extreme values for the bond angle of 127.5(4)° and the angle of 112.2(4)° do not fall within the range previously observed in 1,1′-P-substituted biphenylenes. The best planes of the two phenyl rings of the biphenylene unit intersect at an angle of 64.7°.

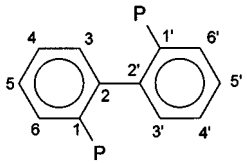


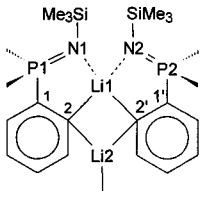
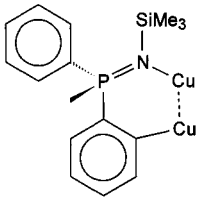
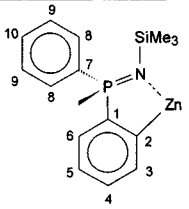
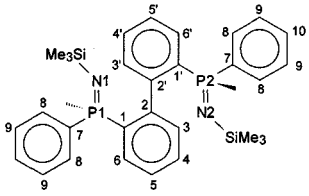
Figure 4

In conclusion, the transmetallation of the *ortho*-lithiated triphenyl(trimethylimino)phosphorane [Li(o-$C_6H_4PPh_2$-$NSiMe_3$)]$_2$·Et_2O gives access to side-arm *N*-donating chelating ligands in organometallic chemistry. The nitrogen donor bond can be as short as a metal−amide bond, as observed in the dimeric copper(I) complex.

Experimental Section

All experiments were performed under nitrogen, either by using modified Schlenk techniques or in a drybox. Solvents were freshly

Table 1. Selected bond lengths [pm] and angles [°] of **2**−**4** compared to those in the starting material **1**

	1 (M = Li)	2 (M = Cu)	3 (M = Zn)	4
				
M–C:	Li1–C2: 233.1(5) Li2–C2: 213.8(6) Li1–C2': 226.3(5) Li2–C2': 212.0(6)	190.7(5)	200.8(5)	–
M–N:	Li1–N1: 203.7(5) Li2–N2: 202.7(4)	191.2(4)	215.8(4)	–
P–N:	P1–N1: 156.2(2) P2–N2: 156.2(3)	159.3(4)	157.4(4)	153.7(5) 153.3(5)
average P–C:	181.2(3)	180.5(6)	181.0(5)	182.9(6)
P–C1:	P1–C1: 180.2(2) P2–C1': 180.4(3)	180.6(6)	181.2(5)	P1–C1: 184.6(5) P1–C1': 181.9(6)
P–N–Si:	P1–N1–Si1: 135.18(13) P2–N2–Si2: 133.47(13)	131.7(3)	127.4(2)	P1–N1–Si1: 145.1(3) P2–N2–Si2: 138.7(3)
N–P–C:	N1–P1–C1: 109.81(11) N2–P2–C1': 110.98(11)	115.0(2)	107.8(2)	N1–P1–C1: 115.1(2) N2–P2–C1': 112.7(2)
M–N–P:	Li1–N1–P1: 107.5(2) Li1–N1–P1: 41.79(11) Li1–N2–P2: 107.9(2) Li1–N2–P2: 41.42(11)	120.4(2)	108.0(2)	–
M–N–Si:	Li1–N1–Si1: 117.3(2)	107.7(2)	120.0(2)	–

distilled from a sodium/potassium alloy prior to use. – ^{1}H-, ^{13}C-, ^{29}Si- and ^{31}P-NMR spectra were recorded in [D_8]THF or C_6D_6 solution using a Bruker AM 250, a Bruker MSL 400 or a Bruker AMX 400 spectrometer. – IR spectra were recorded as Nujol mulls with a Perkin-Elmer 283 spectrometer. – Melting (decomposition) points were determined by using a Laboratory Devices MEL TEMP II melting point apparatus. – EI mass spectra were measured with Finnigan MAT 8230 or Varian MAT CH5 instruments. – Elemental analyses were performed by the analytical laboratory of the Departments of Inorganic Chemistry at Göttingen and Würzburg.

[Li(*o*-$C_6H_4PPh_2NSiMe_3$)]$_2$·OEt_2 (1) was prepared by reaction of $Ph_3P{=}NSiMe_3$ with MeLi in diethyl ether.[10]

[Cu(*o*-$C_6H_4PPh_2NSiMe_3$)]$_2$ (2): To [Li(*o*-$C_6H_4PPh_2NSiMe_3$)]$_2$·OEt_2 (**1**) (1.86 g, 2.37 mmol) in THF (20 ml), a suspension of CuBr (0.34 g, 2.37 mmol) in THF (20 ml) was added dropwise at −78°C. The light-yellow solution was allowed to warm to room temp. and was then stirred overnight. The reaction mixture turned deep yellow. The THF was removed in vacuo until the product precipitated. After filtration, yellow crystals suitable for X-ray analysis were obtained from the mother liquor after storage for several weeks at room temp. Yield: 0.56 g (0.68 mmol, 28.7%); m.p. 148−175°C (decomp.). – IR (Nujol, KBr): $\tilde{\nu}$ = 2894 cm^{-1} (Si−CH_3), 1444 (P−Ph), 1363 (CH_3), 1243 ($SiMe_3$), 1092 (P=N), 965, 823, 711. – ^{1}H NMR (C_6D_6, room temp., TMS): δ = 0.34 (s, 18 H, $SiMe_3$), 6.98−7.73 (m, 28 H, Ph). – ^{13}C NMR (C_6D_6, room temp., TMS): δ = 4.4 (s, $SiMe_3$), 127.8−132.4 (m, Ph). – ^{31}P NMR (C_6D_6, room temp., 85% H_3PO_4): δ = −1.01. – MS (70 eV); *m/z* (%): 824 (2.0) [M^+], 681 (76) [M^+ − 2Cu − Me], 424 (86) [$(C_6H_4PPhN)_2Si$], 334 (100) [$C_6H_4PPh_2NSiMe_2$]. – $C_{42}H_{46}Cu_2N_2P_2Si_2$ (824.00): calcd. C 61.22, H 5.63, N 3.40; found C 61.33, H 5.48, N 3.24.

[Zn(*o*-$C_6H_4PPh_2NSiMe_3$)]$_2$ (3): A mixture of [Li(*o*-$C_6H_4PPh_2$-$NSiMe_3$)]$_2$·Et_2O (**1**) (1.50 g, 1.91 mmol) and $ZnCl_2$ (0.26 g, 1.91 mmol) was dissolved in THF (15 ml), and the pale-yellow solution was stirred for 3 d at room temp. The solvent was then removed in vacuo. Toluene (30 ml) was added to the residue and the mixture was stirred overnight. The insoluble LiCl was removed by filtration and the colourless mother liquor was concentrated until the product precipitated. THF was then added dropwise to redissolve the precipitate. The resulting clear solution was cooled to 0°C for 14 d to afford [Zn(*o*-$C_6H_4PPh_2NSiMe_3$)]$_2$ (**3**) as colourless crystals. The mother liquor was filtered and the solvent was removed from the filtrate in vacuo. The white residue was washed with pentane (30 ml) and dried in vacuo. Spectroscopic data of the crystals and the precipitate were identical. Total yield: 0.70 g (0.92 mmol, 48%); m.p. 234°C (decomp.). – IR (Nujol, KBr): $\tilde{\nu}$ = 2930 cm^{-1} (Si−CH_3), 1440 (P−Ph), 1385 (CH_3), 1261 ($SiMe_3$), 1098 (P=N), 1020, 801, 534. – ^{1}H NMR (C_6D_6, room temp., TMS): δ = 0.43 (s, 18 H, $SiMe_3$), 7.08 (m_c, 14 H), 7.36 (m_c, 4 H), 7.91 (m_c 8 H), 8.27 (d, $^3J_{3,4}$ = 7.0 Hz, 2 H, 3-H). – ^{13}C NMR (C_6D_6, room temp., TMS): δ = 4.7 (d, $^3J_{C\text{-}P}$ = 3.4 Hz, $SiMe_3$), 125.0−140.3 (m, Ph), 172.8 (dd, $^2J_{C\text{-}P}$ = 30.8 Hz, $^3J_{C\text{-}P}$ = 4.1 Hz, 2-P). – ^{29}Si NMR (C_6D_6, room temp., TMS): δ = −0.1 (d, $^2J_{Si\text{-}P}$ = 5.0 Hz). – ^{31}P NMR (C_6D_6, room temp., 85% H_3PO_4): δ = 21.8. – MS (70 eV); *m/z* (%): 763 (23) [M^+], 492 (47) [PPh_3NSiMe_3ZnPh], 488 (100) [$PPh_3NSiMe_3ZnNPSi$], 412 (60) [PPh_3NSiMe_3Zn], 334 (78) [PPh_3NSiMe_2], 318 (86) [PPh_3NSiMe]. – $C_{42}H_{46}N_2P_2Si_2Zn$ (762.30): calcd. C 66.18, H 6.08, N 3.67; found C 66.37, H 5.98, N 3.60.

(*o*-$C_6H_4PPh_2NSiMe_3$)$_2$ (4): A mixture of $CuCl_2$ (0.26 g, 1.93 mmol) and [Li(*o*-$C_6H_4PPh_2NSiMe_3$)]$_2$·Et_2O (**1**) (1.55 g, 1.97 mmol) was stirred in THF (30 ml) for 2 d at room temp. The solvents were then removed in vacuo, toluene (30 ml) was added to the residue, and the suspension was stirred for a further day. The precipitated material was removed from the mother liquor by filtration. The filtrate was concentrated in vacuo until the product precipitated, and then THF was added dropwise until the precipitate redissolved. After storage of the resulting solution at room temp. for 10 d, colourless crystals were obtained. These were filtered off and the

Table 2. Crystal data for **2**−**4**

	2	**3**	**4**
Formula	$C_{42}H_{46}Cu_2N_2P_2Si_2$	$C_{42}H_{46}N_2P_2Si_2Zn$	$C_{42}H_{46}N_2P_2Si_2$
Mol. mass	824.00	762.30	696.93
Cryst. size [mm]	0.2 × 0.2 × 0.1	0.5 × 0.4 × 0.3	0.5 × 0.4 × 0.3
Space group	$P4_32_12$ (no. 96)	*Pbcn* (no. 60)	$P2_1/c$ (no. 14)
a [pm]	1742.31(14)	1441.0(3)	1726.6(4)
b [pm]	1742.31(14)	1663.5(3)	1014.3(2)
c [pm]	1343.4(3)	1699.9(3)	2225.3(5)
β [°]	90	90	92.24(3)
V [nm^3]	4.0748(9)	4.0748(14)	3.8942(14)
Z	4	4	4
T [K]	173(2)	153(2)	153(2)
$\rho_{calcd.}$ [Mgm^{-3}]	1.343	1.243	1.189
μ [mm^{-1}]	1.212	0.771	0.205
F(000)	1712	1600	1480
2Θ range [°]	6−47	8−45	8−45
No. of reflns. measd.	5981	2313	5208
No. of unique reflns.	3095	2313	5066
No. of restraints	24	–	–
Refined param.	226	225	439
$R1$[a] [$I > 2\sigma(I)$]	0.0490	0.0475	0.0667
$wR2$[b] (all data)	0.0795	0.1114	0.1618
$g1$; $g2$[c]	0.0240; 0.0	0.0359; 7.5914	0.0445; 7.6971
Flack *x* param.	−0.01(2)	–	–
Highest diff peak [10^{-6} e pm^{-3}]	0.262	0.314	0.309
Absorpt. corr.	semi-empirical	–	–
Transm. min; max	0.7935; 0.8884		

[a] $R1 = \Sigma||F_o| - |F_c||/\Sigma|F_o|$. – [b] $wR2 = \{\Sigma[w(F_o^2 - F_c^2)^2/\Sigma[w(F_o^2)^2]\}^{1/2}$. – [c] $w = 1/[\sigma^2(F_o^2) + (g1 \cdot \mathbf{P})^2 + g2 \cdot \mathbf{P}]$; $P = (F_o^2 + 2F_c^2)/3$.

solvents were removed from the filtrate in vacuo. The pale-yellow residue was washed with pentane (30 ml) and dried in vacuo. Spectroscopic data of the crystals and the pale-yellow precipitate were identical. Total yield: 0.48 g (0.69 mmol, 35%); m.p. 179°C. – IR (Nujol, KBr): $\tilde{\nu}$ = 3051 cm^{-1} (Ar–CH), 2900 (Si–CH_3), 1442 (P–Ph), 1390 (CH_3), 1271 ($SiMe_3$), 1102 (P=N), 860, 826, 531, 516. – ^{1}H NMR ([D$_8$]THF, room temp., TMS): δ = –0.10 (d, $^4J_{H-P}$ = 0.45 Hz, 18 H, $SiMe_3$), 7.05 (m_c, 4 H), 7.27 (m_c, 10 H), 7.44 (m_c, 6 H), 7.72 (m_c, 8 H). – ^{13}C NMR ([D$_8$]THF, room temp., TMS): δ = 4.0 (d, $^3J_{C-P}$ = 3.3 Hz, $SiMe_3$), 127.2–145.4 (m, Ph). – ^{29}Si NMR ([D$_8$]THF, room temp., TMS): δ = –12.7 (d, $^2J_{Si-P}$ = 21.0 Hz). – ^{31}P NMR ([D$_8$]THF, room temp., 85% H_3PO_4): δ = 1.9. – MS (70 eV); *m/z* (%): 696 (8) [M^+], 681 (76) [$M^+ - CH_3$], 536 (37) [$M^+ - NSiMe_3PPh_2$], 424 (100) [$M^+ - NSiMe_3PPh_2$], 333 (46) [$Ph_3PNSiMe_2$]. – $C_{42}H_{46}N_2P_2Si_2$ (696.93): calcd. C 72.38, H 6.65, N 4.02; found C 72.67, H 6.43, N 3.99.

Crystallographic Measurements: Crystal data for structures **2**–**4** are presented in Table 2. Data of **2** were collected using an Enraf-Nonius CAD4 diffractomer and data of **3** and **4** were collected with a Stoe AED 2 diffractometer fitted with a classical scintillation counter using graphite-monochromated Mo-K_α radiation (λ = 0.71073 Å). All data were collected at low temperatures using oil-coated shock-cooled crystals.[30] A semiempirical absorption correction was applied for structure **2**.[31] The structures were solved by Patterson or direct methods using SHELXS-90.[32] All structures were refined by full-matrix least-squares procedures on F^2, using SHELXL-93.[33] All non-hydrogen atoms were refined anisotropically, and a riding model was employed in the refinement of the hydrogen atom positions. Although the anisotropic displacement parameters of the trimethylsilyl group in **2** indicate slight rotational disorder, refinement to split occupation sites of the methyl groups was not successful. The elongation of the anisotropic displacement parameter of the *ipso*-carbon atom C2 in **3** along the Zn–C bond is due to the lack of absorption correction. Unfortunatelly, the crystal of **3** decomposed right after data collection of the unique set. Further details of the structure investigation may be obtained from CCDC, 12 Union Road, Cambridge CB2 1EZ, U.K., on quoting the supplementary publication nos. CCDC-102400, -102401, -102402.

Acknowledgments

The authors would like to thank the Deutsche Forschungsgemeinschaft, the Fonds der Chemischen Industrie, the Stiftung Volkswagenwerk and the DAAD (PROCOPE German/French exchange program) for financial support. D. S. kindly acknowledges support of Bruker axs-Analytical X-ray Systems, Karlsruhe, and CHEMETALL, Frankfurt/Main.

[1] H. Gilman, R. G. Jones, L. A. Woods, *J. Org. Chem.* **1952**, *17*, 1630.
[2] For a review, see: B. H. Lipshutz, S. Sengupta, *Org. React.* **1992**, *41*, 135.
[3] [3a] N. Krause, A. Gerold, *Angew. Chem.* **1997**, *109*, 195; *Angew. Chem. Int. Ed. Engl.* **1997**, *36*, 186, and references therein. – [3b] G. Boche, F. Bosold, M. Marsch, K. Harms, *Angew. Chem.* **1998**, 110, 1779; *Angew. Chem. Int. Ed. Engl.* **1998**, *37*, 1684.
[4] [4a] G. van Koten, *J. Organomet. Chem.* **1990**, *400*, 283. – [4b] P. P. Power, *Prog. Inorg. Chem.* **1991**, *39*, 75. – [4c] G. van Koten, S. L. James, J. T. B. H. Jastrzebski in *Comprehensive Organometallic Chemistry II* (Eds.: E. W. Abel, F. G. A. Stone, G. Wilkinson), Pergamon, Oxford, **1995**, *3*, 57.
[5] See for example: [5a] S. Gambarotta, C. Floriani, A. Chiesi-Villa, C. Guastini, *J. Chem. Soc., Chem. Commun.* **1983**, 1156. – [5b] S. Gambarotta, S. Strologo, C. Floriani, A. Chiesi-Villa, C. Guastini, *Organometallics* **1984**, *3*, 1444. – [5c] D. M. Knotter, W. J. J. Smeets, A. L. Spek, G. van Koten, *J. Am. Chem. Soc.* **1990**, *112*, 5895. – [5d] B. Lenders, D. M. Grove, W. J. J. Smeets, P. van der Sluis, A. L. Spek, G. van Koten, *Organometallics* **1991**, *10*, 786. – [5e] X. He, M. M. Olmstead, P. P. Power, *J. Am. Chem. Soc.* **1992**, *114*, 9668.
[6] See for example: [6a] H. J. Küppers, K. Wieghardt, Y.-H. Tsay, C. Krüger, B. Nuber, J. Weiss, *Angew. Chem.* **1987**, *99*, 583; *Angew. Chem. Int. Ed. Engl.* **1987**, *26*, 575. – [6b] D. W. Stephan, *Coord. Chem. Rev.* **1989**, *95*, 41. – [6c] H. Maelger, F. Olbrich, J. Kopf, D. Abeln, E. Weiss, *Z. Naturforsch., B* **1992**, *47*, 1276. – [6d] D. L. Reger, M. F. Huff, *Organometallics* **1992**, *11*, 69.
[7] G. van Koten, J. G. Noltes, *Comprehensive Organometallic Chemistry* (Eds.: G. Wilkinson, F. G. A. Stone, F. W. Abel), Pergamon, Oxford **1982**, vol. 3, p. 709.
[8] H. Schmidbaur, G. Jonas, *Chem. Ber.* **1967**, *100*, 1120.
[9] A. Müller, B. Neumüller, K. Dehnicke, *Chem. Ber.* **1996**, *129*, 253.
[10] A. Steiner, D. Stalke, *Angew. Chem.* **1995**, *107*, 1908; *Angew. Chem. Int. Ed. Engl.* **1995**, *34*, 1752.
[11] B. Schiemenz, P. P. Power, *Organometallics* **1996**, *15*, 958.
[12] Cambridge Structural Database, May 1998 release; F. H. Allen, O. Kennard, *Chem. Des. Automation News* **1993**, *8*, 131.
[13] P. Rademacher in *Strukturen organischer Moleküle*, VCH, Weinheim, **1987**.
[14] [14a] R. I. Papasergio, C. L. Raston, A. H. White, *J. Chem. Soc., Chem. Commun.* **1983**, 1419. [14b] R. I. Papasergio, C. L. Raston, A. H. White, *J. Chem. Soc., Dalton. Trans.* **1987**, 3085.
[15] A. Müller, B. Neumüller, K. Dehnicke, *Angew. Chem.* **1997**, *109*, 2447; *Angew. Chem. Int. Ed. Engl.* **1997**, *36*, 2350.
[16] See for example: [16a] H. Hope, P. P. Power, *Inorg. Chem.* **1984**, *23*, 936. – [16b] S. Gambarotta, M. Bracci, C. Floriani, A. Chiesi-Villa, C. Guastini, *J. Chem. Soc., Dalton Trans.* **1987**, 1883. – [16c] H. Chen, M. M. Olmstead, S. C. Shoner, P. P. Power, *J. Chem. Soc., Dalton Trans.* **1992**, 451.
[17] F. Weller, H.-C. Kang, W. Massa, T. Rübenstahl, F. Kunkel, K. Dehnicke, *Z. Naturforsch., B* **1995**, *50*, 1050.
[18] E. Niecke, D. Gudat, *Angew. Chem.* **1991**, *103*, 251; *Angew. Chem. Int. Ed. Engl.* **1991**, *30*, 217.
[19] G. Nardin, L. Randaccio, E. Zangrando, *J. Organomet. Chem.* **1974**, *74*, C23.
[20] [20a] P. K. Mehrotra, R. Hoffmann, *Inorg. Chem.* **1978**, *17*, 2187. – [20b] P. Pyykkö, *Chem. Rev.* **1997**, *97*, 597. – [20c] P. Pyykkö, N. Runeberg, F. Mendizabal, *Chem. Eur. J.* **1997**, *3*, 1451. – [20d] P. Pyykkö, F. Mendizabal, *Chem. Eur. J.* **1997**, *3*, 1458.
[21] A. Heine, D. Stalke, *Angew. Chem.* **1993**, *105*, 90; *Angew. Chem. Int. Ed. Engl.* **1993**, *32*, 121.
[22] A. Heine, R. Herbst-Irmer, D. Stalke, *J. Chem. Soc., Chem. Commun.* **1993**, 1729.
[23] [23a] W. Oppolzer, *Angew. Chem.* **1989**, *101*, 39; *Angew. Chem. Int. Ed. Engl.* **1989**, *28*, 38. – [23b] A. Fürstner, *Synthesis* **1989**, 571. – [23c] K. Soai, S. Niwa, *Chem. Rev.* **1992**, *92*, 833.
[24] G. van Koten, *Pure Appl. Chem.* **1989**, *61*, 1681.
[25] [25a] V. W. Day, D. H. Campbell, C. J. Michejda, *J. Chem. Soc., Chem. Commun.* **1975**, 118. – [25b] M. Weidenbruch, M. Herrndorf, A. Schäfer, S. Pohl, W. Saak, *J. Organomet. Chem.* **1989**, *361*, 139. – [25c] P. R. Markies, G. Schat, O. S. Akkerman, F. Bickelhaupt, W. J. J. Smeets, A. L. Spek, *Organometallics* **1990**, *9*, 2243. – [25d] S. Brooker, N. Bertel, D. Stalke, M. Noltemeyer, H. W. Roesky, G. M. Sheldrick, F. T. Edelmann, *Organometallics* **1992**, *11*, 192.
[26] J. Dekker, J. Boersma, L. Fernholt, A. Haaland, A. L. Spek, *Organometallics* **1987**, *6*, 1202.
[27] A. Haaland, K. Hedberg, P. P. Power, *Inorg. Chem.* **1984**, *23*, 1972.
[28] N. A. Bell, P. T. Moseley, H. M. M. Shearer, C. B. Spencer, *J. Chem. Soc., Chem. Commun.* **1980**, 359.
[29] [29a] A. E. Jukes, *Adv. Organomet. Chem.* **1974**, *12*, 215. – [29b] G. H. Posner, *Org. React.* **1974**, *22*, 253.
[30] D. Stalke, *Chem. Soc. Rev.* **1998**, *27*, 171.
[31] A. C. T. North, D. C. Phillips, F. S. Mathews, *Acta Crystallogr., Sect. A* **1968**, *24*, 351.
[32] G. M. Sheldrick, *Acta Crystallogr., Sect. A* **1990**, *46*, 467.
[33] G. M. Sheldrick, *Program for Crystal Structure Refinement*, Universität Göttingen, **1996**.

Received July 29, 1998
[98249]

Reactions at the $N_2Ni(\mu_2\text{-}SR)_2NiN_2$ Core in Dinuclear Nickel(II) Amine-Thiolate Complexes

Berthold Kersting,*[a] Gunther Steinfeld,[a] and Julia Hausmann[a]

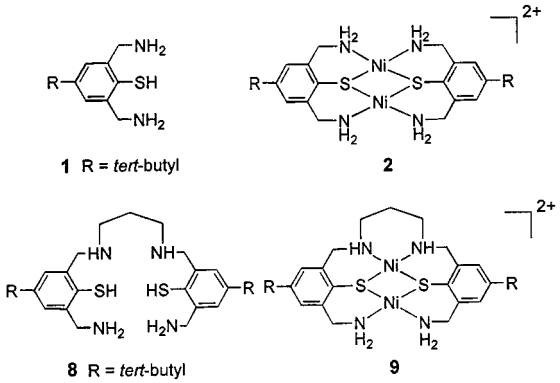
Keywords: Hexadentate N/S-ligand / Dinuclear complexes / Nickel / Redox chemistry

A discrete dinickel complex with a central $N_2Ni^{II}(\mu_2\text{-}SR)_2Ni^{II}N_2$ core has been synthesized and investigated in the context of ligand binding and oxidation state changes. Reaction of the hexadentate amine-thiolate ligand *N,N′*-bis-[2-thio-3-aminomethyl-5-*tert*-butylbenzyl]propane-1,3-diamine (**8**) with $Ni(ClO_4)_2 \cdot 6\ H_2O$ in methanol affords $[Ni^{II}_2\mathbf{8}][ClO_4]_2 \cdot 3\ CH_3OH$ (**9**), the structure of which has been determined by X-ray crystallography. Complex **9** contains a central $N_2Ni(\mu_2\text{-}SR)_2NiN_2$ core with two approximately planar *cis*-N_2S_2Ni coordination polyhedra bridged at the thiolate sulfur atoms. The *cis*-N_2S_2Ni units differ in that one nickel atom forms a six-membered chelate ring with the two secondary amine nitrogen atoms of **8** whereas the other nickel atom is bound to the remaining primary nitrogen atoms. Complex **9** binds a variety of substrates. Binding of anions to the $N_2Ni(\mu_2\text{-}SR)_2NiN_2$ core in **9** occurs selectively at the Ni atom bound to the secondary nitrogen atoms because of a slightly weaker ligand-field strength. This is demonstrated by X-ray structure determination of the isothiocyanate complex $[Ni^{II}_2\mathbf{8}(NCS)_2] \cdot MeOH$ (**10**) formed by the reaction of **9** with 2 equiv. of KSCN in methanol. Complex **10** is the first example of a complex with adjacent octahedral *cis*-N_4S_2Ni and planar *cis*-N_2S_2Ni sites. The overall dinuclear structure of the parent complex **9** is retained in **10**, except for *trans*-axially bound isothiocyanate ions at Ni(1) and an as yet unexplained inversion of configuration at both secondary amine nitrogen atoms. In DMF solution both complexes undergo two successive reductions at potentials of –0.95 V and –1.53 V vs SCE, assigned to the formation of mixed-valent $[Ni^{I}Ni^{II}\mathbf{8}]^{1+}$ and $[Ni^{I}_2\mathbf{8}]^{0}$ species, respectively. The similar electrochemical properties of **9** and **10** suggest that the *trans*-axially bound isothiocyanate ions in **10** are replaced by DMF molecules in DMF solution. Upon reduction, these solvent molecules decoordinate to produce an unsolvated $[Ni^{I}Ni^{II}\mathbf{8}]^{1+}$ species with two planar N_2S_2Ni units.

Introduction

Discrete first-row transition-metal complexes featuring central $M(\mu_2\text{-}SR)_xM$ cores ($x = 1-3$) have come under increased investigation in the past several years owing to their unusual electronic and magnetic properties[1] and their occurrence in biological systems.[2–4] There are numerous $M(\mu_2\text{-}SR)_2M$ type complexes,[5] which, for the most part, have been studied in attempts to mimic the bonding, spectral, and redox properties of the active site of certain metalloenzymes.[6–9] By contrast, chemical reactivity studies of such species are extremely rare because of the paucity of stable complexes.[10]

The apparent nonuniformity of dinuclear thiolate complexes of labile metal ions with mono- or bidentate thiolate ligands, especially in the solution state, renders desirable the synthesis of well-defined complexes by use of multidentate thiolate ligands containing additional donor atoms such as amine nitrogen or imine nitrogen atoms. However, the synthesis of such N/S-based ligands is a relatively recent development in coordination chemistry and often involves a multi-step reaction sequence. Thus, there are only few reports in which a $M(\mu_2\text{-}SR)_2M$ core is solely assembled by the donor atoms of a multidentate N/S based ligand. An early example of such a system involved the template synthesis of a dinuclear nickel amine-thiolate complex with formaldehyde and nitroethane in aqueous basic solution to give a hexadentate N_4S_2 ligand.[11] Since then the use of metal-directed template reactions between derivatives of 2,6-diformylthiophenol[12] and α,ω-diamines has been an important new source of macrocyclic Schiff-base ligands containing imine nitrogen and thiolate sulfur donor atoms.[13,14]



Scheme 1. Structures of ligands and complexes **1**, **2**,[15] **8**, and **9**

Recently we reported the syntheses and characterization of dinuclear, dithiolate-bridged nickel complexes of the tridentate amine-thiolate ligand **1** (see Scheme 1).[15] The dicationic nickel complex **2**, for example, was found to react with another one equivalent of the ligand, resulting in the

[a] Institut für Anorganische und Analytische Chemie, Universität Freiburg
Albertstrasse 21, D-79104 Freiburg, Germany
Fax: (internat.) +49 (0)761/ 203-6001
E-mail: kerstber@sun2.ruf.uni-freiburg.de

 © WILEY-VCH Verlag GmbH, D-69451 Weinheim, 1999 1434–1948/99/0101–0179 $ 17.50+.50/0

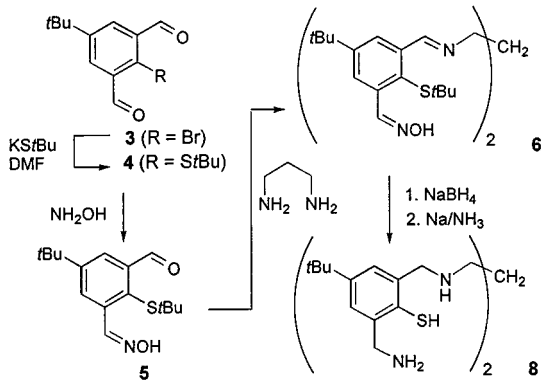
formation of a novel, face-sharing bioctahedral complex with a unique $N_3Ni^{II}(\mu_2\text{-}SR)_3Ni^{II}N_3$ core.[16] While these results unambiguously revealed the ability of the $N_2Ni(\mu_2\text{-}SR)_2NiN_2$ site to expand both nickel coordination spheres from square-planar (*cis*-N_2S_2) to octahedral (*fac*-S_3N_3), an important point that has not been addressed previously was whether unidentate substrates could similarly bind to this dinickel site. Unfortunately, reactions of complex **2** with unidentate substrates did not proceed in a well-defined manner and all attempts to isolate well-defined products have not yet been successful.

In anticipating that a more rigid ligand backbone would allow the dicationic complex to retain its dinuclear structure upon binding of further ligands, we have now prepared the novel hexadentate amine-thiolate ligand **8**, in which two 2,6-bis(aminomethyl)-4-*tert*-butylthiophenolate moieties are joined by one lateral 1,3-propylene chain at the amine nitrogen atoms. We here report the synthesis of **8** and its dinickel complex $[Ni^{II}_2\mathbf{8}][ClO_4]_2 \cdot 3$ MeOH (**9**), the solid-state structure of which has been determined by X-ray structure analysis. We also present the crystal structure of the isothiocyanate complex $[Ni^{II}_2\mathbf{8}(NCS)_2] \cdot$ MeOH (**10**), which is obtained by reaction of **9** with KSCN in methanol. To the best of our knowledge, this result represents the first unambiguous example for substrate binding to a $N_2Ni(\mu_2\text{-}SR)_2NiN_2$ site without affecting the dinuclear structure of the parent complex.[14,17] Both complexes, **9** and **10**, were further characterized by cyclic voltammetry.

Results and Discussion

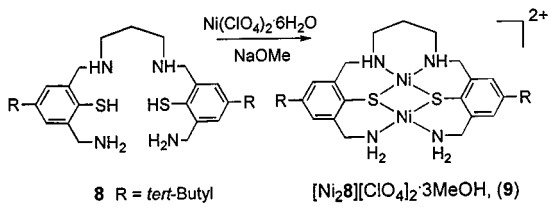
Syntheses

The preparation of the hexadentate N_4S_2 ligand **8** is very similar to that described previously for the tridentate amine-thiolate ligand **1**[15] and required only slight modifications (Scheme 2). In the first step *tert*-butyl-protected thiolate compound **4** was prepared instead of the benzyl-protected derivative benzyl (4-*tert*-butyl-2,6-diformylphenyl)sulfide used in the preparation of **1**, since reductive cleavage of the ArylS$-$C$(CH_3)_3$ bond by Na/NH_3 (last step) was found to proceed more smoothly than cleavage of the ArylS$-$$CH_2$Ph bond (by virtue of higher yields and easier workup conditions). Key step of this reaction sequence is the reaction of dialdehyde **4** with hydroxylamine in a 1:1 molar ratio, which, besides unreacted **4** and the dioxime as side product, affords the desired monoaldehyde **5** in 69% yield. Reaction of **5** with 1,3-propanediamine in a 2:1 molar ratio in ethanol then furnishes the diimine derivative **6**. This compound precipitates from the reaction mixture in analytically pure form. Subsequent reductions employing $NaBH_4$ and Na/NH_3 as reducing agents gave the hexadentate amine-thiolate ligand **8**. The hydrochloride salt **8** $\cdot$ 4 HCl is a pale yellow solid that can be handled in air for short periods of time without any sign of oxidative decomposition. For long term usage the compound was stored under an atmosphere of dry nitrogen.



Scheme 2. Preparation of the hexadentate amine-thiolate ligand **8**

Reaction of $Ni(ClO_4)_2 \cdot 6\ H_2O$ with **8** $\cdot$ 4 HCl in methanol in the presence of sodium methanolate (Scheme 3) in a 2:1:6 molar ratio gives the dinickel(II) complex $[Ni^{II}_2(\mathbf{8})][ClO_4]_2$ as a dark-red microcrystalline solid. Recrystallization from methanol solution affords this complex as the methanol solvate $[Ni^{II}_2(\mathbf{8})][ClO_4]_2 \cdot 3$ MeOH (**9**), the structure of which has been determined by X-ray crystal-structure determination (below).



Scheme 3. Reaction of **8** with $Ni(ClO_4)_2 \cdot 6\ H_2O$

Complex **9** is an air-stable crystalline solid which is very soluble in polar aprotic solvents like acetonitrile and *N*,*N*-dimethylformamide (DMF). It is less soluble in methanol and practically insoluble in H_2O or dichloromethane. In the IR spectrum the most prominent feature is the strong ClO_4^- absorption at 1090 cm^{-1}, and ν(NH) and $\nu(NH_2)$ stretching frequencies also occur as one broad feature at 3222 cm^{-1} in the usual 3170$-$3225 cm^{-1} region.[18] The O$-$H stretching vibrations of the methanol solvates appear as one broad feature at a relatively low frequency of 3415 cm^{-1} which is due to N$-$H$\cdots$O hydrogen bonding interactions in the solid state.

The UV/Vis spectrum of **9** in acetonitrile is very similar to that of **2** and related planar $N_2S_2Ni^{II}$ complexes with an intense ligand-to-metal charge-transfer band at 501 nm (ε = 1005 $M^{-1}cm^{-1}$) (Figure 1).[19] However, a discrete ^{1}H-NMR spectrum for **9** could not be obtained in CD_3CN solution, presumably due to a paramagnetic species which is formed by coordination of the ClO_4^- anions or solvent molecules. This is also supported by distinct UV/Vis spectral changes for **9** in other donor solvents. DMF solutions of **9**, for example, give rise to new absorption bands at 523 nm (ε = 580 $M^{-1}cm^{-1}$) and 616 nm (sh, ε = 269). Under these conditions, **9** is assumed to exist as discrete dinuclear species with at least one nickel atom being five-coordinate (N_2S_2ONi).[13a,b] A six-coordinate structure can be ruled

out, since the spectrum does not reveal the ν_1 ($^3A_{2g} \rightarrow {}^3T_{2g}$) absorption band around 900−1000 nm characteristic for octahedral, six-coordinate Ni^{II} complexes.[20][21]

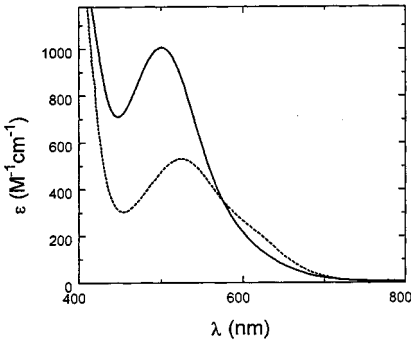


Figure 1. UV/Vis spectra of **9** in CH_3CN (—) and DMF (---) at 295 K

Crystal Structure of $[Ni_2\mathbf{8}][ClO_4]_2 \cdot 3\ CH_3OH$ (9)

The X-ray crystal structure determination of **9** revealed the structure to consist of well-separated molecules of the dinickel complex, two perchlorate anions, and three molecules of methanol of crystallization. Two of the three solvates form hydrogen-bonds with the primary nitrogen atoms of the dication [N(2)−H(2A)···O(9) 2.978 Å, N(4)−H(4A)···O(10) 3.030 Å] whereas the third one is involved in hydrogen-bonding interactions with both secondary nitrogen atoms [N(1)−H(1)···O(11) 3.067 Å, N(3)−H(3)···O(11) 2.987 Å]. However, there are no close contacts between methanol molecules and nickel atoms of the complex cation. Perspective views of the dication of **9** are shown in Figure 2. Bond lengths and angles are summarized in Tables 1 and 2.

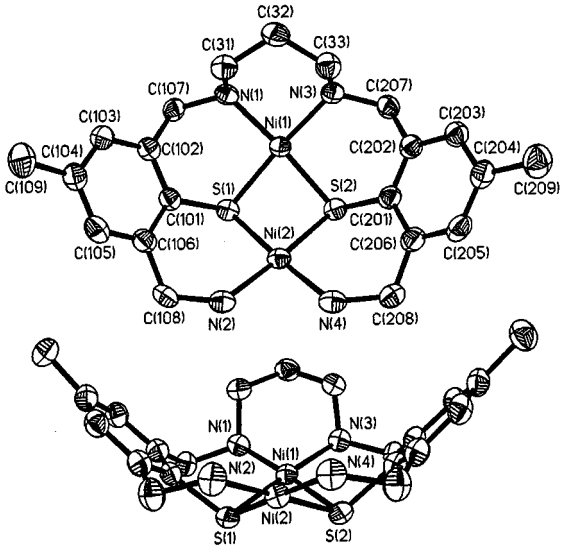


Figure 2. Two different views of the molecular structure of the $[Ni^{II}_2\mathbf{8}]^{2+}$ cation in **9** (50% probability thermal ellipsoids). Hydrogen atoms and *tert*-butyl methyl carbon atoms have been omitted for reasons of clarity. Selected bond lengths and angles are collected in Tables 1 and 2

Table 1. Selected bond lengths [Å] in **9** and **10**

Bond lengths	**9**	**10**		**9**	**10**
Ni(1)−S(1)	2.192(1)	2.412(3)	Ni(2)−S(1)	2.189(1)	2.198(2)
Ni(1)−S(2)	2.193(1)	2.445(3)	Ni(2)−S(2)	2.189(1)	2.217(2)
Ni(1)−N(1)	1.944(4)	2.105(6)	Ni(2)−N(2)	1.933(5)	1.963(7)
Ni(1)−N(3)	1.947(4)	2.082(8)	Ni(2)−N(2)	1.933(5)	1.963(7)
Ni(1)−N(5)	−	2.108(7)			
Ni(1)−N(6)	−	2.095(8)	Ni(1)···Ni(2)	2.973(1)	3.124(1)
S(5)−C(5)	−	1.638(10)	C(5)−N(5)	−	1.162(11)
S(6)−C(6)	−	1.638(10)	C(6)−N(6)	−	1.152(12)

The dication $[Ni_2\mathbf{8}]^{2+}$ possesses idealized C_s symmetry with a pseudo mirror plane passing through the metal atoms and the methylene carbon atom C(32) of the 1,3-diazacyclohexane ring. Its overall structure is very similar to that of **2**,[16] with two approximately planar *cis*-N_2S_2Ni coordination units joined by the thiolate sulfur atoms, with almost identical Ni−N and Ni−S bond lengths, and with a similar bowl-shaped molecular structure. The Ni−N bond lengths at Ni(1) and Ni(2) do not differ significantly, despite the fact that Ni(1) is coordinated by two secondary amine nitrogen atoms. A major structural difference is the six-membered nickela-1,3-diazacyclohexane chelate ring involving the atoms Ni(1), N(1), N(3), C(31), C(32), and C(33). The chelate ring adopts the typical chair conformation[22][23] with enantiomeric configurations (*R*) and (*S*) for asymmetric nitrogen atoms N(1) and N(3), respectively. While this isomer seems to be the thermodynamically most stable form (or the least soluble form), it is likely that the other possible isomers coexist with (*RS*)-**9** in the solution-state (Chart 1). In compound **10**, for example, the 1,3-diazacyclohexane ring adopts the (*S*)-N(1), (*R*)-N(3) set of nitrogen configurations (see below). Similar equilibria between isomers related by (*SR*) ↔ (*RS*) N-inversions within 1,3-diazacyclohexane rings have also been observed in nickel(II) complexes of macrocyclic secondary amine ligands, for example, in $[Ni(cyclam)]^{2+}$ (cyclam = 1,4,8,11-tetraazacyclotetradecane).[24]

Properties of 9

While the molecular structures of **2** and **9** reveal only slight differences, the substitution of two of the tridentate N_2S ligands **1** in **2** by the hexadentate N_4S_2 ligand **8** in **9** affords a kinetically and conformationally more stable complex, as demonstrated by the reactions and electrochemical properties detailed below. Most important, binding of anionic ligands to coordinatively unsaturated **9** does not affect its overall bowl-shaped dinuclear structure. This is in contrast to complex **2** which has been shown to undergo significant structural changes upon coordination of further ligands.[16]

Binding of Anionic Ligands to 9

The red complex **9** reacts cleanly with a variety of substrates such as NaCN, NH_4SCN, NaN_3, or NaHS. In the

Table 2. Selected bond angles [°] in **9** and **10**

Bond angles	**9**	**10**		**9**	**10**
S(1)−Ni(1)−S(2)	79.79(6)	75.09(8)	S(1)−Ni(2)−S(2)	79.94(5)	84.17(9)
S(1)−Ni(1)−N(1)	95.8(1)	95.4(1)	S(1)−Ni(2)−N(2)	96.4(1)	94.02(1)
S(1)−Ni(1)−N(3)	175.5(1)	170.9(2)	S(1)−Ni(2)−N(4)	176.1(1)	176.9(2)
S(2)−Ni(1)−N(1)	175.5(1)	170.4(2)	S(2)−Ni(2)−N(2)	176.2(1)	176.8(2)
S(2)−Ni(1)−N(3)	95.8(1)	95.8(2)	S(2)−Ni(2)−N(4)	96.3(2)	94.8(2)
N(1)−Ni(1)−N(3)	88.5(2)	93.6(3)	N(2)−Ni(2)−N(4)	87.4(2)	86.9(3)
S(1)−Ni(1)−N(5)	−	91.0(2)	S(1)−Ni(1)−N(6)	−	89.2(3)
S(2)−Ni(1)−N(5)	−	91.0(2)	S(2)−Ni(1)−N(6)	−	89.3(3)
N(1)−Ni(1)−N(5)	−	87.4(3)	N(1)−Ni(1)−N(6)	−	92.4(3)
N(3)−Ni(1)−N(5)	−	88.8(3)	N(3)−Ni(1)−N(6)	−	91.1(3)
N(5)−Ni(1)−N(6)	−	179.7(3)			
Ni(1)−S(1)−Ni(2)	86.14(5)	85.20(9)	C(5)−N(5)−Ni(1)	−	159.4(7)
Ni(1)−S(2)−Ni(2)	86.12(5)	84.01(8)	C(6)−N(6)−Ni(1)	−	149.8(7)

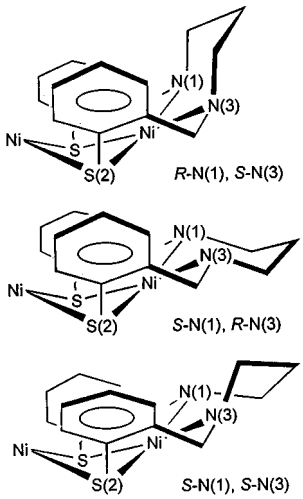


Chart 1. Possible conformations of the six-membered chelate rings in **9** and **10** and the respective configurations at secondary nitrogen atoms N(1) and N(3)

following we will concentrate on the reaction with thiocyanate.[25] Binding of the thiocyanate ion is facile and is accompanied by distinct spectral changes (Figure 3).

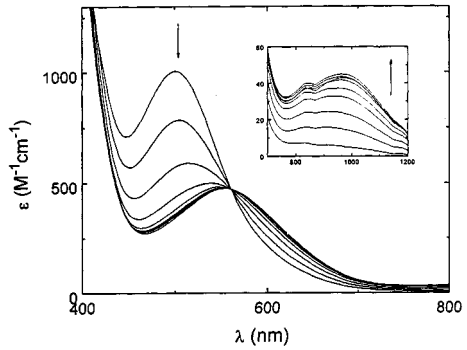
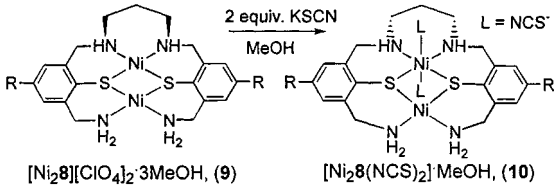


Figure 3. UV/Vis spectral titration of complex **9** ([**9**] = 1×10^{-3} M) with NH_4SCN (0.0−4.0 added equiv.) in acetonitrile at 295 K

Thus, addition of NH_4SCN to **9** in acetonitrile resulted in disappearance of the 501 nm band with concomitant evolution of new absorption bands at 555 nm and 968 nm. An isosbestic point occurred at 561 nm. The 555 nm band exhibited its maximum absorption at a complex to SCN^- ratio of 1:2, and remained essentially unchanged at higher SCN^- concentrations, consistent with binding of two thiocyanate ions. The weak absorption at 968 nm (ε = 48 $M^{-1}cm^{-1}$) is tentatively assigned to the ν_1 band ($^3A_{2g} \rightarrow {}^3T_{2g}$) characteristic for a six-coordinate nickel(II) ion (S = 1), implying that both substrates bind to the same nickel atom. When **9** was allowed to react with KSCN in methanol solution, the complex $[Ni^{II}_2\mathbf{8}(NCS)_2]\cdot CH_3OH$ (**10**) was obtained as a microcrystalline solid (Scheme 4).



Scheme 4. Reaction of **9** with KSCN

Complete replacement of the ClO_4^- anions in **9** by thiocyanate anions in **10** is indicated by the absence of the characteristic ν_3F_2 stretching frequency of the ClO_4^- ion and by the presence of two strong ν(CN) absorptions at 2084 and 2071 cm^{-1}. Compared to the ν(CN) frequencies of KSCN (2053 cm^{-1}),[18] the shift to higher ν(CN) frequencies in **10** clearly indicates the coordination of the thiocyanate ion. However, from the values and numbers of the observed ν(CN) stretching frequencies one cannot a priori distinguish between an S-bonded (thiocyanato complex) or an N-bonded (isothiocyanato complex) or whether both coordination modes occur at the same time. To elucidate the exact bonding mode the crystal structure of **10** was determined.

Crystal Structure of $[Ni_2\mathbf{8}(NCS)_2] \cdot CH_3OH$ (10)

The X-ray crystal structure determination of **10** confirmed coordination of the two thiocyanate anions. Both thiocyanate anions are N-bonded to one nickel atom of the dinuclear isothiocyanate complex. To the best of our knowledge this is the first structurally characterized example of a discrete nickel amine-thiolate complex with adjacent planar *cis*-N_2S_2Ni and octahedral *cis*-N_4S_2Ni units. Figure 4 shows

the molecular structure of the C_s-symmetric neutral complex with the individual atoms displayed as thermal ellipsoids drawn at the 50% probability level. Tables 1 and 2 summarize selected bond lengths and angles.

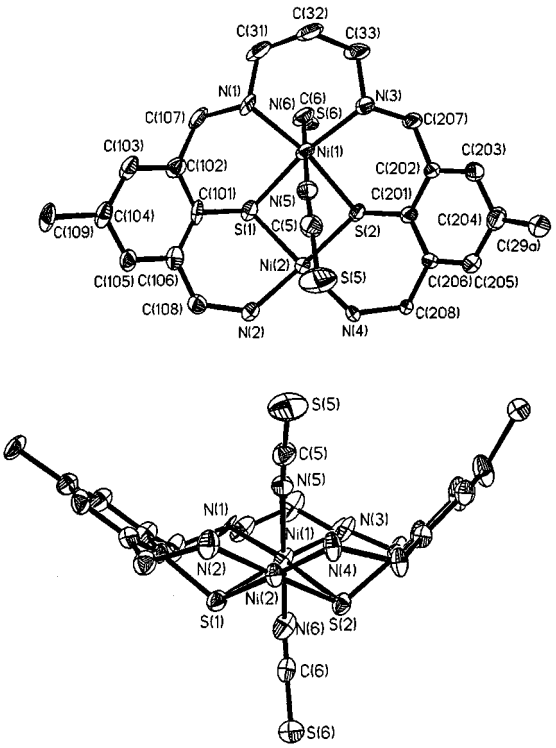


Figure 4. Perspective views of the molecular structure of **10**. Hydrogen atoms and *tert*-butyl methyl carbon atoms are omitted for reasons of clarity. Selected bond lengths and angles are summarized in Tables 1 and 2

The linear isothiocyanate ions occupy *trans*-positions in the $N_4S_2Ni(1)$ octahedron with Ni−N bond lengths of 2.108(7) and 2.095(8) Å, an SCN−Ni−NCS angle of 179.7(3)°, and C−N−Ni angles of 159.4(7) and 149.8(7)°. These values and the average CN and CS distances compare well with those of other isothiocyanato complexes.[26] The remaining coordination sites at Ni(1) are occupied by two bridging thiolate sulfur atoms and by two secondary amine nitrogen atoms. The average Ni−S (2.429 Å) and Ni−N bond lengths (2.098 Å) of six-coordinate Ni(1) are longer than those of four-coordinate Ni(2) and compare well with those of other six-coordinate $N_{6-n}S_nNi^{II}$ complexes. In *cis*-$[Ni(bpy)_2(SPh)_2] \cdot 2\ D_2O$,[27] for example, the average Ni−S and Ni−N bond lengths are at 2.445 Å and 2.091 Å. The average Ni−S (2.208 Å) and Ni−N bond lengths (1.963 Å) for the four-coordinate atom Ni(2), on the other hand, are only slightly longer in comparison with the corresponding values of the four-coordinate nickel atoms in **9**.

As can be seen in Figure 5, the neutral complexes stack in pairs with relatively short [Ni(2)···Ni(2a) 3.904 Å, Ni(2)···S(1a) 3.994 Å, and Ni(2)···S(2a) 3.777 Å] but nonbonding intermolecular interactions. The intramolecular Ni(1)···Ni(2) separation in **10** is shorter at 3.124(1) Å, but likewise out of range of bonding interactions.[28]

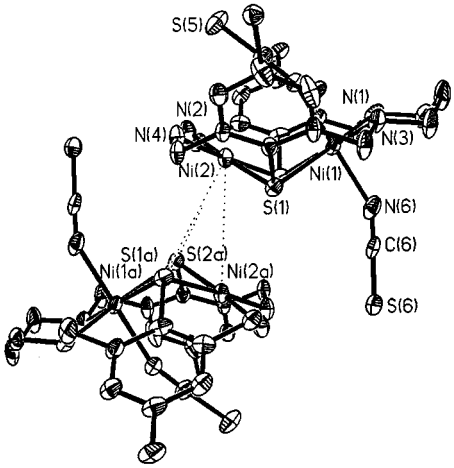


Figure 5. Intermolecular contacts between the neutral molecules in the crystal structure of **10**

It is interesting to note that the isothiocyanate ions have not selected to coordinate to the nickel atom Ni(2). This is surprising because the primary amine nitrogen atoms N(2) and N(4) bound to Ni(2) appear to be sterically less demanding than the secondary nitrogen atoms N(1) and N(3) bound to Ni(1). It thus appears that steric effects play only a minor role for this site-selective binding. This then favors the other explanation that the thiocyanate ions sense the slightly weaker ligand field strength exerted by the secondary amine nitrogen donors at Ni(1) when coordinating to coordinatively unsaturated complex **9**. Consistent with this are observations that the ligand field strength steadily decreases for amine ligands as the number of *N*-alkyl groups is increased.[29]

Another interesting feature is the fact that the 1,3-diazacyclohexane chelate ring now adopts a conformation with (*S*)-N(1) and (*R*)-N(3) nitrogen configurations. That is (*R*)-N(1) and (*S*)-N(3) nitrogen configurations in **9** change to (*S*)-N(1) and (*R*)-N(3) in **10**. However, in the absence of a more detailed kinetic study, one can only hypothesize about the likely mechanism for the inversions.[30,31]

Comparison with other Structures

Compound **10** is unique because it is a crystallographically characterized dinickel(II) amine-thiolate complex where adjacent square-planar N_2S_2Ni and octahedral N_4S_2Ni sites are assembled via the N_4S_2 donor set of a hexadentate N_4S_2 ligand and through the nitrogen atoms of two *N*-bound thiocyanate ions. The dinuclear complex $[Ni(terpy)(SPh)_2]_2 \cdot 6\ H_2O$[17] features a central $N_3SNi(\mu_2\text{-}SR)_2NiSN_3$ core, but this structure is not assembled by a multidentate amine-thiolate ligand. Complex **10** is also an important addition to the series of dinuclear nickel complexes of tridentate aliphatic amine-thiolate,[32] hexadentate macrocyclic amine-thiolate,[11] and imine-thiolate ligands.[13][14] However, these ligands tend to form almost

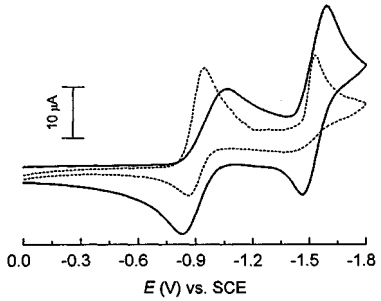


Figure 6. Cyclic voltammograms of complexes **9** (—) and **2** (---) in DMF solution at 295 K. Experimental conditions: [**9**] ca. 1×10^{-3} M, Pt disk working electrode, Ag wire reference electrode, 0.1 M [nBu$_4$N][PF$_6$], scan rate = 200 mV·s^{-1}

exclusively complexes with square-planar N_2S_2Ni units because of the stronger ligand fields of the aliphatic thiolate or the imine donors and, therefore, lack a reactivity pattern similar to that observed for the compounds examined in this study. Binding in the compounds $[Ni_2L(NCCH_3)_2]^{2+}$ and $[Ni_2L(NCS)_2OCN(CH_3)_2]^{2+}$, for example, has been reported to occur only after replacing one half of the N_4S_2 imine-thiolate donor set by an N_2O amine-phenolate donor set.[14c,d] Such compounds have recently attracted interest in connection with the Ni(μ_2-SR)$_2$(X)Fe dinuclear active site in hydrogenase from *Desulfovibrio gigas* (X = unknown ligand).[33]

Electrochemistry

Complexes **9** and **10** were further characterized by cyclic voltammetry. Cyclic voltammograms have been recorded in DMF solution with tetra-*n*-butylammoniumhexafluorophosphate as the supporting electrolyte. All potentials are referenced to the SCE (Table 3).

The CV of **9** in DMF in the cathodic potential region 0.0 to −1.8 V reveals two reduction waves at $E^1_{1/2} = -0.95$ V and at $E^2_{1/2} = -1.53$ V vs SCE. Similar but less well-defined reduction waves were previously observed for complex **2**[15] at −0.97 and −1.48 V (Figure 6). Since the number of observed reduction waves matches with the number of N_2S_2Ni units in **2** and **9** and since the ligands are unlikely to undergo ligand-centered redox reactions, it is assumed that these processes correspond to metal-centered redox reactions with successive formation of mixed valent $Ni^{II,I}$ and $Ni^{I,I}$ species (Eqs. 1a, b). This is also supported by the electrochemical properties of related nickel amine-thiolate complexes featuring planar N_2S_2Ni units which have been reported to undergo $Ni^{II/I}$ reductions at similar potentials.[9a,34]

$$[Ni^{II}_2\mathbf{8}]^{2+} + e^- \rightleftharpoons [Ni^{II}Ni^{I}\mathbf{8}]^{1+} \qquad E^1_{1/2} \qquad (1a)$$

$$[Ni^{II}Ni^{I}\mathbf{8}]^{1+} + e^- \rightleftharpoons [Ni^{I}_2\mathbf{8}]^{0} \qquad E^2_{1/2} \qquad (1b)$$

It is worthwhile to note that the CV of compound **2** is not so well defined in comparison to that of **9**. The second reduction wave at $E^2_{1/2}$, for example, is electrochemically irreversible for **2** (no anodic peak current present) whereas

Table 3. Electrochemical data (E (V)) for **2**,[15] **9**, and **10**[a]

	9	**10**	**2**
$E^1_{1/2}$	−0.95 (230)	−0.96 (192)	−0.97 (irr.)
$E^2_{1/2}$	−1.53 (110)	−1.50 (120)	−1.48 (irr.)
$E^3_{1/2}$		+0.52 (114)	

[a] DMF solutions of **2**, **9**, and **10** were 0.1 M in nBu$_4$NPF$_6$ and ca. 1×10^{-3} M in sample, Pt disk working electrode, Ag wire reference electrode, scan rate 200 mV·s^{-1}, $E^{\times}_{1/2} = (E^{ox}_p + E^{red}_p)/2$ for reversible one-electron-transfer processes; oxidation (E^{ox}_p) or reduction peak potentials (E^{red}_p) are given for irreversible (irr) processes; number in parentheses denote peak-to-peak separations $\Delta E_p = |E^{ox}_p - E^{red}_p|$.

for complex **9** it is quasi-reversible with cathodic and anodic peak potentials separated by 110 mV. It follows that the reduced $[Ni_2\mathbf{8}]^{1+}$ and $[Ni_2\mathbf{8}]^{0}$ species, presumably as a result of a more rigid ligand structure of the hexadentate ligand **8**, exhibit greater stability than the Ni^I species, $[Ni_2\mathbf{1}_2]^{1+}$ and $[Ni_2\mathbf{1}_2]^{0}$, of the tridentate N_2S ligand **1**. The results predict that incorporation of the N_4S_2 donor set into a fully cyclized ligand system would further increase the stability of the dinickel(II,I) or dinickel(I,I) species such as to probably allow for their isolation and an investigation of their properties.

Another important feature of the cyclic voltammogram of complex **9** is the rather broad peak-to-peak separation of the first reduction wave at $E^1_{1/2}$ ($\Delta E_{1/2} = 220$ mV), possibly because of changes in axial ligation upon reduction or oxidation or slight differences in the coordination environments of both nickel ions.[35] This is not unreasonable since the UV/Vis spectral properties of $[Ni_2\mathbf{8}]^{2+}$ in CH_3CN or DMF solution (Figure 2) implicated coordination of solvent molecules to the dinickel(II,II) complex in the latter solvent. It is assumed that these Ni-bound DMF molecules, irrespective of the site of reduction, decoordinate upon the first one-electron-transfer to give a monocationic $[Ni_2\mathbf{8}]^{1+}$ species with unoccupied axial coordination sites at both N_2S_2Ni units (Eq. 2).

$$[Ni_2\mathbf{8}(DMF)_x]^{2+} + e^- \rightleftharpoons [Ni_2\mathbf{8}]^{1+} + x\ DMF \qquad E^1_{1/2} \qquad (2)$$

There are several points which strongly argue for such a structure of the mixed-valent complex. First, the overall charge of the parent complex $[Ni^{II}_2\mathbf{8}(DMF)_\times]^{2+}$ decreases by one unit to give the monocationic complex $[Ni^{I}Ni^{II}\mathbf{8}]^{1+}$ which is expected not to bind substrates as readily as the dicationic $[Ni^{II}_2\mathbf{8}]^{2+}$ species. Second, the rather narrow peak-to-peak separation of the second reduction wave at $E^2_{1/2}$ departs not so strongly from reversibility as observed for the first one-electron-transfer process at $E^1_{1/2}$, implicating that this process does not involve changes in axial ligation. Finally, nearly all structurally characterized Ni^I complexes (d^9 electronic configuration) have been shown to be four-coordinate with a planar coordination around Ni^I.[36] Similar conclusions can be drawn from a comparison of the electrochemical properties of complex **9** and the isothiocyanate complex **10**.

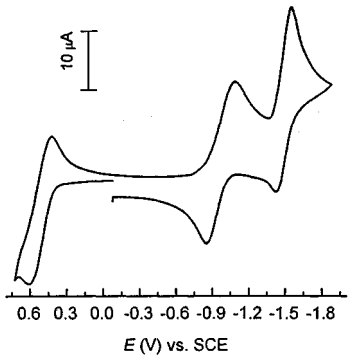


Figure 7. Cyclic voltammogram of complex **10** in DMF solution at 295 K. Experimental conditions: [**10**] ca. 1×10^{-3} M, Pt disk working electrode, Ag wire reference electrode, 0.1 M $[n\text{Bu}_4\text{N}][\text{PF}_6]$, scan rate = 200 mV·s^{-1}

As shown in Figure 7 the CV of complex **10** reveals, besides two reduction waves in the cathodic potential region, an additional oxidation wave at $E^3_{1/2} = 0.52$ V vs SCE in the anodic potential region. Since this feature was not present in the CV of **9**, it is assigned to oxidation of free thiocyanate (Eq. 3b) which is deliberated from **10** by DMF substitution (Eq. 3a). The reported values of $E_{1/2} = 0.77$ V (vs SCE, H_2O) for the process indicated in Eq. 3b is in good agreement with this assignment.[37] It thus appears that in DMF solution the solvent molecules compete successfully with the thiocyanate ions for the axial coordination sites at the dimetal centrum.

$$[\text{Ni}_2\mathbf{8}(\text{NCS})_2]^{2+} + x\ \text{DMF} \rightleftharpoons [\text{Ni}_2\mathbf{8}(\text{DMF})_x]^{2+} + 2\ \text{NCS}^- \quad (3a)$$

$$\text{NCS-SCN} + 2\ e^- \rightleftharpoons 2\ \text{NCS}^- \quad (3b)$$

The fact that complexes **10** and **9** reduce at nearly the same potentials with similar peak-to-peak separation characteristics reveal that both complexes in DMF solution exist presumably as the same DMF-solvated $[\text{Ni}_2\mathbf{8}(\text{DMF})_x]^{2+}$ species. Finally, the presence of free thiocyanate in the electrolyte medium has obviously no effect on the reduction of the mixed-valent $[\text{Ni}^{\text{II}}\text{Ni}^{\text{I}}\mathbf{8}]^{1+}$ species at $E^2_{1/2}$, indicating little, if any, affinity for binding of anions.

Conclusion

Two novel thiolate-bridged dinickel complexes have been synthesized and crystallographically characterized. Both compounds represent important additions to the series of similar structures previously established with hexadentate imine-thiolate ligands. However, the hexadentate N_4S_2 amine-thiolate ligand described in this study exerts a weaker ligand field strength such that binding of exogenous substrates occurs to the central $N_2Ni(\mu_2\text{-}SR)_2NiN_2$ core in **9**. In contrast to **2**, complex **9** represents a thermodynamically and configurationally more stable dinuclear nickel amine-thiolate complex that coordinates further anions without affecting its overall dinuclear structure. We expect further exciting coordination chemistry with **9** and **10** and with other first-row transition metal complexes of this ligand.

Experimental Section

Materials and Methods: Compound **3**[15] was prepared as previously described. All other chemicals were of reagent grade and used without further purification. Solvents were predried over molecular sieves and freshly distilled from appropriate drying agents. − ^{1}H-NMR and ^{13}C{^{1}H}-NMR spectra were recorded on a Bruker AC 200 spectrometer. All chemical shifts are quoted on the δ scale with TMS or the solvent as internal standard. Coupling constants are expressed in Hz. − Melting points were determined in capillaries and are uncorrected. − CHN-Analyses were determined with a Perkin Elmer Elemental Analyzer 240. − IR spectra were recorded on a Bruker IFS25 spectrophotometer as KBr pellets. − Absorption spectra were recorded on a Jasco V-570 UV/VIS/NIR spectrometer. − Cyclic voltammetry measurements were carried out at 25°C with an EG&G Princeton Applied Research Potentiostat/Galvanostat Model 263 A. The cell contained a Pt working electrode, a Pt wire auxiliary electrode, and an Ag wire as reference electrode. Concentration of solutions were 0.1 M in supporting electrolyte ($n\text{Bu}_4\text{NPF}_6$) and ca 1×10^{-3} M in sample. Ferrocenium/ferrocene was used as internal standard. All potentials were converted to the SCE reference.

***tert*-Butyl (4-*tert*-Butyl-2,6-diformylphenyl) Sulfide (4):** To a suspension of *tert*-butylthiol (4.78 g, 53.0 mmol) and K_2CO_3 (8.29 g, 60.0 mmol) in DMF (80 mL) was added solid 1-bromo-4-*tert*-butyl-2,6-diformylbenzene (**3**) (14.3 g, 53.0 mmol). After stirring the reaction mixture for 12 h, the product precipitated upon dropwise addition of water (200 mL). The solid was isolated by filtration, washed with water (100 mL), and dried in vacuum. The crude product was used without further purification. Yield: 14.0 g (95%). − ^{1}H NMR (200 MHz, $CDCl_3$, 25°C, TMS): δ = 10.80 (s, 2 H, C*H*O), 8.18 (s, 2 H, Ar*H*), 1.30 (s, 9 H, CH_3), 1.21 (s, 9 H, CH_3). − ^{13}C{^{1}H} NMR (50.2 MHz, $CDCl_3$, 25°C): δ = 192.4, 153.3, 140.2, 136.4, 130.2, 49.2, 35.0, 30.7.

***tert*-Butyl (4-*tert*-Butyl-2-formyl-6-hydroximinomethylphenyl) Sulfide (5):** To a solution of **4** (27.8 g, 100 mmol) in $CHCl_3$ (300 mL) was added a solution of $NH_2OH\cdot HCl$ (6.95 g, 100 mmol) and NEt_3 (10.1 g, 100 mmol) in $CHCl_3$ (100 mL). The reaction mixture was stirred for 12 h and then reduced in volume to 150−200 mL by evaporation under reduced pressure. As indicated by TLC chromatography, the reaction mixture contains **5** as the main product (second spot), the dioxime as side product (third spot), and unreacted **2** (first spot). For easier workup, most of the dioxime was precipitated by addition of hexanes and separated by filtration. The filtrate was then taken to dryness to leave a pale yellow oil. The oil was loaded on a SiO_2 column and the product (second fraction) eluted by using CH_2Cl_2/C_6H_{12} (1:1, v:v) as eluent. Removal of the solvent afforded 20.2 g (69%) of **5** as colorless crystals. − ^{1}H NMR (200 MHz, $CDCl_3$, 25°C, TMS): δ = 10.77 (s, 1 H, C*H*O), 9.00 (s, 1 H, C*H*N), 8.15 [d, ^4J(H,H) = 2 Hz, 1 H, Ar*H*], 8.01 [d, ^4J(H,H) = 2 Hz, 1 H, Ar*H*], 7.58 (br. s, 1 H, NO*H*), 1.30 (s, 9 H, CH_3), 1.18 (s, 9 H, CH_3). − ^{13}C{^{1}H} NMR (50.2 MHz, $CDCl_3$, 25°C): δ = 193.4, 152.8, 147.3, 140.3, 139.8, 132.0, 127.9, 125.7, 49.5, 35.0, 31.0, 30.9.

***N,N′*-Bis-[2-*tert*-butylsulfanyl-3-hydroximinomethyl-5-*tert*-butylbenzylidene]propane-1,3-diamine (6):** To a solution of **5** (587 mg, 2.00 mmol) in ethanol (10 mL) was added a solution of propane-1,3-diamine (71 mg, 0.96 mmol) in ethanol (3 mL). The solution was heated to 60°C for 10 min. On cooling **6** precipitated as a white solid. The solid was isolated by filtration, washed with ether (3 × 2 mL), and dried in air to give 557 mg (93%, based on 1,3-propanediamine) of analytically pure product. Compound **6** exhibits only poor solubility in organic solvents. − ^{1}H NMR (200 MHz,

[D$_6$]DMSO, 35°C): δ = 11.32 (s, 2 H, NO*H*), 9.10 (s, 2 H, C*H*=N), 8.81 (s, 2 H, C*H*=N), 8.13 [d, ^4J(H,H) = 2 Hz, 2 H, Ar*H*], 8.01 [d, ^4J(H,H) = 2 Hz, 2 H, Ar*H*], 3.71 [t, ^3J(H,H) = 7 Hz, 4 H, NCH_2], 1.98 [qnt, ^3J(H,H) = 7 Hz, 2 H, CH_2], 1.31 (s, 18 H, CH_3), 1.13 (s, 18 H, CH_3).

***N,N′*-Bis-[2-*tert*-butylsulfanyl-3-hydroximinomethyl-5-*tert*-butylbenzyl]propane-1,3-diamine (7):** To a suspension of **6** (5.0 g, 8.0 mmol) in MeOH/CH_2Cl_2 (100 mL, 1:1) was added a solution of $NaBH_4$ (1.06 g, 28.0 mmol) in MeOH (50 mL). After the reaction mixture was stirred for 2 h, the resulting homogeneous solution was acidified with concentrated HCl to destroy the excess reducing agent. Then water (100 mL) was added and the reaction mixture was made alkaline by addition of 6 M KOH solution (final pH = 13). The organic phase was separated, and the aqueous phase extracted with CH_2Cl_2 (3 × 200 mL). The combined organic phases were dried with K_2CO_3, filtered, and the solvent removed in vacuum to give 4.6 g (91%) of the product as a white foam. The product was used without further purification. – ^{1}H NMR (200 MHz, CD_3OD, 25°C): δ = 8.83 (s, 2 H, C*H*=NO), 7.91 [d, ^4J(H,H) = 2 Hz, 2 H, Ar*H*], 7.57 [d, ^4J(H,H) = 2 Hz, 2 H, Ar*H*], 4.84 (s, 4 H, ArCH_2N), 2.66 [t, ^3J(H,H) = 7 Hz, 4 H, NCH_2], 1.75 [qnt, ^3J(H,H) = 7 Hz, 2 H, CH_2], 1.31 (s, 18 H, CH_3), 1.13 (s, 18 H, CH_3). – ^{13}C{^{1}H} NMR (50.2 MHz, CD_3OD, 25°C): δ = 153.1, 151.3, 146.3, 139.5, 129.5, 128.9, 123.0, 53.1, 49.6, 48.2, 35.3, 31.4, 31.2, 29.6

***N,N′*-Bis-[2-thio-3-aminomethyl-5-*tert*-butyl-benzyl]propane-1,3-diamine (8):** A solution of **7** (6.29 g, 10.0 mmol) in THF (50 mL) was added dropwise to a solution of sodium (6.51 g, 28.3 mmol) in liquid ammonia (100 mL). During addition the temp. was kept below −60°C by cooling with a dry ice/2-propanol bath. After the deep blue reaction mixture was stirred for further 3 h at −50°C, solid ammonium chloride was added to destroy excess reducing equivalents. The ammonia was allowed to evaporate at atmospheric pressure, and then the remaining THF was evaporated in vacuum. The solid residue was dissolved in 30 mL of water and the pH of the solution adjusted to 1 by addition of 1 M HCl. After stirring for 30 min, the precipitate was collected by filtration, and recrystallized from 1 M HCl to give 4.32 g (68%) of **8** · 4 HCl as a pale yellow solid. – ^{1}H NMR (200 MHz, D_2O, 25°C): δ = 7.45 (s, 4 H, Ar*H*), 4.26 (s, 4 H, ArCH_2N), 4.16 (s, 4 H, ArCH_2N), 3.31 [t, ^3J(H,H) = 7 Hz, 4 H, NCH_2], 1.75 [qnt, ^3J(H,H) = 7 Hz, 2 H, CH_2], 1.31 (s, 18 H, CH_3). – ^{13}C{^{1}H} NMR (50.2 MHz, D_2O, 25°C): δ = 152.7, 136.3, 134.2, 129.7, 129.2, 127.0, 57.4, 50.4, 44.4, 34.3, 30.2, 22.5.

[Ni_2(8)][ClO_4]$_2$ · 3 MeOH (9): ***Caution! Transition-metal perchlorates are hazardous and may explode. Only small quantities should be prepared and great care taken.*** To a suspension of **8** · 4 HCl (635 mg, 1.00 mmol) in methanol (5 mL) was added a solution of $Ni(ClO_4)_2$ · 6 H_2O (731 mg, 2.00 mmol) in methanol (5 mL). The resulting pale green suspension was allowed to stir for further 10 min. Then a 1.00 M solution of NaOMe in methanol (6.00 mL, 6.00 mmol) was added. The dark red solution was stirred over night to obtain the product as a red microcrystalline powder. Filtration and recrystallization from methanol affords the complex as the methanol solvate **9** · 3 MeOH. Further product may be obtained by addition of $LiClO_4$ to the mother liquor to give a total yield of 580 mg (70%) of **9** · 3 MeOH. The crystals lose the methanol molecules of crystallization upon storage in air at 298 K. – IR (KBr): $\tilde{\nu}$ = 3415s (OH), 3222s (NH), 1090vs cm^{-1} [ClO_4^-, $\nu_3(F_2)$]. – UV/Vis (CH_3CN): λ_{max} (ε): 312 (6858), 374 (5821), 501 nm (1005 M^{-1} cm^{-1}). – $C_{27}H_{42}Cl_2N_4Ni_2O_8S_2$ · 3 CH_3OH (899.18): calcd. C 40.07, H 6.05, N 6.23; found C 39.08, H 5.82, N 5.88.

[Ni_2(8)($NCS)_2$] · MeOH (10): A solution of NH_4SCN (10 mg, 0.13 mmol) in methanol (2 mL) was added to a solution of **9** (45 mg, 0.050 mmol) in methanol (5 mL) resulting in the precipitation of a purple solid. After the suspension was stirred for further 30 min, the product was isolated by filtration, washed with 2 mL of methanol, and dried in air. Single crystals suitable for study by X-ray diffraction were grown by slow evaporation of an acetonitrile/methanol solution (2:1) of **10**. – IR (KBr): $\tilde{\nu}$ = 3277w, 3208sh, 3193 br s, 3150sh (NH), 2084vs, 2072vs cm^{-1} (NCS^-). – UV/Vis (CH_3CN): λ_{max} (ε): 555 (478), 968 nm (45 M^{-1}cm^{-1}). – $C_{29}H_{42}N_6Ni_2S_4$·CH_3OH (752.35): calcd. C 47.89, H 6.16, N 11.17; found C 47.81, H 6.02, N 10.88.

Crystal-Structure Determinations: Crystals of **9** suitable for X-ray structure analysis were obtained by recrystallization from methanol. Black crystals of **10** suitable for single-crystal X-ray determination were obtained by the procedure described above.

Crystal data and refinement details for **9** ($C_{30}H_{54}Cl_2N_4Ni_2O_{11}S_2$, M_r 899.18): crystal size 0.18 × 0.16 × 0.08 mm^3, STOE IPDS diffractometer, T = 213(2) K, monoclinic, space group $P2_1/n$, a = 11.408(2), b = 17.396(3), c = 20.342(4) Å, β = 92.29(3)°, V = 4033.7 Å^3, Z = 4, ρ_{calcd} = 1.48 g·cm^{-3}, μ(Mo-K_α) = 0.64 mm^{-1}, empirical absorption correction, transmission factors 0.92–0.97, 56797 reflections collected, 7806 unique reflections (R_{int} = 0.1058), 6233 observed reflections [$I > 2\sigma(I)$]. The structure was solved by direct methods (SHELXS-86)[38] and refined by full-matrix least-squares techniques against F^2 (SHELXL-93). All non-hydrogen atoms were refined anisotropically except the methyl carbon atoms of one disordered *tert*-butyl group and the oxygen atoms of the disordered perchlorate ions. An isotropic split-atom model was applied for the disordered methyl carbon and oxygen atoms. The multiplicities of the respective orientations [C(110)–C(112)/C(113)–C(115), O(1A)–O(4A)/O(1B)–O(4B), O(5A)–O(8A)/O(5B)–O(8B)] were refined as follows: 0.68/0.32, 0.55/0.45, 0.49/0.51. Hydrogen atoms were placed at calculated positions and were refined using a riding model with isotropic thermal parameters fixed at 1.2 times the equivalent isotropic U of the atom to which they were bonded. Final residuals: $R1$, $wR2$ [$F_o > 4\sigma(F_o)$]: 0.0715, 0.1778, $R1$, $wR2$ (all data): 0.0889, 0.2007, goodness-of-fit on F^2: 1.08, residual electron density: 1.16/-0.79 e·Å^{-3}.

Crystal data and refinement details for **10** ($C_{30}H_{46}N_6Ni_2OS_4$, M_r 752.39): crystal size 0.21 × 0.12 × 0.11 mm^3, Enraf-Nonius CAD4 diffractometer, T = 183(2) K, triclinic, space group $P\bar{1}$, a = 12.051(2), b = 12.117(2), c = 13.139(3) Å, α = 99.39(3), β = 110.88(3), γ = 100.66(3)°, V = 1705.9 Å^3, Z = 2, ρ_{calcd} = 1.47 g·cm^{-3}, μ(Mo-K_α) = 1.38 mm^{-1}, empirical absorption correction based on ψ-scans, transmission factors 0.96–0.91, 7001 reflections collected, 6665 unique reflections (R_{int} = 0.0917), 3891 observed reflections [$I > 2\sigma(I)$]. The structure was solved by the heavy atom method (SHELXS–86) and refined by full-matrix least-squares techniques against F^2 (SHELXL-93). All non-hydrogen atoms were refined anisotropically except the methyl carbon atoms of the disordered *tert*-butyl groups and the atoms of the methanol solvate. An isotropic split-atom model was applied for the disordered methyl carbon atoms of the *tert*-butyl groups. The multiplicities of the respective orientations [C(110)–C(112)/C(113)–C(115), C(220)-C(212)/C(213)-C(215)] were refined as follows: 0.64/0.36 and 0.48/0.52. Hydrogen atoms were placed at calculated positions and were refined using a riding model with isotropic thermal parameters fixed at 1.2 times the equivalent isotropic U of the atom to which they were bonded. Final residuals: $R1$, $wR2$ [$F_o > 4\sigma(F_o)$]: 0.0652, 0.1706, $R1$, $wR2$ (all data): 0.1613, 0.2463, goodness-of-fit on F^2: 1.05, residual electron density: 0.86/–0.97 e·Å^{-3}. Crystallo-

graphic data (excluding structure factors) for the structures reported in this paper have been deposited with the Cambridge Crystallographic Data Centre as supplementary publication no. CCDC-102781 (**10**) and CCDC-102782 (**9**). Copies of the data can be obtained free of charge on application to CCDC, 12 Union Road, Cambridge CB2 1EZ, UK [Fax: +44 (1223) 336-033; E-mail: deposit@cam.ac.uk].

Acknowledgments

This work was supported by the Deutsche Forschungsgemeinschaft. We thank Prof. Dr. H. Vahrenkamp for his generous support, and Prof. Dr. B. Krebs for the use of the STOE-IPDS diffractometer. We are grateful to S. Höck and A. Trösch for help in collecting the X-ray data.

[1] [1a] T. Beissel, T. Glaser, F. Kesting, K. Wieghardt, B. Nuber, *Inorg. Chem.* **1996**, *35*, 3936−3947. − [1b] T. Beissel, F. Birkelbach, E. Bill, T. Glaser, F. Kesting, C. Krebs, T. Weyhermüller, K. Wieghardt, C. Butzlaff, A. X. Trautwein, *J. Am. Chem. Soc.* **1996**, *118*, 12376−12390.

[2] For biological, di(sulfide)-bridged Fe/Fe systems, see: R. Cammack, *Adv. Inorg. Chem.* **1992**, *38*, 281−322.

[3] For biological, dithiolate-bridged Fe/Ni systems, see: [3a] A. Volbeda, M.-H. Charon, C. Piras, E. C. Hatchikian, M. Frey, J. C. Fontecilla-Camps, *Nature* **1995**, *373*, 580−587. − [3b] A. Volbeda, E. Garcin, C. Piras, A. L. de Lacey, V. M. Fernandez, E. C. Hatchikian, M. Frey, J. C. Fontecilla-Camps, *J. Am. Chem. Soc.* **1996**, *118*, 12989−12996. − [3c] M. A. Halcrow, *Angew. Chem.* **1995**, *107*, 1307−1310; *Angew. Chem. Int. Ed. Engl.* **1995**, *34*, 1193−1197.

[4] For biological, dithiolate-bridged Cu/Cu systems, see: [4a] T. Tsukihara, H. Aoyama, E. Yamashita, T. Tomizaki, H. Yamaguchi, K. Shinzawa-Itoh, R. Nakashima, R. Yaono, S. Yoshikawa, *Science* **1995**, *269*, 1069−1074. − [4b] S. Iwata, C. Ostermeier, B. Ludwig, H. Michel, *Nature* **1995**, *376*, 660−669.

[5] [5a] B. Krebs, G. Henkel, *Angew. Chem.* **1991**, *105*, 785−804; *Angew. Chem. Int. Ed. Engl.* **1991**, *30*, 769−788. − [5b] I. G. Dance, *Polyhedron* **1986**, *5*, 1037−1104. − [5c] P. J. Blower, J. R. Dilworth, *Coord. Chem. Rev.* **1987**, *76*, 121−85.

[6] For synthetic, dithiolate-bridged Fe/Fe systems, see: [6a] K. D. Karlin, S. J. Lippard, *J. Am. Chem. Soc.* **1976**, *98*, 6951−6957. − [6b] D. Sellmann, M. Hannakam, F. Knoch, M. Moll, *Z. Naturforsch.* **1992**, *47b*, 1545−1550.

[7] For synthetic, dithiolate-bridged Cu/Cu systems, see: [7a] N. D. J. Branscombe, A. J. Blake, A. Marin-Becerra, W.-S. Li, S. Parsons, L. Ruiz-Ramirez, M. Schröder, *J. Chem. Soc. Chem. Commun.* **1996**, 2573−2574. − [7b] R. P. Houser, V. G. Young, Jr., W. B. Tolman, *J. Am. Chem. Soc.* **1996**, *118*, 2101−2102. − [7c] D. D. LeCloux, R. Davydov, S. J. Lippard, *J. Am. Chem. Soc.* **1998**, *120*, 6810−6811.

[8] For synthetic, dithiolate-bridged Fe/Ni systems, see: D. K. Mills, Y. M. Hsiao, P. J. Farmer, E. V. Atnip, J. H. Reibenspies, M. Y. Darensbourg, *J. Am. Chem. Soc.* **1991**, *113*, 1421−1423.

[9] For synthetic, dithiolate-bridged Ni/Ni systems, see: [9a] H.-J. Krüger, R. H. Holm, *Inorg. Chem.* **1989**, *28*, 1148−1155. − [9b] J. D. Franolic, W. Y. Wang, M. Millar, *J. Am. Chem. Soc.* **1992**, *114*, 6587−6588.

[10] [10a] M. Kumar, R. O. Day, G. J. Colpas, M. J. Maroney, *J. Am. Chem. Soc.* **1989**, *111*, 5974−5976. − [10b] T. Krüger, B. Krebs, G. Henkel, *Angew. Chem.* **1989**, *101*, 54−55; *Angew. Chem. Int. Ed. Engl.* **1989**, *28*, 61−63. − [10c] A. Müller, G. Henkel, *Z. Naturforsch.* **1995**, *50b*, 1464−1468.

[11] G. A. Lawrance, M. Maeder, T. M. Manning, M. A. O′Leary, B. W. Skelton, A. H. White, *J. Chem. Soc. Dalton Trans.* **1990**, 2491−2495.

[12] [12a] J. G. Hughes, R. Robson, *Inorg. Chim. Acta.* **1979**, *35*, 87−92. − [12b] M. Louey, P. D. Nichols, R. Robson, *Inorg. Chim. Acta.* **1980**, *47*, 87−96. − [12c] P. Iliopoulos, K. S. Murray, R. Robson, J. C. Wilson, G. A. Williams, *J. Chem. Soc. Dalton Trans.* **1987**, 1585−1591. − [12d] A. M. Bond, M. Haga, I. S. Creece, R. Robson, J. C. Wilson, *Inorg. Chem.* **1989**, *28*, 559−566. − [12e] B. F. Hoskins, C. J. McKenzie, R. Robson, L. Zhenrong, *J. Chem. Soc. Dalton Trans.* **1990**, 2637−2641. − [12f] B. F. Hoskins, R. Robson, G. A. Williams, J. C. Wilson, *Inorg. Chem.* **1991**, *30*, 4160−4166.

[13] [13a] A. J. Atkins, A. J. Blake, M. Schröder, *J. Chem. Soc. Chem. Commun.* **1993**, 1662−1665. − [13b] A. J. Atkins, D. Black, A. J. Blake, A. Marin-Becerra, S. Parsons, L. Ruiz-Ramirez, M. Schröder, *J. Chem. Soc. Chem. Commun.* **1996**, 457−464.

[14] [14a] S. Brooker, P. D. Croucher, *J. Chem. Soc. Chem. Commun.* **1995**, 1493−1494. − [14b] S. Brooker, P. D. Croucher, *J. Chem. Soc. Chem. Commun.* **1995**, 2075−2076. − [14c] S. Brooker, P. D. Croucher, F. M. Roxburgh, *J. Chem. Soc. Dalton Trans.* **1996**, 3031−3037. − [14d] S. Brooker, P. D. Croucher, *J. Chem. Soc. Chem. Commun.* **1997**, 459−460.

[15] B. Kersting, *Eur. J. Inorg. Chem.* **1998**, 1071−1077.

[16] B. Kersting, D. Siebert, *Inorg. Chem.* **1998**, *37*, 3820−3828.

[17] N. Baidya, M. Olmstead, P. K. Mascharak, *Inorg. Chem.* **1991**, *30*, 929−937.

[18] K. Nakamoto, *Infrared and Raman Spectra of Inorganic and Coordination Compounds*, Wiley, New York, **1978**.

[19] M. A. Halcrow, G. Christou, *Chem. Rev.* **1994**, *94*, 2421−2481.

[20] N. Herron, P. Moore, *Inorg. Chim. Acta* **1979**, *36*, 89−96.

[21] [21a] P. Moore, J. Sachinidis, G. R. Willey, *J. Chem. Soc. Dalton Trans.* **1984**, 1323−1327. − [21b] P. Moore, J. Sachinidis, G. R. Willey, *J. Chem. Soc. Chem. Commun.* **1983**, 522−523.

[22] B. Bosnich, M. L. Tobe, G. A. Webb, *Inorg. Chem.* **1965**, *4*, 1109−1112.

[23] L. G. Warner, D. H. Busch, *J. Am. Chem. Soc.* **1969**, *91*, 4092−4101.

[24] [24a] A. M. Martin, K. J. Grant, E. J. Billo, *Inorg. Chem.* **1986**, *25*, 4904−4906. − [24b] P. J. Connolly, E. J. Billo, *Inorg. Chem.* **1987**, *26*, 3224−3226. − [24c] D. T. Pierce, T. L. Hatfield, E. J. Billo, Y. Ping, *Inorg. Chem.* **1997**, *36*, 2950−2955.

[25] We will report on other reactions in a subsequent paper. G. Steinfeld, J. Hausmann, B. Kersting, unpublished results.

[26] A. H. Norbury, *Adv. Inorg. Chem. Radiochem.* **1975**, *17*, 231−386.

[27] K. Osakada, T. Yamamoto, A. Yamamoto, A. Takenaka, Y. Sasada, *Acta Crystallogr.* **1984**, *C40*, 85−87.

[28] A. Silver, M. Millar, *J. Chem. Soc. Chem. Commun.* **1992**, 948−949.

[29] F. Wagner, E. K. Barefield, *Inorg. Chem.* **1976**, *15*, 408−417.

[30] R. G. Wilkins, *Kinetics and Mechanism of Reactions of Transition Metal Complexes*, 2nd. ed., p. 360 ff., VCH, Weinheim, **1991**.

[31] R. W. Hay, M. Akbar Ali, *Inorg. Chim. Acta* **1985**, *103*, 23−29.

[32] I. Murase, S. Ueno, S. Kida, *Bull. Chem. Soc. Jpn.* **1983**, *56*, 2748−2751.

[33] [33a] C. Lai, J. H. Reibenspies, M. Y. Darensbourg, *Angew. Chem.* **1996**, *108*, 2551−2554; *Angew. Chem. Int. Ed. Engl.* **1996**, *35*, 2390−2392. − [33b] V. E. Kaasjager, R. K. Henderson, E. Bouwman, M. Lutz, A. L. Spek, J. Reedijk, *Angew. Chem.* **1998**, *110*, 1787−1789; *Angew. Chem. Int. Ed. Engl.* **1998**, *37*, 1668−1670.

[34] G. Musie, P. J. Farmer, T. Tuntulani, J. H. Reibenspies, M. Y. Darensbourgh, *Inorg. Chem.* **1996**, *35*, 2176−2183.

[35] M. P. Suh, H. K. Kim, M. J. Kim, K. Y. Oh, *Inorg. Chem.* **1992**, *31*, 3620−3625.

[36] [36a] L. R. Furenlid, M. W. Renner, D. J. Szalda, E. Fujita, *J. Am. Chem. Soc.* **1991**, *113*, 883−892. − [36b] D. J. Szalda, E. Fujita, *Acta. Crystallogr.* **1992**, *C48*, 1767−1771. − [36c] D. J. Szalda, E. Fujita, R. Sanzenbacher, H. Paulus, H. Elias, *Inorg. Chem.* **1994**, *33*, 5855−5863. − [36d] M. S. Ram, C. G. Riordan, R. Ostrander, A. L. Rheingold, *Inorg. Chem.* **1995**, *34*, 5884−5892. − [36e] M. P. Suh, S.-G. Kang, V. L. Goedken, S.−H. Park, *Inorg. Chem.* **1991**, *30*, 365−370.

[37] [37a] F. Seel, E. Müller, *Chem. Ber.* **1955**, *88*, 1747−1755. − [37b] R. C. Weast, *CRC Handbook of Chemistry and Physics*, 51st ed., CRC, Ohio, **1970**.

[38] G. M. Sheldrick, *SHELXS-86*, University of Göttingen, Germany, **1990**; G. M. Sheldrick, *SHELXL-93*, University of Göttingen, Germany, **1993**.

Received September 18, 1998
[I98318]

Preparation, Structure, and Properties of a Mixed-Valent $Ni^{II}Ni^{III}$ Amine-Selenolate Complex

Berthold Kersting*[a] and Dieter Siebert[b]

Dedicated to Prof. Dr. Bernt Krebs on the occasion of his 60th birthday

Keywords: Mixed-valent compounds / Nickel / N_2Se ligand / Cyclic voltammetry / EPR spectroscopy

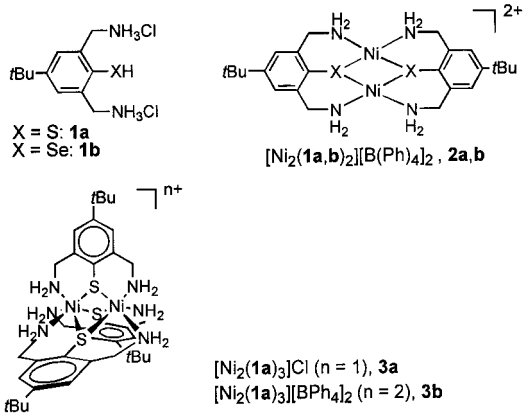
Two dinuclear nickel amine-selenolate complexes of the tridentate amine-selenolate ligand, 4-*tert*-butyl-2,6-di-(aminomethyl)selenophenol (**1b**), have been synthesized and their properties characterized. The green complex $[Ni^{II}_2(\mathbf{1b})_3]Cl$ (**4a**) is readily prepared from **1b**, $NiCl_2 \cdot 6\,H_2O$, and NaOMe in methanol or by reaction of coordinatively unsaturated $[Ni^{II}_2(\mathbf{1b})_2][BPh_4]_2$ (**2b**) with another one equivalent of **1b** in the presence of triethylamine. The face-sharing, bioctahedral structure of **4a** is derived from UV/Vis spectroscopy, cyclic voltammetry, and single-crystal X-ray diffraction of its oxidation product, $[Ni^{II}Ni^{III}(\mathbf{1b})_3]^{2+}$. The dication was prepared by air-oxidation of **4a** in MeOH and isolated as the dark-brown BPh_4^- salt, $[Ni^{II}Ni^{III}(\mathbf{1b})_3][BPh_4]_2 \cdot CH_3OH$ (**4b**). Mixed-valent complex **4b** consists of a dinuclear, face-sharing bioctahedral dication with a central $N_3Ni^{II}(\mu_2\text{-}SeR)_3Ni^{III}N_3$ core and well-separated tetraphenylborate anions. Distortions from D_{3h} symmetry suggest that **4b** is a trapped-valence compound in the solid-state. On the CV time scale complex **4a** undergoes two reversible one-electron oxidations at $E^1_{1/2} = -0.15$ and at $E^2_{1/2} = +0.29$ V vs SCE, affording **4b** and the thermally not stable trication $[Ni^{III}_2(\mathbf{1b})_3]^{3+}$, respectively. The EPR spectrum of a powdered sample of **4b** reveals an $S = {}^3/_2$ ground state of the mixed-valent $Ni^{II}Ni^{III}$ complex.

Introduction

In contrast to the considerable chemistry of nickel thiolate complexes,[1] the coordination chemistry of nickel selenolate complexes has been less extensively developed.[2] The majority of the structurally characterized complexes contain divalent, four-coordinate nickel with planar[3] or tetrahedral coordination environments.[4] Recently, higher coordination numbers have been realized by partial selenolate ligand replacement through multidentate N-based coligands.[5][6] Structurally characterized selenolate complexes of trivalent[7] and quadrivalent[8] nickel are known as well, most of them with unsaturated selenolate ligands, as for instance with benzene-1,2-diselenol.[9] However, attempts to prepare nickel(III) complexes of monodentate aliphatic or aromatic selenolate ligands have not yet been successful.

Recently we have reported the synthesis, solution- and solid-state structures of dinuclear nickel complexes **2a**,**b** of amine-thiolate and -selenolate ligands **1a**,**b**.[10] In contrast to many other $N_2Ni(\mu_2\text{-}SR)_2NiN_2$ type complexes, the amine-thiolate complex **2a** was shown to readily react with another one equivalent of **1a** to afford the dinuclear, face-sharing bioctahedral complex **3a**. Furthermore, complex **3a** could be reversibly oxidized to afford the mixed-valent dication $[Ni^{II}Ni^{III}(\mathbf{1a})_3]^{2+}$ in **3b** with distinct localized Ni^{III} ($S = {}^1/_2$) and Ni^{II} ions ($S = 1$).[11] Such dinuclear, face-sharing octahedral complexes have attracted considerable attention in regards to their electronic structures.[12,13]

We now present the synthesis, structural, spectral, and redox properties of the selenium analogs of **3a**,**b**.



Scheme 1. Structures of ligands and complexes **1a**,**b**, **2a**,**b**, and **3a**,**b**

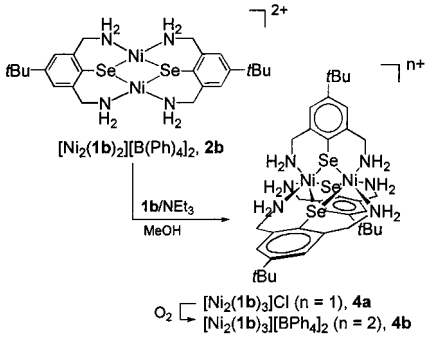
Results and Discussion

Syntheses

The synthesis of amine-selenolate complexes **4a**,**b** is shown in Scheme 2. Analogously to the preparation of amine-thiolate complex **3a**, complex **4a** was obtained by reaction of **2b** with another one equivalent of **1b** in the presence of triethylamine. Alternatively, complex **4a** could also

[a] Institut für Anorganische und Analytische Chemie, Universität Freiburg
Albertstraße 21, D-79104 Freiburg, Germany
Fax: (internat.) +49 (0)761/ 203-6001
E-mail: kerstber@sun2.ruf.uni-freiburg.de
[b] Institut für Physikalische Chemie, Universität Freiburg
Albertstraße 23a, D-79104 Freiburg, Germany

 © WILEY-VCH Verlag GmbH, D-69451 Weinheim, 1999 1434–1948/99/0101–0189 $ 17.50+.50/0



Scheme 2. Preparation of amine-selenolate complexes **4a**,**b**

be obtained by the direct reaction between **1b** and $Ni(ClO_4)_2 \cdot 6\ H_2O$ in a 3:2 molar ratio. The face-sharing, bioctahedral structure of **4a** is derived from UV/Vis spectroscopy, cyclic voltammetry, and single-crystal X-ray diffraction of its oxidation product **4b** (see below).

Complex **4a** is a pale-green, air-sensitive solid that is insoluble in most common organic solvents, but a suspension of **4a** in methanol, when exposed to air, produces a clear deep brown solution. From the resulting clear solution, upon addition of $NaBPh_4$, the dicationic salt $[Ni_2(\mathbf{1b})_3][BPh_4]_2 \cdot MeOH$ (**4b**) is obtained as black crystals.

Crystal Structure of 4b

The crystal structure determination of **4b** confirms the dinuclear structure and the mixed-valent nature of the $[Ni_2(\mathbf{1b})_3]^{2+}$ dication. The crystal structure consists of well-separated dications $[Ni_2(\mathbf{1b})_3]^{2+}$, BPh_4^- anions, and one methanol molecule of crystallization. Complex **4b** is isostructural with the amine-thiolate complex **3b**.[11] The molecular structure of the $[Ni_2(\mathbf{1b})_3]^{2+}$ dication is displayed in Figure 1 along with important bond lengths and angles.

Both nickel ions are facially coordinated to three amine nitrogen atoms and three bridging selenolate selenium atoms of three amine-selenolate ligands. The N_3Se_3 octahedra around Ni(1) and Ni(2) are different, and consequently, the local symmetry of the $[Ni_2(\mathbf{1b})_3]^{2+}$ dication is distorted from D_{3h} symmetry. These distortions are manifested in three different Ni−Se distances at Ni(1) at 2.456(1), 2.427(1), and 2.533(1) Å and similarly at Ni(2) at 2.443(1), 2.391(1), and 2.529(1) Å. Likewise, the Ni−N distances at Ni(1) at 2.042(4), 2.102(4), and 2.061(4) Å and similarly at Ni(2) at 2.011(4), 2.107(4), and 2.087(4) Å are not equidistant. It is noted that the Ni−N and Ni−Se bond lengths appear to be shorter at Ni(2).

As expected, the average Ni−Se bond length at 2.463(1) Å is longer than the average Ni−S bond length in **3b** at 2.380(1) Å. The average Ni−N bond length, on the other hand, has decreased from 2.089(3) Å in **3b** to 2.068(4) Å in **4b**. Both, Ni−Se and Ni−N distances should be compared with Ni−Se and Ni−N distances of 2.440(3) and 2.063(5) Å, respectively, in $[Ni(terpy)(SeC_6H_2\text{-}2,4,6\text{-}Me_3)_2]$, which contains five-coordinate Ni^{II} in a distorted trigonal-bipyramidal coordination environment.[6] As a consequence of

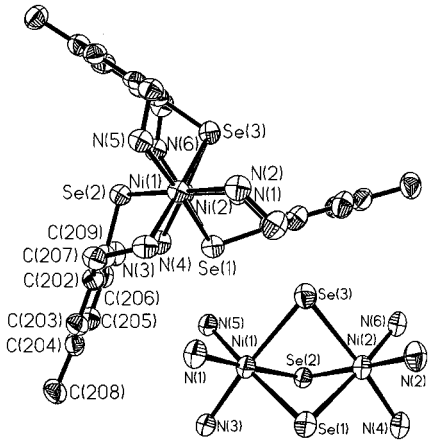


Figure 1. Molecular structure of the $[Ni^{II}Ni^{III}(\mathbf{1b})_3]^{2+}$ dication and the structure of the central $N_3Ni(\mu_2\text{-}SeR)_3NiN_3$ core in **4b** (50% probability thermal ellipsoids). Hydrogen atoms and *tert*-butyl methyl carbon atoms have been omitted for reasons of clarity. Selected bond lengths [Å] and angles [°]: Ni(1)−N(1) 2.042(4), Ni(1)−N(3) 2.102(4), Ni(1)−N(5) 2.061(4), Ni(2)−N(2) 2.011(4), Ni(2)−N(4) 2.107(4), Ni(2)−N(6) 2.087(4), Ni(1)−Se(1) 2.456(1), Ni(1)−Se(2) 2.427(1), Ni(1)−Se(3) 2.533(1), Ni(2)−Se(1) 2.443(1), Ni(2)−Se(2) 2.391(1), Ni(2)−Se(3) 2.529(1); Ni(1)−Se(1)−Ni(2) 80.96, Ni(1)−Se(2)−Ni(2) 82.63(1), Ni(1)−Se(3)−Ni(2) 77.84(1), N−Ni−N 89.0(2)−92.7(2), Se−Ni−Se 80.40(3)−85.99(3), N−Ni−Se_{cis} 91.4(1)−93.8(1), N−Ni−Se_{trans} 172.1(1)−174.7(7), Ni−Se−Ni 77.84(1)−82.63(1)

longer Ni−Se distances, the Ni(1)···Ni(2) separation in **4b** is 3.181(1) Å. The corresponding value in **3b** was determined to be 3.064(1) Å. In both compounds, however, wide Ni−S−Ni [mean 80.16(3)°] and Ni−Se−Ni angles [mean 80.48(3)°] preclude any attraction between the metal atoms.[14]

The individual bond lengths and angles within the three amine-selenolate ligands show no unusual features ruling out the possibility of a ligand-centered oxidation of **4a** with one of the ligands being coordinated as a selenyl radical in **4b**. A metal-centered rather than a ligand-centered oxidation is also supported by infrared spectroscopy. From the apparent distortions from D_{3h} symmetry complex **4b** appears to be a trapped-valence $Ni^{II}Ni^{III}$ compound with distinct localized Ni^{II} and Ni^{III} sites (Class I in Robin and Day's classification of mixed-valent species).[15] A delocalized species would be expected to have structurally identical nickel sites.[16] The greater extent of distortion in Ni−N and Ni−Se distances at Ni(2) may be due to a Jahn−Teller distortion, which is expected for an octahedral Ni^{III} ion with low-spin d^7 electronic configuration. Thus, Ni(2) is presumably a Ni^{III} ion.

Infrared and UV/Vis Spectra of 4a, b

The most characteristic features in the infrared spectrum of **4a** are two strong absorptions at 3328 and 3250 cm^{-1}. These bands are assigned to $\nu_{as}(NH_2)$ and $\nu_s(NH_2)$ stretching vibrations of the RNH_2 groups.[17] In the infrared spectrum of **4b**, the $\nu(NH_2)$ stretching frequencies are shifted by ca. 20 cm^{-1} to lower wavenumbers. This further supports the metal-centered oxidation of **4a** and the ground state of

4b, since the decrease in Ni−N bond lengths upon passing from $Ni^{II}-NH_2$ to $Ni^{III}-NH_2$ is expected to give a more polarized $Ni^{III}N-H$ bond, causing a weakening of the N−H bonds. Furthermore, the increase in the number of $\nu(NH_2)$ stretching vibrations from two in **4a** to five in **4b** nicely corroborates with the notion of distinct localized Ni^{II} and Ni^{III} oxidation states in the mixed-valent compound **4b**.

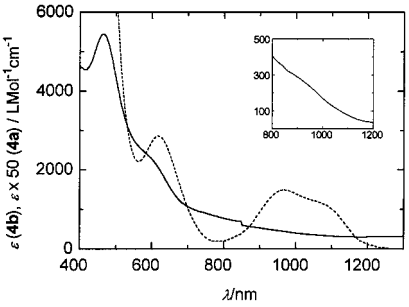


Figure 2. UV/Vis spectra of **4a** (···) and **4b** (—) in DMF at 295 K. The inset displays the spectrum of **4b** in the 800-to-1200 nm region

The pale-green complex **4a** exhibits typical weak d-d transitions of octahedral nickel(II) (d^8) in the 500 to 1200 nm region (Figure 2). Compared to the thiolate complex **3a**, the ligand field transitions ν_2 ($^3A_{2g} \rightarrow {}^3T_{1g}$) at 617 nm and ν_1 ($^3A_{2g} \rightarrow {}^3T_{2g}$) at 966 and 1065 nm (splitting due to lower symmetry) are shifted by 24 and 44 nm to lower energies, consistent with a weaker ligand field strength of the amine-selenolate ligand. The electronic spectrum of **4b** is dominated by two intense, spin-allowed charge transfer (CT) transitions at 465 and 604 nm. Similar intense absorptions were observed for complex **3b** at 473 and 580 nm. Other than the two intense CT bands, the UV/Vis spectrum of **4b** reveals no further characteristic features.

Electrochemistry

The cyclic voltammogram of **4a** in DMF solution reveals two one-electron oxidation waves at $E^1_{1/2} = -0.15$ V and $E^2_{1/2} = +0.29$ V vs SCE both closely approaching the characteristics of reversible charge transfer processes; that of **4b** using the same experimental conditions is identical to that of **4a** (Figure 3).

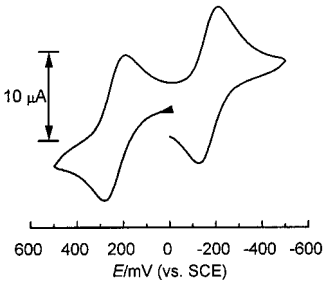


Figure 3. Cyclic voltammogram of **4b** in DMF at 295 K. Experimental conditions: [**4b**] ca. 1×10^{-3} M, 0.1 M [nBu$_4$N][PF_6], Pt disk working electrode, Ag wire reference electrode, scan rate = 200 mV·s^{-1}

At all scan rates (50−500 mV·s^{-1}), the ratio i_{pc}/i_{pa}, $i_p/\nu^{1/2}$ is independent of scan rate, and $\Delta E^1_p = 85$ mV and $\Delta E^2_p =$ 79 mV (at 100 mV·s^{-1}) increase slightly with scan rate. Controlled-potential coulometry of **4a** in DMF at an applied potential of 0.0 V vs SCE consumed $n = 0.96 \pm 2$ e$^-$/complex. The brown solution contains the $[Ni_2(\mathbf{1b})_3]^{2+}$ dication as shown by UV/Vis spectroscopy. Rereduction at −0.45 V vs SCE reforms the pale-green complex **4a**. Accordingly, the respective one-electron-transfer processes are assigned to Eqs. 1a, b producing the mixed-valent complex **4b** and subsequently the thermally instable dinickel(III) selenolate species.

$$[Ni^{III}Ni^{III}(\mathbf{1b})_3]^{3+} + e^- \rightleftharpoons [Ni^{III}Ni^{II}(\mathbf{1b})_3]^{2+} \quad E^2_{1/2} \qquad (1a)$$

$$[Ni^{III}Ni^{II}(\mathbf{1b})_3]^{2+} + e^- \rightleftharpoons [Ni^{II}Ni^{II}(\mathbf{1b})_3]^{1+} \quad E^1_{1/2} \qquad (1b)$$

$$[Ni^{III}Ni^{III}(\mathbf{1b})_3]^{3+} + [Ni^{II}Ni^{II}(\mathbf{1b})_3]^{1+} \rightleftharpoons [Ni^{III}Ni^{II}(\mathbf{1b})_3]^{2+} \quad K_{com}$$

From the redox potentials $E^x_{1/2}$ the comproportionation constant K_{com} is calculated to be 1.1×10^7, which is slightly smaller than the corresponding constant determined for **3b** (1.4×10^8). Relative to the amine-thiolate complexes **3a**,**b**, the $Ni^{III/II}$ redox potentials of the amine-selenolate complexes **4a**,**b** are cathodically shifted by 0.18 V and 0.13 V, respectively.

EPR Spectroscopy

The mixed-valent nature of **4b** is further confirmed by EPR-Spectroscopy. The EPR spectrum of a powdered sample of **4b** at 77 K exhibits a rhombic signal with three resonances at 1230, 2210, and 3350 G, indicating an $S = {}^3/_2$ ground state. Closer inspection reveals a further resonance at 1080 G, which is also present in the single-crystal EPR spectra. This resonance is tentatively assigned to the $M_s = -{}^3/_2$ to $M_s = +{}^3/_2$ transition, which is forbidden in axial environments, but gains intensity by the rhombic distortion. Unfortunately, hyperfine coupling to nitrogen atoms (^{14}N) could not be observed.

Thus, mixed-valent complex **4b** exhibits an $S = {}^3/_2$ ground state, which is most likely attained by an intramolecular ferromagnetic exchange interaction between a low-spin Ni^{III} ion ($S = {}^1/_2$) and a Ni^{II} ion ($S = 1$). It is interesting to note that an intramolecular ferromagnetic exchange interaction between adjacent Ni^{III} and Ni^{II} ions has also been observed in the trinuclear $Co^{III}Ni^{III}Ni^{II}$ complex $[LCo^{III}Ni^{III}Ni^{II}L][PF_6]_2$ [L = 1,4,7-tris(4-*tert*-butyl-2-mercaptobenzyl)-1,4,7-triazacyclononane], which contains a central $N_3Co^{III}(\mu_2\text{-}SR)_3Ni^{III}(\mu_2\text{-}SR)_3Ni^{II}N_3$ core with three face-sharing octahedra.[12] We anticipate a more detailed study of the electronic spin systems of **3b** and **4b** by magnetic susceptibility measurements.

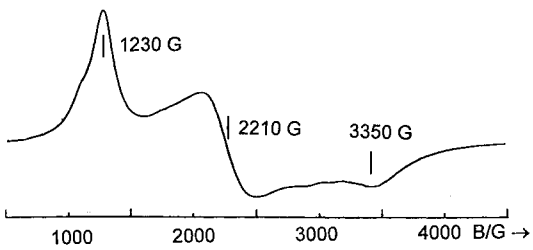


Figure 4. X-Band EPR powder spectrum of **4b** (9 GHz) at 78 K

In the present study it was shown that the coordinatively unsaturated amine-selenolate complex **2b**, upon reaction with **1b**, forms the dinuclear, face-sharing bioctahedral complex **4a** with a central $N_3Ni^{II}(\mu_2\text{-}SeR)_3Ni^{II}N_3$ core. Similarly to the electrochemical properties of isostructural amine-thiolate complex **3a**, complex **4a** undergoes an electrochemically and chemically reversible one-electron oxidation to produce a stable $Ni^{II}Ni^{III}$ amine-selenolate complex. Hence, the amine-chalcogenolate ligands **1a**,**b** both allow for the preparation of discrete dinuclear complexes and the stabilization of unusual nickel oxidation states. Further studies will focus on the isolation of the analogous tellurolate derivatives.

Experimental Section

Materials and Methods: Compounds **1b** and $[Ni_2(\mathbf{1b})_2][BPh_4]_2 \cdot CH_3OH \cdot CH_3CN$[10a] were prepared as previously described. All reactions were carried out under dry nitrogen with standard Schlenk techniques. Solvents were predried over molecular sieves and freshly distilled from appropriate drying agents. – CHN Analyses were determined with a Perkin-Elmer Elemental Analyzer 240. – IR spectra were recorded on a Bruker IFS25 spectrophotometer as KBr pellets. – Electronic spectra were recorded on a Jasco V-570 UV/VIS/NIR spectrometer. – Cyclic voltammetry measurements were carried out at 25°C with an EG&G Princeton Applied Research Potentiostat/Galvanostat Model 263 A. The cell contained a Pt working electrode, a Pt wire auxiliary electrode, and an Ag wire as reference electrode. Concentration of solutions were 0.1 M in supporting electrolyte (nBu$_4$NPF$_6$) and ca 1×10^{-3} M in sample. Ferrocenium/ferrocene was used as internal standard. All potentials were converted to the SCE reference. – EPR spectra were recorded by a conventional Varian X-band spectrometer with 100 kHz modulation.

$[Ni_2(\mathbf{1b})_3][Cl]\cdot EtOH$ (4a). – Method A: To a solution of $[Ni_2(\mathbf{1b})_2][BPh_4]_2 \cdot CH_3OH \cdot CH_3CN$ (137 mg, 0.100 mmol) in acetonitrile (5 mL) was added a solution of **1b** (34 mg, 0.10 mmol) in methanol (2 mL). Addition of 3 drops of NEt_3 initiated the precipitation of a pale-green solid, which was isolated by filtration, washed with methanol (2 mL) and ether (1 mL). The solid was recrystallized from ethanol. Yield: 62 mg (62%). – UV/Vis (DMF): λ_{max} (ε) = 617 (203), 966 (150), 1065 nm (137 $M^{-1}cm^{-1}$). – IR (KBr): $\tilde{\nu}$ = 3328s (NH_2), 3250s cm^{-1} (NH_2). – CV (DMF, 295 K, 0.1 M nBu$_4$NPF$_6$, E [V] vs SCE): $E^1_{1/2} = -0.15$ V, $E^2_{1/2} = +0.29$ V. – $C_{36}H_{57}N_6Se_3Ni_2Cl\cdot EtOH$ (1009.67): calcd. C 45.20, H 6.29, N 8.32; found C 44.83, H 5.87, N 7.94.

Method B: To a solution of $Ni(ClO_4)_2 \cdot 6\,H_2O$ (244 mg, 0.67 mmol) and the hydrochloride salt of the ligand **1b** (344 mg, 1.00 mmol) in ethanol (10 mL) was added a solution of triethylamine (303 mg, 3.00 mmol) in ethanol (3 mL). The mixture was stirred for 30 min at 20°C during which time a pale-green microcrystalline of **4a** formed which was filtered off, washed with ethanol and ether, and dried in vacuum. Yield: 240 mg (72%).

$[Ni_2(\mathbf{1b})_3][BPh_4]_2\cdot MeOH$ (4b): A suspension of **4a** (101 mg, 0.100 mmol) in methanol (30 mL) was stirred for 6h in the presence of air to ensure complete oxidation of **4a**. To the resulting brown solution was added dropwise a solution of $NaBPh_4$ (0.20 g, 0.58 mmol) in methanol (2 mL). The solution was filtered and was allowed to stand for 2d at room temperature during which time **4b** precipitated as black crystals. Yield: 86 mg (54%). – IR (KBr): $\tilde{\nu}$ = 3302 m, 3289 w, 3268 w, 3242 s, 3229 s cm^{-1} (NH_2). – UV/Vis (DMF): λ_{max} (ε) = 350 (8710), 399 (4644), 465 (4978), 604 nm (1554 $M^{-1}cm^{-1}$). – CV (DMF, 295 K, 0.1 M nBu$_4$NPF$_6$, E [V] vs SCE): $E^1_{1/2} = -0.15$ V, $E^2_{1/2} = +0.29$ V. – $C_{85}H_{101}B_2N_6Ni_2OSe_3$ (1598.66): calcd. C 63.86, H 6.37, N 5.26; found C 63.83, H, 6.22, N 5.11.

Crystal-Structure Determination: Black crystals of **4b** suitable for single-crystal X-ray determination were obtained by the procedure described above. Crystal data and refinement details for **4b** ($C_{85}H_{101}B_2N_6Ni_2OSe_3$, M_r 1598.66): crystal size 0.52 × 0.44 × 0.32 mm^3, STOE IPDS diffractometer, T = 193(2) K, monoclinic, space group $P2_1/c$, a = 23.552(5), b = 19.384(4), c = 16.701(3) Å, β = 105.79(3)° , V = 7507(3) Å^3, Z = 4, ρ_{calcd} = 1.41 g·cm^{-3}, μ(Mo-K_α) = 2.007 mm^{-1}, $2\theta_{max}$ = 48.6°, 63669 reflections collected, 11924 unique reflections (R_{int} = 0.1051), 8926 observed reflections [$I > 2\sigma(I)$]. The data were corrected for Lorentz and polarization effects. The structure was solved by direct methods (SHELXS-86)[18] and refined by full-matrix least-squares techniques against F^2 (SHELXL-93). All non-hydrogen atoms were refined anisotropically except the methyl carbon atoms of one disordered *tert*-butyl group. An isotropic split-atom model was applied for the disordered methyl carbon and oxygen atoms. The multiplicities of the respective orientations C(210)–C(212)/C(213)–C(215) were refined as follows: 0.73(1)/0.27(1). Hydrogen atoms were placed at calculated positions and were refined using a riding model with isotropic thermal parameters fixed at 1.2 times the equivalent isotropic U of the atom to which they were bonded. Final residuals: $R1$, $wR2$ [$F_o > 4\sigma(F_o)$]: 0.0446, 0.0963, $R1$, $wR2$ (all data): 0.0701, 0.1137, goodness-of-fit on F^2: 1.05, residual electron density: 0.58/−0.62 e·Å^{-3}. The quality of the structure could not be improved with an absorption correction. Crystallographic data (excluding structure factors) for the structure reported in this paper have been deposited with the Cambridge Crystallographic Data Centre as supplementary publication no. CCDC-102536 (**4b**). Copies of the data can be obtained free of charge on application to CCDC, 12 Union Road, Cambridge CB2 1EZ, UK [Fax: +44 (1223) 336-033; E-mail: deposit@cam.ac.uk].

Acknowledgments

This work was supported by the Deutsche Forschungsgemeinschaft. We thank Prof. Dr. H. Vahrenkamp for his generous support and Prof. Dr. B. Krebs for the use of the STOE-IPDS diffractometer. We are grateful to S. Höck for help in collecting the X-ray data.

[1] [1a] B. Krebs, G. Henkel, *Angew. Chem.* **1991**, *105*, 785–804; *Angew. Chem. Int. Ed. Engl.* **1991**, *30*, 769–788. – [1b] M. A. Halcrow, G. Christou, *Chem. Rev.* **1994**, *94*, 2421–2481.
[2] J. Arnold, *Prog. Inorg. Chem.* **1995**, *43*, 353–417.
[3] [3a] C. A. Marganian, N. Baidya, M. M. Olmstead, P. K. Mascharak, *Inorg. Chem.* **1992**, *31*, 2992–2994. – [3b] S. B. Choudhury, M. A. Pressler, S. A. Mirza, R. O. Day, M. J. Maroney, *Inorg. Chem.* **1994**, *33*, 4831–4839.
[4] [4a] J. M. McConnachie, J. A. Ibers, *Inorg. Chem.* **1991**, *30*, 1770–1773. – [4b] C. M. Marganian, M. M. Olmstead, P. K. Mascharak, *Inorg. Chem.* **1996**, *35*, 2752–2757.
[5] N. Baidya, B. C. Noll, M. M. Olmstead, P. K. Mascharak, *Inorg. Chem.* **1992**, *31*, 2999–3000.
[6] C. A. Marganian, H. Vazir, N. Baidya, M. M. Olmstead, P. K. Mascharak *J. Am. Chem. Soc.* **1995**, *117*, 1584–1594.
[7] [7a] R.-M. Olk, B. Olk, J. Rohloff, J. Reinhold, J. Sieler, K. Trübenbach, R. Kirmse, E. Hoyer, *Z. Anorg. Allg. Chem.* **1992**, *609*, 103–116. – [7b] W. B. Heuer, A. E. True, P. N. Swepston, B. M. Hoffman, *Inorg. Chem.* **1988**, *27*, 1474–1482.
[8] [8a] P. T. Beurskens, J. A. Cras, *J. Cryst. Mol. Struct.* **1971**, *1*,

63−67. − [8b] J. Kaiser, W. Dietzsch, R. Richter, L. Golic, J. Siftar, *Acta Crystallogr.* **1980**, *B36*, 147−150.
[9] D. J. Sandman, G. W. Allen, L. A. Acampora, J. C. Stark, S. Jansen, M. T. Jones, G. J. Ashwell, B. M. Foxman, *Inorg. Chem.* **1987**, *26*, 1664−1669.
[10] [10a] B. Kersting, *Eur. J. Inorg. Chem.* **1998**, 1071−1077. − [10b] B. Kersting, G. Steinfeld, J. Hausmann, *Eur. J. Inorg. Chem.*, 179−187.
[11] B. Kersting, D. Siebert, *Inorg. Chem.* **1998**, *37*, 3820−3828.
[12] T. Beissel, F. Birkelbach, E. Bill, T. Glaser, F. Kesting, C. Krebs, T. Weyhermüller, K. Wieghardt, C. Butzlaff, A. X. Trautwein, *J. Am. Chem. Soc.* **1996**, *118*, 12376−12390.
[13] [13a] S. Drüeke, P. Chaudhuri, K. Pohl, K. Wieghardt, X.-Q. Ding, E. Bill, A. Sawaryn, A. X. Trautwein, H. Winkler, S. J. Gurman, *J. Chem. Soc. Chem. Commun.* **1989**, 59−62. − [13b] D. R. Gamelin, E. L. Bominaar, M. L. Kirk, K. Wieghardt, E. I. Solomon, *J. Am. Chem. Soc.* **1996**, *118*, 8085−8097.
[14] F. A. Cotton, D. A. Ucko, *Inorg. Chim. Acta* **1972**, *6*, 161−172.
[15] M. B. Robin, P. Day, *Adv. Inorg. Chem. Radiochem.* **1967**, *10*, 247−422.
[16] C. Creutz, *Prog. Inorg. Chem.* **1983**, *30*, 1−73.
[17] K. Nakamoto, *Infrared and Raman Spectra of Inorganic and Coordination Compounds*, Wiley, New York, **1978**.
[18] G. M. Sheldrick, *SHELXS-86*, University of Göttingen, Germany, **1990**; G. M. Sheldrick, *SHELXL-93*, University of Göttingen, Germany, **1993**.

Received September 23, 1998
[I98326]

Supramolecular Assemblies of 1,2-Dicarbadodecaborane(12) with Bowl-Shaped Calix[5]arene

Michaele J. Hardie[a] and Colin L. Raston*[a]

Keywords: Calixarene / Carboranes / Host-guest chemistry / Non-classical hydrogen bonding / Supramolecular chemistry

Treatment of globular 1,2-dicarbadodecaborane(12) (*o*-carborane) **1** with the bowl-shaped container molecule calix[5]arene **2** affords either the crystalline 1:1 or 1:2 host-guest complexes (*o*-carborane)(calix[5]arene)(CH_2Cl_2) **3**, (*o*-carborane)(calix[5]arene)(toluene) **4** and (*o*-carborane)-(calix[5]arene)$_2$(CH_2Cl_2)$_{0.5}$ **5**. The three complexes show a remarkable range of different supramolecular interplay beyond the common structural unit, a ball-and-socket nanostructure or supermolecule [(*o*-carborane)∩(calix[5]arene)]. Complex **3** forms dimeric [(*o*-carborane)∩(calix[5]arene)]$_2$ units, and **5** has an additional edge on interaction between the supermolecule and a secondary calix[5]arene host.

Introduction

Carbon-containing polyhedral boranes, the carboranes, are extremely stable cage molecules known for over 30 years. Carboranes and their derivatives have applications in a number of diverse fields such as boron neutron capture therapy, boron carbide-type ceramics, complexing agents for extraction of metal ions, nonlinear optics, conducting polymers and more.[1] The carboranes *o*-, *m*-, and *p*-$C_2B_{10}H_{12}$[1,2-, 1,7-, 1,12-dicarbadodecaborane(12)] (hereafter *o*-, *m*-, and *p*-carborane) are twelve-vertex icosahedral cages whose potential as components or building blocks in supramolecular systems is beginning to be explored.[2−6][9−12] Rigid rod-like and trigonal carborane-based molecular building units have been synthesised,[2] as well as metallodendrimers.[3] A number of carborane derived macrocyles are known, with the clusters linked through their carbon centres by both organic groups[4] and mercury centres.[5] The mercury linked macrocycles show host-guest complexation of halide ions, and the tetrameric macrocycle can complex *closo*-$B_{10}H_{10}^{2-}$.[6]

Carboranes have high C−H acidity[7] and consequently show potential for hydrogen bonding.[8] Supramolecular complexes involving such weak intermolecular interactions are known. The first examples to be reported were the series of inclusion complexes with cyclodextrin host molecules and *o*-carborane as the guest.[9] Thermally stable 1:1 cyclodextrin/carborane complexes were formed with α-, β-, and γ-cyclodextrin, and a 2:1 complex was also found for α-cyclodextrin. More recently the crystal structures of the 1:1 complexes of hexamethylphosphoramide (HMPA) with *o*-, *m*-, and *p*-carboranes have been reported.[10] The three complexes show extensive C−H···O hydrogen bonding and all adopt quite different supramolecular structures, commensurate with their differing arrangement of C−H sites. These complexes represent the first structures of unsubstituted carboranes in a crystal lattice. *o*-Carborane forms 1:1 complexes with diaza-18-crown-6 and aza-18-crown-6 again with distinct supramolecular structures.[11] The (*o*-carborane)(diaza-18-crown-6) complex associates through C−H···O hydrogen bonds at distances similar to those found for the HMPA complexes, whereas the aza-18-crown-6 complex has a layered structure with no close intermolecular contacts. The bowl-shaped container molecule cyclotriveratrylene (CTV) can act as a host for *o*-carborane guest molecules and a 2:1 CTV/*o*-carborane complex is formed.[12] In the solid state one CTV molecule complexes a carborane guest while the other forms a π interaction with the host CTV. Each $C-H_{carborane}$ is directed towards the centroid of an aromatic ring in the cavity of the CTV as a Coulumbic interaction between a polarised C−H bond and the basic π-electrons of an aromatic ring. The energy of such an interaction between benzene with *o*-carborane, shown schematically in Figure 1, is calculated to be energetically favoured by 2.74 kcal mol^{-1},[12] and this type of interaction is usually described as a weak non-classical C−H···π hydrogen bond. NMR studies were uninformative, except to suggest that *o*-carboranes can bind *endo*- and *exo*-to the cavity of the CTV.[12]

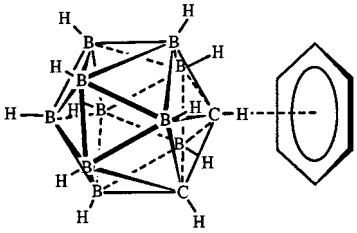


Figure 1. Schematic representation of non-classical hydrogen bonding between *o*-carborane and an aromatic ring

The complexation of *o*-carborane by a bowl-shaped container molecule such as CTV is reminiscent of much of the host-guest chemistry of the fullerene C_{60}[13][14] Both the carboranes and C_{60} are thermally stable, icosahedral clusters with diameters of about 8 and 10 Å respectively. Fullerene C_{60} forms inclusion complexes with the bowl-shaped CTV[13] and a number of calixarenes,[14] indeed the selective

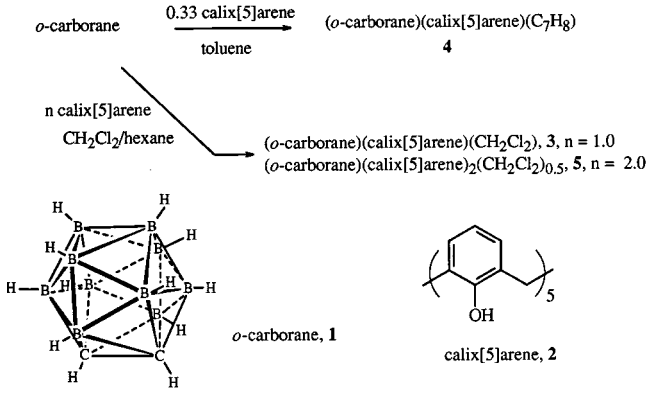
[a] Department of Chemistry, Monash University, Clayton, Melbourne, Victoria 3168, Australia

 © WILEY-VCH Verlag GmbH, D-69451 Weinheim, 1999 1434−1948/99/0101−0195 $ 17.50+.50/0

complexation of C_{60} by *p*-*t*Bu-calix[8]arene is a simple and efficient means of C_{60} extraction from a mixture of fullerenes. The supramolecular chemistry of carboranes with bowl-shaped potential host molecules is, by comparison, in its infancy and may also lead to simplified separation procedures, currently reliant on chromatographic techniques.[7] The work reported herein further develops host-guest chemistry between carboranes and bowl-shaped molecules with the formation of 1:1 and 1:2 complexes of *o*-carborane with calix[5]arene. The solid state structures have been established from low-temperature X-ray diffraction data. These three complexes show a remarkable range of supramolecular interactions and, despite being constructed from similar or the same supramolecular synthons/molecular building blocks, form different nano-structures. The ability to control weak intermolecular interactions underpins much of the basic aims and ideals of supramolecular chemistry,[15] yet the range of possible interactions is often extensive even for simple systems, illustrated by the quite distinct nano-structures formed here.

Results and Discussion

Slow evaporation of toluene solutions of 1:1, 1:2 mixtures of *o*-carborane **1** and calix[5]arene **2**, and subsequent recrystallisation from dichloromethane/hexane affords the colourless crystalline complexes, (*o*-carborane)(calix[5]arene)(CH_2Cl_2) **3** and (*o*-carborane)(calix[5]arene)$_2$-(CH_2Cl_2)$_{0.5}$ **5**, see Scheme 1. Heating a 3:1 mixture of **1** and **2** in toluene at ca. 70°C for one hour and subsequent cooling gave crystals of the toluene solvated 1:1 complex (*o*-carborane)(calix[5]arene)(C_7H_8) **4**. The complexes were characterised by IR spectroscopy, microanalysis and single crystal X-ray crystallography. The IR showed a clear a shift to lower energy (by 11 cm^{-1}) for ν_{C-H} of the carborane in **5**. Similar shifts in the IR were seen for the previously reported 2:1 complex (*o*-carborane)(CTV)$_2$ where the carborane ν_{C-H} shifts 13.5 cm^{-1} to lower energy.[12] Such an energy shift is indicative of the involvement of the carborane C−H in hydrogen bonding, with dispersal of the extra charge on the carbon resulting in the strengthening of the B−H bonds. Smaller shifts of 6 and 3 cm^{-1} respectively were seen in the 1:1 complexes **3** and **4**.



Scheme 1

(*o*-Carborane)(calix[5]arene)(CH_2Cl_2) 3

X-ray diffraction data was collected for **3** at −123(1)°C. The crystal structure was solved in the monoclinic space group $P2_1/n$. As was seen for (*o*-carborane)(CTV)$_2$,[12] a ball-and-socket supermolecule is formed between the host calix[5]arene and guest *o*-carborane.

The calix[5]arene adopts a bowl-conformation, with an average torsion angle between an aromatic ring and the plane formed by hydroxy oxygens of around 50°. The ball-and-socket supermolecule is shown in Figure 2. The carborane guest sits close to the middle of the calixarene cavity, with distances from C or B vertices of the carborane to aromatic ring centroids of the calixarene of 3.44, 3.55, 3.78, 3.93, and 4.08 Å. Both C−H vectors of the carborane are directed towards aromatic rings of the host molecule, albeit in an unsymmetrical fashion. As was seen for (*o*-carborane)(CTV)$_2$,[12] this interaction is most likely non-classical C−H···π hydrogen bonding, with the two interactions having $C_{carborane}$···aromatic centroid separations of 3.55 and 3.44 Å, and $C-H_{carborane}$···centroid angles of 11.8 and 24.8° respectively; the closer contact having the lesser C−H···π interaction, indicated by the greater angle at the hydrogen.

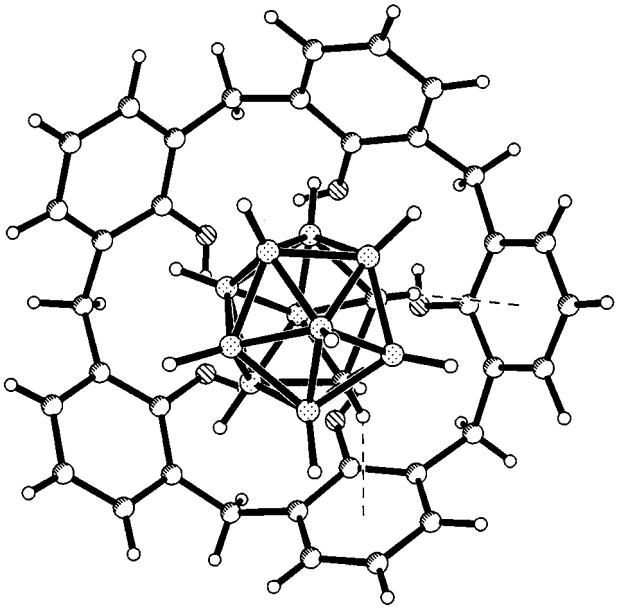


Figure 2. Ball-and-socket (*o*-carborane)∩(calix[5]arene) assembly of (calix[5]arene)(*o*-carborane)(CH_2Cl_2) **3**. Potential non-classical C−H π hydrogen bonds are indicated as dashed lines

The ball-and-socket (*o*-carborane)∩(calix[5]arene) units organise into larger dimeric supramolecules within the crystal lattice. The dimers have the calixarene hydroxy groups facing each other, forming a hydrophilic core shown in Figure 3. The X-ray data obtained did not allow for the location of the hydroxy hydrogens, and those shown in Figures are at calculated positions. This makes it difficult to ascertain the exact hydrogen-bonding pattern. The O···O contacts between the calixarenes are quite close at 2.96, 3.01, 3.09, 3.14, and 3.22 Å. There are no close contacts between dimers within the crystal lattice. The dimers occur in two layers, each running in the *b* direction and alternat-

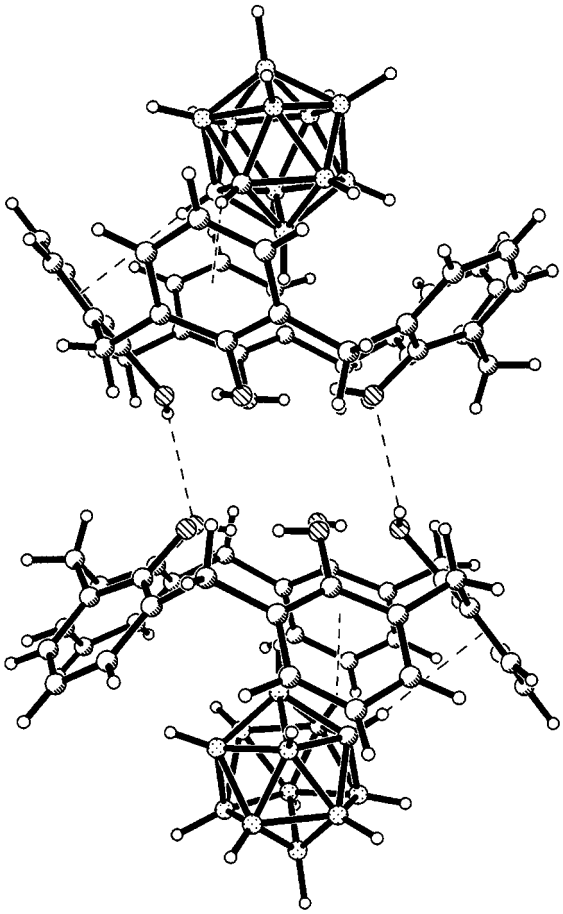


Figure 3. The dimeric [(*o*-carborane)∩(calix[5]arene)]$_2$ nano-structures of **3**. The hydrogen-bonded (calix[5]arene)$_2$ unit can be considered to be acting as a divergent receptor

ing in the *c* direction, with disordered dichloromethane molecules positioned between individual dimers.

(*o*-Carborane)(calix[5]arene)(C_7H_8) 4

X-ray diffraction data was collected for **4** at −150(1)°C. The crystal structure was solved in the monoclinic space group $P2_1/n$. Although the basic structural unit of **4** − a ball-and-socket type (*o*-carborane)∩(calix[5]arene) − is similar to that of **3**, the crystal packing is quite distinct.

The (*o*-carborane)∩(calix[5]arene) supermolecule of **4** is similar to that of **3**, although the *o*-carborane sits slightly closer to the host molecule. The calix[5]arene adopts a bowl-conformation, with an average torsion angle between an aromatic ring and the plane formed by hydroxy oxygens of around 48°. The C−H vectors of the carborane point towards the edges of aromatic rings of the calix[5]arene host at $C_{carborane}$···aromatic centroid separations of 3.40 and 3.49 Å, and $C-H_{carborane}$···centroid angles of 20.2 and 31.4°. The dimeric units evident in **3** are not formed, however, with the (*o*-carborane)∩(calix[5]arene) supermolecules stacking in the same orientation along the *b* direction (Figure 4) to form columns of the supermolecule. The orientation of these columns alternates along the *c* direction. The

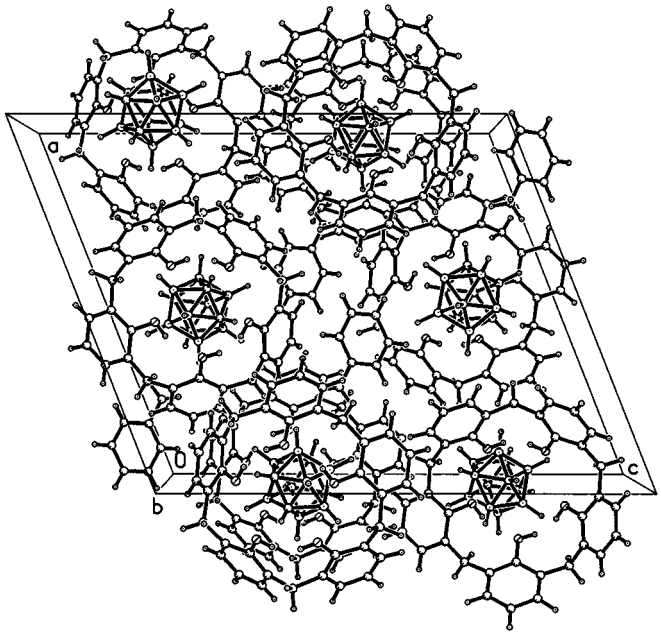


Figure 4. Packing diagram of (calix[5]arene)(*o*-carborane)(C_7H_8) **4** along the *b* axis. Columns of (calix[5]arene)]∩(calix[5]arene) supermolecules are formed along *b*

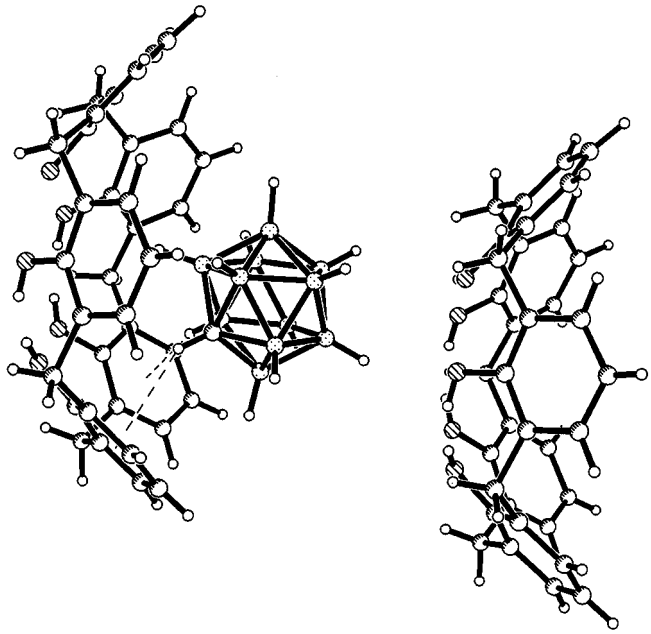


Figure 5. Side view of the ball-and-socket (*o*-carborane)∩(calix[5]arene) supermolecule and calixarene of next supermolecule along *b*, of (calix[5]arene)(*o*-carborane)(C_7H_8) **4**. Potential non-classical C-H π hydrogen bonds are indicated as dashed lines

included *o*-carborane of one supermolecule has contacts to the hydroxy groups of the next (*o*-carborane)∩(calix[5]arene) at a closest B···O distance of 3.55 Å (Figure 5).

Each toluene molecule within the crystal lattice forms close contacts to two calix[5]arene molecules (Figure 6). The plane of the toluene is almost exactly perpendicular to the plane of an aromatic ring of one calix[5]arene (torsion angle 89.1°). An aromatic C−H of the toluene, *ortho* to the methyl group, is directed towards the centre of this arene at

a H···centroid distance of 2.6 Å. One of the toluene C-Hs *meta* to the methyl group is directed towards a hydroxy oxygen of the calix[5]arene at an H···O distance of 2.5 Å. The toluenes effectively bridge between the supramolecular columns in the direction of the *c* axis.

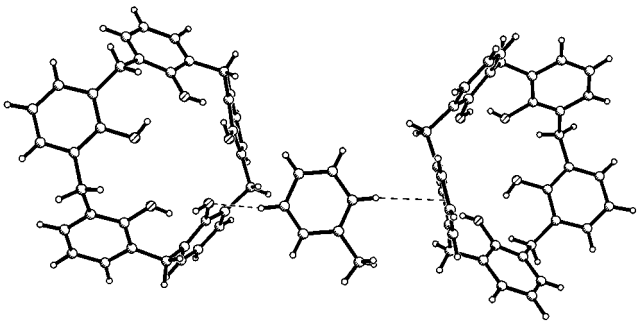


Figure 6. Environment of toluene molecule in (calix[5]arene)(*o*-carborane)(C_7H_8) **4**. Close contacts between the toluene and adjacent calix[5]arene molecules are indicated as dashed lines

(*o*-Carborane)(calix[5]arene)$_2$(CH_2Cl_2)$_{0.5}$ 5

X-ray diffraction data was collected for **5** at room temperature and −100°C. The crystals were observed to undergo a phase change from primitive monoclinic (room temperature, $P2_1/m$: a = 11.679(1), b = 18.128(2), c = 16.394(1) Å, β = 97.12(1)°) to triclinic [−100°C: a = 11.6151(13), b = 16.3617(17), c = 18.014(2) Å, α = 90.699(9), β = 91.612(9), γ = 96.739(9)] on cooling. The room-temperature and low-temperature structures are essentially the same, although the carborane displays some positional disorder in the room temperature structure. Data from the low temperature study is presented here. The structure was solved in space group $P\bar{1}$, and features two types of calixarene molecule and one carborane.

Both calix[5]arene molecules adopt a bowl conformation, and their ability to act as host molecules manifests itself in two distinct manners. The curvature of the two calixarenes is quite different. One calixarene has torsion angle between an aromatic ring and the plane formed by hydroxy oxygens between 46.5 and 49.0° (average 48°). The second calixarene is considerably more puckered with torsion angles between 34.4 and 64.2° (average 49°). The shallower calixarene acts as a host molecule for the *o*-carborane, forming the familar ball-and-socket arrangement seen in **4**. The more puckered calixarene acts as a secondary host for the (*o*-carborane)∩(calix[5]arene) assembly forming the [(*o*-carborane)∩(calix[5]arene)]∩(calix[5]arene) nano-structure illustrated in Figure 7. The complexation of a host-guest species by a secondary host is, to out knowledge, relatively uncommon. Other examples of such supramolecular interactions include the complexation of alkali metal-crown ethers by cyclodextrins.[16] These form entirely different nano-structures to that seen here.

The (*o*-carborane)∩(calix[5]arene) arrangement in **5** is similar to the analogous supermolecule in **3**, with both C−H vectors of the included *o*-carborane directed towards aromatic rings of the host calix[5]arene to form non-classical hydrogen bonds. In the case of **5**, however, the C−H$_{carborane}$ vectors point more directly to the centre of the aromatic rings with C···aromatic centroid separations of 3.51 and 3.57 Å, and a C−H$_{carborane}$···centroid angles of 0.8

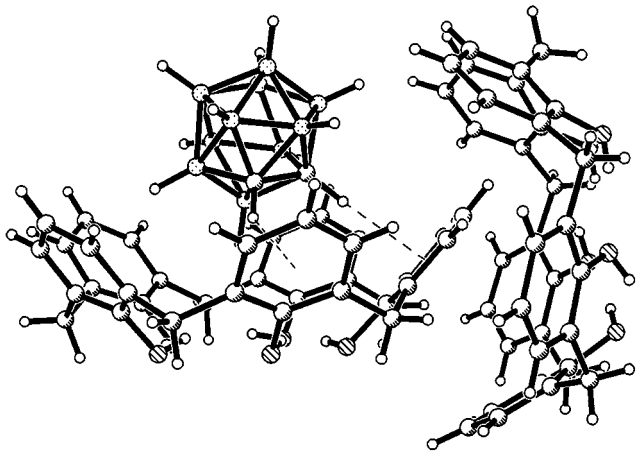


Figure 7. The (*o*-carborane)∩[(calix[5]arene)]∩(calix[5]arene) nano-structure of (calix[5]arene)$_2$(*o*-carborane)(CH_2Cl_2)$_{0.5}$ **5**. Potential non-classical C−H π hydrogen bonds are indicated as dashed lines. The two aromatic rings shown side-on show π-π stacking at a centroid separation of 3.920 Å and torsional angle of 18.8°

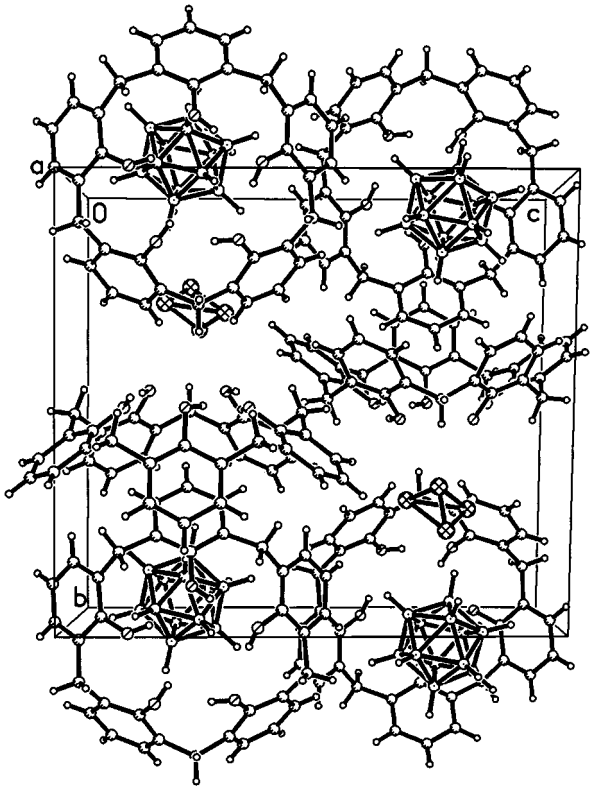


Figure 8. Packing diagram of (calix[5]arene)$_2$(*o*-carborane)(CH_2Cl_2)$_{0.5}$ **5** shown down the *a* axis

and 9.1° (Figure 7). The closest B···aromatic ring centroid distances are 3.80, 3.90, and 4.22 Å. It is evident from this that the carborane is positioned to one side of the calixarene bowl − not surprisingly, the side featuring C-$H_{carborane}$···π interactions (Figure 7). The (*o*-carborane)∩-(calix[5]arene) supermolecule.

The presence and identity of solvent molecules also plays a vital role in determining the crystal packing and overall topology of the systems. The crystallisation from CH_2Cl_2 instead of toluene, for instance, results in a dimer of the 1:1 complex being formed. We also note that calixarenes are known to form inclusion complexes with dichloromethane through the formation of non-classical hydrogen bonds.[17] Chlorinated solvents such as chloroform are known to break up analogous fullerene-calixarene complexes through such bonds competing with fullerene-calixarene associations.[14] In the carborane-based supramolecular systems reported here, however, carborane-calixarene and calixarene-calixarene interactions appear to form the preferred interactions.

Experimental Section

Synthesis of 3 and 5: Calix[5]arene and *o*-carborane were mixed in toluene in 1:1, 2:1, and 1:3 proportions and the solution slowly evaporated to dryness. The residues were taken up in dichloromethane then hexane vapour was diffused into the solutions to give colourless crystals. (*o*-Carborane)(calix[5]arene)(CH_2Cl_2) **3**; $C_{38}H_{44}B_{10}Cl_2O_5$. − IR 3284, 3061, 2577, 1594, 1489, 1451, 1386, 1245, 1212, 1150, 1089, 1016, 907, 841, 803, 754, 714, 637, 559, 472 cm^{-1}; microanalysis C 60.50% (60.07), H 5.91% (5.83); (*o*-carborane)(calix[5]arene)$_2$(CH_2Cl_2)$_{0.5}$. − **5**; IR 3286, 3059, 2946, 2875, 2556, 2280, 1612, 1468, 1450, 1386, 1244, 1210, 1152, 1086, 906, 841, 803, 755, 698, 639, 558, 486; microanalysis C 69.69% (69.78), H 6.07% (5.90). − **4**: Calix[5]arene and *o*-carborane were mixed in toluene in 1:3 proportions and the solution heated at ca. 70°C for one hour then cooled to room temperature to give colourless crystals of (*o*-carborane)(calix[5]arene)(C_7H_8); IR 3260, 3066, 2572, 2362, 1611, 1468, 1449, 1398, 1243, 1210, 1151, 1085, 841, 756, 714, 559, 468 cm^{-1}.

X-ray Crystallography: Details of data collections and structure refinements for **3** to **5** are given in Table 1. All data sets were collected on an Enraf-Nonius KappaCCD diffractometer with MoK_α radiation (λ = 0.71073 Å). Data was corrected for Lorentzian, polarisation but not absorption. The structures were solved by direct methods using SHELXS-97[18] and refined by full matrix least-squares on $|F^2|$ using SHELXL-97.[19] Carbon atoms within the carborane molecules were assigned by analysis of atomic displacement parameters. As the X-ray scattering factors for B and C are very similar these assignments should be regarded as tentative. Only neutron diffraction data would allow for unequivocal discrimination between C and B. Treatment of hydrogen atoms was mixed. The hydroxy hydrogens for **3** to **5** were fixed at geometrically estimated positions with a riding refinement. The hydrogen positions of the disordered CH_2Cl_2 molecule in **3**, and the toluene molecule of **4** were fixed at geometrically estimated positions with a riding refinement. All other hydrogen atoms were fully refined. The disordered CH_2Cl_2 molecule in **3** was modelled with two carbon positions each with an occupancy of 0.5. The disordered CH_2Cl_2 molecule in **5** was refined with an overall occupancy of 0.5, four disordered chlorine positions (with occupancies of 0.15 or 0.35), forming a rough tetrahedron, were modelled, however the central carbon atom was not located. Crystallographic data (excluding structure factors) for the structures reported in this paper have been deposited with the Cambridge Crystallographic Data Centre as supplementary publication nos. CCDC-101900, CCDC-101901, and CCDC-101902 Copies of the data can be obtained free of charge on application to CCDC, 12 Union Road, Cambridge CB2 1EZ, UK [Fax: (+44) 1223/ 336-033; E-mail: deposit@ccdc.cam.ac.uk]

Table 1. Crystal structure data and details of structure refinement for **3**

	3	**4**	**5**
Formula	$C_{38}H_{44}B_{10}Cl_2O_5$	$C_{44}H_{50}B_{10}O_5$	$C_{72}H_{72}B_{10}ClO_{10}$
M_r [g mol^{-1}]	759.73	766.94	1240.85
Crystal system	monoclinic	monoclinic	triclinic
Space group	$P2_1/n$	$P2_1/n$	$P\bar{1}$
a [Å]	12.1605(4)	18.9709(7)	11.6151(13)
b [Å]	12.2485(4)	9.9961(5)	16.3617(17)
c [Å]	27.0023(6)	23.3192(8)	18.014(2)
α [°]	90.0	90.0	90.699(9)
β [°]	100.833(1)	111.369(5)	91.612(9)
γ [°]	90.0	90.0	96.739(9)
V [Å^3], Z	3950.3(2), 4	4118.1(3)	3398.0(7), 2
ρ_{calc} [g cm^{-1}]	1.277	1.237	1.213
crystal size [mm]	0.38 × 0.25 × 0.18	0.38 × 0.35 × 0.25	0.35 × 0.35 × 0.20
μ [mm^{-1}]	0.207	0.074	0.114
T [K]	150(1)	150(1)	173(1)
Scan increment [°], exposure [sec]	1 (φ, ω), 40	1 (φ, ω), 40	1 (φ, ω), 20
2θ range [°]	6.14 to 56.58	5.92 to 56.54	5.82 to 56.36
Reflns collected	21213	25634	24331
Unique reflns	9593	10063	13635
R_{int}	0.049	0.091	0.087
observed refln $I > 2\sigma(I)$	5081	3925	3533
Data/restraints/ parameters	9593/0/653	10063/0/680	13636/0/865
R_1 (obs data)	0.0772	0.0726	0.1082
wR_2 (all data)	0.2398	0.1895	0.3059
weights a[a]	0.1368	0.0866	0.1605
S	1.049	0.945	0.936
max shift/error	0.000	0.000	0.000
$\|\Delta\rho\|_{max}$ [e Å^3]	0.961	0.331	0.636

[a] $w = 1/[\sigma^2(F_o^2) + aP^2]$ where $P = (F_o^2 + 2F_c^2)/3$.

Acknowledgments

This work was supported by the Australian Research Council.

[1] J. Plesek, *Chem. Rev.* **1992**, *92*, 269.
[2] X. Yang, W. Jiang, C. B. Knobler, M. F. Hawthorne, *J. Am. Chem. Soc.* **1992**, *114*, 9717; J. Müller, K. Base, T. F. Magnera, J. Michel, *J. Am. Chem. Soc.* **1992**, *114*, 9721; W. Jiang, C. B. Knobler, M. D. Mortimer, M. F. Hawthorne, *Angew. Chem.* **1995**, *107*, 1470; *Angew. Chem., Int. Ed. Engl.* **1995**, *34*, 1332; W. Jiang, C. B. Knobler, M. F. Hawthorne, *Inorg. Chem.* **1996**, *35*, 3056; W. Jiang, D. E. Harwell, M. D. Mortimer, C. B. Knobler, M. F. Hawthorne, *Inorg. Chem.* **1996**, *35*, 4355.
[3] D. Armspach, M. Cattalini, E. C. Constable, C. E. Housecroft, D. Philips, *Chem. Commun.* **1996**, 1823.
[4] R. N. Grimes, *Angew. Chem.* **1993**, *105*, 1350; *Angew. Chem., Int. Ed. Engl.* **1993**, *32*, 1289; W. Clegg, W. R. Gill, J. A. H. MacBride, K. Wade, *Angew. Chem.* **1993**, *105*, 1402; *Angew. Chem., Int. Ed. Engl.* **1993**, *32*, 1328; I. T. Chizhevsky, S. E. Johnson, C. B. Knobler, F. A. Gomez, M. F. Hawthorne, *J. Am. Chem. Soc.* **1993**, *115*, 6981.

[5] A. A. Zinn, Z. Zheng, C. B. Knobler, M. F. Hawthorne, *J. Am. Chem. Soc.* **1996**, *118*, 70, references therein.
[6] X. Yang, C. B. Knobler, M. F. Hawthorne, *J. Am. Chem. Soc.* **1993**, *115*, 4904.
[7] R. N. Grimes, *Carboranes*, Academic Press, New York, **1970**.
[8] L.A. Leites, *Chem. Rev.* **1992**, *92*, 279; G. Harakas, T. Vu, C. B. Knobler, M. F. Hawthorne, *J. Am. Chem. Soc.*, **1998**, *120*, 6405, references therein.
[9] A. Harada, S. Takahashi, *J. Chem. Soc., Chem. Commun.* **1988**, 1352.
[10] M. G. Davidson, T. G. Hibbert, J. A. K. Howard, A. Mackinnon, K. Wade, *Chem. Commun.* **1996**, 2285.
[11] P. D. Godfrey, W. J. Grigsby, P. J. Nichols, C. L. Raston, *J. Am. Chem. Soc.* **1997**, *119*, 9283.
[12] R. J. Blanch, M. Williams, G. D. Fallon, M. G. Gardiner, R. Kaddour, C. L. Raston, *Angew. Chem.* **1997**, *109*, 520; *Angew. Chem., Int. Ed. Engl.* **1997**, *36*, 504.
[13] J. L. Atwood, M. J. Barnes, R. S. Burkhalter, P. C. Junk, J. W. Steed, C. L. Raston, *J. Am. Chem. Soc.* **1994**, *116*, 10346; J. L. Atwood, M. J. Barnes, M. G. Gardiner, C. L. Raston, *Chem. Commun.*. **1996**, 1449.
[14] R. M. Williams, J. W. Verhoeven, *Recl. Trav. Chim. Pays-Bas* **1992**, *111*, 531; J. L. Atwood, G. A. Koutsantonis, C. L. Raston, *Nature* **1994**, *368*, 229; R. M. Williams, J. M. Zwier, J. W. Verhoeven, *J. Am. Chem. Soc.* **1994**, *116*, 6965; T. Suzuki, K. Nakashima, S. Shinkai, *Chem. Lett.* **1994**, 699; T. Suzuki, K. Nakashima, S. Shinkai, *Tetrahedron Lett.* **1995**, *36*, 249; C. L. Raston, J. L. Atwood, P. J. Nichols, I.B. N. Sudria, *Chem. Commun.* **1996**, 2615; K. Araki, K. Akao, T. Suzuki, S. Shinkai, *Tetrahedron Lett.* **1996**, *37*, 73; A. Ikeda, S. Shinkai, *Chem. Rev.* **1997**, *97*, 1713; T. Haino, M. Yanase, Y. Fukazawa, *Angew. Chem.* **1997**, *109*, 288; *Angew. Chem. Int. Ed. Engl.* **1997**, *36*, 259; T. Haino, M. Yanase, Y. Fukazawa, *Tetrahedron Lett.* **1997**, *38*, 3739; K. Tsubaki, K. Tanaka, T.Kinoshita, K. Fuji, *Chem. Commun.* **1998**, 8955. J. L. Atwood, L. J. Barbour, C. L. Raston, I. B. N. Sudria, *Angew. Chem.* **1998**, *110*, 1028; *Angew. Chem., Int, Ed, Engl.*, **1998**, *37*, 981.
[15] J.-M. Lehn, *Supramolecular Chemistry, Concepts, Perspectives* **1995**,VCH, Weinham.
[16] S. Kamitori, K. Hirotsu, T. Higuchi, *J. Am. Chem. Soc.* **1987**, *109*, 2409; S. Kamitori, K. Hirotsu, T. Higuchi, *Bull. Chem. Soc. Jpn.* **1988**, *61*, 3825.
[17] J. L. Atwood, S. G. Bott, C. Jones, C. L. Raston, *J. Chem. Soc., Chem. Commun.* **1992**, 1349.
[18] G. M. Sheldrick, *SHELXS97. Program for the Solution of Crystal Structures*, **1997**, University of Göttingen, Germany.
[19] G. M. Sheldrick, *SHELXL97. Program for the Refinement of Crystal Structures*, **1997**, University of Göttingen, Germany.

Received August 20, 1998
[I98287]

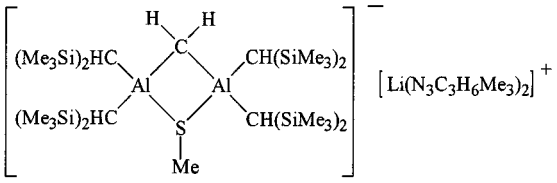
The Reaction of Diazomethane Derivatives with the Dielement Compounds $R_2Al–AlR_2$ and $R_2Ga–GaR_2$ [R = $CH(SiMe_3)_2$] − Insertion versus Fragmentation

Werner Uhl*[a] and Frank Hannemann[a]

Keywords: Aluminium / Gallium / Low-valent compounds / Insertion reactions

Tetrakis[bis(trimethylsilyl)methyl]dialane(4) **1** reacted with trimethylsilyldiazomethane and bis(trimethylsilyl)diazomethane at room temperature by the insertion of the terminal nitrogen atoms into its aluminium–aluminium bond. As shown by a crystal structure determination, one of the aluminium atoms of each product enhanced its coordination number to four by the interaction with the central nitrogen atom of the C=N–N group, which results in the formation of a three-membered AlN_2 heterocycle bearing an exocyclic N=C double bond. The reactions of the corresponding gallium compound (**2**) containing a gallium–gallium single bond needed more drastic conditions. Mixtures of many unknown products were formed, and only on treatment with trimethylsilyldiazomethane two compounds could be isolated after repeated recrystallization in yields below 10%, which were characterized by crystal structure determinations. One was identified as the trimeric dialkylgallium cyanide (**8**) with a nine-membered $Ga_3C_3N_3$ heterocycle, and the other one (**9**) has a dialkylgallium fragment coordinated by both terminal nitrogen atoms of the chelating ligand $NH_2–N=C(SiMe_3)–NH^-$. Due to the NMR spectroscopic characterization, **8** seems to be tetrameric in solution with an asymmetric structure containing four different gallium atoms. With this unusual structure, the IR spectrum of tetrameric dimethylgallium cyanide could now completely be interpreted, which was published more than 20 years ago.

Tetrakis[bis(trimethylsilyl)methyl]dielement(4) compounds with aluminium−aluminium (**1**)[1], gallium−gallium (**2**)[2], and indium−indium bonds (**3**)[3] were isolated and completely characterized for the first time about ten years ago in our group. They showed a remarkable and unprecedented chemical reactivity, and up to now we observed six different types of reaction[4]. Among these, the insertions of atoms, molecules, and molecular fragments are quite outstanding owing to the number and the structural variety of the isolated products. At present, we are much interested in the insertion of carbenes into the element−element bonds, which may lead to the formation of methylene-bridged dielement compounds with two coordinatively unsaturated aluminium, gallium, or indium atoms. Such compounds are of particular interest in current organoelement chemistry, because they are potentially useful as chelating Lewis acids[5]. However, only once before we unexpectedly succeeded in inserting a carbene, when we treated the dialuminium derivative **1** with $LiCH_2SMe$[6]. In the course of this reaction, the thiomethyl compound was cleaved to yield CH_2, which was inserted into the Al−Al bond by the formation of an $Al–CH_2–Al$ group, and the remaining thiomethanolate was coordinated in a chelating manner by both aluminium atoms to give compound **4** (Scheme 1). A similar reaction was not observed for the gallium (**2**) or indium analogues (**3**), which on similar conditions gave a complete fragmentation[6]. In order to obtain the uncoordinated methylene bridged dielement compounds by the insertion of carbenes, we treated **1** to **3** with diazomethane derivatives.



4

Scheme 1

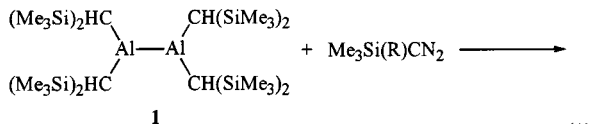
Reactions of the Dialuminium(4) Compound 1 with Trimethylsilyl and Bis(trimethylsilyl) Diazomethane

One equivalent of each of the diazomethane derivatives was added to solutions of **1** in hexane at room temperature, and **1** was completely consumed after stirring for about one day in both cases. Trimethylsilyldiazomethane gave only a highly viscous fluid (**5**), which could not be purified by recrystallization. Its purity was, however, high enough to allow the complete NMR spectroscopic characterization. In contrast, product (**6**) obtained by the reaction of **1** with bis(trimethylsilyl)diazomethane was isolated as a yellow crystalline solid by recrystallization from *n*-hexane. Both products have a similar constitution, as was easily derived from some very characteristic NMR data. In **5**, the resonance of one proton was observed at very low field (δ = 7.95) indicative for a N=C(H)R group, and the protons of the trimethylsilyl groups attached to the diazomethane carbon atom of compound **6** gave two resonances in accord-

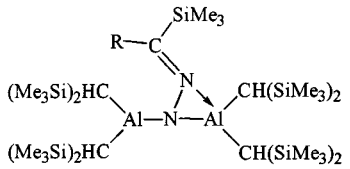
[a] Fachbereich Chemie der Universität,
Postfach 2503, D-26111 Oldenburg, Germany
Fax: (internat.) +49 (0)441/ 798−3352

 © WILEY-VCH Verlag GmbH, D-69451 Weinheim, 1999 1434−1948/99/0101−0201 $ 17.50+.50/0

ance with the differing chemical vicinity at each side of a C=N double bond. The corresponding central carbon atoms revealed ^{13}C-NMR shifts of δ = 152.9 (**5**) and δ = 179.0 (**6**) characteristic of imines[7]. Thus, the diazomethane derivatives did not react as a carbene donor, but they were completely inserted into the Al−Al bond of the starting compound **1** by the formation of energetically favored Al−N bonds (Eq. 1).



1 (1)



5: R = H
6: R = SiMe$_3$

The constitution of **5** and **6** given in Equation (1) was verified also by a crystal structure determination of compound **6** (Figure 1). Bis(trimethylsilyl)diazomethane inserted into the Al−Al bond of **1** with its terminal nitrogen atom N1, and by the interaction of the nitrogen lone pair at N2 with the aluminium atom Al1 a three-membered AlN_2 heterocycle results. The compound may be described as a hydrazone derivative with both N−H hydrogen atoms replaced by dialkylaluminium groups. The shortest Al−N bond is observed to the coordinatively unsaturated exocyclic atom Al2 [183.5(2) pm], while the bond Al1−N1 in the ring is little lengthened to 189.6(2) pm. Both are within the characteristic range of Al−N single bonds[8]. As expected, the dative bond[8] between the imine nitrogen atom N2 and Al1 is much elongated to 198.9(2) pm. The N1−N2 bond [141.7(2) pm] is shorter than in hydrazine or derivatives of hydrazine[9], but similar to some N−N distances observed in hydrazones with a more comparable bonding situation[10]. The length of the C=N double bond (131.5 pm) corresponds to the standard value of 128 pm[11]. The angle Al1−N1−Al2 is 141.5°, an even closer approach to linearity is observed for the group Al1−N2−C including the C=N double bond (159.3°).

The structures of **5** and **6** have two chemically different dialkylaluminium groups, one with a tricoordinated, coordinatively unsaturated and one with a tetracoordinated, saturated aluminium atom. Thus, two different types of bis(trimethylsilyl)methyl groups should be detectable in the NMR spectra. But at room temperature only one singlet was observed for the $SiMe_3$ or methine protons indicating a fast exchange process of the imine nitrogen atom (N2) between both aluminium atoms. The chemical shifts of the methine resonances, which are very indicative for the coordination number at the aluminium atoms[12], are intermediate [δ = −0.51 (**5**) and −0.44 (**6**)] between the range of tetracoordinated (δ < −0.7) and tricoordinated (δ > −0.2) bis(trimethylsilyl)methyl aluminium compounds. On cooling to −70°C a complicated splitting of all resonances was observed indicating, that all bis(trimethylsilyl)methyl groups became different. The signals of the methine protons splitted into four resonances of equal intensity at δ = −0.26, −0.45, −0.47, and −0.78, from which only the last one was in that region characteristic for tetracoordinated aluminium atoms. For the trimethylsilyl groups a multiplet with nine maxima in the range between δ = 0.16 and 0.43 was observed. The behavior of the diazomethane insertion products is thus quite different from that of the related products (**7**) obtained by the insertion of isonitriles into the Al−Al bond of **1**[13]. The structure of **7** in the solid state is quite similar to that of compound **6** with one tricoordinated and one tetracoordinated aluminium atom and a three-membered heterocycle; but a C=N double bond is included in the ring (Scheme 2). This structure was retained in solution, and we observed the resonances of the different $CH(SiMe_3)_2$ groups even at +100°C. The much faster exchange process detected for **5** and **6** is favored by the easy rotation around the N−N single bond of the heterocycle after opening of the Al−N2 bond, while an exchange with the isontrile products requires the energetically unfavorable inversion of the nitrogen atom, which is part of the C=N double bond. Furthermore, it seems, that the dative nitrogen−aluminium interaction in **5** or **6** is weaker than that in the isonitrile insertion products. The Al−N2 distance is much lengthened to 198.9 pm in the hydrazone derivative **6** compared to 186.4 pm of the isonitrile product **7**.

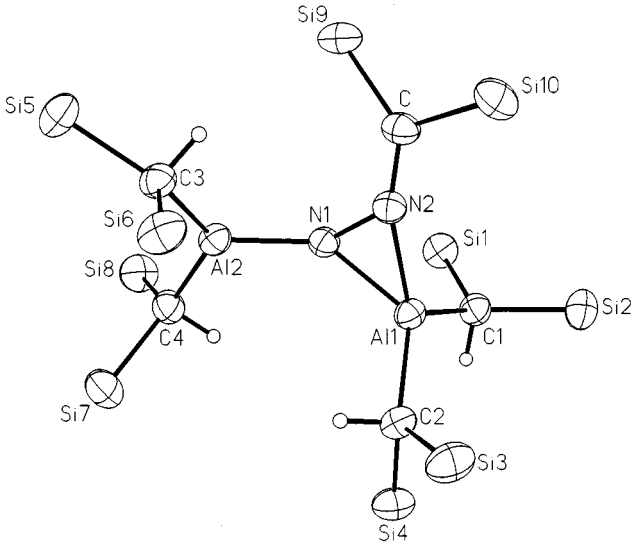
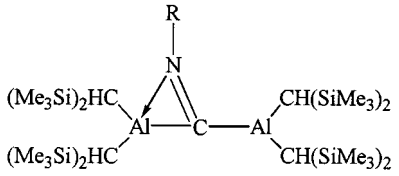


Figure 1. Molecular structure and numbering scheme of compound **6**; the thermal ellipsoids are drawn at the 40% probability level; methyl groups are omitted for clarity; selected bond lengths [pm] and angles [°]: N1−N2 141.7(2), N2−C 131.5(3), Al1−N1 189.6(2), Al1−N2 198.9(2), Al1−C1 199.3(3), Al1−C2 199.1(2), Al2−N1 183.5(2), Al2−C3 198.2(3), Al2−C4 197.6(2), Al1−N1−Al2 141.5(1), Al1−N1−N2 72.2(1), Al1−N2−N1 65.1(1), Al1−N2−C 159.3(2), N1−Al1−N2 42.70(7), Al2−N1−N2 132.9(2), N1−N2−C 127.6(2)



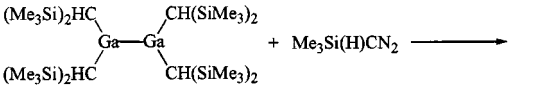
7

Scheme 2

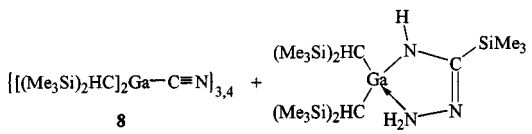
Compound **6** melts at 110°C without decomposition. UV irradiation in *n*-pentane gave no reaction after five minutes. After 60 minutes, complete decomposition occurred with the formation of a mixture of many unknown products, from which no one could be isolated in a pure form.

Reaction of the Digallium(4) Compound 2 with Trimethylsilyldiazomethane

In contrast to the easy reactions of the Al−Al bond, the insertion into the Ga−Ga bond of **2** usually needs more drastic reaction conditions with longer reaction times or does not occur at all[14]. In accordance with these observations, **2** did not react with trimethylsilyl or bis(trimethylsilyl) diazomethane at room temperature. Even in boiling solvents no reaction was observed with the last one, but on UV irradiation in a quartz apparatus **2** was completely consumed within 35 minutes. The main product of the obtained mixture was, however, formed by the disproportionation reaction of **2** and was spectroscopically identified as the trialkylgallium compound $Ga[CH(SiMe_3)_2]_3$[2]. Sterically less shielded trimethylsilyldiazomethane reacted in boiling *n*-hexane with **2**, but the reaction time was 24 h. A complicated mixture of products was formed, from which after repeated recrystallization from toluene two components (**8** and **9**) could reproducibly be isolated in a pure form and in a very low yield below 10% (Eq. 2). They were identified by crystal structure determinations.



2 (2)



8 **9**

Compound **8** was isolated in a yield of 6% and identified as the trimeric dialkylgalliumcyanide (Figure 2). The isotypic aluminium compound was recently obtained in our group[15]. **8** has a nine-membered $Ga_3C_3N_3$ heterocycle, in which three gallium atoms are bridged by three cyanide groups. This is an unusual structure for alkyl metal cyanides, which often polymerize like Me_2In-CN[16] or Me_3Sn-CN[17]. A tetrameric structure was reported for a dialkylgold compound[18]. Some other dialkylelement cyanides with the heavier elements of the third main group are known in literature, their degree of association between four and eight was, however, detected only by mass spectroscopy or molecular weight determinations[19]. The heterocycle of **8** deviates from planarity and adopts almost a boat conformation with the atom Ga1 furthest above the mean plane (34.3 pm). The GaC_2 planes with the central atoms of the $CH(SiMe_3)_2$ groups are not exactly perpendicular to the heterocycle, the angles between their normals are 102.6° (Ga1), 71.7° (Ga2), and 105.2° (Ga3). The bond lengths of the C−N triple bonds is 115.2 pm on average, they lie within the range observed for covalent or ionic cyanides[11][16−18][20]. The cyanide groups are not exactly linear coordinated by the gallium atoms, and angles of 164° on average are detected at the carbon or nitrogen atoms. The bonds Ga−N and Ga−C (208.8 pm on average) are much lengthened compared with the corresponding aluminium compound (202.2 pm)[15], which may be caused by a lower ionic contribution to the Ga−C or Ga−N bonds.

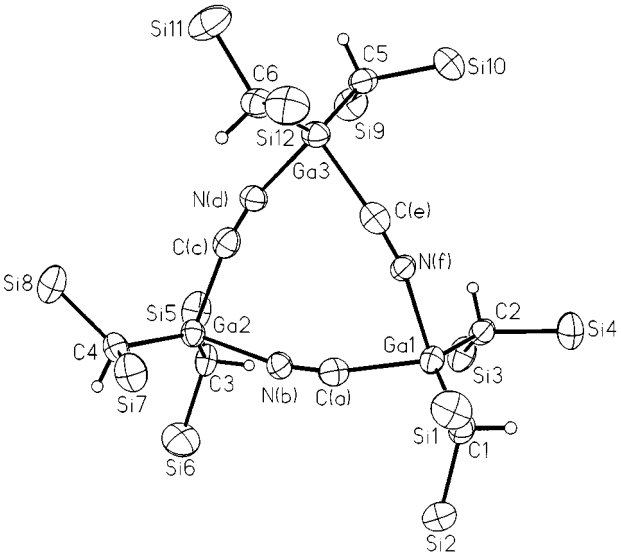
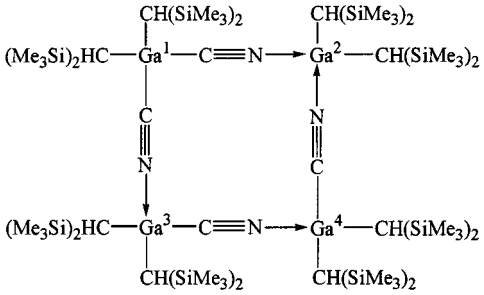


Figure 2. Molecular structure and numbering scheme of compound **8**; the thermal ellipsoids are drawn at the 40% probability level; methyl groups are omitted for clarity; the atoms of the cyanide groups are statistically disordered, the labels of the atoms are idealized; selected bond lengths [pm] and angles [°]: Ga1−C1 197.0(4), Ga1−C2 198.3(3), Ga2−C3 197.4(4), Ga2−C4 197.5(4), Ga3−C5 197.7(4), Ga3−C6 198.2(4), Ga1−(C,N)(a) 208.1(4), Ga1−(C,N)(f) 209.3(4), Ga2−(C,N)(b) 209.5(4), Ga2−(C,N)(c) 207.7(4), Ga3−(C,N)(d) 208.7(4), Ga3−(C,N)(e) 209.2(4), (C,N)(a)−(C,N)(b) 115.0(5), (C,N)(c)−(C,N)(d) 115.7(5), (C,N)(e)−(C,N)(f) 114.9(4), Ga−(C,N)−(C,N) 164.4 (average), (C,N)−Ga−(C,N) 85.1 (average)

The aluminium analogue of **8** was a dimer in solution and showed three resonances in the ^{1}H-NMR spectrum in the ratio of 1 to 2 to 1 for the $SiMe_3$ and methine protons. These observations were interpreted in terms of a different coordination of the aluminium atoms, one by two carbon and one by two nitrogen atoms of the cyanide ligands. Both bis(trimethylsilyl)methyl groups of one aluminium atom

gave two separate resonances possibly owing to a hindered rotation and the usually observed molecular conformation with the methine hydrogen atom of one substituent pointing between both trimethylsilyl groups of the second one[15]. The NMR spectra of **8** are much more complicated. The ^{1}H-NMR spectrum shows four different methine protons of equal intensity at $\delta = -0.23$, -0.33, -0.34, and -0.50 in a range characteristic of tetracoordinated gallium atoms[6][21]. Furthermore, six different $SiMe_3$ groups with the integration ratio of 1 to 1 to 2 to 2 to 1 to 1 are observed; one of the more intensive signals has a shoulder possibly indicating a poorly resolved further splitting. A similar ^{13}C-NMR spectrum is observed with six resonances of the $SiMe_3$ groups and four resonances of the methine carbon atoms. Most striking is the occurrence of four different ^{13}C resonances of the cyanide groups in the characteristic range of about $\delta = 143$; these resonances were difficult to detect due to the low solubility of these dialkyl cyanides. The appearance of the NMR spectra clearly cannot be explained by the formation of a single dimer in solution. For two isomeric dimers in an equilibrium with four different cyanide groups, an even more complicated pattern of resonances of the methine and trimethylsilyl protons has to be expected, and despite their different structures and energy those two isomers must be present in absolutely identical concentrations to account for the observed NMR spectra, which seems to be quite unlikely. A tetrameric structure was formulated for dimethylgallium cyanide owing to molecular mass determinations[19], and a similar structure may be adopted by compound **6** in solution. A complete interpretation of the NMR spectra succeeds, however, only by the assumption of a asymmetric constitution with one gallium atom coordinated by two carbon atoms of cyanide, one by two nitrogen atoms, and the remaining two by one carbon and one nitrogen atom, as shown in Scheme 3. This structure has four different cyanide carbon atoms and four different methine groups. Furthermore, two resonances are expected for those bis(trimethylsilyl)methyl groups, which have diastereotopic trimethylsilyl groups owing to the asymmetric coordination of the gallium atoms by one carbon and one nitrogen atom of the ring. In contrast, only one singlet should be observed for the $CH(SiMe_3)_2$ groups attached to the gallium atoms, which are symmetrically coordinated by two carbon or two nitrogen atoms of the ring with a local mirror plane bisecting the C−Ga−C or N−Ga−N as well as the Si−C−Si angles. All these expectations are in accordance with the experimental ^{1}H- and ^{13}C-NMR spectra described above. The question arose, whether this asymmetry was observed in the IR spectra of dimethylgallium cyanide, too, which was intensively investigated by the group of Dehnicke 23 years ago[19]. Six absorptions were observed for the Ga-(C,N) stretching vibrations of the ring between 316 and 365 cm^{-1}, this number was too high for a symmetric structure. They originally were explained by the intermolecular coupling of vibrations. A calculation now done by Dehnicke with the asymmetric structure proposed by us for compound **6** gave, however, an excellent agreement with the experimental spectrum. It was based on a local C_{2v} symmetry of those gallium atoms coordinated by two carbon or two nitrogen atoms of the heterocycle (Ga^1 and Ga^2), which result in two IR active stretching vibrations (A_1, B_2) for each of the groups $Ga^1-(CN)_2$ and $Ga^2-(NC)_2$. The local C_s symmetry at both gallium atoms asymmetrically coordinated by one carbon and one nitrogen atom of the heterocycle (Ga^3 and Ga^4) leads to two indistinguishable stretching vibrations for Ga−(CN) and Ga−(NC) of the symmetry type A′, which gives a total of six IR active stretching vibrations for the $(GaCN)_4$ group. This result impressively confirms our interpretation of compound **6** as a tetramer in solution and the asymmetric structure of the tetramers.



Scheme 3

Upon heating solutions of **8**, the splitting of the $SiMe_3$ resonances disappeared and only one singulet was observed at $\delta = 0.31$. The methine protons gave three resonances with an intensity ratio of 1 to 2 to 1 with similar chemical shifts as observed at room temperature. The temperature of coalescence was at about 40°C. Probably, the resonances of different $SiMe_3$ groups coincided, and there is not enough information for a sensible interpretation. In the IR spectra, the CN stretching vibration was observed in an expected range[22] at 2172 cm^{-1} similar to the aluminium analogue (2185 cm^{-1})[15].

The second product of the reaction of **2** with trimethylsilyldiazomethane was identified as compound **9**, which was isolated in a yield of 4%. A dialkylgallium fragment is coordinated by the ligand $H_2N-N=C(SiMe_3)-NH-$ (Figure 3), which to the best of our knowledge has never been used before in coordination chemistry. However, few derivatives of the neutral compound with two terminal NH_2 groups (amidrazones) are reported in literature[23]. The gallium atom in **9** has a distorted tetrahedral coordination sphere with normal Ga−C bond lengths of 200.0 pm on average. The Ga−N distances differ with 204.8(2) pm to the nitrogen atom N1 of the NH_2 group and 192.7(2) pm to the amide nitrogen atom N3. The N1−N2 single bond length [149.5(2) pm] is longer than in the diazomethane insertion product **6** discussed above, in which both nitrogen atoms were part of a three-membered heterocycle and coordinated by aluminium. The carbon−nitrogen double bond C3−N2 has a length of 130.9(3) pm in the normal range similar to that observed in compound **6**. Also, the C−N bond between C3 and the NH group (N3) is short [134.0(2) pm] and has some π character due to the delocalization of elec-

tron density. A five-membered heterocycle is formed by the coordination of the gallium atom by both terminal nitrogen atoms of the ligand (N1 and N3), which is almost ideally planar. The atom N1 deviates furthest from the average plane by only 4.9 pm. Also, the silicon atom Si5 bound to the carbon atom C3 and the hydrogen atom at N3 lie within this plane with small deviations of 9.1 and 3.5 pm, respectively.

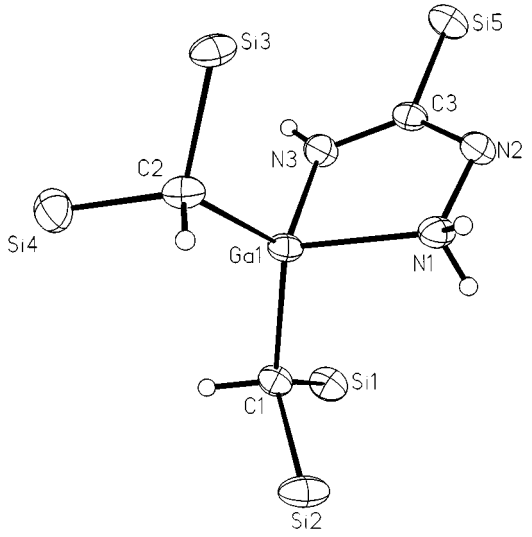


Figure 3. Molecular structure and numbering scheme of compound **9**; the thermal ellipsoids are drawn at the 40% probability level; methyl groups are omitted for clarity; selected bond lengths [pm] and angles [°]: Ga1−N1 204.8(2), Ga1−N3 192.7(2), N1−N2 149.5(2), N2−C3 130.9(3), N3−C3 134.0(2), C3−Si5 190.1(2), Ga1−C1 199.9(2), Ga1−C2 200.0(2), N1−Ga1−N3 80.11(8), Ga1−N1−N2 111.3(1), N1−N2−C3 110.1(2), N2−C3−N3 122.6(2), C3−N3−Ga1 115.3(2)

The trimethylsilyl groups of the $CH(SiMe_3)_2$ substituents are diastereotopic due to the molecular symmetry and give two resonances in the ^{1}H- and ^{13}C-NMR spectra. The methine protons show a resonance at very high field ($\delta = -0.75$), which is characteristic for a coordination number of four at the gallium atom[21], and the N−H protons give two broad signals in the intensity ratio of 1 to 2 at $\delta = 4.51$ and 4.20. The carbon atom of the chelating ligand has, as expected, a resonance at low field ($\delta = 176.7$) similar to the bis(trimethylsilyl)diazomethane product **6** discussed above. In the IR spectrum, two absorptions are observed at 1584 and 1501 cm^{-1}, which can be attributed to the N−C−N moiety with a delocalized π bond in the chelate ligand.

The diindium compound **3** with an In−In single bond did not react with the diazomethane derivatives at room temperature. Complete disproportionation by the formation of elemental indium and the corresponding InR_3 compound occurred upon heating in boiling *n*-hexane or under irradiation with UV light, and no product of a reaction with the diazomethanes could be detected by NMR spectroscopy.

Experimental Section

General: All procedures were carried out under purified argon in dried solvents (toluene with Na/benzophenone, *n*-hexane with $LiAlH_4$). Compounds **1**, **2**, and **3** were synthesized as described in ref.[1−3]. A commercially available solution of trimethylsilyldiazomethane in *n*-hexane was used without further purification; bis(trimethylsilyl)diazomethane was synthesized according to ref.[24].

Reaction of 1 with Trimethylsilyldiazomethane. − Synthesis of 5: A solution of trimethylsilyldiazomethane in *n*-hexane (2 M, 0.77 ml, 1.53 mmol) was added to a solution of dialane(4) **1** (0.960 g; 1.39 mmol) in 50 ml of *n*-hexane at room temperature. The mixture was stirred for 24 h. The color changed from pale-yellow to orange. The solvent was removed in vacuo, and the residue was thoroughly dried in vacuo. The product (**5**) could not be purified by recrystallization. − ^{1}H NMR (C_6D_6, 300 MHz): δ = 7.95 (1 H, CH of azomethane), 0.32 [72 H, $SiMe_3$ of bis(trimethylsilyl)methyl], 0.26 (9 H, $SiMe_3$ of diazomethane), −0.51 (4 H, $AlCHSi_2$). − ^{13}C NMR (C_6D_6, 75.5 MHz): δ = 152.9 (C=N), 6.0 ($SiMe_3$ of diazomethane), 5.2 [$SiMe_3$ of bis(trimethylsilyl)methyl], −0.6 ($AlCSi_2$).

Reaction of 1 with Bis(trimethylsilyl)diazomethane. − Synthesis of 6: A solution of 0.796 g (1.15 mmol) dialane(4) **1** in 60 ml of *n*-hexane was added to 0.294 g (1.58 mmol) bis(trimethylsilyl)diazomethane at room temperature. The mixture was stirred for 18 h. The solvent was removed in vacuo. The residue was recrystallized from *n*-hexane. Yield: 0.761 g (75%), yellow crystals. − M. p. (argon, sealed capillary): 110°C. − ^{1}H NMR (C_6D_6, 300 MHz, 300 K): δ = 0.43 (9 H, $SiMe_3$ of diazomethane), 0.36 [72 H, $SiMe_3$ of bis(trimethylsilyl)methyl], 0.32 (9 H, $SiMe_3$ of diazomethane), −0.44 (4 H, $AlCHSi_2$). − ^{1}H NMR ([D$_8$]toluene, 300 MHz, 203 K): δ = 0.43, 0.40, 0.39, 0.36, 0.34, 0.30, 0.24, 0.19, 0.16 ($SiMe_3$), −0.26, −0.45, −0.47, −0.78 (each 1 H, $AlCHSi_2$). − ^{13}C NMR (C_6D_6, 75.5 MHz): δ = 179.0 (C=N), 5.9 [$SiMe_3$ of bis(trimethylsilyl)methyl], 5.1 ($SiMe_3$ of diazomethane), 4.0 ($AlCSi_2$), 2.1 ($SiMe_3$ of diazomethane). − IR (CsBr, paraffin): $\tilde{\nu}$ = 1289 vw cm^{-1}, 1248 vs δCH_3; 1187 vw, 1154 vw, 1071 w, 1045 m νNN; 1007 m δCH; 951 m, 922 m, 845 vs, 777 m, 752 m, 723 m ρCH_3(Si); 675 s ν_{as}SiC; 646 w, 631 w ν_sSiC; 594 vw, 557 w, 527 w, 515 m, 502 w, 465 w, 451 w νAlC, νAlN; 401 vw, 378 vw, 339 vw δSiC. − UV (*n*-hexane): λmax (lg ε) = 260 nm (br., 3.5), 360 (3.5), 370 (sh, 3.3). − $C_{35}H_{94}N_2Si_{10}Al_2$ (878.0): calcd. Al 6.1, found Al 6.0. − Mol. mass: 825 (cryoscopically measured in benzene).

Reaction of 2 with Trimethylsilyldiazomethane − Synthesis of 8 and 9: A solution of trimethylsilyldiazomethane (2 ml; 2 M; 4.00 mmol) was added to a solution of 0.953 g (1.23 mmol) digallane(4) **2** in 50 ml of *n*-hexane. The mixture was refluxed for 24 h. After cooling to room temperature, the solvent was removed in vacuo, and the brown residue was dissolved in 1.5 ml of toluene. An amorphous solid crystallized on storing the solution at −50°C for 14 d, which was isolated and recrystallized from 2 ml of toluene at −50°C for seven days. Three compounds were detected in the solid by NMR spectroscopy, one could not be isolated in a pure form and was not identified. Compound **8** [$(R_2GaCN)_3$] was isolated after dissolution of the solid in 2.5 ml of toluene and slow cooling to 0°C. The mother liquor was cooled to −50°C to obtain a colorless solid, which was dissolved in *n*-hexane and gave product **9** upon slow cooling to −20°C.

Characterization of 8: Yield: 0.06 g (6%, based on **2**), colorless crystals. − M. p. (argon, sealed capillary): 224−226°C (dec.). − ^{1}H NMR (C_6D_6, 300 MHz, 298 K): δ = 0.369 (9 H), 0.362 (9 H), 0.353 (18 H), 0.346 (sh) and 0.342 (18 H), 0.335 (9 H), 0.325 (9 H, all $SiMe_3$), −0.225, −0.332, −0.339, −0.504 (each 1 H, $GaCHSi_2$).

Table 1. Crystal data, data collection parameters and structure refinement for **6**, **8**, and **9**[a]

	6	**8**	**9**
Formula	$C_{35}H_{94}N_2Al_2Si_{10}$	$C_{45}H_{114}N_3Si_{12}Ga_3$	$C_{18}H_{50}N_3Si_5Ga$
Crystal system	monoclinic	monoclinic	monoclinic
Space group	$P2_1/n$; No.14[25]	$P2_1/n$; No.14[25]	$P2_1/n$; No.14[25]
Z	4	4	4
Temperature [K]	293(2)	293(2)	213(2)
$d_{calc.}$ [g/cm^3]	1.019	1.105	1.110
a [pm]	1916.0(2)	1234.2(2)	1229.7(1)
b [pm]	1506.7(1)	2323.4(5)	1735.1(1)
c [pm]	1997.2(2)	2610.5(5)	1476.8(1)
β [°]	97.01(2)	93.36(2)	99.914(9)
V [10^{-30} m^3]	5722.5(9)	7473(3)	3103.9(4)
μ [mm^{-1}]	0.284	1.294	1.089
Crystal size [mm]	0.8 × 0.8 × 0.9	0.3 × 0.4 × 0.4	0.4 × 0.5 × 0.5
Diffractometer	AED-2	AED-2	Stoe-IPDS
Radiation	Mo-K_α; graphite monochromator		
2Θ range [°]	$3.1 \le 2\Theta \le 50.0$	$3.1 \le 2\Theta \le 45.0$	$4.0 \le 2\Theta \le 51.8$
Index ranges	$-22 \le h \le 22$	$-13 \le h \le 13$	$-14 \le h \le 15$
	$0 \le k \le 17$	$0 \le k \le 25$	$-21 \le k \le 21$
	$0 \le l \le 23$	$0 \le l \le 28$	$-17 \le l \le 16$
Independent reflections	10025	10339	5841
Reflections $F > 4\,\sigma(F)$	7940	7710	4585
Parameters	472	604	270
$R = \Sigma\|\|F_o\| - \|F_c\|\|/\Sigma\|F_o\|$ ($F > 4\,\sigma(F)$)	0.0519	0.0478	0.0300
$wR^2 = \{\Sigma w(\|F_o\|^2-\|F_c\|^2)^2/\Sigma w(F_o^2)^2\}^{1/2}$ (all data)	0.0934	0.0903	0.0562
Max./min. residual [10^{30} e/m^3]	0.296/−0.204	0.336/−0.255	0.353/−0.300

[a] Programmes SHELXL-93; SHELXTL[26]; solutions by direct methods, full matrix refinement with all independent structure factors.

− ^{1}H NMR ([D$_8$]toluene, 300 MHz, 343 K): δ = 0.31 (72 H, $SiMe_3$), −0.25 (1 H), −0.34 (2 H), −0.49 (1 H, all $GaCHSi_2$). − ^{13}C NMR (C_6D_6, 75.5 MHz): δ = 144.4, 143.6, 143.5, 142.7 (cyanide), 6.98, 5.04, 5.00 ($GaCSi_2$), 4.58, 4.50, 4.42, 4.35, 4.25, 4.15 ($SiMe_3$; intensity ratio 1:2:1:1:2:1), 2.44 ($GaCSi_2$). − IR (CsBr, paraffin): $\tilde{\nu}$ = 2172 cm^{-1} νCN; 1462 vs, 1377 vs paraffin; 1294 w, 1260 sh, 1250 vs δCH_3; 1167 vw, 1115 vw; 1022 vs, 1011 vs δCH; 982 s, 970 s; 843 vs, 775 vs, 758 vs, 725 s ρCH_3(Si); 673 vs ν_{as}SiC; 625 w, 615 w ν_sSiC; 513 m, 486 s, 465 w, 407 m νGaC, νGaN; 361 m, 351 m, 332 m δSiC. − $C_{45}H_{114}N_3Si_{12}Ga_3$ (1243.6): calcd. Ga 16.8, found Ga 16.5.

Characterization of 9: Yield: 0.052 g (4%, based on **2**), colorless crystals. − M. p. (argon, sealed capillary): 124°C (dec.). − ^{1}H NMR (C_6D_6, 300 MHz): δ = 4.51 (1 H, AlNH), 4.20 (2 H, $AlNH_2$), 0.22 (9 H, $SiMe_3$ of the chelating ligand), 0.19 and 0.10 [each 18 H, $SiMe_3$ of bis(trimethylsilyl)methyl], −0.75 (2 H, $GaCHSi_2$). − ^{13}C NMR (C_6D_6, 75.5 MHz): δ = 176.7 (C=N), 4.9 ($SiMe_3$ of the chelating ligand), 4.0 and 3.8 [$SiMe_3$ of bis(trimethylsilyl)methyl], −2.4 ($GaCSi_2$). − IR (CsBr, paraffin): $\tilde{\nu}$ = 3428 m, 3273 m, 3185 m, 3098 m νNH; 2922 vs, 2853 vs paraffin; 1584 s cm^{-1}, 1501 s νNCN; 1462 vs, 1373 vs paraffin; 1289 w, 1256 sh, 1246 vs δCH_3; 1192 m, 1155 s νCN; 1017 s δCH; 936 s, 909 m, 843 vs, 785 s, 774 s, 754 s, 725 m ρCH_3(Si); 669 m ν_{as}SiC; 629 w, 619 m ν_sSiC; 583 m, 525 m, 517 m, 498 s νGaC, νGaN; 368 m δSiC. − $C_{18}H_{50}N_3Si_5Ga$ (518.8): calcd. Ga 13.4, found Ga 13.3.

Crystal Structure Determinations: Single crystals of the compounds **6**, **8**, and **9** were obtained by recrystallization from *n*-hexane, toluene, and *n*-hexane, respectively. Crystal data and structure refinement parameters are given in Table 1[27]. In compound **8**, the atoms of the cyanide groups are statistically disordered as often observed before; each position was refined by the occupation with a half nitrogen and a half carbon atom. The positions of the hydrogen atoms bound to nitrogen in **9** were taken from a difference Fourier-map and isotropically refined. All other hydrogen atoms were calculated on ideal positions and refined by using the riding model.

Acknowledgments

We are very indepted to Prof. Dr. K. Dehnicke (University of Marburg) for the discussion of the IR spectra of tetrameric dimethylgallium cyanide. Further, we are grateful to the Deutsche Forschungsgemeinschaft and the Fonds der Chemischen Industrie for generous financial support.

[1] W. Uhl, *Z. Naturforsch., B. Chem. Sci.* **1988**, *43*, 1113−1118.
[2] W. Uhl, M. Layh, T. Hildenbrand, *J. Organomet. Chem.* **1989**, *364*, 289−300.
[3] W. Uhl, M. Layh, W. Hiller, *J. Organomet. Chem.* **1989**, *368*, 139−154.
[4] W. Uhl, *Coord. Chem. Rev.* **1997**, *163*, 1−32.
[5] W. Uhl, F. Hannemann, W. Saak, R. Wartchow, *Eur. J. Inorg. Chem.* **1998**, 921−926. Cited literature.
[6] W. Uhl, R. Gerding, F. Hannemann, *Z. Anorg. Allg. Chem.* **1998**, *624*, 937−944.
[7] H. O. Kalinowski, S. Berger, S. Braun, *13*C-NMR-Spektroskopie, Thieme Verlag, Stuttgart, **1984**.
[8] A. Haaland, in *Coordination Chemistry of Aluminum*, (Ed.: G. H. Robinson), VCH, Weinheim, **1993**.
[9] K. Bode, U. Klingebiel, *Adv. Organomet. Chem.* **1996**, *40*, 1−43. K. Bode, U. Klingebiel, M. Noltemeyer, H. Witte-Abel, *Z. Anorg. Allg. Chem.* **1995**, *621*, 500−505. H. Nöth, H. Sachdev, M. Schmidt, H. Schwenk, *Chem. Ber.* **1995**, *128*, 105−113. B. Gemünd, H. Nöth, H. Sachdev, M. Schmidt, *Chem. Ber.* **1996**, *129*, 1335−1344. J. Knizek, I. Krossing, H. Nöth, H. Schwenk, T. Seifert, *Chem. Ber.* **1997**, *130*, 1053−1062. S. Dielkus, C. Drost, R. Herbst-Irmer, U. Klingebiel, *Angew. Chem.* **1993**, *105*, 1689−1690; *Angew. Chem. Int. Ed. Engl.* **1993**, *32*, 1625−1626. C. Glidewell, D. W. H. Rankin, A. G. Robiette, G. M. Sheldrick, *J. Chem. Soc. A* **1970**, 318−323. Y. Morino, T. Iijima, Y. Murata, *Bull. Chem. Soc. Japan* **1960**, *33*, 46−48.
[10] Acyclic hydrazones, which are not coordinated by transition metal cations: D. L. Cullen, M. M. Mangion, B. V. Crist, D. A. Lightner, *Tetrahedron*, **1983**, *39*, 733−742. I. L. Knunyants, Yu. T. Struchkov, M. D. Bargamova, A. A. Espenbetov, *Izv. Acad. Nauk SSSR, Ser. Khim.* **1985**, 1097−1099. C. R. Hauer, G. S. King, E. L. McCool, W. B. Euler, J. D. Ferrara, W. J. Youngs, *J. Am. Chem. Soc.* **1987**, *109*, 5760 −5765. A. Cousson, F. Nec-

toux, B. Bachet, B. Kokel, M. Hubert-Habart, *Acta Crystallogr., Sect. C* **1994**, *50*, 1753−1756. F. Bachechi, V. M. Coiro, M. Delfini, *Acta Crystallogr., Sect. C* **1996**, *52*, 2915−2918. J. Osterodt, M. Nieger, P.-M. Windscheif, F. Vögtle, *Chem. Ber.* **1993**, *126*, 2331−2336. Hydrazones coordinated to two silicon or germanium atoms similar to **6**: K. Knipping, C. Drost, U. Klingebiel, M. Noltemeyer, *Z. Anorg. Allg. Chem.* **1996**, *622*, 1215−1221. M. Lazraq, C. Couret, J. P. Declercq, A. Dubourg, J. Escudie, M. Riviere-Baudet, *Organometallics* **1990**, *9*, 845−848.

[11] J. March, *Advanced Organic Chemistry*, third edition, Wiley, **1985**, p. 19.

[12] W. Uhl, M. Layh, *Z. Anorg. Allg. Chem.* **1994**, *620*, 856−862. W. Uhl, M. Koch, M. Heckel, W. Hiller, H. H. Karsch, *Z. Anorg. Allg. Chem.* **1994**, *620*, 1427−1433. W. Uhl, M. Koch, A. Vester, *Z. Anorg. Allg. Chem.* **1993**, *619*, 359−366. W. Uhl, M. Koch, J. Wagner, *Z. Anorg. Allg. Chem.* **1995**, *621*, 249−257. W. Uhl, E. Schnepf, J. Wagner, *Z. Anorg. Allg. Chem.* **1992**, *613*, 67−75. W. Uhl, A. Vester, *Chem. Ber.* **1993**, *126*, 941−945.

[13] W. Uhl, U. Schütz, W. Hiller, M. Heckel, *Chem. Ber.* **1994**, *127*, 1587−1592.

[14] W. Uhl, R. Gerding, I. Hahn, S. Pohl, W. Saak, H. Reuter, *Polyhedron* **1996**, *15*, 3987−3992. W. Uhl, I. Hahn, U. Schütz, S. Pohl, W. Saak, J. Martens, J. Manikowski, *Chem. Ber.* **1996**, *129*, 897−901.

[15] W. Uhl, U. Schütz, W. Hiller, M. Heckel, *Z. Anorg. Allg. Chem.* **1995**, *621*, 823−828.

[16] J. Blank, H.-D. Hausen, J. Weidlein, *J. Organomet. Chem.* **1993**, *444*, C4−C6.

[17] E. O. Schlemper, D. Britton, *Inorg. Chem.* **1966**, *5*, 507−510.

[18] R. F. Phillips, H. W. Powell, *Proc. Roy. Chem. Soc. London, Ser. A* **1939**, *173*, 147−148. A. F. Wells, *Structural Inorganic Chemistry*, fifth edition, Clarendon Press, Oxford, **1984**.

[19] G. E. Coates, R. N. Mukherjee, *J. Chem. Soc.* **1963**, 229−233. J. Müller, F. Schmock, A. Klopsch, K. Dehnicke, *Chem. Ber.* **1975**, *108*, 664−672. R. Ehrlich, A. R. Young, *J. Inorg. Nucl. Chem.* **1966**, *28*, 674−676.

[20] A. F. Hollemann, E. Wiberg, N. Wiberg, *Lehrbuch der Anorganischen Chemie*, de Gruyter, Berlin, **1995**.

[21] W. Uhl, I. Hahn, H. Reuter, *Chem. Ber.* **1996**, *129*, 1425−1428. W. Uhl, I. Hahn, R. Wartchow, *Chem. Ber./Recueil* **1997**, *130*, 417−420. W. Uhl, R. Graupner, I. Hahn, T. Spies, W. Frank, *Eur. J. Inorg. Chem.* **1998**, 355−360. W. Uhl, I. Hahn, M. Koch, M. Layh, *Inorg. Chim. Acta* **1996**, *249*, 33−39. W. Uhl, R. Graupner, I. Hahn, *Z. Anorg. Allg. Chem.* **1997**, *623*, 565−572.

[22] J. Weidlein, U. Müller, K. Dehnicke, *Schwingungsfrequenzen I−Hauptgruppenelemente*, Thieme Verlag, Stuttgart, **1981**.

[23] T. Kauffmann, S. Spaude, D. Wolf, *Angew. Chem.* **1963**, *75*, 344. T. Kauffmann, S. Spaude, D. Wolf, *Chem. Ber.* **1964**, *97*, 3436-3443. H. Neunhoeffer, F. Weischedel, *Liebigs Ann. Chem.* **1971**, *749*, 16−23. R. O. Day, R. R. Holmes, H. Tautz, J. H. Weinmaier, A. Schmidpeter, *Inorg. Chem.* **1981**, *20*, 1222−1229. R. O. Day, A. Schmidpeter, R. R. Holmes, *ibid.* **1982**, *21*, 3916−3919 and **1983**, *22*, 3696−3699.

[24] E. Glozbach, J. Lorberth, *J. Organomet. Chem.* **1980**, *191*, 371−379.

[25] T. Hahn (Ed.), *International Tables for Crystallography, Space Group Symmetry*, Kluwer Academic Publishers, Dordrecht-Boston-London, **1989**, vol. A.

[26] *SHELXTL-Plus REL. 4.1*, Siemens Analytical X-RAY Instruments Inc., Madison, USA, **1990**; G. M. Sheldrick *SHELXL-93, Program for the Refinement of Structures*, Universität Göttingen, **1993**.

[27] The crystallographic data of **6**, **8**, and **9** (excluding structure factors) were deposited with the Cambridge Crstallographic Data Centre as supplementary publication no. CCDC-102908 (**6**), −102909 (**8**), and −102910 (**9**). Copies of the data can be obtained free of charge on application to The Director, CCDC, 12 Union Road, GB-Cambridge CB2 1EZ, UK [fax: Int. Code+44 (1223) 336-033; e-mail: deposit@chemcrys.cam.ac.uk].

Received September 14, 1998
[I98311]

An Na_8 Cluster in the Structure of a Novel Oxamato-Bridged Na^ICu^{II} Three-Dimensional Coordination Polymer

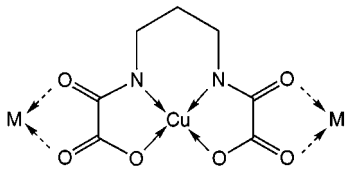
Ally Aukauloo,[a] Xavier Ottenwaelder,[a] Rafael Ruiz,[a][+] Yves Journaux,*[a] Yu Pei,[a] Eric Rivière,[a] Beatriz Cervera,[b] and M. Carmen Muñoz[c]

Keywords: Amides / Chirality / Clusters / Copper / Sodium

The new heterometallic sodium(I)-copper(II) compound Na_4Cu_2 (**2**) · 10.5 H_2O (**3**), where H_8[**2**] stands for *N*,*N*′,*N*″,*N*‴-methanetetrayltetrakismethylenetetrakis(oxamic acid), has been synthesized and its crystal structure determined by single-crystal X-ray diffraction. The structure of **3** consists of cationic $[Cu_2(\eta^4{:}\eta^4\text{-}\mathbf{2})]^{4-}$ dinuclear units, coordinated sodium cations, and water molecules. In the crystal, the dinuclear copper entities are joined through discrete aggregates of eight sodium atoms linked by oxamato and water bridges, leading to a three-dimensional polymeric network.

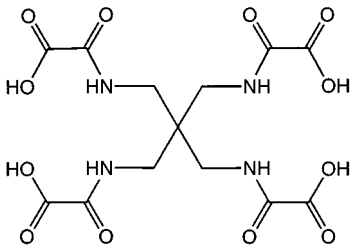
The chemistry of polymetallic coordination compounds (clusters or cages) has received much attention during the last two decades because of their fundamental role in redox metalloenzymes[1] and metal storage proteins.[2] The recent finding that polymetallic complexes could exhibit intrinsically original magnetic properties, such as high-spin molecules (nanomagnets), has further enhanced the interest in cluster chemistry.[3] Metal clusters with different kinds of bridging ligands (both organic and inorganic) are known for almost all transition metals throughout the periodic table,[4] including among them the class of polyoxometalates.[5] The preparation of these clusters has been frequently based on the use of organic terminal ligands to prevent the formation of undesired polymeric solids. Otherwise, the use of metal complexes as ligands in the preparation of cluster compounds is an attractive approach to obtain heterometal aggregates. This can be realized using suitable precursor complexes with exposed donor atoms which ligate another metal site.

We have always been interested in the coordination chemistry of oxamato ligands like H_4[**1**], the parent acid of the polychelating ligand *N*,*N*′-propane-1,3-diylbis(oxamate). The fully deprotonated ligand forms a stable copper(II) complex $[Cu(\eta^4\text{-}\mathbf{1})]^{2-}$, where the tetradentate ligand coordinates to Cu^{II} through the two strongly basic amide-N and the two carboxylate-O atoms,[6] while the four carbonyl-O atoms are still sufficiently basic to coordinate to another metal ion in a bischelate fashion (Scheme 1). That provides diverse examples of heterometallic compounds with both first-row transition[7] and rare-earth lanthanide metal ions.[8] In particular, this family of compounds ranges from discrete mononuclear[6] or small oligonuclear complexes[7b,7c] (dimers and trimers) to extensive infinite chain arrays[7a,8c] and layers,[8a,8b] although no three-dimensional networks are reported.



Scheme 1. Coordination modes of the *N*,*N*′-propane-1,3-diylbis(oxamato) ligand: tetradentate-*N*,*N*,*O*,*O* (full arrows) and bis(bidentate-*O*,*O*) (dashed arrows)

In the scope of our continuous research in this field we prepared the related binucleating ligand H_8[**2**], the parent acid of the ligand *N*,*N*′,*N*″,*N*‴-methanetetrayltetrakismethylenetetrakis(oxamate). Potentially, this ligand can bind two Cu^{II} ions to give a dimeric copper(II) complex $[Cu_2(\eta^4{:}\eta^4\text{-}\mathbf{2})]^{4-}$, which in turn can act as ligand, as its monomeric counterpart. We report herein the synthesis and general physical and structural characterization of the sodium salt of this oxamatocopper(II) complex of formula $Na_4[Cu_2(\eta^4{:}\eta^4\text{-}\mathbf{2})]$ · 10.5 H_2O (**3**).



H_8[**2**]

The structure of **3** comprises dimeric copper(II) complex anions $[Cu_2(\eta^4{:}\eta^4\text{-}\mathbf{2})]^{4-}$, complexed sodium metal cations and solvent water molecules, both coordinated and non-coordinated (Figure 1). Within the dinuclear copper anion,

[a] Laboratoire de Chimie Inorganique, Université de Paris-Sud, F-91405 Orsay, France
Fax: (internat.) 0033-1/69154754
E-mail: jour@icmo.u-psud.fr
[b] Departament de Química Inorgànica, Universitat de València, Dr. Moliner 50, E-46100 Burjassot (València), Spain
[c] Departamento de Física Aplicada, Universidad Politécnica de València, E-46071 València, Spain
[+] Present address: Departament de Química Inorgànica de la Universitat de València.

 © WILEY-VCH Verlag GmbH, D-69451 Weinheim, 1999 1434–1948/99/0202–0209 $ 17.50+.50/0

the Cu(1) and Cu(2) atoms are coordinated to the two deprotonated amide-N and two carboxylate-O atoms of the bistetradentate ligand in a nearly square-planar geometry [metal deviations from the mean basal planes are 0.020(4) and 0.188(5) Å, respectively], with Cu(2) showing a weak axial interaction with the oxygen atom O(16) from water (2.80 Å). The average Cu−N and Cu−O bond lengths (1.92 and 1.97 Å, respectively) and the copper bond angles (84.0−96.6°) are similar to those found for the related monomeric complex $(PPh_4)_2[Cu(\eta^4\text{-}\mathbf{1})] \cdot 2\ H_2O$.[6] The conformation of the ligand is such that the two mean copper basal planes form a dihedral angle of 44.0°, thus a global butterfly-folded shape to the dinuclear copper molecule.

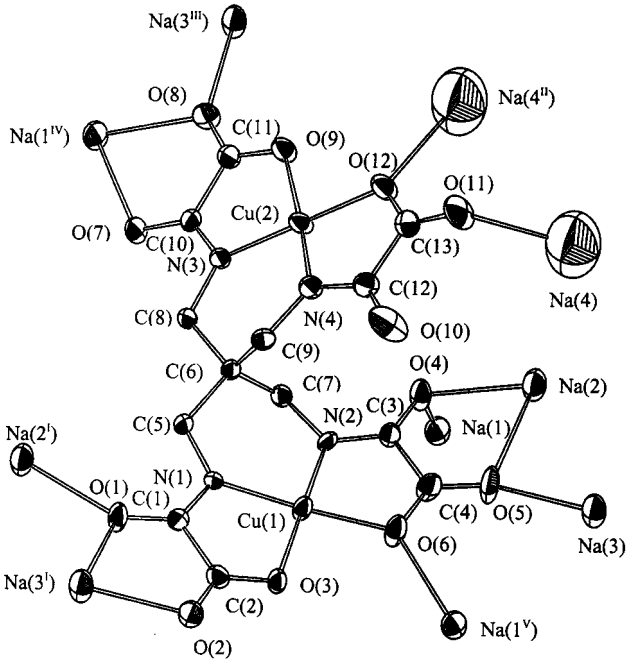


Figure 1. Perspective drawing of the assymetric unit of **3** with the atom-numbering scheme; thermal ellipsoids are representted at the 30% probability level (all hydrogen atoms and oxygen atoms from water molecules have been omitted for clarity); selected bond lengths [Å] and angles [°] with standard deviations in parentheses: Cu(1)−N(1) 1.926(5), Cu(1)−N(2) 1.919(5), Cu(1)−O(3) 1.961(4), Cu(1)−O(6) 1.964(4), Cu(2)−N(3) 1.929(5), Cu(2)−N(4) 1.921(5), Cu(2)−O(9) 1.963(4), Cu(2)−O(12) 1.983(4); N(2)−Cu(1)−N(1) 96.6(2), O(3)−Cu(1)−N(1) 84.5(2), O(6)−Cu(1)−N(1) 173.3(2), N(2)−Cu(1)−O(3) 176.8(2), N(2)−Cu(1)−O(6) 84.2(2), O(6)−Cu(1)−O(3) 95.1(2), N(3)−Cu(2)−N(4) 95.1(2), O(9)−Cu(2)−N(3) 84.4(2), O(12)−Cu(2)−N(3) 178.9(2), N(4)−Cu(2)−O(9) 172.4(2), N(4)−Cu(2)−O(12) 84.0(2), O(12)−Cu(2)−O(9) 96.4(2)

The dinuclear copper anion molecule is dissymmetric both (*R*) and (*S*) optical isomers are present in the crystal due to the existence of an inversion center according to the *P*−1 space group]. In fact, the central carbon atom C(7) connecting the two mononuclear copper fragments turns out to be the center of dissymmetry of the molecule because of the four independent oxamato substituents are involved in distinct coordinative interactions with the metal sodium cations (i.e., the central C atom in the free ligand H_8[**2**] can be seen as being "prochiral"). Actually, almost all twelve oxygen atoms [but O(10)] from the four oxamato groups of the dicopper complex anion participate in coordination of the sodium metal cations. These sodium cations form in turn molecular aggregates comprising of eight Na^+ which are connected through the $[Cu_2(\eta^4\text{:}\eta^4\text{-}\mathbf{2})]^{4-}$ moieties, thus leading to an intricate three-dimensional structure in the solid-state (Figure 2). The Cu(1)···Cu(2) intramolecular separation is 5.92 Å, while the shortest intermolecular ones $Cu(1^V)\cdots Cu(1^{VI})$ and $Cu(2^{II})\cdots Cu(2^{VI})$ are 5.28 and 4.08 Å, respectively (II = 1 − *x*, 2 − *y*, 2 − *z*; V = −*x*, 1 − *y*, 1 − *z*; VI = *x*, 1 + *y*, *z*).

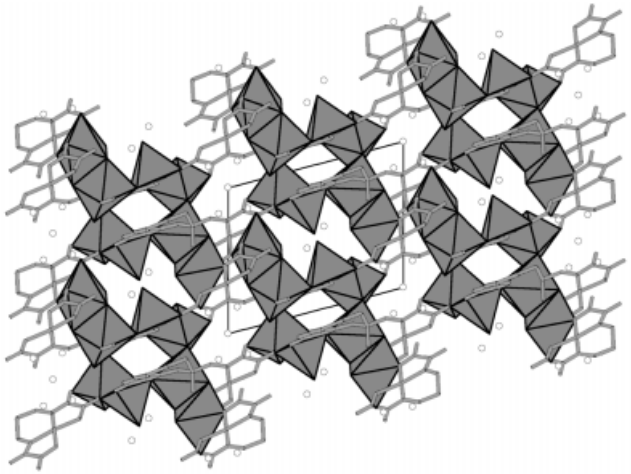


Figure 2. Projection view of the unit cell of **3** along the *b* axis, showing the formation of octanuclear sodium aggregates in the solid state; sodium cations are represented by shaded octahedra and all remaining atoms are represented by spheres of arbitrary radii

The octanuclear sodium cationic entity (Figure 3) is made up of two tetranuclear propeller-like molecular units with an approximate three-fold symmetry related by an inversion center (V = −*x*, 1 − *y*, 1 − *z*). The central tris(chelate) sodium complex of one tetrameric fragment and its symmetry related one have opposite chirality, one isomer being Δ and the other Λ (i.e., the centrosymmetric octanuclear moiety is mesomorphic). Alternatively, the resulting cluster can also be viewed as a ring of six sodium atoms with two edge-bridged sodium atoms. Therefore, all but two pairs of neighboring sodium polyhedra in the aggregate share an edge, while Na(1) and $Na(3^V)$ atoms (and their symmetry-related pair) share a corner. The central hexasodium ring is reminiscent to that found in some cyclic hexairon(III)[9a] and hexamanganese(III) complexes.[9b] The six sodium atoms which form the ring are situated at the vertices of an almost regular hexagon [Na(1)−Na(2), Na(2)−Na(3) and Na(3)−$Na(1^V)$ distances of 3.52, 3.44 and 3.70 Å, respectively, and Na(2)−Na(1)−$Na(3^V)$, Na(3)−Na(2)−Na(1) and Na(2)−Na(3)−$Na(1^V)$ angles of 118.9, 116.9 and 105.4°, respectively], with a diameter of about 6.92 Å (average distance between two opposing symmetry-related sodium atoms). The remaining Na(4) and $Na(4^V)$ atoms are connected to the ring through Na(2) and $Na(2^V)$ atoms, respectively [Na(2)−Na(4) distance of 3.50 Å]. The intraring sodium atoms lie essentially in a plane with a maximum deviation of ±0.467(2) Å for Na(2) and $Na(2^V)$, whereas the extraring ones are ±2.58(1) Å out of the ring plane.

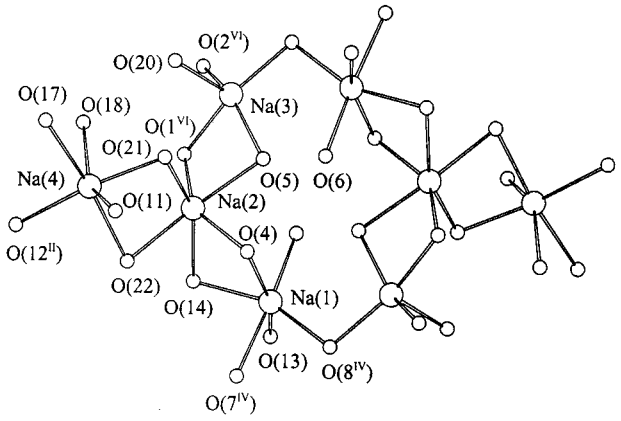


Figure 3. Perspective drawing of the cationic octasodium cluster of **3** with the atom-numbering scheme; an inversion center relates one tetranuclear unit to the other one; atoms are represented by spheres of arbitrary radii; selected bond lengths [Å] and angles [°] with standard deviations in parentheses: Na(1)−O(4) 2.513(6), Na(1^V)−O(6) 2.368(5), Na(1)−O(7^{IV}) 2.384(5), Na(1)−O(8^{IV}) 2.379(5), Na(1)−O(13) 2.421(7), Na(1)−O(14) 2.395(6), Na(2)−O(1^{VI}) 2.299(5), Na(2)−O(4) 2.358(5), Na(2)−O(5) 2.485(5), Na(2)−O(14) 2.463(6), Na(2)−O(21) 2.366(10), Na(2)−O(22) 2.539(9), Na(3)−O(1^{VI}) 2.357(5), Na(3)−O(2^{VI}) 2.386(5), Na(3)−O(5) 2.346(5), Na(3^V)−O(8^{IV}) 2.291(5), Na(3)−O(20) 2.345(10), Na(4)−O(11) 2.532(10), Na(4)−O(12^{II}) 2.615(9), Na(4)−O(17) 2.532(10), Na(4)−O(18) 2.540(14), Na(4)−O(21) 2.302(14), Na(4)−O(22) 2.52(2); Na(2)−O(4)−Na(1) 92.3(2), Na(1)−O(14)−Na(2) 92.7(2), Na(2)−O(1^{VI})−Na(3) 95.4(2), Na(3)−O(5)−Na(2) 90.8(2), Na(4)−O(21)−Na(2) 97.0(5), Na(4)−O(22)−Na(2) 87.4(4), Na(3^V)−O(8^{IV})−Na(1) 104.7(2) [symmetry codes: (II) 1 − x, 2 − y, 2 − z; (IV) − x, 1 − y, 2 − z; (V) − x, 1 − y, 1 − z; (VI) x, 1 + y, z]

Focusing on the core skeleton of the cationic Na_8 cluster, the six sodium atoms which define the central ring are linked by ten bridging oxygen atoms: four carboxylate-O and four carbonyl amide-O atoms from the oxamato groups and only two water molecules. Bis(aquo) bridges connect the two extraring sodium atoms to the central Na_6 skeleton. The remaining sites of the six [NaO_6] octahedra and two [NaO_5] trigonal bipyramids which form the octasodium aggregate are occupied by oxygen atoms from additional water molecules and oxamato ligands. The Na−O bond lengths are not all equivalent (2.29−2.66 Å), and the O−Na−O angles lie in the large range 69.6−166.7°. The architecture of the sodium cluster is issued from the bridging modes of the oxamato groups: each of the two μ_4-O_3C_2NR moieties link four Na^+ ions in the inner rim of the cyclic ring, while each of the four μ_2-O_2C_2ONR moieties link two Na^+ ions in the outer rim. In addition, two bidentate bridging carboxylate moieties from two μ_2-O_2C_2ONR groups connect the extraring Na^+ ions from two neighboring aggregates.

In summary, compound **3** provides a clear evidence of self-assembly in the solid-state of an unprecedent octanuclear sodium cluster which serves as the molecular fragment of a three-dimensional supramolecular complex. In that case, the formation of the octasodium cluster relies on the multidentate character of the novel dicopper oxamato complex $[Cu_2(\eta^4{:}\eta^4\text{-}\mathbf{2})]^{4-}$, acting as both terminal and bridging ligand. We are currently focusing our attention on the ability of this novel organometallic assembling block to bind more relevant cations in the field of magnetochemistry, such as iron and manganese, in order to elaborate new materials with interesting magnetic properties (molecular-based magnets)

Experimental Section

Preparation of H_8[2]: The tetraethyl ester Et_4H_4[**2**] ligand resulted from the condensation of tetrakis(aminomethyl)methane prepared according to a literature procedure[10] and diethyl oxalate in tetrahydrofuran: A solution of the tetraamine (4.0 g, 30 mmol) in THF (100 mL) was added dropwise through a dropping funnel to a large excess of diethyl oxalate (250 mL). The resulting mixture was stirred for 0.5 h at room temp. and then filtered through paper. The solvent was removed in a rotatory evaporator and the remaining oil was treated with diethyl ether to give a white solid which was collected by filtration and dried under vacuum (90%). − ^{1}H NMR ([D_6]DMSO): δ = 1.29 (t, 12 H, CH_3), 3.02 (d, 8 H, CH_2N), 4.27 (q, 8 H, CH_2O), 8.89 (t, 4 H, NH). − IR (KBr): $\tilde{\nu}$ = 3330 cm^{-1} (NH), 1740 and 1695 (C=O).

Synthesis of 3: The sodium salt of the copper(II) complex **3** was obtained by reaction of the tetraethyl ester Et_4H_4[**2**] with Cu^{2+} in basic aqueous media: To a suspension of Et_4H_4[**2**] (1.33 g, 2.5 mmol) in water (50 mL) was added an aqueous solution (25 mL) of NaOH (1.00 g, 25 mmol). After stirring for 15 min at room temp. until complete dissolution, an aqueous solution (25 mL) of $Cu(NO_3)_2 \cdot 3\ H_2O$ (1.20 g, 5 mmol) was added dropwise. The deep-blue solution was then filtered to eliminate the rest of solid particles and the solvent volume was reduced to 25 mL in a rotatory evaporator when a solid began to appear. Slow addition of absolute ethanol to the mother liquor gave a purple-blue crystalline solid which was collected by filtration and air-dried. Upon standing a second crop separated which was also collected and dried (95%). − IR (KBr): $\tilde{\nu}$ = 1640 and 1608 cm^{-1} (C=O). − $C_{13}H_8Cu_2N_4Na_4O_{12} \cdot 8\ H_2O$ (775): calcd. C 20.14, H 3.12, N, 7.23; found C 19.35, H 2.85, N 7.01. − The purple-blue crystalline solid is readily soluble in water but insoluble in common solvents (even in DMSO or DMF). Well-shaped large purple prisms of **3**, suitable for X-ray diffraction, were obtained by recrystallization from concentrated aqueous solutions after two weeks of slow concentration at room temp.

X-ray Crystallographic Study for 3:[11] Crystal data: $C_{13}H_{29}Cu_2Na_4N_4O_{22.5}$, mol. mass = 820, triclinic, space group $P\bar{1}$, a = 10.507(1), b = 10.958(2), c = 13.438(2) Å, α = 109.17(1), β = 99.21(1), γ = 103.11(1)°, V = 1376.3(3) Å^3, d = 1.99 g mL^{-1}, Z = 2. − Data collection: Enraf-Nonius CAD-4 diffractometer, Mo-K_α radiation, λ = 0.71069 Å, graphite monochromator, 293 K, ω-2θ, Lorentz and polarization effects and absorption correction, μ = 1.72 mm^{-1}, 2.0° ≤ θ ≤ 22.5°, crystal size 0.05 × 0.20 × 0.05 mm. 3498 unique reflections, and 3428 assumed as observed with $I > 2\sigma(I)$. Structural analysis and refinement: standard Patterson methods with subsequent full-matrix least-squares method refinement, SHELX93.[12] The hydrogen atoms from the organic ligand were located from a difference synthesis and refined with an overall isotropic thermal parameter. The hydrogen atoms from the water molecules were neither found nor calculated. Refinement of 414 variables with anisotropic thermal parameters for all non-hydrogen atoms gave R = 0.051 and R_w = 0.123 with S = 1.05. The crystal drawings were carried out with the SCHAKAL[13] and CRYSTAL MAKER[14] programs.

Acknowledgments

This work was supported by the CNRS (France) and the DGICYT (Spain) through project PB94-1002. B. C. thanks the Conselleria de Educació i Ciència de la Generalitat Valenciana (Spain) for a grant. We would also like to express our gratitude to Profs. M. Julve and T. Mallah for fruitful discussions during the preparation of this manuscript.

[1] G. Blondin, J. J. Girerd, *Chem. Rev.* **1990**, *90*, 1359.
[2] K. S. Hagen, *Angew. Chem.* **1992**, *104*, 1036; *Angew. Chem. Int. Ed. Engl.* **1992**, *31*, 1010.
[3] D. Gatteschi, A. Caneschi, L. Pardi, R. Sessoli, *Science* **1994**, *265*, 1054.
[4] I. G. Dance in *Comprehensive Coordination Chemistry*, vol. 1 (Eds.: G. Wilkinson, R. D. Gillard, J. A. McCleverty), Pergamon, Oxford, **1987**, pp. 135−177.
[5] A. Muller, F. Peters, M. T. Pope, D. Gatteschi, *Chem. Rev.* **1998**, *98*, 239.
[6] B. Cervera, J. L. Sanz, M. J. Ibañez, G. Vila, F. Lloret, M. Julve, R. Ruiz, X. Ottenwaelder, A. Aukauloo, S. Poussereau, Y. Journaux, M. C. Muñoz, *J. Chem. Soc., Dalton Trans.* **1998**, 781.
[7] [7a] Y. Pei, M. Verdaguer, O. Kahn, J. Sletten, J. P. Renard, *Inorg. Chem.* **1987**, *26*, 138. − [7b] Y. Pei, Y. Journaux, O. Kahn, *Inorg. Chem.* **1988**, *27*, 399. − [7c] J. Ribas, C. Diaz, R. Costa, Y. Journaux, C. Mathonière, O. Kahn, A. Gleizes, *Inorg. Chem.* **1990**, *29*, 2042.
[8] [8a] O. Guillou, P. Bergerat, O. Kahn, E. Bakalbassis, K. Boubekeur, P. Batail, M. Guillot, *Inorg. Chem.* **1992**, *31*, 110. − [8b] O. Guillou, O. Kahn, R. L. Oushoorn, K. Boubekeur, P. Batail, *Inorg. Chim. Acta* **1992**, *119*, 198. − [8c] O. Guillou, R. L. Oushoorn, O. Kahn, K. Boubekeur, P. Batail, *Angew. Chem.* **1992**, *104*, 658; *Angew. Chem. Int. Ed. Engl.* **1992**, *31*, 626.
[9] [9a] A. Caneschi, A. Cornia, S. J. Lippard, *Angew. Chem.* **1995**, *107*, 511; *Angew. Chem. Int. Ed. Engl.* **1995**, *34*, 467. − [9b] G. L. Abbati, A. Cornia, A. C. Fabretti, A. Caneschi, D. Gatteschi, *Inorg. Chem.* **1998**, *37*, 1430.
[10] A. Litherland, F. G. Mann, *J. Chem. Soc.* **1938**, 1588.
[11] Crystallographic data (excluding structure factors) for the structure reported in this paper have been deposited with the Cambridge Crystallographic Data Centre as supplementary publication no. CCDC-101560. Copies of the data can be obtained free of charge on application to CCDC, 12 Union Road, Cambridge CB21EZ, UK (Fax: + 44-1223/336-033; E-mail: deposit@ccdc.cam.ac.uk).
[12] G. M. Sheldrick, *SHELXL93, Program for the Refinement of Crystal Structures*, University of Göttingen, Germany, **1993**.
[13] K. Keller, *SCHAKAL, A Program for the Graphic Representation of Molecular and Crystallographic Models,* University of Freiburg, Germany, **1987**.
[14] D. Palmer, *Crystal Maker*, Cambridge University Technical Services Ltd., Cambridge, UK, **1996**.

Received August 1, 1998
[I98276]

A Unique Fourfold Intramolecular Hydrogen Bonding Stabilises the Structure of *trans*-Bis(2-amino-5,7-dimethyl[1,2,4]triazolo[1,5-*a*]pyrimidine-N^3)-aquatrichlororuthenium(III) Monohydrate

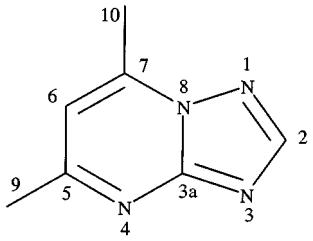
Aldrik H. Velders,[a] Franco Ugozzoli,[b] Marina Biagini-Cingi,[b] Anna M. Manotti-Lanfredi,[b] Jaap G. Haasnoot,[a] and Jan Reedijk*[a]

Keywords: Ruthenium / Nitrogen heterocycles / Hydrogen bonds / Antitumor agents / Crystal structures

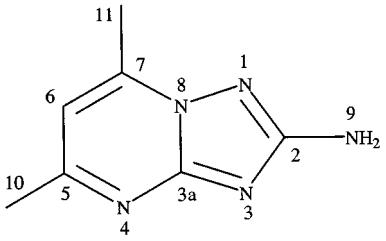
The X-ray structure of the potential antitumour complex *trans*-[$RuCl_3(H_2O)(admtp)_2$] · H_2O (admtp = 2-amino-5,7-dimethyl[1,2,4]triazolo[1,5-*a*]pyrimidine) shows unique and very interesting intramolecular hydrogen-bonding properties with the non-bridgehead pyrimidinic nitrogen atom of admtp acting as hydrogen acceptor and the amino group acting as hydrogen donor.

In the search for new chemotherapeutic antitumour agents, ruthenium(III) complexes of the type *trans*-(LH)[$RuCl_4(L)_2$] (where L is an aromatic N-heterocycle like imidazole or indazole and HL the protonated heterocycle) have shown promising activity in preclinical tests against different (platinum-resistant) tumour models.[1] As yet no clear structure−activity relationship has been reported for ruthenium(III) complexes, like for platinum compounds;[2] therefore, the hydrolysis properties[3] and DNA binding[4] are important factors to analyse. In vivo the ionic *trans*-(LH)[$RuCl_4(L)_2$] complexes with bicyclic ligands like indazole appear to be prodrugs that hydrolyze rapidly to form relatively stable neutral complexes of the type *trans*-[$RuCl_3(H_2O)(L)_2$].[5] However, the consecutive extracellular and intracellular reactions of these monoaquatrichlororuthenium(III) complexes that finally lead to the antitumour activity, and the role of the heterocyclic ligands therein, are not yet understood[3,6] and are currently under investigation.

Recently, we have reported the synthesis and characterisation of the neutral trichlororuthenium(III) complex *trans*-[$RuCl_3(H_2O)(dmtp)_2$] · H_2O, in which the azapurine 5,7-dimethyl[1,2,4]triazolo[1,5-*a*]pyrimidine (dmtp) (Scheme 1), is coordinated to the ruthenium(III) centre through the N(3) nitrogen atom of the triazole moiety, whilst the pyrimidinic (N4) nitrogen atoms of both coordinated ligands are involved in intramolecular hydrogen bonds with the two hydrogen atoms of the coordinated water molecule.[7] The hydrogen-bonding interactions of the dmtp suggested the possibility of fine-tuning in the investigations of the hydrolysis reactions and hydrolysis products of ruthenium(III) antitumour complexes, on use of heterocyclic ligands with the capacity to form intramolecular donor and/or acceptor hydrogen bonds.



dmtp



admtp

Scheme 1

In the past two decades several triazolopyrimidines have been used to synthesise complexes with different metals and purposes,[8,9] and recently a platinum complex with two triazolopyrimidine ligands has been reported which has interesting antimour activity.[9c] To our knowledge, the 2-amino-5,7-dimethyl[1,2,4]triazolo[1,5-*a*]pyrimidine,[10] (admtp) (Scheme 1), has not been reported yet as a ligand for metal coordination. We now present the synthesis and characterisation of a ruthenium complex, in which admtp acts as a monodentate ligand with unique intramolecular hydrogen-bonding properties, and its possible role in the search for a structure−activity relationship of antitumour-active ruthenium(III) complexes is discussed.

[a] Leiden Institute of Chemistry, Gorlaeus Laboratories, Leiden University,
P. O. Box 9502, NL-2300 RA Leiden, The Netherlands
E-mail: reedijk@chem.leidenuniv.nl
[b] Dipartimento di Chimica Generale ed Inorganica, Chimica Analitica, Chimica Fisica, Università di Parma and Centro di Studio per la Strutturistica Diffrattometrica del C.N.R.,
Viale delle Scienze 78, I-43100 Parma, Italy

Supporting information for this article is available on the WWW under http://www.wiley-vch.de/home/eurjic or from the author.

 © WILEY-VCH Verlag GmbH, D-69451 Weinheim, 1999 1434−1948/99/0202−0213 $ 17.50+.50/0

The new neutral monoaquatrichlororuthenium(III) compound *trans*-[$RuCl_3(H_2O)(admtp)_2$] · H_2O (**1**) was synthesised by a procedure analogous to *trans*-[$RuCl_3(H_2O)(dmtp)_2$] · H_2O[7] (**2**) and characterised by elemental analysis, and NMR and IR spectroscopy. The crystal structure of **1** (Figure 1) was determined by X-ray diffraction analysis and shows a six-coordinated ruthenium(III) ion with three chloride ions in a *mer* configuration, two admtp molecules, coordinated by their N(3) nitrogen atoms, in a parallel "face-to-face" *trans* orientation, and a water molecule coordinated in the plane of the chloride ions and lying in between the pyrimidinic rings of the two admtp ligands. The Ru−N, Ru−Cl, and Ru−O bond lengths are comparable with those found in related complexes, like *trans*-[$RuCl_3(H_2O)(dmtp)_2$][7] and *trans*-[$RuCl_3(H_2O)(1\text{-MeInd})_2$][5] which also display a quasi-octahedral stereochemistry with two *trans*-located heterocyclic ligands.

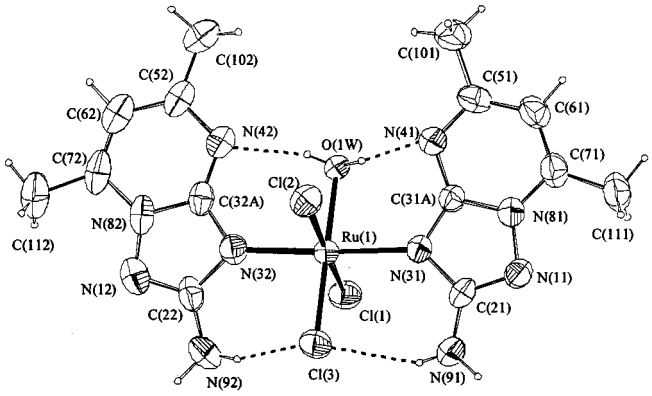


Figure 1. X-ray structure and numbering scheme of **1** with the thermal ellipsoids drawn at a 50% probability level (PLATON); intramolecular hydrogen bondings are indicated with dotted lines; the crystal water is omitted for clarity; selected metal−ligand bond lengths [Å] and angles [°]: Ru(1)−N(31) 2.117(4), Ru(1)−N(32) 2.131(5), Ru(1)−O(1W) 2.098(4), Ru(1)−Cl(1) 2.339(2), Ru(1)−Cl(2) 2.348(2), Ru(1)−Cl(3) 2.358(2), N(32)−Ru(1)−N(31) 175.7(2), Cl(1)−Ru(1)−Cl(2) 175.08(5), Cl(3)−Ru(1)−O(1W) 176.5(1); donor···acceptor (D···A) and hydrogen···acceptor (H···A) distances [Å], and donor−hydrogen···acceptor (D−H···A) angles [°] of the intramolecular hydrogen bonds: O(1W)−H(1WA)···N(41) 2.650(6), 1.81(9), and 154(8); O(1W)−H(1WB)···N(42) 2.662(6), 1.95(7), and 165(8); Cl(3)···H(91A)−N(91) 3.126(6), 2.51(6), and 141(6); Cl(3)···H(92A)−N(92) 3.077(7), 2.35(10), and 155(10)

The most striking feature of the structure of **1** is that a fourfold intramolecular hydrogen-bond system is present. In addition to the hydrogen-bonding acceptor properties of the pyrimidinic N(4) nitrogen atoms to the coordinated water hydrogen atoms, the amino groups of the two admtp ligands are both involved as hydrogen donors in intramolecular hydrogen bonding to the chloride ion Cl(3) lying *trans* to the coordinated water molecule. This special hydrogen bonding is probably also the origin of the elongated Ru(1)−Cl(3) distance (2.358 Å), which is slightly longer than the other two ruthenium−chloride bonds (2.339 and 2.348 Å). It is more difficult to draw conclusions about differences in the stability of the coordinated water molecule from the crystallographic data of **1** and **2** as the water molecule in the former is also involved in intermolecular hydrogen bonds.

Double intramolecular hydrogen bonding of heterocyclic ligands with both hydrogen atoms of a coordinated water molecule has been observed before for metal complexes,[7,9a,11a] and also double intramolecular hydrogen bonding of N−H groups with one coordinated halide ion is not an unknown feature for coordination compounds. However, the combination of (intramolecular) hydrogen-accepting and hydrogen-donating bonds of one ligand in a coordination compound, like in this case for admtp [via the N(4) nitrogen atom and the amine moiety, respectively] is to our knowledge unique.[11b] As both admtp ligands in **1** bind in a similar way, complex **1** is an as yet unique example of a coordination compound in which four square-planar coordinated monodentate ligands, linked to each other by a fourfold intramolecular hydrogen bond, form a pseudo-chelating tetradentate ligand which is organised by the heterocyclic ligand.

Due to the (non-symmetric) intermolecular hydrogen bonds of the two amino groups and the two water molecules in the crystal structure of **1** no twofold symmetry is present. However, it is likely that in solution **1** does have a twofold symmetry, in agreement with the single set of admtp signals found in NMR. Time-dependent UV/Vis absorption, NMR, and conductivity measurements of **1** in coordinating solvents (Solv), like DMSO and acetonitrile, indicate the formation of complexes of the type *trans*-[$RuCl_3(Solv)(admtp)_2$]. This type of reactions is related to those seen in the *trans*-[$RuCl_3(H_2O)(dmtp)_2$] · H_2O chemistry[7] and will be published in detail in a full paper. Preliminary results indicate that the solvolysis of **1**, in acetonitrile for example, is slightly faster than that of **2**, but still much slower than in analogous complexes that do not have double intramolecular hydrogen bonds that can stabilise the coordinated water molecule.[12] Although the water-substitution reactions are not directly correlated to in vivo reactions of this type of ruthenium complexes, these results do indicate that the ruthenium−ligand properties have been slightly changed by a small modification of the ligand.

As hydrolysis properties play a key role in the antitumour mechanism of chemotherapeutic platinum complexes, it is useful to study these properties of ruthenium complexes, too. The structure of complex **1** indicates that the use of the triazolopyrimidine admtp offers the possibility to stabilise, isolate, and study the first hydrolysis product of antitumour-active ruthenium(III) complexes of the type *trans*-(LH)[$RuCl_4(L)_2$]. Furthermore, the intramolecular hydrogen bonds of admtp are likely to influence hydrolysis properties through interactions with incoming (water molecules), as well as with leaving ligands (chloride ions). Also the consecutive in vivo reactions of the aquated ruthenium species, in which the water molecules are thought to be substituted by DNA bases, are likely to be influenced by the presence of hydrogen-donating as well as hydrogen-accepting moieties of the heterocyclic ligands. Finally, the amine group of the ligand admtp is also interesting for its potential intermolecular hydrogen-bonding properties, which for antitumour-active platinum compounds have been proven to be a crucial factor for the in vivo DNA binding and

distortion that finally lead to cell death.[2]

In summary, the hydrogen-bonded stabilised structure of *trans*-[$RuCl_3(H_2O)(admtp)_2$] proves the possibility to design and synthesise new ruthenium complexes with specific ligands that can fine-tune the chemical and physical properties of potential antiumour complexes via multiple intramolecular hydrogen bondings. The easy synthesis and interesting hydrogen-bonding properties of admtp give it promise as a useful ligand for the synthesis of complexes with other transition metals in different fields of coordination chemistry, too. Although the amine group of the admtp is not as reactive as a primary amine, due to the delocalisation of the electron pair in the triazolopyrimidine ring system,[10] it is a useful functional group for the design and synthesis of other triazolopyrimidine derivatives that might also be successful ligands.

Experimental Section

General: NMR: Bruker WM 300 MHz spectrometer. For [D_6]acetone as solvent, δ_H = 2.06 at 295 K. ^{1}H-NMR data of **1** were obtained using an inversion recovery pulse sequence, *π-τ-π/2-acquisition*, with τ (the variable delay time between the inversion and the acquisition pulse, respectively) in the order of 100 ms. The ^{1}H-NMR signals of **1** could be identified as the paramagnetically shifted and broadened signals with relaxation times in the order of ms.

***trans*-[$RuCl_3(H_2O)(admtp)_2$] · H_2O (1):** The ligand 2-amino-5,7-dimethyl[1,2,4]triazolo[1,5-*a*]pyrimidine (admtp) was prepared by a method slightly different method from the one by Kreutzberger[10] by condensation of 3,5-diamino-1,2,4-triazole (Aldrich) with a small excess of 2,4-pentanedione (Merck) in boiling ethylene glycol. After gentle heating at 75°C for 3 h of a ruthenium(III) chloride solution (5 mmol in 50 mL 1 M HCl) with admtp (15 mmol in 50 mL of ethanol), *trans*-[$RuCl_3(H_2O)(admtp)_2$] · H_2O was obtained as a brick-red powder; recrystallisation from acetone/water (5:1) yielded orange-red prismatic crystals. — $C_{14}H_{22}Cl_3N_8O_2Ru$ (569.8): calcd. C 29.50, H 3.86, N 24.58, Cl 18.67; found: C 29.52, H 3.86, N 24.58, Cl 18.6. − The effective magnetic moment, μ_{eff}, of the complex was determined to be 1.9 Bohr magneton at 20°C. − ^{1}H NMR ([D_6]acetone): δ (peak width at half height) = +1.4 (20 Hz) [H(61/62)], +4.7 (35 Hz) and −3.5 (15 Hz) [CH_3(101/102) and CH_3(111/112)], and +53 (2000 Hz) [coordinated H_2O].

X-ray Crystallographic Study of 1: $C_{14}H_{20}Cl_3N_{10}ORu \cdot H_2O$; M = 569.823; monoclinic, space group $P2_1/c$; a = 8.292(5), b = 26.289(5), c = 10.175(5) Å, β = 97.16(2)°; V = 2201(2) Å^3; Z = 4; $D_{calcd.}$ = 1.720 g cm^{-3}; graphite-monochromated Cu-K_α radiation (λ = 1.54178 Å); μ = 9.421 mm^{-1}; T = 293 K. Data were collected with a Siemens AED and corrected for Lorentz and polarisation effects: 4150 unique data in the range 6° < θ < 70°. Refinement on F^2 values of all data with SHELXL96.[13] Final $R1 = \Sigma ||F_o| - |F_c||/\Sigma|F_o| = 0.0566$ for 3140 $F_o > 4\sigma(F_o)$ and 0.0689 for all data, $wR2 = [\Sigma w(F_o^2 - F_c^2)^2/\Sigma wF_o^4]^{1/2} = 0.1605$, $\Sigma = [\Sigma w(F_o^2 - F_c^2)^2/(n - p)]^2 = 1.073$ for 303 parameters. Residual electron density extrema are 2.49 and −1.5 eÅ^{-3}. Crystallographic data (excluding structure factors) for the structure reported in this paper have been deposited with the Cambridge Crystallographic Data Centre as supplementary publication number CCDC-103269. Copies of the data can be obtained free of charge on application to CCDC, 12 Union Road, Cambridge CB2 1EZ, UK [Fax: int. code + 44-1223/336-033; E-mail: deposit@ccdc.cam.ac.uk].

Acknowledgments

The authors thank Johnson & Matthey (Reading, UK) for their generous loan of $RuCl_3 \cdot 3\ H_2O$. This research is sponsored by the Netherlands Organisation for Chemical Research (SON), with financial aid of the Netherlands Organisation for the Advancement of Research (NWO), and support by COST Action D8/0017/97 (Metals in medicine) is also kindly acknowledged. The authors wish to thank the Italian MURST and the Italian C.N.R. (Roma) for the financial support to this work.

[1] [1a] B. K. Keppler, M. Henn, U. M. Juhl, M. R. Berger, R. Niebl, F. E. Wagner, *Prog. Clin. Biochem. Med.* **1989**, *10*, 41−69. − [1b] H. Depenbrock, S. Schmelcher, R. Peter, B. K. Keppler, G. Weirich, T. Block, J. Rastetter, A.-R. Hanauske, *Eur. J. Cancer* **1997**, *33*, 2404−2410.
[2] J. Reedijk, *Chem. Commun.* **1996**, 801-806.
[3] [3a] C. Anderson, A. L. Beauchamp, *Can. J. Chem.* **1995**, *73*, 471−482. − [3b] O. M. Ni Dhubhghaill, W. R. Hagen, B. K. Keppler, K.-G. Lipponer, P. J. Sadler, *J. Chem. Soc., Dalton Trans.* **1994**, 3305−3310.
[4] M. Hartmann, T. J. Einhauser, B. K. Keppler, *Chem. Commun.* **1996**, 1741−1742.
[5] K.-G. Lipponer, E. Vogel, B. K. Keppler, *Metal-Based Drugs* **1996**, *3*, 243−260.
[6] M. Hartmann, K.-G. Lipponer, B. K. Keppler, *Inorg. Chim. Acta* **1998**, ***267***, 137−141.
[7] A. H. Velders, L. Pazderski, F. Ugozzoli, M. Biagini-Cingi, A. M. Manotti-Lanfredi, J. G. Haasnoot, J. Reedijk, *Inorg. Chim. Acta* **1998**, *273*, 259−265.
[8] [8a] J. M. Salas, M. A. Romero, A. Rahmani, R. Faure, G. Alvarez de Cienfuegos, E. R. T. Tiekink, *J. Inorg. Biochem.* **1996**, *64*, 259−271. − [8b] J. A. R. Navarro, J. M. Salas, M. A. Romero, R. Vilaplana, F. Gonzalez-Vílchez, R. Faure, *J. Med. Chem.* **1998**, *41*, 332-338.
[9] [9a] J. G. Haasnoot, T. L. F. Favre, W. Hinrichs, J. Reedijk, *Angew. Chem.* **1988**, *100*, 884−886; *Angew. Chem. Int. Ed. Engl.* **1988**, *27*, 856−858. − [9b] M. Biagini-Cingi, A. M. Manotti-Lanfredi, A Tiripicchio, J. G. Haasnoot, J. Reedijk, *Inorg. Chim. Acta* **1985**, *101*, 49−61. − [9c] T. L. F. Favre, J. G. Haasnoot, J. Reedijk, *Polyhedron* **1986**, *5*, 1405-1411.
[10] A. Kreutzberger, *Chem. Ber.* **1966**, *99*, 2237−2245.
[11] [11a] J. Ochocki, B. Zurowska, J. Mrozinski, H. Kooijman, A. L. Spek, J. Reedijk, *Eur. J. Inorg. Chem.* **1998**, 169−175. − [11b] A search was done in the Cambridge Structural Database for transition-metal (Tr) complexes with (double) intramolecular hydrogen bonds of the type Tr−Cl···H−N and Tr−OH2···N, with H−N and N being part of a ligand coordinated to the metal.
[12] A. H. Velders, in preparation.
[13] G.-M. Sheldrick, University of Göttingen, Germany, **1996**

Received October 12, 1998
[I98348]

Spontaneous Assembly of a Novel Tetranuclear Ni–Fe Complex by Complete Reshuffling of Ligands and Oxidation States

Elisabeth Bouwman,*[a] Richard K. Henderson,[a] Anthony L. Spek,[b] and Jan Reedijk[a]

Keywords: Nickel / Iron / Clusters / Carbonyl complexes / S ligands

Upon reaction of the mononuclear nickel dithiolate complex [Ni(dsdm)] (H_2dsdm = *N*,*N*′-dimethyl-*N*,*N*′-bis(2-sulfanylethyl)ethylenediamine) with K[HFe(CO)$_4$] in ethanol a unique reshuffling of ligands and of oxidation states takes place. This results in the formation of a novel tetranuclear complex [Fe^{II}(dsdm)Ni^0(CO)$_3$]$_2$, in which a linear array of Ni–Fe–Fe–Ni is formed. The inner core of this complex consists of the dinuclear [Fe(dsdm)]$_2$, and two Ni(CO)$_3$ groups are bound at the periphery through one of the thiolate sulfurs.

The [NiFe] hydrogenases consist of enzymes, which, apart from iron, also contain nickel in the active site. The first crystal structure of a [NiFe] hydrogenase enzyme, extracted from *Desulfovibrio gigas*, has been published by Volbeda et al. in 1995.[1] The active site was shown to contain an unexpected disulfur-bridged heterobimetallic Ni−Fe core. There are two further cysteine groups bound to the nickel and three small non-protein ligands bound to the iron. These diatomic ligands are nowadays considered to be one carbon monoxide and two cyanide molecules, based on isotopic enrichment experiments and FT-IR measurements.[2] The publication of the crystal structure has renewed interest in the chemical modelling of the active site of [NiFe] hydrogenases. A large amount of modelling chemistry had already been reported prior to the publication of the X-ray structure,[3][4] when it was believed that the active site contained mononuclear nickel.

The compound described in the present paper was synthesised as part of research in modelling the heterodinuclear Ni−Fe active site of hydrogenases. It was decided that ligands containing mixed N/S donor groups would be used preferentially to provide greater synthetic control. In view of the new structural information, the ligand *N*,*N*′-dimethyl-*N*,*N*′-bis(2-sulfanylethyl)ethylenediamine (H_2dsdm) was considered useful in our synthetic modelling studies. The mononuclear [Ni(dsdm)] and trinuclear [Ni_3(dsdm)$_2$]-Cl_2 complexes with this ligand have previously been reported from this laboratory.[5] The mononuclear nickel compound was reinvestigated as it contains two *cis* sulfur atoms from thiolate groups, which have potential in forming heterodimetallic complexes in which sulfur bridges to iron compounds.[6]

The complex [Fe(dsdm)Ni(CO)$_3$]$_2$ (**1**) was prepared from a reaction of the mononuclear dithiolate complex [Ni(dsdm)] with K[HFe(CO)$_4$], and was characterised by IR spectroscopy, elemental analysis and single-crystal X-ray crystallography. A fully labelled representation of the molecular structure of the tetranuclear compound **1**, is given in Figure 1. The asymmetric unit contains one half of the molecule, the other half is generated by a centre of symmetry. The compound is built up in an array of Ni^0−Fe^{II}−Fe^{II}−Ni^0. The ligand dsdm is folded around the Fe^{II} ion, and one of the thiolate groups of the dsdm ligand bridges to the second (symmetry generated) iron ion, thus forming the dinuclear [Fe(dsdm)]$_2$ core of the complex. The other thiolate group of the ligand is bridging to a Ni^0 tricarbonyl group, thus forming the tetranuclear complex.

Initially, the structure was refined as "[Ni(dsdm)Fe(CO)$_3$]$_2$", in view of the composition of the starting materials. However, substitution of Fe^{II} for Ni^{II}, thus giving a tetranuclear Fe_4 cluster, resulted in significantly better *R* values and lower residual electron densities in the refinement of the structure, and substitution of the peripheral iron by nickel resulted in even better refinement of the crystal data. Ultimately, this also explained the "16-electron" count for the, initially, Fe^0 moieties, which can now be rationalised as 18-electron Ni^0 species. The coordination around the iron is distorted trigonal bipyramidal, and the nickel atoms are in a tetrahedral geometry. The Fe−N and the Fe−S distances in this unique tetranuclear compound are significantly longer than the Ni−N and Ni−S distances observed in the Ni-dsdm trinuclear species characterised by Turner et al.[5] Instead, the Fe−N and Fe−S bond distances and angles in **1** are comparable to those found in [Fe(dsdm)]$_2$,[7] deviating by less than 0.04 Å and 5.6° from this "parent" compound.

Reactivity studies of nickel thiolate complexes in binding with other metal ions have been reported for several years. In particular mononuclear nickel complexes with *cis* dithiolate groups are regarded as very reactive in forming thiolate bridged polynuclear compounds. Reactions of such nickel complexes with $FeCl_2$,[8] Fe(ClO$_4$)$_2$,[9] $Fe_2(CO)_9$,[10] or (norbornadiene)M(CO)$_4$ (with M = Cr, Mo, W)[6] have been carried out at room temperature with stirring only.

[a] Leiden Institute of Chemistry, Gorlaeus Laboratories, Leiden University,
P. O. Box 9502, 2300 RA Leiden, The Netherlands
E-mail: bouwman@chem.leidenuniv.nl
[b] Bijvoet Center for Biomolecular Research, Crystal and Structural Chemistry, Utrecht University,
Padualaan 8, 3584 CH Utrecht, The Netherlands

 © WILEY-VCH Verlag GmbH, D-69451 Weinheim, 1999 1434−1948/99/0202−0217 $ 17.50+.50/0

EurJIC 299/98

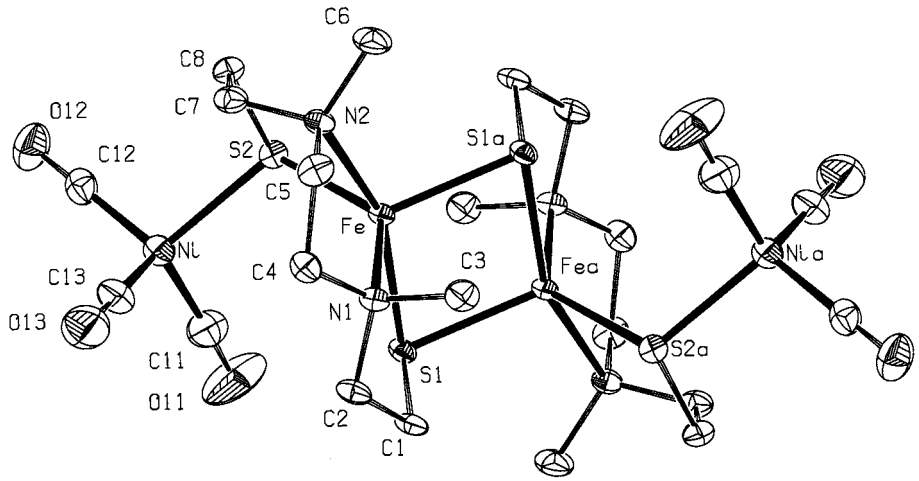


Figure 1. ORTEP view at 50% probability level of the molecular structure of **1** with the atomic labelling. Hydrogen atoms have been omitted for clarity; selected bond lengths [Å] and angles [°]: Ni−Fe 3.899(1), Fe−Fea 3.098(1), Ni−S2 2.317(1), Ni−C11 1.789(6), Ni−C12 1.773(4), Ni−C13 1.786(5), Fe−S1 2.444(1), Fe−S2 2.346(1), Fe−N1 2.168(3), Fe−N2 2.330(3), Fe−S1a 2.363(1), S2−Ni−C11 103.9(2), S2−Ni−C12 104.5(2), S2−Ni−C13 110.8(2), C11−Ni−C12 110.8(2), C11−Ni−C13 113.7(2), C12−Ni−C13 112.5(2), S1−Fe−S2 97.79(4), S1−Fe−N1 83.58(9), S1−Fe−N2 156.20(8), S1−Fe−S1a 99.75(4), S2−Fe−N1 132.48(10), S2−Fe−N2 82.98(8), S2−Fe−S1a 115.56(4), N1−Fe−N2 78.7(1), N1−Fe−S1a 110.87(9), N2−Fe−S1a 101.32(8)

These reactions resulted in various heteropolynuclear complexes, in which the original nickel thiolate complexes act as monodentate or didentate ligands towards the newly introduced metal ion. In our hands, the mononuclear compound [Ni(dsdm)] did not react with either $Fe_2(CO)_9$ or $Fe(CO)_5$ under similar mild reaction conditions. However, more severe conditions such as described above, leads to complete scrambling of the reactants.

Although the initial aim of the reaction was to form a heterodinuclear NiFe compound as a model for hydrogenase, such as the one reported by Darensbourg et al.,[10] the tetranuclear complex which was obtained instead is interesting by itself for other research areas. Numerous examples are known of iron carbonyl compounds, which are bridged by thiolates to other transition metals, but to our knowledge such compounds have not been reported with nickel carbonyl groups. The tetranuclear **1** is the first compound in which a $Ni(CO)_3$ group is bound to a transition metal thiolate complex. Only a few organometallic clusters with bridging inorganic sulfide, in which the nickel monocarbonyl is part of the cluster core, have been reported.[11]

The observation and characterisation of this reshuffled complex may draw the attention to the fact that a tetradentate chelating ligand may not be enough to hold on and stabilize a divalent metal ion. The reshuffling of ligands and oxidation states may have been triggered by the strong reducing power of $K[HFe(CO)_4]$ species, leading to "$[Ni(0)(dsdm)]^{2-}$", which then falls apart and causes a cascade of other reactions. Another scrambled compound which could be isolated from the reaction mixture is the dinuclear [Fe(dsdm)Fe(dmes)$(CO)_2$] (H_2dmes = bis(sulfanylethyl)sulfide).[12]

Experimental Section

General: Infrared spectra (KBr pellets) were recorded in the range 4000−400 cm^{-1} using a Perkin−Elmer FT-IR Paragon spectrophotometer controlled by a PC using PE Grams Analyst software.

Synthesis: All experiments were performed in an argon atmosphere. Solvents were dried according to standard procedures. The ligand H_2dsdm was synthesised according to a literature procedure.[13] [Ni(dsdm)] was synthesized by reaction of $Ni(acac)_2$ with H_2dsdm in toluene.

Iron pentacarbonyl (1 mmol, 0.131 mL) was added to an ethanolic solution of potassium hydroxide (2 mmol, 0.112 g in 5 mL of absolute ethanol) and stirred overnight until a red solution of $K[HFe(CO)_4]$ was obtained.[14] The solution was filtered to remove precipitated $KHCO_3$, which was washed with 10 mL of absolute ethanol. To the red solution was added solid [Ni(dsdm)] (1 mmol, 0.26 g) and the mixture was heated under reflux for 2 hours during which time the solution became very dark. After cooling the reaction mixture was filtered to remove any precipitated solids, and the resulting solution was left to crystallize. Orange-brown crystals suitable for X-ray diffraction were obtained after a few days. − Infrared Spectrum (KBr pellet): 3443 (br) 2919 (m), 2861 (m), 2048 (vs), 1968 (vs), 1949 (vs), 1648 (m,br), 1465 (m), 1295(m), 1273(m), 1079 (m), 1046 (m), 1029 (m), 939 (s), 882 (w), 764 (m), 740 (w), 668 (w), 519 (w), 450 (m) cm^{-1}. The compound gets slightly sticky when in contact with air. Satisfactory elemental analysis was obtained for $[C_{22}H_{36}Fe_2N_4Ni_2O_6S_4] \cdot 3\ H_2O$.

X-ray Crystal Structure Analysis: Crystal data for [Fe(dsdm)Ni$(CO)_3]_2$: $[C_{22}H_{36}Fe_2N_4Ni_2O_6S_4]$, M = 809.89, orange-brown needle (0.12 × 0.12 × 0.55 mm), triclinic, space group $P-1$ with a = 8.2339(17), b = 8.3530(15), c = 12.729(3) Å, α = 79.683(18), β = 74.661(18), γ = 75.532(16)°, U = 811.5(3) $Å^3$, Z = 1, D_c = 1.657 $g \cdot cm^{-3}$, $F(000)$ = 416, μ(Mo-K_α) = 23.2 cm^{-1}, 7392 reflections measured, 3717 independent (R_{av} = 0.05). Mo-K_α radiation, graphite monochromator, λ = 0.71073 Å, θ_{max} = 27.5°, T = 150 K, CAD4T diffractometer on rotating anode. Data were corrected for absorption (analytical). The structure was solved by Patterson techniques (DIRDIF)[15] and refined on F^2 using SHELXL96.[16] Non-hydrogen atoms were refined with anisotropic displacement parameters. Hydrogen atoms were located at calculated positions and refined riding on their carrier atoms. Convergence was reached at R_1 = 0.0415 [for 2653 reflections with $I > 2\sigma(I)$] and wR_2 = 0.0892 (S = 0.98). A final difference map did not show any features outside $-0.54 < \Delta\rho < 0.70$ e·$Å^{-3}$. Structure graphics and checking for higher symmetry were performed with the program PLATON.[17]

Crystallographic data (excluding structure factors) for the structure in this paper have been deposited at the Cambridge Crystallographic Data Centre as supplementary publication no. CCDC-102783. Copies of the data can be obtained free of charge on application to CCDC, 12 Union Road, Cambridge CB2 1EZ, UK [Fax: (internat.) +44(1223) 336-033, E-mail: deposit@ccdc.cam.ac.uk].

Acknowledgments

Financial support for this project has been provided by a Biotech grant (Contract no. BIO2-CT94-2041) from the European Union. The research of E. B. has been made possible by a Fellowship of the Royal Netherlands Academy of Arts and Sciences. The work was in part (A. L. S.) supported by The Netherlands Foundation of Chemical Research (SON) with financial aid from the Netherlands Foundation for Scientific Research (NWO). We are grateful to Mr V. E. Kaasjager for reproduction of the compound.

[1] A. Volbeda, M.-H. Charon, C. Piras, E. C. Hatchikian, M. Frey, J. C. Fontecilla-Camps, *Nature* **1995**, *373*, 580−587.
[2] R. P. Happe, W. Roseboom, A. J. Pierik, S. P. J. Albracht, K. A. Bagley, *Nature* **1997**, *385*, 126.
[3] J. C. Fontecilla-Camps, *J. Bioinorg. Chem*. **1996**, *1*, 91−98.
[4] M. A. Halcrow, G. Christou, *Chem. Rev.* **1994**, *94*, 2421−2481.
[5] M. A. Turner, W. L. Driessen, J. Reedijk, *Inorg. Chem*. **1990**, *29*, 3331−3335.
[6] J. Yoo, J. Ko, S-E. Park, *Bull. Korean. Chem. Soc*. **1994**, *15*, 803−805.
[7] W.-J. Hu, S. J. Lippard, *J. Am. Chem. Soc.* **1974**, *96*, 2366−2372.
[8] D. K. Mills, Y. M. Hsiao, P. J. Farmer, E. V. Atnip, J. H. Reibenspies, M. Y. Darensbourg, *J. Am. Chem. Soc.* **1991**, *113*, 1421−1423.
[9] G. J. Colpas, R. O. Day, M. J. Maroney, *Inorg. Chem*. **1992**, *31*, 5053−5055.
[10] C.-H. Lai, J. H. Reibenspies, M. Y. Darensbourg, *Angew. Chem*. **1996**, *108*, 2551−2554; *Angew. Chem. Int. Ed. Engl*. **1996**, *35*, 2390−2392.
[11] A search of over 181,000 entries in the Cambridge Crystal Structure Database (CSD). Use of the services and facilities of the Dutch National NWO/SURF Expertise Center CAOS/CAMM, under grant numbers SON 326-052 and STW NCH99.1751, is gratefully acknowledged.
[12] V. E. Kaasjager, R. K. Henderson, E. Bouwman, M. Lutz, A. L. Spek, J. Reedijk, *Angew. Chem*. **1998**, *110*, 1787−1789; *Angew. Chem. Int. Ed*. **1998**, *37*, 1668−1670.
[13] A. Avdeef, F. Hartenstein, A. R. Chemotti, J. A. Brown, *Inorg. Chem*. **1992**, *31*, 3701−3705.
[14] J.-J. Brunet, F. B. Kindela, D. Neibecker, *Inorg. Synth*. **1992**, *29*, 151−156.
[15] P. T. Beurskens, G. Admiraal, G. Beurskens, W. P. Bosman, S. Garcia-Granda, R. O. Gould, J. M. M. Smits, C. Smykalla, *The DIRDIF Program System*, Technical Report of the Crystallography Laboratory, University of Nijmegen, Nijmegen, The Netherlands, **1996**.
[16] G. M. Sheldrick SHELXL−96. *Program for Crystal Structure refinement*; University of Göttingen, Germany, **1996**.
[17] A. L. Spek, *Acta Cryst* **1990**, *A46*, C34.

Received September 4, 1998
[I98299]

A μ-η¹-Azavinylidene Complex: Intramolecular Condensation of Two Acetonitrile Ligands at a Dinuclear Molybdenum(III) Site

Philippe Schollhammer,[a] Mael Pichon,[a] Kenneth W. Muir,*[b] François Y. Pétillon,*[a] Roger Pichon,[a] and Jean Talarmin[a]

Keywords: Dimolybdenum(III) complexes / Azavinylidene / C–C coupling / Acetonitrile ligands / X-ray crystal structure

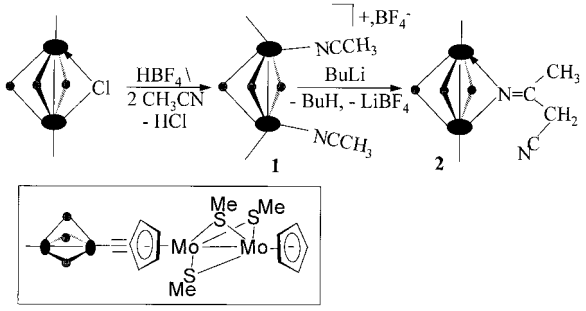
Removal of a proton from one of the two coordinated acetonitrile ligands in $[Mo_2Cp_2(\mu\text{-}SMe)_3(CH_3CN)_2](BF_4)$ (**1**) initiates its intramolecular condensation with the second of the acetonitrile ligands attached to the bimetallic $[Mo_2Cp_2(\mu\text{-}SMe)_3]$ core, thereby giving rise to the novel μ-η¹-azavinylidene complex $\{Mo_2Cp_2(\mu\text{-}SMe)_3[\mu\text{-}\eta^1\text{-}N{=}C(CH_3)\text{-}CH_2CN]\}$ (**2**). Complex **2** has been characterized by NMR and X-ray methods.

Bimetallic complexes with direct M−M bonds permit the simultaneous activation of neighbouring ligands. The ensuing reactions are often different from those that occur with polymetallic systems[1] or with bimetallic species in which there is little or no direct communication between the metal atoms.[1−3] Here, we show that a well-known organic reaction, the self-condensation of an alkyl cyanide, can still occur when both substrate molecules are attached to the neighbouring metal atoms of a binuclear complex. Moreover, the product represents a new type of N-donor bridging ligand.

We are currently extensively developing the chemistry of bimetallic complexes with an $[Mo_2Cp_2(\mu\text{-}SMe)_3]$ core by using the bis(acetonitrile) compound $[Mo_2Cp_2(\mu\text{-}SMe)_3(CH_3CN)_2](BF_4)$ (**1**) as a starting material for the coordination of other substrates, such as alkynes and hydrazines, at the bimetallic site. However, we have found that the coordinated nitriles can themselves undergo reaction. We report here their transformation into a novel bridging azavinylidene ligand in the presence of a base.

Electrophilic abstraction of the chloride bridge in the complex $[Mo_2Cp_2(\mu\text{-}SMe)_3(\mu\text{-}Cl)]$ by HBF_4 proceeded in acetonitrile solution and was followed by the coordination of one acetonitrile molecule to each molybdenum atom (Scheme 1).[4] Reaction of the resulting bis(acetonitrile) compound $[Mo_2Cp_2(\mu\text{-}SMe)_3(CH_3CN)_2](BF_4)$ (**1**) with butyllithium in THF afforded the complex $\{Mo_2Cp_2(\mu\text{-}SMe)_3[\mu\text{-}\eta^1\text{-}N{=}C(CH_3)CH_2CN]\}$ (**2**) which was isolated in good yield (Scheme 1). Complex **2** was characterized by IR, one- and two-dimensional NMR, mass spectrometry, and elemental analysis.

The IR stretching frequency of the C≡N bond was detected at 2220 cm^{-1}, while the ^{1}H-NMR spectrum exhibited a set of resonances characteristic of the $[Mo_2Cp_2(\mu\text{-}SMe)_3]$ core. Two additional signals, a single resonance at δ = 2.05 and an AB spin system at δ = 3.02, could be attributed to the CH_3 and CH_2 groups, respectively, of a fourth bridging ligand. Two-dimensional heteronuclear ^{1}H-^{15}N and ^{1}H-^{13}C inverse-correlation experiments were carried out to further characterize **2**. The correlation peaks in the HMBC ^{1}H-^{15}N spectrum were characteristic of $^3J(^1H\text{-}^{15}N)$ couplings. This spectrum showed the AB pattern at δ = 3.02 to be coupled with two nitrogen atoms with signals at δ = −132.5 and δ = −14.2, relative to nitromethane, and the methyl group with signal at δ = 2.05 to be correlated only with the second nitrogen atom with signal at δ = −14.2. The signal at δ = −132.5 suggested the presence of a free nitrile group in the molecule (see Experimental Section).[5] Such a pattern was consistent with an N≡C−CH_2−C(CH_3)=N backbone. Full assignment of the ^{13}C chemical shifts was achieved by means of HMQC ^{1}H-^{13}C and HMBC ^{1}H-^{13}C experiments, which were also in accord with an N≡C−CH_2−C(CH_3)=N ligand.



Scheme 1. Synthesis of complex **2**

The structure of the new complex was confirmed by X-ray analysis of the orange crystals of **2**, which were obtained by cooling a dichloromethane/pentane/carbon disulfide (1:1:1, v/v/v) solution to −15°C (Figure 1). It was found to consist of a typical $[Mo^{III}_2Cp_2(\mu\text{-}SMe)_3]$ unit[6] bridged by the nitrogen atom of the 3-iminobutyronitrile ligand N≡C−CH_2−C(CH_3)=N, namely an η¹-azavinylidene group. The p orbitals on sp²-hybridized N1 and C5 are seen to overlap [Mo1−N1−C5−C6 = −5.4(5)°], so that the C5−N1

[a] UMR 6521, Chimie, Electrochimie Moléculaires et Chimie Analytique, Faculté des Sciences, Université de Bretagne Occidentale,
B. P. 452, F-29285 Brest Cédex, France
E-mail: francois.petillon@univ-brest.fr
[b] Department of Chemistry, University of Glasgow, Glasgow G12 8QQ, Great Britain

 © WILEY-VCH Verlag GmbH, D-69451 Weinheim, 1999 1434−1948/99/0202−0221 $ 17.50+.50/0

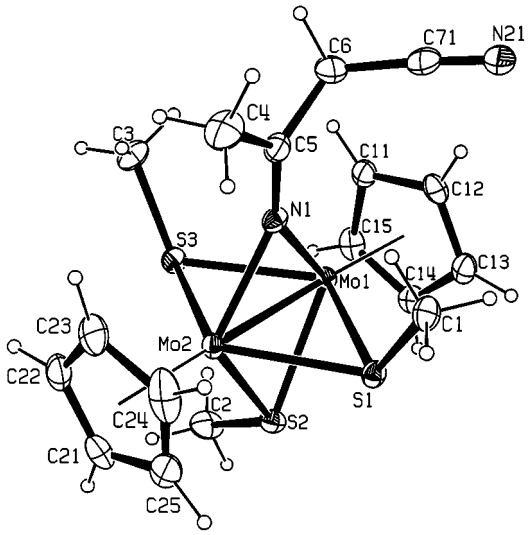
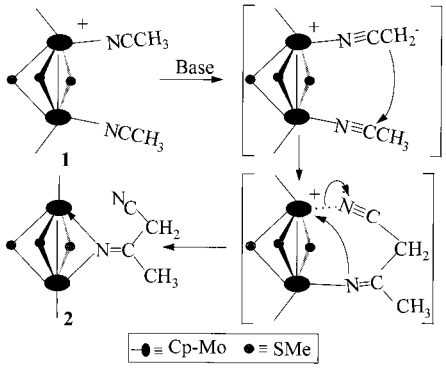


Figure 1. A view of the $\{Cp_2Mo_2(\mu\text{-}SMe)_3[\mu\text{-}\eta^1\text{-}N{=}C(Me)\text{-}CH_2CN]\}$ molecule showing 20% probability ellipsoids; hydrogen atoms are shown as spheres of arbitrary radius; the CN group attached to C6 adopts two orientations with equal probability [N1−C5−C6−C71 92.5(8), N1−C5−C6−C72 −169.6(8)°]; this disorder is not shown for the sake of clarity; selected distances [Å] and angles [°]: Mo1−Mo2 2.574(1), Mo1−N1 2.101(4), Mo1−S1 2.479(1), Mo1−S2 2.448(1), Mo1−S3 2.458(1), Mo2−N1 2.114(4), Mo2−S1 2.466(1), Mo2−S2 2.458(2), Mo2−S3 2.450(1), N1−C5 1.266(6), C5−C6 1.507(8), C6−C71 1.430(13), C6−C72 1.468(13), C71−N21 1.142(14), C72−N22 1.161(14); Mo2−S1−Mo1 62.7(1), Mo2−S2−Mo1 63.3(1), Mo2−S3−Mo1 63.3(1), Mo1−N1−Mo2 75.3(1), Mo1−N1−C5 142.8(4), Mo2−N1−C5 142.0(4), C4−C5−C6 116.1(5), C71−C6−C5 116.3(7), C6−C71−N21 175.5(1)

bond [1.266(6) Å] has appreciable multiple character. The Mo−N1 bond lengths [2.101(4) and 2.114(4) Å] are nearly equal.

A mechanism involving an intramolecular carbon−carbon attack accounts for the formation of the 3-iminobutyronitrile ligand in this reaction (Scheme 2). Initial deprotonation of the methyl group of one of the coordinated acetonitriles by a strong base leads to a resonance-stabilized $[Mo{-}N{\equiv}C{-}CH_2^-]$ carbanion.[7] This is then attacked by the electrophilic nitrile carbon atom of the second acetonitrile ligand $[Mo{-}N{\equiv}C{-}CH_3]$. The imino nitrogen atom moves to a bridging position as the second C≡N group decoordinates, finally giving the bridging azavinylidene ligand $[\mu\text{-}\eta^1\text{-}N{=}C(CH_3)CH_2CN]$ present in **2**. Evidently, coordination to molybdenum does not impair the ability of acetonitrile to undergo Thorpe−Ziegler-type activation through α-hydrogen abstraction, while the electronic and geometric properties of the bimetallic site ensure a specific intramolecular condensation in preference to an intermolecular reaction[2] or other types of coupling.[8] Moreover, the two bonded metal atoms confer stability on the azavinylidene ligand.



Scheme 2. Possible pathway to the formation of **2**

In view of the role of azavinylidene species as postulated intermediates in the reduction of nitriles to amines[9] and the importance of cyanoenamine in the synthesis of heterocycles,[10] we now intend to investigate the redox behaviour of complex **2** and to extend these preliminary results to other bis(nitrile) complexes.

Experimental Section

Experimental Procedure: At −70°C, 0.5 mL of a 2.5 M solution of butyllithium in hexane (1.25 mmol) was added to a red solution of **1** (600 mg, 0.9 mmol) in THF (50 mL). When the temperature reached 25°C, the solution became orange. After evaporation of the solvent, the product **2** was extracted with toluene (5 × 15 mL). The toluene was then removed from the pooled extracts in vacuo, and after washing of the residue with cold pentane, **2** was obtained as an orange powder (424 mg, 85%). − $C_{17}H_{24}N_2Mo_2S_3$ (544.44): calcd. C 37.5, H 4.4, N 5.1; found C 36.9, H 4.4, N 4.9. − MS; *m/z*: 544 [M^+]. − Selected spectroscopic data for **2**: ^{1}H NMR ($CDCl_3$, relative to TMS): δ = 5.46 (s, 5 H, C_5H_5), 5.44 (s, 5 H, C_5H_5), 3.02 [AB, J_{HH} = 16.7 Hz, N≡CCH_2C(CH$_3$)=N], 2.05 [s, 3 H, N≡CCH$_2$C(CH_3)=N], 1.67 (s, 3 H, SCH_3), 1.28 (s, 3 H, SCH_3), 1.23 (s, 3 H, SCH_3). − ^{13}C NMR ($CDCl_3$, relative to TMS): δ = 158.8 [N≡CCH$_2$*C*(CH$_3$)=N], 116.7 [N≡*C*CH$_2$C(CH$_3$)=N], 91.5 (C_5H_5), 31.2 [N≡C*C*H$_2$(CH$_3$)=N], 26.4 [N≡CCH$_2$C(*C*H$_3$)=N], 13.9 (2 × S*C*H$_3$), 10.8 (S*C*H$_3$). − ^{15}N NMR ($CDCl_3$, relative to CH_3NO_2): δ = −132.5 [*N*≡CCH$_2$C(CH$_3$)=N], −14.2 [N≡CCH$_2$C(CH$_3$)=*N*]. − ^{15}N NMR (CD_3COCD_3, relative to CH_3NO_2): δ = −184.9 {(Mo−*N*≡CCH$_3$) in $[Mo_2Cp_2(\mu\text{-}SMe)_3(NCCH_3)_2]BF_4$ (**1**)}, −137 (free *N*≡CCH$_3$).

Crystal Data for 2: $C_{17}H_{24}Mo_2N_2S_3$, M_r = 544.44, monoclinic, space group $P2_1/c$, a = 14.153(1), b = 8.930(1), c = 15.710(1) Å, β = 95.250(6)°, V = 1977.1(3) Å^3, Z = 4, D_c = 1.829 Mg/m^3, $F(000)$ = 1088, Mo-K_α radiation, λ = 0.71073 Å, μ = 1.587 mm^{-1}, orange plate 0.28 × 0.24 × 0.04 mm, CAD4 diffractometer; 5562 absorption-corrected intensities (transmission factors 0.734−0.655) with θ(Mo-K_α) < 27° yielded the 4297 unique F_0^2 values (R_{int} = 0.044) that were used to refine 235 parameters (SHELXL-97). R = 0.081 for all unique data and 0.038 for the 2846 reflections with $I > 2\,\sigma(I)$. The CN group attached to C6 can adopt two equally probable orientations. H atoms were allowed to ride on their parent C atoms.

Acknowledgments

We thank the CNRS, the EPSRC, Glasgow University, and Brest University for financial support.

[1] [1a] D. Coucouvanis, *J. Bioinorg. Chem.* **1996**, *1*, 594. − [1b] M. Hidai, Y. Mizobe, *Chem. Rev.* **1995**, *95*, 5970.
[2] [2a] V. W.-W. Yam, K. M.-C. Wong, K.-K. Cheung, *J. Chem. Soc., Chem. Commun.* **1998**, 135. − [2b] D. Duchateau, T. Tuin-

stra, E. A. C. Brussee, A. Meetsma, P. T. van Duijnen, J. H. Teuben, *Organometallics* **1997**, *16*, 3511.
[3] R. A. Michelin, M. Mozzon, R. Bertani, *Coord. Chem. Rev.* **1996**, *147*, 299 (and refs. therein).
[4] F. Barrière, Y. Le Mest, F. Y. Pétillon, S. Poder-Guillou, P. Schollhammer, J. Talarmin, *J. Chem. Soc., Dalton Trans.* **1996**, 3967.
[5] S. Berger, S. Braun, H.-O. Kalinowski, *NMR Spectroscopy of the Non-Metallic Elements*, John Wiley and Sons, New York, **1997**, p. 111.
[6] [6a] P. Schollhammer, E. Guénin, F. Y. Pétillon, J. Talarmin, K. W. Muir, D. S. Yufit, *Organometallics* **1998**, *17*, 1922. – [6b] P. Schollhammer, E. Guénin, S. Poder-Guillou, F. Y. Pétillon, J. Talarmin, K. W. Muir, P. Baguley, *J. Organomet. Chem.* **1997**, *532*, 193.
[7] [7a] I. N. Juchnovski, I. G. Binev, *J. Organomet. Chem.* **1975**, *99*, 1. – [7b] I. I. Creaser, A. M. Sargeson, *J. Chem. Soc., Chem. Commun.* **1975**, 324. – [7c] D. A. Buckingham, F. R. Keene, A. M. Sargeson, *J. Am. Chem. Soc.* **1973**, *95*, 5649. – [7d] C. Krüger, *J. Organomet. Chem.* **1967**, *9*, 125.
[8] [8a] B. F. Becker, H. P. Fritz, *Liebigs Ann. Chem.* **1976**, 1015. – [8b] B. Bloch, *Ann. Chim.* **1965**, *10*, 583.
[9] [9a] S. G. Feng, J. L. Templeton, *Organometallics* **1992**, *11*, 1295. – [9b] S. G. Feng, P. S. White, J. L. Templeton, *Organometallics* **1993**, *12*, 1765. – [9c] A. J. L. Pombeiro, D. L. Hughes, R. L. Richards, *J. Chem. Soc., Chem. Commun.* **1988**, 1052.
[10] H. Takaya, T. Naota, S. I. Murahashi, *J. Am. Chem. Soc.* **1998**, *120*, 4244.

Received September 14, 1998
[I98300]

Sidechain Functionalizations by Cuprate Additions to Phosphorylallenyl-Substituted Arenetricarbonylchromium Complexes

Markus Ansorge,[a] Kurt Polborn,[a] and Thomas J. J. Müller*[a]

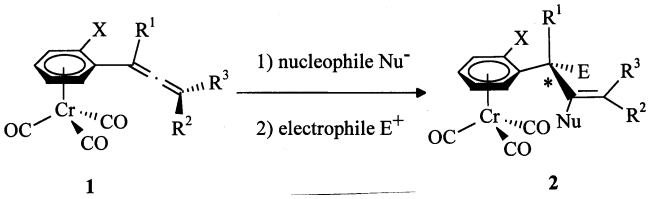
Keywords: Arene complexes / Chromium / Sidechain functionalization / Allenes / Cuprates

The cuprate addition to (arene)$Cr(CO)_3$-substituted phosphorylallenes **1** gives rise to the regioselective formation of complexed allylphosphane oxide derivatives **3a–c** and allylphosphonate derivatives **3d–j** in good yields. In the case of racemic planar chiral *ortho*-substituted complexed (arylallenyl)phosphonates **1c**, **d** the protonation of the intermediate allyl anion proceeds diastereoselectively due to the hindered rotation around the C_{ipso}–C_α bond. This diastereoselective protonation is discussed on the basis of the conformational analysis as deduced from the X-ray structure analyses of the allenylphosphonate **1d** and the allylphosphonates **3i**, **j**.

Introduction

Planar chiral (arene)$Cr(CO)_3$ complexes bear a plethora of opportunities for diastereoselective transformations and thus have become well-established building blocks in natural products syntheses.[1,2] Besides stereochemical issues the carbonylchromium complexation alters the reactivity of the arene ligands significantly and therefore opens new reaction pathways. In particular, the activation of the benzylic position has received the most attention and has been intensively studied.[3] Complexed benzylic anions stabilized by the strong electron-withdrawing nature of the (arene)$Cr(CO)_3$ fragment[4] basically can be generated in two different ways: (a) by deprotonation of toluene complexes[5] or (b) by addition of a nucleophile to the β-position of styrene or dihydronaphthalene complexes.[1b,6] Especially, the addition of nucleophiles to an alkenyl side chain of an arene complex represents an extremely useful reaction allowing a subsequent trapping of the complexed benzylic anion by a suitable electrophile. Unfortunately, this process is only limited to stabilized carbanions.[1b,6] Presumably, the nucleophilic susceptibility of the β-carbon atom in styrene complexes is not very strong. In order to overcome these severe limitations we have started to investigate the syntheses, structure and reactivity of allenyl-substituted arene complexes[7] which upon nucleophilic addition to the β-carbon atom of the allenyl side chain give rise to (arene)$Cr(CO)_3$-stabilized allyl anions. This interesting class of ambident nucleophiles opens new opportunities to extended sidechain functionalizations (Scheme 1).

Recently, we could show that allenylphosphonate complexes **1** [R^1 = $PO(OEt)_2$, R^2 = R^3 = Me, X = H] can be successfully applied to metal-template-directed syntheses of 5- and 6-membered heterocyclic dienes by a nucleophilic addition/intramolecular olefination sequence.[7b] So far,



Scheme 1

there are only very few examples of diastereoselective functionalizations initiated by an attack on the homobenzylic position of the tricarbonylchromium-substituted arene sidechain.[1b,8] Here we report on conformational aspects of allenylphosphonate-substituted (arene)$Cr(CO)_3$ complexes **1** in the solid state, cuprate additions to these allenylphosphonates and subsequent regio- and diastereoselective protonations of the ambident planar chiral complexed arylallyl anions to give allylphosphonate-substituted (arene)$Cr(CO)_3$ complexes. The diastereoselectivity of the protonations is discussed on the basis of conformation analyses as deduced from relative stereochemistry by X-ray crystal structure analyses of the organometallic allylphosphonates.

Results and Discussion

Conformational Aspects of (Arene)$Cr(CO)_3$-Substituted Phosphorylallenes

(Arene)$Cr(CO)_3$-substituted allenes have proven to be easily accessible by displacement rearrangements of the corresponding arene complex substituted propargylic alcohols.[7] Although, the structure in solution of some planar chiral organometallic allenes has been elucidated by NMR spectroscopy,[7b] conformational aspects, i.e. the mutual arrangement of the allenyl substituent and the arene(carbonyl)chromium fragment, have not been addressed yet. In the case of the allene derivatives **1a** and **1d** the crystal structures[9] have been elaborated by X-ray structure analysis.

[a] Institut für Organische Chemie der Ludwig-Maximilians-Universität München
Karlstraße 23, D-80333 München, Germany
E-mail: tom@cup.uni-muenchen.de

 © WILEY-VCH Verlag GmbH, D-69451 Weinheim, 1999 1434–1948/99/0202–0225 $ 17.50+.50/0

The linear allenyl sidechain [C10−C11−C12: 177.1(3)°] of the benzene complex substituted allenylphosphane oxide **1a** (Figure 1, Table 4) is arranged almost coplanarily with the complexed phenyl ring (torsional angle C9−C4−C10−C11: 164.9°) indicating an ideal overlap of the proximate allenic double bond and the complexed arene π-system. One of the phenyl rings on the phosphane oxide group shields the *endo* face of the allenyl substituent. Therefore, a nucleophilic attack to this conformer will occur from the *exo* face.

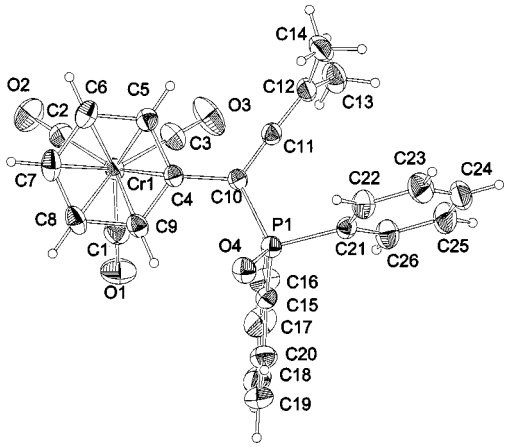


Figure 1. ORTEP plot of **1a**; selected bond lengths [Å], angles [°], and torsional angles [°]: C(10)−C(11) 1.318 (3), C(11)−C(12) 1.291 (4), C(4)−C(10) 1.489(3); C(10)−C(11)−C(12) 177.1(3), C(4)−C(10)−C(11) 122.3(2), C(4)−C(10)−P(1) 119.6(2); C(9)−C(4)−C(10)−P(1) −19.8(3), C(9)−C(4)−C(10)−C(11) 164.9 (2), C(4)−C(10)−P(1)−O(4) −47.4(2), C(7)−C(8)−C(9)−C(4) 0.5(4)

The introduction of a sterically demanding *ortho* substituent into the complexed arene causes significant changes in the mutual arrangement of the allenyl and the arene(carbonyl)chromium fragments. The X-ray structure analysis of **1d** (Figure 2 and Table 4) reveals that the torsion of the allene substructure deviates from coplanarity with the arenetricarbonylchromium fragment by almost 60° (torsional angle C9−C4−C10−C11: 59.3°). Interestingly, the phosphonate group at the linear allenyl fragment (C10−C11−C12: 178°) and carbonylchromium tripod are arranged in an *anti* conformation and the *P*-oxygen atom is arranged *anti* with respect to the acetal group. According to MM2 calculations[10] the *anti* conformer is by 1.0 kcal/mol lower in energy than the corresponding *syn* conformer and the rotation barrier can be estimated by 3.3 kcal/mol. Thus, an attacking nucleophile preferably will add in an *anti* fashion with respect to the carbonylchromium tripod and the *ortho* substituent but with only a small preference for either conformers.

Cuprate Addition and Diastereoselective Protonation

Organocuprates are known to add to allenylphosphonates in a 1,4-fashion to give allylphosphonates.[11] Thus, various Gilman and Normant cuprates easily add to the allenylarene complexes **1** to give after aqueous workup the

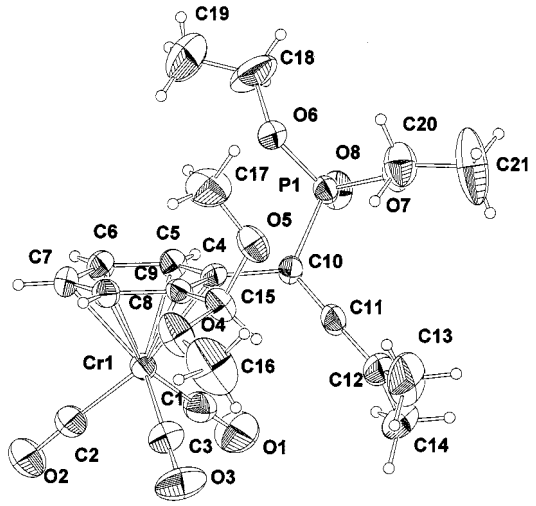
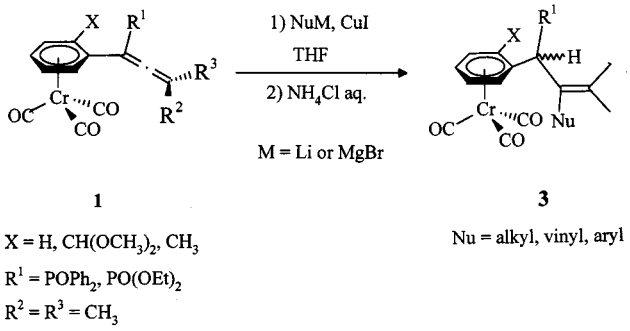


Figure 2. ORTEP plot of **1d**; selected bond lengths [Å], angles [°], and torsional angles [°]: C(10)−C(11) 1.297(9), C(11)−C(12) 1.314(11), C(4)−C(10) 1.492(9); C(10)−C(11)−C(12) 178.2(8), C(4)−C(10)−P(1) 117.9(5), C(4)−C(10)−C(11) 124.3(6); C(9)−C(4)−C(10)−C(11) 59.3(11), C(9)−C(4)−C(10)−P(1) −123.6(6), O(8)−P(1)−C(10)−C(4) −92.4(6), C(4)−C(9)−C(15)−O(5) 69.7(9), C(7)−C(8)−C(9)−C(4) 0.9(10)

regioselectively protonated allylarene complexes **3** in moderate to good yields as light yellow crystalline solids (Scheme 2 and Table 1). All transformations were performed with racemic planar chiral complexes.



Scheme 2. Cuprate addition/protonation sequence

In the NMR spectra the regioselective protonation of the allyl derivatives **3** is supported by the appearance of characteristic $^2J_{P,H}$ and $^1J_{P,C}$ coupling constants of the benzylic protons and carbon atoms. For the phosphane oxide derivatives **3a**−**3c** (R^1 = Ph, X = H) the benzylic methine proton appears in the proton NMR spectra as a doublet ($^2J_{P,H}$ = 10.0−11.6 Hz) at δ ≈ 4.6−4.7. The corresponding signals for the phosphonates **3d**−**3j** [R^1 = OEt, X = H, Me, and $CH(OMe)_2$] are found at δ ≈ 4.1−4.4 as doublets ($^2J_{P,H}$ = 25.2−27.7 Hz). In the proton-decoupled ^{13}C-NMR spectra the benzylic carbon resonances of the phosphane oxides **3a**−**3c** appear as doublets ($^1J_{P,C}$ = 63.0−67.1 Hz) at δ ≈ 46.1−46.8 and the corresponding resonances of the phosphonates **3d**−**3j** at δ ≈ 42.2−45.0 display characteristic large $^1J_{P,C}$ coupling constants (139.9−145.9 Hz).

In addition, the allylphosphonate structure was elaborated and supported by X-ray structure analyses[9] of **3f** and **3j** (Figures 3, 4 and Table 4). The benzylic carbon atom

Table 1. Summarized results of the cuprate additions protonation experiments ($R^2 = R^3 = CH_3$; E = H)

Entry	Allene	R^1	Nu	X	(Phosphorylallyl)-arene complex **3** Yield[a] (ratio of diastereomers)
1	**1a**	$Ph_2P(O)$	Me	H	79% **3a**
2	**1a**	$Ph_2P(O)$	Bu	H	51% **3b**
3	**1a**	$Ph_2P(O)$	Vinyl	H	56% **3c**
4	**1b**	$(EtO)_2P(O)$	Me	H	69% **3d**
5	**1b**	$(EtO)_2P(O)$	Bu	H	57% **3e**
6	**1b**	$(EtO)_2P(O)$	Vinyl	H	79% **3f**
7	**1b**	$(EtO)_2P(O)$	Ph	H	90% **3g**
8	**1c**	$(EtO)_2P(O)$	Me	Me	68% (5:1)[b] **3h**
9	**1c**	$(EtO)_2P(O)$	Ph	Me	68% (> 15:1)[c] **3i**
10	**1d**	$(EtO)_2P(O)$	Me	$CH(OMe)_2$	85% (2:1)[d] **3j**

[a] The yields reported were determined after chromatography on silica gel. – [b] The diastereomers could be separated by chromatography. – [c] The other diastereomer was not detected by NMR spectroscopy. – [d] The major diastereomer can be enriched by recrystallization from dichloromethane/pentane (2:1 to 85:15)

C10 is pyramidalized, in agreement with the formation of an sp^3-hybridized phosphonate moiety upon regioselective protonation of an allyl anion. In the case of the planar chiral complex **3j** only the major of two possible diastereomeric racemates was crystallized and the relative configuration was determined to be (*S*,*S*) or (*R*,*R*). The benzylic and the acetal hydrogen atoms are arranged in a *syn* conformation whilst the 2-isoprenyl substituent is oriented in an antiperiplanar fashion with respect to the tricarbonylchromium tripod.

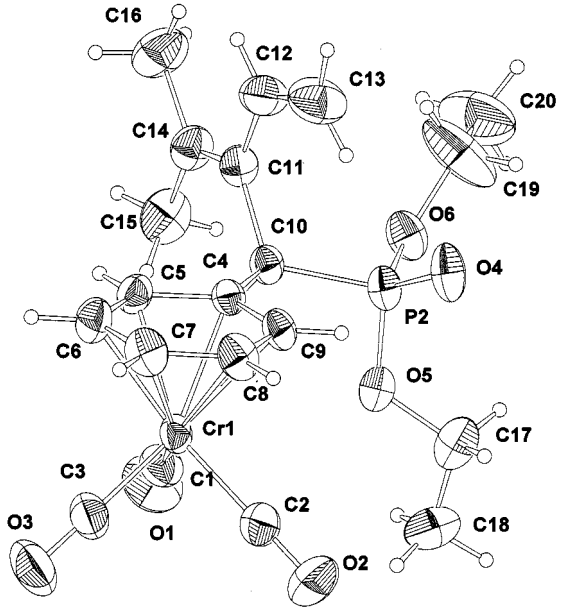


Figure 3. ORTEP plot of **3f**; selected bond lengths [Å], angles [°], and torsional angles [°]: C(4)–C(10) 1.531(4), C(10)–C(11) 1.546(5), C(11)–C(14) 1.332(5); C(4)–C(10)–C(11) 111.3(3), C(11)–C(10)–P(2) 114.2(2); C(9)–C(4)–C(10)–C(11) –122.5(3), C(9)–C(4)–C(10)–P(2) 11.0(4), C(10)–C(11)–C(14)–C(15) –2.5(6), C(6)–C(7)–C(8)–C(9) 0.5(6)

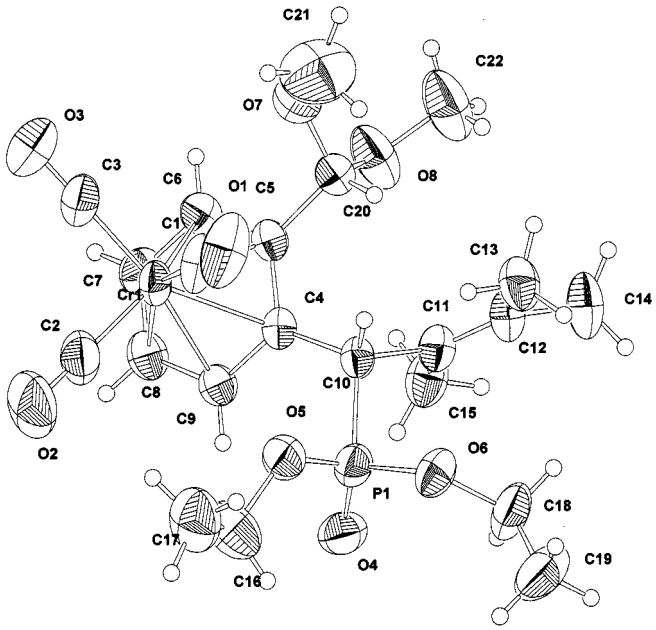
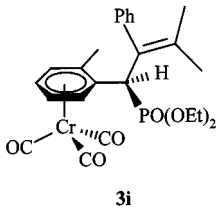


Figure 4. ORTEP plot of **3j**; selected bond lengths [Å], angles [°], and torsional angles [°]: C(4)–C(10) 1.533(6), C(10)–C(11) 1.541(6), C(11)–C(12) 1.329(7); C(4)–C(10)–C(11) 111.4(4), C(11)–C(10)–P(1) 108.5(3), C(9)–C(4)–C(10)–C(11) 110.7(5); C(9)–C(4)–C(10)–P(1) –14.0(6), C(10)–C(11)–C(12)–C(14) –0.7(10), C(7)–C(8)–C(9)–C(4) 0.9(9)

The X-ray crystal structure[9] of the pure racemic diastereomer **3i** (Figure 5 and Table 4) clearly reveals the relative configuration of the product to be (*R*,*R*) or (*S*,*S*). Unfortunately, the ethoxy group in **3i** was strongly disordered and a pentane molecule was incorporated in the crystal lattice both giving rise to an insufficient wR_2 value for all data (Table 4).

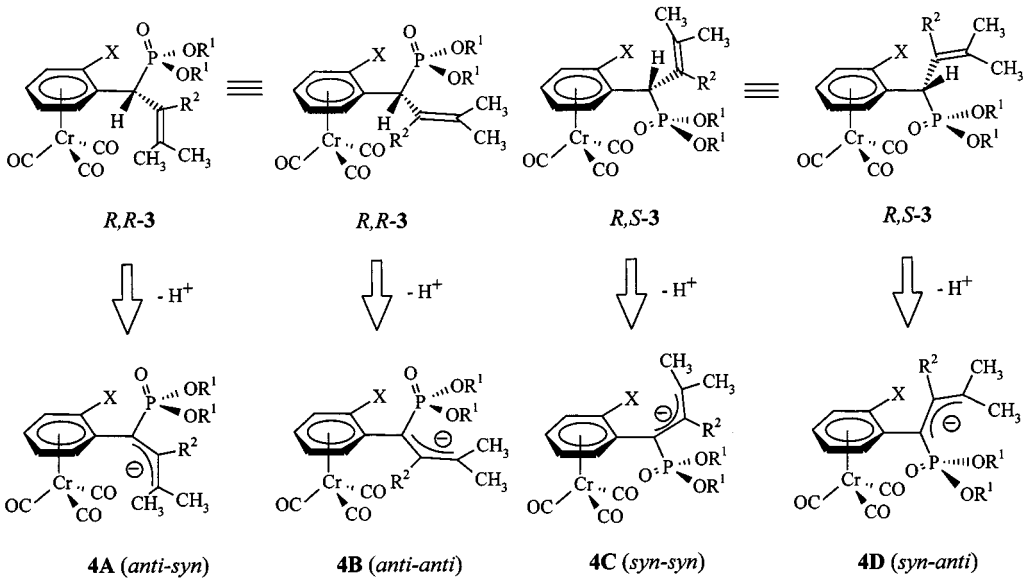


3i

Figure 5. Relative configuration of **3i**

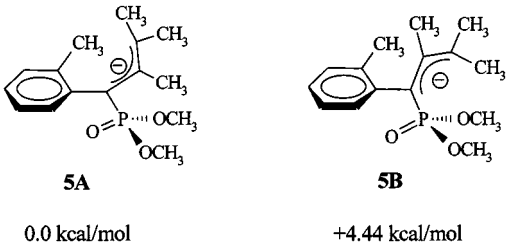
Obviously, the protonation of the allyl anions that form upon the cuprate addition to the allenyl derivatives proceeds with a facial diastereoselection. Aqueous ammonium chloride as proton source guarantees a protonation under kinetic control and excludes a base-catalyzed epimerization at the benzylic carbon atom. Based upon the relative configurations of **3i** and **3j** as established by the X-ray structure analyses the structure of the diastereomeric conformations of the allyl anions can be deduced (Scheme 3).

Assuming a diastereofacial protonation[12] of the allyl anions from the less hindered *endo* face the major diastereomer (*R*,*R*)-**3** (or *S*,*S*-**3**) can be derived from two diastereomeric allyl anions where the phosphonate group



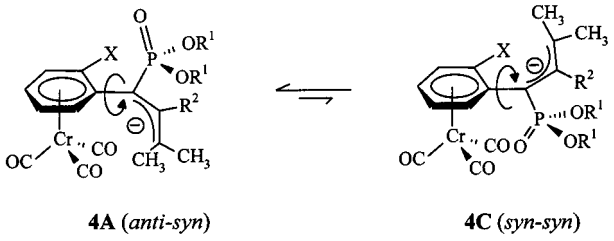
Scheme 3. Stereochemical correlation of the allylphosphonates **3** and the allylphosphonate anions **4**

orientation is *anti* to the carbonylchromium tripod and the mutual stereochemistry of the phosphonate group and the substituent R^2 is either *syn* (**4A**) or *anti* (**4B**). In analogy, the minor diastereomer (*R*,*S*)-**3** (or *S*,*R*-**3**) stems from the protonation of diastereomeric allyl anions **4C** or **4D** where the phosphonate and the chromium fragment are in a *syn* conformation whereas the substituent R^2 can be either *syn* (**4C**) or *anti* (**4D**) with respect the phosphonate group. According to PM3 calculations[10] performed on the free ligands (**5A** and **5B**, Scheme 4) the phosphonate/methyl *syn* isomer (**5A**) is by 4.44 kcal/mol lower in energy than the phosphonate/methyl *anti* isomer (**5B**). The depicted structures are also the corresponding lowest energy conformations of **5A** and **5B**, respectively.



Scheme 4. Relative energies (PM3) of the configurational isomers of the free ligand **5**

The activation enthalpy for the *anti*-*syn* isomerization of these allyl anions is represented by a rotation around the $C_\alpha - C_\beta$ bond and can be estimated to be 2.4 kcal/mol. This relatively low rotation barrier is caused by an efficient resonance stabilization of the benzylic phosphonate carbanion. In turn, the *anti*-*syn* equilibration proceeds rapidly to give the thermodynamically more stable *syn* isomer almost exclusively. Thus, it is reasonable to assume that the corresponding complexed diastereomers **4A** and **4C** (Scheme 5) with a *syn* orientation of the substituent R^2 with respect the phosphonate moiety are also low-energy isomers. Therefore, the cuprate addition to the allenylphosphonates **1** very likely leads to the formation of the diastereomers **4A** and **4C**. Since the allyl anions **4A** and **4C** are diastereomeric conformers their interconversion proceeds by a rotation around the $C_{ipso} - C_\alpha$ bond. Therefore, the temperature dependence of this rotation should be reflected in the **4A**/**4C** ratio, ultimately in the diastereomeric ratio of the protonation products **3**.



Scheme 5. The **4A**/**4C** equilibration by rotation around the $C_{ipso} - C_\alpha$ bond

In a number of cuprate addition/protonation sequences to planar chiral complexes the dependence on the temperature, the reaction time and the cuprate was investigated (Table 2). In case of the *ortho*-methyl-substituted complex **1c** (entries 1–4) the diastereoselectivities depend on the reaction temperature and the nature of the cuprate. Obviously, the fast cuprate addition to the allenylphosphonate **1c** predominantly leads to the kinetically controlled formation of the conformer **4A** (entries 2 and 3). The free rotation of the allyl anion moiety around the $C_{ipso} - C_\alpha$ bond is facilitated as the temperature rises and the allylanion conformers **4A** and **4B** equilibrate to give after protonation the observed thermodynamic diastereoselectivity (entry 1). This indicates that the energy difference between the allyl anion conformers **4A** and **4B** is 0.4 kcal/mol. In the case of complex **1d** (entries 5 and 6) the resulting diastereoselectivity is rather poor and not temperature-dependent. Presumably, the coordinating ability of the *ortho*-acetal facilitates the

thermodynamic equilibration very rapidly, even at low temperatures.

Table 2. Diastereotopic cuprate addition/protonation experiments

Entry	Allene	R	Temperature	Reaction time	Yield (diastereomeric ratio)
1	**1c**	Me	−40 to 20°C	3 h	68% (2:1) **3h**
2	**1c**	Me	−50 to −40°C	3 h	70% (5:1) **3h**
3	**1c**	Me	−78 to −70°C	7 h	67% (5:1) **3h**
4	**1c**	Ph	−78 to −70°C	3 h	68% (> 15:1) **3i**
5	**1d**	Me	−40 to −15°C	3 h	85% (2:1)[a] **3j**
6	**1d**	Me	−78 to −40°C	8 h	80% (2:1)[a] **3j**

[a] The major diastereomer can be enriched by recrystallization (2:1 to 85:15)

Finally, the initial step of this sequence, i.e. the cuprate addition to the allenylphosphonates **1** has to be discussed. According to MM2 calculations[10] the conformers **6A** and **6C** (Scheme 6) are almost equal in energy and are interconverted by a low rotation barrier (i.e. **6B**) indicating a rapid preequilibrium.

The cuprates add to the allenylphosphonates **1** from the *exo* face with respect to the carbonylchromium tripod and the *ortho* substituent to give preferentially the conformer **4A** under kinetic control (vide supra). Considering the bulky nature of a Gilman or Normant cuprate[13] the precoordination to the phosphonate oxygen atoms in conformer **6C** from the *exo* face with respect to the carbonylchromium fragment is sterically less biased than the corresponding attack to conformer **6A** from the *exo* face. Once the phosphonate-substituted allyl anion has formed and the organocopper group has dissociated, the conformational stability and thus the diastereoselective protonation is influenced by the temperature-dependent rotation around the $C_{ipso}-C_{\alpha}$ bond. Thus, the generation and the electrophilic trapping reactions of conformationally and configurationally stable (arene)$Cr(CO)_3$-substituted allyl anions without additional anion-stabilizing functionalities for diastereoselective sidechain functionalizations are currently under investigation.

Conclusion

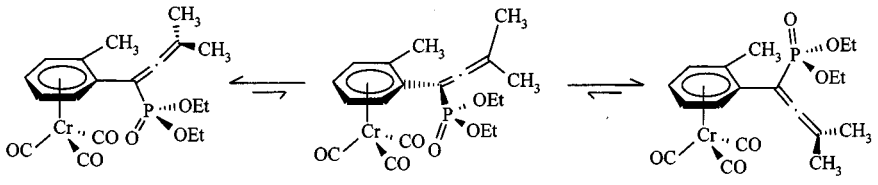
(Arene)$Cr(CO)_3$-substituted allenylphosphane oxides and allenylphosphonates readily react with organocuprates in a 1,4-addition to give after protonation 1-(arene)$Cr(CO)_3$-substituted (2-propen-1-yl)phosphane oxides and (2-propen-1-yl)phosphonates in good yields. With planar chiral *ortho*-substituted complexed allenes this cuprate addition/protonation sequence gives rise to the diastereoselective formation of complexed allylphosphane oxide and allylphosphonate derivatives. The conformation analysis of the intermediate arene complex substituted allyl anions reveals that the crucial origin of the observed diastereoselectivity stems from the hindered rotation around the $C_{ipso}-C_{\alpha}$ bond. Therefore, future studies will be directed towards the study of the reactivity and selectivity of (arene)$Cr(CO)_3$-stabilized allyl anions in intra- and intermolecular electrophilic trapping reactions.

Experimental Section

All reactions involving tricarbonylchromium complexes were carried out in flame-dried Schlenk flasks under nitrogen by using septum and syringe techniques. Solvents were dried and distilled according to standard procedures.[14] − Column chromatography: Silica gel 60 (Merck, Darmstadt), mesh 70−230. TLC: Silica gel plates (60 F_{254} Merck, Darmstadt). Melting points (uncorrected values): Reichert-Jung Thermovar. − The *ortho*-iodobenzaldehyde dimethylacetal complex,[15] the complexed allenylphosphane oxide **1a** and the complexed allenylphosphonates **1b** and **1c** were prepared in analogy to our published procedures.[7] The organolithium and vinylmagnesium chloride solutions were purchased from Aldrich. Chlorodiethoxyphosphane (Aldrich) was used without further purification. Chlorodiphenylphosphane (Aldrich) was distilled under reduced pressure prior to use. All crystalline arenechromium complexes can be handled in air. − ^{1}H-, ^{13}C-, and ^{31}P-NMR spectra: Bruker ARX 300, Varian VXR 400S [D_6]DMSO. The assignments of quaternary C, CH, CH_2, and CH_3 has been made by using DEPT spectra. − IR: Perkin Elmer Models Lambda 16. − MS: Finnigan MAT 90 and MAT 95 Q. − Elemental analyses were carried out in the Microanalytical Laboratory of the Institut für Organische Chemie, Ludwig-Maximilians-Universität München.

X-ray Structure Determination of Compounds 1a, 1d, 3f, 3i, and 3j: Suitable crystals were mounted on a capillary and transferred to an Enraf-Nonius CAD4 diffractometer. The structures were solved by direct methods and refined anisotropically on F^2 (G.M. Sheldrick, SHELXS-86, SHELXL-93 programs, University of Göttingen). Hydrogen atoms were found from differential Fourier synthesis and refined. The data of the X-ray structure analyses are summarized in Table 4.

Tricarbonyl{η^6-1-[3-hydroxy-3-methylbut-1-yn-1-yl]-2-(dimethoxymethyl)benzene}chromium(0): 1.00 g (2.40 mmol) of the *o*-iodobenzaldehyde dimethylacetal complex,[15] 33 mg (0.04 mmol) of bis(triphenylphosphane)palladium dichloride and 5 mg (0.02 mmol) of



Scheme 6. Relative energies (MM2) of the conformations **6A,6B** and **6C**

copper iodide were dissolved in a degassed mixture of 15 mL of THF and 7 mL of triethylamine. A solution of 0.28 mL (2.90 mmol) of 3-methylbutyn-3-ol, dissolved in 10 mL of THF, was added over a period of 1 h. After complete addition, the solution was heated to reflux temperature for 5 h and then cooled to room temperature. Diethyl ether was added, the mixture was filtered and the solvents were evaporated. Chromatography on silica gel with diethyl, ether/pentane afforded 0.65 g (73%) of the propargyl alcohol complex. Recrystallization from pentane gave yellow crystals, m.p. 68−70°C. − ^{1}H NMR ([D$_6$]DMSO, 300 MHz): δ = 1.46 (s, 6 H), 3.33 (s, 3 H), 3.53 (s, 3 H), 5.21 (s, 1 H), 5.54 (s, 1 H), 5.64 (t, *J* = 6.1 Hz, 1 H), 5.71−5.78 (m, 2 H), 5.85 (d, *J* = 6.5 Hz, 1 H). − ^{13}C NMR ([D$_6$]DMSO, 75 MHz): δ = 31.53 (CH$_3$), 54.01 (CH$_3$), 57.18 (CH$_3$), 63.80 (C$_{quat.}$), 74.75 (C$_{quat.}$), 91.27 (C$_{quat.}$), 91.85 (CH), 92.19 (CH), 94.67 (CH), 96.08 (CH), 99.88 (C$_{quat.}$), 101.71 (CH), 109.18 (C$_{quat.}$), 233.07 (C$_{quat.}$, CO). − MS (70 eV, FAB); *m/z* (%): 370 [M$^+$] (7), 314 [M$^+$ − 2 CO] (2), 286 [M$^+$ − 3 CO] (100), 52 [Cr$^+$] (14). − IR (KBr): $\tilde{\nu}$ = 3089 cm^{-1}, 2983, 2935, 2837, 1977, 1898, 1879, 1629, 1527, 1494, 1449, 1418, 1364, 1341, 1271, 1249, 1201, 1187, 1170, 1111, 1096, 1082, 1044, 983, 962, 912, 829, 808, 662, 624, 534, 469. − UV/Vis (DMSO): λ$_{max}$ (ε) = 325 (9500). − $C_{17}H_{18}CrO_6$ (370.31): calcd. C 55.14, H 4.89; found C 55.98, H 5.08.

Tricarbonyl{η^6-1-[1-diethoxyphosphoryl)-3-methylbuta-1,2-dien-1-yl]-2-(dimethoxymethyl)benzene}chromium(0) (1d): In a two-necked round-bottomed flask 0.49 g (1.35 mmol) of the previously prepared propargyl alcohol and 0.20 mL (1.50 mmol) of triethylamine were dissolved in 15 mL of THF under nitrogen. The resulting mixture was cooled to −78°C and 0.19 mL (1.40 mmol) of chlorodiethoxyphosphane, dissolved in 5 mL of THF, was added over a period of 5 min. After 1 h at −78°C, the cooling bath was removed and stirring was continued for further 20 h at room temperature. To the mixture was added 20 mL of water and the aqueous layer was extracted several times with dichloromethane. The combined organic phases were dried with anhydrous magnesium sulfate and the solvents were removed in a rotary evaporator under reduced pressure. After chromatography on silica gel [diethyl ether/pentane (1:1), diethyl ether, methanol/dichloromethane (1:10)], the yellow band was isolated to give 0.55 g (84%) of **1d**. Recrystallization from dichloromethane/pentane afforded yellow crystals, m.p. 70°C. − ^{1}H NMR ([D$_6$]DMSO, 300 MHz): δ = 1.21 (m, 6 H), 1.82 (m, 6 H), 3.11 (s, 3 H, OMe), 3.47 (s, 3 H, OMe), 3.98 (m, 4 H), 5.38 (s, 1 H), 5.68 (m, 2 H), 5.81 (m, 2 H). − ^{13}C NMR ([D$_6$]DMSO, 75 MHz): δ = 16.24 (CH$_3$, *J* = 6.1 Hz), 17.97 (CH$_3$, *J* = 6.1 Hz), 19.69 (CH$_3$, *J* = 6.1 Hz), 50.28 (CH$_3$, OMe), 56.27 (CH$_3$, OMe), 62.43 (CH$_2$, *J* = 6.1 Hz), 62.71 (CH$_2$, *J* = 6.1 Hz), 89.48 (C$_{quat}$, *J* = 191.6 Hz), 90.03 (CH), 92.12 (CH), 95.18 (CH), 97.86 (CH), 98.28 (C$_{quat}$), 98.53 (CH), 105.48 (C$_{quat}$, *J* = 15.8 Hz), 109.27 (C$_{quat}$, *J* = 4.8 Hz), 208.49 (C$_{quat}$, *J* = 4.3 Hz), 233.18 (C$_{quat}$, CO). − ^{31}P NMR ([D$_6$]DMSO, 121 MHz) : δ = 13.46. − MS (70 eV), *m/z* (%): 490 [M$^+$] (1), 434 [M$^+$ − 2 CO] (5), 406 [M$^+$ − 3 CO] (22), 354 [M$^+$ − Cr(CO)$_3$] (3), 52 [Cr$^+$] (12). − IR (KBr): $\tilde{\nu}$ = 3069 cm^{-1}, 2988, 2937, 2910, 2833, 1967, 1886, 1866, 1630, 1525, 1444, 1414, 1392, 1367, 1340, 1254, 1195, 1159, 1112, 1082, 1063, 1029, 975, 925, 907, 874, 834, 801, 753, 717, 679, 665, 627, 579, 553, 534, 479, 427. − UV/Vis (DMSO): λ$_{max}$ (ε) = 324 (8800). − $C_{21}H_{27}CrO_8P$ (490.40): calcd. C 51.43, H 5.55; found C 51.54, H 5.57.

General Procedure (GP) for the Preparation of the Complexed Allylphosphane Oxides and Allylphosphonates 3

1) Preparation of the Cuprate: A stirred suspension of 104 mg (0.550 mmol) of copper iodide in 10 mL of THF was cooled (exact conditions see below) and 1.10 mmol of a solution of a commercially available organolithium or organomagnesium halide was added over a period of 1 min by syringe. The temperature of the solution had to be adjusted exactly due to the thermal lability of some cuprates. For the preparation of the cuprates the solution was cooled to 0°C when methyllithium was used, to −60°C for butyllithium and to −78°C for phenyllithium and for vinylmagnesium chloride. The resulting cuprate solution was stirred for further 40 min at the given temperature.

2) Nucleophilic Addition/Protonation: To the stirred and cooled solution of the cuprate (temperatures see below) a solution of 0.50 mmol of **1** in 5 mL of THF was added over a period of 5 min. Stirring was continued at the indicated temperatures for 3−7 h (Tables 2 and 4). Then 20 mL of saturated ammonium chloride solution was added to the reaction mixture at the final temperature. The aqueous layer was extracted several times with diethyl ether. The combined organic phases were dried with magnesium sulfate, filtered, and concentrated in a rotary evaporator. After chromatography on silica gel (diethyl ether/pentane to diethyl ether) the yellow bands were collected to give the products **3**. The experimental details and yields are summarized in Table 3.

Tricarbonyl{η^6-[1-(diphenylphosphoryl)-2,3-dimethylprop-2-en-1-yl]benzene}chromium(0) (3a): Yellow crystals, m.p. 178−180°C. − ^{1}H NMR ([D$_6$]DMSO, 300 MHz): δ = 1.42 (s, 3 H), 1.73 (s, 3 H), 1.87 (s, 3 H), 4.60 (d, *J* = 10.3 Hz, 1 H), 5.29 (t, *J* = 6.2 Hz, 1 H), 5.51 (t, *J* = 6.3 Hz, 1 H), 5.63 (t, *J* = 6.1 Hz, 1 H), 5.76 (d, *J* = 6.2 Hz, 1 H), 6.01 (d, *J* = 6.4 Hz, 1 H), 7.48−7.88 (m, 10 H). − ^{13}C NMR ([D$_6$]DMSO, 75 MHz): δ = 17.22 (CH$_3$), 20.64 (CH$_3$), 21.31 (CH$_3$), 46.81 (CH, $J_{P,C}$ = 64.5 Hz), 91.07 (CH), 91.86 (CH), 96.29 (CH), 98.29 (CH, $J_{P,C}$ = 4.6 Hz), 99.72 (CH, $J_{P,C}$ = 5.6 Hz), 110.55 (C$_{quat}$), 123.62 (C$_{quat}$, $J_{P,C}$ = 5.5 Hz), 128.51 (CH, $J_{P,C}$ = 11.1 Hz), 128.74 (CH, $J_{P,C}$ = 11.1 Hz), 130.50 (CH, $J_{P,C}$ = 9.0 Hz), 131.25 (CH, $J_{P,C}$ = 9.0 Hz), 131.48 (C$_{quat}$), 131.99 (CH), 132.11 (C$_{quat}$, $J_{P,C}$ = 94.3 Hz), 132.47 (C$_{quat}$, $J_{P,C}$ = 128.3 Hz), 233.63 (C$_{quat}$). − ^{31}P NMR ([D$_6$]DMSO, 121 MHz) : δ = 31.28. − MS (70 eV, *EI*), *m/z* (%): 468 [M$^+$ − CO] (8), 440 [M$^+$ − 2 CO] (9), 412 [M$^+$ − 3 CO] (89), 360 [M$^+$ − Cr(CO)$_3$] (11), 52 [Cr$^+$] (18). − IR (KBr): $\tilde{\nu}$ = 3056 cm^{-1}, 2924, 1964, 1883, 1628, 1590, 1524, 1483, 1456, 1438, 1377, 1312, 1233, 1180, 1116, 1101, 1072, 998, 847, 816, 741, 721, 700, 660, 632, 568, 547, 534, 517, 507, 482, 427. − UV/Vis (DMSO): λ$_{max}$ (ε) = 319 (8900). − $C_{27}H_{25}CrO_4P$ (496.46): calcd. C 65.32, H 5.08; found C 65.14, H 5.10.

{η^6-[2-Butyl-1-(diphenylphosphoryl)-3-methylprop-2-en-1-yl]benzene}tricarbonylchromium(0) (3b): Yellow crystals, m.p. 157−159°C. − ^{1}H NMR ([D$_6$]DMSO, 300 MHz): δ = 0.76−1.74 (m, 15 H), 4.61 (d, *J* = 10.02 Hz, 1 H), 5.32 (m, 1 H), 5.49 (m, *J* = 6.1 Hz, 1 H), 5.68 (m, *J* = 6.1 Hz, 1 H), 5.88 (d, *J* = 6.1 Hz, 1 H), 6.04 (d, *J* = 5.8 Hz, 1 H), 7.50−7.91 (m, 10 H). − ^{13}C NMR ([D$_6$]DMSO, 75 MHz): δ = 13.86 (CH$_3$), 20.80 (CH$_3$), 21.45 (CH$_3$), 22.90 (CH$_2$), 30.55 (CH$_2$), 31.24 (CH$_2$), 46.14 (CH, d, *J* = 67.1 Hz), 90.65 (CH), 91.40 (CH), 96.52 (CH), 98.41 (CH, d, *J* = 7.6 Hz), 99.61 (CH, d, *J* = 4.6 Hz), 110.63 (C$_{quat}$), 128.44 (CH, d, *J* = 12.2 Hz), 128.69 (CH, d, *J* = 10.6 Hz), 129.43 (C$_{quat}$, d, *J* = 6.1 Hz), 130.63 (CH, d, *J* = 7.6 Hz), 131.23 (CH, d, *J* = 9.1 Hz), 131.90 (CH), 132.28 (C$_{quat}$, d, *J* = 94.6 Hz), 132.44 (C$_{quat}$), 133.03 (C$_{quat}$, d, *J* = 109.9 Hz), 233.49 (CO). − ^{31}P NMR ([D$_6$]DMSO, 121 MHz) : 30.15. − MS (70 eV), *m/z* (%): EI: 482 [M$^+$ − 2 CO] (4), 454 [M$^+$ − 3 CO] (44), 402 [M$^+$ − Cr(CO)$_3$] (36), 52 [Cr$^+$] (44); FD: 538 [M$^+$] (100), 510 [M$^+$ − CO] (5), 482 [M$^+$ − 2 CO] (25), 454 [M$^+$ − 3 CO] (5), 402 [M$^+$ − Cr(CO)$_3$] (67). − IR (KBr): $\tilde{\nu}$ = 3059 cm^{-1}, 2932, 1965, 1870, 1458, 1437, 1190, 1114, 750, 720, 700, 662, 631, 525. − UV/Vis (DMSO): λ$_{max}$ (ε) = 319 nm (9200).

Table 3. Experimental details on the cuprate addition/protonation sequence

Phosphorylallene **1** mg (mmol)	Organolithium/magnesium mL (mmol)	Temperature	Yield of **3** mg (%)
0.24 g (0.50 mmol) of **1a**	0.68 mL (1.10 mmol) of methyllithium[a]	−40°C to r.t.	0.19 g (79%) of **3a**
0.24 g (0.50 mmol) of **1a**	0.68 mL (1.10 mmol) of butyllithium[b]	−60°C to r.t.	0.13 g (51%) of **3b**
0.24 g (0.50 mmol) of **1a**	0.64 mL (1.10 mmol) of vinylmagnesium chloride[c]	−78°C to r.t.	0.14 g (56%) of **3c**
0.20 g (0.50 mmol) of **1b**	0.68 mL (1.10 mmol) of methyllithium[a]	−40°C to r.t.	0.14 g (69%) of **3d**
0.20 g (0.50 mmol) of **1b**	0.68 mL (1.10 mmol) of butyllithium[b]	−60°C to r.t.	0.13 g (57%) of **3e**
0.20 g (0.50 mmol) of **1b**	0.64 mL (1.10 mmol) of vinylmagnesium chloride[c]	−78°C to r.t.	0.15 g (70%) of **3f**
0.20 g (0.50 mmol) of **1b**	0.61 mL (1.10 mmol) of phenyllithium[d]	−78°C to r.t.	0.22 g (90%) of **3g**
a) 0.21 g (0.50 mmol) of **1c**	0.68 mL (1.10 mmol) of methyllithium[a]	−40°C to r.t.	98 mg (44%) of (*R*,*R* or *S*,*S*)-**3h** and 53 mg (24%) of (*R*,*S* or *S*,*R*)-**3h**[e]
b) 0.21 g (0.50 mmol) of **1c**	0.68 mL (1.10 mmol) of methyllithium[a]	−50°C to − 40°C	151 mg (68%) (d.r. 5:1)
0.21 g (0.50 mmol) of **1c**	0.61 mL (1.10 mmol) of phenyllithium[d]	−78°C to −70°C	0.17 g (68%) **3i** (d.r. > 15:1)
0.24 g (0.50 mmol) of **1d**	0.68 mL (1.10 mmol) of methyllithium[a]	−40°C to r.t.	0.21 g (85%, d.r. 2:1)[f] **3j**

[a] 1.6 M in diethyl ether. − [b] 1.6 M in hexanes. − [c] 1.7 M in THF. − [d] 1.8 M in cyclohexane/diethyl ether. − [e] Both diastereomers were separated by chromatography on silica gel (diethyl ether/pentane). − [f] After recrystallization from pentane: 160 mg (85:15).

− $C_{30}H_{31}CrO_4P$ (538.5): calcd. C 66.91, H 5.80; found C 66.57, H 5.76.

Tricarbonyl{η^6-[1-(diphenylphosphoryl)-2-ethenyl-3-methylprop-2-en-1-yl]benzene}chromium(0) (3c): Yellow crystals, m.p. 147−150°C. − ^{1}H NMR ([D$_6$]DMSO, 300 MHz): δ = 1.60 (d, *J* = 2.7 Hz, 3 H), 1.83 (s, 3 H), 4.68 (d, *J* = 11.6 Hz, 1 H), 5.18 (d, *J* = 17.6 Hz, 1 H), 5.30 (m, 2 H), 5.56 (m, 2 H), 5.68 (d, *J* = 6.7 Hz, 1 H), 5.91 (d, *J* = 6.0 Hz, 1 H), 6.64−6.74 (m, 1 H), 7.48−7.88 (m, 10 H). − ^{13}C NMR ([D$_6$]DMSO, 75 MHz): δ = 22.12 (CH$_3$), 22.52 (CH$_3$), 46.33 (CH, $J_{P,C}$ = 63.0 Hz), 91.49 (CH), 92.43 (CH), 95.59 (CH), 98.05 (CH, $J_{P,C}$ = 4.6 Hz), 98.82 (CH, $J_{P,C}$ = 3.9 Hz),

Table 4. Crystal data and structure refinements for **1a**, **1d**, **3f**, **3i**, and **3j**

	1a	**1d**	**3f**	**3i**	**3j**
Empirical formula	$C_{26}H_{21}CrO_4P$	$C_{21}H_{27}CrO_8P$	$C_{20}H_{25}CrO_6P$	$C_{25}H_{29}CrO_6P$	$C_{22}H_{31}CrO_8P$
Formula weight	480.4	490.4	444.3	547.5	506.4
Temperature	293(2) K	293(2) K	293(2) K	293(2) K	293(2) K
Radiation	0.71073 Å	0.71073 Å	0.71073 Å	0.71073 Å	0.71073 Å
Crystal system	monoclinic	triclinic	monoclinic	monoclinic	monoclinic
Space group	$P2_1/n$	$P-1$	$P2_1/n$	Pc	$P2_1/n$
Unit cell dimensions [Å]	a = 12.618(2)	a = 9.495(3)	a = 13.985(2)	a = 18.220(9)	a = 11.389(2)
	b = 10.3038	b = 16.535(4)	b = 8.977(2)	b = 11.874(4)	b = 17.153(2)
	c = 18.588(4)	c = 18.522(4)	c = 19.077(4)	c = 13.184(4)	c = 13.705(3)
[°]		α = 64.65(2)			
	β = 105.595	β = 85.68(2)	β = 110.549	β = 97.54(3)	β = 105.079
		γ = 73.77(2)			
Volume [Å^3]	2327.7(7)	2519.8(11)	2242.6(8)	2827.6(19)	2585.2(7)
Z	4	4	4	4	4
Density (calculated)	1.371 g/cm^3	1.293 g/cm^3	1.316 g/cm^3	1.286 g/cm^3	1.301 g/cm^3
Absorption correction	φ scans	φ scans	φ scans	φ scans	φ scans
Absorption coefficient	0.590 mm^{-1}	0.557 mm^{-1}	0.612 mm^{-1}	0.499 mm^{-1}	0.545 mm^{-1}
Max. and min. transmission	−	−	0.9695 and 0.9990	0.9652 and 0.9998	0.8933 and 0.9983
F(000)	992	1024	928	1148	1064
Cystal size [mm]	0.27 × 0.43 × 0.53	0.20 × 0.23 × 0.40	0.30 × 0.43 × 0.53	0.2 × 0.3 × 0.6	0.23 × 0.27 × 0.33
θ range (min./max.)	2.26 to 24.97°	2.44 to 22.55°	2.54 to 22.55°	2.49 to 21.66°	2.20 to 23.98°
Index ranges	$-14 \le h \le 14$	$-10 \le h \le 0$	$-15 \le h \le 14$	$-18 \le h \le 18$	$0 \le h \le 13$
	$-12 \le k \le 0$	$-17 \le k \le 17$	$-9 \le k \le 0$	$0 \le k \le 12$	$-19 \le k \le 0$
	$-22 \le l \le 0$	$-19 \le l \le 19$	$0 \le l \le 20$	$0 \le l \le 13$	$-15 \le l \le 15$
Reflections collected	4219	7104	3052	3500	4270
Independent reflections	4085	6625	2948	3499	4046
	[R(int) = 0.0087]	[R(int) = 0.0218]	[R(int) = 0.0105]	[R(int) = 0.0134]	[R(int) = 0.0271]
Observed reflections	3525 [$I > 2\sigma(I)$]	4675 [$I > 2\sigma(I)$]	2420 [$I > 2\sigma(I)$]	1992 [$I > 2\sigma(I)$]	2553 [$I > 2\sigma(I)$]
Refinement method	SHELXL-93 on F^2	SHELXL-93 on F^2	SHELXL-93 on F^2	SHELXL-93 on F^2	SHELXL-93 on F^2
Data/restraints/parameters	4085/0/291	6625/0/571	2948/0/257	3499/344/605	4046/60/338
Goodness of fit on F^2	1.201	1.126	1.043	1.023	1.078
Final R indices [$I > 2\sigma(I)$]					
R_1	0.0335	0.0728	0.0398	0.0834	0.0640
wR_2	0.1090	0.1496	0.1072	0.2150	0.1468
R indices (all data)					
R_1	0.0409	0.1065	0.0520	0.1368	0.1033
wR_2	0.1137	0.1651	0.1165	0.2630	0.1706
Largest diff. peak and hole (e/Å^3)	0.320 and −0.368	0.326 and −0.352	0.249 and −0.239	0.971 and −0.304	0.362 and −0.216

110.12 (C_{quat}), 120.34 (CH_2), 128.29 (C_{quat}), 128.45 (CH, $J_{P,C}$ = 11.5 Hz), 128.58 (CH, $J_{P,C}$ = 11.6 Hz), 130.64 (CH, $J_{P,C}$ = 8.9 Hz), 131.35 (CH, $J_{P,C}$ = 8.6 Hz), 131.82 (C_{quat}, $J_{P,C}$ = 94.8 Hz), 132.04 (CH), 132.10 (C_{quat}, $J_{P,C}$ = 97.1 Hz), 135.35 (CH), 135.64 (C_{quat}, $J_{P,C}$ = 10.2 Hz), 233.66 (C_{quat}, CO). − ^{31}P NMR ([D$_6$]DMSO, 121 MHz) : δ = 31.28. − MS (70 eV); *m/z* (%): 452 [M^+ − 2 CO] (7), 424 [M^+ − 3 CO] (100), 372 [M^+ − $Cr(CO)_3$] (11), 52 [Cr^+] (18). − IR (KBr): $\tilde{\nu}$ = 1964 cm^{-1}, 1881, 1628, 1524, 1457, 1437, 1383, 1181, 1116, 1073, 998, 925, 746, 722, 701, 660, 631, 545, 532. − UV/Vis (DMSO): λ_{max} (ε) = 320 (7700). − $C_{28}H_{25}CrO_4P$ (508.47): calcd. C 66.14, H 4.95; found C 66.86, H 5.36.

Tricarbonyl{η^6-[1-(diethoxyphosphoryl)-2,3-dimethylprop-2-en-1-yl]benzene}chromium(0) (3d): Yellow crystals, m.p. 100−103°C. − ^{1}H NMR ([D$_6$]DMSO, 300 MHz): δ = 1.21 (m, 6 H), 1.68 (s, 3 H), 1.70 (s, 3 H), 1.80 (s, 3 H), 4.02 (m, 5 H), 5.56 (m, 2 H), 5.69 (m, 2 H), 6.09 (d, *J* = 6.1 Hz, 1 H). − ^{13}C NMR ([D$_6$]DMSO, 75 MHz): δ = 16.20 (CH_3, $J_{P,C}$ = 6.1 Hz), 16.37 (CH_3, $J_{P,C}$ = 5.4 Hz), 20.83 (CH_3), 21.11 (CH_3), 45.01 (CH, $J_{P,C}$ = 140.7 Hz), 61.53 (CH_2, $J_{P,C}$ = 7.3 Hz), 62.65 (CH_2, $J_{P,C}$ = 6.9 Hz), 92.86 (CH), 93.64 (CH), 95.13 (CH), 96.75 (CH, $J_{P,C}$ = 11.9 Hz), 97.24 (CH), 109.72 (C_{quat}), 122.01 (C_{quat}), 131.49 (C_{quat}, $J_{P,C}$ = 12.9 Hz), 233.85 (C_{quat}, CO). − ^{31}P NMR ([D$_6$]DMSO, 121 MHz) : δ = 24.24. − MS (70 eV, EI); *m/z* (%): 376 [M^+ − 2 CO] (18), 348 [M^+ − 3 CO] (100), 296 [M^+ − $Cr(CO)_3$] (2), 52 [Cr^+] (5). − IR (KBr): $\tilde{\nu}$ = 3069 cm^{-1}, 2990, 2928, 1968, 1886, 1871, 1633, 1525, 1455, 1412, 1391, 1249, 1236, 1220, 1160, 1099, 1055, 1027, 974, 867, 823, 801, 761, 661, 630, 618, 586, 536, 515, 487. − UV/Vis (DMSO): λ_{max} (ε) = 316 (9900). − $C_{19}H_{25}CrO_5P$ (432.37): calcd. C 52.78, H 5.83; found C 52.97, H 5.84.

{η^6-[2-Butyl-1-(diethoxyphosphoryl)-3-methylprop-2-en-1-yl]benzene}tricarbonylchromium(0) (3e): Yellow crystals, m.p. 63−65°C.− ^{1}H NMR ([D$_6$]DMSO, 300 MHz): δ = 0.70−2.13 (21 H), 3.96 (m, 5 H), 5.50 (m, 1 H), 5.53 (m, 1 H), 5.70 (m, 2 H), 6.19 (m, 1 H). − ^{13}C NMR ([D$_6$]DMSO, 75 MHz): δ = 13.70 (CH_3), 16.15 (CH_3, $J_{P,C}$ = 7.5 Hz), 16.35 (CH_3, $J_{P,C}$ = 7.5 Hz), 20.90 (CH_3), 21.20 (CH_3), 22.70 (CH_2), 29.60 (CH_2), 31.50 (CH_2), 45.85 (CH, $J_{P,C}$ = 143.4 Hz), 61.35 (CH_2, $J_{P,C}$ = 7.5 Hz), 62.75 (CH_2, $J_{P,C}$ = 7.5 Hz), 92.90 (CH), 93.60 (CH), 94.80 (CH), 96.40 (CH), 97.30 (CH, $J_{P,C}$ = 15.1 Hz), 109.50 (C_{quat}), 127.45 (C_{quat}, $J_{P,C}$ = 7.5 Hz), 132.10 (C_{quat}, $J_{P,C}$ = 15.1 Hz), 233.90 (C_{quat}, CO). − ^{31}P NMR ([D$_6$]DMSO, 121 MHz) : δ = 23.93. − MS (70 eV); *m/z* (%): 474 [M^+] (1), 446 [M^+ − CO] (1), 418 [M^+ − 2 CO] (12), 390 [M^+ − 3 CO] (100), 338 [M^+ − $Cr(CO)_3$] (21), 52 [Cr^+] (4). − IR (KBr): $\tilde{\nu}$ = 2957 cm^{-1}, 2929, 2858, 1966, 1887, 1731, 1601, 1524, 1495, 1455, 1414, 1391, 1249, 1163, 1098, 1055, 1028, 965, 870, 815, 747, 701, 661, 630, 560, 530, 479. − UV/Vis (DMSO): λ_{max} (ε) = 315 (5800). − $C_{22}H_{31}CrO_6P$ (474.45): calcd. C 55.69, H 6.58; found C 55.47, H 6.55.

Tricarbonyl{η^6-[1-(diethoxyphosphoryl)-2-ethenyl-3-methylprop-2-en-1-yl]benzene}chromium(0) (3f): Yellow crystals, m.p. 99−100°C. − ^{1}H NMR ([D$_6$]DMSO, 300 MHz): δ = 1.19 (m, 6 H), 1.89 (m, 6 H), 4.00 (m, 4 H), 4.29 (d, *J* = 27.7 Hz, 1 H), 5.21 (m, 2 H), 5.66 (m, 4 H), 6.10 (m, 1 H), 6.42 (m, 1 H). − ^{13}C NMR ([D$_6$]DMSO, 75 MHz): δ = 16.31 (CH_3), 21.76 (CH_3), 22.47 (CH_3), 43.78 (CH, $J_{P,C}$ = 139.9 Hz), 61.65 (CH_2), 62.81 (CH_2), 93.11 (CH), 93.83 (CH), 94.86 (CH), 96.67 (CH), 97.06 (CH), 109.97 (C_{quat}), 119.56 (CH_2), 126.98 (C_{quat}), 133.57 (CH), 136.24 (C_{quat}), 233.94 (C_{quat}, CO). − ^{31}P NMR ([D$_6$]DMSO, 121 MHz) : δ = 24.17. − MS (70 eV); *m/z* (%): 444 [M^+] (1), 416 [M^+ − CO] (1), 388 [M^+ − 2 CO] (10), 360 [M^+ − 3 CO] (100), 308 [M^+ − $Cr(CO)_3$] (2), 52 [Cr^+] (4). − IR (KBr): $\tilde{\nu}$ = 3084 cm^{-1}, 2982, 1971, 1886, 1867, 1629, 1528, 1458, 1393, 1248, 1221, 1177, 1049, 1026, 976, 902, 764, 668, 633, 618, 571, 529. − UV/Vis (DMSO): λ_{max} (ε) = 316 (9300). − $C_{20}H_{25}CrO_6P$ (444.38): calcd. C 54.06, H 5.67; found C 54.27, H 5.61.

Tricarbonyl{η^6-[1-(diethoxyphosphoryl)-3-methyl-2-phenylprop-2-en-1-yl]benzene}chromium(0) (3g): Yellow crystals, m.p. 146−148°C. − ^{1}H NMR ([D$_6$]DMSO, 300 MHz): δ = 1.25 (m, 6 H), 1.44 (s, 3 H), 1.97 (s, 3 H), 4.07 (m, 4 H), 4.38 (d, *J* = 25.5 Hz, 1 H), 5.36−5.66 (m, 5 H), 6.95−7.29 (m, 5 H). − ^{13}C NMR ([D$_6$]DMSO, 75 MHz): δ = 15.83 (CH_3, *J* = 6.2 Hz), 16.21 (CH_3, *J* = 5.7 Hz), 20.65 (CH_3), 22.89 (CH_3), 44.94 (CH, *J* = 142.3 Hz), 61.21 (CH_2), 62.41 (CH_2, *J* = 6.7 Hz), 91.82 (CH), 93.01 (CH), 94.55 (CH), 97.02 (CH), 97.69 (CH), 108.61 (C_{quat}), 126.49 (CH), 127.26 (CH), 129.30 (C_{quat}), 130.46 (CH), 134.52 (C_{quat}), 138.57 (C_{quat}), 233.91 (C_{quat}, CO). − ^{31}P NMR ([D$_6$]DMSO, 121 MHz) : δ = 23.14. − MS (70 eV); *m/z* (%): 494 [M^+] (1), 466 [M^+ − CO] (1), 438 [M^+ − 2 CO] (2), 410 [M^+ − 3 CO] (100), 358 [M^+ − $Cr(CO)_3$] (14), 52 [Cr^+] (2). − IR (KBr): $\tilde{\nu}$ = 2991 cm^{-1}, 1969, 1882, 1636, 1458, 1254, 1232, 1054, 1028, 972, 767, 702, 662, 631, 595, 531. − UV/Vis (DMSO): λ_{max} (ε) = 317 (9100). − $C_{24}H_{27}CrO_6P$ (494.44): calcd. C 58.30, H 5.50; found C 58.10, H 5.59.

(*R*,*R* or *S*,*S*)-{η^6-1-[2-Butyl-1-(diethoxyphosphoryl)-3-methylprop-2-en-1-yl]-2-methylbenzene}tricarbonylchromium(0) (3h, Major Diastereomer): Yellow crystals, m.p. 108−111°C. − ^{1}H NMR ([D$_6$]DMSO, 300 MHz): δ = 1.18 (t, *J* = 6.9 Hz, 3 H), 1.29 (t, *J* = 6,9 Hz, 3 H), 1.49 (s, 3 H), 1.69 (d, *J* = 5.3 Hz, 3 H), 1.78 (m, 3 H), 1.96 (s, 3 H), 3.73−4.15 (m, 5 H), 5.52 (d, *J* = 6.1 Hz, 1 H), 5.61 (d, *J* = 6.3 Hz, 1 H), 5.74 (t, *J* = 6.4 Hz, 1 H), 6.36 (d, *J* = 6.5 Hz, 1 H). − ^{13}C NMR ([D$_6$]DMSO, 75 MHz): δ = 15.71 (CH_3), 16.12 (CH_3, $J_{P,C}$ = 5.9 Hz), 16.61 (CH_3, $J_{P,C}$ = 4.6 Hz), 18.45 (CH_3), 21.01 (CH_3), 21.31 (CH_3), 42.78 (CH, $J_{P,C}$ = 144.6 Hz), 61.35 (CH_2, $J_{P,C}$ = 7.2 Hz), 63.16 (CH_2, $J_{P,C}$ = 6.6 Hz), 91.48 (CH), 95.25 (CH), 95.61 (CH), 97.30 (CH, $J_{P,C}$ = 4.6 Hz), 107.82 (C_{quat}), 109.76 (C_{quat}, *J* = 15.9 Hz), 119.60 (C_{quat}, *J* = 8.6 Hz), 132.08 (C_{quat}, *J* = 11.9 Hz), 234.25 (C_{quat}, CO). − MS (70 eV, EI); *m/z* (%): 446 [M^+] (2), 418 [M^+ − CO] (1), 390 [M^+ − 2 CO] (12), 362 [M^+ − 3 CO] (100), 310 [M^+ − $Cr(CO)_3$] (6), 52 [Cr^+] (4). − IR (KBr): $\tilde{\nu}$ = 3084 cm^{-1}, 2982, 2928, 1967, 1889, 1872, 1629, 1445, 1380, 1251, 1233, 1213, 1162, 1097, 1047, 1024, 973, 799, 754, 667, 629, 587, 538, 515, 481. − UV/Vis (DMSO): λ_{max} (ε) = 316 nm (9900). − $C_{20}H_{27}CrO_6P$ (446.39): calcd. C 53.81, H 6.09; found C 53.97, H 6.02.

(*R*,*S* or *S*,*R*)-{η^6-1-[2-Butyl-1-(diethoxyphosphoryl)-3-methylprop-2-en-1-yl]-2-methylbenzene}tricarbonylchromium(0) (3h, Minor Diastereomer): Yellow crystals, m.p. 93−95°C. − ^{1}H NMR ([D$_6$]DMSO, 300 MHz): δ = 1.06 (t, *J* = 6.9 Hz, 3 H), 1.16 (t, *J* = 7.0 Hz, 3 H), 1.66 (d, *J* = 3.3 Hz, 3 H), 1.79 (s, 3 H), 2.01 (s, 3 H), 2.28 (s, 3 H), 3.82−3.99 (m, 4 H), 4.15 (d, *J* = 26.5 Hz, 1 H), 5.44−5.49 (m, 2 H), 5.83 (t, *J* = 6.4 Hz, 1 H), 6.06 (d, *J* = 5.8 Hz, 1 H). − ^{13}C NMR ([D$_6$]DMSO, 75 MHz): δ = 16.30 (CH_3), 16.39 (CH_3), 17.65 (CH_3), 19.62 (CH_3), 20.96 (CH_3), 21.31 (CH_3), 40.79 (CH, $J_{P,C} \approx$ 135 Hz, under DMSO multiplet), 61.87 (CH_2, $J_{P,C}$ = 7.2 Hz), 62.57 (CH_2, *J* = 6.6 Hz), 90.16 (CH), 93.45 (CH), 97.28 (CH), 98.92 (CH, $J_{P,C}$ = 3.5 Hz), 109.83 (C_{quat}), 112.40 (C_{quat}, $J_{P,C}$ = 5.3 Hz), 122.65 (C_{quat}, $J_{P,C}$ = 5.9 Hz), 131.31 (C_{quat}, $J_{P,C}$ = 13.9 Hz), 234.01 (C_{quat}, CO). − MS (70 eV, EI); *m/z* (%): 446 [M^+] (1), 390 [M^+ − 2 CO] (12), 362 [M^+ − 3 CO] (100), 310 [M^+ − $Cr(CO)_3$] (6), 52 [Cr^+] (3). − IR (KBr): $\tilde{\nu}$ = 3090 cm^{-1}, 2988, 1955, 1873, 1631, 1444, 1386, 1251, 1213, 1191, 1163, 1097, 1047, 1033, 969, 839, 814, 797, 738, 667, 639, 628, 579, 540, 531, 497, 479. − UV/Vis (DMSO): λ_{max} (ε) = 317 nm (9000). − $C_{20}H_{27}CrO_6P$ (446.39): calcd. C 53.81, H 6.09; found C 53.92, H 6.08.

Tricarbonyl{η⁶-1-[1-(diethoxyphosphoryl)-3-methyl-2-phenylprop-2-en-1-yl]-2-methylbenzene}chromium(0) (3i): Yellow crystals, m.p. 94−97°C. − ^{1}H NMR ([D$_6$]DMSO, 300 MHz): δ = 1.30 (m, 6 H), 1.45 (d, *J* = 4.2 Hz, 3 H), 1.95 (d, *J* = 2.5 Hz, 3 H), 2.13 (s, 3 H), 4.09−4.25 (m, 4 H), 4.38 (d, *J* = 26.7 Hz, 1 H), 5.04 (t, *J* = 6.3 Hz, 1 H), 5.39 (d, *J* = 6.3 Hz, 1 H), 5.58 (t, *J* = 6.3 Hz, 1 H), 5.82 (d, *J* = 6.6 Hz, 1 H), 6.72−7.12 (m, 5 H). − ^{13}C NMR ([D$_6$]DMSO, 75 MHz): δ = 16.03 (CH$_3$), 16.63 (CH$_3$, $J_{P,C}$ = 5.3 Hz), 18.26 (CH$_3$), 20.78 (CH$_3$, $J_{P,C}$ = 2.6 Hz), 23.16 (CH$_3$, $J_{P,C}$ = 2.6 Hz), 42.21 (CH, $J_{P,C}$ = 145.9 Hz), 61.42 (CH$_2$, $J_{P,C}$ = 7.9 Hz), 63.14 (CH$_2$, $J_{P,C}$ = 7.3 Hz), 89.64 (CH), 93.83 (CH), 95.98 (CH), 97.95 (CH, $J_{P,C}$ = 3.9 Hz), 106.74 (C$_{quat}$, $J_{P,C}$ = 1.9 Hz), 110.37 (C$_{quat}$, $J_{P,C}$ = 15.9 Hz), 115.36 (CH), 118.91 (CH), 126.75 (CH), 127.52 (CH), 127.76 (C$_{quat}$, $J_{P,C}$ = 7.9 Hz), 129.48 (CH), 135.45 (C$_{quat}$, $J_{P,C}$ = 11.9 Hz), 139.00 (C$_{quat}$), 234.22 (C$_{quat}$, CO). − MS (70 eV, EI); *m/z* (%): 508 [M$^+$] (1), 480 [M$^+$ − CO] (1), 452 [M$^+$ − 2 CO] (2), 424 [M$^+$ − 3 CO] (100), 372 [M$^+$ − Cr(CO)$_3$] (1), 52 [Cr$^+$] (5). − IR (KBr): $\tilde{\nu}$ = 3079 cm^{-1}, 2984, 2929, 2856, 1955, 1910, 1890, 1640, 1606, 1594, 1491, 1474, 1459, 1441, 1383, 1254, 1235, 1205, 1162, 1097, 1055, 1023, 1010, 970, 830, 808, 770, 755, 723, 701, 663, 629, 596, 552, 526, 477. − UV/Vis (DMSO): λ_{max} (ε) = 317 nm (9300). − $C_{25}H_{29}CrO_6P$ (508.46): calcd. C 59.02, H 5.74; found C 60.32, H 5.84.

{η⁶-1-[2-Butyl-1-(diethoxyphosphoryl)-3-methylprop-2-en-1-yl]-2-(dimethoxymethyl)benzene}tricarbonylchromium(0) (3j): Yellow crystals, m.p. 90−96°C. − ^{1}H NMR ([D$_6$]DMSO, 300 MHz): δ = 1.19 (t, *J* = 7.0 Hz, 3 H), 1.29 (t, *J* = 6.9 Hz, 3 H), 1.48 (m, 3 H), 1.66−1.70 (m, 3 H), 1.82 (m, 3 H), 3.09 (s, 3 H, OMe), 3.42 (s, 3 H, OMe), 3.88−4.10 (m, 4 H), 4.36 (d, *J* = 25.2 Hz, 1 H), 4.91 (s, 1 H), 5.66−5.70 (m, 2 H), 5.78−5.84 (m, 1 H), 6.20−6.23 (m, 1H); additional signals (minor diastereomer): δ = 1.01 (t, *J* = 7.0 Hz, 3 H), 1.15 (t, *J* = 6.9 Hz, 3 H), 3.76−3.84 (m, 4 H), 4.74 (d, *J* = 27.9 Hz, 1 H), 5.21 (s, 1 H). − ^{13}C NMR ([D$_6$]DMSO, 75 MHz): δ = 16.08 (CH$_3$), 16.17 (CH$_3$), 16.66 (CH$_3$), 16.73 (CH$_3$), 21.51 (CH$_3$), 42.20 (CH, $J_{P,C}$ = 141.9 Hz), 53.62 (CH$_3$, OMe), 56.57 (CH$_3$, OMe), 61.30 (CH$_2$, $J_{P,C}$ = 7.3 Hz), 63.20 (CH$_2$, $J_{P,C}$ = 7.3 Hz), 92.74 (CH), 92.96 (CH), 93.98 (CH), 95.79 (CH, $J_{P,C}$ = 4.6 Hz), 100.48 (CH), 107.67 (C$_{quat}$, *J* = 4.6 Hz), 107.91 (C$_{quat}$), 120.79 (C$_{quat}$, *J* = 9.9 Hz), 131.09 (C$_{quat}$, *J* = 11.9 Hz), 233.53 (C$_{quat}$, CO); additional signals (minor diastereomer): δ = 49.27 (CH, $J_{P,C}$ = 141.9 Hz), 55.91 (CH$_3$, OMe), 91.03 (CH), 94.35 (CH), 98.66 (CH), 109.46 (C$_{quat}$), 233.22 (C$_{quat}$, CO). − ^{31}P NMR ([D$_6$]DMSO, 121 MHz) : δ = 23.99; additional signal (minor diastereomer): δ = 25.80. − MS (70 eV, EI); *m/z* (%): 506 [M$^+$] (1), 450 [M$^+$ − 2 CO] (21), 422 [M$^+$ − 3 CO] (100), 52 [Cr$^+$] (5). − IR (KBr): $\tilde{\nu}$ = 3084 cm^{-1}, 2984, 2931, 2832, 1965, 1888, 1635, 1525, 1444, 1416, 1391, 1347, 1252, 1238, 1204, 1162, 1101, 1055, 1024, 969, 859, 796, 762, 742, 665, 628, 586, 531, 481. − UV/Vis (DMSO): λ_{max} (ε) = 318 nm (10100). − $C_{22}H_{31}CrO_8P$ (506.44): calcd. C 52.17, H 6.17; found C 52.43, H 6.18.

Acknowledgments

The financial support of this work by the Fonds der Chemischen Industrie and the Deutsche Forschungsgemeinschaft is gratefully acknowledged. We wish to express our appreciation to Prof. H. Mayr for his generous support.

[1] [1a] M. F. Semmelhack, A. Zask, *J. Am. Chem. Soc.* **1983**, *105*, 2034−2043. − [1b] M. Uemura, T. Minami, Y. Hayashi, *J. Chem. Soc., Chem. Commun.* **1984**, 1193−1194. − [1c] M. F. Semmelhack, *Comprehensive Organometallic Chemistry II* (Eds.: E. W. Abel, F. G. A. Stone, G. Wilkinson), Pergamon, Oxford, UK, **1995**, vol. 12, p. 979−1015. − [1d] M. Uemura in *Advances in Metal-Organic Chemistry* (Ed.: L. S. Liebeskind), JAI Press, London, **1991**, vol. 2, p. 195−240.

[2] [2a] K. Schnellhaas, H.-G. Schmalz, J. W. Bats, *Chem. Eur. J.* **1998**, *4*, 57−66. − [2b] T. Geller, H.-G. Schmalz, J. W. Bats, *Tetrahedron. Lett.* **1998**, *39*, 1537−1540. − [2c] T. Geller, J. Jakupovic, H.-G. Schmalz, *Tetrahedron Lett.* **1998**, *39*, 1541−1544. − [2d] H.-G. Schmalz, M. Arnold, J. Hollander, J. W. Bats, *Angew. Chem.* **1994**, *106*, 77−79; *Angew. Chem. Int. Ed. Engl.* **1994**, *33*, 109−111.

[3] S. G. Davies, T. D. McCarthy, *Comprehensive Organometallic Chemistry II* (Eds.: E. W. Abel, F. G. A. Stone, G. Wilkinson), Pergamon, Oxford, UK, **1995**, vol. 12, p. 1039−1070.

[4] A. Ceccon, A. Gambaro, A. Venzo, *J. Organomet. Chem.* **1985**, *275*, 209−222.

[5] S. G. Davies, S. J. Coote, C. L. Goodfellow, in *Advances in Metal-Organic Chemistry* (Ed.: L. S. Liebeskind), JAI Press, London, **1991**, vol. 2, p. 1−57.

[6] [6a] M. F. Semmelhack, W. Seufert, L. Keller, *J. Am. Chem. Soc.* **1980**, *102*, 6584−6586. − An interesting novel approach utilizes samarium iodide induced SET processes for radical additions to styrene complexes followed by the reduction of the benzylic radical to the benzylic anion, see, e.g.: [6b] H.-G. Schmalz, S. Siegel, D. Bernicke, *Tetrahedron Lett.* **1998**, *39*, 6683−6686. − [6c] H.-G. Schmalz, S. Siegel, J.W. Bats, *Angew. Chem.* **1995**, *107*, 2597−2599; *Angew. Chem. Int. Ed. Engl.* **1995**, *34*, 2383−2385.

[7] [7a] T. J. J. Müller, M. Ansorge, *Chem. Ber.* **1997**, *130*, 1135−1139. − [7b] T. J. J. Müller, M. Ansorge, *Tetrahedron* **1998**, *54*, 1457−1470.

[8] [8a] W. R. Jackson, T. R. B. Mitchell, *J. Chem. Soc. B* **1969**, 1228−1230. − [8b] A. Solladié-Cavallo, E. Tsamo, *J. Organomet. Chem.* **1979**, *172*, 165−169. − [8c] P. Bloem, D. M. David, L. A. Kane-Maguire, S. G. Pyne, B. W. Skelton, A. H. White, *J. Organomet. Chem.* **1991**, *407*, C19−C22.

[9] Crystallographic data (excluding structure factors) for the structures reported in this paper have been deposited with the Cambridge Crystallographic Data Centre as supplementary publication nos. CCDC-102960 (**1a**), -102961 (**1d**), -102962 (**3f**), -102963 (**3j**), and -102964 (**3i**). Copies of the data can be obtained free of charge on application to CCDC, 12 Union Road, Cambridge CB2 1EZ, UK (Fax: + 44-1223/336-033; E-mail: deposit@ccdc.cam.ac.uk).

[10] *Quantum CAChe 3.0 Program*, Oxford Molecular Group, **1997**.

[11] [11a] K. Koosha, J. Berlan, M. L. Capmau, W. Chodkiewicz, *Bull. Soc. Chim. Fr.* **1976**, 1284−1290. − [11b] K. Koosha, J. Berlan, M. L. Capmau, W. Chodkiewicz, *Bull. Soc. Chim. Fr.* **1976**, 1291−1294. − [11c] J. Berlan, K. Koosha, J.-P. Battioni, *Bull. Soc. Chim. Fr.* **1978** (II), 575−580.

[12] For diastereoselective protonations, see e.g.: [12a] N. Krause, S. Ebert, A. Haubrich, *Liebigs Ann.* **1997**, 2409−2418. − [12b] C. Fehr, *Angew. Chem.* **1996**, *108*, 2727−2748; *Angew. Chem. Int. Ed. Engl.* **1996**, *35*, 2566−2587.

[13] See e.g.: [13a] A. Gerold, J. T. B. H. Jastrzebski, C. M. P. Kronenburg, N. Krause, G. van Koten, *Angew. Chem.* **1997**, *109*, 778−780; *Angew. Chem. Int. Ed. Engl.* **1997**, *36*, 755−757. − [13b] G. van Koten, *J. Organomet. Chem.* **1990**, *400*, 283−301. − [13c] P. P. Power, *Prog. Inorg. Chem.* **1991**, *39*, 75−112. − [13d] A. Gerold, N. Krause, *Angew. Chem.* **1997**, *109*, 194−213; *Angew. Chem. Int. Ed. Engl.* **1997**, *36*, 186−204.

[14] Various Editors, *Organikum*, 14th ed., VEB Deutscher Verlag der Wissenschaften, Berlin, **1993**.

[15] T. J. J. Müller, M. Ansorge, K. Polborn, *J. Organomet. Chem.*, in press.

Received September 7, 1998
[I98298]

Nanostructuring Titania: Control over Nanocrystal Structure, Size, Shape, and Organization

Abdelkrim Chemseddine*[a] and Thomas Moritz[b]

Dedicated to Professor J. Rouxel in recognition of his important contributions to the chemistry of solids

Keywords: TiO_2 / Growth / Self-organisation / Polytitanate / Nanocrystals / Nanostructure / Superlattice / Films

Control over crystal structure, size, shape, and organization of TiO_2 nanocrystals has been achieved by means of wet chemistry. Hydrolysis and polycondensation of titanium alkoxide [$Ti(OR)_4$] has been performed in the presence of tetramethylammonium hydroxide (Me_4NOH). This base both catalyzes the reaction and provides an organic cation that stabilizes the anatase polyanionic cores formed in this medium. These anatase clusters are organized so as to favour self-assembly into intermediate nanocrystals, which, in turn, self-assemble into superlattices. This self-assembling process has been exploited for the processing of highly structured titania films. Furthermore, larger anatase TiO_2 nanocrystals of different sizes and shapes have been obtained by adjusting the relative concentrations of titanium alkoxide and Me_4NOH, the reaction temperature, and the pressure. HRTEM, XRD, and EXAFS have been used to characterize the various samples and to elucidate the growth of titania anatase. Our observations are in accordance with theoretically predicted condensation and growth pathways. The formation of mesoscopic structures through a self-assembling process of the multiply charged polytitanate anions in the presence of Me_4N^+ is also discussed.

Introduction

The chemistry of titania has been the subject of much scientific and technological attention. This material is used as a white pigment in making paints and cosmetics, in the electroceramics industry, as a support in catalysis, and as a photocatalyst.[1,2] Nanostructuring of titania is of great interest with regard to the construction of membranes for gas-phase separations,[3] its use as a nanoporous electrode material in the development of new types of solar cells,[4] and its use as an active layer in the design of electrochromic devices.[5] Recently, TiO_2 coatings on glasses have been shown to exhibit interesting antifogging and self-cleaning properties.[6] The performance of titania in applications such as these could be optimized with specific microstructural and macrostructural control over the morphology of the material. Progress in this area depends on our understanding of the fundamental details by which chemical reactivity is related to nucleation and growth of titania. These processes need to be controlled at the earliest stages of production and arrested at the appropriate stage so as to furnish titania particles with the desired crystal structure and a well-defined size, shape, and surface structure. Furthermore, control over the surface chemistry of nanocrystals and their functionalization through the attachment of organic ligands may lead to organized assemblies[7] and provide new types of precursors for the processing of highly nanostructured titania-based materials.[8]

[a] Hahn-Meitner Institut, Bereich Physikalische Chemie, Abt. CD, Glienicker Strasse 100, D-14109 Berlin, Germany
E-mail: chemseddine@hmi.de
[b] Present adress: Atotec, Erasmusstr. 20, D-10553 Berlin, Germany

The fundamental physical properties of such nanoscale materials are of interest, since their small size and large surface area can lead to unexpected or dramatically differing properties.[9] The need for high-quality titania systems in order to achieve a quantitative understanding of size effects on the physical properties is another motivating factor in this work.[9]

In techniques such as CVD, MOCVD, and simple thermal pyrolysis, molecular precursors are allowed to react at rather high temperatures in the gas phase or as molecular solids.[10] Control over particle size, size distribution, shape, and crystalline orientation is inherently difficult to achieve. In contrast, in wet chemical methods, a solvent is used as the reaction medium or vehicle, and the reaction is performed at low temperature. There are many advantages in using wet chemistry for the synthesis of nanomaterials.[7] Reaction, nucleation and growth can be easily monitored and influenced. The growth can be arrested by controlling the stoichiometry or by using appropriate ligands.[11] In contrast to growing clusters on solid substrates or in solid matrices, in the liquid phase the mobility and dynamics of the growing phase is assured, allowing structural arrangement of the core and growth termination by surface restructuring and capping. By variation of the synthesis conditions or reactants and characterization of the materials obtained, the production of nanocrystals can be rationalized.[11,12] Nanocrystals can be isolated according to size in the form of soluble, processable, manageable powders, or used as precursors in the processing of films.[13]

Furthermore, a major line of development of this chemistry concerns the spontaneous generation of well-defined architecture by the self-assembly of suitably designed and functionalized nanocrystals.[7] This issue of ordered nano-

 © WILEY-VCH Verlag GmbH, D-69451 Weinheim, 1999 1434–1948/99/0202–0235 $ 17.50+.50/0

structured arrays of functional nanocrystals is of central importance for the evaluation of the competitiveness of wet chemistry, i.e. sol-gel processes or solution techniques, since through the size, shape, and organization of particles, organic species can be confined within well-defined inorganic structures, allowing control over their thermal removal.[8,14] One of the problems encountered in making titania is the high reactivity of the available precursors, such alkoxides or chlorides, toward water.[15] The reaction invariably leads to a mixture of different polymeric species, which assume a variety of structures and sizes, and finally to an amorphous solid. Although certain chemical modifications have been successful in controlling the reactivity of titanium alkoxides and have permitted the isolation of intermediate polyoxoalkoxides,[16,17] none of these species resemble the structure of the bulk dioxide and any further hydrolysis again leads to gels and amorphous precipitates. In both cases, a peptization process is required to convert these polymers into crystalline particles. Control over size, size distribution, and shape is difficult during these dissolution-growth processes.[3] The present approach involves performing the reaction in a purely aqueous medium in the presence of a base, so as to achieve a complete hydrolysis and to provide conditions similar to those used in the aforementioned peptization process. Thus, hydrolysis and polycondensation of titanium alkoxide [$Ti(OR)_4$] is performed in the presence of tetramethylammonium hydroxide (Me_4NOH). This base both catalyzes the reaction[15,17] and provides an organic cation that is known to stabilize polyanionic cores in basic media, e.g. polyanions of tungsten, molybdenum, and vanadium.[18]

Results

Figure 1 shows an overview image of titania nanocrystals from a first sample, denoted as sample A. The nanocrystals are uniform in shape and are not aggregated. The particles are single nanocrystals and exhibit a triangular prismatic shape with a relatively narrow size distribution. The high resolution micrograph clearly shows lattice planes. All images of sample A show particles with an interplanar distance of 3.52 Å in the tetragonal [101] planes, which corresponds to the anatase phase. The lateral dimensions of the particles can be estimated by counting the number of lattice planes (about 30 LP in this case, which amounts to 10.5 nm). The average length measured directly from the micrograph is about 20 ± 1 nm. A careful analysis of the particles reveals structural features that can be utilized for the study of surface morphologies of small particles and the changes that occur during growth. Thin edges of TEM samples represent surfaces that can be viewed in profile by HRTEM.[20] The steps on the particle edges are in the [101] crystallographic directions and the height of each step can be taken as an indication of a cluster-cluster growth (see below). The triangular shape is in fact due to the presence of stepped [101] surfaces.

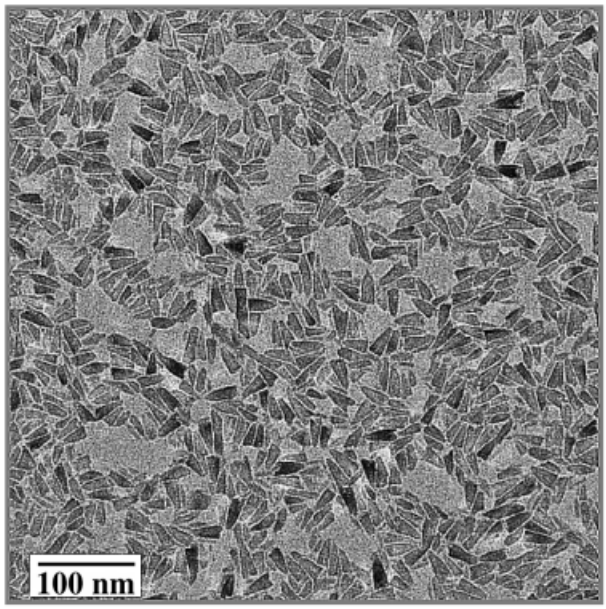


Figure 1. TEM micrograph of TMA-capped TiO_2 particles obtained for $R = 3$; the particles are homogeneous in size and triangular in shape

The X-ray diffraction pattern (Figure 2b) of sample A confirms the single anatase phase. However, all the Bragg peaks are relatively broad due to the finite size of the nanocrystals. The sizes calculated from the half-widths of the peaks using the Scherrer equation amount to 11.1 nm for the [101] peak, 20.8 nm for the [004] peak, and 20.7 nm for the [200] peak. These values are in accordance with the lateral dimensions measured from the TEM micrographs of these triangular prismatic nanocrystals.

Autoclaving of solution A leads to a shape transformation from triangular to rectangular particles, which have lengths of about 28 ± 3 nm and widths of about 12 ± 2 nm (Figure 3). The autoclaving leads to nanocrystals of uniform shape, which are non-aggregated and conform to a single anatase phase, according to TEM and XRD analysis. The morphological transformation of particles can be attributed to the thermal decomposition of the organic cations under the autoclaving conditions. The loss or decomposition of the organic cations probably induces chemical etching, which is followed by further growth and elimination of steps, ultimately leading to a shape transformation from triangular to rectangular.

Figure 4a shows a typical TEM image at low magnification of titania particles obtained in the case of sample B. A homogeneous fibrous or rod-like texture is achieved, although a relatively marked polydispersity in terms of length and width is apparent. Figure 4b shows a high-resolution image of a selected titania nanocrystal from sample B. The nanocrystal is viewed along the [010] direction. The surface profile image of the nanocrystal B shows stepped terraces on the [101] surface, which are marked with arrows. Its height is measured as a multiple of 3.52 Å, in accordance with the $d_{[101]}$. The corrugated sides are structural features that have not previously been observed in the case of titania

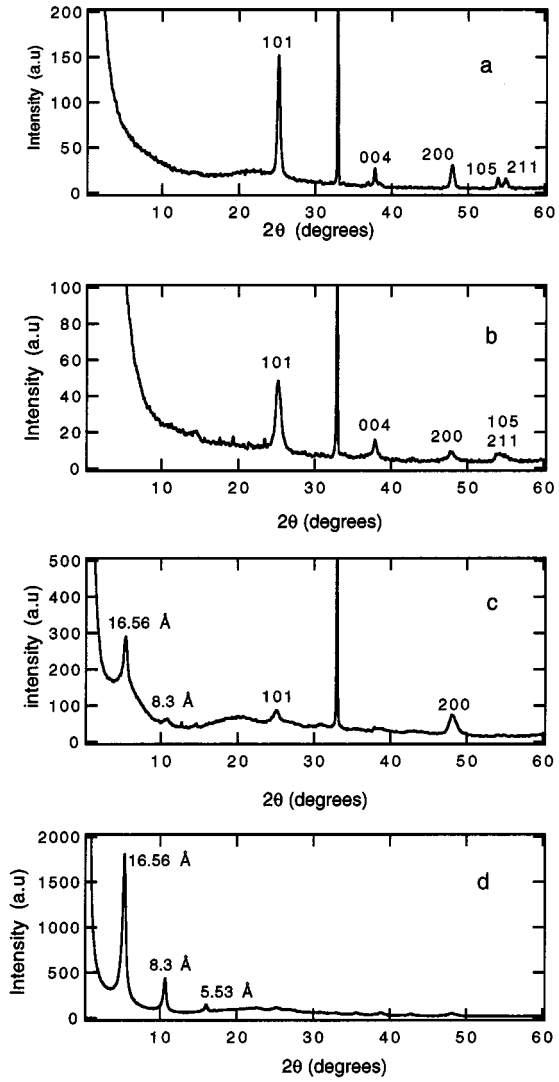


Figure 2. X-ray powder diffractograms of TiO_2 nanocrystals made with various Ti/Me_4N^+ ratios R; Figures b, c, and d correspond to solutions A (R = 4), B (R = 1.25), and E (R = 0.84); Figure a was obtained after autoclaving solution B under a saturated vapor pressure of water at 200°C and 2500 kPa; large-angle peak assignments are based on anatase titania; peak broadening indicates a decrease of nanocrystal size with increasing R; in addition to the perfect organization in the lateral dimensions shown in Figure 10, the series of harmonics in d indicates ordering of the growing anatase cluster in the nanocrystals forming a layered nanostructure; the sharpness of the peaks indicates a high degree of structural communication between the nanocrystals

and are a consequence of cluster-cluster growth and condensation of skewed octahedra in the case of anatase (see Discussion). The two sets of lattice fringes give two interplanar distances, which correspond to the [101] and the [002] of the anatase crystal structure (Figure 5). The elongated particles lie in the [010] plane.

XRD measurements on films obtained by the deposition of sample B solution onto a silicon wafer (Figure 2c) yield further information on the polydispersity of the sample. The low-angle peaks correspond to the presence of smaller titania clusters (cf. sample E). The relatively high intensity of the [200] peaks compared to the [101] peak is indicative

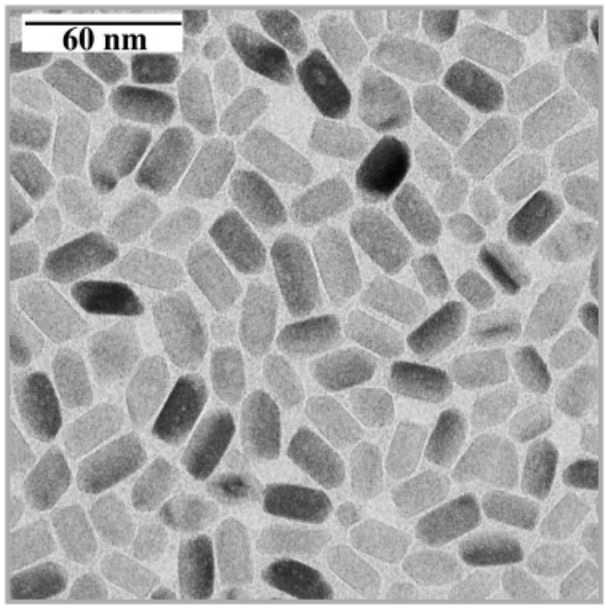


Figure 3. Overview of titania nanocrystals prepared by autoclaving solution A; the nanocrystals are homogeneous in both shape and size

of film anisotropy and confirms a preferred orientation of the crystallites. The Scherrer equation leads to 92.9 Å for the [101] peak and to 79.6 Å for the [200] peak.

Figure 6 shows TEM images of particles obtained after autoclaving sample B. The rod-like morphology is maintained. The diameter of the rods varies between 15 and 20 nm, but a large polydispersity in terms of rod length is apparent ($76 < L < 177$ nm). The adopted procedure of adding the titanium alkoxide solution in a dropwise fashion is mainly responsible for the observed polydispersity. In contrast to sample A, where a shape transformation was seen to occur, further growth in length and diameter takes place during the autoclaving of solution B without a change in the rod-like morphology. However, the structural features on the surface, such as sharp edges and steps, are no longer present. Again, the surface reconstruction can be related to the thermal decomposition of the organic cations under the autoclaving conditions. This confirms the role of the Me_4N^+ cation as a good capping ligand in stabilizing the surface structure of titania nanocrystals.

The size of the particles can also be fine-tuned by changing the autoclave temperature. Autoclaving of portions of sample B at 175°C and 200°C for a duration of 5 h resulted in particle sizes, calculated using the Scherrer equation, of 18 nm and 12 nm, respectively, for the [101] peak, and of 15.6 nm and 14 nm, respectively, for the [200] peak. The average width of nanocrystals measured from the TEM images is of the same order (about 12.32 nm). The average length of 63 nm reflects the nanocrystal dimension in the [002] direction, as shown in Figure 6b.

As mentioned above, the adopted procedure of adding the titanium alkoxide solution in a dropwise fashion accounts for the observed polydispersity in samples A and B. Figures 7a and 7b show two typical images obtained from

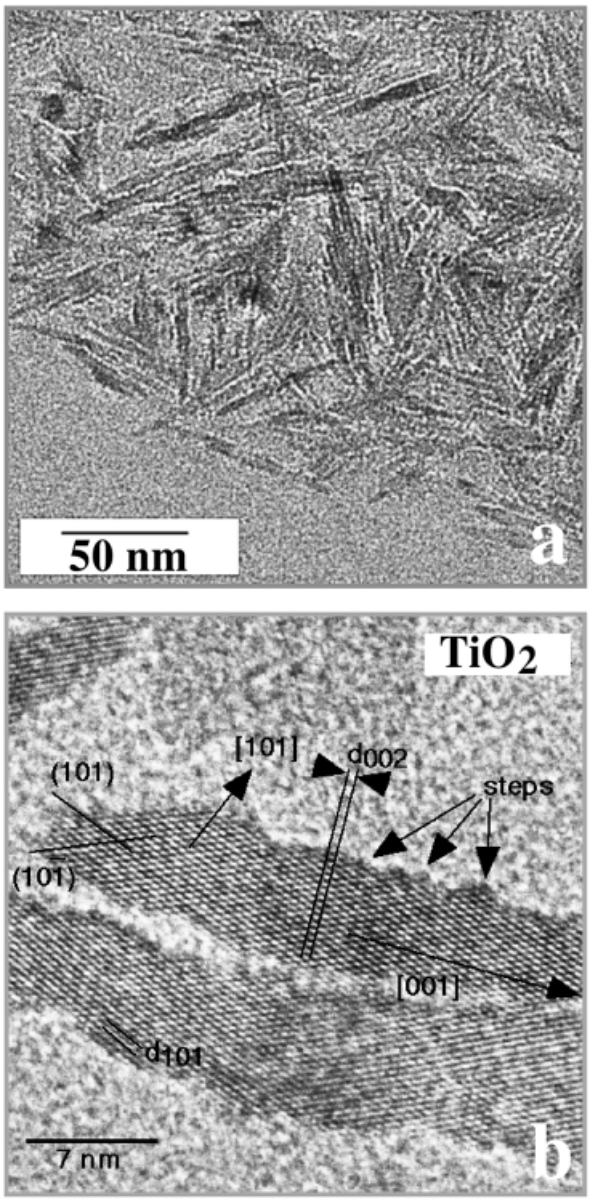


Figure 4. a) Elongated nanocrystals prepared with $R = 1.25$ (solution B); b) HRTEM of nanocrystals lying in the [010] plane and elongated in the [001] direction; the corrugated sides shown by arrows are due to oscillatory repetition of [1 0 1] and [1 0 −1] planes

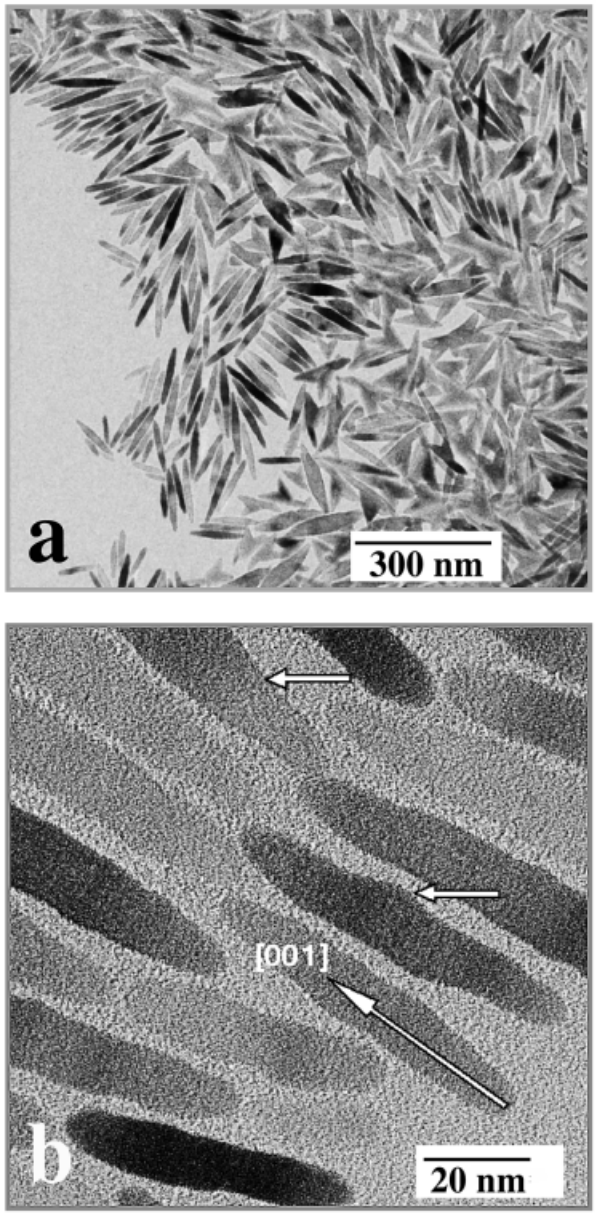


Figure 6. a) Overview of nanocrystals obtained after autoclaving B at 200°C, 2500 pKa for 5 hours; b) HRTEM shows no sharp edges and no clear surface steps after NMe_4^+ decomposition

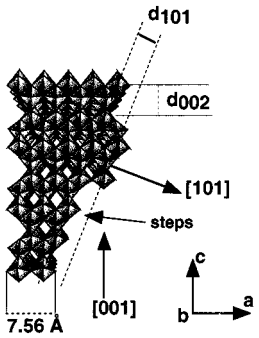


Figure 5. Polyhedral and packing drawing of anatase, TiO_2 in the [010] projection; [101] and [001] growth directions and a stepped [101] surface are shown

sample C ($Ti/Me_4NOH = 2$), made by adding the titanium alkoxide solution in a single portion. The sample has a relatively homogeneous appearance at low magnification. Particles of two distinct shapes are formed. These two particle types represent unique morphologies, in the sense that they are themselves the products of a self-assembling process (aggregation) of smaller elongated titania particles (slabs), as indicated by arrows in Figure 7b.

Particles with a triangular prismatic shape are also present in sample C, as indicated by arrows in Figure 7a. In contrast to sample A, where the particles are single nanocrystals, particles in sample C are composed of smaller ti-

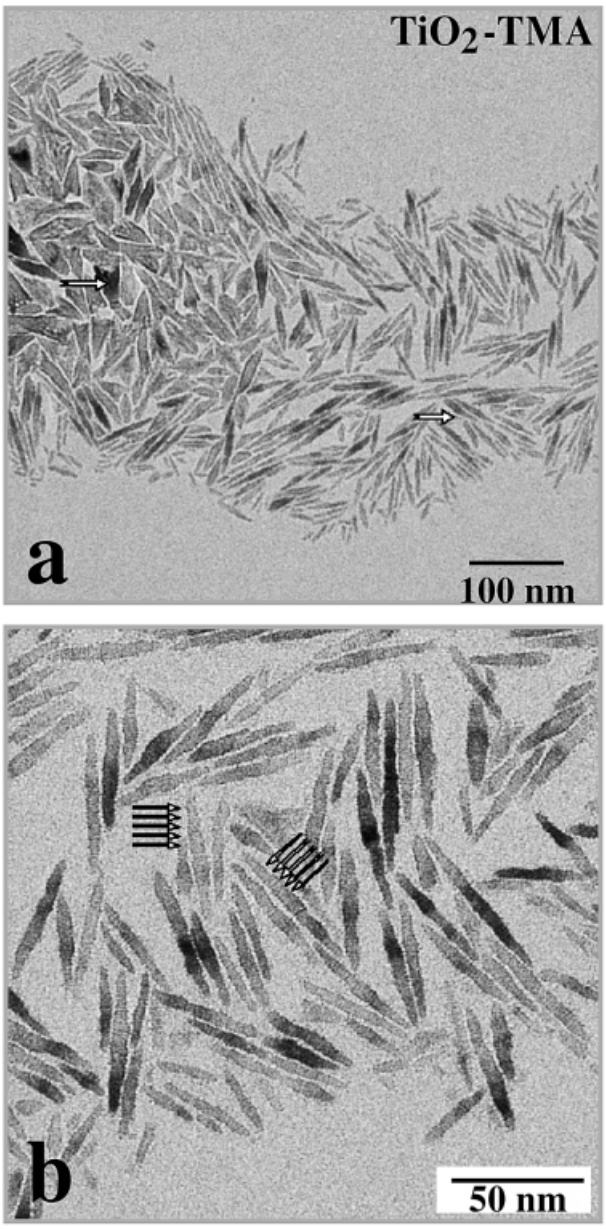


Figure 7. a) Two type of particles, shown by arrows, are obtained in solution C; b) These particles are composed of self-assembled smaller slabs as indicated by arrows

tania particles (slabs) self-assembled into aggregates of triangular shape.

Figure 8 shows images obtained from sample D (Ti/Me_4NOH = 1). At low beam intensities, the particles exhibit an internal structure as that in the case of sample C. Slabs are disposed parallel to one another along the [001] direction. At high magnification (higher electron fluxes), a coalescence (condensation) is induced by the loss of the organic cations (see Figure 8). The nanocrystals are viewed along the [010] axis, oriented parallel to the electron beam. The coalescence of these slabs (building units) leads to particles with corrugated sides or stepped [101] surfaces, as shown by black arrows in Figure 8. In addition to these thin slabs, as already observed in the case of sample C, spherical particles are formed. Particles of this type form at R = Ti/$Me_4NOH \leq 1$ and they show a propensity to self-assemble into organized structures. Their concentration increases, at the expense of their elongation, with the TMA concentration.

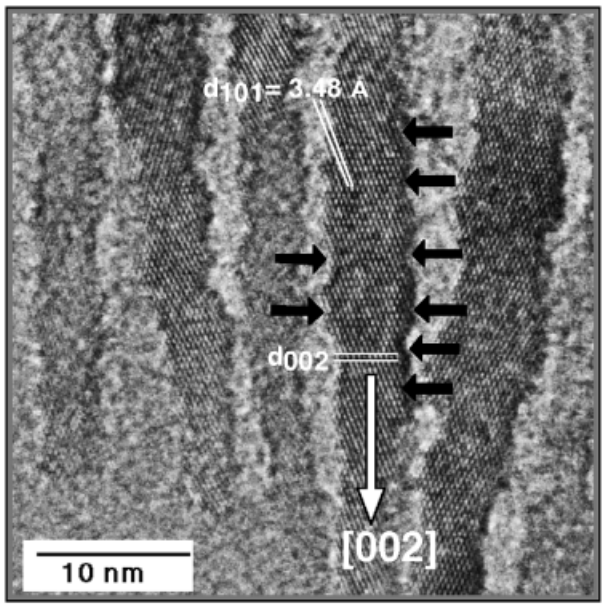


Figure 8. Titania clusters made in solution D; elongated slabs self-assemble into aggregates; at high magnification (higher electron fluxes) the particles coalesce into elongated nanocrystals presenting the same corrugated sides shown by arrows

Figures 9a and 9b show TEM images obtained in the case of sample E. The particles are seen to be organized in an ordered structure (2D superlattice). TEM provides a real-space imaging of the superlattice. In addition, small-angle electron diffraction can be used to probe the superlattice structure on the micrometer scale, while small-angle XRD allows insight into the structures of individual titania/Me_4N^+ nanocrystals on the Ångström scale. Figure 9 shows an array of nanocrystals with a mean inter-particle (center-to-center) distance of 15.7 nm, determined by direct imaging and confirmed from the power spectrum. The high magnification Figure 9b reveals well-faceted hexagonal crystals that form a hexagonal close-packed sheet. The crystals measure 13.5 nm in diameter. The high regularity in terms of size and shape, and long-range translational and orientational order is confirmed by the relatively sharp spots seen in the power spectrum (see inset in Figure 9a).

Further structural information is provided by X-ray diffraction (XRD). Measurements performed on thin films obtained by solution deposition on various supports, particularly on silicon wafers, are very sensitive to the periodicity perpendicular to the substrate (Figure 2d).

The diffraction intensity appears in two distinct scattering regions, the small-angle and large-angle. A series of harmonics at inter-plane distances of 16.56, 8.3, and 5.53 Å indicates an orientation in the direction normal to the substrate. The titania clusters are stacked in columns directly on top of one another, forming a multilayered struc-

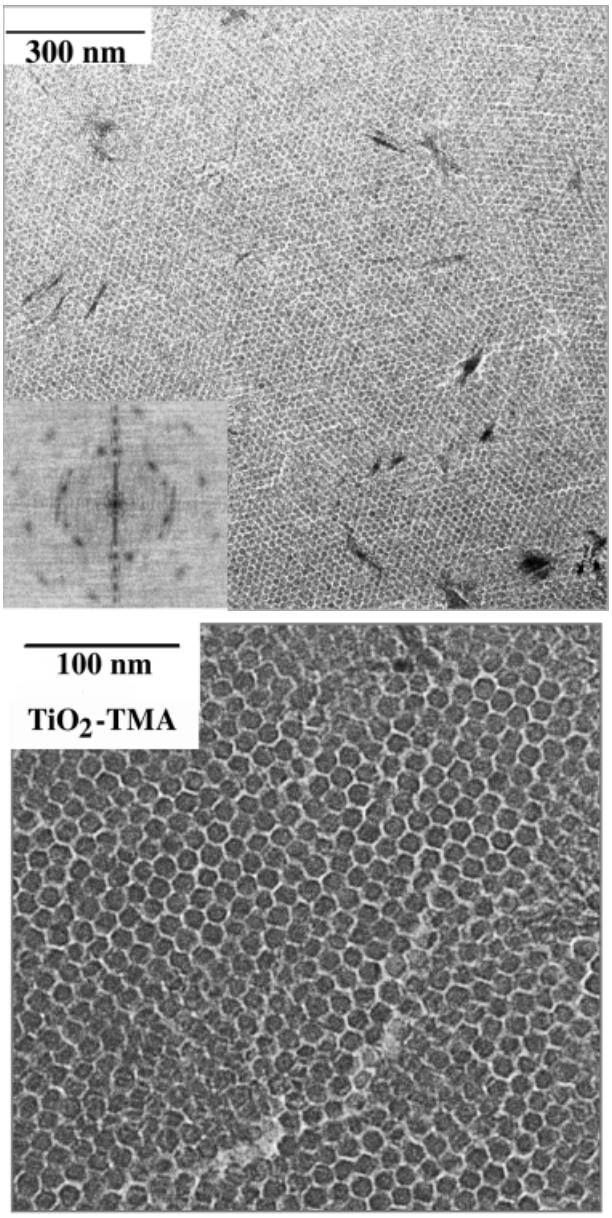


Figure 9. a) Transmission electron micrograph of titania/Me_4N^+ nanocrystals self-assembled into a superlattice with dimensions of the order of μm; the power spectrum (inset) confirms the long-range translational and orientational order of the superlattice; b) high magnification shows well-faceted hexagonal nanocrystals

ture. The majority of the nanocrystallites have the same orientation of their layered structures, which accounts for the sharpness of the XRD peaks.The white space observed around the nanocrystals in Figure 9 is probably occupied by organic cations.

Figure 10 shows TEM images of particles obtained in the case of sample F, which corresponds to solution E kept under reflux for an additional hour. The arrays obtained exhibit less regular geometries on a large scale. In comparison with sample E, changes in particle shape and in their organization, as well as in the internal structures of the nanocrystals are observed. Instead of the hexagonal shape observed in E, the drying leads to a rectangular shape and the nanocrystals are differently packed (Figure 10). Furthermore, two types of internal structures are observed. This can be explained in terms of the presence of two competing structures, since one type of nanocrystal is seen to be composed of slabs disposed parallel to one another, while the other type does not have any discerning features. Another explanation is that in a few nanocrystals a condensation process takes place, leading to slabs. These local transformations will affect the self-assembling process, thereby leading to new structures. A very interesting observation is that the high magnification images reveal that the newly formed slabs adopt a zig-zag structure. This is an indication of the presence of *cis*-skewed chains, characteristic of the anatase crystal structure (Figure 10). In fact, these anatase slabs are the condensation products of smaller ones (sample E), the anatase structure of which was shown by EXAFS and XRD experiments.

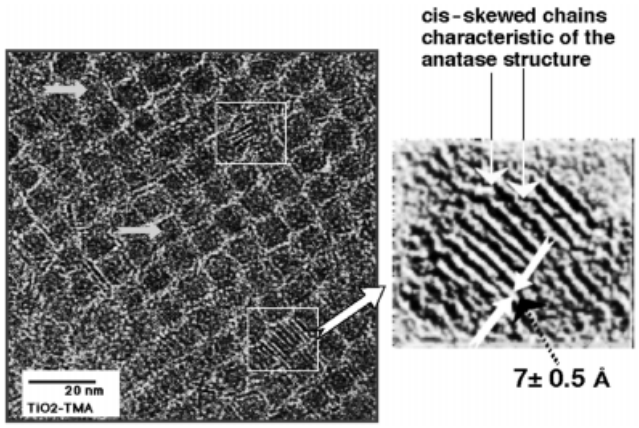


Figure 10. Nanocrystals obtained from solution F: Arrow shows nanocrystal composed of slabs disposed parallel to one another; high magnification indicates structural features that can be related to the *cis*-skewed chains in the [001] direction of the anatase crystal structure; the neighboring nanocrystals do not exhibit the same internal structure; arrows point to small clusters that probably did not condense to give slabs; a competing structure, where the slabs are differently oriented, is present

Figure 11 shows particles obtained in the case of sample G, using the same composition as in sample D, but with $(C_5H_{11})_4NOH$ as the base instead of Me_4NOH. The particles obtained are also elongated and relatively homogeneous, with widths of about 3.6 nm and lengths of about 42 nm. The important difference is the absence of the corrugated sides observed with Me_4N^+. The sharp edges indicate a relatively flat [100] surface. High-resolution microscopy shows most particles to be single nanocrystals, and a structural regularity where only [101] lattice planes are observed for most particles. The use of $(C_5H_{11})_4N^+$ illustrates the influence of cation size on the growth of titania, the larger ion leading to [100] surfaces instead of [101] surfaces.

Figure 12 depicts an electron micrograph of particles of sample H. The particles are almost spherical in shape and display a large size distribution (102 nm < diameter < 5 nm). Besides the spherical particles, a few elongated forms (or slabs) are also present, as indicated in Figure 12. By

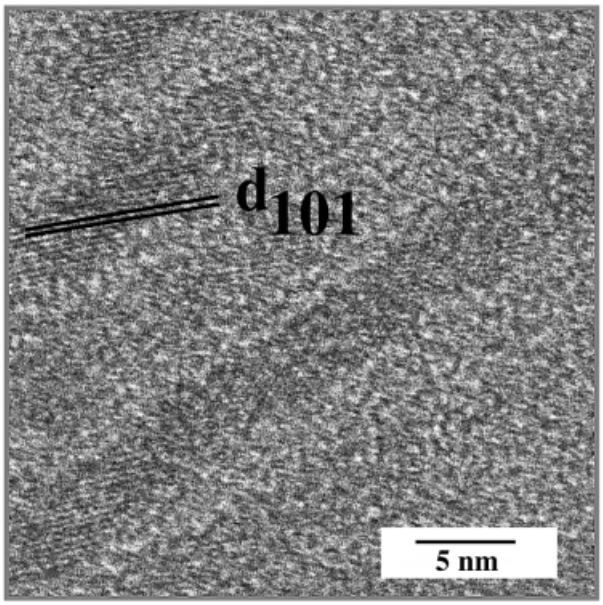


Figure 11. Elongated nanocrystals made with TPA; HRTEM showing no corrugated sides but relatively sharp edges corresponding to flat [100] surfaces

comparison with sample E, this experiment shows the importance of stirring with regard to the size distribution of particles.

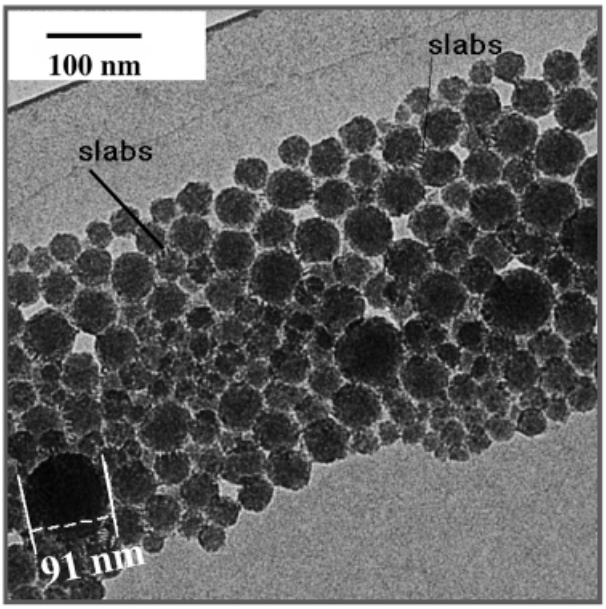


Figure 12. Overview of nanocrystals obtained without continuous stirring; in addition to the wide distribution of sizes, some slabs are observed (arrows), which seem to bridge or to interact with neighboring spherical nanocrystals

Figure 13 shows particles of sample I, made using the same procedure as in the case of sample E but with titanium tetrabutoxide Ti(O*n*Bu)$_4$ as the titanium source in butanol. The particles are almost spherical in shape and display a very narrow size distribution, having a mean diameter of about 7 nm. In this overall view of the particles, some small organized domains can be observed. However, no long-range order is apparent. The difference in size and shape of the particles compared to those in sample E can be attributed to the nature of the alkoxide groups.

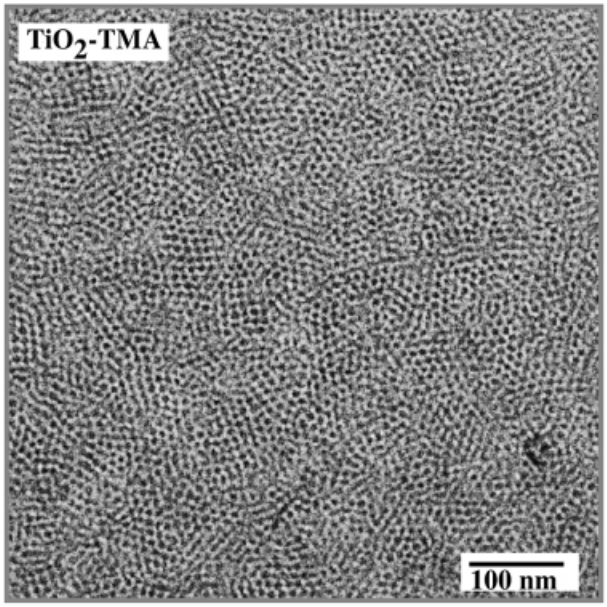


Figure 13. A new type of nanocrystal is obtained with titanium tetrabutoxide in butanol; monodisperity is achieved but the nanocrystals are smaller compared to those in sample E

Sample J was prepared using a 10-fold more concentrated titanium alkoxide solution. The condensation products are titania fibres or slabs of uniform width (7.5 ± 1 Å). However, polydispersity in slab length is in evidence ($1 < L < 18$ nm), as can be seen in Figure 14.

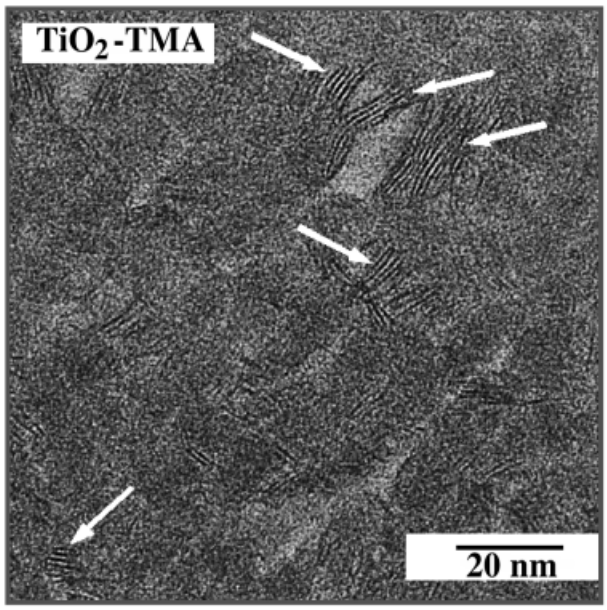


Figure 14. A further increase in titanium concentration leads to the formation of longer and relatively stable slabs, or of polymers with a polydispersity in length; the same width is observed for all polymers

Discussion

As far as we are aware, the work reported herein represents the first incidence of the tailoring of the morphologies of titania nanocrystals with the anatase crystal structure under homogeneous conditions by variation of the hydrolysis conditions and control of the hydrothermal treatment. In this approach, relatively high concentrations of the alkoxide [$Ti(OR)_4$] are used. The hydrolysis is performed in the presence of excess water and a base is employed to catalyze the complete hydrolysis of all OR groups. The effects of unhydrolyzed OR groups on the condensation pathway or on the structure of the primary polycondensed species are therefore avoided. Moreover, hydrolysis and condensation are not separated due to the high titanium concentrations.[17] This methodology leads to a totally new type of clusters and nanocrystals, exhibiting exclusively the anatase crystal structure, with stabilization by tetramethylammonium cations (Me_4N^+).

The hydrolysis and condensation of titanium alkoxide or titanium cations in solution has been the subject of a great deal of attention.[17,21] Particularly relevant to the present results is the theoretical work based on the partial charge model by Henry and Livage, developed to understand and predict inorganic polymerization in the case of transition metal oxide precursors,[21] as well as the work by Bradley on the hydrolysis of titanium alkoxides in the presence of a base.[22] According to these authors, the presence of a base influences the condensation by favouring the formation of the highly nucleophilic TiO^-. This reactive condensation precursor reacts with the positively charged titanium, leading to the formation of polymeric materials.[17]

In the case of a highly dilute alcoholic solution of the alkoxide, the overall hydrolysis reaction after the addition of excess water can be written as:

$$Ti(OR)_4 + 4\ H_2O \rightarrow Ti(OH)_4 + 4\ ROH \quad (a)$$

However, at the high titanium concentrations used in the present study, it is difficult to separate the hydrolysis (Equation a) and condensation (Equation b) processes. These two primary processes are accelerated by the presence of Me_4NOH as a result of the formation of the highly nucleophilic TiO^- according to Equation c. The cation also plays a role in preventing further condensation and stabilizing condensed species according to Equation d.

$$Ti{-}OH + XO{-}Ti \rightarrow Ti{-}O{-}Ti + XOH\ (X = H, R) \quad (b)$$
$$Ti{-}OH + Me_4NOH \rightarrow Ti{-}O^- + Me_4N^+ + H_2O \quad (c)$$
$$Ti_xO_yH_z + Me_4NOH \rightarrow (Ti_xO_yH_{z-1})Me_4N + H_2O \quad (d)$$

The Me_4NOH concentration will also determine the x and y values and therefore the size of the condensed species. According to refs.[17][22] reaction according to Equation c leads to polymers, which is consistent with the formation of stable polymeric material in Figure 14, or of slabs in Figure 7b. In terms of the partial charge model,[21] the formation and stabilization of a totally new type of clusters, slabs, polymers, or nanocrystals, exhibiting exclusively the anatase crystal structure, can be explained by considering a condensation process dominated by an olation pathway, which is seemingly favoured under the present experimental conditions.[17][21] It is generally accepted that early in the condensation process, the coordination number of titanium changes from 4 to 6, and that the basic building unit in the polymerization process is an octahedral arrangement of six oxygen atoms around a titanium centre.[17][21] These octahedra link together by sharing edges, so as to form dimers. According to the partial charge model, these dimers condense to form skewed chains as a result of olation processes, as illustrated in Figure 15.[21] In the presence of Me_4N^+, the condensed species can be stabilized allowing their isolation, or may be forced to condense into larger particles by further heat treatment. In the early stages of condensation, the linear growth (polymerization) leads to skewed chains,[21] which corresponds to growth in the [001] direction of the anatase phase (main stem). Then, through an oxolation process, the nuclei can grow in one of the two equivalent directions.[21] The shape of the particle will be determined by the difference in growth velocities in the [101] and [001] directions, as indicated in Figure 5. At low concentrations of Me_4N^+, growth is favoured in the the [101] direction (Figure 1), while at high concentrations the growth velocity is favoured in the [001] direction (Figure 4). Therefore, the shape of nanocrystals can be fine-tuned by changing the ratio Ti/Me_4NOH, denoted as R.

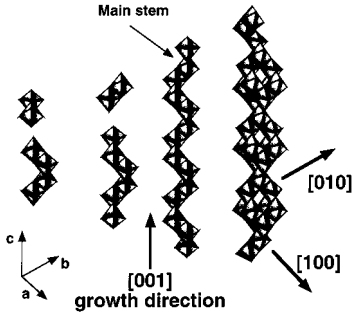


Figure 15. Model to explain condensation and growth of titania anatase; the mode of linking dimers imposes restriction on the growth direction leading to *cis*-skewed chains (main stem) and this is favoured by the physicochemical conditions of the present reaction; [100] and [010] are the first branching directions; then, depending on the organic cation present and its concentration, the secondary branching can be parallel to [101] or can remain parallel to [100] and [010]

The HRTEM micrograph shown in Figure 4b and the illustration in Figure 5 relate to titania nanocrystals where the [101] and [010] are the predominant surfaces. The corrugated sides are due to oscillatory repetition of [1 0 1] and [1 0 −1]. In terms of the mechanism discussed above, the main stem of the nanocrystal is seemingly in the [001] direction. The [100] and [010] directions are equivalent in the case of the anatase crystal phase, and both can be primary branching directions. Sample B, heat-treated for only 2 h, was found to contain small slabs and very thin elongated particles in the [001] crystallographic direction; in Figure 1 nanocrystals also show stepped [101] surfaces. The surface steps are of a height equivalent to the cluster size. Growth

will take place by the building-up of these steps so as to form new cluster layers, and the rate of this process will depend on the concentration of Me_4N^+. The crystal surface in contact with the building units can be influenced by Me_4N^+. This cation seems to interact preferentially with the [101] surface, leading to the favoured development of these surfaces, as shown in Figures 4b.

The decomposition of Me_4N^+ at higher temperatures and pressures leads to surface reconstruction and further growth. The structural features observed on the surface, such as steps, corrugated sides, and sharp edges are, in fact, stabilized by Me_4N^+. However, no corrugated sides or steps are observed in the presence of $(C_5H_{11})_4N^+$ cations (Figure 11). The [100] surfaces of the particles are relatively flat. The observed effect of cation size on nanocrystal shape can be explained in terms of the role of the cations during the early stages of condensation, and thereafter during the crystal growth. Preliminary attempts to stabilize smaller clusters by replacing Me_4N^+ with $(C_5H_{11})_4N^+$ were not successful.

The Me_4N^+-stabilized clusters are able to self-assemble to form nanocrystals, which can be identically replicated in unlimited quantities provided that vigorous stirring of the solution is maintained during the hydrothermal reaction (see Figure 9, and to some extent Figures 10 and 13 as well). Without stirring, a wide size distribution is generally obtained, as shown in Figure 12, where arrows indicate the additional presence of slabs. In fact, the monodispersity of the primary clusters determines the monodispersity of the intermediate nanocrystals formed by a self-assembling process and, therefore, the formation of the superlattice observed in Figures 9 and 10. These results clearly indicate the construction of a superlattice in 3 steps. This was called a progressive condensation process in our preliminary report.[23] The overall process first involves the formation of the monodispersed primary building units. Secondly, they self-assemble into nanocrystals with a diameter of 13.5 nm. Finally, these nanocrystals are made to self-assemble in a uniform manner to form a superlattice. These clusters and nanocrystals are negatively charged and their electrostatic repulsion accounts for the stability of the solutions inasmuch as it prevents flocculation. On the other hand, these interactions and the monodispersity are responsible for the long-range ordering observed after evaporation of the solvent (Figure 10). The charged titania nanocrystals are aligned in a periodic array, rather like in a crystal.[24]

The very broad peaks seen in Figure 2d and the preliminary EXAFS experiments performed on our samples, particularly on sample E, are indicative of the anatase crystal structure.[25] The structural changes observed after an additional heat-treatment of E to make F clearly indicate a further condensation among a few nanocrystals to form slabs, with the *cis*-skewed chains being characteristic of the anatase crystal phase. Further structural information could be gleaned from the XRD pattern of cluster films prepared by simple deposition of solution E onto a silicon wafer followed by drying in air (Figure 2d). A similar procedure was used to obtain TEM measurements, where one drop of the solution was applied to a carbon film. A series of peaks at low angular range with the spacings 16.56 Å, 8.3 Å, and 5.53 Å was observed, attributable to [001], [002], and [003] reflections, respectively, of a spacing of 16.56 Å. These XRD data suggest that the clusters are arranged inside the nanocrystal such as to form a layered structure. Packing of this type has been observed in the case of colloidal nanosheets made from exfoliated titanate. The exfoliation/reassembly process in the presence of tetrabutylammonium hydroxide Bu_4N^+ leads to a comparable XRD pattern.[26] In both cases, drying of the aggregate leads to textured films, in which reflections are suppressed due to the preferred orientation of the nanosheets or, in this case, clusters or slabs. The thickness of the nanosheets is 7.5 Å, which is comparable to the thickness of the slabs (sample F), while their lateral dimension is in the range 0.3−1 μm.[26] Figure 10 shows nanocrystals composed of slabs disposed parallel to one another with a repeating distance of about 16 ± 1 Å. This distance falls within the range of the spacings estimated from the XRD pattern of sample F, which is analogous to Figure 2d.

The observed stepped surfaces in Figures 1 and 4b give indications of a cluster-cluster growth of titania anatase nanocrystals, especially the corrugated sides observed in the case of sample B. According to XRD, these particles are already formed at the reflux stage, i.e. in solution. In the case of samples C and D, particles are seen to be composed of aggregated small slabs at low magnification, which subsequently coalesce into elongated particles also having corrugated sides (Figure 8) like those of sample B grown in solution (Figure 4). This direct observation suggests that a cluster-cluster growth takes place in solution. The coalescence process that takes place under the electron beam still has to be carefully investigated.

The nature of the intermediate nanocrystals observed in Figure 9 proved to be sensitive to the OR group of the alkoxide. Figure 13 shows smaller nanocrystals formed when titanium tetrabutoxide in butanol was used (particle diameter ca. 8−9 nm). The difference in size, and probably in the internal structure as well, highlights the importance of the OR group in the hydrolysis and condensation processes.

The ordering observed in Figure 9 is due to electrostatic interactions between the multiply charged titanium polyanions and the Me_4N^+ cations and leads to intermediate nanocrystals. In turn, through inter-nanocrystal interactions, these form a long-range ordered array, comparable to arrays of pores typically observed in mesophases. In the case of polysilicates, the self-assembly process can be accompanied by a condensation-polymerization process, leading to the formation of three-dimensionally structured arrays, which are stable even after calcination.[27,28]

The present synthetic technique furnishes titania clusters of various sizes and shapes in solution. These clusters may be used to grow transparent thin films, allowing control over both the orientation of superlattices and that of individual nanocrystals. The exact internal structure of the superlattice still has to be determined, and this will be addressed once single crystals are obtained. However, EXAFS

results, XRD, HRTEM, and elemental analysis indicate the presence of anatase clusters and Me_4N^+ cations. Optical measurements and X-ray photoelectron spectroscopy (XPS) indicate dramatic changes in the electronic properties of the titania nanocrystals according to their size and shape.[25]

Conclusion

We have presented a new method for preparing titania nanocrystals with exclusively the anatase crystal structure. Small titania clusters or polytitanate anions have been prepared and stabilized in solution for the first time. Cluster-cluster growth has been shown to take place, leading to larger nanocrystals. The growth can be influenced by controlling the hydrolysis and condensation with Me_4NOH. There is an apparent preference for interaction between [101] surfaces and Me_4N^+, which would account for the differential growth velocities in the [101] and [001] directions. The monodispersity of the negatively charged clusters renders them suitable for the progressive formation of titania/Me_4N^+ superlattices. Thin-film growth allows control over the orientations of superlattices, individual nanocrystals, and individual clusters. The polycondensation and growth processes observed and discussed in this study are in accordance with theoretical predictions. These new results should motivate further investigations of titania and polytitanates in solution.

Experimental Section

General: All hydrolysis reactions were conducted in air, whereas the refluxing of solutions was carried out under argon.

Chemicals: All chemicals used were analytical grade or of the highest purity available and were used as purchased. 2-Propanol and butanol from Merck; titanium isopropoxide $Ti(OiPr)_4$ and butoxide $Ti(OnBu)_4$ from Aldrich, and tetramethylammonium hydroxide Me_4NOH and tetrapentylammonium hydroxide $(C_5H_{11})_4NOH$ from Fluka.

Synthesis of TiO_2 Clusters and Nanocrystallites: A 250-mL three-necked flask was placed in a large crystallizing dish on top of a magnetic stirrer, and the side necks were fitted with a thermometer and a gas inlet tube. A magnetic stirrer bar and 150 mL of aqueous Me_4NOH solution were placed in the flask and the crystallizing dish was filled with ice. When the temperature of the Me_4NOH solution had reached 2°C, a solution of 0.333 mL of titanium isopropoxide in 10 mL of 2-propanol was added dropwise by means of a dropping funnel (1 drop/s) while the mixture was stirred vigorously. During the course of the addition, a white precipitate formed. After the addition was complete, the mixture was left to stand for 10 min, then the ice bath was replaced by a heating mantle, and the mixture was heated. On refluxing, the precipitate dissolved after about 3 h, but after 6 h the solution became slightly turbid once more (sample A).

Sample B was prepared according to the same procedure, but using different concentrations (see Table 1); the mixture became slightly turbid only after all the titanium alkoxide solution had been added (about 5 min). In this case, aliquots were withdrawn from the refluxing solution after 2 h and 6 h in order to carry out TEM observations.

Aliquots of solutions A and B (8 mL each) were heat-treated in a titanium autoclave at 175 and 200°C for a period of 5 h under a saturated vapor pressure of water (about 2500 kPa) in a titanium-coated reactor.

For the preparation of all other samples, the procedure adopted was similar to that described above, except that the titanium alkoxide solution was added in a single portion rather than dropwise to the Me_4NOH solution (see Table 1).

Table 1. Stoichiometry of the reactions

Sample	$Ti(OR)_4$ x µmol[a]	Me_4NOH y µmol[a]	Reflux [h]	Temperature [°C]
A	1.14	0.26	6	90−100
B	1.14	0.82	6	90−100
C	1.14	0.57	6	90−100
D	1.14	1.09	6	90−100
E	1.14	1.36	6	90−100
F	1.14	1.42	7	90−100
G	1.14[b]	1.17	6	90−100
H	1.14	1.36	13 d	50−60
I	1.06[b]	1.42	6	90−100
J	11.4	11.6	6	90−100

[a] x µmol of titanium isopropoxide in 10 mL of 2-propanol, y µmol of Me_4NOH in 150 mL of water. − [b] Sample G was prepared with tetrapentylammonium hydroxide (TPA) and sample I with titanium tetrabutoxide in butanol. Sample H was left for 13 d without stirring.

Elemental Analysis of Sample E was carried out commercially at the microanalytical laboratory Pascher in Remagen-Bahndorf, Germany. Elemental analysis of powder E, dried at room temperature in air: C 18.22, H 5.5, N 4.9, O 42.87, Ti 33.3. The composition can be roughly written as $Ti_4O_{15}[N(CH_3)_4]_2H_{12}$.

Film Growth: The samples were prepared by depositing freshly prepared solutions on a silicon [100] wafer or on glass. In some cases, the solutions were first concentrated in a rotary evaporator prior to deposition in order to accelerate thick-film processing. Optically transparent films of ordered titania nanocrystals could be prepared by controlling the rate of evaporation of the solvent. Slow evaporation leads to thin film growth, which allows orientation of the superlattice and of the individual layered structures. Such deposition on solid substrates produces ordered and oriented films.

The titania clusters and nanocrystals were investigated with a Philips CM12 transmission electron microscope. Samples were prepared by placing a drop of the freshly prepared nanocrystal solution on a carbon film supported on a Cu grid. The advantages of investigating crystal growth in the case of nanocrystals is that the specimens are already thin to the point of electron transparency, and are thus readily amenable to TEM examination. High resolution is quite easily achieved nowadays and image processing is straightforward, allowing a stimulating interplay between synthesis and TEM observation.[19] A careful analysis of the micrographs can provide unique periodical and morphological information to aid in the understanding of the effects of additives on crystal growth. The NIH image-processing program was used to enhance the data obtained from some samples.

X-ray Powder Diffraction and Small-Angle X-ray Scattering were carried out with a Siemens D500/5000 diffractometer, operating with a Cu anode at 45 kV and 30 mA. A secondary graphite monochromator was used to select the K_a1 and K_a2 lines.

Acknowledgments

The authors are indebted to U. Bloeck and D. Su for technical assistance in obtaining TEM images, and to K. Diesner for performing the XRD experiments.

[1] A. Fujishima, K. Honda, *Nature* **1972**, *238*, 37−38.
[2] A. Fujishima, K. Kohayakawa, K. Honda, *J. Electrochem. Soc.* **1975**, *122*, 1487−1489.
[3] B. Kraeutler, A. J. Bard, *J. Am. Chem. Soc.* **1978**, *100*, 5985−5992; A. Chemseddine, H. P. Boehm, *J. Mol. Catal.* **1990**, *60*, 295−311.
[4] B. O. Regan, M. Graetzel, *Nature* **1991**, *353*, 737−739.
[5] C. G. Granqvist, *Handbook of Inorganic Electrochromic Materials*, Elsevier Science, Amsterdam, **1995**.
[6] R. Wang, K. Hashimoto, A. Fujishima, *Nature* **1997**, *388*, 431−432.
[7] A. Chemseddine, H. Jungblut, S. Boulmaaz, *J. Phys. Chem.* **1996**, *100*, 12546−12551.
[8] A. Chemseddine, M. L. Fearheily, *Thin Solid Films* **1994**, *247*, 3−7.
[9] R. D. Andres, R. S. Averback, W. L. Brown, L. E. Brus, W. A. Goddard, A. Kaldo, S. G. Louie, M. Moscovits, P. S. Peercy, S. J. Riley, S. J. Siegel, F. Spaepen, Y. Wang, *J. Mater. Res.* **1989**, *4*, 704−736.
[10] J. Augustynski, J. Hinden, C. Stalder, *J. Electrochem. Soc.* **1977**, *124*, 1063−1064; Y. Takahashi, A. Ogiso, R. Tomodo, K. Sugiyama, H. Minoura, M. Tsuiki, *J. Chem. Soc., Faraday Trans.* **1982**, *78*, 2563−2571.
[11] A. Chemseddine, H. Weller, *Ber. Bunsen Ges. Phys. Chem.* **1993**, *97*, 636−637; A. Chemseddine, *Chem. Phys. Lett.* **1993**, *216*, 265−269; T. Vossmeyer, L. Katsikas, M. Giersig, I. G. Popovic, K. Diesner, A. Chemseddine, A. Eychmüller, H. Weller, *J. Phys. Chem.* **1994**, *98*, 7665−7673.
[12] R. L. Whetten, J. T. Khoury, M. M. Alvarez, S. Murthy, I. Vezmar, Z. L. Wang, P. W. Stephens, C. L. Cleveland, W. D. Luedtke, U. Landman, *Adv. Mater.* **1995**, *8*, 428−433.
[13] A. Chemseddine, *Mat. Res. Soc. Symp. Proc.* **1994**, *346*, 881−886.
[14] A. Chemseddine, M. Fieber-Erdmann, E. Holub-Krappe, S. Boulmaaz, *Z. Phys. D* **1997**, *40*, 566−569.
[15] D. C. Bradley, R. C. Mehrotra, D. P. Gaur, *Metal Alkoxides*, Academic Press, London, **1978**.
[16] V. W. Day, T. A. Eberspacher, Y. Chen, J. Hao, W. G. Klemperer, *Inorg. Chim. Acta* **1995**, *229*, 391−405.
[17] J. Livage, M. Henry, C. Sanchez, *Prog. Solid State Chem.* **1988**, *18*, 259−341.
[18] M. S. Whittingham, J. Li, J. D. Guo, P. Zavalij, *Mater. Sci. Forum* **1994**, *152−153*, 99−108.
[19] R. Sinclair, *MRS Bulletin* **1994**, (June), 26−30.
[20] S. Ijima, *J. Electron Microsc.* **1985**, *34*, 249−265.
[21] M. Henry, J. P. Jolivet, J. Livage, *Struct. Bonding (Berlin)* **1992**, *77*, 155−206.
[22] D. C. Bradley, *Adv. Chem.* **1959**, *23*, 10−17.
[23] T. Moritz, J. Reiss, K. Diesner, D. Su, A. Chemseddine, *J. Phys. Chem. B* **1997**, *101*, 8052−8053.
[24] P. Pieranski, *Contemp. Phys.* **1983**, *24*, 25−73.
[25] A. Chemseddine, D. Tonti, M. Fieber-Erdmann, unpublished results.
[26] [26a] T. Sasaki, M. Watanabe, H. Hashizume, H. Yamada, H. Nakazawa, *J. Chem. Soc., Chem. Commun.* **1996**, 229−230. − [26b] T. Sasaki, M. Watanabe, H. Hashizume, H. Yamada, H. Nakazawa, *J. Am. Chem. Soc.* **1996**, *118*, 8325−8335. − [26c] T. Sasaki, M. Watanabe, *J. Phys. Chem. B* **1997**, *101*, 10159−10161.
[27] A. Firouzi, D. Kumar, L. M. Bull, T. Besier, P. Sieger, Q. Huo, S. A. Walker, J. A. Zasadzinski, C. Glinka, J. Nicol, D. Margolese, G. D. Stucky, B. F. Chmelka, *Science* **1995**, *267*, 1138−1143.
[28] A. Corma, *Chem. Rev.* **1997**, *97*, 2373−2419.

Received August 20, 1998
[I98288]

Electrochemical and Ozone Oxidation of $(CF_3)_3B \cdot NH_3$: Formation and Characterization of Products with Nondegradated $(CF_3)_3B$ Groups

David J. Brauer,[a] Hans Bürger,*[a] Yonas Chebude,[a] and Gottfried Pawelke[a]

Keywords: Boron / Fluorine / Oxidation / Nitrogen / Molecular structures

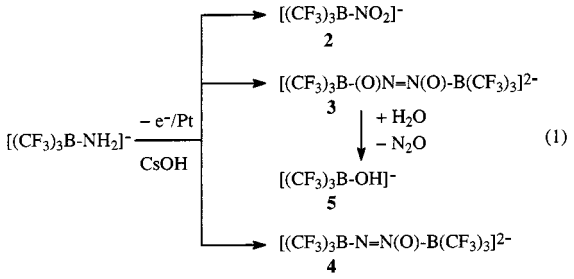
$(CF_3)_3B \cdot NH_3$ (**1**) has been oxidized in aqueous solution using a platinum anode. At pH = 8–9 in $CsOH/Cs_2CO_3$ solution $Cs[(CF_3)_3B–NO_2]$ (**2**), $Cs_2[(CF_3)_3B–N(O)=N(O)–B(CF_3)_3]$ (**3**) and $Cs_2[(CF_3)_3B–N=N(O)–B(CF_3)_3]$ (**4**) are formed. Compound **3** slowly hydrolyses to yield the hydroxyborate $Cs[(CF_3)_3B–OH]$ (**5**). Compound **2** and traces of **3** and **5** were also formed by oxidation of **1** or $(CF_3)_3B \cdot NHEt_2$ with ozone. The constitution of the novel borates has been deduced from multinuclear NMR, IR and mass spectra. The structures of **2**–**5** have been investigated by single-crystal X-ray diffraction.

Introduction

Homoleptic, donor-free (perfluoroalkyl)boranes, e. g. $(R_f)_3B$ (R_f = CF_3, C_2F_5, ...), are still unknown in spite of considerable efforts made in the past towards their synthesis.[1] The simplest species tris(trifluoromethyl)borane, $(CF_3)_3B$, is expected to readily decompose under elimination of difluorocarbene and formation of BF_3. However, various amine adducts of $(CF_3)_3B$ are accessible, and they have been shown to be amazingly stable.[2a–2d] As a result of the presumed high Lewis acidity of the $(CF_3)_3B$ moiety and despite its relative bulkiness, the B–N bond in amine–tris(trifluoromethyl)boranes is thermodynamically extraordinarily strong. Attempts to selectively cleave this bond have failed so far. Such amine–boranes withstand e. g. concentrated hydrochloric acid as well as concentrated solutions of KOH. SbF_5 or superacids like $HSbF_6/HF$ react at 10°C with e. g. $(CF_3)_3B \cdot NHEt_2$ with cleavage of the B–N bond and formation of BF_3, perfluoropropene or HCF_3. Since the isolation of the donor-free tris(trifluoromethyl)-borane remains a challenge, we have focused our continuing interest on the synthesis of alternative promising precursor molecules. We decided to start from ammine–tris-(trifluoromethyl)borane, $(CF_3)_3B \cdot NH_3$ (**1**), the synthesis of which has been improved.[3] We hoped that oxidation of its nitrogen atom might favor low-temperature B–N cleavage reactions.

Results

Ammine–tris(trifluoromethyl)borane (**1**) is a hygroscopic compound which forms a crystalline tetrahydrate when exposed to moist air. Dissolved in water it is a weak acid with a pK_a = 5 and behaves like an ammonium cation. Attempts to electrochemically oxidize the nitrogen atom on platinum anodes in acidic solution failed, only H_2 and O_2 being evolved. On raising the pH to 8–9, the nitrogen atom in **1** is deprotonated to form the aminotris(trifluoromethyl)borate anion $[(CF_3)_3B–NH_2]^-$. In view of planned X-ray crystal studies a $CsOH/Cs_2CO_3$ mixture was used to adjust the pH to 8.5 because cesium salts of the oxidation products were expected to crystallize well. Under these alkaline conditions the nitrogen atom was found to be readily oxidized at a 4.5 V potential difference between electrodes. The progress of the oxidation was monitored by measurement of ^{19}F-NMR spectra of the solution. The electrolysis was interrupted every two hours in order to isolate the insoluble, colorless material which accumulated on the anode and at the bottom of the cell. Work-up of the precipitated material revealed that it consisted mainly of a mixture of cesium azodioxybis[tris(trifluoromethyl)borate] $Cs_2[(CF_3)_3B–N(O)=N(O)–B(CF_3)_3]$ (**3**) and cesium azoxybis[tris(trifluoromethyl)borate] $Cs_2[(CF_3)_3B–N=N(O)–B(CF_3)_3]$ (**4**) (Equation 1).



(1)

The main product of the anodic oxidation, however, was the nitroborate $Cs[(CF_3)_3B–NO_2]$ (**2**) which precipitated when the concentrated solution was cooled to 4°C. Concentration of the solution to dryness gave a residue which contained substantial quantities of $Cs[(CF_3)_3B–OH]$ (**5**). Besides these main products, which according to ^{19}F-NMR spectra account for 95% of all formed from **1**, several other (trifluoromethyl)borates were detected. These include compounds with either three or two CF_3 groups attached to the boron atom. However, separation and characterization of these species failed.

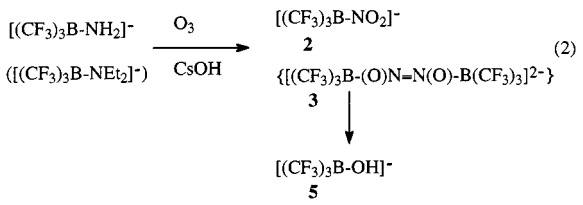
The origin of **5** became apparent from a study of the hydrolysis of **3**. This compound slowly reacts with water at

[a] Anorganische Chemie, FB 9, Universität-GH, D-42097 Wuppertal, Germany

 © WILEY-VCH Verlag GmbH, D-69451 Weinheim, 1999 1434–1948/99/0202–0247 $ 17.50+.50/0

room temperature − the elimination of N_2O, which was confirmed by IR spectroscopy, and formation of **5** being completed within one week. We are sure that this pathway accounts for all of **5** produced.

Besides the electrochemical oxidation, attempts were also undertaken to oxidize compound **1** chemically. The results of such oxidation reactions will be reported later, but one case is mentioned here. Ozone reacts readily with **1** in cesium hydroxide solution to form **2** and **5** in a ratio of 7:2. Moreover, we found that $(CF_3)_3B\cdot NHEt_2$, the precursor molecule for **1**, is also directly converted into similar quantities of **2** and **5** (Equation 2). The fate of the *N*-ethyl groups has not yet been elucidated.



(2)

Spectra and Properties

The NMR chemical shifts and coupling constants of **2**−**5** are set out in Table 1 and are consistent with the proposed structures. For **3** and one of the $B(CF_3)_3$ groups of **4** the resonances of the CF_3 groups were not found in the ^{13}C-NMR spectra due to quadrupolar broadening by the boron nucleus.

Table 1. NMR-spectral data for **2**−**5**

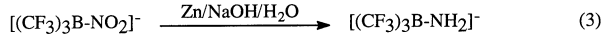
Compound	**2**	**3**	**4**	**5**
^{1}H NMR				
δ(OH)				2.1
^{19}F NMR				
δ(CF_3)	−64.8	−59.6	−60.7	−68.0
^2J(BF)	28.5		25.9	26.8
δ(CF_3)			−63.0	
^{11}B NMR				
δ(B)	−9.8	−10.3	−13.0	−10.6
^2J(BF)	28.5		25.9	26.7
δ(B)			−10.8	
^{13}C NMR				
δ(C)	130.1		134.1	134.7
^1J(BC)	82.0		75.7	75.8
^1J(CF)	301.6		309.2	311.4
^3J(CF)				ca. 2.7
δ(C)			131.2	
^{14}N NMR				
δ(N)	42			

Infrared and Raman spectra of **2**−**5** were recorded. All of these novel borates contain a $(CF_3)_3B-X$ (X = N, O) moiety, the vibrational frequencies of which fall into well-defined ranges. First the bands in the range of 1300−1280 cm^{-1} and 1140−1060 cm^{-1} are assigned to ν(CF_3) vibrations which are associated with very strong infrared absorptions but medium to weak Raman lines. Then, the $\delta_s(CF_3)$ mode is found at ca. 720 and 690 cm^{-1} where the former mode appears as a strong Raman line and the latter as a medium to strong infrared band. Near 500 cm^{-1} $\delta_{as}(CF_3)$ features with medium infrared and weak Raman intensity occur while ρ(CF_3) is associated with weak infrared bands and medium to strong Raman lines at 350−280 cm^{-1}. The BC_3 and B−X stretching vibrations are strongly coupled and may be assigned to several infrared bands between 950 and 860 cm^{-1} showing $^{10/11}$B isotopic patterns. Compound **2** has an NO_2 group, which exhibits characteristic frequencies. Thus, the infrared bands/Raman lines [cm^{-1}] were assigned as follows: 1471 vs/1484 m (ν_{as} NO_2), 1400 w/1400 vs (ν_s NO_2), 795 s/797 s (δ_s NO_2), 595 m/− (δ_{op} BNO_2). Compound **3** has *trans* configuration with C_i symmetry in the crystal. Consequently, backbone vibrations which occur in characteristic ranges obey the mutual exclusion principle of the infrared and Raman frequencies. These vibrations were assigned to infrared bands/Raman lines [cm^{-1}] at: −/1415 vs (ν NN), −/1125 m (ν NO i.p.), 685 −/m (δ NNO), ca. 1100 s/− (ν NO o.p.), 620 s/− (δ NNO). Compound **4** has strongly coupled N−N and N−O stretching vibrations which were assigned to infrared bands/Raman lines [cm^{-1}] at 1511 m/1514 m (ν NN) and 1258 vs/1265 m (ν NO). The N−N−O bending mode is associated with features in the IR and Raman spectrum at 800 m/805 w cm^{-1}. The O−H stretching and B−O−H bending vibrations of **5** were unambiguously assigned to IR bands at 3650 and 1520 cm^{-1}.

The molecular masses of **2** and **5** were determined by ESI/neg. spectra (CH_3CN + 10% H_2O). Compound **2** showed the peak of the anion $[(CF_3)_3B-NO_2]^-$, 100%, and the cluster peak $[Cs[(CF_3)_3B-NO_2]_2]^-$, 10%, whereas **5** gave only the anion peak $[(CF_3)_3B-OH]^-$, 100%.

The cesium borates **2**−**5** are colorless solids. Their approximate decomposition temperatures determined thermogravimetrically are 260°C (**2**), 80°C (**3**), 190°C (**4**), and 150°C (**5**). Because the decomposition of **3** is violent, reliable elemental analyses were difficult to obtain.

Compound **2** is stable towards acids like HCl, H_3PO_4, or H_2SO_4. Dissolved in neat CF_3SO_3H **2** reacts within 1 d under elimination of difluorocarbene. This subsequently inserts into the O−H bond to form the ester $CF_3SO_2OCF_2H$, which was identified by its NMR spectra. Reaction of **2** with ethereal HCl forms the sublimable ether adduct $(CF_3)_3B-NO_2H \times Et_2O$. The latter is hydrolyzed by moist air to form what appears to be a pentahydrate **2a** $(CF_3)_3B-NO_2H \times 5\ H_2O$. Titration of **2a** revealed a pK_a of ca. 1.9 and a molecular mass of 359 g/mol which is in line with a pentahydrate (355.93 g/mol), while elemental analyses were in agreement both with a penta- or a hexahydrate. Compound **2a** is stable at room temperature and decomposes according to thermogravimetric experiments at 75°C without leaving any residue. Compound **2** reacts with zinc in aqueous KOH to form **1** (Equation 3) and it is reduced by sodium amalgam in ether to form, according to NMR spectra, a mixture of **3** and **4** (Equation 4).



(3)

$$[(CF_3)_3B\text{-}NO_2]^- \xrightarrow{Na/Hg} \begin{matrix}[(CF_3)_3B\text{-}N(O)\text{=}N(O)\text{-}B(CF_3)_3]^{2-} \\ + \\ [(CF_3)_3B\text{-}N\text{=}N(O)\text{-}B(CF_3)_3]^{2-}\end{matrix} \quad (4)$$

We were unable to isolate **3** and **4** from this reduction because the ethereal solutions decomposed violently upon concentration. This might be ascribed to precipitation of the salts $Na_2[(CF_3)_3B-N(O)=N(O)-B(CF_3)_3]$ and $Na_2[(CF_3)_3B-N=N(O)-B(CF_3)_3]$ from this sodium-rich system. Such salts might be thermally less stable than their cesium counterparts; that is, small cations are stronger Lewis acids than Cs^+ and tend to abstract fluoride from the CF_3 groups. This is underscored by the rather low decomposition temperature of $Li[(CF_3)_3B-NO_2]$, 70°C, compared with that of $Cs[(CF_3)_3B-NO_2]$, 260°C.

Only little information on the chemical properties of **3** and **4** has been gathered. We have no evidence for an equilibrium $[(CF_3)_3B-N(O)=N(O)-B(CF_3)_3]^{2-} \rightleftarrows 2\,[(CF_3)_3B-N=O]^-$ which is known to exist for aliphatic nitroso compounds. Since monomers of the latter compounds are intensely colored whereas solutions of **3** are colorless, any such equilibrium for **3** must be shifted far to the left. The protonation of **5** has been investigated in more detail. Upon treatment with ethereal HCl, protonation and formation of a sublimable ether adduct $(CF_3)_3B-OH_2 \times Et_2O$, which is analogous to compound **2**, was observed. The ether is readily replaced by water on contact with moist air to form an oily product which, according to thermogravimetric analysis, is a pentahydrate **5a**. This behaves as an acid, with a pK_a of 1.6, and is thermally stable up to 70°C.

Discussion

Hydroxyborate anions of the general formula $[R_3BOH]^-$ with R = F,[4] H,[5] CH_3,[6] C_6H_5[7] are well known, and compound **5** might be regarded as a further homologue with R = CF_3. Unlike **5**, such anions for R = alkyl or aryl are only stable under alkaline conditions, and species with R = F or H are of limited thermal and kinetic stability which decompose upon protonation. Compounds **2**, **3** and **4** have, to our knowledge, no real counterparts in boron chemistry. The formation of the $[F_3BNO_2]^-$ anion in solution has been reported.[8] This anion, only characterized by ^{19}F-NMR spectra, was found prone to disproportionation into $[BF_4]^-$ and $[F_2B(NO_2)_2]^-$. The stability of **2** towards dissociation gives an impression of the Lewis acid strength of illusive free $(CF_3)_3B$.

Borate ions with $N_2O_2^{2-}$ or N_2O^{2-} as coordinating ligands as revealed in **3** and **4** are unknown whereas a Lewis acid/base complex with SO_3, $[O-N=N(O)-SO_3]^{2-}$, has been characterized. The latter anion is formed when NO is introduced into an alkaline SO_3^{2-} solution,[9] and the structure of the ammonium salt has been determined.[10] This salt hydrolyses slowly in water to form SO_4^{2-} and N_2O, and experiments with ^{15}N-labeled material proved that the hyponitrite anion is an intermediate.[11] Therefore the slow hydrolysis of **3** with elimination of N_2O and formation of **5** is in line with the behavior of $[O-N=N(O)-SO_3]^{2-}$.

The stability of the $(CF_3)_3BN$ skeleton towards oxidation is remarkable. This results in part from the steric bulk of three CF_3 groups, which efficiently shield the boron atom, the boron−carbon bonds as well as the boron−nitrogen bond in **1**, **2**, and **4**. In the course of the oxidation reactions, the nitrogen atom changes its oxidation state in alkaline solution from −3 in **1** over "average" ±0 in **4** to +1 in **3** and finally to +3 in **2**. One of the oxidizing reagents that is able to accomplish this oxidation is ozone. Its oxidation strength in alkaline solution is clearly larger than is that of hydrogen peroxide; for example, the standard reduction potential for the half reaction $O_3 + H_2O + 2e^- \rightarrow O_2 + 2OH^-$, +1.24 V, is much larger than for $HO_2^- + H_2O + 2e^- \rightarrow 3OH^-$, +0.87 V. Whereas O_3 readily oxidizes **1** to **2**, concentrated H_2O_2 in alkaline solution is unable to perform an oxidation. Apparently, the lower limit for oxidation of **1** in alkaline solution must lie between +0.87 V and +1.24 V; so in the absence of kinetic hindrance, any other reagent with standard reduction potentials higher than +1.24 V should be able to convert **1** into **2**. Similar to ozone, fluorine reacts in alkaline solution readily with **1** to form **2** whereas in acidic solution only water is oxidized. The oxidation of $Cs[(CF_3)_3B-NH_2]$ in acetonitrile has been studied by cyclic voltammetry. The anion is irreversibly oxidized at a potential against an Ag reference electrode of ca. 1.82 V which is close to the limit dictated by the acetonitrile solvent. This high potential might explain why XeF_2 failed to react with $Cs[(CF_3)_3B-NH_2]$ in acetonitrile.

The oxidation of **1**, which leads ultimately to the formation of a nitro group, resembles the oxidation of aniline to nitrobenzene which also can be performed with ozone[12] or electrochemically.[13] Diazene bis(oxides) R−N(O)=N(O)−R (azodioxy compounds) or diazene *N*-oxides R−N=N(O)−R (azoxy compounds) with R = alkyl, aryl are also formed both by oxidation or reduction of precursor molecules. For example *cyclo*-C_6H_{11}−(O)N=N(O)−*cyclo*-C_6H_{11} is formed from *cyclo*-$C_6H_{11}NH_2$ using peracetic acid[14] while $C_6H_5-N=N(O)-C_6H_5$ is obtained by reduction of nitrobenzene with Zn[15] or Pb.[16] On the other hand azoxybenzene is prepared more conveniently by oxidation of aniline with a mixture of hydrogen peroxide and acetonitrile.[17] In this respect compound **1** behaves like an ammonium cation which is deprotonated in alkaline solution to form an "amine" before it is oxidized. Consequently, compounds **2**, **3** and **4** correspond to a nitroalkane, a diazene bis(oxide) and a diazene *N*-oxide, respectively, bearing overall negative charges.

Crystal Structures

In the anion of **2** (Figure 1) the nitro group is coplanar with the boron atom to within 0.002 Å. Despite the sp^2 hybridization of the nitrogen atom, the B−N bond length [1.606(4) Å] is more typical for a linkage of a $B(CF_3)_3$ group to an sp^3-hybridized nitrogen atom such as in $(CF_3)_3B \cdot NH_3$, 1.595(8) Å,[2d] than to an sp^2-hybridized nitrogen

atom such as in $(CF_3)_3B \cdot NHCHNMe_2$, 1.541(4) Å.[2d] Similarly, an average distance between a nitro group and a quaternary carbon atom is given as 1.533(13) Å,[18] which compares well with the C−N distance reported for the *tert*-butylammonium cation, 1.506(3) Å.[19] The average value of the B−C bond length in **2**, 1.618(10) Å, is normal, as are the respective averages of the C−B−C and N−B−C bond angles, 111.5(8) and 107.4(14)°. The small but significant spread in these angles [1.5(4) and 2.7(4)°, respectively] results in part from the mismatch in the symmetries of the $B(CF_3)_3$ (C_{3v}) and BNO_2 (C_{2v}) groups. Thus, the symmetry of the anion can not exceed C_s, and the magnitude of the O(2)−N−B−C(2) torsion angle, 19.6(5)°, shows that the structure is even less symmetric.

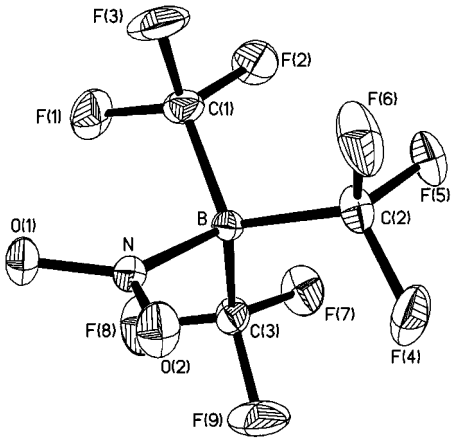


Figure 1. A perspective drawing of the $[(CF_3)_3BNO_2]^-$ anion with 20% probability thermal ellipsoids

While all atoms of **3** occupy general positions in the crystal, the midpoint of the N−N bond of the anion (Figure 2) lies on an inversion center. The $B_2N_2O_2$ fragment is planar to within 0.004 Å, and the N−N′ and N−O bond lengths of 1.30(2) and 1.30(1) Å, respectively, indicate delocalized π bonding in the azodioxy anion. These atom distances agree to within experimental error with the corresponding values for the azodioxysulfonate $[O-N=N(O)-SO_3]^{2-}$.[10] In **3** the B−N bond length is 1.59(2) Å, and the B−N−N′ angle [123(1)°] is significantly larger than the B−N−O angle [117(1)°].

In crystals of **4**, the two crystallographically unique Cs cations as well as the B(1), B(2), C(2), C(4), F(5) and F(10) atoms of the anion (Figure 3) lie on a crystallographic mirror plane. Since the azoxy group is oriented perpendicular to this plane, the positions of its atoms are disordered. A further consequence of this disorder is that the locations found for the $B(CF_3)_3$ groups are superpositions of two distinct orientations; for example, the C_3 axis of the $B(CF_3)_3$ group of the B(1) atom will either lie along the B(1)−N(2) or B(1)−N(2′) directions − the angle between these C_3 axes being 33.7(9)°. Therefore the atom distances and angles in this structure should not be taken too seriously although the agreement factors (Table 2) are acceptable. The N(1)−N(2) bond length [1.25(1) Å] should not be prejudiced by the disorder, and this value does not differ significantly from that of the analogous linkage in *p*-azoxyanisole, 1.218(5) Å.[20]

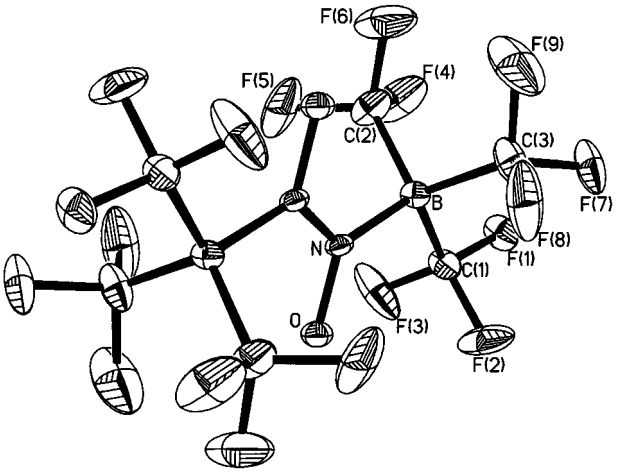


Figure 2. A perspective drawing of the $[(CF_3)_3B-N(O)=N(O)-B(CF_3)_3]^{2-}$ anion with 20% probability thermal ellipsoids

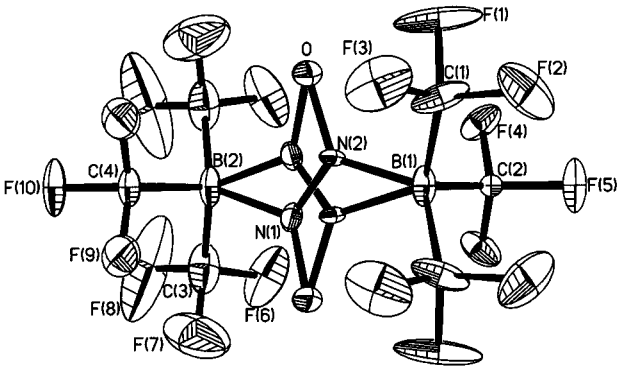


Figure 3. A perspective drawing of the $[(CF_3)_3B-N=N(O)-B(CF_3)_3]^{2-}$ anion with 20% probability thermal ellipsoids showing the disorder of the azoxy group

Crystals of **5** contain the cations Cs(1) and Cs(2) in C_3 and S_6 symmetry sites, respectively, while the H, O, B, C(2) and F(4) atoms of the anion (Figure 4) lie on a mirror plane. The B−O bond length of 1.447(7) Å falls in the range, 1.432(3)−1.465(3) Å, found for hydroxyborates bearing two boron-bonded trifluoromethyl substituents.[21] In **5** the average B−C bond length, 1.617(6) Å, is in excellent agreement with that found in **2**. While the length determined for the O−H bond, 0.76(7) Å, is obviously too short, the B−O−H angle albeit imprecise seems to be acceptable, 109(5)°. No interionic hydrogen bonding is present since no oxygen or fluorine atom in a neighboring ion lies within 2.50 Å of the hydrogen atom even after extension of the O−H bond to 0.973 Å. The hydrogen atom lies in the plane which bisects the C(1)−B−C(1′) angle. The latter angle, 111.7(6)°, is larger than its C(1)−B−C(2) counterpart, 108.0(3)°. Furthermore, the O−B−C(1) angle, 111.4(3)°, is markedly larger than O−B−C(2), 106.1(4)°. Thus, significant deviations from C_{3v} symmetry are apparent at the boron atom, and although they correlate with the orientation of the hydroxy group, they may well have resulted from packing forces.

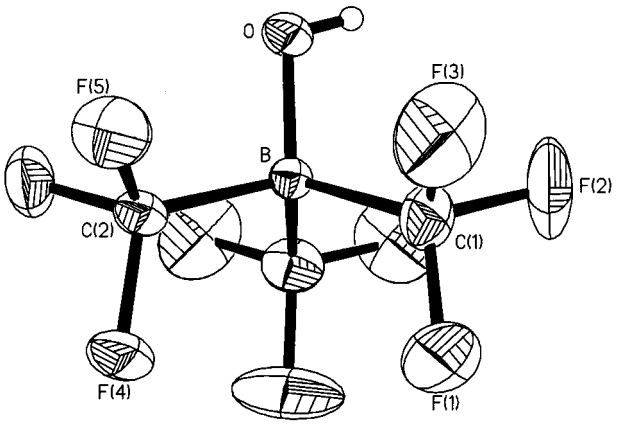


Figure 4. A perspective drawing of the $[(CF_3)_3BOH]^-$ anion with 20% probability thermal ellipsoids for the nonhydrogen atoms

The coordination polyhedra of the cesium cations in **2**−**5** are mostly irregular. The shortest Cs−O and Cs−F contacts are 3.054(9) and 3.049(5) Å, respectively, and most cations form between four and eight contacts shorter than 3.25 Å. If all contacts with oxygen and fluorine atoms which are less than 3.80 Å are counted, then the cation coordination numbers are 12 in **3** and **5** (both cases) and 14 in **2** and **4** (both cases). High coordination numbers imply low bonding strength for the cations,[22] and these weakly acidic centers are apparently well matched to the weakly basic CF_3 donors. The condensation of the coordination polyhedra in **5** is particularly fascinating. First, coordination spheres of the Cs(1) cations are bridged across their O_3 faces to dimers which possess crystallographic C_{3h} symmetry (Figure 5). This bridging gives rise to a Cs−Cs distance [4.616(2) Å], which is shorter than the 5.25 Å value found in the metal. Second, the symmetry of the complexation of the Cs(2) cation is higher (S_6); that is, it is surrounded by two interpenetrating trigonal antiprisms of fluorine atoms. These polyhedra are fused along F_3 faces to form infinite chains of C_3 symmetry parallel to the *c* axis (Figure 6). However, the interactions which bridge the Cs(2) cations [Cs(2)−F(4), 3.518(2) Å] are much longer and weaker than those which link the Cs(1) cations to dimers [Cs(1)−O, 3.182(3) Å]; as a result, the Cs(2)−Cs(2) separations along the chain are much longer, 6.180(2) Å, than the Cs(1)−Cs(1) contacts in the dimers. In addition to the long bridging distances, the other contacts involving the second cation [Cs(2)−F(1), 3.546(6) Å] are also relatively long. Indeed the cavity enclosed by the Cs(2) coordination polyhedron is large enough to allow marked rattling of the cation. Thus, the equivalent isotropic temperature factor of the Cs(2) cation, 0.0881(3) $Å^2$, is much larger than is that of Cs(1), 0.0559 $Å^2$, and is in fact the largest of all cations studied.

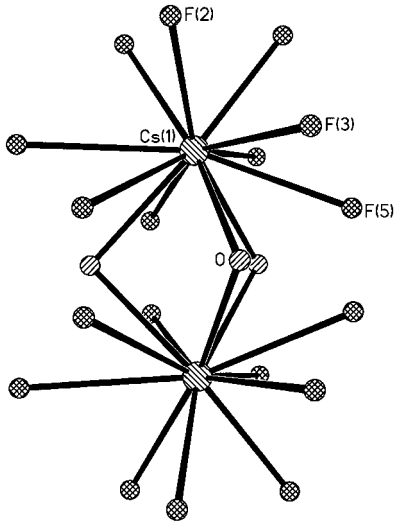


Figure 5. A perspective drawing of a Cs(1) dimer in **5** with atoms not bonded to Cs(1) omitted; selected bond lengths in [Å]: Cs(1)−O 3.182(3), Cs(1)−F(2) 3.131(4), Cs(1)−F(3) 3.599(6), Cs(1)−F(5) 3.440(4)

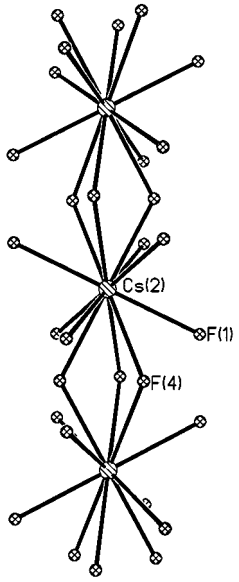


Figure 6. A perspective view of a segment of the infinite Cs(2) chain in **5** with atoms not bonded to Cs(2) omitted; selected distances in [Å]: Cs(2)−F(1) 3.546(6), Cs(2)−F(4) 3.518(2)

Experimental Section

General: NMR: Bruker ARX 400 (400 MHz, 100.6 MHz and 376.5 MHz, for ^1H, ^{13}C and ^{19}F, respectively), Bruker AC 250 (79.8 MHz for ^{11}B). [D_3]acetonitrile as solvent and internal standard ^1H: δ_H = 1.95, ^{13}C: δ_C = 1.30, ^{19}F: external standard $CFCl_3$, ^{11}B: external standard $BF_3 \cdot OEt_2$. − IR: Bruker IFS 25. − Raman: Cary 82 Kr^+ 647.1 nm. − MS: Varian MAT 311 (70 eV). − Thermogravimetry: Mettler TA4000. − Ozone Generator: Fischer 501.

X-ray Crystallographic Studies: Crystals were glued to glass fibers and transferred to a Siemens P3 diffractometer, which was equipped with a graphite monochromator. Intensities were determined from the profiles of the θ-2θ scans and corrected either by integration (**2**, **4** and **5**) or empirically (**3**) for absorption. The structures of **2**, **3** and **5** were solved by direct methods − the hydrogen atom of **5** being located with a difference Fourier synthesis and refined freely. In order to avoid unreasonable geometries for the CF_3 groups of **3**, C_3 restraints were applied to these groups with the C−F bond length and intra-group F···F contact being refined. The heavy-atom method was used to develop the structure of **4** −

Table 2. Crystal data for **2**−**5**

Compound	**2**	**3**	**4**	**5**
Formula	$C_3BCsF_9NO_2$	$C_6B_2Cs_2F_{18}N_2O_2$	$C_6B_2Cs_2F_{18}N_2O$	C_3HBCsF_9O
Mr	396.76	761.52	745.52	367.76
Crystal system	Triclinic	Monoclinic	Orthorhombic	Hexagonal
Space group	$P\bar{1}$	$P2_1/n$	$Cmc2_1$	$P6_3/m$
a [Å]	6.4439(8)	7.3960(10)	7.556(2)	11.365(3)
b [Å]	7.8042(8)	15.241(2)	6.938(5)	11.365(3)
c [Å]	9.7989(13)	9.1755(14)	14.284(3)	12.360(5)
α [°]	91.594(10)	90	90	90
β [°]	97.469(10)	112.651(11)	90	90
γ [°]	91.665(9)	90	90	120
Z	2	2	4	6
D(calcd.) [g cm^{-3}]	2.699	2.650	2.709	2.650
T [K]	294(2)	295(2)	295(2)	294(2)
λ [Å]	0.71073	1.54184	0.71073	0.71073
θ range [°]	2.10−30.08	5.81−57.15	2.40−25.02	2.07−30.05
Index ranges	$-9 \le h \le 9$	$0 \le h \le 8$	$-8 \le h \le 8$	$0 \le h \le 16$
	$-10 \le k \le 10$	$0 \le k \le 16$	$0 \le k \le 20$	$-16 \le k \le 13$
	$0 \le l \le 13$	$-9 \le l \le 9$	$-17 \le l \le 17$	$-17 \le l \le 0$
Reflections collected	3008	1396	2958	4621
unique	2856	1284	1735	1417
R (int)	0.0248	0.0291	0.0303	0.0216
observed [$I > 2\sigma(I)$]	2568	1011	1684	1041
μ(λ) [mm^{-1}]	3.921	31.543	4.166	4.130
Crystal size [mm]	0.40 × 0.14 × 0.09	0.18 × 0.06 × 0.04	0.50 × 0.21 × 0.16	0.60 × 0.14 × 0.14
Transmission	0.5428−0.7363	0.1900−0.6331	0.4126−0.5624	0.5281−0.5904
Parameters	154	148	166	78
S on F^2	1.021	1.017	1.051	1.088
*R*1 (*F*, observed)	0.0290	0.0537	0.0350	0.0371
*wR*2 (F^2, all data)	0.0821	0.1420	0.0890	0.1117
Final Δ*F* [e Å^{-3}]	0.849 to −0.557	1.728 to −1.395	0.726 to −0.612	1.383 to −0.636

the NNO group being disordered over the mirror plane. Treatment of the structure as a pseudo-merohedral twin space group *Cc*, twinning plane (100)] gave comparable final residuals but poor convergence; thus, the disordered model in $Cmc2_1$ will be presented here. The absolute structure parameter for **4**, 0.02(5), implies that the polarity of the *c* axis has been chosen correctly. An extinction correction was only necessary for **3**. The structures were solved, refined and illustrated with the SHELXTL program package. Additional crystal data are given in Table 2. Further details of the crystal-structure investigations may be obtained from the Fachinformationszentrum Karlsruhe, D-76344 Eggenstein-Leopoldshafen, Germany, on quoting the depository numbers CSD-410079, -410078, -410077, and -410076 for **2**, **3**, **4** and **5**, respectively.

Preparation of Compounds: Cesium Tris(trifluoromethyl)nitroborate (2), Cesium Azodioxybis[tris(trifluoromethyl)borate] (3), Cesium Azoxybis[tris(trifluoromethyl)borate] (4), Cesium Tris(trifluoromethyl)hydroxyborate (5): $(CF_3)_3B \cdot NH_3 \times 4\ H_2O$ was prepared from $(CF_3)_3B \cdot NHEt_2$ according to ref.[3] 10 g ($33 \cdot 10^{-3}$ mol) of $(CF_3)_3B \cdot NH_3 \times 4\ H_2O$, 20 g ($61 \cdot 10^{-3}$ mol) of Cs_2CO_3 and 10 g ($60 \cdot 10^{-3}$ mol) of $CsOH \times H_2O$ were dissolved in 300 mL of water. This mixture was electrolyzed at 4.5 V/0.15 A for ca. 2 h using platinum net electrodes (DEGUSSA 303, diameter 35 mm, height 50 mm). Compounds **3** and **4**, which are poorly soluble in water, accumulated at the bottom of the reaction vessel as well as on the anode and were isolated and dried. The electrolysis was then continued until all starting material was consumed as indicated by ^{19}F-NMR spectroscopy. The solution was concentrated and upon cooling in an ice bath most of compound **2** precipitated (plates). After all of **2** had been isolated (ca. 50%), the mother liquor was concentrated in vacuo and the residue stirred with dry acetonitrile. The slurry was filtered, and the filtrate slowly concentrated until **5** crystallized (needles) (ca. 5%).

Separation of 3 and 4: When the mixture of **3** and **4**, dissolved in dry acetonitrile at 20°C, was cooled to −30°C, most of **3** crystallized (ca. 10%). After stripping off the acetonitrile, the residue **4** was recrystallized from methanol/acetone (yield ca. 24%).

Compounds **2** and **5** were formed by oxidation of $(CF_3)_3B \cdot NH_3 \times 4\ H_2O$ or $(CF_3)_3B{\cdot}NHEt_2$ in CsOH solution in a flow of ozone/oxygen in a ratio of 7:2. In a typical experiment $20 \cdot 10^{-3}$ mol of reactant was mixed with 50 mL 25% CsOH solution and a flow of ozone/oxygen (ca. 2 g O_3/h) was introduced into the stirred reaction mixture at 20°C through a Teflon PFA tube. The progress of the reaction was monitored by running ^{19}F-NMR spectra from the solution. In case of $(CF_3)_3B \cdot NHEt_2$, which is only slightly soluble in CsOH solution, the reaction was stopped when a clear solution was obtained. Work-up and separation as described above yielded ca. 65% of **2**. − **2:** $C_3BCsF_9NO_2$ (396.74): calcd. C 9.08, N 3.53; found C 9.0 N, 3.8. − **3:** $C_6B_2Cs_2F_{18}N_2O_2$ (761.48): calcd. C 9.46, N 3.68, F 44.91; found C 9.4, N 3.6, F 46.4. − **4:** $C_6B_2Cs_2F_{18}N_2O$ (745.48): calcd. C 9.67, N 3.76, F 45.87; found C 9.6, N 3.6, F 44.4. − **5:** C_3HBCsF_9O (367.74): calcd. C 9.80, H 0.27; found C 9.3, H 0.3.

Protonation of 2 and 5: To a stirred suspension of $12 \cdot 10^{-3}$ mol (4 g) of **2** in 20 mL of diethyl ether, 5 mL of 1 M ethereal HCl was added dropwise at 20°C. The reaction mixture was stirred for 20 min and the CsCl formed removed by filtration in air. Ether and HCl were removed in vacuo at 0.1 mbar/20°C and **2a** was purified by repeated sublimation at 60°C/10^{-2} mbar, yield 2.7 g (85%). Compound **5** was analogously protonated to yield 88% of **5a**. − MS (70 eV); *m/z*(%): **2a:** 99 (100) [CBF_4^+], 69 (78) [CF_3^+], 81 (36) [$C_2F_3^+$], 47 (13) [HNO_2^+], 246 (11) [$M^+ - F$]; **5a:** 66 (100) [F_2BOH^+], 46 (57) [FBO^+], 96 (20) [CF_3BO^+], 108 (16) [$C_2F_3BO^+$], 216 (16) [$M^+ - HF$]. − IR film: **2a**: $\tilde{\nu}$ = 3669 cm^{-1} (OH), 1624

δ(NOH), 1479 (NO), 1397(NO), 1282 (CF), 1080−1150 (CF_3), 939, 917 (BC_3), 794 $\delta_s(NO_2)$, 718, 707, 700 $\delta_s(CF_3)$, 598 $\delta_{op}(BNO_2)$, 525 $\delta_{as}(CF_3)$; **5a**: $\tilde{\nu}$ = 3664 cm^{-1} (OH), 1666, 1612 δ(BOH), 1273 (CF_3), 1105 (CF_3), 887 (BC_3), 682 $\delta_s(CF_3)$. − **2a:** ^1H NMR (CD_2Cl_2): δ = 7.8. − ^{19}F NMR (CD_2Cl_2): δ = −66.4. − **5a:** ^1H NMR ([D_3]acetonitrile): δ = 6.0. − ^{19}F NMR ([D_3]acetonitrile): δ = −68.0. − **2a:** $C_3H_{13}BF_9NO_8$ (372.93): calcd. C 9.66, H 3.51, N 3.76; $C_3H_{11}BF_9NO_7$ (354.92): calcd. C 10.15, H 3.12, N 3.95; found C 10.89, H 3.42, N 3.73. − **5a:** $C_3H_{12}BF_9O_6$ (325.92): calcd. C 11.06, H 3.71, found C 11.39, H 3.48.

Reduction of 2 to 1: To a stirred solution of $5 \cdot 10^{-3}$ mol (2 g) of **2** in 20 mL of water and 2 mL of 50% CsOH, 0.5 g of Zn powder was added at 60°C. The reaction mixture was stirred for 2 h, filtered, the filtrate concentrated to dryness and **1** extracted with acetonitrile.

Acknowledgments

We thank Dr. D. Stöckigt of the Max-Planck-Institut für Kohlenforschung, Mülheim/Ruhr, for recording the ESI mass spectra and Dr. R. Winter of the Institut für Anorganische Chemie, University of Stuttgart, for measurements. Financial support by the DAAD to Y. C. and by the Fonds der Chemischen Industrie is gratefully acknowledged.

[1] G. Pawelke, H. Bürger, *Applied Organomet. Chem.* **1996**, *10*, 147−174.
[2] [2a] G. Pawelke, *J. Fluorine Chem.* **1989**, *42*, 429−433. − [2b] D. J. Brauer, H. Bürger, F. Dörrenbach, B. Krumm, G. Pawelke, W. Weuter, *J. Organomet. Chem.* **1990**, *385*, 161−172. − [2c] A. Ansorge, D. J. Brauer, H. Bürger, F. Dörrenbach, B. Krumm, G. Pawelke, *Z. Naturforsch.* **1992**, *47b*, 772−782. − [2d] A. Ansorge, D. J. Brauer, H. Bürger, B. Krumm, G. Pawelke, *J. Organomet. Chem.* **1993**, *446*, 25−35.
[3] G. Pawelke, *J. Fluorine Chem.* **1995**, *73*, 51−55.
[4] N. N. Greenwood, R. L. Martin, *Qt. Revs.* **1954**, *8*, 1−39.
[5] J. Goubeau, H. Kallfass, *Z. Anorg. Allgem. Chem.* **1959**, *299*, 160−169.
[6] S. R. Sandler, W. Karo, *Organic Functional Group Preparations*, Academic Press Inc., San Diego, **1986**, vol. 12-II, pp. 456, 414, **1983**, vol. 12-I, p. 498.
[6] J. Goubeau, J. W. Ewers, *Z. Phys. Chem.* **1960**, *25*, 276−282.
[7] D. L. Fowler, C. A. Kraus, *J. Am. Chem. Soc.* **1940**, *62*, 1143−1144.
[8] S. Brownstein, G. Latremouille, *Can. J. Chem.* **1978**, *56*, 2764−2767.
[9] R. S. Drago, *Inorg. Synth.* **1957**, *5*, 117−122.
[10] G. A. Jeffrey, H. P. Stadler, *J. Chem. Soc.* **1951**, 1467−1474.
[11] K. Clusius, H. Schumacher, *Helv. Chim. Acta* **1957**, *40*, 1137−1144.
[12] E. Keinan, Y. Mazur, *J. Org. Chem.* **1977**, *42*, 844−847.
[13] Y. Takahashi, M. Tokuda, M. Itoh, A. Suzuki, *Synthesis* **1976**, 616−618.
[14] W. D. Emmons, *J. Am. Chem. Soc.* **1957**, *79*, 6522−6524.
[15] H. I. Bolker, F. L. Kung, *J. Chem. Soc. C* **1969**, 2298−2304.
[16] J. A. Azoo, J. Grimshaw, *J. Chem. Soc. C* **1968**, 2403−2405.
[17] [17a] G. B. Payne, P. H. Deming, P. H. Williams, *J. Org. Chem.* **1961**, *26*, 659−663. − [17b] F. D. Popp, A. Catala, *Tetrahedron Lett.* **1962**, 1071−1072.
[18] F. H. Allen, O. Kennard, D. G. Watson, L. Brammer, A. G. Orpen, R. Taylor, *J. Chem. Soc., Perkin Trans. 2* **1987**, 1−19.
[19] I. Goldberg, *Acta Crystallogr.* **1975**, *B31*, 2592−2600.
[20] W. R. Krigbaum, Y. Chatani, P. G. Barber, *Acta Crystallogr.* **1970**, *B26*, 97−102.
[21] A. Ansorge, D. J. Brauer, H. Bürger, T. Hagen, G. Pawelke, *J. Organomet. Chem.* **1994**, *467*, 1−11.
[22] I. D. Brown, *Acta Crystallogr.* **1997**, *B53*, 381−393.

Received September 21, 1998
[I98321]

New Azoniaboratacyclopropanes from $(F_3C)_2BNMe_2$ and Diazomethane Derivatives – Structure of *cyclo*-$(F_3C)_2B–CPh_2–NMe_2$ and $HOB(CF_3)_2–CHC_6F_5–NHMe_2$

David J. Brauer,[a] Hans Bürger,*[a] Silke Buchheim-Spiegel,[a] and Gottfried Pawelke[a]

Dedicated to Professor H. D. Lutz on the occasion of his 65th birthday

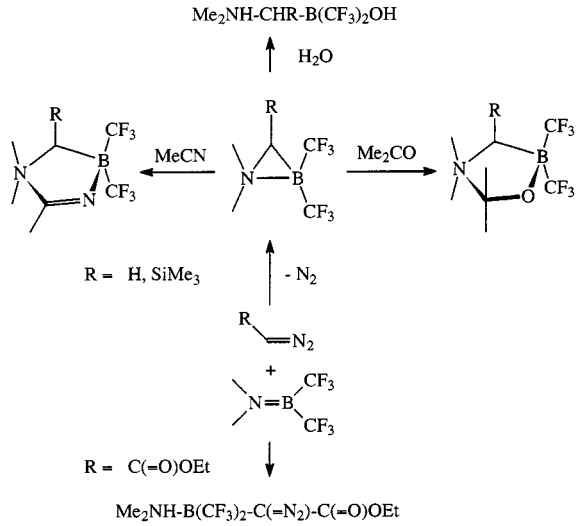
Keywords: Boron / Small rings / Trifluoromethyl group / Crystal structure

1,1-Dimethyl-2,2-bis(trifluoromethyl)azoniaboratacyclopropanes, *cyclo*-$(F_3C)_2B–CR^1R^2–NMe_2$ [$R^1 = R^2 = C_6H_5$ (**2a**); $R^1/R^2 = C_{12}H_8$ (**2b**); R^1 = H, $R^2 = C_6H_5$ (**2c**), 4-FC_6H_4 (**2d**), 3-FC_6H_4 (**2e**), 2-FC_6H_4 (**2f**), C_6F_5 (**2g**), *i*Pr (**2h**), *t*Bu (**2i**); R^1 = Me, R^2 = C(=O)OMe (**2j**), C(=O)OEt (**2k**)] have been obtained from $(F_3C)_2BNMe_2$ (**1**) and diazomethanes $R^1R^2CN_2$. In contrast to compound **2a**, the B–N bonds of **2b**–**2k** hydrolyze to form the zwitterionic species $Me_2NH–CR^1R^2–B(CF_3)_2OH$ (**3b**–**3k**). The diazoacetic acid esters $HC(N_2)C(=O)OMe$ and $HC(N_2)C(=O)OtBu$ react with **1** to form three-membered rings, which hydrolyze rapidly to form $Me_2NH–CR^1R^2–B(CF_3)_2OH$ [R^1 = H, R^2 = C(=O)OMe (**3l**), C(=O)O*t*Bu (**3m**)]. F_3CSiF_3 reacts under elimination of CF_2 with **1** to form the acyclic derivative $(F_3C)_2BF–CF=NMe_2$ (**4**). The structures of **2a** and **3g** have been investigated crystallographically. A nearly eclipsed conformation is found for the central B–C bond of **3g**, which is 0.097(7) Å longer than the B–C bond length in the three-membered ring of **2a**.

(Dimethylamino)bis(trifluoromethyl)borane, $(F_3C)_2BNMe_2$ (**1**), possesses chemical properties that are unique in aminoborane chemistry.[1] Owing to a balance of pronounced electrophilic character and steric protection of the boron atom, the reactivity of its strong B=N bond bears a degree of resemblance to an olefinic C=C bond. On the other hand its polarity is related to that of a C=N bond in a dimethyliminium cation. In a preceding paper we reported on reactions of diazomethane derivatives with **1**.[2] While diazomethane itself, trimethylsilyldiazomethane and trimethylsilyl(benzyl)diazomethane formed novel heterocyclopropane derivatives, diazoacetic acid ethyl ester underwent an ene-type reaction to form an extraordinary stable, borylated diazomethane species (Scheme 1). In contrast to the B−N bond in dimethylamine−bis(trifluoromethyl)boranes, $R(F_3C)_2B \cdot NMe_2H$, which is not only stable to dissociation but also to displacement reactions at room temperature, the B−N bond in the azoniaboratacyclopropanes, which are formed from reactions of **1** with diazomethane or trimethylsilydiazomethane, is rather reactive.

Thus, water cleaves their B−N bonds to form $Me_2NH–CHR–B(CF_3)_2OH$ while nitriles like H_3CCN or carbonyl compounds like acetone insert into the B−N bond to yield the five-membered heterocycles *cyclo*-$Me_2N–CHR–B(CF_3)_2N=CMe$ and *cyclo*-$Me_2N–CHR–B(CF_3)_2O–CMe_2$, respectively.[3] On the other hand *cyclo*-$(F_3C)_2B–C(SiMe_3)(CH_2C_6H_5)–NMe_2$ was far less reactive than the other three-membered rings.

The reasons for the varying reactivity were not fully understood, and there were questions left unanswered: (1) What is the influence of the substituents R^1 and R^2 on the formation, reactivity and stability of azoniaboratacyclopropanes? (2) Can other potential carbene sources (e. g., F_3CSiF_3) be used to form such three-membered rings? (3) Will diazoacetic acid esters other than $HC(N_2)C(=O)OEt$ also enter into ene-type reactions or will they form three-membered rings? Here we report on our results.



Scheme 1. Diazomethane derivatives and (dimethylamino)bis(trifluoromethyl)borane

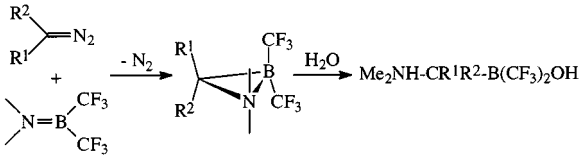
Results

The reactivity of compound **1** towards many solvents and reagents prohibits in situ generation of diazomethanes. Furthermore the diazomethanes must be accessible as neat ma-

[a] Anorganische Chemie, FB 9, Universität-GH, D-42097 Wuppertal, Germany
E-mail: buerger1@wrcs3.urz.uni-wuppertal.de

 © WILEY-VCH Verlag GmbH, D-69451 Weinheim, 1999 1434−1948/99/0202−0255 $ 17.50+.50/0

terial in high purity. These demands limit the number of possible candidates to a small number of stable, isolable diazomethanes. Of these candidates, $R^1R^2CN_2$, those with R^1 and R^2 as defined in Scheme 2 were prepared and dissolved in dry pentane. Compound **1** was condensed onto these frozen solutions at −196°C. Upon warming decolorization and evolution of nitrogen was observed as soon as **1** melted and mixed with the diazomethane solutions.



	R^1	R^2	
2a	C_6H_5	C_6H_5	
2b		$C_{12}H_8$	**3b**
2c	H	C_6H_5	**3c**
2d	H	*4*-FC_6H_4	**3d**
2e	H	*3*-FC_6H_4	**3e**
2f	H	*2*-FC_6H_4	**3f**
2g	H	C_6F_5	**3g**
2h	H	*i*-Pr	**3h**
2i	H	*t*-Bu	**3i**
2j	CH_3	C(=O)OMe	**3j**
2k	CH_3	C(=O)OEt	**3k**
	H	C(=O)OMe	**3l**
	H	C(=O)O*t*-Bu	**3m**

Scheme 2. Formation of azoniaboratacyclopropanes and hydrolytic cleavage of their B−N bond

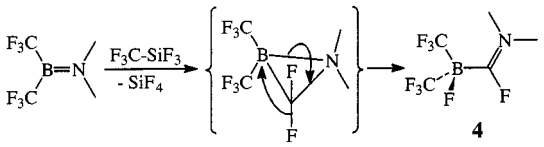
All of the investigated diazomethanes act as carbene sources, and though their reactivity towards **1** varied, no competing reactions were observed. The relatively stable diphenyldiazomethane and fluorenyldiazomethane react less rapidly than the less stable phenyl and alkyldiazomethanes. On the other hand trifluoromethyldiazomethane, F_3CHCN_2, did not react with **1**.

While $HC(N_2)COOEt$ undergoes an ene-type reaction with **1**, the corresponding diazoacetic acid esters $HC(N_2)COOMe$ and $HC(N_2)COOtBu$ reacted differently − three-membered rings were formed with elimination of N_2. Due to their sensitivity towards water, these ring compounds were not isolated in a pure state and therefore are missing in the list of Scheme 2. However, their hydrolysis products **3l** and **3m** were obtained in high yields.

The reactivity of **2a**−**2k** was tested by reaction with water (Scheme 2). Except for compound **2a** all of the three-membered rings hydrolyze within minutes to form the zwitterionic species **3b**−**3m**. Because neat $F_2C{=}N_2$ is difficult to prepare and because all of the diazomethanes tested here reacted as carbene sources, we were interested in testing the reactivity of a suitable difluorocarbene source with compound **1**. Such a difluorocarbene source is trifluoro(trifluoromethyl)silane, F_3CSiF_3, which is known to decompose at 30°C according to Equation 1.[4]

$$F_3C\text{-}SiF_3 \rightarrow \{CF_2\} + SiF_4 \quad (1)$$

Indeed trifluoro(trifluoromethyl)silane reacts rapidly with **1** at −60°C; however, instead of the expected three-membered ring, the acyclic isomer $(F_3C)_2BF{-}CF{=}NMe_2$ (**4**) was obtained (Scheme 3). We assume that difluorocarbene adds primarily to the B=N bond of **1**; however, the three-membered ring is unstable and rearranges by a 1,2-dyotropic shift to form **4**.



Scheme 3. Difluorocarbene and (dimethylamino)bis(trifluoromethyl)borane

Properties and Spectra

Compounds **2a**−**4** are colorless solids. Except for compound **2a** the three-membered heterocycles **2b**−**2k** are sensitive to moisture − their B−N bond being cleaved. At first it is surprising that **2a** is stable to water whereas **2b** hydrolyses readily. In both species two phenyl rings are bonded to the ring carbon atom. However, electronically both groups in the ring are different. Heterolytic breaking of the C−N bond in **2a** and **2b** would generate either a borylated diphenylmethyl (**2a**) or a borylated fluorenyl cation (**2b**). If it is accepted that the diphenylmethyl cation is more stable than the fluorenyl cation and that this is also true for a borylated species, then the $C_{13}H_8$ substituent attracts more electron density from the B−N bond in **2b** than the $C(C_6H_5)_2$ group does in **2a**. Thus, the B−N bond in **2b** is more polar than in **2a** and hence more reactive towards water.

The ^{1}H-, ^{19}F-, ^{11}B- and ^{13}C-NMR spectra of **2a**−**4** were recorded. The shift data which are set out in Table 1 are consistent with the proposed structures, and only a few comments will be necessary. The ^{13}C resonances of the CF_3 groups in **2a**−**2k** are not detectable due to quadrupolar broadening by the boron atom. In **3b**−**4** they appear as extremely broadened signals. Therefore these resonances are not included in Table 1. Compounds **2c**−**2k** and **3c**−**3m** have an asymmetric carbon atom which causes a splitting of the NMR signals of both the $N(CH_3)_2$ and $B(CF_3)_2$ groups. For compound **3g** five ^{19}F and five ^{13}C resonances are found for the pentafluorophenyl ring. This splitting is due to hindered rotation of the ring relative to the NMR time scale which was confirmed by recording the NMR spectra at different temperatures. While **2a**−**2k** show only broad signals for the ring carbon atoms, in the zwitterions **3b**−**3m** the ^{13}C resonances of these carbon atoms appear as 1:1:1:1 quadruplets with ^1J(BC) = 42−51 Hz. The ^{19}F chemical shift of the boron-bonded fluorine atom in **4** occurs at unusually high field, δ = −220.9. This shift is larger than that for $Mes(F_3C)BF{-}CF{=}NMe_2$ [δ(B*F*) = −202.7][5]

Table 1. NMR-spectral data of **2a**−**2k** and **3b**−**4**[a]

	2a	**2b**	**2c**	**2d**	**2e**	**2f**	**2g**	**2h**	**2i**	**2j**	**2k**	**3b**	**3c**	**3d**	**3e**	**3f**	**3g**	**3h**	**3i**	**3j**	**3k**	**3l**	**3m**	**4**
^{1}H																								
δ(NCH_3)	3.00	3.02	2.48 3.04	2.46 3.02	2.51 3.04	2.86 3.03	2.65 3.09	2.77 2.82	2.82 2.91	2.81 2.96	2.85 2.99	2.64	2.59 2.74	2.62 2.77	2.91 3.00	2.88 2.99	2.73 3.02	2.76 2.88	2.88 2.99	2.86 3.10	2.64 2.93	3.16 3.25	2.93 3.08	3.35 3.60
δ(BCH_n)			3.48	3.42	3.44	3.37	3.11	1.82	2.01				3.63	3.66	3.76	4.21	4.03	2.30	2.62			3.62	3.40	
δ(CCH_3)								1.00 1.13	1.17	1.72	1.28 1.75							1.03 1.17	1.17	1.53	1.27 1.46		1.45	
δ(CH_nC)								2.05										2.15						
δ(OCH_n)										3.71	4.20									3.67	4.15	3.64		
δ(C$_6H_n$)	7.25 · 7.45	7.50 · 7.80	7.3 · 7.42	7.07 7.30	7.03 7.08 7.37 7.12 7.37	7.1 · 7.4						7.37 7.47 7.82 7.87	7.49 7.36	7.12 7.56	7.11 7.39 7.45	7.16 7.40 7.93								
δ(NH)												7.2	7.05	7.0	7.68	7.72	7.2	8.4	ca. 8.7	ca. 7.8	ca. 7.2	ca. 8.0	ca. 7.1	
δ(OH)												2.16	1.71	2.2	2.1	2.2	2.30	2.2	ca. 2.3	2.09	ca. 2.2	ca. 2	ca. 1.8	
^{19}F																								
δ(CF_3)	−55.0	−53.8	−55.5 −60.1	−55.5 −60.2	−56.0 −60.7	−56.2 −60.6	−59.6 −60.9	−57.7 −60.5	−53.1 −58.9	−58.2 −60.0	−56.1 −57.5	−65.2	−60.2 −63.7	−66.3 −69.4	−66.1 −69.4	−66.5 −69.6	−69.4 −69.5	−65.1 −68.2	−64.3 −67.3	−64.7 −67.2	−64.9 −66.8	−67.3 −70.7	−65.9 −70.4	−70.5
δ(BF)																								−220.9
δ(=CF)																								−6.6
δ(C$_6F_n$)					−112.3	−112.8	−113.1 −151.6 −161.2	−137.2						−116.3	−115.7	−117.1	−136.2 −143.0 −157.4 −164.8 −165.5							
^{11}B																								
δ(B)	−14.0	−11.6	−15.1	−14.6	−16.8	−16.9	−15.7	−15.5	−17.3	−17.2	−17.1	−6.6	−6.9	−6.8	−8.1	−8.0	−8.0	−9.2	−7.8	−7.4	−7.5	−3.5	−3.5	−4.1
^{13}C																								
δ(NCH$_3$)	45.1	45.2	41.9	41.8	42.0	41.1	41.8	40.1	41.7	42.2	42.7	41.8	41.6	41.6	42.6	42.5	44.4	38.9	ca. 42.5	41.8	42.3	41.7	41.8	40.3
			49.0	48.9	49.1	48.3	48.8	49.2	51.0	45.5	46.0		45.7	45.8	46.8	46.8	47.3	47.8	ca. 48.1	41.9		45.1	44.9	41.0
δ(BC)	69	65	57	56	55.8	50.7	43.6	60.7	65	ca. 55.3	ca. 55.9	75.9	68.7	67.9	69.0	59.1	57.2	70.5	74.7	70.4	70.8	62.6	63.4	ca. 189
δ(CCH$_3$)								20.6 23.9	30.6	15.0	14.1 15.5							21.7 24.7	30.6	11.2	11.5 14.3		27.3	
δ(CCH$_3$)								24.8	33.2									27.3	35.3				81.8	
δ(OCH_n)										52.2	62.2									52.4	62.9	50.7		
δ(C$_6$H$_n$)	127.5 128.5 129.5 139.1	119.8 127.1 128.8 138.3 142.5	128.6 128.8 130.7 131.9	115.6 126.5 133.8 163.0	116.0 118.8 127.7 130.2 133.1 162.6	115.0 118.6 124.5 131.3 134.3 163.4	106.1 137.9 142.0 146.7					120.8 128.0 128.1 129.7 142.8 143.3	128.9 129.2 133.7 134.0	115.6 130.4 135.8 163.8	116.3 120.9 130.5 130.9 138.0 163.8	116.5 122.4 125.1 131.7 135.9 163.5	112.3 138.4 141.4 ca. 146.2 ca. 146.9							
δ(C=O)										171.1	171.4									174.3	174.2	171.4	169.8	

[a] **2a**−**2h**, **2j**, **2k** in $CDCl_3$, **2i** in CD_2Cl_2, **3b**−**3d**, **3g**−**3k**, **3m**, **4** in [D_3]acetonitrile, **3e**, **3f**, **3l** in [D_6]acetone.

which was previously believed to be the upper limit for a fluorine bonded directly to boron.

EI mass-spectral data are set out in Table 2. M^+ peaks are generally weak, but the fragments [$M^+ - CF_3$] and [$M^+ - C_2F_5$] give reliable indications of the molecular mass. The base peak of the three-membered rings **2c**−**2h** is [$(CH_3)_2NCHR^+$], which is less prominent in **2i** due to the instability of the *t*Bu group. In the corresponding hydrolyzed products **3c**−**3h** the fragment [CH_3NHCHR^+] is in general the base peak.

Description of the Crystal Structures of 2a and 3g

The structure of **2a** is shown in Figure 1. The three-membered ring defines a non-crystallographic mirror plane, which is obeyed by the exocyclic bonds to within experimental error and is followed by the angles and the magnitude of the torsion angles to within 4°. The phenyl groups are oriented parallel to the B−N bond and are thus not capable of conjugation with the tangential Walsh ring orbitals.[6]

Several features of the ring geometry deserve comment. Firstly, the B−N bond length [1.568(6) Å] is clearly shorter than those reported between quaternary nitrogen atoms and $(F_3C)_2B$ entities in four-, five- and six-membered rings − all of which exceed 1.61 Å.[7−9] Secondly, the N−C(1) linkage [1.556(5) Å] is markedly longer than the N−CH_3 bonds [av. 1.484(5) Å], but examples of long bonds between quaternary nitrogen and carbon atoms have been registered in five-membered heterocycles involving the $(F_3C)_2B$ group such as *cyclo*-$(F_3C)_2B-NMe_2-CMe_2-S(=O)-O$ [1.543(3) Å[8]] and *cyclo*-$(F_3C)_2B-CH(SiMe_3)-NMe_2-CMe_2-O$ [1.582(4) Å[3]]. In this connection we note that the B−C, B−N and N−C(1) [1.556(5) Å] bond lengths in **2a** agree to within experimental error with the values [1.595(5), 1.560(5) and 1.567(4) Å] found for the corresponding linkages in *cyclo*-$(F_3C)_2B-C(SiMe_3)(CH_2C_6H_5)-NMe_2$ (**5**).[2] Thirdly, the exocyclic substituent planes of the B and C(1) atoms do not bisect the N−B−C(1) and B−C(1)−N angles, respectively, but rather are pivoted away from the bisecting positions by 8.8(5)° and 9.7(5)°, respectively, towards the NMe_2 group. A similar distortion was found in **5**. Fourthly, the bond angles defined at the ring atoms by their two exocyclic substituents average 109.1(8)°, which is similar to the 108.0(3)° value found in **5**. These angles seem small in view of the relatively high s character ascribed to the hybrid orbitals used by a cyclopropyl ring atom in its exocyclic bonds.[10]

A drawing of **3g** is given in Figure 2. The nearly eclipsed conformation about the B−C(3) bond and its great length,

Table 2. EI mass-spectral data for **2a**−**2i** and **3b**−**4**

	m/z (%) [fragment$^+$]
2a	165 (100) [$C_{13}H_9^+$], 74 (43) [$F_2BN(CH_3)_2^+$], 77 (33) [$C_6H_5^+$], 240(31) [$M^+ - C_2F_5$], 91(26) [$C_7H_7^+$], 290(25) [$M^+ - CF_3$], 162(19) [$M^+ - C_2F_5 - C_6H_5$], 359(5) [M^+]
2b	165 (100) [$C_{13}H_9^+$], 91 (15) [$C_7H_7^+$], 74 (12) [$F_2BN(CH_3)_2^+$], 357 (1) [M^+]
2c	134 (100) [$(CH_3)_2NCHC_6H_5^+$], 74 (80) [$F_2BN(CH_3)_2^+$], 42 (77) [CH_3NCH^+], 91 (19) [$C_7H_7^+$], 164 (33) [$M^+ - C_2F_5$], 168 (23) [$C_6H_5BFCFNHCH_3^+$], 77 (17) [$C_6H_5^+$], 214 (15) [$M^+ - CF_3$], 182 (10) [$C_6H_5BFCFN(CH_3)_2^+$], 283 (3) [M^+]
2d	152 (100) [$(CH_3)_2NCHC_6H_4F^+$], 42 (68) [CH_3NCH^+], 74 (60) [$F_2BN(CH_3)_2^+$], 109 (30) [$C_7H_6F^+$], 232 (21) [$M^+ - CF_3$], 182 (15) [$M^+ - C_2F_5$], 301 (3) [M^+]
2e	152 (100) [$(CH_3)_2NCHC_6H_4F^+$], 42 (20) [CH_3NCH^+], 74 (22) [$F_2BN(CH_3)_2^+$], 186 (18) [$FC_6H_4BFCFNHCH_3^+$], 109 (5) [$C_7H_6F^+$], 232 (4) [$M^+ - CF_3$], 182 (4) [$M^+ - C_2F_5$], 301 (2) [M^+]
2f	152 (100) [$(CH_3)_2NCHC_6H_4F^+$], 42 (21) [CH_3NCH^+], 186 (19) [$FC_6H_4BFCFNHCH_3^+$], 74 (18) [$F_2BN(CH_3)_2^+$], 109 (6) [$C_7H_6F^+$], 232 (7) [$M^+ - CF_3$], 182 (4) [$M^+ - C_2F_5$], 301 (3) [M^+]
2g	224 (100) [$(CH_3)_2NCHC_6F_5^+$], 230 (43) [$F_2CCHC_6F_5^+$], 42 (38) [CH_3NCH^+], 258 (29) [$M^+ - C_2F_4 - CH_3$], 74 (27) [$F_2BN(CH_3)_2^+$], 254 (5) [$M^+ - C_2F_5$], 304 (5) [$M^+ - CF_3$]
2h	100 (100) [$(CH_3)_2NCHCH(CH_3)_2^+$], 44 (66) [$(CH_3)_2N^+$], 106 (60) [$M^+ - C_2F_4 - (CH_3)_2CH$], 148 (5) [$F_2BCCH(CH_3)_2N(CH_3)_2^+$]
2i	57 (100) [$(CH_3)_3C^+$], 44 (79) [$(CH_3)_2N^+$], 70 (51) [$(CH_3)_3CCH^+$], 106 (39) [$M^+ - C_2F_4 - (CH_3)_3C$], 114 (21) [$(CH_3)_2NCHC(CH_3)_3^+$], 148 (7) [$F_2BCCH(CH_3)_2N(CH_3)_2^+$], 156 (5) [$M^+ - CF_2 - (CH_3)_3C$], 213 (4) [$M^+ - CF_2$], 263 (2) [$M^+$]
3b	194 (100) [$CH_3NHC_{13}H_8^+$], 209 (76) [$(CH_3)_2NHC_{13}H_8^+$], 211 (64) [$M^+ - C_2F_5 - NH(CH_3)_2$], 165 (46) [$C_{13}H_9^+$], 44 (22) [$(CH_3)_2N^+$], 256 (20) [$M^+ - C_2F_5$], 306 (3) [$M^+ - CF_3$]
3c	42 (100) [CH_3NCH^+], 120 (88) [$CH_3NHCHC_6H_5^+$], 44 (76) [$(CH_3)_2N^+$], 137 (35) [$M^+ - C_2F_5 - NH(CH_3)_2$], 91 (19) [$C_7H_7^+$], 182 (26) [$M^+ - C_2F_5$], 135 (25) [$(CH_3)_2NHCHC_6H_5^+$], 77 (13) [$C_6H_5^+$], 232 (2) [$M^+ - CF_3$]
3d	138 (100) [$CH_3NHCHC_6H_4F^+$], 42 (88) [CH_3NCH^+], 44 (67) [$(CH_3)_2N^+$], 155 (42) [$M^+ - C_2F_5 - NH(CH_3)_2$], 200 (24) [$M^+ - C_2F_5$], 152 (23) [$(CH_3)_2NCHC_6H_4F^+$], 109 (13) [$C_7H_6F^+$], 250 (2) [$M^+ - CF_3$]
3e	138 (100) [$CH_3NHCHC_6H_4F^+$], 44 (66) [$(CH_3)_2N^+$], 42 (45) [CH_3NCH^+], 200 (44) [$M^+ - C_2F_5$], 155 (42) [$M^+ - C_2F_5 - NH(CH_3)_2$], 152 (16) [$(CH_3)_2NCHC_6H_4F^+$], 109 (7) [$C_7H_6F^+$], 250 (3) [$M^+ - CF_3$]
3f	138 (100) [$CH_3NHCHC_6H_4F^+$], 200 (65) [$M^+ - C_2F_5$], 155 (65) [$M^+ - C_2F_5 - NH(CH_3)_2$], 44 (45) [$(CH_3)_2N^+$], 42 (24) [$CH_3NCH^+$], 152 (21) [$(CH_3)_2NCHC_6H_4F^+$], 109 (6) [$C_7H_6F^+$], 250 (6) [$M^+ - CF_3$]
3g	210 (100) [$CH_3NHCHC_6F_5^+$], 44 (86) [$(CH_3)_2N^+$], 272 (77) [$M^+ - C_2F_5$], 225 (55) [$(CH_3)_2NHCHC_6F_5^+$], 227 (34) [$M^+ - C_2F_5 - NH(CH_3)_2$], 42 (30) [$CH_3NCH^+$], 322 (9) [$M^+ - CF_3$]
3h	86 (100) [$CH_3NHCHC_3H_7^+$], 148 (68) [$M^+ - C_2F_5$], 198 (11) [$M^+ - CF_3$]
3i	46 (100) [$(CH_3)_2NH_2^+$], 100 (97) [$CH_3NHCHC_4H_9^+$], 44 (93) [$(CH_3)_2N^+$], 162 (76) [$M^+ - C_2F_5$], 106 (64) [$M^+ - C_2F_5 - (CH_3)_2CCH_2$], 57 (50) [$C_4H_9^+$], 115 (26) [$(CH_3)_2NHCHC_4H_9^+$], 212 (13) [$M^+ - CF_3$]
3j	72 (100) [$CH_3NH_2CHCO^+$], 131 (30) [$(CH_3)_2NHCCH_3CO_2CH_3^+$], 116 (15) [$(CH_3)_2NHCCH_3CO_2^+$], 178 (7) [$M^+ - C_2F_5$], 228 (3) [$M^+ - CF_3$]
3k	72 (100) [$CH_3NH_2CHCO^+$], 116 (43) [$(CH_3)_2NHCCH_3CO_2^+$], 100 (33) [$(CH_3)_2NHCCH_3CO^+$], 192 (24) [$M^+ - C_2F_5$], 145 (15) [$(CH_3)_2NHCCH_3CO_2C_2H_5^+$], 242 (8) [$M^+ - CF_3$]
3l	86 (100) [$(CH_3)_2NHCHCO^+$], 58 (62) [$(CH_3)_2NCH_2^+$], 102 (50) [$(CH_3)_2NHCHCO_2^+$], 164 (38) [$M^+ - C_2F_5$], 117 (35) [$(CH_3)_2NHCHCO_2CH_3^+$], 214 (8) [$M^+ - CF_3$]
3m	86 (100) [$(CH_3)_2NHCHCO^+$], 150 (47) [$M^+ - C_2F_5 - C_4H_8$], 103 (45) [$(CH_3)_2NHCHCO_2H^+$], 57 (26) [$(CH_3)_3C^+$], 58 (14) [$(CH_3)_2NCH_2^+$], 200 (8) [$M^+ - CF_3 - C_4H_8$], 256 (2) [$M^+ - CF_3$], 206 (1) [$M^+ - C_2F_5$]
4	124 (100) [$M^+ - C_2F_5$], 56 (15) [$C_3H_6N^+$], 49 (13) [BF_2^+], 60 (10) [H_3CNCF^+], 108 (6) [$M^+ - C_2F_5 - CH_4$], 174 (1) [$M^+ - CF_3$]

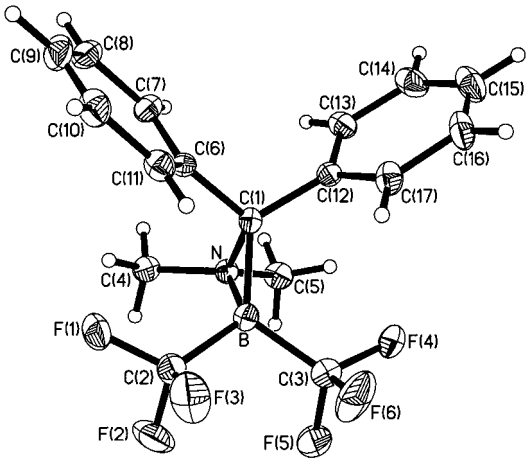


Figure 1. A perspective drawing of **2a**

1.683(4) Å, are reminiscent of the structures reported previously for $B(CF_3)_2(OH)CH(Ph)NH(Bz)(tBu)$ (**6**)[11] and $B(CF_3)_2(OH)CH(SiMe_3)NHMe_2$ (**7**)[3] − the corresponding B−C bond lengths being 1.673(4) and 1.690(4) Å, respectively. Each compound exhibits a synperiplanar O−B−C(3)−N torsion angle − their values of 20.3(5)° and 19.6(5)° in **6** and **7**, respectively, being significantly larger than in **3g**, 11.6(3)°. While the conformation in **6** and **7** is stabilized by moderately strong intramolecular N−H···O hydrogen bonds of 1.88(2) and 1.82(3) Å, respectively, the corresponding distance in **3g**, 2.41(3) Å, is too long to be bonding. Here the nitrogen atom donates its proton to an oxygen atom of an inversion-related molecule, 2.03(3) Å; thus, centrosymmetric, hydrogen-bonded dimers are formed in the solid state. Perhaps the absence of intramolecular hydrogen bonding in **3g** accounts for its O−B−C(3) and B−C(3)−N angles [110.2(2)° and 111.4(2)°, respectively] being on the average 5(1)° larger than the analogous angles of **6** and **7**.

Because hindered rotation was detected by NMR spectroscopy for the C_6F_5 group, we note that the aryl group in **3g** is oriented roughly parallel to the C(3)−H(3) bond − the H(3)−C(3)−C(6)−C(11) torsion angle being 17(2)°. A similar orientation was found for the corresponding phenyl substituent of **6**. In **3g** the aryl group protrudes into a cavity

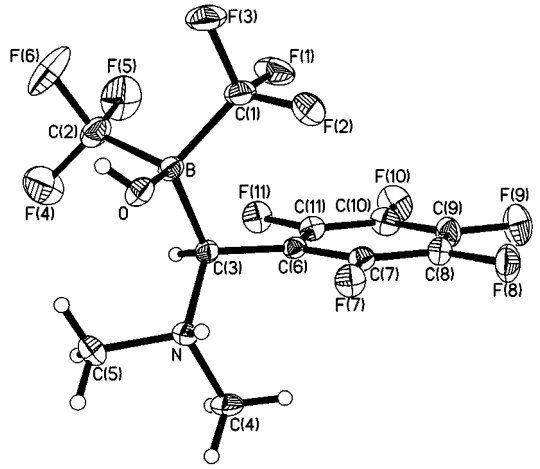
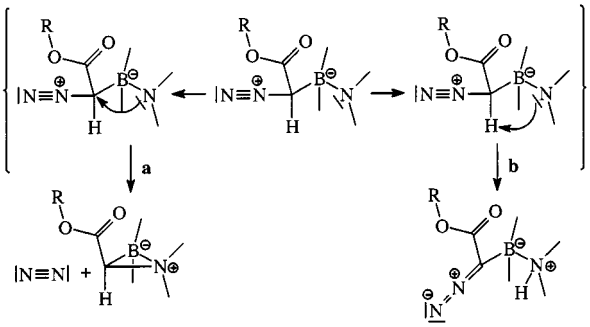


Figure. 2. A perspective drawing of **3g**

in which the CH_3 group of C(4) and the CF_3 group of C(1) are on opposites sides of the ring plane.

Discussion

The divergent behavior of the three diazoacetic acid esters $HC(N_2)COOR$ (R = *t*Bu, Et and Me) is not fully understood. The acetic acid esters H_3CCOOR with R = *t*Bu, Et undergo an ene-type reaction with **1** regardless of their substituent R. Therefore we speculate that the mechanism which leads to ene-type products of acetic acid esters and the diazoacetic acid ethyl ester are different. The reaction of all diazomethane derivatives with **1** is obviously initiated by a nucleophilic attack of boron at the diazo carbon atom (Scheme 4). The transient complex thus formed has two ways to gain stabilization. In pathway **a** the nitrogen lone pair attacks the diazomethane carbon atom, dinitrogen is eliminated and the three-membered ring is fused. In pathway **b** the lone pair abstracts a proton bonded to the diazomethane carbon atom − the diazo group being preserved.



Scheme 4. Formation of azoniaboratecyclopropanes and ene-type reaction products with **1** and diazomethane derivatives

A small conformational change in the transition complex, as determined by the N−B−C−H torsional angle, is presumably responsible for the formation of azoniaboratacyclopropanes (route **a**) or ene-products (route **b**). The conformation about the B−C bond should be affected by the varying shape of the groups R [R = Me, *t*Bu (C_3 symmetry) and R = Et (C_s symmetry)], and the conformation governs the distances between the lone pair, the carbon atom and the hydrogen atom and thus the reaction pathway. Route **b** is, however, also dependent on the acidity of the abstracted proton. Therefore this route is only observed for diazocarbonyl derivatives.

The failure to synthesize the three-membered ring *cyclo*-$(F_3C)_2B-CF_2-NMe_2$ animated us to compare the difference in its calculated energy and that of **4** to the analogous difference of *cyclo*-$(F_3C)_2B-CH_2-NMe_2$ versus $(F_3C)_2BH-CH=NMe_2$. According to semi-empirical AM1 calculations the energy of *cyclo*-$(F_3C)_2B-CH_2-NMe_2$ is ca. 2 kcal/mol lower than that of $(F_3C)_2BH-CH=NMe_2$ while **4** is ca. 30 kcal/mol more stable than *cyclo*-$(F_3C)_2B-CF_2-NMe_2$

Experimental Section

General: NMR: Bruker ARX 400 (400 MHz, 100.6 MHz and 376.5 MHz, for ^1H, ^{13}C and ^{19}F respectively), Bruker AC 250 (79.8 MHz for ^{11}B). [D_3]Acetonitrile as solvent and internal standard (^1H: $\delta_H = 1.95$; ^{13}C: $\delta_C = 1.30$), $CDCl_3$ as solvent and internal standard (^1H: $\delta_H = 7.27$; ^{13}C: $\delta_C = 77.0$), [D_6]acetone as solvent and internal standard (^1H: $\delta_H = 2.05$; ^{13}C: $\delta_C = 29.8$), CD_2Cl_2 as solvent and internal standard (^1H: $\delta_H = 5.35$; ^{13}C: $\delta_C = 53.8$), ^{19}F external standard $CFCl_3$, ^{11}B external standard $BF_3 \cdot OEt_2$. − IR: Bruker IFS 25. − MS: Varian MAT 311 (70 eV).

X-ray Structure Determinations: Crystals of **2a** and **3g** were grown from solutions in $CHCl_3$ and acetone/H_2O, respectively. While crystals of **2a** were sealed in glass capillaries under nitrogen, those of **3g** were glued to glass fibers. The structures were solved and refined using absorption-corrected X-ray data with the SHELXTL program package.[12] While the H(N) and H(O) atoms of **3g** were refined freely, the positions of all other hydrogen atoms were idealized. Crystal data are summarized in Table 3. Crystallographic data (excluding structure factors) have been deposited with the Cambridge Crystallographic Data Centre as supplementary publication no. CCDC-102694 for **2a** and -102695 for **3g**. Copies of the data can be obtained free of charge on application to CCDC, 12 Union Road, Cambridge CB2 1EZ, UK [Fax: int. code + 44(1223)336-033; E-mail: deposit@ccdc.cam.ac.uk].

1,1-Dimethyl-3,3-diphenyl-2,2-bis(trifluoromethyl)-1-azonia-2-boratacyclopropane (2a), 3-Fluorenyl-1,1-dimethyl-2,2-bis(trifluoromethyl)-1-azonia-2-boratacyclopropane (2b), 1,1-Dimethyl-3-phenyl-2,2-bis(trifluoromethyl)-1-azonia-2-boratacyclopropane (2c), 3-(4-Fluorophenyl)-1,1-dimethyl-2,2-bis(trifluoromethyl)-1-azonia-2-boratacyclopropane (2d), 3-(3-Fluorophenyl)-1,1-dimethyl-2,2-bis(trifluoromethyl)-1-azonia-2-boratacyclopropane (2e), 3-(2-Fluorophenyl)-1,1-dimethyl-2,2-bis(trifluoromethyl)-1-azonia-2-boratacyclopropane (2f), 1,1-Dimethyl-3-(pentafluorophenyl)-2,2-bis(trifluoromethyl)-1-azonia-2-boratacyclopropane (2g), 3-Isopropyl-1,1-dimethyl-2,2-bis(trifluoromethyl)-1-azonia-2-boratacyclopropane (2h), 3-*tert*-Butyl-1,1-dimethyl-2,2-bis(trifluoromethyl)-1-azonia-2-boratacyclopropane (2i), 3-(Methoxycarbonyl)-1,1,3-trimethyl-2,2-bis(trifluoromethyl)-1-azonia-2-boratacyclopropane (2j), 3-(Ethoxycarbonyl)-1,1,3-trimethyl-2,2-bis(trifluoromethyl)-1-azonia-2-boratacyclopropane (2k). − General Procedure: 10×10^{-3} mol of the respective neat diazomethane (Scheme 2) and 10−15 ml of pentane (stored over P_4O_{10}) were condensed at −196°C into a U-shaped reaction vessel connected to a vacuum line. By warming the vessel, pentane and the diazomethane were mixed. The vessel was cooled

Table 3. Crystal data and structure refinement

Compound	**2a**	**3g**
Formula	$C_{17}H_{16}BF_6N$	$C_{11}H_9BF_{11}NO$
M_r	359.12	391.00
Crystal system	orthorhombic	monoclinic
Space group	$P2_12_12_1$	$P2_1/n$
a [Å]	7.592(2)	8.409(1)
b [Å]	12.836(3)	14.179(2)
c [Å]	17.539 (4)	12.417(2)
β [°]	90	91.52(1)
Z	4	4
D(calcd.) [g cm^{-3}]	1.396	1.755
T [K]	297(2)	294(2)
Diffractometer	Siemens AED 1	Siemens P3
λ [Å]	0.71073	1.54184
Monochromation	Zr filter	graphite
θ range [°]	2.3−25.0	4.7−69.0
Quadrants	$h, \pm k, \pm l$	$h, k, \pm l$
Reflections collected	3475	2879
Unique	1738	2750
Observed [$I > 2\sigma(I)$]	1028	2184
μ (λ) [mm^{-1}]	0.127	1.890
Crystal size [mm]	0.46 × 0.24 × 0.13	0.36 × 0.34 × 0.11
Transmission	0.971−0.984	0.606−0.825
Parameters	232	243
R_F (observed)	0.044	0.054
wR_F^2 (all data)	0.085	0.158
Final diff. density [e Å^{-3}]	0.15 to −0.16	0.53 to −0.40

again to −196°C and 2 g (11 × 10^{-3} mol) of $(F_3C)_2BNMe_2$ and ca 10 ml of pentane were condensed onto the diazomethane/pentane mixture. The reaction vessel was gassed with dry nitrogen and allowed to warm to room temperature under stirring. After 10 min at 20°C, all volatile material was removed in vacuo. According to NMR spectra the reaction was quantitative and the products were analytically pure.

3-Fluorenyl-5,5,5-trifluoro-4-hydroxy-2-methyl-4-(trifluoromethyl)-2-azonia-4-boratapentane (3b), 5,5,5-Trifluoro-4-hydroxy-2-methyl-3-phenyl-4-(trifluoromethyl)-2-azonia-4-boratapentane (3c), 5,5,5-Trifluoro-3-(4-fluorophenyl)-4-hydroxy-2-methyl-4-(trifluoromethyl)-2-azonia-4-boratapentane (3d), 5,5,5-Trifluoro-3-(3-fluorophenyl)-4-hydroxy-2-methyl-4-(trifluoromethyl)-2-azonia-4-boratapentane (3e), 5,5,5-Trifluoro-3-(2-fluorophenyl)-4-hydroxy-2-methyl-4-(trifluoromethyl)-2-azonia-4-boratapentane (3f), 5,5,5-Trifluoro-4-hydroxy-2-methyl-3-(pentafluorophenyl)-4-(trifluoromethyl)-2-azonia-4-boratapentane (3g), 5,5,5-Trifluoro-4-hydroxy-3-isopropyl-2-methyl-4-(trifluoromethyl)-2-azonia-4-boratapentane (3h), 3-*tert*-Butyl-5,5,5-trifluoro-4-hydroxy-2-methyl-4-(trifluoromethyl)-2-azonia-4-boratapentane (3i), 5,5,5-Trifluoro-4-hydroxy-3-(methoxycarbonyl)-2,3-dimethyl-4-(trifluoromethyl)-2-azonia-4-boratapentane (3j), 3-(Ethoxycarbonyl)-5,5,5-trifluoro-4-hydroxy-2,3-dimethyl-4-(trifluoromethyl)-2-azonia-4-boratapentane (3k), 5,5,5-Trifluoro-4-hydroxy-3-(methoxycarbonyl)-2-methyl-4-(trifluoromethyl)-2-azonia-4-boratapentane (3l), 3-(*tert*-Butoxycarbonyl)-5,5,5-trifluoro-4-hydroxy-2-methyl-4-(trifluoromethyl)-2-azonia-4-boratapentane (3m). − General Procedure: A solution (3 × 10^{-3} mol) of the corresponding azoniaboratacyclopropane in 10 ml of CH_2Cl_2 was stirred with 20 × 10^{-3} mol of H_2O for 12 h at ambient temperature. After removal of the solvent and the water in vacuo, pure **3b**−**3m** were obtained in quantitative yield.

3b: M.p. 160°C. − IR: $\tilde{\nu}$ = 3636 cm^{-1} (OH), 3270 (NH), 1078 (CF).

3c: M.p. 96°C. − IR: $\tilde{\nu}$ = 3638 cm^{-1} (OH), 3278 (NH), 1107, 1083 (CF).

Table 4. Elemental analyses of **2a**−**2c** and **3b**−**3m**

Compound	Formula	found/(calcd.)		
		C	H	N
2a	$C_{17}H_{16}BF_6N$	56.5/(56.86)	4.4/(4.49)	3.9/(3.90)
2b	$C_{17}H_{14}BF_6N$	55.3/(57.18)	4.1/(3.95)	4.0/(3.92)
2c	$C_{11}H_{12}BF_6N$	46.0/(46.68)	4.3/(4.27)	4.7/(4.95)
3b	$C_{17}H_{16}BF_6NO$	54.2/(54.43)	4.6/(4.30)	3.7/(3.73)
3c	$C_{11}H_{14}BF_6NO$	43.8/(43.89)	4.6/(4.69)	4.4/(4.65)
3d	$C_{11}H_{13}BF_7NO$	41.4/(41.41)	4.3/(4.11)	4.6/(4.39)
3e	$C_{11}H_{13}BF_7NO$	40.8/(41.41)	4.3/(4.11)	4.5/(4.39)
3f	$C_{11}H_{13}BF_7NO$	41.1/(41.41)	4.0/(4.11)	4.5/(4.39)
3g	$C_{11}H_9BF_{11}NO$	33.4/(33.79)	2.3/(2.32)	3.2/(3.58)
3h	$C_8H_{16}BF_6NO$	35.0/(35.99)	5.2/(6.04)	5.6/(5.25)
3i	$C_9H_{18}BF_6NO$	36.9/(38.46)	6.0/(6.46)	5.5/(4.98)
3j	$C_8H_{14}BF_6NO_3$	32.4/(32.35)	4.8/(4.75)	4.1/(4.72)
3k	$C_9H_{16}BF_6NO_3$	34.0/(34.76)	5.0/(5.19)	4.7/(4.50)
3l	$C_7H_{12}BF_6NO_3$	29.6/(29.71)	4.3/(4.27)	5.3/(4.95)
3m	$C_{10}H_{18}BF_6NO_3$	36.8/(36.95)	5.4/(5.58)	3.6/(4.31)

3d: M.p. 100°C. − IR: $\tilde{\nu}$ = 3663 cm^{-1} (OH), 3262 (NH), 1092 (CF).

3e: M.p. 104°C. − IR: $\tilde{\nu}$ = 3643 cm^{-1} (OH), 3270 (NH), 1086 (CF).

3f: M.p. 102°C. − IR: $\tilde{\nu}$ = 3646 cm^{-1} (OH), 3272 (NH), 1086, 1025 (CF).

3g: M.p. 110°C. − IR: $\tilde{\nu}$ = 3661 cm^{-1} (OH), 3257 (NH), 1091 (CF).

3h: M.p. 60°C. − IR: $\tilde{\nu}$ = 3671 cm^{-1} (OH), 3277 (NH), 1074, 1021 (CF).

3i: M.p. 92°C. − IR: $\tilde{\nu}$ = 3663 cm^{-1} (OH), 3269 (NH), 1094, 1074 (CF).

3j: M.p. 120°C. − IR: $\tilde{\nu}$ = 3164 cm^{-1} (NH), 1708 (C=O), 1086 (CF).

3k: M.p. 106°C. − IR: $\tilde{\nu}$ = 3161 cm^{-1} (NH), 1705 (C=O), 1106, 1081 (CF).

3l: M.p. 124°C. − IR: $\tilde{\nu}$ = 3670 cm^{-1} (OH), 3082 (NH), 1716 (C=O), 1086 (CF).

3m: M.p. 140°C. − IR: $\tilde{\nu}$ = 3435 cm^{-1} (OH), 3254 (NH), 1688 (C=O), 1088 (CF).

3,4,5,5,5-Pentafluoro-2-methyl-4-(trifluoromethyl)-2-azonia-4-boratapent-2-ene (4): 1 g (6.5 × 10^{-3} mol) of F_3CSiF_3 and 1.25 g (6.5 × 10^{-3} mol) of **1** were condensed at −196°C into an ampoule fitted with a PTFE valve. The ampoule was slowly warmed to room temperature and all volatile material was removed in vacuo. The brown residue was crystallized from a $CH_2Cl_2/CHCl_3$ mixture. Yield 89%; decomp. ca. 40°C. − IR: $\tilde{\nu}$ = 1684 cm^{-1} (C=N), 1112, 1081, 1051 (CF). − For elemental analyses see Table 4.

Acknowledgments

Financial support by the Fonds der Chemischen Industrie is gratefully acknowledged.

[1] G. Pawelke, H. Bürger, *Appl. Organomet. Chem.* **1996**, *10*, 147−174.
[2] A. Ansorge, D. J. Brauer, H. Bürger, T. Hagen, G. Pawelke, *Angew. Chem.* **1993**, *105*, 429−430; *Angew. Chem. Int. Ed. Engl.* **1993**, *32*, 384−385.

[3] A. Ansorge, D. J. Brauer, H. Bürger, T. Hagen, G. Pawelke, *J. Organomet. Chem.* **1994**, *467*, 1−11.
[4] H. Beckers, H. Bürger, *J. Organomet. Chem.* **1990**, *385*, 207−219.
[5] D. J. Brauer, H. Bürger, T. Dittmar, G. Pawelke, *J. Organomet. Chem.* **1996**, *524*, 225−235.
[6] J. W. Lauber, J. A. Ibers, *J. Amer. Chem. Soc.* **1975**, *97*, 561−567.
[7] D. J. Brauer, S. Buchheim-Spiegel, H. Bürger, R. Gielen, G. Pawelke, J. Rothe, *Organometallics* **1997**, *16*, 5321−5330.
[8] D. J. Brauer, H. Bürger, G. Pawelke, J. Rothe, *J. Organomet. Chem.* **1995**, *522*, 129−136.
[9] A. Ansorge, D. J. Brauer, H. Bürger, F. Dörrenbach, T. Hagen, G. Pawelke, W. Weuter, *J. Organomet. Chem.* **1990**, *396*, 253−267.
[10] F. H. Allen, *Acta Crystallogr.* **1981**, *B37*, 890−900.
[11] A. Ansorge, D. J. Brauer, H. Bürger, F. Dörrenbach, B. Krumm, G. Pawelke, *Z. Naturforsch.* **1992**, *47b*, 772−782.
[12] G. M. Sheldrick, *SHELXTL Version 5.03*, Siemens Industrial Automation, Inc., Madison, WI, **1994**.

Received September 21, 1998
[I98322]

Square-Planar and Octahedral Nickel(II) Complexes of Isomeric *cis*-2,9-Bis(aminomethyl)-5,7,7,12,14,14-hexamethyl-1,4,8,11-tetraazacyclotetradecanes

Bohdan Korybut-Daszkiewicz,*[a] Przemysław Gluziński,[a] Janusz Krajewski,[a] Andrejas Kemme,[b] and Anatolij Mishnev[b]

Keywords: Macrocyclic ligands / N ligands / Nickel complexes

Isomeric *cis*-2,9-bis(aminomethyl)-5,7,7,12,14,14-hexamethyl-1,4,8,11-tetraazacyclotetradecanes (**6a** and **6b**) and their octahedral (**4**) and square-planar nickel(II) complexes (**5**) have been prepared and characterized. X-ray crystallographic investigations of the octahedral complexes have confirmed a folded conformation of the macrocyclic ring. Protonation of the pendant amino groups results in a change in the Ni configuration, which is accompanied by a concomitant change of the macrocycle conformation from a folded to a planar one. The structures of the protonated, square-planar complexes and of the free ligands have been established mainly on the basis of their ^{1}H- and ^{13}C-NMR spectra.

Introduction

Tetraaza macrocyclic ligands functionalized with pendant donor groups form diamagnetic square-planar nickel(II) complexes when the donor groups are protonated and cannot coordinate, whereas at higher pH coordination of the pendant donors leads to paramagnetic, octahedral complexes.[1,2] In the case of monosubstituted ligands, coordination of the pendant donor occurs at one of the axial sites, and the second axial site is occupied by an anion or solvent molecule.[3,4] Pendant methylnitronato[5] or carboxylate[6] groups, by virtue of their ability to offer two possible donor oxygen atoms, may also fill this coordination site and act as a bridge between nickel(II) ions forming one-dimensional polymers.

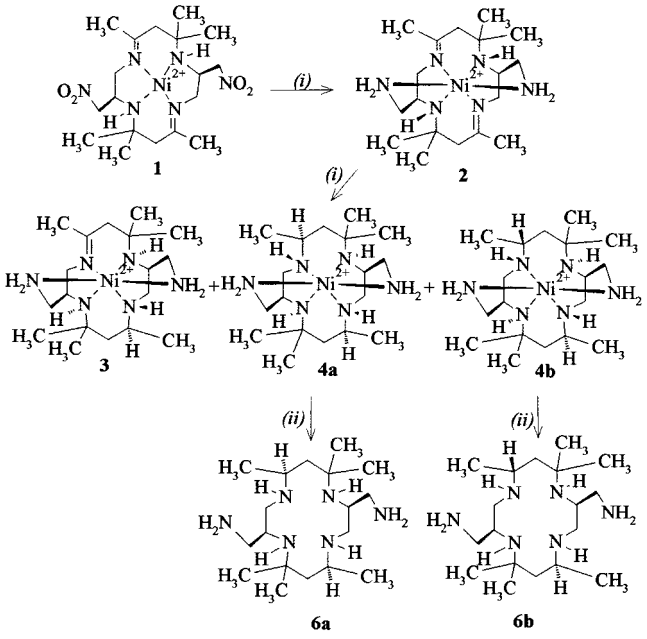
Nickel(II) complexes of cyclam derivatives substituted with two pendant amino groups are subject to similar pH-dependent equilibria. *trans*-Substituted ligands form octahedral complexes, with the nitrogen atoms of the macrocycle occupying an equatorial plane and the pendant groups in axial positions.[7–9] However, coordination of both pendant groups in the case of *cis*-substituted cyclam derivatives requires folding of the macrocycle conformation. Such folding occurs upon coordination of the pendant amino groups in *cis*-2,9-bis(aminomethyl)-5,7,7,12,14,14-hexamethyl-1,4,8,11-tetraazacyclotetradeca-4,11-diene nickel(II) diperchlorate (**2**).[8] Hydrogenation of complex **2** gave two violet nickel(II) complexes of isomeric *cis*-2,9-bis(aminomethyl)-substituted cyclam derivatives, **4a** and **4b**. Crystallographic data for these two octahedral nickel(II) complexes, as well as the spectroscopic characterization of their diamagnetic square-planar protonation products and free ligands, are described in the present paper.

[a] Institute of Organic Chemistry, Polish Academy of Sciences, Kasprzaka 44/52, PL-01224 Warszawa, Poland
E-mail: bkd@ichf.edu.pl
[b] Institute of Organic Synthesis, Latvian Academy of Science, LV-1006 Riga, Latvia

Results and Discussion

Synthesis

The synthesis of the isomeric complexes **4a**, **4b** and the free ligands **6a**, **6b** is outlined in Scheme 1.



Scheme 1. Reagents: (*i*) zinc amalgam and HCl; (*ii*) NaCN in water under reflux

Reduction of the nitro groups in the *cis*-2,9-bis(nitromethyl)-substituted complex **1**, followed by hydrogenation of the C=N double bonds with zinc amalgam and hydrochloric acid led to the isomeric 2,9-bis(aminomethyl)-substituted Ni complexes **4a**, **4b** and the intermediate product **3**. Work-up of the mixture after a shorter reaction time allowed isolation of the previously described, unsaturated complex **2**. The use of zinc amalgam in place of the zinc dust used in published procedures[9,10] proved advantageous

 © WILEY-VCH Verlag GmbH, D-69451 Weinheim, 1999 1434–1948/99/0202–0263 $ 17.50+.50/0

since the degree of decomposition accompanying reduction of the nitro groups was lower. The two isomeric, fully saturated, octahedral Ni^{II} complexes were separated by chromatography on an SP Sephadex C-25 column and were isolated in the form of their diperchlorate salts **4a** and **4b**.

Upon acidification with 72% perchloric acid, violet nitromethane solutions of complexes **4a** and **4b** gave deep-red and orange solutions of the square-planar tetraperchlorates **5aα** and **5b**, respectively, with protonated pendant arms. Complexes **5aα** and **5b** were found to readily undergo isomerization in protic solvents and thus they were characterized only in nitromethane solution. *N*-Isomeric **β** and **γ** forms of complex **5a** were isolated in solid form, but only an oily mixture of isomers was precipitated upon addition of diethyl ether to an ethanolic solution of complex **5b**.

Demetallation of **4a** and **4b** in aqueous solution using an excess of sodium cyanide gave the free ligands **6a** and **6b**.

Crystal Structures of 4a and 4b

Selected bond lengths and valence angles in cations **4a** and **4b**, as shown in Figures 1 and 2, are listed in Table 1.

Table 1. Selected bond lengths [Å] and angles [°] for cations **4a** and **4b**

Bond	**4a**	**4b**	Angle	**4a**	**4b**
N1−Ni	2.135(6)	2.130(6)	N1−Ni−N4	79.8(3)	80.7(3)
N4−Ni	2.104(7)	2.082(7)	N1−Ni−N8	105.9(3)	101.1(3)
N8−Ni	2.141(7)	2.102(8)	N1−Ni−N11	97.5(3)	95.7(3)
N11−Ni	2.115(7)	2.123(8)	N1−Ni−N16	82.8(3)	82.9(3)
N16−Ni	2.122(9)	2.113(8)	N1−Ni−N18	170.7(3)	176.5(3)
N18−Ni	2.126(8)	2.120(8)	N4−Ni−N8	97.7(3)	95.4(3)
C2−N1	1.49(1)	1.484(9)	N4−Ni−N11	175.3(3)	173.7(3)
C14−N1	1.50(1)	1.52(1)	N4−Ni−N16	87.1(4)	85.5(4)
C3−C2	1.53(1)	1.53(1)	N4−Ni−N18	96.0(3)	99.4(4)
C15−C2	1.53(1)	1.51(1)	N8−Ni−N11	79.2(3)	80.2(3)
N4−C3	1.50(1)	1.48(1)	N8−Ni−N16	170.7(3)	176.0(3)
C5−N4	1.47(1)	1.51(1)	N8−Ni−N18	82.9(3)	82.4(4)
C6−C5	1.53(1)	1.51(1)	N11−Ni−N16	96.5(4)	99.2(4)
C19−C5	1.51(1)	1.52(1)	N11−Ni−N18	87.1(3)	84.6(4)
C7−C6	1.53(1)	1.54(1)	N16−Ni−N18	88.7(4)	93.6(4)
N8−C7	1.51(1)	1.52(1)	Ni−N1−C2	96.7(5)	97.0(5)
C20−C7	1.52(1)	1.53(1)	Ni−N1−C14	121.4(5)	121.5(5)
C21−C7	1.54(1)	1.53(2)	Ni−N4−C3	107.2(6)	107.9(6)
C9−N8	1.50(1)	1.51(1)	Ni−N4−C5	119.5(5)	117.6(6)
C10−C9	1.51(1)	1.51(1)	Ni−N8−C7	121.1(5)	127.2(6)
C17−C9	1.52(1)	1.52(1)	Ni−N8−C9	96.1(5)	98.2(6)
N11−C10	1.50(1)	1.49(1)	Ni−N11−C10	107.4(6)	108.0(6)
C12−N11	1.49(1)	1.51(1)	Ni−N11−C12	118.4(5)	122.2(6)
C13−C12	1.50(1)	1.49(1)	Ni−N16−C15	109.0(7)	107.8(6)
C22−C12	1.53(1)	1.50(2)	Ni−N18−C17	108.5(6)	108.8(7)
C23−C14	1.53(1)	1.52(1)	N1−C2−C3	106.0(8)	104.3(7)
C24−C14	1.54(1)	1.57(1)	N1−C2−C15	110.4(7)	110.9(8)
N16−C15	1.47(1)	1.48(1)	N1−C14−C13	111.2(6)	112.3(8)
N18−C17	1.46(1)	1.45(1)	N1−C14−C23	105.6(7)	111.3(9)
			N1−C14−C24	112.3(7)	103.3(8)

Both cations have an irregular octahedral Ni^{II} coordination sphere with the macrocycle coordinated in a folded conformation, with fold angles (N1−Ni−N8) of 106° and 101° in **4a** and **4b**, respectively. All N−Ni−N angles in the five-membered chelate rings are rather small (79−83°). The angles in the six-membered chelate rings incorporating the macrocyclic nitrogen atoms are large (95−98°), while those incorporating the aminomethyl pendant arms are small (84−87°). The Ni−N distances fall in the range typical for octahedral coordination (2.10−2.14 Å for **4a**; 2.08−2.13 Å for **4b**).

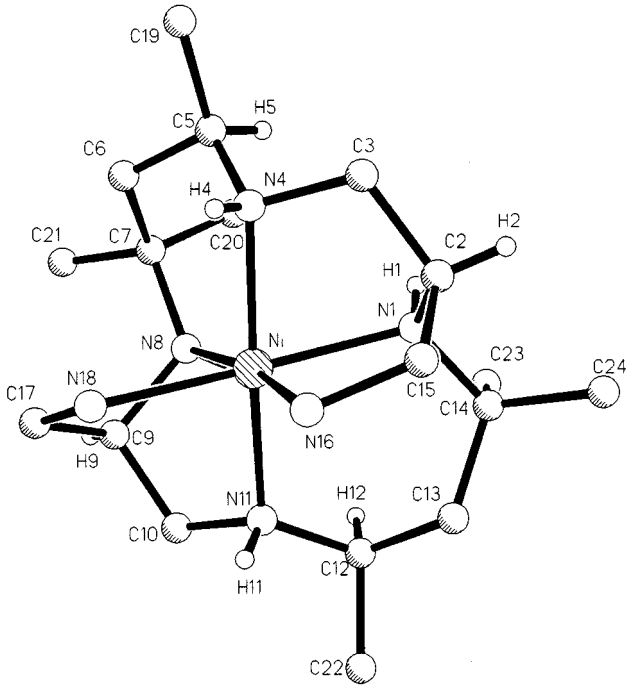


Figure 1. Molecular structure together with atomic labelling for cation **4a**

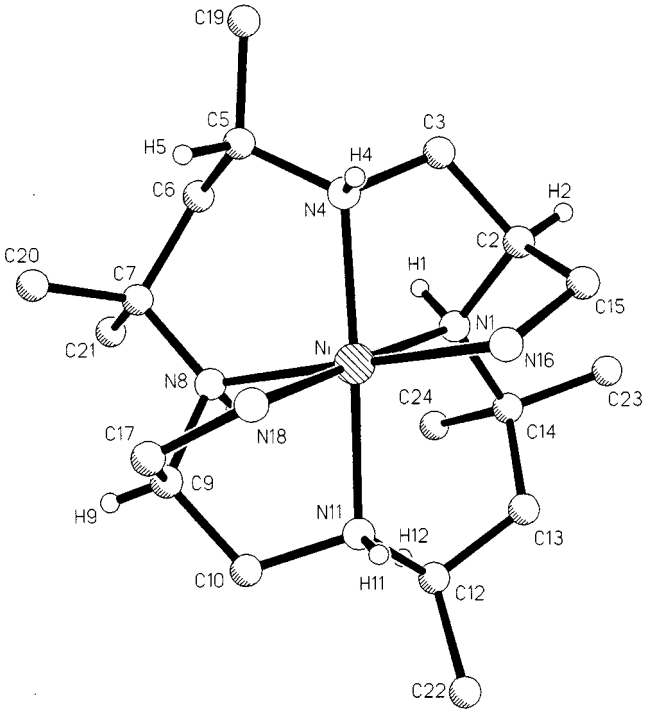


Figure 2. Molecular structure together with atomic labelling for cation **4b**

The shape and symmetry of any given ring is precisely described by its set of endocyclic torsion angles (ETAs) and

the sequence of their signs.[11] The ETAs of complexes **4a** and **4b** are collected in Table 2, together with the appropriate *n*-butane conformational codes.

Table 2. Endocyclic torsion angles [°] and sequences of their configurational codes[a] for **4a** and **4b**

Torsion angles	**4a**		**4b**	
C3−C2−N1−C14	164.8	*a*	163.9	*a*
N4−C3−C2−N1	45.6	*g*	53.1	*g*
C5−N4−C3−C2	−134.5	*−ac*	−145.1	*−ac**
C6−C5−N4−C3	162.5	*a*	81.7	*g**
C7−C6−C5−N4	−77.0	*−g*	81.8	*g**
N8−C7−C6−C5	68.1	*g*	−63.5	*−g*
C9−N8−C7−C6	96.8	*ac**	152.0	*a**
C10−C9−N8−C7	164.4	*a*	154.1	*a**
N11−C10−C9−C8	45.3	*g*	49.5	*g*
C12−N11−C10−C9	−133.7	*−ac*	−145.6	*−ac**
C13−C12−N11−C10	164.6	*a*	150.8	*a**
C14−C13−C12−N11	−79.3	*−g*	−68.8	*−g*
N1−C14−C13−C12	69.7	*g*	69.7	*g*
C13−C14−N1−C2	97.0	*ac**	97.8	*ac**

[a] Codes for torsion angles: *a:* antiperiplanar (180 ± 30°), *ac:* anticlinical (120 ± 30°), *g:* gauche (60 ± 30°), *sp:* synperiplanar (0 ± 30°). − * Deformation > 20°.

The folded macrocycle of cation **4a** has C_2 symmetry and its conformation according to Boeyens notation[12] can be assigned as type V [3434]. The macrocycle forms two five-membered chelate rings in E_2 (*envelope*) and two six-membered rings in ^4E (*sofa*) conformation. In the isomeric cation **4b**, both of the endomacrocyclic five-membered rings and one of the six-membered chelate rings adopt similar E_2 (*envelope*) and ^4E (*sofa*) conformations, respectively. The second six-membered ring [N(4)−N(8)] adopts a $^3H_4$ (*half-chair*) conformation and the folded cyclam macrocycle assumes a type V [21434] form.

The 5,12-dimethyl and 2,9-bis(aminomethyl) substituents in isomer **4a** are located on the same side of the macrocyclic ring and the relative configuration of the chiral N and C atoms, according to Cahn−Ingold−Prelog rules,[13] is assigned as (1*R*2*S*4*R*5*S*8*R*9*S*11*R*). The methyl group attached to C-5 in cation **4b** is located on the opposite side of the macrocycle and the configuration of this isomer is assigned as (1*R*2*S*4*R*5*R*8*R*9*S*11*R*). The 5,12-dimethyl groups assume *equatorial* positions and the coordinated pendant arms are *axially* arranged in both isomeric complexes.

Structures of Square-Planar Complexes 5

The structures of the free ligands and of the diamagnetic complexes were established mainly on the basis of their ^{13}C- and ^{1}H-NMR spectra (Tables 3 and 4).

Under acidic conditions in nitromethane solution, the amino groups on the side-chains of complexes **3**, **4a** and **4b** are protonated, leaving the Ni^{II} ions in a square-planar configuration. This change in the Ni^{II} configuration is accompanied by a concomitant change in the conformation of the macrocycle from a folded to a planar one. However, the secondary nitrogen atoms in the ring retain their configurations in the course of this process. This can clearly be seen in the ^{1}H-NMR spectra of protonated complex **5aα** and its *N*-isomeric forms (**5aβ** and **5aγ**), most notably in the chemical shifts of the 7- and 14-geminal methyl substituent signals (Table 4).

The conformations of the methyl groups and of the six-membered chelate rings can be assigned on the basis of the known deshielding effects observed for axially oriented substituents in the ^{1}H-NMR spectra of square-planar macrocyclic Ni^{II} complexes.[14−17] The 5,12-dimethyl groups retain an *equatorial* arrangement in all the isomeric **5aα**, **5aβ** and **5aγ** complexes (Scheme 2).

The geminal 7,14-dimethyl groups in complex **5aα**, due to the non-chair conformation of the six-membered chelate

Table 3. 125.8-MHz ^{13}C-NMR spectra of complexes **5** and free ligands **6** (δ in ppm relative to TMS)

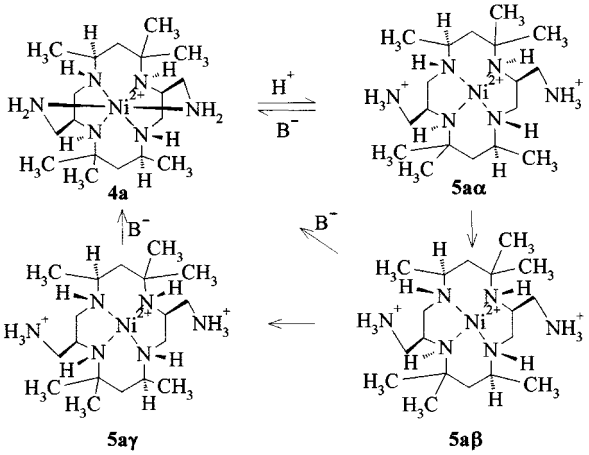
	Compound/Solvent						
Carbon atom	**5aα**[a] CD_3NO_2 + $HClO_4$	**5aβ** CD_3NO_2	**5aγ(ClO$_4$)$_4$**[a] CD_3CN	**5aγCl$_4$**[a] D_2O + DCl	**5b** CD_3NO_2 + $HClO_4$	**6a**[a] $CDCl_3$	**6b**[a] $CDCl_3$
7,14-CH_3	29.3 *ax*	24.8	26.2 *ax*	25.8 *ax*	25.6	25.4	24.5
	29.8 *eq*	26.9	28.2 *eq*	26.3 *eq*	27.3	28.9	28.3
		29.3			28.4		29.5
		29.9			29.5		31.1
5,12-CH_3	21.7	18.9	20.0	18.4	19.7	21.7	21.6
		18.9			19.7		22.0
2,9-CH_2NH_3	40.9	41.0	41.5	40.9	40.0	46.1	46.3
		41.9			41.7		47.2
C-2,9	51.8	54.4	54.5	55.4	55.7	52.9	51.8
		57.0			56.0		54.0
C-3,10	47.6	49.5	52.8	53.5	47.3	51.3	51.4
		52.7			50.2		52.5
C-5,12	55.0	53.8	53.6	53.9	52.1	51.7	50.8
		55.4			52.6		52.2
C-6,13	50.0	50.0	49.3	49.0	49.5	51.8	51.1
		50.0			49.9		52.2
C-7,14	56.5	56.5	59.3	58.7	57.5	54.0	52.6
		61.2			57.8		53.6

[a] Assignments were confirmed by 2D heteronuclear (^{1}H−^{13}C) experiments.

Table 4. 500.13-MHz ^{1}H-NMR spectra of complexes **5** and free ligands **6** (δ in ppm relative to TMS, *J* in Hz)[a]

Assignment	Compound/Solvent **5aα**[b] CD_3NO_2 + $HClO_4$	**5aβ** CD_3NO_2	**5aγ(ClO$_4$)$_4$**[b] CD_3CN	**5aγCl$_4$**[b] D_2O + DCl	**5b** CD_3NO_2 + $HClO_4$	**6a**[b] $CDCl_3$	**6b**[b] $CDCl_3$
7,14-CH_3	1.70 s 1.73 s	1.37 s, 1.47 s 1.74 s, 2.44 s	1.31 s 2.12 s	1.28 s 2.16 s	1.48 s, 1.57 s 1.58 s, 1.63 s	1.07 s 1.09 s	1.06 s, 1.07 s 1.10 s, 1.13 s
5,12-CH_3	1.27 d (5.2)	1.19 d (6.2) 1.26 d (7.0)	1.16 bd (2.6)	1.13 d (6.7)	1.31 d (6.0) 1.42 d (6.2)	0.98 d (6.1)	0.98 d (6.1) 1.04 d (6.4)
5,12-CH	3.87 b	3.65 m 3.58 m	3.76 bm	3.78 m		2.75 m	2.74 m 2.76 m
2,9-CH_2NH_3	3.88 b		3.61 dd (13.3, 4.0)	3.71 dd (13.6, 8.0)		2.66 dd (12.0, 6.9)	2.66 m 2.66 m
	4.55 b	2.6−4.1	3.75 dd (13.3, 10.0)	3.84 dd (13.6, 6.8)		2.76 m	2.58 dd (12.3, 6.9) 2.77 dd (12.3, 3.3)
2,9-CH	3.43 b		3.46 b	3.42 m		2.80 m	2.66 m 2.80 m
6,13-CH_2	1.59 dd (15.3, 9.4) 1.90 d (15.3)	1.52 dd (16.2, 12.2) 1.95 dd (16.2, 2.0) 1.67 dd (15.7, 10.2) 2.02 dd (15.7, 5.3)	1.48 dd (15.6, 11.5) 1.80 d (15.6)	1.53 dd (15.4,11.6) 1.84 d (15.4)	1.5−5.2	1.36 dd (14.7, 1.8) 1.53 dd (14.7, 11.1)	1.34 dd (14.5, 1.7) 1.49 dd (14.5, 9.5) 1.39 dd (14.8, 2.7) 1.46 dd (14.8, 10.9)
3,10-CH_2	2.54 b, 3.81 b	 2.6−4.1	2.72 b 3.13 bd (11.1)	2.74 m 2.90 dd (13.3, 4.3)		2.44 dd (11.3, 3.3) 2.75 m	2.14 dd (10.6, 9.2) 2.82 dd (10.6, 2.9) 2.36 dd (11.1, 3.6) 2.92 dd (11.1, 2.3)
NH	3.20 b 4.19 b		2.47 b 3.08 b	3.75 bm 4.75 bs			
NH_3	7.35 b	7.22 b 7.36 b	6.90 b		7.10 b 7.25 b		

[a] s: singlet, d: doublet, m: multiplet, b: broad; coupling constants in parentheses. − [b] Assignments were confirmed by 2D heteronuclear (^{1}H−^{13}C) experiments.



Scheme 2. Isomerization pathway and configurations of square-planar complexes **5a**

rings, resonate at almost the same frequency. This indicates that the macrocycle in **5aα** retains a type-V conformation. The inversion at N(1) causes a switch in the N(1)−N(11) six-membered chelate-ring conformation to the chair form. This is reflected in the large separation of *axial* and *equatorial* 14-methyl group signals in the spectrum of **5aβ** and indicates a type-II conformation of the macrocycle. The second isomerization, caused by inversion at N(8), followed by conformational change in the second six-membered ring, results in formation of the cation **5aγ**. The macrocycle in **5aγ** adopts a type-I conformation, with all secondary amino protons and substituents in 2,5,9,12-positions on the same side of the ring.

Addition of perchloric acid to a nitromethane solution of the octahedral complex **4b** results in the formation of an orange square-planar complex, **5b**. The chemical shifts of the geminal methyl groups indicate a non-chair conformation of both six-membered chelate rings and a type-V conformation of the macrocycle. This complex also undergoes isomerization upon addition of protic solvents, but attempts to isolate and characterize the individual species as solids were not successful.

Electronic spectra in nitromethane solution, acidified with perchloric acid, show d−d transition bands at 506 nm (ε = 188) and 476 nm (ε = 122) for **5aα** and **5b**, respectively. The wavelengths of the bands are substantially longer and the molar absorption coefficients are higher than typically observed for Ni^{II} complexes of cyclam derivatives ($\lambda_{max} \approx$ 450 nm, ε ≈ 80).[18] This indicates strong distortion of the square-planar $Ni^{II}N_4$ geometry,[19] especially in the case of isomer **5aα**, which has six substituents on the same side of the macrocyclic ring. After isomerization, the less strained complex **5aβ** absorbs at 462 nm and the most stable cation **5aγ** at 454 nm, close to the usual wavelength for Ni^{II} square-planar complexes.

Conclusion

In Ni^{II} complexes of *cis*-2,9-bis(aminomethyl)-5,7,7,12,14,14-hexamethyl-1,4,8,11-tetraazacyclotetradecanes, coordination of the two pendant amino groups located on the same side of the tetraaza macrocyclic ring forces the ring to adopt a folded conformation. Protonation of the pendant donor groups by perchloric acid in nitromethane solution is accompanied by a concomitant return of the macrocycle to a preferred planar arrangement around the central Ni^{II} ion. Steric crowding in **5aα** and **5b**,

as well as the unusual type-V conformation of the cyclam ring, leads to severe distortion of the square-planar geometry and to weakening of the ligand field. In the presence of protic solvents, consecutive inversions at chiral nitrogen atoms, accompanied by conversion of the macrocyclic ring conformation, lead to the more stable isomers **5aβ** and **5aγ**.

Experimental Section

General Remarks: IR spectra (paraffin oil mulls) were recorded with a Perkin-Elmer 1600 FT-IR spectrometer. NMR spectra were obtained with a Bruker AM 500 spectrometer using TMS as internal standard. Electronic spectra were recorded using a Cary 1E UV/Vis spectrophotometer and mass spectra with an AMD 604 spectrometer.

Synthesis: ***Caution! Perchlorate salts are potentially explosive!*** Preparation of complex **1** and its reduction with zinc dust and hydrochloric acid has been described previously.[8−10] Zinc amalgam was prepared according to the standard procedure.[20] Hydrochloric acid, perchloric acid, and solvents were commercial materials and were used without further purification.

Reduction of [5,7,7,12,14,14-Hexamethyl-2,9-*cis*-bis(nitromethyl)-1,4,8,11-tetraazacyclotetradeca-4,11-diene]nickel(II) Diperchlorate (1): Concentrated hydrochloric acid (75 mL) was added dropwise to a vigorously stirred mixture of zinc amalgam (25 g) and complex **1** (35 g) in a 1:1 water/methanol solution (400 mL), while the temperature was maintained below 20°C. After 24 h, the mixture was filtered, the filtrate was diluted with water (400 mL) and applied to a Dowex 50WX2 cation-exchange column (H^+ form). The column was washed with 1 M HCl (1 L) and then eluted with 3 M HCl. An orange eluate was obtained, which was concentrated to dryness. The residue was dissolved in 1 M perchloric acid and the solution was made alkaline by the addition of 50% sodium hydroxide solution. The violet precipitate thus obtained was filtered off, redissolved in 0.02 M perchloric acid, and the resulting orange solution was filtered and applied to an SP Sephadex C-25 column (12 × 60 cm). The column was washed with water and eluted with 0.2 M sodium sulfate solution. Four orange bands were collected, which were each absorbed onto Dowex 50WX2 columns and, after washing with 1 M HCl, were eluted with 3 M HCl. Orange eluates were obtained, which were concentrated to dryness. The respective residues were dissolved in 1 M perchloric acid and neutralized with NaOH (50%). On cooling, violet crystals formed, which were filtered off and recrystallized from water. Minor fractions 1 and 2 were found to contain two isomeric products **4a** (0.5 g, 1.7%) and **4b** (0.3 g, 1%), respectively, in which besides the nitro groups both of the C=N double bonds were reduced. The third fraction contained product **3** (3.2 g, 10%) with two aminomethyl groups and one C=N double bond. The major fourth fraction contained complex **2** (12.5 g, 39%).

[2,9-Bis(aminomethyl)-5,7,7,12,14,14-hexamethyl-1,4,8,11-tetraazacyclotetradecane]nickel(II) Diperchlorates 4a and 4b: Concentrated hydrochloric acid (30 mL) was added dropwise over a period of 30 min to a vigorously stirred mixture of zinc amalgam (10 g) and complex **2** (4 g) in water (200 mL), while the temperature was maintained below 20°C. Stirring was continued for 72 h and then the mixture was applied to a Dowex 50WX2 cation-exchange column (H^+ form). The column was washed with 1 M HCl and eluted with 3 M HCl. An orange eluate was collected, which was concentrated to dryness. The residue was dissolved in water and the resulting solution was applied to an SP Sephadex C-25 column (5 × 50 cm). Four fractions were eluted with 0.2 M sodium sulfate solution and were worked up according to the same procedure as described above. 2.3 g (58%) of **4a**, 0.9 g (22%) of **4b**, 0.5 g (12%) of **3**, and 0.2 g (5%) of **2** were isolated and crystallized from water. − **3**: $C_{18}H_{40}Cl_2N_6NiO_8$ (598.2): calcd. C 36.0, H 6.7, Cl 11.8, N 14.0; found C 35.9, H 7.3, Cl 11.3, N 14.0. − ^{1}H NMR (500.13 MHz, CD_3NO_2 + $HClO_4$): δ = 1.32 (d, J = 6.8 Hz, 12-CH_3), 2.29 (s, 5-CH_3), 1.51, 1.54, 1.59, 1.71 (s, 7,14-CH_3). − ^{13}C NMR (125.8 MHz, CD_3NO_2 + $HClO_4$): δ = 19.2, 24.5, 25.9, 26.5, 28.3, 29.2 (CH_3), 39.4 and 43.1 (CH_2NH_3), 50.0, 50.0, 52.8, 55.3, 55.3, 55.8, 56.0, 56.4, 56.9, 191.9 (macrocyclic ring C atoms). − IR (Nujol): $\tilde{\nu}$ = 3354, 3308, 3280, 3201 cm^{-1} (ν N−H); 1652 (ν C=N), 1622 (δ N−H), 1099 and 624 (ClO_4^-). − UV/Vis (methanol): λ_{max} (ε_{max}) = 331 nm (67 $dm^3cm^{-1}mol^{-1}$), 510 (11.8), 813 (9.5). − **4a**: $C_{18}H_{42}Cl_2N_6NiO_8 \cdot H_2O$ (618.2): calcd. C 35.0, H 7.2, Cl 11.5, N 13.6; found C 34.6, H 7.3, Cl 11.5, N 14.4. − IR (Nujol): $\tilde{\nu}$ = 3612, 3542 cm^{-1} (ν H_2O); 3346, 3306, 3283, 3204 (ν N−H); 1617 (δ N−H), 1110 and 623 (ClO_4^-). − UV/Vis (methanol): λ_{max} (ε_{max}) = 332 nm (13.2 $dm^3cm^{-1}mol^{-1}$), 516 (10.3), 812 (9.8). − **4b**: $C_{18}H_{42}Cl_2N_6NiO_8$ (600.2): calcd. C 36.0, H 7.1, Cl 11.8, N 14.0; found C 36.0, H 7.6, Cl 11.1, N 14.5. − IR (Nujol): $\tilde{\nu}$ = 3348, 3301, 3287 sh, 3276 sh, 3209 cm^{-1} (ν N−H); 1607 (δ N−H), 1099 and 625 (ClO_4^-). − UV/Vis (methanol): λ_{max} (ε_{max}) = 331 nm (14.8 $dm^3cm^{-1}mol^{-1}$), 514 (10.6), 814 (9.8).

[2,9-Bis(ammoniomethyl)-5,7,7,12,14,14-hexamethyl-1,4,8,11-tetraazacyclotetradecane]nickel(II) Tetrachloride (5aγ): The fraction containing **4a** in hydrochloric acid, eluted from the Dowex column as described above, was concentrated to dryness. The remaining oily residue was crystallized from methanol. Orange crystals were filtered off and dried in vacuo. − $C_{18}H_{44}Cl_4N_6Ni \cdot H_2O$ (563.1): calcd. C 38.4, H 8.2, Cl 25.2, N 14.9; found C 38.2, H 8.1, Cl 25.2, N 14.9. − IR (Nujol): $\tilde{\nu}$ = 3401 cm^{-1} (ν O−H), 3106, 3070 (ν N−H); 1607 and 1541 (δ N−H and δ O−H). − UV/Vis (methanol): λ_{max} (ε_{max}) = 452 nm (117 $dm^3cm^{-1}mol^{-1}$).

[2,9-Bis(ammoniomethyl)-5,7,7,12,14,14-hexamethyl-1,4,8,11-tetraazacyclotetradecane]nickel(II) Tetraperchlorate (5aβ): Complex **4a** (0.124 g, 0.2 mmol) was dissolved in 1 mL of nitromethane, acidified with perchloric acid (70%, 0.2 mL). The solution was then diluted with absolute ethanol (10 mL), whereupon the color changed from deep-red to orange. The solvents were removed under reduced pressure to leave an orange solid (ca. 0.10 g), which was washed with ethanol and dried in vacuo. The complex **5aβ** isomerized into **5aγ** (tetraperchlorate tetrahydrate) during recrystallization from ethanol. − **5aβ**: $C_{18}H_{44}Cl_4N_6NiO_{16} \cdot 4\ H_2O$ (873.2): calcd. C 24.8, H 6.0, Cl 16.2, N 9.6; found C 24.3, H 6.2, Cl 17.0, N 9.4. − IR (Nujol): $\tilde{\nu}$ = 3598, 3543 cm^{-1} (ν O−H); 3191 (ν N−H), 1620 and 1531 (δ N−H and δ O−H); 1095, 625 (ClO_4^-). − UV/Vis (nitromethane): λ_{max} (ε_{max}) = 462 nm (115 $dm^3cm^{-1}mol^{-1}$). − **5aγ**: $C_{18}H_{44}Cl_4N_6NiO_{16} \cdot 4\ H_2O$ (873.2): calcd. C 24.8, H 6.0, Cl 16.2, N 9.6; found C 24.9, H 5.9, Cl 16.0, N 9.7. − IR (Nujol): $\tilde{\nu}$ = 3610 sh, 3536 cm^{-1} (ν O−H); 3189 (ν N−H), 1619 sh, 1598, 1521 (δ N−H and δ O−H); 1107, 624 (ClO_4^-). − UV/Vis (nitromethane): λ_{max} (ε_{max}) = 454 nm (120 $dm^3cm^{-1}mol^{-1}$).

2*SR*,9*SR*-Bis(aminomethyl)-5*SR*,7,7,12*SR*,14,14-hexamethyl-1,4,8,11-tetraazacyclotetradecane (6a): A mixture of sodium cyanide (0.75 g, 0.015 mol) and complex **4a** (1.5 g, 2.5 mmol) in 50 mL of water was refluxed for 2 h. After cooling, sodium hydroxide (2 g) was added and the solution was extracted with chloroform. The combined chloroform extracts were dried with magnesium sulfate, filtered, and concentrated to dryness. The oily residue was dissolved in acetonitrile (5 ml) and the resulting solution was stored

Table 5. Crystal data and measurement conditions for **4a** and **4b**

	4a	**4b**
Formula	$C_{18}H_{42}Cl_2N_6NiO_8 \cdot H_2O$	$C_{18}H_{42}Cl_2N_6NiO_8$
Molecular weight	618.19	600.17
Crystal system	monoclinic	orthorhombic
a [Å]	10.692(1)	16.417(2)
b [Å]	20.985(2)	16.039(2)
c [Å]	12.614(1)	20.384(3)
β [°]	99.74(1)	90
V [Å^3]	2789.4(5)	5367.4(12)
Z	4	8
Calculated density [g · cm^{-3}]	1.47	1.49
Space group	$P2_1/n$	*Pbca*
Radiation (graphite-monochromated)	Mo-K_α	Mo-K_α
Wavelength [Å]	0.71069	0.71069
Linear absorption coeff. μ [mm^{-1}]	0.94	0.97
Number of electrons *F*(000)	1312	2544
Crystal size [mm]	0.25 × 0.22 × 0.18	0.27×0.23×0.21
Temperature [°C]	22 ± 1	22 ± 1
Diffractometer	Syntex $P2_1$	Syntex $P2_1$
Scan mode	Θ/2Θ	Θ/2Θ
Scan range (2Θ) [°]	0−54	0−54
Number of collected data:		
totally measured	2666	2739
unique [with $I > 2\sigma(I)$]	2138	2081
*R*1	0.0595	0.0666
*wR*2	0.1140	0.1262
GooF	1.092	1.089

in a refrigerator until crystals formed. After ca. one week, 0.7 g (81%) of colorless crystals were filtered off and dried in vacuo; m.p. 89−90°C. − $C_{18}H_{42}N_6 \cdot 2\ H_2O$ (378.4): calcd. C 57.1, H 12.2, N 22.2; found C 57.7, H 12.1, N 21.8. − HR MS: calcd. for $C_{18}H_{42}N_6$ 342.3471; found 342.3467.

2*SR*,9*SR*-Bis(aminomethyl)-5*RS*,7,7,12*SR*,14,14-hexamethyl-1,4,8,11-tetraazacyclotetradecane (6b): The free ligand was prepared from complex **4b** according to the same procedure as above; m.p. 92−96°C. − Yield 80%. − $C_{18}H_{42}N_6 \cdot H_2O$ (360.4): calcd. C 60.0, H 12.3, N 23.3; found C 60.2, H 12.0, N 23.1. − HR MS: calcd. for $C_{18}H_{42}N_6$ 342.3471; found 342.3457.

X-ray Crystallography: Well-shaped crystals of compounds **4a** and **4b** were selected for X-ray-diffractometric measurements. In both cases, the cell constants were obtained from least-squares refinement based on 25 setting angles. The stabilities of the crystals were checked by monitoring 2 control reflections at 50 reflection intervals; no appreciable decay was observed. Lorentz and polarization corrections were applied to all collected data. No absorption corrections were performed at the measurement stage. Table 5 shows the crystal data and measurement conditions for **4a** and **4b**. Models of the two structures were obtained by direct methods using the program SHELXS-86[21] and a series of subsequent Fourier difference syntheses (program SHELX-93[22]) revealed the positional parameters for all non-hydrogen atoms. The same refinement procedure was applied in both cases: Initially, the positional and isotropic temperature factors for non-hydrogen atoms were refined by full-matrix, least-squares procedures (program SHELX-93). Further refinement steps were performed in anisotropic mode for the non-hydrogen atoms. The positional parameters for *C*-attached hydrogen atoms were calculated from assumed geometries. They were added to parameter sets and refined in isotropic mode in separate blocks. The highest residual electron density peaks observed in each case on final difference maps were below 0.4 eÅ^{-3}.

Crystallographic data (excluding structure factors) for the structures reported in this paper have been deposited with the Cambridge Crystallographic Data Centre as supplementary publication no. CCDC-101460. Copies of the data can be obtained free of charge on application to CCDC, 12 Union Road, Cambridge CB2 1EZ, U.K. [Fax: (internat.) + 44-1223/336033; E-mail: deposit@ccdc.cam.ac.uk].

Acknowledgments

The authors are grateful to Dr. K. Wozniak for assistance in the preparation of X-ray data for publication.

[1] T. A. Kaden, *Top. Curr. Chem.* **1984**, *121*, 157−180.
[2] P. V. Bernhardt, G. L. Lawrance, *Coord. Chem. Rev.* **1990**, *104*, 297−343.
[3] J. W. Krajewski, P. Gluziński, B. Korybut-Daszkiewicz, A. Kemme, A. Mishniov, *Bull. Acad. Polon. Sci., Ser. Sci. Chem.* **1991**, *39*, 279−285.
[4] E. Kimura, *Crown Ethers and Analogous Compounds*, in *Studies in Organic Chemistry*, vol. 45 (Ed.: M. Hiraoka), Elsevier, **1992**, pp. 381−478.
[5] J. W. Krajewski, P. Gluziński, B. Korybut-Daszkiewicz, A. Mishnev, A. Kemme, *J. Chem. Soc., Dalton Trans.* **1991**, 53−56.
[6] T. W. Hambley, G. A. Lawrance, M. Maeder, E. N. Wilkes, *Inorg. Chim. Acta* **1996**, *246*, 65−71.
[7] P. Gluziński, J. W. Krajewski, B. Korybut-Daszkiewicz, A. Mishnev, A. Kemme, *J. Crystallogr. Spectr. Res.* **1993**, *23*, 61−64.
[8] P. Gluziński, J. W. Krajewski, R. A. Koliński, B. Korybut-Daszkiewicz, A. Mishnev, A. Kemme, *Pol. J. Chem.* **1994**, *68*, 2567−2588.
[9] P. Gluziński, J. W. Krajewski, R. A. Koliński, B. Korybut-Daszkiewicz, A. Mishnev, A. Kemme, *Pol. J. Chem.* **1995**, *69*, 350−360.
[10] B. Korybut-Daszkiewicz, *J. Chem. Soc., Dalton Trans.* **1992**, 1673−1679.
[11] R. Bucourt, *Top. Stereochem.* **1974**, *8*, 159−224.
[12] J. C. A. Boeyens, S. M. Dobson, "Stereochemistry of Metallic Macrocyclics" in *Stereochemical and Stereophysical Behaviour of Macrocycles* (Ed.: I. Bernal), Elsevier, New York, **1987**, p. 1−102.
[13] *IUPAC Nomenclature of Organic Chemistry, Section E, Stereochemistry*, Recommendation 1974, *Pure Appl. Chem.* **1976, 45**, 11.
[14] R. A. Koliński, B. Korybut-Daszkiewicz, *Inorg. Chim. Acta* **1975**, *14*, 237−245.
[15] R. A. Koliński, B. Korybut-Daszkiewicz, Z. Kubaj, J. Mroziński, *Inorg. Chim. Acta* **1982**, *57*, 269−280.
[16] L. G. Warner, N. J. Rose, D. H. Busch, *J. Am. Chem. Soc.* **1968**, *90*, 6938−6946.
[17] L. G. Warner, D. H. Busch, *J. Am. Chem. Soc.* **1969**, *91*, 4092−4101.
[18] H. Kobayashi, B. Korybut-Daszkiewicz, *Bull. Chem. Soc. Jpn.* **1972**, *45*, 2485−2490.
[19] S.-G. Kang, M.-S. Kim, D. Whang, K. Kim, *J. Chem. Soc., Dalton Trans.* **1994**, 853−857.
[20] A. I. Vogel, *Textbook of Practical Organic Chemistry*, 5th ed., Wiley, New York, **1989**, p. 487.
[21] G. M. Sheldrick, *SHELXS-86*, University of Göttingen, **1986**.
[22] G. M. Sheldrick, *SHELXL-93*, University of Göttingen, **1993**.

Received May 7, 1998
[98139]

Synthesis and Investigation of Chalcogen Atom Substituted Dinitriles and Porphyrazines

Anthony E. Pullen,* Christophe Faulmann, and Patrick Cassoux*

Keywords: Phthalocyanines / Porphyrazines / Macrocycles / Chalcogen atom substitution

A series of chalcogen atom substituted porphyrazines have been assembled and characterized. Oxygen and sulfur chalcogen atoms have been substituted for peripheral methylene groups. Heteroatom-enriched, seven-membered ring dinitriles (**1**–**3**) were synthesized and characterized by IR, MS, UV-vis, ^{1}H NMR, elemental analysis, and X-ray analysis to examine the ring conformations. They were template cyclized in the presence of Mg^{II} to form the Mg^{II} containing porphyrazine macrocycles. The Mg^{II} and metal-free macrocycles (**4**–**9**) were synthesized for all peripherally substituted porphyrazines. The unchalcogen-substituted Ni^{II}, Cu^{II}, and Zn^{II} containing porphyrazine derivatives (**10**–**12**) were also synthesized because of the higher solubility of the metal-free porphyrazine **7**. The macrocycles were characterized and studied using such techniques as UV-vis, IR, elemental analysis, cyclic voltammetry, and electrical conductivity measurements.

Introduction

Phthalocyanines and porphyrins have received considerable attention due to the number of applications that these two families of compounds have been employed, and also for their interesting properties.[1] Among their many applications, phthalocyanines have often been studied for their electrical conductivity,[2] liquid-crystalline properties[3] and use as pigments.[4] Porphyrins for example, have been studied for their magnetic[5] and catalytic[6] properties and their role in biomolecular processes.[7] Another family of similar conjugated macrocycles that have received considerably less attention than the phthalocyanines or porphyrins, are the porphyrazines (also called tetraazaporphyrazines).[8][9] Recently, a significant amount of work has been made with these systems. Hoffman and coworkers for example, have reported the synthesis of polymetallic porphyrazines and a novel metal-linked porphyrazine dimer.[10–13]

Efforts have also been made studying porphyrazines substituted with long alkyl chains for applications in liquid crystals and Langmuir–Blodgett layers.[14] Hemiporphyrazines, a slightly different class of porphyrazines which exhibit a box-like geometry, have also been recently reported. They have been used in the assembly of Langmuir–Blodgett layers[15] and ladder polymers and oligomers.[16]
Bryce and coworkers have applied porphyrazines in supramolecular chemistry by synthesizing pyrazinoporphyrazines with pendant TTF (tetrathiafulvalene) units.[17] Along a similar line, other modifications to the porphyrazine system may be envisioned, for example, a synthetic goal would be to incorporate chalcogen atoms with large diffuse atomic orbitals directly into the periphery of the planar, conjugated porphyrazine macrocycle. An additional related goal would be also to determine their feasibility for use in chalcogen-rich electrically conducting complexes. Despite the enormous amount of research currently being carried out worldwide in the areas of phthalocyanines, porphyrins, and porphyrazines, to our knowledge only the work recently reported by Swager and coworkers[18] has chalcogen-atom incorporation been investigated for these types of macrocycles. This idea has been extensively utilized in the field of the synthesis of chalcogen-rich, planar and fully conjugated organic donor and acceptor molecules. Such well-known examples are TTF, BEDT-TTF (bisethylenedithiotetrathiafulvalene), and square planar metal bis-dmit (dmit = 2-thione-1,3-dithiole-4,5-dithiolato) complexes, which have been used in the assembly of superconducting partial-oxidation state materials.[19] In this paper, we report the findings of a study of the synthesis and characterization of a series of chalcogen-enriched porphyrazine macrocycles and their possible use for future incorporation into electrically conductive materials. Four methylene groups in the periphery of the porphyrazine molecule have been substituted by oxygen and sulfur atoms. Seven-membered ring dinitrile compounds were first synthesized with a methylene (**1**), sulfur (**2**), or oxygen (**3**) group in the five position. Single crystal X-ray structures were obtained for compounds **1**–**3** to understand the ring conformations. The Mg^{II} and

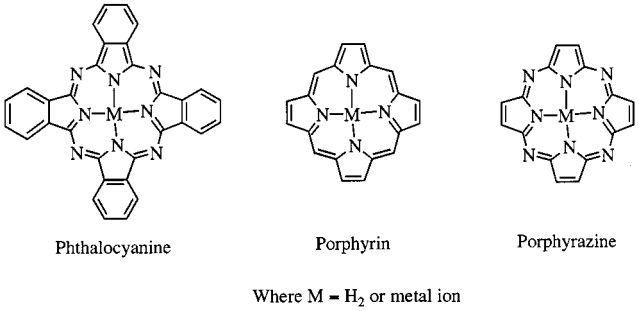
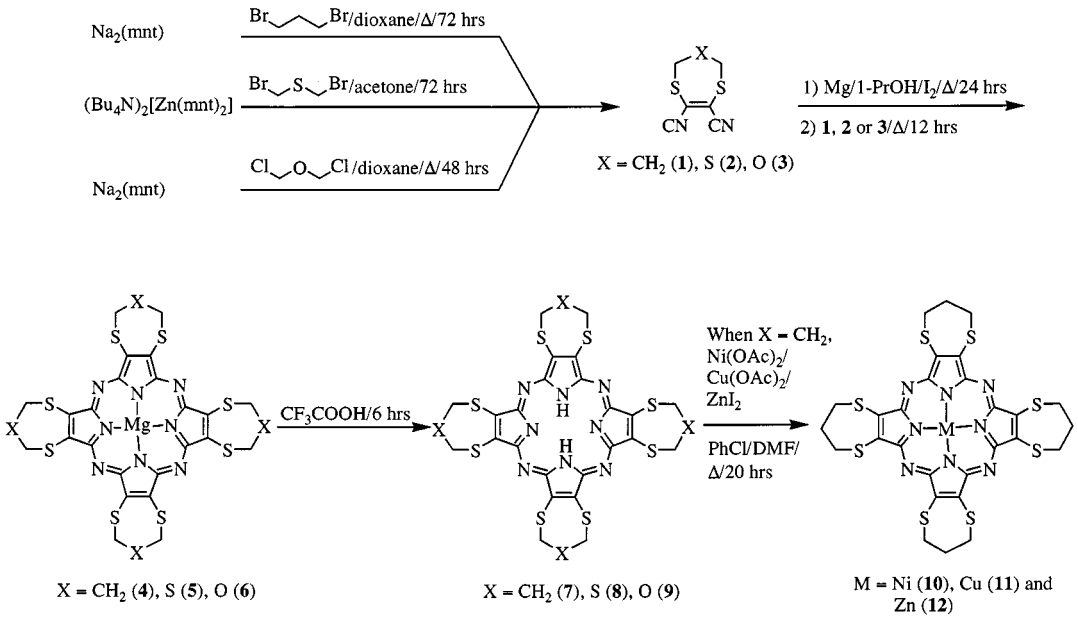


Figure 1. Figure showing general structural differences between phthalocyanines, porphyrins, and porphyrazines

[a] Equipe Précurseurs Moléculaires et Matériaux, Laboratoire de Chimie de Coordination du CNRS,
205 Route de Narbonne, 31077 Toulouse Cédex, France
Fax: (internat.) +33 (0)561/ 553003
E-mail: pullen@lcctoul.lcc-toulouse.fr
cassoux@lcctoul.lcc-toulouse.fr

 © WILEY-VCH Verlag GmbH, D-69451 Weinheim, 1999 1434–1948/99/0202–0269 $ 17.50+.50/0



Scheme 1. Synthesis of chalcogen atom substituted dinitriles and related porphyrazines

H_2 containing porphyrazines (**4**−**9**), which were cyclized from the dinitriles, have been synthesized along with the Ni^{II}, Cu^{II}, and Zn^{II} containing macrocycles of the methylene derivative (**10**−**12**). Their electronic spectra and electrochemical properties have been examined and compared to similar reported systems. Also, two-probe pressed-pellet electrical conductivity measurements have been carried out on some of the compounds.

Synthesis of the Porphyrazine Macrocycles

The syntheses of compounds **1**−**12** are shown in Scheme 1. Dinitriles 3,7-dithiacycloheptamaleonitrile (**1**) and 3,7-dithia-5-oxocycloheptamaleonitrile (**3**) were assembled by the reaction of mnt^{2-} ligand with the corresponding dihalide in high dilution conditions in refluxing dioxane over a period of 3 days to obtain yields of 14 and 25% respectively.

3,5,7-trithiacycloheptamaleonitrile (**2**) was synthesized in 67% yield by the reaction of $S(CH_2Br)_2$ with the labile $(Bu_4N)_2[Zn(mnt)_2]$ complex in acetone at room temperature over the same period of time. All three dinitriles had to be purified by column chromatography due to the large amount of dimeric, trimeric and oligomeric side products with similar solubilities. In a previous paper by Spannenberg et al.,[20] compound **1** was synthesized, isolated, and characterized along with the dimeric and trimeric cyclization products. The dimeric and trimeric forms were not of interest in this work. The crystal structures of the three dinitriles **1**−**3** are shown in Figure 2 and selected bond lengths and angles are listed in Table 1.

Their structures were obtained to examine the conformation of the seven-membered rings due to the inability to obtain crystal structures of the ensuing porphyrazine macrocycles. In Figures 2a for 3,7-dithiacycloheptamaleonitrile (**1**) and 2b for 3,5,7-trithiacycloheptamaleonitrile (**2**), both compounds exhibit similar twisted ring conformations. In compound **1**, the dihedral angle between the S1′−C3′−C3−S1 and C2′−C1−C2 planes is 45.48(8)° while for **2** the dihedral angle between the S1−C1−C2−S2 and C5−S3−C6 planes is almost the same at 45.44(17)°. Figures 2c and d each show a different view of the same compound 3,7-dithia-5-oxocycloheptamaleonitrile (**3**). Figure 2c is in the same perspective as for compounds **1** and **2** while Figure 2d is a profile view down the axis of the C1=C2 bond showing a chair-like conformation of the ring unlike that seen for **1** and **2**. This is in contrast to the twisted ring conformations of compounds **1** and **2**. The S1−C5−C6−S2 plane is folded at the sulfur atoms at an angle of 56.76(6)° from the S1−C1−C2−S2 plane and 70.12(15)° from the C5−C6−O1 plane. The square planar metal complexes $(Et_4N)[Cu(pddt)_2]$ (where pddt = $C_5H_6S_4^{2-}$ = 1,3-propanediyldithioethylene-1,2-dithiolato),[21] $(Bu_4N)[Pd(dtdt)_2]$ (where dtdt = $C_4H_4S_5^{2-}$ = 5,7-dihydro-1,4,6-trithiin-2,3-dithiolato),[22] and $(Ph_4P)[Cu(diod)_2]$ (where diod = $C_4H_4OS_4^{2-}$ = 1,4-dithia-6-oxa-2,3-dithiolato)[23] have been reported and the ligands contain the seven-membered rings as compounds **1**−**3** do respectively. It is interesting to note that in every instance, the rings are in a chair-like conformation like compound **3**. For $(Ph_4P)[Cu(diod)_2]$, the fold angles of the planes at the ring sulfur atoms was reported as 61.2° which is greater than for **3** [56.76°(6)]. The angle of the C−O−C plane reported for $(Ph_4P)[Cu(diod)_2]$ is 65.9°, smaller than that found in compound **3** of 70.12(15)°.[23]

The conversion of the dinitriles to the Mg^{II} porphyrazine macrocycles Mg(dtchp) (**4**), Mg(ttchp) (**5**) and Mg(dochp) (**6**) were achieved following slightly modified procedures by Linstead and Whalley[8b] in refluxing Mg alkoxide suspensions. To remove Mg^{II} and to synthesize the metal-free porphyrazines H_2(dtchp) (**7**), H_2(ttchp) (**8**), and H_2(dochp) (**9**),

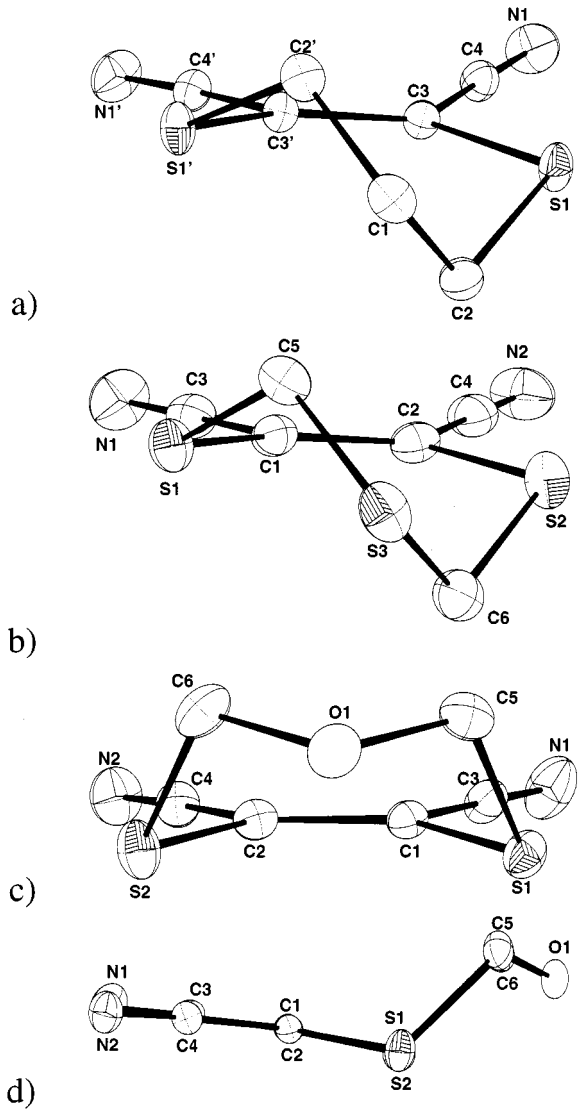


Figure 2. Thermal ellipsoids drawings (30% probability) and numbering schemes for the dinitriles (a) 3,7-dithiacycloheptamaleonitrile (**1**), (b) 3,5,7-trithiacycloheptamaleonitrile (**2**), (c) 3,7-dithia-5-oxocycloheptamaleonitrile (**3**), (d) Profile view down the axis of the C1−C2 double bond of **3** showing the chair-like conformation of the seven-membered ring. Hydrogen atoms have been omitted for clarity.

compounds **4**−**6** were treated with trifluoroacetic acid followed by aqueous precipitation and neutralization with ammonia.[10b] This method resulted in clean demetallation and yielded compounds **7**−**9** in up to 83% yield.

Purification of H_2(dtchp) (**7**) was achieved using column chromatography. The sulfur and oxygen peripherally substituted compounds H_2(ttchp) (**8**) and H_2(dochp) (**9**) could not be purified with column chromatography due to their rather low solubility in common organic solvents. Sublimation was attempted as it has been shown to purify phthalocyanines.[16] In both cases though, black insoluble materials resulted and no sublimation products were observed. Nevertheless, **8** and **9** can be purified through exhaustive washing.

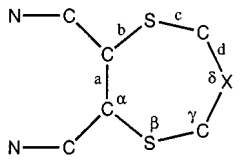
Due to the adequate solubility of H_2(dtchp) (**7**), facile insertion of Ni^{II}, Cu^{II}, and Zn^{II} ions into the core of the macrocycle was accomplished to assemble compounds **10**−**12**. This was completed by refluxing anhydrous $Ni(OAc)_2$, $Cu(OAc)_2$, and ZnI_2 respectively with the metal-free porphyrazine in a mixture of PhCl/DMF over a period of 20 hours.[12]

Electronic Absorption Spectroscopy

Phthalocyanines and porphyrazines give similar and characteristic absorption spectra as it is a valuable tool in determining their synthesis.[4b] This is important in this study due to the inability to obtain single-crystal X-ray structures of the macrocycles. Table 2 lists the electronic band maxima for all compounds synthesized. Figure 3 shows the spectra for compounds **4** and **7** which are representative of all of the Mg^{II} and metal-free compounds assembled in this study along with the Ni^{II}, Cu^{II} and Zn^{II} containing macrocycles of the methylene derivative, **10**−**12**.

The optical spectra for the four-fold symmetric Mg^{II} derivatives Mg(dtchp) (**4**), Mg(ttchp) (**5**), and Mg(dochp) (**6**) are nearly identical. They exhibit an intense single Soret band at approximately 368−370 nm, a weak shoulder absorption at 510−538 nm and an intense Q band at 656−664 nm. This is similar to that seen for metal phthalocyanines.[1] The Soret and Q band region absorptions are attributed to

Table 1. Selected and averaged bond lengths [Å] and angles [°] for compounds **1**−**3** [where X = CH_2 (**1**), S (**2**), or O (**3**)]



	1	2	3		1	2	3
a	1.352(3)	1.367(6)	1.354(3)	α	130.59(5)	130.9(3)	126.38(15)
b	1.7558(15)	1.745(4)	1.7524(19)	β	101.98(7)	102.4(2)	104.15(10)
c	1.8149(16)	1.799(5)	1.818(2)	γ	113.59(10)	115.2(3)	115.28(15)
d	1.5155(19)	1.794(5)	1.403(3)	δ	112.71(18)	98.2(2)	113.70(16)

Table 2. Electronic band maxima (λ_{max}, nm) and log ε values for compounds **4**−**12** along with M(pc) (where M = Mg, H_2, Ni, Cu, or Zn)[4b] values for comparison (measured in CH_2Cl_2 unless noted otherwise)

Compound	λ_{max} (log ε)
Mg(dtchp) (**4**)	370 (4.30), 538 (3.69), 612 (3.82), 664 (4.15)
Mg(ttchp) (**5**)	368 (4.50), 514 (4.10) 610 (4.15), 656 (4.29)
Mg(dochp) (**6**)	370 (4.32), 518 (3.93), 610 (3.99), 656 (4.15)
Mg(pc)[a]	347 (4.73), 610 (4.45), 647 (4.39), 674 (4.94)
H_2(dtchp) (**7**)	358 (4.37), 526 (4.02), 614 (3.99), 700 (3.98)
H_2(ttchp) (**8**)[b]	346 (5.10), 518 (4.81), 610 (4.81), 680 (4.75)
H_2(dochp) (**9**)[b]	346 (6.10), 514 (5.84), 616 (5.84), 686 (5.77)
H_2(pc)[c]	350 (4.74), 602 (4.43), 638 (4.62), 665 (5.18), 698 (5.21)
Ni(dtchp) (**10**)[d]	342 (4.85), 508 (4.55), 640 (4.61)
Ni(pc)[c]	351 (4.57), 643 (4.51), 671 (5.10)
Cu(dtchp) (**11**)[b]	352 (4.80), 536 (4.49), 656 (4.60)
Cu(pc)[c]	351 (4.57), 643 (4.51), 671 (5.10)
Zn(dtchp) (**12**)[b]	372 (4.73), 556 (4.20), 666 (4.56)
Zn(pc)[a]	348 (4.81), 607 (4.59), 646 (4.56), 672(5.45)

[a] Measured in pyridine. − [b] In DMF. − [c] In chloronapthalene. − [d] In chlorobenzene.

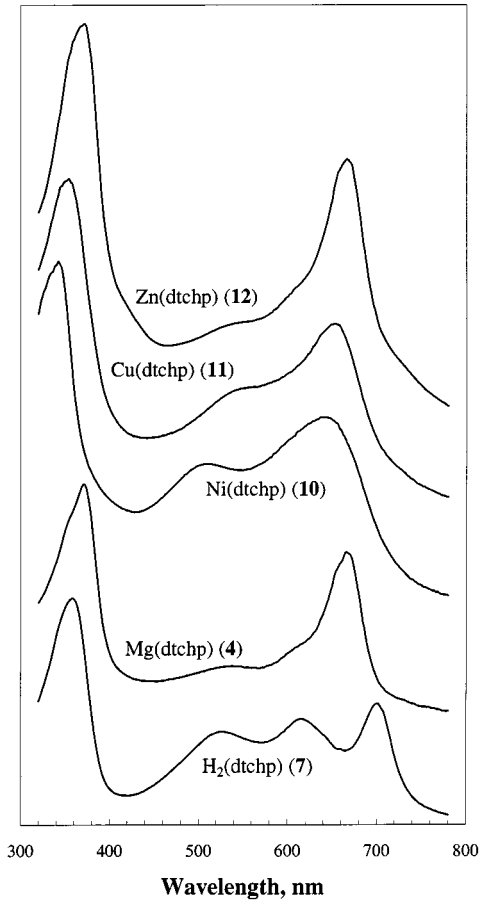


Figure 3. Comparison of the UV-vis absorption spectra for the metal-free derivative H_2(dtchp) (**7**) and metal-containing derivatives Mg(dtchp) (**4**), Ni(dtchp) (**10**), Cu(dtchp) (**11**), and Zn(dtchp) (**12**)

π→π* transitions from the a_{1u}, a_{2u} HOMOs to the doubly degenerate (e_g) LUMOs.[12] The optical spectra of H_2(dtchp) (**7**), H_2(ttchp) (**8**), and H_2(dochp) (**9**) which are also very similar, show a splitting of the Q band found at 656−664 nm for compounds **4**−**6**. This is due to the lowering of symmetry from four-fold (D_{4h}) to two-fold (D_{2h}) symmetry for the metal-free derivatives **7**−**9**, and removal of the degeneracy of the e_g LUMOs.[4b] Also observed in each is a slight red-shift of the Soret band in the metal-free compounds. This behavior observed in the Soret and Q band regions is typical for substituted porphyrazines.[8][10−12][14][24] In difference to metal and metal-free phthalocyanines, we observe a definite broadening of the absorptions in compounds **4**−**9**.[4b] This has also been observed in several instances in other sulfur-containing porphyrazines. With 8 sulfur atoms in the periphery of the CH_2 derivative and more so with 12 sulfur and oxygen atoms in the periphery of the other new porphyrazine derivatives reported here, there are probably significant contributions to the spectra from underlying n→π* transitions from the lone pair electrons of the heteroatoms.[12] Like Mg(dtchp) (**4**), the D_{4h} Ni^{II}, Cu^{II}, and Zn^{II} derivatives, Ni(dtchp) (**10**), Cu(dtchp) (**11**), and Zn(dtchp) (**12**), show similar spectra with an intense Soret band and Q band with a weaker absorption in the 500−560 nm region. In the case of the Ni^{II} derivative, the Soret band at 342 nm, the weak absorption at 508 nm and the Q band region absorption at 640 nm are the most red-shifted absorptions of all the new metal derivatives presented here. In comparison to the Mg^{II} derivative, this is not observed in metal phthalocyanines as the Mg^{II} and Ni^{II} derivatives give absorptions at nearly the same wavelengths (Table 2). This effect has been seen in other thio-substituted porphyrazines.[24]

Redox Properties of H_2(dtchp) (7)

The redox properties of H_2(dtchp) (**7**) have been investigated with cyclic voltammetry. The $E_{1/2}$ values are found in Table 3 along with other related porphyrazine and phthalocyanine systems for comparison. Potentials as high as +0.90 V were reached (vs. SCE, CH_2Cl_2, 0.1 M Bu_4NPF_6) with **7** but no oxidation process were found. Upon scanning cathodically, two low-potential redox couples were observed with $E_{1/2}$ values of −0.95 and −1.29 V (vs. Fc/Fc^+ couple; $E_a - E_c$ = 120 and 250 mV and $i_{p,a}/i_{p,c}$ = 0.80 and 0.91 respectively).

Table 3. Cyclic voltammetric half-wave potentials (V, reported vs. Fc/Fc^+ couple) for the reduction of H_2(dtchp) (**7**)[a] and similarly related compounds for comparison

Compound	$E_{1/2}{}^1$	$E_{1/2}{}^2$
H_2(dtchp) (**7**)	−0.95	−1.29
H_2(obtp)[b]	−0.85	−1.19
H_2(obcbp)[c]	−0.8	−1.2
H_2(pc)[d]	−1.20	−1.54

[a] Conditions: scan rate, 100 mV/s; reference electrode, standard calomel; working electrode, Au plate; 0.1 M Bu_4NPF_6 electrolyte in CH_2Cl_2 under argon at room temperature. − [b] Ref.[11b] − [c] Ref.[12] − [d] Ref.[25]

These values are slightly lower than the tetrathioether-substituted porphyrazines H_2(obcbp) [obcbp = octa(4-butyloxycarbonylbenzylthio) porphyrazine, −0.8 and −1.2 V] and H_2(obtp) [obtp = octa(benzylthio) porphyrazine, −0.85 and −1.19 V] reported by Hoffman and coworkers.[11b][12] These compounds were also reported to exhibit no oxidation processes as seen in the H_2(dtchp) (**7**) system. This is in contrast to phthalocyanines which can exhibit oxidation processes that are typically irreversible along with their reversible reduction couples. The $E_{1/2}$ values for the ring reductions for H_2(pc) (−1.20 and −1.54 V) are lower than the values for the porphyrazines reported and discussed here.[12,25]

Conductivity Measurements

As said above, one side goal of this work was to determine the feasibility for use of the chalcogen-rich porphyrazines studied here in the preparation of electrically conducting complexes. Preliminary electrical conductivity studies have been completed and measurements of compounds H_2(dtchp) (**7**), Ni(dtchp) (**10**), and Cu(dtchp) (**11**) exhibited pressed-pellet conductivities of $<10^{-12}$ S/cm. It is thus clear that this result doesn't live up the expectations. Moreover, even the metal-free H_2(dtchp) is not oxidized at potentials below 0.9 V/SCE, and the lack of solubility of most of the studied porphyrazines severely limits a more detailed analysis.

Conclusions

We have synthesized a series of chalcogen-substituted dinitrile isologues and they have been characterized and investigated using a variety of techniques including single-crystal X-ray analysis. Compounds **1** and **2** show a twisted conformation of the seven-membered rings while **3** exhibits a chair conformation. The dinitriles were cyclized in Mg propoxide suspensions to assemble the macrocyclic Mg^{II} porphyrazines. The metal-free porphyrazines were obtained by treatment with trifluoroacetic acid. The electronic spectra of the Mg^{II} and metal-free porphyrazines show very little variance with the substitution of O or S for a methylene group in the periphery. Due to the low-solubility of the peripherally substituted oxygen and sulfur derivatives, only the higher soluble methylene substituted porphyrazine H_2(dtchp) (**7**) could be further studied. Compound **7** could be purified via column chromatography and cyclic voltammetry studies showed it exhibits two low-potential reduction couples. The Ni^{II}, Cu^{II}, and Zn^{II} containing porphyrazines were then assembled and characterized. Due to the fact that the solubility of the porphyrazines studied here is lowered when chalcogen atoms are incorporated into the structure, future directions must also consist of the addition of solubility improving groups, such as long alkyl chains. This may then allow chalcogen atom enhanced porphyrazine derivatives to be further studied for metal coordination, electrochemical, and electrical conductivity studies.

Experimental Section

General Procedures and Chemicals: All reactions unless otherwise noted were carried out under an argon atmosphere. All solvents were purified following standard procedures. Compounds Na_2mnt and $(Bu_4N)_2[Zn(mnt)_2]$ were synthesized according to Davison et al.[26] Bis(chloromethyl) ether and bis(bromomethyl) thioether were synthesized following Buc[27] and Komoto et al.,[28] respectively. − Column chromatography was carried out using silica gel 60 (Merck, 63−200 μm particle size), and POLGRAM SIL G/UV 254 (Macherey-Nagel, 0.25 mm thickness) was used for TLC experiments. − Elemental analyses were performed by the Microanalysis Service at the LCC-CNRS, Toulouse. − Mass spectra were obtained at the Joint Mass Spectrometry Service at Paul Sabatier University, Toulouse. − Melting points were obtained using a Stuart Scientific SMP1 melting point apparatus and are uncorrected. − UV-vis spectra were recorded on a Hewlett Packard 8452A spectrophotometer. − IR spectra were obtained on a Perkin Elmer 1725X FT-IR spectrometer as KBr pellets. − NMR spectra were recorded on a Bruker AC 200 MHz instrument.

Preparation of 3,7-Dithiacycloheptamaleonitrile (1): Compound **1** was prepared, isolated, and purified according to Spannenberg et al.,[20] and its elemental analysis was in agreement with that reported.

3,5,7-Trithiacycloheptamaleonitrile (2): An 8.0 g ($9.63\cdot10^{-3}$ mol) amount of $(Bu_4N)_2[Zn(mnt)_2]$ was dissolved in 350 ml of acetone. Dropwise was added 4.30 g (0.020 mol) of bisbromomethyl thioether to the rapidly stirring solution. The stirring was continued and the solution turned from a pale yellow to a deep red color after 3 days. At this time, the solvent was evaporated to leave a dark-red oil. The product was isolated with column chromatography using CH_2Cl_2 as eluent (R_f = 0.73). The solid was recrystallized using CH_2Cl_2/hexane to yield 2.60 g of **2** (67%) as yellow platelets, m. p. 91−92°C. − $C_6H_4N_2S_3$ (200.29): calcd. C 35.98, H 2.01, N 13.99; found C 35.95, H 1.55, N 13.69. − ^{1}H NMR ($CDCl_3$): δ = 4.82 (s, 4 H). − IR (KBr): $\tilde{\nu}$ = 2996 cm^{-1} m, 2937 m, 2220 m, 1496 s, 1386 s, 1227 s, 1198 s, 1158 vs, 1117 m, 1033 m, 1008 m, 984 w, 850 m, 780 m, 734 vs, 490 vs. − UV/Vis (CH_2Cl_2): λ_{max} (lg ε) = 256 nm (4.46), 300 (4.46), 364 (4.43), 386 (4.42). − MS (FAB); *m/z* (%): 201 (100) [M + H^+].

3,7-Dithia-5-oxocycloheptamaleonitrile (3): Compound **3** was prepared similar to **1**. A 5.58 g (0.030 mol) sample of Na_2mnt was placed in 600 ml of dioxane under an argon atmosphere allowed to react with 3.45 g (0.030 mol) of bis(chloromethyl) ether. The crude product was purified by column chromatography using CH_2Cl_2 as eluent (R_f = 0.88). The pale yellow microcrystalline product was recrystallized in CH_2Cl_2/hexane to yield 1.09 g (25%) of **3** as cream-colored plates, m. p. 133−134°C. $C_6H_4N_2OS_2$ (184.23): calcd. C 39.12, H 2.19, N 15.21; found C 39.36, H 1.64, N 15.13. − ^{1}H-NMR ($CDCl_3$): δ = 5.45 (s, 4 H). − IR (KBr): $\tilde{\nu}$ = 3006 cm^{-1} m, 2927 m, 2220 m, 1511 s, 1441 vs, 1401 sh, 1335 s, 1322 s, 1242 s, 1147 vs, 1067 vs, 998 s, 970 vs, 932 vs, 682 vs, 510 s. − UV/Vis (CH_2Cl_2): λ_{max} (lg ε) = 258 nm (2.38), 300 (2.40), 358 (2.38). − MS (EI, 70 eV); *m/z* (%): 184 (100) [M^+].

[Tetrakis(dithiacyclohepta)porphyrazinato]magnesium(II) [Mg(dtchp) (4)], [Tetrakis(trithiacyclohepta)porphyrazinato]magnesium(II) [Mg(ttchp) (5)], and [Tetrakis(dithiaoxocyclohepta)porphyrazinato]magnesium(II) [Mg(dochp) (6)]: The synthesis of the following Mg containing derivatives **4**−**6** were completed following previously reported procedures.[8b] Under an argon atmosphere, magnesium (Aldrich, 98%) was refluxed with 15 ml of 1-propanol with

Table 4. Crystallographic and acquisition data and refinement for compounds **1**−**3**

Compound	**1**	**2**	**3**
Formula	$C_7H_6N_2S_2$	$C_6H_4N_2S_3$	$C_6H_4N_2OS_2$
Molecular mass	182.26	200.29	184.23
Crystal system	Tetragonal	Orthorhombic	Monoclinic
Space group	$P4_12_12$	$I2cb$	$P2_1/c$
a [Å]	8.3297(10)	6.7361(9)	6.9920(10)
b [Å]	8.3297(10)	12.1566(18)	13.3750(16)
c [Å]	12.161(2)	20.332(3)	8.9440(12)
α [°]	90	90	90
β [°]	90	90	112.880(15)
γ [°]	90	90	90
U [Å^3]	843.8(2)	1665.0(4)	770.62(18)
Z	4	8	4
ρ (calcd.) [g cm^{-3}]	1.435	1.598	1.588
μ [mm^{-1}]	0.563	0.820	0.627
F (000)	376	816	376
T [K]	180(2)	180(2)	180(2)
Crystal size [mm^3]	0.38 × 0.38 × 0.25	0.45 × 0.40 × 0.13	0.38 × 0.25 × 0.25
θ Range for data collection [°]	3.84→24.23	1.95→24.39	2.90→24.20
hkl range:	$-9 \le h \le 9$; $-9 \le k \le 9$; $-13 \le l \le 14$	$-7 \le h \le 7$; $-14 \le k \le 13$; $-23 \le l \le 23$	$-7 \le h \le 8$; $-15 \le k \le 15$; $-10 \le l \le 10$
Data collected	6643	5120	4772
No. of measured reflections	671	1327	1219
No. of refined parameters	51	100	100
Min./max. height in final Δρ map [eÅ^{-3}]	−0.116/0.120	−0.341/0.325	−0.228/0.263
S : Goodness-of-fit on F^2	1.111	1.190	1.084
Final R [a,b] indices [$I > 2\sigma(I)$]	$R_1 = 0.0173$, $wR_2 = 0.0464$	$R_1 = 0.0356$, $wR_2 = 0.1074$	$R_1 = 0.0289$, $wR_2 = 0.0777$
R indices (all data)	$R_1 = 0.0174$, $wR_2 = 0.0465$	$R_1 = 0.0372$, $wR_2 = 0.1120$	$R_1 = 0.0320$, $wR_2 = 0.0795$
a and b values used in w	0.0243; 0.2028	0.0663; 2.02115	0.0321; 0.2856

[a] $R = \Sigma\ ||F_o| - |F_c||/\Sigma\ F_o$. − [b] $wR_2 = \{\Sigma[\ w(F_o^2-F_c^2)^2\ ]/\Sigma[w(F_o^2)^2\ ]\}^{1/2}$; $w = 1/[\sigma^2(F_o^2) + (aP)^2 + bP\ ]$ where P is $[2\ F_c^2 + \mathrm{Max}(F_o^2,0)\ ]/3$. $S = \mathrm{GoF} = \{\Sigma\ [\ w(F_o^2-F_c^2)^2\ ]/(n-p)\}^{1/2}$ where n is the number of reflections and p is the total number of parameters refined.

a crystal of iodine as initiator for 24 hours. To the grayish suspension was then added the dicyano compound **1**−**3** as a slurry in a small amount of 1-propanol. The mixture was stirred and refluxed for a minimum of 12 hours. The solution was filtered hot and the precipitate was washed with CH_2Cl_2 until the washings were pale blue. The filtrate and washings were combined and evaporated to dryness to give a blue-black product. The product was washed with water until the washings were clear followed by copious amounts of EtOH also until the washings were clear. The solid was dried under vacuum and recrystallized in CH_2Cl_2/2-propanol. − Mg(dtchp) (**4**): Yield 33%, dark-blue microcrystals. − IR (KBr): $\tilde{\nu}$ = 2962 cm^{-1} m, 2926 m, 1654 m, 1560 m, 1459 m, 1384 m, 1300 m, 1255 w, 1220 w, 1104 m, 1026 s, 802 s, 560 w. − $C_{28}H_{24}MgN_8S_8$ (753.34): calcd. C 44.64, H 3.21, N 14.87; found C 44.30, H 2.80, N 14.65. − UV/Vis (CH_2Cl_2): λ_{max} (lg ε) = 370 nm (4.30), 538 (3.69), 612 (3.82), 664 (4.15). − Mg(ttchp) (**5**): Yield 19%, dark-blue microcrystals. − IR (KBr): $\tilde{\nu}$ = 2963 cm^{-1} m, 2930 w, 2073 w, 1617 m, 1459 m, 1384 m, 1262 s, 1097 s, 1022 s, 801 vs, 559 w. − $C_{24}H_{16}MgN_8S_{12}$ (825.47): calcd. C 34.92, H 1.95, N 13.57; found C 34.20, H 1.30, N 13.41. − UV/Vis (CH_2Cl_2): λ_{max} (lg ε) = 368 nm (4.50), 514 (4.10), 610 (4.15), 656 (4.29). − Mg(dochp) (**6**): Yield 27%, dark-blue microcrystals. − IR (KBr): $\tilde{\nu}$ = 2950 cm^{-1} m, 2919 m, 1701 sh, 1623 s, 1472 m, 1372 w, 1310 s, 1245 w, 1215 w, 1034 vs, 897 s, 794 m, 756 m, 661 w, 558 s. − $C_{24}H_{16}MgN_8O_4S_8$ (761.22): calcd. C 37.87, H 2.12, N 14.72; found C 37.20, H 1.71, N 14.56. − UV/Vis (CH_2Cl_2): λ_{max} (lg ε) = 370 nm (4.32), 518 (3.93), 610 (3.99), 656 (4.15).

Tetrakis(dithiacyclohepta)porphyrazine [H_2(dtchp) (7)], Tetrakis(trithiacyclohepta)porphyrazine [H_2(ttchp) (8)], and Tetrakis(dithiaoxocyclohepta)porphyrazine [H_2(dochp) (9)]: The following procedure for the synthesis of the metal free derivatives is similar to that reported by Hoffman and coworkers.[11b] A sample of the Mg containing macrocycles **4**−**6** was dissolved in a minimal amount of trifluoroacetic acid and was placed in the dark for 6 hrs. The solution was filtered, slowly poured into ice water, neutralized with concentrated ammonia, and filtered again. The precipitate was washed extensively with 5% HCl/MeOH, distilled water followed by MeOH until the washings were clear. The product was dried under vacuum and for H_2(dtchp) (**7**), purified with column chromatography (R_f = 0.90) with 5% MeOH/CH_2Cl_2 as eluent. − H_2(dtchp) (**7**): Yield 75%, blue-black powder. − IR (KBr): $\tilde{\nu}$ = 2962 cm^{-1} m, 2924 m, 2347 w, 1711 m, 1697 w, 1560 w, 1412 m, 1301 m, 1261 vs, 1098 s, 1018 vs, 864 m, 798 vs, 739 m, 660 w. − $C_{28}H_{26}N_8S_8$ (731.05): calcd. C 46.00, H, 3.59, N 15.33, S 35.08; found C, 45.70, H 3.40, N 15.25, S 34.94. − UV/Vis (CH_2Cl_2): λ_{max} (lg ε) = 358 nm (4.37), 526 (4.02), 614 (3.99), 700 (3.98). − MS (FAB); *m/z* (%): 731 (100) [M$^+$]. − H_2(ttchp) (**8**): Yield 80%, blue-black powder. − IR (KBr): $\tilde{\nu}$ = 2961 cm^{-1} m, 2928 m, 2347 vw, 1697 m, 1681 m, 1560 w, 1453 w, 1375 m, 1288 m, 1218 s, 1015 vs, 866 m, 798 s, 729 s, 669 m. − $C_{24}H_{18}N_8S_{12}$ (803.18): calcd. C 35.89, H 2.26, N 13.95, S 47.90; found C 36.22, H 2.06, N 13.60, S 47.42. − UV/Vis (DMF): λ_{max} (lg ε) = 346 nm (5.10), 518 (4.81), 610 (4.81), 680 (4.75). − H_2(dochp) (**9**): Yield 83%, blue-black powder. − IR (KBr): $\tilde{\nu}$ = 2961 cm^{-1} m, 2926 m, 1711 m, 1618 m, 1470 m, 1424 s, 1384 m,

1306 s, 1226 s, 1047 vs, 898 vs, 786 s, 739 m, 713 m, 663 m, 483 s. − $C_{24}H_{18}N_8O_4S_8$ (738.93): calcd. C 39.01, H 2.46, N 15.17, O 8.66, S 34.71; found C 38.40, H 2.13, N 14.84, S 34.23. − UV/Vis (DMF): λ_{max} (lg ε) = 346 nm (6.10), 514 (5.84), 616 (5.84), 686 (5.77). − FAB-MS; *m/z* (%): 739 (100) [M^+].

[Tetrakis(dithiacyclohepta)porphyrazinato]nickel(II) [Ni(dtchp) (10)], [Tetrakis(dithiacyclohepta)porphyrazinato]copper(II) [Cu(dtchp) (11)], and [Tetrakis(dithiacyclohepta)porphyrazinato]zinc(II) [Zn-(dtchp) (12)]: Compounds **10**−**12** were synthesized similar to previously reported procedures found in refs.[10−12] After the reaction of **7** with anhydrous $Ni(OAc)_2$, $Cu(OAc)_2$, or ZnI_2 respectively in a 3:1 mixture of PhCl/DMF at 100°C for 20 hours under an argon atmosphere, the solvents were removed under vacuum. The remaining solids were washed thoroughly with water and 5% HCl/MeOH to remove excess metal salts followed by MeOH until the washings were clear then dried under vacuum. − Ni(dtchp) (**10**): Yield 92%, blue-black powder. − IR (KBr): $\tilde{\nu}$ = 2993 cm^{-1} m, 2922 m, 1683 m, 1538 w, 1517 m, 1412 m, 1302 m, 1254 s, 1244 s, 1078 m, 1047 vs, 875 m, 815 s, 750 s, 690 w. − $C_{28}H_{26}NiN_8S_8$ (787.72): calcd. C 42.69, H 3.33, N 14.23, S 32.56; found C 42.21, H 3.04, N 14.13, S 32.40. − UV/Vis (PhCl): λ_{max} (lg ε) = 342 nm (4.85), 508 (4.55), 640 (4.61). − Cu(dtchp) (**11**): Yield 95%, blue-black powder. − IR (KBr): $\tilde{\nu}$ = 2960 cm^{-1} m, 2923 m, 1654 w, 1560 w, 1488 w, 1414 m, 1302 s, 1260 s, 1236 m, 1091 s, 1043 s, 907 w, 864 w, 805 vs, 745 s, 678 w, 503 w. − $C_{28}H_{26}CuN_8S_8$ (792.58): calcd. C 42.43, H 3.05, N 14.14, S 32.36; found C 42.05, H 2.98, N 14.10, S 32.15. − UV/Vis (DMF): λ_{max} (lg ε) = 354 nm (4.80), 550 (4.49), 654 (4.60). − Zn(dtchp) (**12**): Yield 94%, green-black powder. − IR (KBr): $\tilde{\nu}$ = 2963 cm^{-1} m, 1653 m, 1613 m, 1413 w, 1380 w, 1262 s, 1098 s, 1022 s, 864 w, 800 vs, 687 w. − $C_{28}H_{26}N_8S_8Zn$ (794.41): calcd. C 42.33, H 3.05, N 14.11; found C 42.10, H 2.98, N 14.02. − UV/Vis (DMF): λ_{max} (lg ε) = 372 nm (4.73), 556 (4.20), 666 (4.56).

Electrochemical Methods: Cyclic voltammetry was performed using a ISMP Model Elektrokemat 400 potentiostat equipped with microcomputer-controlled instrumentation with positive feedback ohmic resistance compensation following previously described techniques.[29] Methylene chloride was dried, distilled, and degassed with argon prior to use and tetrabutylammonium hexafluorophosphate was used as the supporting electrolyte (0.1 M). A standard calomel electrode was used for the reference electrode with a 2 mm gold plate as the working electrode and the electrochemical experiments were completed under an argon atmosphere.

Electrical Conductivity Measurements: Two-probe pressed powder, AC electrical resistance measurements were carried out with an in-house assembled powder press using a Hewlett Packard 4263A LCR meter.

Crystal Structure Determinations: Suitable crystals of compounds **1** (pale green diamonds), **2** (yellow plates), and **3** (clear hexagons) were obtained from slow evaporation of 1:1 solutions of hexane/dichloromethane. Data were collected on an imaging plate IPDS-STOE diffractometer [Mo-K_α radiation, λ(Mo-K_α) = 0.71073 Å]. The cell parameters were determined from 5000 reflections over the whole θ range. Data for all structures were corrected for Lorentz-polarization effects. Data reduction were performed with X-Red.[30] The structures were solved by direct methods (SHELXS-86)[31] followed by normal heavy-atom procedures. For every compound, full matrix least-squares refinement on F^2 with all non-H atoms anisotropic. H-atoms were placed geometrically at 0.99 Å and included in the calculations as riding the adjacent C atom with an isotropic displacement parameter 50% higher than the one of the adjacent C atom. All crystallographic calculations were performed using SHELXL-97 (Sheldrick, 1997)[32] Neutral atom scattering factors were taken from ref. 33. Molecular graphics were obtained using Cameron.[34] The crystallographic data are compiled in Table 4. Crystallographic data (excluding structure factors) for the structures reported in this manuscript have been deposited with the Cambridge Crystallographic Data Centre. The deposition number for compounds **1**, **2**, and **3** is 101472. Copies of the data can be obtained free of charge on application to The Director, CCDC, 12 Union Road, GB-Cambridge CB12 1EZ [Fax: (internat.) +44 (0)1223/ 336-033, E-mail: deposit@ccdc.cam.ac.uk].

Acknowledgments

Financial support from the Ministère des Affaires Etrangères of the French Government for a Chateaubriand Post-Doctoral Fellowship for A. E. P. is gratefully acknowledged.

[1] [1a] P. Sayer, M. Gouterman, C. R. Connell, *Acc. Chem. Res.* **1982**, *15*, 73−79. − [1b] F. H. Moser and A. L. Thomas in *The Phthalocyanines*; CRC Press, Boca Raton, FL, **1983**, volumes 1 and 2. − [1c] *Phthalocyanines: Properties and Applications*; (Eds. C. C. Leznoff, A. B. P. Lever), VCH Publishers, New York, **1989**.

[2] [2a] J. Metz, M. Hanack, *J. Am. Chem. Soc.* **1983**, *105*, 828−830. − [2b] J. Martinsen, J. L. Stanton, R. L. Greene, J. Tanaka, B. M. Hoffmann, J. A. Ibers, *J. Am. Chem. Soc.* **1985**, *107*, 6915−6920. − [2c] T. J. Marks, *Angew. Chem. Int. Ed. Engl.* **1990**, *29*, 857−879; *Angew. Chem.* **1990**, *102*, 886. − [2d] M. Hanack, M. Lang, *Adv. Mater.* **1994**, *6*, 819−832.

[3] [3a] C. Piechocki, J. Simon, A. Skoulios, D. Guillon, P. Weber, *J. Am. Chem. Soc.* **1982**, *104*, 5245−5247. − [3b] M. Hanack, A. Beck, H. Lehmann, *Synthesis* **1987**, 703−705.

[4] [4a] H. F. Payne in *Organic Coating Technology*; Wiley, New York, **1961**, chapters 1−3. − [4b] A. B. P. Lever, *Adv. Inorg. Chem. Radiochem.* **1965**, *7*, 27−114. − [4c] Kasuga, K.; Tsutsui, M. *Coord. Chem. Rev.* **1980**, *32*, 67−95.

[5] J. S. Miller, A. J. Epstein, *Angew. Chem. Int. Ed. Engl.* **1994**, *33*, 385−415*; Angew. Chem.* **1994**, *106*, 399.

[6] [6a] P. Ortiz de Montellano, *Cytochrome P450. Structure, Mechanism, and Biochemistry*; Plenum: New York, **1995**, 2nd ed. − [6b] H. A. Wagenknecht, W. D. Woggon, *Angew. Chem. Int. Ed. Engl.* **1997**, *36*, 390−392; *Angew. Chem.* **1997**, *109*, 404−407. − [6c] R. J. Cheng, S. H. Lin, H. M. Mo, *Organometallics.* **1997**, *16*, 2121−2126.

[7] [7a] J. P. Collman, *Acc. Chem. Res.* **1977**, *10*, 265−272. − [7b] J. P. Collman, T. R. Holbert, K. S. Suslick in *Metal Ion Activation of Dioxygen*; (Ed. T. G. Spiro) Wiley, New York, **1980**, chapter 1. − [7c] E. C. Niederhoffer, J. H. Timmons, A. E. Martell, *Chem. Rev.* **1984**, *84*, 137−203. − [7d] J. N. H. Reek, A. E. Rowan, R. de Gelder, P. T. Beurskens, M. J. Crossley, S. De Feyter, F. de Schryver, R. J. M. Nolte, *Angew. Chem. Int. Ed. Engl.* **1997**, *36*, 361−363; *Angew. Chem.* **1997**, *109*, 396−399.

[8] [8a] A. H. Cook, R. P. Linstead, *J. Chem. Soc.* **1937**, 929−933. − [8b] R. P. Linstead, M. Whalley, *J. Chem. Soc.* **1952**, 4839−4846. − [8c] G. E. Ficken, R. P. Linstead, *J. Chem. Soc.* **1952**, 4846−4854.

[9] [9a] W. Wolf, E. Degener, S. Petersen, *Angew. Chem.* **1960**, *72*, 963−966. − [9b] G. Manecke, D. Wöhrle, *Makromolekulare Chem.* **1968**, *120*, 176−191. − [9c] W. E. Hahan, A. Kujawski, *Soc. Sci. Lodz. Acta Chim.* **1971**, *16*, 129−136.

[10] [10a] C. S. Velàzquez, W. E. Broderick, M. Sabat, A. G. M. Barret, B. M. Hoffman, *J. Am. Chem. Soc.* **1990**, *112*, 7408−7410. − [10b] C. S. Velàzquez, G. A. Fox, W. E. Broderick, K. A. Andersen, O. P. Anderson, A. G. M. Barrett, B. M. Hoffman, *J. Am. Chem. Soc.* **1992**, *114*, 7416−7424. − [10c] C. S. Velàzquez, T. F. Baumann, M. M. Olmstead, H. Hope, A. G. M. Barrett, B. M. Hoffman, *J. Am. Chem. Soc.* **1993**, *115*, 9997−10003.

[11] [11a] T. F. Baumann, J. W. Sibert, M. M. Olmstead, A. G. M. Barrett, B. M. Hoffman, *J. Am. Chem. Soc.* **1994**, *116*, 2639−2640. − [11b] T. F. Baumann, M. S. Nasir, J. W. Sibert, A. J. P. White, M. M. Olmstead, D. J. Williams, A. G. M. Barrett, B. M. Hoffman, *J. Am. Chem. Soc.* **1996**, *118*, 10479−10486.

[12] J. W. Sibert, T. F. Baumann, D. J. Williams, A. J. P. White, A.

G. M. Barrett, B. M. Hoffman, *J. Am. Chem. Soc.* **1996**, *118*, 10487−10493.
[13] T. F. Baumann, A. G. M. Barrett, B. M. Hoffman, *Inorg. Chem.* **1997**, *36*, 5661− 5665.
[14] [14a] F. Lelj, G. Morelli, G. Ricciardi, A. Roviello, A. Sirigu, *Liq. Cryst.* **1992**, *12*, 941−960. − [14b] F. Bonosi, G. Ricciardi, F. Lelj, G. Martini, *J. Phys. Chem.* **1993**, *97*, 9181−9186. − [14c] F. Bonosi, G. Ricciardi, F. Lelj, G. Martini, *J. Phys. Chem.* **1994**, *98*, 10613−10620. −[14d] G. Ricciardi, A. Bavoso, A. Bencini, A. Rosa, F. Lelj, F. Bonosi, *J. Chem. Soc., Dalton Trans.* **1996**, 2799−2807. − [14e] G. Ricciardi, A. Bencini, A. Bavoso, A. Rosa, F. Lelj, *J. Chem. Soc., Dalton Trans.* **1996**, 3243−3249.
[15] A. Ferencz, R. Ries, G. Wegner, *Angew. Chem. Int. Ed. Engl.* **1993**, *32*, 1184−1187; *Angew. Chem.* **1993**, *105*, 1251.
[16] M. Rack, M. Hanack, *Angew. Chem. Int. Ed. Engl.* **1994**, *33*, 1646−1648*; Angew. Chem.* **1994**, *106*, 1712.
[17] C. Wang, M. R. Bryce, A. S. Batsanov, J. A. K. Howard, *Chem. Eur. J.* **1997**, *3*, 1679−1690.
[18] D. M. Knawby, T. M. Swager, *Chem. Mater.* **1997**, *9*, 535−538.
[19] [19a] P. Cassoux, L. Valade, H. Kobayashi, A. Kobayashi, R. A. Clark, A. E. Underhill, *Coord. Chem. Rev.* **1991**, *110*, 115−160. − [19b] P. Cassoux, L. Valade in *Inorganic Materials*, J. Wiley and Sons, Chichester, England, **1992**, chapter 1. − [19c] J. M. Williams, J. R. Ferraro, R. J. Thorn, K. D. Carlson, U. Geiser, H. H. Wang, A. M. Kini, M. H. Whangbo in *Organic Superconductors (Including Fullerenes);* Prentice Hall, Englewood Cliffs, NJ, **1992**, chapter 1.
[20] A. Spannenberg, H. J. Holdt, K. Praefcke, J. Kopf, J. Teller, *Liebigs Ann.* **1996**, 1005−1007.
[21] R. D. Bereman, H. Lu, *Inorg. Chim. Acta* **1993**, *204*, 53−61.
[22] C. Faulmann, A. Errami, B. Donnadieu, I. Malfant, J.-P. Legros, P. Cassoux, C. Rovira, E. Canadell, *Inorg. Chem.* **1996**, *35*, 3856−3873.
[23] C. F. Cleary, N. Robertson, M. Takahashi, A. E. Underhill, D. E. Hibbs, M. B. Hursthouse, K. M. Abdul Malik, *Polyhedron* **1997**, *16*, 1111−1117.
[24] C. J. Schramm, B. M. Hoffman, *Inorg. Chem.* **1980**, *19*, 383−385.
[25] L. A. Bottomley, W. J. H. Chiou, *J. Electroanal. Chem.* **1986**, *198*, 331−346.
[26] A. Davison, R. H. Holm, *Inorg. Synth.* **1967**, *10*, 8−26.
[27] S. R. Buc, *Org. Synth.* **1964**, *36*, 101−103.
[28] H. Komoto, H. Kobayashi, *Makromol. Chem.* **1968**, *113*, 104−110.
[29] C. Faulmann, P. Cassoux, E. B. Yagubskii, L. V. Vetoshkina, *New. J. Chem.* **1993**, *17*, 385−391.
[30] X-Red, version 1.08, *STOE Data Reduction Programs*; STOE and Cie: GmbH, Darmstadt, Federal Republic of Germany, **1986**.
[31] G. M. Sheldrick, SHELXS86, *Progr. for the Solution of Crystal Structures*, Univ. of Göttingen, Federal Republic of Germany, **1986**.
[32] G. M. Sheldrick, SHELXL-97, *Progr. for Crystal Structure Refinement*, Univ. of Göttingen, Federal Republic of Germany, **1997**.
[33] D. T. Cromer, J. T. Waber, *International Tables for X-Ray Crystallography*; Kynoch Press, Birmingham, UK, **1974**; vol. 4.
[34] D. J. Watkin, C. K. Prout, L. J. Pierce, CAMERON, Chemical Crystallography Laboratory, OXFORD, UK, **1996**.

Received May 8, 1998
[I98145]

Equilibria Between Gas and Liquid Phases for Concentrated Aqueous Solutions of Nitric Acid

Fanny Balbaud,*[a] Gérard Sanchez,[a] Gérard Santarini,[a] and Gérard Picard[b]

Keywords: Nitric acid / Nitrogen oxides / Electrochemistry / Thermodynamics

Calculated diagrams, representing chemical and electrochemical properties of concentrated aqueous nitric acid mixtures, have been drawn for temperatures of 25 °C and 100 °C using vapor pressures and thermochemical data of related gaseous species. Electrochemical measurements have permitted the establishment of an experimental potential scale (referenced to the saturated mercurous sulfate electrode at 25 °C) incorporated in the diagram at 100 °C. These measurements also allowed the determination of the Gibbs free energy of formation of dissolved nitrous acid for various nitric acid solutions at 100 °C, leading to a value of $\Delta G_f(HNO_2)$ = –36.31 kJ mol^{-1}, for the whole nitric acid concentration range.

Introduction

Nuclear fuel reprocessing is achieved in France using nitric acid as the dissolution reaction medium. Nitric acid acts as an oxidizing agent and is currently used over a large range of concentration, e.g. 1 mol L^{-1} to 14.4 mol L^{-1}, and temperature, from room temperature to boiling point (at atmospheric pressure). The corrosive nature of these nitric mixtures leads to the use of corrosion-resistant materials such as austenitic stainless steels and zirconium. Corrosion studies of selected materials have previously been performed in the CEA-CEREM laboratories in an attempt to answer many practical industrial problems.[1,2] A more fundamental study of corrosion in these mixtures was undertaken some years ago[3] and showed the necessity of investigating thoroughly the corrosive nature of the reaction medium as had been performed for fused sodium nitrate−nitrite mixtures.[4a,4b]

The main objective of the study presented in this paper is to build up a synthetic thermodynamic representation of the chemical properties of concentrated nitric media. This representation connects with the Pourbaix diagram[5] for solutions of positive pH and gives a picture of the medium for more concentrated solutions. The construction of this thermodynamic representation involves knowledge of the thermochemical data of all the species present in the medium. As the value of the Gibbs free energy of formation of nitrous acid (one of the major soluble nitrogenous species apart from nitric acid) in nitric acid at 100 °C appeared to be uncertain, electrochemical measurements were performed to determine this datum. These measurements also allowed the establishment of an experimental potential scale for the diagram.

[a] CEA-CEREM, Service de la Corrosion, d′Electrochimie et de Chimie des Fluides,
B. P. 6, F-92265 Fontenay-aux-Roses Cedex, France
E-mail: fbalbaud@teaser.fr and santarini@cyborg.cea.fr
[b] Laboratoire d′Electrochimie et de Chimie Analytique (UMR 7575 du C.N.R.S.), Ecole Nationale Supérieure de Chimie de Paris,
11 rue Pierre et Marie Curie, F-75231 Paris Cedex 05, France
E-mail: picard@ext.jussieu.fr

Analysis of Available Literature Data and Graphic Representation of the Chemical Properties of Nitric Media

Nitric acid and water vapor pressures for acid concentrations varying from 0% to 95% and temperatures from 0 °C to 140 °C may be found from an analysis of literature data [Tables 1 and 2; all the pressures are given in bar (1 bar = 10^5 Pa)].[6−15]

The major interest in considering the gaseous forms of the different substances is that it makes possible the use of thermochemical data associated with the gaseous pure substances instead of those of soluble species which are generally not known with a great accuracy for concentrated media. Thermochemical data used for the calculations are presented in Table 3.[16−19]

Principle of the Construction of a Potential−Acidity-Type Diagram

All species are gaseous, including water and nitric acid, and thermochemical data used are those of pure substances under a pressure of 1 bar. The diagram was drawn using the coordinates $\log(P_{O_2}) = f[-\log(P_{HNO_3})$ or pH]. The curves represent the calculated values of the oxygen pressure for which the partial pressures of the various gaseous species are equal to 1 bar and 0.1 bar. For pH < 0, the x axis is plotted as $-\log(P_{HNO_3})$; this parameter allows the scale to be expanded and avoids the problems of proton activity in a concentrated medium. For pH > 0 the classical pH scale is used and the representation becomes equivalent to a Pourbaix diagram. The y axis is in $\log(P_{O_2})$. This choice allows the exclusive use of gaseous species, without making any approximation concerning the nitric acid dissociation

 © WILEY-VCH Verlag GmbH, D-69451 Weinheim, 1999 1434−1948/99/0202−0277 $ 17.50+.50/0

Table 1. Vapor pressures of water as a function of temperature and nitric acid concentration [wt-%][6−15]

T [°C]	20%	30%	40%	50%	60%	70%	80%	90%
0	0.0052	$4.44\cdot10^{-3}$	$3.72\cdot10^{-3}$	$2.34\cdot10^{-3}$	$2.07\cdot10^{-3}$	$1.32\cdot10^{-3}$	$5.51\cdot10^{-4}$	$1.58\cdot10^{-4}$
10	0.0104	$8.77\cdot10^{-3}$	$7.20\cdot10^{-3}$	$5.17\cdot10^{-3}$	$4.10\cdot10^{-3}$	$2.67\cdot10^{-3}$	$1.31\cdot10^{-3}$	$2.70\cdot10^{-4}$
20	0.0196	0.0165	0.0133	$9.72\cdot10^{-3}$	$7.48\cdot10^{-3}$	$5.13\cdot10^{-3}$	$2.90\cdot10^{-3}$	$8.54\cdot10^{-4}$
30	0.0355	0.0297	0.0238	0.0176	0.0135	$9.37\cdot10^{-3}$	$5.68\cdot10^{-3}$	$2.16\cdot10^{-3}$
40	0.0616	0.0514	0.0409	0.0307	0.0237	0.0164	0.0103	$4.27\cdot10^{-3}$
50	0.1031	0.0859	0.0680	0.0519	0.0402	0.0278	0.0174	$7.15\cdot10^{-3}$
60	0.1669	0.1388	0.1098	0.0849	0.0663	0.0459	0.0282	0.0111
70	0.2621	0.2180	0.1725	0.1350	0.1062	0.0738	0.0448	0.0170
80	0.4003	0.3333	0.2643	0.2094	0.1657	0.1157	0.0704	0.0283
90	0.5964	0.4973	0.3958	0.3174	0.2524	0.1767	0.1076	0.0464
100	0.8680	0.7256	0.5800	0.4705	0.3760	0.2622	0.1597	0.0738
110	1.2358	1.0351	0.8329	0.6833	0.5487	0.3799	0.2290	0.1075
120	1.7214	1.4449	1.1730	0.9735	0.7845	0.5408	0.3257	0.1319

Table 2. Vapor pressures of nitric acid as a function of temperature and nitric acid concentration [wt-%][6−15]

T [°C]	20%	30%	40%	50%	60%	70%	80%	90%
0	$4.17\cdot10^{-6}$	$5.21\cdot10^{-6}$	$8.36\cdot10^{-6}$	$1.52\cdot10^{-5}$	$9.79\cdot10^{-5}$	$1.17\cdot10^{-3}$	$3.12\cdot10^{-3}$	$8.13\cdot10^{-3}$
10	$8.91\cdot10^{-6}$	$1.16\cdot10^{-5}$	$2.80\cdot10^{-5}$	$1.02\cdot10^{-4}$	$3.48\cdot10^{-4}$	$2.32\cdot10^{-3}$	$6.18\cdot10^{-3}$	0.0177
20	$1.86\cdot10^{-5}$	$2.89\cdot10^{-5}$	$7.66\cdot10^{-5}$	$2.71\cdot10^{-4}$	$8.78\cdot10^{-4}$	$4.39\cdot10^{-3}$	0.0115	0.0347
30	$3.46\cdot10^{-5}$	$6.67\cdot10^{-5}$	$1.82\cdot10^{-4}$	$5.85\cdot10^{-4}$	$1.86\cdot10^{-3}$	$8.02\cdot10^{-3}$	0.0207	0.0632
40	$6.18\cdot10^{-5}$	$1.47\cdot10^{-4}$	$3.99\cdot10^{-4}$	$1.18\cdot10^{-3}$	$3.63\cdot10^{-3}$	0.0141	0.0359	0.1081
50	$1.09\cdot10^{-4}$	$3.10\cdot10^{-4}$	$8.19\cdot10^{-4}$	$2.28\cdot10^{-3}$	$6.61\cdot10^{-3}$	0.0239	0.0603	0.1761
60	$2.00\cdot10^{-4}$	$6.37\cdot10^{-4}$	$1.63\cdot10^{-3}$	$4.24\cdot10^{-3}$	0.0115	0.0390	0.0977	0.2739
70	$3.67\cdot10^{-4}$	$1.25\cdot10^{-3}$	$3.09\cdot10^{-3}$	$7.60\cdot10^{-3}$	0.0193	0.0613	0.1527	0.4089
80	$6.66\cdot10^{-4}$	$2.34\cdot10^{-3}$	$5.64\cdot10^{-3}$	0.0131	0.0318	0.0939	0.2305	0.5862
90	$1.22\cdot10^{-3}$	$4.20\cdot10^{-3}$	$9.94\cdot10^{-3}$	0.0218	0.0506	0.1405	0.3389	0.8135
100	$2.45\cdot10^{-3}$	$7.33\cdot10^{-3}$	0.0169	0.0354	0.0787	0.2069	0.4869	1.098
110	$5.81\cdot10^{-3}$	0.0140	0.0282	0.0560	0.1196	0.2997	0.6871	1.450
120	0.0158	0.0287	0.0471	0.0870	0.1793	0.4249	0.9465	1.897

Table 3. Literature values for the Gibbs free energy of formation used in the thermochemical calculations at 25°C and 100°C;[16−19] dissociation constant of nitric acid [$HNO_3(g) \rightleftharpoons H^+ + NO_3^-$]: $K = 3.22 \cdot 10^6$ mol^2 L^{-2} bar^{-1} at 25°C[18] $K = 4.874 \cdot 10^3$ mol^2 L^{-2} bar^{-1} at 100°C[19]

	ΔG^0_f/kJ mol^{-1}; T = 25°C	ΔG^0_f/kJ mol^{-1}; T = 100°C
$HNO_3(g)$	−73.964[16]	−58.634[17]
$NO_2(g)$	51.262[16]	55.872[17]
$N_2O_4(g)$	97.788[16]	120.020[17]
$NO(g)$	86.599[16]	85.621[17]
$N_2O(g)$	104.172[16]	109.768[17]
$H_2O(g)$	−228.620[16]	−225.138[17]

or the proton activity. The partial pressures of the gases are considered to be equal to their fugacities.

Calculated Diagrams at 25°C and 100°C (Involving Only Gaseous Species)

The following equilibria were considered in order to represent the variations of oxygen pressure for the different gases:

$$2\ HNO_3 \rightleftharpoons N_2 + \frac{5}{2}O_2 + H_2O \quad (a)$$

$$2\ HNO_3 \rightleftharpoons N_2O + 2O_2 + H_2O \quad (b)$$

$$2\ HNO_3 \rightleftharpoons 2\ NO + \frac{3}{2}O_2 + H_2O \quad (c)$$

at 100°C: $$2\ HNO_3 \rightleftharpoons 2\ NO_2 + \frac{1}{2}O_2 + H_2O \quad (d)$$

at 25°C: $$2\ HNO_3 \rightleftharpoons N_2O_4 + \frac{1}{2}O_2 + H_2O \quad (e)$$

At 25°C, the dimer N_2O_4 is the predominant form whilst at 100°C the monomer NO_2 is the predominant form for pressures of 1 bar and 0.1 bar.

For each reaction, the equilibrium constant can be written as a function of the pressures of the different gases. For reaction (a), the equilibrium constant may be expressed as:

$$K_a = \frac{P_{N_2} P_{O_2}^{5/2} P_{H_2O}}{P_{HNO_3}^2}$$

For a given temperature, the equilibrium constant K_a can be calculated, as the Gibbs free energies of formation of the different gases are known in the literature. The variation of the logarithm of the oxygen pressure can then be expressed as:

$$\log P_{O_2} = \frac{2}{5}\log K_a - \frac{2}{5}\log P_{H_2O} - \frac{4}{5}\log P_{HNO_3} - \frac{2}{5}\log_{N_2} \quad (7)$$

For given nitric acid concentration and temperature, the nitric acid and water vapor pressures are known and it is

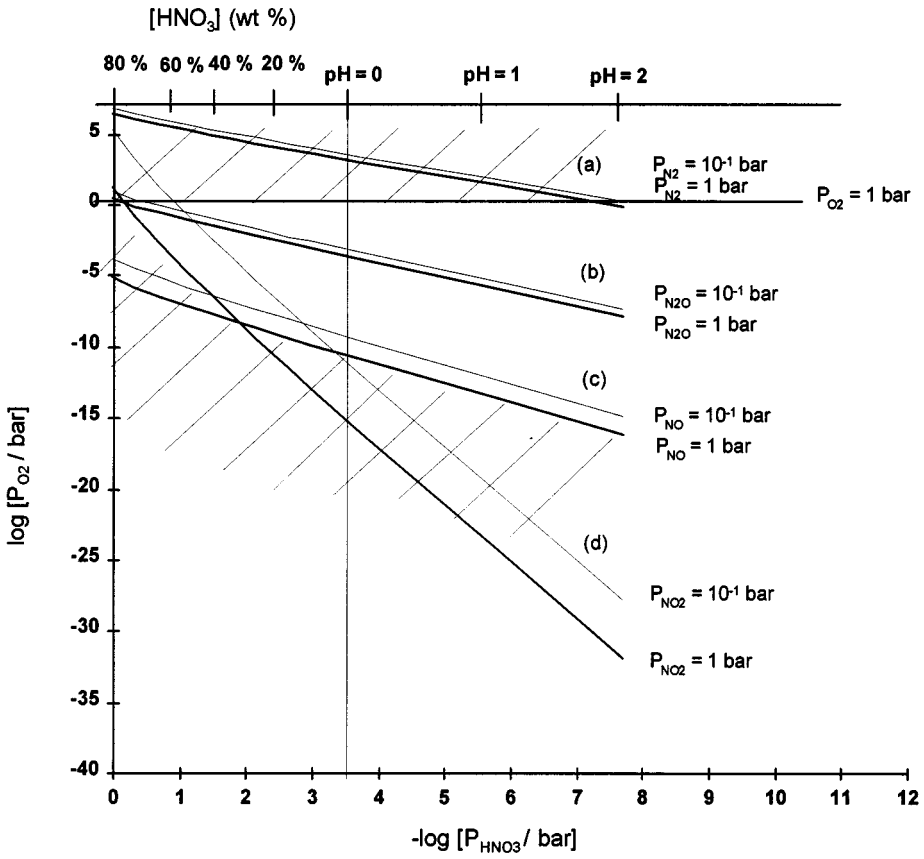


Figure 1. Calculated thermochemical diagram of nitric acid at 100°C involving gaseous species − stability domain of nitric acid under a pressure of 1 bar

therefore possible to determine the variation of the oxygen pressure with the nitric acid vapor pressure, for a given nitrogen pressure. For the other equilibria, the same calculation method may be used.

Theoretical representations in [log (P_{O_2})] − [−log (P_{HNO_3})] were calculated from the thermochemical data available in the literature at 100°C and 25°C (Figures 1 and 2).

Experimental Results and Discussion

In order to determine the missing datum of the free energy of formation of nitrous acid in nitric acid solutions at 100°C, potentiometric measurements were performed. All the measurements were referenced to the saturated mercurous sulfate electrode at 25°C (SSE).

Potentiometric Study; Determination of the Standard Potentials of the HNO_3/HNO_2 Electrochemical System at 100°C

To determine the standard potential of the HNO_3/HNO_2 system, the potential of the platinum electrode was measured at 100°C as a function of the concentration of nitrite (nitrous acid) in different nitric acid solutions (Figure 3). Initially, with no addition of nitrite, the concentration of nitrous acid in the nitric acid solution was approximately of 10^{-6} mol L^{-1}.

Nitrite ions were added as $NaNO_2$ in a 2.3 mol L^{-1} aqueous solution. In concentrated nitric acid, nitrite ions exist in the form of nitrous acid, HNO_2. During the potential measurements, the concentration of nitrous acid in nitric acid solution was considered equal to the concentration of nitrite added. This assumption was verified by analyzing the solutions for an expected value of 10^{-3} mol L^{-1}. The results obtained are given in Table 4 and show a good agreement. The following reduction reaction was considered:

$$HNO_{3(g)} + 2H^+_{(aq.)} + 2\bar{e} \rightleftharpoons HNO_{2(aq)} + H_2O_{(g)} \quad (1)$$

For this reaction, the Nernst equation can be written as:

$$E = E_1^0 + \frac{RT}{2F} \ln\left(\frac{P_{HNO_3}[H^+]^2}{P_{H_2O}[HNO_2]}\right)$$

The experimental measurements of the potential of the platinum electrode, as a function of the nitrous acid concentration, lead to the determination of the apparent standard potential $E_1{}^{0'}$ of the HNO_3/HNO_2 system. This apparent standard potential is the potential measured for a nitrous acid concentration of 1 mol L^{-1}, the concentrations of the other species being fixed by the solution. It can be expressed as:

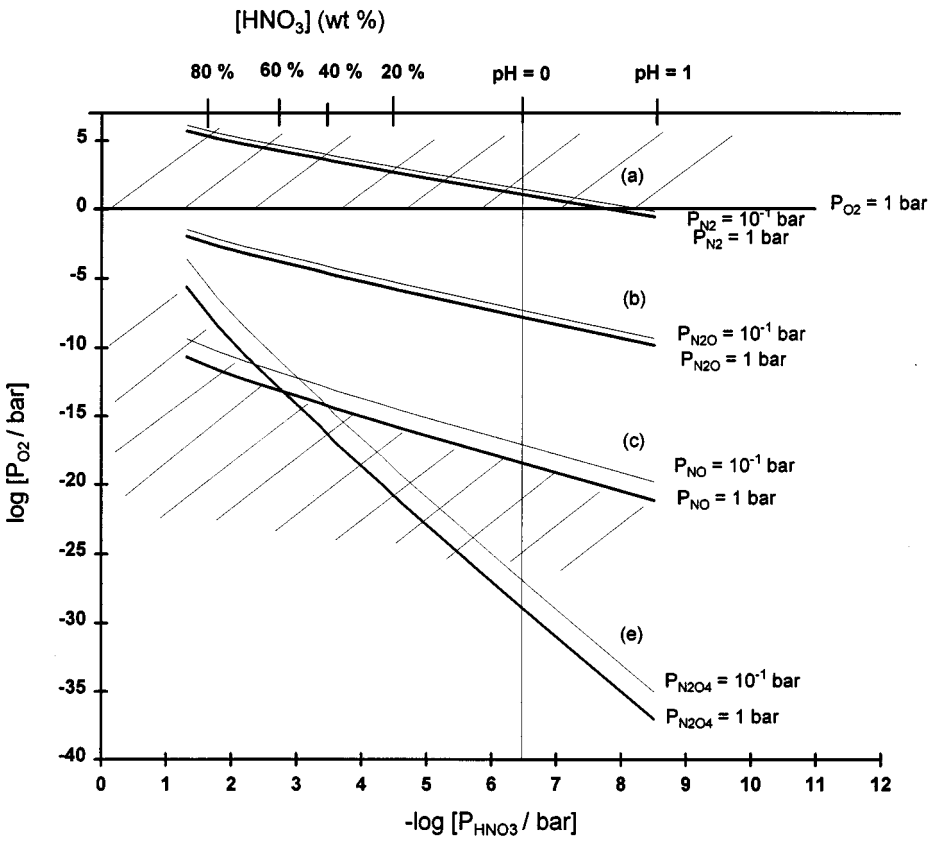


Figure 2. Calculated thermochemical diagram of nitric acid at 25°C involving gaseous species − stability domain of nitric acid under a pressure of 1 bar

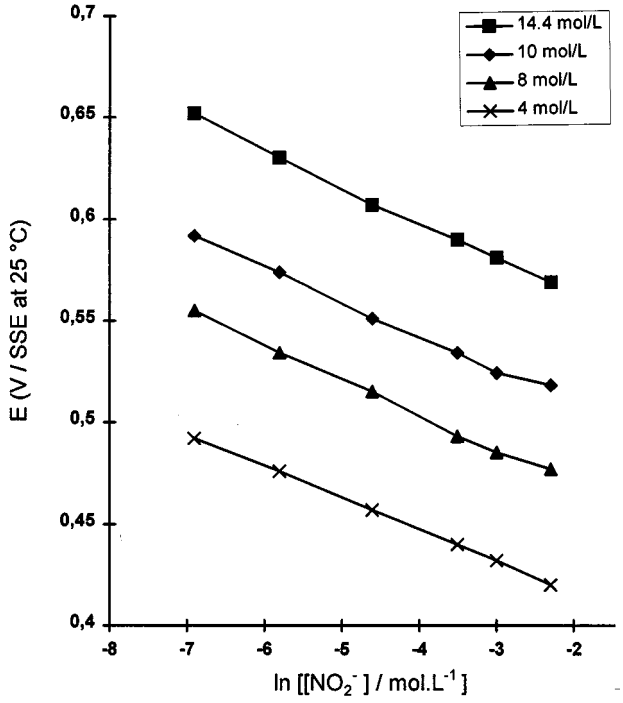


Figure 3. Potential of the platinum working electrode as a function of the concentration of nitrite added in solution and of the nitric acid concentration at 100°C

Table 4. Experimental measurement of the nitrite (nitrous acid) concentration in solution as a function of the nitric acid concentration; $[HNO_2]_{added} = 10^{-3}$ mol L^{-1} (theoretical concentration)

$[HNO_3]$/mol L^{-1}	$[HNO_2]$/mol L^{-1} measured in solution
4	$8.9 \cdot 10^{-4}$
8	$8.7 \cdot 10^{-4}$
10	$9.6 \cdot 10^{-4}$
14.4	$1.2 \cdot 10^{-3}$

$$E_1^{0'} = E_1^0 + \frac{RT}{2F} \ln\left(\frac{P_{HNO_3}[H^+]^2}{P_{H_2O}}\right)$$

The potential can then be written as:

$$E = E_1^{0'} - \frac{RT}{2F} \ln[HNO_2]$$

The variations of the potential of the platinum electrode, as a function of the nitrous acid concentration, are represented in Figure 3 for four nitric acid solutions of concentrations of 4 mol L^{-1}, 8 mol L^{-1}, 10 mol L^{-1}, and 14.4 mol L^{-1}. The experimental slope obtained with the linear regression analysis varies from 0.0178 for 14.4 mol L^{-1} to 0.0156 for 4 mol L^{-1}. The theoretical slope being equal to 0.0161, it can be inferred that the HNO_3/HNO_2 system follows the Nernst law.

Table 5 gives the experimental apparent standard potentials for the different solutions, $E_1{}^{0\prime}$. The values were determined by a linear regression analysis performed by fixing the value of the slope at the Nernst value.

Table 5. Experimental apparent standard potentials of HNO_3/HNO_2 and HNO_3/NO_2 systems as a function of nitric acid concentration at 100°C

$[HNO_3]$ [mol L^{-1}]	$E^0_{app.}(HNO_3/HNO_2)$ (V/SSE) = $E_1{}^{0\prime}$	$E^0_{app.}(HNO_3/NO_2)$ (V/SSE) = $E_2{}^{0\prime}$
14.4	0.535±5 mV	0.615±2 mV
10	0.478±3 mV	–
8	0.440±4 mV	0.474±4 mV
4	0.383±2 mV	0.391±5 mV

Determination of the Standard Potentials of the HNO_3/NO_2 Electrochemical System at 100°C

To determine the standard potential of the HNO_3/NO_2 system, the potential of the platinum electrode was measured at 100°C as a function of the nitrogen dioxide pressure (Figure 4). The nitrogen dioxide pressure was fixed and controlled by a continuous flow of NO_2 in the reactor. The measurement was performed after stabilization of the potential. No measurement was performed for a nitric acid concentration of 10 mol L^{-1}.

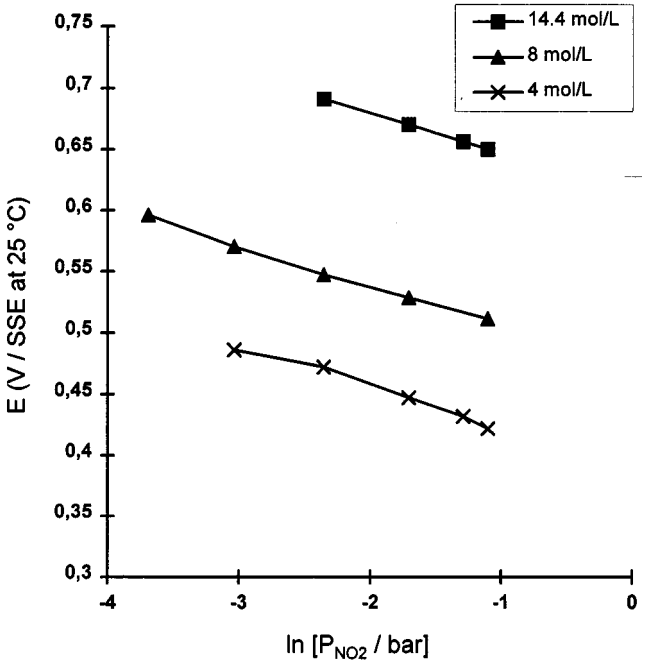


Figure 4. Potential of the platinum working electrode as a function of the nitrogen dioxide pressure and of the nitric acid concentration at 100°C

The following reaction was considered:

$$HNO_{3(g)} + H^+_{(aq.)} + \bar{e} \rightleftharpoons NO_{2(g)} + H_2O_{(g)} \quad (2)$$

According to this reaction, the Nernst equation can be written:

$$E = E_2^0 + \frac{RT}{F} \ln\left(\frac{P_{HNO_3}[H^+]}{P_{H_2O}\, P_{NO_2}}\right)$$

As previously, it is possible to define an apparent standard potential:

$$E_2^{0\prime} = E_2^0 + \frac{RT}{F} \ln\left(\frac{P_{HNO_3}[H^+]}{P_{H_2O}}\right)$$

Then:

$$E = E_2^{0\prime} - \frac{RT}{F} \ln(P_{NO_2})$$

The variations of the potential as a function of the nitrogen dioxide pressure are represented in Figure 4 for three nitric acid concentrations, 4 mol L^{-1}, 8 mol L^{-1}, and 14.4 mol L^{-1}. The experimental slope varies from 0.0325 for 8 mol L^{-1} to 0.0330 for 4 mol L^{-1}. In this case the theoretical slope is equal to 0.0321; therefore HNO_3/NO_2 shows Nernst-like behavior. The values of the apparent standard potentials of HNO_3/NO_2 are reported in Table 5.

Calculation of the Gibbs Free Energy of Formation of Nitrous Acid at 100°C

Combining the expressions of the equilibrium potential obtained for the HNO_3/HNO_2 and for the HNO_3/NO_2 systems, the following equation can be written:

$$E_2^{0\prime} = E_1^{0\prime} + \frac{RT}{2F} \ln\left(\frac{P^2_{NO_2}}{[HNO_2]}\right)$$

The ratio of the square nitrogen dioxide pressure to the nitrous acid concentration (right term) is linked to the equilibrium constant, K_3, of the following reaction, by the ratio of the partial pressure of nitric acid to the partial pressure of water:

$$HNO_{3(g)} + HNO_{2(aq.)} \rightleftharpoons 2\,NO_{2(g)} + H_2O_{(g)} \quad (3)$$

Therefore, the constant K_3, for a given nitric acid solution (concentration and temperature fixed), can be deduced from the apparent standard potentials according to the expression:

$$K_3 = \frac{P_{H_2O}}{P_{HNO_3}} \exp\left(\frac{2F}{RT}(E_2^{0\prime} - E_1^{0\prime})\right)$$

Experimentally, the standard apparent potentials of the systems HNO_3/HNO_2 and HNO_3/NO_2 have been determined for nitric acid concentrations of 4 mol L^{-1}, 8 mol L^{-1}, and 14.4 mol L^{-1}. Therefore the constant K_3 for these concentrations can be easily calculated, without making any assumption of the proton activity or of the reference system used. Moreover, with this calculation method, uncertainties in the potential measurements, linked to an eventual liquid-junction potential, are avoided if this potential is supposed to be constant for all the measurements.

As the Gibbs free energies of formation of gaseous nitric acid, gaseous water and nitrogen dioxide are known, and as for a given nitric acid solution, the partial pressures of water and nitric acid are also known, it is possible to calculate the Gibbs free energy of formation of dissolved nitrous acid in 4 mol L^{-1}, 8 mol L^{-1}, and 14.4 mol L^{-1} solutions. The results are reported in Table 6 in which the three values obtained from the calculations on the apparent standard potentials are given with all the figures obtained. The three values are quite close and therefore a mean value of the Gibbs free energy of formation of nitrous acid at 100°C was determined as $\Delta G_f(HNO_2) = -36.3 \pm 1$ kJ mol^{-1}.

This value is considered constant for the whole nitric acid concentration range. The error of 1 kJ mol^{-1} corresponds to a potential measurement error of ± 5 mV. In Table 6, two literature values corresponding to the Gibbs free energy of formation of dissolved nitrous acid in water at 100°C, are reported.[20,21] These values are quite different and the experimental datum determined above is intermediate between them.

Table 6. Experimental values of the free energy of formation of nitrous acid in various nitric acid solutions (results obtained by a calculation made with the experimental standard potentials); literature values in water at 100°C[20,21]

$[HNO_3]$ [mol L^{-1}]	$\Delta G_f(HNO_2)$ at 100°C [kJ mol^{-1}]
4	−35.703
8	−37.230
14.4	−36.110
Water (literature data)	−38.456[20] and −32.617[21]

Joint Use of Thermochemical and Potentiometric Data for Establishing an Improved Potential−Acidity Diagram for Nitric Media

Calculated Diagrams at 25°C and 100°C

The curves on the diagrams (Figures 1 and 2) represent the calculated values of the oxygen pressure for which the partial pressures of the various gaseous species are equal to 1 bar and 0.1 bar. For concentrated media (around 65%), the curves tend to deviate from a linear evolution; this phenomenon is due to the variation of the water vapor pressure.

The oxygen pressure is directly linked to the oxidizing power of the medium. Therefore, the curves relative to the different gases delimit the stability domain of nitric acid solutions in oxidation and in reduction under a pressure of 1 bar.

According to the diagrams at 25°C, as well as at 100°C, nitric acid should not be stable and should decompose into nitrogen and oxygen. In practice, the curves corresponding to the variation of the oxygen pressure for a pressure of 1 bar of nitrogen, N_2, and for a pressure of 1 bar of dinitrogen monoxide, N_2O, are found at much lower oxygen pressures than the values calculated. Literature results report that nitrogen and dinitrogen monoxide are formed at potentials lower than 0.7 V/NHE i.e. 0 V/SSE.[22] This potential gives a value of the oxygen pressure of $\log(P_{O_2}) \approx -30$, which is much lower than the values obtained by calculations. This behavior is probably due to the slow kinetics of the reactions involving N_2 or N_2O.

If N_2 and N_2O are not considered, the curves relative to the gaseous nitrogen oxides, NO and NO_2, delimit the stability domain of nitric solutions when the medium is reduced (under a pressure of 1 bar). This domain is equivalent to the electroactivity domain for cathodic potentials in a Pourbaix diagram. In oxidation, the domain is limited by the formation of oxygen. In the diagram at 25°C, the reduction of nitric acid leads to the formation of NO for nitric acid concentrations lower than 60 wt-% ($P_{HNO3} = 1.58 \cdot 10^{-3}$ bar) and to the formation of N_2O_4 for higher concentrations. At 100°C, the electroactivity domain of nitric acid in reduction under a pressure of 1 bar is also divided into two parts. The formation of NO limits the stability domain of nitric acid for concentrations lower than 40 wt-% ($P_{HNO3} = 0.0115$ bar) and the formation of NO_2 limits the stability domain for higher concentrations.

The junction between the $[-\log(P_{HNO3})]$ scale and the pH scale is made with the dissociation constant of nitric acid. Consider the equilibrium:

$$HNO_{3(g)} \rightleftharpoons H^+_{(aq.)} + NO^-_{3(aq.)} \quad (4)$$

For pH = 0, the activity of protons is considered to be equal to its concentration, and the equilibrium constant of reaction (4), known in the literature,[18,19] can be written as:

$$K_{diss.} = \frac{[H^+][NO_3^-]}{P_{HNO_3}}$$

This expression leads to:

$$-\log(P_{HNO_3}) = 2\,pH + \log(K_{diss.})$$

Therefore the junction between pH and nitric acid vapor pressure can be established.

Incorporation of Experimental Measurements into the Calculated Diagram at 100°C

In Figure 5, the variation of the oxygen pressure for the various gaseous species is represented. Moreover, the variation of the oxygen pressure is drawn for a concentration of nitrous acid of 10^{-2} mol L^{-1}. To represent this variation, the mean experimental value of the free energy of formation of nitrous acid in a nitric acid solution at 100°C, $\Delta G_f(HNO_2) = -36.3 \pm 1$ kJ mol^{-1}, is used and the equilibrium (f) is considered:

$$HNO_{3(g)} \rightleftharpoons HNO_{2(aq.)} + \frac{1}{2} O_{2(g)}$$

Then, the variation of the oxygen pressure can be written as:

$$\log P_{O_2} = 2\log K_f + 2\log P_{HNO_2} - 2\log[HNO_2]$$

Here all the terms are known for a given nitric acid concentration and temperature. The experimental curve is represented with error bars corresponding to a potential measurement error of ± 5 mV [or 1 kJ mol^{-1} in terms of $\Delta G_f(HNO_2)$].

For pH > 0, the variations of the oxygen pressure, for a concentration of nitrous acid of 10^{-2} mol L^{-1}, obtained with literature values of $\Delta G_f^0(HNO_2)$, are also represented. The experimental variation is located between those curves.

An experimental potential scale, referenced to the saturated sulfate electrode at 25°C, has been superimposed on the $\log(P_{O2})$ scale for each nitric acid concentration. It is necessary to be aware that this experimental potential scale is not a thermodynamic scale because of the temperature gradient. The working electrode was in the nitric acid solution at 100°C and the reference electrode in a compartment of the electrochemical bridge at 25°C for practical considerations. However, all the measurements were performed in the same conditions and are reproducible, and can therefore be compared between with other.

The correspondence between the oxygen pressure and the potential scale is established in the following way. The potential can be expressed according to the system O_2/H_2O:

$$E = E^0_{O_2/H_2O} + \frac{RT}{2F}\ln\frac{P_{O_2}^{1/2}[H^+]^2}{P_{H_2O}}$$

For a given nitric acid concentration and temperature, the concentration of protons and the water vapor pressure are fixed. They can be included in an apparent standard potential, $E^{0\prime}{}_{O2/H2O}$, and the potential can be written as:

$$E = E^{0\prime}_{O_2/H_2O} + 2.303\frac{RT}{4F}\log P_{O_2}$$

For a variation of 1 of the $\log(P_{O2})$ scale for a given nitric acid concentration at 100°C, the apparent standard potential, $E^{0\prime}{}_{O2/H2O}$ is constant and the corresponding variation of the potential is equal to 18.5 mV according to:

$$\Delta E = 2.303\frac{RT}{4F} = 18.5\ \text{mV}$$

The electrochemical measurements led to the determination of the apparent standard potential of the HNO_3/NO_2 system, $E_2{}^{0\prime}$, at nitric acid concentrations of 4 mol L^{-1}, 8 mol L^{-1}, and 14.4 mol L^{-1}. Therefore, the values of $E_2{}^{0\prime}$ could be placed on the diagram, for each nitric acid concentration, on the curve representing the variation of the oxygen pressure for a nitrogen dioxide pressure of 1 bar.

At a given nitric acid concentration, knowing the value of $E_2{}^{0\prime}$, all the other potentials can be determined with the

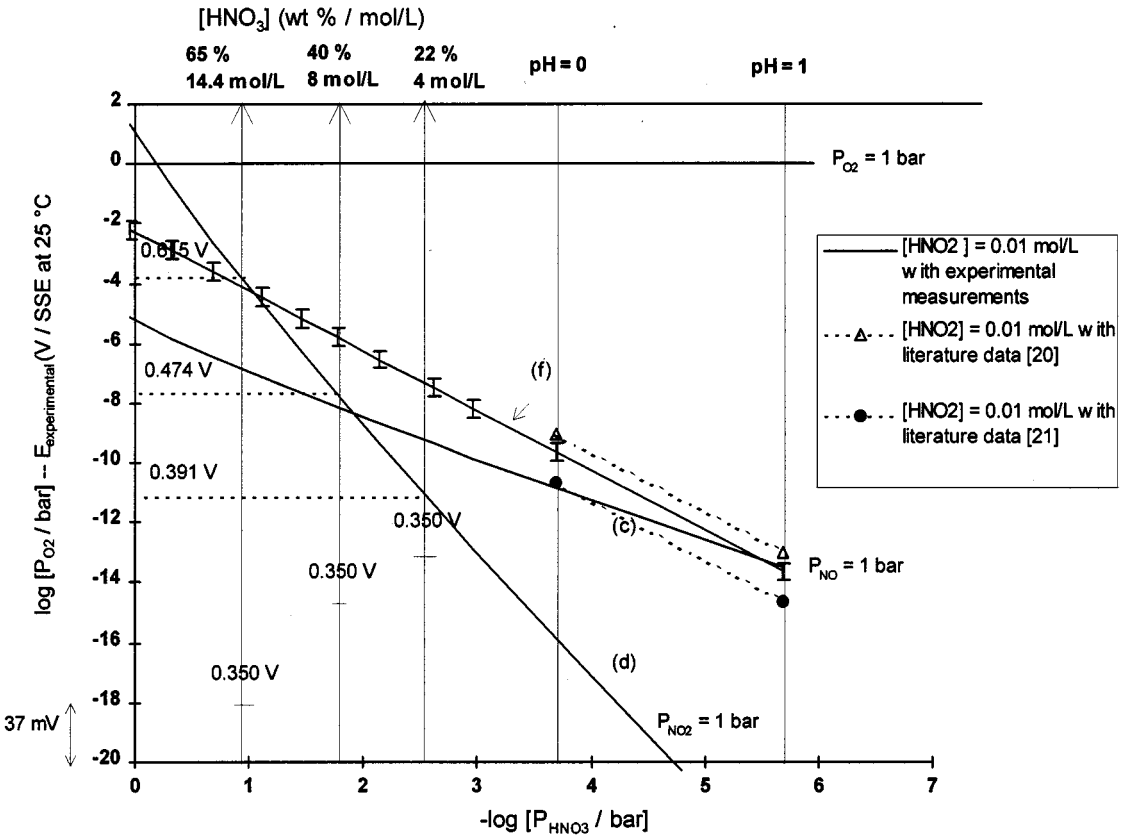


Figure 5. Incorporation of the experimental results into the calculated thermochemical diagram at 100°C; determination of an experimental potential scale referenced on the nitrogen dioxide curve for a pressure of 1 bar

correspondence between the $\log(P_{O2})$ axis and the experimental potential axis.

In Figure 5, the potential value of 0.350 V/(SSE at 25°C) for the three nitric acid concentrations is represented in order to show the variation of the experimental potential scale with the nitric acid concentration. For each nitric acid concentration, an experimental potential scale has then been established. This scale allows any experimental measurement to be placed on the diagram.

Conclusion

The method used in this study to represent the nitric acid chemical properties can be extended to any concentrated medium. The choice of an *x* scale linked to a gaseous species avoids the use of uncertain data on the dissociation of concentrated acid and of thermochemical data of soluble species which are often unknown in the working medium. Moreover, working with vapor pressures in concentrated media allowed us to obtain a more expanded scale.

In the case of nitric acid, the major soluble species apart from nitric acid is nitrous acid. For this substance, uncertainties remained in the value of the Gibbs free energy of formation in solution at 100°C. Values of the free energy of formation of nitrous acid in solution have, however, now been determined experimentally for nitric acid concentrations varying from 4 mol L^{-1} to 14.4 mol L^{-1}. These values led to the determination of the free energy of formation of nitrous acid in solution for the whole nitric acid concentration range. Knowledge of this value allowed us to place the variation of the oxygen pressure for a concentration of nitrous acid of 10^{-2} mol L^{-1} into the diagram.

Finally, the major species found when nitric acid is reduced at potentials close to the equilibrium potential have been determined: NO for nitric acid concentration lower than 40% (ca. 8 mol L^{-1}) and NO_2 for higher concentrations. An experimental potential scale, referenced to the saturated mercurous sulfate electrode at 25°C, was also established with the experimental determination of the HNO_3/HNO_2 and HNO_3/NO_2 systems.

This representation appears to be a useful tool to understand and clarify the behavior of concentrated nitric acid. In the subsequent part of the study, corresponding to an electrokinetic investigation of the reduction of concentrated nitric acid at 100°C, this diagram will help us to understand reduction mechanisms of nitric acid occurring at a platinum electrode.

Experimental Section

Reactor Cell: The reactor was regulated at 100°C and contained 1 L of solution with the volume of the vapor phase approximately 0.6 L. The size of reactor was chosen for the measurements under a flow of nitrogen dioxide as a large volume of solution avoided a significant variation in the composition of the liquid medium with the gaseous flow. The working electrode was a platinum plate of 0.25 cm^2 polished to a mirror finish. The following circuit was set up for measuring the electrode potential: working electrode/HNO_3 solution, 100°C/HNO_3 solution, 25°C/saturated KNO_3 solution, 25°C/saturated K_2SO_4 solution, 25°C/saturated sulfate electrode, 25°C. The reference electrode was a saturated mercurous sulfate electrode and may be described as: Hg/Hg_2SO_4/saturated K_2SO_4 solution. The potential of this reference electrode relative to the standard hydrogen electrode at 25°C is equal to E_{SSE} = 0.640 V/SHE.[23] The difference in temperature between the working electrode and the reference electrode prevented us from measuring thermodynamic potentials: The potential scale established was not a thermodynamic scale but rather, was purely experimental allowing us to compare values obtained in the same conditions.

Electrochemical Apparatus and Procedure: The potential measurements were made with an EG&G PAR Model 273 potentiostat as other electrochemical experiments, which are not presented here, were performed in the same time. Measurements were performed in 22 wt-% (4 mol L^{-1}), 40 wt-% (8 mol L^{-1}), 48 wt-% (10 mol L^{-1}), and 65 wt-% (14.4 mol L^{-1}) nitric acid solutions at 100°C with addition of nitrites (nitrous acid in concentrated medium) in the solution or under a controlled atmosphere performed with a gas flow imposing a specific NO_2 pressure. The NO_2 flow was performed by combining air and NO at specific rates to form NO_2 at the desired pressures according to:

$$NO(g) + {}^1/_2\ O_2(g) \rightleftharpoons NO_2(g)$$

The NO_2 pressure was verified by bubbling NO_2 for one hour through a sodium hydroxide solution and measuring the concentration of nitrites as NO_2 reacts with NaOH to form nitrites according to:

$$2\ NO_2(g) + 2\ NaOH \rightleftharpoons NaNO_2(aq.) + NaNO_3(aq.) + H_2O$$

The concentration of nitrous acid (nitrite ions) in solution was measured by colorimetry with a Perkin−Elmer UV/Vis spectrometer according to the Griess method.[24]

Acknowledgments

The authors are grateful to COGEMA for their financial contribution. They also express thanks to the SGN company and CEA company for their interest in this work and their scientific contribution.

[1] M. Leduc, M. Pelras, J. Sannier, G. Turluer, R. Demay, "Etudes de corrosion sur les matériaux destinés aux usines de retraitement", *RECOD'87*, paper 195, Paris, **1987**.
[2] P. Fauvet, G. Pinard Legry, "Corrosion aspects in reprocessing technology", *EUROCORR'92*, Espoo, Finland, **1992**.
[3] J. P. Schosger, F. Dabosi, R. Demay, P. Fauvet, J. P. Moulin, G. Santarini, "Influence of corrosion products on the passivation of AISI 304 L stainless steel in nitric acid media", *EUROCORR'96*, Nice, France, **1996**, session IX, paper 32.
[4] [4a] G. Picard, H. Lefebvre, B. Tremillon, *J. Electrochem. Soc.* **1987**, *134*, 52−58. − [4b] G. Picard, H. Lefebvre, B. Tremillon, *Molten Salts*, The Electrochemical Society Softbound Proceedings Series, **1987**, *vol. 87−7*, p. 1028−1042.
[5] M. Pourbaix, *Atlas d'équilibres électrochimiques*, Gauthier-Villars & Cie, Paris, **1963**, p. 493−503.
[6] W. Davis, H. J. de Bruin, *J. Inorg. Nucl. Chem.* **1964**, *26*, 1069−1083.
[7] A. Potier, *Ann. Faculté Sci. Univ. Toulouse Sci. Math. Sci. Phys.* **1956**, *20*, 1−98.
[8] R. Vandoni, M. Laudy, *J. Chem. Phys.* **1952**, *49*, 99−102.
[9] W. C. Sproesser, G. B. Taylor, *J. Am. Chem. Soc.* **1921**, *43*, 1782−1787.
[10] W. J. Hamer, Y-C. Wu, *J. Phys. Chem. Ref. Data* **1972**, *1*, 1047−1063.

[11] R. Haase, K. H. Dücker, H. A. Küppers, *Ber. Bunsenges. Phys. Chem*. **1965**, *69*, 97−109.
[12] R. Flatt, F. Benguerel, *Helv. Chim. Acta* **1962**, *45*, 1765−1772.
[13] M. A. Yakimov, V. Y. Mishin, *Sov. Radiochem*. **1964**, *6*, 523.
[14] J. L. Clavelin, P. Mirabel, *J. Chim. Phys*. **1979**, *76*, 533−537.
[15] T. Marnac, M. Enjalbert, *Chim. Ind. Genie Chim*. **1967**, *98*, 1047.
[16] I. Barin, *Thermochemical data of pure substances*, VCH Verlagsgesellschaft, Weinheim, **1993**.
[17] O. Knacke, O. Kubaschewski, K. Hesselmann, *Thermochemical properties of inorganic substances*, Springer-Verlag, Berlin, **1991**.
[18] S. E. Schwartz, W. H. White, *Adv. Environ. Sci. Eng.* **1981**, *4*, 1−45.
[19] H. C. Hegelson, *J. Phys. Chem*. **1967**, *71*, 3121−3136.
[20] H. E. Barner, R. V. Scheuerman, *Handbook of thermochemical data for compounds and aqueous species*, John Wiley & Sons, New York, **1978**.
[21] D. D. Wagman, Evans, Pauker, Schumm, Halow, Bailey, Churney, Nuttall, *J. Phys. Chem. Ref. Data* **1982**, *11*, 2.64−2.65.
[22] V. P. Razygraev, M. V. Lebedeva, S. A. Kabakchi, E. Yu. Ponomareva, R. S. Balovneva, L. P. Lobanova, *J. Appl. Chem. USSR* **1988**, *61*, 71−79.
[23] A. J. Bard, L. R. Faulkner, *Electrochimie: principes et applications*, Masson & Cie, Paris, **1983**, 785.
[24] G. Charlot, *Les méthodes de la chimie analytique − Analyse quantitative minérale*, Masson & Cie, Paris, **1961**, p. 620.

Received May 29, 1998
[I98170]

Interactions Between Cyclodextrins and Tm^{III} Chelates of Polyazamacrocycles as Studied by NMR in Aqueous Solution

Emrin Zitha-Bovens,[a] Herman van Bekkum,[a] Joop A. Peters,*[a] and Carlos F. G. C. Geraldes*[b]

Keywords: MRI contrast agents / Macrocyclic ligands / Cyclodextrins / Host-guest chemistry / Lanthanides

The interactions between α-, β-, and γ-CD and the Tm^{III} chelates of the macrocyclic polyaminopolycarboxylates DOTA and NOTA were studied with the use of ^1H- and ^{13}C-NMR shift and relaxation rate measurements. Interactions were only observed between $Tm(DOTA)^-$ and γ-CD. The structure and the stability of the concerning supramolecular structures was elucidated by fitting of the NMR titration curves to a theoretical model. It appears that an inclusion compound is formed, where the hydrophobic macrocyclic part of the chelate sits in the γ-CD cavity. This inclusion compound binds a second $Tm(DOTA)^-$ molecule at the outside lower rim of the CD cone. The binding occurs probably via hydrogen bonds between non-chelated carboxylate oxygen atoms of the concerning $Tm(DOTA)^-$ and CH_2OH groups of the γ-CD molecule, which are in a favorable position due to opening of the γ-CD cone angle as a result of the inclusion of the first γ-CD.

Introduction

A number of stable lanthanide(III) complexes with polyazamacrocyclic ligands are utilized in biomedical diagnosis, for example as paramagnetic shift reagents for in vivo NMR,[1] and specially as contrast agents for Magnetic Resonance Imaging (MRI).[2−4] One of the currently applied contrast agents is $Gd(DOTA)^-$ (Dotarem®) (H_4DOTA = 1,4,7,10-tetraazacyclododecane-*N*,*N*′,*N*′′,*N*′′′-tetraacetic acid) (For structures of the ligands see Figure 1).[5] The efficacy of MRI contrast agents is determined by their ability to enhance the solvent water proton relaxation rate. Among the strategies to improve this, optimisation of the inner-sphere relaxivity, through slowing down of the rotational dynamics, has proved to be quite useful.[2−4] This has been achieved by either covalent conjugation[2,6] or non-covalent binding[7] of the Gd^{III} complexes to high molecular weight aggregates or macromolecules, such as Human Serum Albumin (HSA).

Cyclodextrins (CDs) are cyclic oligosaccharides made up of six, seven, or eight α-1,4-linked D-glucopyranoside units (α-, β-, and γ-CD, respectively).[8,9] They have a cone-like shape with a hydrophobic cavity, the size of which depends on the number of glucopyranose units constituting the CD. Many NMR studies of the solution thermodynamic stability and structure of host-guest compounds of α-, β-, and γ-CDs with organic molecules have recently been published.[10−14] Several inclusion complexes of γ-CD with crown ethers, azamacrocycles and their complexes with metal cations such as Li^+, Ca^{2+}, and Ba^{2+}, have been characterized.[15−17] Inclusion compounds with cyclodextrins have drawn attention as enzyme model systems and found a wide range of applications, such as in drug delivery systems.[8,9,18] Formation of a stable inclusion compound between a contrast agent and a cyclodextrin would possibly increase its relaxivity and also alter its in vivo biodistribution. Aime et al. have studied inclusion compounds of β-benzyloxy-α-propionic substituted DOTA and DTPA-Gd^{III} complexes.[19] The benzyl groups of these compounds are included in the small CD cavity, which resulted in an increase of the relaxivity. Sherry et al. have observed the formation of weak inclusion compounds between γ-CD and $Tm(DOTP)^{5-}$ (H_8DOTP = 1,4,7,10-tetraazacyclododecane-*N*,*N*′,*N*′′,*N*′′′-tetrakis(methylenephosphonic acid).[20]

The present paper reports an NMR study on the stability and structure of the inclusion compound(s) formed between γ-CD and $Tm(DOTA)^-$. The latter complex has a lower net charge than $Tm(DOTP)^{5-}$ and, therefore, is probably less hydrophilic. Tm^{III} was selected as Ln^{III} ion for these studies because this Ln^{III} ion induces both large chemical shifts and relaxation rate enhancements.[4] The geometry of the inclusion compounds was studied by measuring the cyclodextrin ^1H- and ^{13}C-NMR Lanthanide Induced Shifts (LIS) and spin-lattice (T_1) relaxation rate enhancements induced by the paramagnetic cation in the supramolecular system(s) formed. A one-step procedure is presented for the fitting of the measured LIS data to model the complexes formed. We also investigated the effect of a change in the size of the macrocyclic Tm^{III} complex [by using Tm(NOTA) complexes, H_3NOTA = 1,4,7-triazacyclononane-*N*,*N*′,*N*′′-tri-

[a] Laboratory of Organic Chemistry and Catalysis,
Delft University of Technology,
Julianalaan 136, NL-2628 BL Delft, The Netherlands
Fax: (internat.) + 31-15/278-1415
E-mail: J.A.Peters@stm.tudelft.nl
[b] Department of Biochemistry and Center of Neurosciences,
University of Coimbra,
P. O Box 3126, P-3000 Coimbra, Portugal
Fax: (internat.) + 351-39/85-3607
E-mail: geraldes@cygnus.ci.uc.pt

 © WILEY-VCH Verlag GmbH, D-69451 Weinheim, 1999 1434−1948/99/0202−0287 $ 17.50+.50/0

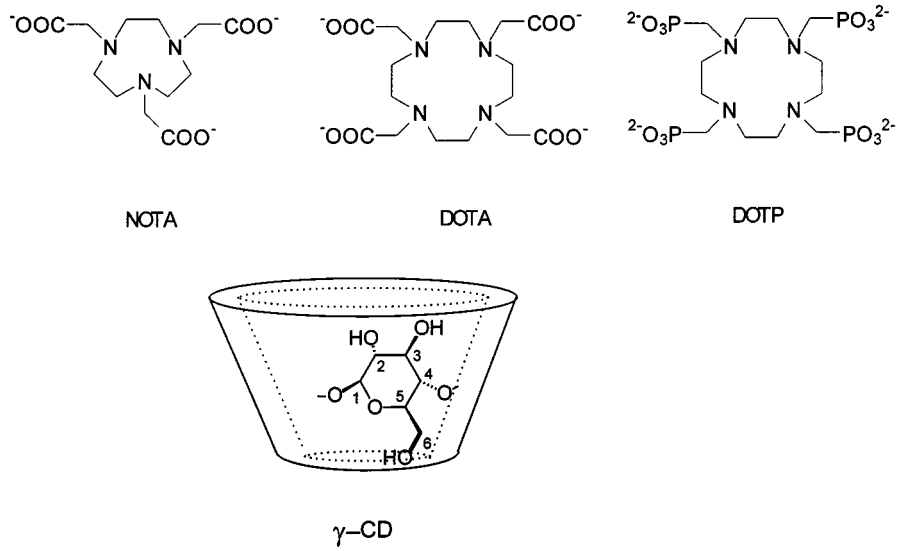


Figure 1. Structures of macrocyclic ligands and γ-CD

acetic acid] and of the cyclodextrin cavity size (by using α-, β-, and γ-CDs) on the stability of the inclusion compound(s) formed.

Results and Discussion

Referencing of NMR Chemical Shifts

Referencing of NMR chemical shifts in a study of the interaction between CDs and a paramagnetic complex is a non-trivial problem. Any internal reference used should not interfere with the equilibria between these species. ^{1}H-NMR spectra of γ-CD referenced with respect to the potential internal references *tert*-butyl alcohol, 1,4-dioxane, pentaerythritol, or tetramethylammonium bromide showed concentration dependence of the chemical shifts, which suggests an interaction between the CD and the "standard". To avoid these problems, we decided to use a solution of TMS in $CDCl_3$ in a coaxial tube inside the sample tube as external standard. Introduction of paramagnetic complexes into the outer compartment of the NMR samples causes large changes of bulk magnetic susceptibility (BMS), which are not felt in the inner tube containing the standard.[21] Therefore, corrections for these BMS effects are required. The BMS for a system with a coaxial cylindrical sample tube parallel to the main magnetic field is given by Equation (1), where Δ_χ is the paramagnetic contribution to the BMS in ppm, c is the concentration of the Tm^{III} complex in mol dm^{-3}, and T is the temperature.[21]

$$\Delta_\chi = 29\,997 \cdot c/T \quad (1)$$

Experimentally determined BMS values, determined with samples containing $Tm(DOTA)^-$ and *tert*-butyl alcohol as internal reference, were, within the experimental error, the same as those calculated with Equation (1). All chemical shifts mentioned below are corrected for BMS contributions.

Screening of the Interactions Between Macrocyclic Tm^{III} Complexes and α-, β-, and γ-Cyclodextrin

We started by titrating Tm(NOTA) or $Tm(DOTA)^-$ into 5 mM solutions of α-, β-, and γ-CD in D_2O at 25°C. Interactions were monitored by the ^{1}H resonances of the CD in question. Only upon addtion of $Tm(DOTA)^-$ to γ-CD, significant induced ^{1}H shifts were observed (after subtraction of the BMS contribution, see above). For all other combinations the induced shifts were less than 0.1 ppm when the concentration of the Tm^{III} chelate was increased up to a molar ratio Tm^{III} complex/CD (ρ) of 10. Only some line broadening was observed in these cases and the longitudinal ^{1}H relaxation rate enhancements were of the same order of magnitude as those observed for *tert*-butyl alcohol in a sample containing the same concentration of the Tm^{III} chelate. For example, ^{1}H relaxation rate enhancements ranging between 2.4 and 4.5 s^{-1} were measured for β-CD in the presence of $Tm(DOTA)^-$ at ρ = 3, whereas for *tert*-butyl alcohol under similar conditions an enhancement of 2.8 s^{-1} was observed. Therefore, it can be concluded that these relaxation rate enhancements are due to intermolecular effects, i.e. to effects resulting from diffusion of substrate molecules past the paramagnetic chelate complexes. Any direct binding of a Tm^{III} chelate to a CD molecule would lead to additional specific and substantial relaxation rate enhancements. Binding of the Tm^{III} chelates to the outer surface of the CD cones, therefore, does not play an important role.

The internal diameters of the three CD cavities are: α-CD: 4.7−5.2 Å; β-CD: 6.0−6.4 Å; γ-CD: 7.5−8.3 Å, where the smaller value is for the ring 5-H and the larger value is for the ring 3-H.[8,22] The size of the Tm^{III} chelates was evaluated by measuring (using standard molecular modelling software) the maximum distance between two ring ethylenediamino protons or acetate arm protons oppositely placed in the chelate structure. For Tm(NOTA) these distances are 5.82 and 6.76 Å, respectively.[23] A comparison of the approximate sizes of the potential host cavities and

the chelate guest indicates that the α-CD and β-CD cavities are too small to accomodate Tm(NOTA), while the γ-CD cavity is already too large to interact with the bottom macrocyclic ring hydrophobic surface of that chelate. Similarly, molecular models show that $Tm(DOTA)^-$ (distances 7.5 and 8.3 Å) fits exactly into the cavity of γ-CD, but is too bulky for inclusion in α- or β-CD.

Thus, the observation of significant Tm^{III}-induced ^1H shifts corresponds with the ability of the Tm^{III} chelate to form a well-fitting inclusion compound with the CD. Apparently, a very fine geometry fitting is needed for a reasonable host-guest interaction, perhaps due to the need of the guest to expel the hydrogen-bonded network of water molecules from inside the host CD cavity. Similar phenomena have been reported for $Tm(DOTP)^{5-}$, which induces paramagnetic ^1H shifts in γ-CD nuclei, but not in β-CD nuclei.[20]

Interactions between $Tm(DOTA)^-$ and γ-CD; Tm^{III}-Induced NMR Shifts

The interaction between $Tm(DOTA)^-$ and γ-CD was studied in more detail. Upon titration of $Tm(DOTA)^-$ into a 25 mM γ-CD solution, all ^1H and ^{13}C resonances of the CD molecule, after correction for the BMS shift contribution (see above), show Tm^{III}-induced shifts, some to high and others to low frequency. The magnitude of each (corrected) LIS was sensitive to the amount of $Tm(DOTA)^-$ added, indicating fast exchange between free and bound γ-CD. Figure 2 illustrates the plots of experimental LIS values versus ρ for some ^1H and ^{13}C CD resonances. In a similar NMR titration performed with the diamagnetic $La(DOTA)^-$ no induced shifts were observed for the γ-CD resonances. Therefore, it can be concluded that diamagnetic contributions to the shifts induced by the Tm^{III} complex are negligible.

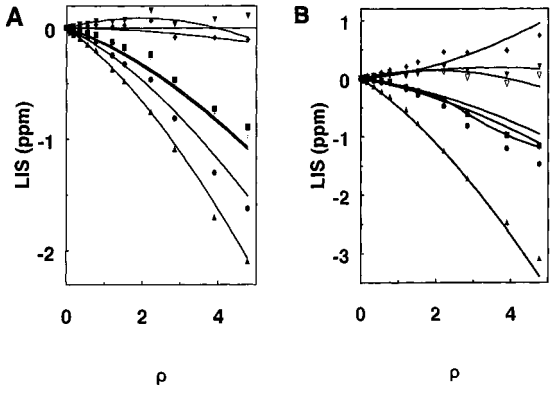


Figure 2. ^{13}C (A) and ^1H-NMR titration curves (B) for the addition of $Tm(DOTA)^-$ to a 25 mM solution of γ-CD in D_2O; the curves are calculated using the parameters given in Table 1 (see text); + C-1/1-H, ● C-2/2-H, ▲ C-3/3-H, ■ C-4/4-H, ◆ C-5/5-H, ▼ C-6/6-H, ▽ 6′-H; the experimental points of 2-H and 4-H coincide

It is known that Ln^{III} ions have only weak interactions with carbohydrates.[24] The Tm^{III} ion in $Tm(DOTA)^-$ is strongly chelated by the bulky macrocyclic ligand in an eight-dentate fashion[25] and, therefore, it may be assumed that additional coordination of a CD in the first coordination sphere of Tm^{III} does not occur. As a result, the contact contributions to the LIS can be neglected; the LIS are determined exclusively by the pseudo-contact mechanism.[4] Furthermore, the $Ln(DOTA)^-$ complexes have 4-fold symmetry and, consequently, the pseudo-contact contributions to the fully bound LIS values (LIS_{pc}) of each ligand nucleus is related to the structure of the chelate through Equation (2).[26] Here, the geometric term G depends on the spherical coordinates r and θ of the nucleus under study with respect to Ln^{III} at the origin and with the principal symmetry axis of the system as the z axis.

$$LIS_{pc} = D \cdot G = D \cdot \frac{3\cos^2\theta - 1}{r^3} \qquad (2)$$

The magnetic proportionality constant D is characteristic of the Ln^{III} ion and the chelate. Brittain and Desreux have reported that the D value for the major isomer of $Yb(DOTA)^-$ is 5082 ± 209 ppm·Å^3.[27] The ratio of the pseudocontact shifts of isostructural Yb^{III} and Tm^{III} complexes is known to be 53:22.[4][28] Therefore, the value of D of the major $Tm(DOTA)^-$ complex can be estimated to be 12243 ppm·A^3 (= 5082×53/22). From Equation (2) it follows that the magnitude and direction of the LIS is determined by the position of the nucleus relative to the paramagnetic center. The LIS is zero in spatial positions on a cone centered on the metal, with an axis coinciding with the magnetic axis of the chelate and with a cone angle of 54.7°, where the geometrical factor G and the shift change sign. We assume that the position of the principal axis and the value of D of adducts of the Tm^{III} chelates and γ-CD are the same as those in the free $Tm(DOTA)^-$ complexes, and also that binding to γ-CD does not affect the isomer equilibrium of $Tm(DOTA)^-$.[25]

The initial slopes of the titration curves of protons 1-H to 4-H, as well as the corresponding carbon atoms C-1 to C-4 are negative (shifts to lower frequencies, negative LIS values), whereas the atoms 5-H, 6-H, 6′-H, C-5, and C-6 have positive LIS values. This change in sign of the LIS between the C-4-H and C-5-H moieties of the γ-CD ring determines, through the change of sign of the geometrical term for the $Tm(DOTA)^-$ (see Equation 2), the depth at which the chelate sits inside the γ-CD cavity, and thus gives a qualitative picture about the relative position of the chelate and the cyclodextrin molecule (see Figure 3). This is quite similar to what has been previously found for $Tm(DOTP)^{5-}$/γ-CD.[20]

Surprisingly, almost all titration curves of Figure 2 show an increase of slope upon an increase of ρ, whereas for $Tm(DOTP)^{5-}$ the titration curves have been reported to to be linear up to ρ = 50.[20] Therefore, it can be concluded that besides the 1:1 adduct of $Tm(DOTA)^-$ and γ-CD [ML, M = $Tm(DOTA)^-$, L = γ-CD] another species is present, most likely M_2L. Furthermore, it can be noted from Figure 2 that, even at ρ = 5, the LIS values have not reached a

limiting value. This indicates that the association constant for the stability constants of the adducts are very low.

The most common procedure for the elucidation of solution structures of Ln^{III} complexes in the case of fast exchange between the free and bound substrate on the NMR time scale involves two steps.[4,29] First fully bound shifts of the ligand nuclei are evaluated from fitting titration curves or relative bound shifts are determined from the initial slopes of the titration curves. The bound shifts are then entered into a fitting to, for example, Equation (2) to give the molecular structure. In the present case, however the determination of bound shifts is difficult because of the curvature of the plots and because the limiting values of the shifts are not reached at high ρ-values. Therefore, we performed the two fitting procedures simultaneously. Since both the geometries of the host and the guest are rather rigid and well-known, structural constraints can be applied in the fitting procedure, which results indirectly in constraints on the calculated bound shifts. In a simultaneous fitting these constraints, on their turn, reduce the uncertainty in the resulting stability constants.

The experimental LIS data for the titration of γ-CD with $Tm(DOTA)^-$ were fitted with a model taking into account the ML and M_2L adducts. It was assumed that the ML adduct is an inclusion compound in which the main symmetry axis of the host and the guest coincide. Any location of the second chelate M at the surface of the CD cone is less likely, because then averaging over the various equivalent positions in the eight sugar units would lead to averaging out of the angular term in Equation (2) and, therefore, to very small LIS values. Most likely, the second M is near one of the rims and its position probably coincides with the main symmetry axis of γ-CD. For this situation, equivalent nuclei of the various sugar units have equal θ values and averaging out of the induced shifts does not occur.

Reported crystal coordinates for γ-CD[30] were submitted to molecular mechanics with the MM+ force field, after docking of a model of the $Eu(DOTA)^-$ structure obtained from reported crystal coordinates[31] in the cavity. The geometry of the guest was fixed during these calculations. The resulting coordinates of the γ-CD moiety were used in the elucidation of the solution structure of ML and M_2L. From an initial guess of the location of the two Tm^{III} ions on the symmetry axis of γ-CD, the bound shifts of the γ-CD nuclei of ML and M_2L (Δ_{ML} and Δ_{M2L}) were calculated using Equation (2). The *D* value in Equation (2) was fixed at 12243 ppm·Å^3 (see above). It is assumed that the *D* values of the adducts ML and M_2L are the same as that of the parent compound M. The equilibrium constants of the species in question were defined as in Equations (3) and (4).

$$\beta_{ML} = \frac{[ML]}{[M][L]} \quad (3)$$

$$\beta_{M_2L} = \frac{[M_2L]}{[M]^2[L]} \quad (4)$$

From an initial guess of β_{ML} and β_{M2L}, Equations (3) and (4) and the mass balances, the concentrations of the various species were obtained by an iteration following a procedure outlined previously.[32] With these concentrations the fractions of L bound as ML and M_2L were calculated (f_{ML} and f_{M2L}, respectively). Then the induced shifts $\delta_{calcd.}$ at the various ρ values were calculated using Equation (5).

$$\delta_{calcd.} = f_{ML}\Delta_{ML} + f_{M2L}\Delta_{M2L} \quad (5)$$

The agreement between the calculated and experimental shifts was optimized using an iteration with the location of the two Tm^{III} centers on the symmetry axis of the γ-CD host, and β_{ML} and β_{M2L} as variables. An optimal fit was obtained for the parameters reported in Table 1. The corresponding bound shifts for ML and M_2L calculated with these parameters are included in Table 1. The Tm^{III} of the included $Tm(DOTA)^-$ chelate is located 2.7 Å above the plane formed by the anomeric oxygen atoms of the glucose units of the CD host. A similar position of Tm^{III} has been reported for $Tm(DOTP)^{5-}$ included in γ-CD.[20] The second Tm^{III} ion in the M_2L complex is found 5.1 Å below this plane, the second $Tm(DOTA)^-$ molecule is thus located at the lower rim of the host (see Figure 3). An inspection of molecular models of this complex shows that such a location is favorable for the formation of hydrogen bonds between the non-chelated carboxylate oxygens of the $Tm(DOTA)^-$ molecule and CH_2OH functions of the glucose units of γ-CD.

Table 1. Stabilities of 1:1 and 2:1 $Tm(DOTA)^-$: γ-CD complexes as obtained from Tm^{III}-induced shift measurements,[a] location of the Tm^{III} cations, and calculated bound shifts

	ML	M_2L
β [M^{-1}]	0.33 ± 0.03	3.4 ± 0.3
distance Tm^{III}−O-1 plane [Å][c]	2.67 ± 0.05	−5.14 ± 0.09
bound shifts [ppm]		
C-1	−14.5	−15.5
C-2	−22.4	−20.3
C-3	−32.6	−26.0
C-4	−16.3	−14.4
C-5	−0.3	−3.1
C-6	12.4	−13.1
1-H	−11.1	−15.5
2-H	−15.0	−16.3
3-H	−55.3	−41.2
4-H	−11.3	−15.3
5-H	6.1	19.7
6-H	19.5	−20.9
6′-H	14.1	−7.9

[a] Calculated with *D* = 12243 (see text). Agreement factor *R* = 0.16. − [b] M = $Tm(DOTA)^-$, L = γ-CD. − [c] Plane through the anomeric oxygen atoms of the glucose units of γ-CD, the direction towards the upper (wide) rim of γ-CD is denoted positive.

The calculated locations of the Tm^{III} centers are not very sensitive to the choice of the value of *D* in Equation (2). If the value of this parameter was fixed at 7434, a value derived from that reported for the minor isomer of $Yb(DOTA)^-$,[27] positions 2.6 Å above and 5.2 Å below the plane of the anomeric glucose oxygen atoms were obtained.

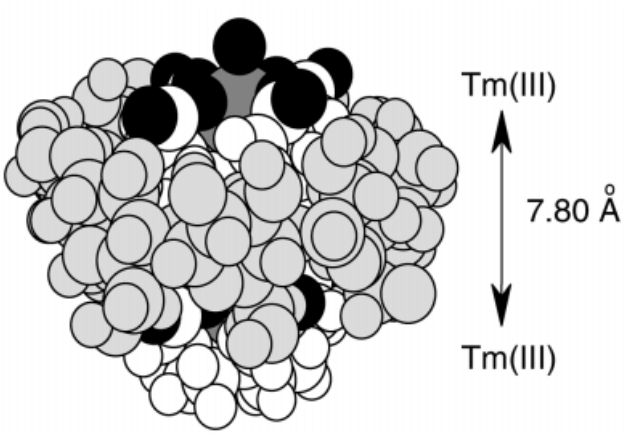


Figure 3. Schematic representation of the M_2L complex [M = $Tm(DOTA)^-$, L = γ-CD]

The calculated formation constants were, however, somewhat higher (β_{ML} = 0.51 M^{-1}; β_{M2L} = 6.6 M^{-2}).

Iterations with a model including a second 1:1 adduct with M bound at the outside of the cone at the lower rim rather than inside the CD cavity, did not lead to a better agreement between the calculated and observed titration curves. Furthermore, the resulting stability constant for the concerning complex was relatively small (β = 0.10 ± 0.05 M^{-1}). This is in line with the observation that α- and β-CD, which are not able to include $Tm(DOTA)^-$, also do not show interaction with this chelate at the outside surface of their cones. Furthermore, it should be noted that the stepwise formation constant of M_2L is larger than the formation constant of ML. Apparently, inclusion of the first $Tm(DOTA)^-$ chelate leads to a situation that is favorable for binding of the second one. It is known that inclusion of bulky guests into CDs results in adaption of the cone-angle of the CD host.[17] We assume that the inclusion of $Tm(DOTA)^-$ in γ-CD brings the CH_2OH functions of the CD in a position that is more favorable for the formation of multiple hydrogen bonds with a second $Tm(DOTA)^-$ molecule. This also explains, why an M_2L complex was not observed with $Tm(DOTP)^{5-}$,[20] as the distance between the oxygen atoms of the phosphonate functions is too large for the formation of hydrogen bonds with CH_2OH functions. Also the high negative charge of the Tm(DOTP) chelate (about −3 at pH = 7) causes it to hinder the binding of the second one at the lower rim through electrostatic repulsion.

Interactions between $Tm(DOTA)^-$ and γ-CD; Tm^{III}-Induced Relaxation Rate Enhancements

The longitudinal ^1H relaxation rate enhancements of γ- and β-CD upon addition of $Tm(DOTA)^-$ at ρ = 3 are given in Table 2. The ^{13}C relaxation rate enhancements are at least an order of magnitude smaller and are not taken into consideration. Various relaxation enhancing mechanisms contribute to the total effect. Two contributions resulting from the binding of the $Tm(DOTA)^-$ to the CD molecule should be envisaged: (i) a dipolar one ($1/T_{1,p}$) caused by through space interactions due to the random fluctuations of the electronic field of Tm^{III}[33,34] and (ii) the Curie contribution ($1/T_{1,Curie}$), which arises from the interaction of the nuclear spin with the thermal average of the electronic spins[35−38] (Equation 6).

Table 2. Contributions to the Tm^{III}-induced longitudinal relaxation rate enhancements of a 0.023 M solution of γ-CD nuclei in D_2O at ρ = 2.8[a]

	$1/T_{1,p} + 1/T_{1,Curie}$ [s^{-1}][a]	$1/T_{1,inter}$ [s^{-1}][b]	$1/T_{1,calcd.}$ [s^{-1}][c]	$1/T_{1,exp}$ [s^{-1}]
1-H	0.51	5.79	6.30	5.23
2-H	0.41	4.95	5.36	7.25
3-H	4.39	7.15	11.54	12.44
4-H	0.64	4.16	4.80	4.59
5-H	4.05	4.41	8.46	5.01
6-H/6′-H	3.03	3.85	6.88	4.90

[a] Calculated with Equations 6−9 (see text). − [b] Estimated from relaxation rate measurements on a 0.013 M solution of β-CD in D_2O at ρ = 3.0. A correction for the difference in the $Tm(DOTA)^-$ concentrations between the two samples was applied. − [c] Sum of $1/T_{1,p}$, $1/T_{1,Curie}$, and $1/T_{1,inter}$.

$$\frac{1}{T_{1,b}} = \frac{1}{T_{1,p}} + \frac{1}{T_{1,Curie}} \tag{6}$$

Tm^{III} has a very short electronic relaxation time ($T_{1e} \approx 10^{-13}$ s). If zero-field splitting (ZFS) effects are neglected,[38] $1/T_{1,p}$ can be given by the simplified Solomon-Bloembergen Equation (7).[33,34]

$$\frac{1}{T_{1,p}} = \frac{4}{3}\left(\frac{\mu_0}{4\pi}\right)^2 \frac{\gamma_I^2 \mu_{eff}^2 \beta^2}{r^6} T_{1e} \tag{7}$$

Here, $\mu_0/4\pi$ is the magnetic permeability of a vacuum, γ_I is the magnetogyric ratio of the nucleus under study, μ_{eff} is the effective magnetic moment of Tm^{III}, β is the Bohr magneton, and r is the distance between the nucleus under study and Tm^{III}. The Curie spin contribution can be expressed by Equation (8) where H_0 is the magnetic field strength, k is the Boltzmann constant, T is the temperature, τ_R is the rotational tumbling time of the complex and ω_I is the Larmor frequency of the nucleus under study.[35,36]

$$\frac{1}{T_{1,Curie}} = \frac{6}{5}\left(\frac{\mu_0}{4\pi}\right)^2 \left(\frac{\gamma_I^2 H_0^2 \mu_{eff}^4 \beta^4}{(3kT)^2 r^6}\right)\left(\frac{\tau_R}{1+\omega_I^2 \tau_R^2}\right) \tag{8}$$

Merbach et al. have reported a value of 77 ps for the rotational correlation time (τ_R) of $Gd(DOTA)^-$ at 298 K[39] and Aime et al. have reported values of 72 and 80 ps for the Gd^{III} and Lu^{III} complexes of DOTA, respectively.[40] The rotational correlation times are, according to the Debye-Stokes-Einstein equation, proportional to a^{-3} for spherical complexes, where a is the molecular diameter. On this basis, we have used 80, 268, and 339 ps as estimates for the τ_R values of M, ML, and M_2L, respectively. Values of T_{1e} of lanthanides other than Gd^{III} are usually not very

dependent on the structure of bound ligands. The T_{1e} values reported by Aime et al. for DOTA chelates of Tb^{III}, Dy^{III}, and Ho^{III}[40] are close to those tabulated for the aquo complexes.[41] It should be noted, however, that T_{1e} values obtained with data processing including ZFS effects are about 2−3 times higher,[38] although the same nuclear relaxation rates were calculated as with a procedure in which ZFS effects were neglected. Therefore, we have used T_{1e} = 0.369 ps for $Tm(DOTA)^-$ and its complexes with γ-CD. With the use of these parameters and Equations (5−8) the $1/T_{1,b}$ values for ML, and M_2L were calculated. The exchange of γ-CD between ML, M_2L, and L is fast on the NMR time scale and, therefore, the relaxation rate enhancement due to binding of $Tm(DOTA)^-$ to γ-CD can be estimated with Equation (9).

$$\frac{1}{T_{1,calc}} = \frac{f_{ML}}{T_{1,ML}} + \frac{f_{M_2L}}{T_{1,M_2L}} \qquad (9)$$

The relaxation rates have no angular dependence, and therefore, in contrast to the LIS values the effects of random diffusion controlled encounters between the paramagnetic complexes and the γ-CD moieties do not average out. These intermolecular contributions ($1/T_{1,inter}$) were estimated from the longitudinal relaxation rate enhancements of β-CD upon addition of $Tm(DOTA)^-$ (see Table 2), since inclusion does not occur there. It can be seen that this mechanism plays a major role in the present case. After inclusion of $1/T_{1,inter}$ the order of magnitude of the resulting calculated relaxation rates is the same as that of the experimental ones and the large relative value of the relaxation rate of 3-H is reproduced. The agreement between the calculated and experimental values is reasonable, considering the many assumptions that have been made in the course of these calculations.

Conclusion

$Tm(DOTA)^-$ forms a weak inclusion complex with γ-CD. The hydrophilic carboxylate groups remain outside the cavity. The resulting inclusion compound is able to bind a second $Tm(DOTA)^-$ chelate at the outer surface of the CD molecule at the lower rim. The binding occurs probably by hydrogen bonding between the carboxylate oxygen atoms of $Tm(DOTA)^-$ and the CH_2OH functions of the glucose units of γ-CD. Similar complexes are not formed with α- or β-CD or with the less bulky chelate $Tm(NOTA)^-$. Apparently, a good spatial fit of the guest in the cavity of the CD is required for the formation of an inclusion compound. The stability of the inclusion compound is even lower than that of the previously reported inclusion compound of $Tm(DOTP)^{5-}$ and γ-CD.[20] For that compound, however, binding of a second chelate molecule was not observed. Because of the low stability constants of the inclusion compounds, it can be concluded that inclusion of $Gd(DOTA)^-$ into γ-CD is not a useful approach to increase its efficacy as contrast agent for MRI.

Experimental Section

General Remarks: $TmCl_3 \cdot 6\ H_2O$ was purchased from Aldrich, and α-, β-, and γ-cyclodextrin from Fluka. All reagents were used without further purification. The macrocyclic ligands H_4DOTA and H_3NOTA were synthesized according to known procedures.[42−44] The respective Tm^{III} complexes [$Tm(DOTA)^-$ and Tm(NOTA)] were prepared by adding stoichiometric amounts of $TmCl_3 \cdot 6\ H_2O$ to a ligand solution, while maintaining the pH at about 6. The solution was kept at 80°C for about 6 h to ensure complete complex formation, and was tested for free lanthanide ions using xylenol orange and arsenazo III as indicators.[45,46] Salts were removed by nanofiltration through a Toray "Romembra" UTC-60 membrane under 20 bar nitrogen pressure. The final solutions were freeze-dried. The Tm^{III} content of the products was determined from the induced Bulk Magnetic Susceptibility (BMS) shift.[47,48] The latter was measured in a 5-mm sample tube equipped with a 2-mm coaxial inner cell (New Era Enterprises, Vineland, NJ, USA). The inner cell was filled with a 1% solution of TMS in $CDCl_3$ and the outer compartment with a 1% solution of *tert*-butyl alcohol in D_2O. The BMS was determined from the increase of the separation between the TMS and *tert*-butyl alcohol signals upon addition of the Tm^{III} complex.

The NMR titrations were performed by adding weighted amounts of the Tm^{III} complexes to 5 mM or 25 mM CD solutions in D_2O at pH = 6−7, using 10-mm NMR tubes. A 2-mm coaxial tube containing a solution of TMS in $CDCl_3$ was used as external reference for ^1H- and ^{13}C-NMR shifts.

All pH measurements were made at room temperature using a Corning 125 pH meter and a calibrated microcombination electrode purchased from Aldrich Chemical Co. Adjustments of the pH of the solutions were made with DCl and NaOD solutions in D_2O (all supplied by Merck), and no correction was made for the deuterium isotope effect.

NMR spectra were obtained with Varian VXR-400S or Unity 500 spectrometers. Spin-lattice relaxation rates were measured using the inversion recovery method. The ^1H- and ^{13}C-NMR spectra of γ-CD were assigned by two-dimensional homonuclear (COSY) and heteronuclear (HETCOR) correlated spectra, and agreed with the literature.[10−15,20] Molecular mechanics was performed with the use of the HyperChem program (version 3, MM+ force field, HyperCube Inc., Gainsville, FL, USA).Computer fitting of the LIS data was carried out with a homemade computer program using the Micromath Scientist version 2.0 (Salt Lake City, UT, USA) program. The speciations used in this program were evaluated following procedures outlined previously.[32] The equation file used in this program is available from the authors upon request.

Acknowledgments

This investigation was carried out with the support of the EC BIOMED 2 program (MACE project), The EC Erasmus program is thanked for funding the stay of E. Z.-B. at the University of Coimbra. This research has been done in the framework of the EC COST D8 program "Rational Design of Lanthanide Chelates for Biomedical Applications". C. F. G. C. G. acknowledges the support of FCT, Portugal (projects Praxis 2/2.2/SAU/1194/95 and PCEX/C/QUI/67/96).

[1] N. Bansal, M. J. Germann, V. Seshan, G. T. Shires III, C. R. Malloy, A. D. Sherry, *Biochemistry* **1993**, *32*, 5638−5643.
[2] R. B. Lauffer, *Chem. Rev.* **1987**, *87*, 901−927.
[3] M. F. Tweedle in *Lanthanide Probes in Life, Chemical and Earth Sciences* (Eds: J.-C. G. Bünzli, G. R. Choppin), Elsevier, Amsterdam, **1989**, chapter 5.
[4] J. A. Peters, J. Huskens, D. J. Raber, *Progr. NMR Spectrosc.* **1996**, *28*, 283−350.
[5] J. C. Bousquet, S. Saini, D. D. Stark, P. F. Hahn, M. Nigam, J. Wittenberg, J. T. Ferrucci, *Radiology* **1988**, *166*, 693−698.
[6] S. H. Koenig, R. D. Brown, III, *Progr. NMR Spectrosc.* **1990**, *22*, 487−567.
[7] S. Aime, M. Botta, M. Fasano, S. G. Crich, E. Terreno, *J. Biol. Inorg. Chem*. **1996**, *1*, 312−319.
[8] W. Saenger, *Angew. Chem. Int. Ed. Engl.* **1980**, *19*, 344−362.
[9] J. Szejtli, *Cyclodextrins and their Inclusion Complexes*, Akademiai Kiado, Budapest, **1982**.
[10] S. Divakar, *J. Agric. Food Chem*. **1990**, *38*, 940−944.
[11] C. Jaime, J. Redondo, F. Sánchez-Ferrando, A. Virgili, *J. Org. Chem*. **1990**, *55*, 4772−4776.
[12] M. Watabane, H. Nakamura, T. Matsuo, *Bull. Chem. Soc. Jpn.* **1992**, *65*, 164−169.
[13] M. V. Rekharsky, R. N. Goldberg, F. P. Schwarz, Y. B. Tewari, P. D. Ross, Y. Yamashoji, Y. Inoue, *J. Am. Chem. Soc*. **1995**, *117*, 8830−8840.
[14] K. A. Udachin, J. A. Ripmeester, *J. Am. Chem. Soc*. **1998**, *120*, 1080−1081.
[15] F. Vögtle, W. M. Muller, *Angew. Chem. Int. Ed. Engl*. **1979**, *18*, 623−624.
[16] S. Kamitori, K. Hirotsu, T. Higuchi, T., *J. Chem. Soc., Chem. Commun*. **1986**, 690−691.
[17] S. Kamitori, K. Hirotsu, T. Higuchi, *J. Am. Chem. Soc*. **1987**, *109*, 2409−2414.
[18] R. Breslow, N. Greenspoon, T. Guo, R. Zarzycki, *J. Am. Chem. Soc*. **1989**, *111*, 8296−8297.
[19] S. Aime, M. Botta, M. Panero, M. Giandi, F. Uggeri, *Magn. Res. Chem*. **1991**, *29*, 923−927.
[20] A. D. Sherry, R. Zarzycki, C. F. G. C. Geraldes, *Magn. Res. Chem*. **1994**, *32*, 361−365.
[21] S. C.-K. Chu, Y. Xu, J. A. Balschi, C. S. Springer, Jr., *Magn. Reson. Med*. **1990**, *13*, 239−262.
[22] R. J. Clarke, J. H. Coates, S. F. Lincoln, *Adv. Carbohydr. Chem. Biochem*. **1988**, *46*, 205−249.
[23] A. D. Sherry, M. Singh, C. F. G. C. Geraldes, *J. Magn. Reson.* **1986**, *66*, 511−524.
[24] S. J. Angyal, *Adv. Carbohdr. Chem. Biochem*. **1989**, *47*, 1−43.
[25] S. Aime, M. Botta, M, M. P. M. Marques, C. F. G. C. Geraldes, D. Pubanz, A. E. Merbach, *Inorg. Chem*. **1997**, *36*, 2059−2068, and references therein.
[26] J. M. Briggs, G. P. Moss, E. W. Randall, K. D. Sales, *J. Chem. Soc., Chem. Commun*. **1972**, 1180−1182.
[27] H. G. Brittain, J. F. Desreux, *Inorg. Chem*. **1984**, *23*, 4459−4466.
[28] B. Bleaney, *J. Magn. Reson*. **1972**, *8*, 91−100.
[29] D. J. Raber in *Lanthanide Shift Reagents in Stereochemical Analysis* (Ed.: T. C. Morrill), VCH, New York, **1986**, chapter 3.
[30] J. Ding, T. Steiner, V. Zabel, B. E. Hingerty, S. A. Mason, W. Saenger, *J. Am. Chem. Soc.* **1991**, *113*, 8081−8089.
[31] M. Spirlet, J. Rebizant, J. F. Desreux, *Inorg. Chem*. **1984**, *23*, 359−363.
[32] J. Huskens, H. van Bekkum, J. A. Peters, *Comp. Chem*. **1995**, *19*, 409−416.
[33] I. Solomon, *Phys. Rev.* **1955**, *99*, 559−565.
[34] N. Bloembergen, *J. Chem. Phys.* **1957**, *27*, 572−573.
[35] M. Gueron, *J. Magn. Reson*. **1975**, *19*, 58−66.
[36] A. J. Vega, D. Fiat, *Mol. Phys.* **1976**, *31*, 347−355.
[37] R.E. Lenkinski, *Biol. Magn. Reson*. **1984**, *6*, 23−71.
[38] I. Bertini, F. Capozzi, C. Luchinat, G. Nicastro, Z. Xia, *J. Phys. Chem*. **1993**, *97*, 6351−6354.
[39] D. H. Powell, O. M. Ni Dhubghghaill, D. Pubanz, L. Helm, Y. S. Lebedev, W. Schlaepfer, A. E. Merbach, *J. Am. Chem. Soc.* **1996**, *118*, 9333−9346.
[40] S. Aime, L. Barbero, M. Botta, G. Ermondi, *J. Chem. Soc., Dalton Trans.* **1992**, 225−228.
[41] B. M. Alsaadi, F. J. C. Rossotti, R. J. P. Williams, *J. Chem. Soc., Dalton Trans.* **1980**, 2147−2154.
[42] J. F. Desreux, *Inorg. Chem*. **1980**, *19*, 1319−1324.
[43] C. F. G. C. Geraldes, M. C. Alpoim, M. P. M. Marques, A. D. Sherry, M. Singh, M., *Inorg. Chem*. **1985**, *24*, 3876−3881.
[44] I. Lazar, D. C. Hrncir, W. D. Kim, G. E. Kiefer, A. D. Sherry, *Inorg. Chem*. **1992**, *31*, 4422−4424.
[45] G. Brunisholz, M. Randin, *Helv. Chim. Acta* **1959**, *42*, 1927−1938.
[46] D. F. Evans, *J. Chem. Soc.* **1959**, 2003−2005.
[47] D. M. Corsi, H. van Bekkum, J. A. Peters, to be published.

Received July 1, 1998
[I98210]

Tetracarboxylatodirhenium Complexes Linked by Axial Cyano Bridges to Metalpentacarbonyl Ligands − Synthesis and Characterization

Fritz E. Kühn,*[a] Isabel S. Gonçalves,[b,c] André D. Lopes,[b] João P. Lopes,[b] Carlos C. Romão,[b] Wolfgang Wachter,[a] Janos Mink,[d,e] Làszló Hajba,[e] A. Jorge Parola,[f] Fernando Pina,[f] and João Sotomayor[f]

Keywords: Chromium / Carboxylate complexes / Metal–metal multiple bonds / Molybdenum / Rhenium / Tungsten

Reaction of $Re_2\{\mu\text{-}O_2CC(CH_3)_3\}_4Cl_2$ with $[(CO)_5M–CN]Na$ (M = Cr, Mo, W) leads to tetranuclear complexes of formula $Re_2\{\mu\text{-}O_2CC(CH_3)_3\}_4[–NC–M(CO)_5]_2$ (M = Cr, Mo, W). These complexes were characterized by ^1H-, ^{13}C-, and ^{95}Mo-NMR, IR and Raman spectroscopy, elemental analysis and examined by cyclic voltammetry. The applied methods show the donor capabilities of the $[(CO)_5M–CN]^-$ ligands which shift electron density towards the Re centers weakening the Re–Re quadruple bond. The Re–Re bond lengths and the ν(Re–Re) force constants are estimated based on the FT-IR and Raman examinations. Photochemical examinations and TG/MS experiments have also been conducted. The latter method shows that the product complexes decompose around 100 °C, by first loosing their carbonyl substituents; as do the Cr, Mo, W precursor compounds. The dirhenium tetrapivalate unit decomposes only at higher temperatures in a distinct second step.

Introduction

Dirhenium carboxylates of the general formula $Re_2(\mu\text{-}O_2CR)_4X_2$ were among the first molecules containing metal−metal quadruple bonds to be correctly described.[1] Their recognition followed closely upon the heels of the structural characterization of the $[Re_2Cl_8]^{2-}$ anion and the correct treatment of its bonding.[2] However, the first reports of rhenium carboxylates appeared before this, but failed to take into account the possibility of metal−metal bonding.[3] In the interim a very extensive chemistry of $Re_2(\mu\text{-}O_2CR)_4X_2$ complexes has been developed.[1] Nevertheless, the variation of the ligands in axial position (X) remained rather limited. In particular, halides and pseudohalides, e.g. Cl, Br, I, NCS etc. have been reported.[4] Ligands containing transition metals are rare. To our knowledge, only one such compound with perrhenate as axial ligand has been structurally characterized.[4c] During the course of our own work on mixed transition metal complexes linked by nitrile and cyano groups[5] we came to examine the reactivity of $Re_2\{\mu\text{-}O_2CC(CH_3)_3\}_4Cl_2$ with $[(CO)_5M–CN]Na$ (M = Cr, Mo, W). The latter complexes have gained considerable interest in recent times due to their ability to form cyano bridges to other molecules.[6] The results of these reactions and the characterization of the products are reported in this work.

[a] Anorganisch-chemisches Institut der Technischen Universität München,
Lichtenbergstraße 4, D-85747 Garching bei München, Germany
[b] Instituto de Tecnologia Química e Biológica da Universidade Nova de Lisboa,
Quinta do Marquês, EAN, Apt 127, 2780 Oeiras, Portugal
[c] Departamento de Química, Universidade de Aveiro,
Campus de Santiago, 3810 Aveiro, Portugal
[d] Institute of Isotope and Surface Chemistry of the Hungarian Academy of Sciences,
P. O. Box 77, H-1525 Budapest, Hungary
[e] Department of Analytical Chemistry, University of Veszprém,
Egyetem Utca 10, P. O. Box 158, H-8203 Veszprém, Hungary
[f] Departamento de Química, Centro de Química Fina e Biotecnologia,
Faculdade de Ciências e Tecnologia, Universidade Nova de Lisboa,
2825 Monte de Caparica, Portugal

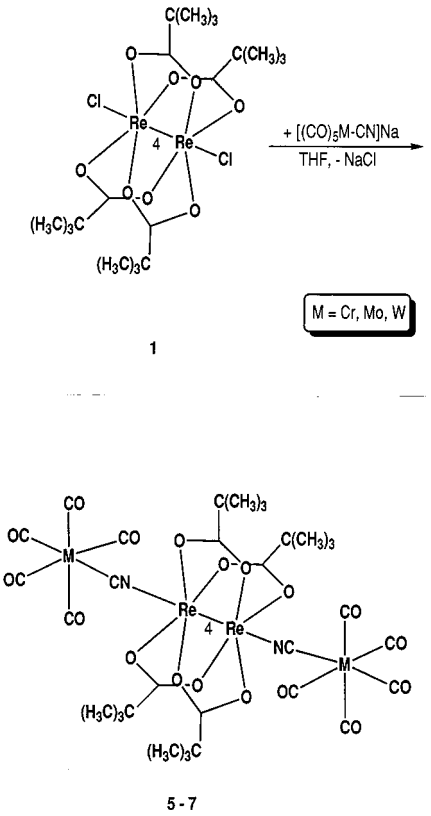
Results and Discussion

Synthesis and Spectroscopic Characterization

Mixing of a suspension of dichlorodirhenium tetrapivalate (**1**) with $[(CO)_5M–CN]Na$ [M = Cr (**2**) , Mo (**3**), W (**4**)] in THF at room temperature leads to a color change from brown to very dark red. A white precipitate is formed. According to Scheme 1, molecules of composition $Re_2\{\mu\text{-}O_2CC(CH_3)_3\}_4[–NC–M(CO)_5]_2$ [M = Cr (**5**), Mo (**6**), W (**7**)] and sodium chloride as stoichiometric byproduct are formed. After extraction with dichloromethane to remove the NaCl, the compounds **5**−**7** can be precipitated by the addition of *n*-pentane. The yields of isolated compounds obtained in this way are nearly quantitative. Compounds **5**−**7** can be handled in air at room temperature.

As it might be expected, the ^1H-NMR spectra are not very informative. Both complex **1** and complexes **5**−**7** display a singlet at $\delta(^1H) = 1.52$. The ^{13}C-NMR spectra clearly indicate the formation of the complexes **5**−**7**. The ^{13}C-NMR data are summarized in Table 1. All signals are influenced by the coordination. The strongest shift difference can be seen in the signal corresponding to the carbon atom of the bridging cyano group. This signal is shifted ca. 15−25 ppm to higher field, depending on the central metal atom of the coordinating axial ligand. Interestingly, the shifts of the corresponding signals are very similar in all product molecules in remarkable contrast to the Cr, Mo, W

 © WILEY-VCH Verlag GmbH, D-69451 Weinheim, 1999 1434−1948/99/0202−0295 $ 17.50+.50/0



Scheme 1

precursor compounds. The carboxylate carbon atoms are nearly uninfluenced by the coordination, the ^{13}C signals of the carbonyl C atoms are only slightly (ca. 5 ppm) shifted upfield. The influence of the coordination is also clearly reflected in the ^{95}Mo-NMR spectrum of compound **6** when compared with that of compound **3**. The signal is shifted more then 270 ppm to lower field and is significantly broadened (ca. 130 Hz in the starting material **3**, more than 5000 Hz in compound **6**). The ^{95}Mo-NMR data also display a temperature dependence as depicted in Table 2. A temperature decrease of 100°C causes a downfield shift of ca. 100 ppm in the complex **6**. This seems to be due to the somewhat reduced electron-transfer capability of the complexes at elevated temperatures, probably due to an increase of the thermal movements of the ligands. The latter is reflected in the significantly increasing half widths of the ^{95}Mo-NMR signals at higher temperatures. As can be also concluded from the ^{13}C NMR the electron density in compound **6** is withdrawn from the Mo core. The axial Cr, Mo, W ligands therefore act as donors, which is in good agreement with the expectations and earlier examinations of the behavior of the $[(CO)_5M-CN]^-$ moiety.[6]

Table 2. ^{95}Mo-NMR data for $Re_2\{\mu\text{-}O_2CC(CH_3)_3\}_4[-NC-Mo(CO)_5]_2$ (**6**, in CD_2Cl_2) and $[(CO)_5Mo-CN]Na$ (**2**, in CD_3OD)

Temp. [°C]	δ(^{95}Mo) [ppm]	$\Delta\nu_{1/2}$ [Hz]
	$[(CO)_5Mo-CN]Na$	
−25	−1892	190
+25	−1882	130
+60	−1875	190
	$Re_2\{\mu\text{-}O_2CC(CH_3)_3\}_4[-NC-Mo(CO)_5]_2$	
−85	−1580	5000
−40	−1610	5300
±0	−1620	5900
+25	−1690	6300
+35	−1700	6700

IR and Raman Spectroscopy

The characteristic IR and Raman bands of the complexes **2**−**7** are summarized in Table 3. The vibrational symmetry of the complexes **5**−**7** is D_{4h} which leads to the alternativity of the IR and Raman bands especially for the skeletal modes involving displacements of the Re atoms. The infrared spectra of the starting pentacarbonylmetal complexes **2**−**4** are also tabulated for a better understanding of the vibrational assignment. According to theoretical considerations of the vibrations, the very characteristic and important stretching modes of the linear CN−ReRe−NC moiety has no interaction with the ReO vibrations which involve displacements perpendicular to the linear molecular axis. According to the selection rules the Re−Re and the inphase symmetric stretchings of the Re−N and C−N are Raman-active and the antisymmetric contribution of Re−N and C−N stretches are IR-active. Since the vibrational interactions via the heavy Re atoms should be very weak, the IR and Raman stretching frequencies are expected to be rather close to each other. Because of the above-mentioned very weak or negligible vibrational coupling through Re−Re groups, the assignment of the $[NC-M(CO)_5]^-$ moieties can be performed on the basis of C_{4v} local symmetry (see Table 3). The general features reflected by the experimental observations can be summarized as follows:

The IR data of the complexes **5**−**7** show that the ν(CO) vibrations are shifted to higher wavenumbers relative to the starting materials **2**−**4**. However, in both types of complexes the carbonyl−metal bond is dominated by the back donation of the metal core to the carbonyl groups. The

Table 1. ^{13}C-NMR data of complexes **1**−**7** [ppm]

	1 ($NCCD_3$)	**2** ($NCCD_3$)	**3** ($NCCD_3$)	**4** ($NCCD_3$)	**5** (CD_2Cl_2)	**6** (CD_2Cl_2)	**7** (CD_2Cl_2)
$C(CH_3)_3$	29.3	–	–	–	27.5	27.4	27.4
$C(CH_3)_3$	42.8	–	–	–	41.1	41.2	41.1
NCMCO	–	221.5	211.1	206.0	217.9	207.9	201.0
OCMCO	–	218.5	206.8	201.4	215.5	204.4	195.2
OC(R)O	207.3	–	–	–	205.6	205.7	200.5
NC	–	153.8	149.2	140.0	124.6	124.3	124.7

back-donating effect to the π* orbitals of the carbonyl groups is decreased in the product molecules because part of the electron density at the metal centers is now shifted towards the CN units.[7] Accordingly, the ν(CN) vibrations are shifted ca. 10−20 cm^{-1} to lower wavenumbers. Electron density is withdrawn from the C≡N bond to the rhenium atoms.

The vibrational frequencies of the $Re_2\{\mu\text{-}O_2CC(CH_3)_3\}_4$ unit are only slightly influenced by the new metalpentacarbonyl ligands. Characteristic bands were observed at 1550 (w), 1430 (s) and 1220 (vs) cm^{-1}, referring to one asymmetric and two symmetric COO stretching vibrations, respectively. The COO deformational mode is observed as a strong IR band at 630 cm^{-1}. The ReO stretching modes appear in the range of 360−480 cm^{-1} assigned to a_{1g}, e_u, a_{2u} and e_g species (see Table 3).

The very strong Raman bands at 275, 277 and 288 cm^{-1} can unambiguously be assigned to stretching frequencies of the quadruple bond between the rhenium atoms for the complexes **5**−**7**. The position and intensity of this Raman bands[8] suggests that coupling occurs between the metal−metal stretching mode and the rhenium−cyanide stretching mode. The Re−Re stretching vibraton of these complexes are shifted to higher energies relative to that of $Re_2\{\mu\text{-}O_2CC(CH_3)_3\}_4Cl_2$ (**1**) in accord with the occurrence of less ReRe→(N≡CR) π back-bonding. We can observe a slight strengthening of the Re−Re bond in the Re-Re←N≡CM(CO)$_5$ moiety in the order M = Cr < Mo < W.

Simplified force-constant calculations have been performed using the linear CN−ReRe−NC moiety of the complexes. On the basis of literature values of bond lengths and Re−Re stretching frequencies the metal−metal stretching force constants have been calculated for the compounds shown in Table 4. A clear correlation has been observed between bond lengths and force constants. This relation can be used to predict bond lengths for the newly synthesized complexes **5**−**7**. As the Re−Re force constants are increasing from 4.15 to 4.55 Ncm^{-1}, consequently the predicted bond lengths are shortened from 226 to 223.6 pm for complexes **5**−**7** (see Table 4).

Electrochemical Studies

Complexes **5**−**7** have a chain of 12 atoms along the Re−Re axis, with four triple bonds (2 C≡O and 2 C≡N) and one quadruple Re−Re bond which will show some degree of conjugation due to π back-donation. Cyclovoltammetric studies have shown that both the organometallic ligands $[(CO)_5M-CN]^-$, and the $Re_2\{\mu\text{-}O_2CC(CH_3)_3\}_4X_2$ moiety are electrochemically active. The former undergo 1-e^- oxidations which are only reversible for M = Cr.[9a] The latter undergo 1-e^- reduction to give the paramagnetic anions $[Re_2\{\mu\text{-}O_2CC(CH_3)_3\}_4X_2]^-$ possessing a $(\sigma)^2(\pi)^4(\delta)^2(\delta^*)^1$ electronic configuration.[9b] These facts suggested the possibility of obtaining interesting redox activities for such complexes and, therefore, an electrochemical survey was carried out. The cyclic voltammograms (CV) of the tetranuclear complexes **5**−**7** were measured in a CH_2Cl_2 solution in the presence of $N[CC(CH_3)_3]_4BF_4$ as supporting electrolyte and the data are presented in Table 5. For sake of comparison, the same table presents the data collected for the organometallic ligands **2**−**4**. These could not be obtained in the same solvent due to insolubility and were, therefore, measured in $NCCH_3$ in good agreement with reported values.[9a] The values obtained under our conditions for complex **1** in CH_2Cl_2 are also in agreement with those reported in ref.[9b]

The voltammograms of **6** and **7** are essentially similar. They only present a totally irreversible oxidation wave at $E_{pa} \approx 1.15$ V without any cathodic response. In the case of **5**, this wave is better defined and a small cathodic response at $E_{pa} = 0.82$ V is already present, as depicted in Figure 1. A second irreversible oxidation in the CV of **5** is indicated by the anodic peak at $E_{pa} = 1.39$ V. Lowering of the temperature to −50°C increases the reversibility of the former wave ($i_a/i_c \approx 1$) suggesting that its lack of reversibility at room temperature results from a chemical decomposition process taking place after oxidation. In agreement, the anodic peak at $E_{pa} = 1.39$ V disappears completely at −50°C. No wave was present in the region expected for the oxidation of free, uncoordinated ligands $[(CO_5)M-CN]^-$ which attests to the stability of the adducts **5**−**7**.

In complex systems like these tetranuclear species it is obviously difficult to assign the part of the molecule whereupon the oxidation is based. However, we assign these oxidations to the $[(CO_5)M-CN]$ center (M = Cr, Mo, W), in the case of the Cr derivative **5** ($E_{pa} = 1.15$ V) this corresponds to a shift of the E_{pa} signal to more positive potentials by ca. 0.3 V since the anion **2** undergoes a reversible oxidation in that region at $E_{pa} = 0.73$ in $NCCH_3$. The irreversible anodic waves of **3** and **4** also undergo a similar shift towards higher potentials in their corresponding complexes **6** and **7**. In this case a more accurate comparison of potentials is not possible because of the insolubility of the complexes **2**−**4** are in CH_2Cl_2. Although the lack of reversibility does not allow an accurate interpretation, these results suggest that the organometallic ligands $[M(CO)_5-CN]^-$ (**2**−**4**) donate electronic density to the ReRe core, therefore becoming more difficult to be oxidized.

As we mentioned above, the complexes $Re_2\{O_2CC(CH_3)_3)\}_4X_2$ undergo a 1-e^- reduction to their monoanions. This reduction presents a linear dependence on the nature of the halogen X, being more difficult in the case of X = Cl relative to X = I by only 0.1 V.[9b] In view of the reversible voltammetric behavior of these halides and the ready acceptance of an anti-bonding electron by the Re−Re quadruple bond molecular orbital framework, the absence of a corresponding reduction wave in all three complexes **5**−**7** is quite surprising. All experimental modifications attempted (lowering the temperature to −70°C, changing the sweep rate, increasing the sample concentration) failed to reveal any reduction wave. At present we cannot offer a sound explanation for the absence of this reduction although it may be considered consistent with a significant electron transfer from the axial ligands capable of modifying the

Table 3. Selected characteristic vibrational frequencies [cm^{-1}] for complexes **2**−**7**

5		**2**	**6**		**3**	**7**		**4**	assignments
IR	Raman	IR	IR	Raman	IR	IR	Raman	IR	
2976 w			2976 w			2974 w			CH_3 asym str
			2936 vw			2938 vw			CH_3 asym str
			2906 vw			2906 vw			CH_3 sym str
2101 m			2101 m			2105 m			CN str $[a_{2u}]$[a]
		2111 m			2099 s			2099 w	CN str $[a_{1g}]$
		2054 w			2066 m			2058 m	CO sym str (a_1)[b]
2041 vs		1996 s	2038 s		1986 s	2029 s		1983 s	CO asym str (b_1)
1931 vs		1911 vs	1933 vs		1921 vs	1929 vs		1908 vs	CO asym str (e)
		1826 s			1846 s			1815 sh	CO sym str (a_1)
1221 vs			1219 vs			1221 vs			COO sym str $[e_u]$
	630 vw			630 w			630 w		COO bend $[a_{1g}]$
627 m			629 s			627 s			COO bend $[e_u]$
679 m	665 w	683 m	606 s	600 w	612 m	594 s		600 m	M−CO bend (a_1)
660 vs	650 w	654 vs	590 vs		591 vs	581 s	580 w	581 s	M−CO bend (e)
		550 w			533 w			541 w	M−CO bend (e)
		474 m							
	480 m			470 w			460 m		Re−O str. $[a_{1g}]$
			468 m			464 m			Re−O str $[e_u]$
	445 m	450 m	450 m	450 w	435 w		435 m	444 w	M−CO str (e)
	384 s			411 m			435 m		M−CO str (a_1)
390 s			375 s			377 vs			Re−O str $[a_{2u}]$
	(384 s)			360 w			386 w		Re−O str $[e_g]$,
346 w				345 w			334 w		M−CN str. (a_1)
330 w				330 w			312 w		M−CN bend (e)
	275 s			277 s			288 s		ReRe str $[a_{1g}]$
243 w			237 w			235 w			Re−CN str (a_{2u})
	225 w,b			230 w,b			245 w,b		Re−CN str (a_{1g})
185 sh			187 m			184 m			ReReN bend $[e_u]$
	175 sh			175 sh			200 sh		ReReN bend $[e_g]$
173 m			170 m			168 m			CMC bend (?)[c]

[a] In square brackets are the predicted symmetry species are included referring to D_{4h} general (idealized) point group of the whole molecule. − [b] In round brackets are the suggested symmetry species due to C_{4v} local symmetry of the metalpentacarbonyl moiety. − [c] The C−M−C bond-angle deformation modes are strongly overlapping vibrations and can be attributed to all IR-active species (a1 and e) of the metalpentacarbonyl fragment.

Table 4. Bond lengths [pm], stretching frequencies ν [cm^{-1}] and force constants K [10^2 Nm^{-1}] of selected complexes with Re−Re quadruple bonds

compound and reference	Re−Re bond lengths	ν(M−M)	K(M−M)[b]
$Re_2OCl_5(O_2CCH_2CH_3)_2 \cdot (PPh_3)_2$[8b]	252.0	216	2.559
Re_2Cl_5(2,5-dithiahexane)[8b]	229.0	267	3.011
$Re_2(O_2CCH_3)_4Cl_2$[8b,8c]	223.6(1)	288	4.550
$[Re_2F_8][NBu_4] \cdot 2\ Et_2O$[8d,8e,8f]	218.8(3)	318	5.547
1	223.6(1)	288	4.550
5	226.0[a]	275	4.149
6	225.5[a]	277	4.202
7	223.5[a]	288	4.550

[a] Estimated bond lengths (see text): occuracy ca. 0.5 pm. − [b] The simplified calculation gives overestimated values.

electronic framework of the Re−Re bond to such an extent as to shift the reduction potential to the outside of the solvent window. A more detailed study of the electrochemical behavior of axially substituted ReRe complexes of type $[Re_2\{\mu\text{-}O_2CC(CH_3)_3\}_4L_2]^{n+}$ as well as a theoretical investigation of the orbital interactions in complexes **5**−**7** is currently under way. Preliminary results show that the analogous nitrile complexes $[Re_2\{\mu\text{-}O_2CC(CH_3)_3\}_4(NCR)_2]^{2+}$ (R = Me, Ph) undergo irreversible reductions in the expected region, ca. $E_{pa} \approx -0.5$ V.

Thermogravimetry and Thermal Decomposition

The Re precursor compound **1** is thermally very stable, subliming at ca. 380°C (onset temperature) leaving a residue of only 3.6%. Possibly only those parts of the compound decompose which cannot sublime quickly enough. Lowering the amount of compound in the crucible also lowers the amount of the remaining residue. The mass spectrometer we used, which is able to detect only masses of $m/z < 400$, does not record any species.

The Mo precursor **3**, of which the thermal decomposition behavior was examined, starts to decompose quickly at ca. 160°C (onset 158.3°C). Carbonyl ligands can be detected as volatile fragments in the mass spectrometer. Only traces of $[Mo(CO)_6]^+$ (m/z = 264) have been detected. This molecule has also been detected during the thermal decomposition of related complexes.[6e] The remaining residue contains 54.6% of the original mass of the compound. Thus, 45.4% of the sample mass is lost during the heating process. This is in good agreement with the total mass of CO in the starting material (48.8%).

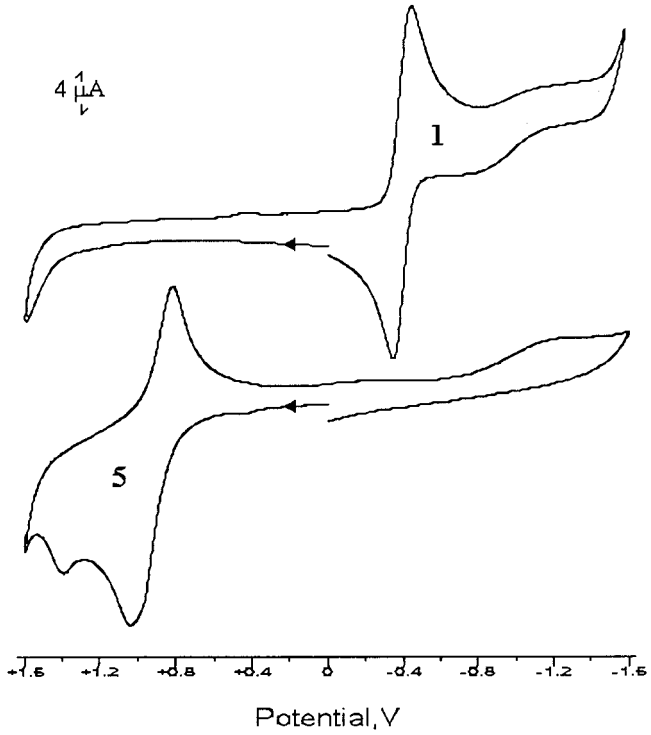


Figure 1. Cyclic voltammogram of $Re_2\{\mu\text{-}O_2CC(CH_3)_3\}_4Cl_2$ (**1**) and $Re_2\{\mu\text{-}O_2CC(CH_3)_3\}_4[-NC-Cr(CO)_5]_2$ (**5**)

Table 5. Cyclovoltammetric data (recorded in CH_2Cl_2)

compound		E_{pa} [V][a]	E_{pc} [V][b]	comment
$Re_2\{\mu\text{-}O_2CC(CH_3)_3\}_4Cl_2$	**1**	−0.35	−0.45	reversible
$[(CO)_5Cr-CN]Na$	**2**	0.73[c]	0.65[c]	reversible
$[(CO)_5Mo-CN]Na$	**3**	0.85[c]	–	irreversible
$[(CO)_5W-CN]Na$	**4**	0.82[c]	–	all irreversible
		1.11[c]	–	
$Re_2\{\mu\text{-}O_2CC(CH_3)_3\}_4[-NC-Cr(CO)_5]_2$	**5**	1.03	0.82	all irreversible
		1.39	–	
$Re_2\{\mu\text{-}O_2CC(CH_3)_3\}_4[-NC-Mo(CO)_5]_2$	**6**	1.14	–	irreversible
$Re_2\{\mu\text{-}O_2CC(CH_3)_3\}_4[-NC-W(CO)_5]_2$	**7**	1.20	–	irreversible

[a] E_{pa}: Anodic sweep (peak potencials, Volts). – [b] E_{pc}: Cathodic sweep (peak potencials, Volts). – [c] Recorded in $NCCH_3$.

The decomposition behavior of the product molecules **5**−**7** is rather similar and the appearance of the curve depends on the total mass of the metal atoms (Figure 2). All product compounds first loose their carbonyl ligands. The total mass loss during the first decomposition step is roughly comparable to the CO content of the molecules, as also observed in the case of the $[NCMo(CO)_5]Na$ precursor molecule. The onset temperatures for the first decomposition step are ca. 100, 110 and 160°C respectively, in the case of **5**, **6** and **7**. In the first decomposition step no indication for the formation of $M(CO)_6$ as a thermal decomposition product has been detected. During the second decomposition step fragments of the pivalate ligand can be observed, especially $[C(CH_3)_3]^+$, $[H_2CCCH_2]^+$, $[H_2CCH]^+$ and $[CH_3]^+$. Carbon dioxide can also be found in significant amounts during the second decomposition step. Trace amounts of HCN^+ (m/z = 27) have also been detected during the second decomposition step of the complexes **5**−**7**. The onset temperatures for the second step are ca. 360, 390 and 270°C, respectively, for **5**, **6** and **7**. A small amount of pivalate fragments, however, can already be found during the first decomposition step. The intensity is nearly one order of magnitude smaller than during the second decomposition step. The remaining mass at the end of the measurement at 550°C is 44.6%, 49.3% and 61.9%, respectively. The mass of the metal atoms and the CN groups together is 43.5%, 47.4% and 53.7% in the cases of **5**−**7**. Taking into account the results of the simultaneous mass spectrometry this shows that the majority of the CO and the pivalate ligands is removed during the heating process. Replacement of the axial Cl ligands by $[(CO)_5M-CN]^-$ ligands clearly lowers the thermal stability of the resulting complex in comparison to its precursor.

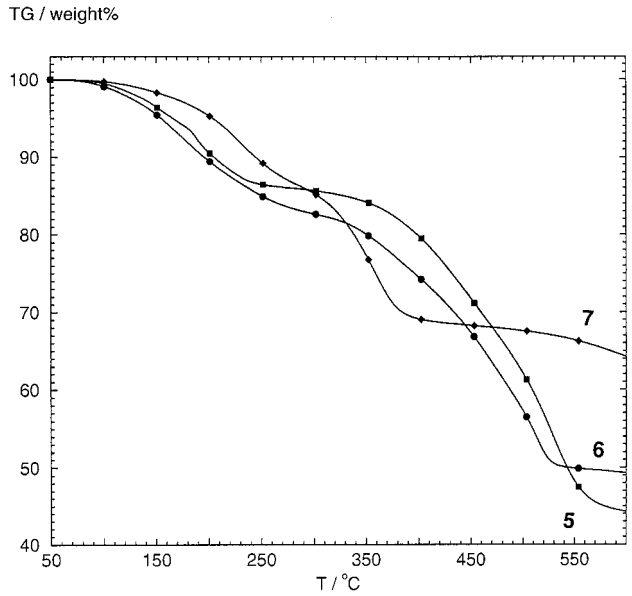


Figure 2. TG curves of $Re_2\{\mu\text{-}O_2CC(CH_3)_3\}_4[-NC-M(CO)_5]_2$ [M = Cr (**5**), Mo (**6**), W (**7**)]

Absorption Spectra

The UV/Vis absorption spectra of the compounds **5**−**7** are represented in Figure 3. The trace lines correspond to the absorption spectrum of the dichlorodirhenium tetrapivalate **1**, the point lines to the absorption spectra of the mononuclear complexes $[(CO)_5M-CN]Na$ [M = Cr (**2**), Mo (**3**), W (**4**)], and the full lines to the respective tetranuclear compounds. Comparison of the absorption spectra of these last species with the sum of the spectra of their components (two $[(CO)_5M-CN]^-$ units plus the dirhenium moiety) shows the appearence of new absorption bands that extend to the near-infrared region. These types of bands have been observed in similar compounds[6j] and can be attributed to MMCT transitions from the $[(CO)_5M-CN]^-$

units to the Re^{III} centers, on the basis of the NMR, IR and CV data.

Irradiation on these MMCT bands does not give any significant reaction followed in the visible spectral region.

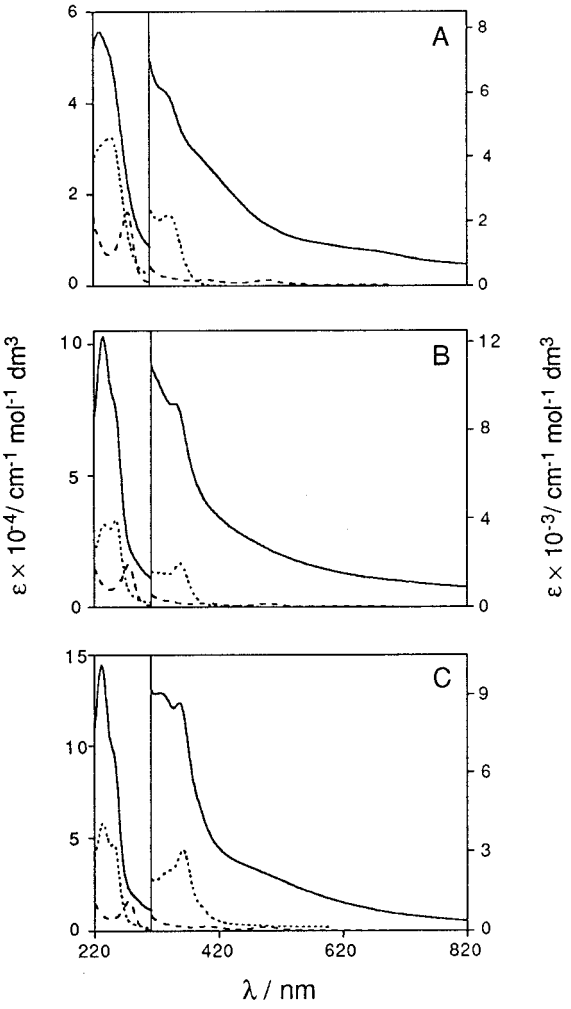


Figure 3. Absorption spectra of compounds **5** (**A**, full line), **6** (**B**, full line) and **7** (**C**, full line and their components **1** (**A**,**B**,**C**, point line), **2** (**A**, trace line), **3** (**B**, trace line) and **4** (**C**, trace line), in CH_3CN

Conclusions

Molecules of the type $[(CO)_5M-CN]^-$ not only form complexes with mononuclear metal centers, as described in the literature during the recent years, but also with dinuclear complexes containing metal−metal multiple bonds. Charge transfer between the ligands and the multiple bonded core unit takes place as can be judged from the optical absorption spectra. Significant charge donation from the $[(CO)_5M-CN]^-$ ligands to the ReRe core is also implied by ^{13}C- and ^{95}Mo-NMR as well as by cyclic voltammetry data. The Re−Re quadruple bond is only slightly weakened due to the donor influence of the organometallic ligand in the axial position. The synthesis of the described molecules is straightforward. An introduction of more NC functions in the ligands could therefore lead to long chained molecules with conjugated multiple bonds. It can also be assumed that it is easily possible to substitute other compounds of the type $[M_2(O_2CR)_4][X_2]$ or $[M_2(CH_3CN)_{10}][X_4]$ (M = Re, Rh, Mo, Tc, etc., X = BF_4, SF_6 etc.) with $[(NO)_xM(CO)_{6-x}]^-$ ligands. Work in this direction is currently under way in our laboratories and will be reported elsewhere.

Experimental Section

General: All preparations and manipulations were performed with standard Schlenk techniques under oxygen- and water-free argon. Solvents were dried by standard procedures: THF, Et_2O, *n*-pentane, and *n*-hexane with sodium benzophenone ketyl; acetonitrile and dichloromethane were distilled from P_2O_5 after refluxing for several hours. Acetone was distilled from K_2CO_3 and kept over 4-Å molecular sieves. − Microanalyses were performed at the ITQB (Oeiras). −^1H-NMR spectra were obtained with a Bruker CXP 300 spectrometer, ^{13}C-NMR spectra were measured at 100.28 MHz with a JEOL JNM GX-400 and a Bruker Avance DPX-400, ^{95}Mo-NMR spectra were measured at 26.07 MHz with a Bruker Avance DPX-400. − Infrared spectra were recorded with a Unican Mattson Mod 7000 FTIR spectrophotometer using KBr pellets and/or solutions. − The TG/MS studies were performed using a Perkin Elmer TGA 7 thermobalance coupled with a Balzers QMG 420 mass spectrometer. The thermolysis experiments were carried out in a dynamic helium atmosphere (purity 5.0, 45 sccm) using a 50 to 600°C temperature program at a rate of 10°C/min. The temperature of the capillary interface was 280°C. − The electrochemical instrumentation consisted of a BAS CV 50W−1000 Voltammetric Analyzer connected to BAS/Windows data acquisition software. All the electrochemical experiments were run under argon at room temperature. Tetrabutylammonium hexafluorophosphate (Aldrich) was used as supporting electrolyte after being recrystallized from ethanol. Cyclic voltammetry experiments were performed in a glass cell MF-1082 from BAS in a C-2 cell enclosed in a Faraday cage. The reference electrode was SSC (MF-2063 from BAS). In all cases the calibration of the reference eletrode was performed with a solution of ferrocene (1mM) to obtain a potential in agreement with the literature value. The auxiliary electrode was a 7.5-cm platinum wire (MW-1032 from BAS) with a gold-plated connector. The working electrode was a disk of platinum (MF-2013 from BAS) with ca. 0.022 cm^2 sealed in Kel-F plastic. Solvents were dried as previously described.

Photochemical Studies: All solutions (ca. 10^{-3} M) were prepared and handled in the dark. Electronic absorption spectra were run using a Perkin Elmer lambda 6 UV/Vis spectrophotometer. The photochemical reactivity was initially tested at $\lambda \geqslant 600$ nm, $\lambda \geqslant 540$ nm. Even after longer irradiation times (> 24 h), no significant spectral changes were observed. Further irradiations were than carried out to check the photochemical reactivity at $\lambda = 436$ nm and $\lambda = 366$ nm. Irradiation experiments at $\lambda \geqslant 600$ nm and $\lambda \geqslant 540$ nm were carried out with a tungsten lamp and filters with cut-off at 600 and 540 nm, respectively. Irradiation experiments at 436 nm and 366 nm, were carried out in PTI instrumentation, using a medium-pressure Hg lamp (HBO 100 W) mounted in a lamphouse (Model A1010) connected to an LPS-220 Lamp Arc Supply. The light, whose intensity was of the order of 10^{-7} Einstein min^{-1},was isolated from the medium-pressure Hg lamp by means of interference filters P/N 56450 with $\lambda_{max} = 435.8$ nm, and P/N 56430 9 BAGT with $\lambda_{max} = 367$ nm, both from Allied Electro Optics

(Italy). − Raman spectra were measured at room temperature with a Renishaw imaging microscope 2000, equipped with a 25-mW Spectra Physics 127 HeNe excitation laser (632.8 nm); resolution of 1 cm^{-1}. − $[(CO)_5M-CN]Na$ (M = Mo, Cr, W)[10] and $Re_2\{\mu\text{-}O_2CC(CH_3)_3\}_4Cl_2$[11] complexes were prepared as described in the literature.

Spectroscopic data already given in the Tables 1−5 are not repeated in the Experimental Section.

Preparation of Complexes of General Formula $Re_2\{\mu\text{-}O_2CC(CH_3)_3\}_4[-CN-M(CO)_5]_2$ [M = Cr (5), Mo (6), W (7): A suspension of $Re_2\{\mu\text{-}O_2CC(CH_3)_3\}_4Cl_2$ (0.43 g, 0.50 mmol) in THF (15 mL), was treated with 1.00 mmol of $[(CO)_5M-CN]Na$ (M=Mo, Cr, W). The mixture turned dark red. After 90 min at room temperature, the resulting solution was concentrated to dryness, extracted with dichoromethane and concentrated. Upon addition of *n*-pentane, a dark red microcrystalline powder precipitated The mother liquor was filtered off and the remaining solid was dried in oil-pump vaccuum. Yield: 91% (**5**), 89% (**6**), 86% (**7**).

$Re_2\{\mu\text{-}O_2CC(CH_3)_3\}_4[-CN-Cr(CO)_5]_2$ (5): $C_{32}H_{36}Cr_2N_2O_{18}Re_2$ (1213.05): calcd. C 31.69, H 2.99, N 2.31; found C 31.78, H 3.13, N 2.02. − ^1H NMR (CD_2Cl_2, 300 MHz, +25°C): δ = 1.52 (s, 9 H, 3 Me).

$Re_2\{\mu\text{-}O_2CC(CH_3)_3\}_4[-CN-Mo(CO)_5]_2$ (6): $C_{32}H_{36}Mo_2N_2O_{18}Re_2$ (1300.91): calcd. C 29.54, H 2.79, N 2.15; found C 29.77; H 3.10; N 2.06. − ^1H NMR (CD_2Cl_2, 300 MHz, room temp.): δ = 1.52 (s, 9 H, 3 Me). − ^{95}Mo NMR (CD_2Cl_2, 400 MHz, +25°C): δ = −1690.

$Re_2\{\mu\text{-}O_2CC(CH_3)_3\}_4[-CN-W(CO)_5]_2$ (7): $C_{32}H_{36}N_2O_{18}Re_2W_2$ (1476.76): calcd. C 26.03, H 2.46, N 1.90; found C 26.09; H 2.65; N 1.83. − ^1H NMR (CD_2Cl_2, 300 MHz, +25°C): δ = 1.52 (s, 9 H, 3 Me).

Acknowledgments

This work was supported by PRAXIS XXI, Project (2/2.1/QUI/316/94) and Project (2/2.1/QUI/419/94). The authors want to thank the DAAD (INIDA, Accões Integradas and Keretében Megvalósuló Program), the BMFT/JNICT Protokoll and Professor W. A. Herrmann for generous support. A. D. L. (BD) thanks PRAXIS XXI for a grant, F. E. K. acknowledges the Alexander von Humboldt foundation for financial support. We also thank OTKA T025278, AKP 9793-2,4/29 and COST-DS for support.

[1] F. A. Cotton, R. A. Walton, *Multiple Bonds between Metal Atoms*, 2nd ed., Oxford University Press, Oxford, **1993**.
[2] [2a] F. A. Cotton, C. B. Curtis, C. B. Harris, B. F. G. Johnson, S. J. Lippard, J. T. Mague, W. R. Robinson, J. S. Wood, *Science* **1964**, *145*, 1305. − [2b] F. A. Cotton, *Inorg. Chem.* **1965**, *4*, 334−336. − [2c] F. A. Cotton, C. B. Harris, *Inorg. Chem.* **1965**, *4*, 330−333.
[3] [3a] A. S. Kotel′nikova, V. G. Tronev, *Zh. Neorg. Khim.* **1958**, *3*, 1016; *Russ. J. Inorg. Chem.* **1958**, *3*, 268. − [3b] A. S. Kotel′nikova, G. A. Vinogradova, *Zh. Neorg. Khim.* **1964**, *9* , 303−305; *Russ. J. Inorg. Chem.* **1964**, *9*, 168−170. − [3c] A. S. Kotel′nikova, G. A. Vinogradova, *Zh. Neorg. Khim* . **1964**, *9*, 307−309; *Russ. J. Inorg. Chem.* **1964**, *9*, 166−168.
[4] [4a] F. Taha, G. Wilkinson, *J. Chem. Soc.* **1963**, 5406−4512. − [4b] C. Calvo, N. C. Jayadevan, C. J. L. Lock, *Can. J. Chem.* **1969**, *47*, 4213−4220. − [4c] C. Calvo, N. C. Jayadevan, C. J. L. Lock, R. Restivo, *Can. J. Chem.* **1970**, *48*, 219−224.
[5] [5a] M. G. B. Drew, V. Felix, I. S. Gonçalves, F. E. Kühn, A. D. Lopes, C. C. Romão, *Polyhedron* **1998**, *17*, 1091−1102. − [5b] I. S. Gonçalves, F. E. Kühn, A. D. Lopes, A. J. Parola, F. Pina, J. Sotomayor, C. C. Romão, *J. Organomet. Chem.* **1998**, *560*, 117−124. − [5c] F. E. Kühn, E. Herdtweck, J. J. Haider, W. A. Herrmann, I. S. Gonçalves, A. D. Lopes, C. C. Romão, *J. Organomet. Chem.*, in press.
[6] [6a] N. Zhu, H. Vahrenkamp, *Angew. Chem.* **1994**, *106*, 2166−2167; *Angew. Chem. Int. Ed. Engl.* **1994**, *33*, 2090−2091. − [6b] N. Zhu, H. Vahrenkamp, *J. Organomet. Chem.* **1994**, *472*, C5−C7. − [6c] N. Zhu, J. Pebler, H. Vahrenkamp, *Angew. Chem.* **1996**, *108*, 984−985; *Angew. Chem. Int. Ed. Engl.* **1996**, *35*, 894−895. − [6d] G. A. Carriedo, N. G. Conelly, S. Alvarez, E. Pérez-Carreño, S. García-Granada, *Inorg. Chem.* **1993**, *32*, 272−276. − [6e] M. Fritz, D. Rieger, E. Bär, G. Beck, J. Fuchs, G. Holzmann, W. P. Fehlhammer, *Inorg. Chim. Acta* **1992**, *198*, 513−526. − [6f] A. Vogler, A. H. Osman, H. Kunkely, *Coord. Chem. Rev.* **1985**, 159−163. − [6g] A. Vogler, A. H. Osman, H. Kunkely, *Inorg. Chem.* **1987**, *26*, 2337−2340. − [6h] G. A. Carriedo, N. G. Connelly, M. C. Crespo, I. C. Quarmby, V. Riera, H. G. Worth, *J. Chem. Soc., Dalton Trans.* **1991**, 315−323. − [6i] P. Braunstein, B. Oswald, A. Tiripicchio, M. T. Camellini, *Angew. Chem.* **1990**, *102*, 1206−1209; *Angew. Chem. Int. Ed. Engl.* **1990**, *29*, 1140−1143. − [6j] H. Vahrenkamp, A. Geiß, G. N. Richardson, *J. Chem. Soc., Dalton Trans.* **1997**, 3643−3651 and references cited therein. − [6k] E. Bär, W. P. Fehlhammer, D. K. Breitinger, J. Mink, *Inorg. Chim. Acta* **1984**, *82*, L17−L19.
[7] H. Willner, F. Aubke, *Angew. Chem.* **1997**, *109*, 2506−2530; *Angew. Chem. Int. Ed. Engl.* **1997**, *36*, 2402−2530.
[8] [8a] C. Oldham, J. E. D. Davies, A. P. Ketteringham, *Chem. Commun.* **1971**, 572−573. − [8b] J. S. Filippo, H. J. Sniadoch, *Inorg. Chem.* **1973**, *12*, 2326. − [8c] D. M. Collins, F. A. Cotton, L. D. Gage, *Inorg. Chem.* **1979**, *18*, 1712−1715. − [8d] R. J. H. Clark, M. J. Stead, *Inorg. Chem.* **1983**, *22*, 1214−1220. − [8e] S. D. Conradson, A. P. Sattelberger, W. H. Woodruff, *J. Am. Chem. Soc.* **1988**, *110*, 1309−1311. − [8f] G. Henkel, G. Peters, W. Preetz, J. Skowronek, *Z. Naturforsch.* **1990**, *45b*, 469−475.
[9] [9a] W. P. Fehlhammer, C. Moinet, *J. Organomet. Chem.* **1979**, *174*, C55. − [9b] V. Srinivasan, R. A. Walton, *Inorg. Chem.* **1980**, *19*, 1635−1640.
[10] [10a] R. B. King, *Inorg. Chem.* **1967**, *6*, 25−29. − [10b] J. K. Ruff, *Inorg. Chem.* **1968**, *7*, 1821−1825.
[11] F. A. Cotton, C. Oldham, W. R. Robinson, *Inorg. Chem.* **1966**, *5*, 1798−1802.

Received July 8, 1998
[98218]

Comparison of Electrochemically and Photochemically Induced Electron-Transfer Processes of a Series of Copper(II) Schiff Base Complexes with Thiolate Coordination

Stephan Knoblauch,[a] František Hartl,*[b] Derk J. Stufkens,[b] and Horst Hennig*[a]

Dedicated to Professor Arnd Vogler on the occasion of his 60th birthday

Keywords: Spectroelectrochemistry / Cyclic voltammetry / Photochemistry / Copper(II) complexes / Thiolate complexes

The electrochemical and photoredox properties of copper(II) thiopyrazolone Schiff base complexes **1**–**9** with imine and thiolate coordination, showing variable degrees of tetrahedral distortion, were investigated by means of combined electrochemical and spectroscopic techniques in the temperature range of 193−293 K. The cyclic voltammograms of **1**–**9** in butyronitrile revealed that the reduction and oxidation paths are strongly dependent on the geometry of the CuN_2S_2 moiety. Due to the strong delocalization of the singly occupied redox orbital (SOMO) the oxidations and reductions occur in a narrow potential range. The one-electron-reduced **1(r)**–**9(r)** and oxidized **1(o)**–**9(o)** products were electrogenerated and stabilized inside optically transparent thin-layer electrochemical (OTTLE) cells at variable temperatures and could be characterized for the first time by UV/Vis spectroscopy. The reduced formal d^{10} copper(I) species absorb only weakly in the visible region. The oxidized products **1(o)**–**9(o)** show several strong absorptions in the visible region due to the presence of formal d^8 copper(III) species. The spectral information allowed assignment of the initial photoproducts. Irradiations in donor media such as THF or EtOH initially produces **1(r)**–**9(r)**. No photoreduction was observed in *t*BuOH which cannot liberate reducing H_α. The primary oxidized species **1(o)**–**9(o)** were formed in chlorinated acceptor solvents ($CHCl_3$) on UV irradation. Fast relaxation to the ground state prevents the photoredox reactions from CT or LF excited states.

Introduction

Recently we have shown that the photocatalytic oxygenation of terpenes like α-pinene induced by iron(III) porphyrins leads in the presence of copper(II) complexes with $[CuN_2S_2]$ constitution to rearrangement of α-pinene to limonene (beside the formation of oxygenation products).[1] $[CuN_2S_2]$ complexes containing Schiff base ligands with imine and thiolate coordination sites (Figure 1) are of particular significance in that photocatalytic rearrangement. Because it is assumed that photoinduced electron-transfer processes between iron(III) porphyrins, $[CuN_2S_2]$ complexes and α-pinene occur, the spectroscopic, electrochemical, and photochemical properties of the copper(II) complexes themselves were investigated to obtain more insight into the rather intricate function of these complexes. This paper summarizes results obtained from combined electrochemical and photochemical investigations of copper(II) complexes of Schiff base ligands with imine and thiolate coordination sites.

The well-known procedure of the synthesis of these ligands by condensation of the 4-benzoyl-5-mercapto-3-methyl-1-phenylpyrazole with selected diamines has been applied to derivatives of phenylene-1,2-diamine[2][3] with the intention of studying the influence of a coupling π-system between the pyrazole units on the redox behavior. The investigated systems complete a series of tetrahedrally distorted complexes reported by L. Hennig et al.[4]. The reduction potentials were expected to be strongly dependent on the geometry of the donor sphere surrounding the copper ion but this trend could not be experimentally confirmed by L. Hennig et al. It appeared, therefore, necessary to extend the series by more planar complexes to recognize the trends in the redox properties and reactivity of the singly reduced and oxidized species.

The investigated complexes **1**−**9** belong to the comparatively few examples of stable copper(II) thiolate complexes studied so far.[5] In general, previous research done on these compounds was focused on aspects of biomimetic modelling of the active site behavior of biological *Type I* copper centres with regard to their structural and reduction properties. However, oxidation of these compounds has recieved little attention. Further investigation is required in this field. Notably, the first stable copper(III) thiolate complex [Cu(phmi)](PPh_4)] [phmi = 1,2-phenylenebis(2-mercapto-2-methylpropionamide)] has recently been described in the literature.[6]

Ferraudi and Muralidharan reviewed the photochemistry of copper complexes in 1981.[7] A review of research until the early 1990s is given by Horváth and Stevenson.[8] Only little is known, however, about photochemical properties of

[a] Institut für Anorganische Chemie, Universität Leipzig
Talstraße 35, D-04103 Leipzig, Germany
Fax: (internat.) + 49(0)341/9604600
E-mail: hennigho@sonne.tachemie.uni-leipzig.de
[b] Institute of Molecular Chemistry, Universiteit van Amsterdam
Nieuwe Achtergracht 166, NL-1018 WV Amsterdam,
The Netherlands
Fax: (internat.) + 31-20/525-6456
E-mail: hartl@anorg.chem.uva.nl

 © WILEY-VCH Verlag GmbH, D-69451 Weinheim, 1999 1434−1948/99/0202−0303 $ 17.50+.50/0

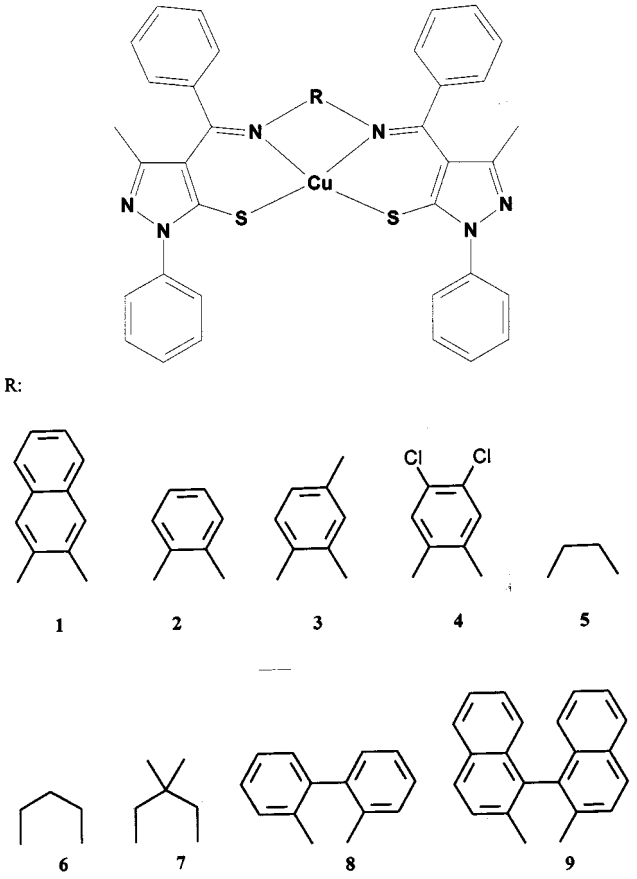


Figure 1. Structural scheme of the Cu^{II} Schiff base complexes used displaying the different backbones R

copper(II) thiolate complexes with large chelating ligands.[9] To our knowledge, only copper(II) complexes with thioethers[10] or dithiolate derivatives (dithiocarbamate,[11–14] maleonitriledithiolate,[15–19] dithiooxalate[20,21] etc.) have been studied photochemically so far.

The detailed spectroscopic and photochemical characterization of large systems like the studied Schiff base complexes **1**–**9** is complicated by strong delocalization of the frontier orbitals and low symmetry.[22] Nevertheless, the presence of intense low-energy charge-transfer absorption bands and the accessibility of two or more oxidation states suggest a variety of photoredox reactions. A redshift of the CT absorptions correlated to the tetrahedral distortion of the CuN_2S_2 moiety is observed.[3] Due to the better separation of the charge-transfer bands, it was important to find out whether redox reactions can be initiated by electronic excitation into the corresponding electronic transitions, or from other excited states, with regard to potential application of these light-sensitive compounds as catalysts in homogeneous photocatalytic systems.[1]

Results and Discussion

Electronic Absorption Spectra

The electronic absorption spectra of the Schiff base ligands employed feature an intense band system in the UV region (see Figure 1). The spectral data of the ligands are listed in Table 1. These transitions are, in accordance with their intensities, attributable to $\pi\rightarrow\pi^*$ transitions within the aromatic system and the azomethine or the thiolate chromophores. They occur at lower energies for the Schiff bases with aromatic coupling between the two imine groups linked by phenylene or biphenylene units. The less intense bands in the near ultraviolet may also arise from $\pi\rightarrow\pi^*$ transitions since they are too intense to be assigned to $n\rightarrow\pi^*$ bands. These absorptions disappear on deprotonation of the ligands during coordination of the metal ion.

Table 1. UV/Vis-spectroscopic data of the free ligands $\mathbf{H}_2$**1**–$\mathbf{H}_2$**9** in $CHCl_3$ at 293 K

Ligand	Band λ_{max} [nm] (ε [$M^{-1}cm^{-1}$])
$\mathbf{H}_2$**1**	271 (37300), 321 (34000), 419 (11700)
$\mathbf{H}_2$**2**	276 (35500), 318 (35800), 421 (11900)
$\mathbf{H}_2$**3**	275 (34800), 317 (35100), 419 (12300)
$\mathbf{H}_2$**4**	271 (36000), 321 (36000), 426 (10900)
$\mathbf{H}_2$**5**	277 (26100), 314 (31200), 399 (11700)
$\mathbf{H}_2$**6**	281 (24500), 310 (29900), 394 (11100)
$\mathbf{H}_2$**7**	282 (25600), 311 (31200), 394 (11400)
$\mathbf{H}_2$**8**	271 (32800), 321 (26300), 419 (10600)
$\mathbf{H}_2$**9**	284 (37900), 344 (28300), 446 (12100)

The electronic absorption spectra of the copper(II) complexes **1**–**9** exhibit UV absorption bands that can be assigned to intraligand (IL) transitions. They are only slightly shifted relative to those of the corresponding uncoordinated Schiff base ligands (Table 2). The UV/Vis region displays bands or shoulders which have been assigned to ligand-to-metal (σ,π-SR$\rightarrow Cu^{II}$) charge-transfer transitions (LMCT)[4] as reviewed by Schugar.[37] For example, **5** shows a shoulder at 346 nm and a relatively strong and broad absorption at 438 nm with a shoulder at 520 nm. In contrast to that, two intense bands in the visible region are observed for **9** (530 nm and 659 nm), together with a shoulder at 355 nm (Table 2). These bands exhibit a red shift on going from a square-planar to a pseudotetrahedral geometry of the CuN_2S_2 chromophores, i.e. from **1** to **9**.[22,29] It should be recalled that strict assignment cannot be given due to strong delocalization of the frontier orbitals.[22]

Ligand field transitions (LF or d-d) at Cu^{II} could not be localized due to strong overlap with CT bands in the visible region. This is not surprising, as the LF transitions are also expected to shift to lower energy with increasing tetrahedral distortion.[30,33]

Cyclic Voltammetry

Cyclic voltammograms of the complexes **1**–**9** were recorded in butyronitrile, as this solvent is also suitable for spectroelectrochemical studies at variable temperatures (described hereinafter). In selected cases THF was employed. All complexes **1**–**9** can be oxidized and reduced within the

Table 2. UV/Vis-spectroscopic data of the complexes **1**−**9** and their redox products

Complex[a]	Band λ_{max} [nm] (ε [in $M^{-1}cm^{-1}$])
1[a]	476, 410 (sh), 328, 273
1[b]	484 (sh) (4300), 410 (sh) (16200), 336 (41600), 275 (41400)
1(ir)[b][c]	400 (sh) (5100), 310 (sh) (29700), 250 (65800)
1(io)[b][c]	350 (sh) (10700), 270 (sh) (39500), 208 (61200)
2[a]	500 (sh) (2500), 405 (sh) (11900), 344 (32900), 275 (37500)
2[b]	480 (sh), 460(sh), 375 (sh), 323, 256
2(ir)[b][c]	390 (sh) (2100), 280 (sh) (23800), 233 (48800)
2(io)[b][c]	331 (sh) (7200), 240 (sh) (32500)
2(r)·[b][c]	510 (sh) (1000), 420(sh), 330 (sh) (13800), 275 (sh), 234 (46200)
2(o)[b][c]	750 (sh) (1800), 628 (2500), 516 (5100), 439 (5000), 375 (sh), 330 (30900), 262 (34800), 239 (34200)
3[a]	500 (sh) (2500), 410 (sh) (12200), 345 (33600), 277 (39400)
4[a]	505 (sh) (2500), 410 (sh) (14100), 350 (33700), 317 (28400), 279 (34000)
5[a]	520 (sh) (1600), 438 (3500), 346 (sh) (10800), 275 (35600)
5[b]	500 (sh), 420, 330 (sh), 275
5(r)[b,c]	390 (sh) (3400), 330 (sh), 270 (36100)
5(o)[b,c]	> 900, 556 (1400), 432 (10100), 270 (sh) (15000), 251 (35900)
6[a]	610 (sh) (1900), 476 (3900), 339 (12100), 274 (36700)
6[b]	580, 473, 350 (sh), 322, 269, 224
6(r)[b,c]	440 (sh) (900), 330 (sh) (1200), 263 (39400)
6(o)[b,c]	800 (2900), 550 (sh) (1800), 449 (9900), 340 (sh) (5900), 280 (sh) (24700), 250 (45400)
7[a]	599 (1900), 473 (3700), 341 (11500), 272 (35500)
8[a]	630 (sh) (1400), 522 (2100), 350 (sh) (10800), 279 (35500)
9[a]	659 (1600), 530 (1800), 355 (sh) (17000), 290 (51800)
9[b]	660, 511, 375 (sh), 334, 290
9(r)[b,c]	440 (sh) (2100), 350 (sh), 272 (32800)
9(o)[b,c]	733 (2600), 570 (sh), 469 (3900), 330 (sh) (15600), 290 (sh) (38900), 276 (39200)

[a] In $CHCl_3$ at 293 K. − [b] In butyronitrile containing $3\cdot10^{-1}$ M Bu_4NPF_6 at 293 K. − [c] Abbreviation **(ir)** denotes the secondary reduction products, **(r)** the primary one-electron reduction products, **(io)** the secondary oxidation products, and **(o)** the primary one-electron oxidation products.

Table 3. Electrochemical data of the complexes **1**−**9**[a]

Complex	$E_{p,c}$(red)	ΔE_p	$E_{p,a}$(ox)	ΔE_p	ΔE_p(Fc/Fc$^+$)
Butyronitrile					
1	−1.03[b]	−	0.31[b]	0.105	0.100
1[d]	−1.05[b]	0.130	0.28[e]	0.100	0.100
1(ir)	−	−	−0.30[b]	−	
1(ir)[e]	−	−	−0.20[b]	−	
2	−1.04[b]	−	0.34[b]	0.095	0.105
2[d]	−0.96[e]	0.175	0.27[e]	0.100	0.100
2(ir)	−	−	−0.30[b]	−	
3	−1.06[b]	−	0.32[b]	0.100	0.105
3[d]	−1.08[b]	0.110	0.25[e]	0.100	0.100
3[e]	−1.06[e]	0.125	0.30[e]	0.100	0.100
3(ir)	−	−	−0.32[b]	−	
4	−0.94[b]	−	0.42[b]	0.110	0.105
4[d]	−0.98[b]	0.110	0.37[e]	0.100	0.100
4[e]	−0.99[e]	0.150	0.35[e]	0.110	0.100
4(ir)	−	−	−0.26[b]	−	
4(ir)[e]	−	−	−0.24[b]	−	
5	−1.23[e]	0.130	0.27[e]	0.115	0.105
6	−1.04[e]	0.110	0.23[b]	−	0.100
6[d]	−1.06[e]	0.175	0.21[e]	0.150	0.110
7	−1.02[e]	0.110	0.24[b]	−	0.110
7[d]	−0.97[e]	0.100	0.28[b]	0.150	0.100
8	−0.89[e]	0.100	0.25[b]	−	0.100[g]
8[f]	−0.81[e]	0.100	0.30[b]	0.140	0.105[g]
9	−0.84[e]	0.100	0.29[b]	−	0.100
9[e]	−0.80[e]	0.100	0.28[e]	0.150	0.090
THF					
2	−1.19[b]	−	0.37[e]	0.100	0.100
2(ir)	−	−	−0.36[b]	−	
6	−1.08[e]	0.110	0.31[e]	0.110	0.110
9	−0.95[e]	0.110	0.30[e]	0.110	0.110

[a] Cyclic voltammetry, $5\cdot10^{-4}$ M solutions of the complexes in butyronitrile or THF containing $3\cdot10^{-1}$ M Bu_4NPF_6, T = 293 K (unless stated otherwise), Pt disk electrode (0.42 mm^2 apparent surface area), scan rate v = 100 mV/s. Redox potentials given vs. $E_{1/2}$(Fc/Fc$^+$) = 0.43 V and 0.57 V vs. SCE in butyronitrile and THF, respectively. Abbreviation **(ir)** denotes the secondary reduction products of **1**−**4**, oxidizable back to the parent complexes. − [b] Chemically irreversible redox process. − [c] T = 213 K. − [d] T = 230 K. − [e] Chemically reversible redox process. − [f] T = 250 K. − [g] $CoCp_2^{+/0}$ employed as internal standard redox system ($E_{1/2}$ = −1.34 V vs. Fc/Fc$^+$). −

potential window available in these solvents. The corresponding redox potentials (vs. Fc/Fc$^+$) are summarized in Table 3. The representative cyclic voltammograms of **2**, **5**, and **9** in butyronitrile are shown in Figures 2A−C, respectively. The cathodic and anodic steps will be described separately.

Reduction

In *butyronitrile*, the reduction of the complexes **5**−**9** on the time scale defined by scan rates $v \geq 50$ mV/s is chemically reversible already at room temperature (see Figure 2C). The electron transfer is electrochemically reversible for **7**−**9**, but quasi-reversible for **5** and **6** (see Figure 2B and Table 3). On the other hand, the reduction of the complexes **1**−**4** at room temperature is chemically totally irreversible, as no anodic counterpeak was observed on the reverse anodic scan (see Figure 2A). The reduction in the latter case produces species, denoted **1(ir)**−**4(ir)** in Table 3, which oxidize on the reverse scan ca. 0.7 V more positively in comparison with the reduction potentials of the parent complexes **1**−**4**. The complexes **1**−**9** could be reduced completely with one equivalent of cobaltocene, which agrees with the transfer of one electron. The cobaltocenium salts of the anionic products **5(r)**−**9(r)** persisted in the solution for several minutes without any decomposition and could be oxidized back completely to parent **5**−**9** by one equiva-

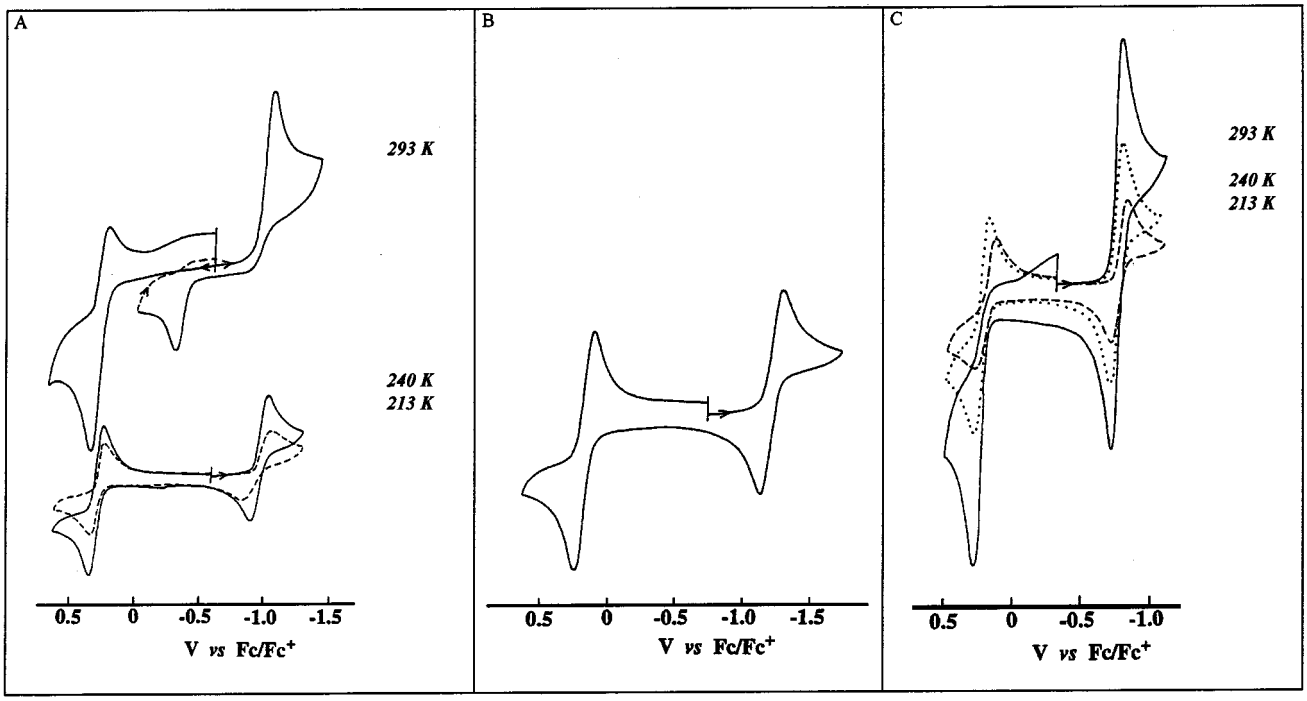


Figure 2. Cyclic voltammograms of the complexes (A) **2** at 293, 240, and 213 K; (B) **5** at 293 K; (C) 9 at 293, 240, and 213 K (butyronitrile/ $3 \cdot 10^{-1}$ M Bu_4NPF_6, Pt disk microelectrode with 0.42 mm^2 disk area, scan rate v = 100 mV/s)

lent of $FcBF_4$. The secondary anionic reduction products **1(ir)−4(ir)** are also inherently stable, as confirmed by cyclic voltammetry. Scan reversal beyond their anodic peaks (see Table 3) led to the reappearance of the cathodic peaks due to the reduction of **1**−**4**. The recovery of **1** and **2** on oxidation of **1(ir)** and **2(ir)**, respectively, was further documented by corresponding UV/Vis spectroelectrochemical experiments (see below). This behavior points to rapid conversion of the primary one-electron reduction products **1(r)−4(r)** to **1(ir)−4(ir)** at room temperature, resulting in a reversible conformational change (see below). Oligomerization or polymerization reactions induced by the reduction are less likely due to the limited conformational flexibility of the ligand framework in the parent complexes **1**−**4** (see Figure 1). As reported recently by Rasmussen et al.,[34] a tetranuclear cluster (Cu_4L_4) is produced in the course of the reaction between the more flexible deprotonated ligand *N*,*N*′-(2,2′-biphenyldiyl)bis(4-aminomethyl-1,3-diphenyl-5-thiopyrazole) and $[Cu(CH_3CN)]^+$ in DMF.

All stable reduction products **1(ir)−4(ir)** and **5(r)−9(r)** are EPR-silent. This result is consistent with the formation of one-electron-reduced, formal Cu^I complexes; although, the Extended-Hückel calculations on the fragments of the parent complexes **2**, **5**, and **6** and the average imine N−C distances (1.31 Å for **8**[3,14]) in the middle of the N=C/N−C bond-length range[38] (1.25−1.39 Å) show that the singly occupied redox orbital (SOMO) is strongly delocalized over the *cis*-CuN_2S_2 moiety.[22] It cannot be excluded, however, that in the anionic reduction products **1(r)−9(r)** the added electron density resides more on the central Cu atom, for example due to the mixing of the HOMO of the anions with close-lying empty orbitals (LUMO and LUMO +1) which are largely localized[22] on the electron-withdrawing imine functions and the thiopyrazolone rings.

Within the series of the parent compounds **1**−**9** the geometry around the central ion strongly depends on the flexibility of the backbone R connecting the two imine nitrogen atoms (see Figure 1). Thus, the rather rigid naphthylene and phenylene backbones in **1**−**4** impose only slightly distorted square planar geometry, as documented by the crystal structures of **1** and **2** showing θ = 3.3° and 9.3°, respectively (θ is the dihedral angle between the two N−Cu−S planes in the crystal). In contrast to this, in **5** and **6** with the more flexible ethylene and propylene backbones, the value for θ increases to 34.7° and 42.5°, respectively, and θ = 52.1° was determined for **8** (L. Hennig et al.[4]) with the flexible 2,2′-biphenylene backbone enforcing a large tetrahedral twist on the coordination polyhedron. Even larger tetrahedral distortion from the planar geometry was recently observed for a novel complex **10** with the backbone R = butylene, where θ = 56°.[36] In general, Cu^I complexes will prefer the tetrahedral coordination, which also applies for the studied primary one-electron reduction products **1(r)−9(r)**. We have indeed observed that the one-electron reduction at room temperature is chemically irreversible for the nearly square planar complexes **1**−**4**, while the thermal stability of **5(r)−9(r)** nicely correlates with the increased tetrahedral distortion in **5**−**9**. We therefore propose that the secondary chemical reactivity of **1(r)−4(r)** producing **1(ir)−4(ir)** has its origin in a tetrahedral twist induced by the electron-transfer step. The electrochemically quasireversible character of the reduction of **5** at room temperature may indicate some small conformational change on going to **5(r)** while the geometry of the

coordination polyhedron of **6(r)−9(r)** with respect to that of the parent complexes **6−9** remains unchanged. It is noteworthy that the size of the chelate ring, the nature (aromatic, aliphatic) and steric demands of the bridging system in **1−7** possess rather limited influence on the reduction potential. Only for the pseudotetrahedral complexes **8** and **9** an apparent positive shift of the reduction potential was observed (see Table 3). This shift may arise from a stabilizing overlap between the π systems of the twisted 2,2′-biphenylene and 2,2′-binaphthylene backbones, respectively, and the π system of the "4-benzyl" substituent at the thiopyrazolone rings, as judged from the crystal structure of **8**.[4,35] For example, the tetrahedrally most twisted complex **10** with the aliphatic butylene backbone R reversibly reduces at $E_{p,c} = -1.03$ V,[36] i.e. again more negatively than **8** and **9** but identical to nearly planar **1−3** and less twisted **6** and **7**.

Cyclic voltammetry performed at moderate scan rates has revealed that the reduction of **2** becomes chemically reversible at $T = 230$ K, as judged from $I_{p,a}/I_{p,c} = 1$ and disappearance of the anodic peak due to the oxidation of **2(ir)** on the reverse scan. Between 243 and 213 K the ΔE_p value gradually increases relative to that of the Fc/Fc^+ internal standard and the voltammetric response broadens, while $I_{p,a}/I_{p,c}$ again becomes less than 1 and $I_p v^{-1/2}$ is virtually independent of v (see Figure 2A). This behavior is characteristic for an electrochemically quasireversible charge transfer and suggests that, likewise **5(r)** and **6(r)** (see above), also **2(r)** and parent **2** may slightly differ in the coordination geometry. A similar temperature dependent voltammetric response was recorded for **3** and **4**; chemical reversibility of the reduction in the latter cases was, however, only achieved at $T = 213$ K (see Table 3). In contrast to this, the one-electron reduction of the nearly square planar complex **1** ($\theta = 3.3°$) remains chemically irreversible even at $T = 213$ K.

No significant difference in the reduction path was observed when cyclic voltammograms of **2**, **6**, and **9** were recorded in *THF* at $T = 293$ K, besides a shift of the reduction potentials to lower values by 40−160 mV (see Table 3).

Oxidation

Oxidation of **1−9** in *butyronitrile* occurs, independently of the geometry of the CuN_2S_2 core, in a narrow potential range (see Table 3). At $v = 100$ mV/s oxidation of the nearly square planar complex **1**, in contrast to its reduction, is a both chemically and electrochemically reversible one-electron process independently of the applied temperature between 293 and 213 K. Of course, at $T = 330$ K for example, the oxidized species of **1** will decompose. In consequence of the increasing tetrahedral distortion of the coordination polyhedron, the oxidation of the complexes **2−10** at $T = 293$ K is chemically irreversible at $v = 100$ mV/s (see Table 3). The oxidation of the complexes **2−4** on this subsecond time scale is still an one-electron process and the primary oxidation products **2(o)−4(o)** are detectable on the reverse anodic scan ($I_{p,c}/I_{p,a} \approx 0.4-0.5$). At $T = 255$ K the secondary chemical reactivity of **2(o)−4(o)** becomes completely suppressed, as judged from $I_{p,c}/I_{p,a} = 1$ (see Figure 2A). The one-electron-oxidized complex **5(o)** does not fit within the series, being exceptionally stable even at room temperature (see Figure 2B). On the other hand, complex **6** is oxidized in a chemically totally irreversible step which corresponds with transfer of two electrons ($n_{app} = 2$). Proceeding to **7−9** the oxidation remains chemically irreversible but the number of transferred electrons at $v = 100$ mV/s again decreases to $n_{app} \approx 1.5$ for **7** and $n_{app} = 1$ for **8** and **9** (see Figure 2C). Scanning at low temperatures revealed that the oxidation of **6** at $T = 230$ K becomes chemically reversible ($n_{app} = 1$) while for **9** $T = 220$ K is required to stabilize the cation **9(o)** at $v = 100$ mV/s. The corresponding cations **7(o)** and **8(o)** remain unstable even at $T = 213$ K. It is noteworthy that, opposite to **1−4**, the one-electron oxidation of **6−9** producing **6(o)−9(o)** is electrochemically quasireversible while the one-electron reduction of these complexes under identical conditions is electrochemically reversible (see Table 3). This redox behavior may indicate that, likewise **1−4** and **1(r)−4(r)** (see above), also **6−9** and **6(o)−9(o)** in butyronitrile slightly differ in the coordination geometry of the CuN_2S_2 core. In the case of **5** the little conformational change applies both for **5(r)** and **5(o)**.

In sharp contrast to the cyclic voltammetric response in butyronitrile, the complexes **2**, **6**, and **9** oxidize in THF at room temperature in a both chemically and electrochemically reversible one-electron step (see Table 3). Addition of an excess of PPh_3 to the THF solution of **9** converts the oxidation of the latter complex to a chemically totally irreversible two-electron process while the chemically reversible one-electron reduction remains unaffected.

The one-electron-oxidized complexes **1(o)−9(o)** can be viewed in first approach formally as d^8-Cu^{III} species. Their preference for the square-planar geometry of the CuN_2S_2 polyhedron may explain the electrochemically quasireversible character of the one-electron oxidation of the strongly tetrahedrally distorted parent complexes **5−9**. This description is, however, too oversimplified as the SOMO of **1−9** is known to be strongly delocalized over the whole CuN_2S_2 moiety, with a major contribution from the two sulfur atoms.[22] For example, oxidation of the derivative of **2** with the thiolate donors replaced by oxygen functions occurs significantly more positively [**2-O**: $E_{p,a}(ox) = 0.9$ V and $E_{p,c}(red) = -1.38$ V vs. Fc/Fc^+ in butyronitrile at $T = 293$ K; the one-electron reduction is chemically reversible at $v = 100$ mV/s]. It can therefore be accepted that the one-electron oxidation mainly affects the stability of the Cu−S bond(s). The chemical irreversibility of the oxidation and its overall two-electron character have probably its origin in the cleavage of the Cu−S bonds, followed by closure of intra- or intermolecular disulfide S−S bonds in **1(io)−9(io)**, the secondary oxidation products. The latter processes become significantly accelerated for the tetrahedrally twisted complexes **6−9**, pointing to the role of conformational change induced by the electron transfer to the anode, and

in the presence of strongly coordinating ligands like butyronitrile or PPh_3, which may occupy the coordination sites abandoned by the sulfur atoms. This anodic path explains the increased chemical reversibility of the primary one-electron oxidation step in weakly coordinating THF.

UV/Vis Spectroelectrochemistry

UV/Vis spectra of primary and secondary redox products of **1**−**9**, detected by cyclic voltammetry were recorded in situ at variable temperatures by using appropriate OTTLE cells. The main goal of these experiments was to obtain spectroscopic information needed for correct assignment of species generated on photo-induced reduction and oxidation of selected complexes under study. The UV/Vis spectroelectrochemical data are collected in Table 2.

Reduction

The one-electron reduction of **5** (Figure 3A), **6** and **9** (Figure 3B) in butyronitrile at 293 K, and **2** in butyronitrile at 190 K (Figure 3C) in the course of the OTTLE experiments yielded the stable species **5(r)**, **6(r)**, **9(r)**, and **2(r)** as single products. This assignment was based on the thin-layer cyclic voltammograms recorded during the reduction and reverse reoxidation steps, which corresponded with the chemically reversible redox couples observed in ordinary cyclic voltammograms under identical conditions. In all of these cases retention of isosbestic points was observed and the reoxidation of the anionic products resulted in full recovery of the parent complexes. The UV/Vis spectra of the anions are characterized by the presence of an intense band between 230 and 275 nm with an apparent shoulder at ca. 330 nm. The charge-transfer absorption bands of the parent complexes in the visible region disappeared. Instead, the anions **2(r)**, **5(r)**, **6(r)**, and **9(r)** absorb only weakly between 380 and 500 nm.

The UV/Vis spectrum of square-planar **2(r)** also shows a weak absorption at 510 nm (see the insert to Figure 3C). This band is missing in the UV/Vis spectrum of the secondary reduction product **2(ir)** generated during the one-electron reduction of **2** in butyronitrile at 293 K (see Figure 3C). The rest of the UV/Vis spectrum of **2(ir)** closely resembles that of **2(r)**, pointing to a very similar bonding situation in both anions. For example, oxidation at the positively shifted anodic potential of **2(ir)** (see Table 3) also led to the complete reappearance of the UV/Vis spectrum of **2**, in agreement with the cyclic voltammetric behavior (see above). Almost identical spectroscopic responses were observed for the chemically irreversible one-electron reduction of nearly square planar **1** at 293 K and for the reverse oxidation of **1(ir)** (see Table 2 and Figure 3C).

Oxidation. Electrochemical oxidation of **2**, **5**, **6**, and **9** in butyronitrile at 193 K within the UV/Vis OTTLE cell produced stable cations **2(o)**, **5(o)**, **6(o)**, and **9(o)**. As depicted in Figure 4 and summarized in Table 2, the electronic absorption spectra of these cations typically exhibit several

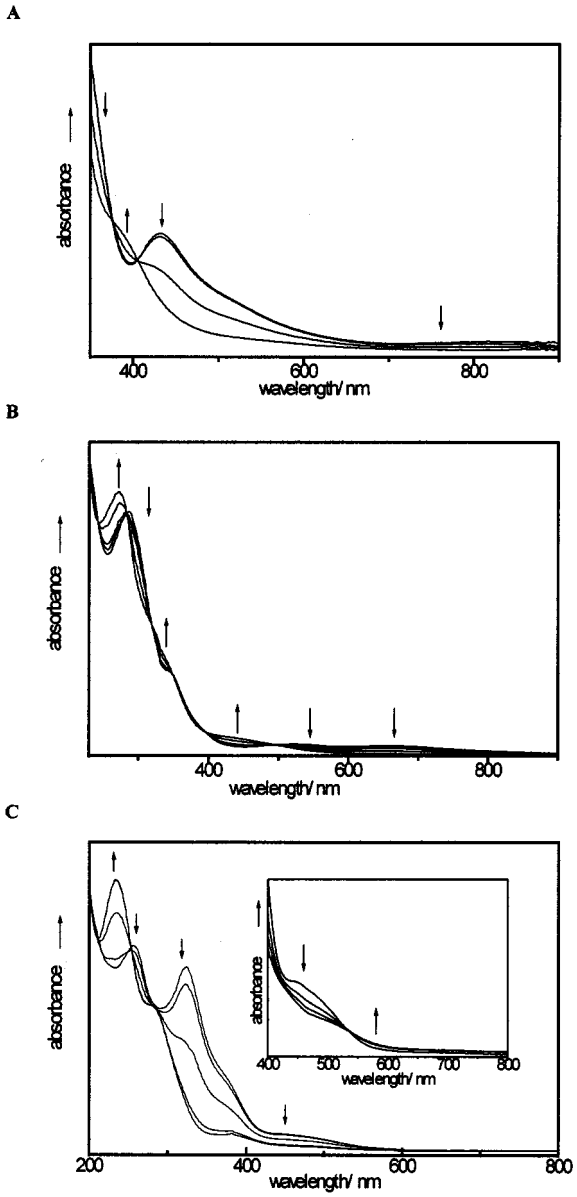


Figure 3. UV/Vis-spectroscopic changes accompanying electrochemical reduction of **5** (A), **9** (B), and **2** (C) in butyronitrile at 293 and 193 K (inset) within an OTTLE cell[27,28]

absorption bands covering the whole visible region between 400 and 900 nm. Their assignment was not attempted, particularly due to the strong electronic delocalization of the parent complexes, which probably also persists in the one-electron-oxidized species. The cation **2(o)** was still observable at 230 K whereas **5(o)** existed a few minutes even at 293 K. The oxidation of **2** at room temperature only yielded the stable secondary product **2(io)** which does not absorb in the visible region (see Table 2). Interestingly, reverse reduction of **2(io)** directly resulted in full recovery of the parent complex **2**. The same result was obtained for the corresponding planar complex **1**, regardless of the chemically reversible one-electron oxidation of the latter complex at 293 K on the subsecond time scale of cyclic voltammetry. Provided **1(io)**−**9(io)** contain intra- or intermolecular disulfide linkages, as argued above, their reduction is then largely

localized on this function, resulting in rapid recoordination of the reduced thiolate appendages and the recovery of **1**−**9**.

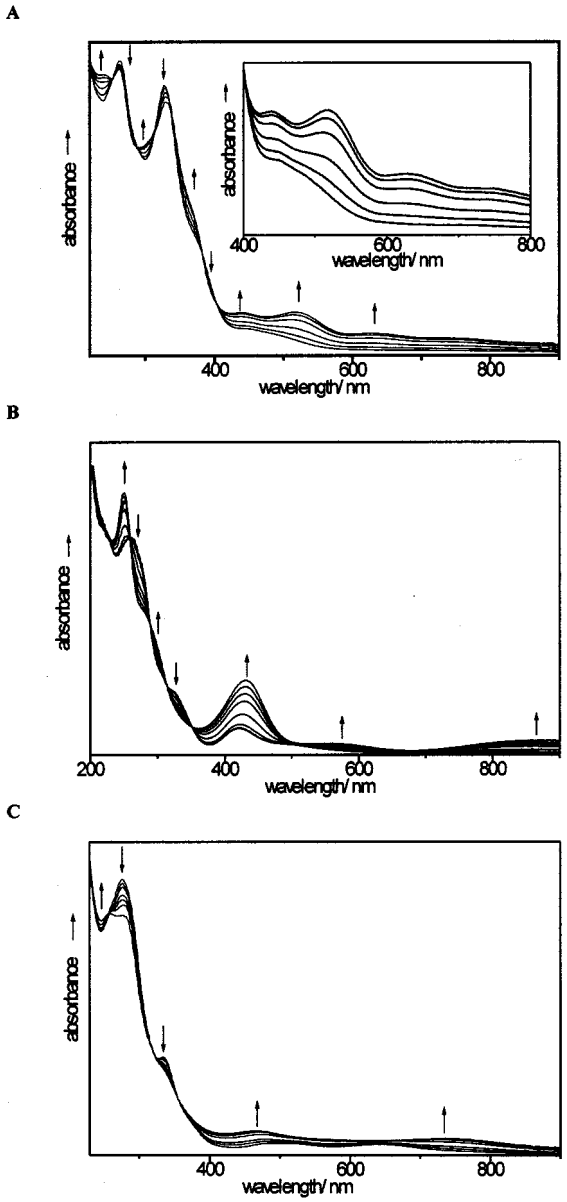


Figure 4. UV/Vis-spectroscopic changes accompanying electrochemical oxidation of **2** (A), **5** (B), and **9** (C) in butyronitrile at 193 K within an OTTLE cell[28]

Photochemistry

The photochemical experiments have been carried out to investigate the possibility to initiate photoinduced electron-transfer processes producing oxidized or reduced species from the parent copper(II) complexes.

Photoreduction

Continuous photolysis of complexes **1**−**9** with full output of the mercury lamp in donor solvents EtOH or THF at room temperature led to bleaching of the bands in the visible region within approximately 30 min. Identical spectral changes were monitored when wavelengths $\lambda_{irr} < 310$ nm were excluded. The photoreactions became accelerated in the presence of electron donors such as $N(CH_2CH_2OH)_3$ (TEA). No photoreduction took place in *t*BuOH within 30 min ($T = 303$ K), presumably because this solvent does not liberate α-hydrogen atoms, in contrast to THF and EtOH.

The UV/Vis-spectral changes accompanying the photoreduction of complex **9** at 293 K are depicted in Figure 5A ($\lambda_{irr} > 315$ nm). Identical spectral changes were monitored upon the electrochemical one-electron reduction of this complex within the OTTLE cell. The same behavior was observed for **8**. The increase of absorbance around 450 nm is a characteristic feature of the primary reduced anions **8(r)** and **9(r)**. The conversion is complete within ca. 60 min. The photoreduction requires strictly anaerobic conditions. Full recovery of the starting complexes was observed on air exposure of the photogenerated anions **8(r)** and **9(r)** if the irradiation was stopped before side reactions started.

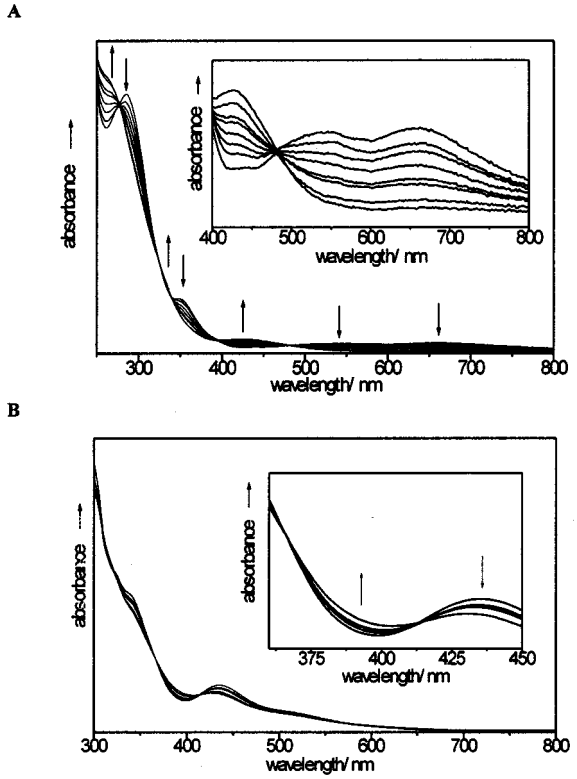


Figure 5. UV/Vis-spectroscopic changes accompanying continuous photolysis of **9** (A) at 293 K, **5** (B) at 193 K in THF ($\lambda_{irr} > 310$ nm, $t_{irr} = 0, 10, 20, 35, 50, 70$ s)

Photochemical generation of the reduced complexes **5(r)**−**7(r)** failed at room temperature, though the spectroelectrochemical investigations reveal their thermal stability. Continuous photolysis in THF at low temperatures ($T \leq 213$ K), however, yielded the expected anionic complexes. The formation of **5(r)** at $T = 193$ K is shown in Figure 5B.

The application of low temperature was not successful in the case of **2(r)**. The absence of the weak absorption of **2(r)** at 500 nm arising in the course of the electrochemical

reduction, reveals that only the secondary product **2(ir)** was formed on irradiation of **2** in EtOH and THF, even at T = 193 K. This finding obviously fits with the lower stability of the primary reduced complex **2(r)** in comparison with **5(r)−9(r)**, as discussed in previous sections.

Photooxidation

Irradiation of **1**−**9** in $CHCl_3$ at 546, 436, and 366 nm did not lead to any measurable photoreaction, although intense CT absorption bands dominate in this region (see Table 2). With λ_{irr} = 332 nm only minor spectral changes could be detected within 60 min. A considerable acceleration of the photoreaction was observed when shorter irradiation wavelengths (λ_{irr} = 313 , 302 , and 254 nm) were applied, though the absorbance of **1**−**9** does not deviate significantly at the latter wavelengths from that at 334 or 366 nm. Notably, a week absorbance ($A \approx 0.004$ vs. H_2O; d = 1 cm) of the solvent $CHCl_3$ was measurable already at λ = 313 nm (cut off at ca. 250 nm).

Continuous photolysis (λ_{irr} = 254 , 302 , and 313 nm) of the complexes **1**−**9** in $CHCl_3$ only resulted in disappearance of the visible and UV absorption bands. The bleaching reactions may indicate formation of secondary oxidized products as studied in the course of the corresponding UV/Vis-spectroelectrochemical experiments (see Table 2).

In order to obtain evidence for the formation of the primary one-electron-oxidized species **1(o)**−**9(o)** upon irradiation in $CHCl_3$, flash photolysis experiments were carried out at room temperature. The samples were excited with 266 nm and 355 nm laser pulses. The ns transient absorption spectra were recorded in 10-nm steps for deaerated, as well as oxygen-saturated solutions (Figure 6). The expected increase of absorption in the visible region due to the cationic species **1(o)**−**9(o)** was indeed observed independent of the exclusion of oxygen, as displayed in Figure 7 for **2**. Following the decay of this transient absorption on the ns time scale showed that the cationic complexes exist at room temperature only a few hundred ns. The lifetimes τ of **1(o)**−**9(o)** in oxygen-free $CHCl_3$ were estimated assuming a first- or pseudo-first-order decay. Values for τ are given in Table 4. The longer lifetimes of **2(o)** and particularly **1(o)** relative to those of **6(o)**, **9(o)**, and particularly **8(o)** nicely agree with the cyclic voltammetric trends (see above).

In general, the photochemical reactivity of **1**−**9** in $CHCl_3$ tracks the absorbance spectrum of the solvent $CHCl_3$. The observed reactions are therefore assigned to be solvent initiated or to take place from CTTS excited states, which are not manifested in the electronic spectrum of these compounds in $CHCl_3$.[38]

No spectral changes could be monitored on excitation of the complexes **1**−**9** with visible light (λ > 400 nm) within 30 min. This behavior appears to be a result of relaxation processes from CT excited states via LF excited states.

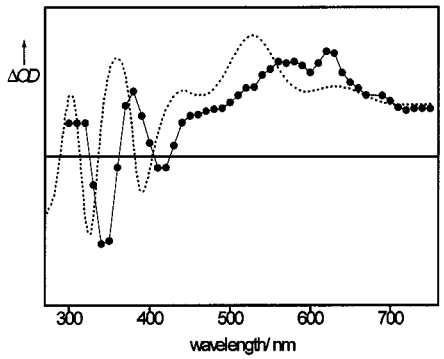


Figure 6. Transient absorption spectrum of **2** in *CHCl*$_3$ measured point-by-point 0.4 μs after laser excitation at 266 nm (••••), compared with UV/Vis absorbance difference spectrum recorded on one-electron oxidation of **2** in *butyronitrile* at 193 K (----) (see also Figure 3C)

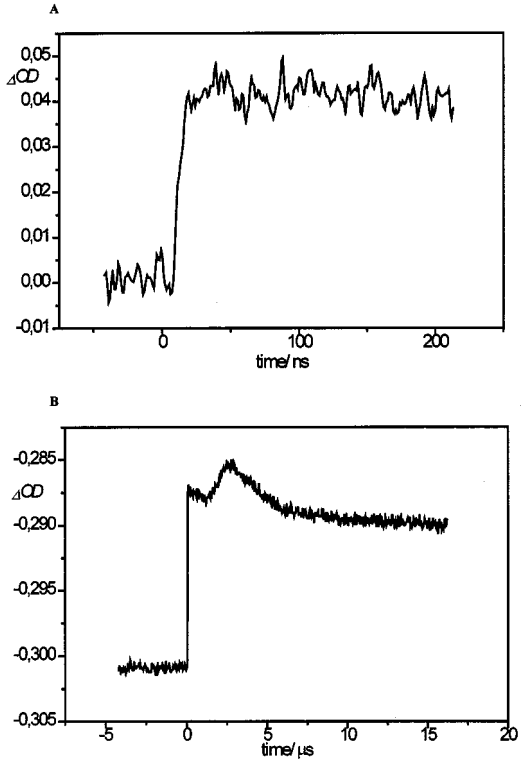


Figure 7. Transient decay following flash excitation of **2** in $CHCl_3$ at 266 nm on nanosecond (A) and microsecond (B) time scales

Table 4. Estimated lifetimes τ of the photooxidized complexes

Cation	**1(o)**	**2(o)**	**5(o)**[a]	**6(o)**	**8(o)**	**9(o)**
τ [μs]	3.1	1.2	–	0.5	0.2	1.0

[a] The lifetime of **5(o)** could not be estimated due to very weak decrease of optical density accompanying the formation of secondary product sfrom **5(o)**.

Conclusions

The thiolate sulfur atom of the complexes under study is bound to an sp^2-hybridized carbon atom. The coupling of the pyrazole-ring carbon atom and the sulfur p-orbitals provides an easily conjugable framework to stabilize the thiolato copper(II) linkage. This electronic coupling results in a strong delocalization crucially influencing the electro-

chemical and photochemical properties of **1**−**9**. This kind of strong delocalization seems to be responsible that photochemical reactions can only be initiated by exciting intraligand excited states whilst excitation of low-energy electronically excited states leads to fast radiationless deactivation via d-d excited states.

Both thermally and photochemically induced reaction pathways of **1**−**9** are summarized in Scheme 1. In general, the same primary redox products, as studied by spectroelectrochemistry, are initially formed on photolysis in the appropriate reducing and/or oxidizing media. Photoreduction occurs in solvents bearing H_α atoms. Photooxidation in chlorinated solvents like $CHCl_3$ are solvent-initiated or initiated by population of CTTS-excited states.

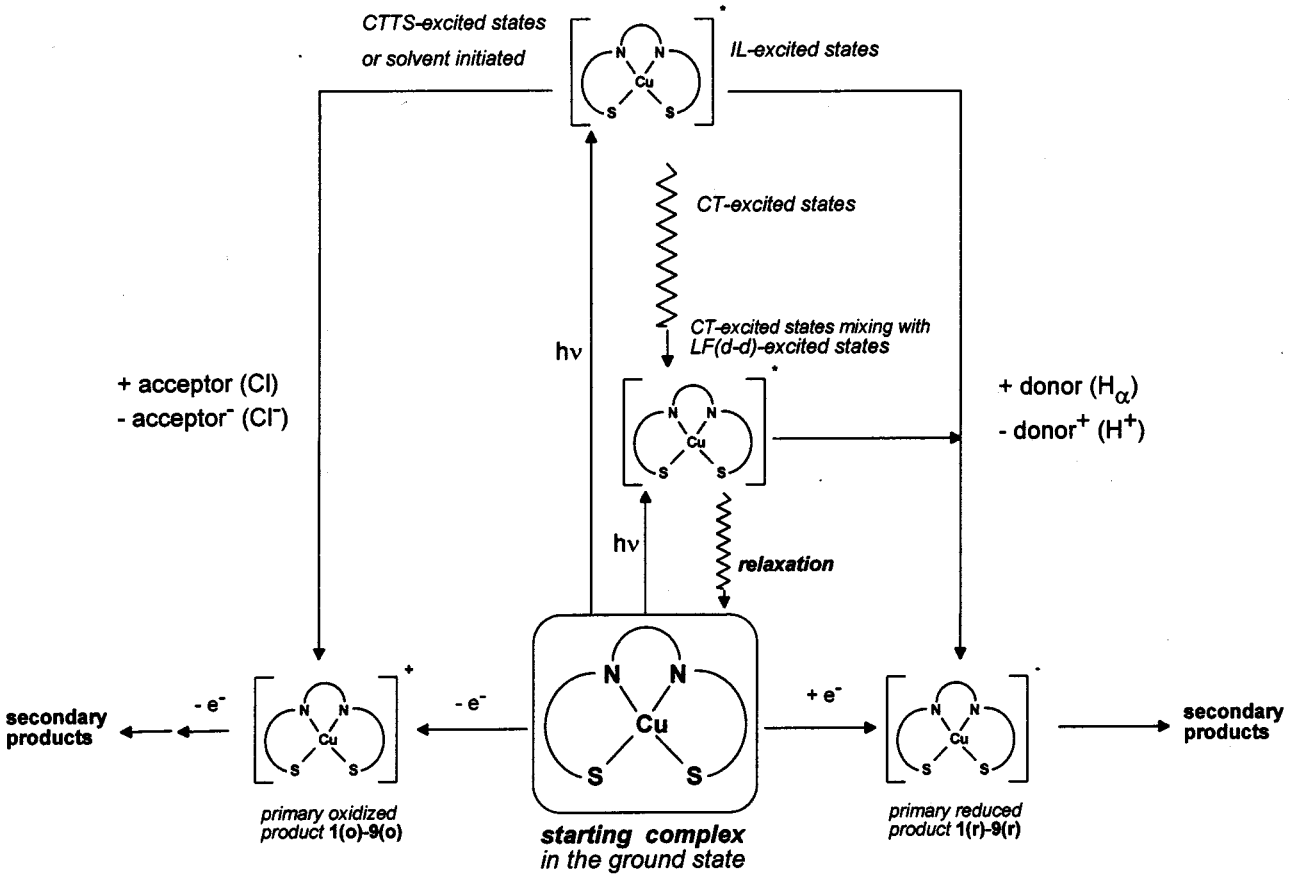
The oxidation takes place on the copper−sulfur moiety. Obviously, the strong delocalization is responsible for the similar values of the oxidation potentials. The primary one-electron-oxidized products of copper(II) thiolate complexes could be characterized by UV/Vis spectroscopy at low temperature.

The reduction behavior is strongly dependent on the geometry of the pseudotetrahedral N_2S_2 donor set surrounding the Cu^{II} ion. The stability of the primary one-electron-reduced products increases with stronger tetrahedral distortion. An opposite trend applies for the primary one-electron-oxidized species (formally d^8-Cu^{III}) which prefer square-planar geometry of the coordination sphere.

The effect of different substituents on the redox behavior of the nearly planar complexes **1**−**4** containing aromatic backbones is not significant. The influence of the ligand flexibility on the reduction of the complexes with aliphatic backbones is reflected in the two-electron oxidation of the complexes **6** and **7** in comparison with **8** and **9** on the time scale of cyclic voltammetry. The oxidation path is significantly influenced by the kind of donor solvents used. Thus, strongly coordinating butyronitrile facilitates cleavage of the Cu−S bonds in the primary one-electron-oxidized species, followed by transfer of a second electron. This reactivity can be supressed in weakly coordinating THF.

Experimental Section

Synthetic Methods and Materials: All chemicals were of analytical grade and were used as received from Aldrich [Bu_4NPF_6, ferrocene (Fc), cobaltocene ($CoCp_2$), cobaltocenium hexafluorophosphate ($CoCp_2PF_6$), PPh_3]. Ferrocenium tetrafluoroborate ($FcBF_4$) was prepared according to a literature procedure.[23] THF (Acros) was dried with NaOH pellets, followed by distillation from Na/benzophenone under nitrogen. Butyronitrile (Fluka) was freshly distilled from CaH_2 under nitrogen. Solvents for photoredox reactions ($CHCl_3$, ethanol), from Merck (Uvasol) or Aldrich (*t*BuOH), were degassed by means of ultrasound or bubbling solvent-saturated N_2 through the solutions before use. The complexes **1**−**9** (Figure 1) were synthesized according to literature procedures.[2,4,22] Their purity was checked by elemental analysis and mass spectrometry.



Scheme 1. General scheme of the electron-transfer pathway of the complexes **1**−**9**

Instrumentation

Spectroelectrochemistry: Cyclic voltammetry was performed in butyronitrile or THF using a standard vacuum-tight single-compartment cell equipped with a Pt disk working electrode of 0.42 mm^2 apparent surface area polished carefully with a 0.25 μm diamond paste. Pt gauze auxiliary and coiled Ag wire pseudoreference electrodes were used. The redox potentials are reported versus the $E_{1/2}$ potential of the ferrocene/ferrocenium (Fc/Fc^+) couple used as the recommended internal standard.[24] Occasionally, the cobaltocene/cobaltocenium ($CoCp_2^{+/0}$) couple was employed instead of Fc/Fc^+, using $E_{1/2}(CoCp_2^{+/0}) = -1.34$ V vs. Fc/Fc^+.[25] In butyronitrile $E_{1/2}(Fc/Fc^+) = +0.43$ V vs. SCE.[26] The cyclic voltammetric samples contained one of the $5\cdot10^{-4}$ M complexes **1**−**9** and $3\cdot10^{-1}$ M Bu_4NPF_6 as supporting electrolyte. UV/Vis spectroelectrochemistry at variable temperatures was carried out with previously described optically transparent thin-layer electrochemical (OTTLE) cells[27][28] placed into a Perkin-Elmer Lambda 5 spectrophotometer equipped with a 3600 data station. The solutions were typically $5\cdot10^{-3}$ M in the copper complexes **1**−**7** or less concentrated (near saturation) due to limited solubility of **8** and **9**, and $3\cdot10^{-1}$ M in the supporting electrolyte. Potential control during spectroelectrochemical experiments was achieved with a PA4 potentiostat (*EKOM*, Czech Republic).

Photochemistry: The photochemical experiments were carried out in 1-cm quartz cuvettes. The solutions typically contained ca. $5\cdot10^{-5}$ M **1**-**9**. As light source served a high-pressure mercury lamp USH 102DH (Ushio) equipped with appropriate filters or a monochromator (AMKO). Electronic absorption spectra were recorded in the course of the photochemical experiments with Cary 3 (Varian) and Perkin-Elmer Lambda 900 spectrophotometers.

Time-Resolved Spectroscopy: The third or fourth harmonic outputs (355 or 266 nm) of an Nd-Yag laser (GCR-11, Quanta-ray) were used for photoexcitation and a Xenon lamp (XBO 500, Narva) for probing the transient absorption in the ns and μs experiments. The light source for the ms experiments were two high-pressure mercury flash lamps operating parallel (Narva). The absorption was probed with an HBO 500 lamp (Narva). After each pulse, the sample solutions were replaced to avoid accumulation of photoproducts.

Acknowledgments

Financial support by the Deutsche Forschungsgemeinschaft, the Netherlands Foundation for Chemical Research (SON) and the Netherlands Organization for Pure Research (NWO) is gratefully acknowledged. We wish to thank Prof. O. Brede and his group (University of Leipzig) for the ns and μs time-resolved spectroscopic experiments.

[1] H. Hennig, S. Knoblauch, D. Scholz, *New J. Chem*. **1997**, *21*, 701−708; H. Hennig, M. Ecke, S. Knoblauch, *J. Inf. Rec.* **1996**, *23*, 131−134.
[2] L. Hennig, G. Mann, *Z. Chem*. **1988**, *28*, 364−365.
[3] H. Toftlund, J. Becher, P. H. Olesen, J. Z. Pedersen, *Isr. J. Chem*. **1985**, *21*, 56−65.
[4] L. Hennig, R. Kirmse, O. Hammerich, S. Larsen, H. Frydendahl, H. Toftlund, J. Becher, *Inorg. Chim. Acta* **1995**, *234*, 67−74.
[5] S. Mandal, G. Das, R. Singh, R. Shukla, P. K. Bharadwaj, *Coord. Chem. Rev.* **1997**, *160*, 191−235.
[6] J. Hanss, H.-J. Krüger, *Angew. Chem*. **1996**, *108*, 2989−2991; *Angew. Chem. Int. Ed. Engl.* **1996**, *35*, 2827−2830.
[7] G. Ferraudi, S. Muralidharan, *Coord. Chem. Rev.* **1981**, *36*, 45−88.
[8] O. Horváth, K. L. Stevenson, *Charge transfer photochemistry of coordination compounds*, VCH Publishers, New York, **1993**, chapter 4.1., p. 35−62.
[9] B. G. Jeliazkova, J. K. Panajotova, *Z. Naturforsch., B: Chem. Sci.* **1995**, *50*, 524−528.
[10] P. L. Verheijdt, J. G. Haasnoot, J. Reedijk, *Inorg. Chim. Acta* **1983**, *76*, L43−L46.
[11] B. G. Jeliazkova, N. D. Yordanov, *Inorg. Chim. Acta* **1993**, *203*, 201−204.
[12] B. G. Jeliazkova, M. A. Doicheva, *Polyhedron* **1996**, *15*, 1277−1282.
[13] B. G. Jeliazkova, G. C. Sarova, *J. Photochem. Photobiol. A* **1996**, *97*, 5−9.
[14] B. G. Jeliazkova, G. C. Sarova, *Polyhedron* **1997**, *16*, 3967−3975.
[15] D. M. Dooley, B. M. Patterson, *Inorg. Chem*. **1982**, *21*, 4330−4332.
[16] A. Vogler, H. Kunkely, *Inorg. Chem*.**1982**, 21, 1172−1175.
[17] A. Vogler, H. Kunkely, *J. Am. Chem. Soc.* **1981**, *103*, 1559−1560.
[18] A. Vogler, H. Kunkely, *Angew. Chem*. **1981**, *93*, 399−400; *Angew. Chem. Int. Ed. Engl.* **1981**, *20*, 386−387.
[19] R. Henning, W. Schlamann, H. Kisch, *Angew. Chem*. **1980**, *92*, 664−665; *Angew. Chem. Int. Ed. Engl*. **1980**, *19*, 645−646.
[20] W. Dietzsch, P. Strauch, E. Hoyer, *Coord. Chem. Rev.* **1992**, *121*, 43−130.
[21] T. Imamura, M. Ryan, G. Gordon, D. Coucouvanis, *J. Am. Chem. Soc.* **1984**, *106*, 984−990.
[22] H. Hennig, S. Knoblauch, R. Benedix, J. Sieler, S. Jelonek, F. Somoza, publication in preparation
[23] D. W. Hendrickson, Y. S. Sohn, H. B. Gray, *Inorg. Chem*. **1971**, *10*, 1559−1563.
[24] R. R. Gagné, C. A. Koval, G. C. Lisensky, *Inorg. Chem*. **1980**, *19*, 2854−2855.
[25] R. S. Stojanovic, A. M. Bond, *Anal. Chem*. **1993**, *65*, 56−64.
[26] B. D. Rossenaar, F. Hartl, D. J. Stufkens, C. Amatore, E. Maisonhaute, J. N. Verpeaux, *Organometallics* **1997**, *16*, 4675−4685.
[27] M. Krejcík, M. Danek, F. Hartl, *J. Electroanal. Chem., Interfacial Electrochem*. **1991**, *317*, 179−187.
[28] F. Hartl, H. Luyten, H. A. Nieuwhuis, G. Schoemaker, *Appl. Spectrosc.* **1994**, *48*, 1522−1528.
[29] T. Yamabe, K. Hori, T. Minato, K. Fukui, Y. Sugiura, *Inorg. Chem*. **1982**, *21*, 2040−2046.
[30] R. L. Harlow, W. J. Wells III, G. W. Watt, S. H. Simonsen, *Inorg. Chem*. **1975**, *14*, 1768−1773.
[31] P. K. Bharadwaj, J. A. Potenza, H. J. Schugar, *J. Am. Chem. Soc.* **1986**, *108*, 1351−1352.
[32] M. Gulliotti, L. Casella, A.Pintar, E. Suardi, P. Zanello, S. Mangani, *J. Chem. Soc., Dalton Trans.* **1989**, 1979−1986.
[33] R. D. Bereman, G. D. Shields, J. Bordner, J. Dorfman, *Inorg. Chem*. **1981**, *20*, 2165−2169.
[34] J. C. Rasmussen, H. Toftlund, A. N. Nivorizhkin, J. Bourassa, P. C. Ford, *Inorg. Chim. Acta* **1996**, *251*, 291−298.
[35] In contrast to our electrochemical findings, L. Hennig et al. found the reduction potential of **8** at a mercury film electrode in acetonitrile to be more negative by 0.33 V and 0.43 V than those of more planar **5** and **6**, respectively[4].
[36] S. Knoblauch, F. Somoza, unpublished results.
[37] H. J. Schugar, *Copper Coordination Chemistry: Biochemical and Inorganic Perspectives* (Eds.: K. D. Karlin, J. Zubieta), Adenine Press, New York, **1983**, p. 43−74.
[38] P. E. Hoggard, *Coord. Chem. Rev.* **1997**, *159*, 235−243.

Received July 9, 1998
[I98221]

Synthesis, Electrochemistry, and Oxygen-Atom Transfer Reactions of Dioxotungsten(VI) and -molybdenum(VI) Complexes with N_2O_2 and N_2S_2 Tetradentate Ligands

Yee-Lok Wong,[a] Jian-Fang Ma,[a] Wing-Fong Law,[a] Yan Yan,[a] Wing-Tak Wong,[b] Ze-Ying Zhang,[a] Thomas C. W. Mak,[a] and Dennis K. P. Ng*[a]

Keywords: Tungsten complexes / Molybdenum complexes / Tetradentate ligands / Oxygen-atom transfer

A series of N_2O_2 tetradentate ligands with a range of substituents attached to the nitrogen atoms have been prepared (H_2L^n) (n = 1–9). Treatment of these ligands and the N_2S_2 tetradentate ligand H_2L^{10} with [WO_2Cl_2(DME)] (DME = 1,2-dimethoxyethane) in the presence of triethylamine leads to the formation of *cis*-dioxotungsten(VI) complexes [$WO_2(L^n)$] (n = 1–10). Reaction of the N_2O_2 tetradentate ligands H_2L^n (n = 1, 3–7) with ammonium molybdate tetrahydrate and dilute hydrochloric acid gives the corresponding molybdenum(VI) analogs [$MoO_2(L^n)$] (n = 1, 3–7). These compounds have been spectroscopically characterized and the molecular structures of [$WO_2(L^n)$] (n = 1, 2, 9) and [$MoO_2(L^5)$] have been established by X-ray diffraction analysis. These high-valent compounds participate in oxygen-atom transfer reactions and can catalyze the oxidation of benzoin with dimethyl sulfoxide. The complex [$WO_2(L^{10})$], which contains an S-donor ligand, has lower reduction potential and higher reactivity toward oxo-transfer reactions than analogous tungsten complexes having N_2O_2 ligands. The kinetics of these catalytic processes along with the structure and electrochemistry of these dioxotungsten and -molybdenum complexes are described and compared.

Introduction

Atom-transfer chemistry of tungsten has recently attracted considerable attention because of its relevance to some important oxidation processes promoted by high-valent tungsten species[1] and biological reactions mediated by tungsten oxotransferase enzymes, which catalyze the oxo-transfer reactions for a range of substrates such as aldehydes and carbon dioxide.[2] In contrast to the related molybdenum chemistry that has been well documented,[3] tungsten-mediated atom-transfer reactions have been little studied and, to our knowledge, not more than a dozen examples have been reported so far.[4] Of much current interest are those containing bidentate dithiolene-type ligands which mimic the pterin cofactors found in the tungstoenzymes.[4][5] Although the oxomolybdenum complexes with tetradentate N-, O- and S-donor ligands have been studied extensively and some of them participate in various atom-transfer reactions,[6] very little has been accomplished with regard to the analogous tungsten chemistry.[7] We describe herein the synthesis and characterization of a new series of dioxotungsten(VI) complexes with N_2O_2 and N_2S_2 tetradentate ligands. These compounds undergo an irreversible reduction at highly negative potentials, but are still active toward oxygen-atom transfer reactions. The structural, electrochemical and oxo-transfer properties of these tungsten complexes are discussed and compared with those of their molybdenum counterparts, some of which have also been synthesized for the first time.

[a] Department of Chemistry, The Chinese University of Hong Kong,
Shatin, N.T., Hong Kong
Fax: (internat.) + 852/2603-5057
E-mail: dkpn@cuhk.edu.hk
[b] Department of Chemistry, The University of Hong Kong, Pokfulam Road, Hong Kong

Supporting information for this article is available on the WWW under http://www.wiley-vch.de/home/eurjic or from the author.

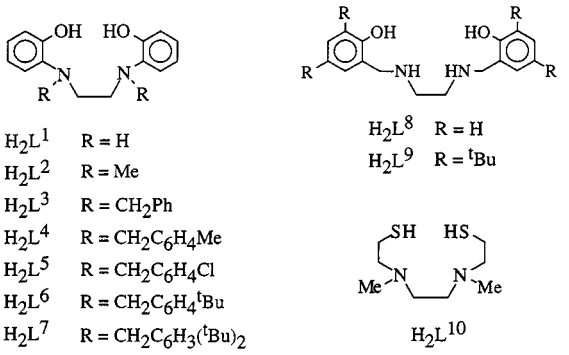
Results and Discussion

Synthesis and Characterization

Deprotonation of the readily available tetradentate ligand H_2L^1[8] with *n*BuLi followed by *N*-methylation with methyl iodide or *N*-benzylation with various benzyl bromides led to the formation of a series of N_2O_2 tetradentate ligands H_2L^n (n = 2−7) in good yield (Scheme 1). These substituents, having different steric and electronic properties, were introduced to the nitrogen atoms with the goal of examining their effects on complex formation and properties of the resulting complexes. The ligand H_2L^2 was prepared previously by reductive amination from formaldehyde and glyoxalbis(2-hydroxyanil).[9] The new ligands H_2L^n (n = 3−7) were found to be rather unstable and the yellow oily liquids darkened gradually upon exposure to air over 1−2 days. The ligands should therefore be freshly prepared for complex formation. The ligands H_2L^n (n = 8−10) were synthesized according to literature methods.[10,11]

Treatment of these ligands with [WO_2Cl_2(DME)] in the presence of triethylamine gave the corresponding dioxo complexes [$WO_2(L^n)$] (n = 1−10, Scheme 2). In contrast to the commonly used starting material [WO_2Cl_2],[12] this DME adduct, which can be prepared readily from [$WOCl_4$], $(Me_3Si)_2O$ and DME,[13] possesses good solubility in or-

 © WILEY-VCH Verlag GmbH, D-69451 Weinheim, 1999 1434−1948/99/0202−0313 $ 17.50+.50/0



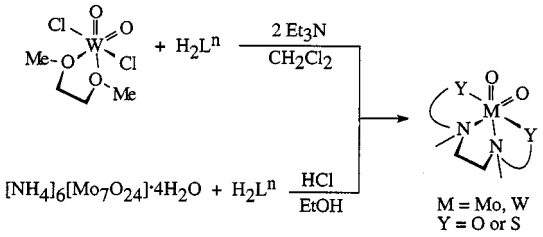
H_2L^1 R = H
H_2L^2 R = Me
H_2L^3 R = CH_2Ph
H_2L^4 R = $CH_2C_6H_4Me$
H_2L^5 R = $CH_2C_6H_4Cl$
H_2L^6 R = $CH_2C_6H_4{}^tBu$
H_2L^7 R = $CH_2C_6H_3({}^tBu)_2$

H_2L^8 R = H
H_2L^9 R = ^tBu

H_2L^{10}

Scheme 1. Structures of tetradentate ligands

ganic solvents and undergoes facile ligand-substitution reactions.[14] It therefore appears to be a more versatile precursor to other high-valent tungsten complexes. The molybdenum counterparts $[MoO_2(L^n)]$ (n = 1, 3−7) were also prepared in moderate yield by treating ammonium molybdate tetrahydrate with the ligands H_2L^n (n = 1, 3−7) in the presence of HCl and EtOH (Scheme 2).[15] The complex $[MoO_2(L^1)]$ was prepared previously from $[MoO_2(acac)_2]$ (acac = acetylacetonate) and H_2L^1 by Spence et al.[16] All these air-stable dioxotungsten and -molybdenum complexes could be purified by column chromatography and/or recrystallization, and were characterized with elemental analyses or accurate mass measurements, along with a range of spectroscopic methods.



Scheme 2. Preparation of dioxotungsten(VI) and -molybdenum(VI) complexes

All the tungsten compounds showed two characteristic *cis*-dioxo $[WO_2]$ vibrational bands at 895−921 and 936−958 cm^{-1} in their IR spectra,[17] except $[WO_2(L^8)]$ the IR spectrum of which exhibited only the higher frequency band at 941 cm^{-1} while the lower frequency band was embedded in a broad signal at 885 cm^{-1}. The IR spectra of the molybdenum analogs showed similar asymmetric and symmetric Mo=O stretches at 905−919 and 928−938 cm^{-1}, respectively; the latter band occurred at a 15−25 cm^{-1} lower frequency than that for the tungsten congeners. The ^{1}H- and ^{13}C-NMR spectra of these dioxo compounds were in accord with an octahedral structure having a C_2 rotation axis. Take compounds $[WO_2(L^n)]$ (n = 8, 9) as examples; the two methylene protons next to the aromatic ring are no longer equivalent. Two doublets with a geminal coupling constant of ca. 14 Hz appeared at $\delta \approx 3.9$ and 4.7 in their ^{1}H-NMR spectra recorded in [D$_6$]DMSO. The two methylene protons in the benzyl groups in $[MO_2(L^n)]$ (M = Mo, W; n = 3−6) are also diastereotopic and an AB quadruplet was observed for these protons in all the spectra. All these dioxo compounds were also characterized by fast atom bombardment (FAB) or liquid secondary ion (LSI) mass spectrometry. The M^+ or $[M+H]^+$ species were identified in all cases with predicted isotopic distribution pattern.

Molecular Structures

Single-crystal X-ray diffraction studies of $[WO_2(L^2)]$ and $[MoO_2(L^5)]$ revealed that the asymmetric unit consists of two crystallographically independent molecules. The former also contains solvated dichloromethane. Figures 1 and 2 display the molecular structure of one of the independent molecules for $[WO_2(L^2)]$ and $[MoO_2(L^5)]$, respectively. For $[WO_2(L^9)]$ (Figure 3), the tungsten atom lies on a crystallographic 2-fold axis so that one-half of the molecule is present in the asymmetric unit. A perspective view of $[WO_2(L^1)]$ is also presented in Figure 4. Each of these structures possesses C_2 {for $[WO_2(L^9)]$} or approximate C_2 symmetry and adopts distorted octahedral geometry, with the N atoms *trans* to the terminal oxo groups. The bond lengths and angles of these complexes are unexceptional and resemble those found in other six-coordinate dioxo−W^{VI}[12d,14a,17b,18] and −Mo^{VI} complexes.[9,10,19] Selected bond lengths and angles for these compounds, along with a brief description is available as Supporting Information on the WWW or from the author.

Electrochemistry

The electrochemical behavior of $[MoO_2(L^1)]$ in *N*,*N*-dimethylformamide (DMF) was studied previously by cyclic voltammetry.[16] The voltammogram displayed an irreversible one-electron reduction peak at −1.41 V vs. SCE coupled to an oxidation peak at −0.02 V, together with a reversible one-electron reduction peak at −1.70 V assignable to the Mo^{VI}/Mo^V and Mo^V/Mo^{IV} couples, respectively. An oxo−Mo^V species with deprotonated amino ligand was postulated as the intermediate. The electrochemistry of $[MoO_2(L^n)]$ (n = 4, 5, 7), which do not have ionizable protons, is somewhat different. Their voltammograms recorded in DMF showed only one redox couple attributable to a metal-based reduction. A weak cathodic peak at around −1 V was also observed for $[MoO_2(L^n)]$ (n = 5, 7) but its origin is unclear at this stage. The electrochemical data are summarized in Table 1. Ferrocene was added in all measurements as an internal reference and its half-wave potential ($E_{1/2}$ = 0.08 V vs. Ag/Ag^+ in MeCN) remained virtually unchanged. By comparing the values of ΔE_p of the reduction couples of $[MoO_2(L^n)]$ (n = 4, 5, 7) (102−160 mV) with that of ferrocene which ranges from 66 to 71 mV, and on considering the i_{pa}/i_{pc} values which are less than unity, these couples can be described as quasi-reversible processes. It is worth noting that the substituents attached to the nitrogen atoms of the ligands only have marginal effects on the redox potentials. The $E_{1/2}$ values follow the order

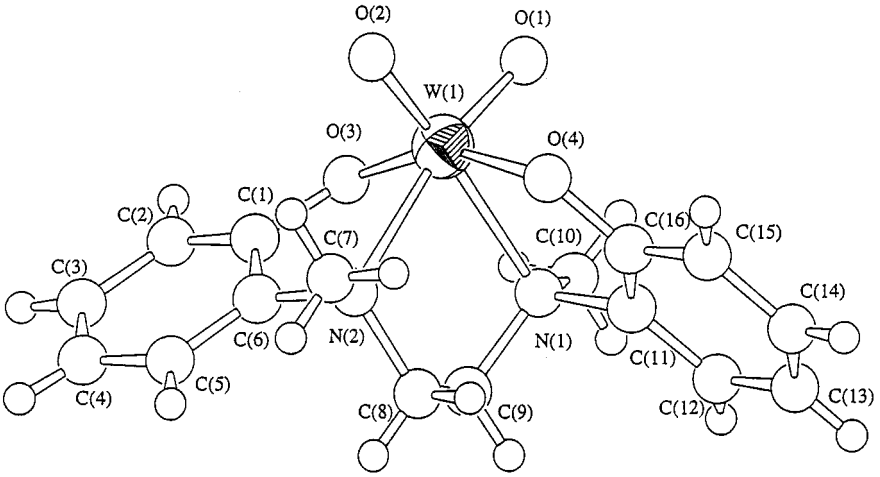


Figure 1. Molecular structure and atom-labeling scheme for $[WO_2(L^2)]$; the hydrogen atoms are shown with small arbitrary radii

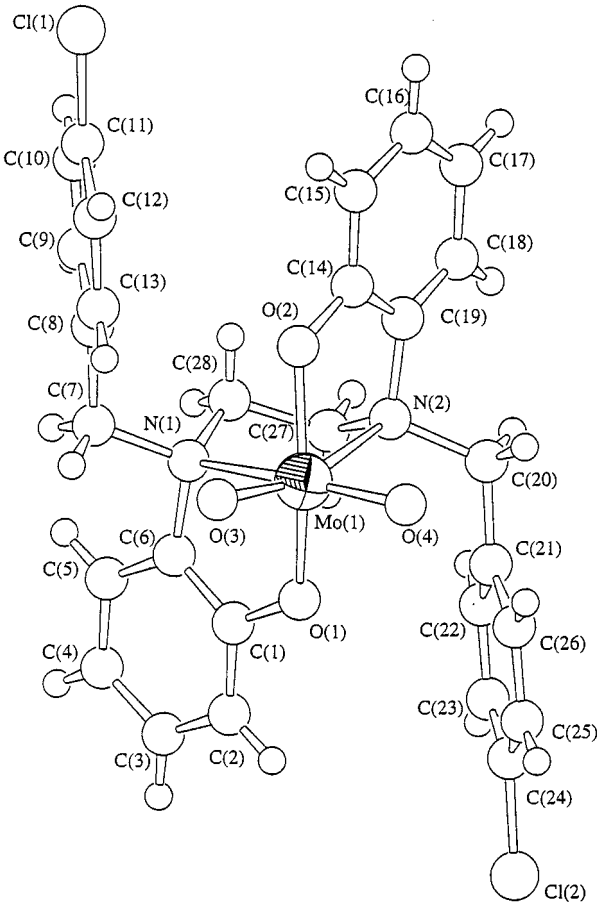


Figure 2. Molecular structure and atom-labeling scheme for $[MoO_2(L^5)]$; the hydrogen atoms are shown with small arbitrary radii

$[MoO_2(L^5)] > [MoO_2(L^4)] > [MoO_2(L^7)]$ as a result of the different electron-withdrawing abilities (Cl > Me > *t*Bu).

The voltammograms of the tungsten analogs $[WO_2(L^n)]$ (n = 1, 4, 5, 8) revealed a major irreversible process at highly negative potentials (E_{pc} ranged from −2.07 to −2.32 V vs. SCE) assignable to the reduction of the W^{VI} metal center. Some weak and unidentified signals were also seen for some of these complexes (Table 1). In accordance with previous studies,[5a,17b,20] the metal-based reduction potentials for the tungsten complexes were more negative than those of the corresponding molybdenum counterparts and the redox processes were less reversible.

The electrochemical behavior of $[WO_2(L^{10})]$ was remarkably different from that of other tungsten analogs. Its voltammogram recorded at a scan rate of 100 mV s^{-1} showed a reduction couple centered at −1.90 V and an oxidation peak at −0.06 V, both vs. SCE (Figure 5a). The anodic peak for the reduction couple was not observed at slower scan rates but this peak emerged and the peak current ratio (i_{pa}/i_{pc}) for this couple approached unity as the scan rate was increased. The peak-to-peak separation (ΔE_p) fell in the region 100 to 105 mV at scan rates between 100 and 700 mV s^{-1}. The value increased gradually to 197 mV with increasing scan rate to 10,000 mV s^{-1}. These results suggested that the reduction changed from an irreversible to a quasi-reversible process as the scan rate was increased. The peak current function ratio {peak current function: $i_p\nu^{-1/2}C^{-1}$, where i_p = peak current [A], ν = scan rate [V s^{-1}], C = concentration [M]} for the reduction of $[WO_2(L^{10})]$ with respect to the one-electron oxidation of ferrocene under identical conditions was 1.25 at 20 mV s^{-1}, which decreased to 0.76 at 800 mV s^{-1}. These data together with the plot showing the variation of $i_{pc}\nu^{-1/2}$ with ν (Figure 6) indicated that the process approaches an overall two-electron reduction at slow scan rates. This plot implied that the one-electron reduction product is somewhat unstable and a further removal of one electron occurs readily to the W^{IV} state. This will happen if the $W^{VI/V}$ potential is more negative than the $W^{V/IV}$ potential, as was observed for related molybdenum complexes.[10,21] It is also worth noting that the intensity of the oxidation peak at −0.06 V decreases with increasing scan rate and eventually vanishes at 800 mV s^{-1} (Figure 5b). This peak may thus be attributed to an electrochemically generated W^{IV} species and a purely one-electron quasi-reversible reduction seems to occur at scan rates over 800 mV s^{-1}. This behavior is very similar to that of the molybdenum counterpart $[MoO_2(L^{10})]$ with the ex-

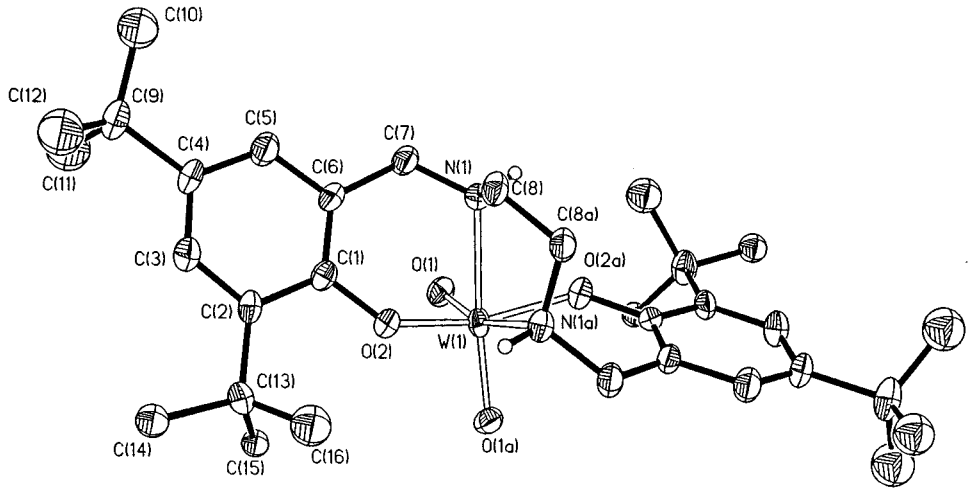


Figure 3. Perspective view and atom-labeling scheme for $[WO_2(L^9)]$

Table 1. Electrochemical data for selected dioxomolybdenum and -tungsten complexes[a]

Compound	E_{pc}	E_{pa}	$E_{1/2}$	ΔE_p[b]	$\lvert i_{pa}/i_{pc}\rvert$	Other processes
$[MoO_2(L^4)]$	−1.42	−1.32	−1.37	102	0.84	nil
$[MoO_2(L^5)]$	−1.43	−1.27	−1.35	160	0.48	$E_{pc} = -0.99$
$[MoO_2(L^7)]$	−1.48	−1.33	−1.41	156	0.85	$E_{pc} = -1.11$
$[WO_2(L^1)]$	−2.30	–	–	–	–	$E_{pc} = -1.57, -2.00$; $E_{pa} = -0.59$
$[WO_2(L^4)]$	−2.32	–	–	–	–	$E_{pa} = 0.94$
$[WO_2(L^5)]$	−2.27	–	–	–	–	$E_{pa} = 0.91$
$[WO_2(L^8)]$	−2.07	–	–	–	–	nil
$[WO_2(L^{10})]$	−1.96	−1.84	−1.90	118	0.51	$E_{pa} = -0.06$

[a] Recorded with $[Bu_4N][ClO_4]$ as electrolyte in DMF (0.1 M) at ambient temp. Scan rate = 100 mV s^{-1}. Potentials are expressed in V vs. SCE. – [b] $\Delta E_p = \lvert E_{pc} - E_{pa}\rvert$ in mV.

ception that the reduction of the latter occurs at a much more positive potential (−1.34 V vs. SCE).[22] It is interesting to note that incorporation of sulfur-containing ligand such as L^{10} lowers the reduction potential of the complex and increases its reversibility relative to the analogous oxygen-containing ligands. The reduction potential of $[WO_2(L^{10})]$ (E_{pc} = −1.96 V vs. SCE or −2.27 V vs. Ag/Ag^+ in MeCN), however, is still more negative than those of the synthetic models for tungstoenzymes such as $[Et_4N]_2[WO_2(bdt)_2]$ (bdt = 1,2-benzenedithiolate) (E_{pc} = −1.34 V vs. SCE)[5a] and $[Et_4N]_2[WO_2(mnt)_2]$ (mnt = 1,2-dicyanoethylenedithiolate) (E_{pc} = −1.50 V vs. Ag/Ag^+ in MeCN).[5c] It appears that these unsaturated dithiolene-type ligands are crucial for the complexes to reach physiologically accessible potentials.

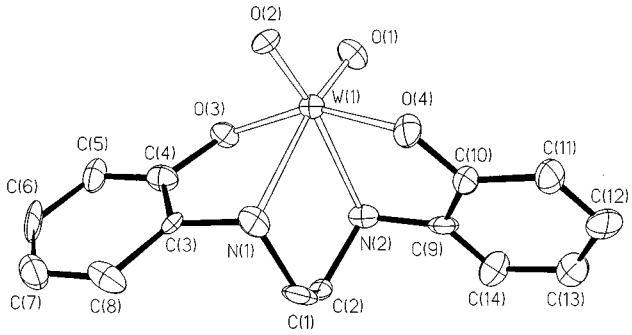


Figure 4. Molecular structure of $[WO_2(L^1)]$ showing the atom-labeling scheme

Oxo-Transfer Reactions

As tungsten-mediated oxo-transfer reactions had been little studied, we were interested to examine the oxo-transfer properties of some of these dioxotungsten(VI) compounds, namely $[WO_2(L^n)]$ (n = 1, 8, 10) using benzoin as the common reductant. Typically, 7×10^{-3} mmol of the complexes and 20 equiv. of benzoin were dissolved in deoxygenated $[D_6]$DMSO (0.5 ml). The mixtures were sealed in NMR tubes and heated at 100°C. The kinetics of the systems were analyzed by ^{1}H-NMR spectroscopy which allowed the quantification of benzoin and its oxidized product, benzil, as well as the complexes. The concentration ratios of {[benzoin] + [benzil]} to $\{[WO_2(L^n)]\}$ (n = 1, 8, 10) remained constant during the course of the reactions. In the absence of the complexes, no reaction between benzoin and $[D_6]$DMSO was detected. The percentage conversion of benzoin to benzil was about 90% after 36 h when compound $[WO_2(L^{10})]$ was used. Reactions involving complexes $[WO_2(L^n)]$ (n = 1, 8) proceeded slowly and only ca. 50% of benzoin was consumed after 1 week. These results indicated that these dioxotungsten(VI) complexes can catalyze the

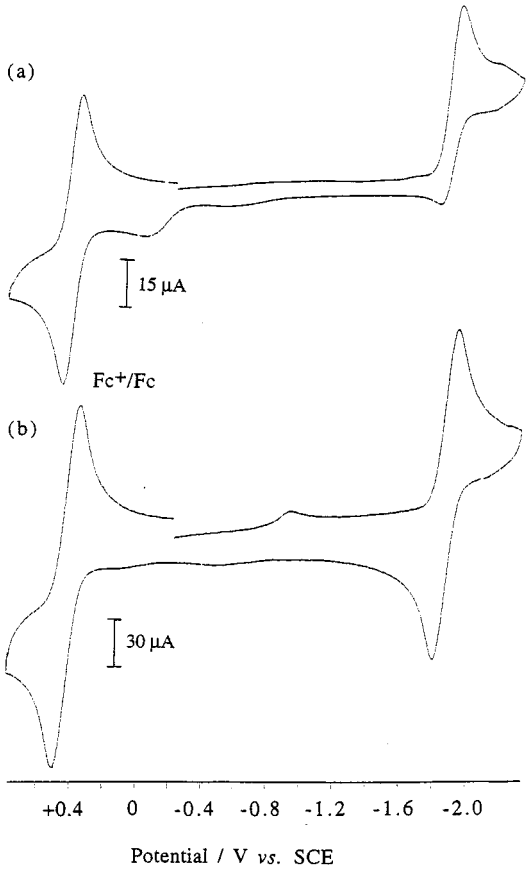


Figure 5. Cyclic voltammograms of $[WO_2(L^{10})]$ in DMF containing 0.1 M $[Bu_4N][ClO_4]$ recorded at (a) 100 mV s^{-1} and (b) 800 mV s^{-1}

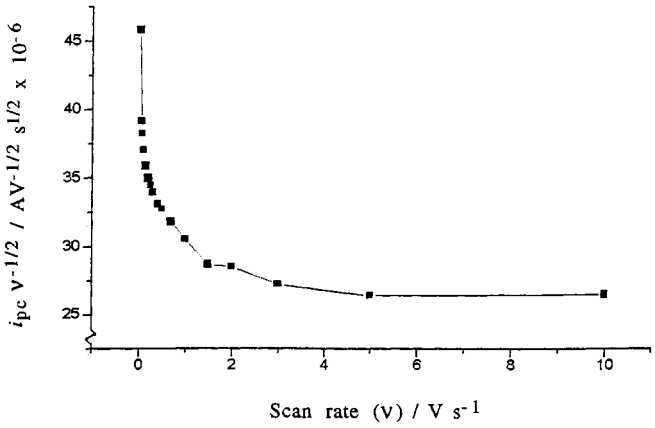
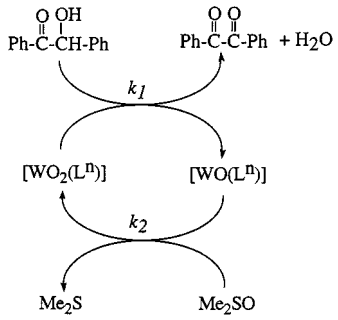


Figure 6. Plot of $i_{pc}v^{-1/2}$ vs. v for $[WO_2(L^{10})]$

oxidation of benzoin with $[D_6]$DMSO. The use of DMSO as oxo donor in this study has biological relevance to the molybdenum-containing DMSO reductases, which are able to utilize a variety of dialkyl- and alkylarylsulfoxides as oxidizing substrate.[23]

A plausible mechanism for this oxidation is suggested in Scheme 3 by analogy to that proposed for related catalytic systems.[24] Presumably, the W^{VI} complexes are reduced by benzoin to yield monomeric oxotungsten(IV) species, benzil and water. The W^{IV} complexes are then oxidized back to their parent dioxo compounds with $[D_6]$DMSO. Assuming that the regeneration of the W^{VI} species is fast ($k_2 \gg k_1$), their concentration should be essentially constant throughout the reactions. The rate of consumption of benzoin can thus be regarded as a pseudo-first-order reaction ($-$d[benzoin]/dt = k_{obs} [benzoin], where k_{obs} = k_1 {[WO(L^n)]}). Figure 7 shows the variation of ln{[benzoin]$_o$/[benzoin]} with time for $[WO_2(L^{10})]$, where [benzoin]$_o$ is the initial concentration of benzoin. From the slope of the best-fit straight line (1.86×10^{-5} s^{-1}), the value of k_1 can be determined (1.31×10^{-3} M^{-1} s^{-1}). For the other two N_2O_2 complexes $[WO_2(L^n)]$ (n = 1, 8), a gradual decrease in the catalytic activities was observed after prolonged heating. The respective k_1 values were calculated to be 1.28×10^{-4} and 9.43×10^{-5} M^{-1} s^{-1} based on the data collected in the first 85 h. The *S*-ligated complex $[WO_2(L^{10})]$ is therefore a better oxo donor than the *O*-ligated complexes $[WO_2(L^n)]$ (n = 1, 8) which is fully consistent with the electrochemical data (Table 1). A comparison of these dioxo complexes shows that the anionic complexes $[WO_2(bdt)_2]^{2-}$[5a,25] and $\{WO_2[O_2CC(S)Ph_2]_2\}^{2-}$[24a] are very efficient in promoting the oxidation of benzoin, while the complexes $[WO_2LX]$ [L = hydrotris(3,5-dimethyl-1-pyrazolyl)borate; X = OPh, S_2PPh_2-*S*] are inert toward oxygen-atom transfer reactions.[17b]



Scheme 3. Proposed mechanism for the oxidation of benzoin with DMSO using $[WO_2(L^n)]$ as a catalyst

In order to reveal whether the W^{IV} species $[WO(L^{10})]$ or the W^V dimer $[W_2O_3(L^{10})_2]$ were actually formed, a mixture of $[WO_2(L^{10})]$ and one equiv. of benzoin in deoxygenated $[D_7]$DMF was sealed in an NMR tube and heated at 100°C. The reaction was monitored by ^{1}H-NMR spectroscopy. Surprisingly, the spectra were essentially unchanged and no significant amount of benzil was detected even after 1 week.

The oxo-transfer properties of the molybdenum analogs $[MoO_2(L^n)]$ (n = 5, 6) were also investigated under identical conditions for comparison. These molybdenum-mediated reactions proceeded considerably faster and ca. 75% of benzoin was consumed after 25 h at 100°C. However, the {[benzoin] + [benzil]}-to-{$[MoO_2(L^n)]$} (n = 5, 6) ratios increased gradually during the course of the reactions indicating that part of the catalysts was deactivated and consumed. Some unidentified signals were also observed in the NMR spectra which precluded a detailed kinetic analysis. Lowering the temperature to 50°C greatly retarded the oxo-transfer reactions; the benzoin conversion was only 5−7% after 95 h. The higher oxo-transfer reactivity of molybdenum

complexes relative to their tungsten counterparts may be attributed to their lower reduction potentials and weaker M=O bond (bond dissociation energy = ca. 410 kJ mol^{-1} for Mo=O and > 580 kJ mol^{-1} for W=O).[4,17b]

In summary, we have synthesized a new series of dioxotungsten complexes with N_2O_2 and N_2S_2 tetradentate ligands which represent rare examples of tungsten compounds showing oxo-transfer activity. The S-donor atoms in the ligand seem to play an important role in lowering the reduction potential of the complex and thereby increasing its oxo-transfer reactivity toward the oxidation of benzoin with DMSO. The analogous molybdenum complexes are more active in this oxygen-atom transfer reaction which is in accord with the electrochemical data.

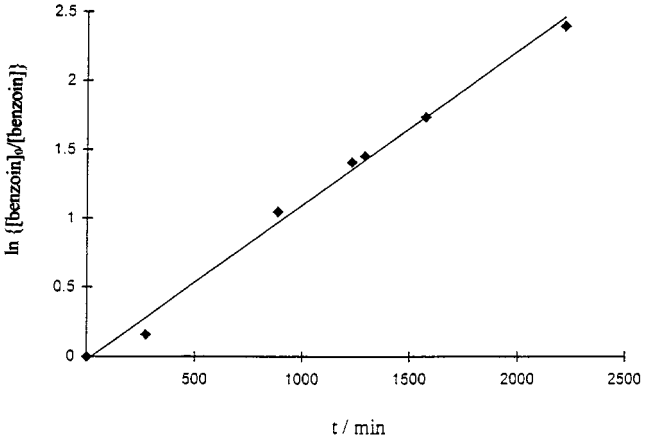


Figure 7. Plot of ln{[benzoin]$_o$/[benzoin]} vs. time for a system containing initially 0.28 M benzoin and 0.014 M [$WO_2(L^{10})$] in [D_6]DMSO at 100°C

Experimental Section

All reactions were carried out with standard Schlenk-line techniques under nitrogen; workups were performed in air. Dichloromethane was dried with 4-Å molecular sieves and distilled from calcium hydride. Tetrahydrofuran (THF) was distilled from sodium benzophenone ketyl. DMF for voltammetric studies was dried with barium oxide and distilled under reduced pressure. The electrolyte [Bu_4N][ClO_4] was recrystallized from dry acetone three times prior to use. All other reagents and solvents were of reagent grade and used as received. The ligands H_2L^n (n = 1,[8] 8, 9,[10] 10[11]) and the tungsten complex [WO_2Cl_2(DME)][13] were prepared by previously described methods. − NMR: Bruker WM 250 (^{1}H, 250; ^{13}C, 62.9 MHz), Bruker DPX 300 (^{1}H, 300; ^{13}C, 75.4 MHz) and Bruker ARX 500 (^{1}H, 500; ^{13}C, 125.8 MHz), $CDCl_3$ as solvent and TMS as internal standard unless otherwise stated, for [D_6]DMSO as solvent δ_H = 2.50, δ_C = 39.7, coupling constant J in Hz. − IR: Perkin Elmer 1600 FT-IR and Nicolet 550 FT-IR as KBr pellets. − MS: Hewlett Packard 5989B (FAB) and Bruker APEX 47e FT-ICR (LSI) with 3-nitrobenzyl alcohol as matrix. − Elemental analyses: Shanghai Institute of Organic Chemistry, Chinese Academy of Sciences. − Electrochemical measurements were carried out with a BAS CV-50W voltammetric analyzer. The cell comprised inlets for a platinum-sphere working electrode, a silver-wire counter electrode and an Ag/$AgNO_3$ (0.1 M in MeCN) reference electrode which was connected to the solution by a Luggin capillary whose tip was placed close to the working electrode.[26] Typically, a 0.1 M solution of [Bu_4N][ClO_4] in DMF containing 1.0 mM of sample was purged with nitrogen for 20 min, then the voltammograms were recorded at scan rates ranging from 20 to 3000 mV s^{-1} at ambient temp. unless otherwise stated. All potentials were referred internally to the ferrocene/ferrocenium couple at +0.39 V vs. SCE.[27]

General Procedure for the Preparation of H_2L^n (n = 2−7): To a colorless solution of H_2L^1 (0.24 g, 1.0 mmol) in THF (10 ml) was added *n*BuLi (1.6 M solution in *n*-hexane, 2.6 ml, 4.1 mmol) dropwise at 0°C. The mixture was stirred at this temp. for 1 h, then allowed to warm to room temp. Iodomethane (0.13 ml, 2.0 mmol) or differently substituted benzyl bromides (2.0 mmol) were added slowly and stirring was continued for 18 h (only 6 h was required for the reaction with iodomethane). The volatiles were removed under reduced pressure and water (20 ml) was added. The mixture was extracted with CH_2Cl_2 (3 × 50 ml) and the combined extracts were dried with sodium sulfate and the solvent was removed using a rotary evaporater. The ligand H_2L^2 was collected as a white solid by washing the residual light brown solid with CH_2Cl_2/hexane (1:3), while the other ligands were purified by column chromatography using hexane followed by CH_2Cl_2 as eluent. These ligands were obtained as a pale yellow oil.

***N,N′*-Bis(2-hydroxyphenyl)-*N,N′*-dimethyl-1,2-diaminoethane (H_2L^2):** 0.20 g (73%); m.p. 110−112°C (ref.[9] 112°C). − ^{1}H NMR (250 MHz): δ = 2.87 (s, 6 H, CH_3), 3.02 (s, 4 H, CH_2), 6.86 (dt, J = 1.5, 7.6, 2 H, ArH), 6.94 (dd, J = 1.5, 8.0, 2 H, ArH), 7.06 (dt, J = 1.5, 7.6, 2 H, ArH), 7.17 (dd, J = 1.5, 8.0, 2 H, ArH).

***N,N′*-Dibenzyl-*N,N′*-bis(2-hydroxyphenyl)-1,2-diaminoethane (H_2L^3):** 0.30 g (71%). − ^{1}H NMR (300 MHz): δ = 2.90 (s, 4 H, CH_2CH_2), 3.84 (s, 4 H, PhCH_2), 6.73−6.79 (m, 2 H, ArH), 6.88 (dd, J = 1.5, 8.1, 2 H, ArH), 6.96−7.04 (m, 8 H, ArH), 7.13−7.20 (m, 6 H, ArH). − ^{13}C{^{1}H} NMR (75.4 MHz): δ = 52.1, 60.9, 114.5, 119.9, 123.3, 126.8, 127.3, 128.2, 129.1, 136.0, 136.8, 152.9. − HRMS (LSI): m/z = 425.2216 {calcd. for [M + H]$^+$ 425.2229}.

***N,N′*-Bis(2-hydroxyphenyl)-*N,N′*-bis(4-methylbenzyl)-1,2-diaminoethane (H_2L^4):** 0.35 g (77%). − ^{1}H NMR (300 MHz): δ = 2.38 (s, 6 H, CH_3), 3.02 (s, 4 H, CH_2CH_2), 3.93 (s, 4 H, ArCH_2), 6.86−6.91 (m, 2 H, ArH), 6.99−7.19 (m, 14 H, ArH). − ^{13}C{^{1}H} NMR (75.4 MHz): δ = 21.0, 52.1, 60.5, 114.4, 119.8, 123.3, 126.7, 128.8, 129.0, 133.8, 136.2, 136.8, 152.9. − HRMS (LSI): m/z = 453.2553 {calcd. for [M + H]$^+$ 453.2542}.

***N,N′*-Bis(4-chlorobenzyl)-*N,N′*-bis(2-hydroxyphenyl)-1,2-diaminoethane (H_2L^5):** 0.39 g (79%). − ^{1}H NMR (300 MHz): δ = 2.88 (s, 4 H, CH_2CH_2), 3.83 (s, 4 H, ArCH_2), 6.78 (dt, J = 1.5, 7.6, 2 H, ArH), 6.89 (dd, J = 1.5, 8.1, 2 H, ArH), 6.93−6.96 (m, 4 H, ArH), 6.99 (dd, J = 1.5, 8.0, 2 H, ArH), 7.02−7.07 (m, 2 H, ArH), 7.11−7.16 (m, 4 H, ArH). − ^{13}C{^{1}H} NMR (75.4 MHz): δ = 52.3, 60.3, 114.8, 120.1, 123.2, 127.1, 128.4, 130.4, 133.2, 135.1, 135.4, 152.9. − HRMS (LSI): m/z = 493.1458 {calcd. for [M + H]$^+$ based on ^{35}Cl 493.1449}.

***N,N′*-Bis(4-*tert*-butylbenzyl)-*N,N′*-bis(2-hydroxyphenyl)-1,2-diaminoethane (H_2L^6):** 0.40 g (75%). − ^{1}H NMR (300 MHz): δ = 1.27 (s, 18 H, *t*Bu), 2.87 (s, 4 H, CH_2CH_2), 3.80 (s, 4 H, ArCH_2), 6.76 (dt, J = 1.5, 7.6, 2 H, ArH), 6.90−7.06 (m, 10 H, ArH), 7.20−7.23 (m, 4 H, ArH). − ^{13}C{^{1}H} NMR (75.4 MHz): δ = 31.3, 34.4, 51.3, 60.5, 114.5, 119.8, 123.2, 125.2, 126.7, 128.7, 133.8, 136.4, 150.2, 152.8. − HRMS (LSI): m/z = 537.3480 {calcd. for [M + H]$^+$ 537.3481}.

***N,N′*-Bis(3,5-di-*tert*-butylbenzyl)-*N,N′*-bis(2-hydroxyphenyl)-1,2-diaminoethane (H_2L^7):** 0.45 g (69%). − ^{1}H NMR (300 MHz): δ = 1.22 (s, 36 H, *t*Bu), 2.95 (s, 4 H, CH_2CH_2), 3.89 (s, 4 H, ArCH_2), 6.75 (dt, J = 1.2, 7.7, 2 H, ArH), 6.85−6.87 (m, 6 H, ArH), 6.92

(dd, J = 1.2, 7.7, 2 H, Ar*H*), 7.00 (dt, J = 1.2, 7.7, 2 H, Ar*H*), 7.23−7.24 (m, 2 H, Ar*H*). − $^{13}C\{^1H\}$ NMR (75.4 MHz): δ = 31.3, 34.6, 52.3, 61.4, 114.4, 119.7, 121.1, 123.7, 124.2, 126.7, 128.9, 135.5, 150.4, 153.1. − HRMS (LSI): *m/z* = 649.4773 {calcd. for $[M + H]^+$ 649.4733}.

General Procedure for the Preparation of $[WO_2(L^n)]$ (n = 1−10): To a mixture of $[WO_2Cl_2(DME)]$ (0.38 g, 1.0 mmol) and H_2L^n (n = 1−10, 1.0 mmol) in CH_2Cl_2 (30 ml) was added triethylamine (0.28 ml, 2.0 mmol). The mixture was allowed to reflux overnight then the volatiles were removed in vacuo. The complex $[WO_2(L^2)]$ was purified by chromatography with CH_2Cl_2/ethyl acetate (1:1) as eluent followed by recrystallization from acetone/hexane. The complexes $[WO_2(L^n)]$ (n = 3−7) were purified by chromatography with $CHCl_3$ as eluent. The remaining complexes were obtained by washing the residue with ethanol and hexane followed by recrystallization from MeCN {for $[WO_2(L^9)]$} or CH_2Cl_2 {for $[WO_2(L^{10})]$}, or diffusion of water into a DMF solution of the crude product {for $[WO_2(L^n)]$ (n = 1, 8)}.

$[WO_2(L^1)]$: 0.22 g (50%), light pink solid. − ^1H NMR ([D$_6$]DMSO, 250 MHz): δ = 2.85−3.01 (m, 4 H, CH_2CH_2), 6.83 (d, J = 7.5, 2 H, Ar*H*), 6.91 (t, J = 7.5, 2 H, Ar*H*), 7.20 (d, J = 7.5, 2 H, Ar*H*), 7.21 (t, J = 7.5, 2 H, Ar*H*), 8.04 (br s, 2 H, N*H*). − $^{13}C\{^1H\}$ NMR ([D$_6$]DMSO, 125.8 MHz): δ = 50.4, 117.0, 121.4, 125.6, 129.0, 134.1, 161.6. − IR: ν(WO$_2$) = 911 s, 951 s cm^{-1}. − MS (LSI): Cluster peak at *m/z* = 459 (27%) $[M + H]^+$. − $C_{14}H_{14}N_2O_4W$ (458.13): calcd. C 36.70, H 3.08, N 6.11; found C 36.68, H 3.00, N 5.88.

$[WO_2(L^2)]$: 0.34 g (70%), white crystals. − ^1H NMR ([D$_6$]DMSO, 300 MHz): δ = 2.62 (d, J = 10.0, 2 H, CH_2), 3.06 (d, J = 10.0, 2 H, CH_2), 3.26 (s, 6 H, CH_3), 6.94 (dd, J = 1.5, 8.1, 2 H, Ar*H*), 7.02 (dt, J = 1.5, 7.7, 2 H, Ar*H*), 7.30 (dt, J = 1.5, 7.7, 2 H, Ar*H*), 7.60 (dd, J = 1.5, 8.1, 2 H, Ar*H*). − $^{13}C\{^1H\}$ NMR ([D$_6$]DMSO, 75.4 MHz): δ = 48.3, 59.5, 117.8, 122.3, 122.7, 129.7, 138.6, 159.6. − IR: ν(WO$_2$) = 914 s, 950 s cm^{-1}. − MS (FAB): Cluster peak at *m/z* = 487 (24%) $[M + H]^+$. − $C_{16}H_{18}N_2O_4W$ (486.18): calcd. C 39.53, H 3.73, N 5.76; found C 40.09, H 4.05, N 5.13.

$[WO_2(L^3)]$: 0.46 g (72%), white crystals. − ^1H NMR (300 MHz): δ = 2.90 (d, J = 9.0, 2 H, CH_2CH_2), 3.06 (d, J = 9.0, 2 H, CH_2CH_2), 4.91−5.04 (AB q, 4 H, ArCH_2), 6.66 (d, J = 8.1, 2 H, Ar*H*), 6.75 (t, J = 7.7, 2 H, Ar*H*), 6.83 (d, J = 8.1, 2 H, Ar*H*), 7.21 (t, J = 7.7, 2 H, Ar*H*), 7.34−7.41 (m, 10 H, Ar*H*). − $^{13}C\{^1H\}$ NMR (75.4 MHz): δ = 56.2. 64.9, 118.7, 121.3, 124.4, 128.4, 128.9, 129.6, 132.4, 133.8, 137.1, 160.5. − IR: ν(WO$_2$) = 916 s, 953 s cm^{-1}. − MS (FAB): Cluster peak at *m/z* = 639 (100%) $[M + H]^+$. − $C_{28}H_{26}N_2O_4W$ (638.38): calcd. C 52.68, H 4.11, N 4.39; found C 52.95, H 4.05, N 4.12.

$[WO_2(L^4)]$: 0.47 g (71%), white crystals. − ^1H NMR (300 MHz): δ = 2.37 (s, 6 H, CH_3), 2.91 (d, J = 9.0, 2 H, CH_2CH_2), 3.04 (d, J = 9.0, 2 H, CH_2CH_2), 4.87−4.98 (AB q, 4 H, ArCH_2), 6.69 (dd, J = 1.5, 8.1, 2 H, Ar*H*), 6.74 (dt, J = 1.5, 7.7, 2 H, Ar*H*), 6.82 (dd, J = 1.5, 8.1, 2 H, Ar*H*), 7.13 (d, J = 7.7, 4 H, Ar*H*), 7.17−7.22 (m, 6 H, Ar*H*). − $^{13}C\{^1H\}$ NMR (75.4 MHz): δ = 21.1, 56.1, 64.5, 118.4, 121.2, 124.6, 129.0, 129.4, 130.6, 132.2, 137.1, 138.6, 160.4. − IR: ν(WO$_2$) = 918 s, 956 s cm^{-1}. − MS (FAB): Cluster peak at *m/z* = 667 (63%) $[M + H]^+$. − $C_{30}H_{30}N_2O_4W$ (666.43): calcd. C 54.07, H 4.54, N 4.20; found C 53.98, H 4.59, N 4.21.

$[WO_2(L^5)]$: 0.46 g (65%), silvery grey crystals. − ^1H NMR (300 MHz): δ = 2.84 (d, J = 9.0, 2 H, CH_2CH_2), 3.04 (d, J = 9.0, 2 H, CH_2CH_2), 4.81−4.95 (AB q, 4 H, ArCH_2), 6.71−6.82 (m, 6 H, Ar*H*), 7.20−7.25 (m, 2 H, Ar*H*), 7.32 (s, 8 H, Ar*H*). − $^{13}C\{^1H\}$ NMR (75.4 MHz): δ = 55.8, 64.0, 118.7, 121.5, 123.7, 128.6, 129.8, 131.9, 133.8, 135.1, 136.8, 160.3. − IR: ν(WO$_2$) = 908 s, 949 m cm^{-1}. − HRMS (LSI): *m/z* = 707.0688 {calcd. for $[M + H]^+$ based on ^{35}Cl and ^{184}W 707.0680}.

$[WO_2(L^6)]$: 0.50 g (67%), white crystals. − ^1H NMR (300 MHz): δ = 1.33 (s, 18 H, *t*Bu), 2.85 (d, J = 9.3, 2 H, CH_2CH_2), 3.05 (d, J = 9.3, 2 H, CH_2CH_2), 4.83−5.00 (AB q, 4 H, ArCH_2), 6.74−6.77 (m, 6 H, Ar*H*), 7.15−7.19 (m, 2 H, Ar*H*), 7.27−7.36 (m, 8 H, Ar*H*). − $^{13}C\{^1H\}$ NMR (75.4 MHz): δ = 31.3, 34.6, 55.9, 64.4, 118.6, 121.2, 124.2, 125.2, 129.4, 130.5, 132.3, 137.4, 151.8, 160.4. − IR: ν(WO$_2$) = 919 s, 958 s cm^{-1}. − HRMS (LSI): *m/z* = 751.2749 {calcd. for $[M + H]^+$ based on ^{184}W 751.2712}.

$[WO^2(L^7)]$: 0.54 g (63%), white crystals. − ^1H NMR (300 MHz): δ = 1.27 (s, 36 H, *t*Bu), 2.86 (d, J = 9.3, 2 H, CH_2CH_2), 3.06 (d, J = 9.3, 2 H, CH_2CH_2), 4.93 (s, 4 H, ArCH_2), 6.54 (dd, J = 1.2, 8.1, 2 H, Ar*H*), 6.69 (dt, J = 1.2, 7.7, 2 H, Ar*H*), 6.80 (dd, J = 1.2, 8.1, 2 H, Ar*H*), 7.14 (s, 2 H, Ar*H*), 7.15 (s, 2 H, Ar*H*), 7.19 (dt, J = 1.2, 7.7, 2 H, Ar*H*), 7.42 (s, 2 H, Ar*H*). − $^{13}C\{^1H\}$ NMR (75.4 MHz): δ = 31.4, 34.7, 56.1, 65.7, 118.5, 120.8, 122.3, 124.7, 126.9, 129.5, 132.7, 137.1, 150.7, 160.7. − IR: ν(WO$_2$) = 921 s, 956 s cm^{-1}. − MS (FAB): Cluster peak at *m/z* = 862 (11%) $[M^+]$. − $C_{44}H_{58}N_2O_4W$ (862.81): calcd. C 61.25, H 6.78, N 3.25; found C 61.36, H 6.98, N 3.05.

$[WO^2(L^8)]$: 0.36 g (74%), white crystalline solid. − ^1H NMR ([D$_6$]DMSO, 250 MHz): δ = 2.32 (br s, 2 H, N*H*), 2.87 (br s, 2 H, CH_2), 3.87 (d, J = 14.3, 2 H, CH_2), 4.74 (d, J = 14.3, 2 H, CH_2), 5.46 (br s, 2 H, CH_2), 6.76 (d, J = 8.0, 2 H, Ar*H*), 6.83 (t, J = 7.5, 2 H, Ar*H*), 7.11 (d, J = 7.5, 2 H, ArH), 7.18 (t, J = 7.5, 2 H, ArH). − $^{13}C\{^1H\}$ NMR ([D$_6$]DMSO, 62.9 MHz): δ = 46.1, 52.6, 119.2, 120.3, 122.4, 128.0, 129.5, 158.2. − IR: ν(WO$_2$) = 941 s cm^{-1}. − MS (LSI): Cluster peak at *m/z* = 487 (17%) $[M + H]^+$. − $C_{16}H_{18}N_2O_4W$ (486.18): calcd. C 39.53, H 3.73, N 5.76; found C 39.63, H 3.42, N 5.74.

$[WO^2(L^9)]$: 0.42 g (59%), colorless crystals. − ^1H NMR (250 MHz): δ = 1.28 (s, 9 H, *t*Bu), 1.45 (s, 9 H, *t*Bu), 2.79 (br s, 2 H, N*H*), 3.00 (br s, 4 H, CH_2CH_2), 3.95 (d, J = 13.6, 2 H, ArCH_2), 5.22 (d, J = 13.6, 2 H, ArCH_2), 6.86 (s, 2 H, Ar*H*), 7.32 (s, 2 H, Ar*H*). − $^{13}C\{^1H\}$ NMR (62.9 MHz): δ = 30.0, 31.6, 34.3, 35.2, 46.7, 54.3, 120.7, 123.6, 124.1, 138.9, 142.9, 154.9. − IR: ν(WO$_2$) = 897 s, 939 s cm^{-1}. − MS (LSI): Cluster peak at *m/z* = 711 (21%) $[M + H]^+$. − $C_{32}H_{50}N_2O_4W$ (710.62): calcd. C 54.09, H 7.09, N 3.94; found C 53.49, H 7.14, N 3.74.

$[WO^2(L^{10})]$: 0.14 g (33%), yellow crystals. − ^1H NMR (250 MHz): δ = 3.26 (s, 6 H, CH_3), 3.04−3.39 (m, 10 H, CH_2), 3.54−3.64 (m, 2 H, CH_2). − $^{13}C\{^1H\}$ NMR ([D$_6$]DMSO, 125.8 MHz): δ = 27.6, 52.0, 56.2, 67.0. − IR: ν(WO$_2$) = 895 s, 936 s cm^{-1}. − MS (LSI): Cluster peak at *m/z* = 423 (15%) $[M + H]^+$. − $C_8H_{18}N_2O_2S_2W$ (422.21): calcd. C 22.76, H 4.30, N 6.63, S 15.19; found C 23.00, H 4.21, N 6.56, S 15.74.

General Procedure for the Preparation of $[MoO_2(L^n)]$ (n = 1, 3−7): A mixture of ammonium molybdate tetrahydrate $[NH_4]_6[Mo_7O_{24}] \times 4\ H_2O$ (0.18 g, 0.14 mmol), H_2L^n (n = 3−7, 1.0 mmol) and dilute hydrochloric acid (0.1 M, 5 ml, 0.5 mmol) in ethanol (30 ml) was stirred at room temp. overnight. $[MoO_2(L^1)]$ was collected by filtration as a yellow solid which was washed with ethanol and hexane, and dried in vacuo. For the other molybdenum complexes, the solid was collected by filtration and the filtrate was extracted with CH_2Cl_2 (3 × 20 ml). The solid and the extracts were combined, dried with sodium sulfate and the solvent removed using a rotary evaporator. The residue was chromatographed with $CHCl_3$ as eluent to develop a bright yellow band which was collected and evaporated to give a yellow solid.

[$MoO_2(L^1)$]:[16] 0.26 g (70%). − ^{1}H NMR ([D$_6$]DMSO, 300 MHz): δ = 2.78−2.91 (m, 4 H, CH_2CH_2), 6.79 (dd, *J* = 1.2, 8.0, 2 H, Ar*H*), 6.89 (dt, *J* = 1.2, 7.6, 2 H, Ar*H*), 7.16−7.22 (m, 4 H, Ar*H*), 7.78 (s, 2 H, N*H*). − ^{13}C{^{1}H} NMR ([D$_6$]DMSO, 75.4 MHz): δ = 50.0, 115.7, 121.0, 125.4, 128.6, 134.2, 162.7. − IR: ν(MoO_2) = 910 s, 932 m cm^{-1}. − MS (LSI): Cluster peak at *m/z* = 373 (13%) [M + H]$^+$.

[$MoO_2(L^3)$]: 0.30 g (55%). − ^{1}H NMR (300 MHz): δ = 2.77 (d, *J* = 9.0, 2 H, CH_2CH_2), 3.05 (d, *J* = 9.0, 2 H, CH_2CH_2), 4.87−5.02 (AB q, 4 H, ArCH_2), 6.66−6.82 (m, 6 H, Ar*H*), 7.17 (t, *J* = 7.5, 2 H, Ar*H*), 7.33−7.38 (m, 10 H, Ar*H*). − ^{13}C{^{1}H} NMR (75.4 MHz): δ = 55.9, 64.6, 117.4, 120.8, 124.5, 128.3, 128.7, 129.2, 132.3, 134.1, 137.1, 161.5. − IR: ν(MoO_2) = 905 s, 928 m cm^{-1}. − MS (FAB): Cluster peak at *m/z* = 553 (54%) [M + H]$^+$. − $C_{28}H_{26}MoN_2O_4$ (550.47): calcd. C 61.10, H 4.76, N 5.09; found C 61.03, H 4.80, N 4.88.

[$MoO_2(L^4)$]: 0.39 g (67%). − ^{1}H NMR (300 MHz): δ = 2.37 (s, 6 H, CH_3), 2.74 (d, *J* = 9.9, 2 H, CH_2CH_2), 3.02 (d, *J* = 9.9, 2 H, CH_2CH_2), 4.86−5.00 (AB q, 4 H, ArCH_2), 6.68 (dd, *J* = 1.2, 8.4, 2 H, Ar*H*), 6.74 (dt, *J* = 1.2, 7.6, 2 H, Ar*H*), 6.84 (dd, *J* = 1.2, 8.4, 2 H, Ar*H*), 7.11−7.22 (m, 10 H, Ar*H*). − ^{13}C{^{1}H} NMR (75.4 MHz): δ = 21.2, 56.0, 64.4, 117.4, 120.7, 124.7, 129.0, 129.2, 131.2, 132.2, 137.2, 138.5, 161.7. − IR: ν(MoO_2) = 919 s, 938 s cm^{-1}. − MS (FAB): Cluster peak at *m/z* = 581 (45%) [M + H]$^+$. − $C_{30}H_{30}MoN_2O_4$ (578.52): calcd. C 62.29, H 5.23, N 4.84; found C 61.98, H 5.27, N 4.72.

[$MoO_2(L^5)$]: 0.44 g (71%). − ^{1}H NMR (300 MHz): δ = 2.71 (d, *J* = 9.0, 2 H, CH_2CH_2), 3.02 (d, *J* = 9.0, 2 H, CH_2CH_2), 4.77−4.94 (AB q, 4 H, ArCH_2), 6.71−6.81 (m, 6 H, Ar*H*), 7.19 (dt, *J* = 1.5, 7.6, 2 H, Ar*H*), 7.30 (s, 8 H, Ar*H*). − ^{13}C{^{1}H} NMR (75.4 MHz): δ = 55.6, 63.7, 117.5, 121.0, 123.8, 128.5, 129.4, 132.2, 133.7, 134.9, 136.8, 161.4. − IR: ν(MoO_2) = 911 s, 934 m cm^{-1}. − MS (FAB): Cluster peak at *m/z* = 620 (63%) [M$^+$]. − $C_{28}H_{24}Cl_2MoN_2O_4$ (619.36): calcd. C 54.30, H 3.91, N 4.52; found C 53.95, H 3.79, N 4.28.

[$MoO_2(L^6)$]: 0.43 g (65%). − ^{1}H NMR (300 MHz): δ = 1.33 (s, 18 H, *t*Bu), 2.70 (d, *J* = 9.6, 2 H, CH_2CH_2), 3.04 (d, *J* = 9.6, 2 H, CH_2CH_2), 4.79−4.99 (AB q, 4 H, ArCH_2), 6.72−6.79 (m, 6 H, Ar*H*), 7.12−7.17 (m, 2 H, Ar*H*), 7.29−7.35 (m, 8 H, Ar*H*). − ^{13}C{^{1}H} NMR (75.4 MHz): δ = 31.3, 34.6, 55.7, 64.2, 117.4, 120.8, 124.2, 125.1, 129.1, 131.0, 132.2, 137.5, 151.7, 161.6. − IR: ν(MoO_2) = 916 s, 937 m cm^{-1}. − MS (FAB): Cluster peak at *m/z* = 664 (18%) [M$^+$]. − $C_{36}H_{42}MoN_2O_4$ (662.69): calcd. C 65.25, H 6.39, N 4.23; found C 65.73, H 6.71, N 3.94.

[$MoO_2(L^7)$]: 0.46 g (59%). − ^{1}H NMR (300 MHz): δ = 1.26 (s, 36 H, *t*Bu), 2.71 (d, *J* = 10.5, 2 H, CH_2CH_2), 3.04 (d, *J* = 10.5, 2 H, CH_2CH_2), 4.92 (s, 4 H, ArCH_2), 6.56 (d, *J* = 8.1, 2 H, Ar*H*), 6.68 (t, *J* = 7.7, 2 H, Ar*H*), 6.79 (d, *J* = 8.1, 2 H, Ar*H*), 7.12 (s, 2 H, Ar*H*), 7.13 (s, 2 H, Ar*H*), 7.15 (t, *J* = 7.8, 2 H, Ar*H*), 7.40 (s, 2 H, Ar*H*). − ^{13}C{^{1}H} NMR (75.4 MHz): δ = 31.4, 34.7, 55.8, 65.5, 117.3, 120.4, 122.2, 124.7, 126.8, 129.1, 133.1, 137.1, 150.6, 161.8. − IR: ν(MoO_2) = 913 s, 935 s cm^{-1}. − MS (FAB): Cluster peak at *m/z* = 777 (3%) [M + H]$^+$. − $C_{44}H_{58}MoN_2O_4$ (774.90): calcd. C 68.20, H 7.54, N 3.62; found C 68.31, H 7.74, N 3.53.

X-ray Crystallographic Analysis of [$WO_2(L^1)$] and [$WO_2(L^9)$] · MeCN · EtOH: Crystal data and data-processing parameters are given in the Supporting Information on the WWW or may be obtained from the author. Data collection was performed in the variable ω-scan mode with a Rigaku AFC7R diffractometer using Mo-K_α radiation (λ = 0.71073 Å) at 294 K. Unit-cell parameters were calculated from least-squares fitting of the 2θ angles for 25 selected strong reflections. Three standard reflections were monitored periodically after every 150 reflections and showed no significant decay during the data collection. The tungsten atom {of site symmetry 2 for [$WO_2(L^9)$] · MeCN · EtOH} was located by the Patterson method and the remaining non-hydrogen atoms were derived from subsequent Fourier difference syntheses. For [$WO_2(L^9)$] · MeCN · EtOH, both *tert*-butyl groups exhibit twofold orientational disorder, and the ethanol molecule is likewise twofold disordered with a common methylene group. The acetonitrile molecule lies on a crystallographic twofold axis. All non-hydrogen atoms were refined with anisotropic thermal parameters by full-matrix least-squares procedures. The hydrogen atoms were placed in idealized positions (C−H 0.96 Å, N−H 0.90 Å) with fixed isotropic thermal parameters and allowed to ride on their respective parent carbon and nitrogen atoms. All calculations were performed with a PC-486 computer using the SHELXL-PLUS program package.[28] Analytical expressions of neutral-atom scattering factors were employed, and anomalous dispersion corrections were incorporated.[29]

X-ray Crystallographic Analysis of [$WO_2(L^2)$ · 1/4CH_2Cl_2] and [$MoO_2(L^5)$]: All pertinent crystallographic data and other experimental details are also summarized in the Supporting Information. Intensity data were collected at 298 K with an Enraf-Nonius diffractometer using graphite monochromated Mo-K_α radiation and the ω-2θ scan technique. Three checked reflections were monitored periodically throughout data collection and showed no significant variations. All intensity data were corrected for Lorentz and polarization effects. An absorption correction by the ψ-scan method[30] was applied for [$WO_2(L^2)$ · 1/4CH_2Cl_2]. Both structures were solved by direct methods (SIR 92)[31] and expanded using Fourier techniques.[32] Some non-hydrogen atoms were refined anisotropically, while the rest was refined isotropically by full-matrix least-squares analysis. Hydrogen atoms were generated in their idealized positions but not refined. All calculations were performed with a Silicon-Graphics computer using the program package TEXSAN.[33]

Crystallographic data (excluding structure factors) for the structures reported in this paper have been deposited with the Cambridge Crystallographic Data Center as supplementary publication nos. CCDC-102337 {for [$WO_2(L^2)$]}, 101953 {for [$WO_2(L^2)$ · 1/4CH_2Cl_2]}, 102338 {for [$WO_2(L^9)$] · MeCN · EtOH} and 101952 {for [$MoO_2(L^5)$]}. Copies of the data can be obtained free of charge on application to CCDC, 12 Union Road, Cambridge CB2 1EZ, UK [Fax: int.code + 44(1223)336-033; E-mail: deposit@ccdc.cam.ac.uk].

Acknowledgments

This work was supported by The Hong Kong Research Grants Council (Earmarked Grant: CUHJ 464/95P).

[1] [1a] R. A. Sheldon, J. K. Kochi, *Metal-catalysed Oxidation of Organic Compounds*, Academic Press, New York, **1981**. − [1b] J.-Y. Piquemal, S. Halut, J.-M. Brégeault, *Angew. Chem.* **1998**, *110*, 1149−1152; *Angew. Chem. Int. Ed. Engl.* **1998**, *37*, 1146−1149 and references therein.
[2] M. K. Johnson, D. C. Rees, M. W. W. Adams, *Chem. Rev.* **1996**, *96*, 2817−2839.
[3] [3a] R. H. Holm, *Chem. Rev.* **1987**, *87*, 1401−1449. − [3b] R. H. Holm, *Coord. Chem. Rev.* **1990**, *100*, 183−221. − [3c] R. H. Holm, J. P. Donahue, *Polyhedron* **1993**, *12*, 571−589.
[4] G. C. Tucci, J. P. Donahue, R. H. Holm, *Inorg. Chem.* **1998**, *37*, 1602−1608 and references therein.
[5] [5a] N. Ueyama, H. Oku, A. Nakamura, *J. Am. Chem. Soc.* **1992**, *114*, 7310−7311. − [5b] H. Oku, N. Ueyama, A. Nakamura,

Bull. Chem. Soc. Jpn. **1996**, *69*, 3139−3150. − [5c] S. K. Das, D. Biswas, R. Maiti, S. Sarkar, *J. Am. Chem. Soc.* **1996**, *118*, 1387−1397. − [5d] J. P. Donahue, C. Lorber, E. Nordlander, R. H. Holm, *J. Am. Chem. Soc.* **1998**, *120*, 3259−3260. − [5e] C. Lorber, J. P. Donahue, C. A. Goddard, E. Nordlander, R. H. Holm, *J. Am. Chem. Soc.* **1998**, *120*, 8102−8112.

[6] [6a] J. H. Enemark, C. G. Young, *Adv. Inorg. Chem.* **1993**, *40*, 1−87. − [6b] A. G. Wedd, *Coord. Chem. Rev.* **1996**, *154*, 5−11.

[7] [7a] K. R. Barnard, R. W. Gable, A. G. Wedd, *J. Biol. Inorg. Chem.*, submitted. − [7b] Y.-L. Wong, Y. Yan, E. S. H. Chan, Q. Yang, T. C. W. Mak, D. K. P. Ng, *J. Chem. Soc., Dalton Trans.* **1998**, 3057−3064.

[8] H. H. Freedman, A. E. Frost, *J. Chem. Soc.* **1958**, *23*, 1292−1298.

[9] C. J. Hinshaw, G. Peng, R. Singh, J. T. Spence, J. H. Enemark, M. Bruck, J. Kristofzski, S. L. Merbs, R. B. Ortega, P. A. Wexler, *Inorg. Chem.* **1989**, *28*, 4483−4491.

[10] P. Subramanian, J. T. Spence, R. Ortega, J. H. Enemark, *Inorg. Chem.* **1984**, *23*, 2564−2572.

[11] K. D. Karlin, S. J. Lippard, *J. Am. Chem. Soc.* **1976**, *98*, 6951−6957.

[12] [12a] K. Yamanouchi, S. Yamada, *Inorg. Chim. Acta* **1974**, *11*, 223−226. − [12b] A. C. McDonell, S. G. Vasudevan, M. J. O′Connor, A. G. Wedd, *Aust. J. Chem.* **1985**, *38*, 1017−1024. − [12c] A. A. Eagle, E. R. T. Tiekink, C. G. Young, *J. Chem. Soc., Chem. Commun.* **1991**, 1746−1748. − [12d] A. A. Eagle, C. G. Young, E. R. T. Tiekink, *Organometallics* **1992**, *11*, 2934−2938. − [12e] F. M. Hornung, W. Kaim, *J. Chem. Soc., Faraday Trans.* **1994**, *90*, 2909−2912.

[13] K. Dreisch, C. Andersson, C. Stålhandske, *Polyhedron* **1991**, *10*, 2417−2421.

[14] [14a] K. Dreisch, C. Andersson, C. Stålhandske, *Polyhedron* **1992**, *11*, 2143−2150. − [14b] K. Dreisch, C. Andersson, C. Stålhandske, *Polyhedron* **1993**, *12*, 303−311. − [14c] K. Dreisch, C. Andersson, C. Stålhandske, *Polyhedron* **1993**, *12*, 1335−1343. − [14d] K. Dreisch, C. Andersson, M. Håkansson, S. Jagner, *J. Chem. Soc., Dalton Trans.* **1993**, 1045−1049.

[15] W. P. Griffith, T. Y. Koh, D. J. Williams, *J. Chem. Soc., Dalton Trans.* **1993**, 3459−3462.

[16] O. A. Rajan, J. T. Spence, C. Leman, M. Minelli, M. Sato, J. H. Enemark, P. M. H. Kroneck, K. Sulger, *Inorg. Chem.* **1983**, *22*, 3065−3072.

[17] [17a] S. Lee, D. L. Staley, A. L. Rheingold, N. J. Cooper, *Inorg. Chem.* **1990**, *29*, 4391−4396. − [17b] A. A. Eagle, E. R. T. Tiekink, C. G. Young, *Inorg. Chem.* **1997**, *36*, 6315−6322.

[18] [18a] A. A. Eagle, G. N. George, E. R. T. Tiekink, C. G. Young, *Inorg. Chem.* **1997**, *36*, 472−479. − [18b] V. S. Sergienko, V. A. Abramenko, A. B. Ilyukhin, *Russ. J. Inorg. Chem.* **1995**, *40*, 1740−1743.

[19] [19a] J. M. Berg, R. H. Holm, *J. Am. Chem. Soc.* **1985**, *107*, 917−925. − [19b] J. A. Craig, E. W. Harlan, B. S. Snyder, M. A. Whitener, R. H. Holm, *Inorg. Chem.* **1989**, *28*, 2082−2091.

[20] [20a] C. A. Rice, P. M. H. Kroneck, J. T. Spence, *Inorg. Chem.* **1981**, *20*, 1996−2000. − [20b] J. R. Bradbury, A. F. Masters, A. C. McDonell, A. A. Brunette, A. M. Bond, A. G. Wedd, *J. Am. Chem. Soc.* **1981**, *103*, 1959−1964. − [20c] G. Backes-Dahmann, K. Wieghardt, *Inorg. Chem.* **1985**, *24*, 4049−4054.

[21] [21a] R. D. Taylor, J. P. Street, M. Minelli, J. T. Spence, *Inorg. Chem.* **1978**, *17*, 3207−3211. − [21b] J. T. Spence, M. Minelli, P. Kroneck, *J. Am. Chem. Soc.* **1980**, *102*, 4538−4541. − [21c] U. Küsthardt, R. W. Albach, P. Kiprof, *Inorg. Chem.* **1993**, *32*, 1838−1843.

[22] C. Pickett, S. Kumar, P. A. Vella, J. Zubieta, *Inorg. Chem.* **1982**, *21*, 908−916.

[23] R. Hille, *Chem. Rev.* **1996**, *96*, 2757−2816.

[24] [24a] A. Cervilla, E. Llopis, A. Ribera, A. Doménech, E. Sinn, *J. Chem. Soc., Dalton Trans.* **1994**, 3511−3513. − [24b] P. Barbaro, T. R. Belderrain, C. Bianchini, G. Scapacci, D. Masi, *Inorg. Chem.* **1996**, *35*, 3362−3368.

[25] H. Oku, N. Ueyama, A. Nakamura, *Chem. Lett.* **1996**, 1131−1132.

[26] D. T. Sawyer, A. Sobkowiak, J. L. Roberts, Jr., *Electrochemistry for Chemists*, 2nd ed., Wiley, New York, **1995**, chapter 6.

[27] J. K. Bashkin, P. J. Kinlen, *Inorg. Chem.* **1990**, *29*, 4507−4509.

[28] [28a] G. M. Sheldrick in *Computational Crystallography* (Ed.: D. Sayre), Oxford University Press, New York, **1982**, p. 506. − [28b] G. M. Sheldrick in *Crystallographic Computing 3: Data Collection, Structure Determination, Proteins, and Databases* (Eds.: G. M. Sheldrick, C. Krüger, R. Goddard), Oxford University Press, New York, **1985**, p. 175.

[29] *International Tables for X-ray Crystallography*, vol. 4, Kynoch, Birmingham, **1974**, pp. 55, 99, and 149 (present distributer: Kluwer, Dordrecht).

[30] A. C. T. North, D. C. Phillips, F. S. Mathews, *Acta Crystallogr., Sect. A* **1968**, *24*, 351−359.

[31] A. Altomare, M. C. Burla, M. Camalli, M. Cascarano, C. Giacovazzo, A. Guagliardi, G. Polidori, *J. Appl. Crystallogr.* **1994**, *27*, 435.

[32] P. T. Beurskens, G. Admiraal, G. Beurskens, W. P. Bosman, R. de Gelder, R. Israel, J. M. M. Smits, *The DIRDIF-94 program system*, Technical Report of the Crystallography Laboratory, University of Nijmegen, The Netherlands, **1994**.

[33] *TEXSAN, Crystal Structure Analysis Package*, Molecular Structure Corporation, Houston, **1985** and **1992**.

Received July 23, 1998
[I98246]

An Experimental and Theoretical Study of Gaseous Products in the Radiolysis of Germane/Ethylene Mixtures

Paola Antoniotti,[a] Paola Benzi,[a] Mario Castiglioni,[a] and Paolo Volpe*[a]

Keywords: Semiconductors / Germanium carbide / Radiolysis / Ab initio calculations / Gas-phase reactions

Gas-phase radical reactions of germane/ethylene mixtures have been investigated using theoretical calculations and radiolysis techniques. Ab initio quantum chemical calculations have been performed on reactions starting from GeH_x (x = 0–3) radicals and C_2H_4. The geometrical structure and relative stability of isomeric GeC_2H_n (n = 4–7) radicals have been investigated and restricted to the species in which a C–C bond is present, at the MP2(FROZEN) level of calculation with double-ζ quality basis sets. To better evaluate the relative stability of the investigated species, single-point calculations at the QCISD(T) level were performed with a 6-311G(3df,2p) basis set. Reaction enthalpies and heats of formation of the species have also been determined using theoretical calculations. From irradiation of GeH_4/C_2H_4 mixtures, condensed products and volatile species were obtained. Composition, amount, and characteristics of the condensed phase products are reported. The volatile compounds were identified and their amounts determined. From experimental results and theoretical calculations some hypotheses on the reaction mechanisms are presented.

Introduction

In the last few years much work has been done on the photovoltaic applications of amorphous materials, as they are less expensive and more direct in use than the crystalline ones. Amorphous alloys, such as Si−C, Si−Ge, and Ge−C, are very interesting because they can be obtained with variable compositions, and hence with tunable physical properties, by varying the nature and concentration of the reagents. Si−C and Si−Ge have been widely studied[1−9] while Ge−C has been generally neglected, even though the Davis and Mott equation[10] suggests that amorphous Ge−C can have good photovoltaic properties, depending on the Ge/C ratio.[11] This is probably due to the difficulties encountered in its preparation using simple methods, although many different synthetic paths have been exploited.[12−18] One of these methods is the radiolysis of gas mixtures of GeH_4 and hydrocarbons. The use of high-energy radiation (namely X-rays) overcomes the problem of the activation of compounds having very different bond energies (Ge−H, C−H, and C−C).

In our laboratory, studies on the decomposition of gas-phase mixtures of germane and saturated hydrocarbons using high-energy radiation have been performed. By this method, powders and thin films of materials containing Ge and C in different ratios have been obtained,[19−21] but even at high mol fraction of alkane in the reacting mixture, the C content of the solids is generally low.[22] A study of radiolysis of germane/unsaturated hydrocarbon mixtures is now in progress which has been undertaken because of the presence of the more reactive double bond which may lead to an increase in the number of carbon atoms incorporated into the solid.

[a] Dipartimento di Chimica Generale ed Organica Applicata, Università di Torino,
C.so Massimo D'Azeglio, 48, I-10125 Torino, Italy

This paper will deal with the gas-phase reactivity of monogermane/ethylene mixtures. In order to find a relationship between the gaseous reactant molar fraction and the abundance of the corresponding atoms in the solid, it is of fundamental importance to know the gas-phase behaviour of the reacting molecules. The combination of experimental and theoretical investigations is becoming a useful approach to the study of gas-phase chemistry.[23,24] In fact, in this paper, we report results of ab initio theoretical calculations to determine the structure, relative stability, and thermochemical data of the ground state of some products of the more probable gas-phase reactions proposed as a consequence of the experimental results. These calculations can help in some qualitative speculation on the whole mechanism involved.

Radiolysis of GeH_4/C_2H_4 Mixtures

Following irradiation of germane/ethylene mixtures gaseous and solid products are obtained, the latter being deposited on the bottom of the irradiation ampoules. For the samples containing more than of 15% ethylene, small amounts of a viscous liquid phase are formed which easily dissolve some of the volatile products making sampling and analysis of the gas phase products difficult.

Besides unreacted germane and ethylene, analysis of the gas-phase products indicates the presence of variable amounts of species containing both Ge and C. Only traces of volatile hydrocarbons, formed by polymerization of ethylene and mainly containing eight C atoms, is sometimes observed. The amounts of volatile species (other than GeH_4 and C_2H_4) as a function of ethylene percentage are reported in Table 1.

From Table 1 it appears that (i) apart from in the 30% ethylene mixture, the percentage of Ge found in the gas-

 © WILEY-VCH Verlag GmbH, D-69451 Weinheim, 1999 1434−1948/99/0202−0323 $ 17.50+.50/0

Table 1. Amounts of gaseous species formed upon irradiation of GeH_4/C_2H_4 mixtures with different compositions; note that the μmol values are affected by an error of 20%

Species	Amount of ethylene [μmol] 3%	5%	8%	15%	30%
GeC_2H_8	1.40	4.31	6.4	7.45	1.89
Ge_2H_6	5.38	3.03	2.92	$9.45\cdot10^{-1}$	n.d.[a]
GeC_4H_{12}	$2.56\cdot10^{-1}$	$2.90\cdot10^{-1}$	$8.05\cdot10^{-1}$	1.26	$9.74\cdot10^{-1}$
$Ge_2C_2H_{10}$	$3.22\cdot10^{-1}$	1.05	$8.42\cdot10^{-1}$	$2.86\cdot10^{-1}$	$6.11\cdot10^{-2}$
Ge_3H_8	$2.92\cdot10^{-1}$	$3.12\cdot10^{-1}$	$3.06\cdot10^{-2}$	n.d.[a]	n.d.[a]
GeC_6H_{16}	$9.70\cdot10^{-2}$	$6.98\cdot10^{-2}$	$4.17\cdot10^{-2}$	$8.60\cdot10^{-2}$	$1.33\cdot10^{-1}$
$Ge_2C_4H_{14}$	$1.71\cdot10^{-2}$	$9.15\cdot10^{-2}$	$6.09\cdot10^{-1}$	$8.19\cdot10^{-1}$	$3.05\cdot10^{-2}$
$Ge_3C_2H_{12}$	$2.81\cdot10^{-3}$	$1.03\cdot10^{-2}$	$1.58\cdot10^{-2}$	$3.03\cdot10^{-3}$	n.d.[a]
$Ge_2C_6H_{18}$	n.d.[a]	$1.07\cdot10^{-2}$	$3.62\cdot10^{-2}$	$1.08\cdot10^{-2}$	$3.29\cdot10^{-2}$
$Ge_3C_4H_x$	n.d.[a]	n.d.[a]	$1.25\cdot10^{-2}$	$6.31\cdot10^{-3}$	$5.14\cdot10^{-3}$
n.i.[b] (> Ge_3C_4)	$7.65\cdot10^{-2}$	n.d.[a]	$6.78\cdot10^{-1}$	$3.31\cdot10^{-2}$	$7.00\cdot10^{-2}$

[a] n.d.: not detected. – [b] n.i.: not identified.

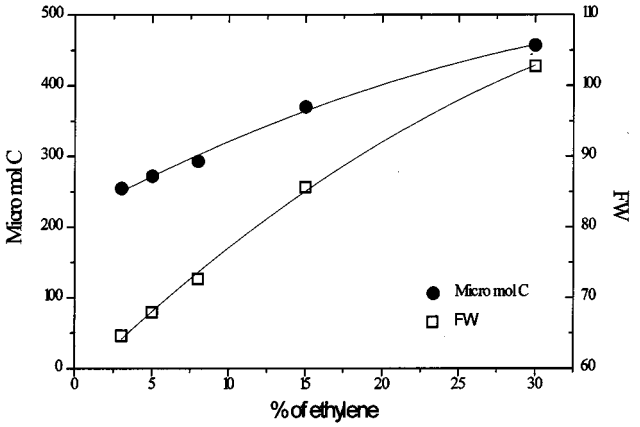


Figure 1. Absolute amounts of carbon and formula weight (FW) of the condensed-phase products vs. C_2H_4 percentage

phase products compared with Ge present in the reacting mixture is quite constant at about 0.1%, probably because of the formation of compounds of very low volatility and/or the solubility of the gases in the liquid phase; and (ii) the percentage of C found in the volatile products with respect to its starting amount is constant at about 0.6%, except for the samples at 30% ethylene, for the same reasons given above. The volatile products may be obtained from addition of GeH_x ($x = 1-3$) species with germane molecules or with ethylene or ethylene derivatives. It can be observed that with increasing amounts of ethylene in the reacting mixture, the amounts of the products containing only Ge and H decrease. In contrast, the amounts of the compounds containing both Ge and C increase, though for the latter the quantity decreases as the number of Ge atoms in the compound increases.

The low amounts of volatile products observed seems to indicate that the reactions which lead to condensed-phase products are favoured. In Table 2, amounts, composition and other characteristics of the condensed phases products obtained by irradiation of GeH_4/C_2H_4 mixtures with various ethylene percentages are reported. Ge/C and H/(Ge + C) atomic ratios observed for the condensed phase products are also reported.

Table 2 and Figure 1 show that both the absolute amount and the formula weight of the condensed-phase products increase as C_2H_4 increases. Moreover from Table 2 it can be observed that the Ge/C ratio decreases while the H/(Ge + C) ratio increases as the ethylene percentage is enhanced.

It is noteworthy that even if both volatile compounds and condensed-phase products (reported in Table 1 and 2) are considered, the decomposition of the GeH_4 is low with respect to the analogous germane/alkane mixtures.[22] In fact, the percentage of germane decomposed with respect to the germane initially present in the mixture varies from 0.5% to 2.0% when ethylene ranges from 3.0% to 30.0% corresponding to G ($-GeH_4$) values (μM/J) ranging from 1.4 to 5.2. In the GeH_4/alkane systems previously studied, the G ($-GeH_4$) values are 11.7 and 10.7 with ethane and propane, respectively, for mixtures with 25% of alkane. To explain this decomposition with respect to that observed when GeH_4 is irradiated alone, G ($-GeH_4$) = 1.26, the poor energy transfer between excited molecules of GeH_4 and hydrocarbon molecules has been invoked.[22] In fact, in such conditions the collisional quenching decreases and an excited GeH_4 molecule may therefore suffer decomposition after a few collisions. In the present study, ethylene is generally a minor component of the irradiated mixture and it is

Table 2. Characterization of the condensed-phase products obtained from irradiation of GeH_4/C_2H_4 mixtures with different compositions

	3% C_2H_4	5% C_2H_4	8% C_2H_4	15% C_2H_4	30% C_2H_4
Weight [mg]	5.0 ± 0.8	7.0 ± 1.4	10.0 ± 2.0	15.0 ± 1.2	20.0 ± 2.0
Description	brown orange dusty solid	dark orange dusty solid	orange dusty solid	range waxy solid	viscous colourless liquid
% of the original carbon[a]	5.5	5.7	5.6	5.8	5.8
% of the original germanium[b]	0.39	0.61	0.88	1.30	1.95
Empirical formula	$GeC_{0.88}H_{2.39}$	$GeC_{0.99}H_{2.74}$	$GeC_{1.13}H_{3.13}$	$GeC_{1.66}H_{4.46}$	$GeC_{2.26}H_{5.92}$
% of carbon[c]	20.6	20.9	21.4	23.3	24.6
Ge/C atomic ratio	1.14	1.01	0.88	0.60	0.44
H/(Ge + C) atomic ratio	1.27	1.37	1.47	1.67	1.81

[a] Percentage of C atoms in the condensed-phase products with respect to the C atoms present in the reacting mixture. – [b] Percentage of Ge atoms in the condensed-phase products with respect to the Ge atoms present in the reacting mixture. – [c] Percentage of carbon atoms in condensed-phase products.

generally present in too low percentage to prevent the energy transfer from excited germane molecules to germane molecules in the ground state.

As far as the condensed-phase products are concerned, it is interesting to study the hydrogen content as a function of the C_2H_4 percentage in the starting mixture, as shown in Figure 2.

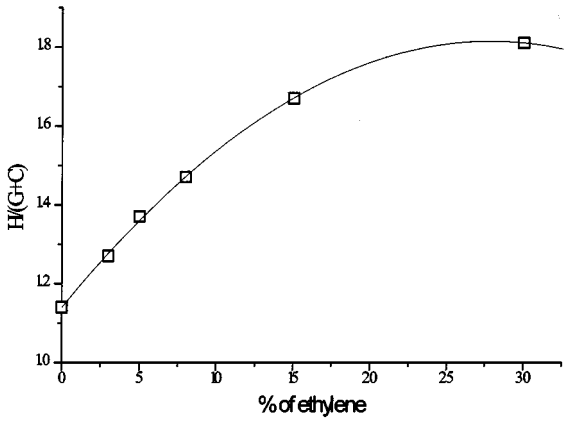


Figure 2. H/(Ge + C) atomic ratio in the condensed-phase obtained by irradiation of GeH_4/C_2H_4 mixtures with different ethylene percentages; the point on the *y* axis is an extrapolated value

Extrapolation to 0% ethylene, gives a value of H/Ge = 1.14 which is very close to the 1.29 value found in the γ radiolysis of pure GeH_4, measured using a radioisotopic technique.[25] The agreement improves considering the higher irradiation dose used in those experiments and that the extent of hydrogenation slowly increases with the dose.

During the irradiation both ionic and radical species may be involved in the formation of volatile and condensed-phase products. The ionic contribution to these processes can be investigated by mass-spectrometric experiments of both single reactants and their mixtures. The most important ions in the mass spectrum of pure ethylene are $C_2H_4^+$, $C_2H_3^+$, and $C_2H_2^+$ with abundances of 38, 23, and 22%, respectively, and other ions such as $C_2H_5^+$,$C_3H_n^+$ (n = 5, 7), and $C_5H_n^+$ (n = 7, 9) are also formed by ion−molecule reactions.[27] In germane the most abundant ionic species are GeH_3^+, GeH_2^+, GeH^+, and Ge^+. In addition, the formation of dimeric, trimeric, and tetrameric ions in ion−molecule reactions has been also observed.[28,29]

In a Fourier-transform mass-spectrometric study[27] of GeH_4/C_2H_4 mixtures it has been observed that reaction between $C_2H_4^+$ ions and GeH_4 molecules gives GeH_3^+ and, to a lesser extent, GeH_2^+ ions. Further reactions of GeH_3^+ ion species with GeH_4 or C_2H_4 neutrals lead to the formation of mixed species or ions containing two Ge atoms, respectively (Equations. 1, 2, and 3).

$$GeH_3^+ + GeH_4 \rightarrow Ge_2H_3^+ + 2\,H_2 \quad (1)$$
$$GeH_3^+ + GeH_4 \rightarrow Ge_2H_5^+ + H_2 \quad (2)$$
$$GeH_3^+ + C_2H_4 \rightarrow GeC_2H_5^+ + H_2 \quad (3)$$

Moreover, it is reasonable to suppose that ions obtained from the above reactions react further with GeH_4 and/or C_2H_4 leading to products with longer chains. This hypothesis is supported by the finding that in mass-spectrometric experiments performed under chemical ionization conditions on GeH_4/C_2H_4 mixtures, several ions containing one Ge and up to four C atoms were detected with relatively high abundance. Ions with two Ge and two to four C atoms were also observed.[27]

In summary, the ionic reaction mechanisms reported in a previous study,[27] using Fourier-transform and high-pressure mass-spectrometric methods, are in satisfactory agreement with the observations of this work.

In the radiolysis a great contribution to the products is, however, given by radical species. In order to evaluate the relative contribution of ions and radicals, the energy required for ionization and for the formation of a radical should be considered. The average energy absorbed for the formation of an *ion pair* (W)[26] in GeH_4 is about 22.0 eV ($8.41 \cdot 10^{-22}$ kcal)[22] and because the ionization potential (I) of GeH_4 is only 10.7 eV ($4.08 \cdot 10^{-22}$ kcal),[25,31] there is an excess energy ($W - I$) of about 11.3 eV ($4.33 \cdot 10^{-22}$ kcal) available for the formation of excited molecules and/or radicals. Considering the germylene radical (which from energetic data reported below, is the more probable primary radical) the energy required is 2.16 eV ($8.27 \cdot 10^{-23}$ kcal).[32] It follows that about four radicals can be formed in addition to each ion. It can therefore be concluded that radical reactions should give the major contribution to the product formation.

In previous experiments on GeH_4/alkane mixtures, high amounts of gaseous products were obtained and none of the product yields seemed to be affected by the addition of oxygen as a radical scavenger.[22] In contrast, in mixtures where ethylene is used instead of an alkane, a very low abundance of volatile products is formed. In particular, the amount of Ge_2H_6 is low and decreases with increasing concentration of ethylene, whereas the amount of GeC_2H_8 species increases with ethylene pressure showing that ethylene strongly competes with germane in the reactions with the GeH_x (x = 1−3) radicals and that germane−alkene reactions are mainly scavenging processes.

This hypothesis is supported by the data of Tables 1 and 2 which show that while the fraction of carbon in the products (gas and condensed phase) is about 6% of carbon in the reactant over the whole range of ethylene concentration, the fraction of germanium present in the products increases from about 0.5 to about 2% with increasing concentration of C_2H_4.

The radicals formed during the germane radiolysis are germyle, GeH_3, and germylene, GeH_2; it has been proposed that their formation occurs by decomposition of excited molecules according to the Equations 4 and 5.[33]

$$GeH_4^* \rightarrow GeH_3 + H \quad (4)$$
$$GeH_4^* \rightarrow GeH_2 + H_2 \quad (5)$$

The formation of GeH_3 and GeH_2 radicals requires an activation energy of $2.27 \cdot 10^{24}$ eV mol^{-1} (87.20 kcal mol^{-1})

and $1.30 \cdot 10^{24}$ eV mol^{-1} (49.80 kcal mol^{-1}), respectively,[32] so the reaction forming GeH_2 radicals should be energetically favoured. Moreover, it has been observed that GeH_2 further decomposes according to Equations 6 and 7, which compete with each other in the ratio 9:1[32] and suggest that the Ge and GeH species must also be considered in the products formation.

$$GeH_2 + M \rightarrow Ge + H_2 + M \quad (6)$$
$$GeH_2 + M \rightarrow GeH + H + M \quad (7)$$
M = neutral molecule

Therefore, it can be proposed that the germane radicals react with ethylene molecules leading to mixed species according to Equations (8) to (15). In these reactions ethylene addition or addition followed by elimination of hydrogen molecules or atoms occurs.

$$Ge + C_2H_4 \rightarrow GeC_2H_4 \quad (8)$$
$$GeH + C_2H_4 \rightarrow GeC_2H_5 \quad (9)$$
$$GeH_2 + C_2H_4 \rightarrow GeC_2H_4 + H_2 \quad (10)$$
$$GeH_2 + C_2H_4 \rightarrow GeC_2H_5 + H \quad (11)$$
$$GeH_2 + C_2H_4 \rightarrow GeC_2H_6 \quad (12)$$
$$GeH_3 + C_2H_4 \rightarrow GeC_2H_5 + H_2 \quad (13)$$
$$GeH_3 + C_2H_4 \rightarrow GeC_2H_6 + H \quad (14)$$
$$GeH_3 + C_2H_4 \rightarrow GeC_2H_7 \quad (15)$$

Because the long-chain products derive from the light ones, the same mechanisms for beginning a chain may be invoked to explain the formation of both volatile species and condensed-phase products. In fact, the species obtained from the above reactions may further react (by analogous mechanisms) with germane or ethylene with chain propagation leading to condensed-phase products, but the chain can be stopped by reaction with hydrogen radicals leading to the observed volatile species.

Considering the hydrogenation extent of the condensed-phase products, two hypotheses on the product formation can be proposed: (i) the main radicals which contribute to the Ge−C mixed compounds are the ones poor in hydrogen (Ge and GeH) and (ii) if germyle and germylene are the reactants, then in the reactions H (or H_2) is released. Some evidence supports the first hypothesis; in fact Figure 2 shows that the extent of condensed-phase hydrogenation increases with the carbon content. It is possible to think that the hydrogen enters in the chain mainly bonded to carbon atoms. This is because when an ethylene molecule leads upon a radical addition reaction it incorporates four hydrogen atoms, i.e. two hydrogen atoms for each carbon atom. To reach the empirical formula reported in Table 2 any germanium atom must lead, on average, to less then two hydrogen atoms. Moreover, even if from the above energetic considerations the germylene is the more probable primary radical, it must undergo an extensive decomposition leading to Ge and GeH. Thus, even Ge and GeH radicals have an important function in chain propagation leading to condensed-phase products which should, as a result, be poor in hydrogen.

Theoretical Study of the GeC_2H_n ($n = 4-7$) Species

In order to determine the most probable reaction pathways leading to the formation of the condensed-phase products, ab initio theoretical calculations on the products obtained from the previous reactions have been performed. Since in the radiolysis of ethylene the products maintaining the C−C bond predominate,[34] only the GeC_2H_n ($n = 4-7$) species in which such a bond is present were considered.

The enthalpies[35] of reactions leading to the most stable isomer have been calculated at the QCISD(T)/6-311G(3df,2p) level of theory and are reported in Table 3. Formation enthalpies $\Delta H°_f$ for the most stable GeC_2H_n ($n = 4-7$) species considered in this paper have also been computed and are reported in Table 4. They have been obtained by the method proposed by Pople et al.[36] The method was used with the following modifications: (i) The QCISD(T)/6-311G(3df,2p) energies (reported in Table 5) have been directly used throughout in order to evaluate the energy difference relevant to the isogyric reaction; (ii) instead of the ZPE correction to the energy, the full thermal correction at the MP2/BS level of theory has been applied (as outlined in ref.[35]).

Table 3. Enthalpies of reactions leading to the most stable products [kcal mol^{-1}]

Equation	Reaction	$\Delta H°$
(8)	$Ge + C_2H_4 \rightarrow GeC_2H_4$	−31.5
(10)	$GeH_2 + C_2H_4 \rightarrow GeC_2H_4 + H_2$	−3.0
(9)	$GeH + C_2H_4 \rightarrow GeC_2H_5$	−19.4
(11)	$GeH_2 + C_2H_4 \rightarrow GeC_2H_5 + H$	49.0
(13)	$GeH_3 + C_2H_4 \rightarrow GeC_2H_5 + H_2$	5.8
(12)	$GeH_2 + C_2H_4 \rightarrow GeC_2H_6$	−35.2
(14)	$GeH_3 + C_2H_4 \rightarrow GeC_2H_6 + H$	23.6
(15)	$GeH_3 + C_2H_4 \rightarrow GeC_2H_7$	−25.2

Table 4. Heats of formation for the most stable GeC_2H_n ($n = 4-7$) species [kcal mol^{-1}]

	Species	$\Delta H°_f$
3a	GeC_2H_4	74.0
4a	GeC_2H_5	76.2
5a	GeC_2H_6	42.1
6a	GeC_2H_7	45.4

GeC_2H_4

The investigation of the potential-energy surface of singlet and triplet GeC_2H_4 radicals suggested the existence of three distinct species. The geometrical parameters are shown in Figure 3 and the total and relative energies are reported in Table 5. The structure **3a**, a singlet species with C_S symmetry, obtained from the reaction of the Ge radical with the ethylene molecule (reaction 8), is the global minimum on the potential-energy surface. This structure contains a Ge atom bridging the two carbon atoms. The exo-

thermicity of the reaction (-31.5 kcal mol^{-1}) suggests that the formation of these radicals are rather probable. The structure **3b,** also with C_S symmetry, is a triplet state, less stable than structure **3a** by 17.6 kcal mol^{-1} at the QCI level of theory. Once again, the results of the calculations suggest that reaction is rather probable. The structure **3c** can probably be obtained from the reaction of the GeH_2 radical with the ethylene molecule with a subsequent elimination of a hydrogen molecule. Structure **3c** is a cyclic species calculated to lie 38.4 kcal mol^{-1} above **3a** at the highest level of calculation. Results for the enthalpy calculations for the **3c** formation reaction show that more than 35.4 kcal mol^{-1} are necessary to overcome the barrier for dissociation of a H_2 molecule.

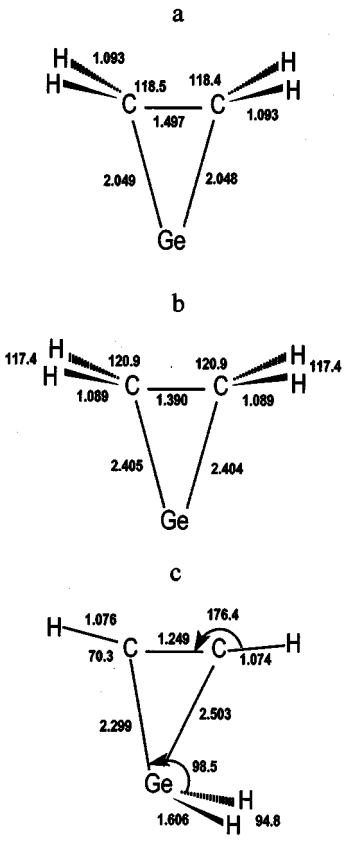


Figure 3. MP2/BS geometrical parameters of the GeC_2H_4 isomers with bond lengths [Å] and bond angles [°]

GeC_2H_5

Six different critical points have been located on the GeC_2H_5 potential-energy surface corresponding to a minimum or first-order saddle point. The optimized geometries and the total and relative energies of GeC_2H_5 isomers are reported in Figure 4 and Table 5.

The allyl-like structure **4c** with C_S symmetry, obtained most easily from Equation (11) (endothermic by 49.0 kcal mol^{-1}), was found to be a first-order saddle point corresponding to a transition structure for the rotation of the germylene group around the Ge−C bond. The activation energy of the rotation process was computed as 3.3 kcal mol^{-1} at the QCI level of calculation. This is not in agreement with that found for $GeC_2H_5^+$ ions where the allyl-like planar structure corresponds to the most stable absolute minimum.[37] The other two structures **4a** and **4b**, which can be obtained from Equation (11), have been characterized as minima on the potential-energy surface. The **4a** species, with C_1 symmetry, the most stable at the MP2 level of theory, becomes less stable by 1 kcal mol^{-1} at the QCI level with respect to **4b** which has C_S symmetry. Although these isomers are stable, the calculated enthalpy change for Equation (11) is very high (49.0 kcal mol^{-1}) and it follows that formation of these radicals from the reaction considered becomes more difficult than from Equations (9) or (13).

Only one 1-propenyl-like species, corresponding to a minimum, has been located on the potential-energy surface, indicated as **4f**. This product, derived probably from Equation (13) (endothermic by 5.8 kcal mol^{-1} compared to species **4a**), was found to be the less stable isomer at all levels of calculation. In fact, it is 27.2 kcal mol^{-1} less stable than **4b** at the QCI level. Moreover, in order to obtain this product it is probably necessary to overcome a barrier for dissociation of a H_2 molecule.

The 2-propenyl-like species **4e** has been located and characterized as a minimum on the potential-energy surface of GeC_2H_5 radicals, as a product of Equation (13). In this case too, in addition to the reaction endothermicity, the energy of this species was found to be rather high (22.5 kcal mol^{-1} with respect to the species **4a**). This is probably due to the contamination of the spin state (see Table 5).

The only thermally allowed reaction according to Equation (9) (-19.4 kcal mol^{-1}), which follows from the junction of a GeH radical and an ethylene molecule, gives rise to the species **4d**. Although this product was found to be less stable by 21.2 kcal mol^{-1} with respect to structure **4a**, the reaction remains feasible.

GeC_2H_6

Five critical points have been located on the potential-energy surface of the singlet GeC_2H_6 species. The geometrical parameters are shown in Figure 5 and the absolute and relative energies are collected in Table 5.

The staggered and eclipsed (C_s symmetry) conformations of vinylgermane have been located on the potential-energy surface. They are indicated as **5b** and **5c**, respectively. The former corresponds to a minimum and the latter corresponds to a first-order saddle point for rotation of GeH_3 around the Ge−C bond. The energy difference between **5b** and **5c** is computed to be as large as 1.2 kcal mol^{-1} at the QCI level of calculation. Moreover, the staggered conformation of vinylgermane results to be more stable than **5a** by 4.3 kcal mol^{-1} at the QCI level of theory and the global minimun on the GeC_2H_6 potential-energy surface. The species **5b** can probably be obtained from Equation (14) (but this process is endothermic) following a hydrogen atom dissociation, or from equation (12) (exothermic by 35.2 kcal

Table 5. Total and relative energies [Hartree and kcal mol^{-1}] of the investigated GeC_2H_n ($n = 4-7$) radicals

Species (NIMAG[a])	UMP2 (FROZEN)/BS[b]	ΔE	$<S^2>$[c]	QCISD(T)/6-311G(3df, 2p)	ΔE	ZPE[d]
3a (0)	2151.666487	0.0	0.0	−2153.832970	0.0	32.6
3b (0)	−2151.644778	13.6	2.0226	−2153.804955	17.6	33.4
3c (0)	−2151.597615	43.2	0.0	−2153.771804	38.4	26.0
4a (0)	−2152.221537	0.0	0.7528	−2154.415308	1.0	35.7
4b (0)	−2152.218953	1.6	0.8276	−2154.416910	0.0	36.3
4c (1)	−2152.207728	8.7	0.9267	−2154.410043	4.3	35.1
4d (0)	−2152.196235	15.9	0.7662	−2154.383159	21.2	35.5
4e (0)	−2152.166337	34.6	0.9272	−2154.380980	22.5	32.8
4f (0)	−2152.162187	37.2	0.9153	−2154.373585	27.2	32.6
5a (0)	−2152.850449	0.0	0.0	−2155.048495	0.0	44.8
5b (0)	−2152.840411	6.3	0.0	−2155.055417	−4.3	40.6
5c (1)	−2152.838854	7.3	0.0	−2155.053513	−3.1	40.4
5d (0)	−2152.833696	10.5	0.0	−2155.039476	5.7	42.8
5e (0)	−2152.825597	15.6	0.0	−2155.031992	10.4	42.7
5f (0)	−2152.816532	21.3	2.0044	−2155.009337	24.6	45.3
5g (0)	−2152.777011	46.1	2.0196	−2154.980569	42.6	41.1
5h (1)	−2152.771834	49.3	2.0161	−2154.975185	46.0	40.5
5i (0)	−2152.735584	72.1	2.0157	−2154.952319	60.3	37.8
6a (0)	−2153.431692	0.0	0.7528	−2155.646408	0.0	50.3
6b (0)	−2153.394454	23.4	0.7653	−2155.619322	17.0	46.5
6c (0)	−2153.392628	24.5	0.7653	−2155.620345	16.4	46.7
6d (1)	−2153.389900	26.2	0.7636	−2155.614387	20.1	46.7

[a] Number of imaginary frequencies. − [b] For the specification of the basis set BS, see the Computational Details section. − [c] Eigenvalues of spin operator at the UHF/BS level of theory. − [d] Zero-point energies [kcal mol^{-1}] at the UMP2 (FROZEN)/BS level of theory.

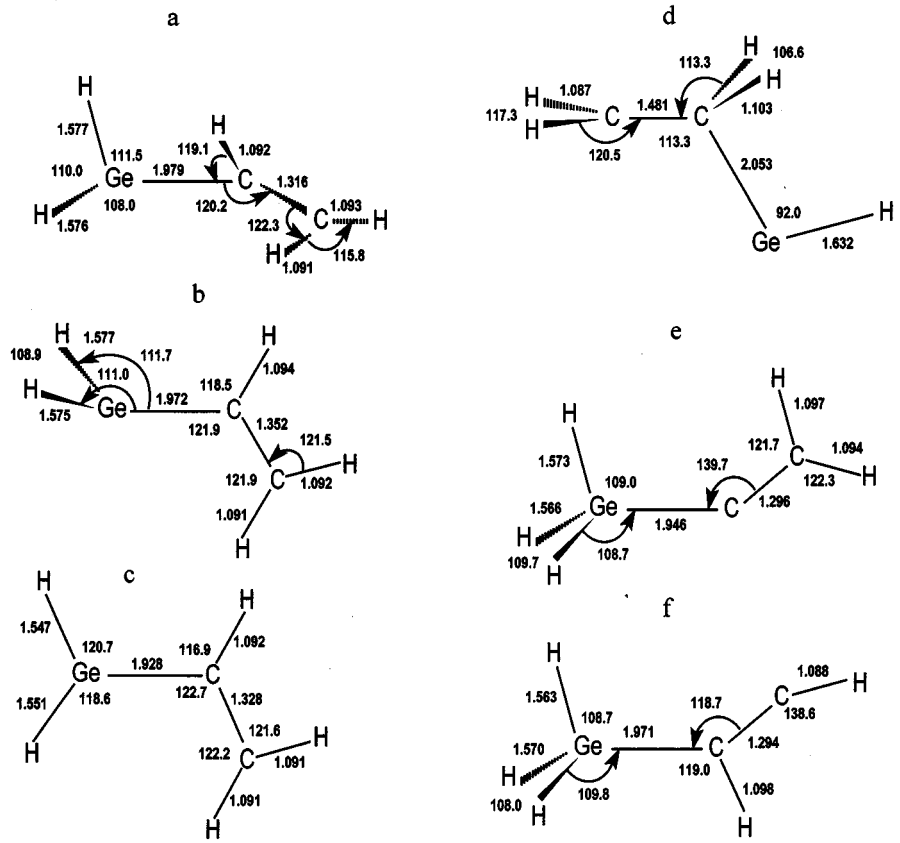


Figure 4. MP2/BS geometrical parameters of the GeC_2H_5 isomers with bond lengths [Å] and bond angles [°]

mol^{-1}) through a hydrogen-atom migration. The ethylgermylene **5a**, the most stable at the MP2 level of theory, becomes less stable at the QCI level. This product cannot be obtained directly from the exothermic reaction according to Equation (12), but through a rearrangement of the structure after this reaction or a rearrangement and a loss of a

hydrogen atom after the reaction according to Equation (14). The 2-methyl-1-germaethylene **5e** was found to be 14.7 kcal mol^{-1} above the most stable species **5b**. This structure, which can be derived from the more feasible process according to Equation (12), requires a transposition of a hydrogen atom. The germacyclopropane **5d** can only be obtained directly from the thermally favoured formation reaction of GeC_2H_6. Although the energy of the germacyclopropane was found to be higher by 10.0 kcal mol^{-1} with respect to that of **5a**, the reaction remains thermally allowed.

The investigation of the potential-energy surface of the triplet GeC_2H_6 species provides four other structures that are shown also in Figure 5 (**5f** to **5i**). The total and relative energies are collected in Table 5. The products obtained directly from the process according to Equation (12) correspond to the species **5g** and **5h**, the former being a minimum on the potential-energy surface, the latter a first-order saddle point for rotation of a methylene group around the C−C bond. The activation energy of the rotation process was calculated to be 3.4 kcal mol^{-1}. The energy of the minimum **5g** was found to be 42.6 kcal mol^{-1} higher than that of the most stable GeC_2H_6 species **5a**.

The other two species **5f** and **5i** can be obtained from the exothermic reaction according to Equation (12) only through rearrangements of the molecular structure that require overcoming energy barriers. Moreover, if the energy of the **5f** species was found to be only 24.6 kcal mol^{-1} higher than that of **5a**, the **5i** species is 60.3 kcal mol^{-1} higher in energy. The energy required for these reactions is very high which therefore are the least feasible.

GeC_2H_7

Four different critical points have been located on the potential-energy surface of the GeC_2H_7 radical obtained from Equation (15). The main geometrical parameters are shown in Figure 6, absolute and relatives energies are collected in Table 5.

Two different 1-propyl-like structures can be conceived, i.e. $CH_3CH_2GeH_2$ and $GeH_3CH_2CH_2$.

Both the bisected and the eclipsed conformations of $GeH_3CH_2CH_2$, henceforth indicated as **6d** and **6b**, have been located in the C_S symmetry on the potential-energy surface. The bisected conformation (Figure 6d) has been characterized as a first-order saddle point for rotation of the methylene group around the C−C bond, the activation energy of this process being computed as 3.1 kcal mol^{-1} at the QCI level of calculation. The eclipsed conformation **6b** was found to be a minimum on the potential-energy surface with an energy 17.0 kcal mol^{-1} higher with respect to the most stable $CH_3CH_2GeH_2$ radical **6a** in the C_1 symmetry. Since the reaction enthalpy corresponds to −25.2 kcal mol^{-1} this process is thermochemically feasible. However, species **6a**, the global minimum on the potential-energy surface of the GeC_2H_7 radical, cannot be obtained directly from Equation (15) but only through a rearrangement of an H atom from a Ge to a C atom.

Only one 2-propyl-like structure can be conceived for the GeH_3CHCH_3 radicals. The structure obtained is reported in Figure 6c; the energy was found 16.4 kcal mol^{-1} higher than that of **6a**. In this case, the structure cannot be obtained directly from Equation (15) but a migration of an H atom over a C−C bond is necessary.

Comparing these results with those for the $GeC_2H_7^+$ ions[38] the 1-propyl-like species appears to be the most stable structure, which is in agreement with the available data concerning the $GeC_2H_7^+$ ions. However, there is a difference between the ions and radicals as, in the latter case, a cyclic structure has not been obtained.

Conclusions

The results of the mass-spectrometric study outlined above, together with the composition of the condensed-phases products and the low yield of volatile species observed in the radiolysis of GeH_4/C_2H_4 mixtures seem to suggest a propensity for ethylene to react with both neutral or ionic GeH_x species. The above findings appear to solve the problems regarding the poor content of carbon of the solid obtained from GeH_4/alkane mixtures.

The theoretical calculations indicate that, among the considered reactions, the most probable are those which take place without atomic or molecular hydrogen dissociation. Moreover, among the reactions whose products are obtained by addition of the two reagent species, the processes without molecular rearrangements are favoured. In particular, for the species GeC_2H_4 and GeC_2H_5 the **3a**, **3b**, and **4d** isomers, from Equations (8) and (9), can be easily obtained. With regard to the GeC_2H_6 species, the structure **5d** is the most probable isomer which originates from Equation (12), but it is a closed-shell structure without free electrons. The most probable GeC_2H_7 radical obtained from reaction 15 is the **6b** isomer.

As reported above, the more abundant radical species derived from GeH_4 radiolysis seem to be Ge and GeH and so the most abundant primary mixed compounds are the GeC_2H_4 isomers **3a** and **3b**obtained from Equation (8) and the GeC_2H_5 isomer **4d** from Equation (9). These mixed products are probably the species which result from reactions with germane radicals and/or with ethylene molecules, leading to formation of condensed-phase products and also to volatile compounds with longer chains. This is consistent with the low hydrogen content of the products in the condensed phase and it is in agreement with the trend of the H/(Ge + C) ratio as a function of ethylene percentage, reported in Figure 2. It seems to indicate that the hydrogen atoms present in the chain are those of ethylene which remain bonded to carbon atoms.

Experimental Section

Radiolysis: Monogermane was prepared according to the literature[39] and purified by bulb-to-bulb distillation. Ethylene was high-purity SIAD (Società Italiana Acetilene e Derivati) gas and was

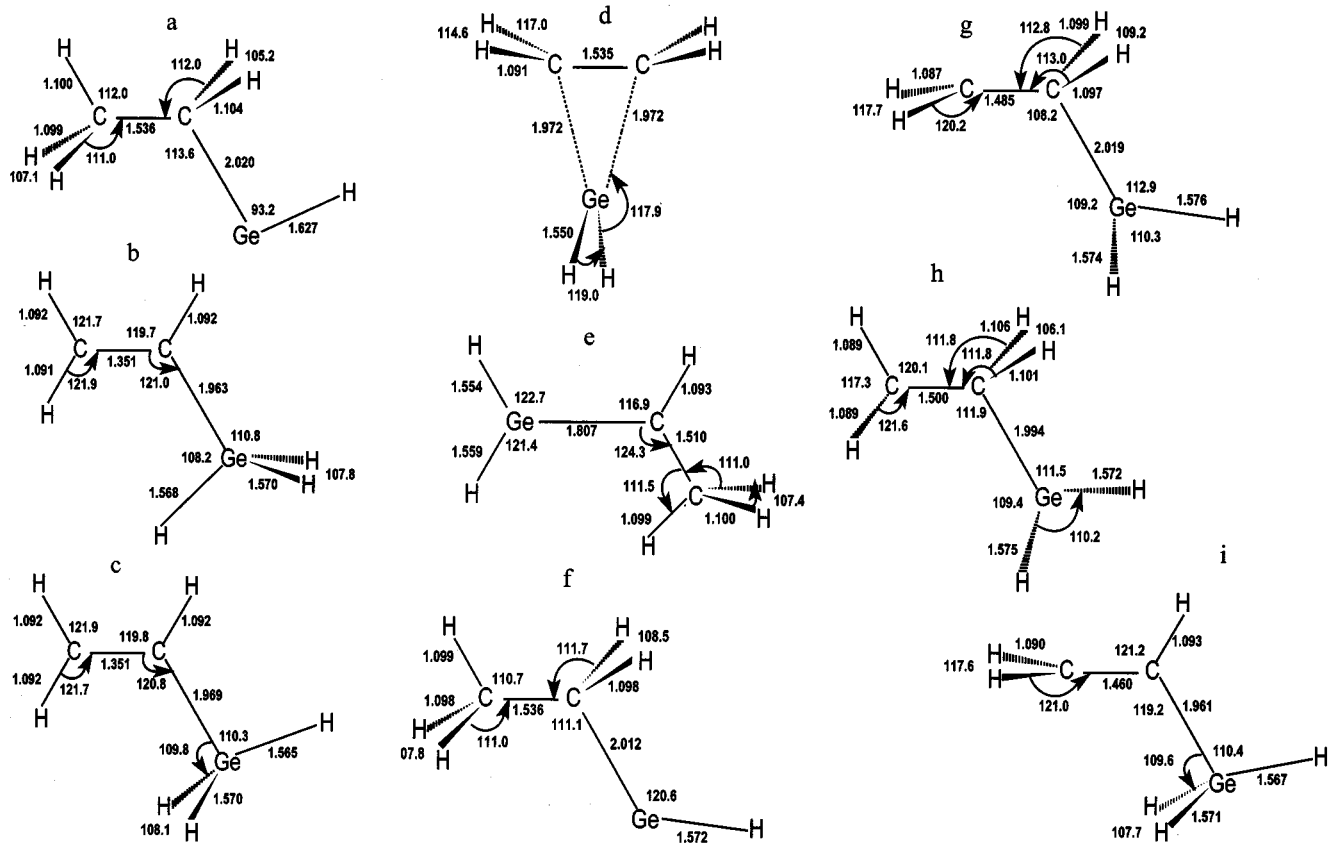


Figure 5. MP2/BS geometrical parameters of the GeC_2H_6 isomers with bond lengths [Å] and bond angles [°]

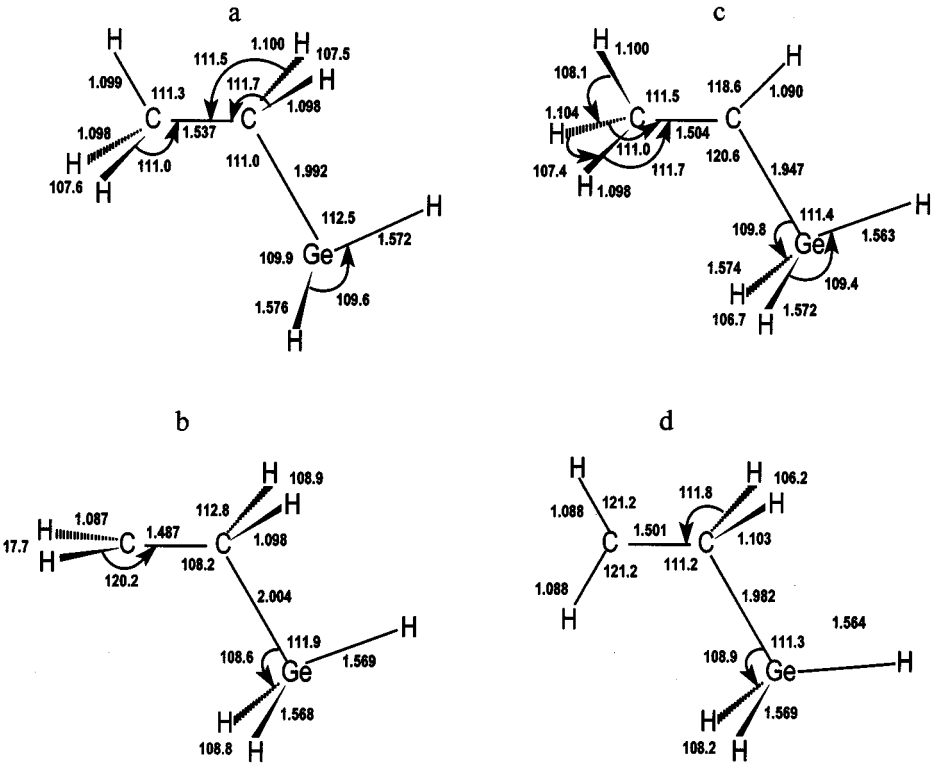


Figure 6. MP2/BS geometrical parameters of the GeC_2H_7 isomers with bond lengths [Å] and bond angles [°]

used without purification. Samples of GeH_4/C_2H_4 mixtures of different compositions were irradiated with 250-keV X-rays in 365-ml Pyrex vessels at a total pressure of 700 Torr. Standard vacuum techniques were used to handle both reactants and gaseous products. The X-ray source was a CPXT-320 tube (GILARDONI) with a maximum output of 320-keV X-ray. The dose absorbed by each sample was evaluated to be $5.0 \cdot 10^4$ Gy at a rate of $1.0 \cdot 10^4$ Gy h^{-1}. During the irradiation the temperature did not exceed 320 K. The gaseous product analysis was performed by gas chromatography and mass spectrometry using a VARIAN 3400/Finnigan ITD instrument equipped with Alltech AT-1 chromatographic column (polydimethylsiloxane, length 30 m, i.d. 0.25 mm, film thickness 1.0 μm). The temperature ranged from 243 to 523 K at 10 K/min. A 10 psi He carrier front column was used. Ionisation in the ion trap was achieved by electron impact at 70eV and acquisition of ions was obtained in the 20−650 unit mass range. Quantitative determination of volatile compounds was effected by calibrating the gas chromatograph with GeH_4. The values reported are the averages of at least four experiments.

Computational Details: Ab initio quantum-mechanical calculations were performed using an IBM RISC/6000 and a DIGITAL α STATION version of Gaussian 94 set of programs.[40] The geometries of investigated species were optimized by gradient-based techniques[41] at the unrestricted Möller−Plesset level of theory[42] truncated at the second order and with the frozen-core approximation (UMP2/FROZEN). The basis set (BS) used was obtained as follows. For the germanium atoms, starting with Huzinaga (4333/433/4) basis,[43] the last s and p atomic orbitals were decontracted to the double-ζ level to give (43321/4321/4); in addition, a set of polarization functions[43] was added with exponent α = 0.246. For the carbon atom, starting with the Huzinaga (43/4/1) basis, the last s and p atomic orbitals were decontracted to the double-ζ level to give (421/31/1). For the hydrogen atom, the 6-31G basis set was employed.[44] The critical points were characterized as minima at this level through diagonalization of analytically calculated Hessian matrices (vibrational frequencies calculation). The UMP2/(FROZEN)/BS geometries were employed to recompute the relative energies by quadratic configuration-interaction calculations at the QCISD(T) level[45] with the more extended basis set 6-311G (3df,2p).[46a−46d] Zero-point vibrational energies were computed at the UMP2(FROZEN)/BS level.[47]

Acknowledgments

The authors thank MURST and the University of Torino for financial support.

[1] H. Wieder, M. Cardona, C. R. Guarnieri, *Phys. Status Solidi* **1979**, *92*, 99.
[2] H. Rübel, B. Schröder, W. Fush, J. Krauskopf, T. Rupp, K. Bethge, *Phys. Status Solidi* **1987**, *139*, 131.
[3] N. Saito, *J. Non-Cryst. Solids* **1989**, *108*, 211.
[4] T. Drüsedau, A. Panckow, W. Herms, H. Sobotta, V. Riede, R. Böttcher, A. Witzmann, *J. Non-Cryst. Solids* **1993**, *155*, 195.
[5] L. Mariucci, F. Ferrazza, D. Della Sala, M. Capizzi, F. Evangelisti, U. Coscia, *J. Non-Cryst. Solids* **1987**, *97/98*, 1075.
[6] A. Morimoto, M. Kumeda, T. Shimizu, *J. Non-Cryst. Solids* **1983**, *59/60*, 537.
[7] Y. Katayama, K. Usami, T. Shimada, *Philos. Mag.* **1981**, *43*, 283.
[8] J. Robertson, *Philos. Mag.* **1992**, *66*, 615.
[9] Y. Tawada, K. Tsuge, M. Kondo, H. Okamoto, Y. Hamakawa, *J. Appl. Phys.* **1982**, *53*, 5273.
[10] E. A. Davis, N.-F. Mott, *Philos. Mag.* **1970**, *22*, 903.
[11] P. Mazerolles, R. Morancho, A. Reynes, *Silicon, Germanium, Tin Lead Compd.* **1986**, *9*, 243.
[12] J. Shinar, H. S. Wu, R. Shinar, H. R. Shanks, *J. Appl. Phys.* **1987**, *62*, 808.
[13] S. Kumar, S. C. Kashyap, K. L. Chopra, *J. Non-Cryst. Solids* **1988**, *101*, 287.
[14] T. Drüsedau, A. Andreas, B. Schröder, H. Freisted, *Philos. Mag.* **1994**, *69*, 1.
[15] H. Yuan, R. S. Willams, *Chem. Mater.* **1993**, *5*, 479.
[16] D. A. Anderson, W. E. Spear, *Philos. Mag.* **1977**, *35*, 1.
[17] D. C. Booth, K. J. Voss, *J. Phys.* **1981**, *42*, C4-1033.
[18] M. Gazicki, A. Jachimowicz, R. Shallauer, K. Pirker, W. Fallmann, F. Kohl, F. Olcaytug, G. Urban, *J. Appl. Polym. Sci.: Appl. Polym. Symp.***1990**, *46*, 137.
[19] P. Antoniotti, P. Benzi, M. Castiglioni, L. Operti, P. Volpe, *Chem. Mater.* **1992**, *4*, 717.
[20] P. Benzi, M. Castiglioni,P. Volpe, *J. Mater. Chem.* **1994**, *4*, 1067.
[21] P. Benzi, M. Castiglioni, E. Truffa, P. Volpe, *J. Mater. Chem.* **1996**, *6*, 1507.
[22] P. Antoniotti, P. Benzi, M. Castiglioni, L. Operti, P. Volpe, *Radiat. Phys. Chem.* **1996**, *48*, 457.
[23] [23a] M. L. Mandich, W. D. Reents Jr., M. F. Jarrold, *J. Chem. Phys.* **1988**, *88*, 1703. − [23b] M. L. Mandich, W. D. Reents, Jr., K. D. Kolenbrander, *J. Chem. Phys.* **1990**, *92*, 437. − [23c] M. L. Mandich, W. D. Reents, Jr., *J. Chem. Phys.* **1991**, *95*, 7360. − [23d] M. L. Mandich, W. D. Reents, Jr., *J. Chem. Phys.* **1992**, *96*, 4429.
[24] [24a] P. Antoniotti, L. Operti, R. Rabezzana, G. A. Vaglio, P. Volpe, J. F. Gal, R. Grover, P. C. Maria, *J. Phys. Chem.* **1996**, *100*, 155. − [24b] P. Antoniotti, L. Operti, R. Rabezzana, M. Splendore, G. Tonachini, G. A. Vaglio, *J. Chem. Phys.* **1997**, *107*, 1491.
[25] R. Belluati, M. Castiglioni, P. Volpe, M. C. Gennaro, *Polyhedron* **1987**, *6*, 441.
[26] The energy for *ion pair* (W) formation is related to the process: $GeH_4 \rightarrow GeH_4^+ + e$; J. W. T. Spinks, R. J. Woods, *An Introduction To Radiation Chemistry*, 3rd ed. Wiley, New York, **1990**, p. 236.
[27] P. Benzi, L. Operti, G. A. Vaglio, P. Volpe, M. Speranza, R. Gabrielli, *J. Organomet. Chem.* **1989**, *373*, 289.
[28] J. K. Northrup, F. W. Lampe, *J. Phys. Chem.* **1973**, *77*, 30.
[29] P. Benzi, L. Operti, G. A. Vaglio, P. Volpe, M. Speranza, R. Gabrielli, *J. Organomet. Chem.* **1989**, *354*, 39.
[30] F. E. Saalfeld, H. J. Svec, *Inorg. Chem.* **1963**, *2*, 46.
[31] P. P. Gaspar, J. J. Frost, *J. Am. Chem. Soc.* **1973**, *95*, 6567.
[32] C. G. Newman, J. Dzarnoski, M. A. Ring, H. E. O'Neal, *Int. J. Chem. Kinetics* **1980**, *XI*, 661.
[33] Y. Rousseau, G. J. Mains, *J. Phys. Chem.* **1966**, *70*, 3158.
[34] R. O. Bolt, J. G. Carrol, *Radiation Effect on Organic Chemistry*, Academic Press, New York and London, **1963**, p.77.
[35] J. B. Foresman, M. J. Frisch, *Exploring Chemistry with Electronic Structure Methods*, Gaussian, Pittsburgh, **1996**, p.166.
[36] J. A. Pople, B. T. Luke, M. J. Frish, J. S. Binkley, *J. Phys. Chem.* **1985,** *89*, 2198.
[37] P. Antoniotti, P. Benzi, F. Grandinetti, P. Volpe, *J. Phys. Chem.* **1993**, *97*, 4945.
[38] P. Antoniotti, F. Grandinetti, P. Volpe, *J. Phys. Chem.* **1995**, *99*, 17724.
[39] A. J. Jolly, J. E. Drake, *Inorg. Synth.* **1963**, 7, 37.
[40] M. J. Frisch, G. W. Trucks, H. B. Schlegel, P. M. W. Gill, B. G. Johnson, M. A. Robb, J. R. Cheeseman, T. Keith, G. A. Petersson, J. A. Montgomery, K. Raghavachari, M. A. Al-Laham V. G. Zakrzewski, J. V. Ortiz, J. B. Foresman, J. Cioslowski, B. B. Stefanov; A. Nanayakkara, M. Challacombe, C. Y. Peng, P. Y. Ayala, W. Chen, M. W. Wong, J. L. Andres, E. S. Reploge, R. Gomperts, R. L. Martin, D. J. Defrees, J. Baker, J. P. Stewart, M. Head-Gordon, C. Gonzalez, J. A. Pople, *GAUSSIAN 94*, Gaussian Inc., Pittsburgh, PA, **1995**.
[41] H. B. Schlegel, *J. Comput. Chem.* **1982**, *3*, 214.
[42] C. Möller, M. S. Plesset, *Phys. Rev.* **1934**, *46*, 618.
[43] S. Huzinaga, J. Andzelm, M. Klobukowski, E. Radzio-Andzelm, Y Sakai, H Tatewaki, *Gaussian basis sets for molecular calculations*, Elsevier, Amsterdam, **1984**.
[44] W. J. Hehre, R. Ditchfield, J. A. Pople, *J. Chem. Phys.* **1972**, *56*, 2257.
[45] J. A. Pople, M Head-Gordon, K. Raghavachari, *J. Chem. Phys.* **1987**, *87*, 5968.
[46] [46a] W. J. Hehre, R. Ditchfield, J. A. Pople, *J. Chem. Phys.* **1972**,

56, 2257. – [46b] P. C. Hariharan, J. A. Pople, *Theor. Chim. Acta* **1973**, *28*, 213. – [46c] M. M. Francl, W. J. Pietro, W. J. Hehre, J. S. Binkley, M. S. Gordon, D. J. Defrees, J. A. Pople, *J. Chem. Phys.* **1982**, *77*, 3654. – [46d] K. J. Raghavachari, J. S. Binkley, R. Seeger, J. A. Pople, *J. Chem. Phys.* **1980**, *72*, 650. – [46e] A. D. McLean, G. S. Chandler, *J. Chem. Phys.* **1980**, *72*, 5639.

[47] J. A. Pople, A. P. Scott, M. W. Wong, L. Radom, *Isr. J. Chem.* **1993**, *33*, 345.

Received August 5, 1998
[I98266]

Transition Metal Complexes with Sulfur Ligands, 134[+]

Synthesis of the Tetradentate Thioether Amine and Thioether Thiolate Ligands ′tpS$_2$(NH$_2$)$_2$′ and ′tpS$_4$′-H$_2$ and Some Representative Six-Coordinate Ruthenium and Osmium Complexes [′tpS$_2$(NH$_2$)$_2$′ = 1,2-Bis(2-aminophenylthio)phenylene; ′tpS$_4$′$^{2-}$ = 1,2-Bis(2-mercaptophenylthio)phenylene(2–)]

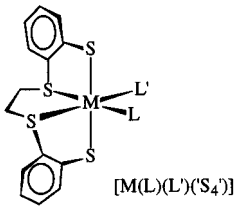
Dieter Sellmann,*[a] Klaus Engl,[a] Torsten Gottschalk-Gaudig,[a] and Frank W. Heinemann[a]

Dedicated to Professor Bernt Krebs on the occassion of his 60th birthday

Keywords: Cleavage reactions / C–S cleavage / Ligand synthesis / Osmium / Ruthenium / S ligands

In search of a tetradentate thioether thiolate ligand that is more stable toward reductive C–S bond cleavage than the parent ligand ′S$_4$′-H$_2$ [′S$_4$′-H$_2$ = 1,2-bis(2-mercaptophenylthio)ethane], the novel tris-phenylene ligand ′tpS$_4$′-H$_2$ (**3**) [′tpS$_4$′-H$_2$ = 1,2-bis(2-mercaptophenylthio)phenylene] was synthesized via the nitro and amine compounds ′tpS$_2$(NO$_2$)$_2$′ (**1**) and ′tpS$_2$(NH$_2$)$_2$′ (**2**). The coordination of ′tpS$_4$′$^{2-}$ to ruthenium centers resulted in the formation of six-coordinate [Ru(L)(PR$_3$)(′tpS$_4$′)] complexes (R = Et, L = PEt$_3$ **4**; R = Ph, L = PPh$_3$ **5**, CO **6**, DMSO **7**). The X-ray structure analyses of **4** and **6** revealed that the thiolate donors occupy trans positions; consequently the ′tpS$_4$′$^{2-}$ ligand coordinates in the same way as the ′S$_4$′$^{2-}$ ligand. The stability of the ′tpS$_4$′$^{2-}$ ligand toward reductive C–S cleavage reactions was shown by the synthesis of [Os(PEt$_3$)$_2$(′tpS$_4$′)] (**8**). In contrast to [Os(PEt$_3$)$_2$(′S$_4$′)], **8** is stable for unlimited periods of time. The X-ray structure analysis of [Ru(Cl)$_2$(PPh$_3$)(′tpS$_2$(NH$_2$)$_2$′)] (**9**) demonstrates that the potentially tetradentate ligand ′tpS$_2$(NH$_2$)$_2$′ coordinates in **9** through three donors leaving one NH$_2$ donor dangling.

The tetradentate thioether thiolate ligand ‘S$_4$’−H$_2$ [= 1,2-bis(2-mercaptophenylthio)ethane] exhibits a rich coordination chemistry. It binds to numerous transition metals, e.g. Fe, Ru, Os, Cr, Mo, W, Ni, and the resulting [M(′S$_4$′)] complex fragments are able to coordinate a large variety of coligands to give six-coordinate complexes of the type [M(L)(L′)(′S$_4$′)].[1]



[M(L)(L')('S$_4$')]

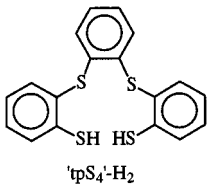
The coligands L or L′ range from hard ligands such as halides or oxide to soft ligands such as CO or phosphanes. The coligands also include a large number of biologically relevant small species, for example, N$_2$H$_2$, N$_2$H$_3$, N$_2$H$_4$, NH$_3$, NO$^+$, NO, NH$_2$O, H$_2$, H$^-$, CH$_3^-$, CH$_3$CO$^-$, H$_2$S, or S$_2$. The activation or stabilization and the reactivity of these small species is strongly influenced by the [M(′S$_4$′)] cores. In some of these reactions, the ′S$_4$′$^{2-}$ ligand appears to behave as a ′spectator′ ligand only, yielding a robust [M(′S$_4$′)] core, although in all reactions involving protons, the Brønsted basicity of the thiolate donors has been shown to be pivotal.[1b,1g,2,3] In other reactions, the ′S$_4$′$^{2-}$ ligand can experience severe changes. Coordination of the ′S$_4$′$^{2-}$ ligand to very electron-rich metal centers and UV irradiation or treatment of [M(′S$_4$′)] complexes with strongly reducing reagents frequently causes the reductive elimination of the C$_2$H$_4$ bridge as ethylene. For example, the reaction of ′S$_4$′$^{2-}$ with [MoCl$_2$(PMe$_3$)$_4$] gives the Mo^{IV} complex [Mo(PMe$_3$)$_2$(S$_2$C$_6$H$_4$)$_2$] and C$_2$H$_4$,[4] [Os(PEt$_3$)$_2$(′S$_4$′)] readily releases C$_2$H$_4$ to give [Os(PEt$_3$)$_2$(S$_2$C$_6$H$_4$)$_2$],[1e] UV irradiation of [Ru(CO)(PCy$_3$)(′S$_4$′)] yields [Ru(PCy$_3$)(S$_2$C$_6$H$_4$)$_2$] and C$_2$H$_4$,[5] and the reduction of [Fe(CO)$_2$(′S$_4$′)] by metallic sodium gives the Fe^{II} complex [Fe(S$_2$C$_6$H$_4$)$_2$]$^{2-}$ and C$_2$H$_4$.[6] The partial cleavage of S−C bonds is observed when [Ru(PPh$_3$)$_2$(′S$_4$′)] is treated with NO.[7] In this case, [Ru(NO)(PPh$_3$)(S$_2$C$_6$H$_4$)(CH$_2$=CH−SC$_6$H$_4$S)] forms, which contains a vinyl thioether thiolate ligand. All these reactions represent the reversal of the ′S$_4$′$^{2-}$ formation, which is synthesized via template alkylation of S$_2$C$_6$H$_4^{2-}$ by 1,2-C$_2$H$_4$Br$_2$.[1a] The ′S$_4$′$^{2-}$ cleavage reactions are usually unwanted. They can be traced back to the π acidity of the thioether donor functions and the partial occupation of antibonding C−S(thioether) σ* orbitals by metal d-electrons.[8] We have now tried to synthesize a ligand which

[+] Part 133: D. Sellmann, S. Emig, F. W. Heinemann, F. Knoch, *Z. Naturforsch.*, in press.

[a] Institut für Anorganische Chemie der Universität Erlangen-Nürnberg
Egerlandstraße 1, D-91058 Erlangen, Germany
Fax: (internat.) + 49(0)9131/8527367
E-mail: sellmann@anorganik.chemie.uni-erlangen.de

 © WILEY-VCH Verlag GmbH, D-69451 Weinheim, 1999 1434−1948/99/0202−0333 $ 17.50+.50/0

maintains the donor functions and coordination pattern of the $'S_4'^{2-}$ ligand, but is stable toward strong reducing reagents and photolysis. For this purpose, the C_2H_4 bridge in $'S_4'^{2-}$ has been replaced by an *o*-phenylene bridge. In order to clearly distinguish the target from the parent ligand and for indicating the presence of the phenylene entities, we use the acronym $'tpS_4'$-H_2.

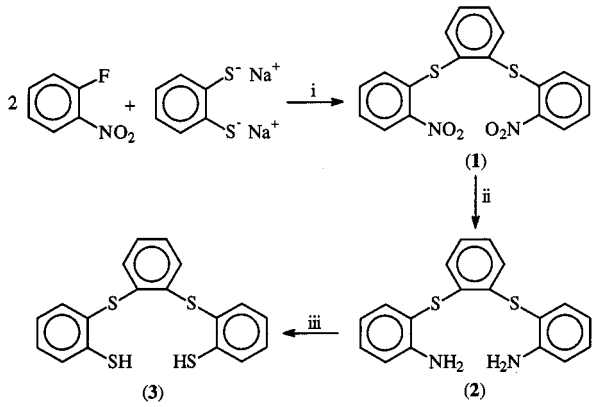


$'tpS_4'$-H_2

In orienting experiments, the coordination of $'tpS_4'^{2-}$ to electron-rich Ru^{II} and Os^{II} complexes was tested.

Results

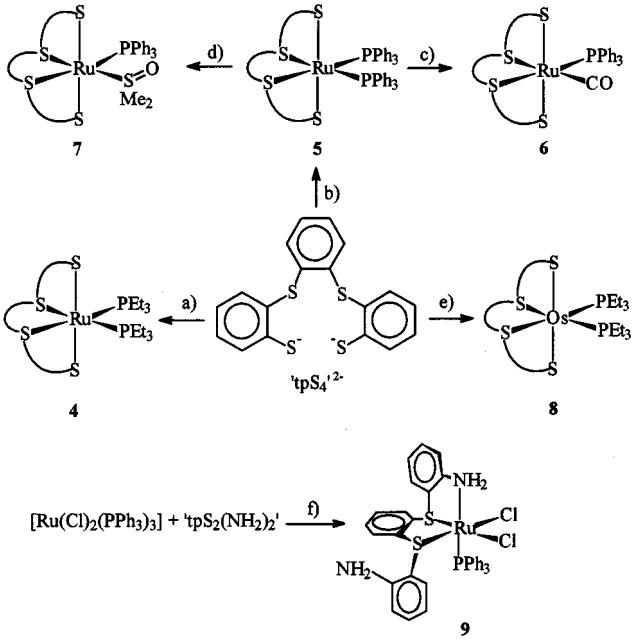
The target ligand $'tpS_4'$-H_2 (**3**) was synthesized by the route given in Scheme 1.



Scheme 1. Synthesis of $'tpS_4'$-H_2; i: MeOH/12 h/reflux; ii: Zn/NH_4Cl/THF/12 h/reflux; iii: 1. $NaNO_2/H_2SO_4/H_2O$/0°C; 2. KSC(S)OEt/H_2O/85°C; 3. KOH/EtOH/12 h/reflux; 4. HCl/H_2O, 5. LiOMe/$Niac_2 \cdot 4\ H_2O$, 6. HCl

Nucleophilic substitution of fluorine in 1,2-C_6H_4(F)-(NO_2)[9] by the thiolate functions of $Na_2S_2C_6H_4$ yielded the tris-phenylene nitro compound $'tpS_2(NO_2)_2'$ (**1**) in practically quantitative yield. Reduction of the nitro groups in **1** by Zn/NH_4Cl[10] gave the diamine-dithioether $'tpS_2(NH_2)_2'$ (**2**). Diazotisation of the NH_2 groups of **2** and subsequent reaction of the resulting bis-diazonium salt with KSC(S)(OEt), hydrolysis and acidification[11] yielded a brown oil containing $'tpS_4'$-H_2 (**3**) and a mixture of other compounds. Purification of this brown oil proved difficult. After many unsuccessful attempts applying conventional techniques, isolation of pure $'tpS_4'$-H_2 (**3**) was finally achieved by coordination to Ni^{II} salts and subsequent hydrolysis of the resulting nickel complex. Treatment of the brown oil with LiOMe and $Niac_2 \cdot 4\ H_2O$ yielded a red-brown microcrystalline solid which was analyzed as $[Ni('tpS_4')]_2 \cdot THF \cdot 0.5$ MeOH. Hydrolysis with hydrochloric acid gave a colorless analytically pure oil of $'tpS_4'$-H_2 (**3**). The compounds **1**, **2**, and **3** were characterized by elemental analysis and spectroscopic methods. The molecular structures of **1** and **2** were determined by X-ray diffraction.

Scheme 2 summarizes the syntheses of ruthenium and osmium complexes which were obtained with $'tpS_4'^{2-}$. In one experiment also the coordination of $'tpS_2(NH_2)_2'$ (**2**) was investigated.



Scheme 2. Synthesis of $'tpS_4'^{2-}$ ruthenium and osmium complexes and of $[Ru(Cl)_2(PPh_3)('tpS_2(NH_2)_2')]$; (a) $[Ru(Cl)_2(DMSO)_4]$/PEt_3/MeOH/1 h reflux; (b) $[RuCl_2(PPh_3)_3]$/THF/4 h at room temperature/5 min reflux; (c) CH_2Cl_2/CO/12 h/room temperature; (d) DMSO/5 min at 40°C; (e) $OsCl_3 \cdot \mathbf{x}\ H_2O$/$PEt_3$/MeOH/2 h reflux; (f) THF/1 h reflux

The reaction of dianionic $'tpS_4'^{2-}$, which was routinely obtained from $'tpS_4'$-H_2 (**3**) and NaOMe or BuLi, with $[Ru(Cl)_2(DMSO)_4]$ in the presence of excess PEt_3 yielded $[Ru(PEt_3)_2('tpS_4')]$ (**4**). Heating to reflux was necessary in order to drive the reaction to completeness. Treatment of $[RuCl_2(PPh_3)_3]$ with $'tpS_4'$-Li_2 in boiling THF gave $[Ru(PPh_3)_2('tpS_4')]$ (**5**). Complex **5** shows that also two sterically demanding phosphanes can bind to the $[Ru('tpS_4')]$ fragment. One PPh_3 ligand in **5** is labile and readily exchanges for CO at ambient temperatures to give $[Ru(CO)(PPh_3)('tpS_4')]$ (**6**). The PPh_3 ligand also exchanges for DMSO at slightly elevated temperature (40°C) to give $[Ru(DMSO)(PPh_3)('tpS_4')]$ (**7**). The DMSO ligand in **7** is also labile. ^{1}H-NMR spectra of **7** in [D_6]DMSO show only one DMSO signal at $\delta = 2.57$ indicating exchange of coordinated DMSO and [D_6]DMSO solvent molecules, which is rapid on the NMR time-scale.

A critical test for the inertness of $'tpS_4'^{2-}$ toward C−S cleavage reactions was its reaction with $OsCl_3 \cdot \mathbf{x}\ H_2O$ in the presence of excess PEt_3. It yielded, although in low yield, $[Os(PEt_3)_2('tpS_4')]$ (**8**). Subsequent NMR spectroscopic investigations showed that **8** is stable in solution for unlimited periods of time and contrasts $[Os(PEt_3)_2('S_4')]$

which rapidly releases C_2H_4 to give $[Os(PEt_3)_2(S_2C_6H_4)_2]$.[1e]

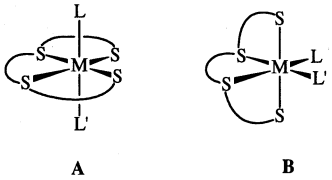
The comparison of the reactions b) and f) in Scheme 2 shows that $'tpS_2(NH_2)_2'$ (**2**) has poorer coordinating capabilities than $'tpS_4'^{2-}$ (**3**). Even after prolonged heating to reflux, the THF mixture of $RuCl_2(PPh_3)_3$ and $'tpS_2(NH_2)_2'$ yielded exclusively $[Ru(Cl)_2(PPh_3)('tpS_2(NH_2)_2')]$ (**9**) in which the potentially tetradentate $'tpS_2(NH_2)_2'$ (**2**) utilizes only three of its four donor functions.

Characterization of the Compounds and Complexes

All compounds were characterized by elemental analysis and spectroscopic methods, the molecular structures of $'tpS_2(NO_2)_2'$ (**1**), $'tpS_2(NH_2)_2'$ (**2**), $[Ru(PEt_3)_2('tpS_4')]$ (**4**), $[Ru(CO)(PPh_3)('tpS_4')]$ (**6**), and $[Ru(Cl)_2(PPh_3)('tpS_2(NH_2)_2')]$ (**9**) were also determined by X-ray diffraction.

Characteristic IR absorptions of the nitro compound **1** are ν(NO) bands of the asymmetric and symmetric ν(NO) vibrations at 1511, 1333, and 1303 cm^{-1}. The $'tpS_4'$-H_2 ligand (**3**) exhibits a medium intensity ν(SH) band at 2526 cm^{-1}. All $[M('tpS_4')]$ complexes show a nearly identical IR pattern for the $[M('tpS_4')]$ cores. Strong ν(CO) (1965 cm^{-1}) and ν(SO) (1087 cm^{-1}) bands are suited to readily identify $[Ru(CO)(PPh_3)('tpS_4')]$ (**6**) and $[Ru(DMSO)(PPh_3)('tpS_4')]$ (**7**). The ν(SO) band of **7** indicates *S*-bound DMSO.[12a]

A major concern was the coordination mode of the $'tpS_4'^{2-}$ ligand and the question whether, despite of the rigid phenylene bridge, $[M('tpS_4')]$ cores assume the same helical configuration as $[M('S_4')]$ cores. Formulas A and B schematically show the two potential configurations of $[M('tpS_4')]$ cores.



The X-ray structure analysis of **4** and **6** revealed that configuration B is assumed. When the $[M('tpS_4')]$ cores bind two different coligands L and L′ also ^{13}C-NMR spectra allow to distinguish between A and B.

Identical coligands L = L′ result in any case either in C_{2v} (formula A) or in C_2 symmetrical structures (formula B). When L ≠ L′, formula A exhibits (approximately) C_S symmetry, formula B, however, C_1 symmetry. Consequently, in complexes assuming the structure B, all aromatic C atoms are chemically non equivalent. The ^{13}C-NMR spectrum of $[Ru(CO)(PPh_3)('tpS_4')]$ (**6**) exhibits 22 aromatic ^{13}C signals and thus allows to unambiguously assign structure B. In contrast, the ^{13}C-NMR spectrum of **4** exhibits only 9 aromatic ^{13}C signals which do not allow to distinguish between structures A and B.

The coordination of $'tpS_2(NH_2)_2'$ (**2**) in $[Ru(Cl)_2(PPh_3)('tpS_2(NH_2)_2')]$ (**9**) leaving one amino donor dangling could be concluded from the ^1H-NMR spectrum of **9**. The protons of the uncoordinated NH_2 group give rise to a singlet, while the protons of the coordinated NH_2 group give rise to two doublets, because the NH protons are nonequivalent in C_1-symmetrical **9**. In addition, only the uncoordinated NH_2 group shows H^+/D^+ exchange with D_2O.

The molecular structures of $'tpS_2(NO_2)_2'$ (**1**), $'tpS_2(NH_2)_2'$ (**2**) $[Ru(Cl)_2(PPh_3)('tpS_2(NH_2)_2')]$ (**9**), $[Ru(PEt_3)_2('tpS_4')] \cdot 0.5\ Et_2O$ (**4** · 0.5 Et_2O), and $[Ru(CO)(PPh_3)('tpS_4')] \cdot CH_2Cl_2$ (**6** · CH_2Cl_2) are depicted in Figure 1. Table 1 lists selected distances and angles.

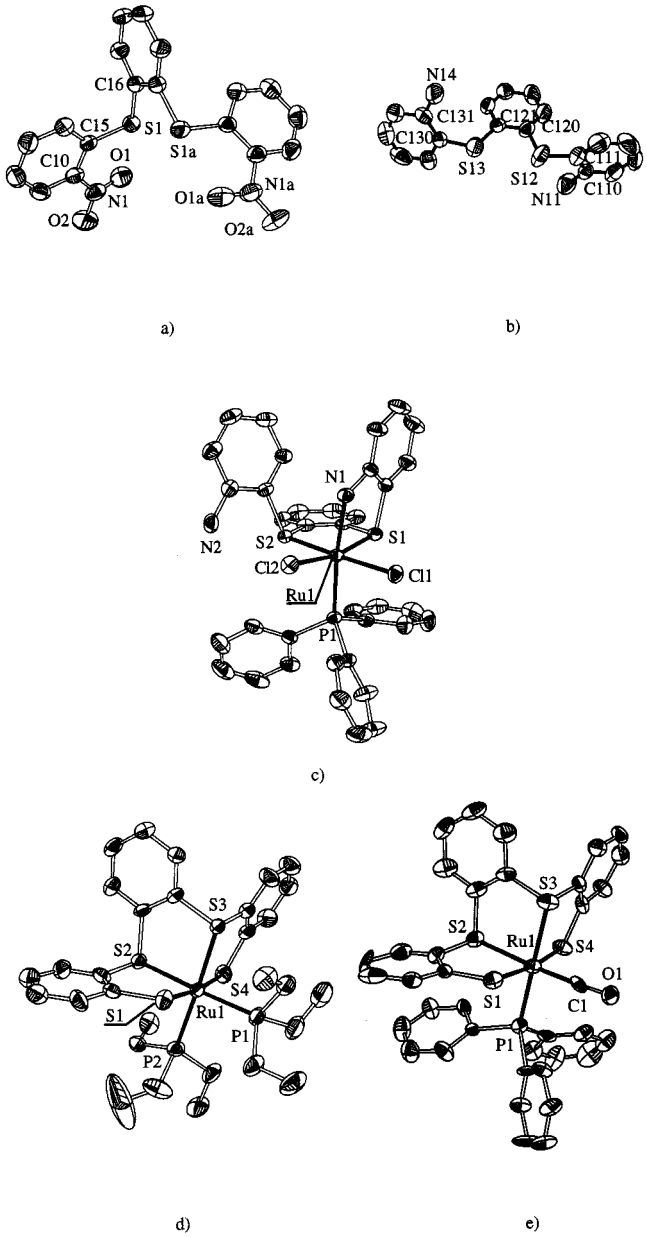


Figure 1. Molecular structures of (a) $'tpS_2(NO_2)_2'$ (**1**), (b) $'tpS_2(NH_2)_2'$ (**2**), (c) $[Ru(Cl)_2(PPh_3)('tpS_2(NH_2)_2')]$ (**9**), (d) $[Ru(PEt_3)_2('tpS_4')] \cdot 0.5\ Et_2O$ (**4** · 0.5 Et_2O), and (e) $[Ru(CO)(PPh_3)('tpS_4')] \cdot CH_2Cl_2$ (**6** · CH_2Cl_2) (50% probability ellipsoids, H atoms and solvent molecules omitted)

The compound $'tpS_2(NO_2)_2'$ (**1**) exhibits crystallographically imposed C_2 symmetry and shows that the two thioether S atoms lead to a helical preorganization of the three

Table 1. Selected distances [pm] and angles [°] of $'tpS_2(NO_2)_2'$ (**1**), $'tpS_2(NH_2)_2'$ (**2**), $[Ru(Cl)_2(PPh_3)('tpS_2(NH_2)_2')]$ (**9**), $[Ru(PEt_3)_2('tpS_4')] \cdot 0.5\ Et_2O$ (**4** · 0.5 Et_2O), and $[Ru(CO)(PPh_3)('tpS_4')] \cdot CH_2Cl_2$ (**6** · CH_2Cl_2)

1			**2**		
S1−C15	177.7(2)	S12−C111	177.0(5)	S22−C211	177.8(5)
S1−C16	178.5(2)	S12−C120	177.1(4)	S22−C220	177.4(4)
N1−C10	145.8(3)	N11−C110	137.9(5)	N21−C210	136.8(5)
N1−O1	122.4(2)	−	−	−	−
N1−O2	123.3(2)	−	−	−	−
C15−S1−C16	100.93(8)	C111−S12−C120	103.1(2)	C211−S22−C220	104.1(2)
C15−C10−N1	120.7(2)	C111−C110−N11	122.9(6)	C211−C210−N21	122.6(6)
O1−N1−O2	122.7(2)				

9			**4** · 0.5 Et_2O	**6** · CH_2Cl_2
Ru1−Cl1	243.8(2)	Ru1−S1	239.2(3)	241.5(3)
Ru1−Cl2	242.9(2)	Ru1−S2	236.1(2)	241.8(3)
Ru1−S1	227.9(1)	Ru1−S3	234.3(2)	238.6(3)
Ru1−S2	228.9(1)	Ru1−S4	239.0(3)	238.2(3)
Ru1−N1	216.3(3)	Ru1−P1	233.0(3)	233.8(3)
Ru1−P1	230.6(1)	Ru1−P2	234.1(3)	−
−	−	Ru1−C1	−	179.5(11)
S1−Ru1−S2	88.54(5)	S1−Ru1−S4	173.2(1)	172.4(1)
Cl1−Ru1−S1	91.97(5)	S2−Ru1−S3	86.81(8)	86.4(1)
Cl2−Ru1−S2	88.59(5)	P1−Ru1−P2	94.2(1)	−
−	−	P1−Ru1−C1	−	90.2(3)
N1−Ru1−P1	173.4(1)	S1−Ru1−P1	90.9(1)	−
−	−	S1−Ru1−C1	−	95.9(3)

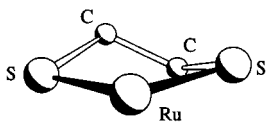
phenylene units as found in **4** and **6**. The NO_2 groups bind approximately coplanar to the phenylene rings. Distances and angles show no anomalies.

The thioetheramine compound $'tpS_2(NH_2)_2'$ crystallizes with 2 independent molecules per asymmetric unit, having practically identical distances and angles. The thioether distances and angles compare with those of **1**, and **2** is also characterized by well-approximated C_2 symmetry.

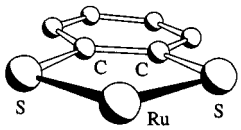
The metal centers of all three ruthenium complexes exhibit pseudo-octahedral coordination. The molecular structure of **9** unambiguously shows that one NH_2 group remains uncoordinated. Distances and angles of **9** lie in the same range as found in other Ru^{II} thioether ammine complexes, for example, $[Ru(Br)(PPh_3)('Bz_2S_2N_2H_2')]Br$ ($'Bz_2S_2N_2H_2'$ = 1,10-dibenzyl-2,3,8,9-dibenzo-1,10-dithia-4,7-diazadecane).[12b]

The $'tpS_4'^{2-}$ ligand in **4** and **6** coordinates in the same helical configuration as the $'S_4'^{2-}$ ligand in analogous $[Ru('S_4')]$ complexes. As a result, the thiolate donors assume trans positions. Also worth being noted is that the distances of **4** and **6** are virtually identical to those found in the analogous $[Ru(PR_3)_2('S_4')]$[1d] or $[Ru(L)(PR_3)('S_4')]$ complexes (L = Cl, I).[13] For example, C_2-symmetrical $[Ru(PnBu_3)_2('S_4')]$ exhibits Ru−S(thiolate) [239.8(2) pm] and Ru−S(thioether) [236.8(2) pm] distances.[1d] This suggests that the small difference in the Ru−S(thioether) distances of **4** [236.1(2) pm; 234.3(2) pm] is due to crystal packing effects. It is further noted that the differences either in the Ru−S(thiolate) or the Ru−S(thioether) distances of C_1-symmetrical **6** remain very small and are certainly due to coligand effects.

The only significant difference between $[Ru('S_4')]$ and $[Ru('tpS_4')]$ cores thus is the central five-membered chelate ring formed by the metal, the two thioether donors and the C_2H_4 or C_6H_4 bridge. In $[Ru('S_4')]$ cores, this chelate ring invariably assumes the chair conformation C, in both $[Ru('tpS_4')]$ complexes it is found to be virtually planar (D). The deviation of the two phenylene C atoms from the plane defined by the Ru and the two S atoms is only 7(1) pm and 12(1) pm in **4** · 0.5 Et_2O and 7(1) and 11(1) pm in **6** · CH_2Cl_2 respectively.



C



D

Concluding Discussion

Aim of this work was the synthesis of a tetradentate thioether thiolate ligand which shows a coordination chemistry as rich as that of the $'S_4'^{2-}$ ligand but is stable toward the reductive elimination of the C_2 bridge connecting the $C_6H_4S_2$ units. The new ligand $'tpS_4'^{2-}$ coordinates to metal centers in six-coordinate complexes in the same way as the $'S_4'^{2-}$ ligand. The resulting $[M('tpS_4')]$ cores exhibit two *trans*-positioned thiolate donors and two *cis* positions which can be occupied by ligands such as PEt_3, PPh_3, CO,

or DMSO. Orienting experiments indicate that, for example, $[Ru(PPh_3)_2('tpS_4')]$ shows a PPh_3 substitution chemistry similar to that of $[Ru(PPh_3)_2('S_4')]$. X-ray structure analyses further demonstrate that the RuS_4 distances and core angles remain invariant when the C_2H_4 bridge in $[Ru('S_4')]$ is replaced by a phenylene bridge in $[Ru('tpS_4')]$. The only and significant difference of $[Ru('S_4')]$ and $[Ru('tpS_4')]$ fragments is the central $[RuS_2C_2]$ chelate ring, which is virtually planar in $[Ru('tpS_4')]$, but exhibits a chair conformation in $[Ru('S_4')]$. The stability of the $'tpS_4'^{2-}$ ligand toward reductive cleavage could be demonstrated by the synthesis of $[Os(PEt_3)_2('tpS_4')]$ (**8**). Complex **8** is stable in solution for unlimited periods of time and thus contrasts $[Os(PEt_3)_2('S_4')]$ which readily eliminates ethylene.

Experimental Section

General Methods: Unless noted otherwise, all reactions and operations were carried out under nitrogen using standard Schlenk techniques. Solvents were dried and distilled before use. As far as possible, reactions were monitored by IR or NMR spectroscopy. − Spectra were recorded with the following instruments: IR (KBr discs or CaF_2 cuvettes, solvent bands were compensated): Perkin Elmer 983, 1620 FT IR, and 16PC FT-IR. − NMR: Jeol FT-JNM-GX 270, EX 270, and Lambda LA 400 with the protio-solvent signal used as a reference. Chemical shifts are quoted on the δ scale (downfield shifts are positive) related to tetramethylsilane (^1H, $^{13}C\{^1H\}$ NMR) or 85% H_3PO_4 ($^{31}P\{^1H\}$ NMR). Spectra were recorded at 25°C. − Mass spectra: Varian MAT 212 and Jeol MSTATION 700 spectrometers. − Elemental analysis: Carlo Erba EA 1106 or 1108 analyzer. − $[RuCl_2(DMSO)_4]$,[14] $[RuCl_2(PPh_3)_3]$,[15] and *o*-benzenedithiol ($'S_2'$-H_2)[16] were prepared as described in the literature, potassiumethylxanthogenate, 1-fluoro-2-nitrobenzene, LiOMe, and *n*BuLi (2.5 M in *n*-hexane) were purchased from Aldrich.

$'tpS_2(NO_2)_2'$ (1): A red-orange solution containing NaOMe (2.70 g, 50 mmol), $'S_2'$-H_2 (3 mL, 23.7 mmol), and 1-fluoro-2-nitrobenzene (5 mL, 47.4 mmol) in MeOH (100 mL) was heated under reflux for 20 h. A bright yellow solid precipitated that was separated, washed with MeOH (100 mL) and H_2O (150 mL), and dried in vacuo. Yield: 9.00 g of **1** (99%). − $C_{18}H_{12}N_2O_4S_2$, **1** (384.42): calcd. C 56.24, H 3.15, N 7.29, S 16.68; found C 56.41, H 3.12, N 7.33, S 16.28. − IR (KBr): $\tilde{\nu}$ = 1511, 1333, 1303 cm^{-1} ν(NO). − ^1H NMR (269.6 MHz, CD_2Cl_2): δ = 8.20 (m, 2 H, C_6H_4), 7.70−7.20 (m, 8 H, C_6H_4), 6.90 (m, 2 H, C_6H_4). − $^{13}C\{^1H\}$ NMR (67.7 MHz, CD_2Cl_2): δ = 137.52, 137.10, 136.55, 133.57, 131.15, 129.39, 129.35, 125.96, 125.78 [C(aryl)]. − EI MS (70 eV); *m/z*: 385 $['tpS_2(NO_2)_2']^+$.

$'tpS_2(NH_2)_2'$ (2): A yellow-grey suspension of **1** (6.0 g, 15.6 mmol), zinc powder (15.4 g, 235.5 mmol), and NH_4Cl (8.0 g, 149.6 mmol) in THF (120 mL) was heated under reflux for 20 h yielding a grey suspension. The grey solid was filtered off and washed with hot THF (100 mL), the colorless filtrate was concentrated to dryness. The remaining oily residue was recrystallized from hot EtOH (20 mL) yielding white crystals that were washed with EtOH (15 mL) and dried in vacuo. Yield: 4.00 g of **2** (79%). − $C_{18}H_{16}N_2S_2$, **2** (324.46): calcd. C 66.63, H 4.97, N 8.63, S 19.76; found C 66.67, H 5.21, N 8.65, S 19.37. − IR (KBr): $\tilde{\nu}$ = 3448, 3360 cm^{-1} ν(NH). − ^1H NMR (269.6 MHz, CD_2Cl_2): δ = 7.45 (m, 2 H, C_6H_4), 7.25 (m, 2 H, C_6H_4), 6.95 (m, 2 H, C_6H_4), 6.80−6.70 (m, 6 H, C_6H_4), 4.35 (s, 4 H, NH_2). − $^{13}C\{^1H\}$ NMR (67.7 MHz, CD_2Cl_2): δ = 149.32, 137.25, 135.49, 131.42, 128.01, 126.73, 118.94, 115.69, 114.69 [C(aryl)]. − FD MS (CH_2Cl_2); *m/z*: 324 $['tpS_2(NH_2)_2']^+$.

Synthesis of Crude $'tpS_4'$-H_2 (3): At 0°C, $'tpS_2(NH_2)_2'$ (**2**) (3.0 g, 18.5 mmol) was suspended in a mixture of H_2SO_4 (2.2 g, 22.4 mmol) and H_2O (35 mL). After addition of ice (12 g), a solution of $NaNO_2$ (1.34 g, 19.4 mmol) in H_2O (12 mL) was added dropwise to the suspension. The resulting yellow suspension was stirred for 1 h at 0°C and subsequently added slowly to a hot solution (85°C) of KSC(S)OEt (12.0 g, 74.9 mmol) in H_2O (30 mL), whereupon a red oil separated. The mixture was stirred for 45 min at 85°C, cooled to room temperature, and extracted with CH_2Cl_2 (150 mL). The CH_2Cl_2 extract was evaporated in vacuo. The remaining red oil was dissolved in EtOH (50 mL), solid KOH (6.0 g) was added, and the mixture was heated under reflux for 12 h. Evaporation of the solvent yielded a yellow residue which was suspended in H_2O (100 mL) and extracted with CH_2Cl_2 (75 mL). To the remaining aqueous solution hydrochloric acid was added until pH = 1 was reached and an orange oil separated. The oil was extracted from the aqueous phase with CH_2Cl_2 (125 mL), and the CH_2Cl_2 extract was dried with Na_2SO_4. Removal of CH_2Cl_2 yielded a brown oil. Yield: 1.5 g of **3** (46%). − IR (Film): $\tilde{\nu}$ = 2526 cm^{-1} (SH). − ^1H NMR (269.6 MHz, CD_2Cl_2): δ = 7.40 (m, 2 H, C_6H_4), 7.30 (m, 2 H, C_6H_4), 7.35−6.95 (m, 8 H, C_6H_4), 4.20 (s, 2 H, S*H*). − $^{13}C\{^1H\}$ NMR (67.7 MHz, CD_2Cl_2): δ = 137.43, 135.94, 134.54, 131.42, 130.67, 130.04, 129.32, 128.05, 126.71 [C(aryl)]. − FD MS (CH_2Cl_2); *m/z*: 358 $['tpS_4'$-$H_2]^+$.

Purification of Crude $'tpS_4'$-H_2 (3)

$[Ni('tpS_4')]_2$: The brown oil containing crude $'tpS_4'$-H_2 (1.5 g, 4.2 mmol) was dissolved in THF (40mL). LiOMe (8.4 mL, 8.4 mmol of a 1 M solution in MeOH) was added and stirred for 1 h. Removal of the THF yielded a yellow brown solid which turned into a white powder upon digestion with CH_2Cl_2 (150 mL). After drying, the white powder was characterized as $Li_2'tpS_4'$ by ^1H- and ^{13}C-NMR spectroscopy. − $Li_2'tpS_4'$ (330 mg, 0.89 mmol) in 20 mL of THF and $Niac_2 \cdot 4\ H_2O$ (222 mg, 0.89 mmol) in 20 mL MeOH were combined and stirred for 12 h. A microcrystalline red brown solid resulted which was separated, washed with MeOH (20 mL), THF (50 mL), Et_2O (20 mL), and dried in vacuo. It analyzed as $[Ni('tpS_4')]_2 \cdot THF \cdot 0.5\ MeOH$. Yield: 290mg (70%). − $C_{40.5}H_{34}O_{1.5}S_8Ni_2$ (918.60): calcd. C 52.95, H 3.74, S 27.92; found C 52.98, H 3.64, S 27.93.

$'tpS_4'$-H_2 (3): A red brown suspension of $[Ni('tpS_4')]_2 \cdot THF \cdot 0.5$ MeOH (280 mg, 0.30 mmol) in CH_2Cl_2 (15 mL) was combined with concentrated aqueous hydrochlorid acid (10 mL) and stirred for 1 h. A colorless CH_2Cl_2 and a light-green aqueous phase formed. The CH_2Cl_2 phase was separated, dried with Na_2SO_4, and concentrated to dryness, yielding a colorless oil of **3**. Yield: 120 mg of **3** (56%).− $C_{18}H_{14}S_4$, **3** (358.55): calcd. C 60.30, H 3.94, S 35.77; found C 60.51, H 3.99, S 35.47.

$[Ru(PEt_3)_2('tpS_4')]$ (4): A yellow suspension of $'tpS_4'$-H_2 (**3**) (120 mg, 0.33 mmol), NaOMe (38 mg, 0.7 mmol), and $[Ru(Cl)_2(DMSO)_4]$ (161 mg, 0.33 mmol) in MeOH (10 mL) was combined with PEt_3 (0.23 mL, 1.69 mmol) and heated under reflux for 1 h. After cooling to room temperature, the precipitated yellow solid was separated, washed with MeOH (10 mL) and Et_2O (10 mL), dried in vacuo for 5 min, and redissolved in CH_2Cl_2 (5 mL). The yellow CH_2Cl_2 solution was layered with MeOH (15 mL) and stored at room temperature. In the course of 4 d, yellow crystals precipitated that were separated, washed with MeOH (10 mL) and Et_2O (10 mL), and dried in vacuo. Yield: 100 mg of **4** · 0.5 CH_2Cl_2 (41%). − $C_{30.5}H_{43}ClP_2RuS_4$, **4** · 0.5 CH_2Cl_2 (736.41): calcd. C 49.75, H 5.89, S 17.42; found C 49.70, H 6.26, S 17.13. − IR (KBr):

$\tilde{\nu}$ = 1086 cm^{-1} δ(PCH). − ^1H NMR (269.6 MHz, CD_2Cl_2): δ = 7.90 (m, 2 H, C_6H_4), 7.75 (m, 2 H, C_6H_4), 7.30 (m, 2 H, C_6H_4), 7.20 (m, 2 H, C_6H_4), 6.90−6.70 (m, 4 H, C_6H_4), 1.85 (m, 12 H, PCH_2), 1.05 (m, 18 H, CH_3). − $^{13}C\{^1H\}$ NMR (67.7 MHz, CD_2Cl_2): δ = 159.02, 138.48, 136.66, 132.00, 131.58, 130.10, 129.68, 128.81, 121.06 [C(aryl)], 19.23 (vt, PCH_2CH_3), 8.49 (PCH_2CH_3). − $^{31}P\{^1H\}$ NMR (109.38 MHz, CD_2Cl_2): δ = 18.5 (s). − FD MS (CH_2Cl_2, ^{102}Ru); *m/z*: 694 $[Ru(PEt_3)_2('tpS_4')]^+$.

[Ru(PPh$_3$)$_2$('tpS$_4$')] (5): A yellow solution of 'tpS$_4$'-H$_2$ (**3**) (102 mg, 0.28 mmol) in THF (15 mL) was combined with *n*BuLi (0.23 mL, 0.58 mmol) at −78 °C and subsequently warmed to room temperature. Addition of $[Ru(Cl)_2(PPh_3)_3]$ (281 mg, 0.28 mmol) resulted in an orange solution which was stirred for 4 h at room temperature, heated to reflux for 5 min, and cooled to room temperature. Yellow microcrystals precipitated which were separated, washed with THF (20 mL) and Et_2O (10 mL), dried in vacuo for 5 min, and redissolved in CH_2Cl_2 (15 mL). The yellow CH_2Cl_2 solution was filtered, THF (50 mL) was added to the filtrate, and the mixture was reduced in volume to 10 mL. The precipitated yellow microcrystals were separated, washed with THF (20 mL), MeOH (20 mL), and Et_2O (20 mL), and dried in vacuo. Yield: 145 mg of **5** · 0.25 CH_2Cl_2 (51%). − $C_{54.25}H_{42.5}Cl_{0.5}P_2RuS_4$, **5** · 0.25 CH_2Cl_2 (1003.44): calcd. C 64.94, H 4.27, S 12.78; found C 65.18, H 4.42, S 12.55. − ^1H NMR (269.6 MHz, CD_2Cl_2): δ = 7.60 (m, 2 H, C_6H_4), 7.30 (m, 14 H, C_6H_4), 7.25 (m, 6 H, C_6H_4), 7.15 (m, 2 H, C_6H_4), 7.05 (m, 14 H, C_6H_4), 6.85 (m, 2 H, C_6H_4), 6.60 (m, 2 H, C_6H_4). − $^{13}C\{^1H\}$ NMR (67.9 MHz, CD_2Cl_2): δ = 157.70, 138.50, 137.35, 135.20, 131.45, 130.90, 129.80, 129.60, 129.40, 128.95, 128.25, 121.40 [C(aryl)]. − $^{31}P\{^1H\}$ NMR (109.38, CD_2Cl_2) δ = 27.0 (s). − FD MS (CH_2Cl_2, ^{102}Ru); *m/z*: 982 $[Ru(PPh_3)_2('tpS_4')]^+$.

[Ru(CO)(PPh$_3$)('tpS$_4$')] (6): CO gas was bubbled through a yellow suspension of $[Ru(PPh_3)_2('tpS_4')]$ (**5**) (147 mg, 0.15 mmol) in CH_2Cl_2 (15 mL) for 3 h. A yellow solution resulted which was stirred for another 12 h under CO, reduced in volume to 3 mL, and layered with MeOH (50 mL). In the course of 3 d, yellow crystals precipitated which were separated, washed with MeOH (20 mL) and Et_2O (10 mL), and dried in vacuo. Yield: 85 mg of **6** (73%). − $C_{37}H_{27}OPRuS_4$, **6** (747.90): calcd. C 59.42, H 3.64, S 17.15; found C 59.43, H 3.80, S 16.83. − IR (KBr): $\tilde{\nu}$ = 1964 cm^{-1} (CO). − ^1H NMR (269.6 MHz, CD_2Cl_2): δ = 7.90 (m, 1 H, C_6H_4), 7.75 (m, 1 H, C_6H_4), 7.60 (m, 7 H, C_6H_4), 7.35 (m, 10 H, C_6H_4), 7.20 (m, 2 H, C_6H_4), 7.10−6.85 (m, 4 H, C_6H_4), 6.70 (m, 1 H, C_6H_4), 6.55 (m, 1 H, C_6H_4). − $^{13}C\{^1H\}$ NMR (100.40 MHz, CD_2Cl_2): δ = 200.81 (d, *C*O); 155.89 (d), 155.28, 138.57 (d), 136.20 (d), 135.36 (d), 134.45 (d), 134.07, 133.09, 132.93 (d), 132.80, 132.62, 131.86, 131.80 (d), 130.83, 130.52 (t), 130.30, 130.19, 129.81, 129.15, 128.16 (d), 122.60, 122.01 [C(aryl)]. − $^{31}P\{^1H\}$ NMR (161.70 MHz, CD_2Cl_2): δ = 38.98 (s). − FD MS (CH_2Cl_2, ^{102}Ru); *m/z*: 748 $[Ru(CO)(PPh_3)('tpS_4')]^+$.

[Ru(DMSO)(PPh$_3$)('tpS$_4$')] (7): $[Ru(PPh_3)_2('tpS_4')]$ (**5**) (170 mg, 0.17 mmol) was dissolved in warm DMSO (6 mL, 40 °C) and the resulting yellow solution was cooled to room temperature. After addition of MeOH (45 mL), a yellow solid precipitated which was separated, washed with MeOH (50 mL) and Et_2O (20 mL), and dried in vacuo. Yield: 105 mg of **7** (77%). − $C_{38}H_{33}OPRuS_5$, **7** (798.02): calcd. C 57.19, H 4.17, S 20.09; found C 57.12, H 4.10, S 20.01. − IR (KBr): $\tilde{\nu}$ = 1087 cm^{-1} (SO). − ^1H NMR (269.6 MHz, CD_2Cl_2): δ = 7.95 (m, 1 H, C_6H_4), 7.80−7.50 (m, 9 H, C_6H_4), 7.40−7.15 (m, 11 H, C_6H_4), 7.10−6.95 (m, 2 H, C_6H_4), 6.90−6.70 (m, 3 H, C_6H_4), 6.50 (m, 1 H, C_6H_4), 3.00 (s, 3 H, CH_3), 2.70 (s, 3 H, CH_3). − $^{13}C\{^1H\}$ NMR (67.9 MHz, CD_2Cl_2): δ = 157.20 (d), 155.03, 137.79 (t), 135.25, 135.00 (d), 134.62, 132.36, 132.20, 132.10, 131.84, 131.44, 130.95, 130.79, 130.47, 130.12, 129.92, 129.54, 129.14, 128.93, 128.75, 127.40 (d), 122.17, 121.63 [C(aryl)],

Table 2. Selected crystallographic data of $'tpS_2(NO_2)_2'$ (**1**), $'tpS_2(NH_2)_2'$ (**2**), $[Ru(Cl)_2(PPh_3)('tpS_2(NH_2)_2')]$ (**9**), $[Ru(PEt_3)_2('tpS_4')]$ · 0.5 Et_2O (**4** · 0.5 Et_2O), and $[Ru(CO)(PPh_3)('tpS_4')]$ · CH_2Cl_2 (**6** · CH_2Cl_2)

Compound	**1**	**2**	**9**	**4** · 0.5 Et_2O	**6** · CH_2Cl_2
formula	$C_{18}H_{12}N_2O_4S_2$	$C_{18}H_{16}N_2S_2$	$C_{36}H_{31}Cl_2N_2PRuS_2$	$C_{32}H_{47}O_{0.5}P_2RuS_4$	$C_{38}H_{29}Cl_2OPRuS_4$
M_r[g/mol]	384.42	324.45	758.69	1461.89	832.79
crystal size [mm]	0.6 × 0.5 × 0.4	0.40 × 0.30 × 0.25	0.6 × 0.6 × 0.6	0.7 × 0.5 × 0.4	0.5 × 0.4 × 0.2
F(000)	792	680	1544	3048	1688
space group	*Pccn*	*P*−1	$P2_1/n$	$Pna2_1$	$P2_1/c$
crystal system	orthorhombic	triclinic	monoclinic	orthorhombic	monoclinic
a [pm]	2210.3(12)	1101.9(3)	940.8(6)	3073.7(4)	1802.3(5)
b [pm]	518.6(3)	1105.4(3)	1877.4(6)	1511.0(2)	1142.6(5)
c [pm]	1481.0(4)	1519.1(5)	1866.7(6)	1491.8(2)	1888.3(4)
α [°]	90	109.65(2)	90	90	90
β [°]	90	105.88(2)	98.62(4)	90	110.70(2)
γ [°]	90	90.22(2)	90	90	90
V [nm^3]	1.698(1)	1.6667(8)	3.260(3)	6.929(2)	3.638(2)
Z	4	4	4	8	4
$D_{calcd.}$ [g/cm^3]	1.504	1.293	1.546	1.401	1.521
μ [mm^{-1}]	0.341	0.317	0.852	0.808	0.882
diffractometer	Nicolet R3m/V	Nicolet R3m/V	Siemens P4	Siemens P4	Siemens P4
radiation [pm]	Mo-K_α (λ = 71.073)	Mo-K_α (λ = 71.073)	Mo-K_α (λ = 71.073)	Mo-K_α (λ = 71.073)	Mo-K_α (λ = 71.073)
temperature [K]	293	298	200	200	200
scan technique	ω scan	ω scan	ω scan	ω scan	ω scan
$2\Theta_{range}$ [°]	3−54	3−54	4−54	4−55	4−52
scan speed [°/min]	3.0−15.0	10	3.0−30.0	3.0−30.0	30.0 (fixed)
meas. reflections	3847	8111	9382	9870	8666
indep. reflections	1825	7272	7105	8870	7132
R_{int} [%]	3.85	7.53	5.42	4.21	13.12
obs. reflections	1271	1270	5499	6068	2190
σ criterion	$F_o > 4\sigma(F_o)$	$F_o > 4\sigma(F_o)$	$F_o > 4\sigma(F_o)$	$F_o > 4\sigma(F_o)$	$F_o > 4\sigma(F_o)$
*R*1; *wR*2 [%]	3.70; 9.59	3.95; 7.76	3.59; 12.56	5.70; 16.41	6.38; 15.32
ref. parameters	142	397	521	726	424
abs. struct. param.[19]	−	−	−	−0.03(5)	−

49.78, 44.52 (SCH_3). – $^{31}P\{^1H\}$ NMR (109.38 MHz, CD_2Cl_2): δ = 34.8 (s).

[Os(PEt$_3$)$_2$('tpS$_4$')] (8): A solution of 'tpS$_4$'-H$_2$ (**3**) (190 mg, 0.53 mmol) and LiOMe (40 mg, 1.06 mmol) in THF (20 mL) was stirred for 1 h. Removal of the solvent yielded a yellow residue. It was dissolved in MeOH (20 mL) and combined with $OsCl_3 \cdot \mathbf{x}\ H_2O$ (158 mg, 0.53 mmol) and PEt_3 (1.60 mL, 11.8 mmol). The resulting yellow-brown solution was heated under reflux for 2 h, cooled to room temperature, reduced in volume to 10 mL, and Et_2O (10 mL) was added. A yellow solid precipitated, which was separated, washed with MeOH (15 mL), Et_2O (5 mL), and H_2O (10 mL), and dried in vacuo. Yield: 20 mg of **8** · 2 H_2O (5%). – $C_{30}H_{46}O_2OsP_2S_4$, **8** · 2 H_2O (819.08): calcd. C 43.99, H 5.66, S 15.66; found C 44.27, H 5.53, S 15.63. – ^1H NMR (269.6 MHz, CD_2Cl_2): δ = 7.90 (m, 2 H, C_6H_4), 7.85 (m, 2 H, C_6H_4), 7.20 (m, 4 H, C_6H_4), 6.85 (m, 2 H, C_6H_4), 6.55 (m, 2 H, C_6H_4), 1.95 (m, 12 H, PCH_2), 1.00 (m, 18 H, CH_2CH_3). – $^{13}C\{^1H\}$ NMR (67.9 MHz, CD_2Cl_2): δ = 158.98 (d), 139.35, 137.75, 131.54, 131.29, 130.02, 129.90, 129.62, 128.99, 121.26 [C(aryl)], 18.95 (vq, PCH_2CH_3), 8.51 (PCH_2CH_3). – $^{31}P\{^1H\}$ NMR (109.38 MHz, CD_2Cl_2): δ = −25.0 (s). – FD MS (CH_2Cl_2, ^{192}Os); *m/z*: 784 [Os(PEt$_3$)$_2$('tpS$_4$')]$^+$.

[Ru(Cl)$_2$(PPh$_3$)('tpS$_2$(NH$_2$)$_2$')] (9): 'tpS$_2$(NH$_2$)$_2$' (**2**) (168 mg, 0.52 mmol) was added to a brown solution of [Ru(Cl)$_2$(PPh$_3$)$_3$] (495 mg, 0.52 mmol) in THF (25 mL). An orange solution formed which was heated under reflux for 1 h, cooled to room temperature, and reduced in volume to 15 mL. Yellow microcrystals precipitated which were separated, washed with THF (15 mL) and Et_2O (25 mL), and dried in vacuo. Yield: 330 mg of **9** · THF (76%). – $C_{40}H_{39}Cl_2N_2OPRuS_2$, **9** · THF (759.93): calcd. C 57.83, H 4.73, N 3.37, S 7.72; found C 57.90, H 4.64, N 3.37, S 7.45. – IR (KBr): $\tilde{\nu}$ = 1616 cm^{-1} δ(NH). – ^1H NMR (269.6 MHz, $CDCl_3$): δ = 7.85 (m, 7 H, C_6H_5), 7.15 (m, 1 H, C_6H_4), 7.40–7.05 (m,13 H, C_6H_4), 7.00 (m, 1 H, C_6H_4), 6.75 (m, 1 H, C_6H_4), 6.00 (m, 1 H, N*H*), 5.95 (m, 1 H, C_6H_4), 5.00 (s, 2 H, N*H*), 4.80 (m, 1 H, C_6H_4), 4.50 (m, 1 H, N*H*). – $^{13}C\{^1H\}$ NMR (67.7 MHz, $CDCl_3$): δ = 148.03, 144.16, 142.12, 139.86, 138.60, 135.90, 135.24, 134.50 (d), 133.38, 132.09, 131.56, 131.50, 131.24, 130.86, 130.45, 129.83, 129.02, 128.22 (d), 119.31, 119.11, 119.03 [C(aryl)]. – $^{31}P\{^1H\}$ NMR (109.38 MHz, CD_2Cl_2): δ = 43.5 (s). – FD MS (CH_2Cl_2, ^{102}Ru); *m/z*: 721 [Ru(Cl)(PPh$_3$)('tpS$_2$(NH$_2$)$_2$') − 2 H]$^+$.

X-ray Structure Analyses of 'tpS$_2$(NO$_2$)$_2$' (1), 'tpS$_2$(NH$_2$)$_2$' (2), [Ru(Cl)$_2$(PPh$_3$)('tpS$_2$(NH$_2$)$_2$')] (9), [Ru(PEt$_3$)$_2$('tpS$_4$')] · 0.5 Et$_2$O (4 · 0.5 Et$_2$O), and [Ru(CO)(PPh$_3$)('tpS$_4$')] · CH$_2$Cl$_2$ (6 · CH$_2$Cl$_2$): Yellow cubes of **1** crystallized from a hot saturated solution of **1** in THF upon cooling to room temperature, colorless cubes of **2** from a satured $CHCl_3$ solution. Orange cubes of **9** formed in the course of 7 d, when a saturated CH_2Cl_2 solution of **9** was stored at room temperature. Yellow plates of **4** and **6** were grown by layering CH_2Cl_2 solutions of **4** and **6** with Et_2O and MeOH, respectively, at room temperature. In the case of **4**, spontaneous separation of racemic **4** occured. Both independent molecules present in the asymmetric unit of **4** · 0.5 Et_2O represent the same enantiomer. Distances and angles of the two independent molecules differ only marginally. Suitable single crystals were sealed under N_2 in glass capillaries. Data were corrected for Lorentz and polarization effects, no absorption correction. The structures were solved by direct methods (SHELXTL 5.03[17]). Full-matrix least-squares refinement was carried out on F^2 (SHELXTL 5.03). All non-hydrogen atoms were refined anisotropically, the positions of the hydrogen atoms of **1**, **2**, and **9** were taken from the difference Fourier map and were either refined isotropically (**1**, **9**) or kept fixed with a common isotropic displacement parameter (**2**). In the case of **4** and **6** the hydrogen atoms were geometrically positioned with isotropic displacement parameters fixed at 1.5 times *U*(eq) of the preceding carbon atom. In the case of **2** and **4**, there are two crystallographically independent molecules per asymmetric unit. Selected crystallographic data are summarized in Table 2.[18]

Acknowledgments

Support of these investigations by the Deutsche Forschungsgemeinschaft and Fonds der Chemischen Industrie is gratefully acknowledged.

[1] [1a] D. Sellmann, H.-E. Jonk, H.-R. Pfeil, G. Huttner, J. v. Seyerl, *J. Organometal. Chem.* **1980**, *191*, 171–179. – [1b] D. Sellmann, H. Friedrich, F. Knoch, M. Moll, *Z. Naturforsch.* **1994**, *49b*, 76–88. – [1c] D. Sellmann, E. Böhlen, *Z. Naturforsch.* **1982**, *37b*, 1026–1033. – [1d] D. Sellmann, T. Gottschalk-Gaudig, F. W. Heinemann, F. Knoch, *Chem. Ber.* **1997**, *130*, 571–579. – [1e] D. Sellmann, A. C. Hennige, F. W. Heinemann, *Eur. J. Inorg. Chem.* **1998**, 819–826. – [1f] D. Sellmann, B. Seubert, W. Kern, F. Knoch, M. Moll, *Z. Naturforsch.* **1991**, *46b*, 1435–1448. – [1g] D. Sellmann, H.-J. Kremitzl, F. Knoch, M. Moll, *J. Biol. Inorg. Chem.* **1996**, *1*, 127–135. – [1h] D. Sellmann, W. Kern, G. Pöhlmann, F. Knoch, M. Moll, *Inorg. Chim. Acta* **1991**, *185*, 155–162. – [1i] D. Sellmann, S. Fünfgelder, G. Pöhlmann, F. Knoch, M. Moll, *Inorg. Chem.* **1990**, *29*, 4772–4778.

[2] D. Sellmann, G. H. Rackelmann, F. W. Heinemann *Chem. Eur. J.* **1997**, 3, 2071–2080.

[3] D. Sellmann, T. Gottschalk-Gaudig, F. W. Heinemann, *Inorg. Chem.* **1998**, *37*, 3982–3988.

[4] D. Sellmann, W. Reißer, *J. Organometal. Chem.* **1985**, *294*, 333–346.

[5] T. Gottschalk, Diplomarbeit, Universität Erlangen-Nürnberg, **1994**.

[6] D. Sellmann, W. Reißer, *J. Organometal. Chem.* **1985**, *297*, 319–329.

[7] D. Sellmann, I. Barth, F. Knoch, M. Moll, *Inorg. Chem.* **1990**, *29*, 1822–1826.

[8] G. E. Mullen, M. J. Went, S. Wocadlo, A. K. Powell, P. J. Blower, *Angew. Chem.* **1997**, *109*, 1254–1256; *Angew. Chem. Int. Ed. Engl.* **1997**, *36*, 1205–1207 and literature cited therein.

[9] J. F. K. Wilshire, *Aust. J. Chem.* **1988**, *41*, 995–1001.

[10] R. C. Larock, *Comprehensive Organic Transformations*, VCH, New York, **1989**, pp. 411–415.

[11] [11a] G. E. Hilbert, T. B. Johnson, *J. Am. Chem. Soc.* **1929**, *51*, 1526–1533. – [11b] D. S. Tarbell, D. K. Fukushima, *Org. Synth. Coll. Vol.* **1951**, *3*, 809–811.

[12] [12a] K. Nakamoto, *Infrared Spectra of Inorganic and Coordination Compounds*, 4th ed., Wiley and Sons, New York, **1986**, p. 270. – [12b] D. Sellmann, R. Ruf, F. Knoch, M. Moll, *Inorg. Chem.* **1995**, *34*, 4745–4755.

[13] D. Sellmann, T. Gottschalk-Gaudig, F. W. Heinemann, *Inorg. Chim. Acta* **1998**, 269, 63–72.

[14] I. P. Evans, A. Spencer, G. Wilkinson, *J. Chem. Soc., Dalton Trans.* **1973**, 204–209.

[15] T. A. Stephenson, G. Wilkinson, *J. Inorg. Nucl. Chem.* **1966**, *28*, 945–956.

[16] J. Degani, R. Fochi, *Synthesis* **1976**, *7*, 471–472.

[17] *SHELXTL 5.03 for Siemens Crystallographic Research Systems*, Siemens Analytical X-ray Instruments Inc., Madison, WI, U.S.A., **1995**.

[18] Crystallographic data (excluding structure factors) for the structures reported in this paper have been deposited with the Cambridge Crystallographic Data Centre as CCDC-102376 (**1**), -102377 (**2**), -102378 (**4**), -102379 (**6**), -102380 (**9**). Copies of the data can be obtained free of charge on application to CCDC, 12 Union Road, Cambridge CB2 1EZ, UK [Fax: int. code + 44-1223/336-033; E-mail: deposit@ccdc.cam.ac.uk].

[19] H. D. Flack, *Acta Crystallogr.* **1983**, *A39*, 876–881.

Received August 7, 1998
[I98268]

Transition Metal Complexes with Sulfur Ligands, 135[+]

Electron-Rich Fe and Ru Complexes with the New Trisamine Dithiolate Ligand $'N_3H_3S_2'$-H_2 [2,2′-Bis(2-mercaptophenylamino)diethylamine]

Dieter Sellmann,*[a] Jürgen Utz,[a] and Frank W. Heinemann[a]

Keywords: N ligands / S ligands / Iron / Ruthenium / Pentadentate ligands

In order to obtain iron and ruthenium complexes which are analogous to [M(L)($'NHS_4'$)] and [M(L)($'N_2H_2S_3'$)] complexes [$'NHS_4'^{2-}$ = 2,2′-bis(2-mercaptophenylthio)diethylamine(2–), $'N_2H_2S_3'^{2-}$ = 2,2′-bis(2-mercaptophenylamino)diethylsulfide-(2–)] but have electron-richer metal centers, the new pentadentate amine thiolate ligand $'N_3H_3S_2'$-H_2 [= 2,2′-bis(2-mercaptophenylamino)diethylamine] (**4**) was synthesized. The dianion $'N_3H_3S_2'^{2-}$ reacted with Fe^{II} salts to give high-spin [Fe($'N_3H_3S_2'$)] (**5**) [μ_{eff} (293 K) = 3.94 μ_B], which yielded diamagnetic [Fe(CO)($'N_3H_3S_2'$)] (**6**) upon reaction with CO. Complex **6** exhibits a low-frequency ν(CO) band (1934 cm^{-1} in THF) indicating an electron-rich Fe center and a strong Fe–CO bond. In spite of this, **6** readily dissociated in solution to **5** and CO. The reaction of $[RuCl_2(PPh_3)_3]$ with $'N_3H_3S_2'^{2-}$ yielded [Ru(PPh_3)($'N_3H_3S_2'$)] (**7**), which proved inert with respect to PPh_3 substitution but could be methylated at the thiolate donors. The resulting [Ru(PPh_3)($'N_3H_3S_2'$-Me_2)]I_2 (**8**) proved as inert towards substitution as **7**. Complex **8** could reversibly be deprotonated to give [Ru(PPh_3)($'N_3H_2S_2'$-Me_2)]I (**11**), in the course of which the $[RuPN_3S_2]$ cores rearrange from C_S to C_1 symmetry. Reversible protonation/deprotonation was also found with [Ru(NO)($'N_3H_2S_2'$)] (**9**) which formed from $[RuCl_3(NO)(PPh_3)_2]$ and $'N_3H_3S_2'^{2-}$ in the presence of one additional equivalent of LiOMe. Protonation of **9** with HBF_4 gave [Ru(NO)($'N_3H_3S_2'$)]BF_4 (**10**). The NMR spectra and the X-ray structure analysis of **8** proved that the $[RuPN_3S_2]$ cores of **7** and **8** exhibit a C_S-symmetrical *meso* structure. In all other complexes, however, the $[MLN_3S_2]$ cores exhibit a C_1-symmetrical structure. It results from the *fac-mer* coordination mode of the $'N_3H_3S_2'^{2-}$ ligand and favors the planarization of amide donors when NH functions are reversibly deprotonated.

Structure–function relationships of transition metal complexes are primarily determined by the metal oxidation state, type and number of the donor atoms, and the structure of the metal ligand core.[1] In quest of metal complexes that combine structural (metal sulfur sites) and functional (reactivity) features of nitrogenase centers, our interest focusses on complexes with multidentate ligands which contain amine N, thioether S, and thiolate S donors. In this search the [Fe($'NHS_4'$)] fragment (Scheme 1) was found to exist in the diastereomeric forms **A** and **B** and to bind N_2H_2, N_2H_4, NH_3, and CO, but not N_2.[2] As high electron densities at the metal centers usually favor the coordination of N_2,[3] we tried to increase the iron electron density in the [Fe($'NHS_4'$)] cores through a systematic substitution of σ-donor–π-acceptor thioether functions by σ-donor amine functions.

The first target ligand $'N_2H_2S_3'$-H_2[4] yielded the CO complex [Fe(CO)($'N_2H_2S_3'$)], whose ν(CO) frequency of 1932 cm^{-1} indicated a higher Fe electron density when compared with to that of [Fe(CO)($'NHS_4'$)] (1960 cm^{-1}). However, despite the low-frequency ν(CO) indicating strong Fe–CO π-back-bonding, [Fe(CO)($'N_2H_2S_3'$)] proved much more labile than [Fe(CO)($'NHS_4'$)], and neither N_2 nor N_2H_2, N_2H_4, or NH_3 complexes could be obtained with the [Fe($'N_2H_2S_3'$)] fragment. Beyond that all [Fe(L)($'N_2H_2S_3'$)] and corresponding [Ru(L)($'N_2H_2S_3'$)] complexes were shown to exhibit the core structure **C** having thiolate donor atoms in *cis* positions. The core structure **C** distinctly differs from the [Fe($'NHS_4'$)] core structure **B** having *trans*-thiolate donors. *trans*-Thiolate donors, however, proved to be essential for the stabilization of molecules such as N_2H_2 in [μ-N_2H_2{Fe($'NHS_4'$)}$_2$], because only a *trans* coordination of thiolate donors allows the formation of strong N–H···$(S)_2$ bridges.[2a,2c]

In the series of systematically varied ligands, our next target ligand was $'N_3H_3S_2'$-H_2. It is comparable with the $'NHS_4'^{2-}$ ligand in so far as all thioether donors are exchanged for amine donors. Simultaneously, the terminal thiolate donors are maintained in a coordination mode that enables them to occupy, at least in principle, *trans* positions in six-coordinate metal complexes.

Results

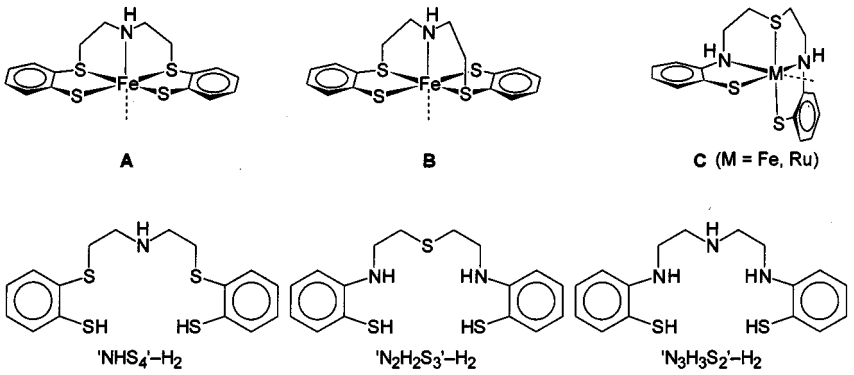
Ligand Synthesis

As in the case of the $'N_2H_2S_3'^{2-}$ ligand synthesis, the requirement of terminal thiolate functions in the target ligand $'N_3H_3S_2'^{2-}$ necessitated a specific synthetic route (Scheme 2).

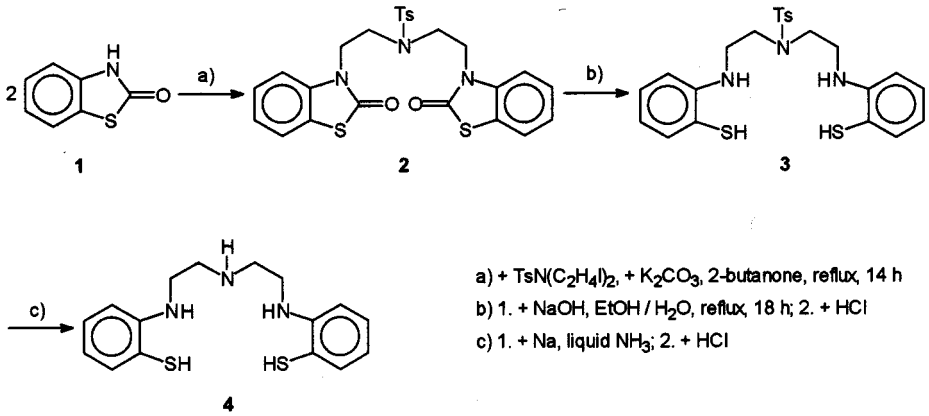
[+] Part 134: D. Sellmann, K. Engl, T. Gottschalk-Gaudig, F. W. Heinemann, *Eur. J. Inorg. Chem.* **1999**, 333–339

[a] Institut für Anorganische Chemie der Universität Egerlandstraße 1, D-91058 Erlangen, Germany
Fax: (internat.) + 49(0)9131/8527367
E-mail: sellmann@anorganik.chemie.uni-erlangen.de

 © WILEY-VCH Verlag GmbH, D-69451 Weinheim, 1999 1434–1948/99/0202–0341 $ 17.50+.50/0



Scheme 1. Ligands and core structures of metal complex fragments



Scheme 2. Synthesis of $'N_3H_3S_2'$-H_2 (**4**)

Alkylation of 2(3*H*)-benzothiazolone (**1**) with $TsN(C_2H_4I)_2$ in the presence of K_2CO_3 yielded **2** as major product. The rather unusual N-lost derivative $TsN(C_2H_4I)_2$ had to be applied because all other and more common alkylation reagents such as $NH(C_2H_4Br)_2$ or amides of the type $R(CO)N(C_2H_4Br)_2$ failed. For example, $NH(C_2H_4Br)_2$ gave piperazine derivatives[5] instead of alkylating **1**, the amides $R(CO)N(C_2H_4Br)_2$ rearranged.[6] From the crude product of **2**, traces of by-products resulting from oxygen alkylation of **1**[7] could readily be removed by extraction with EtOH. Compound **2** is soluble in CH_2Cl_2 and THF and moderately soluble in EtOH or MeOH; it was characterized by the usual spectroscopic methods and by elemental analysis. The $^{13}C\{^1H\}$-NMR CO signal (δ = 170.6) and the IR ν(CO) band (1678 cm^{-1} in KBr) are particularly suited to confirm alkylation of the N atom in **1** and to identify **2**.

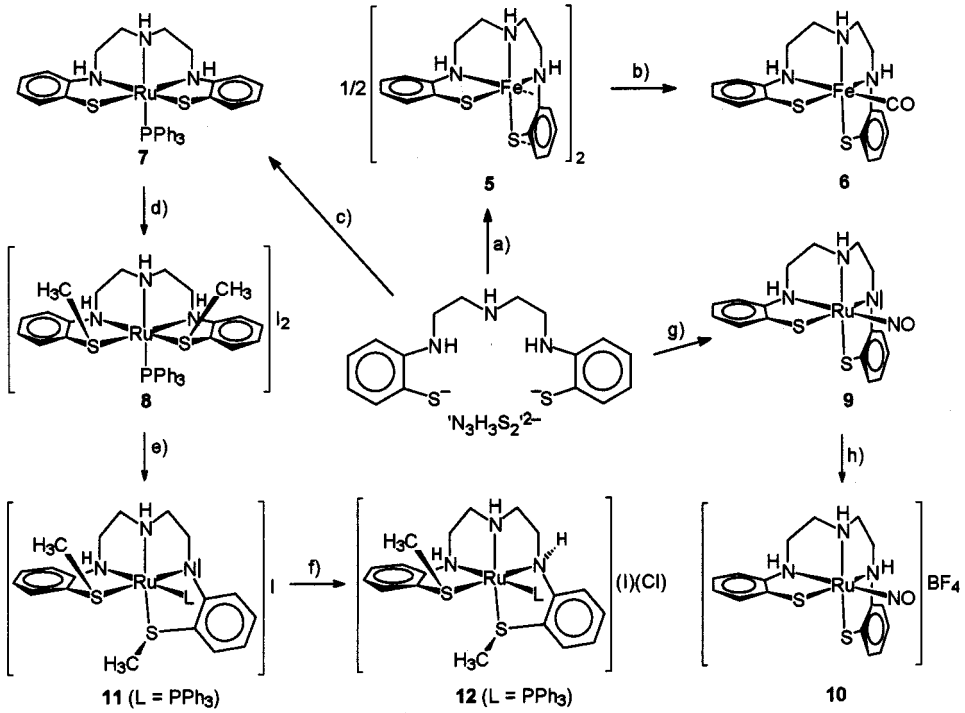
Alkaline hydrolysis of **2** by aqueous NaOH in EtOH and subsequent acidification with hydrochloric acid yielded **3** as yellow powder in nearly quantitative amounts. The final step, the reductive detosylation of the central N atom in **3** with sodium in liquid NH_3 gave **4**, which was isolated after recrystallization from EtOH in form of beige needles.

Syntheses of Fe and Ru Complexes

Scheme 3 summarizes the syntheses and reactions of $[M('N_3H_3S_2')]$ complexes.

The reaction a) of Fe^{II} salts with $'N_3H_3S_2'^{2-}$, which was routinely obtained from $'N_3H_3S_2'$-H_2 and two equivalents of LiOMe, gave grey-white $[Fe('N_3H_3S_2')]$ (**5**). The structure of **5** remains unknown, but in analogy to the closely related dinuclear $[Fe('N_2H_2S_3')]_2$ complex, **5** is suggested to exhibit a dinuclear structure resulting from thiolate bridging. In solid state, **5** is paramagnetic [μ_{eff} (293 K) = 3.94 μ_B]. The μ_{eff} value is compatible with four unpaired electrons per Fe center, which are partially coupled antiferromagnetically through Fe−S−Fe bridges.

All attempts to obtain $[Fe(L)('N_3H_3S_2')]$ derivatives by treating **5** with N_2H_4, NEt_4N_3, or PMe_3 in MeOH or THF solutions remained unsuccessful and yielded only the starting complex **5**. Exclusively CO could be added to give red $[Fe(CO)('N_3H_3S_2')]$ (**6**) (Scheme 3, reaction b). Complex **6** is diamagnetic and probably exhibits the C_1-symmetric structure indicated in Scheme 3. The C_1 symmetry is concluded from the NMR spectra of **6** (see below), and it corresponds with that of the related $[Fe(CO)('N_2H_2S_3')]$ whose structure has been determined by X-ray diffraction. Complex **6** exhibits a low-frequency ν(CO) IR band at 1934 cm^{-1} (in THF) indicating strong Fe−CO π-back-bonding. In accordance with this, solid **6** is stable at room temperature for unlimited periods of time. In solution, however, **6** rather unexpectedly readily loses CO within a few hours and yields the starting complex **5**. In this respect, the properties of **6** resemble very closely those of the related



Scheme 3. Syntheses and reactions of [M('$N_3H_3S_2$')] complexes (M = Fe, Ru)

[Fe(CO)('$N_2H_2S_3$')]. For this reason, we tried to obtain the kinetically less labile ruthenium homologue of **6**. As in the case of the '$N_2H_2S_3$'$^{2-}$ ligand, all efforts to obtain the corresponding monocarbonyl complex [Ru(CO)('$N_3H_3S_2$')] remained unsuccessful. The composition of the complexes resulting from reactions of precursors such as $[Ru(H)(Cl)(CO)(PCy_3)_2]$[8] or $[Ru(Cl)_2(CO)_3(THF)]$[9] with '$N_3H_3S_2$'$^{2-}$ suggested that only four of the five '$N_3H_3S_2$'$^{2-}$ donors had become coordinated.

However, coordination of all five '$N_3H_3S_2$'$^{2-}$ donors could be achieved when $[RuCl_2(PPh_3)_3]$ was treated with '$N_3H_3S_2$'$^{2-}$ in refluxing THF (Scheme 3, reaction c). Yellow [Ru(PPh_3)('$N_3H_3S_2$')] (**7**) resulted, which interestingly also formed when $[RuCl_2(PPh_3)_3]$ was treated with the *N*-tosylated ligand '$^{Ts}N_3H_2S_2$'$^{2-}$ (**3**). This indicates that coordination of **3** facilitates its detosylation. Detosylation of amides normally needs much more drastic reaction conditions.[10] The C_S symmetry of **7** indicated in Scheme 3 is concluded from the ^{1}H-NMR signal pattern of the aliphatic '$N_3H_3S_2$'$^{2-}$ protons. It consists of two pseudo triplets and a multiplet and characteristically differs from the pattern observed consisting of two pseudo triplets. This signal pattern characteristically differs from that observed for the aliphatic protons in C_1-symmetrical [Fe(CO)('$N_3H_3S_2$')]. A ^{13}C-NMR spectrum confirming this conclusion could not be recorded due to insufficient solubility of **7**. However, the C_S symmetry assumed for **7** is further supported by the C_S-symmetrical structure of the *S*-methylated derivative of **7**. Alkylation of **7** by CH_3I yielded [Ru(PPh_3)('$N_3H_3S_2$'-Me_2)]I_2 (**8**) (reaction d), whose molecular structure could be determined by X-ray structure analysis.

Coordination of the '$N_3H_3S_2$'$^{2-}$ ligand to (nitrosyl)ruthenium complexes resulted in deprotonation of one aromatic amine function. Treatment of $[RuCl_3(NO)(PPh_3)_2]$ with '$N_3H_3S_2$'$^{2-}$ and LiOMe yielded neutral, deep green [Ru(NO)('$N_3H_2S_2$')] (**9**), which exhibits one amide donor (reaction g). The formation of the amide could further be substantiated by protonation of **9** with HBF_4 (reaction h). It yielded red [Ru(NO)('$N_3H_3S_2$')]BF_4 (**10**). The protonation is accompanied by a shift of the ν(NO) band from 1779 cm^{-1} in **9** to 1855 cm^{-1} in **10**. The ^{1}H- and ^{13}C-NMR spectra indicate that **10** exists in two diastereomeric forms (see below).

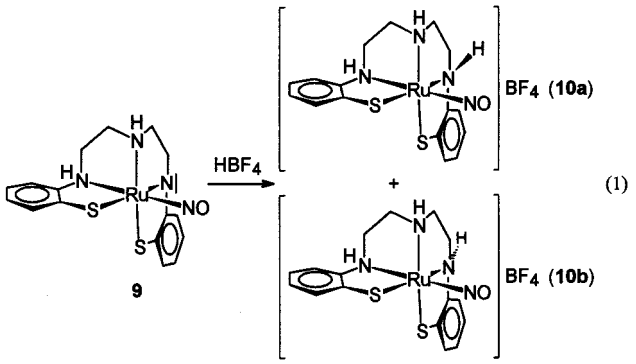
Substitution and Acid−Base Reactions

The reactivity of the complexes containing [M('$N_3H_3S_2$')] or [M('$N_3H_2S_2$')] cores paralleled that of complexes with [M('$N_2H_2S_3$')] or [M('N_2HS_3')] cores. The [Fe(CO)('$N_3H_3S_2$')] complex proved unexpectedly labile with respect to CO loss.

The ruthenium complexes proved extremely inert towards substitution. For example, the PPh_3 ligand in [Ru(PPh_3)('$N_3H_3S_2$')] (**7**) could neither be substituted by CO (50 bar, 2 d, THF) nor by N_2H_4 which was used as solvent (40°C, 1 d). With the intention to labilize the Ru−PPh_3 bond by converting the thiolate into thioether

functions, **7** was alkylated. The resulting [Ru(PPh_3)-($'N_3H_3S_2'$-Me_2)]I_2 (**8**) proved to be as inert towards substitution as **7**.

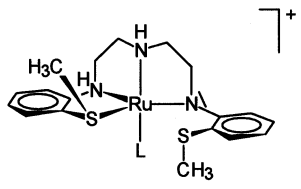
As in the case of [M($'N_2H_2S_3'$)] complexes, protonation−deprotonation reactions of the [M($'N_3H_3S_2'$)] cores could be observed. Protonation of the amide donor in [Ru(NO)($'N_3H_2S_2'$)] yielded two diastereomers of [Ru(NO)($'N_3H_3S_2'$)]BF_4. The formation of two diastereomers could be concluded from the $^{13}C\{^1H\}$-NMR spectrum and is explained by the stereogenicity of the amine function that results from either a "front"- or a "back"-side attack of the proton upon the prochiral amide donor (Equation 1).



(1)

The protonation−deprotonation reactions of [Ru(PPh_3)($'N_3H_3S_2'$-Me_2)]I_2 (**8**) differ from those of the analogous [Ru(PPh_3)($'N_2H_2S_3'$-Me_2)]I_2. The ^{1}H-NMR spectrum and X-ray structure determination established that **8** formed in isomerically pure form as C_S-symmetrical species when synthesized from **7** and CH_3I. Complex **8** can be deprotonated by bases such as N_2H_4 to give [Ru(PPh_3)($'N_3H_2S_2'$-Me_2)]I (**11**), which is converted into [Ru(PPh_3)($'N_3H_3S_2'$-Me_2)](I)(Cl) (**12**) when treated with HCl. The ^{1}H- and ^{13}C-NMR spectra unambiguously show that **11** and **12** have C_1 symmetry only. Thus, the deprotonation−protonation reactions [steps e) and f) in Scheme 3] lead to a configurational rearrangement of **8**.

The rearrangement could occur via the five-coordinate intermediate [Ru(PPh_3)($'N_3H_2S_2'$-Me_2)]$^+$ in which one thioether donor has dissociated. Driving force of this rearrangement probably is the planarization tendency of amide N atoms[11] and, in addition, the capability of amide donors to stabilize five-coordinate intermediates by π donation.[2e] The rearrangement further indicates that, like [M($'N_2H_2S_3'$)] cores, also [M($'N_3H_3S_2'$)] cores prefer the C_1-symmetrical configuration. It is noteworthy that the protonation of **11** yields only one diastereomer of **12** (cf. ref.[4]).



Characterization of Complexes

All complexes except [Fe($'N_3H_3S_2'$)]$_2$ (**5**) are diamagnetic and exhibit similar solubilities. They are soluble in DMF and DMSO, moderately soluble in CH_2Cl_2, THF, and acetone, and virtually insoluble in all other common organic solvents. The phosphane complex [Ru(PPh_3)($'N_3H_3S_2'$)] (**7**) is only very moderately soluble even in DMSO. All complexes have been characterized by elemental analysis, IR, NMR, and mass spectra. The FD mass spectra of the complexes showed the molecular ions except in the case of **6** in which only the decarbonylated species [Fe($'N_3H_3S_2'$)]$^+$ could be observed. As expected the IR (KBr) spectra show numerous bands. One broad or up to three weak- to medium-intensity ν(NH) bands in the region of 3293 to 3102 cm^{-1} can be used as an IR probe for the complexes containing [M($'N_3H_3S_2'$)] cores. In contrast, [Ru(NO)($'N_3H_2S_2'$)] (**9**) containing one amide donor gives rise to two medium ν(NH) bands at 3245 and 3224 cm^{-1}. The complexes **6**, **9**, and **10** can further readily be identified by their strong ν(CO), ν(NO), and ν(BF_4) bands which appear at 1934 cm^{-1} (**6** in THF), 1779 cm^{-1} (**9** in KBr), and 1855 and 1084 cm^{-1}, respectively (**10** in KBr). $^{13}C\{^1H\}$-NMR spectra are the most suitable probe for distinguishing between C_1 or C_S symmetry of the complexes[4][12]. Twelve aromatic ^{13}C-NMR signals in the range δ = 160−108 and four aliphatic ^{13}C-NMR signals of the *N*-bonded C atoms in the range δ = 65−45 indicate C_1 symmetry of the complexes **6** and **9** containing [M($'N_3H_3S_2'$)] or [M($'N_3H_2S_2'$)] cores. Two sets of this signal pattern in the $^{13}C\{^1H\}$-NMR spectrum of **10** suggest the presence of two diastereomers. Only six aromatic and two aliphatic (*N*-bonded C_2H_4 groups) ^{13}C-NMR signals for the [M($'N_3H_3S_2'$)] core indicate the C_S symmetry of **8**, which was confirmed by X-ray structure analysis. The C_S symmetry of **8** is also reflected in the appearance of only one SCH_3 singlet in the ^{1}H-NMR spectrum.

X-ray Structure Analysis of [Ru(PPh_3)($'N_3H_3S_2'$-Me_2)]I_2 · 2 CH_2Cl_2 (**8** · 2 CH_2Cl_2)

The molecular structure of [Ru(PPh_3)($'N_3H_3S_2'$−Me_2)]I_2 · 2 CH_2Cl_2 (**8** · 2 CH_2Cl_2) (Figure 1) was determined by X-ray structure analysis. Table 1 lists selected distances and angles.

The ruthenium center of **8** is pseudo-octahedrally surrounded by the phosphane and the $'N_3H_3S_2'$-Me_2 donors. Both the aromatic amine and the thioether donor atoms assume *cis* positions, and the aliphatic amine donor N3 and the phosphane donor occupy *trans* positions such that **8** exhibits approximate C_S symmetry. Distances and angles show no anomalies and are typical for this type of Ru^{II} complexes.[4,13] Within the crystal, the complex cations, iodide anions, and CH_2Cl_2 solvate molecules are connected by hydrogen bonds. The shortest interionic contact is observed between the N2, H2, and I2 atoms [N2−H2···I2: N2−H2 86(6), N2···I2 352.8(4), H2···I2 274(5) pm; N2−H2···I2 153(4)°].

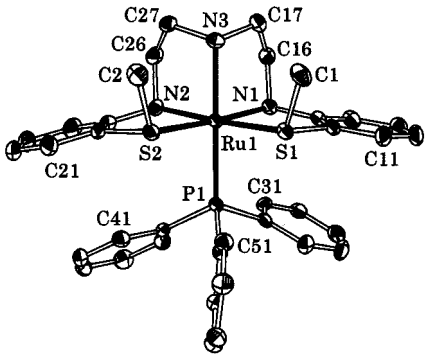


Figure 1. Molecular structure of the cation of $[Ru(PPh_3)('N_3H_3S_2'\text{-}Me_2)]I_2 \cdot 2\ CH_2Cl_2$ (**8** · 2 CH_2Cl_2) (50% probability ellipsoids, H atoms and solvate molecules omitted)

Table 1. Selected distances [pm] and angles [°] of $[Ru(PPh_3)('N_3H_3S_2'\text{-}Me_2)]I_2 \cdot 2\ CH_2Cl_2$ (**8** · 2 CH_2Cl_2)

Ru1−N1	217.6(3)	N1−Ru1−N3	80.5(1)
Ru1−N2	215.9(3)	N2−Ru1−N3	80.6(1)
Ru1−N3	216.4(3)	P1−Ru1−N3	173.4(1)
Ru1−P1	234.3(1)	S1−Ru1−N3	96.0(1)
Ru1−S1	231.5(1)	S2−Ru1−N3	96.2(1)
Ru1−S2	231.3(1)	N1−Ru1−N2	96.0(1)

Concluding Discussion

In the course of a study aiming at the series of $'NHS_4'^{2-}$, $'N_2H_2S_3'^{2-}$, and $'N_3H_3S_2'^{2-}$ ligands and transition metal complexes with increasing electron density at the transition metal centers, the new pentadentate ligand $'N_3H_3S_2'\text{-}H_2$ was prepared.

A special synthetic route which warranted the NH and the terminal thiolate donors of $'N_3H_3S_2'\text{-}H_2$ was developed. The low-frequency ν(CO) of $[Fe(CO)('N_3H_3S_2')]$ (**6**) (1934 cm^{-1}) shows that the iron center indeed exhibits a high electron density. However, the Fe electron density is not higher than in the related $[Fe(CO)('N_2H_2S_3')]$ (1932 cm^{-1}), the CO ligand is very labile and no small molecules other than CO could be coordinated to the $[Fe('N_3H_3S_2')]$ fragment. With respect to $[Fe('NHS_4')]$ fragments, a further serious shortcoming of $[M(L)('N_3H_3S_2')]$ complexes is their core structure. Like $[M(L)('N_2H_2S_3')]$ complexes, $[M(L)('N_3H_3S_2')]$ complexes appear to prefer C_1-symmetrical structures and thiolate donors in *cis* position. Only $[Ru(PPh_3)('N_3H_3S_2')]$ (**7**) and its *S*-methylated derivative $[Ru(PPh_3)('N_3H_3S_2'-Me_2)]I_2$ (**8**) exhibit C_S-symmetrical structures which are comparable with the C_S-symmetrical diastereomer of the $[Fe('NHS_4')]$ fragment. However, the deprotonation−protonation reactions of **8** lead to the C_1-symmetrical diastereomer **12** and indicate that also the $[Ru('N_3H_3S_2')]$ fragment prefers the C_1-symmetrical core structure. Thus, with respect to structure, $[M(L)('N_3H_3S_2')]$ and $[M(L)('N_2H_2S_3')]$ complexes show largely similar properties. The same holds for the electronic and reactivity features. The corresponding carbonyliron complexes exhibit high electron density at the metal centers, but are labile. The ruthenium complexes are virtually substitution inert. The reversible deprotonation of one amine NH function to give an amide donor is their only significant reaction. It has previously been discussed in detail that this formation of π-donor amides can lead to either labilization or stabilization of *trans*-metal−ligand bonds.[4,14]

Experimental Section

General: Unless noted otherwise, all procedures were carried out under N_2 at room temperature by using Schlenk techniques. Solvents were dried and distilled before use. As far as possible the reactions were monitored by IR spectroscopy. − Spectra were recorded with the following instruments: IR: Perkin Elmer 16 PC FT-IR. − NMR: JEOL JNM-GX 270 and JNM-EX 270 [^{1}H NMR (269.6 MHz) and ^{13}C NMR (67.7 MHz): The protio-solvent signal was used as an internal reference. Chemical shifts are quoted on the δ scale (downfield shifts are positive) relative to tetramethylsilane; ^{31}P NMR (109.38 MHz): external standard H_3PO_4]. − Mass spectra: Varian MAT 212 and JEOL JMS 700. − Magnetic moments: Johnson Matthey magnetic susceptibility balance (293K). − $[RuCl_3(NO)(PPh_3)_2]$,[15] $[RuCl_2(PPh_3)_3]$,[16] *N*,*N*-bis[2-(*p*-tolylsulfonyloxy)ethyl]-*p*-toluolsulfonamide,[17] and 2(3*H*)-benzothiazolone[18] were prepared by literature methods. *N*,*N*-bis(2-iodoethyl)-*p*-toluenesulfonamide[19] was prepared in situ and directly used afterwards. Hydrazine was obtained by twofold distillation of $N_2H_4 \cdot H_2O$ over solid potassium hydroxide under reduced pressure.

Alkylation of 2(3*H*)-Benzothiazolone (1) with *N*,*N*-Bis(2-iodoethyl)-*p*-toluenesulfonamide To Give 2: A solution of *N*,*N*-bis[2-(*p*-tolylsulfonyloxy)ethyl]-*p*-toluenesulfonamide (2.03 g, 3.58 mmol) and NaI (2.50 g, 10.68 mmol) in acetone (40 mL) was refluxed for 14 h and concentrated to dryness. The resulting residue was dissolved in CH_2Cl_2 (30 mL), insoluble material was removed by filtration, and the filtrate was concentrated to dryness, yielding *N*,*N*-bis(2-iodoethyl)-*p*-toluenesulfonamide (1.52 g, 89%). − A suspension of 2(3*H*)-benzothiazolone (0.96 g, 6.35 mmol) and K_2CO_3 (0.88 g, 6.37 mmol) in 2-butanone (20 mL) was refluxed for 30 min and then combined with a solution of *N*,*N*-bis(2-iodoethyl)-*p*-toluenesulfonamide (1.52 g, 3.17 mmol) in 2-butanone (10 mL). The resulting white suspension was refluxed for 14 h and concentrated to dryness to give a foamy white residue. It was redissolved in EtOH (30 mL). Addition of water (50 mL) precipitated a white powder, which was separated, digested with EtOH (30 mL), and dried in vacuo. Yield: 1.39 g (74%). − $C_{25}H_{23}N_3O_4S_3$ (525.67): calcd. C 57.12, H 4.41, N 7.99, S 18.30; found C 56.71, H 4.47, N 7.98, S 18.11. − IR (KBr): $\tilde{\nu}$ = 1678 vs ν(CO), 1327, 1153 w ν(SO_2) cm^{-1}. − MS (FD, CH_2Cl_2); *m/z*: 525 [**2**]$^+$. − ^{1}H NMR ($CDCl_3$): δ = 7.59 (d, 2 H, C_6H_4), 7.40 (d, 2 H, C_6H_4), 7.34 (d, 2 H, C_6H_4), 7.25−7.10 (m, 6 H, C_6H_4), 4.14 (t, 4 H, C_2H_4), 3.50 (t, 4 H, C_2H_4), 2.35 (s, 3 H, CH_3, Ts). − ^{13}C{^{1}H} NMR ($CDCl_3$): δ = 170.6 (CO), 144.6, 137.3, 135.8, 130.6, 127.7, 127.4, 124.0, 123.4, 123.3, 111.3 (C, aryl), 46.9, 42.2 (C_2H_4), 22.2 (CH_3, Ts).

$'^{Ts}N_3H_2S_2'\text{-}H_2$ (3): A suspension of **2** (1.83 g, 3.48 mmol) in EtOH (20 mL) was combined with a solution of NaOH (1.39 g, 34.8 mmol) in H_2O (20 mL) and refluxed for 18 h. Concentrated hydrochloric acid was added until pH = 3 was reached, the solution was concentrated in volume to one half, diluted with H_2O (60 mL), and extracted with CH_2Cl_2 (60 mL). The combined CH_2Cl_2 phases were dried with anhydrous Na_2SO_4 and concentrated to dryness, yielding **3** as a yellow powder. Yield: 1.60 g (97%). − $C_{23}H_{27}N_3O_2S_3$ (473.69): calcd. C 58.32, H 5.75, N 8.87, S 20.31; found: C 58.10, H 5.90, N 8.91, S 19.99. − IR (KBr): $\tilde{\nu}$ = 3385, 3364 w ν(NH), 2522 w ν(SH), 1323 s, 1159 vs ν(SO_2) cm^{-1}. − MS (FD, CH_2Cl_2);

m/z: 474 [$'^{Ts}N_3H_2S_2'$-H_2]$^+$. – ^{1}H NMR ($CDCl_3$): δ = 7.62 (d, 2 H, C_6H_4, Ts, *ortho* to SO_2), 7.23 (d, 2 H, C_6H_4, *ortho* to SH), 7.17 (d, 2 H, C_6H_4, Ts, *meta* to SO_2), 7.03 (dd, 2 H, C_6H_4, *para* to SH), 6.50 (dd, 2 H, C_6H_4, *para* to NH), 6.42 (d, 2 H, C_6H_4, *ortho* to NH), 4.80 (s, br., 2 H, NH), 3.27 (s, 8 H, C_2H_4), 2.70 (s, br., 2 H, SH), 2.30 (s, 3 H, CH_3, Ts). – ^{13}C{^{1}H} NMR ($CDCl_3$): δ = 147.6, 143.7, 135.5, 135.2, 129.8, 129.4, 127.1, 117.2, 111.6, 109.8 (C, aryl), 48.8, 42.9 (C_2H_4), 21.4 (CH_3, Ts).

$'N_3H_3S_2'$-H_2 (4): Metallic sodium was added in small portions to a solution of $'^{Ts}N_3H_2S_2'$-H_2 (**3**) (1.0 g, 2.1 mmol) in refluxing liquid NH_3 (100 mL) until the blue color of dissolved sodium persisted for 10 min. Ammonium chloride was added until the blue color disappeared, and the liquid NH_3 was allowed to evaporate. The resulting beige residue was dissolved in aqueous NaOH (0.4 g NaOH in 100 mL H_2O). The resulting H_2O solution was extracted with CH_2Cl_2 (70 mL) and filtered through filter pulp. Concentrated hydrochloric acid was added to the H_2O filtrate. When pH = 8 was reached, a white solid precipitated which was separated and washed with H_2O (40 mL). Recrystallization from EtOH yielded beige needles of **4**. The pH = 8 proved critical, because further lowering of the pH led to formation of yellow material, which had a gummy consistency, proved insoluble in all common organic solvents, and was not characterized in detail. Yield: 0.51 g (66%) of **4** · EtOH. – $C_{18}H_{27}N_3OS_2$ (365.57): calcd. C 59.14, H 7.44, N 11.49, S 17.54; found C 58.86, H 7.61, N 11.74, S 17.69. – IR (KBr): $\tilde{\nu}$ = 3376, 3317 m ν(NH), 2588 w, br. ν(SH) cm^{-1}. – MS (FD, CH_2Cl_2); *m/z*: 319 [$'N_3H_3S_2'$-H_2]$^+$. – ^{1}H NMR (CD_2Cl_2): δ = 7.35 (d, 2 H, C_6H_4), 7.15 (t, 2 H, C_6H_4), 6.68–6.53 (m, 4 H, C_6H_4), 3.50–3.10 (s, br., superimposed by t, 9 H, SH, NH, C_2H_4), 2.97 (t, 4 H, C_2H_4). – ^{13}C{^{1}H} NMR (CD_2Cl_2): δ = 148.8, 135.1, 129.3, 117.3, 110.8, 110.8 (C_6H_4), 48.4, 43.6 (C_2H_4).

[Fe($'N_3H_3S_2'$)]$_2$ (5): A yellow solution of $'N_3H_3S_2'$-H_2 · EtOH (**4** · EtOH) (0.22 g, 0.60 mmol) and LiOMe (1.20 mmol, 1.20 mL of a 1 M solution in MeOH) in THF (10 mL) was combined with a solution of $FeCl_2 \cdot 4\ H_2O$ (0.12 g, 0.60 mmol) in MeOH (10 mL). A white solid precipitated which was separated, washed with MeOH (15 mL), and dried in vacuo, in the course of which the color of the solid changed from white to grey. Yield: 0.20 g (89%). – $C_{32}H_{38}Fe_2N_6S_4$ (746.66): calcd. C 51.48, H 5.13, N 11.26, S 17.18; found C 51.19, H 5.29, N 11.17, S 16.98. – IR (KBr): $\tilde{\nu}$ = 3145 m, br. ν(NH) cm^{-1}. – MS (FD, DMSO); *m/z*: 373 [Fe($'N_3H_3S_2'$)]$^+$. – μ_{eff} (293 K) = 3.94 μ_B.

[Fe(CO)($'N_3H_3S_2'$)] (6): CO was continuously bubbled through a solution of $'N_3H_3S_2'$-H_2 · EtOH (**4** · EtOH) (0.135 g, 0.37 mmol) and LiOMe (0.75 mmol, 0.75 mL of a 1 M solution in MeOH) in MeOH (15 mL). A solution of $FeCl_2 \cdot 4\ H_2O$ (0.074 g, 0.37 mmol) in MeOH (15 mL) was added and a red suspension formed. After 15 min, the resulting red solid was separated, washed with MeOH (20 mL), and dried in vacuo. Yield: 0.15 g (97%) **6** · 0.5 MeOH. – $C_{17.5}H_{21}FeN_3O_{1.5}S_2$ (417.36): calcd. C 50.36, H 5.07, N 10.07, S 15.37; found C 50.35, H 4.88, N 10.27, S 15.59. – IR (KBr): $\tilde{\nu}$ = 3241, 3157, 3102 w ν(NH), 1930 s, 1910 vs ν(CO) cm^{-1}. – IR (THF): $\tilde{\nu}$ = 1934 vs ν(CO) cm^{-1}. – MS (FD, DMSO); *m/z*: 373 [Fe($'N_3H_3S_2'$)]$^+$, 317 [($'N_3H_3S_2'$)]$^+$. – ^{1}H NMR ([D$_6$]DMSO): δ = 7.26–6.50 (m, 9 H, C_6H_4 and NH superimposed), 5.86 (s, br., 1 H, NH), 5.78 (s, br., 1 H, NH), 3.70–2.20 (m, 8 H, C_2H_4). – ^{13}C{^{1}H} NMR ([D$_6$]DMSO): δ = 221.3 (CO), 153.6, 152.1, 151.1, 149.1, 129.0, 128.2, 124.7, 124.5, 122.4, 119.5, 119.4, 119.0 (C_6H_4), 62.2, 58.9, 46.2, 45.0 (C_2H_4).

[Ru(PPh$_3$)($'N_3H_3S_2'$)] (7): [$RuCl_2(PPh_3)_3$] (0.79 g, 0.82 mmol) was added to a solution of $'N_3H_3S_2'$-H_2 · EtOH (**4** · EtOH) (0.30 g, 0.82 mmol) and LiOMe (1.65 mmol, 1.65 mL of a 1 M solution in MeOH) in THF (30 mL). The reaction mixture was stirred for 24 h and then refluxed for 3 h. The yellow solid precipitating from the green solution was separated, washed with THF (15 mL) and MeOH (60 mL), and dried in vacuo. [Compound **7** was obtained in equally high yields, when instead of **4** · EtOH the ligand $'^{Ts}N_3H_2S_2'$-H_2 (**3**) was used]. Yield: 0.18 g (32%). – $C_{34}H_{34}N_3PRuS_2$ (680.84): calcd. C 59.98, H 5.03, N 6.17, S 9.42; found C 59.63, H 5.19, N 6.29, S 9.34. – IR (KBr): $\tilde{\nu}$ = 3288 w, 3258, 3247 m ν(NH) cm^{-1}. – MS (FD, DMSO, ^{102}Ru); *m/z*: 681 [Ru(PPh$_3$)($'N_3H_3S_2'$)]$^+$. – ^{1}H NMR ([D$_6$]DMSO): δ = 7.35–6.17 [m, 23 H, C_6H_4 and P(C_6H_5) superimposed], 5.77 (d, 2 H, NH), 4.41 (s, br., 1 H, NH), 3.75 (pseudo-t, 2 H, C_2H_4), 2.90 (pseudo-t, 2 H, C_2H_4), 2.75–2.20 (m, 4 H, C_2H_4). – ^{31}P{^{1}H} NMR ([D$_6$]DMSO): δ = 52.6 [s, P(C_6H_5)].

[Ru(PPh$_3$)($'N_3H_3S_2'$-Me$_2$)]I$_2$ (8): Addition of MeI (0.50 mL, 8.0 mmol) to a yellow suspension of [Ru(PPh$_3$)($'N_3H_3S_2'$)] (**7**) (0.13 g, 0.19 mmol) in THF (20 mL) yielded a beige suspension. The beige solid was separated after 2 d, washed with THF (10 mL), and dried in vacuo. Yield: 0.19 g (96%) **8** · THF. – $C_{40}H_{48}I_2N_3OPRuS_2$ (1036.83): calcd. C 46.34, H 4.67, N 4.05, S 6.19; found C 46.18, H 4.85, N 3.92, S 6.48. – IR (KBr): $\tilde{\nu}$ = 3284 w, br. ν(NH) cm^{-1}. – MS (FD, CH_2Cl_2, ^{102}Ru); *m/z*: 838 {[Ru(PPh$_3$)($'N_3H_3S_2'$–Me$_2$)](I)}$^+$, 711 [Ru(PPh$_3$)($'N_3H_3S_2'$-Me$_2$)]$^+$. – ^{1}H NMR ([D$_6$]DMSO): δ = 7.73–6.96 [m, 23 H, C_6H_4 and P(C_6H_5) superimposed], 6.85 (d, 2 H, NH arom.), 6.46 (s, br., 1 H, NH aliphat.), 4.06 (m, 2 H, C_2H_4), 2.92 (s, 6 H, SCH_3), 2.87–2.72 (m, 6 H, C_2H_4). – ^{13}C{^{1}H} NMR ([D$_6$]DMSO): δ = 148.3 (C_6H_4), 133.2, 132.7 [d, P(C_6H_5)], 131.7, 131.2, 130.6 (C_6H_4), 129.8 [s, br., P(C_6H_5)], 128.2 (C_6H_4), 127.8 [d, P(C_6H_5)], 126.4 (C_6H_4), 60.0, 51.8 (C_2H_4), 25.3 (d, SCH_3). – ^{31}P{^{1}H} NMR ([D$_6$]DMSO): δ = 37.5 [s, P(C_6H_5)].

[Ru(PPh$_3$)($'N_3H_2S_2'$-Me$_2$)]I (11): [Ru(PPh$_3$)($'N_3H_3S_2'$-Me$_2$)]I_2 · THF (**8** · THF) (0.10 g, 0.10 mmol) was suspended in N_2H_4 (1.0 mL). The yellow reaction mixture was stirred for 4 h and then concentrated to dryness. The resulting yellow residue was dissolved in CH_2Cl_2 (5 mL), insoluble material was removed by filtration, and the filtrate was concentrated to dryness yielding a yellow powder. Yield: 0.07 g (84%). – IR (KBr): $\tilde{\nu}$ = 3275 m ν(NH) cm^{-1}. – MS (FD, DMSO, ^{102}Ru); *m/z*: 694 [Ru(PPh$_3$)($'N_3H_2S_2'$-CH$_2$)]$^+$. – ^{1}H NMR (CD_2Cl_2): δ = 7.57 [t, 2 H, CH(aryl)], 7.47–7.19 [m, 17 H, CH(aryl)], 6.97 [t, 1 H, CH(aryl)], 6.75 [d, 1 H, CH(aryl)], 6.31 [d, 1 H, CH(aryl)], 6.09 [t, 1 H, CH(aryl)], 5.72 (t, br., 1 H, NH), 5.46 (t, br., 1 H, NH), 3.46–2.60 (m, 8 H, C_2H_4), 2.36 (s, 3 H, CH_3), 1.75 (s, 3 H, CH_3). – ^{13}C{^{1}H} NMR (CD_2Cl_2): δ = 158.6, 147.3, 138.1 (d) (C_6H_4), 133.8, 133.6 [d, P(C_6H_5)], 131.9, 131.3, 131.0 (C_6H_4), 130.1 [s, br., P(C_6H_5)], 130.0, 129.6 (C_6H_4), 129.2 [d, P(C_6H_5)], 127.2, 120.0, 111.4, 110.7 (C_6H_4), 58.7, 57.4, 55.8, 49.2 (C_2H_4), 28.2, 23.1 (d) (SCH_3). – ^{31}P{^{1}H} NMR (CD_2Cl_2): δ = 43.7 [s, P(C_6H_5)].

[Ru(PPh$_3$)($'N_3H_3S_2'$-Me$_2$)](I)(Cl) (12) by Protonation of 11: Hydrochloric acid (0.50 mmol, 5 mL of a 0.1 M solution of HCl in H_2O) was added to a yellow suspension of [Ru(PPh$_3$)($'N_3H_2S_2'$-Me$_2$)]I (**11**) (0.04 g, 0.05 mmol) in MeOH (15 mL). The reaction mixture was stirred for 5 min. Removal of the solvents yielded a yellow powder (0.04 g). – MS (FD, CH_2Cl_2, ^{102}Ru); *m/z*: 711 [Ru(PPh$_3$)($'N_3H_3S_2'$-Me$_2$)]$^+$, 695 [Ru(PPh$_3$)($'N_3H_2S_2'$-Me)]$^+$, 681 [Ru(PPh$_3$)($'N_3H_3S_2'$)]$^+$. – ^{1}H NMR (CD_2Cl_2): δ = 9.57 (t, br., 1 H, NH arom.), 9.37 (s, br., 1 H, NH arom.), 7.80–7.04 [m, 24 H, C_6H_4, P(C_6H_5) and NH superimposed], 3.96–2.82 (m, 8 H, C_2H_4), 2.29 (s, 3 H, SCH_3), 1.84 (s, 3 H, SCH_3). – ^{13}C{^{1}H} NMR (CD_2Cl_2): δ = 151.9, 151.4, 136.8, 134.3, 134.1 (d), 133.5 (d), 132.1, 131.9, 131.8, 131.2, 130.9, 129.6 (d), 129.2 (d), 128.8, 125.4, 125.1

Table 2. Selected crystallographic data of [Ru(PPh$_3$)('$N_3H_3S_2$'-Me$_2$)]I$_2$ · 2 CH$_2$Cl$_2$ (**8** · 2 CH$_2$Cl$_2$)

Compound	**8**·2 CH$_2$Cl$_2$
Formula	$C_{38}H_{44}Cl_4I_2N_3PRuS_2$
M_r [g/mol]	1134.52
Crystal size [mm]	0.7 × 0.5 × 0.4
F(000)	2232
Space group	$P2_1/c$
Cryst. system	monoclinic
a [pm]	1602.7(4)
b [pm]	1738.8(4)
c [pm]	1695.5(4)
β [°]	110.67(2)
Z	4
V [nm^3]	4.421(2)
$d_{calcd.}$ [g/cm^{-3}]	1.705
μ [mm^{-1}]	2.154
Diffractometer	Siemens P4
Radiation [pm]	Mo-K_α (λ = 71.073)
Temperature [K]	163
Scan technique	ω scan
2θ range [°]	4.6−54.2
Scan speed [°/min]	3.0−30.0
Meas. reflections	13956
Indep. reflections	9702
Obsd. reflections	7037
σ criterion	$F \geq 4\sigma(F)$
Refined parameters	620
R_1, wR_2 (%)	3.34, 9.18

(C, aryl), 59.1, 54.4, 53.6, 46.3 (NCH_2), 28.4, 26.4 (d) (SCH_3). − $^{31}P\{^1H\}$ NMR (CD_2Cl_2): δ = 36.0 [s, P(C_6H_5)].

[Ru(NO)('$N_3H_2S_2$')] (9): [$RuCl_3$(NO)(PPh_3)$_2$] (0.42 g, 0.55 mmol) was added to a solution of '$N_3H_3S_2$'-H_2 · EtOH (**4** · EtOH) (0.20 g, 0.55 mmol) and LiOMe (1.64 mmol, 1.64 mL of a 1 M solution in MeOH) in THF (20 mL). The resulting black solution was stirred for 48 h, during which time a green solid precipitated. The solid was separated, washed with MeOH and THF (20 mL each), and dried in vacuo. Yield: 0.14 g (57%). − $C_{16}H_{18}N_4ORuS_2$ (447.55): calcd. C 42.94, H 4.05, N 12.52, S 14.33; found C 42.96, H 4.22, N 12.37, S 14.09. − IR (KBr): $\tilde{\nu}$ = 3245, 3224 m ν(NH), 1779 vs ν(NO) cm^{-1}. − MS (FD, DMSO, ^{102}Ru); *m/z*: 448 [Ru(NO)('$N_3H_2S_2$')]$^+$. − ^{1}H NMR ([D$_6$]DMSO): δ = 7.83 (s, br., 1 H, NH), 7.20 (d, 1 H, C_6H_4), 6.97−6.29 (m, 8 H, C_6H_4 and NH superimposed), 3.89−2.77 (m, 8 H, C_2H_4). − $^{13}C\{^1H\}$ NMR ([D$_6$]DMSO): δ = 158.5, 146.6, 146.1, 137.9, 129.0, 127.0, 126.3, 125.0, 122.6, 121.7, 114.7, 108.3 (C_6H_4), 59.0, 57.7, 52.5, 50.5 (C_2H_4).

[Ru(NO)('$N_3H_3S_2$')]BF_4 (10): Addition of HBF_4 (0.30 mL of a 54% solution in Et_2O) to a green suspension of [Ru(NO)('$N_3H_2S_2$')] (**9**) (0.94 g, 2.12 mmol) in a 1:1 mixture (20 mL) of MeOH and Et_2O yielded a red suspension. The resulting red solid was separated after 3 h, washed with MeOH (5 mL), and dried in vacuo. Yield: 0.67 g (59%). − $C_{16}H_{19}BF_4N_4ORuS_2$ (535.36): calcd. C 35.90, H 3.58, N 10.47, S 11.98; found C 36.12, H 3.56, N 10.42, S 11.69. − IR (KBr): $\tilde{\nu}$ = 3293, 3238, 3219 w ν(NH), 1855 vs ν(NO), 1084 s ν(BF_4) cm^{-1}. − MS (FD, DMSO, ^{102}Ru); *m/z*: 448 [Ru(NO)('$N_3H_2S_2$')]$^+$. − ^{1}H NMR ([D$_6$]DMSO): δ = 10.04 (m, 0.6 H, NH arom.), 8.42 (m, 0.3 H, NH arom.), 8.24 (s, br., 0.3 H, NH arom.), 8.05 (s, br., 0.6 H, NH arom.), 7.67−6.87 (m, 8 H, C_6H_4), 4.41 (m, 0.3 H, NH aliphat.), 4.10 (m, 0.6 H, NH aliphat.), 3.94−2.95 (m, 8 H, C_2H_4). − $^{13}C\{^1H\}$ NMR ([D$_6$]DMSO): δ = 150.9, 148.5, 147.4, 147.3, 145.0, 143.1, 142.2, 141.3, 129.7, 129.2, 129.1, 128.0, 127.6, 127.0, 125.2, 124.3, 123.8, 123.7, 123.6, 123.4, 122.5 (C_6H_4), 62.5, 58.5, 57.6, 57.1, 54.2, 52.0, 51.7, 51.4 (C_2H_4).

X-ray Structure Analysis of [Ru(PPh$_3$)('$N_3H_3S_2$'-Me$_2$)]I$_2$ · 2 CH$_2$Cl$_2$ (8 · 2 CH$_2$Cl$_2$): Bright green columns of [Ru(PPh$_3$)('$N_3H_3S_2$'-Me$_2$)]I$_2$ · 2 CH$_2$Cl$_2$ (**8** · 2 CH$_2$Cl$_2$) were grown from a saturated CH_2Cl_2 solution of **8** which was layered with *n*-hexane. A suitable single crystal was sealed under N_2 in a glass capillary, and data were collected with a Siemens P4 diffractometer. The structure was solved by direct methods (SHELXTL-PLUS).[20] Full-matrix least-squares refinement was carried out on F^2 values (SHELXL-93).[21] The hydrogen atoms were located in a difference Fourier synthesis and isotropically refined. The hydrogen atoms of the CH_2Cl_2 solvate molecules were calculated for ideal geometries. Their isotropic temperature factors were fixed at 1.5 times the value for the C atoms attached to them. For the atom Cl41, an obvious alternative position exists, which, however, could not be refined. Table 2 contains selected crystallographic data for [Ru(PPh$_3$)('$N_3H_3S_2$'-Me$_2$)]I$_2$ · 2 CH$_2$Cl$_2$ (**8** · 2 CH$_2$Cl$_2$).[22]

Acknowledgments

Support of these investigations by the Deutsche Forschungsgemeinschaft and Fonds der Chemischen Industrie is gratefully acknowledged.

[1] [1a] D. P. Mellor in *Chelating Agents and Metal Chelates* (Eds.: F. P. Dwyer, D. P. Mellor), Academic Press, New York, London, **1964**, p. 44. − [1b] K. Burger, in *Biocoordination Chemistry* (Ed.: K. Burger), Ellis Horwood, New York, **1990**, p. 11.
[2] [2a] D. Sellmann, J. Sutter, *Acc. Chem. Res.* **1997**, *30*, 460−469. − [2b] D. Sellmann, W. Soglowek, F. Knoch, G. Ritter, J. Dengler, *Inorg. Chem.* **1992**, *31*, 3711−3717. − [2c] D. Sellmann, W. Soglowek, F. Knoch, M. Moll, *Angew. Chem.* **1989**, *101*, 1244−1245; *Angew. Chem. Int. Ed. Engl.* **1989**, *28*, 1271−1272. − [2d] D. Sellmann, H. Kunstmann, F. Knoch, M. Moll, *Inorg. Chem.* **1988**, *27*, 4183−4190. − [2e] D. Sellmann, T. Hofmann, F. Knoch, *Inorg. Chim. Acta* **1994**, *224*, 61−71.
[3] R. A. Henderson, G. J. Leigh, C. J. Picket, *Adv. Inorg. Chem. Radiochem.* **1983**, *27*, 245.
[4] D. Sellmann, J. Utz, F. W. Heinemann, *Inorg. Chem.*, submitted.
[5] Cf.: A. F. Childs, L. J. Goldsworthy, G. F. Harding, F. E. King, A. W. Nineham, W. L. Norris, S. G. P. Plant, B. Selton, A. L. L. Tompsett, *J. Chem. Soc.* **1948**, 2174−2177.
[6] Cf.: W. C. J. Ross, J. G. Wilson, *J. Chem. Soc.* **1959**, 3616−3622.
[7] Cf.: G. Klein, B. Prijs, *Helv. Chim. Acta* **1954**, *37*, 2057−2067.
[8] D. Sellmann, R. Ruf, F. Knoch, M. Moll, *Inorg. Chem.* **1995**, *34*, 4745−4755.
[9] M. I. Bruce, F. G. A. Stone, *J. Chem. Soc. A* **1967**, 1238−1241.
[10] R. C. Roemmele, H. Rapoport, *J. Org. Chem.* **1988**, *53*, 2367−2371.
[11] B. R. Cameron, D. A. House, A. McAuley, *J. Chem. Soc., Dalton Trans.* **1993**, 1019−1022.
[12] [12a] D. Sellmann, H. Kunstmann, F. Knoch, M. Moll, *Inorg. Chem.* **1988**, *27*, 4183−4190. − [12b] D. Sellmann, C. Rohm, M. Moll, F. Knoch, *Z. Naturforsch.* **1995**, *50b*, 1229−1244.
[13] [13a] D. Sellmann, R. Ruf, F. Knoch, M. Moll, *Inorg. Chem.* **1995**, *34*, 5963−5972. − [13b] D. Sellmann, O. Käppler, F. Knoch, M. Moll, *Z. Naturforsch.* **1990**, *45b*, 803−816.
[14] M. L. Tobe, *Adv. Inorg. Bioinorg. Mech.* **1983**, *2*, 1.
[15] J. J. Levison, S. D. Robinson, *J. Chem. Soc. A* **1970**, 2947−2954.
[16] T. A. Stephenson, G. Wilkinson, *J. Inorg. Nucl. Chem.* **1966**, *28*, 945−956.
[17] L. Qian, Z. Sun, M. P. Mertes, K. Bowman Mertes, *J. Org. Chem.* **1991**, *56*, 4904−4907.
[18] R. F. Hunter, *J. Chem. Soc.* **1930**, 125−147.
[19] F. P. Schmidtchen, *Chem. Ber.* **1980**, *113*, 2175−2182.
[20] *SHELXTL-PLUS for Siemens Crystallographic Research Systems, Release 4 21/V*, Siemens Analytical X-ray Instruments Inc., Madison, WI, **1990**.

[21] G. M. Sheldrick, *SHELXL-93, Program for crystal structure refinement*, Universität Göttingen, **1993**.
[22] Crystallographic data (excluding structure factors) for the structure of $[Ru(PPh_3)('N_3H_3S_2'\text{-}Me_2)]I_2 \cdot 2\ CH_2Cl_2$ have been deposited with the Cambridge Crystallographic Data Centre as supplementary publication no. CCDC-100956. Copies of the data can be obtained free of charge on application to CCDC, 12 Union Road, Cambridge CB2 1EZ, UK [Fax: int.code + 44-1223/336-033; E-mail: deposit@ccdc.cam.ac.uk].

Received August 7, 1998
[I98278]

Local Density Functional Study of Copper Clusters: A Comparison between Real Clusters, Model Surface Clusters, and the Actual Metal Surface

Xavier Crispin,*[a] Christophe Bureau,*[b] Victor Geskin,[a] Roberto Lazzaroni,[a] and Jean-Luc Brédas*[a]

Keywords: Copper clusters / Cu(100) surface / Chemical hardness / Relaxation energy / Size effect

Density Functional Theory is used to study the influence of the size of copper clusters modeling the Cu(100) surface, on the electronic properties: ionization potential, electron affinity, electronic chemical potential, and chemical hardness. The model clusters are chosen to have a bilayer structure and range in size from 9 to 20 copper atoms. The chemical hardness being identified as the relaxation energy of the frontier levels when an electron is removed or added to the system, a simple expression is proposed to estimate its value from the eigenenergies of the frontier levels in neutral and partially ionized systems. A detailed comparison of the geometric and electronic structures is made between the model surface copper clusters, real copper clusters, and the actual metal surface; it is seen that the model surface clusters provide an easy extrapolation to the properties of the metal surface.

Introduction

Metal clusters are increasingly exploited as surface models to study surface reactions. The size dependence of their electronic properties and reactivities therefore attracts major interest from both fundamental and applied standpoints, especially since clusters provide a bridge between the properties of metal atoms and those of the infinite metallic solid, between homogeneous catalysis and heterogeneous catalysis.[1−6] To study the mesoscopic world between the metal atom and the metal solid, a traditional approach is to evaluate the properties of *real* metal clusters with intermediate sizes and to build a rationalization of the evolution of these properties. With real metal clusters, direct comparison between theory and experiment is possible; however, real clusters are shape-distorted spheres and thus present geometric structures (interatomic distances, packing structures) and electronic properties that can be much different from those of (infinite) metal surfaces. As we ultimately aim at studying reactions at metal surfaces, we have investigated size effects for metal clusters modeling metal surfaces; the geometric structure of such *model* clusters is chosen to represent a portion of the surface: they are flat (generally bilayered) and extended into two dimensions. The comparison between such an approach based on flat *model* clusters and the traditional approach using *real* clusters is interesting since both must extrapolate to the same limit at infinite size.

Among transition metal clusters, copper clusters are probably those that are most studied because of the apparent simplicity of the copper atom, which can be seen in a first approximation as monovalent (the 3d bonding and antibonding orbitals in a copper cluster are all filled). Numerous experimental measurements and theoretical studies of increasing sophistication have been performed on the size evolution of the properties of real copper clusters, such as ionization potential, electron affinity, and band gap.[7−12] Early theoretical approaches, such as the corrected classical model,[13] in which the cluster is considered as a perfect conducting sphere, fail to reproduce the behavior of electron affinity and ionization potential with cluster size.[14] Hence, a quantum mechanical treatment is needed to obtain a reliable average evolution of cluster properties, as shown in the semi-classical model of Brack.[14,15] The latter method is able to explore the properties of huge clusters (up to 10^6 atoms) since the nuclei are not explicitly considered; however, it only gives an average evolution of the properties as a function of the cluster size, fails for small clusters, and does not provide other electronic features (bond description, charge distributions, etc.). The semi-classical model can be refined within jellium models to take into account shell effects, where the valence electrons move in a spherical or a perturbed spherical potential modeling the positive charge due to the nucleus screened by core electrons, such as the Clemenger−Nilsson model.[3,4,16] Such jellium methods reproduce the shell effect and even-odd oscillations typical of real copper clusters,[7,9,12] which are not explained by the classical or semi-classical models; however, they are not reliable for very small metallic clusters (< 7 atoms) since the nuclei cannot be modeled with a jellium. Methods that take into account the positions of the nuclei are therefore necessary; they are more computationally demanding but adequate to study small copper clusters. Among these are the effective-medium methods[17] and other semi-empirical methods[18,19] as well as Hartree−Fock ab initio methods[20−23] and density functional theory-based methods.[24−29]

In the first part of this work, a density functional approach is used to analyze the size evolution of electronic

[a] Service de Chimie des Matériaux Nouveaux, Centre de Recherche en Electronique et Photonique Moléculaires, Université de Mons-Hainaut,
Place du Parc 20, B-7000 Mons, Belgium
Fax: (internat.) + 32(0)65/37.33.66
E-mail: Xavier@averell.umh.ac.be
[b] DSM-DRECAM-SRSIM (bât 466), CEA-Saclay,
F-91191 Gif-sur-Yvette Cedex, France
Fax: (internat.) + 33-1/69.08.64.62
E-mail: bureau@DRECAM.cea.fr

 © WILEY-VCH Verlag GmbH, D-69451 Weinheim, 1999 1434−1948/99/0202−0349 $ 17.50+.50/0

properties (ionization potential and electron affinity) of copper clusters as surface models. In contrast to previous theoretical works,[23,24,28,29] the clusters studied here are designed to model an adsorption site of the Cu(100) surface. Therefore, copper cluster systems studied here do not have the quasi-spherical shape of real copper clusters. The consequences of such a difference are analyzed, on the one hand, on the validity of the surface model, and on the other hand, on the ability to extrapolate the evolution of ionization potential and electron affinity with cluster size.

In the second part, the copper clusters are characterized in terms of global properties as defined within Density Functional Theory (DFT): the electronic chemical potential (μ) and chemical hardness (η). One of the highlights of the present work is to point out the relationship between hardness and relaxation energy of the valence levels when one electron is removed or added to the system; an estimate of hardness is proposed on the basis of the eigenenergies of the frontier levels of neutral and partially ionized systems. The evolutions of the chemical potential and hardness are analyzed with respect to the size of the clusters. Bureau et al.[30] have shown that the DFT chemical potential, μ, is particularly relevant to describe the interaction of a molecule with a metallic surface, should it be polarized or not: μ is the pertinent parameter both for mimicking the setting of a metallic surface under voltage under electrochemical conditions, and for the description of the charge transfer between the adsorbed species and the surface. The latter aspect is based on the relationship between DFT and the Lewis concept of acids and bases, as introduced by Pearson and Parr;[31,32] within this scheme, the hardness of the surface and the molecule, and the difference in their chemical potentials are essential parameters for the understanding of adsorption phenomena.[32–34] It is thus of primary interest to analyze the behavior of these properties (chemical potential, chemical hardness) with cluster size since we ultimately aim at using metal clusters as surface models to study the interaction between an organic molecule and a metal surface.

We emphasize that we have deliberately chosen to adopt a very pedagogical pace to introduce the concepts touched upon in this work. The validity and merits of our methodological approach can in this way be best assessed.

Methodology

The (100) Copper Surface

An adsorption site of the fcc crystal (100) surface is modeled with various copper clusters by considering sizes ranging from nine to twenty copper atoms (Figure 1). The interatomic distances are fixed at the bulk crystal values, so that all reconstruction phenomena are neglected. This choice of interatomic distances for the copper clusters designed to model the surface is obviously taken to simulate at best a site on the surface. Indeed, it is well known that the atomic density at the surface and thus the interatomic

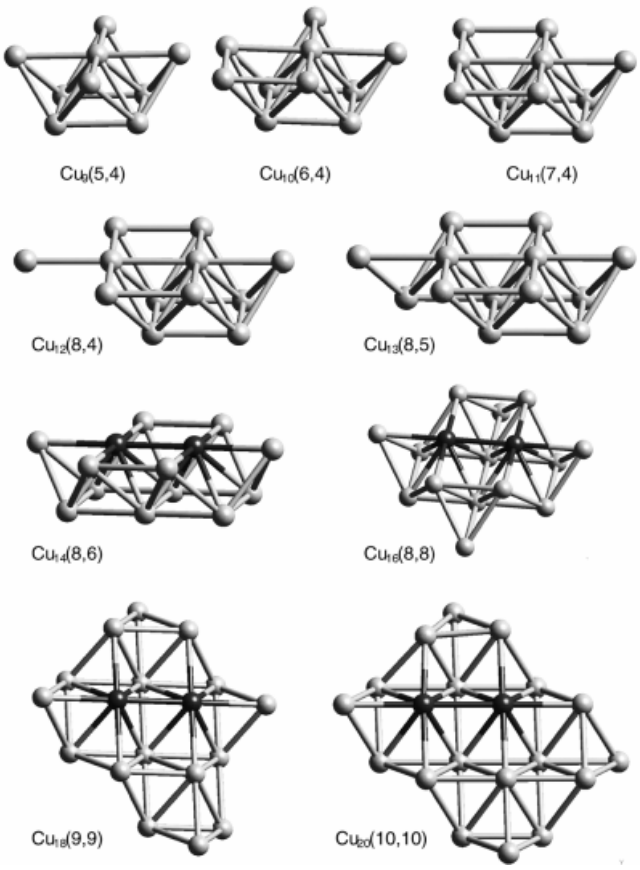


Figure 1. Representation of the copper clusters $Cu_n(y,w)$ used as models of the Cu(100) surface. The clusters are composed of two atomic layers; one containing *y* atoms and the other *w* atoms; from the fourteen-atom cluster, the two copper atoms in dark have the same nearest neighbors as a surface atom on the actual Cu(100) surface

distances can have a strong influence on the chemisorption energy of an adsorbate. This is illustrated by the different reactivities of different crystalline surfaces of transition metals.[35–37]

The clusters are bilayered; the smallest one is $Cu_9(5,4)$ (where the subscript indicates the total number of copper atoms in the cluster and the numbers in parentheses denote the composition of its layers, in this case, 5 atoms in the upper layer and 4 in the bottom layer); in $Cu_9(5,4)$, the central atom of the upper layer has the same number of nearest neighbors as on the actual (100) surface. Clusters $Cu_{10}(6,4)$, $Cu_{11}(7,4)$, and $Cu_{12}(8,4)$ are obtained by extending the upper layer; extending the bottom layer then leads to $Cu_{13}(8,5)$ and $Cu_{14}(8,6)$; $Cu_{14}(8,6)$ has two central atoms which have the same number of nearest neighbors as on the actual (100) surface. Larger clusters built from $Cu_{14}(8,6)$ are also considered: $Cu_{16}(8,8)$, $Cu_{18}(9,9)$, and $Cu_{20}(10,10)$.

Computational Approach

The calculations are performed in the framework of the density functional theory.[38,39] This method is a nonempirical approach, alternative to Hartree–Fock-based theories,

that presently enjoys a wide range of applications to chemical problems due to the possibility of including a significant part of the electron correlation energy; correlation is essential for a correct description of transition metal compounds. An extension of the Kohn−Sham theory describes the energy as a continuous function of the occupation of the monoelectronic levels;[40,41] this allows one to use fractional occupations to evaluate the derivatives of energy with respect to the number of electrons in the system. The evaluation of such derivatives is a way to estimate the electronic chemical potential and chemical hardness of copper clusters.

All the calculations were performed with the DMol program.[42,43] The basis set is DNP (double zeta numeric with polarization). The core orbitals are frozen during the SCF iterations and we choose a "MEDIUM" mesh size of the numerical grid for the calculations.[42,44,45] The calculations are performed within the local spin density approximation (LSD) with the Vosko−Wilk−Nusair exchange-correlation potential.[46] The ionization potential and electron affinity are calculated from total energy differences: $IP(n) = E_{tot}(Cu^+) - E_{tot}(Cu_n)$ and $EA(n) = E_{tot}(Cu_n) - E_{tot}(Cu^-_n)$ [note that, when using this convention, $EA(n) > 0$ means the anionic species is more stable than the neutral species]; the ions are maintained in the same geometry as the neutral copper clusters. The LSD approximation is known to give electron affinities and ionization potentials that are better than those obtained with Hartree−Fock methods[47,48] and in reasonable agreement with experimental data. Therefore, reliable trends for the evolution of electronic properties with respect to the size of the copper clusters can be expected from LSD calculations. Note that since the method is less computationally demanding than the gradient-corrected approximations, it allows us to consider relatively large clusters with all 3d, 4s and 4p atomic orbitals of Cu included in the basis set. The charge analysis used in this work comes from the Hirshfeld scheme, which is directly based on electronic density.[49,50]

Results and Discussion

The presentation of the results is divided into two parts. Firstly, we compare the electronic properties of the model clusters [representing a site of the copper (100) surface] to those of real copper clusters; the evolution of ionization potential (*IP*) and electron affinity (*EA*) as a function of cluster size is analyzed. Secondly, the electronic chemical potential (μ) and the chemical hardness (η) of copper clusters are evaluated and their evolution with cluster size is discussed.

Comparison between Real Copper Clusters, Surface-Model Clusters, and the Metal Surface

In this section, the $Cu_n(y,w)$ clusters modeling the Cu(100) surface are compared to the corresponding real clusters Cu_n, in terms of geometric structure and behavior of *EA* and *IP* with cluster size. The main geometric differences are the interatomic distances and the overall shape of the clusters; their consequences on the electronic properties are described below.

Small real copper clusters (<10 atoms) have significantly shorter interatomic distances[22,27,28] than those in the bulk (nearest-neighbor distance of 2.55 Å). The mean interatomic distance in real copper clusters tends to increase when the cluster grows. As far as the atomic packing is concerned, the fcc structure is found to be the most stable for clusters larger than thirteen atoms with interatomic distances close to those of the bulk metal.[51] Hence, the contraction of the interatomic distances is significant only for small clusters.

The interatomic distances used in the model clusters are the same as those in the bulk (thus larger than the distances of the corresponding real clusters), and their structure is fcc. Note that the use of non-optimized clusters has some unexpected consequences: in the spin-unrestricted calculations, some clusters with an even number of atoms are more stable in their triplet state, whereas real copper clusters with an even number of atoms are expected to be singlet. The total spin of the most stable states found in the odd-clusters (i.e., having an odd number of atoms), namely Cu_9(5,4), Cu_{11}(7,4), and Cu_{13}(8,5), is always 1/2. For the even-clusters, the spin of the most stable state is one for Cu_{10}(6,4), zero for Cu_{12}(8,4), one for Cu_{14}(8,6), one for Cu_{16}(8,8), and zero for Cu_{18}(9,9) and Cu_{20}(10,10). Nevertheless, it must be noted that the total energy of the first singlet state for Cu_{10}(6,4), Cu_{14}(8,6), and Cu_{16}(8,8) is always very close to that of the first triplet state. The fact that we obtain triplet states for these clusters results from the quasi-degeneracy of the one-electron levels near the highest occupied molecular orbital, which is a consequence of the large interatomic distances used and the non quasi-spherical symmetry of the clusters, as explained below.

The ionic species Cu^-_n and Cu^+_n used to calculate $EA(n)$ and $IP(n)$ are more stable in a state having a spin multiplicity of either one or two. The spin multiplicity is one for the anionic or cationic odd-clusters, and two when the ionic species have an even number of copper atoms. No spin-multiplicity difference among the charged even-clusters is observed, in contrast to the neutral clusters.

1. Size Dependence of EA and IP: We now consider the evolution of electron affinity and ionization potential with the size of copper clusters. These two properties are expected to converge on increasing the cluster size since both become equal to the workfunction at infinite size where the cluster is truly metallic, with no electronic gap. In Figure 2, we compare the *EA* values calculated for the $Cu_n(y,w)$ clusters to those measured experimentally from the ionization threshold of real anionic clusters.[7,9] In the experimental work, the energy needed to remove an electron from the anionic cluster was associated to the opposite of the electron affinity of the neutral cluster; as it is a vertical evaluation of *EA*, these experiments in fact provide the *EA* of the neutral cluster in the geometry of the anionic cluster. Note that the presence of an extra electron globally increases the interatomic distances; this is closer to our theo-

retical situation since the interatomic distances of the $Cu_n(y,w)$ clusters are those of the bulk (known to be larger than in small neutral clusters). It can be seen in Figure 2 that the theoretical values of *EA* and the experimental data lie in the same energy range; such an overall agreement is an indication of the ability of our method to evaluate *EA*.

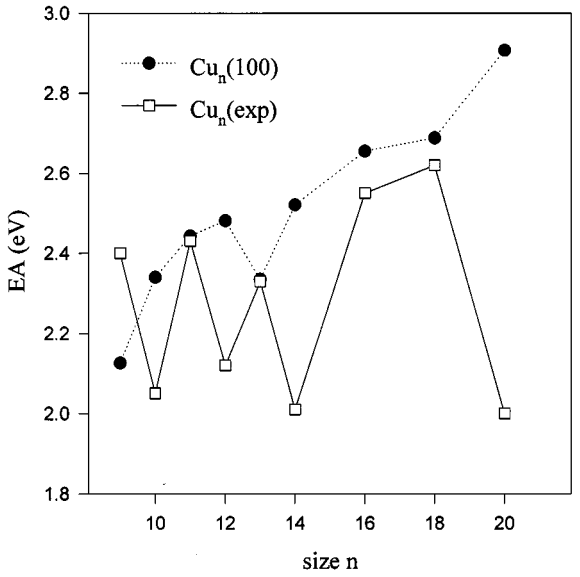


Figure 2. Comparison between the calculated electronic affinities (*EA*) of the copper clusters $Cu_n(y,w)$ ($n = 9 - 20$) modeling the (100) surface and the experimental values for the corresponding real copper clusters

Some errors are expected to be introduced by the LSD and frozen-core approximations used in our calculations. The magnitude of this error can be estimated by comparing the experimental vertical *EA* provided by ultraviolet photoelectron spectroscopy (UPS) measurements on the anionic copper dimer[8] to the calculated value EA_{cal}. EA_{cal} is the difference between the total energy of the anionic copper dimer whose geometry was optimized and the total energy of the neutral copper dimer in the geometry of the anionic species. The experimental vertical *EA* of Cu_2 is 0.89 ±0.01 eV, while the calculated *EA* is 0.80 eV. That the error in the evaluation of the electron affinity for Cu_2 is small (0.1 eV), again illustrates the ability of the method we apply to calculate such a property.

The most striking feature of Figure 2 is the oscillating behavior of the experimental curve, which is not reproduced in the calculations. In order to understand this difference, it is necessary to briefly recall basic theoretical models describing real copper clusters. Real copper clusters (>7 atoms) tend to adopt an equilibrium geometry consisting of either a sphere or a distorted sphere. This was demonstrated theoretically for copper clusters up to 29 atoms by searching the most stable geometry using a simulated annealing approach coupled to an effective-medium method.[17] Although strong 3d-4s hybridization occurs for some small copper clusters, which affects their electronic structure and geometry,[27] it has been shown that the Cu−Cu bonds are mainly due to the overlap of 4s atomic orbitals, as mentioned for Cu_2.[26,52] Various theoretical studies aiming at explaining experimental data have used the following crude but reasonable approximation (e.g. refs.[9] and[12]): copper atoms are considered as monovalent in clusters; as a consequence, the number of valence electrons involved in a cluster is the same as the number of copper atoms in the cluster. In this approximation, the 4s valence electrons of an ideal spherical copper cluster are confined in a spherically symmetric potential (spherical jellium model). Because of its symmetry, such a potential gives rise to a spherical shell structure where the valence electrons successively fill the degenerate levels. The electronic system of a cluster with exactly the right number of electrons to complete a shell is very stable. This is the case when the number of 4s electrons is for instance 8 or 20; the corresponding clusters (Cu_8, Cu_{20}) are thus very stable: this is called the "shell effect" and the numbers 8 and 20 are called "magic numbers (n_g)". This can be experimentally related to the high relative abundance in the mass spectrum for the anionic species of ($n_g - 1$) atoms, like 7 and 19,[7,8] and for cationic species of ($n_g + 1$) copper clusters, like 9 and 21;[53] such stable ions have a completely filled shell. When one atom is added to a Cu_8 or Cu_{20} neutral cluster, its valence electron occupies a degenerate state with considerably higher energy, and hence the stability of the cluster is reduced. In such a case, the cluster symmetry is reduced into a distorted sphere in order to minimize the energy (Jahn−Teller-like effect).[17,54] For each system, the structure distorts to maximize the gap at the Fermi level under the constraints set up by other energy contributions. For even-numbered clusters, there are two electrons in the HOMO and thus the energy gain due to the distortion is larger, resulting in a larger gap.[17] This interplay between the electronic system and the geometry of the cluster allows some clusters to be very stable without having a "magic number" of atoms.

As shown by Pettiette et al.,[9] the low electron affinity of magic-size copper clusters with respect to the *EA* of the neighboring sizes, as well as the even-odd oscillations of experimental *EA* values, can be explained qualitatively within a monoelectronic scheme with Koopmans' theorem thanks to jellium models:

(i) The sudden decrease in *EA* for magic sizes (Cu_{20}) can be understood by considering the shell structure appearing when valence electrons move in a spherical potential; the *EA* for $n = 20$ is lower than that for size $n - 1 = 19$, since an additional electron must occupy a new shell of higher energy. For surface models $Cu_n(y,w)$, no shell structure is expected since the shape is not spherical but flat. This explains why $Cu_{20}(10,10)$, corresponding to a magic size for real clusters, does not have a low calculated *EA*. As a consequence, *EA* for size 20 differs most importantly with respect to experiment (ca. 1 eV) (Figure 2).

(ii) The magnitude of the even-odd oscillations is about 0.5 eV in small real copper clusters; these oscillations decrease when the size increases and disappear at the bulk limit. To qualitatively understand the even-odd oscillations, Taylor et al.[12] refer to the case of monovalent, non-fully symmetrical clusters, thus with no degeneracy in the energy levels. In the even-numbered neutral clusters, the HOMO is

doubly occupied while the odd-numbered neutral clusters are open-shell species. To a first approximation, the extra electron, which makes the cluster negative, would either occupy the lowest unoccupied molecular orbital (LUMO) of the even-numbered clusters or fill the HOMO of the odd-numbered clusters. Such an effect will result into lower *EA* for the even-atom clusters.

The lack of even-odd oscillations in the theoretical curve (Figure 2) can be understood on the basis of the density of valence states (DOS) of the $Cu_n(y,w)$ surface models. The calculated DOS of the model $Cu_{10}(6,4)$ cluster and that of the real $Cu_{10}^{D_{4d}}$ cluster (both shown in Figure 3), as well as the experimental photoemission spectrum of Cu(100),[19,55] are presented in Figure 4 [the DOS of the copper clusters are obtained by enveloping the DFT eigenvalue spectrum with Gaussians of width 0.1 eV and we use Löwdin's decomposition[56] to obtain local DOS (LDOS); note also that the Fermi level is set at zero energy]. The comparison between these DOS and the experimental spectrum shows, on the one hand, strong differences between the DOS of $Cu_{10}^{D_{4d}}$ and that of $Cu_{10}(6,4)$, and, on the other hand, the similarity between the DOS of $Cu_{10}(6,4)$ and the experimental photoemission spectrum of Cu(100). For both copper clusters, the most important region of d monoelectronic states lies in the −4,0 to −1,3 eV range, between hybridized s-p states. Two main differences appear between the DOS of the two copper clusters: the global shape and the electronic gap. The DOS spectrum of the real cluster $Cu_{10}^{D_{4d}}$ shows weakly overlapping peaks, while the DOS of the 3 d states of $Cu_{10}(6,4)$ is non-vanishing in the entire −3 to −1 eV energy range, where these states are almost exclusively concentrated; these features are present in the total DOS of all $Cu_n(y,w)$ clusters studied here. The lower symmetry of $Cu_n(y,w)$ relative to spherical clusters, is responsible for the more uniform, in general, distribution of the monoelectronic states, i.e. the absence of the degenerate levels. The fact that the 3d states of $Cu_{10}(6,4)$ are mainly localized at higher energy is related to the chemical saturation (the number of the nearest neighbors) of the copper atoms in the clusters. Indeed, Figure 5 shows that the lower the saturation of the copper atoms, the more they are involved in 3d states of high energy: the local DOS corresponding to molecular orbitals involving 3d atomic orbitals centered on the peripheral atoms of the top layer (3 or 4 nearest neighbors) are mainly in a range of higher energy than the local DOS related to the peripheral atoms of the bottom layer (5 or 6 nearest neighbors); it is the local DOS related to the most saturated atom, i.e. the central atom with 8 nearest neighbors, that spreads over the widest range of energy. Hence, since every atom is saturated almost equally in $Cu_{10}^{D_{4d}}$, its DOS does not display the specific concentration of 3d valence states in a range of high energy as for $Cu_{10}(6,4)$.

The other main difference between the eigenvalue spectrum of $Cu_{10}^{D_{4d}}$ and that of $Cu_{10}(6,4)$ is the significant electronic gap for the real cluster (Figure 4), while for our surface model the electronic gap is vanishingly small; extremely small gaps are actually observed for all $Cu_n(y,w)$ surface models, since these clusters do not have spherical or quasi-spherical symmetry. This is why the evolution of $IP(n)$ and $EA(n)$ for these clusters does not show shell effects and even-odd oscillations. The removal of such strong oscillations in $EA(n)$ [and also in $IP(n)$] is actually a major advantage when the average behavior of these properties needs to be extrapolated to larger cluster sizes.

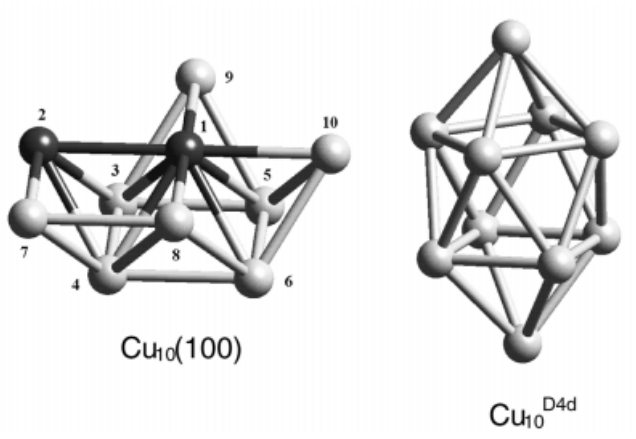


Figure 3. Geometric structures of the surface model $Cu_{10}(6,4)$ and of the corresponding real cluster $Cu_{10}^{D_{4d}}$

In Figure 4, we observe a narrower distribution of the 3d and 4s states in the DOS of $Cu_{10}(6,4)$, relative to that in the experimental spectrum of Cu(100). This is due to two major reasons: first, the model cluster is not large enough to represent the metal; secondly, the application of Koopmans' theorem is not strictly valid for the DFT eigenvalues, since Janak has shown that these eigenvalues rather correspond to the derivative of the total energy with respect to the occupation of orbitals[40]. However, the striking similarity between the DOS of $Cu_{10}(6,4)$ and the experimental spectrum for Cu(100), along with the difference relative to the DOS of $Cu_{10}^{D_{4d}}$, is a favorable argument for considering the $Cu_n(y,w)$ surface models appropriate (and better than real clusters) to model the (100) copper surface.

2. Exploration of the Mesoscopic Size Copper Clusters: Here, we take advantage of the weak oscillations observed in the evolution of $EA(n)$ and $IP(n)$ for the $Cu_n(y,w)$ surface models to explore the mesoscopic region. Properties of large copper clusters are thus deduced from the properties calculated for small model copper clusters.

It has been shown that the evolution of the properties of real clusters, such as the cohesive energy, ionization potential, and electron affinity, can be described with a convergent series whose variable is the number of atoms (n) in the cluster.[57] When neglecting high-order terms, the truncated expansion contains only one unknown coefficient (A) and shows that a property G(n) evolves as a function of $n^{-1/3}$:

$$G(n) = G(\infty) + A \cdot n^{-1/3} \quad (1)$$

The exponent of n is thought to be related to the ratio between the surface and the volume of the cluster, as suggested by Müller et al.[57]. The exponent is therefore ap-

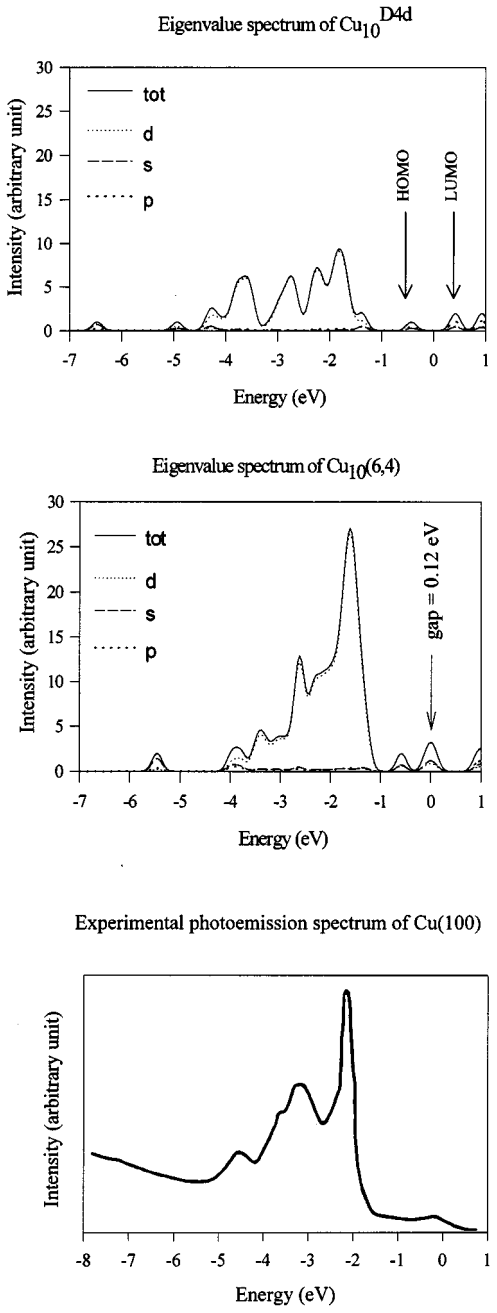


Figure 4. Comparison between the calculated total density of valence states (DOS) of $Cu_{10}^{D_{4d}}$, that of $Cu_{10}(6,4)$ and the experimental photoemission spectrum of Cu(100).[19,55] The total densities of valence states are enveloped with Gaussians of width 0.1 eV and their decomposition in local density of states (LDOS) is obtained from the scheme by Löwdin. The local density of states corresponding to molecular orbitals including 4s atomic orbitals is shown as a dashed line, the 4p component as a thick-dotted line and the 3d component as a thin-dotted line. The Fermi level is set at zero energy.

proximately $-1/3$ for real clusters, which are often almost spherical. Although the $Cu_n(y,w)$ surface models are not spherical, we also use $-1/3$ as the exponent, for the sake of simplicity and to allow a comparison with previous work dealing with real copper clusters[7–9,11]. The average behavior of $IP(n)$ or $EA(n)$ as a function of size (n) of the clusters can thus be expressed as follows: $EA(n) = W_{Cu} + B \cdot n^{-1/3}$ and $IP(n) = W_{Cu} + C \cdot n^{-1/3}$, where W_{Cu} is the workfunction of polycrystalline copper (4.65 eV).

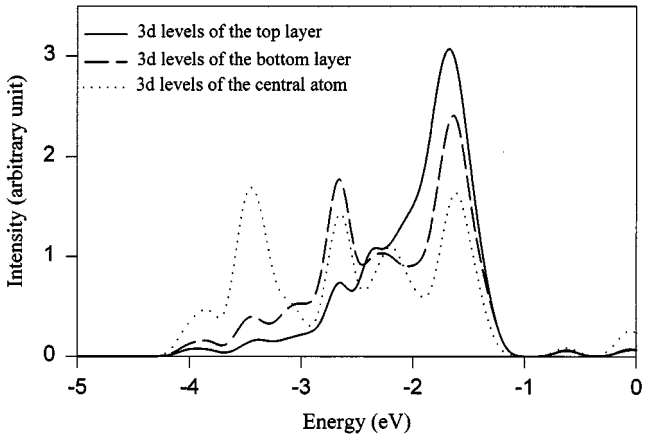


Figure 5. Local density of states (LDOS) from the d component of $Cu_{10}(6,4)$ localized on different regions of the cluster: (i) the peripheral atoms of the top layer (atoms labeled 2, 7, 8, 9, 10 in Figure 3) (full line); (ii) the peripheral atoms of the bottom layer (3, 4, 5, 6) (dashed line); and (iii) the central atom (1) (dotted line).

Accurate descriptions of the average evolution of $EA(n)$ and $IP(n)$ are obtained by imposing the condition that the curves $EA(n) = W_{Cu} + B{*}n^{-1/3}$ and $IP(n) = W_{Cu} + C \cdot n^{-1/3}$ pass through the experimental bulk limit ($n^{-1/3} = 0$, $W_{Cu} = 4.65$ eV), see Figure 6. Coefficients B and C are determined from linear regressions, which yields the following expressions:

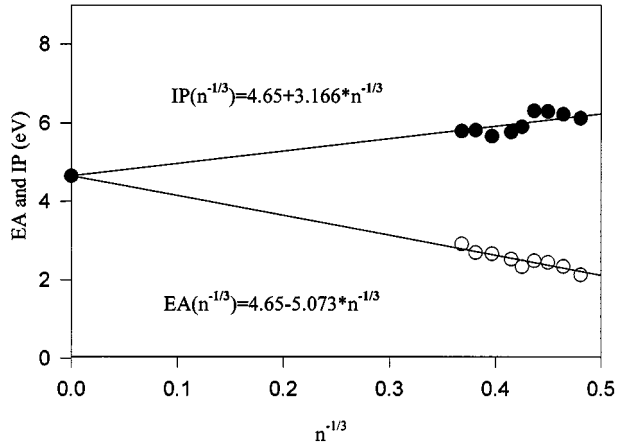


Figure 6. Evolution of calculated $EA(n)$ (open circles) and $IP(n)$ (full circles) with the size n of the cluster $Cu_n(y,w)$. The straight lines represent the average evolution of these properties with size, as obtained by the method described in the text. The intersection point between the average evolution of $IP(n)$ and that of $EA(n)$ is set at the workfunction of polycrystalline copper ($W_{Cu} = 4.65$ eV).

$$EA(n) = 4.65 - 5.073 \cdot n^{-1/3} \quad (2a)$$

$$IP(n) = 4.65 + 3.166 \cdot n^{-1/3} \quad (2b)$$

Note that if the linear regressions are performed without imposing the curve to pass through ($n^{-1/3} = 0$, $W_{Cu} = 4.65$ eV), the extrapolated values for the workfunction of copper is found to be 4.34 eV; this is as good an estimate as those found for the workfunction of other metals from jellium calculations in the LSD approximation (VWN func-

tional).[58,59] Since oscillations are very weak for large copper clusters, the average evolution of $EA(n)$ or $IP(n)$ given by these expressions is expected to follow closely the real evolution. Therefore, we believe that calculations on small copper clusters can provide valuable estimates of the properties of large copper clusters, by means of the above interpolation formulae.

An argument in favor of the validity of the calculated coefficients is that the ratio between coefficient B for $EA(n)$ and C for $IP(n)$, i.e. B/C = −5.073/3.166, is very close to that observed in various experimental studies (−5/3)[8,11]. The average behavior of $IP(n)$ and $EA(n)$ can be evaluated from the limited sample of $Cu_n(y,w)$ (n = 9−20) clusters studied here because the absence of spherical symmetry induces small electronic gaps and thus a rather linear evolution of $IP(n)$ and $EA(n)$ vs. $n^{-1/3}$. The simple expressions describing the average evolution of $IP(n)$ and $EA(n)$ will thus be used below to describe the behavior of the chemical potential of the clusters.

Size Dependence of Chemical Potential μ(n) and Hardness η(n)

1. Evaluation of Chemical Potential and Hardness; Relation with Other Electronic Properties: The chemical potential and the hardness or softness of the clusters are important parameters for describing the physics and chemistry of metal clusters. Firstly, various studies have shown that the softness, a global property measuring the response of a system to the change in the number of electrons at fixed external potential, is directly related to the static dipole polarizability α, a measure of the response of the electron cloud to the change in external potential (modification of external electric field) at a fixed number of electrons.[60−66] Secondly, the chemical potential and the hardness are related to the reactivity and the charge transfer between the metal cluster and an adsorbate upon chemical bond formation.[34,67] Moreover, Ghanty et al. noticed that the condition of maximum hardness, which can be regarded as a criterion of stability,[68] can in general be associated to the minimum polarizability.[69] Thus, the chemical reactivity could be guided by the evolution of hardness or polarizability upon reaction.

In this section, we show the relation between hardness and relaxation of valence levels when an electron is added or removed from the electronic system. We then propose various ways to estimate these properties and calculate the hardness $\eta(n)$ and chemical potential $\mu(n)$ for the $Cu_n(y,w)$ copper clusters.

We first consider a neutral cluster containing n copper atoms, with N_0 electrons explicitly taken into account in the calculations; here, $N_0 = 11 \cdot n$, since 11 electrons per atom are not frozen. Janak showed that the DFT total energy can be seen as a continuous function of the occupation vector and thus of the number of electrons, N, in the system.[40] The total energy of Cu_n^{+x}, $E(n, N = N_0 - x)$, obtained by the removal of a negative charge $x|e|$ (x is not necessarily an integer), can be expressed from the total energy of the neutral cluster, $E(n,N_0)$, by means of a series:[38,67]

$$E(n, N = N_0 - x) = E(n, N_0) - x\left(\frac{\partial E}{\partial N}\right)_{N=N_0} + (x^2/2)\left(\frac{\partial^2 E}{\partial N^2}\right)_{N=N_0} - R(x^3) \quad (3)$$

$R(x^3)$ contains the higher-order terms of the series. An analogous expression can be written when considering the addition of a partial charge x. We recall that, in DFT, the first derivative of the expansion, $(\delta E/\delta N)_{N = N_0}$, considering either charge removal or addition, is defined as the electronic chemical potential $\mu(n)$;[70] while half of the second derivative, $1/2(\delta^2 E/\delta N^2)_{N = N_0}$, corresponds to the absolute hardness[32] $\eta(n)$ or half of the inverse of the softness $[2S(n)]^{-1}$. The chemical potential, i.e., the opposite of the electronegativity, and the hardness can also be obtained in the finite difference approximation:[32]

$$\mu(n) \approx -\frac{IP(n) + EA(n)}{2} \; ; \quad \eta(n) \approx \frac{IP(n) - EA(n)}{2} \quad (4)$$

As discussed by several authors,[41,71−74] electronic open-shell systems have a single chemical potential while closed-shell systems do not have a unique chemical potential. Indeed, for the latter, the removed electron comes from the HOMO level while the added electron goes to the LUMO level. As a consequence, the derivative (at x = 0) of the energy with respect to the charge removed from the system, i.e. the chemical potential denoted μ^+, corresponds to the HOMO energy, according to Janak′s theorem;[40] similarly, the derivative of the energy with respect to the charge added to the system, i.e. μ^-, corresponds to the LUMO energy.

$$\mu^+(n) = \left(\frac{\partial E(n,N)}{\partial(N_0 - x)}\right)_{N_0^+} = \varepsilon_{HOMO}(n, N_0) \quad (5a)$$

$$\mu^-(n) = \left(\frac{\partial E(n,N)}{\partial(N_0 + x)}\right)_{N_0^-} = \varepsilon_{LUMO}(n, N_0) \quad (5b)$$

For closed-shell systems, the injection of Equations 5 into Equation 3 allows the definition of the ionization potential and electron affinity:

$$IP(n) = E(n,N_0 - 1) - E(n,N_0) = -\varepsilon_{HOMO}(n,N_0) + E^+_{rel}(n) \quad (6a)$$
$$-EA(n) = E(n,N_0 + 1) - E(n,N_0) = \varepsilon_{LUMO}(n,N_0) + E^-_{rel}(n) \quad (6b)$$

$E^+_{rel}(n)$ and $E^-_{rel}(n)$ are the relaxation energy when an electron is removed from the HOMO level and the relaxation energy when an electron is added to the LUMO of the cluster of size n, respectively. The relaxation energies, as defined here, are expressed as follows:

$$E^+_{rel(n)} = \eta^+(n) + R^+(n) = IP(n) + \varepsilon_{HOMO}(n,N_0) \quad (7a)$$
$$E^-_{rel(n)} = \eta^-(n) + R^-(n) = -EA(n) + \varepsilon_{LUMO}(n,N_0) \quad (7b)$$

where $R^+(n)$ and $R^-(n)$ are the values of the higher-order terms $R(x^3)$ in the series (Eq. 3) for $x = 1$ when the electron is removed or added to the system, respectively:

$$R^+(n) = \sum_{i=3} \frac{(-1)^i}{i!} \left(\frac{\partial^i E}{\partial N^i} \right)_{N=N_0} \quad (8a)$$

$$R^-(n) = \sum_{i=3} \frac{1}{i!} \left(\frac{\partial^i E}{\partial N^i} \right)_{N=N_0} \quad (8b)$$

When $R^+(n)$ and $R^-(n)$ can be neglected, the relaxation energy of the valence levels is directly related to the hardness of the electronic system. In this approximation, *we propose a new expression for the hardness*, which can be written as:

$$\eta_{ED}{}^+(n) = \frac{1}{2} \left(\frac{\partial^2 E(n,N)}{\partial (N_0 - x)^2} \right)_{N_0^+} \cong IP(n) + \varepsilon_{HOMO}(n,N_0) \quad (9a)$$

$$\eta_{ED}{}^-(n) = \frac{1}{2} \left(\frac{\partial^2 E(n,N)}{\partial (N_0 + x)^2} \right)_{N_0^-} \cong -EA(n) - \varepsilon_{LUMO}(n,N_0) \quad (9b)$$

The hardnesses estimated using Equation 9 are denoted $\eta_{ED}(n)$, since the ionization potential and electron affinity are evaluated as total energy differences (ED).

The *IP* and *EA* values can also be calculated using Slater's transition state concept;[75−77] the simplest approach is to consider the opposite of the eigenenergy of the HOMO-[LUMO] coming from the neutral system, when this orbital is occupied by half of an electron, as the value of the ionization potential [electron affinity]. Consequently, the hardnesses of a system can be estimated only from the eigenvalues of the frontier orbitals for neutral and partially ionized systems:

$$\eta^-{}_{Slater}(n) \approx -\varepsilon_{HOMO}(n,N_0 - 1/2) - \varepsilon_{HOMO}(n,N_0) \quad (10a)$$
$$\eta^+{}_{Slater}(n) \approx -\varepsilon_{LUMO}(n,N_0 + 1/2) - \varepsilon_{LUMO}(n,N_0) \quad (10b)$$

Since, for the copper clusters we study here, the HOMO −LUMO gap is very small (as discussed above), we may consider in a first good approximation that unique (average) first and second derivatives of the energy can satisfactorily characterize the chemical potential and absolute hardness of the copper clusters (closed-shell and open-shell). Hence, the HOMO and LUMO eigenenergies written in the above relations can be replaced by the chemical potential of the copper clusters. This approximation becomes increasingly accurate for closed-shell systems as the size of the cluster expands, the electronic structure then approaching that of the metal, for which the chemical potential of the electrons and hardness are well-defined concepts[33]. Taking this approximation and neglecting the high-order terms $R(x^3)$ of the series in Eq. 3, the total energy difference, $[E(n, N_0 - x) - E(n, N_0)]$, displays a parabolic dependence on charge x:

$$[E(n,N_0 - x) - E(n.N_0)] = -\mu(n)x + \eta(n)x^2 \quad (11)$$

For $x = -1|e|$ and $x = 1|e|$, i.e. in the finite-difference approximation, Equation 11 provides $EA(n)$ and $IP(n)$ values that can be recombined to express $\mu(n)$ and $\eta(n)$ as in Equation 4. In order to improve on the accuracy of $\mu(n)$ and $\eta(n)$ with respect to the definitions given in Equation 4, we have considered a set of charges x ($x = -1|e|$; $x = -0.5|e|$; $x = 0|e|$; $x = 0.5|e|$; $x = 1|e|$) and interpolated the SCF total energy difference $[E(n,N_0 - x) - E(n,N_0)]$ through the second-order polynomial of Equation 11, for each size n of the clusters. The chemical potential and hardness of $Cu_n(y,w)$ clusters resulting from the above interpolation are denoted below $\mu(n)$ and $\eta(n)$ (without any indices).

Figure 7 shows the calculated $[E(n,N_0 - x) - E(n,N_0)]$ for $Cu_{20}(10,10)$ carrying different charges, together with the second-order fit. The value of the first derivative of this expression for $x = 0$ gives an estimate of the electronic chemical potential of the cluster $[-\mu(20)]$ while the curvature of the parabola (Eq. 10) is an estimate of the hardness of the cluster $[\eta(20)]$. The graph of Figure 7 provides the values of *EA*, *IP*, and μ for $Cu_{20}(10,10)$: respectively 2.9 eV, 5.8 eV, and −4.4 eV. We obtain the trend that the differences between $IP(20)$ and $-\mu(20)$ or between $-EA(20)$ and $\mu(20)$ are mainly related to the hardness $\eta(20)$ and only weakly depend on the higher terms R in the expressions 7a and 7b: $\{IP(20) - [-\mu(20)]\} = 1.43$ eV and $[-\mu(20) - EA(20)] = 1.45$ eV are both very close to the curvature of the parabola $\eta(20) = 1.44$ eV.

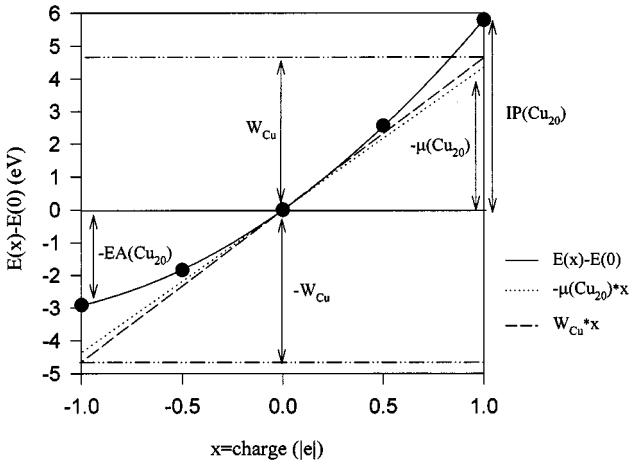


Figure 7. Calculated total energy of $Cu_{20}(10,10)$ as a function of charge x (full circles). The parabola interpolated from the calculated points (Equation 11) is represented by a full line. The dotted line represents the tangent of the parabola at the origin, which corresponds to $[-\mu(Cu_{20}) \cdot x]$, and the dashed line represents $[W_{Cu} \cdot x]$. The arrows point to specific values, such as $IP(Cu_{20})$, $EA(Cu_{20})$, and $\mu(Cu_{20})$.

We now apply the relations defined above and compare the results to those obtained from the interpolation using Equation 11. Table 1 lists the energies of the HOMO and LUMO levels as a function of cluster size as well as the chemical potentials estimated from the slope at the origin of the interpolated parabola (Eq. 11). The μ values are very close to the HOMO or LUMO energies of the neutral $Cu_n(y,w)$ clusters. This confirms that Equation 11 is a

reasonable way to determine the chemical potential [we note that both frontier orbital energies are given in Table 1 since: (i) the calculations were performed at the unrestricted level; and (ii) the copper clusters having an even number of atoms are not necessarily closed-shell systems].

Table 1. Comparison between the chemical potential $\mu(n)$, estimated as the slope at the origin of the interpolated parabola described by Equation 11, and the eigenenergies of the frontier orbitals of the neutral copper clusters $Cu_n(y,w)$ with $n = 9-20$. All the electronic properties are given in eV.

n	$\mu(n)$	$\varepsilon_{HOMO}(n,N_0)$	$\varepsilon_{LUMO}(n,N_0)$
9	−4.13	−4.13	−4.02
10	−4.29	−4.30	−4.18
11	−4.37	−4.41	−4.26
12	−4.36	−4.51	−4.19
13	−4.12	−4.16	−4.03
14	−4.16	−4.18	−4.15
16	−4.17	−4.21	−4.07
18	−4.25	−4.23	−4.17
20	−4.36	−4.41	−4.38

Table 2 compares the energies of the frontier levels when they are occupied by half an electron with the electron affinity and ionization potential coming from total energy differences. The results show that the use of Slater′s transition state gives the right order of magnitude for the ionization potential and electron affinity. However, this simple approximation introduces some inaccuracy in the estimates of EA [err$|EA - \varepsilon_{LUMO}| = 0.28$ eV] and IP [err$|IP - \varepsilon_{HOMO}| = 0.14$ eV] and, consequently, also in Equations 10 which gives the hardness η_{Slater}.

Table 2. Comparison between the electron affinity (EA) and ionization potential (IP) of the $Cu_n(y,w)$ clusters, calculated using total energy differences and with the eigenenergies of the HOMO and LUMO levels occupied by half of an electron and coming from those of the neutral system (Err is the mean error). All the electronic properties are given in eV.

n	$EA(n)$	$\varepsilon_{LUMO}(n,N_0 + 1/2)$	$IP(n)$	$\varepsilon_{HOMO}(n,N_0 - 1/2)$
9	2.13	−2.82	6.12	−6.22
10	2.34	−2.38	6.22	−6.13
11	2.44	−3.06	6.29	−5.97
12	2.48	−2.42	6.31	−6.20
13	2.33	−2.77	5.90	−5.75
14	2.52	−2.54	5.77	−5.81
16	2.66	−2.46	5.66	−5.67
18	2.69	−2.60	5.82	−5.83
20	2.91	−3.26	5.79	−6.21
Err $\lvert EA - \varepsilon_{LUMO}\rvert = 0.28$ eV $\lvert IP - \varepsilon_{HOMO}\rvert = 0.14$ eV				

In Table 3, we compare the hardness values calculated in various ways. These all provide the right order of magnitude. However, the results from Equation 10 miss what appears as the reasonable evolution of the relaxation energy and hardness, i.e. their decrease with cluster size; it is likely that an improved approximation, such as the Generalized Slater′s Transition State method,[76] would give the right evolution.

A relationship between the polarizability and the electronic relaxation of valence levels also exists since, as we have mentioned above, the hardness is related to the polarizability. In fact, a low relaxation energy implies a low energy cost of the deformation of the electronic cloud. Hence, the smaller the relaxation energy of valence molecular orbitals, the smaller the hardness and the higher the polarizability of the system.

Table 3. Comparison among: (i) the hardness, η, evaluated as the curvature of the interpolated parabola described by Equation 11; (ii) the hardness, η^+_{ED} and η^-_{ED}, estimated from Equations 9a and 9b; and (iii) the hardness, η^+_{Slater} and $\eta^-_{Slater}(n)$, coming from Equations 10a and 10b. The values are in eV.

n	$\eta^+_{ED}(n)$	$\eta^-_{ED}(n)$	$\eta^+_{Slater}(n)$	$\eta^-_{Slater}(n)$	$\eta(n)$
9	1.99	1.89	2.09	1.20	2.00
10	1.92	1.84	1.83	1.80	1.96
11	1.89	1.82	1.57	1.20	1.93
12	1.80	1.71	1.69	1.77	1.91
13	1.74	1.69	1.59	1.26	1.79
14	1.59	1.63	1.63	1.61	1.62
16	1.45	1.41	1.46	1.61	1.48
18	1.58	1.48	1.60	1.57	1.57
20	1.39	1.47	1.81	1.12	1.44

2. Evolution of the Chemical Potential and Hardness with the Size of Copper Clusters: The knowledge of the chemical potential and hardness of the copper clusters allows us to characterize the evolution of these properties with size, from a small metal cluster to bulk metal. Since the relationship between hardness, polarizability, and relaxation energy of the valence levels has been pointed out above, we also discuss the evolution of these properties.

The evolution of the parameters μ and η of the parabola (Equation 11) has been analyzed as a funtion of the size of the cluster. The results are presented in Figure 8. We first discuss the behavior of the first derivative in the expansion, $-\mu(n)$. Figure 8 indicates that $-\mu$ remains close to the value of W_{Cu} whatever the size; it slowly converges towards the workfunction of the metal surface for an infinite size, as found within the jellium model.[78] The oscillation of the chemical potential of the metal clusters is weaker than that of IP or EA since the chemical potential can be seen as an average of these properties (Eq. 4). Hence, the slope of the average evolution of $IP(n)$, $EA(n)$ and $-\mu(n)$ should also be correlated. The average evolutions were found above for $EA(n) = 4.65 - 5.073 \cdot n^{-1/3}$ and $IP(n) = 4.65 + 3.166 \cdot n^{-1/3}$. The slope D of $-\mu(n) = 4.65 - D \cdot n^{-1/3}$ can be directly evaluated by using the interpolation formulae (Eq. 2) of $IP(n)$ and $EA(n)$ in Equation 4; it appears that $D = (5.073 - 3.166)/2 = 0.954$, which is in good agreement with the value of $D = 0.938$ calculated from a linear regression of $-\mu(n)$ for $n = 9-20$:

$$-\mu(n) = 4.65 - 0.954 \cdot n^{-1/2} \quad (12)$$

The small value of coefficient D leads to a relatively weak dependence of μ on n, in the range of n studied; this rationalizes the proximity between $-\mu$ and W_{Cu} and the slow convergence of $-\mu$ towards W_{Cu}, i.e. the quasi-constant character of μ in the clusters studied here. The HOMO energy of copper clusters (Table 1), and thus the chemical potential as calculated here (since the gap is very small), is then a

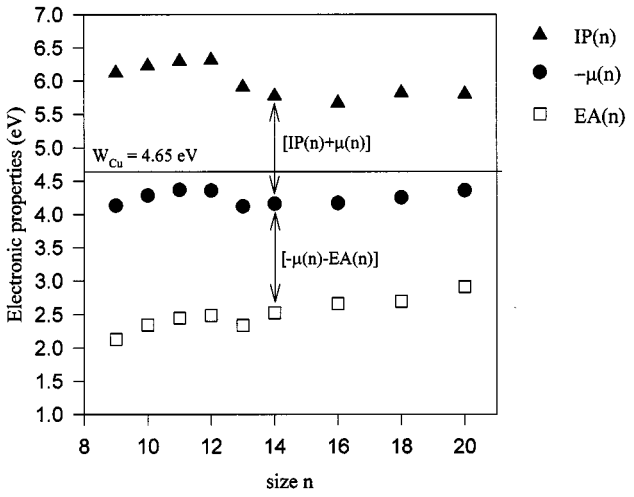


Figure 8. Evolution of the electronic properties of $Cu_n(y,w)$ with size n: (i) opposite of the chemical potential $-\mu(n)$ (full circles); (ii) $IP(n)$ (full triangles); and (iii) $EA(n)$ (open squares). The solid line indicates the workfunction of the metal.

good approximation of the workfunction of the metal. This result was first observed by Russier et al. for other transition metal clusters such as those of palladium.[79]

The hardness, $\eta(n)$, decreases as a function of size of the cluster (Figure 9). This trend is similar to that found for sodium clusters (Na_n).[63,65] The curvature of the parabola $\eta(n)$ (represented in Figure 7 for $n = 20$) decreases with increasing size n, hence the edges of the parabola for $x = -1$ and 1, i.e. EA and IP respectively, tend to become equal to the workfunction W, as shown in Figure 6. The decrease in hardness with cluster size is fully consistent with the expected evolution of the polarizability and relaxation energy. As the copper clusters grow, the number of valence levels that are close in energy increases, which induces a smaller relaxation energy and a higher polarizability.[63,80]

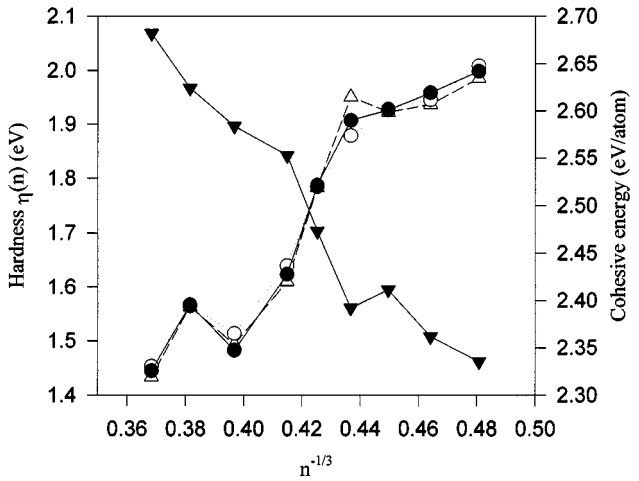


Figure 9. Evolution of the cohesive energy per atom (full triangles) and chemical hardness of the copper clusters $Cu_n(y,w)$. The full circles represent the hardness evaluated from the curvature of the polynomial expression (Eq. 11, Figure 7); the other two curves represent the evolution of $[IP(n) + \mu(n)]$ (open triangles) and $[-\mu(n) - EA(n)]$ (open circles).

For bulk metals, n is considered to be infinite and the relaxation energy when removing an electron at the Fermi energy is zero [for $n = \infty$, IP becomes the workfunction and the HOMO level corresponds to the Fermi level; Equation 7a then becomes: $E^+_{rel}(n = \infty) = 0$]. Equation 7a shows that the non-zero value of the hardness of a metal surface exactly corresponds to the opposite of the higher-order terms in the series of Eq. 3, $-R^+(n = \infty)$. Hence, as the hardness is also the inverse of the density of states at the Fermi level $g(E_F)$,[33] we obtain the following equalities:

$$\eta(n = \infty) = -R^+(n = \infty) = 1/[2g(E_F)] \quad (13)$$

This shows the direct relationship, for a bulk metal, between the higher-order terms in the series of Eq. 3 and the density of states at the Fermi level.

It has been demonstrated that hardness modifications with size are related to the shell structure in atoms or metal clusters.[65,81] The hardness of real copper clusters possessing a magic size is expected to be larger than that of the neighboring sizes, as observed for Li_n clusters;[82] clusters with a magic size adopt a geometric structure such that a shell is filled, so that hardness is maximized according to the maximum hardness principle.[68] Consequently, as for the other properties [$IP(n)$, $EA(n)$], the absence of shell structure in the model copper clusters can be advantageous to evaluate the average evolution of hardness with size. Figure 9 indicates that the $[-\mu(n) - EA(n)]$ and $[IP(n) + \mu(n)]$ curves are similar to that of $\eta(n)$; this shows that the simple relation (Eq. 4) defining the hardness from EA and IP is valuable for finite copper clusters $Cu_n(y,w)$. Of course, Equation 4 is not valid for infinite metal clusters (according to it, the hardness would be zero, whereas the hardness of a metal is non-zero); nevertheless, since the hardness of a metal is small [$g(E_F)$ is large], it is reasonable to use Equations 4 and 2 to estimate the hardness of large clusters; injecting Equation 1 into 3 gives the following relation:

$$\eta(n) = 4.120 \cdot n^{-1/3} \quad (14)$$

The comparison between the evolutions of chemical potential (Eq. 12) and hardness (Eq. 14) illustrates that the hardness varies much more strongly than the chemical potential with size. In the expression of the total energy as a series (Eq. 3), it is the second-derivative term, related to the relaxation energy (Eq. 8) and hardness, that is mostly responsible for the variation of $IP(n)$ and $EA(n)$ when the size n is changed, as already indicated for IP by Russier[41].

We have also calculated the cohesive energy of the $Cu_n(y,w)$ copper clusters (binding energy per atom); it is found to evolve in a roughly linear manner with respect to $n^{-1/3}$ (Figure 9). This is in good agreement with the previous study by Delley et al. on quasi-spherical copper clusters.[25] Figure 9 clearly shows that when the cluster size increases, the cohesive energy increases while the hardness decreases. The same kind of observation was made by Ghanty et al.[63] for Na_n clusters; these authors pointed out a polarizability increase as well as a cohesive energy increase with size of the Na_n clusters. To the best of our

knowledge, no analytical relation between cohesive energy and hardness has been established. Such a relationship would probably be linked to another concept (which is not related to size dependence): the maximum hardness principle,[68] which is a stability criterion and could be associated to a minimum polarizability condition, as has been suggested by Ghanty.[69]

Synopsis

Density Functional Theory has been used to study the dependence of the size of copper clusters $Cu_n(y,w)$ (n = 9−20) modeling the Cu(100) surface on their electronic properties. A comparison has been made between real quasi-spherical clusters, flat clusters modeling the surface, and the actual metal surface. We can draw the following major conclusions:

(i) The electronic structure of the copper clusters modeling the surface involves the absence of shell effect and even-odd oscillation in the evolution of *EA* and *IP* with size. Consequently, the evolution of *IP* and *EA* with $n^{-1/3}$ is quasi-linear, which allows the extrapolation of these properties to large copper clusters, for which such DFT calculations are intractable.

(ii) The DOS analysis of the model $Cu_{10}(6,4)$ cluster, compared to that of the quasi-spherical $Cu_{10}^{D_{4d}}$, shows that the absence of shell structure in the flat copper clusters is due to their geometric structure. The DOS of the surface-modeling clusters are similar to the photoemission spectrum of the actual Cu(100) surface, indicating the better adequacy of such surface models to simulate the metal surface, compared to real copper clusters.

(iii) Another important feature of the electronic structure of the $Cu_n(y,w)$ model surfaces is the small HOMO-LUMO gap. This allows one to consider energy derivatives with respect to charge removal or addition to be equal for closed-shell systems. Hence, it is possible to define global properties such as the chemical potential, μ, and the absolute hardness, η, whatever the size and the closed or open shell character. These properties are estimated as derivatives of the total energy versus charge, where the energy function is a second-order polynomial interpolated from SCF total energies calculated for partially negatively and positively charged clusters.

(iv) By exploiting the newly established relationship between hardness and relaxation energy of the valence levels when an electron is added to or removed from the system, it becomes possible to estimate the hardness from the eigenenergies of the frontier levels of the neutral and partially ionized systems.

(v) The average evolutions of the chemical potential and hardness can be extrapolated vs. $n^{-1/3}$ from the expressions of *IP* and *EA* vs. $n^{-1/3}$. The chemical potential of small copper clusters is close to the workfunction of a polycrystalline copper surface and is already a good estimate of this macroscopic property. The hardness decreases significantly with size; this is directly related to the decrease in relaxation energy of the valence levels and the increase in polarizability when increasing the size towards the metal.

In a forthcoming paper, we intend to exploit the knowledge base obtained in the present work to study the influence of the copper cluster size on the adsorption of organic molecules such as acrylonitrile; the adsorption of acrylonitrile on copper surfaces and copper electrodes has indeed been identified as the initial step leading to the grafting of polyacrylonitrile on a copper cathode through electropolymerization, a process that holds much promise for the surface protection of commodity metals.[83−85]

Acknowledgments

The Mons−Saclay collaboration is conducted in the framework of the "TOURNESOL" bilateral programme between Belgium and France (contract 98.026). The work in Mons is partly supported by the Belgian Federal Government "Service des Affaires Scientifiques, Techniques et Culturelles (SSTC)" in the framework of the "Pôle d'Attraction Interuniversitaire en Chimie Supramoléculaire et Catalyse Supramoléculaire (PAI 4/11)", FNRS-FRFC, and an IBM Academic Joint Study. XC is a grant holder of "Fonds pour la Formation à la Recherche dans l'Industrie et dans l'Agriculture (FRIA)". RL is Maître de Recherches of the Belgian "Fonds National de la Recherche Scientifique (FNRS)".

[1] G. Schmid, *Chem. Rev.* **1992**, *92*, 1709−1727.
[2] R. S. Berry, *Chem. Rev.* **1993**, *93*, 2379−2394.
[3] W. A. d. Heer, *Rev. Mod. Phys.* **1993**, *65*, 611−676.
[4] M. Brack, *Rev. Mod. Phys.* **1993**, *65*, 677−732.
[5] H. Haberland (Ed.) *Clusters of Atoms and Molecules*, Springer Series in Chemical Physics, 52 (Germany, **1995**).
[6] J. Shi, S. Gider, K. Babcock, D. D. Awschalom, *Science* **1996**, *271*, 937−941.
[7] L. S. Zheng, C. M. Kraner, P. J. Brucat, S. H. Yang, C. L. Pettiette, M. J. Craycraft, R. E. Smalley, *J. Chem. Phys.* **1986**, *85*, 1681−1688.
[8] D. G. Leopold, J. Ho, W. C. Lineberger, *J. Chem. Phys.* **1987**, *86*, 1715−1726.
[9] C. L. Pettiette, S. H. Yang, M. J. Craycraft, J. Conceicao, R. T. Laaksonen, O. Cheshnovsky, R. E. Smalley, *J. Chem. Phys.* **1988**, *88*, 5377−5382.
[10] M. F. Jarrold, K. M. Creegan, *Int. J. Mass Spectrom. Ion Processes* **1990**, *102*, 161−181.
[11] J. Ho, K. M. Ervin, W. C. Lineberger, *J. Chem. Phys.* **1990**, *93*, 6987−7002.
[12] K. J. Taylor, C. L. Pettiette, O. Cheshnovsky, R. E. Smalley, *J. Chem. Phys.* **1992**, *96*, 3319−3329.
[13] G. Makov, A. Nitzan, L. E. Brus, *J. Chem. Phys.* **1988**, *88*, 5076−5085.
[14] M. Seidl, K. H. Meiwes-Broer, M. Brack, *J. Chem. Phys.* **1991**, *95*, 1295−1303.
[15] M. Brack, *Phys. Rev. B* **1989**, *39*, 3533−3542.
[16] K. Clemenger, *Phys. Rev. B* **1985**, *32*, 1359−1362.
[17] O. B. Christensen, K. W. Jacobsen, J. K. Norskov, M. Manninen, *Phys. Rev. Lett.* **1991**, *66*, 2219−2222.
[18] R. C. Baetzold, R. E. Mack, *J. Chem. Phys.* **1975**, *62*, 1513−1520.
[19] A. B. Anderson, *J. Chem. Phys.* **1978**, *68*, 1744−1751.
[20] C. Bachmann, J. Demuynck, A. Veillard, *Faraday Symp.* **1980**, *14*, 170−179.
[21] J. Demuynck, M. M. Rohmer, A. Strich, A. Veillard, *J. Chem. Phys.* **1981**, *75*, 3443−3453.
[22] J. Flad, G. Igelmann, H. Preuss, H. Stoll, *Surf. Sci.* **1985**, *156*, 379−385.
[23] D.-W. Liao, K. Balasubramanian, *J. Chem. Phys.* **1992**, *97*, 2548−2552.
[24] R. P. Messmer, S. K. Knudson, K. H. Johnson, J. B. Diamond, C. Y. Yang, *Phys. Rev. B* **1976**, *13*, 1396−1415.

[25] B. Delley, D. E. Ellis, A. J. Freeman, E. J. Baerends, D. Post, *Phys. Rev. B* **1983**, *27*, 2132−2144.
[26] G. S. Painter, F. W. Averill, *Phys. Rev. B* **1983**, *28*, 5536−5547.
[27] K. Jackson, *Phys. Rev. B* **1993**, *47*, 9715−9722.
[28] C. Massobrio, A. Pasquarello, R. Car, *Chem. Phys. Lett.* **1995**, *238*, 215−221.
[29] P. Calaminci, A. M. Köster, N. Russo, D. R. Salahub, *J. Chem. Phys.* **1996**, *105*, 9546−9556.
[30] C. Bureau, G. Lécayon, *J. Chem. Phys.* **1997**, *106*, 8821−8829.
[31] R. G. Pearson, *J. Am. Chem. Soc.* **1963**, *85*, 3533−3539.
[32] R. G. Parr, R. G. Pearson, *J. Am. Chem. Soc.* **1983**, *105*, 7512−7516.
[33] W. Yang, R. G. Parr, *Proc. Natl. Acad. Sci. USA*. **1985**, *82*, 6723−6726.
[34] R. F. Nalewajski, *J. Am. Chem. Soc.* **1984**, *106*, 944−945.
[35] C. F. Zinola, A. J. Arvia, G. L. Estiu, E. A. Castro, *J. Phys. Chem.* **1994**, *98*, 7566−7576.
[36] S. Seong, A. B. Anderson, *J. Phys. Chem.* **1996**, *100*, 11744−11747.
[37] J. T. Stuckless, C. E. Wartnaby, N. Al-Sarraf, S. J. B. Dixon-Warren, M. Kovar, D. A. King, *J. Chem. Phys.* **1997**, *106*, 2012−2030.
[38] R. G. Parr, W. Yang, *Density-Functional Theory of Atoms and Molecules*; Oxford University Press (New York, **1989**).
[39] D. P. Chong, *Recent Advances in Density Functional Methods*; World Scientific (Singapore, **1995**), Vol. 1.
[40] J. F. Janak, *Phys. Rev. B* **1978**, *18*, 7165−7168.
[41] V. Russier, *Phys. Rev. B* **1992**, *45*, 8894−8901.
[42] B. Delley, *J. Chem. Phys.* **1990**, *92*, 508−517.
[43] B. Delley, *New. J. Chem.* **1992**, *16*, 1103−1107.
[44] D. Ellis, G. Painter, *Phys. Rev. B.* **1968**, *56*, 2887−2895.
[45] Biosym/MSI. DMol 95.0/3.0.0, *Quantum Chemistry User Guide* (San Diego, **1995**).
[46] H. Vosko, L. Wilk, M. Nusair, *Can. J. Phys.* **1980**, *58*, 1200−1211.
[47] T. Ziegler, *Chem. Rev.* **1991**, *91*, 651−667.
[48] R. O. Jones, O. Gurnnarsson, *Rev. Mod. Phys.* **1989**, *61*, 689−746.
[49] F. L. Hirshfeld, *Theoret. Chim. Acta.* **1977**, *44*, 129−138.
[50] B. Delley, *Chem. Phys.* **1986**, *110*, 329−338.
[51] P. A. Montano, G. K. Shenoy, E. E. Alp, W. Schulze, J. Urban, *Phys. Rev. Lett.* **1986**, *56*, 2076−2079.
[52] E. A. Rohlfing, J. J. Valentini, *J. Chem. Phys.* **1986**, *84*, 6560−6566.
[53] I. Katakuse, T. Ichihara, Y. Fujita, T. Matsuo, T. Sakurai, H. Matsuda, *Int. J. Mass Spectrom. Ion Processes* **1985**, *67*, 229−236.
[54] M. Brack, O. Genzken, K. Hansen, *Z. Phys.* **1990**, *D 19*, 51−53.
[55] J. M. Burkstrand, G. G. Kleiman, G. G. Tibetts, J. C. Tracy, *J. Vac. Sci. Tech.* **1976**, *13*, 291−295.
[56] P. O. Löwdin, *J. Chem. Phys.* **1950**, *18*, 365−375.
[57] H. Müller, H. G. Fritsche, L. Skala, Chap 2.5: Analytic Cluster Models and Interpolation Formulae for Clusters Properties, In *Clusters of Atoms and Molecules I*; Haberland, H., (Germany, **1995**); pp 114−140.
[58] Z. Y. Zhang, D. C. Langreth, J. P. Perdew, *Phys. Rev. B* **1990**, *41*, 5674−5684.
[59] R. Monnier, J. P. Perdew, *Phys. Rev. B* **1978**, *17*, 2595−2611.
[60] P. J. Politzer, *J. Chem. Phys.* **1987**, *86*, 1072−1073.
[61] A. Vela, J. L. Gazquez, *J. Am. Chem. Soc.* **1990**, *112*, 1490−1492.
[62] J. K. Nagle, *J. Am. Chem. Soc.* **1990**, *112*, 4741−4747.
[63] T. K. Ghanty, S. K. Ghosh, *J. Phys. Chem.* **1993**, *97*, 4951−4953.
[64] T. K. Ghanty, S. K. Ghosh, *J. Phys. Chem.* **1994**, *98*, 9197−9201.
[65] S. Hati, D. Datta, *J. Phys. Chem.* **1994**, *98*, 10451−10454.
[66] S. Hati, D. Datta, *J. Phys. Chem.* **1995**, *99*, 10742−10746.
[67] W. J. Mortier, S. K. Ghosh, S. Shankar, *J. Am. Chem. Soc.* **1986**, *108*, 4315−4320.
[68] R. G. Parr, P. K. Chattaraj, *J. Am. Chem. Soc.* **1991**, *113*, 1854−1857.
[69] T. K. Ghanty, S. K. Ghosh, *J. Phys. Chem.* **1996**, *100*, 12295−12298.
[70] R. G. Parr, R. A. Donnelly, M. Levy, W. E. Palke, *J. Chem. Phys* **1978**, *68*, 3801−3807.
[71] J. P. Perdew, R. G. Parr, M. Levy, J. L. Balduz, *Phys. Rev. Lett.* **1982**, *49*, 1691−1694.
[72] R. G. Parr, L. J. Bartolotti, *J. Phys. Chem.* **1983**, *87*, 2810−2815.
[73] J. Cioslowski, B. B. Stefanov, *J. Chem. Phys.* **1993**, *99*, 5151−5162.
[74] M. H. Cohen, M. V. Ganduglia-Pirovano, J. Kudrnovsky, *J. Chem. Phys.* **1994**, *101*, 8988−8997.
[75] J. C. Slater, *Adv. Quantum Chem.* **1972**, *6*, 1.
[76] A. R. Williams, R. A. deGroot, C. B. Sommers, *J. Chem. Phys.* **1975**, *63*, 628−631.
[77] D. P. Chong, *Chem. Phys. Lett.* **1995**, *232*, 486−490.
[78] E. Engel, J. P. Perdew, *Phys. Rev. B* **1991**, *43*, 1331−1337.
[79] V. Russier, D. R. Salahub, C. Mijoule, *Phys. Rev. B.* **1990**, *42*, 5046−5056.
[80] D. E. Beck, *Phys. Rev. B* **1984**, *30*, 6935−6942.
[81] R. Parr, Z. Zhou, *Acc. Chem. Res.* **1993**, 256−258.
[82] M. K. Harbola, *Proc. Natl. Acad. Sci. USA* **1992**, *89*, 1036−1039.
[83] G. Lécayon, Y. Bouizem, C. Le Gressus, C. Reynaud, C. Boiziau, C. Juret, *Chem. Phys. Lett.* **1982**, *91*, 506−510.
[84] C. Bureau, G. Deniau, P. Viel, G. Lécayon, J. Delhalle, *J. Adhesion* **1996**, *58*, 101−121.
[85] X. Crispin, R. Lazzaroni, V. Geskin, N. Baute, P. Dubois, R. Jérôme, J. L. Brédas, *J. Am. Chem. Soc.*, in press.

Received August 27, 1998
[I98292]

Modification of the Adsorption and Catalytic Properties of Molecular Sieves by Reaction with Organometallic Complexes

Frédéric Lefebvre,[a] Aimery de Mallmann,[a] and Jean-Marie Basset*[a]

Keywords: Zeolites / Transition metals / Organometallic compounds / Adsorption properties

Molecular sieves can be modified by organometallic complexes using two different methods: (i) OMCVD (organometallic chemical vapor deposition), where a multilayered organometallic fragment is calcined and transformed into an oxide of rather indefinite composition, and (ii) SOMC (surface organometallic chemistry), where an organometallic fragment is grafted with retention of its molecular integrity. Both methods may lead to a grafting, which can occur at the external surface and/or inside the channels of the zeolites. In the case of SOMC, by judicious choice of both the reaction conditions and the organometallic complexes, it is possible to modify only the external surface of the sieve, for example, of a mordenite. This can lead to a decrease of the surface acidity, allowing greater selectivity in catalytic reactions (such as xylene isomerization). Another application is the modification of the pore openings of the channels by grafting organometallic compounds near the pore entrances. This results in a modification of the adsorption characteristics of the molecular sieve, allowing a fine tuning of its properties. Depending on the size of the adsorbed molecule, two effects can be observed: (i) a total exclusion of the molecule from the channels of the molecular sieve, due to steric effects ("thermodynamic" control); (ii) a modification of the adsorption kinetics of the adsorbed molecule, depending greatly on its size and on the size of the organometallic fragment ("kinetic" control). Finally, the grafting reaction can, in some cases, occur inside the channels, thereby leading to effects similar to those described above and to a reduction of the adsorption capacity due to the presence of the grafted organometallic moieties within the pores.

[a] Laboratoire de Chimie Organométallique de Surface, UMR CNRS − CPE 9986,
43, Bd. du 11 Novembre 1918, F-69616 Villeurbanne Cedex, France
Fax: (internat.) + 33-4/72431795



Jean-Marie Basset was born in 1943. After studies at the ESCIL, he joined the Institut de Recherches sur la Catalyse at Lyon in 1965. He received his PhD in 1969 from the University of Lyon. After a postdoctoral period at the University of Toronto in 1969−1970 he returned to the Institut de Recherches sur la Catalyse where he developed a research group on olefin metathesis and organometallic chemistry on surfaces. He created an new laboratory called L.C.O.M.S. (Laboratoire de Chimie Organométallique de Surface) at the ESCPE-Lyon in 1993. His was elected to the French Academy of Sciences as Correspondent Member at the same period. He is at present developing the application of Surface Organometallic Chemistry to the design of catalysts and to new reactions such as alkanes metathesis.



Frédéric Lefebvre was born in Arras, France in 1956. He received the Agrégation in Chemistry in 1979. He worked first in the field of heteropolyanions with Prof. Hervé and after a 3rd cycle thesis he washired by CNRS and joined the Institut de Recherches sur la Catalyse in 1981 where he received his PhD in 1985. After a postdoctoral period at the University of Namur (Belgium) with Prof. Derouane, he returned to the Institut de Recherches sur la Catalyse where he was responsible of the solid-state NMR group until 1993. At this period he joined the group of Dr. Basset. He is actually in charge of the solid-state NMR and of the SOMC on zeolites and metathesis groups in the L.C.O.M.S. laboratory.



Aimery de Mallmann was born in Paris, France in 1960. He worked in the field of zeolites with Denise Barthomeuf and, after a 3rd cycle thesis in 1986, he was hired by CNRS and received a new thesis from University Paris VI in 1989. After a postdoctoral period at Texas A&M University with Jack Lunsford and one year spent at an industrial research center for Elf-Atochem, he joined L.C.O.M.S. group in 1993. His research in the field of zeolite, catalysis and organometallic chemistry is aimed at the rational design of heterogeneous catalysts for a variety of chemical transformations.

MICROREVIEWS: This feature introduces the readers to the authors' research through a concise overview of the selected topic. Reference to important work from others in the field is included.

 © WILEY-VCH Verlag GmbH, D-69451 Weinheim, 1999 1434−1948/99/0303−0361 $ 17.50+.50/0

Introduction

Molecular sieves, and more specifically zeolites, offer many applications, including catalysis (e.g. catalytic cracking, isomerization of xylenes, alkylation of aromatic compounds), separation processes (e.g. the preparation of oxygen or the removal of water from gases, solvents, etc.), not to mention one of their most important applications as bulk materials to replace phosphate compounds in detergents. Their cage-like structures of precise geometry, with pores of uniform shape running throughout the entire crystal, render them very useful for all these applications. Indeed, the limited size of the channels may prevent the formation of certain intermediates in catalytic reactions, thereby leading to unexpected selectivities (shape−form selectivity). Furthermore, the fixed dimensions of the channels lead to similar properties over the whole crystal.

Although more than fifty naturally occurring species have been characterized and more than 120 synthetic zeolites have been prepared,[1] it is not yet possible to vary the size of the pores and of the cages in a continuous, systematic manner. A zeolite is mainly composed of SiO_4 and AlO_4 tetrahedra and has a well-defined crystallographic structure. For a given zeolite, the size of the pores can be varied by cation exchange or by replacement of the Si or Al atoms by other atoms. This has led to numerous techniques for modification of the zeolitic pore system in a controlled manner, with the aim of improving their performances in catalysis and/or molecular separations. These techniques can generally be classified into three groups:[2]

(i) Modification by a Cation-Exchange Process: The zeolitic pore size can be altered, in a controlled manner, by a replacement of the exchangeable cations, which are normally located near the pore openings. This can lead to a significant alteration of the zeolitic pore structure.[3] A typical example is the adsorption of 2-methylpentane and 2,2-dimethylbutane on mordenite: both alkanes are adsorbed on a calcium mordenite, but only 2-methylpentane is adsorbed on a strontium- or barium-exchanged mordenite.[4] This observation can be simply explained in terms of a pore size reduction on going from the calcium-exchanged mordenite to the strontium and barium ones. As 2,2-dimethylbutane has a kinetic diameter slightly larger than that of 2-methylpentane, it will be excluded from the strontium- and barium-exchanged mordenites.

(ii) Modification by Preadsorption of Polar Molecules: Another method for modifying the molecular sieving effect of a zeolite is to preadsorb polar molecules. Indeed, these molecules will bind around the exchangeable cations and thereby modify the diffusion of adsorbed hydrocarbons. A typical example is the adsorption of butanes on a CaA zeolite, which shows a marked dependence on the amount of preadsorbed water or amines.[5]

(iii) Modification of the Zeolite Framework: Finally, pore size "engineering" in zeolites can be achieved by a modification of the zeolitic framework. This can be performed in various ways:

(a) Firstly, crystallographic changes can be obtained by thermal treatment. For example, thermal treatment of zeolites in the presence of water results in a modification of the pore sizes.[6] Indeed, steam treatment leads to migration and hydrolysis of the exchangeable cations. We will not describe this process in more detail here, as such modifications are not relevant in the realm of organometallic compounds.

(b) Another method is the internal and external structure modification of the zeolite framework by the incorporation of additional atom groups. Various methods have been described in the literature[7] such as silylation, disilylation, boration, etc. As silanes are organometallic compounds, we will briefly discuss these methods in the final part of this review, but we will describe more extensively the reactions of organotin compounds with cloverite, a recently discovered gallophosphate.[8]

(c) A third way of modifying the zeolite framework is to selectively modify the external surface of the zeolite crystal, leaving the internal channels or cavities unaffected. This is typically achieved by reaction with organometallic compounds (including silicon compounds) and will be reported in detail in the next section, in particular the modification of mordenite by reaction with organotin or -germanium compounds.

Modification of the External Surface of Zeolite Crystals

The first example of a variation of the properties of a zeolite by modification of the external surface was reported by Niwa et al. in 1984.[9] The principle of the method was relatively simple, its purpose being the deposition of an organometallic moiety on the zeolite surface that could not enter the pore system. The great advantage of this modification method was that the internal properties of the zeolite remained unchanged after the grafting reaction, in contrast to what was observed when the modification occurred inside the pores as well (see the next part of this review). In most cases, the zeolite used in these studies was mordenite. Indeed, mordenite has monodimensional channels (Figure 1)[6] and so, even if not all the pore openings were modified, an effect could still be observed. Indeed, modification of only 50% of the pore openings should lead, statistically, to 25% of the channels remaining unmodified, 25% of them being modified at both ends, and 50% of them having only one extremity modified. For zeolites with bi- or tri-dimensional channel systems (e.g. ZSM-5 or faujasite), modification of 50% of the channel apertures will have no effect on the adsorption properties since the molecules can enter via the unmodified channel apertures and occupy all the voids in the solid. Significant effects can only be observed when more than 95% of the pore openings are modified, a result which in practice is difficult to achieve. This accounts for the fact that, in most cases, the studies have been carried out on mordenite.

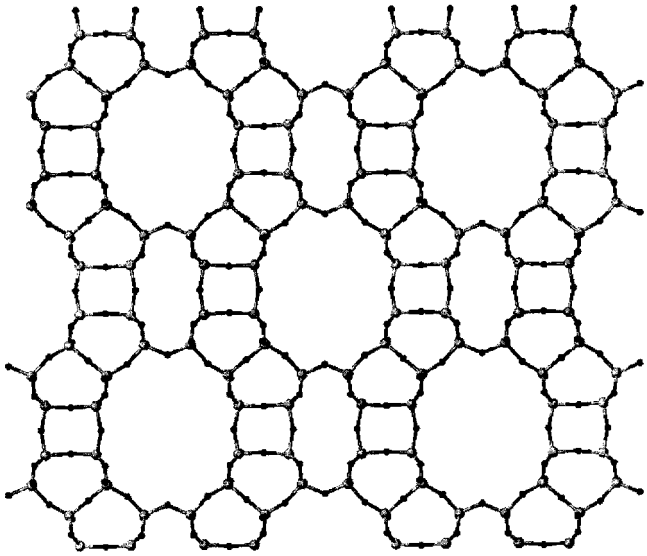


Figure 1. Schematic representation of the channels of mordenite

Niwa et al.[9] deposited $Si(OCH_3)_4$ on mordenite by chemical vapor deposition (C.V.D.). The C.V.D. technique differs quite significantly from surface organometallic chemistry (S.O.M.C.), which will be discussed later. In C.V.D., there is no control of the grafting process at the molecular level. Once one, or more typically, several layers of an organometallic have been grafted on a surface, thermal or chemical treatment leads to an inorganic material (usually an oxide, but possibly also a carbide, a nitride, etc.), which has a definite composition. In S.O.M.C., only one (or less than one) monolayer of an organomolecular fragment is grafted onto the surface, which thus retains, at least in part, its molecular integrity. In the case of the Niwa approach by OMCVD, $Si(OCH_3)_4$ was allowed to react with the hydroxy groups present on the external surface of the zeolite, thereby leading to a surface organometallic complex:

$$\equiv T-OH + Si(OCH_3)_4 \rightarrow \equiv T-O-Si(OCH_3)_3 + CH_3OH$$

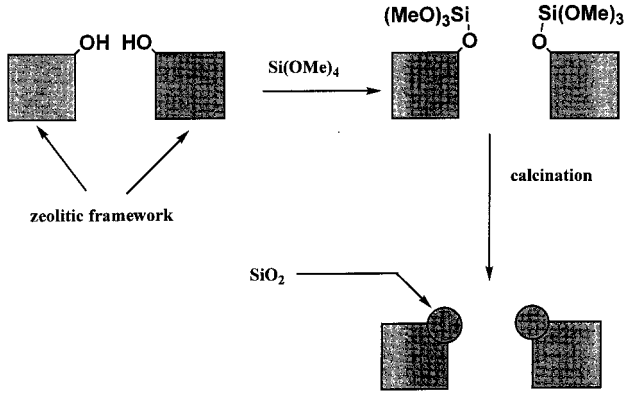
where T represents a framework atom such as Si or Al. This surface complex was then able to undergo further reactions with the hydroxy groups of the surface, leading to multigrafted species:

$$\equiv T-O-Si(OCH_3)_3 + x \equiv T-OH \rightarrow (\equiv T-O)_{1+x}Si(OCH_3)_{3-x} + x\ CH_3OH$$

$$T = Si, Al;\ x = 1, 2$$

The resulting materials were subsequently calcined under oxygen, leading to the formation of silica-coated zeolites by the elimination of the hydrocarbon residues (ligand and alcohol) as shown in Scheme 1.

Repetition of this process reduced the dimensions of the pore entrances by 0.1 nm for a single-step modification or by 0.2 nm for a multistep OMCVD modification. Adsorption of *p*-xylene was greatly modified on these materials;



Scheme 1. Modification of the pore entrance of a zeolite by reactions with $Si(OMe)_4$

while this molecule was easily adsorbed on unmodified mordenite (Large pore from Norton), it was totally excluded from the same zeolite modified by grafting $Si(OCH_3)_4$ (2.7 wt.-% complex) and subsequent calcination. A study of the reaction on the surface of mordenites with various Si/Al ratios was carried out, the results of which showed that the amount of adsorbed methoxysilane depended on this parameter, the "epitaxial" growth of the SiO_2 layer on the external surface being perturbed by the aluminium atoms.[10]

Various other silicon-containing molecules have been used, for example $(C_3H_7)_3Si(OCH_3)$, which led only to a monografted complex, the Si−C bond being very stable,[11] or chlorosilanes.[12] With the latter, the reaction led to the formation of hydrochloric acid, thus it was necessary to use zeolites with a high Si/Al ratio in order to avoid the local destruction of the framework by HCl.

As these modifications did not affect the internal catalytic properties of the zeolites, the modified solids could be used in catalysis, often showing increased selectivity for the desired products. There have been numerous reports of such applications, although most of them deal with the formation of dibranched aromatic compounds and the production of *para*-substituted aromatic compounds. For example, such systems are used in the alkylation of toluene by methanol.[13] The deposition of silica onto the zeolite leads to a large decrease in the catalytic activity, but to a concomitant marked increase in the *p*-xylene selectivity. These results were explained in terms of a decrease of the diffusivity inside the channels due to the silica deposit, together with a deactivation of the acid sites on the external surface due to reaction with the silicon compound. Similar results were obtained for toluene disproportionation and *o*-xylene isomerization;[9c] the larger the amount of silica deposited on the catalyst, the higher the selectivity towards *p*-xylene and the lower the catalytic activity.

However, the main problem of these studies was that the reaction of the organometallic compound with the surface was performed by OMCVD, which does not offer control at the molecular level. Numerous surface species were most probably obtained which, by calcination and migration,

gave rise to poorly defined solids. It was thus difficult to correlate the catalytic properties with the modification of the zeolite.

More recently, numerous studies have been undertaken using the SOMC technique, which preserves the molecular structure on the surface. Various organometallic compounds have been reacted with mordenite and the grafted fragments thus obtained have been fully characterized by in situ IR spectroscopy, volumetric measurements, elemental analysis, and ^{13}C-CP-MAS solid-state NMR.[14−18] The grafting of organometallic derivatives of various metals has also been studied, including magnesium ($MgNp_2$), zirconium ($ZrNp_4$), germanium ($GeBu_4$), and, most thoroughly, tin (SnR_4 compounds with R = Me, Et, *i*Pr, *n*Pr, *n*Bu, Ph, Cy; $HSnBu_3$). In the case of the alkyltin compounds, the solids were also characterized by ^{119}Sn-MAS-NMR. In each case, reaction of the organometallic compound with the external surface hydroxy groups occurred, which can be described in terms of the following equations:

$$\equiv Si-OH + MR_4 \rightarrow \equiv Si-O-MR_3 + RH$$
$$M = Sn, Ge, Zr; R = Me, Et, nPr, iPr, nBu, Np, Cy, Ph$$
$$\equiv Si-OH + HSnBu_3 \rightarrow \equiv Si-O-SnBu_3 + H_2$$
$$\equiv Si-OH + MgNp_2 \rightarrow \equiv Si-O-MgNp + NpH$$

These results were confirmed by further studies on various oxides (silica, alumina, silica/alumina, etc.).[19] For all organometallic compounds, the reaction occurred only at the external surface and near the pore entrances, the starting organometallic compounds being too large to enter inside the channels (with the sole exception of $SnMe_4$, which probably reacted very rapidly at the pore entrances, thereby preventing other molecules of tetramethyltin from penetrating inside the channels, XPS showing a considerable tin enrichment on the surface). The main interest in this approach stemmed from the fact that the organometallic compounds were not calcined after the grafting reaction. As a consequence, the reduction of the pore openings was under a *strict molecular control* and was also much larger than that achieved in the previously mentioned studies, where calcination and formation of an oxide layer typically resulted in only a ca. 5% decrease in the dimensions of the pore entrance. Figure 2 shows a pore entrance of mordenite after grafting of a tributyltin organometallic fragment. It can readily be seen that the pore entrance is reduced by ca. 30−40%. This significant obstruction of the pore entrance results in a marked change in the adsorption properties of the modified zeolite. In studies of these systems, the adsorption capacities were determined by a dynamic method, the apparatus being shown in Figure 3. It could be described as a chromatographic method, the zeolite being placed in a small chromatographic column. Pulses of the desired hydrocarbon were introduced at the entrance of the column and the gaseous phase was analyzed at the output. The adsorption capacity was determined from the quantity of hydrocarbon present in the pulses that did not appear in the output from the column.

Figure 4 shows the adsorption capacities for *n*-hexane, 2-methylpentane, 2,3-dimethylbutane, and isooctane (2,2,4-trimethylpentane) of mordenite and of mordenite modified by grafting various organometallic complexes. Clearly, the adsorption capacities (as determined by this method) were greatly modified after the grafting reaction, although the data were not so easy to explain quantitatively. In principle, the role of the organometallic fragment should be very simple; the incoming molecule either can or cannot enter the pore system, depending on the bulkiness of the organometallic fragment. This may be evaluated, for example by molecular modelling. Experimentally, however, the results are more complicated:

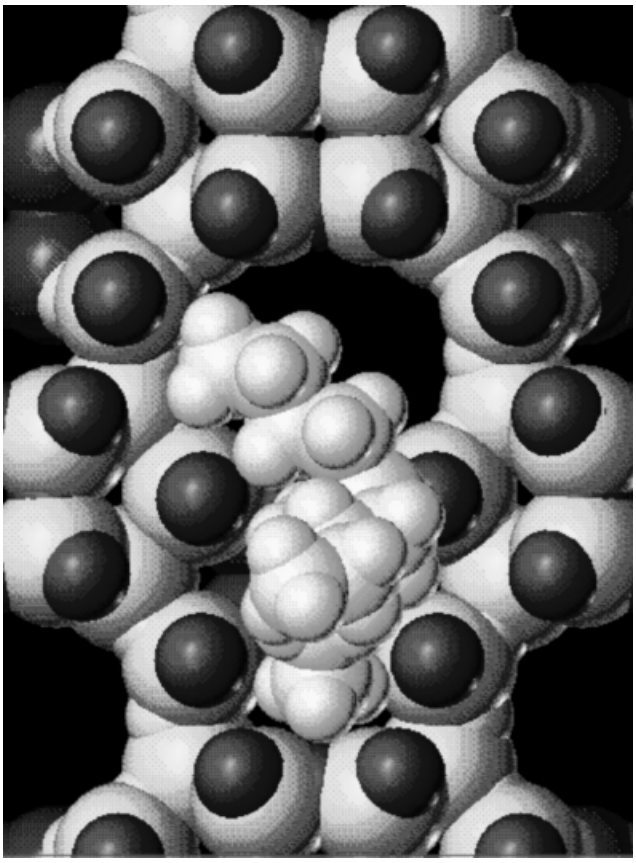


Figure 2. Molecular modelling representation of the pore entrance of mordenite after the grafting reaction of an organometallic tributyltin fragment

In some cases, molecules which were experimentally found to enter into the pore system of mordenite (e.g. isooctane) could no longer penetrate into mordenites modified by bulky organotin compounds (e.g. SnR_3; R = Cy, *n*Bu).

In other cases, molecules experimentally found to enter the pore system of mordenite were also found to penetrate mordenite modified by organotin fragments, albeit more slowly. This was the case for 2,3-dimethylbutane. Here, the actual adsorption capacity of the mordenite was not modified by the grafting reaction, which occurred only on the external surface of the solid without modification of the bulk.

These results are best explained as follows:

(a) A "thermodynamic" effect is observed when a hydrocarbon molecule, which can be adsorbed by the unmodified

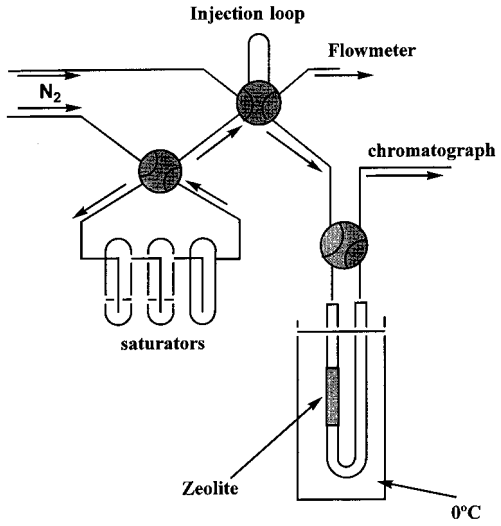


Figure 3. Schematic representation of the apparatus used for the determination of adsorption capacities by a dynamic method ("pulse" method)

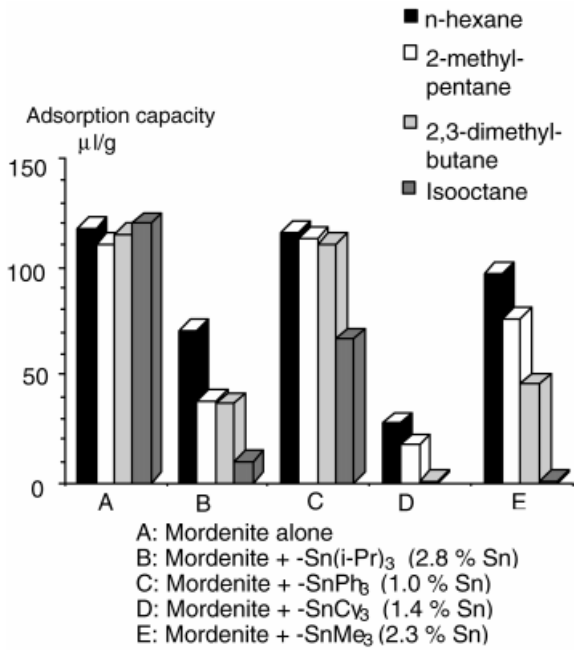
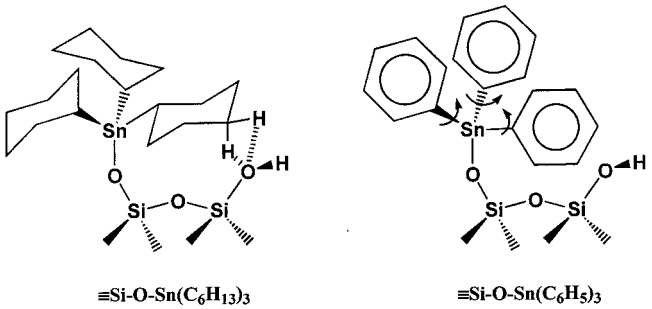


Figure 4. Adsorption capacities (determined by the pulse method) of *n*-hexane, 2-methylpentane, 2,3-dimethylbutane, and isooctane in unmodified mordenite and in mordenite modified by grafting various organometallic complexes

zeolite, can no longer pass through the partially obstructed pore entrance following grafting of the complex, due to steric interactions. A typical example is provided by isooctane, which is adsorbed by mordenite, but is totally excluded from mordenite modified by trimethyltin or tricyclohexyltin. In this case, the new adsorption capacity is zero.

(b) A "kinetic" effect, which is attributable to a decrease in the diffusion rate of molecules able to pass through the modified pore entrances. Indeed, at the pore entrances, the hydrocarbon molecules can interact with the alkyl ligands of the grafted organometallic complexes, resulting in a decrease of their diffusion rate and so to an apparently lower adsorption capacity. These effects were relatively straightforwardly predicted by Monte Carlo theoretical calculations.[20]

Another interesting conclusion of these studies was obtained by comparing the effects of the tricyclohexyltin and triphenyltin grafted fragments (Figure 4). While mordenite modified by tetracyclohexyltin readily discriminated the four hydrocarbons, no effect was observed for the samples modified by reaction with tetraphenyltin. This was explained by assuming, in agreement with ^{13}C-CP-MAS NMR data,[19c] that the phenyl ligands were able to rotate freely about the C−Sn bonds, while the cyclohexyl moieties interacted with remaining hydroxy groups on the surface, thereby leading to a more efficient reduction of the dimensions of the pore entrances (Scheme 2).



Scheme 2. Structure of ≡Si−O−SnR_3 (R = C_6H_{13}, C_6H_5) grafted on mordenite

Most of the modified zeolites were found to be unstable at high temperature (decomposition of the organometallic fragment at temperatures above 200 °C). However, a significant exception to this rule was observed with mordenite modified by organogermanes; the grafted fragment was stable up to ca. 400 °C, allowing the possibility of using this material for practical applications.[15]

These materials were also studied with regard to the direct separation of a mixture of the aforementioned four hydrocarbons. For this purpose, a different experimental setup was used (Figure 5). The mixture of hydrocarbons was passed continuously through the zeolite in the form of chromatographic column and the gases were analysed sequentially by GC. Figure 6 shows typical results obtained by this method: while the four hydrocarbons (*n*-hexane, 2-methylpentane, 2,3-dimethylbutane and isooctane) were not discriminated by unmodified mordenite, they were easily separated by mordenite modified by grafting organometallic complexes. These experiments thus represented a real case of separation of hydrocarbon mixtures by a zeolite. It should be pointed out that, with the exception of isooctane, even if the hydrocarbons could enter the pores, they were discriminated by their van der Waals interactions with the grafted organometallic fragment (combination of thermodynamic and kinetic effects).

Finally, a study was undertaken of the zeolite properties as a function of the organometallic loading, in order to gain a better understanding of the grafting mechanism.[21] Vari-

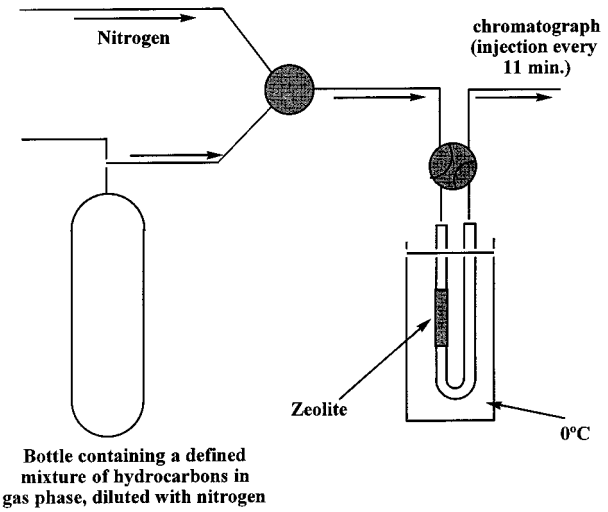


Figure 5. Schematic representation of the apparatus used for the separation of mixtures of hydrocarbons

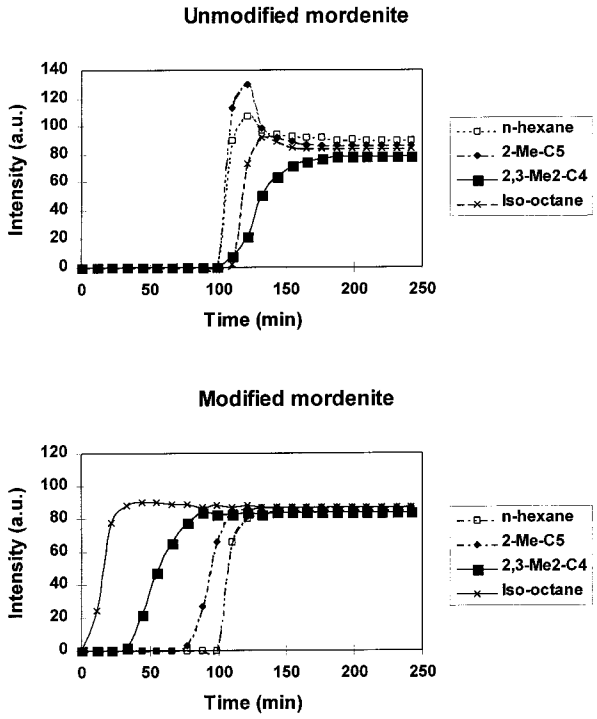


Figure 6. Separation of a mixture of hydrocarbons (*n*-hexane, 2-methylpentane, 2,3-dimethylbutane, and isooctane) by unmodified mordenite and by mordenite modified by grafting tributyltin fragments

ous organometallic complexes of tin (SnR_4; R = Me, Et, *n*Pr, *n*Bu) were used. The adsorption properties of these modified materials towards *n*-hexane, 2-methylpentane, 2,3-dimethylbutane, and isooctane were studied (Figure 7).

It was shown that a total exclusion of isooctane could be achieved with tin loadings greater than 0.5 wt.-%, while 2-methylpentane and 2,3-dimethylbutane were only discriminated with tin loadings in excess of 0.9 wt.-%. No detectable effect was observed in the case of *n*-hexane, even with tin loadings as high as 1.5 wt.-%. These results can be interpreted by assuming that the grafting reaction of the tin fragments occurs on different hydroxy sites of the mordenite, depending on the degree of tin loading. There are four possible grafting sites on an idealized external surface of mordenite (Figure 8), reaction at which should lead to differential reductions of the pore sizes. It has been proposed that for low tin loadings (below 0.5 wt.-%), the grafting reaction occurs only at site 1. A molecular modelling study showed that under these conditions only isooctane would be totally excluded and that the other hydrocarbons would still be able to enter. For tin loadings between 0.5 and 1.0 wt.-%, it is proposed that the grafting reaction occurs at sites 3 or 4, resulting in the exclusion of both 2-methylpentane and 2,3-dimethylbutane.

These modified mordenites have also been used in catalysis experiments, for the selective isomerization of C_8 aromatic mixtures to xylenes.[16] These C_8 aromatic mixtures contained *ortho*-, *meta*- and *para*-xylenes and a non-negligible amount of ethylbenzene (10−40%), of which *para*-xylene is the most useful component. This is removed from the reaction mixture in an aromatic separation unit and the *p*-xylene-depleted mixture is then fed to a unit where the *o*- and *m*-xylenes are isomerized into an equilibrium mixture of *p*-, *o*- and *m*-xylenes. This mixture is then recycled to the *p*-xylene recovery unit together with fresh feed. As the C_8 mixture contains ethylbenzene, the catalyst has to be able to convert it with a minimum loss of xylenes, in order to avoid an increase of its concentration in the recycle loop. Consequently, the objectives of the isomerization units are to isomerize xylenes and to convert ethylbenzene into valuable products. Usually, this is accomplished industrially by the use of a bifunctional catalyst consisting of a large-pore acid zeolite (typically mordenite) and a hydrogenating metal (platinum). It was thus interesting to study the applicability of mordenites modified by organometallic complexes in this reaction. However, such reactions are performed at high temperatures (410°C) and under these conditions the organometallic fragment is not stable: a dealkylation of the grafted species occurs, resulting in a mordenite bearing only dealkylated species. The modified mordenites were therefore calcined prior to use. They were then mixed mechanically with a hydrogenation catalyst, in the form of Pt/Al_2O_3 (0.3 wt.-% Pt). Mordenites modified by various organometallic complexes [$MgNp_2$, $ZrNp_4$, $Sn(n\text{Bu})_4$, $Ge(n\text{Bu})_4$] were used. It was observed that the disproportionation reactions, which lead to undesirable products and to a loss of some of the xylenes, were, in some cases, greatly reduced compared to the situation using an unmodified mordenite. When the mordenite was modified by $Ge(n\text{Bu})_4$ or $ZrNp_4$, the isomerization selectivity (between xylenes, and for the transformation of ethylbenzene into xylenes) was increased, while the disproportionation reactions became less significant. When mordenite was modified by $Sn(n\text{Bu})_4$ or $MgNp_2$, no difference was observed compared to unmodified mordenite.

These results were compared to XPS data: XPS showed that in the case of magnesium and tin complexes there was migration of these metals into the interior of the zeolite

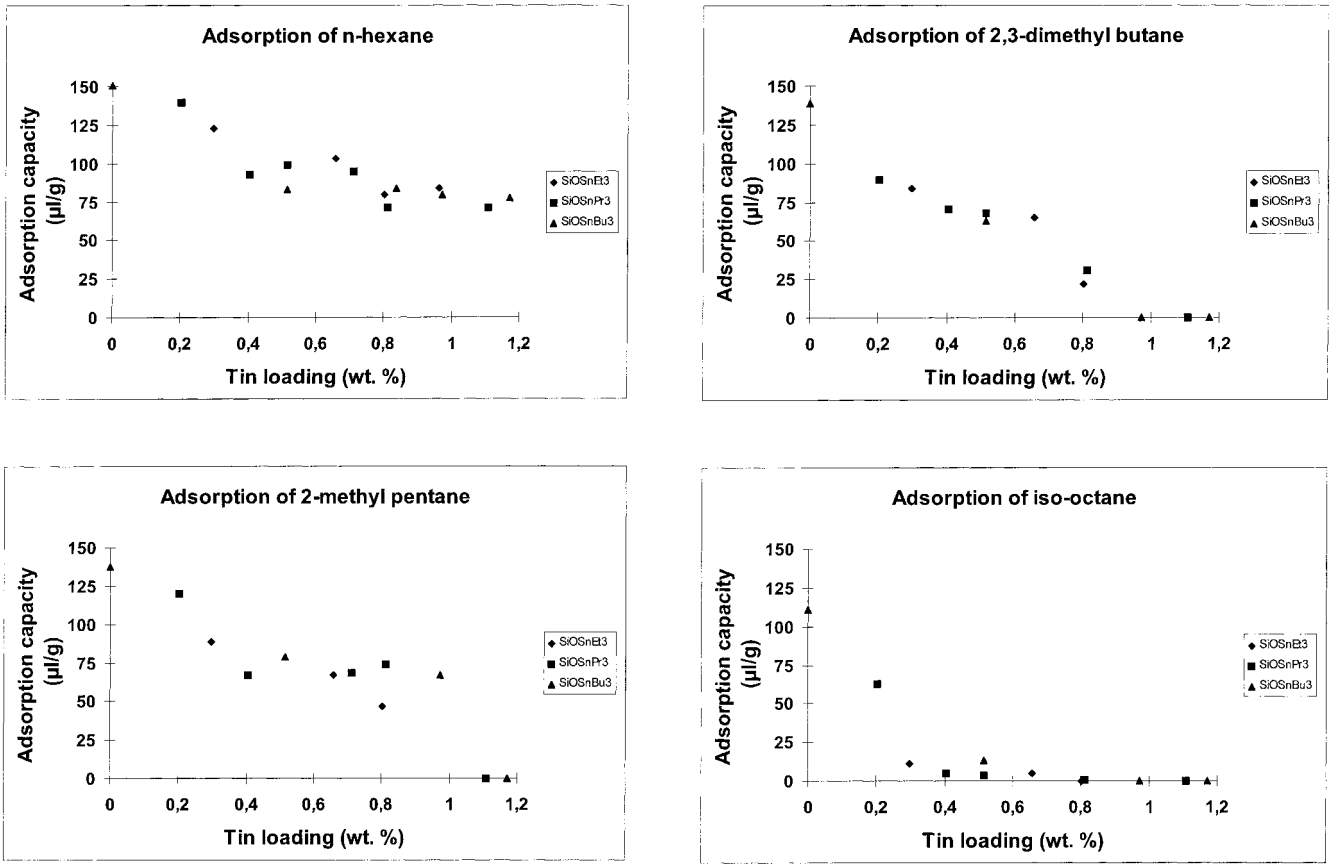


Figure 7. Adsorption capacities towards various hydrocarbons, determined by the pulse method, of mordenite modified by reaction with tetraalkyltin complexes, as a function of the tin loading

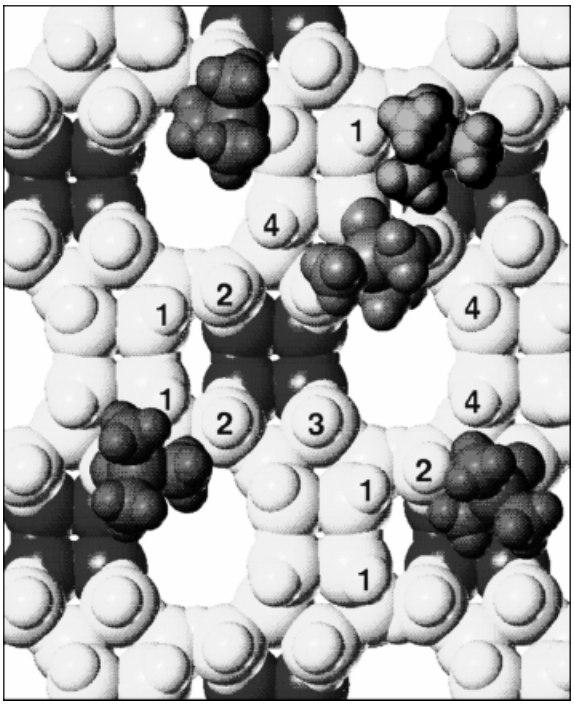


Figure 8. Grafting sites at the pore entrances of mordenite

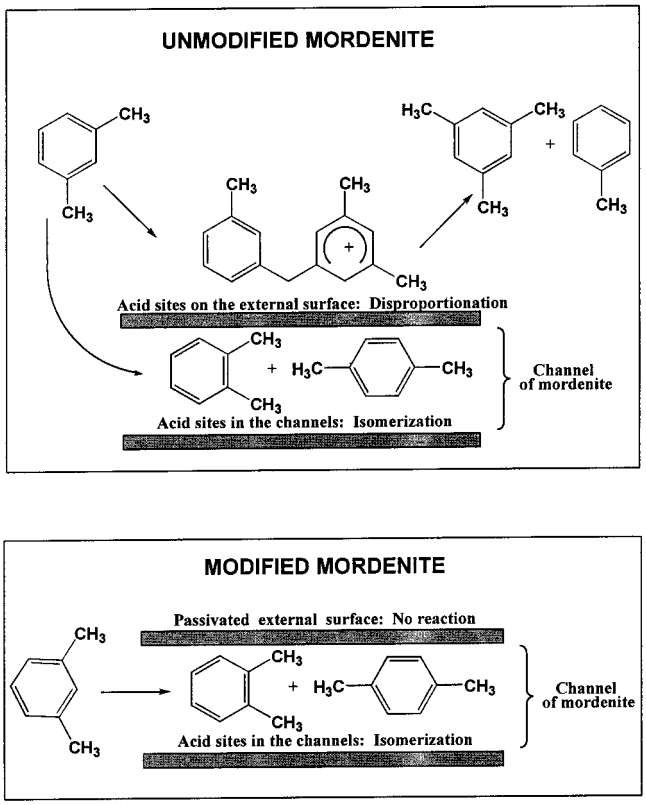
grains during calcination, whereas in the case of germanium and zirconium there was no migration, resulting in the formation of a disperse layer of Ge or Zr "oxide" on the external surface of the zeolite crystals. It was thus logical to suppose that the disperse layer was responsible for the observed decrease in disproportionation.

The interpretation of this experimental correlation between catalytic and XPS results is shown in Scheme 3. The disproportionation reaction is bimolecular; it requires the formation of a bulky reaction intermediate. This intermediate, in view of the channel dimensions of the mordenite zeolite framework, should be formed preferentially by the intervention of the acid sites present at the channel entrances, or preferably at the external surface of the zeolite crystals. The grafting of the organometallic complexes at the external surface leads to the elimination or poisoning of such "non-selective" acid sites, which leads to an overall reduction of the disproportionation reactions.

These studies were also extended to other microporous materials, such as mesoporous silicas and cloverite. However, in these cases, the modification occurred not only on the external surface but also inside the channels. These results are presented in the following part of this review.

Modification of the Internal and External Surfaces of Molecular Sieves

Before describing the modification of the properties of molecular sieves by true organometallic compounds, we will



Scheme 3. Isomerization of xylenes on unmodified and modified mordenite

briefly overview the modification by the other compounds, essentially silanes and boranes.[2,22]

Acidic zeolites can be modified by reaction with silanes, due to the reactivity of the Si−H bond. Reactions with hydroxy groups of the zeolite can thus be written as:

$$\equiv T{-}OH + SiH_4 \rightarrow \equiv T{-}O{-}SiH_3 + H_2$$
$$\equiv T = Si, Al$$

This chemisorbed group can react further with another hydroxy group, resulting in a silicon dihydride species linked to the surface via two σ-bonded oxygen atoms:

$$\equiv T{-}OH + \equiv T{-}O{-}SiH_3 \rightarrow (\equiv T{-}O)_2SiH_2 + H_2$$
$$\equiv T = Si, Al$$

In all cases, the samples were further hydrolyzed in order to obtain stable compounds that could not react with the adsorbents:

$$(4-x)\,H_2O + (\equiv T{-}O)_xSiH_{4-x} \rightarrow (\equiv T{-}O)_xSi(OH)_{4-x} + (4-x)\,H_2$$
$$\equiv T = Si, Al;\ x = 1, 2$$

Thus, a total of 4 hydrogen molecules were evolved per grafted silicon. In principle, the greatest number of silanes that could react with the zeolite (very often a mordenite) could not exceed the number of hydroxy groups (typically around 2 mmol per gram). In practice, the experimental value was invariably lower, owing to several factors: (i) heterogeneous reactivity of the hydroxy groups (depending on their crystallographic localization), (ii) a decrease of the diffusion rate of the silane molecules in the channels, following the reduction of the dimensions of the pore openings after modification by an initial SiH_4 molecule (this effect is somewhat analogous to that described above as a kinetic effect in the case of zeolites modified only at the external surface).

Another modification method involved the use of disilanes such as $H_3Si{-}SiH_3$ rather than simple silanes of the type SiR_4. Two reactions occurred simultaneously, depending on whether the Si−Si or an Si−H bond was broken:

$$2 \equiv T{-}OH + Si_2H_6 \rightarrow H_2 + 2 \equiv T{-}O{-}SiH_3$$
$$\equiv T{-}OH + Si_2H_6 \rightarrow H_2 + \equiv T{-}O{-}Si_2H_5$$

In the case of silanes, the chemisorbed species could undergo further reactions with the hydroxy groups, leading to multigrafted species. Finally, the residual ≡Si−H and ≡Si−Si≡ bonds were hydrolysed to ≡Si−OH groups:

$$\equiv Si{-}H + H_2O \rightarrow H_2 + \equiv Si{-}OH$$
$$\equiv Si{-}Si\equiv + 2\,H_2O \rightarrow H_2 + 2 \equiv Si{-}OH$$

The resulting solids were often characterized by adsorption kinetics of Xe, Kr, O_2 or N_2. In all cases, a pore size reduction was observed, leading to a decrease of the pore volume. It was also observed that the hydrolysis reaction led to a marked decrease in the pore volume, resulting, in some cases, in a complete exclusion of *n*-butane. This was not due to a destruction of the framework, since smaller molecules such as rare gases and oxygen could still fill the pores, but solely due to the reduction of the pore size by the grafted fragments (thermodynamic effect).

Similar modifications of zeolites were carried out using B_2H_6 but, as above, changes in the adsorption properties were only significant after treatment under severe conditions.[2]

Recently, the reaction of organometallic compounds with the internal hydroxy groups of molecular sieves has been studied. Due to the non-negligible size of the organometallic complexes, only some molecular sieves could be used, namely cloverite[23] and mesoporous silica (MCM-41 or MS-1).[24]

Cloverite is a synthetic microporous gallophosphate with a 20-tetrahedral pore opening, the synthesis and structure of which was reported in 1991.[8] Its crystal structure contains two non-intersecting channel systems with 8-ring (8-T, 3.8 Å) and 20-ring (20-T, 13.2 Å) pore openings. The diagonal dimension of the supercages formed at the intersections of the 20-ring channels amounts to 23−30 Å (Figure 8).[25] Furthermore, hydroxy groups can only be found at the windows of these supercages (4 hydroxy groups per window, 6.2 Å apart). The reactions of $SnMe_4$, $SnEt_4$ and $HSnBu_3$ with this solid were studied by numerous methods and the resulting materials were fully characterized by physicochemical techniques such as ^{13}C-CP-MAS- and ^{119}Sn-MAS-NMR, EXAFS, X-ray powder diffraction, XPS, etc.[23] In all cases, it was shown that the grafting reaction had occurred both on the external surface and inside

the channels, most of the tin being found in the bulk. Depending on the starting organometallic species, different solids were obtained, with a mean value of one grafted organometallic fragment per window of the supercages when $SnEt_4$ or $HSnBu_3$ were used (corresponding to ca. 3.5 wt.-% tin) or four grafted organometallic fragments per window in the case of $SnMe_4$ (corresponding to ca. 14 wt.-% tin). In the latter case, all hydroxy groups in the solid had reacted. For all samples, the grafted organometallic fragment was fully characterized as a $\equiv T-O-SnR_3$ complex, in which tin was tetracoordinated. The reaction was not selective and both $\equiv P-OH$ and $\equiv Ga-OH$ hydroxy groups reacted:

$$\equiv T-OH + SnR_4 \rightarrow \equiv T-O-SnR_3 + RH$$
$$R = Me, Et$$
$$\equiv T-OH + HSnBu_3 \rightarrow \equiv T-O-SnBu_3 + H_2$$

As an example, Figure 9 shows a molecular modelling representation of a supercage window before and after modification by $SnEt_4$.

The adsorption properties of unmodified cloverite and of cloverite modified by grafted $-SnR_3$ fragments were studied. The adsorption properties towards *n*-hexane, benzene and isooctane were determined using a static method. The apparatus used for these studies is shown schematically in Figure 10. The cloverite sample was connected to a pressure gauge and a vacuum line via a break-seal. A known amount of the appropriate hydrocarbon was introduced into the system as a liquid and immediately vaporized. The break-seal was then broken and the variation of the hydrocarbon pressure was analyzed as a function of time, thereby allowing determination of the adsorption capacity.

The values obtained for unmodified cloverite showed that benzene and isooctane filled only the 20-T channel system, while *n*-hexane filled both the 8-T and 20-T channel systems. When cloverite was modified by tetramethyltin (14 wt.-%), tetraethyltin, or tributyltin hydride (3.5 wt.-%), the following features were observed: (a) Total exclusion of isooctane from all materials. (b) Reduction of the adsorption capacities towards *n*-hexane and benzene, which became very similar after the grafting reaction.

The exclusion of isooctane was explained in terms of the reduction of the size of the windows of the supercages, which prevented passage of this molecule. This was also the case for butane after reaction with disilane. These observations are nicely predictable by molecular modelling.

The reduction of the adsorption capacities towards *n*-hexane and benzene was due to two factors: (i) *n*-Hexane could only fill the 20-T channel system, owing to a blocking of the pore openings of the 8-T channels by the organometallic fragments grafted onto the external surface. (ii) The decrease of the adsorption capacity corresponds to a reduction in the pore volume due to the presence of the grafted organometallic complexes inside the channels. This effect was also predictable by simple molecular modelling calculations.

Unfortunately, no difference was observed between cloverites modified by reaction with tetramethyltin, tetraethyltin, or tributyltin hydride, even though the sizes of the windows were reduced to varying extents. This was probably related to the limited range of hydrocarbons adsorbed on these materials. However, such a modification of the adsorption characteristics of a molecular sieve is very interest-

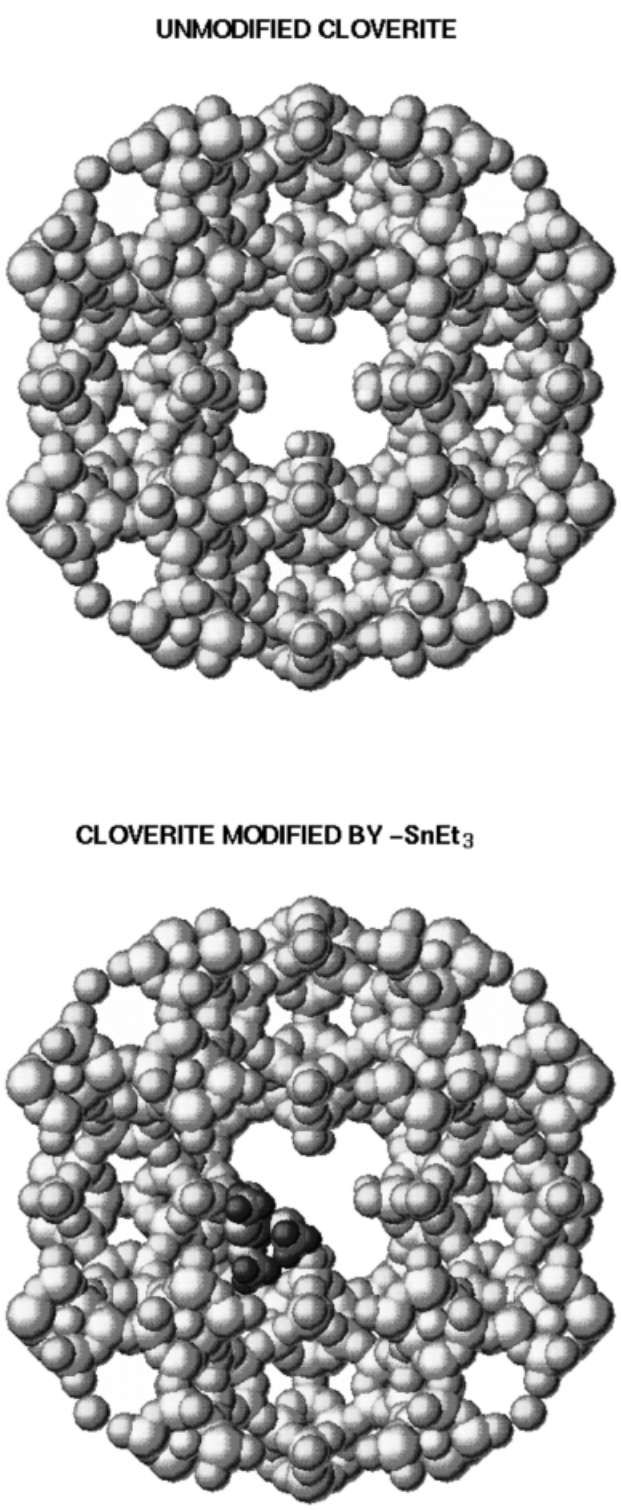


Figure 9. Molecular modelling representation of a supercage window of cloverite before and after modification by reaction with tetraethyltin

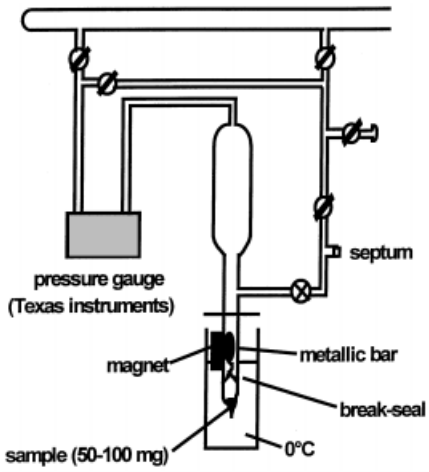


Figure 10. Schematic representation of the apparatus used for the determination of the adsorption capacities by a static method

ing as there are many more steric interactions between the adsorbed molecule and the grafted organometallic complex than in the case of mordenite, where the grafting reaction occurs only on the external surface (there is not just one interaction with the organometallic compound as the hydrocarbon is adsorbed onto the solid, but numerous interactions along the channels).

Analogous studies were also performed on MCM-41, a recently discovered mesoporous silica.[26] MCM-41 has pores with a very sharp diameter distribution, rendering this material useful for separation processes of large molecules. Depending on the template used during the synthesis, the diameter of the pores can be varied from ca. 20 to 100 Å. The reactions of various alkyltin complexes with this solid were studied using the same physicochemical techniques as mentioned above.[24] As with mordenite and cloverite, a reaction was observed with the surface hydroxy groups. However, in contrast to what was observed in the previous examples, the main surface product when the mesoporous silica was pretreated at 200°C was not $\equiv Si-O-SnR_3$ but $(\equiv Si-O)_2SnR_2$, obtained by reaction of two hydroxy groups with SnR_4. This result was tentatively attributed to the concavity of the walls in the pores, which probably induced a stabilization of the multi-grafted species. When the mesoporous silica was initially dehydroxylated at 500°C, the mono-grafted species was predominant (more than 90% of the tin was present in the form of $\equiv Si-O-SnR_3$ species) and all the hydroxy groups were consumed. For this material, the grafting reaction completely modified the shapes of the hydrocarbon adsorption isotherms (Figure 11). Indeed, the isotherm of unmodified mesoporous silica showed a great increase of the adsorbed alkane (for example, *n*-hexane) at low P/P_0 ratios, while the isotherm of the modified material increased only slowly as a function of P/P_0. This phenomenon was independent of the hydrocarbon, all alkanes with the same number of carbon atoms giving the same curves. It was explained by assuming that for the unmodified material the adsorption curve was due to hydrogen bonding between the

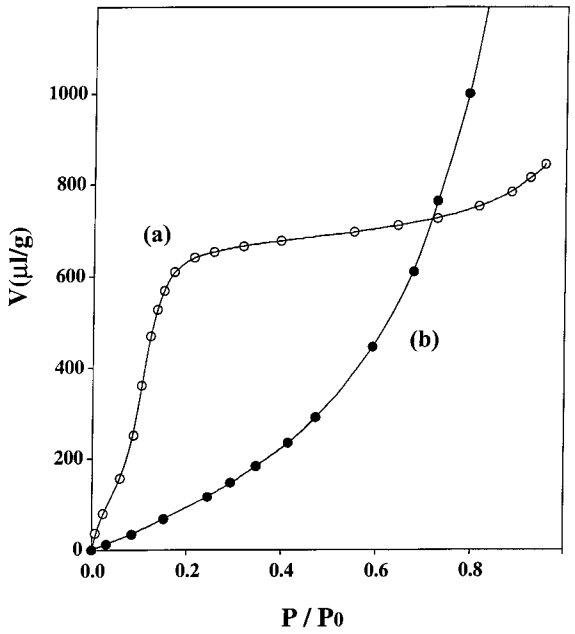


Figure 11. Adsorption isotherms at 0°C of *n*-hexane on MCM-41 dehydroxylated at 500°C before (a) and after (b) reaction with tetrabutyltin

hydroxy groups of the surface and the C−H bonds of alkanes, while in the modified material the hydroxy groups were absent and the aforementioned interactions were replaced by van der Waals interactions between the alkyl groups of the grafted organometallic fragments and the hydrocarbons.

Conclusion

This short review article has shown the great advantages of the modification of molecular sieves by grafting organometallic compounds. Two different methods can be used: OMCVD, where the grafted organometallic fragment is calcined and transformed into an oxide of rather indefinite composition, and SOMC, where the grafted organometallic fragment is well-characterized and retains its molecular integrity. Both methods can lead either to a grafting reaction only on the external surface, or to grafting inside the channels of the molecular sieve as well, depending on the reaction conditions and on the size of the organometallic complex used for the modification. In the case of SOMC, it is possible to modify only the external surface of molecular sieves such as mordenites, leading to an increased selectivity, e.g., in xylene isomerization. Grafting of the organometallic complex near the pore entrances permits a fine tuning of the adsorption properties of the zeolite. Two effects can be observed, depending on the size of the adsorbed molecule: (i) a total exclusion of the molecule from the channels of the molecular sieve, due to steric constraints ("thermodynamic effect"); (ii) a retardation of the adsorption kinetics of the adsorbed molecule, due to steric interactions with the grafted organometallic fragments at the pore entrances ("kinetic control").

These properties of the modified materials can be envisaged as being useful in catalysis. For this purpose, it would be necessary to first introduce the catalytically active species into the channels of the molecular sieve and then to graft the organometallic complex onto the external surface in order to reduce the dimensions of the pore entrances. Two effects could then be expected: (i) The leaching of the catalyst could be completely avoided, allowing easy recycling. (ii) By judicious choice of the organometallic complex, only some reaction products could be desorbed from the molecular sieve containing the homogeneous catalyst, resulting, in line with the principle of microreversibility, to an increase in the selectivity towards these products.

[1] W. M. Meier, D. H. Olson, *Atlas of Zeolite Structure Types*, 3rd ed., Butterworth, London, **1992**.
[2] E. F. Vansant, *Pore Size Engineering in Zeolites*, John Wiley & Sons, New York, **1990**.
[3] [3a] E. F. Vansant, G. Peeters, C. Michelena, *J. Chem. Res.* **1978**, *90*, 1165. – [3b] D. W. Breck, W. G. Eversole, R. M. Milton, T. B. Reed, T. L. Thomas, *J. Am. Chem. Soc.* **1956**, *78*, 5963.
[4] S. Namba, A. Yoshimura, T. Yashima, *Chem. Lett.* **1979**, 759.
[5] [5a] R. M. Barrer, L. V. C. Rees, *Trans. Faraday Soc.* **1954**, *50*, 852. – [5b] V. N. Choudhary, R. V. Jasra, T. S. G. Bhat, *J. Chem. Soc., Faraday Trans. 1* **1992**, *88*, 3111.
[6] D. W. Breck, *Zeolite Molecular Sieves*, John Wiley & Sons, New York, **1974**.
[7] [7a] R. M. Barrer, E. F. Vansant, G. Peeters, *J. Chem. Soc., Faraday Trans. 1* **1978**, *74*, 1871. – [7b] A. Thijs, G. Peeters, E. F. Vansant, I. Verhaert, P. de Bièvre, *J. Chem. Soc., Faraday Trans. 1* **1983**, *79*, 2835. – [7c] A. Thijs, G. Peeters, E. F. Vansant, I. Verhaert, P. de Bièvre, *J. Chem. Soc., Faraday Trans. 1* **1983**, *79*, 2821. – [7d] A. Thijs, G. Peeters, E. F. Vansant, I. Verhaert, *J. Chem. Soc., Faraday Trans. 1* **1986**, *82*, 963. – [7e] J. Philippaerts, E. F. Vansant, *Surf. Interfaces* **1987**, *2*, 271. – [7f] Y. Yan, J. Verbiest, P. de Hulsters, E. F. Vansant, *J. Chem. Soc., Faraday Trans. 1* **1989**, *85*, 3087. – [7g] Y. Yan, J. Verbiest, P. de Hulsters, E. F. Vansant, *J. Chem. Soc., Faraday Trans. 1* **1989**, *85*, 3095.
[8] M. Estermann, L. B. McCusker, C. Baerlocher, A. Merrouche, H. Kessler, *Nature* **1991**, *352*, 320.
[9] [9a] M. Niwa, S. Kato, T. Hattori, Y. Murakami, *J. Chem. Soc., Faraday Trans. 1* **1984**, *80*, 3135. – [9b] M. Niwa, S. Kato, T. Hattori, Y. Murakami, *J. Phys. Chem.* **1986**, *90*, 6233. – [9c] H. Hibino, M. Niwa, Y. Murakami, *J. Catal.* **1991**, *128*, 551.
[10] T. Hibino, M. Niwa, Y. Kawashita, Y. Murakami, in *Chemistry of Microporous Crystals*, Kodansha-Elsevier, Tokyo, **1991**, p. 151.
[11] J. H. Kim, A. Ishida, M. Okajima, M. Niwa, *Shokubai (Catalyst)* **1995**, *37*, 156.
[12] [12a] B. A. Morrow, I. A. Cody, *J. Phys. Chem.* **1973**, *77*, 1465. – [12b] C. P. Tripp, M. L. Hair, *Langmuir* **1992**, *8*, 1120.
[13] H. Vasques, Ph.D. Thesis, Lisbon (Portugal), **1991**.
[14] A. Théolier, E. Custodero, A. Choplin, J.-M. Basset, F. Raatz, *Angew. Chem. Int. Ed. Engl.* **1990**, *29*, 805.
[15] [15a] C. Nédez, A. Choplin, J. Corker, J.-M. Basset, J. F. Joly, E. Benazzi, *J. Mol. Catal.* **1994**, *92*, L239. – [15b] A. Choplin, *J. Mol. Catal.* **1994**, *86*, 501.
[16] [16a] E. Benazzi, S. de Tavernier, P. Beccat, J. F. Joly, C. Nédez, A. Choplin, J.-M. Basset, *ChemTech* **1994**, 13. – [16b] E. Benazzi, S. de Tavernier, P. Beccat, J. F. Joly, C. Nédez, J.-M. Basset, A. Choplin, *Proc. Symp. on Chemically Modified Molecular Sieves*, 206th A.C.S. National Meeting, Chicago, **1993**, p. 561. – [16c] E. Benazzi, G. Hotier, J.-M. Basset, A. Choplin, A. Théolier, C. Nédez, European Patent 559510, **1993**; *Chem. Abstr.* **1993**, *113*, 229921.
[17] C. Nédez, A. Théolier, F. Lefebvre, A. Choplin, J.-M. Basset, J. F. Joly, E. Benazzi, *Microporous Mater.* **1994**, *2*, 51.
[18] A. Théolier, A. Choplin, J.-M. Basset, E. Benazzi, *Stud. Surf. Sci. Catal.* **1994**, *84*, 1293.
[19] [19a] C. Nédez, A. Choplin, F. Lefebvre, J.-M. Basset, *Inorg. Chem.* **1994**, *33*, 1575. – [19b] C. Nédez, A. Choplin, F. Lefebvre, J.-M. Basset, E. Benazzi, *Inorg. Chem.* **1994**, *33*, 1099. – [19c] C. Nédez, F. Lefebvre, A. Choplin, J.-M. Basset, *New J. Chem.* **1994**, *18*, 1215. – [19d] C. Nédez, F. Lefebvre, A. Choplin, J.-M. Basset, E. Benazzi, *J. Am. Chem. Soc.* **1994**, *116*, 3039. – [19e] C. Nédez, F. Lefebvre, A. Choplin, G. P. Niccolai, J.-M. Basset, E. Benazzi, *J. Am. Chem. Soc.* **1994**, *116*, 8638. – [19f] C. Nédez, A. Théolier, F. Lefebvre, A. Choplin, J.-M. Basset, J. F. Joly, *J. Am. Chem. Soc.* **1993**, *115*, 722. – [19g] C. Nédez, F. Lefebvre, J.-M. Basset, *Langmuir* **1996**, *12*, 925. – [19h] C. Nédez, F. Lefebvre, F. Humblot, J.-M. Basset, E. Benazzi, *J. Chem. Soc., Faraday Trans.* **1996**, *92*, 3419.
[20] [20a] V. H. Peuch, Ph.D. Thesis, Lyon (France), **1996**. – [20b] B. Bigot, V. H. Peuch, *J. Phys. Chem.*, in press.
[21] F. Lefebvre, M. O. Grand, F. Bayard, A. de Mallmann, J.-M. Basset, *Proc. ECTOC-3 Conf.* **1997**, in press.
[22] E. F. Vansant, *Stud. Surf. Sci. Catal.* **1988**, *37*, 143.
[23] [23a] M. Adachi, F. Lefebvre, C. Schott-Darie, H. Kessler, J.-M. Basset, *Appl. Surf. Sci.* **1997**, *121/122*, 355. – [23b] M. Adachi, J. Corker, H. Kessler, A. de Mallmann, F. Lefebvre, J.-M. Basset, *Microporous Mater.*, in press.
[24] X. X. Wang, F. Lefebvre, A. de Mallmann, H. Kessler, J.-M. Basset, to be published.
[25] P. L. Bedard, C. L. Bowes, N. Combs, A. J. Holmes, T. Jiang, S. J. Kirkby, P. M. McDonald, A. M. Malek, G. A. Ozin, S. Petrov, N. Plavac, R. A. Ramik, M. R. Steele, D. Young, *J. Am. Chem. Soc.* **1993**, *115*, 2300.
[26] C. T. Kresge, M. E. Leonowicz, W. J. Roth, J. C. Vartuli, J. S. Beck, *Nature* **1992**, *359*, 710.

Received September 14, 1998
[I98310]

Some Silicon, Germanium, Tin, and Lead Analogues of Carbenes, Alkenes, and Dienes

Manfred Weidenbruch[a]

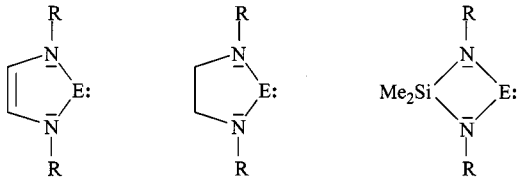
Keywords: Silicon / Germanium / Tin / Lead / Carbene analogues / Multiple bonds

The isolation and characterization of thermally stable diaminocarbenes and diaminosilylenes has reawakened interest in the low-coordinated compounds of group-14 elements. The existence of these species is presumably due to interactions between the free electron pairs on the nitrogen atoms and the carbene carbon atom or the silicon atom. The present review is mainly concerned with the heavier analogues R_2Ge**:**, R_2Sn**:**, and R_2Pb**:**, systems without intramolecular donor stabilization that owe their existence principally to steric shielding by the voluminous alkyl or aryl groups R. Dimerizations of these electron-sextet molecules give rise to the double-bond systems of the digermenes, distannenes, and diplumbenes; the latter species have for a long time been considered as being incapable of existence. The properties of these molecules are compared with the results of quantum chemical calculations. A separate section is devoted to the isomers of Si_4R_6, which include novel tetrasilacyclobutenes and the diene analogues, the tetrasilabuta-1,3-dienes.

Introduction

One of the most interesting developments in organo-element chemistry of the past few years has been the preparation and complete characterization of the diaminocarbenes **1**, which were soon supplemented by the saturated ring compounds **4** and even the corresponding acyclic compounds.[1] Shortly thereafter, the stable or marginally stable silylenes **2** and **5**,[2] as well as germylenes with the same substitution pattern,[1] were successfully prepared. The diaminogermylenes **7**, -stannylenes **8**, and -plumbylenes **9** have been known for a longer time and have since been shown to possess an extensive chemistry.[3] A correspondingly substituted silylene has now also been detected, although it is only stable in a matrix up to 77 K.[4]

A common feature of all these compounds is the presence of a free electron pair on the nitrogen atom, or on other donor atoms as well, which can either allow delocalization, as in the five-membered rings of **1**−**3** or, in the case of saturated systems, can participate in π-interactions with electron-deficient centers, as in compounds **4**−**9**.[5] As a result, the tendency of these species to undergo dimerization with formation of homonuclear double bonds is rather low. The dialkyl, diaryl, or disilyl derivatives of silicon, germanium, tin, and lead behave differently: They do not experience any intramolecular donor stabilization and can thus undergo dimerization to afford the homonuclear double-bond systems of the disilenes, digermenes, and distannenes with varying degrees of ease.



1 2 3 E = C, Si, Ge

4 5 6 E = C, Si, Ge

7 8 9 E = Ge, Sn, Pb

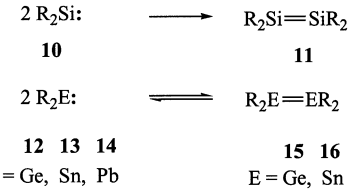
[a] Fachbereich Chemie, Universität Oldenburg,
Carl-von-Ossietzky-Straße 9−11, D-26111 Oldenburg, Germany
Fax: (internat.) + 49(0)441/798-3352

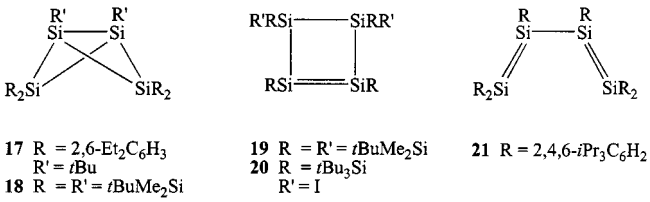


Manfred Weidenbruch studied chemistry at the Technical University of Aachen and received his Dr. rer. nat. in 1965 under the guidance of the late Professor Martin Schmeisser. After his habilitation at Aachen in 1971 he was appointed Außerplanmäßiger Professor in 1973. In 1978 he moved as Full Professor of Inorganic Chemistry to the University of Oldenburg. His research interests lie in the general field of main-group chemistry, particularly group-14 compounds, with emphasis on synthetic and structural studies.

MICROREVIEWS: This feature introduces the readers to the authors' research through a concise overview of the selected topic. Reference to important work from others in the field is included.

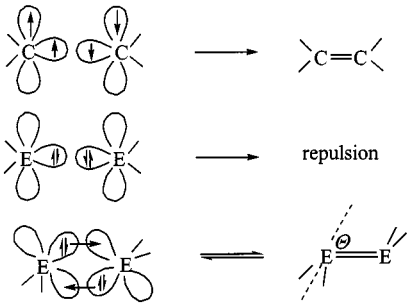
 © WILEY-VCH Verlag GmbH, D-69451 Weinheim, 1999 1434−1948/99/0303−0373 $ 17.50+.50/0





17 R = 2,6-$Et_2C_6H_3$, R' = *t*Bu
18 R = R' = *t*$BuMe_2Si$
19 R = R' = *t*$BuMe_2Si$
20 R = *t*Bu_3Si, R' = I
21 R = 2,4,6-*i*$Pr_3C_6H_2$

While most disilenes **11** are sufficiently stable towards dissociation into the silylenes **10**,[6] the tendency of the double-bond systems in **15** and **16** to undergo cleavage to the carbene analogues **12**–**14** increases on descending group 14 towards the heavier elements.[7] Thus, for example, only one distannene that retains its structural integrity in solution is known. In the case of lead, until recently merely a few dialkyl-, disilyl-, and diarylplumbylenes, but no diplumbenes $R_2Pb{=}PbR_2$, had been isolated. This behavior – which clearly deviates from that of alkenes – has been explained theoretically in terms of the varying nature of the double bond on descending the series. Thus, carbenes have either a triplet ground state (T) or a singlet ground state (S), with relatively small S → T transition energies. The familiar picture of a C–C double bond results from the approach of two triplet carbenes in the manner shown in Scheme 1.



Scheme 1. Double-bond formation from two carbenes and their analogues

In contrast to the carbenes, all silylenes, germylenes, stannylenes, and plumbylenes characterized to date have exclusively singlet ground states, with the energy of the S → T separation increasing with increasing atomic mass of the group-14 element.[8] Thus, approach of two such singlet species in the manner shown in Scheme 1 should result in repulsion rather than in bond formation. However, if the two electron-sextet species are rotated with respect to one another, interactions between the doubly-occupied s orbitals and the vacant p orbitals can also lead to the creation of a double bond, which, in contrast to that in alkenes, arises by way of a double donor–acceptor adduct formation. This is accompanied by a *trans* bending of the substituents about the E=E vector, with the *trans*-bending angle Θ increasing appreciably on going to heavier elements.[9–12]

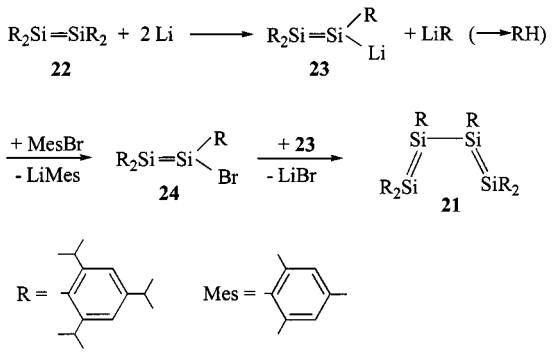
Since the results obtained up to 1994/1995 in the field of multiple bonding of group-14 elements have been covered in numerous review articles,[6,7] only some more recent developments, including the first diplumbene, the first tetrasilabutadiene, and some other isomers with the composition Si_4R_6, are included in the present survey.

The Si_4R_6 Isomers

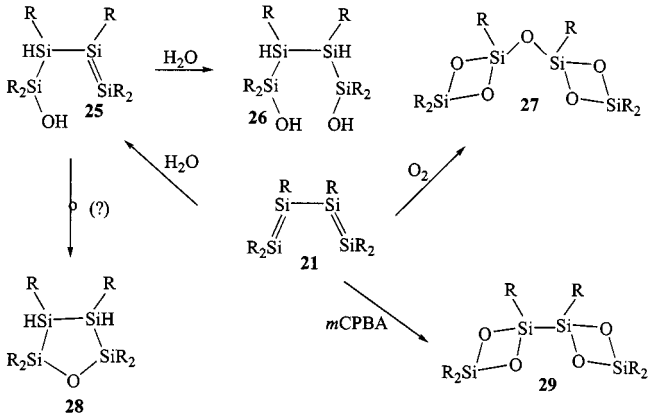
Since the isolation of tetramesityldisilene as the first molecule containing an Si–Si double bond in 1981,[13] numerous other compounds belonging to this class have been reported, although fundamentally new bonding systems are still rare. Recently, Kira et al. described the isolation of the first thermally stable cyclooligosilene **19** incorporating an Si=Si bond in the ring, albeit in very low yield, which was obtained by coupling of two oligosilanes.[14] Although compound **19** was found to be stable in the dark for an indefinite period, the action of visible light resulted in conversion to the tetrasilabicyclo[1.1.0]butane derivative, the butterfly-like skeleton of which had been described about 15 years earlier by Masamune et al. in relation to compound **17**.[15] Trapping experiments at low temperature indicated that the primary product of the coupling reaction was not the tetrasilacyclobutene **19**, but rather the tetrasilabicyclobutane **18**, which underwent conversion to **19** by 1,2-silyl group migration during work-up.[16] Although ring systems of this type are relatively new in molecular chemistry, the corresponding butterfly anions have long been known in solid-state chemistry. Thus, addition of two electrons to the tetrahedral anion $[Si_4]^{4-}$ leads smoothly to the tetrasilabicyclobutane system $[Si_4]^{6-}$ through cleavage of one bond, as is realized in the compound Ba_3Si_4.[17] By way of the same principle, Wiberg et al. recently obtained the tetrasilacyclobutene **20** in almost quantitative yield by reaction of the *tetrahedro*-tetrasilane $(tBu_3SiSi)_4$[18] with iodine.[19]

The isomer formed seemingly depends strongly not only on the nature of the substituents but also on the chosen synthetic route. The missing link in the series of simple compounds with the composition Si_4R_6, i.e. the tetrasilabuta-1,3-diene **21**, has been prepared in this laboratory in the following way. The action of excess lithium on the disilene **22**,[20] prepared photolytically from the trisilane $R_2Si(SiMe_3)_2$ by the method of West and co-workers,[21] presumably furnishes the disilenyllithium compound **23**. Half of the formed **23** is converted by reaction with mesityl bromide to the bromodisilene **24**, which spontaneously reacts with the remainder of the formed **23** through intermolecular cleavage of LiBr to afford the tetrasilabutadiene **21** in 60% yield.[22,23]

Interestingly, a crystal structure analysis of the brownish-red compound **21** revealed that it adopts the *s-cis* arrangement in the solid state, which is rather less favorable[24] than the *s-trans* form, with a dihedral angle of 51° within the Si_4 skeleton. The Si–Si double bonds are slightly lengthened in comparison with the corresponding bonds in disilenes, while the formal single bond is markedly shortened in spite



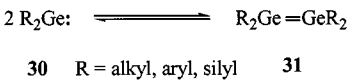
of the bulky substituents. These data, together with the electronic spectrum in solution, which reveals a bathochromic shift of the longest wavelength absorption of 100 nm compared with that of the tetraaryldisilenes, indicate that a conjugation between the Si−Si double bonds is present in both phases.



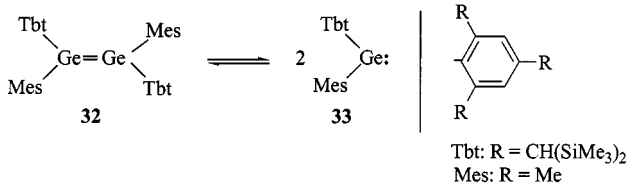
Although the *s-cis* form of compound **21** would appear to be ideally suited for Diels−Alder reactions, all attempts to achieve a [4 + 2] cycloaddition with C−C multiple bonds have failed.[25] The reason for this is probably the high steric shielding of the Si atoms in **21**, as well as the large 1,4 separation of about 540 pm. However, compound **21** does react readily with small molecules, as illustrated. For example, an initial 1,2-addition to furnish compound **25** occurs with water, which can be followed by a second 1,2-addition to afford **26**. Somewhat surprisingly, however, compound **26** does not exhibit any tendency to undergo condensation. Although the constitution of compound **28** has been confirmed by an X-ray crystal structure analysis, it cannot as yet be stated whether it is formed by rearrangement of **25** or by another route. The reaction of *meta*-chloroperbenzoic acid (*m*CPBA) with **21** proceeds through a three-membered ring intermediate [a bis(disilaoxirane)] to furnish bis(2,4-disila-1,3-dioxetane) **29** as the final product. With atmospheric oxygen, an additional insertion of oxygen into the formal Si−Si single bond with formation of **27** occurs; considering the steric shielding of this bond, this is a somewhat unexpected reaction.[23,26]

Germylenes, Digermenes

Stable dialkyl- or diarylgermylenes R_2Ge**:** (**30**), apart from Lappert's compound[27] $[(Me_3Si)_2CH]_2Ge$**:**, have only become known in the past few years. Examples include, among others, the structurally confirmed molecules $(Me_3Si)_3C[(Me_3Si)_2CH]Ge$**:**[28] and $(2,4,6\text{-}tBu_3C_6H_2)_2Ge$**:**[29], of which the latter is converted in the presence of a Lewis acid or at high temperatures to a germaindane derivative by insertion of the germanium atom into one of the methyl groups of the *ortho-tert*-butyl substituents,[30] as well as the sterically extremely crowded $(2,6\text{-}Mes_2C_6H_3)_2Ge$**:** (Mes = $2,4,6\text{-}Me_3C_6H_2$).[31] The compound $[2,4,6\text{-}(CF_3)_3C_6H_2]_2Ge$**:** can only be mentioned with reservations since it has to be classified as an intramolecularly donor-stabilized germylene on account of the weak F···Ge contacts between the electron-poor germanium atom and the fluorine atoms of the *ortho*-CF_3 groups.[32]

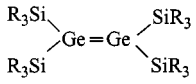


A comparatively large number of germylenes are stable in solution since some of the digermenes **31**, although stable in the solid state, dissociate to germylene molecules in solution. Whether monomeric germylenes with larger Ge···Ge separations or digermenes with a formal Ge−Ge double bond exist in the solid state probably depends on both the spatial requirements of the substituents bonded to the germanium atom and the possible donor properties of these groups. Thus, the aforementioned germylenes either bear very bulky substituent groups or, as in the case of the 2,4,6-$(CF_3)_3C_6H_2$-substituted compound, experience a weak donor stabilization. Lappert's germylene is an exception: It is stable in solution but exists as a digermene in the crystalline state in spite of the presence of very bulky substituents.[33]

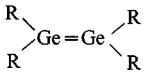


The usually facile cleavage of the Ge−Ge double bond to furnish two germylene molecules is most probably due to the low bond dissociation energy. Thus, a bond dissociation energy of merely 61.5 kJ mol^{-1} has recently been determined for the cleavage **32** → 2 **33** by variable-temperature electronic spectroscopy.[34] This is in accord with the variable Ge−Ge bond lengths in digermenes, which range from 221 to 246 pm, as well as with the *trans*-bent angles, which range from 45° to almost 0° (i.e. a planar structure). The shortest Ge−Ge bond length is observed in the digermene $Dep_2Ge{=}GeDep_2$ (Dep = $2,6\text{-}Et_2C_6H_3$), where the substituents have the lowest spatial requirements.[35] The *trans*-bent angle in this compound, 12°, is also small, and represents one of the lowest values yet found for a tetraaryldigermene. Even the slightest changes in the spatial require-

ments of the substituents can result in markedly different bond lengths and angles: Thus, the compound (*E*)-MesDipGe=GeMesDip (Dip = 2,6-$iPr_2C_6H_3$) has a Ge−Ge bond length of 230.1(1) pm and a bending angle of 36°.[36] These examples illustrate the difficulties in predicting the lengths and deformations of Ge−Ge double bonds, which can again be explained in terms of the flat potentials for bending angles and E=E bond lengths in homonuclear multiple bonds between the heavier elements of group 14.

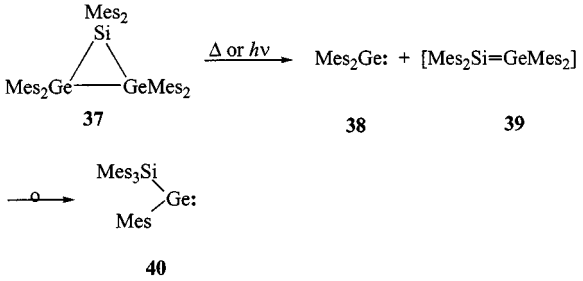


34 $SiR_3 = iPr_2MeSi$
35 $SiR_3 = iPr_3Si$



36 R = 2-*t*Bu-4,5,6-Me_3C_6H

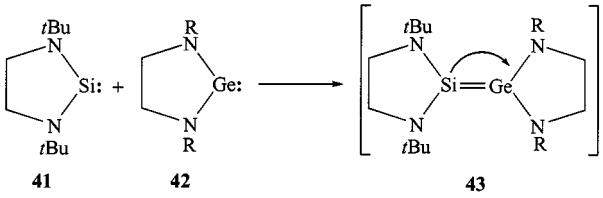
Recently, Kira et al. described some tetrasilyldigermenes, among which the structures of compounds **34** and **35** were characterized by X-ray crystallography. In agreement with theoretical calculations, which predict that electropositive substituents should favor a planar arrangement, these molecules exhibit small bending angles of 5.9° and 16.4°, while the Ge−Ge double bond lengths are surprisingly short in view of the bulky substituents, 226.8(1) pm in **34** and 229.8(1) pm in **35**.[37] However, the presence of electropositive substituents is not an essential prerequisite for such an arrangement, as demonstrated by the tetraaryldigermene **36**, which has an almost planar structure and a short Ge−Ge bond length of 225.21(8) pm.[38]



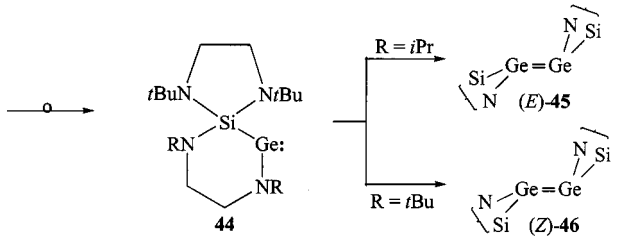
37 **38** **39**

40

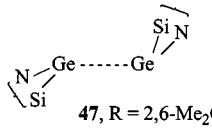
These examples further illustrate how difficult it is to correlate the substitution pattern about the Ge−Ge double bond with the molecular structure. Nevertheless, the existence of Si−Si and Ge−Ge double bonds cannot be questioned. On the other hand, stable compounds with heteronuclear double bonds between these elements are still unknown. In a series of papers, Baines et al. reported on the photolysis and thermolysis of the siladigermirane **37**, which resulted in regioselective conversion to the germylene **38** and the germasilene **39**, although the latter compound underwent rapid isomerization to the silylgermylene **40**. The presence of compounds **38**, **39**, and **40** in the reaction mixture was confirmed by isolation of the corresponding products of trapping reactions.[39−42]



41 **42** **43**



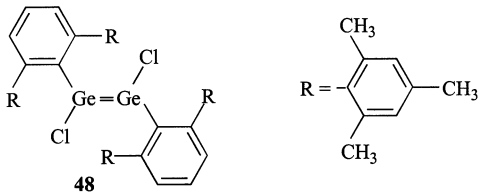
44 **(*E*)-45** **(*Z*)-46**



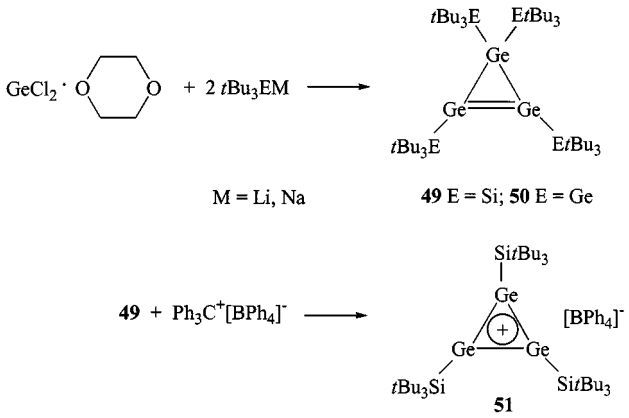
47, R = 2,6-$Me_2C_6H_3$

The potentially promising idea of allowing the marginally stable diaminosilylene **41**[2] to react with various diaminogermylenes **42**[1] as an approach to germasilenes yielded surprising results. It seems that in all cases an initial, loosely bound adduct **43** is formed between the electron-sextet species, which is then transformed into the novel aminosilylgermylenes **44** by insertion of the silicon atom into one of the Ge−N bonds. The conceivable subsequent reactions are again strongly influenced by the nature of the substituents R at the germanium atom. In the case of R = *t*Bu, the digermene (*Z*)-**46** is formed; this compound has a very long Ge−Ge bond of 245.4(2) pm and pronounced *trans*-bent angles of 41.3° and 42.3°, which clearly exceed all previously known θ values.[43] On the other hand, with R = *i*Pr the digermene (*E*)-**45** is obtained, which has an even longer Ge−Ge bond length than that in (*Z*)-**46**, as well as a markedly larger bending angle.[44] Finally, with the aryl substituent R = 2,6-$Me_2C_6H_3$, the germylene **47** is isolated. The Ge−Ge separation of 410 pm and the *trans*-bent angle of 14° are indicative of weak dispersive forces between neighboring germylene molecules.[44] In parallel to the investigations performed in this laboratory, Lappert et al. reported on an analogous insertion of a diaminosilylene into one of the Ge−N bonds of $Ge[N(SiMe_3)_2]_2$; the final product in this case being a germane.[45] The large Ge−Ge bond lengths in (*E*)-**45** and (*Z*)-**46**, and the only very weak interactions in **47**, are probably attributable to the substitution patterns in these compounds. Although the Ge−Si bond in the intermediate **44** promotes the formation of a Ge−Ge double bond, the Ge−N bonds also present hinder Ge−Ge contacts, with the overall result that the structural param-

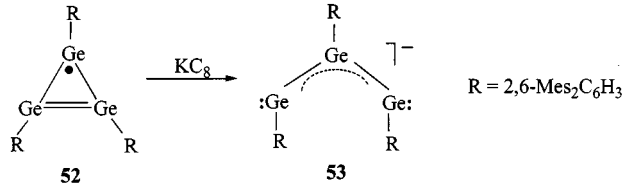
eters described above represent a compromise between these opposing effects.



A similar situation is found in compound **48**, where each germanium atom bears an aryl group and a chlorine atom; in the solid state it exists as a dimer with a Ge−Ge bond length of 244.3(2) pm and a *trans*-bending angle of Θ = 39°.[31] A further candidate for an analogous dimer could be the germylene RGeCl (R = 2,4,6-tBu$_3$C$_6$H$_2$), which is monomeric in solution but has yet to be examined in the solid state by X-ray crystallography.[46]



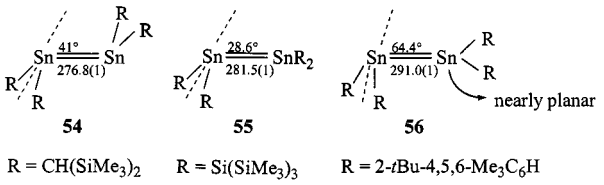
The cyclotrigermenes **49** and **50**, the first compounds with endocyclic Ge−Ge double bonds, were reported by Sekiguchi et al.,[47] who also generated and isolated the cation **51** from compound **49** by treatment with trityl tetraphenylborate.[48] An X-ray crystal structure analysis of the cyclotrigermenium salt revealed the presence of free germyl cations with a delocalized 2π-electron system, reminiscent of the cyclopropenium ion, with an equilateral triangular form.[48] The Ge−Ge bond lengths of 232.5 pm are intermediate between those of a single and a double bond.



Power et al. obtained another unusual compound similar to the cation **51** by dehalogenation of RGeCl (R = 2,6-Mes$_2$C$_6$H$_3$) with KC$_8$; the reaction furnished the cyclotrigermyl radical **52**. Although X-ray crystal structure analysis of **52** provided only limited details because of disorder problems, the EPR spectrum of the compound indicated the localization of the unpaired electron on one germanium atom. Further action of KC$_8$ on **52** led to the trigermyl anion **53**, with a structure comparable to that of the allyl anion but with a very large Ge−Ge−Ge angle of 159.2°.[49]

Stannylenes, Distannenes

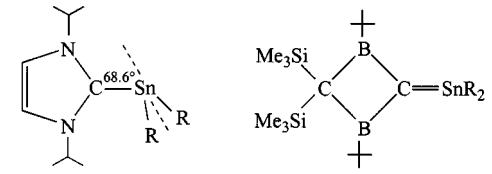
Lappert's distannene **54** was the first compound with a homonuclear multiple bond between two heavier atoms of group-14 elements to be prepared; however, its classification was at first difficult on account of the lack of suitable data for comparison.[9,50] The successful syntheses of stable disilenes and digermenes,[6,7] as well as the results of quantum chemical calculations,[9−12] were additionally needed to show that this molecule, with its *trans* bending of the substituents by 41° and the Sn−Sn bond length of 276.8(1) pm, a value approaching that of an Sn−Sn single bond, fits almost ideally into the series of homonuclear bonds between atoms of elements of this group.



Although compound **54** was first prepared and characterized by X-ray crystallography in 1976,[50] almost twenty years passed before the isolation of **55** and **56**, two further distannenes that are also stable in the solid state. These three distannenes differ considerably in their spatial structures. While the parameters for **54** are akin to those theoretically calculated for the parent compound Sn_2H_4, the highly distorted compound **55** avoids the strain arising from the bulky substituents by means of a considerable torsion about the double bond of 63.2° and a small *trans*-bent angle of 28.6°.[51] The structure of **56** is even more unusual: The long Sn−Sn bond, the length of which even exceeds that of an Sn−Sn single bond by about 13 pm, as well as the differing environments of the substituents on the two tin atoms, are indicative of a zwitterionic character of the molecule according to $R_2Sn^+ \rightarrow {}^-SnR_2$, which may arise through a single donor−acceptor interaction between the fully occupied s orbital of one tin atom and the empty p orbital of the other. This hypothesis is supported by the observation that the Sn−C bond lengths at the formally negatively charged tin atom are appreciably longer than those at the tin atom bearing the positive charge.[52] However, these observations are apparently at variance with the ^{119}Sn CP-MAS NMR spectrum of crystalline **56**, which features only one signal at δ_{iso} = 819.[53]

In order to simulate the bonding situation in solid **56**, a nucleophilic carbene of the Arduengo type[1] was prepared in this laboratory according to the method of Kuhn and Kratz,[54] and was allowed to react with a diarylstannylene. In spite of the different binding partners, the resulting compound **57** exhibited great similarity to the distannene **56**.

Thus, the tin atom in **57** exhibits a strong pyramidalization, with a bending angle of 68.6°, and the molecule has



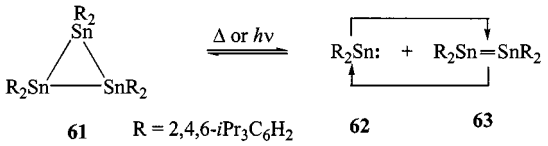
57 R = 2,4,6-*i*Pr$_3$C$_6$H$_2$ **58** R = 2-*t*Bu-4,5,6-Me$_3$C$_6$H

an extremely stretched Sn−C bond length of 237.9(5) pm.[55] In contrast, the stannaethene **58**, prepared for comparison purposes from an electrophilic cryptodiborylcarbene and a diarylstannylene, has completely planar environments at both the tin and the carbon atoms, with an Sn−C bond length of only 203.2(5) pm.[56]

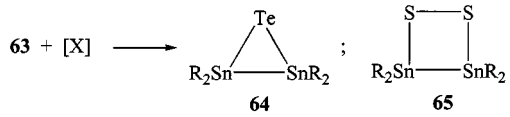
$R_2Sn{=}SnR_2 \rightleftharpoons 2\ R_2Sn:$

59 crystal **60** solution

A common feature of all distannenes **59**, including the recently reported compound RR′Sn=SnRR′ [R = Si(SiCH$_3$)$_3$, R′ = 2,4,6-(CF$_3$)$_3$C$_6$H$_2$],[57] is their stability in the crystalline state, even though they largely dissociate into stannylenes **60** in solution. An exception is the distannene **63**, first prepared by Masamune and Sita by thermolysis or photolysis of the cyclotristannane **61**, which retains its structural integrity in solution.[58]



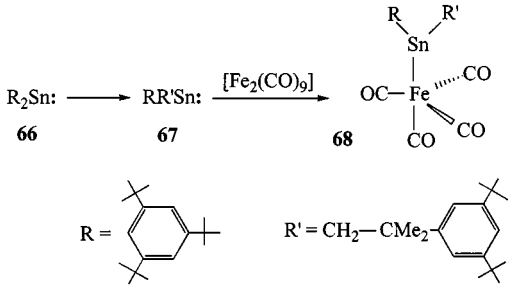
61 R = 2,4,6-*i*Pr$_3$C$_6$H$_2$ **62** **63**



64 **65**

The existence of the Sn−Sn double bond in solution was demonstrated not only by variable-temperature ^{119}Sn-NMR spectroscopy,[58,61] but also by trapping reactions with the heavier chalcogens to give, for example, the new ring systems of the telluradistannirane **64,**[59] or the unusual 1,2-dithiadistannetane **65**.[60] However, compound **63** cannot be isolated as a solid because at room temperature there is invariably some reversion to cyclotristannane **61** through generation of the stannylene **62** and its addition to **63**. Since the steric crowding of the aryl groups in distannene **63** is insufficient to prevent this reversion to cyclotristannane **61**, the isopropyl substituents in **63** were replaced by *tert*-butyl groups, and, after numerous unsuccessful attempts, dark-red crystals of the stannylene **66** were obtained by reaction of 2,4,6-*t*Bu$_3$C$_6$H$_2$Li with Sn[N(SiMe$_3$)$_2$]$_2$. This compound was found to exist as the monomeric stannylene both in solution and in the solid state. The spatial requirements of the substituents are apparently too great to allow a dimerization to the distannene in this case.[62]

Although the diarylstannylene **66** is stable in the crystalline state for an indefinite length of time, in solution a slow

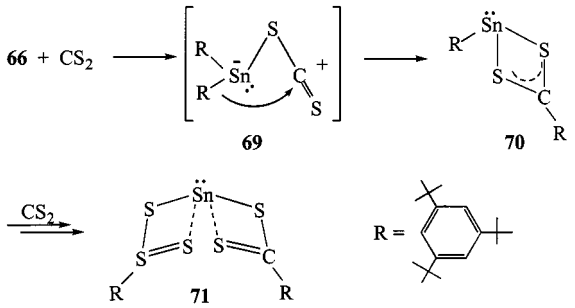


66 **67** **68**

R = R′ = CH$_2$—CMe$_2$

isomerization occurs, leading to the alkylarylstannylene **67**. Accordingly, all reactions with heavier chalcogens or transition metal substrates furnish exclusively products containing an aryl/alkyl-isomerized group R′.[63] One unusual result arose from the reaction of the stannylene with [Fe$_2$(CO)$_9$] or [Fe$_3$(CO)$_{12}$]: In the resulting iron complex **68** the stannylene **67** occupies an axial site, indicative of a strong σ-donor but weak π-acceptor character.[64,65]

It is of interest to note that **66** represents the first structurally characterized diarylstannylene that lacks donor stabilization. However, the stannylene [2,4,6-(CF$_3$)$_3$C$_6$H$_2$]$_2$Sn:, stabilized by weak F···Sn contacts, was known previously and had been observed in a second crystalline form involving weak Sn···Sn interactions.[66,67] Recently, Power et al. described the sterically crowded stannylene (2,6-Mes$_2$C$_6$H$_3$)$_2$Sn:, which, like **66**, cannot form a distannene in the solid state for steric reasons.[31] Structurally confirmed dialkylstannylenes are also rare, of which the cyclic compound SnC(SiMe$_3$)$_2$[CH$_2$]$_2$C^a(SiMe$_3$)$_2$(*Sn*−*C*^{a}) is mentioned as an example.[68]



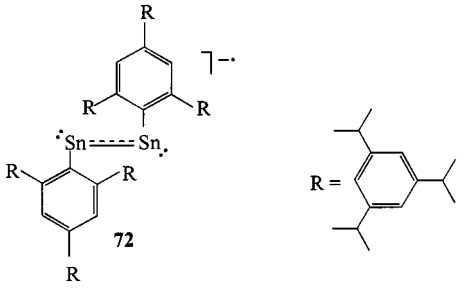
69 **70**

71

The only reaction of **66** to proceed without isomerization is that with carbon disulfide. This is probably due to the primary formation of an end-on or side-on adduct of the reacting species, **69**, followed by an aryl group migration to afford the tricoordinated stannylene **70**. A repetition of this process then leads to the final product, the tetracoordinated stannylene **71**; the structures of both compounds **70** and **71** were confirmed by X-ray crystallography.[69]

The trend towards decreasing E=E bond energies, which first becomes apparent in the digermenes, becomes more pronounced in the distannenes with the result that all distannenes, with the exception of compound **63**,[58] largely exist as the corresponding stannylenes in solution. Accordingly, the activation barrier determined for the equilibrium **59** ⇄ **60** (R = 2-*t*Bu-4,5,6-Me$_3$C$_6$H) amounts to just 34 kJ mol^{-1}.[53] As illustrated by the facile isomerization of **66**,

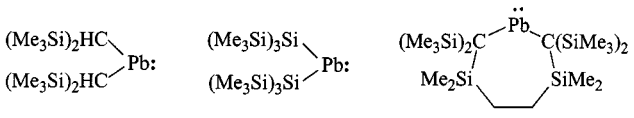
the Sn−C bonds are also appreciably more labile on account of their relatively large bond lengths.



Power et al. have recently reported on a novel Sn−Sn bonding situation: Reaction of a sterically extremely crowded arylchlorostannylene with KC_8 furnished the radical anion **72**, which could be crystallized with $[K(THF)_6]^+$ or $[K(dibenzo\text{-}18\text{-}crown\text{-}6)(THF)_3]^+$ as the counterion. The anion exhibits an Sn−Sn bond length of 281.2(1) pm and a *trans*-bent angle of 95.2°. Together with the spectral data, these values are indicative of a molecular ion with an Sn−Sn bond order of 1.5 and a localization of the free electron pairs on the two tin atoms.[70]

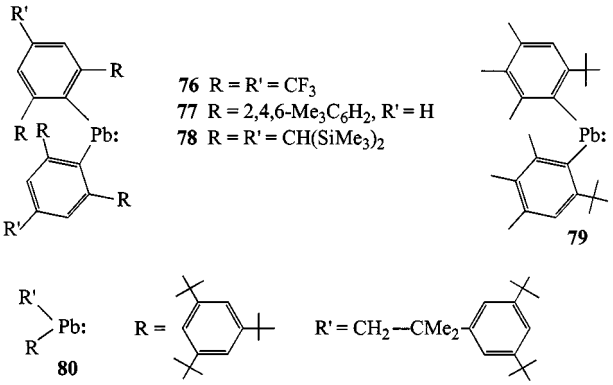
The Elusive Diplumbenes

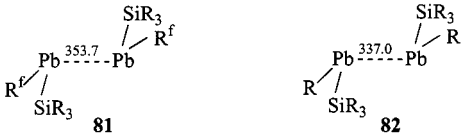
On account of their thermal lability and sensitivity to light, dialkyl- and diarylplumbanes were virtually unknown until recently. Although Lappert et al.[27][71] reported the isolation of the purple plumbylene **73** as early as 1973, its structure has only recently been determined.[72] In the solid state, compound **73** exists as a loosely bound dimer with a second plumbylene molecule and has a Pb···Pb separation of 412.9 pm with a *trans*-bent angle of 34.2°.



In contrast, the not too dissimilar cyclic plumbylene **75**[73] and the disilyl compound **74**[51] are strictly monomeric. The same holds for the diarylplumbylene **76**, which represents a borderline case between non-stabilized and donor-stabilized systems as a consequence of its weak Pb···F contacts,[74] and for the sterically extremely crowded diarylplumbylenes **77**[31] and **78**.[75]

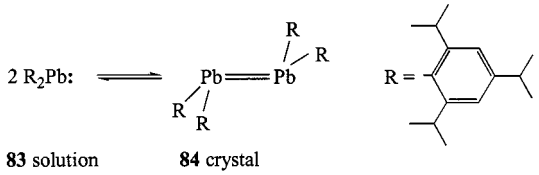
The sterically less crowded diarylplumbylene **79** and the heteroleptic alkylarylplumbylene **80** do not interact with neighboring plumbylene molecules either.[76] The formation of **80** is of interest since it allows a comparison to be made with the molecules $(2,4,6\text{-}t\text{Bu}_3C_6H_2)_2\text{Ge:}$[29] and **66**,[62] which were prepared by similar routes. The germanium compound is only stable at low temperature, while **66**, although stable for an indefinite length of time in the solid state, undergoes a slow isomerization in solution to furnish an alkylarylstannylene with the same substitution pattern as that in **80**. There is some evidence that the diarylplumbylene is formed initially in the reaction of $2,4,6\text{-}t\text{Bu}_3C_6H_2MgBr$ with lead(II) chloride, but then undergoes rearrangement to compound **80** at temperatures above −30°C.[76]





$SiR_3 = Si(SiMe_3)_3$; $R^f = 2,4,6\text{-}(CF_3)_3C_6H_2$; R = 2-*t*Bu-4,5,6-$Me_3C_6H$

The plumbylenes **73**−**80** all exist as V-shaped monomers in the crystal, with C−Pb−C angles ranging from 96.5° (**80**) to 117.1° (**75**). A first breakthrough with regard to lead−lead contacts between plumbylene molecules was realized with the recent isolation of the heteroleptic plumbylene dimer **81**, which has a Pb···Pb separation of 353.7(1) pm and a *trans*-bent angle of 40.8°.[57] Since intramolecular interactions between the fluorine atoms of the *ortho*-CF_3 groups and the lead atoms should weaken rather than favor a possible lead−lead interaction, another heteroleptic plumbylene has been prepared in this laboratory by reaction of the plumbylenes **74** and **79**. In the solid state, the thus formed plumbylene dimer **82** exhibits a short lead−lead separation of 337.0(1) pm and a *trans*-bent angle of 46.5°.[76] However, the observed lead−lead separations in **82**, and especially in **81**, are still markedly larger than the bond length of 295−300 pm calculated for the parent compound $H_2Pb{=}PbH_2$.[10,12,57]



Since sterically less demanding aryl groups apparently favor lead−lead contacts between plumbylene molecules, the reaction of $2,4,6\text{-}i\text{Pr}_3C_6H_2MgBr$ with lead(II) chloride at low temperature has been examined. This led to a violet solution of the plumbylene **83**, from which red crystals of the diplumbene **84** could be obtained. The existence of the first molecule with a lead−lead double bond is supported by the Pb−Pb bond length of 305.15(3) pm and the *trans*-

bent angles of 43.9° and 51.2°, which agree rather well with the calculated values.[77] Thus, with the discovery of compound **84**, homonuclear double bonds between all elements of group 14 are now known.

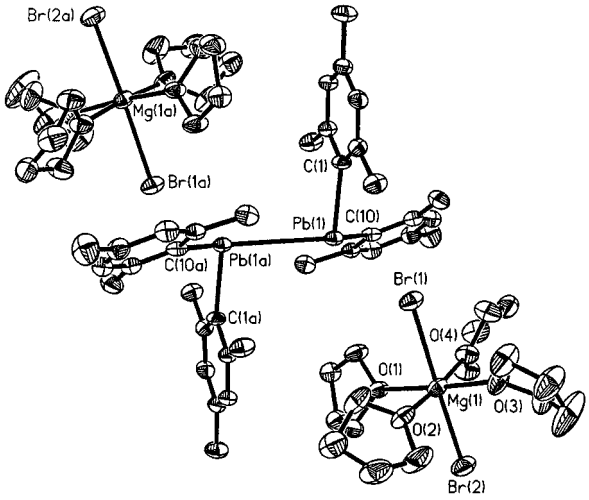


Figure 1. Molecular structure of the $MgBr_2(thf)_4$-stabilized plumbylene dimer $(Mes_2Pb)_2$

In order to examine whether even smaller aryl groups are capable of protecting a possible diplumbene from subsequent reactions, 2,4,6-$Me_3C_6H_2MgBr$ was allowed to react with lead(II) chloride under otherwise identical conditions. Black crystals of compound **85** were obtained, a plumbylene dimer stabilized by $MgBr_2(THF)_4$, as shown in Figure 1. Although the Pb···Br contact is about 50 pm longer than a Pb−Br bond, it does have an appreciable influence on the molecular structure of **85**, as manifested in the *trans*-bent angle of 71.2° and the Pb···Pb separation of 335.49(6) pm.[78] These examples indicate that more interesting results may be expected in the field of plumbylene dimers and diplumbenes.

Acknowledgments

Financial support of our work by the Deutsche Forschungsgemeinschaft and the Fonds der Chemischen Industrie is gratefully acknowledged.

[1] [1a] Review: W. A. Herrmann, C. Köcher, *Angew. Chem.* **1997**, *109* 2256−2282; *Angew. Chem. Int. Ed. Engl.* **1997**, *36*, 2162−2187. − See also: [1b] M. K. Denk, A. Thadani, H. Hatano, A. L. Lough, *Angew. Chem.* **1997**, *109*, 2719−2721; *Angew. Chem. Int. Ed. Engl.* **1997**, *36*, 2607−2609. − [1c] A. J. Arduengo III, F. Davidson, H. V. R. Dias, J. R. Goerlich, D. Khasmis, W. J. Marshall, T. K. Prakasha, *J. Am. Chem. Soc.* **1997**, *119*, 12742−12749.

[2] [2a] M. Denk, R. Lennon, R. Hayashi, R. West, A. V. Belyakov, H. P. Verne, A. Haaland, M. Wagner, N. Metzler, *J. Am. Chem. Soc.* **1994**, *116*, 2691−2692. − [2b] M. Denk, J. C. Greene, N. Metzler, M. Wagner, *J. Chem. Soc., Dalton Trans.* **1994**, 2405−2410. − [2c] B. Gerhus, M. F. Lappert, J. Heinicke, R. Boese, D. Bläser, *J. Chem. Soc., Chem. Commun.* **1995**, 1931−1932. − [2d] R. West, M. Denk, *Pure Appl. Chem.* **1996**, *68*, 785−788.

[3] Review: M. Veith, *Angew. Chem.* **1987**, *99*, 1−14; *Angew. Chem. Int. Ed. Engl.* **1987**, *26*, 1−14.

[4] M. Veith, E. Werle, R. Lisowsky, R. Löppe, H. Schnöckel, *Chem. Ber.* **1992**, *125*, 1375−1377.

[5] [5a] C. Heinemann, T. Müller, Y. Apeloig, H. Schwarz, *J. Am. Chem. Soc.* **1996**, *118*, 2023−2038. − [5b] C. Boehme, G. Frenking, *J. Am. Chem. Soc.* **1996**, *118*, 2039−2046. − [5c] R. West, J. J. Buffy, M. Haaf, T. Müller, B. Gerhus, M. F. Lappert, Y. Apeloig, *J. Am. Chem. Soc.* **1998**, *120*, 1639−1640.

[6] [6a] Reviews: R. West, *Angew. Chem.* **1987**, *99*, 1231−1241; *Angew. Chem. Int. Ed. Engl.* **1987**, *26*, 1202−1211. − [6b] G. Raabe, J. Michl, in *The Chemistry of Organic Silicon Compounds, Part 2* (Eds.: S. Patai, Z. Rappoport), Wiley, Chichester, U.K., **1989**, p. 1015−1142. − [6c] T. Tsumuraya, S. A. Batcheller, S. Masamune, *Angew. Chem.* **1991**, *103*, 916−944; *Angew. Chem. Int. Ed. Engl.* **1991**, *30*, 902−930. − [6d] M. Weidenbruch, *Coord. Chem. Rev.* **1994**, 275−300. − [6e] R. Okazaki, R. West, in *Multiply-Bonded Main Group Metals and Metalloids* (Eds.: R. West, F. G. A. Stone), Academic Press, San Diego, U.S.A., **1996**, p. 232−273.

[7] [7a] Reviews: M. Driess, H. Grützmacher, *Angew. Chem.* **1996**, *108*, 900−929; *Angew. Chem. Int. Ed. Engl.* **1996**, *35*, 827−856. − [7b] K. M. Baines, W. G. Stibbs, in *Multiply Bonded Main-Group Metals and Metalloids* (Eds.: R. West, F. G. A. Stone), Academic Press, San Diego, U.S.A. **1996**, p. 275−324. − [7c] For a recent review on "Homonuclear multiple bonding in heavier main group elements" see: P. P. Power, *J. Chem. Soc., Dalton Trans.* **1998**, 2939− 2951.

[8] Review: Y. Apeloig, in *The Chemistry of Organic Silicon Compounds, Part 1* (Eds. S. Patai, Z. Rappoport), Wiley, Chichester, U.K., **1989**, p. 57−225.

[9] D. E. Goldberg, P. B. Hitchcock, M. F. Lappert, K. M. Thomas, A. J. Thorne, T. Fjeldberg, A. Haaland, B. E. R. Schilling, *J. Chem. Soc., Dalton Trans.* **1986**, 2387−2394.

[10] [10a] G. Trinquier, J. P. Malrieu, *J. Am. Chem. Soc.* **1987**, *109*, 5303−5315. − [10b] G. Trinquier, *J. Am. Chem. Soc.* **1990**, *112*, 2130−2137.

[11] T. L. Windus, M. S. Gordon, *J. Am. Chem. Soc.* **1992**, *114*, 9559−9568.

[12] H. Jacobsen, T. Ziegler, *J. Am. Chem. Soc.* **1994**, *116*, 3667−3679.

[13] R. West, M. J. Fink, J. Michl, *Science* **1981**, *214*, 1343−1344.

[14] M. Kira, T. Iwamoto, C. Kabuto, *J. Am. Chem. Soc.* **1996**, *118*, 10303−10304.

[15] [15a] S. Masamune, Y. Kabe, S. Collins, D. J. Williams, R. Jones, *J. Am. Chem. Soc.* **1985**, *107*, 5552−5553. − [15b] R. Jones, D. J. Williams, Y. Kabe, S. Masamune, *Angew. Chem.* **1986**, *98*, 176−177; *Angew. Chem. Int. Ed. Engl.* **1986**, *25*, 173−174.

[16] T. Iwamoto, M. Kira, *Chem. Lett.* **1998**, 277−278.

[17] Review: H. G. von Schnering, *Angew. Chem.* **1981**, *93*, 44−63; *Angew. Chem. Int. Ed. Engl.* **1981**, *20*, 33−51.

[18] Review: N. Wiberg, *Coord. Chem. Rev.* **1997**, *163*, 217−252.

[19] N. Wiberg, H. Auer, H. Nöth, J. Knizek, K. Polborn, *Angew. Chem.* **1998**, *110*, 3030−3033; *Angew. Chem. Int. Ed.* **1998**, *37*, 2869−2872.

[20] H. Watanabe, K. Takeuchi, N. Fukawa, M. Kato, M. Goto, Y. Nagai, *Chem. Lett.* **1987**, 1341−1344.

[21] A. J. Millevolte, D. R. Powell, S. G. Johnson, R. West, *Organometallics* **1992**, *11*, 1091−1095.

[22] M. Weidenbruch, S. Willms, W. Saak, G. Henkel, *Angew. Chem.* **1997**, *109*, 2612−2613; *Angew. Chem. Int. Ed. Engl.* **1997**, *36*, 2503−2504.

[23] S. Willms, M. Weidenbruch, in *Organosilicon Chemistry IV - From Molecules to Materials* (Eds.: N. Auner, J. Weis), Wiley-VCH, Weinheim, in press.

[24] T. Müller, Frankfurt, personal communication. − Highlight: T. Müller, *Angew. Chem.* **1998**, *110*, 71−73; *Angew. Chem. Int. Ed.* **1998**, *38*, 68−70.

[25] S. Willms, M. Weidenbruch, unpublished results.

[26] S. Willms, W. Saak, M. Weidenbruch, unpublished results.

[27] P. J. Davidson, D. H. Harris, M. F. Lappert, *J. Chem. Soc., Dalton Trans.* **1976**, 2268−2274.

[28] P. Jutzi, A. Becker, H. G. Stammler, B. Neumann, *Organometallics* **1991**, *10*, 1647−1648.

[29] P. Jutzi, H. Schmidt, B. Neumann, H. G. Stammler, *Organometallics* **1996**, *15*, 741−746.

[30] L. Lange, B. Meyer, W.-W. du Mont, *J. Organomet. Chem.* **1987**, *329*, C17−C20.

[31] R. S. Simons, L. Pu, M. M. Olmstead, P. P. Power, *Organometallics* **1997**, *16*, 1920−1925.

[32] J. E. Bender, M. M. Banaszak Holl, J. W. Kampf, *Organometallics* **1997**, *16*, 2743−2745.
[33] P. B. Hitchcock, M. F. Lappert, S. J. Miles, A. J. Thorne, *J. Chem. Soc., Chem. Commun.* **1984**, 480−482.
[34] K. Kishikawa, N. Tokitoh, R. Okazaki, *Chem. Lett.* **1998**, 239−240.
[35] J. T. Snow, S. Murakami, S. Masamune, D. J. Williams, *Tetrahedron Lett*. **1984**, *25*, 4191−4194.
[36] S. A. Batcheller, T. Tsumuraya, O. Tempkin, W. A. Davis, S. Masamune, *J. Am. Chem. Soc.* **1990**, *112*, 9394−9395.
[37] M. Kira, T. Iwamoto, T. Maruyama, C. Kabuto, H. Sakurai, *Organometallics* **1996**, *15*, 3767−3769.
[38] M. Weidenbruch, M. Stürmann, H. Kilian, S. Pohl, W. Saak, *Chem. Ber.* **1997**, *130*, 735−738.
[39] K. M. Baines, J. A. Cooke, *Organometallics* **1992**, *11*, 3487−3488.
[40] K. M. Baines, J. A. Cooke, C. E. Dixon, H. W. Liu, M. R. Netherton, *Organometallics* **1994**, *13*, 631−634.
[41] K. M. Baines, J. A. Cooke, J. J. Vittal, *Heteroatom Chem.* **1994**, *5*, 293−303.
[42] C. E. Dixon, H. W. Liu, C. M. Vander Kant, K. M. Baines, *Organometallics* **1996**, *15*, 5701−5705.
[43] A. Schäfer, W. Saak, M. Weidenbruch, H. Marsmann, G. Henkel, *Chem. Ber.* **1997**, *130*, 1733 −1737.
[44] A. Schäfer, W. Saak, M. Weidenbruch, *Z. Anorg. Allg. Chem.* **1998**, *624*, 1405−1408.
[45] B. Gehrhus, P. B. Hitchcock, M. F. Lappert, *Angew. Chem.* **1997**, *109*, 2624−2626; *Angew. Chem. Int. Ed. Engl.* **1997**, *36*, 2514−2516.
[46] P. Jutzi, C. Leue, *Organometallics* **1994**, *13*, 2898−2899.
[47] A. Sekiguchi, H. Yanazaki, C. Kabuto, H. Sakurai, *J. Am. Chem. Soc.* **1995**, *117*, 8025−8026.
[48] [48a] H. Sekiguchi, M. Tsukamoto, M. Ichinohe, *Science* **1997**, *275*, 60−61.– [48b] M. Ichinohe, N. Fukaya, A. Sekiguchi, *Chem. Lett.* **1998**, 1045−1046.
[49] M. M. Olmstead, L. Pu, R. S. Simons, P. P. Power, *J. Chem. Soc., Chem. Commun.* **1997**, 1595−1596.
[50] D. E. Goldberg, D. H. Harris, M. F. Lappert, K. M. Thomas, *J. Chem. Soc., Chem. Commun.* **1976**, 261−262.
[51] K. W. Klinkhammer, W. Schwarz, *Angew. Chem.* **1995**, *107*, 1448−1451; *Angew. Chem. Int. Ed. Engl.* **1995**, *34*, 1334−1336.
[52] M. Weidenbruch, H. Kilian, K. Peters, H. G. von Schnering, H. Marsmann, *Chem. Ber.* **1995**, *128*, 983−985.
[53] M. A. Della Bona, M. C. Cassani, J. M. Keates, G. A. Lawless, M. F. Lappert, M. Stürmann, M. Weidenbruch, *J. Chem. Soc., Dalton Trans.* **1998**, 1187−1190.
[54] N. Kuhn, T. Kratz, *Synthesis* **1993**, 561−562.
[55] A. Schäfer, M. Weidenbruch, W. Saak, S. Pohl, *J. Chem. Soc., Chem. Commun.* **1995**, 1157−1158.
[56] M. Weidenbruch, H. Kilian, M. Stürmann, S. Pohl, W. Saak, H. Marsmann, D. Steiner, A. Berndt, *J. Organomet. Chem.* **1997**, *530*, 255−257.
[57] K. W. Klinkhammer, T. F. Fässler, H. Grützmacher, *Angew. Chem.* **1998**, *110*, 114−116; *Angew. Chem. Int. Ed.* **1998**, *37*, 124−126.
[58] S. Masamune, L. R. Sita, *J. Am. Chem. Soc.* **1985**, *107*, 6390−6391.
[59] A. Schäfer, M. Weidenbruch, W. Saak, S. Pohl, H. Marsmann, *Angew. Chem.* **1991**, *103*, 873−874; *Angew. Chem. Int. Ed. Engl.* **1991**, *30*, 834−836.
[60] A. Schäfer, M. Weidenbruch, W. Saak, S. Pohl, H. Marsmann, *Angew. Chem.* **1991**, *103*, 978−979; *Angew. Chem. Int. Ed. Engl.* **1991**, *30*, 962−964.
[61] M. Weidenbruch, A. Schäfer, H. Kilian, S. Pohl, W. Saak, H. Marsmann, *Chem. Ber.* **1992**, *125*, 563−566.
[62] M. Weidenbruch, J. Schlaefke, A. Schäfer, K. Peters, H. G. von Schnering, H. Marsmann, *Angew. Chem.* **1994**, *106*, 1938−1939; *Angew. Chem. Int. Ed. Engl.* **1994**, *33*, 1846−1848.
[63] [63a] M. Weidenbruch, A. Stilter, J. Schlaefke, K. Peters, H. G. von Schnering, *J. Organomet. Chem.* **1995**, *501*, 67−70. – [63b] M. Weidenbruch, A. Stilter, K. Peters, H. G. von Schnering, *J. Organomet. Chem.* **1998**, *560*, 125−129.
[64] M. Weidenbruch, A. Stilter, K. Peters, H. G. von Schnering, *Chem. Ber.* **1996**, *129*, 1565−1567.
[65] A. R. Rossi, R. Hoffmann, *Inorg. Chem.* **1975**, *14*, 365−374.
[66] H. Grützmacher, H. Pritzkow, F. T. Edelmann, *Organometallics* **1991**, *10*, 23−25.
[67] U. Lay, H. Pritzkow, H. Grützmacher, *J. Chem. Soc., Chem. Commun.* **1992**, 260−262.
[68] M. Kira, R. Yauchibara, R. Hirano, C. Kabuto, H. Sakurai, *J. Am. Chem. Soc.* **1991**, *113*, 7785−7787.
[69] M. Weidenbruch, U. Grobecker, W. Saak, E.-M. Peters, K. Peters, *Organometallics* **1998**, *17*, 5206−5209.
[70] M. M. Olmstead, R. S. Simons, P. P. Power, *J. Am. Chem. Soc.* **1997**, *119*, 11705−11706.
[71] P. J. Davidson, M. F. Lappert, *J. Chem. Soc., Chem. Commun.* **1973**, 317.
[72] K. W. Klinkhammer, W. Schwarz, unpublished results. The author thanks Dr. K. W. Klinkhammer for advance communication.
[73] C. Eaborn, T. Ganicz, P. B. Hitchcock, J. D. Smith, S. E. Sözerli, *Organometallics* **1997**, *16*, 5621−5622.
[74] S. Brooker, J.-K. Buijink, F. T. Edelmann, *Organometallics* **1991**, *10*, 25−26.
[75] Review: N. Kano, N. Tokitoh, R. Okazaki, *Yuki Gosei Kagaku Kyokai Shi* **1998**, in press. The author thanks Professor R. Okazaki for advance communication.
[76] M. Stürmann, M. Weidenbruch, K. W. Klinkhammer, F. Lissner, H. Marsmann, *Organometallics* **1998**, *17*, 4425−4428.
[77] M. Stürmann, W. Saak, H. Marsmann, M. Weidenbruch, *Angew. Chem.*, in press.
[78] M. Stürmann, W. Saak, M. Weidenbruch, unpublished results.

Received October 5, 1998
[I98339]

Efficient and Selective Photochemical Labilization of a Given Bidentate Ligand in Mixed Ruthenium(II) Complexes of the $Ru(phen)_2L^{2+}$ and $Ru(bipy)_2L^{2+}$ Family (L = Sterically Hindering Chelate)

Anne-Chantal Laemmel,[a] Jean-Paul Collin,*[a] and Jean-Pierre Sauvage*[a]

Keywords: Ruthenium / Photochemistry / Photosubstitution / Diimine chelates / Sterically hindered ligands

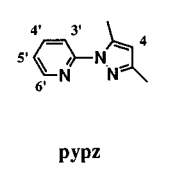
Mixed ruthenium(II) complexes containing 1,10-phenanthroline (or 2,2′-bipyridine) and a sterically congested bidentate ligand such as 2,9-diphenyl-1,10-phenanthroline, 6,6′-dimethyl- or 6,6′-diphenyl-2,2′-bipyridine, or 1-(2′-pyridyl)-3,5-dimethylpyrazole undergo clean and selective ligand substitution under irradiation with visible light. For instance, $Ru(phen)_2(dmbp)^{2+}$ in CH_3CN is quantitatively converted to $Ru(phen)_2(CH_3CN)_2{}^{2+}$ in a photochemical reaction accompanied by expulsion of the sterically hindering chelate dmbp (phen = 1,10-phenanthroline; dmbp = 6,6′-dimethyl-2,2′-bipyridine). Interestingly, 2,2′-bipyridine was found to be photochemically ejected in one case, probably as a consequence of its greater flexibility.

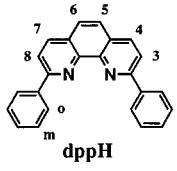
The development of new molecular devices relying on electronic and photonic processes is an attractive challenge. Signal processing and information storage at the molecular level could be based on molecules able to exist in two stable states,[1] with the interconversion between these states having to be fast and quantitative.

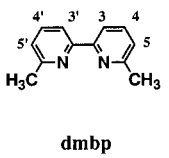
Ruthenium(II) complexes display photochemical properties that permit their use as photoactive electron- or energy-transfer components,[2] photochemical stability of the complex being an essential requirement. On the other hand, *the photolabilization of a ligand followed by its recoordination in the dark could be the key steps in the construction of photoswitchable molecular devices.* Interesting photochemically labile ruthenium(II) complexes have been reported, some of which are capable of clean photo-expulsion of a given ligand with a high quantum efficiency.[3]

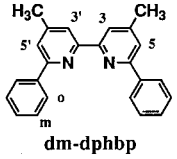
Herein, we describe the quantitative photosubstitution reactions that occur in four tris-chelated ruthenium(II) complexes. These complexes (**1**, **2**, **5**, **6**), incorporating two identical bidentate ligands (bipy or phen; bipy = 2,2′-bipyridine, phen = 1,10-phenanthroline) and a suitable third ligand, are shown in Scheme 1.

The choice of the third ligand was made with the help of models, which predicted that photolabilization would be most likely to occur on the weakest ligand field axis.[4] Hindering bidentate ligands such as dppH, dmbp, and dm-dphbp (dppH = 2,9-diphenyl-1,10-phenanthroline; dmbp = 6,6′-dimethyl-2,2′-bipyridine; dm-dphbp = 4,4′-dimethyl-6,6′-diphenyl-2,2′-bipyridine) or disymmetrical ligands with poor σ-donor character such as pypz [pypz = 1-(2′-pyridyl)-3,5-dimethylpyrazole] are considered to decrease the ligand field. Excitation in the MLCT region leads to a charge-transfer excited state, allowing the thermal









$Ru(bipy)_2(pypz)(PF_6)_2$	**1**
$Ru(bipy)_2(dppH)(PF_6)_2$	**2**
$Ru(bipy)(dppH)(CH_3CN)_2(PF_6)_2$	**3**
$Ru(bipy)(dpp)(CH_3CN)(PF_6)$	**4**
$Ru(phen)_2(dmbp)(PF_6)_2$	**5**
$Ru(phen)_2(dm\text{-}dphbp)(PF_6)_2$	**6**

Scheme 1. The various ligands used and the ruthenium(II) complexes made and studied

population of low-lying dissociative d-d states.[5] As expected, visible (300 nm ≤ λ ≤ 800 nm) light irradiation of **1**, **2**, **5**, and **6** in degassed acetonitrile led very selectively to a substitution of one bidentate ligand by two molecules of solvent (reactions 1, 2, and 3 in Scheme 2). The photoproduct was unambiguously identified as $[Ru(bipy)_2(CH_3CN)_2](PF_6)_2$ or $[Ru(phen)_2(CH_3CN)_2](PF_6)_2$ depending on the starting complex.

However, contrasting behavior between the various complexes could also be observed. Since the tris complex $Ru(pypz)_3{}^{2+}$, previously studied by Marzin et al.,[6] undergoes photosubstitution in acetonitrile to produce $Ru(pypz)_2(CH_3CN)_2{}^{2+}$,[7] it was not unexpected that irradiation of **1** led efficiently to $Ru(bipy)_2(CH_3CN)_2{}^{2+}$. On the contrary,

[a] Laboratoire de Chimie Organo-minérale, Institut Le Bel, Université Louis Pasteur,
4 rue Blaise Pascal, F-67070 Strasbourg, France
E-mail: sauvage@chimie.u-strasb.fr

 © WILEY-VCH Verlag GmbH, D-69451 Weinheim, 1999 1434−1948/99/0303−0383 $ 17.50+.50/0

$$Ru(bipy)_2(pypz)^{2+} \xrightarrow[CH_3CN]{h\nu} Ru(bipy)_2(CH_3CN)_2{}^{2+} + pypz \quad (1)$$

$$Ru(bipy)_2(dppH)^{2+} \xrightarrow[CH_3CN]{h\nu} Ru(bipy)(dppH)(CH_3CN)_2{}^{2+} + bipy \quad (2)$$

$$Ru(phen)_2(L)^{2+} \xrightarrow[CH_3CN]{h\nu} Ru(phen)_2(CH_3CN)_2{}^{2+} + L \quad (3)$$

L = dmbp or dm-dphbp

Scheme 2. Photochemical subtitution of a given bidentate chelate by CH_3CN

compound **2** formed from the same $Ru(bipy)_2$ core and disubstituted 1,10-phenanthroline (dppH) displayed unexpected behavior. In this case, a bipyridine was photolabilized rather than the hindering dppH ligand. This finding may be related to the distorted structure of the complex. Indeed, the coordination of dppH in this complex may be quite normal in terms of Ru−N distances and the N−Ru−N angle. On the other hand, strong steric interactions between the phenyl groups and the bipy ligands could result in extension of the Ru−N(bipy) distances or to a twisting of the pyridine moieties. Such a distortion has been found in the solid state for the closely analogous complex $Ru(phen)_2(dmp)^{2+}$ (dmp = 2,9-dimethyl-1,10-phenanthroline).[8] An alternative argument hinges on the different rigidities of the bipyridine and phenanthroline ligands. Intuitively, the decoordination of phenanthroline must be more difficult than that of bipyridine, since after the first Ru−N bond breaking, the pyridine ring can rotate about the $C^2-C^{2'}$ bond in the case of bipy, whereas the aromatic plane of phen is almost impossible to distort. Indeed, intermediates with η^1-bipyridine ligands have been previously postulated[3a,5b] and recently identified[9] in the photosubstitution of $Ru(bipy)_2(3,3'\text{-dmbp})^{2+}$ in acidic media (3,3′-dmbp = 3,3′-dimethyl-2,2′-bipyridine). Unfortunately, complex **2** does not fulfil the requirements of reversibility because the photoproduct $Ru(bipy)(dppH)(CH_3CN)_2{}^{2+}$ is highly base-sensitive. During its attempted purification on an alumina column or in the presence of a trace of base, an orthometallation reaction takes place at one phenyl group leading to the very stable $Ru(bipy)(dpp)(CH_3CN)^+$ complex. This complex was fully characterized by ^{1}H NMR, FAB MS, and cyclic voltammetry. In order to avoid this reaction, and in view of the behavior of the disubstituted phenanthroline in complex **2**, complexes **5** and **6**, based on the $Ru(phen)_2$ core and incorporating a disubstituted bipyridine (dmbp or dm-dphbp), were prepared and irradiated in acetonitrile. These two systems were found to undergo very efficient photolabilization of the hindering bipyridine ($t_{1/2}$ = 28 and 390 s for **5** and **6**, respectively). As illustrated in Figure 1, after 140 s of irradiation, the electronic spectrum of a degassed acetonitrile solution of **5** is transformed to the characteristic spectrum of the $Ru(phen)_2(CH_3CN)_2{}^{2+}$ species.[10]

The presence of marked isosbestic points at 342 and 404 nm demonstrates the selectivity of the photosubstitution.

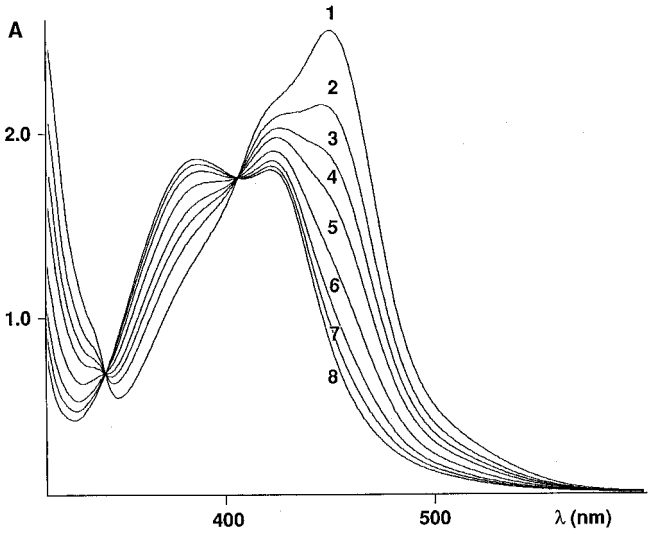


Figure 1. Visible spectra of a CH_3CN solution of **5** (1-cm cell; [**5**] = $2.4\cdot10^{-4}$ molL^{-1}) after various irradiation times: 0 s (1), 15 s (2), 25 s (3), 35 s (4), 55 s (5), 80 s (6), 105 s (7), 140 s (8)

The same result was also obtained by ^{1}H-NMR spectroscopy with direct light irradiation of the NMR tube. As suggested by the behavior of **2** and confirmed in the case of **5** and **6**, phenanthrolines are seen to be much more difficult to photolabilize than bipyridine ligands, regardless of which type of ligand is the hindering one. This conclusion can be related to the different quantum yields of photoanation found for $Ru(bipy)_3Cl_2$ and $Ru(phen)_3Cl_2$ (0.1 and 0.014, respectively) in CH_2Cl_2, which differ almost by one order of magnitude.[5b]

In conclusion, we have shown that by combining ligands with precisely defined electronic and steric properties in the same ruthenium(II) complex, it is possible to prepare photochemically active compounds that undergo quantitative and selective decoordination of a given ligand under light irradiation. Work currently in progress is concerned with the use of the present photolabile complexes as building blocks and their incorporation into multi-component systems. Preliminary experiments demonstrate that the recoordination reaction of dmbp onto the ruthenium centre, starting from $Ru(phen)_2(CH_3CN)_2{}^{2+}$ is indeed quantitative.

Experimental Section

Physical Measurements: ^{1}H NMR: Bruker WP200 SY (200 MHz) and Bruker AM 400 (400 MHz) instruments; the reported chemical shifts are referenced to Me_4Si as an internal standard. − UV/Vis: Kontron Uvikon 860. − MS: VG ZAB-HF, Thomson THN 208. − Irradiation: Hanimex slide projector (150-W halogen lamp). − Cyclic voltammetry: PAR model 273A potentiostat, Pt disc as working electrode, CH_3CN solution, 0.1 M Bu_4NBF_4 as supporting electrolyte, Pt wire as auxiliary electrode, SCE as reference electrode.

Photolysis Experiments − Representative Photolysis of 1: In a round-bottomed Pyrex Schlenk flask, 30 mg (0.034 mmol) of **1** was dissolved in 50 mL of CH_3CN. The resulting solution was stirred under argon and irradiated for 8 h. In order to obtain a crystalline

product, the solution was first concentrated to half of its original volume, 30 mL of toluene was added, and then the remaining CH_3CN was evaporated with the temperature not exceeding 40°C. Orange crystals were obtained, which were filtered off on a porosity grade 4 glass frit and washed with diethyl ether. The product was dried in vacuo to give 26 mg of $[Ru(bipy)_2(CH_3CN)_2](PF_6)_2$ (96%). The remaining 4% was accounted for by recovered starting material **1**. − UV/Vis (CH_3CN): λ_{max} (ε) = 425 nm (8460 $Lmol^{-1}cm^{-1}$). − ^1H NMR ([D_6]acetone, 200 MHz): δ = 9.7 (d, *J* = 5.05 Hz, 2 H, 6-H), 8.9 (d, *J* = 7.88 Hz, 2 H, 6′-H), 8.76 (d, *J* = 7.87 Hz, 2 H, 3-H), 8.51 (td, *J* = 7.93, 1.55 Hz, 2 H, 5-H), 8.19 (td, *J* = 7.87, 1.48 Hz, 2 H, 4-H), 8.07 (td, *J* = 6.58, 1.35 Hz, 2 H, 5′-H), 7.96 (d, *J* = 4.92 Hz, 2 H, 3′-H), 7.52 (td, *J* = 6.64, 1.47 Hz, 2 H, 4′-H), 2.59 (s, 6 H, 2 CH_3CN). − The photolysis of **2** was performed following the same method (yield 81%). The photolyses of **5** and **6** were realized in a Schlenk cell on an analytical scale.

Synthesis of Ligands and Complexes: The ligands dppH,[11] pypz,[6] dmbp,[12] and dm-dphbp,[13] and the complexes *cis*-$Ru(L)_2Cl_2$ (L = bipy or phen),[14] were prepared according to literature procedures.

$[Ru(bipy)_2(pypz)](PF_6)_2$ (1): The complex *cis*-$Ru(bipy)_2Cl_2$ (145 mg, 0.3 mmol) was dissolved in 20 mL of EtOH/H_2O (3:1) and the resulting solution was refluxed for 1 h. The ligand pypz (52 mg, 0.3 mmol) was then slowly added and refluxing was continued for a further 4 h, in the course of which the colour of the solution changed from purple-red to orange-red. The mixture was then filtered, the filtrate was concentrated to dryness, and the residue was redissolved in water (20 mL). The complex was precipitated as the hexafluorophosphate by the dropwise addition of concentrated KPF_6 solution. The product was filtered off (grade 4 glass frit) and recrystallized from EtOH/H_2O to give an orange-red microcrystalline powder (210 mg), yield 80%. − UV/Vis (CH_3CN): λ_{max} (ε) = 449 nm (9200 $Lmol^{-1}cm^{-1}$). − ^1H NMR (CD_3CN, 200 MHz): δ = 8.45 (m, 4 H), 8.2−7.9 (m, 7 H), 7.77 (m, 2 H), 7.60 (d, *J* = 5.42 Hz, 1 H), 7.53−7.28 (m, 5 H), 7.22−7.14 (m, 1 H), 6.35 (s, 4-H), 2.82 (s, 5-CH_3), 1.48 (s, 3-CH_3).

$[Ru(bipy)_2(dppH)](PF_6)_2$ (2): In a 100-mL round-bottomed flask fitted with a reflux condenser, a mixture of 145 mg (0.3 mmol) of *cis*-$Ru(bipy)_2Cl_2$ and 120 mg (0.36 mmol) of dppH in 25 mL of ethylene glycol was heated under reflux for 3 h. After cooling to room temperature, the orange solution was filtered through a porosity grade 4 glass frit. Then, at 100°C, the filtrate was treated dropwise with a saturated aqueous solution of KPF_6. The resulting solution was allowed to cool and left to stand overnight at 0°C, whereupon the complex crystallized. It was filtered off, washed with a copious amount of water, and air-dried. The crude red product was purified by chromatography on silica gel, eluting with acetonitrile/water/saturated aqueous KNO_3 (100:5:0.5). After anion exchange, 243 mg (76%) of **2** was obtained. − UV/Vis (CH_3CN): λ_{max} (ε) = 451 nm (13300 $Lmol^{-1}cm^{-1}$). − ^1H NMR (CD_3CN, 400 MHz): δ = 8.66 (d, *J* = 8.04 Hz, 4-H, 7-H), 8.34 (s, 5-H, 6-H), 8.24 (d, *J* = 7.76 Hz, 2 H), 8.05 (td, *J* = 7.88, 1.53 Hz, 2 H), 7.89 (d, *J* = 5.08 Hz, 2 H), 7.84 (d, *J* = 7.76 Hz, 2 H), 7.54 (d, *J* = 8.28 Hz, 3-H, 8-H), 7.45 (t, *J* = 7.9 Hz, 2 H), 7.34 (t, *J* = 6.44 Hz, 2 H), 7.13 (br. s, 2 H, *o*-H), 7.02 (t, *J* = 7.5 Hz, 2 H, *p*-H), 6.86 (br. s, 2 H, *o*-H), 6.74 (br. s, 2 H, *m*-H), 6.66 (d, *J* = 5.64 Hz, 2 H), 6.56 (td, *J* = 6.68, 1.5 Hz, 2 H), 6.12 (br. s, 2 H, *m*-H). − Redox potential (V vs. SCE): $E°(Ru^{III/II})$ = 1.3 V, $E°(Ru^{II/I})$ = −1.3 V, irreversible wave.

$Ru(bipy)(dppH)(CH_3CN)_2(PF_6)_2$ (3): In a round-bottomed Schlenk flask, 20 mg (0.019 mmol) of **2** was dissolved in 30 mL of acetonitrile and the resulting orange-red solution was stirred under argon and irradiated for 8 h. The yellow solution thus obtained was chromatographed on a silica gel column, eluting with acetonitrile/water/saturated aqueous KNO_3 (100:5:0.5). After anion exchange, 0.15 g of **2** (81%) was obtained. − UV/Vis (CH_3CN): λ_{max} (ε) = 401 nm (4720 $Lmol^{-1}cm^{-1}$), 424 nm (4690 $Lmol^{-1}cm^{-1}$). − ^1H NMR (CD_2Cl_2, 200 MHz): δ = 8.80 (d, *J* = 8.36 Hz, 7-H or 4-H), 8.37 (d, *J* = 8.36 Hz, 4-H or 7-H), 8.27 (d, *J* = 8.62 Hz, 5-H or 6-H), 8.25 (d, *J* = 6.4 Hz, 1 H), 8.10 (t, *J* = 8.12, 8.36 Hz, 3-H or 8-H, 6-H or 5-H), 8.02 (d, 7.88 Hz, 1 H), 7.92 (d, *J* = 7.62 Hz, 1 H), 7.83−7.71 (m, 4 H), 7.58 (m, 4 H), 7.44 (d, *J* = 8.36 Hz, 8-H or 3-H), 7.36 (td, *J* = 3.66, 1.47 Hz, 2 H), 7.14 (td, *J* = 6.64, 1.48 Hz, 2 H), 7.05 (td, *J* = 6.4, 1.48 Hz, 1 H), 6.95 (t, *J* = 7.62 Hz, 1 H), 6.70 (d, *J* = 5.66 Hz, 1 H), 6.44 (d, *J* = 7.62 Hz, 1 H), 2.77 (s, 3 H, CH_3CN), 1.50 (s, 3 H, CH_3CN). − Redox potential (V vs. SCE): $E°(Ru^{III/II})$ = 1.49 V, $E°(Ru^{II/I})$ = −1.3 V, irreversible wave.

$Ru(bipy)(dpp)(CH_3CN)(PF_6)$ (4): 40 mg (0.039 mmol) of **3** was subjected to chromatography on 5 successive alumina columns, eluting with CH_2Cl_2/MeOH (99.3:0.7), to give 25.5 mg of **4** (85%). − UV/Vis (CH_3CN): λ_{max} (ε) = 458 nm (7900 $Lmol^{-1}cm^{-1}$), 520 (9681 $Lmol^{-1}cm^{-1}$). − ^1H NMR (CD_3CN, 200 MHz): δ = 8.99 (d, *J* = 6.4 Hz, 1 H), 8.47 (d, *J* = 8.38 Hz, dpp-H), 8.40 (d, *J* = 8.86 Hz, dpp-H), 8.28 (d, *J* = 8.86 Hz, dpp-H), 8.15 (d, *J* = 8.86 Hz, dpp-H), 8.07 (d, *J* = 8.84 Hz, dpp-H), 8.03 (t, *J* = 7.12, 7.64 Hz, 2 H), 7.89 (m, 1 H), 7.85 (dd, *J* = 7.74, 1.35 Hz, 1 H), 7.76 (td, *J* = 7.75, 1.48 Hz, 1 H), 7.61 (d, *J* = 8.36 Hz, dpp-H), 7.54 (td, *J* = 7.5, 1.48 Hz, 1 H), 7.36 (m, 2 H), 7.20 (d, *J* = 4.92 Hz, 1 H), 7.01 (m, 3 H), 6.87−6.62 (m, 4 H), 5.95 (d, *J* = 6.4 Hz, 1 H), 1.99 (s, 3 H, CH_3CN). − FAB-MS; *m*/*z*: 589 [M^+ − bipy], 630.1 [M^+ − bipy + CH_3CN]. − Redox potential (V vs. SCE): $E°(Ru^{III/II})$ = 0.5 V, $E°(Ru^{II/I})$ = −1.68 V.

$Ru(phen)_2(dmbp)(PF_6)_2$ (5): A mixture of *cis*-$Ru(phen)_2Cl_2$ (0.2 g, 0.38 mmol), dmbp (0.1 g, 0.54 mmol), and degassed ethylene glycol (5 mL) was heated at 160°C under argon for 4 h. After cooling to room temperature, 20 mL of saturated aqueous KPF_6 solution was added. The yellow precipitate thus obtained was collected by filtration, washed with water (30 mL), and redissolved in the minimum volume of CH_3CN. This solution was subjected to column chromatography on silica, using CH_2Cl_2/MeOH (0 to 4%) as eluent. Complex **5** was obtained as a red powder (0.18 g, 51%). − UV/Vis (CH_3CN): λ_{max} (ε) = 449 nm (12200 $Lmol^{-1}cm^{-1}$). − ^1H NMR (CD_3CN, 200 MHz): δ = 8.71 (dd, *J* = 8.37, 1.23 Hz, 2 H, 2-H), 8.43 (dd, *J* = 7.62 Hz, 1.23 Hz, 2 H, 9-H), 8.40 (dd, *J* = 5.41, 1.23 Hz, 2 H, 4-H), 8.38 (m, 2 H, bipy-H), 8.28 (d, *J* = 8.86 Hz, 2 H, 5-H or 6-H), 8.17 (d, *J* = 8.84 Hz, 2 H, 6-H or 5-H), 7.92 (m, 2 H, bipy-H), 7.88 (dd, *J* = 8.24, 5.3 Hz, 2 H, 8-H or 3-H), 7.58 (dd, *J* = 5.16, 1.22 Hz, 2 H, 7-H), 7.31 (dd, *J* = 8.24, 5.3 Hz, 2 H, 3-H or 8-H), 7.21 (dd, *J* = 7.62, 0.98 Hz, 2 H, bipy-H), 1.46 (s, 6 H, 2 CH_3).

$Ru(phen)_2(dm\text{-}dphbp)(PF_6)_2$ (6): A mixture of *cis*-$Ru(phen)_2Cl_2$ (0.15 g, 0.28 mmol), dm-dphbp (0.93 g, 0.28 mmol), and degassed ethylene glycol (5 mL) was refluxed under argon for 3 h. After cooling, addition of aqueous KPF_6 solution (20 mL) afforded a brown precipitate, which was collected by filtration, washed with water (50 mL) and diethyl ether (50 mL), and finally dried. The product was purified by chromatography (silica gel) using CH_2Cl_2/MeOH (0 to 2%) as eluent, to give a red powder (0.25 g, 81%). − UV/Vis (CH_3CN): λ_{max} (ε) = 454 nm (12100 $Lmol^{-1}cm^{-1}$). − ^1H NMR (CD_3CN, 200 MHz): δ = 8.67 (dd, *J* = 5.29, 1.23 Hz, 2 H, 2-H), 8.70 (dd, *J* = 8.24, 1.12 Hz, 2 H, 4-H), 8.54 (s, 2 H, bipy-H), 8.15 (d, *J* = 8.86 Hz, 5-H), 7.96 (dd, *J* = 8.23, 4.66 Hz, 2 H, 3-H), 7.88 (d, *J* = 8.86 Hz, 2 H, 6-H), 7.87 (dd, *J* = 8.11, 1.23 Hz, 2 H, 7-H), 7.05 (br. s, 2 H, phenyl-H), 6.98 (s, 2 H, bipy-H), 6.64

(m, 4 H, phenyl-H), 6.60 (dd, J = 8.12, 5.42 Hz, 2 H, 8-H), 6.47 (dd, J = 5.29, 1.24 Hz, 2 H, 9-H), 6.11 (br. s, 2 H, phenyl-H), 5.36 (br. s, 2 H, phenyl-H), 2.54 (s, 6 H, 2 CH_3).

Acknowledgments

This work was performed with the aid of financial support from the CNRS. We thank C. O. Dietrich-Bucheker and G. Mieslin for providing a sample of dm-dphbp.

[1] U. Kölle, *Angew. Chem.* **1991**, *103*, 970−972; *Angew. Chem. Int. Ed. Engl.* **1991**, *30*, 956−958; M. Sano, H. Taube, *J. Am. Chem. Soc.* **1991**, *113*, 2327−2328; O. Kahn, C. J. Martinez, *Science* **1998**, *279*, 44−48.

[2] A. Juris, V. Balzani, F. Barigelletti, S. Campagna, P. Belser, A. Von Zelewsky, *Coord. Chem. Rev.* **1988**, *84*, 85−277; J.-P. Sauvage, J.-P. Collin, J.-C. Chambron, S. Guillerez, C. Coudret, V. Balzani, F. Barigelletti, L. De Cola, L. Flamigni, *Chem. Rev.* **1994**, *94*, 993−1019.

[3] Representative examples: [3a] B. Durham, J. L. Walsh, C. L. Carter, T. J. Meyer, *Inorg. Chem.* **1980**, *19*, 860−865. − [3b] R. J. Crutchley, A. B. L. Lever, *Inorg. Chem.* **1982**, *21*, 2276−2282. − [3c] D. V. Pinnick, B. Durham, *Inorg. Chem.* **1984**, *23*, 1140−1445. − [3d] G. H. Allen, R. P. White, D. P. Rillema, T. J. Meyer, *J. Am. Chem. Soc.* **1984**, *106*, 2613−2620. − [3e] H. F. Suen, S. W. Wilson, M. Pomerantz, J. L. Walsh, *Inorg. Chem.* **1989**, *28*, 786−791. − [3f] R. Wang, J. G. Vos, R. H. Schmehl, R. Hage, *J. Am. Chem. Soc.* **1992**, *114*, 1964−1970.

[4] L. G. Vanquickenborne, A. Ceulemans, *Coord. Chem. Rev.* **1983**, *48*, 157−202.

[5] [5a] J. Van Houten, R. J. Watts, *Inorg. Chem.* **1978**, *17*, 3381−3385. − [5b] B. Durham, J. V. Caspar, J. K. Nagle, T. J. Meyer, *J. Am. Chem. Soc.* **1982**, *104*, 4803−4810.

[6] P. J. Steel, F. Lahousse, D. Lerner, C. Marzin, *Inorg. Chem.* **1983**, *22*, 1488−1493.

[7] G. M. Brown, R. W. Callahan, T. J. Meyer, *Inorg. Chem.* **1975**, *14*, 1915−1921.

[8] H. Hichida, S. Tachiyashiki, Y. Sasaki, *Chem. Lett.* **1989**, 1579−1580.

[9] S. Tachiyashiki, H. Ikezawa, K. Mizumachi, *Inorg. Chem.* **1994**, *33*, 623−625.

[10] P. Bonneson, J. L. Walsh, W. T. Pennington, A. W. Cordes, B. Durham, *Inorg. Chem.* **1983**, *22*, 1761−1765.

[11] C. O. Dietrich-Bucheker, P. A. Marnot, J.-P. Sauvage, *Tetrahedron Lett.* **1982**, *23*, 5291−5294.

[12] G. R. Newkome, D. C. Pantaleo, W. E. Puckett, P. L. Ziefle, W. A. Deutsh, *J. Inorg. Nucl. Chem.* **1981**, *43*, 1529−1531.

[13] C. O. Dietrich-Bucheker, G. Mieslin, W. Hosseini, unpublished results.

[14] B. P. Sullivan, D. J. Salman, T. J. Meyer, *Inorg. Chem.* **1978**, *17*, 3334−3341.

Received October 1, 1998
[I98335]

Organometallic Compounds Containing the *cis*-$[MoO(NNPhR)]^{2+}$ Core (R = Me, Ph) – X-ray Structures of $[MoO(NNPh_2)Me_2(o\text{-phen})]$ and $[MoO(NNPh_2)Ph_2(o\text{-phen})]$

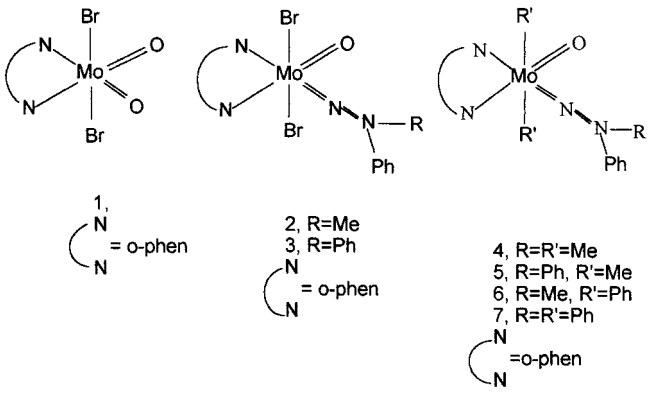
Ana M. Galindo,[a] Macarena Mardones,[a] Carolina Manzur,[a] Daphne Boys,*[b] Jean-René Hamon,*[c] and David Carrillo*[a]

Keywords: Molybdenum / Hydrazido complexes / Organometallic complexes / Phenanthroline / X-ray structure determination

New organometallic compounds containing the *cis*-$[MoO(NNPhR)]^{2+}$ core have been synthesized by means of a two-step procedure involving: (i) functionalization of the precursor $[MoO_2Br_2(o\text{-phen})]$ (**1**) with $MePhNNH_2$ and Ph_2NNH_2 to afford the intermediates $[MoO(NNMePh)Br_2(o\text{-phen})]$ (**2**) and $[MoO(NNPh_2)Br_2(o\text{-phen})] \cdot MeCN$ (**3**), respectively, and (ii) reaction of these intermediates with Grignard reagents to give $[MoO(NNPhR)Me_2(o\text{-phen})]$ [R = Me (**4**), R = Ph (**5**)], $[MoO(NNPhMe)Ph_2(o\text{-phen})]$ (**6**), and $[MoO(NNPh_2)Ph_2(o\text{-phen})] \cdot CH_2Cl_2$ (**7**). These compounds have been characterized by ^{1}H-NMR, IR, and UV/Vis spectroscopy and the crystal and molecular structures of **5** and **7** have been determined by X-ray diffraction analysis.

Much of the current interest in coordination of the hydrazido ligand, NNH_2, at transition-metal centers stems from the expectation that its geometric and electronic structure, as well as its reactivity, may provide some insight into the mechanism of metal-catalysed reduction of dinitrogen into ammonia.[1−6] Organohydrazido ligands, NNRR′ (RR′ = alkyl and/or aryl; H and alkyl/aryl), are considered as potential models of NNH_2 because of their structural similarities. Accordingly, in the last few years increasing attention has been paid to transition-metal complexes containing NNRR′ ligands and, consequently, several studies have been carried out involving chemical and electrochemical cleavage of the N−N bond,[7−11] *N*-alkylation,[10,12] protonation−deprotonation reactions,[13,14] and hydrolysis of the Mo−NNRR′ group.[15] Very recently, we have studied the electronic structures of hydrazido and organohydrazido ligands using Extended Hückel Molecular Orbital (EHMO) and ab initio calculations, with the aim of resolving uncertainties regarding the assignment of hydrazido(2−) or isodiazene character to NNH_2 and NNRR′ groups (RR′ = alkyl and/or aryl) in coordination compounds.[16]

As part of an ongoing investigation into (organohydrazido)molybdenum complexes, we have previously described the synthesis, characterization, and the chemical properties of a number of inorganic complexes containing the *cis*-$[Mo(NNPhR)_2]^{2+}$ and *cis*-$[MoO(NNPhR)]^{2+}$ cores with a wide range of ancillary ligands, e.g. acetylacetonate,[14,17−21] tertiary phosphanes,[14,21,22] 2,2′-bipyridine,[15] 1,10-phenanthroline,[15] hydridotris(pyrazolyl)borate,[23,24] hydridotris(3,5-dimethylpyrazolyl)borate,[23] and mercaptobenzoate.[25] However, recent work in our laboratories has focused on the synthesis of organometallic molybdenum compounds containing these cores; the new piano-stool compounds formulated as $[(\eta^5\text{-}C_5H_5)Mo(NNPhR)_2(PPh_3)]^+CF_3SO_3^-$ (R = Me, Ph) represent the first two members of this new class of organometallic compounds.[26] This paper deals with a convenient synthesis of the first members of a new class of organometallic molybdenum compounds containing the *cis*-$[MoO(NNPhR)]^{2+}$ core. Functionalization of the novel precursor $[MoO_2Br_2(o\text{-phen})]$ (**1**) with neutral organohydrazines leads to the stable intermediates $[MoO(NNMePh)Br_2(o\text{-phen})]$ (**2**) and $[MoO(NNPh_2)Br_2(o\text{-phen})] \cdot MeCN$ (**3**). Subsequent reaction of these with Grignard reagents affords the organometallic compounds formulated as $[MoO(NNPhR)Me_2(o\text{-phen})]$ [R = Me (**4**), R = Ph (**5**)], $[MoO(NNPhMe)Ph_2(o\text{-phen})]$ (**6**), and $[MoO(NNPh_2)Ph_2(o\text{-phen})] \cdot CH_2Cl_2$ (**7**). We also report the X-ray crystal and molecular structures of compounds **5** and **7**.



[a] Laboratorio de Química Inorgánica, Universidad Católica de Valparaíso,
Av. Brasil 2950, Valparaíso, Chile,
E-mail: dcarrill@aix1.ucv.cl
[b] Departamento de Física, Facultad de Ciencias Físicas y Matemáticas, Universidad de Chile, Santiago, Chile
[c] UMR CNRS 6509, Organométalliques et Catalyse: Chimie et Eléctrochimie Moléculaires, Université de Rennes 1,
Campus de Beaulieu, F-35042 Rennes Cedex, France

 © WILEY-VCH Verlag GmbH, D-69451 Weinheim, 1999 1434−1948/99/0303−0387 $ 17.50+.50/0

Results and Discussion

The preparations of the organometallic compounds **4**−**7** were carried out starting from the inorganic precursor $[MoO_2Br_2(o\text{-phen})]$ (**1**), according to a two-step procedure: (i) functionalization of complex **1** with neutral 1,1-disubstituted hydrazines, $PhRNNH_2$ (R = Me, Ph), to obtain the inorganic intermediates $[MoO(NNMePh)Br_2(o\text{-phen})]$ (**2**) and $[MoO(NNPh_2)Br_2(o\text{-phen})] \cdot MeCN$ (**3**), and (ii) reaction of the intermediate complexes **2** and **3** with Grignard reagents R′MgBr (R′ = Me, Ph), to afford the organometallic compounds formulated as $[MoO(NNPhR)Me_2(o\text{-phen})]$ [R = Me (**4**), R = Ph (**5**)], $[MoO(NNMePh)Ph_2(o\text{-phen})]$ (**6**), and $[MoO(NNPh_2)Ph_2(o\text{-phen})] \cdot CH_2Cl_2$ (**7**).

Precursor **1** was synthesized in excellent yield (86%) by oxidation of $[Mo(CO)_6]$ with bromine in the presence of 1,10-phenanthroline, using a mixture of CH_2Cl_2/EtOH (1:1) as solvent (for further details, see Experimental Section). This one-pot procedure, developed in our laboratories, is essentially a modification of that described in the literature for obtaining $[MoO_2Br_2(bpy)]$[27] (bpy = 2,2′-bipyridine) through: (i) photochemical reaction of $[Mo(CO)_6]$ with bpy in hexane[28] to generate the precursor $[Mo(CO)_4(bpy)]$, and (ii) oxidation of this precursor with an excess of bromine in CH_2Cl_2/EtOH (1:1).

Step 1. Synthesis and Characterization of the Intermediate Complexes $[MoO(NNMePh)Br_2(o\text{-phen})]$ (2) and $[MoO(NNPh_2)Br_2(o\text{-phen})] \cdot MeCN$ (3)

The syntheses of complexes **2** and **3** were performed in acetonitrile by reaction of precursor **1** with the neutral 1,1-disubstituted hydrazines $PhRNNH_2$ (R = Me, Ph), respectively, in a 1:2 molar ratio (Equation 1).

$$[MoO_2Br_2(o\text{-phen})] + PhRNNH_2 \rightarrow [MoO(NNPhR)Br_2(o\text{-phen})] + H_2O \quad (1)$$

We have found that the use of an excess of organohydrazine in these reactions does not lead to the bis(organohydrazido) complexes, but rather the yields of **2** and **3** are increased somewhat. We have observed that in similar molybdenum complexes the *cis*-$[Mo(NNPhR)_2]^{2+}$ group undergoes hydrolysis with loss of one NNPhR ligand if water is present.[15] As is apparent from Equation 1, the formation of the *cis*-$[MoO(NNPhR)]^{2+}$ group is accompanied by the elimination of one water molecule.

Complexes **2** and **3** were obtained as orange, air-stable crystalline solids in yields of 91% and 80%, respectively, and were characterized by ^{1}H-NMR, IR, and UV/Vis spectroscopy (see Experimental Section). The ^{1}H-NMR spectra of both complexes feature a complex multiplet in the range δ = 6.85−10.20, attributable to the phenyl and phenanthroline proton resonances. The spectrum of complex **2** containing the NNMePh ligand, which had to be recorded in [D$_6$]DMSO solution owing to the low solubility of this complex in $CDCl_3$, CD_3COCD_3, and CD_3NO_2, exhibits three proton resonances in the region δ = 3.65−4.50. These resonances may be attributed to the unmodified complex, $[MoO(NNMePh)Br_2(o\text{-phen})]$, and the cationic species $[MoO(NNMePh)Br(Me_2SO)(o\text{-phen})]^+$ and $[MoO(NNMePh)(Me_2SO)_2(o\text{-phen})]^{2+}$, formed by successive substitutions of the Br^- ligands by Me_2SO solvent molecules.

Step 2. Synthesis and Characterization of the Organometallic Compounds $[MoO(NNPhR)Me_2(o\text{-phen})]$ [R = Me (4), R = Ph (5)], $[MoO(NNMePh)Ph_2(o\text{-phen})]$ (6), and $[MoO(NNPh_2)Ph_2(o\text{-phen})] \cdot CH_2Cl_2$ (7)

The syntheses of the organometallic compounds **4**−**7** were carried out at 0°C in dry THF by reaction of the inorganic intermediates **2** and **3** with the corresponding Grignard reagents, R′MgBr (R′ = Me, Ph; Equation 2). Under the experimental conditions used, an excess of the Grignard reagent was added to the solution in order to solubilize the inorganic intermediates **2** and **3**.

$$[MoO(NNPhR)Br_2(o\text{-phen})] + 2R'MgBr \rightarrow [MoO(NNPhR)R'_2(o\text{-phen})] + 2MgBr_2 \quad (2)$$

Compounds **4**, **5** and **7** were obtained in yields of 41−80%, while compound **6** was isolated in only 17% yield. All compounds were obtained as orange, air-stable crystalline solids, and were characterized by ^{1}H-NMR, IR, and UV/Vis spectroscopy. The ^{1}H-NMR spectra each feature a complex multiplet in the range δ = 6.65−10.15, attributable to the phenyl proton resonances of the NNMePh ligand and the proton resonances of the *o*-phenanthroline ligand. The spectra of compounds **6** and **7** are more complicated than those of **4** and **5** owing to the proton resonances of the phenyl ligands bonded to the molybdenum center in *trans* positions (vide infra). The spectra of compounds **4** and **6** also feature methyl proton resonances due to the NNMePh ligand at δ = 4.00 and δ = 4.23, respectively. In addition, the spectra of **4** and **5** exhibit methyl proton resonances at δ = 0.17 and δ = 0.19, attributable to the methyl ligands bonded to the molybdenum center in *trans* positions. The spectrum of compound **7**, which crystallizes with a CH_2Cl_2 solvent molecule, exhibits a methylene proton resonance at δ = 5.30.

Structural Results

ORTEP drawings of $[MoO(NNPh_2)Me_2(o\text{-phen})]$ (**5**) and $[MoO(NNPh_2)Ph_2(o\text{-phen})]$ (**7**), in similar perspectives for the sake of comparison, are presented in Figures 1 and 2. In both compounds, the molybdenum center displays distorted octahedral geometry, with the two methyl and two phenyl ligands occupying mutually *trans* positions, and with the equatorial plane being defined by the oxo group, the N(1) and N(2) atoms of the *o*-phenanthroline, and the N(3) atom of the organohydrazido ligand. The geometric parameters observed in the *cis*-$[MoO(NNPhR)]^{2+}$ cores of these com-

pounds are quite similar to those reported in the literature for other (organohydrazido)oxomolybdenum complexes.[16,29] An extensive delocalization of the electron density throughout the $Mo(NNPh_2)$ units is supported by (i) the short Mo−N(3) and N(3)−N(4) bond lengths of 1.770(3) and 1.330(4) Å in **5**, and of 1.770(6) and 1.307(9) Å in **7**; (ii) the almost linear Mo−N(3)−N(4) bond angles of 171.7(2)° and 173.6(5)° in **5** and **7**, respectively, and (iii) the almost planar Mo−N(3)−N(4)C(31)C(41) moiety, the sum of the bond angles about N(4) being 358.7(3)° and 360.0(5)° in **5** and **7**, respectively. On the other hand, the Mo−O bond lengths of 1.711(2) and 1.711(4) Å in **5** and **7**, respectively, fall within the normal range[29] and, in line with expectation,[15] the *trans* influence exerted by this group is clearly far more important than that exerted by the organohydrazido ligands, e.g. Mo−N(2) = 2.361(3) Å vs. Mo−N(1) = 2.302(3) Å for **5**, and Mo−N(2) = 2.368(5) Å vs. Mo−N(1) = 2.302(6) Å for **7**. Finally, one more salient feature of the structures of these compounds is the preferential inclination of the two methyl (**5**) and the two phenyl (**7**) ligands toward the N(2) atom of the *o*-phenanthroline ligand; thus, in **5** the C(51)−Mo−N(2) and C(61)−Mo−N(2) bond angles are 74.5(1) and 76.1(1)° while the C(51)−Mo−N(1) and C(61)−Mo−N(1) bond angles are 84.7(1) and 79.8(1)°; likewise, in **7** the C(51)−Mo−N(2) and C(61)−Mo−N(2) bond angles are 76.7(2) and 78.6(2)° while the C(51)−Mo−N(1) and C(61)−Mo−N(1) bond angles are 89.5(2) and 81.5(2)°. These differences can most probably be ascribed to repulsions between the methyl and phenyl ligands and the oxo group. As a further consequence of these repulsions, the C(51)−Mo−C(61) bond angles are 149.9(1) and 155.3(2)° in compounds **5** and **7**, respectively. For comparison purposes, it is noteworthy that the methyl and *p*-anisyl ligands in the related organometallic compounds $[MoO_2R_2(bpy)]$ (R = Me,[30] C_6H_4OMe[31]) are also bent toward the midpoint of the N,N vector of the bpy ligand, the C−Mo−C bond angles in these cases amounting to 149.03(10) and 153.6(1)°, respectively. On the other hand, in the related inorganic complexes $[MoO(NNPh_2)Cl_2(o\text{-phen})]$ and $[MoO(NNPh_2)Cl_2(bpy)]$, this folding effect is less pronounced and the Cl−Mo−Cl

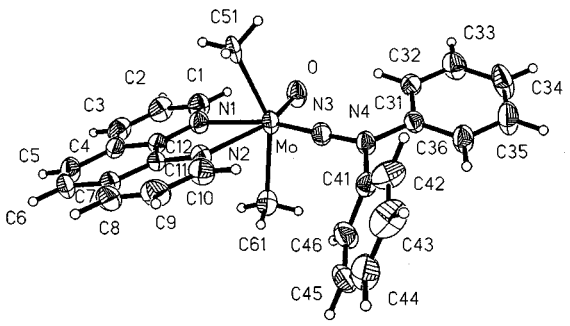


Figure 1. Molecular structure of compound **5** with thermal ellipsoids drawn at a 40% probability level; selected bond lengths (Å) and angles (°): Mo−O 1.711(2), Mo−N(1) 2.302(3), Mo−N(2) 2.361(3), Mo−N(3) 1.770(3), Mo−C(51) 2.331(3), Mo−C(61) 2.226(4), N(3)−N(4) 1.330(4); Mo−N(3)−N(4) 171.7(2), N(3)−N(4)−C(31) 119.4(2), N(3)−N(4)−C(41) 117.5(3), C(31)−N(4)−C(41) 121.8(3), C(51)−Mo−C(61) 149.9(1)

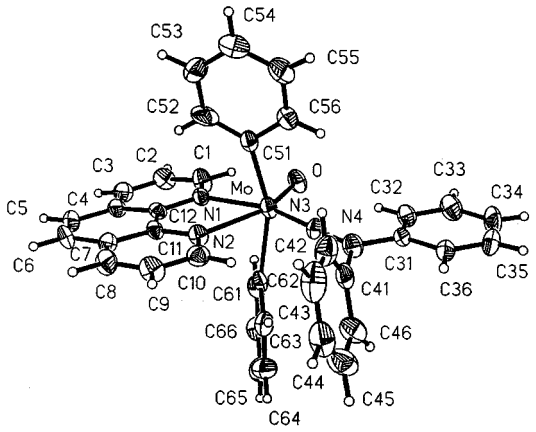


Figure 2. Molecular structure of compound **7** with thermal ellipsoids drawn at a 40% probability level; selected bond lengths (Å) and angles (°): Mo−O 1.711(4), Mo−N(1) 2.302(6), Mo−N(2) 2.368(5), Mo−N(3) 1.770(6), Mo−C(51) 2.240(7), Mo−C(61) 2.220(8), N(3)−N(4) 1.307(9); Mo−N(3)−N(4) 173.6(5), N(3)−N(4)−C(31) 121.3(5), N(3)−N(4)−C(41) 119.1(5), C(31)−N(4)−C(41) 119.6(6), C(51)−Mo−C(61) 155.3(2)

bond angles are found to be 161.5(1)° and 160.2(1)°, respectively.[15]

With reference to our recent study concerned with molecular orbital analysis of hydrazido(2−)−metal bonding in coordination chemistry,[16] if formally considered as a dianion, the hydrazido ligand represents a six-electron donor when it is coordinated in a linear mode in monohydrazido complexes. Accordingly, the molybdenum center in the organometallic compounds described herein attains an 18-electron configuration.

Conclusion

The present study highlights the potential utility of the new inorganic precursor $[MoO_2Br_2(o\text{-phen})]$ (**1**) for the preparation of organometallic *trans*-dialkyl and *trans*-diaryl compounds containing the *cis*-$[MoO(NNPhR)]^{2+}$ core, where R = Me, Ph. The readiness with which the *cis*-MoO_2^{2+} fragment can be monofunctionalized with neutral 1,1-disubstituted hydrazines opens a facile synthetic route for the preparation of stable inorganic intermediates, further reaction of which with Grignard reagents, as in the present investigation, allows access to organometallic compounds formulated as $[MoO(NNPhR)Me_2(o\text{-phen})]$ and $[MoO(NNPhR)Ph_2(o\text{-phen})]$ (R = Me, Ph). These derivatives containing the *cis*-$[MoO(NNPhR)]^{2+}$ core represent the first members of a new class of organometallic molybdenum compounds, the chemical and electrochemical properties of which, associated with cleavage of the N−N bond, will be the subject of further investigations in our laboratories.

Experimental Section

General: All operations were performed under inert atmosphere using standard vacuum/nitrogen line (Schlenk) techniques. Hexacarbonylmolybdenum, bromine, 1-methyl-1-phenylhydrazine, 1,1-

diphenylhydrazine hydrochloride, methylmagnesium bromide (3.3 M in diethyl ether), phenylmagnesium bromide (0.79 M in THF), and 1,10-phenanthroline, were purchased from commercial sources and used as received. Solvents were dried and distilled under nitrogen by standard methods prior to use. − Microanalytical data were obtained with a Perkin-Elmer Model 2400 elemental analyzer. − IR spectra were obtained from KBr disks with a Perkin-Elmer Model 1600 FT-IR spectrophotometer. − Electronic spectra were recorded in CH_2Cl_2 solutions with a Hewlett Packard 8452A spectrophotometer. − ^{1}H-NMR spectra were recorded in $CDCl_3$ or [D_6]DMSO with a Bruker FT AC/200P spectrometer; chemical shifts are reported in ppm relative to tetramethylsilane, with the residual solvent proton resonances as internal standards. − Melting points were determined using a Kofler apparatus.

Preparation of [MoO_2Br_2(*o*-phen)] (1): To a vigorously stirred solution of [$Mo(CO)_6$] (3.95 g, 15.0 mmol) and 1,10-phenanthroline (2.70 g, 15.0 mmol) in 200 mL of CH_2Cl_2/EtOH (1:1), excess bromine was added dropwise. Following the addition, the mixture was warmed to 40°C and stirred for 45 min, whereupon a microcrystalline orange solid was deposited. The crude material was filtered off, washed with diethyl ether, dried in vacuo, and finally recrystallized from CH_3CN. Yield before recrystallization: 6.04 g (86%), m.p. 195°C (dec.). − $C_{12}H_8Br_2MoN_2O_2$ (467.96): calcd. C 30.80, H 1.72, N 5.99; found C 29.83, H 1.76, N 5.89. − UV/Vis (CH_2Cl_2): λ_{max} (log ε) = 266 nm (4.47). − IR (KBr): $\tilde{\nu}$ = 3052 cm^{-1} (vw), ν(CH); 2921 (vw), ν(CH); 2818 (vw), ν(CH); 935 (vs) and 901 (vs), ν(MoO_2). − ^{1}H NMR ($CDCl_3$): δ = 9.90 (dd, 2 H, $^3J_{HH}$ = 8.2 Hz), 8.67 (dd, 2 H, $^3J_{HH}$ = 4.9 Hz), 8.12 (s, 2 H), 8.06 (dd, 2 H, $^3J_{HH}$ = 1.4 Hz).

Preparation of [MoO(NNMePh)Br_2(*o*-phen)] (2): To 1.83 g (3.91 mmol) of **1**, dissolved in 180 mL of acetonitrile, was added 0.96 g (7.82 mmol) of 1-methyl-1-phenylhydrazine, $MePhNNH_2$. The mixture was stirred vigorously under reflux for 2 h, in the course of which a microcrystalline solid was deposited. The pink solid was filtered off, washed with acetonitrile and diethyl ether, and dried in vacuo. Yield 2.04 g (91%), m.p. 315°C (dec.). − $C_{19}H_{16}Br_2MoN_4O$ (572.11): calcd. C 39.89, H 2.81, N 9.79; found C 38.66, H 2.70, N 9.76. − UV/Vis (CH_2Cl_2): λ_{max} (log ε) = 535 (4.13), 388 (4.60), 298 sh (5.13), 276 (5.40). − IR (KBr): $\tilde{\nu}$ = 3052 cm^{-1} (w), ν(CH); 2932 (w), ν(CH); 2856 (vw), ν(CH); 1583 (m), ν(NN); 902 (s), ν(MoO). − ^{1}H NMR ([D_6]DMSO): δ = 10.17−6.87 (m, 13 H, $C_{12}H_8N_2$ and C_6H_5), 4.47, 4.42, 3.67 (s, 3 H, CH_3).

Preparation of [MoO($NNPh_2$)Br_2(*o*-phen)]·MeCN (3): The procedure adopted was similar to that described for **2**, using in this case 1.34 g (6.08 mmol) of 1,1-diphenylhydrazine hydrochloride, $Ph_2NNH_3^+Cl^-$, previously neutralized with triethylamine, and 1.42 g (3.04 mmol) of **1**. The product was obtained as a red microcrystalline solid. Yield 2.16 g (80%), m.p. 290°C. − $C_{26}H_{21}Br_2MoN_5O$ (675.23): calcd. C 46.25, H 3.13, N 10.37; found C 46.44, H 3.10, N 9.38. − UV/Vis (CH_2Cl_2): λ_{max} (log ε) = 520 nm (3.28), 388 (3.70), 298 sh (4.19), 278 (4.48). − IR (KBr): $\tilde{\nu}$ = 3044 cm^{-1} (w), ν(CH); 2922 (vw), ν(CH); 2856 (vw), ν(CH); 1585 (m), ν(NN); 899 (s), ν(MoO). − ^{1}H NMR ($CDCl_3$): δ = 10.19−6.99 (m, 18 H, $C_{12}H_8N_2$ and 2 C_6H_5 hydrazido), 2.01 (s, 3 H, CH_3CN).

Preparation of [MoO(NNMePh)Me_2(*o*-phen)] (4): To 0.30 g (0.52 mmol) of **2** suspended in 20 mL of dry THF at 0°C, 0.38 g (3.15 mmol) of methylmagnesium bromide in Et_2O was added dropwise. After stirring for 1 h, the reaction mixture was allowed to warm to room temperature and then concentrated to dryness in vacuo. The residue was partitioned between 20 mL of CH_2Cl_2 and 20 mL of saturated aqueous ammonium chloride solution, the aqueous phase was extracted with further CH_2Cl_2, and the combined organic extracts were dried with magnesium sulfate. After concentrating the dried extract to a volume of 10 mL, it was allowed to stand at −18°C, resulting in the deposition of an orange microcrystalline solid. This was filtered off, washed with diethyl ether, dried in vacuo, and finally recrystallized from CH_2Cl_2 layered with diethyl ether. Yield before recrystallization: 0.094 g (41%), m.p. 173°C. − $C_{21}H_{22}MoN_4O$ (442.37): calcd. C 56.96, H 4.97, N 12.65; found C 56.11, H 5.09, N 12.19. − UV/Vis (CH_2Cl_2): λ_{max} (log ε) = 380 nm br (3.83), 326 (4.24), 270 (4.60). − IR (KBr): $\tilde{\nu}$ = 3056 cm^{-1} (w), ν(CH); 2945 (m), ν(CH); 2878 (w), ν(CH); 1592 (s), ν(NN); 886 (vs), ν(MoO). − ^{1}H NMR ($CDCl_3$): δ = 10.17−6.97 (m, 13 H, $C_{12}H_8N_2$ and C_6H_5 hydrazido), 4.00 (s, 3 H, CH_3 hydrazido), 0.17 (s, 6 H, $2CH_3$).

Preparation of [MoO($NNPh_2$)Me_2(*o*-phen)] (5): The synthesis of this yellow crystalline complex was carried out using a procedure similar to that described for complex **4**, adding in this case 0.56 g (4.66 mmol) of methylmagnesium bromide to 0.49 g (0.73 mmol) of **3** in 20 mL of dry THF. Suitable single crystals for X-ray diffraction studies were obtained from CH_2Cl_2 layered with diethyl ether. Yield 0.58 g (80%), m.p. 215°C. − $C_{26}H_{24}MoN_4O$ (504.44): calcd. C 61.91, H 4.80, N 11.11; found C 61.22, H 4.70, N 10.98. − UV/Vis (CH_2Cl_2): λ_{max} (log ε) = 380 nm br. (4.32), 310 (4.92), 270 (5.32). − IR (KBr): $\tilde{\nu}$ = 3056 cm^{-1} (vw), ν(CH); 2951 (w), ν(CH); 2889 (w), ν(CH); 1586 (m), ν(NN); 892 (vs), ν(MoO). − ^{1}H NMR ($CDCl_3$): δ = 10.20−7.20 (m, 18 H, $C_{12}H_8N_2$ and 2 C_6H_5 hydrazido), 0.19 (s, 6 H, 2 CH_3).

Preparation of [MoO(NNMePh)Ph_2(*o*-phen)] (6): To 0.31 g (0.54 mmol) of **2**, dissolved in 20 mL of dry THF, 0.59 g (3.20 mmol) of phenylmagnesium bromide in THF was added dropwise. After stirring for 1 h at 0°C, the reaction mixture was allowed to warm to room temperature and then concentrated to dryness in vacuo. The residue was partitioned between 20 mL of CH_2Cl_2 and 20 mL of saturated aqueous ammonium chloride solution. The CH_2Cl_2 solution containing the product was dried with magnesium sulfate and concentrated to a volume of 10 mL. On leaving the concentrated solution to stand at −18°C, a brown crystalline solid was deposited, which was filtered off, washed with diethyl ether, and dried in vacuo. Yield 0.052 g (17%), m.p. 165°C. − $C_{31}H_{26}MoN_4O$ (566.51): calcd. C 65.73, H 4.63, N 10.07; found C 64.85, H 4.48, N 9.82. − UV/Vis (CH_2Cl_2): λ_{max} (log ε) = 420 nm br. (4.27), 334 (4.90), 270 (5.33). − IR (KBr): $\tilde{\nu}$ = 3041 cm^{-1} (w), ν(CH); 2964 (vw), ν(CH); 2922 (vw), ν(CH); 1592 (m), ν(NN); 896 (s), ν(MoO). − ^{1}H NMR ($CDCl_3$): δ = 10.48−6.67 (m, 23 H, $C_{12}H_8N_2$, C_6H_5 hydrazido and 2 C_6H_5), 4.23 (s, 3 H, CH_3 hydrazido).

Preparation of [MoO($NNPh_2$)Ph_2(*o*-phen)]·CH_2Cl_2 (7): This yellow crystalline complex was synthesized according to the procedure described above, adding in this case 1.08 g (5.95 mmol) of phenylmagnesium bromide to 0.31 g (0.46 mmol) of **3** in 20 mL of dry THF. Suitable single crystals for X-ray diffraction studies were obtained from CH_2Cl_2 layered with hexane. Yield before recrystallization: 0.22 g (67%), m.p. 185°C. − $C_{37}H_{30}Cl_2MoN_4O$ (713.52): calcd. C 62.28, H 4.24, N 7.85; found C 61.46, H 4.23, N 7.99. − UV/Vis (CH_2Cl_2): λ_{max} (log ε) = 368 nm br. (4.07), 332 (4.45), 256 (4.75). − IR (KBr): $\tilde{\nu}$ = 3047 cm^{-1} (w), ν(CH); 3000 (vw), ν(CH); 2956 (vw), ν(CH); 1586 (m), ν(NN); 889 (vs), ν(MoO). − ^{1}H NMR ($CDCl_3$): δ = 10.52−6.68 (m, 28 H, $C_{12}H_8N_2$, 2 C_6H_5 hydrazido and 2 C_6H_5), 5.30 (s, 2 H, CH_2Cl_2).

X-ray Structure Determination for 5: $C_{26}H_{24}MoN_4O$, M_r = 504.4 g mol^{-1}, unit cell dimensions: a = 9.346(2), b = 20.936(4), c = 12.389(2) Å, β = 106.26(2)°, V = 2327(1) $Å^3$, monoclinic, $P2_1/n$, Z = 4, $D_{calcd.}$ = 1.440 g cm^{-3}, μ(Mo-K_α) = 0.589 mm^{-1}, F(000) =

Table 1. Crystal data for $[MoO(NNPh_2)Me_2(o\text{-phen})]$ (**5**) and $[MoO(NNPh_2)Ph_2(o\text{-phen})]\cdot CH_2Cl_2$ (**7**)

	5	**7**
Empirical formula	$C_{26}H_{24}MoN_4O$	$C_{37}H_{30}Cl_2MoN_4O$
Crystal size [mm]	0.50 × 0.28 × 0.20	0.20 × 0.18 × 0.06
Crystal system	Monoclinic	Monoclinic
Space group	$P2_1/n$	$P2_1/n$
a [Å]	9.346(2)	11.951(2)
b [Å]	20.936(4)	19.850(3)
c [Å]	12.389(3)	14.135(2)
β [°]	106.26(2)	100.97(1)
Volume [Å^3]	2327(1)	3292(1)
Z	4	4
Molecular mass	504.4	713.5
Density (calcd.) [Mg/m^3]	1.440	1.440
F(000)	1032	1456
Absorption coefficient [mm^{-1}]	0.589	0.597
max./min. transmission factors	0.6708/0.5782	0.9518/0.9053
Reflections collected	4338	4562
2θ range [°]	3 → 50	3 → 45
Index ranges	$0 \le h \le 11$ $0 \le k \le 24$ $-14 \le l \le 14$	$0 \le h \le 12$ $0 \le k \le 21$ $-15 \le l \le 14$
Independent reflections	4077	4324
R_{int}	0.0245	0.0229
Observed reflections [$F > 4\sigma(F)$]	3435	2261
Weighting scheme g [$w^{-1} = \sigma^2(F) + gF^2$]	0.0014	0.0006
Number of parameters refined	289	406
Final R indices [R/(obsd. data) wR]	0.0355/0.0526	0.0387/0.0378
Goodness-of-fit S	1.19	0.81
Residual ρ_{max}/ρ_{min} [eÅ^{-3}]	0.70/−0.34	0.32/−0.31

1032, crystal size [mm]: 0.50 × 0.28 × 0.20. Siemens R3m/V four-circle diffractometer; Mo-K_α radiation (λ = 0.71073, graphite monochromator), 2θ range 3.0−50.0° at 298 K, scan type θ-2θ, reflections collected 4338, independent reflections 4077 (R_{int} = 2.45%), observed reflections 3435 [$F > 4.0\sigma(F)$]. Convergence at R = 0.0355, R_w = 0.0526, $w^{-1} = \sigma^2(F) + gF^2$. Cell parameters were determined from least-squares fits of 25 reflections with 15° ≤ 2θ ≤ 30°. Two standard reflections, monitored every 98 reflections, showed no significant variation of intensity during data collection. Intensities were corrected for Lorentz and polarization effects, and semiempirical corrections based on ψ scans were applied for absorption.

X-ray Structure Determination for 7: $C_{37}H_{30}Cl_2MoN_4O$, M_r = 713.5 g mol^{-1}, unit cell dimensions: a = 11.951(2), b = 19.850(3), c = 14.135(2) Å, β = 100.97(1)°, V = 3292(1) Å^3, monoclinic, $P2_1/n$, Z = 4, $D_{calcd.}$ = 1.440 g cm^{-3}, μ(Mo-K_α) = 0.597 mm^{-1}, F(000) = 1456, crystal size [mm]: 0.20 × 0.18 × 0.06. Siemens R3m/V four-circle diffractometer; Mo-K_α radiation (λ = 0.71073 Å, graphite monochromator), 2θ range 3.0−45.0° at 298 K, scan type θ-2θ, reflections collected 4562, independent reflections 4324 (R_{int} = 2.29%), observed reflections 2261 [$F > 4.0\sigma(F)$]. Convergence at R = 0.0387, R_w = 0.0378, $w^{-1} = \sigma^2(F) + gF^2$. Cell parameters were determined from least-squares fits of 30 reflections with 15° ≤ 2θ ≤ 30°. Two standard reflections, monitored every 98 reflections, showed no significant variation of intensity during data collection. Intensities were corrected for Lorentz and polarization effects, and semiempirical corrections based on ψ scans were applied for absorption.

Both structures were solved by direct methods and refined on F by full-matrix least-squares calculations (see Table 1). The function minimized was $\Sigma w(F_o - F_c)^2$. All non-H atoms were refined anisotropically. A riding model was applied to H atoms, which were placed at calculated positions with C−H = 0.96 Å, with the equivalent isotropic thermal parameters of their parent C atoms. All calculations were performed with the Siemens SHELXTL-PLUS system of programs.[32] Crystallographic data (excluding structure factors) for the structures reported in this paper have been deposited with the Cambridge Crystallographic Data Centre as supplementary publication no. CCDC-102552 (**5**) and -102553 (**7**). Copies of the data can be obtained free of charge on application to CCDC, 12 Union Road, Cambridge CB2 1EZ, UK [Fax: (int. code) + 44-1223/336-033, E-mail: deposit@ccdc.cam.ac.uk].

Acknowledgments

This work was supported by the Fondo Nacional de Desarrollo Científico y Tecnológico, FONDECYT-CHILE, Grant No. 1951088 and the Dirección General de Investigación y Postgrado, Universidad Católica de Valparaíso, Chile (D. C. and C. M.). A. M. G. thanks the Instituto de Cooperación Iberoamericana, Spain, for support of a graduate fellowship. D. B. gratefully acknowledges the Fundación Andes for funding the purchase of a single-crystal diffractometer.

[1] R. A. Henderson, G. J. Leigh, C. J. Pickett, *Adv. Inorg. Chem. Radiochem.* **1983**, *27*, 197−203.
[2] J. A. McCleverty, *Transition Met. Chem.* **1987**, *12*, 282−287.
[3] B. F. G. Johnson, B. L. Haymore, J. R. Dilworth, in *Comprehensive Coordination Chemistry* (Eds.: G. Wilkinson, R. D. Gillard, J. A. McCleverty), Pergamon Press, Oxford, **1987**, vol. 2, p. 130−141.
[4] D. J. Evans, R. A. Henderson, B. E. Smith, *Bioinorganic Catalysis* (Ed.: J. Reedijk), Marcel Dekker, Inc., **1993**, p. 89−130.
[5] D. Sutton, *Chem. Rev.* **1993**, *93*, 995−1022.
[6] M. Hidai, Y. Mizobe, *Chem. Rev.* **1995**, *95*, 1115−1133.
[7] R. A. Henderson, G. J. Leigh, C. J. Pickett, *J. Chem. Soc., Dalton Trans.* **1989**, 425−430.
[8] P. J. Walsh, M. J. Carney, R. G. Bergman, *J. Am. Chem. Soc.* **1991**, *113*, 6343−6345.
[9] J. R. DeBord, T. A. George, Y. Chang, Q. Chen, J. Zubieta, *Inorg. Chem.* **1993**, *32*, 785−786.

[10] M. G. Vale, R. R. Schrock, *Inorg. Chem.* **1993**, *32*, 2767−2772.
[11] M. Retboll, E. R. Möller, R. G. Hazell, A. Jörgensen, *Acta Chem. Scand.* **1995**, *49*, 278−290.
[12] J. D. Niemoth-Anderson, J. R. D. Debord, T. A. George, C. R. Ross II, J. J. Stezowski, *Polyhedron* **1996**, *15*, 4031−4040.
[13] R. A. Henderson, K. E. Oglieve, *J. Chem. Soc., Dalton Trans.* **1990**, 1093−1096.
[14] C. Bustos, C. Manzur, D. Carrillo, F. Robert, P. Gouzerh, *Inorg. Chem.* **1994**, *33*, 4937−4944.
[15] C. Manzur, C. Bustos, D. Carrillo, D. Boys, J.-R. Hamon, *Inorg. Chim. Acta* **1997**, *255*, 73−80.
[16] S. Kahlal, J.-Y. Saillard, J.-R. Hamon, C. Manzur, D. Carrillo, *J. Chem. Soc., Dalton Trans.* **1998**, 1229−1240.
[17] C. Bustos, C. Manzur, H. Gonzalez, R. Schrebler, D. Carrillo, C. Bois, Y. Jeannin, P. Gouzerh, *Inorg. Chim. Acta* **1991**, *185*, 25−31.
[18] D. Carrillo, F. Robert, P. Gouzerh, *Inorg. Chim. Acta* **1992**, *197*, 209−215.
[19] C. Bustos, C. Manzur, D. Carrillo, F. Robert, P. Gouzerh, *Inorg. Chem*. **1994**, *33*, 1427−1433.
[20] C. Manzur, C. Bustos, D. Carrillo, F. Robert, P. Gouzerh, *Inorg. Chim. Acta* **1996**, *249*, 245−250.
[21] C. Manzur, D. Carrillo, R. Baggio, M. T. Garland, *J. Chem. Crystallogr*. **1997**, *27*, 339−342.
[22] C. Manzur, D. Carrillo, A. Vega, M. T. Garland, *Bol. Soc. Chil. Quím.*, in press.
[23] C. Manzur, D. Carrillo, D. Boys, *Acta Crystallogr*. **1997**, *C53*, 1401−1403.
[24] C. Manzur, D. Carrillo, D. Boys, P. Hamon, J.-R. Hamon, *Inorg. Chim. Acta* **1998**, *268*, 199−204.
[25] J. Li-Kao, O. Gonzalez, R. Mariezcurreña, R. Baggio, M. T. Garland, D. Carrillo, *Acta Crystallogr.* **1995**, *C51*, 2486−2489.
[26] C. Manzur, D. Carrillo, F. Robert, P. Gouzerh, J.-R. Hamon, *Organometallics* **1998**, *17*, 3728−3732.
[27] C. G. Hull, M. H. B. Stiddard, *J. Chem. Soc. A* **1966**, 1633−1635.
[28] D. M. Manuta, A. J. Lees, *J. Chem. Educ.* **1987**, *64*, 637−638.
[29] W. A. Nugent, J. M. Mayer, *Metal−Ligand Multiple Bonds*, Wiley-Interscience, New York, **1988**.
[30] G. N. Schrauzer, L. A. Hughes, N. Strampach, P. R. Robinson, E. O. Schlemper, *Organometallics* **1982**, *1*, 44−47.
[31] G. N. Schrauzer, X. Zhang, N. H. Liu, E. O. Schlemper, *Organometallics* **1988**, *7*, 279−282.
[32] G. M. Sheldrick, *SHELXTL-Plus, Release 4.2 for Siemens Crystallographic Research Systems*, Siemens Analytical X-ray Instruments, Inc., Madison, USA, **1992**.

Received September 15, 1998
[I98312]

Syntheses, Structures, and Coordination of Diborylbipyridines and Bipyridinediborates

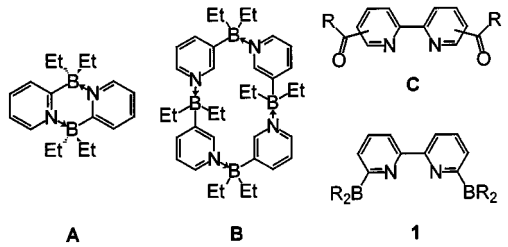
Norbert Weis,[a] Hans Pritzkow,[a] and Walter Siebert*[a]

Dedicated to Prof. Dr. Günter Wächtershäuser on the occasion of his 60th birthday

6,6′-Bis(diethylboryl)-2,2′-bipyridine (**1a**) was obtained in low yield by in situ deprotonation of 2,2′-bipyridine in the presence of diethyl(methoxy)borane. 6,6′-Dilithio-2,2′-bipyridine reacts with various alkoxyboranes leading to bipyridinediborates **2** in good yields. The derivatives **2b** and **2c** allow the formation of the free diborylbipyridines **1b** and **1c**. The coordination properties of the diboryl–bipyridines as tetrafunctional donor–acceptor compounds have been used for the formation of the copper complex **4** and of the adduct **5** which is built from diborylbipyridine and a dihydroxydiboroxan derivative. The composition of the products follows from spectroscopic data and from X-ray structure analyses for **2f**, **4**, and **5**.

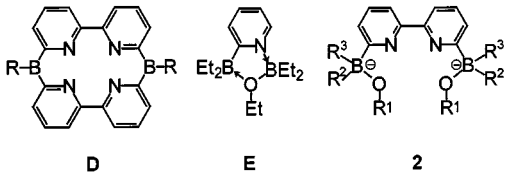
Introduction

The intramolecular presence of Lewis basic (nitrogen) and Lewis acidic centers (boron) results in interesting properties of borylated pyridines and bipyridines. A small number of borylpyridines has been reported,[1] which were synthesized as starting compounds for Suzuki coupling reactions.[2] 2-(Diethylboryl)pyridine[3] and 3-(diethylboryl)-pyridine[4] are known for their stability towards moisture and oxygen. The reason for this is their assembly by intermolecular boron−nitrogen coordination. 2-(Diethylboryl)-pyridine exists as a dimer (**A**) in solution and in the solid state,[5] and 3-(diethylboryl)pyridine as a cyclic tetramer (**B**).



Scheme 1

Bipyridines have been the subject of many studies.[6][7] The π-acceptor properties of this bidentate σ-donor are weak. By introducing electron-withdrawing groups the π*-level is lowered as has been demonstrated with acyl- and carboxybipyridines (**C**).[8] The dπ→π* absorption bands in L_3Ru^{II} complexes (L = bipyridines) are shifted toward the red region of the spectra and this shift increases the quality of these metal complexes as sensitizers in solar energy converting processes.[9] 6,6′-Diboryl-2,2′-bipyridines **1** should also have increased π-acceptor qualities relative to that of non-substituted bipyridines. We are in particular interested in 6,6′-diborylated bipyridines with respect to their donor-acceptor properties and their potential of forming the macrocycle **D**.



Scheme 2

From spectroscopic data the formation of the cyclic adduct **E**, based on the donor−acceptor pattern of 2-(diethylboryl)pyridine was postulated.[3] For the tetrafunctional 6,6′-diboryl-2,2′-bipyridines **1** one may expect a complex donor−acceptor behavior due to their geometric requirements. In the following the coordination properties of the donor−acceptor molecules **1** will be presented. In addition the formation of bipyridinediborates **2** and their behavior as N_2O_2 tetradentate ligands are studied, of which numerous examples have been reported.[10−13]

Results and Discussion

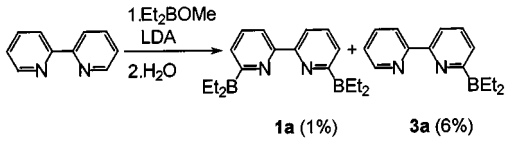
Synthesis

Following a general procedure,[14] we synthesized the diborylbipyridine **1a** by in situ deprotonation of 2,2′-bipyridine with lithium diisopropylamide (LDA) in the presence of an excess of diethyl(methoxy)borane. In this reaction **1a** was obtained in very low yield (1%) besides the monoborylated product **3a** (6%). **1a** is a colorless, high-melting solid of low solubility whereas **3a** is a viscous oil. Both substances are stable toward moisture and air. Their ^{11}B-NMR spectra (δ = 3) indicate tetracoordinate boron atoms in as yet unknown assembly, most likely **1a** and **3a** form donor−acceptor compounds similar to **A**. In the EI mass spectra the fragments of the monomeric species with loss of one

[a] Anorganisch-Chemisches Institut der Universität,
Im Neuenheimer Feld 270, D-69120 Heidelberg, Germany
Fax: (internat.) + 49(0)6221/54-5609
E-mail: ci5@ix.urz.uni-heidelberg.de

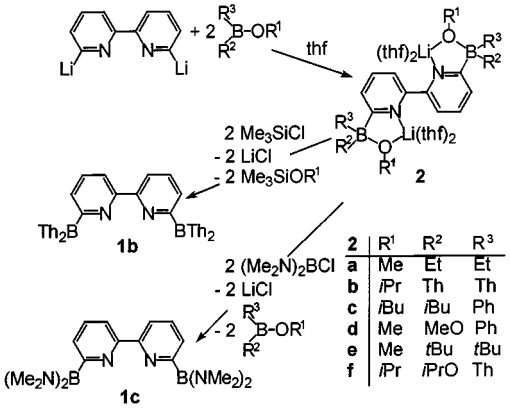
 © WILEY-VCH Verlag GmbH, D-69451 Weinheim, 1999 1434−1948/99/0303−0393 $ 17.50+.50/0

ethyl group appear as highest masses at m/z = 263 [**1a** − Et]$^+$ and 195 [**3a** − Et]$^+$.



Scheme 3

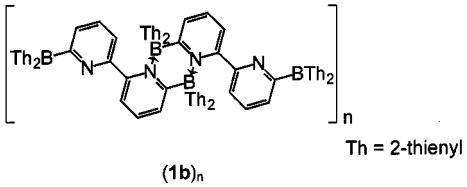
To improve the yields a stepwise synthesis was carried out. 6,6′-Dilithio-2,2′-bipyridine, obtained by a metal/halogen exchange,[15] was treated with various alkoxyboranes to give the borate derivatives **2a−f**.



Scheme 4

Regardless of the steric and electronic properties of the substituents, the products **2a−f** are thermally stable and isolated in 64−89% yields. All are colorless, crystalline substances, which, however, are very sensitive toward hydrolysis to give bipyridine and the corresponding boron compounds. They are characterized by ^{1}H-, ^{13}C-, ^{11}B-NMR spectroscopy and by an X-ray structure analysis of **2f** (see below). In these molecules the expected leaving groups LiOR are bound to the diborylbipyridines. There are interactions between the acceptor function (boron) with the alkoxy group and between the donor function (nitrogen) with the lithium ion. The formation of this five-membered heterocyclic arrangement enhances the stability of the adducts.

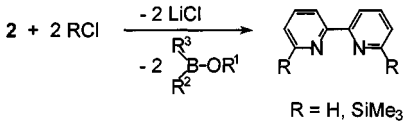
Attempts to synthesize **1a** from **2a** failed. Reaction of **2b** with $ClSiMe_3$ yields the 6,6′-bis-di(2-thienyl)boryl]-2,2′-bipyridine (**1b**) in 36% yield. The combination of steric (*i*Pr) and electronic effects (thienyl) of the substituents destabilizes the coordination in the dianionic borate **2b** and thus allows the formation of the free diborylbipyridine **1b**. Based on the ^{11}B-NMR spectrum in thf (δ = −1), its low solubility and high melting point (> 250°C) we propose an aggregation via N−B donor acceptor interactions to give an oligomer of unknown structure and number of diborylbipyridine units. The appearence of only one ^{11}B-NMR signal may indicate a cyclic arrangement. In a chain-like donor−acceptor compound $(\mathbf{1b})_n$ the two terminal BTh_2 groups could be stabilized by thf molecules forming donor−acceptor adducts.



Scheme 5

The reaction of the diisobutoxy derivative **2c** with chlorobis(dimethylamino)borane results in the formation of 6,6′-bis[bis(dimethylamino)boryl]-2,2′-bipyridine (**1c**). It is obtained in 64% yield as a red oil of limited solubility in thf. In comparison to bis(dimethylamino)organoboranes (δ = 34−36)[16] the ^{11}B-chemical shift of **1c** appears at higher field (δ = 31). Most likely this is caused by π-interaction between the p_z orbital of the boron atom and the π system of the heterocycle. In the ^{1}H NMR there is only one signal for the dimethylamino groups which indicates a free rotation around the B−N and the B−C bonds on the NMR time scale.

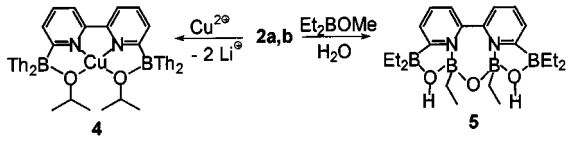
In general the reactivity of **2a−f** is high toward HCl/Et_2O and $ClSiMe_3$ (except **2b**), resulting in the cleavage of the boron−bipyridine bond. Because of their high sensitivity toward moisture, no satisfactory C,H,N analysis could be obtained.



Scheme 6

Complex Formation

In the borates **2** the bipyridine has an *anti* conformation and acts as a tetradentate ligand toward two lithium cations. Treatment of **2b** with one equivalent of $(Et_4N)_2CuCl_4$ results in the formation of the deep green-blue coordination compound **4**. The copper ion is coordinated by two nitrogen and two oxygen atoms of the alkoxy groups. Because of the paramagnetism of the d^9-Cu^{II} ion the NMR spectra of **4** could not be used for characterization. The cyclovoltammetry of **4** shows a reversible oxidation at $E_{1/2}$ = 0.65 V and an irreversible reduction at −1.1 V.



Scheme 7

An unprecedented coordination mode is observed in the adduct **5**. It is formed by the interaction of **1a** with 1,3-diethyl-1,3-dihydroxydiboroxane. The unknown dihydroxy-

diboroxane molecule is stabilized by the intermolecular aggregation. Treatment of 6,6′-dilithio-2,2′-bipyridine with an excess of diethyl(methoxy)borane and aqueous workup leads to **5** in 42% yield. The Lewis donor−acceptor pattern of **1a** induces the formation of the matching partner with the inverted Lewis functionality. Hydrolysis of the diethyl(methoxy)borane yields 1,3-diethyl-1,3-dihydroxydiboroxane coordinated to the diborylbipyridine **1a**. The free dihydroxydiboroxane is unstable and is expected to give give cyclic 1,3,5-boroxine. **5** is characterized by ^{1}H-, ^{13}C-, ^{11}B-NMR spectroscopy and an X-ray structure analysis (see below). In the ^{11}B-NMR spectrum appears only one broad signal at $\delta = 9$. Therefore all four boron atoms are quaternized. The Lewis acidic diethylboryl groups act as acceptor for the terminal oxygen atoms and the electron pair of the nitrogen atoms donate to the boron atoms of the dihydroxydiboroxane. The chemical shift of the methylene groups of the diethylboroxane at $\delta = -0.2$ corresponds with the high electron density at the boron atoms.

Crystal Structures

Single crystals of **2f** were grown from a tetrahydrofuran solution at room temperature. Figure 1 shows a molecule of **2f**, its lithium centers are tetracoordinated. Besides the bonding to the oxygen atom of the alkoxy group [Li−O: 1.87(1) Å] there is an interaction with the nitrogen atom [Li−N: 2.08(1) Å] of the bipyridine unit. The coordination sphere is completed by two thf molecules [Li−O: 1.97(1) Å]. The five-membered heterocycles are approximately planar with deviations from the best plane being less than 0.02 Å. The bond length B1−C1 is 1.64 Å. The two pyridine units are twisted by 149.6°.

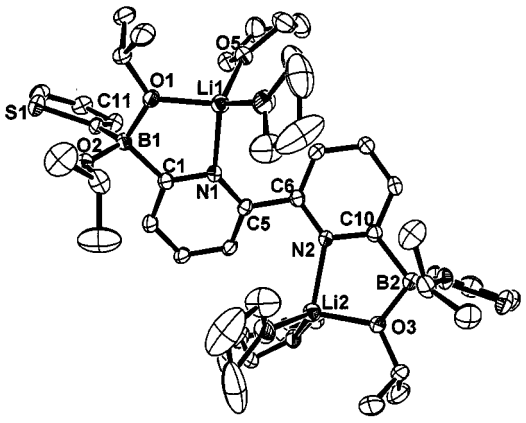


Figure 1. Structure of **2f** in the crystal; selected bond lengths [Å] and angles [°]: B1−C1 1.642(8), B1−O1 1.506(7), B1−O2 1.479(7), Li1−O1 1.87(1), Li1−N1 2.08(1), Li1−O5 1.97(1), C1−B1−O1 106.4(4), C1−B1−O2 112.5(5), C1−B1−C11 107.0(4), N1−C5−C6−N2 30.6

The large variety of possible coordination modes of Cu^{II}[17] are known. Therefore it is of interest to obtain structural information on the copper coordination in **4**. Single crystals suitable for an X-ray diffraction study were grown by slow diffusion of *n*-hexane into the solution of **4** in CH_2Cl_2. Figure 2 shows its structure in the crystal. The copper center has a distorted square-planar coordination by two nitrogen and two oxygen atoms. One of the oxygen atoms (O2) deviates strongly from the plane. The geometry around O2 differs much from that around O1. The distance Cu1−O2 [2.016(3) Å] is larger than Cu1−O1 [1.962(3) Å]. The oxygen atom O1 shows a planar coordination, while O2 is pyramidalized. The five-membered cycle of O1 is planar, that of O2 has an envelope form. The isopropyl group at O1 lies approximately symmetrical to the plane through the ring, while in the case of O2 it is strongly bent to one side, and one of the methyl groups reaches a position above the copper ion. A weak agostic interaction with one of its hydrogen atoms to the copper ion [Cu1−H 2.48(4) Å] is observed. The distances between the boron atoms and the bridging oxygen atoms [1.558(5), 1.575(5) Å] are about 0.1 Å longer than in regular B−O bonds of uncoordinated borates.

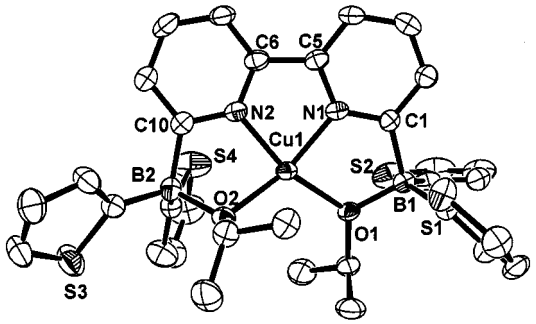


Figure 2. Structure of **4** in the crystal; selected bond lengths [Å] and angles [°]: B1−C1 1.630(6), B1−O1 1.558(5), B2−O2 1.575(5), Cu1−N1 1.938(3), Cu1−N2 1.938(3), Cu1−O1 1.962(3), Cu1−O2 2.016(3), C5−C6 1.483(6), C1−B1−O1 103.7(3), C10−B2−O2 104.8(3), N1−Cu1−N2 80.8(1), N1−Cu1−O1 83.1(1), O1−Cu1−O2 114.8(1), O2−Cu1−N2 83.4(1), B1−O1−C27 116.6(3), C27−O1−Cu1 126.5(3), Cu1−O1−B1 116.9(2), N1−C5−C6−N2 7.4, N1−C1−B1−O1 2.1, N2−C10−B2−O2 23.7

Figure 3 shows the molecule structure of **5** in the crystal. Crystals suitable for X-ray structure analysis were obtained by slow diffusion of *n*-hexane in a CH_2Cl_2 solution of **5**. The molecules of **5** form dimers in the solid state by hydrogen bonds. There are two independent dimers (four molecules) in the cell. They may be described as a donor−acceptor coordination product of **1a** with 1,3-diethyl-1,3-dihydroxydiboroxane, with the nitrogen atoms of the bipyridine and the hydroxy groups of the boroxane acting as donors to the boron atoms. All boron atoms are tetrahedrally coordinated. Three groups of B−O bonds are found, which are clearly distinguished in their distances: One type in the seven-membered ring with the two-coordinated oxygen atoms varying from 1.415−1.445 Å, two types in the five-membered rings with three-coordinated oxygen atoms, where they differ in the coordination of the boron atoms; 1.503−1.536 Å for the boron atoms connected to the nitrogen atoms, and 1.561−1.620 Å for the boron atoms connected to three carbon atoms.

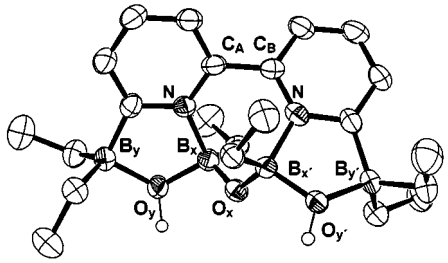


Figure 3. Structure of **5** in the crystal; selected bond lengths [Å] [mean values and range given (esd. 0.006−0.009 Å)]: B_X-O_X 1.440 (1.415−1.445), B_X-O_Y 1.525 (1.503−1.536), B_Y-O_Y 1.595 (1.561−1.620), B_X-N 1.626 (1.611−1.650), C_A-C_B 1.486 (1.479−1.494)

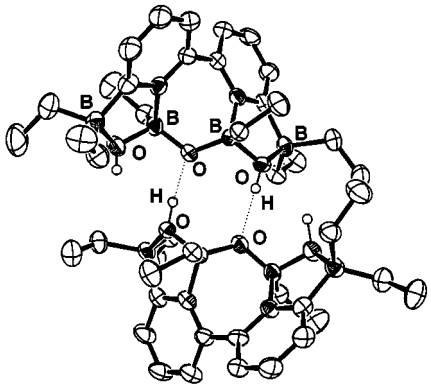


Figure 4. Hydrogen-bridged dimer of **5** in the crystal

Experimental Section

General: Reactions were carried out under dry argon, using standard Schlenk techniques. Solvents were dried, distilled, and saturated with nitrogen. Glassware was dried with a heat-gun in high vaccum. − ^{1}H, ^{13}C, ^{11}B NMR: Bruker AC 200 spectrometer, NMR references are $(CH_3)_4Si$ and $BF_3 \cdot Et_2O$. − Mass spectra were obtained with a Finnigan MAT 8200 plus spectrometer using EI technique. − Melting points (uncorrected) were obtained with a Büchi apparatus, using capillaries which were filled under argon and sealed.

Crystal-Structure Determination: Unique sets of intensity data were collected at −70°C with a four-circle diffractometer (Mo-K_α radiation λ = 0.71073 Å, graphite monochromator, ω-scan). Empirical absorption corrections (ψ-scans) for **2f** and **4** were applied. The structures were solved by direct methods [SHELXS86][18] and refined by least-squares methods based on F^2 with all measured reflections [SHELXL97].[19] All non-hydrogen atoms were refined anisotropically.

Crystallographic data (excluding structure factors) for the structures reported in this paper have been deposited with the Cambridge Crystallographic Data Center: CCDC-102722 (**2f**), -102723 (**4**), and -102724 (**5**). Copies of the data can be obtained free of charge and by application to CCDC, 12 Union Road, Cambridge CB2 1EZ, UK [Fax: int. code + 44-1223/336-001; E-mail: deposit@ccdc.cam.ac.uk].

6,6′-Bis(diethylboryl)-2,2′-bipyridine (1a) and 6-Diethylboryl-2,2′-bipyridine (3a): 3.00 g (30 mmol) of Et_2BOMe and 900 mg (7.5 mmol) of 2,2′-bipyridine were dissolved in 30 ml of Et_2O and cooled to −75°C. 15 mmol of $LiNiPr_2$ in 30 ml of Et_2O was added dropwise within 1 h. The resulting yellow solution was stirred for 6 h at −75°C and was allowed to warm up to room temp. overnight. The red solution was hydrolysed with 100 ml of brine (saturated NaCl solution) and the organic layer was extracted with ethyl acetate (3 × 100 ml). The combined extracts were dried with anhydrous sodium sulfate and the solvent was removed in high vacuo. The residue was column-chromatographed with silica gel (2 × 30 cm) with a mixture of *n*-hexane and ethyl acetate (4:1) to give 27 mg (0.09 mmol, 1%) **1a** and 97 mg (0.4 mmol, 6%) of **3a**. − **1a:** ^{1}H NMR (200.1 MHz, [D$_8$]thf): δ = 0.55 (t, 12 H, CH_2CH_3), 0.82 (q, 8 H, CH_2CH_3), 6.93 (m, 2 H, $C_{10}H_6N_2$), 7.63 (m, 2 H, $C_{10}H_6N_2$), 8.02 (m, 2 H, $C_{10}H_6N_2$). − ^{11}B NMR (64.2 MHz, $CDCl_3$): δ = 3.2. − ^{13}C NMR (50.3 MHz, [D$_8$]thf): δ = 8.7 (CH_2CH_3), 10.5 (CH_2CH_3), 16 (br., CH_2CH_3), 123.8, 127.7, 139.0, 147.4 ($C_{10}H_6N_2$). − MS (70 eV, EI); *m*/*z* (%): 263 (26) [M − Et]$^+$, 235 (8) [M − Et − C_2H_4]$^+$, 167 (100) [M − BEt_2 − HCN]$^+$, 78 (16) [C_5H_4N]$^+$. − M. p. > 250°C. − **3a:** ^{1}H NMR (200.1 MHz, [D$_8$]thf: δ = 0.50 (t, 6 H, CH_2CH_3), 0.78 (q, 4 H, CH_2CH_3), 7.24 (m, 1 H, $C_{10}H_7N_2$), 7.50 (m, 1 H, $C_{10}H_7N_2$), 7.96 (m, 1 H, $C_{10}H_7N_2$), 8.06 (m, 1 H, $C_{10}H_7N_2$), 8.40 (m, 2 H, $C_{10}H_7N_2$), 8.52 (m, 1 H, $C_{10}H_7N_2$). − ^{13}C NMR (50.3 MHz, $CDCl_3$): δ = 9.9 (CH_2CH_3), 13.4 (br., CH_2CH_3), 118.9, 123.1, 124.5, 136.9, 138.1, 139.8, 141.9, 146.9, 149.2 ($C_{10}H_7N_2$). − ^{11}B NMR (64.2 MHz, $CDCl_3$): δ = 3.4. − MS (70 eV, EI); *m*/*z* (%): 195 (40) [M − Et]$^+$, 180 (3) [M − Et − Me]$^+$, 167 (100) [M − HCN − C_2H_4]$^+$,78 (4) [$C_5H_4N^+$].

6,6′-Bis-di(2-thienyl)boryl]-2,2′-bipyridine (1b): 630 mg (0.68 mmol) of **2b** was dissolved in 5 ml of CH_2Cl_2. 147 mg (1.36 mmol) of $ClSiMe_3$ in 5 ml of CH_2Cl_2 was added dropwise at 0°C. The yellow solution was stirred at room temp. for 15 h. The mixture was filtered and 20 ml of thf was added to the precipitate. The mixture was again filtered from LiCl. After recrystallisation in thf, 124 mg (0.24 mmol, 36%) of **1b** was obtained as an amorphus solid. − ^{1}H NMR (200.1 MHz, [D$_8$]thf): δ = 7.39 (dd, 2 H, C_4H_3S), 7.65 (dd, 1 H, $C_{10}H_6N_2$), 7.82−7.89 (m, 3 H, $C_{10}H_6N_2/C_4H_3S$), 8.05 (dd, 2 H, C_4H_3S), 8.42 (dd, 1 H, $C_{10}H_6N_2$). − ^{13}C NMR (50.3 MHz, $CDCl_3$): δ = 120.4, 126.1, 131.0, 133.5, 138.5, 140.1, 141.6 ($C_{10}H_6N_2/C_4H_3S$). − ^{11}B NMR (64.2 MHz, [D$_8$]thf): δ = 1.0. − MS (70 eV, EI): *m*/*z* (%): 342 (28) [M − 2 (C_4H_3S)]$^+$, 259 (11) [M − 3 (C_4H_3S)]$^+$, 84 (100) [$C_4H_4S^+$]. − MS (FAB); *m*/*z* (%): 509 [M + 1$^+$]. − M.p. > 250°C.

6,6′-Bis[bis(dimethyamino)boryl]-2,2′-bipyridine (1c): To a solution of 500 mg (0.79 mmol) of **2c** in 5 ml of thf 211 mg (2 mmol) of $ClB(NMe_2)_2$ in 5 ml of Et_2O was added dropwise at room. temp. After some min, a red solid started to precipitate. After stirring at room temp. overnight, the mixture was filtered. The residue was destilled in high vacuo (10^{-2} mbar, 220°C) yielding 179 mg (0.51 mmol, 64%) of **1c** as a red oil. − ^{1}H NMR (200.1 MHz, [D$_8$]thf): δ = 2.52 (s, 12 H, NMe_2), 7.60 (d, 2 H, $C_{10}H_6N_2$), 7.76 (dd, 2 H, $C_{10}H_6N_2$), 8.38 (d, 2 H, $C_{10}H_6N_2$). − ^{13}C NMR (50.3 MHz, [D$_8$]thf): δ = 40.4, [$N(CH_3)_2$], 120.9, 129.8, 140.8, 142.6 ($C_{10}H_6N_2$). − ^{11}B NMR (64.2 MHz, [D$_8$]thf): δ = 31.0. − EI-MS; *m*/*z* (%): 253 (25) [M − $B(NMe_2)_2$]$^+$, 226 (46) [M − $B(NMe_2)_2$ − HCN]$^+$, 79 (100) [$C_5H_5N^+$].

2,2′-Bipyridine-6,6′-diborates 2: 1.57g (5 mmol) of 6,6′-dibromo-2,2′-bipyridine, dissolved in 75 ml of thf, was added dropwise within 20 min to a solution of 10 mmol *n*BuLi in 50 ml of thf at −80°C. After stirring for 45 min, the alkoxyborane, dissolved in 30 ml of Et_2O, was added dropwise within 30 min to the red solution The mixture was allowed to warm up to room temp. overnight. Half of the solvent was removed in vacuo and 30 ml of *n*-hexane was added. After 36 h at 0°C, the mixture was filtered. The borates were obtained as colorless solids.

2a: (2.10 g, 3.2 mmol, 64%). − ^{1}H NMR (200.1 MHz, [D$_8$]thf): δ = 0.19 (q, 4 H, CH_2CH_3), 0.71 (t, 6 H, CH_2CH_3), 3.14 (s, 3 H,

Table 1. Crystal data and structure refinement for **2f**, **4**, and **5**

	2f	**4**	**5**
Empirical formula	$C_{46}H_{72}B_2Li_2N_2O_8S_2$	$C_{32}H_{32}B_2Cu_1N_2O_2S_4$	$C_{22}H_{38}B_4N_2O_3$
Formula weight	880.7	690.0	421.8
Crystal system	monoclinic	triclinic	triclinic
Space group	$P2_1$	$P\bar{1}$	$P\bar{1}$
Unit cell			
a [Å]	10.418(6)	9.950(5)	13.051(7)
b [Å]	14.443(7)	13.434(7)	17.295(9)
c [Å]	17.001(8)	13.389(7)	22.120(11)
α [°]	90	82.29(4)	89.28(3)
β [°]	90.66(4)	68.38(3)	79.56(3)
γ [°]	90	76.47(4)	88.84(3)
V [Å^3]	2558(2)	1615(1)	4909(4)
Z	2	2	8
Calcd. density [g/cm^3]	1.14	1.42	1.14
Absorp.coeff. [mm^{-1}]	0.15	0.97	0.07
F(000)	948	714	1824
Crystal size [mm]	0.2 × 0.9 × 1.0	0.1 × 0.3 × 0.7	0.4 × 0.4 × 0.7
Θ_{max} [°]	25	25	24
Index ranges	−12/+12, 0/+17, 0/+20	−10/+11, −15/+15, 0/+15	−14/+14, −19/+19, 0/+25
No. of reflections			
Unique	4711	5660	15383
Observed [$I > 2\sigma(I)$]	3129	4285	8919
Transmission	0.91−1.00	0.82−1.00	−
Parameters	562	469	1188
Final R indices			
$R1$ [$I > 2\sigma(I)$]	0.052	0.047	0.086
$wR2$	0.140	0.123	0.274
Largest diff.peak/hole [e/Å^3]	0.27/−0.25	0.56/−0.42	0.39/−0.40

OCH_3), 7.26−7.41 (m, 1 H, $C_{10}H_6N_2$), 7.80−7.89 (m, 1 H, $C_{10}H_6N_2$), 8.42−8.46 (m, 1 H, $C_{10}H_6N_2$). − ^{13}C NMR (50.3 MHz, [D$_8$]thf): δ = 9.6 (br., *C*H$_2$CH$_3$), 11.1(CH$_2$*C*H$_3$), 49.5 (OCH_3), 121.0, 124.5, 137.4, 149.9 ($C_{10}H_6N_2$). − ^{11}B NMR (64.2 MHz, [D$_8$]thf): δ = 8.1. − M. p. 212−215°C.

2b: (4.08 g, 4.4 mmol, 87%). − ^{1}H NMR (200.1 MHz, [D$_8$]thf): δ = 0.91 (d, 6 H, CH_3), 3.93 [sept, 1 H, C*H*(CH$_3$)$_2$], 7.04−7.56 (m, 10 H, CH). − ^{13}C NMR (50.3 MHz, [D$_8$]thf): δ = 18.9 (CH_3), 61.3 [*C*H(CH$_3$)$_2$], 111.3 ($C_{10}H_6N_2$), 118.3 (C_4H_3S), 120.6 (C_4H_3S), 122.1 ($C_{10}H_6N_2$), 123.4 (C_4H_3S), 128.0 ($C_{10}H_6N_2$), 148.9 ($C_{10}H_6N_2$). − ^{11}B NMR (64.2 MHz, [D$_8$]thf): δ = 0.7. − M. p. 189−191°C.

2c: (3.49 g, 3.9 mmol, 78%). − ^{1}H NMR (200.1 MHz, [D$_8$]thf): δ = 0.83 (d, 6 H, CH_3), 0.90 [d, 6 H, CH$_2$CH(C*H*$_3$)$_2$], 1.70 [m, 2 H, CH$_2$C*H*(CH$_3$)$_2$], 3.00−3.19 [m, 4 H, C*H*$_2$CH(CH$_3$)$_2$], 6.81−7.02 (m, 3 H, CH), 7.37−7.61 (m, 5 H, CH). − ^{13}C NMR (50.3 MHz, $CDCl_3$): δ = 19.6 (CH_3), 32.2 [OCH$_2$*C*H(CH$_3$)$_2$], 69.8 [O*C*H$_2$CH(CH$_3$)$_2$], 124.6, 126.7, 133.9, 157.8 ($C_{10}H_6N_2$). − ^{11}B NMR (64.2 MHz, [D$_8$]thf): δ = 6.6. − M. p. 242−244°C.

2d: (2.95 g, 4.1 mmol, 82%). − ^{1}H NMR (200.1 MHz, [D$_8$]thf): δ = 3.06 (s, 6 H, CH_3), 6.79−7.00 (m, 3 H, ar), 7.34−7.52 (m, 5 H, ar). − ^{13}C NMR (50.3 MHz, [D$_8$]thf): δ = 49.7 (OCH_3), 118.8, 124.8, 126.9, 129.3, 133.6, 135.1, 158.3 (ar). − ^{11}B NMR (64.2 MHz, [D$_8$]thf]): δ = 6.7. − M. p. > 250°C (dec.).

2e: (3.49 g, 4.5 mmol, 89%). − ^{1}H NMR (200.1 MHz, [D$_8$]thf): δ = 0.84 (s, 18 H, CH_3), 3.61 (s, 3 H, OCH_3), 7.29−7.45 (m, 2 H, $C_{10}H_6N_2$), 7.65−7.70 (m, 1 H, $C_{10}H_6N_2$). − ^{13}C NMR (50.3 MHz, [D$_8$]thf): δ = 34.2 (CH_3), 32.8 (CH_3), 53.8 [br., B*C*(CH$_3$)$_3$], 53.9 (OCH_3), 117.7 [br., BC($C_{10}H_6N_2$)], 129.2, 130.6, 132.2, 132.7 ($C_{10}H_6N_2$). − ^{11}B NMR (64.2 MHz, [D$_8$]thf): δ = 5.1. − M. p. 212−214°C.

2f: (2.91g, 3.3 mmol, 65%). − ^{1}H NMR (200.1 MHz, [D$_8$]thf): δ = 0.86 (d, 6 H, CH_3), 1.07 (d, 6 H, CH_3), 3.91 [sept, 2 H, C*H*(CH$_3$)$_2$], 6.80 (m, 2 H, ar), 7.09 (d, 1 H, ar), 7.50 (m, 2 H, ar), 7.76 (dd, 1 H, ar). − ^{13}C NMR (50.3 MHz, [D$_8$]thf): δ = 26.3 (CH_3), 26.5 (CH_3), 62.8 [*C*H(CH$_3$)$_2$], 118.9, 124.3, 126.4, 128.6, 130.9, 133.8, 156.9 (ar). − ^{11}B NMR (64.2 MHz, [D$_8$]thf): δ = 5.1. − M. p. 199−201°C.

{2,2′-Bipyridine-6,6′-bisdiisopropoxydi(2-thienyl)borato]}-copper(II) (4): 928 mg (1 mmol) of **2b** and 456 mg (1 mmol) of $(Et_4N)_2CuCl_4$ were dissolved in 10 ml of CH_2Cl_2 at room temp. After stirring for 12 h, the green-blue solution was filtered from Et_4NCl. The solvent was removed in vacuo yielding 650 mg (0.95 mmol, 95%) of **4** as a deep green-blue air-sensitive solid. m. p. > 250°C. Cyclic voltammetry data (EG&G PARC 175 potentiostat): Pt disc (1 mm) working electrode, CH_2Cl_2 solution, 0.1 M Bu_4NPF_6 as supporting electrolyte, Pt wire as auxiliar electrode, SCE as reference electrode. Reversible oxidation at $E_{1/2}$ = 0.65 V, irreversible reduction at −1.1 V.

1,3-Diethyl-1,3-dihydroxydiboroxane Adduct 5 of 1a: 1.57g (5 mmol) of 6,6′-dibromo-2,2′-bipyridine, dissolved in 75 ml of thf, was added dropwise within 20 min to a solution of 10 mmol of *n*BuLi in 50 ml of thf at −80°C. After stirring for 45 min, 2.50 g (25 mmol) of diethyl(methoxy)borane, dissolved in 30 ml of Et_2O, was added dropwise within 30 min to the red solution. The mixture was allowed to warm up to room temp. overnight. The red solution was hydrolysed with 100 ml of brine and the organic layer was extracted with ethyl acetate (3 × 100 ml). The combined extracts were dried with anhydrous sodium sulfate and the solvent was removed in vacuo. The residue was dissolved in 20 ml of thf and 10 ml of *n*-hexane was added. After 40 h at 0°C, the mixture was filtered yielding 884 mg (2.1 mmol, 42%) of **5**. − ^{1}H NMR (200.1 MHz, CD_2Cl_2): δ = −0.21 [q, 2 H, OB(OH)C*H*$_2$CH$_3$], 0.52 [q, 4 H, OB(C*H*$_2$CH$_3$)$_2$], 0.64 [t, 3 H, OB(OH)CH$_2$C*H*$_3$], 0.79 [t, 6 H, OB(CH$_2$C*H*$_3$)$_2$], 3.93 (br., 0.8 H, OH), 7.45−7.67 (m, 2 H, $C_{10}H_6N_2$), 7.93 (t, 1 H, $C_{10}H_6N_2$). − ^{13}C NMR (50.3 MHz, CD_2Cl_2): δ = 7.8 (CH$_2$*C*H$_3$), 9.6 (CH$_2$*C*H$_3$), 9.8 (CH$_2$*C*H$_3$), 15 (br.,

CH_2CH_3), 123.4, 127.9, 139.6, 146.1 ($C_{10}H_6N_2$). – ^{11}B NMR (64.2 MHz, CD_2Cl_2): δ = 9.2 (br.). – M. p. 156–160°C (dec.).

Acknowledgments

This work was supported by the Graduiertenkolleg "Selektivität und Reaktivität in der organischen und metallorganischen Synthese und Katalyse" and the DFG (SFB 247).

[1] B. M. Michailov, A. V. Bazhenova, *Izvest. Akad. Nauk S.S.S.R, Otdel. Khim. Nauk* **1959**, 80–84 (*Chem. Abstr.* **1959**, *53*, 1628; F. C. Fischer, E. Havinga, *Recl. Trav. Chim. Pays-Bas* **1974**, *93*, 21–24; H. C. H. A. van Riel, F. C. Fischer, J. Lugtenburg, E. Havinga, *Tetrahedron Lett.* **1969**, 3085.
[2] N. Miyaura, A. Suzuki, *J. Chem. Soc., Chem. Commun.* **1982**, 866.
[3] M. Isikura, T. Mano, I. Oda, M. Terashima, *Heterocycles* **1984**, *22*, 2471–2474.
[4] Y. Sugihara, R. Mijatake, T. Katsuto, Y. Shigenobu, *J. Chem. Soc., Chem. Commun.* **1994**, 1925–1926.
[5] M. Ishikura, M.Kamada, M. Terashima, *Synthesis* **1994**, 936.
[6] P. Homanen, M. Haukka, M. Ahlgrén, T. A. Pakkanen, *Inorg. Chem.* **1997**, *36*, 3794–3797.
[7] A. Togni, L. Venanzi, *Angew. Chem* **1994**, *106*, 517–547, *Angew. Chem.*, *Int. Ed. Engl.* **1994**, *33*, 497–526.
[8] P.A. Anderson, T.J. Meyer et al., *Inorg. Chem.* **1994**, *33*, 3863–3864.
[9] B. O′Regan, M. Grätzel, *Nature* **1991**, *353*, 737–740.
[10] C. Bolm, M. Zender, D. Bur, *Angew. Chem.* **1990**, *102*, 206–208; *Angew. Chem. Int. Ed. Engl.* **1990**, *29*, 205.
[11] C. Bolm, G. Schlingloff, K. Harms, *Chem. Ber.* **1992**, *125*, 1191–1203.
[12] W. Zhang, J.L Loebach, S.R. Wilson, E.N. Jacobsen, *J. Am. Chem. Soc.* **1990**, *112*, 2801–2803.
[13] R. Irie, K. Noda, Y. Ito, N. Matsumaoto, T. Katsuki, *Tetrahedron Lett.* **1990**, *31*, 7345–7348.
[14] T. Murafuji, R. Mouri, Y Sugihara, *Tetrahedron* **1996**, *52*, 13933–13938.
[15] J. E. Parks, B. E. Wagner and R. H. Holm, *J. Organomet. Chem.* **1973**, *56*, 53–66.
[16] H. Nöth, B.Wrackmayer, *NMR Spectroscopy on Boron Compounds*, Springer Verlag Berlin, Heidelberg, **1978**.
[17] B. J. Hathaway, D. E. Billing, *Coord. Chem. Rev.* **1970**, *5*, 143; B. J. Hathaway in *Comprehensive Coordination Chemistry*, vol. 5 (Eds.: G. Wilkinson, R. D. Gillard, J. A. McCleverty), Pergamon, Oxford, **1987**, p. 533.
[18] G. M. Sheldrick, *SHELXS86*, Univ. Göttingen, **1986**.
[19] G. M. Sheldrick, *SHELXL97*, Univ. Göttingen, **1997**.

Received August 28, 1998
[I98294]

Syntheses, Structures, and Reactivity of 2,5-Diboryl-1-alkylpyrroles and Di(1-alkyl-2-pyrrolyl)boranes

Jürgen Faderl,[a] Bernd Deobald,[a,b] Roger Guilard,[b] Hans Pritzkow,[a] and Walter Siebert*[a]

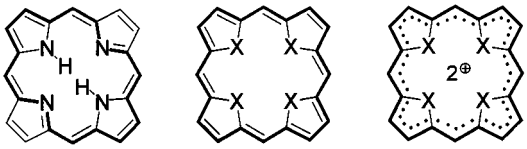
Dedicated to Prof. Wolfgang Sundermeyer on the occasion of his 70th birthday

Keywords: Boranes / 1-Alkylpyrroles / Porphyrinogenes / Lithiation / Tin–boron exchange

Reactions of 2,5-dilithiated 1-methylpyrrole (**1a**) with $ClB(NR_2)_2$ lead to the novel 2,5-diboryl-1-methylpyrroles **2a** and **2b**. Accordingly, 2,5-diboryl-1-benzylpyrrole **2d** is obtained. **1a** and Cl_2BNiPr_2 form the aminochloroboryl-substituted derivative **2c** and the di(5-boryl-2-pyrrolyl)borane **4** in 29% and 15% yield, respectively. The 2,5-distannyl-1-methylpyrrole **1c** is used for the synthesis of the aryloxy-boryl derivative **2e**. Reacting monolithiated 1-methyl- and 1-benzylpyrroles with Cl_2BNiPr_2 yields the di(2-pyrrolyl)boranes **3e** and **3f**, respectively. NMR and MS data are in agreement with the compositions of the compounds, which are confirmed by X-ray structure analyses for **2a**, **2b**, **2d**, und **3e.**

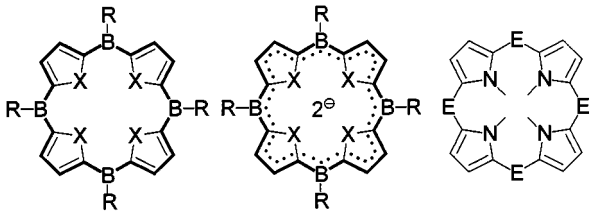
Introduction

Since 1960 the hypothetical isophlorin (*N,N′*-dihydroporphyrin) **B**, X = NH,[1] as well as its heteroatom analogs have become a matter of interest. They may be regarded as bridged [20]annulenes. While the [18]annulene porphyrin **A** is very stable and shows a diatropic ring current[2] the tetraoxa macrocycle **B**, X = O, is less stable and exhibits a paratropic ring current.[3] Its dicationic precursor **C**, X = O, is an aromatic compound with a diatropic ring current.[4] In the octaethyl, tetramethyl derivatives of the tetraaza compounds **B** and **C**, X = NMe, the steric interference of the methyl groups causes non-planarity of both molecules. This yields for **C**, X = NMe, only to a small diatropic ring current,[5] whereas the paratropic ring current of **B**, X = NMe, is almost zero.[3]



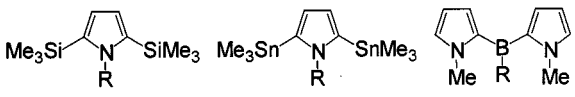
A **B** X = NH, NR, O, S **C** X = NH, NR, O, S

We are interested in the electronic structure and ligand properties of the tetrabora porphyrinogenes **D**, which formally derive from **B** by exchange of the *meso*-carbon for boron atoms. In **D** the empty p_z orbitals of the boron atoms may allow macrocyclic conjugation, when **D** (16 π electrons) is reduced to the dianion **E**. As a first example of a tetrabora porphyrinogene **D** we recently synthesized the tetrathia macrocycle **D**, X = S, R = N*i*Pr$_2$.[6] The formation of the silyl- and stannyl-bridged macrocycles **F**, E = $SiMe_2$, $SnMe_2$, has been reported.[7]



D X = NH, NR, O, S **E** X = NH, NR, O, S **F** E = $SiMe_2$, $SnMe_2$

Possible building blocks for the synthesis of **D**, X = NR, may be 2,5-diborylpyrroles **2** and di(2-pyrrolyl)boranes **3**, which when suitably functionalized should be precursors for ring-closure reactions. However, 2,5-diborylpyrroles **2** are not yet known. Only a few 2,5-disilylpyrroles **G**[8] and the 2,5-distannylpyrrole **H**[9] have been reported. The di(1-methyl-2-pyrrolyl)boranes **3a–d** were synthesized via tin–boron exchange and characterized by NMR.[10] In the following we report on the syntheses of novel 2,5-diborylpyrroles **2** as well as the preparation of the di(2-pyrrolyl)boranes **3e** and **3f** via lithiated 1-alkylpyrroles.



G R = Me, CO_2tBu, CONH*t*Bu **H** R = CO_2tBu **3a-d** R = NMe_2, Et, Cl, C_4H_3NMe

[a] Anorganisch-Chemisches Institut der Universität, Im Neuenheimer Feld 270, D-69120 Heidelberg, Germany
Fax: (internat.) +49(0)6221/54-5609
E-mail: ci5@ix.urz.uni-heidelberg.de
[b] Université de Bourgogne, LIMSAG (UMR 5633), Faculté des Sciences, 6 Boulvard Gabriel, F-21100 Dijon, France

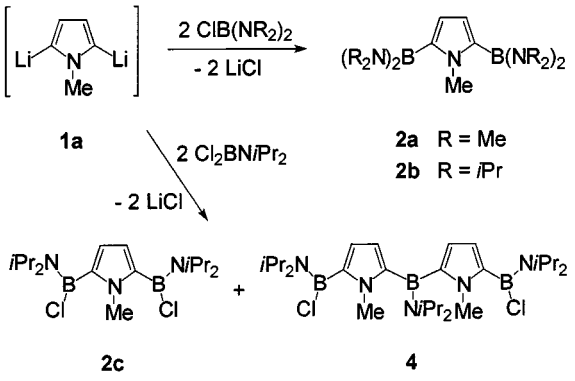
 © WILEY-VCH Verlag GmbH, D-69451 Weinheim, 1999 1434–1948/99/0303–0399 $ 17.50+.50/0

Results and Discussion

Syntheses and Reactivity

2,5-Dilithio-1-methylpyrrole (**1a**) is formed by treating 1-methylpyrrole with 2.4 equivalents of *n*-butyllithium in the presence of *N,N,N′,N′*-tetramethylethylendiamine (tmeda) in refluxing hexane. The grey-brown suspension of **1a** is very sensitive and immediately turns dark on air contact. Due to its high reacticity **1a** was used in situ for the preparation of the compounds **2a−c**. Presumably the lithium centers of **1a** are coordinated and stabilized with tmeda.

The reaction of **1a** with $ClB(NMe_2)_2$ leads to the novel 2,5-bis[bis(dimethylamino)boryl]-1-methylpyrrol (**2a**) in 47% yield as colorless, crystalline solid, which is sensitive to air and moisture. The composition of **2a** follows from spectroscopic data and is confirmed by an X-ray structure analysis (see below). The ^{1}H-NMR spectrum shows the expected three singulets. The ^{11}B-NMR spectrum exhibits a signal at $\delta = 30.1$, which corresponds with that of 2-bis(dimethylamino)boryl-1-methylpyrrole ($\delta = 29.8$).[10a] In the ^{13}C-NMR spectrum the signals of the ring carbon atoms appear at $\delta = 116.2$ for those in 3- and 4-position and at $\delta = 137$ as a broadened signal[11] for the boron-bound ring atoms. The ^{13}C signals of the ring atoms reveal a low-field shift of 7 and 15 ppm compared with those of 1-methylpyrrole,[12] which may be explained by π-interaction of the heterocycle with the boryl substituent as discussed by Nöth et al.[10] A thermogravimetric analysis of **2a** shows a continuous loss of mass with no hint for condensation reactions, expected to be accompanied with elimination of $B(NMe_2)_3$. An analogous reaction is known to occur with 2,5-bis(dimethylboryl)thiophene[13] even at room temperature. Treatment of **2a** with $AlMe_3$, MeOH, or PCl_5 did not lead to the projected exchange of substituents at the boron atoms.



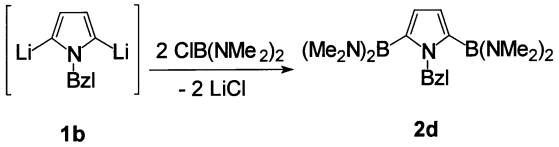
Scheme 1

The reaction of **1a** with $ClB(N\textit{i}Pr_2)_2$ yields only 6% of 2,5-bis[bis(diisopropylamino)boryl]-1-methylpyrrole (**2b**) as a colorless, crystalline solid, which is sensitive to air and moisture. The difference in the yield of **2a** and **2b** is probably caused by the greater steric impact of the diisopropylamino in comparison to the dimethylamino group. The spectroscopic and structural data of **2b** are similar to those of **2a**. Treatment of **2b** with BCl_3 did not yield the appropriate bis(dichloroboryl) derivative.

By adding the suspension of **1a** slowly into a cooled solution of $Cl_2BN\textit{i}Pr_2$ the 2,5-bis(chlorodiisopropylaminoboryl)-1-methylpyrrole (**2c**) is obtained in 29% together with 15% of bis[5-(chlorodiisopropylaminoboryl)-1-methyl-2-pyrrolyl]diisopropylaminoborane (**4**). Most likely the latter is formed, when the intermediate 5-(chlorodiisopropylamino)-2-lithio-1-methylpyrrole reacts with **2c** to give **4**.

2c is a colorless, crystalline solid, sensitive to air and moisture. Its ^{1}H-, ^{11}B-, and ^{13}C-NMR shifts are very similar to that of **2b** with exception of the shifts for the isopropyl groups. They appear in the ^{1}H-NMR spectrum as two sets of broadened signals with equal intensity, which indicates a B−N double bond.

4 is a colorless, air- and moisture-sensitive crystalline solid, which decomposes when heated to 130°C. The ^{1}H-NMR spectrum of **4** shows three sets of isopropyl groups in equal intensity. The signals for the aminochloroboryl substituents are identical with that of **2c**, the third set belongs to the isopropylamino group between the two heterocycles and is resolved as doublet and septet. The ring protons appear as two doublets at $\delta = 6.51$ and 6.63 with a coupling constant of 3.5 Hz. The ^{11}B-NMR spectrum shows one broad unsymmetrical signal at $\delta = 35$, formed by superposition of the two signals of the different boron atoms. In the ^{13}C-NMR spectrum only one broad signal at $\delta = 23$ for the two methyl groups of the outer isopropyl group is found, the corresponding methyne signals are separated. For the heterocycles four signals are found, two at $\delta = 114.1$ and 116.7 for the carbon atoms in 3- and 4-position and two broad ones[11] at $\delta = 137$ and 141 for the two different boron-bound carbon atoms. The composition of **4** is confirmed by a high resolution mass spectrum.



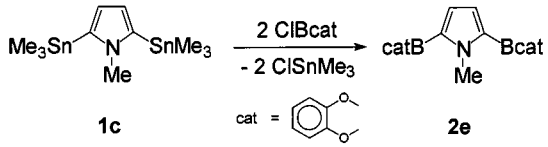
Scheme 2

Treating 1-benzylpyrrole with 2.4 equivalents of *n*-butyllithium and tmeda in refluxing hexane leads to the formation of 1-benzyl-2,5-dilithiopyrrole (**1b**). It is in situ treated with $ClB(NMe_2)_2$ to yield 34% of 2,5-bis[bis(dimethylamino)boryl]-1-benzylpyrrole (**2d**) as a colorless, crystalline solid, which is sensitive to air and moisture. Beside the benzyl group its spectroscopic data are similar to **2a**. A high resolution mass spectrum and an X-ray structure analysis confirm the composition of **2d**.

Attempts to synthesize 2,5-bis(dimethylboryl)-1-methylpyrrole (**2f**) from **1a** and Me_2BBr failed. The alternative route via the ditin derivative **1c** was tested to obtain **2e** as precursor for **2f**. Reaction of **1a** with trimethyltinbromide leads to the formation of 2,5-bis(trimethylstannyl)-1-methylpyrrole (**1c**), a colorless solid, characterized by multinuclear NMR spectroscopy (^{1}H, ^{13}C, and ^{119}Sn) and mass spectrometry. It is transformed into 2,5-bis(1,3,2-benzodioxaborol-2-yl)-1-methylpyrrole (**2e**) by the reaction of **1c**

with 2-chloro-1,3,2-benzodioxaborole. The tin−boron exchange leads to colorless **2e** in 75% yield.

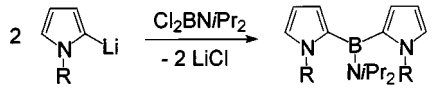
The 200-MHz ^{1}H-NMR spectrum of **2e** shows only two multiplets in the aromatic region. A 300-MHz spectrum reveals that the singulet for the pyrrole ring protons (δ = 7.09) superposes with one of the multiplets of the benzo ring protons at δ = 7.11. The ^{11}B-NMR shift of **2e** is δ = 30. In the ^{13}C-NMR spectrum a signal for the boron-bound carbon atoms could not be observed.[11] As recently shown the benzodioxaborole ring is easily cleaved by LiMe or $AlMe_3$ to yield dimethylboryl groups.[14] The reaction of **2e** with $AlMe_3$ at −70°C indicated the formation of 2,5-bis(dimethylboryl)-1-methylpyrrole (**2f**), which could not be isolated. Most likely a polycondensation of the projected **2f** occured with elimination of BMe_3.



1c **2e**

Scheme 3

The reaction of monolithiated 1-methylpyrrole (**1d**) with Cl_2BNiPr_2 yields diisopropylaminodi(1-methyl-2-pyrrolyl)-borane (**3e**) as a colorless, crystalline solid. **3e** is stable up to 210°C, but sensitive to air and moisture. The ^{1}H-NMR spectrum shows next to the signals of the isopropyl group and the ring methyl group three multiplets for the ring protons at δ = 6.31, 6.48, and 6.56. The signal at δ = 6.31 is resolved as doublet of doublets with coupling constants of 2.4 and 3.5 Hz. They are ^3J coupling constants and hence the signal is assigned to the ring proton in 4-position. According to Nöth et al.[10b] the signals for the ring atoms in 4-position (proton and carbon atom) appear at high field, compared with those of the other ring atoms. This fact is based on the mesomeric effect of the boryl group in 2-position, which leads to partially postive charged 1-, 3-, and 5-positions. Accordingly, in the ^{13}C-NMR spectrum the signal for the carbon atom in 4-position appears at δ = 107.7 with the other ring signals at δ = 116.7, 125.4, and 138, the latter being the broadened signal[11] for the boron-bound carbon atoms. The ^{11}B-NMR spectrum shows a signal at δ = 35.6, which is comparable to dimethylamino derivative **3a** (δ = 31.8).[10a] The composition of **3e** is confirmed by a high resolution mass spectrum and an X-ray structure analysis.



1d R = Me **3e** R = Me
1e R = Bzl **3f** R = Bzl

Scheme 4

Analogously, di(1-benzyl-2-pyrrolyl)diisopropylamino-borane (**3f**) is synthesized from **1e**. The colorless solid is sensitive to air and moisture. Its chemical shifts are very similar to those of **3e** with exception of the benzyl group.

Crystal Structures

To elucidate the structure of the novel 2,5-diborylpyrroles **2** X-ray diffraction studies of the amino-substituted derivatives **2a**, **2b**, and **2d** were carried out (crystal data and structure refinement including **3e** are shown in Table 1).

The molecule of **2a** has almost C_s-symmetry with the mirror plane perpendicular to the ring plane. The bond lengths and angles are equal within the *esd*s.

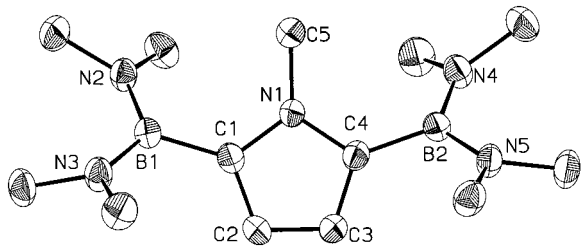


Figure 1. Molecular structure of **2a** in the crystal; selected bond lengths [Å] and angles [°]: N1−C1 1.390(2), N1−C4 1.391(2), C1−C2 1.383(3), C4−C3 1.381(3), C2−C3 1.402(3), N1−C5 1.457(2), C1−B1 1.577(3), C4−B2 1.575(3), B1−N2 1.419(2), B1−N3 1.429(3), B2−N4 1.429(3), B2−N5 1.424(3), C4−N1−C1 111.0(1), N1−C1−C2 105.6(1), C1−C2−C3 108.8(2), C2−C3−C4 108.8(2), C3−C4−N1 105.7(1), N1−C1−B1 127.8(1), N1−C4−B2 127.4(1).

2b has a crystallographic two-fold axis through the molecule and **2d** a crystallographic mirror plane perpendicular to the pyrrole ring.

The geometries of the three molecules are very similar. The distances and angles of the pyrrole rings are almost equal (within 3σ), but show significant deviations from the unsubstituted pyrrole ring,[12] especially for the endocyclic angles (values for the unsubstituted pyrrole in parantheses): C−N−C 111.0−111.6° (109.8°), N−C−C 105.4−105.7° (107.7°), C−C−C 108.7−108.8° (107.4°). The reason for this difference is not clear.

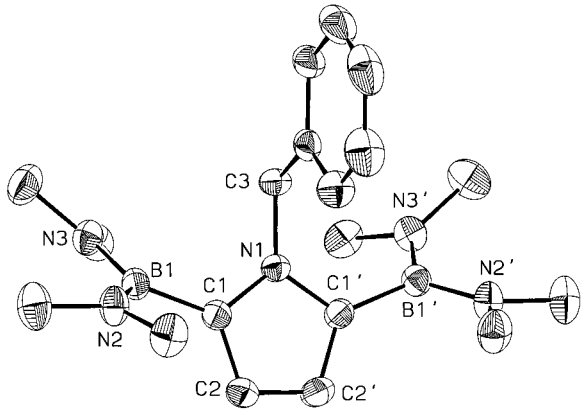


Figure 2. Molecular structure of **2d** in the crystal. − Selected bond lengths [Å] and angles [°] of **2d**: N1−C1 1.390(2), C1−C2 1.382(2), C2−C2′ 1.411(4), N1−C3 1.456(3), C1−B1 1.578(2), B1−N2 1.419(2), B1−N3 1.427(2), C1′−N1−C1 111.4(2), N1−C1−C2 105.6(1), C1−C2−C2′ 108.7(1), N1−C1−B1 125.5(1). − Selected bond lengths [Å] and angles [°] of **2b**: N1−C1 1.384(3), C1−C2 1.373(3), C2−C2′ 1.405(5), N1−C3 1.447(4), C1−B1 1.584(4), B1−N2 1.425(4), B1−N3 1.438(4), C1′−N1−C1 111.6(3), N1−C1−C2 105.4(2), C1−C2−C2′ 108.7(1), N1−C1−B1 127.0(2).

The pyrrole rings are almost planar with max. deviations of 0.006 Å for **2a** and 0.010 Å for **2b** and **2d**. The substituents deviate only slightly from the ring plane. The boron atoms have an almost planar coordination, but the CBNN planes are twisted against the ring planes. The interplanar angles increase from 43.0 and 48.2° for **2a** to 57.8° for **2d** (caused by the benzyl ligand) and up to 71.5° for **2b** with the bulky isopropyl groups. The planes through the amino groups are not coplanar with the CBNN planes, but rotated by 19.0−35.1°. The B−N distances (1.419−1.438 Å) are somewhat greater than in other aminoboranes.[15]

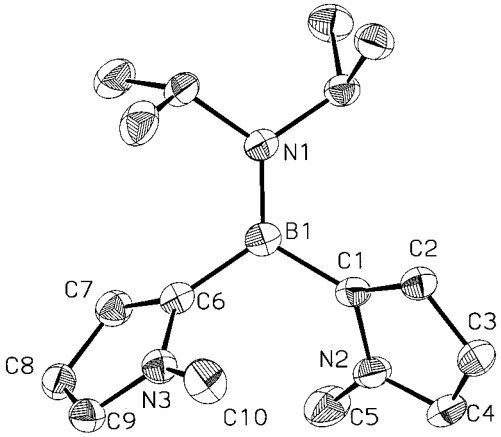


Figure 3. Molecular structure of **3e** in the crystal; selected bond lengths [Å] and angles [°]: N2−C1 1.389(2), N3−C6 1.392(2), C1−C2 1.387(2), C6−C7 1.384(2), C2−C3 1.409(3), C7−C8 1.406(3), C3−C4 1.357(3), C8−C9 1.363(3), C4−N2 1.366(2), C9−N3 1.367(2), N2−C5 1.456(3), N3−C10 1.456(3), C1−B1 1.577(3), C6−B1 1.574(3), B1−N1 1.406(2), C4−N2−C1 109.7(1), C9−N3−C6 110.3(1), N2−C1−C2 105.3(1), N3−C6−C7 105.0(2), C1−C2−C3 109.2(2), C6−C7−C8 109.5(2), C2−C3−C4 106.5(2), C7−C8−C9 106.9(2), C3−C4−N2 109.1(2), C8−C9−N3 108.3(2), N2−C1−B1 124.6(1), N3−C6−B1 122.5(1).

3e is the first di(2-pyrrolyl)borane, whose structure was determined. The coordination at the boron and the N1 nitrogen center is almost planar, but the molecule ist twisted by 17.8° around the B−N bond. The B−N distance is smaller than in the 2,5-diborylpyrroles **2**. The two pyrrole rings show only small deviations (max. 0.008 Å) from planarity and are rotated by 45.9 and 58.1° against the plane through B1, C1, C6, and N1. The pyrrole rings are not symmetrically substituted and show significant differences of the distances and angles compared with the unsubstituted pyrrole[12] and the 2,5-diborylpyrroles **2**.

Experimental Section

General: Reactions were carried out under dry nitrogen using standard Schlenk techniques. Solvents and chemicals were dried, distilled, and saturated with nitrogen. Glassware was dried with a heat-gun in high vacuum. − ^{1}H, ^{11}B, ^{13}C, ^{119}Sn NMR: Bruker AC 200 spectrometer, shift references are $(CH_3)_4Si$, $BF_3 \cdot Et_2O$, and $(CH_3)_4Sn$. − Mass spectra were obtained with a Varian MAT CH7 spectrometer, high resolution mass spectra with a Jeol JMS-700 spectrometer both using the EI technique. − Melting points (uncorrected) were measured with a Büchi apparatus using a capillary, which was filled under nitrogen and sealed. − 1-Benzylpyrrole,[16a] $ClB(NMe_2)_2$,[16b] $ClB(NiPr_2)_2$,[16c] Cl_2BNiPr_2,[16d] 2-chloro-1,3,2-benzodioxaborole (ClBcat),[16e] and $(CH_3)_3SnBr$[16f] were prepared according to literature procedures.

2,5-Dilithio-1-methylpyrrole (1a): To a solution of 3.6 mL (24.0 mmol) of tmeda in 40 mL of hexane 9.6 mL (24.0 mmol) of *n*-butyllithium (2.5 M in hexane) were added with cooling and stirred for 15 min at room temp. After the addition of 0.9 mL (10.1 mmol) of 1-methylpyrrole the mixture was refluxed for 9 h. A grey-brown suspension was formed.

2,5-Bis(trimethylstannyl)-1-methylpyrrole (1c): To a suspension of **1a** (10.3 mmol) in 50 mL of hexane a solution of 5.86 g (24.0 mmol) of $(CH_3)_3SnBr$ in 10 mL of hexane was added dropwise at −30°C. The mixture was allowed to warm to room temp. and stirred for 15 h. Volatile compounds were removed in vacuum, the residue was dissolved in hexane and filtered. The solvent was evaporated in vacuum and the colorless solid obtained was recrystallized from hexane at −80°C. Yield: 2.88 g (69%) colorless **1c**. − ^{1}H NMR (C_6D_6, 200.1 MHz): δ = 0.22 [s, 18 H, ^2J(H,^{117}Sn) = 53.4 Hz (7,1%), ^2J(H,^{119}Sn) = 55.9 Hz (7,7%), SnCH_3], 3.41 (s, 3 H, $^4J_{H,Sn}$ = 2.4 Hz, NCH_3), 6.65 (s, 2 H, $^3J_{H,Sn}$ = 10.5 Hz, C*H*). − ^{13}C NMR (C_6D_6, 50.3 MHz): δ = −8.8 ($^1J_{C,Sn}$ = 348.3 Hz and 364.3 Hz, Sn*C*H$_3$), 39.4 (N*C*H$_3$), 120.1 ($^2J_{C,Sn}$ = 50.5 Hz and 60.5 Hz, *C*H), 136.3 (ring-*C*Sn). − ^{119}Sn NMR (C_6D_6, 74.6 MHz): δ = −33.0. − MS: *m*/*z* (%): 407 (26) [M$^+$], 392 (62) [M$^+$ − Me], 230 (100).

2,5-Bis[bis(dimethylamino)boryl]-1-methylpyrrole (2a): To a suspension of **1a** (10.1 mmol) in 50 mL of hexane a solution of 2.75 g (20.5 mmol) of $ClB(NMe_2)_2$ in 15 mL of hexane was added within 25 min at −30°C. The mixture was allowed to warm to room temp. and stirred for 14 h. After 20 min of refluxing the volatile compounds were evaporated in vacuum, the residue was dissolved in hexane and filtered. The solvent was removed in vacuum and **2a** was sublimed. A single crystal was grown from a pentane solution at −30°C. Yield: 1.32 g (47%) colorless **2a**, subl.p.: 72°C/5·10^{-2} mbar. − ^{1}H NMR (C_6D_6, 200.1 MHz): δ = 2.65 (s, 24 H, BNCH_3), 3.44 (s, 3 H, CNCH_3), 6.52 (s, 2 H, C*H*). − ^{11}B NMR (C_6D_6, 64.2 MHz): δ = 30.1. − ^{13}C NMR (C_6D_6, 50.3 MHz): δ = 34.4 (CN*C*H$_3$), 40.8 (BN*C*H$_3$), 116.2 (*C*H), 137 (br, *C*B). − MS: *m*/*z* (%): 277 (7) [M$^+$], 233 (3) [M$^+$ − NMe_2], 58 (100).

2,5-Bis[bis(diisopropylamino)boryl]-1-methylpyrrole (2b): To a suspension of **1a** (10.1 mmol) in 50 mL of hexane a solution of 5.10 g (20.7 mmol) of $ClB(NiPr_2)_2$ in 20 mL of hexane was added within 20 min at room temp. The mixture was stirred for 14 h and refluxed for 8 h. Volatile compounds were removed in vacuum, the residue was dissolved in hexane and filtered. The solvent was evaporated in vacuum and **2b** was sublimed. A single crystal was grown from a hexane solution at −30°C. Yield: 0.30 g (6%) colorless **2b**, subl.p.: 140°C/1.2·10^{-2} mbar. − ^{1}H NMR (C_6D_6, 200.1 MHz): δ = 1.17 [d, 48 H, $^3J_{H,H}$ = 6.9 Hz, CH(CH_3)$_2$], 3.58 [sept, 8 H, $^3J_{H,H}$ = 6.9 Hz, C*H*(CH$_3$)$_2$], 3.70 (s, 3 H, NCH_3), 6.39 (s, 2 H, ring-C*H*). − ^{11}B NMR (C_6D_6, 64.2 MHz): δ = 33.7. − ^{13}C NMR (C_6D_6, 50.3 MHz): δ = 25.1 [CH(*C*H$_3$)$_2$], 37.3 (N*C*H$_3$), 47.8 [*C*H(CH$_3$)$_2$], 116.7 (ring-*C*H), *C*B signal not observed. − MS: *m*/*z* (%): 501 (47) [M$^+$], 458 (39) [M$^+$ − *i*Pr], 401 (43) [M$^+$ − N*i*Pr$_2$], 211 (100) [B(N*i*Pr$_2$)$_2^+$].

2,5-Bis(chlorodiisopropylaminoboryl)-1-methylpyrrole (2c) and Bis[5-(chlorodiisopropylaminoboryl)-1-methyl-2-pyrrolyl]diisopropylaminoborane (4): To a solution of 4.43 g (24.3 mmol) of Cl_2BNiPr_2 in 20 mL of hexane a suspension of **1a** (10.3 mmol) in 50 mL hexane was added dropwise at −50°C. The mixture was allowed to warm to room temp. and stirred for 15 h. Volatile compounds were removed in vacuum, the residue was dissolved in hexane and fil-

tered. The solvent was evaporated and the residue treated with 20 mL of hexane. **4** was crystallized from the solution at −30°C, filtered, and dried. The remaining solution was evaporated in vacuum to half the volume and **2c** was crystallized at −30°C, separated, and dried. Yield: 1.12 g (29%) of colorless **2c**. − ^{1}H NMR (C_6D_6, 200.1 MHz): δ = 0.84, 1.34 [each br, 12 H, CH(CH_3)$_2$], 3.38, 4.07 [each br, 2 H, CH(CH$_3$)$_2$], 3.81 (s, 3 H, NCH_3), 6.48 (s, 2 H, ring-CH). − ^{11}B NMR (C_6D_6, 64.2 MHz): δ = 33.8. − ^{13}C NMR (C_6D_6, 50.3 MHz): δ = 22.1, 23.0 [each CH(*C*H$_3$)$_2$], 37.1 (N*C*H$_3$), 47.0, 51.6 [each *C*H(CH$_3$)$_2$], 115.0 (ring-*C*H), 137 (br, *C*B). − MS: *m*/*z* (%): 371 (13) [M$^+$], 328 (18) [M$^+$ − *i*Pr], 84 (100). − Yield: 422 mg (15%) of colorless **4**, m.p.: 187°C (decomp.). − ^{1}H NMR (C_6D_6, 200.1 MHz): δ = 0.94, 1.32 [each br, 12 H, CH(CH_3)$_2$ (outer)], 1.17 [d, 12 H, $^3J_{H,H}$ = 6.8 Hz, CH(CH_3)$_2$ (inner)], 3.31 (s, 6 H, NCH_3), 3.37 [br, 2 H, CH(CH$_3$)$_2$ (outer)], 4.07 [sept, 2 H, $^3J_{H,H}$ = 6.8 Hz, CH(CH$_3$)$_2$ (inner) and br, 2 H, CH(CH$_3$)$_2$ (outer)], 6.51, 6.63 (each d, 2 H, $^3J_{H,H}$ = 3.5 Hz, ring-CH). − ^{11}B NMR (C_6D_6, 64.2 MHz): δ = 35. − ^{13}C NMR (C_6D_6, 50.3 MHz): δ = 23 [br, both CH(*C*H$_3$)$_2$ (outer)], 24.8 [CH(*C*H$_3$)$_2$ (inner)], 36.2 (N*C*H$_3$), 46.9, 51.5 [each *C*H(CH$_3$)$_2$ (outer)), 49.1 (*C*H(CH$_3$)$_2$ (inner)], 114.1, 116.7 (each ring-*C*H), 137, 141 (each br, *C*B). − MS: *m*/*z* (%): 561 (56) [M$^+$], 518 (27) [M$^+$ − *i*Pr], 292 (100). − HR-MS: *m*/*z* (%): 561.3915 (9) [M$^+$, calc. for $^{12}C_{28}$ $^1H_{52}$ $^{11}B_3$ $^{35}Cl_2$ $^{14}N_5$: 561.3879].

2,5-Bis[bis(dimethylamino)boryl]-1-benzylpyrrole (2d): To a solution of 3.6 mL (24.0 mmol) of tmeda in 50 mL of hexane 9.2 mL (23.0 mmol) of *n*-butyllithium (2.5 M in hexane) was added with cooling. After stirring for 20 min at room temp. 1.58 g (10.0 mmol) of 1-benzylpyrrole was added with cooling and the mixture was heated under reflux for 14 h. To the resulting suspension 2.77 g (20.6 mmol) of ClB(NMe$_2$)$_2$ in 20 mL of hexane was added dropwise at −30°C. After the mixture was allowed to warm to room temp. and stirred for 4 h, it was refluxed for 2 h. Volatile compounds were evaporated in vacuum, the residue was dissolved in hexane and filtered. The solvent was removed in vacuum and the colorless solid washed with pentane. A single crystal was grown from a solution of pentane and CH_2Cl_2 (4:1) at −30°C. Yield: 1.21 g (34%) colorless **2d**, m.p.: 103°C. − ^{1}H NMR ($CDCl_3$, 200.1 MHz): δ = 2.59 (s, 24 H, CH_3), 4.91 (s, 2 H, CH_2), 6.17 (s, 2 H, pyrrole-CH), 6.92 (m, 2 H, phenyl-CH), 7.17 (m, 3 H, phenyl-CH). − ^{11}B NMR ($CDCl_3$, 64.2 MHz): δ = 30.8. − ^{13}C NMR ($CDCl_3$, 50.3 MHz): δ = 40.6 (*C*H$_3$), 51.1 (*C*H$_2$), 116.1 (pyrrole-*C*H), 126.5, 127.2, 127.9 (each phenyl-*C*H), 141.4 (phenyl-*C*$_{ipso}$), *C*B signal not observed. − MS: *m*/*z* (%): 353 (69) [M$^+$], 309 (9) [M$^+$ − NMe$_2$], 99 (100) [B(NMe$_2$)$_2^+$]. − HR-MS: *m*/*z* (%): 353.2907 (22) [M$^+$, calc. for $^{12}C_{19}$ $^1H_{33}$ $^{11}B_2$ $^{14}N_5$: 353.2922].

2,5-Bis(1,3,2-benzodioxaborol-2-yl)-1-methylpyrrole (2e): A solution of 1.13 g (2.8 mmol) of **1c** in 10 mL of toluene was cooled to −75°C and the solution of 878 mg (5.7 mmol) of ClBcat in 10 mL of toluene was added. The mixture was allowed to warm to room temp. and stirred for 15 h. After 1 h of refluxing the resulting solid was separated by filtration, washed with hexane and CH_2Cl_2, and dried. Yield: 661 mg (75%) colorless **2e**. − ^{1}H NMR ([D$_8$]thf, 200.1 MHz): δ = 4.38 (s, 3 H, CH_3), 7.09 (s, 2 H, pyrrole-CH), 7.11, 7.31 (each m, 4 H, benzo-CH). − ^{11}B NMR ([D$_8$]thf, 64.2 MHz): δ = 30. − ^{13}C NMR ([D$_8$]thf, 50.3 MHz): δ = 37.3 (*C*H$_3$), 113.3, 123.9 (each benzo-*C*H), 124.2 (pyrrole-*C*H), 149.6 (*C*O), *C*B signal not observed. − MS: *m*/*z* (%): 317 (28) [M$^+$], 58 (100).

Diisopropylaminodi(1-methyl-2-pyrrolyl)borane (3e): To a solution of 2.6 mL (29.2 mmol) of 1-methylpyrrole in 20 mL of thf 12.5 mL (31.2 mmol) of *n*-butyllithium (2.5 M in hexane) was added at −35°C. After the mixture was allowed to warm for 1 h, and stirred at room temp. for 3 h. At −70°C a solution of 2.60 g (14.3 mmol) of Cl_2BNiPr_2 in 10 mL of thf was added. The mixture was allowed to warm to room temp. and stirred for 16 h. Volatile compounds were removed in vacuum, the residue was dissolved in hexane and filtered. The solvent was evaporated in vacuum and the colorless

Table 1. Crystal data and structure refinement for **2a**, **2b**, **2d**, and **3e**

	2a	**2b**	**2d**	**3e**
Formula	$C_{13}H_{29}B_2N_5$	$C_{29}H_{61}B_2N_5$	$C_{19}H_{33}B_2N_5$	$C_{16}H_{26}BN_3$
Molecular weight	277.03	501.46	353.13	271.22
Crystal system	orthorhombic	monoclinic	orthorhombic	triclinic
Space group	*P*bca	*C*2/c	*P*bnm	$P\bar{1}$
Unit cell				
a [Å]	12.500(9)	22.925(4)	9.492(5)	7.697(4)
b [Å]	16.070(11)	12.651(2)	13.721(8)	9.678(5)
c [Å]	16.796(15)	12.773(2)	16.263(9)	12.324(6)
α [°]	90	90	90	72.93(3)
β [°]	90	111.03(1)	90	74.62(3)
γ [°]	90	90	90	81.94(3)
Volume [Å^3]	3374(4)	3457.7(11)	2118(2)	844.2(7)
Z	8	4	4	2
Calc. density [g/cm^3]	1.09	0.96	1.11	1.07
Adsorption coeff. [mm^{-1}]	0.07	0.06	0.07	0.06
F(000)	1216	1120	768	296
Crystal size [mm]	0.5×0.5×0.7	0.5×0.55×0.8	0.25×0.5×0.7	0.3×0.4×0.4
Θ_{max} [°]	25	25	30	25
Index ranges	0/+14, 0/+19, 0/+19	0/+29, 0/+16, −16/+15	0/+13, 0/+19, 0/+22	−8/+7, −10/+11, 0/+14
Number of reflections				
unique	2970	3008	3187	2798
observed [$I > 2\sigma(I)$]	2195	1884	1929	2138
Transmission	0.891−0.999	0.736−0.786	0.886−0.999	0.930−0.996
Parameters	201	181	202	285
Final *R* indices				
*R*1 [$I > 2\sigma(I)$]	0.044	0.072	0.053	0.043
*wR*2	0.115	0.207	0.157	0.113
Max. diff. peak / hole [e/Å^3]	+0.15 / −0.20	+0.17 / −0.19	+0.34 / −0.27	+0.15 / −0.23

solid recrystallized from hexane at −30°C. A single crystal was grown from a solution of hexane and CH_2Cl_2 (6:1) at room temp.. Yield: 1.50 g (38%) colorless **3e**, m.p. > 210°C. − ^{1}H NMR (C_6D_6, 200.1 MHz): δ = 1.17 [d, 12 H, $^3J_{H,H}$ = 6.7 Hz, CH(CH_3)$_2$], 2.82 (s, 6 H, NCH_3), 4.07 [sept, 2 H, $^3J_{H,H}$ = 6.7 Hz, CH(CH$_3$)$_2$], 6.31 [dd, 2 H, $^3J_{H,H}$ = 2.4 Hz, $^3J_{H,H}$ = 3.5 Hz, ring-CH(C4)], 6.48 (m, 2 H, ring-CH), 6.56 (dd, 2 H, $^3J_{H,H}$ = 3.5 Hz, $^4J_{H,H}$ = 1.5 Hz, ring-CH). − ^{11}B NMR (C_6D_6, 64.2 MHz): δ = 35.6. − ^{13}C NMR (C_6D_6, 50.3 MHz): δ = 24.8 [CH(*C*H$_3$)$_2$], 35.3 (N*C*H$_3$), 49.0 [*C*H(CH$_3$)$_2$], 107.7 [ring-*C*H(C4)], 116.7, 125.4 (each ring-*C*H), 138 (br, *C*B). − MS: *m*/*z* (%): 271 (65) [M$^+$], 147 (100). − HR-MS: *m*/*z* (%): 271.2226 (38) [M$^+$, calc. for $^{12}C_{16}$ $^1H_{26}$ ^{11}B $^{14}N_3$: 271.2220].

Di(1-benzyl-2-pyrrolyl)diisopropylaminoborane (3f): To a solution of 1.8 mL (12.0 mmol) of tmeda in 40 mL of hexane 4.8 mL (12.0 mmol) of *n*-butyllithium (2.5 M in hexane) was added with cooling and stirred for 30 min at room temp.. After the addition of 1.55 g (9.9 mmol) of 1-benzylpyrrole the mixture was refluxed for 2 h. To the brown suspension a solution of 1.04 g (5.7 mmol) of Cl_2BNiPr_2 in 25 mL of hexane was added within 45 min at −30°C. After the mixture was allowed to warm to room temp. and stirred for 18 h, it was refluxed for 30 min. Volatile compounds were removed in vacuum, the residue was dissolved in toluene and filtered. The solvent was evaporated in vacuum and the colorless solid recrystallized from pentane at −80°C. Yield: 662 mg (31%) colorless **3f**. − ^{1}H NMR ($CDCl_3$, 200.1 MHz): δ = 1.11 [d, 12 H, $^3J_{H,H}$ = 6.8 Hz, CH(CH_3)$_2$], 4.04 [sept, 2 H, $^3J_{H,H}$ = 6.8 Hz, CH(CH$_3$)$_2$], 4.57 (s, 4 H, CH_2), 6.28 [dd, 2 H, $^3J_{H,H}$ = 2.4 Hz and 3.4 Hz, pyrrole-CH(C4)], 6.47 (dd, 2 H, $J_{H,H}$ = 3.4 Hz, $^4J_{H,H}$ = 1.5 Hz, pyrrole-CH), 6.85 (dd, 2 H, $^3J_{H,H}$ = 2.4 Hz, $^4J_{H,H}$ = 1.5 Hz, pyrrole-CH), 7.08 (m, 4 H, phenyl-CH), 7.26 (m, 6 H, phenyl-CH). − ^{11}B NMR ($CDCl_3$, 64.2 MHz): δ = 36.4. − ^{13}C NMR ($CDCl_3$, 50.3 MHz): δ = 24.6 [CH(*C*H$_3$)$_2$], 48.9 [*C*H(CH$_3$)$_2$], 51.7 (*C*H$_2$), 107.4 [pyrrole-*C*H(C4)], 116.7, 124.5 (each pyrrole-*C*H), 126.9, 127.3, 128.1 (each phenyl-*C*H), 137 (br, *C*B), 139.5 (phenyl-C_{ipso}). − MS: *m*/*z* (%): 423 (100) [M$^+$], 408 (18) [M$^+$ − Me], 91 (88) [CH$_2$ − Ph$^+$].

X-ray Structure Determinations of 2a, 2b, 2d, and 3e: Crystal data and details of the stucture determinations are listed in Table 1. Unique sets of intensity data for **2a**, **2d**, and **3e** were collected at −70°C with a Siemens Stoe AED2 diffractometer and for **2b** at room temp. with a Syntex R3 diffractometer (Mo-K_α radiation, λ = 0.7107 Å, graphite monochromator, ω-scan). Empirical absorption corrections (ψ-scans) were applied. The structures were solved by direct methods (SHELXS-86)[17a] and refined by least-squares methods based on F^2 with all measured reflections (SHELXL-93)[17b]. All non-hydrogen atoms are refined anisotropically. For **2a** and **2b** hydrogen atoms were inserted in calculated positions, for **2d** and **3e** they were located in difference Fourier maps and refined isotropically.

Crystallographic data (excluding structure factors) for the structures reported in this paper have been deposited with the Cambridge Crystallographic Data Center as supplementary publications no. CCDC-102879 (**2a**), CCDC-102880 (**2b**), CCDC-102881 (**2d**), and and CCDC-102882 (**3e**). Copies of the data can be obtained free of charge on application to CCDC, 12 Union Road, Cambridge CB2 1EZ, UK; Fax: int. code +44 (0)1223/ 336-001; E-mail: deposit@ccdc.cam.ac.uk

Acknowledgments

Support of this work by the Deutsche Forschungsgemeinschaft (SFB 247), the Fonds der Chemischen Industrie and the BASF AG is gratefully acknowledged. J. F. thanks the Graduiertenkolleg "Selektivität in der Organischen und Metallorganischen Synthese und Katalyse" for support.

[1] R. B. Woodward, *Angew. Chem.* **1960**, *72*, 651−662.
[2] K. M. Smith in *Comprehensive Heterocyclic Chemistry Vol. 4* (Ed.: A. R. Katritzky, C. W. Rees), Pergamon Press Oxford **1984**, 378−419.
[3] M. Pohl, H. Schmickler, J. Lex, E. Vogel, *Angew. Chem.* **1991**, *103*, 1737−1741; *Angew. Chem. Int. Ed. Engl.* **1991**, *30*, 1693−1697.
[4] E. Vogel, W. Haas, B. Knipp, J. Lex, H. Schmickler, *Angew. Chem.* **1988**, *100*, 445−448; *Angew. Chem. Int. Ed. Engl.* **1988**, *27*, 406-409.
[5] E. Vogel, P. Röhrig, M. Sicken, B. Knipp, A. Herrmann, M. Pohl, H. Schmickler, J. Lex, *Angew. Chem.* **1989**, *101*, 1683−1687; *Angew. Chem. Int. Ed. Engl.* **1989**, *28*, 1651−1655.
[6] F. H. Carré, R. J.-P. Corriu, T. Deforth, W. E. Douglas, W. Siebert, W. Weinmann, *Angew. Chem.* **1998**, *110,* 654−656; *Angew. Chem. Int. Ed.* **1998**, 37, 652−654.
[7] [7a] B. König, M. Rödel, P. Bubenitschek, P. G. Jones, *Angew. Chem.* **1995**, *107*, 752−754; *Angew. Chem. Int. Ed. Engl.* **1995**, *34*, 661−663. − [7b] B. König, M. Rödel, P. Bubenitschek, P. G. Jones, I. Thondorf, *J. Org. Chem.* **1995**, *60*, 7406−7410.
[8] [8a] W. Chen, M. P. Cava, *Tetrahedron Lett.* **1987**, *28*, 6025−6026. − [8b] T. J. Barton, G. P. Hussmann, *J. Org. Chem.* **1985**, *50*, 5881−5882. − [8c] M. Gharpure, A. Stoller, F. Bellamy, G. Firnau, V. Snieckus, *Synthesis* **1991**, 1079−1082.
[9] S. Martina, V. Enkelmann, G. Wegner, A.-D. Schlüter, *Synthesis* **1991**, 613−615.
[10] [10a] B. Wrackmeyer, H. Nöth, *Chem. Ber.* **1976**, *109*, 1075−1088. − [10b] J. D. Odom, T. F. Moore, R. Goetze, H. Nöth, B. Wrackmeyer, *J. Organomet. Chem.* **1979**, *173*, 15−32.
[11] The fact that signals for boron-bound carbon atoms in standard proton-decoupled ^{13}C-NMR spectra measured at room temperature normally are broadened or even cannot be observed is based on relaxation effects of the boron nucleii. For details see: H. Nöth, B. Wrackmeyer, *NMR Spectroscopy of Boron Compounds*, Springer Verlag Heidelberg **1978**, 6−104.
[12] R. A. Jones in *The Chemistry of Heterocyclic Compounds Vol. 48*, Wiley & Sons New York **1990**, 22−42.
[13] W. Siebert, *Chem. Ber.* **1970**, *103*, 2308−2313.
[14] [14a] A. Maderna, H. Pritzkow, W. Siebert, *Angew. Chem.* **1996**, *108*, 1664−1666; *Angew. Chem. Int. Ed. Engl.* **1996**, *35*, 1501−1503. − [14b] C. Ester, A. Maderna, H. Pritzkow, W. Siebert, *Eur. J. Inorg. Chem.* to be published. − For reactions with Grignard reagents see: S. Cabiddu, A. Maccioni, M. Secci, *Gazz. Chim. Ital.* **1972**, *102*, 555−556.
[15] A. Meller in *Gmelin Handbook B 4th Suppl. Vol. 3a*, Springer-Verlag Heidelberg **1991**, 152−261 and references cited therein.
[16] [16a] C. F. Hobbs, C. K. McMillin, E. P. Papapdopoulos, C. A. VanderWerf, *J. Am. Chem. Soc.* **1962**, *84*, 43−51. − [16b] R. J. Brotherton, A. L. McCloskey, L. L. Petterson, H. Steinberg, *J. Am. Chem. Soc.* **1960**, *82*, 6242−6245. − [16c] D. W. Aubrey, M. F. Lappert, M. K. Majumdar, *J. Chem. Soc.* **1962**, 4088−4094. − [16d] W. Gerrard, H. R. Hudson, E. F. Mooney, *J. Chem. Soc.* **1960**, 5168−5172. − [16e] W. Gerrard, M. F. Lappert, B. A. Mountfield, *J. Chem. Soc.* **1959**, 1529−1535. − [16f] S. Sorriso, A. Ricci, R. Danieli, *J. Organomet. Chem.* **1975**, *87*, 61−65.
[17] [17a] G. M. Sheldrick, *SHELXS-86*, Universität Göttingen **1986**. − [17b] G. M. Sheldrick, *SHELXL-93*, Universität Göttingen **1993**.

Received September 21, 1998
[I98323]

Preparation of Enantiomerically Pure Chelate Ligands L_2 = $XCH_2CH(OH)CH_2Y$ from Epichlorohydrin – Conformation of Their $L_2Rh(COD)^+$ Derivatives and Enantioselective Hydrogenation by $L_2Rh(COD)^+$

Jörg Karas,[a] Gottfried Huttner,*[a] Katja Heinze,[a] Peter Rutsch,[a] and Laszlo Zsolnai[a]

In memoriam of Laszlo Zsolnai

Keywords: Epichlorohydrin / Chiral diphos ligands / Diphos rhodium complexes / Conformation analysis / Chelates / Asymmetric synthesis

Enantiomerically pure chelate ligands L_2 = $XCH_2CH(OH)CH_2Y$ (**1**) are obtained from epichlorohydrin in a two-step synthesis. X and Y may be different types of R_2P donor groups, NR_2 or SR donors. The OH function of **1** may be transformed into an ether function under specialized conditions. Ligands **1** react with $[Rh(COD)Cl]_2$ in the presence of KPF_6 to give the coordination compounds **2**, $[L_2Rh(COD)]^+PF_6^-$, as orange, microcrystalline salts. The structures adopted by compounds **2** in the solid state have been analysed by X-ray crystallography in selected cases, and it has been found that the six-membered chelate cycles adopt twist as well as chair conformations depending on the nature of X and Y. In solution, compounds **2** generally show dynamic behaviour, which is in part due to the conformational flexibility of the six-membered cycles. In cases where one of the PR_2 donor groups contains *ortho*-substituted phenyl substituents, rotational isomerism of these groups is an additional dynamic process. For some of these compounds, the nature of the dynamic behaviour has been analysed by variable-temperature NMR experiments. Compounds **2** are found to be precatalysts in the hydrogenation of (*Z*)-2-acetamidocinnamic acid. The rate of conversion is strongly influenced by the steric bulk of the substituents, with smaller substituents leading to higher rates. Enantiomeric discrimination is high only for those ligands that contain *ortho*-substituted aryl groups at their PR_2 donors. The maximum enantiomeric excess observed was 85% for X = PPh_2, Y = $P(2\text{-MeOPh})_2$.

Introduction

Enantioselective hydrogenation mediated by chiral bis(phosphane)rhodium templates is a well-established process.[1,2] Even though the major steps of the relevant catalytic cycles are well known,[3] there is still no means of predicting which properties of the ligands will induce a high enantioselectivity. It has been found that chelate diphosphane ligands are generally a good choice.[4,5] From the data available to date, it appears that five-membered and seven-membered cycles are superior to six-membered chelate rings in this respect.[2] In almost all of the relevant chelate ligands, chirality is embedded in the backbone, and this again appears to be a good principle, in particular because building blocks for the chiral backbones are often readily available from the chiral pool.[5] Despite the existence of a large amount of relevant literature,[6] there is no straightforward way of predicting the efficiency of a specific ligand.

As far as six-membered chelate cycles are concerned, their generally low efficiency has been attributed to the particular conformational flexibility of these cycles, which allows both chair and twist conformations, although only the twist conformations induce strong enantiomeric discrimination.[7] In solid-state structures, both conformations have been observed, even with the same chelate ligand. Thus, (2*S*,4*S*)-2,4-bis(diphenylphosphanyl)pentane $Ph_2PCH(CH_3)CH_2CH(CH_3)PPh_2$ (skewphos) forms a chelate chair with norbornadiene (NBD) as a coligand in the catalyst precursor skewphosRh(NBD)$^+$, while it is found in the twist conformation with cyclooctadiene (COD) as a coligand in skewphosRh(COD)$^+$.[8,9] Even though the chair conformation is thus available to this specific chelate cycle, it holds the record for enantioselectivity (*ee* > 90%) achieved in hydrogenation experiments.[8,9] From an analysis of the conformational properties of chirally substituted 1,3-diaminopropanes, it has been argued that with these amino ligands, which have a substitution pattern equivalent to that of skewphos, the twist conformation should be preferred on energetic grounds.[10] For chiral 1,3-diphosphanylpropane chelate cycles, the experimental material available so far[6,9] is not sufficient to deduce any general trends in this respect, nor are reliable force-field calculations available for isolated cycles.[11] In an attempt to create a structural database of chirally substituted 1,3-bis(phosphanyl)propane chelate cycles, with the ultimate aim of deriving a reliable force-field description by global optimization[12] of the relevant force-field parameters, a series of chiral 1,3-bis(phosphanyl)propanes (L_2) has been synthesized. Their rhodium complexes $[L_2Rh(COD)]PF_6$ (**2**) have been prepared and, where possible, structurally characterized as

[a] Anorganisch-Chemisches Institut der Universität Heidelberg, Im Neuenheimer Feld 270, D-69120 Heidelberg, Germany
Fax: (internat.) + 49(0)6221/545707

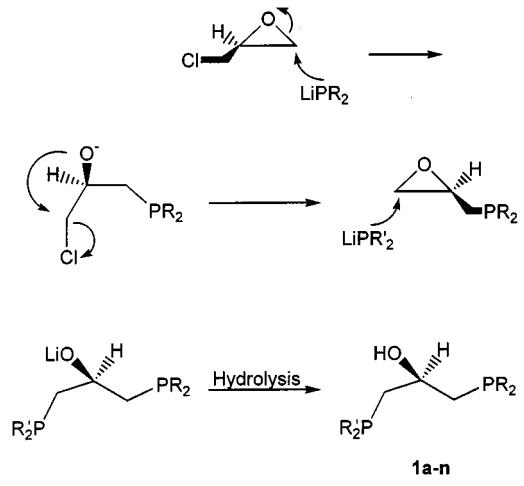
 © WILEY-VCH Verlag GmbH, D-69451 Weinheim, 1999 1434–1948/99/0303–0405 $ 17.50+.50/0

well. The catalytic activities of these complexes and the associated enantioselectivities have been probed and it has been found that [(**1g**)Rh(COD)]PF_6 [**1g** = $Ph_2PCH_2CH(OH)CH_2P(2\text{-}MeOPh)_2$] permits up to 85% *ee* in the rhodium-mediated hydrogenation of (*Z*)-2-acetamidocinnamic acid (AAC).

Results and Discussion

Ligands

It has been reported that epichlorohydrin $H_2C(O)CHCH_2Cl$ (**A**) permits a simple and fully stereoselective synthesis of chiral tripod ligands $X_2POCH(CH_2PR_2)(CH_2PR'_2)$.[13] The corresponding tripod rhodium compounds, on the other hand, have been shown to be rather sluggish catalysts offering only slight enantiomeric discrimination.[14] Their reduced reactivity and low enantioselectivity has been explained on the basis of the hypothesis that in order to form active catalyst precursors, η^2-diphos species first have to be generated from the η^3-coordinated compounds by dissociation of one of the "legs" of the tripod ligands.[14,15] This hypothesis is well supported by a series of observations made for catalytic systems involving tripod metal entities.[14–17] In the light of this hypothesis, a logical course of action is to probe diphos ligands $HOCH(CH_2PR_2)(CH_2PR'_2)$, which differ from the above tripod ligands simply by the absence of the third oxygen-supported "leg". Such ligands are easily accessible by the same sequence of reactions as that used for the synthesis of the above tripod ligands.



Scheme 1. Reaction scheme

The reaction scheme shown for the consecutive addition of two phosphorus-centred nucleophiles (**1a–1l**) may be adapted to allow the incorporation of sulfur- or nitrogen-centred nucleophiles as well (**1m**, **1n**). Compounds **1** were purified by column chromatography and were obtained as colourless oils of modest to low viscosity. In no case could a crystalline product be obtained. In most cases it proved difficult to completely remove the solvent and successive cycles of freezing and drying had to be applied to overcome this problem. The microanalytical data were in agreement with the assigned constitutions with only a few exceptions (Tables 8 and 11). In these cases, high-resolution mass spectrometry was used as an analytical tool (Tables 8 and 11).

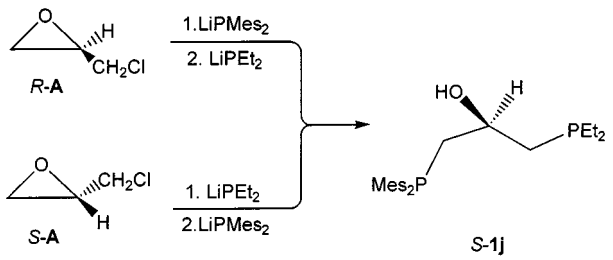
Table 1. Ligands **1a–1n**

	R	R′[a]
1a: (*S*)-	Ph	3,5-Me_2Ph
1b: (*R*)-	*o*-Tol	Ph
1c: (*S*)-	*o*-Tol	DBP
1d: (*S*)-	Ph	Mes
1e: (*S*)-	Mes	DBP
1f: (*R*)-	2-MeOPh	Mes
1g: (*S*)-	Ph	2-MeOPh
1h: (*S*)-	Ph	2-EtPh
1i: (*S*)-	Ph	2-Me_2NPh
1j: (*S*)-	Et	Mes
1k: (*S*)-	Et	*o*-Tol
1l: (*S*)-	Et	2-MeOPh
1m: (*S*)-	Ph	SPh
1n: (±)-	Ph	NPh_2

[a] R′ in PR'_2 for **1a–1l**, donor group for **1m**, **1n**.

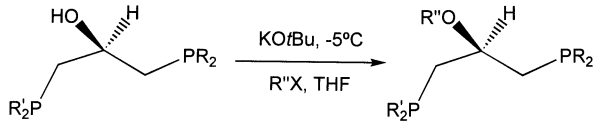
The ^{31}P-, ^{13}C-, and ^{1}H-NMR spectra provided further unequivocal evidence for the identity of the compounds (Tables 9, 10, 12, and 13). The assignment of the individual signals was in part based on the observation that chemically different PR_2 groups give rise to ^{31}P resonances in distinct and different ranges [dibenzophospholyl (DBP): δ = −20 to −23; PPh_2: δ = −21 to −25; PEt_2: δ = −26 to −30; $PMes_2$: δ = −30 to −33; $P(C_6H_4OMe)_2$: δ = −41 to −45; $P(o\text{-}Tol)_2$: δ = −44 to −47 (Tables 10 and 13)]. Comparing the whole set of spectra of compounds **1**, assignments based on these shift ranges were thus possible, whereas owing to the narrow range of shifts of specific organic groups, individual assignments of all the ^{13}C and ^{1}H resonances were not possible in all cases. The shifts and patterns observed leave no doubt as to the identity of **1** (Tables 9, 10, 12, and 13). The chirality of **1** gives rise to a range of specific rotations of $|[\alpha]_D^{20}| = 1–79$ (Tables 8 and 11).

With the donor groups $PMes_2/PEt_2$ (**1j**) and $P(o\text{-}Tol)_2/PEt_2$ (**1k**), the synthesis was performed by two alternative routes, as shown for **1j** in Scheme 2.



Scheme 2. Alternative syntheses of (*S*)-**1j**

Either (*R*)-**A** was used as the starting compound and the phosphane donors were introduced in the sequence: 1. $PMes_2$, 2. PEt_2, to obtain **1j** [or: 1. $P(o\text{-}Tol)_2$, 2. PEt_2, to produce **1k**], or alternatively (*S*)-**A** was used with the inverse



Scheme 3. Synthesis of ether derivatives **1**

sequence of addition. Both reactions lead to the same compound with the same chirality provided they are, as documented,[13,18] fully stereoselective. In line with expectation, the optical rotations of the two pairs of samples prepared by these two routes were in fact equal (**1j**: $[\alpha]_D^{20} = +46.2$, **1k**: $[\alpha]_D^{20} = +15.7$, Table 8).

All of the ligands **1a−1n** contain a hydroxy function. Etherification of this type of function in the presence of phosphane groups may be problematic.[19] For tripod ligands $HOCH_2C(CH_2PPh_2)_3$, a strategy that circumvents the problems caused by the nucleophilicity of the phosphorus functions in the course of a Williamson-type etherification has been developed.[20] The same type of reaction protocol works equally well with the diphos ligands **1**. The compound $Ph_2PCH_2CH(OH)CH_2PPh_2$, prepared by literature methods,[13] reacts with methyl iodide after depro-

Table 2. Ligands **1o−1u**

	R	R′	R′′	X
1o:	Ph	Ph	CH_3	I
1p: (*R*)-	*o*-Tol	Ph	CH_3	I
1q: (*R*)-	*o*-Tol	Ph	$SiMe_3$	Cl
1r: (*R,S*)-	*o*-Tol	Ph	(*S*)-$H_3CCH_2CH(CH_3)CH_2$	OTs
1s: (*S*)-	Ph	2-MeOPh	$SiMe_3$	Cl
1t: (*S,S*)-	Ph	2-MeOPh	(*S*)-$H_3CCH_2CH(CH_3)CH_2$	OTs
1u: (*S*)-	Ph	Mes	$H_2CCH[CH_2]_9$	OTs

Table 3. Synthesis and analytical data of complexes **2**

	R	R′[a]	R′′	yield (%)	MS (FAB) [M^+], [M^+ − COD]	$[\alpha_D^{20}]$	$C_{calcd.}H_{calcd.}P_{calcd.}$ $C_{found}H_{found}P_{found}$	M.p.[f] [°C]
2a: (*S*)-	Ph	3,5-Me_2Ph	H	92	695, 586	8.1 ± 1.5	54.29, 5.91, 11.35 54.57, 5.52, 10.38	167
2b: (*R*)-	*o*-Tol	Ph	H	83	667, 559	−19.0 ± 0.1	54.69, 5.21, 11.44 53.66, 5.69, 10.45	173
2c: (*S*)-	*o*-Tol	DBP	H	86	664, 557	−22.4 ± 1.1	54.83, 4.97, 11.46 55.13, 5.32, 11.10	175 (dec.)
2d: (*S*)-	Ph	Mes	H	93	723, 615	−61.8 ± 0.1	56.69, 5.80, 10.70 55.72, 6.08, 10.16	200
2e: (*S*)-	Mes	DBP	H	95	721, 613	39.2 ± 0.9	52.99, 5.30, 9.76[b] 53.01, 5.30, n.d.	208 (dec.)
2f: (*R*)-	2-MeOPh	Mes	H	74	783, 675	29.2 ± 0.5	52.14, 5.57, 9.17[b] 51.76, 5.63, 8.73	226
2g: (*S*)-	Ph	2-MeOPh	H	84	699, 591	10.7 ± 0.1	52.62, 5.01, 11.00 51.84, 5.10, n.d.	207
2h: (*S*)-	Ph	2-EtPh	H	91	695, 584	12.4 ± 0.1	55.72, 5.52, 11.05 56.47, 6.07, n.d.	140
2i: (*S*)-	Ph	2-Me_2NPh	H	See Experimental Section				
2j: (*S*)-	Et	Mes	H	97	627, 519	8.0 ± 0.1	51.30, 6.52, 12.03 50.83, 6.57, 11.99	136
2k: (*S*)-	Et	*o*Tol	H	88	571, 463	−74.5 ± 2.8	48.62, 5.91, 12.97 48.41, 5.97, 13.05	201
2l: (*S*)-	Et	2-MeOPh	H	81	603, 495	−47.4 ± 2.9	46.54, 5.66, 12.41 46.60, 5.71, n.d.	164 (dec.)
2m: (*S*)-	Ph	SPh	H	77	563, 455	79.1 ± 0.2	49.16, 4.69, 8.74 48.30, 4.71, 7.78	180
2n: (±)-	Ph	NPh_2	H	See Experimental Section				
2o:	Ph	Ph	CH_3	86	653, 545	−	52.13, 4.91, 11.05[c] 51.83, 5.08, n.d.	206 (dec.)
2p: (*R*)-	*o*-Tol	Ph	CH_3	81	681, 572	10.4 ± 1.4	55.22, 5.37, 11.24 53.41, 5.33, n.d.	174
2q: (*R*)-	*o*-Tol	Ph	$SiMe_3$	83	739, 631	18.6 ± 1.6	54.30, 5.71, 10.50 52.16, 5.79, n.d.	173
2r: (*R,S*)-	*o*-Tol	Ph	X[d]	89	737, 629	−5.8 ± 0.1	57.15, 5.94, 10.53 56.69, 5.87, n.d.	210 (dec.)
2s: (*S*)-	Ph	2-MeOPh	$SiMe_3$	79	771, 663	−7.9 ± 1.1	52.41, 5.50, 11.00 52.12, 5.51, n.d.	208 (dec.)
2t: (*S,S*)-	Ph	2-MeOPh	X[d]	87	769, 661	11.6 ± 0.5	55.15, 5.73, 10.16 54.87, 5.70, n.d.	134
2u: (*S*)-	Ph	Mes	Y[e]	46	875, 763	−39.2 ± 1.5	61.18, 6.91, 9.10 58.52, 7.19, n.d	180 (dec.)
2v:	Ph	Ph	H	89	639, 531	−	53.56, 4.88, 11.85 53.16, 5.14, 11.63	193
2w: (*R*)-	*p*-Tol	Ph	H	74	667, 559	−5.4 ± 0.9	54.69, 5.21, 11.44 53.92, 5.48, 10.67	188

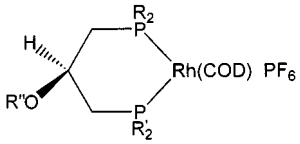
[a] R′ in PR'_2 for **2a−2l** and **2o−2w**, donor group for **2m**, **2n**. − [b] = M · CH_2Cl_2. − [c] = M · 0.5 CH_2Cl_2. − [d] X = (*S*)-$H_3CCH_2CH(CH_3)CH_2$. − [e] Y = $H_2CCH[CH_2]_9$. − [f] dec. = decomposition.

tonation with KO*t*Bu at temperatures below 20°C to produce **1o**. In the same way, **1b** is transformed into **1p**. Stringent temperature control is necessary to avoid alkylation at the phosphorus atom.[20] With **1g** as the starting material, however, exclusive methylation at the oxygen position with methyl iodide proved impossible, even under these controlled conditions. The increased nucleophilicity of the $(2\text{-MeOPh})_2P$ function leads to partial quaternization of this phosphorus centre during the course of the reaction. On the other hand, etherification by the tosylate H_3CCH_2-$CH(CH_3)CH_2OTs$ could be achieved both for **1b** (→ **1r**) and for **1g** (→ **1t**). Silylation (**1b** → **1q**, **1g** → **1s**) did not present any problems of this kind.

With longer-chain tosylates, problems tend to arise in the separation of the ligands from the long-chain alcohols. Thus, when **1d** was treated with $H_2C{=}CH(CH_2)_9OTs$, the corresponding ether derivative (**1u**) was obtained, which could, however, not be obtained in an analytically pure state as such (Table 11), but was unequivocally characterized by the data obtained for its coordinated derivative **2u** (Table 3).

Coordination Compounds

Ligands **1** react with $[Rh(COD)Cl]_2$ under standard conditions to give the coordination compounds **2** [(**1a**–**u**)Rh-(COD)]PF_6.



Scheme 4. Constitution of compounds **2**

The labelling scheme used is such that coordination compound **2**"label" contains ligand **1**"label". Coordination compounds **2v** (R = R′ = Ph) and **2w** (R = *p*-Tol, R′ = Ph) were obtained from the appropriate ligands, the preparation of which has been described previously.[13] Compounds **2** were obtained as orange, microcrystalline solids.

The identities of compounds **2** were evident from their analytical data (Table 3), as well as from several X-ray analyses (see below). Elemental analyses, as well as the mass numbers as determined by FAB mass spectrometry, were in agreement with the constitutions as given. The optical rotations of the chiral compounds (all compounds except **2o**, **2v**) were found to be in the absolute range $|[\alpha]_D^{20}| = 5.4-79$ (Table 3).

The ^{1}H-NMR spectra are cumbersome to interpret. In most cases, broad signals are found at room temperature and the spectra are strongly temperature-dependent, indicating a dynamic behaviour of the chelate cycles. This is clearly borne out by analysis of the ^{31}P-NMR spectra (see

Table 4. $^{31}P\{^1H\}$-NMR data of complexes **2**[a]

	R	R′[b]	*T* [K]	PR_2 δ ($^1J_{PRh}$, $^2J_{PP}$)		PR'_2 δ ($^1J_{PRh}$, $^2J_{PP}$)
2a: (*S*)-	Ph	3,5-Me_2Ph	298	15.6 (141, 44)		16.8 (143, 44)
2b: (*R*)-	*o*-Tol	Ph	388[c]	15.9 (145, 43)		19.3 (141, 43)
2c: (*S*)-	*o*-Tol	DBP	403[c]	14.3 (142, 46)		18.3 (br) (140, 46)
2d: (*S*)-	Ph	Mes	340[c]	8.0 (br) (148, 36)		−2.4 (133, 37)
			298	I) 7.0 (148, 36)		I) −2.2 (133, 37)
				II) 11.2 (150, 36)		II) −4.5 (132, 36)[d]
					I:II = 4.5:1	
2e: (*S*)-	Mes	DBP	298[e]	I) −0.7 (135, 37)		I) 7.0 (144, 37)
				II) 0.2		II) 11.8 (146, 39)[d]
					I:II = 7:1	
2f: (*R*)-	2-MeOPh	Mes	298[e]	I) 12.3 (151, 34)		I) −6.7 (34, 133)
				II) 8.5 (149, 34)		II) −3.5 (35, 134)[d]
					I:II = 1:3	
2g: (*S*)-	Ph	2-MeOPh	378[c]	12.6 (142, 46)		16.5 (145, 46)
2h: (*S*)-	Ph	2-EtPh	388[c]	18.5 (br)		16.1 (145, 43)
2j: (*S*)-	Et	Mes	298	I) 2.9 (35, 141)		I) −3.0 (37, 136)
				II) 7.6 (36, 140)		II) −2.0 (37, 135)[d]
					I:II = 7:1	
2k: (*S*)-	Et	*o*-Tol	298	22.7 (br)		8.0 (br)
2l: (*S*)-	Et	2-MeOPh	298[e]	19.4 (br)		8.7 (br)
2m: (*S*)-	Ph	SPh	298	18.1 (143)		
2o:	Ph	Ph	298	15.1 (145.8)		
2p: (*R*)-	*o*-Tol	Ph	298	10.0−20.0 (br)		
2q: (*R*)-	*o*-Tol	Ph	298	5.0−10.0 (br)		
2r: (*R,S*)-	*o*-Tol	Ph	298	11.0−19.3 (br)		
2s: (*S*)-	2-MeOPh	Ph	368[c]	17.2 (46, 145)		13.3 (46, 142)
2t: (*S,S*)-	2-MeOPh	Ph	298	9.0−17.9 (br)		
2u: (*S*)-	Ph	Mes	298	I) 7.6 (147, 37)		I) −3.3 (134, 37)
				II) 11.1 (150, 37)		II) −2.9[d]
					I:II = 8:1	
2v:	Ph	Ph	298	15.8 (144)		
2w: (*R*)-	*p*-Tol	Ph	298	14.5 (45, 141)		18.8 (45, 144)

[a] br = broad; for complexes **2i**, **2n** see Experimental Section. – [b] R′ in PR'_2 for **2a**–**2l** and **2o**–**2w**, donor group for **2m**. – [c] High temperature limit. – [d] I, II: two conformational isomers at the temperature of observation. – [e] Decomposition upon heating.

below). Individual assignment of groups of signals is nevertheless possible in the ^1H- (Table 14) as well as in the ^{13}C-NMR spectra (Table 15). Full interpretation of the spectra would, however, require an intricate analysis of the dynamic behaviour. The spectra of **2a**, **2m**, **2o**, **2v**, **2w** are comparatively sharp at room temperature and indicate the presence of one single species, at least over the time average. Sharp signals are also observed for compounds **2d−f**, **2j**, and **2u**, which contain $PMes_2$ groups. For these species, however, the presence of two different conformers (see below) leads to an overlap of signals, which hampers the unambiguous assignment of their ^1H and ^{13}C data.

The most clear-cut information is provided by the ^{31}P-NMR spectra. They are in agreement with the given constitutions in that they show the appropriate signals for each of the differently substituted PR_2 entities within the chelate cycle (Table 4). The signal pattern characteristic for each of the phosphorus nuclei consists of a doublet of doublets with $^1J_{PRh} \approx 140$ Hz, $^2J_{PP} \approx 40$ Hz (Table 4). There are only two compounds where the PR_2 groups are equal (**2o**, **2v**), and only one kind of phosphorus signal (doublet, $^1J_{PRh} \approx 145$ Hz) is observed in these cases at 293 K (Table 4).

The dynamic behaviour of the compounds is in some cases already apparent at or above room temperature, and is a rather general phenomenon. In the cases of **2d−f**, **2j**, and **2u**, which contain $PMes_2$ groups, the behaviour is static already at room temperature, where two different conformers give rise to two sets of signals. Two conformers are sometimes observed for compounds **2** in the solid state as well (see below).

The kind of dynamic behaviour is not always directly evident from the spectra, since there are a number of conceivable dynamic processes. In some cases, hindered rotation of *ortho*-substituted aryl groups as well as conformational changes of the chelate cycles seem to be simultaneously operative in the same system. Not all of the dynamic processes have yet been delineated, hence the types of process will be described here only for especially clear-cut cases.

With **2b**, the only dynamic process observed on the timescale of the experiment is the hindered rotation of the *ortho*-tolyl groups of the P(*o*-Tol)$_2$ moiety. At 273 K, broad multiplets are observed (Figure 1). Upon heating, one clear doublet of doublets structure is observed (Figure 1), which indicates that one of the phosphorus nuclei is not influenced by a change of the environment. The signal of the other phosphorus atom, however, is completely broadened into the baseline at 313 K; its signal starts to reappear at 328 K and a clear doublet of doublets pattern is observed at 388 K. Above this temperature, the compound starts to decompose and so the high-temperature limit can only be approached (Figure 1). The structure of the new signal observed at 388 K leaves no doubt that it has to be assigned to the second phosphorus atom ($^1J_{PRh} = 145$ Hz, $^2J_{PP} = 43$ Hz).

The signals also sharpen at temperatures below 273 K, giving rise to two patterns, each composed of two doublet of doublets structures. The innermost pattern (Figure 1, 213 K) corresponds to one set of two chemically different phosphorus nuclei, and the outer one characterizes another pair of chemically different phosphorus atoms. The coherence of the outer set of signals is evident from PPCOSY experiments (Figure 2). The inner set of signals is of higher order, and its coherence is clear from the type of pattern as well as from the coupling constants.

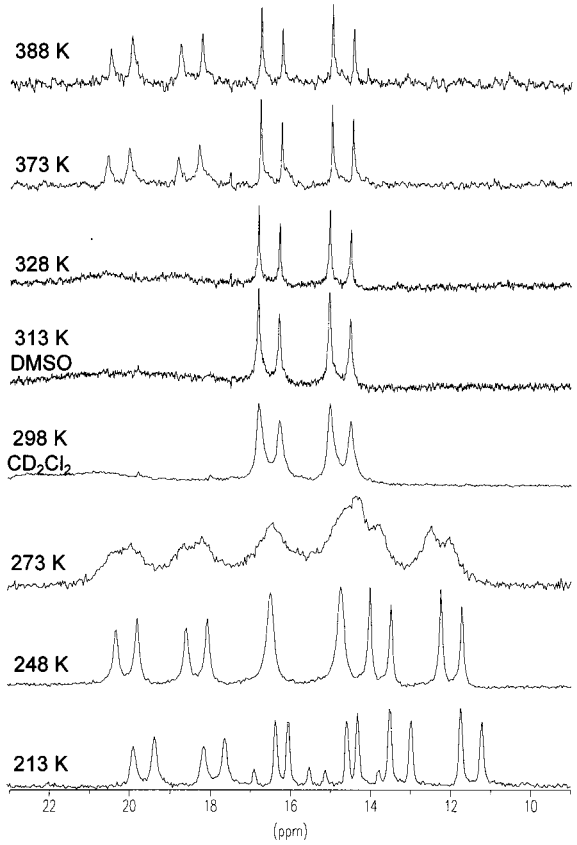


Figure 1. Temperature dependence of the $^{31}P\{1H\}$-NMR spectrum of **2b**

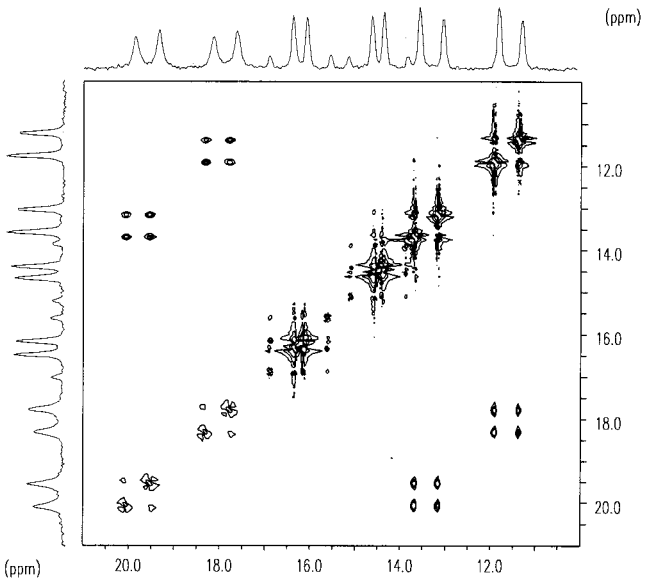


Figure 2. ^{31}P-^{31}P COSY experiment on **2b** at 213 K

These observations can be interpreted as follows. The tolyl groups of the P(*o*-Tol)$_2$ fragment of the compound are fixed in two different positions at the low temperature limit and are, focusing only on a single P(*o*-Tol)$_2$ group, mirror images of one another. Either the left-hand aryl group has its methyl substituent pointing forward while the right-hand group has it pointing backwards (Figure 3), or vice versa. Thus, there are two conformers present at the low-temperature limit. Evidently, the conformation of the chelate cycle is either still fully dynamic at this temperature, or the different conformations which it might adopt (chair, twist) do not significantly influence the phosphorus resonances.

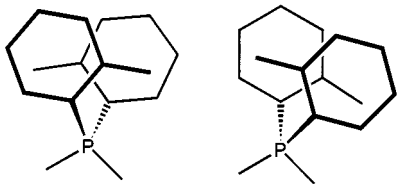


Figure 3. Conformations of the P(*o*-Tol)$_2$ fragment

The conformational enantiomerization of the P(*o*-Tol)$_2$ group, which is the rationale for the fact that two different species are observed at the low-temperature limit, also accounts for the changes observed in the spectra at higher temperatures. Just above 273 K (Figure 1), a clear doublet of doublets structure evolves for one of the constitutionally different PR_2 groups. The second one is not observable at all. This indicates that the environment of the "unobservable" phosphorus atom changes at such a rate that no signal is observed. At higher temperatures, this change speeds up and the signal appears as a doublet of doublets. The change of environment is due to the enantiomerization of the P(*o*-Tol)$_2$ conformation. The phosphorus atom of the P(*o*-Tol)$_2$ group itself does not take much notice of this conformational change, whereas the PPh_2 "spectator" group well feels it.

The validity of the above interpretation is corroborated by the observation of analogous behaviour in a case where there is no doubt as to which phosphorus signal is from which group. The ^{31}P-NMR spectra of the whole series of compounds $H_3C(CH_2PPh_2)_n[CH_2P(o\text{-}Tol)_2]_{3-n}Mo(CO)_3$ have been thoroughly analysed with regard to their dynamic behaviour.[21] The conformational enantiomerization (see above) of the P(*o*-Tol)$_2$ groups lies at the basis of the dynamic processes observed for these species. For $H_3C(CH_2PPh_2)_2[CH_2P(o\text{-}Tol)_2]Mo(CO)_3$, it has been found that the signal of the phosphorus atom of the P(*o*-Tol)$_2$ group is undisturbed by the enantiomerization of the P(*o*-Tol)$_2$ conformation, while the phosphorus nuclei at the two spectator PPh_2 groups are strongly influenced.[21]

Compound **2c** is an analogue of **2b**, the only difference being that the phenyl groups of the PPh_2 moiety of **2b** are linked by a carbon−carbon bond in its dibenzophosphole donor group. The dynamic behaviour of **2c** is found to be qualitatively analogous to that of **2b** in the high-temperature range (Figure 4). In the low-temperature range between 298 K and 218 K, the behaviour is again similar with the signals of two different species gradually evolving. At the lowest accessible temperature (185 K), however, there is seemingly only one species. This implies that one of the diastereomers generated by the conformational isomerism of the P(*o*-Tol)$_2$ group is decidedly more stable than its epimeric form.

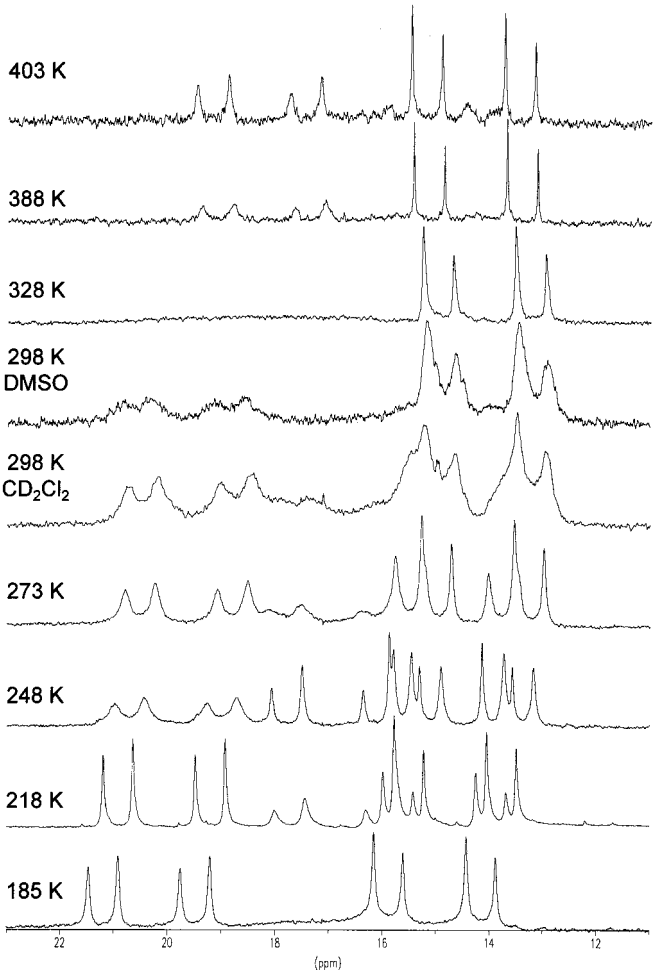


Figure 4. Temperature dependence of the $^{31}P\{^1H\}$-NMR spectrum of **2c**

X-ray Analyses

The kind of dynamic behaviour indicated by the NMR observations has not yet been fully delineated for all compounds **2**. It will in part be associated with the conformational flexibility of the chelate cycles, and the X-ray data obtained for **2** (Table 5) clearly show that these can adopt chair as well as twist conformations.

Considering structurally equivalent moieties, the scalar properties (distances, angles) are rather similar for the whole group of compounds (Table 6). The real difference between the compounds is apparent from the torsion angles (Table 5). There are five independent molecules that adopt chair conformations (Table 5), with the crystal structure of **2b** containing two crystallographically independent molecules of this type. The torsion angles within this group of

conformationally similar molecules are not too dissimilar within each set of conformationally equivalent groups (cf. columns φ_{2345}, φ_{6543} in Table 5; these angles should be equal in size but opposite in sign for a mirror-symmetric chair. The signs of the torsion angles of **2c** are the opposite of those of **2b**; this is not a physically relevant difference but arises because of the priority rules used to assign chirality). The different conformational classes are most clearly apparent from the pseudo torsion angle φ_{3265} (Table 5), which is close to zero for the chair conformations and +/−51−56° for the δ or λ conformations (Table 5).

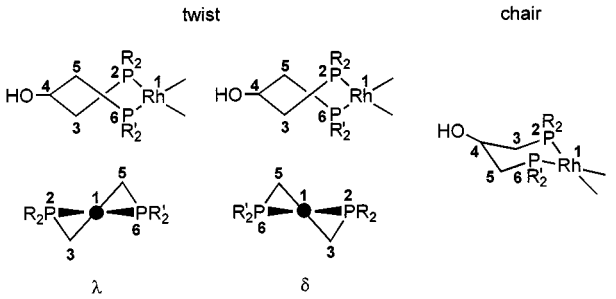


Figure 5. Schematic illustration of the conformations adopted by the chelate cycles in **2**

To illustrate the twist conformation the structures of the δ and λ conformations, both of which are found in the crystal of **2d**, are illustrated in Figure 6. The two molecules are conformational diastereomers. Even though the chirality defined by the substitution pattern at the ligand is the same for both molecules, the additional chirality induced by the twist of the chelate cycle is opposite in sense for the two

Table 5. Torsion angles for the chelate cycles of compounds **2**[a]

	R	R′	conf.	φ_{1234}	φ_{1654}	φ_{2345}	φ_{6543}	φ_{6123}	φ_{2165}	φ_{3265}
2v	Ph	Ph	chair	52	−57	−74	82	−32	32	1
2o	Ph	Ph	chair	64.9	−58.7	−75.3	71.3	−42.2	40.5	−2.5
2b	Ph	*o*-Tol	chair	48.6	−51.9	−73.9	74.6	−23.0	24.6	1.3
	Ph	*o*-Tol	chair	57.8	−58.8	−74.6	74.5	−36.0	36.6	0.5
2d	Ph	Mes	δ	−73.9	−69.3	40.4	32.1	28.2	28.1	54.3
	Ph	Mes	λ	67.2	79.9	−20.7	−53.7	−30.8	−24.9	−54.3
2g	Ph	2-MeOPh	δ	−74.1	−62.8	45.5	22.8	27.3	27.8	51.6
	Ph	2-MeOPh	λ	65.3	74.2	−24.1	−45.8	−27.9	−25.6	−51.2
2f	Mes	2-MeOPh	δ	−72.6	−72.5	30.9	42.9	33.7	23.6	55.6
	Mes	2-MeOPh	λ	79.5	65.7	−46.7	−28.1	−30.9	−23.9	−54.6
2e	Mes	DBP	δ	−81.6	−59.5	42.4	28.5	37.2	15.9	51.8
2c	*o*-Tol	DBP	chair	−53.9	45.9	74.2	−71.2	27.1	−23.2	3.5

[a] The numbering scheme adopted refers to Figure 5 throughout and is different from the schemes used to label individual atoms in the deposited data.[36]

Table 6. Distances and angles in compounds **2**[a]

	R R′	conf.	Rh−PR_2 Rh−PR'_2	Rh−C_{COD} (R)[b]	Rh−C_{COD} (R′)[b]	PR_2−C3 PR'_2−C5	C4−C3 C4−C5	PRhP
2v[c]	Ph	chair	226.5(4)					91.2(2)
	Ph		228.2(5)					
2o	Ph	chair	230.6(2)	226.2(6)	222.9(6)	183.9(5)	152.5(8)	88.6(5)
	Ph		229.6(6)	223.6(5)	222.6(6)	184.0(5)	153.1(7)	
2b	Ph	chair	230.0(2)	225.2(7)	230.6(7)	183.2(7)	154.7(11)	91.6(1)
	o-Tol		232.8(2)	225.4(8)	224.8(8)	184.7(7)	152.0(10)	
	Ph	chair	231.1(2)	228.2(8)	226.0(9)	182.8(9)	151.7(12)	89.6(1)
	o-Tol		232.2(2)	225.4(8)	222.9(8)	184.5(7)	150.4(12)	
2d	Ph	δ	230.4(2)	222.4(10)	225.8(8)	181.3(9)	153.6(13)	87.8(1)
	Mes		233.4(2)	223.1(9)	226.1(9)	184.7(10)	151.6(13)	
	Ph	λ	229.6(2)	219.4(9)	225.4(9)	186.9(8)	151.5(13)	88.3(1)
	Mes		232.1(2)	226.3(8)	219.8(8)	184.9(9)	157.8(13)	
2g	Ph	δ	228.8(3)	223.9(8)	228.0(11)	182.2(7)	154.6(13)	87.7(1)
	2-MeOPh		231.3(2)	222.7(9)	223.9(10)	183.0(11)	156.2(16)	
	Ph	λ	229.3(2)	224.3(11)	223.3(13)	184.5(7)	153.6(11)	87.7(1)
	2-MeOPh		231.4(2)	222.7(9)	225.7(11)	185.4(9)	148.0(13)	
2f	Mes	δ	235.6(3)	217.9(17)	219.5(15)	184.5(2)	161.3(2)	87.7(1)
	2-MeOPh		234.6(4)	225.1(15)	229.1(12)	180.8(2)	153.7(2)	
	Mes	λ	231.2(4)	228.3(18)	225.2(16)	185.6(13)	149.8(2)	88.9(1)
	2-MeOPh		230.1(4)	225.2(13)	221.6(14)	182.9(12)	148.3(2)	
2e	Mes	δ	232.0(1)	225.3(3)	224.6(3)	186.4(3)	153.5(4)	87.2(3)
	DBP		229.9(1)	224.1(3)	225.8(3)	184.0(4)	153.7(5)	
2c	*o*-Tol	chair	231.3(1)	223.9(5)	229.5(4)	185.5(4)	152.0(6)	91.3(4)
	DBP		227.2(1)	226.4(4)	224.0(4)	183.4(4)	152.8(6)	

[a] The numbering scheme adopted refers to Figure 5 throughout and is different from the schemes used to label individual atoms in the deposited data.[36] − [b] C_{COD} *cis* to PR_2 (PR'_2). − [c] The structure of **2v** is rather inaccurate, disorder is observed for the COD ligand and for the aryl substituents of one of the PPh_2 groups. Only items involving solely P and Rh are therefore given in the table. The overall geometry is nevertheless clearly evident, as is the chair-type conformation of the chelate cycle (Table 5).

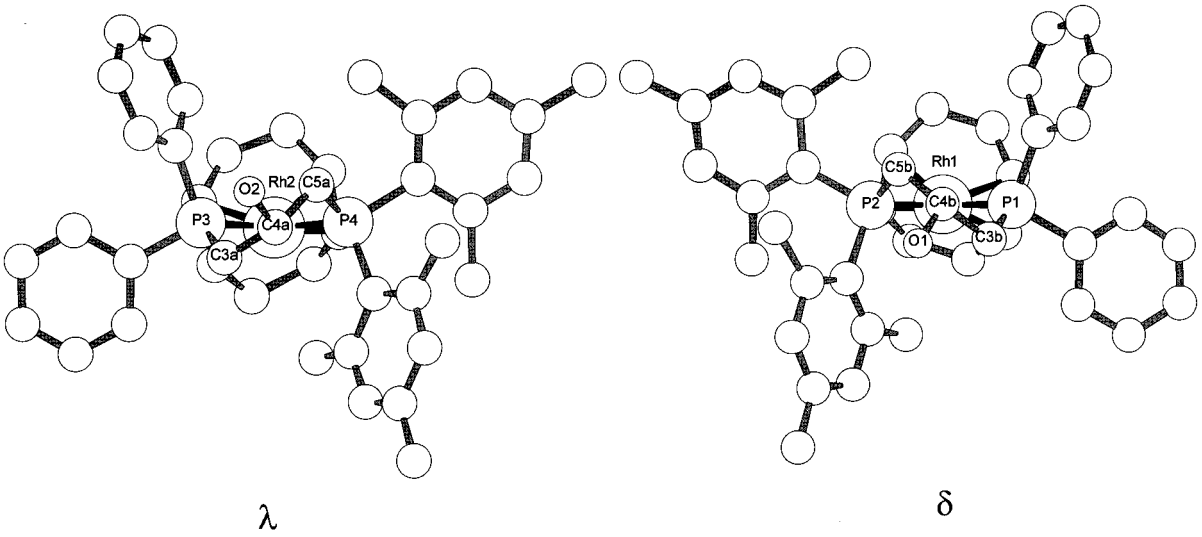


Figure 6. Conformations of the cation of **2d** as observed in the solid state; the numbering scheme refers to Figure 5; the designators *a* and *b* are used to differentiate between the two different molecules in the crystal of **2d**

species. It appears that with the substituents used, enantioselective discrimination is not sufficient to make one of the ring conformations much more stable than the other. The ^{31}P-NMR spectra of **2d** (see above, Table 4) show that two conformers are also present in solution at room temperature. In contrast to **2b**, **2c** (see above), it is not clear, however, whether the conformational isomerism observed in solution is due to an inversion of the ring conformation or to the hindered rotation of the mesityl groups.

The results presented in Table 5 suggest that sterically more demanding substituents at the phosphorus centres favour twist conformations. Chair conformations are found for **2b**, **2c**, **2o**, **2v**, and their overall geometry is illustrated for **2b** (Figure 7). Only one of the two geometrically almost equivalent independent molecules in the crystal of **2b** is shown in Figure 7. Despite the fact that **2b** adopts a chair conformation in the solid state, two conformers are observed in solution at low temperatures, which are attributed to a rotational isomerism of the P(*o*-Tol)$_2$ group (see above). In the crystal, the P(*o*-Tol)$_2$ groups of the two independent molecules adopt the same orientation.

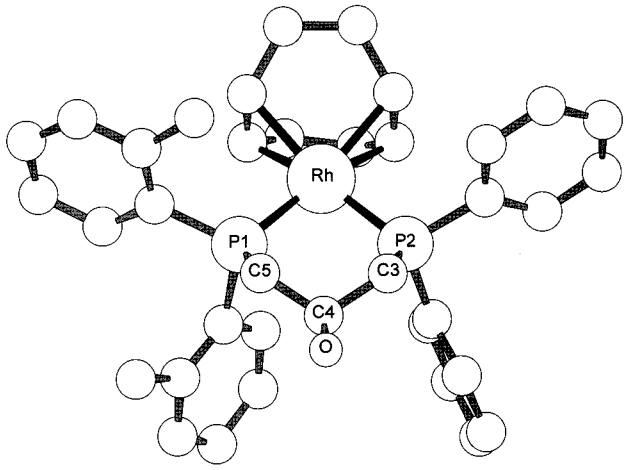


Figure 7. Conformation of the cation of **2b** as observed in the solid state; the numbering scheme refers to Figure 5

Catalysis

Compounds **2** act as precatalysts in the catalytic hydrogenation of (*Z*)-2-acetamidocinnamic acid (AAC). Table 7 shows the relative efficiencies of the various compounds **2**, together with the *ee* values observed in each case. The highest rate is observed for **2v**, i.e. for the sterically least demanding ligand, $Ph_2PCH_2CH(OH)CH_2PPh_2$, of the series. The activity of **2v** is similar to that observed for $[Ph_2PCH_2C(CH_3)_2CH_2PPh_2]Rh(COD)^+$.[22] The reactivity is not significantly reduced by *para* substitution of one of the PPh_2 groups [P(*p*-Tol)$_2$, **2w**], nor by *meta* substitution [P(*m*-Xyl)$_2$, **2a**], see Table 7. The enantiodiscriminating influence of this type of substitution is also low (*ee* = 3% and 6%, respectively). Replacing one of the PPh_2 groups by a P(*o*-Tol)$_2$ group (**2b**) has virtually no effect on the reactivity, but the enantiomeric excess is found to rise to 36% (*S*) at 20°C, 40% at 50°C, and 49% at 30 bar, 25°C. To examine the influence of the OH substituent on the backbone of the ligand, *O*-alkylated and *O*-silylated derivatives of **2b** were analysed. It was found that **2p** (substituent OCH_3), **2q** (substituent $OSiMe_3$), and **2r** [substituent (*S*)-H_3CCH_2-$CH(CH_3)CH_2O$] required longer reaction times in order to reach full conversion (Table 7). The enantiomeric excess, however, proved to be almost independent of this type of substitution (Table 7).[22]

Replacing the PPh_2 group in **2b** by a DBP group (**2c**) greatly reduces the reactivity. The enantioselectivity becomes inverted such that the product is of (*R*) configuration. Increasing either the temperature or the pressure results in reduced selectivity. Replacing one of the PPh_2 groups in **2v** by an SPh donor (**2m**) also reduces the reactivity, with the observed *ee* value lying at the lower end of the range. Although the large difference between the properties

Table 7. Catalytic activity of compounds **2** in the hydrogenation of (*Z*)-2-acetamidocinnamic acid[a]

	1 bar								30 bar[b]		
	0°C			20°C			50°C			25°C	
	t	yield (%)	*ee*	*t*	yield (%)	*ee*	*t*	yield (%)	*ee*	*t*	yield (%)	*ee*
2v				20 min	100	0						
2w				30 min	100	3 (*R*)						
2a				25 min	100	6 (*R*)	15 min	100	0			
2b				30 min	100	36 (*S*)	25 min	100	40 (*S*)	48 h	100	49(*S*)
2p				2.5 h	100	38 (*S*)						
2q				5 h	100	35 (*S*)						
2r				22 h	100	40 (*S*)						
2c				7 h	100	23 (*R*)	1 h	100	20 (*R*)	48 h	30	4 (*S*)
2m				10 h	100	14(*R*)						
2d				4 d	< 10	n.d.	5 d	16	31 (*R*)	60 h	52	40 (*R*)
2u										5 d	100	40 (*R*)
2e										48 h	12	n.d.
										5 d	90	64 (*R*)
2h	4 h	100	56 (*R*)	2 h	100	48 (*R*)				16 h	100	62 (*R*)
2g				40 h	100	77 (*S*)				48 h	100	67 (*S*)
	2.5 h[c]	100	85 (*S*)	1 h[c]	100	77 (*S*)						
2s				2 h[c]	100	77 (*S*)						
2t	20 h[c]	100	82 (*S*)	2.5 h[c]	100	79 (*S*)						
2f							4 d	< 10	n.d.	5 d	90	64 (*S*)

[a] 1 mol-% catalyst. – [b] For the high-pressure experiments the reaction time was set to the values given and thus has no immediate relation to the reactivity of the catalyst. – [c] 4 mol-% catalyst.

of the donor groups PPh_2 and SPh might be expected to increase enantiomeric discrimination, this expectation is counterbalanced by the fact that the reaction "pocket" accessible to the substrate with the SPh substituent will be larger than that formed by a PPh_2 substituent. Moreover, the coordinated sulfur centre is itself a centre of chirality, the configuration of which could be such as to counteract enantioselectivity.

When one of the PPh_2 groups in **2v** is replaced by a $PMes_2$ group (**2d**), the reactivity is drastically reduced, such that complete conversion could not be achieved under any of the conditions employed (Table 7). Enantioselectivity leading to favoured formation of the (*R*) product is found. Etherification of the OH position (**2u**) again has no significant influence. Replacing the PPh_2 group of **2d** by DBP (**2e**) results in reduced reactivity, but the enantiomeric excess is found to increase to 64% (*R*).

The results of the experiments described so far indicate that in order to obtain sufficient reactivity, a low degree of substitution at the PR_2 entities is favourable. With regard to the enantiomeric excess, it appears that *ortho* substitution of the aryl groups is effective. Etherification at the OH position of the ligands does not appear to have strong influence on the *ee*, but it is found to reduce the reactivity.

With these findings in mind, **2h**, the ethyl-substituted analogue of **2b**, was prepared and screened for its catalytic activity. The reactivity was found to be somewhat lower than that observed with **2b**, but higher enantioselectivity was achieved, rising to 62% *ee* at 30 bar (Table 7). Replacing the ethyl substituents in **2h** by methoxy groups (**2g**) reduces the reactivity, but increases selectivity (Table 7); 77% *ee* (*S*) is observed at 20°C, 1 bar H_2. Increasing the pressure reduces the selectivity to 67% (*S*) at 30 bar H_2. Reducing the temperature to 0°C and compensating for the reduced reactivity by using 4 mol-% catalyst instead of the standard 1 mol-% leads to quantitative conversion in less than 3 h, with an *ee* of 85% (*S*) (Table 7). While enantioselectivities much higher than this have been observed with analogous rhodium complexes derived from five- or seven-membered chelate ligands, to the best of our knowledge there has only been one report to date where a six-membered chelate cycle has led to an *ee* in excess of 80%. The corresponding ligand was skewphos, $Ph_2PCH(CH_3)CH_2CH(CH_3)PPh_2$, which contains two chiral carbon centres in its backbone. On the other hand, the efficiency of *ortho*-alkyloxy substitution in phosphorus-bound aryl groups with regard to enantiomeric discrimination has been known for a long time.[23] In **2g**, both effects, i.e. the skew of the chelate cycle and the activity of the methoxy substituent, may lie at the basis of its enantioselectivity. Further modifications of **2g** by either etherification of its OH group (**2s**, **2t**) or by replacing the PPh_2 group by a $PMes_2$ group (**2f**) did not increase enantioselectivity, but reduced the reactivity to varying extents (Table 7).

Conclusion

The following conclusions can be drawn from the results presented in this paper:

1. Enantiomerically pure chelate ligands $L_2 = XCH_2CHOHCH_2Y$ are easily accessible for a broad range of donor groups X and Y by a two-step synthesis starting from epichlorohydrin. Under specialized conditions, ether derivatives of L_2, $XCH_2CHORCH_2Y$ may be prepared, even with X, Y = PR_2.

2. The chelate cycles in $L_2Rh(COD)^+$ may adopt twist or chair conformations with dynamic equilibria between the different conformations being operative in solution.

3. Compounds $L_2Rh(COD)^+$ act as precatalysts for the homogeneous hydrogenation of AAC. Depending on the nature of the donor groups X and Y, *ee* values of up to 85% can be achieved.

Table 8. Synthesis and analytical data of ligands **1a−1n**

	A[a]	H-Nuc^1 (*t*) H-Nuc^2 (*t*)	eluent (R_f)	yield (%)	α_D^{20}	MS (*m*/*z*) [M^+][M^+ − Frag.]	$C_{calcd.}H_{calcd.}$ $C_{found}H_{found}$	HR-MS $M^+_{calcd./found}$
1a	(*S*)-	$HPPh_2$ (0.5 h) P(*m*-Xylyl)$_2$ (1.5 h)	PE/Et_2O 2:1 (0.28)	82	0.8 ± 0.2	484 407 [−C_6H_5]	76.84, 7.07 75.44, 7.35	
1b	(*S*)-	HP(*o*-Tol)$_2$ (1.5 h) $HPPh_2$ (2 h)	PE/Et_2O 2:1 (0.31)	77	−21.6 ± 3.2	456 379 [−C_6H_5]	76.30, 6.62 76.15, 6.98.	
1c	(*S*)-	HP(*o*-Tol)$_2$ (0.5 h) DBPH (2 h)	PE/Et_2O 3:1 (0.30)	86	−38.7 ± 0.9	454 363 [−$C_6H_4CH_3$]	76.64, 6.21 75.05, 6.46	
1d	(*S*)-	$HPPh_2$ (0.5 h) $HPMes_2$ (1.5 h)	PE/Et_2O 2:1 (0.25)	70	79.3 ± 0.2	512 393 [−C_9H_{11}]	77.32, 7.47 76.55, 7.77	
1e	(*S*)-	$HPMes_2$ (0.5 h) DBPH (2 h)	PE/Et_2O 3:1 (0.28)	56	−92.9 ± 0.7	510 391 [−C_9H_{11}]	77.63, 7.11 77.90, 7.50	
1f	(*R*)-	$HPMes_2$ (0.5 h) HP(2-MeOPh)$_2$ (16 h)	PE/Et_2O 2:1 (0.15)	37	−37.4 ± 0.7	572 453 [−C_9H_{11}]	73.41, 7.39 70.16, 7.56	572.26093 572.26226
1g	(*S*)-	$HPPh_2$ (0.5 h) HP(2-MeOPh)$_2$ (16 h)	PE/Et_2O 1:2 (0.26)	51	3.9 ± 0.2	488 411[−C_6H_5]	71.30, 6.19 69.79, 6.33	488.16702 488.16710
1h	(*S*)-	$HPPh_2$ (2 h) HP(2-EtPh)$_2$ (2 h)	PE/Et_2O 4:1 (0.24)	71	2.9 ± 0.4	484 379 [−C_6H_4Et]	76.84, 7.07 75.21, 7.10	484.20850 484.20882
1i	(*S*)-	$HPPh_2$ (1 h) HP(2-Me_2NPh)$_2$ (16 h)	PE/Et_2O 3:2 (0.31)	53	−6.8 ± 0.4	514 394 [−$C_6H_4NMe_2$]	72.36, 7.05 72.01, 7.01	
1j	(*S*)-	$HPEt_2$ (0.5 h) $HPMes_2$ (1.5 h)	PE/Et_2O 1:2 (0.24)	67	46.2 ± 0.2	416	72.09, 9.20	
1j	(*R*)-	$HPMes_2$ (0.5 h) $HPEt_2$ (1.5 h)	PE/Et_2O 1:2 (0.24)	64		387 [−C_2H_5]	71.43, 9.08	
1k	(*S*)-	$HPEt_2$ (0.5 h) HP(*o*-Tol)$_2$ (2 h)	PE/Et_2O 1:2 (0.24)	57	15.7 ± 0.5	360	69.98, 8.39	360.17719
1k	(*R*)-	HP(*o*-Tol)$_2$ (0.5 h) $HPEt_2$ (1.5 h)	PE/Et_2O 1:2 (0.24)	63		331 [−C_2H_5]	66.42, 8.71	360.17496
1l	(*S*)-	$HPEt_2$ HP(2-MeOPh)$_2$	PE → Et_2O (0.30, Et_2O)	68	0.8 ± 0.2	393 364 [−C_2H_5]	−	−
1m	(*S*)-	$HPPh_2$ HSPh	PE/Et_2O 1:1 (0.39)	84	−29.0 ± 0.2	352 275 [−C_6H_5]	71.57, 6.01 71.66, 6.25	
1n	(±)-	$HPPh_2$ $HNPh_2$	PE/Et_2O 1:2 (0.44)[b]	80	−	411 334 [−C_6H_5]	78.80, 6.37 78.67, 6.65	

[a] Configuration of epichlorohydrin (**A**). − [b] Solid phase for chromatography Al_2O_3 (neutral).

Table 9. ^{1}H-NMR data of ligands **1a−1n**[a]

	R	R′[a]	CH_2PR_2 δ, ($^2J_{HH}$, $^3J_{HH}$)	$CH_2PR'_2$ δ, ($^2J_{HH}$, $^3J_{HH}$)	C*H*−O δ	H_{Ar} δ	aryl subst. δ	other δ
1a: (*S*)-	Ph	3,5-Me_2Ph	2.5−2.7		3.9	7.0−7.5	2.4	
1b: (*R*)-	*o*-Tol	Ph	2.3−2.7		3.9	7.1−7.55	2.46	
1c: (*S*)-	*o*-Tol	DBP	2.2−2.6		4.0	7.1−7.9	2.38	
1d: (*S*)-	Ph	Mes	2.7−2.85 [3 H]	3.2 (13.5, 3.0) [1 H]	3.7	6.8 (Mes) 7.3−7.5	2.3	
1e: (*S*)-	Mes	DBP	3.05 (13.3, 3.1) [1 H]	2.7−2.8 [3 H]	3.82	6.9 (Mes) 7.4−8.0	2.1−2.4	
1f: (*R*)-	2-MeOPh	Mes	2.4−2.7 [3 H]	2.96 (13.7, 3.8) [1 H]	3.7	6.8−7.5	2.25, 3.76 (OMe)	
1g: (*S*)-	Ph	2-MeOPh	2.25−2.65		3.92	6.8−7.5	3.70	2.83 (OH)
1h: (*S*)-	Ph	2-EtPh	2.5−2.75		4.0	7.3−7.6	1.3, 3.0	
1i: (*S*)-	Ph	2-Me_2NPh	2.1−2.5		3.65	6.9−7.45	2.6, 2.8	
1j: (*S*)-	Et	Mes	1.75 [2 H] 2.4−2.7 [2 H]	2.74 3.0 (12.0, 3.4) [1 H]	3.7	6.8	2.3	1.0, 1.4 (Et)
1k: (*S*)-	Et	*o*-Tol	1.8	2.2	3.9	7.2−7.4	2.5	1.0, 1.4 (Et)
1l: (*S*)-	Et	2-MeOPh	1.8	2.2	3.9	6.9−7.45	3.84	1.1, 1.45 (Et)
1m: (*S*)-	Ph	SPh	3.04 (13.7, 7.8)	2.43 (6.6)	3.85	7.05−7.6		2.74 (O*H*)
1n: (±)-	Ph	NPh_2	3.73 (15.3, 9.1)	2.36 (6.2)	4.0	6.8−7.5		

[a] R′ in PR'_2 for **1a−1l**, donor group of **1m**, **1n**.

Experimental Section

General: All manipulations involving phosphanes were carried out under argon by means of standard Schlenk techniques and were monitored by TLC (Macherey Nagel Co., Polygram SIL G/UV_{254}). All solvents were dried by standard methods[24] and distilled under argon. The solvents $CDCl_3$, CD_2Cl_2, [D_6]DMSO, and [D_8]THF used for NMR-spectroscopic measurements were degassed by three successive "freeze-pump-thaw" cycles and dried with 4-Å molecular sieves. − NMR: Bruker Avance DPX 200 at 200.12 MHz (^{1}H), 50.323 MHz (^{13}C{^{1}H}), 81.015 MHz (^{31}P{^{1}H}), T = 298 K, unless stated otherwise; chemical shifts (δ) in ppm with respect to $CHCl_3$ (^{1}H: δ = 7.27; ^{13}C: δ = 77.0) and CH_2Cl_2 (^{1}H: δ = 5.32; ^{13}C: δ = 53.5) as internal standards. ^{31}P chemical shifts (δ) in ppm with

Table 10. ^{31}P{^{1}H}- and ^{13}C{^{1}H}-NMR data of ligands **1a−1n**[a]

	R	R′[a]	PR_2 δ (^{31}P)	PR'_2 δ (^{31}P)	CH_2PR_2 δ, $^3J_{CP}$, $^1J_{CP}$	$CH_2PR'_2$ δ, $^3J_{CP}$, $^1J_{CP}$	CH−O δ, $^2J_{CP}$,$^2J_{CP}$	C_{Ar} δ	C_{Ar}−P δ, $^1J_{CP}$	C_{Ar}−Z[b] δ, $^2J_{CP}$	aryl subst. δ
1a: (*S*)-	Ph	3,5-Me_2Ph	−25.3	−26.1	38.5−39.0		68.1, 17	128.9−133.6	138.1−138.4		21.8
1b: (*R*)-	*o*-Tol	Ph	−47.1	−25.0	37.8, 7, 13	39.4, 7, 13	67.9, 17	126.7−134.1	136.6, 11 138.8, 11	141.8, 22	21.6
1c: (*S*)-	*o*-Tol	DBP	−47.3	−22.9	37.9, 7, 14	40.1, 7, 22	68.5	125.9−131.7	136.4	143.6	
1d: (*S*)-	Ph	Mes	−24.6	−33.1	39.2, 8, 14	38.6, 9, 15	68.6	128.8−133.6		138−143	21−24
1e: (*S*)-	Mes	DBP	−31.1	−20.3	38.5, 8, 15	40.4, 8, 21	69.0	121.7−143.2			21−24
1f: (*S*)-	2-MeOPh	Mes	−41.4	−29.8	36.5, 8, 14	38.8, 8, 15	68.3	111.0−134.1	125.8	138−143 161.6, 13	20.9−23.6 (Mes) 55.8 (OMe)
1g: (*S*)-	Ph	2-MeOPh	−22.4	−42.5	38.8, 8, 14	36.7, 8, 14	68.3, 17	110.9−134.1	139.3, 13	161.6	55.5
1h: (*S*)-	Ph	2-EtPh	−23.0	−48.7	38.9, 9, 13	39.4, 10, 14	68.0	126.5−133.0	136.4, 13 139.1, 13	148.9, 24	15.9, 28.0
1i: (*S*)-	Ph	2-Me_2NPh	−21.0	−41.7	40.1, 8, 16	38.7, 7, 14	67.7, 13	119.2−133.7	137.4, 139.6	157.7	45.3
1j: (*S*)-	Et	Mes	−30.0	−32.9	37.4, 7, 15	38.7, 9, 15	69.0, 15	130.3−133.0		138−143	21−23
1k: (*S*)-	Et	*o*-Tol	−27.5	−43.9	37.5−38.0		68.3	126.5−131.8	136.6	142.8	21.5, 22.0
1l: (*S*)-	Et	2-MeOPh	−25.8	−45.2	36.5, 7, 13	36.5, 8, 14	68.7, 15, 18	110.9−133.4	126.0, 15	161.8	
1m: (*S*)-	Ph	SPh	−24.0		35.8, 13	42.4, 9	67.6, 17	126.2−132.8	137.9, 135.1		
1n: (±)-	Ph	NPh_2	−24.8		34.3, 15	59.3, 9	66.9, 15	117.6−132.7	148.1		

[a] R′ in PR'_2 for **1a−1l**, donor group of **1m**, **1n**. − [b] Z = aryl substituent.

Table 11. Synthesis and analytical data of ligands **1o−1u**

	electrophile	eluent (R_f)	yield (%)	α_D^{20}	MS (*m*/*z*) [M^+][M^+ − Frag.]	$C_{calcd.}H_{calcd.}$ $C_{found}H_{found}$	MS (EI) [M^+ calcd./found]
1o:	H_3CI	−	76		442 365 [$-C_6H_5$]	76.01, 6.38 74.99, 6.57	
1p: (*R*)-	H_3CI	−	71	−	470 379 [$-C_7H_7$]	−	
1q: (*R*)-	Me_3SiCl	−	88	4.3 ± 0.8	528 437 [$-C_7H_7$]	72.70, 7.24 71.54, 7.30	
1r: (*R,S*)-	X[a]	PE/Et_2O 3:1 (0.8)	40	11.6 ± 0.5	526 435 [$-C_7H_7$]	77.54, 7.66 76.14, 7.64	526.2565 526.2560
1s: (*S*)-	Me_3SiCl	PE/Et_2O 2:1 (0.69)	44	−11.5 ± 0.6	560 483 [$-C_6H_5$]	68.55, 6.83 63.37, 7.39	560.2103 560.2084
1t: (*S,S*)-	X[a]	PE/Et_2O 4:1 (0.18)	45	−20.0 ± 0.5	559 452 [$-C_7H_7O$]	73.10, 7.22 72.25, 7.10	
1u[b]: (*S*)-	Y[c]	PE/Et_2O 2:1 (0.46)	53	−	665 546 [$-C_9H_{11}$]	−	

[a] X = $H_3CCH_2CH(CH_3)CH_2OSO_2C_6H_4CH_3$. − [b] See Experimental Section. − [c] Y = $H_2C{=}CH(CH_2)_9OSO_2C_6H_4CH_3$.

Table 12. ^{1}H-NMR data of ligands **1o−1u**

	R	R′	R″	CH_2P δ	CH−O δ	H_{Ar} δ	aryl subst. δ	(R″)H δ
1o:	Ph	Ph	CH_3	2.74−2.9	3.59	7.48−7.71		3.34
1p: (*R*)-	*o*-Tol	Ph	CH_3	2.2−2.4	3.36	7.14−7.41	2.5	3.15
1q: (*R*)-	*o*-Tol	Ph	$SiMe_3$	2.55−2.85	4.14	7.2−7.7	2.55	0.02
1r: (*R,S*)-	*o*-Tol	Ph	X[a]	2.5−2.7	3.6	7.25−7.58	2.51, 2.59	0.9−1.5, 3.2
1s: (*S*)-	Ph	2-MeOPh	$SiMe_3$	2.5−2.85	4.19	7.0−7.6	3.85	0.05
1t: (*S,S*)-	Ph	2-MeOPh	X[a]	2.54−2.73	3.6	6.9−7.6	3.83	0.9−1.5, 3.3
1u: (*S*)-	Ph	Mes	Y[b]	3.0−3.4	3.5	7.2−7.4	2.28	1.36, 5.0, 5.81

[a] X = (*S*)-$H_3CCH_2CH(CH_3)CH_2$. − [b] Y = $H_2C{=}CH[CH_2]_9$.

respect to 85% H_3PO_4 (^{31}P: δ = 0) as external standard. – MS (EI): Finnigan MAT 8320: Fast-atom bombardment (FAB) xenon, matrix: 4-nitrobenzyl alcohol. – HR-MS(EI): Jeol JMS-700. – Melting points: Gallenkamp MFB-595010; uncorrected values. – Optical rotations: Jasco DIP310, 10-cm cell, Na-D line (λ = 589 nm). – GC/MS: HP 5890II (GC) interfaced to an HP5981 (MS) (Hewlett Packard). – Elemental analyses: Microanalytical Laboratory of the Organisch-Chemisches Institut, Universität Heidelberg.

Table 13. $^{31}P\{^1H\}$- and $^{13}C\{^1H\}$-NMR data of ligands **1o–1u**

	R	R′	R″	PR_2 δ (^{31}P)	PR'_2 δ (^{31}P)	CH_2PR_2 δ, $^3J_{CP}$, $^1J_{CP}$	$CH_2PR'_2$ δ, $^3J_{CP}$, $^1J_{CP}$	CH–O δ, $^2J_{CP}$, $^2J_{CP}$	C_{Ar} δ	C_{Ar}–P δ, $^1J_{CP}$	C_{Ar}–Z[d] δ, $^2J_{CP}$	aryl subst. δ	R″ δ
1o:	Ph	Ph	CH_3	–23.6		33.8, 8, 15	77.6	128.9–133.8	139.8			56.9	
1p: (*R*)-	*o*-Tol	Ph	CH_3	–46.3	–23.9	34.5, 8, 15	35.8, 8, 15	77.3	126.3–133.6	137.3, 139.1, 13	142.7	21.4, 21.9	56.7
1q: (*R*)-	*o*-Tol	Ph	$SiMe_3$	–44.6	–21.6	37.9, 8, 15	39.3, 9, 14	69.5, 18	126.4–133.5	137.6, 14 149.8	142.7, 26	21.5	0.4
1r: (*R,S*)-	*o*-Tol	Ph	X[a]	–44.6	–21.7	34.8, 9, 15	36.7, 8, 15	76.3	126.4–133.6	137.6, 13 139.8, 13	142.6, 26	21.3	11.7, 16.9, 26.6, 35.7, 74.6
1s: (*S*)-	Ph	2-MeOPh	$SiMe_3$	–39.1	–21.3	38.9, 9, 14	36.2, 9, 15	70.2, 17, 22	110.9–134.1	140.1	161.8, 13	55.9	0.05
1t: (*S,S*)-	Ph	2-MeOPh	X[a]	–38.2	–21.4	36.2, 9, 14	32.7, 8, 15	76.9	110.9–134.0	126.2, 12 139.9, 14	161.7, 13	55.8	11.7, 16.9, 26.6, 35.7, 74.5
1u[b]: (*S*)-	Ph	Mes	Y[c]	–22.8	–30.6								

[a] X = (*S*)-$H_3CCH_2CH(CH_3)CH_2$. – [b] See Experimental Section. – [c] Y = $H_2C{=}CH[CH_2]_9$. – [d] Z = aryl substituent.

Table 14. ^1H-NMR data of complexes **2**[a,b]

	CH_2 δ	CH–O δ	CH_{COD} δ	H_{Ar} δ	CH_3/other δ
2a: (*S*)-	2.1–3.1	3.78	4.37, 5.0	6.9–7.7	2.32, 2.35
2b: (*R*)-	2.1–3.0	3.9	4.2–4.9	7.3–7.7	2.38, 2.41
2c: (*S*)-	2.0–3.2	3.9	4.0–4.7	7.0–8.1	2.17, 2.20
2d: (*S*)-	2.1–2.6 3.1 [1 H] CH_2PMes_2	3.6	3.97, 4.37, 4.47, 4.79	6.8–7.3 (Mes) 7.1–8.2 (Ph)	1.76, 2.05, 2.31, 2.41, 2.71, 3.56
2e: (*S*)-	1.9–2.6, 3.38 [1 H] CH_2PMes_2	3.8	4.23, 4.74	6.8–7.3 (Mes) 7.6–8.1 (DBP)	1.78, 2.20, 2.37, 2.41, 3.0, 3.72
2f: (*R*)-	2.1–2.9 2.93 [1 H] CH_2PMes_2	4.15	4.1–4.4	6.6–7.5, 7.78 + 9.22 (Mes)	1.70, 2.05, 2.32, 2.43, 2.62, 3.66, 3.73, 4.01 (OCH_3)
2g: (*S*)-	2.1–2.5, 2.55, 3.0 [1 H] $CH_2PR'_2$	3.71	4.25–4.6	7.1–7.8	3.86, 3.93
2h: (*S*)-	2.1–3.0		3.9–4.9	7.3–8.2	1.1–1.5, H_3CCH_2
2j: (*S*)-	1.7–2.8	3.69	4.0, 4.6	6.8–7.1	1.68, 2.2–2.4, 2.83, 1.2–1.4 (Et)
2k: (*S*)-	1.0–3.0	3.5	4.72, 5.2	6.8–7.8	1.2–1.4 (Et)
2l: (*S*)-	2.0–2.8		4.1–4.4	7.0–7.7	3.9, 1.1–1.7 (Et)
2m: (*S*)-	2.91–3.35, 2.0–2.5 (COD)	4.25	4.25	7.44–8.0	
2o:	2.25–2.8	3.33	4.43, 4.97	7.4–7.8	3.23 (H_3CO)
2p: (*R*)-	2.1–3.0	3.45	4.1–4.9	7.4–7.8	3.11 (H_3CO)
2q: (*R*)-	1.8–3.0		3.9–4.9	7.0–8.1	–0.1 $(H_3C)_3Si$
2r: (*R,S*)-	2.0–3.1		3.9–5.0	7.0–8.4	0.8 (H_3C) 0.96 (CH), 1.22 (CH_2)
2s: (*S*)-	2.3–2.8		4.45	7.16–7.6	–0.1 (H_3CSi) 3.9 (OCH_3)
2t: (*S,S*)-	2.1–2.8	3.55	4.3–4.7	7.1–7.9	0.8 (H_3C), 0.96 (CH), 1.29 (CH_2)
2u: (*S*)-	2.1–2.8		4.01, 4.38, 4.51, 4.82	6.9–8.2	0.9–1.5 (CH_2), 1.7, 2.1–2.8, 3.4–3.7 (Mes) 5.0 (H_2C), 5.9 (CH)
2v:	2.1–2.6, 2.85	3.80	4.41, 4.96	7.2–7.8	–
2w: (*R*)-	2.8–2.85	3.80	4.40, 4.98	7.24–7.75	2.40

[a] Due to dynamic phenomena (see text) most of the signals are rather broad. Depending on the appearance of the spectra, either ranges are given in the table, or, if predominant peaks are observed in the corresponding ranges, the shifts of these peaks are given. – [b] For complexes **2i**, **2n** see Experimental Section.

− Catalytic hydrogenations were performed in a hydrogenation apparatus according to Marhan (Normag) (1 bar) or in an HR 250 stainless steel high-pressure laboratory reactor (Berghof/Maasen GmbH) (30 bar). Yields were determined by ^{1}H-NMR analysis; the *ee* values were determined by GC/MS (column: Chirasil L-Val, Chrompack GmbH).

Materials: Silica gel (Kieselgel z.A. 0.06−0.2 mm, J. T. Baker Chemicals B.V.) used for chromatography was degassed at 1 mbar for 24 h and saturated with argon. A solution of 2.5 M *n*BuLi in hexanes was used for deprotonations. (*S*)- and (*R*)-epichlorohydrin (A) (Aldrich, 97% *ee*) were degassed (see above) and checked for optical purity by measurement of their specific rotations ($|[\alpha]_D^{20}|$ = 34.3[25]). $HPEt_2$,[26] $HPPh_2$,[27] HP(*p*-Tol)$_2$,[27] HP(*o*-Tol)$_2$,[28] HP(*m*-Xyl)$_2$,[29] $HPMes_2$,[30] HP(2-EtPh)$_2$,[31] HP(2-MeOPh)$_2$,[32] HP(2-Me_2NPh)$_2$,[32,33] DBPH,[34] and [Rh(COD)Cl]$_2$[35] were prepared according to or by adaptation of literature procedures. All other chemicals were obtained from commercial suppliers and used without further purification.

Ligand Synthesis

General Procedure for the Synthesis of Ligands 1a−1n: 5−12 mmol of phosphane R_2PH for the generation of nucleophile I (Table 8) was dissolved in 30 mL of THF and deprotonated by the dropwise addition of *n*BuLi at −70°C. This solution was stirred for 10 min. Meanwhile, 5−12 mmol of epichlorohydrin was dissolved in 20 mL of THF and the solution was cooled to −70°C. At this temperature, the previously prepared phosphide solution was added in a dropwise manner over a period of 30 min. After warming to room

Table 15. $^{13}C\{^1H\}$-NMR data of complexes **2**[a]

	CH_2 ($^1J_{CP}$, $^3J_{CP}$)	CH−O δ	CH_{COD} δ	C_{Ar}[b] δ	CH_3/other δ
2a: (*S*)-	30.8 (COD) 34.6 (8,12) 35.1 (8,12)	64.4	98.3, 99.1, 103.7, 104.5	129.0−134.3, 139.3 (C_q)	21.5
2b: (*R*)-	27.0−33.0	65.3	99.0−104.0	126.5−133.5, 143.0 (C_q)	23.1, 23.8
2c: (*S*)-	30.3, 33.2	66.0	101.3, 106.3	122.4−135.8, 142.8 (C_q)	23.9
2d: (*S*)-	30.1−35.4	65.7	92.3, 94.8, 99.4, 106.7	129.5−136.2, 124.3 [C_i(Mes)], 141.4−144.3 (C_q)	20.8−27.1
2e: (*S*)-	28−28.6 (COD), 32.0, 38.2	65.4	95.6, 96.9, 98.4, 108.5	122.0−132.0 140.0−145.0 (C_q)	20.9, 21.0, 22.5, 24.7, 26.4, 27.7
2f: (*R*)-	28.1−33.3	66.2	89.7, 94.9, 98.6, 104.6	112.3−144.3 117.2 (C_r-Anisyl) 160.1−162.3 (C_q)	20.8−26.9, 56.0 (OCH_3)
2g: (*S*)-	30.3−32.7	65.4	97.9−102.7	112.3−121.4 (Anisyl) 129.6−136.0 160.9 (C_q−OCH_3)	56.1
2h: (*S*)-	28−29.5 (COD) 31.0−33.0	65.2	98.0−104.5	126.4−134.5 149.3 (C_q−Et)	14.4, 32.0
2j: (*S*)-	18.6−35.3	69.0	93.5, 106.3	130.0−142.0	
2k: (*S*)-	28.8−33.0	64.7	97.1, 99.2, 103.3	126.2−133.3 140.7−143.1 (C_q)	8.4, 21.0 (Et) 23.2, 23.9
2l: (*S*)-	29.9−32.6	66.2	96.2, 97.0 112.2, 116.7	121.1 ($C_{Ar}C_qOCH_3$), 131−134.7, 160.8 (C_q)	8.6, 19.5 (Et) 56.0
2m: (*S*)-	30.0−31 (COD) 35.1 (23) 44.5 (CH_2S)	65.8		129.2−135.3	
2o:	30.6, 31.5	73.2	99.8, 104.2	129.1−134.2	56.0 (OCH_3)
2p: (*R*)-	27.0−33.5	74.5	98.0−104.0	126.5−133.3 141.7 (C_q)	23.1−23.7 56.2 (H_3CO)
2q: (*R*)-	27.0−33.5	65.9	97.0−104.5	126.5−133.3 140.3 (C_q)	−0.1 (C−Si) 23.3
2r: (*R,S*)-	27.0−33.3	72.9	99.0−104.5	126.6−134.2 141.3 (C_q)	11.4, 16.6, 26.3, 35.3, 74.0 (R′′) 23.1 (Tol)
2s: (*S*)-	30.1−33.6	66.0	99.5, 102.5	112.2 ($C_{Ar}C_qOCH_3$), 121.4−134.1 160.8 (C_q)	−0.2 (C−Si), 56.1 (OCH_3)
2t: (*S,S*)-	27.0−31.0	73.1	98.0−103.0	121.2−134.5 160.9 (C_q)	11.4, 16.6, 26.3, 35.2, 73.9 (R′′) 56.0 (OCH_3)
2u: (*S*)-	20.8−34.2	68.7	92.4, 94.9, 97.8, 107.0	129.4−139.6	72.9 (H_2C), 114.3 (CH) (R′′)
2v:	30.6 (COD), 34.6	64.2	99.1, 104.2	129.4−134.1	−
2w: (*R*)-	30.6 (COD), 34.6	65.3	98.8, 103.9	125.7−134.5 143.0 (C_q)	21.5

[a] For complexes **2i**, **2n** see Experimental Section. − [b] C_q = C_{Ar}−C, C_i = C_{Ar}−P.

temperature, the orange solution was stirred for 30−120 min (Table 8) and then cooled to −70°C once more. Then, a solution of 1 equiv. of nucleophile II (phosphane, thiol, or amine), generated by a deprotonation procedure analogous to that described for nucleophile I, was added in a dropwise manner to the cooled reaction mixture over a period of 30 min. The resulting mixture was stirred at room temperature for 2−16 h (Table 8). The solvent was then evaporated in vacuo (10^{-1} mbar) and the residue was suspended in 30 mL of diethyl ether. 20 mL of acetate buffer was added, the organic phase was separated, and the aqueous layer was extracted with three 20-mL portions of diethyl ether. The combined organic phases were dried with Na_2SO_4, the solvent was evaporated in va-

Table 16. Crystal data[a]

Compound	**2v**[b]	**2o**·CH_2Cl_2	**2b**[c]·CH_2Cl_2·1/2Et_2O	**2d**·Et_2O
Formula	$C_{35}H_{38}F_6OP_3Rh$	$C_{36}H_{40}F_6OP_3Rh$	$C_{37}H_{42}F_6OP_3Rh$	$C_{41}H_{50}F_6OP_3Rh$
Molecular mass	784.470	798.530	812.550	868.660
Crystal system	orthorhombic	monoclinic	triclinic	triclinic
Space group	$Pna2_1$	$C2/c$	$P1$	$P1$
Lattice constants	a = 1852.9(3)	a = 3129.9(5)	a = 1042.1 (1)	a = 1205.8(2)
	b = 1131.9(2)	b = 1280.9(1)	b = 1243.0 (2)	b = 1267.4(2)
	c = 1628.3(3) pm	c = 1901.9(1) pm	c = 1708.7 (2) pm	c = 1706.3(3) pm
	α = 90	α = 90	α = 79.27 (1)	α = 87.23(1)
	β = 90	β = 88.56(1)	β = 77.38 (1)	β = 70.44(1)
	γ = 90°	γ = 90°	γ = 67.31 (1)°	γ = 63.05(1)°
Cell volume	3415 × 10^6 pm^3	7623 × 10^{-6} pm^3	1980 × 10^6 pm^3	2174 × 10^6 pm^3
Molecular units per cell	Z = 4	Z = 8	Z = 2	Z = 2
Density (calculated)	1.526 g/cm^3	1.536 g/cm^3	1.453 g/cm^3	1.439 g/cm^3
Temperature	200 K	200 K	200 K	200 K
Number of reflections for cell refinement	30	32	34	25
Scan range	4.2° < 2Θ < 56.0°	3.4° < 2Θ < 50.0°	4.1° < 2Θ < 54.0°	3.6° < 2Θ < 48.0°
Method	ω scan, Δω = 0.47°	ω scan, Δω = 0.60°	ω scan, Δω = 0.60°	ω scan, Δω = 0.50°
scan speed [° min^{-1}]	8.0	15.0	10.0	12.0
Number of measured reflections	4263	6641	9131	11043
unique reflections	4263	6511	9131	10613
observed reflections ($I \geq 2\sigma$)	3070	4437	8324	10044
Number of parameters refined	382	489	898	1019
Maximum of residual Electron density	1.23 × 10^{-6} e/pm^3	0.51 × 10^6 e/pm^3	1.26 × 10^{-6} e/pm^3	0.59 × 10^{-6} e/pm^3
Agreement factors (F^2 refinement)	R_1 = 0.087	R_1 = 0.052	R_1 = 0.047	R_1 = 0.032
	R_w = 0.286	R_w = 0.132	R_w = 0.132	R_w = 0.094

Compound	**2g**[c]	**2f**[d]·CH_2Cl_2	**2e**[d]·CH_2Cl_2	**2c**·Et_2O
Formula	$C_{37}H_{42}F_6O_3P_3Rh$	$C_{43}H_{54}F_6O_3P_3Rh$	$C_{41}H_{48}F_6OP_3Rh$	$C_{37}H_{40}F_6OP_3Rh$
Molecular mass	844.530	928.70	866.650	810.540
Crystal system	monoclinic	monoclinic	orthorhombic	monoclinic
Space group	$P2_1$	$P2_1$	$P2_12_12_1$ #19	$P2_1$
Lattice constants	a = 1485.0(3)	a = 1516.5(4)	a = 1072.9(2)	a = 982.4(1)
	b = 1311.3(2)	b = 1522.9(3)	b = 1433.8(2)	b = 1630.5(2)
	c = 2041.2(4) pm	c = 2050.4(5) pm	c = 2695.3(3) pm	c = 1275.2(1) pm
	α = 90	α = 90.	α = 90	α = 90
	β = 108.72(1)	β = 110.49(2)	β = 90	β = 71.60(1)
	γ = 90°	γ = 90°	γ = 90°	γ = 90°
Cell volume	3764 × 10^6 pm^3	4435 × 10^6 pm^3	4146 × 10^6 pm^3	1938 × 10^6 pm^3
Molecular units per cell	Z = 4	Z = 4	Z = 4	Z = 2
Density (calculated)	1.490 g/cm^3	1.452 g/cm^3	1.524 g/cm^3	1.512 g/cm^3
Temperature	298 K	200 K	200 K	200 K
Number of reflections for cell refinement	31	31	30	29
Scan range	2.1° < 2Θ < 47.0°	2.1° < 2Θ < 50.2°	3.0° < 2Θ < 51.0°	4.2° < 2Θ < 50.1°
Method	ωscan, Δω = 0.43°	ωscan, Δω = 0.50°	ωscan, Δω = 0.54°	ωscan, Δω = 0.45°
scan speed [° min^{-1}]	12.0	8.0	8.0	10.0
Number of measured reflections	12137	7629	8612	7538
unique reflections	11117	7386	7565	6634
observed reflections ($I \geq 2\sigma$)	8730	6477	7189	6427
Number of parameters refined	853	1063	572	496
Maximum of residual electron density	0.59 × 10^{-6} e/pm^3	2.23 × 10^{-6} e/pm^3	0.45 × 10^{-6} e/pm^3	0.46 × 10^{-6} e/pm^3
Agreement factors (F^2 refinement)	R_1 = 0.045	R_1 = 0.067	R_1 = 0.027	R_1 = 0.030
	R_w = 0.113	R_w = 0.218	R_w = 0.062	R_w = 0.087

[a] The crystals of **2** tend to contain solvate molecules. The number and type of solvate molecules found per formula unit is given in the column header. − [b] Disorder of the COD ligand and of two of the aryl groups greatly reduces the accuracy of the structure determination. − [c] Disorder of the two PF_6 counterions. − [d] Disorder of one PF_6 counterion.

cuo, and the oily white residue was purified by column chromatography (silica gel, eluent and R_f as given in Table 8). Analytical difficulties arose in part due to the hygroscopic nature and the sensitivity to oxidation of the ligands when analytical samples were prepared without inert gas protection.

General Procedure for the Etherification of Ligands 1a−1n: 1 mmol of ligand was dissolved in 50 mL of freshly dried THF and the resulting solution was cooled to −5°C. At this temperature, 2 equiv. of KO*t*Bu were added and the solution was stirred for 2 min.

Methylation: 2 equiv. of methyl iodide were added to the above solution and the progress of the reaction was monitored by TLC. After completion of the reaction (maximum reaction time 30 min), the solvent and excess methyl iodide were evaporated in vacuo. The residue was dissolved in 30 mL of diethyl ether and the solution was filtered to remove potassium chloride. Removal of the solvent yielded the methylated ligands in an analytically pure state (Table 11).

Silylation: 1.6 equiv. of Me_3SiCl were added to the above solution and the progress of the reaction was monitored by TLC. After completion of the reaction (maximum reaction time 30 min), the solvent and excess Me_3SiCl were evaporated in vacuo. The residue was dissolved in 30 mL of CH_2Cl_2 and the solution was filtered to remove potassium chloride. If, after removal of the solvent, the products were not found to be analytically pure, they were further purified by column chromatography (Table 11).

Alkylation: 1.5 equiv. of alkyl tosylate were added to the reaction mixture and the ensuing reaction was monitored by TLC. The solution was stirred for 30 min, allowed to warm to room temperature, and then stirred for 6 h. If the conversion was not complete, the reaction mixture was cooled to −5°C once more, 0.5 equiv. of KO*t*Bu and alkyl tosylate were added and, after warming to room temperature, the solution was stirred for a further 4 h. The solvent was then evaporated in vacuo and the residue was purified by column chromatography (silica gel, eluent and R_f as given in Table 11). Compound **1u** could not be obtained in an analytically pure state because of identical R_f values for both the product and the corresponding long-chain alcohol. Therefore, the crude product **1u** was used to synthesize **2u**, which could be purified by column chromatography.

General Procedure for the Synthesis of Complexes 2: 0.5 equiv. of di-μ-chlorobis(η^4-1,5-cyclooctadiene)dirhodium(I) ($[Rh(COD)Cl]_2$) was dissolved in 10 mL of CH_2Cl_2 and a solution of 1.2 equiv. of potassium hexafluorophosphate in 5 mL of THF/acetone (1:1) was added. The mixture was stirred for 2 min. 1 mmol (1 equiv.) of the appropriate ligand was dissolved in 30 mL of CH_2Cl_2 and the resulting solution was added to the above mixture in a dropwise manner. After stirring for 30 min, the solvent was evaporated in vacuo, the residue was redissolved in 5 mL of CH_2Cl_2, and the solution was filtered through Na_2SO_4. Complexes **2** were precipitated as orange powders upon addition of 20 mL of diethyl ether. Further purification was generally not necessary but could be achieved by washing with diethyl ether, by recrystallization, or by chromatography. Chromatography on silica gel was possible when CH_2Cl_2 solutions of **2** were applied to a column with CH_2Cl_2 as the mobile phase. Elution with CH_2Cl_2 removed contaminants while compounds **2** did not noticeably migrate under these conditions. They were subsequently eluted with CH_2Cl_2/Et_2O or THF/Et_2O mixtures. On evaporation of the solvent from the eluate, the purified compounds **2** were obtained in microcrystalline form. The syntheses of the complexes containing an amine donor function (**2i**, **2n**), even under varied reaction conditions, invariably resulted in a mixture of different coordination products, as was clearly evident from the ^{31}P-NMR spectra. In none of these cases could a single product be separated by recrystallization or column chromatography.

X-ray Structure Determinations:[36] Single crystals were obtained by the layering technique. Exploratory experiments with various solvents (CH_2Cl_2, THF, Et_2O) and mixtures thereof had to be performed in order to obtain crystals of sufficient quality. Suitable crystals were taken directly from the mother liquor, immersed in perfluorinated polyether oil, and fixed to a glass rod at 200 K. In the case of **2g**, for which the data were collected at 298 K, the crystal was fixed in a Lindemann capillary. The measurements were made with a Siemens P4 four-circle diffractometer (equipped with a low-temperature device) using graphite-monochromated Mo-K_α radiation. All calculations were performed using the SHELXTPLUS[37] software package. Structures were solved by direct methods with the SHELXS-86 program[37a] and refined with the SHELX-93 program.[37b] Graphical handling of the structural data during solution and refinement was performed with XPMA.[38] Absorption corrections (ψ scan, $\Delta\psi = 10°$) were applied to the data. Atomic coordinates and anisotropic parameters of the non-hydrogen atoms were refined by full-matrix least-squares calculations. Data pertaining to the structure determinations are compiled in Table 16.

Acknowledgments

We are indebted to the Deutsche Forschungsgemeinschaft and the Fonds der Chemischen Industrie for financial support. A generous loan of rhodium(III) chloride by the DEGUSSA AG is gratefully acknowledged. We wish to thank T. Jannack for mass-spectrometric analysis and Dr. J. Groß for his help with high-resolution mass spectra. The continued enthusiasm and patience of Dr. Laszlo Zsolnai in solving crystal structures over more than two decades has helped a lot. Dr. Zsolnai died April 26, 1998.

[1] V. Caplar, G. Comisso, V. Sunjic, *Synthesis* **1981**, 85−116.
[2] M. Nógradi, *Stereoselective Synthesis*, VCH, Weinheim, **1995**.
[3] [3a] J. Halpern, D. P. Riley, A. S. Chan, J. J. Pluth, *J. Am. Chem. Soc.* **1977**, *99*, 8055−8057. − [3b] A. S. Chan, J. Halpern, *J. Am. Chem. Soc.* **1980**, *102*, 838−840. − [3c] P. S. Chua, N. K. Roberts, B. Bosnich, S. J. Okrasinski, J. Halpern, *J. Chem. Soc., Chem. Commun.* **1981**, 1278−1280. − [3d] J. M. Brown, P. A. Chaloner, *Tetrahedron Lett.* **1978**, *21*, 1877−1880. − [3e] C. R. Landis, J. Halpern, *J. Am. Chem. Soc.* **1987**, *109*, 1746−1754.
[4] H. B. Kagan, T. B. Dang, *J. Chem. Soc., Chem. Commun.* **1971**, 481−483.
[5] H. B. Kagan, T. B. Dang, *J. Am. Chem. Soc.* **1972**, *94*, 6429−6433.
[6] H. Brunner, *Handbook of Enantioselective Catalysis with Transition Metal Compounds*, VCH, Weinheim, **1993**.
[7] J. M. Brown, P. A. Chaloner, B. A. Murrer, D. Parker, *A. C. S. Symp. Ser.* **1980**, *119*, 169−194.
[8] P. McNeil, N. K. Roberts, B. Bosnich, *J. Am. Chem. Soc.* **1981**, *103*, 2273−2280.
[9] J. Bakos, I. Tóth, B. Heil, G. Szalontai, L. Párkányi, V. Fülöp, *J. Organomet. Chem.* **1989**, *370*, 263−276.
[10] [10a] S. R. Niketic, F. Woldbye, *Acta. Chem. Scand.* **1973**, *27*, 621−642. − [10b] M. Kojima, M. Fufita, J. Fujita, *Bull. Chem. Soc. Jpn.* **1977**, *50*, 898−906.
[11] See however modelling of tripod metal templates: S. Beyreuther, J. Hunger, G. Huttner, S. Mann, L. Zsolnai, *Chem. Ber.* **1996**, *129*, 745−757.
[12] J. Hunger, S. Beyreuther, G. Huttner, K. Allinger, U. Radelof, L. Zsolnai, *Eur. J. Inorg. Chem.* **1998**, *6*, 693−702.
[13] J. Scherer, G. Huttner, M. Büchner, *Chem. Ber.* **1996**, *129*, 697−713.
[14] J. Scherer, G. Huttner, M. Büchner, J. Bakos, *J. Organomet. Chem.* **1996**, *520*, 45−58.
[15] E. G. Thaler, K. G. Caulton, *Organometallics* **1990**, *9*, 1871−1876.

[16] E. G. Thaler, K. Folting, K. G. Caulton, *J. Am. Chem. Soc.* **1990**, *112*, 2664−2672.
[17] W. O. Siegl, S. J. Lapporte, J. P. Collmann, *Inorg. Chem.* **1971**, *10*, 2158−2165.
[18] H. Brunner, A. Sicheneder, *Angew. Chem.* **1988**, *100*, 730−731, *Angew. Chem. Int. Ed. Engl.* **1988**, *27*, 718−719.
[19] [19a] Th. Seitz, A. Muth, G. Huttner, Th. Klein, O. Walter, M. Fritz, L. Zsolnai, *J. Organomet. Chem.* **1994**, *469*, 155−162. − [19b] Th. Seitz, G. Huttner, M. Büchner, *Z. Naturforsch. B* **1994**, *49*, 1813−1817.
[20] P. Schober, R. Soltek, G. Huttner, L. Zsolnai, K. Heinze, *Eur. J. Inorg. Chem.* **1998**, 1407−1415.
[21] [21a] A. Frick, Diplomarbeit, Universität Heidelberg, **1996**. − [21b] Publication in preparation.
[22] A. Jacobi, G. Huttner, U. Winterhalter, *J. Organomet. Chem.*, in press. It thus appears that with six-membered chelate cycles, hydroxy or alkoxy functionalization at the chelate backbone does not drastically influence reactivity. This is in contrast to the observations made for larger, more flexible chelate cycles, where this type of substitution interferes with reactivity as well as selectivity. For a review see: J. Holz, M. Quirmbach, A. Börner, *Synthesis* **1997**, 983−1006.
[23] [23a] W. S. Knowles, B. D. Vineyard, M. J. Sabacky, *J. Chem. Soc., Chem. Commun*. **1972**, 10−11. − [23b] B. D. Vineyard, W. S. Knowles, M. J. Sabacky, D. J. Weinkauff, *J. Am .Chem. Soc.* **1975**, *97*, 2567−2568. − [23c] B. D. Vineyard, W. S. Knowles, M. J. Sabacky, G. L. Bachmann, *J. Am. Chem. Soc.* **1977**, *99*, 5946−5952.
[24] *Organikum*, Deutscher Verlag der Wissenschaften, Berlin, **1990**.
[25] J. Baldwin, A. Raab, K. Mensler, B. Arison, D. McClure, *J. Org. Chem.* **1978**, *43*, 4876−4878.
[26] K. Issleib, A. Tzack, *Chem. Ber.* **1959**, *92*, 704−711.
[27] K. Issleib, H. O. Fröhlich, *Z. Naturforsch. B* **1959**, *14*, 349−350.
[28] [28a] F. G. Mann, E. J. Chaplin, *J. Chem. Soc.* **1937**, 527−535. − [28b] G. P. Schiemenz, *Angew. Chem.* **1968**, *80*, 559−560; *Angew. Chem. Int. Ed. Engl.* **1968**, *7*, 544−545. − [28c] C. A. Tolman, *J. Am. Chem. Soc.* **1970**, *92*, 2956−2965.
[29] M. Culcasi, Y. Berchadsky, G. Groncho, P. Tordo, *J. Org. Chem.* **1991**, *56*, 3537−3542.
[30] J. B. Lambert, J. H. So, *J. Org. Chem.* **1991**, *56*, 5960−5962.
[31] [31a] G. Schiemenz, H. Kack, *Liebigs Ann. Chem.* **1973**, 1494−1504. − [31b] C. Ziegler, R. Heck, *J. Org. Chem.* **1978**, *43*, 2941−2946.
[32] P. Budzelaar, J. Doorn, N. Meijboom, *Recl. Trav. Chim. Pays-Bas* **1991**, *110*, 420−432.
[33] L. Horner, G. Simons, *Phosphorus Sulfur* **1983**, *15*, 165−175.
[34] [34a] J. Cornforth, R. H. Cornforth, R. T. Grey, *J. Chem. Soc., Perkin Trans. 1* **1982**, 2289−2297. − [34b] E. H. Braye, I. Chaplier, R. Saussez, *Tetrahedron* **1971**, *21*, 5523−5537.
[35] G. Giordano, R. H. Crabtree, *Inorg. Synth.* **1990**, *28*, 88−90.
[36] Tables of the fractional atomic cordinates are available from the author on request. Further details of the crystal structure investigations may be obatined from the Fachinformationszentrum Karlsruhe, D-76344 Eggenstein-Leopoldshafen on quoting the depository numbers CSD-410021 (**2o**), -410022 (**2c**), -410023 (**2f**), -410024 (**2g**), -410025 (**2e**), -410026 (**2v**), -410027 (**2d**), and -410028 (**2b**).
[37] [37a] G. M. Sheldrick, *SHELX(S)-86*, University of Göttingen, **1986**. − [37b] G. M. Sheldrick, *SHELXL-93*, University of Göttingen, **1993**. − [37c] *International Tables for X-ray Crystallography*, vol. 4, Kynoch Press, Birmingham, U.K., **1974**.
[38] L. Zsolnai, G. Huttner, *XPMA*, University of Heidelberg, **1994**.

Received August 19, 1998
[I98285]

Addition of Stabilized Carbanions to Cationic (η^6-Arene)tricarbonylmanganese Complexes: Syntheses of Homo (Mn–Mn) and Hetero (Mn–Cr) Dinuclear Complexes

Eric Rose,*[a] Claudine Le Corre-Susanne,[a] Françoise Rose-Munch,[a] Christophe Renard,[a] Vanessa Gagliardini,[a] Fatima Teldji,[a] and Jacqueline Vaissermann[b]

Keywords: Arene complexes / Chromium / Cyclohexadienyl complexes / Dinuclear complexes / Manganese

The reaction of secondary α-cyano or α-sulfonyl carbanions with cationic (η^6-arene)tricarbonylmanganese complexes affords neutral mono- and dinuclear tricarbonyl(η^5-cyclohexadienyl)manganese complexes. The X-ray analyses of three (η^5-cyclohexadienyl)Mn complexes (two mononuclear and one dinuclear) obtained by addition of α-cyano carbanion to cationic (η^6-arene)manganese complexes are reported. The addition of benzylic carbanions of (η^6-arene)tricarbonylchromium complexes to cationic (η^6-arene)manganese complexes gives rise to the formation of the corresponding heterodinuclear [(η^5-cyclohexadienyl)-manganese–(η^6-arene)chromium] complexes.

Introduction

The air-stable [(η^6-arene)$Mn(CO)_3$] cations are quite electrophilic and the addition of nucleophiles to the arene ring affording thermally stable cyclohexadienyl complexes has been the subject of numerous studies.[1] Among them, a mere handful of papers describes the use of organometallic derivatives as nucleophiles[2−4] towards (η^6-arene)tricarbonylmanganese complexes giving rise to the formation of homo- and heteropolymetallic complexes.

Our studies concerning the structure and reactivity of (η^6-arene)tricarbonylmanganese complexes and their application in organic synthesis, led us to discover the possibility of synthesizing di- or even trinuclear complexes by the simple addition of stabilized carbanions to cationic manganese complexes. In particular, during the course of our work on the synthesis of mescaline (**1**), a natural product with hallucinogenic properties, we undertook the study of the regioselectivity of the addition of primary and secondary stabilized carbanions to tricarbonyl(1,2,3-trimethoxybenzene)manganese complex **2**[5] (Equation 1). We observed the formation of mononuclear complex **3** and unexpected dinuclear complex **4**.

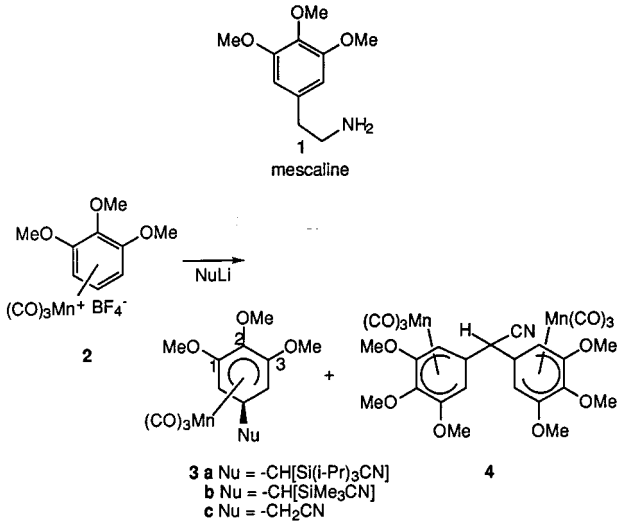
We report an extension of this work as well as a complete study of the addition of stabilized carbanions, α-cyano and α-sulfonyl carbanions to the simplest complex: the benzene manganese complex, and the structures of one dinuclear and two mononuclear complexes obtained by this method. In addition, we describe an extension of this method to the preparation of new heteropolymetallic Mn−Cr complexes.

[a] Laboratoire de Synthèse Organique et Organométallique, UMR CNRS 7611, Université P. et M. Curie, Tour 44 − 1er étage, 4, Place Jussieu, F-75252 Paris Cedex 05, France
Fax: (internat.) + 33(0)1/44277089
E-mail: rose@ccr.jussieu.fr
[b] Laboratoire de Chimie des Métaux de Transition, URA CNRS 409, Université P. et M. Curie, Bâtiment F, 4, Place Jussieu, F-75252 Paris Cedex 05, France

Results and Discussion

Addition of Silylated α-Cyano Carbanions to (1,2,3-Trimethoxybenzene)manganese Complex

Our first attempt at functionalizing the trisubstituted arene ring of complex **2**, in order to synthesize a precursor of mescaline (**1**), involved the reaction of lithioacetonitrile (Equation 1). Unfortunately, the reaction mixture turned black and decomposition occured very quickly. Since more substituted carbanions have previously been shown to be nucleophiles of optimum reactivity for addition to arene−Cr complexes,[6] we anticipated that the same would apply to Mn complexes. We thus decided to study the reactivity of more crowded nucleophiles such as silylated α-cyano carbanions.



Equation 1. Nucleophilic addition of a nucleophile to tricarbonyl(1,2,3-trimethoxybenzene)manganese complex **2**

2-Lithio-2-(triisopropylsilyl)acetonitrile, prepared in situ by addition of lithium (diisopropyl)amide, LDA, to a solu-

 © WILEY-VCH Verlag GmbH, D-69451 Weinheim, 1999 1434−1948/99/0303−0421 $ 17.50+.50/0

tion of one equivalent of (triisopropylsilyl)acetonitrile in THF under N_2 at −78°C, reacted with complex **2** to give the neutral complex **3a**, Equation 1, in 38% yield. An analogous reaction occured with the anion of (trimethylsilyl)acetonitrile as nucleophile, yielding complex **3b** as the major product. Unexpectedly, a silicon−carbon bond cleavage occurred after silica gel column chromatography, affording complex **3c**. We noticed also the formation of a minor dinuclear complex **4** in 12% yield, whose formation will be discussed later (vide infra, mechanism involved in the synthesis of complex **7a**).

In the case of the two mononuclear neutral complexes **3a** and **3c** we were able to obtain crystals suitable for X-ray determinations. The structures appear in Figures 1 and 2 whereas the crystallographic data, selected bond lengths and bond angles can be found in Table 1.

Table 1. Selected bond lengths [Å] and bond angles [°] for **3a** and **3c**

Bond lengths	Complex **3a**	Complex **3c**
Mn−C1	2.178(6)	2.19(1)
Mn−C2	2.143(6)	2.15(1)
Mn−C3	2.194(6)	2.19(1)
Mn−C4	2.169(6)	2.18(1)
Mn−C6	2.201(6)	2.20(1)
Bond angles	**Complex 3a**	**Complex 3c**
C4−C5−C6	104.3(5)	103.8(9)
C2−Mn−C6	68.1(2)	67.8(4)
C2−Mn−C4	68.3(2)	68.4(4)
C2−O2−C8	118.0(2)	113.8(10)

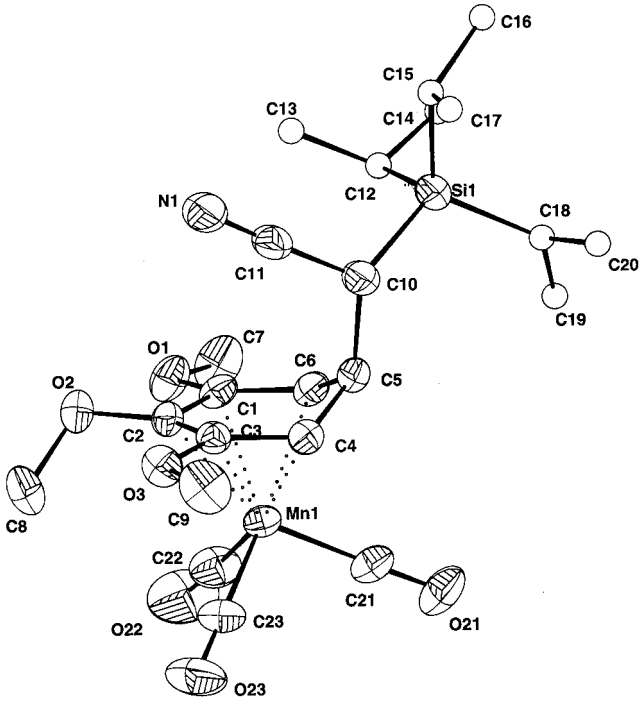


Figure1. ORTEP diagram of complex **3a**

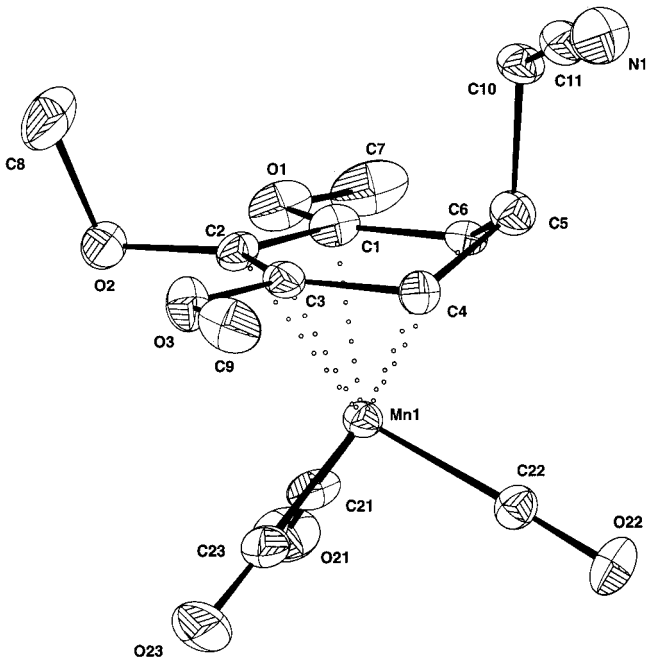


Figure 2. ORTEP diagram of complex **3c**

The ORTEP views show classical (η^5-cyclohexadienyl) structures with the five ring atoms C^1, C^2, C^3, C^4, C^5, almost coplanar while the remaining atom C^6 lies in a $C^4-C^5-C^6$ plane making an angle of 40° with the other one (in both complexes). It is worth noting the completely different position adopted by the OMe groups attached to the C^2 atoms: in the case of complex **3a**, this methoxy group is pointing away from the bulky silylated substituent attached to the sp^3 carbon atom, and thus it is located on the same side of the ring plane with respect to the $Mn(CO)_3$ moiety. The reverse is observed for the corresponding methoxy group of complex **3c**: it is opposite to the organometallic entity.

The ^{1}H- and ^{13}C-NMR data of complexes **3a**, **3b**, **3c**, and **4** are presented in Tables 2 and 3. We noticed that the ^{13}C-NMR data of the C^1, C^2, C^3 atoms of the four complexes (Table 3) were in good agreement with those observed in the case of unsubstituted neutral η^5-cyclohexadienyl−Mn complexes[7] or even in the case of η^5-Cr complexes.[8] This feature was attributed to a strong charge alternation in such η^5 systems as it was shown by charge density calculations at the individual carbon atoms.[9] Thus, the C^2 signals are shielded by roughly 20 ppm with respect to the C^1 and C^3 signals (Table 3).

Also interesting to note are the more shielded signals of H^4, H^5, H^6 of dinuclear complex **4** when compared to the corresponding proton signals of the mononuclear complex **3c** (Table 2).

No significant effect could be dectected comparing the chemical shifts of the OMe groups attached to the C^2 atoms of the complexes **3a** and **3c** (δ = 4.02 and 4.06, respectively, Table 2). Therefore, it was clear that the methoxy groups did not keep the same orientation in solution as in the solid state because of the free rotation of the methoxy groups.

Table 2. ^{1}H-NMR data of complexes **3a**, **3b**, **3c**, **4** (in $CDCl_3$)

	$H^{4[a]}$	$H^{6[a]}$	H^5	H^7	OMe^2	$OMe^{1[b]}$	$OMe^{3[b]}$
3a	2.83	3.14	2.93	1.44	4.02	3.43	3.58
3b	2.84	3.09	2.77	1.28	4.06	3.47	3.58
3c	2.90	2.90	2.90	1.67	4.06	3.48	3.48
4	2.66	2.76	2.52	0.98	3.99	3.50	3.59

[a] H^4 or H^6. – [b] OMe^1 or OMe^3.

In order to better understand the mechanism of formation of dinuclear complexes such as **4**, we extended this study to the reactivity of α-cyano carbanions towards the simplest arene−Mn complex: that of benzene.

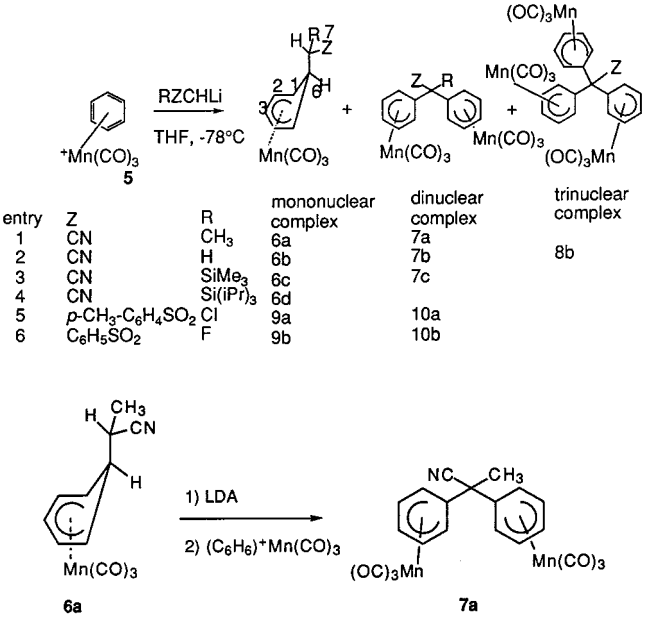
Addition of α-Cyano Carbanions to the (η^6-Benzene)manganese Complex 5

2-Lithiopropionitrile (prepared in situ by addition of LDA to a solution of one equivalent of propionitrile in THF under N_2 at −78°C) reacted with one equivalent of (η^6-benzene)tricarbonylmanganese complex **5** to give the mononuclear complex **6a** and the dinuclear complex **7a** (Table 4) in 76% and 11% yield, respectively. These complexes were purified by flash chromatography on an alumina column. An analogous reaction in the presence of an excess of **5** (two equivalents) and an excess of LDA (two equivalents) allowed us to isolate complex **7a** as the major product (61% yield) as well as complex **6a** (24% yield). It is interesting to note that, although some additions of α-cyano carbanions to (η^6-arene)manganese complexes have already been reported,[10−12] no formation of dinuclear complexes was described.

The formation of the dinuclear complex **7a** was easily explained. Indeed, in this basic medium, the acidic proton, α to the cyano group of complex **6a** could be abstracted, giving rise to a new carbanion which could, in turn, add to the arene ring of complex **5**. Two points support this mechanism: 1. The higher yield of complex **7** obtained when an excess of complex **5** and LDA were used; this is in good agreement with our mechanism proposal. 2. In a separate experiment which was carried out starting from complex **6a** itself, the addition of one equivalent of LDA to complex **6a** and further reaction with cationic complex **5**, gave complex **7a** in almost quantitative yield (Equation 2).

The ^{1}H-NMR spectrum of complex **6a** in $CDCl_3$ showed expected signals at δ = 5.80 (H^3), δ = 4.97 and 4.92 (diastereotopic protons H^2 and H^4), δ = 3.34 and 3.15 (diastereotopic protons H^1 and H^5) whose multiplicities could be unambigously interpreted (Table 5). The difference between the chemical shifts of the H^1 and H^5 signals is larger than the one between the H^2 and H^4 signals, certainly due to the proximity of the chiral center.

Table 4. Nucleophilic addition of a nucleophile to benzenetricarbonylmanganese complex



Equation 2. Preparation of dinuclear complex **7a**

The ^{1}H-NMR spectrum of complex **7a** showed the same features due to the η^5-cyclohexadienyl structure but two points warranted comment (Table 5): 1. An overall deshielding effect was observed for the protons of the dinuclear structure relative to those of the mononuclear structure. This effect can reach 1.44 ppm in the case of the H^1 signal. An opposite effect was noticed in the case of complexes **3c** and **4**, clearly showing the effect of the three methoxy groups. 2. Although the H^2 and H^4 atoms did not present distinct signals for complex **7a**, the H^1 and H^5 atoms showed two signals with a very important difference − a shift of 1.43 ppm was observed instead of 0.19 ppm for the corresponding protons of complex **6a**.

Recrystallization of complex **7a** in an acetone/ether mixture afforded yellow single crystals suitable for X-ray analysis. As can be seen from the ORTEP view in Figure 3 the structure showed a classical (η^5-cyclohexadienyl) struc-

Table 3. ^{13}C-NMR data of complexes **3a**, **3b**, **3c**, **4** (in $CDCl_3$)

	C^{1a}	C^{3a}	C^{2b}	OMe^2	OMe^{1c}	OMe^{3c}	C^5	C^{4d}	C^{6d}
3a	136.2	136.9	115.8	66.3	54.7	55.3	35.8	35.7	36.4
3b	136.3	136.7	116.5	66.3	54.8	55.3	35.9	35.5	36.2
3c	137.1	137.1	115.4	66.8	55.3	55.3	34.4	33.8	33.8
4	137.2	137.5	115.1	66.2	55.4	55.6	35.3	32.3	33.2

[a] C^1 or C^3 – [b] CN or C^2 – [c] OMe^1 or OMe^3 – [d] C^4 or C^6.

Table 5. ^{1}H-NMR data of complexes **6a**, **7a** (in [D_6]acetone)

	H^3	H^2 or H^4	H^4 or H^2	H^1 or H^5	H^5 or H^1
Complex **6a**	5.80, t J = 6.1	4.97, t J = 6.1	4.92, t J = 6.1	3.34, tt J = 6.1 and 1.5	3.15, tt J = 6.1 and 1.5
Complex **7a**	5.98, tt J = 5.7 and 1.3	5.25, m	5.25, m	4.78, tt J = 5.7 and 1.3	3.35, tt J = 5.7 and 1.3

ture.[7] The sp^3 carbon atoms (C^6 and $C^{6'}$) of the rings are each eclipsed by a Mn−CO bond. The anion added on the *exo* face with respect to the manganese atom. The cyclohexadienyl rings are nearly planar and fold about $C^1C^6C^5$ and $C^{1'}C^{6'}C^{5'}$ with the same angle of 36°. The two metal centers are 7.556(6) Å apart. Crystallographic data, selected bond lengths and bond angles are listed in Table 6. It is worth noting that the two metal centers are not directly bonded to each other and could not be linked: our trials to form a metal−metal bond by irradiating, for example, complex **7a**, failed.

2-Lithioacetonitrile (prepared by addition of LDA to a solution of acetonitrile in THF under nitrogen at −78°C) reacted with (η^6-benzene)manganese complex **5** giving rise to the formation of three compounds (Table 4, entry 2) (overall yield 58%): the mononuclear complex **6b**, the dinuclear complex **7b** and the unexpected complex **8b** in a 80:18:2 ratio. This "caroussel-like" complex **8b** was very dif-

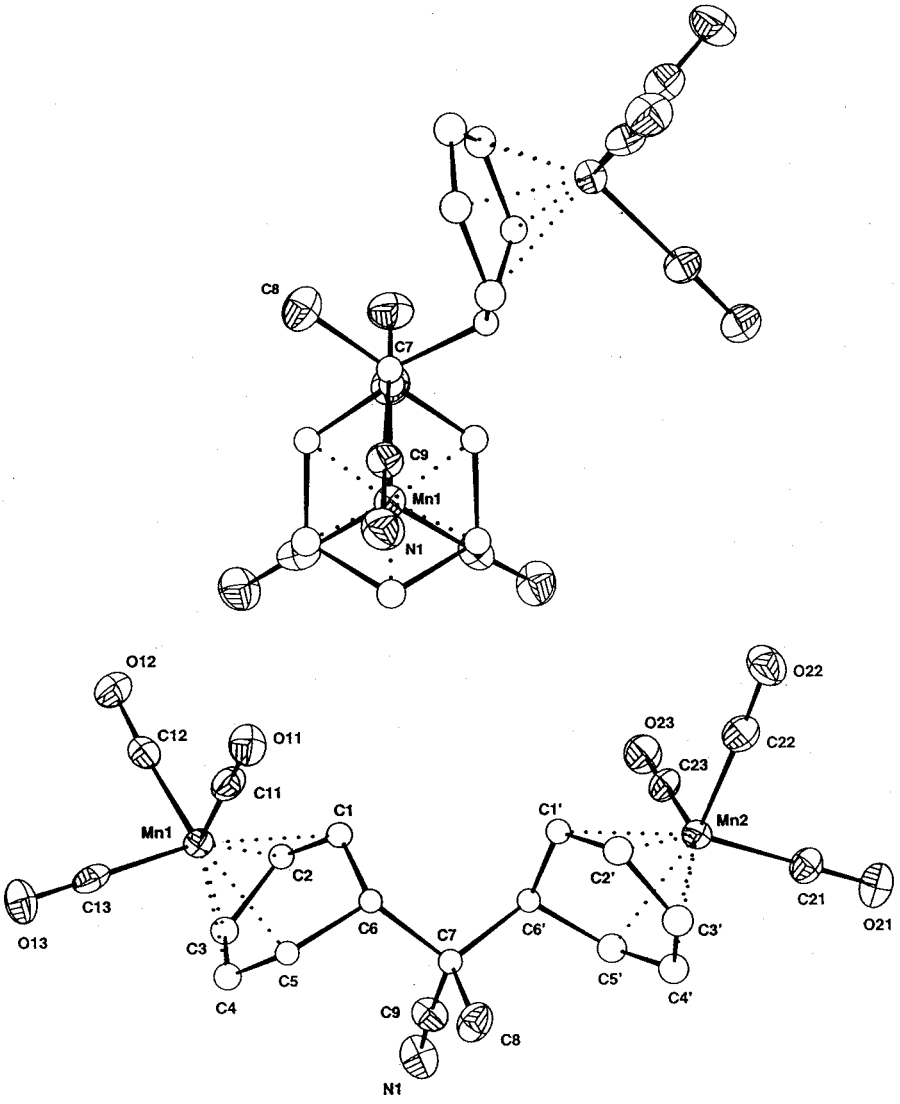


Figure 3. ORTEP diagram of complex **7a**

Table 6. Selected bond lengths [Å] and bond angles [°] for **7a**

Bond lengths	Bonds angles
Mn1−C3: 2.14 (1)	C8−C7−C9: 108.5 (11)
Mn2−C3′: 2.12 (1)	C1−C6−C5: 103.1 (10)
C7−C6: 1.58 (2)	C1′−C6′−C5′: 103.6 (10)
C7−C6′: 1.57 (2)	

ficult to isolate from the mixture of **6b** and **7b**; nevertheless we succeeded in obtaining **8b** in 11% yield by using 1.2 equivalents of LDA and 0.4 equivalents of nitrile. All attempts to obtain crystals of **8b** suitable for X-ray crystallography were unsuccessful: the sharp needles obtained so far are too small to be studied.

In solution, the ^{1}H-NMR spectrum of the "caroussel" complex **8b** showed also the atom H^3 as the less shielded one at $\delta = 5.85$, the atoms $H^{2,4}$ at $\delta = 5.04$ and the atoms $H^{1,5}$ at $\delta = 3.12$ in $CDCl_3$ (Table 7). The ^{13}C-chemical shifts of the carbon atom bearing the cyano group are in good agreement with the substitution of this bridge carbon atom. Indeed this carbon atom, which resonates at $\delta = 29$ in the case of complex **6b**, is deshielded by 26.4 ppm in the case of complex **7b** ($\delta = 55.4$) and by 37.2 ppm in the case of **8b** ($\delta = 66.2$) (Table 8).

Table 7. ^{1}H-NMR data of complexes **6b**, **7b**, **8b** (in $CDCl_3$)

	H^3	H^4	H^5	H^6
6b	5.84	4.94	3.23	2.94
7b	5.81	4.93	3.12	2.68
8b	5.85	5.04	3.12	2.79

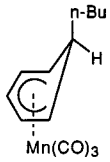
Table 8. ^{13}C-NMR data of complexes **6b**, **7b**, **8b** (in [D_6]acetone)

	C^1	C^2	C^3	C^6	CN	C(CN)
6b	53.2	96.9	80.7	31.7	116.7	29.0
7b	54.3	99.2	83.5	34.6	119.7	55.4
	56.4	99.0				
8b	55.4	98.0	81.7	36.7	120.0	66.2

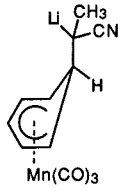
Under the same conditions, 2-lithio-2-(trimethylsilyl)-acetonitrile (2.2 equivalents) reacted with one equivalent of complex **5** (Table 4, entry 3) to give a mixture of complexes **6c**, **7c**, **6b**, and **7b** in a 64:28:7:1 ratio in 66% overall yield after a very fast silica gel column chromatography to avoid C−Si bond cleavage. Using a bulkier anion such as 2-lithio-2-(triisopropylsilyl)acetonitrile (2.2 equivalents), the same reaction gave only complex **6d** (Table 4, entry 4). No C−Si bond scission was noticed, even after silica gel column chromatography.

Addition of α-Sulfonyl Carbanions to the (η^6-Benzene)manganese Complex 5

Lithiation of chloromethyl *p*-tolyl sulfone $CH_3-C_6H_4-SO_2-CH_2Cl$ with *n*BuLi gave the corresponding α-sulfonyl carbanion[13,14] which reacted with one equivalent of complex **5** in a THF suspension. Two complexes **9a** and **10a** were isolated in a 1:1 ratio (73% yield) (Table 4, entry 5). The ^{1}H-NMR spectra were in good agreement with an η^5-cyclohexadienyl mononuclear structure for complex **9a** and with a dinuclear structure for complex **10a**. Indeed, in the case of complex **9a**, the atom H^7 attached to the sp^3 carbon atom resonates as a doublet at $\delta = 3.65$ and is absent in the case of complex **10a**. With the phenylsulfonylfluoromethyl carbanion $C_6H_5-SO_2-CHFLi$,[15] analogous results were obtained: Two complexes **9b** and **10b** were isolated in a 9:1 ratio (48% yield) (Table 4, entry 6). When two equivalents of complex **5** and two equivalents of *n*BuLi were used, three complexes **9b**, **10b**, and **11** were isolated in 3, 52, and 16% yield, respectively. The less polar complex **11**, which was eluted first by silica gel flash column chromatography, appeared to be the neutral 6-*exo*-butyl-η^5-cyclohexadienyl derivative whose preparation by a different method was previously reported by Chung et al.[16] In a separate experiment, complex **11** could be obtained in almost quantitative



11



12

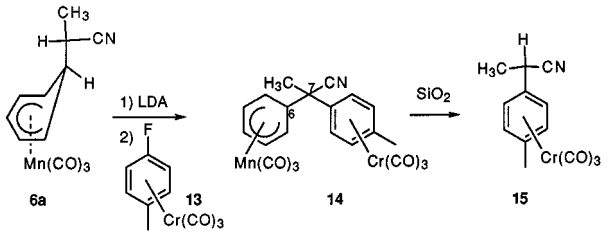
yield by treating one equivalent of *n*BuLi with complex **5**.[4]

We thus demonstrated the high reactivity of the α-cyano carbanion of complex **6a** towards benzene complex **5** (Equation 2), allowing us to synthesize, by this original way, homonuclear dimetallic complexes. We then tried to take advantage of these results in treating the same carbanion with other organometallic electrophilic complexes, such as chromium complexes, to obtain an access to heterodinuclear complexes.

Heterodinuclear Complex Syntheses

It is well known that arenes coordinated to the tricarbonylchromium entity are very electrophilic and the corresponding complexes, substituted by a good leaving group, readily undergo *ipso*,[17] *cine*,[18] or *tele*[19] nucleophilic aromatic substitutions. Addition of tricarbonyl(*p*-fluorotoluene)chromium complex **13** to the carbanion **12** of complex **6a** yielded the heterodinuclear complex **14**, detected by NMR spectroscopy in the crude mixture. However, when the reaction mixture was filtered through a silica gel chromatography column, a new unexpected *para*-disubstituted arenetricarbonylchromium complex **15** was isolated (Equation 3). This tricarbonyl[2-(*para*-tolyl)propionitrile]chromium complex **15** was obtained by cleavage of the C^6-C^7 bond and subsequent rearomatization of the (η^5-cyclohexadienyl)manganese part of complex **14**. It is worth noting that this complex **14** could be obtained in 37% yield along with complex **15** (63% yield) by adding the lithium salt of

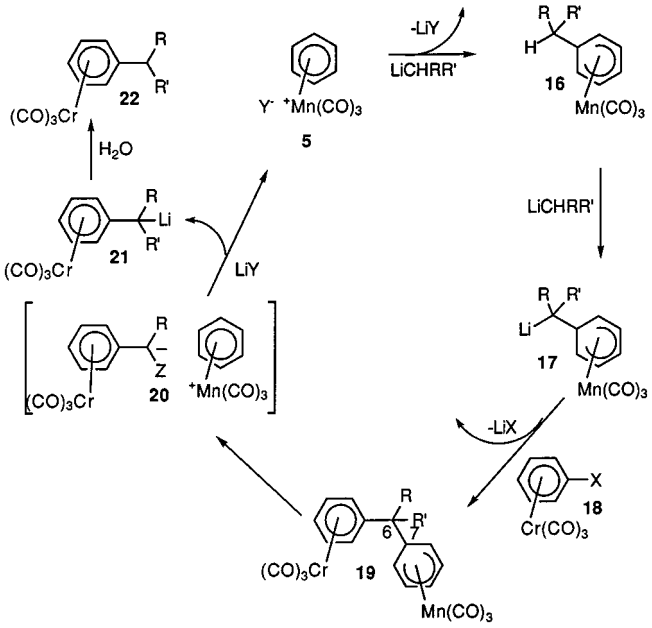
complex **15** to the arene complex **5**, followed by a simple extraction without further purification. When the mixture was subjected to chromatography, only complex **15** was obtained.



Equation 3. Synthesis of *para*-disubstituted complex **15** from **6a** and **13**

Treating the tricarbonyl(*p*-flurorotoluene)chromium complex **13** with the lithium salt **12** gave a new *para*-disubstituted arenetricarbonylchromium complex **15** and the cationic benzene complex **5**. The carbanion **12** plays an unexpected role because it is an unusual way to render the reaction of the propionitrile carbanion with (η^6-benzene)tricarbonylmanganese cation **5** reversible, by an indirect process! We can point out that *ipso* substitution of the fluoro group of **13** by a propionitrile carbanion can also give complex **15**. Thus, the carbanion **12** is a formal precursor of the carbanion of the propionitrile. It is obvious that this reaction would be of great interest if we could apply it to the addition of anions which do not react with arenechromium complexes but which react easily with arenemanganese complexes. Indeed it is well known that manganese complexes are much more reactive than chromium complexes. The reaction could maybe work in the presence of a catalytic amount of complex **5** according to the mechanism represented in Scheme 1. Indeed a primary or secondary carbanion LiCHRR′ in the presence of complexes **5** (catalytic amount) and **18** (X being a good leaving group) could react faster with the more electrophilic complex **5**, giving a catalytic amount of complex **16**. Complex **16**, in this medium, could be deprotonated yielding a catalytic amount of the complex **17** which could react with complex **18** giving complex **19** and LiX. Cleavage of the C^6-C^7 bond of the binuclear complex **19** could afford the zwitterionic complex **20**. In the presence of LiY, the complexes **22** (after hydrolysis of **21**) and **5** could be obtained; thus **5** might play a catalytic role in this process.

Having thus established the easy addition of benzylic anions such as **15-Li** to complex **5**, we turned our attention to modifications of the nature of the substituents at the bridgehead carbon atom of dinuclear complexes such as **14**, so as to increase the stability of the newly-formed C^6-C^7 bond. For this purpose, we assumed that it would be interesting to replace the electron-withdrawing cyano group by an electron-donating group such as methoxy.[20] For this reason, we treated the benzylic carbanion **23** (Z = OMe, R′ = R″ = H) with the cationic benzene complex **5** (Table 9, entry 1). We were pleased to find that the dinuclear complex **24a** could be obtained almost quantitatively (according to the ^{1}H-NMR spectrum of the crude mixture), and that



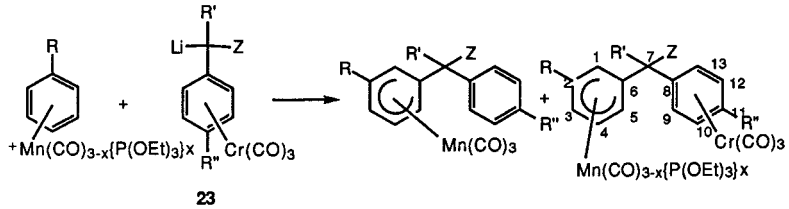
Scheme 1. Tranformation of **18** into **22**: possible mechanism for the carbon−carbon bond formation catalyzed by benzenetricarbonylmanganese complex **5**

it could be purified by silica gel chromatography without any cleavage of the C^6-C^7 bond. However, some decoordination of chromium occured giving rise to the formation of the product **25** (29%), free of Cr, besides the expected complex **24a** (41%). It is thus clear that the nature of the substituent at the benzylic position of the nucleophile plays an important role with respect to the stability of the bridge of these dinuclear complexes.

We were interested in the fate of this reaction (Table 9) when other ligands around the manganese atom were used. Indeed, it has been demonstrated that substitution of one or two CO ligands of arene manganese complexes by phosphane or phosphite could lead to cleaner reactions during the nucleophilic addition process[4,7a,24,25] and, in some cases, could even modify the regioselectivity of the addition.[23] We thus prepared complexes $\mathbf{5P}_1$ and $\mathbf{5P}_2$ by substituting one and two carbonyl groups by one and two triethyl phosphito groups, respectively. After addition of carbanion **23** (Z = OMe, R′ = R″ = H) to $\mathbf{5P}_1$ (or $\mathbf{5P}_2$), we isolated, after column chromatography, the complex **24b** in 55% yield (or **24c** in 47% yield) and starting Cr complex **23** in 16% yield (28% in the case of $\mathbf{5P}_2$) (Table 9, entries 2 and 3). In both cases, no sign of chromium decoordination was detected. The NMR study of the η^5-cyclohexadienyl rings of complexes **24** reflected the electronic influence of the phosphito ligands on the cycle coordinated to the Mn entity. A shielding effect was detected in the ^{1}H- and ^{13}C-NMR spectra (Table 10). No modification of chemical shifts of chromium ring proton signals was observed.

The role of the phosphito ligands with respect to the manganese atom could thus be two-fold: 1. The phosphito ligands, being weaker π-acceptors than CO ligands, lead to an increase of the electron density of the cycle and lower the activation of the manganese complex towards nucleophilic

Table 9. Addition of benzylic anions prepared from tricarbonylchromium complexes to cationic Mn complexes



		Cr complex			mononuclear	dinuclear
entry	Mn complex	Z	R'	R"	complex	complex
1	5 R=H, x=0	OMe	H	H	25	24a
2	$5P_1$ R=H, x=1	OMe	H	H		24b
3	$5P_2$ R=H, x=2	OMe	H	H		24c
4	26a R=OMe, x=0	OMe	CH_3	H		27a
5	26b R=OMe, x=1	OMe	CH_3	H		27b

Table 10. Shielding effect of phosphito ligands on the η^5-cyclohexadienyl ring of complexes **24**

Complexes **24**	**24a**	**24b**	**24c**
H^1 and H^5	3.30, 2.83	3.04, 2.54	2.61, 2.05
H^2 and H^4	4.91	4.73	4.53
H^3	5.79	5.53	5.18
H^6	2.60	2.62	2.51
C^1 and C^5	51.7, 54.6	48.5, 51.4	45.2, 47.8
C^2 and C^4	96.8, 97.0	95.3, 95.5	93.2, 93.7
C^3	80.4	79.5	76.8
C^6	87.0	87.0	87.2

addition. Thus, 16% and 28% of starting material was recovered when $\mathbf{5P_1}$ and $\mathbf{5P_2}$, respectively, were used. 2. Although the phosphito−manganese complexes were less electrophilic, better yields in **24b** and **24c** were observed (55% and 47%, respectively) due to an overall stabilization of these dinuclear complexes, which is as yet difficult to explain.

To further investigate the regioselectivity of the addition of α-benzylic carbanions to manganese complexes, we treated the carbanion **23** (Z = OMe, R′ = CH_3, R′′ = H) with the cationic (η^6-anisole) complex **26a**. We observed the formation of only one regioisomer **27a** in 47% yield as a mixture of two diastereoisomers in a 1:1 ratio (measured by integrating the methoxy protons at C2), and some Cr complex starting material (26%) (Table 9, entry 4). Addition occured, as expected, *meta* to the methoxy group.[21,22] No formation of a mononuclear Mn complex due to the decoordination of the chromium entity was observed.

An analogous reaction was carried out with the anisole dicarbonyl mono-phosphito complex **26b** in order to gain insight into the influence of the nature of manganese ligands. Thus, complex **26b** treated with the benzylic carbanion **23** (Z = OMe, R′ = CH_3, R′′ = H) yielded complex **27b** as a unique regioisomer in 64% yield (2 diastereoisomers in a 1:1 ratio) (Table 9, entry 5) and some Cr starting material was recovered. In this example again, substitution of a CO ligand by a phosphito ligand led to a significant increase of the yield of the dinuclear complex. As already observed for complexes **24**, the ^{1}H- and ^{13}C-NMR spectra of complex **27b** showed shielded signals compared to those of complex **27a**: for example, the H^3 and H^4 atoms are shielded by 0.34 and by 0.26 ppm and the C^3 and C^4 atoms are shielded by 1.3 and 0.9 ppm, respectively.

Conclusion

The reaction of stabilized carbanions with cationic (η^6-arene)tricarbonylmanganese complexes gives, as expected, neutral mononuclear tricarbonyl(η^5-cyclohexadienyl)manganese complexes. But, depending on the amount of carbanion, these reactions can also lead to dinuclear tricarbonyl(η^5-cyclohexadienyl)manganese complexes. With a primary carbanion, it was even possible to isolate a "caroussel-like" trinuclear tricarbonyl(η^5-cyclohexadienyl)manganese complex, whose formation, as well as that of the dinuclear complex, was easily explained.

We have extended this reaction to the synthesis of heterodinuclear complexes with η^5 and η^6 hapticities by using other electrophiles, such as tricarbonyl(halogenoarene)chromium derivatives. In one case, we have observed a spectacular cleavage of the bond between an (η^5-cyclohexadienyl)manganese unit and a benzylic carbon atom of an arene-tricarbonylchromium entity.

An alternative method to these heterodinuclear complexes involves the reaction of electrophilic Mn complexes with nucleophilic benzylic carbanions of Cr complexes.

Experimental Section

General: All reactions were carried out under dry nitrogen. All experiments were always protected from exposure to light and oxygen. Workup procedures were done in air. Tetrahydrofuran (THF) and dibutyl ether (DBE) used were distilled from sodium benzophenone ketyl under dry nitrogen. − ^{1}H- and ^{13}C-NMR spectra were obtained with Bruker AC 200 and ARX 400 spectrometers. Infrared spectra were recorded with Perkin-Elmer 1420 and Bruker FT spectrometers. Elemental analyses were performed by Le Service de Microanalyses de l′Université P. et M. Curie. Melting points were measured with a Reichert apparatus.

Preparation of (η^6-Arene)manganese and -chromium Complexes

Tricarbonyl(η^6-1,2,3-trimethoxybenzene)manganese Tetrafluoroborate (2): Prepared according to a literature method, yield: 95%, ref.[5]: 95%. − IR ($CHCl_3$): $\tilde{\nu}$ = 2058 cm^{-1}, 1997 (CO). − ^1H NMR (200 MHz, [D_6]acetone): δ = 7.00 (t, J = 7 Hz, 1 H, H^5), 6.25 (t, J = 7 Hz, 2 H, H^4 and H^6), 4.27 (s, OCH_3 at C^1 and C^3), 4.08 (s, OCH_3 at C^2). − ^{13}C NMR (50 MHz, [D_6]acetone): δ = 217.6 (CO), 146.6 (C^1 and C^2), 120 (C^2), 74.1 (C^4 and C^6), 65.2 (OCH_3 at C^2), 59.3 (OCH_3 at C^1 and C^3). − $C_{12}H_{12}BF_4MnO_6$ (392.07): calcd. C 36.58, H 3.07; found C 36.54, H 2.99.

(η^6-Benzene)tricarbonylmanganese Hexafluorophosphate Complex 5: Prepared according to a literature method, yield: 92%; ref.[26] 72%.

(η^6-Benzene)dicarbonylphosphitomanganese Hexafluorophosphate Complex $5P_1$: Prepared according to a literature method, yield: 54%, ref.[28a] 88%.

(η^6-Benzene)carbonyldiphosphitomanganese Hexafluorophosphate Complex $5P_2$: Prepared according to a modified literature method[28a] from complex **5**. Yield: 54%, yellow solid. − IR ($CHCl_3$): $\tilde{\nu}$ = 1940 cm^{-1} (CO). − ^1H NMR (200 MHz, [D_6]acetone): δ = 5.00 (t, J = 2.1 Hz, 6 H), 4.15 (m, 12 H), 1.34 (t, J = 7.1 Hz, 18 H). − ^{13}C NMR (50 MHz, [D_6]acetone): δ = 227.0 (d, J_{CP} = 37.5 Hz), 94.7 (CH), 63.1 (CH_2), 16.2 (CH_3). − ^{31}P NMR (162 MHz, [D_6]acetone): δ = 181.5. − $C_{19}H_{36}F_6MnO_7P_3$ (638.34): calcd. C 35.75, H 5.68; found C 35.85, H 5.71.

(η^6-Anisole)tricarbonylmanganese Hexafluorophosphate Complex 26a: Prepared according to a literature method, yield 70%; ref.[27] 56%.

(η^6-Anisole)dicarbonylphosphitomanganese Hexafluorophosphate Complex 26b: In a typical procedure[28b] cationic complex **26a** (500 mg, 1.27 mmol) was dissolved in freshly distilled acetone (50 mL). $P(OEt)_3$ (430 μL, 2.50 mmol), then Me_3NO (a pinch) were added and mixed at room temperature for 3 h. Solvents were removed under reduced pressure. The crude oil was washed with ether and the complex was recrystallised in an acetone/diethyl ether mixture to give orange-yellow needles of complex **26b** (457 mg, 0.86 mmol, 68% yield). − IR ($CHCl_3$): $\tilde{\nu}$ = 1960 cm^{-1}, 2005 (CO). − ^1H NMR (200 MHz, $CDCl_3$): δ = 6.32 (t, J = 5.6 Hz, 2 H, H^3 and H^5), 5.71 (d, J = 5.6 Hz, 2 H, H^2 and H^6), 5.58 (t, J = 5.6 Hz, 1 H, H^4), 4.02 [m, 6 H, $P(OCH_2CH_3)$], 3.92 (s, 3 H, CH_3), 1.35 [t, J = 7.0 Hz, 9 H, $P(OCH_2CH_3)$]. − ^{13}C NMR (100 MHz, $CDCl_3$): δ = 219.9 (CO−Mn), 146.1 (C^1), 101.4 (C^3 and C^5), 87.5 (C^4), 80.5 (C^2 and C^6), 63.6 [d, J = 7.0 Hz, $P(OCH_2CH_3)$], 57.3 (CH_3), 16.0 [d, J = 7.0 Hz, $P(OCH_2CH_3)$]. − ^{31}P NMR (162 MHz, $CDCl_3$): δ = 176.0. − $C_{15}H_{23}F_6MnO_6P_2$ (530.20): calcd. C 31.16, H 4.01; found C 31.51, H 4.42.

Tricarbonyl(η^6-*p*-fluorotoluene)chromium Complex 13: Prepared according to literature methods described for tricarbonyl(*o*- and *m*-fluorotoluene)chromium complexes.[29] Yield: 42%. − IR (CCl_4): $\tilde{\nu}$ = 1910 cm^{-1}, 1980 (CO). − ^1H NMR (200 MHz, [D_6]acetone): δ = 5.81 (d, J = 4.1 Hz, 4 H, H^2, H^3, H^5, and H^6), 2.11 (s, 3 H, CH_3). − ^{13}C NMR (50 MHz, [D_6]acetone): δ = 233.7 (Cr−CO), 145.8 (C^1, d, J = 260.4 Hz), 105.5 (C^4), 95.9 (C^3 and C^5, d, J = 7.1 Hz), 82.2 (C^2 and C^6, d, J = 20.4 Hz), 19.6 (CH_3). − $C_{10}H_7CrFO_3$ (246.16): calcd. C 48.79, H 2.87, N 21.13; found C 48.83, H 2.85, N 21.19.

(η^6-Benzyl methyl ether)tricarbonylchromium Complex 23: Prepared according to a literature method, yield 62%, ref.[30] 84%.

Syntheses of Complexes 3a, 3b, 3c, 4, 6a, 7a, 6b, 7b, 8b, 6c, 7c

Typical Procedure. − Complex 3a: To a solution of $LiN(CHMe_2)_2$ (1.2 mmol) [obtained by addition of *n*BuLi (755 μL, 1.2 mmol) in a solution of $HN(CHMe_2)_2$ (154 μL, 1.2 mmol) in THF at −78°C] in THF (10 mL) were added $(iPr)_3SiCH_2CN$ (220 μL, 1.2 mmol) and TMEDA (905 μL, 6 mmol). The mixture was stirred for 5 min at −78°C, then added, through a canula, to a solution of complex **2** (394 mg, 1 mmol) in THF (5 mL). The resulting solution was stirred for 3 min at −78°C then treated with distilled water, then with Et_2O. After extraction, the organic phase was washed with brine and dried with $MgSO_4$. Concentration of the organic layer gave a yellow solid. Flash chromatography on basic alumina gave compound **3a** (yield 38%). m.p. 113°C. − IR ($CHCl_3$): $\tilde{\nu}$ = 2010 cm^{-1}, 1935 (CO), 2210 (CN). − ^1H NMR (200 MHz, $CDCl_3$): δ = 4.02 (s, 3 H, OCH_3 at C^2), 3.58 (s, 3 H, OCH_3 at C^1 or C^3), 3.43 (s, 3 H, OCH_3 at C^3 or C^1), 3.14 (dd, J = 6 and 1.9 Hz, 1 H, H^4 or H^6), 2.93 (q, J = 6 Hz, 1 H, H^5), 2.83 (dd, J = 6 and 1.9 Hz, 1 H, H^6 or H^4), 1.44 (d, J = 6 Hz, 1 H, C*H*CN), 1.22 [m, 3 H, $Si(CH-Me_2)$], 1.09 {d, 18 H, $[(CH_3)_2CH]_3Si$}. − ^{13}C NMR (100 MHz, $CDCl_3$): δ = 219.3 (CO), 136.9 (C^1 or C^3), 136.2 (C^3 or C^1), 119.8 (CN or C^2), 115.8 (C^2 or CN), 66.3 (OCH_3 at C^2), 55.3 (OCH_3 at C^1 or C^3), 54.7 (OCH_3 at C^3 or C^1), 36.4 (C^4 or C^6), 35.8 (C^5), 35.7 (C^6 or C^4), 29.2 (CH), 18.6 (CH_3), 11.9 (CH). − $C_{23}H_{34}MnNO_6Si$ (503.54): calcd. C 54.86, H 6.80, N 2.78; found C 54.91, H 6.79, N 2.72.

Crystal Structure of 3a: $[Mn(CO)_3(C_{20}H_{34}O_3NSi)]$, M = 503.5, μ = 0.548 mm^{-1}, $F(000)$ = 1064, ρ = 1.24 $g.cm^{-3}$, monoclinic, $P2_1/n$, Z = 4, a = 13.264(3), b = 12.120(4), c = 17.246(6) Å, β = 104.41(2)°, V = 2685(15) $Å^3$, from 25 reflections (30° < 2θ < 30.5°). Cell dimensions and intensities were measured at 295 K with a Nonius CAD4 diffractometer with graphite-monochromated Mo-K_α radiation (λ = 0.71069 Å). ω/2θ scans, two standard reflections measured every hour showed no significant variation. 1° < θ < 28° (−17 < h < 16, 0 < k < 15, 0 < l <22); 6984 measured reflections, 6461 unique reflections of which 3385 were observed [$|F_o|^2 > 3\sigma(|F_o|^2)$]; R_{int} = 0.021 for equivalent reflections. Data were corrected for Lorentz and polarization effects and for absorption[31] (transmission factors min. 0.9, max. 1). The structure was solved by direct methods using SHELXS,[32] all other calculations used CRYSTALS.[33] Atomic scattering factors and anomalous dispersion terms were taken from ref.[34] Full-matrix least-squares refinement based on $|F|$ and a Chebychev weighting scheme gave final values R = 0.0576, wR = 0.0707, and s = 1.00 for 301 variables and 3385 contributing reflections. The maximum shift/esd of the last cycle was 1.32. Non-hydrogen atoms were anisotropically refined. Hydrogen atoms were introduced in calculated positions, except for hydrogen atoms of methoxy groups which were located in a difference Fourier map; their coordinates were left in fixed positions, only an overall isotropic thermal parameter was refined. The final difference electron density map showed a maximum of 0.43 and a minimum of −0.34 $eÅ^{-3}$.

Complexes 3b, 3c, and 4: Same method as for complex **3a**. Preparation from $LiN(CHMe_2)_2$ (1.2 mmol), Me_3SiCH_2CN (164 μl, 1.2 mmol), complex **2** (393.96 mg, 1 mmol). Overall yield 60%. After a fast silica gel column chromatography, complexes **3b**, **3c**, and **4** could be isolated in a 82:12:4 ratio (50.4%, 7.2%, 2.4% yield, respectively).

Complex 3b: M.p.103°C. − IR ($CHCl_3$): $\tilde{\nu}$ = 2210 cm^{-1} (CN), 2010,1930 (CO). − ^1H NMR (200 MHz, $CDCl_3$): d = 4.06 (s, 3 H, OCH_3 at C^2), 3.58 (s, 3 H, OCH_3 at C^1 or C^3), 3.47 (s, 3 H, OCH_3 at C^3 or C^1), 3.09 (d, J = 6.2 Hz, 1 H, H^4), 2.84 (m, 2 H, H^6, H^4 and H^5), 2.77 (q, J = 6.3 Hz, 1 H, H^5), 1.28 (d, J = 6.2

Hz, 1 H, C*H*CNSiMe$_3$), 0.19 [s, 9 H, (CH$_3$)$_3$Si]. − ^{13}C NMR (CDCl$_3$, 100 MHz): δ = 219.3 (CO), 136.7 (C^1 or C^3), 136.3 (C^3 or C^1), 119.5 (CN or C^2), 116.5 (C^2 or CN), 66.4 (OCH$_3$ at C^2), 55.4 (OCH$_3$ at C^1 or C^3), 54.8 (OCH$_3$ at C^3 or C^1), 36.2 (C^4 or C^6), 36 (C^5), 35.5 (C^6 or C^4), 34.3 (C*H*CNSiMe$_3$), − 2.06 (CH$_3$ at SiMe$_3$). − $C_{17}H_{22}MnNO_6Si$ (419.4): calcd. C 48.68, H 5.28, N 3.33; found C 48.83, H 5.32, N 3.37.

Complex 3c: M.p. 91°C. − IR (CHCl$_3$): $\tilde{\nu}$ = 2242 cm^{-1} (CN), 2010, 1935 (CO). − ^{1}H NMR (200 MHz, CDCl$_3$): δ = 4.06 (s, 3 H, OCH$_3$ at C^2), 3.48 (s, 6 H, OCH$_3$ at C^1 and C^3), 2.90 (m, 3 H, H^4, H^5 and H^6), 1.67 (d, *J* = 5.8 Hz, 2 H, CH$_2$CN). − ^{13}C NMR (50 MHz, CDCl$_3$,): δ = 212.1 (CO), 137.1 (C^1 and C^3), 116.4 (CN or C^2), 115.4 (C^2 or CN), 66.8 (OCH$_3$ at C^2), 55.3 (OCH$_3$ at C^1 and C^3), 34.4 (C^5), 33.8 (C^4 or C^6), 29.9 (CH$_2$CN). − $C_{14}H_{14}MnNO_6$ (347.2): calcd. C 48.43, H 4.06, N 4.03; found C 49.68, H 4.58, N 4.05.

Crystal Structure of 3c: [Mn(CO)$_3$(C$_{11}$H$_{14}$O$_3$N)], *M* = 347.2, μ = 0.811 mm^{-1}, *F*(000) = 712, ρ = 1.43 g cm^{-3}, monoclinic, *P*2$_1$/*n*, *Z* = 4, *a* = 13.198(6), *b* = 12.691(6), *c* = 9690(2) Å, (= 97.17(3)°, *V* = *1*610 Å^3, from 25 reflections (30° < 2θ < 32°). Cell dimensions and intensities were measured at 295 K with a Philips PW1100 diffractometer with graphite-monochromated Mo-K_α radiation (λ = 0.71069Å). ω/2θ scans, two standard reflections measured every two hours showed no significant variation. 2° < θ < 25° (−15 < *h* < 15, 0 < *k* < 15, 0 < *l* <11); 3134 measured reflections, 2804 unique reflections of which 1124 were observed [$|F_o|^2 > 2.5\sigma(|F_o|^2)$]; R_{int} = 0.025 for equivalent reflections. Data were corrected for Lorentz and polarization effects and for absorption[31] (transmission factors min = 0.75, max = 1). The structure was solved by direct methods using SHELXS,[32] all other calculations used CRYSTALS.[33] Atomic scattering factors and anomalous dispersion terms were taken from ref.[34] Full-matrix least-squares refinement based on |*F*| and a Chebychev weighting scheme gave final values *R* = 0.0666, *wR* = 0.0627, and *s* = 1.13 for 200 variables and 3385 contributing reflections. The maximum shift/esd of the last cycle was 0.26. Non-hydrogen atoms were anisotropically refined. Hydrogen atoms were located in a difference Fourier map; their coordinates were left in fixed positions, only an overall isotropic thermal parameter was refined. The final difference electron density map showed a maximum of 0.31 and a minimum of − 0.39 eÅ^{-3}.

Complex 4: M.p. 191°C. − IR (CHCl$_3$): $\tilde{\nu}$ = 2225 cm^{-1} (CN), 2010,1935 (CO). − ^{1}H NMR (200 MHz, CDCl$_3$): δ = 3.99 (s, 6 H, 2 OCH$_3$ at C^2), 3.59 (s, 6 H, 2 OCH$_3$ at C^1 or C^3), 3.50 (s, 6 H, 2 OCH$_3$ at C^3 or C^1), 2.76 (dd, *J* = 6.1 and 1.4 Hz, 2 H, 2 H^4 or 2 H^6), 2.66 (dd, *J* = 6.1 and 1.4 Hz, 2 H, 2 H^6 or 2 H^4), 2.52 (q, *J* = 6.1 Hz, 2 H, 2H^5), 0.98 (t, *J* = 6.1 Hz, 1 H, CHCN). − ^{13}C NMR (100 MHz, CDCl$_3$,): δ = 218.5 (CO), 137.5 (C^1 or C^3), 137.2 (C^3 or C^1), 117.8 (CN or C^2), 115.1 (C^2 or CN), 66.2 (OCH$_3$ at C^2), 55.6 (OCH$_3$ at C^1 or C^3), 55.4 (OCH$_3$ at C^3 or C^1), 55.1 (*C*HCN), 35.2 (C^5), 33.2 (C^4 or C^6), 32.3 (C^6 or C^4). − $C_{26}H_{25}Mn_2NO_{12}$ (653.35): calcd. C 47.75, H 3.82, N 2.14; found C 47.95, H 3.95, N 2.19.

Complexes 6b, 7b and 8b:

Typical Procedure: To a solution of LiN(CHMe$_2$)$_2$ (1.1 mmol) [obtained by addition of *n*BuLi (687 μL, 1.1 mmol) in a solution of HN(CHMe$_2$)$_2$ (140μL, 1.1 mmol) in THF at −78°C] in THF (10 mL) was added acetonitrile (55 μL, 1.05 mmol). The mixture was stirred for 5 min at −78°C , then added, through a canula, to a solution of complex **5** (362 mg, 1 mmol) in THF (5 mL). The resulting solution was stirred for 3 min at −78°C then treated with distilled water followed by Et$_2$O. After extraction, the organic phase was washed with brine and dried with MgSO$_4$. Concentration of the organic layer gave a yellow oil. Flash chromatography on basic alumina gave compounds **8b** (the less polar), then **7b** and **6b** (overall yield: 58%) in a 2:18:80 ratio.

Complex 6b: M.p. 95°C. − IR (CCl4): $\tilde{\nu}$ = 2240 cm^{-1} (CN), 1945, 2005 (CO). − ^{1}H NMR (200 MHz, CDCl3): δ = 5.84 (t, *J* = 6.0 Hz, 1 H, H^3), 4.94 (t, *J* = 6.0 Hz, 2 H, H^2 and H^4), 3.23 (t, *J* = 6.0 Hz, 2 H, H^1 and H^5), 2.94 (m, 1 H, H^6), 1.69 (d, *J* = 6.7 Hz, 2 H, CH$_2$). − ^{13}C NMR (50 MHz, [D$_6$]acetone): δ = 221.7 (Mn−CO), 116.7 (CN), 96.9 (C^2 and C^4), 80.7 (C^3), 53.2 (C^1 and C^5), 31.7 (C^6), 29.0 (CH$_2$). − $C_{11}H_8MnNO_3$ (257.13) calcd. C 51.38, H 3.14, N 5.45; found C 51.42, H 3.30, N 5.43.

Complex 7b: M.p. 201°C. − IR (CHCl$_3$): $\tilde{\nu}$ = 2230 cm^{-1} (CN), 1940, 2100 (CO). − ^{1}H NMR (400 MHz, [D$_6$]acetone): δ = 6.04 (tt, *J* = 6.5 and 1.2 Hz, 2 H, 2 H^3), 5.17 (m, 4 H, 2 H^2 and 2 H^4), 3.42 (tdd, *J* = 6.5, 3.3 and 1.2 Hz, 2 H, 2 H^1 or 2 H^5), 3.33 (tdd, *J* = 6.5, 3.3 and 1.2 Hz, 2 H, 2 H^5 or 2 H^1), 2.85 (q, *J* = 6.5 and 6.7 Hz, 2 H, 2 H^6), 1.32 (t, *J* = 6.5 Hz, 1 H, H^7). − ^{13}C NMR (100 MHz, [D$_6$]acetone): δ = 224.5 (Mn−CO), 119.7 (CN), 99.0 and 99.2 (C^2 and C^4), 83.5 (C^3), 55.4 (C^7), 54.3 and 56.4 (C^1 and C^5), 34.6 (C^6). − $C_{20}H_{13}Mn_2NO_6$ (473.21) calcd. C 50.77, H 2.77, N 2.96; found C 50.90, H 2.71, N 3.02.

Complex 8b: M.p. 204°C. − IR (CCl4): $\tilde{\nu}$ = 2330 cm^{-1} (CN), 2020, 1950 (CO). − ^{1}H NMR (200 MHz, [D$_6$]acetone): δ = 6.01 (t, *J* = 5.8 Hz, 3 H, H^3), 5.26 (t, *J* = 5.8 Hz, 6 H, H^2 and H^4), 3.46 (t, *J* = 5.8 Hz, 6 H, H^1 and H^5), 2.93 (t, *J* = 5.8 Hz, 3 H, H^6). − ^{13}C NMR (50 MHz, [D$_6$]acetone): δ = 222.9 (Mn−CO), 120 (CN), 98 (C^2 and C^4), 81.7 (C^3), 66.2 (*C*-CN), 55.4 (C^1 and C^5), 36.7 (C^6). − $C_{29}H_{18}Mn_3NO_9$ (689.27) calcd. C 50.53, H 2.63, N 2.03; found C 50.95, H 2.77, N 3.16.

Complexes 6a and 7a: Same method as for complexes **6b**, **7b**, and **8b**: Starting from 1 equiv. of complex **5**, 1 equiv. of CH$_3$CH$_2$CN and 1 equiv. of LDA, complexes **6a** and **7a** were obtained (overall yield: 87%) in a 87:13 ratio. Starting from 2 equiv. of complex **5**, 1 equiv. of CH$_3$CH$_2$CN and 2 equiv. of LDA, complexes **6a** and **7a** were obtained (overall yield 85%) in a 28:72 ratio.

Complex 6a: M.p. 139°C. − IR (CCl$_4$): $\tilde{\nu}$ = 2240 cm^{-1} (CN), 1950, 2010 (CO). − ^{1}H NMR (200 MHz, CDCl$_3$): δ = 5.80 (t, 1 H, *J* = 6.1 Hz, H^3), 4.97 (t, *J* = 6.1 Hz, 1 H, H^2 or H^4), 4.92 (t, *J* = 6.1 Hz, 1 H, H^4 or H^2), 3.34 (tt, *J* = 6.1 and 1.5 Hz, 1 H, H^1 or H^5), 3.15 (tt, *J* = 6.1 and 1.5 Hz 1 H, H^5 or H^1), 2.64 (m, 1 H, H^6), 1.69 (q, *J* = 7.2 Hz, 1 H, H^7), 1.01 (d, *J* = 7.2 Hz 3 H, CH$_3$). − ^{13}C NMR (50 MHz, [D$_6$]acetone): δ = 225.4 (Mn−CO), 124.8 (CN), 99.9 (C^2 and C^4), 84.0 (C^3), 54.3 (C^1 and C^5), 38.9 (C^6), 38.7 (C^7), 14.9 (CH$_3$). − $C_{12}H_{10}MnNO_3$ (271.16): calcd. C 53.16, H 3.72, N 5.07; found C 53.06, H 3.81, N 5.17.

Complex 7a: M.p. 194°C. − IR (CCl4): $\tilde{\nu}$ = 2240 cm^{-1} (CN), 1945, 2005 (CO). − ^{1}H NMR (200 MHz, [D$_6$]acetone): δ = 5.98 (tt, *J* = 5.7 and 1.3 Hz, 2 H, H^3), 5.25 (m, 4 H, 2 H^2 and 2 H^4), 4.78 (tt, *J* = 5.7 and 1.3 Hz, 2 H, 2 H^1 or 2 H^5), 3.35 (tt, *J* = 5.7 and 1.3 Hz, 2 H, 2 H^5 or 2 H^1), 2.84 (m, 2 H, 2 H^6), 0.74 (s, 3 H, CH$_3$). − ^{13}C NMR (50 MHz, [D$_6$]acetone): δ = 225.5 (Mn−CO), 124.7 (CN), 101.1 (C^2 and C^4), 84.0 (C^3), 56.0 and 57.4 (C^1 and C^5), 40.9 (C^6), 39.6 (C^7), 18.1 (CH$_3$). − $C_{21}H_{15}Mn_2NO_6$ (487.23): calcd. C 51.77, H 3.10, N 2.87; found C 52.15, H 3.09, N 2.84.

Crystal Structure of 7a: [(CO)$_3$Mn(C$_{15}$H$_{15}$N)Mn(CO)$_3$], *M* = 487.21, μ = 0.126 mm^{-1}, *F*(000) = 492, ρ = 1.26 g.cm^{-3}, triclinic, *P*$\bar{1}$, *Z* = 2, *a* = 6.735(6), *b* = 12.779(8), *c* = 13.425(12) Å, α = 116.11(6), β = 92.21(1), γ = 103.94(8)°, *V* = 993 Å^3, from 25 reflections (20° < 2θ < 22°). Cell dimensions and intensities were measured at 295 K with a Philips PW1100 diffractometer with graphite-monochromated Mo-K_α radiation (λ = 0.71069 Å). ω/2θ scans, two

standard reflections measured every two hours showed no significant variation. $2° < \theta < 20°$ ($-6 < h < 6$, $-12 < k < 11$, $0 < l < 12$); 1960 measured reflections, 1816 unique reflections of which 1232 were observed [$|F_o|^2 > 1.5\sigma(|F_o|^2)$]; $R_{int} = 0.035$ for equivalent reflections. Data were corrected for Lorentz and polarization effects and for absorption[31] (transmission factors min = 0.8, max = 1). The structure was solved by direct methods using SHELXS,[32] all other calculations used CRYSTALS.[33] Atomic scattering factors and anomalous dispersion terms were taken from ref.[34] Full-matrix least-squares refinement based on $|F|$ and a Chebychev weighting scheme gave final values $R = 0.0591$, $Rw = 0.0616$, and $s = 1.18$ for 207 variables and 1232 contributing reflections. The maximum shift/esd in the last cycle was 0.22. $Mn(CO)_3$, CN, and methyl C atoms were anisotropically refined, other C atoms were left isotropic in order to reduce the number of variables. Hydrogen atoms were introduced in calculated positions; their coordinates were left in fixed positions, only an overall isotropic thermal parameter was refined. The final difference electron density map showed a maximum of +0.52 and a minimum of −0.45 eÅ^{-3}.

Crystallographic data (excluding structure factors) have been deposited with the Cambridge Crystallographic Data Center as supplementary publication no. CCDC-101517 (**3a**), -101518 (**3c**), -101519 (**7a**). Copies of the data can be obtained free of charge on application to CCDC, 12 Union Road, Cambridge CB2 1 EZ, UK [Fax: (internat.) + 44-1223/336-033; E-mail: deposit@ccdc.cam.ac.uk].

Complexes 6c and 7c: Same method as for complexes **6b**, **7b**, and **8b**: prepared from $LiN(CHMe_2)_2$ (1.2 mmol), Me_3SiCH_2CN (164 µL, 1.2 mmol), and complex **5** (362.04 mg, 1 mmol). Overall yield: 66%. A fast silica gel chromatography gave complexes **6c**, **7c**, **6b**, and **7b** in a 64:28:7:1 ratio.

Complex 6c: M.p. 93°C. − IR ($CHCl_3$): $\tilde{\nu}$ = 2205 cm^{-1} (CN), 2015 and 1945 (CO). − ^{1}H NMR (400 MHz, $CDCl_3$): δ = 5.86 (t, J = 6.2 Hz, 1 H, H^3), 5.00 (t, J = 6.2 Hz, 1 H, H^2 or H^4), 4.93 (t, J = 6.2 Hz, 1 H, H^4 or H^2), 3.40 (t, J = 6.2 Hz, 1 H, H^1 or H^5), 3.16 (t, J = 6.2 Hz, 1 H, H^5 or H^1), 2.85 (q, J = 6.2 Hz 1 H, H^6), 1.33 (d, J = 6.2 Hz, 1 H, C*H*CNSiMe$_3$), 0.19 (s, 9 H, $(CH_3)_3Si$). − ^{13}C NMR (100 MHz, $CDCl_3$): δ = 222.3 (CO), 120.1 (CN), 96.6 (C^2 or C^4), 96.3 (C^4 or C^2), 81.3 (C^3), 55.1 (C^1 or C^5), 55.0 (C^5 or C^1), 33.5 (*C*HCNSiMe$_3$), 33.4 (C^6), −1.72 (CH_3 of $SiMe_3$). − $C_{14}H_{16}MnNO_3Si$ (329.31): calcd. C 51.06, H 4.89, N 4.25; found C 51.06, H 4.92, N 4.14.

Complex 7c: M.p. 163°C. − IR ($CHCl_3$): $\tilde{\nu}$ = 2200 cm^{-1} (CN), 2100 and 1945 (CO). − ^{1}H NMR (400 MHz, $CDCl_3$): δ = 5.86 (t, J = 6 Hz, 2 H, H^3), 5.10 (t, J = 6 Hz, 2 H, 2 H^2 or 2 H^4), 4.93 (t, J = 6 Hz, 2 H, 2 H^4 or 2 H^2), 3.32 (t, J = 6 Hz, 2 H, 2 H^1 or 2H^5), 3.16 (t, J = 6 Hz, 2 H, 2 H^5 or 2 H^1), 2.93 (t, J = 6 Hz, 2 H, 2 H^6), 0.24 (s, 9 H, $SiMe_3$). − ^{13}C NMR (200 MHz, [D$_6$]acetone): δ = 223.7 (CO), 122.5 (CN), 98.6 (C^2 and C^4), 82.4 (C^3), 58.4 (C^1 or C^5), 56.5 (C^5 or C^1), 53.3 (*C*CNSiMe$_3$), 37.7 (C^6), −0.40 ($SiMe_3$). − $C_{23}H_{21}Mn_2NO_6$ (545.38): calcd. C 50.65, H 3.88, N 2.57; found C 50.61, H 3.79, N 2.45.

Complex 6d: Same method as for complexes **6b**, **7b**, **8b**: prepared from $LiN(CHiPr_2)_2$ (1.2 mmol), iPr_3SiCH_2CN (220µL, 1.2 mmol), and complex **5** (362.04 mg, 1 mmol). Yield: 49%. − M.p. 88°C. − IR (CHCl3): $\tilde{\nu}$ = 2210 cm^{-1} (CN), 2010 and 1945 (CO). − ^{1}H NMR (200 MHz, $CDCl_3$): δ = 5.85 (tt, J = 6 and 1 Hz, 1 H, H^3), 5.02 (t, J = 6 Hz, 1 H, H^2 or H^4), 4.90 (t, J = 6 Hz, 1 H, H^4 or H^2), 3.46 (tt, J = 6 and 1 Hz, 1 H, H^1 or H^5), 3.19 (tt, J = 6 and 1 Hz, 1 H, H^5 or H^1), 2.96 (q, J = 6 Hz 1 H, H^6), 1.50 (d, J = 6 Hz, 1 H, C*H*CNSi*i*Pr$_3$), 1.22 [m, 3 H, $(Me_2CH)_3Si$], 1.09 {d, 18 H, $[(CH_3)_2CH]_3Si$}. − ^{13}C NMR (100 MHz, $CDCl_3$): δ = 222.1 (CO), 120.3 (CN), 96.5 (C^2 or C^4), 96.1 (C^4 or C^2), 81.1 (C^3), 55.2 (C^1 or C^5), 33.0 (C^6), 28.2 {$[(CH_3)_2CH]_3SiCHCN$}, 18.7 and 18.6 {$[(CH_3)_2CH]_3Si$}, 11.9 {$[(CH_3)_2CH]_3Si$}. − $C_{20}H_{28}MnNO_3Si$ (413.47): calcd. C 58.09, H 6.82, N 3.38; found C 58.11, H 6.81, N 3.36.

Addition of α-Sulfonyl Carbanions to Benzenetricarbonylmanganese Complex 5: Typical procedure: *n*BuLi (692 µL of a solution 1.6 M in hexane; 1.1 mmol) was added under nitrogen to a solution of chloromethyl *p*-toluenesulfonate (204.6 mg; 1.0 mmol) in THF (10 mL). After 30 min of stirring, this solution was transferred at −78°C under nitrogen through a canula into a flask containing benzenetricarbonylmanganese complex **5** (364.5 mg; 1 mmol) and THF (10 mL). After 30 min, the reaction temperature was increased progressively to room temperature. The mixture was extracted with water and diethyl ether, the organic layer was washed with brine, and dried with $MgSO_4$. Concentration of the ether layer gave a yellow oil. After chromatography on a silica gel column, two fractions were obtained: the first one was a yellow powder consisting of a 2:1 mixture of complex **9a** (149.5 mg; 0.35 mmol; yield 35%) and starting sulfone (eluent: petroleum ether/diethyl ether, 80:20); dinuclear complex **10a** (241.9 mg; 0.38 mmol; yield 38%) was obtained from the second fraction.

Complex 9a: IR (CCl_4): $\tilde{\nu}$ = 1940 cm^{-1}, 1950, and 2010 (CO), 1150 and 1350 (SO_2). − ^{1}H NMR (400 MHz, $CDCl_3$): δ = 7.86 (d, J = 9.3 Hz, 1 H, H^9 or H^{13}), 7.54 (d, 1 H, J = 9.3 Hz, H^{13} or H^9), 7.18 (m, 2 H, H^{10} and H^{12}), 5.83 (t, J = 5.4 Hz, 1 H, H^3), 4.99 (m, 2 H, H^2 and H^4), 3.65 (d, J = 9.3 Hz, 1 H, H^7), 3.49 (m, 1 H, H^1 or H^5), 3.30 (m, 1 H, H^6), 3.12 (m, 1 H, H^5 or H^1), 2.46 (s, 3 H, CH_3). − ^{13}C NMR (50 MHz, $CDCl_3$): δ = 221.8 (Mn−CO), 145.9 (C^8), 133.1 (C^{11}), 130.1 (C^{10} and C^{12}), 129.5 (C^9 and C^{13}), 96.5 (C^2 and C^4), 81.2 (C^7), 78.1 (C^3), 48.9 and 53.9 (C^1 and C^5), 36.2 (C^6), 21.8 (CH_3). − MS (CI) (NH_3); *m*/*z*: 438 [MNH_4]$^+$.

Complex 10a: IR (CCl_4): $\tilde{\nu}$ = 1945 cm^{-1} and 2005 (CO), 1140 and 1325 (SO_2). − ^{1}H NMR (400 MHz, $CDCl_3$): δ = 7.74 (d, J = 9.5 Hz, 2 H, H^9 and H^{13}), 7.38 (m, 2 H, H^{10} and H^{12}), 5.78 (t, J = 5.3 Hz, 2 H, 2 H^3), 5.09 (m, 2 H, 2 H^2 or 2 H^4), 4.89 (t, J = 5.3 Hz, 2 H, 2 H^4 or 2 H^2), 3.34 (m, 4 H, 2 H^1 and 2 H^5), 3.15 (m, 2 H, 2 H^6), 2.48 (s, 3 H, CH_3). − ^{13}C NMR (50 MHz, $CDCl_3$): δ = 222.0 (Mn−CO), 146.1 (C^8), 133.0 (C^{11}), 130.6 (C^{10} and C^{12}), 129.7 (C^9 and C^{13}), 97.7 and 97.9 (2 C^2, 2 C^4), 93.1 (C^7), 80.1 (C^3), 54.5 (2 C^1, 2 C^5), 39.8 (C^6), 21.8 (CH_3). − $C_{26}H_{19}ClMn_2O_8S$ (636.83): calcd. C 49.01, H 2.98; found C 49.00, H 2.96.

Complexes 9b and 10b: Same method as for **9a** and **10a**: starting from *n*BuLi (692 µL; 1.1 mmol), fluoromethyl benzenesulfonate (174.2 mg; 1 mmol), and complex **5** (364.5 mg; 1 mmol). A fast silica gel column chromatography gave complexes **9b** (43%) and a mixture of complex **10b** (5%) and some starting sulfone. If 2 equiv. of *n*BuLi and 2 equiv. of complex **5** were used, after chromatography, complexes **11** (16%), **9b** (3%), and a mixture of **10b** (52%) and starting sulfone were obtained.

Complex 9b: IR (CCl_4): $\tilde{\nu}$ = 1905 cm^{-1}, 1945, 1975, and 2005 (CO), 1155 and 1347 (SO_2). − ^{1}H NMR (400 MHz, $CDCl_3$): δ = from 7.42 to 7.92 (several m, H^9, H^{10}, H^{11}, H^{12}, and H^{13}), 5.78 (t, J = 5.6 Hz, 1 H, H^3), 4.90 (m, 2 H, H^2 and H^4), 3.91 (dd, J_{HF} = 47.5 Hz, J_{HH} = 7.5 Hz, 1 H, H^7), 3.44 (m, 1 H, H^6), 3.06 (m, 1 H, H^1 or H^5), 2.95 (t, J = 5.6 Hz, 1 H, H^5 or H^1). − ^{13}C NMR (50 MHz, $CDCl_3$): δ = 222.4 (Mn−CO), 134.8 (C^8), 129.6 (C^{11}), 129.4 (C^{10} and C^{12}), 129.2 (C^9 and C^{13}), 97.3 and 97.6 (C^2 and C^4), 99.9 and 104.3 (C^7), 80.8 (C^3), 47.8 and 48.6 (C^1 and C^5), 33.5 and 33.9 (C^6). − MS (CI) (NH_3); *m*/*z*: 408 [MNH_4^+], 391 [MH^+].

Complex 10b: IR (CCl_4): $\tilde{\nu}$ = 1905 cm^{-1}, 1945, 1975, and 2005 (CO), 1155 and 1347 (SO_2). − ^1H NMR (400 MHz, $CDCl_3$): δ = 7.42−7.92 (several m, H^9, H^{10}, H^{11}, H^{12} and H^{13}), 5.71 (t, *J* = 6.0 Hz, 2 H, $2H^3$), 4.90 (m, 2 H, H^2 and H^4), 4.58 (t, *J* = 6.0 Hz, 2 H, H^2 and H^4), 3.29 (t, *J* = 6.0 Hz, 1 H, H^6), 3.24 (t, *J* = 6.0 Hz, 1 H, H^6), 3.06 (m, 2 H, H^1 and H^5), 2.76 (t, *J* = 6.0 Hz, 2 H, H^1 and H^5). − ^{13}C NMR (50 MHz, $CDCl_3$): δ = 222.4 (Mn−CO), 134.9 (C^8), 129.4 (C^{11}), 129.2 (C^{10} and C^{12}), 129.0 (C^9 and C^{13}), 97.5 and 97.7 (C^2 and C^4), 93.1 (C^7), 80.5 (C^3), 49.9 and 50.7 (C^1 and C^5), 36.7 and 37.2 (C^6). − MS(CI)(NH_3); *m*/*z*: 624 [MNH_4^+], 607 [MH^+].

Complex 15: $LiN(CHMe_2)_2$ (1.1 mmol) was added at −78°C, under nitrogen to a solution of complex **6a** (388.8 mg; 1.43 mmol) in 5 mL of THF. After 15 min, this red solution was transferred through a canula to another flask containing a solution of tricarbonyl(*p*-fluorotoluene)chromium complex **13** (369.2 mg; 1.50 mmol) in 5 mL of THF. After 30 min of stirring at room temperature, the mixture was extracted with water and diethyl ether. The ether layer was washed with brine, dried with $MgSO_4$, concentrated, and purified by chromatography on a silica gel column. Eluting with a mixture of diethyl ether/petroleum ether (2:98) gave tricarbonyl(*p*-fluorotoluene)chromium complex **13** (160.6 mg, 0.65 mmol, 43% yield); elution with a mixture of diethyl ether/petroleum ether (60:40) gave complex **15** (157.3 mg, 0.56 mmol, 40% yield). M.p. 123°C. − IR ($CHCl_3$): $\tilde{\nu}$ = 1900 cm^{-1} and 1945 (CO), 2220 (CN). − ^1H NMR (400 MHz, [D_6]acetone): δ = 5.89 (d, *J* = 6.2 Hz, 2 H, H^3 and H^5), 5.58 (d, *J* = 6.2 Hz, 1 H, H^2 or H^6), 5.55 (d, *J* = 6.2 Hz, 1 H, H^6 or H^2), 4.01 (q, *J* = 7.2 Hz, 1 H, H^7), 2.24 (s, 3 H, CH_3), 1.66 (d, *J* = 7.2 Hz, 3 H, CH_3). − ^{13}C NMR (50 MHz, [D_6]acetone): δ = 233.8 (Cr−CO), 120.5 (CN), 111.3 (C^1), 106.8 (C^4), 94.5 and 95.5 (C^3 and C^5), 93.8 and 94.0 (C^2 and C^6), 28.6 (C^7), 21.4 (CH_3), 20.2 (CH_3). − $C_{13}H_{11}CrNO_3$ (281.23): calcd. C 55.52, H 3.94, N 4.98; found C 55.74, H 3.75, N 4.31.

Complex 14: $LiN(CHMe_2)_2$ (1.1 mmol) was added at −78°C under nitrogen to a solution of complex **15** (39.6 mg; 0.14 mmol) in 10 mL of THF. After 10 min, this solution was transferred through a canula to a suspension of benzenetricarbonylmanganese complex **5** (57.9 mg; 0.16 mmol) in 5 mL of THF. After 5 min at room temperature, the mixture was extracted with water and diethyl ether, the organic layer was washed with brine and concentrated to give 52.3 mg of a yellow powder, consisting of a mixture of compounds **14** (yield 37%) and **15** (yield 63%). Chromatography of this mixture on silica gel 15 μ column, leads only to the recovery of complex **15**. − IR ($CHCl_3$): $\tilde{\nu}$ = 1905 cm^{-1} and 1920 (Cr−CO), 1945 and 2010 (Mn−CO), 2240 (CN). − ^1H NMR (200 MHz, [D_6]acetone): δ = 5.84 (dd, *J* = 6.8 and 1.6 Hz, 1 H, H^{10} or H^{12}), 5.76 (dd, *J* = 6.8 and 1.6 Hz, 1 H, H^{12} or H^{10}), 5.50 (dd, *J* = 6.8 and 1.6 Hz, 1 H, H^9 or H^{13}), 5.43 (d, *J* = 6.8 Hz, 1 H, H^{13} or H^9), 5.30 (m, 2 H, H^2 and H^4), 3.54 (t, *J* = 5.9 Hz, 1 H, H^3), 3.40 (m, 1 H, H^1 or H^5), 3.32 (t, *J* = 5.9 Hz, 1 H, H^5 or H^1), 3.12 (t, *J* = 5.9 Hz, 1 H, H^6), 2.33 (s, 3 H, CH_3), 1.47 (s, 3 H, CH_3). − ^{13}C NMR (50 MHz, [D_6]acetone): δ = 233.8 (Cr−CO), 223.2 (Mn−CO), 124.5 (CN), 112.5 (C^8), 106.1 (C^{11}), 99.3 and 99.4 (C^2 and C^4), 97.0 (C^{10} and C^{12}), 92.4 and 92.5 (C^9 and C^{13}), 54.7 (C^3), 54.1 (C^1 and C^5), 47.1 (C^6), 21.4 (C^7), 20.6 (CH_3), 20.2 (CH_3). − MS(CI)(NH_3); *m*/*z*: 515 [MH_4^+], 498 [MH^+].

Reaction of the Anion of (Benzyl methyl ether)tricarbonylchromium Complex 23 with Complexes 5, $5P_1$, $5P_2$. − Typical Procedure: 750 μl of *n*BuLi (1.2 mmol) was added at −40°C to a solution of (benzyl methyl ether)tricarbonylchromium complex **23** (258.2 mg; 1.00 mmol) in THF (20 mL). After 1 h, this solution was transferred under nitrogen through a canula to a suspension of benzenetricarbonylchromiummanganese complex **5** (434.4 mg; 1.2 mmol) in 5 mL of THF. The mixture was extracted with water and diethyl ether. The organic phase was washed with brine, dried with $MgSO_4$ and concentrated to give an oil which was purified by chromatography on a silica gel (15 μ) column. Elution with a mixture of petroleum ether/diethyl ether (92:8) gave complex **25** (96.4 mg; 0.285 mmol, 29% yield); with a mixture of petroleum ether/diethyl ether (78:22), complex **24a** (193.5 mg; 0.408 mmol, 41% yield) was isolated.

Complex 24a: Yellow oil. − IR ($CHCl_3$): $\tilde{\nu}$ = 1940 cm^{-1} and 2010 (Mn−CO), 1895 and 1970 (Cr−CO). − ^1H NMR (200 MHz, $CDCl_3$): δ = 5.79 (t, *J* = 6.0 Hz, 1 H, H^3), 5.39 [m, 2 H, H^{10} and H^{12} (or H^9 and H^{13})], 5.23 (t, *J* = 6.3 Hz, 1 H, H^{11}), 5.11 [m, 2 H, H^9 and H^{13} (or H^{10} and H^{12})], 4.91 (m, 2 H, H^2 and H^4), 3.44 (s, 3 H, OMe), 3.30 (t, *J* = 6.0 Hz, 1 H, H^1 or H^5), 3.03 (s, 1 H, H^7), 2.83 (t, *J* = 6.0 Hz, 1 H, H^5 or H^1), 2.60 (m, 1 H, H^6). − ^{13}C NMR (50 MHz, $CDCl_3$): δ = 232.7 (Cr−CO), 222.2 (Mn−CO), 107.1 (C^8), 96.8 and 97.0 (C^2 and C^4), 90.7 (C^{11}), 89.8, 90.9, 93.1 and 94.1 (C^9, C^{10}, C^{12} and C^{13}), 87.0 (C^6), 80.4 (C^3), 59.9 (OMe), 56.7 (C^7), 51.7 and 54.6 (C^1 and C^5). − $C_{20}H_{15}CrMnO_7$ (474.27) calcd. C 50.65; H 3.19; found C 51.09, H 3.45.

Complex 25: Yellow oil. − IR ($CHCl_3$): $\tilde{\nu}$ = 1940 cm^{-1} and 2010 (CO). − ^1H NMR (200 MHz, $CDCl_3$): δ = from 7.08 to 7.37 (several m, H^9, H^{10}, H^{11}, H^{12} and H^{13}), 5.78 (tt, 1 H, H^3, *J* = 5.9 and 1.1 Hz), 4.89 [tt, 1 H, H^2 (or H^4), *J* = 5.9 and 1.1 Hz], 4.80 [tt, 1 H, H^4 (or H^2), *J* = 5.9 and 1.1 Hz], 3.48 [m, 1 H, H^1 (or H^5)], 3.05 (s, 3 H, OMe), 3.01 (d, 1 H, H^7, *J* = 8.7 Hz), 2.76 (m, 1 H, H^6), 2.52 [tt, 1 H, H^5 (or H^1), *J* = 5.9 and 1.1 Hz]. − ^{13}C NMR (50 MHz, $CDCl_3$): δ = 222.8 (Mn−CO), 137.8 (C^8), 127.6 and 128.4 (C^9, C^{10}, C^{12} and C^{13}), 128.0 (C^{11}), 96.4 and 96.7 (C^2 and C^4), 90.5 (C^7), 80.0 (C^3), 56.7 (OMe), 52.5 and 56.8 (C^1 and C^5), 41.6 (C^6). − $C_{17}H_{15}MnO_4$ (338.21): calcd. C 60.37, H 4.47; found C 59.80, H 4.90.

Complex 24b: Same method as for **24a** (yield 55%), yellow oil. − IR ($CHCl_3$): $\tilde{\nu}$ = 1965 cm^{-1}, 1945, 1880 (CO). − ^1H NMR (400 MHz, $CDCl_3$): δ = 5.53 (t, *J* = 3.6 Hz, 1 H, H^3), 5.40 (m, 2 H, H^{10}, H^{12} or H^9, H^{13}), 5.26 (t, J = 6.6 Hz, 1 H, H^{11}), 5.18 (m, 2 H, H^9, H^{13} or H^{10}, H^{12}), 4.73 (m, 2 H, H^2 and H^4), 3.92 [m, 6 H, $P(OCH_2CH_3)$], 3.47 (s, 3 H, OCH_3), 3.04 (m, 1 H, H^5 or H^1), 2.62 (m, 2 H, H^6 and H^7), 2.54 (m, 1 H, H^1 or $H^{5)}$, 1.27 [t, *J* = 7.0 Hz, 9 H, $P(OCH_2CH_3)$]. − ^{13} C NMR (100 MHz, $CDCl_3$): δ = 233.1 (CO−Cr), 229.0 (d, *J* = 31.1 Hz, CO−Mn), 108.3 (C^8), 95.3 and 95.5 (C^2 and C^4), 93.6, 94.1, 91.1, 90.0 (C^9, C^{10}, C^{11}, C^{12}, C^{13}), 87.0 (C^6), 79.5 (C^3), 60.3 [$P(OCH_2CH_3)_3$], 59.8 (OCH_3), 48.5 and 51.4 (C^1 and C^5), 42.7 (C^7), 16.2 and 16.5 [$P(OCH_2CH_3)_3$]. − $C_{25}H_{30}CrMnO_9P$ (612.43): calcd. C 49.03, H 4.94; found C 48.81, H 4.85.

Complex 24c: Same method as for **24a** (yield 47%), yellow oil. − IR ($CHCl_3$): $\tilde{\nu}$ = 1950 cm^{-1}, 1850, 1810. − ^1H NMR (200 MHz, $CDCl_3$): δ = 5.33, 5.18 (2 m, 6 H, H^9, H^{10}, H^{11}, H^{12}, H^{13}, and H^3), 4.53 (m, 2 H, H^2 and H^4), 3.92 [m, 12 H, $P(OCH_2CH_3)$], 3.41 (s, 3 H, OCH_3), 2.61 (m, 1 H, H^5 or H^1), 2.51 (m, 1 H, H^6), 2.15 (m, 1 H, H^7), 2.05 (m, 1 H, H^1 or H^5), 1.20 [t, *J* = 7.0 Hz, 18 H, $P(OCH_2CH_3)$]. − ^{13}C NMR (50 MHz, $CDCl_3$): δ = 233.4 (CO−Cr), 230.4 (m, CO−Mn), 109.6 (C^8), 93.2 and 93.7 (C^2 and C^4), 89.9, 91.0, 91.2, 93.9, 94.1 (C^9, C^{10}, C^{11}, C^{12}, C^{13}), 87.2 (C^6), 76.8 (C^3), 59.7 [$P(OCH_2CH_3)$ and OCH_3], 45.2 and 47.8 (C^1 and C^5), 42.3 (C^7), 16.4 [$P(OCH_2CH_3)_3$]. − $C_{30}H_{45}CrMnO_{11}P_2$ (750.58): calcd. C 48.01, H 6.04; found C 48.06, H 6.09.

Reaction of the Anion of (Benzyl methyl ether)tricarbonylchromium Complex 23 with Anisolemanganese Complexes 26a and 26b. − Typical Procedure: To a solution of complex **23** (258 mg, 1 mmol)

in THF (20 mL) at −78° C was added *n*BuLi (1.2 mmol). After stirring for 1 h at −40°C, this solution was added through a canula to cationic complex **26a** (470 mg, 1.2 mmol), dissolved in freshly distilled THF (5 mL). The reaction mixture turned orange and was stirred at room temperature for 15 min, then treated with distilled water and Et_2O. After extraction, the organic phase was washed with brine and dried with $MgSO_4$. Concentration of the organic phase under a nitrogen flow gave a yellow oil which was separated by chromatography. Dinuclear complex **27a** (2 diastereoisomers in a 1:1 ratio) was isolated first by eluting with an Et_2O/petroleum ether (15:100) mixture (239 mg, 0.47 mmol, 47% yield). Then starting complex **23** (123 mg, 0.26 mmol, 26% yield) was obtained by eluting with an Et_2O/petroleum ether (20:100) mixture.

Complex 27a: Yellow oil. − IR ($CHCl_3$): $\tilde{\nu}$ = 2005 cm^{-1}, 1930 (CO−Mn), 1970, 1890 (CO−Cr). − ^1H NMR (200 MHz, $CDCl_3$): δ = 5.67 (m, 2 H, H^3), 5.38 (m, 4 H, H^9 and H^{13}), 5.20 (m, 4 H, H^{10} and H^{12}), 5.07 (t, *J* = 6.0 Hz, 2 H, H^{11}), 4.92 (m, 2 H, H^4), 3.51 and 3.49 (s, 6 H, OCH_3 at C_2), 3.44 (s, 6 H, OCH_3 at C^7), 4.19 (m, 4 H, H^1 or H^7), 2.72 (m, 8 H, H^1, H^5, H^6 and H^{11}). − ^{13}C NMR (100 MHz, $CDCl_3$): δ = 232.9 (CO−Cr), 222.2 (CO−Mn), 143.5 (C^2), 110.8 (C^8), 94.2 (C^9 and C^{13}), 93.3 and 93.7 (C^4) 93.0 (C^{11}) 90.9 (C^9, C^{13}, C^{10}, C^{12}), 90.0 (C^{10}, C^{12}), 87.0 and 87.3 (C^6), 67.9 and 68.5 (C^3), 59.9 (OCH_3 at C^7), 55.0 (C^7), 54.4 (OCH_3 at C_2), 52.4 (C^7), 45.1 (C^5), 38.3 and 40.0 (C^1). − $C_{21}H_{17}CrMnO_8$ (504.30): calcd. C 50.02, H 3.40; found C 50.09, H 3.35.

Complex 27b: Same procedure as for **27a**. Yield: 64% of **27b** (2 diastereoisomers in a 1:1 ratio), yellow oil. − IR ($CHCl_3$): $\tilde{\nu}$ = 1965 cm^{-1}, 1870 (CO−Cr), 1940, 1880 (CO−Mn). − ^1H NMR (400 MHz, $CDCl_3$): δ = 5.33 (m, 5 H, 2 H^3, 2 H^9 and 1 H^{13}), 5.13 (m, 7 H, 2 H^{10} 2 H^{11}, 2 H^{12}, and 1 H^{13}), 4.67 (m, 2 H, H^4), 3.85 [m, 12 H, $P(OCH_2CH_3)$], 3.39 (s, 6 H, OCH_3 at C^7), 3.38 (s, 3 H, OCH_3 at C^2), 3.37 (s, 3 H, OCH_3 at C^2: the other diast.), 3.04 (m, 1 H, H^1) 2.75 (m, 1 H, H^7), 2.65 (m, 2 H, H^5), 2.54 (m, 3 H, H^2 and H^6), 2.27 (m, 1 H, H^7), 1.27 [m, 18 H, $P(OCH_2CH_3)$]. − ^{13}C NMR (100 MHz, $CDCl_3$): δ = 232.0 (CO−Cr), 223.3 and 230.4 (m, CO−Mn), 139.5 (C^2), 107.2 (C^8), 93.0 (C^9, C^{13}), 92.5 and 92.7 (C^4) 92.4 (C^{11}), 89.9 and 90.1 (C^9 and C^{13}), 88.8, 89.0 and 89.8 (C^{10} and C^{12}), 86.0 and 86.4 (C^6), 66.7 and 67.1 (C^3), 59.2 [$P(OCH_2CH_3)$], 58.7 (OCH_3 at C^7), 53.1 and 52.8 (OCH_3 at C^2), 48.1 and 50.9 (C^7), 43.8 and 43.9 (C^5), 34.4 and 36.6 (C^1), 15.2 [$P(OCH_2CH_3)$]. − ^{31}P NMR (162 MHz, $CDCl_3$): δ = 196.7, 198.0. − $C_{26}H_{32}MnCrO_{10}P$ (642.45): calcd. C 48.61, H 5.02; found C 48.66, H 5.16.

Acknowledgments

This work was supported by the CNRS and by a grant from the French Ministry of University and Scientific Research to C. R. and V. G.

[1] See, for example, the following reviews: [1a] L. A. P. Kane-Maguire, E. D. Honig, D. A. Sweigart, *Chem. Rev.* **1984**, *84*, 525−543. − [1b] L. Balas, D. Jhurry, L. Latxague, S. Grelier, Y. Morel, M. Hamdani, N. Ardoin, D. Astruc, *Bull. Soc. Chim. Fr.* **1990**, *127*, 401−426. − [1c] F. J. Mc Quillin, D. G. N. Parker, G. R. Stephenson, *Transition Metal in Organic Synthesis*, University Press, Cambridge, **1991**. − [1d] M. F. Semmelhack in *Comprehensive Organometallic Chemistry II*, vol. 12 (Eds.: E. N. Abel, F. G. A. Stone, G. Wilkinson), Pergamon, Oxford, **1995**, pp. 979−1015. − [1e] S. Sun, C. A. Dulloghan, D. A. Sweigart, *J. Chem. Soc., Dalton Trans.* **1996**, 4493−4507. − [1f] F. Rose-Munch, V. Gagliardini, C. Renard, E. Rose, *Coord. Chem. Rev.*, in press.

[2] [2a] B. Niemer, M. Steinmann, W. Beck, *Chem. Ber.* **1988**, *121*, 1767−1769. − [2b] W. Beck, B. Niemer, J. Breimair, J. Heidrich, *J. Organomet. Chem.* **1989**, *372*, 79−83. − [2c] J. Breimair, T. Weidman, B. Wagner, W. Beck, *Chem. Ber.* **1991**, *124*, 2431−2434. − [2d] B. Niemer, J. Breimair, T. Völkel, B. Wagner, K. Polborn, W. Beck, *Chem. Ber.* **1991**, *124*, 2237−2244. − [2e] M. Wieser, K. Sünkel, C. Robl, W. Beck, *Chem. Ber.* **1992**, *125*, 1369−1373. − [2f] J. Breimair, M. Wieser, W. Beck, *J. Organomet. Chem.* **1992**, *441*, 429−439. − [2g] M. Wieser, K. Karaghiosoff, W. Beck, *Chem. Ber.* **1993**, *126*, 1081−1089. − [2h] W. Beck, B. Niemer, M. Wieser, *Angew. Chem. Int. Ed. Engl.* **1993**, *32*, 923−1110. − [2i] J. Milke, K. Sünkel, W. Beck, *J. Organomet. Chem.* **1997**, *543*, 39−46.

[3] [3a] F. Rose-Munch, C. Susanne, F. Balssa, E. Rose, *J. Organomet. Chem.* **1994**, *476*, C25−C26. − [3b] F. Rose-Munch, C. Le Corre-Susanne, F. Balssa, E. Rose, J. Vaisserman, E. Licandro, A. Papagni, S. Maiorana, W. Meng, R. Stephenson, *J. Organomet. Chem.* **1997**, *9*, 545−546.

[4] C. Renard, R. Valentic, F. Rose-Munch, E. Rose, *Organometallics* **1998**, *17*, 1587−1594.

[5] V. Gagliardini, F. Balssa, F. Rose-Munch, E. Rose, C. Susanne, Y. Dromzee, *J. Organomet. Chem.* **1996**, *519*, 281−283.

[6] [6a] M. F. Semmelhack, G. R. Clark, J. L. Garcia, J. J. Harrison, Y. Thebtaranonth, W. Wulff, A. Yamashita, *Tetrahedron* **1981**, *37*, 3957−3965. − [6b] M. F. Semmelhack *Comprehensive Organic Synthesis*, vol. 4 (Eds: B. M. Trost, I. Fleming), Pergamon, Oxford, **1991**, 517.

[7] [7a] R. D. Pike, D. A. Sweigart, *Synlett* **1990**, 565. − [7b] F. Balssa, V. Gagliardini, C. Le Corre-Susanne, F. Rose-Munch, E. Rose, J. Vaisserman, *Bull. Soc. Chim. Fr.* **1997**, *134*, 537−541 and ref. therein; see also refs.[2a,3b]

[8] [8a] E. P. Kündig, A. F. Cunningham, P. Paglia, D. P. Simmons, G. Bernardinelli, *Helv. Chim. Acta* **1990**, *73*, 386−404. − [8b] J. P. Djukic, F. Rose-Munch, E. Rose, Y. Dromzee, *J. Am. Chem. Soc.* **1993**, *11*, 6434−6435.

[9] R. Hoffmann, P. Hofmann, *J. Am. Chem. Soc.* **1976**, *98*, 598−604.

[10] E. Jeong, Y. K. Chung, *J. Organomet. Chem.* **1992**, *434*, 225−233.

[11] W. J. Ryan, P. E. Peterson, Y. Cao, P. G. Williard, D. A. Sweigart, C. D. Baer, C. F. Thompson, Y. K. Chung, T. M. Chung, *Inorg. Chim. Acta* **1993**, *211*, 1−3.

[12] T. Y. Lee, S. S. Lee, Y. K. Chung, S. W. Lee, *J. Organomet. Chem.* **1995**, *486*, 141−145.

[13] F. Rose-Munch, K. Aniss, *Tetrahedron Lett.* **1990**, *31*, 6351−6354.

[14] R. Khourzom, F. Rose-Munch, E. Rose, *Tetrahedron Lett.* **1990**, *31*, 2011−2014.

[15] We thank Dr. M. Imbeaux and Pr. C. Rolando (Ecole Normale Supérieure de Paris, France) for a gift of a fluoro(phenylsulfonyl)methane sample.

[16] [16a] Y. K. Chung, H. K Bae, I. N. Jung, *Bull. Korean Chem. Soc.* **1988**, *9*, 349−352. − [16b] See also ref.[4]

[17] For *ipso* substitutions, see for example: [17a] J. C. Boutonnet, F. Rose-Munch, E. Rose, A. Semra, *Bull. Soc. Chim. Fr.* **1987**, 640−648. − [17b] F. Rose-Munch, K. Aniss, E. Rose *J. Organomet. Chem.* **1990**, *385*, C1−C3. − [17c] F. Rose-Munch, K. Aniss, E. Rose, J. Vaisserman, *J. Organomet. Chem.* **1991**, *415*, 223−255. − [17d] M. Persson, V. Hacksell, I. Csöregh, *J. Chem. Soc., Perkin Trans. 1* **1991**, 1453−1459. − [17e] F. Rose-Munch, R. Khourzom, J. P. Djukic, E. Rose, *J. Organomet. Chem.* **1993**, *456*, C8-C10. − [17f] F. Rose-Munch, R. Khourzom, J. P. Djukic, A. Perrotey, E. Rose, J. Brocard, *J. Organomet. Chem.* **1994**, *467*, 195−206; see also ref.[1c]

[18] For *cine* substitutions, see: [18a] F. Rose-Munch, E. Rose, A. Semra, *J. Chem. Soc., Chem. Commun.* **1986**, 1551−1552. − [18b] F. Rose-Munch, E. Rose, A. Semra, *J. Organomet. Chem.* **1989**, *377*, C9−C12.

[19] For *tele-meta* substitutions, see for example: [19a] J. C. Boutonnet, F. Rose-Munch, E. Rose, *Tetrahedron Lett.* **1985**, *26*, 3989−3992. − [19b] F. Rose-Munch, E. Rose, A. Semra, *J. Chem. Soc., Chem. Commun.* **1986**, 1108−1109. − [19c] F. Rose-Munch, E. Rose, A. Semra, Y. Jeannin, F. Robert, *J. Organomet. Chem.* **1988**, *353*, 53−64. − [19d] F. Rose-Munch, E. Rose, A. Semra, J. Garcia-Oricain, C. Knobler, *J. Organomet. Chem.* **1989**, *363*, 297−309. − [19e] F. Rose-Munch, E. Rose, A. Semra, C. Bois, *J. Organomet. Chem.* **1989**, *363*, 103−121. − [19f] R. Khourzom, F. Rose-Munch, E. Rose, *Tetrahedron Lett.* **1990**, *31*, 2011−2014. − [19g] F. Rose-Munch, J. P. Djukic, E. Rose, *Tetra-*

hedron Lett. **1990**, *31*, 2589−2590. − [19h] J. P. Djukic, F. Rose-Munch, E. Rose, *J. Chem. Soc., Chem. Commun.* **1991**, *22*, 1634−1635. − [19i] J. P. Djukic, P. Geysermans, F. Rose-Munch, E. Rose, *Tetrahedron Lett.* **1991**, *32*, 6703−6704. − [19j] J. P. Djukic, F. Rose-Munch, E. Rose, Y. Dromzee, *J. Am. Chem. Soc.* **1993**, *115*, 6434−6435. − [19k] J. P. Djukic, F. Rose-Munch, E. Rose, *Organometallics* **1995**, *14*, 2027−2038. − [19l] H.-G. Schmalz, K. Schellhaas, *Tetrahedron Lett.* **1995**, *36*, 5511−5514. − [19m] F. Balssa, V. Gagliardini, F. Rose-Munch, E. Rose, *Organometallics* **1996**, *15*, 4373−4382. − [19n] H.-G. Schmalz, K. Schellhaas, *Angew. Chem. Int. Ed. Engl.* **1996**, *35*, 2146−2148. − [19o] V. Gagliardini, V. Onnikian, F. Rose-Munch, E. Rose, *Inorg. Chim. Acta* **1997**, *259*, 265−271. −
For *tele-para* substitutions, see: [19p] F. Rose-Munch, E. Rose, A. Semra, *J. Chem. Soc., Chem. Commun.* **1987**, 942−943. − [19q] F. Rose-Munch, E. Rose, A. Semra, M. Philoche-Levisalles, *J. Organomet. Chem.* **1989**, *363*, 123−130.

[20] For some examples of additions of benzylic anions from complexes such as μ-(diphenylmethane)bis(tricarbonylchromium) complexes see ref.[2g]

[21] A. J. Pearson, P. R. Bruhn, F. Gouzoules, S. H. Lee, *J. Chem. Soc., Chem. Commun*. **1989**, 659−661.

[22] [22a] W. H. Miles, P. M. Smiley, H. R. Brinkman, *J. Chem. Soc., Chem. Commun*. **1989**, 1897−1899. − [22b] W. H. Miles, H. R. Brinkman, *Tetrahedron Lett*. **1992**, *33*, 589−592.

[23] F. Rose-Munch, C. Susanne, C. Renard, E. Rose, J. Vaisserman, *J. Organomet. Chem*. **1996**, *519*, 253−259.

[24] D. B. Snyder, S. J. Schauer, D. P. Eyman, J. L. Moles, J. J. Weers, *J. Am. Chem. Soc.* **1993**, *115*, 6718−6729.

[25] S. G. Lee, J. A. Kim, Y. K. Chung, T. S. Yoon, N. J. Kim, W. Shin, *Organometallics* **1995**, *14*, 1023−1029.

[26] G. Winkhaus, L. Pratt, G. Wilkinson, *J. Chem. Soc.* **1961**, 3807−3813.

[27] P. L. Pauson, J. A. Segal, *J. Chem. Soc., Dalton Trans.* **1975**, 1677−1682.

[28] [28a] D. A. Brown, W. K. Glass, K. M. Kreddan, *J. Organomet. Chem.* **1991**, *413*, 233−242. − [28b] D. B. Snyder, S. J. Schauer, D. B. Eyman, J. L. Moler, J. Weers, *J. Am. Chem. Soc*. **1993**, *115*, 6718−6729.

[29] F. Rose-Munch, E. Rose, A. Semra, L. Mignon, J. Garcia-Oricain, C. Knobler, *J. Organomet. Chem.* **1989**, *363*, 297−309.

[30] J. Blagg, S. G. Davies, N. H. Holman, C. A. Laughton, B. E. Mobbs, *J. Chem. Soc., Dalton Trans.* **1986**, 1581−1589.

[31] N. Walker, D. Stuart, "DIFABS", *Acta Crystallogr.* **1983**, A39, 158−166.

[32] G. M. Sheldrick, *SHELXS-86, Program for Crystal Structure Solution*, University of Göttingen, **1986**.

[33] D. J. Watkin, C. K. Prout, J. R. Carruthers, P. W. Betteridge, *Crystals*, issue 10, Chemical Crystallography Laboratory, University of Oxford, U.K.**1996**

[34] D. T. Cromer, *International Tables for X-ray Crystallography*, vol IV, Kynoch Press, Birmingham, U.K., **1974**.

Received September 14, 1998
[I98309]

Complex Catalysis 55[+]

Oxidative Addition Reactions of Organorhodium(I) Complexes Containing the Tridentate Ligand 2,6-Bis(diphenylphosphanylmethyl)pyridine [Rh(PNP)R] ($R = CH_3$, C_6H_5) with Iodine and Methyl Iodide and Investigation of the Reductive Elimination

Christine Hahn,[a] Michael Spiegler,[b] Eberhardt Herdtweck,[b] and Rudolf Taube*[b]

Dedicated to Professor Helmut Werner on the occasion of his 65th birthday

Keywords: Rhodium(III) complexes / Tridentate ligand / Oxidative addition / Reductive elimination / C–C coupling

As part of studies aimed at delineating the mechanism of the rhodium complex-catalyzed hydroamination of olefins, the model complexes [Rh(PNP)R] (R = CH_3 **1a**, C_6H_5 **1b**) have been investigated with regard to oxidative addition reactions. The reaction of I_2 with **1a** leads to both *trans*- and *cis*-[Rh(PNP)(CH_3)I_2] (*trans*: **2a**, *cis*: **2a′**), whereas with **1b** only *trans*-[Rh(PNP)(C_6H_5)I_2] (**2b**) is obtained. The rhodium(III) complexes [Rh(PNP)(CH_3)RI] (**3a**,**b**) are formed by the reaction of **1a**,**b** with CH_3I. The new organorhodium(III) complexes **2a**,**b** and **3a**,**b** have been characterized by ^{31}P-, ^{1}H-, and ^{13}C-NMR spectrometry, as well as by EI mass spectrometry. The hydrocarbons RCH_3 are reductively eliminated in the reaction of [Rh(PNP)(CH_3)RI] (**3a**,**b**) with $TlBF_4$ in acetone, while the reaction of **3b** and $TlBF_4$ in THF/CH_3CN leads to the stable rhodium(III) complex [Rh(PNP)(CH_3)(C_6H_5)(CH_3CN)]BF_4 (**5**). Complex **5** has been characterized by X-ray crystallography.

Introduction

Detailed model studies have been initiated aimed at elucidating the reaction mechanism of the rhodium complex-catalyzed hydroamination of ethylene.[1] For the first time, the process was shown to be catalyzed by a cationic ethylene rhodium(I) complex under normal conditions.[2] For these studies, model complexes containing the 2,6-bis(diphenylphosphanylmethyl)pyridine-rhodium(I) fragment [Rh(PNP)]$^+$ as a stable structural unit were synthesized and characterized.[3]

Since the formation and cleavage of an Rh−C σ-bond is expected to play an essential role in this catalytic cycle, organorhodium(I) complexes [Rh(PNP)R] (R = CH_3, C_6H_5) were synthesized and investigated with regard to the coordination of ethylene and protolysis. It was found that with protic acids such as HSO_3CF_3 and [$HN(CH_3)_3$]Cl, these organorhodium(I) complexes react by immediate release of the hydrocarbon HR, presumably via reductive elimination from an initially formed hydrido organorhodium(III) complex.[4]

While a hydrido organorhodium(III) complex, which might have been expected to be formed by oxidative addition of the protic acid, could not be isolated or detected in these cases, a stable monohydrido chloro rhodium(III) complex [Rh(PNP)HCl(CH_3CN)]SO_3CF_3 is accessible by oxidative addition of HSO_3CF_3[4] to the related chloro rhodium(I) complex [Rh(PNP)Cl].[3b,5] Since the oxidative addition and the reductive elimination involved in numerous other rhodium-complex catalyzed processes are of general importance[6] it seemed therefore interesting to study these reaction steps at the [Rh(PNP)]$^+$ fragment.

In this paper, we report on oxidative addition reactions of the organorhodium(I) complexes [Rh(PNP)R] (R = CH_3, C_6H_5) with I_2 and CH_3I, as well as on the conditions under which the obtained diorganorhodium(III) complexes [Rh(PNP)(CH_3)RI] undergo reductive elimination.

Results and Discussion

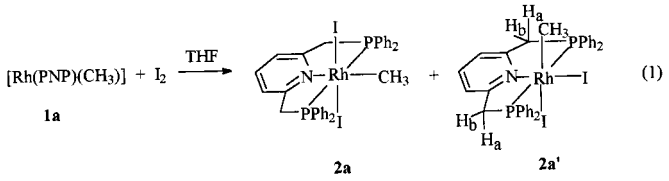
Oxidative Addition Reactions of [Rh(PNP)R] ($R = CH_3$, C_6H_5) with I_2 and CH_3I

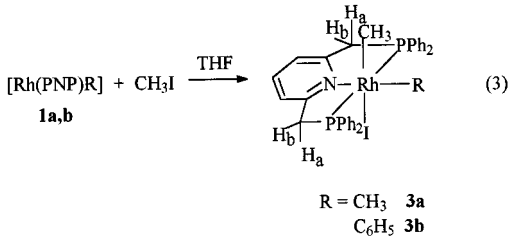
In order to show that stable PNP-organorhodium(III) complexes are accessible, the reactivity of organorhodium(I) complexes **1a**,**b** with iodine and methyl iodide, which are known as suitable reagents for oxidative addition to rhodium(I) complexes,[7] was investigated. Both organorhodium(I) complexes **1a**,**b** were found to react smoothly with iodine to give the corresponding rhodium(III) complexes [Rh(PNP)I_2R] **2** [Eqs. (1) and (2)], which were isolated as brown, air-stable solids.

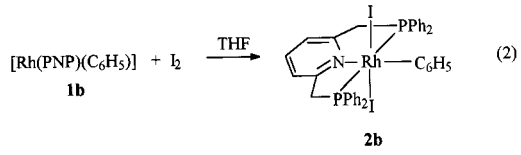
[+] Part 54: See ref.[4]

[a] Dipartimento di Chimica, Università di Napoli "Federico II"
via Mezzocannone 4, I-80134 Napoli, Italy
E-mail: chahn@chemna.dichi.unina.it
[b] Anorganisch-Chemisches Institut, Technische Universität München
Lichtenbergstraße 4, D-85747 Garching, Germany
Fax: (internat.) +49 (0)89/28913473

 © WILEY-VCH Verlag GmbH, D-69451 Weinheim, 1999 1434−1948/99/0303−0435 $ 17.50+.50/0







In the case of the methyl complex, the formation of the *trans* as well as of the *cis* addition product (**2a** and **2a′**, respectively) was established by NMR spectrometry. The two isomers constantly crystallize as a mixture, however, no further attempts were made to separate **2a** and **2a′** by other methods. In the ^{31}P-NMR spectrum, two doublets are observed at δ = 14.3 (J_{P-Rh} = 99 Hz) for **2a** and at δ = 23.3 (J_{P-Rh} = 106 Hz) for **2a′**, in an intensity ratio of 3:2. The phosphorus-rhodium coupling constants are markedly lower in comparison to those in the organorhodium(I) complexes **1a**,**b**, indicating the Rh^{III} oxidation state.[8] Accordingly, in the ^{1}H-NMR spectrum, two discrete methyl group signals are observed at δ = 1.99 for **2a** and at δ = 0.43 for **2a′**, with the same relative intensities of 3:2. The corresponding characteristic signal patterns of the methylene protons of the PNP ligand, a pseudo triplet at δ = 4.84 for **2a** and two doublets of pseudo triplets at δ = 4.49 and 4.80 for **2a′**, are consistent with the symmetry of these *trans* and *cis* isomers. In the ^{13}C-NMR spectrum, two discrete signals at δ = −18.4 and δ = 8.7 are observed for the methyl groups, while for the methylene groups of the PNP ligand, two signals appear at δ = 44.7 and δ = 46.7, showing slightly different intensities.

The phenyl complex **1b** forms exclusively the *trans* addition product **2b** on reaction with iodine [Eq. (2)]. The ^{31}P-NMR spectrum exhibits only one doublet at δ = 18.8 (J_{P-Rh} = 105 Hz). The pseudo triplet for the methylene group is seen at δ = 4.90 in the ^{1}H-NMR spectrum, consistent with the C_2 symmetry of the *trans*-diiodo complex **2b**. The ^{1}H-NMR signals of the phenyl moiety in **2b** are slightly downfield shifted compared to those found for **1b**, appearing at δ = 6.88 and 7.96.

In the mass spectra of **2a**,**a′** (analyzed as an isomeric mixture) and of **2b**, peaks are observed corresponding to the fragments $[M - I]^+$, $[M - R]^+$, $[M - I - R]^+$, $[M - I - I]^+$, and $[M - I - I - R]^+$. Additionally in the mass spectrum of **2a**,**a′**, a peak at *m*/*z* = 142 is found, which can be assigned to $[CH_3I]^+$ as the product of reductive elimination.

The reactions of **1a**,**b** with methyl iodide [Eq. (3)] led to the diorganorhodium(III) complexes [Rh(PNP)(CH_3)RI] **3a**,**b**, which were isolated as pale-yellow air-stable solids and characterized by ^{31}P-, ^{1}H-, and ^{13}C-NMR spectrometry, as well as by mass spectrometry.

The ^{31}P-NMR signals observed at δ = 26.5 (J_{P-Rh} = 120 Hz) for **3a** and at δ = 30.5 (J_{P-Rh} = 119 Hz) for **3b** are downfield shifted in comparison to the signals of the corresponding diiodo complexes **2a** and **2b**. The increased phosphorus-rhodium coupling constants in **3a**,**b** in comparison to those in **2a**,**b** may be arised by coordination of the more basic methyl ligand instead of one iodo ligand, respectively. In the ^{1}H-NMR spectrum of the dimethyl complex **3a**, two discrete methyl signals are observed at δ = −0.35 and δ = 1.02, suggesting the coordination of two distinct methyl groups in a mutual *cis*-arrangement. This is confirmed by the resonances of the methylene protons of the PNP ligand, which appear as two doublets of pseudo triplets at δ = 4.31 and 4.66, consistent with the inequivalence of the methylene protons arising from the *cis* orientation of the methyl groups. Accordingly, in the ^{13}C-NMR spectrum, two discrete signals for the methyl groups are observed at δ = −14.5 and 6.9.

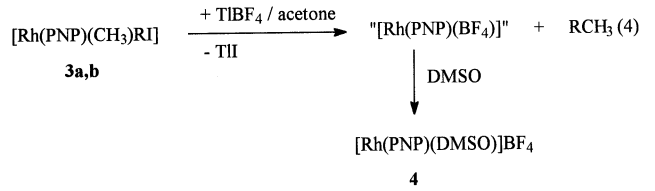
The ^{1}H-NMR signal of the methyl group in the methyl phenyl complex **3b** appears at δ = 0.35, while the phenyl group gives rise to multiplets at δ = 6.90 and 7.68. The typical signal pattern for the non-equivalent methylene protons, as observed for **3a**, is seen in the spectrum of **3b** at δ = 4.34 and 4.80. The ^{13}C-NMR signal for the methyl group in **3b** appears at δ = 8.8, while the phenyl group signals are seen at δ = 121.5, 125.9, and 142.3.

In the mass spectra of **3a** and **3b**, peaks are observed corresponding to the fragments $[M - CH_3]^+$, $[M - CH_3 - R]^+$, and $[M - CH_3 - R - I]^+$. Additionally, in the mass spectrum of **3b**, a peak at *m*/*z* = 91 can be observed, attributable to $[C_7H_7]^+$. This suggests that toluene is reductively eliminated from the methyl phenyl complex **3b** following C−C bond formation.

Investigation of the Reductive Elimination of Hydrocarbons by C−C Bond Formation from [Rh(PNP)(CH_3)RI]BF_4 3a,b

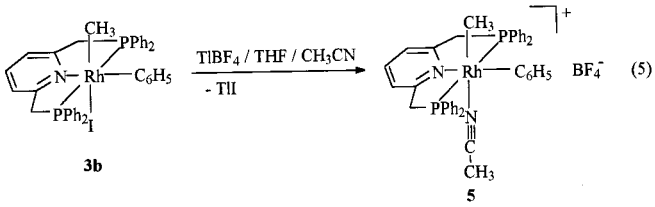
In a manner analogous to the reductive elimination of the hydrocarbon from the proposed hydrido organorhodium(III) intermediates by formation of a C−H bond,[4,9] the reactivity of the diorganorhodium(III) complexes **3a**, **b** was investigated. The aforementioned mass spectral observation of toluene generation from **3b** gave a prior indication of C−C bond formation between the two organo moieties. After addition of $TlBF_4$ to a solution of **3a** or **3b** in acetone, TlI precipitated while the solution changed colour from pale yellow to dark-red during 1−2 days indicating the

change of the oxidation state from Rh^{III} to Rh^{I}. Indeed, the hydrocarbon which is formed by reductive elimination from **3a** and **3b**, respectively [Eq. (4)], has been proved. Carrying out the reaction of **3a** and $TlBF_4$ in [D_6]acetone in a sealed NMR tube the singlet of the liberated ethane could be observed in the ^{1}H-NMR spectrum while the signals of complex **3a** disappeared. Whereas the toluene reductively eliminated from **3b** was detected in the filtrate of the reaction solution by gas chromatography. The dark colour of the solutions indicated a decomposition reaction, most likely as a consequence of the weak coordination of the acetone, which does not have sufficient donor strength to stabilize the remaining $[Rh^{I}(PNP)]^+$ fragment. In order to prove that the rhodium was present in the +I oxidation state, some DMSO was added to the solution. The corresponding stable rhodium(I) complex $[Rh(PNP)(DMSO)]BF_4$ **4** was obtained, which was identified by comparison of its ^{31}P-NMR spectrum with that of an authentic sample (cf. ref.[3b]).



Clearly, the cleavage of the iodo ligand from the octahedral diorganorhodium(III) complex **3a**,**b** leads to a kinetically unstable five-coordinate complex, which cannot be stabilized by the weakly coordinating acetone used as solvent. This confirms the dissociative mechanism of the reductive elimination.[9]

However, when the reaction of **3b** with $TlBF_4$ was carried out in the presence of the more strongly coordinating acetonitrile, a stable six-coordinate methyl phenyl acetonitrile rhodium(III) complex $[Rh(PNP)(CH_3)(C_6H_5)(CH_3CN)]BF_4$ **5** was obtained [Eq. (5)], which was isolated as an air-stable, white, crystalline solid and characterized by ^{31}P-, ^{1}H-, and ^{13}C-NMR spectrometry, as well as by X-ray crystal structure analysis.



In the ^{31}P-NMR spectrum of **5**, the doublet at $\delta = 32.7$ ($J_{P-Rh} = 117$ Hz) is somewhat downfield shifted compared to the corresponding signal in the iodo complex **3b**. While the ^{1}H- and ^{13}C-NMR signals of the phenyl moiety appear at approximately the same chemical shifts as found for **3b**, the signals for the methyl moiety of **5** are somewhat upfield shifted in both the ^{1}H- ($\delta = 0.09$) and the ^{13}C-NMR spectra ($\delta = 2.0$), compared to those in **3b**. This may be interpreted in terms of the differential *trans* influence of the respective *trans*-coordinated ligands (I^- **3b**; CH_3CN **5**).

For the coordinated acetonitrile in **5**, a singlet is observed at $\delta = 1.45$ in the ^{1}H-NMR spectrum, while in the ^{13}C-NMR spectrum, two signals are observed at $\delta = 2.0$ and 128.5. In the IR spectrum, the two bands characteristic of end-on coordinated acetonitrile[9] are seen at $\tilde{\nu} = 2281$ and 2376 cm^{-1}. The coordination of the pyridine of the PNP ligand is indicated by two bands at $\tilde{\nu} = 1574$ and 1606 cm^{-1},[11] while a strong band at $\tilde{\nu} = 1062$ cm^{-1} is characteristic of the non-coordinated BF_4^- anion.[12]

Single crystals of **5** of X-ray quality were obtained from a solution of the complex in acetone overlayered with diethyl ether. X-ray crystal structure analysis confirmed the *cis*-arrangement of the organo moieties in the octahedral complex cation of **5**, which is an essential structural prerequisite for the reductive elimination of toluene. The molecular structure of the complex cation $[Rh(PNP)(CH_3)(C_6H_5)(CH_3CN)]^+$ is shown in Figure 1.

Comparing the rhodium-carbon distances of the σ-bonded methyl and phenyl groups [Rh−C(3) 2.085(3), Rh−C(11) 2.049(3)], only a very slight difference is apparent. The small difference in bond lengths of the two types of Rh−C bond may be viewed as reflecting the differential *trans* influence of the N(sp^2) and N(sp) atoms of the coordinated pyridine moiety and acetonitrile ligand, respectively, which gives rise to an extension of the Rh−C(sp^2) bond and a shortening of the Rh−C(sp^3) bond. However, it may also be viewed as merely following the expected trend that the sp^2 carbon atom has a shorter distance to the rhodium atom than the sp^3 carbon atom.

Furthermore, it is interesting to compare the molecular structure of **5** with that of the related cationic Rh^{III} complex $[Rh(PNP)ClH(CH_3CN)]SO_3CF_3$,[4] which contains the same structural unit $[Rh^{III}(PNP)(CH_3CN)]^+$, but with the hydrido ligand coordinated *trans* to the acetonitrile ligand. In both complexes, the N atom of the coordinated acetonitrile shows an identical distance to the rhodium atom of 2.14 Å, as a result of the comparable *trans* influence of the methyl and hydrido ligands. However, the distance of the pyridine N atom to the rhodium atom in **5** is significantly longer [Rh−N(2) 2.152(2) Å] than the corresponding Rh−N(py) distance in the hydrido chloro Rh^{III} complex [Rh−N(2) 2.0656(17) Å].[4] This is consistent with the expected stronger *trans* influence of the phenyl group, which has a lower electronegativity than the chloro ligand coordinated *trans* to the pyridine. The end-on coordinated acetonitrile shows an almost linear arrangement of Rh−N(1)−C(1)−C(2) [C(1)−N(1)−Rh 172.0(2)°, N(1)−C(1)−C(2) 178.4(4)°], as was also found in the cationic Rh^{III} complex $[Rh(PNP)ClH(CH_3CN)]SO_3CF_3$,[4] as well as in the cationic rhodium(I) complex $[Rh(PNP)(CH_3CN)]BF_4$.[3b]

Conclusions

The organorhodium(I) complexes [Rh(PNP)R] smoothly undergo oxidative addition reactions with I_2 and CH_3I to give the stable organorhodium(III) complexes $[Rh(PNP)RI_2]$ and $[Rh(PNP)(CH_3)RI]$, respectively.

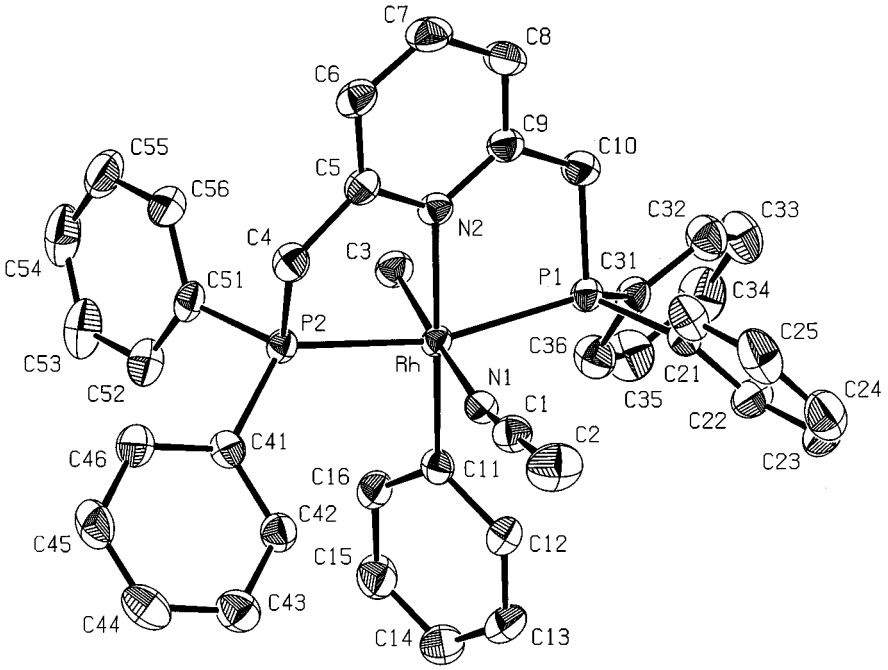


Figure 1. PLATON[13] drawing of the structure of the complex cation of $[Rh(PNP)(C_6H_5)(CH_3)(CH_3CN)]BF_4$ **5**. Selected bond lengths [Å] and angles [°]: Rh−N(1) 2.142(3), Rh−N(2) 2.152(2), Rh−C(3) 2.082(3), Rh−C(11) 2.049(3), Rh−P(1) 2.2913(9), Rh−P(2) 2.3098(8), P(1)−C(10) 1.848(5), P(2)−C(4) 1.835(3); P(1)−Rh−P(2) 164.58(3), N(1)−Rh−P(1) 93.92(7), N(1)−Rh−P(2) 89.55(7), N(1)−Rh−N(2) 88.56(9), C(3)−Rh−C(11) 91.77(12), N(1)−Rh−C(3) 176.65(11), N(2)−Rh−C(11) 179.9(2), C(1)−N(1)−Rh 172.0(2), N(1)−C(1)−C(2) 178.4(4).

It was shown that the diorganorhodium(III) complexes $[Rh(PNP)(CH_3)RI]$, in which the organo moieties are coordinated in a *cis* arrangement, C−C bond formation leading to the reductive elimination of the hydrocarbons RCH_3 is possible. This was realized by cleavage of the iodo ligand with $TlBF_4$ in the presence of acetone. Acetone is too weakly coordinating as a ligand to stabilize the resulting five-coordinate diorganyl rhodium(III) complex. However, when the reaction is carried out in the presence of the more strongly coordinating CH_3CN, the stable six-coordinate acetonitrile complex $[Rh(PNP)(CH_3)(C_6H_5)(CH_3CN)]BF_4$ is formed, confirming the dissociative mechanism of the reductive elimination.

The smooth oxidative addition reactions of the model compounds [Rh(PNP)R], and the stability as well as the reactivity of the Rh-C σ-bond in the rhodium-PNP complexes suggests that rhodium(I) has the potential to catalyze the hydroamination of olefins according to the proposed catalytic reaction mechanism.[4]

Experimental Section

All reactions were carried out under dry argon. Acetone, [D$_6$]acetone, CD_2Cl_2, and $CDCl_3$ were refluxed over 4-Å molecular sieves and purged of oxygen by bubbling argon. THF and diethyl ether were refluxed over Na/benzophenone. Acetonitrile, DMSO, and methyl iodide were dried over 4-Å molecular sieves and distilled prior to use.

Infrared spectra were recorded from KBr pellets on a Perkin-Elmer FT-IR 16 spectrometer. − The ^{1}H-, ^{13}C{^{1}H}-, and ^{31}P{^{1}H}-NMR spectra were recorded at 300, 75, and 121 MHz, respectively, on a Varian Gemini 300 NMR spectrometer. The ^{1}H- and ^{13}C-NMR shifts were referenced to the solvent signals, while the ^{31}P-NMR shifts were referenced to external 85% H_3PO_4. − A Chrompack CP 9000 gas chromatograph was used for the identification of liquid organic compounds. − EI mass spectra were recorded on an AMD 402 spectrometer (AMD Intectra) at 70 eV. − C,H,N elemental analyses were carried out on a LECO CHN 932 analyzer, while Rh was determined using a photometric method.[14]

Synthesis of $[Rh(PNP)RI_2]$ (R = CH_3 *trans:* 2a, *cis*: 2a′; C_6H_5 2b): 237 mg of I_2 (0.93 mmol) in 2 mL of THF was added to a solution of 552 mg (0.93 mmol) of **1a** in 4 mL of THF. After a few seconds, a brown, microcrystalline solid precipitated, and the reaction mixture was stirred for 10 min. After a further 30 min (without stirring), the solid was filtered off and washed with THF and diethyl ether. The crude product was recrystallized from refluxing THF. The recrystallized product was washed twice with THF and twice with diethyl ether and dried in vacuo.

2a (*trans*)/2a′ (*cis*): Yield: 498 mg (0.59 mmol, 63%); m.p. 295−298°C (dec.). − $C_{32}H_{30}I_2NP_2Rh$ (846.90): calcd. C 45.34, H 4.52, N 1.90, Rh 12.15; found C 45.43, H 4.33, N 1.73, Rh 12.03. − ^{31}P NMR (CD_2Cl_2): δ = 14.3 (d, J_{P-Rh} = 99 Hz, *trans*), 23.3 (d, J_{P-Rh} = 106 Hz, *cis*). − ^{1}H NMR (CD_2Cl_2): δ = 0.43 (td, J_{H-P} = 6.2 Hz, J_{H-Rh} = 2.2 Hz, 3 H, CH_3, *cis*), 1.99 (td, J_{H-P} = 4.8 Hz, J_{H-Rh} = 2.2 Hz, 3 H, CH_3, *trans*), 4.49 (d ps. t, J_{Ha-Hb} = 17.3 Hz, N_{H-P} = 4.4 Hz, 2 H, CH_a, *cis*), 4.80 (d ps. t, J_{Ha-Hb} = 17.3 Hz, N_{H-P} = 5.6 Hz, 2 H, CH_b, *cis*), 4.84 (vt, N_{H-P} = 4.6 Hz, 4 H, CH_a, *trans*), 7.36−8.20 (m, PPh, py, *trans*/*cis*). − ^{13}C NMR (CD_2Cl_2): δ = −18.4 (dt, J_{C-P} = 8.9 Hz, J_{C-Rh} = 16.1 Hz, *C*H_3, *trans*), 8.7 (dt, J_{C-P} = 4.0 Hz, J_{C-Rh} = 20.2 Hz, *C*H_3, *cis*), 44.7 (ps. t, *N* = 13.0 Hz, *C*H_2, *trans*), 46.7 (ps. t, *N* = 15.5 Hz, *C*H_2, *cis*), 121.3 (ps. t, *N* = 5.0 Hz, $C_{3,5\text{-py}}$), 121.5 (ps. t, *N* = 5.0 Hz, $C_{3,5\text{-py}}$), 127.9 (ps. t, *N* = 5.6 Hz, PC_{meta}, *trans*) 127.9 (ps. t, *N* = 5.0 Hz, PC_{meta}, *cis*), 128.3 (ps. t, *N* = 4.6 Hz, PC_{meta}, cis), 130.0 (s,

PC_{para}, *trans*), 130.2 (s, PC_{para}, cis), 130.5 (s, PC_{para}, cis), 132.3 (ps. t, N = 4.7 Hz, PC_{ortho}, cis), 132.9 (ps. t, N = 5.0 Hz, PC_{ortho}, *trans*), 133.9 (ps. t, N = 5.0 Hz, PC_{ortho}, cis), 138.2 (s, $C_{4\text{-py}}$, *cis*), 138.5 (s, $C_{4\text{-py}}$, *trans*), 159.3 (ps. t, N < 3 Hz, $C_{2,6\text{-py}}$, *cis*), 162.1 (ps. t, N < 3 Hz, $C_{2,6\text{-py}}$, *trans*). − EI-MS: *m/z* (%): 832 (0.1) $[M - CH_3]^+$, 719 (1.2) $[M - I]^+$, 705 (100) $[M - CH_3 - I]^+$, 578 (21) $[M - CH_3 - I - I]^+$, 142 (16) $[CH_3I]^+$.

The synthesis of **2b** was carried out in the same manner as described for **2a/a′**, starting from 572 mg (0.87 mmol) of **1b** in 4 mL of THF and 222 mg of I_2 dissolved in 2 mL of THF. Yield: 565 mg (0.62 mmol, 71%); m.p. 293°C (dec.). − $C_{37}H_{32}I_2NP_2Rh$ (909.33): calcd. C 48.87, H 3.55, N 1.54, Rh 11.32; found C 49.05, H 3.95, N 1.31, Rh 11.42. − ^{31}P NMR (CD_2Cl_2): δ = 18.8 (d, J_{P-Rh} = 105 Hz). − ^{1}H NMR (CD_2Cl_2): δ = 4.90 (ps. t, N_{H-P} = 4.7 Hz, 4 H, CH_2), 6.88 (m, 3 H, Ph), 7.26−7.38 (m, 20 H, PPh), 7.60 (d, J_{H-H} = 7.7 Hz, 2 H, 3,5-py), 7.82 (t, J_{H-H} = 7.7 Hz, 1 H, 4-py), 7.96 (m, 2 H, Ph). − ^{13}C NMR (CD_2Cl_2): δ = 48.1 (ps. t, N = 15.7 Hz, *C*H_2), 121.5 (ps. t, N = 5.3 Hz, $C_{3,5\text{-py}}$), 122.7 (s, Ph), 125.9 (s, Ph), 127.7 (ps. t, N = 5.0 Hz, PC_{meta}), 130.3 (s, PC_{para}), 134.3 (ps. t, N = 4.7 Hz, PC_{ortho}), 135.9 (ps. t, N = 24.5 Hz, PC_{ipso}), 138.8 (s, $C_{4\text{-py}}$), 147.2 (ps. t, N = 4.3 Hz, Ph), 160.4 (ps. t, N < 3 Hz, $C_{2,6\text{-py}}$). − EI-MS: *m/z* (%): 832 (0.4) $[M - C_6H_5]^+$, 781 (12.5) $[M - I]^+$, 705 (100) $[M - I - C_6H_5]^+$, 655 (1.4) $[M - I - I]^+$, 578 (27) $[M - I - I - C_6H_5]^+$.

Synthesis of [Rh(PNP)(CH$_3$)RI] (R = CH_3 **3a**, C_6H_5 **3b**): To a solution of 571 mg (0.96 mmol) of **1a** in 6 mL of THF was added 60 µl of CH_3I (Rh/CH_3I = 1:1). After a few seconds, a pale-yellow microcrystalline solid precipitated and the reaction mixture was stirred for 10 min. After a further 30 min (without stirring), the solid was filtered off and washed with THF and diethyl ether. The crude product was recrystallized by extraction with refluxing THF. The recrystallized product was washed twice with THF, twice with diethyl ether, and dried in vacuo.

3a: Yield: 390 mg (0.53 mmol, 55%); m.p. 214−220°C (dec.). − $C_{33}H_{33}INP_2Rh$ (735.39): calcd. C 53.90, H 4.52, N 1.90, Rh 13.99; found C 53.62, H 4.46, N 1.79, Rh 14.36. − ^{31}P NMR (CD_2Cl_2): δ = 26.5 (d, J_{P-Rh} = 120 Hz). − ^{1}H NMR (CD_2Cl_2): δ = −0.35 (td, J_{H-P} = 6.4 Hz, J_{H-Rh} = 2.2 Hz, 3 H, CH_3), 1.02 (td, J_{H-P} = 5.2 Hz, J_{H-Rh} = 2.1 Hz, 3 H, CH_3), 4.31 (d ps. t, J_{Ha-Hb} = 16.6 Hz, N_{H-P} = 4.2 Hz, 2 H, CH_a), 4.66 (d ps. t, J_{Ha-Hb} = 16.6 Hz, N_{H-P} = 4.9 Hz, 2 H, CH_b), 7.32−7.41 (m, 12 H, PPh), 7.50 (d, J_{H-H} = 7.6 Hz, 2 H, 3,5-py), 7.73 (t, J_{H-H} = 7.6 Hz, 1 H, 4-py), 7.79 (m, 8 H, PPh). − ^{13}C NMR (CD_2Cl_2): δ = −14.5 (dt, J_{C-P} = 7.1 Hz, J_{C-Rh} = 22.4 Hz, *C*H_3), 6.9 (dt, J_{C-P} = 6.3 Hz, J_{C-Rh} = 26.0 Hz, *C*H_3), 44.9 (ps. t, N = 13.6 Hz, *C*H_2), 120.8 (ps. t, N = 5.0 Hz, $C_{3,5\text{-py}}$), 127.9 (ps. t, N = 5.0 Hz, PC_{meta}), 128.2 (ps. t, N = 4.3 Hz, PC_{meta}), 129.4 (s, PC_{para}), 130.1 (s, PC_{para}), 131.8 (ps. t, N = 4.8 Hz, PC_{ortho}), 134.3 (ps. t, N = 5.8 Hz, PC_{ortho}), 137.4 (s, $C_{4\text{-py}}$), 159.3 (ps. t, N < 3 Hz, $C_{2,6\text{-py}}$). − EI-MS: *m/z* (%): 719 (2) $[M - CH_3]^+$, 705 (100) $[M - CH_3 - CH_3]^+$, 578 (15) $[M - CH_3 - CH_3 - I]^+$.

3b: The complex was obtained in the same manner as described for **3a**, starting from 692 mg (1.05 mmol) of **1b** and 66 µl of CH_3I in 7 mL of THF. − Yield: 528 mg (0.66 mmol, 63%); m.p. 186−195°C (dec.). − $C_{38}H_{35}INP_2Rh$ (797.46): calcd. C 57.23, H 4.42, N 1.76, Rh 12.90; found C 56.75, H 4.60, N 1.56, Rh 12.46. − ^{31}P NMR (CD_2Cl_2): δ = 30.5 (d, J_{P-Rh} = 119 Hz). − ^{1}H NMR (CD_2Cl_2): δ = 0.35 (td, J_{H-P} = 6.4 Hz, J_{H-Rh} = 2.2 Hz, 3 H, CH_3), 4.34 (d ps. t, J_{Ha-Hb} = 16.9 Hz, N_{H-P} = 4.3 Hz, 2 H, CH_a), 4.80 (d ps. t, J_{Ha-Hb} = 16.6 Hz, N_{H-P} = 4.8 Hz, 2 H, CH_b), 6.90 (m, 3 H, Ph), 7.11−7.38 (m, 20 H, PPh), 7.56 (d, J_{H-H} = 7.7 Hz, 2 H, 3,5-py), 7.68 (m, 2 H, Ph). 7.83 (t, J_{H-H} = 7.7 Hz, 1 H, 4-py). − ^{13}C NMR (CD_2Cl_2): δ = 8.8 (dt, J_{C-P} = 5.5 Hz, J_{C-Rh} = 26.7 Hz, *C*H_3), 46.3 (ps. t, N = 14.1 Hz, *C*H_2), 121.1 (ps. t, N = 5.1 Hz, $C_{3,5\text{-py}}$), 121.5 (s, Ph), 125.9 (s, Ph), 127.5 (ps. t, N = 5.0 Hz, PC_{meta}), 128.2 (ps. t, N = 4.7 Hz, PC_{meta}), 129.9 (s, PC_{para}), 130.0 (s, PC_{para}), 133.1 (ps. t, N = 5.1 Hz, PC_{ortho}), 134.2 (ps. t, N = 5.6 Hz, PC_{ortho}), 138.0 (s, $C_{4\text{-py}}$), 142.3 (ps. t, N = 4.0 Hz, Ph), 159.7 (ps. t, N < 3 Hz, $C_{2,6\text{-py}}$). − EI-MS: *m/z* (%): 781 (0.1) $[M - CH_3]^+$, 719 (0.8) $[M - C_6H_5]^+$, 705 (100) $[M - CH_3 - C_6H_5]^+$, 578 (17) $[M - CH_3 - C_6H_5 - I]^+$, 91 (57) $[C_7H_8 - H]^+$.

Reactivity of 3a and 3b Toward TlBF$_4$: (a) A mixture of 20 mg (0.027 mmol) of **3a** and 8 mg (0.027 mmol) of $TlBF_4$ in 0.7 mL of [D_6]acetone was shaken in a sealed NMR tube over 2 days. While TlI precipitated the solution changed colour to dark-red. In the ^{1}H-NMR spectrum a singlet is found at δ = 0.82 for ethane, whereas the signals of **3a** completely disappeared.

78 mg (0.27 mmol) of $TlBF_4$ was added to a solution of 215 mg (0.27 mmol) of **3b** in 5 mL of acetone. After stirring overnight, a yellow precipitate of TlI was filtered off. Toluene was detected in the dark-red filtrate by means of gas chromatography. Upon addition of 0.5 mL of DMSO, the solution became orange-red in colour. The DMSO−rhodium(I) complex [Rh(PNP)(DMSO)]BF_4 (**4**) was detected by ^{31}P-NMR spectroscopy (in acetone/external C_6D_6: δ = 40.2, J_{P-Rh} = 148 Hz). This was consistent with an authentic sample, which was prepared from [Rh(PNP)(C_2H_4)]BF_4 and DMSO.[3b]

(b) In the Presence of CH$_3$CN: 322 mg (0.4 mmol) of **3b** was suspended in a mixture of 7 mL of THF and 1 mL of acetonitrile. To this was added 120 mg of $TlBF_4$ and the mixture was stirred overnight. A yellow precipitate of TlI was deposited, which was filtered off. Diethyl ether was added dropwise to the pale-yellow filtrate, resulting in the precipitation of a white, crystalline solid. This was filtered off, washed with diethyl ether, and dried in vacuo. The solid was characterized as [Rh(PNP)(CH_3)(C_6H_5)(CH_3CN)]BF_4 (**5**): Yield: 271 mg (0.34 mmol, 85%); m.p. 146°C (dec.). − $C_{40}H_{38}BF_4N_2P_2Rh$ (798.41): calcd. C 60.17, H 4.80, N 3.51, Rh 12.89; found C 60.30, H 5.28, N 3.75, Rh 12.57. − ^{31}P NMR ($CDCl_3$): δ = 32.7 (d, J_{P-Rh} = 117 Hz). − ^{1}H NMR ($CDCl_3$): δ = 0.09 (td, J_{H-P} = 6.6 Hz, J_{H-Rh} = 1.5 Hz, 3 H, CH_3), 1.45 (s, 3 H, NCH_3), 4.30 (d ps. t, J_{Ha-Hb} = 17.5 Hz, N_{H-P} = 4.3 Hz, 2 H, CH_a), 4.47 (d ps. t, J_{Ha-Hb} = 17.5 Hz, N_{H-P} = 4.2 Hz, 2 H, CH_b), 6.95 (m, 3 H, Ph), 7.07−7.40 (m, 22 H, PPh, Ph), 7.75 (d, J_{H-H} = 7.7 Hz, 2 H, 3,5-py), 7.99 (t, J_{H-H} = 7.7 Hz, 1 H, 4-py). − ^{13}C NMR ($CDCl_3$): δ = 2.03 (s, N*C*H_3), 2.03 (m, overlapped with the N*C*H_3 signal, *C*H_3), 44.7 (ps. t, N = 13.7 Hz, *C*H_2), 120.4 (s, Ph), 122.5 (ps. t, N = 5.6 Hz, $C_{3,5\text{-py}}$), 127.2 (s, Ph), 128.5 (br, *C*N), 128.7 (br, PC_{meta}), 130.7 (s, PC_{para}), 130.8 (s, PC_{para}), 131.7 (ps. t, N = 18.3 Hz, PC_{ipso}), 132.7 (ps. t, N = 5.7 Hz, PC_{ortho}), 132.9 (ps. t, N = 5.6 Hz, PC_{ortho}), 138.1 (ps. t, N < 4.0 Hz, Ph), 139.6 (s, $C_{4\text{-py}}$), 159.1 (ps. t, N < 3 Hz, $C_{2,6\text{-py}}$). − IR (KBr): $\tilde{\nu}$ = 2281, 2376 cm^{-1} (CH_3CN); 1574, 1606 (py); 1062 (BF_4).

Crystal Structure Determination of Compound 5: *Crystal Data:* $C_{40}H_{38}BF_4N_2P_2Rh \cdot (C_4H_{10}O)_{0.8}$, formula weight 857.79 g mol^{-1}, monoclinic, $P2_1/n$ (No. 14), a = 12.6065(6), b = 24.5689(10), c = 13.5059(9) Å, β = 102.356(6)°, V = 4086.3(4) Å^3, Z = 4, d_{calc} = 1.394 g cm^{-3}, F(000) = 1767. − *Data Collection:* STOE-IPDS,[14] Mo-K_α radiation (graphite monochromator, λ = 0.71073 Å), crystal size 0.34 × 0.30 × 0.26 mm^3, T = 193(2) K, scan range 2.0 < θ < 25.7°; intensities were measured for 31092 reflections with 7411 unique reflections, of which 5469 were considered observed [$I \geq 2\sigma(I)$]. The reflections were corrected for Lorentz and polarization effects; μ = 0.55 mm^{-1}, no absorption correction. − *Structural Analysis and Refinement:* Preliminary positions of heavy atoms

were found by direct methods,[16] while positions of the other non-hydrogen atoms were determined from subsequent difference Fourier synthesis coupled with initial isotropic least-squares refinement.[17] An additional diethyl ether solvent molecule was located in the asymmetric unit and refined with 80% partial occupancy. With the exception of those of the solvent molecule, all hydrogen atoms were found in a difference Fourier map and refined with individual isotropic temperature parameters. Refinement: Full-matrix least-squares on F^2; 7070 reflections; 649 refined parameters; final $R_1 = 0.0333$, $wR_2 = 0.0806$, goodness-of-fit on $F^2 = 1.040$.

Crystallographic data (excluding structure factors) for the structure reported in this paper have been deposited with the Cambridge Crystallographic Data Centre (CCDC-100736). Copies of the data can be obtained free of charge on application to CCDC, 12 Union Road, Cambridge CB2 1EZ, U.K. [Fax: (internat.) + 44-1223/336033; E-mail: deposit@ccdc.cam.ac.uk].

Acknowledgments

We thank the Deutsche Forschungsgemeinschaft (Sonderforschungsbereich 347 of the University of Würzburg) for financial support.

[1] [1a] R. Taube in *Applied Homogeneous Catalysis with Organometallic Compounds* (Eds.: B. Cornils, W. A. Herrmann), Verlag Chemie, Weinheim, **1996**, vol. 1, pp. 507. – [1b] D. Steinborn, R. Taube, *Z. Chem.* **1986**, *26*, 349–359. – [1c] J.-J. Brunet, D. Neibecker, F. J. Niedercorn, *J. Mol. Catal.* **1989**, *49*, 235–259. – [1d] J.-J. Brunet, *Gazz. Chim. Ital.* **1997**, *127*, 111–118. – [1e] T. E. Müller, M. Beller, *Chem. Rev.* **1998**, *98*, 675–703.

[2] E. Krukowka, R. Taube, D. Steinborn, DD 296 909 A5 (10.11.88), **1988**; *Chem. Abstr.* **1992**, 213993b.

[3] [3a] C. Hahn, J. Sieler, R. Taube, *Chem. Ber.* **1997**, 130, 939–945. – [3b] C. Hahn, J. Sieler, R. Taube, *Polyhedron* **1998**, 17, 1183–1193.

[4] C. Hahn, M. Spiegler, E. Herdtweck, R. Taube, *Eur. J. Inorg. Chem.* **1998**, 1425–1432.

[5] G. Vasapollo, P. Giannoccaro, C. F. Nobile, A. Sacco, *Inorg. Chim. Acta* **1981**, *48*, 125–128.

[6] J. P. Collman, L. S. Hegedus, J. R. Norton, R. G. Finke, *Principles and Aplications of Organotransition Metal Chemistry*, University Science Books, Mill Valley, CA, **1987**.

[7] [7a] T. E. Nappler, D. W. Meek, R. M. Kirchner, J. A. Ibers, *J. Am. Chem. Soc.* **1973**, *95*, 4194–4210. – [7b] J. A. Tiethof, J. L. Peterson, D. W. Meek, *Inorg. Chem.* **1976**, *15*, 1365–1370.

[8] P. S. Pregosin, R. W. Kunz in *^{31}P and ^{13}C NMR of Transition Metal Phosphine Complexes* (Eds.: P. Diehl, E. Fluck, R. Kosfeld), Springer-Verlag, Berlin, Heidelberg, New York, **1979**, vol. 16.

[9] D. Milstein, *Acc. Chem. Res.* **1984**, *17*, 221–226.

[10] B. N. Storhoff, H. C. Lewis, *Coord. Chem. Rev.* **1977**, *23*, 1–29.

[11] W. V. Dahlhoff, S. M. Nelson, *J. Chem. Soc. (A)* **1971**, 2184–2190.

[12] W. Beck, K. Sünkel, *Chem. Rev.* **1988**, *88*, 1405–1421.

[13] A. L. Spek, "PLATON-92", *Acta Crystallogr. Sect. A* **1990**, *46*, C34.

[14] B. Lange, Z. J. Vejdelek, *Kolorimetrische Analyse*, Verlag Chemie, Weinheim, **1982**, p. 232.

[15] *IPDS Operating System Version 2.8., STOE & CIE GmbH*, Darmstadt, Germany, **1997**.

[16] A. Altomare, G. Cascarano, C. Giacovazzo, A. Guargliardi, M. C. Burla, G. Polidori, M. Camalli, *SIR-92*, University of Bari, Italy, **1992**.

[17] G. M. Sheldrick, *SHELXL-93*, in *Crystallographic Computing 3* (Ed.: G. M. Sheldrick, C. Krüger, R. Goddard), Oxford University Press, England, **1993**, pp. 175–189.

Received June 6, 1998
[I98181]

Singly *anti-anti* Carboxylate-Bridged Zig-Zag Chain Complexes from a Carboxylate-Containing Tridentate Schiff Base Ligand and $M(hfac)_2$ [M = Mn^{II}, Ni^{II}, and Cu^{II}]: Synthesis, Crystal Structure, and Magnetic Properties

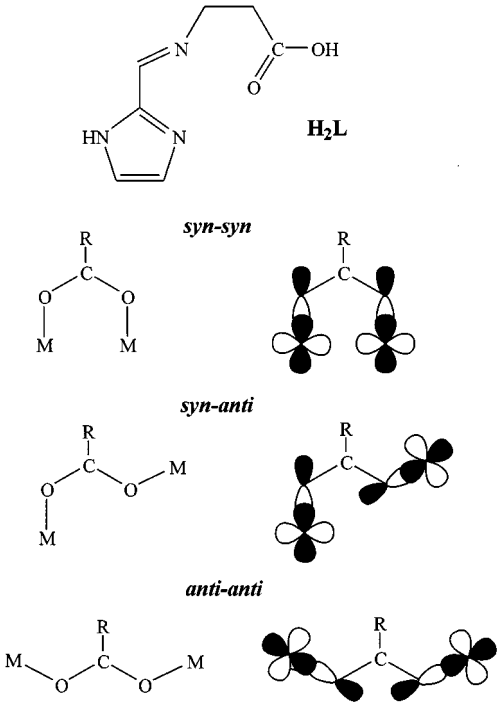
Enrique Colacio,*[a] Jose M. Domínguez-Vera,[a] Mustapha Ghazi,[a] Raikko Kivekäs,[b] Martti Klinga,[b] and José M. Moreno[a]

Keywords: Copper / Nickel / Manganese / Carboxylate bridge / Metal complexes / Magnetic properties

The reaction of $M(hfac)_2$ with the tridentate Schiff base H_2L (where H_2L stands for the 1:1 condensation product of 2-imidazolecarboxaldehyde with β-alanine) leads to the complexes $[M(HL)(hfac)]_n$ [M = Mn^{II}, Ni^{II}, and Cu^{II}; hfac = hexafluoroacetylacetonate anion] (**1**–**3**). The structures of the complexes **1** and **3** have been solved by X-ray crystallographic methods. The structures are very similar and consist of infinite zig-zag chains, running parallel to the *b* axis, in which the metal ions are bridged sequentially by *anti-anti* carboxylate groups with intrachain metal–metal distances of 6.134 Å for **1** and 6.239 Å for **3**. Each monodeprotonated HL ligand acts as a tridentate one to a metal(II) ion and as a monodentate one to a neighbouring metal(II) centre. Metal atoms exhibit distorted octahedral coordination spheres comprised of two oxygen atoms from the hexafluoroacetylacetonate ligand, three donor atoms from the HL ligand and the oxygen atom belonging to the carboxylate group of an adjacent molecule. The complexes **1–3** have been confirmed to be isomorphous and isostructural on the basis of X-ray powder diffraction and IR spectra. The magnetic properties of the three compounds were studied by susceptibility measurements as a function of the temperature and successfully analyzed in terms of the isotropic spin Hamiltonian for one-dimensional infinite chain systems to give the coupling parameters J = –0.91 cm^{-1}, g = 2.03 (**1**); J = –13.2 cm^{-1}, g = 2.24 (**2**); and J = 0.40 cm^{-1}, g = 2.11 (**3**). The magnetic behaviour for all three complexes can be satisfactorily explained in terms of the conformation of the bridge and the interaction between the d orbitals of the metal centre and the bridge.

Polynuclear complexes containing bridging carboxylate groups are of current interest due to the fact that the carboxylate ions play a key role as a ligand in many biochemical systems involving mono- and polymetallic active sites.[1,2] In addition, polynuclear metal carboxylates are good candidates for the investigation of exchange-coupling interaction between adjacent metal ions.[3–6] Carboxylate is a versatile anion that can assume many types of bridging conformations, the most important being monoatomic and triatomic *syn-syn*, *syn-anti*, and *anti-anti*[5,6] (see Scheme 1). Copper(II) complexes with monoatomic or *syn-anti* triatomic conformations exhibit very weak magnetic exchange interactions,[5,7] whereas triatomic *syn-syn* and *anti-anti* conformations mediate large and weak to medium antiferromagnetic interactions, respectively.[8,9] Among metal(II) carboxylate polymers, structurally and magnetically characterized singly carboxylate-bridged chain complexes are rare[4,10–12] and those adopting the *anti-anti* conformation are rarer still. To our knowledge, they are limited to three Mn^{III} Schiff base chain complexes[11,13,14] and one Fe^{II}[15] and one Cu^{II}[9] two-dimensional complex.

Polydentate ligands with carboxylate groups are good candidates to undergo self-assembly processes based on complexation reactions. In fact, we have previously shown that the tridentate ligand 1,3-dimethyl-5-[(2-carboxyphen-



Scheme 1. The H_2L ligand and some of the bridging conformations for the carboxylate group

[a] Departamento de Química Inorgánica, Universidad de Granada, Facultad de Ciencias, E-18071 Granada, Spain
[b] Department of Chemistry, Laboratory of Inorganic Chemistry, P.O. Box 55, FIN-00014 University of Helsinki, Finland

 © WILEY-VCH Verlag GmbH, D-69451 Weinheim, 1999 1434–1948/99/0303–0441 $ 17.50+.50/0

yl)azo]barbituric acid reacts with copper(II) leading to a *syn-anti* carboxylate-bridged helix chain copper(II) complex through a self-assembly reaction.[4] Following a similar strategy we succeeded in obtaining a series of *anti-anti* singly carboxylate-bridged chain complexes from the reaction of the precursors $M(hfac)_2$ [M = Mn^{II}, Ni^{II}, and Cu^{II}, hfac = hexafluoroacetylacetonato anion] with the tridentate Schiff base H_2L, where H_2L stands for the 1:1 condensation product of 2-imidazolecarboxaldehyde and β-alanine (see Scheme 1). The present paper is devoted to the structural and magnetochemical studies of these complexes.

When the square-planar complexes $M(hfac)_2$ [M = Mn^{II}, Ni^{II}, and Cu^{II}] react with the tridentate Schiff base H_2L, the ligand loses the carboxylic proton and replaces one of the hfac ligands of the precursor complex to give rise, in principle, to a pentacoordinated complex. Because the metal ion is able to additionally receive the non-coordinated oxygen atom of the carboxylate group belonging to another pentacoordinated molecule, a spontaneous self-assembly reaction occurs leading to singly carboxylate-bridged chain complexes $[M(HL)(hfac)]_n$. It should be pointed out that chemical analyses, IR spectra and powder X-ray data confirm that compounds **1**−**3** are isomorphous and isostructural.

Crystal Structures

Complexes **1** and **3** are isostructural and consist of infinite zig-zag chains, running parallel to the *b* axis, in which the metal ions are bridged sequentially by *anti-anti* carboxylate groups. A perspective view of the zig-zag chain for **3**, together with the corresponding atom labelling scheme, is given as an example in Figure 1. Selected bond lengths and angles are listed in Table 1.

Each monodeprotonated HL ligand acts as a tridentate one to a metal(II) ion and as monodentate one to a neighbouring metal(II) centre. Metal atoms exhibit distorted octahedral coordination spheres comprised of two oxygen atoms from the hexafluoroacetylacetonate ligand, three donor atoms from the HL ligand, and the oxygen atom belonging to the carboxylate group of an adjacent molecule. As expected, the three donor atoms of HL occupy in-plane coordination positions and then the carboxylate bridges have to be oriented in a mutually *cis* fashion. The tridentate behaviour of the HL ligand results in the formation of one five- and one six-membered rings having the M−N(7) bond in common. For **3**, the *anti-anti* carboxylate group bridges two Cu^{II} ions in equatorial-axial positions and the surrounding of each copper ion is (4+2), the octahedron being elongated along the O(17)−Cu(1)−$O(12)^{ii}$ axis (*ii* = 1 − *x*, 0.5 + *y*, 1.5 − *z*). In the M−O−C−O−M fragment of **3**, the metal ions are pushed out of the COO plane by 0.214 and 0.806 Å. In **1** the metal ions are also out of the COO plane by 0.620 and 0.652 Å. For both compounds large deviations from the idealized orthogonal geometry are found at the metal atom in the five-membered M−N(1)−C(2)−C(6)−N(7)−M rings [N(1)−Mn−N(7) = 74.33(18)° for **1** and N(1)−Cu−N(7) = 81.45° for **3**]. Such deviations are expected to be due to the small bite distance of this part of the HL ligand. Bond lengths of M(hfac) moieties are in agreement with those reported for other hfac-

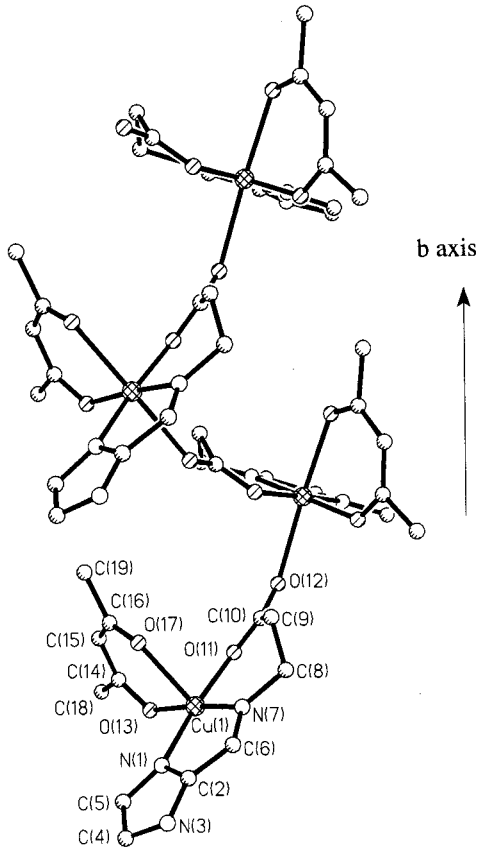


Figure 1. Perspective view of complex **3** along the *b* axis

Table 1. Selected bond lengths [Å] and angles [°] for **1** and **3**

Complex **1**			
Mn(1)−$O(12)^{i}$	2.111(5)	Mn(1)−O(17)	2.218(5)
Mn(1)−O(13)	2.134(4)	Mn(1)−N(1)	2.230(5)
Mn(1)−O(11)	2.142(5)	Mn(1)−N(7)	2.262(5)
$O(12)^{i}$−Mn(1)−O(13)	91.90(17)	O(11)−Mn(1)−N(1)	156.59(18)
$O(12)^{i}$−Mn(1)−O(11)	89.15(18)	O(17)−Mn(1)−N(1)	93.42(18)
O(13)−Mn(1)−O(11)	101.64(17)	$O(12)^{i}$−Mn(1)−N(7)	92.39(19)
$O(12)^{i}$−Mn(1)−O(17)	172.84(17)	O(13)−Mn(1)−N(7)	174.24(18)
O(13)−Mn(1)−O(17)	81.61(16)	O(11)−Mn(1)−N(7)	82.28(18)
O(11)−Mn(1)−O(17)	89.21(19)	O(17)−Mn(1)−N(7)	94.29(18)
$O(12)^{i}$−Mn(1)−N(1)	90.85(18)	N(1)−Mn(1)−N(7)	74.33(18)
O(13)−Mn(1)−N(1)	101.76(18)		
Complex **3**			
Cu(1)−O(11)	1.933(3)	Cu(1)−N(7)	2.007(3)
Cu(1)−O(13)	1.969(3)	Cu(1)−O(17)	2.359(3)
Cu(1)−N(1)	1.984(3)	Cu(1)−$O(12)^{ii}$	2.446(3)
O(11)−Cu(1)−O(13)	91.80(12)	N(1)−Cu(1)−O(17)	94.41(13)
O(11)−Cu(1)−N(1)	173.05(12)	N(7)−Cu(1)−O(17)	96.15(12)
O(13)−Cu(1)−N(1)	94.70(13)	N(1)−Cu(1)−$O(12)^{ii}$	88.60(12)
O(11)−Cu(1)−N(7)	91.99(12)	N(7)−Cu(1)−$O(12)^{ii}$	89.64(12)
O(13)−Cu(1)−N(7)	175.92(13)	O(11)−Cu(1)−$O(12)^{ii}$	89.06(12)
N(1)−Cu(1)−N(7)	81.46(13)	O(13)−Cu(1)−$O(12)^{ii}$	88.89(11)
O(11)−Cu(1)−O(17)	88.55(14)	O(17)−Cu(1)−$O(12)^{ii}$	173.81(9)
O(13)−Cu(1)−O(17)	85.48(11)		

i = 1 − *x*, 0.5 + *y*, 0.5 − *z*; *ii* = 1 − *x*, 0.5 + *y*, 1.5 − *z*.

containing Mn^{II} and Cu^{II} complexes.[16] The *anti-anti* bridging mode for **3** affords an intrachain metal−metal distance of 6.239 Å, whereas for **1** the metal−metal distance is 6.134 Å; they are similar to those found for singly *anti-anti* carboxylate-bridged Mn^{III}[11,13,14] and Fe^{III}[15] complexes. The shortest interchain metal separations are 7.412 and 6.854 Å for **1** and **3**, respectively. The polymeric chains are held together by pairs of complementary hydrogen bonds between the N(3)−H group and the carboxylate oxygen atoms of a neighbouring chain.

Magnetic Properties

The EPR spectrum of complex **1** at 100 K exhibits a featureless broad resonance at $g = 2.00$ with a half-height width of 400 G. The broadness of this EPR signal is characteristic of polynuclear manganese(II) complexes. The frozen methanol solution spectrum at 100 K exhibits an allowed hyperfine sextuplet centred at $g = 2.0$ ($A = 88.10^{-4}$ cm^{-1}) with forbidden hyperfine lines corresponding to transitions between levels with different nuclear magnetic quantum numbers. This spectrum is typical of electronically isolated Mn^{II} species, thus suggesting either that the chain structure of complex **1** is not retained in solution or that the small antiferromagnetic interaction operating between the Mn^{II} ions does not modify appreciably the EPR spectrum of the complex. Neither polycrystalline powder nor solution EPR spectra could be detected for complex **2**. At 100 K the spectrum of a polycrystalline sample of **3** looks like that expected for a copper(II) ion in a d(x^2-y^2) ground state. Two main features are attributable to paralell ($g_{||} = 2.24$) and perpendicular ($g_{\perp} = 2.11$) components of an axially symmetrical spectrum. In addition, signals of low intensity are observed between these two features. The spectrum is devoid of any hyperfine structure or half-field signal and does not show any appreciable temperature dependence. Analogous spectra have also been observed for other ferromagnetic chain copper complexes with oxalate[17] and *syn-anti* carboxylate bridges.[4] The frozen methanol solution spectrum of **3** at 100 K is typical of electronically isolated Cu^{II} species, thus suggesting that the chain structure is not retained in dilute methanol solution or that the magnetic exchange interaction does not appreciably affect the EPR spectrum.

The magnetic properties of the complexes **1**−**3** are given in Figure 2 in the form $\chi_M T$ versus T. The $\chi_M T$ products per metal atom at 290 K for complexes **1**−**3** are 4.41, 1.15, and 0.425 cm^3·mol^{-1}·K, respectively, which correspond well with those expected for isolated metal ions. For complexes **1** and **2**, $\chi_M T$ continuously decreases upon cooling and reaches values, at 4.2 K, of 1.225 and 0.056 cm^3·mol^{-1}·K, respectively, thus revealing the existence of an antiferromagnetic exchange interaction between metal ions through the carboxylate bridging group. The occurrence of susceptibility maximum around 5 and 25 K for **1** and **2**, respectively, is the signature of the antiferromagnetic interaction. The absence of a Curie-like tail at the lowest temperatures allows one to assume the absence of impurities in these products. For **3**, the $\chi_M T$ product steadily increases when the temperature decreases to a value of 0.63 cm^3·mol^{-1}·K at 2 K, thus suggesting a weak ferromagnetic interaction between the copper(II) ions. The experimental magnetization values as a function of the applied field at 5 K are higher than those predicted by the Brillouin function for $S = 1/2$, thus confirming the existence of weak ferromagnetic interaction between copper(II) ions.

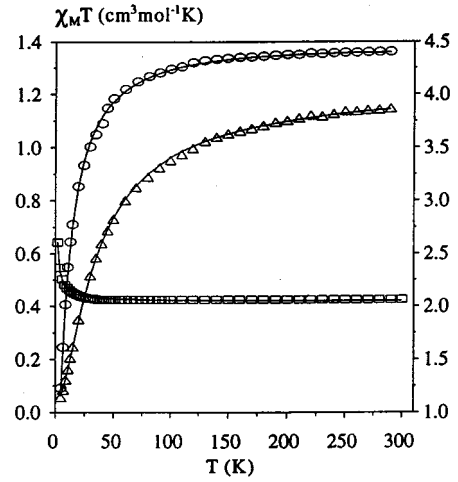


Figure 2. Magnetic plots ($\chi_M T$ vs T) of complexes: **1** (○) (right axis), **2** (△) (left axis) and **3** (□) (left axis)

We fitted the data of **1** using the analytical expression derived by Fisher for an infinite chain of classical spin scaled to $S = 5/2$;[18] for **2** we used the expression derived by Weng from calculations performed on ring systems of increasing lengths, where the nickel ion is assumed to be magnetically isotropic;[18] while the expression used to fit the magnetic data of **3** was that of Baker et al.,[18] which is based on the high-temperature Padé expansion technique.

Very good fits of the data of the complexes **1**−**3** to the corresponding theoretical equations can be obtained with $J = -0.91$ cm^{-1}, $g = 2.03$ (**1**); $J = -13.2$ cm^{-1}, $g = 2.24$ (**2**); $J = 0.40$ cm^{-1}, $g = 2.11$ (**3**).

The difference in the magnitude and sign of the magnetic exchange interactions found for **1**, **2**, and **3** can be satisfactorily explained in terms of the conformation of the bridge and the interaction between the d orbitals of the metal centre and the bridge. It is noteworthy that despite the larger separations found in complexes containing *anti-anti* bridges this configuration is more favourable for transmitting the interaction through the carboxylate bridge than the *syn-anti* one. The reason of these different magnetic behaviours lies in the fact that the contributions of the 2p oxygen orbitals belonging to the magnetic orbital centred on the metal ions are much more favourably oriented to give an effective overlap in the *anti-anti* than in the *syn-anti* configuration (see Scheme 1), thus leading to stronger magnetic exchange couplings.

In good accord with this, complexes **1** and **2** exhibit significant antiferromagnetic couplings with J values that are larger than those observed for singly bridged *syn-anti* car-

boxylate Mn^{II}[19] and alternating *syn-anti* and *anti-anti* carboxylate chain Mn^{II} and Ni^{II} complexes.[20] The *J* value for complex **1** is much smaller than that of complex **2**. Nevertheless, to deal with comparable values, the $n^2|J|$ relation (*n* is the number of unpaired electrons on each paramagnetic centre) should be taken into account. From the *J* values of **1** and **2** and the $n^2|J|$ relation we see that $|J_{Ni}|$ (13.2 cm^{-1}) >> 25/4 $|J_{Mn}|$ (5.7 cm^{-1}), thus illustrating the ability of Ni^{II} as compared to Mn^{II} to yield antiferromagnetic interactions, everything being equal. Similar *J* values have been reported for Mn^{II} (−1.1 cm^{-1}) and Ni^{II} (14 cm^{-1}) complexes with 2,2′-bipyrimidine,[21,22] a ligand that has been shown to transmit intermediate magnetic exchange couplings. Several reasons may contribute to the higher efficiency of the superexchange for the nickel(II) complex: (i) the larger spin delocalization on the bridge in the case of the Ni^{II}, since the energies of the $3d_{Ni}$ orbitals are lower and the M−O distances generally shorter than those of the Mn^{II}; (ii) small structural differences affecting either the carboxylate bridges or M^{II}−N,O bond lengths, and (iii) the possibility of more ferromagnetic contributions in the case of Mn^{II}.

In the case of **3**, the copper(II) ion exhibits a tetragonal elongated geometry, in which the unpaired electron is adequately described by a $d(x^2-y^2)$ orbital pointing toward the nitrogen and oxygen atoms of the basal equatorial plane, O(11)N(1)O(13)N(7). In light of the structural features of **3**, it is evident that these copper(II) orbitals are mismatched for interaction to take place between them through the carboxylate group, since the exchange pathway Cu−O−C−O−Cu involves an equatorial position on one copper [$d(x^2-y^2)$ direction] and an axial position on the other copper atom [$d(z^2)$ direction]. Departures from the idealized symmetry might allow some mixture with the $d(z^2)$ orbital, but in any case the overlap would be very weak. This would lead to a negligible antiferromagnetic contribution so that the ferromagnetic one becomes predominant. It should be noted that other carboxylate-bridged copper complexes having similar topology of the bridges also exhibit weak ferromagnetic interactions.[17]

Experimental Section

General: Elemental analyses were carried out with a Fisons-Carlo Erba analyzer, model EA 1108. − IR: Perkin−Elmer 983 G (KBr pellets). − Variable-temperature magnetic susceptibility data of **1** and **2** were collected on powdered samples of the compounds with the use of a pendulum-type magnetometer (MANICS DSM8) equipped with a helium continuous-flow cryostat working in the 300−4.2 K range and a Drusch EAF 164E electromagnet, whereas those of **3** (2−290 K) were obtained with a SQUID-based sample magnetometer using a Quantum Design Model MPMS instrument. Data were corrected for the diamagnetism of the ligands using Pascal′s constants. − EPR: Bruker ESP 300E (solid state: 300 and 100 K, methanol solution: 110 K).

Preparation of [M(HL)(hfac)] (1−3): These complexes were all prepared using the same method as described in detail for complex **1** as an example. This complex was prepared by refluxing 2-imidazolecarboxaldehyde (0.15 g, 1.56 mmol) and β-alanine (0.14 g, 1.56 mmol) for 1 h in 30 mL of an MeOH/H_2O mixture (4:1, v/v). To the cold, filtered yellow solution was added $Mn(hfac)_2$ (0.73 g, 1.56 mmol) in 30 mL of MeOH dropwise with stirring. The resulting yellow solution was kept at room temperature for 2 d and provided yellow prism-like crystals, which were filtered and air-dried. Yield: 0.60 g (90%). − $C_{12}H_9F_6MnN_3O_4$ (427.93): calcd. C 33.66, H 2.12, N 9.81; found C 33.49, H 1.96, N 10.15. − IR (KBr): $\tilde{\nu}$ = 3141 cm^{-1} (N_{im}−H), 1649, 1602 (C=O), 1257, 1217, 1144 (F−C).

2: Green powder. − Yield: 0.54 g (80%). − $C_{12}H_9F_6N_3NiO_4$ (431.71): calcd. C 33.41, H 2.10, N 9.75; found C 33.79, H 1.91, N 9.45. − IR (KBr): $\tilde{\nu}$ = 3137 cm^{-1} (N_{im}−H), 1649, 1600 (C=O), 1259, 1221, 1144 (F−C). − Powder X-ray diffraction:[23] monoclinic, *Pc*, *a* = 11.900(63), *b* = 8.462(24), *c* = 16.578(104) Å, β = 102.92(44)°.

3: Green plate-like crystals. − Yield: 0.44 g (65%). − $C_{12}H_9CuF_6N_3O_4$ (436.54): calcd. C 33.03, H 2.08, N 9.64; found C 32.98, H 2.09, N 9.53. − IR (KBr): $\tilde{\nu}$ = 3142 (N_{im}−H), 1664, 1625 (C=O), 1259, 1209, 1141 (F−C).

X-ray Crystallographic Study: Crystallographic data are listed in Table 2. The unit-cell parameters were determined and the data collected with a Rigaku AFC7S diffractometer at −80°C for complex **1** and with a Siemens P4 diffractometer at 20°C for **3**. The data were corrected for Lorentz polarisation effects and for dispersion, and an empirical absorption correction, using the programs TEXSAN[24a] and SHELXTL V5[24b] for **1** and **3**, respectively. The structures were solved by Direct methods using the SHELXS-86 program[24c] and refined (full-matrix least squares on F^2) by using the SHELX-97 and SHELXL-93 programs.[24d] For **1**, all non-hydrogen atoms were refined anisotropically, while for **3**, all non-hydrogen atoms were refined anisotropically except the F atoms, which were disordered and refined isotropically. In both cases, H atoms were included in calculated positions and treated as riding atoms using the SHELX-97 (for **1**) and SHELXL-93 (for **3**) default parameters.

Table 2. Crystal data and structure refinement for **1** and **3**

	Complex **1**	Complex **3**
Molecular formula	$C_{12}H_9N_3O_4F_6Mn$	$C_{12}H_9N_3O_4F_6Cu$
Mass	428.16	436.76
Unit-cell dimensions		
a [Å]	11.797(3)	11.290(5)
b [Å]	8.611(3)	8.685(5)
c [Å]	16.564(3)	16.799(5)
β [°]	104.49(3)	105.598(5)
Z	4	4
$d_{calcd.}$ [g cm^{-3}]	1.746	1.829
Crystal system	monoclinic	monoclinic
Space group	*P*2(1)/*c* (no. 14)	*P*2(1)/*c* (no. 14)
Crystal size [mm]	0.15 × 0.12 × 0.06	0.40 × 0.30 × 0.06
Absorption coeff. [mm^{-1}]	0.899	1.468
θ range data collection [°]	2.54−25.00	1.87−30.00
Reflections collected	3016	5663
Independent reflections	2868	4440
Data/restraints/parameters	2868/6/235	4419/0/295
*R*1 [*I* > 2 (*I*)]	0.0714	0.0442
w*R*2 [*I* > 2 (*I*)]	0.1433	0.1203
Goodness-of-fit on F^2	1.033	0.731

Acknowledgments

Financial support from the Dirección General de Investigación Científica y Técnica (DGICYT) through project PB94−0764 is

acknowledged. We thank Dr. A. Mari from the Laboratoire de Chimie de Coordination (C.N.R.S.), Toulouse, France, for his contribution to the magnetic measurements. Academy of Finland is acknowledged by R. K.; M. G. thanks the Ministère de L′Education Nationale Marocaine − Enseignement Superieur for a grant.

[1] *Manganese Redox Enzymes* (Ed.: V. L. Pecoraro), VCH, New York, **1992**, p. 1−28.
[2] K. Wieghardt, *Angew. Chem.* **1989**, *101*, 1179−1198; *Angew. Chem. Int. Ed. Engl.* **1989**, *28*, 1153−1172.
[3] E. Coronado in *Magnetic Molecular Materials* (Eds.: D. Gatteschi, O. Khan, J. E. Miller, F. Palacio), Nato ASI Series, E198, Kluwer Academic Publisher, Dordrecht, **1991**, p. 267−279.
[4] E. Colacio, J. M. Dominguez-Vera, J. P. Costes, R. Kivekäs, J. P. Laurent, J. Ruiz, M. Sundberg, *Inorg. Chem.* **1992**, *31,* 774−778 and references therein.
[5] E. Colacio, J. M. Dominguez-Vera, R. Kivekäs, J. M. Moreno, A. Romerosa, J. Ruiz, *Inorg. Chim. Acta* **1993**, *212*, 115−121 and references therein.
[6] Z. N. Chen, S. X. Liu, J. Qiu, Z. M. Wang, J. L. Huang, W. X. Tang, *J. Chem. Soc., Dalton Trans.* **1994**, 2989−2993.
[7] J. P. Costes, F. Dahan, J. P. Laurent, *Inorg. Chem.* **1985**, *24,* 1018−1022.
[8] M. Kato, Y. Muto, *Coord. Chem. Rev.* **1988**, *92*, 45.
[9] M. Inoue, M. Kubo, *Inorg. Chem.* **1970**, *9*, 2310−2314.
[10] D. K. Towle, S. K. Hoffmann, W. E. Hatfield, P. Singh, P. Chaudhuri, *Inorg. Chem.* **1988**, *27*, 394−399.
[11] J. E. Davies, B. M. Gatehouse, K. S. Murray, *J. Chem. Soc., Dalton Trans.* **1973**, 2523−2527.
[12] K. K. Nanda, A. W. Addison, E. Sinn, L. K. Thompson, *Inorg. Chem.* **1996**, *35*, 5966−5967.
[13] J. A. Bonadies, M. L. Kirk, M. S. Lah, D. P. Kessissoglou, W. E. Hatfield, V. L. Pecoraro, *Inorg. Chem.* **1989**, *28*, 2037−2044.
[14] N. Aurangzeb, C. E. Hulme, C. A. McAuliffe, R. G. Pritchard, M. Watkinson, A. García-Deibe, M. R. Bermejo, A. Sousa, *J. Chem. Soc., Chem. Commun.* **1992**, 1524−1526.
[15] M. A. Martínez-Lorente, J. P. Tuchagues, V. Pétrouléas, J. M. Savariault, R. Poinsot, M. Drillon, *Inorg. Chem.* **1991**, *30*, 3587−3589.
[16] C. J. O′Connor, D. P. Freyberg, E. Sinn, *Inorg. Chem.* **1979**, *18*, 1077−1088.
[17] J. Suárez-Varela, J. M. Dominguez-Vera, E. Colacio, J. C. Avila-Rosón, M. A. Hidalgo, D. Martín-Ramos, *J. Chem. Soc., Dalton. Trans.* **1995**, 2143−2146 and references therein.
[18] O. Kahn, *Molecular Magnetism*, VCH, New York, **1993**.
[19] V. Tangoulis, G. Psomas, C. Dendrinou-Samara, C. P. Raptopoulou, A. Terzis, D. P. Kessissoglou, *Inorg. Chem.* **1996**, *35*, 7655−7660.
[20] J. J. Borrás-Almenar, E. Coronado, C. J. Gómez-García, L. Ouahab, *Angew. Chem.* **1993**, *105*, 637−639; *Angew. Chem. Int. Ed. Engl.* **1993**, *32,* 561−563.
[21] G. De Munno, M. Julve, F. Lloret, A. Derory, *J. Chem. Soc., Dalton Trans.* **1993**, 1179−1184.
[22] G. De Munno, R. Ruiz, F. Lloret, J. Faus, R. Sessoli, M. Julve, *Inorg. Chem.* **1995**, *34*, 408−411.
[23] D. Martín-Ramos, *PLV, A program for PXRD evaluation*, Departamento de Mineralogia y Petrologia, Universidad de Granada, E-18071 Granada, Spain, **1995**; available from the author.
[24] [24a] *TEXSAN: Single Crystal Structure Analysis Software*, Molecular Structure Corp., The Woodlands, TX, USA, **1993**. − [24b] *SHELXTL PC, version 5.0*, Siemens Analytical X-ray Instruments, Madison, WI, **1995**. − [24c] *SHELXS-86:* G. M. Sheldrick, *Acta Crystallogr.* **1990**, *A46,* 467−473. − [24d] G. M. Sheldrick, *SHELXL-93* and *SHELX-97*, Universität Göttingen, **1993** and **1997**.

Received July 9, 1998
[I98223]

Multistep Oxidation Kinetics of [Fe^{II}(cdta)] [cdta = *N,N′,N′′,N′′′*-(1,2-Cyclohexanediamine)tetraacetate] with Molecular Oxygen

Sabine Seibig[a] and Rudi van Eldik*[a]

Keywords: Kinetics / Oxidations / Iron / Oxygen / High pressure

The complicated oxidation kinetics of the reaction of [Fe^{II}(cdta)] [cdta = 1,2-(*N,N′*- cyclohexanediamine)tetraacetate] with molecular oxygen was investigated as a function of [Fe^{II}], [O_2], pH, temperature and pressure. In the presence of an excess of [Fe^{II}(cdta)] three steps could be observed, for which the following rate constants were found at 25°C; k_1 = 1080 ± 16 M^{-1} s^{-1}, k_2 = 103 ± 4 M^{-1} s^{-1} and k_3 = 59 ± 5 M^{-1} s^{-1}. These reaction steps can be accounted for in terms of the following mechanism: (1) [Fe^{II}(cdta)H_2O]$^{2-}$ reacts with O_2 by a substitution process to form [Fe^{II}(cdta)O_2]$^{2-}$; (2) electron-transfer to form an Fe^{III}-superoxo species; (3) subsequent bridge formation followed by electron-transfer to give [(cdta)Fe^{III}-O_2^{2-}-Fe^{III}(cdta)]$^{4-}$; and (4) a fast decomposition of the peroxide intermediate yielding the monomeric [Fe^{III}(cdta)] and H_2O_2. Rate and activation parameters for these steps are reported and discussed in terms of the postulated mechanism and in reference to available literature data.

Introduction

During the past decades there has been a continued interest in the study of oxidation reactions of [Fe^{II}(aminopolycarboxylato)] complexes, especially with dioxygen or hydrogen peroxide.[1−12] Of particular interest in the present context was their importance in several biochemical processes, for example the cleavage of DNA, the decomposition of H_2O_2 or the dismutation of superoxide.[13−20] Many investigators have tried to solve these complicated reactions before, but in most cases they could only observe a single reaction step spectroscopically, even when more than one step was postulated in the mechanism.[1−12,21]

We recently reported a detailed kinetic study of the oxidation kinetics of [Fe^{II}(edta)] with molecular oxygen.[22] For the first time we could observe three steps spectroscopically and could investigate two of them in detail. The first step was so fast that we were not able to analyse it systematically on the stopped-flow time scale. We have therefore searched for a ligand, which would tune the reactivity of the complex in such a way, that this first step would become slower. Since the cdta ligand (cdta = *N,N′*-(1,2-cyclohexanediamine)tetraacetate) is known to stabilize its metal complexes, we thought that it would also affect their reactivity.[23−27] Moreover, it is known from several kinetic investigations that the cdta complex always reacts slower than the corresponding edta complex.[28−30] We, therefore, performed detailed kinetic measurements on the rather complicated oxidation reactions of [Fe^{II}(cdta)] with dioxygen.

The present work describes how the selected chelate can tune the reactivity of the complex. We were now able to investigate three reaction steps in detail. A mechanism is presented that accounts for all spectroscopic and kinetic observations, and is discussed in reference to our earlier work on the [Fe^{II}(edta)] system[22] and work reported in the literature.[4,6,7,10,12,21]

Results and Discussion

Spectral Observations

A number of test experiments on the [Fe^{II}(cdta)] system showed that its spectroscopic behavior is very similar to the [Fe^{II}(edta)] system, which we investigated recently.[22] Typical spectra indicate that both [Fe^{II}(cdta)] and [Fe^{III}(cdta)] exhibit an absorbance maximum at 260 nm and that the molar extinction coefficient for [Fe^{III}(cdta)] is significantly higher than for the [Fe^{II}(cdta)] complex. Since the overall oxidation reaction is accompanied by a significant decrease in [H^+], it was necessary to use buffers for pH ≥ 3 throughout the study.[31] The reaction of [Fe^{II}(cdta)] with molecular oxygen can best be followed at 370 nm in the presence of an excess of [Fe^{II}(cdta)] and at 260 nm in the presence of an excess of O_2 using a 1 cm cuvette. All kinetic traces were measured over more than 5 half-lives.

Kinetic Measurements

Kinetic traces measured in the presence of an excess of [Fe^{II}(cdta)] showed a complicated multistep process. In contrast to the [Fe^{II}(edta)] system, we could now fit the kinetic traces in most cases to three exponential functions (see Figure 1). This means we were able to confirm our earlier observations, where we only had limited evidence for the first

[a] Institute for Inorganic Chemistry, University of Erlangen-Nürnberg,
Egerlandstraße 1, 91058 Erlangen, Germany
Fax: (internat.) +49 (0)9131/ 85-27387
E-mail: vanEldik@anorganik.chemie.uni-erlangen.de

Supporting information for this article is available on the WWW under http://www.wiley-vch.de/home/eurjic or from the author.

 © WILEY-VCH Verlag GmbH, D-69451 Weinheim, 1999 1434−1948/99/0303−0447 $ 17.50+.50/0

fast step.[22] For the present system the fast step was only about a factor of ten faster than the subsequent steps. According to the data analysis this step is accompanied by a small decrease in absorbance which results in the non-linear increase in absorbance seen in Figure 1b. The two subsequent steps differ by a factor of ca. two, which is in good agreement with the data we obtained for the [Fe^{II}(edta)] system. However, in comparison, the rate constants for the [Fe^{II}(edta)] system are two times faster than for the [Fe^{II}(cdta)] system. The values of k_{obs} for all three reaction steps vary linearly with [Fe^{II}(cdta)] over the investigated concentration range (see Figure 2). The dependence for the first step shows a significant intercept, whereas the two other lines go through the origin. At pH = 6.0, the three reaction steps have the following second-order rate constants, $k_1 = 1080 \pm 16$ M^{-1} s^{-1}, $k_2 = 103 \pm 4$ M^{-1} s^{-1} and $k_3 = 59 \pm 5$ M^{-1} s^{-1} at 25°C, which are assigned to the reaction steps outlined in (2), (4), and (6), respectively (see further Discussion).

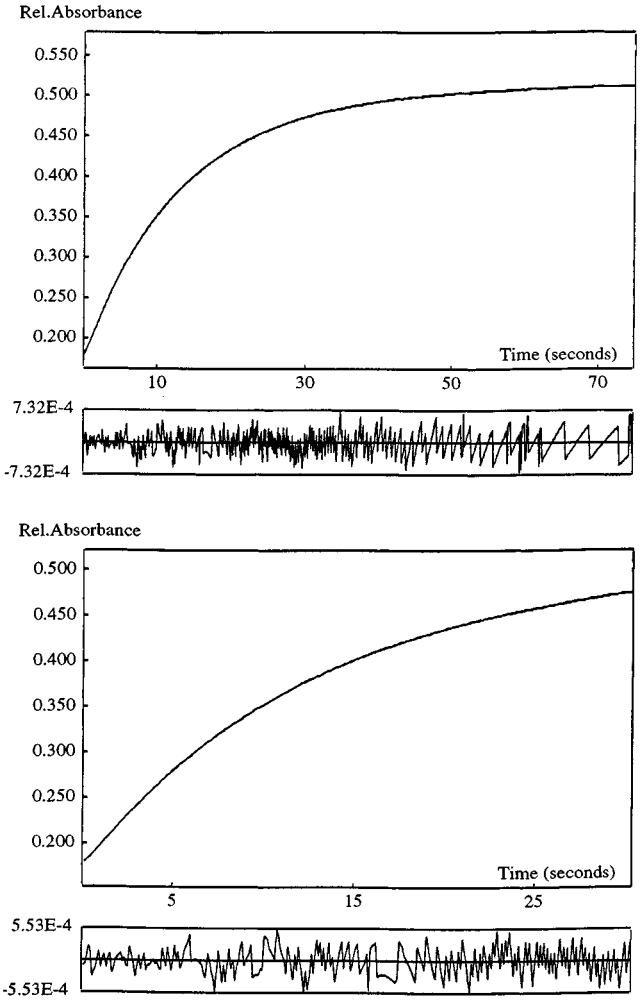


Figure 1. Typical absorbance time trace obtained in an excess of [Fe^{II}(cdta)] fitted with three exponential functions. – Experimental conditions: [Fe^{II}(cdta)] = $2.5 \cdot 10^{-3}$ M, [O_2] = $1.25 \cdot 10^{-4}$ M, ionic strength = 0.5 M, [acetate buffer] = 0.1 M, pH = 6, T = 25°C, λ = 370 nm

The pH dependence of the reaction in the presence of an excess [Fe^{II}(cdta)] was studied in the range pH = 2 to 7 (see

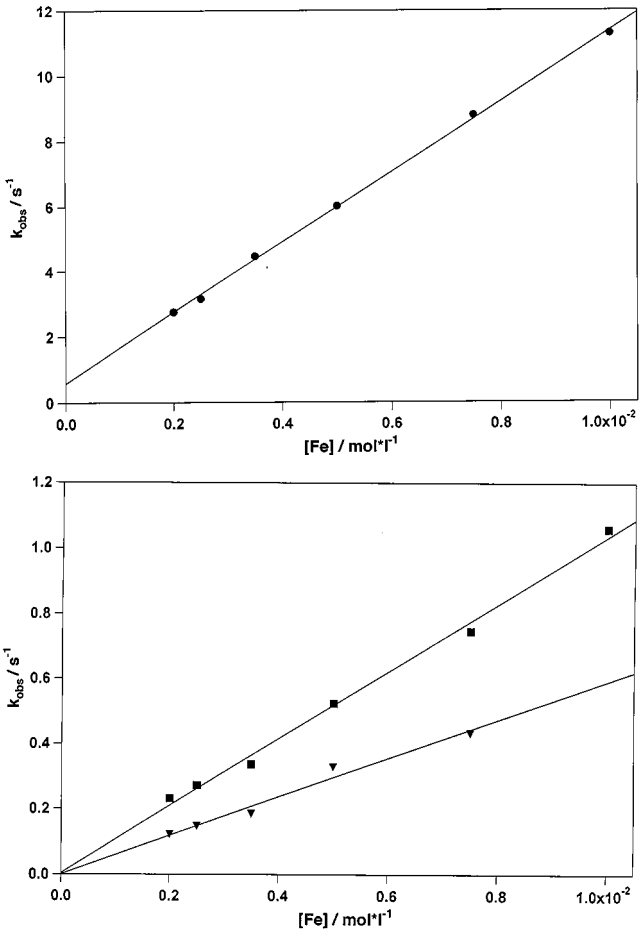


Figure 2. a: k_{obs1} (•) as a function of [Fe^{II}(cdta)] for the oxidation of [Fe^{II}(cdta)]. – b: k_{obs2} (■) as a function of [Fe^{II}(cdta)] for the oxidation of [Fe^{II}(cdta)]. – c: k_{obs3} (▼) as a function of [Fe^{II}(cdta)] for the oxidation of [Fe^{II}(cdta)]
Experimental conditions: [O_2] = $1.25 \cdot 10^{-4}$ M, ionic strength = 0.5 M, [acetate buffer] = 0.1 M, pH = 6, T = 25°C, λ = 370 nm.

Figure 3). The resolution of the time traces at a pH > 4 showed a more complicated kinetic behavior, but we were able to analyze the three main steps. All three steps show a bell-shaped pH dependence with a maximum around pH = 2.5. The maximum rate of all three observed steps corresponds quite well to the distribution of species in solution (see Figure 4). The kinetic pH dependence indicates that the monoprotonated species in solution is the most reactive one. This behavior was also observed for different [Fe^{II}(edta)] reactions before. For example, the oxidation kinetics of [Fe^{II}(edta)] with molecular oxygen showed the same pH dependence.[21,22] But, moreover, kinetic studies of the reaction of [Fe^{II}(edta)] with HONO or NO_2^- also showed the same pH dependence,[35,36] which supports our suggestion that the observed bell-shaped curves are due to the distribution of species in solution and not due to an acid-catalyzed process, as suggested in an earlier study.[21]

The increase in rate at pH > 6 (see Figure 3a) is not expected on the basis of the distribution of species in solution. This may be an effect of the selected buffer and we therefore selected other buffers. This, however, did not solve the problem. It was noticed that a precipitate occurred at

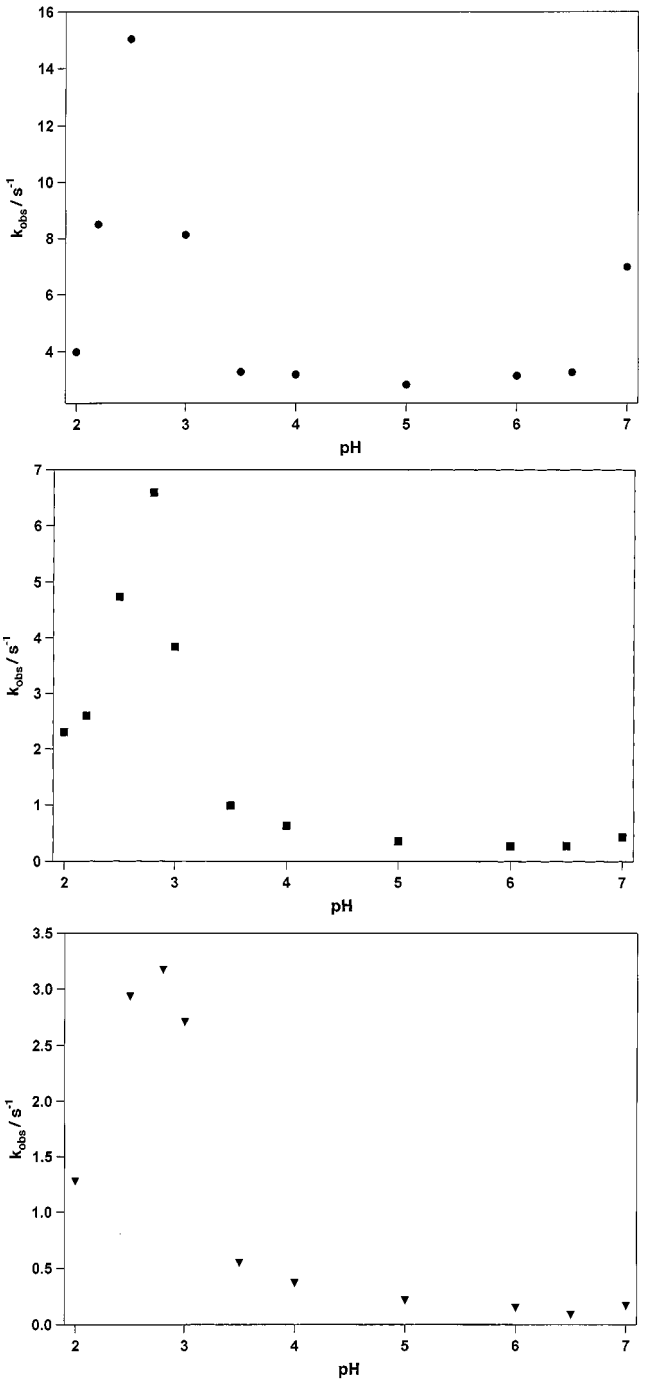


Figure 3. a: pH dependence of k_{obs1} (●) for the oxidation of [Fe^{II}(cdta)] in the presence of an excess of [Fe^{II}(cdta)]. – b: pH dependence of k_{obs2} (■)for the oxidation of [Fe^{II}(cdta)] in the presence of an excess of [Fe^{II}(edta)]. – c: pH dependence of k_{obs3} (▼) for the oxidation of [Fe^{II}(cdta)] in the presence of an excess of [Fe^{II}(cdta)]
Experimental conditions: [Fe^{II}(cdta)] = $2.5 \cdot 10^{-3}$ M, [O_2] = $1.25 \cdot 10^{-4}$ M, ionic strength = 0.5 M, [acetate buffer] = 0.1 M for pH > 3, [Tris buffer] = 0.1 M or [MOPS buffer] = 0.1 M for pH > 6 , T = 25°C, λ = 370 nm.

pH = 7.5, which prevented measurements in a higher pH range. The precipitate suggested that the investigated [Fe^{II}(cdta)] complex is not as stable as reported in the literature[38] and that some free Fe^{II} may be present in solution.

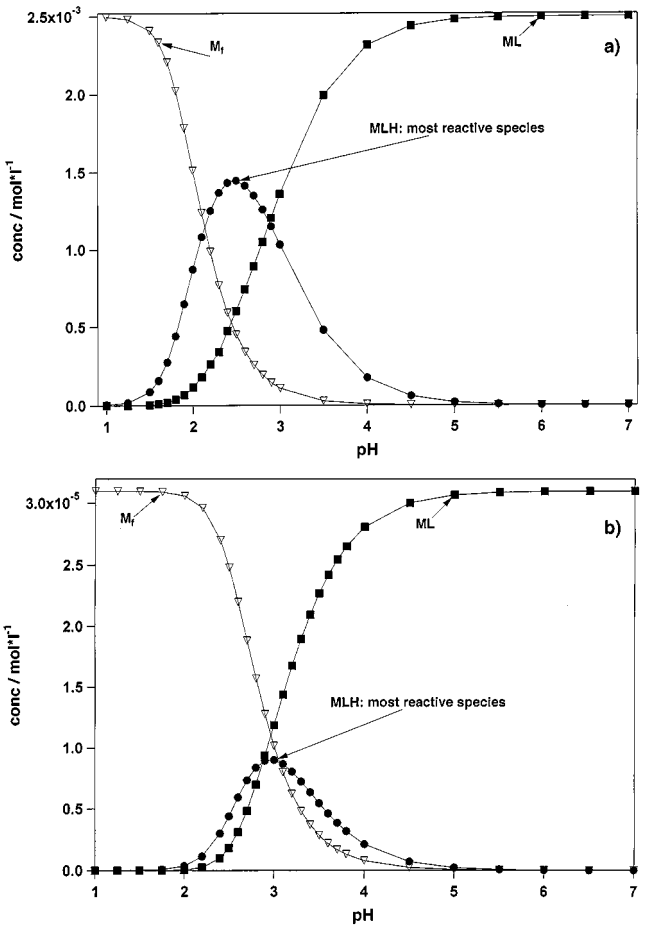


Figure 4. a: Distribution of [Fe^{II}(cdta)] species in solution, [Fe^{II}(cdta)] = 2.5×10^{-3} M. – b: Distribution of [Fe^{II}(cdta)] species in solution, [Fe^{II}(cdta)] = 3.0×10^{-5} M; M_f = free Fe_2+, ML = [Fe^{II}(cdta)$(H_2O)]^{2-}$, MLH = [Fe^{II}(cdtaH)$(H_2O)^-$

The addition of $FeSO_4 \cdot 7\ H_20$ to the test solution accelerated the observed reactions with dioxygen, and the presence of free Fe^{II} can therefore account for the unexpected increase in rate at pH > 6.

Reactions in the presence of an excess of oxygen could in most cases be fitted to two exponential functions between pH = 6.0 and pH = 2.0. However, near the maximum reactivity, the kinetic behavior was even more complicated, so that it was sometimes necessary to fit the kinetic traces to three exponential functions. In these cases we only report rate constants for the two main reaction steps for reason of comparison with the other pH data. The complicated kinetic behavior in more acidic medium is also reflected by the difficulties encountered to fit our data in the presence of an excess of [Fe^{II}(edta)] in that pH region (vide supra). The studied pH dependence exhibits a maximum at pH = 3 (see Figure 5), which is in good agreement with the data obtained for the pH dependence in an excess of [Fe^{II}(cdta)] (see Figure 3) and corresponds also quite well to the distribution of species in solution at the appropriate concentration of [Fe^{II}(cdta)] (see Figure 4b).

Various efforts were made to study the oxygen concentration dependence under these conditions, especially to

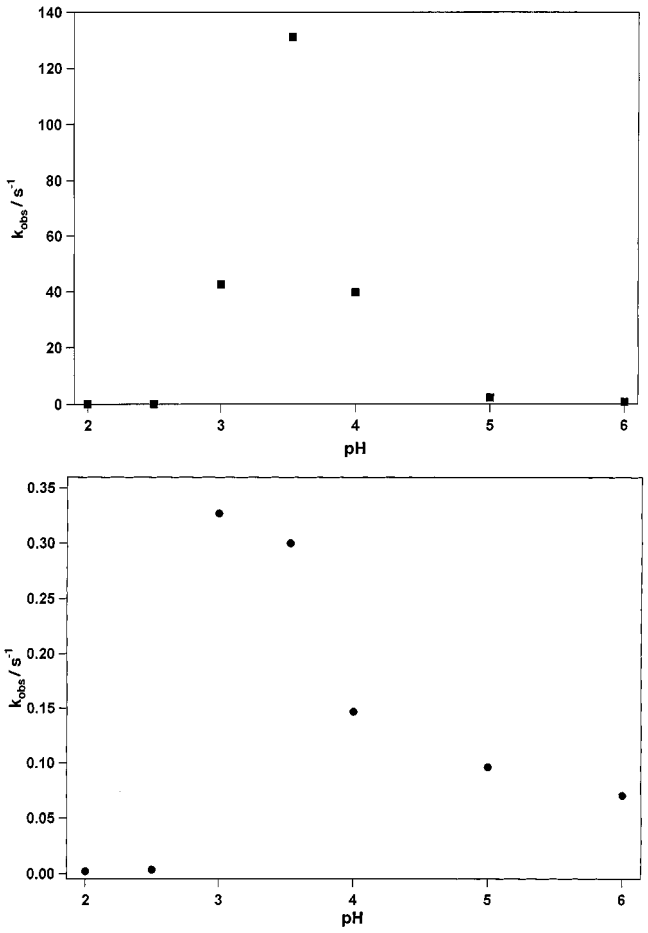


Figure 5. a: pH dependence of k_{obs1} (■) for the oxidation of [Fe^{II}(cdta)] in the presence of an excess of O_2. – b: pH dependence of k_{obs2} (•) for the oxidation of [Fe^{II}(cdta)] in the presence of an excess of O_2
Experimental conditions: [O_2] = $6.25 \cdot 10^{-4}$ M, [Fe^{II}(cdta)] = $3.0 \cdot 10^{-5}$ M, ionic strength = 0.5 M, [acetate buffer] = 0.1 M for pH > 3, T = 25°C, λ = 260 nm

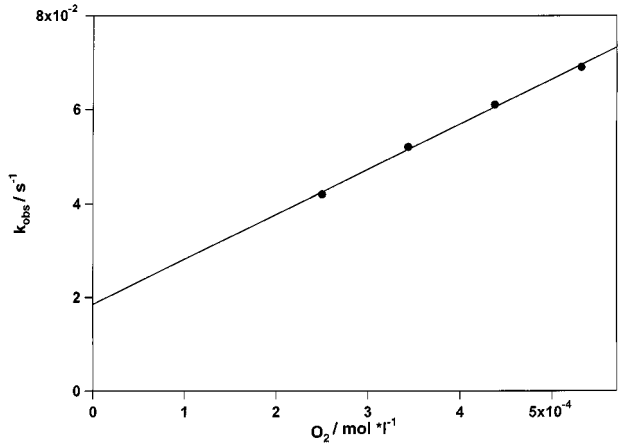


Figure 6. k_{obs2} (•) as a function of [O_2] for the oxidation of [Fe^{II}(cdta)]
Experimental conditions: [Fe^{II}(cdta)] = $3.0 \cdot 10^{-5}$ M, ionic strength = 0.5 M, [acetate buffer] = 0.1 M, pH = 6, T = 25°C, λ = 260 nm

analyse the mentioned additional faster reaction step, which could also be observed in the case of the [Fe^{II}(edta)] system.[22] First we used a concentration range where we worked in a 10- to 20-fold excess of oxygen. We could fit the obtained traces quite well to two exponential functions. The k_{obs} values for the second step observed under these conditions varied linearly with the O_2 concentration at pH = 6.0 (see Figure 6). The slope of the line, viz. 96 ± 3 M^{-1} s^{-1}, is in very close agreement with that observed for the second reaction step in the presence of an excess of [Fe^{II}(cdta)], viz. k_2 = 103 ± 4 M^{-1} s^{-1} under similar conditions.

In general the obtained kinetic traces were of a too poor quality to allow analysis of the fast step, due to the relatively low [Fe^{II}(cdta)] concentration that had to be selected in order to have the oxygen in a large enough excess. We, therefore, tried to increase the concentration of [Fe^{II}(cdta)] and measured in a 6- to 10-fold excess of oxygen. Under these conditions the data could best be fitted to three exponential functions. The initial fast rate constant showed, within experimental error limits, no meaningful dependence on the oxygen concentration. In principle such a reaction step could involve ring-opening of the cdta ligand prior to or following the binding of dioxygen. Unfortunately, it was not possible to determine within reasonable accuracy the thermal activation parameters for this reaction. The second subsequent step exhibited a decrease in absorbance comparable to the first fast step observed in the presence of an excess of [Fe^{II}(cdta)]. The determined second order rate constant for this step is k_1 = 611 ± 234 M^{-1} s^{-1} , which is of the same order as k_1 = 1080 ± 16 M^{-1} s^{-1} determined in the presence of an excess of [Fe^{II}(cdta)]. It follows that the data obtained in the presence of an excess of oxygen, despite their relatively poor quality, do support the overall trends observed in the presence of an excess of [Fe^{II}(cdta)].

Mechanistic Interpretation

pH titrations for the [Fe^{II}(cdta)] complex[37] show a similar behavior as reported for the [Fe^{II}(edta)] complex.[38] As these complexes are very similar, it is reasonable that [Fe^{II}(cdta)] shows a similar behavior like [Fe^{II}(edta)] in solution and in the solid state. It is known from X-ray data for the [Fe^{II}(edta)] complex, which was crystallized from neutral solution, that it exists as a seven coordinate [Fe^{II}-(edta)H_2O]$^{2-}$ species with a mono-capped trigonal-prismatic geometry (MCP).[39] The edta chelate can be protonated when the solution is acidified.[4,40,41] This results in a monoprotonated species [Fe^{II}(edtaH)(H_2O)]$^-$, which has a pentagonal bipyramidal geometry (PB) in the solid state.[41] Although such X-ray data are not available for the [Fe^{II}(cdta)] complex, it is quite realistic to expect that [Fe^{II}(cdta)] behaves in a similar way, and that the structure in solution is comparable to the structure in the solid state. For example, from NMR and Raman studies,[42–46] it is known for the [Fe^{III}(edta)] complex, that the structure in solution is the same as in the crystalline state.[47–49]

The increase in k_{obs} with increasing [H^+] at pH < 5 could result from the protonation of the cdta ligand which is ac-

companied by a change in geometry from MCP to PB. The PB geometry has a higher reactivity due to the greater bite angle in the PB form such that the incoming oxygen molecule has more space to enter the coordination sphere and to substitute the coordinated water. On further acidification, another changeover in geometry occurs which is associated with the diprotonation of the complex as shown in (1). This diprotonated form of the complex results again in a mono-capped trigonal-bipyramidal geometry.[41] Here the $Fe-OH_2$ bond of the $[Fe^{II}(edta)(H_2O)]^{2-}$ complex is shortened as a result of protonation of two acetate arms. The decrease in reactivity can therefore also be due to a shortening of the $Fe-OH_2$ bond of the corresponding $[Fe^{II}(cdtaH_2)(H_2O)]$ complex at pH < 2.5.

For the deprotonation of the monoprotonated complex a pK_a of 2.88 was reported in the literature.[37] The resulting distribution diagramms (see Figure 4) correlate very well with the found kinetic pH dependencies, such that these titration data strongly support our assumption that the monoprotonated form of the complex is the reactive one.

$$\underset{\text{MCP}}{[Fe^{II}(cdta)(H_2O)]^{2-}} + H^+ \overset{K_{a1}}{\rightleftharpoons} \underset{\text{PB}}{[Fe^{II}(cdtaH)(H_2O)]^-} \quad (1)$$

$$\underset{\text{PB}}{[Fe^{II}(cdtaH)(H_2O)]^-} + H^+ \overset{K_{a2}}{\rightleftharpoons} \underset{\text{MCP}}{[Fe^{II}(cdtaH_2)(H_2O)]}$$

All three complexes can react with O_2 to produce $[Fe^{II}(cdta)(O_2)]^{2-}$, $[Fe^{II}(cdtaH)(O_2)]^-$, and $[Fe^{II}(cdtaH_2)(O_2)]$, respectively, as shown in (2). We believe that these reactions account for the first fast step, especially because they correlate with the pH-dependent profile (see Figure 3a). Moreover, the substitution of coordinated H_2O by O_2 on the $[Fe^{II}(cdta)]$ complexes is not expected to cause a significant UV-Vis spectral change. The concentration dependence in Figure 2a suggests that the process is reversible. From the slope and the intercept an apparent equilibrium constant was calculated to be $K_1 = 1862\ M^{-1}$. However, this is based on the assumption that the intercept in Figure 2a is entirely due to the back reaction, which does not have to be the case.

$$[Fe^{II}(cdta)(H_2O)]^{2-} + O_2 \underset{k_{-1}}{\overset{k_1}{\rightleftharpoons}} [Fe^{II}(cdta)(O_2)]^{2-} + H_2O$$

$$[Fe^{II}(cdtaH)(H_2O)]^- + O_2 \underset{k'_{-1}}{\overset{k'_1}{\rightleftharpoons}} [Fe^{II}(cdtaH)(O_2)]^- + H_2O \quad (2)$$

$$[Fe^{II}(cdtaH_2)(H_2O)] + O_2 \underset{k''_{-1}}{\overset{k''_1}{\rightleftharpoons}} [Fe^{II}(cdtaH_2)(O_2)] + H_2O$$

The reactions in (2) are reversible substitution processes in which the protonated pentagonal bipyramidal species can bind O_2 more rapidly than the nonprotonated and diprotonated mono-capped trigonal-prismatic species.

The following rate law for the forward reactions can account for the bell shaped pH dependence at pH = 2.0:

$$k_{obs1} = \left\{ \frac{k_1 + k'_1 K_{a1}[H^+] + k''_1 K_{a1}K_{a2}[H^+]^2}{1 + K_{a1}[H^+] + K_{a1}K_{a2}[H^+]^2} \right\} [Fe^{II}(cdta)] \quad (3)$$

The subsequent redox reactions (4) to produce superoxo complexes of $[Fe^{III}(cdta)]$ will induce a significant spectral change and are suggested to account for the first slower reaction step. Thus electron transfer is the rate-determining step following the rapid coordination of O_2 in (2). The observed rate constants, k_{obs2}, are expected to depend on pH since the different species produced in (2) are expected to undergo oxidation at different rates.

$$[Fe^{II}(cdta)(O_2)]^{2-} \xrightarrow{k_2} [Fe^{III}(cdta)(O_2^-)]^{2-}$$

$$[Fe^{II}(cdtaH)(O_2)]^- \xrightarrow{k'_2} [Fe^{III}(cdtaH)(O_2^-)]^- \quad (4)$$

$$[Fe^{II}(cdtaH_2)(O_2)] \xrightarrow{k''_2} [Fe^{III}(cdtaH_2)(O_2^-)]$$

The given rate law (5), derived under conditions that $[Fe^{II}(cdta)] >> [O_2]$, can account for the bell shaped pH dependence observed at pH = 2.0 in Figure 3b. Furthermore, this rate law is also in agreement with the linear dependence on the concentration of $[Fe^{II}(cdta)]$ as found in Figure 2b.

$$k_{obs2} = \left\{ \frac{k_2K_1 + k'_2 K'_1 K_{a1}[H^+] + k''_2 K'_1 K_{a1}K_{a2}[H^+]^2}{1 + K_{a1}[H^+] + K_{a1}K_{a2}[H^+]^2} \right\} [Fe^{II}(cdta)] \quad (5)$$

The subsequent reaction step, k_{obs3}, exhibits a similar pH profile (Figure 3c) and is on the average ca. two times slower than k_{obs2}. Since these experiments are performed in the presence of an excess of $[Fe^{II}(cdta)]$, we suggest that equilibrium (1) must also account for the pH dependence found for this reaction step. Thus the superoxo species produced in (4) may react further as shown in (6). The rate law for these reactions will be similar to that in (5), as summarized in (7).

$$[Fe^{III}(cdta)(O_2^-)]^{2-} + [Fe^{II}(cdta)(H_2O)]^{2-} \xrightarrow{k_3} [(cdta)Fe^{III}(O_2^{2-})Fe^{III}(cdta)]^{4-} + H_2O$$

$$[Fe^{III}(cdtaH)(O_2^-)]^- + [Fe^{II}(cdtaH)(H_2O)]^- \xrightarrow{k'_3} [(cdtaH)Fe^{III}(O_2^{2-})Fe^{III}(cdtaH)]^{2-} + H_2O \quad (6)$$

$$[Fe^{III}(cdtaH_2)(O_2^-)] + [Fe^{II}(cdtaH_2)(H_2O)] \xrightarrow{k''_3} [(cdtaH_2)Fe^{III}(O_2^{2-})Fe^{III}(cdtaH_2)] + H_2O$$

$$k_{obs3} = \left\{ \frac{k_3 + k'_3 K_{a1}[H^+] + k''_3 K_{a1}K_{a2}[H^+]^2}{1 + K_{a1}[H^+] + K_{a1}K_{a2}[H^+]^2} \right\} [Fe^{II}(cdta)] \quad (7)$$

The temperature and pressure dependence of the reactions were also studied in the presence of an excess of [Fe^{II}(cdta)]. As the concentration dependence of the first fast step exhibits a significant intercept, it was neccessary to measure the temperature dependence as a function of concentration in order to separate the contribution of the intercept from the slope (see Supplementary Table S1). The volumes of activation could only be obtained for the second and the third step (see Supplementary Figure S1). Since the first fast step exhibits only very small absorbance changes and is ca. ten times faster in comparison to the subsequent steps, our instrumentation did not allow a determination of the associated volume of activation. All obtained rate and activation parameters are summarized in Table 1.

Table 1. Rate constants and activation parameters determined in the presence of an excess of [Fe^{II}(cdta)] for the oxidation by dioxygen

	1. Reaction	2. Reaction	3. Reaction
rate constant ($M^{-1} s^{-1}$)	1080 ± 16	103 ± 4	59 ± 5
$\Delta H^{\#}$ (kJ mol^{-1})	44.1 ± 2.3	66.5 ± 0.9	67.1 ± 0.8
$\Delta S^{\#}$ (J $mol^{-1} K^{-1}$)	−236 ± 8	18.7 ± 2.4	18.0 ± 2.7
$\Delta V^{\#}$ (cm^3 mol^{-1})	not determined	−20.2 ± 2.3	−23.0 ± 3.9

Experimental conditions: [Fe^{II}(cdta)] = $2.5 \cdot 10^{-3}$ M, [O_2] = $1.25 \cdot 10^{-4}$ M, ionic strength = 0.5 M, [acetate buffer] = 0.10 M, pH = 6.0, λ = 370 nm.

Overall Suggested Mechanism

All three reaction steps could be resolved during the interaction of dioxygen with an excess of [Fe^{II}(cdta)]. These include at first substitution of a coordinated water molecule by dioxygen, where this process probably follows an associative mechanism as a result of the strongly negative entropy of activation (see Table 1). This step is then followed by an intramolecular electron-transfer reaction to produce an Fe^{III}-superoxo complex, which in the third step reacts with another [Fe^{II}(cdta)] species to produce a dimeric [$Fe^{III}-O_2^{2-}-Fe^{III}$] complex, which is postulated to dissociate rapidly to form the monomeric [Fe^{III}(cdta)] complex and H_2O_2. The latter species was shown to react considerably faster with [Fe^{II}(cdta)] than dioxygen (typical rate constants of $k_1 = 1.9 \cdot 10^4$ $M^{-1}s^{-1}$ and $k_2 = 1.6 \cdot 10^3$ $M^{-1}s^{-1}$ were found at $T = 25°C$ and pH = 6). In principle, it should be possible to observe four reaction steps of which two are associated with substitution and electron-transfer of the first [Fe^{II}(cdta)] complex, and two associated with similar reactions of the second [Fe^{II}(cdta)] complex. With the aid of a Global Analysis Program it could be shown that the fit with a three-step mechanism is not perfect. But due to the similarity of the two postulated substitution processes, we were not successful to separate it into four rate constants. The fact that all three observed concentration dependences are linear means that the substitution equilibria for the first and third steps must be unfavorable in order to result in a linear concentration dependence of the second and fourth reaction steps.

The extinction coefficient of [Fe^{II}(cdta)] at pH = 6 was found to be 743 $M^{-1} cm^{-1}$ at 261 nm, which is much lower than for the corresponding [Fe^{II}(edta)] complex.[22] The extinction coefficient of [Fe^{III}(cdta) H_2O]$^-$ under similar conditions was found to be 7817 $M^{-1} cm^{-1}$ and for [Fe^{III}(cdta) OH]$^{2-}$ to be 7644 $M^{-1} cm^{-1}$. From this data a final spectrum could be calculated. Due to our assumption that only the monomeric [Fe^{III}(cdta)] species is formed, the stoichiometry of the reaction is only between 2:1 and 3:1 (Fe/O_2). That leads to the result that the applied model could be too simple and that a small amount of free Fe^{II} (vide supra) or bridged species affect the final absorbance.

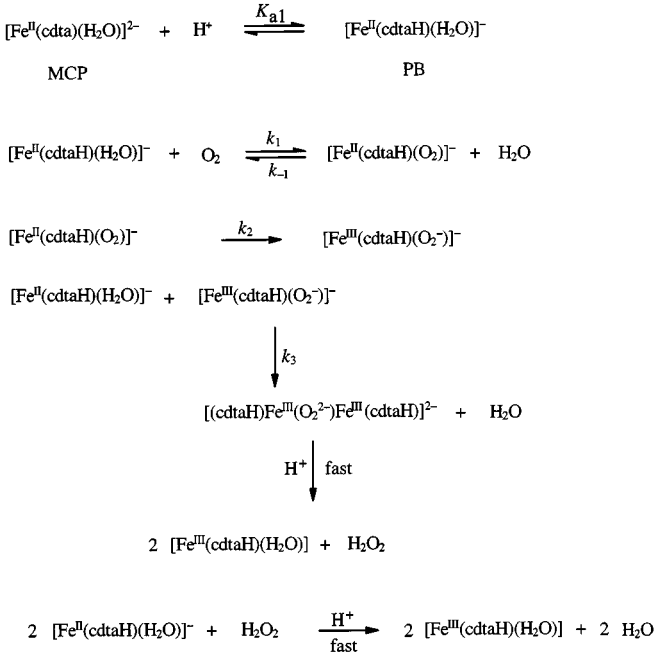
The rate constants clearly show that the substitution processes are very fast and are followed by the rate-determining electron-transfer processes. This is one of the reasons, why we were unable to detect the postulated intermediates as the superoxo or peroxo species, since they immediately react once they are formed. Furthermore, for the related [Fe(edta)] complex it was reported that the characteristic bands for the [Fe^{III}(edta)O_2]$^{2-}$ complex at 287 nm (ε = 6100 $M^{-1} cm^{-1}$) and 520 nm (ε = 530 $M^{-1} cm^{-1}$) show, in comparison to [Fe^{III}(edta)H_2O]$^-$ with ε = 9290 $M^{-1} cm^{-1}$ (256 nm),[15,16,50] low extinction coefficients, such that the spectra of the intermediates would be hidden by the product spectrum. Such data are presently not available for the corresponding [Fe(cdta)] complexes.

The reaction with dioxygen proceeds via a fast substitution process on the [Fe^{II}(cdta)H_2O]$^{2-}$ complex. For this process only $\Delta H^{\#}$ and $\Delta S^{\#}$ could be determined, where $\Delta S^{\#}$ is strongly negative (see Table 1). Our assumption that this first fasty step is a substitution process is strongly supported by these activation parameters. They are rather similar to related substitution processes on corresponding Ru complexes.[51−53] The subsequent slower intramolecular electron-transfer process must be controlled by a reorganization barrier in order to convert [$Fe^{II}-O_2$] to [$Fe^{III}-O_2^-$]. This reaction is characterized by a significantly negative $\Delta V^{\#}$ value (Table 1), which must be related to the oxidation of Fe^{II} to Fe^{III} and the reduction of O_2 to O_2^-. The corresponding value for $\Delta S^{\#}$, however, is small and positive; this apparent discrepancy can be explained by the large experimental error of $\Delta S^{\#}$. Both these processes are expected to involve a significant decrease in partial molar volume and an increase in electrostriction.[54−56] The efficiency of the ligand substitution process is controlled by the nature of the [Fe^{II}(cdta)H_2O]$^{2-}$ complex, which on protonation produces a more labile [Fe^{II}(cdtaH)H_2O]$^-$ species. The latter accounts for the drastic increase in observed rate constant on decreasing the pH in the range from 5 to 3.

The reaction of the second [Fe^{II}(cdta)H_2O]$^{2-}$ species results in very similar concentration, pH, temperature and pressure dependencies, which are once again interpreted in terms of a rapid complex-formation reaction followed by a rate-determining electron-transfer process. This reaction is once again characterized by a significantly negative $\Delta V^{\#}$ value for the same reasons as outlined above. A comparison with the data reported in our last study,[22] indicates that the determined $\Delta V^{\#}$ values are very similar for both com-

plexes, which confirms our assumption that they are due to electron-transfer processes. The very similar activation parameters observed for both oxidation processes indicate that a similar reorganization barrier must exist. When oxygen is used in excess, only one electron transfer reaction is observed since a peroxo-bridged complex cannot be formed under these conditions. This is in good agreement with the second reaction step observed in the presence of an excess of [Fe^{II}(cdta)]. Again the reaction is controlled by electron-transfer and the associated reorganization barrier. The additional fast process which was observed in an excess of [O_2] may be related to ring-opening of the cdta ligand when dioxygen enters the coordination sphere as mentioned above.

The results of this study have shown that a change in the chelate ligand has decelerated the fast substitution process, which could not be studied in detail in our recent paper.[22] The change in reactivity can be due to the different geometry of the here employed ligand,[23−30] which has its acetate arms in the trans position. This seems to lead to a less reactive binding of O_2. We are now able to suggest a detailed multistep mechanism for the reaction in the presence of an excess of [Fe^{II}(cdta)] as shown in Scheme 1. At high pH (pH = 6), mostly the nonprotonated form will react, whereas at low pH (pH = 4) the more reactive monoprotonated form will react. The mechanism in Scheme 1 is given for the more reactive protonated species



Scheme 1. Multistep mechanism for the reaction of [Fe^{II}(cdta)] with molecular oxygen

Experimental Section

Materials: Chemicals of analytical reagent grade and ultrapure water were used throughout this study. [Fe^{II}(cdta)] was prepared in solution from $FeSO_4 \cdot 7\ H_2O$ and H_4(cdta). NaOH, $HClO_4$, and NaOAc were used to adjust the pH of the test solutions.[31] The ionic strength of the medium was adjusted with $NaClO_4$.

Preparation of Solutions: [Fe^{II}(cdta)] is extremely oxygen sensitive and is rapidly oxidized to [Fe^{III}(cdta)].[32] Test solutions were therefore prepared under the exclusion of oxygen as described in our earlier report.[22] The ionic strength was adjusted with $NaClO_4$ to 0.50 M for all solutions. Acetate buffer was employed for 3 < pH < 6 and Tris or MOPS buffer was used for 6 < pH < 7. Test measurements showed that the employed buffers had no significant effect on the observed kinetics. Test solutions were transferred to the stopped-flow unit by using gastight syringes.

Instrumentation: The kinetic experiments were performed on a Applied Photophysics SX.18MV stopped-flow unit, to which an online data acquisition system was connected. Rapid scan spectra were obtained with the Applied Photophysics Instrument by addition of obtained absorbance-time traces over the investigated wavelength range. Kinetic measurements at pressures up to 120 MPa were performed on a homemade high-pressure stopped-flow unit.[3,34] UV-Vis spectra were recorded on a Hewlett-Packard HP 8452A diode array spectrophotometer. The pH of the stock solutions was measured with the aid of a Mettler Delta 340 pH meter. The reference electrode was filled with NaCl instead of KCl in order to prevent precipitation of $KClO_4$. All kinetic traces were analyzed by using OLIS KINFIT (OLIS, Bogart, Georgia, USA) and Applied Photophysics Kinfit (Applied Photophysics Limited, Leatherhead, UK) software. For Global Analysis, spectra were recorded on the Applied Photophysics Instrument and fitted with the aid of the Applied Photophysics Software Package.

Supporting Information

Figure S1 reports pressure dependences obtained in the presence of an excess of [Fe^{II}(cdta)]. Table S1 reports second-order rate constants as a function of temperature. This material is available on the WWW under http://www.wiley-vch.de/home/eurjic or from the authors.

Acknowledgments

The authors gratefully acknowledge financial support from the Deutsche Forschungsgemeinschaft and the Volkswagen-Stiftung.

[1] M. Cher, N. Davidson, *J. Am. Chem. Soc.* **1955**, *77*, 793.
[2] R. E. Huffman, N. Davidson, *J. Am. Chem. Soc.* **1956**, *78*, 4836.
[3] T. Kaden, S. Fallab, *Chelate Catalysed Autoxydation of Iron(II) Complexes*; Mcmillan Company: New York, **1961**.
[4] Y. Kurimura, R. Ochiai, N. Matsuura, *Bull. Chem. Soc. Jpn.* **1968**, *41*, 2234.
[5] A. P. Purmal, Y. I. Skurlatov, S. O. Travin, *Bull. Acad. Sci. USSR Div. Chim. Sci. (Engl. Transl.)* **1980**, *29*, 315.
[6] E. Sada, H. Kumazawa, H. Machida, *Ind. Eng. Chem. Res.* **1987**, *26*, 1468.
[7] E. R. Brown, J. D. Mazzarella, *J. Electroanal. Chem.* **1987**, *222*, 173.
[8] M. Rahhal, H. W. Richter, *J. Chem. Soc.* **1988**, *110*, 3126.
[9] J. D. Rush, W. H. Koppenol, *J. Am. Chem. Soc.* **1988**, *110*, 1957.
[10] H. J. Wubs, A. A. C. M. Beenackers, *Ind. Eng. Chem. Res.* **1993**, *32*, 2580.
[11] L. Liang, J. A. McNabb, J. M Paulk,. B. Gu, J. F. McCarthy, *Environ. Sci. Technol.* **1993**, *27*, 1864.
[12] D. W. King, H. A. Lounsbury, F. J. Millero, *Environ. Sci. Technol.* **1995**, *29*, 818.
[13] W. Krapp Pogozelski, T. J. McNeese, T. D. Tullius, *J. Am. Chem. Soc.* **1995**, *117*, 6428.

[14] M. Fontecave, J. L. Pierre, *Bull. Soc. Chim. France* **1993**, *130*, 77.
[15] G. J. McClune, J. A. Fee, G. McCluskey, J. T. Groves, *J. Am. Chem. Soc.* **1977**, *99*, 5220.
[16] C. Bull, G. J. McClune, J. Fee, A. *J. Am. Chem. Soc.* **1983**, *105*, 5290.
[17] R. P. Hertzberg, P. B. Dervan, *Biochemistry* **1984**, *23*, 3934.
[18] R. S. Youngquist, P. B. Dervan, *J. Am. Chem. Soc.* **1985**, *107*, 5528.
[19] P. D. Dervan, *Science* **1986**, *232*, 464.
[20] I. Yamazaki, L. H. Piette, *J.Am Chem Soc.* **1991**, *113*, 7588.
[21] V.Zang, R. van Eldik, *Inorg. Chem.* **1990**, *29*, 1705.
[22] S.Seibig, R. van Eldik, *Inorg. Chem.* **1997**, *36*, 4115.
[23] H. A. Weakliem, J.L. Hoard, *Inorg. Chem.* **1959**, *28*, 549.
[24] N. Okaku, K. Toyoda, Y. Moriguchi, K. Ueno *Bull. Chem. Soc. Jpn.* **1967**, *40*, 2326.
[25] A. S. de Sousa, G. J. B. Croft, C. A. Wagner; J. P. Michael; R. D. Hancock, *Inorg. Chem.* **1991**, *30*, 3525.
[26] G. Schwarzenbach, R. Gut, G. Anderegg, *Helv. Chim. Acta*, **1954**, *37*, 937.
[27] M. W. Brechbiel, O. A. Gansow, C. G. Pippin , R. D. Rogers, R. P. Planalp, *Inorg. Chem.* **1996**, *35*, 6343.
[28] W. H. Woodruff, D. C. Weatherburn, D. W. Margerum; *Inorg. Chem.* **1971**, *10*, 2102.
[29] W. H. Woodruff, B. A. Burke, D. W. Margerum, *Inorg. Chem.* **1974**, 13, 2573.
[30] W. H. Woodruff, D. W. Margerum, *Inorg. Chem.* **1974**, *13*, 2578.
[31] D. D. Perrin, D. Dempsey, *Buffers for pH and Metal Ion Control*; Chapman and Hall: London, **1974**.
[32] H. Ogino, T. Nagata, K.Ogino, *Inorg. Chem.* **1989**, *28*, 3656.
[33] R. van Eldik, D. A. Palmer, R. Schmidt, H. Kelm, *Inorg. Chim. Acta* **1981**, *50*, 131.
[34] R. van Eldik, W. Gaede, S. Wieland, J. Kraft, M. Spitzer, D. A. Palmer, *Rev. Sci. Instrum.* **1993**, *64*, 1355.
[35] V. Zang, M. Kotowski, R. van Eldik, *Inorg. Chem.* **1988**, *27*, 3279.
[36] V. Zang, R. van Eldik, *Inorg. Chem.* **1990**, *29* 4462.
[37] J. A. M. Ahmad, W. C. E. Higginson, *J. Chem. Soc. Dalton Trans.* **1983**, 1449.
[38] N. H. Clark, A. E. Martell, *Inorg. Chem.* **1988**, *27*, 1297.
[39] T. Mizuta, J. Wang, K. Miyoshi, *Bull. Chem. Soc. Jpn.* **1993**, *66*, 2547.
[40] A. Marton, N. Süksösd-Rozlosnik, A. Vertes, I. Nagy-Czako, K. Burger, *Inorg. Chim. Acta* **1987**, *137*, 173.
[41] T. Mizuta, J. Wang, K. Miyoshi, *Inorg. Chim. Acta* **1995**, *230*, 119.
[42] J. F. Whidbey, D. E. Leyden, *Anal. Chim. Acta* **1970**, *51*, 25.
[43] C. Manley, *Z. Angew. Phys.* **1971**, *32*, 187.
[44] J. Bloch, G. Navon, *J. Inorg. Nucl. Chem.* **1980**, *42*, 693.
[45] J. Oakes, E. G. Smith, *J. Chem. Soc. Faraday Trans. 1* **1983**, *79*, 543.
[46] K. Kanamori, H. Dohniwa, N. Ukita, I. Kanesaka, K. Kawai, *Bull. Chem. Soc. Jpn.* **1990**, *63*, 1447.
[47] C. H. L. Kennard, *Inorg. Chim. Act.* **1967**, *1*, 347.
[48] X. Solans, M. Font Alba, *Acta Cryst.* **1984**, *C40*, 635.
[49] T. Mizuta, T. Yamamoto, K. Miyoshi, Y. Kushi, *Inorg. Chim. Acta* **1990**, 121.
[50] K. C. Francis, D. Cummnis, J. Oakes, *J. Chem. Soc., Dalton Trans.* **1985**, 493.
[51] H. C Bajaj,. R. van Eldik, *Inorg. Chem.* **1988**, *27*, 4052.
[52] H. C. Bajaj, R. van Eldik, *Inorg. Chem.* **1989**, *28*, 1980.
[53] H. C. Bajaj, R. van Eldik, *Inorg. Chem.* **1990**, *29*, 2855.
[54] R. van Eldik, T. Asano, W. J. le Noble, *Chem Rev.* **1989**, *89*, 549; A. Drljaca, C. D. Hubbard, R. van Eldik, T. Asano, M. V. Basilevsky, W. J. le Noble, *Chem. Rev.* **1998**, *98*, 2167.
[55] M. Zhang, R. van Eldik, J. H. Espenson, , A. Bakac, *Inorg. Chem.* **1994**, *33*, 130.
[56] H.-D. Projahn, S. Schindler, R. van Eldik, D. G. Fortier, C. R. Andrew, A. G. Sykes *Inorg. Chem.* **1995**, *34*, 5935.

Received July 14, 1998
[I98232]

Searching for New Luminescent Sensors: Synthesis and Photophysical Properties of a Tripodal Ligand Incorporating the Dansyl Chromophore and of Its Metal Complexes

Luca Prodi,*[a] Fabrizio Bolletta,[a] Marco Montalti,[a] and Nelsi Zaccheroni[a]

Keywords: Chemosensors / Fluorescence / Tripodal ligands

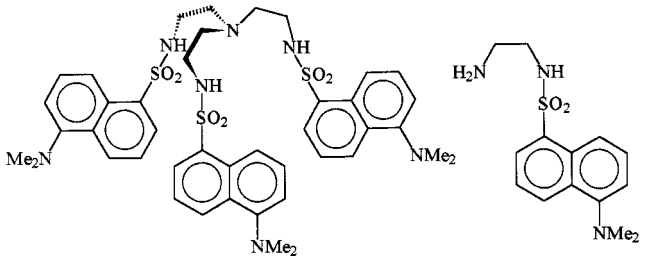
The new tripodal ligand **1** containing the dansyl chromophore has been synthesized and characterized. The intense luminescence characteristic of the chromophore is maintained in the ligand structure, showing that no intramolecular interactions are present. This ligand has been shown to complex in acetonitrile/water solutions only with Cu^{2+}, Co^{2+}, Zn^{2+}, and Cd^{2+} ions, with concomitant pronounced changes in the fluorescence spectra. The complexation is controlled by pH conditions: at neutral pH this ligand shows a remarkable selectivity towards Cu^{2+} ions, suggesting a possible use for **1** as a luminescent chemosensor for this ion.

Photoluminescence spectroscopy has recently attracted increasing attention in the scientific community as it has been finding applications in growing fields of great economic and social impact, such as medical diagnostics, environmental sciences, cell biology and molecular electronics.[1−5] In particular, the synthesis, characterization, and application of many luminescent sensors has opened up many opportunities for solving complex analytical problems. The sensitivity and versatility of luminescence spectroscopy make it a particularly suitable technique for analytical applications, giving for example the possibility of monitoring analyte concentrations in real-time and real-space.[2−5]

Of particular interest is the measurement of the concentrations of transition-metal ions, since many of these are also pollutants in environmental systems and essential trace elements in biological systems. For these reasons, many fluorescent sensors for these metal ions have been synthesized and characterized.[3−5] In this context, we have synthesized the ligand tris[2-(5-dimethylamino-1-naphthalenesulphonamido)ethyl]amine (**1**), a new tripodal ligand incorporating the dansyl chromophore. Its luminescent properties have been widely used in order to obtain fluorescent sensors and labels,[6−15] especially in the field of biochemistry for peptides and amino acids. We report here the synthesis and the luminescence properties of this ligand and its metal complexes, as well as luminescence studies of (dansylethylenediamine)metal complexes **2** to provide a more in-depth investigation of the photophysics of such a widely used chromophore.

Results

All the photophysical experiments were carried out in acetonitrile/water (1:1, v/v) solutions. The absorption spectrum of **1** (Figure 1) was very similar in shape to the absorption spectrum of **2**, but it was three times more intense, as would be expected given the presence of three chromophoric groups in **1**. As far as the fluorescence properties are concerned, as can be seen from Table 1, compounds **1** and **2** have very similar spectra and exhibit similar lifetimes and quantum yields. The absorption spectra and fluorescence properties of **1** and **2** do not depend on the pH conditions in the range 3−11.



1 2

Scheme 1

As can be seen from Figure 2 and Table 1, strong changes in the luminescence properties of **1** were indeed observed upon addition of Cu^{2+}, Co^{2+}, Zn^{2+}, and Cd^{2+} at pH = 9.5. In particular, for the first two metal ions, a strong quenching (I_{rel} = 1%, Table 1) of the fluorescence intensity was observed, while for Zn^{2+} and Cd^{2+} a blue shift, accompanied by an enhancement of the quantum yield, could be detected.

Smaller, but non-negligible changes could also be observed at these pH conditions in the absorption bands of **1** upon addition of Co^{2+}, Zn^{2+}, Cd^{2+}, and Cu^{2+} (Figure 1). A blue shift of the fluorescence band of **1** was also observed upon addition of Ag^{+} and Hg^{2+} metal ions; however, precipitation of the metal ions before reaching complete complexation prevented further investigations. Similar effects caused by addition of Cu^{2+} ions were observed in the absorption and luminescence spectra of compound **2**, while

[a] Dipartimento di Chimica "G. Ciamician", Università di Bologna, Via Selmi 2, I-40126 Bologna, Italy
Fax: (internat.) + 39(0)51/259456
E-mail: lprodi@ciam.unibo.it

 © WILEY-VCH Verlag GmbH, D-69451 Weinheim, 1999 1434−1948/99/0303−0455 $ 17.50+.50/0

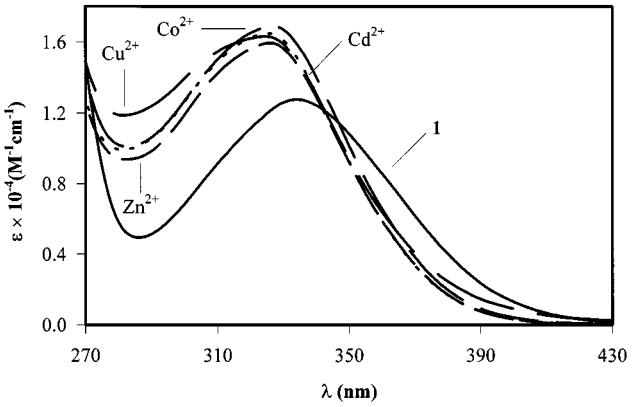


Figure 1. Absorption spectra of **1** and of its complexes with Cu^{2+}, Co^{2+}, Cd^{2+}, and Zn^{2+} in acetonitrile/water (1:1, v/v) solutions at pH = 9.5

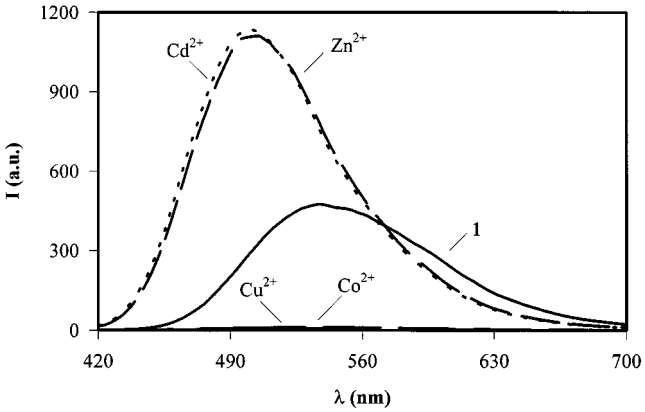


Figure 2. Fluorescence spectra (λ_{exc} = 340 nm) of **1** and of its complexes with Cu^{2+}, Co^{2+}, Cd^{2+}, and Zn^{2+} in acetonitrile/water (1:1, v/v) solutions at pH = 9.5

Table 1. Photophysical properties of ligands **1** and **2** and of their complexes with transition-metal ions in water/acetonitrile (1:1, v/v) at pH = 9.5

	Absorption		Luminescence room temp.			77 K	
	λ_{max} [nm]	ε_{max} [$M^{-1}cm^{-1}$]	λ_{max} [nm]	τ [ns]	I_{rel}	λ_{max} [nm]	I_{rel}
1	334	12700	540	10	100	536	100
$[Cu(\mathbf{1})]^-$	324	16300	540	10	1[a]	536	2[a]
$[Co(\mathbf{1})]^-$	327	16900	540	10	1[a]	536	2.5[a]
$[Zn(\mathbf{1})]^-$	326	16000	500	12	370	495	250
$[Cd(\mathbf{1})]^-$	326	16500	500	12	370	495	250
2	334	4300	540	10	100	536	100
$[Cu(\mathbf{2})_2]$	325	5200	540	< 0.5	< 1	536	< 1

[a] This residual luminescence can be ascribed to an impurity of a luminescent dansyl derivative present in the sample. For more details, see text.

addition of Co^{2+} ions did not cause any change in its photophysical properties. An increase in the luminescence intensity of **2** was observed upon addition of Zn^{2+} and Cd^{2+}, but the formation of the metal hydroxide prevented the formation of the complex.

Addition to a 5×10^{-5} M solution of **1** and **2** of up to 10 molar equiv. of Na^+, K^+, Ca^{2+}, Sr^{2+}, Ba^{2+}, Eu^{3+}, Ni^{2+}, Mn^{2+}, Pb^{2+}, Fe^{2+}, Fe^{3+}, and Cr^{3+} did not lead to any change in the absorption and emission spectra of the dansyl derivatives in all the pH range examined (3−11). Furthermore, no effects were found on the absorption and luminescence spectra upon addition of up to 10 equiv. of the aforementioned metal ions to a solution containing equimolar amounts of **1** and Zn^{2+} or Cu^{2+} ions.

The observed changes for **1** and **2**, as can be seen from Figures 3 and 4, respectively, were very sensitive to the pH conditions: They were almost negligible at pH values lower than 4, and reached a plateau at higher pH, the pattern being characteristic for the ligand and the metal ion. This behavior is fully reversible; superimposable titration profiles have been obtained starting from pH = 11 upon addition of acid.

Titration experiments were performed in order to investigate the stoichiometry of the complexes formed, by adding

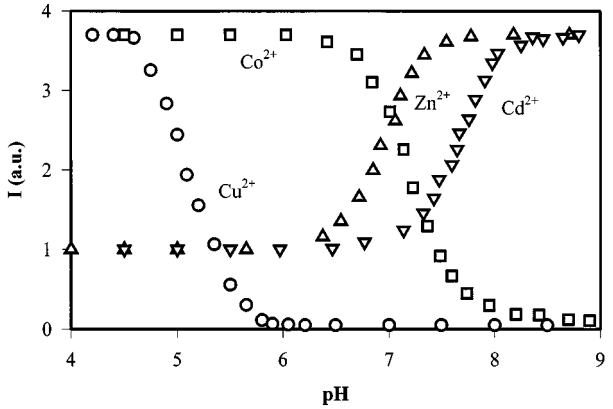


Figure 3. pH dependence of the fluorescence intensity (λ_{exc} = 340 nm) for solutions containing equimolar amounts (8×10^{-5} M) of **1** and (i) Cu^{2+} ions (λ_{em} = 540 nm), (ii) Co^{2+} ions (λ_{em} = 540 nm), (iii) Zn^{2+} ions (λ_{em} = 500 nm), and (iv) Cd^{2+} ions (λ_{em} = 500 nm); superimposable titration profiles have been obtained starting from pH = 11 upon addition of acid

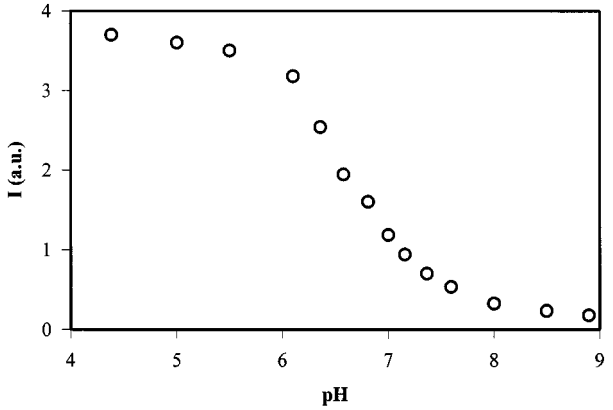


Figure 4. pH dependence of the fluorescence intensity (λ_{exc} = 340 nm, λ_{em} = 540 nm) for a solution containing equimolar (8×10^{-5} M) amounts of **2** and Cu^{2+}; superimposable titration profiles have been obtained starting from pH = 11 upon addition of acid

the metal ion to a basic (pH = 9.5) solution of the ligand. Titrations of **1** and **2** with Cu^{2+} are shown in Figure 5. These experiments always indicate a 1:1 (metal/ligand) stoichiometry for **1**, while for **2** there is evidence of a 1:2 (metal/

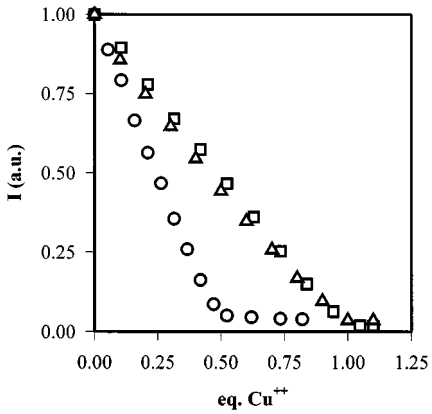


Figure 5. Dependence of the fluorescence intensity (λ_{exc} = 340 nm, λ_{em} = 540 nm) of a solution (i) containing **2** (8×10^{-5} M) at pH = 9.5 (open circles), (ii) containing **1** (8×10^{-5} M) at pH = 9.5 (open triangles), and (iii) containing **1** (8×10^{-5} M), Zn^{2+}, Co^{2+}, and Cd^{2+} (1.6×10^{-4} M) at pH = 6.5 (open squares) upon addition of Cu^{2+}

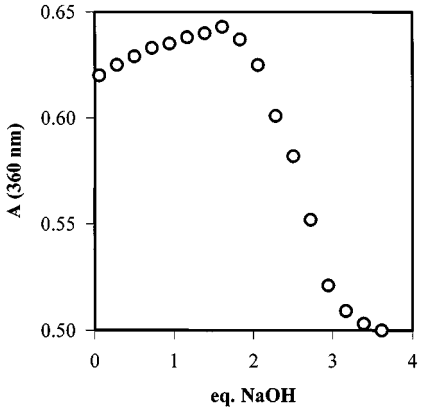


Figure 7. Dependence of the absorbance at 360 nm of a solution containing **1** and Cu^{2+} (8×10^{-5} M) upon addition of NaOH

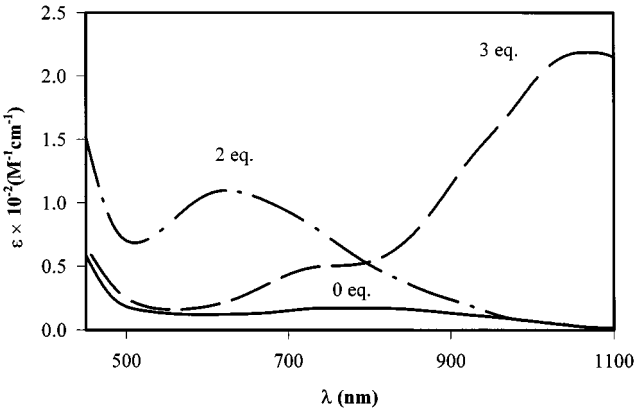


Figure 8. Cu^{2+}-centered absorption bands in the presence of one equiv. of **1** in acetonitrile/water (1:1, v/v) after the addition of various amounts of NaOH

ligand) stoichiometry. On adding up to 2 equiv. of Co^{2+}, Zn^{2+}, and Cd^{2+} ions to a solution of **1** at pH = 6.5 no changes in the luminescence properties of the ligand were observed. Titration of the same solution containing the aforementioned ions with Cu^{2+} ions led to the same pattern as shown for the titration at pH = 9.5 (Figure 5). These results clearly indicate that under these conditions only the copper ions can induce changes in the luminescence properties of **1**, and no interferences come from the other metal ions.

Addition of NaOH to a solution containing an equimolar amount of metal ion and ligand **1** (Figure 6) showed that for Co^{2+}, Zn^{2+}, and Cd^{2+} the plateau of the luminescence intensity vs. added base is reached after addition of 3 equiv. of base. For Cu^{2+}, the complete quenching of the luminescence was observed after addition of 2 equiv. of base while further changes were observed in the absorption bands of the dansyl chromophores until the addition of 3 equiv. (Figure 7). Strong changes were also observed for the metal-centered absorption bands of the copper ion in the 450−1100 nm region (Figure 8). Addition of up to 2 equiv. of base to an equimolar (1×10^{-3} M) solution of **1** and Cu^{2+} led to the appearence of a band with maximum at 620 nm, while addition of a third equivalent caused the disappearence of such a band with the concomitant formation of a band centered at 1050 nm.

By contrast, for **2** and Cu^{2+} complete quenching of the luminescence was observed after addition of 1 equiv. of base relative to the ligand.

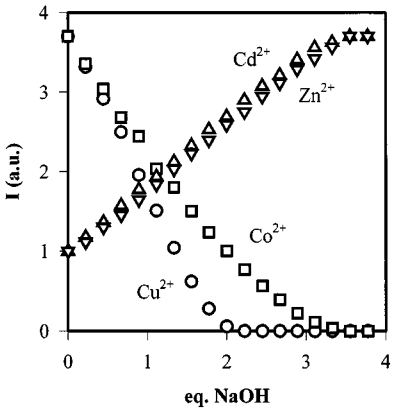


Figure 6. Dependence of the fluorescence intensity (λ_{exc} = 340 nm) for solutions containing equimolar amounts (8×10^{-5} M) of **1** and (i) Cu^{2+} ions (λ_{em} = 540 nm), (ii) Co^{2+} ions (λ_{em} = 540 nm), (iii) Zn^{2+} ions (l_{em} = 500 nm), and (iv) Cd^{2+} ions (λ_{em} = 500 nm) upon addition of NaOH

Discussion

Dansylamide and its derivatives typically show intense and large luminescence bands in the 400−600-nm region. These bands are very sensitive to the polarity of the solvent and have considerable charge-transfer character, caused by mixing of the ^1L_a and ^1L_b states of naphthalene with a charge-transfer state arising from the promotion of a lone-pair electron on the amino group into a π antibonding orbital of the naphthalene ring.[16] The photophysical behavior of **1** and **2** is in agreement with the data obtained with other dansyl derivatives.[6−16] The constancy of the

photophysical properties on passing from compound **1** to dansylamide and the ligand **2** shows that intramolecular interactions between the three chromophores in **1** are negligible.

Complexes with Cu^{2+}

Addition of Cu^{2+} ions to a neutral water/acetonitrile (1:1, v/v) solution of **1** and **2** caused a strong decrease in the fluorescence intensity and lifetime of the ligands. The quenching observed for **2** has been explained, as already reported for other dansyl derivatives, as being due to the complex formation by the amino group, followed by abstraction of the sulphonamide hydrogen atom.[9−10,17] For compound **2** (Figure 5) evidence for the formation of a complex with a 2:1 (ligand/metal ion) stoichiometry could be seen, although a 1:1 stoichiometry at higher metal concentration cannot be ruled out.[11] The observation of a plateau after addition of an equimolar amount of base in respect to the ligand is further evidence for the mechanism involving the deprotonation of the sulphonamide group for obtaining the quenched species.

A similar complexation/deprotonation mechanism can also be invoked for **1**, but with some differences. The first one is the evidence, from titration experiments, of the formation of a complex with 1:1 stoichiometry between **1** and Cu^{2+}. In addition, the pattern shown by the fluorescence spectra clearly indicates that an almost complete quenching is reached after addition of two equiv. of base (Figure 6), i.e. with the formation of a neutral complex obtained with the deprotonation of only two dansyl moieties. Under these conditions a residual luminescence with a relative intensity of 1% is observed that has an unquenched lifetime. This residual luminescence can be ascribed to an impurity of a luminescent dansyl derivative present in the sample. The further deprotonation of the third side arm, demonstrated by the changes in the absorption spectra (Figures 7 and 8), is obtained only in a second step at pH > 7.5 with the addition of the third equivalent of base.

In principle, the quenching effect after the formation of the complex can be ascribed for both **1** and **2** to either a dansyl-to-metal energy-transfer (ET) or a metal-to-dansyl electron-transfer (eT) mechanism. From the intensity data obtained, lower limits of the quenching rate constants at room temperature and at 77 K can be calculated for **1** by using Equation 1, and are 1×10^{-10} s^{-1} and 5×10^{-9} s^{-1}, respectively. The high value of the estimated quenching rate constant at 77 K suggests at least a contribution from the ET mechanism.

$$k_q = 1/\tau^\circ(I^\circ/I - 1) \quad (1)$$

The almost complete quenching of **1** after deprotonation of only two dansyl derivatives suggests that under these conditions the third side arm lies in close contact to the metal ion.

It is important to note that the formation of the Cu complex occurs at lower pH values for **1** than for **2**. This observation, together with the different stoichiometry observed for the two ligands, confirms the co-operative effect of the three side arms of the tripodal ligand **1**.

Complexes with Co^{2+}

As reported above, no changes in absorption and fluorescence spectra were observed on adding Co^{2+} ions to a solution of **2**. In contrast, at pH values higher than 7, a quenching (I_{rel} = 1%, Table 1) of the fluorescence intensity of **1** is observed, and titration experiments revealed a 1:1 (ligand/metal) stoichiometry of the complex. In this case, a simultaneous deprotonation of all the three dansyl moieties is observed from titration experiments (Figure 6). As discussed previously, a dansyl-to-Co energy-transfer (ET) or a Co-to-dansyl electron-transfer (eT) mechanism can be invoked to explain the observed fluorescence quenching, although its high efficiency at 77 K (Table 1) again suggests a contribution from the energy-transfer mechanism. As proposed for the Cu^{2+} complex, a co-operative effect of the three arms of the ligand **1** has to be invoked in order to explain the different behaviour of the two ligands examined.

Complexes with Zn^{2+} and Cd^{2+}

As reported above, addition of Zn^{2+} and Cd^{2+} ions to basic water/acetonitrile solutions of **1** caused a noticeable blue-shift in their fluorescence bands, with a concomitant increase in the quantum yield and lifetime. This effect can also be explained in terms of the formation of a complex by the amino group, followed by the deprotonation of the sulphonamide hydrogen atoms. As already known, complexation with d^{10}-Zn^{2+} and -Cd^{2+} ions does not usually introduce low-energy metal-centered or charge-separated excited states into the molecule, so that ET and eT processes cannot usually occur. However, the deprotonation/complexation process increases the electronic density on the naphthalene ring, moving towards higher energy the amine-to-naphthalene charge-transfer state present in the dansyl chromophore. A hypsochromic shift with a concomitant increase of the luminescence intensity is also observed for dansyl derivatives upon raising the energy of this excited state using low-polar solvents.[16] Complexes with a 1:1 (ligand/metal ions) stoichiometry are obtained for **1** with both Zn^{2+} and Cd^{2+}, and as observed for the Co^{2+} ions, a simultaneous deprotonation of all the three dansyl groups takes place (Figure 6). For ligand **2**, formation of the complexes occurs at higher pH values, but the competitive formation and precipitation of the metal hydroxide prevents the complete formation of the complexes.

The results obtained with Na^+, K^+, Ca^{2+}, Sr^{2+}, Ba^{2+}, Eu^{3+}, Ni^{2+}, Mn^{2+}, Pb^{2+}, Fe^{2+}, Fe^{3+}, and Cr^{3+}, both by direct and by competition experiments, indicate that these metal ions do not interfere with the complexation of Cu^{2+}, Co^{2+}, Zn^{2+} and Cd^{2+} ions. Finally, it is worth noting that among the latter ions, **1** shows a remarkable affinity and selectivity towards the Cu^{2+} ions, as can be seen from the

titration experiment performed in the presence of the other possible interfering metal ions (Figure 5). The pH window in which the complete quenching occurs is quite large (Figure 3) compared with that of other chemosensors for Cu^{2+}.[18−20] All these features make **1** a good candidate for a possible use as chemosensor for copper ions.

Conclusions

Tris[2-(5-dimethylamino-1-naphthalenesulphonamido)-ethyl]amine (**1**), a new tripodal ligand, has been synthesized and characterized, and the results compared with dansylethylenediamine (**2**), a compound that has been widely used as a reference for many other dansyl derivatives. The fluorescence properties of **1** are not unexpected considering the presence of three non-interacting dansyl moieties. Strong changes were observed upon addition of Cu^{2+}, Co^{2+}, Zn^{2+}, and Cd^{2+}, indicating a strong complexation leading to deprotonation of the sulphonamide groups of the dansyl moieties for all of them. For Cu^{2+} and Co^{2+}, a strong quenching was observed both at room temperature and at 77 K, that can be ascribed to energy- or electron-transfer processes, although the first possibility seems to be the most likely. For Zn^{2+} and Cd^{2+}, a shift of the fluorescence band toward lower wavelengths was observed with a concomitant increase of fluorescence quantum yield and lifetime. This phenomenon can be explained by a higher electronic density on the naphthalene ring of the dansyl groups after the deprotonation/complexation process. For all the metal ions, **1** was found to form stronger complexes than **2**, indicating a co-operative effect of the three arms of the tripodal ligand. Furthermore, **1** shows a remarkable affinity and selectivity towards the Cu^{2+} ions at pH > 4, suggesting a possible use of this ligand as luminescent chemosensor for these ions.

Experimental Section

General: The following materials were used: dansyl chloride (Aldrich), tris(2-aminoethyl)amine, "TREN" (Aldrich), triethylamine (Aldrich); sodium hydroxide, copper(II) nitrate hemipentahydrate, cobalt(II) and zinc(II) hexahydrate, and cadmium(II) nitrate tetrahydrate were obtained from Fluka. − Dansylethylenediamine (**2**) was a gift from Prof. Marchelli and Dr. Corradini of the University of Parma, and was available from previous work.[9] − Thin-layer-chromatographic analysis was performed using precoated TLC silica gel plates (60 F-254, Merck). − ^{1}H-NMR and ^{13}C-NMR spectra were recorded at 20°C with a Varian 500 FT spectrometer.

Tris[2-(5-dimethylamino-1-naphthalenesulphonamido)ethyl]amine (1): To a stirred solution of dansyl chloride (0.2 g, 0.74 mmol) in anhydrous $CHCl_3$ (8 ml) was added triethylamine (0.1 ml, 0.75 mmol) and TREN (35 ml, 0.25 mmol); the solution turned from dark yellow to fluorescent in less than 2 min. After stirring for another 2 h, the reaction mixture was quenched (ethyl acetate, 0.1 M in water) and extracted (CH_2Cl_2, 3 × 30 ml). Purification by flash chromatography on silica gel (CH_2Cl_2/diethyl ether, 1:1) allowed the isolation of **1** (120 mg, 59%) as a highly fluorescent yellow dense oil. − ^{1}H NMR (500 MHz, $CDCl_3$): δ = 8.51 (d, 3 H, J = 8.5 Hz), 8.44 (d, 3 H, J = 8.5 Hz), 8.26 (d, 3 H, J = 7.0 Hz), 7.52 (m, 6 H), 7.05 (d, 3 H, J = 7.5 Hz), 6.56 (br. s, 3 H, NH), 2.84 (m, 24 H, NCH_3, NCH_2CH_2NH), 2.42 (br. s, 6 H, NCH_2CH_2NH). − ^{13}C NMR ($CDCl_3$): δ = 152.19, 130.58, 130.31, 130.07, 129.55, 129.06, 123.74, 119.98, 115.75, 53.14 (NCH_2CH_2NH), 45.93 (NCH_3), 42.02 (NCH_2CH_2NH).

Spectroscopic Measurements: The solvents used for photophysical measurements were acetonitrile (Merck UVASOL) and Millipore grade water, both without further purification. The solutions of the ligands were prepared in a concentration range between 4×10^{-5} M and 1×10^{-4} M unless otherwise noted. Absorption spectra were recorded with Perkin−Elmer lambda 16 and lambda 40 spectrophotometers. Corrected emission and excitation spectra were obtained with a Perkin−Elmer LS50 spectrofluorimeter. The fluorescence lifetimes (uncertainty, ± 5%) were obtained with an Edinburgh single-photon-counting apparatus (D_2-filled flash lamp). Luminescence quantum yields (uncertainty ± 15%) were determined using quinine sulphate (Φ = 0.546[21] in 1 N H_2SO_4 aqueous solution) as standard. Emission spectra in a rigid matrix at 77 K were recorded using quartz tubes immersed in a quartz Dewar filled with liquid nitrogen. In order to allow comparison of emission intensities, corrections for instrumental response, inner filter effects, and phototube sensitivity were performed.[22]

Metal-Ion Binding: Titration experiments of **1** and **2** with the different metal ions were carried out on 3 ml of 5×10^{-5} M solutions, adding 10 ml each time of a 2.5×10^{-3} M solution of the metal ion. These experiments were performed at pH = 6.5 using a 10^{-2} M lutidine buffer and at pH = 9.5 using a 10^{-2} M borate buffer. The pH dependence of the complexation processes were followed by adding 10 ml each time of a 5×10^{-3} M solution of NaOH to a solution containing **1** or **2** (5×10^{-5} M) and the metal ion (5.2×10^{-5} M).

Acknowledgments

This work was financially supported by the Ministero dell'Università e della Ricerca Scientifica e Tecnologica (Progetto Disposition Supramolecolan), by the University of Bologna (Funds for Selected Research Topics). The authors thank Professor Rosangela Marchelli and Dr. Roberto Corradini for supplying the sample of dansylethylenediamine (**2**), and Maria Cristina Fiorini for performing experimental measurements.

[1] A. Mayer, S. Neuenhofer, *Angew. Chem. Int. Ed. Engl.* **1994**, *33*, 1044−1072.
[2] *Fluorescent Chemosensors for Ion and Molecule Recognition* (Ed.: A. W. Czarnik), American Chemical Society, Washington, DC, **1992**.
[3] A. P. de Silva, H. Q. N. Gunaratne, T. Gunnlaugsson, A. J. M. Huxley, C. P. McCoy, J. T. Rademacher, T. E. Rice, *Chem. Rev.* **1997**, *97*, 1515−1566, and references therein.
[4] L. Fabbrizzi, A. Poggi, *Chem. Soc. Rev.* **1995**, 197−202, and references therein.
[5] A. P. de Silva, H. Q. N. Gunaratne, T. Gunnlaugsson, A. J. M. Huxley, C. P. McCoy, J. T. Rademacher, T. E. Rice, *Advances in Supramolecular Chemistry*, vol. 4, Jai Press. Inc., **1997**, p. 1−53.
[6] M. Shuster, M. Sandor, *Fresenius J. Anal. Chem.* **1996**, *356*, 326−330.
[7] K. Hamasaki, S. Usui, H. Ikeda, T. Ikeda, A. Ueno, *Supramol. Chem.* **1997**, *8*, 125−135.
[8] M. Nakamura, T. Ikeda, A. Nakamura, H. Ikeda, A. Ueno, F. Toda, *J. Chem. Soc., Chem. Commun.* **1995**, 721.
[9] R. Corradini, A. Dossena, G. Galaverna, R. Marchelli, A. Panagia, G. Sartor, *J. Org. Chem.* **1997**, *62*, 6283−6289.
[10] R. Corradini, A. Dossena, R. Marchelli, A. Panagia, G. Sartor, M. Saviano, A. Lomabardi, V. Pavone, *Chem. Eur. J.* **1996**, *2*, 373.

[11] R. F. Chen, J. Kernohan, *J. Biol. Chem.* **1967**, *242*, 5813−5823.
[12] W.-Y. Lin, H. E. van Wart, *J. Inorg. Biochem.* **1988**, *32*, 21−38.
[13] R. B. Thompson, E. R. Jones, *Anal. Chem.* **1993**, *65*, 730−734.
[14] [14a] G. K. Walkup, B. Imperiali, *J. Am. Chem. Soc.* **1996**, *118*, 3053−3054. − [14b] G. K. Walkup, B. Imperiali, *J. Am. Chem. Soc.* **1997**, *119*, 3443−3450.
[15] E. Kimura, T. Koike, *Chem. Soc. Rev.* **1998**, *27*, 179.
[16] Y.-H. Li, L.-M. Chan, L. Tyer, R. T. Moody, C. M. Himel, D. M. Hercules, *J. Am. Chem. Soc.* **1975**, *97*, 3118−3126.
[17] G. Battistuzzi Gavioli, G. Grandi, L. Menabue, G. C. Pellacani, M. Sola, *J. Chem. Soc., Dalton Trans.* **1985**, 2363−2368.
[18] R. Kramer, *Angew. Chem. Int. Ed. Engl.* **1998**, *37*, 772.
[19] [19a] L. Fabbrizzi, M. Licchelli, P. Pallavicini, A. Perrotti, A. D. Sacchi, *Angew. Chem. Int. Ed. Engl.* **1994**, *33*, 1975. − [19b] L. Fabbrizzi, M. Licchelli, P. Pallavicini, A. Perrotti, A. Taglietti, D. Sacchi, *Chem. Eur. J.* **1996**, *2*, 75−82.
[20] D. Y. Sazaki, D. R. Shnek, D. W. Pack, F. H. Arnold, *Angew. Chem. Int. Ed. Engl.* **1995**, *34*, 905−907.
[21] S. R. Meech, D. Phillips, *J. Photochem.* **1983**, *23*, 193.
[22] A. Credi, L. Prodi, *Spectrochim. Acta, Part A* **1998**, *54*, 159.

Received August 4, 1998
[I98260]

Distorted Germyllithium Induced by Intramolecular Coordination of an Amino Group: Synthesis and Structures of {Tris[2-(dimethylamino)phenyl]germyl}lithium

Atsushi Kawachi,*[a] Yoko Tanaka,[a] and Kohei Tamao*[a]

Keywords: Germyllithium / 2-(Dimethylamino)phenyl ligand / Chelates / Solid-state structures / Solution structures

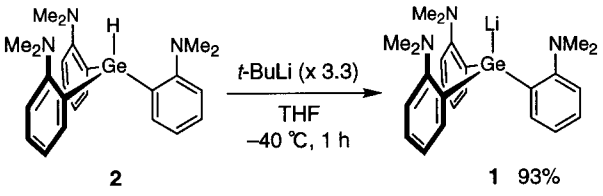
{Tris[2-(dimethylamino)phenyl]germyl}lithium (**1**) has been prepared. The X-ray analysis shows that **1** exists as a monochelated monomer in the solid state, where the lithium atom is coordinated to one of the amino groups and two THF molecules. The interaction between the lithium atom and the amino group induces the distortion of the geometry around the germanium atom. In solution, however, two species exist as evidenced by ^{1}H-, ^{7}Li-, and ^{13}C-NMR spectra. The temperature-dependent behavior of these two species has been analyzed by variable-temperature NMR studies.

Introduction

Among a variety of Group-14 element−alkali metal compounds, germyllithium compounds have been well studied from the synthetic point of view,[1] but structural studies are still scarce; only six structures of germyllithium compounds have been determined by X-ray analysis[2] and the substituents have been limited to the tris(trimethylsilyl)silyl group and germole skeletons. We report here the preparation of {tris[2-(dimethylamino)phenyl]germyl}lithium (**1**) and its structure in the solid state and in solution, focusing on the interaction between the lithium atom and the amino group[3] as well as on the germanium−lithium bonding character.

Results and Discussion

The germyllithium **1** was prepared by deprotonation of the hydrogermane[4] **2** with *tert*-butyllithium (3.3 equiv.) in THF at −40°C in 93% yield, as shown in Scheme 1; the yield was estimated by quenching with D_2O. When **2** was treated with a deficient amount of *tert*-butyllithium (1.2 equiv.), **1** could be isolated as pale yellow crystals in 33% yield after recrystallization from toluene at −20°C.



Scheme 1

[a] Institute for Chemical Research, Kyoto University, Uji, Kyoto 611-0011, Japan
E-mail: tamao@scl.kyoto-u.ac.jp
kawachi@scl.kyoto-u.ac.jp

Structure in the Solid State

X-ray analysis of the crystal reveals that **1** has a monomeric structure in the solid state, as shown in Figure 1. The selected bond lengths, bond angles, and torsion angles are listed in Table 1. The most striking feature is the highly distorted geometry around Ge(1) due to the unsymmetrical interaction of Li(1) with the amino group. Li(1) bonded to Ge(1) is coordinated to N(1) of one of the three NMe_2 groups, forming a five-membered chelate ring consisting of Li(1), Ge(1), C(1), C(2), and N(1). Li(1) is also coordinated to O(1) and O(2) of two THF molecules arising from the reaction solvent. The Li(1)−Ge(1) bond length [2.598(9) Å] is the shortest among those of the characterized germyllithium compounds [2.613(3)−2.759(24) Å].[2] The Li(1)−N(1) bond length [2.15(1) Å] is longer than the sum of the covalent radii (Li 1.23 Å; N 0.70 Å),[5] but normal as coordinative Li−N bonds (2.01−2.17 Å).[3] The intramolecular coordination of N(1) to Li(1) reduces the angle of Li(1)−Ge(1)−C(1) to 83.9(3)°. As a result, Li(1), Ge(1), C(9), and C(17) are almost coplanar; the sum of the three angles of Li(1)−Ge(1)−C(9), Li(1)−Ge(1)−C(17), and C(9)−Ge(1)−C(17) is 359.5°. In spite of the distorted geometry, however, there are no significant differences among the three Ge−C bonds [2.042(6), 2.030(5), and 2.054(5) Å] and the three C−Ge−C angles [96.8(2), 99.2(2), and 98.4(2)°]. It is also noted that the sum of the latter (294.4°) is strongly reduced from the sp^3 tetrahedral value (328°). Thus, the geometry of **1** may be designated pyramidal rather than distorted tetrahedral.

In order to obtain information about the electronic structure, we performed an ab initio calculation of **1**·$(THF)_2$ at HF level using the 6-311+G* basis set on Li and Ge atoms and the 6-31G basis set on H, C, N, and O atoms,[6] based on the geometry of the crystal structure. The natural bond orbital analysis reveals that the anionic electrons on Ge(1) have a considerably higher s character (s 57.3%; p 42.6%; d 0.1%) than the sp^3-hybrid orbitals,[7] whereas the three Ge−C bonds have a higher p character [Ge(1)−C(1), 86.7%; Ge(1)−C(9), 84.0%; Ge(1)−C(17), 85.2%]. These p

 © WILEY-VCH Verlag GmbH, D-69451 Weinheim, 1999 1434−1948/99/0303−0461 $ 17.50+.50/0

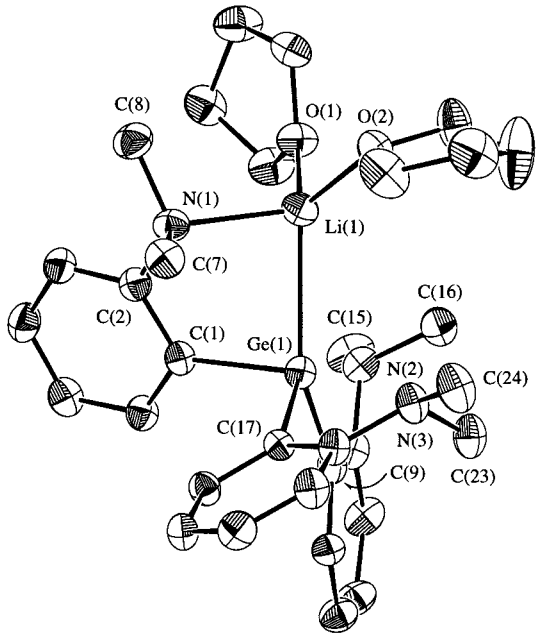


Figure 1. Molecular structure of **1**·$(THF)_2$ with 30% probability ellipsoids (H atoms omitted for clarity); selected bond lengths [Å] and angles [°]: Ge(1)−Li(1) 2.598(9), Ge(1)−C(1) 2.042(6), Ge(1)−C(9) 2.030(5), Ge(1)−C(17) 2.054(5), Li(1)−N(1) 2.15(1), Li(1)···N(2) 4.11(1), Li(1)···N(3) 4.43(1), Ge(1)−Li(1)−N(1) 83.7(3), Li(1)−Ge(1)−C(1) 83.9(3), Li(1)−Ge(1)−C(9) 138.3(3), Li(1)−Ge(1)−C(17) 122.8(3), C(1)−Ge(1)−C(9) 96.8(2), C(1)−Ge(1)−C(17) 99.2(2), C(9)−Ge(1)−C(17) 98.4(2)

Table 1. Selected bond lenghts [Å], bond angles [°], and torsion angles [°] for **1**·$(THF)_2$

Ge(1)−C(1)	2.598(9)
Ge(1)−C(9)	2.042(6)
Ge(1)−C(17)	2.030(5)
Li(1)−N(1)	2.15(1)
Li(1)···N(2)	4.11(1)
Li(1)···N(3)	4.43(1)
Li(1)−Ge(1)−C(1)	83.9(3)
Ge(1)−Li(1)−N(1)	83.7(3)
Li(1)−Ge(1)−C(9)	138.3(3)
Li(1)−Ge(1)−C(17)	122.8(3)
C(9)−Ge(1)−C(17)	98.4(2)
C(1)−Ge(1)−C(9)	96.8(2)
C(1)−Ge(1)−C(17)	99.2(2)
Li(1)−Ge(1)−C(1)−C(2)	−23.5(4)
Li(1)−Ge(1)−C(9)−C(10)	−9.1(7)
Li(1)−Ge(1)−C(17)−C(18)	−66.1(5)
Ge(1)−C(1)−C(2)−N(1)	−10.4(6)
Ge(1)−C(9)−C(10)−N(2)	6.1(8)
Ge(1)−C(17)−C(18)−N(3)	−5.8(7)

characters are almost equivalent to each other, in agreement with the similarity of the Ge−C bond lengths. The molecular orbital analysis of the anionic electrons (HOMO) indicates that the lithium atom is located not along the vector of the anionic electrons but aside from it, as shown in Figure 2. This may be represented as an intramolecular separated ion pair, which is not unusual if the Ge−Li interaction is weak while the N−Li coordinative interaction is relatively strong.

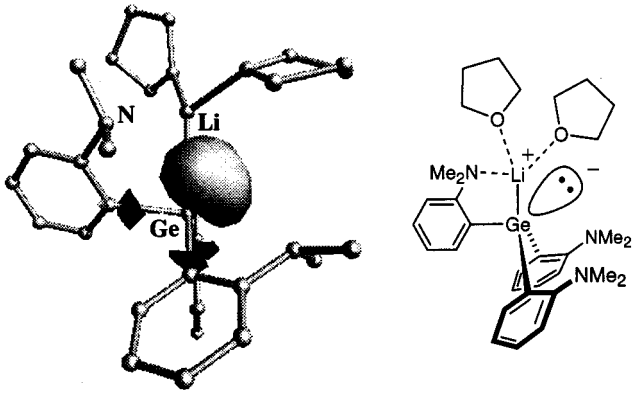


Figure 2. HOMO of **1**·$(THF)_2$ calculated at HF level using the 6-311+G* basis set on Li and Ge atoms and the 6-31G basis set on H, C, N, and O atoms; geometry is based on the crystal structure; its schematic representation is also shown

Structures in Solution

In contrast to the single structure in the solid state, the structure of **1** in solution is not simple. Crystalline **1** involving two solvated THF molecules was dissolved in $[D_8]$toluene, and the behavior was examined by variable-temperature ^{1}H-, ^{7}Li-, and ^{13}C-NMR spectroscopy. The results of the latter two analyses are shown in Figure 3. The analysis of the spectra reveals that **1** exists as a mixture of two species in the solution and their integral ratio reversibly changes as the temperature changes. Thus, the ^{7}Li-NMR spectra display two distinct signals at $\delta = 1.20$ and $\delta = 2.88$. The ^{13}C-NMR spectra show two kinds of signals at $\delta = 46.1$ and $\delta = 47.0$ for the NMe_2 carbon atoms. The ^{1}H-NMR spectra also show two kinds of signals at $\delta = 2.31$ and $\delta = 2.59$ for the NMe_2 protons, analogously to the ^{13}C-NMR signals.

Based on the temperature-dependent behavior of these two species, we assumed that the monomer **1a**, arising from the crystals, dimerizes to the dimer **1b** and they are in equilibrium in the solution, as shown in Scheme 2. Whereas the monomer **1a** is favored at higher temperatures in terms of the entropy effect,[3g] the dimer **1b** is favored at lower temperatures in terms of the electrostatic interaction,[8] through which the anionic electrons are efficiently stabilized by the two lithium cations. Based on this assumption, the thermodynamic parameters for the monomer−dimer equilibrium between **1a** and **1b** were estimated from a series of ^{1}H-NMR spectra. The equilibrium is described as $K_{eq} = [\mathbf{1b}]/[\mathbf{1a}]^2$ according to Scheme 2. From a van′t Hoff plot of $\ln(K_{eq})$ vs $1/T$, we obtained $\Delta H° = -34.5 \pm 1.7$ kJ/mol, $\Delta S° = -135 \pm 7$ J/mol·K, $\Delta G°_{293} = 5.1 \pm 3.8$ kJ/mol, and $\Delta G°_{213} = -5.8 \pm 3.2$ kJ/mol. These thermodynamic data, especially the large negative entropy, strongly support the proposed monomer−dimer equilibrium and formation of the dimer at lower temperatures.

To confirm the monomer/dimer assignment and rule out other assignments for the higher aggregate, we performed a variable concentration study.[9] A plot of log[dimer] vs log[monomer] (integration of ^{1}H-NMR spectra at 233 K) has a slope of 2.1 ± 0.2, confirming that the two species

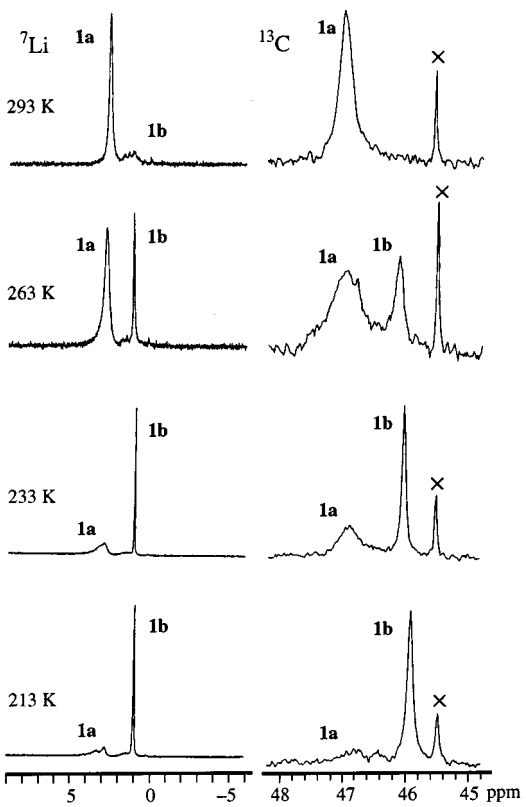
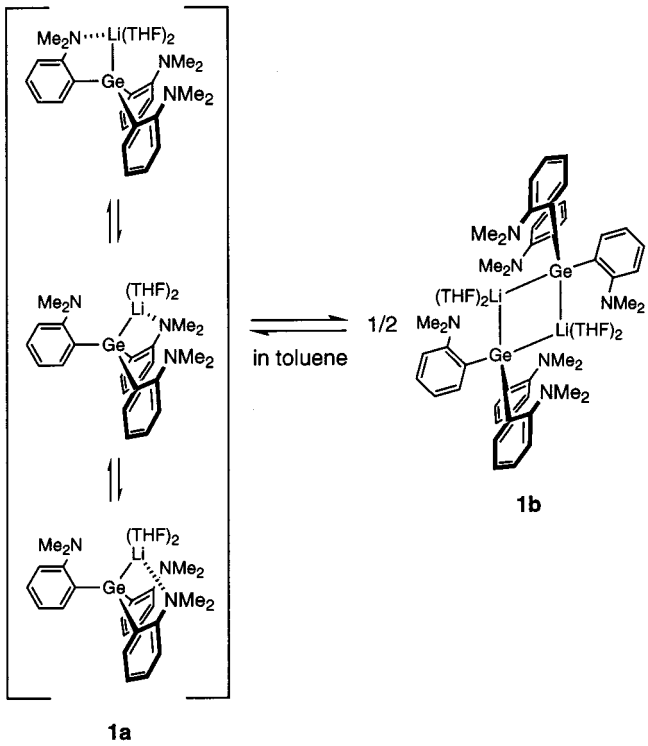


Figure 3. ^{7}Li- and ^{13}C-NMR spectra of **1** in [D_8]toluene at different temperatures; peaks marked with × are due to the hydrogermane **2**



Scheme 2

differ in aggregation state by a factor of 2. It is also found that the ^{7}Li-chemical shift of **1a** (δ = 2.88) is consistent with the GIAO calculated shift of **1**·$(THF)_2$ (δ = 3.06), based on the geometry of the crystal structure.[6,10,11] Thus, the two species **1a** and **1b** are represented as monomer and dimer, respectively.

Accordingly, the signals at δ = 2.88 (^{7}Li) and δ = 47.0 (^{13}C) can be attributed to **1a** while the signals at δ = 1.20 (^{7}Li) and δ = 46.1 (^{13}C) can be attributed to **1a** at 263 K in Figure 3. Some aspects require a comment: (i) In the hydrocarbon solvent, the monomer **1a** is expected to be chelated by the NMe_2 group(s), as observed in the crystal structure. However, the NMe_2 groups might equilibrate on the NMR time scale, because they appear as a broad ^{13}C resonance upon cooling to 213 K. (ii) In the dimer **1b**, the NMe_2 groups may not interact with the lithium atom, because they appear as a sharp ^{13}C resonance upon cooling to 213 K. (iii) The smaller line width of the ^{7}Li resonance[3g,12] of **1b** than that of **1a** may reflect the more symmetrical environment around the lithium atom in the former.

In conclusion we have revealed the structure of the germyllithium **1** in the solid state and in solution. While in the solid state the intramolecular coordination of the amino group induces the distorted geometry of the monomeric **1a**, **1a** tends to dimerize in solution.

Experimental Section

General: ^{1}H (270 MHz), ^{7}Li (105.01 MHz), and ^{13}C (67.94 MHz) NMR spectra were recorded with a JEOL EX-270 spectrometer. ^{1}H- and ^{13}C-chemical shifts were referenced to internal [D_8]toluene (^{1}H: δ = 2.10; ^{13}C: δ = 20.40), [D_6]benzene (^{1}H: δ = 7.20), and $CDCl_3$ (^{13}C: δ = 77.00). ^{7}Li-chemical shifts were referenced to external lithium chloride (δ = 0) in methanol. − Mass spectra were measured at 70 eV with a JEOL JMS-700 mass spectrometer equipped with an MS-SEPU data processing system. − Melting points were measured with a Yanaco-MP-S3 apparatus and are uncorrected. − Infrared spectra were recorded with a JASCO IR-810 spectrophotometer. − *tert*-Butyllithium in pentane was purchased from Kanto Chemical Co., Inc. THF was distilled under nitrogen from sodium benzophenone ketyl and then lithium aluminium hydride or sodium potassium alloy. Toluene was distilled under nitrogen from sodium. All reactions were carried out under an inert atmosphere.

Preparation of {Tris[2-(dimethylamino)phenyl]germyl}lithium (1) and Trapping with D_2O. − Formation of Tris[2-(dimethylamino)phenyl]-deuteriogermane (3): To a solution of tris[2-(dimethylamino)phenyl]hydrogermane (**2**)[4] (217 mg, 0.50 mmol) in THF (1.0 mL) was added *tert*-butyllithium in pentane (1.64 M, 1.0 mL, 1.64 mmol) at −40°C. The reaction mixture was stirred at −40°C for 1 h to give a yellow suspension of **1**. To the suspension was added deuterium oxide (0.3 mL, 17 mmol) at −40°C and the mixture was stirred at room temperature for 4 h. After the solvent was removed under reduced pressure, the residue was diluted with benzene (10 mL) and filtered. The filtrate was concentrated to give **3** as a solid. The yield was estimated by means of NMR analysis (93%) using mesitylene as the internal standard. Recrystallization of the solid from hexane (0.4 mL) gave **3** as colorless crystals (178 mg, 82% yield based on **2**), m.p. 96.5−97.0°C. − ^{1}H NMR ([D_6]benzene): δ = 2.57 (s, 18 H), 6.94−6.99 (m, 3 H), 7.07−7.10 (m, 3 H), 7.20−7.25 (m, 3 H), 7.40−7.43 (m, 3 H). − ^{13}C NMR ($CDCl_3$): δ = 45.68, 119.30,

123.40, 129.49, 135.53, 136.57, 159.44. − IR (KBr): $\tilde{\nu}$ = 1530 cm^{-1} (Ge−D). − MS (70 eV); *m/z* (%): 436 (2) [M^+], 434 (1) [M^+ − D], 314 (85) [$(Me_2NC_6H_4)_2Ge$], 194 (56) [$Me_2NC_6H_4Ge$], 120 (100) [$Me_2NC_6H_4$].

Table 2. Summary of X-ray diffraction data for **1**·$(THF)_2$

Empirical formula	$C_{32}H_{46}GeLiN_3O_2$
Formula mass	584.27
Color	pale yellow
Crystal size [mm]	0.4 × 0.30 × 0.30
Crystal system	monoclinic
Space group	$P2_1/c$ (no. 14)
a [Å]	16.222(2)
b [Å]	10.1011(9)
c [Å]	20.715(2)
β [°]	111.897(3)
V [$Å^3$]	3149.5100
Z	4
D(calcd.) [g/cm^3]	1.232
μ (Mo-K_α) [$^{-1}$]	10.03
$2\theta_{max}$ [°]	55.3
Temp. [K]	173
No. of reflections collected	6355
No. of obsd. reflections, $I > 3\sigma(I)$	4370
No. of variables	353
R	0.093
R_w	0.121
Goodness of fit	1.68
Max/min peak in final diff. map [$e/Å^3$]	1.13/−1.17

Crystals of 1·$(THF)_2$: To a solution of **2** (210 mg, 0.49 mmol) in THF (1.4 mL) was added *tert*-butyllithium in pentane (1.56 M, 0.38 mL, 0.59 mmol) at −40°C. The reaction mixture was stirred at −40°C for 1 h. The solvent was removed under reduced pressure at 0°C to give a yellow solid. Recrystallization of the solid from toluene (0.5 mL) at −20°C gave **1**·$(THF)_2$ as pale yellow crystals (92 mg, 33% yield based on **2**), m.p. 270.0−271.0°C (sealed tube, decomp.).

X-ray Structure Determination for 1·$(THF)_2$: All crystal data and refinement parameters are summarized in Table 2. The crystal was sealed in a capillary tube under argon. Data were collected with a Rigaku RAXIS-IV imaging plate area detector with filtered Mo-K_α radiation. The structure was solved by direct methods (SIR92)[13] and expanded using Fourier techniques (DIRDIF94)[14] and refined on $|F|^2$. Empirical absorption corrections based on azimuthal scans of several reflections were applied**.** The non-hydrogen atoms were anisotropically refined. All hydrogen atoms were located at the expected positions by a geometrical calculation and fixed at these positions. Crystallographic data (excluding structure factors) for the structure reported in this paper have been deposited with the Cambridge Crystallographic Data Centre as supplementary no. CCDC-102693. Copies of the data can be obtained free of charge on application to CCDC, 12 Union Road, Cambridge CB2 1EZ, UK [Fax: int. code + 44-1223/336-033; E-mail: deposit@ccdc.cam.ac.uk].

Acknowledgments

We thank the Ministry of Education, Science, Sports and Culture, Japan, for the Grants-in-Aid for Scientific Research (Grant Nos. 07405043 and 09239103). Y. T. thanks the Japan Society for the Promotion of Science (Fellowship for Japanese Junior Scientists).

[1] P. Riviere, M. Riviere-Baudet, J. Satge in *Comprehensive Organometallic Chemistry II* (Ed.: A. G. Davies), Elsevier Science, Ltd., Oxford, **1995**, vol. 2, chapter 5, and references cited therein.

[2] Based on the Cambridge Structural Database, Update April **1998**. [2a] S. Freitag, R. Herbst-Irmer, L. Lameyer, D. Stalke, *Organometallics* **1996**, *15*, 2839−2841. − [2b] J.-H. Hong, H. Pan, P. Boudjouk, *Angew. Chem.* **1996**, *108*, 213−216; *Angew. Chem. Int. Ed. Engl.* **1996**, *35*, 186−188. − [2c] R. West, H. Sohn, D. R. Powell, T. Müller, Y. Apeloig, *Angew. Chem.* **1996**, *108*, 1095−1097; *Angew. Chem. Int. Ed. Engl.* **1996**, *35*, 1002−1004. − [2d] A. Heine, D. Stalke, *Angew. Chem.* **1994**, *106*, 121−123; *Angew. Chem. Int. Ed. Engl.* **1994**, *33*, 113−115.

[3] Silyllithium compounds with nitrogen donors: − [3a] J. Belzner, U. Dehnert, D. Stalke, *Angew. Chem.* **1994**, *106*, 2580−2582; *Angew. Chem. Int. Ed. Engl.* **1994**, *33*, 2450−2452. Organolithium compounds with nitrogen donors: − [3b] D. Hüls, H. Günther, G. van Koten, P. Wijkens, J. T. B. H. Jastrzebski, *Angew. Chem.* **1997**, *109*, 2743−2744; *Angew. Chem. Int. Ed. Engl.* **1997**, *36*, 2629−2631. − [3c] H. J. Reich, B. Ö. Gudmundsson, *J. Am. Chem. Soc.* **1996**, *118*, 6074−6075. − [3d] P. Wijkens, E. M. van Koten, M. D. Janssen, J. T. B. H. Jastrzebski, A. L. Spek, G. van Koten, *Angew. Chem.* **1995**, *107*, 239−242; *Angew. Chem. Int. Ed. Engl.* **1995**, *34*, 219−222. − [3e] M. H. P. Rietveld, I. C. M. Wehman-Ooyevaar, G. M. Kapteijn, D. M. Grove, W. J. J. Smeets, H. Kooijman, A. L. Spek, G. van Koten, *Organometallics* **1994**, *13*, 3782−3787. − [3f] J. T. B. H. Jastrzebski, G. van Koten, M. Konijin, G. H. Stam, *J. Am. Chem. Soc.* **1982**, *104*, 5490−5492. Lithium amides with nitrogen donors: [3g] G. Hilmersson, Ö. Davidsson, *J. Org. Chem.* **1995**, *60*, 7660−7669. − [3h] D. Sato, H. Kawasaki, I. Shimada, Y. Arata, K. Okamura, T. Date, K. Koga, *J. Am. Chem. Soc.* **1992**, *114*, 761−763.

[4] A. Kawachi, Y. Tanaka, K. Tamao, *Organometallics* **1997**, *16*, 5102−5107.

[5] J. Emsley, in *The Elements*, 2nd ed., Clarendon Press, Oxford, **1992**.

[6] M. J. Frisch, G. W. Trucks, H. B. Schlegel, P. M. W. Gill, B. G. Johnson, M. A. Robb, J. R. Cheeseman, T. Keith, G. A. Petersson, J. A. Montgomery, K. Raghavachari, M. A. Al-Laham, V. G. Zakrzewski, J. V. Ortiz, J. B. Foresman, J. Cioslowski, B. B. Stefanov, A. Nanayakkara, M. Challacombe, C. Y. Peng, P. Ayala, W. Chen, M. W. Wong, J. L. Andres, E. S. Replogle, R. Gomperts, R. L. Martin, D. J. Fox, J. S. Binkley, D. J. Defrees, J. Baker, J. P. Stewart, M. Head-Gordon, C. Gonzalez, J. A. Pople, *Gaussian 94, Revision D.3*, Gaussian, Inc., Pittsburgh, PA, **1995**.

[7] C. Lambert, P. v. R. Schleyer, *Angew. Chem.* **1994**, *106*, 1187−1199; *Angew. Chem. Int. Ed. Engl.* **1994**, *33*,1129−1140, and references cited therein.

[8] A.-M. Sapse, D. C. Jain, K. Raghavachari, in *Lithium Chemistry* (Eds.: A.-M. Space, P. v. R. Schleyer), John Wiley & Sons, New York, **1995**, chapter 2, and references cited therein.

[9] H. J. Reich, D. P. Green, M. A. Medina, W. S. Goldenberg, B. Ö. Gudmundsson, R. R. Dykstra, N. H. Phillips, *J. Am. Chem. Soc.* **1998**, *120*, 7201.

[10] Basis set: Ge (6-311+G*/ECP), Li (6-311+G*), H, C, N, O (6-31G). The calculated shift is reported relative to that of $Li^+ \cdot MeOH$.

[11] A recent example of the GIAO calculation of ^{7}Li-chemical shift: D. H. Barich, T. Xu, J. Zhang, J. F. Haw, *Angew. Chem.* **1998**, *110*, 2607; *Angew. Chem. Int. Ed.* **1998**, *37*, 2530.

[12] R. Benn, A. Rufin′ska, *Angew. Chem.* **1986**, *98*, 851−871; *Angew. Chem. Int. Ed. Engl.* **1986**, *25*, 861−881.

[13] SIR92: A. Altomare, M. C. Burla, M. Camalli, M. Cascarano, C. Giacovazzo, A. Guagliardi, G. Polidori, *J. Appl. Crystallogr.* **1994**, *27*, 435.

[14] DIRDIF94: P. T. Beurskens, G. Admiraal, G. Beurskens, W. P. Bosman, R. de Gelder, R. Israel, J. M. M. Smits, *The DIRDIF-94 Program System, Technical Report of the Crystallography Laboratory*, University of Nijmegen, The Netherlands, **1994**.

Received August 24, 1998
[I98291]

Metal Complexes of Biologically Important Ligands, CXII[+]

Bis(dipeptide ester–H^+) Complexes of Palladium(II) – Precursors for the Formation of Cyclotetrapeptides

Katharina Haas,[a] Eva-Maria Ehrenstorfer-Schäfers,[a] Kurt Polborn,[a] and Wolfgang Beck*[a]

Dedicated to Professor Peter Jutzi on the occasion of his 60th birthday

Keywords: Dipeptide ester / Cyclic tetrapeptides / Palladium complexes / Coordination chemistry

trans-Bis(dipeptide ester)palladium **1**–**6** complexes with a deprotonated amide group were obtained by dehydrochlorination of *trans*-Cl_2Pd(dipeptide ester)$_2$ or by direct reaction of Na_2PdCl_4 with dipeptide ester in the presence of sodium methoxide. The structure of $Pd(NH_2CH_2CONCH_2CH_2CO_2CH_3)_2$ (**3**) was determined by X-ray diffraction. Addition of $NaOCH_3$ to $Pd[NH_2C(H)(R)NCH_2CH_2CO_2CH_3]_2$ [R = $CH(CH_3)_2$ **4**, CH_2Ph **5**] results in the formation of the corresponding complexes **7**, **8** with cyclic tetrapeptides which also can be directly synthesized from the dipeptide ester and Na_2PdCl_4.

Introduction

Palladium(II) and platinum(II) complexes of amino acids and peptides have found considerable attraction due to their potential antitumor activity. Amino acid and peptide ligands may act as carriers for cyctotoxic metal fragments.[2] The chemistry of palladium(II)[3−5] and platinum(II)[3,6] with α-amino acids and peptides has been reviewed. Palladium(II) has many attractive features as a Lewis acid due to its fixed coordination number 4, its high Lewis acidity, its high formation constants with N,O donor ligands and its intermediate kinetic lability.[7] A particular feature of palladium(II) is its ability to deprotonate peptide NH groups, which in free peptides have pK_a values of ca. 15. The pK_a value of the Pd^{II}-induced ionization of peptide NH bonds is about 3.5[8], which is much lower than that of other metal ions such as Cu^{2+}, Ni^{2+} and Zn^{2+}.[9−11] Thus, Pd^{2+} ions show a nonspecific binding to the peptide backbone involving a destabilization of the secondary structure of peptides, i.e. α-helices.[12] The palladium ion promoted hydrolysis of peptides[13−15] and esters[7,15] has attracted attention due to the relevance of these systems to the function of metalloenzymes.[16] Ternary palladium complexes with peptides and nucleic acids were synthesized as models for the interaction between proteins and nucleic acids with the intervention of metal ions.[5,17,18] Several palladium complexes of peptides have been structurally characterized.[19−21]

Mogilevkina et al.[22] reported the synthesis of platinum(II) complexes $Pt(NH_2CH_2CONCH_2COOH)_2$ and $[Pt(NH_2CH_2CONCH_2CO_2)_2]^{2-}$ from Cl_2Pt(gly−glyOH)$_2$[23]. Margerum et al. studied the formation of (tripeptide)platinum complexes in solution.[24] From IR data a structure with N,N′ chelate rings was derived, like that found for the structurally characterized (Cl)Pt(gly−L-met).[25]

Results and Discussion

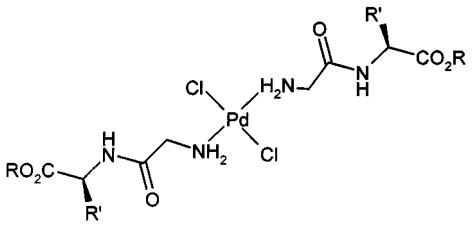
Recently we reported the metal-assisted formation of cyclic tetrapeptides from dipeptide esters.[26] In the course of our continuing studies on the formation of peptides at metal centres,[27−29] including the use of platinum(II) and palladium(II) as amino protecting group [6,30,31] we describe the synthesis and characterization of bis(dipeptide ester) complexes of palladium(II), which are precursors for the formation of cyclic peptides. The *trans*-bis(dipeptide ester) complexes of palladium(II) were obtained by two routes: a) by dehydrochlorination of *trans*-dichlorobis(dipeptide ester)palladium(II) with NEt_3 in dichloromethane to give **1** and **2** and b) by direct reaction of the dipeptide ester hydrochloride, consisting of α- and β-amino acids, with Na_2PdCl_4 in the presence of two equivalents of NaOMe in methanol to give **3**−**6**.

In the IR spectra the intensive absorptions at 1559−1580cm^{-1} and at 1722−1731 cm^{-1} are characteristic for the deprotonated and coordinated amide group and the ester group. The ^{1}H- and ^{13}C-NMR spectra show the expected signals. In accordance with *trans* configuration (C_2 symmetry) of **1**−**6** the peptide ligands show only one set of signals in the ^{1}H- and ^{13}C-NMR spectra. All compounds contain two supramolecularly bound equivalents of water

[+] Part CXI: see ref.[1]

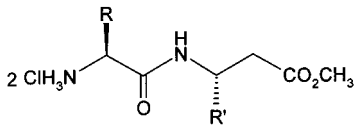
[a] Institut für Anorganische Chemie der Ludwig-Maximilians-Universität,
Meiserstraße 1, D-80333 München, Germany
E-mail: wbe@anorg.chemie.uni-muenchen.de

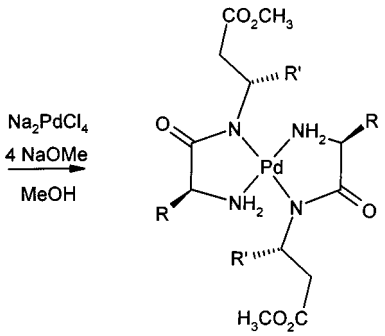
 © WILEY-VCH Verlag GmbH, D-69451 Weinheim, 1999 1434−1948/99/0303−0465 $ 17.50+.50/0



	R	R′
1	*t*Bu	H
2	Et	CH_2Ph

Scheme 1. Synthesis of *trans*-bis(dipeptide ester)Pd^{II} complexes by dehydrochlorination of *trans*-dichlorobis(dipeptide ester)Pd^{II} complexes





	R	R′
3	H	H
4	$CH(CH_3)_2$	H
5	CH_2Ph	H
6	H	CO_2CH_3

Scheme 2. Synthesis of *trans*-bis(dipeptide ester)Pd^{II} complexes by direct reaction of the dipeptide ester hydrochloride and Na_2PdCl_4

which can be observed in the ^{1}H-NMR spectra by a broad signal at $\delta \approx 4.6$.

Crystals of **3** were obtained by slow cooling of a saturated solution in methanol. The environment of the palladium atom is strictly planar (sum of the angles around the Pd atom is 360°). The X-ray crystal structure analysis of **3** × 4 H_2O shows the expected *trans* configuration with

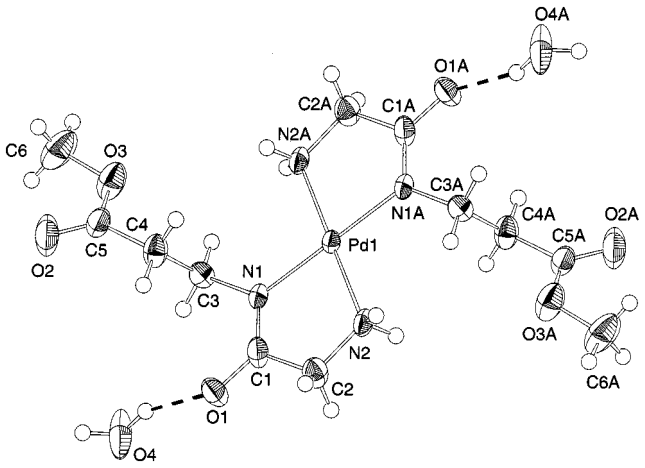


Figure 1. Molecular structure of **3** in the crystal; selected bond lengths [Å] and angles [°]: Pd−N(1) 2.010(6), Pd−N(2) 2.033(5), Pd−N(1A) 2.010(6), Pd−N(2A) 2.033(5), N(1)−C(1) 1.289(9), N(1)−C(3) 1.481(8), N(2)−C(2) 1.500(9), C(1)−C(2) 1.501(9), C(3)−C(4) 1.529(10), C(4)−C(5) 1.498(10), O(1)−C(1) 1.267(9), O(2)−C(5) 1.203(9), O(3)−C(5) 1.324(9), O(3)−C(6) 1.446(10); N(1A)−Pd−N(1) 180.0, N(1A)−Pd−N(2A) 81.5(2), N(1)−Pd−N(2A) 98.5(2), N(1A)−Pd−N(2) 98.5(2), N(1)−Pd−N(2) 81.5 (2), N(2A)−Pd−N(2) 180.0(1)

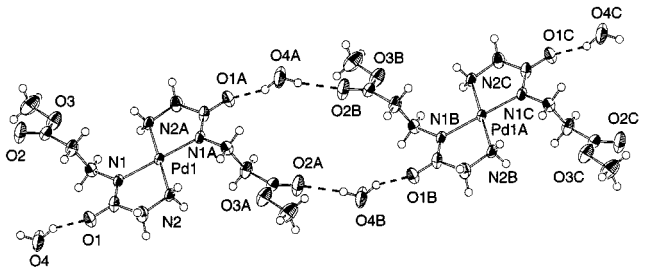


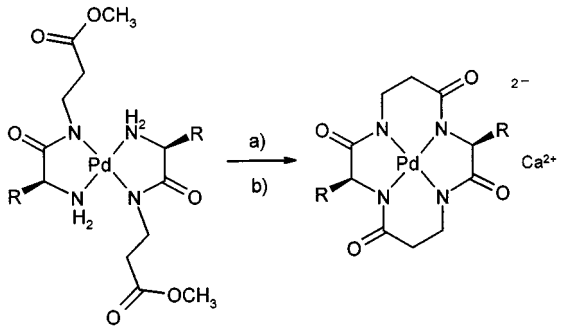
Figure 2. Part of the chain structure formed by the molecules of **3**

coordination of the amino and the deprotonated amide groups and with palladium as inversion centre (Figure 1). In the crystal lattice the molecules of **3** form chains via hydrogen bonds between the water molecules and the carbonyl groups of the amide and the ester groups (distance O1B···HO4B 1.856 Å, O2A···HO4B 2.023 Å, Figure 2). Similar hydrogen bonds between water molecules and carbonyl groups have been observed in the palladium complex [cyclo(gly−ß-ala)$_2$Pd](PPN)$_2$ × 8 H_2O × 3 CH_3CN which lead to the formation of layers.[26]

Addition of two equivalents of NaOMe to **4** and **5** results in the formation of the palladium complexes of cyclic tetrapeptides **7** and **8** which can also be directly obtained from a dipeptide ester and Na_2PdCl_4 (Scheme 3). Thus, the suggested mechanism[26] for the formation of cyclic tetrapeptides at some metal centres from dipeptide esters is proven.

The IR spectra of **7** and **8** show the characteristic intensive absorption for the amide group at 1560−1670 cm^{-1}. The ^{1}H-NMR spectra of **7** and **8** reveal broad signals according to a coordination of the calcium cation to the cyclic tetrapeptide.

A similar chelate complex of platinum(II) with two deprotonated tripeptide ligands **10** has been obtained by dehydrochlorination of *trans*-Cl_2Pt(gly−gly−glyOH)$_2$ (**9**) with

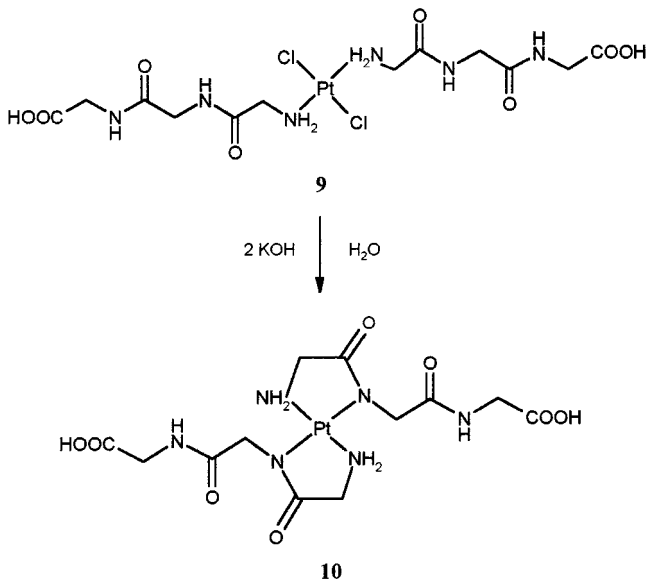


4, 5

	R
7	$CH(CH_3)_2$
8	CH_2Ph

Scheme 3. Formation of cyclotetrapeptide complexes: a) 2 NaOMe, MeOH, 24 h, 65°C; b) $CaCl_2$, acetone, H_2O

KOH. The latter was analogously synthesized as described for $Cl_2Pt(gly-alaOH)_2$.[32] Complex **10** can be further deprotonated with NaOH in aqueous solution to give $Na_2[Pt(NH_2CH_2CONCH_2CONHCH_2CO_2)_2]$ (**11**).



9

10

Scheme 4. Formation of complex **10**

Experimental Section

The *trans*-dichlorobis(dipeptide ester)Pd^{II} complexes were prepared as previously described.[33] Dipeptide ester hydrochlorides were prepared according to standard methods.[34,35] All operations were carried out under nitrogen using Schlenk techniques. Solvents were dried by distillation from Mg (MeOH), calcium hydride (CH_2Cl_2) or Na (Et_2O). − NMR spectra: Jeol EX 400 (^1H: 399.78 MHz; ^{13}C: 100.53 MHz). − IR: Perkin Elmer 841, Nicolet 520 FT-IR. − X-ray: NONIUS CAD4 diffractometer.

General Procedure for the Synthesis of 1 and 2: To a solution of *trans*-dichlorobis(dipeptide ester)palladium(II) (0.2 mmol) in 10 mL of dichloromethane NEt_3 (0.4 mmol) was slowly added. The solution was stirred for 3 d at room temperature, while the colour changed to light yellow. After concentration, the solid residue was washed twice with a small amount of water. The precipitate was centrifuged off and dried in vacuo.

1: Light yellow powder, yield 42%; m.p. 176°C (dec). − IR (KBr, cm^{-1}): $\tilde{\nu}$ = 3280 s, 3230 s (NH_2), 1730 vs (ester), 1673 m, 1570 vs, br. (amide I). − $C_{16}H_{30}N_4O_6Pd$ (480.9): calcd. C 39.96, H 6.29, N 11.65; found C 39.70, H 6.39, N 10.41.

2: Light yellow powder, yield 25%; m.p. 110°C (dec). − IR (KBr, cm^{-1}): $\tilde{\nu}$ = 3280 s, 3240 s (NH_2), 1720 vs (ester), 1670 m, 1570 vs, br. (amide I). − $C_{26}H_{34}N_4O_6Pd$ (605.0): calcd. C 51.61, H 5.66, N 9.26; found C 51.28, H 5.68, N 8.37.

General Procedure for the Synthesis of 3−6: In a typical experiment the dipeptide ester hydrochloride (0.2 mmol) and Na_2PdCl_4 (0.1 mmol) were dissolved in methanol (5 mL) and NaOMe (0.4 mmol) was slowly added to the solution. The light yellow reaction mixture was stirred for 1 h at room temperature. Then the solvent was evaporated in vacuo and the residue was dissolved in 10 mL of absolute dichloromethane. To achieve complete dissolution a minimum volume of absolute methanol was added. After centrifugation, the solution was concentrated to a volume of approximately 2 mL and the *trans*-bis(dipeptide ester)palladium(II) complexes were precipitated by addition of 40 mL of Et_2O as colourless powders, which were dried in vacuo.

3: Light yellow platelets, yield 76%; m.p. 165°C (dec.). − IR (KBr, cm^{-1}): $\tilde{\nu}$ = 3332.5 vs, 3299.2 s (NH_2), 1731.3 vs (ester), 1564.1 vs, br. (amide I). − ^1H NMR (400 MHz, CD_3OD/D_2O): δ = 3.73 (s, 3 H, CO_2H_3), 3.35 (s, 2 H, CH_2), 3.04 (pseudo t, $^2J = {}^3J$ = 6.64 Hz, 2 H, NCH_2CH_2CO), 2.52 (pseudo t, $^2J = {}^3J$ = 6.64 Hz, 2 H, NCH_2CH_2CO). − ^{13}C NMR (100 MHz, CD_3OD/D_2O): δ = 183.00 (CONR), 176.86 (CO_2CH_3), 53.30 (CH_2), 42.46 (NCH_2CH_2CO), 35.65 (NCH_2CH_2CO). − $C_{12}H_{22}N_4O_6Pd \times H_2O$ (442.77): calcd. C 32.55, H 5.46, N 12.65; found C 33.35, H 5.47, N 12.04.

4: Colourless powder, yield 67%; m.p. 125°C (dec.). − IR (KBr, cm^{-1}): $\tilde{\nu}$ = 3230 s, 3125 s (NH_2), 1728.8 vs (ester), 1559.4 vs, br. (amide I). − ^1H NMR (300 MHz, CD_3OD): δ = 3.63 (s, 6 H, CO_2CH_3), 3.47 [pseudo quint, ^2J = 5 Hz, ^3J = 7 Hz, 2 H, $CHCH(CH_3)_2$], 3.11−3.16 (m, 4 H, $NCH_2CH_2CO_2CH_3$), 2.53−2.46 [m, 2 H, $CHCH(CH_3)_2$], 2.36−2.30 (m, 4 H, $NCH_2CH_2CO_2CH_3$), 1.10 [d, ^3J = 7 Hz, 6 H, $CHCH(CH_3)_2$]. − ^{13}C NMR (300 MHz, CD_3OD): δ = 183.16 (CONR), 174.72 (CO_2CH_3), 66.09 [$CHCH(CH_3)_2$], 52.31 (CO_2CH_3), 41.93, 36.83 (CH_2CH_2), 32.59 [$CHCH(CH_3)_2$], 20.01, 18.09 [$CHCH(CH_3)_2$]. − $C_{18}H_{34}N_4O_6Pd \times 3\ H_2O$ (562.96): calcd. C 38.40, H 7.16, N 10.16; found C 37.99, H 6.40, N 9.95.

5: Colourless powder, yield 68%; m.p. 158°C (dec.). − IR (KBr, cm^{-1}): $\tilde{\nu}$ = 3385.0 s, 3274.8 s, 3232.9 s (NH_2), 1721.7 vs (ester), 1568.9 vs, br. (amide I). − ^1H NMR (300 MHz, CD_3OD): δ = 7.36−7.17 (m, 10 H, Ph), 3.53 (dd, ^3J = 3.59 Hz, ^3J = 9.34 Hz, 2 H, $CHHCH$), 3.23 (dd, ^3J = 3.59 Hz, ^2J = 14.23 Hz, 2 H, $CHHCH$), 3.15 (pseudo t, $^3J = {}^2J$ = 7.48 Hz, 4 H, NCH_2CH_2CO), 3.03 (dd, ^3J = 9.34 Hz, ^2J = 14.23 Hz, 2 H, $CHHCH$), 2.46 (pseudo t, $^3J = {}^2J$ = 7.48 Hz, 4 H, NCH_2CH_2CO). − ^{13}C NMR (300 MHz, CD_3OD): δ = 182.38 (CONR), 174.52 (CO_2CH_3), 138.27, 130.68, 129.90, 128.14 (Ph), 62.02 ($CHCH_2$), 42.03, 41.08, 36.68 ($CHCH_2$ and CH_2CH_2). − $C_{26}H_{34}N_4O_6Pd \times 2.5\ H_2O$ (650.04): calcd. C 48.04, H 6.04, N 8.62; found C 47.91, H 5.68, N 8.70.

6: Colourless powder, yield 63%; m.p. 121°C (dec.). − IR (KBr, cm^{-1}) : $\tilde{\nu}$ = 3293.7 s, 3223.6 s (NH_2), 1721.8 vs (ester), 1580.4 vs,

br. (amide I). − ^{1}H NMR (300 MHz, CD_3OD): δ = 3.75, 3.70 (2 s and m, 14 H, 2 CO_2CH_3 and $CHCH_2$), 3.35 (d, 2 H, *H*CH), 3.2 (d, 2 H, HC*H*), 3.06 (dd, ^3J = 5.57 Hz, ^2J = 16.93 Hz, 2 H, CH*H*CH), 2.84 (dd, ^3J = 8.02 Hz, ^2J = 16.93 Hz, 2 H, CHHC*H*). − ^{13}C NMR (300 MHz, CD_3OD): δ = 183.42 (CONR), 175.45, 174.99 (2 CO_2CH_3), 57.50 ($CHCH_2$), 53.16, 53.08, 52.97 (CH_2, 2 CO_2CH_3), 37.06 ($CHCH_2$). − $C_{16}H_{26}N_4O_{10}Pd \times 2\ H_2O$ (576.86): calcd. C 33.31, H 5.24, N 9.71; found C 33.02, H 4.87, N 9.43.

X-ray Structure Determination of 3:[36] $C_{12}H_{22}O_6N_4Pd \times 2\ H_2O$, M = 460.77, T = 21(2)°C, NONIUS CAD4 diffractometer, crystal size, 0.17 × 0.27 × 0.50 mm, monoclin $P2_1/c$ (no. 14), a = 11.939(5), b = 7.814(3), c = 10.250(4), β = 96.38(2)°, V = 950.3(7) Å^3, Z = 2, d(calcd.) = 1.620 g/cm^3, λ(Mo-K_α) = 0.71073 Å, μ(Mo-K_α) = 1.021 mm^{-1}, F(000) = 472, 2θ range: 3.12−22.96°, index ranges: $-13 \le h \le 13$, $0 \le k \le 8$, $-11 \le l \le 0$, reflections collected: 1219, independent reflections: 1144 [R(int) = 0.0401], observed reflections: 941, semiempirical absorption correction from ψ scans, max./min. transmission: 0.9594/0.5076, data/restraints/parameters: 1144/0/116, refinement method: full-matrix least squares on F^2, goodness-of-fit on F^2: 1.077; final R indices [$I > 2\ \sigma(I)$]: $R1$ = 0.0491, $wR2$ = 0.1379; R indices (all data): $R1$ = 0.0579, $wR2$ = 0.1506, largest diff. peak/hole: 0.833/−0.787 eÅ^{-3}.

General Procedure for the Synthesis of 7 and 8: The *trans*-bis(dipeptide ester)Pd^{II} complex **4** or **5** (0.1 mmol) is dissolved in 10 mL of methanol. A solution of NaOMe (0.2 mmol) in methanol is added and the solution is heated to 65°C for 24 h, after which $CaCl_2$ (0.1 mmol) is added. Upon the addition of acetone the white precipitate is collected and for purification recrystallized from water/acetone (1/5), twice washed with acetone and dried in vacuo.

7: White powder, yield 89%. − IR (KBr, cm^{-1}): ṽ = 1560 vs, br. (amide I), 1417 s (amide II). − ^{1}H NMR (400 MHz, D_2O/CD_3OD): δ = 3.62−3.75 [m, br., 2 H, C*H*CH$(CH_3)_2$], 3.53−3.59 (m, br., 2 H, N*H*CHHCHCO), 3.5−2.92 (m, br., 4 H, NHC*HH*CHCO), 2.86−2.69 [m, br., 2 H, CHC*H*$(CH_3)_2$], 2.55−2.22 (m, br., 2 H, NHCHHC*H*CO), 1.10−1.14 [m, br., 12 H, CHCH$(CH_3)_2$]. − $C_{24}H_{24}CaN_4O_4Pd \times 8\ H_2O$ (683.025): calcd. C 39.86, H 5.58, N 7.75; found C 39.19 H 4.66, N 7.45.

8: White powder, yield 92%. − IR (KBr, cm^{-1}): ṽ = 1569 vs, br. (amide I), 1448 s, 1428 s, 1413 s (amide II). − ^{1}H NMR (400 MHz, D_2O/CD_3OD): δ = 6.98−7.45 (m, 10 H, C_6H_5), 4.20−4.45 (m, br., 2 H, C*H*CH_2Ph), 3.18−2.63 (m, br., 6 H, N*H*CHCH$_2$CO, CHC*H*$_2$Ph), 2.44−1.87 (m, br., 6 H, NHC*HCH*$_2$CO). − $C_{16}H_{24}CaN_4O_4Pd \times 3\ H_2O$ (536.938): calcd. C 35.79, H 5.63, N 10.43; found C 35.83 H 5.59, N 9.98.

9: The synthesis of **9** was accomplished according to Mogilevkina et al.[32] K_2PtCl_4 (420 mg, 1 mmol) and gly−gly−glyOH (760 mg, 4 mmol) were dissolved in 10 mL of 0.25 N NaOH (4 mmol) and the mixture was stirred for 40 min at 60°C in a water bath, while the colour of the solution changed from red to light yellow. After ice cooling the solution was combined with 2.5 mL of concentrated HCl and stirred for another 3 d at room temperature. The light yellow precipitate was collected and washed with HCl (2 N), ethanol and diethyl ether and dried in vacuo. − Light yellow powder, yield 34%; m.p. 196°C (dec.). − IR (KBr, cm^{-1}): ṽ = 3330 s, 3270 sh, 3230 sh (NH_2), 1720 m (COOH), 1650 vs (amide I), 1535 s (amide II). − $C_{12}H_{22}Cl_2N_6O_8Pt$ (644.3): calcd. C 22.27, H 3.44, N 13.04; found C 21.91, H 3.90, N 12.96.

10: A solution of 215 mg (0.33 mmol) of **9** in 1.33 mL of 0.5 N KOH (0.66 mmol) was stirred for 3.5 h at 70°C using a water bath. After stirring for 24 h at room temperature, the white precipitate was collected, washed with water, ethanol and diethyl ether and dried in vacuo. − Colourless powder, yield 21%; m.p. 206°C (dec.). − IR (KBr, cm^{-1}): ṽ = 3340 s, 3260 s (NH_2), 1700 vs (COOH), 1633 m, 1575 vs (amide I). − $C_{12}H_{20}N_6O_8Pt \times 2\ H_2O$ (607.5): calcd. C 23.73, H 3.98 N, 13.84; found C 23.82, H 3.69, N 13.61.

11: 170 mg (0.26 mmol) of **10** in 10.4 mL of 0.1 N NaOH (1.04 mol) was heated at 60°C for 8 h. After cooling to room temperature, the solution was added to acetone dropwise, whereby the white product precipitated, was collected and washed with acetone and dried in vacuo. − Yield 50%; m.p. 283°C (dec.). − IR (KBr): ṽ = 3280, 3230 sh (NH), 1633 s, 1575 w (amide), 1605 sh (CO_2^-). − $C_{12}H_{30}Na_2N_6O_{14}Pt \times 6\ H_2O$ (723.5): calcd. C 19.90, H 4.18, N 11.60; found C 19.87, H 3.71, N 11.49.

Acknowledgments

We thank the Deutsche Forschungsgemeinschaft, the Fonds der Chemischen Industrie, the Wacker-Chemie, München, for generous support, and the Degussa AG, Hanau, for gifts of chemicals.

[1] D. Koch, K. Sünkel, W. Beck, *Z. Naturforsch.*, in press.
[2] W. Beck, H. Bissinger, M. Girnth-Weller, B. Purucker, G. Thiel, H. Zippel, H. Seidenberger, B. Wappes, H. Schönenberger, *Chem. Ber.* **1982**, *115*, 2256−2270.
[3] L. M. Volshtein, *Sov. J. Coord. Chem. (Engl.)* **1975**, *1*, 483−509; T. G. Appleton, *Coord. Chem. Rev.* **1997**, *166*, 313−359; A. Iakovidis, N. Hadjiliadis, *Coord. Chem. Rev.* **1994**, *135*, 17−63.
[4] L. D. Pettit, M. Bezer, *Coord. Chem. Rev.* **1985**, *61*, 97.
[5] S. Kasselouri, A. Garoufis, M. Lamera-Haldjiliadis, N. Hadjiliadis, *Coord. Chem. Rev.* **1990**, *104*, 1−12.
[6] W. Beck, *Pure Appl. Chem.* **1988**, *60*, 1357−1362.
[7] R. W. Hay, M. P. Pujari, *Inorg. Chim. Acta* **1986**, *123*, 47−51.
[8] E. W. Wilson, R. B. Martin, *Inorg. Chem.* **1970**, *9*, 528.
[9] E. W. Wilson, R. B. Martin, *Inorg. Chem.* **1971**, *10*, 1197.
[10] M. S. Michailidis, R. B. Martin, *J. Am. Chem. Soc.* **1969**, *91*, 4683.
[11] H. Sigel, R. B. Martin, *Chem. Rev.* **1982**, *82*, 385−426.
[12] R. Ghadiri, C. Choi, *J. Am. Chem. Soc.* **1990**, *112*, 1630−1632.
[13] X. Chen, L. Zhu, H. Yan, X. You, N. M. Kostic, *J. Chem. Soc., Dalton Trans.* **1996**, 2653−2658.
[14] T. N. Parac, N. M. Kostic, *J. Am. Chem. Soc.* **1996**, *118*, 5946−5951; **1996**, *118*, 51−58.
[15] R. W. Hay, P. Banerjee, *J. Chem. Soc., Dalton Trans.* **1981**, 362−365; R. W. Hay, M. P. Pujari, *Inorg. Chim. Acta* **1986**, *123*, 175−179; M.-C. Lim, *J. Chem. Soc., Dalton Trans.* **1983**, 1675−1677; R. W. Hay in *Comprehensive Coordination Chemistry* (Eds.: G. Wilkinson, R. D. Gillard, J. A. McCleverty), vol. 6, sect. 61.4, p. 411, Pergamon, Oxford, **1987**.
[16] L. Zhu, R. Bakhtiar, N. M. Kostic, *J. Biol. Inorg. Chem.* **1998**, *3*, 383−391 and references therein.
[17] M. Sabat, K. A. Satyshur, M. Sundaralingham, *J. Am. Chem. Soc.* **1983**, *105*, 976.
[18] E. Katsarou, A. Troganis, N. Hadjiliadis, *Inorg. Chim. Acta* **1997**, *256*, 21−28.
[19] B. T. Khan, S. Shamsuddin, K. Venkatasubramanian, *Polyhedron* **1992**, *11*, 671.
[20] M. Wienken, E. Zangrado, L. Randaccio, S. Menzer, B. Lippert, *J. Chem. Soc., Dalton Trans.* **1993**, 3349.
[21] S. L. Best, T. K. Chattopadhyay, M. I. Djuran, R. A. Palmer, P. J. Sadler, I. Sóvágó, K. Varnagy, *J. Chem. Soc., Dalton Trans.* **1997**, 2578−2596.
[22] M. F. Mogilevkina, V. I. Bessenov, I. M. Cheremisina, *Russ. J. Inorg. Chem.* **1973**, 1396−1398.
[23] L. M. Volshtein, G. G. Motyagina, *Russ. J. Inorg. Chem.* **1965**, *10*, 721−723.
[24] G. E. Kirvan, D.W. Margerum, *Inorg. Chem.* **1985**, *24*, 3017−3021.
[25] H. Freeman, M. L. Golomb, *Chem. Commun.* **1970**, 1523−1524.
[26] K. Haas, W. Ponikwar, H. Nöth, W. Beck, *Angew. Chem.* **1998**, *110*, 1200−1203; *Angew. Chem. Int. Ed. Engl.* **1998**, *37*, 1086−1089.

[27] W. Beck, R. Krämer, *Angew. Chem.* **1991**, *103*, 1492−1493; *Angew. Chem. Int. Ed. Engl.* **1991**, *30*, 1467−1469.
[28] R. Krämer, M. Maurus, K. Polborn, K. Sünkel, C. Robl, W. Beck, *Chem. Eur. J.* **1996**, *2*, 1518−1526.
[29] W. Hoffmüller, M. Maurus, K. Severin, W. Beck, *Eur. J. Inorg. Chem.* **1998**, 729−731.
[30] N. Steiner, E. Ehrenstorfer, J. Chen, W. Beck, *Chem. Ber.* **1988**, *121*, 275.
[31] W. Beck, H. Bissinger, T. Castrillo de Castro, L. Olgemöller, B. Purucker, *Chem. Ber.* **1985**, *118*, 3135−3142.
[32] M. F. Mogilevkina, I. B. Usmanov, I. K. Korobeinicheva, V. A. Logvinenko, *Russ. J. Inorg. Chem.* **1985**, *30*, 385−388.
[33] U. Taubald, U. Nagel, W. Beck, *Chem. Ber.* **1984**, *117*, 1003−1012.
[34] M. Bodanszky, *Principles of Peptide Synthesis*, 2nd ed., Springer, Berlin, **1994**.
[35] V. Dourtoglou, B. Gross, V. Lambropoulou, C. Zioudrou, *Synthesis* **1984**, 572−574.
[36] Crystallographic data (excluding structure factors) for the structures reported in this paper have been deposited with the Cambridge Crystallographic Data Center as supplementary publication no. CCDC-108443. Copies of the data can be obtained free from charge on application to CCDC, 12 Union Road, Cambridge CB2 1EZ, UK [Fax: int. code + 44-1223/336-033: E-mail: deposit@ccdc.cam.ac.uk].

Received September 10, 1998
[I98302]

Metal Complexes of Biologically Important Ligands, CXIII[+]

Cinchona Alkaloids as Versatile Ambivalent Ligands – Coordination of Transition Metals to the Four Potential Donor Sites of Quinine

Roland Hubel,[a] Kurt Polborn,[a][2] and Wolfgang Beck*[a]

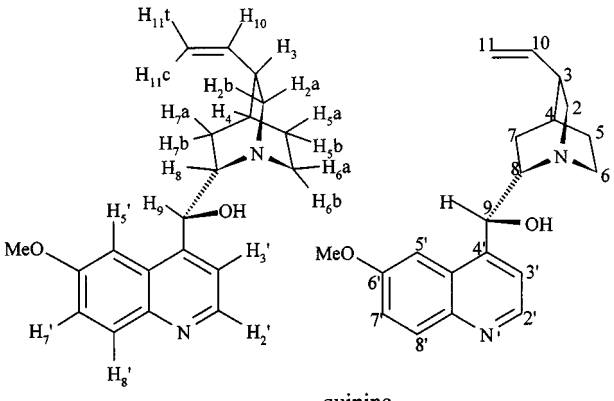
Dedicated to Professor Helmut Werner on the occasion of his 65th birthday

Keywords: Quinine / Cinchonine / Palladium / Platinum / Silver / Gold

A series of metal complexes in which quinine (L^1) and cinchonine (L^2) are coordinated via the four possible donor atoms was prepared and characterized. Coordination of the tertiary N atom of quinine is observed in $[L^1MPPh_3]^+NO_3^-$ [M = Au (**1**), Ag (**2**)], $[L^1Pd(COD)(Cl)]^+$ NO_3^- (**3**) and $L^1Pd(Cl)(allyl)$ (**4**). The mono anion of quinine functions as N,O chelate ligand in $(L^1–H^+)M(Cl)(PR_3)$ (M = Pd, Pt, **5**–**10**), $[(L^1–H^+)Pd(en)]^+NO_3^-$ (**11**) and $(L^1–H^+)_2TiCl_2$ (**12**). Protection of the tertiary N atom of quinine by methylation or protonation allows the synthesis of the quinoline complexes $[(L^1CH_3^+)M(Cl)_2(PR_3)]^+$ BF_4^- (M = Pd, Pt, **14**–**18**), $[(L^1CH_3^+)Ir(Cl)_2(Cp^*)]^+$ BF_4^- (**19**), $[(L^1+H^+)M(Cl)_2(PR_3)]^+$ $CF_3SO_3^-$ (M = Pd, Pt, **20**–**22**) and $(L^2+H^+)(ZnCl_3^-)$ (**23**). Quinine and cinchonine act as N,O–N bridge in the complexes $(R_3P)(Cl)M(\mu\text{-}L^1–H^+)M(Cl)_2(PR_3)$ (M = Pd, Pt, **24**, **25**, **27**, **28**), $(Cp^*)(Cl)Ir(\mu\text{-}L^1–H^1)Ir(Cl)_2(Cp^*)$ (**29**), $(EtP_3)(Cl)Pd(\mu\text{-}L^2–H^+)Pd(Cl)_2(PEt_3)$ (**26**), and as N–N bridge in the complexes $[(Ph_3P)Au(\mu\text{-}L^1)Au(PPh_3)]^+NO_3^-$ (**30**) and $(allyl)(Cl)Pd(\mu\text{-}L^1)Pd(Cl)(allyl)$ (**31**). Coordination of quinine via the C=C double bond occurs in $[(L^1+2\ H^+)PtCl_3]^+Cl^-$ (**32**). The structures of **11**, **13**, **19**, **23**, **26** and **32** were determined by X-ray diffraction. In most cases the coordination mode and the conformation of quinine can also be derived from the ^{1}H-NMR spectra.

Quinine is a widely used antimalaria drug and its derivatives are applied as optically active auxiliaries in asymmetric synthesis.[3] Most important is the Sharpless asymmetric dihydroxylation of olefins with osmium tetroxide and cinchona alkaloids.[4]

Recently, the interesting mechanism of this reaction was extensively analysed by Sharpless[5] and Corey.[6] The mechanism involves coordination of the tertiary N atom of the quinuclidine residue and the structure of the OsO_4 complex with the tertiary *N*-coordinated dihydroquinidine derivative was established by Sharpless et al.[7] To our knowledge only few metal complexes of cinchona alkaloids have been described.[8] In our group several organometallic compounds of cinchona alkaloids were synthesized and the first N,O-chelate complexes of cinchonidine and cinchonine were characterized by X-ray crystallography.[9] In continuation of these studies we now report on the synthesis of quinine complexes using all four potential donor sites of quinine (OH group, tertiary N and pyridine N atoms, olefinic C=C bond). In most cases analysis of the ^{1}H-NMR spectra of the various complexes gives information which donor atom is involved in coordination. The ^{1}H-NMR spectra of the free ligands have been previously interpreted.[10,11]



quinine

Results and Discussion

1. Coordination at the Quinuclidine N Atom

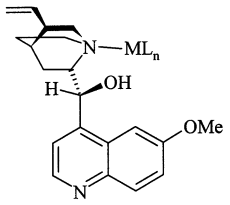
The most basic donor site of quinine is the quinuclidine N atom and coordination at this donor occurs in the reaction of quinine with in situ prepared Ph_3PAuNO_3, Ph_3PAgNO_3, $(COD)Pd(Cl)(NO_3)$ and with $(\eta^3\text{-}C_3H_5)Pd(\mu\text{-}Cl)_2Pd(\eta^3\text{-}C_3H_5)$ to give the complexes **1**–**4**.

The mode of coordination can be unambiguously derived from the ^{1}H-NMR spectra. The signals (which were assigned by 2D-COSY experiments) of the hydrogen atoms situated near the tertiary N atom show a considerable

[+] Part CXII: Ref.[1]

[a] Institut für Anorganische Chemie der Universität München, Meiserstraße 1, D-80333 München, Germany

 © WILEY-VCH Verlag GmbH, D-69451 Weinheim, 1999 1434–1948/99/0303–0471 $ 17.50+.50/0

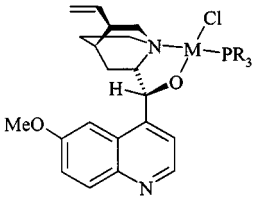


	ML_n
1	$AuPPh_3^+NO_3^-$
2	$AgPPh_3^+NO_3^-$
3	$PdCl(COD)^+NO_3^-$
4	PdCl(allyl)

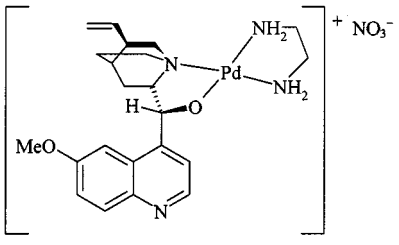
downfield shift in comparison to those of the free quinine. A detailed study of the conformations of cinchona alkaloides has been carried out by Wynberg and Sharpless[11] and four conformers were defined ("closed conformation 1 and 2, open conformation 3 and 4"). The "open conformation 3" in **1**−**4** which was also found for the OsO_4 complex[7] and some complexes of Ru, Ir, and Au[9] follows from the downfield shift of the signal of 7b-H as a consequence of the change of the position of 7b-H relative to the aromatic system: In the "open conformation 3" the 7b-H atom lies in the same plane with the quinoline ring and is no longer shielded by the anisotropic cone of the heteroaromatic ring. Hydrogen 7a-H, which is positioned above the quinoline ring, suffers a small upfield shift. In contrast to **5**−**10** (see below) the signals of the aromatic protons are almost not shifted which means that they do not interact with the d_{z^2} orbital of Pd^{II},[12] a further hint for the "open conformation 3".

2. N,O-Chelate Complexes

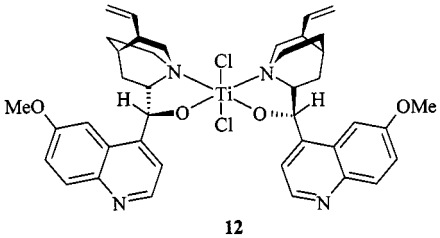
From the chloro-bridged complexes $(R_3P)(Cl)M(\mu\text{-}Cl)_2M(Cl)(PR_3)$ (M = Pd, Pt) and quinine in the presence of NaOMe in methanol the compounds **5**−**10** are obtained.



	M	R
5	Pt	Et
6	Pt	Bu
7	Pd	Et
8	Pd	Pr
9	Pd	Bu
10	Pd	Ph



11



12

In order to avoid coordination of the pyridine N atom the reaction was carried out at −78 °C. We assume that the *trans*-P−M−N isomers are formed as main products. Presumably the reaction proceeds stepwise as was found, for example, for the reaction of $[PtCl_3(C_2H_4)]^-$ with α-amino carboxylates.[13] The first step is the opening of the chloro bridge by the quinuclidine N atom and building of the M−N bond. This step is followed by the closure of the chelate ring with displacement of the *cis*-chloride by the oxy group. The P−M−N isomer was also found e.g. for $(Cl)(Ph_3P)Pt[NH_2C(Me)_2CO_2]$.[14] Two further ^{31}P-NMR signals of low intensity (< 5%) which were only observed for the Pd^{II} complexes may indicate formation of the *cis* isomer and of a complex with quinine coordinated via the pyridine N atom as minor products.

The reaction of $[(en)Pd(OH_2)_2]^{2+}(NO_3^-)_2$ with quinine affords the N,O-chelate complex **11**. The formation of the five-membered chelate ring in **5**−**11** is confirmed by the downfield shift of the ^{1}H-NMR signal of 9-H and by the disappearance of the ν(OH) absorption in the IR spectrum.

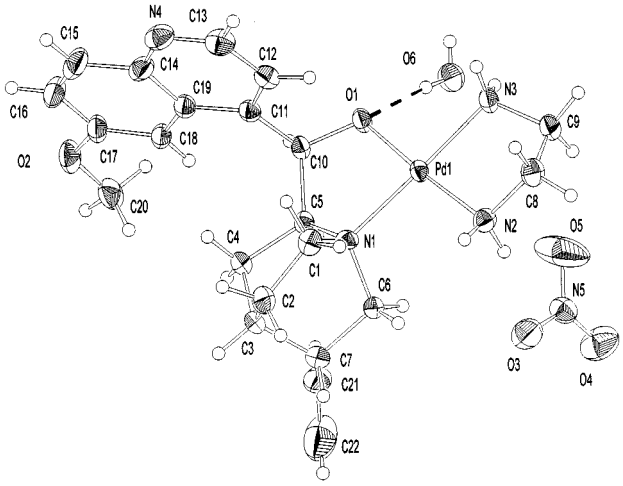


Figure 1. Molecular structure of **11** in the crystal; selected bond lengths [Å] and angles [°]: Pd1−O1 1.982(3), Pd1−N1 2.040(3), Pd1−N3 2.043(3), Pd1−N2 2.041(4), O1−C10 1.406(5), N1−C1 1.485(8), N1−C5 1.505(5) N1−C6 1.518(7), N2−C8 1.474(6), N3−C9 1.481(6), C8−C9 1.505(7), C5−C10 1.543(6), C10−C11 1.525(7); O1−Pd1−N1 85.30(13), O1−Pd1−N3 92.84(13), N1−Pd1−N3 178.0(2), O1−Pd1−N2 175.05(14), N1−Pd1−N2 98.79(15), N3−Pd1−N2 83.11(15), N1−C5−C10 111.2(4), N1−Pd1−O1−C10 6.8(3), N1−Pd1−N2−C8 −163.0(4), N1−C5−C10−O1 40.7(6), N1−C5−C10−C11 −86.9(5)

The conformation of quinine in **5**−**11** can be described as "open conformation 4".[11] The signal of the 3′-H atom in **5**−**11** suffers a downfield shift up to 1.8 ppm which is due to interaction with the d_{z^2} orbital.[12] This is ascertained by the X-ray structure determination of **11**.

Reaction of $TiCl_4$ and quinine in CH_2Cl_2 afforded a complex **12** for which − from analytic and ^{1}H-NMR data − we assume the shown structure.

3. Coordination at the Quinoline N Atom

The quinuclidine N atom of quinine was selectively protected by alkylation with Me_3O^+ BF_4^- [15] and from the reaction of the methylquininium tetrafluoroborate **13** with chloro-bridged complexes $(Cl)(R_3P)M(\mu\text{-}Cl)_2M(Cl)(PR_3)$ (M = Pd, Pt) and $(Cl)(Cp^*)Ir(\mu\text{-}Cl)_2Ir(Cl)(Cp^*)$ the compounds **14**−**19** were isolated.

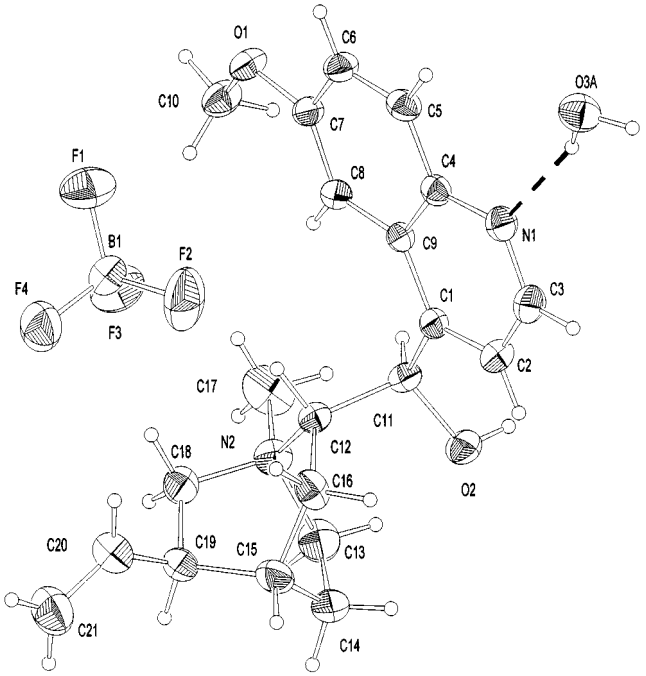


Figure 2. Molecular structure of **13** in the crystal; selected bond lengths [Å] and angles [°]: N2−C17 1.495(4), C1−C11 1.520(4), C11−C12 1.528(4), O2−C11 1.413(3), C1−C11 1.520(4); O2−C11−C1 111.5(2), O2−C11−C12 108.5(2), O2−C11−C12−N2 −68.9(2), C2−C1−C11−C12 106.9(3), C1−C11−C12−N2 168.5(2)

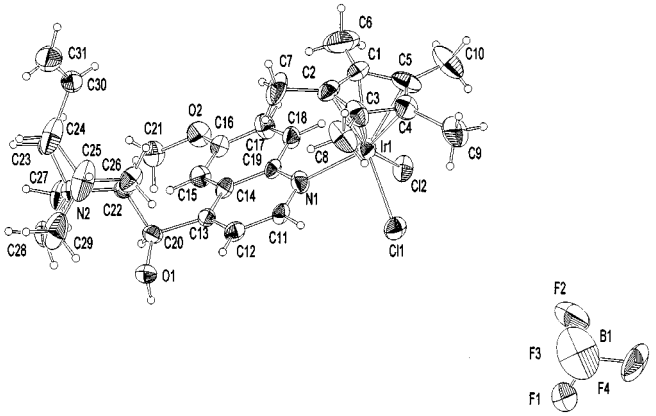
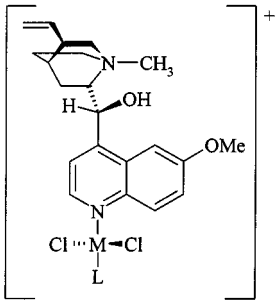
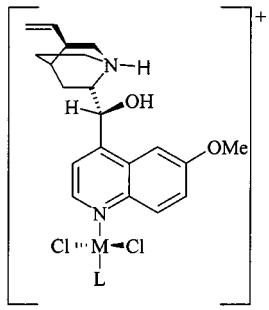


Figure 3. Molecular structure of **19** in the crystal; selected bond lengths [Å] and angles [°]: Ir1−N1 2.139(9), Ir1−Cl2 2.402(3), Ir1−Cl1 2.442(3), Ir1−C1 2.125(12), O1−C20 1.414(13), Ir1−C2 2.144(10), N1−Ir1−Cl1 88.8(3), N1−Ir1 Cl2 91.9(3); O1−C20−C13 112.5(9), N2−C22−C20 114.4(8), C12−C13−C20−O1 −20.2(13), O1−C20−C22−N2 −77.0(11), C13−C20−C22−N2 161.3(9)

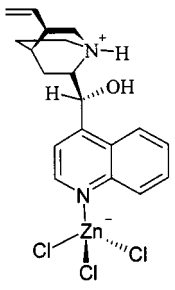
Protection of the quinuclidine N atom is even more easily achieved by protonation of quinine with F_3CSO_3H, and the



	M	L
14	Pt	PEt_3
15	Pt	PBu_3
16	Pd	PEt_3
17	Pd	PPr_3
18	Pd	PBu_3
19	Ir	Cp*



	M	L
20	Pt	PEt_3
21	Pd	PEt_3
22	Pd	PPr_3



23

obtained ammonium salt (which was not isolated) reacted with the chloro-bridged Pd and Pt complexes to give compounds **20**−**22**. Attempts to deprotonate **20**−**22** in order to yield neutral complexes gave mixtures which were not separated.

In the ^{1}H-NMR spectra of **14**−**19** and **20**−**22** a downfield shift is observed for the signals of 2′-H and 8′-H, which indicates coordination of the metal center to the quinoline N atom. For **14**, **15** and **20**−**22** a ^4J(2′-H,P) coupling can be detected. The "open-conformation 3" of coordinated quinine is found for **14**−**22**, like in **1**−**4**. In the IR spectra of **20**−**22** the ν(NH) absorption at 2600−2700 cm^{-1} and the ν(OH) band at ca. 3400 cm^{-1} are characteristic.

A zwitterionic structure is found for the product **23** from cinchonine and $ZnCl_2$ in methanol. Complex **23** may be compared with a molecular L-histidinium trichlorozincate (L-histidineH^+) $ZnCl_3$.[16]

4. Dinuclear Complexes

The bimetallic complexes **24**−**29** were obtained in two steps using first a stoichiometric ratio of 1/1/0.5 of NaOMe,

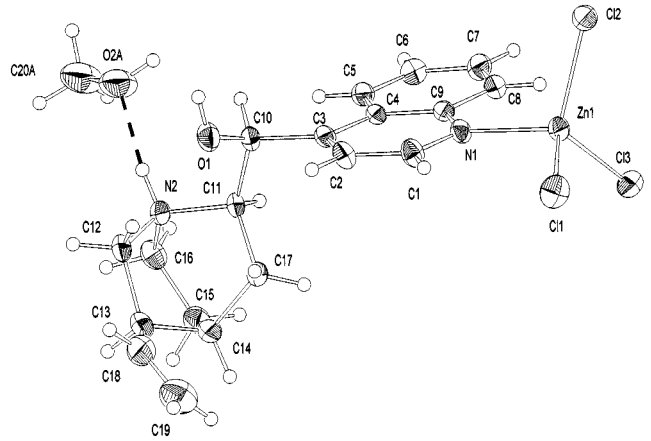
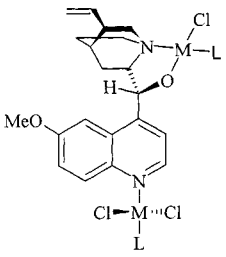
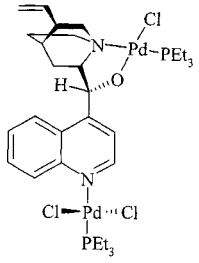


Figure 4. Molecular structure of **23** in the crystal; selected bond lengths [Å] and angles [°]: Zn1−N1 2.088(2), Zn1−Cl2 2.2340(8), Zn1−Cl3 2.2497(10), Zn1−Cl1 2.2732(11), O1−C10 1.418(5), C3−C10 1.524(3), C10−C11 1.540(4), N2−C11 1.520(3); N1−Zn1−Cl2 105.82(6), N1−Zn1−Cl3 109.94(8), Cl2−Zn1−Cl3 112.51(4), N1−Zn1−Cl1 105.57(8), Cl2−Zn1−Cl1 115.81(5), Cl3−Zn1−Cl1 106.90(4), O1−C10−C3 110.8(3), O1−C10−C11 109.4(2), Cl3−Zn1−N1−C1 128.7(2), Cl1−Zn1−N1−C1 13.8(2), Cl2−Zn1−N1−C9 69.4(2), Zn1−N1−C9−C8 0.1(3), O1−C10−C11−N2 52.4(3), C2−C3−C10−O1 21.3(3), C3−C10−C11−N2 174.3(3)

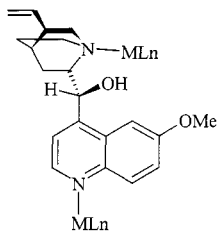
quinine or cinchonine and $[LMCl_2]_2$ to give the N,O-chelates which were not isolated and which by addition of another 0.5 equivalent of $[LMCl_2]_2$ afforded the desired products.



	M	L
24	Pt	PEt_3
25	Pd	PEt_3
27	Pd	PPr_3
28	Pd	PBu_3
29	Ir	Cp*



26



	ML_n
30	$AuPPh_3^+NO_3^-$
31	PdCl(allyl)

Heterobimetallic complexes could only be obtained as mixtures by this route. The "open conformation 4" of quinine and cinchonine in **24**−**29** is analogous to that in **5**−**10**. The downfield shift of the 2′-H and 8′-H ^{1}H-NMR signals caused by the interaction with the d_{z^2} orbital of the metal ion[12] indicates that the chloro ligands in **24**−**29** as in **14**−**19** lie perpendicular to the quinoline plane.

In the dinuclear complexes **30**−**31** quinine functions as a bis(monodendate) bridge. The characteristic ^{1}H-NMR signals of **30**−**31** are consistent with an "open conformation 3" of the ligand.

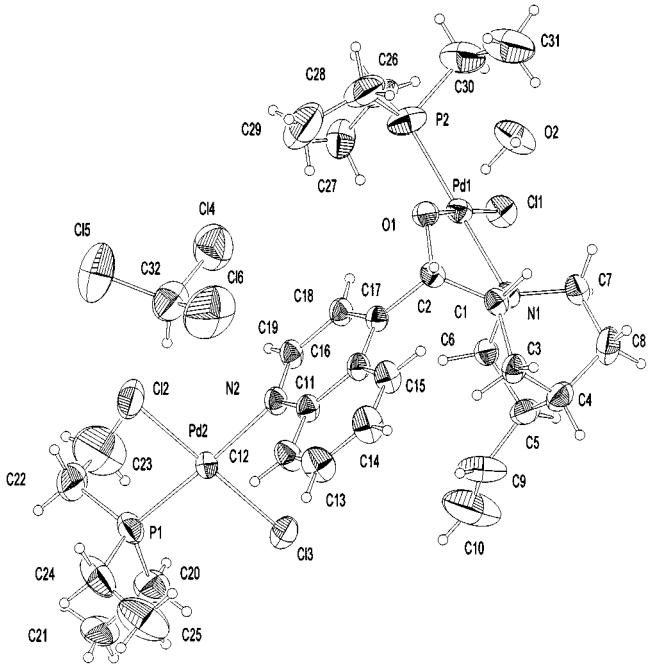


Figure 5. Molecular structure of **26** in the crystal; selected bond lengths [Å] and angles [°]: Pd1−O1 1.989(4), Pd1−N1 2.120(4), Pd1−P2 2.237(2), Pd1−Cl1 2.314(2), Pd2−N2 2.116(4), Pd2−P1 2.2288(15), Pd2−Cl2 2.287(2), Pd2−Cl3 2.291(2), O1−C2 1.402(6), C1−C2 1.534(7), C2−C17 1.524(7), C9−C10 1.109(15); O1−Pd1−N1 84.35(14), O1−Pd1−P2 89.90(12), N1−Pd1−P2 173.86(13), N2−Pd2−P1 176.32(12), N2−Pd2−Cl2 89.69(12), P1−Pd2−Cl2 88.28(7), N2−Pd2−Cl3 89.01(12), N2−Pd2−P1 176.32(12), O1−Pd1−Cl1 177.44(11), N2−Pd2−P1 176.32(12), Cl2−Pd2−Cl3 176.99(9), Cl2−Pd2−N2−C11 98.4(4), Cl3−Pd2−N2−C11 −78.9(4), O1−Pd1−N1−C1 −7.8(3), O1−C2−C17−C18 28.3(6), C1−C2−C17−C18 −98.4(5), N1−C1−C2−C17 81.4(5)

5. Coordination at the Olefinic Group

Finally we proved the coordination of a metal ion at the C=C double bond of quinine using the general method[17] for preparing (olefin)platinum complexes.

The reaction of double protonated quinine with K_2PtCl_4 in aqueous hydrochloride acid gives the (also thermally) stable complex **32**, which is an analogue of the Zeise salt $K[PtCl_3(C_2H_4)]$. As a consequence of complexation of the C=C double bond an upfield shift is observed for the three ^{1}H-NMR signals of the olefinic protons. In the ^{1}H-NMR spectrum of **32** two sets of signals in the ratio 1:1 are observed. By coordination of the prochiral C=C double bond the C-10 atom becomes a stereogenic centre, and two diastereoisomers are formed. In contrast to various Pt^{II} complexes with coordinated olefins and optically active amino acids[18] or amines[19] no diastereoselectivity is observed in our case.

Metal complexes of C=C-coordinated quinine may be useful for the derivativization of quinine at the C=C double bond.

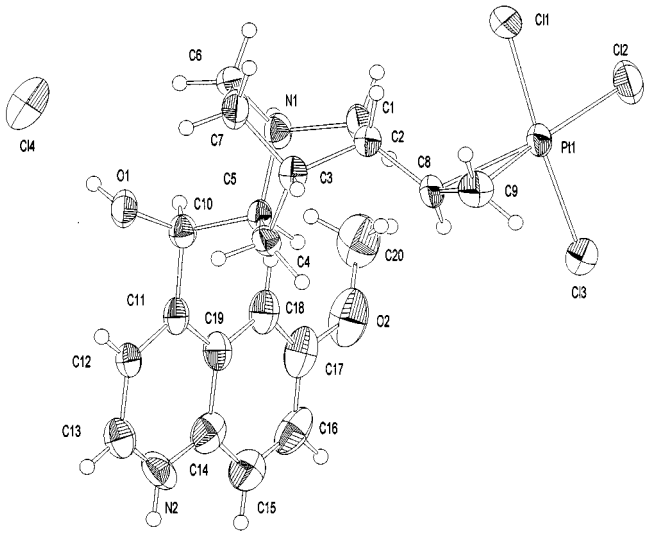
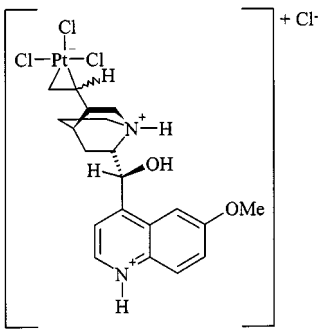


Figure 6. Molecular structure of **32** in the crystal; selected bond lengths [Å] and angles [°]: Pt1−C8 2.164(8), Pt1−Cl3 2.277(3), Pt1−Cl1 2.293(3), Pt1−Cl2 2.321(3), C8−C9 1.396(14), O1−C10 1.399(11), C10−C11 1.524(14), C5−C10 1.537(12); C8−Pt1−Cl1 94.7(3), C8−Pt1−Cl2 154.9(3), Cl3−Pt1−Cl2 90.34(13), Cl1−Pt1−Cl2 88.13(13), O1−C10−C11 110.4(7), O1−C10−C5 111.0(7), N1−C5−C10 111.0(7), Cl3−Pt1−Cl1 175.13(11), O1−C10−C11−C12 −14.6(11), N1−C5−C10−O1 −74.6(9), Cl3−Pt1−C8−C9 93.3(6), Cl1−Pt1−C8−C9 −83.1(6), N1−C5−C10−C11 163.4(7)



32

6. X-ray Structural Determinations of 11, 13, 19, 23, 26 and 32[28]

Of interest is the conformation of the coordinated cinchona alkaloid in the various complexes which can be derived from the torsion angle C4′−C9−C8−N. The "open conformation 3" is found in the complexes **19**, **23**, **32** and in **13** according to the ^{1}H-NMR spectra. The torsion angles of these compounds are in the range of 161−176°. For the "free" cinchonidine a torsion angle of 158° was reported.[20] The formation of the N,O-chelate in **11** and **26** affords a torsion angle C4′−C9−C8−N of 81−85° ("open conformation 4").

In the Pd^{II} complexes **11** and **26** the Pd atoms have a strictly planar environment with distortion of the square. The ligands at the Zn^{2+} ion of **23** form a distorted tetrahedron.

The analysed crystal of **32** contained the diastereoisomer [*S*(C10), *S*(C8), *R*(C9), *S*(C4), *R*(C3)]. The olefinic C=C double bond lies perpendicular to the $PtCl_3$ plane as in $K[PtCl_3(C_2H_4)]$. Also the C=C, Pt−C and Pt−Cl lengths are similar to that of the Zeise salt.[21]

Experimental Section

Where appropriate, the reactions were carried out in dry solvents under nitrogen. − NMR: Jeol GSX 270 or Jeol EX 400, using the solvent as internal standard. − IR: Nicolet 520 FT-IR. − The starting materials were prepared according to literature procedures: Ph_3PAuCl,[22] $[(C_3H_5)PdCl]_2$,[23] $(COD)PdCl_2$,[24] $[R_3PPtCl_2]_2$,[25] $[R_3PPdCl_2]_2$,[24] $(en)PdCl_2$,[26] $[Cp^*IrCl_2]_2$.[27] Quinine and cinchonine were used as supplied (Fluka). $ZnCl_2$ was dried for 2 d at 80°C. PE = polyethylene.

1: To a solution of 49.5 mg (0.1 mmol) of PPh_3AuCl in 3 mL of CH_2Cl_2 a solution of 17 mg (0.1 mmol) of $AgNO_3$ in 3 mL of methanol was added. After 1 h of vigorous stirring with exclusion of light, AgCl was centrifuged off and 32.4 mg (0.1 mmol) of quinine was added. The light yellow solution was stirred for another 1 h to give a clear colourless solution which was concentrated to about 1 mL and added to 20 mL of pentane. The white precipitate was washed twice with Et_2O and dried in vacuo for a few days. − IR (KBr): $\tilde{\nu}$ = 3379 cm^{-1} m br. (OH), 3074 w (CH_{arom}), 2935 m (CH_{aliph}). − ^{1}H NMR (400 MHz, $CDCl_3$): δ = 8.71 (d, 1 H, $^3J_{3'}$ = 4.61 Hz, 2′), 8.10 (d, 1 H, $^3J_{7'}$ = 9.37 Hz, 8′), 7.74 (d, 1 H, $^3J_{2'}$ = 4.35 Hz, 3′), 7.57−7.43 [m. 16 H, $P(C_6H_5)_3$, 5′], 7.35 (dd, 1 H, $^3J_{8'}$ = 9.31 Hz, $^4J_{5'}$ = 2.45 Hz, 7′), 6.02 (s, br., 1 H, 9), 5.77 (ddd, 1 H, $^3J_{11c}$ = 17.47 Hz, $^3J_{11t}$ = 10.15 Hz, $^3J_3$ = 7.32 Hz, 10), 5.02 (d, 1 H, $^3J_{10}$ = 17.43 Hz, 11*c*), 4.98 (d, 1 H, $^3J_{10}$ = 10.03 Hz, 11*t*), 4.0−3.6 (m, 1 H, 6b*), 3.75 (s, 3 H, OCH_3), 3.37 (m, 1 H, 2b), 2.93 (m, 1 H, 8), 2.43−1.20 (5m, 8 H, 2a, 6a, 3, 4, 5b, 7b, 5a, 7a). − ^{31}P NMR (109.3 MHz): δ = 29.8. − $C_{38}H_{39}AuN_3O_5P \times CH_2Cl_2$ (866.9): calcd. C 52.99, H 4.59, N 4.85; found C 52.87, H 5.02, N 4.40.

2: To a solution of 34 mg (0.2 mmol) of $AgNO_3$ in 10 mL of methanol a solution of 65 mg (0.2 mmol) of quinine in 5 mL of CH_2Cl_2 was added with exclusion of light. After 1 h of vigorous stirring at room temperature, a white precipitate was obtained which was dissolved again by the addition of 52.5 mg (0.2 mmol) of PPh_3. The colourless solution was stirred for another 1 h, concentrated to about 0.5 mL and added to 20 mL of Et_2O to give the product as white light-sensitive solid which was washed twice with Et_2O and dried in vacuo for 2 d. − IR (KBr): $\tilde{\nu}$ = 3397 cm^{-1} m br. (OH), 3071 w (CH_{arom}), 2939 s (CH_{aliph}). − ^{1}H NMR (400 MHz, $CDCl_3$): δ = 8.75 (d, 1 H, $^3J_{3'}$ = 4.38 Hz, 2′), 7.82 (d, 1 H, $^3J_{7'}$ = 9.36 Hz, 8′), 7.68 (d, 1 H, $^3J_{2'}$ = 4.76 Hz, 3′), 7.52−7.30 [m, 15 H, $P(C_6H_5)_3$], 7.07 (dd, 1 H, $^3J_{8'}$ = 9.19 Hz, $^4J_{5'}$ = 2.04 Hz, 7′), 6.99 (s, 1 H, 5′), 6.06 (s, 1 H, 9), 5.57 (ddd, 1 H, $^3J_{11c}$ = 17.33 Hz, $^3J_{11t}$ = 10.53 Hz, $^3J_3$ = 6.80 Hz, 10), 5.05 (d, 1 H, $^3J_{10}$ = 10.12 Hz, 11*t*), 5.02 (d, 1 H, $^3J_{10}$ = 17.85 Hz, 11*c*), 4.35 (m, 1 H, 6b), 3.77 (s, 3 H, OCH_3), 3.56 (dd, 1 H, *J* = 10.66 Hz, *J* = 13.19 Hz, 2b), 3.40 (m, 1 H, 8), 3.23 (m, 2 H, 2a, 6a), 2.70 (m, 1 H, 3), 2.24−2.10 (m, 3 H, 4, 5b, 7b), 1.90- 1.79 (m, 1 H, 5a), 1.42 (m, 1 H, 7a). − ^{31}P NMR (109.3 MHz): δ = 12.4. − $C_{38}H_{39}AgN_3O_5P \times 0.5\ CH_2Cl_2$ (799.1): calcd. C 57.87, H 5.05, N 5.28; found C 57.93, H 5.15, N 5.63.

3: To a solution of 86 mg (0.30 mmol) of $(COD)PdCl_2$ in 10 mL of CH_2Cl_2 a solution of 51 mg (0.30 mmol) of $AgNO_3$ in 15 mL of methanol was added. After 1 h of vigorous stirring with exclusion of light, AgCl was centrifuged off and 97 mg (0.30 mmol) of quinine was added. The solution was stirred for another 1 h to give a clear colourless solution which was concentrated to about

Table 1. Crystal data and structure refinement for **11**, **13** and **19**

	11	**13**	**19**
Empirical formula	$C_{22}H_{31}N_4O_2Pd^+ NO_3^- \times H_2O$	$2\,C_{21}H_{27}N_2O_2^+ \,2\,BF_4^- \times H_2O$	$C_{31}H_{42}Cl_2IrN_2O_2^+ BF_4^-$
Formula weight	569.93	870.53	824.58
T [K]	293(2)	293(2)	293(2)
Crystal system	monoclinic	monoclinic	monoclinic
Space group	$P2_1$ (no. 4)	$P2_1$ (no. 4)	$P2_1$ (no. 4)
Unit cell dimensions			
a [Å]	11.2430(13)	8.1347(12)	14.428(4)
b [Å]	8.0008(13)	15.769(3)	11.875(3)
c [Å]	27.100(4)	16.602(2)	22.727(10)
α [°]	90	90	90
β [°]	93.974(11)	97.883(14)	92.30(3)
γ [°]	90	90	90
Volume [Å^3]	2431.9(6)	2109.6(7)	3890.8(23)
Z	4	2	4
Density (calcd.) [g/cm^3]	1.557	1.370	1.408
μ (Mo-K_α) [mm^{-1}]	0.810	0.112	3.614
F(000)	1176	916	1640
Crystal size [mm]	0.33 × 0.37 × 0.53	0.43 × 0.53 × 0.53	0.57 × 0.50 × 0.27
2θ range [°]	4.88−45.94	4.96−47.96	4.66−47.94
Index ranges	$\pm h \pm k -l$	$-h \pm k \pm l$	$-h \pm k \pm l$
Reflections collected	6885	7496	12718
Independent reflections	6724 [R(int) = 0.0159]	6611 [R(int) = 0.0086]	12178 [R(int) = 0.0237]
Absorption correction	semiempirical from ψ scan	semiempirical from ψ scan	semiempirical from ψ scan
Max./min. transmission	0.9974/0.9265	0.9983/0.9754	0.9995/0.6639
Data/parameters	6724/629	6611/576	12178/878
Goodness-of-fit on F^2	0.971	1.047	1.101
Final R indices [$I > 2\sigma(I)$]	$R1$ = 0.0261, $wR2$ = 0.0713	$R1$ = 0.0394, $wR2$ = 0.0975	$R1$ = 0.0477, $wR2$ = 0.1314
R indices (all data)	$R1$ = 0.0308, $wR2$ = 0.0764	$R1$ = 0.0487, $wR2$ = 0.1063	$R1$ = 0.0656, $wR2$ = 0.1465
Largest diff. peak and hole [eÅ^{-3}]	0.575 and −0.422	0.312 and −0.192	1.222 and −0.460

Table 2. Crystal data and structure refinement for **23**, **26** and **32**

	23	**26**	**32**
Empirical formula	$C_{19}H_{23}Cl_2N_2OZn^+ Cl^- \times CH_4O$	$C_{31}H_{51}Cl_3N_2OP_2Pd_2 \times CHCl_3 \times H_2O$	$C_{20}H_{26}Cl_3N_2O_2Pt^+ Cl^- \times H_2O \times 1.5\,O$
Molecular mass	499.16	986.21	705.33
T [K]	293(2)	293(2)	293(2)
Crystal system	monoclinic	triclinic	monoclinic
Space group	$P2_1$ (no. 4)	$P1$ (no. 1)	$C2$ (no. 5)
Unit cell dimensions			
a [Å]	9.2510(11)	7.772(2)	24.663(3)
b [Å]	12.957(3)	12.002(2)	12.447(4)
c [Å]	9.2976(9)	12.364(3)	9.591(2)
α [°]	90	97.99(2)	90
β [°]	93.147(9)	94.89(2)	105.049(13)
γ [°]	90	107.33(2)	90
V [Å^3]	1112.8(3)	1080.5(4)	2843.3(11)
Z	2	1	4
d (calcd.) [g/cm^3]	1.490	1.516	1.645
μ (Mo-K_α) [mm^{-1}]	1.482	1.306	5.338
F(000)	516	500	1372
Crystal size [mm]	0.27 × 0.50 × 0.53	0.03 × 0.50 × 0.53	0.20 × 0.33 × 0.53
2θ range [°]	5.4−48	5.34−47.94	4.82−47.98
Index ranges	$\pm h \pm k +l$	$\pm h \pm k \pm l$	$+h \pm k \pm l$
Reflections collected	3728	6740	4540
Independent reflections	3497 [R(int) = 0.0170]	6738 [R(int) = 0.0138]	4431 [R(int) = 0.0123]
Absorption correction	semiempirical from ψ scan	semiempirical from ψ scan	semiempirical from ψ scan
Max./min. transmission	0.9991/0.9257	0.9991/0.6908	0.9994/0.8415
Data/parameters	3497/255	6738/545	4431/291
Goodness-of-fit on F^2	1.031	1.200	1.081
Final R indices [$I > 2\sigma(I)$]	0.0243, 0.0654	0.0260, 0.0814	0.0351, 0.1004
R indices (all data)	0.0267, 0.0680	0.0287, 0.0844	0.0388, 0.1050
Largest diff. peak and hole [eÅ^{-3}]	0.217 and −0.186	0.422 and −0.374	1.175 and −0.457

0.5 mL and added to 20 mL of Et_2O. The white precipitate was washed twice with Et_2O and dried in vacuo for a few days. − IR (KBr): $\tilde{\nu}$ = 3313 cm^{-1} vs br. (OH), 3073 m (CH_{arom}), 2939 s (CH_{aliph}). − IR (PE): $\tilde{\nu}$ = 351 cm^{-1} m (M−Cl). − ^{1}H NMR (400 MHz, $CDCl_3$): δ = 10.72 (s, br., 1 H, OH), 8.73 (d, 1 H, $^3J_{3'}$ = 4.63 Hz, 2′), 8.19 (s, br., 1 H, 8′), 7.73 (d, 1 H, $^3J_{2'}$ = 4.72 Hz, 3′), 6.98 (d, 1 H, $^3J_{8'}$ = 8.81 Hz, 7′), 6.64 (d, 1 H, $^4J_{7'}$ = 2.17 Hz, 5′), 6.16 [pd, 4 H, J = 16.74 Hz, NPd($C_8H_8H_{4olef}$)], 5.93 (s, br., 1 H,

9), 5.53 (ddd, 1 H, $^3J_{11c}$ = 17.16 Hz, $^3J_{11t}$ = 10.43 Hz, $^3J_3$ = 6.74 Hz, 10), 5.01 (d, 1 H, $^3J_{10}$ = 10.09 Hz, 11*t*), 4.98 (d, 1 H, $^3J_{10}$ = 17.67 Hz, 11*c*), 4.39−4.33 (m, 1 H, 6b), 3.29 (s, 3 H, OCH_3), 3.67−1.30 [9m, 6a, 2a, 2b, 8, 4, 5a, 5b, NPd($C_8H_{8aliph}H_4$), 7a, 7b]. − $C_{28}H_{36}ClN_3O_5Pd \times 0.15\ CH_2Cl_2$ (649.2): calcd. C 52.08, H 5.64, N 6.47; found C 52.06, H 5.89, N 6.59.

4: To a solution of 66 mg (0.2 mmol) of quinine in 8 mL of CH_2Cl_2, which was cooled to −78°C, 37 mg (0.10 mmol) of $[(allyl)PdCl]_2$ was added. After stirring for 1.5 h, the solvent was removed in vacuo to obtain a white solid which was washed twice with 15 mL of Et_2O and dried in vacuo. − IR (KBr): $\tilde{\nu}$ = 3383 cm^{-1} vs br. (OH), 3070 w (CH_{arom}), 2937 vs (CH_{aliph}). − IR (PE): $\tilde{\nu}$ = 276 cm^{-1} w (M−Cl). − ^{1}H NMR (400 MHz, CD_2Cl_2): δ = 8.61 (d, 1 H, $^3J_{3'}$ = 4.16 Hz, 2′), 8.20 (s, br., 1 H, 8′), 7.56 (s, br., 1 H, 3′), 7.43 (s, br., 1 H, 5′), 7.32 (dd, 1 H, $^3J_{8'}$ = 9.22 Hz, $^4J_{5'}$ = 2.65 Hz, 7′), 5.76−5.62 [m, 1 H, NPdC*H*$(CH_2)_2$], 5.62−5.50 (m, 1 H, 10), 5.1 (s, br., 1 H, 9), 4.97 (d, 1 H, $^3J_{10}$ = 17.13 Hz, 11c), 4.88 (d, 1 H, $^3J_{10}$ = 10.43 Hz, 11t), 4.0−3.8 [m, 5 H, 6b*, 8*, 2b*, NPdCH(CH_2*H*$_{endo}$)$_2$*], 3.93 (s, 3 H, OCH_3), 3.2−2.5 [4 m, 5 H, 2a, 6a, OH, NPdCH(CH_2*H*$_{exo}$)$_2$], 2.26 (m, 1 H, 3), 1.74−1.2 (3 m, 5 H, 4, 7b, 5b, 7a, 5a). − $C_{23}H_{29}ClN_2O_2Pd \times 0.3\ CH_2Cl_2$ (532.8): calcd. C 52.52, H 5.60, N 5.26; found C 52.56, H 6.05, N 5.02.

General Procedure for the Preparation of 5−10: A solution of quinine in 10 mL of CH_2Cl_2 and the appropriate amount of a solution of NaOMe in methanol was cooled to −78°C. After the addition of $[R_3PMCl_2]_2$, the solution was allowed to warm up to room temperature for 16 h and stirred for another 2 h. The solvent of the light yellow suspension was removed in vacuo and the residue was dissolved again in CH_2Cl_2 and stirred for 10 min. The suspension was filtered through Celite to remove NaCl and the resulting clear yellow solution was concentrated to dryness. The yellow solid was washed twice with pentane and once with 10 mL of cold Et_2O and dried in vacuo for 2 d.

5: 65 mg (0.2 mmol) of quinine, 0.2 mmol of NaOMe in MeOH and 77 mg (0.1 mmol) of $[(PEt_3)PtCl_2]_2$ were used. − IR (KBr): $\tilde{\nu}$ = 3076 cm^{-1} m (CH_{arom}), 2963 s, 2935 s (CH_{aliph}). − IR (PE): $\tilde{\nu}$ = 333 cm^{-1} m (M−Cl). − ^{1}H NMR (400 MHz, $CDCl_3$): δ = 9.30 (d, 1 H, $^3J_{2'}$ = 4.53 Hz, 3′), 8.89 (d, 1 H, $^3J_{3'}$ = 4.52 Hz, 2′), 8.06 (d, 1 H, $^3J_{7'}$ = 9.16 Hz, 8′), 7.37 (dd, 1 H, $^3J_{8'}$ = 9.16 Hz, $^4J_{5'}$ = 2.69 Hz, 7′), 7.12 (d, 1 H,$^4J_{7'}$ = 2.71 Hz, 5′), 5.97 (ddd, 1 H, $^3J_{11c}$ = 17.21 Hz, $^3J_{11t}$ = 10.31 Hz, $^3J_3$ = 6.87 Hz, 10), 5.76 (dd, 1 H, ^4J_P = 9.78 Hz, $^3J_8$ = 6.67 Hz, 9), 5.24 (d, 1 H, $^3J_{10}$ = 10.37 Hz, 11*t*), 5.20 (d, 1 H, $^3J_{10}$ = 17.12 Hz, 11*c*), 4.09 (m, 1 H, 8), 3.92 (s, 3 H, OCH_3), 3.79 (d, 1 H, *J* = 12.99 Hz, 2b), 3.52 (m, 1 H, 2a), 3.25 (m, 1 H, 6b), 2.94 (pt, 1 H, ^3J = 12.09 Hz, 6a), 2.41 (m, 1 H, 3), 2.26−2.16 (m, 1 H, 7b), 2.10−1.84 [m, 6 H, P(CH_2CH_3)$_3$], 1.81 (m, 1 H, 4), 1.29 [dt, 9 H, ^3J_P = 16.44 Hz, $^3J_{CH2}$ = 7.58 Hz, P(CH_2CH_3)$_3$], 1.41−1.21 (m, 3 H, 5b*, 7a*, 5a*). − ^{31}P NMR (109.3 MHz): δ = −4.12 ($^1J_{P\text{-}Pt}$ = 3430 Hz). − $C_{26}H_{38}ClN_2O_2PPt \times 0.5\ CH_2Cl_2$ (714.6): calcd. C 44.54, H 5.50. N 3.92; found C 44.54, H 5.67, N 3.79.

6: 39.5 mg (0.122 mmol) of quinine, 0.122 mmol of NaOMe in MeOH and 57 mg (0.061 mmol) of $[(PBu_3)PtCl_2]_2$ were used. − IR (KBr): $\tilde{\nu}$ = 3072 cm^{-1} m (CH_{arom}), 2955 s, 2931 s (CH_{aliph}). − IR (PE): $\tilde{\nu}$ = 330 cm^{-1} m (M−Cl). − ^{1}H NMR (400 MHz, $CDCl_3$): δ = 9.34 (d, 1 H, $^3J_{2'}$ = 4.51 Hz, 3′), 8.88 (d, 1 H, $^3J_{3'}$ = 4.72 Hz, 2′), 8.06 (d, 1 H, $^3J_{7'}$ = 9.41 Hz, 8′), 7.37 (dd, 1 H, $^3J_{8'}$ = 9.09 Hz, $^4J_{5'}$ = 2.54 Hz, 7′), 7.12 (d, 1 H,$^4J_{7'}$ = 2.33 Hz, 5′), 5.99 (ddd, 1 H, $^3J_{11c}$ = 17.13 Hz, $^3J_{11t}$ = 10.46 Hz, $^3J_3$ = 6.78 Hz, 10), 5.75 (dd, 1 H, ^4J_P = 9.42 Hz, $^3J_8$ = 6.48 Hz, 9), 5.27 (d, 1 H, $^3J_{10}$ = 10.53 Hz, 11*t*), 5.22 (d, 1 H, $^3J_{10}$ = 17.10 Hz, 11*c*), 4.09 (m, 1 H, 8), 3.95 (s, 3 H, OCH_3), 3.1 (d, 1 H, *J* = 12.70 Hz, 2b), 3.55−3.46 (m, 1 H, 2a), 3.23 (m, 1 H, 6b), 2.98−2.90 (m, 1 H, 6a), 2.46−2.39 (m, 1 H, 3), 2.26−2.17 (m, 1 H, 7b), 1.93−1.79 [m, 6 H, P($CH_2C_3H_7$)$_3$], 1.77−1.62 [m, 6 H, P($CH_2CH_2C_2H_5$)$_3$], 1.59−1.54 [m, 6 H, P($C_2H_4CH_2CH_3$)$_3$], 1.29 [t, 9 H, $^3J_{P(C2H4\text{-}CH2\text{-}CH3)3}$ = 6.85 Hz, P($C_3H_6CH_3$)$_3$], 1.93−1.54 (m, 4 H, 4*, 5b*, 7a*, 5a*). − ^{31}P NMR (109.3 MHz): δ = −11.93 ($^1J_{P\text{-}Pt}$ = 3420 Hz). − $C_{32}H_{50}N_2ClO_2PPt \times CH_2Cl_2$ (841.2): calcd. C 47.12, H 6.23, N 3.33; found C 46.80, H 6.37, N 3.16.

7: 65 mg (0.2 mmol) of quinine, 0.2 mmol of NaOMe in MeOH and 59 mg (0.1 mmol) of $[(PEt_3)PdCl_2]_2$ were used. − IR (KBr): $\tilde{\nu}$ = 3077 cm^{-1} w (CH_{arom}), 2975 s, 2931 m (CH_{aliph}). − IR (PE): $\tilde{\nu}$ = 327 cm^{-1} m (M−Cl). − ^{1}H NMR (400 MHz, $CDCl_3$): δ = 9.12 (d, 1 H, $^3J_{2'}$ = 4.71 Hz, 3′), 8.86 (d, 1 H, $^3J_{3'}$ = 4.77 Hz, 2′), 8.06 (d, 1 H, $^3J_{7'}$ = 9.37 Hz, 8′), 7.36 (dd, 1 H, $^3J_{8'}$ = 9.32 Hz, $^4J_{5'}$ = 2.77 Hz, 7′), 7.06 (d, 1 H,$^4J_{7'}$ = 2.66 Hz, 5′), 5.99 (ddd, 1 H, $^3J_{11c}$ = 17.18 Hz, $^3J_{11t}$ = 10.31 Hz, $^3J_3$ = 6.97 Hz, 10), 5.46 (d, 1 H, $^3J_8$ = 6.59 Hz, 9), 5.19−5.15 (2m, 2 H, 11*c*, 11*t*), 3.94−3.80 (m, 1 H, 8), 3.99 (s, 3 H, OCH_3), 3.66 (dd, 1 H, *J* = 13.72 Hz, *J* = 10.22 Hz, 2b), 3.43 (d, 1 H, ^3J = 13.59 Hz, 2a), 3.22−3.04 (m, 2 H, 6b, 6a), 2.40 (m, 1 H, 3), 2.12−2.01 (m, 2 H, 7b, 5b), 1.94−1.83 [m, 6 H, P(CH_2CH_3)$_3$], 1.77 (m, 1 H, 4), 1.35 [dt, 9 H, ^3J_P = 16.92 Hz, $^3J_{CH2}$ = 7.60 Hz, P(CH_2CH_3)$_3$], 1.20−1.0 (m, 2 H, 7a*, 5a). − ^{31}P NMR (109.3 MHz): δ = 34.89 (0.05 N′PdP), 31.28 (0.05 NPdP$_{cis}$), 30.82 (NPdP$_{trans}$). − $C_{26}H_{38}ClN_2O_2PPd \times 0.25\ CH_2Cl_2$ (603.7): calcd. C 52.23, H 6.43, N 4.64; found C 52.12, H 6.66, N 4.43.

8: 76 mg (0.234 mmol) of quinine, 0.234 mmol of NaOMe in MeOH and 79 mg (0.117 mmol) of $[(PPr_3)PdCl_2]_2$ were used. − IR (KBr): $\tilde{\nu}$ = 3077 cm^{-1} w (CH_{arom}), 2960 s, 2923 s (CH_{aliph}). − IR (PE): $\tilde{\nu}$ = 352 cm^{-1} m, 328 w (M−Cl). − ^{1}H NMR (400 MHz, $CDCl_3$): δ = 9.05 (d, 1 H, $^3J_{2'}$ = 4.49 Hz, 3′), 8.82 (d, 1 H, $^3J_{3'}$ = 4.51 Hz, 2′), 8.01 (d, 1 H, $^3J_{7'}$ = 9.24 Hz, 8′), 7.32 (dd, 1 H, $^3J_{8'}$ = 9.23 Hz, $^4J_{5'}$ = 2.87 Hz, 7′), 7.03 (d, 1 H,$^4J_{7'}$ = 2.60 Hz, 5′), 5.95 (ddd, 1 H, $^3J_{11c}$ = 17.22 Hz, $^3J_{11t}$ = 10.23 Hz, $^3J_3$ = 6.99 Hz, 10), 5.41 (d, 1 H, $^3J_8$ = 6.72 Hz, 9), 5.15−5.10 (2m, 2 H, 11*c*, 11*t*), 3.84 (s, 3 H, OCH_3), 3.80 (m, 1 H, 8*), 3.60 (dd, 1 H, $^2J_3$ = 13.62 Hz, $^3J_{2a}$ = 10.34 Hz, 2b), 3.37 (pd, 1 H, ^3J = 13.39 Hz, 2a), 3.16−3.01 (m, 2 H, 6b, 6a), 2.34 (m, 1 H, 3), 2.07−1.94 (m, 1 H, 7b), 1.86−1.64 [m, 8 H, P(CH_2CH_3)$_3$, 5b*, 4*], 1.32 (m, 1 H, 7a), 1.07 [t, 9 H, $^3J_{CH2CH3}$ = 6.83 Hz, P($C_2H_4CH_3$)$_3$, 5a*]. − ^{31}P NMR (109.3 MHz): δ = 25.73 (0.04 N′PdP), 22.44 (0.05 NPdP$_{cis}$), 22.25 (NPdP). − $C_{29}H_{44}ClN_2O_2PPd$ (624.5): calcd. C 55.77, H 7.10, N 4.49; found C 55.23, H 7.06, N 4.41.

9: 47 mg (0.145 mmol) of quinine, 0.145 mmol of NaOMe in MeOH and 55 mg (0.072 mmol) of $[(PBu_3)PdCl_2]_2$ were used. − IR (KBr): $\tilde{\nu}$ = 3076 cm^{-1} w (CH_{arom}), 2959 s, 2920 s (CH_{aliph}). − IR (PE): $\tilde{\nu}$ = 326 cm^{-1} m, 306 w (M−Cl). − ^{1}H NMR (400 MHz, $CDCl_3$): δ = 9.11 (d, 1 H, $^3J_{2'}$ = 4.53 Hz, 3′), 8.84 (d, 1 H, $^3J_{3'}$ = 4.42 Hz, 2′), 8.03 (d, 1 H, $^3J_{7'}$ = 9.25 Hz, 8′), 7.34 (dd, 1 H, $^3J_{8'}$ = 9.30 Hz, $^4J_{5'}$ = 2.68 Hz, 7′), 7.05 (d, 1 H,$^4J_{7'}$ = 2.67 Hz, 5′), 5.97 (ddd, 1 H, $^3J_{11c}$ = 17.25 Hz, $^3J_{11t}$ = 10.26 Hz, $^3J_3$ = 6.99 Hz, 10), 5.43 (d, 1 H, $^3J_8$ = 6.61 Hz, 9), 5.18−5.11 (2m, 2 H, 11*c*, 11*t*), 3.87 (s, 3 H, OCH_3), 3.84 (m, 1 H, 8*), 3.62 (dd, 1 H, $^2J_3$ = 13.69 Hz, $^2J_{2a}$ = 10.26 Hz, 2b), 3.39 (pd, 1 H, ^3J = 13.17 Hz, 2a), 3.19−2.99 (m, 2 H, 6b, 6a), 2.44−2.30 (m, 1 H, 3), 2.11−1.96 (m, 1 H, 7b), 1.89−0.9 (m, 5b*, 4*, 5a*, 7a*), 1.89−1.60 [m, 12 H, P($C_2H_4C_2H_5$)$_3$], 1.54−1.41 [m, 6 H, P($C_2H_4CH_2CH_3$)$_3$], 0.98 [t, 9 H, $^3J_{CH2CH3}$ = 6.83 Hz, P($C_3H_6CH_3$)$_3$]. − ^{31}P NMR (109.3 MHz): δ = 26.75 (0.05 N′PdP), 23.16 (0.05 NPdP$_{cis}$), 22.89 (NPdP). − $C_{32}H_{50}ClN_2O_2PPd \times 0.25\ CH_2Cl_2$ (687.8): calcd. C 56.32, H 7.40, N 4.07; found C 56.58, H 7.48, N 4.05.

10: 65 mg (0.2 mmol) of quinine, 0.2 mmol of NaOMe in MeOH and 88 mg (0.1 mmol) of $[(PPh_3)PdCl_2]_2$ were used. − IR (KBr): $\tilde{\nu}$ = 3075 cm^{-1} w (CH_{arom}), 2969 w, 2940 m (CH_{aliph}). − IR (PE): $\tilde{\nu}$ = 329 cm^{-1} w (M−Cl). − ^1H NMR (400 MHz, $CDCl_3$): δ = 8.87 (d, 1 H, $^3J_{2'}$ = 4.64 Hz, 3′), 8.37 (d, 1 H, $^3J_{3'}$ = 4.73 Hz, 2′), 8.00 (d, 1 H, $^3J_{7'}$ = 9.03 Hz, 8′) 7.74−7.67 [m, 5 H, $P(C_6H_5)(C_6H_5)_2$], 7.50−7.44 [m, 5 H, $P(C_6H_5)(C_6H_5)_2$], 7.42−7.36 [m, 5 H, $P(C_6H_5)(C_6H_5)_2$], 7.33 (dd, 1 H, $^3J_{8'}$ = 9.20 Hz, $^4J_{5'}$ = 2.60 Hz, 7′), 7.01 (d, 1 H,$^4J_{7'}$ = 2.57 Hz, 5′), 5.96 (ddd, 1 H, $^3J_{11c}$ = 17.19 Hz, $^3J_{11t}$ = 10.43 Hz, $^3J_3$ = 6.76 Hz, 10), 5.29 (d, 1 H, $^3J_8$ = 6.56 Hz, 9), 5.18 (d, 1 H, $^3J_{10}$ = 10.65, 11*t*), 5.14 (m,1 H, 11*c*), 4.00 (dt, 1H ^3J = 14.6 Hz, ^3J = 8.74 Hz, 8), 3.87 (s, 3 H, OCH_3), 3.79 (dd, 1 H, *J* = 13.80 Hz, *J* = 10.28 Hz, 2b), 3.53 (d, 1 H, ^3J = 13.82 Hz, 2a), 3.40 (d, 1 H, ^3J = 11.92 Hz, 6b), 3.17−3.08 (m, 1 H, 6a), 2.45−2.35 (m, 1 H, 3), 2.10−1.99 (m, 1 H, 7b), 1.80−1.72 (m, 1 H, 4), 1.38 (m, 1 H, 5b), 1.24−1.16 (m, 1 H, 7a), 1.13−1.04 (m, 1 H, 5a). − ^{31}P NMR (109.3 MHz): δ = 29.05 (0.05 N′PdP), 26.11 (0.05 $NPdP_{cis}$), 25.70 (NPdP). − $C_{38}H_{38}ClN_2O_2PPd \times 0.25\ CH_2Cl_2$ (748.8): calcd. C 61.35, H 5.18, N 3.74; found C 61.03, H 5.63, N 3.63.

11: 24 mg (0.1 mmol) of $(en)PdCl_2$ were added to a solution of 34 mg (0.2 mmol) of $AgNO_3$ in 5 mL of water and stirred at 40°C for 4 h in the dark. After AgCl was centrifuged off, the solution was concentrated to 2 mL and added to a solution of 32.5 mg (0.1 mmol) of quinine and 0.1 mmol NaOMe in 3 mL of methanol. After 12 h of vigorous stirring, the solvent was removed in vacuo. The slight yellow residue was crystallized twice from water to give slightly yellow crystals. − IR (KBr): $\tilde{\nu}$ = 3432 cm^{-1} s, 3271 s, 3217 s, 3133 s (NH), 3074 s (CH_{arom}), 2980 s, 2945 s, 2915 s (CH_{aliph}). − ^1H NMR (400 MHz, D_2O): δ = 8.98 (d, 1 H, $^3J_{2'}$ = 4.25 Hz, 3′), 8.74 (d, 1 H, $^3J_{3'}$ = 4.76 Hz, 2′), 7.87 (d, 1 H, $^3J_{7'}$ = 9.18 Hz, 8′), 7.34 (dd, 1 H, $^3J_{8'}$ = 9.52 Hz, $^4J_{5'}$ = 2.59 Hz, 7′), 7.06 (d, 1 H,$^4J_{7'}$ = 2.62 Hz, 5′), 5.93 (ddd, 1 H, $^3J_{11c}$ = 16.67 Hz, $^3J_{11t}$ = 10.40 Hz, $^3J_3$ = 6.27 Hz, 10), 5.30 (d, 1 H, $^3J_8$ = 6.85 Hz, 9), 5.09 (d, 1 H, $^3J_{10}$ = 17.68 Hz, 11*c*), 5.08 (d, 1 H, $^3J_{10}$ = 9.29 Hz, 11*t*), 4.75 [$Pd(H_4N_2C_2H_4$*], 3.82−3.70 (m, 1 H, 8), 3.78 (s, 3 H, OCH_3), 3.55 (d, 1 H, *J* = 15.72 Hz, 2b), 3.16−3.08 (m, 1 H, 2a), 3.04−2.95 (m, 1 H, 6b), 2.76−2.6 [m, 5 H, 6a, $Pd(H_4N_2C_2H_4)$], 2.39−2.31 (m, 1 H, 3), 2.11−2.01 (m, 1 H, 7b), 1.66−1.59 (m, 1 H, 4), 1.29−1.19 (m, 1 H, 5b), 0.96−0.90 (m, 2 H, 7a, 5a). − $C_{22}H_{31}N_5O_5Pd \times 2\ H_2O$ (587.0): calcd. C 45.01, H 6.01, N 11.93; found C 45.31, H 5.66, N 11.69.

12: To a solution of 116 mg (0.358 mmol) of quinine in 10 mL of CH_2Cl_2, 178 μL (0.179 mmol) of $TiCl_4$ in CH_2Cl_2 was added. At once a light orange precipitate was obtained which was dissolved again by vigorous stirring. After 2 d of stirring, the solution was concentrated to about 0.5 mL and added to 20 mL of Et_2O. The white precipitate was washed twice with 15 mL of Et_2O and dried in vacuo for several days. − ^1H NMR (400 MHz, CD_3OD): δ = 8.77 (d, 1 H, $^3J_{3'}$ = 4.75 Hz, 2′), 8.01 (d, 1 H, $^3J_{7'}$ = 9.19 Hz, 8′), 7.91 (d, 1 H, $^3J_{2'}$ = 5.08 Hz, 3′), 7.57 (d, 1 H, $^4J_{7'}$ = 2.73 Hz, 5′), 7.52 (dd, 1 H, $^3J_{8'}$ = 9.25 Hz, $^4J_{5'}$ = 2.63 Hz, 7′), 6.28 (s, 1 H, 9), 5.77 (ddd, 1 H, $^3J_{11c}$ = 17.33 Hz, $^3J_{11t}$ = 10.31 Hz, $^3J_3$ = 7.02 Hz, 10), 5.12 (dt, 1 H, $^3J_{10}$ = 17.37 Hz, $^2J_{11t}$ = $^4J_3$ = 2.43 Hz, 11*c*), 5.03 (dt, 1 H, $^3J_{10}$ = 10.29 Hz, $^2J_{11c}$ = $^4J_3$ = 2.41 Hz, 11*t*), 4.33−4.24 (m, 1 H, 6b), 4.07 (s, 3 H, OCH_3), 3.68−3.58 (m, 2 H, 8, 2b), 3.34−3.26 (m, 2 H, 2a, 6a), 2.88−2.78 (m, 1 H, 3), 2.30−2.16 (m, 2 H, 7b, 5b), 2.12−2.09 (m, 1 H, 5a), 2.03−1.9 (m, 1 H, 5a), 1.60−1.53 (m, 1 H, 7a). − $C_{40}H_{46}Cl_2N_4O_4Ti \times 0.5\ CH_2Cl_2$ (808.1): calcd. C 60.20, H 6.11, N 6.93; found C 60.03, H 6.27, N 6.87.

13: 2 g (6.16 mmol) of quinine was dissolved in 50 mL of CH_2Cl_2 and cooled to −78°C. After addition of 740 mg (5 mmol) of $(CH_3)_3O^+BF_4^-$, the mixture was stirred for 16 h and was allowed to warm up to room temp. A white precipitate was obtained which was centrifuged off, washed three times with 10 mL of CH_2Cl_2 and dried in vacuo at 80°C for 1 d. Crystallization from water gave colourless plates. − IR (KBr): $\tilde{\nu}$ = 3122 cm^{-1} s br. (OH), 3070 w (CH_{arom}), 3010 m, 2971 m, 2954 m, 2885 m, 2842 m, (CH_{aliph}). − ^1H NMR (400 MHz, [D_6]acetone): δ = 8.81 (d, 1 H, $^3J_{3'}$ = 4.31 Hz, 2′), 8.03 (d, 1 H, $^3J_{7'}$ = 9.18 Hz, 8′), 7.83 (dd, 1 H, $^3J_{2'}$ = 4.38 Hz, *J* = 0.7 Hz, 3′), 7.46 (dd, 1 H, $^3J_{8'}$ = 9.21 Hz, $^4J_{5'}$ = 2.69 Hz, 7′), 7.30 (d, 1 H, $^4J_{7'}$ = 2.72 Hz, 5′), 6.58 (s, 1 H, 9), 5.84 (s, 1 H, $OH^{not\ sure}$), 5.80 (ddd, 1 H, $^3J_{11c}$ = 17.31 Hz, $^3J_{11t}$ = 10.48 Hz, $^3J_3$ = 6.84 Hz, 10), 5.16 (d, 1 H, $^3J_{10}$ = 18.63 Hz, 11*c*), 5.01 (d, 1 H, $^3J_{10}$ = 11.44 Hz, 11*t*), 4.54−4.45 (m, 1 H, 6b), 4.02 (s, 3 H, OCH_3), 3.91 (m, 1 H, 2b), 3.84−3.79 (m, 1 H, 8), 3.71−3.60 (m, 2 H, 2a*, 6a*), 3.69 (s, 3 H, NCH_3), 3.07 (m, 1 H, 3), 2.45−2.25 (m, 2 H, 4, 5b), 2.25−2.11 (m, 2 H, 7b, 5a), 1.64−1.54 (m, 1 H, 7a). − $C_{21}H_{27}BF_4N_2O_2 \times CH_2Cl_2$ (511.2): calcd. C 51.69, H 5.72, N 5.48; found C 52.08, H 5.79, N 5.45.

General Procedure for the Preparation of 14−19: To a solution of **13** in methanol, the chloro-bridged metal complex was added. After 16 h of vigorous stirring, the clear solution was concentrated to 1 mL and added to 20 mL of cold Et_2O. The precipitate was centrifuged off and washed twice with 15 mL of Et_2O and dried in vacuo for 2 d.

14: 65 mg of **13** (0.127 mmol) and 49 mg (0.064 mmol) of $[(PEt_3)PtCl_2]_2$ were used. − IR (KBr): $\tilde{\nu}$ = 3466 cm^{-1} s br. (OH), 3078 w (CH_{arom}), 2964 m, 2938 w (CH_{aliph}). − IR (PE): $\tilde{\nu}$ = 342 cm^{-1} s (M−Cl). − ^1H NMR (270 MHz, CD_3OD): δ = 9.40 (d, 1 H, $^3J_{7'}$ = 9.49 Hz, 8′), 8.96 (dd, 1 H, $^3J_{3'}$ = 5.37 Hz, ^4J_P = 3.53 Hz, 2′), 7.95 (d, 1 H, $^3J_{2'}$ = 5.35 Hz, 3′), 7.62 (dd, 1 H, $^3J_{8'}$ = 9.48 Hz, $^4J_{5'}$ = 2.57 Hz, 7′), 7.27 (d, 1 H, $^4J_{7'}$ = 2.56 Hz, 5′), 6.33 (s, br., 1 H, 9), 5.73 (ddd, 1 H, $^3J_{11c}$ = 17.32 Hz, $^3J_{11t}$ = 10.36 Hz, $^3J_3$ = 6.96 Hz, 10), 5.13 (dt, 1 H, $^3J_{10}$ = 16.01 Hz, $^2J_{11t}$ = $^4J_3$ = 0.95 Hz, 11*c*), 5.04 (dt, 1 H, $^3J_{10}$ = 10.37 Hz, $^2J_{11c}$ = $^4J_3$ = 1.15 Hz, 11*t*), 4.42−4.28 (m, 1 H, 6b), 4.06 (s, 3 H, OCH_3), 3.76−3.50 (m, 3 H, 2a, 2b, 8), 3.43 (s, 4 H, NCH_3, 6a*), 2.94−2.81 (m, 1 H, 3), 2.33−2.20 (m, 2 H, 7b, 4), 2.14−2.08 (m, 1 H, 5b), 2.05−1.91 [m, 6 H, $P(CH_2CH_3)_3$], 1.55−1.41 (m, 1 H, 7a), 1.15 [dt, 9 H, ^3J_p = 17.17 Hz, $^3J_{CH2}$ = 7.56 Hz, $P(CH_2CH_3)_3$], 1.38−1.10 (m, 1 H, 5a*). − ^{31}P NMR (109.3 MHz): δ = 1.05 ($^1J_{P\text{-}Pt}$ = 3391 Hz). − $C_{27}H_{42}BCl_2F_4N_2O_2PPt \times 0.5\ H_2O$ (819.4): calcd. C 39.58, H 5.29, N 3.42; found C 39.67, H 5.43, N 3.50.

15: 61 mg of **13** (0.119 mmol) and 56 mg (0.060 mmol) of $[(PBu_3)PtCl_2]_2$ were used. − IR (KBr): $\tilde{\nu}$ = 3430 cm^{-1} s br. (OH), 3077 w (CH_{arom}), 2957 s, 2931 w (CH_{aliph}). − IR (PE): $\tilde{\nu}$ = 342 cm^{-1} s (M−Cl). − ^1H NMR (270 MHz, [D_6]acetone): δ = 9.45 (d, 1 H, $^3J_{7'}$ = 9.42 Hz, 8′), 9.01 (dd, 1 H, $^3J_{3'}$ = 5.38 Hz, ^4J_P = 3.38 Hz, 2′), 8.05 (d, 1 H, $^3J_{2'}$ = 5.12 Hz, 3′), 7.62 (dd, 1 H, $^3J_{8'}$ = 9.52 Hz, $^4J_{5'}$ = 2.60 Hz, 7′), 7.38 (d, 1 H, $^4J_{7'}$ = 2.41 Hz, 5′), 6.64 (s, br., 1 H, 9), 5.81 (ddd, 1 H, $^3J_{11c}$ = 17.34 Hz, $^3J_{11t}$ = 10.30 Hz, $^3J_3$ = 7.03 Hz, 10), 5.15 (dt, 1 H, $^3J_{10}$ = 17.18 Hz, $^2J_{11t}$ = $^4J_3$ = 1.15 Hz, 11*c*), 5.01 (dt, 1 H, $^3J_{10}$ = 10.42 Hz, $^2J_{11c}$ = $^4J_3$ = 1.11 Hz, 11*t*), 4.50−4.41 (m, 1 H, 6b), 4.10−3.60 (m, 2a*, 2b*, 8*, 6b*), 4.06 (s, 3 H, OCH_3), 3.70 (s, 3 H, NCH_3,), 3.09−2.90 (m, 1 H, 3), 2.83 (s, br., 1 H, OH), 2.47−2.27 (m, 2 H, 7b, 4), 2.2−0.97 (5b*, 7a*, 5a*), 2.07−1.48 [3 m, 18 H, $P(C_3H_6CH_3)_3$], 1.00 [t, 9 H, $^3J_{CH2}$ = 7.28 Hz, $P(C_3H_6CH_3)_3$]. − ^{31}P NMR (109.3 MHz): δ = −6.65 ($^1J_{P\text{-}Pt}$ = 3426 Hz). − $C_{33}H_{54}BCl_2F_4N_2O_2PPt$ (894.6): calcd. C 44.31, H 6.08, N 3.13; found C 44.56, H 6.10, N 3.38.

16: 86 mg of **13** (0.168 mmol) and 50 mg (0.084 mmol) of $[(PEt_3)PdCl_2]_2$ were used. − IR (KBr): $\tilde{\nu}$ = 3450 cm^{-1} s br. (OH), 3077 w (CH_{arom}), 2975 m, 2938 m (CH_{aliph}). − IR (PE): $\tilde{\nu}$ = 352 cm^{-1} m (M−Cl). − ^1H NMR (400 MHz, CD_3OD): δ = 9.13 (s, br., 1 H, 8′), 8.88 (s, br., 1 H, 2′), 7.85 (d, 1 H, $^3J_{2'}$ = 4.88 Hz, 3′), 7.55 (dd, 1 H, $^3J_{8'}$ = 9.06 Hz, $^4J_{5'}$ = 1.53 Hz, 7′), 7.19 (d, 1 H, $^4J_{7'}$ = 2.23 Hz, 5′), 6.27 (s, 1 H, 9), 5.65 (ddd, 1 H, $^3J_{11c}$ = 17.15 Hz, $^3J_{11t}$ = 10.40 Hz, $^3J_3$ = 6.76 Hz, 10), 5.09 (d, 1 H, $^3J_{10}$ = 17.25 Hz, 11*c*), 4.97 (d, 1 H, $^3J_{10}$ = 10.53 Hz, 11*t*), 4.28 (m, 1 H, 6b), 4.00 (s, 3 H, OCH_3), 3.67−3.51 (m, 3 H, 2a, 2b, 8), 3.36 (s, 4 H, NCH_3, 6a*), 2.81 (m, 1 H, 3), 2.26−2.02 (m, 2 H, 7b, 4), 2.00−1.92 [m, 6 H, $P(CH_2CH_3)_3$], 1.72−1.10 (5b*, 7a*, 5a*), 1.30 [dt, 9 H, ^3J_P = 17.87 Hz, $^3J_{CH2}$ = 7.33 Hz, $P(CH_2CH_3)_3$]. − ^{31}P NMR (109.3 MHz): δ = 37.48. − $C_{27}H_{42}BCl_2F_4N_2O_2PPd \times H_2O$ (738.8): calcd. C 43.90, H 6.00, N 3.79; found C 44.21, H 5.91, N 3.62.

17: 88 mg of **13** (0.172 mmol) and 58 mg (0.086 mmol) of $[(PPr_3)PdCl_2]_2$ were used. − IR (KBr): $\tilde{\nu}$ = 3431 cm^{-1} s br. (OH), 3084 w (CH_{arom}), 2963 s, 2934 m (CH_{aliph}). − IR (PE): $\tilde{\nu}$ = 349 cm^{-1} m (M−Cl). − ^1H NMR (270 MHz, CD_3OD): δ = 9.15 (s, br., 1 H, 8′), 8.91 (d, 1 H, $^3J_{3'}$ = 5.24 Hz, 2′), 7.89 (d, 1 H, $^3J_{2'}$ = 5.18 Hz, 3′), 7.59 (dd, 1 H, $^3J_{8'}$ = 9.38 Hz, $^4J_{5'}$ = 2.42 Hz, 7′), 7.23 (d, 1 H, $^4J_{7'}$ = 2.47 Hz, 5′), 6.32 (s, 1 H, 9), 5.70 (ddd, 1 H, $^3J_{11c}$ = 17.21 Hz, $^3J_{11t}$ = 10.33 Hz, $^3J_3$ = 6.89 Hz, 10), 5.13 (d, 1 H, $^3J_{10}$ = 17.23 Hz, 11*c*), 5.02 (d, 1 H, $^3J_{10}$ = 10.44 Hz, 11*t*), 4.40−4.25 (m, 1 H, 6b), 4.05 (s, 3 H, OCH_3), 3.77−3.52 (m, 3 H, 2a, 2b, 8), 3.50−3.30 (m, 1 H, 6a*), 3.40 (s, 3 H, NCH_3), 2.93−2.79 (m, 1 H, 3), 2.33−2.16 (m, 2 H, 7b, 4), 2.01−1.73 [m, 13 H, $P(C_2H_4CH_3)_3$, 5b*], 1.51−1.37 (m, 1 H, 7a), 1.15 [t, 9 H, $^3J_{CH2}$ = 7.08 Hz, $P(C_2H_4CH_3)_3$], 0.95−0.90 (m, 1 H, 5a). − ^{31}P NMR (109.3 MHz): δ = 27.48. − $C_{30}H_{48}BCl_2F_4N_2O_2PPd \times 0.5\ H_2O$ (771.8): calcd. C 46.69, H 6.40, N 3.63; found C 46.61, H 6.37, N 3.64.

18: 79 mg of **13** (0.155 mmol) and 58 mg (0.077 mmol) of $[(PBu_3)PdCl_2]_2$ were used. − IR (KBr): $\tilde{\nu}$ = 3450 cm^{-1} s br. (OH), 3084 w (CH_{arom}), 2956 m, 2932 m (CH_{aliph}). − IR (PE): $\tilde{\nu}$ = 352 cm^{-1} m (M−Cl). − ^1H NMR (270 MHz, CD_3OD): δ = 9.14 (s, br., 1 H, 8′), 8.91 (d, 1 H, $^3J_{3'}$ = 4.96 Hz, 2′), 7.90 (d, 1 H, $^3J_{2'}$ = 5.22 Hz, 3′), 7.57 (dd, 1 H, $^3J_{8'}$ = 9.38 Hz, $^4J_{5'}$ = 2.57 Hz, 7′), 7.23 (d, 1 H, $^4J_{7'}$ = 2.52 Hz, 5′), 6.32 (s, 1 H, 9), 5.72 (ddd, 1 H, $^3J_{11c}$ = 17.23 Hz, $^3J_{11t}$ = 10.39 Hz, $^3J_3$ = 6.85 Hz, 10), 5.14 (dt, 1 H, $^3J_{10}$ = 16.00 Hz, $^2J_{11t}$ = $^4J_3$ = 0.85 Hz, 11*c*), 5.03 (dt, 1 H, $^3J_{10}$ = 10.36 Hz, $^2J_{11c}$ = $^4J_3$ = 1.15 Hz, 11*t*), 4.39−4.26 (m, 1 H, 6b), 4.05 (s, 3 H, OCH_3), 3.78−3.52 (m, 3 H, 2a, 2b, 8), 3.52−3.32 (m, 1 H, 6a*), 3.38 (s, 3 H, NCH_3), 2.91−2.80 (m, 1 H, 3), 2.36−2.18 (m, 2 H, 7b, 4), 2.12−0.90 (5b*, 7a*, 5a*), 2.05−1.90 [m, 6 H, $P(CH_2C_3H_7)_3$], 1.86−1.70 [m, 6 H, $P(CH_2CH_2C_2H_5)_3$], 1.66 −1.37 [m, 6 H, $P(C_2H_4CH_2CH_3)_3$], 1.02 [t, 9 H, $^3J_{CH2}$ = 7.35 Hz, $P(C_3H_6CH_3)_3$]. − ^{31}P NMR (109.3 MHz): δ = 28.67. − $C_{33}H_{54}BCl_2F_4N_2O_2PPd$ (804.9): calcd. C 49.24, H 6.76, N 3.48; found C 48.99, H 6.75, N 3.43.

19: 74.5 mg of **13** (0.146 mmol) and 58 mg (0.073 mmol) of $[Cp^*IrCl_2]_2$ were used. Slow concentration of a solution in acetone gave orange crystals. − IR (KBr): $\tilde{\nu}$ = 3395 cm^{-1} s br. (OH), 3083 w (CH_{arom}), 2963 m, 2922 m (CH_{aliph}). − IR (PE): $\tilde{\nu}$ = 281 cm^{-1} s, 254 m (M−Cl). − ^1H NMR (400 MHz, [D$_6$]acetone): δ = 9.26 (d, 1 H, $^3J_{3'}$ = 5.65 Hz, 2′), 9.01 (d, 1 H, $^3J_{7'}$ = 9.89 Hz, 8′), 7.55 (d, 1 H, $^3J_{2'}$ = 5.64 Hz, 3′), 7.24 (dd, 1 H, $^3J_{8'}$ = 9.60 Hz, $^4J_{5'}$ = 2.44 Hz, 7′), 6.51 (s, 1 H, 5′), 6.26 (s, 1 H, 9), 5.59 (ddd, 1 H, $^3J_{11c}$ = 17.39 Hz, $^3J_{11t}$ = 10.33 Hz, $^3J_3$ = 7.06 Hz, 10), 5.00 (d, 1 H, $^3J_{10}$ = 17.16 Hz, 11*c*), 4.88 (d, 1 H, $^3J_{10}$ = 10.49 Hz, 11*t*), 4.35−4.21 (m, 1 H, 6b), 4.02 (s, 3 H, OCH_3), 3.85 (dd, ^3J = 12.96 Hz, ^3J = 10.55 Hz, 2b), 3.67 (s, 3 H, NCH_3), 3.62−3.45 (m, 2 H, 2a, 8), 3.45−3.33 (m, 1 H, 6a), 2.98−2.78 (m, 1 H, 3), 2.34−2.20 (m, 1 H, 7b), 2.15−1.95 (m, 1 H, 4), 1.68−1.57 (m, 1 H, 5b), 1.38−1.09 (m, 7a*, 5a*), 1.27 [s, 15 H, $C_5(CH_3)_5$]. − $C_{31}H_{42}BCl_2IrF_4N_2O_2 \times H_2O$ (842.6): calcd. C 44.19, H 5.26, N 3.32; found C 44.29, H 5.22, N 3.16.

General Procedure for the Preparation of 20−22: To a solution of quinine in 10 mL of CH_2Cl_2 and the equivalent amount of CF_3SO_3H the chloro-bridged metal complex was added. After 16 h of stirring, the solvent of the yellow solution was removed in vacuo and the residue was washed twice with 5 mL of cold Et_2O. The yellow powder was dried in vacuo for 2 d.

20: 53 mg (0.163 mmol) of quinine, 14.3 μL (0.163 mmol) of CF_3SO_3H and 62.7 mg (0.082 mmol) of $[(PEt_3)PtCl_2]_2$ were used. − IR (KBr): $\tilde{\nu}$ = 3409 cm^{-1} vs br. (OH), 3083 m,sh (CH_{arom}), 2971 s, 2938 m (CH_{aliph}), 2692 w, 2665 w br. (N^+−H). − IR (PE): $\tilde{\nu}$ = 343 cm^{-1} s (M−Cl). − ^1H NMR (270 MHz, $CDCl_3$): δ = 9.33 (d, 1 H, $^3J_{7'}$ = 9.52 Hz, 8′), 8.92 (dd, 1 H, $^3J_{3'}$ = 5.30 Hz, ^4J_P = 3.43 Hz, 2′), 7.74 (d, 1 H, $^3J_{2'}$ = 5.25 Hz, 3′), 7.44 (dd, 1 H, $^3J_{8'}$ = 9.53 Hz, $^4J_{5'}$ = 2.39 Hz, 7′), 7.05 (d, 1 H, $^4J_{7'}$ = 2.32 Hz, 5′), 6.02 (s, 1 H, 9), 5.55 (ddd, 1 H, $^3J_{11c}$ = 17.12 Hz, $^3J_{11t}$ = 10.40 Hz, $^3J_3$ = 6.72 Hz, 10), 5.06 (d, 1 H, $^3J_{10}$ = 10.40 Hz, 11*t*), 5.03 (d, 1 H, $^3J_{10}$ = 16.93 Hz, 11*c*), 4.61 (s, br., 1 H, OH), 4.01−3.96 (m, 1 H, 6b), 3.74 (s, 3 H, OCH_3), 3.52 (dd, 1 H, *J* = 13.15 Hz, *J* = 10.90 Hz, 2b), 3.30 (pt, 1 H, *J* = 8.70 Hz, 8), 3.18−2.98 (m, 2 H, 2a, 6a), 2.75−2.64 (m, 1 H, 3), 2.11−1.74 (5b*, 5a*, 4*, 7b*), 2.01−1.88 [m, 6 H, $P(CH_2CH_3)_3$], 1.38 (m, 1 H, 7a), 1.28 [dt, 10 H, ^3J_P = 17.04 Hz, $^3J_{CH2}$ = 7.63 Hz, $P(CH_2CH_3)_3$]. − ^{31}P NMR (109.3 MHz): δ = 0.17 ($^1J_{P\text{-}Pt}$ = 3403 Hz). − $C_{27}H_{40}Cl_2F_3N_2O_5PPtS$ (858.6): calcd. C 37.77, H 4.70, N 3.26; found C 37.62, H 4.86, N 3.18.

21: 108 mg (0.333 mmol) of quinine, 29.2 μL (0.333 mmol) of CF_3SO_3H and 98 mg (0.166 mmol) of $[(PEt_3)PdCl_2]_2$ were used. − IR (KBr): $\tilde{\nu}$ = 3442 cm^{-1} vs br. (OH), 2970 m, 2938 m (CH_{aliph}), 2692 w, 2665 w, 2606 w (N^+−H). − IR (PE): $\tilde{\nu}$ = 352 cm^{-1} s (M−Cl). − ^1H NMR (270 MHz, $CDCl_3$): δ = 9.11 (d, 1 H, $^3J_{7'}$ = 9.22 Hz, 8′), 8.89 (dd, 1 H, $^3J_{3'}$ = 5.21 Hz, ^4J_P = 3.41 Hz, 2′), 7.71 (d, 1 H, $^3J_{2'}$ = 5.29 Hz, 3′), 7.43 (dd, 1 H, $^3J_{8'}$ = 9.30 Hz, $^4J_{5'}$ = 2.41 Hz, 7′), 7.02 (d, 1 H, $^4J_{7'}$ = 1.95 Hz, 5′), 5.95 (s, 1 H, 9), 5.23 (ddd, 1 H, $^3J_{11c}$ = 17.01 Hz, $^3J_{11t}$ = 10.40 Hz, $^3J_3$ = 6.64 Hz, 10), 5.04 (d, 1 H, $^3J_{10}$ = 10.24 Hz, 11*t*), 5.01 (d, 1 H, $^3J_{10}$ = 16.64 Hz, 11*c*), 4.65 (s, br., 1 H, OH), 3.99−3.85 (m, 1 H, 6b), 3.79 (s, 3 H, OCH_3), 3.50 (dd, 1 H, *J* = 13.04 Hz, *J* = 10.98 Hz, 2b), 3.27 (pt, 1 H, *J* = 8.95 Hz, 8), 3.13−2.98 (m, 2 H, 2a, 6a), 2.68 (m, 1 H, 3), 2.1−1.2 (5b*, 4*, 7b*, 5a*, 7a*), 2.07−1.90 [m, 6 H, $P(CH_2CH_3)_3$], 1.32 [dt, 9 H, ^3J_P = 17.83 Hz, $^3J_{CH2}$ = 7.60 Hz, $P(CH_2CH_3)_3$]. − ^{31}P NMR (109.3 MHz): δ = 36.15. − $C_{27}H_{40}Cl_2F_3N_2O_5PPdS$ (770.0): calcd. C 42.12, H 5.24, N 3.64; found C 41.62, H 5.66, N 3.49.

22: 316 mg (0.974 mmol) of quinine, 85.5 μL (0.974 mmol) of CF_3SO_3H and 328 mg (0.487 mmol) of $[(PPr_3)PdCl_2]_2$ were used. − IR (KBr): $\tilde{\nu}$ = 3402 cm^{-1} s br. (OH), 2964 s, 2930 m (CH_{aliph}), 2692 m, 2665 m br. (N^+−H). − IR (PE): $\tilde{\nu}$ = 350 cm^{-1} s (M−Cl). − ^1H NMR (270 MHz, $CDCl_3$): δ = 9.18 (s, br., 1 H, NH), 9.11 (d, 1 H, $^3J_{7'}$ = 9.37 Hz, 8′), 8.90 (dd, 1 H, $^3J_{3'}$ = 5.21 Hz, ^4J_P = 3.49 Hz, 2′), 7.71 (d, 1 H, $^3J_{2'}$ = 5.31 Hz, 3′), 7.44 (dd, 1 H, $^3J_{8'}$ = 9.43 Hz, $^4J_{5'}$ = 2.53 Hz, 7′), 7.02 (d, 1 H, $^4J_{7'}$ = 2.24 Hz, 5′), 5.98 (d, 1 H, ^3J = 3.09 Hz, 9), 5.54 (ddd, 1 H, $^3J_{11c}$ = 17.25 Hz, $^3J_{11t}$ = 10.49 Hz, $^3J_3$ = 6.76 Hz, 10), 5.06 (d, 1 H, $^3J_{10}$ = 10.04 Hz, 11*t*), 5.02 (d, 1 H, $^3J_{10}$ = 16.77, 11*c*), 4.58 (d, 1 H, ^3J = 3.54 Hz, $OH^{not\ sure}$), 4.01−3.88 (m, 1 H, 6b), 3.78 (s, 3 H, OCH_3), 3.52 (pt, 1 H, *J* = 12.03 Hz, 2b), 3.28 (pt, 1 H, *J* = 8.73 Hz, 8), 3.12−3.01 (m, 2 H, 2a, 6a), 2.68 (s, br., 1 H, 3), 2.07−1.1 (5b*, 4*, 7b*, 5a*,

7a*), 2.07−1.70 [2 m, 12 H, P($C_2H_4CH_3$)$_3$], 1.13 [t, 9 H, $^3J_{CH2}$ = 6.96 Hz, P($C_2H_4CH_3$)$_3$]. − ^{31}P NMR (109.3 MHz): δ = 26.94. − $C_{30}H_{46}Cl_2F_3N_2O_5PPdS$ (811.1): calcd. C 44.43, H 5.72, N 3.45; found C 43.90, H 5.99, N 3.32.

23: To a solution of 261 mg (1.90 mmol) of $ZnCl_2$ in 10 mL of methanol a solution of 621 mg (2.11 mmol) of cinchonine in 10 mL of methanol was added and stirred for 1 h. At once a white precipitate was obtained which was crystallized by slow concentration of a solution in MeOH/CH_3CN to give clear colourless crystals which were powdered and dried in vacuo for 2 d. − IR (KBr): $\tilde{\nu}$ = 3389 cm^{-1} vs br. (OH), 3084 m (CH_{arom}), 2944 s (CH_{aliph}), 2600 m br. (N^+−H). − ^{1}H NMR (400 MHz, [D_6]acetone): δ = 12.27 (s, br., 1 H, NH), 8.88 (d, 1 H, $^3J_{3'}$ = 4.44 Hz, 2′), 8.49 (d, 1 H, $^3J_{7'}$ = 8.36 Hz, 8′), 7.95 (d, 1 H, $^3J_{6'}$ = 9.87 Hz, 5′), 7.54 (ddd, 1 H, $^3J_{5'}$ = 8.32 Hz, $^3J_{7'}$ = 6.93 Hz, $^4J_{8'}$ = 1.38 Hz, 6′), 7.30 (ddd, 1 H, $^3J_{8'}$ = 8.25 Hz, $^3J_{6'}$ = 6.90 Hz, $^4J_{5'}$ = 1.35 Hz, 7′), 6.78 (d, 1 H, *J* = 3.53 Hz, 9), 6.32 (d, 1 H, *J* = 4.05 Hz), 6.17 (ddd, 1 H, $^3J_{11c}$ = 17.63 Hz, $^3J_{11t}$ = 10.25 Hz, $^3J_3$ = 7.38 Hz, 10), 5.27 (dt, 1 H, $^3J_{10}$ = 17.48 Hz, $^2J_{11t}$ = $^4J_3$ = 1.38 Hz, 11*c*), 5.21 (dt, 1 H, $^3J_{10}$ = 10.27 Hz, $^2J_{11c}$ = $^4J_3$ = 1.16 Hz, 11*t*), 4.29−4.24 (m, 1 H, 2b), 3.60−1.18 (7m, 11 H, 6b, 2a, 8, OH, 3, 6a, 5b, 4, 7b, 7a, 5a).

General Procedure for the Preparation of 24−29: A solution of quinine in 10 mL of CH_2Cl_2 and the equivalent amount of a solution of NaOMe in methanol was cooled to −78°C. After the addition of 0.5 equivalents of [R_3PMCl_2]$_2$ or of [Cp*$IrCl_2$]$_2$, the solution was allowed to warm up to room temp. for 16 h and stirred for another 2 h. To the yellow solution again 0.5 equivalents of [R_3PMCl_2]$_2$ or of [Cp*$IrCl_2$]$_2$ were added. After 16 h of stirring, the solvent was removed in vacuo, the residue was dissolved in CH_2Cl_2 and the mixture was filtered through Celite to remove NaCl. The solvent was removed again in vacuo and the residue was washed twice with 5 mL of cold Et_2O to give a yellow powder which was dried in vacuo for several days.

24: 59 mg (0.182 mmol) of quinine, 0.182 mmol of NaOMe in MeOH and 140 mg (0.182 mmol) of [(PEt_3)$PtCl_2$]$_2$ were used. − IR (KBr): $\tilde{\nu}$ = 3073 cm^{-1} w (CH_{arom}), 2962 s, 2935 m (CH_{aliph}). − IR (PE): $\tilde{\nu}$ = 340 cm^{-1} s, 331 s sh (M−Cl). − ^{1}H NMR (400 MHz, $CDCl_3$): δ = 9.40 (d, 1 H, $^3J_{7'}$ = 9.65 Hz, 8′), 9.27 (d, 1 H, $^3J_{2'}$ = 5.11 Hz, 3′), 8.99 (dd, 1 H, $^3J_{3'}$ = 5.52 Hz, ^4J_P = 3.42 Hz, 2′), 7.49 (dd, 1 H, $^3J_{8'}$ = 9.44 Hz, $^4J_{5'}$ = 2.54 Hz, 7′), 7.05 (d, 1 H, $^4J_{7'}$ = 2.48 Hz, 5′), 5.96 (ddd, 1 H, $^3J_{11c}$ = 17.22 Hz, $^3J_{11t}$ = 10.37 Hz, $^3J_3$ = 6.85 Hz, 10), 5.22−5.15 (m, 3 H, 9, 11*c*, 11*t*), 3.94−3.75 (m, 2 H, 8*, 2b*), 3.81 (s, 3 H, OCH_3), 3.45−3.41 (m, 1 H, 2a), 3.27−3.21 (m, 1 H, 6b), 3.01−2.92 (m, 1 H, 6a), 2.44 (m, 1 H, 3), 2.20−2.09 (m, 1 H, 7b), 2.09−1.20 (4*, 5b*, 7a*, 5a*) 2.05−1.98 [m, 6 H, N′PtP(CH_2CH_3)$_3$], 1.92−1.83 [m, 6 H, (N,O)PtP(CH_2CH_3)$_3$], 1.37−1.23 (m, 18 H, N′PtP(CH_2CH_3)$_3$, (N,O)PtP(CH_2CH_3)$_3$]. − ^{31}P NMR (109.3 MHz): δ = 6.18 (N′PtP, $^1J_{P\text{-}Pt}$ = 3636 Hz), −0.20 [(N,O)PtP, $^1J_{P\text{-}Pt}$ = 3382 Hz]. − $C_{32}H_{53}Cl_3N_2O_2P_2Pt_2$ × 0.5 CH_2Cl_2 (1098.7): calcd. C 35.53, H 4.95. N 2.55; found C 35.16, H 5.19, N 2.54.

25: 67 mg (0.207 mmol) of quinine, 0.207 mmol of NaOMe in MeOH and 122 mg (0.207 mmol) of [(PEt_3)$PdCl_2$]$_2$ were used. − IR (KBr): $\tilde{\nu}$ = 3077 cm^{-1} w (CH_{arom}), 2964 s, 2931 m (CH_{aliph}). − IR (PE): $\tilde{\nu}$ = 356 cm^{-1} s, 328 m (M−Cl). − ^{1}H NMR (270 MHz, $CDCl_3$): δ = 9.20 (d, 1 H, $^3J_{7'}$ = 9.38 Hz, 8′), 9.11 (d, 1 H, $^3J_{2'}$ = 4.92 Hz, 3′), 9.01 (dd, 1 H, $^3J_{3'}$ = 5.24 Hz, ^4J_P = 3.50 Hz, 2′), 7.48 (dd, 1 H, $^3J_{8'}$ = 9.46 Hz, $^4J_{5'}$ = 2.54 Hz, 7′), 7.03 (d, 1 H, $^4J_{7'}$ = 2.71 Hz, 5′), 5.96 (ddd, 1 H, $^3J_{11c}$ = 17.12 Hz, $^3J_{11t}$ = 10.25 Hz, $^3J_3$ = 6.77 Hz, 10), 5.44 (d, 1 H, $^3J_8$ = 6.85 Hz, 9), 5.19 −5.12 (2m, 2 H, 11*c*, 11*t*), 3.94−3.78 (m, 1 H, 8*), 3.86 (s, 3 H, OCH_3), 3.64 (dd, 1 H, *J* = 13.74 Hz, *J* = 10.32 Hz, 2b), 3.38 (pd, 1 H, *J* = 14.28 Hz, 2a), 3.23−2.93 (m, 2 H, 6b, 6a), 2.39 (m, 1 H, 3), 2.14−1.71 (m, 3 H, 7b*, 5b*, 4*), 2.14−1.95 [m, 6 H, N′PdP(CH_2CH_3)$_3$], 1.91−1.71 [m, 6 H, (N,O)PdP(CH_2CH_3)$_3$], 1.48−1.22 (m, 18 H, N′PdP(CH_2CH_3)$_3$, (N,O)PdP(CH_2CH_3)$_3$], 1.48−1.02 (m, 2 H, 7a*, 5a*). − ^{31}P NMR (109.3 MHz): δ = 35.01 (N′PdP), 31.39 [(N,O)PdP]. − $C_{32}H_{53}Cl_3N_2O_2P_2Pd_2$ (878.9): calcd. C 43.73, H 6.08, N 3.13; found C 43.45, H 6.08, N 3.18.

26: 188 mg (0.639 mmol) of cinchonine, 0.639 mmol of NaOMe in MeOH and 377 mg (0.639 mmol) of [(PEt_3)$PdCl_2$]$_2$ were used. Crystals were obtained from a $CHCl_3$/hexane solution. − IR (KBr): $\tilde{\nu}$ = 3084 cm^{-1} w (CH_{arom}), 2957 s, 2938 s (CH_{aliph}). − IR (PE): $\tilde{\nu}$ = 359 cm^{-1} s, 324 m (M−Cl). − ^{1}H NMR (270 MHz, $CDCl_3$): δ = 9.28 (d, 1 H, $^3J_{3'}$ = 8.31 Hz, 8′), 9.21−9.13 (m, 2 H, 2′, 5′), 7.78 (t, 1 H, ^3J = 7.84 Hz, 7′), 7.76 (3′*), 7.49 (t, 1 H, ^3J = 7.30 Hz, 6′), 5.52 (d, 1 H, $^3J_8$ = 6.77 Hz, 9), 4.77 (ddd, 1 H, $^3J_{11c}$ = 16.88 Hz, $^3J_{11t}$ = 10.51 Hz, $^3J_3$ = 6.27 Hz, 10), 4.52 (d, 1 H, $^3J_{10}$ = 10.59 Hz, 11*t*), 4.11 (d, 1 H, $^3J_{10}$ = 17.12 Hz, 11*c*), 3.78−3.69 (m, 1 H, 8), 3.44−3.20 (m, 3 H, 6b, 2b, 6a), 2.71−2.61 (m, 1 H, 2a), 2.13−1.07 (3*, 4*, 7a*, 5a*, 5b*), 2.08−1.95 [m, 6 H, N′PdP(CH_2CH_3)$_3$], 1.88−1.72 [m, 6 H, (N,O)PdP(CH_2CH_3)$_3$], 1.41−1.22 [m, 18 H, N′PdP(CH_2CH_3)$_3$, (N,O)PdP(CH_2CH_3)$_3$]. − ^{31}P NMR (109.3 MHz): δ = 34.99 (N′PdP), 31.33 [(N,O)PdP]. − $C_{31}H_{51}Cl_3N_2OP_2Pd_2$ × 0.75 $CHCl_3$ (938.4): calcd. C 40.64, H 5.56, N 2.98; found C 40.58, H 5.55, N 2.94.

27: 60 mg (0.185 mmol) of quinine, 0.185 mmol of NaOMe in MeOH and 124 mg (0.185 mmol) of [(PPr_3)$PdCl_2$]$_2$ were used. − IR (KBr): $\tilde{\nu}$ = 3077 cm^{-1} w (CH_{arom}), 2957 vs, 2931 s (CH_{aliph}). − IR (PE): $\tilde{\nu}$ = 352 cm^{-1} s, 330 m (M−Cl). − ^{1}H NMR (400 MHz, $CDCl_3$): δ = 9.16 (d, 1 H, $^3J_{7'}$ = 9.53 Hz, 8′), 9.05 (d, 1 H, $^3J_{2'}$ = 5.21 Hz, 3′), 8.97 (dd, 1 H, $^3J_{3'}$ = 5.26 Hz, ^4J_P = 3.49 Hz, 2′), 7.45 (dd, 1 H, $^3J_{8'}$ = 9.28 Hz, $^4J_{5'}$ = 2.49 Hz, 7′), 7.00 (d, 1 H, $^4J_{7'}$ = 2.51 Hz, 5′), 5.92 (ddd, 1 H, $^3J_{11c}$ = 17.25 Hz, $^3J_{11t}$ = 10.38 Hz, $^3J_3$ = 6.88 Hz, 10), 5.44 (d, 1 H, $^3J_8$ = 6.78 Hz, 9), 5.14−5.10 (2 m, 2 H, 11*c*, 11*t*), 3.88−3.76 (m, 1 H, 8*), 3.84 (s, 3 H, OCH_3), 3.60 (dd, 1 H, *J* = 13.54 Hz, *J* = 10.34 Hz, 2b), 3.33 (pd, 1 H, *J* = 13.93 Hz, 2a), 3.15−3.09 (m, 1 H, 6b), 3.00−2.92 (m, 1 H, 6a), 2.34 (m, 1 H, 3), 2.04−1.60 (m, 3 H, 7b*, 5b*, 4*), 2.04−1.92 [m, 12 H, N′PdP($CH_2C_2H_5$)$_3$, (NO)PdP($CH_2C_2H_5$)$_3$], 1.92−1.60 [m, 12 H, N′PdP($CH_2CH_2CH_3$)$_3$ (N,O)PdP($CH_2CH_2CH_3$)$_3$], 1.36−1.00 (m, 2 H, 7a*, 5a*), 1.2−1.0 [m, 18 H, N′PdP($C_2H_4CH_3$)$_3$, (N,O)PdP($C_2H_4CH_3$)$_3$]. − ^{31}P NMR (109.3 MHz): δ = 28.67 (0.05 $NPdCl_2P^{not\ sure}$), 25.69 (N′PdP), 22.39 [(N,O)PdP]. − $C_{38}H_{65}Cl_3N_2O_2P_2Pd_2$ (963.1): calcd. C 47.39, H 6.80, N 2.91; found C 47.92, H 7.04, N 2.89.

28: 52 mg (0.160 mmol) of quinine, 0.160 mmol of NaOMe in MeOH and 121 mg (0.121 mmol) of [(PBu_3)$PdCl_2$]$_2$ were used. The residue was washed twice with 10 mL of cold hexane. − IR (KBr): $\tilde{\nu}$ = 3076 cm^{-1} w (CH_{arom}), 2960 s, 2930 m (CH_{aliph}). − IR (PE): $\tilde{\nu}$ = 355 cm^{-1} s, 327 m (M−Cl). − ^{1}H NMR (400 MHz, $CDCl_3$): δ = 9.15 (d, 1 H, $^3J_{7'}$ = 9.20 Hz, 8′), 9.07 (d, 1 H, $^3J_{2'}$ = 5.19 Hz, 3′), 8.94 (dd, 1 H, $^3J_{3'}$ = 5.09 Hz, ^4J_P = 3.68 Hz, 2′), 7.42 (dd, 1 H, $^3J_{8'}$ = 9.35 Hz, $^4J_{5'}$ = 2.63 Hz, 7′), 6.98 (d, 1 H, $^4J_{7'}$ = 2.21 Hz, 5′), 5.91 (ddd, 1 H, $^3J_{11c}$ = 17.15 Hz, $^3J_{11t}$ = 10.24 Hz, $^3J_3$ = 6.91 Hz, 10), 5.38 (d, 1 H, $^3J_8$ = 6.60 Hz, 9), 5.11 (d, 1 H, $^3J_{10}$ = 16.07 Hz, 11*c*), 5.10 (d, 1 H, $^3J_{10}$ = 11.69 Hz, 11*t*), 3.88−3.78 (m, 1 H, 8*), 3.82 (s, 3 H, OCH_3), 3.58 (dd, 1 H, *J* = 13.43 Hz, *J* = 10.50 Hz, 2b), 3.33 (pd, 1 H, *J* = 13.59 Hz, 2a), 3.14−3.08 (m, 1 H, 6b), 2.99−2.92 (m, 1 H, 6a), 2.32 (m, 1 H, 3), 2.09−0.90 (7b*, 5b*, 4*, 7a*, 5a*), 2.09−0.90 [4 m, 54 H, N′PdP(C_4H_9)$_3$, (NO)PdP(C_4H_9)$_3$]. − ^{31}P NMR (109.3 MHz): δ = 26.98 (N′PdP), 23.40 [(N,O)PdP]. − $C_{44}H_{77}Cl_3N_2O_2P_2Pd_2$ (1047.4): calcd. C 50.46, H 7.41, N 2.67; found C 50.44, H 7.71, N 2.65.

29: 67 mg (0.207 mmol) of quinine, 0.207 mmol of NaOMe in MeOH and 165 mg (0.207 mmol) of $[Cp^*IrCl_2]_2$ were used. − IR (KBr): $\tilde{\nu}$ = 3071 cm^{-1} w (CH_{arom}), 2961 m, 2918 s (CH_{aliph}). − IR (PE): $\tilde{\nu}$ = 288 cm^{-1} m (M−Cl). − ^1H NMR (270 MHz, $CDCl_3$): δ = 9.55 (d, 1 H, $^3J_{3'}$ = 5.20 Hz, 2′), 9.13 (d, 1 H, $^3J_{7'}$ = 8.56 Hz, 8′), 7.96 (d, 1 H, $^3J_{2'}$ = 5.58 Hz, 3′), 7.31 (dd, 1 H, $^3J_{8'}$ = 9.80 Hz, $^4J_{5'}$ = 2.74 Hz, 7′), 6.87 (d, 1 H, $^4J_{7'}$ = 2.85 Hz, 5′), 6.03 (d, 1 H, ^3J = 9.74 Hz, 9), 5.28−5.11 (m, 1 H, 10), 4.63 (d, 1 H, $^3J_{10}$ = 18.81 Hz, 11*c*), 4.53−4.35 (m, 1 H, 11*t*), 3.95−3.69 (8*, 2b*), 3.84 (s, 3 H, OCH_3), 3.37−3.31 (m, 3 H, 2a, 6a, 6b), 2.11 (m, 1 H, 3), 1.7−1.2 (7b*, 4*, 5b*, 7a*), 1.68 {s, 15 H, N′$IrCl_2[C_5(CH_3)_5]$}, 1.41 {s, 15 H, (N,O)$IrCl[C_5(CH_3)_5]$}, 0.78−0.65 (m, 1 H, 5a). − $C_{40}H_{53}Cl_3Ir_2N_2O_2$ (1084.7): calcd. C 44.29, H 4.93, N 2.58; found C 44.40, H 5.24, N 2.31.

30: To a solution of 142 mg (0.287 mmol) of PPh_3AuCl in 5 mL of CH_2Cl_2 a solution of 49 mg (0.287 mmol) of $AgNO_3$ in 10 mL of methanol was added. After 1 h of vigorous stirring with exclusion of light, AgCl was centrifuged off and 46.5 mg (0.144 mmol) of quinine was added. The solution was stirred for another 3 h to give a clear colourless solution which was concentrated to about 0.5 mL and added to 20 mL of Et_2O. The white precipitate was washed twice with Et_2O and dried in vacuo for 2 d. − IR (KBr): $\tilde{\nu}$ = 3430 cm^{-1} vs br. (OH), 3077 m (CH_{arom}), 2938 m (CH_{aliph}). − ^1H NMR (400 MHz, $CDCl_3$): δ = 8.82 (d, 1 H, $^3J_{3'}$ = 5.12 Hz, 2′), 8.33 (d, 1 H, $^3J_{7'}$ = 9.54 Hz, 8′), 8.03 (d, 1 H, $^3J_{2'}$ = 5.01 Hz, 3′), 7.65−7.30 (m, 32 H, 2 PPh_3, 5′, 7′), 6.50 (s, br., 1 H, 9), 5.77 (ddd, 1 H, $^3J_{11c}$ = 17.21 Hz, $^3J_{11t}$ = 9.81 Hz, $^3J_3$ = 7.32 Hz, 10), 5.05 (d, 1 H, $^3J_{10}$ = 18.59 Hz, 11*c*), 5.01 (d, 1 H, $^3J_{10}$ = 10.47 Hz, 11*t*), 4.39 (s, br., 1 H, OH), 3.75−3.55 (6b*), 3.63 (s, 3 H, OCH_3), 3.5−3.2 (m, 4 H, 2b, 8, 2a, 6a), 2.59 (m, 1 H, 3), 2.24−1.2 (4m, 5 H, 5b, 4, 7b, 5a, 7a). − ^{31}P NMR (109.3 MHz): δ = 28.54. − $C_{56}H_{54}AuN_4O_8P_2 \times CH_2Cl_2$(1451.9): calcd. C 47.15, H 3.89. N 3.86; found C 47.32, H 3.95, N 3.91.

31: 46 mg (0.126 mmol) of $[(allyl)PdCl]_2$ and 41 mg (0.126 mmol) of quinine were dissolved in 15 mL of CH_2Cl_2. After stirring for 3 h, the solvent was removed in vacuo and the grey-green solid was washed twice with pentane and dried in vacuo for 2 d. − IR (KBr): $\tilde{\nu}$ = 3358 cm^{-1} vs br. (OH), 3070 w (CH_{arom}), 2934 m (CH_{aliph}). − IR (PE): $\tilde{\nu}$ = 276 cm^{-1} s (M−Cl). − ^1H NMR (400 MHz, CD_2Cl_2): δ = 8.74 (d, 1 H, $^3J_{3'}$ = 5.09 Hz, 2′), 8.45 (d, 1 H, $^3J_{7'}$ = 9.60 Hz, 8′), 7.72 (d, 1 H, $^3J_{2'}$ = 5.24 Hz, 3′), 7.58 (s, br., 1 H, 5′), 7.40 (dd, 1 H, $^3J_{8'}$ = 9.27 Hz, $^4J_{5'}$ = 2.51 Hz, 7′), 6.51 (s, br., 1 H, 9), 5.67−5.47 [m, 3 H, 10, NPdC*H*$(CH_2)_2$, N′PdC*H*$(CH_2)_2$], 5.00 (d, 1 H, $^3J_{10}$ = 17.09 Hz, 11*c*), 4.86 (d, 1 H, $^3J_{10}$ = 10.60 Hz, 11*t*), 4.68 (s, br., 1 H, OH), 4.27 (s, br., 1 H, 6b), 4.01 (s, 3 H, OCH_3), 3.91 [m, 6 H, 8*, 2b*, N′PdCH($CH H_{endo}$)$_2$, NPdCH($CH H_{endo}$)$_2$], 3.38−3.30 (m, 1 H, 2a), 3.20−3.10 (m, 1 H, 6a), 3.10−2.90 [m, 4 H, N′PdCH($CH H_{exo}$)$_2$, NPdCH($CH H_{exo}$)$_2$], 2.31 (m, 1 H, 3), 1.75−1.65 (m, 3 H, 4, 7b, 5b), 1.55−1.50 (m, 1 H, 5a), 1.07−1.00 (m, 1 H, 7a). − $C_{26}H_{34}Cl_2N_2O_2Pd_2 \times 0.25\ CH_2Cl_2$ (711.5): calcd. C 44.31, H 4.89, N 3.94; found C 44.29, H 5.10, N 3.66.

32: To a solution of 410 mg (1.26 mmol) of quinine in 20 mL of aqueous 0.1 N HCl 524 mg (1.26 mmol) of K_2PtCl_4 were added. At once a light red precipitate was obtained which was dissolved again by the addition of 10 mL of 2 N HCl. The red solution was stirred for several hours at 90°C until a yellow precipitate was formed which was washed twice with 10 mL of water, once with 10 mL of ethanol and once with 10 mL of Et_2O and was dried in vacuo. Yellow crystals were obtained from 1 N HCl. − IR (KBr): $\tilde{\nu}$ = 3418 cm^{-1} vs br. (OH), 2827−2448 vs br. (N^+−H). − IR (PE): $\tilde{\nu}$ = 332 cm^{-1} s, 304 m (M−Cl). − ^1H NMR (400 MHz, [D_7]DMF): δ = 12.55 (s, 0.5 H, NH^+), 12.35 (s, 0.5 H, NH^+), 9.315 (d, 0.5 H, $^3J_{3'}$ = 5.64 Hz, 2′), 9.298 (d, 0.5 H, $^3J_{3'}$ = 5.91 Hz, 2′), 8.45−8.38 (m, 2 H, 3′, 8′), 8.10 (pt, 1 H, $^4J_{7'}$ = 2.64 Hz, 5′), 7.82−7.78(m, 1 H, 7′), 7.20 (s, br., 1 H, N′H), 6.87 (s, 0.5 H, 9), 6.83 (s, 0.5 H, 9), 4.92−4.77 (m, 1 H, 10), 4.26−4.01 (11*t**,11*c**, 8*, 6b*), 4.19 (s, 1.5 H, OCH_3), 4.17 (s, 1.5 H, OCH_3), 3.72−3.66 (m, 1 H, 2b), 3.42−3.28 (m, 2 H, 2a, 6a), 3.18 (s, br., 0.5 H, 3), 2.8−2.7 (0.5 H, 3), 2.38−1.80 (5m, 5 H, 5b, 4, 5a, 7b, 7a). − $C_{20}H_{26}Cl_4N_2O_2Pt$ (663.3): calcd. C 36.21, H 3.95, N 4.22; found C 35.68, H 4.30, N 4.02.

Acknowledgments

We thank the Deutsche Forschungsgemeinschaft, the Fonds der Chemischen Industrie, the Wacker Chemie, München, for generous support and the Degussa AG, Hanau, for gifts of chemicals.

[1] Part CXII: K. Haas, E. M, Ehrenstorfer-Schäfers, K. Polborn, W. Beck, *Eur. J. Inorg. Chem.* **1998**, 465−469.
[2] X-ray structure analyses.
[3] O. Cervinka, J. Fusek, *Collect. Czech. Chem. Commun.* **1973**, *38*, 441−446; O. Cervinka, O. Kriz, *Collect. Czech. Chem. Commun.* **1973**, *38*, 294−297; R. M. Lequan, M. Lequan, *Tetrahedron Lett*. **1981**, *22*, 1323−1326; M. Lequan, R. M. Lequan, *J. Organomet. Chem.* **1982**, *226*, 35−40; K. Kobayashi, T. Okamoto, T. Oida, S. Tanimoto, *Chem. Lett*. **1986**, 2031−2034; E. N. Jacobsen, I. Marko, M. B. France, J. S. Svendsen, K. B. Sharpless, *J. Am. Chem. Soc.* **1989**, *111*, 737−739; J. T. Wehrli, A. Baiker, D. M. Monti, H. U. Blaser, H. P. Jalett, *J. Mol. Catal.* **1989**, *57*, 245−257; M. Garland, H. U. Blaser, *J. Am. Chem. Soc.* **1990**, *112*, 7048−7050; W. A. H. Vermeer, A. Fulford, P. Johnston, P. B. Wells, *J. Chem. Soc., Chem. Commun.* **1993**, *13*, 1053−1054; O. Riant, H. B. Kagan, L. Ricard, *Tetrahedron* **1994**, *50*, 4543−4554; Y. Nitta, K. Kobiro, *Chem. Lett.* **1996**, 897−898; H. Brunner, B. Kimel, *Monatsh. Chem*. **1996**, *127*, 1063−1072; H. Bönnemann, G. A. Braun, *Angew. Chem.* **1996**, *108*, 2120−2122; *Angew. Chem. Int. Ed. Engl.* **1996**, *35*, 1992−1995; H. Okamura, Y. Nakamura, T. Iwagawa, M. Nakatani, *Chem. Lett* **1996**, *3*, 193; B. Lygo, P. G. Wainwright, *Tetrahedron Lett.* **1997**, *38*, 8595−8598; A. Baiker, *J. Mol. Catal. A: Chem.* **1997**, *115*, 473−493; *Spec. Publ. R. Soc. Chem.* (Eds.: B. K. Hodnett, A. P. Kybett, J. H. Clark, K. Smith,), Royals Society at Chemistry, Cambridge, UK, **1998**, p. 216; I. E. Marko, J. S. Svendsen in *Comprehensive Organometallic Chemistry II* (Eds.: E. W. Abel, F. G. A. Stone, G. Wilkinson), Pergamon, **1995**, vol. 12, p. 1137−1176; M. Schürch, T. Heinz, R. Acchimann, T. Mallat, A. Pfaltz, A. Baiker, *J. Catal.* **1998**, *173*, 187−195; M. Bartók, K. Feldöldi, B. Török, T. Bartók, *Chem. Commun.* **1998**, 2605−2606.
[4] M. G. Finn, K. B. Sharpless, *Asymmetric Synthesis* (Ed.: J. D. Morrison), Academic Press, New York, **1985**, vol. 5, p. 259; H. C. Kolb, M. S. VanNieuwenhze, K. B. Sharpless, *Chem. Rev.* **1994**, *94*, 2483−2547; B. J. Berriesford, C. Bolm, K. B. Sharpless, *Angew. Chem.* **1995, 107**, 1159−1171; *Angew. Chem. Int. Ed. Engl.* **1995**, *34*, 1050−1064 and references therein.
[5] H. C. Kolb, P. G. Andersson, K. B. Sharpless, *J. Am. Chem. Soc.* **1994**, *116*, 1278−1291; P.-O. Norrby, H. C. Kolb, K. B. Sharpless, *J. Am. Chem. Soc.* **1994**, *116*, 8470−8478 and references therein.
[6] C. Noe, E. J. Corey, *J. Am. Chem. Soc.* **1996**, *118*, 11038−11053.
[7] J. S. Svendsen, I. Markó, E. N. Jakobsen, Ch. P. Rao, S. Bott, K. B. Sharpless, *J. Org. Chem.* **1989**, *54*, 2263−2264.
[8] Z. Foldi, T. Foldi, A. Foldi, *Acta Chim. Acad. Sci. Hung.* **1958**, *16*, 185; J. M. Tsangaris, G. T. Baxevanidis, *Z. Naturforsch.* **1974**, *29b*, 532−537; J. M. Tsangaris, T. A. Kabanos, *Monatsh. Chem*. **1982**, *113*, 1393−1398.
[9] C. Missling, S. Mihan, K. Polborn, W. Beck, *Chem. Ber.* **1996**, *129*, 331−335.
[10] R. Verpoorte in *The Chemistry of Heterocyclic Compounds − Monoterpenoid Indole Alkaloids* (Ed.: J. E. Saxton), J. Wiley, Cichester, supplement to part 4, **1994**, p. 647−687; J. Schripsema, R. Verpoorte, A. B. Svendsen, *Tetrahedron Lett.* **1986**, *27*, 2523−2526; R. Verpoorte, J. Schripsema, T. van der Leer, A. Brossi, *Alkaloids (Academic Press)* **1988**, *34,* 331; R. Verpoorte, *J. Nat. Prod.* **1986**, *49*, 1.

[11] G. D. H. Dijkstra, R. M. Kellogg, H. Wynberg, *J. Org. Chem.* **1990**, *55*, 6121−6131; G. D. H. Dijkstra, R. M. Kellogg, H. Wynberg, J. S. Svendsen, I. Marko, K. B. Sharpless, *J. Am. Chem. Soc.* **1989**, *111*, 8069−8076.
[12] See e. g. J. M. Casas, L. R. Falvello, J. Forniés, A. Martin, *Inorg. Chem.* **1996, 35**, 6009−6014; W. Yao, O. Eisenstein, R. H. Crabtree, *Inorg. Chim. Acta* **1997**, *254*, 105−111.
[13] G. Carturan, P. Uguagliati, U. Belluco, *Inorg. Chem.* **1974**, *13*, 542−546; J. Fujita, K. Konya, K. Nakamoto, *Inorg. Chem.* **1970**, *9*, 2794−2796.
[14] A. Lombardi, O. Maglio, V. Pavone, B. Di Blasio, M. Saviano, F. Nastri, C. Pedone, E. Benedetti, *Inorg. Chim. Acta* **1993**, *204*, 87−92.
[15] The alkylation of quinine with CH_3I and $PhCH_2Cl$ gives alkylquininium halides which were used as clathrates for the separation of racemic 2-butanol: D. Worsch, F. Vögtle, *Naturwissenschaften* **1984**, *71*, 423−424.
[16] M. Förster, R. Burth, A. K. Powell, T. Eiche, H. Vahrenkamp, *Chem. Ber.* **1993**, *126*, 2643−2648.
[17] For a $PtCl_3$ complex with a protonated amino olefin ligand see: D. B. Brown, A. R. Khokhar, M. P. Hacker, J. J. McCormack, *Inorg. Chim. Acta* **1982**, *67*, 45−52; R. G. Denning, L. M. Venanzi, *J. Chem. Soc*. **1963**, 3241−3247; F. R. Hartley, *The Chemistry of Platinum and Palladium*, Applied Science Publishers LTP, London, **1973**, p. 361−397.
[18] Y. Terai, H. Kido, K. Kashiwabara, K. Saito, *Bull. Chem. Soc. Jpn.* **1978**, *51*, 3245−3250; K. Saito, K. Kashiwabara, *J. Organomet. Chem.* **1987**, *330*, 291−303; L. E. Erickson, G. S. Jones, J. L. Blanchard, K. J. Ahmed, *Inorg. Chem.* **1991**, *30*, 3147−3155.
[19] A. C. Cope, C. R. Ganellin, H. W. Johnson, Jr., *J. Am. Chem. Soc.* **1962**, *84*, 3191−3192; G. Paiaro, A. Panunzi, *J. Am. Chem. Soc.* **1964**, *86*, 5148−5152; A. Panunzi, G. Paiaro, *J. Am. Chem. Soc.* **1966**, *88*, 4843−4847; F. R. Hartley in *Comprehensive Organometallic Chemistry* (Eds.: G. Wilkinson, F. G. A. Stone, E. W. Abel), Pergamon, Oxford, **1982**, vol. 6, p. 659.
[20] B. J. Oleksyn, *Acta Crystallogr.* **1982**, *B38*, 1832−1834.
[21] J. A. J. Jarvis, B. T. Kilbourn, P. G. Owston, *Acta Crystallogr.* **1971**, *B 27,* 366−372.
[22] B. J. Gregory, C. K. Ingold, *J. Chem. Soc. B* **1969**, 276−289.
[23] Y. Tatsuno, T. Yoshida, Seiotsuka, *Inorg. Synth.* **1979**, *19*, 220−221.
[24] F. R. Hartley, *Organomet. Chem. Rev.* **1970**, *A6*, 119−137.
[25] W. Baratta, P. S. Pregosin, *Inorg. Chim. Acta* **1993**, *209*, 85−87.
[26] J. McCormick, E. N. Jaynes, Jr., R. J. Kaplan, *Inorg. Synth.* **1972**, *13*, 216−218.
[27] C. White, A. Yates, P. M. Maitlis, *Inorg. Synth.* **1992**, *29*, 228−230.
[28] Further details of crystallographic data (excluding structure factors) for the structures reported in this paper have been deposited with the Cambridge Crystallographic Data Center as supplementary publication no. CCDC-102785 (**11**), -102786 (**13**), -102787 (**19**), -102788 (**23**), -102789 (**26**) -102790 (**32**). Copies of the data can be obtained free of charge on application to CCDC, 12 Union Road, Cambridge CB2 1EZ, UK [Fax: + 44-1223/336-033; E-mail: deposit@ccdc.cam.ac.uk].

Received September 10, 1998
[I98303]

Synthesis and Nonlinear Optical Properties of Carbonylrhenium Bromide Complexes with Conjugated Pyridines

Oliver Briel,[a] Karlheinz Sünkel,[a][+] Ingo Krossing,[a][+] Heinrich Nöth,[a][+] Elmar Schmälzlin,[b][++] Klaus Meerholz,[b][++] Christoph Bräuchle,[b][++] and Wolfgang Beck*[a]

Dedicated to Professor Klaus-Jürgen Range on the occasion of his 60th birthday

Keywords: Rhenium / N Ligands / Nonlinear optics

Carbonylrhenium bromide complexes *fac*-$Br(OC)_3ReL_2$ (**3a**,**b**, **4a**,**b**) and *cis*-$Br(OC)_4ReL$ (**5a**,**b**) with conjugated pyridines L = Fc–CH=CH–*p*-C_5H_4N (**1a**), Fc–CH=CHC-(CH_3)=CHCH=CHCH=C(CH_3)CH=CH–*p*-C_5H_4N (**1b**), 1,1′-Fc(–CH=CH–*p*-$C_5H_4N)_2$ (**1c**), *p*-Me_2N–C_6H_4–CH=CHCH= CH–*p*-C_5H_4N (**2a**), and *p*-Me_2N–C_6H_4–CH=CHC(CH_3)= CHCH=CHCH=C(CH_3)–CH=CH–*p*-C_5H_4N (**2b**) have been synthesized. The structures of **4a** and **5a** have been determined by X-ray diffraction analysis. Compound **4a** exhibits a remarkable quadratic hyperpolarizability.

1. Introduction

Following the discovery of a marked first hyperpolarizability of *cis*-[1-ferrocenyl-2-(4-nitrophenyl)ethylene] by Green et al.[1] in 1987, organometallic materials with nonlinear optical properties have attracted increasing attention. Compared to organic substances, metal complexes have some definitive advantages such as tunability of the polarizability by changing the oxidation state of the metal atom or by variation of the ligands.[2a] In a recent article by Whittall et al.,[2b] the scope of various nonlinear optical organometallic complexes was reviewed.

Kanis et al.[3] have performed ZINDO-SOS calculations for substituted pyridine complexes of the type (py)ML_5 (py = substituted pyridine derivative; ML_5 = d-metal fragment) in order to determine their hyperpolarizabilities β. They found that the metal fragments in complexes bearing donor-substituted pyridines as ligands contribute as inductive acceptors to the β response of the materials. A series of conjugated pyridine-containing nonlinear optical (NLO) metal complexes have been reported.[3–5] Furthermore, some carbonylrhenium compounds $X(OC)_3ReL_2$ incorporating aromatic N-donors have been studied as NLO materials.[6] Carbonylrhenium compounds,[7] including those of the type $X(OC)_3ReL_2$[8] and $[(OC)_3ReL_2L']^+$, have frequently been used in investigations of other photophysical or electron-transfer processes.

In continuation of our studies of metal complexes with polyene-containing ligands,[9] we have used new pyridine-containing ligands with an olefinic backbone and electron-donating organic or organometallic substituents to construct and investigate complexes of the type $(R-py)_nRe(CO)_{5-n}Br$ (n = 1, 2). We chose to prepare complexes of this type because of their stability and ease of handling.

As the molecular structures of our complexes fulfilled the basic requirements for NLO active materials, HRS measurements were performed.

Complexes of the type *cis*/*trans*-$LRe(CO)_4X$ have been investigated by several research groups, with L being some kind of phosphane.[10] To the best of our knowledge, only one complex of this type has been reported with an N-donor.[11] We have obtained new stable complexes of the type $(R-py)Re(CO)_4Br$ by reaction of $Re(CO)_5Br$ with pyridyl ligands.

2. Results and Discussion

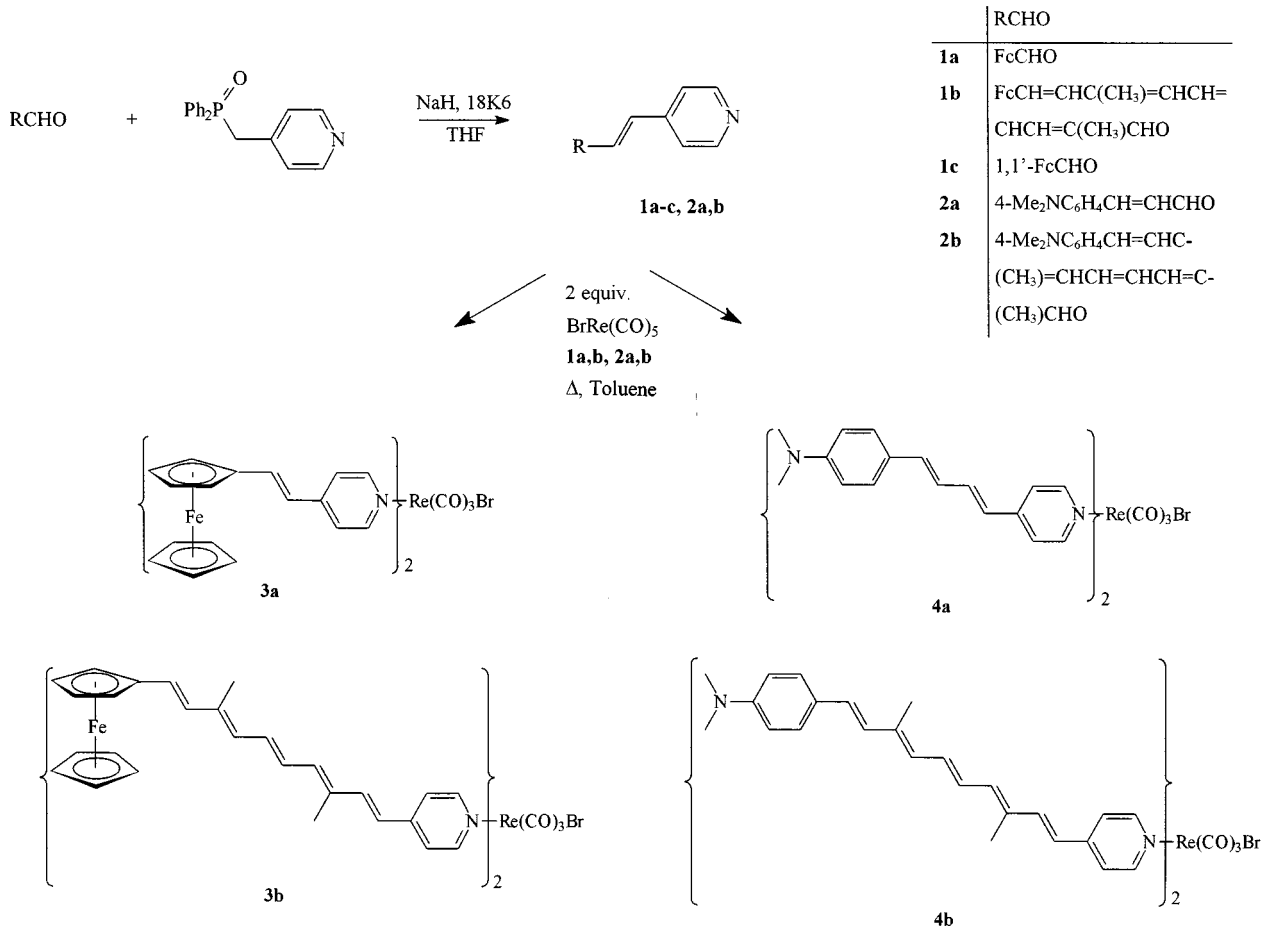
2.1 Synthesis

Pyridine derivatives bearing extended conjugated olefinic substituents **1a–c**, **2a**,**b** in all-*trans* configuration were obtained by Wittig–Horner reaction of aldehydes with diphenyl(4-picolyl)phosphane oxide in yields of up to 70% according to the procedure of Effenberger et al.[12] We used formylferrocene, 1,1′-diformylferrocene, 9-ferrocenyl-2,7-dimethylnonatetraenal,[13] *p*-(dimethylamino)cinnamaldehyde, and 9-(*p*-dimethylaminophenyl)-2,7-dimethylnonatetraenal[13] as aldehyde components. The new compounds were purified by column chromatography on grade-III Al_2O_3 using dichloromethane as eluent. The ligand **1a** has previously been synthesized by other routes[5] and complexes $[(\mathbf{1a})M(CO)_5]$ (M = Cr, W, Mn^+, Re^+) have been prepared as NLO materials.

By reaction of $Re(CO)_5Br$ with two equivalents of the pyridine-containing ligands **1a**,**b** and **2a**,**b** in boiling tolu-

[a] Institut für Anorganische Chemie der Ludwig-Maximilians-Universität,
Meiserstraße 1, D-80333 München, Germany
[b] Institut für Physikalische Chemie der Ludwig-Maximilians-Universität,
Sophienstraße 11, D-80333 München, Germany
[+] X-ray structure analysis.
[++] NLO measurements.

 © WILEY-VCH Verlag GmbH, D-69451 Weinheim, 1999 1434–1948/99/0303–0483 $ 17.50+.50/0



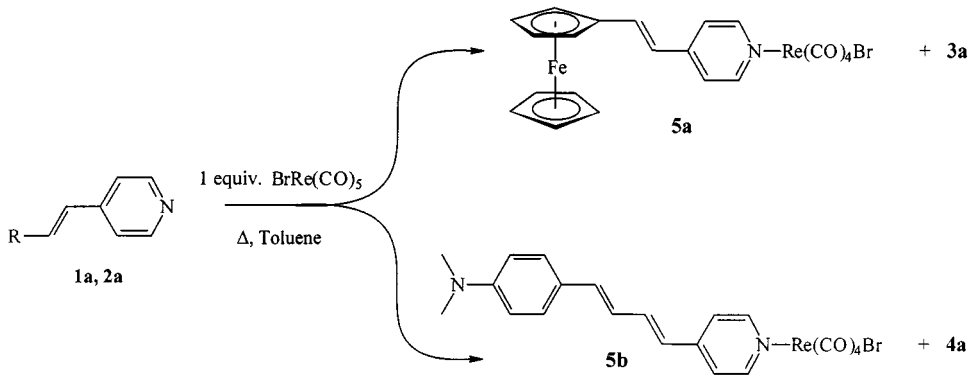
	RCHO
1a	FcCHO
1b	FcCH=CHC(CH_3)=CHCH=CHCH=C(CH_3)CHO
1c	1,1'-FcCHO
2a	4-$Me_2NC_6H_4$CH=CHCHO
2b	4-$Me_2NC_6H_4$CH=CHC(CH_3)=CHCH=CHCH=C(CH_3)CHO

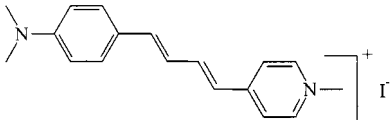
ene, two carbonyl ligands were substituted to give the *fac*-tricarbonylrhenium complexes **3a**,**b** and **4a**,**b**. These complexes were isolated by column chromatography of the crude reaction mixtures on silica gel using dichloromethane as eluent. Upon reaction of **1c** with $Re(CO)_5Br$, a red powder was obtained, presumably of the polymeric structure $[Re(CO)_3BrL]_n$.

Reaction of only one equivalent of the pyridine derivatives **1a** and **2a** with $Re(CO)_5Br$ led to the formation of a mixture of monosubstituted *cis*-(R−py)$Re(CO)_4Br$ (**5a**,**b**) and disubstituted complexes (R−py)$_2Re(CO)_3Br$ (**3a**, **4a**), which could be separated by column chromatography.

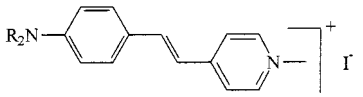
2.2 Characterization

For the complexes **3a**−**c** and **4a**,**b**, three CO absorptions of similar intensity are observed in the IR spectra, which is typical for *fac*-$L_2Re(CO)_3X$ complexes.[10] The CO band at the highest frequency is the one most sensitive to the nature of the ligand L. This absorption appears at lower energies compared with existing data for similar substituted pyridyl complexes.[6,10c] This indicates that the π-donor strength of our pyridine ligands is larger. For the complexes (R−py)Re(CO)$_4$Br (**5a** and **5b**), four CO absorptions are detected, in accordance with their *cis* configuration.

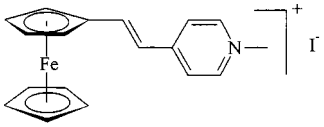




6



7a : R= CH_3; **7b**: R= $C_{16}H_{33}$



8

In agreement with the results of McCleverty et al.,[5b] the pyridyl protons H^2 and H^6 as well as H^3 and H^5 in **3**−**5** are equivalent and thus each pair gives rise to just one signal in the room-temperature ^{1}H-NMR spectra. This implies rapid rotation of the pyridyl rings in relation to the vinyl group to which they are attached; if the pyridyl ring were coplanar with the rest of the conjugated system, it could not have two-fold symmetry.

Several intense absorption bands are seen in the UV/Vis spectra in CH_2Cl_2. For the ferrocene-containing compounds, the following transitions are expected: two ferrocene-based MLCT absorptions between 350 and 500 nm and an intense π→π* absorption around 300 nm.[5a] Furthermore, π→π* or intense ILCT absorptions for the olefinic backbones, as well as MLCT bands of d(Re)→π* (py−R) around 340 nm are observed. The intense π→π* absorption of **1a**[5a] (313 nm) is red-shifted upon complexation (**3a**: 342 nm) and becomes superimposed by the expected MLCT band. A further weaker absorption appears at 501 nm. The principal absorption band of compound **3b** is a π→π* absorption of the olefinic backbone at 443 nm. Weaker absorptions of **3b** give bands at 334 nm and as a shoulder at 521 nm. Compounds **4a** (438 nm) and **5b** (444 nm) show strong and broad ILCT absorptions, which cover the MLCT [d(Re)→π*(py−R)] absorptions.

For compound **2a**, an emission spectrum is observed. The fluorescence band may be attributed to a long-distance intramolecular charge transfer (ICT).[14] This emission band is red-shifted in complexes **4a** and **5b**, in accordance with the inductive electron-accepting effect of the complex fragment.[3] For the other compounds, no fluorescence could be observed at $\lambda_{em} \leq 630$ nm with excitation between 350 and 450 nm.

Table 1. UV/Vis data for compounds **1a**,**b**, **2a**,**b**, **3a**,**b**, **4a**,**b** and **5a**,**b** in CH_2Cl_2

	λ_{max} [nm] (lg ε)
1a	313 (4.47), 374 (3.67), 464 (3.47)
1b	417 (4.99), 493 sh (4.35)
2a	394 (4.58)
2b	448 (4.85)
3a	343 (4.72), 501 (3.99)
3b	443 (4.98), 521 sh (4.69)
4a	438 (5.11)
4b	328 (4.49), 484 (5.01)
5a	341 (4.66), 508 (3.89)
5b	307 (4.59), 444 (5.00)

2.3 X-ray Crystallography

X-ray quality crystals of **4a** and **5a** were obtained by diffusion of *n*-pentane into solutions of the complexes in CH_2Cl_2. The structures are essentially as expected and confirm the expected structures of the complexes. Crystal parameters are given in Table 2.[15]

Both compounds crystallize in centrosymmetric space groups (**4a** in *C*2/*c* and **5a** in *R*−3). Both crystal structures contain relatively large channels, which extend along the C_2 (in **4a**) or C_3 axes (in **5a**), and which constitute 17% and 5.4% of the respective cell volumes. The cavities in **4a** are surrounded by bromine atoms with distances of 3.89 Å, while in **5a** they are surrounded by the oxygen atoms of two carbonyl ligands with distances of 3.68 Å (O1) and 3.20 Å

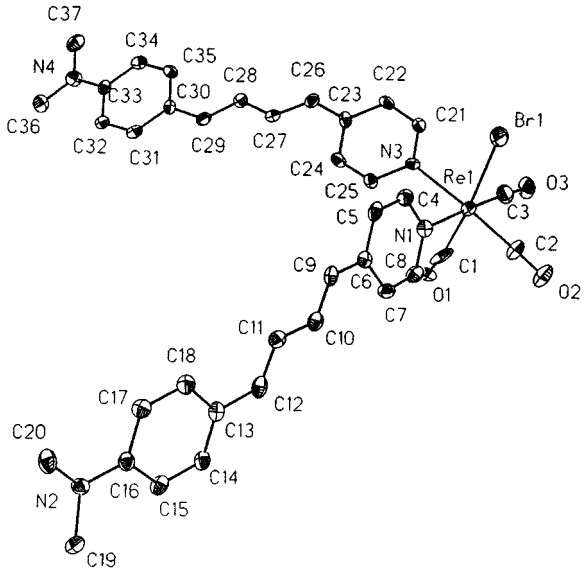


Figure 1. Molecular structure of complex **4a** × $(CH_2Cl_2)_{1.5}$; selected bond lengths [Å] and angles [°]: Re(1)−C(2) 1.89(1), Re(1)−C(3) 1.90(2), Re(1)−C(1) 1.8900(1), Re(1)−N(3) 2.21(1), Re(1)−N(1) 2.21(1), Re(1)−Br(1) 2.614(2), O(1)−C(1) 1.1701(2), O(2)−C(2) 1.18(1), O(3)−C(3) 1.17(2), C(6)−C(9) 1.46(2), C(9)−C(10) 1.31(2), C(10)−C(11) 1.44(2), C(11)−C(12) 1.36(2), C(12)−C(13) 1.47(2), C(23)−C(26) 1.45(2), C(26)−C(27) 1.33(2), C(27)−C(28) 1.42(2), C(28)−C(29) 1.33(2), C(29)−C(30) 1.45(2); C(10)−C(9)−C(6) 125(1), C(9)−C(10)−C(11) 126(1), C(12)−C(11)−C(10) 122(1), C(11)−C(12)−C(13) 129(1), C(27)−C(26)−C(23) 126(1), C(26)−C(27)−C(28) 129(1), C(29)−C(28)−C(27) 124(1), C(28)−C(29)−C(30) 130(1)

(O2).[16] In compound **4a**, a molecule of CH_2Cl_2 was found to be localized in the "void channel" and could be refined (besides a further CH_2Cl_2 molecule in a general position). No solvent molecules were found in the crystal structure of **5a**, which might in part be due to the incompatibility of

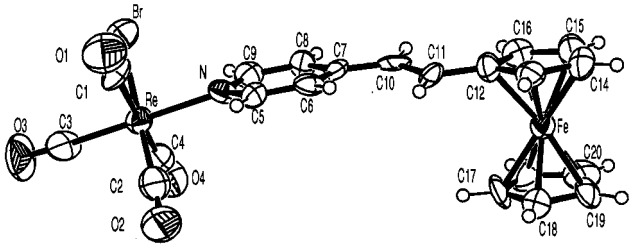


Figure 2. Molecular structure of complex **5a**; selected bond lengths [Å] and angles [°]: Re−C(2) 1.89(2), Re−C(3) 1.97(2), Re−C(4) 2.01(2), Re−C(1) 2.06(2), Re−N 2.187(13), Re−Br 2.595(2), O(1)−C(1) 1.00(2), O(2)−C(2) 1.17(2), O(3)−C(3) 1.11(2), O(4)−C(4) 1.10(2), C(7)−C(10) 1.46(2), C(10)−C(11) 1.29(2), C(11)−C(12) 1.43(2); C(4)−Re−C(1) 75.8(7), C(1)−Re−Br 85.7(5), N−Re−Br 86.4(3), C(11)−C(10)−C(7) 127(2), C(10)−C(11)−C(12) 127(2)

CH_2Cl_2 symmetry with the trigonal symmetry of the void.

In both compounds, the rhenium atoms are very close to ideal octahedral geometry, with Re−Br and Re−N distances in the expected ranges.[6c]

In **4a**, the pyridine ligands are mutually *cis* oriented, with an interplanar angle of 72°. In both compounds, the pyridine ligands are in a staggered orientation with respect to the $Re(CO)_2BrN$ fragments: The interplanar angles are 38° and 50° in **4a**, and 49° in **5a**. This indicates that minimization of steric interactions prevails over electronic π-delocalization.[5b]

The π-system in compound **5a** is less twisted than that in compound **4a**. The angle between the cp ligand and the pyridyl ring is only 4°, which results from two mutually cancelling torsions at the double bond (C6−C7−C10−C11 −9.3°/C10−C11−C12−C13 −170.3°). In **4a**, however, the torsions are additive and lead to interplanar angles of 17° between the terminal planes containing N1, and of 7° between the termini in the second pyridyl ligand (C5−C6−C9−C10 −174.8°/C9−C10−C11−C12 −173.0° and C22−C23−C26−C27 −178.4°/C26−C27−C28−C29 −177.8°).

The small twist in the ferrocenyl derivative **5a** permits additional intermolecular interactions between a cyclopentadienyl ring and a pyridine ring of a neighbouring molecule. The distance between the ring centroids is 3.68 Å, and with a vertical plane distance of 3.42 Å; this leads to a β angle of 18°, indicative of effective π-stacking of the molecules.[16]

2.4 NLO Properties of 3a and 4a

The first hyperpolarizabilities of **3a** and **4a** were determined by hyper Rayleigh scattering (HRS)[17] To circum-

Table 2. Crystallographic data for complexes **4a** and **5a**

	4a	**5a**
Empirical Formula	$C_{38.50}H_{37}BrC_{13}N_4O_3Re$	$C_{21}H_{15}BrFeNO_4Re$
Molecular mass	976.18	667.30
Crystal color, habit	orange plate	redbrown needles
Crystal dimensions [mm]	0.20 × 0.15 × 0.05	0.20 × 0.175 × 0.075
Crystal system	monoclinic	rhombohedral
Space group	*C*2/*c*	*R*−3
a [Å]	18.3826(1)	30.357(4)
b [Å]	15.1048(1)	30.357(4)
c [Å]	28.5866(1)	12.398(2)
β [°]	92.848(1)	90
V [Å^3]	7927.71(7)	9895(2)
Z	8	18
$D_{calcd.}$ [gcm^{-3}]	1.636	2.016
Absorption coefficient [mm^{-1}]	4.317	8.003
F(000)	3848	5688
θ range for data collection	2.86−58.46° (2θ)	2.26−24.96°
Index ranges	$-23 \le h \le 23$, $-18 \le k \le 18$, $-35 \le l \le 35$	$-2 \le h \le 27$, $-30 \le k \le 29$, $-13 \le l \le 12$
Reflections collected	18304	3679
Independent reflections	7804 [*R*(int) = 0.0728]	2930 [*R*(int) = 0.0715]
Absorption correction	semi-empirical	ψ scan
Max. and min. transmission	0.492 and 0.598	0.177 and 0.130
Refinement method	full-matrix least squares on F^2	full-matrix least squares on F^2
Data/restraints/parameters	7804/9/480	2929/0/262
Goodness-of-fit on F^2	1.216	1.036
Final *R* indices [$I > 2\sigma(I)$]	$R1 = 0.0726$, $wR^2 = 0.1723$	$R1 = 0.0578$, $wR^2 = 0.1048$
R indices (all data)	$R1 = 0.1044$, $wR^2 = 0.1964$	$R1 = 0.1250$, $wR^2 = 0.1302$
Structure solution program	*SHELXS-97* (G. M. Sheldrick, **1997**)	*SHELXS-93* (G. M. Sheldrick, **1993**)
Refinement details:		
Program used	*SHELXL-97* (G. M. Sheldrick, **1997**)	*SHELXL-97* (G. M. Sheldrick, **1997**)
	Distances Re1−C1 and C1−O1 were fixed. In free refinement the C1−O1 distance was too short (0.9 Å) and the Re1−C1 distance too long (1.98 Å).	
CifRtf version used	2.0	

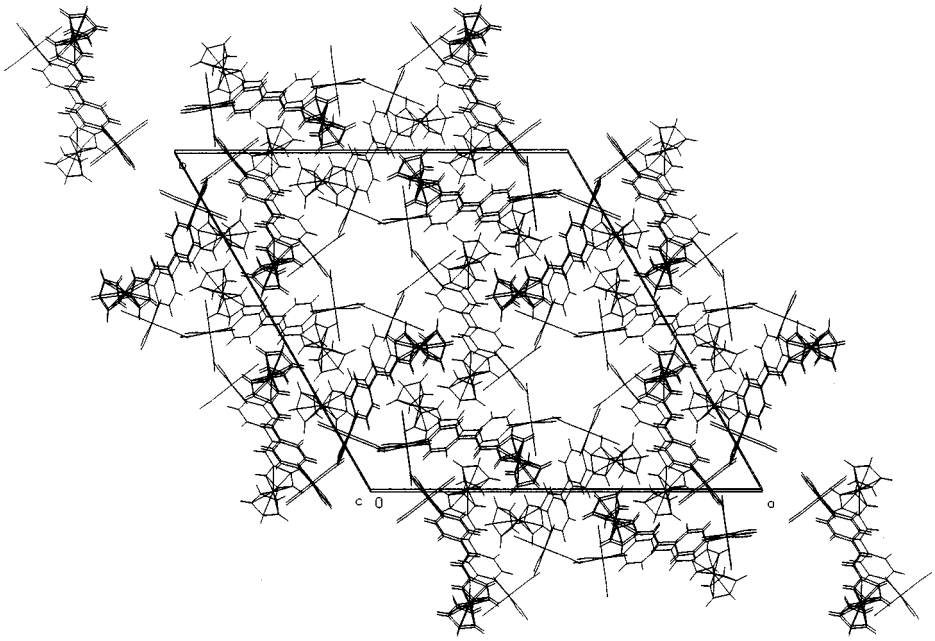


Figure 3. Crystal structure of complex **5a** view down the *c* axis

vent problems associated with reabsorption of the second harmonic and enhancement of β by multiphoton-induced fluorescence,[18] the measurements were carried out at fundamental wavelengths of 1300 nm (**3a**) and 1500 nm (**4a**), respectively. Descriptions of the HRS apparatus and of the method of data analysis have been given previously,[19,20] thus we describe here in brief only the key features. As an external standard, *p*-dimethylaminocinnamaldehyde (DMAZ) was used ($\beta_{zzz} = 41 \times 10^{-30}$ esu at 1300 nm, and 35×10^{-30} esu at 1500 nm in $CHCl_3$).[21] A plot of $I(2\omega)$, the intensity of the measured second harmonic, versus the number density for both sample and reference leads to the ratio $<\beta_{HRS}^2>_{sample}/<\beta_{HRS}^2>_{reference}$, from which specific components of the β tensor may be determined. Depending on the molecular symmetry, only some tensor elements contribute to $\langle\beta_{HRS}^2\rangle$. For 1D molecules such as DMAZ:

$$\langle\beta_{HRS}^2\rangle = \frac{6}{35}\beta_{zzz}^2 \qquad (1)$$

3a and **4a** have approximate C_2 symmetry, therefore:

$$\langle\beta_{HRS}^2\rangle = \frac{6}{35}\beta_{zzz}^2 + \frac{4}{7}\beta_{xyz}^2 + \frac{38}{105}\left(\beta_{xxz}^2 + \beta_{yyz}^2\right) + \frac{16}{105}\left(\beta_{xxz}\beta_{yyz} + \beta_{xxz}\beta_{zzz} + \beta_{yyz}\beta_{zzz}\right) \qquad (2)$$

Since it is not possible to deduce β_{xxz}, β_{xyz}, β_{yyz} and β_{zzz} of **3a** and **4a** from the measured $<\beta_{HRS}^2>$ value, a theoretical ratio $\beta_{xxz}/\beta_{xyz}/\beta_{yyz}/\beta_{zzz}$ was calculated by tensor addition.[20,22] For the sake of simplicity, **3a** and **4a** were assumed to consist of two non-interacting 1D subunits. From X-ray crystallography measurements on **4a**, a 90° angle between the subunits was derived. For **3a**, the same angle was assumed. Electron transitions within the Re complex were neglected. As a result, β_{xyz} and β_{yyz} vanish, and β_{xxz} and β_{zzz} were found to be equal. Together with Eq. 2, this yields:

$$\langle\beta_{HRS}^2\rangle = \frac{24}{35}\beta_{zzz}^2; \quad \beta_{zzz} = \beta_{xxz} \qquad (3)$$

The results of the HRS measurements and the β values of the subchromophores **6** and **8** given in the literature are summarized in Table 2. The modulus

$$\|\beta\| = \sqrt{\sum_{ijk}\beta_{ijk}^2}$$

was used to compare the hyperpolarizabilities of molecules with different specific components of the β tensor.

Table 3. First hyperpolarizabilities of **3a**, **4a**, **6**−**8**; hyperpolarizabilities are given in 10^{-30} esu; 1×10^{-30} esu = 3.713×10^{-51} Cm^3V^{-2}; the HRS measurements were carried out in $CHCl_3$

	λ_{max} [nm]	β_{xxz}	β_{zzz}	$\|\beta\|$	fundamental wavelength [nm]
3a	501[e]	12	12	24	1300
4a	438[e]	104	104	208	1500
6	526[a]		343[a]	343	1910
7a	509[e]/479[a]		178[a]	178	1910
7b	515[d]		140[b]	140	1910
8	521[c]		68[c]	68	1910

[a] ZINDO-derived value, ref.[23] – [b] HRS measurement at 1500 nm,[25] converted to 1910 nm by the two-level model.[26] – [c] ZINDO-derived value, ref.[24] – [d] In $CHCl_3$. – [e] In CH_2Cl_2.

Taking the β values of the 1D molecules **6** and **8** as starting points, the theoretical moduli $\|\beta\|$ of angled clusters consisting of two equal 1D subchromophores were calculated by tensor addition. For a 90° angle, this yielded $\|\beta\| = 96 \times 10^{-30}$ esu (subchromophore **8**) and $\|\beta\| = 485 \times 10^{-30}$ esu (subchromophore **6**), respectively, at 1910 nm. Although comparison of the calculated and experimental data for **7a** and **7b** indicates an overestimation of the β values by ZINDO, the hyperpolarizabilities of the complexes **3a** and **4a** are much smaller than those calculated for the angled clusters consisting of the corresponding subchromophores **6** and **8**, respectively. Therefore, replacement of the methyl

moiety by the Re complex leads to a noticeable reduction of the acceptor properties of the pyridinium moiety. Nevertheless, **4a** shows a remarkably high first hyperpolarizability. Even higher quadratic hyperpolarizabilities have recently been reported for the complexes $[(\mathbf{1a})M(CO)_5]^+$ (M = Mn, Re).[5d]

Experimental Section

All operations were carried out under nitrogen using the Schlenk technique. $Re(CO)_5Br$ was synthesized according to a literature procedure.[27] Solvents were dried by distillation from sodium/benzophenone, $LiAlH_4$, or CaH_2 as appropriate. − NMR spectra were recorded with a Jeol GSX 270 (^1H: 270.17 MHz; ^{13}C: 67.94 MHz; ^{31}P: 109.38 MHz) or a Jeol EX 400 spectrometer (^1H: 399.78 MHz; ^{13}C: 100.53 MHz). − IR: Perkin−Elmer 841, Nicolet 520 FT-IR. − UV/Vis: Philips PU 8710. − Luminescence: Perkin−Elmer Luminescence Spectrometer LS 50B.

Ligands 1a−c, 2a,b: Essentially the same procedures were followed to synthesize **1a−c** and **2a**,**b**. Thus, only the preparation of **1a** is described here in detail.

***trans*-Fc−CH=CH−C_5H_4N (1a):** A mixture of 275 mg (0.94 mmol) of diphenyl(4-picolyl)phosphane oxide, 200 mg (0.94 mmol) of ferrocene aldehyde, 250 mg (0.96 mmol) of 18-crown-6, and 55 mg (1.2 mmol; 55% in paraffin; washed twice with pentane) of NaH was stirred in 40 mL of THF at room temperature for 3 h. At the beginning of the reaction, 25 μL of H_2O was added to activate the NaH. The resulting red suspension was then filtered through a G3 glass funnel. The solvent was removed from the filtrate in vacuo, and the crude product was chromatographed on grade-III Al_2O_3. The first fraction (R_f = 0.5) was identified as the product, and furnished a red powder upon evaporation of the solvent. Yield 136 mg (50%). − IR (KBr): ṽ(C=C, C=N) = 1632 (s), 1594 cm^{-1} (vs). − ^1H NMR (270 MHz, $CDCl_3$): δ = 8.53 (d, 2 H, ^3J = 6.2 Hz, NC*H*), 7.28 (d, 2 H, ^3J = 6.0 Hz, NCHC*H*), 7.13 (d, 1 H, ^3J = 15.7 Hz, H_{ol}), 6.60 (d, 1 H, ^3J = 16.1 Hz, H_{ol}), 4.51 (t, 2 H, ^3J = 1.9 Hz, C_5H_4), 4.36 (t, 2 H, ^3J = 2.2 Hz, C_5H_4), 4.16 (s, 5 H, C_5H_5). − UV/Vis (CH_2Cl_2) (lg ε): λ_{max} = 313 (4.47), 374 (3.67), 464 nm (3.47). − $C_{17}H_{15}FeN$ (289.1): calcd. C 70.61, H 5.22, N 4.84; found C 69.31, H 5.30, N 4.48.

all-*trans*-(C_5H_5)Fe(C_5H_4)CH=CHC(CH_3)=CHCH=CHCH=C(CH_3)CH=CHC_5H_4N (1b): Dark-red powder, yield 150 mg (37%). − IR (KBr): ṽ(C=C, C=N) = 1618 (m), 1598 (s), 1588 (s), 1556 cm^{-1} (vs). − ^1H NMR (270 MHz, $CDCl_3$): δ = 8.53 (d, 2 H, ^3J = 5.9 Hz, NC*H*), 7.28 (d, 2 H, ^3J = 6.0 Hz, NCHC*H*), 7.07 (d, 1 H, ^3J = 15.6 Hz, H_{ol}), 6.74−6.24 (m, 6 H, H_{ol}), 6.48 (d, 1 H, ^3J = 15.9 Hz, H_{ol}), 4.42 (t, 2 H, ^3J = 1.9 Hz, C_5H_4), 4.29 (t, 2 H, ^3J = 1.8 Hz, C_5H_4), 4.12 (s, 5 H, C_5H_5), 2.02 (s, 6 H, CH_3). − UV/Vis (CH_2Cl_2) (lg ε): λ_{max} = 417 (4.99), 493 nm (sh, 4.35). − $C_{27}H_{27}FeN$ (421.2): calcd. C 76.93, H 6.46, N 3.32; found C 76.30, H 6.46, N 3.29.

***trans*-Fe[(C_5H_4)CH=CHC_5H_4N]$_2$ (1c):** Red powder, yield 263 mg (70%). − IR (KBr): ṽ(C=C, C=N) = 1629 (s), 1593 cm^{-1} (vs). − ^1H NMR (270 MHz, $CDCl_3$): δ = 8.44 (d, 4 H, ^3J = 6.3 Hz, NC*H*), 7.08 (d, 4 H, ^3J = 6.5 Hz, NCHC*H*), 6.93 (d, 2 H, ^3J = 16.1 Hz, H_{ol}), 6.47 (d, 2 H, ^3J = 16.1 Hz, H_{ol}), 4.48 (t, 4 H, ^3J = 2.0 Hz, C_5H_4), 4.35 (t, 4 H, ^3J = 2.1 Hz, C_5H_4). − $C_{24}H_{20}N_2Fe$ (392.1): calcd. C 73.49, H 5.14, N 7.14; found C 72.48, H 5.06, N 6.95.

all-*trans*-($H_3C)_2N(C_6H_4$)CH=CHCH=CHC_5H_4N (2a): Bright-yellow needles, yield 140 mg (57%). − IR (KBr): ṽ(C=C, C=N) = 1601 (s), 1588 cm^{-1} (s). − ^1H NMR (270 MHz, $CDCl_3$): δ = 8.51 (d, 2 H, ^3J = 6.1 Hz, NC*H*), 7.36 (d, 2 H, ^3J = 8.7 Hz, C_6H_4), 7.26 (d, 2 H, ^3J = 6.0 Hz, NCHC*H*), 7.07 (dd, 1 H, ^3J = 15.3, ^3J = 9.7 Hz, H_{ol}), 6.82−6.73 (m, 2 H, H_{ol}), 6.69 (d, 2 H, ^3J = 9.0 Hz, C_6H_4), 6.46 (d, 1 H, ^3J = 15.3 Hz, H_{ol}), 3.00 [s, 6 H, ($H_3C)_2N$]. − UV/Vis (CH_2Cl_2) (lg ε): λ_{max} = 394 nm (4.58). − Emission spectrum (CH_2Cl_2, λ_{ex} = 350 nm): $\lambda_{em,max}$ = 511 nm. − $C_{17}H_{18}N_2$ (250.1): calcd. C 81.55, H 7.25, N 11.20; found C 79.26, H 6.70, N 10.80.

($H_3C)_2N(C_6H_4$)CH=CHC(CH_3)=CHCH=CHCH=C(CH_3)CH=CHC_5H_4N (2b): Orange powder, yield 120 mg (35%). − IR (KBr): ṽ(C=C, C=N) = 1609 (vs, sh), 1604 (s), 1597 cm^{-1} (vs). − ^1H NMR (400 MHz, $CDCl_3$): δ = 8.52 (d, 2 H, ^3J = 5.8 Hz, NC*H*), 7.35 (d, 2 H, ^3J = 8.6 Hz, C_6H_4), 7.27 (d, 1 H, NCHC*H*), 7.07 (d, 1 H, ^3J = 15.9 Hz, H_{ol}), 6.83−6.30 (m, 7 H, H_{ol}), 6.70 (d, 2 H, ^3J = 9.0 Hz, C_6H_4), 2.98 [s, 6 H, ($H_3C)_2N$], 2.05/2.03 (each s, each 3 H, CH_3). − UV/Vis (CH_2Cl_2) (lg ε): λ_{max} = 448 nm (4.85). − $C_{25}H_{28}N_2$ (356.2): calcd. C 84.22, H 7.92, N 7.86; found C 83.82, H 7.71, N 7.79.

Complexes 3a−c, 4a,b, 5a,b: All the compounds were found to be moderately stable as solids and did not decompose significantly upon exposure to air for several days. Essentially the same procedures were followed to synthesize **3a−c** and **4a**,**b**, thus only the preparation of **4a** is described here in detail.

[all-*trans*-($H_3C)_2N(C_6H_4$)CH=CHCH=CHC_5H_4N]$_2$Re(CO)$_3$Br (4a): 100 mg (0.4 mmol) of **2a** and 80 mg (0.2 mmol) of $Re(CO)_5Br$ were allowed to react in refluxing toluene for 1 h. The solvent was then evaporated from the resulting orange solution. The crude product was chromatographed on silica gel using CH_2Cl_2 as eluent. The first fraction was found to contain the product. Bright-orange powder, yield 85 mg (77%). − IR (KBr): ṽ(C=O) = 2019 (vs), 1919 (vs), 1878 cm^{-1} (vs). − ^1H NMR (270 MHz, $CDCl_3$): δ = 8.63 (d, 4 H, ^3J = 6.9 Hz, NC*H*), 7.37 (d, 4 H, ^3J = 9.2 Hz, C_6H_4), 7.21 (d, 4 H, ^3J = 6.9 Hz, NCHC*H*), 7.16 (m, 2 H, H_{ol}), 6.79−6.77 (m, 4 H, H_{ol}), 6.69 (d, 4 H, ^3J = 9.0 Hz, C_6H_4), 6.42 (d, 2 H, ^3J = 15.3 Hz, H_{ol}), 3.00 [s, 12 H, ($H_3C)_2N$]. − ^{13}C NMR (68 MHz, $CDCl_3$): δ = 195.39/192.20 (CO), 154.04, 147.59, 138.95, 137.85, 130.67, 129.11, 128.51, 124.96, 121.73, 112.30 (C_{ar}, C_{ol}), 40.31 [$N(CH_3)_2$]. − UV/Vis (CH_2Cl_2) (lg ε): λ_{max} = 438 nm (5.11). − Emission spectrum (CH_2Cl_2, λ_{ex} = 350 nm): $\lambda_{em,max}$ = 564 nm. − $C_{37}H_{36}BrN_4O_3Re$ (850.7): calcd. C 52.23, H 4.27, N 6.59; found C 51.85, H 3.92, N 6.45.

(*trans*-Fc−CH=CH−$C_5H_4N)_2$Re(CO)$_3$Br (3a): Red powder, yield 60 mg (67%). − IR (KBr): ṽ(C=O) = 2021 (vs), 1914 (vs), 1884 cm^{-1} (vs). − ^1H NMR (270 MHz, $CDCl_3$): δ = 8.66 (d, 4 H, ^3J = 6.6 Hz, NC*H*), 7.30 (m, 2 H, H_{ol}), 7.22 (d, 4 H, ^3J = 8.2 Hz, C_6H_4), 7.21 (d, 4 H, ^3J = 6.9 Hz, NCHC*H*), 6.56 (d, 2 H, ^3J = 15.6 Hz, H_{ol}), 4.53 (t, 4 H, ^3J = 1.9 Hz, C_5H_4), 4.43 (t, 4 H, ^3J = 1.9 Hz, C_5H_4), 4.16 (s, 10 H, C_5H_5). − UV/Vis (CH_2Cl_2) (lg ε): λ_{max} = 343 (4.72), 501 nm (3.99). − $C_{37}H_{30}BrFe_2N_2O_3Re$ (928.0): calcd. C 47.85, H 3.26, N 3.02; found C 47.80, H 3.43, N 2.87.

[(C_5H_5)Fe(C_5H_4)CH=CHC(CH_3)=CHCH=CHCH=C(CH_3)-CH=CHC_5H_4N]$_2$Re(CO)$_3$Br (3b): Dark-red powder, yield 80 mg (67%). − IR (KBr): ṽ(C=O) = 2021 (vs), 1916 (vs), 1882 cm^{-1} (vs). − ^1H NMR (270 MHz, $CDCl_3$): δ = 8.64 (d, 4 H, ^3J = 6.4 Hz, NC*H*), 7.23 (d, 4 H, ^3J = 6.8 Hz, NCHC*H*), 7.11 (d, 2 H, ^3J = 15.8 Hz, H_{ol}), 6.86−6.25 (m, 12 H, H_{ol}), 6.43 (d, 2 H, ^3J = 16.3 Hz, H_{ol}), 4.46 (t, 4 H, ^3J = 1.8 Hz, C_5H_4), 4.30 (t, 4 H, ^3J = 1.9 Hz, C_5H_4), 4.12 (s, 10 H, C_5H_5), 2.02/2.01 (each s, each 6 H, CH_3). − UV/Vis (CH_2Cl_2) (lg ε): λ_{max} = 443 (4.98), 521 nm (sh, 4.69). − $C_{57}H_{54}BrFe_2N_2O_3Re$ (1192.2): calcd. C 57.37, H 4.57, N 2.35; found C 57.51, H 4.39, N 2.19.

{trans-Fe[(C_5H_4)CH=CHC_5H_4N]$_2$Re(CO)$_3$Br}$_n$ (3c): Dark-red powder, washing with CH_2Cl_2 furnished the product; yield 30 mg (23%). − IR (KBr): $\tilde{\nu}$(C=O) = 2020 (vs), 1912 (vs), 1884 cm^{-1} (vs). − ^{1}H NMR (270 MHz, $CDCl_3$): δ = 8.70−8.60 (m, 4 H, NC*H*), 7.37−7.15 (m, 6 H, NCHC*H*, H_{ol}), 6.58−6.42 (m, 2 H, H_{ol}), 4.55−4.35 (m, 8 H, C_5H_4). − ($C_{27}H_{20}BrFeN_2O_3Re)_n$ (1/*n* M = 741.96): calcd. C 43.67, H 2.72, N 3.77; found C 42.79, H 2.89, N 3.65.

[($H_3C)_2$N(C_6H_4)CH=CHC(CH_3)=CHCH=CHCH=C(CH_3)CH=CHC_5H_4N]$_2$Re(CO)$_3$Br (4b): Dark-red powder, yield 40 mg (67%). − IR (KBr): $\tilde{\nu}$(C=O) = 2019 (vs), 1915 (vs), 1880 cm^{-1} (vs). − ^{1}H NMR (270 MHz, $CDCl_3$): δ = 8.65 (d, 4 H, ^3J = 6.7 Hz, NC*H*), 7.37 (d, 4 H, ^3J = 8.7 Hz, C_6H_4), 7.23 (d, 4 H, ^3J = 6.5 Hz, NCHC*H*), 7.12 (d, 1 H, ^3J = 15.8 Hz, H_{ol}), 6.88−6.32 (m, 14 H, H_{ol}), 6.71 (d, 4 H, ^3J = 8.6 Hz, C_6H_4), 3.00−2.99 [m, 12 H, ($H_3C)_2$N], 2.05/2.02 (each s, each 6 H, CH_3). − UV/Vis (CH_2Cl_2) (lg ε): λ_{max} = 328 (4.49), 485 nm (5.01). − $C_{53}H_{56}BrN_4O_3Re$ (1062.3): calcd. C 59.87, H 5.31, N 5.27; found C 59.53, H 5.81, N 5.63.

***trans*-Fc−CH=CH−C_6H_4N−*cis*-Re(CO)$_4$Br (5a):** 58 mg (0.2 mmol) of *trans*-Fc−CH=CH−C_6H_4N was added to 81 mg (0.2 mmol) of $Re(CO)_5Br$ in toluene and the mixture was heated until a solution was obtained. The solvent was then evaporated and the residue was subjected to column chromatography on silica gel using CH_2Cl_2 as eluent. Two main fractions were collected, the first containing **5a** (32 mg, 25%) and the second **4a** (52 mg, 28%). Dark-red powder. − IR (KBr): $\tilde{\nu}$(C=O) = 2105 (m), 2002 (vs), 1988 (vs), 1946 cm^{-1} (vs). − ^{1}H NMR (270 MHz, $CDCl_3$): δ = 8.84 (d, 2 H, ^3J = 7.0 Hz, NC*H*), 7.39 (d, 2 H, ^3J = 8.9 Hz, C_6H_4), 7.30 (d, 2 H, ^3J = 6.8 Hz, NCHC*H*), 7.26−7.20 (m, 1 H, H_{ol}), 6.83 (m, 2 H, H_{ol}), 6.70 (d, 2 H, ^3J = 8.7 Hz, C_6H_4), 6.45 (d, 1 H, ^3J = 15.6 Hz, H_{ol}), 3.03 [s, 6 H, ($H_3C)_2$N]. − ^{13}C NMR (109 MHz, $CDCl_3$): δ = 195.47, 192.17 (CO), 154.07, 147.27, 136.73 (C_{ar}), 121.44/120.92 (C_{ol}), 80.47, 70.64, 69.55, 67.93 (Fc). − UV/Vis (CH_2Cl_2) (lg ε): λ_{max} = 341 (4.66), 508 nm (3.89). − $C_{21}H_{15}BrFeNO_4Re$ (666.9): calcd. C 37.79, H 2.27, N 2.10; found C 38.15, H 2.49, N 2.13.

[all-*trans*-($H_3C)_2$N(C_6H_4)CH=CHCH=CHC_5H_4N]−*cis*-Re(CO)$_4$-Br (5b): Orange powder, yield 55 mg (22%). − IR (KBr): $\tilde{\nu}$(C=O) = 2108 (m), 2024 (vs), 1990 (vs), 1938 cm^{-1} (vs). − ^{1}H NMR (270 MHz, $CDCl_3$): δ = 8.87 (d, 2 H, ^3J = 6.8 Hz, NC*H*), 7.34 (d, 2 H, ^3J = 6.9 Hz, NCHC*H*), 7.30 (d, 1 H, ^3J = 16.1 Hz, H_{ol}), 6.59 (d, 1 H, ^3J = 16.1 Hz, H_{ol}), 4.56 (t, 2 H, ^3J = 1.8 Hz, C_5H_4), 4.46 (t, 2 H, ^3J = 1.9 Hz, C_5H_4), 4.18 (s, 5 H, C_5H_5). − UV/Vis (CH_2Cl_2) (lg ε): λ_{max} = 307 (4.59), 444 nm (5.00). − Emission spectrum (CH_2Cl_2, λ_{ex} = 350 nm): $\lambda_{emi,max}$ = 573 nm. − $C_{21}H_{18}BrN_2O_4Re$ (628.0): calcd. C 40.13, H 2.89, N 4.46; found C 39.53, H 2.90, N 4.27.

Acknowledgments

Generous support by the Fonds der Chemischen Industrie is gratefully acknowledged. We thank the BASF AG, Ludwigshafen, and the F. Hoffmann-LaRoche AG, Basel, for gifts of carotenoid dialdehydes.

[1] M. L. H. Green, S. R. Marder, M. E. Thompson, J. A. Bandy, D. Bloor, P. V. Kolinsky, R. J. Jones, *Nature* **1987**, *330*, 360−362.

[2] [2a] N. J. Long, *Angew. Chem.* **1995**, *107*, 37−56; *Angew. Chem. Int. Ed. Engl.* **1995**, *34*, 21. − [2b] I. R. Whittall, A. M. McDonagh, M. G. Humphrey, M. Samoc, *Adv. Organomet. Chem.* **1998**, *42*, 291−362.

[3] D. R. Kanis, P. G. Lacroix, M. A. Ratner, T. J. Marks, *J. Am. Chem. Soc.* **1994**, *116*, 10089−10102.

[4] [4a] B. J. Coe, J. A. Harris, L. J. Harrington, J. C. Jeffery, L. H. Rees, S. Houbrechts, A. Persoons, *Inorg. Chem.* **1998**, *37*, 3391−3399. − [4b] R. H. Naulty, A. M. McDonagh, I. R. Whittall, M. P. Cifuentes, M. G. Humphrey, S. Houbrechts, J. Maes, A. Persoons, G. A. Heath, D. C. R. Hockless, *J. Organomet. Chem.* **1998**, *563*, 137−146. − [4c] S. L. W. McWhinnie, J. A. Thomas, T. A. Hamor, C. J. Jones, J. A. McCleverty, D. Collison, F. E. Mabbs, C. J. Harding, L. J. Yellowlees, M. G. Hutchings, *Inorg. Chem.* **1996**, *35*, 760−774. − [4d] S. Houbrechts, K. Clays, A. Persoons, V. Cadierno, M. P. Gamasa, J. Gimeno, *Organometallics* **1996**, *15*, 5266−5268. − [4e] D. W. Bruce, A. Thornton, B. Chaudret, S. Sabo-Etienne, T. L. Axon, G. H. Cross, *Polyhedron* **1995**, *13−14*, 1765−1770. − [4f] W.-Y. Wong, W.-T. Wong, K.-K. Cheung, *J. Chem. Soc., Dalton Trans.* **1995**, 1379−1387. − [4g] B. J. Coe, J. P. Essex-Lopresti, J. A. Harris, S. Houbrechts, A. Persoons, *J. Chem. Soc., Chem. Commun.* **1997**, 1645−1646. − [4h] J. T. Lin, J. J. Wu, C.-S. Li, Y. S. Wen, K.-J. Lin, *Organometallics* **1996**, *15*, 5028−5034.

[5] [5a] M. M. Bhadhade, A. Das, J. C. Jeffery, J. A. McCleverty, J. A. Navas Badiola, M. D. Ward, *J. Chem. Soc., Dalton Trans.* **1995**, 2769−2777. − [5b] S. Sakanishi, D. A. Bardwell, S. Couchman, J. C. Jeffery, J. A. McCleverty, M. D. Ward, *J. Organomet. Chem.* **1997**, *528*, 35−45. − [5c] J. Mata, S. Uriel, E. Peris, R. Llusar, S. Houbrechts, A. Persoons, *J. Organomet. Chem.* **1998**, *562*, 197−202. − [5d] I. S. Lee, S. S. Lee, Y. K. Chung, D. Kim, N. W. Song, *Inorg. Chim. Acta* **1998**, *279*, 243−248.

[6] [6a] V. W.-W. Yam, K.-Z. Wang, C.-R. Wang, Y. Yang, K.-K. Cheung, *Organometallics* **1998**, *17*, 2440−2446. − [6b] V. W.-W. Yam, V. C.-Y. Lau, K.-Z. Wang, K.-K. Cheung, C.-H. Huang, *J. Mater. Chem.* **1998**, *8*, 89−97. − [6c] J. T. Lin, S.-S. Sun, J. J. Wu, Y.-C. Liaw, K.-J. Lin, *J. Organomet. Chem.* **1996**, *517*, 217−226. − [6d] J. C. Calabrese, W. Tam, *Chem. Phys. Lett.* **1987**, *133*, 244−245. − [6e] M. Bourgault, K. Baum, H. Le Bozec, G. Pucetti, I. Ledoux, J. Zyss, *New. J. Chem.* **1998**, 517−522.

[7] [7a] B. D. Rossenaar, E. Lindsay, D. J. Stufkens, A. Vlcek, Jr., *Inorg. Chim. Acta* **1996**, *250*, 5−14. − [7b] E. Schutte, J. B. Helms, S. M. Woessner, J. Bowen, B. P. Sullivan, *Inorg. Chem.* **1998**, *37*, 2618−2619. − [7c] G. F. Strouse, J. R. Schoonover, R. Duesing, T. J. Meyer, *Inorg. Chem.* **1995**, *34*, 2725−2734. − [7d] A. P. Zipp, L. Sacksteder, J. Streich, A. Cook, J. N. Demas, B. A. DeGraff, *Inorg. Chem.* **1993**, *32*, 5629−5632. − [7e] L. Wallace, D. P. Rillema, *Inorg. Chem.* **1993**, *32*, 3836−3843. − [7f] L. Sacksteder, M. Lee, J. N. Demas, B. A. DeGraff, *J. Am. Chem. Soc.* **1993**, *115*, 8230−8238.

[8] [8a] A. I. Baba, J. R. Shaw, J. A. Simon, R. P. Thummel, R. H. Schmehl, *Coord. Chem. Rev.* **1998**, *171*, 43−59. − [8b] B. D. Rossenaar, D. J. Stufkens, A. Vlcek, *Inorg. Chem.* **1996**, *35*, 2902−2909. − [8c] R. Ziessel, A. Juris, M. Venturi, *J. Chem. Soc., Chem. Commun.* **1997**, 1593−1594. − [8d] H. Hori, F. P. A. Johnson, K. Koike, K. Takeuchi, T. Ibusuki, O. Ishitani, *J. Chem. Soc., Dalton Trans.* **1997**, 1019−1023. − [8e] F. P. A. Johnson, M. W. George, F. Hartl, J. J. Turner, *Organometallics* **1996**, *15*, 3374−3387. − [8f] M. Wrighton, D. L. Morse, *J. Am. Chem. Soc.* **1974**, *96*, 998−1003; P. J. Giordano, S. M. Fredericks, M. S. Wrighton, D. L. Morse, *J. Am. Chem Soc.* **1978**, *100*, 2257−2259; C.-F. Shu, M. S. Wrighton, *Inorg. Chem.* **1988**, *27*, 4326−4329.

[9] A. Fehn, O. Briel, W. Beck, *Chem. Ber.* **1997**, *130*, 1467−1473; O. Briel, A. Fehn, K. Polborn, W. Beck, *Polyhedron*, in press; O. Briel, A. Fehn, W. Beck, *J. Organomet. Chem.*, in press.

[10] [10a] P. W. Jolly, F. G. A. Stone, *J. Chem. Soc.* **1965**, 5259−5261. − [10b] P. Braunstein, L. Douce, F. Balegroune, D. Grandjean, D. Bayeul, Y. Dusausoy, P. Zanello, *New J. Chem.* **1992**, *16*, 925−929. − [10c] T. M. Miller, K. J. Ahmed, M. S. Wrighton, *Inorg. Chem.* **1989**, *28*, 2347−2355. − [10d] P. J. Giordano, M. S. Wrighton, *J. Am. Chem. Soc.* **1979**, *101*, 2888−2997. − [10e] F. Zingales, U. Sartorelli, F. Canziani, M. Raveglia, *Inorg. Chem.* **1966**, *6*, 154−157; M. Schweiger, W. Beck, *Z. Anorg. Allg. Chem.* **1991**, *595*, 203−210.

[11] W. Hieber, L. Schuster, *Z. Anorg. Allg. Chem.* **1956**, *287*, 214−222.

[12] F. Effenberger, C.-P. Niesert, *Synthesis* **1992**, 1137−1144.

[13] F. Effenberger, H. Schlosser, *Synthesis* **1990**, 1085−1094.

[14] A. Salma-Schwok, M. Blanchard-Desce, J.-M. Lehn, *J. Phys. Chem.* **1990**, *94*, 3894−3902.

[15] Crystallographic data (excluding structure factors) for the structures reported in this paper have been deposited with the Cambridge Crystallographic Data Centre as supplementary publication no. CCDC-112120 (**4a**) and -111966 (**5a**). Copies of the data can be obtained free of charge on application to CCDC, 12 Union Road, Cambridge CB2 1EZ, U.K. [Fax: (internat.) + 44-1223/336033; E-mail: deposit@ccdc.cam.ac.uk].
[16] *PLATON 98* (ver. 170698, by A. Spek, L. Farrugia).
[17] K. Clays, A. Persoons, *Phys. Rev. Lett.* **1991**, *66*, 2980−2987.
[18] [18a] S. Stadler, G. Bourhill, C. Bräuchle, *J. Phys. Chem.* **1996**, *100*, 6927−6934. − [18b] M. C. Flipse, R. de Jonge, R. H. Woudenberg, A. W. Marsman, C. A. von Walree, L. W. Jenneskens, *Chem. Phys. Lett.* **1995**, *245*, 297−303.
[19] S. Stadler, R. Dietrich, G. Bourhill, C. Bräuchle, *Opt. Lett.* **1996**, *21*, 251.
[20] C. Lambert, E. Schmälzlin, K. Meerholz, C. Bräuchle, *Chem. Eur. J.* **1998**, *4*, 512−521.
[21] E. Schmälzlin, K. Meerholz, S. Stadler, C. Bräuchle, H. Patzelt, D. Oesterhelt, *Chem. Phys. Lett.* **1997**, *280*, 551−555.
[22] [22a] J. L. Oudar, J. Zyss, *Phys. Rev.* **1982**, *A26*, 2016. − [22b] J. Zyss, J. L. Oudar, *Phys. Rev.* **1982**, *A26*, 2028.
[23] D. R. Kanis, M. A. Ratner, T. J. Marks, *Chem. Rev.* **1994**, *94*, 195−242.
[24] D. R. Kanis, M. A. Ratner, T. J. Marks, *J. Am. Chem. Soc.* **1992**, *114*, 10338−10357.
[25] [25a] S. Stadler, G. Bourhill, C. Bräuchle, *Proc. SPIE* **1996**, *2852*, 142. − [25b] S. Stadler, Ph. D. Thesis, Ludwig-Maximilians-Universität München, **1996**.
[26] J. L. Oudar, D. S. Chemla, *J. Chem. Phys.* **1977**, *66*, 2664−2668.
[27] W. P. Fehlhammer, W. A. Herrmann, K. Öfele, *Handbuch der präparativen Anorganischen Chemie* (Ed.: G. Brauer), 3rd. ed., Enke-Verlag, Stuttgart, **1981**.

Received September 11, 1998
[I98304]

Synthesis and Structure of 2-Hydro-, 2-Alkyl-, 2-Alkynyl-, and 2-Stannyl-2,3-dihydro-1*H*-1,3,2-diazaboroles

Lothar Weber,*[a] Eckhard Dobbert,[a] Hans-Georg Stammler,[a] Beate Neumann,[a] Roland Boese,[b] and Dieter Bläser[b]

Dedicated to Professor Dietmar Seyferth on the occasion of his 70th birthday

Keywords: Boron / Diazaboroles / Hydrides / Tin / Heterocycles

1,3-Di-*tert*-butyl-2,3-dihydro-1*H*-1,3,2-diazaborole (**4a**) and 1,3-bis(2,6-dimethylphenyl)-2,3-dihydro-1*H*-1,3,2-diazaborole (**4b**) were formed by the reaction of the corresponding 2-bromo or 2-iodo derivatives **1a** and **2b** with $LiAlH_4$. Treatment of **1a** with *n*-butyllithium afforded 2-*n*-butyl-1,3-di-*tert*-butyl-2,3-dihydro-1*H*-1,3,2-diazaborole (**5a**), whereas 1,3-di-*tert*-butyl-2-cyano-2,3-dihydro-1*H*-1,3,2-diazaborole (**3a**) was converted into the 2-*tert*-butyl derivative **6a** or the 2-ethynyl-1,3,2-diazaborole **7a** by means of *tert*-butyllithium or by the ethylenediamine adduct of lithium acetylide. Similarly, 1,3-di-*tert*-butyl-2-trimethylstannyl-2,3-dihydro-1*H*-1,3,2-diazaborole (**8a**) and 1,3-bis(2,6-dimethylphenyl)-2-trimethylstannyl-2,3-dihydro-1*H*-1,3,2-diazaborole (**8b**) were accessible from **1a** or **2b** and trimethylstannyllithium. In the complex **9a** the compound **3a** serves as an η^1 ligand towards the $[Cr(CO)_5]$ unit via the cyano group. These novel compounds were characterized by ^1H-, ^{11}B-, ^{13}C-, and ^{119}Sn-NMR spectroscopy, as well as by X-ray structure analyses of **4b**, **8a**, and **9a**.

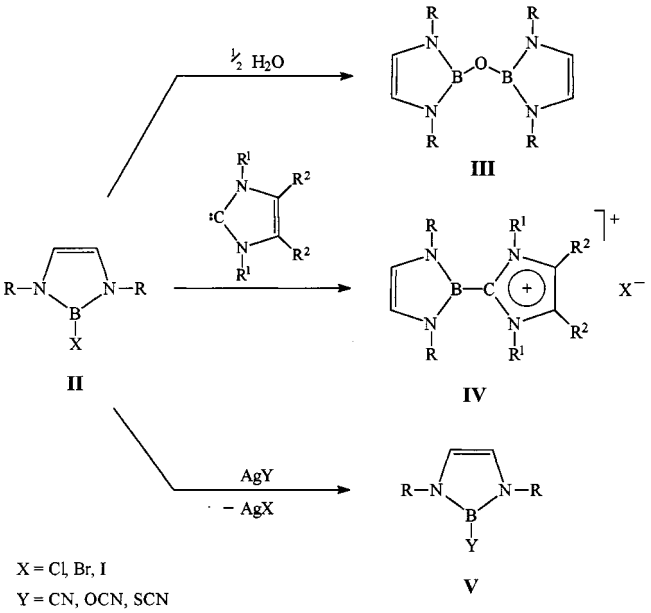
The synthesis of the first 2,3-dihydro-1*H*-1,3,2-diazaboroles **I** dates back to the early 1970s,[1,2] and since then a series of papers concerned with the synthesis, structure, and bonding of such heterocycles has been published.[3,4] A thorough investigation of the chemical reactivity of 2,3-dihydro-1*H*-1,3,2-diazaboroles was primarily hampered by the lack of functionalities at the core of the molecules.[5,6]

Recently, we started a program for the synthesis of the 2-halo-2,3-dihydro-1*H*-1,3,2-diazaboroles **II** as starting materials for further chemical transformations.[7] Treatment of **II** with water, imidazol-2-ylidenes, AgCN, AgOCN, and AgSCN afforded a series of novel 1,3,2-diazaboroles **III**–**V**.[7,8]

The intention of the work described herein is to provide efficient syntheses for 2-hydro-, 2-alkyl-, 2-alkynyl-, and 2-stannyl-2,3-dihydro-1*H*-1,3,2-diazaboroles.

Results and Discussion

One general route to 2,3-dihydro-1*H*-1,3,2-diazaboroles involves the formation of borolium salts from suitable 1,4-diazabutadienes and organoboron halides prior to reduction with sodium amalgam.[2,3,7,8] Accordingly, in the early attempts to synthezise 2,3-dihydro-1*H*-1,3,2-diazaboroles a 1,4-diazabutadiene derivative was treated with $Me_2NH \cdot BH_3$, which led to an inseparable 1:4 mixture of the desired diazaborole **4a** and the corresponding saturated 2-bora-1,3-diazacyclopentane **VI**.[9]

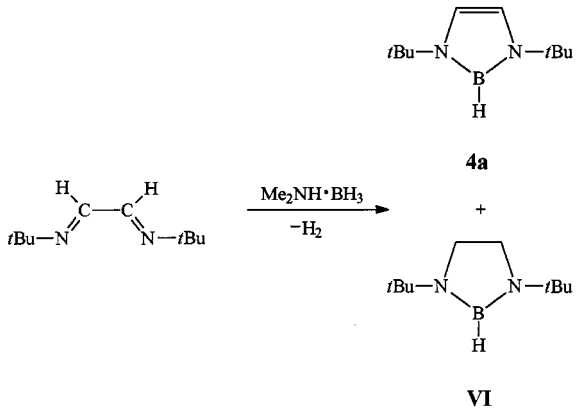


Scheme 1. Chemical transformations of **II**

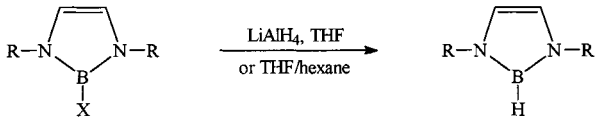
However, the availability of 2-halo-functionalized 2,3-dihydro-1*H*-1,3,2-diazaboroles provides an alternative approach to 2,3-dihydro-1*H*-1,3,2-diazaboroles. Thus, the treatment of the 2-bromo derivative **1a** and the 2-iodo derivative **2b** with equimolar amounts of $LiAlH_4$ in a hexane/THF mixture or in THF, led cleanly to the 2,3-dihydrodiazaboroles **4a** and **4b**, respectively, in high yields and within a few min.

[a] Fakultät für Chemie der Universität Bielefeld, Universitätsstraße 25, D-33615 Bielefeld, Germany
Fax: (internat.) +49(0)5201/106-6146
E-mail: lothar.weber@uni-bielefeld.de
[b] Institut für Anorganische Chemie der Universität–Gesamthochschule Essen, Universitätsstraße 5–7, D-45117 Essen, Germany

 © WILEY-VCH Verlag GmbH, D-69451 Weinheim, 1999 1434–1948/99/0303–0491 $ 17.50+.50/0



Scheme 2. Borane reduction of a 1,4-diazabutadiene

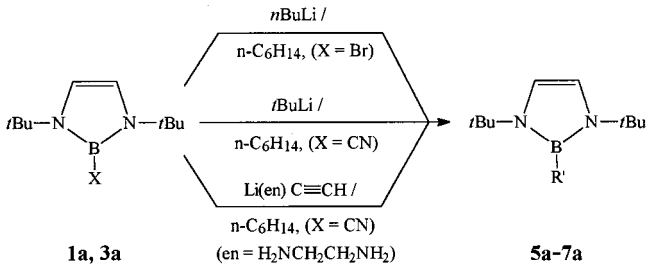


Comp.	R	X
1, 4a	*t*Bu	Br
2, 4b	2,6-$Me_2C_6H_3$	I

Scheme 3. Formation of **4a,b**

The crude products were purified by sublimation at 50°C and 10^{-3} Torr (**4a**) or 210°C and 10^{-4} Torr (**4b**) to give colorless air- and moisture-sensitive solids. In the proton-coupled ^{11}B-NMR spectra (C_6D_6 solution) compounds **4a** and **4b** exhibit doublets at δ = 18.9 ($^1J_{B,H}$ = 149 Hz) and 21.9 ($^1J_{B,H}$ = 158 Hz). The former value compares well with results given in Schulze′s thesis for **4a** (δ = 18.9, d, $^1J_{B,H}$ = 152 Hz), which was dissolved in the four-fold amount of the corresponding saturated compound **VI** (δ = 26.1, d, $^1J_{B,H}$ = 136 Hz).[9] Niedenzu et al. observed for the 1,3,2-diazaboracyclopentane (Me)N^{a}CH$_2$CH$_2$N^b(Me)BH(*N*^{a}−B) and the diazaboracyclohexane (Me)N^{a}CH$_2$CH$_2$CH$_2$N^b-(Me)BH(*N*^{a}−B) ^{11}B-NMR signals at δ = 28.3 (d, $J_{B,H}$ = 131 Hz) and 26.0 (d, $J_{B,H}$ = 132 Hz).[10,11]

The ^{1}H-NMR spectrum of **4a** shows a quadruplet resonance at δ = 4.78 ($^1J_{B,H}$ = 150 Hz) for a boron-ligated hydrogen atom. A medium intense band at $\tilde{\nu}$ = 2594 cm^{-1} and a weak band at $\tilde{\nu}$ = 2623 cm^{-1} in the IR spectrum of **4a** are attributed to the stretching vibrations ν(^{11}B−H) and ν(^{10}B−H). The IR spectrum of **4b** shows a medium intense band at $\tilde{\nu}$ = 2607 cm^{-1} for this mode of vibration. Alkyl substituents at the boron atom of diazaboroles were usually introduced with the organodihaloborane in the condensation step of the synthesis. With 2-halo- and 2-pseudohalo-1,3,2-diazaboroles an inverse approach to such species, namely the replacement of the halide (pseudohalide) by carbanions is now available.



Comp.	R'
5a	*n*-Bu
6a	*t*-Bu
7a	C≡CH

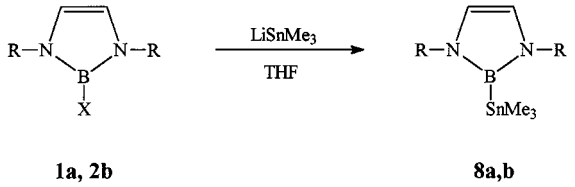
Scheme 4. Nucleophilic substitutions at the B atom of **1a,3a**

The reaction of 2-bromo-1,3,2-diazaborole **1a** with an equimolar amount of *n*-butyllithium in hexane at ambient temp. cleanly afforded **5a** as a colorless hygroscopic solid after distillation at 200−250° and 10^{-3} Torr (84%).

Similarly the 2-cyano-1,3,2-diazaborole **3a** was converted in high yield into the 2-*tert*-butyl- and the 2-ethynyl-1,3,2-diazaboroles **6a** and **7a**, respectively, by treatment with *t*BuLi or the ethylenediamine adduct of lithium acetylide. In the case of **7a** the employment of the 2-cyano-1,3,2-diazaborole as a starting material was crucial since the bromo derivative and the organolithium component gave rise to the formation of (*t*Bu)N^{a}CH=CHN^b(*t*Bu)B^a−N^c(H)CH$_2$-CH$_2$N^d(H)B^{b}N^e(*t*Bu)CH=CH−N^f(*t*Bu)(*N*^{a}−B^a)(*B*^{b}−N^f) instead of **7a**.[12] The ^{11}B{^{1}H}-NMR signals of **5a** (δ = 26.4) compare well with those of (*t*Bu)N^a−CH=CHN^b(*t*Bu)B−CH$_3$(*N*^{a}−B) (δ = 26.2),[3,9] whereas the ^{11}B-NMR resonance of the *tert*-butyl derivative **6a** appeared slightly deshielded (δ = 30.1). In a series of bis(aminoboryl-)acetylenes, the ^{11}B-NMR resonances were registered in the narrow range of δ = 23.8−24.9 regardless of the remaining substituents at the C≡C triple bond.[13] In comparison to this the ^{11}B-NMR signal of **7a** (δ = 15.7) is shielded markedly. This observation may be explained by the aromaticity of the heterocyclic system under discussion. In the ^{1}H-NMR spectrum of **7a** the chemical shift of the ethynyl proton (δ^{1}H = 2.72, s) is identical with those in ($R_2N)_2$B(C≡CH) (R = Me or Et).[13]

The resonance for the α-C atom of the ethynyl unit could not be located in the ^{13}C{^{1}H}-NMR spectrum of the compound. The signal of C_β was registered as a singlet at δ = 96.2, and thus this carbon atom is more deshielded than the corresponding ^{13}C nuclei in Et_2N−B(C≡CH)$_2$ (δ = 85.0), whereas the signal of C_β in (*n*BuO)$_2$B−C≡CH (δ = 91.4) is better comparable with that of **7a**.

The first stannylated 2,3-dihydro-1*H*-1,3,2-diazaboroles were synthesized from **1a** and **2b** and equimolar amounts of trimethylstannyllithium in a THF/hexane mixture at ambient temp.



Comp.	R
1a, 8a	*t*Bu
2b, 8b	2,6-$Me_2C_6H_3$

Scheme 5. Stannylation of **1a,2b**

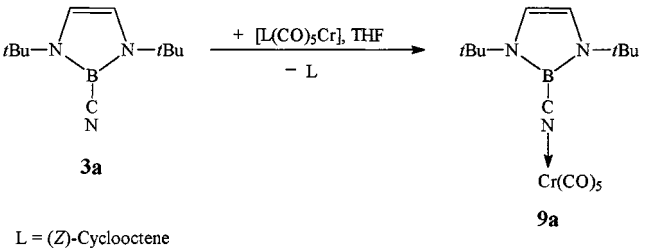
Purification of the colorless solid **8a** was achieved by distillation at 190°C and 10^{-3} Torr and subsequent crystallization of the distillate from *n*-hexane at −30°C (89% yield). The colorless crystalline **8b** precipitated from a hexane solution at −10°C (60% yield).

The $^{11}B\{^1H\}$-NMR spectrum of **8a** is characterized by a singlet at δ = 25.8, with ^{119}Sn satellites ($^1J_{Sn,B}$ = 1031 Hz). In accordance to this, a quadruplet at δ = 152 ($^1J_{Sn,B}$) was encountered in the $^{119}Sn\{^1H\}$-NMR spectrum of the compound. Similarly, the ^{11}B chemical shift of **8b** (δ = 28.2) shows a ^{119}Sn-^{11}B coupling of ^1J = 960 Hz. The $^{119}Sn\{^1H\}$-NMR resonance of **8b** is observed as a quadruplet at δ = 146 with $^1J_{Sn,B}$ = 960 Hz. The saturated compound (Me)-$N^a-CH_2CH_2N^b$(Me)B($SnMe_3$)(N^a−B) displayed a ^{11}B signal at markedly lower field (δ = 36.5, $^1J_{Sn,B}$ = −930 Hz) and a ^{119}Sn-NMR resonance at δ = 152.[14]

The mass spectra of **8a** and **8b** showed, in addition to the peak of the molecular ion, peaks of high intensity at *m*/*z* = 194 (80%) and *m*/*z* = 290 (100%), respectively, which are attributed to the corresponding 2-methyl-2,3-dihydro-1*H*-1,3,2-diazaboroles.

Principally, the 2-cyano-2,3-dihydro-1*H*-1,3,2-diazaborole **3a** is a polyfunctional ligand with different donor sites. Formation of the complex **9a** featuring η^1 coordination of the ligand via the cyano group was achieved by treatment of **3a** with an equimolar amount of [(*Z*)-cyclooctene]$Cr(CO)_5$ in THF at room temp. The product was isolated as yellow needles after crystallization from *n*-hexane at −10°C (83% yield). The ^{11}B-NMR signal of the complex is shielded by Δδ = 2.5 with respect to that of the free ligand. Four ν(CO) bands in the IR spectrum of **9a** ranging from $\tilde{\nu}$ = 2053 to 1888 cm^{-1}, and singlets in the $^{13}C\{^1H\}$-NMR spectrum at δ = 214.4 (CO_{eq}) and 218.9 (CO_{ax}), are consistent with the presence of a $Cr(CO)_5$ group and thus clearly point to a η^1 coordination of **3a**.

In addition to the significant high-field shifts of the ^{11}B-NMR signals of the 2,3-dihydro-1*H*-1,3,2-diazaboroles presented here, in comparison to their saturated analogs, the ^1H- and ^{13}C-NMR resonances of the CH=CH building block (δ^1H = 6.00−6.39 and $\delta^{13}C$ = 112.7−115.5 in **4a−9a**) sustain the argument for the heteroaromatic nature of the rings under discussion.



Scheme 6. Formation of complex **9a**

X-ray Structural Analysis of 8

The molecular structure of **8a** (Figure 1) features a planar 1,3,2-diazaborole ring with a trimethylstannyl substituent which is linked to the boron atom via a B−Sn single bond of 2.274(5) Å. Structurally documented atomic distances between tricoordinate boron and tetravalent tin atoms are rare. The Sn−B bond lengths in the 1,2-bis(organostannylboryl)ethenes **VII** and **VIII** amount to 2.305(7)−2.323(7) and 2.286(17), and 2.277(17) Å, respectively.[15]

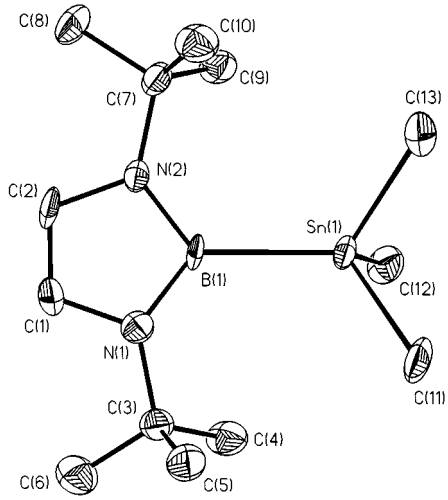
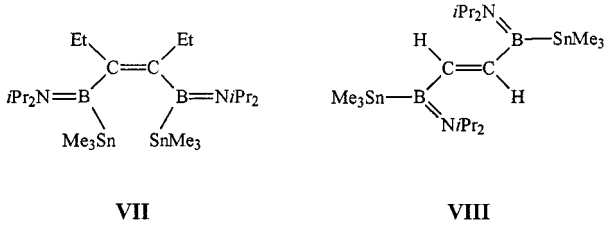


Figure 1. Molecular structure of **8a** in the crystal; selected bond lengths [Å] and angles [°]: B(1)−Sn(1) 2.274(5), B(1)−N(1) 1.439(7), N(1)−C(1) 1.379(7), C(1)−C(2) 1.344(8), N(2)−C(2) 1.399(7), B(1)−N(2) 1.450(7), N(1)−C(3) 1.500 (7), N(2)−C(7) 1.497(7); N(1)−B(1)−N(2) 105.0(4), N(1)−B(1)−Sn(1) 127.5(4), N(2)−B(1)−Sn(1) 127.5(4), B(1)−N(1)−C(1) 108.1(4), B(1)−N(2)−C(2) 107.1(4), B(1)−N(1)−C(3) 131.1(5), B(1)−N(2)−C(7) 130.7(4), N(1)−C(1)−C(2) 110.2(5), N(2)−C(2)−C(1) 109.7(5), B(1)−Sn(1)−C(11) 116.7(2), B(1)−Sn(1)−C(12) 111.7(3), B(1)−Sn(1)−C(13) 119.2(3)



VII **VIII**

Scheme 7. Stannylboranes **VII** and **VIII**

A boron−tin bond length of 2.237(5) Å was measured in the boratobenzene complex (C_5Me_5)Fe(C_5H_5B−$SnMe_3$).[16] In the anion $[B_{11}H_{11}SnMe]^-$ boron−tin con-

tacts of comparable lengths [2.288(3)−2.306(3) Å] were encountered.[17]

Atomic distances and valence angles within the diazaborole ring are in good agreement with the equivalent data for the borolylimidazolium cation **IV**.[7] In **8a** the B−N bond lengths [1.439(7), 1.450(7) Å] indicate multiple bond character. In a series of diazaboroles the B−N bond lengths range from 1.407(3) to 1.450(2) Å. The atomic distance C(1)−C(2) [1.344(8) Å] and the N−C(sp^2) bond lengths [1.379(7) and 1.399(7) Å] also indicate multiple bonding. For the N(sp^2)−C(sp^3) single bonds N(1)−C(3) and N(2)−C(7) bond lengths of 1.500(7) and 1.497(7) Å are measured. The endocyclic angles in **8a** N(1)−B(1)−N(2) [105.0(4)°], B(1)−N(1)−C(1) [108.1(4)°], B(1)−N(2)−C(2) [107.1(4)°], N(1)−C(1)−C(2) [110.2(5)°], and N(2)−C(2)−C(1) [109.7(5)°] resemble those in **2b**:[8] N−B−N [106.9(4)°], B−N−C [107.5(3)°], and N−C−C [109.1(2)°] and **IV** [107.1(6), 105.9(4) and 110.5(3)°]. This also applies to the exocyclic angles N(1)−B(1)−Sn(1) and N(2)−B(1)−Sn(1) [127.5(4)°] in **8a**, and the corresponding angle in **2b** [126.6(2)°]. The angles B(1)−Sn(1)−C(13) [119.2(3)°] and B(1)−Sn(1)−C(11) [116.7(2)°] are significantly widened as compared to the angle B(1)−Sn(1)−C(12) [111.7(3)°], which reflects steric interactions between the *tert*-butyl substituents and methyl groups C(11)H_3 and C(13)H_3.

X-ray Structural Analysis of 4

The molecular structure of **4b** (Figure 2) features a planar 1,3,2-diazaborole ring with two nearly orthogonally oriented *ortho*-xylyl substituents at the nitrogen atoms (interplanar angles between the heterocycle and the arene rings: ψ = 85.9 and 86.5°). Atomic distances and valence angles within the diazaborole ring (see caption of Figure 2) are in excellent agreement with those of **8a**, **2b**, and **IV**.

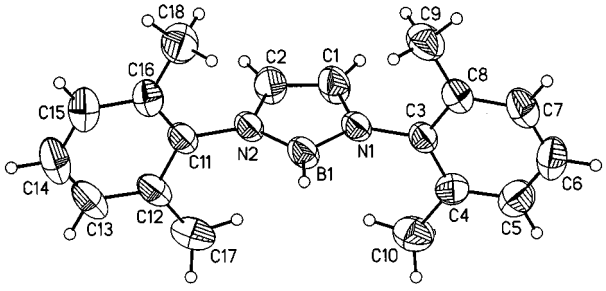


Figure 2. Molecular structure of **4b** in the crystal; selected bond lengths [Å] and angles [°]: B(1)−H(1A) 1.04(3), B(1)−N(1) 1.395(4), N(1)−C(1) 1.377(3), N(1)−C(3) 1.427(3), B(1)−N(2) 1.398(4), N(2)−C(2) 1.374(3), N(2)−C(11) 1.421(3), C(1)−C(2) 1.323(4); N(1)−B(1)−N(2) 106.8(2), N(1)−B(1)−H(1A) 124(2), N(2)−B(1)−H(1A) 129(2), B(1)−N(1)−C(1) 106.9(2), B(1)−N(1)−C(3) 130.9(2), N(1)−C(1)−C(2) 109.8(3), C(1)−N(1)−C(3) 122.1(2), B(1)−N(2)−C(2) 107.3(2), B(1)−N(2)−C(11) 130.6(2), C(2)−N(2)−C(11) 122.1(2), N(2)−C(2)−C(1) 109.2(3)

X-ray Structural Analysis of 9

The molecular structure determination of the pentacarbonylchromium adduct **9a** reveals a nearly undistorted octahedron, one apex of which is occupied by the η^1-2-cyano-2,3-dihydro-1*H*-1,3,2-diazaborole. Thus the atoms B(1), C(1), N(1), Cr(1), C(14), and O(14) are in a linear arrangement. The plane of the heterocycle is staggered with respect to the plane defined by the metal center and the four equatorial carbonyl groups. The bond Cr(1)−C(14) in *trans* disposition to the ligand [1.825(7) Å] is markedly shortened as compared to the remaining Cr(1)−C(CO) bond lengths [1.899(6)−1.917(6) Å], which reveals the 2-cyanodiazaborole as a donor ligand without appreciable π-back bonding. The bond Cr(1)−N(1) of 2.051(5) Å is close to sum of the covalent radii of Cr^0 (1.48 Å)[18] and sp-hybridized N (0.55 Å)[19a]. The C(1)−N(1) bond length of 1.140(6) Å resembles that in cyanogen (1.15 Å).[19b] Due to the presence of an sp-hybridized carbon atom, the bond length B(1)−C(1) [1.547(8) Å] is shorter than the B(sp^2)−C(sp^2) bond in the borolylimidazolium ion **IV** [1.580(11) Å], and it is comparable with the C(sp^2)−B(sp) distance in Li^+-[2,4,6-$Me_3C_6H_2$−B=C−B(2,4,6-$Me_3C_6H_2$)CH($SiMe_3$)$_2$]$^-$ [1.543(6) Å].[20] The bonding parameters within the 1,3,2-diazaborole ring largely resemble those of **4b**, **IV**, and **2b**, and merit no further discussion.

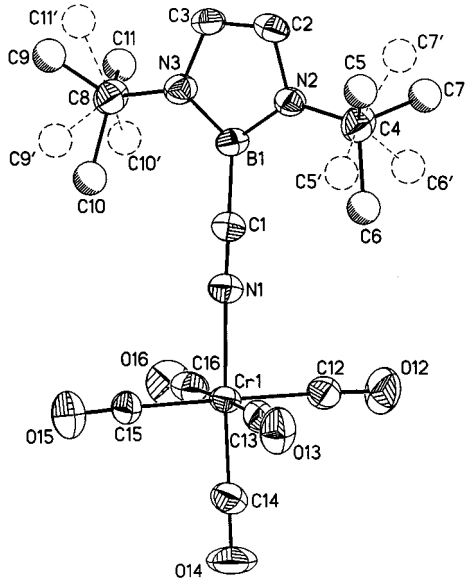


Figure 3. Molecular structure of **9a** in the crystal; selected bond lengths [Å] and angles [°]: B(1)−N(2) 1.416(7), N(2)−C(2) 1.389(7), N(2)−C(4) 1.477(5), B(1)−N(3) 1.433(7), N(3)−C(3) 1.373(6), N(3)−C(8) 1.478(5), C(2)−C(3) 1.312(8), B(1)−C(1) 1.547(8), C(1)−N(1) 1.140(6), Cr(1)−N(1) 2.051(5), Cr(1)−C(12) 1.906(7), Cr(1)−C(13) 1.899(6), Cr(1)−C(14) 1.825(7), Cr(1)−C(15) 1.906(6), Cr(1)−C(16) 1.917(6); N(2)−B(1)−N(3) 107.5(4), B(1)−N(2)−C(4) 133.5(4), B(1)−N(3)−C(8) 132.9(4), B(1)−N(2)−C(2) 105.6(4), C(2)−N(2)−C(4) 120.9(4), B(1)−N(3)−C(3) 105.1(4), C(3)−N(3)−C(8) 122.0(4), N(2)−C(2)−C(3) 110.2(5), N(3)−C(3)−C(2) 111.5(5), B(1)−C(1)−N(1) 178.2(5), C(1)−N(1)−Cr(1) 177.5(5), N(1)−Cr(1)−C(12) 89.0(2), N(1)−Cr(1)−C(13) 90.4(2), N(1)−Cr(1)−C(14) 177.5(3), N(1)−Cr(1)−C(15) 91.7(2), N(1)−Cr(1)−C(16) 92.0(2), Cr(1)−C(14)−O(14) 177.9(6)

Experimental Section

General: All manipulations were performed under dry argon. Solvents were rigorously dried with an appropriate drying agent and freshly distilled before use. − The following compounds were prepared as described in the literature: (*t*Bu)N^a−CH=CH−N^b(*t*Bu)-BBr(*N*^{a}−B) (**1a**),[7] (*t*Bu)N^a−CH=CH−N^b(*t*Bu)BCN(*N*^{a}−B) (**3a**),[8] (2,6-Me$_2$C$_6$H$_3$)N^a−CH=CH−N^b(2,6-Me$_2$C$_6$H$_3$)BI(*N*^{a}−B) (**2b**),[8] [(*Z*)-cyclooctene]Cr(CO)$_5$.[21] LiAlH$_4$, Me$_3$SnCl, Li(H$_2$NCH$_2$CH$_2$NH$_2$)C≡CH, Li metal, *n*-butyllithium, *tert*-butyllithium were purchased. − IR spectra: Bruker FTIR IFS66. − ^{1}H-, ^{11}B-, ^{13}C-, and ^{119}Sn-NMR spectra: C$_6$D$_6$ at room temp.; Bruker AC 100 (^{1}H, 100.13 MHz); Bruker Avance DRX 500 (^{1}H, 500.13 MHz, ^{11}B, 160.46 MHz, ^{13}C, 125.75 MHz, ^{119}Sn, 186.51 MHz); references: SiMe$_4$ (^{1}H, ^{13}C), BF$_3$ · OEt$_2$ (^{11}B), SnMe$_4$ (^{119}Sn). − Mass spectra (EI): VG Autospec sector-field mass spectrometer (Micromass) 70 eV.

(*t*Bu)N^a−CH=CH−N^b(*t*Bu)BH(*N*^{a}−*B*) (4a): A sample of solid LiAlH$_4$ (0.114 g, 3.0 mmol) was added to a solution of **1a** (0.777 g, 3.0 mmol) in a mixture of *n*-hexane (20 mL) and THF (20 mL). After 2 min of stirring at 20°C, the solution was decanted from the solid components and concentrated to dryness. The residue was taken up in *n*-pentane (30 mL) and filtered. The filtrate was freed from solvent, and the colorless residue was sublimed (40−45°C, 10^{-3} Torr) to afford 0.475 g (88%) of colorless solid **4a**. M.p. 51−53°C. − IR (nujol): $\tilde{\nu}$ = 2623 cm^{-1} w [ν(^{10}B−H)], 2594 m [ν(^{11}B−H)], 1410 s, 1366 s, 1316 m, 1290 m, 1282 m, 1247 s, 1221 w, 1147 m, 1092 w, 922 m, 818 w, 664 s, 633 w, 553 m. − ^{1}H NMR: δ = 1.30 (s, 18 H, *t*Bu), 4.78 (q, $^1J_{B,H}$ = 150 Hz, 1 H, BH), 6.39 (s, 2 H, CH). − ^{13}C{^{1}H} NMR: δ = 31.9 [s, C(*C*H$_3$)$_3$], 51.4 [s, *C*(CH$_3$)$_3$], 114.2 (s, CH). − ^{11}B NMR: δ = 18.9 (d, $^1J_{B,H}$ = 149 Hz). − MS/EI: *m*/*z* (%) = 180 (67) [M$^+$], 165 (100) [M$^+$ − CH$_3$]. − C$_{10}$H$_{21}$BN$_2$ (180.12): calcd. C 66.67, H 11.77, N 15.54; found C 66.73, H 12.04, N 15.28.

(2,6-Me$_2$C$_6$H$_3$)N^a−CH=CH−N^b(2,6-Me$_2$C$_6$H$_3$)BH(*N*^{a}−*B*) (4b): A sample of solid LiAlH$_4$ (0.100 g, 2.6 mmol) was added to a solution of 0.820 g (2.0 mmol) of **2b** in 80 mL of THF at room temp., and the mixture was vigorously stirred. After 5 min, the colorless solution was decanted and liberated from solvent in vacuo. The oily residue was taken up in *n*-hexane (40 mL) and filtered. The solvent was removed from the filtrate, and the residue was sublimed at 210°C (10^{-3} Torr). The product was crystallized from *n*-pentane at −10°C to yield 0.490 g (89%) of colorless **4b**. M.p. 112°C. − IR (KBr): $\tilde{\nu}$ = 3104 cm^{-1} w, 3022 w, 2953 m, 2921 m, 2854 w, 2607 [ν(BH)], 1594 w, 1555 w, 1479 s, 1438 m, 1402 m, 1376 sh, 1281 m, 1258 m, 1246 w, 1190 w, 1126 m, 1107 w, 1089 w, 1033 w, 902 m, 808 w, 770 s, 749 w, 687 s, 583 w, 552 w, 514 w, 455 w. − ^{1}H NMR: δ = 2.20 (s, 12 H, CH$_3$), 6.03 (s, 2 H, CH=CH), 7.01 (s, 6 H, H−aryl). − ^{13}C{^{1}H} NMR: δ = 18.2 (s, CH$_3$), 118.4 (s, CH=CH), 126.5 (s, C-*p* aryl), 135.2 (s, C-*o* aryl), 141.8 (s, C-*i* aryl). − ^{11}B{^{1}H} NMR: δ = 21.9 (d, $^1J_{B,H}$ = 158 Hz). − MS/EI: *m*/*z* (%) = 276 (100) [M$^+$]. − C$_{18}$H$_{21}$BN$_2$ (276.19): calcd. C 78.28, H 7.66, N 10.14; found C 78.28, H 7.86, N 10.12.

(*t*Bu)N^a−CH=CH−N^b(*t*Bu)B(*n*Bu)(*N*^{a}−*B*) (5a): A solution of 0.518 g (2.0 mmol) of **1a** in *n*-hexane (30 mL) was treated with 1.25 mL (2.0 mmol) of a 1.6 M *n*-butyllithium solution in *n*-hexane at room temp. After 30 min of stirring, it was filtered. The filtrate was freed from the solvent, and the residue was distilled (10^{-3} Torr, 200−250°C) to give **5a** as a colorless hygroscopic solid. The crude material was crystallized from *n*-pentane at −10°C (yield 0.400 g, 84%). M.p. 95−100°C. − IR (KBr): $\tilde{\nu}$ = 2956 cm^{-1} vs, 2929 s, 2913 s, 2869 s, 2766 m, 1628 s, 1610 s, 1464 s, 1437 sh, 1395 m, 1368 s, 1234 s, 1210 s, 1134 w, 1095 w, 967s, 754 w, 558 w, 473 m. − ^{1}H NMR: δ = 0.99 (t, $^3J_{H,H}$ = 7.3 Hz, 3 H, CH$_2$C*H*$_3$), 1.36(s, 18 H, *t*Bu), 1.48 (m, 4 H, C*H*$_2$C*H*$_2$CH$_3$), 1.66 (m, 2 H, BCH$_2$), 6.33 (s, 2 H, CH). − ^{13}C{^{1}H} NMR: δ = 14.0 (s, CH$_2$*C*H$_3$), 26.9 (s, *C*H$_2$CH$_3$), 31.1 (s, *C*H$_2$CH$_2$CH$_3$), 32.1 [s, C(*C*H$_3$)$_3$], 52.9 [s, *C*(CH$_3$)], 112.7 (s, CH). − ^{11}B{^{1}H} NMR: δ = 26.4 s. − MS/EI: *m*/*z* (%) = 236 (65) [M$^+$]. − C$_{14}$H$_{29}$BN$_2$ (236.21): calcd. C 71.19, H 12.37, N 11.86; found C 70.92, H 12.56, N 10.98.

(*t*Bu)N^a−CH=CH−N^b(*t*Bu)B(*t*Bu)(*N*^{a}−*B*) (6a): A chilled solution (−30°C) of **3a** (0.615 g, 3.0 mmol) in *n*-hexane (30 mL) was treated with 2 mL of 1.5 M solution of *tert*-butyllithium (3.0 mmol) in *n*-pentane. It was allowed to warm up to 20°C, and the resultant slurry was filtered. Removal of the solvent and distillation of the residue gave **6a** as a light yellow oil (bp 150−170°C, 10^{-3} Torr), which slowly solidified at 0°C. M.p. 54−56°C. Yield: 0.623 g (88%). − IR (KBr): $\tilde{\nu}$ = 2970 cm^{-1}, s, 1660 m, 1631 m, 1478 s, 1460 sh, 1419 sh, 1396 s, 1365 s, 1310 m, 1228 m, 1133 w, 1057 m, 934 w, 748 w, 713 w, 631 w. − ^{1}H NMR: δ = 1.41 [s, 9 H, B(*t*Bu)], 1.42 [s, 18 H, N(*t*Bu)], 6.32 (s, 2 H, CH). − ^{13}C{^{1}H} NMR: δ = 33.4 [s, NC(*C*H$_3$)$_3$], 33.9 [s, BC(*C*H$_3$)$_3$], 53.8 [s, N*C*(CH$_3$)$_3$], 113.6 (s, CH)). − ^{11}B{^{1}H} NMR: δ = 30.1 s. − MS/EI: *m*/*z* (%) = 236 (6) [M$^+$], 179 (10) [M$^+$ − *t*Bu]. − C$_{14}$H$_{29}$BN$_2$ (236.21): calcd. C 71.19, H 12.37, N 11.86; found C 70.78, H 12.25, N 11.65.

(*t*Bu)N^a−CH=CH−N^b(*t*Bu)B−C≡CH(*N*^{a}−*B*) (7a): A sample of Li(H$_2$N−CH$_2$CH$_2$−NH$_2$)C≡CH (0.370 g, 2.0 mmol) was added to a solution of 0.420 g (2.0 mmol) of **3a** in *n*-hexane (50 mL). Stirring at ambient temp. was continued for 24 h. Then the colorless hexane phase was decanted from a precipitate, and subsequently concentrated to dryness (10^{-3} Torr). The colorless residue was recrystallized from *n*-hexane to give pure **7a** as colorless needles. M.p. 77−85°C (dec.). Yield 0.347 g (85%). − IR (film, CsI): $\tilde{\nu}$ = 3299 cm^{-1} w [ν(≡CH)], 2972 s, 2936 w, 2910 w, 2872 w, 2067 w [ν(C≡C)], 1629 w, 1478 w, 1463 w, 1398 s, 1367 s, 1345 s, 1284 m, 1235 s, 1143 m, 947 w, 824 w, 652 s. − ^{1}H NMR: δ = 1.47 (s, 18 H, *t*Bu), 2.72 (s, 1 H, ≡C−H), 6.25 (s, 2 H, =CH). − ^{13}C{^{1}H} NMR: δ = 31.7 [s, C(*C*H$_3$)$_3$], 53.3 [s, *C*(CH$_3$)$_3$], 96.2 [s, BC≡*C*H], 112.8 (s, =*C*H). − ^{11}B{^{1}H} NMR: δ = 15.7 s. − MS/EI: *m*/*z* (%) = 204 (27) [M$^+$], 92 (100) [M$^+$ − 2 Me$_2$C=CH$_2$]. − C$_{12}$H$_{21}$BN$_2$ (204.16): calcd. C 70.59, H 10.29, N 13.70; found C 70.14, H 10.15, N 13.82.

(*t*Bu)N^a−CH=CH−N^b(*t*Bu)BSnMe$_3$(*N*^{a}−*B*) (8a): 0.100 g (14.4 mmol) of lithium sand was added to a solution of 0.770 g (3.9 mmol) of chlorotrimethylstannane in THF (40 mL), and the slurry was stirred under ultrasonic activation for 30 min. Then 1.00 g (3.9 mmol) of **1a** was added with vigorous stirring. After 1 h, the reaction mixture was filtered, and the solvent was removed from the filtrate by distillation. The residue was dissolved in 20 mL of *n*-hexane. The cloudy solution was filtered and the filtrate was subjected to distillation. The product was obtained as a fraction at 190°C (10^{-3} Torr). Recrystallization from *n*-hexane at −30°C afforded 0.117 g (89%) of **8a** as a colorless solid. M.p. 59°C. − IR (nujol): $\tilde{\nu}$ = 1630 cm^{-1} w, 1574 w, 1394 m, 1365 s, 1296 s, 1263 w, 1230 s, 1196 w, 1185 w, 1136 m, 1026 w, 953 w, 928 w, 824 w, 772 s, 670 m, 642 w, 615 m, 508 s. − ^{1}H NMR: δ = 0.41 (s, $^2J_{Sn,H}$ = 44 Hz, 9 H, SnMe$_3$), 1.31 (s, 18 H, *t*Bu), 6.50 (s, $^4J_{Sn,H}$ = 14 Hz, 2 H, CH). − ^{13}C{^{1}H} NMR: δ = −4.6 (s, $^1J_{Sn,C}$ = 283 Hz, SnCH$_3$), 33.1 [s, C(*C*H$_3$)$_3$], 53.3 [s, *C*(CH$_3$)$_3$], 114.8 (s, $^3J_{Sn,C}$ = 43 Hz, CH). − ^{11}B{^{1}H} NMR: δ = 25.8 (s, $^1J_{Sn,B}$ = 1031 Hz). − ^{119}Sn{^{1}H} NMR: δ = 152 (q, $^1J_{Sn,B}$ = 1032 Hz). − MS/EI: *m*/*z* (%) = 344 (4) [M$^+$], 329 (75) [M$^+$ − CH$_3$], 194 (80) [(*t*Bu)N^{a}CH=CH−N^b(*t*Bu)BCH$_3$(*N*^{a}−B)$^+$]. − C$_{13}$H$_{29}$BN$_2$Sn (342.89): calcd. C 45.54, H 8.52, N 8.17; found C 45.38, H 8.52, N 7.82.

(2,6-Me$_2$C$_6$H$_3$)N^a−CH=CH−N^b(2,6-Me$_2$C$_6$H$_3$)BSnMe$_3$(*N*^{a}−*B*) (8b): A quantity of 0.297 g (1.5 mmol) of Me$_3$SnCl was treated

Table 1. Crystal data and data collection parameters

Compound	**4b**	**8a**	**9a**
formula	$C_{18}H_{21}BN_2$	$C_{13}H_{29}BN_2Sn$	$C_{16}H_{20}BCrN_3O_5$
M_r	276.18	342.88	397.16
crystal dimensions [mm]	0.33×0.21×0.18	0.9×0.4×0.2	0.15×0.13×0.03
crystal system	monoclinic	triclinic	orthorhombic
space group	$P2(1)/n$	$P\bar{1}$	$P2(1)2(1)2(1)$
a [Å]	8.4986(2)	8.998(5)	6.4166(1)
b [Å]	16.9200(3)	9.357(6)	16.3958(1)
c [Å]	11.7980(1)	11.225(7)	20.0326(2)
α [°]	90	90.71(5)	90
β [°]	98.723(1)	93.26(5)	90
γ [°]	90	116.86(4)	90
V [Å^3]	1676.89(5)	841.0(9)	2107.54(4)
Z	4	2	4
$\rho_{calcd.}$ [Mg m^{-3}]	1.094	1.354	1.252
μ [mm^{-1}]	0.063	1.504	0.570
$F(000)$	592	352	824
T [K]	296	173	296
2θ [°]	2.8−48.4	3.6−55.0	5.4−56.8
no. refl. recorded	8226	3769	18627
no. refl. unique	2437	3551	4388
no. refl. obs. $I > 2\sigma(I)$	1645	3145	3193
R (int)	0.0407	0.0629	0.0488
refined parameters	194	163	232
GOF	1.035	1.108	1.024
$R(2\sigma)$	0.0676	0.0618	0.0699
w$R2$	0.2230	0.1685	0.2101
$\Delta\rho_{max}$ [e Å^{-3}]	0.234	1.88	0.675

with 0.100 g (14.4 mmol) of lithium sand in 30 mL of THF with ultrasonic activation. At room temp. a solution of 0.600 g of **2b** in 20 mL of *n*-hexane was added dropwise. After 1 h of stirring, the solvent was removed, and 20 mL of *n*-hexane was added to the residue. It was filtered, and the light yellow filtrate was concentrated to initiate crystallization. Completion of the crystallization was achieved by storing the solution overnight at −10°C. Yield: 0.395 g (60%) of colorless crystalline **8b**. M.p. 43−45°C. − IR (KBr): $\tilde{\nu}$ = 3023 cm^{-1} w, 2976 m, 2911 m, 1621 w, 1594 w, 1477 s, 1438 m, 1378 s, 1277 w, 1263 w, 1246 w, 1183 w, 1102 w, 907 w, 767 s, 695 w, 518 s, 498 m. − ^{1}H NMR: δ = −0.19 (s, $^2J_{Sn,H}$ = 77.4 Hz, 9 H, Sn Me_3), 2.16 (s, 12 H, Me−aryl), 6.13 (s, $J_{Sn,H}$ = 10 Hz, HC=CH), 6.99 (m, 6 H, H−aryl). − ^{13}C{^{1}H} NMR: δ = −12.3 (s, $^1J_{Sn,C}$ = 293 Hz), 18.0 (s, CH_3−aryl), 120.0 (s, $^3J_{Sn,C}$ = 34 Hz, HC=CH), 127.0 (C-*p* aryl), 135.8 (C-*o* aryl), 142.6 (C-*i* aryl). − δ^{11}B{^{1}H} NMR: δ = 28.2 (s, $^1J_{Sn,B}$ = 960 Hz). − δ^{119}Sn{^{1}H} NMR: δ = 146.0 (q, $^1J_{Sn,B}$ = 960 Hz. − MS/EI: *m*/*z* (%) = 425 (45) [$M^+ - CH_3$]; 290 (100) [(2,6-$Me_2C_6H_3$)N^a−CH=CH−N^b(2,6-$Me_2C_6H_3$)BMe(N^a−B)$^+$]. − $C_{21}H_{29}BN_2Sn$ (438.97) calcd. C 57.46, H 6.66, N 6.38; found: C 57.58, H 6.72, N 6.30.

(*t*Bu)N^a−CH=CH−N^b(*t*Bu)BCN→Cr(CO)$_5$(*N*^{a}−*B*) (9a): A solution of [(*Z*)-cyclooctene]Cr(CO)$_5$ (0.440 g, 14.5 mmol) in 5 mL of THF was added dropwise at room temp. to a stirred solution of **3a** (0.300 g, 14.6 mmol) in 30 mL of THF. After 1 h, the brown reaction mixture was concentrated to dryness. The residue was dissolved in 30 mL of hexane. It was filtered, and the filtrate was stored at −10°C. Product **9a** was isolated as yellow needles. Yield: 0.480 g (83%). M.p. 45−50°C (dec.). − IR (KBr): $\tilde{\nu}$ = 2975 cm^{-1} m, 2206 w, 2120 w, 2053 m [ν(CO)], 1987 sh [ν(CO)], 1927 vs [ν(CO)], 1888 sh [ν(CO)], 1632 m, 1529 w, 1467 w, 1432 w, 1404 w, 1369 m, 1305 w, 1262 w, 1208 w, 1170 w, 1067 m, 1027 m, 803 m, 697 m, 663 s, 552 w, 449 w. − ^{1}H NMR: δ = 1.11 (s, 18 H, *t*Bu), 6.00 (s, 2 H, CH). − ^{13}C{^{1}H} NMR: δ = 31.2 [s, C(CH_3)$_3$], 53.8 [s, $C(CH_3)_3$], 115.5 (s, CH), 214.4 (s, CO_{eq}), 218.9 (s, CO_{ax}). − ^{11}B{^{1}H} NMR: δ = 9.4 s. − MS/EI: *m*/*z* (%) = 397 (0.2) [M^+], 285 (0.4) [M^+ − 4 CO], 257 (5) [M^+ − 5 CO], 205 (30) [M^+ − Cr(CO)$_5$]. − $C_{16}H_{20}BCrN_3O_5$ (397.16): calcd. C 48.39, H 5.08, N 10.58; found: C 48.39, H 5.02, N 10.60.

X-ray Crystallography: For **4b** and **9a** crystallographic data were collected with a Siemens CCD-Smart three-axis goniometer using graphite-monochromated Mo-K_α radiation with a full-sphere scan covering more than 98% of the data. An empirical absorption correction (Siemens-SADABS) was applied, for structure solution with Direct Methods and refinements on F^2; Siemens SHELTL-Plus software (Vers. 5.01) was used. Hydrogen atoms were treated as riding groups with U values at the 1.2 fold (1.5 fold for methyl groups) of the corresponding C atoms. − For **8a** the data were collected with a Bruker P2$_1$ four-circle diffractometer. Crystallographic programs used for structure solution and refinement were from SHELXTL PLUS and SHELXL-97. The structure was solved by using Direct Methods and was refined by using full-matrix least squares on F^2 of all unique reflexions with anisotropic thermal parameters for all non-hydrogen atoms. Hydrogen atoms were included at calculated positions with U(H) = 1.2 U_{eq} for groups, U(H) = 1.5 U_{eq} for CH_3 groups. Crystal data of the compounds are listed in Table 1.[22]

Acknowledgments

This work was financially supported by the Fonds der Chemischen Industrie, Frankfurt/Main, and the Deutsche Forschungsgemeinschaft, Bonn, which are gratefully acknowledged.

[1] [1a] K. Niedenzu, J. S. Merriam, *J. Organomet. Chem.* **1973**, *51*, C1−C2. − [1b] K. Niedenzu, J. S. Merriam, *Z. Anorg. Allg. Chem.* **1974**, *406*, 251−259.
[2] L. Weber, G. Schmid, *Angew. Chem.* **1974**, *86*, 519; *Angew. Chem. Int. Ed. Engl.* **1974**, *13*, 467.
[3] G. Schmid, J. Schulze, *Chem. Ber.* **1977**, *110*, 2744−2750.

[4] G. Schmid, M. Polk, R. Boese, *Inorg. Chem.* **1990**, *29*, 4421−4429.
[5] [5a] G. Schmid, J. Schulze, *Angew. Chem.* **1977**, *89*, 258−259; *Angew. Chem. Int. Ed. Engl.* **1977**, *16*, 249. − [5b] G. Schmid, J. Schulze, *Chem. Ber.* **1981**, *114*, 495−504.
[6] G. Schmid, J. Lehr, M. Polk, R. Boese, *Angew. Chem.* **1991**, *103*, 1029−1031; *Angew. Chem. Int. Ed. Engl.* **1991**, *30*, 1015.
[7] L. Weber, E. Dobbert, H.-G. Stammler, B. Neumann, R. Boese, D. Bläser, *Chem. Ber.* **1997**, *130*, 705−710.
[8] L. Weber, E. Dobbert, R. Boese, M. T. Kirchner, D. Bläser, *Eur. J. Inorg. Chem.* **1998**, 1145−1152.
[9] J. Schulze, Dissertation, Universität Essen, **1980**.
[10] E. F. Rothgery, P. J. Busse, K. Niedenzu, *Inorg. Chem.* **1971**, *10*, 2343−2345.
[11] E. B. Bradley, R. H. Herber, P. J. Busse, K. Niedenzu, *J. Organomet. Chem.* **1973**, *52*, 297−306.
[12] L. Weber, E. Dobbert, H.-G. Stammler, B. Neumann, *Z. Naturforsch.*, in press.
[13] B. Wrackmeyer, H. Nöth, *Chem. Ber.* **1977**, *110*, 1086−1094.
[14] W. Biffar, H. Nöth, H. Pommerening, R. Schwerthöffer, W. Storch, B. Wrackmeyer, *Chem. Ber.* **1981**, *114*, 49−60.
[15] F. Frankhauser, H. Pritzkow, W. Siebert, *Z. Naturforsch.* **1994**, *49b*, 250−254,
[16] G. E. Herberich, personal communication.
[17] R. W. Chapman, J. G. Kester, K. Folting, W. E. Streib, L. J. Todd, *Inorg. Chem.* **1992**, *31*, 979−983.
[18] F. A. Cotton, D. C. Richardson, *Inorg. Chem.* **1966**, *5*, 1851.
[19]
[19a] Holleman−Wiberg, *Lehrbuch der Anorganischen Chemie*, 101st ed., de Gruyter, Berlin, **1995**, p. 1839.
[19b] Holleman−Wiberg, *Lehrbuch der Anorganischen Chemie*, 101st ed., de Gruyter, Berlin, **1995**, p. 873.
[20] R. Hunold, J. Allwohn, G. Baum, W. Massa, A. Berndt, *Angew. Chem.* **1988**, *100*, 961−963; *Angew. Chem. Int. Ed. Engl.* **1988**, *27*, 961.
[21] F.-W. Grevels, V. Skibbe, *J. Chem. Soc., Chem. Commun.* **1984**, 681.
[22] Further details of the crystal structure investigations are available on request from Fachinformationszentrum Karlsruhe, D-76344 Eggenstein-Leopoldshafen, on quoting the depository numbers CSD-410214 (**4b**), -410215 (**9**), and from the Cambridge Crystallographic Data Centre, CCDC, 12 Union Road, Cambridge CB21EZ, UK, [Fax: int.code +44-1223/336-0335, E-mail: deposit@ccdc.cam.nc.uk], on quoting the depository numbers CCDC-103177 (**8a**), the names of the authors, and the journal citation.

Received September 23, 1998
[I98327]

Reactions of 1,8-Diheterocyclotetradeca-4,11-diynes with (η^4-Cycloocta-1,5-diene)(η^5-cyclopentadienyl)cobalt

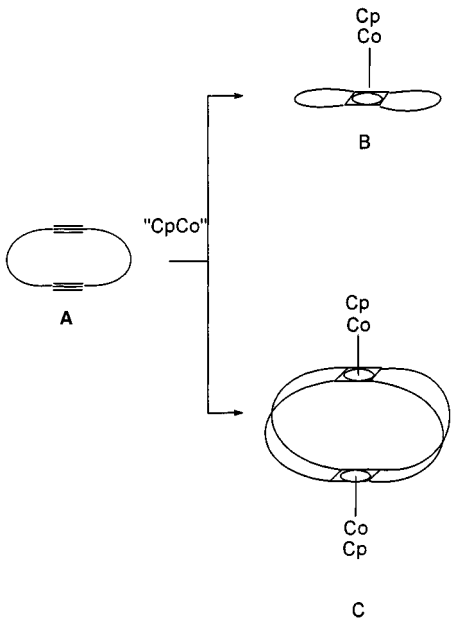
Volker Wolfart,[a] Matthias Ramming,[a] Rolf Gleiter,*[a] Bernhard Nuber,[b] Hans Pritzkow,[b] and Frank Rominger[a]

Keywords: Alkynes / Heterocycles / Cyclizations / Cobalt

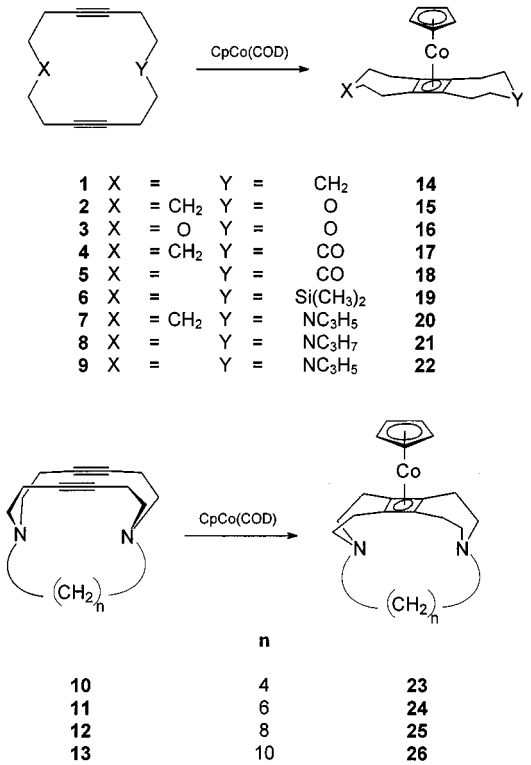
The following monocyclic and bicyclic 14-membered diynes were treated with [CpCo(cod)]: 1-oxacyclotetradeca-4,11-diyne (**2**), 1,8-dioxacyclotetradeca-4,11-diyne (**3**), cyclotetradeca-4,11-diynone (**4**), cyclotetradeca-4,11-diyne-1,8-dione (**5**), 1,1,8,8-tetramethyl-1,8-disilacyclotetradeca-4,11-diyne (**6**), 1-allyl-1-azacyclotetradeca-4,11diyne (**7**), 1,8-dipropyl-1,8-diazacyclotetradeca-1,11-diyne (**8**), 1,8-diallyl-1,8-diazacyclotetradeca-4,11-diyne (**9**), 1,8-diazabicyclo[6.6.4]-octadeca-4,11-diyne (**10**), 1,8-diazabicyclo[6.6.6]eicosa-4,11-diyne (**11**), 1,10-diazabicyclo[8.6.6]docosa-13,19-diyne (**12**) and 1,12-diazabicyclo[10.6.6]tetracosa-15,21-diyne (**13**). In all cases we obtained an intramolecular cyclobutadiene complex stabilized with a CpCo fragment (**15**–**26**). For **3** we could isolate, besides the cyclobutadiene complex **16**, the trimerization product **28**. In the cases of **15**, **16**, **18**, **20**, **23**, **25**, and **26** the structure of the cylobutadiene complexes could be confirmed by X-ray studies. Common to all structures is a boat-like conformation of the tricyclic unit containing the cyclobutadiene ring. The two cycloheptene units adopt a chair conformation in which the heteroatom is removed from the metal center.

The cobalt-mediated cycloaddition of alkynes proceeds either in a [2+2] fashion to yield cyclobutadiene (Cbd) complexes or in a [2+2+2] fashion to give aromatic systems.[1−7] In the case of cyclic diynes the cyclobutadiene complexes dominate.[5−7] Depending on the length of the chain between the triple bonds one obtains either the tricyclic intramolecular cyclobutadiene complexes **B** or the superphanes **C** which are generated in an intermolecular pathway.[6,7] The latter path was preferred in the case of 1,6-cyclodecadiyne and in disilabridged cyclic diynes, while larger rings favored the intramolecular path.[6,7]

In order to extend our knowledge to the 14-membered rings we synthesized a number of hetero derivatives of 1,8-



Scheme 1. Possible reaction paths between cycloalkynes and a CpCo fragment



Scheme 2. Numbering of starting materials of cyclic (**1**−**9**) and bicyclic (**10**−**13**) dynes and tricyclic (**14**−**22**) as well as tetracyclic (**23**−**26**) products

[a] Organisch-Chemisches Institut der Universität Heidelberg, Im Neuenheimer Feld 270, D-69120 Heidelberg, Germany
[b] Anorganisch-Chemisches Institut der Universität Heidelberg, Im Neuenheimer Feld 270, D-69120 Heidelberg, Germany

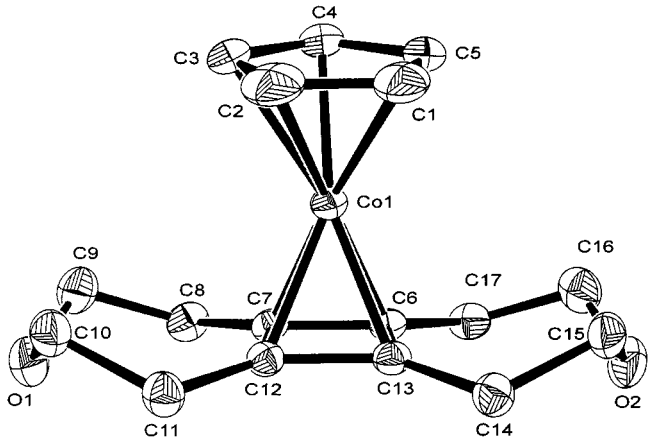
 © WILEY-VCH Verlag GmbH, D-69451 Weinheim, 1999 1434−1948/99/0303−0499 $ 17.50+.50/0

cyclotetradecadiyne (**1**) and explored their reaction with (η^4-cycloocta-1,5-diene)(η^5-cyclopentadienyl)cobalt ([CpCo(cod)]). As model systems we either chose monocyclic systems with O and NR as electron-donating heteroatoms and dimethylsilyl groups as bulky substituents, or we chose bicyclic 1,8-diaza-substituted systems. By varying the chain length we were able to influence the conformation of the 14-membered ring system.

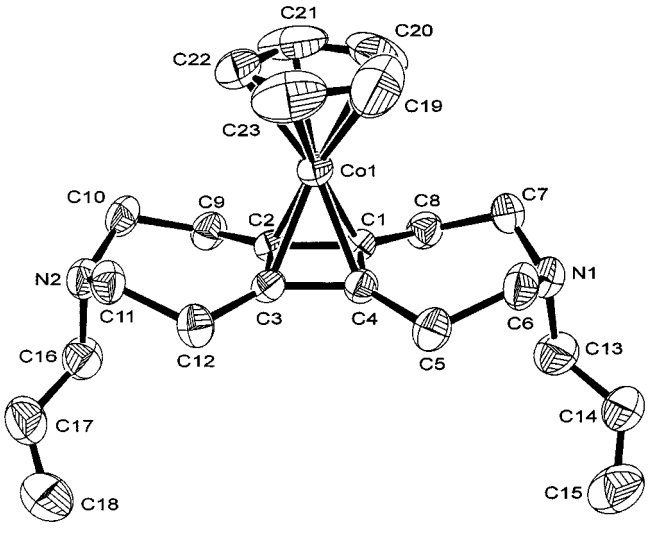
We chose the following congeners of **1**: 1-oxacyclotetradeca-4,11-diyne (**2**),[8] 1,8-dioxacyclotetradeca-4,11-diyne (**3**),[8] cyclotetradeca-4,11-diynone (**4**),[8] cyclotetradeca-4,11-diyne-1,8-dione (**5**),[8] 1,1,8,8-tetramethyl-1,8-disilacyclotetradeca-4,11-diyne (**6**),[9] 1-allyl-1-azacyclotetradeca-4,11-diyne (**7**),[10] 1,8-dipropyl-1,8-diazacyclotetradeca-4,11-diyne (**8**),[10] 1,8-diallyl-1,8-diazacyclotetradeca-4,11-diyne (**9**),[10] 1,8-diazabicyclo[6.6.4]octadeca-4,4-diyne (**10**),[10] 1,8-diazabicyclo[6.6.6]eicosa-4,11-diyne (**11**),[10] 1,10-diazabicyclo[8.6.6]docosa-13,19-diyne (**12**)[10] and 1,12-diazabicyclo[10.6.6]tetracosa-15,20-diyne (**13**)[10] (see Scheme 2).

Results and Discussion

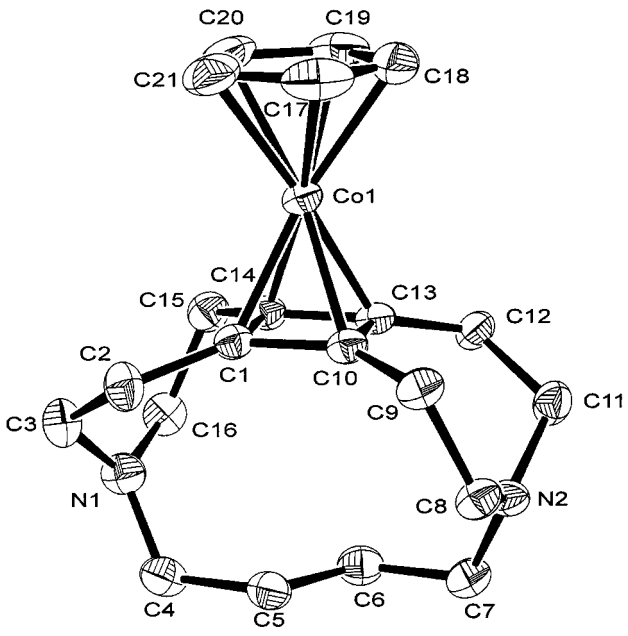
The reactions of **2**−**13** were carried out by heating the diynes in nonane with [CpCo(cod)] until no starting material could be detected. In most cases we could only observe the corresponding intramolecular products **15**−**26** in yields



16



22



23

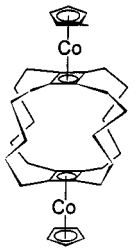
Figure 1. Molecular structure of **16**, **22** and **23**; selected bond lengths [Å] and angles [°]: **16**: Co−C6 1.980(2), Co−C7 1.991(2), Co−C1 2.058(2), Co−C3 2.082(2), C6−C7 1.462(2), C7−C12 1.463(2); C7−C8 1.485(2), C9−O1 1.433(2), C9−O1−C10 115.2(2), C8−C9−O1 113.4(2); **22**: Co−C1 1.977(3), Co−C2 1.983(3), Co−C19 2.035(5), Co−C20 2.041(5), C1−C2 1.466(4), C2−C3 1.452(4), C1−C8 1.477(4), C7−N1 1.459(5), N1−C13 1.448(5), C13−C14 1.493(6), C14−C15 1.298(6); C6−N1−C7 116.9(3), C6−N1−C13 115.0(3), C13−C14−C15 125.6(5); **23**: Co−C1 1.983(3), Co−C10 1.978(3), Co−C19 2.058(3), Co−C20 2.065(4), C1−C10 1.465(5), C1−C14 1.448 (5), C1−C2 1.495(5), C3−N1 1.441(4), N1−C4 1.448(4); C3−N1−C16 118.8(2), C3−N1−C4 119.0(3)

between 3 and 70% (see Table 1). The exceptions were the parent system **1**, in which besides the intramolecular product **14** a superphane **27** could be observed in 7% yield,[11] and **3**, for which in addition to **16** the trimer **28** was obtained in 6% yield. In the case of **15**, **16**, **18**, **22**, **23**, **25**, and **26** we were able to grow single crystals which allowed the study of the molecular structure of these molecules in the solid state. In Figure 1 we show the X-ray-structures of **16**, **22**, and **23** as examples. In all cases we observed that together with the two carbon atoms of the cyclobutadiene unit the bridges with five main-group atoms between the former triple bonds adopt a chair conformation in which the heteroatom is removed from the metal center. This holds whether the heteroatoms are tethered with a short (C_4 in **23**), a long (C_{10} in **26**) or no chain (**15**, **16**, **18**, **22**). The substituents at the nitrogen atoms adopt the axial position whether they are tethered (**23**, **25**, **26**) or not (**22**).

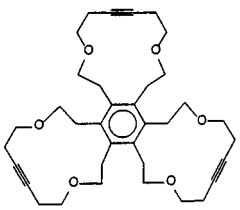
Table 1. Yields of the intramolecular cyclobutadiene complexes **14**−**26** by treating **1**−**13** with [CpCo(cod)]

starting material		**1**	**2**	**3**	**4**	**5**	**6**
product		**14**	**15**	**16**	**17**	**18**	**19**
yield (%)		29	11	14	48	60	68
starting material	**7**	**8**	**9**	**10**	**11**	**12**	**13**
product	**20**	**21**	**22**	**23**	**24**	**25**	**26**
yield (%)	5	39	3	71	25	38	50

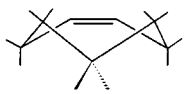
The chair conformation is expected because for cycloheptene systems a chair conformation **29** is reported in the literature.[12] The axial position of the allylic groups in **22** we ascribe to packing effects in the crystal because there are clearly two 1,3 interactions in the chair form.



27

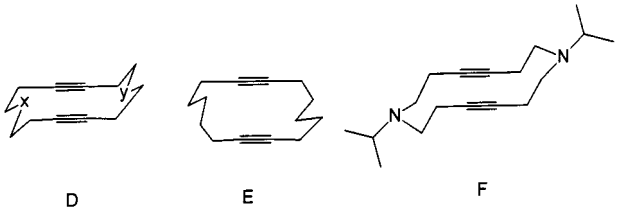


28



29

The uniformity of the conformations of the products is contrasted by a variety of conformations of the starting diynes. The structures of **1**, **3**−**5**,[8] 1,8-diisopropyl-1,8-diazacyclotetradeca-4,11-diyne (**30**),[10] **10**,[10] and **12**[10] have been studied in the solid state by means of X-ray techniques. For **3**−**5** the 14-membered ring adopts a chair conformation with a zig-zag arrangement of the chains between the triple bonds. This gives rise to two *anti* and two *gauche* interactions in the chain (**D**). In the case of **1**[8,13] an arrangement of the methylene groups with three *gauche* and one *anti* interaction is found (**E**). AM1[14] and MNDO[15] calculations show only a small energy difference (2 kcal/mol) between the two conformations. In the case of **30** a chair conformation was found in which the chains adopt a half-envelope conformation (**F**). In this conformation there are two *gauche* and two *eclipsed* interactions. The energy difference between conformations **F** and **D** was calculated (AM1, MNDO) to be 20 kcal/mol. In the cases of the bicyclic diynes **10** and **12** a twist-boat conformation was encountered.



D E F

X = Y = O
X = Y = CO
X = CO Y = O

The different conformations provide different transannular distances between the triple bonds: **1**: 4.64 Å; **3**: 4.71 Å; **5**: 5.20 Å; **29**: 3.85 Å; **10**: 4.19 Å; **12**: 3.77 Å. Our experiments provide no correlation between conformations of the starting material and yield of the products. This can be interpreted by assuming either that steric effects are important at a later stage of the multi-step reaction, or that at the reaction temperature all conformations mentioned above interconvert rapidly.

Experimental Section

General Methods: Reactions were conducted in oven-dried (150°C) glassware under argon. Solvents were distilled and dried under argon before use: *n*-nonane and cyclooctane from sodium, DME from potassium. − Melting points: Dr. Tottoli apparatus (Büchi), uncorrected values. − Materials used for column chromatography: Neutral alumina (Aldrich, Macherey-Nagel), Kieselgel 60 (Merck, Macherey-Nagel), Florisil (Acros). GLC: HP 5890A instrument connected to a Shimadzu C-R3A integrator. A capillary column Ultra 2 (PhMeSilicone, 25 m × 0.32 mm × 0.52 μm) was used with nitrogen carrier gas and a flame-ionization detector (FID). − ^{1}H and ^{13}C NMR: Bruker WH 300 (^{1}H at 300 MHz and ^{13}C at 75.47 MHz) and Bruker WH 200 (^{1}H at 200 MHz and ^{13}C at 50.33 MHz) by using the solvent as internal standard. If not otherwise mentioned spectra were determined at 300 MHz and 75.47 MHz, respectively. − IR: Perkin Elmer 580B, Bruker IFS 66, Bruker IFS 88 and Bruker Vector 22. − UV: Hewlett Packard HP 8452A. − High-resolution MS: ZAB high-resolution mass spectrometer (Fa. Vacuum Generators). − Elemental analyses were carried out by the Mikroanalytisches Laboratorium der Universität Heidelberg.

General Procedure for the Reactions of the Cyclic and Bicyclic Diynes 2−13 with [CpCo(cod)]: If not otherwise mentioned the diynes and [CpCo(cod)] were dissolved in *n*-nonane and the mixtures were heated under reflux. When the diyne could not be detected any more by TLC the mixture was cooled. In the case of the carbocyclic cobalt complexes **17** and **18** the solvent was removed under vacuum. The residue was dissolved in CH_2Cl_2, adsorbed on Al_2O_3 (neutral, 6% H_2O) and chromatographed on Al_2O_3 (neutral, 6% H_2O). For the other cobalt complexes excess [CpCo(cod)] and *n*-nonane were removed by flash chromatography on Al_2O_3 (neutral, 6% H_2O) with petroleum ether as solvent. Afterwards the cobalt complex was eluted with petroleum ether or petroleum ether/diethyl ether mixtures as eluent.

(η^5-Cyclopentadienyl){(η^4-1,2,8,9)-5-oxatricyclo[7.5.0.0^{2,8}]tetradeca-1,8-diene}cobalt (15): To a refluxing solution of 800 mg (5.0 mmol) of 1-oxacyclotetradeca-4,11-diyne (**2**) in 80 mL of *n*-nonane 1.66 g (10.0 mmol) of [CpCo(cod)] in 20 mL of *n*-nonane was added within 60 min and refluxing was continued for 4 h. Column chromatography of the cooled mixture with petroleum ether/pentane (5:1) as eluent yielded 330 mg, (21%) of **15** as orange crystals, m.p. 143°C. − ^{1}H NMR ($CDCl_3$): δ = 4.72 (s, 5 H, H_{Cp}), 4.19 (m, ^2J = 12.5 Hz, 2 H, CH_2−O), 3.42 (m, 2 H, CH_2−O), 1.97 (m, 4 H, C_{Cbd}−CH_2, 1.58 (m, 5 H, CH_2). − ^{13}C NMR ($CDCl_3$): δ = 79.9 (C_{Cbd}), 78.8 (C_{Cp}), 76.8 (C_{Cbd}), 74.4 (CH_2−O), 30.4, 30.2, 30.0, 27.8 (CH_2). − IR (KBr): $\tilde{\nu}$ = 3436 cm^{-1}, 3094, 2922, 2860, 2811, 1112, 1002, 809. − UV (CH_2Cl_2): λ_{max} (lg ε) = 292 nm (3.09), 272 (4.35), 222 (4.05). − $C_{18}H_{23}CoO$ (314.31): calcd. C 68.78, H 7.38; found C 68.67, H 7.45.

(η^5-Cyclopentadienyl){(η^4-1,2,8,9)-5,12-dioxatricyclo-[7.5.0.0^{2,8}]tetradeca-1,8-diene}cobalt (16): Starting material: 800 mg (4.2 mmol) of 1,8-dioxacyclotetradeca-4,11-diyne (**3**) and 966 mg (4.2 mmol) of [CpCo(cod)] in 50 mL of *n*-nonane. Reaction time: 4 h. The warm reaction mixture was chromatographed with petroleum ether/diethyl ether (1:1) to yield the intramolecular complex **16** (180 mg, 14%). Afterwards the trimerization product **28** (51 mg, 6%) could be isolated by using diethyl ether as eluent. − **16**: Yellow-orange crystals, m.p. 193°C. − ^{1}H NMR (CD_2Cl_2): δ = 4.70 (s, 5 H, H_{Cp}), 4.15 (m, 4 H, CH_2−O), 3.63 (m, 4 H, CH_2−O), 1.94 (m, 8 H, C_{Cbd}−CH_2). − ^{13}C NMR (CD_2Cl_2): δ = 79.3 (C_{Cp}), 30.6 (C_{Cbd}−CH_2), 77.8 (CH_2−O), 74.5 (C_{Cbd}). − IR (KBr): $\tilde{\nu}$ = 3440 cm^{-1}, 2938, 2866, 2816, 1632, 1108. − UV (CH_2Cl_2): λ_{max} (lg ε) = 386 nm (2.35), 298 (2.87), 266 (4.37), 222 (4.04). − HRMS (EI, 70 eV): $C_{17}H_{21}CoO_2$: calcd. 316.0874, found 316.0841. − **28**: Colorless needles. − ^{1}H NMR ($CDCl_3$): δ = 3.71 (t, 12 H, CH_2−O), 3.62 (t, 12 H, CH_2−O), 3.08 (t, 12 H, CH_2−Ph), 2.40 (t, 12 H, CH_2−C≡). − ^{13}C NMR ($CDCl_3$): δ = 135.5 (C_{ar}), 79.5 (C≡C), 20.8 (CH_2−C≡C), 71.4 (CH_2−O), 69.0 (CH_2−O), 31.5 (CH_2−Ph). − IR (KBr): $\tilde{\nu}$ = 3441 cm^{-1}, 2864, 1632, 1483, 1365, 1131, 799. − UV (CH_2Cl_2): λ_{max} (lg ε): 232 nm (3.3). − HRMS (EI, 70 eV): $C_{36}H_{48}O_6$: calcd. 576.3451, found 576.3465.

(η^5-Cyclopentadienyl){(η^4-1,2,8,9)-tricyclo[7.5.0.0^{2,8}]tetradeca-1,8-dien-5-one}cobalt (17): Starting material: 400 mg (2.0 mmol) of cyclotetradeca-4,11-diynone (**4**) and 504 mg (2.2 mmol) of [CpCo(cod)] in 30 mL of *n*-nonane. Reaction time: 3 d. The reaction mixture was chromatographed with *n*-hexane/diethyl ether (8:1). For elemental analysis it was necessary to subject **17** to further column chromatography on silica gel with the solvent mixture mentioned above. Yield: 314 mg (48%) of **16** as yellow crystals, m.p. 124°C. − ^{1}H NMR ($CDCl_3$): δ = 4.80 (s, 5 H, H_{Cp}), 2.98 (td, ^2J = $^3J_1$ = 11.3, $^3J_2$ = 5.2 Hz, 2 H, O=C−CH_2), 2.54 (d, 2 H, O=C−CH_2, ^2J = 11.3 Hz), 2.12−1.80 (m, 10 H, CH_2), 1.58 (m, 4 H, CH_2). − ^{13}C NMR ($CDCl_3$): δ = 214.4 (CO), 80.7 (C_{Cbd}), 79.2 (C_{Cp}), 76.4 (C_{Cbd}), 44.1, 30.4, 30.3, 27.5, 22.4 (CH_2). − IR (KBr): $\tilde{\nu}$ = 2920 cm^{-1}, 2821, 2812, 1701, 1444, 1321, 1295, 798. − UV/Vis (CH_2Cl_2): λ_{max} (lg ε) = 224 nm (4.05), 266 (4.29). − $C_{19}H_{23}CoO$ (326.32): calcd. C 69.93, H 7.11; found C 69.84, H 7.10.

(η^5-Cyclopentadienyl){(η^4-1,2,8,9)-tricyclo[7.5.0.0^{2,8}]tetradeca-1,8-diene-5,12-dione}cobalt (18): Starting material: 500 mg (2.3 mmol) of cyclotetradeca-4,11-diyne-1,8-dione (**5**) and 580 mg (2.5 mmol) of [CpCo(cod)] in 35 mL of *n*-nonane. Reaction time: 5 d. The reaction mixture was chromatographed with $CHCl_3$/ethyl acetate (20:1). For elemental analysis it was necessary to subject **18** to further column chromatography on silica gel with the solvent mixture mentioned above. Yield: 470 mg (60%) of **18** as yellow crystals, m.p. 177°C. − ^{1}H NMR (200 MHz, $CDCl_3$): δ = 4.85 (s, 5 H, H_{Cp}), 2.95 (td, ^2J = $^3J_1$ = 11.6, $^3J_2$ = 5.2 Hz, 4 H, O=C−CH_2,), 2.57 (m, 4 H, O=C−CH_2), 2.12 (ddd, 4 H, C_{Cbd}−CH_2, ^2J = 15.9, $^3J_1$ = 5.2, $^3J_2$ = 4.2 Hz), 1.88 (ddd, 4 H, C_{Cbd}−CH_2, ^2J = 15.9, $^3J_1$ = 11.6, $^3J_2$ = 4.3 Hz). − ^{13}C NMR (50.33 MHz, $CDCl_3$): δ = 208.7 (CO), 79.8 (C_{Cp}), 77.7 (C_{Cbd}), 44.0, 22.1 (CH_2). − IR (KBr): $\tilde{\nu}$ = 1695 cm^{-1}, 1321, 1295, 1165, 1104, 803. − UV/VIS (CH_2Cl_2): λ_{max} (lg ε) = 224 nm (4.03), 268 (4.26). − $C_{19}H_{21}CoO_2$ (340.31): calcd. C 67.06, H 6.22; found C 66.75, H 6.25.

(η^5-Cyclopentadienyl){(η^4-1,2,8,9)-5,5,12,12-tetramethyl-5,12-disilatricyclo[7.5.0.0^{2,8}]tetradeca-1,8-diene}cobalt (19): Starting material: 106 mg (0.38 mmol) of 1,1,8,8-tetramethyl-1,8-disilacyclotetradeca-4,11-diyne (**6**) and 159 mg (0.69 mmol) of [CpCo(cod)] in 25 mL of *n*-nonane. Reaction time: 130 h. The reaction mixture was poured on a column, which was filled with 5 cm of Al_2O_3 (neutral, 6% water) and SiO_2 on top. Quick flash chromatography, with petroleum ether as eluent, yielded **19** (105 mg, 68%) as yellow crystals, m.p. 120°C (dec.). − ^{1}H NMR (C_6D_6): δ = 4.92 (s, 5 H, H_{Cp}), 2.25−1.86 (m, 8 H, C_{Cbd}−CH_2), 1.07−0.88 (m, 8 H, Si−CH_2), 0.12 (s, 6 H, Si−CH_3), −0.02 (s, 6 H, Si−CH_3). − ^{13}C NMR (C_6D_6): δ = 81.4 (C_{Cbd}), 79.2 (C_{Cp}), 21.0 (CH_2), 16.9 (Si−CH_2), −1.6 (Si−CH_3), −6.2 (Si−CH_3). − IR (KBr): $\tilde{\nu}$ = 3449 cm^{-1}, 3101, 3080, 2947, 2915, 2893, 2874, 2821, 1622, 1439, 1394, 1246, 1001, 834, 679. − UV (CH_2Cl_2): λ_{max} (lg ε) = 224 nm (4.01), 266 (4.29), 296 (3.15), 362 (2.60). − HRMS (EI, 70 eV): $C_{21}H_{33}CoSi_2$: calcd. 400.14527, found 400.14529.

{(η^4-1,2,8,9)-*N*-Allyl-5-azatricyclo[7.5.0.0^{2,8}]tetradeca-1,8-diene}-(η^5-cyclopentadienyl)cobalt (20): Starting material: 800 mg (3.5 mmol) of *N*-allyl-1-azacyclotetradeca-4,11-diyne (**7**) and 810 mg (3.5 mmol) of [CpCo(cod)] in 40 mL of *n*-nonane were heated at reflux for 4 h. After 10 h of additional stirring at room temperature (r.t.), the mixture was subjected to column chromatography with petroleum ether/diethyl ether (3:1) as eluent. Yield: 60 mg (5%) of **20** as orange crystals, m.p. 102°C. − ^{1}H NMR ($CDCl_3$): δ = 5.83 (m, 1 H, CH_2=C*H*−), 5.13 (m, 2 H, C*H*$_2$=CH−), 4.78 (s, 5 H, H_{Cp}), 3.28−2.95 (m, 4 H, CH_2−N), 2.13−1.57 (m, 8 H, C_{Cbd}−CH_2, CH_2). − ^{13}C NMR ($CDCl_3$): δ = 136.6 (CH_2=*C*H), 116.7 (*C*H_2=CH−), 79.5 (C_{Cbd}), 78.9 (C_{cp}), 78.0 (C_{Cbd}), 55.5, 54.7 (CH_2−N), 30.6, 30.4, 28.0, 26.9, 26.2, 24.6 (CH_2). − IR (KBr): $\tilde{\nu}$ = 3440 cm^{-1}, 3074, 2913, 1636, 1442, 1351, 1112, 1000, 803, 566. − UV (CH_2Cl_2): λ_{max} (lg ε) = 222 nm (4.1), 266 (4.37), 300 (3.07). − $C_{20}H_{28}CoN$ (353.39): calcd. C 71.37, H 7.99; N 3.96; found C 71.42, H 7.86, N 3.77.

(η^5-Cyclopentadienyl){(η^4-1,2,8,9)-*N*,*N*′-di-*n*-propyl-5,12-diazatricyclo[7.5.0.0^{2,8}]tetradeca-1,8-diene}cobalt (21): Starting material: 850 mg (3.7 mmol) of [CpCo(cod)] in 50 mL of *n*-nonane, which was refluxed for 45 min; 945 mg (3.45 mmol) of *N*,*N*′-di-*n*-propyl-1,8-diazacyclotetradeca-4,11-diyne (**8**) was added. The mixture was heated to 160°C for 20 h. After cooling to r.t., column chromatography of the reaction mixture on Al_2O_3 [neutral, 6% water, petroleum ether/diethyl ether (5:1)] gave 537 mg, (39%) of **21** as orange crystals, m.p. 40°C. − ^{1}H NMR ($CDCl_3$): δ = 4.75 (s, 5 H, H_{Cp}), 3.24−3.00 (m, 8 H, CH_2−N), 2.44 (m, 4 H, CH_2−N), 2.04 (m, 4 H, C_{Cbd}−CH_2), 1.75−1.70 (m, 4 H, C_{Cbd}−CH_2),1.44 (m, 4 H, CH_2), 0.86 (t, ^3J = 7.4 Hz, 6 H, CH_3). − ^{13}C NMR ($CDCl_3$): δ = 79.0 (C_{Cp}), 77.9 (C_{Cbd}), 55.4 (CH_2−N), 52.4 (CH_2−N), 26.1, 20.6 (CH_2), 11.9 (CH_3). − IR (KBr): $\tilde{\nu}$ = 3440 cm^{-1}, 3094, 3066, 2952, 2899, 2869, 2828, 1624, 1449, 1348, 1117, 1091, 1024, 999, 807, 587, 438. − UV (CH_2Cl_2): λ_{max} (lg ε) = 222 nm (4.3), 266 (4.4), 294 (3.5), 358 (3.2). − HRMS (EI, 70 eV): $C_{23}H_{36}CoN_2$: calcd. 398.2148, found 398.2132.

Table 2. Crystallographic data of **15**, **16**, **18**, **22**, **23**, **25** and **26**

	15	**16**	**18**	**22**	**23**	**25**	**26**
Empirical formula	$C_{18}H_{23}CoO$	$C_{17}H_{21}CoO_2$	$C_{19}H_{21}CoO_2$	$C_{23}H_{31}CoN_2$	$C_{21}H_{29}CoN_2$	$C_{25}H_{37}CoN_2$	$C_{27}H_{41}CoN_2$
Molecular mass [g/mol]	314.29	316.27	340.29	394.43	368.40	424.50	452.56
Crystal size [mm]	0.5 × 0.35 × 0.2	0.38 × 0.27 × 0.21	0.95 × 0.90 × 0.35	0.8 × 0.2 × 0.05	0.15 × 0.4 × 0.55	0.32 × 0.25 × 0.9	0.25 × 0.35 × 0.8
Crystal color	orange-yellow	yellow-orange	orange	yellow-orange	yellow	orange-yellow	yellow
Crystal system	monoclinic	orthorhombic	orthorhombic	triclinic	triclinic	monoclinic	triclinic
Space group	$P2_1/c$	$P2_12_12_1$	$P2_12_12_1$	$P\bar{1}$	$P\bar{1}$	$C2/c$	$P\bar{1}$
a [Å]	13.601(2)	7.7984(2)	8.235(2)	6.912(3)	8.686(4)	16.004(3)	10.281(3)
b [Å]	8.9720(10)	11.1670(1)	11.243(2)	9.844(4)	9.529(5)	11.725(3)	10.682(2)
c [Å]	13.688(2)	16.1573(3)	16.800(3)	15.067(7)	11.359(6)	12.533(3)	12.307(3)
α [°]	90	90	90	96.42(4)	86.91(2)	90	75.04(2)
β [°]	115.320(10)	90	90	92.29(4)	85.77(3)	109.40(3)	78.58(2)
γ [°]	90	90	90	96.34(4)	69.64(2)	90	72.63(2)
V [Å^3]	1509.9(4)	1407.05(5)	1555.4(5)	1011.1(8)	878.6(8)	2218.3(8)	1235.5(5)
$D_{calcd.}$ [g/cm^3]	1.383	1.493	1.453	1.296	1.392	1.271	1.217
Z	4	4	4	2	2	4	2
F(000)	664	664	712	420	392	912	488
T [K]	293(2)	200(2)	293(2)	293(2)	293(2)	293(2)	293(2)
μ [mm^{-1}]	1.130	1.218	1.107	0.857	0.980	0.786	0.710
Refl. collected	3778	6452	5259	4627	4595	2888	4351
Refl. unique	3641	2365	4775	4627	4595	2888	4351
Refl. observed [$I > 2\sigma(I)$]	2740	2229	3940	3438	3234	2107	3191
Variables	273	265	261	360	333	191	417
$(\Delta/\sigma)_{max}$							
$R1$ [$I > 2\sigma(I)$]	0.052	0.020	0.053	0.058	0.041	0.042	0.057
$wR2$	0.127	0.0499	0.1386	0.115	0.1103	0.1042	0.1232
S (Gof)	1.131	1.056	1.045	1.112	1.021	1.022	1.110
$(\Delta\rho)_{max}$ [e Å^{-3}]	0.547	0.181	0.589	0.409	0.739	0.805	0.250
$(\Delta\rho)_{min}$ [e Å^{-3}]	−0.382	−0.284	−0.404	−0.261	−0.564	−0.504	−0.206

(η^5-Cyclopentadienyl){(η^4-1,2,8,9)-*N*,*N*′-diallyl-5,12-diazatricyclo[7.5.0.0^{2,8}]tetradeca-1,8-diene}cobalt (22): 1.0 g (3.7 mmol) of *N*,*N*′-diallyl-1,8-diazacyclotetradeca-4,11-diyne (**9**) and 860 mg (3.7 mmol) of [CpCo(cod)] in 20 mL of *n*-nonane were heated at reflux for 3 h. After 10 h of additional stirring at r.t., the mixture was subjected to column chromatography with petroleum ether/diethyl ether (3:1) as eluent. Yield: 50 mg (3%) of **22** as orange crystals, m.p. 102°C. − ^{1}H NMR ($CDCl_3$): δ = 5.83 (m, 2 H, CH_2=C*H*−), 5.13 (m, 4 H, C*H*$_2$=CH−), 4.77 (s, 5 H, H_{Cp}), 3.24 (m, 4 H, CH_2N), 3.17 (m, 4 H, CH_2−N), 2.98 (dt, 4 H, ^3J = 16 Hz, CH_2−N), 1.90 (m, 8 H, C_{Cbd}−CH_2). − ^{13}C NMR ($CDCl_3$): δ = 136.5 (CH_2=*C*H−), 116.8 (*C*H$_2$=CH−), 79.0 (C_{Cp}), 77.9 (C_{Cbd}), 55.5 (CH_2−N), 54.0 (CH_2−N), 26.4 (CH_2). − IR (KBr): $\tilde{\nu}$ = 3431 cm^{-1}, 3073, 3004, 2906, 2868, 2818, 1639. − UV (CH_2Cl_2): λ_{max} (lg ε) = 382 nm (1.70), 300 (2.72), 266 (4.18), 224 (3.97). − $C_{23}H_{31}CoN_2$ (394.44): calcd. C 70.04, H 7.92; N 7.10; found C 69.57, H 8.15, N 6.86.

(η^5-Cyclopentadienyl){(η^4-4,5,11,12)-1,8-diazatetracyclo[6.6.4.0^{4,12}.0^{5,11}]octadeca-4,11-diene}cobalt (23): Starting material: 168 mg (0.69 mmol) of 1,8-diazabicyclo[6.6.4]octadeca-4,11-diyne (**10**) and 176 mg (0.76 mmol) of [CpCo(cod)] in 80 mL of *n*-nonane. Reaction time: 66 h. The reaction mixture was chromatographed with petroleum ether/diethyl ether (5:2). Yield: 187 mg (71%) of **23** as a yellow-orange solid, decomposition at 205°C. − ^{1}H NMR: ($CDCl_3$): δ = 4.63 (s, 5 H, H_{Cp}), 2.84 (t, 8 H, CH_2−N), 2.75 (t, 4 H, CH_2−N), 2.30−1.98 (m, 8 H, C_{Cbd}−CH_2), 1.39 (q, 4 H, CH_2). − ^{13}C NMR: ($CDCl_3$): δ = 79.1 (C_{Cp}), 74.1 (C_{Cbd}), 55.4, 48.7 (CH_2−N), 27.7, 25.7 (CH_2). − IR (KBr): $\tilde{\nu}$ = 2903 cm^{-1}, 2827, 2225, 2044, 2014, 1620, 1427, 1357, 1159, 1128, 1031, 740. − UV (CH_2Cl_2): λ_{max} (lg ε) = 224 nm (4.25), 274 (4.36), 312 (960), 392 (2.60). − HRMS (EI, 70 eV): $C_{21}H_{29}CoN_2$: calcd. 369.1741; found 369.1799.

(η^5-Cyclopentadienyl){(η^4-4,5,11,12)-1,8-Diazatetracyclo[6.6.6.0^{4,12}0^{5,11}]eicosa-4,11-diene}cobalt (24): Starting material: 440 mg (1.6 mmol) of 1,8-diazabicyclo[6.6.6]eicosa-4,11-diyne (**11**) and 400 mg (1.7 mmol) of [CpCo(cod)] in 100 mL of cyclooctane at 150°C. Reaction time: 6 d. The reaction mixture was chromatographed with petroleum ether/diethyl ether (10:1). Yield: 160 mg (25%) of **24** as yellow-orange colored solid, m.p. > 250°C. − ^{1}H NMR (200 MHz, CD_2Cl_2): δ = 4.60 (s, 5 H, H_{Cp}), 2.64 (m, 8 H, CH_2−N), 2.10 (m, 8 H, CH_2), 1.33 (m, 8 H, C_{Cbd}−CH_2). − ^{13}C NMR (50.33 MHz, CD_2Cl_2): δ = 79.3 (C_{Cp}), 79.3 (C_{Cbd}), 58.4, 53.3 (CH_2−N), 29.8, 29.3, 27.6 (CH_2). − IR (KBr): $\tilde{\nu}$ = 2924 cm^{-1}, 2848, 1631, 1371, 1349, 1105, 797. − UV (CH_2Cl_2): λ_{max} (lg ε) = 222 nm (4.2), 273 (4.3). − $C_{23}H_{33}CoN_2$ (396.46): calcd. C 69.68, H 8.39; N 7.07; found C 69.21, H 8.41, N 6.62.

(η^5-Cyclopentadienyl){(η^4-13,14,19,20)-1,10-diazatetracyclo-[8.6.6.0^{13,20}.0^{14,19}]docosa-13,19-diene}cobalt (25): Starting material: 370 mg of (1.2 mmol) 1,10-diazabicyclo[8.6.6]docosa-13,19-diyne (**12**) and 280 mg (1.2 mmol) of [CpCo(cod)] in 100 mL of *n*-nonane. Reaction time: 35 h. The reaction mixture was chromatographed with petroleum ether/diethyl ether (5:1). Yield: 194 mg (38%) of **25** as yellow crystals m.p. 120°C. − ^{1}H NMR (200 MHz, $CDCl_3$): δ = 4.67 (s, 5 H, H_{Cp}), 2.95 (m, 8 H, CH_2−N), 2.73 (m, 4 H, CH_2−N), 2.00 (m, 8 H, C_{Cbd}−CH_2), 1.27 (m, 12 H, CH_2). − ^{13}C NMR (50.33 MHz, $CDCl_3$): δ = 79.0 (C_{Cp}), 76.3 (C_{Cbd}), 55.5, 53.4 (CH_2−N), 30.6, 29.3, 29.1, 26.8 (CH_2). − IR (KBr): $\tilde{\nu}$ = 3440 cm^{-1}, 3089, 2895, 1602, 1442, 1375, 1344, 1144, 1125, 798. − UV (CH_2Cl_2): λ_{max} (lg ε) = 224 nm (4.31), 268 (4.41), 300 (3.24), 378 (3.02). − HRMS (EI, 70 eV): $C_{25}H_{37}CoN_2$: calcd. 425.2367; found 425.2330.

(η^5-Cyclopentadienyl){(η^4-15,16,21,22)-1,12-diazatetracyclo-[10.6.6.0^{15,22}0^{16,21}]tetracosa-15,21-diene}cobalt (26): Starting material: 126 mg (0.38 mmol) of 1,12-diazabicyclo[10.6.6]tetracosa-15,21-diyne (**13**) and 89 mg (0.38 mmol) of [CpCo(cod)] in 50 mL of *n*-nonane. Reaction time: 5 d. The reaction mixture was chromatographed with petroleum ether/diethyl ether (5:2). Yield: 85 mg

(50%) of **26** as yellow solid, m.p. 130°C. − ^{1}H NMR ($CDCl_3$): δ = 4.71 (s, 5 H, H_{Cp}), 3.25−2.95 (m, 8 H, CH_2−N), 2.65 (t, 4 H, CH_2−N), 2.15−1.81 (m, 8 H, C_{Cbd}−CH_2), 1.44−1.21 (m, 16 H, CH_2). − ^{13}C NMR ($CDCl_3$): δ = 79.0 (C_{Cp}), 76.7 (C_{Cbd}), 55.4, 52.2 (CH_2−N), 29.4, 29.3, 29.2, 28.9, 27.0 (CH_2). − IR (KBr): $\tilde{\nu}$ = 3091 cm^{-1}, 2925, 2898, 2848, 1597, 1442, 1361, 1136, 799. − UV (CH_2Cl_2): λ_{max} (lg ε) = 224 nm (4.18), 266 (4.36), 304 (2.98). − $C_{27}H_{41}CoN_2$ (452.56): calcd. C 71.66, H 9.13, N 6.19; found C 71.29, H 9.15, N 6.19.

X-ray Crystallographic Studies: Crystal data are given in Table 2. Intensity data were collected for **16** at −73°C with a Siemens CCD system, for all other compounds with a Syntex R3 diffractometer (Mo-K_α radiation, graphite monochromator, ω scan). Intensities were corrected for Lorentz and polarization effects. An empirical absorption correction was applied. All structures were solved by direct methods (SHELXS-86)[16] and refined by least-squares methods based on F^2 with all measured reflections (SHELXL-97).[17] All non-hydrogen atoms were refined anisotropically, hydrogen atoms were located in difference Fourier maps and refined isotropically. The cyclopentadienyl rings in **18** and **25** were disordered. The positions of the Cp hydrogen atoms in the latter compounds and in **26** were calculated and not refined. Crystallographic data (excluding structure factors) for the structures reported in this paper have been deposited with the Cambridge Crystallographic Data Centre as supplementary publication no. CCDC-103160 (**15**), -103161 (**16**), -103162 (**18**), -103163 (**22**), -103164 (**23**), -103165 (**25**), -103166 (**26**). Copies of the data can be obtained free of charge on application to the CCDC, 12 Union Road, Cambridge CB2 1EZ, UK [Fax: int. code + 44-1223/336-0335, E-mail: deposit@ccdc.cam.uc.uk].

Acknowledgments

We are grateful to the Deutsche Forschungsgemeinschaft (SFB 247), the Fonds der Chemischen Industrie and the BASF Aktiengesellschaft, Ludwigshafen, for financial support.

[1] A. Efraty, *Chem. Rev.* **1977**, *77*, 691.
[2] N. E. Shore, *Chem. Rev.* **1988**, *88*, 1081.
[3] K. P. C. Vollhardt, *Acc. Chem. Res.* **1977**, *10*, 1; *Angew. Chem.* **1984**, *96*, 525; *Angew. Chem. Int. Ed. Engl.* **1984**, *23*, 531.
[4] H. Bönnemann, *Angew. Chem.* **1985**, *97*, 264; *Angew. Chem. Int. Ed. Engl.* **1985**, *24*, 284.
[5] R. B. King, A. Efraty, *J. Am. Chem. Soc.* **1972**, *94*, 3021.
[6] R. Gleiter, *Angew. Chem.* **1992**, *104*, 29; *Angew. Chem. Int. Ed. Engl.* **1992**, *31*, 27.
[7] R. Gleiter, M. Merger, *Angew. Chem.* **1997**, *109*, 2532; *Angew. Chem. Int. Ed. Engl.* **1997**, *36*, 2426.
[8] R. Gleiter, M. Ramming, H. Weigl, V. Wolfart, H. Irngartinger, T. Oeser, *Liebigs Ann.* **1997**, 1545.
[9] G. Haberhauer, R. Gleiter, to be published.
[10] V. Wolfart, R. Gleiter, H. Irngartinger, T. Oeser, C. Krieger, *Eur. J. Org. Chem.* **1998**, 2803.
[11] R. Gleiter, B. Treptow. D. Kratz. B. Nuber, *Tetrahedron Lett.* **1992**, *33*,1733.
[12] I. Ermolcera, V. S. Mastryukov. N. L. Allinger, A. Almeningen, *J. Mol. Struct.* **1989**, *196*, 151; E. L.Eliel, S. H. Wilen, *Stereochemistry of Organic Compounds*, J. Wiley, New York, **1994**, p. 764.
[13] J. Dale, A. J. Hubert, G. S. D. King, *J. Chem. Soc.* **1963**, *73*.
[14] M. J. S. Dewar, G. E. Zoebisch, E. F. Healy, J. P. Stewart, *J. Am. Chem. Soc.* **1985**, *107*, 3902.
[15] M. J. S. Dewar, W. Thiel, *J. Am. Chem. Soc.* **1977**, *99*, 4899.
[16] G. M. Sheldrick, *SHELXS-86*, Universität Göttingen, Germany, **1997**.
[17] G. M. Sheldrick, *SHELXL-97*, Universität Göttingen, Germany, **1997**.

Received October 8, 1998
[I98331]

A Dimeric Tetranuclear Copper(II) Compound Assembled through Pentacoordinating Carbonate Anions

Richard H. Bode,[a] Willem L. Driessen,*[a] Frans B. Hulsbergen,[a] Jan Reedijk,[a] and Anthony L. Spek[b]

Keywords: Macrocycle / Pyrazole / N-Heterocycle / Carbonate / Copper

The 22-membered macrocycle, spanning four endocyclic pyrazole groups, viz. 1,4,9,14,17,22,27,28,29,30-decaaza-5,13,18,26-tetramethylpentacyclo[24.2.1.1^{4,7}.1^{11,14}.1^{17,20}]-triacontane-5,7(28),11(29),12,18,20(30),24(27),25-octaene (**22Pz**), rendered the tetranuclear compound [Cu_4(22Pz)$_2$-(CO_3)$_2$($MeOH$)$_2$](ClO_4)$_4$($MeOH$)$_4$. The copper(II) ions are in distorted octahedral N_3O_3 environments. All four pyrazole groups of each macrocycle participate in the coordination of the copper(II) ions. The cationic part of this compound is in fact a dimer of two macrocyclic ligands, each containing two copper(II) ions bridged by two carbonate ions in the highly unusual pentacoordinating fashion.

Introduction

In the course of our investigations towards model compounds[1−4] for type-3 site copper proteins, like the important dioxygen processing enzymes hemocyanin and tyrosinase,[5−7] the macrocyclic ligand 9,22-di(pyridin-2-ylmethyl)-1,4,9,14,17,22,27,28,29,30-decaaza-5,13,18,26-tetramethylpentacyclo[24.2.1.1^{4,7}.1^{11,14}.1^{17,20}]triacontane-5,7(28),11(29),12,18,20(30),24(27),25-octaene (**MePy22Pz**) which contains four endocyclic pyrazole groups and two exocyclic pyridine groups, has been synthesised in an eleven-step procedure.[8,9] Several dinuclear coordination compounds have been prepared with this macrocyclic ligand, notably some copper(I) complexes which were found to bind one equivalent of dioxygen between the two copper ions as an O_2^{2-} anion in an end-on *trans*-μ-1,2-peroxo fashion inside the 22-membered cavity.[10] This appeared to be the first example of a dinuclear copper complex capable of binding dioxygen at room temperature in a protic solvent.

While processing a solution of this ligand with a copper(II) salt and sodium carbonate, with the objective to obtain a carbonate-bridged dinuclear copper(II) compound, the pendent pyridine arms were hydrolysed and a unique tetranuclear copper(II) compound resulted in which the carbonate groups indeed bridge the copper ions, but in an uncommon pentacoordinating fashion. The present paper reports the structure of this unusual carbonate-bridged tetranuclear copper compound.

[a] Leiden Institute of Chemistry, Gorlaeus Laboratories, Leiden University
P.O. Box 9502, NL-2300 RA Leiden, The Netherlands
E-mail: driessen@chem.leidenuniv.nl
[b] Bijvoet Centre for Biomolecular Research,
Crystal and Structural Chemistry Utrecht University
Padualaan 8, NL-3584 CH Utrecht, The Netherlands

Results and Discussion

Synthetic Aspects

The tetranuclear copper(II) compound [Cu_4(22Pz)$_2$-(CO_3)$_2$($MeOH$)$_2$](ClO_4)$_4$($MeOH$)$_4$ has been obtained by treating a solution of MePy22Pz and copper(II) perchlorate in methanol/water with a solution of sodium carbonate in water. During this process hydrolysation at the tertiairy nitrogen of the macrocycle resulted in the loss of the pendent pyridine groups and the formation of the "bare" 22-membered macrocycle **22Pz**. Vapor diffusion with diethylether resulted in the growth of single crystals of the coordination compound suitable for X-ray diffraction. The ligand field spectrum of this compound shows an asymmetric band at 16500 cm^{-1} in compliance with the distorted N_3O_3 environments of the copper(II) ions (vide supra). NMR spectra of the compound in solution could not be obtained due to linebroadening paramagnetism.

Description of the Structure

A PLUTON[11] plot of the cationic part is given in Figure 1. The asymmetric unit comprises half a molecule [Cu_4-(22Pz)$_2$(CO_3)$_2$($MeOH$)$_2$](ClO_4)$_4$($MeOH$)$_4$, the other half of the molecule is generated through a center of symmetry.

Firstly it is to be remarked that the ligand in this tetranuclear compound is a derivative of the macrocycle MePy22Pz,[8−10] viz. 1,4,9,14,17,22,27,28,29,30-decaaza-5,13,18,26-tetramethylpentacyclo[24.2.1.1^{4,7}.1^{11,14}.1^{17,20}]triacontane-5,7(28),11(29),12,18,20(30),24(27),25-octaene (**22Pz**) as during the synthesis of the coordination compound the pyridine groups and spacers were lost through hydrolysis. Also, all pyrazole groups are involved in the coordination of the copper ions, which appeared not to be the

 © WILEY-VCH Verlag GmbH, D-69451 Weinheim, 1999 1434−1948/99/0303−0505 $ 17.50+.50/0

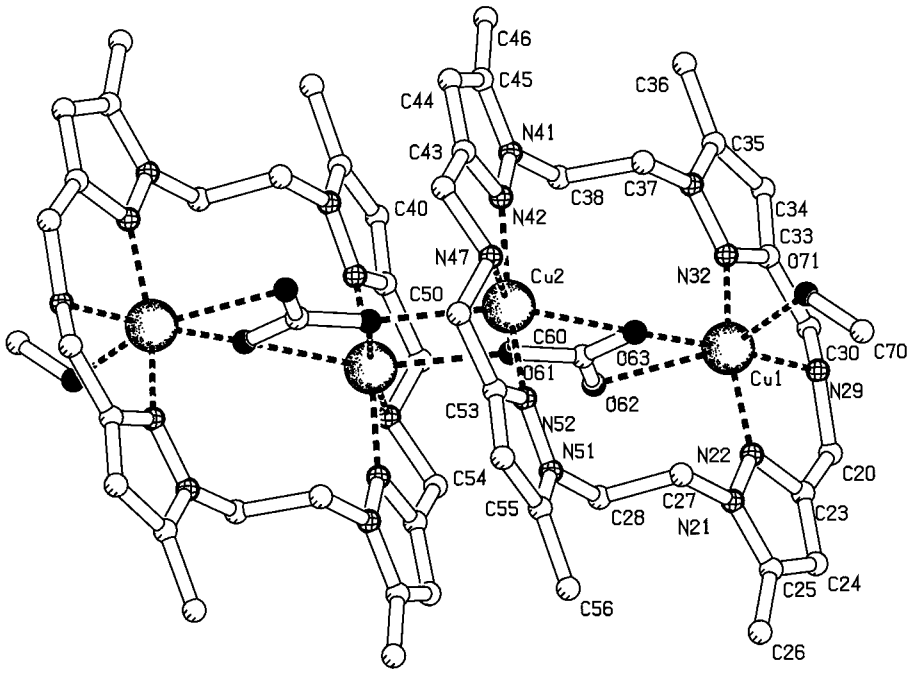


Figure 1. A PLUTON[11] projection of $[Cu_4(22Pz)_2(CO_3)_2(MeOH)_2]^{4+}$; hydrogen atoms are omitted for clarity

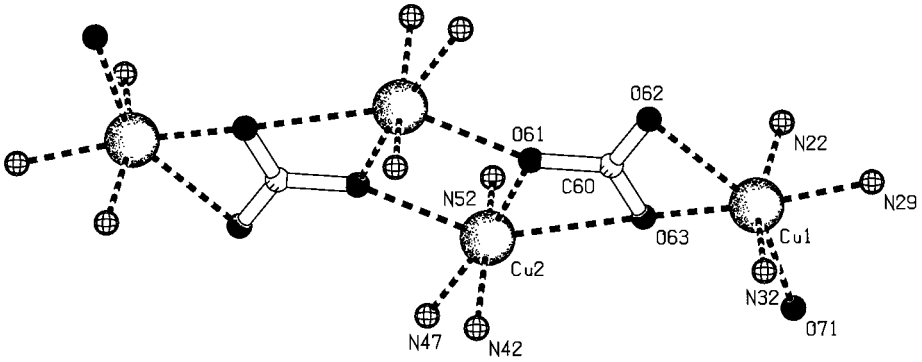


Figure 2. A PLUTON[11] projection of the coordination environments of the four copper(II) ions in the tetranuclear dimeric cation, showing the pentacoordination of the carbonate ions

case with the parent ligand MePy22Pz.[12] The most remarkable feature, however, is the penta-coordination mode of the carbonate ions (see Figure 2) with regular copper to oxygen bonds of 1.934(5) and 1.905(5) Å between respectively Cu(1) and O(63) and between Cu(2) and O(61), while the Cu(1) to O(62), the Cu(2) to O(61)a, and the Cu(2) to O(63) distances of respectively 2.589(8), 2.453(6), and 2.668(5) Å are regarded as *semi*-bonding distances (see Table 1).

O(62) binds to Cu(1), O(63) bridges between Cu(1) and Cu(2) in the same macrocyclic ring, while O(61) bridges between Cu(2) and Cu(1) in different macrocyclic rings. So, the two carbonate ions are bridging both intramolecularly and intermolecularly, thereby effecting that the tetranuclear cation is in fact a dimer of two dinuclear parts, viz. $[\{Cu_2(22Pz)(CO_3)(MeOH)\}^{2+}]_2$. Multiple bridging of carbonate groups in coordination compounds is not a rare phenomenon,[13,14] but only one compound has been reported so far,[13] viz. a trinuclear nickel compound,[15] in which the carbonate ion also bridges in a pentacoordinating fashion, in this case with five regular nickel to oxygen bonding distances (varying between 2.14 and 2.22 Å).

The coordination geometries of both copper ions are roughly the same. Each copper(II) ion is in a distorted, more or less elongated, octahedral N_3O_3 environment, with N(22), N(29), N(32), and O(63) equatorial and O(71) and O(62) axial for Cu(1) and with N(42), N(47), N(52), and O(61) equatorial and O(63) and O(61)a axial for Cu(2). The largest distortion from regular octahedral symmetry is of course caused by the didentate carbonate oxygens, imposing O−Cu−O angles of about 55° (see Table 1 and Figure 2).

The three-bond ligand bites contribute also to the deviation from regular octahedral symmetry. The two copper ions in the same macrocyclic ring, viz. Cu(1) and Cu(2), are at a distance of 4.601(2) Å, a distance suitable for the binding of a small molecule like dioxygen in a bridging fashion between the two copper ions. Two of the copper ions in different macrocyclic rings, viz. Cu(2) and Cu(2)a, are even

Table 1. Selected bond lengths [Å] and angles [deg] for $[Cu_4(22Pz)_2(CO_3)_2(MeOH)_2](ClO_4)_4(MeOH)_4$

Cu(1)−N(32) 1.979(7)	Cu(2)−N(52) 2.004(7)
Cu(1)−N(29) 2.039(7)	Cu(2)−O(61) 1.905(5)
Cu(1)−N(22) 2.000(7)	Cu(2)−N(42) 2.006(7)
Cu(1)−O(63) 1.934(5)	Cu(2)−N(47) 2.007(7)
Cu(1)−O(71) 2.294(5)	Cu(2)−O(61)a 2.453(6)
Cu(1)−O(62) 2.589(8)	Cu(2)−O(63) 2.668(5)
Cu(1)−Cu(2) 4.601(2)	Cu(2)−Cu(2)a 3.240(2)
O(63)−Cu(1)−N(29) 173.0(3)	O(61)−Cu(2)−N(47) 171.9(3)
O(63)−Cu(1)−O(71) 94.8(2)	O(61)−Cu(2)−N(52) 100.3(3)
O(63)−Cu(1)−N(32) 99.0(3)	O(61)−Cu(2)−N(42) 98.2(3)
O(63)−Cu(1)−N(22) 99.0(3)	O(61)−Cu(2)−O(61)a 84.8(2)
O(71)−Cu(1)−N(32) 93.3(3)	N(42)−Cu(2)−N(47) 80.7(3)
O(71)−Cu(1)−N(29) 92.2(3)	N(42)−Cu(2)−N(52) 161.0(3)
O(71)−Cu(1)−N(22) 93.0(3)	N(42)−Cu(2)−O(61)a 90.6(3)
N(22)−Cu(1)−N(32) 160.4(3)	N(47)−Cu(2)−N(52) 81.6(3)
N(22)−Cu(1)−N(29) 80.8(3)	N(47)−Cu(2)−O(61)a 87.3(3)
N(29)−Cu(1)−N(32) 80.4(3)	N(52)−Cu(2)−O(61)a 95.4(3)
O(62)−Cu(1)−O(63) 56.9(2)	O(63)−Cu(2)−O(61) 55.0(2)
O(62)−Cu(1)−O(71) 151.5(2)	O(63)−Cu(2)−N(42) 93.6(2)
O(62)−Cu(1)−N(22) 93.9(3)	O(63)−Cu(2)−N(47) 132.9(3)
O(62)−Cu(1)−N(29) 116.2(3)	O(63)−Cu(2)−N(52) 93.4(2)
O(62)−Cu(1)−N(32) 89.2(3)	O(63)−Cu(2)−O(61)a 139.7(2)

a = 1−*x*, −*y*, −*z*.

on a smaller distance [3.240(2) Å] of course resulting from the bridging of O(61) (see Figure 2).

Experimental Section

Synthesis of $[Cu_4(22Pz)_2(CO_3)_2(MeOH)_2](ClO_4)_4(MeOH)_4$: To a solution of 25.0 mg of 9,22-di(pyridin-2-ylmethyl)-1,4,9,14,17,22,27,28,29,30-decaaza-5,13,18,26-tetramethylpentacyclo-[24.2.1.1^{4,7}.1^{11,14}.1^{17,20}]triacontane-5,7(28),11(29),12,18,20(30),24(27),25-octaene (**MePy22Pz**)[9][12] (38.8 mmol) in 5 mL of MeOH and 1 mL of H_2O, two equivalents (1.3 mL) of a solution of $Cu(ClO_4)_2 \cdot 6\ H_2O$ in MeOH (59 mmol) were added. A clear green solution was obtained after gentle warming and subsequent filtration. Addition of one equivalent Na_2CO_3 (77.6 mmolar solution in H_2O) invoked a blue colorisation for only a few seconds. After filtration a clear green solution was obtained. Vapour diffusion with Et_2O at 298 K resulted after three weeks in light-blue crystals, suitable for X-ray diffraction, of $[Cu_4(22Pz)_2(CO_3)_2(MeOH)_2](ClO_4)_4(MeOH)_4$, with **22Pz** being 1,4,9,14,17,22,27,28,29,30-decaaza-5,13,18,26-tetramethylpentacyclo[24.2.1.1^{4,7}.1^{11,14}.1^{17,20}]triacontane-5,7(28),11(29),12,18,20(30),24(27),25-octaene.

Materials and Methods: FT-IR spectra were recorded on a Perkin Elmer paragon 1000 FT-IR spectrometer as KBr disks (4000−400 cm^{-1}). Ligand field spectra were registered on a Perkin Elmer lambda 900 UV/Vis/NIR spectrometer.

X-ray Structure Analysis of $[Cu_4(22Pz)_2(CO_3)_2(MeOH)_2](ClO_4)_4(MeOH)_4$: $C_{51}H_{84}Cl_4Cu_4N_{20}O_{30}$, M = 1901.39, light-blue prismatic crystal (0.12 × 0.37 × 0.37 mm), Enraf-Nonius CAD4T diffractometer with rotating anode, λ(Mo-*K*α) = 0.71073 Å, T = 290 K, monoclinic, $P2_1/c$, a = 12.419(3), b = 23.058(4), c = 14.743(4) Å, β = 109.98(2)°, V = 3968(2) Å^3, Z = 2, D_c = 1.592 gcm^{-3}, μ(Mo-*K*α) = 12.8 cm^{-1}, F(000) = 1956, θ max = 26.5°, h, k, l range = −14/14, −27/27, 0/17, a total of 15281 reflections, of which 7462 unique, with R_{int} = 0.139 (poor crystal quality) and 3263 observed [I>2σ(I)], R = 0.087 (*wR* 0.23, *S* 0.89), ρ min/max = −0.47/1.05 e/Å^3, n(pars) = 561, correction for Lorentz and polarization, no absorption correction. Structure solved with automated Patterson techniques (DIRDIF/PATT[16]), refined on F^2, full-matrix least-squares (SHELXL-97.[17,18]) All non-hydrogen atoms refined with anisotropic displacement parameters, hydrogen atoms introduced on calculated positions and refined riding on their carrier atoms. The disordered perchlorate anions were isotropically refined with the oxygens on partly occupied positions, as were the non-hydrogens of the lattice solvent molecules without calculated hydrogens. Geometric calculations and molecular graphics were performed with PLATON.[11] Table 1 contains selected bond lengths and angles.

Crystallographic data (excluding structure factors) for the structure reported in this paper have been deposited with the Cambridge Crystallographic Data Centre as supplementary publication no. CCDC-103045. Copies of the data can be obtained free of charge on application to CCDC, 12 Union Road, Cambridge CB2 1EZ, UK (Fax: +44-1223/ 336-033; E-mail: deposit@ccdc.cam.ac.uk).

Acknowledgments

The authors are indebted to the EU for a grant as Host Institute in the EU Programme Human Capital and Mobility (1994−1997). Use of the services and facilities of the Dutch National NWO/ SURF Expertise Center CAOS/CAMM, under grant numbers SON 326-052 and STW NCH99.1751, is gratefully acknowledged.

[1] P. J. Baesjou, W. L. Driessen, G. Challa, J. Reedijk, *J. Mol. Catalysis A* **1996**, *110*, 195.
[2] G. J. A. A. Koolhaas, W. L. Driessen, J. Reedijk, J. L. van der Plas, R. A. G. de Graaff, D. Gatteschi, H. Kooijman, A. L. Spek, *Inorg. Chem.* **1996**, *35*, 1509.
[3] G. Tabbì, W. L. Driessen, J. Reedijk, R. P. Bonomo, N. Veldman, A. L. Spek, *Inorg. Chem.* **1997**, *36* 1168.
[4] W. L. Driessen, R. A. G. de Graaff, F. J. Parlevliet, J. Reedijk, R. M. de Vos, *Inorg. Chim. Acta* **1994**, *216*, 43.
[5] W. Kaim, J. Rall, *Angew. Chem.* **1996**, *108*, 47; *Angew. Chem., Int. Ed. Engl.* **1996**, *35*, 43.
[6] K. A. Magnus, H. Ton-That, J. Carpenter, *Chem. Rev.* **1994**, *94*, 727.
[7] E. I. Solomon, M. D. Lowery, *Science* **1993**, *259*, 1575.
[8] J. E. Bol, *Synthetic models for dinuclear copper proteins.* Ph.D. Thesis, Leiden University, **1997**.
[9] J. E. Bol, B. Maase, G. Gonesh, W. L. Driessen, K. Goubitz, J. Reedijk, *Heterocycles* **1997**, *45*, 1477.
[10] J. E. Bol, W. L. Driessen, R. Y. N. Ho, B. Maase, L. Que, J. Reedijk, *Angew. Chem.* **1997**, *109*, 1022; *Angew. Chem. Int. Ed. Engl.* **1997**, *36*, 998.
[11] A. L. Spek, *Acta Crystallogr.* **1990**, *A46*, C-34.
[12] R. H. Bode, F. B. Hulsbergen, W. L. Driessen, J. Reedijk, A. L. Spek, *Inorg. Chem.*, submitted.
[13] A search of over 181,000 entries in the Cambridge Crystal Structure Database (CSD).
[14] See for instance: [14a] C. Bazzicalupi, A. Bencini, A. Bencini, A. Bianchi, F. Corana, V. Fusi, C. Giorgi, P. Paoli, P. Paoletti, B. Valtancoli, C. Zanchini *Inorg. Chem.* **1996**, *35*, 5540. − [14b] C. Bazzicalupi, A. Bencini, A. Bianchi, V. Fusi, P. Paoletti, B. Valtancoli, *J. Chem. Soc., Chem. Comm.* **1995**, 1555. − [14c] A. Escuer, F. A. Mautner, E. Penalba, R. Vicente, *Inorg. Chem.* **1998**, *37*, 4190.
[15] A. Escuer, R. Vicente, S. B. Kumar, X. Solans, M. Font-Bardia, A. Caneschi *Inorg. Chem.* **1996**, *35*, 3094.
[16] P. T. Beurskens, G. Admiraal, G. Beurskens, W. P. Bosman, S. Garcia-Granda, R. O. Gould, J. M. M. Smits, C. Smykalla, *The DIRDIF program system*, Technical Report of the Crystallography Laboratory, University of Nijmegen, The Netherlands **1992**.
[17] G. M. Sheldrick, *SHELXL97: Program- for the Refinement of Crystal Structures*, University of Göttingen, Germany **1997**.
[18] A. J. C. Wilson, Ed. *International Tables for Crystallography*, Volume C, Kluwer Academic Publishers, Dordrecht, The Netherlands, **1992**.

Received September 25, 1998
[I98332]

Isomerism in Copper(I)-Induced Folding of Homoditopic Macrocyclic Ligands with Bis(dithiadiimine) Donor Sets

Peter Comba*[a] and Andreas Kühner[a]

Keywords: Macrocyclic ligands / Molecular modeling / Schiff bases / Helical structures / Copper

The structural properties of the dicopper(I) compounds of the two large macrocyclic Schiff base ligands *para*-222 and *meta*-222 with two dithiadiimine coordination sites, where the two sites are linked by two *para*- or two *meta*-xylylene spacer groups and all bridges between the donors of each site are ethylene groups (32- and 30-membered macrocycles for the *para*- or *meta*-xylylen-bridged *para*-222 and *meta*-222 species, respectively) are studied, in solution and by computer modeling. Solid-state structural data have been reported elsewhere. The coordination of the 32-membered macrocycle *para*-222 to two copper(I) centers leads to a helical figure-of-eight-shaped structure. Two diastereomeric pairs of enantiomers have been observed for this type of compound in solution. The crystallized form is more stable than the second isomer by approximately 6–10 kJ/mol (solution-NMR spectroscopy and force-field calculations). Both experimentally detected isomers are more than 15 kJ/mol more stable than the other five possible configurations (force-field calculations). For the *meta*-222 macrocycle (30-membered ring) an achiral structure has been observed in the solid while two of the 21 possible isomers have been detected in solution (3:1, NMR spectroscopy). The computed structures and isomer distributions (force-field calculations) are compared with the solid-state structures and with observed isomer distributions from NMR experiments, and dynamic processes are analyzed in detail.

Introduction

The coordination of the paracyclophane-based preorganized double-helical $(N_2S_2)_2$ bis(dithiadiimine) ligand (phane-222, see Figure 1) to copper(I) yields a dicopper(I) complex that, based on the observed structure, is not much strained.[1] Indeed, the coordination of copper(I) to analoguous macrocyclic ligands, where the two $(N_2S_2)_2$ donor sites are linked by two *para*-xylylene groups (*para*-222, see Figure 1) leads to a very similar figure-of-eight-shaped structure.[2–4] That is, copper(I) induces an identical folding, and this indicates that phane-222 is highly preorganized for copper(I).[5–7] The isomer with *meta*-xylylene-bridged donor groups (30- instead of 32-membered macrocyclic ring, *meta*-222, see Figure 1) leads to an achiral dicopper(I) compound but the overall shape of the structure ("squeezed" instead of "twisted" figure-of-eight shape) and, in particular, the geometry of the chromophores are very similar.[3] Plots of the observed structures of the three dicopper(I) compounds are shown in Figure 1 and relevant parameters are assembled in Table 1.

From solid-state structural studies of an extended series of dicopper(I) compounds of Schiff base $(N_2S_2)_2$ ligands of the general type shown in Figure 1 (variation of the aromatic spacer groups, variation of the chelate ring sizes) it emerges that, for the chiral compounds with *para*-substituted spacer groups (e.g. *para*-222), only one of seven possible diastereoisomeric pairs of enantiomers is observed, that is, one of the two forms that have identical configuration for all four coordinated thioether-S donors (see below and Figure 1); for the *meso* form (*meta*-222) the thioether-S configurations are (*R*)(*R*)(*S*)(*S*) and only one of three theoretically possible isomers with respect to the orientation of the xylylene spacer groups is observed in the crystal structural analysis (see Figure 1).[3,4]

Solution-NMR studies indicate that the geometries in solution are identical to those observed in the solid, that is figure-of-eight-shaped ("twisted" or "squeezed" for *para*- and *meta*-substituted xylylene spacer groups, respectively), and that dynamic processes occur. The dicopper(I) compounds of *para*-222 and of derivatives with larger chelate ring sizes have been studied in detail by solution-NMR spectroscopy.[4] An intramolecular dynamic process leads to helix inversion (epimerization, that is, retention of the configuration of the S donors), and a solvent-dependent intermolecular process leads to full racemization.[4] For the derivative of *para*-222 with two seven-membered chelate rings (*para*-242) there is spectroscopic evidence for an equilibrium with a less stable isomer, and this is attributed to the helix inversion (epimerization) product.[4] The solution chemistry of *meta*-222 is addressed here. We also present a full conformational analysis of the two isomers $[Cu_2(para\text{-}222)]^{2+}$ and $[Cu_2(meta\text{-}222)]^{2+}$, based on force-field calculations, and these are compared to observed solid-state and solution data.

Results and Discussion

Isomerism

The helical dinuclear compounds, that is, the dicopper(I) compounds of phane-222 and *para*-222, have the same shape and the same idealized symmetry (D_2) while the achiral dicopper(I) compound, that is, that of *meta*-222 has ide-

[a] Anorganisch-Chemisches Institut der Universität Heidelberg, Im Neuenheimer Feld 270, D-69120 Heidelberg, Germany
Fax: (internat.) +49(0)6221-54 66 17
E-mail: comba@akcomba.oci.uni-heidelberg.de

 © WILEY-VCH Verlag GmbH, D-69451 Weinheim, 1999 1434–1948/99/0303–0509 $ 17.50+.50/0

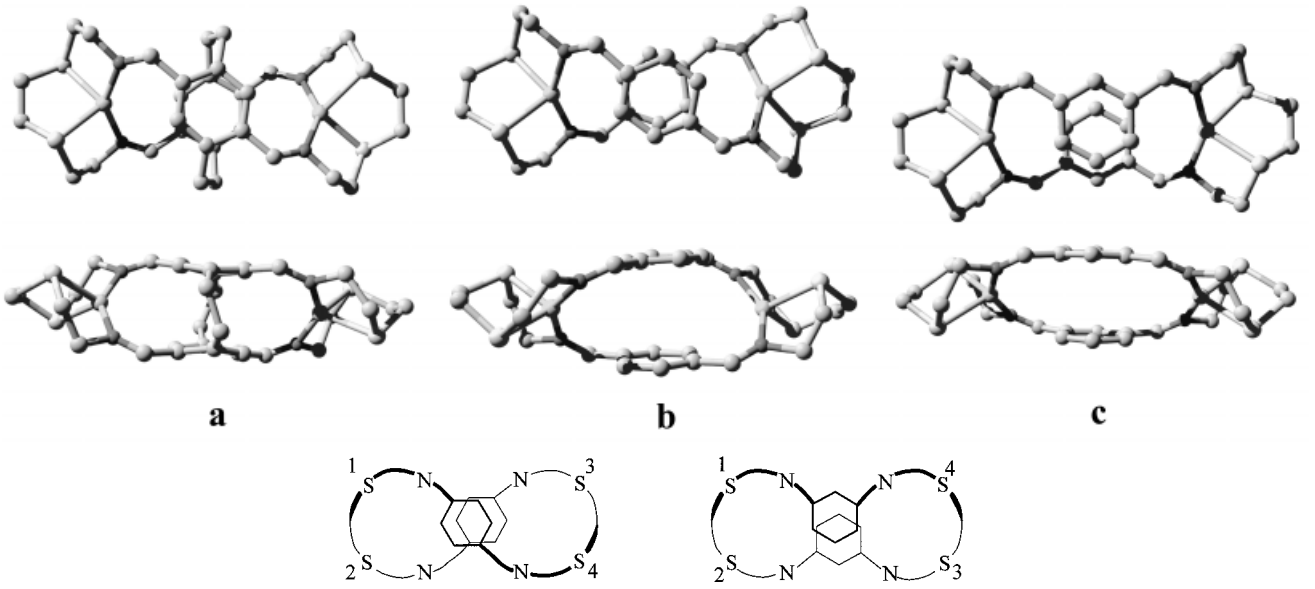


Figure 1. Plots of the molecular cations of the experimentally observed solid-state structures of (a) $[Cu_2(phane\text{-}222)]^{2+}$,[1] (b) $[Cu_2(para\text{-}222)]^{2+}$,[3] (c) $[Cu_2(meta\text{-}222)]^{2+}$[3] and sketches of the " helical" and "squeezed" folding of the macrocycles with numbering scheme

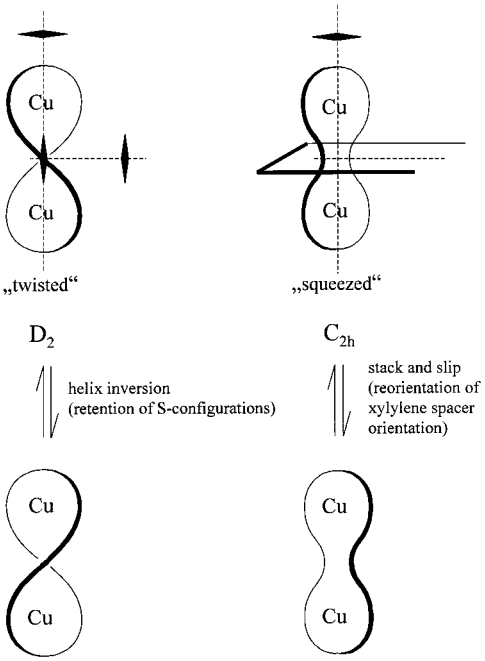
Table 1. Structural parameters of $[Cu_2(phane\text{-}222)]^{2+}$[1], $[Cu_2(para\text{-}222)]^{2+}$[3] and $[Cu_2(meta\text{-}222)]^{2+}$[3]

Ligand	phane-222	*para*-222	*meta*-222
Cu−S	2.42	2.38	2.43
Cu−N	1.96	2.01	1.99
Cu ··Cu	8.22	7.83	8.15
Cxyl···Cxyl	−	3.43	3.26; 3.43
xyl···xyl	3.09	3.59	3.39
S−Cu−S	91.51	91.0	88.2
S−Cu−N	117.4	115.1	113.3
S−Cu−N^{bite}	90.2	90.8	89.7
N−Cu−N	141.2	144.1	148.5
$C^{imine}-C^{xyl}$[a]	32	31	27
θ[b]	71	73	73

[a] Torsional angle around the imine bond. − [b] Tetrahedral twist angle (S−Cu−S; N−Cu−N planes; tetrahedral: 90°).

alized C_{2h} symmetry (see Scheme 1). For $[Cu_2(para\text{-}222)]^{2+}$ there are eleven elements of asymmetry, the helix, the four thioether-S donors and the six five-membered chelate rings. The experimentally determined structure has Λ-(*S*)(*S*)(*S*)(*S*)-λλλλλλ geometry (the order of the thioether-S configurations and of the five-membered chelate ring conformations is based on the numbering scheme given in Figure 1; the same conformation is observed in all other structurally determined derivatives[4]). There are seven diastereomeric pairs of enantiomers with different sequences of thioether-S configurations [Λ-helices: (*S*)(*S*)(*S*)(*S*), (*S*)(*S*)(*S*)(*R*), (*S*)(*S*)(*R*)(*R*), (*S*)(*R*)(*R*)(*S*), (*S*)(*R*)(*S*)(*R*), (*R*)(*R*)(*R*)(*S*) and (*R*)(*R*)(*R*)(*R*)]. For each there is a number of possible sequences of the five-membered chelate ring conformations, leading to 350 non-degenerate isomers.

The $[Cu_2(meta\text{-}222)]^{2+}$ ion has twelve stereochemical elements, the four thioether-S donors, the six five-membered chelate ring conformations and the orientation of the two *meta*-xylylene spacer groups. The crystallized molecule has



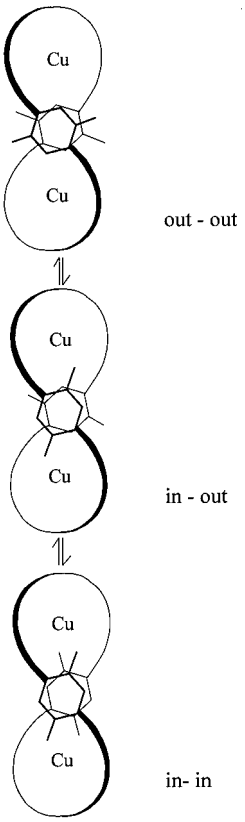
Scheme 1

tail-to-tail-(*S*)(*S*)(*R*)(*R*)-λλλδδδ geometry (the nomenclature follows the numbering scheme given in Figure 1; tail-to-tail refers to the orientation of the *meta*-xylylene bridges, see Scheme 3, below). There are 72 non-degenerate isomers in this system.

Dynamics − Experimental Observations

High-resolution ^{1}H-NMR spectroscopy indicates that, for both structural types, the figure-of-eight-shaped geometry is retained in solution.[1−4] For the helical dicop-

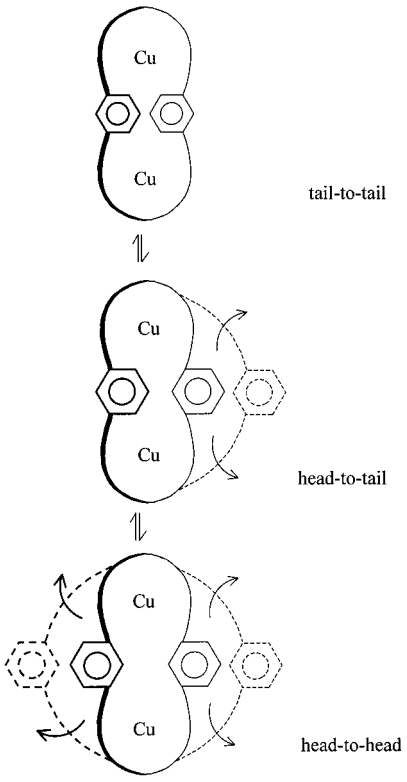
per(I) compounds (e.g. $[Cu_2(para\text{-}222)]^{2+}$) there is evidence for two independent dynamic processes.[4] The first is helix inversion with full retention of the thioether-S configuration (epimerization). This is observed at low temperature in solvents with little affinity to copper(I) (intramolecular reaction, observed in nitromethane) in the low-field region of the ^{1}H-NMR spectrum (non-equivalent aromatic protons, see Scheme 2).[4] For a derivative of *para*-222 (i.e. *para*-242) there is spectroscopic evidence for the second diastereoisomer that emerges from helix inversion [Δ-(*S*)(*S*)(*S*)(*S*) versus Λ-(*S*)(*S*)(*S*)(*S*)]. For *para*-222 the helix inversion has a lower energy barrier and the spectra were therefore not fully resolved at the lowest temperature available in nitromethane.[4] The comparison of the temperature-dependent ^{1}H-NMR data of the dicopper(I) compounds of *para*-222 with those of ligands with substituted benzene spacer groups (e.g. Me-*para*-222, see Scheme 2, dimethylated spacer group) suggests that along the helix inversion mode there is rotation of the xylylene groups around the C1···C4 axes (in/out isomerism, see Scheme 2).[4] The rate of this rotation depends on the size of the xylylene substituents.



Scheme 2

The second dynamic process leads to full racemization, that is, it involves inversion of the helix *and* inversion at each of the four thioether-S donors [Λ-(*S*)(*S*)(*S*)(*S*) versus Δ-(*R*)(*R*)(*R*)(*R*)]. This reaction is only observed in acetonitrile for which copper(I) has a strong affinity. It occurs at significantly higher temperatures than the helix inversion, and it was assigned on the basis of temperature-dependent ^{1}H-NMR spectra in the high-field region (methylene protons).[4] The solvent dependence and the fact that inversion at the thioether-S donors involves copper(I)−S bond breaking suggest that full racemization is an intermolecular process. This was supported by crystallization and the structural analysis of a putative intermediate with two coordinated acetonitrile molecules.[4]

The solution ^{1}H-NMR spectroscopic behavior of the achiral $[Cu_2(meta\text{-}222)]^{2+}$ cation is strikingly different. In both solvents, acetonitrile and nitromethane, there are, in dependence of the temperature, two types of spectra: a well-resolved low-temperature spectrum (for the region of aromatic and imine protons, see Figure 2) and a high-temperature spectrum that has coupling patterns identical to those of the metal-free ligand but chemical shifts (methylene protons, high-field region) that indicate copper(I) coordination. In analogy to the observations and interpretations with the helical compounds[4] (see above), the high-temperature spectrum is attributed to a species, where a dynamic process leads to full scrambling which may involve a "stack-and-slip" process (Scheme 1), reorientation of the *meta*-xylylene spacer groups (Scheme 3) and inversion at the thioether-S centers.



Scheme 3

In contrast to observations with the "twisted" geometries (helical compounds, e.g. $[Cu_2(para\text{-}222)]^{2+}$, see above[4]) with the "squeezed" geometry ($[Cu_2(meta\text{-}222)]^{2+}$) this process occurs in acetonitrile *and* in nitromethane {$[Cu_2(meta\text{-}222)]^{2+}$: coalescence temperatures for the aromatic protons: 330 K (nitromethane), 300 K (nitromethane/acetonitrile, 10:1), 250 K (acetonitrile); $[Cu_2(para\text{-}222)]^{2+}$, aromatic pro-

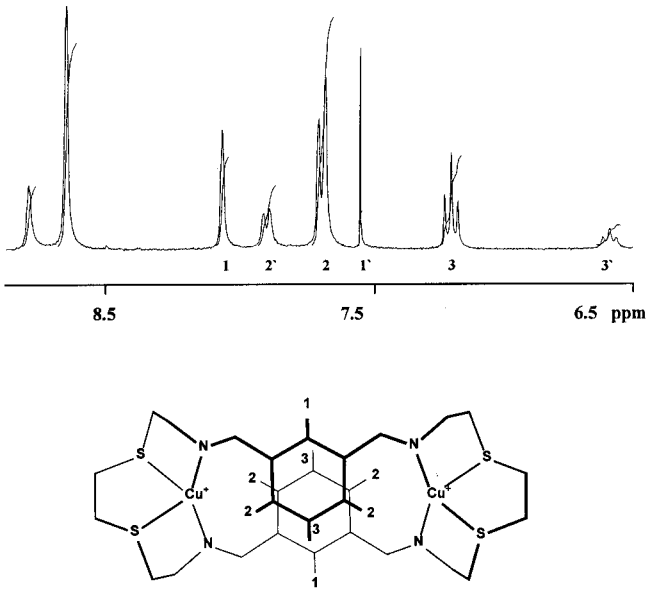


Figure 2. Region of the signals of the aromatic protons in the ^{1}H-NMR spectrum (200 MHz, 290K, CD_3NO_2) of $[Cu_2(meta\text{-}222)]^{2+}$; the numbering of the protons of the *meta*-xylylene groups is given in the sketch

tons: < 230 K, solvent-independent; methylene protons (only in acetonitrile): 300 K}. This suggests that intramolecular processes for $[Cu_2(meta\text{-}222)]^{2+}$ have significantly higher activation barriers. Based on the structural features of the "squeezed" geometry this is not unexpected: The stack-and-slip process (Scheme 1) must lead to a significant amount of unfolding and strain in the copper(I)−donor bonds, especially for the experimentally observed tail-to-tail rotamer; the reorientation of the *meta*-xylylene spacer groups (tail-to-tail/head-to-tail/head-to-head isomerization) involves a rotation around the C1···C3 axis, and this is sterically less favorable than the corresponding rotation of the *para*-xylylene spacer groups (C1···C4 axis). The fact that the high-temperature dynamic process is only moderately dependent on the solvent for $[Cu_2(meta\text{-}222)]^{2+}$ suggests that Cu^I-S bond breaking has a more dissociative activation than for $[Cu_2(para\text{-}222)]^{2+}$, and this is supported by the higher activation barrier of the low-temperature dynamics, that is, these processes involve highly strained transition states. Further support for this interpretation emerges from the observation that the air stability of the $[Cu_2(meta\text{-}222)]^{2+}$ species is considerably lower than that of $[Cu_2(para\text{-}222)]^{2+}$, that is, oxygenation of the dicopper(I) compound is probably also activated along the intramolecular dynamic process.

In the region of the aromatic and imine proton signals one expects a singlet for the imine protons and three signals for the aromatic protons (singlet, doublet, triplet) in the ratio 2:1:2:1. The experimetal ^{1}H-NMR spectrum at 298 K (Figure 2) suggests that two isomeric $[Cu_2(meta\text{-}222)]^{2+}$ species in the ratio of approximately 3:1 are present in solution. There is only one set of signals in the region of aliphatic protons, suggesting that the coordination geometries of the two isomers are close to identical [the sum of the integrals of the signals in the aromatic region (both isomers) corresponds to that expected from the sum of integrals of the aliphatic protons]. Possible isomeric forms [tail-to-tail (observed in the solid state, see Figure 1), head-to-tail, head-to-head] are shown in Scheme 3. The experimental spectrum suggests that only two species are stable in solution. Also, the head-to-tail isomer has a lower symmetry, and additional splitting in the aromatic region would be expected for this species, unless a fast dynamic exchange occured.

Further structural information emerges from a qualitative analysis of the chemical shifts in the aromatic region (Table 2; see structural sketch in Figure 2 for proton numbering). Based on the solid-state structure (Figure 1; the *meta*-xylylene rings are stacked with a xylylene···xylylene distance of 3.39 Å and a horizontal displacement of the two rings by 1.06 Å[3]) one expects that signals of protons 2 and especially 3 are shifted to higher field due to dipole-dipole interactions with the other aromatic ring, while there is less interaction with protons 1. The observed signals of the major species are in agreement with these expectations (shift with respect to the chemical shift of the metal-free ligand of $\Delta\delta = +0.07, -0.11, -0.31$ for signals 1, 2, 3, respectively). In the less abundant isomer (primed resonances in Figure 2), the signals for proton 1′ and 3′ are shifted to higher field with respect to those in the major isomer ($\Delta\delta = -0.53$ and -1.52), indicating that there is a very strong interaction with the other aromatic ring. For protons 2′ there is a decreasing interaction ($\Delta\delta = +0.21$). This behavior may be interpreted by a tilt of the two aromatic planes with respect to each other (see rotation of the xylylene rings above). The relative symmetry (number of symmetry-related protons) suggests that a fast equilibrium between various sites must be involved, that is, in average, both *meta*-xylylene rings are equivalent.

Modeling Studies

Empirical force-field calculations in combination with experimental data (isomer distributions, reduction potentials, EPR, NMR and electronic spectra) have been used extensively to determine structures of transition metal compounds in solution.[8−11] The MOMEC program[12] and force field[13] have been tested successfully in this field, and in various areas they have demonstrated to lead also to accurate predictions of conformational equilibria and energy barriers for conformer interconversions.[14] This is not necessarily expected since the force field is primarily based on solid-state structural data.[14] However, the parameter sets used for the ligand backbones are transferable, and from the fact that some of these parameters were fitted to thermodynamic observables it emerges that the steepnesses of the potentials are approximately realistic. Published studies, primarily in the fields of (hexaamine)cobalt(III) and -nickel(II) compounds support this suggestion.[8−11,14] The new parameters necessary to model the conformational

Table 2. ^{1}H-NMR data of *meta*-222 and $[Cu_2(meta\text{-}222)]^{2+}$ [200 MHz, CD_3NO_2, 290 K (and 350 K), low-field region, δ (ppm)]; for atom numbering, see Figure 2

		$[Cu_2(meta\text{-}222)]^{2+}$		
	Metal-free ligand 290 K	Major isomer 290 K	Minor isomer 290 K	Fast exchange 350 K
imine proton	8.3	8.68	8.82	8.70
aromatic proton 1	8.0	8.07	7.54	8.01
aromatic proton 2	7.8	7.69	7.90	7.75
aromatic proton 3	7.5	7.19	5.57	7.05

space of $[Cu_2(para\text{-}222)]^{2+}$ and $[Cu_2(meta\text{-}222)]^{2+}$ include copper(I)−thioether-S interactions and a few parameters involving the substituents of the thioether and Schiff base donors (see Experimental Section). These were fitted to the published experimental structures in this series.[1−4] Thus, the expectation was that, together with the experimental data discussed above, a full conformational analysis of the two isomers $[Cu_2(para\text{-}222)]^{2+}$ and $[Cu_2(meta\text{-}222)]^{2+}$ would lead to some insight into the dynamic processes in these systems.

$[Cu_2(para\text{-}222)]^{2+}$

The conformation observed in the solid {Λ-(*S*)(*S*)(*S*)(*S*)-λλλλλλ-$[Cu_2(para\text{-}222)]^{2+}$} is the most stable structure (U_{strain} = 28 kJ/mol). Inversion of a five-membered chelate ring costs approximately 5 kJ/mol and inversion of a coordinated thioether-S center leads to a destabilization of approximately 16 kJ/mol. These effects are not additive but the next lowest energy structure (five-membered ring inversions alone excluded; these have activation barriers of approximately 25 kJ/mol,[15,16] i.e. their interconversion will not be frozen at the low-temperature limits of our experimental studies) is that of the helix inversion product, i.e. Δ-(*S*)(*S*)(*S*)(*S*)-λλλλλλ-$[Cu_2(para\text{-}222)]^{2+}$ with U_{strain} = 34 kJ/mol. The strain energy minimization of structures with constrained pseudo-torsional angles ϕ around the centroids of the two *para*-xylylene rings (helix inversion; ϕ = 80° to ϕ = −80°) was not as straight forward as one might anticipate. Without any further constraints there was a considerable distortion in the stacking of the *para*-xylylene rings that lead to intermediate structures at the transition state (pseudo-torsional angle ϕ = 0°) with horizontal translations or tilts of the two *para*-xylylene rings. This supports the interpretation based on the solution ^{1}H-NMR studies that, along the helix inversion, there is a low-energy rotation of the *para*-xylyene rings (see above). Also, with constrained stacking, the distance between the *para*-xylylene rings increases at the transition state (ϕ = 0°) from approximately 3.3 Å to approximately 4.9 Å.The energy barrier of the helix inversion process with constrained stacking of the *para*-xylylene rings is approximately 50 kJ/mol (see Figure 3). This upper limit of the activation energy for the helix inversion process is in good qualitative agreement with the temperature-dependent ^{1}H-NMR data.[4]

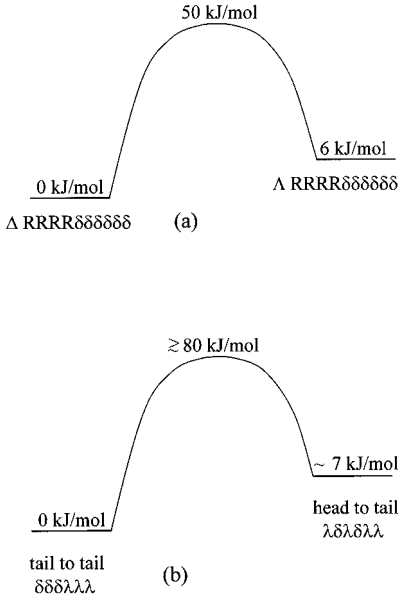


Figure 3. Energy profile of the dynamic processes of (a) $[Cu_2(meta\text{-}222)]^{2+}$ and (b) $[Cu_2(para\text{-}222)]^{2+}$

$[Cu_2(meta\text{-}222)]^{2+}$

Only two of the three putative rotamers of $[Cu_2(meta\text{-}222)]^{2+}$ (Scheme 3) converged to a stable structure. The experimentally observed geometry {tail-to-tail-(*R*)(*R*)(*S*)(*S*)-δδδλλλ-$[Cu_2(meta\text{-}222)]^{2+}$} was that with the lowest strain energy (U_{strain} = 40 kJ/mol; that is, the isomer with *meta*-xylylene spacer groups is approximately 12 kJ/mol less stable than that with *para*-xylylene spacer groups). The energy differences to species with inverted five-membered chelate rings and inverted thioether-S donor groups are similar to those of the *para* isomer (see above). Optimization of the head-to-tail isomer leads to a structure with one of the two aromatic rings tilted with respect to the other (see Figure 4). Optimization of the third rotamer (head-to-head) converged to either of the two other structures (head-to-tail or tail-to-tail), that is, this is not a minimum on the energy surface. The most stable head-to-tail conformer is head-to-tail-(*R*)(*R*)(*S*)(*S*)-λδλδλλ-$[Cu_2(meta\text{-}222)]^{2+}$ with U_{strain} = 47 kJ/mol.[17] The strain energy difference between the two rotamers (7 kJ/mol) is in good agreement with the isomer distribution observed in the ^{1}H-NMR spectrum (3:1, Figure 2). The optimized structure of the less abundant head-to-tail isomer is of particular interest since it is as expected

from the solution ^{1}H-NMR spectroscopic data, that is, the two aromatic spacer groups are tilted with respect to each other (see above). The sketches shown in Scheme 3 indicate that this might be due to the relieve of some strain related to the geometry around the C-1 and C-3 bridgehead carbon atoms of the *meta*-xylylene spacer group.

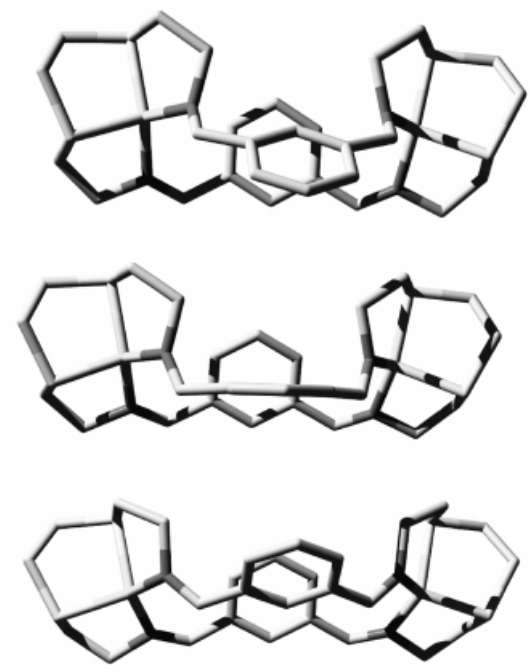


Figure 4. Visualization of the low-temperature dynamic process of the head-to-tail isomer of $[Cu_2(meta\text{-}222)]^{2+}$

Constraints were used to map the interconversion of the two rotamers of $[Cu_2(meta\text{-}222)]^{2+}$. The qualitative picture (see Figure 3) is that there is an activation energy between the two isomers of at least 80 kJ/mol. This is consistent with the observation that, at low temperature (< 300 K) there is no fast interconversion of the two isomers. Especially interesting is the observation that, for the tilted head-to-tail isomer there is a very shallow energy surface with at least three minima where the tilt angle between the two xylylene planes varies from approximately 30° to approximately 120° (see Figure 4). In the enforced structure of the head-to-tail isomer with parallel aromatic rings (transition state) the two *meta*-xylylene rings are symmetry-related, that is, there is a wagging mode of the two rings with an energy barrier of less than approximately 25 kJ/mol, and this is consistent with the observed ^{1}H-NMR spectra (see above). That is, the observed chemical shifts are due to the tilt of one of the xylylene planes with respect to the other and the shallow energy minima with various structural modes is in agreement with the observed high symmetry averaged structure.

Experimental Section

The syntheses have been described before.[1−4] − NMR spectra were obtained with a Bruker AS200 instrument at 200 MHz. − MOMEC97[12,13] with a published force field[12] was used to compute the optimized structures and minimized strain energies. Parameters not published before are given in Table 3.

Table 3. MOMEC force-field parameters[a]

Bond lengths			
Type 1	Type 2	k [mdyn Å^{-1}]	r_o [Å]
N_{imine}	C_{methyl}	3.4	1.48
Cu^I	$S_{thioether}$	0.1	2.30
$C_{benzene}$	O_{ether}	5.0	1.36
$C_{benzene}$	$S_{thioether}$	4.0	1.42
$C_{benzene}$	N_{imine}	4.0	1.42

Torsion angles				
Type 1	Type 2	k [mdyn A]	m	ϕ_0 [rad]
C_{imine}	$C_{benzene}$	0.005 (0.025)[b]	2	1.571
$C_{benzene}$	$C_{benzene}$	0.060	2	1.571

Valence angles				
Type 1	Type 2	Type 3	k [mdyn Å rad^{-2}]	θ_0 [rad]
$S_{thioether}$	CU(I)	N_{amine}	0	0
N_{imine}	CU(I)	N_{imine}	0	0
Cu^I	$S_{thioether}$	C_{methyl}	0.10	1.745
Cu^I	$S_{thioether}$	$C_{benzene}$	0.10	1.571
Cu^I	N_{imine}	$C_{benzene}$	0.10	2.094
$C_{benzene}$	$S_{thioether}$	C_{methyl}	0.50	1.740
$C_{benzene}$	$C_{benzene}$	$S_{thioether}$	0.45	2.094
$C_{benzene}$	N_{imine}	C_{imine}	0.50	2.094
$C_{benzene}$	$C_{benzene}$	N_{imine}	0.50	2.094
$C_{benzene}$	O_{ether}	C_{methyl}	0.75	2.094
$C_{benzene}$	$C_{benzene}$	O_{ether}	0.75	2.094
O_{ether}	C_{methyl}	H	0.36	1.911
C_{methyl}	$O_{alcohol}$	H	0.35	1.870

[a] All other parameters have been published before.[13] − [b] See ref.[17]

Acknowledgments

Generous financial support by the German Science Foundation (DFG) and the Fund of the Chemical Industry (FCI) are gratefully acknowledged.

[1] P. Comba, A. Fath, G. Huttner, L. Zsolnai, *Chem. Commun.* **1996**, 1885.
[2] P. Comba, A. Fath, T. W. Hambley, D. T. Richens, *Angew. Chem. Int. Ed. Engl.* **1995**, *34*, 1883.
[3] P. Comba, A. Fath, T. W. Hambley, A. Vielfort, *J. Chem. Soc., Dalton Trans.* **1997**, 1691.
[4] P. Comba, A. Fath, T. W. Hambley, A. Kühner, D. T. Richens, A. Vielfort, *Inorg. Chem.* **1998**, *37*, 4389.
[5] D. J. Cram, T. Kamda, R. L. Helgeson, G. M. Liu, *J. Am. Chem. Soc.* **1979**, *99*, 948.
[6] D. J. Cram, G. M. Liu, *J. Am. Chem. Soc.* **1985**, *107*, 3657.
[7] P. Comba, *Coord. Chem. Rev.*, in press.
[8] P. Comba, in *Fundamental priciples of molecular modeling* (Eds.: W. Gans, A. Amann, J. C. A. Boeyens), Plenum Press, New York, **1996**, p 167.
[9] P. Comba, in *Molecular modeling and dynamics of bioinorganic systems* (Eds.: L. Banci, P. Comba), Kluwer Dorderecht, Boston, **1997**, p 21.
[10] P. Comba, in *Intermolecular Interactions* (Eds.: W. Gans, J. C. A. Boeyens), Plenum Press, New York, **1998**, p. 97.
[11] P. Comba, in *Implications of Molecular and Materials Structure for New Technologies* (Eds.: J. K. A. Howard, F. H. Allen), Kluwer, Dordrecht, **1998**.

[12] P. Comba, T. W. Hambley, N. Okon, G. Lauer, *MOMEC, a molecular modeling package for inorganic compounds*, CVS, E-mail: cvs@t-online.de, Heidelberg, **1997**.
[13] J. E. Bol, C. Buning, P. Comba, J. Reedijk, M. Ströhle, *J. Comput. Chem.* **1998**, *19*, 512.
[14] P. Comba, T. W. Hambley, *Molecular Modeling of Inorganic Compounds*, VCH, Weinheim, **1995**.
[15] T. W. Hambley, *J. Comput. Chem.* **1987**, *8*, 651.
[16] Y. Kuroda, N. Tanaka, M. Goto, T. Sakai, *Inorg. Chem.* **1989**, *28*, 997.
[17] Detailed studies that involved the reported structures and isomer distributions of all figure-of-eight-shaped dicopper(I) compounds indicate that some of the force-field parameters need some further tuning. One of the critical parameters was the torsional angle force constant for the $C_{xylylene}-C_{imine}$ bond. The steepness of this potential is probably overestimated, and an optimum fit was obtained when this parameter was reduced from $k = 0.025$ mdyn·A by a factor of up to 5. This observation is based on the very restricted class of compounds discussed here, and future studies with other types of compounds are needed to establish this parameter on a more general basis.

Received September 29, 1998
[I98334]

Self-Assembly, Crystal Structure, and Magnetic Properties of a Phenoxo-Bridged Tetranuclear Cu^{II} Complex of the [2 × 2] Grid Type

Javier Rojo,[a] Jean-Marie Lehn,*[a] Gerhard Baum,[b] Dieter Fenske,*[b] Oliver Waldmann,[c] and Paul Müller[c]

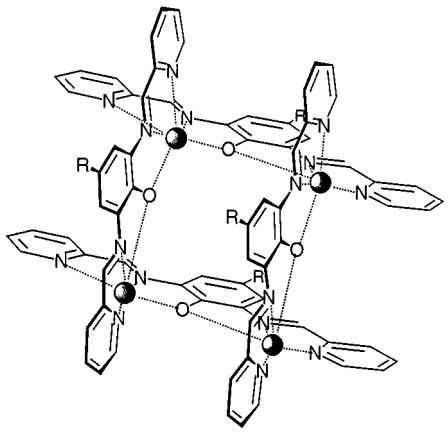
Keywords: Self-assembly / Tetranuclear Cu^{II} complex / [2 × 2] grid-type complex / Crystal structure / Magnetic properties

The ditopic ligand **3** has been synthesized. In its deprotonated form, it reacts with copper(II) ions to form a tetranuclear complex **1** of the [2 × 2] Cu^{II}_4 grid type, the structure of which has been confirmed by X-ray crystallography. Magnetic studies of complex **1** indicate a very weak antiferromagnetic coupling between the phenoxo-bridged Cu^{II} ions.

Self-assembly of suitably designed ligands with transition-metal ions allows the creation of inorganic architectures with well-defined structures in a spontaneous but directed manner.[1] One of the aims of supramolecular chemistry is the formation of assemblies that may possess interesting physical properties.

Previously, we have reported the self-assembly of metal complexes of rack-[2] and grid-type[3] geometries, where the metal ions are bridged by pyrimidine rings. The metallic centers in these arrays are located at appropriate distances (6.16−6.50 Å) such as to allow electronic interaction, which is manifested in the physical properties of the complexes such as redox potentials,[2,3] optical,[4] and magnetic[5] features. In order to enhance the coupling between the metal-ion centers compared to that provided by a pyrimidine group, and to obtain inorganic architectures exhibiting new properties, we have explored the use of ligands that introduce oxygen bridges between the coordination binding sites.

Oxo-bridged binuclear copper(II) complexes have been extensively studied as a result of the magnetic properties arising from ferromagnetic or antiferromagnetic spin-coupling between the copper ions,[6] which depend strongly on the geometry of the Cu−O−Cu bridge (Cu−Cu distances and bridge angles). While a linear correlation of the magnetic exchange parameter J with bridge angle Φ is well-established for dihydroxo-bridged copper(II) complexes with square-pyramidal $d_{x^2-y^2}$ electronic ground states, this might not be the case for monohydroxo-bridged complexes with a different electronic ground state (i.e. trigonal-bipyramidal, d_{z^2}).[7] The antiferromagnetic coupling observed for most monohydroxo-bridged complexes is larger than that found for di-μ-hydroxocopper(II) complexes and normally occurs through a super-exchange mechanism, with the hydroxo bridge acting as the primary pathway for exchange.[8] Most hydroxo-bridged copper(II) complexes are pentacoordinated and typically exhibit square-pyramidal or trigonal-bipyramidal geometries. Here, we report the synthesis, structural details, and magnetic properties of **1**, $[\mathbf{L}Cu]_4(CF_3SO_3)_4$, a tetrametallic copper(II) complex of the [2 × 2] grid type, where the copper atoms adopt a distorted bipyramidal geometry and are bridged by the phenolate oxygen atom of the ionized form $\mathbf{L}^-$ of ligand **3**. Recently, an Mn^{2+} complex of the [2 × 2] grid type with a ligand similar to **3**, but where the metal centers are bridged by non-conjugated alkoxide-type oxygen atoms, has been reported.[9]



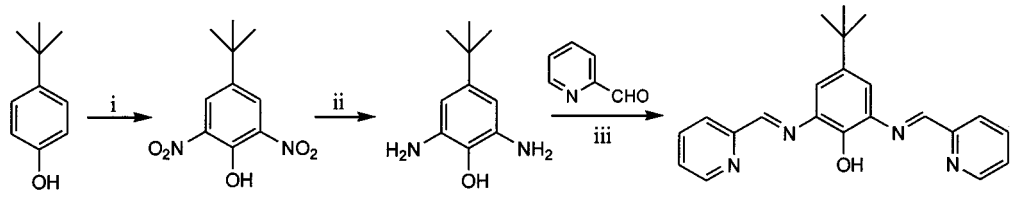
1

Results and Discussion

Ligand **3** was prepared by condensation of two equivalents of 2-pyridinecarboxaldehyde with one equivalent of 2,6-diamino-4-*tert*-butylphenol in methanol solution in the

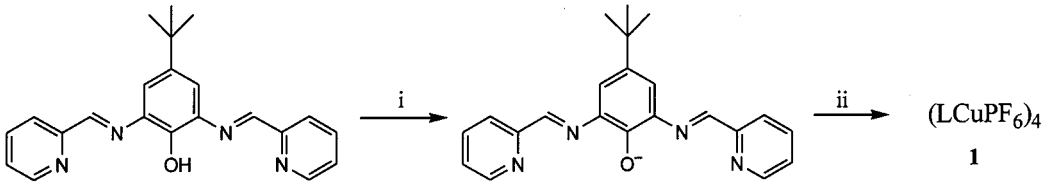
[a] Laboratoire de Chimie Supramoléculaire, ISIS, Université Louis Pasteur, ESA CNRS 7006,
F-67000 Strasbourg, France
Fax: (internat.) + 33(0)3/88411020
E-mail: lehn@chimie.u-strasbg.fr
[b] Institut fur Anorganische Chemie, Universität Karlsruhe, D-76128 Karlsruhe, Germany
[c] Physikalisches Institut III, Universität Erlangen-Nürnberg, D-91058 Erlangen, Germany

 © WILEY-VCH Verlag GmbH, D-69451 Weinheim, 1999 1434−1948/99/0303−0517 $ 17.50+.50/0



2 3 LH

Scheme 1. Synthesis of ligand **3**, **LH**: i) HNO_3, HOAc, −15°C to room temp. − ii) Pd/C, H_4NHCO_2. − iii) 4-Å molecular sieves



LH L^- 1

Scheme 2. Formation of the tetranuclear copper(II) complex **1**: i) NaOMe, MeOH, room temp. − ii) $Cu(CF_3SO_3)_2$; NH_4PF_6

presence of 4-Å molecular sieves. The latter was obtained by dinitration of 4-*tert*-butylphenol[10] to give **2** and subsequent reduction of the nitro groups to amino groups[11] (Scheme 1). Reaction of ligand **3** with one equivalent of sodium methoxide in anhydrous methanol at ambient temperature led to the immediate formation of a deep-red colour, characteristic of the ligand anion $\mathbf{L}^-$, which consists of two tridentate coordination subunits. One equivalent of copper triflate was then added, resulting in a colour change to purple, indicating complex formation (Scheme 2). After 3 h, the copper complex was precipitated by adding a saturated methanolic solution of ammonium hexafluorophosphate, isolated by centrifugation, purified by recrystallization from acetonitrile/diethyl ether, and characterized by its spectral and analytical properties. Its structure was confirmed by X-ray crystallography.

Crystal Structure of Complex 1

Single crystals of complex **1** were obtained by slow vapor diffusion of diethyl ether into an acetonitrile solution of the complex. Crystal structure determination by X-ray diffraction analysis (Figure 1) revealed that the complex consists of a metallic core composed of four copper(II) atoms, four ligands placed in an orthogonal orientation defining a distorted square, and four counteranions (PF_6^-) delocalized in the unit cell, along with two CH_3CN solvent molecules. The arrangement of the metal ions shows approximate C_4 symmetry and is of the [2 × 2] grid type, analogous to the recently described Co_4 grids.[3]

Each copper atom has a distorted bipyramidal geometry and is bound to two pyridine nitrogen atoms, two imine nitrogen atoms, and two phenoxo oxygen atoms belonging to two orthogonal ligands. The Cu−O distances in the complex correspond to those in other Cu^{II}−O(phenolate) complexes, amounting to 2.29 Å for the phenolate in the apical position and 1.98 Å for the phenolate in the equatorial position. Cu−N bond lengths are between 2.06 and 1.96 Å for the equatorial nitrogen atoms and 2.38 Å for the apical nitrogen atoms (Table 1). The tetranuclear center is characterized by metal−metal separations of 4.04 Å for the μ-phenoxo-bridged copper atoms Cu(1)−Cu(2) and of 5.35 Å for Cu(1)−Cu(3), and a bridge angle Cu−O−Cu of 140.58°.

The metal−metal separations and the oxygen bridge angle are larger than those typically found in bridged bimetallic copper(II) complexes.[6] However, there are other cases where longer distances of 4.09 and 4.13 Å have been reported.[7c,7d]

Electronic Absorption Spectrum of Complex 1

The electronic absorption spectrum of complex **1** in acetonitrile solution shows two maxima centered at 224 nm ($\varepsilon = 5.6 \times 10^4$ $M^{-1}cm^{-1}$) and 328 nm ($\varepsilon = 6.1 \times 10^4$ $M^{-1}cm^{-1}$), corresponding to ligand-centered (LC) π-π* transitions. An absorption band in the visible region at 521 nm ($\varepsilon = 4.7 \times 10^4$ $M^{-1}cm^{-1}$) can be ascribed to a metal−ligand charge-transfer transition (MLCT). The strong intensity of this MLCT band suggests a good overlap between the phenolate and the metal orbitals. It is known that charge-transfer transitions of phenolate−Cu^{II} groups are more intense when the phenolate oxygen orbital overlaps with the copper $d_{x^2-y^2}$ orbital.[7c]

Magnetic Studies

Figure 2 depicts the temperature dependence of the susceptibility of **1** plotted as χT (Figure 2a) and the field dependence of the magnetic moment at $T = 2$ K (Figure 2b).

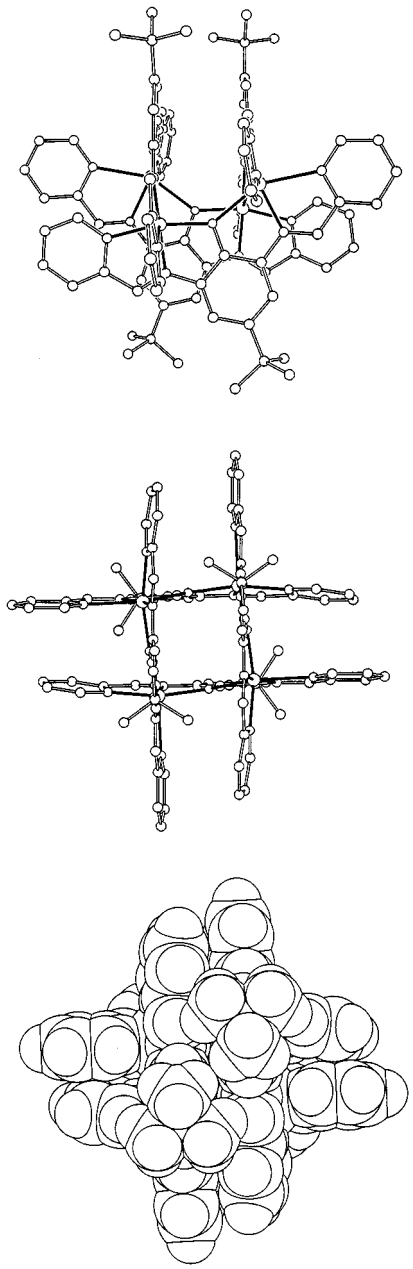


Figure 1. X-ray structure of the [2 × 2] Cu^{II}_4 grid-type complex **1**: (top) side view, (center) top view, (bottom) top view in space-filling representation

The data can be characterized by the following three features:

1. χT decreases slightly with decreasing temperature. The effective moment per copper ion is determined to be μ_{eff} = 1.913 at 250 K and μ_{eff} = 1.786 at 30 K, corresponding to g = 2.21 and g = 2.06, respectively. However, this decrease in χT cannot simply be ascribed to a temperature-independent paramagnetic contribution μ_0 as the decrease is not linear, as can be seen in Figure 2a. Furthermore, the value of μ_0 would have to be of the order of 10^{-3} cm^3 mol^{-1}, a value which is far beyond the scope of experimental uncertainty.

Table 1. Selected bond lengths [Å] and angles [°] from the X-ray structure of the grid complex **1**; the numbering of the atoms corresponds to that given in Figure 3

Cu−N(2)	1.9650	O−Cu−N(1)	160.54
Cu−O	1.9872	N(3)#1−Cu−N(1)	101.94
Cu−N(3)#1	2.0390	N(2)−Cu−O#1	118.33
Cu−N(1)	2.0600	O−Cu−O#1	93.36
Cu−O#1	2.2973	N(3)#1−Cu−O#1	76.71
Cu−N(4)#1	2.3890	N(1)−Cu−O#1	87.21
O−Cu#2	2.2973	N(2)−Cu−N(4)#1	90.01
N(3)−Cu#2	2.0390	O−Cu−N(4)#1	94.92
N(4)−Cu#2	2.3890	N(3)#1−Cu−N(4)#1	75.00
		N(2)−Cu−O	82.68
		N(1)−Cu−N(4)#1	93.81
		N(2)−Cu−N(3)#1	164.96
		O#1−Cu−N(4)#1	151.28
		O−Cu−N(3)#1	97.11
		Cu−O−Cu#2	140.58
		N(2)−Cu−N(1)	79.96

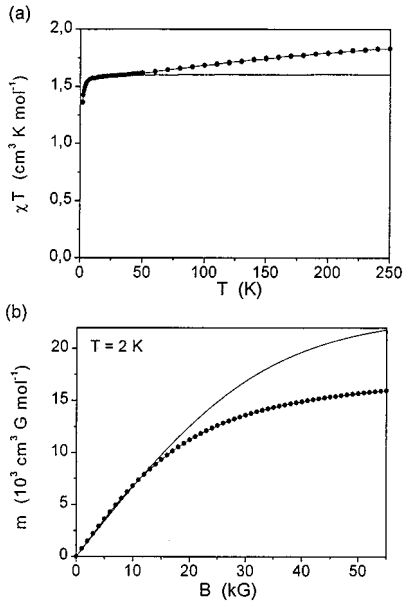


Figure 2. (a) Temperature dependence of the susceptibility of **1** plotted as χT and (b) field dependence of the magnetic moment at T = 2 K; the solid lines represent the curves calculated for the hamiltonian (Equation 1) with parameters J = −0.4 cm^{-1} and g = 2.07

2. Below ca. 10 K, the onset of a sharp decrease of χT can be seen (Figure 2a), indicating a weak antiferromagnetic coupling of the copper ions. In order to obtain an estimate of the coupling strength, we fitted the data below 25 K to the susceptibility given by the spin hamiltonian:

$$H = -J(S_1 \cdot S_2 + S_2 \cdot S_3 + S_3 \cdot S_4 + S_4 \cdot S_1) + \mu_B g B \cdot S \quad (1)$$

The parameters were determined to be J = −0.4 cm^{-1} and g = 2.07. The calculated susceptibility is drawn as a solid line in Figure 2a.

3. The magnetic moment at T = 2 K exhibits a strong field dependence, resulting in unusually low values of the magnetic moment at high fields (Figure 2b). This can clearly be seen if the data are compared to the curve calculated for the hamiltonian (Equation 1) using the above parameters. However, the field dependence is paramagnetic-

like, indicating that the magnetic coupling of the copper ions is at best of the order of -0.1 to -1 cm^{-1}.

As yet, we have been unable to provide a satisfactory interpretation of the magnetic data that would explain both the slight decrease of χT and the unusually strong magnetic field dependence. Nevertheless, although these two peculiarities of the data obviously necessitate further investigation, it can be unambiguously concluded that the exchange coupling in **1** is very weak.

Considering the coupling strengths, monohydroxo-bridged copper(II) dimers may be roughly divided into two classes. The systems belonging to the first class exhibit strong antiferromagnetic coupling of the order of several -100 cm^{-1}. This can be attributed to the arrangement of the square-pyramidal coordination spheres of the copper ions, which leads to $d_{x^2-y^2}$ ground states with the orbital lobes directed towards each other, thereby providing a good σ-type exchange pathway.[7a,8b,12,13] Dimers of the second class are characterized by very weak ferro- or antiferromagnetic couplings of just a few cm^{-1}. In these systems, several coordination geometries are realized, e.g. two square pyramids with the bridging oxygen atom in the apical position,[7c] two trigonal bipyramids with the oxygen atom in the equatorial planes,[13] or a combination of a square pyramid and a trigonal bipyramid with the oxygen atom in the equatorial planes,[12] which lead to negligible overlap and thus to weak coupling.

In the [2 × 2] grid **1** a new situation is seen, which leads to negligible exchange coupling. The coordination geometries of the copper ions can be described as distorted bipyramidal, with the equatorial planes lying perpendicular to the plane of the grid. The ground state of the copper ions is thus $d_{x^2-y^2}$, with the lobes directed towards N_1, N_2, N_3 and the equatorial phenoxy oxygen atom (Figure 3). However, in view of the approximate C_4 symmetry of the grid, the bipyramids of neighboring copper ions are rotated by 90°, such that the overlap of the orbitals is negligible (Figure 3). This accounts for the almost zero exchange coupling found for the present Cu^{II}_4 grid complex **1**. On this basis, we predict that exchange coupling in the analogous nickel grid should be quite strong, as in this case both $d_{x^2-y^2}$ and d_{z^2} would be occupied and thus a $d_{x^2-y^2}$ – d_{z^2} exchange path would exist.

Conclusions

A [2 × 2] Cu^{II}_4 grid-type complex **1** has been synthesized and characterized. The crystal structure data reveal a complex of C_4 symmetry, where the copper centers adopt a distorted bipyramidal geometry. Cu−N bond lengths and Cu−O−Cu bridge angles are typical for complexes of this type, which usually exhibit antiferromagnetic spin coupling. However, in the present case, magnetic measurements indicate only a very weak antiferromagnetic coupling of the copper ions due to insufficient overlap of the orbitals, which can be rationalized by considering the crystal structure of this grid complex.

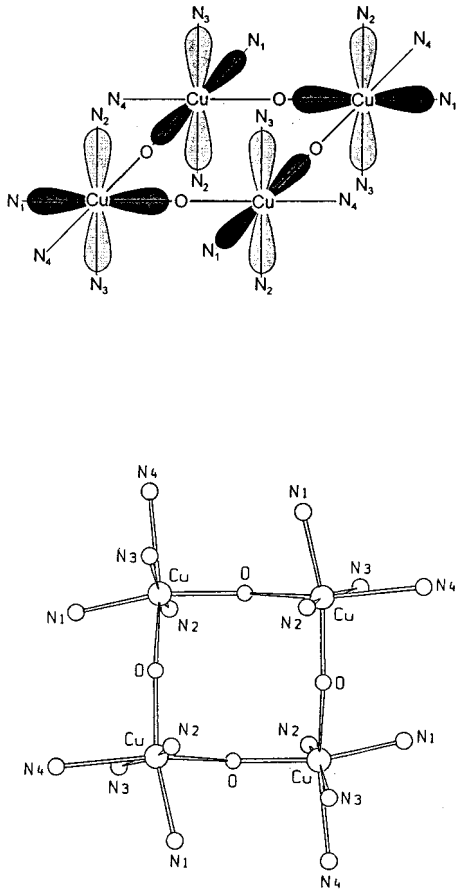


Figure 3. Schematic representation of the orientation of the magnetic $d_{x^2-y^2}$ orbitals in the [2 × 2] grid **1** (top) and X-ray structure of the metallic core of complex **1** and the N,O heteroatoms coordinated to the Cu^{II} ions (bottom)

Experimental Section

Unless otherwise noted, ^{1}H-NMR spectra were recorded in $CDCl_3$ solution with respect to the residual solvent peak at 200 MHz with a Bruker AC 200 spectrometer. − Melting points were obtained with a digital Thomas Hoover (Electrotherma) apparatus and are uncorrected. − Infrared absorption spectra were recorded with a Perkin-Elmer 1600 series FT-IR spectrometer and electronic absorption spectra with a Cary 219 spectrometer in acetonitrile; λ_{max} in nm and ε in M^{-1} cm^{-1}. − Fast-atom bombardment (FAB) mass spectrometry was performed with a ZAB-HF VG spectrometer with *m*-nitrobenzyl alcohol as the matrix; electronic impact (EI) was performed with a Fisons Instruments VG trio 2000 spectrometer, and electrospray (ES) mass spectrometry with a ZAB-HF VG spectrometer. All spectroscopic studies were performed in spectroscopic-grade solvents. All other solvents were reagent grade and were used without further purification.

Magnetic Measurements: Magnetic moments of powdered samples of complex **1** were measured with a commercial SQUID magnetometer (Quantum Design). Measurements were made over the temperature range 2−250 K at a maximum field of 5.5 T. Susceptibility was determined on the basis of measurements made at fields of 10 KG. The powder samples were fixed with apiezon grease on a plastic straw. The background signal of the plastic straw was found to be below the resolution of the magnetometer. The signal of the grease was measured independently and the data were corrected accordingly. The data were also corrected for a diamagnetic contri-

bution of -1.5×10^{-3} cm^3 mol^{-1}, taking into account the contribution of the ligands, which was estimated using Pascal's constants and the TIP of the copper(II) ions. The weight of the powder sample used was typically 1.2 mg. The magnetization of the hamiltonian (Equation 1) was calculated in the following way. The well-known formula for the susceptibility of the hamiltonian $-\Sigma J_{ij} S_i \cdot S_j + \mu_B g B \cdot S$[14] can be easily generalized to

$$m = N\mu_B g \frac{\sum_s \Omega(S) \sinh[(2S+1)y] S B_S(Sy) \exp[-\beta E(S)]}{\sum_s \Omega(S) \sinh[(2S+1)y] \exp[-\beta E(S)]}$$

for the magnetization at arbitrary magnetic field. Here $y = g\mu_B B/(k_B T)$, $B_S(Sy)$ is the Brillouin function,[15] $\beta = 1/(k_B T)$, $\Omega(S)$ denotes the degeneracy of the states E(S), and other symbols have their usual meanings. For the hamiltonian (Equation 1), the energies E(S) and degeneracies $\Omega(S)$ can be easily calculated using Kambe's vector coupling model.[15,16] The final result for the magnetization is

$$m = N\mu_B g \frac{\sinh(3/2y)\, B_1(y)\,(x + 2x^2) + \sinh(5/2y)\, B_2(2y) 2x^3}{\sinh(1/2y)\,(1 + x^2) + \sinh(3/2y)\,(x + 2x^2) + \sinh(5/2y)\, 2x^3}$$

with $x = \exp(\beta J)$.

4-*tert*-Butyl-2,6-dinitrophenol (2): A solution of 4-*tert*-butylphenol (0.1797 mol, 27 g) in glacial acetic acid (60 mL) was added dropwise with constant stirring to a mixture of nitric acid 65% (40 mL) and glacial acetic acid (75 mL) cooled to −15°C. After the addition, the mixture was allowed to slowly warm to room temperature over a period of 30 min and then poured onto crushed ice. The resulting yellow solid was filtered off, redissolved in chloroform, and this solution was washed several times with water. The organic phase was dried (Na_2SO_4) and the solvent was removed under reduced pressure. The residue was chromatographed on silica gel, eluting with ethyl acetate/hexane (1:6), to give **2** as a yellow solid (30 g, 70% yield); m.p. 96−97°C (ref.[10] 95°C). − IR (KBr): $\tilde{\nu}$ = 3448, 3173, 2961, 1640, 1533, 1368, 1309, 1266, 922, 729, 651 cm^{-1}. − ^{1}H NMR: δ = 8.32 (s, 2 H, Ar), 1.37 (s, 9 H, *t*Bu). − ^{13}C NMR: δ = 147.2, 143.0, 137.2, 34.7, 30.8. − MS (EI); *m/z* (%): 239.9 (40) [M$^+$], 224.9 (100) [M$^+$ − Me]. − $C_{10}H_{12}N_2O_5$ (240.22): calcd. C 50.00, H 5.04, N 11.66; found C 50.18, H 5.09, N 11.79.

Ligand LH 3: To 4-*tert*-butyl-2,6-dinitrophenol (**2**, 4.2 mmol, 1.0 g) in ethyl acetate (10 mL) and dry methanol (20 mL), 5% Pd/C (0.4 g) and 9 equiv. of anhydrous ammonium formate (37.5 mmol, 2.36 g) were added. The resulting mixture was stirred at room temperature under argon for 15 min, according to the standard literature procedure.[11] The catalyst was then removed by filtration through a Celite pad and washed with dry methanol. The combined filtrate and washings were concentrated to dryness, the resulting residue was triturated with water (10 mL), and extracted with chloroform (3 × 50 mL). The combined organic extracts were dried (Na_2SO_4) and the solvent was removed under reduced pressure to leave a dark solid (670 mg). This solid was redissolved in dry THF (10 mL), two equivalents of 2-pyridinecarboxaldehyde (7.4 mmol, 0.7 mL) were added, and the resulting mixture was stirred in the presence of 4-Å molecular sieves for 7 h. The solvent was then removed and the residual oil was triturated with hexane to give **3** as a brownish-yellow solid, which was filtered off and washed with further hexane. Ligand **3** (1.01 g, 81% yield, m.p. 103−105°C) was used without further purification for the complexation studies. − IR (KBr): $\tilde{\nu}$ = 3354, 2954, 1629, 1586, 1467, 1435, 1362, 1288, 1247, 989, 778, 550, 406 cm^{-1}. − ^{1}H NMR: δ = 8.87 (s, 2 H, CH=N), 8.72 (d, 2 H, *J* = 4.3 Hz, Ar), 8.28 (d, 2 H, *J* = 8.0 Hz, Ar), 7.89 (dt, 2 H, *J* = 7.7, 1.4 Hz, Ar), 7.39 (ddd, 2 H, *J* = 7.4, 4.9, 1.0 Hz, Ar), 7.28 (s, 2 H, Ar), 1.35 (s, 9 H, *t*-Bu). − ^{13}C NMR: δ = 159.5, 154.3, 149.5, 143.5, 136.9, 136.6, 136.1, 125.1, 121.6, 115.2, 34.4, 31.3. − MS (FAB): *m/z* (%) = 359.1 (100) [M$^+$ + 1]. − HRMS ($C_{22}H_{23}N_4O$): calcd. 359.1867; found 359.1872. − UV/Vis: λ_{max} (ε × 10^4) = 226 (0.13), 282 (0.12), 500 nm (0.05).

$(LCu)_4(PF_6)_4$ 1: To ligand LH **3** (0.2789 mmol, 100 mg) in anhydrous methanol (15 mL), 1 equiv. of NaOMe (0.2789 mmol, 15 mg) was added at room temperature. To the deep-red solution obtained, 1 equiv. of $Cu(CF_3SO_3)_2$ (0.2789 mmol, 100 mg) was added, resulting in a color change to purple. The mixture was stirred for 3 h and then filtered through cotton. Addition of a saturated methanolic solution of ammonium hexafluorophosphate led to the precipitation of a solid, which was collected by centrifugation and recrystallized from acetonitrile/diethyl ether to give complex **1** as a deep-purple solid (158 mg, 80% yield); m.p. 240°C (calcination). − IR (KBr): $\tilde{\nu}$ = 3142, 1598, 1484, 1400, 1281, 1248, 838, 559 cm^{-1}. − MS (ES); *m/z*: 2119.3 [M − PF_6], 987 [M − 2 PF_6]. − $C_{88}H_{84}Cu_4F_{24}N_{16}O_4P_4$ (2263.78): calcd. C 46.69, H 3.74, N 9.90; found C 46.68, H 3.82, N 9.73. − UV/Vis: λ_{max} (ε × 10^4) = 224 (5.6), 328 (6.1), 521 nm (4.7).

Crystal Structure Determination: Crystal data for $C_{88}H_{84}Cu_4F_{24}N_{16}O_4P_4 \cdot (MeCN)_2$, M_r = 2592.18, tetragonal, space group *I*4(1)/*a* (no. 88), *a* = *b* = 26.325(4), *c* = 16.980(3) Å, *V* = 11767(3) Å^3, *Z* = 4, D_c = 1.463 Mg m^{-3}, *F*(000) = 5296, *T* = 200 K, crystal dimensions 0.3 × 0.2 × 0.2 mm, purple; 28039 reflections, of which 5952 were unique (R_{int} = 0.0457), were recorded with an Enraf−Nonius CAD4 diffractometer. Final *R* indices: R_1 = 0.0451, wR_2 = 0.1195; (all data) R_1 = 0.0554, wR_2 = 0.1260 for 463 parameters. Goodness of fit on F^2 = 1.020. Largest diff. peak and hole 0.750 and −0.599 Å^{-3}. Crystallographic data for complex **1** have been deposited at the Cambridge Crystallographic Data Centre (CCDC) as supplementary publication CCDC-112945. Copies of the data can be obtained free of charge on application to CCDC, 12 Union Road, Cambridge CB2 1EZ, U.K. [Fax: (internat.) + 44-1223/336033; E-mail: deposit@ccdc.cam.ac.uk].

Acknowledgments

We thank the French Government (J. R.) and the Deutsche Forschungsgemeinschaft (O. W.) for financial support.

[1] [1a] J.-M. Lehn, *Supramolecular Chemistry: Concepts and Perspectives*, VCH, Weinheim, **1995**. − [1b] *Comprehensive Supramolecular Chemistry* (Eds.: J. L. Atwood, J. E. D. Davies, D. D. MacNicol, F. Vögtle, J.-M. Lehn), Pergamon, Oxford, **1996**; P. N. W. Baxter, vol. 9, ch. 5, p. 165; M. Fujita, vol. 9, ch. 7, p. 253.
[2] G. S. Hanan, C. R. Arana, J.-M. Lehn, G. Baum, D. Fenske, *Chem. Eur. J.* **1996**, *2*, 1292.
[3] G. S. Hanan, D. Volkmer, U. S. Schubert, J.-M. Lehn, G. Baum, D. Fenske, *Angew. Chem. Int. Ed. Engl.* **1997**, *36*, 1842.
[4] A. Credi, V. Balzani, S. Campagna, G. S. Hanan, C. R. Arana, J.-M. Lehn, *Chem. Phys. Lett.* **1995**, *243*, 102.
[5] O. Waldmann, J. Hassmann, P. Müller, G. S. Hanan, D. Volkmer, U. S. Schubert, J.-M. Lehn, *Phys. Rev. Lett.* **1997**, *78*, 3390; O. Waldmann, J. Hassmann, P. Müller, D. Volkmer, U. S. Schubert, J.-M. Lehn, *Phys. Rev. B* **1998**, *58*, 3277.
[6] [6a] A. R. Davis, F. W. B. Einstein, N. F. Curtis, J. W. L. Martin, *J. Am. Chem. Soc.* **1978**, *100*, 6258. − [6b] Y. Agnus, R. Louis, R. Weiss, *J. Am. Chem. Soc.* **1979**, *101*, 3381. − [6c] L. K. Thompson, F. W. Hartstock, P. Robichaud, A. W. Hanson, *Can. J. Chem.* **1984**, *62*, 2755. − [6d] H. P. Berends, D. W. Stephan, *Inorg. Chem.* **1987**, *26*, 749. − [6e] L. J. Farrugia, P. A. Lovatt, R. D. Peacock, *J. Chem. Soc., Dalton Trans.* **1997**, 911. − [6f] E. Escrivá, J. Server-Carrió, L. Lezama, J. V. Folgado, J. L.

Pizarro, R. Ballesteros, B. Abarca, *J. Chem. Soc., Dalton Trans.* **1997**, 2033. – [6g] E. Ruiz, P. Alemany, S. Alvarez, J. Caro, *Inorg. Chem.* **1997**, *36*, 3683.
[7] [7a] P. L. Burk, J. A. Osborn, M.-T. Youinou, Y. Agnus, R. Louis, R. Weiss, *J. Am. Chem. Soc.* **1981**, 103, 1273. – [7b] M. S. Haddad, S. R. Wilson, D. J. Hodgson, D. N. Hendrickson, *J. Am. Chem. Soc.* **1981**, *103*, 384. – [7c] K. J. Oberhausen, J. F. Richardson, R. M. Buchanan, J. K. McCuster, D. N. Hendrickson, J.-M. Latour, *Inorg. Chem.* **1991**, *30*, 1357. – [7d] Y. Nishida, H. Shimo, H. Maehara, S. Kida, *J. Chem. Soc., Dalton Trans.* **1985**, 1945.
[8] [8a] T. N. Doman, D. E. Williams, J. F. Banks, R. M. Buchanan, H.-R. Chang, R. J. Webb, D. N. Hendrickson, *Inorg. Chem.* **1990**, *29*, 1058. – [8b] E. Spodine, J. Manzur, M. T. Garland, M. Kiwi, O. Peña, D. Grandjean, L. Toupet, *J. Chem. Soc., Dalton Trans.* **1991**, 365.
[9] A. Gelasco, A. Askenas, V. L. Pecoraro, *Inorg. Chem.* **1996**, *35*, 1419.
[10] G. G. S. Dutton, T. I. Briggs, B. R. Brown, M. E. D. Hillman, *Can. J. Chem.* **1953**, *31*, 685.
[11] S. Ram, R. E. Ehrenkaufer, *Tetrahedron Lett.* **1984**, *25*, 3414.
[12] T. N. Sorrell, C. J. O′Connor, O. P. Anderson, J. H. Reibenspies, *J. Am. Chem. Soc.* **1985**, *107*, 4199.
[13] V. McKee, M. Zvagulis, J. V. Dagdigian, M. G. Patch, C. A. Reed, *J. Am. Chem. Soc.* **1984**, *106*, 4765.
[14] F. E. Mabbs, D. J. Machin, *Magnetism and Transition Metal Complexes*, Chapman and Hall, London, **1973**.
[15] O. Kahn, *Molecular Magnetism*, VCH, USA, **1993**.
[16] D. Gatteschi, A. Bencini, *Electron Paramagnetic Resonance of Exchange-Coupled Systems*, Springer-Verlag, Berlin, **1990**.

Received October 5, 1998
[I98340]

Characterization of Palladium(II) Azide and Crystal Structure of Bis(azido)bis(pyridine)palladium(II) and Tetramminepalladium Tetraazidopalladate(II)

Wolfgang Beck,[a] Thomas M. Klapötke,*[a] Jörg Knizek,[a][+] Heinrich Nöth,[a][+] and Thomas Schütt[a]

Keywords: Palladium / Azide / Pyridine

Palladium(II) azide **(1)** was synthesized by reaction of palladium nitrate and sodium azide. **1** was characterized by AAS, IR, and ^{14}N-NMR spectroscopy. Bis(azido)bis(pyridine)-palladium(II) (**2**) and tetramminepalladium tetraazidopalladate(II) (**3**) were synthesized by a high-yield reaction. Both were characterized by X-ray structural analysis, IR, Raman, and NMR spectroscopy.

Introduction

In the early 1960s Sherif et al. examined the first palladium azide complexes in solution photometrically. The existence of $[Pd(N_3)_2Cl_2]^{2-}$, $[Pd(N_3)_4]^{2-}$, and $Pd(N_3)^+$ was postulated in accordance with absorption measurements.[1] Palladium(II) azide was first synthesized by Clem et al.[2] Spectroscopic studies failed because the compound exploded. In this work palladium(II) azide has been characterized by AAS, IR, and ^{14}N-NMR spectroscopy. Beck et al. synthesized some interesting palladium azide compounds in the late 1960s.[3−5] Tetraphenylarsonium tetraazidopalladate(II) has been synthesized as shown in Equation 1. In this study the structure of the tetraazidopalladate(II) anion has been determinated by X-ray structure investigation.

$$Pd(NO_3)_2 + 4\,NaN_3 + 2\,As(C_6H_5)_4Cl \xrightarrow[-\,2\,NaNO_3\ -\,2\,NaCl]{H_2O} [As(C_6H_5)_4]_2[Pd(N_3)_4] \quad (1)$$

Results and Discussion

Synthesis of 1

Palladium(II) azide (**1**) can be synthesized by reaction of two equivalents of sodium azide with palladium nitrate in water (Equation 2). A black-brown compound precipitates which is highly explosive if dried in air. Attempts to dry the product in the desiccator failed because of the explosivity of **1**. The compound detonates at 117°C. The palladium determination with AAS spectroscopy shows a result of 46.55% of palladium. For coordinated water the calculated palladium percentage is 46.98%, so it can be expected that there is water coordinated. The IR spectrum of the explosion gases shows a weak absorption at 3650 cm^{-1} for OH streching vibrations. An IR spectrum has been measured on a KBr plate. It was not possible to measure in Nujol because of the explosivity of the compound. The IR spectrum shows five absorptions at 3450 cm^{-1} for OH streching vibrations, at 2067 cm^{-1} for the antisymmetric stretching vibration of the azide group, 1205 cm^{-1} for the symmetric stretching vibration of the azide group, 559 cm^{-1} for the deformation vibration of the azide group and at 438 cm^{-1} for the palladium−nitrogen stretching vibration. The strong intensity of the symmetric stretching vibration which is not allowed for the azide ion, points to a covalent palladium−azide bond.[3] The fact that there is only one signal for the antisymmetric streching vibration of the azide group concludes that the palladium atom is surrounded by chemically equivalent azide groups as shown in Figure 1.

$$Pd(NO_3)_2 + 2\,NaN_3 \xrightarrow[-\,2\,NaNO_3]{H_2O} Pd(N_3)_2 \quad (2)$$

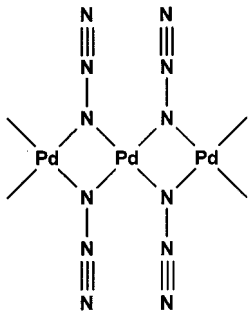


Figure 1. Structure model of **1**

Compound **1** crystallizes probably in chains in which the palladium atom is surrounded in a square-planar fashion by bridging azide groups. The ^{14}N-NMR spectrum of **1** shows the expected signals for covalently bonded azides. The N2 atom shows a resonance at $\delta = -129$, the N3 atom at $\delta = -226$, and the N1 atom a very weak resonance at $\delta = -328$. The solution of **1** in pyridine shows the same

[+] X-ray structure investigations.
[a] Institut für Anorganische Chemie der Ludwig-Maximilians-Universität,
Meiserstr. 1, D-80333 München, Germany
Fax: (internat.) + 49(0)89/590-2382
E-mail: tmk@anorg.chemie.uni-muenchen.de

 © WILEY-VCH Verlag GmbH, D-69451 Weinheim, 1999 1434−1948/99/0303−0523 $ 17.50+.50/0

resonances as for **2** in the ^{14}N-NMR spectrum. Probably pyridine coordinates at the palladium center to form **2**.

Synthesis of 2

Palladium nitrate reacted with an excess of pyridine and sodium azide to form orange-yellow prisms of bis(azido)-bis(pyridine)palladium(II) (Equation 3). The compound is not explosive. At a temperature of 165°C the compound decomposes.

$$Pd(NO_3)_2 + 2\,py + 2\,NaN_3 \xrightarrow[-\,2\,NaNO_3]{H_2O} Pd(py)_2(N_3)_2 \qquad (3)$$

Crystal Structure of 2

Crystals of **2** (Figure 2) are monoclinic, space group *C*2/*c* with 4 molecules in the unit cell. The palladium atom is surrounded by four nitrogen atoms, two of the azide group and two of the pyridine rings. All eight nitrogen atoms lie in plane. The pyridine rings are out of this plane. The distance between two palladium atoms is 3.86 Å. The crystals form chains in which all molecules are congruent. The plane of the nitrogen atoms of the next chain is twisted 90° to the nitrogen plane of the other chain. Bond lengths and bond angles are compiled in Table 1.

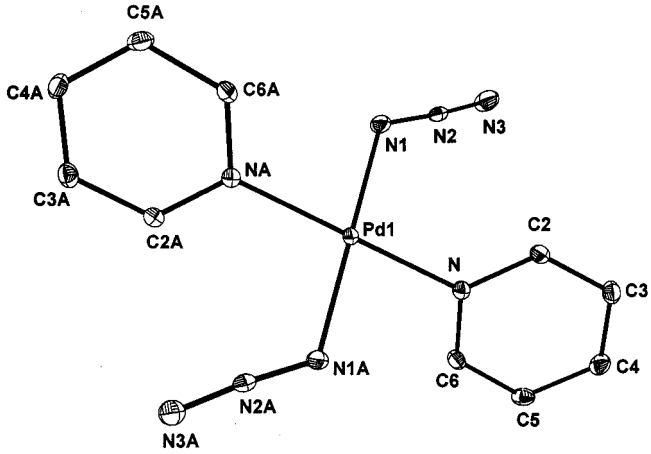


Figure 2. Molecular structure of **2** (the thermal ellipsoids represent a 25% probability)

Table 1. Selected bond lengths [Å] and angles [°] for **2**

Pd(1)−N(1)	2.037(2)	N(1)−N(2)	1.203(2)
Pd(1)−N(A)	2.0417(18)	N(2)−N(3)	1.150(3)
Pd(1)−N(1A)	2.037(2)	C(2)−C(3)	1.387(4)
Pd(1)−N	2.0417(18)	C(3)−C(4)	1.378(4)
N−C(6)	1.334(3)	C(4)−C(5)	1.384(4)
N−C(2)	1.356(4)	C(5)−C(6)	1.388(3)
N(1)−Pd(1)−N(1A)	180	N(1)−Pd(1)−N(A)	85.78(8)
N(1A)−Pd(1)−N(A)	94.21(8)	N(1)−Pd(1)−N	94.21(8)
N(1A)−Pd(1)−N	85.79(8)	N(A)−Pd(1)−N	180
C(6)−N−C(2)	118.6(2)	C(6)−N−Pd(1)	120.0(2)
C(2)−N−Pd(1)	121.3(2)	N(2)−N(1)−Pd(1)	125.5(2)
N(3)−N(2)−N(1)	175.2(2)	N−C(2)−C(3)	121.6(3)
C(4)−C(3)−C(2)	119.5(3)	C(5)−C(4)−C(3)	118.8(2)
C(4)−C(5)−C(6)	119.0(2)	N−C(6)−C(5)	122.5(2)

The N1−N2 bond length is 1.203(2) Å; thus, the bond order is between one and two. The covalent radius[6] for a single-bonded nitrogen atom is r_{cov} = 0.7 Å, 0.6 Å for a double-bonded nitrogen atom, and 0.55 Å for a triple-bonded nitrogen atom. The bond order for the N2−N3 [1.150(3) Å] is between two and three. The angle of the azide group (N1−N2−N3) is 175.2(2)°, the angle between the palladium atom and the azide group (Pd1−N1−N2) is 125.5(2)°.

Synthesis of 3

Compound **3** was synthesized by reaction of $Pd(NH_3)_4Cl_2$ with sodium azide in water (Equation 4). The compound can be handled, but it detonates by shock or by friction. It has been fully characterized by IR, Raman, and ^{14}N-NMR spectroscopy. An X-ray structure determination was also performed for this compound.

$$2\,Pd(NH_3)_4Cl_2 + 4\,NaN_3 \xrightarrow[-\,4\,NaCl\\-\,4\,NH_3]{H_2O} [Pd(NH_3)_4][Pd(N_3)_4] \qquad (4)$$

The ^{14}N-NMR spectrum shows the expected signals for covalently bonded azides.[7−9] But two signals can be seen for the N3 nitrogen atom at δ = −231 and −234. The crystal structure determination shows only equivalent N3 nitrogen atoms, so that only one signal for the N3 atom is expected. Consequently, there are no equivalent N3 nitrogen atoms in solution. There may be a coordination between half of the N3 nitrogen atoms and the electrophilic center of the tetramminepalladium cation. This coordination would lead to different N3 nitrogen atoms.

Crystal Structure of 3

Compound **3** crystallizes in the othorhombic space group *I*4/*m* with two molecules in the unit cell (Figure 3). The crystallographic data and refinement details for compound **3** are summarized in the Experimental Section. The bond lengths and bond angles are compiled in Table 2.

Compound **3** displays a salt-like structure with a Pd−Pd interaction between cation and anion. The Pd−Pd distance is 3.0420 Å. The dihedral angle between the ammine and the azide ligands is 45°. The cation and anion are both ideal square-planar. The N1−N2 distance of the azide group is 1.211(4) Å. This corresponds with a bond order between one and two. The N2−N3 distance is 1.143(4) Å. The bond order of this bond lies between two and three. The azide group is nearly linear with an N1−N2−N3 angle of 178.3(3)°. The angle between the palladium atom and the N2 atom of the azide group is 116.8(2)°. Therefore the structure of the anion looks like a "wind wheel" (Figure 4). The bond lengths and angles are similar to the valence-isoelectronic $[Au(N_3)_4]^-$ anion which shows the same wind-wheel-like structure. This compound crystallizes even with

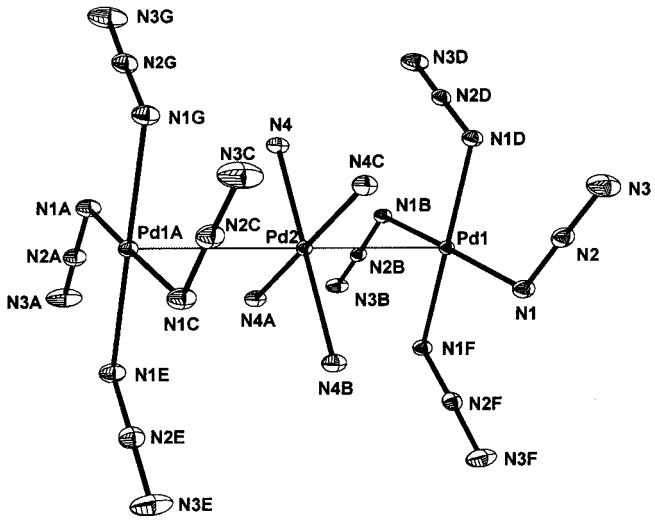


Figure 3. Molecular structure of **3** (the thermal ellipsoids represent a 25% probability)

Table 2. Selected bond lengths [Å] and angles [°] for **3**

Pd(1)−N(1)	2.056(2)	Pd(2)−N(4)	2.039(3)
Pd(1)−Pd(2)	3.0420(2)	N(1)−N(2)	1.211(4)
N(1A)−Pd(1)−N(1)	90	N(2)−N(3)	1.143(4)
N(2)−N(1)−Pd(1)	116.8(2)	N(3)−N(2)−N(1)	178.3(3)

the same coordination number like **3** and not as reported with $Z = 1$.[10]

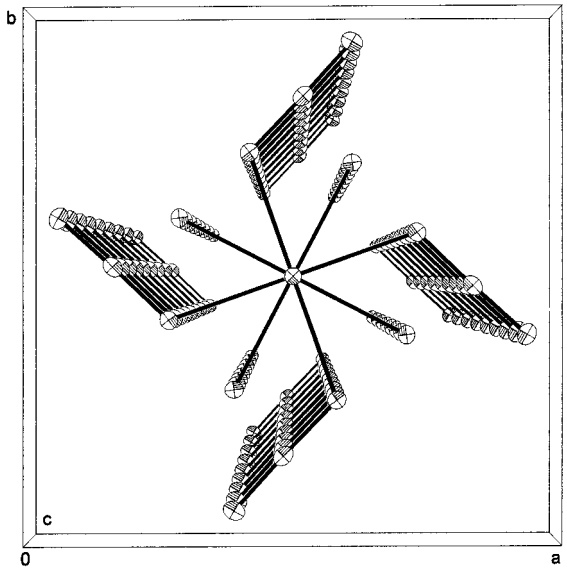


Figure 4. Perspective view of **3** along the *c* axis (the thermal ellipsoids represent a 25% probability)

Experimental Section

General Remarks: ***CAUTION:*** Palladium azide compounds are explosive! **1** is highly explosive. It detonates immediately by touching. Only PE equipment should be used during the preperation and handling of palladium azides. Safety equipment like leather gloves and face-shield is recommended.

NMR: Jeol EX400 Delta [^{1}H, ^{13}C, chemical shifts refer to δ_{TMS} = 0.00 according to the chemical shifts of residual solvent signals; ^{14}N, external standard: $\delta(CH_3NO_2) = 0.00$]. − IR: Nicolet 520 FT-IR (as KBr pellets or on a KBr plate). − Raman: Perkin Elmer Spectrum 2000R NIR FT. − CHN analyses: Analysator Elementar Vario EL. − AAS: Spectrometer 1100B. − MS: Finnigan MAT 90. − Compound **1** was prepared according to the procedure given in the literature.[3]

Palladium(II) Azide (1): A solution of 0.078 g ($1.2 \cdot 10^{-3}$ mol) of NaN_3 in 3 mL of water was added slowly under stirring at room temperature to a solution of 0.138 g ($0.6 \cdot 10^{-3}$ mol) of $Pd(NO_3)_2$ in 10 mL of water. A black-brown compound precipitated. The compound was filtered off after 5 h of stirring and washed with water. The compound was dried in air. Yield: 90.0 mg (80%), black-brown compound; m.p. 117°C (dec.). − IR (KBr): $\tilde{\nu}$ = 3450 (OH) (vw), 2388 [2 × $\nu_s(N_3)$] (m), 2067 [$\nu_{as}(N_3)$] (s), 1617 (w), 1400 (vw), 1205 [$\nu_s(N_3)$] (s), 734 (w), 551 [$\delta(N_3)$] (w), 438 (PdN) (s). − ^{14}N NMR (pyridine, 29 MHz, 25°C): δ = −64 (s, $N_{pyridine}$), −129 (s, N2), −226 (s, N3), −328 (s, N1). − PdN_6 (190.46): calcd. Pd 55.88; $PdN_6 \cdot 2\ H_2O$ (226.49): calcd. Pd 46.98; found Pd 46.53.

Bis(azido)bis(pyridine)palladium(II) (2): 5 mL ($6.18 \cdot 10^{-2}$ mol) of pyridine and a solution of 0.078 g ($1.2 \cdot 10^{-2}$ mol) of NaN_3 in 3 mL of water were added slowly under stirring at room temperature to a solution of 0.138 g ($0.6 \cdot 10^{-3}$ mol) of $Pd(NO_3)_2$ in 15 mL of water. An orange compound precipitated. Compound **2** was filtered off after 5 h of stirring and washed with water. The compound was recrystallized from hot pyridine and dried in vacuo. Yield: 196.0 mg (94%), orange crystals; m.p. 165°C (dec.). − IR (KBr): $\tilde{\nu}$ = 3094 (CH) (w), 2030 [$\nu_{as}(N_3)$] (s), 1606 (CC) (s), 1451 (s), 1291 [$\nu_s(N_3)$] (s), 1153 (m), 766 (m), 693 (s), 581 [$\delta(N_3)$] (w), 460 (PdN) (s). − Raman (400 scans, 40 mW, 180°, 20°C): $\tilde{\nu}$ = 3084 (CH) (3), 2044 [$\nu_{as}(N_3)$] (1.5), 1570 (1.5), 1294 [$\nu_s(N_3)$] (2), 1152 (1.5), 1024 (8), 372 (7.5), 215 (7), 121 (10). − ^{1}H NMR ([D$_6$]acetone, 400 MHz, 25°C): δ = 8.77 (d, NC*H*), 8.10 (m, NCHCHC*H*), 7.67 (m, NCHC*H*). − ^{13}C NMR ([D$_6$]acetone, 101 MHz, 25°C): δ = 152.5 (s, N*C*H), 140.5 (s, NCHCH*C*H), 127.0 (s, NCH*C*H). − ^{14}N NMR ([D$_6$]acetone, 29 MHz, 25°C): δ = −129 (s, N2), −158 (s, $N_{pyridine}$), −225 (s, N3), −328 (s, N1). − MS (EI, 70 eV); *m/z* (%): 79 (100) [$C_5H_5N^+$], 52 (50). − $C_{10}H_{10}N_8Pd$ (348.66): calcd. C 34.45, H 2.89, N 32.14; found C 33.92, H 2.89, N 31.85.

Crystal Structure Analysis of 2: $C_{10}H_{10}N_8Pd$, M = 348.66, crystal size: 0.3 × 0.2 × 0.2 mm, orange-yellow prism, monoclinic, space group *C*2/*c*, a = 16.1667(2), b = 3.855(2), c = 20.3238(2) Å, β = 101.494(1), V = 1241.26(2) Å^3, Z = 4, $d_{calcd.}$ = 1.866 Mg/m^3, μ = 1.495 mm^{-1}, F(000) = 688. Siemens CCD Area detector, scan type: hemisphere, Mo-K_α, λ = 0.71073 Å, T = 193 K, 2θ range = 4.10−58.04° in $-18 \le h \le 18$, $-4 \le k \le 4$, $-26 \le l \le 25$, reflections collected: 1650, independent reflections: 1019 (R_{int} = 0.0132), observed reflections: 943 [$F > 4\sigma(F)$]. Structure solution and refinement program: SHELXS-97 (G. M. Sheldrick, University of Göttingen, Germany, **1997**), direct methods, data-to-parameter ratio: 9.3:1 {8.7:1 [$F > 4\sigma(F)$]}, final R indices [$F > 4\sigma(F)$]: $R1$ = 0.0204, $wR2$ = 0.0557, $R1$ = 0.0220, $wR2$ = 0.0564 (all data), GOF on F^2 = 1.080, largest and mean Δ/σ: 0.001, 0.000, largest difference peak/hole: 0.449, −0.566 e Å^{-3}. Crystallographic data (excluding structure factors) for the structure(s) reported in this paper have been deposited with the Cambridge Crystallographic Data Centre as supplementary publication no. CCDC-107249. Copies of the data can be obtained free of charge on application to CCDC, 12 Union Road, Cambridge CB2 1EZ, UK [Fax: int. code + 44-1223/336-033; E-mail: deposit@ccdc.cam.ac.uk].

Tetramminepalladium Tetraazidopalladate(II) (3): A solution of 0.078 g ($1.2 \cdot 10^{-3}$ mol) of NaN_3 in 5 mL of water was added slowly

under stirring at room temperature to a solution of 0.147 g ($0.6 \cdot 10^{-3}$ mol) of $Pd(NH_3)_4Cl_2$ in 30 mL of water. The solution was concentrated in air. Orange-brown needles precipitated. Compound **3** was filtered off and washed with water. The compound was dried in vacuo. Yield: 127.0 mg (94%), orange-brown needles; m.p. 146°C (dec.). − IR (KBr): $\tilde{\nu}$ = 3293 (NH) (br.), 3146 (NH) (sh), 2017 [$\nu_{as}(N_3)$] (s), 1622 (w), 1287 [$\nu_s(N_3)$] (vs), 1248 [$\nu_s(N_3)$] (sh), 755 (s), 587 [$\delta(N_3)$] (w), 398 (PdN) (s). − Raman (810 scans, 30 mW, 180°, 20°C): $\tilde{\nu}$ = 3124 (NH) (1.5), 2054 [$\nu_{as}(N_3)$] (3.5), 1274 [$\nu_s(N_3)$] (2), 1056 (2), 495 (3.5), 386 (PdN) (10), 185 (7), 146 (7). − ^{14}N NMR ([D$_6$]acetone, 29 MHz, 25°C): δ = −129 (s, N2), −231 (s, N3), −234 (s, N3), −338 (s, N1), −414 (s, NH_3). − MS (EI, 70 eV); *m*/*z* (%): 212 (25) [Pd_2^+], 69 (83), 55 (100), 45 (57). − $H_{12}N_{16}Pd_2$ (449.06): calcd. H 2.69, N 49.91; found H 2.45, N 49.00.

Crystal Structure Analysis of 3: $H_{12}N_{16}Pd_2$, M = 449.06, crystal size: 0.20 × 0.12 × 0.10 mm, orange-brown needle, orthorhombic, space group *I*4/*m*, a = 9.8789(2), b = 9.8789(2), c = 6.0840(2) Å, V = 593.75(3) Å^3, Z = 2, $d_{calcd.}$ = 2.512 Mg/m^3, μ = 3.045 mm^{-1}, F(000) = 432. Siemens CCD Area detector, scan type: hemisphere, Mo-K_α, λ = 0.71073 Å, T = 183 K, 2θ range = 5.84−54.86° in $-12 \le h \le 12$, $-12 \le k \le 12$, $-6 \le l \le 5$, reflections collected: 1650, independent reflections: 327 (R_{int} = 0.0144), observed reflections: 282 [$F > 4\sigma(F)$]. Structure solution and refinement program: SHELXS-97 (G. M. Sheldrick, University of Göttingen, Germany, **1997**), direct methods, data-to-parameter ratio: 9.1:1 {7.8:1 [$F > 4\sigma(F)$]}, final R indices [$F > 4\sigma(F)$]: $R1$ = 0.0134, $wR2$ = 0.0369, $R1$ = 0.0161, $wR2$ = 0.0376 (all data), GOF on F^2 = 1.172, largest and mean Δ/σ: 0.000, 0.000, largest difference peak/hole: 0.315, −0.583 e Å^{-3}. Further details of the crystal-structure investigation may be obtained from the Fachinformationszentrum Karlsruhe, D-76344 Eggenstein-Leopoldshafen, Germany, on quoting the depository number CSD-410384.

[1] F. G. Sherif, K. F. Michail, *J. Inorg. Nucl. Chem.* **1963**, *25*, 999.
[2] R. G. Clem, E. H. Huffman, *J. Inorg. Nucl. Chem.* **1965**, *27*, 365.
[3] W. Beck, W. P. Fehlhammer, P. Pöllmann, E. Schuirer, K. Feldl, *Chem. Ber.* **1967**, *100*, 2335.
[4] C. J. Oetker, W. Beck, *Spectrochim. Acta* **1973**, *29A*, 1975.
[5] W. Beck, W. Becker, K. F. Chew, W. Derbyshire, N. Logan, D. M. Revitt, D. B. Sowerby, *J. Chem. Soc. Dalton Trans.* **1972**, 245.
[6] T. M. Klapötke, I. C. Tornieporth-Oetting, *Nichtmetallchemie*, Verlag Chemie, Weinheim, **1994**.
[7] T. M. Klapötke, A. Schulz, J. McNamara, *J. Chem. Soc., Dalton Trans.* **1996**, 2985.
[8] I. C. Tornieporth-Oetting, T. M. Klapötke, *Angew. Chem. Int. Ed. Engl.* **1995**, *34*, 511.
[9] T. M. Klapötke, P. Geissler, *J. Chem. Soc., Dalton Trans.* **1995**, 3365.
[10] W. Beck, H. Nöth, *Chem. Ber.* **1984**, *117*, 3365.

Received October 8, 1998
[I98343]

Synthesis and Structural Study by Wide-Angle X-ray Scattering (WAXS) of Polymeric $\{Ln_2[M(opba)]_3\}\cdot S$ Compounds Containing 4f Ln^{III} and 3d M^{II} $\{Ln_2[M(opba)]_3\}\cdot S$ Ions [opba = *ortho*-Phenylenebis(oxamato), S = Solvent Molecules]

Myrtil L. Kahn,[a] Marc Verelst,[b] Pierre Lecante,[b] Corine Mathonière,[a] and Olivier Kahn*[a]

Keywords: Lanthanides / WAXS / Ladder polymers / Rare-earth compounds / Supramolecular chemistry

The compounds of formula $Ln_2[M(opba)]_3\cdot xH_2O\cdot yDMSO$ containing 4f Ln^{III} and 3d M^{II} ions have been synthesized; opba stands for *ortho*-phenylenebis(oxamato). These compounds crystallize poorly, and hence structural information has been obtained from the wide angle X-ray scattering (WAXS) technique. It has been shown that the compounds present the same ladder-like motif as that previously described for $Tm_2[Cu(opba)]_3\cdot 4H_2O\cdot 10DMF$. Changing the Ln^{III} and/or M^{II} ions results in more or less pronounced distortions of the ladders. For a given M^{II} ion, changing the Ln^{III} ion from La^{III} to Lu^{III} results in a decrease of the Ln–M distance parallel to the lanthanide contraction. In the same way, for a given rare earth, changing the M^{II} ion from Cu^{II} to Ni^{II} and Zn^{II} ions also results in the decrease of the Ln–M distance in accord with the decreasing radii of the M^{II} ions. The structural details have been analyzed and discussed.

Introduction

For one decade or so, we have been concerned with the chemistry and physics of molecular compounds containing both 4f and 3d metal ions. We first focused on the $Ln^{III}-[Cu(pba)]^{2-}$ systems where Ln^{III} stands for a trivalent lanthanide ion and pba for the bisbidentate ligand 1,3-propylenebis(oxamato). Depending on the $Ln^{III}/[Cu(pba)]^{2-}$ stoichiometry and the synthetic conditions, three structures have been found, namely tube-like motifs, double sheet layers, and ladder-like motifs. Subsequently, we used the $[Cu(opba)]^{2-}$ precursor where opba stands for *ortho*-phenylenebis(oxamato). So far, one- and two-dimensional compounds have been characterized, some of them exhibiting a long-range magnetic ordering at low temperature.[1]

It is now well established that the interaction between Gd^{III} and Cu^{II} ions is ferromagnetic. On the other hand, the nature of the interaction when Gd^{III} is replaced by another magnetic Ln^{III} ion is still an open question. The presence of an orbital momentum makes the theoretical approach very difficult. Recently, we decided to tackle this problem, and to utilize a chemical approach.[2] Let us consider a compound involving both 4f Ln^{III} and 3d M^{II} magnetic ions. The magnetic behavior of such a system is governed by two factors, namely the coupling between Ln^{III} and M^{II} magnetic centres on the one hand, and the thermal population of the Stark levels of Ln^{III} on the other hand. Our approach consists of replacing the magnetic 3d M^{II} ion by a diamagnetic one, such as Zn^{II}. The magnetic behavior of a $Ln^{III}Zn^{II}$ compound is governed only by the thermal population of the Stark levels. Comparing the magnetic properties of the $Ln^{III}M^{II}$ and $Ln^{III}Zn^{II}$ compounds results in a qualitative estimation of the nature of the $Ln^{III}-M^{II}$ interaction, provided that the $Ln^{III}M^{II}$ and $Ln^{III}Zn^{II}$ compounds have similar structures.

In this paper we describe the synthesis and the structural characterization of polymeric compounds of formula $Ln_2[M(opba)]_3\cdot xH_2O\cdot yDMSO$ where M^{II} may be Cu^{II}, Ni^{II} or Zn^{II} and DMSO is dimethyl sulfoxide. Most of these compounds crystallize poorly, and we used the wide-angle X-ray scattering (WAXS) technique to obtain structural information. Even if the WAXS technique cannot give the exact structure as an X-ray diffraction study in principle does, it has been successfully utilized to structurally characterize inorganic polymers.[3] Furthermore, for one of our compounds, a structure determined from X-ray diffraction is available. This structure may be utilized as a starting guess to interpret the WAXS data for the other compounds.

Results

First Approach

Figure 1 (top) shows the reduced intensities for three selected compounds, and Figure 1 (bottom) shows the RDFs. The reduced intensity represents the structural part of the scattering phenomenon after the full correction procedure. The Fourier transform of this spectrum gives the RDF which can be considered as a histogram of ordered distances weighted by the distance multiplicity and the

[a] Laboratoire des Sciences Moléculaires, Institut de Chimie de la Matière Condensée de Bordeaux, UPR No 9048,
F-33608 Pessac, France
Fax: (internat.) + 33(0)556842649
E-mail: kahn@icmcb.u-bordeaux.fr
[b] Centre d'Elaboration de Matériaux et d'Etudes Structurales, UPR CNRS No 8011,
BP 4347, 29 rue Jeanne Marvig, F-31055 Toulouse, France

 © WILEY-VCH Verlag GmbH, D-69451 Weinheim, 1999 1434–1948/99/0303–0527 $ 17.50+.50/0

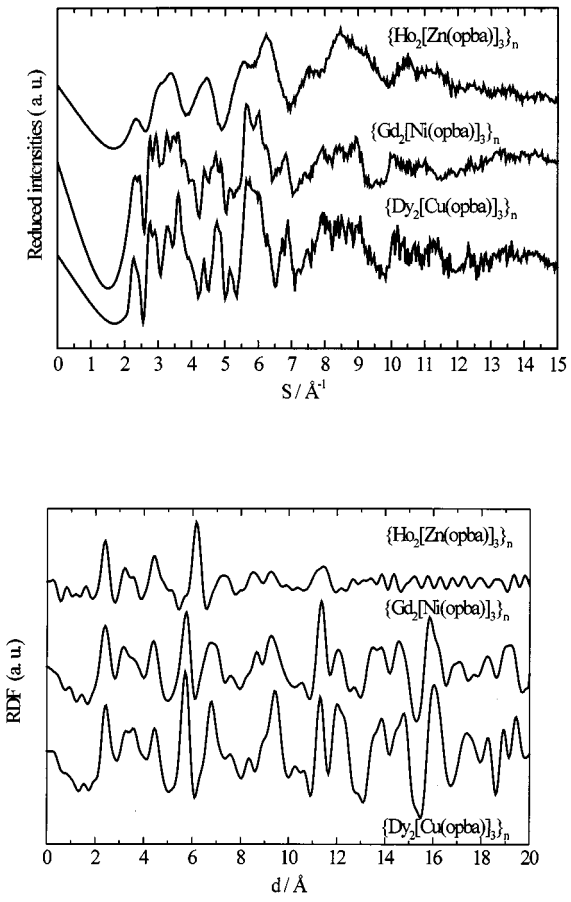


Figure 1. Overview of the experimental reduced intensities (top) and the Radial Distribution Function (RDF, bottom) for three selected samples

number of electrons engaged in these distances. Thus, an intense peak on the RDF indicates a frequent distance between two atoms.

A first qualitative look shows that the spectra are very similar to each other. The spectra of nickel- and copper-containing compounds are almost identical. The few small differences which can be detected will be discussed below. The spectra of the zinc-containing compounds differ a little bit more. This is mainly due to two factors: First, the $\{Ln_2[Zn(opba)]_3\}\cdot S$ compounds are more poorly crystallized; second, a systematic shift of each RDF peak towards longer distances is observed. The coherence length is limited to approximately 12 Å, as revealed by the collapse of ordered distances beyond this limit in the RDF of $\{Ho_2[Zn(opba)]_3\}\cdot S$.

The structures of a few oxamato-bridged $Ln^{III}Cu^{II}$ compounds were determined by X-ray diffraction on single crystals: $Gd_2[Cu(pba)]_3[Cu(H_2O)_5]\cdot 20H_2O$ presents a layered structure,[1] $Sm_2[Cu(pba)]_3\cdot 23H_2O$ shows infinite tube-like motifs,[1] and $Dy_2[Cu(pba)]_3\cdot 23H_2O$[1] and $Tm_2[Cu(opba)]_3\cdot 4H_2O\cdot 10DMF$[4] adopt a ladder-type structure. The theoretical RDFs were calculated for these three different architectures and compared to the experimental RDFs. In all cases, the best fit was obtained for the ladder-type structure. As shown in Figure 2, the uprights are made of Ln[M(opba)] units, with M = Cu, Ni or Zn, and the rungs are made of [M(opba)] units bridging Ln atoms from each upright. When seen along the direction of a rung, the two edges of the ladder are in an eclipsed conformation. Each Ln^{III} ion is surrounded by three $[M(opba)]^{2-}$ groups, its coordination sphere being completed by solvent molecules. Let us consider a specific example: $Dy_2[Cu(opba)]_3\cdot 3H_2O\cdot 9DMSO$. Figure 3 compares the experimental RDF for $Dy_2[Cu(opba)]_3\cdot 3H_2O\cdot 9DMSO$ with the RDF calculated from the X-ray diffraction data for $Tm_2[Cu(opba)]_3\cdot 4H_2O\cdot 10DMF$. The fit is fairly good up to 18 Å, which strongly suggests that $Dy_2[Cu(opba)]_3\cdot 3H_2O\cdot 9DMSO$ also has a ladder-type structure. The main difference between experimental and calculated RDFs is the shift of the peak centred at 9.85 Å in $Tm_2[Cu(opba)]_3\cdot 4H_2O\cdot 10DMF$ which is located around 9.40 Å in $Dy_2[Cu(opba)]_3\cdot 3H_2O\cdot 9DMSO$. In $Tm_2[Cu(opba)]_3\cdot 4H_2O\cdot 10DMF$ this peak corresponds to the *a* lattice parameter, i.e. to the distance between two ladders [see Figure 2 (bottom)]. Apparently, this distance is smaller in $Dy_2[Cu(opba)]_3\cdot 3H_2O\cdot 9DMSO$ than in $Tm_2[Cu(opba)]_3\cdot 4H_2O\cdot 10$ DMF, suggesting that the packing distance between two ladders is smaller in $Dy_2[Cu(opba)]_3\cdot 3H_2O\cdot 9DMSO$ than in $Tm_2[Cu(opba)]_3\cdot 4H_2O\cdot 10DMF$. This difference may be attributed to the fact that the volume of 4 H_2O and 10 DMF molecules is larger than that of 3 H_2O and 9 DMSO molecules. Beyond 18 Å the quality of the fitting decreases somewhat, but for such long distances inter-ladder packing interactions involving non-coordinated solvent molecules become important.

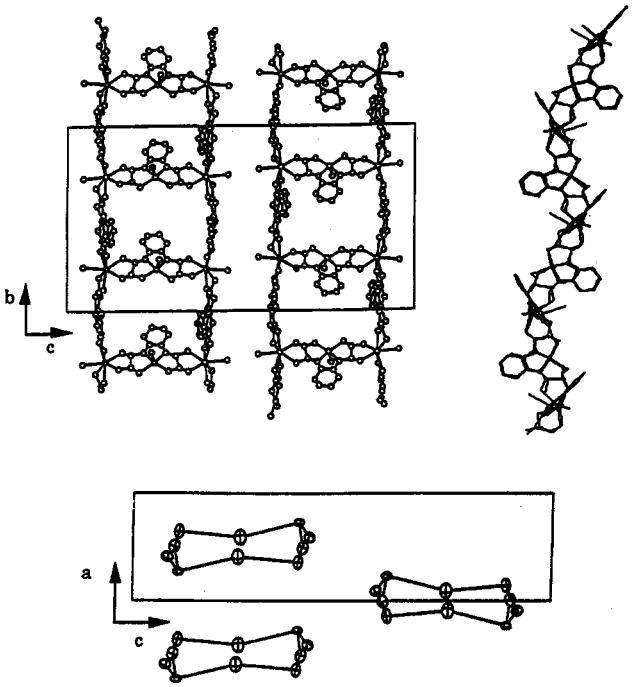


Figure 2. Structure of $Tm_2[Cu(opba)]_3\cdot 4H_2O\cdot 10DMF$ determined from X-ray diffraction; top left: view of two neighboring ladders in the *bc* plane; top right: view of one of the ladders rotated by 90°; bottom: schematic view of the ladders projected in the *ac* plane

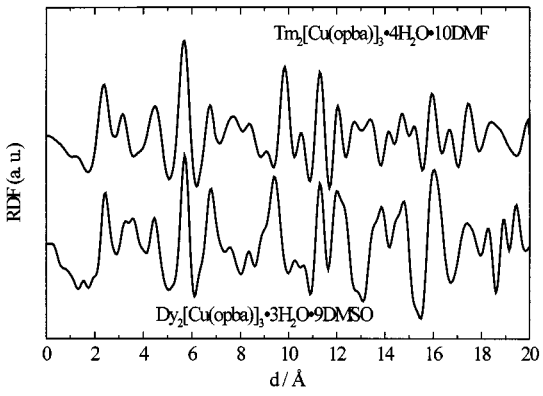


Figure 3. Comparison of the experimental RDF for $Dy_2[Cu(opba)]_3\cdot 3H_2O\cdot 9DMSO$ and the theoretical RDF for $Tm_2[Cu(opba)]_3\cdot 4H_2O\cdot 10DMF$ calculated from the structural data of ref.[4]: space group $P2_12_12_1$, a = 9.864 Å, b = 20.855 Å, c = 39.101 Å

Modeling of the $Dy_2[Cu(opba)]_3$ Ladder

Even if the structures of $Dy_2[Cu(opba)]_3\cdot 3H_2O\cdot 9DMSO$ and $Tm_2[Cu(opba)]_3\cdot 4H_2O\cdot 10$ DMF appear to be very similar, systematic shifts around 0.1 to 0.2 Å can be detected on the RDF peaks, and we decided to go further in the interpretation of the WAXS data. The starting model is a single ladder of $Tm_2[Cu(opba)]_3$ generated from crystallographic data, in which the inter-ladder contributions are obviously ignored. It follows that some slight distortions are imposed on the model in order to obtain a perfect agreement between theoretical and experimental RDF's. The final model is shown in Figure 4. Figure 5 shows the reduced intensities (top) and the RDF (bottom) computed from both experimental data and the model of Figure 4. We can notice that the Ln−Cu distances through the oxamato bridge are found to be slightly larger in $Dy_2[Cu(opba)]_3\cdot 3H_2O\cdot 9DMSO$ than in $Tm_2[Cu(opba)]_3\cdot 4H_2O\cdot 10DMF$ (Dy−Cu = 5.74 Å and Tm−Cu = 5.59 Å).

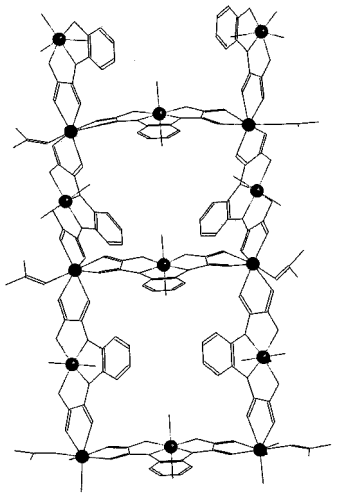


Figure 4. Structure of $Dy_2[Cu(opba)]_3\cdot 3H_2O\cdot 9DMSO$ as deduced from the WAXS study (see text); main distances: Cu−O and Cu−N: 1.95 to 2.1 Å; Dy−O: 2.27 to 2.38 Å; Dy−S: 3.55 Å; Dy−Cu: 5.72 to 5.76 Å; Dy−Dy: 11.21 to 11.36 Å

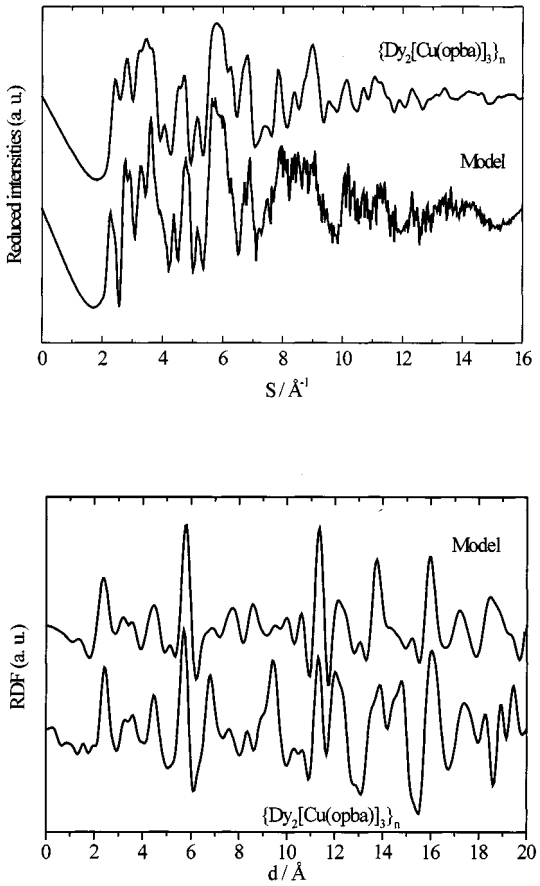


Figure 5. Reduced intensities (top) and experimental and theoretical RDFs (bottom) for $Dy_2[Cu(opba)]_3\cdot 3H_2O\cdot 9DMSO$

An interesting feature is the presence of a RDF peak centered around 3.55 Å in all the compounds containing DMSO molecules. This peak does not appear in the RDF calculated from the crystallogaphic data for $Tm_2[Cu(opba)]_3\cdot 4H_2O\cdot 10DMF$ (compare Figures 3 and 5). A simulation suggests that this distance could correspond to a Ln−S separation associated with a DMSO molecule coordinated to the Ln^{III} ion through an oxygen atom. This hypothesis is strengthened by the fact that the intensity of this peak corresponds approximately to one sulfur atom per lanthanide atom.

The agreement between experimental and calculated RDFs suggests that our model is essentially valid. However, two peaks, at 9.4 Å and 14.7 Å, are not expected in our model. These two peaks arise from intermolecular distances which are not at all modeled. Probably, the peak centred around 9.4 Å is due to the a cell parameter whereas the second one centered at 14.7 Å is the packing distance between two ladders in a same cell (see Figure 2). This hypothesis is strengthened by the fact that these two distances are equal to 9.86 Å and 14.75 Å, respectively, in $Tm_2[Cu(opba)]_3\cdot 4H_2O\cdot 10DMF$.

Ladder Distortions Induced by Metal-Ion Substitutions

Performing the modeling-distortion-fitting procedure for all the compounds would be extremely cumbersome. Such a work was carried out in one case (DyCu compound) in order to demonstrate that the compound has the ladder-type structure found for $Tm_2[Cu(opba)]_3 \cdot 4H_2O \cdot 10DMF$, with some weak distortions of the ladders. Precise assignment of the RDF peaks was also one of our goals. It is possible to determine accurately some structural characteristics such as the Ln−M (5.74 Å for the DyCu compound) and Ln−Ln (11.3 Å for the DyCu compound) distances through the opba bridge as Ln and M are changed. The results are shown in Figure 6. The two curves of Figure 6 confirm that the nickel- and copper-containing compounds have very similar structures. For a same Ln^{III} ion, the width of the ladders is slightly smaller in the copper derivatives, which is in line with the difference in ionic radius between Cu^{II} and Ni^{II} (0.72 and 0.78 Å, respectively). The width of the ladders is even larger in the zinc derivatives, in agreement with an ionic radius of 0.83 Å for Zn^{II}. In a similar way, for a same M^{II} ion the width of the ladders decreases as the atomic number of Ln increases. This observation is obviously in line with the contraction of the atomic radius from the left to the right of the lanthanide series, from 1.22 Å for La^{III} to 0.85 Å for Lu^{III}. It can be noticed that in the LnZn series two compounds, GdZn and TbZn, show larger Ln−Ln distances, 11.65 and 11.75 Å, respectively, than those for the other LnZn compounds (11.45 Å in average). This might result from the relative flexibility of the Ln−Zn−Ln alignment, i.e. the deviation of ρ (the angle between the two Ln−Zn bonds) from 180° (see below).

To obtain further information on the linearity of the Ln−[M(opba)]−Ln network in the various compounds, we calculated the ratios of the distances, ρ = Ln−Ln/Ln−M. If this network is strictly planar, ρ should be equal to 2; a ρ value smaller than 2 reveals a distortion of the network. For the compounds with M = Ni and Cu, ρ is in the range 1.96−1.98, i.e. very close to 2. On the other hand, for the compounds with M = Zn, ρ ranges between 1.80 and 1.85. Probably, the ladders in the zinc-containing compounds are more distorted than in the nickel- and copper-containing derivatives. However, as shown in Figure 6, two compounds of the Zn series (GdZn and TbZn) seem to deviate from linearity less than the other compounds of this series. In any case, this distortion would explain why the zinc derivatives are less crystalline than the nickel and copper ones. In these zinc compounds, this distortion probably induces a statistical disorder which reduces the coherence length to about 12 Å.

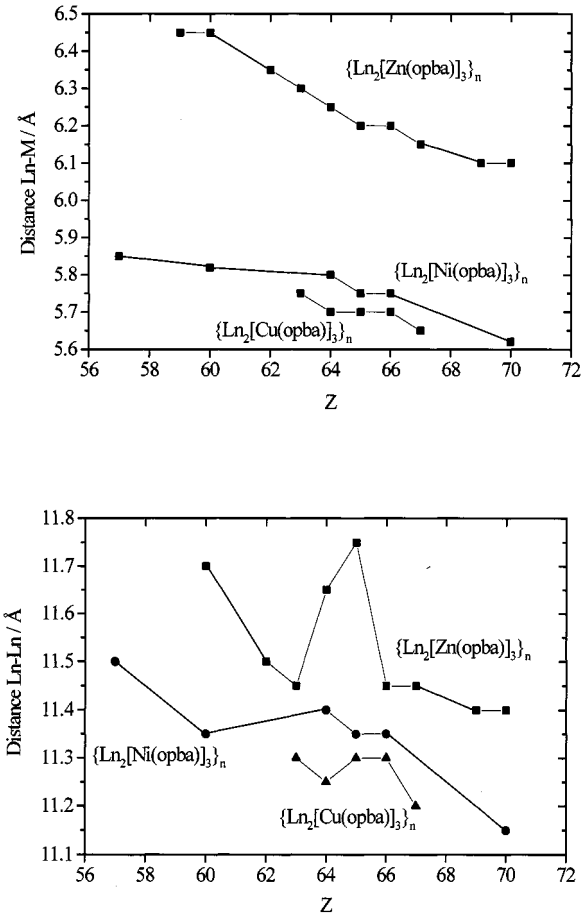


Figure 6. Evolution of M−Ln (top) and Ln−Ln (bottom) distances as a function of the atomic number of the Ln and M elements

Conclusion

This WAXS study on a new series of 4f−3d compounds proves without doubt that all the $\{Ln_2[M(opba)]_3\} \cdot S$ compounds have similar structures. These compounds crystallize poorly. However, the coherence length is important enough to strongly suggest that the structures consist of ladder-like motifs, very similar to those found in $Tm_2[Cu(opba)]_3 \cdot 4H_2O \cdot 10DMF$. These WAXS studies allow us not only to confirm the ladder-type structure but also to determine precisely important distances such as Ln−M, Ln−Ln and Ln−S. The Ln−M separations across the oxamato bridge range from 5.60 to 6.45 Å, and the separation between two Ln^{III} ions connected in the transverse direction range from 11.15 to 11.75 Å depending on the nature of the Ln^{III} and M^{II} ions. The packing distances between two ladders range from 9.0 to 9.5 Å (*a* lattice parameter) and is around 14.7 Å between two ladders in the same cell. For a given M^{II} ion, changing Ln^{III} from La^{III} to Lu^{III} ion results in the decrease of the Ln−M distance in accord with the lanthanide contraction. In the same way, for a given rare earth, changing the M^{II} ion from Cu^{II} to Ni^{II}, and then Zn^{II} results also in the decrease of the Ln−M distance in accord with the decreasing radii of the M^{II} ions. These studies confirm that the determination of the structure of polymeric compounds is possible with the WAXS technique and that precise structural information can be obtained.

Systematic magnetic measurements are in progress and will be published in a subsequent paper. This structural

study was a prerequisite to discussing and interpreting the magnetic data.

Experimental Section

Syntheses. – Starting Materials: $Ln(NO_3)_3\cdot xH_2O$,[5] Et_2H_2opba and $(NMe_4)_2[Cu(opba)]$,[6] were synthesized according to described procedures. The Zn^{II} precursor, $(NBu_4)_2[Zn(opba)]$, was synthesized as follows: A solution of Et_2H_2opba (1.545 g, 5 mmol) and NBu_4OH (2.62 ml, 40 wt.-% sol. in water, 4 mmol) in MeOH was stirred at 60°C for 30 min. A methanolic solution of $Zn(Ac)_2\cdot 2H_2O$ (0.219 g, 1 mmol) was added dropwise. A white precipitate was immediately formed. The solid was collected by centrifugation of the mixture, washed three times with MeOH and dried under vacuum (2.8 g, yield 70%). – ^{1}H NMR [D$_6$]DMSO: δ = 7.94 (br. s, 2 H, *aromatic*); 6.57 (br. s, 2 H, *aromatic*); 3.16, 1.55, 1.29 [3 br. m, 48 H, $N(CH_2)_3CH_3$]; 0.91 (br. m, 24 H, CH_3). – IR (principal vibrations; KBr; cm^{-1}): $\tilde{\nu}$ = 2961.7 (w), 2874.0 (w): ν(C–H); 1598.1 (s), 1572.5 (s): ν(C=O); 753.5 (w): aromatic ring. – $C_{42}H_{96}N_4O_{16}Zn$ (978.6): calcd. C 51.5, H 9.9, N 5.7, Zn 6.7; found C 50.8, H 8.9, N 5.4, Zn 7.3.

Ni^{II} Precursor $(NMe_4)_2[Ni(opba)]$: A solution of Et_2H_2opba (1.545 g, 5 mmol) and NMe_4OH (7.18 ml, 25 wt.-% sol. in water, 20 mmol) in MeOH was stirred at 60°C for 30 min. A methanolic solution of $Ni(ClO_4)_2\cdot 6H_2O$ (1.828 g, 5 mmol) was added dropwise. The solution was filtered and the solvent was removed. The addition of a small amount of distilled MeOH gave a precipitate of $(NMe_4)(ClO_4)$. The reaction mixture was then kept at –18°C for 12 h, then filtered. The solvent was removed under reduced pressure to give an orange oil which crystallized by addition of diethyl ether (3.4 g, yield 85%). – ^{1}H NMR ([D$_6$]DMSO): δ = 7.80 (br. s, 2 H, *aromatic*); 6.55 (br. s, 2 H, *aromatic*); 3.10 (s, 24 H,CH_3). – IR (principal vibrations; KBr; cm^{-1}): $\tilde{\nu}$ = 3018.9 (w): ν(C–H); 1663.8 (s), 1636.1 (s): ν(C=O); 618.5 (w) aromatic. – $C_{22}H_{44}N_4NiO_{10}$ (583.3): calcd. C 45.3, H 7.6, N 9.6, Ni 10.0; found C 45.6, H 7.1, N 11.8, Ni 9.6.

$\{Ln_2[M(opba)]_3\}\cdot S$: All the $\{Ln_2[M(opba)]_3\}\cdot S$ compounds were synthesized by using the same general procedure. Here is described the general procedure. A solution of $Ln(NO_3)_3\cdot xH_2O$ (33 mmol), dissolved in 5 mL of DMSO, was added dropwise to a solution of $(Cat^+)_2[M(opba)]$ (50 mmol), dissolved in 10 mL of DMSO solution. A precipitate was formed and the mixture was stirred for 3 h. The solid was collected by centrifugation, washed three times with DMSO and three times with ether, then dried under vacuum. – IR (principal vibrations; KBr; cm^{-1}): $\tilde{\nu}$ = $\{Dy_2[Cu(opba)]_3\}\cdot S$: 1626.4 (s), 1596.1 (s), 1572.5 (s): ν(C=O); 1014.5 (s), 951.1 (m): ν(S=O). $\{Ho_2[Zn(opba)]_3\}\cdot S$: 1590.4 (s), 1560.4 (s): ν(C=O); 1016.8 (s), 954.3 (m) ν(S=O). $\{Gd_2[Ni(opba)]_3\}\cdot S$: 1618.0 (s), 1572.5 (s): ν(C=O); 1014.8 (s), 953.0 (m): ν(S=O). – $C_{48}H_{72}Cu_3Dy_2N_6O_{30}S_9$ (2017.3): calcd C 28.6, H 3.6, Cu 9.4, N 4.2, S 14.3; found C 28.3, H 2.8, Cu 8.5, N 5.8, S 14.5; $C_{31}H_{45}Gd_2N_6Ni_3O_{33.5}S_{0.5}$ (1544.3): calcd C 24.1, H 2.9, Gd 20.4, N 5.4, S 1.0, Ni 11.4; found C 25.3, H 2.9, Gd 20.0, N 5.3, S 0.4, Ni 10.5; $C_{44}H_{64}Ho_2N_6O_{30}S_7Zn_3$ (1907.5): calcd C 27.7, H 3.4, Ho 17.3, N 4.4, S 11.8; found C 29.6, H 3.9, Ho 17.4, N 4.3, S 11.7.

WAXS Studies: A typical experiment was performed as follows: The sample was sealed in a Lindeman capillary. The diffusion spectrum scattered by the sample irradiated with graphite-monochromatized molybdenum K_α radiation (λ = 0.71069 Å) was obtained using a LASIP diffractometer.[7] 457 intensities corresponding to equidistant points [$s = 4\pi(\sin\theta/\lambda)$; Δs = 0.035 Å^{-1}] were collected in the 0° < θ < 65° range. Measurements of air and Lindeman capillary diffusion were carried out exactly under the same conditions. The raw sample scattered intensity (sample + air + capillary) was corrected for air and capillary contributions by spectra subtraction taking into account absorption from sample, then corrected for polarization and self absorption effects. Normalization was performed using Norman and Krogh-Moe's method.[8] The atomic scattering factors were taken from Cromer and Waber.[9] The reduced experimental Radial Distribution Function (RDF) was calculated similarly as described in ref.[10] Theoretical structural models were built up using the CERIUS2 program.[11] The theoretical RDF was computed from the structural models by Fourier transform of the theoretical intensities calculated according to the Debye formula[12] using the KURVLR program.[13] Debye–Waller factors commonly observed in related crystalline structures were used for the computation.

[1] O. Guillou, O. Kahn, R. L. Oushoorn, K. Boubekeur, P. Batail, *Inorg. Chim. Acta* **1992**, *198–200*, 119–131.
[2] M. L. Kahn, C. Mathonière, O. K ahn, *International Conference on f Elements*, September 14–18, **1997**, Paris, France.
[3] M. Verelst, L. Sommier, P. Lecante, A. Mosset, O. Kahn, *Chem. Mater.* **1998**, *10*, 980.
[4] R. L. Oushoorn, K. Boubekeur, P. Batail, O. Guillou, O. Kahn, *Bull. Soc. Chim. Fr.* **1996**, *133*, 777.
[5] J.-C. G. Bünzli, G. R.Choppin, *Lanthanide Probes in Life, Chemical and Earth Sciences*, Elsevier, Amsterdam, The Netherlands, **1989**.
[6] H. O. Stumpf, Y. Pei, O. Kahn, J. Sletten, J.-P. Renard, *J. Am. Chem. Soc.* **1993**, *115*, 6738.
[7] The LASIP diffractometer has a geometry especially set up for scattering measurements. It minimizes every external parasite scattering phenomenon.
[8] [8a] N. Norman, *Acta Crystallogr.* **1957**, *10*, 370. – [8b] Krogh-Moe, *Acta. Crystallogr.* **1956**, *9*, 951.
[9] D. Cromer, T. Waber, *J. International Tables for X-ray Crystallography*: Kynoch Press, Birmingham, **1974**, vol. 4.
[10] See for example: [10a] A. Mosset, P. Lecante, J. Galy, *J. Phil. Mag. B* **1982**, *46*, 137. – [10b] A. Burian, P. Lecante, A. Mosset, J. Galy, *J. Non-Crystalline Solids* **1987**, *90*, 633. – [10c] C. Laberty, M. Verelst, P. Lecante, A. Mosset, P. Alphonse, A. Rousset, *J. Solid-State Chem.* **1997**, *129*, 271–276. – [10d] M. Verelst, L. Sommier, P. Lecante, A. Mosset, O. Kahn, *Chem. Mater.* **1998**, *10*, 980.
[11] CERIUS2 molecular simulation program is supplied by BIOSYM technologies and runs on an Indy Silicon Graphics workstation.
[12] P. Debye, *Ann. Physik (Leipzig)* **1915**, *46*, 809.
[13] G. Johansson, M. Sandström, *Chem. Scr.* **1973**, *4*, 195.

Received October 9, 1998
[I98346]

The Structures of a Tetracarba-*nido*-octaborane(8) and a Novel Spiro Derivative of a 2,3,5-Tricarba-*nido*-hexaborane(7)

Bernd Wrackmeyer,*[a] Hans-Jörg Schanz,[a] Matthias Hofmann,[b] Paul von R. Schleyer,[b] and Roland Boese[c]

Keywords: Ab initio calculations / Carboranes / NMR / X-ray analysis

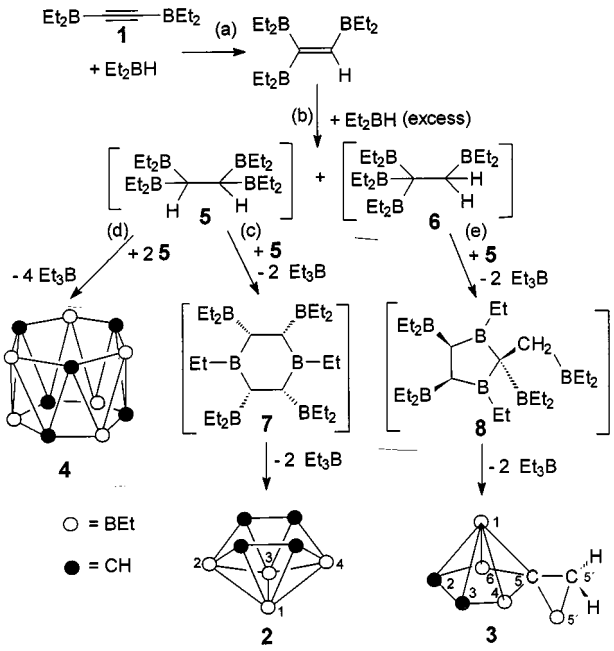
Hydroboration of bis(diethylboryl)ethyne (**1**) with tetraethyldiborane(6) leads to a *B*-ethyl-substituted tetracarba-*nido*-octaborane **2**, a spiro-carborane **3**, which belongs to the 2,3,5-tricarba-*nido*-carborane family, and a hexacarba-*arachno*-dodecaborane(12) **4**, along with polymeric material. The X-ray structure analysis of carborane **2**, determined here, is fully consistent with the structure deduced earlier from NMR data. The structure of **3** in solution was established by theoretical analysis of its NMR data. Ab initio calculations of the structures of **2b** and **3b** (**b** denotes the *B*-metyhl-substituted derivatives) and the comparison of calculated with experimental NMR data support the suggested structures of **2** and **3** in solution. The calculated structure of the carborane cage of **2a** also agrees with the experimental geometry of **2**.

Introduction

Tetracarba-*nido*-octaboranes(8) are reported to result from transition metal complex promoted reactions[1,2] or from the reduction of organo-substituted 1,2,5-thiadiborolenes with potassium.[3] However, the evidence for structural assignments is not firm, and the chemistry of these carboranes has not been explored. We prepared the *B*-ethyl-substituted tetracarba-*nido*-octaborane(8) **2** by hydroboration of bis(diethylboryl)ethyne (**1**); the structure was inferred from NMR data in solution along with an X-ray structural analysis of the hexacarbonyldiiron complex of **2**.[4] The hydroboration of **1** (Scheme 1) also leads to other products, e.g. the hexacarba-*arachno*-dodecaborane(12) derivative **4**,[5] and **3**, a spiro-carborane isomer of **2**.[5] We now report the first X-ray-structural analysis of the *nido*-C_4B_4 cage, and our finding of an isomer of **2** with a carborane cage different from that of **2**. We employ the ab initio/GIAO-IGLO/NMR method[6] to elucidate the structures.

Results and Discussion

The routes to the carboranes **2**−**4** are shown in Scheme 1. The mechanism is speculative. The suggested intermediates **5**−**8** were not detected, but are inferred [as associated diborane(6) species due to the excess of tetraethyldiborane(6)] from the products. The formation of polymeric material is suggested if the diethylboryl groups in **7** or **8** are not in the correct positions for BH-catalyzed intramolecular elimination of Et_3B (these isomers of **7** or **8** are not shown in Scheme 1). In the case of **8** intramolecular elimination of Et_3B from the $Et_2BCH-CHBEt_2$ moiety leads to the apical BEt group and therefore, it can be predicted that a second intramolecular elimination of Et_3B, forming the spiro compound, should give the three-membered ring with an endocyclic C5−B5′ bond as in **3**. The proposed structure of **3** is unique in carborane chemistry and therefore, extensive NMR studies and ab initio MO calculations were per-



Scheme 1. Hydroboration of bis(diethylboryl)ethyne (**1**) using an excess of Et_2BH: formation of polymers and of the carboranes **2**, **3** and **4**

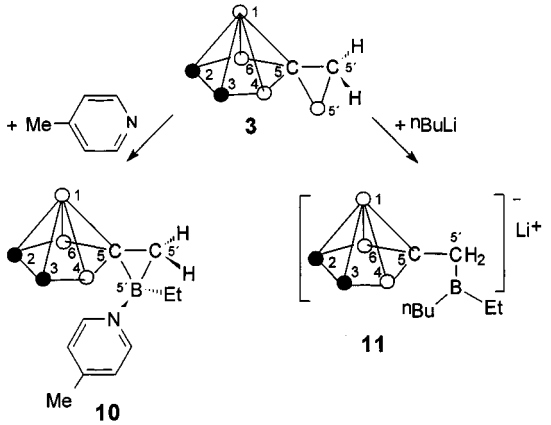
[a] Laboratorium für Anorganische Chemie, Universität Bayreuth, D-95440 Bayreuth, Germany
Fax: (internat.) + 49(0)921/552157
E-mail: b.wrack@uni-bayreuth.de
[b] Center for Computational Quantum Chemistry, University of Georgia, 1004 Cedar Street, Athens, GA 30602-2525, USA
Fax: (internat.) + 1-706/542-0406
E-mail: schleyer@paul.chem.uga.edu
[c] Institut für Anorganische Chemie, FB 8, Universität-GH Essen, Universitätsstraße 5−7, D-45117 Essen
Fax: (internat.) + 49(0)201/1832535
E-mail: boese@structchem.uni-essen.de

 © WILEY-VCH Verlag GmbH, D-69451 Weinheim, 1999 1434−1948/99/0303−0533 $ 17.50+.50/0

formed to prove its existence, in particular in the absence of direct structural evidence.

In contrast to **2** and **4**, the carborane **3** is extremely sensitive towards oxygen. It is therefore not observed when the usual work-up procedures are used. However, if the reaction mixtures are not oxidized or hydrolyzed, **3** can be obtained in a mixture with **2** by fractional distillation, and a complete set of NMR data of **3** can be recorded. The ^{11}B-NMR signal at $\delta = -28.9$ with relative intensity 1 indicates the presence of a boron atom (B1) in apical position, and the signal at $\delta = +23.3$ with relative intensity 2 is typical of boron atoms B4,6 in basal positions. A third ^{11}B-NMR signal at rather low field ($\delta = +64.0$), much more typical of triorganoboranes than of carboranes is assigned to the boron atom in the three-membered ring. The connectivity between the ^{11}B4,6 and ^{13}C2,3 nuclei is evident from the sharpening of relevant ^{13}C-NMR signals as the result of selective ^{11}B decoupling experiments (see Figure 1). Irradiation of the ^{11}B resonance at $\delta = +64.0$ sharpens two $^{13}C(CH_2)$ signals, one due to the BEt group and the other to the unique CH_2 moiety in the three-membered ring. The carborane **3** is the first 2,3,5-tricarba-*nido*-hexaborane derivative[7,8] without an *endo*-C5−H bond. For the parent carborane a hyperconjugative interaction of the *endo*-C5−H bond with B4 (or B6) was found computationally.[9] This participation in the cluster bonding satisfies the electron counting rules.[10] In comparison with the δ^{11}B data of hexaethyl-2,3,5-tricarba-*nido*-hexaborane(7) **9** (Table 1) the apical ^{11}B nucleus in **3** is deshielded by 8 ppm. This can be the result of the different substituents linked to C5 (vide infra), and it can also be caused (however, less likely) by the missing ethyl groups at C2,3 in **3**.

Two reactions of **3** (Scheme 2) provide further evidence for its unique structure. If γ-picoline is added to the mixture of **2** and **3**, the ^{11}B-NMR signal at $\delta = +64.0$ disappears, and a new broad signal at $\delta = +13.5$ is observed. The spiro cage structure of **3** appears to be retained, since the effect on all other ^{11}B and ^{13}C(cage) signals is small. The carborane **2** does not react. Treatment of the mixture of **2** and **3** with BuLi also does not affect **2**, but **3** reacts by ring opening to give the 2,3,5-tricarba-*nido*-hexaborate(1−) derivative **11**. The reaction can be controlled by using slightly less then one equivalent of BuLi. The ^{11}B-NMR spectrum shows signals with correct integral intensities for B(1) and B(4,6) at $\delta = -38.5$ and $+21.7$, respectively, and a signal at $\delta = +86.7$ for the Et(Bu)B group in the typical range of non-cyclic trialkylboranes.[11] The δ^{11}B(1,4,6) values are close to those determined for corresponding 2,3,5-tricarba-*nido*-hexaborates(1−) [e.g. *nido*-Et_6-2,3,5-C_3B_3-hexaborate(1−): δ^{11}B1 = −44.2 and δ^{11}B(4,6) = +17.2.[8]]



Scheme 2. Reactivity of the spiro-carborane **3** towards γ-picoline and BuLi

The NMR data of **2** in solution discussed previously,[4] are fully consistent with the molecular structure of **2** in the solid state.[12] The X-ray data of **2** confirm the proposed[4,13] hexagonal open face formed by the four carbon atoms, linked in pairs, and two boron atoms (Figure 2). In

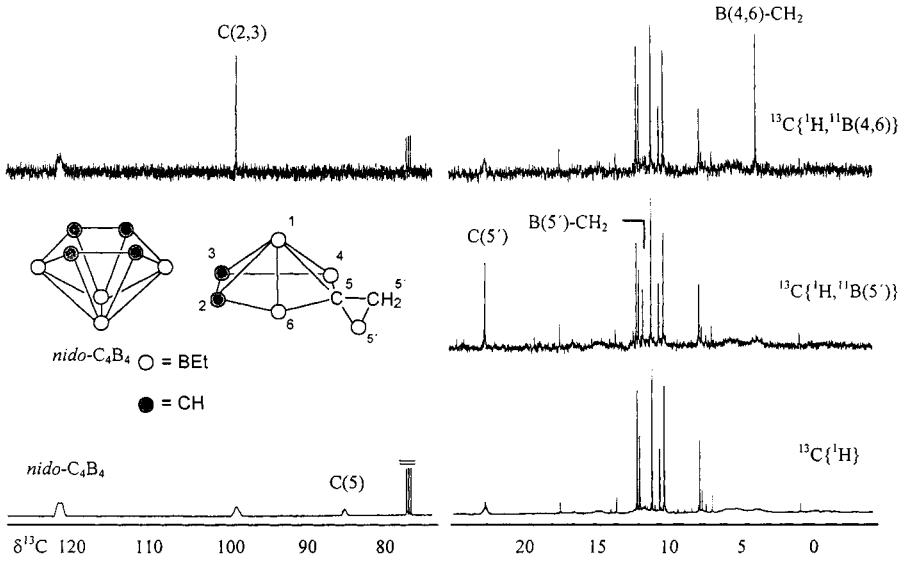


Figure 1. 125.8-MHz ^{13}C-NMR spectra of a mixture of **2** and **3** (ca. 10 mg in 0.5 mL of $CDCl_3$); **A**: normal $^{13}C\{^1H\}$-NMR spectrum spectrum; **B**: the selective heteronuclear $^{13}C\{^1H,^{11}B(4,6)\}$ triple-resonance experiment shows sharpening of the B(4,6)-$^{13}CH_2$, and ^{13}C(2,3) signals; **C**: the selective heteronuclear $^{13}C\{^1H,^{11}B(1)\}$ triple-resonance experiment only gives rise to sharpening of the $^{13}CH_2$-B(1) signal

the cage, the short distances d_{CC} [138.0(3), 138.5(3) pm] and rather short distances d_{B4C} and d_{B2C} [157.7(4), 159.0(4), 158.4(4), 158.6(4) pm] characterize the bonding situation in the open face. In particular, d_{B4B1} = 189.5(4) and d_{B2B3} = 190.5(4) pm are long when compared with the short d_{B1B3} = 171.0(4) pm separation. The other d_{BC} distances in the cage are similar to the known deltahedral B−C bond lengths. Variations of bond lengths in the hexacarbonyldiiron complex of **2** are less significant. The B−C−C angles in the BEt groups are 116.0(3)° (mean value), in the same range as in pentaethyl-1,5-dicarba-*closo*-pentaborane,[14] in which the B−C−C angles were interpreted in terms of hyperconjugational effects.[15]

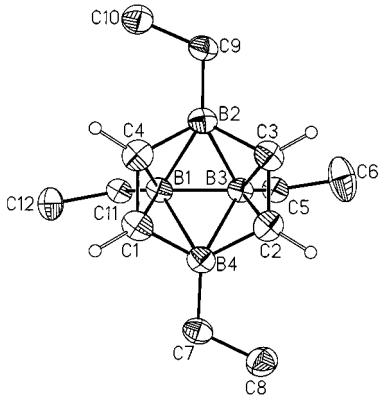


Figure 2. Presentation of the molecular structure of **2** with 50% thermal ellipsoids (ethyl hydrogen atoms are omitted for clarity); selected bond lengths [pm] and angles [°]: B1−C1 172.5(3), B1−C4 172.6(3), B1−B3 171.0(4), B1−B4 189.5(4), B1−C11 157.6(3), B2−C3 158.4(4), B2−C4 158.6(4), B2−C9 159.6(4), B2−B3 190.5(4), C1−C4 138.0(3), C2−C3 138.5(3); C1−B4−C2 109.9(2), C3−B2−C4 110.2(2), C10−C9−B2 115.4(2), C12−C11−B1 116.5(2)

Geometries were optimized at the MP2(fc)/6-31G* level of theory using the Gaussian 94 program.[16] Chemical shifts were evaluated from GIAO-SCF/6-31G* computations of chemical shieldings employing B_2H_6 (σ = 107.0) as a primary reference. Reported values are converted to the experimental standard, $BF_3 \cdot OEt_2$ using $\delta(B_2H_6)$ = 16.6.[17]

The parent $C_4H_8B_4$ spiro-carborane, optimized assuming a classical C_2B three-membered ring attached to a C_2B_3 cluster by two C−B connections, gave a C_s-symmetric geometry **12**. This was characterized as a transition structure at RHF/6-31G*. (Optimization without symmetry constraints converged to a spirocyclic structure with a six- and a three-membered ring.) Computed ^{11}B-NMR-chemical shifts for **12** of +32.5 (B1), +3.2 (B4,5) and +84.6 ppm are in gross disagreement with experimental data (−28.9, +23.3, +64.0 ppm). An alternative starting geometry whose larger B4−B5 separation allows the spiro carbon atom to become part of the cluster optimized to structure **3a**, 63.9 kcal mol^{-1} lower in energy than **12**. Chemical shifts computed for **3a** (B1: −34.0, B4,6: 8.7, B5′: 40.2; C2,3: 108.6, C5: 93.6, C5′: 10.4) are in acceptable agreement with measured values (see Table 1) when substituent effects are

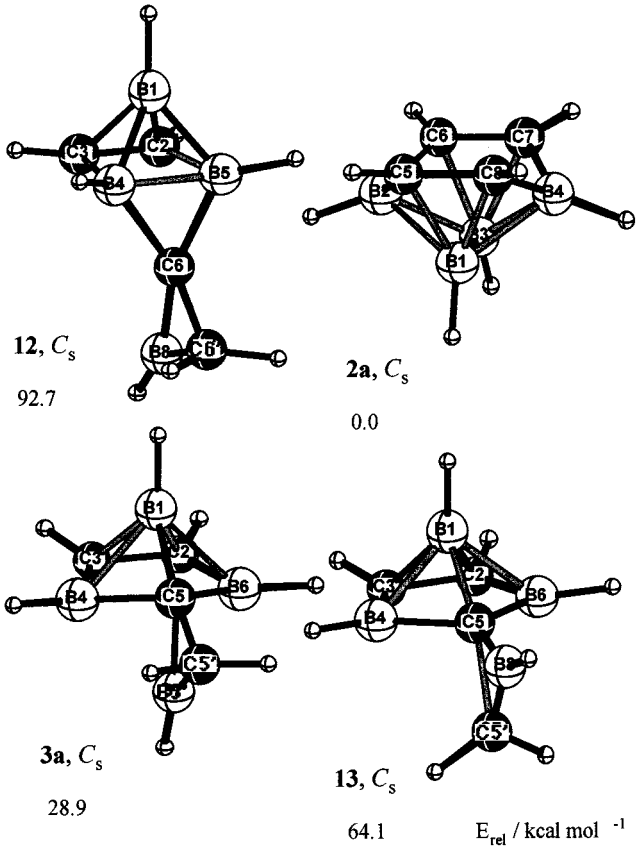


Figure 3. Structures and relative energies [MP2(fc)/6-31G* + 0.89 ZPE(HF/6-31G*] of some $C_4B_4H_8$ isomers

Table 1. Experimental chemical shifts[a] of the cage nuclei of **2**, **3**, **9**, **10** and **11** in comparison to values computed for model compounds **2b** and **3b**[b] (compare Figure 4) at GIAO-SCF/6-31G*//MP2(fc)/6-31G*

	2	**3**	**9**[c]	**10**	**11**	**2b**	**3b**
δ^{11}B(1,3)	0.6					−3.0	
δ^{11}B(1)		−28.9	−36.9	−30.2	−38.5		−30.0
δ^{11}B(2,4)	−4.5					−7.9	
δ^{11}B(4,6)		+23.3	+22.1	+25.0	+21.7		+17.6
δ^{13}C	120.8					128.9	
δ^{13}C(2,3)		98.9	105.9	94.0	n.m.		98.5
δ^{13}C(5)		85.1	55.2	83.6	n.m.		82.5
δ^{13}C(5′)		22.5	16.5	23.0	n.m.		7.2
δ^{11}B(5′)		+64.0		+13.5	+86.7		+49.8

[a] Solution of a mixture of **2** and **3** in $CDCl_3$ (25°C); solutions of mixtures of **2** and **9** and **2** and **10** in C_6D_6 (25°C); n.m.: not measured. − [b] **2b** and **3b** are the *B*-methyl-substituted analogs of **2** and **3**. − [c] Hexaethyl-2,3,5-tricarba-*nido*-hexaborane(7).[8]

taken into account. A model better than **3a**, the tetrakis(*B*-methylated) structure **3b**, gives satisfactory overall agreement although the B5′ chemical shift is 14.2 ppm too low. We compute a B4,6−B5′ separation of 206.2 pm for the parent **3a**. But this distance is increased to 211.6 pm for the better per(*B*-methylated) model (and probably is even larger with ethyl substitution). The $C_4B_4H_8$ tetracarba-*nido*-octaborane structure **2a** is 28.9 kcal mol^{-1} more stable than **3a**. The difference between the tetrakis(*B*-methyl) derivatives **2b** and **3b** is 26.2 kcal mol^{-1} (//MP2(fc)/6-31G*).

Compound **3a** is a derivative of 2,3,5-tricarbahexaborane(7), for which the *endo*-C5−H bond was shown to be asymmetrically bent towards one neighboring boron atom (partially bridging).[9] For **3a**, no evidence for a similar bending of the *endo*-C5−B5 bond was found; the C_s structure is a minimum and the C5−B5 distance is not significantly elongated (150.9 pm). However, the *endo*-B atom does interact with the cage: Hyperconjugative donation from the cage results in a 0.34-electron population of the formally empty p(B5′) orbital according to an NBO analysis (0.31 for **3b**).[18] As a consequence, the NLMO/NPA[18] bond order between the *exo*-B5′ atom and the basal B4,6 atoms is 0.23 (0.31 for **3b**). This compares with 0.73 and 0.87 (0.62 and 0.70 for **3b**) between B5′ and C5 and the methylene C5′ atom, respectively. This hyperconjugation confers considerable stabilization. Thus, **13**, where B5′ is in *exo* position, is 35.3 kcal mol^{-1} less stable than **2a**. The B4,6−B5′ bond order in **3** is only 0.06 and the p(B5′) orbital has a population of only 0.06 electrons. (The *exo*-B5′ isomer related to **12** is only 4.9 kcal mol^{-1} higher in energy than **12**.)

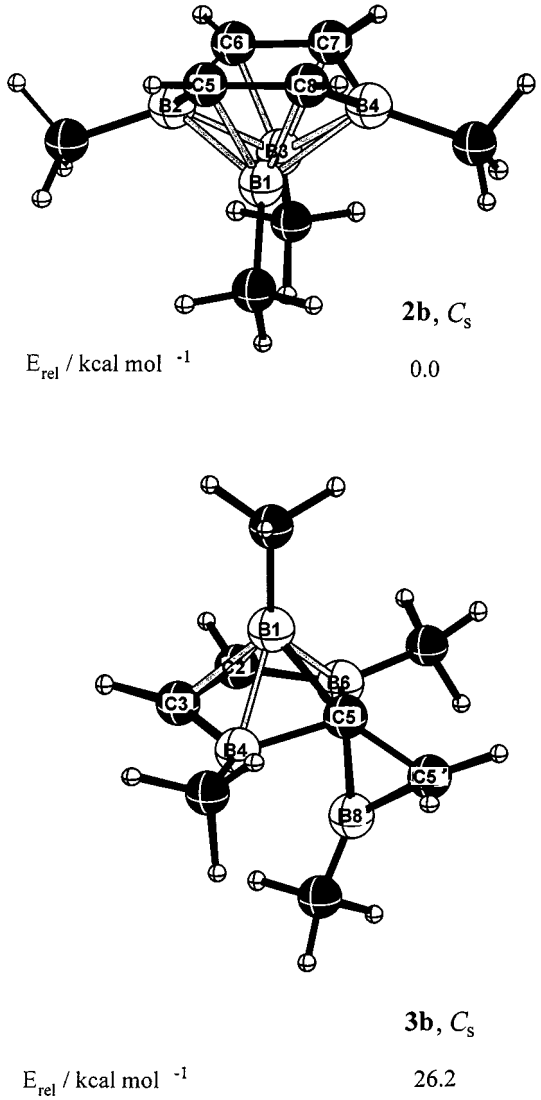


Figure 4. Geometries (bond lengths in pm) of model compounds **2b** (B1−C2 172.8, B1−B4 184.9, B1−C5 161.0, C2−C3 144.5, C2−B6 152.0, B4−C5 161.4, C5−C5′ 150.8, C5−B5 151.1, C5′−B5 158.3) and **3b** (B1−B2 186.5, B1−B3 172.9, B1−C5 170.7, B2−C4 158.5, C5−B8 139.3), optimized at MP2(fc)/6-31G*

Experimental Section

General: The preparation and the handling of samples was carried out under N_2 or Ar, observing all necessary precautions to exclude traces of oxygen or moisture. Commercial starting materials were employed (γ-picoline, BuLi in hexane (1.6 M)] or were prepared as described [Et_2BH,[19] $Et_2B-C\equiv C-BEt_2$[4]]. − NMR spectra: Bruker ARX 250 and DRX 500 spectrometers; the latter was equipped with a triple-resonance probehead for $^{13}C\{^1H,^{11}B\}$ experiments; chemical shifts are given with respect to Me_4Si [δ^1H ($CHCl_3/CDCl_3$) = 7.24; δ^1H ($C_6C_5CD_2H$) = 2.03; $\delta^{13}C$ ($CDCl_3$) = 77.0; $\delta^{13}C$ ($C_6D_5CD_3$) = 20.4] and $Et_2O \cdot BF_3$ [$\delta^{11}B$ = 0 for $\Xi(^{11}B)$ = 32.083971 Mhz].

1,2,3,4-Tetraethyl-5,6,7,8-tetracarba-*nido*-octaborane(8) (2) and Its Spiro Isomer 3: After heating of a solution of 3.57 g (21.7 mmol) of bis(diethylboryl)ethyne in 5.0 mL of Et_2BH (57.1 mmol hydride[20]) at 80°C for a period of 24 h, it was saturated with ethene (reactive B−H are converted into B−Et bonds). Fractional distillation under reduced pressure first gave 0.97 g (21%) of a mixture (65:35) of compounds **2** and **3** (b.p. 75−85°C/10^{-4} Torr). The residue contained polymeric material and **4** which could be isolated as described.[5] Repeated distillation did not lead to further separation of **2** and **3**, and a small amount of this mixture was used to obtain the NMR data of **3** and to carry out the reactions of **3** with γ-picoline and BuLi (by adding the γ-picoline and BuLi to the carborane mixture at −78°C, warming to room temperature and removing all volatile material in vacuo). Treatment of 0.9 g (4.2 mmol) of the carborane mixture with a solution of Na[Et_3BH] in hexane (6 M; 0.5 mL; 3 mmol of hydride) at room temperature gave, after filtration and washing of the insoluble material with hexane (15 mL), a colorless solution containing only Et_3B and the carborane **2** (^{11}B NMR). Compound **2** (0.41 g; 9% relative to **1**; b.p. 82°C/10^{-4} Torr) was obtained as a colorless liquid in high purity (suitable for growing single crystals for X-ray analysis; vide infra) after threfold fractional distillation (see ref.[4] for NMR and MS data of **2**).

3: ^1H NMR (500.1 MHz, 25°C, $CDCl_3$): δ = 5.24 (s, 2 H, C2,3-H), 1.64 (s, 2 H, C5−CH_2), 0.19, 0.56 (q, t, 5 H, B1−Et), 0.83, 0.69, 1.06 (m, m, t, 10 H, B4,6−Et), 1.20, 1.01 (m, t, 5 H, C5−BEt). − ^{11}B NMR (80.3 MHz, 25°C, $CDCl_3$): δ = −28.9 (B1), 23.3 (B4,6), 64.0 (B5′). − ^{13}C NMR (125.8 MHz, 25°C, $CDCl_3$): δ = 98.9 (br., C2,3), 85.1 (br., C5), 22.5 (br., CH_2), −0.4 (br.), 10.6 (B1−Et), 4.0 (br.), 11.2 (B4,6−Et), 11.7 (br.), 12.0 (BEt).

Structure Determination of 2: Compound **2**, $C_{12}H_{24}B_4$, formula weight 211.55, crystallized from the colorless neat liquid by cooling

to 168 K and application of a miniature zone-melting procedure using a CO_2 laser beam[21] as a cylindrical crystal (diameter 0.3 mm) which was measured at 120 K with a Nicolet R3 diffractometer with graphite-monochromized Mo-K_α radiation. Cell dimensions of the triclinic system: a = 8.044(4), b = 9.114(4), c = 10.557(5) Å, α = 71.89(3), β = 88.79(4), γ = 70.13(3)°, V = 688.7(5) Å^3, Z = 2, space group $P\bar{1}$, $\rho_{calcd.}$ = 1.020 gcm^{-3}, μ = 0.052 mm^{-1}, ω-scan data collection of 2567 intensities ($2\Theta_{max}$ = 50°), 2422 independent (R_{merg} = 0.0388), 1756 observed [$F_o \geq 4\sigma(F)$], structure solution with direct methods and refinement on F^2 with Siemens SHELXTL-Plus program package (version 5.03), $R1$(obsd. data) = 0.0577, $wR2$(all data) = 0.1866, GOF = 1.060, $w^{-1} = \sigma^2(F_o^2) + (0.0558 \cdot P)^2 + 0.55 \cdot P$), where $P = [(\max F_o^2) + (2\ F_c^2)]/3$, maximum/minimum residual electron density 0.208/−0.196 e Å^{-3}.

Acknowledgments

Support of this work by the Deutsche Forschungsgemeinschaft and the Fonds der Chemischen Industrie is gratefully acknowledged.

[1] [1a] T. P. Fehlner, *J. Am. Chem. Soc.* **1977**, *99*, 8355−8356. − [1b] T. P. Fehlner, *J. Am. Chem. Soc.* **1986**, *102,* 3426−3430.
[2] [2a] M. G. L. Mirabelli, L. G. Sneddon, *Organometallics* **1986**, *5*, 1510−1511. − [2b] R. N. Grimes, personal communication, **1998**.
[3] W. Siebert, M. E. M. El-Esawi, *Chem. Ber.* **1979**, *112*, 1480−1481.
[4] B. Wrackmeyer, H.-J. Schanz, W. Milius, *Angew. Chem.* **1997**, *109*, 1145−1147; *Angew. Chem. Int. Ed. Engl.* **1997**, *36*, 1117−1119.
[5] B. Wrackmeyer, H.-J. Schanz, M. Hofmann, P. v. R. Schleyer, *Angew. Chem.* **1998**, *110*, 1329−1331; *Angew. Chem. Int. Ed. Engl.* **1998**, *37*, 1245−1247.
[6] [6a] M. Bühl, in *Encyclopedia of Computational Chemistry* (Ed.: P. v. R. Schleyer), Wiley, Chichester, in press. − [6b] M. Bühl, P. v. R. Schleyer, *J. Am. Chem. Soc.* **1992**, *114*, 477−491. − [6c] M. Bühl, J. Gauss, M. Hofmann, P. v. R. Schleyer, *J. Am. Chem. Soc.* **1993**, *115*, 12385−12390. For an extensive list of references to ab initio/IGLO/NMR applications see: [6d] M. Diaz, J. Jaballas, D. Tran, H. Lee, J. Arias, T. Onak, *Inorg. Chem.* **1996**, *35*, 4536.
[7] [7a] A. Feßenbecker, A. Hergel, R. Hettrich, V. Schäfer, W. Siebert, *Chem. Ber.* **1993**, *126*, 2205. − [7b] T. Kuhlmann, H. Pritzkow, U. Zenneck, W. Siebert, *Angew. Chem*. **1984**, *96*, 994−996; *Angew. Chem. Int. Ed. Engl*. **1984**, *23*, 965−967. − [7c] J. Zwecker, T. Kuhlmann, H. Pritzkow, W. Siebert, U. Zenneck, *Organometallics* **1988**, *7*, 2316. − [7d] W. Siebert, *Pure Appl. Chem.* **1988**, *60*, 1345. − [7e] W. Siebert, in *Current Topics in the Chemistry of Boron* (Ed.: G.W. Kabalka), Royal Society of Chemistry, Cambridge, **1994**, pp. 269−274.
[8] B. Wrackmeyer, H.-J. Schanz, *Main Group Met. Chem.* **1998**, *21*, 29−32.
[9] M. Hofmann, M. A. Fox, R. Greatrex, R. E. Williams, P. v. R. Schleyer, *J. Organomet. Chem.* **1998**, *550*, 331−340.
[10] [10a] K. Wade, *J. Chem. Soc., Chem. Commun*. **1971**, 792−793. − [10b] K. Wade, *Adv. Inorg. Chem. Radiochem*. **1976**, *18*, 1−67. − [10c] R. E. Williams, *Adv. Inorg. Chem. Radiochem*. **1976**, *18*, 67.
[11] H. Nöth, B. Wrackmeyer, "NMR Spectroscopy of Boron Compounds" in *NMR − Principles and Progress* (Eds.: P. Diehl, E. Fluck, R. Kosfeld), vol. 14, Springer, Berlin, **1978**.
[12] Crystallographic data (excluding structure factors) have been deposited with the Cambridge Crystallographic Data Centre as supplementary publication no. CCDC-101626. Copies of these data can be obtained free of charge on application to CCDC, 12 Union Road, Cambridge, CB21EZ, UK [Fax: int. code + 44-1223/336-033; E-mail: deposit@ccdc.cam.ac.uk].
[13] R.E. Williams, in *Electron Deficient Boron and Carbon Clusters* (Eds.: G.A. Olah, K. Wade, R.E. Williams), Wiley, New York, **1991**, chapter 2.
[14] M. Antipin, R. Boese, D. Bläser, A. H. Maulitz, *J. Am. Chem. Soc.* **1997**, *119*, 326−333.
[15] R. Boese, D. Bläser, N. Niederprüm, M. Nüsse, W. A. Brett, P. von Ragué Schleyer, M. Bühl, N. J. R. van Eikema Hommes, *Angew. Chem.* **1992**, *104*, 356−358; *Angew. Chem. Int. Ed. Engl.* **1992**, *31*, 314−316.
[16] Geometries have been optimized at the MP2(fc)/6-31G* level of theory using the Gaussian 94 program: M. J. Frisch, G. W. Trucks, H. B. Schlegel, P. M. W. Gill, B. G. Johnson, M. A. Robb, J. R. Cheeseman, T. Keith, G. A. Petersson, J. A. Montgomery, K. Raghavachari, M. A. Al-Laham, V. G. Zakrzewski, J. V. Ortiz, J. B. Foresman, J. Cioslowski, B. B. Stefanov, A. Nanayakkara, M. Challacombe, C. Y. Peng, P. Y. Ayala, W. Chen, M. W. Wong, J. L. Andres, E. S. Replogle, R. Gomperts, R. L. Martin, D. J. Fox, J. S. Binkley, D. J. Defrees, J. Baker, J. P. Stewart, M. Head-Gordon, C. Gonzalez, and J. A. Pople, *Gaussian 94, Revision E.2*, Gaussian, Inc., Pittsburgh PA, **1995**.
[17] T. P. Onak, H. L. Landesman, R. E. Williams, *J. Phys. Chem.* **1959**, *63*, 1533.
[18] A. E. Reed; L. A. Curtis; F. Weinhold, *Chem. Rev.* **1988**, *88*, 899.
[19] R. Köster, P. Binger, *Inorg. Synth.* **1974**, *15*, 141−149.
[20] B. Wrackmeyer, H.-J. Schanz, W. Schüßler, R. Köster, *Fresenius J. Anal. Chem.*, in the press.
[21] [21a] R. Boese, M. Nussbaumer, in *Correlations, Transformations, and Interactions in Organic Crystal Chemistry*, vol. 7 (Ed.: D. W. Jones, A. Katrusiak), Oxford University Press, Oxford, England, **1994**, p. 20−37. − [21b] V. R. Thalladi, H.-C. Weiss, D. Bläser, R. Boese, A. Nangia, G. R. Desiraju, *J. Am. Chem. Soc.*, in press.

Received October 13, 1998
[I98352]

Models for Terminal Ni(S-Cysteine) Modification in [NiFe]Hydrogenases by Iodoacetamide and Iodoacetate

Jason J. Smee,[a] Dawn C. Goodman,[a] Joseph H. Reibenspies,[a] and Marcetta Y. Darensbourg*[a]

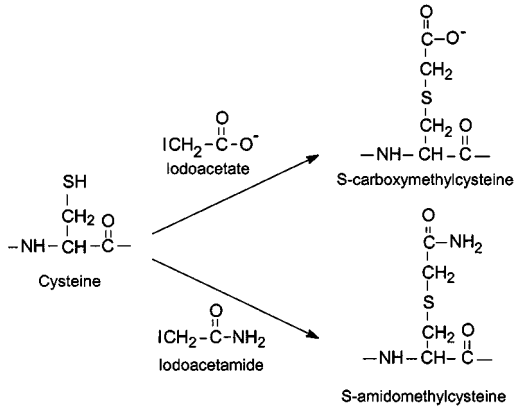
Keywords: Nickel / Sulfur ligands / Hydrogenases / Bioinorganic chemistry

The *cis*-dithiolate complex [*N*,*N*′-bis(2-mercaptoethyl-2-methylpropyl)-1,5-diazacyclooctane]nickel(II) (**Ni-1***) **reacts with stoichiometric amounts of iodoacetamide to yield *S*-alkylated, mono- and diacetamide complexes, [(AA)Ni-1*][I] and [$(AA)_2$Ni-1*][$I]_2$. Their molecular structures are established by X-ray crystallography and find the former in pseudo-square planar geometry with no additional coordination of the amide functionality, while the latter is an octahedral $N_2S_2O_2Ni^{II}$ complex. The assignment of the axial coordination ligands as amide oxygen atoms is consistent with IR-spectroscopic ν(C=O) results both in the solid and solution states. The complexes are further characterized by UV/Vis spectroscopy, conductance measurements, and electrochemical studies. Comparisons are drawn between the alkylation of these simple dithiolate complexes and the loss of [NiFe]hydrogenase activity upon addition of alkylating agents.**

Introduction

Cysteine modification reagents such as sodium iodoacetate ($ICH_2CO_2^-Na^+$) and iodoacetamide [$ICH_2C(=O)NH_2$] are widely used to probe the involvement of cysteine residues in enzymatic systems.[1] S_N2 attack by the nucleophilic cysteinate sulfur atom produces *S*-(carboxymethyl)cysteine and *S*-(amidomethyl)cysteine, respectively (Scheme 1), which typically results in loss of catalytic activity. While Scheme 1 represents the reactive S as sulfhydryl, it is well known that deprotonated cysteines are more reactive towards alkylating agents. In some cases, the modified cysteine unit has been tracked by radiolabelling, thus permitting identification of the active site position in the protein. For example, the zinc metalloenzyme cobalamin-independent methionine synthase (MetE) contains a reactive zinc cysteinate residue at position 726 that is required for enzymatic activity.[2]

Iodoacetamide and acetylene were shown to inhibit the catalysis of H/D exchange of H_2/D_2O by the [NiFe]hydrogenase enzyme of *Thiocapsa roseopersicina*, the former irreversibly.[3] Inhibition by acetylene is reversible; upon removal of the acetylene, nearly maximal activity is restored. On placing the enzyme under acetylene and subsequently treating it with iodoacetamide, the H/D exchange was inhibited, but the activity could be partially restored by removing both the iodoacetamide and the acetylene. Notably, the irreversible inhibition by iodoacetamide occurs only in the reduced, active form of the enzyme. Alkylation with iodoacetamide in the oxidized, inactive form followed by reductive activation of the enzyme showed maximal H/D exchange activity. Although the alkylated residues were not identified, experiments which monitored the levels of ^{14}C-labeled *S*-(amidomethyl)cysteine indicated that the reduced enzyme contained a greater amount of cysteine modification in the portion of the protein containing the active site. These results suggest the possibility of active site modification.[3]



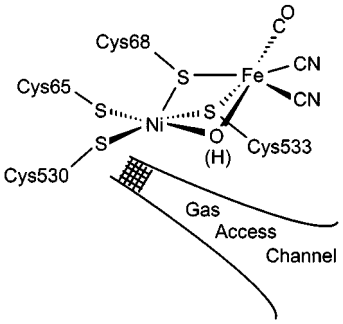
Scheme 1. Products resulting from alkylation of the cysteine sulfhydryl groups with iodoacetate and iodoacetamide; the other product, HI, is not shown

The X-ray crystal structure of an analogous [NiFe]H_2ase, isolated from *Desulfovibrio gigas* was recently solved[4a] and contains an $Ni(S-Cys)_4$ unit comprised of two terminal cysteines and two cysteines which bridge to an $Fe(CN)_2(CO)$ unit.[4b,4c] The oxidized state also contains a bridging ligand tentatively assigned as an oxo or hydroxo species, which is expected to be absent in the reduced or active form of the enzyme.[4b] Analysis of the X-ray crystal structure of *D. gigas* also reveals that the active site is buried ca. 30 Å from the protein surface with several cavities that converge on a unique entrance to the active site.[4b] In a separate study, xenon pressurization of crystals derived from *Desulfovibrio fructosovorans*, a [NiFe]H_2ase with sig-

[a] Department of Chemistry, Texas A&M University, College Station, TX 77843-3255, USA
Fax: (internat.) + 1-409/845-0158
E-mail: marcetta@mail.chem.tamu.edu

 © WILEY-VCH Verlag GmbH, D-69451 Weinheim, 1999 1434–1948/99/0303–0539 $ 17.50+.50/0

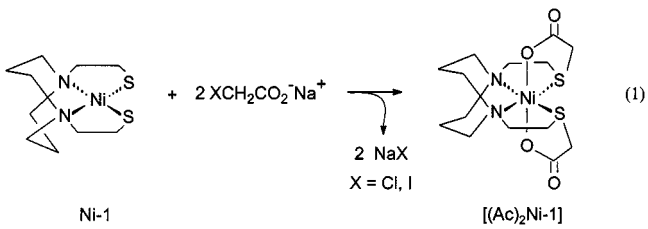
nificant homology to *D. gigas*, confirmed the cavities to be a gas access channel.[5] It is thus tempting to conclude that the channel provides a means for H_2 molecules, as well as acetylene or iodoacetamide, to reach the active site. Experimentally, i.e., by the location of the Xe atoms, this channel was found to approach the active site at the terminal Ni(S−Cys) ligands, specifically $Ni-S-Cys_{530}$, to within 4 to 5 Å (Scheme 2). Electron density maps suggest that there are protein residues or water molecules which prevent closer contact. Molecular dynamics calculations find that H_2 molecules can, however, penetrate to within 1.4 and 1.8 Å of the nickel and iron atoms, respectively.[5] Since EPR and IR spectroscopies of [NiFe]H_2ases derived from various bacteria[4b,6,7] are similar to one another, it is reasonable to expect a similar active site composition, although gas access routes to the active site could differ.



Scheme 2. A representation of the hydrophobic channel leading to the active site of *D. fructosovorans* [NiFe]H_2ase

Thus, the structural studies on [NiFe]H_2ases suggest some, and at most, limited, access to the active-site metal-bound cysteine. Indeed the specific residues alkylated by iodoacetamide in *T. roseopersicina* [NiFe]H_2ase have not been identified. Nevertheless there are examples of metal-bound cysteine modification at the active sites of other metalloproteins such as the zinc-containing MetE protein described above.[2] A fundamental question to be addressed by small molecule biomimics is, assuming active site access, will nickel-bound cysteines be alkylated by iodoacetamide or iodoacetate, and, if so, what are the structural, spectroscopic and electrochemical consequences?

One appropriate study, designed for other purposes, used the N_2S_2Ni square planar complex, *N*,*N*′-bis(mercaptoethyl)-1,5-diazacyclooctanenickel(II) (**Ni-1**).[8] The *cis*-dithiolate sulfur atoms of **Ni-1** are highly reactive with alkylating reagents, and in the case of sodium haloacetate salts, the **Ni-1** species yielded the octahedral $N_2S_2O_2$ complex shown in Equation 1.[8]

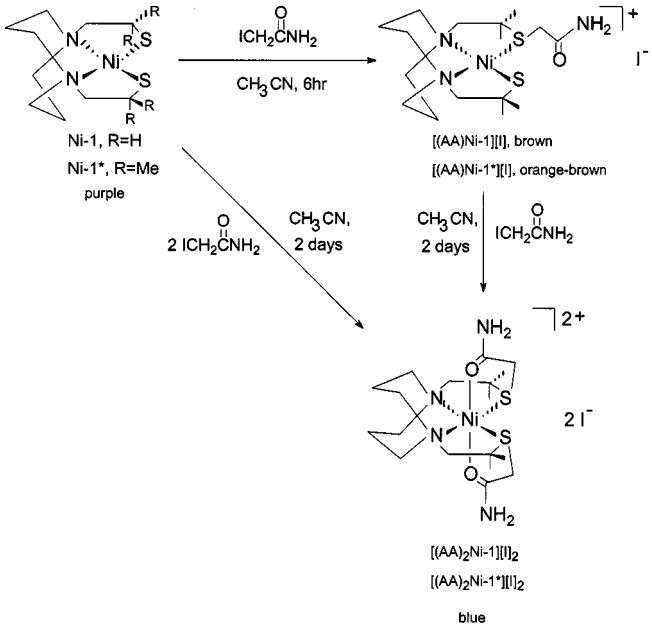


Given the relevance of these results to the [NiFe]H_2ase cysteine modification described above, we have explored similar reactions of **Ni-1** as well as the sterically more hindered *N*,*N*′-bis(2-mercapto-2-methylpropane)-1,5-diazacyclooctanenickel(II) (**Ni-1***) with iodoacetamide. Described below are the fully characterized products of **Ni-1*** reactions with one and two equivalents of iodoacetamide. The X-ray crystal structures will show the two possibilities of S-modification, i.e., with and without additional coordination of functional groups.

Results and Discussion

Syntheses and Solution Properties

In contrast to the reactions[8] of $XCH_2CO_2^-Na^+$ (X = Cl, I) with the parent (bme-daco)Ni (**Ni-1**) complex for which a monoalkylated complex could not be isolated (Equation 1), both the mono- and dialkylated species of **Ni-1** and the sterically encumbered **Ni-1*** have been isolated using iodoacetamide as the alkylating agent. Scheme 3 summarizes the synthetic procedures and stick-drawn structures resulting from structural characterization in the solid state (vida infra).



Scheme 3. Reactions of **Ni-1** and **Ni-1*** with one and two equivalents of iodoacetamide

As depicted in Scheme 3, the monoacetamide derivative of **Ni-1***, **[(AA)Ni-1*][I]**, is a four-coordinate pseudo-square planar complex and is soluble in most polar solvents including H_2O, MeOH and MeCN, all of which result in green solutions. In contrast, the brown solid **[(AA)Ni-1][I]** yields brown solutions in the same solvents. Minor differences in color are also seen for the **[(Me)Ni-1*][I]**[9] and **[(Me)Ni-1][I]**[10] species and are reflected in the d-d transitions as seen in Table 1 (see entries 3, 5, 7 and 9). The molar conductivities of **[(AA)Ni-1*][I]** and **[(AA)Ni-1][I]**,

measured in MeCN, are 166 and 161 S/cm·mol respectively, extrapolated to infinite dilution; these values fall in the range of uni-uni electrolyte solutions in CH_3CN[13] and indicate complete ionization of iodide in solution. Thus, we conclude that both **[(AA)Ni-1*][I]** and **[(AA)Ni-1][I]** are four-coordinate monocations in solution and the difference in color results from differences in ligand fields (see below).

The dialkylated products **[$(AA)_2$Ni-1*][I_2]** and **[$(AA)_2$Ni-1][I_2]** were isolated as blue solids with UV/Vis-spectral properties similar to those of **[$(Ac)_2$Ni-1]** (see entries 4, 6 and 11 of Table 1). For comparison, the dimethylated, four-coordinate derivatives **[$(Me)_2$Ni-1*][I_2]** and **[$(Me)_2$Ni-1][I_2]** have significantly different UV/Vis properties (entries 8 and 10 in Table 1) consistent with the conclusion that **[$(AA)_2$Ni-1*][I_2]** and **[$(AA)_2$Ni-1][I_2]** are six-coordinate complexes with Ni^{2+} in an $N_2S_2O_2$ coordination environment. **[$(AA)_2$Ni-1*][I_2]** and **[$(AA)_2$Ni-1][I_2]** are only slightly soluble in MeCN and are quite soluble in H_2O and MeOH, all of which yield blue solutions.

Table 1. UV/Vis[a] and IR[b] spectroscopic data (AA = *S*-acetamide; Ac = *S*-acetate; sh = shoulder)

Entry	Compound	λ_{max} [nm] (ε)	ν(C=O) [cm^{-1}]
1	Ni-1*[c,d]	353 sh, 498 (91)	–
2	Ni-1[c,e]	506 (640), 602 sh	–
3	[(AA)Ni-1*][I]	604 (51), 456 (124)	1684 (1692)
4	$[(AA)_2$Ni-1*][$I]_2$	580 (23), 356 (29)	1646s, 1591m[f] (1663s)
5	[(AA)Ni-1][I]	592 sh, 472 (137)	1676 (1713)
6	$[(AA)_2$Ni-1][$I]_2$	580 (36), 362 (51)	1649s, 1590m[f] (1663s)
7	[(Me)Ni-1*][I][c]	606 sh, 458 (150)	–
8	$[(Me)_2$Ni-1*][$I]_2$[c,g]	466 (115)	–
9	[(Me)Ni-1][I][c,e]	616 sh, 460 (130)	–
10	$[(Me)_2$Ni-1][$I]_2$[c,e]	656 (90), 428 (930)	–
11	$[(Ac)_2$Ni-1][h]	600 (49), 364 (31)	1593s, 1385m[d,f]
12	$CH_3C(=O)NH_2$	–	1690

[a] Data obtained in CH_3OH unless otherwise noted. – [b] IR data collected as KBr pellets, and, in parentheses, acetonitrile solution. – [c] Data obtained in CH_3CN. – [d] Ref.[11] – [e] Ref.[10] – [f] Assigned as an asymmetric carbonyl stretch. – [g] Ref.[12] – [h] Ref.[8]

Infrared Spectroscopy

Table 1 also lists the ν(C=O) stretching frequencies for acetamide, $CH_3C(=O)NH_2$, and for the complexes derivatized with iodoacetamide. The monoacetamide derivatives exhibit ν(C=O) values similar to free acetamide (entries 3, 5 and 12 in Table 1) whereas the diacetamide derivatives (entries 4 and 6 in Table 1) show a decrease of ca. 35 cm^{-1} in ν(C=O) relative to the monoacetamide complexes. This is consistent with the UV/Vis-spectroscopic results which suggest that oxygen binds to the nickel only in the case of the dialkylates **[$(AA)_2$Ni-1][I_2]** and **[$(AA)_2$Ni-1*][I_2]**. Thus, ν(C=O) is diagnostic for amide oxygen coordination to a metal center. Such shifts in the carbonyl stretching frequencies have been observed for other complexes with ligating amido groups.[14]

Electrochemistry

The cyclic voltammogram of **[(AA)Ni-1*][I]**, Figure 1, shows an irreversible cathodic event at $E_{pc} = -1.30$ V (vs NHE) and two oxidations ascribed to iodide electrochemistry. Figure 2, the cyclic voltammogram of **[$(AA)_2$Ni-1*][I_2]**, shows a quasi-reversible cathodic event at $E_{1/2} = -0.89$ V as well as a quasi-reversible anodic event at $E_{1/2} = +1.44$ V; two oxidations and one reduction due to iodide (or I_3^-) are also present.

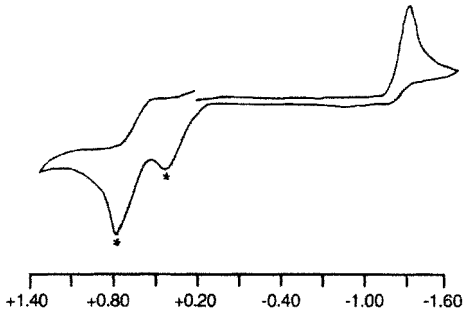


Figure 1. Cyclic voltammogram of **[(AA)Ni-1*][I]** in CH_3CN; all potentials referenced to NHE (* = peaks arising from iodide counterion)

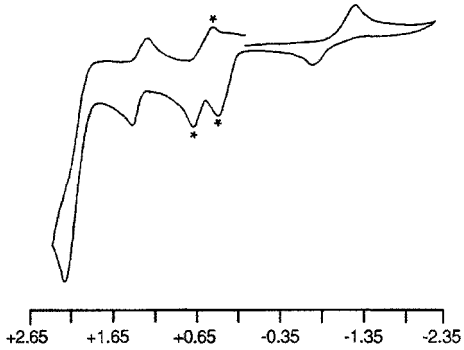
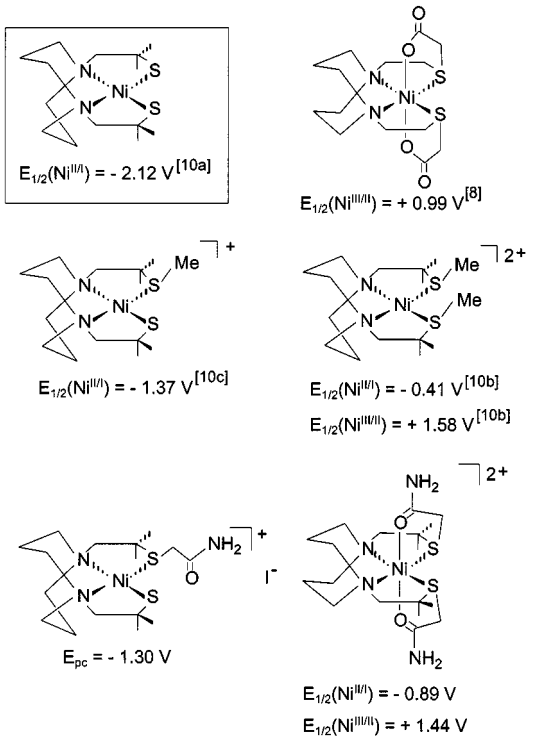


Figure 2. Cyclic voltammogram of **[$(AA)_2$Ni-1*][I_2]** in CH_3CN; all potentials referenced to NHE (* = peaks arising from iodide counterion)

Scheme 4 presents the previously well-defined redox couples of the four-coordinate methyl thioether derivatives **[(Me)Ni-1*][I]**[9] and **[$(Me)_2$Ni-1*][I_2]**[12] and the six-coordinate diacetate derivative **[$(Ac)_2$Ni-1]** for comparison to those of the acetamide complexes **[(AA)Ni-1*][I]** and **[$(AA)_2$Ni-1*][I_2]**.[15] The square planar monomethyl derivative has an $Ni^{II/I}$ redox couple ca. 750 mV more positive than that of the **Ni-1*** dithiolate precursor, while the dimethyl derivative, the dication, shows an additional positive gain of +960 mV. The enhanced accessibilities of the $Ni^{II/I}$ redox couples are attributed mainly to the positive charge resulting from successive *S*-methylations and the transformation of anionic thiolates into neutral thioether donors.[10] Consistent with this is the observation that the $Ni^{II/I}$ reduction of the neutral **[$(Ac)_2$Ni-1]** complex is not observed

when scanned to −2.0 V in CH_3CN. The increased electron density on the nickel center provided by the two anionic axial donors accounts for the negative shift.



Scheme 4. Comparison of the $Ni^{II/I}$ reduction potentials ($E_{1/2}$ vs. NHE) of **[(AA)Ni-1*][I]** and **$[(AA)_2$Ni-1*$][I]_2$** with those of **[(Me)Ni-1*][I]**, **$[(Me)_2$Ni-1*$][I]_2$**, and **$[(Ac)_2$Ni-1]**

The similarity in reduction potentials of **[(AA)Ni-1*][I]** and the $Ni^{II/I}$ redox couple of **[(Me)Ni-1*][I]** suggests that the ligand environments, geometries, and charges are nearly the same in the two complexes. The dialkylated compounds differ. The increased electron density on the nickel center in the octahedral complex accounts for the relative difficulty (by ca. 480 mV) in the reduction of **$[(AA)_2$Ni-1*$][I]_2$** as compared to the four-coordinate **$[(Me)_2$Ni-1*$][I]_2$**, Scheme 4. Nevertheless, the $Ni^{II/I}$ couple of the dication is at minimum 1.1 V more positive than that of the neutral **$[(Ac)_2$Ni-1]** complex.

The anodic events for the **$[(Me)_2$Ni-1*$][I]_2$**, **$[(AA)_2$Ni-1*$][I]_2$** and **$[(Ac)_2$Ni-1]** complexes, Scheme 4, are assigned as metal-based oxidation, presumably $Ni^{II/III}$. The quasi-reversible oxidation wave for **$[(AA)_2$Ni-1*$][I]_2$** is closer in value to **$[(Me)_2$Ni-1*$][I]_2$** (ca. 140 mV more accessible) than to **$[(Ac)_2$Ni-1]** (ca. 440 mV less accessible). These results indicate that both the $Ni^{II/I}$ and the $Ni^{II/III}$ redox potentials are predominantly determined by the charge of the complex, with the addition of axial donor groups providing a lesser perturbation. The greater difference in the $E_{1/2}$ of the $Ni^{II/I}$ couples in **$[(Me)_2$Ni-1*$][I]_2$** and **$[(AA)_2$Ni-1*$][I]_2$** as compared to the difference in $E_{1/2}$ of the $Ni^{II/III}$ couples may be attributed to the following: 1) unlike the hexadentate ligand, the tetradentate N_2S_2 ligand has some capability to distort toward tetrahedral which eases the $Ni^{II/I}$ reduction; and 2) little, if any, ligand distortion is required to accommodate Ni^{3+}.

Molecular Structures

A portion of the crystal packing for **[(AA)Ni-1*][I]** is given in Figure 3 to highlight the intermolecular N···H···O interactions. Each complex cation is H-bonded to an adjacent cation via the carbonyl oxygen atoms and amide hydrogen atoms with N···O distances of 2.60(1) Å. These cations are stacked such that the pseudo six-membered cyclic structures form a channel through the lattice. The cyclic structure itself bonds externally to two iodide ions as seen in the N···I distance of 3.365(1) Å.

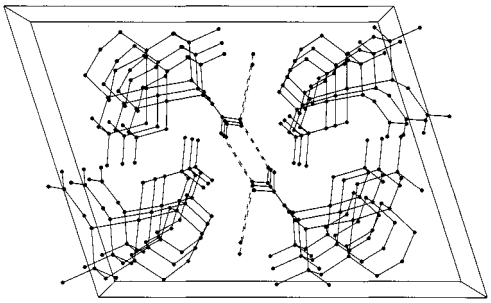


Figure 3. A portion of the crystal packing diagram of **[(AA)Ni-1*][I]** showing intermolecular hydrogen bonding; the hydrogen atoms have been omitted for clarity

Two iodide counterions and one CH_3CN solvent molecule co-crystallize with the complex cation **$[(AA)_2$Ni-1*$]^{2+}$**. The packing diagram for this salt indicates that a weak hydrogen bonding array exists between the amide hydrogen atoms and the iodide ions [I···N distances of 3.55(1) and 3.53(1) Å]; the solvent of crystallization does not appear to be involved in H-bonding.

Figures 4 and 5 display the molecular structures of the coordination complex cations of **[(AA)Ni-1*][I]** and **$[(AA)_2$Ni-1*$][I]_2$**; selected bond lengths and angles for each complex are given in Table 2. The singly alkylated compound, **[(AA)Ni-1*][I]** is four-coordinate and greatly distorted from the regular square planar geometry of the parent dithiolate complex, **Ni-1***. Despite the rigidity of the bme*-daco ligand, this distortion, a 13.6° tetrahedral twist (see Table 2 footnote), is among the largest observed for the collection of **Ni-1** and **Ni-1*** four-coordinate derivative complexes.[10−12,16] The Ni−S(2) (thioether S) distance is only slightly elongated from the Ni−S(1) (thiolate S) distance and from the average Ni−S distance [2.152(1) Å] in **Ni-1***.[11] There is no significant difference in the average Ni−N distances between **[(AA)Ni-1*][I]** and **Ni-1*** [1.995(3) Å]. Like most four-coordinate **Ni-1** and **Ni-1*** derivatives, the diazacyclooctane backbone in **[(AA)Ni-1*][I]** adopts a chair-boat configuration.

The expansion in the coordination sphere of the octahedral **$[(AA)_2$Ni-1*$][I]_2$** relative to the four-coordinate **[(Me)Ni-1*][I]** complex is seen primarily in the Ni−S dis-

Table 2. Selected bond lengths [Å], angles [°], and distortion in N_2S_2 plane [°] for **[(AA)Ni-1*][I]** and **[$(AA)_2$Ni-1*][I]$_2$**

	[(AA)Ni-1*][I]	**[$(AA)_2$Ni-1*][I]$_2$**
Ni(1)−N(1)	1.963(13)	2.100(4)
Ni(1)−N(2)	2.051(12)	2.092(4)
Ni(1)−S(1)	2.088(5)	2.402(1)
Ni(1)−S(2)	2.167(5)	2.427(1)
Ni(1)−O(1)	−	2.040(3)
Ni(1)−O(2)	−	2.052(3)
O(1)−C(16)	1.22(2)	1.238(5)
O(2)−C(18)	−	1.246(5)
C(16)−N(3)	1.330(9)	1.303(6)
C(18)−N(4)	−	1.296(6)
N(1)−Ni(1)−N(2)	89.6(5)	86.02(15)
S(1)−Ni(1)−S(2)	94.7(2)	96.44(5)
N(1)−Ni(1)−S(1)	92.3(4)	89.46(11)
N(1)−Ni(1)−S(2)	163.3(4)	172.33(12)
N(2)−Ni(1)−S(1)	175.4(4)	173.71(11)
N(2)−Ni(1)−S(2)	84.6(3)	88.45(11)
O(1)−Ni(1)−O(2)	−	167.59(13)
O(1)−C(16)−C(15)	123.3(12)	122.8(4)
O(2)−C(18)−C(17)	−	120.7(4)
N(1)−Ni(1)−O(1)	−	87.89(15)
N(1)−Ni(1)−O(2)	−	101.51(14)
N(2)−Ni(1)−O(1)	−	100.60(14)
N(2)−Ni(1)−O(2)	−	88.24(14)
S(1)−Ni(1)−O(1)	−	83.58(9)
S(1)−Ni(1)−O(2)	−	88.38(10)
S(2)−Ni(1)−O(1)	−	87.91(10)
S(2)−Ni(1)−O(2)	−	83.60(10)
N_2S_2 plane distortion[a]	13.6	6.5

[a] The N_2S_2 plane distortion angles are measured as the angle of intersection of the normals of the S(1)−X−S(2) and N(1)−X−N(2) planes, where X is the centroid of the N_2S_2 plane. As the nickel atom is not necessarily equidistant from the nitrogen and sulfur atoms, the centroid rather than Ni is used to define the planes.

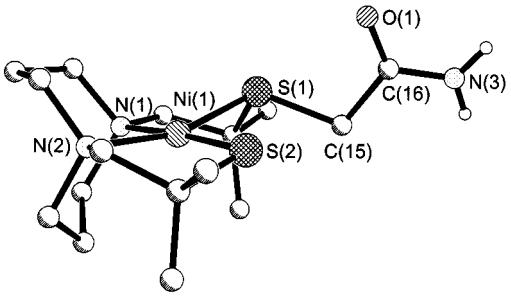


Figure 4. Ball-and-stick structure of **[(AA)Ni-1*][I]**; the iodide counterion and hydrogen atoms bonded to carbon atoms are omitted

tances (lengthened by ca. 0.3 Å). The axial atom that is bound to the nickel center also forms the shortest bond to the amide carbon atom and is thus assumed, consistent with the IR assignment above, to be O. In both **[$(AA)_2$Ni-1*][I]$_2$** and **[$(Ac)_2$Ni-1]** the diazacyclooctane framework adopts the chair-chair configuration commonly seen in other six-coordinate **Ni-1** and **Ni-1*** derivatives in which the central methylene carbon atoms are oriented towards each other and away from the $N_2S_2O_2Ni$ coordination sphere.[8,16b,17−19]

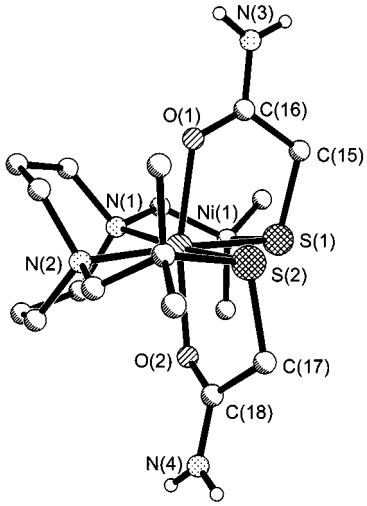


Figure 5. Ball-and-stick structure of **[$(AA)_2$Ni-1*][I]$_2$**; the iodide counterions, the solvent of crystallization and hydrogen atoms bonded to carbon atoms are omitted

Exposure to Acetylene

There are several reports of reactions of metal sulfides with acetylene to produce enedithiolates.[20] Thus, acetylene was bubbled through a CH_3CN solution of **Ni-1*** and the resultant mixture was monitored by UV/Vis spectroscopy. After 25 minutes, the spectrum of the solution was nearly identical to that of a solution containing only **Ni-1***. At that point, the addition of one equivalent of iodoacetamide caused a color change from purple to brown; the UV/Vis spectrum was found to be identical to that of **[(AA)Ni-1*][I]**. The implication is that acetylene does not inhibit or block alkylation by iodoacetamide in the Ni^{II} dithiolate complex.

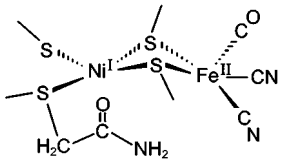
Conclusion

The *cis*-dithiolates **Ni-1** and **Ni-1*** demonstrate S-nucleophilicity with iodoacetate and iodoacetamide, forming S−C bonds and at least the potential for extending the denticity of the modified N_2S_2 ligand. In all cases the thioether S-donors remain coordinated to the nickel center. Both acetamide derivatives of **Ni-1*** show positive $Ni^{II/I}$ redox couple shifts relative to the parent dithiolate, accountable mainly to increased positive charge on the complexes. In the diacetamide derivatives of **Ni-1** and **Ni-1*** the identity of the axial donor atoms as the amide oxygen atoms was suggested by X-ray crystallography and confirmed by IR spectroscopy.

Despite the excellent nucleophilicity of the *cis*-dithiolates of **Ni-1***, the presence of acetylene did not inhibit alkylation by iodoacetamide. Two possible explanations for the reported[3] protection by acetylene of the nickel-iron heterometallic site of *T. roseopersicina* [NiFe]H_2ase from iodoacetamide deactivation are as follows: 1) acetylene might serve as a molecular block which prevents iodoacetamide access to the active site; or 2) in the reduced state of the enzyme,

presumably containing Ni^{I}, acetylene might reversibly bind to the cysteine thiolates or the nickel center to prevent alkylation.

The model study above finds that terminal thiolates bound to nickel(II) are reactive with alkylating agents and maintain Ni−S(thioether) coordination. It is expected that thiolates bound to Ni^{I}, the presumed oxidation state of Ni in the reduced active form, will show similar if not enhanced reactivity. It should be noted that the structural and molecular dynamics studies[5] of the [NiFe]H_2ase enzyme were performed on coordinates derived from the oxidized, inactive form. The active, reduced form of the enzyme could have a modified access channel, one that is more accessible to larger molecules. Thus, *assuming* the iodoacetamide moiety can reach the active site Ni(S−Cys)$_2$ unit, a possible structure of the iodoacetamide-alkylated, heterobimetallic site is depicted in Scheme 5. Amide-O coordination to the nickel center forming a distorted square pyramid (not shown), could be another possible consequence of alkylation. Additionally, the open site of the d^6 iron center expected in the reduced form of the enzyme (i.e., the μ-OH group is lost)[4] could present another amide-O binding site. In any case, *S*-alkylation would disrupt the 4 to 5 Å segment which blocks access to the active site from the gas access channel. The fact that the H/D exchange reaction of H_2/D_2O is lost in the chemically modified protein is consistent with proposals that hydrogen activation takes place at the terminal Ni(S−Cys)$_2$ unit,[21] or at the open site on the iron center. On the other hand, our studies have shown that a dramatic change in redox potentials occurs upon conversion of a thiolate to a thioether by iodoacetamide alkylation. Such a redox change is expected to overwhelm the entire range of [NiFe]H_2ase activity, influencing whatever site and mechanism is operative for H_2/H^+ catalysis.



Scheme 5. One possible structural consequence of iodoacetamide alkylation at a terminal Ni(S-Cys) residue in [NiFe]H_2ase

It is noteworthy that the iodoacetamide deactivation of the zinc-metalloenzyme MetE occurs at a particular cysteine unit (Cys726), known to be bound to zinc.[2] In this case a similar chemical process of *S*-alkylation undoubtedly blocks the transfer of the methyl group from 5-methyltetrahydrofolate to homocysteine. That is, changes in redox properties are not mechanistic options.

While the Vignais study[3] suggests the possibility of active-site cysteine modification, the identity of the modified residues was not determined in the [NiFe]H_2ase examined. Histidine and carboxylate residues, reasonably good nucleophiles, are known to be somewhat reactive with alkylating agents. The modification of these and/or cysteine residues far remote from the active site could cause structural changes in the protein which might severely disrupt the active site or prevent substrate from binding. Thus, despite the clear-cut evidence offered above and elsewhere for nickel-bound thiolate reactivity, there may be factors other than active-site modification which can lead to enzyme deactivation.

Experimental Section

General Procedures: Although the products are air-stable, they are somewhat hygroscopic and should be handled using standard Schlenk or syringe techniques using N_2 (passed through a drying tube of $CaSO_4$, molecular sieves and NaOH) or an Ar-filled glovebox (Vacuum Atmospheres). Solvents were dried according to published procedures[22] and distilled under N_2. Acetonitrile was distilled once from CaH_2 and twice from P_2O_5 and freshly distilled from CaH_2 immediately before use. Reagent grade iodoacetamide (Aldrich) was used as received.

Physical Measurements: UV/Vis spectra were measured with a Hewlett-Packard 8452A diode array spectrophotometer and quartz cells of path length 1.00 cm. Infrared spectra were recorded as KBr pellets (unless otherwise specified) using an IBM IR/32 Fourier transform single-beam spectrophotometer. Elemental analyses were performed by Canadian Microanalytical Services, Delta, British Columbia, Canada. Conductance measurements were performed with an Orion Model 160 conductance meter. − Cyclic voltammograms were recorded with a BAS-100A electrochemical analyzer using $Ag^0/AgNO_3$ reference and glassy carbon working electrodes with 0.1 M tetra-*n*-butylammonium hexafluorophosphate (TBAHFP) supporting electrolyte in CH_3CN with a platinum wire auxiliary electrode. The potentials were referenced to NHE using ferrocene (+400 mV vs NHE).

Syntheses: The **Ni-1*** and **Ni-1** complexes were synthesized and purified according to published procedures.[23] Iodoacetamide was stored inside a glovebox refrigerator (−30°C) and weighed out in the glovebox immediately before use. Unless otherwise stated all reactions were performed under N_2 and at ambient temperature (22°C).

[(AA)Ni-1*][I]: Iodoacetamide (10 mg, 0.054 mmol) was dissolved in dry CH_3CN (5 mL) and transferred to a purple 5-mL acetonitrile solution containing one equivalent of **Ni-1*** (19 mg, 0.055 mmol). A color change from purple to green was immediately observed. The solution was stirred for 6 h during which time no further color change occurred. The reaction mixture was transferred via cannula to a double test tube for ether diffusion. Red brown crystals of suitable for X-ray diffraction were obtained (yield 34%). − $C_{16}H_{32}IN_3NiOS_2$ (532.18): calcd. (found) C 36.1 (36.1), H 6.06 (5.89), N 7.90 (7.85). − FT IR (KBr): ν [$^{-1}$] = 3304, 3140, 1684. − UV/Vis (MeOH): λ_{max} [nm] (ε) = 224 (20626), 264 (7967), 308 (7262), 456 (124), 604 (51).

1,5-Diazacyclooctane-1,5-diylbis(2,2-dimethyl-3-thiapentanamide)-nickel(II) Iodide {[(AA)$_2$Ni-1*][I]$_2$}: As described above, iodoacetamide (20 mg, 1.08 mmol) in 5 mL of CH_3CN was transferred to a 5-mL CH_3CN solution containing 1/2 equivalent of **Ni-1*** (19 mg, 0.055 mmol). A color change from purple to green was observed and the solution was stirred for 48 h to assure complete reaction. The green solution was transferred via cannula to a double test tube for ether diffusion. Dark blue crystals suitable for X-ray diffraction were obtained (yield 27%). − $C_{18}H_{36}I_2N_4NiO_2S_2 \cdot CH_3CN$ (758.19): calcd. (found) C 31.7 (31.7), H 5.18 (5.10), N 9.23 (9.08). − FT IR (KBr): ν [$^{-1}$] = 3236, 3100, 1645, 1591. − UV/Vis

Table 3. Crystallographic data for **[(AA)Ni-1*][I]** and **[$(AA)_2$-Ni-1*][$I]_2$**

	[(AA)Ni-1*][I]	**[$(AA)_2$Ni-1*][$I]_2$**
Emp. formula	$C_{16}H_{32}IN_3NiOS_2$	$C_{18}H_{36}I_2N_4NiO_2S_2 \cdot CH_3CN$
Mol. mass [g/mol]	532.18	758.19
Space group	monoclinic	monoclinic
	$P2_1/c$	$P2_1/c$
a [Å]	14.892(3)	19.722(4)
b [Å]	7.903(2)	8.5270(17)
c [Å]	18.896(4)	18.766(4)
β [°]	107.86(3)	112.99(3)
V [Å^3]	2116.7(7)	2905.2(10)
Z	4	4
ρ(calcd.) [g cm^{-3}]	1.670	1.733
T [K]	298(2)	293(2)
Radiation (λ [Å])	Mo-K_α (0.71073)	Mo-K_α (0.71073)
Total no. of reflns.	3874	5271
No. of obsd. reflns.[a]	3719	5095
	$I \geq 2.0\sigma I$	$I \geq 2.0\sigma(I)$
μ [$^{-1}$]	0.2581	0.2962
$R(F)$ [$I \geq 2.0\sigma(I)$][a]	6.91%	3.65%
$S(F^2)$[a]	1.153	1.042

[a] Residuals: $R(F) = \Sigma|F_o - F_c|/\Sigma F_o$; $S(F^2) = \{\Sigma w(F_o^2 - F_c^2)^2]/[N_{data} - N_{parameters}]\}^{1/2}$.

(MeOH): λ_{max} [nm] (ε) = 220 (19914), 258 (7158), 356 (29), 580 (23).

[(AA)Ni-1][I]: As described above a 10-mL CH_3CN solution of iodoacetamide (140 mg, 0.76 mmol) was transferred to a 40-mL CH_3CN solution of **Ni-1** (220 mg, 0.76 mmol). A color change from purple to dark brown was observed and the solution was stirred for 6 h. The solvent was removed in vacuo. The remaining brown solid was dissolved in dry MeOH (ca. 10 mL) and orange-brown crystals were formed from diethyl ether diffusion (yield 5.6%). − $C_{12}H_{24}IN_3NiOS_2$ (476.07): calcd. (found) C 30.3 (30.5), H 5.08 (5.05), N 8.83 (8.73). − FT IR (KBr): ν [$^{-1}$] = 3362, 3244, 3167, 1676, 1604. − UV/Vis (MeOH): λ_{max} [nm] (ε) = 224 (20048), 304 (7970), 472 (137), 592 (53).

1,5-Diazacyclooctane-1,5-diylbis(3-thiapentamide)nickel(II) Iodide {[$(AA)_2$Ni-1][$I]_2$}: Similarly, a 10-mL CH_3CN solution of iodoacetamide (195 mg, 1.05 mmol) was transferred to a solution of **Ni-1** (153 mg, 0.525 mmol) in 40 mL of CH_3CN. An immediate color change from purple to dark brown was followed by development of a blue color and then a precipitate formed over the course of 12 h. The supernatant was removed via cannula and the precipitate washed twice with dry acetonitrile (2 × 10 mL). The product was dissolved in dry MeOH (ca. 10 mL) and dark blue crystals were formed upon diethyl ether diffusion (yield 49%). − $C_{14}H_{28}I_2N_4NiO_2S_2 \cdot CH_3OH$ (693.08): calcd. (found) C 26.0 (25.8), H 4.65 (5.10), N 8.08 (8.16). − FT IR (KBr): ν [$^{-1}$] = 3240, 3125, 1649, 1590. − UV/Vis (MeOH): λ_{max} [nm] (ε) = 220 (18836), 254 (7182), 362 (51), 580 (36).

Iodoacetamide Addition to Ni-1 in the Presence of Acetylene: A 2.5-mL aliquot of a 5 mM MeCN solution of **Ni-1*** (4.3 mg, 12.5 μmol) was transferred via cannula to a UV/Vis cell. The cell was stoppered with a rubber septum and acetylene was bubbled through the solution for 25 min and the UV/Vis spectrum was recorded; it was identical to that of **Ni-1***. A 0.2-mL portion of a 62.5 mM MeCN solution of iodoacetamide (2.3 mg, 12.5 μmol) was added to the cell via syringe; the acetylene purge was resumed. After ca. 20 min, the solution color had changed from purple to brown; the acetylene bubbling was discontinued and the UV/Vis spectrum was taken. The final UV/Vis spectrum of the **Ni-1***, acetylene and iodoacetamide mixture was identical with that of isolated **[(AA)Ni-1*][I]**.

X-ray Crystallography and Structure Solution: The X-ray crystal structure analyses were carried out at the Crystal & Molecular Structure Laboratory Center for Chemical Characterization and Analysis at Texas A&M University. Crystallographic data for the complexes **[(AA)Ni-1*][I]** and **[$(AA)_2$Ni-1*][$I]_2$** are listed in Table 3; selected parameters are listed in Table 2. Preliminary examinations and data collections were performed with a Siemens P4 X-ray diffractometer. The structures were solved by direct methods [SHELXS, SHELXTL-93].[24] Both compounds crystallize in the monoclinic space group $P2_1/c$. **[(AA)Ni-1*][I]** crystallizes with two orthogonal orientations of the Ni complex relative to the iodide positions in the asymmetric unit. This produces a disordered structure. The Ni position is common to both disordered structures. The disordered portions of the Ni complex are related by a pseudo two-fold axis parallel to the a^* axis and running through the Ni atoms. Crystallographic data (excluding structure factors) for the structures reported in this paper have been deposited with the Cambridge Crystallographic Data Center as supplementary publication nos. CCDC-102633 and -102634. Copies of the data can be obtained free of charge on application to CCDC, 12 Union Road, Cambridge CB2 1EZ, UK [Fax: int. code + 44-1223/336-033; E-mail: deposit@ccdc.cam.ac.uk].

Acknowledgments

Financial support from the National Science Foundation (CHE 94−15901) with contributions from the R. A. Welch Foundation for the work and NSF-CHE 85−13273 for the X-ray diffractometer and crystallographic computing system are gratefully acknowledged.

[1] R. L. Lundblad, *Chemical Reagents for Protein Modification*, 2nd ed., CRC Press, Boca Raton, Florida, **1991**, pp. 59−93.
[2] [2a] J. C. Gonzalez, R. V. Banerjee, S. Huang, J. S. Sumner, R. G. Matthews, *Biochemistry* **1992**, *31*, 6045. − [2b] J. C. Gonzalez, K. Peariso, J. E. Penner-Hahn, R. G. Matthews, *Biochemistry* **1996**, *35*, 12228.
[3] N. A. Zorin, B. Dimon, J. Gagnon, J. Gaillard, P. Carrier, P. M. Vignais, *Eur. J. Biochem*. **1996**, *241*, 675.
[4] [4a] A. Volbeda, M.-H. Charon, C. Piras, E. C. Hatchikian, M. Frey, J. C. Fontecilla-Camps, *Nature* **1995**, *373*, 580. − [4b] A. Volbeda, E. Garcin, C. Piras, A. L. de Lacey, V. M. Fernandez, E. C. Hatchikian, M. Frey, J. C. Fontecilla-Camps, *J. Am. Chem. Soc*. **1996**, *118*, 12989. − [4c] A. L. de Lacey, E. C. Hatchikian, A. Volbeda, M. Frey, J. C. Fontecilla-Camps, V. M. Fernandez, *J. Am. Chem. Soc*. **1997**, *119*, 7181. − [4d] M. Frey, *Struct. Bonding* **1998**, *9*, 97, and references therein. − [4e] J. C. Fontecilla-Camps, *J. Biol. Inorg. Chem.* **1996**, *1*, 91, and references therein.
[5] Y. Montet, P. Amara, A. Volbeda, X. Vernede, E. C. Hatchikian, M. J. Field, M. Frey, J. C. Fontecilla-Camps, *Nat. Struct. Biol*. **1997**, *4*, 523.
[6] [6a] R. Cammack, C. Bagyinka, K. L. Kovacs, *Eur J. Biochem*. **1989**, *182*, 357. − [6b] S. P. J. Albracht, *Biochim. Biophys. Acta* **1994**, *1188*, 167.
[7] R. P. Happe, W. Roseboom, A. J. Plerik, S. P. J. Albracht, K. A. Bagley, *Nature* **1997**, *385*, 126. K. A. Bagley, E. C. Duin, W. Roseboom, S. P. J. Albracht, W. H. Woodruff, *Biochemistry* **1995**, *34*, 5527.
[8] D. C. Goodman, T. Tuntulani, P. J. Farmer, M. Y. Darensbourg, J. H. Reibenspies, *Angew. Chem. Int. Ed. Engl.* **1993**, *32*, 116.
[9] This complex has been previously characterized by X-ray crystallography. A more detailed report of its properties will be presented in another paper.

[10] P. J. Farmer, J. H. Reibenspies, P. A. Lindahl, M. Y. Darensbourg, *J. Am. Chem. Soc*. **1993**, *115*, 4665.
[11] M. Y. Darensbourg, I. Font, M. Pala, J. H. Reibenspies, *J. Coord. Chem*. **1994**, *32*, 39.
[12] G. Musie, J. H. Reibenspies, M. Y. Darensbourg, *Inorg. Chem*. **1998**, *37*, 302.
[13] W. J. Geary, *Coord Chem Rev.* **1971**, *7*, 81.
[14] [14a] L. A. Scheich, P. Gosling, S. J. Brown, M. M. Olmstead, P. K. Mascharak, *Inorg. Chem*. **1991**, *20*, 1677. – [14b] H. C. Freeman, N. D. Hutchinson, *Acta Crystallogr., Sect. B.* **1979**, *35*, 2045. – [14c] D. Fenske, N. Mronga, K. Dehnicke, *Z. Anorg. Allg. Chem*. **1981**, *482*, 106. – [14d] J.-L. Du, S. J. Rettig, R. C. Thompson, J. Trotter, P. Betz, A. Bino, *Can. J. Chem*. **1992**, *70*, 732. – [14e] M. S. Konigs, W. C. Dow, D. B. Love, K. N. Raymond, S. C. Quay, S. M. Rocklage, *Inorg. Chem*. **1990**, *29*, 1488. – [14f] D. J. McCabe, E. N. Dueslar, R. T. Paine, *Inorg. Chem*. **1988**, *27*, 1220.
[15] While the diacetate derivative of **Ni-1*** has not been isolated in significant yield, its spectroscopic properties are very similar to those of **[(Ác)$_2$Ni-1]**.
[16] [16a] D. K. Mills, J. H. Reibenspies, M. Y. Darensbourg, *Inorg. Chem*. **1990**, *29*, 4364. – [16b] D. C. Goodman, R. M. Buonomo, P. J. Farmer, J. H. Reibenspies, M. Y. Darensbourg, *Inorg Chem*. **1996**, *35*, 4029. – [16c] R. M. Buonomo, I. Font, M. J. Maguire, J. H. Reibenspies, T. Tuntulani, M. Y. Darensbourg, *J. Am. Chem. Soc*. **1995**, *117*, 963.
[17] D. C. Goodman, P. J. Farmer, M. Y. Darensbourg, J. H. Reibenspies, *Inorg. Chem.* **1996**, *35*, 4989.
[18] R. M. Buonomo, J. H. Reibenspies, M. Y. Darensbourg, *Chem. Ber*. **1996**, *129*, 779.
[19] D. C. Goodman, J. H. Reibenspies, N. Goswami, S. Jurrison, M. Y. Darensbourg, *J. Am. Chem. Soc*. **1997**, *119*, 4955.
[20] M. Rakowski DuBois, B. R. Jagirdar, S. Dietz, B. C. Noll, *Organometallics* **1997**, *16*, 294, and references therein.
[21] L. M. Roberts, P. A. Lindahl, *Biochemistry* **1994**, *33*, 14339.
[22] A. J. Gordon, R. A. Ford, *The Chemist's Companion*, Wiley and Sons, New York, **1972**, pp. 429–436.
[23] D. K. Mills, I. Font, P. J. Farmer, Y.-M. Hsiao, T. Tuntulani, R. B. Buonomo, D. C. Goodman, G. Musie, C. A. Grapperhaus, M. J. Maguire, C.-H. Lai, M. L. Hatley, J. J. Smee, J. A. Bellefeuille, M. Y. Darensbourg, *Inorg. Synth.* **1998**, *32*, 89.
[24] [24a] G. M. Sheldrick, *SHELXS-86*, Institut für Anorganische Chemie der Universitat, Göttingen, Germany, **1986**. – [24b] G. M. Sheldrick, *SHELXL-93*, Institut für Anorganische Chemie der Universitat, Göttingen, Germany, **1993**.

Received August 19, 1998
[I98281]

Multinuclear NMR Study of the Conformational Changes in Me*p*dG and dG*p*Me upon Interaction with Mg^{2+}, Zn^{2+} and Hg^{2+} Ions Reveals the Strengthening of the Anomeric Effect by Soft M^{2+} Ions

Matjaž Polak[a] and Janez Plavec*[a]

Keywords: Nucleotides / Conformation analysis / NMR spectroscopy / Pseudorotational equilibrium / Anomeric effect

A conformational study is reported on 2′-deoxyguanosine 5′-methylmonophosphate [Me*p*dG (**1**)] and 2′-deoxyguanosine 3′-methylmonophosphate [dG*p*Me (**2**)] and their interactions with Mg^{2+}, Zn^{2+} and Hg^{2+} ions. The conformation of Me*p*dG (**1**) and dG*p*Me (**2**) in D_2O solution was inferred from vicinal proton-proton, proton-phosphorus and carbon-phosphorus NMR coupling constants and nuclear Overhauser effects (NOE). The chemical shift changes showed that hard Mg^{2+} ions interact preferentially with the phosphate oxygen atoms in Me*p*dG (**1**), whereas in the case of dG*p*Me (**2**) the interaction with the phosphate oxygen atoms competes with the interaction to the C6=O carbonyl group. Softer Zn^{2+} and Hg^{2+} ions were found to show strong binding affinity towards N7 in both Me*p*dG (**1**) and dG*p*Me (**2**). Analysis of *J* coupling constants and NOEs measured as a function of metal ion concentration revealed that: (i) N $\rightleftarrows$ S pseudorotational equilibria are biased towards C2′-*endo* pseudorotamers in M^{2+}-free Me*p*dG (**1**) and dG*p*Me (**2**) by 68% and 75% at 298K, respectively. Titration of Me*p*dG (**1**) and dG*p*Me (**2**) with Mg^{2+} ions caused no observable changes in N $\rightleftarrows$ S pseudorotational equilibrium, whereas the interactions of Zn^{2+} and Hg^{2+} ions with N7 resulted in the shift towards N-type pseudorotamers which can be explained by the strengthening of the anomeric effect as softer metal ions bind to N7 and make the imidazole moiety less electron-rich. (ii) The binding of divalent metal ions to Me*p*dG (**1**) and dG*p*Me (**2**) causes a shift of the *syn* $\rightleftarrows$ *anti* equilibrium towards *anti*, which is larger for softer Zn^{2+} than for harder Mg^{2+} ions. (iii) The conformational equilibrium across the C4′–C5′ bond (γ torsion) in dG*p*Me (**2**) is not affected by the increased concentration of M^{2+} ions. (iv) β^t conformers are preferred by ca. 77% in aqueous solution of Me*p*dG (**1**) and only small changes of ca. 1 percentage point in β^t population have been found upon metal ion binding to Me*p*dG (**1**). (v) The two-state $\varepsilon^t \rightleftarrows \varepsilon^-$ conformational equilibrium is biased towards ε^t rotamers by 63.5% in dG*p*Me (**2**). Interaction of hard Mg^{2+} and softer Zn^{2+} or Hg^{2+} ions with dG*p*Me (**2**) resulted in the minor increase (< 3 percentage points) in the population of ε^t conformers.

Introduction

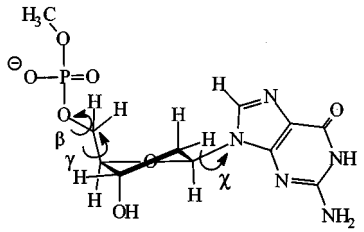
The structure and function of nucleic acids depend on metal ions. A knowledge of the effects of metal species on DNA structures is important in understanding the natural role of metal species.[1] Monovalent alkaline cations and divalent alkaline-earth metal cations interact preferentially with the phosphate groups, which stabilizes the DNA double duplex by neutralizing the negatively charged sugar-phosphate backbone, and to a lesser extent with the bases.[2] Interactions of divalent cations with nucleobases are involved in many biophysical processes and can cause polarization of nucleobases associated with the stabilization of certain hydrogen bonds between A=T and G≡C Watson-Crick base pairs as well as Hoogsteen base pairs in triplex DNA. Little is, however, known in the literature about how the interaction of metal ions with particular nucleotide in oligomeric fragment affects its conformation and how this local conformational change is transmitted into reorganization of the three-dimensional structure. In order to study local conformational changes induced by metal ions we have prepared two simple mononucleotide models of DNA, Me*p*dG (**1**) and dG*p*Me (**2**), which consist of all the essential structural elements of DNA to which metal ions can interact: β-D-2′-deoxyribofuranose, the phosphodiester fragment and the heterocyclic moiety.

The phosphodiester groups in Me*p*dG (**1**) and dG*p*Me (**2**) carry one negative charge at neutral pH and are expected not to overestimate the effect of electrostatic association of metal ions and a nucleotide on the structural change of nucleic acids. With the use of high-field multinuclear ^{1}H-, ^{13}C-, ^{15}N- and ^{31}P-NMR spectroscopy we were able to identify the binding sites for the individual metal ions on Me*p*dG (**1**) and dG*p*Me (**2**), and to examine the conformational changes along the glycosyl bond (*syn* $\rightleftarrows$ *anti* equilibrium, torsion angle χ), pseudorotational equilibrium of sugar moiety between North- and South-type conformers, reorientation along C4′−C5′ bond (torsion angle γ) and the conformational equilibria along phosphodiester fragments with torsion angles β[P−O5′−C5′−C4′] and ε[C4′−C3′−O3′−P] in Me*p*dG (**1**) and dG*p*Me (**2**), respectively.

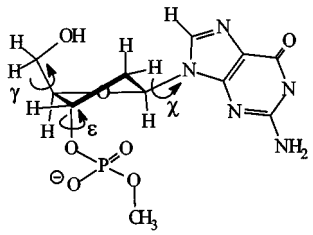
According to the pseudorotation concept[3] the furanosyl ring in nucleosides and nucleotides[4,5] is involved in interconversions of puckered envelope and twist forms. The puckering mode can be defined by Altona−Sundaralingam parameters[4,5] which are the phase angle of pseudorotation (*P*) and the maximum puckering amplitude (Ψ_m). *P* defines

[a] National Institute of Chemistry,
Hajdrihova 19, SI-1115 Ljubljana, Slovenia
Fax: (internat.) + 386-61/125-9244
E-mail: janez.plavec@ki.si

 © WILEY-VCH Verlag GmbH, D-69451 Weinheim, 1999 1434−1948/99/0303−0547 $ 17.50+.50/0



MepdG (**1**)



dGpMe (**2**)

Figure 1. Structural formula of MepdG (**1**) and dGpMe (**2**)

the part of the ring which is most puckered and Ψ_m indicates the extent of the puckering. In a survey of X-ray crystal structures[6] of nucleosides and nucleotides sugar moieties were found in both North (N) and South (S) conformations. The former range ($0° < P < 36°$) is centered around $P = 18°$ (C3′-*endo*), whereas the latter ($144° < P < 180°$) is centered around $P = 162°$ (C2′-*endo*). The values of Ψ_m were found in a range from 30° to 46°.[6] A large collection of NMR data is consistent with the conformational equilibrium between two distinctly identifiable N and S conformations which are dynamically interconverting in solution. Two-state N $\rightleftharpoons$ S pseudrotational equilibrium is controlled by the competing anomeric and *gauche* effects.[7] The 3′-OH or 3′-phosphate groups in 2′-deoxynucleos(t)ides drive the N $\rightleftharpoons$ S equilibrium towards S-type conformation through the tendency to adopt a *gauche* orientation of the [O4′−C4′−C3′−O3′] torsion angle.[7,8] The heterocyclic bases are involved in the anomeric effect which results in the energetic preference of N-type (pseudoaxial nucleobase) over S-type (pseudoequatorial nucleobase) conformation in terms of the anomeric effect alone. The anomeric effect in nucleosides involves the interaction between the non-bonded lone pairs of O4′ and the antibonding σ* orbital of the glycosyl bond (*i.e.* $n_{O4'} \rightarrow \sigma^*_{C1'\text{-}N}$ orbital overlap) and its strength is closely related to the electronic nature of the aglycone.[7,9−15] The protonation of the nucleobase facilitates the $n_{O4'} \rightarrow \sigma^*_{C1'\text{-}N}$ interactions, thereby resulting in the increased population of N-type conformers.[12−14,16] We have already shown in our preliminary study on the conformational changes induced by metal ion binding to 2′-dG that Zn^{2+} and Hg^{2+} bind to N7 and shift the N $\rightleftharpoons$ S pseudorotational equilibrium towards N by 0.8 percentage points ($R = 2.0$) and 4.1 percentage points ($R = 0.2$), respectively.[17] In the present study we have chosen three divalent metal ions (Mg^{2+}, Zn^{2+} and Hg^{2+}) which differ in their soft-hard nature and are known to have distinct binding modes to nucleic acids. Hard metal ions like Mg^{2+} are expected to bind to phosphate oxygen atoms in MepdG (**1**) and dGpMe (**2**), which would alter the strength of the [O4′−C4′−C3′−O3′] *gauche* effect in dGpMe (**2**) in particular and should change the population of S-type conformers in dGpMe (**2**). On the other hand, possible binding of Mg^{2+} to C6=O of guanine ring[18] would change the electron distribution in the purine moiety and thus specifically affect the N $\rightleftharpoons$ S pseudorotational equilibrium through the modulation of the anomeric effect. Soft metal ions like Hg^{2+} will bind to N7 of the guanine ring which is expected to increase the population of the N-type conformers due to the strengthening of the anomeric effect. It is, however, hard to predict how the increase in the steric bulk due to soft metal ion binding to N7 of MepdG (**1**) and dGpMe (**2**) would additionally shift the N $\rightleftharpoons$ S pseudorotational equilibrium towards S. Zn^{2+} is expected to have affinities for both the nucleobase and the phosphate groups and is therefore expected to change both the anomeric effect as well as the strength of the [O4′−C4′−C3′−O3′] *gauche* effect.

Results and Discussion

Binding Sites

The affinity of metal ions towards the specific electron-rich sites in MepdG (**1**) and dGpMe (**2**) has been studied by monitoring the changes in their ^1H, ^{13}C, ^{15}N and ^{31}P NMR chemical shifts as the concentration of Mg^{2+}, Zn^{2+} and Hg^{2+} ions was gradually increased to 0.1, 0.2, 0.5, 1.0 and 2.0 molar equivalents. Titration of MepdG (**1**) and dGpMe (**2**) with two molar equivalents of Mg^{2+} ions resulted in a very small chemical shift change of a few ppb for the H8 signal (Figure 2), which indicates the absence, or possibly very weak interaction of Mg^{2+} with N7 of the guanine moiety.[19] In addition, the small ^1H-, ^{13}C- and ^{15}N-NMR$\Delta\delta$ values reported in Table 1 for MepdG (**1**) indicate a very weak interaction of Mg^{2+} ions with the pentofuranose moiety, phosphodiester or the heterocyclic ring in MepdG (**1**). On the other hand, the addition of two molar equivalents of Mg^{2+} ions to dGpMe (**2**) caused a downfield shift of 0.143 ppm for the C6 signal, which suggests an interaction of Mg^{2+} ions with the C6=O carbonyl oxygen atom under neutral pH. We have furthermore detected changes of 0.4 Hz in $^2J_{PC5'}$ and $^2J_{PCH3}$ coupling constants for MepdG (**1**), which indicate that Mg^{2+} ions interact with oxygen atoms of the phosphate group and possibly influence rotamer population across β (vide infra).

Titration of MepdG (**1**) and dGpMe (**2**) with up to two molar equivalents of Zn^{2+} ions resulted in the progressive downfield shift of the H8 signal (Figure 2). The affinity of Zn^{2+} aqua ions to bind to N7 of the nucleobase[20] has been independently confirmed with ^{13}C- and ^{15}N-NMR data (Table 1). The ^{31}P chemical shifts of MepdG (**1**) and

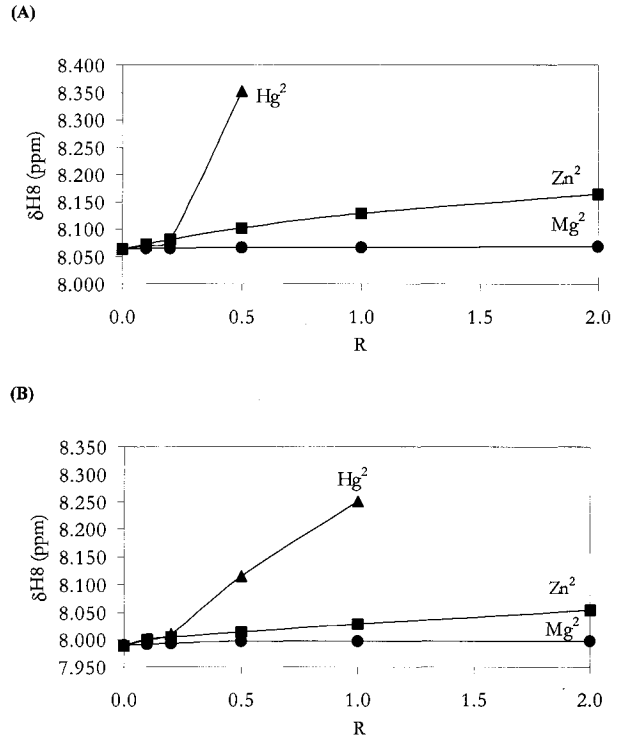


Figure 2. Changes of H8 chemical shifts as a function of increasing metal ion concentration in D_2O solution of Me*p*dG (**1**) (panel A) and dG*p*Me (**2**) (panel B); in the case of Hg^{2+} ions the precipitation precludes the extraction of NMR chemical shifts above R = $[M^{2+}]$/[nucleotide] = 1.0

dG*p*Me (**2**) moved upfield by 0.095 ppm and 0.018 ppm, respectively, upon addition of two molar equivalents of Zn^{2+} ions which suggests that the coordinative interaction between Zn^{2+} and phosphate oxygen atoms is negligible. It is noteworthy that chelation[21−26] of N7 and α-PO_4 monoester in 6-oxopurine nucleotide monophosphates by Pt^{2+} resulted in a downfield Δδ(^{31}P) shift of 3.5 ppm.[21] The ^{31}P chemical shifts are, however, sensitive[27] to bond angle changes, conformational changes along α and ζ and environmental effects, and are therefore difficult to correlate with the strength of binding of metal ions with phosphate groups. The addition of more than 0.2 molar equivalents of Hg^{2+} ions to the aqueous solutions of Me*p*dG (**1**) or dG*p*Me (**2**) resulted in the broadening of ^{1}H-NMR signals probably due to macrochelation, which was followed by precipitation after the addition of one molar equivalent of Hg^{2+} ions. The downfield shifts of H8 resonances upon addition of Hg^{2+} ions were much larger than in the case of Zn^{2+} (Figure 2) which is in agreement with the softer nature of Hg^{2+} ions and indicates strong binding affinity towards N7 (Table 1).

North ⟺ South Pseudorotational Equilibrium

The analysis of the solution conformation of the 2′-deoxy-β-D-ribofuranosyl moiety in Me*p*dG (**1**) and dG*p*Me (**2**) is based on five ($^3J_{1'2'}$, $^3J_{1'2''}$, $^3J_{2'3'}$, $^3J_{2''3'}$ and $^3J_{3'4'}$) proton-proton coupling constants (Table 2) which have been interpreted in terms of a two-state N ⟺ S pseudorotational equilibrium, as is normal for 2′-deoxyribose rings (see Experimental Section).[4,5,29−31] The titration of both Me*p*dG (**1**) and dG*p*Me (**2**) with Mg^{2+} ions caused no observable changes in $^3J_{HH}$ coupling constants (Table 2). In the case of Zn^{2+} and Hg^{2+} ions, we observed considerable changes in $^3J_{HH}$ coupling constants, which indicated that the N ⟺ S pseudorotational equilibrium were perturbed

Table 1. The comparative effects of Mg^{2+}, Zn^{2+} and Hg^{2+} ions on the ^{1}H-, ^{13}C-, ^{31}P- and ^{15}N-NMR chemical shifts[a] of Me*p*dG (**1**) and dG*p*Me (**2**)

	Me*p*dG (**1**)				dG*p*Me (**2**)			
	M^{2+}-free	Mg^{2+} (R = 2.0)	Zn^{2+} (R = 2.0)	Hg^{2+} (R = 0.2)	M^{2+}-free	Mg^{2+} (R = 2.0)	Zn^{2+} (R = 2.0)	Hg^{2+} (R = 0.2)
H8	8.064	0.003	0.100	0.016	7.990	0.008	0.064	0.021
H1′	6.333	−0.002	0.022	0.005	6.344	−0.001	0.007	0.002
H2′	2.847	−0.008	−0.030	−0.010	2.875	0.000	−0.001	0.001
H2″	2.542	0.002	0.031	0.040	2.678	0.004	0.014	0.008
H3′	4.717	−0.003	0.011	−0.010	4.937	0.001	0.002	0.000
H4′	4.246	−0.001	0.013	0.013	4.320	−0.001	−0.001	−0.012
H5′	4.040	0.000	0.019	0.014	3.860	0.000	0.004	−0.009
H5″					3.805	0.000	0.004	−0.010
C6	161.846	0.005	−0.107	−0.032	161.912	0.143	−0.040	−
C8	140.409	0.062	0.482	0.128	140.826	0.005	0.323	0.072
C4′	88.550	0.016	0.072	0.097	89.218	−0.025	0.001	−0.003
C1′	86.475	0.040	0.232	0.176	87.055	−0.010	0.064	0.013
C3′	74.113	0.014	−0.180	0.039	78.559	−0.043	−0.137	−0.034
C5′	67.981	0.048	−0.126	0.053	64.451	−0.002	−0.047	−0.008
Me	55.620	0.054	0.062	0.078	55.758	0.030	0.055	0.018
C2′	41.364	0.085	0.317	0.115	40.687	0.001	0.045	0.003
P	2.342	−0.064	−0.095	−0.020	1.593	−0.037	−0.018	−0.023
N7	−145.3	−0.6	−8.4	−1.5	−146.4	0.0	−4.2	−0.5
N9	−207.2	0.0	0.9	−	−209.1	0.5	1.0	−

[a] Chemical shifts for free Me*p*dG (**1**) and dG*p*Me (**2**), and Δδ [= $\delta_M{}^{2+}$(R) − δ_{free}] values for each of the metal ions are given in ppm. The positive Δδ value indicates that the particular resonance is shifted downfield upon addition of the metal ion. ^{1}H- and ^{13}C-NMR chemical shifts are referenced relative to trimethylsilylpropionic acid.

Table 2. Experimental J_{HH}, J_{HP} and J_{CP} coupling constants as a function of metal ion concentration in aqueous solution of Me*p*dG (**1**) and dG*p*Me (**2**) at 298 K[a]

Metal	Me*p*dG (**1**)				dG*p*Me (**2**)			
	M^{2+}-free	Mg^{2+}	Zn^{2+}	Hg^{2+}	M^{2+}-free	Mg^{2+}	Zn^{2+}	Hg^{2+}
R	0.0	2.0	2.0	0.2	0.0	2.0	2.0	0.2
$^3J_{H1'H2'}$	7.4	7.4	6.7	7.2	8.1	8.1	7.7	7.9
$^3J_{H1'H2''}$	6.4	6.5	6.5	6.4	6.1	6.1	6.3	6.2
$^3J_{H2'H3'}$	6.2	6.2	6.2	6.3	6.1	6.1	6.1	6.1
$^3J_{H2''H3'}$	3.6	3.7	4.0	3.6	2.8	2.8	3.0	2.9
$^3J_{H3'H4'}$	3.1	3.1	3.1	2.9	2.6	2.7	2.8	2.6
$^3J_{H4'H5'}$	3.9	3.9	3.5	3.9	3.4	3.4	3.4	3.4
$^3J_{H4'H5''}$					4.5	4.5	4.6	4.6
$^3J_{H2'P3'}$					0.8	0.8	0.7	0.8
$^3J_{H3'P3'}$					7.2	7.2	7.1	7.2
$^3J_{H4'P5'}$	1.7	1.6	2.0	1.6				
$^3J_{H5'/5''P5'}$	5.0	5.0	4.9	5.0				
$^3J_{C2'P3'}$					3.5	3.5	3.3	3.2
$^3J_{C4'P3'}$					5.8	6.0	5.7	6.0
$^3J_{C4'P5'}$	8.6	8.5	8.7	8.5				
$^3J_{C5'P5'}$	5.5	5.1	5.4	5.2				
$^2J_{C3'P3'}$					5.3	5.2	5.1	4.9
$^2J_{CH3P3'}$					5.8	5.6	5.6	6.1
$^2J_{CH3P5'}$	6.1	5.7	5.9	5.8				

[a] Coupling constants are listed only at two limiting concentrations ($R = 0$ and $R = 2.0$ or 0.2), whereas they have been collected as a function of increasing R. The coupling constants at all concentrations of metal ions ($0.0 < R < 2.0$) have been used in the conformational analysis. The signals for H5′ and H5" were isochronous for Me*p*dG (**1**). $^2J_{2'2''}$ was 14.0 and 14.2 Hz for Me*p*dG (**1**) and dG*p*Me (**2**), respectively. $^2J_{5'5''}$ was 12.5 Hz for dG*p*Me (**2**). $^2J_{2'2''}$ and $^2J_{5'5''}$ did not change by increasing the concentration of metal ions.

as the softer metal ions interacted with Me*p*dG (**1**) and dG*p*Me (**2**).

In the elaboration of the experimental $^3J_{HH}$ coupling constants at various metal ion concentrations we have used the computer program PSEUROT,[31] which calculates the least-squares fit of the five parameters defining the two-state N $\rightleftharpoons$ S pseudorotational equilibrium (P_N, $\Psi_m{}^N$, P_S, $\Psi_m{}^S$ and x_S) to the set of experimental $^3J_{HH}$ coupling constants. Our analysis incorporated 30 (i.e. 6×5) $^3J_{HH}$ coupling constants in the case of Mg^{2+} and Zn^{2+} ions, 15 (i.e. 3×5) $^3J_{HH}$ coupling constants in the case of Hg^{2+} ions and five $^3J_{HH}$ coupling constants for metal-free aqueous solutions of Me*p*dG (**1**) and dG*p*Me (**2**). As $^3J_{HH}$ coupling constants in Me*p*dG (**1**) and dG*p*Me (**2**) indicated a bias of N $\rightleftharpoons$ S pseudorotational equilibrium towards S-type conformers, the maximum puckering amplitude of the minor N-type component ($\Psi_m{}^N$) was constrained in the iterative procedure to find the best fit between experimental and calculated coupling constants. All other parameters were freely optimized (see the Experimental Section for details). The final convergence resulted in the global minima for each metal ion data set with root-mean-square error below 0.3 Hz and the maximum discrepancy between experimental and calculated coupling constants (ΔJ_{max}) below 0.5 Hz. The results in Table 3 show that the geometry of the minor N conformer is characterized by C2′-*exo* puckering ($-32.1° < P_N < -22.0°$, $37.3° < \Psi_m{}^N < 38.2°$), whereas the major S conformer is characterized by C2′-*endo* puckering ($161.5° < P_S < 166.5°$, $37.3° < \Psi_m{}^S < 38.2°$). Two important conclusions can be drawn from the data in Table 3. First, the interaction of Me*p*dG (**1**) and dG*p*Me (**2**) with divalent metal ions results in only a minute variation in the geometry of the pseudorotamers in both N and S regions of conformational space. The differences in the pseudorotational parameters P and Ψ_m are certainly a matter of degree, not of kind. Second, the gradual increase in the concentration of metal ions has direct influence on the population of N- and S-type conformers in Me*p*dG (**1**) and dG*p*Me (**2**) (Figure 3). The largest shift of N $\rightleftharpoons$ S pseudorotational equilibrium towards N-type conformers was 5 percentage points upon addition of two molar equivalents of Zn^{2+} to Me*p*dG (**1**). The binding of metal ions to N7 makes the imidazole moiety less electron-rich which strengthens the anomeric effect of the heterocyclic nucleobase in Me*p*dG (**1**) and dG*p*Me (**2**). Note that the changes in the N $\rightleftharpoons$ S pseudorotational equilibrium are smaller than changes caused by N7 protonation.[12] The smaller drive towards N-type sugar conformation due to the interaction of divalent metal ions with N7 of guanine in Me*p*dG (**1**) and dG*p*Me (**2**) relative to that due to protonation could be explained by the solvation of the metal ions. Water molecules, which mediate M^{2+} interactions with nucleotides reduce the effect of the metal ion on the redistribution of electron density in guanine. The increase in the population of N-type conformers upon interaction with two molar equivalents of Zn^{2+} is larger for Me*p*dG (**1**) than for dG*p*Me (**2**). The interaction of Zn^{2+} with the 5′-phosphodiester in Me*p*dG (**1**) is not expected to affect the N $\rightleftharpoons$ S pseudorotational equilibrium directly. The N7-phosphate chelation in Me*p*dG (**1**) could, however, affect its N $\rightleftharpoons$ S pseudorotational equilibrium and result in higher conformational purity. On the other hand, the interaction of Zn^{2+} ions with the 3′-phosphodiester group in dG*p*Me (**2**) changes the strength of the [O4′−C4′−C3′−O3′] *gauche* effect which should be observed through the specific shift of the N $\rightleftharpoons$ S pseudorotational equilibrium towards the S-type conformers. It is, however, clear from the $\Delta\delta$ values given in Table 1 that Zn^{2+} ions interact predominantly with N7 in dG*p*Me (**2**) which strengthens the anomeric effect and drives the N $\rightleftharpoons$ S pseudorotational equilibrium towards N-type pseudorotamers. As the [O4′−C4′−C3′−O3′] *gauche* effect and the anomeric effect counteract each other in the drive of the N $\rightleftharpoons$ S pseudorotational equilibrium, the overall increase in the population of N-type pseudorotamers is larger in Me*p*dG (**1**) than in dG*p*Me (**2**).

The ^{1}H-NMR chemical shift changes of the H8, H1′ and H2′ resonances for Me*p*dG (**1**) at seven concentrations in the range from 60 mM to 1 mM afforded the average association constant ($K_{av} = 3.5 \pm 1.6$ M^{-1}) which suggested the presence of 94% (±3) of unstacked molecules at a 10 mM concentration. Similar evaluation of self-association of Me*p*dG (**1**) after titration with Mg^{2+} ions ($R = 1.0$) with the use of the chemical shift changes of the H8, H1′, H2′ and H2″ signals gave a K_{av} value of 3.0 ± 1.5 M^{-1} corresponding to 94% (±3) of unstacked molecules at a 10 mM concentration. The interpretation of the chemical shifts of

Table 3. The comparative effect of metal ions on the N ⇌ S pseudorotational equilibrium of Me*p*dG (**1**) and dG*p*Me (**2**)[a]

Metal	*R*	P_N	$\Psi_m{}^N$	P_S	$\Psi_m{}^S$	% S_{free}	% $S_M{}^{2+}$	ΔJ_{max}	r.m.s.
				Me*p*dG (**1**)					
M^{2+}-free	0.0	−23.2	37.5	163.9	37.5	67.7	–	0.43	0.202
Mg^{2+}	2.0	−22.0	37.3	164.9	37.3	67.9	67.4	0.45	0.189
Zn^{2+}	2.0	−26.4	37.6	166.5	37.6	67.4	62.4	0.50	0.232
Hg^{2+}	0.2	−28.4	37.6	165.4	37.6	67.1	66.6	0.45	0.215
				dG*p*Me (**2**)					
Metal	*R*	P_N	$\Psi_m{}^N$	P_S	$\Psi_m{}^S$	% S_{free}	% $S_M{}^{2+}$	ΔJ_{max}	r.m.s.
M^{2+}-free	0.0	−32.1	38.2	162.0	38.2	74.6	–	0.32	0.276
Mg^{2+}	2.0	−30.5	38.1	161.5	38.2	74.7	74.5	0.31	0.282
Zn^{2+}	2.0	−26.9	37.7	163.0	37.6	75.1	72.0	0.38	0.304
Hg^{2+}	0.2	−32.0	38.1	163.5	38.1	74.7	73.3	0.36	0.274

[a] Phase angle of pseudorotation and maximum puckering amplitude for N-(P_N and $\Psi_m{}^N$) and S-type (P_S and $\Psi_m{}^S$) pseudorotamers are in degrees, root-mean-square error (r.m.s.) and the maximum individual discrepancy between experimental and calculated coupling constants (ΔJ_{max}) are in Hz.

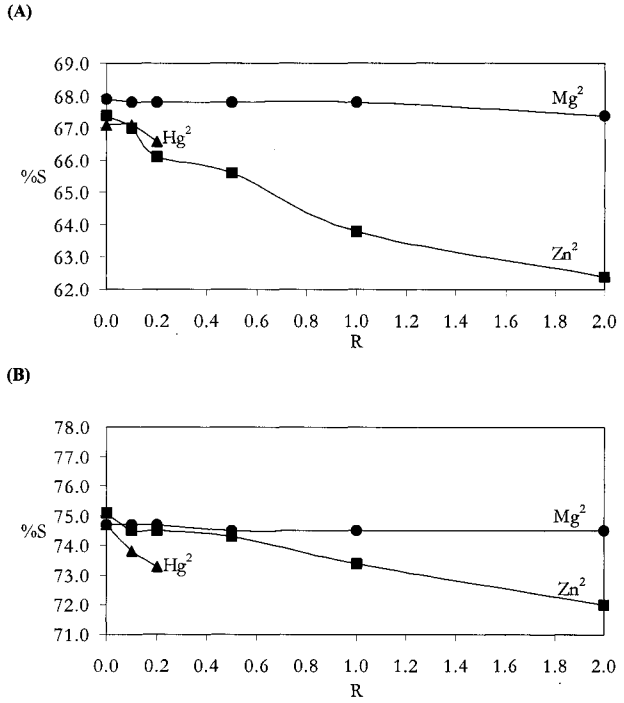


Figure 3. The N ⇌ S pseudorotational equilibrium in Me*p*dG (**1**) (panel A) and dG*p*Me (**2**) (panel B) as a function of increasing metal ion concentration

the H8, H2′ and H2″ signals in Me*p*dG (**1**) in the presence of Zn^{2+} ions (R = 1.0) resulted in a K_{av} value of 27.2 ± 17.0 M^{-1} which corresponds to 67% (± 14) of unstacked species at a 10 mM concentration of Me*p*dG (**1**). The additional titration of Me*p*dG (**1**) with Zn^{2+} ions from R = 0.0 to R = 2.0 was performed at a 1 mM concentration, where 95% (±3) of species was found to be unstacked. The comparison of the results at the two concentrations showed that the geometries of both major and minor conformers and their respective populations differed only slightly (for 1 mM: P_N = −24.9°, $\Psi_m{}^N$ = 37.4°, P_S = 165.3°, $\Psi_m{}^S$ = 37.4°,%S_{free} = 68.1 and %$S_{Zn^{2+}}$ = 65.5 at R = 2.0, r.m.s. error = 0.217 Hz, ΔJ_{max} = 0.4 Hz; for 10 mM see Table 3). Although the fraction of unstacked species decreases from 95% at 1 mM to 67% at 10 mM concentration, the Zn^{2+}-promoted drive of the N ⇌ S pseudorotational equilibrium towards N changes by only 2 percentage points which is within the error limits. There is therefore a definite M^{2+}-promoted drive of the N ⇌ S pseudorotational equilibrium towards N which is not affected considerably by the extent of self-association and the conclusions on the tuning of the N ⇌ S equilibrium by M^{2+} interactions with N7 of the nucleobase at a 10 mM concentration remain unchanged.

The comparison of the temperature-dependent shift of the N ⇌ S pseudorotational equilibrium from 278 K to 338 K at 1 and 10 mM Me*p*dG (**1**) upon interaction with Zn^{2+} (R = 1.0) has shown the following: (i) the geometries of the interconverting N and S conformers are nearly identical [for 1 mM: (P_N = −28.0°, $\Psi_m{}^N$ = 37.5°) ⇌ (P_S = 166.0°, $\Psi_m{}^S$ = 37.5°); for 10 mM: (P_N = −25.2°, $\Psi_m{}^N$ = 37.3°) ⇌ (P_S = 166.5°, $\Psi_m{}^S$ = 37.3°)], and (ii) the decrease in the population of S-type pseudorotamers with the increase of temperature is smaller at a 10 mM than at a 1 mM concentration (for 1 mM: $\%S^{278K}$ = 68.5, $\%S^{338K}$ = 64.0 and for 10 mM: $\%S^{278K}$ = 66.8, $\%S^{338K}$ = 63.8). The increase in temperature from 278 K to 338 K caused the upfield shift of the H8 signal from δ = 8.125 to δ = 8.069 at 10 mM, and from δ = 8.097 to δ = 8.043 at 1 mM Me*p*dG (**1**). The ^{1}H-NMR Δδ values between 278K and 338K are indeed very similar for all resonances at 1 and 10 mM Me*p*dG (**1**). The shift of the N ⇌ S pseudorotational equilibrium is slightly different, which indicates that as more nucleotide becomes unstacked with the increase of temperature, the Zn^{2+}-promoted drive towards N-type sugar conformation becomes comparable at the two concentrations. The temperature-dependent population changes, however, do not allow us to dissect the effect of enthalpy and entropy contributions to the Zn^{2+}-promoted drive towards N-type sugar conformation from the drive of the

N ⟷ S equilibrium due to the variation of the stability constant of labile M^{2+}−nucleotide species with temperature.

syn ⟷ *anti* Equilibrium

The semiquantitative information about the conformational equilibrium across the glycosyl bond (χ) in Me*p*dG (**1**) and dG*p*Me (**2**) upon the interactions with metal ions has been calculated from H8 ↔ H1′ NOEs.[32] Me*p*dG (**1**) showed a preference of 62% for *anti* conformation, whereas dG*p*Me (**2**) showed a preference of 69% for *syn* conformation (Figure 4). The higher tendency for *anti* conformation in Me*p*dG (**1**) relative to that in dG*p*Me (**2**) can be explained by the unfavorable steric interactions between the 5′-phosphodiester group and the nucleobase which are both on the β side in Me*p*dG (**1**). The binding of divalent metal ions to Me*p*dG (**1**) and dG*p*Me (**2**) caused a shift of the *syn* ⟷ *anti* equilibrium towards *anti*, except in the case of Mg^{2+} interactions with dG*p*Me (**2**) which caused a slight shift of 2 percentage points (within experimental error) towards *syn* (Figure 4). The steric bulk of the phosphate group on the β side of the furanosyl moiety in Me*p*dG (**1**) increases with the (electrostatic) interaction of Mg^{2+} ions with the phosphate oxygen atoms, which forces the nucleobase to adopt an *anti* conformation where the steric hindrance is reduced.

It is interesting to note that the shift of the *syn* ⟷ *anti* equilibrium in both Me*p*dG (**1**) and dG*p*Me (**2**) towards *anti* upon binding of Zn^{2+} ions is correlated with the increased population of N-type pseudorotamers. Similar correlations have already been reported.[16,33]

Conformational Equilibrium Across the C4′−C5′ Bond (γ)

The isochronicity of H5′ and H5′′ in Me*p*dG (**1**) prevented the measurement of individual $^3J_{4'5'}$ and $^3J_{4'5''}$ coupling constants. Analysis of the experimental $^3J_{4'5'}$ and $^3J_{4'5''}$ coupling constants (Table 2) in dG*p*Me (**2**) has shown 56% population of γ^+, 28% of γ^t and 16% of γ^- rotamers. Note, that the small changes in the experimental $^3J_{4'5'}$ and $^3J_{4'5''}$ coupling constants of 0.1 Hz (Table 2) upon interaction of M^{2+} ions with dG*p*Me (**2**) indicate negligible redistribution of the conformational equilibrium across γ.

Conformational Equilibrium Across the C5′−O5′ (β) and C3′−O3′ (ε) Bonds

The conformational equilibrium across the torsion angle β[C4′−C5′−O5′−P] has been assessed on the basis of experimental $^3J_{C4'P}$ coupling constants[34] alone as the isochronicity of H5′ and H5′′ protons in Me*p*dG (**1**) prevented the determination of the individual $^3J_{H5'P}$ and $^3J_{H5''P}$ coupling constants. It turned out that β^t conformers are preferred by 76.7% in M^{2+}-free solution of Me*p*dG (**1**). The

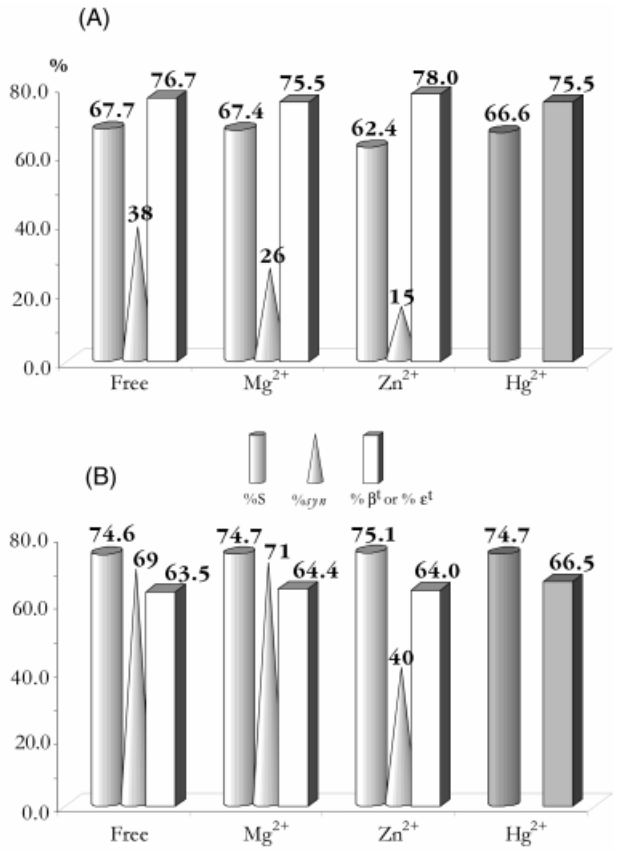


Figure 4. Changes in the conformational equilibria upon interaction of Mg^{2+}, Zn^{2+} and Hg^{2+} ions with Me*p*dG (**1**) (panel A) and dG*p*Me (**2**) (panel B); the population of S-type conformers (% S) is represented with cylinders, population of *syn* conformers (% *syn*) with cones, and population of β^t rotamers (% β^t) in Me*p*dG (**1**) and ε^t rotamers (% ε^t) in dG*p*Me (**2**) with square blocks; note that different levels of shading illustrate that data for Mg^{2+} and Zn^{2+} correspond to the addition of two molar equivalents ($R = 2.0$) of metal ions, whereas data for Hg^{2+} ions correspond to $R = 0.2$

increase in metal ion concentration showed only small changes of ca. 1 percentage point in β^t population, which is well within the range of experimental error (Table 4), and suggests that the conformation along the torsion angle β is not affected by metal ion binding to Me*p*dG (**1**).

Table 4. The effect of metal ions on the conformational equilibria across the C5′−O5′ bond (β torsion) in Me*p*dG (**1**) and across the C3′−O3′ bond (ε torsion)[a] in dG*p*Me (**2**)

	Me*p*dG (**1**)			dG*p*Me (**2**)		
	% β^t	ε^t	ε^-	% ε^t	ΔJ_{max}	r.m.s.
M^{2+}-free	76.7	209.5	270.8	63.5	0.44	0.39
Mg^{2+}	75.5	209.0	270.9	64.4	0.29	0.31
Zn^{2+}	78.0	209.4	270.7	64.0	0.81	0.52
Hg^{2+}	75.5	209.6	270.7	66.5	0.53	0.42

[a] Torsion angles ε^t and ε^- are in degrees, root-mean-square error (r.m.s.) and maximum discrepancy between the experimental and calculated $^3J_{C4'P}$, $^3J_{C2'P}$ and $^3J_{H3'P}$ coupling constants (ΔJ_{max}) are in Hz.

The experimental $^3J_{H3'P}$, $^3J_{C4'P}$ and $^3J_{C2'P}$ coupling constants (Table 2) have been used for the determination of the conformational equilibrium across the C3′−O3′ bond

(torsion angle ε[C4′−C3′−O3′−P]) in dG*p*Me (**2**) in terms of a two-state $\varepsilon^t \rightleftharpoons \varepsilon^-$ conformational equilibrium.[35−38] The ε^t rotamer is preferred by 63.5% in M^{2+}-free dG*p*Me (**2**) (Table 4). Interaction of hard Mg^{2+} and softer Zn^{2+} or Hg^{2+} ions with dG*p*Me (**2**) resulted in the minor increase (< 3 percentage points) in the preference for ε^t conformers which is not correlated with the relatively higher affinity of Mg^{2+} ions for the interaction with phosphate oxygen atoms (Table 4). Additionally, $^4J_{H2'P}$ coupling constants have been used for the qualitative assessment of the population of ε^- rotamers[39] and the results from both methods are in nice agreement (Table 4).

Conclusions

Me*p*dG (**1**) and dG*p*Me (**2**), which consist of all three structural elements of single-stranded DNA, have been chosen as simple model compounds for the evaluation of metal ion binding sites and related conformational changes in the absence of intermolecular interactions. The metal ion concentrations have been gradually increased by titration of aqueous solutions of Me*p*dG (**1**) and dG*p*Me (**2**). Multinuclear ^{1}H-, ^{13}C-, ^{15}N- and ^{31}P-NMR spectroscopy has been used to evaluate all rotational degrees of freedom across the sugar-phosphate backbone and glycosyl torsion angles.

The chemical shift changes showed that hard Mg^{2+} ions interact preferentially with the phosphate oxygen atoms in Me*p*dG (**1**), whereas in the case of dG*p*Me (**2**) the interaction of Mg^{2+} ions with the phosphate oxygen atoms competes with the interaction to the C6=O carbonyl group. Softer Zn^{2+} and Hg^{2+} ions were found to show a strong binding affinity for N7 in both Me*p*dG (**1**) and dG*p*Me (**2**).

The interpretation of $^3J_{HH}$ coupling constants in Me*p*dG (**1**) and dG*p*Me (**2**) has shown the bias of their N $\rightleftharpoons$ S pseudorotational equilibria towards S-type conformers. At 298 K the population of C2′-*endo* pseudorotamers in M^{2+}-free aqueous solutions of Me*p*dG (**1**) and dG*p*Me (**2**) were 68% and 75%, respectively. Titration of Me*p*dG (**1**) and dG*p*Me (**2**) with Mg^{2+} ions caused no observable changes in the N $\rightleftharpoons$ S pseudorotational equilibrium. On the other hand, the interaction of Zn^{2+} and Hg^{2+} ions with N7 strengthens the anomeric effect which is apparent from the increase in the population of N-type pseudorotamers. The shift of the N $\rightleftharpoons$ S pseudorotational equilibrium towards N-type conformers upon addition of two molar equivalents of Zn^{2+} was 5 percentage points for Me*p*dG (**1**) and 3 percentage points for dG*p*Me (**2**). The changes in the N $\rightleftharpoons$ S pseudorotational equilibrium are small compared to the changes caused by protonation which can be explained by the solvation of metal ions with water molecules, which mediate the interaction and thus reduce the effect of labile metal ion interaction on the redistribution of π-electron density of the guanine residue in Me*p*dG (**1**) and dG*p*Me (**2**).

The binding of divalent metal ions to Me*p*dG (**1**) and dG*p*Me (**2**) causes a shift of the *syn* $\rightleftharpoons$ *anti* equilibrium towards *anti*, which is larger for softer Zn^{2+} than harder Mg^{2+} ions. The increase in the population of *anti* conformers in both Me*p*dG (**1**) and dG*p*Me (**2**) upon binding of Zn^{2+} ions is correlated with the increased population of N-type pseudorotamers.

The small changes in the experimental $^3J_{4'5'}$ and $^3J_{4'5''}$ coupling constants in dG*p*Me (**2**) upon interaction with M^{2+} ions indicate negligible redistribution of the conformational equilibrium across C4′−C5′ bond (γ torsion).

The interpretation of $^3J_{C4'P}$ coupling constant has shown that β^t conformers are preferred by ca. 77% in M^{2+}-free aqueous solution of Me*p*dG (**1**). Only small changes of ca. 1 percentage point in the β^t population have been found upon metal ion binding to Me*p*dG (**1**).

The two-state $\varepsilon^t \rightleftharpoons \varepsilon^-$ conformational equilibrium is biased towards ε^t rotamers by 63.5% in dG*p*Me (**2**). The interaction of hard Mg^{2+} and softer Zn^{2+} or Hg^{2+} ions with dG*p*Me (**2**) resulted in the minor increase below 3 percentage points in the population of ε^t conformers.

Experimental Section

Synthesis: The synthesis of Me*p*dG (**1**) and dG*p*Me (**2**) has been carried out by procedures reported by Khorana[48,49] and Marzilli.[20] 2′-Deoxyguanosine-3′-monophosphate and 2′-deoxyguanosine-5′-monophosphate have been suspended in dry methanol. After addition of three molar equivalents of dicyclohexylcarbodiimide (DCC), the suspension was stirred at room temperature for 72 h. The solvent was evaporated under reduced pressure and water was added to precipitate DCC and its byproducts. The filtrate was extracted with petroleum ether and water removed by lyophilization.

NMR Measurements: ^{1}H- and ^{31}P-NMR spectra were recorded with a Varian Unity-plus 300 at 299.858 MHz and at 121.384 MHz, respectively. ^{13}C- and ^{15}N-NMR were acquired at 150.909 MHz and 60.817 MHz, respecitvely, with a Varian Unity Inova 600 NMR spectrometer at the National NMR Center of Slovenia. Spectra were acquired in D_2O (99.9% deuterium) at neutral pH (pH* = 7.5) at a 10 mM concentration, which is a compromise between the extent of self-association and the sensitivity of NMR measurements of rare nuclei like ^{15}N. Trimethylsilylpropionic acid was used as internal standard for ^{1}H- and ^{13}C-NMR (δ = 0) spectra, MeCN (δ = −135.8) as external reference for ^{15}N-NMR spectra, and 85% aq. H_3PO_4 (δ = 0) as external reference for ^{31}P-NMR spectra. The sample temperature was 298K ± 0.5K. Metal ion concentration was gradually increased by simple titration of nucleotides with 0.1, 0.2, 0.5, 1.0 and 2.0 molar equivalents of nitrate salts of Mg^{2+}, Zn^{2+} and Hg^{2+} ions. 1D-^{1}H measurements were performed under identical spectral and processing conditions: 9 ppm sweep width, 32K time domain, zero filling to 128K, and slight Gaussian apodization to give enhanced resolution. In order to obtain accurate *J* coupling data and chemical shifts ^{1}H-NMR spectra were simulated with a standard computer simulation algorithm, which is integrated into the Varian software package (VNMR rev. 5.3B).[28] The error in $^3J_{HH}$ is 0.1 Hz as estimated from the comparison of the experimental and simulated spectra. 1D-NOE experiments were run with 5 s irradiation time and with saturation of individual lines within the multiplet. NOE difference spectra were obtained by internal subtraction of on- and off-resonance spectra. Proton-decoupled ^{13}C-NMR spectra were recorded with 220 ppm sweep, 96K time domain, zero filling to 512K. Proton-

decoupled ^{31}P-NMR spectra were acquired with 100 ppm sweep, 56K time domain, zero filling to 64K. ^{15}N-NMR chemical shifts were obtained from 2D-HMBC experiments using gradients for coherence selection; 4096 (ω2) × 128 (ω1) data points, 320 scans per FID, 16 dummy scans, appropriate delays were calculated according to $^{1}J_{NH}$ = 90 Hz and $^{n}J_{NH}$ = 4 Hz, 6 kHz (ω2) × 15 kHz (ω1) spectral width, transformed after multiplication with a sine bell filter shifted by π/2 in both ω2 and ω1 to give an 8K × 1K matrix. Digital resolutions were 0.05 Hz in ^{1}H-NMR spectra, 0.1 Hz in ^{13}C-NMR spectra, 0.3 Hz in ^{31}P-NMR spectra and 30 Hz along the ^{15}N(*f*1) axis of 2D-HMBC spectra. − The chemical shift measurements at seven concentrations in the range from 60 mM (solubility limit) to 1 mM were employed to study self association with the isodesmic model.[53] In this model, the assumption is made that all the equilibrium constants for the $N_n + N \rightleftarrows N_{n+1}$ equilibria are equal. The observed chemical shift (δ_{obs}) is defined by Equation 1 where *c* is the total concentration of a nucleotide, δ_0 represents the chemical shift at infinite dilution, δ_∞ is the chemical shift at infinitely long stack, and *K* is the association constant.

$$\delta_{obs} = \delta_\infty + \frac{(\delta_\infty - \delta_0)\cdot(1-\sqrt{4Kc+1})}{2Kc} \quad (1)$$

Conformational Analysis: The conformational analysis of the sugar moiety was performed by the computer program PSEUROT[31] with the use of λ electronegativities for the substituents along H−C−C−H fragments and the six-parameter set from 1994 for the generalized Karplus-type equation.[29] The following λ electronegativity values were used: 0.0 for H, 0.58 for heterocycle, 1.26 for OH, 0.62 for C1′, C3′ and C4′, 0.74 for C2′, 1.27 for O4′ and 0.68 for C5′. The analysis of $^{3}J_{HH}$ coupling constants consists of three standard translation steps. First step translates experimental proton−proton coupling constants to proton-proton torsion angles and is covered by the generalized Karplus−Altona equation. Second step is the translation of proton−proton torsion angles into the corresponding endocyclic torsion angles and is formulated with the set of linear equations $\Phi_{HH} = A\nu_j + B$. Φ_{HH} is the torsion angle between two vicinal protons and ν_j is the corresponding endocyclic torsion angle. Parameters A and B were determined from a large collection of X-ray data. Third translational step of endocyclic torsion angles into the pseudorotational parameters is described by a simple cosine function $\nu_j = \Psi_m \cdot \cos[P + (j - 2) \cdot 4\pi/5]$, where *P* is the phase angle of pseudorotation and Ψ_m is the maximum puckering amplitude. In the following optimization procedure the geometries and populations of N and S pseudorotamers are varied to obtain the best fit between experimental and calculated coupling constants. Our optimization procedure was started with the following input values: P_N = 18°, $\Psi_m{}^N$ = 36°, P_S = 156°, $\Psi_m{}^S$ = 36°. The puckering amplitude of the minor N conformer ($\Psi_m{}^N$) was kept frozen during individual iterative least-squares optimization, while all other parameters were freely optimized. The best fits are given in Table 3 together with error evaluation in terms of maximum individual Δ*J* and root-mean-square error. − The population of the β^t rotamers was calculated with the following equation: $x_{\beta t} = [^3J_{C4'P}(expt) - {}^3J_{C4'P}(60°)]/[^3J_{C4'P}(180°) - {}^3J_{C4'P}(60°)] = (^3J_{PC4'}(expt) - 0.7)/10.3$, where the values of 11.0 Hz and 0.7 Hz have been used as the limiting coupling constants for $^3J_{C4'P}(180°)$ and $^3J_{C4'P}(60°)$, respectively.[34] − The population across the C4′−C5′ bond was evaluated on the basis of experimental $^3J_{4'5'}$ and $^3J_{4'5''}$ coupling constants which were interpreted with the assumption of the conformational equilibrium between three staggered conformers.[50] The limiting coupling constants were calculated[29] with the use of the torsion angles γ from a survey of X-ray crystallographic data (*gauche*-plus, γ = 53° ⇌ *gauche*-trans, γ = 180° ⇌ *gauche*-minus, γ = −70°).[50] The limiting coupling constants and populations of the three rotamers are related with the following equations: $^3J_{4'5'} = 1.64\ x_{\gamma+} + 2.86\ x_{\gamma t} + 10.40\ x_{\gamma-}$ and $^3J_{4'5''} = 1.84\ x_{\gamma+} + 10.78\ x_{\gamma t} + 2.71\ x_{\gamma-}$. − The interpretation of the experimental $^3J_{C4'P}$, $^3J_{C2'P}$ and $^3J_{H3'P}$ coupling constants has been performed with the assumption of a two-state $\varepsilon^t \rightleftarrows \varepsilon^-$ conformational equilibrium across the C3′−O3′ bond in dG*p*Me (**2**). The three-parameter Karplus equations[37,38] for $^3J_{CP} = 9.1 \cdot \cos^2\Phi - 1.9 \cdot \cos\Phi + 0.8$ and $^3J_{HP} = 15.3 \cdot \cos^2\Phi - 6.2 \cdot \cos\Phi + 1.5$ have been used in the calculation of $^3J_{CP}$ and $^3J_{HP}$ from ε^t and ε^- torsion angles and their respective populations, which were iterated to find the best fit with the experimental $^3J_{C4'P}$, $^3J_{C2'P}$ and $^3J_{H3'P}$ coupling constants. An additional semiquantitative estimation of the population of ε^- rotamers was done with the equation $x_{\varepsilon^-} = {}^4J_{H2'P}(expt)/2.3$,[39] which showed that population of ε^- rotamers is in the range from 30 to 35 percentage points. − The populations of *syn* and *anti* conformers could be estimated with the use of 1D-NOE difference spectroscopy by saturating H8 and measuring the NOE at H1′ for *syn*, and the sum of NOEs at H2′ and H3′ for the *anti* conformers.[32] As the signal for H3′ is overlapping with the signal of residual HOD for both Me*p*dG (**1**) and dG*p*Me (**2**) and its suppresion could introduce considerable error in our evaluation of *syn* ⇌ *anti* equilibrium we have only used H8 ↔ H1′ NOEs. Nuclear Overhauser enhancements upon saturation of H8 were 4.3% and 7.8% for free Me*p*dG (**1**) and dG*p*Me (**2**), respectively, 2.9% and 8.1% for Mg^{2+} (*R* = 2.0) and 1.7% and 4.5% for Zn^{2+} (*R* = 2.0). The NOE enhancements were used to calculate the population of *syn* conformers with the following equation: %*syn* = 100 · ηH1′/11.3.[32]

Acknowledgments

We thank the Ministry of Science and Technology of Republic of Slovenia (Grant No. Z1−8609−0104) and Krka, Pharmaceutical and Chemical Works, Novo mesto, Slovenia for the financial support and for their financial contribution for the purchase of 300- and 600-MHz Varian NMR spectrometers.

[1] For a recent review on the studies of metal ion interactions with nucleic acid constituents see: "Interactions of Metal Ions with Nucleotides, Nucleic Acids, and Their Constituents", in *Metal Ions in Biological Systems* (Eds.: A. Sigel, H. Sigel), vol. 32, M. Dekker, New York, **1996**, pp. 814.
[2] R. M. Smith, A. E. Martell, Y. Chen, *Pure Appl. Chem.* **1991**, *63*, 1015−1080.
[3] J. E. Kilpatrick, K. S. Pitzer, R. Spitzer, *J. Am. Chem. Soc.* **1947**, *69*, 2483−2488.
[4] C. Altona, M. Sundaralingam, *J. Am. Chem. Soc.* **1972**, *94*, 8205−8212.
[5] C. Altona, M. Sundaralingam, *J. Am. Chem. Soc.* **1973**, *95*, 2333−2344.
[6] H. P. M. de Leeuw, C. A. G. Haasnoot, C. Altona, *Isr. J. Chem.* **1980**, *20*, 108−126.
[7] J. Plavec, W. Tong, J. Chattopadhyaya, *J. Am. Chem. Soc.* **1993**, *115*, 9734−9746.
[8] J. Plavec, C. Thibaudeau, G. Viswanadham, C. Sund, J. Chattopadhyaya, *J. Chem. Soc., Chem. Commun.* **1994**, 781−783.
[9] J. Plavec, L. H. Koole, J. Chattopadhyaya, *J. Biochem. Biophys. Methods* **1992**, *25*, 253−272.
[10] C. Thibaudeau, J. Plavec, K. A. Watanabe, J. Chattopadhyaya, *J. Chem. Soc., Chem. Commun.* **1994**, 537−540.
[11] C. Thibaudeau, J. Plavec, J. Chattopadhyaya, *J. Am. Chem. Soc.* **1994**, *116*, 8033−8037.
[12] C. Thibaudeau, J. Plavec, J. Chattopadhyaya, *J. Org. Chem.* **1996**, *61*, 266−286.
[13] I. Luyten, C. Thibaudeau, J. Chattopadhyaya, *J. Org. Chem.* **1997**, *62*, 8800−8808.

[14] I. Luyten, C. Thibaudeau, A. Sandström, J. Chattopadhyaya, *Tetrahedron* **1997**, *53*, 6433−6464.
[15] M. Polak, B. Mohar, J. Kobe, J. Plavec, *J. Am. Chem. Soc.* **1998**, *120*, 2508−2513.
[16] C. Thibaudeau, A. Foldesi, J. Chattopadhyaya, *Tetrahedron* **1997**, *53*, 14043−14072.
[17] M. Polak, J. Plavec, *Nucleosides Nucleotides* **1998**, *17*, 2011−2020.
[18] L. G. Marzilli, B. de Castro, C. Solorzano, *J. Am. Chem. Soc.* **1982**, *104*, 461−466.
[19] T. Theophanides, M. Polissiou, *Inorg. Chim. Acta* **1981**, *56*, L1-L3.
[20] S. K. Miller, D. G. VanDerveer, L. G. Marzilli, *J. Am. Chem. Soc.* **1985**, *107*, 1048−1055.
[21] M. D. Reily, L. G. Marzilli, *J. Am. Chem. Soc.* **1986**, *108*, 8299−8300.
[22] E. Alessio, Y. Xu, S. Cauci, G. Mestroni, F. Quadrifoglio, P. Viglino, L. G. Marzilli, *J. Am. Chem. Soc.* **1989**, *111*, 7068−7071.
[23] M. C. F. Magalhaes, S. S. Massoud, N. A. Corfu, H. Sigel, *J. Inorg. Biochem.* **1989**, *36*, 295−295.
[24] H. Sigel, S. S. Massoud, N. A. Corfu, *J. Am. Chem. Soc.* **1994**, *116*, 2958−2971.
[25] H. Sigel, *Chem. Soc. Rev.* **1993**, *22*, 255−267.
[26] The generalized all-atom AMBER force-field parameters[51] as implemented in the computer program InsightII[52] has been used to perform a simple energy minimization of dGpMe (**2**). The starting conformation was built in such a way that it agrees with our NMR-derived conformational preferences: South sugar coformation, γ^+, ε^t, *anti*. The distances between N7 and phosphate oxygen atoms in the energy-minimized conformer ($P = 148°$, $\Psi_m = 39°$, $\gamma = 67°$, $\varepsilon = 187°$, $\chi = 244°$) were: 6.54, 6.81, 7.85 and 8.70 Å.
[27] D. G. Gorenstein, *Chem. Rev.* **1994**, *94*, 1315−1338.
[28] *VNMR*™ data acquisition and processing software, Revision 5.3B, Varian, Palo Alto, **1997**.
[29] C. Altona, R. Francke, R. de Haan, J. H. Ippel, G. J. Daalmans, A. J. A. Westra Hoekzema, J. van Wijk, *Magn. Reson. Chem.* **1994**, *32*, 670−678.
[30] C. A. G. Haasnoot, F. A. A. M. de Leeuw, C. Altona, *Tetrahedron* **1980**, *36*, 2783−2792.
[31] F. A. A. M. de Leeuw, C. Altona, *J. Comput. Chem.* **1983**, *4*, 428−437.
[32] H. Rosemeyer, G. Toth, B. Golankiewicz, Z. Kazimierczuk, W. Bourgeois, U. Kretschmer, H.-P. Muth, F. Seela, *J. Org. Chem.* **1990**, *55*, 5784−5790.
[33] W. Saenger Principles of Nucleic Acid Structure (Ed.: C. R. Cantor), Springer Verlag, New York, **1984**.
[34] P. P. Lankhorst, C. A. G. Haasnoot, C. Erkelens, C. Altona, *J. Biomol. Struct. Dyn.* **1984**, *1*, 1387−1405.
[35] P. P. Lankhorst, C. A. G. Haasnoot, C. Erkelens, H. P. Westerink, G. A. van der Marel, J. H. van Boom, C. Altona, *Nucleic Acids Res.* **1985**, *13*, 927−942.
[36] J. Plavec, C. Thibaudeau, G. Viswanadham, A. Sandstöm, J. Chattopadhyaya, *Tetrahedron* **1995**, *51*, 11775−11792.
[37] J. Plavec, J. Chattopadhyaya, *Tetrahedron Lett.* **1995**, *36*, 1949−1952.
[38] M. M. W. Mooren, S. S. Wijmenga, G. A. van der Marel, J. H. van Boom, C. W. Hilbers, *Nucleic Acids Res.* **1994**, *22*, 2658−2666.
[39] M. J. J. Blommers, D. Nanz, O. Zerbe, *J. Biomol. NMR* **1994**, *4*, 595−601.
[40] D. P. Bancroft, C. A. Lepre, S. J. Lippard, *J. Am. Chem. Soc.* **1990**, *112*, 6860−6871.
[41] D. Yang, S. S. G. E. van Boom, J. Reedijk, J. H. van Boom, A. H.-J. Wang, *Biochemistry* **1995**, *34*, 12912−12920.
[42] F. Reeder, F. Gonnet, J. Kozelka, J. C. Chottard, *Chem. Eur. J.* **1996**, *2*, 1068−1076.
[43] J. Kasparkova, K. J. Mellish, Y. Qu, V. Brabec, N. Farrell, *Biochemistry* **1996**, *35*, 16705−16713.
[44] G. Admiraal, M. Alink, C. Altona, F. J. Dijt, C. J. van Garderen, R. A. G. de Graaf, J. Reedijk, *J. Am. Chem. Soc.* **1992**, *114*, 930−938.
[45] F. Reeder, Z. J. Guo, P. D. Murdoch, A. Corazza, T. W. Hambley, S. J. Berners-Price, J. C. Chottard, P. J. Sadler, *Eur. J. Biochem.* **1997**, *249*, 370−382.
[46] M. Iwamoto, S. Mukundan, L. G. Marzilli, *J. Am. Chem. Soc.* **1994**, *116*, 6238−6244.
[47] M. J. Bloemink, E. L. M. Lempers, J. Reedijk, *Inorg. Chim. Acta* **1990**, *176*, 317−320.
[48] H. G. Khorana, *J. Am. Chem. Soc.* **1959**, *81*, 4657−4660.
[49] M. Smith, J. G. Moffatt, H. G. Khorana, *J. Am. Chem. Soc.* **1958**, *80*, 6204−6212.
[50] C. A. G. Haasnoot, F. A. A. M. de Leeuw, H. P. M. de Leeuw, C. Altona, *Recl. Trav. Chim. Pays-Bas* **1979**, *98*, 576−577.
[51] S. J. Weiner, P. A. Kollman, D. T. Nguyen, D. A. Case, *J. Comput. Chem.* **1986**, *7*, 230−252.
[52] *Insight II*, BIOSYM/Molecular Simulations, San Diego, CA, **1995**.
[53] R. B. Martin, *Chem. Rev.* **1996**, *96*, 3043−3064.

Received April 28, 1998
[I98265]

Synthesis of Two Acridine Conjugates of the Bis(phenanthroline) Ligand "Clip-Phen" and Evaluation of the Nuclease Activity of the Corresponding Copper Complexes

Steven A. Ross,[a] Marguerite Pitié,[a] and Bernard Meunier*[a]

Keywords: Bioinorganic chemistry / Copper / DNA cleavage / Intercalation

The synthesis of three novel derivatives [*N*-acetyl-Clip-Phen (**1**), Clip-Phen-hexylaminoacridine (**4**) and Clip-Phen-hexylchloromethoxyaminoacridine (**5**)] of the bis(phenanthroline) ligand "**Clip-Phen**", are described. Complexation of these ligands with copper(II) afforded the 1:1 complexes as hexafluorophosphate salts. The relaxation of ϕX 174 DNA was used as a DNA cleavage assay, with the following results. $[Cu(\mathbf{1})]^{2+}$ was found to show a diminished activity relative to the parent complex $[Cu(\mathbf{Clip\text{-}Phen})]^{2+}$. However, the acridine-containing complexes $[Cu(\mathbf{4})H]^{3+}$ and $[Cu(\mathbf{5})H]^{3+}$ exhibited significantly enhanced cleavage efficiencies, which has been attributed to increased affinity of the complexes for DNA. UV/Vis-spectral data of the complexes in the presence of calf-thymus DNA was consistent with an intercalative mode of binding.

Introduction

The artificial nuclease capability of redox-active copper complexes of the chelating ligand 1,10-phenanthroline (Phen) is well established.[1][2] Single-strand cleavage of nucleic acids is observed in the presence of dioxygen and a reductant, by oxidative attack on deoxyribose units from the DNA minor groove.[1] The reactive species $(Phen)_2Cu^{I}$ is significantly more active than the $(Phen)Cu^{I}$ species,[3] although the association constant for the second Phen ligand[4] is only $10^{5.5}$ M^{-1}. Competitive binding of copper can thus be a problem in cleavage experiments, and may hamper the use of (Phen)copper compexes in vivo. With these concepts in mind, we recently reported the synthesis of the novel bis(phenanthroline) ligand "Clip-Phen", whereby two Phen ligands are linked at the 2′ position by a serinol bridge.[5] The artificial nuclease activity of this new ligand was found to be higher than Phen itself (by a factor of 2) and, in addition, the serinol bridge contains an exogenous amine group, which allows further functionalisation.

Attachment of the natural polyamine spermine to Clip-Phen also afforded a new conjugate with even greater nuclease efficiency.[6] This was attributed to the high affinity of the spermine moiety for nucleic acids, through electrostatic interactions with the anionic phosphate backbone.[7] Cleavage reactions on restriction fragment DNA showed that there was very little sequence specificity of this Clip-Phen-spermine bioconjugate.

Attachment of an intercalating agent to Clip-Phen was the motivation for the current work. DNA binding by intercalation of polyaromatic species between adjacent base pairs was first proposed by Lerman[8] in 1961. Efficient intercalators must be planar and often contain three fused six-membered rings. The presence of a positive charge usually aids in the binding process.[9] Although intercalation has been studied by various groups, the overall binding process is complex, partly due to ambiguities in the actual binding mode (intercalation, minor-groove binding, or electrostatic interactions) and difficulties in measuring association constants.[10] Certain intercalators, such as daunomycin, adriamycin, and *m*-AMSA exhibit anti-tumour activity, in a process which is believed to involve the disruption of topoisomerase activity in vivo.[11] Association constants for intercalation are broadly comparable, normally between 10^5 and 10^6 M^{-1}, and there is a general lack of correlation between affinity and pharmacological efficacy. Overall, there is little sequence specificity observed in the interactions of intercalators with DNA.[9]

We wished to quantify the nuclease efficiency of an intercalator−Clip-Phen hybrid, such that the reactive Clip-Phen fragment would be anchored to the DNA. We chose to attach acridine derivatives for several reasons. Firstly, acridines are one of the most studied of the intercalating groups. Secondly, acridines are known to rapidly enter cells and accumulate in the nucleus,[12] which is an important consideration with regard to in vivo activity. For example, a netropsin−acridine hybrid has been reported to accumulate in the cell nucleus, using the acridine moiety as the cell-penetration vector,[13] whereas netropsin itself exhibits slow kinetics of cell penetration and poor uptake by the nucleus.[14] Finally, conjugation to acridines was considered to be the most straightforward and least expensive synthetic route available. Synthetic strategies to oligonucleotide-intercalator hybrids[15] and minor-groove binder-intercalator hybrids[16] have been reviewed recently in the literature.

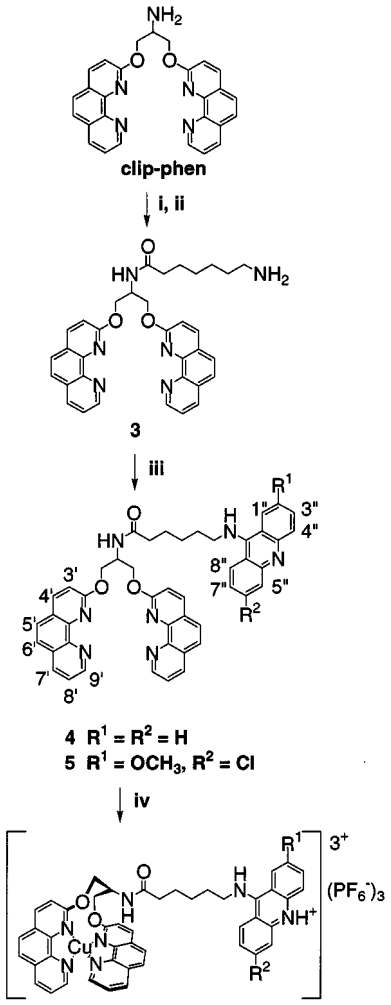
[a] Laboratoire de Chimie de Coordination du CNRS,
205 route de Narbonne, F-31077, Toulouse cedex 4, France
E-mail: bmeunier@lcc-toulouse.fr

 © WILEY-VCH Verlag GmbH, D-69451 Weinheim, 1999 1434−1948/99/0303−0557 $ 17.50+.50/0

Results and Discussion

Ligand Synthesis

Clip-Phen was readily prepared according to the previously reported procedure.[5] The primary amine of Clip-Phen presents a convenient site for further functionalisation. However, previous reports[17] have suggested that the reactive fragments in intercalator hybrids show greater efficacy if separated by a polymethylene linker. We chose, therefore, to protect the amine function of 6-aminohexanoic acid (with the BOC group) allowing facile attachment of the carboxylate to Clip-Phen by amide bond formation. Deprotection of Clip-Phen-hexyl-BOC (**2**) proceeded smoothly to afford Clip-Phen-hexylamine (**3**) in 80% yield (see Scheme 1).



Scheme 1. Synthesis of ligands **4** and **5**, and their corresponding Cu^{II}/PF_6^- complexes; conditions: (i) 6-BOC-amino-1-hexanoic acid, EtOCOCl; (ii) 25% CF_3COOH in CH_2Cl_2; (iii) appropriate 9-phenoxyacridine, CH_3CN, 10 equiv. CH_3COOH; (iv) $Cu(OAc)_2 \cdot 2\,H_2O$, MeOH, then NH_4PF_6

Primary amines are known to react with 9-chloroacridine derivatives in hot phenol (by in situ 9-phenoxyacridine formation) to give the 9-amino acridines in high yield.[18] We encountered several problems with this reaction, only being able to isolate products in very low yield after chromatographic separation. ^{1}H-NMR data from side-products obtained suggested that this was due to decomposition of the Clip-Phen fragment in hot phenol, possibly due to nucleophilic attack of phenol at the C-2′ position of the phenanthroline. We chose, therefore, to isolate the 9-phenoxyacridine derivatives prior to reaction with **3**. Reaction of 9-phenoxyacridine with **3** in refluxing acetonitrile afforded the Clip-Phen-hexylaminoacridine (**4**) in 30−40% yield after chromatography. However, the corresponding reaction between 6-chloro-9-phenoxy-2-methoxyacridine and **3** proceeded in very poor yield. Addition of 5−10 equivalents of acid (usually acetic acid) was found to greatly improve the yield by increasing the electrophilicity of the C-9′′ carbon atom.[19] Subsequent addition of acid to the reaction between 9-phenoxyacridine and **3** also led to a significant enhancement in yield (to 74%). Products **4** and **5** (see Scheme 1) were bright yellow, fluorescent solids, which made chromatographic purification simple, and gave satisfactory ^{1}H-NMR and mass spectra and analytical data.

Since the Clip-Phen fragments of both **4** and **5** contain an amide function in place of the primary amine, we also wished to prepare an analogous Clip-Phen amide derivative (without an intercalating group) to allow direct comparison of reactivities. This was readily achieved by reaction of acetic anhydride with Clip-Phen in CH_2Cl_2, to afford *N*-acetyl Clip-Phen (**1**) (see Figure 1) in 94% yield. The DNA cleavage reactivity of (phenathroline)Cu^{II} derivatives necessitates reduction to Cu^{I}, and thus formation of a tetrahedral intermediate. By converting the amine of Clip-Phen to the amide in **1**, we would thus avoid any differences in the coordination sphere or any steric constraints upon reduction.

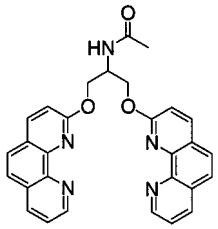


Figure 1. *N*-Acetyl Clip-Phen (**1**)

Complex Formation with Cu^{II} Salts

The coordination chemistry of the Clip-Phen family of ligands (L) with Cu^{II} is not straightforward.[20] The 5-atom bridge between the two phenanthrolines leads to little thermodynamic stability of the mononuclear species $[Cu(L)]^{2+}$, with respect to higher nuclearity species $[Cu_n(L)_n]^{2n+}$, in a process that may be dependent upon concentration and solvent. Complexes with a Cu/L ratio of 2:1 have also been observed when the Cu^{II} concentration is higher than that of the ligand. In general, we found that isolation of solid products of overall stoichiometry 1:1 (L/Cu) was problematic when $CuCl_2 \cdot 2\,H_2O$ or $Cu(SO_4) \cdot 4\,H_2O$ were used as the starting copper salts (data not

shown). We found that a reproducible procedure for complex formation with **1**, **4**, and **5** was to treat one equivalent of $Cu(OAc)_2 \cdot H_2O$ with one equivalent of ligand in warm methanol for two hours. Addition of an excess of NH_4PF_6 gave a precipitate which was redissolved by addition of acetone. Upon concentration of this solution, the products precipitated and could be isolated by centrifugation. Analytical data and mass spectra were consistent with the formation of L/Cu^{II} 1:1 complexes. The pK_a of the acridine fragment (> 10) is sufficiently high to allow proton transfer from the ammonium ion of NH_4PF_6 ($pK_a = 9.3$), such that the intercalator is present as an acridinium hexafluorophophate in the complexes of both **4** and **5** (see Scheme 1). This did not present a problem, however, since the intercalators are also protonated under biological conditions, and under the conditions used for the DNA experiments described (phosphate buffer, pH = 7.2). The UV/Vis spectra of the complexes exhibited the expected ligand absorptions between 200 and 450 nm, in addition to a broad Cu^{II} d-d band at circa 810 nm ($\varepsilon \approx 150\ M^{-1}\ cm^{-1}$).

The 1:1 copper complex of Clip-Phen was prepared by using the previously reported synthesis of [Cu(Clip-Phen]Cl_2.[5] After equimolar quantities of Clip-Phen and anhydrous $CuCl_2$ were stirred in DMF for 4 h, the chloride salt was precipitated with ether. This was redissolved in MeOH and an excess of NH_4PF_6 was added to afford a green precipitate, which was isolated by centrifugation. The analytical data was consistent with the overall stoichiometry [Cu(Clip-Phen)]$(PF_6)_2$. The absence of a third hexafluorophosphate anion in this complex indicates that the exogenous primary amine of Clip-Phen is not protonated.

DNA Cleavage Activity

Relaxation of supercoiled circular Φx 174 DNA (form I) into relaxed circular (form II) and linear (form III) conformations was the assay used to assess the relative cleavage efficiency of the four complexes. The redox activity of the Cu^{II} centres was initiated by the addition of 5 mM mercaptopropionic acid (MPA) in the presence of air.

Reactions were carried out by using either the isolated hexafluorophosphate salts described, or by premetallating the ligands with $CuCl_2$ in DMF/H_2O (40:60, 1 mM in ligand, 1 mM in $CuCl_2$) for 2 h prior to dilution and addition to DNA. The DNA/complex mixtures were allowed to equilibrate for 30 min at room temperature prior to addition of MPA. Several reactions were also carried out by pre-equilibration of the ligand (1 μM, 15 min) with DNA, followed by $CuCl_2$ (1 μM, 15 min), or by pre-equilibration of $CuCl_2$ (1 μM, 15 min) with DNA, followed by ligand (1 μM, 15 min). The choice of counterion (chloride or hexafluorophosphate) or order of addition was found to have a negligible effect upon the degree of reactivity (within experimental error). Since stock solutions of the hexafluorophosphate salts appeared to decompose over time (becoming an orange-brown colour), we chose to freshly prepare our complexes by metallation with $CuCl_2$ prior to reaction.

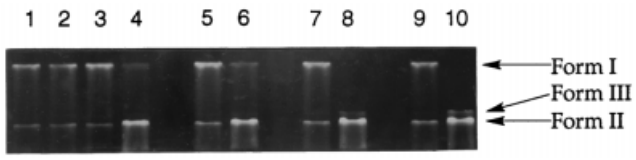


Figure 2. Comparison of Φx 174 cleavage efficiency between Clip-Phen, **1**, **4**, and **5** (1 μM) in the presence of $CuCl_2$ (1 μM) and MPA (5 mM); lane 1: control, no complex, no MPA; lane 2: control, no complex, with MPA; lanes 3, 5, 7, and 9: Clip-Phen, **1**, **4**, and **5**, respectively, without addition of Cu; lanes 4, 6, 8, and 10: Clip-Phen, **1**, **4** and **5**, respectively, in the presence of Cu

Figure 2 shows a representative gel illustrating the relative reactivities of the 4 complexes at 1 μM concentration. The reactivity of Clip-Phen-copper (1.4 ± 0.1 strand breaks per plasmid) is consistent with the previously reported data,[5] showing a cleavage activity which is approximately twice that of phenanthroline itself. However, *N*-acetyl Clip−Phen−copper shows a diminished reactivity (0.9 ± 0.1 strand breaks per plasmid), either due to the lack of a primary amine to coordinate or due to the steric effects of the bulkier amide group. The lack of protonation of the primary amine in the [Cu(Clip-Phen)]$(PF_6)_2$ complex is consistent with coordination to the Cu^{II} centre, although it is unlikely to be coordinated upon reduction to Cu^{I}. The copper complexes of the acridine-containing ligands **4** and **5** both exhibit cleavage activities of circa 4 ± 1, which is significantly higher than the two non-acridine-containing ligands. A direct comparison between **1** and **4** suggests an approximate fourfold increase in reactivity. Since the estimation of cleavage efficiency is less accurate after the disappearance of form 1, the variation in reactivity with concentration was also measured for **1** and **4**, this data being presented in Figure 3. Enhanced reactivity is thus observed at all concentrations.

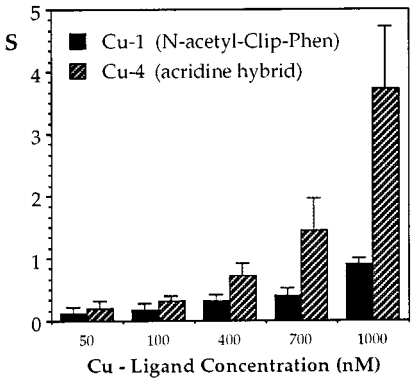


Figure 3. Concentration dependence of Φx 174 cleavage efficiency for **1** (solid) and **4** (hatched) in the presence of equimolar $CuCl_2$

Spectrophotometric Studies of DNA Binding

The binding of the complexes and ligands described herein to DNA is expected to be complex, since both moieties (the acridine fragment and the Cu−Clip-Phen frag-

ment) each have a separate affinity for DNA. Intercalative binding of acridine derivatives is well established, and gives rise to small (but significant) bathochromic and hypochromic shifts in the visible spectrum.[21] This technique was therefore used as a guide to whether intercalation was taking place with derivatives **4** and **5**. The alkylamino derivatives 9-(3-methoxyprop-1-ylamino)acridine (**6**) and 6-chloro-2-methoxy-9-(3-methoxyprop-1-ylamino)acridine (**7**) (see Figure 4) were also prepared and studied, since these analogues should have the same chromophores as **4** and **5**, without containing the clip-phen fragment.

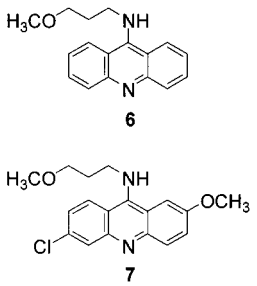


Figure 4. Alkylaminoacidire derivatives **6** and **7**

The spectrophotometric studies were carried out under identical buffer and salt conditions to the DNA cleavage experiments. Spectral shifts were recorded for DNA base-pair ratios of 0, 1, 4, 12, and 20 equivalents. We did not attempt to interpret this data in terms of binding constants, since the Cu−Clip-Phen fragment may also be binding in the minor groove.

Compounds **4**, **4** + $CuCl_2$, and **6** all gave bathochromic shifts of around 4 nm and hypochromic shifts of around 30% upon the addition of calf-thymus DNA (see Table 1), which were in good agreement with data previously reported in the literature.[21] We conclude from these results that the binding process of the free ligand (**4**), its copper complex (**4** + $CuCl_2$) and a related alkylaminoacridine (**6**) all involve intercalative binding of the acridine fragment. The spectral shifts of **4** + $CuCl_2$ and **6** upon titration with calf-thymus DNA are shown in Figure 5.

The data obtained from the 9-amino-6-chloro-2-methoxyacridine derivatives was more complex, as can be evidenced from the data in Table 1. Compounds **5**, **5** + $CuCl_2$, and **7** all show similar λ_b and ε_b in the presence of excess DNA, suggesting that the acridine fragment is in a similar environment for all three upon DNA binding. However, in the absence of DNA, whilst the free acridine compound **7** exhibits the expected behaviour, **5** and its copper complex show anomalous behaviour. This is probably due to stacking interactions of the acridine fragment with the phenanthroline rings in the absence of DNA, particularly with free **5**, which shows a 12-nm red-shift, relative to its Clip-Phen-free analogue **7**.

The in vivo activity of compounds **4** and **5** is currently being investigated and will be reported in due course.

Table 1. UV/Vis data in the region 370−470 nm for **4**, **5**, **4** + $CuCl_2$, **5** + $CuCl_2$, **6**, and **7** (10 μM) in phosphate buffer (pH = 7.2): ε_f and λ_f are the values in the absence of calf-thymus DNA; ε_b and λ_b are the values in the presence of 20 base-pair equivalents of calf-thymus DNA

	λ_f (ε_f)	λ_b (ε_b)
4	396 (7000) 415 (8600) 437 (8100)	398 (4400) 419 (5700) 440 (5400)
4 + $CuCl_2$	394 (4200) 414 (6800) 437 (5500)	397 (2700) 417 (4100) 440 (3700)
6	395 (4500) 410 (8100) 432 (6900)	398 (2900) 416 (5800) 436 (5000)
5	433 (7800) 455 (7700)	428 (9700) 450 (9500)
5 + $CuCl_2$	426 (2900) 444 (2700)	427 (8100) 451 (7700)
7	420 (13300) 443 (12700)	429 (6800) 451 (6900)

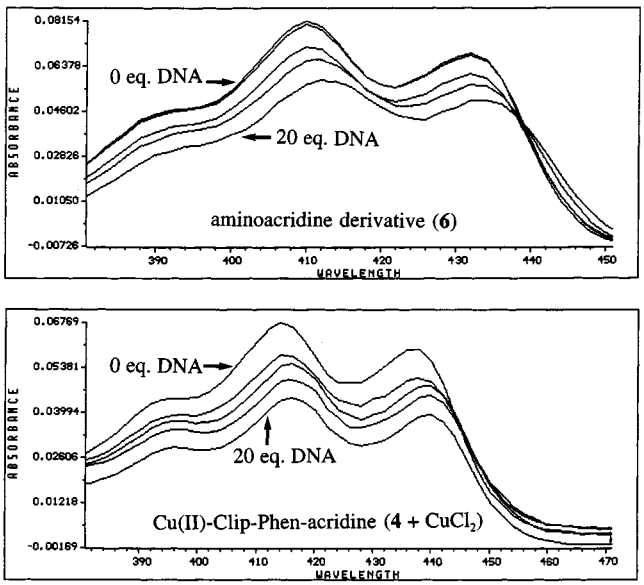


Figure 5. UV/Vis titration of **6** (top) and **4** + $CuCl_2$ (bottom) (all 10 μM) against calf-thymus DNA (0, 1, 4, 12, and 20 base-pair equivalents) in phosphate buffer (pH = 7.2) in the presence of NaCl (50 mM) and $MgCl_2$ (10 mM)

Conclusions

We have described the synthesis of two novel conjugate ligands (**4** and **5**) and their copper(II) complexes, which contain a reactive DNA cleavage unit attached to an intercalating DNA recognition unit. The presence of the intercalator has been shown to significantly enhance the DNA cleavage activity, in spite of the diminished activity which is found upon blockage of the exogenous primary amine of

the parent Clip-Phen from which they are derived. Thus, these species are of potential interest for in vivo applications.

Experimental Section

Warning: Acridines and ethidium bromide are mutagenic and should always be handled with appropriate precautions.

General: Reactions were monitored by thin-layer chromatography using Macherey-Nagel Alugram Sil G/UV 254 plates and spots were visualized with UV light. − Proton NMR spectra were recorded with a Bruker 250 MHz instrument and referenced to deuterated solvent. Aromatic proton signals due to phenanthroline are denoted by a single prime (′), those due to acridine are denoted by double prime (′′). − UV/Vis spectra were recorded with a Hewlett-Packard 8452A diode-array spectrophotometer in cuvettes of 1 cm path length. − Electrospray mass spectra were recorded with a Perkin-Elmer SCIEX API 100 instrument. − Ligand metallation and DNA reactions were carried out in Nanopure deionized water. DMF was dried with calcium sulfate. Other commercial reagents were used without purification.

Syntheses

2-Amino-1,3-bis(1′,10′-phenanthrolin-2′-yloxy)propane (Clip-Phen) was prepared by reaction of 2-chloro-1,10-phenathroline with serinol according to the method described previously.[5]

6-(Butoxycarbonylamino)-1-hexanoic Acid: 6-Aminohexanoic acid (1 g, 7.6 mmol), MgO (296 mg, 7.6 mmol), and NaOH (305 mg, 7.6 mmol) were added to 40 mL of dioxane/H_2O (6:1). Di-*tert*-butyl dicarbonate (1.83 g, 8.39 mmol) was then added in portions over 20 min, the solution was stirred for 18 h at room temperature, filtered, and concentrated in vacuo. The residue was dissolved in H_2O (20 mL), washed with diethyl ether (20 mL), acidified to pH = 3 with acetic acid (10%), and extracted with ethyl acetate (2 × 50 mL). The organic was then dried ($MgSO_4$) and concentrated to afford the product as a colourless oil (1.56 g, 89%). − ^{1}H NMR (CD_2Cl_2): δ = 1.41 [s, 9 H, C(CH_3)$_3$], 1.3−1.5 (m, 4 H, CH_2CH_2), 1.59 (m, 2 H, CH_2), 2.34 (t, 2 H, *J* = 7.5 Hz, CH_2COOH), 3.06 [m, 2 H, CH_2NHC(O)O], 4.67 (br. s, 1 H, CH$_2$N*H*). − DCI MS; *m*/*z* (%): 232 (63) [MH$^+$], 249 (56) [MNH$_4^+$]. − $C_{11}H_{21}NO_4$ (231.3): calcd. (+ 0.5 H_2O) C 54.9, H 9.15, N 5.82; found C 55.5, H 8.91, N 5.84.

***N*-Acetyl Clip-Phen (1):** Clip-Phen (447 mg, 1 mmol) was dissolved in CH_2Cl_2, to which was added Et_3N (1 mL) and acetic anhydride (1 mL). Upon standing for 2 h at room temperature, the solvent was removed in vacuo, the residue redissolved in CH_2Cl_2 (10 mL), washed with aqueous NaOH (10 mL, 1 M), and dried ($MgSO_4$). The solution was then concentrated to ca. 2 mL, and hexane was added to precipitate the product as a white solid (460 mg, 94%), which was filtered off and dried in vacuo. − ^{1}H NMR (CD_2Cl_2): δ = 2.03 (s, 3 H, CH_3), 4.84 (m, 3 H, serinol bridge), 5.04 (m, 2 H, serinol bridge), 7.15 (d, 2 H, *J* = 8.5 Hz, 3′-H), 7.59 (dd, 2 H, *J* = 8, 4.25 Hz, 8′-H), 7.70 (d, 2 H, *J* = 8.75 Hz, 6′-H), 7.77 (d, 2 H, *J* = 8.75 Hz, 5′-H), 8.14 (d, 2 H, *J* = 8.5, 4′-H), 8.27 (dd, 2 H, *J* = 1.5, 8 Hz, 7′-H), 9.07 [br. s, 1 H, CH_3C(O)N*H*], 9.07 (dd, 2 H, *J* = 1.5, 4.25 Hz, 9′-H). − DCI MS; *m*/*z* (%): 490 (100) [MH$^+$]. − $C_{29}H_{23}N_5O_3$ (489): calcd. (+ 0.33 $CHCl_3$, 0.5 H_2O) C 65.4, H 4.43, N 13.1; found C 65.4, 4.49, N 13.4.

Clip-Phen-hexyl-BOC (2): 6-Butoxycarbonylamino-1-hexanoic acid (1.3 g, 5.62 mmol) was dissolved in CH_2Cl_2 (10 mL) at 0°C, to which was then added Et_3N (567 mg, 5.62 mmol) and EtOC(O)Cl (609 mg, 5.62 mmol). After stirring for 30 min, the solvent was removed in vacuo, the residue dissolved in CH_2Cl_2, Clip-Phen (1 g, 2.23 mmol) added, and the solution stirred at room temperature for 3 h. The solvent was removed in vacuo, the residue redissolved in CH_2Cl_2 (50 mL), and the solution was washed with aqueous $KHCO_3$ (5%, 3 × 50 mL), H_2O (3 × 50 mL), dried ($MgSO_4$), and concentrated in vacuo to afford the product as an oily solid (1.22 g, 83%). − ^{1}H NMR (CD_2Cl_2): δ = 1.0−1.2 (m, 4 H, CH_2CH_2), 1.38 [s, 9 H, C(CH_3)$_3$] 1.41 (m, 2 H, CH_2), 2.24 [t, 2 H, *J* = 7.5 Hz, CH_2C(O)NH], 2.88 [m, 2 H, CH_2NHC(O)O], 4.55 [br. s, 1 H, OC(O)N*H*], 4.84 (m, 3 H, serinol bridge), 5.06 (m, 2 H, serinol bridge), 7.14 (d, 2 H, *J* = 8.5 Hz, 3′-H), 7.62 (dd, 2 H, *J* = 8, 4.25 Hz, 8′-H), 7.71 (d, 2 H, *J* = 8.75 Hz, 6′-H) 7.77 (d, 2 H, *J* = 8.75 Hz, 5′-H), 8.14 (d, 2 H, *J* = 8.5 Hz, 4′-H), 8.27 (dd, 2 H, *J* = 1.5, 8 Hz, 7′-H), 8.69 [d, 1 H, *J* = 5.8 Hz, CH$_2$C(O)N*H*], 9.10 (dd, 2 H, *J* = 1.5, 4.25 Hz, 9′-H). − DCI MS; *m*/*z* (%): 661 (72) [MH$^+$]. − $C_{38}H_{40}N_6O_5$ (660).

Clip-Phen-hexylamine (3): 2 (1 g, 1.52 mmol) was dissolved in 25% (v/v) of CF_3COOH/CH_2Cl_2 (40 mL) and the solution stirred for 1 h at room temperature. The solvent was then removed in vacuo, the residue dissolved in H_2O, and the pH adjusted to 12 (1 M NaOH). Extraction of this solution with CH_2Cl_2, followed by drying ($MgSO_4$) and concentration in vacuo afforded the product as a pale yellow solid (823 mg, 97%). − ^{1}H NMR (CD_2Cl_2): δ = 1.0−1.2 (m, 4 H,CH_2CH_2), 1.41 (m, 2 H, CH_2), 2.05 (br. s, 2 H, CH$_2$NH_2), 2.21 [t, 2 H, *J* = 7.8 Hz, CH_2C(O)NH], 2.44 (t, 2 H, *J* = 6.5 Hz, CH_2NH$_2$), 4.85 (m, 3 H, serinol bridge), 5.06 (m, 2 H, serinol bridge), 7.14 (d, 2 H, *J* = 8.5 Hz, 3′-H), 7.58 (dd, 2 H, *J* = 8, 4.25 Hz, 8′-H), 7.69 (d, 2 H, *J* = 8.75 Hz, 6′-H), 7.76 (d, 2 H, *J* = 8.75 Hz, 5′-H), 8.13 (d, 2 H, *J* = 8.5 Hz, 4′-H), 8.26 (dd, 2 H, *J* = 1.5, 8 Hz, 7′-H), 8.69 [d, 1 H, *J* = 5.8 Hz, CH$_2$C(O)N*H*], 9.06 [dd, 2 H, *J* = 1.5, 4.25 Hz, 9′-H]. − DCI MS; *m*/*z* (%): 561 (100) [MH$^+$].

9-Chloroacridine: Acridone (2 g, 10.3 mmol) and $POCl_3$ (20 mL) were placed in a round-bottomed flask and heated at reflux for 1 h. The unused $POCl_3$ was then removed by distillation under vacuum, the residue cooled to 50°C, diluted with $CHCl_3$ (20 mL), and poured into aqueous ammonia (30%, 10 mL) and ice (25 g). After the organic layer was separated and the aqueous further extracted with $CHCl_3$ (3 × 50 mL), the organic layers were combined, dried ($MgSO_4$), and concentrated to 10 mL, and then hexane was added. Filtration afforded the product as a yellow solid (1.99 g, 91%). − ^{1}H NMR (CD_2Cl_2): δ = 7.67 (dd, 2 H, *J* = 9.9 Hz, 2′′-H or 3′′-H), 7.82 (dd, 2 H, *J* = 9.9 Hz, 2′′-H or 3′′-H), 8.20 (d, 2 H, *J* = 9 Hz, 1′′-H or 4′′-H), 8.44 (d, 2 H, *J* = 9 Hz, 1′′-H or 4′′-H). − DCI MS; *m*/*z* (%): 214 (100) [MH$^+$]. − $C_{13}H_8ClN$ (213): calcd. C 73.0, H 3.77, N 6.56; found C 72.7, H 3.35, N 6.41.

9-Phenoxyacridine: 9-Chloroacridine (680 mg, 3.2 mmol) was added to a solution of NaOH (200 mg, 5 mmol) in phenol (3 g, 32 mmol), the mixture was stirred at 100°C for 2 h, then poured into NaOH solution (2 M, 50 mL). The solution was then extracted with $CHCl_3$ (3 × 50 mL) and the solution dried ($MgSO_4$) and concentrated in vacuo. Recrystallisation of the residue from hot MeOH/H_2O (50:50) afforded the product as pale yellow needles (770 mg, 89%). − ^{1}H NMR (CD_2Cl_2): δ = 6.87 (m, 2 H, phenoxy 2-H), 7.05 (m, 1 H, phenoxy 4-H), 7.27 (m, 2 H, phenoxy 3-H) 7.47 (dd, 2 H, *J* = 9.9 Hz, 2′′-H or 3′′-H), 7.78 (dd, 2 H, *J* = 9, 9 Hz, 2′′-H or 3′′-H), 8.11 (d, 2 H, *J* = 9 Hz, 1′′-H or 4′′-H), 8.25 (d, 2 H, *J* = 9 Hz, 1′′-H or 4′′-H). − DCI MS; *m*/*z* (%): 272 (100) [MH$^+$]. $C_{19}H_{13}NO$ (271).

6-Chloro-2-methoxy-9-phenoxyacridine: 6,9-Dichloro-2-methoxyacridine (2 g, 7 mmol) was added to a solution of NaOH (400 mg, 10 mmol) in phenol (10 g, 106 mmol), the mixture was stirred at

100°C for 2 h and then poured into NaOH solution (2 M, 50 mL). After this solution had been extracted with $CHCl_3$ (3 × 50 mL), the combined organic layers were dried ($MgSO_4$) and concentrated in vacuo. Recrystallisation of the residue from hot MeOH afforded the product as yellow needles (2.02 g, 84%). − ^{1}H NMR (CD_2Cl_2): δ = 3.79 (s, 3 H, OC*H*$_3$), 6.86 (d, 2 H, *J* = 12 Hz, phenoxy 2-H), 7.06 (t, 1 H, *J* = 7 Hz, phenoxy 4-H), 7.16 (d, 1 H, *J* = 2.75 Hz, 1′′-H or 5′′-H), 7.26 (m, 2 H, phenoxy 3-H), 7.37 (dd, 1 H, *J* = 9.25, 2 Hz, 3′′-H or 7′′-H), 7.45 (dd, 1 H, *J* = 2.75, 9.5 Hz, 3′′-H or 7′′-H), 7.97 (d, 1 H, *J* = 9.25 Hz, 4′′-H or 8′′-H), 8.08 (d, 1 H, *J* = 9.5 Hz, 4′′-H or 8′′-H), 8.17 (d, 1 H, *J* = 2 Hz, 1′′-H or 5′′-H). − DCI MS; *m*/*z* (%): 336 (100) [MH$^+$].

Clip-Phen-hexylaminoacridine (4): Compound **3** (200 mg, 0.36 mmol), 9-phenoxyacridine (195 mg, 0.72 mmol), and acetic acid (216 mg , 3.6 mmol) were added to CH_3CN (15 mL) and the solution was heated at reflux for 18 h. The solvent was then removed in vacuo, the residue was dissolved in H_2O and the pH adjusted to 12 (1 M NaOH). The solution was extracted with $CHCl_3$ (2 × 50 mL), the combined organic layers dried ($MgSO_4$), concentrated in vacuo, and the residue was purified by column chromatography (CH_2Cl_2/MeOH/Et_3N, 92:7:1) on silica gel to afford the product (R_f = 0.3) as a bright yellow solid (194 mg, 74%). − UV/Vis (phosphate buffer, pH = 7.2): λ_{max} (ε M^{-1}cm^{-1}) = 226 (87500), 268 (90600), 396 (7000), 415 (8600) and 437 (8100). − ^{1}H NMR (CD_2Cl_2): δ = 1.23 (m, 2 H, NHCH$_2$CH$_2$C*H*$_2$CH$_2$CH$_2$), 1.51 (m, 4 H, NHCH$_2$C*H*$_2$CH$_2$C*H*$_2$CH$_2$), 2.31 (t, 2 H, *J* = 7.25 Hz, NHCH$_2$CH$_2$CH$_2$CH$_2$C*H*$_2$), 3.57 (t, 2 H, *J* = 7 Hz, NHC*H*$_2$-CH$_2$CH$_2$CH$_2$CH$_2$), 4.84 (m, 3 H, serinol bridge), 4.99 (m, 3 H, serinol bridge), 7.08 (d, 2 H, *J* = 8.5 Hz, 3′-H), 7.25 (m, 2 H, 2′′-H or 3′′-H), 7.51 (dd, 2 H, *J* = 8, 4.25 Hz, 8′-H), 7.58 (d, 2 H, *J* = 8.75 Hz, 6′-H), 7.59 (m, 2 H, 2′′-H or 3′′-H), 7.65 (d, 2 H, *J* = 8.75 Hz, 5′-H), 7.96 (d, 2 H, *J* = 8.75 Hz, 1′′-H or 4′′-H), 8.04 (d, 2 H, *J* = 8.5 Hz, 4′-H), 8.06 (d, 2 H, *J* = 8.75 Hz, 1′′-H or 4′′-H), 8.16 (dd, 2 H, *J* = 1.5, 8 Hz, 7′-H), 8.92 (br. d, 1 H, *J* = 5.75 Hz, N*H*CO), 9.02 (dd, 2 H, *J* = 1.5, 4.25 Hz, 9′-H). − DCI MS; *m*/*z* (%): 738 (18) [MH$^+$], 542 (38) [MH$^+$ − phenanthrolyloxy], 197 (100) [hydroxyphenathrolineH$^+$]. − $C_{46}H_{39}N_7O_3$ (737): calcd. (+ 2 H_2O) C 71.4, H 5.56, N 12.6; found C 71.6, H 5.39, N 12.5.

Clip-Phen-hexylchloromethoxyaminoacridine (5): Compound **3** (200 mg, 0.36 mmol), 6-chloro-2-methoxy-9-phenoxyacridine (241 mg, 0.72 mmol), and acetic acid (216 mg , 3.6 mmol) were added to CH_3CN (15 mL) and the solution was heated at reflux for 18 h. The solvent was then removed in vacuo, the residue was dissolved in H_2O and the pH was adjusted to 12 (1 M NaOH). The solution was extracted with $CHCl_3$ (2 × 50 mL), the combined organic layers dried ($MgSO_4$), concentrated in vacuo, and the residue was purified by column chromatography (CH_2Cl_2/MeOH/Et_3N, 92:7:1) on silica gel to afford the product (R_f = 0.35) as a bright yellow solid (189 mg, 66%). − UV/Vis (phosphate buffer, pH = 7.2): λ_{max} (ε M^{-1}cm^{-1}) = 228 (112000), 272 (101400), 433 (7800) and 455 (7700). − ^{1}H NMR (CD_2Cl_2): δ = 1.25 (m, 2 H, NHCH$_2$CH$_2$-C*H*$_2$CH$_2$CH$_2$), 1.51 (m, 4 H, NHCH$_2$C*H*$_2$CH$_2$C*H*$_2$CH$_2$), 2.32 (t, 2 H, *J* = 7.25 Hz, NHCH$_2$CH$_2$CH$_2$CH$_2$C*H*$_2$), 3.45 (t, 2 H, *J* = 7 Hz, NHC*H*$_2$CH$_2$CH$_2$CH$_2$CH$_2$), 3.83 (s, 3 H, OC*H*$_3$), 4.84 (m, 3 H, serinol bridge), 4.98 (m, 3 H, serinol bridge), 7.05 (d, 2 H, *J* = 8.5 Hz, 3′-H), 7.12 (dd, 1 H, *J* = 2.25, 9.25 Hz, 3′′-H or 7′′-H), 7.20 (d, 1 H, *J* = 2.5 Hz, 1′′-H or 5′′-H), 7.30 (dd, 1 H, *J* = 2.5, 9.25 Hz, 3′′-H or 7′′-H), 7.49 (dd, 2 H, *J* = 8, 4.25 Hz, 8′-H), 7.54 (d, 2 H, *J* = 8.75 Hz, 6′-H), 7.61 (d, 2 H, *J* = 8.75 Hz, 5′-H), 7.86 (d, 1 H, *J* = 9.25 Hz, 4′′-H or 8′′-H), 7.91 (d, 1 H, *J* = 2 Hz, 1′′-H or 5′′-H), 7.96 (d, 1 H, *J* = 9.25 Hz, 4′′-H or 8′′-H), 8.01 (d, 2 H, *J* = 8.5 Hz, 4′-H), 8.13 (dd, 2 H, *J* = 1.5, 8 Hz, 7′-H), 8.99 (br. s, 1 H, N*H*CO), 9.00 (dd, 2 H, *J* = 1.5, 4.25 Hz, 9′-H). − DCI MS; *m*/*z* (%): 802 (1.5) [MH$^+$], 606 (100) [MH$^+$ − phenanthrolyloxy], 197 (89) [hydroxyphenathrolineH$^+$]. − $C_{47}H_{40}ClN_7O_3$ (801.5): calcd. (+ CH_2Cl_2) C 64.9, H 4.73, N 11.1; found C 65.1, H 4.50, N 11.2.

9-(3-Methoxyprop-1-ylamino)acridine (6): 3-Methoxypropylamine (50 mg, 0.56 mmol), 9-phenoxyacridine (140 mg, 0.52 mmol), and acetic acid (100 mg) were added to CH_3CN (5 mL) and the solution was heated at reflux for 1 h. The solvent was then removed in vacuo and the residue purified by column chromatography (CH_2Cl_2/MeOH/NH_4OH, 90:9:1) on silica gel to afford the product as a bright yellow solid (104 mg, 76%). − ^{1}H NMR (CD_2Cl_2): δ = 2.15 (m, 2 H, C*H*$_2$), 3.41 (s, 3 H, C*H*$_3$), 3.62 (t, 2 H, *J* = 5.5 Hz, C*H*$_2$), 3.99 (t, 2 H, *J* = 7 Hz, C*H*$_2$), 7.09 (dd, 2 H, *J* = 9, 9 Hz, 2′′-H or 3′′-H), 7.41 (dd, 2 H, *J* = 9, 9 Hz, 2′′-H or 3′′-H), 7.72 (d, 2 H, *J* = 9 Hz, 1′′-H or 4′′-H), 8.09 (d, 2 H, *J* = 9 Hz, 1′′-H or 4′′-H). − DCI MS; *m*/*z* (%): 331 (100) [MH$^+$].

6-Chloro-2-methoxy-9-(3-methoxyprop-1-ylamino)acridine (7): 3-Methoxypropylamine (50 mg, 0.56 mmol), 6-chloro-2-methoxy-9-phenoxyacridine (100 mg, 0.30 mmol), and acetic acid (100 mg) were added to CH_3CN (5 mL) and the solution was heated at reflux for 1 h. The solvent was then removed in vacuo and the residue was purified by column chromatography (CH_2Cl_2/MeOH/NH_4OH, 90:9:1) on silica gel to afford the product as a bright yellow solid (80 mg, 81%). − ^{1}H NMR (CD_2Cl_2): δ = 1.97 (m, 2 H, C*H*$_2$), 3.45 (s, 3 H, C*H*$_3$), 3.67 (t, 2 H, *J* = 5.5 Hz, C*H*$_2$), 3.88 (t, 2 H, *J* = 6 Hz, C*H*$_2$), 3.93 (s, 3 H, OC*H*$_3$), 7.27 (dd, 1 H, *J* = 2, 9 Hz, 3′′-H or 7′′-H), 7.30 (d, 1 H, *J* = 2 Hz, 1′′-H or 5′′-H), 7.38 (dd, 1 H, *J* = 2, 9 Hz, 3′′-H or 7′′-H), 7.92 (d, 1 H, *J* = 9 Hz, 4′′-H or 8′′-H), 7.99 (d, 1 H, *J* = 2 Hz, 1′′-H or 5′′-H) and 8.12 (d, 1 H, *J* = 9 Hz, 4′′-H or 8′′-H). − DCI MS; *m*/*z* (%): 267 (100) [MH$^+$].

[(Clip-Phen)Cu^{II}](PF$_6$)$_2$: $CuCl_2$ (3 mg, 0.022 mmol) and Clip-Phen (10 mg, 0.022 mmol) were dissolved in DMF (2 mL) and the solution was stirred for 4 h. Diethyl ether was then added and the solution left at −20°C for 18 h. The green precipitate which had formed was isolated by centrifugation, washed with ether, and dried. This solid was then dissolved in MeOH (2 mL) and a solution of NH_4PF_6 (15.9 mg, 0.1 mmol) in MeOH/H_2O (2 mL, 50:50) was added to give immediately a green precipitate. This was isolated by centrifugation, washed with H_2O and dried in vacuo (11.8 mg, 78%). − UV/Vis (CH_3CN): λ_{max} (ε M^{-1}cm^{-1}) = 226 (71800), 272 (49800), 810 (132). − ES MS; *m*/*z* (%): 510 (26) [Cu(Clip-Phen)]$^+$. − $C_{27}H_{21}CuF_{12}N_5O_2P_2$ (800.5): calcd. (+ 2 H_2O) C 38.7, H 2.98, N 8.37; found C 38.7, H 2.61, N 8.21.

Complex Formation with Ligands 1, 4, and 5: Molar equivalents of ligand and $Cu(OAc)_2 \cdot 2\ H_2O$ were dissolved separately in a small volume (1−2 mL) of warm methanol, then the solutions were mixed and left to stand for 2 h. A fivefold excess of NH_4PF_6 was then added as an aqueous solution to afford a precipitate. Acetone was slowly added until the solid dissolved and the solution was left open to the air for 24−48 h. Evaporation of the acetone afforded the product as a precipitate, which was isolated by centrifugation, washed with water and dried in vacuo.

[(1)Cu^{II}](PF$_6$)$_2$: Reaction of **1** and $Cu(OAc)_2 \cdot H_2O$ on a 0.024-mmol scale afforded 14.9 mg (74%) of product as a pale green solid. − UV/Vis (CH_3CN): λ_{max} (ε M^{-1}cm^{-1}) = 226 (55900), 276 (44400), 818 (135). − ES MS; *m*/*z* (%): 550.9 (100) [Cu(**1**)]$^+$. − $C_{29}H_{23}CuF_{12}N_5O_3P_2$ (842.5): calcd. (+ 0.5 CH_3COCH_3) C 41.9, H 2.97, N 8.03; found C 42.2, H 3.00, N 8.31.

[(4)Cu^{II}](PF$_6$)$_2$ · HPF$_6$: Reaction of **4** and $Cu(OAc)_2 \cdot H_2O$ on a 0.025-mmol scale afforded 17.0 mg (55%) of product as a bright

yellow solid. − UV/Vis (phosphate buffer, pH = 7.2): λ_{max} (ε $M^{-1}cm^{-1}$) = 226 (97600), 274 (89900), 394 (4200), 414 (6800), 437 (5500) and 814 (180). − ES MS; *m/z* (%): 799.3 (73) $[Cu(\mathbf{4})]^+$. − $C_{46}H_{40}CuF_{18}N_7O_3P_3$ (1236.5): calcd. C 44.6, H 3.23, N 7.88; found C 45.0, H 3.22, N 7.92.

$[(5)Cu^{II}](PF_6)_2 \cdot HPF_6$: Reaction of **5** and $Cu(OAc)_2 \cdot H_2O$ on a 0.025-mmol scale afforded 20.2 mg (62%) of product as a bright yellow solid. − UV/Vis (phosphate buffer, pH = 7.2): λ_{max} (ε $M^{-1}cm^{-1}$) = 226 (122000), 274 (122000), 426 (2900), 444 (2700) and 818 (146). − ES MS; *m/z* (%): 865.3 (100) $[Cu(\mathbf{5})]^+$. − $C_{47}H_{41}ClCuF_{18}N_7O_4P_3$ (1301): calcd. (+ CH_3COCH_3) C 44.2, H 3.45, N 7.21; found C 44.2, H 3.30, N 7.46.

DNA Cleavage Experiments: Reactions were carried out in a total volume of 20 μL (10 μL DNA and buffer + 5 μL complex + 5 μL MPA) containing 250 ng of Φx174 viral DNA (7nM, 19 μM in base pairs) in 40 mM sodium phosphate (pH = 7.2), 50 mM NaCl and 10 mM $MgCl_2$ (final concentrations). Complexes were prepared as 1mM stock solutions in DMF, which were then diluted to 4 μM with water, prior to being added to DNA solutions for 30 min at room temperature. DNA cleavage was initiated by addition of mercaptopropionic acid (5 μL, 20mM, final concentration 5mM) and samples were incubated at 37°C for 1 h. 7.5 μL of a solution of 50% (v/v) glycerol/40 mM Tris. HCl buffer (pH = 8) and 0.05% bromophenol blue (w/v) was then added and the samples were immediately loaded on agarose gel (0.8%) containing 1 μg/mL of ethidium bromide. Electrophoresis was carried out at constant current (25 mA) for 15 h in TBE buffer. Bands were located by UV light, photographed, and quantified by microdensity, rates being averaged from at least 3 different sets of experimental data. The correction coefficient 1.47 was used for the decrease in stainability of form I DNA versus forms II and III.[22] The average number of single-strand scissions per DNA molecule, expressed as μ, was considered to be equal to −ln(fraction of form I) according to a Poisson distribution.[23]

UV/Vis-Spectrophotometric Titrations: Solutions were prepared with the appropriate acridine derivative (4 μL of a 2.5 mM solution in DMF), calf-thymus DNA (diluted from a 1 mg/mL solution), NaCl (final concentration 50 mM), $MgCl_2$ (final concentration 10 mM) and phosphate buffer (pH = 7.2, final concentration 40 mM) and diluted with H_2O to a total volume of 1 mL. After equilibration for 24 h, spectra were recorded against an analogous blank solution containing the same concentration of DNA/NaCl/$MgCl_2$ and phosphate buffer. The $CuCl_2$ complexes of **4** and **5** were preformed for 30 min (4 μL of 2.5 mM ligand solution and 1 μL of 10 mM $CuCl_2$ solution) prior to dilution with the appropriate salts and DNA.

Acknowledgments

We thank the European Commission for a Marie Curie Fellowship (Training and Mobility of Researchers: Grant No. ERBFMBICT972447) to SAR.

[1] D. S. Sigman, *Biochemistry* **1990**, *29*, 9097; D. S. Sigman, T. W. Bruice, A. Mazumder, C. L. Sutton, *Acc. Chem. Res.* **1993**, *26*, 98; D. S. Sigman, A. Mazumder, D. M. Perrin, *Chem. Rev.*, **1993**, *93*, 2295; O. Zelenko, J. Gallagher, D. S. Sigman, *Angew. Chem. Int. Ed. Engl*. **1997**, *36*, 2776; M. M. Meiljer, O. Zelenko, D. S. Sigman, *J. Am. Chem. Soc*. **1997**, *119*, 1135; T. Chen, M. M. Greenberg, *J. Am. Chem. Soc.* **1998**, *120*, 3815.
[2] B. Meunier (Ed), *DNA and RNA Cleavers, and Chemotherapy of Cancer and Viral Diseases*, Kluwer, Dordrecht, **1996**; G. Pratviel, J. Bernadou, B. Meunier, *Adv. Inorg. Chem.* **1998**, *45*, 251.
[3] L. E. Marshall, D. R. Graham, K. A. Reich, D. S. Sigman, *Biochemistry* **1981**, *20*, 244; J. M. Veal, K. Merchant, R. L. Rill, *Biochemistry* **1991**, *30*, 1132; J. M. Veal, K. Merchant, R. L. Rill, *Nucleic Acids Res.* **1991**, *19*, 3383.
[4] B. R. James, R. J. P. Williams, *J. Chem. Soc*. **1961**, 2007.
[5] M. Pitié, B. Meunier, *Inorg. Chem*. **1998**, *37*, 3486.
[6] M. Pitié, B. Meunier, *Bioconj. Chem*. **1998**, *9*, 604.
[7] B. G. Feuerstein, N. Pattabiraman, J. Marton, *Nucleic Acids Res.* **1990**, *18*, 1271; M. L. Edwards, R. D. Snyder, D. M. Stermerick, *J. Med. Chem*. **1991**, *34*, 2414; M. Musso, T. Thomas, A. Shirahata, L. H. Sigal, M. W. Van Dyke, T. J. Thomas, *Biochemistry* **1997**, *36*, 1441.
[8] L. S. Lerman, *J. Mol. Biol*. **1961**, *3*, 18.
[9] S. Neidle, Z. Abraham, *CRC Crit. Rev. Biochem*. **1985**, *17*, 73.
[10] J. Sartorius, H-J. Schneider, *J. Chem. Soc., Perkin Trans. 2* **1997**, 2319; H. W. Zimmermann, *Angew. Chem. Int. Ed. Engl*. **1986**, *25*, 115; E. C. Long, J. K. Barton, *Acc. Chem. Res.* **1990**, *23*, 271.
[11] G. Marx, H. Zhou, D. E. Graves, N. Osheroff, *Biochemistry* **1997**, *36*, 15884.
[12] P. Lemay, J. L. Bernier, J. P. Hénichart, J. P. Catteau, *Biochem. Biophys. Res. Commun.* **1983**, *111*, 1074.
[13] C. Bailly, J. P. Hénichart, *Biochem. Biophys. Res. Commun*. **1990**, *167*, 798.
[14] C. Bailly, J. P. Catteau, J. P. Hénichart, K. Reszka, R. G. Shea, K. Krowicki, J. W. Lown, *Biochem. Pharmacol*. **1989**, *38*, 1625.
[15] U. Asseline, N. T. Thuong, C. Hélène, *New. J. Chem*. **1997**, *21*, 5.
[16] C. Bailly, J. P. Hénichart, *Bioconj. Chem*. **1991**, *2*, 379.
[17] L. Ding, G. Etemad-Moghadam, B. Meunier, *Biochemistry* **1990**, *29*, 7868; A. Eliadis, D. R. Philips, J. A. Reiss, A. Skorobogaty, *J. Chem. Soc., Chem. Commun.* **1988**, 1049; G. J. Atwell, W. Leupin, S. J. Twigden, W. A. Denny, *J. Am. Chem. Soc.* **1985**, *107*, 4335; H. D. King, W. D. Wilson, E. J. Gabby, *Biochemistry* **1982**, *21*, 4982; L. P. G. Wakelin, N. Romanos, T-K. Chen, D. Glaubiger, E. S. Canellakis, M. J. Waring, *Biochemistry* **1978**, *17,* 5057.
[18] A. Albert, *The Acridines*, 2nd ed., E. Arnold, London, **1966**, p. 306−307.
[19] Caudrey, I. C. I., B. Pat. 583,220 (*Chem. Abstr*. **1947**, *41*, 330).
[20] M. Pitié, B. Meunier, unpublished results.
[21] A. R. Peacocke, J. N. H. Skerrett, *Trans. Faraday. Soc*. **1956**, *52*, 261; S. C. Zimmerman, C. R. Lamberson, M. Cory, T. A. Fairley, *J. Am. Chem. Soc*. **1989**, *111*, 6805; K. Fukui, K. Iwane, T. Shimidzu, K. Tanaka, *Tetrahedron Lett*. **1996**, *37*, 4983; R. Kuroda, M. Shinomiya, *Biochem. Biophys. Res. Commun*. **1991**, *181*, 1266; K. W. Kohn, M. J. Waring, D. Glaubiger, C. A. Friedman, *Cancer Res.* **1975**, *35*, 71.
[22] J. Bernadou, G. Pratviel, F. Bennis, M. Girardet, B. Meunier, *Biochemistry* **1989**, *28,* 7268.
[23] R. P. Hertzberg, P. B. Dervan, *Biochemistry* **1984**, *23*, 3934; D. Freifelder, B. Trumbo, *Biopolymers* **1969**, *7*, 681.

Received September 21, 1998
[I98320]

Transition Metal Ions in Microporous Crystalline Aluminophosphates: Isomorphous Substitution

Bert M. Weckhuysen,*[a] R. Ramachandra Rao,[a] Johan A. Martens,[a] and Robert A. Schoonheydt[a]

Keywords: Microporous crystalline aluminophosphates / Isomorphous substitution / Synthesis / Spectroscopy / Heterogeneous catalysis / Transition metal ion

Microporous crystalline metalloaluminophosphates (MeAPO-*n*) represent an important group of molecular sieves because of their potential catalytic and adsorptive properties. Many transition metal ions are claimed to incorporate in the framework of these molecular sieves. Here, the concept of isomorphous substitution, and the different indirect and direct tools available to verify this substitution process for Co, Cr, V, Fe and Mn are reviewed taking the $AlPO_4$-5 structure as an example. In addition, it will be shown that transition metal ions can be used as a probe to follow the hydrothermal synthesis process of microporous aluminophosphates.

[a] Centrum voor Oppervlaktechemie en Katalyse, Departement Interfasechemie, K.U. Leuven, Kardinaal Mercierlaan 92, B-3001 Heverlee (Leuven), Belgium
E-mail: Bert.Weckhuysen@agr.kuleuven.ac.be





Bert M. Weckhuysen was born in Aarschot, Belgium in 1968. In 1991 he received his M.S. degree from the Faculty of Agronomy and Applied Biological Sciences, Catholic University of Leuven, Belgium. From 1991 to 1995 he was employed as a doctoral student at the Center for Surface Chemistry and Catalysis under the supervision of Professor Robert A. Schoonheydt. There he gained experience in spectroscopic techniques, zeolite synthesis, catalyst design, and characterization. After obtaining his Ph.D. in Applied Biological Sciences in 1995, he has worked as a visiting research scientist with Professor Israel E. Wachs at the Zettlemoyer Center for Surface Studies of Lehigh University, USA. From 1996 to 1997 he has worked as a postdoc with Professor Jack H. Lunsford in the Chemistry Department of Texas A&M University, USA. Presently, he is a postdoctoral research fellow of the National Fund of Scientific Research at the Catholic University of Leuven. He is author of more than 50 scientific papers.

Ramachandra R. Rao was born in Kanigiri, India in 1968. In 1991 he received his M.S. degree from the A.P.S. University, Rewa, India. After obtaining his Ph.D. in Chemistry from the Osmania University, Hyderabad, India under the supervision of Dr. S. J. Kulkarni in 1996, he moved to the Catholic University of Leuven, Belgium. Presently, he is a postdoctoral fellow at the Department of Interphase Chemistry. His research interests are in the synthesis, characterization and applications of zeolite-based materials. He has authored more than 15 scientific publications.



Johan A. Martens was born in Jette, Belgium in 1958. He obtained his Ph.D. in Applied Biological Sciences at the Catholic University of Leuven, Belgium in 1985. After a research career at the National Fund of Scientific Research, he became full professor in environmental catalysis at the Department of Interphase Chemistry of the Catholic University of Leuven. His teaching assignments are in the fields of "Synthesis of the highly divided solids", "Adsorption" and "Catalysts, adsorbents and colloids for industry and environment". He is author of the book "Synthesis of high-silica aluminosilicate zeolites", editor of two conference proceedings and has published 120 scientific papers. In 1995, he was granted the Exxon Chemical Biannual Science and Engineering Award, for "pioneering research in heterogeneous catalysis for hydrocarbon and natural feedstocks". His current research themes are environmental catalysis, surface chemistry, sol-gel processes, synthesis of oxides, zeolites, adsorption and separation processes, petroleum refining and DeNOx processes.



Robert A. Schoonheydt received his M.S. degree in 1966 and his Ph.D. in 1970, both under the supervision of Professor Jan B. Uytterhoeven at the Catholic University of Leuven, Belgium. After one year as a postdoc with Professor Jack H. Lunsford in the Chemistry Department of Texas A&M University, USA, he returned to the Catholic University of Leuven as a National Fund of Scientific Researchresearcher. He became full professor in 1989. His teaching responsibilities include physical chemistry, analytical chemistry, and general thermodynamics for engineering students at the Faculty of Agricultural and Applied Biological Sciences. His research is concentrated in three areas: (1) spectroscopy and chemistry of surface transition metal ions; (2) molecular organization on clay surfaces, and (3) theoretical modeling of molecule-surface interactions. He has authored more than 170 scientific papers, and is the editor of the book "Developments in the theory of chemical reactivity and heterogeneous catalysis". Presently, he is secretary-general of AIPEA and dean of the Faculty of Agricultural and Applied Biological Sciences. He also serves on the editorial board of Microporous and Mesoporous Materials, Applied Clay Science and European Journal of Inorganic Chemistry.

MICROREVIEWS: This feature introduces the readers to the authors' research through a concise overview of the selected topic. Reference to important work from others in the field is included.

 © WILEY-VCH Verlag GmbH, D-69451 Weinheim, 1999 1434–1948/99/0404–0565 $ 17.50+.50/0

Contents

1. Introduction
2. Isomorphous substitution
3. Indirect tools to verify isomorphous substitution
4. Direct tools to verify isomorphous substitution
4.1. Cobalt
4.2. Chromium
4.3. Vanadium
4.4. Iron
4.5. Manganese
5. Probing the early stages of the crystallization process
6. Heterogeneous catalysis
7. Concluding remarks and look into the future
Acknowledgments
List of abbreviations
References

1. Introduction

Material scientists usually subdivide the family of microporous crystalline oxides into silicate-based and phosphate-based materials[1] (Figure 1). Although this distinction has a historical origin because phosphate-based molecular sieves have been discovered after their silicate-based counterparts, it is often very arbitrary, as some molecular sieves contain both silicon and phosphorus; i.e., the silicoaluminophosphates (SAPO′s). In addition, two other classes of materials recently emerged, which includes the family of e.g. octahedral molecular sieves.

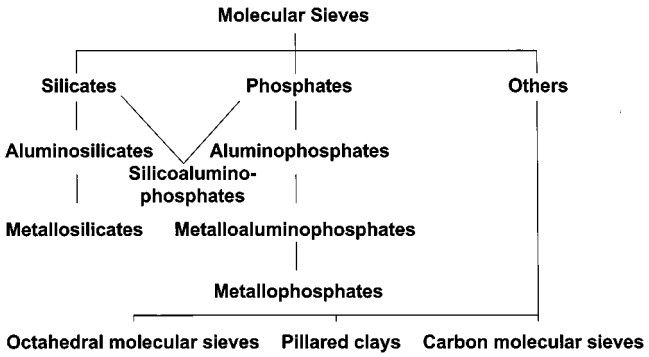


Figure 1. Molecular sieves can be split into three main families, the silicate-based materials containing the aluminosilicates or zeolites and the metallosilicates; the phosphate-based materials containing the aluminophosphates, silicoaluminophosphates, metalloaluminophosphates, and metallophosphates; and finally a remaining group of materials, such as the octahedral molecular sieves

Aluminophosphates consist of tetrahedra of Al^{3+} and P^{5+}, which are corner-sharing an oxygen atom, and building up a three-dimensional framework with channels and/or pores of molecular dimensions.[2,3] This is schematically illustrated in Figure 2. A well-known example is $AlPO_4$-5 (Figure 3), which has one-dimensional channels with 12-ring apertures of 7.3 Å diameter. The acronym $AlPO_4$-*n* is usually used for denoting the different framework structures, and actually more than 35 different topologies of $AlPO_4$-*n* materials are known in the literature.[1−3] All these materials are crystallized from aqueous or non-aqueous solutions at temperatures up to 473 K in the presence of organic structure-directing agents, called templates. Since the first publication on microporous crystalline aluminophosphates in 1982,[4] these materials have attracted a lot of attention mainly because of the promising catalytic and adsorptive properties. Recently, the family of phosphate-based molecular sieves has been further expanded towards mesoporous materials with channel dimensions up to 50 Å.[5]

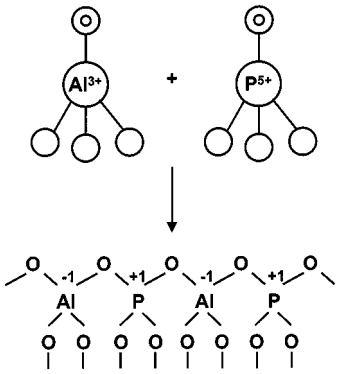


Figure 2. Assembly of a microporous aluminophosphate material (after ref.[1])

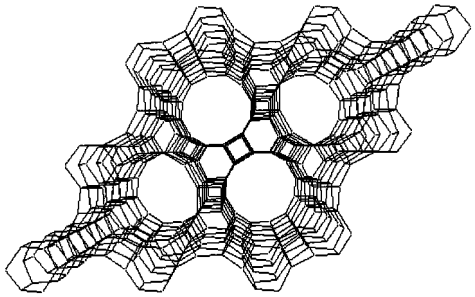


Figure 3. Pictorial representation of the $AlPO_4$-5 structure

In topological models of $AlPO_4$-*n* materials, Al^{3+} and P^{5+} are mostly considered to be both in tetrahedral coordination (Figure 2). This is generally true for dehydrated materials, but important framework distortions or coordination changes may occur in actual $AlPO_4$-*n* crystals in the presence of adsorbed molecules. Indeed, NMR experiments have revealed the formation of five- or six-fold coordinated Al^{3+} in $AlPO_4$-*n* (with n = 5, 11, 21, and 25) materials by interaction with water, ammonia, methanol and acetonitrile.[6] The adsorption of e.g. water may also result in the hydrolysis of Al−O−P bonds with the formation of hydroxy groups. Thus, interrupted frameworks can be formed, in which Al−O−P bonds are systematically missing. These aspects of crystal chemistry of microporous crystalline aluminophosphates seem to be essential in understanding the concept of isomorphous substitution.

Isomorphous substitution in dense oxides is defined as the replacement of an element in the crystalline framework by another element with similar cation radius and coordination requirements.[1c,1d] The concept of isomorphous substitution can be handled for molecular sieves as well, and is

very important because it may result in novel materials with special redox and catalytic properties. Although isomorphous substitution in $AlPO_4$-*n* materials is generally considered as a complex phenomenon, currently 17 elements are reported to replace Al^{3+} and/or P^{5+}; i.e., Be, B, Mg, Si, Ti, V, Cr, Mn, Fe, Co, Ni, Cu, Zn, Zr, Ge, Ga, and As.[1,7] Furthermore, the synthesis of multi-element phases containing up to six different elements has also been claimed.[12]

The only experimental limitation up to now was the substitution degree, which was set to about 38% of the Al^{3+} sites replaced by a particular transition metal ion (TMI).[8] However, very recently Stucky and co-workers were able to increase the substitution degree up to 90% by applying novel synthesis routes.[9] These results suggest that there exists no upper limit to the amount of a particular TMI incorporating in the framework of MeAPO-*n* materials. Indeed, the synthesis of microporous metallophosphates containing no aluminum is also reported in the literature. Some examples are UCSB-6GaCo, a microporous $Co_xGa_{1-x}PO_4$ material synthesized at the University of California at Santa Barbara,[9] DAF-2, a microporous $CoPO_4$ material discovered in the Davy Faraday Research Laboratory[10] and a microporous $ZnPO_4$.[11]

The aim of this review is to give an overview of the evidence currently available in the literature whether a TMI is isomorphously substituted in the framework of MeAPO-*n* materials or not. We will limit ourselves to CoAPO-5 (Co), CrAPO-5 (Cr), VAPO-5 (V), FAPO-5 (Fe), and MnAPO-5 (Mn) because of their well-documented literature. The paper starts with a brief review of the general concepts of isomorphous substitution. These concepts will then be applied to the different TMIs under study, and the obtained information will be compared with the available spectroscopic data. Both indirect and direct tools to verify isomorphous substitution will be discussed. In a third part, it will be shown that TMIs can be used as a probe to monitor the synthesis process of microporous crystalline aluminophosphates. In a final part, the application of microporous crystalline aluminophosphates in the field of heterogeneous catalysis will be briefly discussed. Special emphasis will be placed on possible leaching and mobility of the TMI. The review closes with some concluding remarks, and an outlook into the future.

2. Isomorphous Substitution

As mentioned above, isomorphous substitution in microporous crystalline aluminophosphates is complex, and two different substitution mechanisms can be envisaged for TMIs.[1] This is schematically illustrated in Figure 4. Substitution mechanism (SM) I involves the substitution of an Al atom for a TMI with valence +1 (Ia), +2 (Ib), or +3 (Ic), whereas SM II consists of the replacement of a P atom by a TMI with valence +4 (IIa) or +5 (IIb). Other types of substitutions not mentioned in Figure 4 seem to be very unlikely because they would lead either to positively charged frameworks or to a too high negative charge density. In the case of Si^{4+}, both P^{5+} and Al^{3+} are simultaneously replaced, and, as a consequence, silicon islands are formed in SAPO-5 materials. It is also clear from Figure 4 that SM Ia, Ib, and IIa lead to negatively charged frameworks, which must be balanced by an equivalent number of positively charged extra-framework species such as quaternary ammonium cations, protonated amines, hydroxonium ions or TMIs. On the other hand, SM Ic and IIb lead to electroneutral frameworks, and no charge balancing ions are involved. Finally, it is important to notice that TMI occurring in the synthesis medium under different oxidation states may be simultaneously incorporated according to different substitution mechanisms.

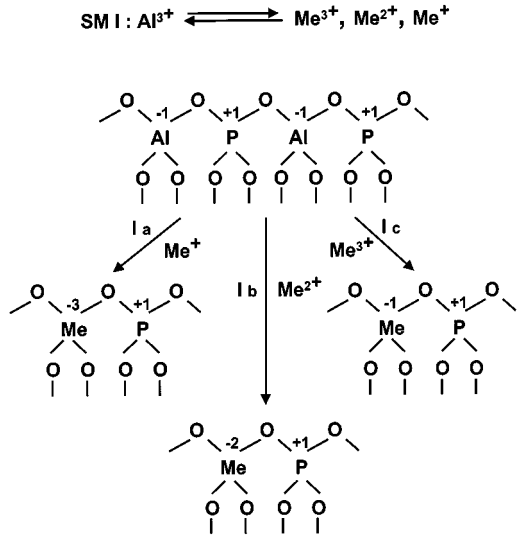


Figure 4A. Isomorphous substitution mechanism I (denoted as SM I) of $AlPO_4$-*n* molecular sieves (after ref.[1])

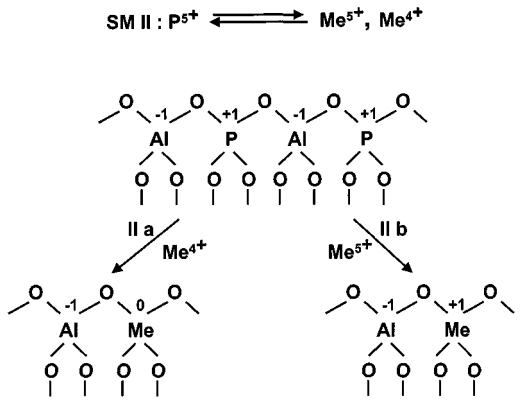


Figure 4B. Isomorphous substitution mechanism II (denoted as SM I) of $AlPO_4$-*n* molecular sieves (after ref.[1])

Four criteria are important for isomorphous substitution of a TMI in $AlPO_4$-5 materials:

(1) The formal charge and the ionic radius of the TMI to be incorporated. In the ionic bonding theory the limited ratios r_+/r_- for tetrahedral and octahedral coordination are

0.225 and 0.414, respectively, [with $r_- = r(O^{2-}) = 1.33$ Å and $r_+ = r$(cation) = 0.299 or 0.551 Å for tetrahedral or octahedral substitution, respectively]. According to Table 1, divalent transition metal ions are too large; trivalent cations are on the limit of tetrahedral coordination, while higher valency would in principle lead to isomorphous substitution.

(2) The solution chemistry of the TMI as a function of the pH of the synthesis gel. Here, it is crucial to avoid precipitation of insoluble transition metal hydroxides or oxides during the synthesis process because they may prevent that the TMI becomes available for isomorphous subsitution.

(3) The ligand field stabilization energy (LFSE) of the TMI. In the cases under study octahedral coordination is always the preferred one.

(4) The thermodynamic stability of the resulting microporous aluminophosphate framework.

Table 1. Ionic cation radii [Å] for different coordination geometries of P, Al, and transition metal ions

Cation	4	5	6	Cation	4	5	6
P^{5+}	0.17	–	–	Mn^{4+}	–	–	0.54
Al^{3+}	0.39	–	0.53	Mn^{3+}	–	0.58	0.65
Co^{2+}	0.57	–	0.74	Mn^{2+}	–	–	0.82
Co^{3+}	–	–	0.61				
Fe^{2+}	0.63	–	0.78				
Fe^{3+}	0.49	–	0.65	Cr^{6+}	0.30	–	–
V^{5+}	0.355	0.46	0.54	Cr^{5+}	0.35	–	–
V^{4+}	–	–	0.59	Cr^{3+}	–	–	0.615
V^{3+}	–	–	0.64	Cr^{2+}	–	–	0.82

Based on the cation radii and valence states it is then likely to assume that Co^{2+}, Fe^{2+}, and Fe^{3+} are substituting for Al^{3+} in the $AlPO_4$-5 framework according to SM Ib or Ic, whereas for example V^{5+} may replace P^{5+}. In any case, the possible incorporation of e.g. octahedrally coordinated Cr^{3+} and Mn^{2+} ions can only be explained by the flexibility of the aluminophosphate framework, and specific interactions with e.g. the organic template molecule. An additional explanation can be found in the unique possibility to increase the coordination number from four to five or six by interaction with additional ligands not being part of the framework; e.g., H_2O or OH groups, as was already discussed above for framework aluminum in $AlPO_4$-5 materials.[6] In addition, TMIs may also exist as oxides or extra-framework cations at the surface of the molecular sieves. Thus, the goal is then to develop direct and indirect tools which are able to verify isomorphous substitution.

3. Indirect Tools to Verify Isomorphous Substitution

The incorporation of TMIs into the framework of $AlPO_4$-5 materials would lead to an increase in unit cell volume of the crystal structure, all other factors remaining invariant (symmetry, etc.). This is expected because the radii of high-spin tetrahedral TMI, in a *T*-O matrix, is larger than that of Al^{3+} or P^{5+} (Table 1), and this expansion can be directly measured by X-ray diffraction techniques (XRD), according to

$$4/3\ [(h^2 + hk + k^2)/a^2] + l^2/c^2 = (4 \sin^2\theta)/\lambda^2$$

with *a* and *c*, the cell parameters of the unit cell of a hexagonal system; θ, the diffraction angle; and λ, the wavelength of the incident X-rays. An example of such a lattice expansion is shown for VAPO-5 materials in Figure 5.[12] However, such lattice expansions are not always observed, and no lattice expansions or even lattice contractions are reported in the literature for MeAPO-5 systems.[13] One of the explanations is that the amount of TMI is not sufficient to change the unit cell dimensions within the experimental error of the system.

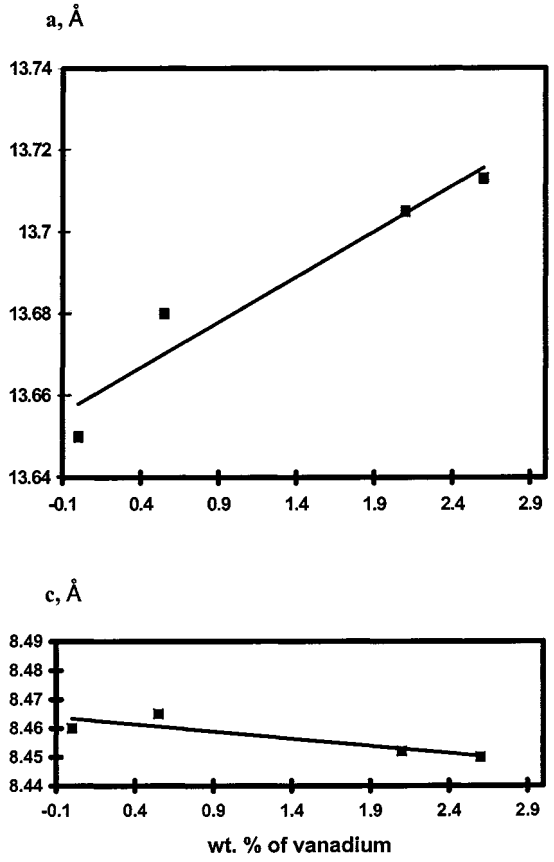


Figure 5. Lattice expansion as observed for VAPO-5 materials: variation of the *a* and *c* cell parameters as a function of the vanadium content (after ref.[12])

Isomorphous substitution can also be verified by chemical analysis. One expect then that the molar ratio of ([TMI] + [Al])/[P] (if the TMI is replacing Al) or ([TMI] + [P])/[Al] (if the TMI is replacing P) is equal to 1. Although this method is still very useful, it is very arbitrary and often inaccurate. Indeed, unreasonable values will be obtained if extra-framework TMI is present or if different substitution mechanisms simultaneously occur in the synthesis medium.

Another method to verify isomorphous substitution is by measuring the weight loss, associated with the burning of the template molecule. In the case of the template molecule Et_3NH^+, one can write the following combustion reaction:

$Et_3NH^+ + 11\ O_2 \rightarrow 6\ CO_2 + 8\ H_2O + NO_2$. It is then assumed that for every TMI^{n+} ($n = 2$) substituting for Al in the lattice, one template molecule is needed to compensate for the negative charge of the framework. It is important to notice that the combustion process of an occluded and positively charged template molecule usually occurs at a higher temperature than that of an adsorbed neutral template molecule.

The formation of extra-framework TMI can be indirectly probed by comparing the volume of intrachannel void space of MeAPO-5 and $AlPO_4$-5. Indeed, the generation of extra-framework species in channels and cavities would reduce the available void space of the $AlPO_4$-5 crystals.

Finally, if Me^{2+} (e.g., Co^{2+}, Fe^{2+}, and Mn^{2+}) substitute for Al^{3+}, one expects the formation of Brønsted acid sites in a concentration equal to that of Me^{2+}. The amount of Brønsted acid sites can be measured by performing TPD with e.g. a secondary amine, such as isopropylamine. Another interesting method is IR spectroscopy in conjunction with ammonia and acetonitrile as probe molecules. One of the problems here is to distinguish between the different forms of acidity (Lewis vs. Brønsted acidity).

The results of the application of these indirect measurements for isomorphous substitution to MeAPO-5 materials (with Me = Co, Cr, V, Fe, and Mn) are summarized in Table 2. It is clear that there is indirect evidence for the isomorphous substitution of Co^{2+}, $Fe^{2+/3+}$, and Mn^{2+} into the framework of $AlPO_4$-5 molecular sieves. Another problem with indirect methods, besides that they being indirect, is the lack of sensitivity. As a consequence, relatively high amounts of framework TMI are necessary to observe characteristic changes with the techniques mentioned.

4. Direct Tools to Verify Isomorphous Substitution

It can be concluded from the previous section that other more direct − preferably spectroscopic − techniques have to be called in to distinguish between framework and extra-framework TMI. Because each spectroscopic technique has its own sensitivity and application domain, a whole battery of complementary spectroscopic techniques has been applied to obtain detailed information of the coordination environment of TMI. Another disadvantage is the occurrence of complex and overlapping spectra, and chemometrical techniques have to be called in to obtain fingerprint spectra of framework and extra-framework TMI.

4.1. Cobalt

CoAPO-5 is probably the most studied MeAPO-*n* system ever. This can be easily explained by the fact that almost all scientists agree that Co^{2+} is substituting − at least partially − for Al^{3+} in the framework. This has been evidenced by applying a combination of DRS, ES, and EXAFS spectroscopies.

As mentioned above, the TMI content that can be incorporated into the $AlPO_4$-5 structure is still limited, and attempts to synthesize CoAPO-5 with high Co content usually lead to low-crystalline products contaminated with impurities.[15] An explanation for the failure in obtaining a pure CoAPO-5 phase from Co-rich gels can be the more favorable crystallization of other competing crystalline phases, such as the chabazite structure of CoAPO-34.[16,17] In addition, when attempting to incorporate large amounts of Co^{2+} in the framework, some of the Co^{2+} is present as octahedral Co^{2+}, clustered CoO and/or a $CoAl_2O_4$ phase.[18]

CoAPO-5 materials have been studied in detail by DRS spectroscopy, and an example of a set of DRS spectra is shown in Figure 6. The absorption bands for the blue, as-synthesized CoAPO-5 are typical for a perfect tetrahedron $[CoO_4]$ with two triplets centered at $\nu_2 = 6700\ cm^{-1}$ and $\nu_3 = 17300\ cm^{-1}$. This observation, together with the linear dependency of the band intensities with the Co^{2+} content are taken as proof of incorporation of Co^{2+} in the lattice. This is surprising because (1) the Co^{2+} radius of 0.57 Å is on the limit of tetrahedral and octahedral coordination and (2) the Co^{2+} radius is significantly larger than that of Al^{3+} (Table 1). As a consequence, a distortion of the $[CoO_4]$ tetrahedron is expected, and this strain is relieved in the lattice by interaction with adsorbed molecules in the 12-ring channels of the $AlPO_4$-5 structure.

This is proven by the DRS spectra taken after calcination in O_2 (Figure 6). A yellow-green sample is obtained with a distorted Co^{2+} species with two triplets centered at $\nu_2 = 5500\ cm^{-1}$ and $\nu_3 = 15150\ cm^{-1}$. These frequencies are indicative of a weaker ligand field, too. The distortion and strain of the zeolite lattice is reflected by the instability of the framework Co^{2+}. Indeed, part of the Co^{2+} is expelled from the lattice to give extra-framework pseudo-tetrahedral Co^{2+} ($\nu_2 = 5500$ and $\nu_3 = 16500\ cm^{-1}$) and octahedral Co^{2+} ($\nu_2 = 8100$ and $\nu_3 = 19550\ cm^{-1}$). A fraction of the Co remaining in the lattice is oxidized to high-spin tetrahedral Co^{3+} with its characteristic d-d transition at around

Table 2. Indirect criteria to verify isomorphous substitution of TMI in $AlPO_4$-5 molecular sieves

TMI	Lattice expansion	Chemical analysis	Template burning	Void space	Brønsted acidity
Co^{2+}	+	+	+	+	+/−
Cr^{3+}	nd	+/−	nd	nd	ne
V^{4+}	+/−	+/−	+	+	nd
$Fe^{2+/3+}$	+	+	nd	nd	−, ne (Fe^{3+})
Mn^{2+}	+	+	nd	nd	+

+: positive evidence; −: negative evidence; +/−: mixed opinions in the literature; nd: not determined; ne: not expected.

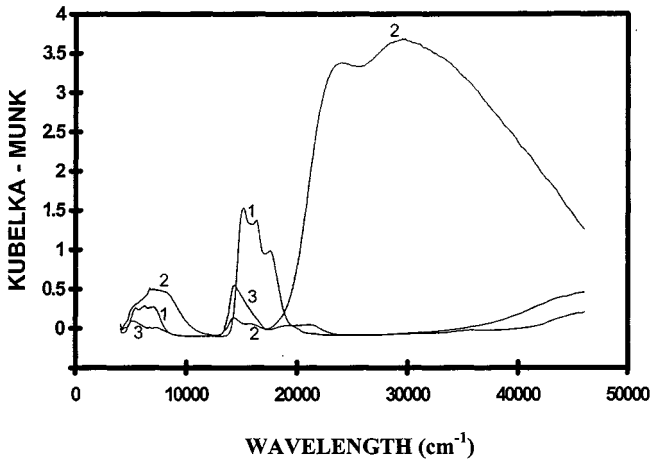


Figure 6. DRS spectra of CoAPO-5 materials as a function of the pretreatment: (1) in as-synthesized form; (b) after calcination overnight at 773 K and (3) after reduction with H_2 at 623 K (after ref.[16])

9000 cm^{-1}, and very intense $O \rightarrow Co^{3+}$ charge transfer transitions around 25000 and 31500 cm^{-1}.

The redox chemistry of Co is reversible. Co^{3+} is quantitatively reduced to Co^{2+} by H_2 at high temperatures, but also by CO, NO, methanol, acetone, and toluene.[16,19–25] The overall scheme of this reaction is given in Figure 7. Additional evidence comes from the observation of a weak OH stretching band at 3540 cm^{-1} after reduction and its disappearance upon oxidation. Whether the presence of a DRS spectrum of tetrahedral Co^{2+} is still a sufficient proof of lattice-substituted Co^{2+} is questionable. Indeed, one might envisage octahedral lattice Co^{2+} by analogy with Al^{3+}, or the presence of extra-framework Co oxides in different forms.

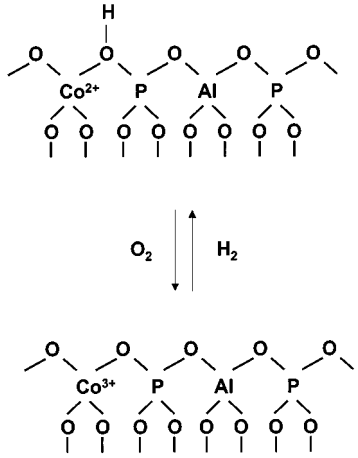


Figure 7. Schematic representation of the oxidation/reduction cycle of CoAPO-5 molecular sieves

Further evidence for the oxidation of Co^{2+} to Co^{3+} during calcination is found by ESR. A significantly reduced ESR signal in calcined CoAPO-5 was explained by a partial oxidation of Co^{2+} to the ESR invisible Co^{3+}.[20,21] Lee and Chon proved the oxidative abilities of CoAPO-5 with ESR by the formation of radicals upon interaction with alkenes.[26] However, this interpretation has been challenged by Kurshev et al.[27] These authors propose a distortion of the tetrahedral Co^{2+} environment to a dihedral symmetry resulting from the interaction of Co^{2+} with two O_2 molecules. Finally, Co K-edge EXAFS studies of CoAPO-5 recorded after synthesis and during calcination and reduction have only revealed small changes in bond lengths and coordination numbers of $Co^{2+/3+}$, suggesting an incomplete oxidation of the Co^{2+}.[28]

4.2. Chromium

The synthesis of CrAPO-5 molecular sieves has also been extensively studied in the literature, but the question remains if Cr^{3+} really substitutes for Al^{3+} in the framework, and to what extent.[29] Indeed, tetrahedral Cr^{3+} is difficult to obtain as evidenced by the scarcity of tetrahedral Cr^{3+} complexes and the absence of reported inorganic structures with tetrahedral Cr^{3+}.[30]

Figure 8 shows the DRS spectra of the green colored as-synthesized CrAPO-5 samples with increasing Cr content, which are characterized by two absorption bands at 15900 and 21800 cm^{-1}.[29][31] The intensities of both bands almost linearly increase with increasing Cr content, and they are assigned to the ν_1 and ν_2 transitions of octahedral Cr^{3+}. In addition, the 15900 cm^{-1} band has two weak shoulders, which are both spin-forbidden transitions. It is important to notice that during synthesis there is no indication for a transformation of Cr^{3+} (O_h) to Cr^{3+} (T_d). A similar conclusion can be made from dehydration experiments in vacuo of as-synthesized CrAPO-5 taking into account that dehydrated $AlPO_4$-5 does not possess octahedral Al^{3+} in the framework (vide supra). Thus, there is no unambiguous experimental evidence to propose an octahedral lattice Cr^{3+} species. Nevertheless, some authors have proposed such lattice Cr^{3+} (O_h) with two H_2O molecules completing its first coordination sphere:[32] $Cr^{3+}(O)_4(H_2O)_2$.

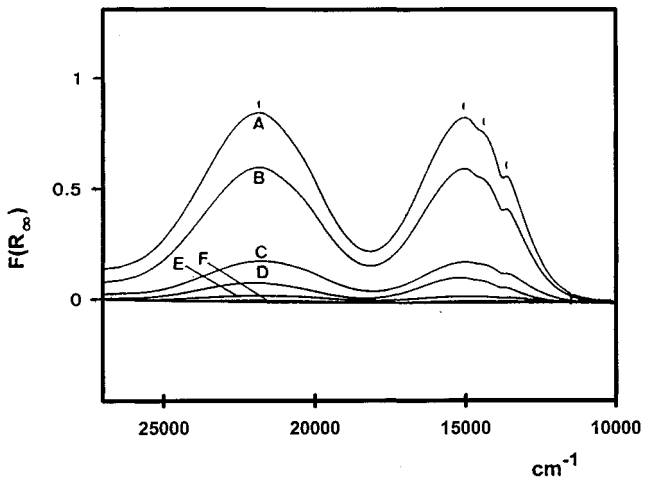


Figure 8. DRS spectra of as-synthesized CrAPO-5 materials as a function of the chromium content: 0.75 $R.(Cr_xAl_yP_z)O_4 \cdot 20\ H_2O$ with x = (A) 0.08; (B) 0.04; (C) 0.02; (D) 0.004; (E) 0.002, and (F) 0.0 (after ref.[29a])

Evidence for the presence of extra-framework Cr^{3+} comes from ESR experiments. The ESR spectra of as-synthesized CrAPO-5 are dominated by two characteristic signals: (1) a broad isotropic signal with $g = 2$ and (2) a rhombic signal with a positive lobe at $g_{eff} = 4.3$ and a weaker isotropic contribution at $g_{eff} = 2$. The zero-field parameters D and E are equal to 0.490 and 0.163 cm^{-1}, respectively. The former signal is typical for clustered Cr^{3+} in octahedral symmetry, which are most probably located as small oxidic particles at the outer surface or in the channels or pores of the molecules sieve. The latter signal is typical for Cr^{3+} in a strongly distorted environment, and because this signal is also observed for Cr^{3+} ions at the surface of amorphous supports (Al_2O_3, ...), one can assign it to distorted Cr^{3+} at the surface of $AlPO_4$-5.[33] By using other techniques, such as photoluminescence and single-crystal UV/Vis spectroscopy, others came to similar conclusions.[34−37]

Calcination in O_2 results in a color change from green to yellow-green. Both DRS and ESR spectroscopies indicate an incomplete oxidation of Cr^{3+} to Cr^{6+} with traces of Cr^{5+}. This suggests that some of the oxidic/isolated Cr^{3+} in the channels or pores of $AlPO_4$-5 resists oxidation. The formed Cr^{6+} is most probably attached to the surface of $AlPO_4$-5 as a chromate species with two extra-framework oxygen ions.[29,31]

4.3. Vanadium

VAPO-5 can be synthesized hydrothermally with different vanadium sources and template molecules, although the final oxidation state of vanadium largely depends on the vanadium source used.[12,13,38]. If V_2O_5 is used, some V^{5+} will be reduced to V^{4+} during hydrothermal synthesis, and a mixture of V^{4+} and V^{5+} is observed in the final solid products. The nature and properties of these vanadium sites are still a subject of debate. Up to now, it has not been proven unambiguously that vanadium really incorporates in the framework of $AlPO_4$-5 crystals, and the incorporation mechanism of $V^{4+/5+}$ is considered to be more complex than in the case of Co^{2+}.[39] This is not only due to the charge difference (proposal of substitution by SM II), but also because vanadium is prone to condensation reactions in solution, which lead to a variety of oligomeric species.

According to Montes et al.[13] and Jhung et al.[38] V^{4+} substitutes for P^{5+}, whereas Rigutto and van Bekkum[40] suggested the replacement of Al^{3+} by V^{4+}. Substitution of P^{5+} by V^{4+} is mainly proposed in view of a priori arguments such as the similarities between vanadium and phosphorus chemistry, and the existence of the mineral Schoderite, which contains both VO_4^{3-} and PO_4^{3-}.[41] The replacement of Al^{3+} by a $V{=}O^{2+}$ cation seems to be more convincing since the presence of the latter species is supported by spectroscopic evidence,[39,40,42] and no tetrahedral V^{4+} was ever detected by spectroscopic means. Indeed, combined DRS-ESR measurements have shown that V^{4+} is always present as a (pseudo-)octahedral species in VAPO-5.[39]

The above-mentioned models have in common that the vanadium sites are considered as monomeric. The key argument used for this assumption is that highly resolved ESR spectra are observed for as-synthesized VAPO-5 materials. However, clustered V^{4+} ions may be invisible due to line broadening as caused by spin-spin coupling of strongly interacting V^{4+} ions. If the vanadium ions tend to cluster one would expect that the amount of isolated V^{4+} ions as determined by quantitative ESR is lower than that expected from chemical analysis. This is indeed the case, and only 10% of the vanadium contributes to the ESR spectrum of VAPO-5.[39] Thus, V^{4+} is present as both isolated and clustered species, but it is uncertain whether both species substitute in the lattice. Finally, it is important to stress that two slightly different ESR signals are observed, which suggest the presence of two distinct V^{4+} ions, most probably located at defect sites.

Upon calcination in O_2, V^{4+} is almost completely oxidized to V^{5+} as evidenced by the weak V^{4+}-ESR signal and the observation of tetrahedrally coordinated V^{5+} (vanadate) by DRS and ^{51}V-NMR spectroscopies.[39,40,43] Reduction with CO or H_2 results in a partial regeneration of V^{4+}, and most probably lower oxidation states, such as V^{3+}, are formed.

4.4. Iron

FAPO-5 molecular sieves, discovered by Messina et al. in 1985,[44] can be synthesized using a variety of template molecules, typically amines or quaternary ammonium hydroxides, and either a Fe^{2+} or Fe^{3+} salt may be used as iron source. Regardless of the iron salt used, mostly both Fe^{2+} and Fe^{3+} are observed in the as-synthesized samples. Two reasons have to be invoked: (1) The oxidation of Fe^{2+} to Fe^{3+} in the initial synthesis gel. Indeed, by flushing the synthesis gel with nitrogen the oxidation to Fe^{3+} could be suppressed; and (2) the reduction of Fe^{3+} to Fe^{2+} by reaction with the amine template, according to $2\ Fe^{3+} + R_3N + H_2O \rightarrow 2\ Fe^{2+} + R_3NO + 2\ H^+$. The same reaction is responsible for the reduction of V^{5+} to V^{4+} during hydrothermal synthesis (vide supra). At low metal content, more than 90% of the iron is reduced, and with increasing iron content, the amount of reduced iron decreases only slowly. The reduction of Fe^{3+} can only be minimized by hydrothermal synthesis at lower temperature using e.g. tetraethylammonium hydroxide as template.

Several papers have appeared in the literature on the spectroscopic characterization of FAPO-5 molecular sieves.[45−55] The main techniques used were DRS, ESR, XPS, and Mössbauer spectroscopy. Especially ESR and Mössbauer spectroscopy seem to be very powerful, although their spectral interpretation is still a matter of debate.

As-synthesized FAPO-5 samples are characterized by a weak absorption at 23500 cm^{-1}, and an intense shoulder at around 26500 cm^{-1} in DRS. The former band is the spin-forbidden transition ν_3 of high-spin Fe^{3+} in tetrahedral coordination, while the latter is a charge-transfer transition of the type $O{\rightarrow}Fe^{3+}$.[46] It is assumed that the band at 23500

cm^{-1} is typical for Fe^{3+} in framework positions. No absorption bands of Fe^{2+} are detected. After calcination in O_2, the material turned from white to off-white, and the corresponding spectrum has characteristic absorption bands at 20800, 23000, 24400, and 26500 cm^{-1}. The transitions at 20800 and 23000 cm^{-1} are assigned to the spin-forbidden transitions ν_1 and ν_2, respectively, of high-spin Fe^{3+} in tetrahedral coordination.[46] Reduction with H_2 does not result in any spectral changes.

The co-existence of Fe^{2+} and Fe^{3+} in as-synthesized samples was unambiguously revealed by XPS. The binding energies of $Fe2p_{3/2}$ at 712.3 and 708.4 eV are assigned to framework Fe^{3+} and Fe^{2+}, respectively, while the presence of non-framework Fe^{3+} was evidenced by the $Fe2p_{3/2}$ peak at 710.5 eV. Calcination results in a total oxidation of Fe^{2+} to Fe^{3+}, and as a consequence, the disappearance of the $Fe2p_{3/2}$ peak at 708.4 eV. More detailed information can be obtained by Mössbauer spectroscopy. Four characteristic quadrupole doublets are observed, which are assigned to framework $Fe^{3+}(T_d)$; extra-framework $Fe^{3+}(O_h)$; framework $Fe^{2+}(T_d)$ and extra-framework $Fe^{2+}(T_d)$, their relative amounts depending on the treatment condition and the preparation method. For example, Schubert et al. found that as-synthesized FAPO-5 contains about 70% of Fe^{3+} and 30% of Fe^{2+}, and the amount of Fe^{3+} gradually increases with increasing calcination temperature.[51b]

Finally, ESR spectroscopy has been used to characterize the state of Fe^{3+} in FAPO-5 materials, and an example of an X-band ESR spectrum is given in Figure 9. Five different ESR signals can be observed: $g_1 = 2.0$; $g_2 = 2.2-2.3$; $g_3 = 4.3$; $g_4 = 5.2$ and $g_5 = 8.4$.[45] The two most intense signals are g_1 and g_2, and their assignments are still controversial. The traditional assignment is that g_1 is due to extra-lattice oxidic Fe^{3+}, whereas g_2 is due to framework Fe^{3+}. The three other signals would then be due to extra-lattice Fe^{3+} in various forms, although no detailed assignments have been given up to now. In light of recent work of Goldfarb et al.,[50] g_1 is due to both framework and extra-framework Fe^{3+}, whereas g_2 is typical for Fe^{3+} in a distorted tetrahedral coordination at defect sites. Thus, ESR alone will not be able to discriminate between framework and extra-framework Fe^{3+}.

It is important to notice that the relative intensity of g_2 decreases with increasing Fe loading, suggesting that Fe^{3+} will first coordinate to defect sites of the $AlPO_4$-5 crystals, while at higher loading, Fe^{3+} will incorporate in the framework or is present as small oxide particles. Upon calcination, the five ESR signals remain visible, suggesting that Fe^{3+} is relatively stable in the FAPO-5 material. Reduction results in a relative increase of the intensity of the g_1 signal, which can be explained by the formation of oxidic Fe^{3+}, and thus a migration and clustering of iron.

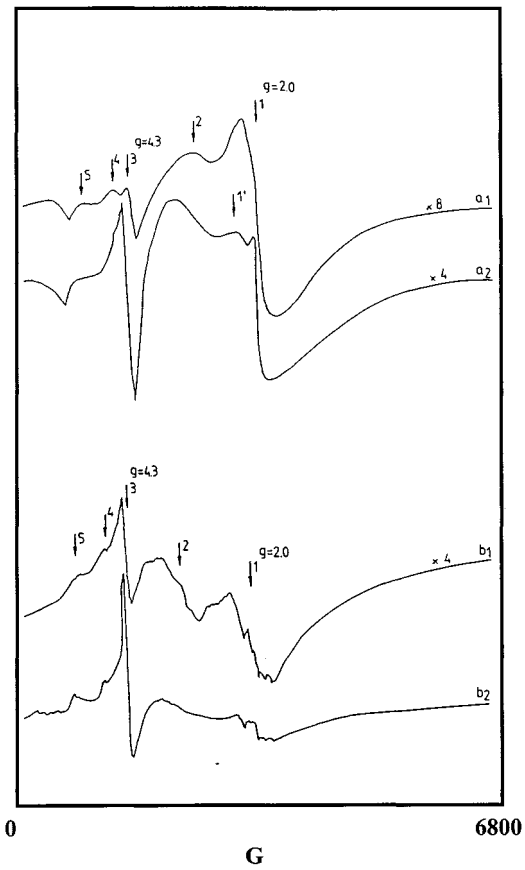


Figure 9. ESR spectra of FAPO-5 materials as a function of the pretreatment: (a) in as-synthesized form and (b) after calcination overnight at 773 K and helium flushing for 15 min at room temperature; the samples were measured at room temperature (1) and at 120 K (2) (after ref.[45])

4.5. Manganese

The evidence for the incorporation of Mn^{2+} into the framework of $AlPO_4$-5 is scarce. One of the reasons is the current discrepancy between the results obtained by indirect and direct tools to verify isomorphous substitution (Table 2). In addition, only ESR and its pulsed variant ESEEM have been applied to probe Mn^{2+} in $AlPO_4$-5 systems.[56–62] Thus, there is clearly a need to use other characterization techniques, such as DRS.

ESR spectroscopy of MnAPO-5 with a low manganese content shows six resolved hyperfine lines ($I = 5/2$) with a hyperfine coupling constant A of 90 G and a small zero-field splitting parameter D. Such ESR spectrum is typical for a slightly distorted octahedral Mn^{2+} species. In addition, ESEEM experiments showed that the isolated Mn^{2+} species interact through weak dipolar interactions with an average of six ^{31}P nuclei at a distance of 5 Å.[56][57] All these observations do not agree with a model in which Mn^{2+} is substituting for framework Al. As a consequence, it was concluded that the majority of Mn^{2+} in MnAPO-5 systems was present as extra-framework Mn^{2+}.

Dehydration of MnAPO-5 systems stimulates migration of the Mn^{2+} cations, resulting in an increase in spin exchange interaction, and only a single ESR line is observed. X-band and Q-band ESR spectra reveal that the 6-line hyperfine splitting is superimposed on a broader ESR signal, which has been assigned to transitions other than $-1/2 \rightarrow$

1/2 of Mn^{2+} with $I = 5/2$ or to another Mn^{2+} species by Levi et al.[57] Removal of water at increasing temperatures up to 400°C significantly broadens the hyperfine line and finally the resolution is completely lost and only one broad line is observed. Rehydration usually restores the 6-lines ESR spectrum of the hydrated MnAPO-5 sample completely.

The redox behavior of Mn^{2+} in MnAPO-5 materials has been investigated by Katzmarzyk et al.[59] Calcination in O_2 changes the color from white to deep blue or violet, and this color change is associated with an overall decrease of the Mn^{2+} ESR intensity. This decrease in signal intensity is attributed by the same authors to a partial oxidation of Mn^{2+} to the ESR inactive Mn^{3+}. Oxidation to Mn^{4+} can be ruled out because new ESR signals cannot be detected at the low measurement temperature (93 K). Addition of polar molecules, such as water and ammonia, causes a color change from blue to pink or even gray. Reduction of the sample with H_2 at temperatures below 450 K does not change the ESR spectrum, while after reduction at 475 K the ESR signal becomes narrower and more intense. A possible explanation is that reduction of Mn^{3+} to Mn^{2+} under these conditions leads to more ESR active spins.

Although the above-described ESR interpretations are challenged by several authors (e.g., the presence of cluster-like arrangements of the type $Mn^{2+}-O-P-O-Mn^{2+}$),[62,63] it is obvious that clear spectroscopic evidence of framework Mn^{2+} is still lacking in the literature.

5. Probing the Early Stages of the Crystallization Process

The synthesis of microporous crystalline aluminophosphates generally starts with a gel phase which is digested during synthesis at high temperatures. Several attempts have been made to elucidate the chemistry of this gel, and its hydrothermal digestion. A whole variety of characterization techniques, such as liquid-phase NMR, IR and Raman spectroscopy, have been applied. For example, the existence of aluminum phosphate entities in solution has been demonstrated by NMR.[64–66]

Another approach is to probe the coordination geometry of TMI during hydrothermal synthesis. Indeed if the TMI is incorporated in the lattice, the synthesis gel with octahedral $TMI(H_2O)_6^{n+}$ ions will be transformed during synthesis into a solid material containing tetrahedral framework and/or non-framework TMI. One way to study this synthesis process is to use spectroscopy to probe the TMI during synthesis. In this respect, DRS has been used to characterize the synthesis of CoAPO-5 from its early precursors to the formation of a crystalline phase.[67–69] This is possible because: (1) Co^{2+} is, as discussed above, relatively easily incorporated in the $AlPO_4$-5 framework during hydrothermal synthesis, and a distinction between tetrahedral and octahedral Co^{2+} can be made; (2) the DRS spectra have excellent quality; and (3) the DRS technique is applicable to both wet gels and dried solids, amorphous and crystalline as well.

Figure 10 shows the XRD and DRS intensities of the solid materials versus synthesis time. The DRS intensities of tetrahedral Co^{2+} increase concomitantly with the XRD intensities. Thus, as crystallization proceeds, Co^{2+} is incorporated in the structure. In the nucleation stage of the synthesis, the nuclei are too small to be detected by XRD, and DRS can then be used to probe the coordination of Co^{2+}. This is illustrated in Figure 11, where the DRS spectra of four distinct gel stages as a function of synthesis time are given.

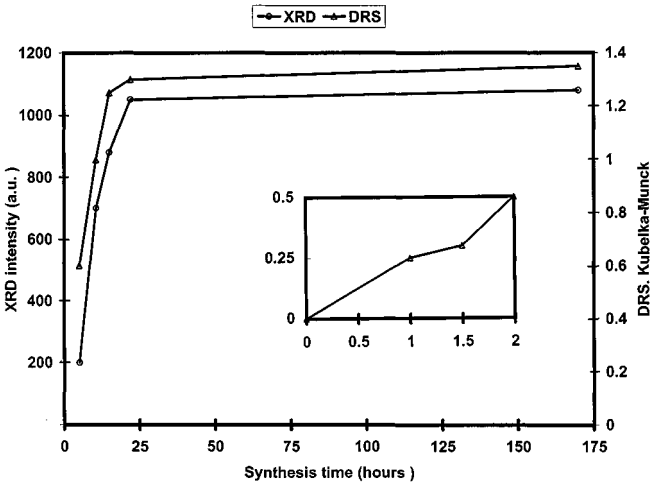


Figure 10. XRD and DRS intensities of the solid materials versus the synthesis time for CoAPO-5 materials (after ref.[67])

These gels were isolated from the autoclaves, and measured at room temperature. S_1 is the hydration-gelation phase, and nucleation has not yet started. Co^{2+} is octahedrally coordinated and not yet incorporated. It can be washed off by centrifugation. The DRS spectrum of gel S_2 consists of a weak triplet of tetrahedral Co^{2+}, superimposed on a broad band of (pseudo-)octahedral Co^{2+}. The latter is interpreted as cobalt with two water molecules in the first coordination sphere; i.e., $[CoO_4(H_2O)_2]$ taken up in the solid gel. Stage 3, which is attained after two hours of synthesis, is characterized by a dramatic increase of the band intensities of tetrahedral Co^{2+} at the expense of octahedral Co^{2+}. This means that Co^{2+} is being taken up by the CoAPO-5 material as $Co(OP)_4$. Further evidence for this transformation process comes from the decrease of the water bands in the NIR region. In stage S_4, the sample contains no water peak, indicating a full transformation of the gel into a crystalline phase. The peaks of tetrahedral cobalt are very intense and well resolved, which is indicative for Co^{2+} in identical crystallographic sites. The overall picture of the uptake of Co^{2+} can then schematically be shown as:

$$Co(H_2O)_6^{2+}\ \text{(liquid phase)} \rightarrow [CoO_4(H_2O)_6]\ \text{(gel phase)} \rightarrow [CoO_4]\ \text{(crystalline)}$$

This scheme is valid for CoAPO-5, but not for all structure types. Thus, CoAPO-34 synthesis is favoured at high template and Co contents; i.e., less water. This means that

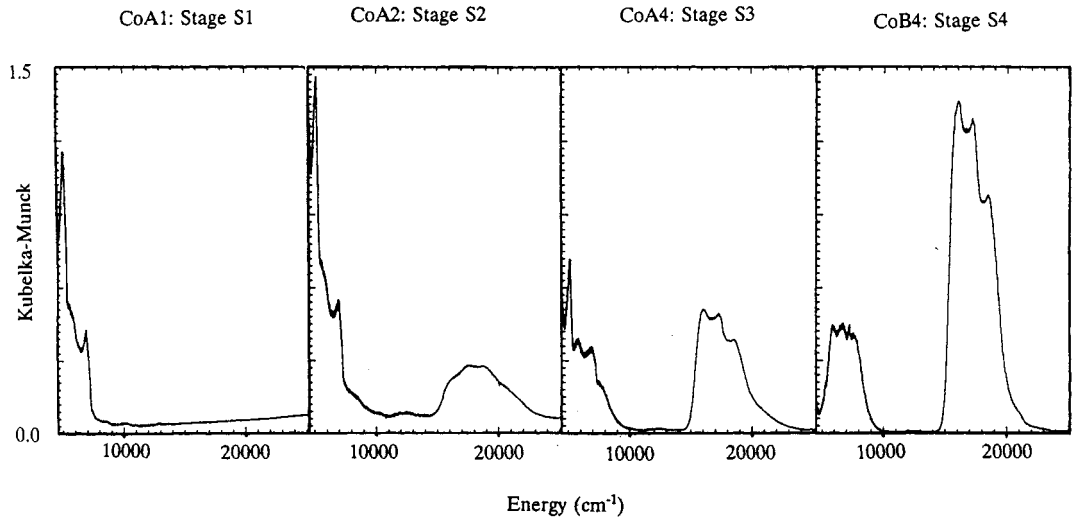


Figure 11. Four distinct gel stages for the synthesis of CoAPO-5, as recorded by DRS (after ref.[67])

upon interaction with the gel phase Co^{2+} is immediately transformed into a tetrahedral species:

$$Co(H_2O)_6^{2+}\ (\text{liquid phase}) \rightarrow [CoO_4]\ (\text{gel}) \rightarrow [CoO_4]\ (\text{crystal})$$

One observes that the template does not intervene directly in both schemes, but through its pH-regulating role it certainly influences indirectly the chemistry going on in the synthesis mixture.

6. Heterogeneous Catalysis

As mentioned above, MeAPO-5 molecular sieves have been explored as promising heterogeneous catalysts for both liquid-phase and gas-phase reactions. Their applications have been recently reviewed by Bellussi and Rigutto[70] and Arends et al.[71] Rather than summarizing the main results described, we would like to focus on the potential problems associated with their use in catalytic applications.

The catalytic activity of MeAPO-5 materials originates from the (co-)presence of Brønsted acid sites and/or redox centers, and thus in principle both acid- and redox-catalyzed reactions can be performed. Indeed, the activation of e.g. CoAPO-5 involves the calcination to remove template molecules. Simultaneously, part of the lattice TMI is oxidized to higher oxidation states (vide supra):

$$\text{CoAPO-5-}(Et)_3NH^+ \rightarrow (Co^{2+}{}_x,Co^{3+})H_x\text{-APO-5}$$

Protons are necessary for charge balance, and thus two catalytic functions are formed (Figure 7). If both Co^{2+} and Co^{3+} are in the lattice, they are expected to be in high-spin and in tetrahedral coordination. Redox catalysis requires free coordination sites, and this is impossible in such an ideal situation. Therefore, such type of catalysis can only be explained by (1) the presence of less than four lattice oxygen atoms around the TMI; (2) the lattice oxygen atoms, which are indirectly involved in redox chemistry or (3) the presence of extra-lattice TMI.

In addition, shape selectivity can be introduced in these molecular sieves because reactive substrates with a kinetic diameter larger than the pore size of the molecular sieve cannot react, whereas the reaction with a smaller molecule may proceed within the pore system. Another important advantage of such materials over their homogeneous counterparts is that the TMI is embedded in an inorganic microporous structure, which prevents or suppresses catalyst deactivation. Indeed, the most common deactivation mechanisms of homogeneous catalysts are the degradation of the (organic) ligands, and oligomerization of the active TMI.

Although the concept "reaction in micropores" generally leads to less catalyst deactivation, it is important to mention that other deactivation mechanisms may come into play; i.e., leaching of the active TMI and blocking of the microporous structure by a strong adsorption of reactants or products. Leaching of the active TMI is often severe, especially in the case of V and Cr, and several authors have attributed their observed catalytic activity solely to the presence of TMI leached in the reaction mixture.[72,73] In this respect, the composition of the reaction mixture is critical. Indeed, for CoAPO-5 molecular sieves it is proven that the molecular sieve dissolves during the oxidation of organic compounds in strong alkaline medium. On the other hand, in a strong apolar solvent (e.g. cyclohexane) an extremely low concentration of Co could be detected in solution, and the autoxidation activity of CoAPO-5 could not be attributed to this dissolved cobalt.[72] Another striking observation was recently found by Haanepen et al.[73] They observed that the leaching process of VAPO-5 molecular sieves only occurred in the beginning of the catalytic reaction, and that the heterogeneous contribution steadily stopped due to a strong adsorption of organic molecules in the pore system of $AlPO_4$-5. Removal of the VAPO-5 material from the reaction mixture after a short reaction time showed an ongo-

ing reaction in the filtrate. Similar results were obtained for CrAPO-5 molecular sieves.[74] Surely, the most promising direction for heterogeneous catalysis seems to be gas-phase reactions.[75] In this respect, the oxidative dehydrogenation of alkanes has received the most attention, and both VAPO-5 and MnAPO-5 are efficient catalysts for this type of reaction.[12,76,77]

7. Concluding Remarks and Look into the Future

The chemistry of TMIs in microporous aluminium phosphates is complex. The synthesis conditions of the materials do not favour incorporation of TMI in the lattice. In addition, the size of the TMI with respect to that of Al or P is such that substitution introduces strain in the structure. The following conclusions can be drawn from this microreview:

(1) Even at low metal loading, TMIs seem to be present under different coordination geometries; i.e.:

(a) Truly isomorphous substituted TMI possessing a (pseudo-)tetrahedral coordination. This has been spectroscopically proven for Co^{2+}, and to a lesser extent for $Fe^{2+/3+}$. It is important to notice that the presence of framework TMI with a higher coordination number (5 or 6) cannot be excluded (e.g., Cr^{3+}). Indeed, NMR studies have clearly shown the presence of octahedrally coordinated Al^{3+} in the framework of $AlPO_4$-*n* materials.

(b) Defect sites, which originate from interrupted frameworks in which Al−O−P bonds are missing. It is anticipated that Co^{2+}, Cr^{3+}, V^{4+}, $Fe^{2+/3+}$, and Mn^{2+} may coordinate to these defects, which will give rise to a (pseudo-)octahedral coordination. In this respect, it is remarkable to see that the overall crystallinity of the MeAPO-5 materials decreases with increasing metal loading. This suggests a continuous creation of defect sites in the framework with increasing incorporation of TMI.

(c) Extra-framework transition metal oxides, which are most probably located at the outer surface or occluded within the micropores of the molecular sieve. Spectroscopic evidence is available that Cr_2O_3, Fe_2O_3, and V_2O_4 clusters are formed during the synthesis of MeAPO-5 materials.

(2) More advanced synthesis procedures have to be developed which selectively increase the amount of framework TMI. The synthesis of nanosized transition metal oxides within the micropores could be another scientific challenge because of their possible quantum size properties.

(3) Both indirect and direct criteria to evaluate isomorphous substitution have been established. It is obvious that positive evidence via indirect criteria is not sufficient to claim a truly isomorphous substituted TMI. There is clearly a need to develop more refined spectroscopic tools to discriminate between framework and extra-framework TMI.

(4) Co^{2+} can be used as a probe for the synthesis mechanisms of microporous aluminium phosphates. Other TMIs, for which there is still no direct spectroscopic proof of lattice substitution, cannot be used as synthesis probes. Another approach, the in situ spectroscopy, might be a useful additional tool to extend this research direction.

(5) Only for Co^{3+}/Co^{2+} in the lattice has a clear redox chemistry been achieved, not yet for the other TMIs. Whether this is indicative for no incorporation of Fe, V, Cr, Mn in the lattice has still to be proven.

(6) The creation of Brønsted acid sites and redox centers makes MeAPO-5 interesting heterogeneous catalysts. However, the careful choice of the catalytic conditions is of paramount importance for the development of a successful catalytic application. In this respect, gas-phase catalysis seems to be a promising new direction.

The authors anticipate that the above-described remarks are also applicable to the isomorphous substitution of TMI in other molecular sieves.

Acknowledgments

B. M.W. is a postdoctoral fellow of the Fonds voor Wetenschappelijk Onderzoek − Vlaanderen (F.W.O), while R. R. R is thankful for a junior postdoctoral fellowship of the K. U. Leuven. This work was financially supported by the Geconcerteerde Onderzoeksacties (G.O.A.) of the Flemish Government.

List of Abbreviations

$AlPO_4$-*n* = microporous crystalline aluminophosphate

DRS = diffuse reflectance spectroscopy

ESEEM = electron spin echo envelope modulation

ESR = electron spin resonance

EXAFS = extended X-ray absorption fine structure

IR = infrared

LFSE = ligand field stabilization energy

MeAPO-*n* = microporous crystalline aluminophosphate containing a transition metal ion, Me

NMR = nuclear magnetic resonance

TMI = transition metal ion

TPD = temperature programmed desorption

XPS = X-ray photoelectron spectroscopy

XRD = X-ray diffraction

[1] [1a] J. A. Martens, P. A. Jacobs, *Stud. Surf. Sci. Catal.* **1994**, *85*, 653. − [1b] J. A. Martens, P. A. Jacobs, in *Catalysis and Zeolites* (Eds.: J. Weitkamp, L. Puppe), Springer Verlag, Berlin, in press. − [1c] M. Tielen, M. Geelen, P. A. Jacobs, in *Proc. Int. Symp Zeolite Catal.* (Eds.: P. Fejes, D. Kallo), *Acta Phys. Chem. Szegediensis* **1985**, *0*, 11. − [1d] D. W. Breck, in *Zeolite Molecular Sieves*, J. Wiley, New York, **1974**, p. 320.

[2] [2a] E. M. Flanigen, R. L. Patton, S. T. Wilson, in *Innovation in Zeolite Materials Science* (Eds.: P. J. Grobet, W. J. Mortier, E. F. Vansant, G. Schulz-Ekloff), Elsevier Science Publishers, B. V., Amsterdam, **1988**, p. 13. − [2b] R. E. Morris, S. J. Weigel, *Chem. Soc. Rev.* **1997**, *26*, 309. − [2c] S. T. Wilson, B. M. Lok, C. A. Messina, T. R. Cannan, E. M. Flanigen, in *ACS Series 218*, American Chemical Society, Washington, **1983**, p. 79.

[3] S. T. Wilson, E. M. Flanigen, in *ACS Series 234*, American Chemical Society, Washington, DC, **1989**, p. 329.

[4] [4a] S. T. Wilson, B. M. Lok, C. A. Messina, T. R. Cannan, E.

M. Flanigen, *U. S. Patent* **1984**, 4,440,871. – [4b] S. T. Wilson, B. M. Lok, C. A. Messina, T. R. Cannan, E. M. Flanigen, *J. Am. Chem. Soc.* **1982**, *104*, 1146.
[5] [5a] P. Feng, Y. Xia, J. Feng, X. Bu, G. Stucky, *Chem. Commun.* **1997**, 949. – [5b] D. Zhao, Z. Luan, L. Kevan, *Chem. Commun.* **1997**, 1009. – [5c] B. Chakraborty, A. C. Pilikottil, S. Das, B. Viswanathan, *Chem. Commun.* **1997**, 911.
[6] [6a] M. P. J. Peeters, L. J. M. van de Ven, J. W. de Haan, J. H. C. van Hooff, *J. Phys. Chem.* **1993**, *97*, 8254. – [6b] M. P. J. Peeters, J. W. de Haan, L. J. M. van de Ven, J. H. C. van Hooff, *J. Chem. Soc., Chem. Commun.* **1992**, 1560. – [6c] M. P. J. Peeters, J. W. de Haan, L. J. M. van deVen, J. H. C. van Hooff, *J. Phys. Chem.* **1993**, *97*, 5363. – [5d] R. Jelinek, B. F. Chmelka, Y. Wu, P. J. Grandinetti, A. Pines, P. J. Barrie, J. Klinowski, *J. Am. Chem. Soc.* **1991**, *113*, 4097.
[7] [7a] S. T. Wilson, B. M. Lok, E. M. Flanigen, *U. S. Patent* **1982**, 4,310,440. – [7b] S. T. Wilson, E. M. Flanigen, *U. S. Patent* **1986**, 4,567,029.
[8] I. M. Bennes, B. K. Marcus, in *Innovation of Zeolite Materials Science* (Eds.: P. J. Grobet, W. J. Mortier, E. F. Vansant, G. Schulz-Ekloff), Elsevier Science Publishers, B. V., Amsterdam, **1988**, p. 269.
[9] [9a] P. Feng, X. Bu, G. D. Stucky, *Nature* **1997**, *388*, 735. – [9b] X. Bu, P. Feng, G. D. Stucky, *Science* **1997**, *278*, 2080. – [9c] M. Jacoby, *Chem. Eng. News* **1997**, September 1, p. 11.
[10] J. Chen, R. H. Jones, S. Natarajan, M. B. Hursthous, J. M. Thomas, *Angew. Chem.* **1994**, *106*, 667; *Angew. Chem. Int. Ed. Engl.* **1994**, *33*, 639.
[11] T. E. Gier, G. D. Stucky, *Nature* **1991**, *349*, 508.
[12] T. Blasco, P. Concepcion, J. M. Lopez Nieto, J. Perez-Pariente, *J. Catal.* **1995**, *152*, 1.
[13] C. Montes, M. E. Davis, B. Murray, M. Narayana, *J. Phys. Chem.* **1990**, *94*, 6431.
[14] [14a] G. Lischke, B. Parlitz, U. Lohse, E. Schreier, R. Fricke, *Appl. Catal. A: General* **1998**, *166*, 351. – [14b] U. Lohse, R. Bertram, K. Jancke, I. Kurzawski, B. Parlitz, E. Loffler, E. Schreier, *J. Chem. Soc., Faraday Trans.* **1995**, *91*, 1163. – [14c] N. J. Tapp, N. B. Milestone, D. M. Bibby, in *Innovation in Zeolite Materials Science*, Elsevier Science Publishers, B. V., Amsterdam, **1988**, p. 393.
[15] V. P. Shiralkar, C. H. Saldarriaga, J. O. Perez, A. Clearfield, M. Chen, R. G. Anthony, J. A. Donohue, *Zeolites* **1989**, *9*, 474.
[16] A. A. Verberckmoes, M. G. Uytterhoeven, R. A. Schoonheydt, *Zeolites* **1997**, *19*, 180.
[17] A. A. Verberckmoes, B. M. Weckhuysen, R. A. Schoonheydt, *Microporous Mesopor. Mater.* **1998**, *22*, 165.
[18] J. H. Ashley, P. C. H. Mitchell, *J. Chem. Soc. A* **1968**, 2861.
[19] R. A. Schoonheydt, R. De Vos, J. Pelgrims, H. Leeman, in *Zeolites: Facts, Figures, Future* (Eds.: P. A. Jacobs, R. A. Vansanten), Elsevier, Amsterdam, **1989**, p. 559.
[20] L. E. Iton, I. Choi, J. A. Desjardins, V. A. Maroni, *Zeolites* **1989**, *9*, 535.
[21] C. Montes, M. E. Davis, B. Murray, M. Narayana, *J. Phys. Chem.* **1990**, *94*, 6425.
[22] B. Kraushaar-Czarnetzki, W. G. M. Hoogervorst, R. R. Andréa, C. A. Emeis, W. H. J. Stork, *J. Chem. Soc., Faraday Trans.* **1991**, *87*, 891.
[23] M. P. J. Peeters, J. H. C. van Hooff, R. A. Sheldon, V. L. Zholobenko, L. M. Kustov, V. B. Kazansky, *Proc. 9th Internat. Zeolite Confer.* (Eds.: R. von Ballmoos, J. B. Higgens, M. M. J. Treacy), Butterworth-Heinemann, New York, **1992**, p. 651.
[24] J. W. Couves, G. Sankar, J. M. Thomas, J. Chen, Catlow, C. R. A;R. Xu, G. N. Greaves, *Proc. 9th Internat. Zeolite Confer.* (Eds.: R. von Ballmoos, J. B. Higgens, M. M. J. Treacy), Butterworth-Heinemann, New York, **1992**, p. 627.
[25] [25a] K. Nakashiro, Ono, Y. *Bull. Chem. Soc. Jpn.* **1993**, *66*, 9. – [25b] J. Jänchen, M. P. J. Peeters, J. H. M. C. vanWolput, J. P. Wolthuizen, J. H. C. van Hooff, U. Lohse, *J. Chem. Soc., Faraday Trans.* **1994**, *90*, 1033.
[26] Y. J. Lee, H. Chon, *J. Chem. Soc., Faraday Trans.* **1996**, *92*, 3453.
[27] V. Kurshev, L. Kevan, D. J. Parillo, C. Pereira, G. T. Kokotailo, R. J. Gorte, *J. Phys. Chem.* **1994**, *98*, 10160.
[28] P. A. Barrett, G. Sankar, C. R. A. Catlow, J. M. Thomas, *J. Phys. Chem.* **1996**, *100*, 8977.
[29] [29a] B. M. Weckhuysen, R. A. Schoonheydt, *Zeolites* **1994**, *14*, 360. – [29b] B. M. Weckhuysen, R. A. Schoonheydt, *Stud. Surf. Sci. Catal.* **1994**, *84*, 965.
[30] [30a] A. B. P. Lever, *Inorganic Electronic Spectroscopy*, 2nd ed., Elsevier, Amsterdam, **1984**. – [30b] D. Reinen, *Struct. Bond.* **1969**, *6*, 30.
[31] B. M. Weckhuysen, I. E. Wachs, R. A. Schoonheydt, *Chem. Rev.* **1996**, *96*, 3327.
[32] [32a] J. D. Chen, R. A. Sheldon, *J. Catal.* **1995**, *153*, 1. – [32b] J. D. Chen, J. Dakka, E. Neeleman, R. A. Sheldon, *J. Chem. Soc., Chem. Commun.* **1993**, 1379.
[33] B. M. Weckhuysen, R. A. Schoonheydt, F. E. Mabbs, D. Collison, *J. Chem. Soc., Faraday Trans.* **1996**, *92*, 2431.
[34] N. Rajic, D. Stojakovic, S. Hocevar, V. Kaucic, *Zeolites* **1993**, *13*, 384.
[35] D. Demuth, K. K. Unger, F. Schüth, G. D. Stucky, V. I. Srdanov, *Adv. Mater.* **1994**, *6*, 931.
[36] D. Demuth, K. K. Unger, F. Schüth, V. I. Srdanov, G. D. Stucky, *J. Phys. Chem.* **1995**, *99*, 479.
[37] S. Thiele, K. Hoffman, R. Vetter, F. Marlow, S. Radaev, *Zeolites* **1997**, *19*, 190.
[38] S. H. Jhung, Y. S. Uh, H. Chon, *Appl. Catal.* **1990**, *62*, 61.
[39] B. M. Weckhuysen, I. P. Vannijvel, R. A. Schoonheydt, *Zeolites* **1995**, *15*, 482.
[40] M. S. Rigutto, H. vanBekkum, *J. Mol. Catal.* **1993**, *81*, 77.
[41] D. M. Hausen, *Am. Mineral.* **1962**, *47*, 637.
[42] B. I. Whittington, J. R. Anderson, *J. Phys. Chem.* **1993**, *97*, 1032.
[43] A. Miyamoto, Y. Iwamoto, H. Matsuda, T. Inui, in *Zeolites, Facts, Figures, Future* (Eds.: P. A. Jacobs, R. A. van Santen), Elsevier Science Publishers, B. V., Amsterdam, **1989**, p. 1233.
[44] C. A. Messina, B. M. Lok, E. M. Flanigen, *Eur. Pat.* **1984**, 131,946.
[45] G. Catana, J. Pelgrims, R. A. Schoonheydt, *Zeolites* **1995**, *15*, 475.
[46] J. W. Park, H. Chon, *J. Catal.* **1992**, *133*, 159.
[47] R. Hoppe, G. Schulz-Ekloff, S. Wohlrab, D. Wohrle, *Chem. Ing. Tech.* **1995**, *67*, 350.
[48] S. Prasad, R. F. Shinde, I. Balakrshnan, *Microporous Mater.* **1994**, *2*, 159.
[49] J. Das, V. V. Satyanaryana, D. K. Chakrabarty, S. N. Piramanayagam, S. N. Shringi, *J. Chem. Soc., Faraday Trans.* **1992**, *88*, 3255.
[50] D. Goldfarb, M. Bernardo, K. G. Strohmaier, D. E. W. Vaughan, H. Thomann, *J. Am. Chem. Soc.* **1994**, *116*, 6344.
[51] [51a] H. X. Li, J. A. Martens, P. A. Jacobs, S. Schubert, F. Schmidt, H. M. Ziethen, A. X. Trautwein, *Stud. Surf. Sci. Catal.* **1988**, *37*, 75. – [51b] S. Shubert, H. M. Ziethen, A. X. Trautwein, F. Schmidt, H. X. Li, J. A. Martens, P. A. Jacobs, in *Zeolites as Catalysts, Sorbents and Detergent Builders*, Elsevier Science Publishers, B. V., Amsterdam, **1989**, p. 735.
[52] J. Ma, B. Fan, R. Li, J. Cao, *Catal. Lett.* **1994**, *23*, 189.
[53] L. E. Iton, R. B. Beal, D. T. Hodul, *J. Mol. Catal.* **1983**, *21*, 151.
[54] D. H. Lin, G. Coudurier, J. C. Vedrine, *Stud. Surf. Sci. Catal.* **1989**, *49*, 227.
[55] A. Brückner, U. Lohse, H. Mehner, *Microporous Mesopor. Mater.* **1998**, *20*, 207.
[56] D. Goldfarb, *Zeolites* **1989**, *9*, 509.
[57] Z. Levi, A. M. Raitsimring, D. Goldfarb, *J. Phys. Chem.* **1991**, *95*, 7830.
[58] D. J. Parrillo, C. Pereira, G. T. Kokotailo, R. J. Gorte, *J. Catal.* **1992**, *138*, 377.
[59] A. Katzmarzyk, S. Ernst, J. Weitkamp, H. Knözinger, *Catal. Lett.* **1991**, *9*, 85.
[60] R. Roque-Malherbe, R. Lopez-Cordero, J. A. Gonzales-Morales, J. Onate-Martinez, M. Carreras-Gracial, *Zeolites* **1993**, *13*, 481.
[61] B. Z. Wan, K. Huang, *Appl. Catal.* **1991**, *73*, 113.
[62] U. Lohse, A. Brückner, E. Schreier, R. Bertram, J. Jänchen, R. Fricke, *Microporous Mater.* **1996**, *7*, 139.
[63] G. Brouet, X. Chen, C. W. Lee, L. Kevan, *J. Am. Chem. Soc.* **1992**, *114*, 3720.
[64] R. F. Mortlock, A. T. Bell, C. J. Radke, *J. Phys. Chem.* **1991**, *95*, 372.
[65] R. F. Mortlock, A. T. Bell, C. J. Radke, *J. Phys. Chem.* **1991**, *95*, 7847.
[66] J. Twu, P. K. Dutta, Kresge, C. T. *J. Phys. Chem.* **1991**, *95*, 5267.
[67] M. G. Uytterhoeven, W. A. VanKeyenberg, R. A. Schoonheydt, *Mat. Res. Soc. Symp. Proc.* **1991**, *233*, 57.
[68] M. G. Uytterhoeven, Schoonheydt, R. A. *Microporous Mater.* **1994**, *3*, 265.

[69] M. G. Uytterhoeven, R. A. Schoonheydt, *Proc. 9th Internat. Zeolite Conf.* (Eds.: R. von Ballmoos, J. B. Higgens, M. M. J. Treacy), Butterworth-Heinemann, Boston, **1993**, vol. 1, p. 329.
[70] G. Belussi, M. S. Rigutto, *Stud. Surf. Sci. Catal.* **1994**, *85*, 177.
[71] I. W. C. E. Arends, R. A. Sheldon, M. Wallau, U. Schuchardt, *Angew. Chem.* **1997**, *109*, 1190; *Angew. Chem. Int. Ed. Engl.* **1997**, *36*, 1144.
[72] D. L. Vanoppen, D. E. DeVos, M. J. Genet, P. G. Rouxhet, P. A. Jacobs, *Angew. Chem.* **1995**, *106*, 637; *Angew. Chem. Int. Ed. Engl.* **1995**, *34*, 560.
[73] M. J. Haanepen, A. M. Elemans-Mehring, J. H. C. vanHooff, *Appl. Catal. A: General* **1997**, *152*, 203.
[74] H. E. B. Lempers, R. A. Sheldon, *J. Catal.* **1998**, *175*, 62.
[75] L. H. Gielgens, I. H. E. Veenstra, V. Ponec, M. J. Haanepen, J. H. C. vanHooff, *Catal. Lett.* **1995**, *32*, 195.
[76] P. Concepcion, J. M. Lopez Nieto, J. Perez-Pariente, *J. Mol. Catal. A: Chemical* **1995**, *99*, 173.
[77] B.-Z. Wan, K. Huang, *Appl. Catal.* **1991**, *73*, 113.

Received August 5, 1998
[I98263]

Compounds of Germanium, Tin, and Lead, 30[+]

A Heteroleptic Diplumbene and a Magnesium Dibromide Stabilized Plumbylene Dimer

Martin Stürmann,[a] Wolfgang Saak,[a] Manfred Weidenbruch,*[a] and Karl W. Klinkhammer[b]

Keywords: Lead / Plumbylenes / Plumbanediyles / Diplumbene / Plumbylene dimers / Double-bond systems

Treatment of the diarylplumbylene R_2Pb**:** (R = 2,4,6-*i*$Pr_3C_6H_2$) with the disilylplumbylene R'_2Pb**:** [R′ = $Si(SiMe_3)_3$] furnishes the heteroleptic plumbylene RR′Pb**:** which exists as the diplumbene RR′Pb=PbRR′ (**7**) in the solid state. The X-ray structure analysis of **7** reveals a *trans*-bent angle of 42.7° and a Pb–Pb bond length of 298.99(5) pm, the shortest observed so far for diplumbenes with a lead–lead double bond. Reaction of mesitylmagnesium bromide with $PbCl_2$ yielded black crystals of an $MgBr_2$ stabilized dimesitylplumbylene dimer with a large *trans*-bent angle of 71°, a lead–lead separation of 335.49(6) pm, and long Pb···Br contacts of 315.71(8) pm.

Dialkyl-[1][2] and diarylplumbylenes[3−5] without intra- or intermolecular donor stabilization have become known and their structures have been elucidated only in the past few years.[6] They predominantly exist as V-shaped molecules without any contacts between the lead atoms of neighboring plumbylene molecules. The low tendency for dimerization (Figure 1) is probably a consequence of the available mechanism for bond formation which, unlike that for carbon, for example, is through donor-acceptor interactions between the doubly occupied 6s orbitals and the empty 6p orbitals of two singlet plumbylene molecules. This is corroborated by the low bond-dissociation energy, which was calculated to be merely 24 kJ mol^{-1}.[7]

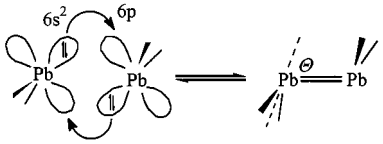
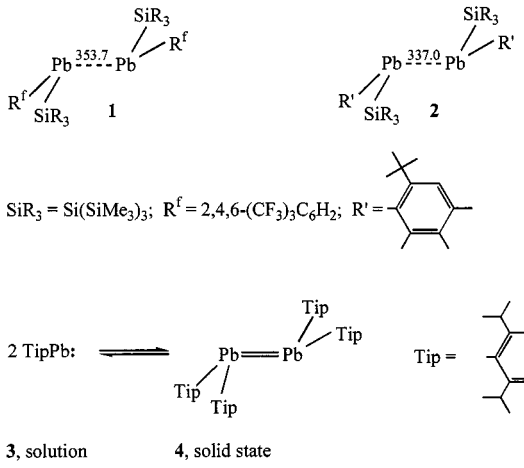
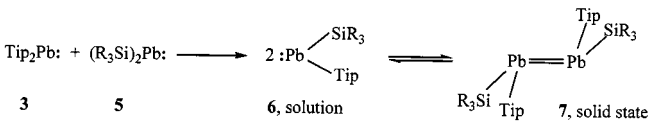


Figure 1. Formation of a diplumbene from two singlet plumbylenes

The first advances in the direction of lead−lead interactions were realized with the syntheses of compounds **1**[7] and **2**[5] which exhibited the theoretically required *trans*-bent arrangements. However, the observed Pb···Pb separations of 353.7(1) pm in **1** and 337.0(1) pm in **2** were markedly larger than the calculated values of around 295 pm for the parent compound $H_2Pb{=}PbH_2$ with a Pb−Pb double bond. Values of about 55° were determined for the corresponding *trans*-bent angles θ.[7−9] With the preparation of compound **4** we recently obtained the first diplumbene with a Pb−Pb bond length [305.15(3) pm] and *trans*-bent angles θ [43.9° and 51.2°] in good agreement with the theoretical predictions.[10]



We now describe the first heteroleptic diplumbene with a Pb−Pb bond even shorter than that of **4** as well as a plumbylene dimer stabilized by magnesium dibromide.



In the syntheses of the plumbylene dimers **1** and **2** the diarylplumbylene was allowed to react with the disilylplumbylene[11] to furnish the heteroleptic molecules **1** and **2** by substituent exchange. An analogous reaction of the plumbylene **3**, existing in solution, with the disilylplumbylene **5** also proceeded through rapid substituent exchange to afford a greenish-blue solution of the plumbylene **6** from

[+] Part 29: U. Fooken, W. Saak, M. Weidenbruch, *J. Organomet. Chem.*, in press.

[a] Fachbereich Chemie der Universität Oldenburg, Carl-von-Ossietzky-Straße 9−11, D-26111 Oldenburg, Germany
[b] Institut für Anorganische Chemie der Universität Stuttgart, Pfaffenwaldring 55, D-70569 Stuttgart, Germany

 © WILEY-VCH Verlag GmbH, D-69451 Weinheim, 1999 1434−1948/99/0404−0579 $ 17.50+.50/0

which reddish-brown crystals of the diplumbene **7** were isolated.

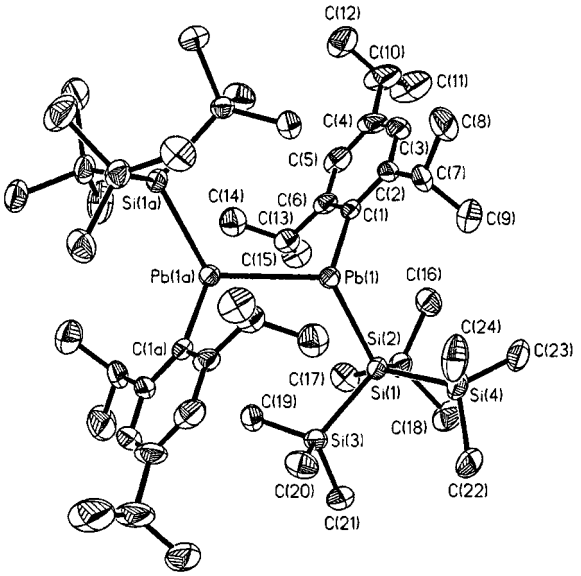
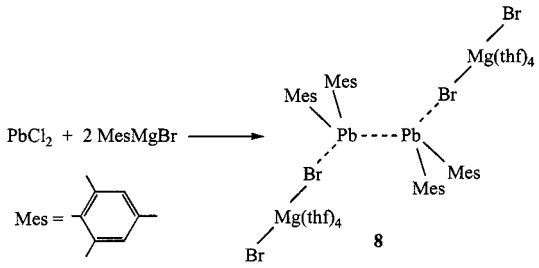


Figure 2. Molecular structure of **7** in the crystal (hydrogen atoms omitted); ellipsoids are drawn at 50% probability; selected bond lengths [pm] and angles [°]: Pb(1)−Pb(1a) 298.99(5), Pb(1)−C(1) 229.6(4), Pb(1)−Si(1) 271.7(1); C(1)−Pb(1)−Si(1) 108.8(1), C(1)−Pb(1)−Pb(1a) 109.5(1), Si(1)−Pb(1)−Pb(1a) 120.72(3)

An X-ray crystal-structure analysis of compound **7** (Figure 2) revealed the existence of a centrosymmetrical molecule having a lead−lead bond length of 298.99(5) pm, a value even shorter than that of **4** and very close to the theoretically calculated value for the parent compound. The *trans*-bent angle θ in **7** of 43.7° (see Figure 1) is somewhat smaller than those of **4**, presumably as a consequence of the different substitution pattern. Thus, compound **7** is not only the second diplumbene ever to be prepared but is also the first heteroleptic molecule of this type.

It has been found for disilenes, digermenes, and distannenes that the steric requirements of the substituents must increase with increasing length of the element−element double bond in order to effectively shield the compounds from further reactions.[12][13] Thus, for example, the compounds $Tip_2Si{=}SiTip_2$ and $Tip_2Ge{=}GeTip_2$ (Tip = 2,4,6-iPr$_3$C$_6$H$_2$) are thermally stable while $Tip_2Sn{=}SnTip_2$, although it can be generated thermally or photochemically from the cyclotristannane $(Tip_2Sn)_3$, reverts to the three-membered ring compound at room temperature.[14] The existence of compounds **4** and **7**, however, seems to suggest that steric shielding of the Pb−Pb double bond does not play such a dominating role. We have thus examined whether the use of smaller aryl groups would also permit the formation of this structural element or whether subsequent reactions would occur.

Reaction of the Grignard reagent MesMgBr with solid lead(II) chloride at low temperature in THF furnished a red-brown solution from which, among other products, black crystals of a very sensitive, thermolabile compound



were isolated. Satisfactory characterization of this product by spectroscopic methods was not possible on account of its properties.

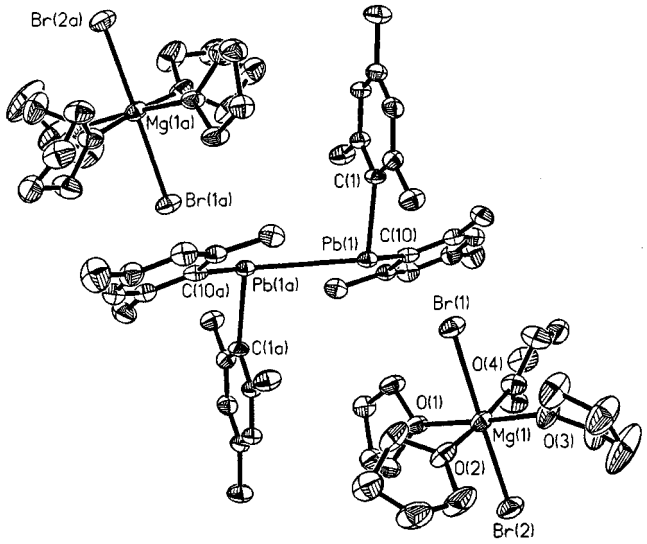


Figure 3. Molecular structure of **8** in the crystal (hydrogen atoms omitted); ellipsoids are drawn at 50% probability; selected bond lengths [pm] and angles [°]: Pb(1)···Pb(1a) 335.49(6), Pb(1)−C(1) 232.2(5), Pb(1)−C(10) 230.4(6), Mg(1)−Br(2) 262.6(2), Mg(1)−Br(1) 279.7(2), Pb(1)···Br(1) 315.71(8); C(1)−(Pb1)−Pb(1a) 99.6(2), C(10)−Pb(1)−Pb(1a) 118.0(2), Br(1)−Pb(1)−Pb(1a) 133.44(2), Br(2)−Mg(1)−Br(1) 178.04(9)

However, a low-temperature X-ray crystallographic analysis of these black crystals revealed that a magnesium bromide stabilized plumbylene dimer **8** had been formed (Figure 3). The Pb···Pb separation of 335.49(6) pm is in the same range as that for compound **2**. The *trans*-bent angle θ of 71° is unusually large. A further surprising feature is that a bromine atom of an $MgBr_2(thf)_4$ molecule experiences a weak interaction with each lead atom and not the THF present in a large excess. Although the respective Pb···Br separations are about 50 pm larger than those of a Pb−Br single bond,[15] these interactions are characterized not only by a large *trans* arrangement but also by the Mg−Br bond lengths within the almost linear Br−Mg−Br units. Thus, the Br−Mg bond weakly coordinated to the lead atom is around 17 pm longer than the other Mg−Br bond.

The novel molecules **7** and **8** described here indicate that further interesting and unexpected results may be expected in the field of low-coordinated lead compounds.

Experimental Section

General: All manipulations were performed by using standard Schlenk techniques under dry argon. − ^{1}H and ^{13}C NMR: Bruker AM 300. − MS: Finnigan MAT 212. − UV/Vis: ComSpec with fiber optics. − Elemental analyses: Analytische Laboratorien, D-51789 Lindlar, Germany.

(2,4,6-Triisopropylphenyl)[tris(trimethylsilyl)silyl]plumbylene (6) and (*E*)-1,2-Bis(2,4,6-triisopropylphenyl)-1,2-bis[tris(trimethylsilyl)silyl]diplumbene (7): A solution of the plumbylenes **3** (0.34 g, 0.55 mmol) and **5** (0.39 g, 0.55 mmol) in 15 mL of *n*-pentane was stirred in the dark for 20 min at room temperature. The greenish-blue solution was concentrated to a volume of 15 mL and cooled at −65°C for 24 h. After this time, 0.53 g (73% yield) of reddish-brown crystals (green in thin layers) of **7** were isolated. M.p. 90°C (decomp.). − Spectroscopic data for **6** in solution: ^{1}H NMR ([D$_8$]toluene, 298 K): δ = 0.44 (s, 27 H), 1.34 (d, 6 H, ^3J = 6.85 Hz), 1.35 (d, 12 H, ^3J = 6.7 Hz), 2.15 (m, 2 H), 2.86 (m, 1 H), 7.29 (s, 2 H). − ^{13}C NMR ([D$_8$]toluene, 298 K): δ = 7.07, 24.50, 24.99, 33.81, 35.52, 124.74, 125.39, 127.58, 147.33, 158.53, 259.12. − ^{29}Si NMR ([D$_8$]toluene, 298 K): δ = −16.4 [*Si*(SiMe$_3$)$_3$], −4.3 (*Si*Me$_3$). − The ^{207}Pb-NMR signal could not be observed. − MS (CI, isobutane); *m*/*z* (%): 660 (5) [**6**$^+$]. − UV/Vis: λ_{max}(ε) = 350 (670), 591 (80), 770 (175) nm. − $C_{48}H_{100}Pb_2Si_8$ (**8**) (1316.4): calcd. C 43.79, H 7.64; found C 43.48, H 7.43.

Bis(2,4,6-trimethylphenyl)plumbylene Dimer·2 MgBr$_2$(thf)$_4$ (8): At −110°C, solid PbCl$_2$ (4.7 g, 16.8 mmol) was added to the Grignard compound, prepared in turn from 1-bromo-2,4,6-trimethylphenylbenzene (6.8 g, 34 mmol) and magnesium turnings (3.2 g, 120 mmol) in 100 mL of THF. The mixture was allowed to warm to room temperature over a period of 30 min with vigorous stirring. THF was distilled off and the residue extracted with 10 mL of *n*-hexane in order to remove small amounts of 1,3,5-trimethylbenzene. The remaining residue was extracted with two portions of toluene (50 mL each), and the magnesium salts were filtered off. Concentration of the reddish-brown toluene solution to a volume of 60 mL and cooling at −50°C furnished 3.72 g (18% yield) of thermally unstable, black crystals of **8**. − ^{1}H NMR (C$_6$D$_6$, 298 K): δ = 2.15 (s, 6 H), 2.62 [s, 12 H, ^4J(^{1}H,^{207}Pb) = 5 Hz], 6.78 (s, 4 H); minor signals for THF at δ = 1.38 (m), 3.69 (m).

Table 1. Crystallographic data for **7** and **8**

	7	**8**
Empirical formula	$C_{48}H_{100}Pb_2Si_8$	$C_{68}H_{108}Br_4Mg_2O_8Pb_2$
Molecular mass	1316.38	1836.18
Crystal dimensions [mm]	0.55×0.50×0.42	0.50×0.50×0.30
Crystal system	monoclinic	triclinic
Space group	$P2_1/c$	$P-1$
a [pm]	1089.4(1)	1262.1(1)
b [pm]	2313.6(2)	1274.3(1)
c [pm]	1368.9(2)	1357.2(2)
α [°]	90	77.59(1)
β [°]	112.80(1)	81.11(1)
γ [°]	90	70.93(1)
V [× 10^6 pm^3]	3180.5(5)	2006.3(4)
Z	2	1
$d_{calcd.}$ [g cm^{-3}]	1.375	1.520
T [K]	193(2)	213(2)
μ [mm^{-1}]	5.464	6.242
$2\theta_{max}$ [°]	52	52
No. of reflections	23407	27054
No. of unique reflections	6156	7351
No. of observed reflections	4552	6151
No. of parameters	262	379
R_1 [$I > 2\sigma(I)$]	0.0263	0.0361
wR_2 (all data)	0.0553	0.1031
GOF on F^2	0.895	1.008

X-ray Structure Analyses of 7 and 8: Crystal data and numerical data of the structure determinations are given in Table 1. In each case, the crystal was mounted in an inert oil. Data collection was performed with an STOE IPDS diffractometer using graphite-monochromated Mo-K_α radiation (λ = 71.073 pm). The structures were solved by direct phase determination and refined by full-matrix least squares against F^2 with the SHELXL-97 program system.[16] Hydrogen atoms were placed in calculated positions, and all other atoms were refined anisotropically.[17]

Acknowledgments

Financial support of our work by the Deutsche Forschungsgemeinschaft and the Fonds der Chemischen Industrie is gratefully acknowledged.

[1] Pb[CH(SiMe$_3$)$_2$]$_2$: Synthesis: P. J. Davidson, M. F. Lappert, *J. Chem. Soc., Chem. Commun.* **1973**, 317; P. J. Davidson, D. H. Harris, M. F. Lappert, *J. Chem. Soc., Dalton Trans.* **1976**, 2268−2274. − Structure: K. W. Klinkhammer, W. Schwarz, unpublished results.
[2] C. Eaborn, T. Ganicz, P. B. Hitchcock, J. D. Smith, S. E. Sözerli, *Organometallics* **1997**, *16*, 5621−5622.
[3] S. Brooker, J.-K. Buijink, F. T. Edelmann, *Organometallics* **1991**, *10*, 25−26.
[4] R. S. Simons, L. Pu, M. M. Olmstead, P. P. Power, *Organometallics* **1997**, *16*, 1920−1925.
[5] M. Stürmann, M. Weidenbruch, K. W. Klinkhammer, F. Lissner, H. Marsmann, *Organometallics* **1998**, *17* 4425−4428.
[6] Review: M. Weidenbruch, *Eur. J. Inorg. Chem.* **1999**, 373−381.
[7] K. W. Klinkhammer, F. T. Fässler, H. Grützmacher, *Angew. Chem.* **1998**, *110*, 114−116; *Angew. Chem. Int. Ed.* **1998**, *37*, 124−126.
[8] G. Trinquier, *J. Am. Chem. Soc.* **1990**, *112*, 2130−2137.
[9] H. Jacobsen, T. Ziegler, *J. Am. Chem. Soc.* **1994**, *116*, 3667−3679.
[10] M. Stürmann, W. Saak, H. Marsmann, M. Weidenbruch, *Angew. Chem.* **1999**, *111*, 145−147; *Angew. Chem. Int. Ed.* **1999**, *38*, 187−189.
[11] K. W. Klinkhammer, W. Schwarz, *Angew. Chem.* **1995**, *107*, 1448−1451; *Angew. Chem. Int. Ed. Engl.* **1995**, *34*, 1334−1336.
[12] Disilenes: reviews: [12a] R. West, *Angew. Chem.* **1987**, *99*, 1231−1241; *Angew. Chem. Int. Ed. Engl.* **1987**, *26*, 1202−1211. − [12b] G. Raabe, J. Michl, in *The Chemistry of Organic Silicon Compounds, Part 2* (Eds.: S. Patai, Z. Rappoport), Wiley, Chichester, U.K., **1989**, p. 1015−1152. − [12c] T. Tsumuraya, S. A. Batcheller, S. Masamune, *Angew. Chem.* **1991**, *103*, 916−944; *Angew. Chem. Int. Ed. Engl.* **1991**, *30*, 902−930. − [12d] M. Weidenbruch, *Coord. Chem. Rev.* **1994**, 275−300. − [12e] R. Okazaki, R. West, in *Multiply Bonded Main Group Metals and Metalloids* (Eds.: R. West, F. G. A. Stone), Academic Press, San Diego, U.S.A., **1996**, p. 232−273.
[13] Digermenes, distannenes: Reviews: [13a] . Driess, H. Grützmacher, *Angew. Chem.* **1996**, *108*, 900−929; *Angew. Chem. Int. Ed. Engl.* **1996**, *35*, 827−856. − [13b] K. M. Baines, W. G. Stibbs, in *Multiply Bonded Main Group Metals and Metalloids* (Eds.: R. West, F. G. A. Stone), Academic Press, San Diego, U.S.A., **1996**, p. 275−324. − [13c] P.P. Power, *J. Chem. Soc., Dalton Trans.* **1998**, 2939−2951. − [13d] See also ref.[12c]
[14] S. Masamune, L. R. Sita, *J. Am. Chem. Soc.* **1985**, *107*, 6390−6391.
[15] N. Kano, N. Tokitoh, R. Okazaki, *Organometallics* **1997**, *16*, 2748−2750 and references cited therein.

[16] G. M. Sheldrick, *SHELXL-97, Program for crystal structure refinement*, Universität Göttingen, Germany, **1997**.
[17] Crystallographic data (excluding structure factors) for the structures reported in this paper have been deposited with the Cambridge Crystallographic Data Centre as supplementary publication no. CCDC-111750 (**7**) and -111751 (**8**). Copies of the data can be obtained free of charge on application to CCDC, 12 Union Road, Cambridge CB2 1EZ, UK [Fax: (internat.) + 44-1223/336-093; E-mail: deposit@ccdc.cam.ac.uk].

Received December 18, 1998
[I98441]

Solubility and Solvation of Carbon Dioxide in the Molten $Li_2CO_3/Na_2CO_3/K_2CO_3$ (43.5:31.5:25.0 mol-%) Eutectic Mixture at 973 K I. Experimental Part

Paul Claes,*[a] Dominique Moyaux,[a] and Daniel Peeters[b]

Keywords: Dicarbonate ion / Autodissociation constant / Electrochemistry / Potentiometric titration / Acidity / Basicity / Anions

The solubility of CO_2 in the molten ternary eutectic mixture Li_2CO_3–Na_2CO_3–K_2CO_3 (43.5, 31.5, 25.0 mol.%) at 973 K has been determined by a titration technique. From the obtained titration curve, the solubility has been found to amount to $9.5\cdot10^{-2}$ mol·L^{-1} (σ = 1.0) under a pressure of CO_2 of 1 atm and the pK_d value of the carbonate melt has been evaluated to 5.37 (σ_5 = 0.24) if the concentrations of the solutes are expressed in mol·L^{-1}. This pK_d value is in good agreement with literature data but the solubility value reported in this work is much higher than most of those reported in the literature. A chemical dissolution of CO_2 as $C_2O_5^{2-}$ is proposed and the consequences of the occurrence of this species on the acidobasic properties of molten carbonates are discussed. It appears from the experimental results that the $CO_2/C_2O_5^{2-}$ equilibrium in the carbonate melt is a slow process.

1. Introduction

The use of molten carbonates as reaction media for chemical or electrochemical applications needs a deep understanding of their chemical properties and particularly of their acidobasic and redox behaviour. Carbonate melts are amphoteric oxoacidobasic liquids whose autodissociation equilibrium is generally written as follows:[1]

$$CO_3^{2-} \rightleftharpoons CO_2 + O^{2-}{}_{solv} \quad (1)$$

where $O^{2-}{}_{solv}$ represents a solvated oxide ion.

The corresponding autodissociation constant (K_d) is then written:

$$K_d = a(O^{2-}{}_{solv}) \cdot P(CO_2) \quad (2)$$

where $a(O^{2-}{}_{solv})$ and $P(CO_2)$ are the activity of solvated oxide ions in the melt and the partial pressure of carbon dioxide in the gas phase in equilibrium with the liquid phase. According to this, the solvated oxide ion is the strongest base available in the melt, while CO_2 is the strongest acid.

Acidity scales may be based on pO^{2-} values [$pO^{2-} = -\log a(O^{2-}{}_{solv})$] or on $-\log P(CO_2)$ values. The two scales are, of course, related:

$$pK_d = pO^{2-} - \log P(CO_2) \quad (3)$$

These scales extend from $pO^{2-} = pK_d$ or $-\log P(CO_2) = 0$ for the most acidic media to $pO^{2-} = 0$ or $-\log P(CO_2) = pK_d$ for the most basic media.

The scales described in this way are quite satisfactory from a thermodynamic point of view but fail to give a sound and complete explanation of chemical or electrochemical behaviours. The concentration of CO_2 physically dissolved in a melt is indeed related to its partial pressure according to Henry's law:

$$C(CO_2) = k_H \cdot P(CO_2) \quad (4)$$

where k_H is the Henry's constant. For a given partial pressure of carbon dioxide, depending on the value of Henry's constant, significant differences might occur in the kinetics of chemical and electrochemical reactions whose rates are limited by the diffusion of CO_2.

Surprisingly, solubility data for CO_2 in carbonate melts are scarce and scattered as shown in Table 1 which presents some literature data for Henry's constant in three carbonate melts. Nevertheless, the knowledge of the correct value of the solubility of carbon dioxide is essential to a complete understanding of phenomena occurring in molten carbonates.

Table 1. Henry's constant for CO_2 in carbonate melts

Melt	T [K]	k_H [mol·L^{-1}·atm^{-1}]	Ref.
Na_2CO_3	1153	$9.6\cdot10^{-3}$	[2]
$(NaK)_2CO_3$	1073	$1.83\cdot10^{-1}$	[3]
$(LiNaK)_2CO_3$	973	$3.6\cdot10^{-3}$	[4]
	973	$1.19\cdot10^{-2}$	[5]
	833	10^{-1}	[6]

The aim of this work is to determine the Henry's constant of CO_2 in a carbonate melt (its solubility under a partial pressure of carbon dioxide of 1 atmosphere) by carrying out a potentiometric titration of a saturated carbonate melt at high temperature. This kind of experiment is probably

[a] Laboratory of Inorganic and Analytical Chemistry,
[b] Laboratory of Quantum Chemistry,
Catholic University of Louvain, Department of Chemistry,
Pl. Louis Pasteur 1, B-1348 Louvain-la-Neuve, Belgium
Fax: (internat.) +32-10/472330
E-mail: claes@inan.ucl.ac.be

 © WILEY-VCH Verlag GmbH, D-69451 Weinheim, 1999 1434–1948/99/0404–0583 $ 17.50+.50/0

the most direct way to the determination of the solubility of carbon dioxide; it does not need any assumption nor any calibration nor any change of temperature or physical state of the system and gives thus, in our opinion, the best confidence about the accuracy of the results.

2. Titration Procedure

The principle of the method is very simple. An accurately known amount of carbonate melt previously saturated with carbon dioxide under a pressure of 1 atmosphere is neutralized by adding to the liquid weighed portions of sodium oxide. The potential of an oxygen electrode dipped into the molten salt is measured after the complete dissolution and reaction of the added sodium oxide. The titration curve is obtained by plotting the measured potentials as a function of the amount of added sodium oxide. The end point of the titration allows to calculate the solubility of carbon dioxide and the pK_d value may be computed from the experimental solubility and from the amplitude of the titration curve.

The melt contained in an alumina crucible was saturated with carbon dioxide by flowing pure CO_2 through the cell for 24 hours. The time needed to reach equilibrium conditions after the addition of a given amount of Na_2O was about 6 hours. On the other hand, the potential difference underwent a slight potential shift which precluded to carry out a complete titration in one continuous experiment by adding successive amounts of Na_2O to one carbonate sample and by measuring the potential difference after each addition. An example of the evolution of the potential difference after addition of a given amount of sodium oxide to a CO_2 saturated melt is shown in Figure 1. The first part of the graph shows the effect of the neutralization reaction which is followed by a regular shift of the potential.

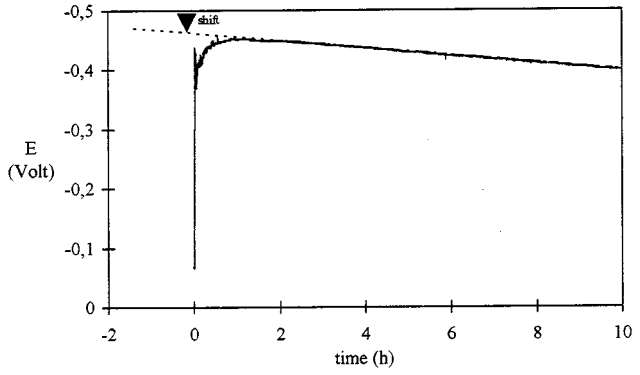


Figure 1. Evolution of the potential difference between the working and the reference electrodes as a function of the time elapsed from the addition of Na_2O to an acidic melt (1.1739 g of Na_2O added to 170.4 ml of melt)

In order to prevent too long observation times, each point of the titration curve was the result of one experiment where a given amount of sodium oxide was added to a freshly saturated sample. By increasing the amount of added Na_2O from one experiment to another, it was possible to construct the complete titration curve.

The neutralization reaction consumed not only the carbon dioxide dissolved in the melt but also the carbon dioxide contained in the free volume of the cell. Each titration point must thus be corrected for this extra consumption. Therefore, the amount of carbon dioxide contained in the cell was accurately measured in the following way. The cell containing an empty crucible was filled with carbon dioxide under a pressure of 1 atmosphere. The gas was then flushed out of the cell by a stream of pure nitrogen and allowed to bubble through a given volume of a standard solution of sodium hydroxide. The amount of absorbed carbon dioxide was determined by titration of the excess sodium hydroxide with a standard solution of hydrogen chloride. Three independent determinations have been carried out. The number of moles of CO_2 contained under a pressure of 1 atmosphere in the cell containing an empty crucible was found to be 0.0290 mol with a standard deviation of $2.9 \cdot 10^{-4}$ mol.

When the experimental results were plotted in order to construct the titration curve, the amounts of sodium oxide added to the melt were corrected for the number of moles of CO_2 contained in the gas phase at equilibrium $n(CO_2)_{gas}$ calculated according to:

$$n(CO_2)_{gas} = 0.0290 - \frac{PV_{melt}}{RT} \quad (5)$$

where P and V_{melt} are the pressure at equilibrium (1 atm) and the volume of the carbonate melt. Due to this procedure, the number of moles of Na_2O is plotted on a scale where it remains negative as long as the total amount of Na_2O added to the system is lower than the quantity required to neutralize the CO_2 contained in the free volume of the cell. The number of moles of sodium oxide calculated in this way was further divided by V_{melt} expressed in liters in order to normalize all the data to 1 liter of carbonate melt. This number $n_{norm}(Na_2O)$ was finally plotted as abscissa.

With the experimental set-up used in this investigation, the number of moles of CO_2 dissolved in the melt amounted to about 20% of the total number of moles introduced into the cell for each experiment.

Another procedure, less accurate than the preceding one, was also used. In this case, when the melt was saturated with CO_2, the cell was connected to the vacuum device for a short time (10 sec) in order to remove the carbon dioxide contained in the free volume. After that time, the residual pressure in the cell was about 1 cm Hg. It is of course impossible to state whether the extraction time was correctly choosen or not. It seems however highly probable that some positive (incomplete exhaustion of the CO_2 from the free volume) or negative (degassing of the melt) occurred in this procedure.

3. Results

Figures 2 and 3 show respectively a titration curve obtained by the first and by the second procedure. From the first graph, the solubility of carbon dioxide at 700°C in the

ternary eutectic under a pressure of 1 atmosphere is found to be 9.5 $10^{-2} \pm 1.0 \times 10^{-2}$ mol·L^{-1}atm^{-1} (this value was obtained by fifth-order polynomial fit with a correlation factor of 0.95). The equivalent point of the titration curve of the second graph corresponds to a solubility of $5.5 \cdot 10^{-2}$ mol·L^{-1}atm^{-1}. The agreement between these two values is reasonable if the difference between the two experimental procedures is taken into account. The observed difference may be attributed to a partial degassing of the melt during the emptying of the free volume.

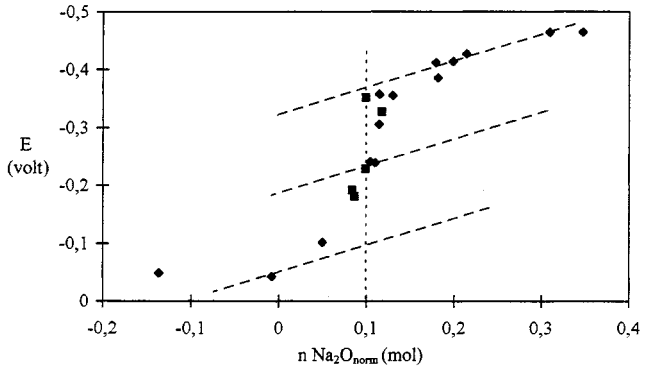


Figure 2. Titration curve obtained after correction for the neutralization of the amount of CO_2 contained in the free volume of the cell

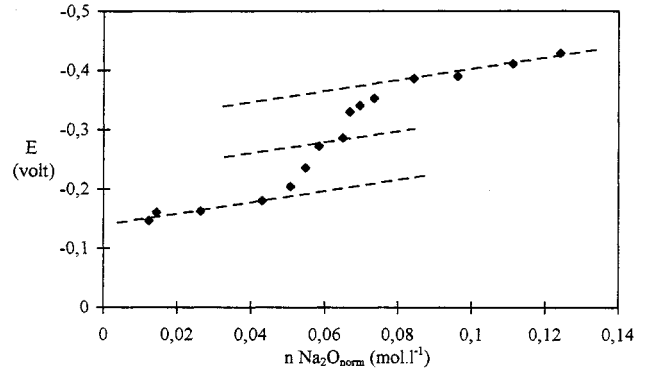


Figure 3. Titration curve obtained after the possibly incomplete removal of the CO_2 contained in the free volume of the cell

The pK_d value of the ternary eutectic at 700°C can be calculated from the value of the potential of the working electrode characteristic of the melt saturated with CO_2 under a pressure of 1 atm on the one hand and from the potential obtained for equilibrium conditions when an excess of sodium oxide has been added to the liquid on the other hand. The excess concentration of sodium oxide must of course be lower than the solubility of sodium oxide in the ternary eutectic at 700°C. According to White and Twardoch, this concentration limit amounts to 0.054 mol·L^{-1} [7].

Equations (6) and (7) describe the electrode reactions of the oxygen redox system respectively in basic and in acidic conditions:

$$O_2 + 4\ e^- \rightleftharpoons 2\ O^{2-} \quad (6)$$
$$O_2 + 2\ CO_2 + 4\ e^- \rightleftharpoons 2\ CO_3^{2-} \quad (7)$$

The corresponding Nernst equations are written:

$$E = E^\circ_{O2/O^{2-}} + (RT/4F)\ \ln P(O_2) - (RT/4F)\ \ln a(O^{2-}) \quad (8)$$
$$E = E^\circ_{O2/O^{2-}} + (RT/4F)\ \ln P(O_2) - (RT/4F)\ \ln K_d + (RT/4F)\ \ln P(CO_2) \quad (9)$$

If the partial pressure of oxygen, which is the residual pressure of oxygen, is considered as a constant, Equations (7) and (8) may be rewritten:

$$E = A - (RT/4F)\ \ln a(O^{2-}) \quad (10)$$
$$E = A - (RT/4F)\ \ln K_d + (RT/4F)\ \ln P(CO_2) \quad (11)$$

The potential value for the excess Na_2O concentration was corrected for the potential shift which occurred in basic media. Therefore, the electrodes were allowed to rest in the melt after the neutralization of the carbon dioxide by the introduced sodium oxide and the potential difference was measured as a function of the time. Using this shift per unit time measured experimentally for each neutralization experiment, the value of the potential obtained for the basic melt was corrected considering the time elapsed between the introduction of sodium oxide and the end of the experiment. Taking into account Equations (10) and (11) as well as the correction for the potential drift $[(\Delta E)_{drift}]$ and assuming that the activity of oxide ions in Equation (10) may be replaced by the excess concentration of sodium oxide $[C(Na_20)_{exc}]$ (the concentration corresponding to the amount of Na_2O introduced in the saturated melt less the solubility of carbon dioxide), one finds for the difference between the initial and the final potentials (ΔE):

$$\Delta E = -(RT/4F)\ \ln K_d - (RT/4F)\ \ln C(Na_2O)_{exc} - (\Delta E)_{drift} \quad (12)$$

The pK_d values were determined from five independent experiments whose results are shown in Table 2. This table gives successively the normalized amount of sodium oxide introduced into the saturated melt $[n_{norm}(Na_2O)]$, the excess concentration of sodium oxide $[C(Na_2O)_{exc}]$, the potential of the gold electrode measured at the beginning of the experiment ($E_{t=0}$) and 8 hours later ($E_{t=8}$), the experimental drift correction $[(\Delta E)_{drift}]$, the potential difference (ΔE) and the calculated pK_d value.

The mean value is pK_d = 5.37 with a standard deviation of σ_5 = 0.24

4. Discussion

4.1. Comparison with the Literature

The Henry's constant determined in this work is one order of magnitude higher than those measured by Appleby[4] and by Broers[5] but it agrees with the value given by Dubois.[6] This disagreement might be due to differences between experimental techniques used in these investigations. Appleby deduced his solubility data using a melt-chilling method based on the measurement of the quantity of dissolved gas released on freezing of the melt. This technique is certainly suitable for the determination of physical solu-

Table 2. Determination of the pK_d value

$n_{norm}(Na_2O)$ [mol·L^{-1}]	$C(Na_2O)_{exc}$ [mol·L^{-1}]	$E_{t=0}$ [Volt]	$E_{t=8h}$ [Volt]	$(\Delta E)_{drift}$ [Volt]	ΔE [Volt]	pK_d
0.179	0.084	0.043	0.412	0.033	0.402	5.24
0.115	0.020	0.043	0.357	0.056	0.370	5.53
0.114	0.019	0.043	0.306	0.096	0.359	5.44
0.130	0.035	0.043	0.355	0.031	0.343	5.01
0.118	0.023	0.069	0.327	0.130	0.388	5.65

bilities but might lead to underestimations in the case of chemical solubilities if the chemical reactions which take place in the dissolution process are slow. Broers used a procedure based on impedance determinations at a stationary $CO,CO_2/CO_3^{2-}$/Au electrode over a range of $P(CO)/P(CO_2)$ ratios which allows the CO_2/CO solubility ratio to be calculated. The CO_2 solubility is then deduced from the solubility of CO measured by an amperometric titration method. The interpretation of impedance spectroscopy determinations is much more complex than our measurements and needs that dissolved CO_2 and CO both occur in the melt as definite species reacting at the electrode at a well defined potential.

The pK_d value obtained in this work ($pK_d = 5.37 \pm 0.24$) is in reasonable agreement with the result obtained by Andersen ($pK_d = 5.8$)[8]. A small lack of accuracy might occur in our determinations due to the fact that the residual partial pressures of oxygen in the carbon dioxide and in the nitrogen used to generate the gaseous atmosphere in equilibrium respectively with the acidic and basic melts are not exactly the same. The accuracy might probably be improved by adding a small constant partial pressure of oxygen to the gaseous atmospheres successively imposed above the melt during the determinations in place of using "pure" carbon dioxide and "pure" nitrogen.

4.2. Comparison with the Electrochemical Behaviour of Carbon Dioxide

Earlier results have shown that CO_2 is electroactive in molten carbonates and that the corresponding CO_2/CO redox system exhibits a reversible behaviour[3,9−11]. The proposed electrochemical reaction is:

$$2\ CO_2 + 2\ e^- \rightleftharpoons CO + CO_3^{2-} \quad (13)$$

This was indeed confirmed in this work since a cathodic peak occurs at about −0.8 V versus the reference electrode in the linear sweep voltammograms of CO_2 saturated melts. Such a voltammogram is shown in Figure 4. The current density of this signal was allways very small, of the order of magnitude of 1 mA·cm^{-2}.

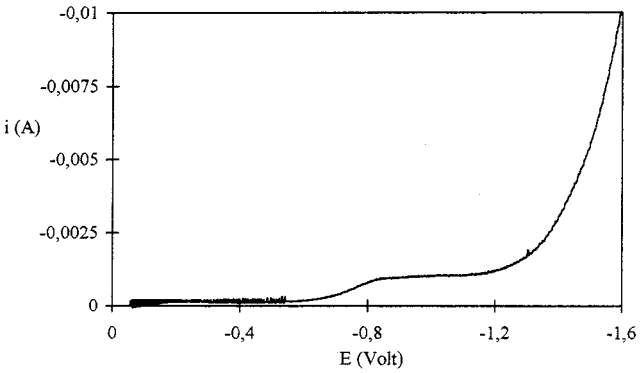


Figure 4. Voltammogram of a CO_2 saturated carbonate melt. ($\nu = 1$ V·s^{-1})

$$i_p = 0.4463(\nu D/RT)^{1/2}(nF)^{3/2}\ SC \quad (14)$$

From the Randles−Sevcikc Equation (14) in which $i_p = 10^{-3}$ A, $n = 1$, $S = 1$ cm^2, $T = 973$ K, $\nu = 1$ Vs^{-1} and $D = 10^{-5}$ cm^{2}s^{-1}, which is the order of magnitude of diffusion coefficients in molten carbonates in the temperature range 873−973 K[3,7,11−13], a concentration value of $2\cdot10^{-3}$ mol·L^{-1} is calculated. This calculation is in agreement with the results of Peelen[11] who reports a value of $0.95\cdot10^{-8}$ mol·cm^{-2}s$^{-1/2}$ for the product $s \times D^{1/2}$ (where s is the solubility) relative to CO_2 in a molten Li/K carbonate mixture at 848 K. From this, with the same diffusion coefficient, the value of the solubility s is found to be $3\cdot10^{-3}$ mol·L^{-1}. These solubilities are lower by about two orders of magnitude than the Henry's constant measured by the titration technique.

In order to make the experimental solubility compatible with the electrochemical observations, it may be assumed that most of the carbon dioxide dissolved in the carbonate melt is so strongly solvated that it should react at the cathode at a potential at which the reduction of carbonate ions still occurs. The formation of dicarbonate ions may be proposed:

$$CO_2 + CO_3^{2-} \rightleftharpoons C_2O_5^{2-} \quad (15)$$

with an equilibrium constant:

$$K = \frac{a(C_2O_5^{2-})}{P(CO_2)} \quad (16]$$

According to this assumption, a small proportion of CO_2 dissolves physically in the melt, yielding "free" CO_2 responsible for the observed electrochemical reduction. As calculated above, this physical dissolution accounts for only about 2% of the dissolved CO_2. The largest part of the dissolution occurs chemically yielding dicarbonate ions. Furthermore, these dicarbonate ions have to be inactive in the electrochemical window. The "complexation" of CO_2 by CO_3^{2-} or the overpotential for the reduction of $C_2O_5^{2-}$ must therefore be strong enough to shift that reaction to potential values where the reduction of CO_3^{2-} still occurs. In order to explain the weakness of the cathodic signal due to the reduction of CO_2, it must also be assumed that the production of CO_2 through equilibrium (15) is slow enough that the consumption of CO_2 in the electrochemical reduction is not compensated by the equilibrium. The sluggishness of the formation−dissociation kinetics of pyrocarbonate ions applies to all phenomena consuming carbon dioxide and the unexpected high solubility of CO_2 contributes little, for instance, to enhance CO_2 mass transfer in MCFC cathodes. The occurrence of a physical and a chemical solubility might also explain, at least partly, the discrepancies between solubility determinations by different techniques.

Unfortunately, we are unable at the moment to propose any experimental evidence for the occurrence of dicarbonate ions in acidic carbonate melts. However, the quantum chemical approach proposed in the second part of this work provides good arguments for the formation of that species.

4.3. Acidobasic Properties of Carbonate Melts

The occurrence of a chemical solubility of carbon dioxide besides its physical solubility leads to a second autodissociation reaction of carbonates, which would be written as Equation (17) and which would occur in the melt besides equilibrium (1).

$$2\ CO_3^{2-} \rightleftharpoons C_2O_5^{2-} + O^{2-} \quad (17)$$

The corresponding autodissociation constant is:

$$K_d' = a(C_2O_5^{2-}) \cdot a(O^{2-}) \quad (18)$$

For practical purposes, this is written:

$$K_d' = [C_2O_5^{2-}]\cdot[O^{2-}] \quad (19)$$

Taking into account equilibrium (16), one finds:

$$K_d' = KP(CO_2)[O^{2-}] = K_dK \quad (20)$$

The neutrality condition for autodissociation, which is a relationship between the concentrations of basic and acidic species in a pure carbonate melt should then be written:

$$[O^{2-}] = [CO_2] + [C_2O_5^{2-}] \quad (21)$$

The titration carried out in this work does not allow the direct measurement of Henry′s constant, which accounts only for the physical solubility. The measured constant is in fact ($k_H + K$) since both chemically and physically dissolved carbon dioxide react with Na_2O:

$$[CO_2] + [C_2O_5^{2-}] = (K+ k_H)\cdot P(CO_2) = 9.5\cdot10^{-2} \pm 1.0\cdot10^{-2}\ mol\cdot L^{-1} \quad (22)$$

The ratio of the concentration of physically and chemically dissolved carbon dioxide depends only on the temperature of the melt:

$$\frac{[CO_2]}{[C_2O_5^{2-}]} = \frac{k_H}{K} \quad (23)$$

An approximative value of this ratio may be proposed from the results obtained in this work: $[CO_2]$ has been evaluated to be $2\cdot10^{-3}$ mol·L^{-1} from the peak current density for the electrochemical reduction of carbon dioxide in a saturated melt and $[C_2O_5^{2-}]$ may be considered as the experimental solubility since, taking into account the level of approximation, the physical solubility may be neglected in comparison with the chemical solubility. The value of $2\cdot10^{-2}$ is thus a good approximation of the ratio of the physical to the chemical solubility.

$C_2O_5^{2-}$ is a weak acid relative to CO_2, which is the strongest acid available in carbonate melts. The respective strengths of these acids are measured by the equilibrium constants (K_1 and K_2) of the reactions of these acids with oxide ions:

$$C_2O_5^{2-} + O^{2-} \rightleftharpoons 2\ CO_3^{2-} \quad (24)$$

$$CO_2 + O^{2-} \rightleftharpoons CO_3^{2-} \quad (25)$$

$$\frac{K_1}{K_2} = \frac{[CO_2]}{[C_2O_5^{2-}]} \quad (26)$$

$C_2O_5^{2-}$ is thus a weaker acid than CO_2 by a factor of about $2\cdot10^{-2}$.

5. Conclusions

The experimental value of the solubility of carbon dioxide in carbonate melts depends on the technique used for the determination. The solubility measured in this work by a titration technique is much higher than those reported in the literature for the same melt at the same temperature. These differences may be explained by the occurrence of a physical and a chemical solubility due to the formation of dicarbonate ions. This chemical solubility is about 50 times more important than the physical solubility. The simultaneous occurrence of CO_2 and $C_2O_5^{2-}$ in carbonate melts means that the autodissociation of carbonate ions occurs in two different ways producing two different conjugated acids of the solvent. The comparison of these two acids from a thermodynamic point of view shows that the strength of the dicarbonate ion is about 50 times lower than that of carbon dioxide, which is the strongest acid available in molten carbonates. Our results do not allow the deduc-

tion of any information about the kinetic properties of these two species, but the occurrence of $C_2O_5^{2-}$ offers a convenient explanation for the slowness of the neutralization reaction of oxide ions in acidic carbonate melts as demonstrated by Lu and Selman[15]. This is a rather speculative consideration but it seems important to pay some attention to this point in the future.

Experimental Section

Chemicals: Lithium-, sodium-, and potassium carbonates were analytical grade reagents from Merck. The lithium salt was dried at 200°C for 24 hours under vacuum before use.

200 g of a dry homogeneous mixture of salts with the composition of the ternary eutectic $Li_2CO_3-Na_2CO_3-K_2CO_3$ (43.5%, 31.5% and 25.0% mol. respectively) was used for each experiment. The sample was progressively heated up to 400°C under a nitrogen pressure of 1 atmosphere in order to remove residual water. After melting, nitrogen was replaced by carbon dioxide and the temperature of the liquid was raised to 700°C.

The gases were supplied by Air Liquide; their purities are certified to be at least 99.999% for nitrogen, 99.99% for O_2, and 99.995% for CO_2. The water content of all these gases is lower than 5 ppm.

When mixtures of gases were needed (reference electrode), the expected proportions were obtained by adjusting the streams of the components with precision valves and flowmeters to a buffer vessel, where the gases were allowed to mix together.

Experimental Set-up: The carbonate melt was contained in an alumina (Al23 Degussa) crucible setted in an alumina (Al23 Degussa) cell located in a vertical furnace whose temperature was regulated to ±2°C. The cell was provided with an airtight cover which allowed to introduce into the melt a working and a reference electrode and with alumina tubings intended to introduce sodium oxide, carbon dioxide and nitrogen into the cell.

Addition of Na_2O was carried out without changing the composition of the gaseous atmosphere in the cell by means of a lock chamber.

During the titration procedure, nitrogen was progressively introduced to compensate for the consumption of carbon dioxide in order to keep constant the total pressure in the cell.

Electrochemical Device: The working electrode used in potentiometric determinations is a 0.5 mm diameter gold wire which acts as an oxygen electrode. The reference electrode is an oxygen electrode in an acidic melt contained in a pythagoras tubing dipped into the investigated melt. The electrochemical arrangement is thus:

Au / CO_2 (0.66 atm), O_2 (0.33 atm) / CO_3^{2-} / pythagoras / CO_3^{2-} sample / CO_2 or O^{2-}, O_2 (res.) / Au

The electrochemical determination have been carried out with a Princeton Applied Research potentiostat/galvanostat model 273.

Acknowledgments

The authors are much indebted to the F.N.R.S. (Fonds National de la Recherche Scientifique de Belgique) for financial assistance in this research.

[1] B. Tremillon, *Electrochimie analytique et réactions en solution*, Tome 1, Masson (Paris, Milan, Barcelone, Bonn) **1993** p. 352.
[2] R. E. Andresen, *J. Electrochem. Soc*. **1979**, *126*, 328.
[3] P. Claes, B. Thirion, J. Glibert, *Electrochimica Acta* **1996**, *41*, 141.
[4] A. J. Appleby, C. Van Drunen, *J. Electrochem. Soc*. **1996,** *127*, 1655.
[5] G. H. J. Broers, *Survey of Basic Research on Fuel Cells with Fused Carbonate Electrolytes*, Internal Rept. 69-0667/1272-7211, Centraal Technisch Instituut TNO, Appeldoorn, Netherlands, **1969**. − G. H. J. Broers, M. Schenke, H. J. J. van Ballegoy, Ext. Abstr. N° 77, 28th Mtg. Internat. Soc. Electrochemistry, Vano, Bulgaria, **1977**, *2*, 313.
[6] J. Dubois, *Ann. Chim*. **1965**, *10*, 145.
[7] S. H. White, U. M. Twardoch, *J. Appl. Electrochemistry* **1965**, *19*, 901.
[8] B. K. Andersen, *Thermodynamic Propereties of molten alkali carbonates*, Ph.D. Thesis, Tech. Un. of Denmark, Lingby **1965**.
[9] A. Borucka, *J. Electrochem. Soc*. **1977**, *124*, 972.
[10] W. M. Vogel, L. J. Bregoli and S. W. Smith, *J. Electrochem. Soc*. **1980**, *127*, 833.
[11] W. Peelen, *Stability and reactivity of oxygen, nickel and cobalt species in molten carbonate*, Ph.D. Thesis, Technische Universiteit Delft, **1997**.
[12] G. Moutiers, M. Cassir and J. Devynck, *J. Electroanal. Chem*. **1992**, *324*, 175.
[13] P. K. Andanuvor, R. E. White, A. J. Appleby, *J. Electrochem. Soc*. **1990**, *137,* 209.
[14] S. H. Lu, J. R. Selman, *Proc. Electrochem. Soc*. **1986**, *86-1*, 584.
Received October 20, 1998
[I98359]

Solubility and Solvation of Carbon Dioxide in the Molten $Li_2CO_3/Na_2CO_3/K_2CO_3$ (43.5:31.5:25.0 mol-%) Eutectic Mixture at 973 K II. Theoretical Part[+]

Daniel Peeters,*[a] Dominique Moyaux,[b] and Paul Claes[b]

Keywords: Ab initio calculations / Dicarbonate anion $C_2O_5^{2-}$ / Dicarbonate structure / Dicarbonate stability

A theoretical study of the structure and stability of the dicarbonate ion has been performed at the Hartree–Fock, MP2, and QCI/SD levels. A flexible 6-31+G(d) basis set was used to allow for the diffuse electron density appearing in the anions. A stable anion corresponding to two CO_2 entities covalently bound to a central oxygen has been found. The formation reaction starting from the carbonate anion and carbon dioxide has also been studied. Its thermodynamic features favour the formation of the dicarbonate anion, which in turn may account for the impressive solubility of carbon dioxide in carbonate melts.

Introduction

In the first part of this work[1] we described the measurement of the solubility of carbon dioxide in the ternary $Li_2CO_3/Na_2CO_3/K_2CO_3$ molten eutectic mixture under a pressure of 1 atm of CO_2. The experimentally determined value amounted to 0.995×10^{-1} mol L^{-1}, which is much higher than the values reported in the literature for the same melt at the same temperature. This solubility value is also 50 times higher than that deduced from the voltammetric peak current density measured for the electrochemical reduction of CO_2 dissolved in the melt under a pressure of 1 atm. In order to rationalize these data, it was suggested that CO_2 might combine with the carbonate ions to yield a strongly stabilized solvated species. The formation of dicarbonate ions has been proposed (Equation 1).

$$CO_2 + CO_3^{2-} \rightleftharpoons C_2O_5^{2-} \quad (1)$$

The free energy change for this reaction was assumed to be sufficiently large to shift the cathodic reaction at potentials where the reduction of carbonate ions yet occurs. Unfortunately, however, the previous investigation did not provide any direct experimental evidence for the occurrence of dicarbonate ions.

The main goal of this study is to analyse by theoretical means the structure, stability and properties, especially thermodynamic properties, of the relevant species. A quantum chemical approach to such a problem remains difficult, even though current computer technology permits access to an explicit and extensive treatment of such systems.

These experiments are carried out by considering a condensed, globally neutral, liquid medium. In such a model approach, the carbonate ions are assumed to be able to move freely through the medium of the molten salt phase while interacting with their neighbours. With this assumption, the study may be reduced to that of a particular molecular event; a single carbonate ion and a single carbon dioxide molecule may be considered in isolation and their mutual interaction can be studied as if they were isolated in the gas phase. We thus explicitly neglect the bulk behaviour as well as the nature of the counterion at this level. These should, of course, be introduced in condensed-phase simulations, but we shall concentrate our study on the most elementary chemical process accessible by quantum chemical means.

At the level used, the main difficulty involved lies in obtaining an adequate description of the behaviour of electrons in anions, especially when multiple excess charges are present. To treat this problem with a suitable degree of accuracy, two criteria need to be fulfilled:

1. As the excess electrons may be delocalized over large domains in space, the basis sets needed to simulate their distribution must offer sufficient flexibility to allow for such a large extension. Theoretical calculations must therefore be based on large basis sets, including polarization functions as well as extra diffuse functions.

2. As the correlation between electrons within the molecular domain is more important than in the case of neutral molecules, theoretical calculations must go beyond the Hartree−Fock level and explicitly include electron correlation.

In the next section, we shall briefly describe the methodology used in this work. The results of our simulation will then be presented. Finally, we shall discuss the chemical properties obtained and their relation to the macroscopic problem of interest.

Method

Owing to the size of the system, we chose to start our calculations at the valence split 6-31G basis set of Pople

[+] Part I: Ref.[1]

[a] Laboratory of Quantum Chemistry,
[b] Laboratory of Inorganic and Analytical Chemistry, Catholic University of Louvain, Department of Chemistry,
Place Louis Pasteur 1, B-1348 Louvain-la-Neuve, Belgium
Fax: (internat.) + 32-10/472707
E-mail: Peeters@cpmc.ucl.ac.be

 © WILEY-VCH Verlag GmbH, D-69451 Weinheim, 1999 1434−1948/99/0404−0589 $ 17.50+.50/0

and co-workers, which was augmented by a set of 6 Cartesian "d" polarization functions.[2] An additional set of diffuse sp functions[3] completed the basis. This led to the 6-31+G(D) basis set, containing some 133 atomic orbitals for the $C_2O_5^{2-}$ system. The ab initio molecular orbital calculations were then performed at restricted Hartree−Fock (RHF) level using the GAUSSIAN series of programs.[4] Post-SCF level computations were subsequently performed to introduce the electron correlation. In these, the inner cores were frozen, but all single and double excitations of the valence orbitals were considered using one of two different approaches: In the first, second-order Moller−Plesset perturbation theory computations (MP2) were performed. Such calculations remain affordable for carrying out a full optimization of the geometry. The second approach involved quadratic configuration interaction (QCI/SD). This latter method was in fact adopted, since it provides, within the variation principle, size-consistent results. This is a prerequisite for obtaining reliable reaction energies.

The geometric structures were derived from a full geometry optimization of all $3N - 6$ internal coordinates, thereby relaxing any a priori symmetry constraints. A conventional gradient technique was used to perform the optimization process.

Analytical computation of the first and second derivatives of the energy hypersurface was completed at the SCF level in order to verify the good behaviour of the minima and maxima found and to obtain a vibrational analysis within the harmonic approximation. This provided some information regarding the ways in which the molecules may be distorted. Knowledge of the geometrical structure and of the related rotational and vibrational frequencies allows further thermodynamic insight into the problem by applying the relationships of conventional statistical thermodynamics. From such an analysis, a simulation of the IR spectrum may even be obtained. At this point, we should mention that the theoretical vibrational frequencies needed to evaluate the zero-point energy and thermal corrections were scaled to adjust theoretical frequencies to experimental ones (Equation 2).[5]

$$\nu(\mathrm{sc}) = 0.9\ \nu(\mathrm{th}) \qquad (2)$$

At post-SCF MP2 level, the analytical gradient was used in conjunction with the analytical SCF Hessian matrix. The same approach was used at the QCI level, although this was not possible for the dicarbonate ion as in this case computation of the analytical gradient remains beyond our computational facilities. For the latter, a single-point energy was obtained at QCI/SD level using the MP2-optimized geometry.

Considering the results obtained for some other systems, we suspect that a correctly optimized structure would induce a further modification of some 0.003 Å in the bond lengths while the energy might be lower by about 2−3 kcal mol^{-1}.

Results

The reactants and product of the reaction were fully optimized as described in the preceding section. The resulting structures and energies for CO_2 and CO_3^{2-} are given in Table 1. Corresponding results for $C_2O_5^{2-}$ are given in Table 2 and its structure is depicted in Figure 1. It is noteworthy that for the latter the potential energy surface around the minimum is very flat and allows a considerable degree of freedom with regard to the position of the central oxygen atom. The absolute minimum has a C_2-symmetric structure at both the RHF and MP2 levels, but an asymmetric adjustment of the central C−O bonds by 0.005 Å leaves the energy almost unchanged.

Table 1. Structures of the reactants at 6-31+G(d) level

Molecule	Method	C−O [Å]	Energy [a.u.]
CO_2	RHF	1.143	−187.6387868
($D_{\infty h}$)	MP2	1.181	−188.1179592
	QCI/SD	1.174	−188.1158356
CO_3^{2-}	RHF	1.286	−262.3193483
(D_{3h})	MP2	1.318	−263.0171893
	QCI/SD	1.313	−263.0184152

Table 2. Structure of the product at 6-31+G(d) level (labels according to Figure 1)

$C_2O_5^{2-}$ (C_2)	C−O [Å]	Angles [°]		Energy [a.u.]
RHF	(1,2) 1.388	C2−O1−C5	138.8	−450.0495857
	(2,3) 1.238	O1−C2−O3	113.6	
	(2,4) 1.230	O1−C2−O4	117.5	
MP2	(1,2) 1.437	C2−O1−C5	134.4	−451.220177
	(2,3) 1.268	O1−C2−O3	112.6	
	(2,4) 1.258	O1−C2−O4	117.4	
QCI/SD[a]				−451.223711

[a] Energy of MP2-optimized structure.

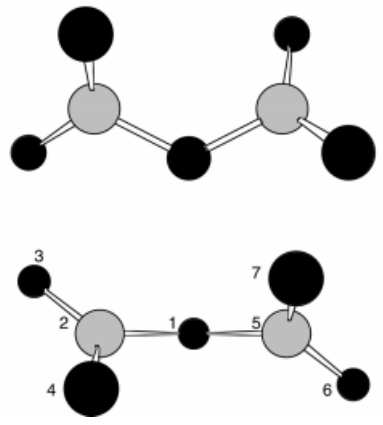


Figure 1. Structure of the $C_2O_5^{2-}$ anion; two views showing the C_2 symmetry of the system

With regard to the charge distribution, it is meaningless to use a conventional Mulliken population analysis with polarized and diffuse atomic basis sets, as their spatial extension and overlap is far too great. Mulliken charges ob-

tained using a 6-31G basis set computation are listed in Table 3.

Table 3. Mulliken charges at 6-31G level for the various molecules

	CO_2	CO_3^{2-}	$C_2O_5^{2-}$
C	+0.86	+0.85	+0.95
O	−0.43	−0.95	(O1) −0.80 (O3) −0.79 (O4) −0.76

Discussion

The collected results offer an insight into the general behaviour of the studied system.

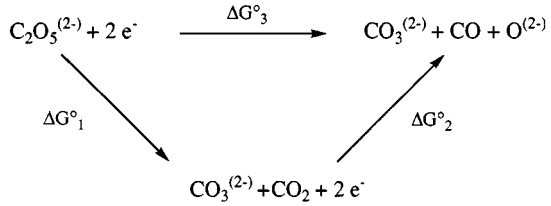
1. From a thermodynamic point of view, starting from the force constants obtained at Hartree−Fock level, one may compute the vibrational frequencies of the reactants and products. Furthermore, the computed energy, the moment of inertia, and scaled frequencies allow us to estimate, using statistical relationships, the reaction enthalpy, the entropy, and the Gibbs′ free energy at various temperatures. The results obtained at 298.15 K are presented in Table 4, along with those at the higher temperatures of 698.15 K and 973.15 K, which are closer to those of molten salts.

Table 4. Thermodynamic reaction properties derived from the theoretical results at 6-31+G(D) level

Method	$\Delta H(T)$ [kcal mol^{-1}]	$\Delta S(T)$ [cal K^{-1}mol^{-1}]	$\Delta G(T)$ [kcal mol^{-1}]
$T = 298.15$ K			
RHF	−56.09	−27.90	−47.77
MP2	−52.05	–	−43.73
QCI/SD	−54.83	–	−46.51
$T = 698.15$ K			
RHF	−55.382	−26.50	−36.87
MP2	−51.342	–	−32.83
QCI/SD	−54.123	–	−35.61
$T = 973.15$ K			
RHF	−54.62	−25.60	−29.71
MP2	−50.58	–	−25.67
QCI/SD	−53.36	–	−28.45

It can readily be seen that the product of this reaction has appreciable thermodynamic stability at any considered temperature. On the one hand, since the structure is not totally optimized at the QCI level, the reaction energies must still be more negative. On the other hand, the theoretical reaction energy of such systems may still be subject to some errors (basis set limitations, electronic correlation). However, we feel that with the presented methodology, especially at QCI level, further sophistication will not lead to a modification of the results by more than a few kcal mol^{-1}, which would be negligible compared to the −54 kcal mol^{-1} enthalpy variation. The reaction entropy is of course negative, but the overall Gibbs′ free energy remains negative, confirming the stability of the dicarbonate species. We may add to the argument that the reaction medium modifies the reaction entropy, generally leading to slightly less negative entropy contributions due to the bulk properties of condensed phase media.[6] This further confirms the thermodynamic stabilization of the dicarbonate ion in the molten medium.

As stated in the introduction, the free energy change for the production of dicarbonate ions from carbon dioxide and carbonate ions must be sufficient to shift the electrochemical reduction at potentials where the reaction of carbonate ions yet occurs. The reduction potential of dicarbonate ions may be calculated from the free energy change associated with reaction according to Equation 1. From the thermodynamic cycle shown in Scheme 1, Equation 3 may be derived.



Scheme 1. Thermodynamic cycle involving $C_2O_5^{2-}$

$$\Delta G^\circ_3 = \Delta G^\circ_1 + \Delta G^\circ_2$$
or
$$\Delta E^\circ_3 = -\Delta G^\circ_1/n\mathrm{F} + \Delta E^\circ_2 \quad (3)$$

Here, ΔG°_1 is the calculated free energy change associated with reaction according to Equation 1, which is given in Table 4 (−28.45 kcal.mol^{-1}); ΔE°_3 and ΔE°_2 are the standard potentials of the $C_2O_5^{2-}$/CO and CO_2/CO redox systems, respectively, and $-\Delta G^\circ_1/n$F is the difference between these two standard potentials. The latter thus represents the difference between the reduction potentials of CO_2 and $C_2O_5^{2-}$.

The value calculated in this way amounts to 617 mV, which is close to the difference between the reaction potential of CO_2 and the cathodic limit of the accessible electrochemical window in the molten ternary eutectic mixture of carbonates, which is of the order of 600 mV. Although the result obtained by our theoretical approach must be treated with caution as no medium effects are taken into consideration, the trend indicated by this estimation is in reasonably good agreement with the assumption made in the first part of this work.

2. From a structural point of view, the association of a CO_2 molecule with a CO_3^{2-} anion does not lead to a molecule−ion complex, as might have been expected, but to a well-defined dicarbonate molecular species. The distances between the C and O atoms correspond to those of covalent bonds. The symmetry of the system indicates that the two CO_2 moieties are equivalent. The integrity of an incoming CO_2 molecule is lost in the formation of the product, in which the central oxygen atom is trapped between two CO_2 units. It is readily conceivable that at the surface of the condensed molten carbonate medium, CO_2 may be absorbed from the gaseous environment forming a $C_2O_5^{2-}$ species,

which will then be able to diffuse inside the molten salt. A possible mechanism for the diffusion could be described in terms of the interchange of oxygen atoms with neighbouring CO_3^{2-} ions (Equation 4).

$$O_2C^* + O'CO_2^{2-} \rightleftharpoons O_2C^*O'CO_2^{2-} \rightleftharpoons O_2C^*O'^{2-} + CO_2 \rightleftharpoons \text{etc.} \quad (4)$$

This description is further supported by the presence in the IR spectrum of a low-energy asymmetric stretch of the central C−O bonds and by the aforementioned observation that the potential energy surface remains almost constant under deformation of the C−O−C arrangement.

Of course, our description only relates to an ideal "gas phase" level, which may indeed be appropriate close to the interface between the gaseous and liquid phases, justifying the solubility of CO_2. However, one must be cautious in generalizing such a mechanism to the bulk, where the nature of the counterions and the existence of high electric fields will presumably modify this mechanism.

Indeed, it was concluded in the first part of this work that the regeneration of CO_2 from the dicarbonate ion should be a slow process, since the electrochemical reduction of CO_2 appears to be restricted to free CO_2. With regard to the proposed transport mechanism, this slowness is unexpected and may highlight an inconsistency.

General Conclusions

We have shown herein that CO_2 interacts with the carbonate anion to produce a stable dicarbonate ion. The latter exhibits C_2 symmetry, the central oxygen atom being covalently bonded by two equivalent CO_2 moieties. Analysis of the potential energy surface, completed by a vibrational analysis, shows that the central oxygen atom has sufficient freedom of motion to undergo ready exchange with the CO_2 species. This leads to the assumption that carbon dioxide should be highly soluble in the molten mixture of carbonates and consequently points to the existence of dicarbonate ions in this medium.

Acknowledgments

The authors are indebted to the Belgian National Fund for Scientific Research and the Fonds de Développement Scientifique of Louvain University for financial support of this research.

[1] P. Claes, D. Moyaux, D. Peeters, *Eur. J. Inorg. Chem.* **1999**, 589−592.
[2] P. C. Hariharan, J. A. Pople, *Theor. Chim. Acta* **1973**, *28*, 213.
[3] T. Clarck, J. Chandrasekhar, G. W. Spitznagel, P. v. R. Schleyer, *J. Comput. Chem.* **1983**, *4*, 294.
[4] M. J. Frisch, G. W. Trucks, H. B. Schlegel, P. M. W. Gill, B. G. Johnson, M. A. Robb, J. R. Cheeseman, T. Keith, G. A. Petersson, J. A. Montgomery, K. Raghavachari, M. A. Al-Laham, V. G. Zakrzewski, J. V. Ortiz, J. B. Foresman, J. Cioslowski, B. B. Stefanov, A. Nanayakkara, M. Challacombe, C. Y. Peng, P. Y. Ayala, W. Chen, M. W. Wong, J. L. Andres, E. S. Replogle, R. Gomperts, R. L. Martin, D. J. Fox, J. S. Binkley, D. J. Defrees, J. Baker, J. P. Stewart, M. Head-Gordon, C. Gonzalez, J. A. Pople, *Gaussian 94*, *Revision C.2*, Gaussian, Inc., Pittsburgh PA, **1995**.
[5] M. Sana in *Computational Organic Chemistry* (Eds.: I. G. Czismadia, R. Daudel), Reidel, Dordrecht, **1981**, p. 183.
[6] P. Migchels, T. Zeegers-Huyskens, D. Peeters, *J. Phys. Chem.* **1991**, *95*, 7599.

[I98360]

Metal–Metal Interactions in Dinuclear (triphos)Cobalt Complexes Exhibiting Mixed Valency

Katja Heinze,[a] Gottfried Huttner,*[a] and Olaf Walter[a]

In memoriam Dr. L. Zsolnai

Keywords: Tripodal ligands / Cobalt / Bridging ligands / Mixed-valence compounds

The spectroscopic and electrochemical properties of a series of dinuclear mixed-valence complexes containing two (triphos)Co units are reported: $[(triphos)Co(L)Co(triphos)]^+$ (L = $C_6O_4X_2$; X = H, Cl, Br, I, Me: **2a–e$^+$**; L = $C_{14}H_4O_4Me_2$: **4$^+$**). Complexes **2a–e$^+$** are bridged by tetraoxybenzene ligands and exhibit very strong metal–metal interaction leading to delocalized class-III behaviour while in **4$^+$** the extended tetraoxoanthracence bridging ligand leads to a partial electron localization. Additionally, the different oxidation behaviour of the parent dicationic complexes **1a–e^{2+}** and **3^{2+}** have been investigated and are explained on the basis of a qualitative MO model.

Introduction

In the frame of a general study of magnetic[1][2] and electronic[3] interactions between two cobalt centres connected through a bridging ligand we have been interested in the investigation of complexes of the type $[(triphos)Co(L)Co(triphos)]^{n+}$. The tridentate terminal ligand triphos [1,1,1-tris(diphenylphosphanylmethyl)ethane] induces a five-fold coordination around each cobalt centre providing two free *cis* coordination sites[4–6] and thus allowing a bis(bidentate) coordination mode of the bridging ligand L within the dinuclear complex. The phosphorus donor set usually splits the metal d orbitals such that low-spin configurations (d^6-Co^{III}; d^7-Co^{II}) with zero or one unpaired electron, respectively, are obtained.[4][5] Antiferromagnetic exchange coupling is observed between the unpaired electrons of two $[(triphos)Co^{II}]$ entities in the complexes $[(triphos)Co(L)Co(triphos)]^{2+}$ with L = di-μ-X (X = Cl,[7][8] Br,[7] OH,[7] NH_2,[9] SMe[10]), 1,4,5,8-tetraoxonaphthalene, 1,4,9,10-tetraoxoanthracene,[1] fumarate and terephthalate.[2] Strong metal−bridging ligand interaction occurs within the dinuclear $[(triphos)Co^{III}]$ complexes $[(triphos)Co(L)Co(triphos)]^{2+}$ with L = 3,6-disubstituted 1,2,4,5-tetraoxybenzenes resulting in unusually intense, low-energy LMCT absorption bands.[3] In all cases the π system of the bridge proved to be essential for the interaction. In the latter complexes a further manifestation of the interaction is the separation of the two metal-centered reduction potentials which is due to the efficient overlap of the metal d(π) orbitals with the π orbitals of the bridging ligand.

We therefore attempted to prepare, isolate and characterize cationic mixed-valence complexes of the type $[(triphos)Co(L)Co(triphos)]^+$ with L = 3,6-disubstituted 1,2,4,5-tetraoxybenzenes in order to address the question of electron delocalization and electron transfer within the dinuclear unit. As the length of the bridging ligand has a remarkable influence on the communication between metal centres, analogous complexes with the extended bridging ligand 1,2,6,7-tetraoxy-9,10-dimethylanthracene are also reported.

[a] Department of Inorganic Chemistry, University of Heidelberg
Im Neuenheimer Feld 270, D-69120 Heidelberg, Germany
Fax: (internat.) + 49(0)6221/545707

Results and Discussion

Preparation of Complexes 1a−e^{2+}, 2a−e$^+$; Thermodynamic Stability and Reactivity of 2a−e$^+$

The complexes $[(triphos)Co(C_6O_4X_2)Co(triphos)]^{2+}$ (X = H, Cl, Br, I, Me), **1a−e^{2+}**, were prepared according to the literature.[3] Their CV data have already been reported but are repeated here for completeness (Table 1). The exceptionally large separation of the two reversible reduction steps shows that the mixed-valence species are thermodynamically stable towards disproportionation into the neutral and dicationic complexes. The green dicationic complexes can be reduced with one equivalent of cobaltocene to the blue cationic complexes **2a−e$^+$** (Figure 1; equation 1) which can be characterized in solution by spectroscopic methods. Reoxidation is possible by reaction with ferrocenium tetrafluoroborate (70−80% recovery).

All attempts to isolate **2a−e$^+$** as pure and crystalline materials failed as the complexes **2a−e$^+$** rapidly decompose on removing the solvent. Furthermore the mixed-valence complexes are highly reactive towards dioxygen leading to decomposition of the complexes (rapid colour change to red-brown yielding the free bridging ligand and phosphane oxides[11]). The reduction of **1a−e^{2+}** to **2a−e$^+$** was also carried out by the reaction with primary and secondary sodium alkoxides (NaOR; R = Me, Et, *i*Pr, CH_2Ph, allyl) yielding the corresponding aldehydes and ketones, respectively (isolated as their 2,4-dinitrophenylhydrazones). No carboxylic acids were detected in the reaction mixture. Ti-

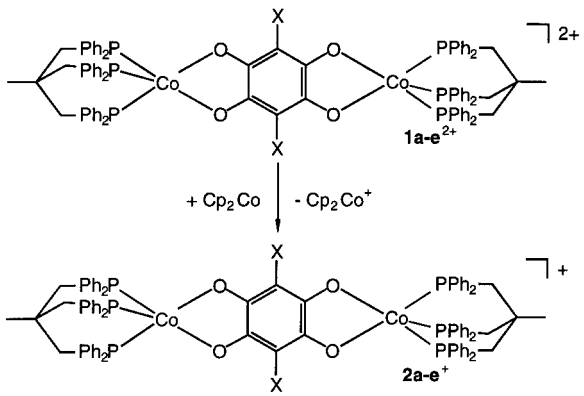
 © WILEY-VCH Verlag GmbH, D-69451 Weinheim, 1999 1434−1948/99/0404−0593v $ 17.50+.50/0

Table 1. Spectroscopic data of **2a−e**$^+$

X =	H (**2a**$^+$)	Cl (**2b**$^+$)	Br (**2c**$^+$)	I (**2d**$^+$)	Me (**2e**$^+$)
UV/Vis[a]					
λ_1 [nm] (ε [M^{-1} cm^{-1}])	300 (25510, sh)	305 (21680, sh)	322 (13750,sh)	303 (20030, sh)	300 (25860, sh)
λ_2 [nm] (ε [M^{-1} cm^{-1}])	394 (5630, sh)	392 (5580, sh)	–	–	394 (6390, sh)
λ_3 [nm] (ε [M^{-1} cm^{-1}])	450 (4450, sh)	447 (4530, sh)	422 (3870, sh)	405 (5300, sh)	456 (4630, sh)
λ_4 [nm] (ε [M^{-1} cm^{-1}])	–	658 (11540, sh)	664 (9560, sh)	658 (10860, sh)	–
λ_5 [nm] (ε [M^{-1} cm^{-1}])	692 (21380)	720 (15240)	720 (12230)	717 (12360)	689 (18800)
λ_6 [nm] (ε [M^{-1} cm^{-1}])	843 (7890, sh)	861 (7050, sh)	855 (5630, sh)	872 (5170, sh)	835 (7660, sh)
Isosbest. point [nm][b]	866	923	923	914	832
CV ($E_{1/2}$)[c]	−105, −1170	+10, −1000	+5, −1000	0, −995	−165, −1250
K_C (CV, 298 K)	11 × 10^{17}	1.2 × 10^{17}	1.0 × 10^{17}	0.6 × 10^{17}	22 × 10^{17}
EPR					
g_{av} (298 K)[a]	2.11	2.11	2.11	2.11	2.11
A_1, A_2 [G] (298 K)	–	–	–	–	40, 29
g_x, g_y, g_z (100 K)[d]	2.21, ?, 2.00	2.21, ?, 2.00	2.21, ?, 2.00	2.21, ?, 2.00	2.21,2.06,2.00[e]
A_x, A_y, A_z (100 K)	40, ?, 34	40, ?, 34	40, ?, 34	40, ?, 34	40, 40, 34

[a] In CH_2Cl_2. – [b] Titration experiment with *i*PrONa in CH_2Cl_2/*i*PrOH (3:1). – [c] In CH_3CN. – [d] In THF/CH_2Cl_2 (2:1). – [e] Simulation.

equation 1



equation 2

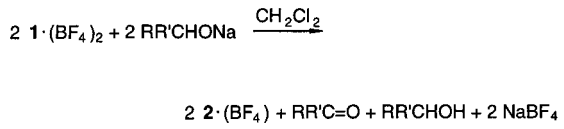


Figure 1. Reduction of **1a−e**$^{2+}$ to **2a−e**$^+$

trations with NaO*i*Pr, monitored by UV/Vis spectroscopy, showed clearly that one equivalent of base is necessary for complete conversion of **1a−e**$^{2+}$ to **2a−e**$^+$ (Table 1). The UV/Vis spectra obtained for the titration of **1c**$^{2+}$ with NaO*i*Pr are shown in Figure 2 as an example.

The intensity of the characteristic LMCT absorption band of **1c**$^{2+}$ at 1195 nm decreases with increasing base concentration, and simultaneously the band pattern of the cationic complex **2c**$^+$ emerges. Three isosbestic points are visible (304, 434 and 923 nm) which show that no UV/Vis-detectable intermediates are present. The net reaction can therefore be written as shown in Figure 1 (equation 2). These solutions are somewhat more stable than solutions of

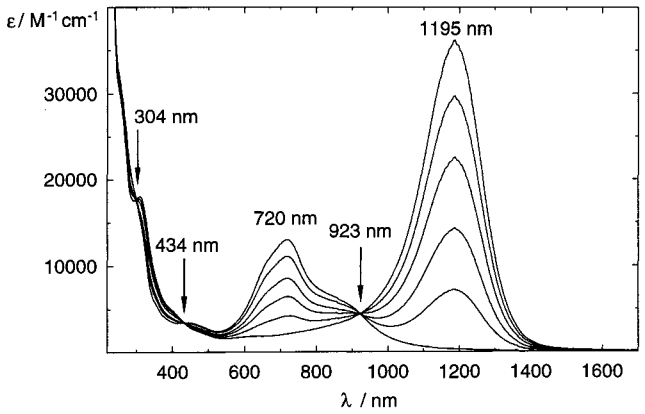


Figure 2. UV/Vis spectra during the titration of **1c**$^{2+}$ with NaO*i*Pr

2a−e$^+$ in pure CH_2Cl_2 and/or THF as long as an excess alcoholate is present.

Spectroscopic Properties of 2a−e$^+$

The isotropic EPR spectra of **2a−e**$^+$ in CH_2Cl_2 at 295 K show a broad, poorly resolved signal at *g* factors of around 2.11 (Table 1). The *g* factor and the width (half width at full height ca. 140 G) of the signal exclude the possibility of a significant spin density located on the bridging ligand. In a THF/CH_2Cl_2 matrix at 100 K the EPR spectrum exhibits a complex line pattern centered around $g = 2.10$. Figure 3 (left) shows the EPR spectrum of **2e**$^+$ as an example.

A 3 × 8 signal pattern would be expected if the unpaired electron were localized at one cobalt centre ($I_{Co} = {}^7/_2$), whereas a coupling with two equivalent cobalt centres should result in a 3 × 15 line pattern. Attempts to simulate the obtained spectra with a coupling to one metal centre failed; on the other hand a satisfactory approximation of the spectra was possible with the assumption of a coupling with two metal centres (Figure 3, right). This leads to the conclusion that the unpaired electron is delocalized over both metal centres, at least on the EPR time scale (10^{-9} s).

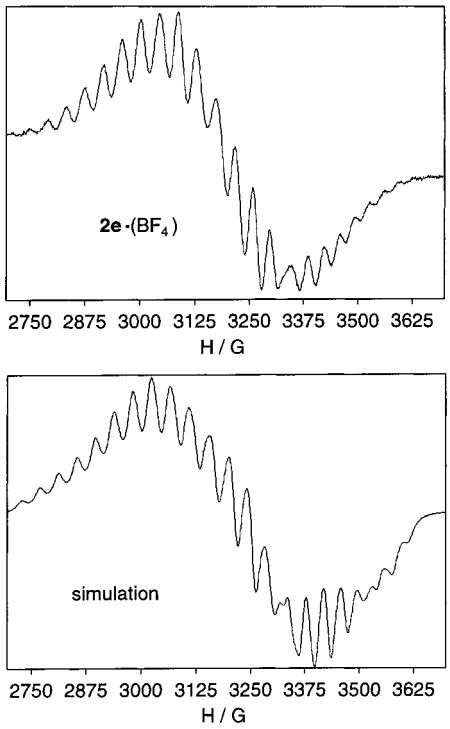


Figure 3. EPR spectrum of $\mathbf{2e}^+$ in THF/CH_2Cl_2 at 100 K and simulated spectrum

The obtained hyperfine coupling constants of $A_x \approx 40$ G, $A_y \approx 40$ G and $A_z \approx 34$ G further corroborate this interpretation. The coupling is significantly smaller than that found in the related mononuclear Co^{II} complexes [(triphos)-Co(L)] (L = substituted catecholate) with the unpaired electron inevitably localized on one metal centre ($A_x \approx 68-74$ G, $A_y \approx 58-60$ G and $A_z \approx 48-53$ G[12][13]).

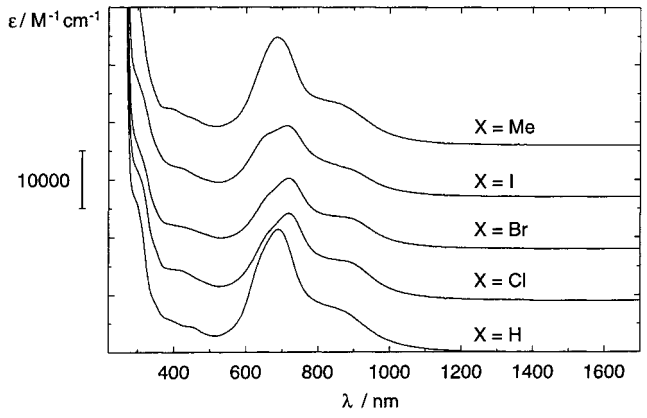


Figure 4. UV/Vis spectra of $\mathbf{2a-e}^+$

In accord with this interpretation of a delocalized system no absorption band which could be assigned to an intervalence transition could be detected up to 1700 nm in the UV/Vis/NIR spectra (Figure 4). In the visible part of the spectra a three-band pattern is observed (Table 1; $\lambda_4-\lambda_6$). The energy of the band maxima depends slightly on the substituents at the central bridge: Halides induce a red shift ($\mathbf{2a-d}^+$), alkyl residues a blue shift ($\mathbf{2e}^+$). This trend was also observed for the parent compounds $\mathbf{1a-e}^{2+}$.[3] The low-energy shoulder λ_6 has a half width at full height of only ca. 1630 cm^{-1} which is more than three times smaller than expected for a partly localized class-II system according to the Hush theory (5150−5260 cm^{-1}[14][15]). This transition might therefore better be described as a $\pi-\pi^*$ transition between delocalized states. Based on the CV, EPR, and UV/Vis data we therefore formulate the complex cations $\mathbf{2a-e}^+$ as delocalized class-III systems.

Crystal Structure of $(\mathbf{2b})_2\cdot(CoCl_4)$

Crystals of the complex salt $(\mathbf{2b})_2 \cdot (CoCl_4)$ were obtained as described in the Experimental Section. $(\mathbf{2b})_2 \cdot (CoCl_4)$ crystallizes in the tetragonal space group *P*4/*n*. The cation possesses crystallographic inversion symmetry, the $CoCl_4^{2-}$ counterion crystallographic S_4 symmetry. The results of the structural analysis are presented in Figure 5 and Table 2. In addition selected bond lengths and angles of the parent dicationic complex $(\mathbf{1b}) \cdot (BF_4)_2$[3] are shown for comparison.

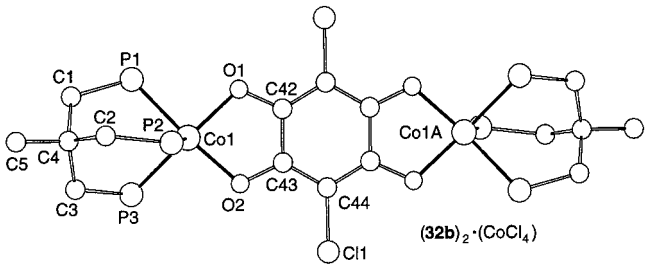


Figure 5. View of the structure of $\mathbf{2b}^+$; phenyl rings of the triphos ligand are omitted for clarity reasons

Neither a ligand dissociation nor a significant distortion of the coordination geometry relative to the structure of $\mathbf{1b}^{2+}$ is observed (maximum angle deviation X−Co−Y is observed for P3−Co1−O2 with 4.4°). Likewise the intraligand bond lengths (C−C, C−O, C−Cl) remain identical within the 2σ limit. Significant changes of the bond lengths are observed for the Co−O and Co−P bonds. The Co1−P2 (Δx = 0.073 Å) and the Co1−O1,2 bonds (Δx = 0.045, 0.053 Å) especially are elongated. As mainly bond lengths and only to a minor extent bond angles are affected by the additional electron the Franck−Condon barrier for the electron transfer can be estimated via $E_{in} = {}^1/_2\, N \Sigma\, k_i\, (\Delta x_i/2)^2$[16] [with k(Co−P) = 200 N m^{-1}; k(Co−O) = 440 N m^{-1}] resulting in about 2.5 kJ mol^{-1} per cobalt centre (i.e. 5 kJ mol^{-1} per complex). For the redox couple $[Co(tacn)_2]^{2+/3+}$ (tacn = 1,4,7-triazacyclononane) E_{in} is calculated as 25 kJ mol^{-1} [k(Co−N) = 170 N m^{-1}; Δx = 0.181 Å].[17] The very low activation barrier for the self-exchange reaction is due to the extremely small changes of the cobalt−ligand bond lengths Δx which might be the result of two effects: first the fact that the electron is delocalized over two metal centres and second that the cobalt centres retain their low-spin state as opposed to the $[Co(tacn)_2]^{2+/3+}$ case (hs-Co^{II}/ls-Co^{III}).

Table 2. Selected bond lengths[a] [Å] and angles[a] [°] for (**1b**) · $(BF_4)_2$ and $(\mathbf{2b})_2$ · $(CoCl_4)$

	1b · $(BF_4)_2$	$(\mathbf{2b})_2$ · $(CoCl_4)$		**1b** · $(BF_4)_2$	$(\mathbf{2b})_2$ · $(CoCl_4)$
Co1−O1	1.873(3)	1.918(5)	O1−Co1−O2	84.2(1)	82.7(2)
Co1−O2	1.881(3)	1.934(5)	C42−O1−Co1	113.6(3)	113.2(4)
Co1−P1	2.200(1)	2.220(2)	C43−O2−Co1	113.0(3)	113.6(4)
Co1−P2	2.178(1)	2.251(2)	O1−C42−C43	114.2(4)	114.4(6)
Co1−P3	2.204(1)	2.225(2)	O2−C43−C42	114.2(4)	114.8(6)
O1−C42	1.311(5)	1.311(8)	P1−Co1−P2	92.29(5)	91.62(9)
O2−C43	1.321(5)	1.311(8)	P1−Co1−P3	90.77(5)	88.59(8)
C42−C43	1.442(6)	1.45(1)	P2−Co1−P3	89.96(5)	91.63(8)
C43−C44	1.385(7)	1.40(1)	P1−Co1−O1	89.8(1)	90.5(2)
C42−C44A	1.390(5)	1.39(1)	P1−Co1−O2	161.7(1)	164.6(2)
C44−Cl1	1.737(5)	1.743(7)	P2−Co1−O1	111.5(1)	108.8(2)
Co1···Co1A	7.56	7.67	P2−Co1−O2	106.0(1)	103.6(2)
			P3−Co1−O1	158.5(1)	159.6(2)
			P3−Co1−O2	88.6(1)	93.0(2)
Co2−Cl2	−	2.301(2)	Cl2−Co2−Cl2A	−	109.60(8)
τ_1[b]	13.6	13.4	φ_1[b]	12.7	5.9
τ_2	15.1	7.9	φ_2	44.4	45.6
τ_3	16.2	16.0	φ_3	15.4	13.5
			φ_4	46.8	33.2
			φ_5	17.6	25.6
			φ_6	16.6	11.0

[a] Estimated standard deviations of the least significant figures are given in parentheses. − [b] The torsion angles τ_x are defined as follows: C4−C_x−P_x−Co (x = 1−3). The torsional arrangement of the six phenyl groups (φ_1−φ_6) is defined with respect to auxiliary vectors Hz_x−P_x (Hz_x is a dummy atom above P_x orthogonal to the plane spanned by the three phosphorus atoms) (x = 1−3): Hz_x−P_x−C_{ipso}−C_{ortho}.

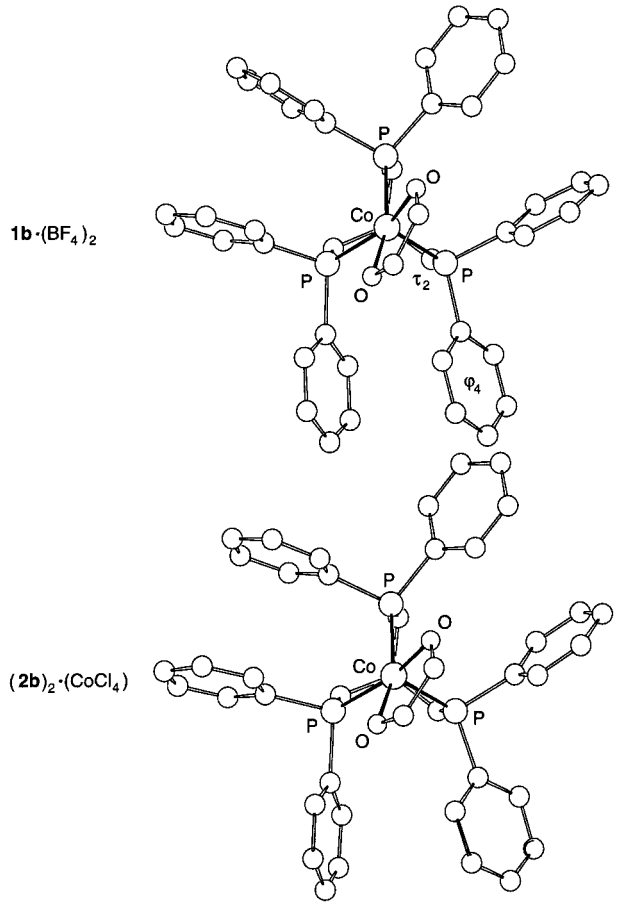


Figure 6. View of one (triphos)Co(O_2C_2) fragment of $\mathbf{1b}^{2+}$ and $\mathbf{2b}^{+}$[3] perpendicular to the plane spanned by the three phosphorus atoms

The conformation of the triphos ligand in the complex cations $\mathbf{1b}^{2+}$ and $\mathbf{2b}^{+}$ as decribed by the torsion angles of the chelate cage τ_{1-3} and the rotational position of the six phenyl rings φ_{1-6}[6] is shown in Figure 6 and Table 2. The only significant changes involve the backbone torsion angle τ_2 ($\Delta\tau_2 \approx 7°$) and the orientation of the fourth phenyl ring ($\Delta\varphi_4 \approx 14°$) both associated with the phosphorus atom P2.

In summary the structural data show that the additional electron in $\mathbf{2b}^{+}$ is neither localized on the bridging ligand nor on the triphos ligand, but on the metal centres. Of course, the X-ray structural analysis does not allow a decision between a localized or delocalized electronic description.

MO Calculations

The results of a molecular orbital calculation on the model compound $[\{(PH_3)_3Co\}_2(C_6H_2O_4)]^{2+}$ by the INDO method are presented in Figure 7,[18] which shows the relative energies and symmetries of the frontier orbitals. Here it suffices to note that in accordance with the EPR results the additional electron occupies a (68%) molecular orbital of b_u symmetry (C_{2h}) centered mainly on both metal atoms and that a filled ligand-centered (99% ligand) MO of b_g symmetry lies *below* the essentially ligand-centered MO of a_g symmetry (70% ligand).

Preparation of Complexes 3^{2+}, 4^{+}, 5^{3+}

The dicationic complex **3** · $(PF_6)_2$ may be obtained from $CoCl_2$, triphos, the bridging ligand 2,3,6,7-tetrahydroxy-9,10-dimethylanthracene and $NaPF_6$ as an analytically pure

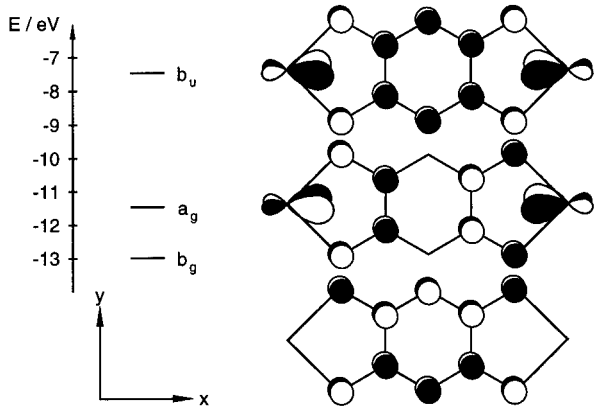


Figure 7. Orbital splitting and orbital symmetry of the model complex $[\{(PH_3)_3Co\}_2(C_6H_2O_4)]^{2+}$; the symmetry labels for the orbitals assume C_{2h} symmetry; the x axis is the Co−Co axis, and the z axis is perpendicular to the plane of the bridging ligand

blue powder. The FAB mass spectrum shows a typical fragmentation pattern[1−3] of dinuclear dicationic (triphos)cobalt complexes (see Experimental Section). The ^{1}H-NMR spectrum of **3** · $(PF_6)_2$ in CD_2Cl_2 shows signals for the CH_3, CH_2 and CH groups of the triphos ligand and signals for the CH and CH_3 groups of the bridging ligand in the correct intensity ratio. The phosphorus atoms of the triphos ligand give rise to a singlet at $\delta = 31.1$ in the ^{31}P-NMR spectrum. The signal of the ^{31}P nucleus of the hexafluorophosphate counterion is observed at $\delta = -144.2$ with the correct intensity ratio[19] of P(PF_6)/P(triphos) = 1:3. Due to the low solubility of **3** · $(PF_6)_2$ no ^{13}C-NMR spectrum could be obtained.

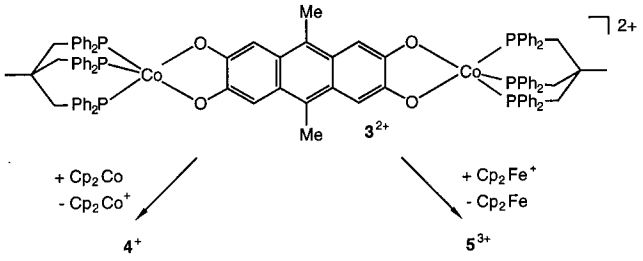


Figure 8. Synthesis of 4^+ and 5^{3+}

The dicationic complex 3^{2+} can be reduced in two reversible steps at −170 mV (Figure 9; 1) and −355 mV (Figure 9; 2), reversibly oxidized at +335 mV (Figure 9; 3) and irreversibly oxidized at $E_p \approx +935$ mV (vs. SCE). The reversible character of both reduction steps and the first oxidation wave precludes any significant structural rearrangement during the redox processes, i.e. all species 3^{2+}, 4^+ and 5^{3+} can be described by the same structure. The reduction to the mixed-valence complex 4^+ can be accomplished with cobaltocene; the oxidation to the trication 5^{3+} with ferrocenium tetrafluoroborate (Figure 8). With the separation of the two reduction potentials of 185 mV the conproportionation constant K_C for 4^+ is estimated to be 1.3×10^3 which is 15 orders of magnitude smaller than K_C of the complex $2e^+$.

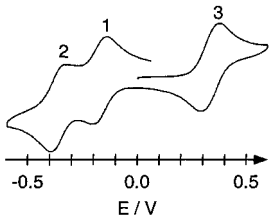


Figure 9. Cyclic voltammogram of **3** · $(PF_6)_2$ in CH_3CN

The UV/Vis spectrum of 3^{2+} (Figure 10, Table 3) shows two intense LMCT bands at 610 and 909 nm and intraligand absorptions around 400 nm as well as a weak absorption at 1250 nm which might have also LMCT character (vide supra).

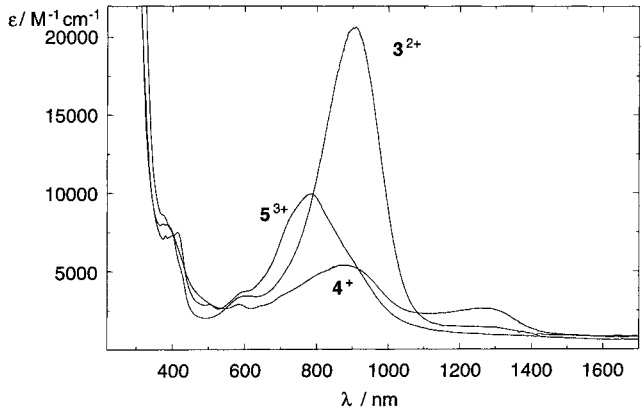


Figure 10. UV/Vis spectra of 3^{2+}, 4^+ and 5^{3+}

Spectroscopic Properties of 4^+

Reduction of 3^{2+} to 4^+ with one equivalent of cobaltocene leads to an orange-brown solution. The UV/Vis spectrum is depicted in Figure 10. Analogous to the mixed-valence complexes **2a**−**e**$^+$ it shows a three-band pattern in the Vis/NIR region. The low-energy absorption is red shifted compared to the corresponding bands of **2a**−**e**$^+$ (Tables 1 and 3). This absorption band might be a candidate for an intervalence transition although its half width at full height (1785 cm^{-1}) is lower than expected for a class-II mixed-valence system according to the Hush theory.[14][15] The characteristic features of this absorption band are quite similar to those of the well-known Creutz−Taube ion.[14] Therefore 4^+ might well be considered a borderline case between a class-II and a class-III system[20] which is also in accord with the thermodynamic data obtained by cyclic voltammetry (Table 3).

Spectroscopic Properties of 5^{3+}

One-electron oxidation of 3^{2+} gives the green tricationic complex 5^{3+}. The stability of 5^{3+} towards dispro-

Table 3. Spectroscopic data of $\mathbf{3}^{2+}$, $\mathbf{4}^{+}$ and $\mathbf{5}^{3+}$

	$\mathbf{4}^{+}$	$\mathbf{3}^{2+}$	$\mathbf{5}^{3+}$
Colour	orange-brown	blue	green
UV/Vis[a]	374 (8060) 584 (2890) 876 (5410)	376 (9450) 404 (6360, sh) 610	382 (7320) 414 (7510) 504 (2880)
λ [nm] (ε [M^{-1} cm^{-1}])	1271 (2640)	(3540) 909 (19140)	598 (3720, sh) 784 (9950)
K_C (CV, 298 K)[b]	1.3×10^3	3.4×10^8	(1.4×10^{10})
EPR (298 K)[a]	silent	diamagnetic	$g = 2.0056$

[a] In CH_2Cl_2. – [b] In CH_3CN.

portionation can only be estimated as the oxidation of $\mathbf{5}^{3+}$ is not reversible. Using the peak potential E_p instead of $E_{1/2\ KC}$ can be estimated to be of the order of 10^8. The UV/Vis spectrum of $\mathbf{5}^{3+}$ is similar to that of $\mathbf{3}^{2+}$ (Figure 10); the charge-transfer bands at 598 and 784 nm are shifted to higher energy and are less intense compared to those of $\mathbf{3}^{2+}$ (Tables 1 and 3). The isotropic EPR spectrum of a CH_2Cl_2 solution of $\mathbf{5}^{3+}$ is shown in Figure 11. The sharp signal centered at $g = 2.0056$ is without observable hyperfine splitting (half width at full height 24 G). This signal is characteristic for organic radicals, showing that the organic part of the dinuclear complex is oxidized.

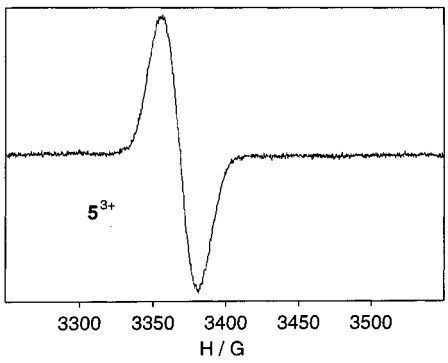


Figure 11. EPR spectrum of $\mathbf{5}^{3+}$ in CH_2Cl_2 at 295 K

MO Calculations

The frontier orbitals of the model complex $[\{(PH_3)_3Co\}_2(C_{14}H_6O_4)]^{2+}$ calculated by the INDO method are shown in Figure 12. As in the case of the complexes $\mathbf{1}^{2+}$ (Figure 7) interaction of the metal fragments with π orbitals of the bridging ligand results in two Co−O π-bonding MOs with large ligand character (b_u: 85%, not shown and a_g: 81% ligand, Figure 12) and in two Co−O π-antibonding MOs which are essentially metal-localized (b_u: 63%, and a_g: 57% metal, not shown, Figure 12). A non-bonding ligand-centered filled π orbital (b_g: 99% ligand) is located energetically between these occupied and empty orbitals. By analogy with the complexes $\mathbf{1a-e}^{2+}$ the intense absorption band at 909 nm can be assigned to the $a_g \rightarrow b_u$ transition and the additional low-energy absorption at 1250 nm to a $b_g \rightarrow b_u$ LMCT transition.

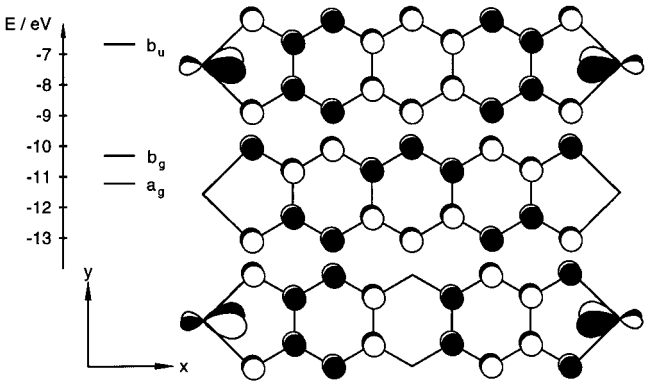


Figure 12. Orbital splitting and orbital symmetry of the model complex $[\{(PH_3)_3Co\}_2(C_{14}H_6O_4)]^{2+}$; the symmetry labels for the orbitals assume C_{2h} symmetry; the x axis is the Co−Co axis, and the z axis is perpendicular to the plane of the bridging ligand

With this MO scheme in mind the interpretation of the redox processes is straightforward: Reduction occurs, as in the case of the redox couple $\mathbf{1}^{2+}/\mathbf{2}^{+}$, at the metal centres leading to mixed-valence species. A reversible oxidation of $\mathbf{3}^{2+}$ which is not observed for $\mathbf{1}^{2+}$, is possible due to the energetically higher Co−O non-bonding ligand-centered b_g molecular orbital. For the complexes $\mathbf{1}^{2+}$ the HOMO of the complexes is Co−O π bonding (Figure 7) and oxidation would weaken the Co−O π bonds.

Concluding Remarks

The mixed-valence (triphos)cobalt complexes $\mathbf{2a-e}^{+}$ with a benzoic system as a bridging ligand ($d_{Co-Co} \approx 7.7$ Å) are shown to belong to class III of the Robin−Day classification, i.e. exhibit complete electron delocalization. In complex $\mathbf{4}^{+}$ with an extended bridging ligand of the anthracence type ($d_{Co-Co} \approx 13$ Å) the delocalization decreases towards a borderline class-II/class-III case. The assignments are corroborated by spectroscopic and theoretical means. In addition, the unexpected oxidation of the dicationic complex $\mathbf{3}^{2+}$ to $\mathbf{5}^{3+}$ leading to a ligand-centered radical is also interpreted in terms of the MO level ordering.

Experimental Section

Computational Details: Calculations were performed with an Apple Macintosh IIfx using the CACHe/ZINDO program Version 3.6 (M. C. Zerner 1990−1994) with INDO/1 parameters. Orbital energies were obtained from an SCF calculation. The geometry of the molecules was idealized to a square-pyramidal polyhedron around the metal centre and a planar bridging ligand. The triphos ligand was replaced by three isoelectronic PH_3 groups. Distances and angles were as follows: Co−P_{eq} 2.14 Å, Co−P_{ax} 2.22 Å, Co−O 1.89 Å, P−H 1.41 Å, O−Co−O 82.8°, P−Co−P 87.5°.

General Methods: Unless noted otherwise all manipulations were carried out under an inert gas by means of standard Schlenk techniques. All solvents were dried by standard methods and distilled under inert gas. − NMR: Bruker AC 200 at 200.13 MHz (^{1}H), 50.323 MHz (^{31}P). − IR: Bruker FTIR IFS-66, as CsI disks. − UV/Vis/NIR: Perkin Elmer Lambda 19. − MS: Finnigan MAT 8230. − EPR: Bruker ESP 300 E, X-band, standard cavity ER 4102, temperature control unit Eurotherm B-VT 2000, external standard diphenylpicrylhydrazyl (DPPH). − Elemental analyses: Microanalytical Laboratory of the Organisch-Chemisches Institut, University of Heidelberg. − Melting points: Gallenkamp MFB-595 010, melting points are not corrected. − Cyclic voltammetry: Metrohm "Universal Meß- und Titriergefäß", Metrohm GC electrode RDE 628, platinum electrode, SCE electrode, Princeton Applied Research potentiostat Model 273, 10^{-3} M in 0.1 M nBu$_4$NPF$_6$/CH_3CN. − Chemicals: 1,1,1-tris(diphenylphosphanylmethyl)-ethane, $CH_3C(CH_2PPh_2)_3$,[21] **1a−e** · $(BF_4)_2$,[3] 2,3,6,7-tetrahydroxy-9,10-dimethylanthracene,[22] (triphos)CoCl.[8,23,24]

Crystallographic Structure Determination: The measurement was carried out with a Siemens P4 (Nicolet Syntex) R3m/v four-circle diffractometer with graphite-monochromated Mo-K_α radiation. All calculations were performed using the SHELXT PLUS software package. The structure was solved by direct methods with the SHELXS-86 program and refined with the SHELX93 program.[25] Graphics were prepared using XPMA and ZORTEP.[26] An absorption correction (ψ scan, Δψ = 10°) was applied to all data. Atomic coordinates and anisotropic thermal parameters of the non-hydrogen atoms were refined by a full-matrix least-squares calculation. $C_{88}H_{78}Cl_4Co_{2.5}P_6O_4$ (· 0.8 Et_2O, 0.5 THF), M = 1674.6 g mol^{-1}, crystal dimensions 0.30 × 0.35 × 0.25 mm, tetragonal, Z = 4, space group $P4/n$ (no. 85), a = 23.773(6) Å, b = 23.776(6) Å, c = 16.301(4) Å, V = 9213(4) Å^3, $\rho_{calcd.}$ = 1.292 g cm^{-3}, T = 293 K, 2θ range = 2.4−54.0°, 25 reflections used for cell parameter refinement, scan speed 4.0−60.0° min^{-1}, 7672 measured reflections, 7198 unique reflections, 3637 observed reflections [$I > 2\,\sigma(I)$], 531 parameters, R_1 = 0.07, $R_w(F^2)$ = 0.224. Further details of the crystal structure determination may be obtained from the Fachinformationszentrum Karlsruhe, D-76344 Eggenstein-Leopoldshafen (Germany), on quoting the depository number CSD-410110.

2a−e · (BF_4): (a) Reduction with cobaltocene: To a dark green solution of the complexes **1a−e** · $(BF_4)_2$ in 20 mL of CH_2Cl_2 [**1a** · $(BF_4)_2$: 8.4 mg; **1b** · $(BF_4)_2$: 8.7 mg; **1c** · $(BF_4)_2$: 9.2 mg; **1d** · $(BF_4)_2$: 9.7 mg; **1e** · $(BF_4)_2$: 8.5 mg; 5 × 10^{-3} mmol] were added 0.5 mL of a Cp_2Co solution (10^{-2} M in CH_2Cl_2). The colour changed to bright blue. This solution was analysed by UV/Vis and EPR spectroscopy. For the low-temperature EPR measurements a mixture of 14 mL of THF and 6 mL of CH_2Cl_2 was used instead of 20 mL of CH_2Cl_2. − (b) Reduction with sodium isopropoxide: To a dark green solution of the complexes **1a−e** · $(BF_4)_2$ in 30 mL of CH_2Cl_2/10 mL of iPrOH [**1a** · $(BF_4)_2$: 16.8 mg; **1b** · $(BF_4)_2$: 17.4 mg; **1c** · $(BF_4)_2$: 18.4 mg; **1d** · $(BF_4)_2$: 19.4 mg; **1e** · $(BF_4)_2$: 17.0 mg; 1 × 10^{-2} mmol] was added 0.5 mL of a solution of iPrONa in CH_2Cl_2 (2 × 10^{-2} M) in 0.1-mL steps. After each addition, a UV/Vis spectrum was recorded. All attempts to isolate crystals from these solutions failed as they rapidly decompose on removing the solvent. Changing the solvents or the counter ions (BF_4^-, PF_6^-, BPh_4^-) was just as unsuccessful. − (c) Crystals of **2b$_2$** · $(CoCl_4)$: To a suspension of (triphos)CoCl (560 mg, 0.78 mmol) in THF (15 mL) was added a solution of 3,6-dichloro-2,5-dihydroxy-1,4-benzoquinone (81 mg, 0.39 mmol) in EtOH (5 mL). The (triphos)CoCl dissolved completely and the solution turned bright blue. After stirring for 30 min, the progress of the reaction was checked by UV/Vis spectroscopy and a solution of $NaBPh_4$ (133.5 mg, 0.39 mmol) in 5 mL of EtOH was added. After filtration and concentration of the solution to approximately 7−8 mL the solution was layered with Et_2O (10 mL). Bright blue crystals of **2b$_2$** · $(CoCl_4)$ suitable for X-ray-crystallographic analysis were obtained within one week.

3 · $(PF_6)_2$: A solution of $CoCl_2$ (130 mg, 1 mmol) in EtOH (15 mL) was added to a solution of the triphos ligand (624 mg, 1 mmol) in THF (15 mL). Addition of solid 2,3,6,7-tetrahydroxy-9,10-dimethylanthracene (135 mg, 0.5 mmol) resulted in a colour change to blue. After the addition of solid $NaPF_6$ (168 mg, 1 mmol), the solution was stirred for 1 h and concentrated to approximately 10 mL. The resulting precipitate was separated by filtration, washed with Et_2O (2 × 10 mL), EtOH (2 × 7 mL) and again with Et_2O (2 × 10 mL). To remove NaCl the blue powder was dissolved in CH_2Cl_2 and filtered through 2 cm of Kieselgur. Addition of Et_2O precipitated **3** · $(PF_6)_2$ in 59% yield (567 mg). − M.p. 240 °C (decomp.). − IR (CsI): $\tilde{\nu}$ = 829 (br., PF). − MS (FAB); m/z (%): 1778 (5) [M^+ + PF_6], 1632 (15) [M^+], 1027 (15) [M^+ − triphos − Co + Ph + 1], 950 (25) [M^+ − triphos − Co], 816 (10) [M^{2+}]. − UV/Vis (CH_2Cl_2): λ_{max} (ε) = 376 nm (9450 M^{-1} cm^{-1}), 404 (6360, sh), 610 (3540), 909 (19140), 1250 (1440, sh). − CV (CH_3CN): $E_{1/2}$ = −0.170 V (rev.), −0.355 V (rev.), +0.335 V (rev.), E_p = +0.935 (irr.). − ^{1}H NMR (CD_2Cl_2): 1.75 (br. s, 3 H, triphos-CH_3), 2.63 (br. s, 6 H, triphos-CH_2), 3.10 (s, 3 H, ligand-CH_3), 7.0−7.5 (m, 30 H, triphos-CH_{ar}), 9.2 (s, 2 H, ligand-CH). − ^{31}P NMR (CD_2Cl_2): 31.1 (s, 3 P, triphos-P), −144.2 (sept., 1 P, PF_6, $^1J_{PF}$ = 713 Hz). − $C_{98}H_{88}Co_2F_{12}O_4P_8$ (1922.3): calcd. for **3** · $(PF_6)_2$ · 0.5 · CH_2Cl_2 C 60.18, H 4.56; found C 60.06, H 5.04.

Reduction of 3 · $(PF_6)_2$ with Cobaltocene to Obtain 4 · (PF_6): To a blue solution of **3** · $(PF_6)_2$ (9.6 mg; 5 × 10^{-3} mmol) in CH_2Cl_2 (20 mL) was added 0.5 mL of a Cp_2Co solution (10^{-2} M in CH_2Cl_2). The colour changed to orange-brown. This solution was analysed by UV/Vis and EPR spectroscopy. Addition of a second equivalent of the Cp_2Co solution (0.5 mL) resulted in a colour change to yellow.

Oxidation of 3 · $(PF_6)_2$ with Ferrocenium Tetrafluoroborate to Obtain 5^{3+}: To a blue solution of **3** · $(PF_6)_2$ (9.6 mg; 5 × 10^{-3} mmol) in CH_2Cl_2 (20 mL) was added 0.5 mL of a $[Cp_2Fe](BF_4)$ solution (10^{-2} M in CH_2Cl_2). The colour changed to green. This solution was analysed by UV/Vis and EPR spectroscopy.

Acknowledgments

This work received support from the Deutsche Forschungsgemeinschaft, the Fonds der Chemischen Industrie and the Volkswagenstiftung.

[1] K. Heinze, S. Mann, G. Huttner, L. Zsolnai, *Chem. Ber.* **1996**, *129*, 1115−1122.
[2] K. Heinze, G. Huttner, P. Schober, *Eur. J. Inorg. Chem.* **1998**, 183−189.

[3] K. Heinze, G. Huttner, L. Zsolnai, A. Jacobi, P. Schober, *Chem. Eur. J.* **1997**, *3*, 732−743.
[4] L. Sacconi, F. Mani, *Transition Met. Chem. (N. Y.)* **1982**, *8*, 179−252, and references cited therein.
[5] R. Morassi, I. Bertini, L. Sacconi, *Coord. Chem. Rev.* **1973**, *11*, 343−402, and references cited therein.
[6] S. Beyreuther, J. Hunger, G. Huttner, S. Mann, L. Zsolnai, *Chem. Ber.* **1996**, *129*, 745−757.
[7] C. Mealli, S. Midollini, L. Sacconi, *Inorg. Chem.* **1975**, *14*, 2513−2521.
[8] K. Heinze, G. Huttner, L. Zsolnai, P. Schober, *Inorg. Chem.* **1997**, *36*, 5457−5469.
[9] K. Heinze, G. Huttner, unpublished results.
[10] C. A. Ghilardi, C. Mealli, S. Midollini, V. I. Nefedov, A. Orlandini, L. Sacconi, *Inorg. Chem.* **1980**, *19*, 2454−2462.
[11] K. Heinze, G. Huttner, L. Zsolnai, *Chem. Ber.* **1997**, *130*, 1393−1403.
[12] C. Bianchini, D. Masi, C. Mealli, A. Meli, G. Martini, F. Laschi, P. Zanello, *Inorg. Chem.* **1987**, *26*, 3683−3693.
[13] V. Körner, A. Asam, G. Huttner, L. Zsolnai, M. Büchner, *Z. Naturforsch.* **1994**, *49b*, 1183−1192.
[14] C. Creutz, *Prog. Inorg. Chem.* **1983**, *30*, 1−73.
[15] N. S. Hush, *Prog. Inorg. Chem.* **1967**, *8*, 391−444.
[16] Y.-D. Gao, K. B. Lipkowitz, F. A. Schulz, *J. Am. Chem. Soc.* **1995**, *117*, 11932−11938.
[17] P. W. Crawford, F. A. Schulz, *Inorg. Chem.* **1994**, *33*, 4344−4350.
[18] M. C. Zerner, *Reviews in Computational Chemistry*, VCH, Weinheim (Germany), **1991**, p. 313−365.
[19] As the phosphorus nuclei of the PF_6^- anion have a significantly lower relaxation rate than the phosphorus nuclei bound to the cobalt centre the relaxation delay between two pulses has to be increased (see ref.[3]). The ^{31}P-NMR spectra were measured with a relaxation delay time of 2.5 s.
[20] M. B. Robin, P. Day, *Adv. Inorg. Chem. Radiochem.* **1967**, *10*, 247−269.
[21] A. Muth, Diplomarbeit, University of Heidelberg, **1989**.
[22] P. Boldt, *Chem. Ber.* **1967**, *100*, 1270−1280.
[23] L. Sacconi, S. Midollini, *J. Chem. Soc., Dalton Trans.* **1972**, 1213−1216.
[24] J. Ellermann, J. F. Schindler, *Chem. Ber.* **1976**, *109*, 1095−1105.
[25] [25a] G. M. Sheldrick, *SHELXS 86*, *Program for Crystal Structure Solution*, University of Göttingen, **1986**. − [25b] G. M. Sheldrick, *SHELXL 93*, *Program for Crystal Structure Refinement*, University of Göttingen, **1993**.
[26] L. Zsolnai, G. Huttner, *XPMA*, *ZORTEP*, University of Heidelberg, **1998**; http://www.rzuser.uni-heidelberg.de/v54.xpm.html

Received September 23, 1998
[I98329]

N-Thiophosphorylated and *N*-Phosphorylated Iminophosphoranes [$R_3P{=}N{-}P(X)R'_2$; X = O, S] as Models for Dendrimers: Synthesis, Reactivity and Crystal Structures

Christophe Larré,[a] Bruno Donnadieu,[a] Anne-Marie Caminade,*[a] and Jean-Pierre Majoral*[a]

Keywords: Phosphorus / Ferrocenes / Phosphorylated iminophosphoranes / Dendrimers / Cations

Several $R_3P{=}N{-}P(X)R'_2$ and $Fe[C_5H_4Ph_2P{=}N{-}P(X)R'_2]_2$ derivatives (X = S, O) are readily obtained from Staudinger reactions between phosphanes and $N_3{-}P(X)R'_2$. The P=N–P=X groups are easily alkylated on the X atom with methyl or isopropyl triflates. The alkylation induces a lengthening of the P–X bond, as shown by X-ray diffraction studies. This corresponds to a weakening of the P–X bond which can be cleaved with $P(NMe_2)_3$ to yield [P=N–P:] linkages. The presence of tricoordinated phosphorus atoms opens the way to a versatile reactivity, including the reaction with alkyl iodides and functionalized azides. These molecules are good models for screening which types of reagents and reactions could be used with macromolecules possessing also P=N–P=X linkages, such as dendrimers.

Introduction

N-Thiophosphorylated iminophosphoranes are known since more than 40 years, but have only attracted a moderate interest up to now as illustrated by the relative small number of $R_3P{=}N{-}P(S)R'_2$ compounds already described[1] (approximately 100). However, we have recently demonstrated the great synthetic interest of the P=N−P=S linkage for the building of very complex hyperbranched nanosized macromolecules, namely dendrimers.[2] Furthermore, the P=N−P=S linkages included in phosphorus-containing dendrimers[3] display a versatile and chemoselective reactivity[4] which leads to the unprecedented grafting of various functional groups[5] or new branches[6] within the dendritic architecture when and where desired.

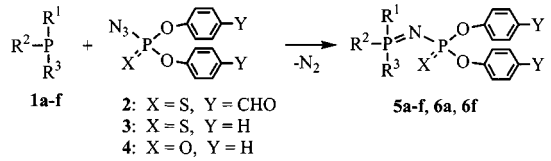
The chemistry of dendrimers is fascinating but generally suffers from two drawbacks: the synthesis requires multistep procedures which are time-consuming, and the reactivity (as well as the synthesis) necessitates to use only reactions with quantitative yields. Thus, it is highly desirable to have models for dendrimers, in order to study the reactivity on small molecules easy to synthesize and to characterize, and to choose the type of reactions and reagents which could be used later with dendrimers. In this paper, we describe the synthesis of various *N*-thiophosphorylated iminophosphoranes, their reactivity toward strong electrophiles such as alkyl triflates, their desulfurization reactions leading to [P=N−P:] linkages, and Staudinger reactions of these linkages with functionalized azides. A few *N*-phosphorylated iminophosphoranes (P=N−P=O linkages) are also described to be compared with their thiophosphorylated analogues. The structure of four derivatives of ferrocene possessing two P=N−P=X or two [P−N−P−X−Me]$^+$ (X = S, O) groups determined by X-ray diffraction is also presented.

[a] Laboratoire de Chimie de Coordination, CNRS,
205, route de Narbonne, F-31077 Toulouse cedex 4, France
Fax: (internat.) + 33-5/61553003
E-mails: majoral@lcc-toulouse.fr or caminade@lcc-toulouse.fr

Results and Discussion

Syntheses

The method of synthesis we have used to obtain the P=N−P=X (X = S, O) linkages is the Staudinger reaction between phosphanes **1a−f** and phosphorylated azides **2−4** (Scheme 1). In all cases, the reaction proceeds rapidly at room temperature with evolution of nitrogen as sole by-product, and leads to compounds **5** (X = S) and **6** (X = O) in quantitative yields as crude products and in very good yields after work up, with the exception of compound **5d** which is isolated only in 70% yield. This lower yield is presumably due to the presence of two C≡C groups in compound **1d**, which are known to undergo cycloaddition reac-



1a-f **2**: X = S, Y = CHO; **3**: X = S, Y = H; **4**: X = O, Y = H **5a-f, 6a, 6f**

Compounds **5** and **6**	R^1	R^2	R^3	X	Y
5a	Ph	Ph	Ph	S	CHO
5b	*p*Cl-C_6H_4	*p*Cl-C_6H_4	*p*Cl-C_6H_4	S	CHO
5c	CH_2CH_2CN	CH_2CH_2CN	CH_2CH_2CN	S	CHO
5d	tBu	C≡C-Ph	C≡C-Ph	S	CHO
5e	Ph			S	H
5f	Me	Ph	Ph	S	H
6a	Ph	Ph	Ph	O	H
6f	Me	Ph	Ph	O	H

Scheme 1. Synthesis of *N*-(thio)-phosphorylated iminophosphoranes

 © WILEY-VCH Verlag GmbH, D-69451 Weinheim, 1999 1434−1948/99/0404−0601 $ 17.50+.50/0

tions with azides,[7] lowering the amount of the desired product **5d**.

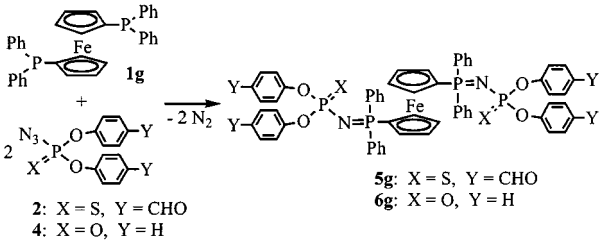
The occurrence of the Staudinger reaction is characterized in the ^{31}P-NMR spectra by the appearance of a system of two doublets, with $^2J_{PP} \approx 30$ Hz for all compounds except for **5d** (Table 1). The chemical shift is $\delta \approx 51$ for the P=S groups, and $\delta \approx -7$ for the P=O groups, for all compounds. The chemical shift of the $R^1R^2R^3P{=}N$ groups strongly depends on the $R^1R^2R^3$ substituents linked to this phosphorus atom, but is almost insensitive to the presence of sulfur or oxygen double bonded to the other phosphorus atom, as shown by the comparison between **5a** [X = S; δ(P=N) = 14.9] and **6a** [X = O; δ(P=N) = 13.7].

Table 1. ^{31}P-NMR data

	Compounds **5**, **6**			Compounds **7**–**11**		
	δ(P=N)	δ(P=X)	$^2J_{PP}$	δ(P=N)	δ(P=X)	$^2J_{PP}$
5a, **7a**	14.9	50.5	30[a]	22.8	23.4	20[a]
9a				22.4*	21.5*	17[a]
5b, **7b**	12.9	50.5	32[b]	26.2	31.4	23[b]
5c, **7c**	30.5	50.5	28[b]	45.7	28.9	10[b]
5d, **7d**	−8.9	52.2	6[a]	−4.7	28.5	5[a]
5e, **7e**	47.9	52.6	29[a]	53.7	24.6	12[a]
5f, **7f**	15.3	52.8	32[a]	24.2*	23.2*	20[a]
5g, **7g**	16.1	49.2	32[a]	25.4	23.9	23[a]
6a, **8a**	13.7	−7.9	32[a]	21.8	−10.0	35[a]
10a				21.7	−12.1	21[a]
6f, **8f**	15.2	−6.2	31[a]	24.2	−9.3	32[a]
11f				23.2	−18.6	33[a]
6g, **8g**	14.5	−8.6	37[a]	25.2	−9.7	35[a]

[a] In $CDCl_3$. – [b] In CD_3COCD_3. – * In these cases, the assignment of the chemical shift to P=N or P–S–R is ambiguous.

Analogous reactions applied to the 4,4′-bis(diphenylphosphanyl)ferrocene **1g** and compounds **2** and **4** lead to the quantitative formation of derivatives **5g** (X = S, Y = CHO) and **6g** (X = O, Y = H) possessing two P=N–P=X linkages (Scheme 2). These compounds display characteristic ^{31}P-NMR data (Table 1).



Scheme 2. Synthesis of bis[*N*-(thio)-phosphorylated iminophosphoranyl]ferrocenes

The structure of both compounds was also determined by X-ray diffraction studies (Table 2). Selected bond lengths and bond angles are gathered in Table 3. Figures 1 and 2 show the molecular structure of compounds **5g** and **6g**, respectively. The dihedral angle between the substituents of the Cp rings is 142.73° for compounds **5g** and 180° for compound **6g**. This position favors a large distance between the "branches", thus compound **5g** has been used as a tetrafunctional core for the synthesis of dendrimers.[8] The P=N–P moieties of the P=N–P=X linkage is very similar for both compounds **5g** and **6g**. Furthermore, the P–N bond lengths are almost equal {*d*[P(1)–N(1)] = 1.559(4) Å and *d*[N(1)–P(2)] = 1.569(4) Å for **5g**; 1.568(2) Å and 1.578(2) Å, respectively, for **6g**}. The P=S [1.918(2) Å] and P=O [1.450(2) Å] bond lengths are classical.

Reactivity

A few alkylations of the sulfur atom of P=N–P=S linkages have already been reported,[9] for instance with methyl iodide,[9a] but this reagent does not react neither with compounds **5**, nor with compounds **6**, so stronger electrophiles are needed. For this purpose, methyl trifluoromethanesulfonate is first used as alkylating agent. The reaction carried out with compounds **5a–g**, **6a**, **6f**, and **6g** leads immediately, and in quantitative yield except for compound **7d**, to the formation of cationic compounds possessing one (**7a–f**, **8a**, **8f**) or two (**7g**, **8g**) $[P{-}N{=}P{-}X{-}Me]^+$ linkages (Scheme 3).

Two different behaviors are observed in the ^{31}P-NMR spectra, depending on the nature of the X atom. The alkylation of the thiophosphoryl groups induces a large shielding of the signal corresponding to the P=S group, from $\delta \approx 51$ to $\delta \approx 25$, while the signal corresponding to the P=N group is deshielded (Table 1). In several cases, the chemical-shift values corresponding to the P=N and P–S–Me groups are very close, but their attribution is unambiguous, on the basis of ^{31}P-NMR spectra with proton couplings, except for compound **7f**. On the other hand, the alkylation of the phosphoryl groups induces only a slight shielding of the signal corresponding to the P=O groups ($\Delta\delta_{max} = 3$) and a deshielding of the signal corresponding to the P=N groups ($\Delta\delta \approx 10$). The value of the $^2J_{PP}$ coupling constant is lowered when X = S (for the transformation **5** → **7**), and slightly increased when X = O (**6** → **8**) (Table 1).

To ascertain the occurrence of the alkylation reaction on the sulfur or oxygen and not on the nitrogen atom or on the aldehyde groups, the structure of compounds **7g** and **8g** was determined by X-ray diffraction (Table 2). Figures 3 and 4 show the molecular structure of the cationic moieties of compounds **7g** and **8g**, respectively. These drawings confirm without any ambiguity that alkylation took place on the sulfur (**7g**) and oxygen atom (**8g**). Selected bond lengths and bond angles for both compounds are gathered in Table 3. The alkylation induces in both cases a lengthening of the P=N [P(1)–N(1)], P=X [P(2)–S(2) or P(2)–O(3)], and O–C(Ar) bond lengths and a shortening of the N–P [N(1)–P(2)] and P–O [P(2)–O(1) and P(2)–O(2)] bond lengths; the six P–O bond lengths are equivalent for compound **8g**. All these phenomena, as well as the deshielding observed for the signal of the P=N groups in the ^{31}P-NMR spectra, indicate that the positive charge is partly localized on this phosphorus atom.

Other triflates can react with the P=N–P=X linkages, for instance isopropyl trifluoromethanesulfonate. The reaction proceeds in the same conditions than with methyl triflate, to afford compounds **9a** and **10a**, from **5a** and **6a**,

Table 2. Crystal data for compounds **5g**, **6g**, **7g** and **8g**

	5g	**6g**	**7g**	**8g**
Emp. formula	$C_{62}H_{48}N_2O_8P_4S_2Fe$	$C_{58}H_{48}N_2O_6P_4Fe$	$C_{64}H_{54}N_2O_8P_4S_2Fe[CF_3SO_3]_2 \cdot 3/2CH_2Cl_2$	$C_{60}H_{54}N_2O_6P_4Fe[CF_3SO_3]_2$
Mol. mass	1192.94	1048.76	1648.52	1376.96
Cryst. system	monoclinic	triclinic	triclinic	monoclinic
Space group	*C*2/*c*	$P\bar{1}$	*P*1	*C*2/*c*
a [Å]	14.420(3)	9.463(2)	10.855(2)	16.844(2)
b [Å]	13.994(4)	10.945(2)	11.091(2)	12.520(2)
c [Å]	28.927(5)	11.961(3)	16.416(2)	29.807(3)
α [°]		88.35(2)	75.41(2)	
β [°]	103.70(2)	86.20(2)	84.91(2)	97.415(9)
γ [°]		89.21(2)	75.84(2)	
V [Å^3]	5673(3)	1235(2)	1854(2)	6233(2)
Z	4	1	1	4

Table 3. Selected bond lengths and bond angles for compounds **5g**, **6g**, **7g** and **8g**

Bond lengths [Å] Bond angles [°]	**5g**	**6g**	**7g**	**8g**
d[P(1)−N(1)]	1.559(4)	1.568(2)	1.60(1)	1.583(4)
d[P(2)−N(1)]	1.569(4)	1.578(2)	1.53(1)	1.535(4)
d[P(2)−S(2)]	1.918(2)		2.045(4)	
d[P(2)−O(3)]		1.450(2)		1.547(4)
d[P(2)−O(1)]	1.630(3)	1.604(2)	1.587(8)	1.553(4)
d[P(2)−O(2)]	1.632(3)	1.607(2)	1.564(9)	1.551(4)
d[O(1)−C(211)]	1.373(6)	1.404(2)	1.38(2)	1.423(6)
d[O(2)−C(221)]	1.389(6)	1.396(2)	1.42(2)	1.421(6)
d[S(2)−C(11)]			1.88(2)	
d[O(3)−C(6)]				1.447(7)
P(1)−N(1)−P(2)	137.2(3)	136.8(1)	140.7(6)	137.5(3)
N(1)−P(2)−S(2)	121.9(2)		113.6(4)	
N(1)−P(2)−O(3)		120.43(9)		117.7(2)
Dihedral angle between the substituents of the Cp rings [°]	142.73	180	148.87	116.95

respectively (Scheme 4, Table 1). An analogous behavior is observed with trimethylsilyl triflate. The oxophilicity of silicon induces the formation of the cationic compound **11f** from **6f** (Scheme 5). The ^{31}P-NMR spectrum displays the expected shielding of the signal corresponding to the PO groups from δ = −6.2 to −18.6 (Table 1). However, it must be noted that this compound is much more sensitive to moisture than the corresponding methylated analogue, thus for practical purposes, the use of trimethylsilyl triflate has not been extended to other compounds, and only the reactivity of cationic compounds **7** and **8** has been explored.

In fact, we have focused our attention on the reactivity of compounds **7**, because the methylation reaction of compounds **5** is more easily monitored by ^{31}P-NMR spectroscopy than that of compounds **6**. The lengthening of the P=S bond after methylation [1.918(2) Å for **5g**, 2.034(5) and 2.040(5) Å for **7g**] should induce a weakening of this bond which could be cleaved, leading to the formation of [P=N−P:] linkages incorporating a tricoordinated phosphorus atom. First experiments are conducted with compound **7f** which is the best model for dendrimers. The desulfurization reaction occurs easily at room temperature when tris(dimethylamino)phosphane is added to a solution of **7f** in CH_2Cl_2.[10] The reaction proceeds with a transfer of the S−Me$^+$ group from **7f** to $P(NMe_2)_3$, leading to compound **12f** and $[MeS-P(NMe_2)_3]^+$ (Scheme 6).

The reaction is monitored by ^{31}P-NMR spectroscopy, which shows the appearance of two doublets at δ = 143.9 (P:) and 9.9 (P=N) ($^2J_{PP}$ = 32 Hz) for **12f** and one singlet at δ = 68 for $[MeS-P(NMe_2)_3]^+$. These data indicate that only the P−S bond is cleaved, and not the P−O or P−N bonds. Compound **12f** is very sensitive toward oxidation, therefore it is not really isolated but only cleared of $[MeS-P(NMe_2)_3][CF_3SO_3]$. The presence of a tricoordinated phosphorus atom in compound **12f** should lead to a versatile reactivity. For instance, compound **12f** can react with electrophiles such as allyl iodide (Scheme 6). The formation of the phosphonium salt **13f** is characterized by ^{31}P-NMR spectroscopy, with the appearance of two doublets at δ = 27.3 and 28.9 ($^2J_{PP}$ = 20 Hz). This reaction, which allows the grafting of functional groups, has been extended to the reactivity of the internal layers of dendrimers.[5b]

Compound **12f** also reacts with azides, such as 4-azidophenyl isothiocyanate. The Staudinger reaction occurs readily to give compound **14f**, characterized in the ^{31}P-NMR spectrum by the presence of two doublets at δ = 15.3 (P=N) and −7.7 (N−P=N) ($^2J_{PP}$ = 16 Hz). This compound can be isolated to be characterized also by ^{1}H- and ^{13}C-NMR spectroscopy, but it decomposes within a few days when left in solution, to give compound **5f** as the sole phosphorus-containing compound. The decomposition probably proceeds by an aza Wittig reaction between the P=N and

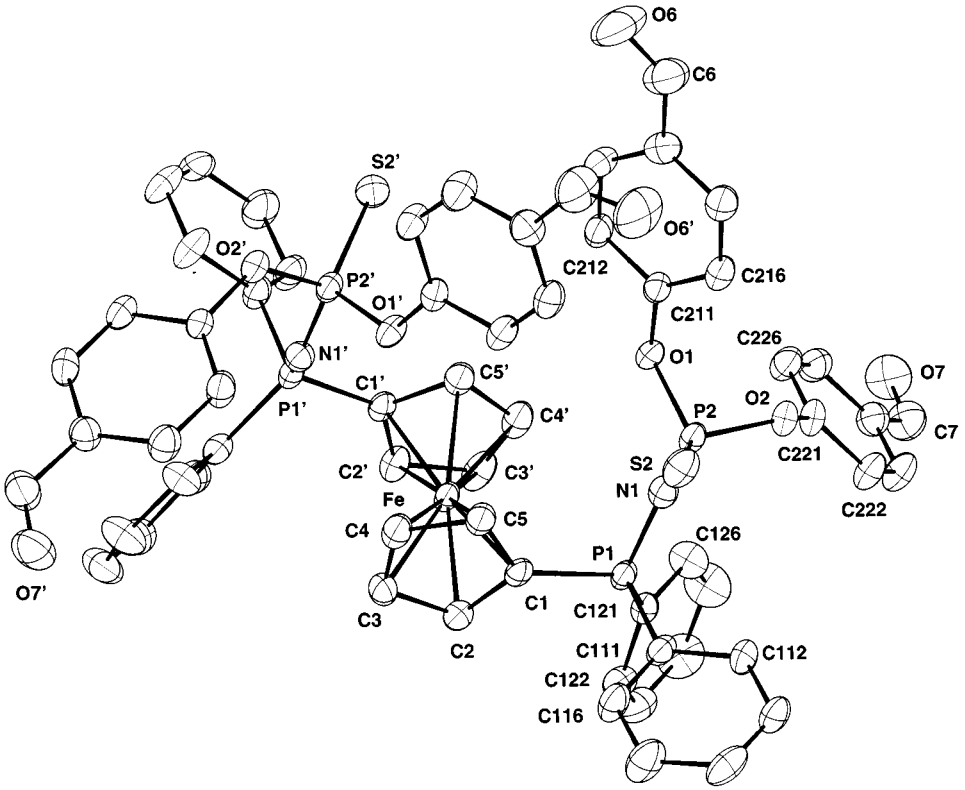


Figure 1. Molecular structure of compound **5g**

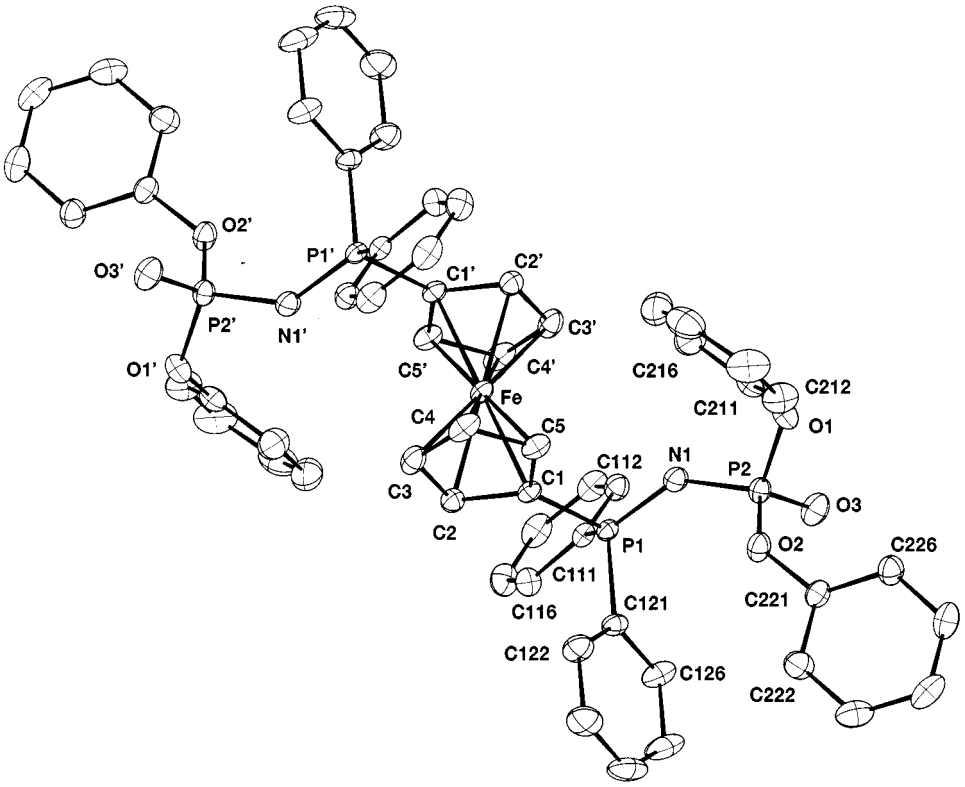
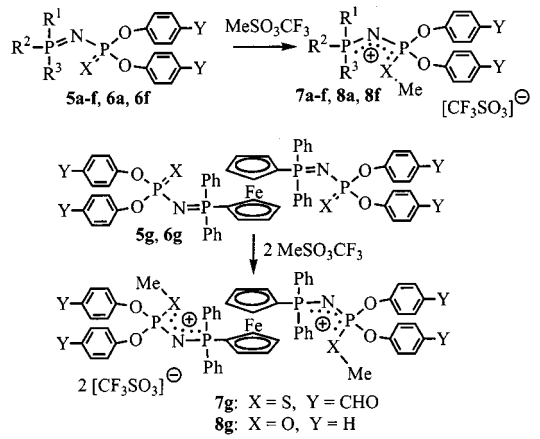


Figure 2. Molecular structure of compound **6g**

C=S bonds. This reaction is presumably intermolecular; indeed, the intramolecular reaction is unlikely from a geometric point of view. Furthermore, the use of the same azide in the internal layers of dendrimers gives stable com-



Scheme 3. Methylation of P=N−P=X linkages

(δ = 17.9, $^2J_{PP}$ = 23 Hz, *P*=N−P=N−P=S; δ = 45.9, $^2J_{PP}$ = 63 Hz, P=N−P=N−*P*=S) and one doublet of doublet (δ = −14.3, P=N−*P*=N−P=S) in the ^{31}P-NMR spectrum. The sequence of reactions **5g** → **7g** → **12g** → **15g** which allows the grafting of aldehyde groups is of crucial importance for the growing of new branches within a dendritic framework.[6]

The P=S group of the P=N−P=N−P=S linkage possesses the same properties than those included in P=N−P=S linkages. Indeed, methylation with $MeSO_3CF_3$ occurs on the sulfur atom, as shown by the large shielding of the doublet corresponding to the P=S groups in the ^{31}P-NMR spectrum from δ = 45.9 ($^2J_{PP}$ = 63.5 Hz) for **15g** to δ = 20.0 ($^2J_{PP}$ = 51 Hz) for **16g**. The slight deshielding observed for the doublet corresponding to the *P*=N−P=N−P=S groups from δ = 17.9 ($^2J_{PP}$ = 23.2 Hz) for **15g** to δ = 21.5

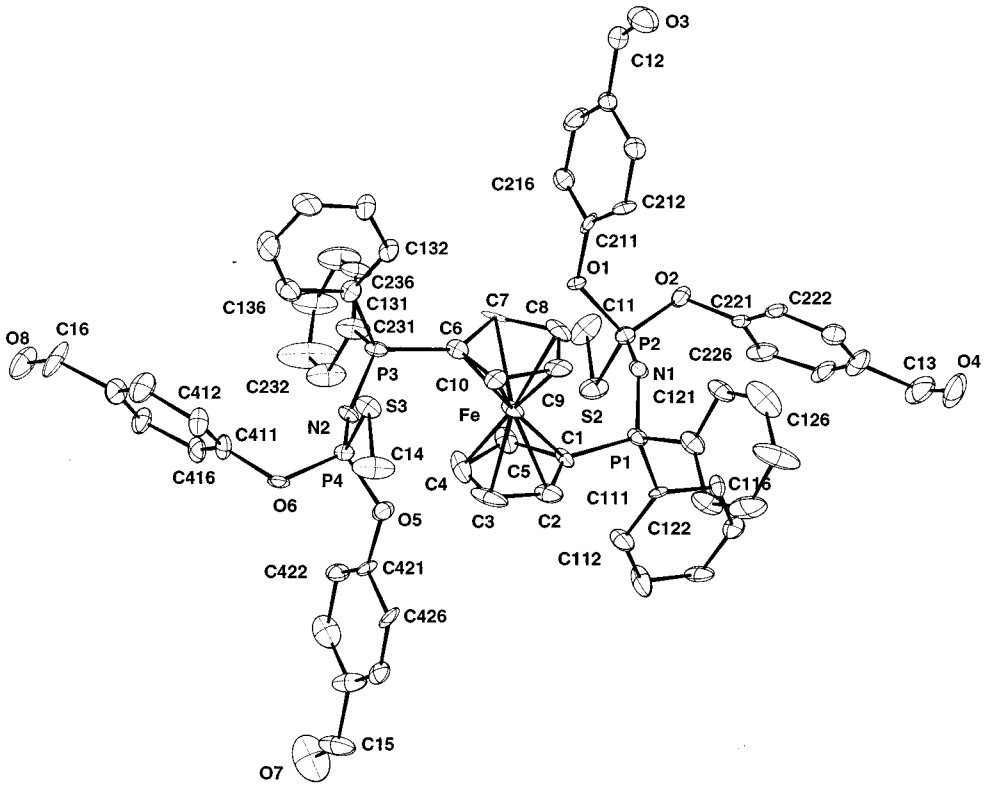


Figure 3. Molecular structure of compound **7g**; the anionic counterion is omitted for clarity

pounds which do not decompose within several days in solution. One can presume that the P=N and C=S bonds of the internal layers of two molecules of dendrimer cannot interact for steric reasons, and that the reaction between two branches of one dendrimer is also unlikely for geometric and topographic reasons.[5b]

The desulfurization reaction can be applied also to the dicationic ferrocene derivative **7g**, leading to the formation of compound **12g** (Scheme 7). The Staudinger reaction of two equivalents of the azide **2** with the ferrocene derivative **12g** affords compound **15g** in quantitative yield. The formation of both P=N−P=N−P=S linkages induces the appearance of a very characteristic system of two doublets ($^2J_{PP}$ = 30 Hz) for **16g**, indicates a delocalization of the positive charge all along this linkage. The chemical shift of the doublet of doublet corresponding to P=N−*P*=N−P=S is almost insensitive to this reaction (δ = −14.3 for **15g**, δ = −16.9 for **16g**).

Conclusion

Various compounds possessing P=N−P=X (X = S, O) linkages have been prepared and their reactivity toward various electrophiles has been tested, leading in all cases to the alkylation of the X atom of this linkage, as shown by

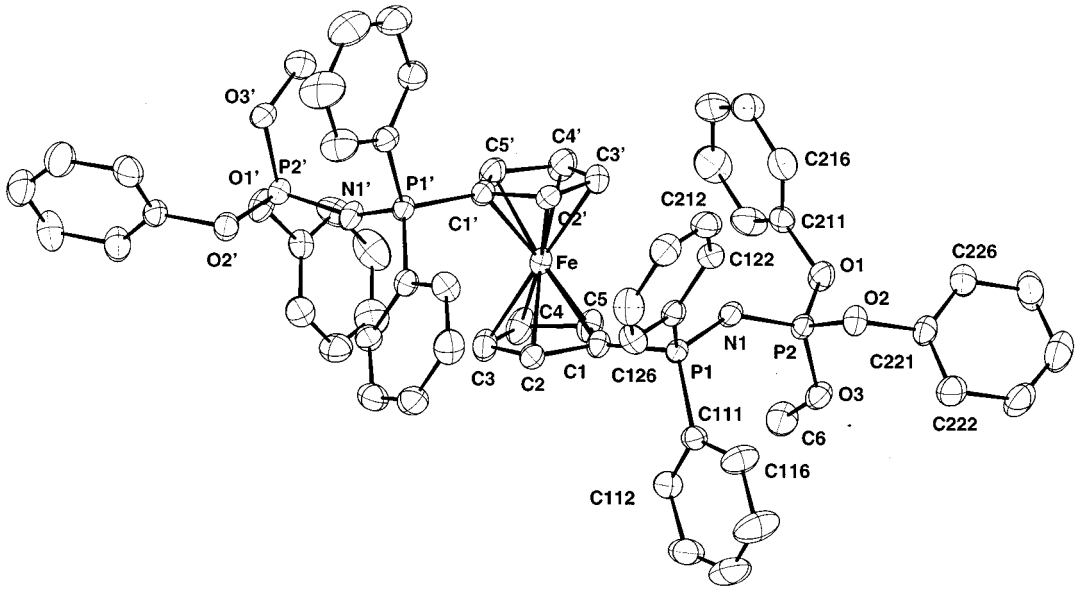
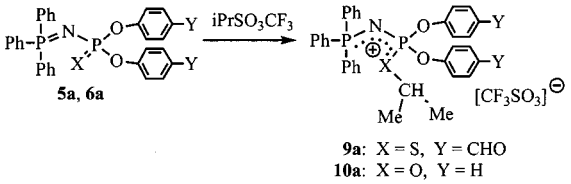
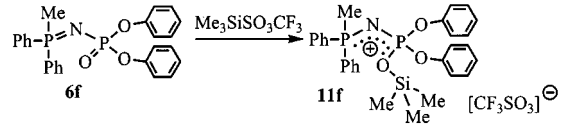


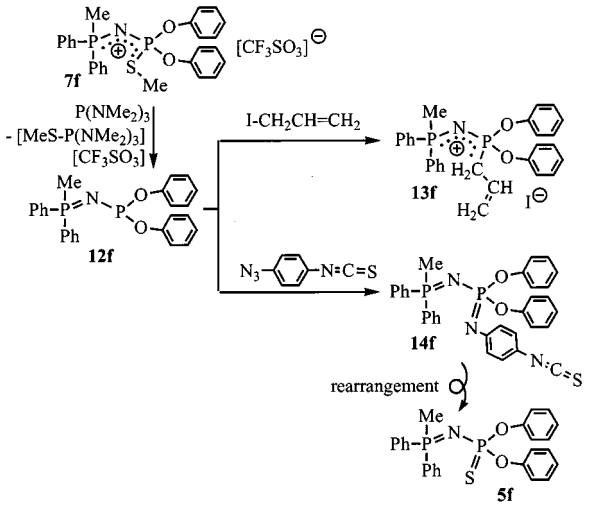
Figure 4. Molecular structure of compound **8g**; the anionic counterion is omitted for clarity



Scheme 4. Alkylation of P=N−P=X lnkage with $iPr_2SO_3CF_3$

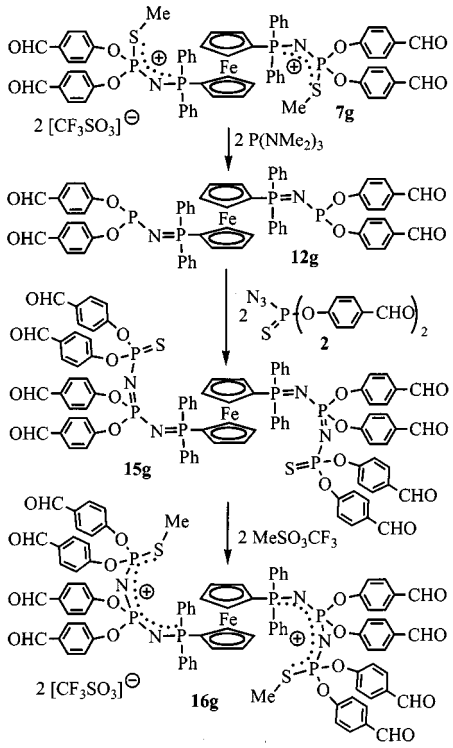


Scheme 5. Alkylation of P=N−P=O linkage with $Me_3SiSO_3CF_3$



Scheme 6. Desulfurization of a P−N−P−S−Me linkage and subsequent reactions

^{31}P-NMR and X-ray diffraction studies. These compounds, particularly $Ph_2MeP{=}N{-}P(S)(OPh)_2$ (**5f**), and $Fe[C_5H_4P\text{-}Ph_2{=}NP(S)(OC_6H_4CHO)_2]_2$ (**5g**) are interesting models to check what type of reactions and reagents could be applied later to dendrimers possessing also P=N−P=S linkages. In this perspective, the desulfurization leading to tricoordinated phosphorus atoms has a great synthetic interest, and has opened the way to a very original field of the chemistry of dendrimers: the grafting of various functional groups and branches in the internal layers of dendrimers after their construction.[5][6]



Scheme 7. Desulfurization of compound **7g** and subsequent reactions

Experimental Section

General: All manipulations were carried out with standard high-vacuum and dry-argon techniques. – ^{1}H-, ^{13}C-, ^{31}P-, and ^{19}F-NMR spectra were recorded with Bruker AC200, AC250 or AMX 400 spectrometers. References for NMR chemical shifts are: $SiMe_4$ for ^{1}H and ^{13}C NMR, 85% H_3PO_4 for ^{31}P NMR, CF_3COOH for ^{19}F NMR. The numbering used for NMR assignments is depicted in Figure 5. – Melting points are uncorrected. – Compounds $N_3P(S)(OC_6H_4CHO)_2$,[11] *t*BuP(C≡CPh)$_2$,[11] Ph(C_4H_6P)[12] and CF_3SO_3*i*Pr,[13] were synthesized according to published procedures. – CF_3SO_3*i*Pr was freshly prepared each time.

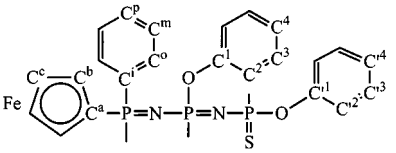


Figure 5. Numbering used for NMR

General Procedure for 5a, 5b, 5d, 5e, 5f, 6a, 6f: To a solution of 3 mmol of compound **2**, **3**, or **4** in THF (10 mL) was added at room temperature a solution of 3 mmol of phosphane **1a,b,d–f** in THF (5 mL). The resulting solution was stirred at room temperature (or at 55°C for **5d**) until the evolution of nitrogen ceases. The solution was concentrated to dryness under vacuum. The residue was washed with ether, then with pentane to afford **5a**, **5b**, **5f**, **6a**, **6f** as powders and **5d**, **5e** as oils.

Synthesis of Compound 5c: The procedure is analogous to the previous one, using CH_3CN instead of THF. Compound **5c** was isolated as an oil.

General Procedure for 5g and 6g: To a solution of 3 mmol of compound **2** or **4** in THF (10 mL) was added at room temperature a solution of 1.5 mmol of 4,4′-bis(diphenylphosphanyl)ferrocene **1g** in THF (10 mL). The resulting solution was stirred at room temperature until the evolution of nitrogen ceased. The solution was concentrated to dryness under vacuum. The residue was washed with ether, then with pentane to give **5g**, **6g** as orange powders. Crystallization at −30°C in CH_2Cl_2 for **5g** and in CH_2Cl_2/pentane (1:1) for **6g** afforded single crystals suitable for X-ray diffraction.

Compound 5a: 97% yield, white powder, m.p. 131°C. – ^{31}P{^{1}H} NMR ($CDCl_3$): δ = 14.9 (d, $^2J_{PP}$ = 30.0 Hz, P=N), 50.1 (d, $^2J_{PP}$ = 30.0 Hz, P=S). – ^{1}H NMR ($CDCl_3$): δ = 7.27–7.78 (m, 23 H, C_6H_4, C_6H_5), 9.90 (s, 2 H, CHO). – ^{13}C{^{1}H} NMR ($CDCl_3$): δ = 121.8 (d, $^3J_{CP}$ = 5.5 Hz, C^2), 128.0 (dd, $^1J_{CP}$ = 106.5 Hz, $^3J_{CP}$ = 3.8 Hz, C^i), 128.5 (d, $^3J_{CP}$ = 13.0 Hz, C^m), 130.9 (s, C^3), 132.4 (d, $^2J_{CP}$ = 10.5 Hz, C^o), 132.6 (br. s, C^4, C^p), 156.6 (d, $^2J_{CP}$ = 9.6 Hz, C^1), 190.8 (s, CHO). – IR (KBr): $\tilde{\nu}$ = 1701 cm^{-1} (C=O). – $C_{32}H_{25}N_1O_4P_2S$ (581.6): calcd. C 66.09, H 4.33, N 2.41; found C 66.30, H 4.49, N 2.36.

Compound 5b: 95% yield, white powder, m.p. 102°C. – ^{31}P{^{1}H} NMR (CD_3COCD_3): δ = 12.9 (d, $^2J_{PP}$ = 32.0 Hz, P=N), 50.5 (d, $^2J_{PP}$ = 32.0 Hz, P=S). – ^{1}H NMR (CD_3COCD_3): δ = 7.56–8.04 (m, 20 H, C_6H_4), 10.10 (s, 2 H, CHO). – ^{13}C{^{1}H} NMR (CD_3COCD_3): δ = 122.2 (d, $^3J_{CP}$ = 5.0 Hz, C^2), 129.3 (d, $^3J_{CP}$ = 14.0 Hz, C^m), 131.0 (s, C^3), 133.2 (s, C^4), 134.0 (dd, $^1J_{CP}$ = 58.3 Hz, $^3J_{CP}$ = 12.0 Hz, C^i), 134.4 (d, $^2J_{CP}$ = 12.5 Hz, C^o), 139.4 (d, $^4J_{CP}$ = 4.8 Hz, C^p), 156.5 (d, $^2J_{CP}$ = 8.5 Hz, C^1), 190.7 (s, CHO). – IR (KBr): $\tilde{\nu}$ = 1696 cm^{-1} (C=O). – $C_{32}H_{22}Cl_3N_1O_4P_2S$ (684.9): calcd. C 56.09, H 3.21, N 2.04; found C 56.39, H 3.31, N 1.97.

Compound 5c: 94% yield, white viscous oil. – ^{31}P{^{1}H} NMR (CD_3COCD_3): δ = 30.5 (d, $^2J_{PP}$ = 28.0 Hz, P=N), 50.5 (d, $^2J_{PP}$ = 28.0 Hz, P=S). – ^{1}H NMR (CD_3COCD_3): δ = 2.68–3.00 (m, 12 H, CH_2–CH_2), 7.57 (m, 4 H, C_6H_4), 8.97 (m, 4 H, C_6H_4), 10.0 (s, 2 H, CHO). – ^{13}C{^{1}H} NMR (CD_3COCD_3): δ = 21.5 (d, $^1J_{CP}$ = 3.0 Hz, *C*H$_2$P), 22.7 (s, *C*H$_2$CH$_2$P), 118.7 (s, C≡N), 122.1 (d, $^3J_{CP}$ = 4.7 Hz, C^2), 131.1 (br. s, C^3), 133.3 (s, C^4), 156.2 (d, $^2J_{CP}$ = 8.4 Hz, C^1), 191.0 (s, CHO). – IR (THF): $\tilde{\nu}$ = 2210 (C≡N), 1701 (C=O) cm^{-1}. – $C_{23}H_{22}N_4O_4P_2S$ (512.5): calcd. C 53.91, H 4.33, N 10.93; found C 53.67, H 4.43, N 10.81.

Compound 5d: 70% yield, yellow viscous oil. – ^{31}P{^{1}H} NMR ($CDCl_3$): δ = −8.9 (d, $^2J_{PP}$ = 6.0 Hz, P=N), 52.2 (d, $^2J_{PP}$ = 6.0 Hz, P=S). – ^{1}H NMR ($CDCl_3$): δ = 1.30 (d, $^3J_{HP}$ = 21.0 Hz, 9 H, CH_3), 7.24–7.94 (m, 18 H, C_6H_4, C_6H_5), 9.83 (s, 2 H, CHO). – ^{13}C{^{1}H} NMR ($CDCl_3$): δ = 22.7 (d, $^2J_{CP}$ = 1.9 Hz, CH_3), 34.1 (dd, $^1J_{CP}$ = 103.1 Hz, $^3J_{CP}$ = 7.0 Hz, *C*-CH_3), 76.7 (d, $^1J_{CP}$ = 186.9 Hz, ≡C–P), 106.4 (d, $^2J_{CP}$ = 31.5 Hz, *C*≡C–P), 118.7 (d, $^3J_{CP}$ = 4.4 Hz, C^i), 121.9 (d, $^3J_{CP}$ = 5.1 Hz, C^2), 128.4 (s, C^m), 130.8 (s, C^3), 131.4 (s, C^p), 132.4 (br. s, C^4, C^o), 156.5 (d, $^2J_{CP}$ = 8.3 Hz, C^1), 190.7 (s, CHO). – IR (THF): $\tilde{\nu}$ = 2170 (C≡C), 1701 (C=O) cm^{-1}. – $C_{34}H_{29}N_1O_4P_2S$ (609.6): calcd. C 66.99, H 4.79, N 2.30; found C 66.93, H 4.59, N 2.24.

Compound 5e: 90% yield, white viscous oil. – ^{31}P{^{1}H} NMR ($CDCl_3$): δ = 47.9 (d, $^2J_{PP}$ = 29.0 Hz, P=N), 52.6 (d, $^2J_{PP}$ = 29.0 Hz, P=S). – ^{1}H NMR ($CDCl_3$): δ = 2.34 (md, $^2J_{HP}$ = 136.0 Hz, 2 H, CH_2P), 2.73 (m, 2 H, CH_2CH$_2$P), 6.14 (ddt, $^3J_{HP}$ = 26.7 Hz, $^3J_{HH}$ = 8.1 Hz, $^3J_{HH}$ = 1.7 Hz, 1 H, C*H*=CH–P), 7.08 (ddt, $^2J_{HP}$ = 45.9 Hz, $^3J_{HH}$ = 8.1 Hz, $^4J_{HH}$ = 1.3 Hz, 1 H, =CH–P), 7.27–7.81 (m, 13 H, C_6H_4, C_6H_5), 9.80 (s, 2 H, CHO). – ^{13}C{^{1}H} NMR ($CDCl_3$): δ = 22.2 (d, $^1J_{CP}$ = 68.9 Hz, CH_2P), 30.5 (d, $^2J_{CP}$ = 9.5 Hz, *C*H$_2$CH$_2$P), 121.4 (d, $^3J_{CP}$ = 4.8 Hz, C^2), 121.6 (d, $^1J_{CP}$ = 90.9 Hz, =CH–P), 128.4 (d, $^3J_{CP}$ = 13.5 Hz, C^m), 128.6 (dd, $^1J_{CP}$ = 110.3 Hz, $^3J_{CP}$ = 9.7 Hz, C^i), 130.2 (d, $^2J_{CP}$ = 11.7 Hz, C^o), 130.7 (s, C^3), 132.1 (s, C^4), 132.2 (s, C^p), 154.9 (d, $^2J_{CP}$ = 23.8 Hz, *C*H=CH-P), 156.1 (d, $^2J_{CP}$ = 9.0 Hz, C^1), 190.4 (s, CHO). – IR (THF): $\tilde{\nu}$ = 1701 cm^{-1} (C=O). – $C_{24}H_{21}N_1O_4P_2S_1$ (481.5): calcd. C 59.87, H 4.40, N 2.91; found C 60.01, H 4.55, N 2.85.

Compound 5f: 88% yield, white viscous oil. – ^{31}P {^{1}H} NMR (THF): δ = 15.5 (d, $^2J_{PP}$ = 32.1 Hz, P=N), 53.0 (d, $^2J_{PP}$ = 32.1 Hz, P=S). – ^{1}H NMR ($CDCl_3$): δ = 2.20 (d, $^3J_{HP}$ = 13.3 Hz, 3 H, CH_3), 7.00–7.65 (m, 20 H, C_6H_5). – ^{13}C {^{1}H} NMR ($CDCl_3$): δ 14.6 (d, $^2J_{CP}$ = 67.9 Hz, CH_3), 121.7 (d, $^3J_{CP}$ = 4.3 Hz, C^2), 124.2 (s, C^4), 128.8 (d, $^3J_{CP}$ = 13.1 Hz, C^m), 129.1 (s, C^3), 130.6 (dd, $^1J_{CP}$ = 108.0 Hz, $^3J_{CP}$ = 5.1 Hz, C^i), 131.1 (d, $^2J_{CP}$ = 10.9 Hz, C^o), 132.3 (d, $^4J_{CP}$ = 3.5 Hz, C^p), 152.1 (d, $^2J_{CP}$ = 8.7 Hz, C^1). – $C_{25}H_{23}NO_2P_2S$ (463.5): calcd. C 64.79, H 5.00, N 3.02; found C 64.98, H 4.95, N, 2.97.

Compound 5g: 97% yield, orange powder, m.p. 211°C. – ^{31}P {^{1}H} NMR ($CDCl_3$): δ = 16.1 (d, $^2J_{PP}$ = 32.0 Hz, P=N), 49.2 (d, $^2J_{PP}$ = 32.0 Hz, P=S). – ^{1}H NMR ($CDCl_3$): δ = 4.35 (dd, $^3J_{HH}$ = 1.8 Hz, $^3J_{HP}$ = 3.7 Hz, 4 H, C^{b}H), 4.55 (dd, $^3J_{HH}$ = 1.8 Hz, $^3J_{HP}$ = 3.5 Hz, 4 H, C^{c}H), 7.24–7.82 (m, 36 H, C_6H_4, C_6H_5), 9.90 (s, 4 H, CHO). – ^{13}C{^{1}H} NMR ($CDCl_3$): δ = 71.8 (dd, $^1J_{CP}$ = 122.0 Hz, $^3J_{CP}$ = 3.4 Hz, C^a), 74.1 (d, $^2J_{CP}$ = 13.4 Hz, C^b), 74.1 (d, $^3J_{CP}$ = 11.3 Hz, C^c), 121.6 (d, $^3J_{CP}$ = 5.8 Hz, C^2), 128.3 (d, $^3J_{CP}$ = 13.4 Hz, C^m), 129.1 (dd, $^1J_{CP}$ = 108.6 Hz, $^3J_{CP}$ = 4.0 Hz, C^i), 131.1 (s, C^3), 131.8 (d, $^2J_{CP}$ = 10.9 Hz, C^o), 132.5 (s, C^4), 132.6 (d, $^4J_{CP}$ = 2.3 Hz, C^p), 156.7 (d, $^2J_{CP}$ = 9.3 Hz, C^1), 190.8 (s, CHO). – IR (KBr): $\tilde{\nu}$ = 1699 cm^{-1} (C=O). – $C_{62}H_{48}FeN_2O_8P_4S_2$ (1193.0): calcd. C 62.42, H 4.06, N 2.35; found C 62.60, H 4.19, N 2.25.

Compound 6a: 97% yield, white powder, m.p. 145°C. – ^{31}P {^1H} NMR ($CDCl_3$): δ = −7.9 (d, $^2J_{PP}$ = 32.0 Hz, P=O), 13.7 (d, $^2J_{PP}$ = 32.0 Hz, P=N). – ^1H NMR ($CDCl_3$): δ = 7.01−7.62 (m, 25 H, C_6H_5). – ^{13}C {^1H} NMR ($CDCl_3$): δ = 120.4 (d, $^3J_{CP}$ = 4.4 Hz, C^2), 123.4 (s, C^4), 128.4 (d, $^3J_{CP}$ = 12.9 Hz, C^m), 128.8 (s, C^3), 129.1 (dd, $^1J_{CP}$ = 107.3 Hz, $^3J_{CP}$ = 3.6 Hz, C^i), 132.1 (s, C^p), 132.3 (d, $^2J_{CP}$ = 11.6 Hz, C^o), 152.1 (d, $^2J_{CP}$ = 7.7 Hz, C^1). – $C_{30}H_{25}N_1O_3P_2$ (509.5): calcd. C 70.73, H 4.95, N 2.75; found C 70.90, H 5.03, N 2.68.

Compound 6f: 96% yield, white powder, m.p. 72°C. – ^{31}P {^1H} NMR ($CDCl_3$): δ = −6.2 (d, $^2J_{PP}$ = 31.0 Hz, P=O), 15.2 (d, $^2J_{PP}$ = 31.0 Hz, P=N). – ^1H NMR ($CDCl_3$): δ = 2.07 (d, $^2J_{HP}$ = 13.3 Hz, 3 H, CH_3), 7.02−7.58 (m, 20 H, C_6H_5). – ^{13}C {^1H} NMR ($CDCl_3$): δ = 15.4 (d, $^1J_{CP}$ = 67.9 Hz, CH_3), 120.4 (d, $^3J_{CP}$ = 5.2 Hz, C^2), 123.4 (s, C^4), 128.5 (d, $^3J_{CP}$ = 12.9 Hz, C^m), 128.9 (s, C^3), 130.2 (dd, $^1J_{CP}$ = 107.7 Hz, $^3J_{CP}$ = 5.5 Hz, C^i), 130.5 (d, $^2J_{CP}$ = 10.7 Hz, C^o), 132.0 (s, C^p), 152.0 (d, $^2J_{CP}$ = 7.9 Hz, C^1). – $C_{25}H_{23}N_1O_3P_2$ (447.4): calcd. C 67.11, H 5.18, N 3.13; found C 67.33, H 5.22, N 2.98.

Compound (6g): 96% yield, orange powder, m.p. 174°C. – ^{31}P {^1H} NMR ($CDCl_3$): δ = −8.6 (d, $^2J_{PP}$ = 37.0 Hz, P=O), 14.5 (d, $^2J_{PP}$ = 37.0 Hz, P=N). – ^1H NMR ($CDCl_3$): δ = 4.21 (br. s, 4 H, C^bH), 4.56 (br. s, 4 H, C^cH), 7.02−7.46 (m, 40 H, C_6H_5). – ^{13}C {^1H} NMR ($CDCl_3$): δ = 72.0 (dd, $^1J_{CP}$ = 120.7 Hz, $^3J_{CP}$ = 3.4 Hz, C^a), 73.7 (d, $^2J_{CP}$ = 13.7 Hz, C^b), 75.0 (d, $^3J_{CP}$ = 11.0 Hz, C^c), 120.2 (d, $^3J_{CP}$ = 5.2 Hz, C^2), 123.4 (s, C^4), 128.2 (d, $^3J_{CP}$ = 13.1 Hz, C^m), 128.8 (dd, $^1J_{CP}$ = 50.0 Hz, $^3J_{CP}$ = 4.2 Hz, C^i), 129.0 (s, C^3), 131.5 (d, $^2J_{CP}$ = 11.4 Hz, C^o), 132.0 (d, $^4J_{CP}$ = 1.9 Hz, C^p), 152.3 (d, $^2J_{CP}$ = 7.7 Hz, C^1). – $C_{58}H_{48}FeN_2O_6P_4$ (1048.8): calcd. C 66.42, H 4.61, N 2.67; found C 66.63, H 4.73, N 2.53.

General Procedure for 7a-f, 8a, 8f: To a solution of 1 mmol of compounds **5a**−**f**, **6a**, **6f** in CH_2Cl_2 (10 mL) was added at room temperature 1.05 mmol (slight excess) of $MeSO_3CF_3$. The solution was stirred for 15 min, then concentrated to dryness. The residue was washed twice with ether/pentane (1:1) to afford **7a**−**f**, **8a**, **8f** as oils.

General Procedure for 7g, 8g, and 16g: To a solution of 1 mmol of compound **5g**, **6g** or **15g** in CH_2Cl_2 (10 mL) was added at room temperature 2.1 mmol (slight excess) of $MeSO_3CF_3$. The solution was stirred for 15 min, then concentrated to dryness. The residue was washed twice with ether/pentane (1:1) to afford **7g**, **8g** or **16g** as a powder. Crystallization at −30°C in CH_2Cl_2/pentane (1:1) afforded single crystals of **7g** and **8g** suitable for X-ray diffraction.

Compound 7a: 95% yield, orange viscous oil. – ^{31}P {^1H} NMR ($CDCl_3$): δ = 22.8 (d, $^2J_{PP}$ = 20.0 Hz, P=N), 23.4 (d, $^2J_{PP}$ = 20.0 Hz, P−S−Me). – ^{31}P NMR ($CDCl_3$): δ = 22.8 (m, P=N), 23.4 (qd, $^2J_{PP} \approx {}^3J_{HP} \approx$ 19 Hz, P−S−Me). – ^1H NMR ($CDCl_3$): δ = 2.59 (d, $^3J_{HP}$ = 19.0 Hz, 3 H, CH_3-S), 7.24−7.92 (m, 23 H, C_6H_4, C_6H_5), 9.96 (s, 2 H, CHO). – ^{13}C {^1H} NMR ($CDCl_3$): (CF_3SO_3 not detected) δ = 13.7 (d, $^2J_{CP}$ = 5.5 Hz, CH_3−S), 121.3 (d, $^3J_{CP}$ = 5.5 Hz, C^2), 124.0 (d, $^1J_{CP}$ = 110.9 Hz, C^i), 130.2 (d, $^3J_{CP}$ = 13.1 Hz, C^m), 131.9 (d, $^2J_{CP}$ = 11.0 Hz, C^o), 132.0 (s, C^3), 134.6 (br. s, C^4, C^p), 153.1 (d, $^2J_{CP}$ = 10.1 Hz, C^1), 190.6 (s, CHO). – ^{19}F NMR ($CDCl_3$): δ = −2.2 (s, CF_3SO_3). – IR (KBr): $\tilde{\nu}$ = 1699 (C=O) cm^{-1}. – $C_{34}H_{28}F_3N_1O_7P_2S_2$ (745.7): calcd. C 54.76, H 3.78, N 1.88; found C 54.83, H 3.82, N 1.85.

Compound 7b: 91% yield, red viscous oil. – ^{31}P {^1H} NMR (CD_3COCD_3): δ = 26.2 (d, $^2J_{PP}$ = 23.0 Hz, P=N), 31.4 (d, $^2J_{PP}$ = 23.0 Hz, P−S−Me). – ^{31}P NMR (CD_3COCD_3): δ = 26.2 (m, P=N), 31.4 (qd, $^2J_{PP} \approx {}^3J_{HP} \approx$ 20 Hz, P−S−Me). – ^1H NMR (CD_3COCD_3): δ = 2.95 (d, $^3J_{HP}$ = 18.5 Hz, 3 H, CH_3-S), 7.74−8.19 (m, 20 H, C_6H_4), 10.18 (s, 2 H, CHO). – ^{13}C {^1H} NMR (CD_3COCD_3): δ = 13.6 (d, $^2J_{CP}$ = 4.6 Hz, CH_3−S), 121.4 (q, $^1J_{CF}$ = 319.9 Hz, CF_3SO_3), 122.0 (d, $^3J_{CP}$ = 4.5 Hz, C^2), 123.1 (br. d, $^1J_{CP}$ = 109 Hz, C^i), 130.3 (d, $^3J_{CP}$ = 14.1 Hz, C^m), 132.1 (s, C^3), 134.4 (d, $^2J_{CP}$ = 14.0 Hz, C^o), 135.3 (s, C^4), 141.0 (s, C^p), 153.3 (d, $^2J_{CP}$ = 9.6 Hz, C^1), 190.9 (s, CHO). – ^{19}F NMR (CD_3COCD_3): δ = 2.7 (s, CF_3SO_3). – IR (KBr): $\tilde{\nu}$ = 1698 (C=O) cm^{-1}. – $C_{34}H_{25}Cl_3F_3N_1O_7P_2S_2$ (849.0): calcd. C 48.07, H 2.94, N 1.64; found C 48.13, H 3.00, N 1.58.

Compound 7c: 92% yield, orange viscous oil. – ^{31}P {^1H} NMR (CD_3COCD_3): δ = 28.9 (d, $^2J_{PP}$ = 10.0 Hz, P−S−Me), 45.7 (d, $^2J_{PP}$ = 10.0 Hz, P=N). – ^{31}P NMR (CD_3COCD_3): δ = 28.9 (qd, $^2J_{PP}$ = 10.0 Hz, $^3J_{HP}$ = 19.0 Hz, P−S−Me), 45.7 (m, P=N). – ^1H NMR (CD_3COCD_3): δ = 2.83 (d, $^3J_{HP}$ = 19.0 Hz, 3 H, CH_3-S), 2.84−2.98 (m, 12 H, CH_2−CH_2), 7.78−8.17 (d, $^3J_{HH}$ = 12.0 Hz, 8 H, C_6H_4), 10.09 (s, 2 H, CHO). – ^{13}C {^1H} NMR (CD_3COCD_3): δ = 13.6 (d, $^2J_{CP}$ = 5.3 Hz, CH_3-S), 21.1 (s, CH_2P), 22.4 (s, CH_2CH_2P), 118.7 (s, C≡N), 121.2 (q, $^1J_{CF}$ = 320.7 Hz, CF_3SO_3), 121.9 (d, $^3J_{CP}$ = 4.8 Hz, C^2), 132.1 (s, C^3), 135.3 (s, C^4), 153.6 (d, $^2J_{CP}$ = 11.0 Hz, C^1), 191.1 (s, CHO). – ^{19}F NMR (CD_3COCD_3): δ = 2.5 (s, CF_3SO_3). – IR (THF): $\tilde{\nu}$ = 2211 (CN), 1700 (C=O) cm^{-1}. – MS [FAB$^+$ (MNBA/CH_2Cl_2)]; *m/z* (%): 527 (100) [$M^+ - CF_3SO_3$]. – $C_{25}H_{25}F_3N_4O_7P_2S_2$ (676.6): calcd. C 44.38, H 3.72, N 8.28; found C 44.47, H 3.73, N 8.24.

Compound 7d: 79% yield, orange viscous oil. – ^{31}P {^1H} NMR ($CDCl_3$): δ = −4.7 (d, $^2J_{PP}$ = 5.5 Hz, P=N), 28.5 (d, $^2J_{PP}$ = 5.5 Hz, P-S-Me). – ^{31}P NMR ($CDCl_3$): δ = −4.7 (dec d, $^2J_{PP}$ = 5.2 Hz, $^3J_{HP}$ = 24.0 Hz, P=N), 28.5 (br. q, $^3J_{HP}$ = 18.5 Hz, P−S−Me). – ^1H NMR ($CDCl_3$): δ = 1.25 (d, $^3J_{HP}$ = 22.5 Hz, 9 H, C−CH_3), 2.79 (d, $^3J_{HP}$ = 18.5 Hz, 3 H, CH_3−S), 7.38−7.95 (m, 18 H, C_6H_4, C_6H_5), 9.85 (s, 2 H, CHO). – ^{13}C {^1H} NMR ($CDCl_3$): δ = 13.5 (d, $^2J_{CP}$ = 5.1 Hz, CH_3−S), 22.3 (d, $^2J_{CP}$ = 2.3 Hz, C−CH_3), 35.0 (dd, $^1J_{CP}$ = 94.9 Hz, $^3J_{CP}$ = 6.0 Hz, C−CH_3), 73.2 (d, $^1J_{CP}$ = 201.7 Hz, ≡C−P), 110.5 (d, $^2J_{CP}$ = 36.0 Hz, C≡C-P), 116.7 (d, $^3J_{CP}$ = 4.6 Hz, C^i), 120.7 (q, $^1J_{CF}$ = 320.8 Hz, CF_3SO_3), 121.3 (d, $^3J_{CP}$ = 4.9 Hz, C^2), 129.0 (s, C^m), 132.0 (s, C^3), 132.6 (s, C^p), 132.8 (d, $^4J_{CP}$ = 1.7 Hz, C^o), 134.6 (d, $^5J_{CP}$ = 1.3 Hz, C^4), 152.9 (d, $^2J_{CP}$ = 10.8 Hz, C^1), 190.3 (s, CHO). – ^{19}F NMR ($CDCl_3$): δ = −2.0 (s, CF_3SO_3). – IR (THF): $\tilde{\nu}$ = 2170 (C≡C), 1699 (C=O) cm^{-1}. – $C_{36}H_{32}F_3N_1O_7P_2S_2$ (773.8): calcd. C 55.88, H 4.17, N 1.81; found C 55.95, H 4.19, N 1.77.

Compound 7e: 91% yield, red-orange viscous oil. – ^{31}P {^1H} NMR ($CDCl_3$): δ = 24.6 (d, $^2J_{PP}$ = 12.0 Hz, P−S−Me), 53.7 (d, $^2J_{PP}$ = 12.0 Hz, P=N). – ^{31}P NMR ($CDCl_3$): δ = 24.6 (qd, $^2J_{PP} = {}^3J_{HP}$ = 18.0 Hz, P−S−Me), 53.7 (m, P=N). – ^1H NMR ($CDCl_3$): δ = 2.33 (m, 2 H, CH_2P), 2.91 (m, 2 H, CH_2CH_2P), 2.60 (d, $^3J_{HP}$ = 18.0 Hz, 3 H, CH_3−S), 6.17 (ddt, $^3J_{HP}$ = 29.2 Hz, $^3J_{HH}$ = 8.1 Hz, $^3J_{HH}$ = 2.2 Hz, 1 H, CH=CH-P), 7.24−7.97 (m, 14 H, C_6H_4, C_6H_5, =CH−P), 9.93 (s, 2 H, CHO). – ^{13}C {^1H} NMR ($CDCl_3$): δ = 13.5 (d, $^2J_{CP}$ = 5.4 Hz, CH_3S), 24.3 (d, $^1J_{CP}$ = 71.2 Hz, CH_2P), 30.9 (d, $^2J_{CP}$ = 11.0 Hz, CH_2CH_2P) 118.6 (d, $^1J_{CP}$ = 90.8 Hz, = CH-P), 121.1 (q, $^1J_{CF}$ = 320.5 Hz, CF_3SO_3), 121.2 (d, $^3J_{CP}$ = 4.7 Hz, C^2), 124.9 (dd, $^1J_{CP}$ = 110.1 Hz, $^3J_{CP}$ = 7.4 Hz, C^i), 124.9 (d, $^3J_{CP}$ = 14.1 Hz, C^m), 130.2 (d, $^2J_{CP}$ = 12.5 Hz, C^o), 132.0 (s, C^3), 132.2 (d, $^4J_{CP}$ = 3.2 Hz, C^p), 134.5 (s, C^4), 153.1 (d, $^2J_{CP}$ = 11.3 Hz, C^1), 160.6 (d, $^2J_{CP}$ = 26.3 Hz, CH=CH-P), 190.4 (s, CHO). – ^{19}F NMR ($CDCl_3$): δ = −2.1 (s, CF_3SO_3). – IR (THF): $\tilde{\nu}$ = 1698 (C=O) cm^{-1}. – MS [FAB$^+$ (MNBA/CH_2Cl_2)]; *m/z* (%): 496 (100) [$M^+ - CF_3SO_3$]. – $C_{26}H_{24}F_3N_1O_7P_2S_2$ (645.6): calcd. C 48.37, H 3.75, N 2.17; found C 48.56, H 3.75, N 2.15.

Compound 7f: 92% yield, orange powder. – ^{31}P {^1H} NMR ($CDCl_3$): δ = 23.2 (d, $^2J_{PP}$ = 20 Hz, P=N or P−S−Me), 24.2 (d, $^2J_{PP}$ = 20 Hz, P−S−Me or P=N). – ^1H NMR ($CDCl_3$): δ = 2.18

(d, $^2J_{HP}$ = 13.2 Hz, 3 H, CH_3P), 2.59 (d, $^3J_{HP}$ = 18.5 Hz, 3 H, CH_3−S), 6.85−7.65 (m, 20 H, C_6H_5). − $^{13}C\{^1H\}$ NMR ($CDCl_3$): δ = 13.6 (d, $^2J_{CP}$ = 5.1 Hz, CH_3S), 14.2 (d, $^1J_{CP}$ = 67.8 Hz, CH_3P), 119.8 (d, $^3J_{CP}$ = 4.8 Hz, C^2), 120.6 (q, $^1J_{CF}$ = 320.0 Hz, CF_3SO_3), 126.2 (dd, $^1J_{CP}$ = 108.0 Hz, $^3J_{CP}$ = 4.7 Hz, C^i), 126.5 (s, C^4), 128.9 (d, $^3J_{CP}$ = 13.0 Hz, C^m), 130.0 (s, C^3), 131.1 (d, $^2J_{CP}$ = 14.5 Hz, C^o), 133.1 (br. s, C^p), 148.9 (d, $^2J_{CP}$ = 8.7 Hz, C^1). − ^{19}F NMR ($CDCl_3$): δ = −2.1 (s, CF_3SO_3). − $C_{27}H_{26}F_3N_1O_5P_2S_2$ (627.6): calcd. C 51.67, H 4.17, N 2.23; found C 51.85, H 4.20, N 2.28.

Compound 7g: 95% yield, orange powder, m.p. 196°C. − $^{31}P\{^1H\}$ NMR ($CDCl_3$): δ = 23.9 (d, $^2J_{PP}$ = 23.0 Hz, P−S−Me), 25.4 (d, $^2J_{PP}$ = 23.0 Hz, P=N). − ^{31}P NMR ($CDCl_3$): δ = 23.9 (qd, $^2J_{PP} \approx {}^2J_{HP} \approx$ 20 Hz, P−S−Me), 25.4 (m, P=N). − ^1H NMR ($CDCl_3$): δ = 2.20 (d, $^3J_{HP}$ = 18.5 Hz, 6 H, CH_3−S), 3.65 (br. s, 4 H, C^bH), 4.02 (br. s, 4 H, C^cH), 6.90−7.70 (m, 36 H, C_6H_4, C_6H_5), 9.71 (s, 4 H, CHO). − $^{13}C\{^1H\}$ NMR ($CDCl_3$): δ = 12.6 (d, $^2J_{CP}$ = 5.5 Hz, CH_3−S), 67.8 (dd, $^1J_{CP}$ = 125.2 Hz, $^3J_{CP}$ = 6.3 Hz, C^a), 72.6 (d, $^2J_{CP}$ = 14.4 Hz, C^b), 74.8 (d, $^3J_{CP}$ = 11.5 Hz, C^c), 120.3 (d, $^3J_{CP}$ = 5.0 Hz, C^2), 124.3 (dd, $^1J_{CP}$ = 107.5 Hz, $^3J_{CP}$ = 3.7 Hz, C^i), 128.6 (d, $^3J_{CP}$ = 13.5 Hz, C^m), 130.6 (d, $^2J_{CP}$ = 12.1 Hz, C^o), 131.0 (s, C^3), 133.6 (d, $^4J_{CP}$ = 2.7 Hz, C^p), 133.9 (d, $^5J_{CP}$ = 1.3 Hz, C^4), 152.2 (d, $^2J_{CP}$ = 11.0 Hz, C^1), 189.9 (s, CHO); CF_3SO_3 signal not detected. − ^{19}F NMR ($CDCl_3$): δ = −2.6 (s, CF_3SO_3). − IR (KBr): $\tilde{\nu}$ = 1705 (C=O) cm^{-1}. − MS [FAB^+ (MNBA/CH_2Cl_2)]; *m/z* (%): 584 (100) [(M^{2+} − Fe − 2 CF_3SO_3)/2]. − $C_{66}H_{54}F_6FeN_2O_{14}P_4S_4$ (1521.2): calcd. C 52.11, H 3.58, N 1.84; found C 52.11, H 3.60, N 1.82.

Compound 8a: 96% yield, colorless viscous oil. − $^{31}P\{^1H\}$ NMR ($CDCl_3$): δ = −10.0 (d, $^2J_{PP}$ = 34.8 Hz, P−O−Me), 21.8 (d, $^2J_{PP}$ = 34.8 Hz, P=N). − ^{31}P NMR ($CDCl_3$): δ = −10.0 (qd, $^2J_{PP}$ = 34.0 Hz, $^3J_{HP}$ = 12.2 Hz, P−O−Me), 21.8 (m, P=N). − ^1H NMR ($CDCl_3$): δ = 4.01 (d, $^3J_{HP}$ = 12.5 Hz, 3 H, CH_3−O), 6.86−7.61 (m, 25 H, C_6H_5). − $^{13}C\{^1H\}$ NMR ($CDCl_3$): δ = 57.4 (d, $^2J_{CP}$ = 7.7 Hz, CH_3−O), 119.4 (d, $^3J_{CP}$ = 4.8 Hz, C^2), 120.4 (q, $^1J_{CF}$ = 321.2 Hz, CF_3SO_3), 124.5 (dd, $^1J_{CP}$ = 109.1 Hz, $^3J_{CP}$ = 3.6 Hz, C^i), 126.3 (s, C^4), 129.1 (d, $^3J_{CP}$ = 13.3 Hz, C^m), 129.9 (s, C^3), 131.5 (d, $^2J_{CP}$ = 11.2 Hz, C^o), 133.8 (s, C^p), 148.7 (d, $^2J_{CP}$ = 9.2 Hz, C^1). − ^{19}F NMR ($CDCl_3$): δ = −2.1 (s, CF_3SO_3). − $C_{32}H_{28}F_3N_1O_6P_2S_1$ (673.6): calcd. C 57.06, H 4.19, N 2.08; found C 57.10, H 4.19, N 2.03.

Compound 8f: 96% yield, colorless viscous oil. − $^{31}P\{^1H\}$ NMR ($CDCl_3$): δ = −9.3 (d, $^2J_{PP}$ = 32.5 Hz, P−O−Me), 24.2 (d, $^2J_{PP}$ = 32.5 Hz, P=N). − ^{31}P NMR ($CDCl_3$): δ = −9.3 (qd, $^2J_{PP}$ = 31.6 Hz, $^3J_{HP}$ = 12.3 Hz, P−O−Me), 24.2 (m, P=N). − ^1H NMR ($CDCl_3$): δ = 2.08 (d, $^2J_{HP}$ = 13.2 Hz, 3 H, CH_3P), 4.04 (d, $^3J_{HP}$ = 12.5 Hz, 3 H, CH_3O), 6.96−7.51 (m, 20 H, C_6H_5). − $^{13}C\{^1H\}$ NMR ($CDCl_3$): δ = 14.5 (d, $^1J_{CP}$ = 67.9 Hz, CH_3P), 57.2 (d, $^2J_{CP}$ = 9.0 Hz, CH_3O), 119.5 (d, $^3J_{CP}$ = 4.7 Hz, C^2), 120.4 (q, $^1J_{CF}$ = 319.4 Hz, CF_3SO_3), 126.0 (dd, $^1J_{CP}$ = 107.9 Hz, $^3J_{CP}$ = 4.6 Hz, C^i), 126.4 (s, C^4), 129.1 (d, $^3J_{CP}$ = 12.9 Hz, C^m), 130.0 (s, C^3), 130.1 (d, $^2J_{CP}$ = 14.7 Hz, C^o), 133.3 (s, C^p), 148.9 (d, $^2J_{CP}$ = 8.6 Hz, C^1). − ^{19}F NMR ($CDCl_3$): δ = −2.1 (s, CF_3SO_3). − $C_{27}H_{26}F_3N_1O_6P_2S$ (611.5): calcd. C 53.03, H 4.29, N 2.29; found C 53.08, H 4.29, N 2.27.

Compound 8g: 96% yield, orange powder, m.p. 169°C. − $^{31}P\{^1H\}$ NMR ($CDCl_3$): δ = −9.7 (d, $^2J_{PP}$ = 34.5 Hz, P−O−Me), 25.2 (d, $^2J_{PP}$ = 34.5 Hz, P=N). − ^{31}P NMR ($CDCl_3$): δ = −9.7 (dq, $^2J_{PP}$ = 34.5 Hz, $^3J_{HP}$ = 12.9 Hz, P−O−Me), 25.2 (m, P=N). − ^1H NMR ($CDCl_3$): δ = 4.03 (br. s, 4 H, C^bH), 4.13 (d, $^3J_{HP}$ = 12.4 Hz, 6 H, CH_3−O), 4.39 (br. s, 4 H, C^cH), 7.00−7.64 (m, 40 H, C_6H_5). − $^{13}C\{^1H\}$ NMR ($CDCl_3$): (CF_3SO_3 not detected) δ = 58.1 (d, $^2J_{CP}$ = 9.1 Hz, CH_3−O), 68.5 (dd, $^1J_{CP}$ = 126.8 Hz, $^3J_{CP}$ = 4.7 Hz, C^a), 73.6 (d, $^2J_{CP}$ = 15.1 Hz, C^b), 76.2 (d, $^3J_{CP}$ = 11.8 Hz, C^c), 119.7 (d, $^3J_{CP}$ = 4.3 Hz, C^2), 126.3 (dd, $^1J_{CP}$ = 107.9 Hz, $^3J_{CP}$ = 4.7 Hz, C^i), 126.8 (s, C^4), 129.4 (d, $^3J_{CP}$ = 13.8 Hz, C^m), 130.5 (s, C^3), 131.4 (d, $^2J_{CP}$ = 11.8 Hz, C^o), 134.1 (s, C^p), 149.4 (d, $^2J_{CP}$ = 9.2 Hz, C^1). − ^{19}F NMR ($CDCl_3$): δ = −2.0 (s, CF_3SO_3). − MS [FAB^+ (MNBA/CH_2Cl_2)]; *m/z* (%): 512 (100) [(M^{2+} − Fe − 2 CF_3SO_3)/2]. − $C_{62}H_{54}F_6FeN_2O_{12}P_4S_2$ (1377.0): calcd. C 54.06, H 3.92, N 2.03; found C 54.10, H 3.95, N 2.00.

General Procedure for 9a, 10a: To a solution of 1 mmol of compound **5a** or **6a** in CH_2Cl_2 (10 mL) was added at room temperature a solution of 1.05 mmol (slight excess) of *i*$PrSO_3CF_3$ generated in situ in CCl_4 at 0°C. The resulting solution was allowed to reach room temperature under stirring for 30 min, then concentrated to dryness. The residue was washed twice with ether/pentane (1:1) to afford **9a** or **10a** as oils.

Compound 9a: 90% yield, red viscous oil. − $^{31}P\{^1H\}$ NMR ($CDCl_3$): δ = 21.5 (d, $^2J_{PP}$ = 17.3 Hz, P−S−*i*Pr), 22.4 (d, $^2J_{PP}$ = 17.3 Hz, P=N). − ^1H NMR ($CDCl_3$): δ = 1.43 (d, $^3J_{HH}$ = 6.8 Hz, 6 H, CH_3), 3.83 (septd, $^3J_{HH}$ = 6.8 Hz, $^3J_{HP}$ = 13.6 Hz, 1 H, C*H*Me_2), 7.01−7.96 (m, 23 H, C_6H_4, C_6H_5), 9.91 (s, 2 H, CHO). − $^{13}C\{^1H\}$ NMR ($CDCl_3$): δ = 24.7 (d, $^3J_{CP}$ = 7.4 Hz, CH_3), 42.6 (d, $^2J_{CP}$ = 5.3 Hz, *C*HMe_2), 120.5 (q, $^1J_{CF}$ = 321.4 Hz, CF_3SO_3), 121.1 (d, $^3J_{CP}$ = 5.1 Hz, C^2), 124.0 (dd, $^1J_{CP}$ = 103.6 Hz, $^3J_{CP}$ = 7.2 Hz, C^i), 129.6 (d, $^3J_{CP}$ = 13.3 Hz, C^m), 131.8 (d, $^2J_{CP}$ = 10.7 Hz, C^o), 131.9 (s, C^3), 134.4 (br. s, C^4, C^p), 153.1 (d, $^2J_{CP}$ = 11.7 Hz, C^1), 190.5 (s, CHO). − ^{19}F NMR ($CDCl_3$): δ = −2.0 (s, CF_3SO_3). − IR (KBr): $\tilde{\nu}$ = 1700 (C=O) cm^{-1}. − $C_{36}H_{32}F_3N_1O_7P_2S_2$ (773.8): calcd. C 55.88, H 4.17, N 1.81; found C 55.83, H 4.09, N 1.86.

Compound 10a: 91% yield, colorless viscous oil. − $^{31}P\{^1H\}$ NMR ($CDCl_3$): δ = −12.1 (d, $^2J_{PP}$ = 21.5 Hz, P−O−*i*Pr), 21.7 (d, $^2J_{PP}$ = 21.5 Hz, P=N). − ^1H NMR ($CDCl_3$): δ = 1.33 (d, $^3J_{HH}$ = 6.2 Hz, 6 H, CH_3), 5.04 (septd, $^3J_{HH}$ = 6.2 Hz, $^3J_{HP}$ = 12.6 Hz, 1 H, C*H*Me_2), 6.91−7.69 (m, 25 H, C_6H_5). − $^{13}C\{^1H\}$ NMR ($CDCl_3$): δ = 23.1 (d, $^3J_{CP}$ = 5.2 Hz, CH_3), 79.7 (d, $^2J_{CP}$ = 9.2 Hz, *C*HMe_2), 119.7 (d, $^3J_{CP}$ = 5.4 Hz, C^2), 120.8 (q, $^1J_{CF}$ = 321 Hz, CF_3SO_3), 125.0 (dd, $^1J_{CP}$ = 108.9 Hz, $^3J_{CP}$ = 3.7 Hz, C^i), 126. 6 (s, C^4), 129.5 (d, $^3J_{CP}$ = 13.1 Hz, C^m), 130.2 (s, C^3), 131.9 (d, $^2J_{CP}$ = 12.0 Hz, C^o), 134.2 (s, C^p), 149.3 (d, $^2J_{CP}$ = 9.4 Hz, C^1). − ^{19}F NMR ($CDCl_3$): δ = −2.3 (s, CF_3SO_3). − $C_{34}H_{32}N_1O_6F_3P_2S$ (701.7): calcd. C 58.20, H 4.60, N 2.00; found C 58.32, H 4.69, N 2.05.

Synthesis of Compound 11f: To a solution of 1 mmol of compound **6f** (450 mg) in CH_2Cl_2 (10 mL) was added at room temperature 1.05 mmol (slight excess) of $Me_3SiSO_3CF_3$. The solution was stirred for 15 min, then concentrated to dryness. The residue was not washed, it was directly used for NMR characterization. − 90% yield, colourless viscous oil. − $^{31}P\{^1H\}$ NMR ($CDCl_3$): δ = −18.6 (d, $^2J_{PP}$ = 33.1 Hz, P−O−Si), 23.2 (d, $^2J_{PP}$ = 33.1 Hz, P=N). − ^1H NMR ($CDCl_3$): δ = 0.25 (br. s, 9 H, CH_3Si), 2.12 (d, $^2J_{HP}$ = 12.9 Hz, 3 H, CH_3P), 7.02−7.62 (m, 20 H, C_6H_5). − $^{13}C\{^1H\}$ NMR ($CDCl_3$): δ = 0.0 (s, CH_3Si), 14.6 (d, $^1J_{CP}$ = 73.7 Hz, CH_3P), 119.6 (s, C^2), 119.8 (q, $^1J_{CF}$ = 319.4 Hz, CF_3SO_3), 126.3 (dd, $^1J_{CP}$ = 112.7 Hz, $^3J_{CP}$ = 4.9 Hz, C^i), 126.4 (s, C^4), 129.2 (d, $^3J_{CP}$ = 13.9 Hz, C^m), 130.1 (s, C^3), 130.3 (d, $^2J_{CP}$ = 14.5 Hz, C^o), 133.6 (s, C^p), 149.2 (d, $^2J_{CP}$ = 7.6 Hz, C^1). − ^{19}F NMR ($CDCl_3$): δ = −1.9 (s, CF_3SO_3).

General Procedure for 12f, and 12g: To a solution of 1 mmol of compound **7f**, or 0.5 mmol of compound **7g** in CH_2Cl_2 (10 mL) was added at room temperature 1.1 mmol (slight excess) of $P(NMe_2)_3$. The solution was stirred for 1 hour, then concentrated to dryness. The residue was extracted with toluene (10 mL) and the solution was filtered under argon to give **12f** or **12g** which were

used without further purification, due to their high sensitivity toward air and moisture.

Compound 12f: Not isolated. − $^{31}P\{^1H\}$ NMR (CH_2Cl_2): δ = 9.9 (d, $^2J_{PP}$ = 32 Hz, P=N), 143.9 (d, $^2J_{PP}$ = 32 Hz, P^{III}).

Compound 12g: Not isolated. − $^{31}P\{^1H\}$ NMR (CH_2Cl_2): δ = 12.8 (d, $^2J_{PP}$ = 63 Hz, P=N), 144.4 (d, $^2J_{PP}$ = 63 Hz, P^{III}).

Synthesis of Compound 13f: To a solution of 0.5 mmol of compound **12f** in toluene (10 mL) was added at room temperature 1 mmol (100% excess) of allyl iodide. The solution was stirred for 1 h. The phosphonium salt **13f** precipitated progressively. This precipitate was recovered by filtration, and washed with pentane to afford **13f** as a powder. − 85% yield, white powder. − $^{31}P\{^1H\}$ NMR (CD_3COCD_3): δ = 27.3 (d, $^2J_{PP}$ = 20.3 Hz, P=N), 28.9 (d, $^2J_{PP}$ = 20.3 Hz, P-allyl). − ^{31}P NMR (CD_3COCD_3): δ = 27.3 (m, P=N), 28.9 (dt, $^2J_{PP} \approx {}^2J_{PH} \approx$ 20 Hz, P-allyl). − ^1H NMR (CD_3COCD_3): δ = 2.57 (d, $^2J_{HP}$ = 13.4 Hz, 3 H, CH_3P), 3.87 (dddd, $^2J_{HP}$ = 20.1 Hz, $^3J_{HHA}$ = 7.3 Hz, $^4J_{HHB} \approx {}^4J_{HHC} \approx$ 1.1 Hz, 2 H, CH_2), 5.52 (dddt, $^3J_{HBHA}$ = 10.2 Hz, $^4J_{HBP}$ = 5.1 Hz, $^2J_{HBHC} \approx {}^4J_{HBCH2} \approx$ 1.2 Hz, 1 H, H_B), 5.64 (dddt, $^3J_{HCHA}$ = 16.8 Hz, $^4J_{HCP}$ = 6.1 Hz, $^2J_{HCHB} \approx {}^4J_{HCCH2} \approx$ 1.3 Hz, 1 H, H_C), 6.03 (dddt, $^3J_{HAHC}$ = 16.8 Hz, $^3J_{HAHB}$ = 10.2 Hz, $^3J_{HACH2} \approx {}^3J_{HAP} \approx$ 7.3 Hz, 1 H, H_A), 7.20−7.90 (m, 20 H, C_6H_5). − $^{13}C\{^1H\}$ NMR (CD_3COCD_3): δ = 15.8 (d, $^1J_{CP}$ = 68.0 Hz, CH_3P), 33.2 (d, $^1J_{CP}$ = 133.6 Hz, -CH_2-), 121.6 (d, $^3J_{CP}$ = 4.2 Hz, C^2), 123.3 (d, $^3J_{CP}$ = 16.2 Hz, CH_2=), 125.4 (d, $^2J_{CP}$ = 12.9 Hz, CH_A), 126.9 (s, C^4), 128.2 (dd, $^1J_{CP}$ = 108.0 Hz, $^3J_{CP}$ = 4.5 Hz, C^i), 129.7 (d, $^2J_{CP}$ = 12.2 Hz, C^m), 130.9 (s, C^3), 131.4 (d, $^3J_{CP}$ = 12.0 Hz, C^o), 133.7 (d, $^4J_{CP}$ = 2.7 Hz, C^p), 149.9 (d, $^2J_{CP}$ = 11.6 Hz, C^1). − $C_{28}H_{28}INO_2P_2$ (599.4): C 56.11, H 4.71, N 2.34; found C 55.98, H 4.63, N 2.27.

Synthesis of Compound 14f: A solution of 0.5 mmol of compound **12f** in toluene (10 mL) was added at room temperature to 0.5 mmol of 4-azidophenyl isothiocyanate. Evolution of nitrogen occurred rapidly. After 1 h, the solution was concentrated to dryness, and the residue was washed twice with THF/pentane (1:5) to afford compound **14f** as a viscous oil. This compound is not stable when left in solution. − 91% Yield, orange viscous oil. − $^{31}P\{^1H\}$ NMR ($CDCl_3$): δ = −7.7 (d, $^2J_{PP}$ = 16 Hz, N=P−O), 15.3 (d, $^2J_{PP}$ = 16 Hz, N=P−C). − ^1H NMR ($CDCl_3$): δ = 1.95 (d, $^3J_{HP}$ = 13.3 Hz, 3 H, CH_3), 6.80−7.80 (m, 24 H, C_6H_5, C_6H_4). − $^{13}C\{^1H\}$ NMR ($CDCl_3$): δ = 15.0 (d, $^1J_{CP}$ = 69 Hz, CH_3), 121.0 (d, $^3J_{CP}$ = 4.7 Hz, C^2), 123.3 (d, $^3J_{CP}$ = 21.0 Hz, C'^o), 124.2 (s, C^4), 126.3 (s, C'^m), 126.9 (s, C'^p), 128.7 (d, $^3J_{CP}$ = 13.5 Hz, C^m), 129.3 (s, C^3), 130.6 (dd, $^1J_{CP}$ = 107 Hz, $^3J_{CP}$ = 5 Hz, C^i), 130.8 (d, $^2J_{CP}$ = 10.3 Hz, C^o), 132.3 (br. s, C^p), 133.7 (s, C=S), 149.8 (br. s, C'^i), 151.7 (d, $^2J_{CP}$ = 8.6 Hz, C^1). − $C_{32}H_{27}N_3O_2P_2S$ (579.6): C 54.40, H 3.85, N 5.95; found C 54.29, H 3.80, N 5.84.

Synthesis of Compound 15g: To a solution of 0.5 mmol of compound **12g** in toluene (10 mL) was added at room temperature a solution of 1 mmol of the azide **2** in toluene (10 mL). Evolution of nitrogen occurred rapidly. After 1 h, the solution was concentrated to dryness, and the residue was washed with dichloromethane/pentane (1:5) to afford compound **15g** as a powder. 95% yield, orange powder, m.p. 237°C. − $^{31}P\{^1H\}$ NMR ($CDCl_3$): δ = −14.3 (dd, $^2J_{PP}$ = 63.5 Hz, $^2J_{PP}$ = 23.2 Hz, N−P=N), 17.9 (d, $^2J_{PP}$ = 23.2 Hz, C−P=N), 45.9 (d, $^2J_{PP}$ = 63.5 Hz, P=S). − ^1H NMR ($CDCl_3$): δ = 4.14 (br. s, 4 H, C^bH), 4.53 (br. s, 4 H, C^cH), 7.02−7.69 (m, 52 H, C_6H_4, C_6H_5), 9.86 (s, 8 H, CHO). − $^{13}C\{^1H\}$ NMR ($CDCl_3$): δ = 70.7 (dd, $^1J_{CP}$ = 126.8 Hz, $^3J_{CP}$ = 4.6 Hz, C^a), 73.6 (d, $^2J_{CP}$ = 13.8 Hz, C^b), 75.5 (d, $^3J_{CP}$ = 11.3 Hz, C^c), 121.0 (d, $^3J_{CP}$ = 4.5 Hz, C^2), 121.5 (d, $^3J_{CP}$ = 4.5 Hz, C'^2), 128.5 (dd, $^1J_{CP}$ = 108.5 Hz, $^3J_{CP}$ = 4.3 Hz, C^i), 128.6 (d, $^3J_{CP}$ = 13.5 Hz, C^m), 130.9 (s, C^3), 131.1 (s, C'^3), 131.8 (d, $^2J_{CP}$ = 11.6 Hz, C^o), 132.4 (s, C'^4), 132.9 (d, $^4J_{CP}$ = 5.0 Hz, C^p), 133.0 (s, C^4), 155.6 (d, $^2J_{CP}$ = 9.1 Hz, C^1), 156.5 (d, $^2J_{CP}$ = 9.1 Hz, C'^1), 190.5 (s, CHO), 190.7 (s, CHO). − IR (KBr): $\tilde{\nu}$ = 1699 cm^{-1} (C=O). − $C_{90}H_{68}FeN_4O_{16}P_6S_2$ (1767.4): calcd. C 61.16, H 3.88, N 3.17; found C 61.25, H 3.95, N 3.14.

Synthesis of Compound 16g: To a solution of 0.4 mmol of compound **15g** in CH_2Cl_2 (10 mL) was added at room temperature 0.81 mmol (slight excess) of $MeSO_3CF_3$. The solution was stirred for 30 min, then concentrated to dryness. The residue was washed twice with ether/pentane (1:1) to afford compound **16g** as a powder. − 96% yield, orange powder. − $^{31}P\{^1H\}$ NMR (CD_3COCD_3): δ = −16.9 (dd, $^2J_{PP}$ = 51 Hz, $^2J_{PP}$ = 29 Hz, N−P=N), 20.0 (d, $^2J_{PP}$ = 51 Hz, P−S−Me), 21.5 (d, $^2J_{PP}$ = 29 Hz, C−P=N). − ^1H NMR (CD_3COCD_3): δ = 2.73 (d, $^3J_{PP}$ = 18.4 Hz, 6 H, CH_3−S), 4.00 (br. s, 4 H, C^bH), 4.40 (br. s, 4 H, C^cH), 7.18−8.00 (m, 52 H, C_6H_4, C_6H_5), 10.0 (s, 8 H, CHO). − $^{13}C\{^1H\}$ NMR (CD_3COCD_3): δ = 13.3 (d, $^2J_{CP}$ = 4.6 Hz, CH_3), 70.4 (dd, $^1J_{CP}$ = 126.4 Hz, $^3J_{CP}$ = 6.8 Hz, C^a), 73.9 (d, $^2J_{CP}$ = 14.1 Hz, C^b), 76.0 (d, $^3J_{CP}$ = 11.4 Hz, C^c), 121.5 (d, $^3J_{CP}$ = 4.9 Hz, C^2 or C'^2), 121.6 (d, $^3J_{CP}$ = 4.9 Hz, C'^2 or C^2), 121.7 (q, $^1J_{CF}$ = 321.1 Hz, CF_3SO_3), 127.5 (dd, $^1J_{CP}$ = 108.0 Hz, $^3J_{CP}$ = 4.0 Hz, C^i), 129.7 (d, $^3J_{CP}$ = 13.6 Hz, C^m), 132.0 (d, $^2J_{CP}$ = 11.1 Hz, C^o), 132.1 (s, C'^3, C^3), 134.3 (br. s, C^p), 134.7 (s, C'^4), 135.3 (s, C^4), 153.5 (d, $^2J_{CP}$ = 9.9 Hz, C^1), 154.6 (d, $^2J_{CP}$ = 9.5 Hz, C'^1), 191.0 (s, CHO). − IR (KBr): $\tilde{\nu}$ = 1699 cm^{-1} (C=O). − $C_{94}H_{74}F_6FeN_4O_{22}P_6S_4$ (2095.6): calcd. C 53.87, H 3.56, N 2.67; found C 54.01, H 3.61, N 2.64.

X-ray Structure Determination for Compounds 5g ($C_{62}H_{48}FeN_2O_8P_4S_2$), 6g ($C_{58}H_{48}FeN_2O_6P_4$), 7g {$[C_{64}H_{54}N_2O_8P_4S_2Fe][CF_3SO_3]_2$ 3/2CH_2Cl_2}, and 8g {$[C_{60}H_{54}N_2O_6P_4Fe][CF_3SO_3]_2$}: The data were collected on a Stoe Imaging Plate Diffraction System (I.P.D.S) equipped with an Oxford Cryosystems Cooler Device, for the four compounds. The structures were solved by direct methods (SIR92)[14] and refined by least-squares procedures on F_o. All hydrogen atoms were located on a difference Fourier map, but they were introduced in calculation in idealized positions [d(C−H) = 0.96 Å], their atomic coordinates were recalculated after each cycle of refinement. They were given isotropic thermal parameters 20% higher than those of the carbon atoms to which they were connected. All non-hydrogen atoms were anisotropically refined. Models were easily located and refined for **5g**, **6g** and **8g**; concerning the structure **7g**, the molecule appears as relatively disordered. Moreover, around the molecules of solvent (CH_2Cl_2) the electron density seems to be spread and diffuse. Finally, the difference Fourier synthesis still shows some residual electron density in these regions, which could not be fitted to any model. Least-squares refinement was carried out by minimizing the function $\Sigma w(||F_o| - |F_c||)^2$, where F_o and F_c are the observed and calculated structure factors. A weighting scheme was used in the last refinement cycles, where weights are calculated from the following expression: w = [weight] × [1 − Δ(F)/6 × σ(F)]^2.[15] Models reached convergence with R = $\Sigma(||F_o| - |F_c||)/\Sigma|F_o|$ and Rw = $[\Sigma w(||F_o| - |F_c||)^2/\Sigma w(|F_o|)^2]^{1/2}$. The calculations were performed with CRYSTALS programs[16] running on a PC. The drawing of the molecules was realized with the aid of CAMERON[17] and the atomic scattering factors were taken from International Tables for X-Ray Crystallography.[18] Crystallographic data (excluding structure factors) for the structure(s) reported in this paper have been deposited with the Cambridge Crystallographic Data Centre as supplementary publication no. CCDC-103861 (**5g**), -103862 (**6g**), -103863 (**7g**), -103864 (**8g**). Copies of the data can be obtained free of charge on application to CCDC, 12 Union Road, Cambridge CB2 1EZ, UK [Fax: int. code + 44(1223)336-033; E-mail: deposit@ccdc.cam.ac.uk].

Acknowledgments

Thanks are due to the CNRS for financial support.

[1] See for example: [1a] R. Appel, W. Buchner, E. Goth, *Justus Liebigs Ann. Chem.* **1958**, *618*, 53. – [1b] R. A. Baldwin, R. M. Washburn, *J. Am. Chem. Soc.* **1965**, *30*, 3860. – [1c] H. W. Roesky, L. F. Grimm, *Angew. Chem. Int. Ed. Engl.* **1970**, *9*, 254. – [1d] H. W. Roesky, *Chem. Ber.* **1972**, *105*, 1439. – [1e] J. Högel, A. Schmidpeter, *Z. Naturforsch.* **1979**, *34b*, 915. – [1f] J. Mitjaville, A. M. Caminade, R. Mathieu, J. P. Majoral, *J. Am. Chem. Soc.* **1994**, *116*, 5007. – [1g] L. Riesel, C. Löwe, J. Pauli, *Z. Anorg. Allg. Chem.* **1995**, *621*, 865. – [1h] S. Horstmann, W. Schnick, *Z. Naturforsch.* **1996**, *51b*, 1732.

[2] For reviews, see for example: [2a] D.A. Tomalia, A. M. Naylor, W. A. Goddard III, *Angew. Chem. Int. Ed. Engl.* 1990, *29*, 138. – [2b] J. Issberner, R. Moors, F. Vögtle, *Angew. Chem. Int. Ed. Engl.* **1994**, *33*, 2413. – [2c] N. Ardoin, D. Astruc, *Bull. Soc. Chim. Fr.* **1995**, *132*, 876. – [2d] G. R. Newkome, C. N. Moorefield, F. Vögtle, in *Dendritic Molecules*, VCH, Weinheim, Germany, **1996**. – [2e] D. Gudat, *Angew. Chem. Int. Ed. Engl.* **1997**, *36*, 1951. – [2f] A. M. Caminade, J. P. Majoral, in *Les Dendrimères* (Ed.: Association Ecrin), Paris, **1998**. – [2g] J. P. Majoral, A. M. Caminade, *Top. Curr. Chem.* **1998**, *197*, 79.

[3] C. Galliot, D. Prévôté, A. M. Caminade, J. P. Majoral, *J. Am. Chem. Soc.* **1995**, *117*, 5470.

[4] [4a] C. Larré, A. M. Caminade, J. P. Majoral, *Angew. Chem. Int. Ed. Engl.* **1997**, *36*, 596. – [4b] C. Larré, B. Donnadieu, A. M. Caminade, J. P. Majoral, *Chem. Eur. J.* **1998**, *4*, 2031.

[5] [5a] C. Larré, B. Donnadieu, A. M. Caminade, J. P. Majoral, *J. Am. Chem. Soc.* **1998**, *120*, 4029. – [5b] C. Larré, D. Bressolles, C. Turrin, B. Donnadieu, A. M. Caminade, J. P. Majoral *J. Am. Chem. Soc*, in press. – [5c] V. Cadierno, A. Igau, B. Donnadieu, A. M. Caminade, J. P. Majoral, *Organometallics*, accepted.

[6] C. Galliot, C. Larré, A. M. Caminade, J. P. Majoral, *Science* **1997**, *277*, 1981.

[7] J. Bastide, J. Hamelin, F. Texier, Y. Vo Quang, *Bull. Soc. Chim. Fr.* **1973**, 2555.

[8] C. Turrin, J. Chiffre, D. de Montauzon, A. M. Caminade, E. Manoury, G. Balavoine, J. P. Majoral, to be published.

[9] [9a] A. Schmidpeter, H. Brecht, J. Eberling, *Chem. Ber.* **1968**, *101*, 3902. – [9b] A. A. Khodak, V. A. Gilyarov, M. I. Kabachnik, *J. Gen. Chem. USSR* **1975**, *45*, 248. – [9c] A. A. Khodak, V. A. Gilyarov, M. I. Kabachnik, *J. Gen. Chem. USSR* **1976**, *46*, 1628.

[10] [10a] J. Omelanczuk, M. Mikolajczyk, *Tetrahedron Lett.* **1984**, *25*, 2493. – [10b] J. Omelanczuk, *J. Chem. Soc., Chem. Commun.* **1992**, 1718. – [10c] D. Prévôté, C. Galliot, A. M. Caminade, J. P. Majoral, *Heteroatom Chem.* **1995**, *6*, 313.

[11] G. Märkl, D. Matthes, *Angew. Chem. Int. Ed. Engl.* **1972**, *11*, 1019.

[12] H. Fritzsche, U. Hasserodt, F. Korte, G. Friese, K. Adrian, H. J. Arenz, *Chem. Ber.* **1964**, *97*, 1988.

[13] C. D. Beard, K. Baum, *J. Org. Chem.* **1974**, *39*, 3875.

[14] A. Altomare, G. Cascarano, G. Giacovazzo, A. Guagliardi, M. C. Burla, G. Polidori, M. Camalli, *J. Appl. Crystallogr.* **1994**, *27*, 435.

[15] J. R. Carruthers, D. J. Watkin, *Acta Crystallogr.* **1979**, *A35*, 698.

[16] D. J. Watkin, C. K. Prout, R. J. Carruthers, P. Betteridge, *CRYSTALS*, Chemical Crystallography Laboratory, Oxford, UK, **1996**, issue 10.

[17] D. J. Watkin, C. K. Prout, L. J. Pearce, *CAMERON*, Chemical Crystallography Laboratory, Oxford, UK, **1996**.

[18] *International Tables for X-Ray Crystallography*, vol. IV, Kynoch Press, Birmingham, England, **1974**.

Received October 21, 1998
[I98363]

Vinylidene Transition-Metal Complexes, 48[+]
A Novel Route to Cationic Four-Coordinate Rhodium(I) Complexes with Rh=C Bonds

Bettina Windmüller,[a] Oliver Nürnberg,[a] Justin Wolf,[a] and Helmut Werner*[a]

Dedicated to Professor Michael F. Lappert on the occasion of his 70th birthday

Keywords: Rhodium / Ketone complexes / Vinylidene complexes / Allenylidene complexes / Ligand substitution reactions

The complex $[Rh(acetone)_2(C_8H_{14})_2]PF_6$ (**2**), which is prepared from $[RhCl(C_8H_{14})_2]_2$ and $AgPF_6$ in acetone, reacts with P*i*Pr$_3$ to afford the PF_6 salt **3** of the cation $[Rh(acetone)_2(PiPr_3)_2]^+$ containing the ketone and phosphane ligands in *cis* dispositions. Treatment of **3** with MeC≡CPh leads to the displacement of one acetone ligand and the formation of the corresponding π-alkyne complex **4**. In contrast, from **3** and terminal alkynes such as HC≡CC_6H_4–4-Me or HC≡CCPh_2OH the cationic vinylidenerhodium(I) compounds **5** and **6** are obtained. The latter, with C=CHCPh_2OH as the ligand, is rather labile and even at room temperature eliminates water to give the cationic four-coordinate rhodium allenylidene **7**. The molecular structure of this compound has been determined by X-ray crystallography. In the presence of pyridine or ammonia, the acetone ligand of **5** and **7** is readily displaced and the substitution products **8**–**10** are formed almost quantitatively. Anions such as acetate or hydroxide also displace the ketone unit of **7** and yield the neutral allenylidenerhodium(I) complexes *trans*-$[RhX(=C=C=CPh_2)(PiPr_3)_2]$ with X = OAc (**11**) and OH (**12**).

Following the synthesis of the first square-planar allenylidenerhodium(I) complex *trans*-[RhCl(=C=C=CPh_2)(P*i*Pr$_3$)$_2$],[1] we have recently shown that rhodium allenylidenes of this particular type are useful tools for the generation of metal bound species that are hardly accessible by other preparative routes.[2] After having characterized a series of compounds of the general composition *trans*-[RhX(=C=C=CRR′)(P*i*Pr$_3$)$_2$] (X = Cl, I, CN, OH, OPh, OAc, OTos),[3] we became interested to find out whether also four-coordinate *cationic* allenylidenerhodium(I) complexes $[Rh(L)(=C=C=CRR')(PiPr_3)_2]^+$ (L = two-electron donor ligand) can be obtained. Recent attempts from our laboratory with the aim to prepare the cation *trans*-$[Rh(=C=C=CPh_2)_2(PiPr_3)_2]^+$ unexpectedly led, via a novel C–C coupling, to the formation of two isomeric hexapentaenerhodium(I) compounds of which the isomer having the polyene coordinated in an unsymmetrical fashion is the thermodynamically more stable.[4] However, after we found that carbonyl-, ethene- and even vinylidenerhodium derivatives such as *trans*-$[Rh(py)(L)(PiPr_3)_2]^+$ and *trans*-$[Rh(NH_3)(L)(PiPr_3)_2]^+$ (L = CO, C_2H_4, C=CHR) are accessible and, with BF_4^- or PF_6^- as counterion, stable under ambient conditions,[5] we felt encouraged to prepare also the corresponding species with L = C=C=CRR′.

In this paper we report the synthesis of complexes *trans*-$[Rh(L')(=C=C=CPh_2)(PiPr_3)_2]PF_6$, the first X-ray crystal structure analysis of a *cationic* rhodium compound with Rh=C=C=CPh_2 as a molecular unit, and an alternative preparative route to neutral species with X^- instead of L′ as ligands coordinated to rhodium(I).

Precursors of the General Composition *cis*-$[Rh(acetone)_2(L)_2]^+$

The procedure which we recently used for the synthesis of the above-mentioned compounds *trans*-[Rh(py)(L)-(P*i*Pr$_3$)$_2$]X with L = CO, C_2H_4 and C=CHR[5] turned out to be not the method of choice for L = C=C=CPh_2. Treatment of the mixture of $[Rh(\eta^3\text{-}C_3H_5)(PiPr_3)_2]$ and $[pyH]BF_4$ with the propargylic alcohol HC≡CCPh_2OH in acetone at room temperature led, within a short period of time, to the formation of a deep red solution from which a red, moderately air-sensitive solid was obtained after removal of the solvent. According to the NMR spectra it consisted mainly of our target, the allenylidene complex *trans*-$[Rh(py)(=C=C=CPh_2)(PiPr_3)_2]BF_4$ but also contained some impurities. Despite several attempts these could not be completely separated from the dominating species.

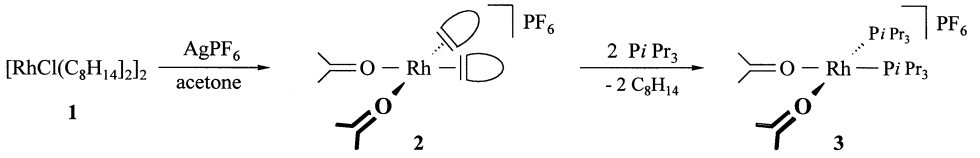
Therefore, we developed an alternative route to the cations $[Rh(L')(=C=C=CPh_2)(PiPr_3)_2]^+$ by using the dimeric bis(cyclooctene)rhodium(I) complex **1** as the starting material. If a suspension of **1** in acetone is treated with a solution of $AgPF_6$ in the same solvent at 0°C, a brownish yellow solution is formed from which the PF_6 salt **2** can be isolated in 74% yield. The yellow microcrystalline solid

[+] Part 47: J. Wolf, W. Stüer, C. Grünwald, O. Gevert, M. Laubender, H. Werner, *Eur. J. Inorg. Chem.* **1998**, 1827–1834.

[a] Institut für Anorganische Chemie der Universität Würzburg, Am Hubland, D-97074 Würzburg, Germany

 © WILEY-VCH Verlag GmbH, D-69451 Weinheim, 1999 1434–1948/99/0404–0613 $ 17.50+.50/0

(which decomposes at 58°C) has been characterized by elemental analysis, conductivity measurements and spectroscopic techniques. Although the ^{1}H-NMR data cannot decide whether the structure proposed in Scheme 1 is correct, in analogy to the related cation $[Rh(acetone)_2(C_8H_{12})]^+$ the *cis* arrangement of the acetone ligands seems most likely.[6] the ^{13}C-NMR spectrum at δ = 75.0 (≡CPh) and 64.5 (≡CMe) and also the IR band at 1885 cm^{-1} assigned to ν(C≡C). The Rh−P coupling of the single ^{31}P-NMR resonance of **4** (116.3 Hz) is considerably smaller than that of **3** (204.9 Hz) which also supports the *trans* position of the two P*i*Pr$_3$ groups.



Scheme 1

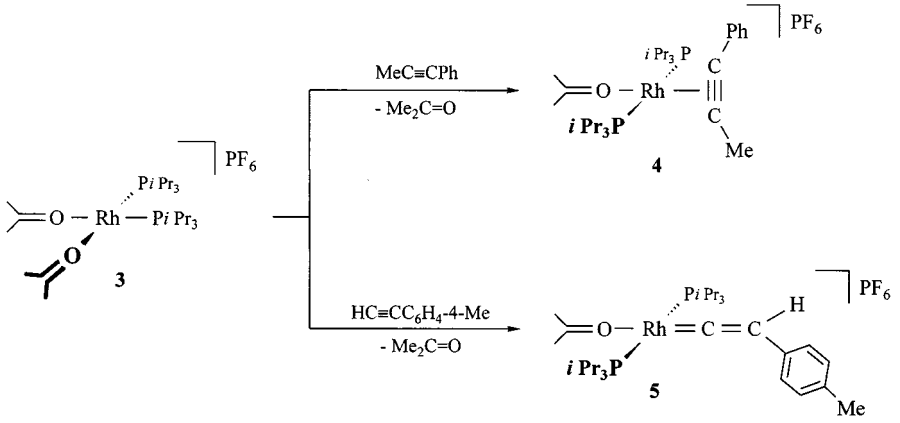
After the isolation of the cationic compound **2** the interesting question arose whether the acetone or the cyclooctene ligands are more weakly bound to the metal center. The experiment revealed that upon treatment of a suspension of **2** in ether/acetone with two equivalents of P*i*Pr$_3$ the olefinic groups are preferentially displaced. Upon recrystallization from acetone/diethyl ether the bis(phosphane) complex **3** was isolated as a violet air-sensitive solid in 98% yield. The ^{31}P-NMR spectrum of **3** displays a doublet at δ = 60.3 with a large Rh−P coupling that is typical for a *cis*-disposed $[Rh(PiPr_3)_2]$ unit.[7]

Cationic Complexes with Rh=C Bonds

The bis(acetone)rhodium(I) complex **3** proved to be an ideal precursor for the preparation of cationic vinylidene and allenylidene rhodium(I) derivatives. In order to test whether one of the metal bound ketones can be selectively replaced by an alkyne ligand, we first carried out the reaction of **3** with MeC≡CPh. It leads to the alkyne complex **4** (Scheme 2) as an orange air-sensitive solid in 75% yield. In contrast to **3**, the ^{1}H-NMR spectrum of **4** displays two resonances for the CH_3 protons of the isopropyl moieties, the virtual coupling of both points to a *trans* arrangement of the phosphane ligands.[8] Typical features of the π-bonded unsymmetrical alkyne unit are the two signals in

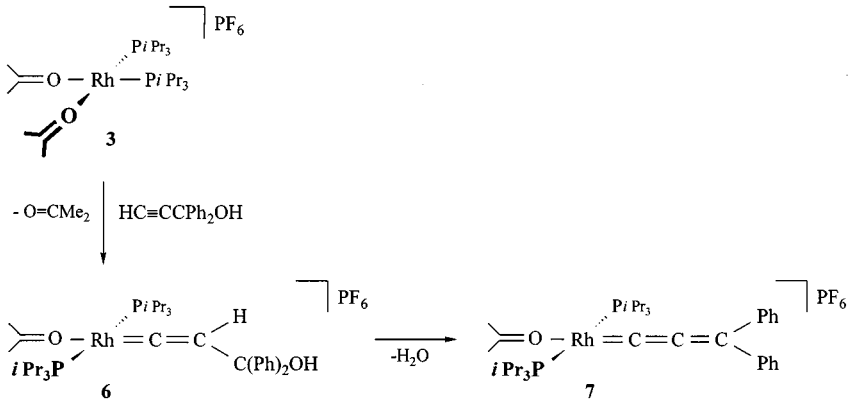
Treatment of compound **3** with HC≡CC_6H_4−4-Me as a representative of a *terminal* acetylene derivative affords instead of an alkyne complex the vinylidene isomer **5** almost quantitatively. If the 1-alkyne is added to a solution of **3** in diethyl ether/acetone at −78°C, a rapid change of color from violet to orange takes place indicating (see: compound **4** is orange) that in the initial step the cation $[Rh(O{=}CMe_2)(HC{\equiv}CR)(PiPr_3)_2]^+$ (R = *p*-tolyl) is probably formed. However, even at −78°C after a few minutes the color of the solution changes again to violet and a violet solid precipitates. Upon warming to room temperature, removal of the solvent and recrystallization of the residue from acetone/diethyl ether the product was obtained in 95% yield. In agreement with the spectroscopic data of other vinylidenerhodium(I) complexes,[5][9][10] the ^{13}C-NMR spectrum of **5** displays two signals (both doublets of triplets) in the low-field region at δ = 309.3 and 113.3 which are assigned to the α- and β-carbon atoms of the vinylidene ligand, respectively.

The course of the reaction of the bis(acetone)rhodium(I) compound **3** with the propargylic alcohol HC≡CCPh_2OH in diethyl ether/acetone is at least in the initial stage quite similar to that of **3** with HC≡CC_6H_4−4-Me (see Scheme 3). If the solution, after it was stirred at −78°C for 2 min and then warmed to 0°C, was quickly worked up an orange-red solid was isolated which based on the NMR spec-



Scheme 2

tra consists of a mixture of the functionalized vinylidene compound **6** and the allenylidene complex **7**, the first being the dominating species. Attempts to obtain **6** as an analytically pure solid failed since the crude product upon dissolution, e.g., in acetone or dichloromethane smoothly converted completely to **7**. In acetone at room temperature, the formation of **7** is completed in ca. 15 min. Removal of the solvent and recrystallization of the residue from acetone/diethyl ether gave orange crystals which were characterized by elemental analysis, conductivity measurements and spectroscopic means. In contrast to the neutral compounds *trans*-[RhCl{=C=C=C(Ph)R}(P*i*Pr$_3$)$_2$],[1][11] in the ^{13}C-NMR spectrum of **7** the resonances of the α-and β-carbon atoms of the Rh=C=C=C moiety could not be observed, even if a saturated solution of **7** in [D$_6$]acetone was used. The signal of the respective γ-carbon atom appears at δ = 150.8 as a singlet.



Scheme 3

In order to confirm the structure proposed for **7** [which is the first *cationic* allenylidenerhodium(I) complex], an X-ray crystal structure analysis was carried out. The result is shown in Figure 1. The coordination geometry around the rhodium center is almost exactly square-planar with bond angles P1−Rh−P2 and O1−Rh−C1 of 176.78(2)° and 178.67(9)°. The Rh−C1 distance is 1.822(2) Å and thus somewhat shorter than in *trans*-[RhCl{=C=C=C(Ph)C$_6$H$_4$−2-Me}(P*i*Pr$_3$)$_2$] [1.855(5) Å].[11] The shortening is surprising insofar as in *cationic* rhodium(I) species the degree of π-back bonding should be smaller compared to structurally related *neutral* derivatives. The bond length C1−C2 [1.267(3) Å] is slightly longer and the bond length C1−C3 [1.343(3) Å] slightly shorter than in the above-mentioned allenylidene(chloro)rhodium(I) compound [C1−C2 = 1.239(8) Å, C2−C3 = 1.370(9) Å], indicating that for the bonding situation the resonance structure **B** (Figure 2) is less important in the cationic complex than in the neutral analog. The Rh−C−C−C chain is nearly linear, with only a slight bending at the carbon atom C2. The planes of the two phenyl groups are not perpendicular to each other like the aryl rings in *trans*-[RhCl{=C=C=C(Ph)C$_6$H$_4$−2-Me}(P*i*Pr$_3$)$_2$] but form a dihedral angle of 68.31(8)°. The atoms O1, C34, C35 and C36 of the acetone ligand lie in a plane which is orthogonal to the central plane [P1, P2, Rh, O1, C1] and we assume that this minimizes the steric repulsion between the O=CMe$_2$ and the P*i*Pr$_3$ ligands.

Ligand Substitution Reactions of Compounds 5 and 7

The observation that in the starting material **3** one of the ketone ligands could be easily replaced by an alkyne, vinylidene or allenylidene unit, led us to try to substitute also the remaining acetone moiety in the cations *trans*-[Rh(O=CMe$_2$)(L)(P*i*Pr$_3$)$_2$]$^+$ by an olefin, alkyne or even a more typical π-acceptor ligand such as CO. However, all these attempts failed. Nevertheless, the displacement of acetone in the vinylidene and allenylidene complexes **5** and **7** can be achieved with *N-donors* such as pyridine or ammonia under very mild conditions. After workup the substitution products **8**−**10** were isolated in 85−90% yield (Scheme 4). The properties of the pyridine- and ammonia-containing cationic compounds are very similar to those of the acetone derivatives **5** and **7** and thus deserve no further comment. It should be mentioned, however, that since for the preparation of **10** aqueous ammonia was used as the substrate, the C=C=CPh$_2$ ligand is *not* attacked by OH$^-$ or H$_2$O as a nucleophile as was observed with a variety of cationic *six-coordinate* allenylidenemetal complexes.[12] The ^{13}C-NMR spectrum of **9** displays the three expected signals for the α-, β- and γ-carbon atoms of the Rh−C−C−C chain at δ = 270.4, 229.6 and 150.9, of which those at lowest fields (assigned to α-C and β-C) are split into doublets of triplets.

In order to illustrate that the acetone ligand of compound **7** can also be displaced by coordinating anions, the known acetato- and hydroxorhodium(I) derivatives **11** and **12** were prepared by this route (Scheme 5). From **7** as the starting material and with CH$_3$CO$_2$Na or KOH as the substrate, the isolated yield of **11** and **12** is ca. 80%. The neutral allenylidene complex **12** with OH in *trans* position to the C$_3$Ph$_2$ unit was originally prepared from the chloro compound *trans*-[RhCl(=C=C=CPh$_2$)(P*i*Pr$_3$)$_2$] and KO*t*Bu in C$_6$H$_6$/*t*BuOH and upon treatment with acetic acid trans-

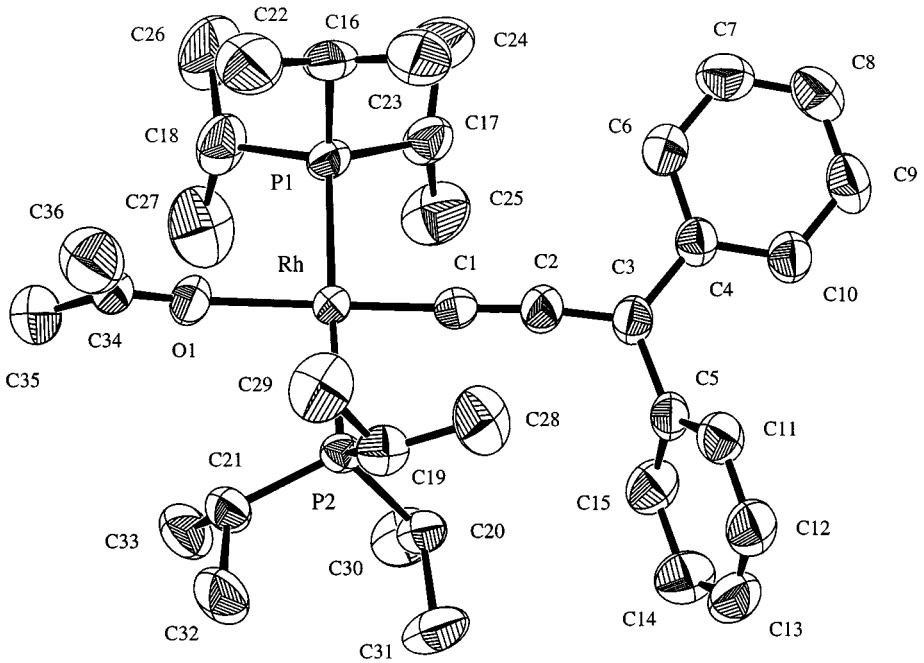


Figure 1. Molecular structure (ORTEP plot) of the cation of compound **7**; the hydrogen atoms are omitted for clarity; selected bond lengths (Å) and angles [°]: Rh−P1 2.3557(6), Rh−P2 2.3513(6), Rh−O1 2.078(2), Rh−C1 1.822(2), C1−C2 1.267(3), C2−C3 1.343(3), C3−C4 1.472(3), C3−C5 1.491(3), O1−C34 1.216(3); P1−Rh−P2 176.78(2), P1−Rh−O1 90.08(5), P1−Rh−C1 90.11(6), P2−Rh−O1 92.41(5), P2−Rh−C1 87.45(6), O1−Rh−C1 178.67(9), Rh−C1−C2 178.1(2), C1−C2−C3 172.6(2), C2−C3−C4 122.8(2), C2−C3−C5 118.2(2), O1−C34−C35 119.1(3), O1−C34−C36 122.4(3)

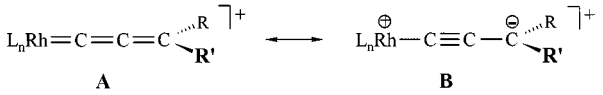
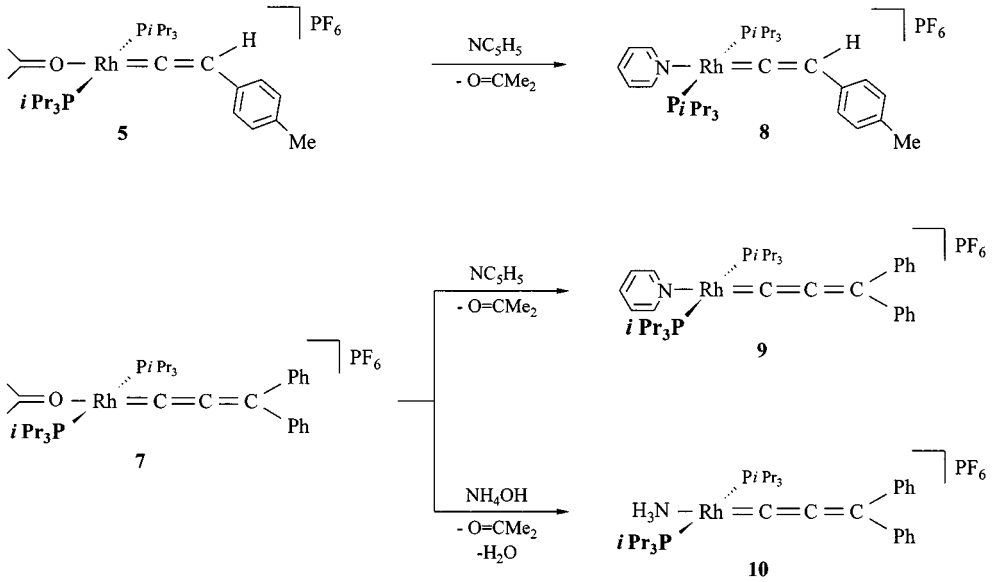


Figure 2. Resonance structures for allenylidenemetal complexes

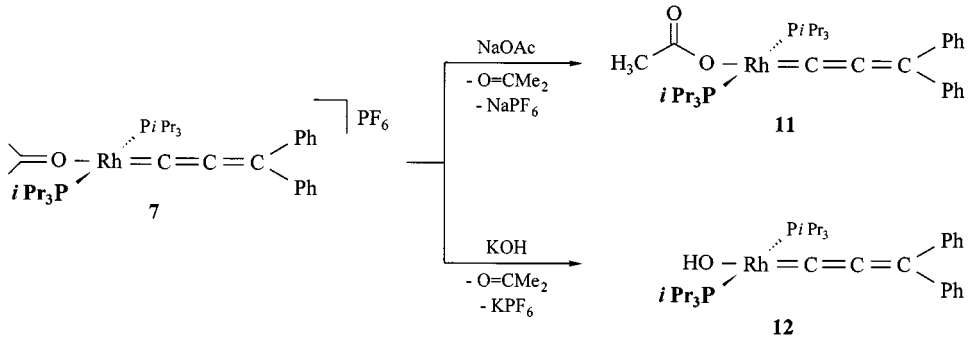
formed to the acetato derivative.[2b][3] Some exploratory studies indicate that it is possible to substitute the acetone ligand of **7** also by C-nucleophiles such as $CH(CN)_2^-$ or CN^- and thus the reaction of **7** with X^- could be an alternative route for the preparation of allenylidenerhodium(I) complexes of the general composition *trans*-[RhX(=C=C=CPh$_2$)(P*i*Pr$_3$)$_2$].

Concluding Remarks

The present investigation has shown that in addition to the well-known neutral rhodium allenylidenes *trans*-[RhX(=C=C=CRR′)(P*i*Pr$_3$)$_2$] structurally related *cationic* complexes *trans*-[Rh(=C=C=CPh$_2$)(L)(P*i*Pr$_3$)$_2$]$^+$ with L = acetone, pyridine or ammonia are also accessible. The



Scheme 4



Scheme 5

method of choice for preparing these compounds (as the PF_6 salts) is the "alkynol route", which was developed by Selegue[13] and later used by us[3][14] and several other groups as well.[15][16] The most remarkable feature is that the starting material **3** (which despite the lability of the acetone-metal bonds has been isolated and fully characterized) reacts with terminal alkynes HC≡CR, including the propargylic alcohol $HC{\equiv}CCPh_2OH$, almost instantaneously to give cationic vinylidene compounds with Rh=C=CHR as the central unit. Since all attempts to detect the corresponding *alkyne*rhodium(I) derivatives assumed to be formed in the initial step failed, we conclude that the metal-assisted isomerization of HC≡CR to C=CHR takes place considerably *faster* in the coordination sphere of a four-coordinate *cationic* than of a related *neutral* d^8 metal center. With regard to the subsequent conversion of the Rh=C=$CHCPh_2OH$ to the Rh=C=C=CPh_2 unit we note that in the case of the *cationic* species the elimination of water also occurs much more readily than for the analogous neutral derivative and that neither the presence of Al_2O_3 nor of Brønsted acids HX is necessary for this process.

Experimental Section

General: All operations were carried out under argon using Schlenk techniques. The starting material $[RhCl(C_8H_{14})_2]_2$ (**1**)[17] and the propargylic alcohol $HC{\equiv}CCPh_2OH$[18] were prepared as described in the literature. The other alkynes were commercial products from ABCR and Aldrich. − IR: Perkin-Elmer 1420. − NMR: Bruker AC 200 and AMX 400 [dvt = doublet of virtual triplets; $N = {}^3J(PH) + {}^5J(PH)$ or ${}^2J(PC) + {}^4J(PC)$, respectively]. − Conductivity measurements in nitromethane with a Schott Konduktometer CG 851. − Melting and decomposition points determined by DTA.

1. Preparation of *cis*-[Rh(O=CMe_2)$_2$(C_8H_{14})$_2$]PF_6 (2): A suspension of 404 mg (0.56 mmol) of **1** in 30 mL of acetone was treated dropwise at 0°C with a solution of 276 mg (1.09 mmol) of $AgPF_6$ in 2 mL of acetone. Under continuous stirring the reaction mixture was slowly warmed to room temp. (ca. 20 min) and after it was stored for 1 h the solution was filtered. The filtrate was concentrated to ca. 5 mL in vacuo and 20 mL of diethyl ether was added. A yellow microcrystalline solid precipitated which was separated from the mother liquor, washed three times with 2-mL portions of diethyl ether and dried; yield 471 mg (74%); dec. temp. 58°C; Λ = 80 $cm^2\Omega^{-1}mol^{-1}$. − ^1H NMR (200 MHz, CD_3NO_2): δ = 2.97 (m, 4 H, =CH of C_8H_{14}), 2.42 (s, 12 H, O=CMe_2), 2.25, 1.62, 1.42 (all m, 24 H, CH_2 of C_8H_{14}). − $C_{22}H_{40}F_6O_2PRh$ (584.4): calcd. C 45.21, H 6.90; found C 44.98, H 6.61.

2. Preparation of *cis*-[Rh(O=CMe_2)$_2$($PiPr_3$)$_2$]PF_6 (3): A suspension of 90 mg (0.15 mmol) of **2** in 10 mL of diethyl ether/acetone (9:1) was treated at −78°C with 62 μL (0.31 mmol) of P*i*Pr_3. Under continuous stirring the reaction mixture was slowly warmed to room temp. (ca. 30 min) which led to a change of color from yellow to dark violet. Moreover, a small amount of a violet solid precipitated. The solution was concentrated to ca. 1 mL in vacuo and then 10 mL of diethyl ether was added. After the mixture was stored for 2 h, the violet precipitate was separated from the mother liquor, washed three times with 2-mL portions of diethyl ether and dried; yield 103 mg (98%); dec. temp. 83°C; Λ = 110 $cm^2\Omega^{-1}mol^{-1}$. − IR (CH_2Cl_2): $\tilde{\nu}$ = 1705, 1653 cm^{-1} (C=O). − ^1H NMR (200 MHz, $(CD_3)_2CO$): δ = 2.08 (s, 12 H, O=CMe_2), 2.03 (m, 6 H, PC*H*CH_3), 1.40 [dd, J(PH) = 13.1, J(HH) = 7.3 Hz, 36 H, PCHC*H*$_3$]. − ^{31}P NMR (81.0 MHz, $(CD_3)_2CO$): δ = 60.3 [d, J(RhP) = 204.9 Hz]. − $C_{24}H_{54}F_6O_2P_3Rh$ (684.5): calcd. C 42.11, H 7.95; found C 42.62, H 7.84.

3. Preparation of *trans*-[Rh(O=CMe_2)(MeC≡CPh)($PiPr_3$)$_2$]PF_6 (4): A suspension of 103 mg (0.15 mmol) of **3** in 10 mL of diethyl ether/acetone (9:1) was treated at −78°C with 19 μL (0.15 mmol) of MeC≡CPh. After the reaction mixture was slowly warmed to room temp. (ca. 30 min), it was worked up analogously as described for **3**. Orange microcrystalline solid; yield 84 mg (75%); dec. temp. 44°C; Λ = 77 $cm^2\Omega^{-1}mol^{-1}$. − IR (CH_2Cl_2): $\tilde{\nu}$ = 1885 (C≡C), 1707 cm^{-1} (C=O). − ^1H NMR (400 MHz, $(CD_3)_2CO$): δ = 7.68 (m, 5 H, C_6H_5), 2.50 (br. s, 3 H, ≡CMe), 2.08 (s, 6 H, O=CMe_2), 1.94 (m, 6 H, PC*H*CH_3), 1.37 [dvt, N = 13.5, J(HH) = 7.0 Hz, 18 H, PCHC*H*$_3$], 1.12 [dvt, N = 13.1, J(HH) = 6.8 Hz, 18 H, PCHC*H*$_3$]. − ^{13}C NMR (100.6 MHz, $(CD_3)_2CO$): δ = 206.2 (s, O=*C*Me_2), 130.9, 129.1, 128.8, 127.7 (all s, C_6H_5), 75.0 (br. m, ≡*C*Ph), 64.5 (br. m, ≡*C*Me), 30.4 (s, O=C*C*H_3), 23.5 (vt, N = 17.7 Hz, P*C*HCH_3), 20.8, 19.6 (both s, PCH*C*H_3), 13.2 (s, ≡C*C*H_3). − ^{31}P NMR (81.0 MHz, $(CD_3)_2CO$): δ = 33.9 [d, J(RhP) = 116.3 Hz]. − $C_{30}H_{56}F_6OP_3Rh$ (742.6): calcd. C 48.52, H 7.60; found C 48.42, H 7.33.

4. Preparation of *trans*-[Rh(O=CMe_2)(=C=CHC_6H_4−4-Me)($PiPr_3$)$_2$]PF_6 (5): A suspension of 103 mg (0.15 mmol) of **3** in 10 mL of diethyl ether/acetone (9:1) was treated at −78°C with 19 μL (0.15 mmol) of $HC{\equiv}CC_6H_4$−4-Me. A rapid change of color from violet to orange occurred which after ca. 5 min was followed by a reverse change of color from orange to violet. Upon continuous stirring a violet solid precipitated. The reaction mixture was slowly warmed to room temp. (ca. 30 min), and after it was stirred for 8 h the solvent was removed in vacuo. The residue was dissolved in 1 mL of acetone and 20 mL of diethyl ether was added to the

solution. Violet crystals were formed which were washed three times with 2-mL portions of diethyl ether and dried; yield 106 mg (95%); dec. temp. 98°C; Λ = 92 $cm^2\Omega^{-1}mol^{-1}$. – ^1H NMR [400 MHz, $(CD_3)_2CO$]: δ = 6.65 (m, 4 H, C_6H_4), 2.46 (m, 6 H, PC*H*CH_3), 2.30 (s, 3 H, C_6H_4C*H*$_3$), 2.08 (s, 6 H, O=CMe_2), 1.38 [dvt, *N* = 14.0, *J*(HH) = 7.0 Hz, 36 H, PCHC*H*$_3$]; signal of =CH proton probably covered by signal of PCHC*H*$_3$ protons. – ^{13}C NMR [100.6 MHz, $(CD_3)_2CO$]: δ = 309.3 [dt, *J*(RhC) = 61.4, *J*(PC) = 17.6 Hz, Rh=C], 206.3 (s, O=*C*Me_2), 136.2, 129.8, 126.8, 120.6 (all s, C_6H_4), 113.3 [dt, *J*(RhC) = 16.1, *J*(PC) = 6.0 Hz, =CH], 30.3 (s, O=C*C*H_3), 24.3 (vt, *N* = 20.9 Hz, P*C*HCH_3), 20.8 (s, C_6H_4*C*H_3), 20.1 (s, PCH*C*H_3). – ^{31}P NMR (162.0 MHz, $(CD_3)_2CO$): δ = 42.5 [d, *J*(RhP) = 135.1 Hz]. – $C_{30}H_{56}F_6OP_3Rh$ (742.6): calcd. C 48.52, H 7.60; found C 48.56, H 7.62.

5. Generation of *trans*-[Rh(O=CMe_2)(=C=CHCPh_2OH)-($PiPr_3$)$_2$]PF_6 (6): A suspension of 103 mg (0.15 mmol) of **3** in 10 mL of diethyl ether/acetone (9:1) was treated at −78°C with 31 mg (0.15 mmol) of HC≡CCPh_2OH. A rapid change of color from violet to orange occurred. After the solution was stirred for 2 min and then warmed to 0°C, it was concentrated to ca. 1 mL in vacuo. Upon dropwise addition of diethyl ether and subsequently of pentane (ca. 10 mL) an orange-red solid precipitated which was separated from the mother liquor, washed three times with 2-mL portions of diethyl ether, then with 2 mL of pentane, and dried. The ^1H- and ^{31}P-NMR spectra revealed that besides **6** also compound **7** was formed. – IR (CH_2Cl_2): $\tilde{\nu}$ = 3410 (OH), 1642 cm^{-1} (C=C). – ^1H NMR [400 MHz, $(CD_3)_2CO$]: δ = 7.57 (m, 10 H, C_6H_5), 3.05 (br. s, 1 H, OH), 2.41 (m, 6 H, PC*H*CH_3), 2.08 (s, 6 H, O=CMe_2), 1.30 [dvt, *N* = 13.9, *J*(HH) = 6.8 Hz, 36 H, PCHC*H*$_3$]; signal of =CH proton probably covered by signal of PCHC*H*$_3$ protons. – ^{13}C NMR [100.6 MHz, $(CD_3)_2CO$]: δ = 206.3 (s, O=*C*Me_2), 130.2, 128.4, 125.9 (all s, C_6H_5), 117.8 [dt, *J*(RhC) = 17.1, *J*(PC) = 6.0 Hz, =CH], 72.0 (s, *C*Ph_2OH), 30.2 (s, O=C*C*H_3), 23.9 (vt, *N* = 20.7 Hz, P*C*HCH_3), 19.8 (s, PCH*C*H_3); signal of Rh=C not exactly located. – ^{31}P NMR [162.0 MHz, $(CD_3)_2CO$]: δ = 42.3 [d, *J*(RhP) = 135.9 Hz].

6. Preparation of *trans*-[Rh(O=CMe_2)(=C=C=CPh_2)($PiPr_3$)$_2$]PF_6 (7): A suspension of 103 mg (0.15 mmol) of **3** in 10 mL of diethyl ether/acetone (9:1) was treated at −78°C with 31 mg (0.15 mmol) of HC≡CCPh_2OH, and upon warming to room temp. was stirred for 15 h. The solvent was removed, the residue was dissolved in 1 mL of acetone and the solution was layered with 20 mL of diethyl ether. Orange crystals were formed which were separated from the mother liquor, washed three times with 2-mL portions of diethyl ether, once with 2 mL of pentane, and dried; yield 93 mg (76%); dec. temp. 62°C; Λ = 87 $cm^2\Omega^{-1}mol^{-1}$. – IR (KBr): $\tilde{\nu}$ = 1873 cm^{-1} (C=C=C). – ^1H NMR [400 MHz, $(CD_3)_2CO$]: δ = 7.73 (m, 10 H, C_6H_5), 2.49 (m, 6 H, PC*H*CH_3), 2.18 (s, 6 H, O=CMe_2), 1.41 [dvt, *N* = 13.8, *J*(HH) = 7.1 Hz, 36 H, PCHC*H*$_3$]. – ^{13}C NMR [100.6 MHz, $(CD_3)_2CO$]: δ = 206.3 (s, O=*C*Me_2), 150.8 (s, Rh=C=C=*C*), 130.5, 130.3, 126.5 (all s, C_6H_5), 30.2 (s, O=C*C*H_3), 24.8 (vt, *N* = 20.6, P*C*HCH_3), 20.0 (s, PCH*C*H_3); signals of α- and β-carbon atoms of Rh=C=C=C unit not exactly located. – ^{31}P NMR [162.0 MHz, $(CD_3)_2CO$]: δ = 41.8 [d, *J*(RhP) = 132.7 Hz]. – $C_{36}H_{58}F_6OP_3Rh$ (816.7): calcd. C 52.94, H 7.16, Rh 12.60; found C 52.51, H 6.87, Rh 13.00.

7. Preparation of *trans*-[Rh(=C=CHC$_6$H$_4$−4-Me)(py)($PiPr_3$)$_2$]PF_6 (8): A suspension of 111 mg (0.15 mmol) of **5** in 10 mL of diethyl ether was treated at −78°C with an excess (ca. 0.5 mL) of pyridine which led to the precipitation of a red-violet solid. After the reaction mixture was warmed under continuous stirring to room temp. (ca. 30 min), it was stored for 1 h. The red-violet solid was separated from the mother liquor, washed three times with 2-mL portions of diethyl ether and dried; yield 86 mg (91%); dec. temp. 96°C. – ^1H NMR (200 MHz, CD_3NO_2): δ = 8.03 (m, 5 H, NC_5H_5), 6.63 (m, 4 H, C_6H_4), 2.42 (m, 6 H, PC*H*CH_3), 2.28 (s, 3 H, C_6H_4C*H*$_3$), 1.39 [dvt, *N* = 14.0, *J*(HH) = 7.0 Hz, 36 H, PCHC*H*$_3$]; signal of =CH proton probably covered by signal of PCHC*H*$_3$ protons. – ^{13}C NMR (50.3 MHz, CD_3NO_2): δ = 309.2 [dt, *J*(RhC) = 61.2, *J*(PC) = 17.4 Hz, Rh=C], 151.8, 140.5, 136.2, 129.7, 127.3, 126.8, 121.5 (all s, NC_5H_5 and C_6H_4), 114.3 [dt, *J*(RhC) = 16.0, *J*(PC) = 6.1 Hz, =CH], 24.6 (vt, *N* = 20.9 Hz, P*C*HCH_3), 21.1 (s, C_6H_4*C*H_3), 20.1 (s, PCH*C*H_3). – ^{31}P NMR [162.0 MHz, $(CD_3)_2CO$]: δ = 40.3 [d, *J*(RhP) = 134.9 Hz]. $C_{32}H_{55}F_6NP_3Rh$ (763.6): calcd. C 50.33, H 7.62, N 1.83; found C 49.56, H 7.62, N 1.50.

8. Preparation of *trans*-[Rh(=C=C=CPh_2)(py)($PiPr_3$)$_2$]PF_6 (9): Analogously as described for **8**, by using 123 mg (0.15 mmol) of **7** and ca. 0.5 mL of pyridine as starting materials. Red-violet solid; yield 109 mg (87%); dec. temp. 98°C. – IR (CH_2Cl_2): $\tilde{\nu}$ = 1916 cm^{-1} (C=C=C). – ^1H NMR (400 MHz, CD_3NO_2): δ = 8.38, 7.48, 7.27 (all m, 5 H, NC_5H_5), 7.92, 7.59, 7.37 (all m, 10 H, C_6H_5), 2.16 (m, 6 H, PC*H*CH_3), 1.24 [dvt, *N* = 13.7, *J*(HH) = 6.6 Hz, 36 H, PCHC*H*$_3$]. – ^{13}C NMR (100.6 MHz, CD_3NO_2): δ = 270.4 [dt, *J*(RhC) = 56.0, *J*(PC) = 19.0 Hz, Rh=C], 229.6 [dt, *J*(RhC) = 15.0, *J*(PC) = 9.0 Hz, Rh=C=*C*], 153.2, 140.3, 131.1, 129.7, 128.1, 127.3, 126.5 (all s, NC_5H_5 and C_6H_5), 150.9 (s, =*C*Ph_2), 26.4 (vt, *N* = 20.0 Hz, P*C*HCH_3), 20.5 (s, PCH*C*H_3). – ^{31}P NMR (162.0 MHz, CD_3NO_2): δ = 38.2 [d, *J*(RhP) = 134.0 Hz]. – $C_{38}H_{57}F_6NP_3Rh$ (837.7): calcd. C 54.99, H 6.86, N 1.67; found C 54.87, H 7.20, N 1.79.

9. Preparation of *trans*-[Rh(=C=C=CPh_2)(NH_3)($PiPr_3$)$_2$]PF_6 (10): A solution of 123 mg (0.15 mmol) of **7** in 10 mL of CH_2Cl_2 was treated at −20°C with 2.8 mL of a 0.55 M solution of NH_4OH (0.15 mmol) in water. The solution was slowly warmed to room temp. and, after it was continuously stirred for 1 h, concentrated to ca. 1 mL in vacuo. The solution was then layered with 10 mL of diethyl ether and upon storing for 6 h at room temp. red crystals were formed. The crystals were separated from the mother liquor, washed three times with 2-mL portions of diethyl ether and pentane and dried; yield 116 mg (85%); dec. temp. 134°C. – IR (CH_2Cl_2): $\tilde{\nu}$ = 1905 cm^{-1} (C=C=C). – ^1H NMR (400 MHz, CD_3NO_2): δ = 7.89, 7.31 (both m, 10 H, C_6H_5), 2.52 (m, 6 H, PC*H*CH_3), 1.32 [dvt, *N* = 13.4, *J*(HH) = 6.7 Hz, 36 H, PCHC*H*$_3$]. – ^{13}C NMR (100.6 MHz, CD_3NO_2): δ = 269.1 (br. m, Rh=C), 230.5 [dt, *J*(RhC) = 19.0 *J*(PC) = 7.0 Hz, Rh=C=*C*], 151.8 (s, =*C*Ph_2), 152.4, 130.7, 130.1, 127.0 (all s, C_6H_5), 25.5 (vt, *N* = 20.0 Hz, P*C*HCH_3), 20.4 (s, PCH*C*H_3). – ^{31}P NMR (162.0 MHz, CD_3NO_2): δ = 41.6 [*J*(RhP) = 131.0 Hz]. – $C_{33}H_{55}F_6NP_3Rh$ (775.6): calcd. C 51.10, H 7.15, N 1.81; found C 50.87, H 7.12, N 1.78.

10. Preparation of *trans*-[Rh(OAc)(=C=C=CPh_2)($PiPr_3$)$_2$] (11): A suspension of 123 mg (0.15 mmol) of **7** in 10 mL of diethyl ether/acetone (9:1) was treated at −78°C with 12 mg (0.15 mmol) of sodium acetate. A rapid change of color from deep orange to green occurred. Under continuous stirring the reaction mixture was warmed to room temp. and then brought to dryness in vacuo. The residue was extracted with 20 mL of diethyl ether, and the solvent was removed from the extract. The residue was dissolved in 2 mL of acetone and the solution was stored at −20°C for 8 h. Green crystals were formed which were separated from the mother liqour, washed three times with 2-mL portions of acetone (−20°C) and dried; yield 82 mg (81%). Compound **11** was identified by comparison of the IR and NMR data with those of an authentic sample.[2b][19]

11. Preparation of *trans*-[Rh(OH)(=C=C=CPh$_2$)(PiPr$_3$)$_2$] (12): Analogously as described for **11**, by using 123 mg (0.15 mmol) of **7** and 8 mg (0.15 mmol) of KOH as starting materials. Green solid; yield 76 mg (79%). Compound **12** was identified by comparison of the IR and NMR data with those of an authentic sample.[2b][19]

12. Determination of the X-ray Crystal Structure of 7:[20] Single crystals were grown from acetone/diethyl ether at room temp. Crystal data (from 23 reflections, $10° < \Theta < 13°$): triclinic; space group P-1 (No. 2); a = 9.074(6), b = 14.42(1), c = 16.16(1) Å, α = 85.50(5), β = 87.16(5), γ = 77.61(5)°; V = 2057(3) Å^3, Z = 2; $d_{calcd.}$ = 1.32 gcm^{-3}; μ(Mo-K_α) = 5.7 cm^{-1}; crystal size 0.15 × 0.15 × 0.40 mm; Enraf-Nonius CAD-4 diffractometer, Mo-K_α radiation (λ = 0.71073 Å), graphite monochromator, zirconium filter (factor 16.4); T = 293(1) K; ω/Θ-scan, max. 2Θ = 48°; 6904 reflections measured, 6442 independent ($R_{int.}$ = 0.0091), 5779 with $F_o > 2\sigma(F_o)$. Intensity data were corrected for Lorentz and polarization effects and an empirical absorption correction (Ψ-scan method) was applied (min. transmission 96.1%). The structure was solved by direct methods (SHELXS-86).[21] Atomic coordinates and the anisotropic thermal parameters of non-hydrogen atoms were refined by full-matrix least squares on F^2 (SHELXS-93).[22] The PF_6^- anion is disordered. The positions of 18 fluorine atoms (3 × 6) could be located around the central phosphorus atom P3 and refined anisotropically with a weighting factor of 1/3. The positions of all hydrogen atoms could be located in a final difference Fourier synthesis and refined isotropically. Conventional R = 0.0216 [for 5779 reflections with $F_o > 2\sigma(F_o)$], and weighted wR_2 = 0.0612 for all 6442 located reflections; reflection/parameter ratio 10.1; residual electron density +0.20/-0.27 eÅ^{-3}.

Acknowledgments

This work was supported by the Deutsche Forschungsgemeinschaft (SFB 347) and the Fonds der Chemischen Industrie (Promotionsstipendium to O. N.). We are grateful to Mrs. R. Schedl and Mr. C. P. Kneis for performing the elemental analyses and DTA measurements, to Dr. B. Stempfle and Dr. W. Buchner for NMR spectra, and in particular to Mrs. A. Spenkuch for valuable technical assistance. Degussa AG generously supported this work by gifts of chemicals.

[1] H. Werner, T. Rappert, *Chem. Ber.* **1993**, *126*, 669−678.
[2] [2a] R. Wiedemann, P. Steinert, O. Gevert, H. Werner, *J. Am. Chem. Soc.* **1996**, *118*, 2495−2496. − [2b] H. Werner, R. Wiedemann, M. Laubender, J. Wolf, B. Windmüller, *Chem. Commun.* **1996**, 1413−1414. − [2c] H. Werner, M. Laubender, R. Wiedemann, B. Windmüller, *Angew. Chem.* **1996**, *108*, 1330−1332; *Angew. Chem., Int. Ed. Engl.* **1996**, *35*, 1237−1239. − [2d] M. Laubender, Dissertation, Universität Würzburg, to be submitted.
[3] H. Werner, *Chem. Commun.* **1997**, 903−910.
[4] H. Werner, R. Wiedemann, N. Mahr, P. Steinert, J. Wolf, *Chem. Eur. J.* **1996**, *2*, 561−569.
[5] O. Nürnberg, H. Werner, *J. Organomet. Chem.* **1993**, *460*, 163−175.
[6] R. R. Schrock, J. A. Osborn, *J. Am. Chem. Soc.* **1971**, *93*, 3089−3091.
[7] [7a] M. Schäfer, J. Wolf, H. Werner, *J. Chem. Soc., Chem. Commun.* **1991**, 1341−1343. − [7b] H. Werner, M. Schäfer, O. Nürnberg, J. Wolf, *Chem. Ber.* **1994**, *127*, 27−38. − [7c] H. Werner, M. Bosch, M. E. Schneider, C. Hahn, F. Kukla, M. Manger, B. Windmüller, B. Weberndörfer, M. Laubender, *J. Chem. Soc., Dalton Trans.* **1998**, in press.
[8] R. K. Harris, *Can. J. Chem.* **1962**, *42*, 2275−2281.
[9] [9a] H. Werner, F. J. Garcia Alonso, H. Otto, J. Wolf, *Z. Naturforsch., B* **1988**, *43*, 722−726. − [9b] H. Werner, U. Brekau, *Z. Naturforsch., B* **1989**, *44*, 1438−1446. − [9c] H. Werner, T. Rappert, J. Wolf, *Isr. J. Chem.* **1990**, *30*, 377−384. − [9d] T. Rappert, O. Nürnberg, N. Mahr, J. Wolf, H. Werner, *Organometallics* **1992**, *11*, 4156−4164. − [9e] T. Rappert, O. Nürnberg, H. Werner, *Organometallics* **1993**, *12*, 1359−1364. − [9f] H. Werner, M. Baum, D. Schneider, B. Windmüller, *Organometallics* **1994**, *13*, 1089−1097. − [9g] M. Baum, B. Windmüller, H. Werner, *Z. Naturforsch., B* **1994**, *49*, 859−869. − [9h] M. Schäfer, J. Wolf, H. Werner, *J. Organomet. Chem.* **1995**, *485*, 85−100. − [9i] H. Werner, P. Bachmann, M. Laubender, O. Gevert, *Eur. J. Inorg. Chem.* **1998**, 1217−1224.
[10] C. Bianchini, F. Laschi, F. Ottaviani, M. Peruzzini, P. Zanello, *Organometallics* **1988**, *7*, 1660−1661.
[11] H. Werner, T. Rappert, R. Wiedemann, J. Wolf, N. Mahr, *Organometallics* **1994**, *13*, 2721−2727.
[12] [12a] M. A. Esteruelas, A. V. Gomez, F. J. Lahoz, A. M. Lopez, E. Oñate, L. A. Oro, *Organometallics* **1996**, *15*, 3423−3435. − [12b] N. Ruiz, D. Peron, S. Sinbandith, P. H. Dixneuf, C. Baldoli, S. Maiorana, *J. Organomet. Chem.* **1997**, *533*, 213−218.
[13] J. P. Selegue, *Organometallics* **1982**, *1*, 217−218.
[14] [14a] P. Schwab, H. Werner, *J. Chem. Soc, Dalton Trans.* **1994**, 3415−3425. − [14b] T. Braun, P. Steinert, H. Werner, *J. Organomet. Chem.* **1995**, *488*, 169−176. − [14c] H. Werner, A. Stark, P. Steinert, C. Grünwald, J. Wolf, *Chem. Ber.* **1995**, *128*, 49−62. − [14d] B. Windmüller, J. Wolf, H. Werner, *J. Organomet. Chem.* **1995**, *502*, 147−161. − [14e] M. Martin, O. Gevert, H. Werner, *J. Chem. Soc., Dalton Trans.* **1996**, 2275−2283. − [14f] H. Werner, R. Lass, O. Gevert, J. Wolf, *Organometallics* **1997**, *16*, 4077−4088. − [14g] C. Grünwald, M. Laubender, J. Wolf, H. Werner, *J. Chem. Soc., Dalton Trans.* **1998**, 833−839. − [14h] H. Werner, C. Grünwald, P. Steinert, O. Gevert, J. Wolf, *J. Organomet. Chem.* **1998**, *565*, 231−241.
[15] Inter alia: [15a] H. Fischer, D. Reindl, G. Roth, *Z. Naturforsch., B* **1994**, *49*, 1207−1214. − [15b] D. Touchard, N. Pirio, P. H. Dixneuf, *Organometallics* **1995**, *14*, 4920−4928. − [15c] V. Cadierno, M. P. Gamasa, J. Gimeno, M. Gonzalez-Cueva, E. Lastra, J. Borge, S. Garcia-Granda, E. Perez-Carreño, *Organometallics* **1996**, *15*, 2137−2147. − [15d] M. A. Esteruelas, L. A. Oro, J. Schrickel, *Organometallics* **1997**, *16*, 796−799. − [15e] I. de los Rios, M. Jimenes Tenorio, M. C. Puerta, P. Valerga, *J. Organomet. Chem.* **1997**, *549*, 221−232.
[16] M. I. Bruce, *Chem. Rev.* **1991**, *91*, 197−257.
[17] A. van der Ent, A. L. Onderdelinden, *Inorg. Synth.* **1973**, *14*, 92−95.
[18] M. M. Midland, *J. Org. Chem.* **1975**, *40*, 2250−2252.
[19] R. Wiedemann, Dissertation, Universität Würzburg, **1995**.
[20] Crystallographic data (excluding structure factors) for the structures reported in this paper have been deposited with the Cambridge Crystallographic Data Centre as supplementary publication no. CCDC-106914 Copies of the data can be obtained free of charge on application to CCDC, 12 Union Road, Cambridge CB2 1EZ, UK (Fax: internat. + 44−1223/336−033; E-mail: deposit@ccdc.cam.ac.uk).
[21] G. M. Sheldrick, *Acta Crystallogr., Sect. A* **1990**, *46*, 467.
[22] G. M. Sheldrick, *A program for crystal structure refinement*, University of Göttingen, **1993**.

Received November 3, 1998
[I98378]

Syntheses and Insertion Reactions of (η^2-Aldehyde)zirconocene-Supported (Hydrido)zirconocene Cation Systems

Ulrich Blaschke,[a] Frederik Menges,[a] Gerhard Erker,*[a] and Roland Fröhlich[a]

Keywords: (η^2-Aldehyde)zirconocene complexes / Metallaoxirane-stabilized group 4 metallocene hydride cations / Nitrile insertion / Isocyanate insertion

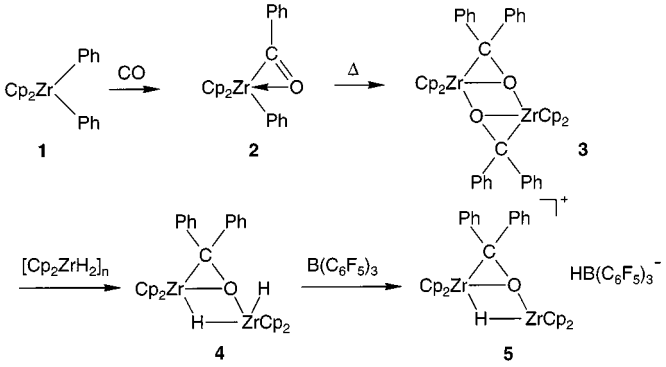
Treatment of the $[Cp_2Zr(\eta^2\text{-acetaldehyde})/H(CH_3)ZrCp_2]$ adduct **8** with $B(C_6F_5)_3$ yields the dimetallabicyclic salt $[Cp_2Zr(\mu\text{-}\eta^1\text{-}O{:}\eta^2\text{-}C,O\text{-}OCHMe)(\mu\text{-}H)(ZrCp_2)]^+[CH_3B(C_6F_5)_3]^-$ **18b**. Similarly, hydride abstraction from the related neutral dimetallabicyclic $[Cp_2Zr(OCHR)/H_2ZrCp_2]$ adducts **11** (R = CH_3) or **14** (R = C_2H_5) with $B(C_6F_5)_3$ yields the systems $[Cp_2Zr(\mu\text{-}\eta^1\text{-}O{:}\eta^2\text{-}C,O\text{-}OCHR)(\mu\text{-}H)(ZrCp_2)]^+[HB(C_6F_5)_3]^-$ (**18a**, **c**) and the reaction of $B(C_6F_5)_3$ with $[Cp_2Zr(OCHCH_2Ph)/H(PhCH_2)ZrCp_2)]^+$ **17** gives $[Cp_2Zr(\mu\text{-}\eta^1\text{-}O{:}\eta^2\text{-}C,O\text{-}(OCHCH_2Ph)(\mu\text{-}H)ZrCp_2]^+[PhCH_2B(C_6F_5)_3]^-$ **18d**. A variety of nitriles $R^2\text{–}C{\equiv}N$ (R = CH_3, CMe_3, *p*-tolyl, or ethyl) cleanly reacts with the cations **18** by addition of the $Zr_2(\mu\text{-}H)$ moiety to the nitrile functionality to yield the respective aldiminium-bridged cations $[Cp_2Zr(\mu\text{-}\eta^1\text{-}O{:}\eta^2\text{-}C,O\text{-}(OCHR^1)(\mu\text{-}N{=}CHR^2)\text{-}ZrCp_2]^+$ (**21**–**24**). Complex **24d** (R^1 = $PhCH_2$, R^2 = C_2H_5) was characterized by an X-ray crystal structure analysis. Similarly, treatment of the systems **18a**–**d** with isocyanates RN=C=O (R = CMe_3, $SiMe_3$, *p*-tolyl, or adamantyl) gave the related μ-formamidato complexes **27**–**30**.

Introduction

It has been shown that (η^2-ketone)- and (η^2-aldehyde)zirconocene complexes structurally and chemically behave as metallaoxiranes.[1] The three-membered metallacycles have a tendency of binding a variety of reactive organometallic species in a specific way by using the nucleophilic character of the metallaoxirane oxygen atom and the strongly electrophilic group 4 metal center in combination. In this way the metallaoxirane template may behave like a molecular metal-oxide model.[2] It has, for instance, been used to bind and stabilize the Cp_2ZrH_2 moiety,[3] that is not persistent as a monomer in solution.[4] The reactivity of the metallaoxirane-template stabilized zirconocene dihydride towards carbon monoxide has been used to devise molecular Fischer–Tropsch models.[5]

Recently we have succeeded in generating a (hydrido)zirconocene cation at a (η^2-diarylketone)zirconocene template.[6] The monomeric $[Cp_2ZrH]^+$ cation is probably an elusive species in solution; but stabilized at this specific metallaoxirane matrix it can readily be generated, characterized and handled. The $[Cp_2Zr(OCPh_2)/(Cp_2Zr{-}H)]^+$ adduct (see Scheme 1) even reacts with ethene to form polyethylene.[6][7]

Unfortunately, we have not been able to experimentally observe and characterize any intermediate insertion products starting from the system **5** so far. Therefore, we have begun to prepare a variety of similarly structured (hydrido)-zirconocene cation systems that are bonded to and stabilized by similar metallaoxirane template frameworks that bear less bulky and sterically demanding substituents at the organometallic three-membered ring. We have succeeded to obtain a number of such systems derived from differently substituted (η^2-aldehyde)zirconocene complexes, and in these cases it was possible to form stable monomeric insertion products by treatment with nitriles and with isocyanates. A series of examples is described in this article.



Scheme 1

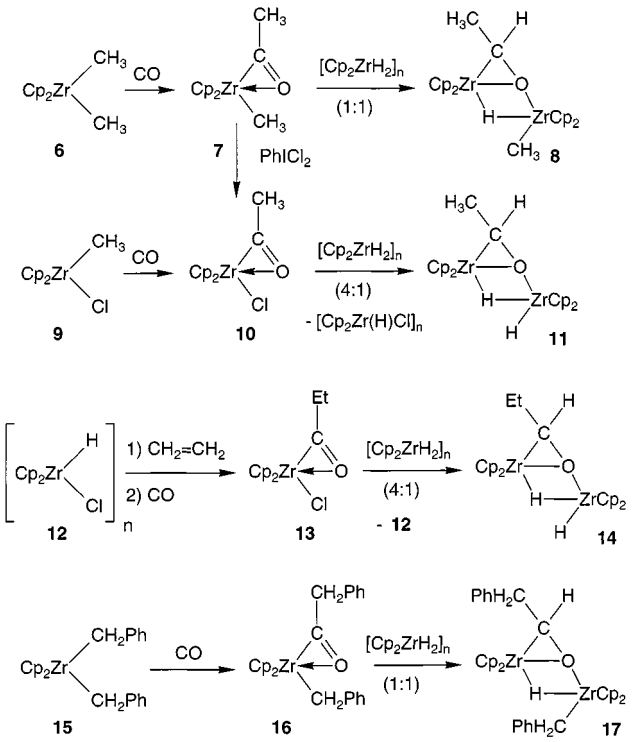
Results and Discussion

Preparation of the (η^2-Aldehyde)zirconocene-Stabilized (Hydrido)zirconocene Cation Systems

Starting materials for the preparation of the $[(\eta^2\text{-aldehyde})ZrCp_2/Cp_2ZrH]^+$ complexes investigated in the course of this study were several neutral metallaoxirane adducts of Cp_2ZrH_2 and of $Cp_2Zr(H)R$ complexes. Three different metallaoxirane templates were used, namely (η^2-acetaldehyde)-, (η^2-propionaldehyde)-, and (η^2-phenylacetaldehyde)zirconocene. The starting materials for the preparation of the dinuclear $[(\mu\text{-}\eta^1\text{-}O{:}\eta^2\text{-}C,O\text{-aldehyde})(\mu\text{-}H)(ZrCp_2)_2]^+$ cations were synthesized as follows (see also Scheme 2).

[a] Organisch-Chemisches Institut der Universität Münster, Corrensstrasse 40, D-48149 Münster, Germany
Fax: (internat.) + 49(0)251/8336503
E-mail: erker@uni-muenster.de

 © WILEY-VCH Verlag GmbH, D-69451 Weinheim, 1999 1434–1948/99/0404–0621 $ 17.50+.50/0



Scheme 2

As previously described by us,[8] the $[Cp_2Zr(OCHMe)/Cp_2Zr(H)Me]$ adduct **8** was prepared by Cp_2ZrH_2 addition to (η^2-acetyl)methyl zirconocene (**7**). The corresponding $[Cp_2Zr(OCHMe)/Cp_2ZrH_2]$ adduct (**11**) was prepared by treatment of (η^2-acetyl)zirconocene chloride (**10**) with excess $[Cp_2ZrH_2]_n$ (4:1 ratio). Under these optimized literature conditions[8] hydride addition to the (η^2-acyl)metallocene moiety is observed and a subsequent chloride vs. hydride exchange reaction is effectively achieved (for details see the Experimental Section). The $[Cp_2Zr(OCHEt)/Cp_2ZrH_2]$ adduct (**14**) was prepared analogously. We have used as an additional starting material the [Cp_2Zr(OCH-benzyl)/Cp_2Zr(H)benzyl] adduct (**17**) that to our knowledge was prepared here for the first time. The reaction sequence employed started from dibenzylzirconocene (**15**). Carbonylation yields the (η^2-phenylacetyl)benzylzirconocene complex **16**. Addition of a stoichiometric quantity of dihydridozirconocene (employed as the oligomeric $[Cp_2ZrH_2]_n$ reagent[4]) then furnished the dinuclear (μ-hydrido)bis(zirconocene) complex **17**.

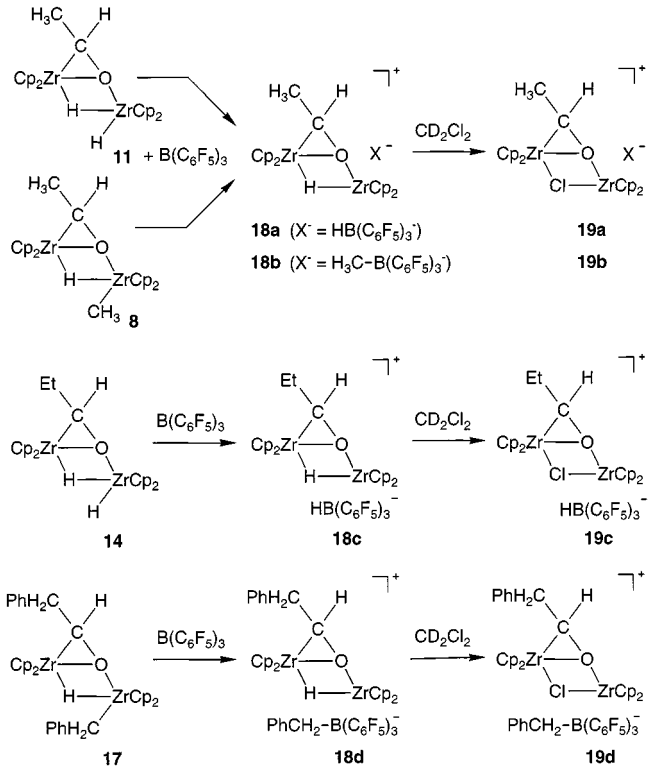
Complex **11** was treated with the organometallic Lewis acid tris(pentafluorophenyl)borane[9] in toluene solution. The reaction between the zirconium hydride and $B(C_6F_5)_3$ takes place instantaneously under these conditions at ambient temperature. The product separates from the solution as a dark colored oil. It dissolves in a [D_8]THF/[D_6]benzene mixture and can thus be characterized spectroscopically. The reaction between **11** and $B(C_6F_5)_3$ has led to abstraction[10] of the terminal hydride ligand at zirconium with formation of the adduct salt $[Cp_2Zr(OCHMe)/Cp_2ZrH]^+[HB(C_6F_5)_3]^-$ (**18a**). The borohydride anion is characterized by its ^{11}B-NMR doublet at δ −24.6 ($^1J_{BH}$ = 82 Hz). The ^{1}H-NMR spectrum of the cation of **18a** shows only a single residual hydride resonance (at δ −1.79) that is very typical of a hydride ligand bridging between two zirconium atoms[11] [see for a comparison: ^{1}H NMR of the bis(zirconocene)dihydride complex **11**: δ 4.32 (terminal Zr−H), δ −1.51 (μ-H), $^2J_{HH}$ = 13.9 Hz].[8] In the complex **18a** the metallaoxirane framework is still intact [^{1}H-NMR signals at δ 3.69 (q, 1 H), 1.48 (d, 3 H, $^3J_{HH}$ = 6.3 Hz); ^{13}C-NMR signals at δ 90.1 (C^1H) and 23.7 (C^1-CH_3)], and both bent metallocene units show diastereotopic splitting of their pairs of Cp-resonances (^{13}C NMR: δ 112.4, 112.1, 106.7, 106.6) due to the adjacent metallaoxirane chirality center (C^1HMeO[Zr]). These NMR features indicate that the chiral dimetallabicyclic framework has remained intact upon treatment of **11** with $B(C_6F_5)_3$. We conclude that this reaction has cleanly resulted in abstraction of the terminal hydride ligand at zirconium by the boron Lewis acid with formation of the dimetallic (η^2-acetaldehyde)zirconocene-template stabilized (hydrido)zirconocene cation complex **18a** (see Scheme 3). Complex **18a** can be dissolved in a halogenated solvent such as [D_2]dichloromethane at low temperature. Its NMR spectra could be recorded at 243 K, but a rather selective reaction with this solvent took place at temperatures above 255 K to replace the μ-hydride ligand by chloride from the solvent to generate **19a**. Surprisingly, dideuteromethane (CD_2H_2) was the only organic product that was detected ^{1}H-NMR spectroscopically (quintett at δ 0.17). The mechanism of this apparently selective double chloride vs. hydride exchange remains to be clarified. An analogous series of reactions was observed upon treatment of the [(η^2-propanal)$ZrCp_2$/H_2ZrCp_2] adduct **14** with $B(C_6F_5)_3$ to yield the cations **18c** and **19c**, subsequently (see Scheme 3).

The salt **18b** was prepared by treatment of **8** with $B(C_6F_5)_3$. In this case, the terminal methyl ligand at the "south-east" zirconocene moiety is selectively removed. The same cation (i.e. $[Cp_2Zr(OCHMe)/Cp_2ZrH]^+$) is obtained from the reaction of **11** with $B(C_6F_5)_3$, only that **18b** contains the $[CH_3B(C_6F_5)_3]^-$ counteranion. Its formation is evident from the respective ^{1}H-NMR (δ 1.03, CH_3B) and ^{11}B-NMR signals (singlet at δ −14.5). The remaining signals of **18a** and **18b** must be considered equivalent, taking into account the pronounced sensitivity of the actual NMR chemical shifts of this charged metallocene system to small changes in solvent polarity (for details see the Experimental Section).

Similarly, treatment of the dinuclear benzyl-substituted metallocene hydride complex **17** with $B(C_6F_5)_3$ results in selective transfer of the σ-benzylligand from zirconium to boron to yield **18d**. Exposure to CD_2Cl_2 at 265 K also leads to H^- vs. Cl^- exchange to generate **19d** and CD_2H_2 (see Scheme 3).

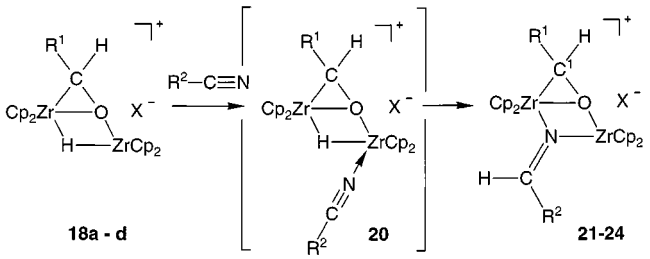
Reaction of the $[Cp_2Zr(OCHR)/Cp_2ZrH]^+$ Cations with Nitriles

The [(μ-acetaldehyde)(μ-hydrido)bis(zirconocene)]$^+$ cation [**18a**, with $HB(C_6F_5)_3^-$ anion] reacts readily with added



Scheme 3

acetonitrile.[12][13] Usually the reaction was carried out by treating a suspension of e.g. **18a** in toluene with $CH_3-C\equiv N$. The addition reaction takes place very rapidly in the two-phase system. After ca. five minutes the oil, that remains separated from the toluene solution, is collected and is shown to consist of the product **21a**. The $HB(C_6F_5)_3^-$ anion is not affected by the treatment with acetonitrile. The cation of **18a** has added its hydride to the acetonitrile $-C\equiv N$ carbon atom with formation of a dimetallated acetaldiminium moiety.[14] In **21a** the iminium nitrogen atom bridges between the two zirconium centers. This leads to the formation of a dimetallabicyclic framework, part of which is the intact (μ-η^1-O:η^2-C,O-acetaldehyde)metallocene template. Consequently, complex **21a** exhibits the typical NMR signals of the metallaoxirane moiety [^{1}H NMR in a [D_8]THF/[D_6]benzene mixture: δ 3.65 (q, 1 H), 1.52 (d, 3 H), $^3J_{HH}$ = 6.1 Hz; ^{13}C NMR: δ 88.5 (C^1-H), 23.9 (C^1-CH_3)]. The presence of the chiral center (C^1) inside the metallaoxirane ring systems results in the observation of the NMR signals of two pairs of diastereotopic Cp ligands at the zirconium centers in complex **21a** (^{13}C NMR in [D_8]THF/[D_6]benzene: δ 113.6, 113.5, 108.8, 108.7). The bridging acetaldiminium moiety shows very typical NMR features; the *H*(Me)*C*=N ^{1}H-/^{13}C-NMR resonances are located at δ 8.67 (^{1}H; q, $^3J_{HH}$ = 4.7 Hz) and δ 187.2 (^{13}C). At such a structural framework two geometrical isomers could in principle be formed that are characterized by having the aldiminium alkyl substituent oriented (*Z*) or (*E*) relative to the metallaoxirane zirconium center. Treatment of **18a** with acetonitrile yielded only a single isomer. In view of an X-ray crystal structure of a related example (see below) we tentatively assign to it the structure of the (*E*)-isomer (see Scheme 4).



R^1	X^-	R^2	CH_3	CMe_3	p-tolyl	Et
CH_3	$HB(C_6F_5)_3^-$	**21**	**a**	**b**	**c**	-
CH_3	$MeB(C_6F_5)_3^-$	**22**	**a**	**b**	**c**	**d**
Et	$HB(C_6F_5)_3^-$	**23**	**a**	**b**	**c**	-
$PhCH_2$	$PhCH_2B(C_6F_5)_3^-$	**24**	**a**	**b**	**c**	**d**

Scheme 4

We have treated most of the complexes **18a−d** (see Scheme 3) with the nitrile reagents R−C≡N with R groups being methyl, ethyl, *tert*-butyl, or *p*-tolyl. In each case a clean 1:1 addition reaction with formation of the respective [(μ-aldiminium)bis(zirconocene)]$^+$ cation complexes (**21−24**) was observed. In each of these cases single isomerically pure products were obtained, that always contained the intact respective metallaoxirane moieties as a part of the dimetallabicyclic framework. Single crystals were obtained of the propionitrile addition product to **18d**. The [(μ-phenylacetaldehyde)(μ-propionaldiminium)bis(zirconocene)]$^+$ cation complex **24d** was characterized by X-ray diffraction. In the crystal there is an enantiomeric disorder at C1 (for details see the Experimental Section). The X-ray crystal structure analysis of complex **24d** shows the presence of a planar dimetallabicyclic framework of the cation. Both zirconium atoms, the C−O part of the μ-aldehyde ligand and the N=CH(R) core are located in the central molecular plane. The (η^2-aldehyde)zirconocene moiety exhibits a very pronounced σ-complex character.[1a,15] Both the Zr1−C1 [2.228(20) Å] and the Zr1−O [2.26(10) Å] linkages are in the σ-bond range. The bond angles inside the Zr1−O−C1 three-membered ring are 71.8(9)° (O−C1−Zr1), 36.2(5)° (C1−Zr1−O) and 72.0(9)° (C1−O−Zr1) (see Figure 1). The C1−O bond length is 1.384(18) Å. The adjacent Zr2−O linkage is very short at 2.007(8) Å. The C1−O−Zr2 angle amounts to 168.7(13)° and Zr1−O−Zr2 angle is at a very typical value of 107.4(5)°. The aldiminium nitrogen bridges between the two zirconium centers [bond lengths Zr2−N 2.187(12) Å, Zr1−N 2.377(11) Å, angle Zr1−N−Zr2 96.7(5)°]. The coordination geometry around the iminium nitrogen atom is trigonally planar. The N−C41 double bond [1.235(19) Å][16] is almost symmetrically arranged in the σ-ligand plane between Zr1 and Zr2 [angles Zr2−N−C41 137.9(11)°, Zr1−N−C41 125.3(12)°], taking into account the rather different coordination environments at Zr2 [angle

O−Zr2−N: 82.2(4)°] and Zr1 [angle O−Zr1−N: 73.6(4)°].[14] Again, there is only a single geometric aldiminium isomer observed in the crystal. It is characterized by having the ethyl substituent ($C^{42}H_2-C^{43}H_3$) at the aldiminium N=C^{41} double bond placed in the (*E*)-orientation relative to the metallaoxirane zirconium center Zr1.

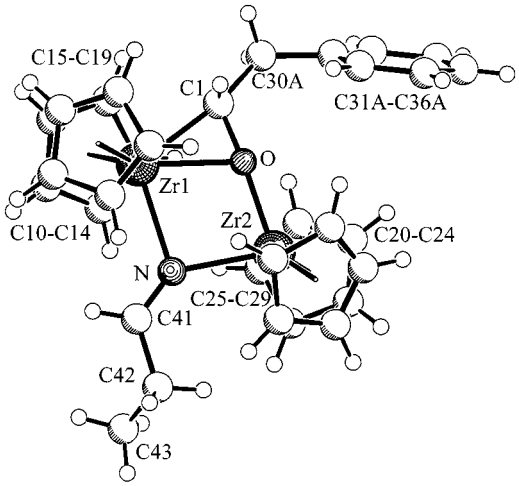
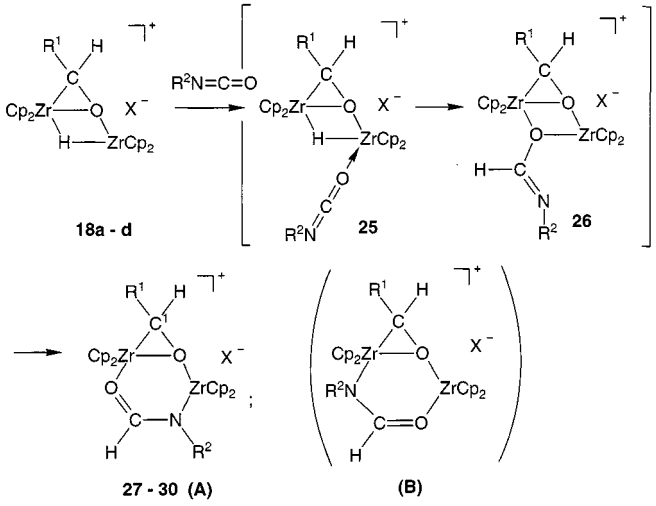


Figure 1. Molecular geometry of complex **24d** (only the cation part is depicted) with selected bond lengths [Å] and angles [°]: Zr1−O 2.26(10), Zr2−O 2.007(8), Zr1−N 2.377(11), Zr2−N 2.187(12), Zr1−C1 2.228(20), O−C1 1.384(18), C1−C30A 1.425(15), C1−C30B 1.423(15), N−C41 1.235(19), C41−C42 1.50(2), C42−C43 1.50(3); Zr1−O−Zr2 107.4(5), Zr1−N−Zr2 96.7(5), Zr1−O−C1 72.0(9), Zr1−C1−O 71.8(9), Zr2−O−C1 168.7(13), C1−Zr1−O 36.2(5), C1−Zr1−N 109.3(5), O−Zr1−N 73.6(4), O−Zr2−N 82.2(4), Zr1−N−C41 125.3(10), Zr2−N−C41 137.9(11), N−C41−C42 127.5(15), C41−C42−C43 113.1(16).

Reactions with Isocyanates

It is mechanistically feasible that an incoming unsaturated reagent may first coordinate to one of the zirconium atoms in the [(μ-aldehyde)(μ-hydride)bis zirconocene]$^+$ cations (**18**) to form an adduct. We assume that coordination probably occurs preferentially at the four-coordinate zirconium and not the five-coordinate zirconium center that is part of the metallaoxirane ring system. Thus, alkyl- or arylnitrile coordination to **18** would be expected to preferentially lead to the reactive intermediate **20** (see Scheme 4). Subsequent hydride shift to the nitrile carbon atom of the activated R−C≡N reagent would in this case directly result in the formation of the (*E*)-stereoisomeric insertion product type that is actually only observed experimentally. It is expected that other unsaturated reagents may follow a similar course when treated with the dinuclear group 4 metallocene hydrido cations **18**. This was in fact observed when the complexes **18** were treated with a series of alkyl or aryl isocyanates RN=C=O (with R being *tert*-butyl, trimethylsilyl, *p*-tolyl, or adamantyl). In each case a single reaction product is formed that was isolated in high yield.

The reaction of **18a** with *tert*-butylisocyanate is a typical example. A single product (**27a**) is obtained, that was isolated as a pale yellow solid in 75% yield. The NMR spectra show that the metallaoxirane moiety inside the dimetallabicyclic framework is retained [^{1}H NMR: δ 3.41 (q, 1 H, C^1-H), 1.53 (d, 3 H, C^1-CH_3), $^3J_{HH}$ = 6.3 Hz; ^{13}C NMR: δ 85.8(C^1), 23.8 (C^1-CH_3)]. Consequently, the signals of two pairs of diastereotopic cyclopentadienyl ligands are registered (^{13}C NMR: δ 114.2, 114.0, 110.0, 109.5 in [D_8]THF/[D_6]benzene solution). The added isocyanate has selectively reacted with the zirconium hydride of the starting material to form a formamidate ligand [^{1}H/^{13}C NMR: δ 7.45/165.1 (O=CH−)].



R^1	X^-	R^2	CMe_3	$SiMe_3$	p-tolyl	1-adamantyl
CH_3	$HB(C_6F_5)_3^-$	**27**	**a**	**b**	**c**	-
CH_3	$MeB(C_6F_5)_3^-$	**28**	**a**	**b**	**c**	**d**
Et	$HB(C_6F_5)_3^-$	**29**	**a**	**b**	**c**	-
$PhCH_2$	$PhCH_2B(C_6F_5)_3^-$	**30**	**a**	**b**	**c**	-

Scheme 5

It is likely that the zirconium hydride addition reaction to the heterocumulene is also initiated by pre-coordination to the more electrophilic four-coordinate zirconium center in **18** (see Scheme 5). The *tert*-butylisocyanate addition to zirconium probably takes place preferentially by means of the heterocumulene oxygen (to generate **25**). Subsequent hydride addition to the sp-carbon atom of the activated RN=C=O reagent then may lead to the formation of the intermediate **26**. In view of the preferred 1,3-κ^2-bonding mode of many related mononuclear amidate or amidinate ligands at the group 4 metallocenes[18] subsequent stabilizing rearrangement of **26** to yield the final [(μ-amidate)bis(zirconocene)]$^+$ cation systems **27**−**30** must be assumed. Unfortunately, we have not been able to characterize any of the RN=C=O reaction products of **18** by X-ray diffraction. Therefore, we cannot definitively decide whether the isomers **27**−**30A** or **B** were formed in the reactions. In each of the examples listed in Scheme 5 a single differently substituted regioisomer of **27**−**30** was formed selectively. From the mechanistic course, preferred formation of the isomers **27**−**30A** would be expected, if the observed reactions are kinetically controlled.

Conclusions

Our study has shown that (η^2-aldehyde)zirconocene moieties are very well suited to serve as templates to accommodate the elusive Cp_2Zr-H^+ cation reagent. Selective σ-ligand abstraction from the readily available dinuclear $[Cp_2Zr(OCHR^1)/Cp_2Zr(H)R^2]$ (R^2 = alkyl or hydride) precursors provides a reliable synthetic entry to the $[Cp_2Zr(OCHR^1)/Cp_2ZrH]^+$ cation systems. The metallaoxirane template seems ideally suited to accommodate the (hydrido)zirconocene cation species since it contains both a strongly electrophilic zirconocene unit and a pronouncedly nucleophilic metallaoxirane oxygen center. This bifunctional characteristic probably results from the pronounced three-membered ring σ-complex properties of the (η^2-aldehyde)$ZrCp_2$ unit, which makes oxygen to zirconium π-backbonding extremely unfavorable.[19] What remains is the inductive effect of the group 16 element that serves to further decrease the electron deficiency at the formally 16 electron metallocene center of the metallaoxirane subunit.

Formal addition of the $[Cp_2Zr-H]^+$ unit to the bifunctional metallaoxirane 1,2-chelate serves to stabilize both the nucleophilic hydride and the electrophilic metallocene of the formally 14-electron cationic reagent. However, binding the (hydrido)metallocene cation to the bifunctional template preserves the principal reactivity pattern of the $[Cp_2Zr-H]^+$ reagent, only in a moderated form. This becomes evident from the course taken in the polar RC≡N or RN=C=O addition reactions, that still follow the typical reaction pattern expected for cationic zirconocene-hydride addition.[12][13] It is remarkable that the 1:1 addition reactions at the template adducts are taking place with very high regioselectivities. Although it is well known that (η^2-aldehyde)$ZrCp_2$ complexes can insert a variety of polar reagents into their zirconium-carbon σ-bond,[17][20] the reactions of the $[Cp_2Zr(OCHR)/Cp_2ZrH^+]$ template adducts selectively involve only the 1,2-coordinated zirconium hydride under the conditions applied in this study. Thus it seems that (η^2-ketone)- and (η^2-aldehyde)zirconocenes serve as very suitable templates for studying otherwise extremely reactive, or even elusive organometallic species, such as the $[Cp_2Zr-H]^+$ cation, stabilized by attachment to the metallaoxirane matrix and moderated in their reactivity, but not completely changed with regard to their typical reactivity pattern. We are hopeful that the favorable template effect of the group 4 metallaoxiranes can be used for accommodating and investigating the typical properties of a variety of other highly reactive organometallic species as well.

Experimental Section

General Information: All reactions were carried out under argon using Schlenk-type glassware or in a glovebox. Solvents, including deuterated solvents, were dried and distilled under argon prior to use. − The following instruments were used for spectroscopic and physical characterization of the compounds: Bruker AC 200P (^{1}H: 200.13, ^{13}C: 50.3 MHz, ^{11}B: 64.2 MHz), Bruker ARX 300 (^{19}F: 282.4 MHz), and Varian Unity Plus (^{1}H: 599.9, ^{13}C: 150.8 MHz) NMR spectrometers (assignments in the ^{1}H- and ^{13}C-NMR spectra were in some example cases confirmed through GCOSY, GHSQC, and GHMBC spectra[21]); Nicolet 5 DXC FT-IR spectrometer; melting points: DSC 2910 (Thermo Analysis/DuPont); elemental analyses: Foss-Heraeus CHN-Rapid. − Tris(pentafluorophenyl)-borane[9], $[Cp_2ZrH_2]_n$[4], $Cp_2ZrMeCl$ **8**[22], bis(η^5-cyclopentadienyl)(η^2-phenylacetyl)benzylzirconium **16**[23], μ-(η^1-O:η^2-C,O-acetaldehyde)-μ-hydrido[bis(η^5-cyclopentadienyl)hydridozirconium][bis(η^5-cyclopentadienyl)zirconium] **11**, μ-(η^1-O:η^2-C,O-acetaldehyde)-μ-hydrido[bis(η^5-cyclopentadienyl)methylzirconium][bis(η^5-cyclopentadienyl)zirconium] **8**, and μ-(η^1-O:η^2-C,O-propionaldehyde)-μ-hydrido[bis(η^5-cyclopentadienyl)hydridozirconium][bis(η^5-cyclopentadienyl)zirconium] **14**[8] were prepared according to literature procedures. In addition, $Cp_2Zr(COMe)Cl$ (**10**) used for the preparation of **8**, was synthesized according to the procedure reported below.

Preparation of Bis(η^5-cyclopentadienyl)(η^2-acetyl)zirconiumchloride (10): 3.15 g (11.6 mmol) of $Cp_2ZrMeCl$ **9** was loaded into a Schlenk tube and dissolved in 60 mL of toluene. Argon was removed by shortly evaporating the Schlenk tube and then the solution was exposed to carbon monoxide under rapid stirring at 0 °C. After two hours the yellow precipitate was isolated by filtration, twice washed with 10 mL of pentane and dried in vacuo, yield 2.60 g (75%).

Preparation of μ-(η^1-O:η^2-C,O-Phenylacetaldehyde)-μ-hydrido-[bis(η^5-cyclopentadienyl)benzylzirconium][bis(η^5-cyclopentadienyl)zirconium] (17): 1.77 g (4.10 mmol) of **16** and 0.90 g (4.03 mmol) of dihydridozirconocene were weighed in a Schlenk vessel, 100 mL of toluene was added and the suspension was stirred for 5 days at room temperature. From the resulting clear yellow solution all volatiles were removed in vacuo. The remaining yellow powder was suspended in 60 mL of a 5:1 mixture of pentane/toluene, the precipitate collected by filtration and washed three times with 20 mL of pentane. After drying in vacuo, **17** was obtained as a slightly yellow solid, yield 1.20 g (46%), mp 146 °C (DSC, decomp.). − $C_{35}H_{36}OZr_2$ (655.1): calcd. C 64.17, H 5.54, found C 62.51, H 5.49. − ^{1}H NMR (599.9 MHz, [D$_6$]benzene): δ = 7.39 (m, 4 H, *o, m*), 7.06 (pst, 1 H, *p*-Zr-CH_2Ph), 7.31 (pst, 2 H, *m*), 7.26 (psd, 2 H, *o*), 7.20 (pst, 1 H, *p*-$CHCH_2$Ph), 5.40, 5.38, 5.37, 5.26 (each s, each 5 H, Cp), 3.11 (dd, 1 H, $^2J_{HH}$ = 14.9 Hz, $^3J_{HH}$ = 3.4 Hz, CHCH_2), 2.83 (dd, 1 H, $^3J_{HH}$ = 9.9 Hz, $^3J_{HH}$ = 3.4 Hz, 1-H), 2.60 (d, 1 H, $^2J_{HH}$ = 9.7 Hz, Zr-CH_2), 2.41 (dd, 1 H, $^2J_{HH}$ = 14.9 Hz, $^3J_{HH}$ = 9.9 Hz, CHCH_2), 2.18 (d, 1 H, $^2J_{HH}$ = 9.7 Hz, Zr-CH_2), −0.61 (br., 1 H, μ-H). − ^{13}C NMR (150.8 MHz, [D$_6$]benzene): δ = 145.0, 128.8, 128.6, 126.0 (*ipso*, *m*, *o*, *p*-$CHCH_2$Ph), 155.2, 127.7, 127.6, 120.7 (*ipso*, *o*, *m*, *p*-Zr-CH_2Ph), 110.5, 110.4, 104.1, 104.1 (each Cp), 82.8 (C1), 45.8 (Zr-CH_2), 44.6 (CHCH_2) .

Generation of the Hydrido Zirconocene Cations 18a−d: General Procedure: A solution of 210 mg (410 μmol) of tris(pentafluorophenyl)borane in 2 mL of toluene was added to a Schlenk flask containing a solution of 293 μmol dimetallic hydride **11**, **8**, **14**, or **17** in 2 mL of toluene. A dark brown oil precipitated immediately. The reaction mixture was stirred for one minute, the oil allowed to settle and then the toluene phase was decanted. The oil was washed with 2 mL of toluene, followed by 2 mL of pentane and then solidified by stirring with 3 mL of pentane. After decanting the solvent and drying the solid in vacuo, the hydrido zirconocene cations were isolated as red-brown powders. Reported below are the quantities of reagents used and yields of products obtained.

Reaction of 11 with Tris(pentafluorophenyl)borane, Preparation of 18a: 200 mg (410 μmol) of **11** was treated with 210 mg (410 μmol) of $B(C_6F_5)_3$ to yield 341 mg (83%) of **18a**, mp 147°C (DSC, decomp.). − $C_{40}H_{26}BF_{15}OZr_2$ (1000.9): calcd. C 48.00, H 2.62, found C 48.46, H 2.74. − ^{1}H NMR (200.1 MHz, [D$_6$]benzene/[D$_8$]tetrahydrofuran, ca. 4:1): δ = 5.78, 5.77, 5.54, 5.46 (each s, each 5 H, Cp), 3.58 (q, 1 H, $^3J_{HH}$ = 6.3 Hz, 1-H), 1.33 (d, 3 H, $^3J_{HH}$ = 6.3 Hz, CHC*H*$_3$), −1.98 (s, 1 H, μ-H), B-*H* resonance not observed. − ^{13}C NMR (50.3 MHz, [D$_6$]benzene/[D$_8$]tetrahydrofuran, ca. 4:1): δ = 149.0, 138.0, 137.1 [each d, each $^1J_{CF}$ = 240 Hz, *o*, *p*, *m*-$B(C_6F_5)_3$], 112.4, 112.1, 106.7, 106.6 (each Cp), 90.1 (C1), 23.7 (CH*C*H$_3$), *ipso*-$B(C_6F_5)_3$ resonance not located. − ^{11}B NMR (64.2 MHz, [D$_6$]benzene/[D$_8$]tetrahydrofuran, ca. 4:1): δ = −24.6 (d, $^1J_{BH}$ = 82 Hz). − ^{19}F NMR (282.4 MHz, [D$_6$]benzene/[D$_8$]tetrahydrofuran, ca. 4:1): δ = −132.0, −163.5, −166.3 [each m, *o*, *p*, *m*-$B(C_6F_5)_3$].

Reaction of 8 with Tris(pentafluorophenyl)borane, Preparation of 18b: 206 mg (410 μmol) of **8** was treated with 210 mg (410 μmol) of $B(C_6F_5)_3$ to yield 320 mg (77%) of **18b**, mp 140°C (DSC, decomp.). − $C_{41}H_{28}BF_{15}OZr_2$ (1014.9): calcd. C 48.52, H 2.78, found C 48.42, H 2.92. − ^{1}H NMR (200.1 MHz, [D$_6$]benzene/[D$_8$]tetrahydrofuran, ca. 4:1): δ = 5.87, 5.85, 5.62, 5.53 (each s, each 5 H, Cp), 3.65 (q, 1 H, $^3J_{HH}$ = 6.2 Hz, 1-H), 1.37 (d, 3 H, $^3J_{HH}$ = 6.2 Hz, CHC*H*$_3$), 1.03 (br, 3 H, B-C*H*$_3$), −1.92 (s, 1 H, μ-H) . − ^{13}C NMR (50.3 MHz, [D$_6$]benzene/[D$_8$]tetrahydrofuran, ca. 4:1): δ = 149.0, 138.0, 137.1 [each d, each $^1J_{CF}$ = 240 Hz, *o*, *p*, *m*-$B(C_6F_5)_3$], 113.0, 112.8, 107.1, 107.0 (each Cp), 90.2 (C1), 23.8 (CH*C*H$_3$) , *ipso*-$B(C_6F_5)_3$ and B-*C*H$_3$ resonances not located. − ^{11}B NMR (64.2 MHz, [D$_6$]benzene/[D$_8$]tetrahydrofuran, ca. 4:1): δ = −14.5. − ^{19}F NMR (282.4 MHz, [D$_6$]benzene/[D$_8$]tetrahydrofuran, ca. 4:1): δ = −132.0, −163.5, −166.3 [each m, *o*, *p*, *m*-$B(C_6F_5)_3$].

Reaction of 14 with Tris(pentafluorophenyl)borane, Preparation of 18c: 206 mg (410 μmol) of **14** was treated with 210 mg (410 μmol) of $B(C_6F_5)_3$ to yield 350 mg (84%) of **18c**, mp 130°C (DSC, decomp.). − $C_{41}H_{28}BF_{15}OZr_2$ (1014.9): calcd. C 48.52, H 2.78, found C 48.27, H 3.01. − ^{1}H NMR (200.1 MHz, [D$_6$]benzene/[D$_8$]tetrahydrofuran, ca. 4:1): δ = 5.87 (double intensity), 5.58, 5.51 (each s, each 5 H, Cp), 3.41 (pst, 1 H, 1-H), 1.75, 1.45 (each m, each 1 H, C*H*$_2$), 0.98 (pst, 3 H, CH$_2$C*H*$_3$), −1.58 (s, 1 H, μ-H), B-*H* resonance not observed. − ^{13}C NMR (50.3 MHz, [D$_6$]benzene/[D$_8$]tetrahydrofuran, ca. 4:1): δ = 149.0, 138.1, 137.2 (each d, each $^1J_{CF}$ = 240 Hz, *o*, *p*, *m*-$B(C_6F_5)_3$), 112.8, 112.6, 106.3 (double intensity) (each Cp), 97.2 (C1), 31.1 (*C*H$_2$), 12.7 (CH$_2$*C*H$_3$), *ipso*-$B(C_6F_5)_3$ resonance not located. − ^{11}B NMR (64.2 MHz, [D$_6$]benzene/[D$_8$]tetrahydrofuran, ca. 4:1): δ = −24.6 (d, $^1J_{BH}$ = 82 Hz). − ^{19}F NMR (282.4 MHz, [D$_6$]benzene/[D$_8$]tetrahydrofuran, ca. 4:1): δ = −132.0, −164.3, −166.9 [each m, *o*, *p*, *m*-$B(C_6F_5)_3$].

Reaction of 17 with Tris(pentafluorophenyl)borane, Preparation of 18d: 269 mg (410 μmol) of **17** was treated with 210 mg (410 μmol) of $B(C_6F_5)_3$ to yield 388 mg (81%) of **18d**, mp 130°C (DSC, decomp.). − $C_{53}H_{36}BF_{15}OZr_2$ (1167.1): calcd. C 54.54, H 3.11, found C 53.89, H 3.18. − ^{1}H NMR (599.9 MHz, [D$_6$]benzene/[D$_8$]tetrahydrofuran, ca. 4:1): δ = 7.26 (pst, 2 H, *m*), 7.19 (pst, 1 H, *p*), 7.09 (psd, 2 H, *o*-CHCH$_2$Ph), 7.16 (psd, 2 H, *o*), 6.98 (pst, 2 H, *m*), 6.85 (pst, 1 H, *p*-B-CH$_2$Ph), 5.76, 5.57, 5.56, 5.46 (each s, each 5 H, Cp), 3.67 (dd, 1 H, $^3J_{HH}$ = 9.1 Hz, $^3J_{HH}$ = 4.0 Hz, 1-H), 3.42 (br, 2 H, B-C*H*$_2$), 2.95 (dd, 1 H, $^2J_{HH}$ = 14.8 Hz, $^3J_{HH}$ = 4.0 Hz, CHC*H*$_2$), 2.46 (dd, 1 H, $^2J_{HH}$ = 14.8 Hz, $^3J_{HH}$ = 9.1 Hz, CHC*H*$_2$), −1.56 (s, 1 H, μ-H). − ^{13}C NMR (150.8 MHz, [D$_6$]benzene/[D$_8$]tetrahydrofuran, ca. 4:1): δ = 149.0, 138.1, 137.2 [each d, each $^1J_{CF}$ = 240 Hz, *o*, *p*, *m*-$B(C_6F_5)_3$], 142.9, 128.9, 128.6, 126.7 (*ipso*, *m*, *o*, *p*-CHCH$_2$Ph), 149.2, 129.3, 127.4, 123.1 (*ipso*, *o*, *m*, *p*-B-CH$_2$Ph), 113.0, 112.8, 106.3, 106.2 (each Cp), 95.6 (C1), 44.8 (CH*C*H$_2$), 32.4 (br, B-*C*H$_2$), *ipso*-$B(C_6F_5)_3$ resonance not located. − ^{11}B NMR (64.2 MHz, [D$_6$]benzene/[D$_8$]tetrahydrofuran, ca. 4:1): δ = −12.3. − ^{19}F NMR (282.4 MHz, [D$_6$]benzene/[D$_8$]tetrahydrofuran, ca. 4:1): δ = −128.1, −164.2, −166.8 [each m, *o*, *p*, *m*-$B(C_6F_5)_3$].

Reaction of 18a−d with [D$_2$]Dichloromethane, Generation of 19a−d. − General Proceedure: 78.1 μmol of dimetallic hydride **11**, **8**, **14**, or **17** and 40 mg (78.1 μmol) of tris(pentafluorophenyl)borane were mixed as solids in a NMR tube, the tube sealed with a septum and cooled to −78°C. Using a syringe, 1 mL of −78°C cold CD_2Cl_2 was added through the septum. The solids slowly dissolved to form a dark red solution which was allowed to warm to room temperature. Above −20°C, gas evolution took place and the color changed to red-orange. NMR spectra were then collected and in all cases CH_2D_2 was observed by ^{1}H NMR at 0.17 (quint.). Reported below are the quantities of reagents used.

Characterization of 19a: 38.1 mg (78.1 μmol) of **11** was treated with 40.0 mg (78.1 μmol) of $B(C_6F_5)_3$ in CD_2Cl_2. − ^{1}H NMR (200.1 MHz, [D$_2$]dichloromethane): δ = 6.47, 6.41, 6.00, 5.96 (each s, each 5 H, Cp), 4.33 (q, 1 H, $^3J_{HH}$ = 6.0 Hz, 1-H), 1.83 (d, 3 H, $^3J_{HH}$ = 6.0 Hz, CHC*H*$_3$), B-*H* resonance not observed. − ^{13}C NMR (50.3 MHz, [D$_2$]dichloromethane): δ = 148.2, 137.9, 136.9 [each d, each $^1J_{CF}$ = 240 Hz, *o*, *p*, *m*-$B(C_6F_5)_3$], 116.5, 116.4, 109.7, 109.6 (each Cp), 91.0 (C1), 24.9 (CH*C*H$_3$), *ipso*-$B(C_6F_5)_3$ resonance not located. − ^{11}B NMR (64.2 MHz, [D$_2$]dichloromethane): δ = −25.6 (d, $^1J_{BH}$ = 82 Hz). − ^{19}F NMR (282.4 MHz, [D$_2$]dichloromethane): δ = −130.6, −163.0, −165.4 [each m, *o*, *p*, *m*-$B(C_6F_5)_3$].

Characterization of 19b: 39.2 mg (78.1 μmol) of **8** was treated with 40.0 mg (78.1 μmol) of $B(C_6F_5)_3$ in CD_2Cl_2. − ^{1}H NMR (200.1 MHz, [D$_2$]dichloromethane): δ = 6.50, 6.42, 6.02, 5.98 (each s, each 5 H, Cp), 4.36 (q, 1 H, $^3J_{HH}$ = 6.0 Hz, 1-H), 1.86 (d, 3 H, $^3J_{HH}$ = 6.0 Hz, CHC*H*$_3$), 0.53 (br, 3 H, B-C*H*$_3$). − ^{13}C NMR (50.3 MHz, [D$_2$]dichloromethane): δ = 149.0, 138.0, 137.1 [each d, each $^1J_{CF}$ = 240 Hz, *o*, *p*, *m*-$B(C_6F_5)_3$], 116.8, 116.7, 110.0, 109.9 (each Cp), 91.7 (C1), 25.4 (CH*C*H$_3$), *ipso*-$B(C_6F_5)_3$ and B-*C*H$_3$ resonances not located. − ^{11}B NMR (64.2 MHz, [D$_2$]dichloromethane): δ = −15.3. − ^{19}F NMR (282.4 MHz, [D$_2$]dichloromethane): δ = −130.5, −162.7, −165.4 [each m, *o*, *p*, *m*-$B(C_6F_5)_3$].

Characterization of 19c: 39.2 mg (78.1 μmol) of **14** was treated with 40.0 mg (78.1 μmol) of $B(C_6F_5)_3$ in CD_2Cl_2. − ^{1}H NMR (200.1 MHz, [D$_2$]dichloromethane): δ = 6.48, 6.43, 6.03, 5.98 (each s, each 5 H, Cp), 4.08 (dd, 1 H, 1-H), 2.2−1.6 (m, 2 H, C*H*$_2$), 1.10 (pst, 3 H, CH$_2$C*H*$_3$), B-*H* resonance not observed. − ^{13}C NMR (50.3 MHz, [D$_2$]dichloromethane): δ = 148.2, 137.9, 136.9 [each d, each $^1J_{CF}$ = 240 Hz, *o*, *p*, *m*-$B(C_6F_5)_3$], 116.7, 116.5, 109.7, 109.5 (each Cp), 98.0 (C1), 32.3 (*C*H$_2$), 13.3 (CH$_2$*C*H$_3$), *ipso*-$B(C_6F_5)_3$ resonance not located. − ^{11}B NMR (64.2 MHz, [D$_2$]dichloromethane): δ = −25.6 (d, $^1J_{BH}$ = 82 Hz). − ^{19}F NMR (282.4 MHz, [D$_2$]dichloromethane): δ = −130.6, −163.0, −165.4 [each m, *o*, *p*, *m*-$B(C_6F_5)_3$].

Characterization of 19d: 51.2 mg (78.1 μmol) of **17** was treated with 40.0 mg (78.1 μmol) of $B(C_6F_5)_3$ in CD_2Cl_2. − ^{1}H NMR (599.9 MHz, [D$_2$]dichloromethane): δ = 7.49 (pst, 2 H, *m*), 7.40 (pst, 1 H, *p*), 7.29 (psd, 2 H, *o*-CH$_2$Ph), 6.88 (pst, 2 H, *m*), 6.80 (pst, 1 H, *p*), 6.76 (psd, 2 H, *o*-B-CH$_2$Ph), 5.76, 5.57, 5.56, 5.46 (Cp), 4.47 (dd, 1 H, $^3J_{HH}$ = 10.6 Hz, $^3J_{HH}$ = 2.8 Hz, 1-H), 3.60 (dd, 1 H, $^2J_{HH}$ = 15.0 Hz, $^3J_{HH}$ = 2.8 Hz, CHC*H*$_2$), 2.92 (dd, 1 H, $^2J_{HH}$ = 15.0 Hz, $^3J_{HH}$ = 10.6 Hz, CHC*H*$_2$), 2.84 (br, 2 H, B-C*H*$_2$). − ^{13}C NMR (150.8 MHz, [D$_2$]dichloromethane): δ = 147.8, 137.5, 135.8 [each d, each $^1J_{CF}$ = 240 Hz, *o*, *p*, *m*-$B(C_6F_5)_3$], 140.6, 128.7, 127.7, 126.8 (*ipso*, *m*, *o*, *p*-CH$_2$Ph), 148.3, 128.3, 126.4, 122.1 (*ipso*, *o*, *m*, *p*-B-CH$_2$Ph), 116.4, 115.9, 109.6, 109.2 (each Cp), 94.8 (C1), 44.4 (CH*C*H$_2$), 30.2 (br, B-*C*H$_2$), *ipso*-$B(C_6F_5)_3$ resonance not located.

– ^{11}B NMR (64.2 MHz, [D$_2$]dichloromethane): δ = −12.9. – ^{19}F NMR (282.4 MHz, [D$_2$]dichloromethane): δ = −128.7, −163.8, −165.4 [each m, *o*, *p*, *m*-B(C_6F_5)$_3$].

Reaction of 18a–d with Nitriles and Isocyanates. – General Procedure: Cation **18** was formed in situ by addition of 4 mL of toluene to a Schlenk flask containing 293 μmol of the dimetallic hydride complex **11**, **8**, **14**, or **17** and 210 mg (293 μmol) of B(C_6F_5)$_3$. The two compounds dissolved and within a few seconds, compound **18** precipitated as a dark brown oil. The solution was decanted and the oil washed with 2 mL of toluene. Then 1.1 equiv. of the respective nitrile or isocyanate reagent was added and the reaction mixture was stirred for five minutes. The resulting yellow or orange oil was washed with 2 mL of toluene, followed by 2 mL of pentane, and then solidified by stirring with 3 mL of pentane. After decanting the solvent and drying the solid in vacuo, the insertion products were isolated as yellow or orange powders. Reported below are the quantities of reagents actually used and the yields of products obtained.

Reaction of 18a with Acetonitrile: Preparation of 21a: Reaction of 200 mg (410 μmol) of **11** with 210 mg (410 μmol) of B(C_6F_5)$_3$ and subsequent reaction of the such in situ prepared **18a** with 23.9 μL (18.5 mg, 450 μmol) of acetonitrile gave **21a** as a yellow powder, yield 320 mg (75%), mp 184°C (DSC, 213°C decomp.). – $C_{42}H_{29}BF_{15}NOZr_2$ (1039.0): calcd. C 48.42, H 2.81, N 1.34, found C 48.40, H 3.00, N 1.52. – ^{1}H NMR (200.1 MHz, [D$_6$]benzene/[D$_8$]tetrahydrofuran, ca. 4:1): δ = 8.67 (q, 1 H, $^3J_{HH}$ = 4.7 Hz, N=C*H*), 5.88, 5.81, 5.44, 5.43 (each s, each 5 H, Cp), 3.65 (q, 1 H, $^3J_{HH}$ = 6.1 Hz, 1-H), 1.81 (d, 3 H, $^3J_{HH}$ = 4.7 Hz, N=CHCH_3), 1.52 (d, 3 H, $^3J_{HH}$ = 6.1 Hz, CHCH_3), B-*H* resonance not observed. – ^{13}C NMR (150.8 MHz, [D$_6$]benzene/[D$_8$]tetrahydrofuran, ca. 4:1): δ = 187.2 (N=*C*H) 149.0, 138.0, 136.9 [each d, each $^1J_{CF}$ = 240 Hz, *o*, *p*, *m*-B(C_6F_5)$_3$], 113.6, 113.5, 108.8, 108.7 (each Cp), 88.5 (C1), 33.3 (N=CH*C*H$_3$), 23.9 (CH*C*H$_3$), *ipso*-B(C_6F_5)$_3$ resonance not located. – ^{11}B NMR (64.2 MHz, [D$_6$]benzene/[D$_8$]tetrahydrofuran, ca. 4:1): δ = −24.6 (d, $^1J_{BH}$ = 82 Hz). – ^{19}F NMR (282.4 MHz, [D$_6$]benzene/[D$_8$]tetrahydrofuran, ca. 4:1): δ = −132.0, −163.5, −166.3 [each m, *o*, *p*, *m*-B(C_6F_5)$_3$].

Reaction of 18a with *tert*-Butyl Cyanide: Preparation of 21b: Reaction of 200 mg (410 μmol) of **11** with 210 mg (410 μmol) of B(C_6F_5)$_3$ and subsequent reaction of the in situ prepared **18a** with 49.7 μL (37.4 mg, 450 μmol) *tert*-butyl cyanide gave **21b** as a yellow powder, yield 342 mg (77%), mp 170°C (DSC, decomp.). – $C_{45}H_{35}BF_{15}NOZr_2$ (1084.0): calcd. C 49.86, H 3.25, N 1.29, found C 48.99, H 3.53, N 1.35. – ^{1}H NMR (200.1 MHz, [D$_6$]benzene/[D$_8$]tetrahydrofuran, ca. 4:1): δ = 8.87 (s, 1 H, N=C*H*), 5.91, 5.84, 5.44, 5.43 (each s, each 5 H, Cp), 3.55 (q, 1 H, $^3J_{HH}$ = 6.0 Hz, 1-H), 1.49 (d, 3 H, $^3J_{HH}$ = 6.0 Hz, CHCH_3), 0.85 [s, 9 H, C(CH_3)$_3$], B-*H* resonance not observed. – ^{13}C NMR (50.3 MHz, [D$_6$]benzene/[D$_8$]tetrahydrofuran, ca. 4:1): δ = 197.5 (N=*C*H), 149.0, 138.0, 136.9 [each d, each $^1J_{CF}$ = 240 Hz, *o*, *p*, *m*-B(C_6F_5)$_3$], 114.0, 113.8, 109.2 (double intensity) (each Cp), 90.0 (C1), 41.6 [*C*(CH$_3$)$_3$], 25.3 [C(*C*H$_3$)$_3$], 23.4 (CH*C*H$_3$), *ipso*-B(C_6F_5)$_3$ resonance not located. – ^{11}B NMR (64.2 MHz, [D$_6$]benzene/[D$_8$]tetrahydrofuran, ca. 4:1): δ = −24.6 (d, $^1J_{BH}$ = 82 Hz). – ^{19}F NMR (282.4 MHz, [D$_6$]benzene/[D$_8$]tetrahydrofuran, ca. 4:1): δ = −132.0, −163.5, −166.3 [each m, *o*, *p*, *m*-B(C_6F_5)$_3$].

Reaction of 18a with *p*-Tolunitrile: Preparation of 21c: Reaction of 200 mg (410 μmol) of **11** with 210 mg (410 μmol) of B(C_6F_5)$_3$ and subsequent reaction of the in situ prepared **18a** with 52.7 mg (450 μmol) of *p*-tolunitrile gave **21c** as a yellow powder, yield 325 mg (71%), mp 169°C (DSC, decomp.). – $C_{48}H_{33}BF_{15}NOZr_2$ (1118.0): calcd. C 51.57, H 2.98, N 1.25, found C 51.77, H 3.57, N 1.86. – ^{1}H NMR (200.1 MHz, [D$_6$]benzene/[D$_8$]tetrahydrofuran, ca. 4:1): δ = 9.59 (s, 1 H, N=C*H*), 7.22, 7.15 (each psd, each 2 H, *m*, *o*-PhCH$_3$), 5.92, 5.88, 5.49 (double intensity) (each s, each 5 H, Cp), 3.62 (q, 1 H, $^3J_{HH}$ = 6.1 Hz, 1-H), 2.23 (s, 3 H, PhCH_3), 1.51 (d, 2 H, $^3J_{HH}$ = 6.1 Hz, CHCH_3), B-*H* resonance not observed. – ^{13}C NMR (50.3 MHz, [D$_6$]benzene/[D$_8$]tetrahydrofuran, ca. 4:1): δ = 184.4 (N=*C*H), 149.0, 138.1, 137.2 [each d, each $^1J_{CF}$ = 240 Hz, *o, p, m*-B(C_6F_5)$_3$], 145.7, 134.2, 130.2, 129.7 (*p*, *ipso*, *m*, *o*-PhCH$_3$), 113.7, 113.5, 109.1, 109.0 (each Cp), 89.7 (C1), 23.6 (CH*C*H$_3$), 21.3 (Ph*C*H$_3$), *ipso*-B(C_6F_5)$_3$ resonance not located. – ^{11}B NMR (64.2 MHz, [D$_6$]benzene/[D$_8$]tetrahydrofuran, ca. 4:1): δ = −24.6 (d, $^1J_{BH}$ = 82 Hz). – ^{19}F NMR (282.4 MHz, [D$_6$]benzene/[D$_8$]tetrahydrofuran, ca. 4:1): δ = −132.0, −164.3, −166.9 [each m, *o*, *p*, *m*-B(C_6F_5)$_3$].

Reaction of 18b with Acetonitrile: Preparation of 22a: Reaction of 206 mg (410 μmol) of **8** with 210 mg (410 μmol) of B(C_6F_5)$_3$ and subsequent reaction of the in situ prepared **18b** with 23.9 μL (18.5 mg, 450 μmol) of acetonitrile gave **22a** as a yellow powder, yield 273 mg (63%), mp 180°C (DSC, 231°C decomp.). – $C_{43}H_{31}BF_{15}NOZr_2$ (1056.0): calcd. C 48.91, H 2.96, N 1.33, found C 48.74, H 3.11, N 1.62. – ^{1}H NMR (200.1 MHz, [D$_6$]benzene/[D$_8$]tetrahydrofuran, ca. 4:1): δ = 8.69 (q, 1 H, $^3J_{HH}$ = 4.8 Hz, N=C*H*), 5.95, 5.88, 5.51, 5.50 (each s, each 5 H, Cp), 3.71 (q, 1 H, $^3J_{HH}$ = 6.0 Hz, 1-H), 1.80 (d, 3 H, $^3J_{HH}$ = 4.8 Hz, N=CHCH_3), 1.53 (d, 3 H, $^3J_{HH}$ = 6.0 Hz, CHCH_3), 1.17 (br, 3 H, B-CH_3). – ^{13}C NMR (150.8 MHz, [D$_6$]benzene/[D$_8$]tetrahydrofuran, ca. 4:1): δ = 186.9 (N=*C*H), 149.0, 138.0, 136.9 [each d, each $^1J_{CF}$ = 240 Hz, *o*, *p*, *m*-B(C_6F_5)$_3$], 113.6, 113.4, 108.7, 108.6 (each Cp), 88.4 (C1), 33.2 (N=CH*C*H$_3$), 23.8 (CH*C*H$_3$), *ipso*-B(C_6F_5)$_3$ and B-*C*H$_3$ resonances not located. – ^{11}B NMR (64.2 MHz, [D$_6$]benzene/[D$_8$]tetrahydrofuran, ca. 4:1): δ = −14.8. – ^{19}F NMR (282.4 MHz, [D$_6$]benzene/[D$_8$]tetrahydrofuran, ca. 4:1): δ = −132.0, −163.5, −166.3 [each m, *o*, *p*, *m*-B(C_6F_5)$_3$].

Reaction of 18b with *tert*-Butyl Cyanide: Preparation of 22b: Reaction of 206 mg (410 μmol) of **8** with 210 mg (410 μmol) of B(C_6F_5)$_3$ and subsequent reaction of the in situ prepared **18b** with 49.7 μL (37.4 mg, 450 μmol) of *tert*-butyl cyanide gave **22b** as a yellow powder, yield 320 mg (71%), mp 169°C (DSC, decomp.). – $C_{46}H_{37}BF_{15}NOZr_2$ (1098.0): calcd. C 50.32, H 3.40, N 1.28, found C 50.58, H 3.69, N 1.44. – ^{1}H NMR (200.1 MHz, [D$_6$]benzene/[D$_8$]tetrahydrofuran, ca. 4:1): δ = 8.84 (s, 1 H, N=C*H*), 5.88, 5.81, 5.42 (double intensity) (each s, each 5 H, Cp), 3.54 (q, 1 H, $^3J_{HH}$ = 6.0 Hz, 1-H), 1.48 (d, 3 H, $^3J_{HH}$ = 6.0 Hz, CHCH_3), 1.17 (br, 3 H, B-CH_3), 0.84 (s, 9 H, C(CH_3)$_3$). – ^{13}C NMR (50.3 MHz, [D$_6$]benzene/[D$_8$]tetrahydrofuran, ca. 4:1): δ = 197.5 (N=*C*H), 149.0, 138.0, 136.9 [each d, each $^1J_{CF}$ = 240 Hz, *o*, *p*, *m*-B(C_6F_5)$_3$], 113.9, 113.8, 109.2 (double intensity) (each Cp), 90.0 (C1), 41.6 [*C*(CH$_3$)$_3$], 25.3 [C(*C*H$_3$)$_3$], 23.4 (CH*C*H$_3$), *ipso*-B(C_6F_5)$_3$ and B-*C*H$_3$ resonances not located. – ^{11}B NMR (64.2 MHz, [D$_6$]benzene/[D$_8$]tetrahydrofuran, ca. 4:1): δ = −14.8. – ^{19}F NMR (282.4 MHz, [D$_6$]benzene/[D$_8$]tetrahydrofuran, ca. 4:1): δ = −132.0, −163.5, −166.3 [each m, *o*, *p*, *m*-B(C_6F_5)$_3$].

Reaction of 18b with *p*-Tolunitrile: Preparation of 22c: Reaction of 206 mg (410 μmol) of **8** with 210 mg (410 μmol) of B(C_6F_5)$_3$ and subsequent reaction of the in situ prepared **18b** with 52.7 mg (450 μmol) of *p*-tolunitrile gave **22c** as a yellow powder, yield 320 mg (68%), mp 188°C (DSC, decomp.). – $C_{49}H_{35}BF_{15}NOZr_2$ (1148.1): C 51.99, H 3.12, N 1.24, found C 52.45, H 3.47, N 1.44. – ^{1}H NMR (200.1 MHz, [D$_6$]benzene/[D$_8$]tetrahydrofuran, ca. 4:1): δ = 9.52 (s, 1 H, N=C*H*), 7.22, 7.15 (each psd, each 2 H, *m*, *o*-PhCH$_3$), 5.84, 5.81, 5.43 (double intensity) (each s, each 5 H, Cp), 3.62 (q, 1 H, $^3J_{HH}$ = 6.1 Hz, 1-H), 2.23 (s, 3 H, PhCH_3), 1.48 (d, 2 H,

$^3J_{HH}$ = 6.1 Hz, CHCH_3), 1.26 (br, 3 H, B-CH_3). − ^{13}C NMR (50.3 MHz, [D$_6$]benzene/[D$_8$]tetrahydrofuran, ca. 4:1): δ = 184.4 (N=*C*H), 149.0, 138.1, 137.2 [each d, each $^1J_{CF}$ = 240 Hz, *o*, *p*, *m*-B(C_6F_5)$_3$], 144.3, 134.3, 130.2, 129.7 (*p*, *ipso*, *m*, *o*-PhCH$_3$), 113.7, 113.6, 109.2, 109.1 (each Cp), 89.7 (C1), 23.6 (CH*C*H$_3$), 21.2 (Ph*C*H$_3$), *ipso*-B(C_6F_5)$_3$ and B-*C*H$_3$ resonances not located. − ^{11}B NMR (64.2 MHz, [D$_6$]benzene/[D$_8$]tetrahydrofuran, ca. 4:1): δ = −14.4. − ^{19}F NMR (282.4 MHz, [D$_6$]benzene/[D$_8$]tetrahydrofuran, ca. 4:1): δ = −132.0, −164.3, −166.9 [each m, *o*, *p*, *m*-B(C_6F_5)$_3$].

Reaction of 18b with Propionitrile: Preparation of 22d: Reaction of 206 mg (410 μmol) of **8** with 210 mg (410 μmol) of B(C_6F_5)$_3$ and subsequent reaction of the in situ prepared **18b** with 32.1 μL (24.7 mg, 450 μmol) of propionitrile gave **22d** as a yellow powder, yield 298 mg (68%), mp 146°C (DSC, 205°C decomp.). − $C_{44}H_{33}BF_{15}NOZr_2$ (1070.0): calcd. C 49.39, H 3.11, N 1.31, found C 48.86, H 3.33, N 1.31. − ^{1}H NMR (200.1 MHz, [D$_6$]benzene/[D$_8$]tetrahydrofuran, ca. 4:1): δ = 8.66 (m, 1 H, N=C*H*), 6.02, 5.96, 5.55 (double intensity) (each s, each 5 H, Cp), 3.75 (q, 1 H, $^3J_{HH}$ = 6.1 Hz, 1-H), 1.95 (m, 2 H, CH_2), 1.54 (d, 3 H, $^3J_{HH}$ = 6.1 Hz, CHCH_3), 1.29 (br, 3 H, B-CH_3), 1.08 (pst, 3 H, CH$_2$CH_3). − ^{13}C NMR (150.8 MHz, [D$_6$]benzene/[D$_8$]tetrahydrofuran, ca. 4:1): δ = 191.8 (N=*C*H), 149.0, 138.0, 136.9 [each d, each $^1J_{CF}$ = 240 Hz, *o*, *p*, *m*-B(C_6F_5)$_3$], 113.8, 113.6, 108.9, 108.8 (Cp), 88.6 (C1), 41.1 (*C*H$_2$), 23.8 (CH*C*H$_3$), 8.6 (CH$_2$*C*H$_3$), *ipso*-B(C_6F_5)$_3$ and B-*C*H$_3$ resonances not located. − ^{11}B NMR (64.2 MHz, [D$_6$]benzene/[D$_8$]tetrahydrofuran, ca. 4:1): δ = −14.7. − ^{19}F NMR (282.4 MHz, [D$_6$]benzene/[D$_8$]tetrahydrofuran, ca. 4:1): δ = −132.0, −163.5, −166.3 [each m, *o*, *p*, *m*-B(C_6F_5)$_3$].

Reaction of 18c with Acetonitrile: Preparation of 23a: Reaction of 206 mg (410 μmol) of **14** with 210 mg (410 μmol) of B(C_6F_5)$_3$ and subsequent reaction of the in situ prepared **18c** with 23.9 μL (18.5 mg, 450 μmol) of acetonitrile gave **23a** as a yellow powder, yield 320 mg (75%), mp 164°C (DSC, 198°C decomp.). − $C_{43}H_{31}BF_{15}NOZr_2$ (1056.0): calcd. C 48.91, H 2.96, N 1.33, found C 48.93, H 3.30, N 1.39. − ^{1}H NMR (200.1 MHz, [D$_6$]benzene/[D$_8$]tetrahydrofuran, ca. 4:1): δ = 8.63 (q, 1 H, $^3J_{HH}$ = 4.7 Hz, N=C*H*), 5.81, 5.76, 5.40, 5.38, (each s, each 5 H, Cp), 3.37 (dd, 1 H, 1-H), 1.76 (d, 3 H, $^3J_{HH}$ = 4.7 Hz, N=CHCH_3), 1.6-1.5 (m, 2 H, CH_2), 0.94 (pst, 3 H, CH$_2$CH_3), B-*H* resonance not observed. − ^{13}C NMR (50.3 MHz, [D$_6$]benzene/[D$_8$]tetrahydrofuran, ca. 4:1): δ = 187.1 (N=*C*H), 149.0 (double intensity), 138.1, 137.2 [each d, each $^1J_{CF}$ = 240 Hz, *o*, *p*, *m*-B(C_6F_5)$_3$], 113.6, 108.7, 108.5 (each Cp), 95.5 (C1), 33.3 (NCH*C*H$_3$), 31.6 (*C*H$_2$), 13.2 (CH$_2$*C*H$_3$), *ipso*-B(C_6F_5)$_3$ resonance not located. − ^{11}B NMR (64.2 MHz, [D$_6$]benzene/[D$_8$]tetrahydrofuran, ca. 4:1): δ = −24.6 (d, $^1J_{BH}$ = 82 Hz). − ^{19}F NMR (282.4 MHz, [D$_6$]benzene/[D$_8$]tetrahydrofuran, ca. 4:1): δ = −132.0, −164.3, −166.9 [each m, *o*, *p*, *m*-B(C_6F_5)$_3$].

Reaction of 18c with *tert*-Butyl Cyanide: Preparation of 23b: Reaction of 206 mg (410 μmol) of **14** with 210 mg (410 μmol) of B(C_6F_5)$_3$ and subsequent reaction of the in situ prepared **18c** with 49.7 μL (37.4 mg, 450 μmol) of *tert*-butyl cyanide gave **23b** as a yellow powder, yield 347 mg (77%), mp 167°C (DSC, decomp.). − $C_{46}H_{37}BF_{15}NOZr_2$ (1098.0): calcd. C 50.32, H 3.40, N 1.28, found C 50.57, H 3.44, N 1.50. − ^{1}H NMR (200.1 MHz, [D$_6$]benzene/[D$_8$]tetrahydrofuran, ca. 4:1): δ = 8.88 (s, 1 H, N=C*H*), 5.89, 5.84, 5.45, 5.43 (each s, each 5 H, Cp), 3.35 (dd, 1 H, 1-H), 1.7-1.4 (m, 2 H, CH_2), 0.96 (pst, 3 H, CH$_2$CH_3), 0.86 [s, 9 H, C(CH_3)$_3$], B-*H* resonance not observed. − ^{13}C NMR (50.3 MHz, [D$_6$]benzene/[D$_8$]tetrahydrofuran, ca. 4:1): δ = 197.6 (N=*C*H), 149.0, 138.1, 137.2 [each d, each $^1J_{CF}$ = 240 Hz, *o*, *p*, *m*-B(C_6F_5)$_3$], 114.0 (double intensity), 109.3, 109.1 (each Cp), 97.1 (C1), 41.6 (*C*(CH$_3$)$_3$), 31.3 (*C*H$_2$), 25.3 (C(*C*H$_3$)$_3$), 13.7 (CH$_2$*C*H$_3$), *ipso*-B(C_6F_5)$_3$ resonance not located. − ^{11}B NMR (64.2 MHz, [D$_6$]benzene/[D$_8$]tetrahydrofuran, ca. 4:1): δ = −24.6 (d, $^1J_{BH}$ = 82 Hz). − ^{19}F NMR (282.4 MHz, [D$_6$]benzene/[D$_8$]tetrahydrofuran, ca. 4:1): δ = −132.0, −164.3, −166.9 [each m, *o*, *p*, *m*-B(C_6F_5)$_3$].

Reaction of 18c with *p*-Tolunitrile: Preparation of 23c: Reaction of 206 mg (410 μmol) of **14** with 210 mg (410 μmol) of B(C_6F_5)$_3$ and subsequent reaction of the in situ prepared **18c** with 52.7 mg (450 μmol) of *p*-tolunitrile gave **23c** as a yellow powder, yield 344 mg (73%), mp 142°C (DSC, 168°C decomp.). − $C_{49}H_{35}BF_{15}NOZr_2$ (1148.1): calcd. C 51.99, H 3.12, N 1.24, found C 51.76, H 3.46, N 1.15. − ^{1}H NMR (200.1 MHz, [D$_6$]benzene/[D$_8$]tetrahydrofuran, ca. 4:1): δ = 9.65 (s, 1 H, N=C*H*), 7.22, 7.15 (each psd, each 2 H, *m*, *o*-PhCH$_3$), 5.99, 5.98, 5.69, 5.57 (each s, each 5 H, Cp), 3.5 (m, 1 H, 1-H), 2.25 (s, 3 H, PhCH_3), 1.8-1.5 (m, 2 H, CH_2), 1.00 (pst, 3 H, CH$_2$CH_3), B-*H* resonance not observed. − ^{13}C NMR (50.3 MHz, [D$_6$]benzene/[D$_8$]tetrahydrofuran, ca. 4:1): δ = 184.6 (N=*C*H), 149.0, 138.1, 137.2 [each d, each $^1J_{CF}$ = 240 Hz, *o*, *p*, *m*-B(C_6F_5)$_3$], 145.7, 134.3, 130.3, 129.7 (*p*, *ipso*, *m*, *o*-PhCH$_3$), 113.8, 113.8, 109.2, 109.0 (each Cp), 96.7 (C1), 31.5 (*C*H$_2$), 21.3 (Ph*C*H$_3$), 13.6 (CH$_2$*C*H$_3$), *ipso*-B(C_6F_5)$_3$ resonance not located. − ^{11}B NMR (64.2 MHz, [D$_6$]benzene[D$_8$]tetrahydrofuran, ca. 4:1): δ = −24.6 (d, $^1J_{BH}$ = 82 Hz). − ^{19}F NMR (282.4 MHz, [D$_6$]benzene/[D$_8$]tetrahydrofuran, ca. 4:1): δ = −132.0, −164.3, −166.9 [each m, *o*, *p*, *m*-B(C_6F_5)$_3$].

Reaction of 18d with Acetonitrile: Preparation of 24a: Reaction of 269 mg (410 μmol) of **17** with 210 mg (410 μmol) of B(C_6F_5)$_3$ and subsequent reaction of the in situ prepared **18d** with 23.9 μL (18.5 mg, 450 μmol) of acetonitrile gave **24a** as a yellow powder, yield 376 mg (76%), mp 239°C (DSC, decomp.). − $C_{55}H_{39}BF_{15}NOZr_2$ (1208.2): calcd. C 54.68, H 3.25, N 1.16, found C 54.50, H 3.65, N 1.01. − ^{1}H NMR (599.9 MHz, [D$_6$]benzene/[D$_8$]tetrahydrofuran, ca. 4:1): δ = 8.51 (q, 1 H, $^3J_{HH}$ = 4.7 Hz, N=C*H*), 7.31 (pst, 2 H, *m*), 7.22 (pst, 1 H, *p*), 7.10 (psd, 2 H, *o*-CH$_2$Ph), 7.19 (psd, 2 H, *o*), 6.98 (pst, 2 H, *m*), 6.84 (pst, 1 H, *p*-B-CH$_2$Ph), 5.63, 5.59, 5.45, 5.42 (each s, each 5 H, Cp), 3.82 (dd, 1 H, $^3J_{HH}$ = 10.2 Hz, $^3J_{HH}$ = 3.2 Hz, 1-H), 3.42 (br, 2 H, B-CH_2), 3.14 (dd, 1 H, $^2J_{HH}$ = 15.2 Hz, $^3J_{HH}$ = 3.2 Hz, CHCH_2), 2.58 (dd, 1 H, $^2J_{HH}$ = 15.2 Hz, $^3J_{HH}$ = 10.2 Hz, CHCH_2), 1.67 (d, 3 H, $^3J_{HH}$ = 4.7 Hz, N=CHCH_3). − ^{13}C NMR (150.8 MHz, [D$_6$]benzene/[D$_8$]tetrahydrofuran, ca. 4:1): δ = 186.9 (N=*C*H), 149.0, 138.1, 137.2 [each d, each $^1J_{CF}$ = 240 Hz, *o*, *p*, *m*-B(C_6F_5)$_3$], 142.0, 128.9, 128.4, 126.8 (*ipso*, *m*, *o*, *p*-CH$_2$Ph), 149.2, 129.3, 127.4, 123.1 (*ipso*, *o*, *m*, *p*-B-CH$_2$Ph), 113.8, 113.5, 108.9, 108.7 (each Cp), 91.6 (C1), 44.1 (CH*C*H$_2$), 33.2 (N=CH*C*H$_3$), 32.4 (br, B-*C*H$_2$), *ipso*-B(C_6F_5)$_3$ resonance not located. − ^{11}B NMR (64.2 MHz, [D$_6$]benzene/[D$_8$]tetrahydrofuran, ca. 4:1): δ = −12.3. − ^{19}F NMR (282.4 MHz, [D$_6$]benzene/[D$_8$]tetrahydrofuran, ca. 4:1): δ = −128.1, −164.2, −166.8 [each m, *o*, *p*, *m*-B(C_6F_5)$_3$].

Reaction of 18d with *tert*-Butyl Cyanide: Preparation of 24b: Reaction of 269 mg (410 μmol) of **17** with 210 mg (410 μmol) of B(C_6F_5)$_3$ and subsequent reaction of the in situ prepared **18d** with 49.7 μL (37.4 mg, 450 μmol) of *tert*-butyl cyanide gave **24b** as a yellow powder, yield 364 mg (71%), mp 166°C (DSC, decomp.). − $C_{58}H_{45}BF_{15}NOZr_2$ (1250.2): calcd. C 55.72, H 3.63, N 1.12, found C 55.05, H 4.16, N 1.63. − ^{1}H NMR (599.9 MHz, [D$_6$]benzene/[D$_8$]tetrahydrofuran, ca. 4:1): δ = 8.89 (s, 1 H, N=C*H*), 7.33 (pst, 2 H, *m*), 7.23 (pst, 1 H, *p*), 7.18 (psd, 2 H, *o*-CH$_2$Ph), 7.08 (psd, 2 H, *o*), 6.91 (pst, 2 H, *m*), 6.77 (pst, 1 H, *p*-B-CH$_2$Ph), 5.79, 5.72, 5.58, 5.55 (each s, each 5 H, Cp), 3.87 (dd, 1 H, $^3J_{HH}$ = 10.3 Hz, $^3J_{HH}$ = 3.0 Hz, 1-H), 3.30 (br, 2 H, B-CH_2), 3.18 (dd, 1 H, $^2J_{HH}$ = 15.2 Hz, $^3J_{HH}$ = 3.0 Hz, CHCH_2), 2.67 (dd, 1 H, $^2J_{HH}$ = 15.2 Hz, $^3J_{HH}$ = 10.3 Hz, CHCH_2), 0.87 [s, 9 H, C(CH_3)$_3$]. − ^{13}C NMR

(150.8 MHz, [D$_6$]benzene/[D$_8$]tetrahydrofuran, ca. 4:1): δ = 197.2 (N=*C*H), 149.0, 138.1, 137.2 [each d, each $^1J_{CF}$ = 240 Hz, *o*, *p*, *m*-B(C$_6$F$_5$)$_3$], 142.0, 128.5, 128.0, 126.4 (*ipso*, *m*, *o*, *p*-CH$_2$Ph), 148.7, 128.8, 126.7, 122.4 (*ipso*, *o*, *m*, *p*-B-CH$_2$Ph), 113.7, 113.5, 109.1, 108.8 (each Cp), 93.3 (C1), 43.5 (CH*C*H$_2$), 41.2 [*C*(CH$_3$)$_3$], 31.9 (br, B-*C*H$_2$), 24.8 [C(*C*H$_3$)$_3$], *ipso*-B(C$_6$F$_5$)$_3$ resonance not located. − ^{11}B NMR (64.2 MHz, [D$_6$]benzene/[D$_8$]tetrahydrofuran, ca. 4:1): δ = −12.3. − ^{19}F NMR (282.4 MHz, [D$_6$]benzene/[D$_8$]tetrahydrofuran, ca. 4:1): δ = −128.1, −164.2, −166.8 [each m, *o*, *p*, *m*-B(C$_6$F$_5$)$_3$].

Reaction of 18d with *p*-Tolunitrile: Preparation of 24c: Reaction of 269 mg (410 μmol) of **17** with 210 mg (410 μmol) of B(C$_6$F$_5$)$_3$ and subsequent reaction of the in situ prepared **18d** with 52.7 mg (450 μmol) of *p*-tolunitrile gave **24c** as a yellow powder, yield 347 mg (66%), mp 222°C (DSC, decomp.). − C$_{61}$H$_{43}$BF$_{15}$NOZr$_2$ (1284.3): calcd. C 57.05, H 3.37, N 1.09, found C 56.41, H 3.62, N 1.18. − ^{1}H NMR (599.9 MHz, [D$_6$]benzene/[D$_8$]tetrahydrofuran, ca. 4:1): δ = 9.54 (s, 1 H, N=C*H*), 7.28 (pst, 2 H, *m*), 7.18 (m, 1 H, *p*), 7.14 (psd, 2 H, *o*-CH$_2$Ph), 7.18 (m, 2 H, *m*), 7.07 (psd, 2 H, *o*-PhCH$_3$), 7.02 (psd, 2 H, *o*), 6.84 (pst, 2 H, *m*), 6.70 (pst, 1 H, *p*-B-CH$_2$Ph), 5.77, 5.60, 5.57 (double intensity) (each Cp), 3.88 (dd, 1 H, $^3J_{HH}$ = 10.2 Hz, $^3J_{HH}$ = 2.8 Hz, 1-H), 3.24 (br, 2 H, B-C*H*$_2$), 3.17 (dd, 1 H, $^2J_{HH}$ = 15.0 Hz, $^3J_{HH}$ = 2.8 Hz, CHC*H*$_2$), 2.67 (dd, 1 H, $^2J_{HH}$ = 15.0 Hz, $^3J_{HH}$ = 10.2 Hz, CHC*H*$_2$), 2.19 (s, 3 H, PhC*H*$_3$). − ^{13}C NMR (150.8 MHz, [D$_6$]benzene/[D$_8$]tetrahydrofuran, ca. 4:1): δ = 184.0 (N=*C*H), 149.0, 138.1, 137.2 [each d, each $^1J_{CF}$ = 240 Hz, *o*, *p*, *m*-B(C$_6$F$_5$)$_3$], 145.2, 133.9, 129.8, 129.1 (*p*, *ipso*, *m*, *o*-PhCH$_3$), 142.0, 128.5, 128.0, 126.3 (*ipso*, *m*, *o*, *p*-CH$_2$Ph), 148.7, 128.7, 126.8, 122.4 (*ipso*, *o*, *m*, *p*-B-CH$_2$Ph), 113.5, 113.2, 109.0, 108.7 (each Cp), 93.0 (C1), 43.7 (CH*C*H$_2$), 31.9 (br, B-*C*H$_2$), 20.8 (Ph*C*H$_3$), *ipso*-B(C$_6$F$_5$)$_3$ resonance not located. − ^{11}B NMR (64.2 MHz, [D$_6$]benzene/[D$_8$]tetrahydrofuran, ca. 4:1): δ = −12.3. − ^{19}F NMR (282.4 MHz, [D$_6$]benzene/[D$_8$]tetrahydrofuran, ca. 4:1): δ = −128.1, −164.2, −166.8 [each m, *o*, *p*, *m*-B(C$_6$F$_5$)$_3$].

Reaction of 18d with Propionitrile: Preparation of 24d: Reaction of 269 mg (410 μmol) of **17** with 210 mg (410 μmol) of B(C$_6$F$_5$)$_3$ and subsequent reaction of the in situ prepared **18d** with 32.1 μL (24.7 mg, 450 μmol) of propionitrile gave **24d** as an orange powder, yield 376 mg (75%), mp 195°C (DSC, 259°C decomp.). − C$_{56}$H$_{41}$BF$_{15}$NOZr$_2$ (1222.2): calcd. C 55.03, H 3.38, N 1.15, found C 54.21, H 3.67, N 1.34. − ^{1}H NMR (599.9 MHz, [D$_6$]benzene/[D$_8$]tetrahydrofuran, ca. 4:1): δ = 8.45 (pst, 1 H, N=C*H*), 7.26 (pst, 2 H, *m*), 7.16 (pst, 1 H, *p*), 7.07 (psd, 2 H, *o*-CH$_2$Ph), 7.09 (psd, 2 H, *o*), 6.89 (pst, 2 H, *m*), 6.76 (pst, 1 H, *p*-B-CH$_2$Ph), 5.64, 5.60, 5.46, 5.43 (each s, each 5 H, Cp), 3.80 (dd, 1 H, $^3J_{HH}$ = 10.4 Hz, $^3J_{HH}$ = 3.4 Hz, 1-H), 3.32 (br, 2 H, B-C*H*$_2$), 3.10 (dd, 1 H, $^2J_{HH}$ = 15.4 Hz, $^3J_{HH}$ = 3.4 Hz, CHC*H*$_2$), 2.56 (dd, 1 H, $^2J_{HH}$ = 15.4 Hz, $^3J_{HH}$ = 10.4 Hz, CHC*H*$_2$), 1.75, 1.68 (each m, each 1 H, N=CHC*H*$_2$), 0.96 (pst, 3 H, CH$_2$C*H*$_3$). − ^{13}C NMR (150.8 MHz, [D$_6$]benzene/[D$_8$]tetrahydrofuran, ca. 4:1): δ = 186.9 (N=*C*H), 149.0, 138.1, 137.2 [each d, each $^1J_{CF}$ = 240 Hz, *o*, *p*, *m*-B(C$_6$F$_5$)$_3$], 142.0, 128.5, 127.8, 126.3 (*ipso*, *m*, *o*, *p*-CH$_2$Ph), 149.2, 128.8, 126.9, 122.5 (*ipso*, *o*, *m*, *p*-B-CH$_2$Ph), 113.8, 113.5, 108.9, 108.7 (each Cp), 91.6 (C1), 44.1 (CH*C*H$_2$), 33.2 (N=CH*C*H$_2$), 31.5 (br, B-*C*H$_2$), 8.2 (CH$_2$*C*H$_3$), *ipso*-B(C$_6$F$_5$)$_3$ resonance not located. − ^{11}B NMR (64.2 MHz, [D$_6$]benzene/[D$_8$]tetrahydrofuran, ca. 4:1): δ = −12.3. − ^{19}F NMR (282.4 MHz, [D$_6$]benzene/[D$_8$]tetrahydrofuran, ca. 4:1): δ = −128.1, −164.2, −166.8 [each m, *o*, *p*, *m*-B(C$_6$F$_5$)$_3$].

X-ray Crystal Structure Analysis of 24d: Pentane was allowed to diffuse through the gas phase into a solution of **24d** in a 6:1 mixture of toluene/tetrahydrofuran. After two days a yellow oil precipitated, standing for 1.5 months, single crystals grew out of this oil: formula C$_{56}$H$_{41}$BF$_{15}$NOZr$_2$, M = 1222.15, yellow crystal, 0.30 × 0.20 × 0.10 mm, a = 10.134(1), b = 19.063(1), c = 12.952(2) Å, β = 98.71(1)°, V = 2473.3(5) Å^3, ρ_{calc} = 1.641 g cm^{-3}, F(000) = 1224 e, μ = 5.21 cm^{-1}, empirical absorption correction via φ scan data (0.859 ≤ T ≤ 0.950), Z = 2, monoclinic, space group $P2_1$ (No. 4), λ = 0.71073 Å, T = 223 K, ω/2θ scans, 4757 reflections collected (+h, -k, ±l), [(sinθ)/λ] = 0.59 Å^{-1}, 4492 independent and 2955 observed reflections [$I \geq 2\,\sigma(I)$], 666 refined parameters, R = 0.067, wR^2 = 0.154, max. residual electron density 0.88 (−2.00) e Å^{-3}, Flack parameter 0.05(9), disorder in the benzyl group C30-C36 (55:45(3)%), distances C1−C30(a,b) and C30(a,b)−C31(a,b) refined with restraints, groups C30(a,b)−C36(a,b) refined as rigid groups, hydrogens calculated and refined as riding atoms. The data set was collected with an Enraf Nonius MACH3 diffractometer. Programs used: data reduction MolEN, structure solution SHELXS-86, structure refinement SHELXL-97, graphics SCHAKAL-92. Crystallographic data (excluding structure factors) for the structure reported in this paper have been deposited with the Cambridge Crystallographic Data Centre as supplementary publication no. CCDC-106600. Copies of the data can be obtained free of charge on application to The Director, CCDC, 12 Union Road, Cambridge CB2 1EZ, UK [fax: int. code +44(1223)336-033, e-mail: deposit@ccdc.cam.ac.uk].

Reaction of 18a with *tert*-Butylisocyanate. − Preparation of 27a: Reaction of 200 mg (410 μmol) of **11** with 210 mg (410 μmol) of B(C$_6$F$_5$)$_3$ and subsequent reaction of the in situ prepared **18a** with 52.8 μL (44.6 mg, 450 μmol) of *tert*-butylisocyanate gave **27a** as a yellow powder, yield 338 mg (75%), mp 205°C (DSC, decomp.). − C$_{45}$H$_{35}$BF$_{15}$NO$_2$Zr$_2$ (1100.0): calcd. C 49.14, H 3.21, N 1.27, found C 49.14, H 3.35, N 1.42. − ^{1}H NMR (200.1 MHz, [D$_6$]benzene/[D$_8$]tetrahydrofuran, ca. 4:1): δ = 7.45 (s, 1 H, O=C*H*), 6.04, 5.95, 5,78, 5.74 (each s, each 5 H, Cp), 3.41 (q, 1 H, $^3J_{HH}$ = 6.3 Hz, 1-H), 1.53 (d, 3 H, $^3J_{HH}$ = 6.3 Hz, CHC*H*$_3$), 1.05 [s, 9 H, C(C*H*$_3$)$_3$], B-*H* resonance not observed. − ^{13}C-NMR (50.3 MHz, [D$_6$]benzene/[D$_8$]tetrahydrofuran, ca. 4:1): δ = 165.1 (O=*C*H), 149.0, 138.0, 136.9 [each d, each $^1J_{CF}$ = 240 Hz, *o*, *p*, *m*-B(C$_6$F$_5$)$_3$], 114.2, 114.0, 110.0, 109.5 (each Cp), 85.8 (C1), 56.1 [*C*(CH$_3$)$_3$], 31.0 [C(*C*H$_3$)$_3$], 23.8 (*C*H$_3$), *ipso*-B(C$_6$F$_5$)$_3$ resonance not located. − ^{11}B NMR (64.2 MHz, [D$_6$]benzene/[D$_8$]tetrahydrofuran, ca. 4:1): δ = −24.6 (d, $^1J_{BH}$ = 82 Hz). − ^{19}F NMR (282.4 MHz, [D$_6$]benzene/[D$_8$]tetrahydrofuran, ca. 4:1): δ = −132.0, −163.5, −166.3 [each m, *o*, *p*, *m*-B(C$_6$F$_5$)$_3$].

Reaction of 18a with Trimethylsilylisocyanate: Preparation of 27b: Reaction of 200 mg (410 μmol) of **11** with 210 mg (410 μmol) of B(C$_6$F$_5$)$_3$ and subsequent reaction of the in situ prepared **18a** with 59.8 μL (51.8 mg, 450 μmol) of trimethylsilylisocyanate gave **27b** as a yellow powder, yield 307 mg (67%), mp 158°C (DSC, decomp.). − C$_{44}$H$_{35}$BF$_{15}$NO$_2$SiZr$_2$ (1116.1): calcd. C 47.35, H 3.16, N 1.25, found C 47.05, H 3.26, N 1.52. − ^{1}H NMR (200.1 MHz, [D$_6$]benzene/[D$_8$]tetrahydrofuran, ca. 4:1): δ = 7.41 (s, 1 H, O=C*H*), 5.91, 5.82, 5,72, 5.68 (each s, each 5 H, Cp), 3.38 (q, 1 H, $^3J_{HH}$ = 6.3 Hz, 1-H), 1.49 (d, 3 H, $^3J_{HH}$ = 6.3 Hz, CHC*H*$_3$), 0.08 [s, 9 H, Si(C*H*$_3$)$_3$], B-*H* resonance not observed. − ^{13}C NMR (50.3 MHz, [D$_6$]benzene/[D$_8$]tetrahydrofuran, ca. 4:1): δ = 170.7 (O=*C*H), 149.0, 138.0, 136.9 [each d, each $^1J_{CF}$ = 240 Hz, *o*, *p*, *m*-B(C$_6$F$_5$)$_3$), 114.0, 113.8, 110.0, 109.4 (each Cp), 86.7 (C1), 23.9 (CH*C*H$_3$), −0.1 [Si(*C*H$_3$)$_3$], *ipso*-B(C$_6$F$_5$)$_3$ resonance not located. − ^{11}B NMR (64.2 MHz, [D$_6$]benzene/[D$_8$]tetrahydrofuran, ca. 4:1): δ = −24.6 (d, $^1J_{BH}$ = 82 Hz). − ^{19}F NMR (282.4 MHz, [D$_6$]benzene/[D$_8$]tetrahydrofuran, ca. 4:1): δ = −132.0, −163.5, −166.3 [each m, *o*, *p*, *m*-B(C$_6$F$_5$)$_3$].

Reaction of 18a with *p*-Tolylisocyanate: Preparation of 27c: Reaction of 200 mg (410 μmol) of **11** with 210 mg (410 μmol) of

$B(C_6F_5)_3$ and subsequent reaction of the in situ prepared **18a** with 56.6 µL (59.9 mg, 450 µmol) of *p*-tolylisocyanate gave **27c** as a yellow powder, yield 335 mg (72%), mp 161°C (DSC, decomp.). – $C_{48}H_{33}BF_{15}NO_2Zr_2$ (1134.0): calcd. C 50.84, H 2.93, N 1.24, found C 51.24, H 3.39, N 1.04. – ^{1}H NMR (200.1 MHz, [D$_6$]benzene/[D$_8$]tetrahydrofuran, ca. 4:1): δ = 7.61 (s, 1 H, O=C*H*), 7.07, 6.72 (m, each 2 H, *m*, *o*-PhCH$_3$), 6.02, 5.79 (double intensity), 5.74 (each s, each 5 H, Cp), 3.47 (q, 1 H, $^3J_{HH}$ = 6.3 Hz, 1-H), 2.19 (s, 3 H, PhC*H*$_3$), 1.50 (d, 3 H, $^3J_{HH}$ = 6.3 Hz, CHC*H*$_3$), B-*H* resonance not observed. – ^{13}C NMR (50.3 MHz, [D$_6$]benzene/[D$_8$]tetrahydrofuran, ca. 4:1): δ = 166.4 (O=*C*H), 149.0, 138.1, 137.2 [each d, each $^1J_{CF}$ = 240 Hz, *o*, *p*, *m*-B(C$_6$F$_5$)$_3$], 139.9, 138.0, 130.8, 121.5 (*ipso*, *p*, *m*, *o*-PhCH$_3$), 114.5, 114.1, 110.2, 109.6 (each Cp), 87.9 (C1), 24.1 (CH*C*H$_3$), 20.7 (Ph*C*H$_3$), *ipso*-B(C$_6$F$_5$)$_3$ resonance not located. – ^{11}B NMR (64.2 MHz, [D$_6$]benzene/[D$_8$]tetrahydrofuran, ca. 4:1): δ = –24.6 (d, $^1J_{BH}$ = 82 Hz). – ^{19}F NMR (282.4 MHz, [D$_6$]benzene/[D$_8$]tetrahydrofuran, ca. 4:1): δ = –132.0, –163.5, –166.3 [each m, *o*, *p*, *m*-B(C$_6$F$_5$)$_3$].

Reaction of 18b with *tert*-Butylisocyanate: Preparation of 28a: Reaction of 206 mg (410 µmol) of **8** with 210 mg (410 µmol) of $B(C_6F_5)_3$ and subsequent reaction of the in situ prepared **18b** with 52.8 µL (44.6 mg, 450 µmol) of *tert*-butylisocyanate gave **28a** as a yellow powder, yield 306 mg (67%), mp 203°C (DSC, decomp.). – $C_{46}H_{37}BF_{15}NO_2Zr_2$ (1114.0): calcd. C 49.60, H 3.35, N 1.26, found C 48.61, H 3.38, N 1.10. – ^{1}H NMR (200.1 MHz, [D$_6$]benzene/[D$_8$]tetrahydrofuran, ca. 4:1): δ = 7.31 (s, 1 H, O=C*H*), 5.93, 5.86, 5,70, 5.66 (each s, each 5 H, Cp), 3.36 (q, 1 H, $^3J_{HH}$ = 6.3 Hz, 1-H), 1.50 (d, 3 H, $^3J_{HH}$ = 6.3 Hz, CHC*H*$_3$), 1.18 (br, 3 H, B-C*H*$_3$), 1.00 [s, 9 H, C(C*H*$_3$)$_3$]. – ^{13}C NMR (50.3 MHz, [D$_6$]benzene/[D$_8$]tetrahydrofuran, ca. 4:1): δ = 165.6 (O=*C*H), 149.0, 138.0, 136.9 [each d, each $^1J_{CF}$ = 240 Hz, *o*, *p*, *m*-B(C$_6$F$_5$)$_3$], 114.0, 113.8, 109.8, 109.3 (each Cp), 85.9 (C1), 56.0 [*C*(CH$_3$)$_3$], 31.0 [C(*C*H$_3$)$_3$], 23.8 (CH*C*H$_3$), *ipso*-B(C$_6$F$_5$)$_3$ and B-*C*H$_3$ resonances not located. – ^{11}B NMR (64.2 MHz, [D$_6$]benzene/[D$_8$]tetrahydrofuran, ca. 4:1): δ = –14.5. – ^{19}F NMR (282.4 MHz, [D$_6$]benzene/[D$_8$]tetrahydrofuran, ca. 4:1): δ = –132.0, –163.5, –166.3 [each m, *o*, *p*, *m*-B(C$_6$F$_5$)$_3$).

Reaction of 18b with Trimethylsilylisocyanate: Preparation of 28b: Reaction of 206 mg (410 µmol] of **8** with 210 mg (410 µmol) of $B(C_6F_5)_3$ and subsequent reaction of the in situ prepared **18b** with 59.8 µL (51.8 mg, 450 µmol) of trimethylsilylisocyanate gave **28b** as a yellow powder, yield 283 mg (61%), mp 157°C (DSC, decomp.). – $C_{45}H_{37}BF_{15}NO_2SiZr_2$ (1130.1): calcd. C 47.83, H 3.30, N 1.24, found C 47.82, H 3.30, N 1.55. – ^{1}H NMR (200.1 MHz, [D$_6$]benzene/[D$_8$]tetrahydrofuran, ca. 4:1): δ = 7.48 (s, 1 H, O=C*H*), 6.05, 5.97, 5.85, 5.80 (each s, each 5 H, Cp), 3.53 (q, 1 H, $^3J_{HH}$ = 6.3 Hz, 1-H), 1.62 (d, 3 H, $^3J_{HH}$ = 6.3 Hz, CHC*H*$_3$), 1.18 (br, 3 H, B-C*H*$_3$), 0.20 [s, 9 H, Si(C*H*$_3$)$_3$]. – ^{13}C NMR (150.8 MHz, [D$_6$]benzene/[D$_8$]tetrahydrofuran, ca. 4:1): δ = 170.6 (O=*C*H), 149.0, 138.0, 136.9 [each d, each $^1J_{CF}$ = 240 Hz, *o*, *p*, *m*-B(C$_6$F$_5$)$_3$], 114.0, 113.8, 110.0, 109.4 (each Cp), 86.7 (C1), 23.9 (CH*C*H$_3$), 11.4 (br, B-*C*H$_3$), 0.1 [Si(*C*H$_3$)$_3$], *ipso*-B(C$_6$F$_5$)$_3$ resonance not located. – ^{11}B NMR (64.2 MHz, [D$_6$]benzene/[D$_8$]tetrahydrofuran, ca. 4:1): δ = –14.6. – ^{19}F NMR (282.4 MHz, [D$_6$]benzene/[D$_8$]tetrahydrofuran, ca. 4:1): δ = –132.0, –163.5, –166.3 [each m, *o*, *p*, *m*-B(C$_6$F$_5$)$_3$].

Reaction of 18b with *p*-Tolylisocyanate: Preparation of 28c: Reaction of 206 mg (410 µmol) of **8** with 210 mg (410 µmol) of $B(C_6F_5)_3$ and subsequent reaction of the in situ prepared **18b** with 56.6 µL (59.9 mg, 450 µmol) of *p*-tolylisocyanate gave **28c** as a yellow powder, yield 334 mg (71%), mp 165°C (DSC, decomp.). – $C_{49}H_{35}BF_{15}NO_2Zr_2$ (1148.1): calcd. C 51.26, H 3.07, N 1.22, found C 52.00, H 3.30, N 1.43. – ^{1}H NMR (200.1 MHz, [D$_6$]benzene/[D$_8$]tetrahydrofuran, ca. 4:1): δ = 7.36 (s, 1 H, O=C*H*), 7.11, 6.69 (m, each 2 H, *m*, *o*-PhCH$_3$) 5.99, 5.78, 5,76, 5.70 (each s, each 5 H, Cp), 3.49 (q, 1 H, $^3J_{HH}$ = 6.3 Hz, 1-H), 2.20 (s, 3 H, PhC*H*$_3$), 1.51 (d, 3 H, $^3J_{HH}$ = 6.3 Hz, CHC*H*$_3$), 1.21 (br, 3 H, B-C*H*$_3$). – ^{13}C NMR (50.3 MHz, [D$_6$]benzene/[D$_8$]tetrahydrofuran, ca. 4:1): δ = 166.0 (O=*C*H), 149.0, 138.1, 137.2 [each d, each $^1J_{CF}$ = 240 Hz, *o*, *p*, *m*-B(C$_6$F$_5$)$_3$], 139.8, 138.2, 130.9, 121.5 (*ipso*, *p*, *m*, *o*-PhCH$_3$), 114.5, 114.1, 110.1, 109.5 (each Cp), 88.2 (C1), 24.1 (CH*C*H$_3$), 20.7 (Ph*C*H$_3$), *ipso*-B(C$_6$F$_5$)$_3$ and B-*C*H$_3$ resonances not located. – ^{11}B NMR (64.2 MHz, [D$_6$]benzene/[D$_8$]tetrahydrofuran, ca. 4:1): δ = –14.6. – ^{19}F NMR (282.4 MHz, [D$_6$]benzene/[D$_8$]tetrahydrofuran, ca. 4:1): δ = –132.0, –163.5, –166.3 [each m, *o*, *p*, *m*-B(C$_6$F$_5$)$_3$].

Reaction of 18b with 1-Adamantylisocyanate: Preparation of 28d: Reaction of 206 mg (410 µmol) of **8** with 210 mg (410 µmol) of $B(C_6F_5)_3$ and subsequent reaction of the in situ prepared **18b** with 79.8 mg (450 µmol) of 1-adamantylisocyanate gave **28d** as a yellow powder, yield 354 mg (66%), mp 208°C (DSC, decomp.). – $C_{52}H_{43}BF_{15}NO_2Zr_2$ (1192.2): calcd. C 52.39, H 3.64, N 1.17, found C 51.90, H 4.22, N 1.05, found C 52.69, H 3.91, N 1.93. – ^{1}H NMR (599.9 MHz, [D$_6$]benzene/[D$_8$]tetrahydrofuran, ca. 4:1): δ = 7.36 (s, 1 H, O=C*H*), 5.97, 5.89, 5.73, 5.69 (each s, each 5 H, Cp), 3.37 (q, 1 H, $^3J_{HH}$ = 6.3 Hz, 1-H), 1.96 (br, 3 H, AdC*H*), 1.7-1.4 (m, 18 H, AdC*H*$_2$, CHC*H*$_3$, B-C*H*$_3$). – ^{13}C NMR (150.8 MHz, [D$_6$]benzene/[D$_8$]tetrahydrofuran, ca. 4:1): δ = 165.0 (O=*C*H), 149.0, 138.0, 136.9 [each d, each $^1J_{CF}$ = 240 Hz, *o*, *p*, *m*-B(C$_6$F$_5$)$_3$], 114.0, 113.8, 119.9, 109.4 (each Cp), 85.7 (C1), 57.4 (Ad*C*), 44.4, 35.8 (Ad*C*H$_2$), 30.0 (Ad*C*H), 23.8 (CH*C*H$_3$), *ipso*-B(C$_6$F$_5$)$_3$ and B-*C*H$_3$ resonances not located. – ^{11}B NMR (64.2 MHz, [D$_6$]benzene/[D$_8$]tetrahydrofuran, ca. 4:1): δ = –14.6. – ^{19}F NMR (282.4 MHz, [D$_6$]benzene/[D$_8$]tetrahydrofuran, ca. 4:1): δ = –132.0, –163.5, –166.3 [each m, *o*, *p*, *m*-B(C$_6$F$_5$)$_3$].

Reaction of 18c with *tert*-Butylisocyanate: Preparation of 29a: Reaction of 206 mg (410 µmol) of **14** with 210 mg (410 µmol) of $B(C_6F_5)_3$ and subsequent reaction of the in situ prepared **18c** with 52.8 µL (44.6 mg, 450 µmol) of *tert*-butylisocyanate gave **29a** as a yellow orange powder, yield 297 mg (65%), mp 176°C (DSC, decomp.). – $C_{46}H_{37}BF_{15}NO_2Zr_2$ (1114.0): calcd. C 49.60, H 3.35, N 1.26, found C 49.45, H 3.56, N 1.27. – ^{1}H NMR (200.1 MHz, [D$_6$]benzene/[D$_8$]tetrahydrofuran, ca. 4:1): δ = 7.39 (s, 1 H, O=C*H*), 5.95, 5.89, 5.71, 5.69 (each s, each 5 H, Cp), 3.15 (dd, 1 H, 1-H), 1.8–1.4 (m, 2 H, C*H*$_2$), 1.01 [s, 9 H, C(C*H*$_3$)$_3$], 0.89 (pst, 3 H, CH$_2$C*H*$_3$), B-*H* resonance not observed. – ^{13}C NMR (50.3 MHz, [D$_6$]benzene/[D$_8$]tetrahydrofuran, ca. 4:1): δ = 165.8 (N=*C*H), 149.0, 138.1, 137.2 [each d, each $^1J_{CF}$ = 240 Hz, *o*, *p*, *m*-B(C$_6$F$_5$)$_3$], 114.1 (double intensity), 119.8, 109.5 (each Cp), 93.2 (C1), 56.1 [*C*(CH$_3$)$_3$], 31.7 (*C*H$_2$), 31.1 [C(*C*H$_3$)$_3$], 14.4 (CH$_2$*C*H$_3$), *ipso*-B(C$_6$F$_5$)$_3$ resonance not located. – ^{11}B NMR (64.2 MHz, [D$_6$]benzene/[D$_8$]tetrahydrofuran, ca. 4:1): δ = –24.6 (d, $^1J_{BH}$ = 82 Hz). – ^{19}F NMR (282.4 MHz, [D$_6$]benzene/[D$_8$]tetrahydrofuran, ca. 4:1): δ = –132.0, –164.3, –166.9 [each m, *o*, *p*, *m*-B(C$_6$F$_5$)$_3$].

Reaction of 18c with Trimethylsilylisocyanate: Preparation of 29b: Reaction of 206 mg (410 µmol) of **14** with 210 mg (410 µmol) of $B(C_6F_5)_3$ and subsequent reaction of the in situ prepared **18c** with 59.8 µL (51.8 mg, 450 µmol) of trimethylsilylisocyanate gave **29b** as a yellow powder, yield 297 mg (64%), mp 185°C (DSC, decomp.). – $C_{45}H_{37}BF_{15}NO_2SiZr_2$ (1130.1): calcd. C 47.83, H 3.30, N 1.24, found C 47.90, H 3.42, N 1.37. – ^{1}H NMR (200.1 MHz, [D$_6$]benzene/[D$_8$]tetrahydrofuran, ca. 4:1): δ = 7.45 (s, 1 H, O=C*H*), 6.00, 5.94, 5.78, 5.76 (each s, each 5 H, Cp), 3.27 (dd, 1 H, 1-H), 1.9-1.7, 1.7-1.4 (each m, each 1 H, C*H*$_2$), 0.90 (pst, 3 H,

CH_2CH_3), 0.13 [s, 9 H, Si(CH_3)$_3$], B-*H* resonance not observed. – ^{13}C NMR (50.3 MHz, [D$_6$]benzene/[D$_8$]tetrahydrofuran, ca. 4:1): δ = 170.7 (O=*C*H), 149.0, 138.1, 137.2 [each d, each $^1J_{CF}$ = 240 Hz, *o*, *p*, *m*-B(C_6F_5)$_3$], 114.1 (double intensity), 119.9, 109.5 (each Cp), 93.9 (C1), 31.8 (CH_2), 14.5 (CH_2CH_3), −0.1 [Si(CH_3)$_3$], *ipso*-B(C_6F_5)$_3$ resonance not located. – ^{11}B NMR (64.2 MHz, [D$_6$]benzene/[D$_8$]tetrahydrofuran, ca. 4:1): δ = −24.6 (d, $^1J_{BH}$ = 82 Hz). – ^{19}F NMR (282.4 MHz, [D$_6$]benzene/[D$_8$]tetrahydrofuran, ca. 4:1): δ = −132.0, −164.3, −166.9 [each m, *o*, *p*, *m*-B(C_6F_5)$_3$].

Reaction of 18c with *p*-Tolylisocyanate: Preparation of 29c: Reaction of 206 mg (410 μmol) of **14** with 210 mg (410 μmol) of B(C_6F_5)$_3$ and subsequent reaction of the in situ prepared **18c** with 56.6 μL (59.9 mg, 450 μmol) of *p*-tolylisocyanate gave **29c** as a yellow powder, yield 353 mg (75%), mp 170°C (DSC, decomp.). – $C_{49}H_{35}BF_{15}NO_2Zr_2$ (1148.1): calcd. C 51.26, H 3.07, N 1.22, found C 50.90, H 3.32, N 1.52. – ^{1}H NMR (200.1 MHz, [D$_6$]benzene/[D$_8$]tetrahydrofuran, ca. 4:1): δ = 7.75 (s, 1 H, O=C*H*), 7.16, 6.78 (each psd, each 2 H, *m*, *o*-PhCH$_3$), 6.16, 5.96, 5.92, 5.90 (each s, each 5 H, Cp), 3.37 (dd, 1 H, 1-H), 2.28 (s, 3 H, PhCH_3), 1.9-1.6 (m, 2 H, CH_2), 0.98 (pst, 3 H, CH_2CH_3), B-*H* resonance not observed. – ^{13}C NMR (50.3 MHz, [D$_6$]benzene/[D$_8$]tetrahydrofuran, ca. 4:1): δ = 166.0 (O=*C*H), 149.0, 138.1, 137.2 [each d, each $^1J_{CF}$ = 240 Hz, *o*, *p*, *m*-B(C_6F_5)$_3$], 139.8, 138.0, 130.8, 121.4 (*ipso*, *p*, *m*, *o*-PhCH$_3$), 114.5, 114.3, 110.1, 109.6 (each Cp), 94.7 (C1), 31.9 (CH_2), 24.8 (Ph*C*H$_3$), 14.5 (CH_2CH_3), *ipso*-B(C_6F_5)$_3$ resonance not located. – ^{11}B NMR (64.2 MHz, [D$_6$]benzene/[D$_8$]tetrahydrofuran, ca. 4:1): δ = −24.6 (d, $^1J_{BH}$ = 82 Hz). – ^{19}F NMR (282.4 MHz, [D$_6$]benzene/[D$_8$]tetrahydrofuran, ca. 4:1): δ = −131.9, −164.3, −166.6 [each m, *o*, *p*, *m*-B(C_6F_5)$_3$].

Reaction of 18d with *tert*-Butylisocyanate: Preparation of 30a: Reaction of 269 mg (410 μmol) of **17** with 210 mg (410 μmol) of B(C_6F_5)$_3$ and subsequent reaction of the in situ prepared **18d** with 52.8 μL (44.6 mg, 450 μmol) of *tert*-butylisocyanate gave **30a** as a yellow powder, yield 358 mg (69%), mp 180°C (DSC, decomp.). – $C_{58}H_{45}BF_{15}NO_2Zr_2$ (1266.3): calcd. C 55.02, H 3.58, N 1.11, found C 55.59, H 3.87, N 1.50. – ^{1}H NMR (599.9 MHz, [D$_6$]benzene/[D$_8$]tetrahydrofuran, ca. 4:1): δ = 7.26 (s, 1 H, O=C*H*), 7.34 (pst, 2 H, *m*), 7.22 (pst, 1 H, *p*), 7.18 (m, 2 H, *o*-CH_2Ph), 6.98 (pst, 2 H, *m*), 6.84 (pst, 1 H, *p*-B-CH_2Ph), 5.85, 5.77, 5.69, 5.52 (each s, each 5 H, Cp), 3.68 (dd, 1 H, $^3J_{HH}$ = 9.9 Hz, $^3J_{HH}$ = 3.1 Hz, 1-H), 3.41 (br, 2 H, B-CH_2), 3.01 (dd, 1 H, $^2J_{HH}$ = 14.7 Hz, $^3J_{HH}$ = 3.1 Hz, CHCH_2), 2.67 (dd, 1 H, $^2J_{HH}$ = 14.7 Hz, $^3J_{HH}$ = 9.9 Hz, CHCH_2), 0.98 (s, 9 H, C(CH_3)$_3$). – ^{13}C NMR (150.8 MHz, [D$_6$]benzene/[D$_8$]tetrahydrofuran, ca. 4:1): δ = 165.3 (O=*C*H), 149.0, 138.1, 137.2 [each d, each $^1J_{CF}$ = 240 Hz, *o*, *p*, *m*-B(C_6F_5)$_3$], 143.8, 129.0, 128.7, 126.8 (*ipso*, *m*, *o*, *p*-CH_2Ph), 149.2, 129.3, 127.4, 123.1 (*ipso*, *o*, *m*, *p*-B-CH_2Ph), 114.1, 114.0, 109.8, 109.5 (each Cp), 91.8 (C1), 56.1 [*C*(CH_3)$_3$], 45.0 (CH*C*H$_2$), 32.4 (br, B-*C*H$_2$), 31.0 [C(*C*H$_3$)$_3$], *ipso*-B(C_6F_5)$_3$ resonance not located. – ^{11}B NMR (64.2 MHz, [D$_6$]benzene/[D$_8$]tetrahydrofuran, ca. 4:1): δ = −12.3. – ^{19}F NMR (282.4 MHz, [D$_6$]benzene/[D$_8$]tetrahydrofuran, ca. 4:1): δ = −128.1, −164.2, −166.8 [each m, *o*, *p*, *m*-B(C_6F_5)$_3$].

Reaction of 18d with Trimethylsilylisocyanate: Preparation of 30b: Reaction of 269 mg (410 μmol) of **17** with 210 mg (410 μmol) of B(C_6F_5)$_3$ and subsequent reaction of the in situ prepared **18d** with 59.8 μL (51.8 mg, 450 μmol) of trimethylsilylisocyanate gave **30b** as a yellow-orange powder, yield 342 mg (65%), mp 167°C (DSC, decomp.). – $C_{57}H_{45}NBF_{15}O_2SiZr_2$ (1282.3): calcd. C 53.39, H 3.54, N 1.09, found C 53.36, H 3.85, N 1.13. – ^{1}H NMR (599.9 MHz, [D$_6$]benzene/[D$_8$]tetrahydrofuran, ca. 4:1): δ = 7.30 (s, 1 H, O=C*H*), 7.28 (pst, 2 H, *m*), 7.17 (pst, 1 H, *p*),7.16 (psd, 2 H, *o*-CH_2Ph), 7.09 (psd, 2 H, *o*), 6.90 (pst, 2 H, *m*), 6.76 (pst, 1 H, *p*-B-CH_2Ph), 5.81, 5.77, 5.68, 5.46 (each s, each 5 H, Cp), 3.71 (dd, 1 H, $^3J_{HH}$ = 9.9 Hz, $^3J_{HH}$ = 3.1 Hz, 1-H), 3.32 (br, 2 H, B-CH_2), 2.98 (dd, 1 H, $^2J_{HH}$ = 14.8 Hz, $^3J_{HH}$ = 3.1 Hz, CHCH_2), 2.64 (dd, 1 H, $^2J_{HH}$ = 14.8 Hz, $^3J_{HH}$ = 9.9 Hz, CHCH_2), 0.01 [s, 9 H, Si(CH_3)$_3$]. – ^{13}C NMR (150.8 MHz, [D$_6$]benzene/[D$_8$]tetrahydrofuran, ca. 4:1): δ = 170.4 (O=*C*H), 149.0, 138.1, 137.2 [each d, each $^1J_{CF}$ = 240 Hz, *o*, *p*, *m*-B(C_6F_5)$_3$], 144.0, 129.0, 128.8, 126.8 (*ipso*, *m*, *o*, *p*-CH_2Ph), 149.2, 129.3, 127.3, 123.0 (*ipso*, *o*, *m*, *p*-B-CH_2Ph), 114.1, 114.0, 109.9, 109.6 (each Cp), 92.7 (C1), 45.0 (CH*C*H$_2$), 32.4 (br, B-*C*H$_2$), −0.1 [Si(*C*H$_3$)$_3$], *ipso*-B(C_6F_5)$_3$ resonance not located. – ^{11}B NMR (64.2 MHz, [D$_6$]benzene/[D$_8$]tetrahydrofuran, ca. 4:1): δ = −12.3. – ^{19}F NMR (282.4 MHz, [D$_6$]benzene/[D$_8$]tetrahydrofuran, ca. 4:1): δ = −128.1, −164.2, −166.8 [each m, *o*, *p*, *m*-B(C_6F_5)$_3$].

Reaction of 18d with *p*-Tolylsilylisocyanate: Preparation of 30c: Reaction of 269 mg (410 μmol) of **17** with 210 mg (410 μmol) of B(C_6F_5)$_3$ and subsequent reaction of the in situ prepared **18d** with 56.6 μL (59.9 mg, 450 μmol) of *p*-tolylisocyanate gave **30c** as a yellow-orange powder, yield 341 mg (64%), mp 168°C (DSC, decomp.). – $C_{61}H_{43}BF_{15}NO_2Zr_2$ (1300.3): calcd. C 56.35, H 3.33, N 1.08, found C 56.08, H 3.46, N 1.44. – ^{1}H NMR (599.9 MHz, [D$_6$]benzene/[D$_8$]tetrahydrofuran, ca. 4:1): δ = 7.27 (s, 1 H, O=C*H*), 7.27 (pst, 2 H, *m*), 7.16 (pst, 1 H, *p*), 7.14 (psd, 2 H, *o*-CH_2Ph), 7.09 (psd, 2 H, *o*), 6.85 (pst, 2 H, *m*), 6.75 (pst, 1 H, *p*-B-CH_2Ph), 7.04, 6.63 (each psd, each 2 H, *m*, *o*-PhCH$_3$), 5.90, 5.81, 5.71, 5.37 (each s, each 5 H, Cp), 3.75 (dd, 1 H, $^3J_{HH}$ = 10.1 Hz, $^3J_{HH}$ = 2.7 Hz, 1-H), 3.31 (br, 2 H, B-CH_2), 2.97 (dd, 1 H, $^2J_{HH}$ = 14.7 Hz, $^3J_{HH}$ = 2.7 Hz, CHCH_2), 2.62 (dd, 1 H, $^2J_{HH}$ = 14.7 Hz, $^3J_{HH}$ = 10.1 Hz, CHCH_2), 2.13 (s, 3 H, PhCH_3). – ^{13}C NMR (150.8 MHz, [D$_6$]benzene/[D$_8$]tetrahydrofuran, ca. 4:1): δ = 165.6 (O=*C*H), 149.0, 138.1, 137.2 [each d, each $^1J_{CF}$ = 240 Hz, *o*, *p*, *m*-B(C_6F_5)$_3$], 139.8, 138.3, 130.9, 121.5 (*ipso*, *p*, *m*, *o*-PhCH$_3$), 144.0, 129.0, 128.8, 126.8 (*ipso*, *m*, *o*, *p*-CH_2Ph), 149.2, 129.3, 127.4, 123.0 (*ipso*, *o*, *m*, *p*-B-CH_2Ph), 114.5, 114.3, 110.1, 109.7 (each Cp), 93.7 (C1), 45.1 (CH*C*H$_2$), 31.8 (br, B-*C*H$_2$), 20.7 (Ph*C*H$_3$), *ipso*-B(C_6F_5)$_3$ resonance not located. – ^{11}B NMR (64.2 MHz, [D$_6$]benzene/[D$_8$]tetrahydrofuran, ca. 4:1): δ = −12.3. – ^{19}F NMR (282.4 MHz, [D$_6$]benzene/[D$_8$]tetrahydrofuran, ca. 4:1): δ = −128.1, −164.2, −166.8 [each m, *o*, *p*, *m*-B(C_6F_5)$_3$].

Acknowledgements

Financial support from the Fonds der Chemischen Industrie and the Deutsche Forschungsgemeinschaft is gratefully acknowledged.

[1] [1a] G. Erker, F. Rosenfeldt, *J. Organomet. Chem*. **1982**, *224*, 29. K. Kropp, V. Skibbe, G. Erker, C. Krüger, *J. Am. Chem. Soc*. **1983**, *105*, 3353. G. Erker, U. Hoffmann, R. Zwettler, P. Betz, C. Krüger, *Angew. Chem*. **1989**, *101*, 644, *Angew. Chem. Int. Ed. Engl.* **1989**, *28*, 630. G. Erker, M. Mena, M. Bendix, *J. Organomet. Chem*. **1991**, *410*, C5. F. R. Askam, K. M. Carroll, P. M. Briggs, A. L. Rheingold, B. S. Haggerty, *Organometallics* **1994**, *13*, 2139. D. H. Gibson, J. O. Franco, B. A. Sleadd, W. Naing, M. S. Mashuta, J. F. Richardson, *Organometallics* **1994**, *13*, 4570. N. Peulecke, A. Ohff, A. Tillack, W. Baumann, R. Kempe, V. V. Burlakov, U. Rosenthal, *Organometallics* **1996**, *15*, 1340. B. Thiyagarajan, L. Michalczyk, J. C. Bollinger, J. C. Huffman, J. W. Bruno, *Organometallics* **1996**, *15*, 1989. D. A. Gately, J. R. Norton, *J. Am. Chem. Soc.* **1996**, *118*, 3479. Y. Huang, N. Etkin, R. R. Heyn, T. T. Nadashi, D. W. Stephan, *Organometallics* **1996**, *15*, 2320. D. Röttger, S. Schmuck, G. Erker, *J. Organomet. Chem*. **1996**, *508*, 263. A. V. Firth, D. W. Stephan, *Organometallics* **1997**, *16*, 2183. – [1b] G. S. Bristow, P. B. Hitchcock, M. F. Lappert, *J. Chem. Soc., Chem. Commun.* **1982**, 162. For related early examples see: K. L. Brown, G. R. Clark, C. E. L. Headford, K. Marsden, W. R. Roper, *J. Am. Chem. Soc.* **1979**, *101*, 503. H. Berke, G. Huttner, G. Weiler, L. Zsolnai, *J. Organomet. Chem*. **1981**, *219*, 353. S. Gambarotta,

C. Floriani, A. Chiesi-Villa, C. Guastini, *J. Am. Chem. Soc.* **1982**, *24*, 405.
[2] G. Erker, S. Schmuck, M. Bendix, *Angew. Chem*. **1994**, *106*, 2043, *Angew. Chem. Int. Ed. Engl*. **1994**, *33*, 1955. F. R. Askam, K. M. Carroll, S. J. Alexander, A. L. Rheingold, B. S. Haggerty, *Organometallics* **1994**, *12*, 4810. S. Schmuck, G. Erker, S. Kotila, *J. Organomet. Chem*. **1995**, *502*, 75.
[3] G. Erker, K. Kropp, *Chem. Ber*. **1982**, *115*, 2437.
[4] [4a] P. C. Wailes, H. Weigold, *J. Organomet. Chem.* **1970**, *24*, 405, 413. H. Weigold, A. P. Bell, R. I. Willing, *J. Organomet. Chem*. **1974**, *73*, C23. – [4b] S. B. Jones, J. L. Petersen, *Inorg. Chem*. **1981**, *20*, 2889. K. P. Reddy, J. L. Petersen, *Organometallics* **1989**, *8*, 547. R. Choukroun, F. Dahan, A.-M. Larsonneur, E. Samuel, J. L. Petersen, P. Meunier, C. Sornay, *Organometallics* **1991**, *10*, 374. A.-M. Larsonneur, R. Choukroun, J. Jaud, *Organometallics* **1993**, *12*, 3216. B. Gautheron, G. Tainturier, *J. Organomet. Chem*. **1980**, *195*, 291. – [4c] See also: M. F. Lappert, C. L. Raston, *J. Chem. Soc., Chem. Commun*.**1981**, 173. S. L. Buchwald, S. J. LaMaire, R. B. Nielsen, B. T. Watson, S. M. King, *Tetrahedron Lett*. **1987**, *28*, 3895. G. Erker, R. Schlund, C. Krüger, *Organometallics* **1989**, *8*, 2349. P. Wipf, H. Jahn, *Tetrahedron* **1996**, *52*, 12853.
[5] G. Erker, *Acc. Chem. Res.* **1984**, *17*, 103. G. Erker, *Angew. Chem*. **1989**, *101*, 411, *Angew. Chem. Int. Ed. Engl*. **1989**, *28*, 397. G. Erker, S. Schmuck, U. Hoffmann, *J. Am. Chem. Soc*. **1991**, *113*, 2330. See also: G. Erker, U. Dorf, J. L. Atwood, W. E. Hunter, *J. Am. Chem. Soc.* **1986**, *108*, 2251.
[6] U. Blaschke, G. Erker, M. Nissinen, E. Wegelius, R. Fröhlich, *Organometallics*, in press.
[7] For various other examples of donor ligand stabilized hydrido metallocene cations see: R. F. Jordan, R. E. LaPointe, P. K. Bradley, N. Baenziger, *Organometallics* **1989**, *8*, 2892. R. B. Grossman, R. A. Doyle, S. L. Buchwald, *Organometallics* **1991**, *10*, 1501. Z. Guo, P. K. Bradley, R. F. Jordan, *Organometallics* **1992**, *11*, 2690. X. Yang, C. L. Stern, T. J. Marks, *Angew. Chem.* **1992**, *104*, 1406; *Angew. Chem. Int. Ed. Engl*. **1992**, *31*, 1375. R. F. Jordan, C. S. Bajgur, W. E. Dasher, A. L. Rheingold, *Organometallics* **1987**, *6*, 1041. See also: Y.-X. Chen, T. J. Marks, *Organometallics* **1997**, *16*, 3649.
[8] G. Erker, K. Kropp, C. Krüger, A.-P. Chiang, *Chem. Ber*. **1982**, *115*, 2447.
[9] A. G. Massey, A. J. Park, F. G. A. Stone, *Proceedings Chem. Soc*. **1963**, 212. A. G. Massey, A. J. Park, *J. Organomet. Chem.* **1964**, *2*, 245. A. G. Massey, A. J. Park, in *Organometallic Synthesis* (Eds. R. B. King, J. J. Eisch), Elsevier, New York, **1986**, Vol. 3, p. 461.
[10] X. Yang, C. L. Stern, T. J. Marks, *J. Am. Chem. Soc.* **1994**, *116*, 10015.
[11] C. P. Pez, C. F. Putnik, S. L. Suib, G. D. Stucky, *J. Am. Chem. Soc.* **1979**, *101*, 6933. G. P. Pez, J. N. Armor, *Adv. Organomet. Chem*. **1981**, *19*, 1.
[12] For examples of reactions of neutral zirconium hydrides with nitriles see: G. Erker, W. Frömberg, J. L. Atwood, W. E. Hunter, *Angew. Chem.* **1984**, *96*, 72, *Angew. Chem. Int. Ed. Engl*. **1984**, *23*, 68. G. Erker, K. Engel, U. Korek, P. Czisch, H. Berke, P. Caubère, P. Vanderesse, *Organometallics* **1985**, *4*, 1531.
[13] For reactions of cationic zirconium hydride and alkyl complexes with nitriles see e.g.: R. F. Jordan, R. E. LaPointe, C. S. Bajgur, S. F. Echols, R. Willett, *J. Am. Chem. Soc.* **1987**, *109*, 4111. M. Bochmann, L. M. Wilson, M. B. Hursthouse, M. Motevalli, *Organometallics* **1988**, *7*, 1148. R. F. Jordan, R. E. LaPointe, N. Baenziger, G. D. Hinch, *Organometallics* **1990**, *9*, 1539. R. F. Jordan, *Adv. Organomet. Chem*. **1991**, *32*, 325. Z. Guo, D. C. Swenson, A. S. Guram, R. F. Jordan, *Organometallics* **1994**, *13*, 766.
[14] For a related dimetallic example see: W. Ahlers, G. Erker, R. Fröhlich, U. Peuchert, *Chem. Ber.* **1997**, *130*, 1069.
[15] G. Fachinetti, C. Biran, C. Floriani, A. Chiesi-Villa, C. Guastini, *J. Am. Chem. Soc.* **1978**, *100*, 1921; *Inorg. Chem*. **1978**, *17*, 2995. D. A. Straus, R. H. Grubbs, *J. Am. Chem. Soc.* **1982**, *104*, 5499. E. J. Moore, D. A. Straus, J. Armantrout, B. D. Santarsiero, R. H. Grubbs, J. E. Bercaw, *J. Am. Chem. Soc.* **1983**, *105*, 2068. S. C. H. Ho, D. A. Straus, J. Armantrout, W. P. Schaefer, R. H. Grubbs, *J. Am. Chem. Soc.* **1984**, *106*, 2210. R. M. Waymouth, B. D. Santarsiero, R. H. Grubbs, *J. Am. Chem. Soc.* **1984**, *106*, 4050. G. Erker, U. Dorf, P. Czisch, J. L. Petersen, *Organometallics* **1986**, *5*, 668.
[16] F. H. Allen, O. Kennard, D. G. Watson, L. Brammer, A. G. Orpen, R. Taylor, *J. Chem. Soc.; Perkin Trans II* **1987**, S1.
[17] For examples of reactions of metallaoxiranes with heterocumulenes or isonitriles see: G. Erker, M. Mena, S. Werner, C. Krüger, *J. Organomet. Chem*. **1990**, *390*, 323. G. Erker, M. Mena, U. Hoffmann, B. Menjón, J.L. Petersen, *Organometallics* **1991**, *10*, 291. G. Erker, M. Mena, C. Krüger, R. Noe, *Organometallics* **1991**, *10*, 1201. G. Erker, M. Mena, C. Krüger, R. Noe, *J. Organomet. Chem*. **1991**, *402*, 67. M. Bendix, M. Grehl, R. Fröhlich, G. Erker, *Organometallics* **1994**, *13*, 3366.
[18] R. Duchateau, A. Meetsma, J. H. Teuben, *Organometallics* **1996**, *15*, 1656. R. Duchateau, C. T. van Wee, A. Meetsma, P. T. van Duijnen, J. H. Teuben, *Organometallics* **1996**, *15*, 2279. R. Kempe, S. Brenner, P. Arndt, *Organometallics* **1996**, *15*, 1071. D. Walther, R. Fischer, M. Friedrich, P. Gebhardt, H. Görls, *Chem. Ber*. **1996**, *129*, 1389. A. Littke, N. Sleiman, C. Bensimon, D. S. Richeson, G. P. A. Yap, S. J. Brown, *Organometallics* **1998**, *17*, 446. J. R. Hagadorn, J. Arnold, *Angew. Chem.* **1998**, *110*, 1813; *Angew. Chem., Int. Ed. Engl*. **1998**, *37*, 1729.
[19] In contrast, π-backdonation is very effective in open chain systems and in Cp_2Zr-O-containing metallacycles of ring sizes ≥6. For typical examples see: [19a] G. Erker, U. Dorf, C. Krüger, Y.-H. Tsay, *Organometallics* **1987**, *6*, 680, and references cited therein. W. Spaether, G. Erker, M. Rump, C. Krüger, J. Kuhnigk, *Organometallics* **1995**, *14*, 2621. W. Spaether, M. Rump, G. Erker, R. Fröhlich, J. Hecht, C. Krüger, J. Kuhnigk, *Anales de Quimica Int. Ed*. **1997**, *93*, 394. – [19b] G. Erker, K. Engel, J. L. Atwood, W. E. Hunter, *Angew. Chem*. **1983**, *95*, 506, *Angew. Chem. Int. Ed. Engl*. **1983**, *22*, 494. G. Erker, F. Sosna, R. Zwettler, C. Krüger, *Organometallics* **1989**, *8*, 450. G. Erker, R. Petrenz, *J. Chem. Soc., Chem. Commun*. **1989**, 345. G. Erker, R. Petrenz, C. Krüger, F. Lutz, A. Weiß, S. Werner, *Organometallics* **1992**, *11*, 1646. G. Erker, R. Petrenz, C. Krüger, M. Nolte, *J. Organomet. Chem*. **1992**, *431*, 297.
[20] G. Erker, P. Czisch, R. Schlund, K. Angermund, C. Krüger, *Angew. Chem*. **1986**, *98*, 356, *Angew. Chem. Int. Ed. Engl*. **1986**, *25*, 364. G. Erker, U. Hoffmann, R. Zwettler, C. Krüger, *J. Organomet. Chem*. **1989**, *367*, C15.
[21] S. Braun, H. Kalinowski, S. Berger, *100 and More Basic NMR Experiments*; VCH: Weinheim, 1996 and references cited therein.
[22] J. R. Surtress, *J. Chem. Soc., Chem.Comm.* **1965**, 567.
[23] G. Fachinetti, G. Fochi, C. Floriani, *J. Chem. Soc., Dalton Trans.* **1977**, *20*, 1946.

Received November 5, 1998
[I98382]

Hard Acid and Soft Base Stabilisation of Di- and Trimercury Cations in Benzene Solution – A Spectroscopic, X-ray Scattering, and Quantum Chemical Study

Stefan Ulvenlund,[a] Jan Rosdahl,[b] Andreas Fischer,[b] Peter Schwerdtfeger,[c] and Lars Kloo*[b]

Dedicated to Prof. Warren R. Roper on the occation of his 60th birthday

Keywords: Mercury cations / Subvalent compounds / Ab initio calculations / Liquid X-ray scattering

Hg_2Cl_2 dissolves in $GaCl_3$/benzene solution to yield Hg_2^{2+} and chlorogallate(III) ions, $Ga_nCl_{3n+1}^-$. In such solutions, Hg_2^{2+} can be reduced to Hg_3^{2+} by metallic mercury. Solubility measurements show that one mol of Hg is oxidised per mol of Hg_2^{2+}. The Hg_3^{2+} ion gives a strong band at 110 cm^{-1} in the Raman spectrum and Hg–Hg correlations at about 2.60 and 5.15 Å in the radial distribution function obtained by liquid X-ray scattering. – Hg_3^{2+} can also be synthesised in high yield by direct oxidation of metallic mercury by Ga^{III} in $GaCl_3$/benzene solution. In contrast, mercury is insoluble in neat liquid $GaCl_3$ and only sparingly soluble in $GaCl_3$/KCl melts. It therefore seems likely that the thermodynamic stabilisation of subvalent mercury species in benzene solution not only relies on the traditional acid stabilisation provided by the hard Lewis acid $GaCl_3$, but also on a "soft-base stabilisation" provided by interactions between the aromatic molecules and the cations. Evidence for such specific interactions between Hg_m^{2+} cations and C_6H_6 are observed in the Raman spectra: The totally symmetric C_6H_6 band at 991 cm^{-1} is found to split in the presence of Hg_m^{2+} ions and to give new peaks at 978 (m = 2) and 982 (m = 3) cm^{-1}. – In order to further elucidate the cluster–arene interactions, ab initio and density functional calculations were performed for the model compounds $Hg_m(C_6H_6)_2^{2+}$ and $Hg_mCl_2(C_6H_6)_2$, m = 2 and 3. The calculations show that both models represent coordinations modes which are feasible for Hg_m^{2+} ions. However, the calculated vibrational frequencies for the $Hg_m(C_6H_6)_2^{2+}$ models with η^1/*quasi*-η^3 coordination of the benzene molecules along the Hg–Hg vector are most consistent with the body of experimental and literature data. The counterions are thus suggested to occupy secondary coordination sites.

Introduction

Mercury displays a rich and unusual subvalent chemistry. In addition to the well-known dimer Hg_2^{2+}, previously reported metal−metal-bonded, subvalent mercury species include the linear cations Hg_3^{2+} and Hg_4^{2+}, which have been structurally characterised as salts of the weakly coordinating anions $AlCl_4^-$,[1] AsF_6^-,[2−4] $Ta_2F_{11}^-$,[5] and $[(MF_5)_2SO_4]^{2-}$ (M = Nb, Ta).[5] Mercury also forms infinite, one-dimensional chains in the non-stoichiometric compounds Hg_xTiS_2[6][7] and $Hg_{3-\delta}MF_6$ (M = As,[8−10] Sb,[11] Nb or Ta[12]), some of which transform into stoichiometric, layered compounds $Hg_3(MF_6)$ under appropriate conditions.[13] The fascinating physical properties of these anisotropic compounds have been investigated in considerable detail,[14−19] and are highlighted by the recent assignment of the well-known orange luminescence of calomel to Hg_3^{2+}, presumably formed by disproportionation of Hg_2Cl_2.[20]

As is the case with the vast majority of subvalent post-transition element species (apart from the anomalously stable Hg_2^{2+} cation), the traditional synthetic routes to subvalent mercury cations are based on molten-salt solutions, superacid media, or solutions of strongly oxidising fluorides in liquid SO_2. These highly Lewis-acidic solvent systems have been considered necessary in order to impede the disproportionation of the subvalent cations to higher, more acidic oxidation states and the parent metal.[21] However, triangular Hg_3^{4+} and $AgHg_2^{3+}$ species have recently been stabilised by diphosphanes in the direct reduction of divalent mercury in the presence of the phosphane ligand.[22−24] This route involves reaction media which are immensly more Lewis-basic than the traditional ones. In addition, it comprises *soft*, rather than hard, donors.

In recent publications we have described the syntheses of bismuth clusters and subvalent gallium species by a novel route employing solutions of $GaCl_3$ in organic (aromatic) solvents as reaction media.[25−28] The spectroscopic data for these systems suggest substantial interactions between subvalent metal species and aromatic donors. These donors have, of course, a pronounced soft character. Considering the recent success of stabilising subvalent mercury species in systems comprising other soft donors (i.e. diphosphanes), the $GaCl_3$/arene route is thus of great potential interest for

[a] Department of Explorative Pharmaceutics, Astra Draco AB, P. O. Box 34, S-22100 Lund, Sweden
[b] Inorganic Chemistry, Royal Institute of Chemistry, S-10044 Stockholm, Sweden
[c] Department of Chemistry, The University of Auckland, Private Bag 92019, Auckland, New Zealand

 © WILEY-VCH Verlag GmbH, D-69451 Weinheim, 1999 1434−1948/99/0404−0633 $ 17.50+.50/0

the synthesis of such mercury species. In addition, the interaction between the mercury species and the solvent, i.e. gallates and arene, is of interest because of the unusual coordination chemistry displayed by the previously investigated metal−metal-bonded bisarene compounds $[Pd_2(AlCl_4)_2](C_6H_6)_2$, $[Pd_2(Al_2Cl_7)_2](C_6H_6)_2$,[29−31] and $[Hg_2(C_9H_{12})_2](AlCl_4)_2$ (C_6H_6 = benzene; C_9H_{12} = mesitylene).[32] In the Pd compounds, the aluminates occupy the primary coordination site along the Pd−Pd bond vector and the benzene molecules sandwich the Pd_2^{2+} core. Surprisingly, the opposite is true for the dimercury compound, where mesitylene occupies the primary coordination site. In the case of mercury, this site is normally occupied by anionic, hard bases with donor atoms such as oxygen, nitrogen, and halogens.[33−35] Nevertheless, the compound $[Hg_2(CO)_2](Sb_2F_{11})_2$ has recently been studied by vibrational spectroscopy and seems to provide another example of linear C−Hg−Hg−C coordination.[36] However, the only isolated, solid compound containing Hg_2^{2+} ions and benzene is $[Hg_2(AlCl_4)_2](C_6H_6)_2$.[37] Unfortunately, this compound has never been completely structurally characterised and thus does not shed any light on the Hg_2^{2+}−benzene interaction and the competition between benzene and chloroaluminate ions for the primary coordination sites of the cation.

The aim of the present work is twofold: firstly, to investigate the stability of subvalent mercury species in aromatic solvents and, secondly, to elucidate the coordination of aromatic molecules by such species.

Experimental Results and Discussion

Throughout this work the abbreviation X°(A;B) will be used to denote the mol fraction of component A with respect to component B in ternary or higher order systems; i.e. $X°(A;B) = n_A/(n_A + n_B)$.

The $Hg_2Cl_2/GaCl_3$/Benzene System

The solubility of Hg_2Cl_2 in a 30 mol-% $GaCl_3$/benzene solution approximately corresponds to $X°(Hg_2Cl_2;GaCl_3) = 0.15$. Solutions saturated with Hg_2Cl_2 consist of two liquid phases in equilibrium with solid Hg_2Cl_2. The less dense, colourless phase constitutes only a minor part of the total volume and Raman and NMR spectra indicate that it essentially consists of pure benzene. The Raman spectrum of the denser, faintly yellow liquid phase is more informative (Figure 1, Table 1) and the bands are readily assigned. The strong band at 154 cm^{-1} coincides with the Hg−Hg stretch frequency of Hg_2Cl_2 in Hg−$HgCl_2$ melts.[38] In addition, the band at 368 cm^{-1} (the symmetrical, terminal $GaCl_3$ stretch in $Ga_nCl_{3n+1}^-$)[25] and the lack of bands belonging to Ga_2Cl_6 unambigously show that $GaCl_3$ acts as a chloride acceptor in the dissolution of Hg_2Cl_2 in $GaCl_3$/benzene solution (Equation 1).

$$Hg_2Cl_2 + 2n\ GaCl_3 \rightarrow Hg_2^{2+} + 2\ Ga_nCl_{3n+1}^- \quad (1)$$

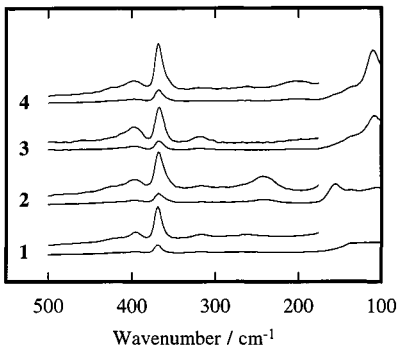


Figure 1. The Raman spectra of (1) the $Ga/GaCl_3/C_6H_6$ system, $X°(Ga;GaCl_3) = 0.191$; (2) the denser liquid phase of the $Hg_2Cl_2/GaCl_3/C_6H_6$ system saturated with Hg_2Cl_2; (3) the $Hg/GaCl_3/C_6H_6$ system saturated with mercury metal; (4) the denser liquid phase of the $Hg/Hg_2Cl_2/GaCl_3/C_6H_6$ system saturated with Hg_2Cl_2 and metallic mercury; $X°(GaCl_3;C_6H_6) = 0.300$ in all systems; the top spectrum of each pair is shown on an expanded scale

The band at 368 cm^{-1} is markedly skew-symmetric relative to the corresponding band observed in $Ga/GaCl_3$/benzene solutions,[25] which suggests a lowering of the local symmetry of the terminal $GaCl_3$ groups in the presence of Hg_2^{2+}. Such a lowering of the $GaCl_3$ symmetry is presumably caused by an interaction between the anions and Hg_2^{2+}. Further inspection of the Raman spectra reveals other indications of strong interactions between Hg_2^{2+} and chlorogallate ions. Thus, the band at 241 cm^{-1} is found near the position of the Ga−Cl−Ga stretch frequency of $Ga_2Cl_7^-$ in $Ga(Ga_2Cl_7)$/benzene solutions (264 cm^{-1}),[25] but the intensity of the 241 cm^{-1} band is much higher relative to that of the symmetrical, terminal $GaCl_3$ stretch vibration. It therefore seems reasonable to assume that this region of the spectrum contains contributions from modes other than the Ga−Cl−Ga stretch. The Hg−Cl stretch vibration (ν_2, Σ_g^+) in Hg_2Cl_2 has been reported at 260 cm^{-1} in $Hg/HgCl_2$ melts and at 279 cm^{-1} in solid Hg_2Cl_2.[38] A shift of the Hg−Cl band towards lower wavenumbers is to be expected when Cl^- is substituted for the more weakly coordinating $Ga_nCl_{3n+1}^-$ ions. It is therefore plausible that the band at 241 cm^{-1} contains contributions also from Hg−Cl modes. Indeed, a distinct Hg−Cl interaction between Hg_2^{2+} and $Ga_nCl_{3n+1}^-$ is expected since Hg_2^{2+} has previously been shown to form Hg−X bonds with weak Lewis bases such as trifluoroacetate and perchlorate.[39][40] However, it has to be remembered that $Ga_nCl_{3n+1}^-$ ions are not the only Lewis bases present in the $Hg_2Cl_2/GaCl_3$/benzene system; the solvent itself, benzene, is a Lewis base and must be accounted for when discussing the coordination of Hg_2^{2+} in this system. Evidence for an interaction between benzene and Hg_2^{2+} are also found in the Raman data. The totally symmetric, ring-breathing mode (of A_{1g} symmetry in the D_{6h} point group) of C_6H_6 at 993 cm^{-1} is split in the spectra of the $Hg_2Cl_2/GaCl_3$/benzene system and a new band is observed at 978 cm^{-1} (Figure 2). This spectral effect could be the result of a symmetry-lowering of C_6H_6 coordinated to Hg_2^{2+} in a $(Hg_2^{2+})(C_6H_6)_k$ complex, but an activation of the most probable candidate, the C−H bending mode of E_{2u} symmetry, is unlikely to produce such a strong Raman

Table 1. Comparison of Raman bands observed in the $Hg_2Cl_2/GaCl_3$/benzene, $Hg/Hg_2Cl_2/GaCl_3$/benzene and $Hg/GaCl_3$/benzene systems with literature data on the molten Hg-$HgCl_2$ system;[38] the intensity and appearance of the bands are indicated by the following abbreviations: s = strong, m = medium, w = weak, v = very, br = broad, sh = shoulder; the assignments for bands of Ga_2Cl_6 and $Ga_nCl_{3n+1}^-$ are based on data from the $Ga/GaCl_3$ system[25][42]

$Hg_2Cl_2/GaCl_3/C_6H_6$	$Hg/Hg_2Cl_2/GaCl_3/C_6H_6$	$Hg/GaCl_3/C_6H_6$	$Hg/HgCl_2$ (melt)	Assignment
ca. 420 sh	ca. 420 sh			$Ga_2Cl_7^-$
		ca. 410 sh		Ga_2Cl_6
395 m	396 m	398 m		$Ga_nCl_{3n+1}^-$
368 s	368 s	367 s		$Ga_nCl_{3n+1}^-$
317 mw		319 m		$Ga_3Cl_{10}^-$
	254 vw			$Ga_2Cl_7^-$
241 m, br	201 m, br		260 vw	Hg−Cl stretch
		ca. 190 sh, br		?
154 vs			154 vs	Hg−Hg, Hg_2X_2
ca. 135 sh	ca. 135 sh	ca. 135 sh		Ga−Cl deform.
	110 vs	109 vs	100 vs	Hg−Hg, Hg_3X_2

band. Instead, the new peak shifted about 15 cm^{-1} to lower wavenumbers is interpreted as arising from the benzene breathing mode of molecules coordinated to the Hg_2^{2+} core, thus reflecting the difference in C−C bonding between coordinated and noncoordinated benzene molecules.

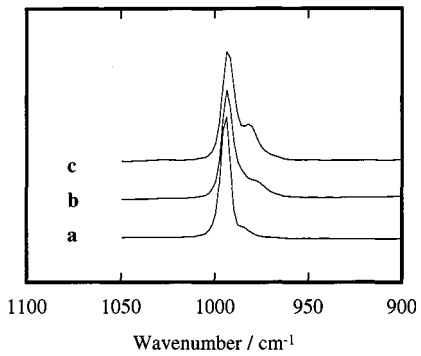


Figure 2. The Raman-spectroscopic effect of Hg_m^{2+} ions on the totally symmetric C_6H_6 ring breathing mode: (a) neat benzene; (b) Hg_2^{2+} in $Hg_2Cl_2/GaCl_3/C_6H_6$ saturated with Hg_2Cl_2; (c) Hg_3^{2+} in $Hg/Hg_2Cl_2/GaCl_3/C_6H_6$ saturated with Hg and Hg_2Cl_2. $X°(GaCl_3;C_6H_6) = 0.300$ in b and c

The IR-active, all-in-phase, out-of-plane C−H bending mode (A_{2u} symmetry) observed at 673 cm^{-1} in benzene, is a sensitive indicator of benzene substitution[41] and, as we will see, coordination. In $GaCl_3$/benzene solution two peaks at 672 and 697 cm^{-1} appear in the IR spectra. The former is identified as the pure benzene A_{2u} band, and the latter is consistent with a shift (+25 cm^{-1}) in frequency of the same vibration mode when benzene is $^1\pi$-coordinated to Ga_2Cl_6.[42] The dissolution of Hg_2Cl_2 in the $GaCl_3$/benzene reaction medium follows Equation 1, where the predominant gallate species formed are $Ga_2Cl_7^-$ and $Ga_3Cl_{10}^-$. In the $Hg_2Cl_2/GaCl_3$/benzene system, we thus expect a strong band at 672 cm^{-1} from noncoordinated benzene, a weak peak at 697 cm^{-1} from benzene coordinated to a small amount of remaining Ga_2Cl_6 and finally a peak from benzene coordinated to Hg_2^{2+}. These expectations are verified and a new band, assigned to benzene in a complex with Hg_2^{2+}, appears at 721 cm^{-1} (shift: +48 cm^{-1} relative to neat benzene).

In ^{13}C-NMR spectra of $Hg_2Cl_2/GaCl_3$/benzene solutions the effects of the inferred complex formation are small and amount to a minor (0.7 ppm in solutions saturated with Hg_2Cl_2) downfield shift of the ^{13}C resonance of C_6H_6 relative to neat benzene. The interaction between aromatic molecules and Hg_2^{2+} has previously been studied by ^{13}C-NMR and Raman spectroscopy in SO_2 solution and a few $(Hg_2^{2+})(arene)_k$ complexes have been isolated from such solution as their hexafluoroarsenate(V) salts.[43][44] No direct structural data were derived, but the results were interpreted in terms of a localized η^2 coordination of C_6H_6 by Hg_2^{2+}. However, the trends in ^{13}C-NMR shifts cannot unambigously be interpreted as coordination effects.

In order to shed further light on the structure of $Hg_2Cl_2/GaCl_3$/benzene solutions, a liquid X-ray scattering investigation (LXS) was performed. Due to the high linear absorptivity of the systems, the data do not allow for a full refinement of a structure model, but the reduced radial distribution function (rRDF, Figure 3) can be evaluated semiquantitatively. The most prominent feature of the rRDF is a strong peak at 2.58 Å which can be assigned to the Hg−Hg correlation. This strong Hg−Hg peak probably overlaps and hides any Hg−Cl or Hg−C correlations. In solid Hg_2Cl_2 the two shortest Hg−Cl distances are found at 2.43 Å,[45] but these can be expected to be somewhat longer for the $Hg_2^{2+}-Ga_nCl_{3n+1}^-$ contacts because of the weaker Lewis basicity of the gallates. The Hg−Hg bond length inferred by the rRDF (2.58 Å) is somewhat longer than in solid Hg_2Cl_2 (2.53 Å)[46] and in aqueous solutions of Hg^I perchlorate (2.52 Å).[47] Unfortunately, the suggested overlap between the Hg−Hg and Hg−Cl (or Hg−C) correlations in the rRDF makes the determination of the Hg−Hg distance uncertain. A detailed interpretation of the inferred bond elongation in terms of coordination effects on Hg_2^{2+} is therefore difficult.

On the basis of the known structural data for the $[Pd_2(AlCl_4)_2](C_6H_6)_2$ and $[Hg_2(C_9H_{12})_2](AlCl_4)_2$ compounds,[29−32] two structural models can be constructed that realistically rationalize the peaks in the rRDF for r values smaller than 5 Å. The two models are depicted schematically in Figures 4a and 4b and are compared with ex-

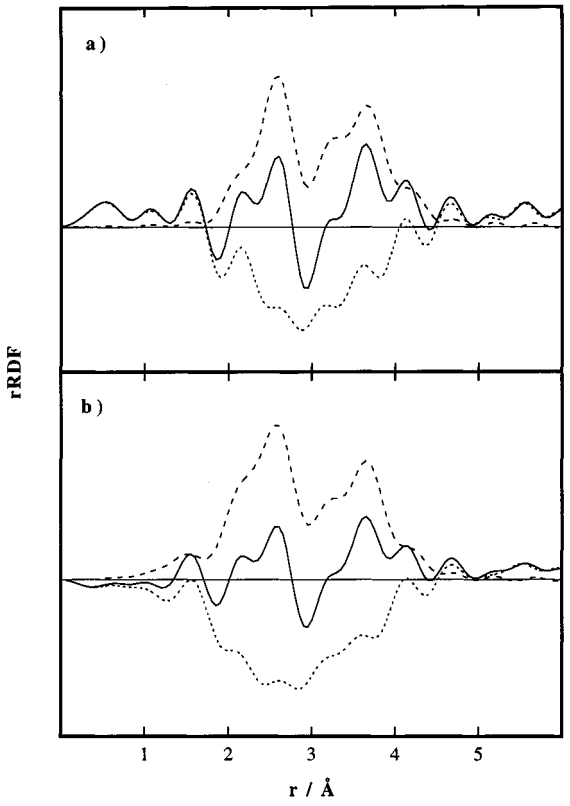


Figure 3. The rRDFs of the $Hg_2Cl_2/GaCl_3/C_6H_6$ (saturated with Hg_2Cl_2) system; X°($GaCl_3$;C_6H_6) = 0.300; the experimental functions are shown as solid lines. The sum of the calculated peak shapes of the two models shown in Figure 4a and 4b are shown as dashed and the difference curves (between experimental data and structural model) as dotted lines in the (a) and (b) figures, respectively

perimental data in the corresponding Figures 3a and 3b. In addition to Hg−Hg and Hg−Cl distances, the models include Ga−Ga, Cl···Cl, terminal Ga−Cl distances, and interaromatic C−C contacts, in agreement with those in benzene solutions of $Ga(Ga_2Cl_7)$.[25] As seen in the Figures 3a and 3b, X-ray scattering alone or in conjunction with spectroscopic data cannot be used to unambigously distinguish between the two structural models. Therefore, we also have to consider the results from quantum-chemical calculations before arriving at a conclusion. These results are reported below, together with those for the Hg_3^{2+} ion.

The $Hg/Hg_2Cl_2/GaCl_3$/Benzene System

The reduction of a $Hg_2Cl_2/GaCl_3$/benzene solution with an excess of metallic mercury yields a dark brown solution. $Hg/Hg_2Cl_2/GaCl_3$/benzene systems saturated with both Hg and Hg_2Cl_2 display two liquid phases, of which the less dense one consists of virtually pure benzene as is evident from its Raman and NMR spectra. The spectral characteristics of the denser liquid phase differ from the corresponding one of the $Hg_2Cl_2/GaCl_3$/benzene solution in several ways:

1. The Hg−Hg Raman band of Hg_2^{2+} at 154 cm^{-1} is replaced by a very strong band at 110 cm^{-1}. This band

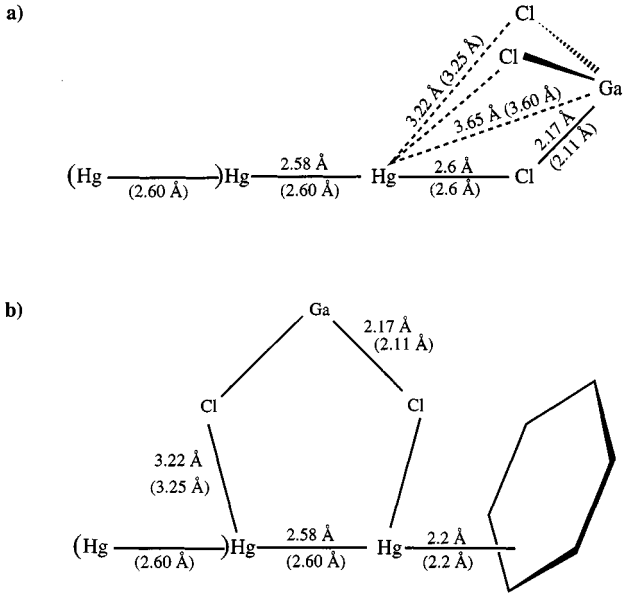


Figure 4. General structural models for (a) the $Hg_m^{2+}-Ga_nCl_{3n+1}^-$ coordination, and (b) the $Hg_m^{2+}-C_6H_6$ coordination compatible with LXS data; distances shown in brackets are those for $m = 3$; those without brackets are for $m = 2$; all distances correspond to peaks in the rRDFs

nearly coincides with that of the Hg_3^{2+} ion in SO_2 solution, reported at 113 cm^{-1}.[2]

2. The band at 241 cm^{-1} is replaced by a less intense band at 201 cm^{-1}. Considering the assignment of this band to Hg−Cl modes, the shift to lower wavenumbers and the decreased intensity suggest a weaker coordination of $Ga_nCl_{3n+1}^-$ to Hg_3^{2+} as compared to Hg_2^{2+}.

3. The ^{199}Hg-NMR resonance at δ = −2103 (relative to $HgMe_2$) observed in $Hg_2Cl_2/GaCl_3$/benzene solutions disappears upon reduction with an excess of metallic Hg. The same NMR-spectroscopic characteristics of Hg_2^{2+} and Hg_3^{2+} have been reported from studies in fluorosulphuric acid and liquid SO_2 solution at room temperature. In these studies, the observation of mercury signals from Hg_3^{2+} was complicated by the enormous Hg−Hg coupling constant and low-temperature experiments were needed to indentify the coupling satellites.[48] Due to the relatively high melting point of benzene, such experiments cannot be performed in this study.

The rRDF of the dense liquid phase from a $GaCl_3$/benzene solution equilibrated with an excess of Hg_2Cl_2 and Hg (Figure 5) is very similar to that of the $Hg_2Cl_2/GaCl_3$/benzene solution at $r < 4$ Å and thus suggests a very similar coordination of the benzene and chlorogallate ions and a nearest neighbour Hg−Hg distance of 2.60 Å. However, a notable feature which is not present in the rRDF of the $Hg_2Cl_2/GaCl_3$/benzene system is the strong peak at 5.15 Å. This value is in good agreement with what should be expected for the correlation between the terminal Hg atoms in a linear Hg_3^{2+} cation with a nearest neighbour Hg−Hg distance of about 2.60 Å. The two alternative general structure models for the rRDF are shown in Figures 4a and 4b, and they are compared with the experimental data in Figures 5a and 5b.

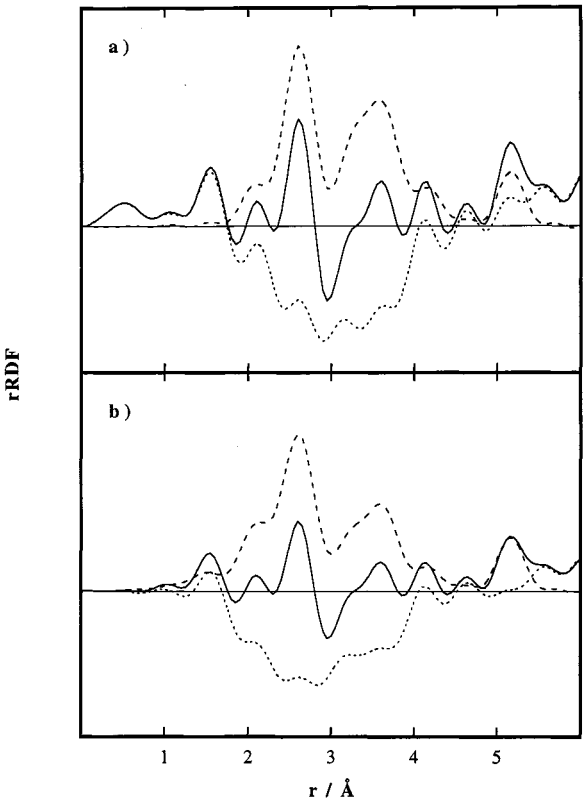


Figure 5. The rRDFs of the $Hg/Hg_2Cl_2/GaCl_3/C_6H_6$ (saturated with Hg and Hg_2Cl_2) systems; $X°(GaCl_3;C_6H_6) = 0.300$; the experimental functions are shown as solid lines; the sum of the calculated peak shapes of the two models shown in Figures 4a and 4b are shown as dashed and the difference curves (between experimental data and structural model) as dotted lines in the (a) and (b) figures, respectively

In the solid state, the Hg_3^{2+} ion has been found to be linear[2] (or very nearly so)[1][5] with Hg−Hg distances ranging between 2.551 and 2.562 Å. The Hg−Hg distance of Hg_3^{2+} in benzene solution (2.60 Å) is thus implied to be somewhat longer than in the solid state and the data therefore parallels the results for the Hg_2^{2+} ion in benzene solution. The $Hg_3^{2+}-C_6H_6$ interaction also seems to parallel that of the Hg_2^{2+} ion. The splitting of the C_6H_6 band at 993 cm^{-1} gives rise to a new band at 982 cm^{-1} in the $Hg/Hg_2Cl_2/GaCl_3$/benzene system (Figure 2), whereas the ^{13}C-NMR resonance in $GaCl_3$/benzene solutions saturated with Hg_2Cl_2 and Hg occurs 0.6 ppm downfield relative to neat benzene. In the IR spectra, the all-in-phase C−H out-of-plane bending mode is shifted to 713 cm^{-1} (shift: +40 cm^{-1}). The spectrum also contains the previously discussed peaks from benzene (673 cm^{-1}) and remaining Ga_2Cl_6−benzene complexes (697 cm^{-1}).

Solubility measurements substantiate the conclusion that Hg_3^{2+} is formed by the oxidation of mercury by Hg_2^{2+}. The solubility measurements were performed in systems where Hg_2Cl_2 was added to transfer essentially all Ga^{III} into $Ga_2Cl_7^-$, according to Equation 1. The only oxidising agent present is thus Hg_2^{2+}, and the solubility was found to be $X°(Hg;Hg_2Cl_2) = 0.958\pm0.005$, thus supporting the interpretation of the spectroscopic data in terms of the reaction $Hg(l) + Hg_2^{2+} \rightarrow Hg_3^{2+}$.

The $Hg/GaCl_3$/Benzene and $Hg/GaCl_3$ Systems − Experimental Evidence for "Soft-Base Stabilisation" of Subvalent Mercury Species

In previous investigations of the reaction between bismuth metal and $GaCl_3$, it transpired that the reactions taking place in $GaCl_3$/benzene solution at room temperature paralleled those in the liquid $GaCl_3$ and $NaCl/GaCl_3$ systems at elevated temperatures.[26][27] In all these solvents, the oxidation of excess bismuth was found to yield concentrated solutions of Bi_5^{3+}, Ga^+, and chlorogallate(III) ions. In stark contrast, the reaction between mercury metal and $GaCl_3$ seems to be thermodynamically dependent on the presence of benzene. Thus, mercury is very soluble in $GaCl_3$/benzene [$X°(Hg;GaCl_3) = 0.226$; $X°(GaCl_3;C_6H_6) = 0.300$], but is insoluble in neat, liquid $GaCl_3$ and only sparingly soluble in liquid $KCl/GaCl_3$ [$X°(Hg;GaCl_3) = 0.024$; $X°(KCl;GaCl_3) = 0.10$]. If an excess of mercury metal is added to a $GaCl_3$/benzene solution, a single, brown liquid phase in equilibrium with mercury metal rapidly is obtained. The Raman spectrum of this solution at low wavenumbers (Figure 1) is very similar to that of the $Hg/Hg_2Cl_2/GaCl_3$/benzene system and confirms the formation of Hg_3^{2+}. In addition, the Raman band at 322 cm^{-1} and the observation of a $^{71}Ga^I$-NMR signal at $\delta = -994$ (relative aqueous $GaCl_4^-$) reveal the concomitant formation of Ga^+ and $Ga_3Cl_{10}^-$ ions, in analogy with the results from $Bi/GaCl_3$/benzene solutions.[26][27] Taken together, these observations strongly suggest Equation 2 to be the predominant reaction between mercury metal and $GaCl_3$ in benzene solution. Assuming a complete reaction between mercury and $GaCl_3$ according to Equation 2, mercury would be soluble to $X°(Hg;GaCl_3) = 0.231$ in the $Hg/GaCl_3$/benzene system. This is in excellent agreement with the experimental value (0.226). In solutions not saturated with Hg metal also Hg_2^{2+} can be synthesised in an analogous manner.

$$3\ Hg + 10\ GaCl_3 \rightarrow Hg_3^{2+} + Ga^+ + 3\ Ga_3Cl_{10}^- \quad (2)$$

It is not feasible to assign the low solubility of mercury metal in liquid $GaCl_3$ and $KCl/GaCl_3$ to a thermal instability of Hg_3^{2+}, since this species has been detected in the chloroaluminate melts at temperatures around 200°C and isolated as tetrachloroaluminate salt from such systems.[1][44] It is therefore tempting to assign the efficient formation of Hg_3^{2+} in $GaCl_3$/benzene solution and the lack of such in liquid $GaCl_3$ and $KCl/GaCl_3$ to stabilising interactions between the arene and the mercury cation. Such interactions, together with those between Ga^+ and benzene, clearly have the potential to push Equation 2 to the right through a formation of $(Hg_3^{2+})(C_6H_6)_k$ complexes and would provide a "base stabilisation" of the subvalent mercury cation. However, Hg_3^{2+} is of course still to be regarded as "acid-stabilised" in the sense that the strongly Lewis-acidic environment ensured by the coordinatively unsaturated $Ga_nCl_{3n+1}^-$ anions prohibits the stabilisation of the Hg^{II} oxidation state through complex formation with chloride and therefore hinders disproportionation. This fact infers a superficially contradictory notion of base stabilis-

ation acting side by side with acid stabilisation. However, the concept of acid stabilisation, as it is normally formulated, is applicable *only* to acid−base equilibria involving hard or intermediate donors and acceptors. This, in turn, is a consequence of the fact that most of the work previously done has involved fluoride and chloride systems. In the present system, the presence of the pronounced *soft* donor C_6H_6 must also be taken into account.

Theoretical Calculations on the Coordination of Hg_m^{2+} Ions

Theoretical calculations were used in an attempt to resolve the experimental ambiguities regarding the coordination of the Hg_m^{2+} ions in $GaCl_3$/benzene media and to substantiate the indications that the subvalent mercury ions are to be regarded as "soft-base-stabilised" in such media. The benzene coordination to the Hg_m^{2+} (m = 2, 3) cores were theoretically investigated in two types of models. In the first type, only interactions between Hg_m^{2+} and two benzene molecules were included; in the second type, also interactions with two chloride ions (as models for gallates/aluminates in the primary coordination site along the Hg−Hg bond vector) were considered. In addition, the separate Hg_m^{2+} and Hg_mCl_2 (m = 2, 3) units where investigated. Models for the coordination of gallates in the secondary site were not considered. The reason is both the ambiguous potential coordination mode and the calculationally huge systems that would emerge.

The quantum-chemical calculations were performed with the GAUSSIAN94 program package.[49] Several potential coordination models for $Hg_m(C_6H_6)_2^{2+}$ and $Hg_mCl_2(C_6H_6)_2$, m = 2 and 3, were optimised at Hartree-Fock level using basis sets of double-zeta quality, viz. LANL2DZ for Hg and 3-21G for the lighter elements. The geometries shown in Figures 6 and 7 represent points of zero gradients on the hypersurface and were identified using the LANL2DZ basis sets (only used for pre-optimisation), later optimised using larger basis sets. The more extended basis sets used for the lighter elements were of augmented 3-21G type; (10s7p)/[5s4p] for Cl, (7s4p)/[4s3p] for C, and (3s)/[2s] for H. The valence space of Hg was optimized at both HF and MP2 level, employing a 60-electron ARECP for Hg,[50] and contracted to (9s9p6d2f)/[6s6p3d1f], where the original f function was omitted because of the lack of gradients for f functions in the combination with ECPs in all common theoretical program packages. Although these basis sets are of moderate size for an atom, the calculations for the molecules were elaborate in computer time and disk space requirements for the full geometry optimisations and frequency calculations, which were performed for all systems at Hartree−Fock (HF) and hybrid density-functional (B3LYP) levels.[51] All systems, except the trimercury ones, were also studied at MP2 level. The HF-optimised basis sets were used for the HF calculations. However, for the correlated calculations the Hg basis set was re-optimised by minimising the MP2 total energy. This has the advantage that basis set superposition errors (BSSE) are suppressed and the bonding involving Hg atoms therefore better described.

The structures in Figure 6 display the $Hg_m(C_6H_6)_2^{2+}$ models in which the chloride ions were not explicitly included and benzene occupies the primary coordination site along the Hg−Hg bond vector. As can be seen from the summary in Tables 2, the energy differences between the η^6, η^2, and η^1/*quasi*-η^3 coordination modes are small but significant. The most stable configuration is the η^1/*quasi*-η^3 one, in good agreement with the crystal structure of $[Hg_2(C_9H_{12})_2](AlCl_4)_2$ (C_9H_{12} = mesitylene).[32] For the $Hg_2(C_6H_6)_2^{2+}$ complex the η^2 mode is 18 kJ mol^{-1} and the η^6 mode 119 kJ mol^{-1} higher in energy (B3LYP level), and the corresponding values for the $Hg_3(C_6H_6)_2^{2+}$ complex are 23 and 99 kJ mol^{-1}. Furthermore, as is obvious from a study of the Hessians, the optimised structures of $Hg_m(\eta^2\text{-}C_6H_6)_2^{2+}$ and $Hg_m(\eta^6\text{-}C_6H_6)_2^{2+}$ (Figure 6) are somewhat too restricted to be considered as proper minima in the strict sense. Negative eigenvalues of the Hessian for these structures correspond to distortions towards the η^1/(*quasi*-η^3) structures. The Hg−Hg bonds are slightly elongated upon coordination to the benzene molecules, and the elongation seems to increase as the hapticity decreases. The charge transfer in the $Hg_m(C_6H_6)_2^{2+}$ complexes is small; the terminal Hg atoms have a formal charge close to +2/m, according to an NBO population analysis. The electron density donation to the terminal Hg atoms seems to be smaller in the trimer than in the dimer, and also the Hg−C distances longer.

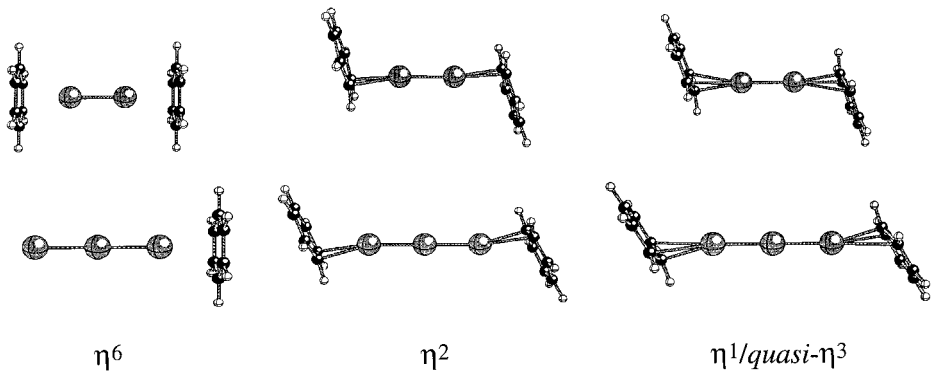


Figure 6. Optimised structures (B3LYP level) of the η^6-, η^2- and η^1/*quasi*-η^3-benzene coordination models for Hg_2^{2+} and Hg_3^{2+}

Table 2. Calulational results including selected atom-atom distances, NLMO/NPA bond orders,[59][60] NBO atom charges[61] and the total energy

System	Method	Distances [Å] Hg−Hg	Hg−Cl	Hg−C	Bond orders Hg−Hg	Hg−Cl	Hg−C	Charges Hg	Cl	bz[a]	Total energy [a.u.]
Hg_2^{2+}											
	HF	2.492			1.00			+1.00			−304.20016
	B3LYP	2.531			1.00			+1.00			−306.15647
	MP2	2.487			1.00			+1.00			−304.56485
Hg_3^{2+}											
	HF	2.495			0.62			+0.67, +0.67[b]			−456.68797
	B3LYP	2.518			0.57			+0.63, +0.68[b]			−459.70361
	MP2	2.477			0.63			+0.64, +0.68[b]			−457.27755
Hg_2Cl_2											
	HF	2.488	2.351		0.83	0.20		+0.87	−0.87		−1219.65913
	B3LYP	2.506	2.357		0.76	0.27		+0.79	−0.79		−1223.09703
	MP2	2.471	2.327		0.80	0.24		+0.81	−0.81		−1220.16356
Hg_3Cl_2											
	HF	2.490	2.376		0.64	0.19		+0.47, +0.71[b]	−0.94		−1372.06080
	B3LYP	2.506	2.380		0.50	0.24		+0.41, +0.66[b]	−0.86		−1376.54366
	MP2	2.470	2.347		0.55	0.22		+0.42, +0.67[b]	−0.88		−1372.78548
bz[a]											
	HF									+0.00	−229.43935
	B3LYP									+0.00	−230.99729
	MP2									+0.00	−229.96685
$Hg_2(bz)_2^{2+}$											
η^6	HF	2.532		2.761	0.91		0.03[c]	+0.99		+0.01	−763.30212
	B3LYP	2.530		2.721	0.88		0.04[c]	+0.94		+0.06	−768.40616
	MP2	2.510		2.661	0.88		0.04[c]	+0.97		+0.03	−764.77296
η^2	HF	2.556		2.452[d]	0.85		0.12[d]	+0.93		+0.07	−763.33120
	B3LYP	2.584		2.438[d]	0.77		0.17[d]	+0.85		+0.15	−768.44496
	MP2	2.538		2.380[d]	0.82		0.09[d]	+0.90		+0.10	−764.80092
η^1	HF	2.571		2.297[e]	0.83		0.17[e]	+0.92		+0.08	−763.33664
	B3LYP	2.599		2.279[e]	0.74		0.23[e]	+0.83		+0.17	−768.45165
	MP2	2.552		2.236[e]	0.79		0.20[e]	+0.88		+0.12	−764.80488
$Hg_3(bz)_2^{2+}$											
η^6	HF	2.523		2.800	0.61		0.03[c]	+0.70, +0.70[b]		−0.05	−915.77249
	B3LYP	2.536		2.761	0.57		0.01[c]	+0.63, +0.69[b]		−0.01	−921.92264
η^2	HF	2.543		2.468[d]	0.65		0.10[d]	+0.65, +0.70[b]		−0.02	−915.79738
	B3LYP	2.557		2.446[d]	0.48		0.12[d]	+0.56, +0.67[b]		+0.05	−921.95179
η^1	HF	2.557		2.299[e]	0.65		0.16[e]	+0.64, +0.71[b]		−0.03	−915.80556
	B3LYP	2.570		2.271[e]	0.48		0.31[e]	+0.55, +0.68[b]		+0.05	−921.96042
$Hg_2Cl_2(bz)_2$											
	HF	2.600	2.459	3.177[d]	0.81	0.11	−0.01[d]	+0.93	−0.84	−0.09	−1678.63180
	B3LYP	2.617	2.461	3.107[d]	0.74	0.15	−0.01[d]	+0.84	−0.75	−0.09	−1685.18161
	MP2	2.582	2.438	3.011[d]	0.77	0.13	−0.01[d]	+0.88	−0.77	−0.11	−1680.21800
$Hg_3Cl_2(bz)_2$											
	HF	2.636	2.465	3.170[f]	0.60	0.10	0.04[f]	+0.62, +0.78[b]	−0.86	−0.23	−1831.12024
	B3LYP	2.636	2.461	3.114[f]	0.50	0.14	−0.05[f]	+0.55, +0.70[b]	−0.77	−0.21	−1838.70274

[a] bz = benzene. − [b] Charge on central Hg atom (first value) and terminal ones (second value). − [c] Average value for all six Hg−C correlations. − [d] Shortest two Hg−C distances and the corresponding average bond order. − [e] Shortest Hg−C distance and the corresponding bond order. − [f] Shortest two Hg−C distances from the central Hg atom and the corresponding average bond order.

In the optimized $Hg_mCl_2(C_6H_6)_2$ models (with chlorides in the primary coordination sites, Figure 7), the electron donation to Hg is substantially larger than in $Hg_m(C_6H_6)_2^{2+}$ (Table 2). Also, the Hg−C bonds are considerably longer, and the benzene coordination is best characterised as η^2 for both $m = 2$ and $m = 3$. In $Hg_2Cl_2(C_6H_6)_2$, the two Hg atoms coordinate in an identical manner, whereas in $Hg_3Cl_2(C_6H_6)_2$ the main benzene coordination is to the central atom of lowest positive charge. In both cases, the coordination mode and distances are very similar to the arene complexes of Pd_2^{2+}, Cu^+, and Ag^+ ions.[29−31,52−54] Inclusion of benzene molecules to the Hg_mCl_2 structures causes a weakening of the Hg−Cl interaction, and a substantial elongation of the Hg−Hg bonds to about 2.6 Å. Furthermore, in $Hg_3Cl_2(C_6H_6)_2$, the charge transfer from benzene to the central Hg atom is substantial, giving the central atom almost the same positive charge as the terminal ones.

According to the calculations, the energy changes for the Equations 3a and 3b are all strongly favourable. At B3LYP level the changes in energy are −789 ($m = 2$) and −688 kJ mol^{-1} ($m = 3$) for Equation 3a, and −236 ($m = 2$) and −432 kJ mol^{-1} ($m = 3$) for Equation 3b.

$$Hg_m^{2+} + 2\ C_6H_6 \rightarrow Hg_m(\eta^1\text{-}C_6H_6)_2^{2+} \quad (3a)$$

$$Hg_mCl_2 + 2\ C_6H_6 \rightarrow Hg_mCl_2(\eta^2\text{-}C_6H_6)_2 \quad (3b)$$

From the calculations, a few general trends regarding the benzene coordination can be discerned: The coordination of benzene to Hg_2^{2+} is more favourable than to Hg_3^{2+}, but this trend is reversed for Hg_mCl_2 (with chlorides in the primary coordination sites). As indicated by the Hg−C bond

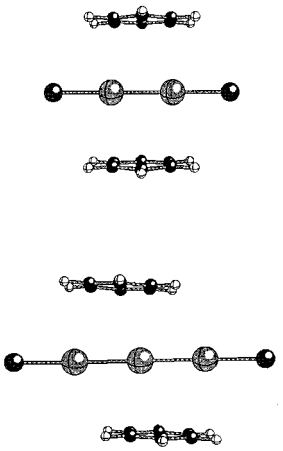


Figure 7. Optimised structures (B3LYP level) of the benzene/gallate coordination models for Hg_2^{2+} and Hg_3^{2+}

lengths, the interaction seems to be energetically stronger between the Hg_m^{2+} ions and benzene, than between the Hg_mCl_2 units and benzene. However, this is a highly simplified analysis, totally disregarding the difference in direct gallate/aluminate−mercury interaction.

Conclusions Based on the Conjunction of Experimental and Theoretical Results

The LAXS data for the Hg_m^{2+} cores in $GaCl_3$/benzene media indicate an elongation of the Hg−Hg distance in such media relative to that in the solid state and molten-salt systems. This evidence finds support in the theoretical calculations, in so far as the calculations suggest that the coordination of benzene to both Hg_m^{2+} and Hg_mCl_2 increase the Hg−Hg distance by a magnitude in good agreement with the experimental results. The calculated Hg−Hg stretch frequencies of the model compounds $Hg_mCl_2(\eta^2\text{-}C_6H_6)_2$ are close to those observed experimentally (Table 3). This is also true for the $Hg_m(C_6H_6)_2^{2+}$ models, irrespective of hapticity, and the influence of benzene coordination on the Hg−Hg stretch frequency thus cannot be used to elucidate the preferred coordination of benzene and chloride by the Hg_m cores.

According to the calculations, the inclusion of benzene molecules to the Hg_mCl_2 structures causes a weakening of the Hg−Cl interaction, consistent with the experimentally observed shift of the Hg−Cl stretch frequencies in benzene media as compared with Hg_mCl_2 melts. The calculated Hg−Cl stretch frequencies (Table 3) are slightly too high at all levels relative to the experimental ones, indicating that the current level of approximation overbind the Hg−Cl interaction. This is expected and unavoidable in the present models, since $Ga_nCl_{3n+1}^-$ ions are weaker Lewis bases than chlorides.

The LAXS and NMR data cannot distinguish between the benzene coordination modes in Figures 6 and 7, although the lack of distinct Hg−C correlations in the rRDFs can be taken as a primitive indication for a low hapticity of the benzene coordination. Nevertheless, the relatively small energy differences between the different coordination modes may indicate a fluxional behavior in solution, consistent with the lack of detailed NMR-spectroscopic data for the benzene interaction. A frontier orbital analysis is consistent with the experimentally observed shift in frequency of the benzene ring breathing mode to lower wavenumbers, assuming an electron-density donation from the bonding benzene π system to the s-dominated, Hg−Hg-antibonding LUMO of the Hg_m^{2+} units. However, of most interest are the calculated shifts in C−C breathing and C−H all-in-phase, out-of-plane mode frequencies of the coordinated benzene molecules for the eight structure models in Figures 6 and 7 (Table 3). It seems clear from the calculations that *only* the end-on coordination of benzene (Figure 6) produces a shift in the C−C mode of a magnitude comparable to the experimental values. The strong and clear effect for the benzene ring breathing mode is a rather convincing evidence for a benzene coordination in the Hg−Hg direction. Also the shift in C−H bending frequencies is best in agreement with the experimental results for the $Hg_m(C_6H_6)_2^{2+}$ models. However, the calculations suggest that the energy of two monomeric $Hg(\eta^2\text{-}C_6H_6)^+$ complexes has about the same energy as $Hg_2(\eta^2\text{-}C_6H_6)_2^{2+}$ at both HF and B3LYP level (Table 2). This indicates that the benzene-coordinated dimer requires the extra stabilisation provided by gallates in the secondary (sandwiching) coordination site. Consequently, it seems that both the presence of benzene *and* gallate anions are important for the stabilisation of subvalent mercury species in benzene solution. This is in good agreement with our experimental data, which are consistent with a strong interaction between both the anionic, hard gallates and the neutral, soft benzene molecules, of which the latter clearly is a fundamental prerequisite for the formation of subvalent mercury ions in the Hg/$GaCl_3$/benzene system.

To conclude, both coordination models proposed for Hg_2^{2+} and Hg_3^{2+} are theoretically feasible, and the current systems are thus highly interesting in terms of the competition between hard and soft donor ligands for the primary coordination site. However, in view of the experimental and quantum-chemical results we are inclined to favour the coordination model with η^1/*quasi*-η^3-benzene along the Hg−Hg bond vector and the gallates confined to a secondary coordination site (Figure 6). The possible "base stabilisation" of subvalent clusters by aromatics definitely deserves further experimental and theoretical investigation since interactions with hetero groups (carbonyl transition metal compounds) recently have been shown to be a way to stabilise new and unprecedented clusters of the post-transition elements.[55−58] However, results derived for the subvalent Hg_m^{2+} ions must be applied with considerable care on other subvalent post-transition element clusters, since the mercury species are unique in their strong interaction with the counterions.

Experimental Section

General: All sample preparations were performed in a glove box under dried, deoxygenated nitrogen (< 1 ppm H_2O). All glassware

Table 3. Calulated vibrational frequencies for the Hg−Hg, Hg−Cl, and important internal benzene modes

System	Method	Hg−Hg stretch [cm^{-1}] symm	Hg−Hg stretch [cm^{-1}] asymm	Hg−Cl stretch [cm^{-1}] symm	Hg−Cl stretch [cm^{-1}] asymm	C−C breathing[a] [cm^{-1}] average	C−C breathing[a] [cm^{-1}] Δ[c]	C−H bending[b] [cm^{-1}] average	C−H bending[b] [cm^{-1}] Δ[c]
Hg_2^{2+}									
($D_{\infty h}$)	HF	222(Σ_g^+)							
	B3LYP	193(Σ_g^+)							
	MP2	216(Σ_g^+)							
Hg_3^{2+}									
($D_{\infty h}$)	HF	158(Σ_g^+)	273(Σ_u^+)						
	B3LYP	142(Σ_g^+)	252(Σ_u^+)						
	MP2	158(Σ_g^+)	276(Σ_u^+)						
Hg_2Cl_2									
($D_{\infty h}$)	HF	203(Σ_g^+)		379(Σ_g^+)	352(Σ_u^+)				
	B3LYP	186(Σ_g^+)		372(Σ_g^+)	347(Σ_u^+)				
	MP2	205(Σ_g^+)		394(Σ_g^+)	367(Σ_u^+)				
Hg_3Cl_2									
($D_{\infty h}$)	HF	148(Σ_g^+)	261(Σ_u^+)	350(Σ_g^+)	350(Σ_u^+)				
	B3LYP	136(Σ_g^+)	248(Σ_u^+)	349(Σ_g^+)	346(Σ_u^+)				
	MP2	150(Σ_g^+)	268(Σ_u^+)	367(Σ_g^+)	366(Σ_u^+)				
bz[d]									
(D_{6h})	HF					1067(A_{1g})		794(A_{2u})	
	B3LYP					1006(A_{1g})		708(A_{2u})	
	MP2					980(A_{1g})		686(A_{2u})	
	exp					993(A_{1g})		673(A_{2u})	
$Hg_2(bz)_2^{2+}$									
(D_{6h}), η^6	HF	134(A_{1g})				1044(A_{1g},A_{2u})	−23	840(A_{1g},A_{2u})	+46
	B3LYP	133(A_{1g})				999(A_{1g},A_{2u})	−7	755(A_{1g},A_{2u})	+48
	MP2	140(A_{1g})				955(A_{1g},A_{2u})	−25	744(A_{1g},A_{2u})	+58
(C_{2h}), η^2	HF	183(A_g)				1038(A_g,B_u)	−29	865(A_g,B_u)	+71
	B3LYP	167(A_g)				983(A_g,B_u)	−23	779(A_g,B_u)	+71
	MP2	180(A_g)				951(A_g,B_u)	−29	762(A_g,B_u)	+76
(C_{2h}), η^1	HF	177(A_g)				1025(A_g,B_u)	−42	869(A_g,B_u)	+75
	B3LYP	160(A_g)				961(A_g,B_u)	−45	783(A_g,B_u)	+75
	MP2	182(A_g)				955(A_g,B_u)	−25	745(A_g,B_u)	+59
$Hg_3(bz)_2^{2+}$									
(D_{6h}), η^6	HF	109(A_{1g})	262(A_{2u})			1050(A_{1g},A_{2u})	−17	818(A_{1g},A_{2u})	+24
	B3LYP	105(A_{1g})	252(A_{2u})			987(A_{1g},A_{2u})	−19	739(A_{1g},A_{2u})	+31
(C_{2h}), η^2	HF	144(A_g)	226(B_u)			1049(A_g,B_u)	−11	861(A_g,B_u)	+67
	B3LYP	135(A_g)	218(B_u)			986(A_g,B_u)	−20	772(A_g,B_u)	+64
(C_{2h}), η^1	HF	137(A_g)	222(B_u)			1046(A_g,B_u)	−21	861(A_g,B_u)	+67
	B3LYP	127(A_g)	212(B_u)			977(A_g,B_u)	−29	772(A_g,B_u)	+64
$Hg_2Cl_2(bz)_2$									
(D_{2h})	HF	157(A_1)		313(A_1)	287(A_1)	1064(A_1,B_2)	−3	821(A_1,B_2)	+27
	B3LYP	146(A_1)		306(A_1)	284(A_1)	1002(A_1,B_2)	−4	740(A_1,B_2)	+32
$Hg_3Cl_2(bz)_2$									
(C_{2h})	HF	104(A_g)	186(B_u)	302(A_g)	295(B_u)	1065(A_g,B_u)	−2	824(A_g,B_u)	+30
	B3LYP	99(A_g)	182(B_u)	301(A_g)	295(B_u)	1003(A_g,B_u)	−3	739(A_g,B_u)	+31

[a] The average benzene ring breathing mode (ν_2). In the mercury compounds, the two benzene rings can vibrate in and out of phase, thus giving rise to two modes with frequencies that normally only differ by a few wavenumbers. Formally, only the A-symmetry mode is Raman-active, but in order to minimise the effect of extensive mixing with other modes in the lower symmetries the average of the two are used. − [b] The all-in-phase C−H bending mode perpendicular to the benzene plane, normally sensitive to ring substitution and coordination. In the mercury complexes, the H atoms in the two benzene rings can vibrate in and out of phase, giving rise to two bands with very similar frequencies. − [c] The difference with respect to the corresponding calculated frequency for free benzene. − [d] bz=benzene.

was dried at 300°C in vacuo prior to use. After sample preparation all sample cells were sealed under vacuum. Hg_2Cl_2 (Merck, p.A. grade) was dried at 150°C for several weeks prior to use. Benzene was distilled and stored over sodium. $GaCl_3$ (ALFA, 99.999%) and mercury metal (Merck, p.A. grade) were used as received. KCl (Merck. p.A.) was dried for several days at 130°C before use. The solubility measurements were made gravimetrically, monitoring the amount of dissolved mercury metal at equilibrium with known amounts of Hg_2Cl_2, $GaCl_3$, and benzene.

Liquid X-ray Scattering (LXS): The LXS experiments were performed at room temperature using Mo-K_α radiation and a Seifert GSD θ−θ diffractometer equipped with a liquid-nitrogen-cooled solid-state detector (Ortec EG&G). The samples were enclosed in sealed Lindemann capillaries with an outer diameter of 1 mm. The experimental procedure and data evaluation have previously been described in detail.[62] The nominal composition of the solvent was $X°(GaCl_3;C_6H_6)$ = 0.29 and the samples were saturated with Hg_2Cl_2 or Hg/Hg_2Cl_2 in order to maximise the contributions from mercury species to the intensity function $s{\cdot}i(s)$ ($s = 4\pi\sin\theta/\lambda$). Data were collected in the s range 0.200−13.00 $Å^{-1}$. In the data evaluation, corrections for spurious peaks in the reduced radial distribution function were applied for $r < 1.0$ Å and the value of k in the damping function $\exp(-ks^2)$ was set to 0.012.

Vibrational Spectroscopy: Raman spectra were recorded with a Bruker IFS-66/FRA-106 FT Raman spectrometer equipped with a low-power Nd:YAG laser (λ = 1064 nm) and a liquid-nitrogen-cooled, solid-state Ge diode detector. The samples were contained in 5-mm NMR tubes sealed under vacuum. The IR spectra were recorded with a Bio-Rad FTS 6000 FT-IR spectrometer, using a Globular radiation source and KBr beamsplitter and DTGS detector, and 6.25 μm Mylar beamsplitter and PE-DTGS detector for the mid-IR and far-IR spectra, respectively. The resolution in both

Raman and IR spectra was 4 cm^{-1}. The samples were prepared in a glove box (vide supra) and contained in polyethylene bags in the far-IR and between Teflon-coated KBr pellets in mid-IR experiments.

NMR Spectroscopy: The NMR measurements were performed with a Varian Unity 300-MHz spectrometer. TMS was used as a reference for the ^{13}C-NMR spectra, whereas ^{199}Hg- and ^{71}Ga-NMR shifts were determined relative to $HgMe_2$ and $GaCl_4^-$ in hydrochloric acid, respectively.

Acknowledgments

This work has been supported by the Swedish Natural Science Research Council and the Human Capital and Mobility (contract no. CHRX CT93 0277). The PDC at the Royal Institute of Technology in Stockholm and the NSC at Linköping University are acknowledged for their allocation of computer resources. P. S. thanks the Marsden Fund (Wellington) for financial support.

[1] R. D. Ellison, H. A. Levy, K. W. Fung, *Inorg. Chem.* **1972**, *11*, 833−836.
[2] B. D. Cutforth, C. G. Davies, P. A. W. Dean, P. R. Ireland, P. K. Ummat, *Inorg. Chem.* **1973**, *12*, 1343−1347.
[3] B. D. Cutforth, R. J. Gillespie, P. R. Ireland, *J. Chem. Soc., Chem. Comm.* **1973**, 723−724.
[4] B. D. Cutforth, R. J. Gillespie, P. R. Ireland, J. F. Sawyer, P. K. Ummat, *Inorg. Chem.* **1983**, *22*, 1344−1347.
[5] I. D. Brown, R. J. Gillespie, K. R. Morgan, J. F. Sawyer, K. J. Schmidt, Z. Tun, P. K. Ummat, J. E. Vekris, *Inorg. Chem.* **1987**, *26*, 689−693.
[6] P. Ganal, P. Moreau, G. Ouvrard, M. Sidorov, M. McKelvy, W. Glaunsinger, *Chem. Mater.* **1995**, *7*, 1132−1139.
[7] M. Sidorov, M. McKelvy, R. Sharma, W. Glaunsinger, P. Ganal, P. Moreau, G. Ouvrard, *Chem. Mater.* **1995**, *7*, 1140−1145.
[8] A. J. Schulz, J. M. Williams, N. D. Miro, A. G. MacDiarmid, A. J. A. Heeger, *Inorg. Chem.* **1978**, *17*, 646−649.
[9] I. D. Brown, B. D. Cutforth, C. G. Davies, R. J. Gillespie, P. R. Ireland, J. E. Vekris, *Can. J. Chem.* **1974**, *52*, 791−793.
[10] N. D. Miro, A. G. MacDiarmid, A. J. Heeger, A. F. Garito, C. K. Chiang, A. J. Schultz, J. M. Williams, *J. Inorg. Nucl. Chem.* **1978**, *40*, 1351−1355.
[11] Z. Tun, I. D. Brown, *Acta Crystallogr., Sect. B* **1982**, *38*, 2321−2324.
[12] Z. Tun, I. D. Brown, P. K. Ummat, *Acta Crystallogr., Sect. C* **1984**, *40*, 1301−1303.
[13] W. R. Datars, P. K. Ummat, R. J. Gillespie, *Mater. Res. Bull.* **1985**, *20*, 865−869.
[14] E. Batalla, W. R. Datars, D. Chartier, R. J. Gillespie, *Solid State Commun.* **1981**, *38*, 1203−1205.
[15] I. J. Dinser, W. R. Datars, D. Chartier, R. J. Gillespie, *Solid State Commun.* **1979**, *32*, 1041−1043.
[16] W. R. Datars, A. van Schyndel, J. S. Lass, D. Chartier, R. J. Gillespie, *Phys. Rev. Lett.* **1978**, *40*, 1184−1187.
[17] E. Batalla, W. R. Datars, D. Chartier, R. J. Gillespie, *Solid State Commun.* **1981**, *40*, 711−714.
[18] D. Chartier, W. R. Datars, R. J. Gillespie, *Can. J. Phys.* **1983**, *61*, 71−75.
[19] F. S. Razavi, W. R. Datars, D. Chartier, R. J. Gillespie, *Phys. Rev. Lett.* **1979**, *42*, 1182−1185.
[20] H. Kunkely, A. Vogler, *Chem. Phys. Lett.* **1995**, *240*, 31−34.
[21] J. D. Corbett, *Prog. Inorg. Chem.* **1976**, *21*, 129−159.
[22] A. Mühlecker-Knoepfler, E. Ellmerer-Müller,R. Konrat, K.-H. Ongania, K. Wurst, P. Peringer, *J. Chem. Soc., Dalton Trans.* **1997**, 1607−1610.
[23] W. R. Mason, *Inorg. Chem.* **1997**, *36*, 1164−1167.
[24] A. Knoepfler, K. Wurst, P. Peringer, *J. Chem. Soc., Chem. Commun.* **1995**, 131−132.
[25] S. Ulvenlund, A. Wheatley, L. A. Bengtsson, *J. Chem. Soc., Dalton Trans.* **1995**, 245−254.
[26] S. Ulvenlund, A. Wheatley, L. A. Bengtsson, *J. Chem. Soc., Chem.* Commun. **1995**, 59−60.
[27] S. Ulvenlund, K. Ståhl, L. Bengtsson-Kloo, *J. Chem. Soc., Faraday Trans.* **1995**, *91*, 4223−4233.
[28] S. Ulvenlund, K. Ståhl, L. Bengtsson-Kloo, *Inorg. Chem.* **1996**, *35*, 223- 230.
[29] G. Allegra, A. Immirzi, L. Porri, *J. Am. Chem. Soc.* **1965**, *87*, 1394−1395.
[30] G. Allegra, G. Tettamanti Casagranda, A. Immirtzi, L. Porri, G. Vitulli, *J. Am. Chem. Soc.* **1970**, *92*, 289−293.
[31] G. Nardin, P. Delise, G. Allegra, *Gazz. Chim. Ital.* **1975**, *105*, 1047−1053.
[32] W. Frank, B. Dincher, *Z. Naturforsch., B* **1987**, *42*, 828−834.
[33] M. Taylor, in *Metal-to-Metal Bonded States of the Main-Group Elements*, Academic Press, New York, **1975**, ch. 2, p. 20−24.
[34] A. F. Wells, *Structural Inorganic Chemistry*, 5th ed., Clarendon Press, Oxford, **1984**, p. 1157−1158.
[35] *Inorganic Reactions and Methods*, vol. 13 (Ed.: A. P. Hagen), VCH, Weinheim, **1991**, p. 363−374.
[36] M. Bodenbinder, G. Balzer-Jöllenbeck, H. Willner, R. J. Batchelor, F. W. B. Einstein, C. Wang, F. Aubke, *Inorg. Chem.* **1996**, *35*, 82−92.
[37] R. W. Turner, E. L. Amma, *J. Inorg. Nucl. Chem.* **1966**, *28*, 2411−2413.
[38] G. A. Voyiatzis, G. N. Papatheodorou, *Inorg. Chem.* **1992**, *31*, 1945- 1951.
[39] M. Sikirica, D. Grdenic, *Acta Crystallogr., Sect. B* **1974**, *30*, 144−146.
[40] G. Johansson, *Acta Chem. Scand.* **1966**, *20*, 553−562.
[41] G. Herzberg, in *Molecular Spectra and Molecular Structure*, Krieger Publishing Co., Malabar, **1991**, vol. II, p. 362−369.
[42] L. Bengtsson-Kloo, S. Ulvenlund, *Spectrochim. Acta, Part A* **1997**, *53*, 2129−2138.
[43] P. A. W. Dean, D. G. Ibbott, J. B. Stothers, *J. Chem. Soc., Chem. Commun.* **1973**, 626−627.
[44] P. A. W. Dean, D. G. Ibbott, J. B. Stothers, *Can. J. Chem.* **1976**, *54*, 166- 176.
[45] E. Dorm, *J. Chem. Soc., Chem. Commun.* **1971**, 466−467.
[46] A. Haaland, *Angew. Chem.* **1989**, *101*, 1017−1032; *Angew. Chem. Int. Ed. Engl.* **1989**, *28*, 992−1007.
[47] E. Biehl, H. J. Deiseroth, *Z. Kristallogr.* **1996**, *211*, 630.
[48] R. J. Gillespie, P. Granger, K. R. Morgan, G. J. Schrobilgen, *Inorg.* Chem. **1984**, *23*, 887−891.
[49] M. J. Frisch, G. W. Trucks, H. B. Schlegel, P. M. W. Gill, B. G. Johnson, M. A. Robb, J. R. Cheeseman, T. A. Keith, G. A. Petersson, J. A. Montgomery, K. Raghavshari, M. A. Al-Laham, V. G. Zakrzewski, J. V. Ortiz, J. B. Foresman, J. Cioslowski, B. B. Stefanov, A. Nanayakkara, M. Challacombe, C. Y. Peng, P. Y. Ayala, W. Chen, M. W. Wong, J. L. Andres, E. S. Replogle, R. Gomperts, R. L. Martin, D. J. Fox, J. S. Binkley, D. J. Defrees, J. Baker, J. P. Stewart, M. Head-Gordon, C. Gonzalez, J. A. Pople, GAUSSIAN94, Gaussian Inc., Pittsburgh PA, **1995**.
[50] U. Häussermann, M. Dolg, H. Stoll, H. Preuss, P. Schwerdtfeger, R. M. Pitzer, *Molec. Phys.* **1993**, *78*, 1211−1224.
[51] A. D. Becke, *J. Chem. Phys.* **1993**, *98*, 5648−5652.
[52] R. W. Turner, E. L. Amma, *J. Am. Chem. Soc.* **1966**, *88*, 1877−1882.
[53] H. G. Smith, R. E. Rundle, *J. Am. Chem. Soc.* **1958**, *80*, 5075−5080.
[54] E. A. H. Griffith, E. L. Amma, *J. Am. Chem. Soc.* **1971**, *93*, 3167−3172.
[55] S. Charles, B. W. Eichhorn, A. L. Rheingold, S. G. Bott, *J. Am. Chem.* Soc. **1994**, *116*, 8077−8086.
[56] A. Seigneurin, T. Makani, D. J. Jones, J. Roziére, *J. Chem. Soc., Dalton Trans.* **1987**, 2111−2116.
[57] B. Schiementz, G. Huttner, *Angew. Chem.* **1993**, *105*, 295−296; *Angew. Chem. Int. Ed. Engl.* **1993**, *32*, 297−298.
[58] B. W. E. Eichhorn, R. C. Haushalter, *J. Chem. Soc., Chem. Commun.* **1990**, 937−938.
[59] A. E. Reed, F. Weinhold, *J. Chem. Phys.* **1985**, *83*, 1736−1740.
[60] A. E. Reed, P. von Rague Schleyer, *J. Am. Chem. Soc.* **1990**, *112*, 1434−1445.
[61] E. D. Glenning, A. E. Reed, J. E. Carpenter, *Gaussian94*, NBO version 3.1.
[62] S. Ulvenlund, L. A. Bengtsson, L.A. *J. Mol. Struct.* **1994**, *326*, 181−191.

Received November 11, 1998
[I98390]

Kinetics and Mechanism of Base Hydrolysis in Cobalt(III) Complexes − The Case of a Complex $CoLCl^{2+}$ where L has the Novel Topology of a Square-Pyramidal NN_4 Coordination Cap

Tilo Poth,[a] Helmut Paulus,[a][+] Horst Elias,*[a] Rudi van Eldik,[b] and Andreas Grohmann*[b]

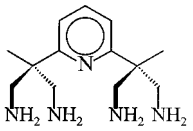
Keywords: Cobalt(III) complexes / Tetrapodal pentadentate ligand / Hydrolysis / Kinetics / Mechanism

Multi-wavelength stopped-flow spectrophotometry was used to study the kinetics of base hydrolysis of the octahedral cobalt(III) complex $CoLCl^{2+}$ (**2**), in which the tetrapodal pentadentate ligand L has an NN_4 donor set and forms a square-pyramidal coordination cap [L = 2,6-bis(1′,3′-diamino-2′-methylprop-2′-yl)pyridine, **1**]. The kinetic investigation, carried out at different temperatures, pressures and ionic strengths I, led to second-order kinetics, rate = k_{OH} [**2**][OH^-], with $k_{OH} = 0.139 \pm 0.001$ $M^{-1}s^{-1}$ (I = 0.1 M) and $k_{OH} = 0.0570 \pm 0.0004$ $M^{-1}s^{-1}$ (I = 1.0 M) at 298 K. The temperature and pressure dependence of k_{OH} resulted in $\Delta H^{\ddagger} = 119 \pm 3$ kJmol^{-1} (I = 0.1 M) and $\Delta H^{\ddagger} = 123 \pm 3$ kJmol^{-1} (I = 1.0 M), $\Delta S^{\ddagger} = +130 \pm 13$ Jmol^{-1}K^{-1} (I = 0.1 M) and $\Delta S^{\ddagger} = +151 \pm 15$ Jmol^{-1}K^{-1} (I = 1.0 M) and $\Delta V^{\ddagger} = +27.6 \pm 0.6$ cm^{3}mol^{-1} (I = 1.0 M). The kinetic results support the operation of the conjugate base mechanism, D_{cb}, with intermediate deprotonation occuring *cis* to the leaving chloride ion. The observed inertness of complex **2** towards base hydrolysis is discussed on the basis of the special structural features of the ligand L. The pK_a of the coordinated water in the aqua species $CoL(H_2O)^{3+}$(**3**) was determined to be pK_a = 6.0 ± 0.1 at I = 0.1 M. The X-ray crystal structure analysis of the hydroxo complex $[CoL(OH)](ClO_4)_2$ (**4**) shows a mononuclear terminal (hydroxo)Co^{III} complex, in which the ligand provides a regular square-pyramidal NN_4 donor cap for the octahedrally six-coordinate Co^{III} ion [**4**, monoclinic, space group $C2/m$, a = 16.841(6) Å, b = 8.541(3) Å, c = 15.112(5) Å, β = 109.13(1)°, Z = 4]. Coordination of L is accompanied by the formation of 6 six-membered chelate rings, all of which adopt a boat conformation. In the crystal lattice, pairs of cations are associated via four (hydroxo)O···H–N(primary amine) hydrogen bonds and related through an inversion center. Full spectroscopic data for **4** (^{1}H-, ^{13}C-NMR, IR, MS) are presented.

Introduction

Tetrapodal pentadentate ligands designed to provide a square-pyramidal coordination cap for octahedrally coordinating transition metal ions were until recently unknown.[1−3] This coordination mode requires a ligand to have an apical donor atom with a lone pair oriented towards the center of the octahedron, while four donor groups are juxtaposed to occupy the equatorial positions. The interest in ligands of this type arises from their potential stabilization of free coordination sites in otherwise octahedrally coordinated complexes. Suitable derivatization of the equatorial positions may then provide an environment for a monodentate substrate or reagent (such as metal-coordinated hydroxide) in which it shows modulated reactivity.[4]

The coordination behavior of the prototypical NN_4 coordination cap **1** (≡ L) towards nickel(II) and cobalt(III) has been the subject of recent work.[2,5,6] The ligand acts as a podand in all cases (including a $Co^{III}-CH_3$ complex), and



1 (≡ L)

a polynuclear coordination mode has not been observed. Given the similarity of pyridine and ammine ligands with respect to their position in the spectrochemical series, **1** may be considered a highly symmetrical chelating analogue of the classical pentaammine donor set, and complexes of **1** are expected to show similar reactivity, e.g. with respect to ligand exchange. In order to substantiate this assumption and obtain mechanistic data relevant to future use of the ligand as a mononucleating head group in functional metal complexes, we chose to study the kinetics of a classical exchange reaction of cobalt(III), viz. the base-assisted hydrolysis of $CoLCl^{2+}$ (**2**).

Base-assisted hydrolysis of the octahedral Werner-type complex $Co(NH_3)_5Cl^{2+}$ according to Equation 1, following the simple rate law of Equation 2, has initiated an impressive number of kinetic studies on reactions of Equation 3.[7]

$$Co(NH_3)_5Cl^{2+} + OH^- \rightarrow Co(NH_3)_5(OH)^{2+} + Cl^- \quad (1)$$

$$\text{rate} = k_{OH}[Co^{III}][OH^-] \quad (2)$$

$$Co(\text{'}N_5\text{'})Cl^{2+} + OH^- \rightarrow Co(\text{'}N_5\text{'})(OH)^{2+} + Cl^- \quad (3)$$

[+] Technische Universität Darmstadt, Fachbereich Materialwissenschaft
[a] Institut für Anorganische Chemie, Technische Universität Darmstadt,
Petersenstraße 18, D-64287 Darmstadt, Germany
E-mail: elias@hrz1.hrz.tu-darmstadt.de
[b] Institut für Anorganische Chemie, Universität Erlangen-Nürnberg,
Egerlandstraße 1, D-91058 Erlangen, Germany
E-mail: grohmann@anorganik.chemie.uni-erlangen.de

 © WILEY-VCH Verlag GmbH, D-69451 Weinheim, 1999 1434−1948/99/0404−0643 $ 17.50+.50/0

These reactions are now commonly agreed to proceed by the so-called "conjugate base mechanism", D_{cb} (formerly S_N1CB), which involves the intermediate formation of a substitutionally labile amide complex.[8,9] The symbol 'N_5' in Equation 3 stands for a set of five N donor atoms in the form of either five monodentate ligands or combinations of monodentate and chelate ligands, such as ($N + N_2 + N_2$), ($N_2 + N_3$), ($N + N_4$), and (N_5).

Such variations in the 'N_5' set of ligands were made in order to allow meaningful conclusions concerning, for example, the question of deprotonation and amide bond formation *cis* or *trans* to the leaving group. An interesting outcome of these studies was that the nature of the ligands making up 'N_5' has a pronounced effect on the magnitude of the second-order rate constant k_{OH}, which reflects the kinetic significance of the structural features in the 'N_5' coordination sphere.

The NN_4 topology of L in the octahedral chlorocobalt complex $[CoLCl]Cl(ClO_4) \cdot H_2O$[2] represents a novel type of 'N_5' unit. In view of the individual steps associated with the D_{cb} mechanism, the situation in this complex is remarkable for several reasons. Firstly, the nitrogen atom *trans* to the leaving group is tertiary, hence cannot be deprotonated. Since pyridine donors coordinated *cis* to the leaving group were found to increase the rate of base hydrolysis markedly,[10] species in which pyridine is coordinated *trans* to the leaving group have long been called for for the purpose of comparison.[11,12] Secondly, the ligand L enforces a rigid square-pyramidal coordination cap containing four equivalent $Co-NH_2R$ bonds, which raises the question whether the internal steric strain associated with the deprotonation of one of the NH_2 groups is possibly too high to allow intermediate amide bond formation at all.

The present contribution provides the kinetic data obtained for the reaction according to Equation 3 at different temperatures, pressures and ionic strengths, as well as spectroscopic and X-ray structural data for the hydroxo complex $[CoL(OH)](ClO_4)_2$ (**4**). The pK_a value of the aqua complex $CoL(H_2O)^{3+}$ (**3**) is also reported.

Results and Discussion

Properties of the Complexes

Table 1 summarizes the UV/Vis absorption data of the cations **2**, **4**, and **3**. The spectra show two absorption maxima, which can be assigned to the transitions $^1T_{1g} \leftarrow {}^1A_{1g}$ and $^1T_{2g} \leftarrow {}^1A_{1g}$, commonly observed in Co^{III} complexes of this type. The variation of the sixth ligand ($Cl^- \rightarrow OH^- \rightarrow H_2O$) causes a blue shift of both maxima ($\lambda_{max} = 356 \rightarrow 343 \rightarrow 335$ nm and $\lambda_{max} = 512 \rightarrow 480 \rightarrow 480$ nm), which is in accord with the position of the ligands in the spectrochemical series.

Table 1. Visible absorption {λ_{max} [nm] (ε_{max} [$M^{-1}cm^{-1}$])} of the complex cations in aqueous solution at 293 K

$CoL(Cl)^{2+}$ (**2**)	356(101)	512(67)
$CoL(OH)^{2+}$ (**4**)	343(128)	480(95)
$CoL(H_2O)^{3+}$ (**3**)	335(100)	480(56)

Figure 1 shows the spectral changes following the stepwise deprotonation of the species **3** according to Equation 4 and, as an example, the plot of A_{483} vs pH. Multi-wavelength fitting of the (A, [H^+]) data (350−600 nm) with Equation 5 leads to $pK_a = 6.0 \pm 0.1$. The pK_a found for complex **3** is very similar to the pK_a reported for other (amine)(monoaqua)cobalt(III) complexes.[13] From its magnitude it follows that even at pH = 5−6 appreciable amounts of the hydroxo species **4** are present.

$$CoL(H_2O)^{3+} \overset{K_a}{\rightleftharpoons} CoL(OH)^{2+} + H^+ \quad (4)$$

$$A = \{A_{H_2O} + A_{OH}(K_a)^{-1}[H^+]\}/\{1 + (K_a)^{-1}[H^+]\} \quad (5)$$

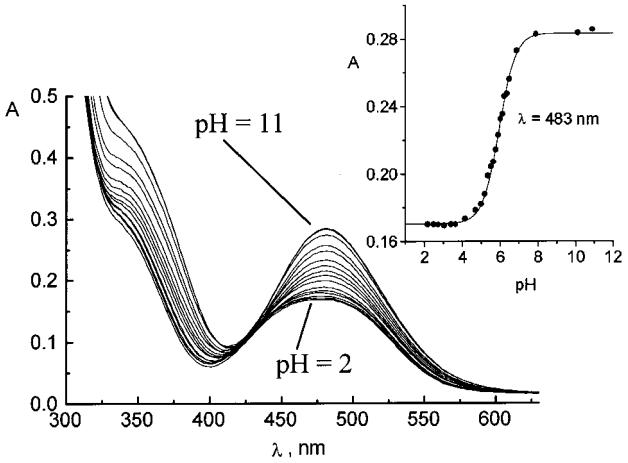


Figure 1. Spectral changes associated with the titration of complex **3** ($3 \cdot 10^{-3}$ M) with 0.1 M NaOH at 298 K and $I = 0.1$ M ($NaNO_3$); insert: plot of A_{483} vs. pH and fit (solid line) with Equation 5

The ^1H- and ^{13}C-NMR spectra of **4** (r.t.; amount of sample: 20 mg; solvent: anhydrous [D_6]DMSO; amount of solvent: 0.6 mL) largely resemble those of the parent chloro complex $[CoLCl]Cl(ClO_4) \cdot H_2O$ in terms of chemical shift and signal multiplicity.[2] A few features deserve special mention. In the ^1H-NMR spectrum of **4**, the resonances of the diastereotopic amine protons ($\delta = 4.52$ and 4.70) are shielded by ca. 0.8 ppm and 1.2 ppm, respectively, relative to the corresponding resonances in $[CoLCl]Cl(ClO_4) \cdot H_2O$ ($\delta = 5.29$ and 5.85). There is a broad singlet at high field, viz. −2.60 (sweep width −20 to +30 ppm; $W_{1/2} = 7.1$ Hz), which we assign to the proton of the hydroxo ligand. The observed high-field shift is presumably a consequence of the OH proton being solitary, i.e. not involved in hydrogen bonding under the given conditions. Hydrogen bonding, if present, as well as the electronegative nature of the heteroatom carrying this proton, would lead one to expect a significant *downfield* shift of its resonance. The signal disappears owing to exchange when water is allowed to diffuse into the sample. We are not aware of reliable previous NMR data of structurally characterised Co^{III} complexes containing a terminal hydroxo ligand. In a structurally characterised monomeric terminal hydroxo complex of zinc, the $Zn-OH$ resonance is observed at similarly high field ($\delta = -0.06$; solvent: [D_6]benzene).[14] In the ^{13}C-NMR spectrum of **4**, the resonance assigned to the methylene carbon atoms

shows fine structure. An asymmetric three-line signal is observed (J = 7.8 Hz), of which the line towards low field is not well resolved but is visible as a shoulder. We attribute this splitting to partially resolved coupling with the ^{14}N nucleus (I = 1), which is usually only observable in highly symmetric species such as tetraalkylammonium ions, in which the electric field gradient at ^{14}N is zero or sufficiently small.[15]

In the IR spectrum of **4**, there is a sharp ν(OH) str band of medium intensity at 3578 cm^{-1}. A band below 1200 to 700 cm^{-1}, characteristic of a hydroxo complex and due to the M−O−H bending vibration,[16] cannot be assigned with certainty as this region is obscured by the very broad absorption of the ClO_4^- counterions.

Structure of the Complex $[CoL(OH)](ClO_4)_2$ (4)

The X-ray structure analysis unequivocally confirms the presence of a mononuclear terminal (hydroxo)Co^{III} complex, making **4** one of the very few examples of such complexes that have been structurally characterised.[17] The molecular structure of the cation, which has crystallographically imposed mirror symmetry, is shown in Figure 2. Selected bond lengths and angles are given in Table 2. The mirror plane contains the pyridine ring, the quaternary and methyl carbon atoms of the pentaamine ligand backbone, one of the protons on each exocyclic methyl group, the cobalt atom, and the oxygen and hydrogen atoms of the hydroxo ligand. All hydrogen atoms have been located in the difference Fourier map. Specifically, the location of electron density corresponding to *one* proton bound to the hydroxo oxygen atom is clearly discernible at a reasonable distance and angle relative to that atom [d(O−H) = 0.863(2) Å, ∠Co−O−H = 109.9(2)°]. There is no residual electron density in the vicinity of the hydroxo ligand.

The pentaamine ligand coordinates to cobalt(III) in pyramidal fashion, with the pyridine nitrogen atom occupying an axial position of the overall coordination octahedron, while the four equivalent amino nitrogen atoms take the equatorial positions. This mode of coordination leads to the formation of 6 six-membered chelate rings, all of which adopt a boat conformation. The hydroxo ligand occupies the remaining axial position. The coordination octahedron is close to regular, with angles N_{ax}−Co−N_{eq} and N_{eq}−Co−N_{eq} ranging from 84.91(10)° to 93.16(7)°. The arrangement of atoms along the principal axis of the octahedron (N11, Co1, O1) is linear [179.77(8)°], and the angles between diametrically disposed pairs of NH_2 substituents (N12, N13′; N12′, N13) at Co are close to 180° [175.94(7)°]. The cobalt atom is displaced from the plane defined by the four equatorial amino nitrogen atoms towards the pyridine N atom by only 0.044(1) Å. The pyridine ring is a regular hexagon. Thus, the tetrapodal pentadentate amine ligand provides a square-pyramidal coordination cap for the metal center in the same way as in a related chloro[2] and methyl complex.[6] The cobalt−pyridine bond length in **4** [1.934(2) Å] is the same within experimental error as that in the chloro complex $[CoLCl]Cl(ClO)_4 \cdot H_2O$ [1.928(3) Å],[2] as opposed to a value of 2.018(2) Å for the corresponding bond in the methyl complex $[CoL(CH_3)]S_2O_6$.[6] This reflects *trans* influences of comparable magnitude for OH^- and Cl^-, as opposed to the significantly larger *trans* influence exerted by the CH_3^- ligand.[18] The Co1−O1 distance in **4** [1.897(2) Å] is comparable to the value obtained for another terminal Co^{III}−OH complex [1.894(10) Å],[17b] while the value determined for a third complex [2.190(3) Å] is so large as to have been considered at odds with the formulation as a hydroxo species.[17a]

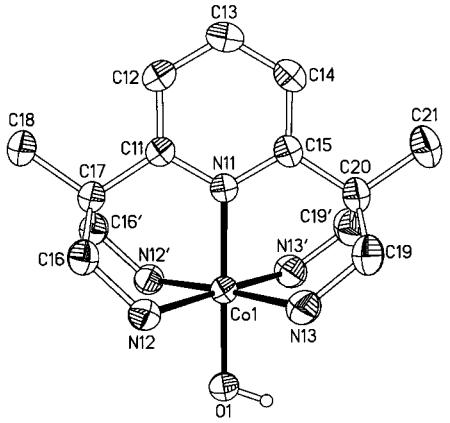


Figure 2. Molecular structure of **4** with thermal ellipsoids drawn at the 50% probability level; the position of the hydroxo hydrogen atom H1 is indicated by a sphere of arbitrary diameter; all other hydrogen atoms have been omitted for clarity

Table 2. Selected distances and angles for $[CoL(OH)](ClO_4)_2$ (**4**)

Atoms	Distance [Å]	Atoms	Distance [Å]
Co1−N11	1.934(2)	Co1−N13	1.958(2)
Co1−N12	1.963(2)	Co1−O1	1.897(2)
O1−H1	0.863(2)		
Atoms	**Angle [°]**	**Atoms**	**Angle [°]**
N11−Co1−O1	179.77(8)	C12−C11−C17	122.8(3)
Co1−O1−H1	109.9(2)	C14−C15−C20	122.2(3)
N11−Co1−N12	93.16(7)	C11−C17−C18	110.9(2)
N11−Co1−N13	89.53(7)	C15−C20−C21	112.3(3)
O1−Co1−N12	87.01(7)	C11−C17−C16	109.9(1)
O1−Co1−N13	90.31(7)	C15−C20−C19	109.8(2)
N12−Co1−N12′	84.92(10)	C16−C17−C18	107.0(1)
N12−Co1−N13	91.91(9)	C19−C20−C21	107.1(2)
N13−Co1−N13′	91.15(12)	C16−C17−C16′	112.0(2)
N12−Co1−N13′	175.94(7)	C19−C20−C19′	110.8(3)
C11−N11−Co1	120.1(2)	C17−C16−N12	112.9(2)
C15−N11−Co1	119.8(2)	C20−C19−N13	113.7(2)
N11−C11−C17	116.7(2)	C16−N12−Co1	117.5(1)
N11−C15−C20	117.5(2)	C19−N13−Co1	118.7(2)

In the crystal lattice, pairs of cations are associated via (hydroxo)O···H−N(primary amine) hydrogen bonds and related through an inversion center as follows: Both lone pairs on the hydroxo ligand of cation 1(2) receive hydrogen bonds from one proton each on two adjacent amino groups in cation 2(1). The distance O1···N12 is 2.874(2) Å, and the angle at H12A is 151.8(1)° (sum of the van der Waals radii of O and N: 3.07 Å[19]). The hydroxo protons of cation 1 and 2 point away from each other and do not participate

in hydrogen bonding. The crystallographic inversion center is located at the midpoint of the vector connecting the hydroxo oxygen atoms of cation 1 and 2. The other non-bonded distances in the crystal packing fall outside the range where significant hydrogen bonding may be inferred. The two perchlorate counterions show rotational disorder which has been resolved, but otherwise have normal structural parameters. The residual electron density in the overall structure is located at ClO_4^-.

Kinetics of Base Hydrolysis

As shown in Figure 3 for pH ≈ 12, base hydrolysis of complex **2**, as obtained by dissolving $[CoLCl]Cl(ClO_4) \cdot H_2O$ in water, is associated with substantial spectral changes and occurs with a half-life of several minutes (T = 298 K). The (A, t) data can be fitted very satisfactorily to one exponential (Equation 6) for the whole wavelength range. Experiments carried out in the presence of a thirtyfold excess of NaCl guaranteed that non-coordinated chloride ions, as introduced with the complex $[CoLCl]Cl(ClO_4) \cdot H_2O$, have no effect on the magnitude of the experimental rate constant k_{obsd}.

$$A = (A_0 - A_\infty)[\exp(-k_{obsd}t)] + A_\infty \quad (6)$$

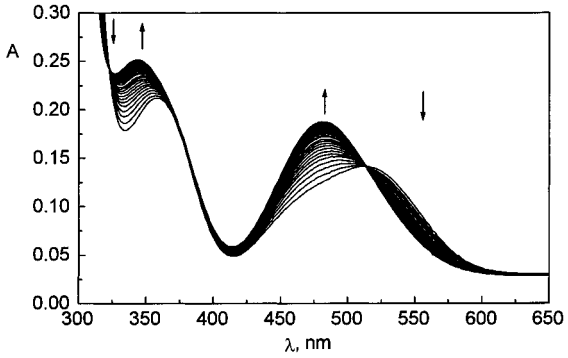


Figure 3. Spectral changes associated with the base hydrolysis of complex **2** ($2.2 \cdot 10^{-3}$ M) at pH ≈ 12 and 293 K (the spectra, taken at time intervals of 19.8 s, cover a reaction time of 990 s)

Figure 4 shows that the dependence of k_{obsd} on $[OH^-]$ is linear, which leads to the rate law of Equation 7 and second-order rate constant k_{OH}.

$$\text{rate} = -d[CoLCl^{2+}]/dt = d[CoL(OH)^{2+}]/dt = k_{OH}[CoLCl^{2+}][OH^-] \quad (7)$$

In addition, Figure 4 documents that the rate of base hydrolysis increases with decreasing ionic strength, as expected for the reaction between species of opposite charge.[20] The observed ratio for k_{OH} (I = 0.1 M)/k_{OH} (I = 1.0 M) = 2.4 is in accord with the averaged value k_{OH} (I = 0.1 M)/k_{OH} (I = 1.0 M) = 2.2, as reported earlier for a number of $Co'N_5'X^{2+}$ complexes.[11]

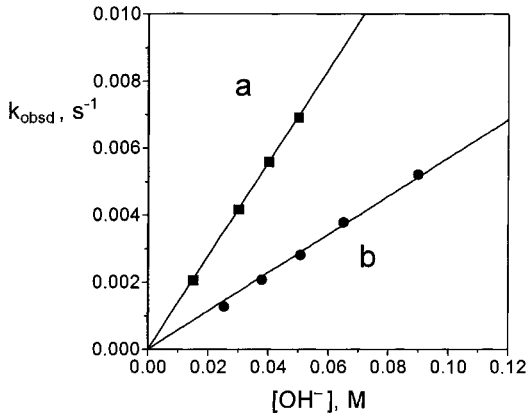


Figure 4. Plot of the experimental rate constant k_{obsd} vs. $[OH^-]$ for base hydrolysis of complex **2** ($2.2 \cdot 10^{-3}$ M) according to Equation 7 at I = 0.1 M $NaClO_4$ (a) and I = 1.0 M $NaNO_3$ (b), (T = 298 K)

Least-squares fitting of the data shown in Figure 3 leads to k_{OH} = 0.139 $M^{-1}s^{-1}$ (I = 0.1 M) and k_{OH} = 0.0570 $M^{-1}s^{-1}$ (I = 1.0 M). These rate constants are amongst the lowest ever reported for base hydrolysis reactions of Equation 3.[21]

The D_{cb} mechanism is based on the reaction sequence of Equations 8a–8c, with Equation 8a being a fast deprotonation/protonation equilibrium and Equation 8b being the rate-determining step which, as pointed out, is very slow in the present system (the symbol L_{-H} stands for the ligand L, mono-deprotonated at one of the four primary amino groups).

$$CoLCl^{2+} + OH^- \overset{K}{\rightleftharpoons} CoL_{-H}Cl^+ + H_2O \quad (8a)$$

$$CoL_{-H}Cl^+ \xrightarrow[\text{rds}]{k} CoL_{-H}^{2+} + Cl^- \quad (8b)$$

$$CoL_{-H}^{2+} + H_2O \xrightarrow{\text{fast}} CoL(OH)^{2+} \quad (8c)$$

Assuming the equilibrium according to Equation 8a to be established and $[complex]_o << [OH^-]$, one can derive the rate law of Equation 9 which suggests that the dependence $k_{obsd} = f([OH^-])$ should come to saturation for $K[OH^-] >> 1$.

$$d[CoL(OH)^{2+}]/dt = \{k \cdot K[OH^-]/(1 + K[OH^-])\} \cdot [CoLCl^{2+}] = k_{obsd}[CoLCl^{2+}] \quad (9)$$

As shown in Figure 4, k_{obsd} increases linearly with $[OH^-]$ up to $[OH^-]$ = 0.09 M. This means that the estimate $K[OH^-] << 1$ can be made, for which condition the rate law of Equation 9 takes the simple form of Equation 10 which corresponds to the experimentally found rate law of Equation 2 with $k_{OH} \equiv k \cdot K$.

$$d[CoL(OH)^{2+}]/dt = k \cdot K[OH^-] \cdot [CoLCl^{2+}] \quad (10)$$

It is noteworthy that a linear dependence of k_{OH} on $[OH^-]$ is generally observed for the base hydrolysis of cobalt(III) complexes.[9]

Table 3. Kinetic parameters for the base hydrolysis of some cobalt(III) complexes of the type Co'N_5'Cl^{2+} according to Equation 3

Complex	I [M]	k_{OH}^{298} [$M^{-1}s^{-1}$]	$\Delta H^{\neq}$ [kJ mol^{-1}][a]	$\Delta S^{\neq}$ [$Jmol^{-1}K^{-1}$][a]	$\Delta V^{\neq}_{exptl}$ [cm^3 mol^{-1}][a]	Ref.
$Co(NH_3)_5Cl^{2+}$	0.1	0.86	118	+155	+33.8 ± 1.0	[28][33]
$Co(L)Cl^{2+}$ (**2**)	0.1	0.1389 ± 0.0009	119 ± 3	+130 ± 13	–	this work
	1.0	0.0570 ± 0.0004	123 ± 3	+151 ± 15	+27.6 ± 0.6	this work
cis-$Co(en)_2(NH_3)Cl^{2+}$[b]	–	54.0	–	–	+31.8 ± 0.6	[24][33]
t-$Co(tren)(NH_3)Cl^{2+}$[c]	1.0	0.02 ± 0.003	–	–	–	[34]
p-$Co(tren)(NH_3)Cl^{2+}$[c]	1.0	3.8 ± 0.2	–	–	–	[34]
a-$Co(tmd)(dien)Cl^{2+}$[d]	0.1	(5.02 ± 0.14)×10^5	81 ± 3	+135 ± 4	–	[25]
d-$Co(tmd)(dien)Cl^{2+}$[d]	0.1	138	89 ± 2	+94 ± 3	–	[25]
h-$Co(tmd)(dien)Cl^{2+}$[d]	0.1	10.6	120 ± 3	+179 ± 6		[25]
$Co(en)_2(py)Cl^{2+}$	0.1	332 ± 4	83.6 ± 0.8	+84 ± 2	–	[10]
$Co(tacn)(amp)Cl^{2+}$[e]	0.1	154 ± 5	–	–	–	[11]
	1.0	66.7 ± 2.3	83.3 ± 1.2	+69 ± 4	–	[11]

[a] $\Delta H^{\neq}$ and $\Delta S^{\neq}$ were obtained from the temperature dependence of k_{OH} at five temperatures in the range T = 285– 318 K. $\Delta V^{\neq}_{exptl}$ was obtained from the pressure dependence of the first-order rate constant k_{obsd} in the range 10–150 MPa at 308 K. – [b] en = 1,2-Diaminoethane ($NH_2[CH_2]_2NH_2$). – [c] tren = Tris(2-aminoethyl)amine [$N(CH_2CH_2NH_2)_3$]; *t* isomer: tertiary nitrogen atom *trans* to coordinated chloride, *p* isomer: tertiary nitrogen atom *cis* to coordinated chloride. – [d] tmd = 1,3-Diaminopropane ($NH_2[CH_2]_3NH_2$); dien = 3-azapentane-1,5-diamine ($NH_2[CH_2]_2NH[CH_2]_2NH_2$); *a* isomer: "flat" nitrogen atom of dien *cis* to coordinated chloride; *d* isomer: "bent" nitrogen atom of dien *cis* to coordinated chloride; *h* isomer: "bent" nitrogen atom of dien *trans* to coordinated chloride. – [e] tacn = 1,4,7-Triazacyclononane; amp = 2-aminomethylpyridine.

It has been shown that anion competition experiments[22,23] and the determination of reaction volume profiles[24] can provide experimental evidence for the validity of the commonly accepted D_{cb} mechanism. In order to substantiate the operation of the D_{cb} mechanism for the base hydrolysis of **2**, experiments at different temperatures (see Table 4) and pressures (see Figure 5) were carried out. The resulting activation parameters $\Delta H^{\neq}$, $\Delta S^{\neq}$, and $\Delta V^{\neq}_{exptl}$ are listed in Table 3, together with the corresponding data reported for other Co'N_5'Cl^{2+} complexes.

Table 4. Rate constants k_{OH} at variable temperature and variable ionic strength[a]

T [K]	$k_{obsd}/[OH^-]$ [$M^{-1}s^{-1}$] (I = 0.1 $NaClO_4$)[b]	$k_{obsd}/[OH^-]$ [$M^{-1}s^{-1}$] (I = 1.0 $NaNO_3$)[c]
288	(2.45 ± 0.01)×10^{-2}	(0.905 ± 0.003)×10^{-2}
293	(5.76 ± 0.08)×10^{-2}	(2.35 ± 0.06)×10^{-2}
298	(13.9 ± 0.1)×10^{-2}	(5.34 ± 0.06)×10^{-2}
308	(75.2 ± 0.2)×10^{-2}	(26.4 ± 0.1)×10^{-2}
318	(335.7± 0.3)×10^{-2}	(124.3 ± 0.5)×10^{-2}

[a] [$CoLCl^{2+}$] = 2.5·10^{-3} M. – [b] [OH^-] = 0.025 M. – [c] [OH^-] = 0.065 M.

The $\Delta H^{\neq}$ and $\Delta S^{\neq}$ values obtained for **2** are conspicuously close to those of the "parent complex" $Co(NH_3)_5Cl^{2+}$, which undergoes base hydrolysis at a similarly low rate.[25] The large positive entropy of activation of ca. 150 $Jmol^{-1}K^{-1}$ has often been discussed as a mechanistic proof for the equilibrium according to Equation 8a.[26] The value of $\Delta V^{\neq}_{exptl}$ = 27.6 ± 0.6 cm^3mol^{-1} (cf. Experimental Section) provides strong evidence that base hydrolysis of complex **2** follows the D_{cb} mechanism. By way of comparison, the average base hydrolysis volume of activation of 11 different dipositive (amine)cobalt(III) complexes is 29.7 cm^3 mol^{-1},[24] and thus close to the value found in the present study. In the same way as $k_{OH} \equiv kK$, $\Delta V^{\neq}_{exptl}$ is a composite parameter, involving the contribution of the pressure dependence of the equilibrium of Equation 8a, $\Delta \bar{V}(K)$, and that of the rate-determining dissociation step of Equation 8b, $\Delta V^{\neq}(k)$, according to Equation 11. For Co^{III} complexes with an overall 2+ charge, the magnitude of $\Delta \bar{V}(K)$ can be estimated[24,27] to be + 19.3 ± 1.5 cm^3 mol^{-1}, resulting in an activation volume $\Delta V^{\neq}(k)$ of 8.3 cm^3 mol^{-1} for the reaction step of Equation 8b.

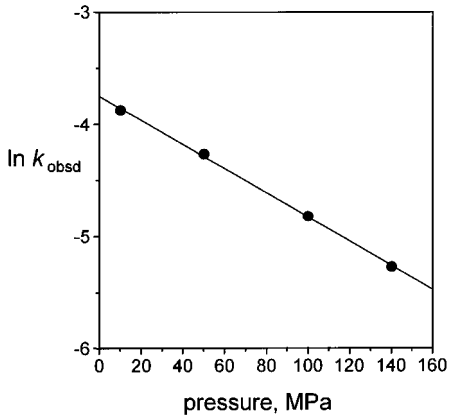


Figure 5. Plot of ln k_{obsd} vs. pressure for base hydrolysis of complex **2** according to Equation 12 at 308 K ([complex] = 2.5·10^{-3} M; [OH^-] = 0.1 M; I = 1.0 M $NaNO_3$)

$$\Delta V^{\neq}_{exptl} = \Delta \bar{V}(K) + \Delta V^{\neq}(k) \quad (11)$$

This value is smaller when compared to $\Delta V^{\neq}(k)$ = 14.5 cm^3 mol^{-1} for the complex $Co(NH_3)_5Cl^{2+}$,[28a] but within the experimental error limits not small enough to indicate convincingly an I_d-controlled reaction of the deprotonated intermediate $CoL_{-H}Cl^+$ (see Equation 8b) as opposed to a D-controlled one.[28b] The overall $\Delta V^{\neq}_{exptl}$ value therefore favors the operation of a D_{cb} mechanism. The difference in $\Delta V^{\neq}(k)$ found for **2** and $Co(NH_3)_5Cl^{2+}$ probably reflects the rigidity of the tetrapodal ligand L, which makes the

formation of a five-coordinate intermediate very unfavorable and hinders the dissociation of the intermediate amide complex according to Equation 8b.

Conclusions Concerning the D_{cb} Mechanism

There has been a lot of controversy as to whether deprotonation in the step of Equation 8a, leading to the conjugate base, occurs at the most acidic amino proton. ^{1}H-NMR studies provided strong evidence that this is not necessarily so.[12,23] It was therefore repeatedly concluded that the differences in the rate of base hydrolysis are mainly governed by the lability of the conjugate base rather than by differences in proton labilities of the parent complex. Questions of this sort need not to be considered for **2**, where the *trans* position is occupied by a 2,6-disubstituted pyridine. Deprotonation can thus occur only at one of the four equivalent amino groups *cis* to the leaving chloride ion.

It is well established that the lability of the amido conjugate base depends significantly on the constraints imposed by the geometry and structure of the ligand(s):

1) A meridional or "flat" secondary nitrogen atom (such as the central nitrogen atom in the ligand dien), *cis* to the leaving group, leads to high base hydrolysis rates. In the case of facial coordination (resulting in a "bent" secondary nitrogen atom), hydrolysis occurs at a notably lower rate.[21]
2) Five-membered chelate rings on either side of a "flat" nitrogen atom favor rapid hydrolysis, especially in the presence of additional six-membered chelate rings.[21]
3) A pyridine ligand *cis* to the leaving group increases the rate of base hydrolysis markedly.[10,11]
4) The geometry and structure of the chelating ligand determine how readily the complex will form a five-coordinate amide intermediate of trigonal bipyramidal geometry, which is considered to be the most favorable geometry.[12,21]

When the first two of these conditions are fulfilled, base hydrolysis can indeed be extraordinarily fast, as in the case of the complex cation Co(tmd)(dien)Cl^{2+}, which has a secondary "flat" nitrogen atom *cis* to the chloride ligand as well as five-membered chelate rings on either side (k_{OH} = $5\cdot10^5$ $M^{-1}s^{-1}$; see Table 3). When the ligand dien in this complex is coordinated facially, with the secondary "bent" nitrogen atom *trans* to chloride, the reaction rate constant is reduced to k_{OH} = 10.6 $M^{-1}s^{-1}$.

According to the four requirements mentioned above, base hydrolysis of complex **2** is expected to be slow, because (i) there are no secondary NH protons at all, (ii) the pyridine ligand is not *cis* to the leaving group, and (iii) the rigid ligand L does not favor the formation of an intermediate of trigonal bipyramidal geometry.

It is interesting to note that base hydrolysis of the complex *t*-Co(tren)$(NH_3)Cl^{2+}$ is also especially slow (k_{OH} = 0.02 $M^{-1}s^{-1}$; see Table 3). The ligand tren in this complex is a tripodal ligand of the type $N(NH_2)_3$ with its tertiary nitrogen donor coordinated *trans* to chloride, whereas in **2** the ligand **L** is tetrapodal and of the type $N(NH_2)_4$. One may argue, therefore, that it is the tripod or tetrapod structural element that causes reduced flexibility and, as a consequence, low base hydrolysis rates. The comparison of the complexes $Co(NH_3)_5Cl^{2+}$ and **2** shows, however, that this argument is of limited value. Both complexes show similarly low base hydrolysis rates and have virtually the same values of $\Delta H^{\neq}$ and $\Delta S^{\neq}$ (see Table 3), while the difference in ligand flexibility could not possibly be greater. Compared to **2**, $Co(NH_3)_5Cl^{2+}$ should easily form the trigonal bipyramidal amide conjugate base. Still, base hydrolysis is practically as slow as in the case of **2**. This may suggest that the rate at which cobalt(III) complexes of the type Co'N_5'Cl^{2+} follow the D_{cb} mechanism will also be affected by the symmetry of the species Co'N_5'Cl^{2+}. In contrast to most of the other complexes listed in Table 3, both $Co(NH_3)_5Cl^{2+}$ and **2** are highly symmetrical in the ground state and deprotonation reduces this high degree of symmetry substantially.

A pseudo-base mechanism has been discussed to account for the rate enhancement which is observed when a pyridine ligand is coordinated *cis* to the leaving group, but there is little experimental evidence to substantiate this assumption.[12,29] A pyridine ligand *trans* to the leaving group is a structural element which had so far been lacking in the chemistry of Co'N_5'Cl^{2+} complexes, despite a number of attempted syntheses.[11,12] The present results clearly prove that a *trans*-coordinated pyridine ligand does not have any significant labilizing effect on the leaving group, and reinforce the analogy between the tetrapodal pentadentate ligand L and the classical pentaammine donor set.

Experimental Section

$AgClO_4$ and $NaClO_4 \cdot H_2O$ (Fluka; reagent grade) were used without further purification. (***CAUTION:*** Perchlorate salts are potentially explosive; they should be handled with caution and in small quantities only!). [CoLCl]$Cl(ClO_4) \cdot H_2O$ was prepared as described.[2] Deionized water was doubly distilled in a quartz apparatus before use.

[CoL(OH)]$(ClO_4)_2$ (4): In non-basic aqueous solution, the removal of coordinated chloride from [CoLCl]$Cl(ClO_4) \cdot H_2O$ by addition of two equivalents of $AgClO_4$ and heating to 80°C for 1 h was not complete. Complex **4** was therefore prepared by keeping a basic aqueous solution of [CoLCl]$Cl(ClO_4) \cdot H_2O$ (110 mg, 0.22 mmol, 10 mL 0.3 M NaOH, pH = 13−14) at 80°C for 1 h. The solution was neutralized with $HClO_4$ (pH = 6−8), and 2 equivalents of $AgClO_4$ were added to remove chloride by precipitation of AgCl, which was separated by filtration. Addition of one equivalent of $NaClO_4 \cdot H_2O$ to the filtrate induced crystallization. Within a few days, **4** separated from solution in the form of orange-red crystals, suitable for X-ray structure analysis (88 mg, 76% yield). − ^{1}H NMR ([D$_6$]DMSO, r.t.): δ = 8.21 [t, ^3J(HH) = 7.9 Hz, 1 H, H^4], 7.73 [d, ^3J(HH) = 7.9 Hz, 2 H, H^{3,5}], 4.70 (m, br., N*H*H), 4.52 (m, br., NH*H*), 2.67 (m, C*H*HNH$_2$, 4 H), 2.26 (m, CH*H*NH$_2$, 4 H), 1.47 (s, 6 H, CH_3), −2.60 [s (br.), $W_{1/2}$ = 7.1 Hz, OH]. − ^{13}C NMR ([D$_6$]DMSO, r.t.): δ = 165.32 (s, C2/6), 140.46 (s, C4), 120.48 (s, C3/5), 46.51 (s, >C<), 44.83 (m, 3 lines, J = 7.8 Hz, CH_2), 21.17 (s, CH_3). − MS (FAB$^+$); *m/z* (relative intensity): 409 (48) [M − OH + ClO_4], 79 (100), C_5H_5N. − MS (ESI$^+$): 326 (100) [M − H], 308 (76) [M − H_2O − H], correct isotope patterns in both cases.

− IR (KBr): $\tilde{\nu}$ = 3578 cm^{-1} (m), 3294 (s), 2972 (m), 1610 (m), 1471 (m), 1093 (vs), 624 (m). − $C_{13}H_{26}Cl_2CoN_5O_9$ (526.22): calcd. C 29.67, H 4.98, N 13.31; found C 29.42, H 4.95, N 13.18.

Instrumentation: UV/Vis spectra, diode array spectrophotometer (Zeiss Specord S10); NMR spectra, FT-NMR spectrometer (JEOL JNM-EX 270); mass spectra, Micromass ZabSpecE spectrometer; IR spectra, FT-IR spectrometer (Nicolet, Impact 400); pH measurements, glass electrode (Schott) in combination with a potentiometer (Metrohm 691), calibrated at I = 0.1 M ($NaNO_3$) and 25°C to yield $-\log[H^+]$ = pH − 0.09; kinetics of base hydrolysis, multi-wavelength stopped-flow spectrophotometer[30] and stopped-flow spectrophotometer in combination with a high-pressure cell.[31]

Spectrophotometric Titration: The acid dissociation constant K_a of **3** according to Equation 4 was determined by spectrophotometric titration of an acid solution of **3** with 0.1 M NaOH. Least-squares fitting of Equation 5 to the (absorbance, $[H^+]$) data led to K_a (A_{H2O} and A_{OH} refer to the absorbance of **3** and **4**, respectively, at the concentration of $[Co]_{tot}$).

Kinetic Measurements: Base hydrolysis of **2** according to Equation 3 in freshly prepared solutions of $[CoLCl]Cl(ClO)_4 \cdot H_2O$ in water was followed by stopped-flow spectrophotometry in the wavelength range 300−600 nm under pseudo-first-order conditions ($[OH^-]$ >> $[complex]_o$) at variable temperature (285−318 K) and variable pressure (10−150 MPa). The reactions were followed for t = 6−8 half-lives. Monitoring at high pressure was done at 480 nm. The ionic strength was set to I = 0.1 M or 1.0 M ($NaClO_4$ or $NaNO_3$). Least-squares fitting of the (absorbance, time) data with Equation 6 led to the experimental rate constant k_{obsd}. The volume of activation was obtained from the pressure dependence of k_{obsd} according to Equation 12. A correction for the pressure dependence of the activity coefficients (less than 0.6 cm^3 mol^{-1} under the given conditions[32]) was not applied.

$$\Delta V^{\neq}_{exptl} = -RT\,(\partial \ln k_{obsd}/\partial P)_T \qquad (12)$$

Crystallography: The crystal of **3** (orange-red platelet, 0.45 × 0.40 × 0.17 mm) was grown as stated above. The measurement was made with a four-circle diffractometer (Stoe-Stadi-4) using graphite-monochromatized Mo-K_α radiation (λ = 0.71069 Å); scan 2θ/ω = 1:1). Cell constants were determined by the least-squares method from the 2θ angles of 50 reflections. The structure was solved by direct methods with SHELXS-86 and refined by least squares to the R values given in Table 5 using the program package SHELXL-93. The non-hydrogen atoms were refined anisotropically. All hydrogen atoms, including that in the hydroxo ligand, were located in the difference Fourier map. The hydrogen atom positions and a uniform isotropic displacement parameter were kept fixed during refinement. An empirical absorption correction was applied (T_{min} = 0.693/T_{max} = 0.799). The residual electron density was +0.624/−0.409 e $Å^{-3}$. Crystal data and data collection parameters are listed in Table 5, and selected distances and angles are given in Table 2. Crystallographic data (excluding structure factors) for the structure reported in this paper have been deposited with the Cambridge Crystallographic Data Centre as supplementary publication no. CCDC-103018. Copies of the data can be obtained free of charge on application to CCDC, 12 Union Road, Cambridge CB2 1EZ, UK [Fax: int. code + 44-1223/336-033; E-mail: deposit@ccdc.cam.ac.uk].

Table 5. Crystallographic data for $[CoL(OH)](ClO_4)_2$ (**4**)

Empirical formula		$C_{13}H_{26}Cl_2CoN_5O_9$	
Formula mass		526.22	
a	16.841(6) Å	space group	$C2/m$ (no. 12)
b	8.541(3) Å	T	299(2) K
c	15.112(5) Å	λ	0.71069 Å
β	109.13(1)°	μ	1.153 mm^{-1}
V	2053.7(12) $Å^3$	$R1$[a] [$I > 2\sigma(I)$]	0.0352
Z	4	$wR2$[b]	0.1070
$D_{calcd.}$	1.702 g cm^3		

[a] $R1 = \Sigma||F_o| - |F_c||/\Sigma|F_o|$. − [b] $wR_2 = \{\Sigma[w(F_o^2 - F_c^2)^2]/\Sigma[w(F_o^2)^2]\}^{1/2}$, where $w = 1/[\sigma^2(F_o^2) + 0.0627\,P^2 + 1.845\,P]$ and $P = (F_o^2 + 2\,F_c^2)/3$.

Acknowledgments

Sponsorship of this work by the Deutsche Forschungsgemeinschaft, the Verband der Chemischen Industrie and the Otto-Röhm-Stiftung is gratefully acknowledged. The authors appreciate the cooperation with Stefan Schmidt (preparation of the chloro complex), Carlos Dücker-Benfer (high-pressure stopped-flow experiments), Frank W. Heinemann (refinement of the X-ray data) and W. Donaubauer (measurement of the mass spectra).

[1] C.-H. Lee, B. Garcia, T. C. Bruice, *J. Am. Chem. Soc.* **1990**, *112*, 6434.
[2] A. Grohmann, F. Knoch, *Inorg. Chem.* **1996**, *35*, 7932.
[3] M. E. de Vries, R. M. La Crois, G. Roelfes, H. Kooijman, A. L. Spek, R. Hage, B. L. Feringa, *J. Chem. Soc., Chem. Commun.* **1997**, 1549.
[4] C. Dietz, S. Schmidt, F. W. Heinemann, A. Grohmann in *Selective Reactions of Metal-Activated Molecules* (Eds.: H. Werner, P. Schreier), Vieweg, Braunschweig, **1998**, p. 217.
[5] C. Dietz, F. W. Heinemann, J. Kuhnigk, C. Krüger, M. Gerdan, A. X. Trautwein, A. Grohmann, *Eur. J. Inorg. Chem.* **1998**, 1041.
[6] A. Grohmann, F. W. Heinemann, P. Kofod, *Inorg. Chim. Acta*, in press.
[7] For an elegant recent study of (cyclen)cobalt(III) complexes, see: D. A. Buckingham, C. R. Clark, A. J. Rogers, J. Simpson, *Inorg. Chem.* **1998**, *37*, 3497.
[8] M. L. Tobe, *Adv. Inorg. Bioinorg. Mech.* **1983**, *2*, 1.
[9] An authoritative, brief summary of the arguments leading to the establishment of the conjugate base mechanism may be found in: R. G. Wilkins, *Kinetics and Mechanism of Reactions of Transition Metal Complexes*, VCH, Weinheim, **1991**, p. 215.
[10] J. McKenzie, D. A. House, *J. Inorg. Nucl. Chem.* **1977**, *39*, 1843.
[11] B. R. Cameron, D. A. House, A. McAuley, *J. Chem. Soc., Dalton Trans.* **1993**, 1019.
[12] E. Ahmed, C. Chatterjee, C. J. Cooksey, M. L. Tobe, G. Williams, M. Humanes, *J. Chem. Soc., Dalton Trans.* **1989**, 645.
[13] J. Burgess, *Metal Ions in Solution*, Wiley, Chichester, **1978,** p. 271.
[14] [14a] A. Looney, R. Han, K. McNeill, G. Parkin, *J. Am. Chem. Soc.* **1993**, *115*, 4690. − [14b] R. Alsfasser, M. Ruf, S. Trofimenko, H. Vahrenkamp, *Chem. Ber.* **1993**, *126*, 703.
[15] H.-O. Kalinowski, S. Berger, S. Braun, *13*C-NMR-Spektroskopie, Thieme, Stuttgart, **1984**, p. 512.
[16] G. Socrates, *Infrared Characteristic Group Frequencies*, Wiley, Chichester, **1994**, p. 223.
[17] A recent search of the Cambridge Crystallographic Data Base for terminal Co^{III}−OH complexes produced 2 hits:
[17a] A. Bigotto, E. Zangrando, L. Randaccio, *J. Chem. Soc. Dalton Trans.* **1976**, 96. − [17b] E. S. Kucharski, B. W. Skelton, A. H.

White, *Aust. J. Chem.* **1978**, *31*, 47.
[18] J. D. Atwood, *Inorganic and Organometallic Reaction Mechanisms*, VCH, New York, **1996**, p. 48.
[19] A. Bondi, *J. Phys. Chem.* **1964**, *68*, 441.
[20] The kinetic data shown in Figure 4 are based on experiments in which $I = 0.1$ M was adjusted with $NaClO_4$ and $I = 1.0$ M with $NaNO_3$, due to limited solubility of the cobalt complex in 1 M $NaClO_4$. It was shown, however, that there is no spectrophotometrically detectable interaction between 1 M $NaNO_3$, and $CoLCl^{2+}$ and $CoLOH^{2+}$ respectively.
[21] R. Henderson, M. L. Tobe, *Inorg.Chem.* **1977**, *16*, 2576.
[22] W. G. Jackson, B. C. McGregor, S. S. Jurrison, *Inorg. Chem.* **1990**, *29*, 4677.
[23] P. Comba, W. G. Jackson, W. Marty, L. Zipper, *Helv. Chim. Acta* **1992**, *75*, 1147.
[24] Y. Kitamura, G. A. Lawrance, R. van Eldik, *Inorg. Chem.* **1989**, *28*, 333.
[25] L. S. Dong, D. A. House, *Inorg. Chim. Acta* **1976**, *19*, 23.
[26] J. O. Edwards, F. Monacelli, G. Ortaggi, *Inorg. Chim. Acta* **1974**, *11*, 47.
[27] Y. Kitamura, R. van Eldik, *Ber. Bunsenges. Chem.* **1984**, *88*, 418.
[28] [28a] Y. Kitamura, R. van Eldik, H. Kelm, *Inorg. Chem.* **1984**, *23*, 2038. – [28b] A. Drljaca, C. D. Hubbard, R. van Eldik, T. Asano, M. V. Basilevsky, W. J. le Noble, *Chem. Rev.* **1998**, *98*, 2167.
[29] D. A. House, P. R. Norman, R. W. Hay, *Inorg. Chim Acta* **1980**, *45*, L117.
[30] H. Elias, F. Sattler, K. J. Wannowius, *GIT Fachz. Lab.* **1985**, *29*, 1138.
[31] R. van Eldik, W. Gaede, S. Wieland, J. Kraft, M. Spitzer, D. A. Palmer, *Rev. Sci. Instrum.* **1993**, *64*, 1355.
[32] R. van Eldik, Y. Kitamura, C. P. Piriz Mac-Coll, *Inorg. Chem.* **1986**, *25*, 4252.
[33] R. G. Pearson, R. E. Meeker, F. Basolo, *J. Am. Chem. Soc.* **1956**, *78*, 709.
[34] D. A. Buckingham, P. J. Cresswell, A. M. Sargeson, *Inorg. Chem.* **1975**, *14*, 1485.

Received September 18, 1998
[I98316]

Hindered Ligand Movements in Transition-Metal Complexes, 46[+]

Facile Hapticity Changes in (1-Hydronaphthalene)manganese Complexes, Ligand Addition and Photochemical Ligand Cleavage

Andreas Georg[a] and Cornelius G. Kreiter*[a]

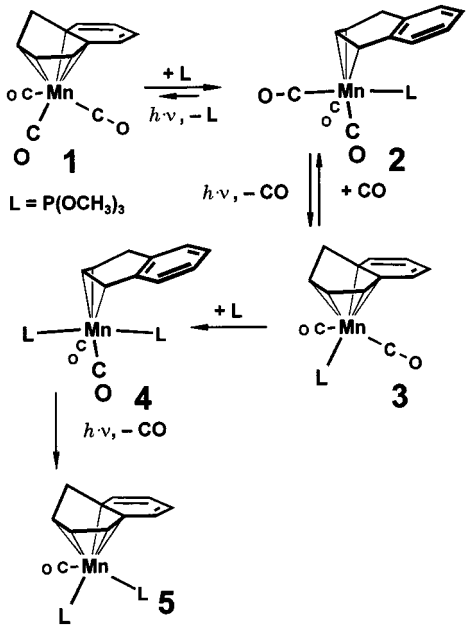
Keywords: Manganese / Coordination modes / 1-Hydronaphthalene complexes / Trimethylphosphite addition / Photochemistry

Tricarbonyl(2–4,4a,8a-η-1-hydronaphthalene)manganese (**1**) reacts readily with trimethyl phosphite to afford tricarbonyl(2–4-η-1-hydronaphthalene)(trimethyl phosphite)-manganese (**2**), by a simultaneous η^5-η^3-hapticity change. Upon UV irradiation, one carbonyl ligand is preferentially cleaved from **2** to yield dicarbonyl(2–4,4a,8a-η-1-hydronaphthalene)(trimethyl phosphite)manganese (**3**), with a η^5-coordinated 1-hydronaphthalene ligand. In a similar fashion **3** also reacts with trimethyl phosphite and forms dicarbonyl(2–4-η-1-hydronaphthalene)bis(trimethyl phosphite)manganese (**4**), which loses carbon monoxide upon UV irradiation to afford carbonyl(2–4,4a,8a-η-1-hydronaphthalene)bis(trimethyl phosphite)manganese (**5**). All compounds were characterized by IR and NMR spectroscopy. The η^5-1-hydronaphthalene complexes **1**, **3** and **5** show hindered 1,4-H shifts of 1-H^{endo}. Considerable energy barriers were also found for the rotation of the 1-hydronaphthalene ligand in **2**–**5**.

Recently, the authors reported the formation of an η^5-1-hydronaphthalene manganese complex as a byproduct of the photochemical reaction of pentacarbonyl(μ-$\eta^{4:6}$-1,4-dimethylnaphthalene)dimanganese with 2-butyne.[2][3] Meanwhile it was found[4] that 1-hydronaphthalene complexes are also formed in high yields by the treatment of cationic tricarbonyl(η^6-naphthalene)manganese complexes[5] with $Li[BEt_3H]$. An analogous behaviour was already known in the case of the corresponding reaction of cationic (η^6-benzene)tricarbonylmanganese complexes.[6–11] In this work the reaction of tricarbonyl(2,3,4,4a,8a-η-1-hydronaphthalene)manganese (**1**) with potential ligands, such as trimethyl phosphite, has been studied in order to learn how the partially weakly coordinated 1-hydronaphthalene ligand influences the reactivity. Even at 203 K **1** adds one equiv. of trimethyl phosphite within seconds to form tricarbonyl(2−4-η-1-hydronaphthalene)(trimethyl phosphite)-manganese (**2**).

The reaction can be carried out in coordinating solvents such as THF or ether, as well as in non-polar hydrocarbon solvents such as *n*-hexane or *n*-pentane. Simultaneously with the coordination of trimethyl phosphite, the C4a−C8a bond is decomplexed and the hapticity of the 1-hydronaphthalene ligand changes from η^5 to η^3.

The π or side-on bonding of unsaturated hydrocarbons to transition metals is described according to the Dewar−Chatt−Duncanson model[12][13] with a so called σ-donor and π-acceptor part. In Lewis formulas of π complexes the interaction between the π system of an unsaturated hydrocarbon and the metal center is normally characterized by an arrow or a (dotted) line from double bonds, circles or circular arches, which symbolize the π system, to the metal center. An alternative formalism, which seems to us more meaningful, uses thin lines between the coordinated carbon atoms and the metal center. It is justified by the bonding model in which each coordinated sp^2-carbon atom donates one electron to the metal center, which then contributes the same number of electrons for back donation. The thin lines in our formulae mark bonding interactions between carbon and metal atoms and do not symbolize localised σ bonds.



Scheme 1

Photolysis of **2** in hexane or THF at room temp. yields 78% of dicarbonyl(2−4,4a,8a-η-1-hydronaphthalene)(trimethyl phosphite)manganese (**3**), in addition to 8% of **1**.

[+] Part 45: Ref.[1]

[a] Fachbereich Chemie der Universität Kaiserslautern, Erwin-Schrödinger-Straße, D-67663 Kaiserslautern, Germany

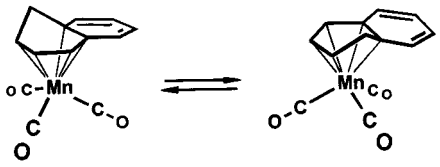
 © WILEY-VCH Verlag GmbH, D-69451 Weinheim, 1999 1434−1948/99/0404−0651 $ 17.50+.50/0

The main reaction is the photochemical cleavage of one carbonyl ligand and the recoordination of the C4a−C8a bond, to afford complex **3**. Byproduct **1** is formed in a back reaction of the addition of trimethyl phosphite to **1**.

The reaction of **3** with CO effects the quantitative back reaction to **2** with decomplexation of the C4a−C8a bond. Treatment of **3** in ether with trimethyl phosphite yields dicarbonyl(2−4-η-1-hydronaphthalene)bis(trimethyl phosphite)manganese (**4**). Due to the steric bulk of the two trimethyl phosphite ligands, this bright yellow complex is only stable at temperatures below 268 K.

By photolysis of **4** one CO ligand is cleaved. The C4a−C8a bond is coordinated again to form the dark red carbonyl(2−4,4a,8a-η-1-hydronaphthalene)bis(trimethyl phosphite)manganese (**5**).

For the η^5-1-hydronaphthalene complexes **1**, **3** and **5** hindered 1,4-H shifts of 1-H^{endo} are observed in the temperature-dependent ^{1}H-NMR spectra. The activation parameters were determined by line-shape analysis (**1**: $\Delta H^{\neq}$ = 78.6 kJ·mol^{-1}, $\Delta S^{\neq}$ = 14.9 J·mol^{-1}·K^{-1}; **3**: $\Delta H^{\neq}$ = 66.7 kJ·mol^{-1}, $\Delta S^{\neq}$ = 0.1 J·mol^{-1}·K^{-1}; **5**: $\Delta H^{\neq}$ = 43.7 kJ·mol^{-1}, $\Delta S^{\neq}$ = 26.9 J·mol^{-1}·K^{-1} with maximum errors of ± 3 kJ·mol^{-1}, and ± 20 J·mol^{-1}·K^{-1}, respectively).



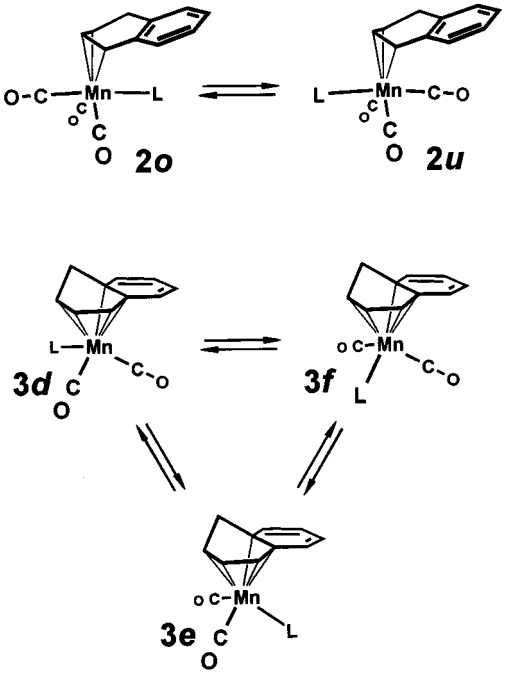
Scheme 2

The low-temperature ^{1}H- and ^{31}P-NMR spectra of **2** show the presence of two isomers with populations of 81:19. They differ due to the position of the trimethyl phosphite ligand in the pseudo-trigonal-bipyramidal coordination sphere of manganese. In [Mn(η^3-enyl)L(CO)$_3$] complexes donor ligands occupy exclusively axial positions from which the *o*-position relative to the enyl ligand is normally more favoured than the *u*-position. In case of sterically demanding enyl ligands the preference of the isomers is inverted. For the η^3-1-hydronaphthalene ligand such a sterical hindrance has to be expected as the trimethyl phosphite ligand is in the *o*-position. For that reason we assign the predominant isomer to ***2u***, and the other to ***2o***, with the trimethyl phosphite close to C-8a of the aromatic ring. In the predominant isomer the trimethyl phosphite shows no sterical interaction with the 1-hydronaphthalene ligand. This assignment is supported by a $^3J_{H,P}$ coupling of 3-H of 15.5 Hz in ***2u***. The isomer ***2o*** shows only a small, unresolved H,P coupling of 3-H. The interconversion of ***2u*** and ***2o*** affords an activation energy of $\Delta H^{\neq}$ = 65.0 kJ·mol^{-1} with $\Delta S^{\neq}$ = 36.0 J·mol^{-1}·K^{-1}.

A comparable ligand movement is found for **4**. The two trimethyl phosphite ligands both occupy axial positions. At 183 K the rotation of the η^3-1-hydronaphthalene ligand is slowed down and two ^{31}P-NMR signals appear. The activation energy was determined to be $\Delta H^{\neq}$ = 51.1 kJ mol^{-1}, $\Delta S^{\neq}$ = 15.5 J K^{-1} mol^{-1}.

The η^5-1-hydronaphthalene complexes **3** and **5** also show a hindered rotation. The ^{31}P-NMR of **3** shows an intense signal at 183 K which is assigned to the less hindered isomer ***3d*** (0.92), a weaker signal is assigned to ***3f*** (0.08). Although a separate signal for the third, strongly hindered isomer is not observed, it can not be excluded with certainty. The activation parameters for the ***3d***/***3f*** isomerization were found to be $\Delta H^{\neq}$ = 47.7 kJ mol^{-1} and $\Delta S^{\neq}$ = 21.0 J K^{-1} mol^{-1}. For **5** all three possible isomers give separate ^{31}P-NMR signals, from which the relative populations 0.89:0.06:0.05 are determined. They were assigned according to the sterical interactions between the trimethyl phosphite ligands and the 1-hydronaphthalene. The activation parameters for the isomerization are $\Delta H^{\geq}$ = 37.6 kJ mol^{-1} and $\Delta S^{\geq}$ = −37.0 J K^{-1} mol^{-1}.

A similar hindered H-shift and ligand rotation was already detected for dicarbonyl($\eta^{4:(2)}$-1,5-*H*-benzocycloheptene)(trimethyl phosphite)chromium(0).[14]



Scheme 3

Experimental Section

All reactions were carried out under dry nitrogen using common Schlenk techniques. THF was dried with potassium, diethyl ether with sodium, *n*-pentane with P_4O_{10} and *n*-hexane with CaH_2. Silica gel for column chromatography was heated to 413 K in vacuo, deactivated with 4% of degassed water and stored under nitrogen. A high-pressure mercury lamp TQ 150 (Heraeus-Noblelight, Kleinostheim) was used for the photolysis reaction. It was immersed in a 120-mL photoreactor of Duran® with a cooling jacket, wrapped with aluminium foil. The photoreactor and the chromatography column were cooled with a cryostat RUL 80 (Lauda), with methanol as the coolant. − IR: Perkin Elmer FT-IR 16 PC. − NMR: Bruker AMX 400 (^{1}H, 400.13 MHz, ^{13}C, 100.62 MHz, ^{31}P, 162.12 MHz), ^{1}H and ^{13}C chemical shifts are given relative to TMS, using

the solvent signals as internal reference ($C_6D_5CHD_2$: δ_H = 2.03, $C_6D_5CD_3$: δ_C = 20.40 , C_6HD_5: δ_H = 7.20, C_6D_6: δ_C = 128), ^{31}P chemical shifts are relative to external 85% phosphorous acid. − Elemental analyses: Perkin Elmer microanalyser 240. − Tricarbonyl(2−4,4a,8a-η-1-hydronaphthalene)manganese (**1**) was synthesized according to the literature[4] using $Li[BEt_3H]$ instead of $Na[BH_3CN]$ as the reducing agent. The activation parameters for the hindered 1,4-H shift of 1-H^{endo} in **1** were determined from the temperature dependence of the ^{1}H-NMR signals of 1-H−4-H; *T* [K], *k* [s^{-1}]: 328, 2; 348, 15; 358, 40; 368, 70; 378, 100. The trimethyl phosphite (Fluka) was used as purchased.

Tricarbonyl(2−4-η-1-hydronaphthalene)(trimethyl phosphite)manganese (2): 175 mg (0.66 mmol) of tricarbonyl(2−4,4a,8a-η-1-hydronaphthalene)manganese (**1**) was dissolved in THF (20 mL). When 0.1 mL (0.85 mmol) of trimethyl phosphite was added dropwise to the orange-red solution the color changed immediately to bright yellow. After 2 min of stirring, $MgSO_4$ (2 g) was added to the solution and the solvent removed in vacuo. Chromatography of the residue on a column packed with silica gel gave two fractions. An orange fraction was eluted with hexane/diethyl ether (50:1). It contained only a small amount of the starting material. **2** was eluted as a bright yellow fraction with *n*-hexane/diethyl ether (20:1). Removal of the solvent and crystallization from *n*-hexane at 243 K gave 158 mg (62%) of **2** as yellow crystals. − IR (*n*-hexane): $\tilde{\nu}$ = 2010 (s) cm^{-1} (CO), 1950 (s), 1944 (sh), 1918 (sh), 1911 (s). The shoulders of the ν_{CO} bands are probably due to the rotamer **2o**. − ^{1}H NMR ([D$_8$]toluene, 333 K): δ = 6.85 (dd, *J* = 7.3, 0.9 Hz, 1 H, 5-H), 6.78 (dd, *J* = 7.3, 6.8 Hz, 1 H, 6-H), 6.70 (ddd, *J* = 7.3, 6.8, 1.3 Hz, 1 H, 7-H), 6.55 (d, 7.3 Hz, 1 H, 8-H), 4.73 (ddd, *J* = 9.5, 6.8, 5.8 Hz, 1 H, 3-H,), 4.15 (d, *J* = 5.8 Hz, 1 H, 4-H), 4.05 (dddd, *J* = 6.8, 4.9, 1.6, 1.6 Hz, 1 H, 2-H), 3.31 (dd, *J* = 21.1, 4.9 Hz, 1 H, 1-H^{endo}), 3.17 [d, *J* = 11.2 Hz, 9 H, $P(OCH_3)_3$], 3.17 (d, *J* = 21.1 Hz, 1 H, 1-H^{exo}) . − ^{1}H NMR ([D$_8$]toluene, 233 K): **2*u*** (81%): δ = 6.90 (d, *J* = 7.5 Hz, 1 H, 5-H), 6.83 (dd, *J* = 7.5, 6.8 Hz, 1 H, 6-H), 6.77 (dd, *J* = 7.3, 6.8 Hz, 1 H, 7-H), 6.60 (d, 7.3 Hz, 1 H, 8-H), 4.76 (ddd, *J* = 15.5, 6.7, 6.1 Hz, 1 H, 3-H,), 4.27 (d, *J* = 6.1 Hz, 1 H, 4-H), 4.02 (br. m, 1 H, 2-H), 3.31 (dd, *J* = 21.8, 7.4 Hz, 1 H, 1-H^{endo}), 3.17 (d, *J* = 21.8 Hz, 1 H, 1-H^{exo}), 3.05 [d, *J* = 10.7 Hz, 9 H, $P(OCH_3)_3$]; **2*o*** (19%): δ = 6.72 (dd, *J* = 6.9, 6.9 Hz, 1 H, 6-H), 6.58 (dd, *J* = 6.9, 6.9 Hz, 1 H, 7-H), 6.52 (d, *J* = 7.1 Hz, 1 H, 8-H), 4.65 (br. dd, *J* = 6.6, 5.6 Hz, 1 H, 3-H), 4.16 (d, *J* = 5.6 Hz, 1 H, 4-H), 3.14 [d, *J* = 10.1 Hz, 9 H, $P(OCH_3)_3$]. − The activation parameters for the hindered interconversion of **2*u*** and **2*o*** were determined from the temperature dependence of the ^{1}H-NMR signals of 3-H of both isomers; *T* [K], *k* [s^{-1}]: 233, 1; 243, 5; 253, 15; 273, 100; 283, 500; 293, 1000; 313, 10000; 333, 30000. − ^{13}C NMR ([D$_8$]toluene, 293 K): δ = 225 (s, 3 C, CO), 143.10 (s, C-4a), 129.01 (s, C-8a), 127.77 (d, *J* = 153 Hz, C-5), 126.54 (d, *J* = 158 Hz, C-6), 125.65 (d, *J* = 158 Hz, C-8), 125.09 (d, *J* = 145 Hz, C-7), 83.84 (d, *J* = 168 Hz, C-3), 61.81 (d, *J* = 180 Hz, C-4 or -2), 59.91 (br. d, *J* = 160 Hz, C-2 or -4), 51.96 (dq, $^1J_{C,H}$ = 147, $^2J_{C,P}$ = 5 Hz, O*C*H$_3$), 34.32 (t, *J* = 127 Hz, C-1) . − ^{31}P NMR ([D$_8$]toluene, 233 K): δ = 194.4 (s, 0.81 P), 185.4 (s, 0.19 P). − $C_{16}H_{18}MnO_6P$ (392.23): calcd. C 49.00, H 4.63; found C 48.9, H 4.4.

Photoreaction of Tricarbonyl(2−4-η-1-hydronaphthalene)(trimethyl phosphite)manganese (2): 106 mg (0.27 mmol) of **2** was dissolved in 100 mL of *n*-hexane in a photoreactor. The yellow solution was irradiated with UV light at room temp. After 10 min, the carbon monoxide bands of **2** had disappeared and the color of the solution turned to orange. The irradiation was stopped, 2 g of $MgSO_4$ added and the solvent removed in vacuo. The orange residue was separated into three fractions by column chromatography on silica gel at 253 K. A bright yellow fraction was obtained with *n*-pentane/toluene (10:1) as eluent. It contained 6 mg (0.02 mmol, 8%) of **1**. The second fraction was eluted with *n*-pentane/diethyl ether (20:1) from which 73 mg (0.21 mmol) of dicarbonyl(2−4,4a,8a-η-1-hydronaphthalene)(trimethyl phosphite)manganese (**3**) was obtained (78%). − IR (*n*-hexane): $\tilde{\nu}$ = 1947 (s) cm^{-1} (CO), 1889 (s). − ^{1}H NMR ([D$_8$]toluene, 293 K): δ = 7.03 (d, *J* = 7.3 Hz, 1 H, 5-H), 6.78 (dd, *J* = 7.5, 7.3 Hz, 1 H, 6-H), 6.72 (d, *J* = 8.2 Hz, 1 H, 8-H), 6.64 (dd, *J* = 8.2, 7.5 Hz, 1 H, 7-H), 5.93 (d, *J* = 5.0 Hz, 1 H, 4-H), 4.85 (ddd, *J* = 5.0, 5.5, 7.0 Hz, 1 H, 3-H), 3.2 [d, *J* = 11.4 Hz, 9 H, $P(OCH_3)_3$], 3.13 (dd, *J* = 13.6, 5.6 Hz, 1 H, 1-H^{endo}), 2.83 (ddd, *J* = 5.8, 5.5, 2.7 Hz, 1 H, 2-H), 2.50 (dd, *J* = 13.6, 2.7 Hz, 1 H, 1-H^{exo}) . − The activation parameters for the hindered 1,4-H shift of 1-H^{endo} in **3** were determined from the temperature dependence of the ^{1}H-NMR signals of 1-H−4-H; *T* [K], *k* [s^{-1}]: 303, 20; 313, 50; 323, 100; 343, 500; 353, 1000. − ^{13}C NMR ([D$_8$]toluene, 293 K): δ = 232.1 (s, CO), 224.5 (s, CO), 134.0 (d, *J* = 161 Hz, C-5), 129.9 (d, *J* = 162 Hz, C-6), 128.3 (d, *J* = 169 Hz, C-7), 126.6 (d, *J* = 162 Hz, C-8), 109.3 (s, C-4a), 96.6 (d, *J* = 164 Hz, C-4), 90.7 (s, C-8a), 72.4 (d, *J* = 173 Hz, C-3), 51.2 [dd, $^1J_{C,H}$ = 145, $^3J_{C,P}$ = 4 Hz, $P(OCH_3)_3$], 46.3 (d, *J* = 165 Hz, C-2), 30.6 (t, *J* = 131 Hz, C-1) . − ^{31}P NMR ([D$_8$]toluene, 183 K): **3*d***: δ = 212.3 (s, 0.92 P), **3*f***: δ = 207.4 (s, 0.08 P). − The activation parameters for the hindered isomerization of **3*d*−3*f*** were determined from the temperature dependence of the ^{31}P-NMR signals of **3*d*** and **3*f***; *T* [K], *k* [s^{-1}]: 183, 1; 203, 30; 223, 500; 233, 1000; 253, 10000; 273, 50000. − $C_{15}H_{18}MnO_5P$ (364.22): calcd. C 49.47, H 4.98; found: C 49.2, H 4.9. − A third red fraction could be eluted with diethyl ether. Removal of the solvent yielded less than 1 mg of a red oil. − IR (*n*-pentane, 293 K): $\tilde{\nu}$ = 1970 (m) cm^{-1},1948 (s), 1889 (m), 1868 (vs).

Reaction of Dicarbonyl(2−4,4a,8a-η-1-hydronaphthalene)(trimethyl phosphite)manganese (3) with Carbon Monoxide: 20 mg of dicarbonyl(2−4,4a,8a-η-1-hydronaphthalene)(trimethyl phosphite)manganese (**3**) was dissolved in 50 mL of diethyl ether. While stirring, carbon monoxide was bubbled through the solution for 5 min, then the reaction solution stirred for another 5 min. The original orange-colored solution changed to bright yellow. In the control IR spectra a quantitative reaction of **3** to **2** was observed. ^{1}H-NMR-spectroscopic measurements confirmed this observation.

Reaction of Dicarbonyl(2−4,4a,8a-η-1-hydronaphthalene)(trimethyl phosphite)manganese (3) with Trimethyl Phosphite: 200 mg (0.55 mmol) of dicarbonyl(2−4,4a,8a-η-1-hydronaphthalene)(trimethyl phosphite)manganese (**3**) was dissolved in 20 mL of *n*-hexane at 243 K. With a syringe 0.2 mL of $P(OMe)_3$ was slowly added dropwise to the solution. Within 10 min the color of the reaction solution changed to a lemon yellow. From the IR control spectra it was seen that **3** had reacted to a dicarbonyl complex nearly quantitatively. This was very temperature-sensitive and decomposed in solution even at 268 K. The solution was concentrated in vacuo at 243 K to about 5 mL and stored for 48 h at 198 K. Bright yellow dicarbonyl(2−4-η-1-hydronaphthalene)bis(trimethyl phosphite)-manganese (**4**) separated as a microcrystalline powder. At 233 K the solvent was removed with a pipette and the residue washed with *n*-pentane (5 ×) and cooled to 233 K. The solid was dried for several days at 243 K in high vacuum. − IR (diethyl ether): $\tilde{\nu}$ = 1947 (s) cm^{-1}, 1848 (vs). − ^{1}H NMR ([D$_8$]toluene, 233 K): δ = 6.99 (d, *J* = 8.3 Hz, 1 H, 5-H), 6.92 (d, *J* = 8.1 Hz, 1 H, 8-H), 6.81 (dd, *J* = 8.3, 6.2 Hz, 1 H, 6-H), 6.74 (dd, *J* = 8.1, 6.2 Hz, 1 H, 7-H), 4.97 (dd, *J* = 6.2, 6.0 Hz, 1 H, 3-H), 4.17 (m, 1 H, 4-H), 4.04 (m,

1 H, 2-H), 3.36 (d, J = 12.4 Hz, 1 H, 1-H^{endo}), 3.32 [d, J = 11.0 Hz, 18 H, P(OCH$_3$)$_3$], 3.18 (d, J = 12.4 Hz, 1 H, 1-H^{exo}). − ^{31}P NMR ([D$_8$]toluene, 183 K): δ = 200.45 (s), 198.25 (s). − $C_{18}H_{27}MnO_8P_2$ (488.30): calcd. C 44.28, H 5.57; found C 45.0, H 5.5.

Photolysis of Dicarbonyl(2−4,4a,8a-η-1-hydronaphthalene)bis-(trimethyl phosphite)manganese (5): In a photolysis vessel 100 mg (0.02 mmol) of dicarbonyl(2−4-η-1-hydronaphthalene)bis(trimethyl phosphite)manganese (**4**) was dissolved at 223 K in 120 mL of diethyl ether. The bright yellow solution was irradiated for 60 min with UV light. One CO ligand was cleaved and an orange-colored monocarbonyl complex formed. The crude product was absorbed at 253 K on 2 g of Na_2SO_4 and placed on a column filled with silica gel. First an orange-colored fraction was eluted with *n*-pentane/diethyl ether (25:1) which contained 10 mg of **1**. A red-brown fraction was eluted with *n*-pentane/diethyl ether (10:1) into a precooled Schlenk tube at 253 K. Removal of the solvent in vacuo at the same temp. yielded carbonyl(2−4-η-1-hydronaphthalene)bis-(trimethyl phosphite)manganese (**5**) as a dark, red-brown oil. − IR (*n*-pentane): $\tilde{\nu}$ = 1869 cm^{-1}. − ^{1}H NMR ([D$_8$]toluene, 183 K): δ = 7.26 (br. s, 1 H, 5-H), 6.91 (br. s, 1 H, 6-H), 6.79 (br. s, 1 H, 8-H), 6.65 (br. s, 1 H, 7-H), 5.88 (br. s, 1 H, 4-H), 5.22 (br. s, 1 H, 3-H), 3.38 [m, 18 H, P(OCH$_3$)$_3$], 3.17(br. s, 1 H, 1-H^{endo}), 3.05 (br. s, 1 H, 2-H), 2.62 (br. s, 1 H, 1-H^{exo}). − ^{31}P NMR ([D$_8$]toluene, 183 K): ***5d,f***: δ = 215.3 (d, J = 82 Hz, 0.89 P), 214.1 (d, J = 82 Hz, 0.89 P); ***5d,e***: δ = 206.7 (br. s, 0.06 P), 193.7 (br. s, 0.06 P); ***5e,f***: δ = 201.5 (br. s, 0.05 P), 198.8 (br. s, 0.05 P). − The activation parameters for the hindered isomerization of ***5d,f***, ***5d,e***, ***5e,f*** were determined from the temperature dependence of the ^{31}P-NMR signals of **5*d***, ***5d,e***, and ***5e,f***; T [K], k [s^{-1}]: 183, 1; 233, 150; 273, 1000. − $C_{17}H_{27}MnO_7P_2$ (460.28): calcd. C 44.36, H 5.91; found C 45.4, H 6.1.

Acknowledgments

Financial support from the Fonds der Chemischen Industrie, the Deutsche Forschungsgemeinschaft and the Land Rheinland-Pfalz (Graduate Stipend) are gratefully acknowledged.

[1] S. Özkar, C.G. Kreiter, M. Kotzian, *J. Organomet. Chem.* **1995**, *494*, 115−121.
[2] C. G. Kreiter, A. Georg, G. J. Reiß, *Chem. Ber.* **1997**, *130*, 1197−1200.
[3] S. Sun, C. A. Dullaghan, G. B. Carpenter, A. L. Rieger, P. H. Rieger, D. A. Sweigart, *Angew. Chem.* **1995**, *107*, 2734−2737; *Angew. Chem. Int. Ed. Engl.* **1995**, *34*, 2540−2542.
[4] S. Sun, C. A. Dullaghan, G. B. Carpenter, D. A. Sweigart, S. S. Lee, Y. K. Chung, *Inorg. Chim. Acta* **1997**, *262*, 213−217.
[5] S. Sun, L. K. Yeung, D. A. Sweigart, T.-Y. Lee, S. S. Lee, Y. K. Chung, S. R. Switzer, R. D. Pike, *Organometallics* **1995**, *14*, 2613−2615.
[6] D. Jones, L. Pratt, G. Wilkinson, *J. Chem. Soc.* **1962**, 4458−4462.
[7] P. J. C. Walker, R. J. Mawby, *Inorg. Chim. Acta* **1973**, *7*, 621−625.
[8] P. L. Pauson, J. A. Segal, *J. Chem. Soc., Dalton Trans.* **1975**, 1683−1686.
[9] Y. K. Cung, D. A. Sweigart, N. G. Connelly, J. B. Sheridan, *J. Am. Chem. Soc.* **1985**, *107*, 2388−2393.
[10] D. B. Snyder, S. J. Schauer, D. P. Eyman, J. L. Moler, J. J. Weers, *J. Am. Chem. Soc.* **1993**, *115*, 6718−6729.
[11] K. Woo, P. G. Willard, D. A. Sweigart, N. W. Duffy, B. H. Robinson, J. Simpson, *J. Organomet. Chem.* **1995**, *487*, 111−118.
[12] M. J. S. Dewar, *Bull. Soc. Chim. Fr.* **1951**, *18*, C79.
[13] J. Chatt, L. A. Duncanson, *J. Chem. Soc.* **1953**, 2939.
[14] C. G. Kreiter, G. Michael, J. Kaub, *J. Organomet. Chem.* **1988**, *355*, 149−162.

Received September 18, 1998
[I98317]

Photochemical Reactions of Transition Metal Organyl Complexes with Olefins, 21[+]

Photolysis of Tricarbonyl(η⁵-cyclohexadienyl)manganese in Tetrahydrofuran, Reactions with Cumulated Dienes

Cornelius G. Kreiter,*[a] Norbert K. Wachter,[a] and Guido J. Reiß[a]

Keywords: Manganese complexes / Organyl complexes / C–C coupling / [5+2] Cycloaddition / Cumulenes / Photochemistry

$[Mn(\eta^5\text{-}C_6H_7)(CO)_3]$ (**1**) forms highly reactive $[Mn(\eta^5\text{-}C_6H_7)(CO)_2(THF)]$ (**2**) upon UV irradiation in THF at 208 K. Solvent complex **2** reacts between 208 and 293 K with 1,1-disubstituted allenes C_3H_2RR' [R, R′ = CH_3, CH_3 (**A**); CH_3, C_6H_5 (**B**); C_2H_5, C_6H_5 (**C**); C_6H_5, C_6H_5 (**D**); OCH_3, $Si(CH_3)_3$ (**E**)] to four different types of complexes: The [5+2] cycloadduct $[Mn(\eta^{3:2}\text{-}C_9H_9RR')(CO)_3]$ (**3E**), rearranged [5+2] cycloadducts $[Mn(\eta^{3:2}\text{-}C_9H_9RR')(CO)_3]$ (**4B**, **4C**, **4D**), 1:2 adducts $[Mn(\eta^{3:2}\text{-}C_{12}H_{11}R_2R'_2)(CO)_3]$ (**5A**–**5E**), and the 1:3 adduct $[Mn\{\eta^{3:2:2}\text{-}C_{15}H_{13}(CH_3)_6\}(CO)_2]$ (**6A**). The constitutions of the products were established by IR and NMR spectroscopy, as well as by C,H elemental analysis and mass spectrometry. The crystal and molecular structure of **6A** was determined by X-ray structure analysis. A formation mechanism for the complexes is proposed.

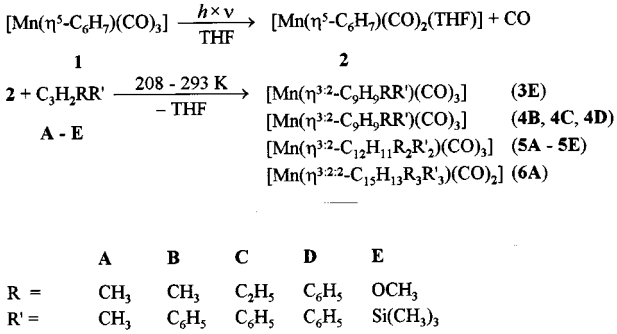
Introduction

Coordination of unsaturated hydrocarbons to transition metals allows pericyclic reactions, that are not allowed for the free hydrocarbons by the Woodward−Hoffmann rules.[2][3] Thus transition-metal-mediated cycloadditions of higher order play an important role in the synthesis of medium-sized carbocyclic and heterocyclic systems. Within the scope of our studies on photochemical reactions of transition metal organyl complexes with olefins we have already reported about light-induced [6+4] cycloadditions of conjugated dienes to tricarbonyl(η⁶-1,3,5-cycloheptatriene)chromium(0)[4−9] and [6+2] cycloadditions of dienes to tricarbonyl(η⁶-cycloocta-1,3,5,7-tetraene)chromium(0).[10]

Further significant advances have been made in recent years.[11−15] The related [6+2] cycloadditions of alkynes to trienes at chromium have also been described by different authors.[16−19] Furthermore we have shown that tricarbonyl(η⁵-pentadienyl)manganese and its derivatives react with conjugated dienes to give tricarbonyl(η$^{3:2}$-cyclonona-2,6-dienyl)manganese complexes in a photochemically induced formal [5+4] cycloaddition.[20−23] Also, photo-assisted cycloadditions of alkynes to η⁵-dienyl ligands have been reported by us[24−28] and others.[29,30] In this respect, the role of cumulenes and heterocumulenes as partners in transition-metal-promoted cycloadditions has so far been described only in a few papers.[31,32] In the following we will discuss our studies upon the reactions of photochemically generated dicarbonyl(η⁵-2,4-cyclohexadienyl)(tetrahydrofuran)manganese (**2**) with selected 1,1-disubstituted cumulenes.

Preparative Results

UV irradiation of tricarbonyl(η⁵-2,4-cyclohexadienyl)-manganese (**1**) at 208 K in THF generates in situ the thermally labile, solvent stabilized dicarbonyl(η⁵-2,4-cyclohexadienyl)(tetrahydrofuran)manganese (**2**). After addition of 3-methyl-1,2-butadiene (**A**), 3-phenyl-1,2-butadiene (**B**), 3-phenyl-1,2-pentadiene (**C**), 1,1-diphenyl-1,2-propadiene (**D**), or 1-methoxy-1-trimethylsilyl-1,2-propadiene (**E**) to the THF solution of **2** at 208 K, the reaction mixture is allowed to warm up slowly to room temperature. Four different types of complexes are formed under these conditions depending on the substituents of the 1,1-disubstituted allenes. Only for **E** is the [5+2] cycloadduct $[Mn\{\eta^{3:2}\text{-}C_9H_9(OCH_3)Si(CH_3)_3\}(CO)_3]$ (**3E**) obtained. Dienes **B**, **C**, and **D** also yield 1:1 adducts with the general formula $[Mn(\eta^{3:2}\text{-}C_9H_9RR')(CO)_3]$ (**4B**, **4C**, **4D**) which are formed from the primary [5+2] cycloadduct by a 1,3 H-shift. All cumulenes used in this study generate 1:2 adducts $[Mn(\eta^{3:2}\text{-}C_{12}H_{11}R_2R'_2)(CO)_3]$ (**5A−5E**), and with **A** a 1:3 adduct $[Mn\{\eta^{3:2:2}\text{-}C_{15}H_{13}(CH_3)_6\}(CO)_2]$ (**6A**) is also obtained.



	A	B	C	D	E
R =	CH_3	CH_3	C_2H_5	C_6H_5	OCH_3
R' =	CH_3	C_6H_5	C_6H_5	C_6H_5	$Si(CH_3)_3$

[+] Part 20: Ref.[1]

[a] Fachbereich Chemie der Universität Kaiserslautern, Erwin Schrödinger-Straße, D-67663 Kaiserslautern, Germany

 © WILEY-VCH Verlag GmbH, D-69451 Weinheim, 1999 1434−1948/99/0404−0655 $ 17.50+.50/0

The reaction mixtures were separated by column and/or HPL chromatography. The complexes are isolated as yellow to red crystals (**4B**, **4C**, **4D**, **6A**) or oils (**3E**, **5A**−**5E**) in moderate to low yields depending upon the substituents R, R′.

^{1}H-NMR and ^{13}C-NMR Spectra

The ^{1}H-NMR-spectroscopic data of the products **3E**−**6A** are given in the Experimental Section. The assignments of the signals to the corresponding protons are based upon homo-decoupling experiments and H,H-COSY-90 spectra. The ^{1}H-NMR spectrum of the [5+2] cycloadduct **3E** shows 11 well-separated signals with the relative intensities 1:1:1:3:1:1:1:1:1:1:9 that prove the addition of one 1-methoxy-1-trimethylsilyl-1,2-propadiene (**E**) to the cyclohexadienyl ligand. The δ,*J* diagram (Figure 1) is in accord with a 6-methylenebicyclo[3.2.1]oct-3-en-2-yl ligand with methoxy and trimethylsilyl groups at the exocyclic sp^2-methylene carbon atom, formed by a [5+2] cycloaddition of the unsubstituted double bond of the cumulene **E** to the cyclohexadienyl ligand of **1**.

The ^{13}C-NMR spectrum of **3E** shows the expected 14 signals. IR, ^{1}H-NMR and ^{13}C-NMR data of **3E** fit well with a tricarbonyl{$\eta^{3:2}$-6-(1-methoxy-1-trimethylsilyl-methylene)bicyclo[3.2.1]oct-3-en-2-yl}manganese complex.

The reactions of **2** with 3-phenyl-1,2-butadiene (**B**), 3-phenyl-1,2-pentadiene (**C**) and 1,1-diphenyl-1,2-propadiene (**D**) yield the 1:1 adducts **4B**, **4C** and **4D**. The ^{1}H-NMR spectra of these complexes are similar with the exception of the substituent signals. The δ-*J* diagram (Figure 1) is in accordance with a 7-methylenebicyclo[3.2.1]oct-2-en-6-yl ligand with methyl and phenyl groups at the exocyclic sp^2-methylene carbon. Like in **3E** it is formed by a [5+2] cycloaddition of the unsubstituted double bond of the cumulene **B** to the cyclohexadienyl ligand followed by a H shift from position 7 to 2.

The ^{13}C-NMR data of **4B** supplement the information from the ^{1}H-NMR spectrum. The ^{1}H-NMR and ^{13}C-NMR spectra of **4C** and **4D** differ from those of **4B** only due to the signals of the substituents. Therefore related structures have to be considered.

All cumulenes used in this study form 2:1 adducts with **1**. The tricarbonyl complexes **5A**−**5E** show similar NMR spectra which differ only in the signals of the respective substituents. The δ,*J* diagram (Figure 1) is closely related to that of **4B** and it is in accordance with a 7-methylenebicyclo[3.2.1]oct-2-en-6-yl ligand with two methyl groups at the exocyclic sp^2-methylene carbon atom and a 3-methyl-2-butenyl group in 4^{endo} position.

The ^{13}C-NMR-spectroscopic data are also in accord with a $\eta^{3:2}$-4-(3-methyl-2-butenyl)-7-(1-methyl-ethylidene)bicyclo[3.2.1]oct-2-en-6-yl-ligand in **5A**.

The ^{1}H-NMR and ^{13}C-NMR spectra of **5B**−**5E** are, with the exception of the signals of the substituents, closely related to those of **5A**. Therefore, in all of them $\eta^{3:2}$-4-(2-propenyl)-7-(methylene)bicyclo[3.2.1]oct-2-en-6-yl-ligands, correspondingly substituted, are present.

The ^{1}H-NMR spectrum of **6A** shows the expected thirteen signals with single and six methyl signals with threefold intensities for a 1:3 adduct of **1** and **A**. Chemical shifts and signal patterns are closely related to those of **5A**, but due

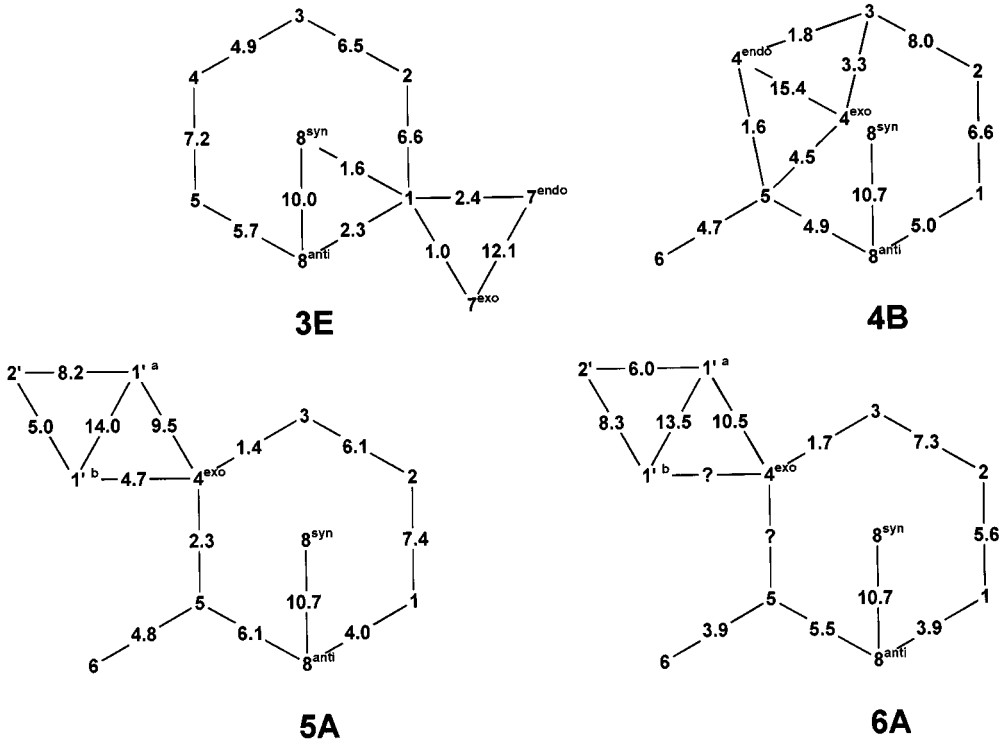


Figure 1. δ,*J* diagrams, showing geminal and vicinal coupling constants, of **3E**, **4B**, **5A** and **6A**

to the overlap of some signals it was not possible to determine all coupling constants. The assignment of the signals was facilitated by a $^1H,^1H$ COSY-90 NMR spectrum, and by the molecular structure of **6A** which was determined by X-ray structure analysis. Two doublets of an AB system at $\delta = 1.00$ and 0.56 ($J = 4.1$ Hz) are due to 1′′*E*-H and 1″*Z*-H of the 2,4-dimethyl-3-methylenepenta-2,4-diyl group. The δ,*J* diagram (Figure 1) of the remaining 11 signals of single intensity is in accord with a 4-(3-methyl-2-butenyl)bicyclo[3.2.1]octa-2,6-dien-7-yl system.

The ^{13}C-NMR spectrum is also consistent with the structure of **6A**.

Crystal and Molecular Structure of 6A

Recrystallization of [Mn{$\eta^{3:2:2}$-$C_{15}H_{12}(CH_3)_6$}$(CO)_2$] (**6A**) from *n*-pentane at 243 K yields red, rhombic crystals. The complex crystallizes in the triclinic space group $P\bar{1}$ with unit cell of $a = 804.8(2)$ pm, $b = 1201.5(4)$ pm, $c = 1222.1(3)$ pm, $\alpha = 61.01(2)°$, $\beta = 81.12(2)°$, $\gamma = 87.47(2)°$. Figure 2 shows an ORTEP projection of the molecule (selected bond lengths and angles are given in the caption). If the coordination sphere of complex **6A** is considered a distorted trigonal bipyramid, the centre of C6, C7 (M2) and C9 occupy the two axial positions. In the equatorial sites the centre of C2, C3 (M1), the centre of gravity of C14−C16 (M3), and C10 are located. The mean value of the six angles between axial and equatorial positions is 90.3° with an msd of 9.0°. For the three angles between equatorial sites the mean value is 119.9° with an msd of 9.5°. Alternatively the coordination sphere can be described as a distorted octahedron with C14−C16 occupying two coordination sites. However, the angle M1−Mn1−C10 with 111.7(5)° makes this description less suited for **6A**.

The plane defined by Mn1, M1, M3, C10 (rmsd 2.69 pm) is cut by M2−Mn1 with 72.6° and by C9−Mn1 with 82.5°. While C2−C3 are virtually parallel to that plane (2.8°), C15−C16 are turned by 28.0° with respect to it. The

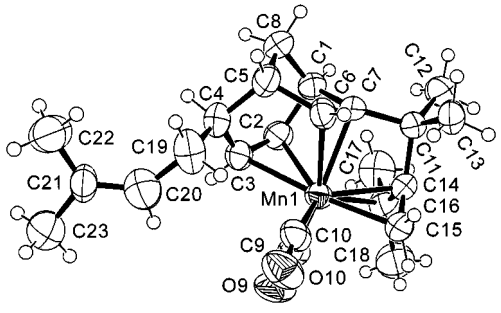


Figure 2. ORTEP projection of dicarbonyl{2,3,6,7,3″,4″,1‴-η-7-(2,4-dimethyl-3-methylenepenta-2,4-diyl)-4-(3-methyl-2-butenyl)-bicyclo[3.2.1]octa-2,6-diene}manganese (**6A**); selected bond lengths [pm] and bond angles [°]: Mn1−C2 213.4(3), Mn1−C3 217.8(3), Mn1−C6 237.2(3), Mn1−C7 226.1(3), Mn1−C9 176.8(3), Mn1−C10 177.9(4), Mn1−C14 212.2(3), Mn1−C15 214.6(3), Mn1−C16 236.5(3), C2−C3 140.4(4), C6−C7 137.4(4), C14−C15 142.6(4), C14−C16 141.5(4), O9−C9 116.2(3), O10−C10 116.3(3); C9−Mn1−C10 84.72(15), O9−C9−Mn1 175.7(3), O10−C10−Mn1 170.6(3), C16−C14−C15 116.3(3)

Mn−C bond lengths of the hydrocarbon chelate ligand differ over a considerable range. For the coordinated sp^2-carbon atoms in the equatorial plane the distances lie between 212.2(3) pm (Mn1−C14) and 217.8(3) pm (Mn1−C3). For Mn1−C16 the distance is distinctly larger [236.5(3) pm] as a result of the steric bulk of the two methyl groups. The C−C double bond in axial position is less tightly coordinated according to Mn1−C6 237.2(3) pm and Mn1−C7 226.1(3) pm. As a consequence of the different extent of coordination the elongation of C2−C3 140.4(4) pm is larger than for C6−C7 with 137.4 (4). A comparable bonding situation has been already found for [$\eta^{3:2:2}$-1-(3-butene-1,2-diyl)-1,3-dimethyl-2,6-cyclononadiene]dicarbonylmanganese with even larger Mn−C distances for the axially coordinated C−C double bond.[20]

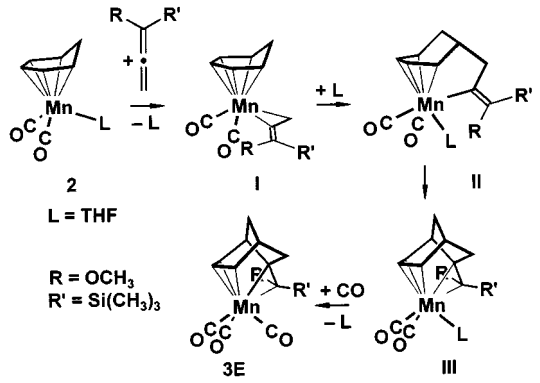
Discussion

Tricarbonyl(η^5-penta-2,4-dienyl)manganese complexes react photochemically with 1,3-dienes in a formal [5+4] cycloaddition to tricarbonyl($\eta^{3:2}$-cyclonona-2,6-dienyl)-manganese complexes. The expected analogous photochemical [5+2] cycloaddition of alkynes to tricarbonyl(η^5-penta-2,4-dienyl)manganese is not observed experimentally.[26] At 208 K in THF, photochemically generated, very reactive dicarbonyl(η^5-2,4-dimethylpenta-2,4-dienyl)(tetrahydrofuran)manganese adds diphenylacetylene or dimethyl butynedioate to yield in a first step the [5+2] cycloadducts with accordingly substituted $\eta^{3:2}$-cyclohepta-2,4-dienyl ligands. These unstable intermediates rearrange by manganese-mediated 1,4-H shifts and form substituted tricarbonyl(η^5-cyclohepta-2,4-dienyl)manganese complexes.

Similarly, irradiation of tricarbonyl(η^5-cyclohexa-2,4-dienyl)manganese (**1**) at 208 K in *n*-pentane in the presence of the cumulenes **A**−**E** causes within 30 minutes only complete decomposition of **1**. The IR spectra, measured during the UV irradiation in regular intervals show no new bands in the region of 2200−1600 cm^{-1} due to the formation of manganese complexes.

Dicarbonyl(η^5-cyclohexa-2,4-dienyl)(tetrahydrofuran)-manganese (**2**), photochemically generated at 208 K, reacts with the 1,2-dienes **A**−**E** when the solution is allowed to warm up to room temperature to four types of complexes. From the constitution of these products their formation can be proposed taking into account the results of other cycloadditions of higher order at metal centres. Prerequisite for a C−C bond formation is the simultaneous presence of reactive hydrocarbon ligands in the coordination sphere. Stable complexes are only formed when one of the ligands is endowed with uncoordinated π-bonds. Each C−C bond formation is accompanied by a loss of two metal−carbon bonds, and produces electronically and coordinatively unsaturated intermediates. Saturation is accomplished by coordination of n-donor or σ-donor-π-acceptor ligands. Metal-mediated C−C bond formation is closely related to reductive elimination, and coordination of olefins to metals centres, by which two metal−carbon bonds are generated, to oxidative addition reactions.

First step of the reaction between **2** and the cumulene **A**−**E** is the substitution of the weakly coordinated THF ligand (**I**) by the cumulene. For stereochemical reasons the hydrocarbons are coordinated through the unsubstituted double bond to the manganese centre. C−C bond formation between C-1 of the cyclohexadienyl and the terminal carbon atom of the coordinated cumulene leads to the dicarbonyl{$\eta^{4:1}$-1-(2-propen-1,2-diyl)cyclohexa-2,3-diene}-manganese intermediates **II** probably stabilized by THF. The second C−C bond is formed between 5-C of the ring and 2-C of the 2-propen-1,2-diyl side chain, and the exocyclic, substituted double bond is coordinated to manganese (**III**). The result of the two C−C bond formations is a formal [5+2] cycloadduct of a cumulene to the cyclohexadienyl ligand. Substitution of the THF ligand by carbon monoxide, dissolved in the solution, completes the reaction of **2** with 1-methoxy-1-trimethylsilyl-1,2-propadiene (**E**) to give **3E**.

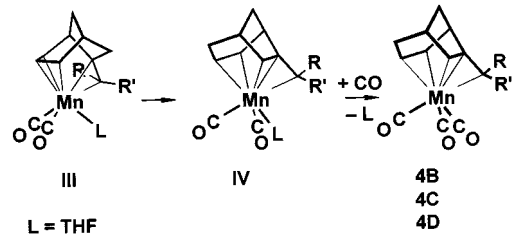


Scheme 1. Proposed formation of tricarbonyl{$\eta^{3:2}$-6-(1-methoxy-1-trimethylsilylmethylene)bicyclo[3.2.1]oct-3-en-2-yl}manganese (**3E**) via intermediates **I**−**III**

With regard to the substituents at the coordinated exocyclic double bond two isomers (*E*, *Z*) are possible. The spectroscopic data of **3E**, however, prove only the formation of one isomer. For stereochemical reasons the bulky $Si(CH_3)_3$ group is proposed to be in *E* position relative to C-5.

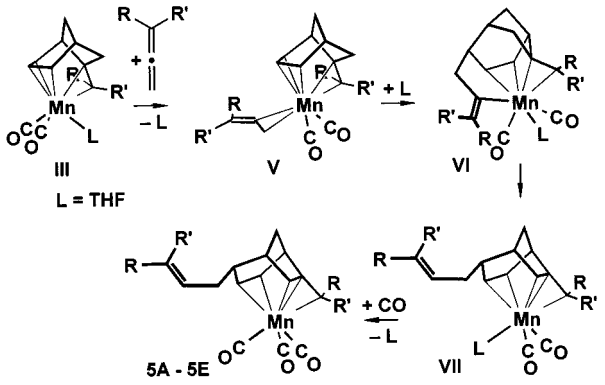
In case of cumulenes with phenyl substituents (**B**, **C**, **D**) from **III** a manganese-mediated 1,3-H shift takes place which results in the THF stabilized dicarbonyl($\eta^{3:2}$-7-methylenebicyclo[3.2.1]oct-2-en-6-yl)manganese complexes **IV**. The exchange of THF by CO completes the reactions to **4B**, **4C** and **4D**. Again, only one regioisomer with the phenyl group in *Z* position relative to C-5 is observed for **4B**, and **4C**.

The formation of the 1:2 adducts **5A**−**5E** is explained by an analogous reaction sequence as for **3E** starting from **III**. Substitution of the THF ligand by a cumulene affords the intermediate **V**. C−C bond formation between C-4 of the 6-methylenebicyclo[3.2.1]oct-3-en-2-yl and the terminal carbon atom of the coordinated cumulene leads to the accordingly substituted dicarbonyl{$\eta^{2:2:1}$-4-(2-propen-1,2-diyl)-6-methylenebicyclo[3.2.1]oct-2-en}(tetrahydrofuran)manganese intermediates **VI**. By a 1,5-H shift (**VII**) and addition of carbon monoxide the tricarbonyl{2,3,6,7,1″-η-7-methyl-



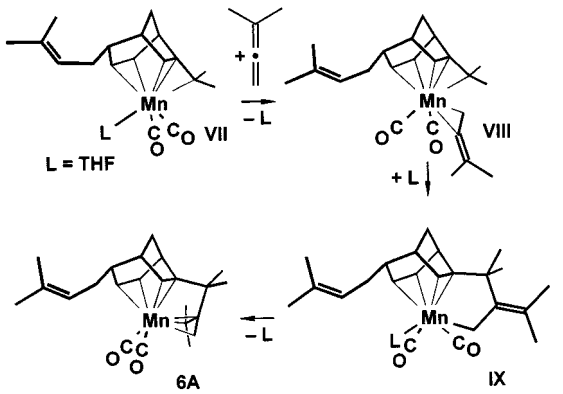
Scheme 2. Proposed formation of tricarbonyl{$\eta^{3:2}$-7-methylenebicyclo[3.2.1]oct-2-en-6-yl}manganese complexes **4B**, **4C**, **4D** by 1,3-H shift in intermediate **III**

ene-4-(2-propenyl)bicyclo[3.2.1]oct-2-en-6-yl}manganese complexes **5A**−**5E** result. Only one regioisomer is obtained for the products from unsymmetrically substituted 1,1-allenes (**5B**, **5C**, **5E**).



Scheme 3. Proposed formation of tricarbonyl{2,3,6,7,1″-η-7-methylene-4-(2-propenyl)bicyclo[3.2.1]oct-2-en-6-yl}mangemese complexes **5A**−**5E** via intermediates **III** and **V**−**VII**

The ligand of **6A** consists of three cumulenes and cyclohexadienyl. A reasonable reaction sequence for **6A** starts from intermediate **VII**. Substitution of THF by **A** gives the cumulene complex **VIII** which rearranges by C−C bond formation between C-1 of the 1-methylethylidene group and C-2 of the 3-methyl-1,2-butadiene unit to intermediate **IX**, stabilized with THF. Finally the 2,4-dimethyl-3-methylenepenta-2,4-diyl side chain is η^3-coordinated to the manganese centre.



Scheme 4. Proposed formation of dicarbonyl{2,3,6,7,3″,4″,1′″-η-7-(2,4-dimethyl-3-methylenepenta-2,4-diyl)-4-(3-methyl-2-butenyl)-bicyclo[3.2.1]octa-2,6-diene}manganese (**6A**)

Experimental Section

All operations and reactions were carried out under dry, oxygen-free nitrogen by common Schlenk techniques. All solvents were purified by standard methods (*n*-pentane, *n*-hexane with CaH_2, THF with potassium, diethyl ether with sodium/benzophenone and CH_2Cl_2 with P_4O_{10}) and stored under nitrogen. Alumina, neutral (Macherey-Nagel GmbH and CO KG, Düren) for column chromatography was degassed under vacuum, deactivated with 4% of water and saturated with nitrogen. UV irradiations were carried out in a 180-mL Duran flask with cooling jacket, wrapped with aluminium foil, with a 150-W mercury lamp TQ 150 (Heraeus-Noblelight, Kleinostheim). The irradiation flask was cooled by a cryostat SK 80 D (Lauda) with methanol as cooling liquid. During the irradiation, nitrogen was bubbled through the solutions to ensure mixing and to remove some of the carbon monoxide from the solutions. HPLC was performed with an Abimed/Gilson appliance consisting of three pumps (type 303), a dynamic mixer (type 811), a high-grade steel column with pre-column (Abimed/Gilson, type Dynamax, l = 25 cm, d = 21.4 mm, silica gel Si 60, 8 μm) and a UV detector (type 116). − IR: Perkin-Elmer FT-IR 16 PC. − NMR: Bruker AC 200 (200.13 MHz for ^{1}H, 50.32 MHz for ^{13}C), Bruker AMX 400 (400.13 MHz for ^{1}H, 100.63 MHz for ^{13}C). Chemical shifts are given relative to TMS, calculated from the solvent as internal standard (C_6HD_5: δ_H = 7.20, C_6D_6: δ_C = 128.0 and CD_2Cl_2: δ_C = 54.0). − C, H elemental analyses: Perkin−Elmer microanalyzer 240. The starting material tricarbonyl(η^5-cyclohexa-2,4-dienyl)manganese (**1**) was prepared from $[Mn(CO)_5Br]$ according to a literature procedure.[33][34] 3-Methyl-1,2-butadiene (**A**), 3-phenyl-1,2-butadiene (**B**), 3-phenyl-1,2-pentadiene (**C**), 1,1-diphenyl-1,2-propadiene (**D**) and 1-methoxy-1-trimethylsilyl-1,2-propadiene (**E**) were also prepared as described in literature.[35]

1. Photoreaction of Tricarbonyl(η^5-cyclohexadienyl)manganese (1) in Tetrahydrofuran: The irradiation flask was loaded with 250 mg (1.15 mmol) of $[Mn(\eta^5\text{-}C_6H_7)(CO)_3]$ (**1**), dissolved in 180 mL of THF. The pale yellow solution was cooled to 208 K and irradiated with UV light. After a few minutes, the colour of the solution turned to red. After 45 minutes, the CO bands of **1** had nearly disappeared and the irradiation was stopped. Dicarbonyl(η^5-cyclohexa-2,4-dienyl)(tetrahydrofuran)manganese (**2**) was identified by IR spectroscopy according to two νCO bands at 1930 (s) und 1861 (s) cm^{-1}.

2. Reaction of Dicarbonyl(η^5-cyclohexa-2,4-dienyl)(tetrahydrofuran)-manganese (2) with 3-Methyl-1,2-butadiene (A): To a THF solution of $[Mn(\eta^5\text{-}C_6H_7)(CO)_2THF]$ (**2**), freshly prepared from 250 mg (1.15 mmol) of $[Mn(\eta^5\text{-}C_6H_7)(CO)_3]$ (**1**), 0.2 mL (3 mmol) of 3-methyl-1,2-butadiene (**A**) was added at 208 K. The reaction mixture was allowed to warm up to room temperature while a slight stream of nitrogen was bubbled through it. During this procedure the colour of the solution changed from carmine to yellow. The solvent was removed in vacuo and the brown, oily residue was dissolved in *n*-pentane and chromatographed at 253 K on alumina with *n*-pentane.

1st Fraction: $[Mn(\eta^5\text{-}C_6H_7)(CO)_3]$ (**1**).

2nd Fraction: Yellow zone, tricarbonyl{2,3,6,7,1″-η-4-(3-methyl-2-butenyl)-7-(1-methylethylidene)bicyclo[3.2.1]oct-2-en-6-yl}manganese (**5A**) with traces of other carbonyl complexes. After purification by HPL chromatography with *n*-hexane as eluent, 105 mg (26%) of **5A**, yellow oil. − IR (*n*-pentane): $\tilde{\nu}$ (CO) = 2005 (s), 1932 (vs), 1922 (vs) cm^{-1}. − ^{1}H NMR (400.13 MHz, C_6D_6, 298 K): δ = 5.32 (m, J = 8.2, 5.0, 1.4, 1.4 Hz, 1 H, 2′-H), 3.82 (ddd, J = 6.1, 2.3, 1.4 Hz, 1 H, 3-H), 2.94 (ddd, J = 14.0, 9.5, 8.2 Hz, 1 H, 1′^{A}-H), 2.89 (d, J = 4.8 Hz, 1 H, 6-H), 2.72 (ddd, J = 14.0, 5.0, 4.7 Hz, 1 H, 1′^{B}-H), 2.64 (dddd, J = 9.5, 4.7, 2.3, 1.4 Hz, 1 H, 4-H), 2.45 (dd, J = 7.4, 4.0 Hz, 1 H, 1-H), 2.30 (dd, 7.4, 6.1 Hz, 1 H, 2-H), 1.99 (s, 3 H, 1″E-CH_3), 1.97 (dddd, J = 6.1, 4.8, 2.3, 2.3 Hz, 1 H, 5-H), 1.76 (d, J = 1.4 Hz, 3 H, 3′-CH_3), 1.69 (d, J = 1.4 Hz, 3 H, 3′-CH_3), 1.57 (ddd, J = 10.7, 6.1, 4.0 Hz,1 H, 8^{anti}-H), 1.28 (s, 3 H, 1″Z-CH_3), 1.21 (d, J = 10.7 Hz, 1 H, 8^{syn}-H). − ^{13}C NMR (50.32 MHz, C_6D_6, 298 K): δ = 226.0 (s, *C*O), 225.3 (s, *C*O), 224.5 (s, *C*O), 133.2 (s, C-3′), 122.9 (d, J = 157 Hz, C-2′), 99.4 (d, J = 158 Hz, C-3), 90.4 (s, C-7 or C-1″), 88.0 (s, C-7 or C-1″), 66.6 (d, J = 166 Hz, C-2), 59.0 (d, J = 119 Hz, C-4), 49.6 (d, J = 165 Hz, C-6), 42.7 (t, J = 132 Hz, C-1′), 39.7 (d, J = 141 Hz, C-1), 35.1 (t, J = 131 Hz, C-8), 33.5 (d, J = 154 Hz, C-5), 27.3 (q, J = 129 Hz, 1″E-*C*H$_3$), 25.9 (q, J = 126 Hz, 3′-*C*H$_3$), 25.6 (q, J = 126 Hz, 3′-*C*H$_3$), 18.1 (q, J = 125 Hz, 1″Z-*C*H$_3$). − $C_{19}H_{23}MnO_3$ (354.33): calcd. C 64.41, H 6.54; found C 64.02, H 6.52.

3rd Fraction: Yellow solution, dicarbonyl{2,3,6,7,3″,4″,1‴-η-7-(2,4-dimethyl-3-methylenepenta-2,4-diyl)-4-(3-methyl-2-butenyl)-bicyclo[3.2.1]octa-2,6-diene}manganese (**6A**). Removal of the solvent and crystallization from *n*-pentane at 243 K yielded 55 mg (12%) of **6A**. Red, rhombic crystals, suitable for X-ray diffraction analysis. − IR (*n*-pentane): $\tilde{\nu}$ (CO) = 1956 (vs), 1900 (vs) cm^{-1}. − ^{1}H NMR (200.13 MHz, C_6D_6, 298 K): δ = 5.56 (m, J = 8.3, 6.0, 1.4, 1.4 Hz, 1 H, 2′-H), 3.54 (dd, J = 3.9, 1.5 Hz, 1 H, 6-H), 3.44 (ddd, J = 7.3, 2.3, 1.7 Hz, 1 H, 3-H), 3.16 (ddd, J = 13.5, 10.5, 6.0, Hz, 1 H, 1′^{A}-H), 2.95 (ddd, J = 13.5, 8.3, ? Hz, 1 H, 1′^{B}-H), 2.95 (m, J = 10.5, 1.7, ? Hz, 1 H, 4-H), 2.52 (ddd, J = 5.6, 3.9, 1.5 Hz, 1 H, 1-H), 2.20 (s, 3 H, CH_3), 2.19 (dd, J = 7.3, 5.6 Hz, 1 H, 2-H), 1.88 (s, 3 H, CH_3), 1.85 (m, J = 5.5, 3.9, 2.3, ? Hz, 1 H, 5-H), 1.80 (s, 3 H, CH_3), 1.39 (s, 3 H, CH_3), 1.35 (ddd, J = 9.4, 5.5, 3.9 Hz, 1 H, 8^{anti}-H), 1.26 (s, 3 H, CH_3), 1.00 (d, J = 4.1 Hz, 1 H, 1‴E-H), 0.99 (d, J = 9.4 Hz, 1 H, 8^{syn}-H), 0.56 (d, J = 4.1 Hz, 1 H, 1‴Z-H), 0.36 (s, 3 H, CH_3). − ^{13}C NMR (50.32 MHz, CD_2Cl_2 298 K) δ = 237 (s, br., 2 C, *C*O), 133.0 (s, C-3′), 123.9 (d, J = 144 Hz, C-2′), 96.8 (d, J = 167 Hz, C-3), 93.7 (s, C-7), 76.2 (d, J = 154 Hz, C-6), 74.4 (s, C-3″), 65.2 (s, C-4″), 56.8 (d, J = 126 Hz, C-4), 46.7 (t, J = 129 Hz, C-1′), 42.8 (d, J = 166 Hz, C-2), 42.0 (d, J = 138 Hz, C-1), 37.4 (d, J = 147 Hz, C-5), 36.0 (s, C-2″), (t, J = 129 Hz, C-8), 32.9 (t, J = 158 Hz, C-1‴), 30.3 (q, J = 130 Hz, 2 C, *C*H$_3$), 27.7 (q, J = 129 Hz, *C*H$_3$), 26.9 (q, J = 130 Hz, *C*H$_3$), 26.1 (q, J = 130 Hz, *C*H$_3$), 18.4 (q, J = 130 Hz, *C*H$_3$). − MS (70 eV); *m/z* (%): 337.8 (100) [M$^+$ − 2 CO], 283.9 (12.67) [M$^+$ − 2 CO, − Mn], 269.9 (53.47) [M$^+$ − 2 CO, − C_5H_8], 201.9 (59.39) [M$^+$ − 2 CO, − 2 C_5H_8]. − $C_{23}H_{31}MnO_2$ (394.44): calcd. C 70.04, H 7.92; found C 69.98, H 8.03.

3. Reaction of Dicarbonyl(η^5-cyclohexa-2,4-dienyl)(tetrahydrofuran)-manganese (2) with 3-Phenyl-1,2-butadiene (B): To a THF solution of $[Mn(\eta^5\text{-}C_6H_7)(CO)_2THF]$ (**2**), freshly prepared from 250 mg (1.15 mmol) of $[Mn(\eta^5\text{-}C_6H_7)(CO)_3]$ (**1**), 0.2 mL (1.5 mmol) of 3-phenyl-1,2-butadiene (**B**) was added at 208 K. After warming up to room temperature, the solvent was removed in vacuo and the residue was separated by HPLC with *n*-hexane.

1st Fraction: $[Mn(\eta^5\text{-}C_6H_7)(CO)_3]$ (**1**).

2nd Fraction: Yellow solution, tricarbonyl{$\eta^{3:2}$-7-(1-phenylethylidene)bicyclo[3.2.1]oct-2-en-6-yl}manganese (**4B**). After crystallization from *n*-pentane, **4B** was isolated as yellow needles 16 mg (4%). − IR (*n*-pentane): $\tilde{\nu}$ (CO) = 2007 (s), 1936 (vs), 1922 (s) cm^{-1}. − ^{1}H NMR (200.13 MHz, C_6D_6, 298 K): δ = 7.61 (d, J = 7.2 Hz, 2 H, *o*-Ph), 7.24 (t, J = 7.2 Hz, 2 H, *m*-Ph), 7.01 (t, J = 7.2 Hz, 1 H, *p*-Ph), 3.66 (dddd, J = 8.0, 3.3, 2.0, 1.8 Hz, 1 H, 3-H), 2.80 (ddd, J = 6.6, 5.0, 1.3 Hz, 1 H, 1-H), 2.70 (dd, J = 4.7, 1.3 Hz, 1 H, 6-H), 2.64 (m, J = 15.4, 4.5, 3.3, 1.5 Hz, 1 H, 4^{exo}-H), 2.39 (dd, J = 8.0, 6.6 Hz, 1 H, 2-H), 2.07 (ddd, J = 15.4, 1.8, 1.6 Hz, 1 H,

4^{endo}-H), 1.99 (m, J = 4.9, 4.7, 4.5, 2.0, 1.6 Hz, 1 H, 5-H), 1.53 (dddd, J = 10.7, 5.0, 4.9, 1.5 Hz, 1 H, 8^{anti}-H), 1.49 (s, 3 H, CH_3), 0.90 (d, J = 10.7 Hz, 1 H, 8^{syn}-H). − ^{13}C NMR (50.32 MHz, C_6D_6, 298 K): δ = 224 (s, br., 3 C, *C*O), 147 (s, 1 C, *ipso*-Ph), 130 (d, 2 C, *o*-Ph), *m*-, *p*-Ph (covered by solvent signals), 97.3 (s, 1 C, 7-C or 1′-C), 95.4 (d, J = 162 Hz, 1 C, 3-C), 93.8 (s, 1 C, 7-C or 1′-C), 64.4 (d, J = 161 Hz, 1 C, 2-C), 59.4 (d, J = 166 Hz, 1 C, 6-C), 46.2 (t, J = 129 Hz, 1 C, 4-C), 41.3 (t, J = 129 Hz, 1 C, 8-C), 35.4 (d, J = 136 Hz, 1 C, 1-C), 34.2 (d, J = 149 Hz, 1 C, 5-C), 28.7 (q, J = 130 Hz, 1 C, *C*H_3). − $C_{19}H_{17}MnO_3$ (348.28): calcd. C 65.52, H 4.92.

3rd Fraction: Yellow solution, tricarbonyl{2,3,6,7,1″-η-4-(3-phenyl-2-butenyl)-7-(1-phenylethylidene)bicyclo[3.2.1]oct-2-en-6-yl}manganese (**5B**), yellow oil, 40 mg (7%). − IR (*n*-pentane): ν̃ (CO) = 2008 (s), 1940 (vs), 1920 (vs) cm^{-1}. − ^{1}H NMR (200.13 MHz, C_6D_6, 298 K): δ = 7.30−7.15 (m, 5 H, Ph-H), 7.10−6.90 (m, 5 H, Ph-H), 5.58 (m, J = 9.0, 5.5, 1.5 Hz, 1 H, 2′-H), 3.63 (ddd, J = 8.0, 2.3, 1.0 Hz, 1 H, 3-H), 3.05 (m, J = 14.7, 9.0, ? Hz, 1 H, $1'^{A}$-H), 3.03 (dd, J = 4.8, 1.0 Hz, 1 H, 6-H), 2.73−2.55 (m, 2 H, $1'^{B}$-H and 4-H), 2.47 (dd, J = 6.1, 5.3, 1.0 Hz, 1 H, 1-H), 2.39 (s, 3 H, CH_3), 2.33 (dd, J = 8.0, 6.1 Hz, 1 H, 2-H), 2.09 (s, 3 H, CH_3), 2.00 (ddd, J = 6.3, 4.8, 2.3 Hz, 1 H, 5-H), 1.71 (ddd, J = 10.9, 6.3, 5.3 Hz, 1 H, 8^{anti}-H), 1.23 (d, J = 10.9 Hz, 1 H, 8^{syn}-H). − ^{13}C NMR (50.32 MHz, C_6D_6, 298 K): δ = 229.0 (s, 1 C, *C*O), 226.0 (s, 1 C, *C*O), 218.7 (s, 1 C, *C*O), 143.9 (s, 1 C, *ipso*-Ph), 142.1 (s, 1 C, *ipso*-Ph), *o*-, *m*-, *p*-Ph (covered by solvent signals), 138.8 (s, 1 C, 3′-C), 125.2 (d, J = 160 Hz, 1 C, 2′-C), 99.6 (d, J = 159 Hz, 1 C, 3-C), 90.7 (s, 1 C, 7-C or 1′′-C), 90.1 (s, 1 C, 7-C or 1′′-C), 70.3 (d, J = 169 Hz, 1 C, 2-C), 58.8 (d, J = 120 Hz, 1 C, 4-C), 50.9 (d, J = 168 Hz, 1 C, 6-C), 42.5 (t, J = 131 Hz, 1 C, 1′-C), 39.3 (d, J = 143 Hz, 1 C, 1-C), 35.9 (t, J = 128 Hz, 1 C, 8-C), 34.4 (d, J = 148 Hz, 1 C, 5-C), 27.8 (q, J = 128 Hz, 1 C, *C*H_3), 25.8 (q, J = 127 Hz, 1 C, *C*H_3). − $C_{29}H_{27}MnO_3$ (478.47): calcd. C 72.80, H 5.69; found C 71.0, H 6.09.

4. Reaction of Dicarbonyl(η^5-cyclohexa-2,4-dienyl)(tetrahydrofuran)-manganese (2) with 3-Phenyl-1,2-pentadiene (C): To a THF solution of [Mn(η^5-C_6H_7)(CO)$_2$THF] (**2**), freshly prepared from 250 mg (1.15 mmol) of [Mn(η^5-C_6H_7)(CO)$_3$] (**1**), 0.2 mL (1.5 mmol) of 3-phenyl-1,2-pentadiene (**C**) was added at 208 K. After warming up to room temperature, the solvent was removed in vacuo and the residue was separated by HPLC with *n*-hexane.

1st Fraction: [Mn(η^5-C_6H_7)(CO)$_3$] (**1**).

2nd Fraction: Yellow solution, tricarbonyl{η$^{3:2}$-7-(1-phenylpropylidene)bicyclo[3.2.1]oct-2-en-6-yl}manganese (**4C**). After crystallization from *n*-pentane, 25 mg (6%) of **4C**, orange red crystals. − IR (*n*-pentane): ν̃ (CO) = 2006 (vs), 1934 (s), 1923 (vs) cm^{-1}. − ^{1}H NMR (200.13 MHz, C_6D_6, 298 K): δ = 7.59 (d, J = 7.0 Hz, 2 H, *o*-Ph), 7.23 (t, J = 7.0 Hz, 2 H, *m*-Ph), 7.10 (t, J = 7.0 Hz, 1 H, *p*-Ph), 3.67 (m, J = 8.0, 3.4, 2.0, 1.8 Hz, 1 H, 3-H), 3.03 (ddd, J = 6.3, 5.6, 1.3 Hz, 1 H, 1-H), 2.79 (dd, J = 4.9, 1.3 Hz, 1 H, 6-H), 2.65 (m, J = 15.4, 4.5, 3.4, 1.5 Hz, 1 H, 4^{exo}-H), 2.32 (dd, J = 8.0, 6.6 Hz, 1 H, 2-H), 2.23 (dq, J = 14.4, 7.2 Hz, 1 H, CH_2), 2.10 (m, J = 15.4, 2.0, 1.5 Hz, 1.5 Hz, 1 H, 4^{endo}-H), 2.02 (m, J = 4.9, 4.8, 4.5, 1.8, 1.5 Hz, 1 H, 5-H), 1.59 (m, J = 10.7, 5.6, 4.8, 1.5, 1.5 Hz, 1 H, 8^{anti}-H), 1.17 (dq, J = 14.4, 7.2 Hz, 1 H, CH_2), 0.97 (d, J = 10.7 Hz, 1 H, 8^{syn}-H), 0.80 (t, J = 7.2 Hz, 3 H, CH_3). − MS (70 eV); *m*/*z* (%): 362.0 (0.94) [M$^+$], 334.0 (6.90) [M$^+$ − CO], 306.0 (9.37) [M$^+$ − 2 CO], 278.0 (100) [M$^+$ − 3 CO], 223.0 (10.11) [M$^+$ − 3 CO, − Mn]. − $C_{20}H_{19}MnO_3$ (362.31): calcd. C 66.30, H 5.29; found C 66.38, H 5.27.

3rd Fraction: Yellow solution, tricarbonyl{2,3,6,7,1″-η-4-(3-phenyl-2-pentenyl)-7-(1-phenylpropylidene)bicyclo[3.2.1]oct-2-en-6-yl}-manganese (**5C**), 60 mg (10%), yellow oil. − IR (*n*-pentane): ν̃(CO) = 2008 (vs), 1940 (vs), 1920 (vs) cm^{-1}. − ^{1}H NMR (200.13 MHz, C_6D_6, 298 K): δ = 7.12−7.20 (m, 5 H, Ph-H), 7.00−6.90 (m, 5 H, Ph-H), 5.58 (dd, J = 9.5, 5.5 Hz, 1 H, 2′-H), 3.64 (ddd, J = 7.8, 2.0, 1.5 Hz, 1 H, 3-H), 3.29 (dq, J = 14.3, 7.2 Hz, 1 H, CH_2) 2.98 (ddd, J = 13.9, 9.5, 9.0 Hz, 1 H, $1'^{A}$-H), 2.98 (d, J = 4.9 Hz, 1 H, 6-H), 2.53−2.68 (m, 2 H, $1'^{B}$-H and 4-H), 2.26−2.48 (m, 5 H, 1-H, 2-H, CH_2), 1.98 (ddd, J = 5.5, 4.9, 2.0 Hz, 1 H, 5-H), 1.71 (ddd, J = 10.7, 5.5, 5.0 Hz, 1 H, 8^{anti}-H), 1.23 (d, J = 10.7 Hz, 1 H, 8^{syn}-H), 1.03 (t, J = 7.2 Hz, 3 H, CH_3), 0.90 (t, J = 7.2 Hz, 3 H, CH_3). − $C_{31}H_{31}MnO_3$ (506.53): calcd. C 73.51, H 6.17.

5. Reaction of Dicarbonyl(η^5-cyclohexa-2,4-dienyl)(tetrahydrofuran)-manganese (2) with 1,1-Diphenyl-1,2-propadiene (D): To a THF solution of [Mn(η^5-C_6H_7)(CO)$_2$THF] (**2**), freshly prepared from 250 mg (1.15 mmol) of [Mn(η^5-C_6H_7)(CO)$_3$] (**1**), 0.3 mL (1.5 mmol) of 1,1-diphenyl-1,2-propadiene (**D**) was added at 208 K. After warming up to room temperature, the solvent was removed in vacuo and the residue was separated by HPLC with *n*-hexane/CH_2Cl_2 (50:1).

1st Fraction: [Mn(η^5-C_6H_7)(CO)$_3$] (**1**).

2nd Fraction: Yellow solution, tricarbonyl{η$^{3:2}$-7-(1,1-diphenylmethylene)bicyclo[3.2.1]oct-2-en-6-yl}manganese (**4D**). After crystallization from *n*-pentane/CH_2Cl_2 (5:1), 15 mg (3%) of **4D** was isolated as red crystals. − IR (*n*-pentane): ν̃ (CO) = 2010 (s), 1945 (vs), 1921 (vs) cm^{-1}. − ^{1}H NMR (400.13 MHz, C_6D_6, 298 K): δ = 7.81 (d, br, 2 H, *o*-Ph), 7.20 (m, 4 H, *o*-, *m*-Ph), 7.10 (t, J = 7.2 Hz, 1 H, *p*-Ph), 6.97 (t, J = 7.2 Hz, 2 H, *m*-Ph), 6.87 (t, J = 7.2 Hz, 1 H, *p*-Ph), 3.80 (dd, J = 8.2, 3.4 Hz, 1 H, 3-H), 3.57 (d, J = 4.8, 1 H, 6-H), 2.97 (dd, J = 8.2, 6.1 Hz, 1 H, 2-H), 2.71 (m, J = 14.7, 3.4, 3.4, 1 H, 4^{exo}-H), 2.21 (ddd, J = 6.1, 4.8, 1 H, 1-H), 2.15 (m, J = 5.5, 4.8, 3.4 Hz, 1 H, 5-H), 2.12 (d, J = 14.75 Hz, 1 H, 4^{endo}-H), 1.60 (ddd, J = 10.8, 5.5, 4.8 Hz, 1 H, 8^{anti}-H), 0.90 (d, J = 10.8 Hz, 1 H, 8^{syn}-H). − MS (70 eV); *m*/*z* (%): 409.8 (< 1) [M$^+$], 381.9 (4.21) [M$^+$ − CO], 353.9 (4.51) [M$^+$ − 2 CO], 325.9 (100) [M$^+$ − 3 CO], 272.0 (23.29) [M$^+$ − 3 CO, − Mn]. − $C_{24}H_{19}MnO_3$ (410.35): calcd. C 70.25, H 4.67.

3rd Fraction: Yellow solution, tricarbonyl{2,3,6,7,1″-η-4-(3,3-diphenyl-2-propenyl)-7-(1,1-diphenyl-methylene)bicyclo[3.2.1]oct-2-en-6-yl}manganese (**5D**). After crystallization from *n*-hexane at 243 K, 35 mg (5%) of **5D**, red needles.− IR (*n*-pentane): ν̃ (CO) = 2010 (s), 1942 (vs), 1920 (vs) cm^{-1}. − ^{1}H NMR (400.13 MHz, C_6D_6, 298 K): δ = 7.79 (d, J = 7.2 Hz, 2 H, *o*-Ph), 7.44 (d, J = 7.2 Hz, 3 H, *o*-Ph), 7.32 (d, J = 7.2 Hz, 3 H, *o*-Ph), 7.28−7.01 (m, 8 H, *m*-Ph), 6.98 (t, J = 7.2 Hz, 3 H, *p*-Ph), 6.90 (t, J = 7.2 Hz, 1 H, *p*-Ph), 6.24 (dd, J = 9.0, 5.8 Hz,1 H, 2′-H), 3.83 (ddd, J = 8.0, 2.5, 1.5 Hz, 1 H, 3-H), 3.26 (dd, J = 6.1, 3.8 Hz, 1 H, 6-H), 3.25 (ddd, J = 14.1, 10.0, 9.0 Hz, 1 H, $1'^{A}$-H), 2.83 (dd, J = 8.0, 6.1 Hz, 1 H, 2-H), 2.80 (ddd, J = 14.1, 5.8, 4.1 Hz, 1 H, $1'^{B}$-H), 2.68 (m, J = 10.0, 4.1, ? Hz, 1 H, 4-H), 2.32 (dd, J = 6.1, 3.4, Hz, 1 H, 1-H), 2.18 (m, J = 6.1, 2.5, ? Hz, 1 H, 5-H), 1.66 (ddd, J = 10.9, 3.4, ? Hz, 1 H, 8^{anti}-H), 1.10 (d, J = 10.9 Hz, 1 H, 8^{syn}-H). − MS (70 eV); *m*/*z* (%): 518.2 (58.17) [M$^+$ − 3 CO], 464.2 (29.77) [M$^+$ − 3 CO, − Mn], 271.1 (76.81) [M$^+$ − 3 CO, − Mn, − $C_3H_3(C_6H_5)_2$], 193.0 (100) [M$^+$ − 3 CO, − Mn, − $C_3H_2(C_6H_5)_2$, − C_6H_5]. − $C_{39}H_{31}MnO_3$ (602.61): calcd. C 77.73, H 5.19; found C 77.07, H 5.07.

6. Reaction of Dicarbonyl(η^5-cyclohexa-2,4-dienyl)(tetrahydrofuran)-manganese (2) with 1-Methoxy-1-trimethylsilyl-1,2-propadiene (E): To a THF solution of [Mn(η^5-C_6H_7)(CO)$_2$THF] (**2**), freshly prepared from 250 mg (1.15 mmol) of [Mn(η^5-C_6H_7)(CO)$_3$] (**1**), 0.3 mL (1.5 mmol) of 1-methoxy-1-trimethylsilyl-1,2-propadiene (**E**)

was added at 208 K. After warming up to room temperature, the solvent was removed in vacuo and the residue was separated by HPLC with *n*-hexane as eluent.

1st Fraction: [Mn(η^5-C_6H_7)(CO)$_3$] (**1**).

2nd Fraction: Yellow solution, tricarbonyl{$\eta^{3:2}$-6-(1-methoxy-1-trimethylsilylmethylene)bicyclo[3.2.1]oct-3-en-2-yl}manganese (**3E**). After removal of the solvent, 50 mg (12%) of **3E**, yellow oil. − IR (*n*-pentane): $\tilde{\nu}$ (CO) = 2006 (w), 1999 (s), 1924 (w), 1912 (vs) cm^{-1}. − ^{1}H NMR (200.13 MHz, C_6D_6, 298 K): δ = 4.71 (ddd, *J* = 6.5, 4.9, 1.1 Hz, 1 H, 3-H), 4.39 (m, *J* = 6.6, 6.5, 2.7, 1.0 Hz, 1 H, 2-H), 4.01 (ddd, *J* = 7.2, 4.9, 2.7 Hz, 1 H, 4-H), 3.59 (s, 3 H, OC*H*$_3$), 3.28 (dddd, *J* = 7.2, 5.7, 1.3, 1.0 Hz, 1 H, 5-H), 2.31 (m, *J* = 6.6, 2.4, 2.3, 1.6 Hz, 1 H, 1-H), 1.73 (ddd, *J* = 12.1, 2.7, 1.3 Hz, 1 H, 7^{exo}-H), 1.35 (dddd, *J* = 12.1, 2.4, 1.1, 1.0 Hz, 1 H, 7^{endo}-H), 0.98 (ddd, *J* = 10.0, 2.7, 1.6 Hz, 1 H, 8^{syn}-H), 0.54 (m, *J* = 10.0, 5.7, 2.3, 1.0 Hz, 1 H, 8^{anti}-H), 0.43 [s, 9 H, Si(C*H*$_3$)$_3$]. − ^{13}C NMR (50 MHz, C_6D_6, 298 K): δ = 229.1 (s, *C*O), 225.2 (s, *C*O), 223.2 (s, *C*O), 128.3 (s, 6-C), 97.0 (d, *J* = 163 Hz, 3-C), 79.2 (s, 1′-C), 73.3 (d, *J* = 161 Hz, 2-C), 57.8 (q, *J* = 144 Hz, O*C*H$_3$), 56.7 (d, *J* = 168 Hz, 4-C), 47.2 (t, *J* = 136 Hz, 7-C), 37.6 (t, *J* = 131 Hz, 8-C), 37.46 (d, *J* = 140 Hz, 1-C or 5-C), 37.3 (d, *J* = 140 Hz, 1-C or 5-C), 1.6 [q, *J* = 120 Hz, 3 C, Si(*C*H$_3$)$_3$]. − $C_{16}H_{21}MnO_4Si$ (360.37): calcd. C 53.33, H 5.87; found C 53.93, H 6.04.

3rd Fraction: Yellow solution, tricarbonyl{2,3,6,7,1″-η-4-(3-methoxy-3-trimethylsilyl-2-propenyl)-7-(1-methoxy-1-trimethylsilylmethylene)bicyclo[3.2.1]oct-2-en-6-yl}manganese (**5E**). After crystallization from *n*-pentane at 243 K 75 mg (13%) of **5E**, yellow crystals. − IR (*n*-pentane): $\tilde{\nu}$ (CO) = 2000 (s), 1920 (vs, br.) cm^{-1}. − ^{1}H NMR (200.13 MHz, C_6D_6, 298 K): δ = 5.15 (dd, *J* = 9.6, 5.4 Hz, 1 H, 2′-H), 4.01 (ddd, *J* = 7.8, 2.2, 1.6 Hz, 1 H, 3-H), 3.80 (s, 3 H, OC*H*$_3$), 3.52 (ddd, *J* = 5.5, 4.6, 2.2 Hz, 1 H, 1-H), 3.35 (s, 3 H, OC*H*$_3$), 3.09 (ddd, *J* = 14.3, 9.8, 9.6 Hz, 1 H, 1′^{A}-H), 2.81 (ddd, *J* = 14.3, 5.4, 3.5 Hz, 1 H, 1′^{B}-H), 2.75 (dd, *J* = 7.8, 5.5 Hz, 1 H, 2-H), 2.65 (m, *J* = 9.8, 3.5, 1.6, 1.4 Hz, 1 H, 4-H), 2.56 (d, *J* = 5.1 Hz, 1 H, 6-H), 2.21 (dd, *J* = 6.0, 5.1 Hz, 1 H, 5-H), 1.73 (m, *J* = 11.1, 6.0, 4.6, 1.4 Hz, 1 H, 8^{anti}-H), 1.34 (d, *J* = 11.1 Hz, 1 H, 8^{syn}-H), 0.47 [s, 9 H, Si(C*H*$_3$)$_3$], 0.28 [s, 9 H, Si(C*H*$_3$)$_3$]. − MS (70 eV); *m*/*z* (%): 501.6 (4.12) [M$^+$], 417.7 (100) [M$^+$ − 3 CO], 385.7 (69.23) [M$^+$ − 3 CO, − OCH$_3$], 355.7 (10.02) [M$^+$ − 3 CO, − 2 OCH$_3$], 281.8 (12.99) [M$^+$ − 3 CO, − 2 OCH$_3$, − Si(CH$_3$)$_3$]. − $C_{23}H_{35}MnO_5Si_2$ (502.64) calcd. C 54.96, H 7.02; found C 55.20, H 6.94.

7. X-ray-Structural Analysis of Dicarbonyl{2,3,6,7,3″,4″,1‴-η-7-(2,4-dimethyl-3-methylenepenta-2,4-diyl)-4-(3-methyl-2-butenyl)-bicyclo[3.2.1]octa-2,6-diene}manganese (6A):[36] $C_{23}H_{31}MnO_2$, *M* = 394.42 g × mol^{-1}, triclinic space group $P\bar{1}$, *a* = 804.8(2), *b* = 1201.5(4), *c* = 1222.1(3) pm, α = 61.01(2), β = 81.12(2), γ = 87.47(2)°, *V* = 1.0206(5) nm^3, *Z* = 2, ρ(calcd.) = 1.283 g × cm^{-3}. Crystal size 0.01 × 0.45 × 0.45 mm. Using a P4 diffractometer (Siemens), radiation Mo-K_α, graphite monochromator, wavelength λ = 71.073 pm, ω-scan type, 5259 reflections were collected in the θ range 4.16° to 26.50° at *T* = 293 K. After data reduction, 4157 unique reflections (R_{int} = 0.0123) were obtained. The structure was solved by direct methods using SHELXS-97[37] and refined by full-matrix least squares against F^2 with SHELXL-97.[38] 271 parameters were refined to R_1 [$I > 2\sigma(I)$] 0.0547, wR_2 [$I > 2\sigma(I)$] 0.0811.

Acknowledgments

Financial support from the Fonds der Chemischen Industrie and the Deutsche Forschungsgemeinschaft is gratefully acknowledged.

[1] C. G. Kreiter, U. Kern, G. Wolmershäuser, G. Heckmann *Eur. J. Inorg. Chem.* **1998**, 127−135.
[2] R. G. Pearson, *Chem. Ber.* **1976**, *12*, 160−165.
[3] M. J. S. Dewar, *Angew. Chem.* **1971**, *83*, 859−875; *Angew. Chem. Int. Ed. Engl.* **1971**, *10*, 761−776.
[4] S. Özkar, H. Kurz, D. Neugebauer, C. G. Kreiter, *J. Organomet. Chem.* **1978**, *160*, 115−124.
[5] C. G. Kreiter, H. Kurz, *Chem. Ber.* **1983**, *116*, 1494−1505.
[6] E. Michels, W. S. Sheldrick, C. G. Kreiter, *Chem. Ber.* **1985**, *118*, 964−978.
[7] C. G. Kreiter, E. Michels, J. Kaub, *Z. Naturforsch., B* **1986**, *41*, 722−730.
[8] C. G. Kreiter, E. Michels, *J. Organomet. Chem.* **1986**, *312*, 59−66.
[9] C. G. Kreiter, *Adv. Organomet. Chem.* **1986**, *26*, 297−375.
[10] C. G. Kreiter, R. Eckert, *Chem. Ber.* **1997**, *130*, 9−12.
[11] J. H. Rigby, H. S. Ateeq, N. R. Charles, J. A. Henshilwood, K. M. Short, P. M. Sugathapala, *Tetrahedron* **1993**, *49*, 5495−5506.
[12] J. H. Rigby, *Acc. Chem. Res.* **1993**, *26,* 579−585.
[13] J. H. Rigby, J. A. Henshilwood, *J. Am. Chem. Soc.* **1991**, *113*, 5122−5123.
[14] J. H. Rigby, H. S. Ateeq, N. R. Charles, S. V. Cuisiat, M. D. Ferguson, J. A. Henshilwood, A. C. Krueger, C. O. Ogbu, K. M. Short, M. J. Heeg, *J. Am. Chem. Soc.* **1993**, *115,* 1382−1396.
[15] J. H. Rigby, S. Scribner, M. J. Heeg, *Tetrahedron Lett.* **1995**, *36*, 8569−8572.
[16] J. H. Rigby, H. S. Ateeq, *J. Am. Chem. Soc.* **1990**, *112*, 6442−6443.
[17] I. Fischler, F.-W.Grevels, J. Leitich, S. Özkar, *Chem. Ber.* **1991**, *124,* 2857−2861.
[18] K. Chaffee, P. Huo, J. B. Sheridan, A. Barbieri, A. Aistars, R. A. Lalancette, R. L. Ostrander, A. L. Rheingold, *J. Am. Chem. Soc.* **1995**, *117*, 1900−1907.
[19] K. Chaffee, J. B. Sheridan, A. Aistars, *Organometallics* **1992**, *11*, 18−19.
[20] C. G. Kreiter, K. Lehr, M. Leyendecker, W. S. Sheldrick, R. Exner, *Chem. Ber.* **1991**, *124*, 3−12.
[21] C. G. Kreiter, K. Lehr, *J. Organomet. Chem.* **1991**, *406*, 159−170.
[22] C. G. Kreiter, K. Lehr, G. Heeb, *Z. Naturforsch., B* **1991**, *46*, 941−949.
[23] C. G. Kreiter, K. Lehr, *Z. Naturforsch., B* **1991**, *46*, 1377−1383.
[24] C. G. Kreiter, C. Fiedler, W. Frank, G. J. Reiß, *Chem. Ber*. **1995**, *128*, 515−518.
[25] C. G. Kreiter, C. Fiedler, W. Frank, G. J. Reiß, *J. Organomet. Chem.* **1995**, *490*, 133−141.
[26] C. G. Kreiter, E. C. Koch, W. Frank, G. J. Reiß, *Z. Naturforsch., B* **1996**, *51*, 1473−1485.
[27] C. G. Kreiter, E. C. Koch, W. Frank, G. J. Reiß, *J. Organomet. Chem.* **1995**, *490*, 125 −131.
[28] C. G. Kreiter, E.-C. Koch, W. Frank, G. J. Reiß, *Inorg. Chim. Acta* **1994**, *220*, 77−83.
[29] W. Chen, H.-J. Chung, C. Wang, J. B. Sheridan, M. L. Coté, R. A. Lalancette, *Organometallics* **1996**, *15*, 3337−3344.
[30] C. Wang, J. B. Sheridan, H.-J. Chung, M. L. Coté, R. A. Lalancette, A. L. Rheingold, *J. Am. Chem. Soc.* **1994**, *116*, 8966−8972.
[31] R. Aumann, H.-J. Weidenhaupt, *Chem. Ber.* **1987**, *120*, 23−27.
[32] J. H. Rigby, G. Ahmed, *Tetrahedron Lett*. **1993**, *34*, 5397−5400.
[33] M. H. Quick, R. J. Angelici, K. J. Reimer, A. Shaver, *Inorg. Synth*. **1990**, *28*, 156.
[34] G. Winkhaus, L. Pratt, G. Wilkinson, *J. Chem. Soc*. **1961**, 3807.
[35] L. Brandsma, H. D. Verkruijsse, *Studies in Organic Chemistry, Synthesis of Acetylenes, Allenes and Cumulenes*, vol. 8, Elsevier Scientific Publishing Company, Amsterdam, Oxford, New York, **1981**.
[36] Crystallographic data (excluding structure factors) for the structure reported in this paper has been deposited at the Cambridge Crystallographic Data Centre as supplementary publication no. CCDC-103095. Copies of the data can be obtained free of charge on application to CCDC, 12 Union Road, Cambridge CB2 1EZ, UK [Fax: int. code + 44-1223/336-033; E-mail: deposit@ccdc.cam.ac.uk].
[37] G. M. Sheldrick, *SHELXS-97, Program for Crystal Structure Solution*, Universität Göttingen, **1997**.
[38] G. M. Sheldrick, *SHELXL-97, Program for Crystal Structure Refinement*, Universität Göttingen, **1997**.

Received October 28, 1998
[I98373]

Electron-Sink Behaviour of the Carbonylnickel Clusters $[Ni_{32}C_6(CO)_{36}]^{6-}$ and $[Ni_{38}C_6(CO)_{42}]^{6-}$: Synthesis and Characterization of the Anions $[Ni_{32}C_6(CO)_{36}]^{n-}$ (n = 5–10) and $[Ni_{38}C_6(CO)_{42}]^{n-}$ (n = 5–9) and Crystal Structure of $[PPh_3Me]_6[Ni_{32}C_6(CO)_{36}] \cdot 4$ MeCN

Francesca Calderoni,[a] Francesco Demartin,[b] Fabrizia Fabrizi de Biani,[c] Cristina Femoni,[a] M. Carmela Iapalucci,[a] Giuliano Longoni,*[a] and Piero Zanello[c]

Keywords: Nickel / Carbonyl complexes / Carbides / Structure elucidation / Electrochemistry

The hexacarbide clusters $[H_{6-n}Ni_{38}C_6(CO)_{42}]^{n-}$ (n = 3, 4, 5, or 6) have been directly obtained from the reaction of $[Ni_6(CO)_{12}]^{2-}$ with C_3Cl_6, whereas the related anions, $[H_{6-n}Ni_{32}C_6(CO)_{36}]^{n-}$ (n = 5 or 6), have been obtained by degradation under carbon monoxide of $[Ni_{38}C_6(CO)_{42}]^{6-}$, or upon thermal treatment at ca. 110 °C of $[Ni_{10}C_2(CO)_{16}]^{2-}$ salts. The compound $[PPh_3Me]_6[Ni_{32}C_6(CO)_{36}] \cdot 4$ MeCN is triclinic, space group $P\bar{1}$ (No 2), with a = 15.974(3), b = 17.474(3), c = 18.200(4) Å, α = 61.37(2), β = 69.31(2), γ = 72.35(2)° and Z = 1; final R = 0.033. The structure of $[Ni_{32}C_6(CO)_{36}]^{6-}$ has an idealised O_h symmetry and is based on a truncated octahedral $Ni_{32}C_6$ framework, with all edges spanned by bridging carbonyl groups. The six interstitial carbide atoms are lodged in square-antiprismatic cavities. The overall geometry of the $Ni_{32}C_6$ core is very similar to that found previously in $[HNi_{38}C_6(CO)_{42}]^{5-}$, and shows very close interatomic separations. Both $[Ni_{32}C_6(CO)_{36}]^{6-}$ and $[H_{6-n}Ni_{38}C_6(CO)_{42}]^{n-}$ (n = 5 or 6) display electron-sink behaviour. Thus, they have been chemically and electrochemically reduced to their corresponding $[Ni_{32}C_6(CO)_{36}]^{n-}$ (n = 7–10), $[Ni_{38}C_6(CO)_{42}]^{n-}$ (n = 7–9) and $[HNi_{38}C_6(CO)_{42}]^{n-}$ (n = 6–8) derivatives, and several of the involved redox changes show features of electrochemical reversibility. In contrast, both $[Ni_{32}C_6(CO)_{36}]^{6-}$ and $[H_{6-n}Ni_{38}C_6(CO)_{42}]^{n-}$ (n = 5 or 6) support only one partially reversible oxidation step. Their different behaviour upon protonation or oxidation is an indirect, but unambiguous, proof of the hydride nature of $[HNi_{32}C_6(CO)_{36}]^{5-}$ and $[H_{6-n}Ni_{38}C_6(CO)_{42}]^{n-}$ (n = 3, 4, or 5), which could not be validated by ^{1}H-NMR spectroscopy.

Introduction

Homoleptic carbonyl transition metal clusters show little propensity for multiple redox changes.[1−3] Only some exceptional compounds feature different (three or more) oxidation states which are stable, or sufficiently long-lived, to permit isolation or spectroscopic characterisation of the species. Among these exceptions there are examples of both homo-, e.g. $[Ir_{14}(CO)_{27}]^{n-}$ (n = 0, 1, 2),[4] and heterometallic clusters, e.g. $[Fe_3Pt_3(CO)_{15}]^{n-}$ (n = 0, 1, 2),[5,6] $[Ag_{13}Fe_8(CO)_{32}]^{n-}$ (n = 3, 4, 5),[7] and $[AuFe_4(CO)_{16}]^{n-}$ (n = 1, 2, 3);[8] a few more associate group 14−16 elements, e.g. $[Co_{13}C_2(CO)_{30}]^{n-}$ (n = 3, 4, 5, 6),[9,2c] $[Co_9Si(CO)_{23}]^{n-}$ (n = 2, 3, 5),[10] $[Ni_{11}Bi_2(CO)_{18}]^{n-}$ (n = 2, 3, 4),[11] $[Ni_{13}Sb_2(CO)_{24}]^{n-}$ (n = 2, 3, 4),[12] and $[Fe_5S_2(CO)_{14}]^{n-}$ (n = 0, 1, 2),[13] in their cluster cores. EHMO[6,7b,8] as well as LDF[14] calculations suggest that the redox aptitude of some clusters descends from ad hoc electronic conditions such as the presence within the HOMO-LUMO gap of a low-lying delocalised orbital, non-bonding or slightly antibonding in character; this can be filled or depleted of electrons without significant destabilisation of the cluster. In other cases, such as $[Co_{13}C_2(CO)_{30}]^{n-}$ and $[Co_9Si(CO)_{23}]^{n-}$, a synergy between steric (good fit of the cavity) and electronic (extra-stabilisation arising from Co−C or Co−Si bonds) effects seems to be operative.

Only very few homoleptic carbonyl clusters, viz. $[Pt_{19}(CO)_{22}]^{4-}$,[15,2c] $[Pt_{24}(CO)_{30}]^{2-}$,[16] and $[HFe_6Pd_6(CO)_{24}]^{3-}$[17] display a wider redox aptitude. In particular the former two homometallic clusters undergo two consecutive pairs of close-spaced one-electron reductions, as well as two close-spaced one-electron oxidations. Several of the above redox changes display features of electrochemical reversibility, even if most electrogenerated species are only stable on the timescale of cyclic voltammetry.

Multivalent carbonyl metal clusters are of interest for several reasons. First of all, the knowledge of their structural parameters and/or spectroscopic behaviour can validate their theoretical analysis (a procedure defined by L. F. Dahl as 'experimental quantomechanics'). Secondly, the intrinsically paramagnetic odd-electron species are molecular quantum dots.[14] Finally, anionic multivalent clusters in conjunction with cationic multivalent counterparts may give rise to ionic materials, hopefully with interesting electronic and magnetic behaviour. Ionic solids in which both

[a] Diportimento di Chimica Fisida ed Inorganica, University of Bologna,
viale Risorgimento 4, I-40136 Bologna, Italy
Fax: (internat.) +39-051/6443690
E-mail: longoni@ms.fci.unibo.it
[b] Dipartimento di Chimica Strutturale e Stereochimica Inorganica, Univerity of Milano,
via Venezian 21, I-20133 Milano, Italy
[c] Dipartimento di Chimica, University of Siena,
Pian dei Mantellini 44, I-53100 Siena, Italy

 © WILEY-VCH Verlag GmbH, D-69451 Weinheim, 1999 1434−1948/99/0404−0663 $ 17.50+.50/0

the cation and the anion are organometallic clusters have already been prepared.[18]

In the search for new multivalent anionic systems we re-investigated the chemistry of the nickel carbido-carbonyl clusters.[19] As a result, we report the synthesis and chemical and structural characterisation of the $[Ni_{32}C_6(CO)_{36}]^{6-}$ and $[HNi_{32}C_6(CO)_{36}]^{5-}$ clusters. The study of the electrochemical redox behaviour of both $[Ni_{32}C_6(CO)_{36}]^{6-}$ and $[H_{6-n}Ni_{38}C_6(CO)_{42}]^{n-}$ (n = 5 or 6) points out that these clusters show electron-sink features. Both compounds withstand several reversible electrochemical and chemical reduction steps. In contrast, they feature only a single one-electron oxidation step and the resulting species of this exhibits a limited stability. This lack of propensity for oxidation provides indirect but unambiguous proof of the hydride nature of $[HNi_{32}C_6(CO)_{36}]^{5-}$ and $[H_{6-n}Ni_{38}C_6(CO)_{42}]^{n-}$ (n = 3, 4, or 5), which could not be validated by proton NMR experiments.

Preliminary reports on the synthesis and structure of $[Ni_{32}C_6(CO)_{36}]^{6-}$ and $[HNi_{38}C_6(CO)_{42}]^{5-}$ have already appeared.[20][21]

Results and Discussion

Synthesis, Chemical Reactivity, and Spectroscopic Behaviour of $[HNi_{32}C_6(CO)_{36}]^{5-}$, $[Ni_{32}C_6(CO)_{36}]^{n-}$ (n = 5−8), $[H_{6-n}Ni_{38}C_6(CO)_{42}]^{n-}$ (n = 3−5), and $[Ni_{38}C_6(CO)_{42}]^{n-}$ (n = 5−8)

Previous work carried out showed that the reaction of the $[Ni_6(CO)_{12}]^{2-}$ dianion with C_3Cl_6 in THF or acetone as solvent leads to the formation of the $[HNi_{38}C_6(CO)_{42}]^{5-}$ hexacarbide cluster in low yields.[20] A re-investigation of the above reaction has shown that slight modifications of the reaction procedure have beneficial effects on the yields. In particular, the changes include: i) the use of a dild. THF solution of C_3Cl_6 which is slowly added in small portions to a THF solution of $[NEt_4]_2[Ni_6(CO)_{12}]$ up to a 1:2 molar ratio, ii) the continuous removal of the reaction atmosphere with a slow stream of nitrogen to avoid the build-up of a carbon monoxide partial pressure, and iii) the cooling of the reaction solution at ca. −15°C to minimise the stripping of $Ni(CO)_4$ vapour. Under these conditions, IR monitoring of the reaction shows that $[Ni_6(CO)_{12}]^{2-}$ is initially oxidised by C_3Cl_6 to $[Ni_7(CO)_{15}]^{2-}$ and $[Ni_9(CO)_{18}]^{2-}$; this step requires ca. 0.3 moles of C_3Cl_6 per mol of $[Ni_6(CO)_{12}]^{2-}$. The subsequent addition of a similar amount of C_3Cl_6 gives rise to a solution containing $Ni(CO)_4$, a yet uncharacterised brown species [ν_{CO} in THF at 2019 (s), 1856 (mw), and 1829 (sh) cm^{-1}] and a dark precipitate. At this stage the reaction mixture is left to stand for 24−48 hours at room temp. under a static nitrogen atmosphere. During this period it precipitates further. Extraction of the precipitate with acetone, acetonitrile, and DMSO sequentially affords three fractions containing $[H_2Ni_{38}C_6(CO)_{42}]^{4-}$, $[HNi_{38}C_6(CO)_{42}]^{5-}$, and $[Ni_{38}C_6(CO)_{42}]^{6-}$ respectively. Formation of the $[H_{6-n}Ni_{38}C_6(CO)_{42}]^{n-}$ (n = 4, 5) hydrides, in addition to the parent $[Ni_{38}C_6(CO)_{42}]^{6-}$ hexaanion, can probably be ascribed to the intrinsic acidity of the reaction solution owing to formation of Ni^{2+} salts during the reaction, and the presence of humidity. The above mixture can be converted into pure $[NEt_4]_6[Ni_{38}C_6(CO)_{42}]$ by direct extraction of the residue in DMSO and precipitation with water. Other quaternary ammonium or phosphonium salts of $[Ni_{38}C_6(CO)_{42}]^{6-}$ have been isolated by metathesis with their corresponding halides in DMSO and precipitation with water.

Addition of stoichiometric amounts of acids yields further products, e.g. dild. H_2SO_4, to an acetonitrile solution of $[Ni_{38}C_6(CO)_{42}]^{6-}$ sequentially, affords $[HNi_{38}C_6(CO)_{42}]^{5-}$ and $[H_2Ni_{38}C_6(CO)_{42}]^{4-}$, as shown by a progressive shift to higher wavenumbers of the carbonyl absorptions. The latter is obtained in a spectroscopically pure form only on switching to acetone as solvent. In this latter solvent addition of a further amount of acid leads to the formation of $[H_3Ni_{38}C_6(CO)_{42}]^{3-}$, which slowly decomposes to an (as yet) uncharacterised species. The $[H_{6-n}Ni_{38}C_6(CO)_{42}]^{n-}$ (n = 3−5), as well as the related $[Ni_{38}C_6(CO)_{42}]^{n-}$ (n = 5−8) species (see below), share a common characteristic infrared pattern consisting of three equally intense bands, one in the terminal and two in the edge bridging region; the absorptions wavenumbers of all above compounds are collected in Table 1. We have been unable to directly and unambiguously demonstrate the presence of hydride atoms by ^1H NMR spectroscopy in any of the $[H_{6-n}Ni_{38}C_6(CO)_{42}]^{n-}$ (n = 3−5) derivatives, probably as a result of the too low molar concentrations which can be obtained in both acetone and acetonitrile. However, as previously reported, the apparent partial or quantitative reduction occurring on dissolving the $[H_{6-n}Ni_{38}C_6(CO)_{42}]^{n-}$ (n = 3−5) salts in organic solvents with increasing dielectric constants can only be reasonably interpreted as due to the occurrence in solution of protonation-deprotonation equilibria, such as those reported in Eq. (1) and (2).

Table 1. Infrared carbonyl absorptions (± 2 cm^{-1}) of the $[H_{6-n}Ni_{38}C_6(CO)_{42}]^{n-}$ (n = 3−6) and $[Ni_{38}C_6(CO)_{42}]^{n-}$ (n = 5−8) derivatives

Compound	Solvent	ν_{CO} [cm^{-1}]
$[H_3Ni_{38}C_6(CO)_{42}]^{3-}$	acetone	2031 (s), 1920 (s), 1902 (s)
$[H_2Ni_{38}C_6(CO)_{42}]^{4-}$	acetone	2016 (s), 1909 (s), 1892 (s)
$[HNi_{38}C_6(CO)_{42}]^{5-}$	acetone	2006 (s), 1891 (s), 1878 (s)
$[HNi_{38}C_6(CO)_{42}]^{5-}$	acetonitrile	2005 (s), 1890 (s), 1876 (s)
$[Ni_{38}C_6(CO)_{42}]^{5-}$	acetonitrile	2006 (s), 1889 (s), 1875 (s)
$[Ni_{38}C_6(CO)_{42}]^{6-}$	acetonitrile	1992 (s), 1877 (s), 1862 (s)
$[Ni_{38}C_6(CO)_{42}]^{6-}$	DMF	1989 (s), 1874 (s), 1859 (s)
$[Ni_{38}C_6(CO)_{42}]^{7-}$	DMF	1978 (s), 1858 (s), 1847 (s)
$[Ni_{38}C_6(CO)_{42}]^{8-}$	DMF	1960 (s), 1845 (s), 1832 (s)

$$[H_2Ni_{38}C_6(CO)_{42}]^{4-} \xrightleftharpoons{MeCN} [HNi_{38}C_6(CO)_{42}]^{5-} + H^+ \quad (1)$$

$$[HNi_{38}C_6(CO)_{42}]^{5-} \xrightleftharpoons{DMSO} [Ni_{38}C_6(CO)_{42}]^{6-} + H^+ \quad (2)$$

Moreover, the presence of hydride atoms has now been indirectly, but unambiguously, proved by the electrochemical experiments (see below).

The $[Ni_{38}C_6(CO)_{42}]^{6-}$ hexaanion in DMF is sequentially reduced by the addition of a sodium/naphthalene solution to the corresponding $[Ni_{38}C_6(CO)_{42}]^{7-}$ and $[Ni_{38}C_6(CO)_{42}]^{8-}$ polyanions. Both these two new derivatives show the characteristic IR pattern of the parent compound and are apparently stable in solution under a nitrogen atmosphere for several hours. Nevertheless, their attempted isolation by precipitation with quaternary ammonium or phosphonium salts failed owing to their partial or complete reoxidation to the hexaanion. Addition of a further amount of the reducing agent to $[Ni_{38}C_6(CO)_{42}]^{8-}$ causes a further shift of the carbonyl absorptions to lower wavenumber; however, the IR pattern appears less distinctive and this can probably be attributed to a $[Ni_{38}C_6(CO)_{42}]^{9-}$ species, as in this instance the band due to the stretching of edge bridging carbonyls is too close to the carbonyl infrared band of DMF.

The $[Ni_{38}C_6(CO)_{42}]^{8-}$ is sequentially oxidised by stoichiometric amounts of tropylium tetrafluoroborate to $[Ni_{38}C_6(CO)_{42}]^{7-}$, $[Ni_{38}C_6(CO)_{42}]^{6-}$, and $[Ni_{38}C_6(CO)_{42}]^{5-}$. The $[Ni_{38}C_6(CO)_{42}]^{5-}$ pentaanion shows infrared carbonyl absorptions practically coincident with those of $[HNi_{38}C_6(CO)_{42}]^{5-}$; however, the different nature of the two is pointed out by the fact that the former is observed in a highly ionising medium such as DMF, where the latter undergoes a ready deprotonation. Addition of one further equiv. of tropylium tetrafluoroborate to $[Ni_{38}C_6(CO)_{42}]^{5-}$ results in its complete decomposition to $Ni(CO)_4$ and an insoluble amorphous black material. The failure to obtain infrared spectroscopic evidence for the possible existence of $[Ni_{38}C_6(CO)_{42}]^{n-}$ ($n = 3, 4$) upon oxidation with tropylium tetrafluoroborate can also be taken as circumstantial evidence of the hydride nature of the $[H_{6-n}Ni_{38}C_6(CO)_{42}]^{n-}$ ($n = 3, 4, 5$) derivatives resulting upon addition of protonic acids to $[Ni_{38}C_6(CO)_{42}]^{6-}$. The enhanced stability of $[H_{6-n}Ni_{38}C_6(CO)_{42}]^{n-}$ ($n = 3-5$) with respect to their corresponding $[Ni_{38}C_6(CO)_{42}]^{n-}$ ($n = 3-5$) anions can probably be ascribed to the fact that protonation, in contrast to oxidation, leaves unchanged the number of valence electrons of the cluster.

The $[H_{6-n}Ni_{38}C_6(CO)_{42}]^{n-}$ ($n = 4$ and 5) derivative is unstable with respect to carbon monoxide at atmospheric pressure and decomposes principally to a mixture of $Ni(CO)_4$ and an insoluble black material. Only minor amounts of the new $[Ni_{32}C_6(CO)_{36}]^{6-}$ hexaanion could be recovered. For $n = 4$, the decomposition above is probably favoured by the instability of the corresponding $[H_2Ni_{32}C_6(CO)_{36}]^{4-}$ species (vide infra). In contrast, the $[Ni_{38}C_6(CO)_{42}]^{6-}$ hexaanion affords $[Ni_{32}C_6(CO)_{36}]^{6-}$ almost quantitatively according to Eq. (3).

$$[Ni_{38}C_6(CO)_{42}]^{6-} + 18\ CO \underset{CO\ (1\ atm)}{\overset{MeCN,}{\rightleftharpoons}} [Ni_{32}C_6(CO)_{36}]^{6-} + 6\ Ni(CO)_4 \quad (3)$$

The equilibrium (Eq. 3) is shifted to the right by removal of $Ni(CO)_4$ under vacuum and re-exposure of the solution to a carbon monoxide atmosphere. IR monitoring of the reaction initially shows the appearance of $Ni(CO)_4$ and a change in the pattern of the carbonyl absorptions. As the reaction proceeds, the absorption attributed to the terminal carbonyl groups progressively weakens and the two bands attributed to the edge bridging carbonyls collapse into a single absorption centred at slightly higher wavenumber. The intermediate IR patterns are suggestive of the possible formation of $[Ni_{38-x}C_6(CO)_{42-x}]^{6-}$ ($x = 1-5$) species by stepwise loss of Ni(CO) moieties. It should be noted that members of the $[Ni_{38-x}C_6(CO)_{42-x}]^{6-}$ ($x = 0-6$) series of compounds would always have $6N + 19$ filled cluster valence orbitals; therefore each one of them is sterically and electronically feasible. Previously reported examples of such behaviour include the $[Ni_{10}C(CO)_{18}]^{2-}$–$[Ni_8C(CO)_{16}]^{2-}$,[19a] $[Ni_{12}C_2(CO)_{16}]^{4-}$–$[Ni_{11}C_2(CO)_{15}]^{4-}$,[19e] $[Ni_{12}Ge(CO)_{22}]^{2-}$–$[Ni_{10}Ge(CO)_{20}]^{2-}$,[22] and $[Ni_{35}C_4(CO)_{39}]^{6-}$–$[Ni_{34}C_4(CO)_{38}]^{6-}$[19d] sets of compounds. The resulting $[Ni_{32}C_6(CO)_{36}]^{6-}$ hexaanion shows a single sharp carbonyl absorption in the region of edge-bridging carbonyls (see Table 2). Although the $[Ni_{32}C_6(CO)_{36}]^{6-}$ hexaanion is also not indefinitely stable under a carbon monoxide atmosphere, its decomposition is slow. As a result, it has been isolated in yields of ca. 80% by monitoring the reaction with IR, and removal of the carbon monoxide atmosphere and $Ni(CO)_4$ as soon as the equilibrium (Eq. 3) has shifted to the right.

Table 2. Infrared carbonyl absorptions (± 2 cm^{-1}) of the $[HNi_{32}C_6(CO)_{36}]^{5-}$ and $[Ni_{32}C_6(CO)_{36}]^{n-}$ ($n = 5-8$) derivatives

Compound	Solvent	ν_{CO} [cm^{-1}]
$[HNi_{32}C_6(CO)_{36}]^{5-}$	acetone	1911 (s)
$[Ni_{32}C_6(CO)_{36}]^{5-}$	DMF	1905 (s)
$[Ni_{32}C_6(CO)_{36}]^{6-}$	acetonitrile	1888 (s)
$[Ni_{32}C_6(CO)_{36}]^{6-}$	DMF	1889 (s)
$[Ni_{32}C_6(CO)_{36}]^{7-}$	DMF	1872 (s)
$[Ni_{32}C_6(CO)_{36}]^{8-}$	DMF	1851 (s)

Formation of small amounts of $[Ni_{32}C_6(CO)_{36}]^{6-}$ often occurs upon thermal treatment of the majority of nickel carbide clusters, including monocarbides such as $[Ni_9C(CO)_{17}]^{2-}$. However, the best results have been obtained by using the $[Ni_{10}C_2(CO)_{16}]^{2-}$ dicarbide as the starting material.[19b] Thermal decomposition of this dicarbide in diglyme affords $[Ni_{32}C_6(CO)_{36}]^{6-}$, approximately according to Eq. 4.

$$5\ [Ni_{10}C_2(CO)_{16}]^{2-} \xrightarrow{110\ °C} [Ni_{16}C_4(CO)_{23}]^{4-} + [Ni_{32}C_6(CO)_{36}]^{6-} + 2\ Ni(CO)_4 + 13\ CO \quad (4)$$

The salts of $[Ni_{32}C_6(CO)_{36}]^{6-}$ separate out from the reaction solution, together with some insoluble inorganic material, owing to their very low solubility in diglyme. Their tetrasubstituted ammonium and phosphonium salts have been purified by extraction in MeCN and precipitated by layering di-isopropyl ether.

The chemical reactivity of $[Ni_{32}C_6(CO)_{36}]^{6-}$ is similar but not coincident with that of the parent $[Ni_{38}C_6(CO)_{42}]^{6-}$.

The major difference is represented by the decreased propensity of $[Ni_{32}C_6(CO)_{36}]^{6-}$ to partially substitute its free negative charge with hydrogen atoms upon protonation. Thus, addition of acid to an acetonitrile solution of $[Ni_{32}C_6(CO)_{36}]^{6-}$ gives rise only to trace amounts of $[HNi_{32}C_6(CO)_{36}]^{5-}$. This arises from the fact that in acetonitrile the equilibrium (Eq. 5) is shifted to the right, and can be moved to the left only on using acetone as the solvent.

$$[HNi_{32}C_6(CO)_{36}]^{5-} \overset{MeCN}{\rightleftharpoons} [Ni_{32}C_6(CO)_{36}]^{6-} + H^+ \quad (5)$$

In this solvent $[HNi_{32}C_6(CO)_{36}]^{5-}$ is stable and has been isolated in the solid state by precipitation with isopropyl alcohol. Attempts to further protonate $[HNi_{32}C_6(CO)_{36}]^{5-}$ only resulted in decomposition to $Ni(CO)_4$ and as yet uncharacterised materials. The instability of the $[H_{6-n}Ni_{32}C_6(CO)_{36}]^{n-}$ ($n = 3-5$) hydrides is in keeping with the reported failures above to degrade the corresponding $[H_{6-n}Ni_{38}C_6(CO)_{42}]^{n-}$ salts with carbon monoxide.

As with $[Ni_{38}C_6(CO)_{42}]^{6-}$, the $[Ni_{32}C_6(CO)_{36}]^{6-}$ hexaanion is progressively reduced by a solution of sodium/naphthalene in DMF to the corresponding $[Ni_{32}C_6(CO)_{36}]^{7-}$ and $[Ni_{32}C_6(CO)_{36}]^{8-}$ polyanions, as shown by a concomitant shift to lower wavenumber of their unique carbonyl absorption (see Table 2). IR monitoring shows that both species are stable at room temp. for at least several hours. The reaction is perfectly reversible upon addition of a DMF solution of tropylium tetrafluoroborate. The $[Ni_{32}C_6(CO)_{36}]^{7-}$ intermediate and the parent $[Ni_{32}C_6(CO)_{36}]^{6-}$ hexaanion are regenerated quantitatively. So far, all attempts to isolate the $[Ni_{32}C_6(CO)_{36}]^{7-}$ and $[Ni_{32}C_6(CO)_{36}]^{8-}$ salts have met with little success owing to their partial or complete reoxidation to $[Ni_{32}C_6(CO)_{36}]^{6-}$ during the workup. Addition of a further equiv. of tropylium tetrafluoroborate to $[Ni_{32}C_6(CO)_{36}]^{6-}$ causes the appearance of an infrared absorption practically coincident with that of $[HNi_{32}C_6(CO)_{36}]^{5-}$; however, this is assigned to $[Ni_{32}C_6(CO)_{36}]^{5-}$, in view of the fact that Eq. 5 is already shifted to the right in acetonitrile. Furthermore, $[HNi_{32}C_6(CO)_{36}]^{5-}$ salts obtained as above are instantaneously and completely deprotonated to the parent hexaanion once dissolved in DMF.

All $[Ni_{32}C_6(CO)_{36}]^{n-}$, as well as $[Ni_{38}C_6(CO)_{42}]^{n-}$ species with an odd n value contain an odd number of electrons and should, therefore, be paramagnetic. However their solutions in organic solvents such as DMF and *N*-methylpyrrolidinone do not display any significant EPR signal at any temperature (150−300 K). It is worth mentioning that such an unfortunate behaviour is featured by several previously reported odd-electron clusters, e.g. $Ni_3Cp_3S_2$[23] and $[Ni_{11}Bi_2(CO)_{18}]^{3-}$;[11] the latter does exhibit an enormously broad EPR signal but only in the solid state. As a result, their formulation is based exclusively upon their chemical and electrochemical behaviour.

X ray Crystal Structure of $[PPh_3Me]_6[Ni_{32}C_6(\mu\text{-}CO)_{36}]\cdot 4$ MeCN

The unit cell of $[PPh_3Me]_6[Ni_{32}C_6(\mu\text{-}CO)_{36}]\cdot 4$ MeCN contains one molecular anion located on a crystallographic inversion centre, six cations, and four acetonitrile molecules. A view of the structure of the $[Ni_{32}C_6(CO)_{36}]^{6-}$ hexaanion is reported in Figure 1. Selected interatomic distances and angles are given in Table 3. The truncated octahedral $Ni_{32}C_6$ framework of $[Ni_{32}C_6(CO)_{36}]^{6-}$, which shows an overall idealized O_h symmetry (Figure 2), is identical to the corresponding fragment previously found in $[HNi_{38}C_6(CO)_{42}]^{5-}$,[20] with very close interatomic separations. A formal stepwise construction of the metal skeletons of the two is shown in Figure 3. The inner part of both clusters constitutes a Ni_8 empty cube ($Ni-Ni_{av}$ = 2.397 Å, vs. 2.402 Å in $[HNi_{38}C_6(CO)_{42}]^{5-}$) with all six faces capped by carbon atoms, which describe a nonbonded C_6 octahedron. This inner Ni_8C_6 moiety is surrounded by a truncated-octahedral Ni_{24} shell {$Ni-Ni_{av}$ = 2.461 Å vs. 2.459 Å in $[HNi_{38}C_6(CO)_{42}]^{5-}$} in such a way as to generate six square-antiprismatic cavities lodging the six carbide atoms ($Ni-C_{av}$ = 2.062 Å). Each nickel atom of the inner cube lies ca. 0.93 Å underneath the centre of each hexagonal face of the outer Ni_{24} shell {av. $Ni_{inner}-Ni_{outer}$ = 2.634 Å vs. 2.633 Å in $[HNi_{38}C_6(CO)_{42}]^{5-}$} and is 12-coordinate being at a bond distance from 6 nickel atoms of the outer shell, 3 nickel atoms of the inner cube and 3 carbide atoms.

In the solid state, $[Ni_{32}C_6(CO)_{36}]^{6-}$ shows the presence of edge-bridging carbonyl groups only ($Ni-C_{av}$ = 1.917; $C-O_{av}$ = 1.152 Å), which span all Ni−Ni edges of the outer Ni_{24} shell. The above carbonyl stereochemistry is also retained in solution, as shown by the infrared spectrum of $[Ni_{32}C_6(CO)_{36}]^{6-}$, which only consists of one strong absorption in the bridging region.

An interesting structural feature of $[Ni_{32}C_6(CO)_{36}]^{6-}$ is represented by the presence of eight distorted hexagonal cups formed by subsequent concentric rings of oxygen, carbon, and nickel atoms, and ending with a unique nickel atom belonging to the inner cube. Addition of six Ni(CO) fragments to six of the above eight cups generates $[Ni_{38}C_6(CO)_{42}]^{6-}$. It may be questioned as to why two opposite cups have been left empty and whether a $[Ni_{40}C_6(CO)_{44}]^{6-}$ species could be possible or not. It is conceivable that the existence of the latter is unlikely owing to the shrinking of the carbonyl groups on those two empty cups, which releases the steric pressure brought about by the progressive entrance of the six Ni(CO) fragments in the others.

Electrochemical Behaviour of $[Ni_{38}C_6(CO)_{42}]^{6-}$ and $[Ni_{32}C_6(CO)_{36}]^{6-}$

The high redox aptitude of $[Ni_{32}C_6(CO)_{36}]^{6-}$ in acetonitrile solution is illustrated in Figure 4. The cyclic voltammogram displays five sequential electron transfer steps possessing features of chemical reversibility. Voltammetry at a platinum electrode with periodical renewal of the diffusion

Table 3. Interatomic distances [Å] and angles [deg.] within the $[Ni_{32}C_6(CO)_{36}]^{6-}$ anion[a]

a) Metal-metal distances

i) within the inner cubic Ni_8 moiety

Ni1−Ni2	2.391(1)	Ni2−Ni3	2.400(1)
Ni1−Ni3′	2.403(1)	Ni2−Ni4′	2.399(1)
Ni1−Ni4	2.398(1)	Ni3−Ni4	2.392(1)
<Ni−Ni>	2.397		

ii) from the inner cubic Ni_8 moiety to the external Ni_{24} shell

Ni1−Ni7	2.633(1)	Ni3−Ni5	2.650(1)
Ni1−Ni8	2.646(1)	Ni3−Ni6	2.633(1)
Ni1−Ni10	2.630(1)	Ni3−Ni11′	2.640(1)
Ni1−Ni11	2.633(1)	Ni3−Ni12′	2.617(1)
Ni1−Ni13	2.647(1)	Ni3−Ni13′	2.652(1)
Ni1−Ni14	2.614(1)	Ni3−Ni16′	2.620(1)
Ni2−Ni5	2.630(1)	Ni4−Ni6	2.625(1)
Ni2−Ni8	2.639(1)	Ni4−Ni7	2.646(1)
Ni2−Ni9′	2.615(1)	Ni4−Ni9	2.620(1)
Ni2−Ni12′	2.647(1)	Ni4−Ni10	2.634(1)
Ni2−Ni14	2.642(1)	Ni4−Ni15′	2.652(1)
Ni2−Ni15	2.628(1)	Ni4−Ni16′	2.636(1)
<Ni−Ni>	2.634		

iii) within the external Ni_{24} shell

Ni5−Ni6	2.466(1)	Ni9−Ni12	2.464(1)
Ni5−Ni8	2.449(1)	Ni9−Ni15′	2.469(1)
Ni5−Ni12′	2.460(1)	Ni10−Ni11	2.462(1)
Ni6−Ni7	2.457(1)	Ni11−Ni12	2.451(1)
Ni6−Ni16′	2.468(1)	Ni11−Ni13	2.460(1)
Ni7−Ni8	2.468(1)	Ni13−Ni14	2.455(1)
Ni7−Ni10	2.471(1)	Ni13−Ni16	2.465(1)
Ni8−Ni14	2.453(1)	Ni14−Ni15	2.458(1)
Ni9−Ni10	2.464(1)	Ni15−Ni16	2.462(1)
<Ni−Ni>	2.461		

b) Ni−C(carbide)

Ni1−C_a	2.017(4)	Ni9−C_b	2.104(4)
Ni2−C_a	2.009(4)	Ni10−C_b	2.115(3)
Ni3−C_a	2.014(4)	Ni11−C_b	2.119(4)
Ni4−C_a	2.000(4)	Ni12−C_b	2.115(4)
Ni5−C_a	2.115(4)	Ni1−C_c	2.004(4)
Ni6−C_a	2.096(4)	Ni2−C_c	2.016(4)
Ni7−C_a	2.116(4)	Ni3′−C_c	1.999(4)
Ni8−C_a	2.136(4)	Ni4′−C_c	2.031(4)
Ni1−C_b	2.005(4)	Ni13−C_c	2.119(4)
Ni2′−C_b	2.021(4)	Ni14−C_c	2.115(4)
Ni3′−C_b	2.004(3)	Ni15−C_c	2.113(4)
Ni4−C_b	2.007(4)	Ni16−C_c	2.105(4)

c) Ni−C−O(carbonyl)

Ni5−C1	1.923(4)	Ni11−C6	1.929(4)
Ni5−C4	1.926(4)	Ni11−C7	1.903(4)
Ni5−C13	1.888(4)	Ni11−C18	1.915(4)
Ni6−C1	1.923(4)	Ni12−C7	1.910(4)
Ni6−C2	1.918(5)	Ni12−C8′	1.911(4)
Ni6−C14′	1.914(5)	Ni12−C13′	1.906(4)
Ni7−C2	1.926(5)	Ni13−C9	1.933(5)
Ni7−C3	1.907(5)	Ni13−C12	1.912(5)
Ni7−C15	1.921(5)	Ni13−C18	1.895(5)
Ni8−C3	1.942(5)	Ni14−C9	1.922(5)
Ni8−C4	1.919(4)	Ni14−C10	1.902(5)
Ni8−C16	1.893(5)	Ni14−C16	1.910(5)
Ni9−C5′	1.906(5)	Ni15−C10	1.944(5)
Ni9−C8′	1.915(4)	Ni15−C11	1.924(5)
Ni9−C17′	1.936(5)	Ni15−C17	1.902(4)
Ni10−C5′	1.930(5)	Ni16−C11	1.932(5)
Ni10−C6	1.930(4)	Ni16−C12	1.916(4)
Ni10−C15	1.911(5)	Ni16−C14	1.910(5)
C1−O1	1.154(5)	C10−O10	1.145(5)
C2−O2	1.157(5)	C11−O11	1.148(5)
C3−O3	1.160(5)	C12−O12	1.149(5)
C4−O4	1.159(5)	C13−O13	1.152(5)
C5−O5	1.148(5)	C14−O14	1.135(5)
C6−O6	1.152(5)	C15−O15	1.134(5)
C7−O7	1.164(5)	C16−O16	1.164(5)
C8−O8	1.154(5)	C17−O17	1.145(5)
C9−O9	1.161(5)	C18−O18	1.150(5)
Ni5−C1−Ni6	79.8(2)	Ni14−C10−Ni15	79.4(2)
Ni5−C1−O1	140.6(4)	Ni14−C10−O10	140.5(4)
Ni6−C1−O1	139.6(4)	Ni15−C10−O10	140.1(4)
Ni6−C2−Ni7	79.5(2)	Ni15−C11−Ni16	79.4(2)
Ni6−C2−O2	139.6(4)	Ni15−C11−O11	140.2(4)
Ni7−C2−O2	140.9(4)	Ni16−C11−O11	140.4(4)
Ni7−C3−Ni8	79.8(2)	Ni13−C12−Ni16	80.2(2)
Ni7−C3−O3	140.7(4)	Ni13−C12−O12	141.0(4)
Ni8−C3−O3	139.5(4)	Ni16−C12−O12	138.8(4)
Ni5−C4−Ni8	79.1(2)	Ni5−C13−Ni12′	80.8(2)
Ni5−C4−O4	139.1(4)	Ni5−C13−O13	140.6(3)
Ni8−C4−O4	141.6(4)	Ni12′−C13−O13	138.6(3)
Ni9′−C5−Ni10′	79.9(2)	Ni6′−C14−Ni16	80.4(2)
Ni9′−C5−O5	139.7(4)	Ni6′−C14−O14	139.7(4)
Ni10′−C5−O5	140.3(4)	Ni16−C14−O14	139.9(4)
Ni10−C6−Ni11	79.3(2)	Ni7−C15−Ni10	80.3(2)
Ni10−C6−O6	140.0(4)	Ni7−C15−O15	139.6(4)
Ni11−C6−O6	140.6(4)	Ni10−C15−O15	140.1(4)
Ni11−C7−Ni12	80.0(2)	Ni8−C16−Ni14	80.3(2)
Ni11−C7−O7	140.1(4)	Ni8−C16−O16	140.2(4)
Ni12−C7−O7	139.8(4)	Ni14−C16−O16	139.4(4)
Ni9′−C8−Ni12′	80.2(2)	Ni9′−C17−Ni15	80.1(2)
Ni9′−C8−O8	139.3(4)	Ni9′−C17−O17	139.1(4)
Ni12′−C8−O8	140.6(4)	Ni15−C17−O17	140.8(4)
Ni13−C9−Ni14	79.1(2)	Ni11−C18−Ni13	80.4(2)
Ni13−C9−O9	140.8(4)	Ni11−C18−O18	138.5(4)
Ni14−C9−O9	140.0(4)	Ni13−C18−O18	141.0(4)

[a] Primed atoms are related to the unprimed ones by the symmetry operation $1 - x, 1 - y, 2 - z$.

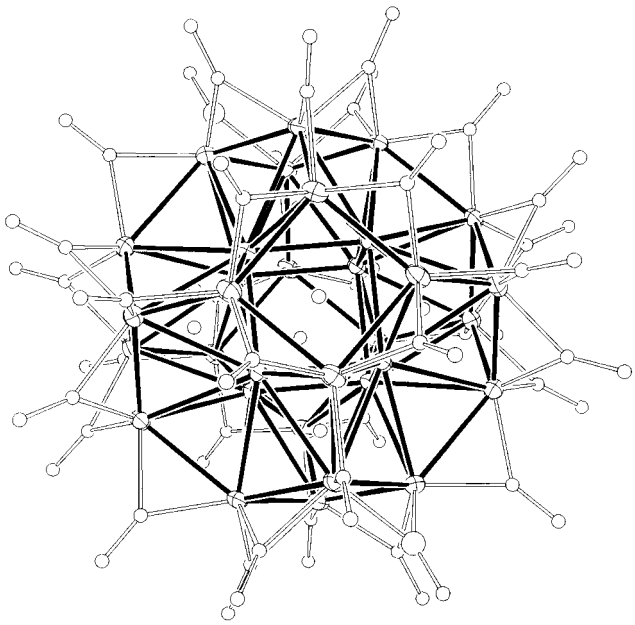


Figure 1. The structure of $[Ni_{32}C_6(CO)_{36}]^{6-}$ (Ni−Ni bonds are black; Ni−$C_{carbide}$ bonds have been omitted for clarity)

layer[24] (direct-current voltammogram) proves that the less cathodic peak-system involves an oxidation process, whereas the subsequent four-peak system is due to reduction processes. Controlled potential coulometric tests

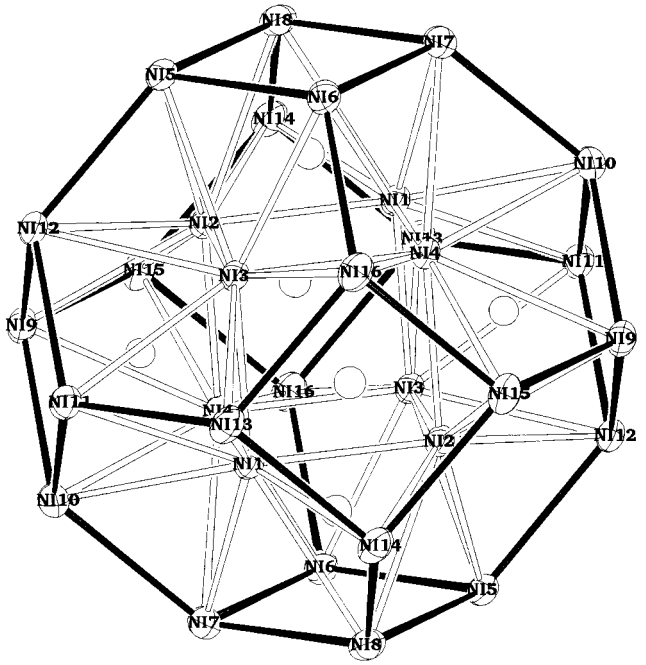


Figure 2. Metal skeleton of $[Ni_{32}C_6(CO)_{36}]^{6-}$ with the atom numbering scheme

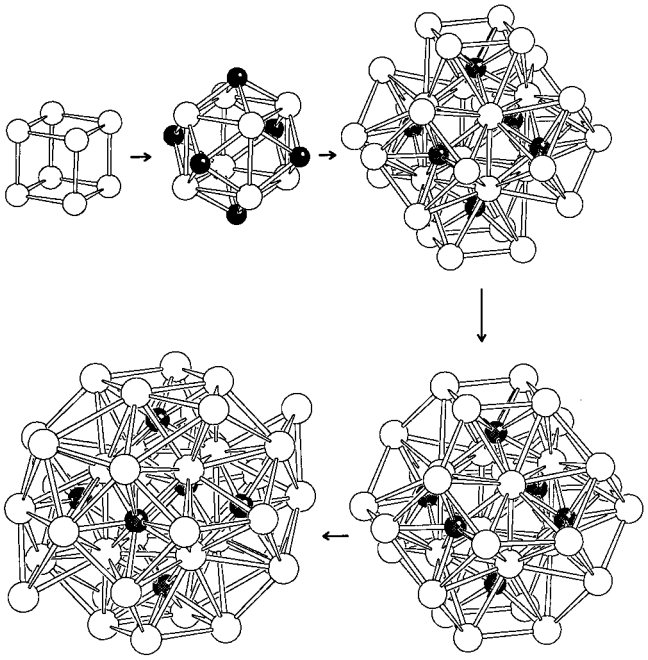


Figure 3. Formal construction of the metal skeletons of $[Ni_{32}C_6(CO)_{36}]^{6-}$ and $[HNi_{38}C_6(CO)_{42}]^{5-}$

performed in correspondence to the first reduction process ($E_w = -0.9$ V) show that it consumes one electron/molecule. The resulting solution displays a cyclic voltammetric profile complementary to the original one, thus testifying to the chemical reversibility of the $[Ni_{32}C_6(CO)_{36}]^{6-/7-}$ redox change. Further exhaustive reduction at the potential of the second reduction process ($E_w = -1.2$ V) also consumes one electron/molecule, but the subsequent cyclic voltammetric monitoring already indicates the partial occurrence of some degradation of the electrogenerated $[Ni_{32}C_6(CO)_{36}]^{8-}$. Based on these results we assume that all the electron transfer processes exhibited by $[Ni_{32}C_6(CO)_{36}]^{6-}$ are one-electron steps generating the corresponding redox congeners (namely $[Ni_{32}C_6(CO)_{36}]^{5-}$, $[Ni_{32}C_6(CO)_{36}]^{7-}$, $[Ni_{32}C_6(CO)_{36}]^{8-}$, $[Ni_{32}C_6(CO)_{36}]^{9-}$, $[Ni_{32}C_6(CO)_{36}]^{10-}$), which are stable under the short times of cyclic voltammetry, but under the longer times of macroelectrolysis only $[Ni_{32}C_6(CO)_{36}]^{7-}$ appears perfectly stable.

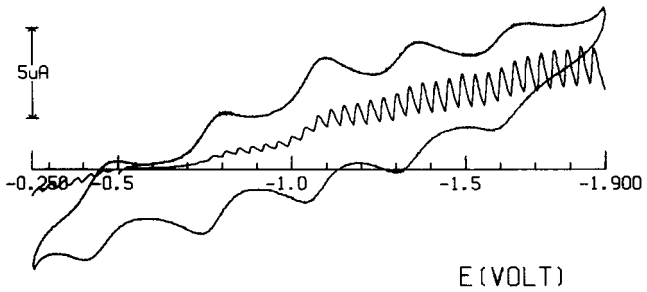


Figure 4. Cyclic and d.c. voltammograms recorded at a platinum electrode on a MeCN solution containing $[Ni_{32}C_6(CO)_{36}]^{6-}$ ($6\cdot10^{-4}$ mol dm^{-3}) and $[NEt_4][ClO_4]$ (0.1 mol dm^{-3}). Scan rates: cyclic voltammogram, 0.2 Vs^{-1}; d.c.voltammogram, 0.02 Vs^{-1}

Figure 5 compares the electrochemical response of $[Ni_{38}C_6(CO)_{42}]^{6-}$ in acetonitrile solution with that of its protonated species $[HNi_{38}C_6(CO)_{42}]^{5-}$. The hexaanion gives rise to four well-defined redox processes, all of which possess features of chemical reversibility in the cyclic voltammetric timescale. In this case too, direct-current voltam-

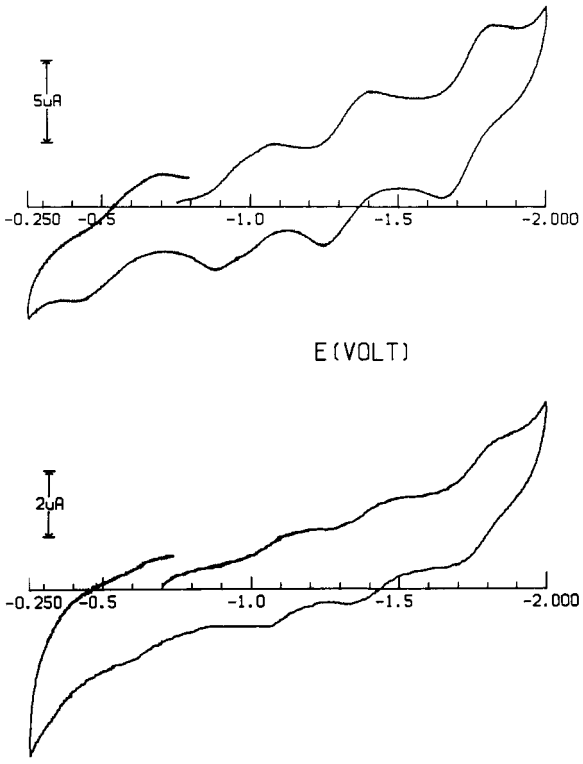


Figure 5. Cyclic voltammograms recorded at a mercury electrode on MeCN solutions containing $[NEt_4][ClO_4]$ (0.1 mol dm^{-3}). Top: $[Ni_{38}C_6(CO)_{42}]^{6-}$ ($4\cdot10^{-4}$ mol dm^{-3}). Bottom: $[HNi_{38}C_6(CO)_{42}]^{5-}$ ($5\cdot10^{-4}$ mol dm^{-3}). Scan rate 0.2 Vs^{-1}

metry shows the occurrence of one oxidation and three subsequent reduction processes. The protonated pentaanion also exhibits an analogous sequence of redox processes, encompassing the $[HNi_{38}C_6(CO)_{42}]^{4-/8-}$ oxidation states; they are, however, less well defined and shifted by about 400 mV towards more negative potential values. To our knowledge, the highest nuclearity clusters which have been previously studied to determine the influence of hydride incorporation on the electrochemical redox behaviour are $[Ru_{10}C(CO)_{24}]^{2-}$ and $[HRu_{10}C(CO)_{24}]^{-}$.[25] These, however, only exhibit a two-electron electrochemically irreversible reduction.

Step-by-step controlled potential coulometry shows that both $[Ni_{38}C_6(CO)_{42}]^{7-}$ and $[Ni_{38}C_6(CO)_{42}]^{8-}$ are stable, whereas $[Ni_{38}C_6(CO)_{42}]^{5-}$ tends to decompose slowly.

Finally, as illustrated in Figure 6, the redox change $[Ni_{38}C_6(CO)_{42}]^{8-/9-}$ in DMF solution is probably masked by the solvent discharge, because of the shift of the redox processes of $[Ni_{38}C_6(CO)_{42}]^{6-}$ towards negative potential values. Furthermore, one more anodic process becomes detectable, even if the instantaneously generated $[Ni_{38}C_6(CO)_{42}]^{4-}$ species is very unstable.

The formal electrode potentials of the redox changes exhibited by the present complexes are compiled in Table 4. From the electrochemical viewpoint it is noteworthy that all the redox changes concerned with the Ni_{38} species exhibit peak-to-peak separations which largely depart from the value of 60 mV, which is the theoretical prediction for electrochemically reversible one-electron processes. It could be speculated that the quasi-reversibility of such redox processes, i.e. their rather slow electron transfer rate, suggests that the Ni_{38} electron exchanges are accompanied by some geometric reorganisations, which are more significant than those accompanying the Ni_{32} redox processes.[2d]

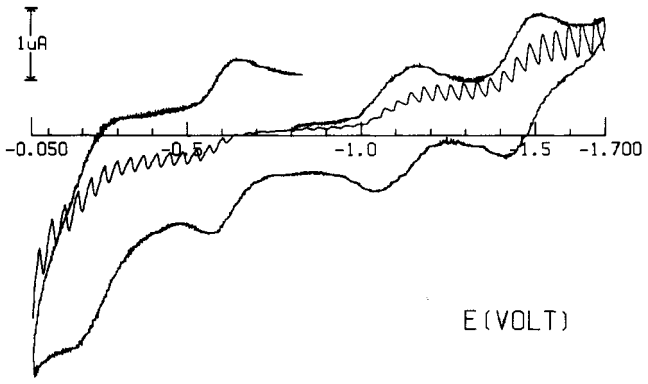


Figure 6. Cyclic and d.c. voltammograms recorded at a mercury electrode on a DMF solution containing $[Ni_{38}C_6(CO)_{42}]^{6-}$ ($3\cdot10^{-4}$ mol dm^{-3}) and $[NEt_4][ClO_4]$ (0.1 mol dm^{-3}). Scan rates: cyclic voltammogram, 0.2 Vs^{-1}; d.c.voltammogram, 0.02 Vs^{-1}.

Conclusion

The most notable property of the $[H_{6-n}Ni_{32}C_6(CO)_{36}]^{n-}$ (n = 5, 6) and $[H_{6-n}Ni_{38}C_6(CO)_{42}]^{n-}$ (n = 4, 5, 6) derivatives is represented by their electron-sink behaviour encompassing up to six different electrochemically reversible oxidation states. Their redox features resemble those of higher valent clusters such the Fe−S cubanes,[2] or fullerenes.[26] In the nickel clusters mentioned above such behaviour probably arises from the presence of highly connected nickel atoms belonging to the inner cube and the extra-stability of the metal core granted by the interstitial carbide atoms. Indeed, the nickel atoms of the inner cubic core of $[Ni_{32}C_6(CO)_{36}]^{6-}$ display coordination number 12, being coordinated to 9 nickel and 3 carbide atoms, whereas the coordination number of six out of eight corresponding nickel atoms of $[Ni_{38}C_6(CO)_{42}]^{6-}$ increases to 13 by intervention of the additional six Ni(CO) fragments. LDF calculations, carried out on $[Ni_{32}C_6(CO)_{36}]^{6-}$ prior to its isolation and characterisation, indicate that its electronic structure begins to bear some qualitative resemblance to that of a metal. In particular, almost degenerate t_{1u}, a_{2g}, and t_{2g} levels, holding a total of ten electrons, were found close to the Fermi energy.[27] This finding is in perfect agreement with the redox behaviour of $[Ni_{32}C_6(CO)_{36}]^{6-}$. Indeed, the progressive one-electron reduction of the latter to the corresponding decaanion corresponds to complete filling of the energy levels mentioned above. Moreover, the differences between the formal electrode potentials of consecutive redox couples of $[Ni_{32}C_6(CO)_{36}]^{6-}$ (range 0.26−0.33 V) is indicative of the presence in the frontier region of almost equally spaced one-electron energy levels with an average energy separation of ca. 0.3 eV. It may be concluded therefore that a metalisation process begins to emerge due to the presence of eight highly-connected nickel atoms.

Experimental Section

General Remarks: All reactions including sample manipulations were carried out under a well ventilated hood with standard Schlenk techniques under nitrogen and in carefully dried solvents.

Table 4. Formal electrode potentials (in V, vs. S.C.E.) and peak-to-peak separations (in mV) for the redox changes exhibited by $[Ni_{32}C_6(CO)_{36}]^{6-}$, $[Ni_{38}C_6(CO)_{42}]^{6-}$, and $[HNi_{38}C_6(CO)_{42}]^{5-}$

Cluster	$E^{\circ\prime}_{4-/5-}$	ΔEp[a]	$E^{\circ\prime}_{5-/6-}$	ΔEp	$E^{\circ\prime}_{6-/7-}$	ΔEp	$E^{\circ\prime}_{7-/8-}$	ΔEp	$E^{\circ\prime}_{8-/9-}$	ΔEp	$E^{\circ\prime}_{9-/10-}$	ΔEp	Solvent
$[Ni_{32}C_6(CO)_{36}]^{6-}$			−0.45	70	−0.77	66	−1.06	66	−1.33	66	−1.61	64	MeCN
$[Ni_{38}C_6(CO)_{42}]^{6-}$			−0.49	160	−0.98	190	−1.33	160	−1.73	178			MeCN
$[Ni_{38}C_6(CO)_{42}]^{6-}$	−0.24b	b	−0.60	85	−1.10	130	−1.47	112					DMF
$[HNi_{38}C_6(CO)_{42}]^{5-}$	−0.6b	b	−1.11	100	−1.42	150	−1.77	120					MeCN

[a] Measured at 0.2 Vs^{-1} − [b] Difficult to be measured.

The $[Ni_6(CO)_{12}]^{2-}$ salts were prepared according to literature.[28] – Elemental analyses: atomic absorption on a Pye-Unicam instrument (Ni), gravimetrically as BPh_4^- salts for the tetrasubstituted ammonium cations. – IR: Perkin-Elmer 1605 interferometer using CaF_2 cells. Materials and apparatus for the electrochemical measurements have been described elsewhere.[29] Potential values are referred to the saturated calomel electrode (SCE).

Synthesis of $[NEt_4]_6[Ni_{38}C_6(CO)_{42}]$: $[NEt_4]_2[Ni_6(CO)_{12}]$ (2.58 g, 2.72 mmol) was dissolved in THF (40 mL) in a 100 mL three-necked round-bottomed flask cooled at −15°C and equipped with a microburette charged with C_3Cl_6 (0.51 g, 2.05 mmol) in THF (5 mL). The C_3Cl_6 solution (4 mL) was added dropwise over a period of six h into the stirred $[NEt_4]_2[Ni_6(CO)_{12}]$ solution while continuously removing the reaction atmosphere with a slow stream of nitrogen. The resulting dark brown suspension was left standing for 2 d at room temp. and under a static nitrogen atmosphere, and then evaporated to dryness under vacuum. The residue was washed in portions with water (30 mL), methanol (20 mL), and THF (20 mL) and extracted with DMSO (30 mL). $[NEt_4]_6[Ni_{38}C_6(CO)_{42}]$ was precipitated from the DMSO solution by addition of a solution of $[NEt_4]Cl$ (1.5 g) in water (30 mL) with stirring, it was then filtered, and washed with methanol (20 mL). The resulting dark brown material was extracted with acetonitrile (20 mL) and filtered. Precipitation by layering of diisopropyl ether (40 mL) gave black crystals of $[NEt_4]_6[Ni_{38}C_6(CO)_{42}]\cdot x$ MeCN (0.61 g). The salt is soluble in acetonitrile, DMF and DMSO, and sparingly soluble or insoluble in acetone, THF, alcohols, and nonpolar solvents. – $[NEt_4]_6[Ni_{38}C_6(CO)_{42}]$: calcd. $[NEt_4]^+$ 18.31, Ni 52.38; found $[NEt_4]^+$ 16.9, Ni 49.07. – Ni/$[NEt_4]^+$ calcd 6.33; found 6.43.

The corresponding $[NBu_4]^+$, $[NMe_3CH_2Ph]^+$, $[PPh_3Me]^+$, $[PPh_3CH_2Ph]^+$, and $[PPh_4]^+$ salts of $[Ni_{38}C_6(CO)_{42}]^{6-}$ have been similarly prepared by metathesis in DMSO with the appropriate quaternary salt.

Synthesis of $[PPh_3Me]_6[Ni_{32}C_6(CO)_{36}]$: A solution of $[PPh_3Me]_6[Ni_{38}C_6(CO)_{42}]$ (0.35 g, 0.067 mmol) in acetonitrile (20 mL) was stirred under a carbon monoxide atmosphere for 15 min and evaporated under vacuum to dryness. The residue was dissolved in acetonitrile (20 mL) and stirred under a carbon monoxide atmosphere for 10 min and dried under vacuum. The resulting dark brown residue was extracted with acetonitrile (20 mL) and filtered. Precipitation by layering of diisopropyl ether (40 mL) gave black crystals of $[PPh_3Me]_6[Ni_{32}C_6(CO)_{36}]\cdot 4$ MeCN (210 mg, 0.043 mmol). The salt is soluble in acetone, acetonitrile, DMF, and DMSO, and insoluble in THF, alcohols, and nonpolar solvents. – $[PPh_3Me]_6[Ni_{32}C_6(CO)_{36}]\cdot 4$ MeCN: calcd. $[PPh_3Me]^+$ 34.74, Ni 39.26; found $[PPh_3Me]^+$ 34.12, Ni 38.87. – Ni/$[PPh_3Me]^+$: calcd 5.33, found 5.37.

The corresponding $[NEt_4]^+$, $[NBu_4]^+$, $[NMe_3CH_2Ph]^+$, $[PPh_3CH_2Ph]^+$, and $[PPh_4]^+$ salts have been similarly prepared using the appropriate starting material.

Synthesis of $[NBu_4]_5[HNi_{38}C_6(CO)_{42}]$: $[NBu_4]_6[Ni_{38}C_6(CO)_{42}]$ (0.91 g) was dissolved in acetonitrile (30 mL), treated with 2.5 mL of a solution obtained by diluting 1 mL of H_2SO_4 (20% in aqueous solution) in acetonitrile (25 mL), and evaporated to dryness under vacuum. The resulting residue was extracted in acetone (20 mL) and precipitated by layering with isopropyl alcohol (45 mL) to give black crystals of $[NBu_4]_5[HNi_{38}C_6(CO)_{42}]$. Yields 0.64 g. The salt is soluble in acetone, sparingly soluble in THF, and insoluble in alcohols and nonpolar solvents. $[NBu_4]_5[HNi_{38}C_6(CO)_{42}]$ is very soluble in acetonitrile, DMF, and DMSO with partial or complete conversion into the corresponding $[Ni_{38}C_6(CO)_{42}]^{6-}$ hexaanion. – $[NBu_4]_5[HNi_{38}C_6(CO)_{42}]$: calcd. $[NBu_4]^+$ 25.80, Ni 47.57; found $[NBu_4]^+$ 25.12, Ni 47.2. – Ni/$[NBu_4]^+$: calcd. 7.6, found 7.74.

Synthesis of $[PPh_3Me]_5[HNi_{32}C_6(CO)_{36}]$: $[PPh_3Me]_6[Ni_{32}C_6(CO)_{36}]$ (0.31 g) was dissolved in acetonitrile (10 mL), treated with 1 mL of a solution obtained by diluting 1 mL of H_2SO_4 (20% in aqueous solution) in acetonitrile (25 mL) and evaporated to dryness under vacuum. The resulting residue was extracted in acetone (15 mL) and precipitated by layering with isopropyl alcohol (30 mL) to give black crystals of $[PPh_3Me]_5[HNi_{32}C_6(CO)_{36}]$. Yields 0.24 g. The salt is soluble in acetone, sparingly soluble in THF, and insoluble in alcohols and nonpolar solvents. $[PPh_3Me]_5[HNi_{32}C_6(CO)_{36}]$ is also soluble in acetonitrile, DMF, and DMSO with complete conversion into the parent $[Ni_{32}C_6(CO)_{36}]^{6-}$ hexaanion. – $[PPh_3Me]_5[HNi_{32}C_6(CO)_{36}]$: calcd. $[PPh_3Me]^+$ 31.88, Ni 43.24; found $[PPh_3Me]^+$ 30.79, Ni 41.57. – Ni/$[PPh_3Me]^+$: calcd 6.4, found 6.37.

X-ray Data Collection and Crystal Structure Determination: Crystal data for $[PPh_3Me]_6[Ni_{32}C_6(CO)_{36}]\cdot 4$ MeCN: triclinic, space group $P\bar{1}$ (No. 2), $a = 15.974(3)$, $b = 17.474(3)$, $c = 18.200(4)$ Å, $\alpha = 61.37(2)$, $\beta = 69.31(2)$, $\gamma = 72.35(2)°$, $V = 4115(1)$ Å^3, $Z = 1$, $D_c = 1.93$ gcm^{-3}, Mo-K_α radiation ($\lambda = 0.71073$ Å), μ (Mo-K_α) = 37.1 cm^{-1}, $T = 298$ K. 14585 reflections with $3° < \theta < 25°$ were measured on a CAD4 diffractometer at room temp. using a crystal with approximate dimensions $0.20 \times 0.15 \times 0.35$ mm. Data were corrected for Lorentz polarisation and absorption effects (empirical absorption, transmission factors in the range 0.56−1.00[30]). The structure was solved by direct methods (SIR 89) and refined using 10639 independent reflections having $I > 3\sigma(I)$, minimising the function $\Sigma w(|Fo|-|Fc|)^2$. Scattering factors were taken from Cromer and Waber.[31] Anomalous dispersion corrections were included.[32] Anisotropic displacement parameters were assigned to all non-hydrogen atoms.The hydrogen atoms were placed at calculated positions (C−H 0.95 Å). The final R value was 0.033 (R_w = 0.043). All the calculations were performed using Personal SDP software.[33]

Crystallographic data (excluding structure factors) for the structure reported in this paper have been deposited with the Cambridge Crystallographic Data Centre as supplementary publication no. CCDC-179-79 Copies of the data can be obtained free of charge on application to The Director, CCDC, 12 Union Road, Cambridge CB2 1EZ, UK [Fax: (internat.) + 44 (1223) 336-033; E-mail: deposit@ccdc.cam.ac.uk].

Acknowledgments

Support from the MURST, the University of Bologna and the HCM program of EU is gratefully acknowledged. P. Z. wishes to thank Mrs. G. Montomoli for technical assistance.

[1] [1a] P. Lemoine, *Coord. Chem. Rev.* **1982**, *47*, 55. – [1b] P. Lemoine, *Coord. Chem. Rev.* **1988**, *83*, 169.
[2] [2a] P. Zanello, *Coord. Chem. Rev.* **1988**, *83*, 199. – [2b] P. Zanello, *Coord. Chem. Rev.* **1988**, *87*, 1. – [2c] P. Zanello, in *Stereochemistry of Organometallic and Inorganic Compounds,* (Ed.: P. Zanello), Elsevier, Amsterdam, **1994**, *5*, 163. – [2d] P. Zanello, *Structure and Bonding*, Spinger-Verlag, Berlin, **1992**, *79*, 101.
[3] G. Longoni, C. Femoni, M. C. Iapalucci, P. Zanello, in *Metal Clusters in Chemistry* (Eds.: P. Braunstein, L. Oro, P. Raithby), Wiley-VCH Verlag, Weinheim, submitted.
[4] R. Della Pergola, L. Garlaschelli, M. Manassero, N. Masciocchi, P. Zanello, *Angew. Chem.* **1993**, *105*, 1415; *Angew. Chem. Int. Ed.* **1993**, *32*, 1347.
[5] [5a] G. Longoni, M. Manassero, M. Sansoni, *J. Am. Chem. Soc.* **1980**, *102*, 7973. – [5b] R. D. Adams, I. Arafa, G. Chen, J-C. Lii, J-G. Wang, *Organometallics* **1990**, *9*, 2350.
[6] R. Della Pergola, L. Garlaschelli, C. Mealli, D. M. Proserpio, P. Zanello, *J. Cluster Sci.* **1990**, *1*, 93.

[7] [7a] V. G. Albano, F. Calderoni, M. C. Iapalucci, G. Longoni, M. Monari, P. Zanello, *J. Cluster Sci.*, **1995**, *6*, 107. – [7b] V. G. Albano, L. Grossi, G. Longoni, M. Monari, S. Mulley, A. Sironi, *J. Am. Chem. Soc.* **1992**, *114*, 5708.
[8] V. G. Albano, R. Aureli, M. C. Iapalucci, F. Laschi, G. Longoni, M. Monari, P. Zanello, *J. Chem Soc., Chem. Comm.* **1993**, 1501.
[9] V. G. Albano, D. Braga, P. Chini, G. Ciani, S. Martinengo, *J. Chem Soc., Dalton Trans.*, **1982**, 645.
[10] [10a] K. M. MacKay, B. K. Nicholson, W. T. Robinson, A. W. Sims, *J. Chem Soc., Chem. Comm.* **1984**, 1276. – [10b] G. C. Barris, D. Phil. Thesis, University of Waikato, New Zealand.
[11] V. G. Albano, F. Demartin, M. C. Iapalucci, G. Longoni, M. Monari, P. Zanello, *J. Chem Soc., Dalton Trans.* **1992**, 497.
[12] V. G. Albano, F. Demartin, M. C. Iapalucci, F. Laschi, G. Longoni, A. Sironi, P. Zanello, *J. Chem Soc., Dalton Trans.* **1991**, 739.
[13] F. Calderoni, F. Demartin, M. C. Iapalucci, G. Longoni, P. Zanello, *Inorg. Chem.* **1996**, *35*, 898.
[14] J. Sinzig, L. J. de Jongh, A. Ceriotti, R. Della Pergola, G. Longoni, M. Stener, K. Albert, N. Rösch, *Phys. Rev. Lett.* **1998**, *81*, 3211.
[15] D. M. Washecheck, E. J. Wucherer, L. F. Dahl, A. Ceriotti, G. Longoni, M. Manassero, M. Sansoni, P. Chini, *J. Am. Chem. Soc.* **1979**, *101*, 6110.
[16] [16a] G. J. Lewis, J. D. Roth, R. A. Montag, L. K. Safford, X. Gao, S-C. Chang, L. F. Dahl, M. J. Weaver, *J. Am. Chem. Soc*. **1990**, *112*, 2831. – [16b] J. D. Roth, G. J. Lewis, L. K. Safford, X. Jiang, L. F. Dahl, M. J. Weaver, *J. Am. Chem. Soc*. **1992**, *114*, 6159
[17] E. Brivio, A. Ceriotti, R. Della Pergola, L. Garlaschelli, F. Demartin, M. Manassero, M. Sansoni, P. Zanello, F. Laschi, B. T. Heaton, *J. Chem Soc., Dalton Trans.* **1994**, 3237.
[18] [18a] J. Podlahová, J. Podlaha, A. Jegorov, J. Hašek, *J. Organomet. Chem*. **1989**, *359*, 401. – [18b] P. Baird, J. A. Bandy, M. L. H. Green, A. Hamnett, E. Marseglia, D. S. Orbetelli, K. Prout, J. Qin, *J. Chem Soc., Dalton Trans.*, **1991**, 2377. – [18c] M. J. Scott, R. H. Holms, *Angew. Chem. Int. Ed. Engl*., **1993**, *32*, 564. – [18d] V. G. Albano, C. Femoni, M. C. Iapalucci, G. Longoni, M. Rauccio, S. Zacchini, *Inorg. Chim. Acta*, submitted.
[19] [19a] A. Ceriotti, G. Longoni, M. Manassero, M. Perego, M. Sansoni, *Inorg. Chem.* **1985**, *24*, 117. – [19b] A. Ceriotti, G. Longoni, M. Manassero, L. Resconi, M. Sansoni, *J. Chem Soc., Chem. Comm.* **1985**, 181. – [19c] A. Ceriotti, G. Longoni, M. Manassero, N. Masciocchi, G. Piro, L. Resconi, M. Sansoni, *J. Chem Soc., Chem. Comm.* **1985**, 1402. – [19d] A. Ceriotti, A. Fait, G. Longoni, G. Piro, L. Resconi, F. Demartin, M. Manassero, N. Masciocchi, M. Sansoni, *J. Am. Chem. Soc.* **1986**, *108*, 5370. – [19e] A. Ceriotti, G. Longoni, G. Piro, M. Manassero, N. Masciocchi, M. Sansoni, *New J. Chem.* **1988**, *12*, 501.
[20] A. Ceriotti, A. Fait, G. Longoni, G. Piro, F. Demartin, M. Manassero, N. Masciocchi, M. Sansoni, *J. Am. Chem. Soc.* **1986**, *108*, 8091
[21] F. Calderoni, F. Demartin, M. C. Iapalucci, G. Longoni, *Angew. Chem. Int. Ed. Engl.* **1996**, *35*, 2225.
[22] A. Ceriotti, F. Demartin, B. T. Heaton, P. Ingallina, G. Longoni, M. Manassero, M. Marchionna, N. Masciocchi, *J. Chem Soc., Chem. Comm.* **1989**, 786.
[23] [23a] H. Vahrenkamp, V. A. Uchtman, L. F. Dahl, *J. Am. Chem. Soc.* **1968**, *90*, 3272. – [23b] L. F. Dahl, J. E. North, J. B. Thoden, B. Spencer, *Organometallics* **1993**, *12*, 1299.
[24] S. Lo Schiavo, G. Bruno, P. Zanello, F. Laschi. P. Piraino, *Inorg. Chem.* **1997**, *36*, 1004.
[25] M. P. Cifuentes, M. G. Humphrey, G. A. Heath, *Inorg. Chim. Acta* **1997**, 259, 273.
[26] I. Noviandri, R. D. Bolskar, P. A. Lay, C. A. Reed, *J. Phys. Chem.* **1997**, *B101*, 6350.
[27] N. Rösch, L. Ackermann, G. Pacchioni, *J. Am. Chem. Soc.* **1992**, *114*, 3549.
[28] A. Ceriotti, G. Longoni, G. Piva, *Inorg. Synth.* **1989**, *26*, 312.
[29] C. Bianchini, F. Laschi, D. Masi, F. M. Ottaviani, A. Pastor, M. Peruzzini, P. Zanello, F. Zanobini, *J. Am. Chem. Soc.* **1993**, *115*, 2723.
[30] A. C. T. North, D. C. Phillips, F. S. Mathews, *Acta Crystallogr.* **1968**, A24, 351.
[31] D. T. Cromer, J. T. Waber, *International Tables for X-ray Crystallography,* Vol IV, Kynoch Press, Birmingham, UK, **1974**, Table 2.2B.
[32] D. T. Cromer, *International Tables for X-ray Crystallography,* Vol IV, Kynoch Press, Birmingham, UK, **1974**, Table 2.3.1.
[33] [33a] B. Frenz, *Comput. Phys.* **1988**, *3*, 42. – [33b] B. Frenz, *Crystallographic Computing*, 5, Oxford University Press, **1991**, Chapter 11, pp. 126–135.

Received September 23, 1998
[I98324]

Bonding Analysis in Inorganic Transition-Metal Cubic Clusters, 4[+] The Distorted $Pd_9(\mu:\eta^5,\eta^2\text{-}As_2)_4(PPh_3)_8$ Architecture

Régis Gautier,[a] Jean-François Halet,*[a] and Jean-Yves Saillard*[a]

Keywords: Electron counting / Electronic structure / Density functional calculations / Extended Hückel calculations / Cluster compounds / Cluster compounds

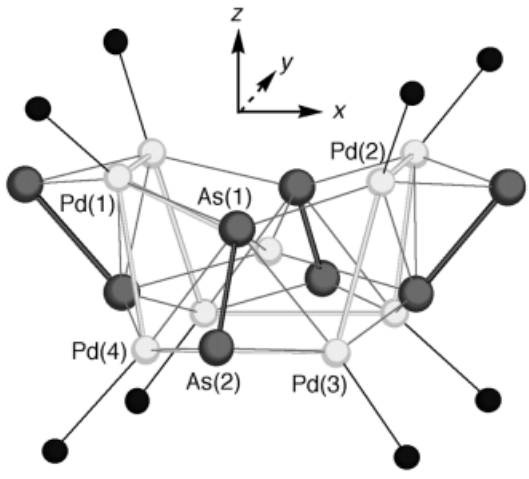
Extended Hückel and density functional calculations were carried out on the title compound **1**. Results indicate that the bonding of the interstitial Pd_i atom with the D_{2d} distorted $(Pd_s)_8(As_2)_4$ cubic host differs from that found in the related metal-centered cubic species $M_9(\mu_4\text{-}E)_6L_8$. Species **1** can be described as an approximate square-planar 16-electron Pd_iL_4 center bound through Pd_i–As rather than Pd_i–Pd_s contacts to a distorted cubic fragment composed of four 30-electron bimetallic Pd_2L_8 units. Although a substantial gap is computed between the highest occupied molecular orbital and the lowest unoccupied molecular orbital for the observed electron count of 130 MVEs, calculations indicate that such an architecture should be observed for different electron counts close to that count. The incorporation of the central Pd atom does not seem to be essential to ensure the stability of the distorded $Pd_8(As_2)_4(PH_3)_8$ cluster. Such empty clusters, with formally four M–M bonds and eight planar 16-electron Pd_s centers, should exist for electron counts close to 120 MVEs.

Introduction

Because of potential applications in nanoelectronics, the miniaturization of solids to cluster size is an area of active research.[1] Initially restricted to metals, this field has rapidly been extended to ligated metal clusters. Among the latter, systems where a metal cube is bridged by different heavy main group atoms constitute now an important and fascinating family, which can be regarded as nanoscaled cutouts of bulk transition metal pnictides and chalcogenides. These cubic arrays may be empty or centered by an interstitial atom.[2−18] Theoretical calculations performed on empty $M_8(\mu_4\text{-}E)_6L_8$ clusters[19] and metal-centered $M_9(\mu_4\text{-}E)_6L_8$[20] (M = transition metal, E = group 14, 15, and 16 element, L = two-electron donor ligand) have shown that such compounds are characterized by an electronic structure which is either "molecular" (closed-shell electron configuration) or "metallic" (open-shell electron configuration) in nature, depending upon the electron count and the nature of the capping ligands.[21]

When omnicapped, such clusters depict generally a rather regular cubic arrangement. Expanding or shrinking of the cube is observed upon variation of the number of metal valence electrons (MVE), which ranges from 99 to 120 MVEs for empty $M_8(\mu_4\text{-}E)_6L_8$ species and from 121 to 130 MVEs for metal-centered $M_9(\mu_4\text{-}E)_6L_8$ clusters so far.[19−21] On the other hand, distorted cubic architectures are encountered when the ligand environment of the metallic cage is nonsymmetrical. This is observed for instance in the 127-MVE species $[Co_9(\mu_5\text{-}Bi)_4(CO)_{16}]^{2-}$, characterized by Eveland and Whitmire.[22] Being viewed as a metal-centered elongated Co_8 cube with four Bi atoms capping the four rectangular faces, such a cluster bears some structural resemblance to the hexacapped cubic $M_9(\mu_4\text{-}E)_6L_8$ compounds. A theoretical analysis of the bonding in this tetracapped compound and in related compounds has been recently published.[21,23]

An alternative distortion of a metal-centered M_9 cube is encountered in the related cluster $Pd_9(\mu:\eta^5,\eta^2\text{-}As_2)_4(PPh_3)_8$ (**1**), characterized by Fenske and Persau some years ago.[14] In this compound, the nine Pd atoms build up an approximate body-centered cube of D_{2d} symmetry, with four short [average Pd(1,2)−Pd(4,3) = 2.88 Å], four long [average Pd(3)−Pd(4) = 3.16 Å], and four very long [average Pd(1)−Pd(2) = 4.45 Å] distances between surface Pd (Pd_s) centers. This D_{2d} distortion of an M_8 cube is sketched in



1

[+] Part 3: Ref.[23]

[a] Laboratoire de Chimie du Solide et Inorganique Moléculaire, UMR CNRS 6511,
Université de Rennes 1, 35042 Rennes Cedex, France
Fax: Int. code + 2 99 38 34 87
E-mail: halet@univ-rennes1.fr

 © WILEY-VCH Verlag GmbH, D-69451 Weinheim, 1999 1434−1948/99/0404−0673 $ 17.50+.50/0

Figure 1. Rather long separations, ca. 3.00−3.09 Å are also observed between Pd_s atoms and the interstitial Pd (Pd_i) atom. Four faces of this highly distorted cube are asymmetrically capped by (μ:η^5,η^2-As_2) dumb-bells. The central Pd_i atom is bound to four As atoms (Pd_i−As = 2.57 Å) in an approximate square-planar arrangement, somewhat distorted toward tetrahedral. The As−As separation is rather short (2.36 Å) suggesting some π-bonding. The atoms constituting each As_2 units have a different environment. The As(1) atoms are connected to five metal atoms, one of them being Pd_i. Among the four As(1)−Pd_s bonds, two of them are shorter [average Pd(1,2)−As(1) = 2.49 Å] while the remaining two are quite long [average Pd(3,4)−As(1) = 2.61 Å]. The pyramidally tricoordinated As(2) atom is bonded to two Pd_s atoms [average Pd(3,4)−As(2) = 2.44 Å].

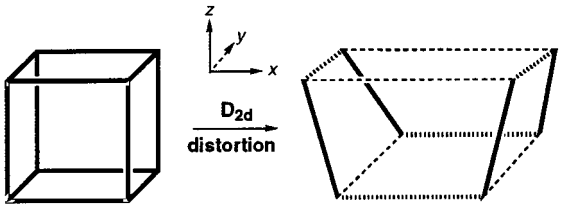


Figure 1. Conceptual formation of the D_{2d} distorted cubic $Pd_8(PH_3)_8$ fragment present in model **1**-H. Dashed lines and dotted lines correspond to long (ca. 3.15 Å) and very long (ca. 4.45 Å) metal−metal contacts, respectively.

Leaving a non-bonding lone pair on As(2), one can count the neutral (μ:η^5,η^2-As_2) units as six-electron donor ligands, which leads to a total of 130 MVEs for **1**. This renders this cluster isoelectronic to the regular cubic $Pd_9(\mu_4\text{-Te})_6(PEt_3)_8$ species.[16] Extended Hückel Theory (EHT) and Density Functional Theory (DFT) calculations were undertaken on the model compound $Pd_9(\mu:\eta^5,\eta^2\text{-}As_2)_4(PH_3)_8$ (**1**-H) to understand the unusual bonding situation in this compound (see the Appendix for the computational details). We discuss the results in this paper.

The Empty Distorted $Pd_8(As_2)_4(PH_3)_8$ Cube

The electronic structure of compound **1**-H can be formally analyzed as resulting from the interaction between the interstitial Pd_i atom and its $Pd_8(As_2)_4(PH_3)_8$ host. On the other hand, the molecular orbital (MO) diagram of the D_{2d} $Pd_8(As_2)_4(PH_3)_8$ fragment itself can be derived from the interaction of the four noninteracting $[As_2]^{4-}$ units (As−As single bonds are assumed) with the distorded $[Pd_8(PH_3)_8]^{16+}$ fragment. The frontier molecular orbitals (FMO) of the latter itself descend from those of a regular cubic cage. Indeed, starting with a regular cube, the metal framework found for **1** can be generated according to a D_{2d} distortion by elongating parallel metal−metal edges of the top and bottom faces of the cube as illustrated in Figure 1. Therefore, it is important to evaluate first the effects of the D_{2d} distortion on the skeletal MOs of an idealized $Pd_8(PH_3)_8$ cube. The qualitative analysis developped below is based on EHT calculations (see Appendix for details).

The MO diagram of the idealized $Pd_8(PH_3)_8$ cube of O_h symmetry (Pd−Pd = 2.88 Å) can be qualitatively obtained by combining the FMOs of the eight $Pd(PH_3)$ units.[19a,21] Such a fragment, as shown on the far left-hand side of Figure 2, presents a block of five d-type orbitals (one, two, and two of σ, π, and δ symmetry, respectively) below a radial σ-type sp hybrid and a set of two tangential π-type orbitals of Pd 5p parentage.[19a] When the cube is built, the three upper diffuse FMOs (sp_σ and p_π) of the eight $Pd(PH_3)$ groups overlap strongly and generate a set of 12 bonding MOs, largely separated from a set of 12 antibonding MOs. The more contracted d-type FMOs give rise to a band of 40 combinations which spreads out over a range of about 1 eV. Unlike for the s and p orbitals, the d-type overlap is not strong enough to create an energy gap separating the in-phase combinations from the out-of-phase ones. In our chosen fragment charge partitioning, the eight upper orbitals of the d-band are formally vacant. The derivation of the MO level ordering of the regular $[Pd_8(PH_3)_8]^{16+}$ cube from the $Pd(PH_3)$ FMOs is sketched in Figure 2a.

Upon D_{2d} distortion which leads to four long and four very long metal−metal separations (see Figure 1), the MO diagram of $[Pd_8(PH_3)_8]^{16+}$ is perturbed as shown in Figure 2b. Because of the lengthening of eight edges of the cube, some antibonding and bonding metal−metal MOs become nonbonding. EHT calculations indicate that the overlap between the s and p Pd FMO's is cancelled along the four 4.45 Å very long edges while it is still significant along the four 3.16 Å long Pd−Pd edges. As a result, four s and p-type antibonding combinations are significantly stabilized, leading to a set of eight antibonding orbitals and a set of 16 bonding/nonbonding orbitals. The overlap between the more contracted d-type orbitals remains significant only on the four 2.88 Å short edges. Whithin the d-band, this leads to the concentration of most of the Pd−Pd bonding character over a set of four orbitals of a_1, b_1, and e symmetry. These four orbitals lie at the very bottom of the band. They are preponderantly localized on the short edges of the distorted cube and have the proper symmetry to be considered as holding four localized Pd−Pd bonding pairs.

With formally a single bond between the As atoms, the seven occupied MOs of an isolated $(As_2)^{4-}$ unit separate into one low-lying σ-bonding orbital and six more or less nonbonding MOs which can be associated with the six lone pairs of the saturated $(As_2)^{4-}$ species. Four of these six orbitals are the in-phase (weakly bonding) and out-of-phase (weakly antibonding) combinations of the 4p(π) As orbitals, the remaining 2 being of σ-type. Because of the large energy separation between the 4s and 4p shells in As, one of the σ-nonbonding combinations, being largely 4s in character, lies at very low energy. Considering that the empty antibonding σ* level is situated at a very high energy, one is left for each $(As_2)^{4-}$ unit with 5 MOs (4 of π-type, 1 of σ-type) lying at a moderate energy and consequently susceptible to significantly interact with the $[Pd_8(PH_3)_8]^{16+}$ cube. These orbitals, all occupied, are sketched on the far right-hand side of Figure 2. When brought together, the frontier orbitals of the $(As_2)^{4-}$ groups give rise to a set of

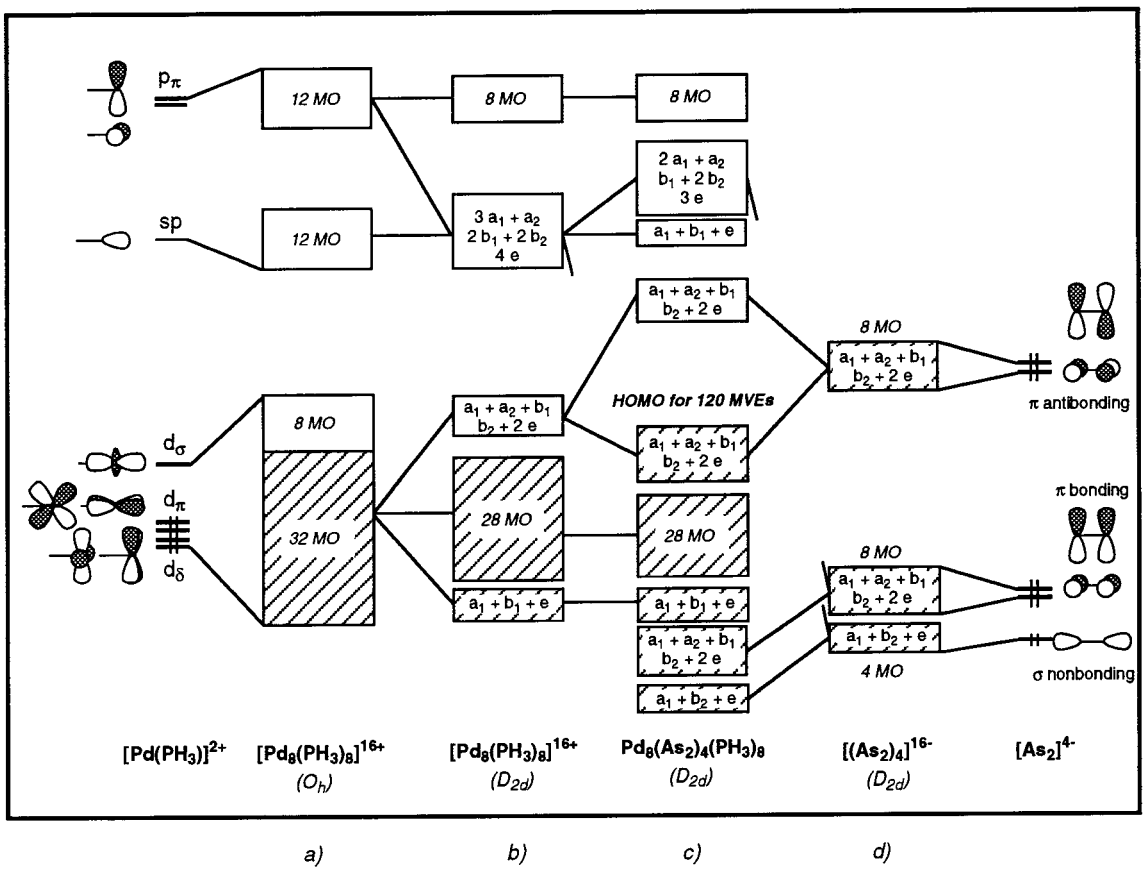


Figure 2. Qualitative MO diagrams based on EHT calculations for the idealized (12 M−M bonds) (a) and distorted (4 M−M bonds) (b) $[Pd_8(PH_3)_8]^{16+}$ fragment, the empty distorted $Pd_8(PH_3)_8(As_2)_4$ cluster (c), and the $[(As_2)_4]^{16-}$ fragment (d). The FMOs of the $Pd(PH_3)$ and As_2 moieties are shown on the far left- and far right-hand sides, respectively.

four combinations of the σ FMOs, lying close to a set of 8 combinations of the π FMOs, separated from the 8 π* combinations, as shown in Figure 2d.

The MO diagram showing the major bonding interactions between the two $[(As_2)_4]^{16-}$ and $[Pd_8(PH_3)_8]^{16+}$ fragments is given in Figure 2c. The twenty occupied FMOs of the former need to find vacant metallic counterparts of the same symmetry in the latter. These twenty metallic FMO's originate from two groups. One of them is made of the 8 d-type vacant orbitals, of symmetry $a_1 + a_2 + b_1 + b_2 + 2\times$ e. The second group, of symmetry $2\times a_1 + a_2 + b_1 + 2\times b_2 + 3\times$ e, is made of 12 among the sixteen s- and p-type bonding/nonbonding combinations. The interaction between the two fragments leads to the formation of twenty bonding and twenty antibonding combinations, as illustrated in Figure 2. Applying the closed-shell requirement to the hypothetical $Pd_8(PH_3)_8(As_2)_4$ model leads to the favored 120-MVE count. For this peculiar electron count, EHT calculations give a gap of 0.90 eV between the highest occupied molecular orbital (HOMO) and the lowest unoccupied molecular orbital (LUMO). The computed overlap population corresponding to the short Pd−Pd distances is rather weak [Pd(1,2)−Pd(3,4) = 0.03], whereas those corresponding to the long and very long Pd−Pd separations are nearly equal to zero. The significant participation to vacant levels of the π* FMOs of the $(As_2)^{4-}$ units provide the As−As single bonds with some additional π-bonding character, as shown by the increase of the As-As overlap population relative to an isolated $(As_2)^{4-}$ unit [0.92 in $Pd_8(PH_3)_8(As_2)_4$ vs 0.53 for the free $(As_2)^{4-}$ group]. The Pd−As overlap populations [Pd(1,2)−As(1) = 0.30, Pd(3,4)−As(1) = 0.18, and Pd(3,4)−As(2) = 0.38] suggest that the As atoms are firmly bonded to the eight Pd atoms.

To gain some confidence in the EHT results, DFT calculations were undertaken on the 120-MVE $Pd_8(PH_3)_8(As_2)_4$ model. Full optimization was made under the D_{2d} symmetry constraint. The optimized bond lengths for this model are given in Table 1 along with those obtained for the 130-MVE metal-centered $Pd_9(\mu{:}\eta^5,\eta^2\text{-}As_2)_4(PH_3)_8$ species. Remarkably, the computed distances are similar overall in the empty and the metal-centered clusters. We shall come back to this point in the next section. A HOMO-LUMO gap of 0.73 eV (comparable to that obtained from EHT calculations) is computed. These results suggest that empty clusters such as $Pd_8(As_2)_4(PH_3)_8$ with a D_{2d} distorted cubic framework may exist.

The fact that each $(As_2)^{4-}$ ligand uses only five FMOs for making six Pd−As "bonds" is typical of hypervalency.[24] However, as for the diamagnetic 120-MVE $M_8(\mu_4\text{-}E)_6L_8$ clusters, it is possible to describe $Pd_8(PH_3)_8(As_2)_4$ with a

simple 2-electron/2-center localized bonding scheme in which the number of bonding electron pairs is necessarily larger than the number of bonding combinations appearing in the delocalized MO diagram.[19] Assuming four Pd−Pd bonds, 24 Pd−As bonds, and four As−As bonds, the triconnected As(2) atoms hold a lone pair and satisfy the octet rule while the hypervalent As(1) atoms are 10-electron centers. Interestingly, within this bonding scheme, the Pd atoms are 16-electron centers, a typical configuration for the planar coordination mode.[24] As a matter of fact, a careful structural analysis of **1** indicates a not-far-from planar ligand environment around the Pd_s atoms. In the $Pd_8(PH_3)_8(As_2)_4$ model, the geometry of which is taken from the idealized geometry of **1**, the two strongest Pd−As bonds and the Pd−P bond are almost in the same plane for each metal center, whereas the weaker Pd−As bond is about 10° away from this plane. From this point of view, the hypothetical 120-MVE $Pd_8(As_2)_4(PH_3)_8$ cluster can be considered as the assemblage of four 30-electron $L_4Pd-PdL_4$ units, made of two 16-electron centers and linked to each other via bridging As_2 ligands (i.e. $4 \times (2 \times 16 - 2) = 120$ MVEs). It is related to a series of 128-MVE Cu_8 clusters which can be described as resulting from the assemblage of eight 16-electron square-planar systems, with no formal metal−metal bonding (except perhaps some $d^{10}-d^{10}$bonding).[26] Adding formally 8 electrons to $Pd_8(PH_3)_8(As_2)_4$ would break the four Pd−Pd bonds, making the system isoelectronic to the Cu_8 species.

Encapsulation of the Interstitial Metal Atom

The qualitative MO diagram of the metal-centered $Pd_9(\mu:\eta^5,\eta^2\text{-}As_2)_4(PH_3)_8$ cluster (**1**-H) illustrating the major interactions between Pd_i and its metallic host is shown in Figure 3. According to EHT calculations, only four among the 9 Pd_i atomic orbitals interact with the empty cage. The 5s and 5p(*x,y*) orbitals (of symmetry a_1 and e, respectively) are strongly destabilized by occupied counterparts of the $Pd_8(PH_3)_8(As_2)_4$ cage. After interaction, the occupation of the 5s and 5p(*x,y*) orbitals is 0.33 and 0.24, respectively. The fourth Pd_i orbital which is involved in the bonding is the low-lying and occupied x^2-y^2 orbital, of b_2 symmetry, which is stabilized by the lowest unoccupied b_2 level of the cage which has a large As−As π* character. After interaction, the x^2-y^2 population is 1.72. The other d-type orbitals of Pd_i do not interact, as well as the 5p(*z*) orbital which remains almost unperturbed with an occupation close to zero (0.03). It is noteworthy that the FMOs of the host which interact with Pd_i are mainly localized on the As(1) atoms overall and rather poorly on the As(2) and Pd_s atoms. This was expected owing to the short Pd_i−As(1) distances (ca. 2.57 Å). Since Pd_i is situated in an approximately square-planar environment of As(1) atoms, it is thus not surprising that it uses its s, *x*,*y*, and x^2-y^2 orbitals for bonding. Four Pd_i−As(1) bonding pairs can be identified. Three of them, of a_1 and e symmetry, are provided by the empty cage and donated to the metal. The fourth bonding pair, of b_2 symmetry, is provided by the metal x^2-y^2 orbital and donated to the cage (mainly to the As−As π* orbitals). Therefore, Pd_i can be described as a d^{10} square-planar 16-electron center. From the point of view of total cluster electron count, it is important to note that the three electron pairs, which are donated by the cage to Pd_i, are already involved in the bonding within the cage. Since they cannot be counted twice, the total MVE count can be formulated as 120 (empty cage) + 16 (Pd_i) − 6 (delocalized bonding electrons) = 130 MVEs.

As expected from the above discussion, the Pd_s-Pd_i overlap population is very weak. On the other hand, the Pd_i−As(1) overlap populations are strong, ca. 0.22, comparable to the Pd_s−As overlap populations which are 0.27 on average. As in the empty $Pd_8(As_2)_4(PH_3)_8$ parent cluster, the overlap populations corresponding to the long and very long Pd_s-Pd_s separations are nearly zero, whereas those corresponding to the short Pd_s-Pd_s contacts are ca. 0.02. The different Pd_s−As overlap populations [Pd(1,2)−As(1) = 0.30, Pd(3,4)−As(1) = 0.16, and Pd(3,4)−As(2) = 0.36] and As−As OP (0.91) are comparable to those computed for the empty parent cluster (vide supra). DFT calculations were carried out on **1**-H in order to support the EHT orbital analysis. The Pd_s-Pd_s and Pd_s−As separations obtained from a full optimization of **1**-H under the D_{2d} symmetry constraint indicate, as suggested from the EHT calculations, that the insertion of the central Pd atom hardly modifies the geometry of the distorted $Pd_8(As_2)_4(PH_3)_8$ cube. The geometries are highly similar

Table 1. Comparison of the calculated and experimental distances [Å] for empty and metal-centered distorted cubic models

Compound	$Pd_8(As_2)_4(PH_3)_8$[a]	$Pd_9(\mu:\eta^5,\eta^2\text{-}As_2)_4(PH_3)_8$[a]	$Pd_9(\mu:\eta^5,\eta^2\text{-}As_2)_4(PPh_3)_8$[b]
Pd_i-Pd_s	−	3.06	3.04
Pd(1-2)−Pd(4-3)	2.98	2.97	2.88
Pd(3)−Pd(4)	3.14	3.06	3.16
Pd(1)−Pd(2)	4.27	4.52	4.46
Pd_i−As(1)	−	2.60	2.57
Pd(1-2)−As(1)	2.49	2.52	2.44
Pd(1-2)−As(2)	2.52	2.53	2.49
Pd(3-4)−As(2)	2.56	2.67	2.61
As(1)−As(2)	2.30	2.31	2.36

[a] Calculated structure. − [b] Experimental structure.

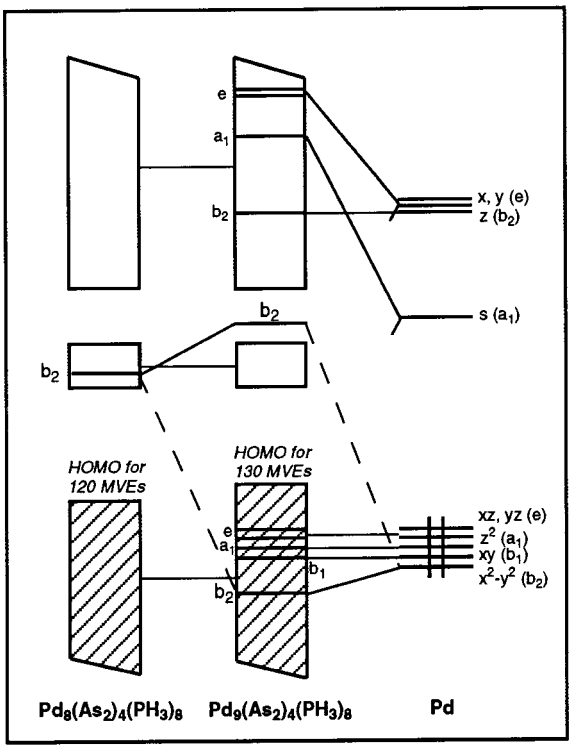


Figure 3. Qualitative MO diagram based on EHT calculations for the metal-centered species **1**-H obtained from the interaction of the distorted cubic $Pd_8(As_2)_4(PH_3)_8$ fragment with the interstitial Pd atom

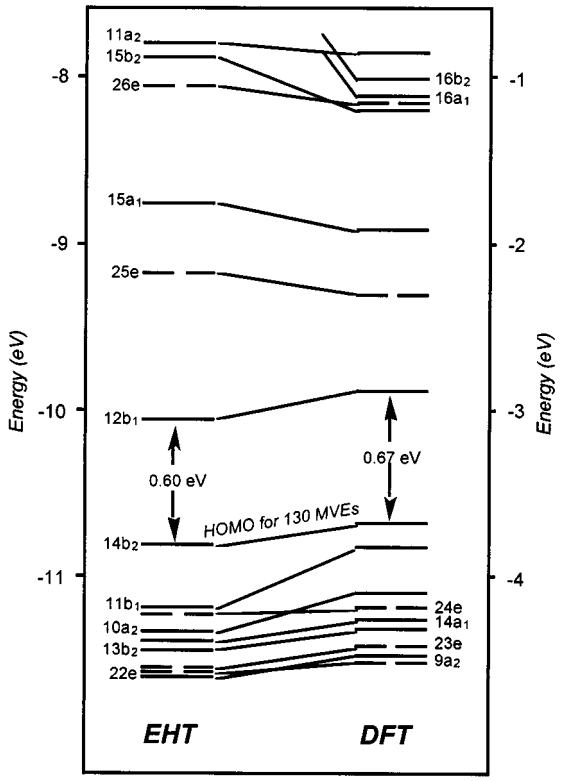


Figure 4. EHT (left) and DFT (right) MO diagrams for **1**-H

(see Table 1). The potential energy surface is particularly flat around the energy minimum, indicating that such an arrangement is rather flexible. A rather good agreement is observed between the optimized geometry of **1**-H and the experimental geometry of **1**. The largest deviation concerns the short Pd_s-Pd_s distance, computed to be 0.09 Å longer than the experimental value. This provides compelling evidence that the DFT approach is reliable for predicting the bond lengths of large inorganic transition metal systems.

The DFT and EHT MO diagrams of **1**-H are compared in Figure 4. They are similar overall, exhibiting the same ground-state electronic configuration. Both calculations predict a closed-shell configuration for the count of 130 MVEs. Note that a single-point DFT calculation on compound **1**, that is in which the PH_3 ligands were replaced by PPh_3 ligands, lead to similar results.

According to Figure 4, several empty MOs lie in the middle of a large energy gap separating the HOMO $14b_2$ from the high-lying 26e MO. One may ask whether reduced species would be stable. EHT calculations indicate that populating the $12b_1$ LUMO hardly changes the nature of the bonding in the cluster. Mono- or di-anionic species should be possible. Conversely, oxidation of compound **1** may be possible since the $14b_2$ HOMO is somewhat Pd_s-Pd_i antibonding. Its complete or partial depopulation should lead to some shrinking of $Pd_8(As_2)_4$ and enhance the Pd_s-Pd_i bonding. In other words, in comparison with other cubic M_8 and M_9 architectures which are observed for a large range of electron counts,[19–21,23] arrangements such as **1** should be observed for different electron counts with either closed- or open-shell electron configurations.

Conclusion

The theoretical analysis of $Pd_9(\mu{:}\eta^5,\eta^2\text{-}As_2)_4(PPh_3)_8$ shows that the bonding of the interstitial Pd atom with the D_{2d} distorded $Pd_8(As_2)_4$ cubic host differs from that found in its related metal-centered cubic species $M_9(\mu_4\text{-}E)_6L_8$ in which the bonding was ensured by strong bonding interactions between the central and surface metal atoms. Indeed, in compound **1** the central atom can be described as a roughly square-planar 16-electron center, bound through Pd_i-As rather than Pd_i-Pd_s contacts to a distorted cubic fragment made of four 30-electron bimetallic Pd_2L_8 units, each Pd_2L_8 unit being made of two approximately planar PdL_4 16-electron centers linked by a Pd–Pd bond. Since six metal-ligand bonding electrons are shared by the cage and the Pd_i center, the cluster electron count can be decomposed as follow: $8 \times (2 \times 16 - 2) + 16 - 6 = 130$ MVEs. A strongly different bonding picture was computed for the isoelectronic 130-MVE $Ni_9Te_6(PEt_3)_8$ species.[20] A substantial HOMO–LUMO gap is computed for the observed electron count of 130 MVEs, a situation generally encountered in stable molecular compounds. However, our calculations indicate that such an architecture should be observed for a range of allowed electron counts around 130 MVEs, a common situation encountered in extended structures.

Appendix

a) Extended Hückel Calculations: Calculations have been carried out within the extended Hückel formalism[26] using the weighted H_{ij} formula[27] with the program CACAO.[28] The exponents (ζ) and the valence shell ionization potentials (H_{ii} in eV) were (respectively): 1.3, −13.6 for H 1s; 1.6, −18.6 for P 3s; 1.6, −14.0 for P 3p; 2.23, −16.22 for As 4s; 1.89, −12.16 for As 4p; 2.19, −7.32 for Pd 5s; 2.152, −3.75 for Pd 5p. H_{ii} value for Pd 4d was set equal to −12.02. A linear combination of two Slater-type orbitals of exponents $\zeta_1 = 5.983$ and $z_2 = 2.613$ with the weighting coefficients $c_1 = 0.5264$ and $c_2 = 0.6373$ was used to represent the Pd 4d atomic orbitals. The different molecular models used were based on the averaged idealized (D_{2d}) experimental structure of **1**. The following bond distances [Å] were used in the $Pd_8(As_2)_4(PH_3)_8$ and $Pd_9(As_2)_4(PH_3)_8$ models: Pd_i-Pd_s = 3.05, Pd(1,2)−Pd(4,3) = 2.88 Å, Pd(3)−Pd(4) = 3.16 Å, Pd(1)−Pd(2) = 4.45 Å, Pd_i−As(1) = 2.57 Å, Pd(1,2)−As(1) = 2.51 Å, Pd(1,2)−As(2) = 2.61 Å, Pd(3,4)−As(2) = 2.43 Å, and Pd−P = 2.26 Å.

b) Density Functional Calculations: Density Functional calculations[29] were carried out on the empty $Pd_8(As_2)_4(PH_3)_8$ and metal-centered $Pd_9(As_2)_4(PH_3)_8$ models using the Amsterdam Density Functional (ADF) program.[30] Electron correlation was treated within the local density approximation (LDA).[31] The numerical integration procedure applied for the calculations was developed by te Velde et al.[29c] The atom electronic configurations were described by a triple-ζ Slater-type orbital (STO) basis set for H 1s, P 2s and 2p, As 3s and 3p, Pd 5s and 4d, and single-z STO function for H 2p, P 3d, As 4d, and Pd 5p. A frozen-core approximation[32] was used to treat the core electrons of P, As, and Pd.

Acknowledgments

The authors thank the Centre de Ressources Informatiques (CRI) of Rennes and the Institut de Développement et de Ressources en Informatique Scientifique (IDRIS-CNRS) of Orsay for computing facilities. Prof. D. Fenske (Karlsruhe, Germany) is thanked for helpful discussions.

[1] *Clusters and Colloids, From Theory to Applications* (Ed.: G. Schmid), VCH, Weinheim, **1994**.
[2] L. D. Lower, L. F. Dahl, *J. Am. Chem. Soc.* **1976**, *98*, 5046.
[3] D. Fenske, R. Basoglu, J. Hachgenei, F. Rogel, *Angew. Chem., Int. Ed. Engl.* **1984**, *23*, 160.
[4] D. Fenske, J. Magull, *Z. Naturforsch.* **1990**, *45b*, 121.
[5] D. Fenske, H. Krautscheid, M. Müller, *Angew. Chem., Int. Ed. Engl.* **1992**, *31*, 321.
[6] D. Fenske, J. Hachgenei, J. Ohmer, *Angew. Chem., Int. Ed. Engl.* **1985**, *24*, 706.
[7] D. Fenske, J. Ohmer, J. Hachgenei, K. Merzweiler, *Angew. Chem., Int. Ed. Eng.* **1988**, *27*, 1277.
[8] D. Fenske, J. Hachgenei, F. Rogel, *Angew. Chem., Int. Ed. Engl.* **1984**, *23*, 982.
[9] G. Christou, K. S. Hagen, J. K. Bashkin, R. H. Holm, *Inorg. Chem.* **1985**, *24*, 1010.
[10] [10a] S. Pohl, U. Opitz, *Angew. Chem., Int. Ed. Engl.* **1993**, *32*, 863. – [10b] S. Pohl, W. Barklage, W. Saak, U. Opitz, *J. Chem. Soc., Chem. Commun.* **1993**, 1251.
[11] C. Junghans, W. Saak, S. Pohl, *J. Chem. Soc., Chem. Commun.* **1994**, 2327.
[12] S. Pohl, W. Saak, *Angew. Chem., Int. Ed. Eng.* **1984**, *23*, 907.
[13] J. P. Zebrowski, R. K. Hayashi, A. Bjarnason, L. F. Dahl, *J. Am. Chem. Soc.* **1992**, *114*, 3121.
[14] D. Fenske, C. Persau, *Z. Anorg. Allg. Chem.* **1991**, *593*, 61.
[15] D. Fenske, J. Ohmer, K. Merzweiler, *Angew. Chem., Int. Ed. Engl.* **1988**, *27*, 1512.
[16] J. G. Brennan, T. Siegrist, S. M. Stuczynski, M. L. Steigerwald, *J. Am. Chem. Soc.* **1989**, *111*, 9240.
[17] D. Fenske, H. Fleischer, C. Persau, *Angew. Chem., Int. Ed. Engl.* **1989**, *28*, 1665.
[18] [18a] D. Fenske, K. Vogt, unpublished results. – [18b] K. Vogt, Ph.D. Dissertation, Univ. of Karlsruhe, Germany, **1994**.
[19] [19a] E. Furet, A. Le Beuze, J.-F. Halet, J.-Y. Saillard, *J. Am. Chem. Soc.* **1994**, *116*, 274. – [19b] N. Rösch, L. Ackerman, G. Pacchioni, *Inorg. Chem.* **1993**, *32*, 2963.
[20] E. Furet, A. Le Beuze, J.-F. Halet, J.-Y. Saillard, *J. Am. Chem. Soc.* **1995**, *117*, 4936.
[21] [21a] J.-F. Halet, J.-Y. Saillard, *Struct. Bond.* **1997**, *87*, 81. – [21b] R. Gautier, J.-F. Halet, J.-Y. Saillard, in *Metal Clusters in Chemistry* (Eds. : P. Braunstein, L. Oro, P. R. Raithby), VCH, Weinheim, **1998**, in press.
[22] K. H. Whitmire, J. R. Eveland, *J. Chem. Soc., Chem. Commun*. **1994**, 1335.
[23] B. Zouchoune, F. Ogliaro, J.-F. Halet, J.-Y. Saillard, J. R. Eveland, K. H. Whitmire, *Inorg. Chem.* **1998**, *37*, 865.
[24] *Orbital Interactions in Chemistry,* T. A. Albright, J. K. Burdett, M-H Whangbo, J. Wiley & Sons, New York, **1984.**
[25] [25a] L. E. Mc Candlish, E. C. Bissell, D. Coucouvanis, J. P. Fackler, K. Knox, *J. Am. Chem. Soc.* **1968**, *90*, 7357. – [25b] F. J. Hollander, D. Coucouvanis, *J. Am. Chem. Soc.* **1974**, *96*, 5646. – [25c] F. J. Hollander, M. L. Cafferty, D. Coucouvanis, 167th National Meeting of the American Chemical Society, Los Angeles, **1974**. – [25d] A. Avdeef, J. P. Fackler, *Inorg. Chem.* **1978**, *17*, 2182.
[26] R. Hoffmann, *J. Chem. Phys.* **1963**, *39*, 1397.
[27] J. H. Ammeter, H.-B. Bürgi, J. C. Thibeault, R. Hoffmann, *J. Am. Chem. Soc.* **1978**,*100*, 3686.
[28] C. Mealli, D. Proserpio, *J. Chem. Educ.* **1990**, *67*, 399.
[29] [29a] E. J. Baerends, D. E. Ellis, P. Ros, *Chem. Phys.* **1973**, *2*, 41. – [29b] E. J. Baerends, P. Ros, *Int. J. Quantum. Chem.* **1978**, *S12*, 169. – [29c] P. M. Boerrigter, G. te Velde, E. J. Baerends, *Int. J. Quantum Chem.* **1988**, *33*, 87. – [29d] G. te Velde, E. J. Baerends, *J. Comput. Phys.* **1992**, *99*, 84.
[30] E. J. Baerends et al., *Amsterdam Density Functional (ADF) program, version 2.0.1*, Vrije Universiteit, Amsterdam, Netherlands, **1996**.
[31] S. D. Vosko, L. Wilk, M. Nusair, *Can. J. Chem.* **1990**, *58*, 1200.
[32] E. J. Baerends, Ph. D. Thesis, Vrije Universiteit, Amsterdam, Netherlands, **1975**.

Received September 24, 1998
[I98325]

Preparation, Properties, and Reactions of Metal-Containing Heterocycles, 99[+]

Cage-Structured Triplatinacyclophanes

Ekkehard Lindner,*[a] Christian Hermann,[a] Gerhard Baum,[b][++] and Dieter Fenske[b][++]

Dedicated to Professor Jochen Ellermann on the occasion of his 65th birthday

Keywords: Cage compounds / Metallacyclophanes / P ligands / Platinum / Supramolecular chemistry

The synthesis of the tris(triflate) **4** (Scheme 1) has been achieved by means of a straightforward three-step reaction sequence. After initial lithiation of mesitylene, treatment of the obtained trilithium compound $C_6H_3(CH_2Li)_3$ (**2**) with oxirane results in the formation of 1,3,5-tris(3-hydroxypropyl)benzene (**3**), which is then transformed to **4** by reaction with $(CF_3SO_2)_2O$ in the presence of pyridine. Whereas **4** reacts with $Na_2[Os(CO)_4]$ in a somewhat complicated manner, similar reactions with $Na[Re(CO)_5]$ and $LiPPh_2$ give the hydrocarbon-bridged tris(rhenium) complex $C_6H_3[(CH_2)_3Re(CO)_5]_3$ (**5**) and the tris(phosphane) $C_6H_3[(CH_2)_3PPh_2]_3$ (**6**), respectively. Employing the high-dilution method, from **6** and $Cl_2Pt(NCPh)_2$ the nanoscaled tri- and hexaplatinacyclophanes **7** and **9** are available. Owing to the optimal geometry and flexibility of the cage in **7**, 1,2-dichloroethane can be reversibly encapsulated. The molecular structure of **7** · 7 1,2-$Cl_2C_2H_4$ was determined by an X-ray structure analysis. The utility of the reactive metal centers in **7** has been demonstrated by replacing the chloro ligands by acetonitrile to give the cationic platinacyclophane **8**, in which, according to NMR studies, the cage-like structure is preserved.

Introduction

Cage-like molecules containing a macrobicyclic skeleton play an important role in host/guest chemistry[1] and as nanoscaled building blocks for the construction of supramolecular assemblies.[2] Attempts to construct such molecules through threefold carbon−carbon couplings necessitate multi-step procedures and high-dilution conditions, and ultimately give only low yields.[3] An attractive alternative, however, is the dimerization of trifunctional molecular precursors. Based on this method, several syntheses of three-dimensional cyclophanes have be realized.[1c,3a,4] Although these cage molecules also incorporated either transition or main-group metal centers, which could serve as anion receptors, they did not possess the classical threefold bridged cyclophane structure with aromatic units at the bottom and the top of the molecule, and where the metal atoms are located in the center of the aliphatic bridges.[5] Since the first typical metallaphanes appeared in the literature in 1994,[6] investigations have been mainly focused on two-dimensional systems.[7] The introduction of tetracarbonyliron and -osmium fragments into the cyclophane framework has a marked effect on the structures of these macrocycles. Moreover, these new reactive centers also permit the insertion of small molecules, such as carbon monoxide, into the metal−carbon σ bonds.

Unlike two-dimensional systems, *bona fide* three-fold bridged metallacyclophanes conforming to the classical cyclophane structure remain rather rare. Of the limited number of examples, most are not suited for host/guest chemistry owing to their rigid structures and/or the absence of an intramolecular cavity.[8] Recently, Fujita et al. introduced a remarkable template synthesis of a palladium-containing cyclophane with the ability to incorporate anions of aromatic carboxylic and sulfonic acids.[9] The same group,[10] as well as Steel[11] and Stang,[12] have also reported on six-fold bridged metallacyclophanes with tetrahedral symmetry. The rigidity of the employed triply functionalized ligands and palladium or platinum complex fragments is an essential prerequisite for this self-assembly. Some of these palladium-containing "nanometer-scale molecular container compounds" are also capable of encapsulating guest molecules.[10,11]

The present investigation relates to a synthetic route recently exploited by Balch et al.[8a] for the synthesis of novel three-fold bridged platinacyclophanes. The objective was to create a flexible ligand system based on an aromatic nucleus with three methylene groups as spacers, functionalized with tertiary phosphane end groups. It is envisaged that two of these ligands should be capable of assembly via three platinum atoms to furnish an elastic, three-dimensional molecular cage, in which the kinetics are sufficiently fast for host/guest complexation and decomplexation.[4c] To meet this re-

[+] Part 98: E. Lindner, I. Krebs, R. Fawzi, M. Steimann, *Organometallics*, in press.

[++] X-ray structure analysis.

[a] Institut für Anorganische Chemie der Universität, Auf der Morgenstelle 18, D-72076 Tübingen, Germany
Fax: (internat.) + 49(0)7071/29-5306
E-mail: ekkehard.lindner@uni-tuebingen.de
[b] Institut für Anorganische Chemie der Universität (TH), Engesserstraße, Geb.-Nr. 30.45, D-76128 Karlsruhe, Germany

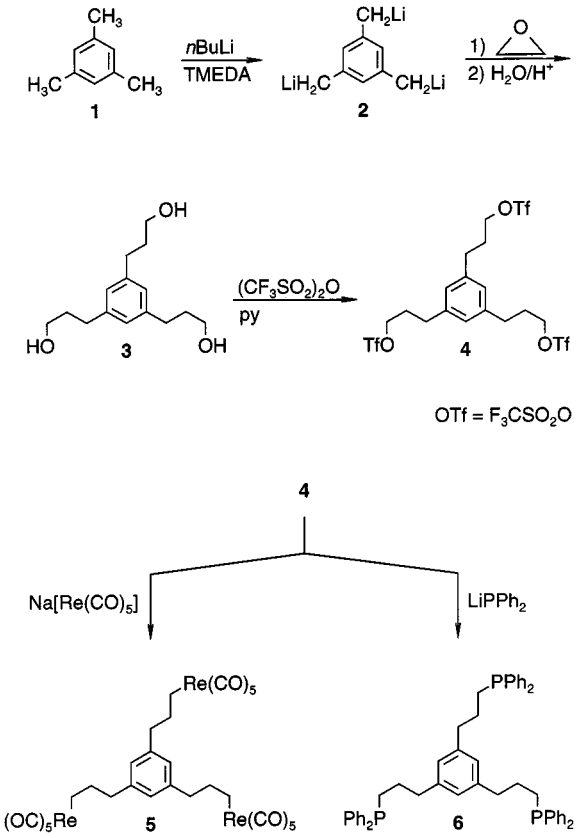
 © WILEY-VCH Verlag GmbH, D-69451 Weinheim, 1999 1434−1948/99/0404−0679 $ 17.50+.50/0

quirement, a symmetrically substituted tris(diphenylphosphanylpropyl)benzene has been synthesized from a suitable tris(triflate).

Results and Discussion

Synthesis of Ligands and Reactions with Metal Lewis Bases

In analogy to previous studies on the generation of osma- and ferracyclophanes,[6,7c,7d] our strategy was to treat the tris(triflate) **4** (Scheme 1) with a suspension of the organometallic Lewis base, $[Os(CO)_4]^{2-}$ or $[Fe(CO)_4]^{2-}$, in dimethyl ether at −25°C, so as to obtain the corresponding triosma- and triferracyclophane species. The tris(triflate) **4** could be obtained by treatment of the triol **3** with $(CF_3SO_2)_2O$[13] in the presence of pyridine at −30°C.[14] In turn, the triol **3**[15] was conveniently prepared by a two-step reaction starting from mesitylene (**1**). Lithiation of **1** with *n*BuLi/TMEDA afforded the trilithium derivative **2**,[16] and subsequent treatment of a suspension of **2** in diisopropyl ether with an equivalent amount of oxirane led directly to the triol **3** (Scheme 1). After purification by column chromatography, the tris(triflate) **4** was obtained as a colorless, viscous, moisture-sensitive, thermally labile oil, which could be stored without any decomposition below −35°C. It was found to be freely soluble in common organic solvents. The molecular composition of **4** was determined from its FD mass spectrum, which showed the molecular ion peak at *m/z* = 647.6.



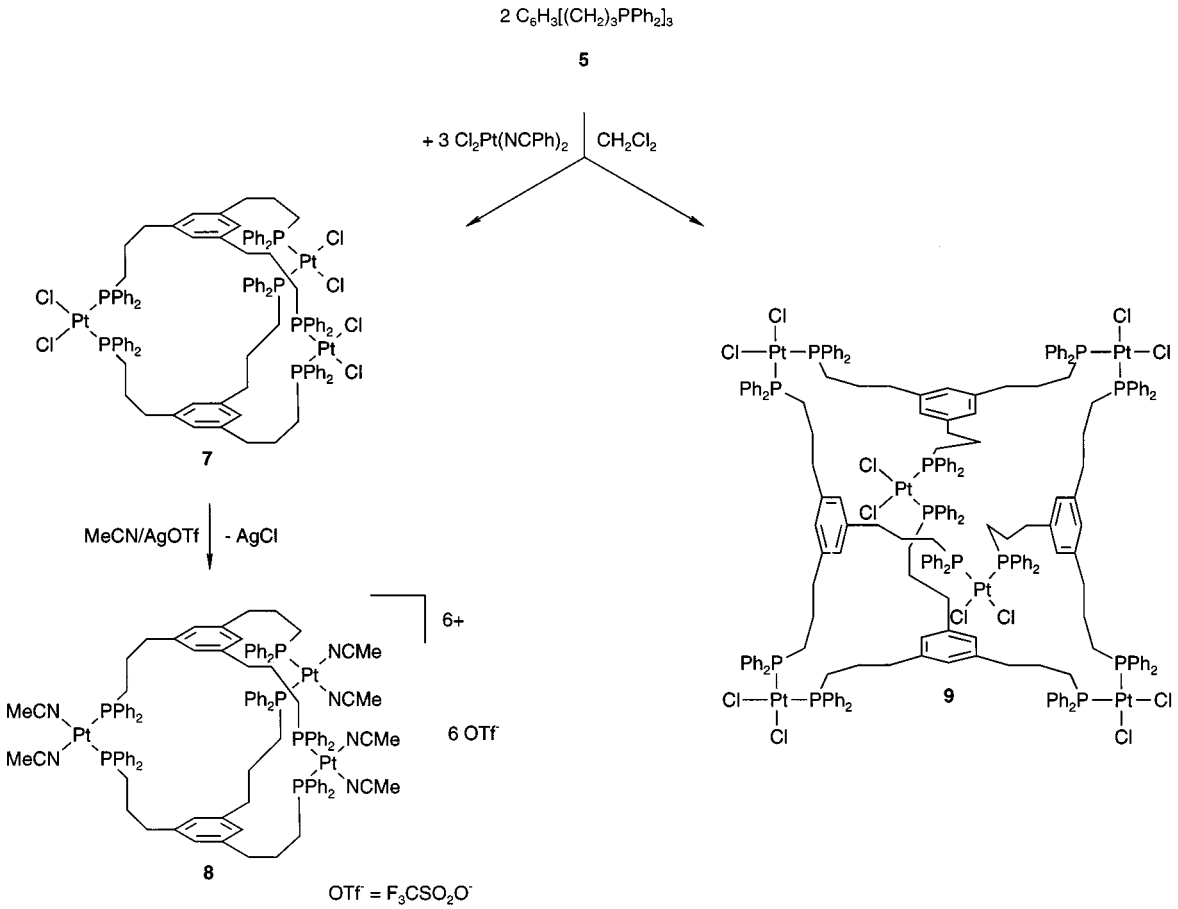
Scheme 1. Synthesis of the rhenium complex **5** and the tris(phosphane) **6**

Reaction of the tris(triflate) **4** with $Na_2[Os(CO)_4]$ in boiling dimethyl ether[6,7c,7d,14] did not lead to the expected triosmacyclophane with D_3 symmetry. Only oligo- or polymeric species precipitated from the reaction mixture. The yellow solid collected exhibited four terminal carbonyl absorptions in its IR spectrum (in KBr: $\tilde{\nu}$ = 2124 cm^{-1}, 2040, 2038, 2009), which are characteristic of *cis*-$Os(CO)_4$ units. The failure of this attempt to gain access to a triosmacyclophane cannot be attributed to any lack of reactivity of the tris(triflate) **4**. When a THF solution of $Na[Re(CO)_5]$ was treated with **4** at −20°C, the colorless, rather stable tris(pentacarbonylrhenium) complex **5** was formed in satisfactory yields. A similar trinuclear rhenium complex with an aromatic unit in the center of the molecule was reported by Beck et al. several years ago.[17] The ^{1}H-NMR spectrum of complex **5** exhibits three complex multiplets at δ = 0.9, 2.0, and 2.5, corresponding to AA′XX′, AA′MM′XX′, and AA′MM′ spin systems for the α-, β-, and γ-methylene protons. This suggests a hindered rotation about the $C_\alpha-C_\beta$ bonds due to the bulky $Re(CO)_5$ fragments at the α-methylene groups.[18]

In our quest to find an alternative approach for the construction of three-dimensional, triply bridged metallaphanes, we considered a cage structure incorporating metal−phosphorus bonds instead of metal−carbon σ linkages. In order to assess this possibility, a prerequisite was the synthesis of the tris(phosphane) **6**, which was achieved by reaction of **4** with $LiPPh_2$ in diethyl ether at −30°C (Scheme 1). After column-chromatographic work-up of the reaction mixture, the phosphane **6** was isolated as a rather air-sensitive, viscous oily liquid, which was found to be freely soluble in common organic solvents. In the FD mass spectrum, the molecular ion peak was observed at *m/z* = 756.9. Such phosphanes represent suitable starting materials for the reaction with substitution-labile platinum complexes to give access to cage-like molecules.[8a]

Platinacyclophanes

Since the discovery of crown ethers by Pedersen[19] in 1967, the chemistry of synthetic hosts for specific complexation of organic and inorganic guest molecules has developed rapidly. In particular, investigations on the use of cyclophanes as hosts have contributed to an understanding of the complexation of neutral organic guest molecules such as arenes or chlorinated hydrocarbons in aqueous and organic media.[20] The introduction of transition metal units into the framework of a cyclophane has an effect on the geometric properties of the cavity formed by the resulting metallacyclophane. In order to achieve the generation of a three-fold bridged metallaphane, the platinum complex $Cl_2Pt(NCPh)_2$ was treated with the tris(phosphane) **6** according to the high-dilution method.[21] Indeed, the hexachlorotriplatinacyclophane **7** was obtained in rather good yields (Scheme 2). Because of entropic factors, the formation of oligomeric and polymeric species was suppressed. The energy cost associated with the loss of several



Scheme 2. Synthesis of the platinacyclophanes **7**–**9**

degrees of freedom for the components of the assembly is not so large for a system with a smaller number of units.[12,22]

The $^{31}P\{^1H\}$-NMR spectrum of **7** reveals a singlet for the six chemical equivalent phosphorus atoms at $\delta = 8.8$ and a doublet for the ^{195}Pt satellites, which is typical for *cis*-$PtCl_2$ fragments. This assignment is confirmed by the ^{195}Pt-NMR spectrum, which displays a triplet at $\delta = -4414$ with a coupling constant of $^1J_{PtP} = 3660$ Hz. Most characteristic for the $^{13}C\{^1H\}$-NMR spectrum of **7** are three complex multiplets with AXX′ spin systems at $\delta = 127.9$, 38.0, and 30.6 which are assigned to the *o*-carbon atoms of the $(C_6H_5)_2P$ units and to the carbon atoms of the α- and β-methylene groups of the hydrocarbon chains, respectively.[5a] To the best of our knowledge, **7** is the first metallacyclophane which is able to encapsulate a lipophilic guest molecule like dichloroethane. In contrast to the cage-like palladium-containing system of Fujita,[9] **7** is also obtainable without a guest (template). The complexation/decomplexation process is reversible, which was proved by microelemental analyses and ^1H- as well as $^{13}C\{^1H\}$-NMR spectra of the complex **7** · 7 $C_2H_4Cl_2$, which in addition to the signals of **7** exhibit the ^{13}C peaks for $C_2H_4Cl_2$. The integration of the ^1H signals in the ^1H-NMR spectrum and the crystal structure analysis corroborate the stoichiometry of **7** · 7 $C_2H_4Cl_2$.[23] One of the dichloroethane molecules is located in the cavity, the others are positioned at the exterior of the cage in interstices of the crystal. In the case of the complexation of exolipophilic guests no specific linkages between guests and hosts are present, but the guests have to fit geometrically into the cavity.[4c] Owing to its alkylene units, the cage **7** is sufficiently flexible to exhibit satisfactorily fast kinetics for complexation and decomplexation reactions. The hexachlorotriplatinacyclophane **7** exhibits an L_2M_3 composition (L = ligand, M = transition metal fragment) with C_3 symmetry of the ring skeleton. In view of the bulky phenyl substituents at the *cis*-platinum-coordinated phosphorus atoms, the trigonal-prismatic cavity of the cage containing the encapsulated 1,2-dichloroethane molecule is well-shielded from the exterior (Figure 1). The length of the edges of this cavity is approximately 8 Å and its height is about 4.8 Å.

Owing to the C_3 axis passing through the phenylene rings of the cyclophane, the embedded dichloroethane had to be refined at three split positions. The centers of both phenylene groups, which are arranged almost parallel, are located approximately one upon the other. All three distorted square-planar coordinated platinum atoms of **7** lie within a circular area, midway between the aromatic rings of the two ligands. The Pt–Cl and Pt–P connections are arranged

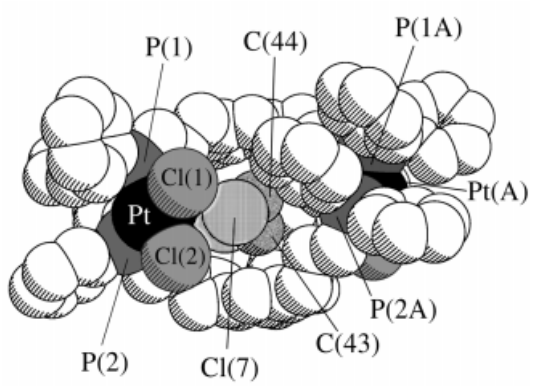


Figure 1. Molecular structure of **7**·7 1,2-$Cl_2C_2H_4$ (space-filling representation); the complete envelopment of 1,2-dichloroethane [gray spheres in center: C(43), C(44), Cl(7)], which is located in one of three possible split positions, is evident

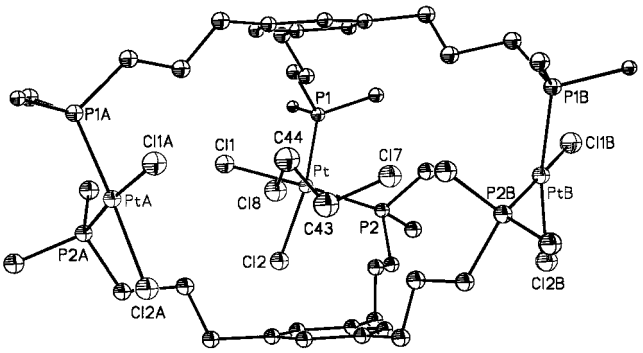


Figure 2. Molecular structure of **7**·7 1,2-$Cl_2C_2H_4$ in the crystal; ORTEP plot with thermal ellipsoids at 20% probability; hydrogen atoms and phenyl groups at the phosphorus atoms are omitted for clarity; selected distances [Å]: Pt−PtA = Pt−PtB = PtA−PtB 9.91(3), P1−P1A = P1−P1B = P1A−P1B 10.94(3), P2−P2A = P2−P2B = P2A−P2B 10.15(2), P1−P2 = P1A−P2A = P1B−P2B 3.44(3), Cl7−Pt 5.98(5), Cl7−PtB 4.30(4), Cl8−Pt 4.03(6), Cl8−PtA 6.12(4), distance between the centers of the phenylene groups of the ligands 8.01(2); torsion angle between the phenylene groups of the ligands 20.0(2)°

above and below this area. The distance between each platinum atom and the center of the circular area is 5.721(3) Å (Figure 2).

According to the considerations of Stang et al.,[12] supramolecular systems containing palladium or platinum complex fragments as that described above are able to form even higher units with the compositions L_4M_6, L_8M_{12}, and $L_{20}M_{30}$ with *T*, *O*, and *I* symmetry, respectively. In fact, in addition to the expected triplatinacyclophane (L_2M_3) **7**, traces of the hexaplatinacyclophane **9** (Scheme 2) with the composition L_4M_6 were also formed in the reaction of **6** with $Cl_2Pt(NCPh)_2$. This system, with a cavity formed by six platinum atoms, was detected in the FAB mass spectrum, which featured the [M^+ − Cl] peak at m/z = 4589. Ideally, such molecules adopt an adamantanoid structure with *T* symmetry.[11,12] Whereas the aromatic rings are placed at the vertices of a tetrahedron, the metal atoms are located at the vertices of an octahedron.

In a subsequent experiment, the triplatinacyclophane **7** was employed as a starting compound in order to obtain a modified cyclophane in which the cage-like structure was preserved, but which exhibited different properties. Thus, by treatment of **7** with silver trifluoromethanesulfonate in a mixture of acetonitrile/dichloromethane (1:1), all the chloro ligands were replaced by acetonitrile and the six-fold positively charged triplatinacyclophane **8** was isolated as a thermally stable white solid (Scheme 2). The composition of this three-fold bridged, cationic macrocycle was confirmed by elemental analysis and by its FAB mass spectrum. In agreement with symmetry requirements, the $^{31}P\{^1H\}$-NMR spectrum of **8** displays a singlet, with appropriate ^{195}Pt satellites, for the six equivalent phosphorus atoms. From the size of the ^1J(Pt,P) couplings, it can be concluded that the phosphorus donors still occupy *cis* positions. The presence of the triflate anions is confirmed by a singlet at δ = −78.8 in the ^{19}F-NMR spectrum of **8**. Although complex, the ^1H- and $^{13}C\{^1H\}$-NMR spectra are not only diagnostic of the proposed structure of **8**, but they are also consistent with the corresponding NMR data of the chloro derivative **7**, the structure of which was elucidated by an X-ray structural determination.[23]

A brief discussion of the $^{13}C\{^1H\}$-NMR spectrum is restricted to the ring skeleton. Two singlets at δ = 141.1 and 126.8 can be assigned to the quaternary (DEPT-135 experiment) and tertiary carbon atoms bonded to the phosphorus atoms of the cage. At higher field (δ = 36.4), an AXX′ pattern can be ascribed to the carbon atoms of the methylene groups adjacent to the phenyl rings. Complex multiplets at δ = 26 are attributable to the remaining methylene functions. Two further singlets at δ = 117.9 and 2.0 are attributable to the nitrile and methyl carbon atoms of the acetonitrile ligands attached to the platinum centers.

Conclusion

Cyclophane chemistry has made a valuable contribution in the field of molecular recognition, since it has led to the development of a multitude of architecturally impressive molecules, with various structural features and functionalities, in which guest molecules can be embedded.[1e,20] The incorporation of transition metals into the aliphatic framework of cyclophanes offers an ingenious means of controlling the inclusion of potential host systems[9−11] and of creating new reactive centers.[7c,7d] Trimetalla- (L_2M_3, L = tripodal ligand, M = transition metal fragment) and even hexametallacyclophanes (L_4M_6), with cavities suitable for the encapsulation of neutral molecules or anions of aromatic carboxylic and sulfonic acids, have hitherto only been prepared by self-assembly, employing nitrogen-containing ligands.[9−12] However, Balch recently succeeded in synthesizing a cage-like molecule composed of aromatic tris(phosphane) ligands,[8a] although due to its rigid structure and limited solubility in nearly all common solvents, this system was not suited for host-guest chemistry. By constructing such a tridentate phosphane around an additional flexible alkane backbone, we have prepared the three-dimensional platinacyclophane **7**, which, by virtue of its size, is able to

reversibly encapsulate 1,2-dichloroethane.[23] Remarkably, in the same reaction, the dodecachlorohexaplatinacyclophane (L_4M_6) **9** was also formed in trace amounts. The ligands attached to the platinum atoms in **7** can easily be exchanged with preservation of the cage-like structure, enabling adaptation of the cyclophane molecules to specific conditions. In this context, the new cationic hexakis(acetonitrile)triplatinacyclophane **8** was prepared, which exhibited quite different properties.

Experimental Section

General: All reactions and manipulations were carried out under dry argon using standard Schlenk techniques. Solvents were dried with appropriate reagents and stored under argon. − Column chromatography: Activated silica gel, 0.063−0.200 mm (Merck); column dimensions are reported in the specific sections describing the synthesis of the compounds. − Elemental analyses: Carlo Erba 1106. − F and S analyses were carried out according to Schöniger[24] and determined as described by Brunisholz and Michod[25], and by Wagner[26], respectively. − Rhenium and platinum were determined with a Varian AA20 spectrometer. − FD and FAB MS: Finnigan 711A (8 kV), modified by AMD. − IR: Bruker IFS 48 FT-IR. − ^{1}H, ^{13}C{^{1}H}, ^{31}P{^{1}H}, ^{19}F, and ^{195}Pt NMR: Bruker DRX 250 spectrometer operating at 250.13, 62.90, 101.26, 235.33, and 53.55 MHz, respectively. ^{1}H chemical shifts were referenced to the residual proton peaks of the solvents and are quoted in ppm downfield from TMS. ^{13}C chemical shifts were calibrated against the deuterated solvent multiplet and referenced to TMS. ^{31}P chemical shifts were measured relative to external 85% H_3PO_4 with downfield values being taken as positive. ^{19}F chemical shifts were measured relative to external 0.05% 1,3,5-trifluorotoluene. ^{195}Pt chemical shifts were measured relative to external 37.5% $Na_2[PtCl_6] \cdot 6\ H_2O$. Oxirane was of commercial grade and was used without further purification; 1,3,5-tris(lithiomethyl)benzene,[16] $(CF_3SO_2)_2O$,[13] $LiPPh_2$,[27] and $Cl_2Pt(NCPh)_2$[28] were synthesized according to literature methods.

1,3,5-Tris(3-hydroxypropyl)benzene (3): Pyrophoric 1,3,5-tris(lithiomethyl)benzene (**2**), prepared from 500 mL of a solution of *n*-butyllithium (1.6 M in *n*-hexane), 92.97 g (800.0 mmol) of TMEDA, and 16.03 g (133.4 mmol) of mesitylene, was filtered off from the reaction mixture (P3) and washed with *n*-pentane until the washings were almost colorless. After drying in vacuo, **2** was suspended in 500 mL of diisopropyl ether and the suspension was cooled to −30°C. Then, 17.62 g (400.0 mmol) of oxirane was condensed into the reaction vessel over a period of 2 h. The resulting mixture was stirred at −30°C for 1 h and then allowed to warm to room temperature. The orange suspension obtained was then rapidly poured into 150 mL of iced water, and 2 N H_2SO_4 was added until pH = 2 was attained. The organic layer was separated and the aqueous phase was washed with diethyl ether (3 × 150 mL). The combined organic phases were dried with Na_2SO_4 and the solvent was evaporated. The product was purified by column chromatography (CH_2Cl_2/MeOH/*n*-hexane, 15:2:1, diameter/length of column 7/50 cm). Yield 7.82 g (24.6%), colorless oil. − ^{1}H NMR ([D$_6$]acetone): δ = 6.87 (s, 3 H, aromatic H), 3.56 (t, $^3J_{HH}$ = 6.4 Hz, 6 H, CH_2OH), 2.61 (t, $^3J_{HH}$ = 7.7 Hz, 6 H, CH_2CH$_2$CH$_2$OH), 1.79 (m, 6 H, CH_2CH$_2$OH). − ^{13}C{^{1}H} NMR ([D$_6$]acetone): δ = 142.7 (s, aromatic C), 126.4 (s, aromatic CH), 61.5 (s, CH$_2$OH), 35.2 (s, *C*H$_2$CH$_2$CH$_2$OH), 32.4 (s, *C*H$_2$CH$_2$OH). − MS (FD, 35°C); *m*/*z*: 252.5 [M$^+$]. − $C_{15}H_{24}O_3$ (252.4): calcd. C 71.39, H 9.59; found C 70.95, H 9.56.

1,3,5-Tris[3-(trifluoromethylsulfonyloxy)propyl]benzene (4): To a suspension of 3.43 g (13.58 mmol) of **3** in 100 mL of dichloromethane, 3.38 g (42.78 mmol) of pyridine was added dropwise. The resulting clear solution was cooled to −30°C and $(CF_3SO_2)_2O$ (12.64 g, 44.81 mmol) was added over a period of 1 h. The reaction mixture was stirred for a further 1 h at −30°C, then filtered (P 3), and washed with water (3 × 50 mL). The organic layer was dried with Na_2SO_4 and then concentrated to a volume of 20 mL under reduced pressure. The product was purified by column chromatography (CH_2Cl_2, diameter/length of column 2/10 cm). Yield 5.92 g (67.2%), colorless oil. − IR (film): $\tilde{\nu}$ = 1412 cm^{-1}, 1246, 1211, 1146, 931 (CH$_2$, CF$_3$, SO$_2$, SOC). − ^{1}H NMR ($CDCl_3$): δ = 6.86 (s, 3 H, aromatic H), 4.49 (t, $^3J_{HH}$ = 6.1 Hz, 6 H, CH$_2$O), 2.70 (t, $^3J_{HH}$ = 7.5 Hz, 6 H, CH_2CH$_2$CH$_2$O), 2.10 (m, 6 H, CH_2CH$_2$O). − ^{13}C{^{1}H} NMR ($CDCl_3$): δ = 141.0 (s, aromatic C), 127.3 (s, aromatic CH), 119.2 (q, $^1J_{FC}$ = 317.7 Hz, CF$_3$), 77.2 (s, CH$_2$O), 31.4 (s, *C*H$_2$CH$_2$CH$_2$O), 31.0 (s, *C*H$_2$CH$_2$O). − MS (FD, 35°C); *m*/*z*: 647.6 [M$^+$]. − $C_{18}H_{21}F_9O_9S_3$ (647.5): calcd. C 33.34, H 3.26, F 26.36, S 14.83; found C 33.49, H 3.62, F 25.94, S 14.59.

1,3,5-Tris[3-(pentacarbonylrhenio)propyl]benzene (5): A solution of $Na[Re(CO)_5]$ in 20 mL of THF, prepared from 502.3 mg (0.77 mmol) of Re_2CO_{10} and sodium amalgam, was added to a solution of 316.8 mg (0.49 mmol) of the tris(triflate) **4** in 50 mL of THF at −20°C. After stirring for 4 h at −20°C, the reaction mixture was allowed to warm to room temperature and the solvent was removed in vacuo. The residue was suspended in 10 mL of a mixture of CH_2Cl_2/*n*-pentane (2:1) and the solid material was filtered off (P4). The filtrate was then purified by column chromatography (CH_2Cl_2/*n*-pentane, diameter/length of column 2/10 cm). The collected product was finally washed with *n*-pentane (5 × 3 mL). Yield 272 mg (47.3%), white solid, m.p. 97°C. − IR (CH_2Cl_2): $\tilde{\nu}$ = 2125 cm^{-1}, 2008, 1981 (CO). − ^{1}H NMR ($CDCl_3$): δ = 6.77 (s, 3 H, aromatic H), 2.49 (m,[29] *N* = 7.7 Hz, 6 H, CH_2CH$_2$CH$_2$Re), 2.00 (m,[30] 6 H, CH_2CH$_2$Re), 0.95 (m,[31] *N* = 17 Hz, 6 H, CH$_2$Re). − ^{13}C{^{1}H} NMR ($CDCl_3$): δ = 186.2 (s, equatorial CO), 181.7 (s, axial CO), 142.7 (s, aromatic C), 126.3 (s, aromatic CH), 44.4 (s, *C*H$_2$CH$_2$CH$_2$Re), 41.7 (s, *C*H$_2$CH$_2$Re), −9.0 (s, CH$_2$Re). − MS (FD, 30°C); *m*/*z*: 1180.0 [M$^+$]. − $C_{30}H_{21}O_{15}Re_3$ (1180.1): calcd. C 30.53, H 1.79, Re 47.34; found C 30.70, H 1.98, Re 47.46.

1,3,5-Tris[3-(diphenylphosphanyl)propyl]benzene (6): To a suspension of $LiPPh_2$ in 50 mL of *n*-pentane, prepared from 2.071 g (11.12 mmol) of $HPPh_2$ and 6.95 mL of a solution of *n*-butyllithium (1.6 M in *n*-hexane), a solution of 2.004 g (3.09 mmol) of **4** in 30 mL of diethyl ether was added at −35°C. The reaction mixture was stirred for 12 h at −35°C and then the LiOTf formed was filtered off by passage through a short silica-gel column (1 cm). After evaporation of the solvent, the product **6** was redissolved in 15 mL of a mixture of *n*-pentane/diisopropyl ether (2:1) and purified by column chromatography (*n*-pentane/diisopropyl ether, 2:1, diameter/length of column 2/20 cm). Yield 1.028 g (44.0%), colorless oil. − ^{1}H NMR ($CDCl_3$): δ = 7.6−7.4 (m, 30 H, C_6H_5), 6.95 (s, 3 H, C_6H_3), 2.85 (t, $^3J_{HH}$ = 7.2 Hz, 6 H, CH_2CH$_2$CH$_2$P), 2.26, 1.97 (m, 12 H, CH$_2$CH$_2$P). − ^{13}C{^{1}H} NMR ($CDCl_3$): δ = 142.5 (s, *quat*-C_6H_3), 139.6 (d, $^1J_{PC}$ = 12.6 Hz, *ipso*-C_6H_5), 133.5 (d, $^2J_{PC}$ = 18.9 Hz, *o*-C_6H_5), 129.3 (s, *m*-C_6H_5), 129.1 (s, *p*-C_6H_5), 127.0 (s, *tert*-C_6H_3), 37.8 (d, $^3J_{PC}$ = 12.6 Hz, *C*H$_2$CH$_2$CH$_2$P), 28.6−28.3 (m, CH$_2$CH$_2$P). − ^{31}P{^{1}H} NMR ($CDCl_3$): δ = −15.0 (s). − MS (FD, 30°C); *m*/*z*: 756.9 [M$^+$]. − $C_{51}H_{51}P_3$ (756.9): calcd. C 80.93, H 6.79; found C 80.77, H 7.11.

5,5,20,20,35,35-Hexachloro-4,4,6,6,19,19,21,21,34,34,36,36-dodecaphenyl-4,6,19,21,34,36-hexaphospha-5,20,35-triplatina[9$_3$](1,3,5)-cyclophane (7): Solutions of $Cl_2Pt(NCPh)_2$ (1.040 g, 2.202 mmol;

−30°C) and of **6** (1.111 g, 1.468 mmol) in 200 mL each of dichloromethane were *simultaneously* added dropwise during 12 h into 500 mL of stirred dichloromethane. Then the solvent was evaporated in vacuo and the residue was extracted with 150 mL of dichloromethane. After concentration of the solvent under reduced pressure to a volume of 20 mL and addition of 100 mL of CCl_4, oligomeric and polymeric fractions were precipitated. The product **7** was precipitated from the remaining solution by addition of diethyl ether. After filtration (P3) the residue was washed three times with 10 mL of diethyl ether to give the pure product. Yield 645.3 mg (38%), white solid, m.p. > 230°C (dec.). − IR (CsCl): $\tilde{\nu}$ = 316 cm^{-1}, 291 (*cis*-$PtCl_2$). − ^1H NMR (CD_2Cl_2): δ = 7.4−7.1 (m, 60 H, C_6H_5), 6.77 (s, 6 H, C_6H_3), 2.49 (t, $^3J_{HH}$ = 7.7 Hz 12 H, $CH_2CH_2CH_2P$), overlapping with 2.38 (br. s, 12 H, CH_2P), 2.11 (br. s, 12 H, CH_2CH_2P). − $^{13}C\{^1H\}$ NMR (CD_2Cl_2): δ = 141.4 (s, *ipso*-C_6H_5), 132.7 (s, *m*-C_6H_5), 130.7 (s, *p*-C_6H_5), 129.8 (s, *quat*-C_6H_3), 127.9 (m[32], *N* = 13 Hz, *o*-C_6H_5), 126.1 (s, *tert*-C_6H_3), 38.0 (m[32], *N* = 17 Hz, CH_2P), 30.6 (m[32], *N* = 44 Hz, CH_2CH_2P), 28.8 (s, $CH_2CH_2CH_2P$). − $^{31}P\{^1H\}$ NMR (CD_2Cl_2): δ = 8.8 (s, d, $^1J_{PtP}$ = 3660 Hz). − ^{195}Pt NMR (CD_2Cl_2): δ = −4414 (t, $^1J_{PtP}$ = 3660 Hz). − MS (FAB, 30°C, positive ions); *m*/*z*: 2331.4 [M^+ + Na], 2274.5 [M^+ − Cl], 2238.6 [M^+ − 2 Cl], 2203.2 [M^+ − 3 Cl]. − MS (FAB, 30°C, negative ions); *m*/*z*: 2344.1 [M^- + Cl], 2311.0 [M^-], 2272.9 [M^- − Cl]. − $C_{102}H_{102}Cl_6P_6Pt_3$ (2311.8): calcd. C 52.99, H 4.45, Cl 9.20, Pt 25.32; found C 52.80, H 4.39, Cl 9.43, Pt 25.06.

5,5,20,20,35,35-Hexachloro-4,4,6,6,19,19,21,21,34,34,36,36-dodecaphenyl-4,6,19,21,34,36-hexaphospha-5,20,35-triplatina[9$_3$](1,3,5)-cyclophane (7) · 7 1,2-$Cl_2C_2H_4$: Complex **7** (60.1 mg, 26.0 mmol) was dissolved in 20 mL of 1,2-dichloroethane. By removal of the excess solvent in vacuo, **7** · 7 1,2-$Cl_2C_2H_4$ was obtained. Yield quantitative, white solid. − ^1H NMR (CD_2Cl_2), additional to the signals of **7**: δ = 3.60 (s, 28 H, 1,2-$Cl_2C_2H_4$). − $^{13}C\{^1H\}$ NMR (CD_2Cl_2), additional to the signals of **7**: δ = 43.7 (s, 1,2-$Cl_2C_2H_4$). − $C_{116}H_{130}Cl_{20}P_6Pt_3$ (3004.5): calcd. C 46.37, H 4.36, Cl 23.60, Pt 19.48; found C 46.11, H 4.08, Cl 23.34, Pt 19.71. − Upon warming **7** · 7 1,2-$Cl_2C_2H_4$ for 12 h to 70°C in vacuo 1,2-$Cl_2C_2H_4$ was removed quantitatively and **7** was obtained without any solvent.

Hexaplatinacyclophane 9: In the course of the reaction of the tris(phosphane) **6** with $Cl_2Pt(NCPh)_2$ in CH_2Cl_2 according to high-dilution techniques, not only the hexachlorotriplatinacyclophane **7** was formed, but also the hexaplatinacyclophane **9**. After evaporation of the solvent and extraction of the product **7** with CCl_4, the remaining residue was subjected to mass-spectrometric analysis, which revealed the presence of the hexaplatinacyclophane **9**. − MS (FAB, 30°C); *m*/*z*: 4653.4 [M^+ + Cl], 4588.5 [M^+ − Cl], 4554.5 [M^+ − 2 Cl].

5,5,20,20,35,35-Hexakis(acetonitrile)-4,4,6,6,19,19,21,21,34,34,36,36-dodecaphenyl-4,6,19,21,34,36-hexaphospha-5,20,35-triplatina-[9$_3$](1,3,5)cyclophane Hexakis(trifluoromethanesulfonate) (8): To a solution of 115.6 mg (0.05 mmol) of the hexachlorotriplatinacyclophane **7** in 60 mL of a mixture of CH_2Cl_2/acetonitrile (1:1), 115.6 mg (0.45 mmol) of silver trifluoromethanesulfonate was added and the reaction mixture was stirred at room temperature for 72 h under exclusion of light. After the addition of 60 mL of CH_2Cl_2, the suspended solid components were centrifuged off, and the supernatant solution was decanted and concentrated under reduced pressure to a volume of 10 mL. Upon addition of *n*-pentane, cage compound **8** was precipitated, which was filtered off and dried in vacuo. Yield: 118.3 mg (73%), white solid, m.p. > 125°C (dec.). − IR (KBr): $\tilde{\nu}$ = 1251 cm^{-1}, 1230, 1178, 1032 (SO_3, CF_3). − ^1H NMR (CD_2Cl_2): δ = 7.5−7.2 (m, 60 H, C_6H_5), 6.99 (s, 6 H, C_6H_3), 2.8−2.3 (br. m, 36 H, $CH_2CH_2CH_2P$), 2.03 (s, CH_3). − $^{13}C\{^1H\}$ NMR (CD_2Cl_2): δ = 141.1 (s, *quat*-C_6H_3), 139.1−129.6 (m, *o*-, *m*-, and *p*-C_6H_5), 126.8 (s, *tert*-C_6H_3), 125.5 (m, *ipso*-C_6H_5), 121.2 (q, $^1J_{FC}$ = 320.8 Hz, CF_3), 117.9 (s, CN), 36.4, 26.4, 24.9 (br. s, $CH_2CH_2CH_2P$), 2.0 (s, CH_3). − $^{31}P\{^1H\}$ NMR (CD_2Cl_2): δ = −2.7 (s, d, $^1J_{PtP}$ = 3617 Hz). − ^{19}F NMR (CD_2Cl_2): δ = −78.8 (s). − MS (FAB, 30°C); *m*/*z*: 3099.7 [M^+ − OTf], 2844.4 [M^+ − OTf − 6 CH_3CN], 2695.2 [M^+ − 2 OTf − 6 CH_3CN], 2542.7 [M^+ − 3 OTf − 6 CH_3CN], 2393.6 [M^+ − 4 OTf − 6 CH_3CN], 2246.4 [M^+ − 5 OTf − 6 CH_3CN]. − $C_{120}H_{120}F_{18}N_6P_6Pt_3O_{18}S_6$ (3239.7): calcd. C 44.49, H 3.73, F 10.56, N 2.59, Pt 18.06, S 5.94; found C 44.06, H 3.52, F 10.97, N 2.41, Pt 17.82, S 6.28.

X-ray Structure Determination of 5,5,20,20,35,35-Hexachloro-4,4,6,6,19,19,21,21,34,34,36,36-dodecaphenyl-4,6,19,21,34,36-hexaphospha-5,20,35-triplatina[9$_3$](1,3,5)cyclophane (7) · 7 1,2-$Cl_2C_2H_4$:[23] Single crystals of **7** · 7 $C_2H_4Cl_2$ were obtained from a 1,2-dichloroethane/*n*-octane solution. Diffractometer STOE IPDS, Mo-K_α radiation, λ = 0.71069 Å. No absorption correction was applied. The structure was solved by direct methods (SHELXS) and refined by last-square methods with the full matrix, based on F_o^2 (SHELXL). Hydrogen atoms bound to carbon atoms are located at calculated positions. − Crystallographic data: $C_{102}H_{102}Cl_6P_6Pt_3 \cdot 7\ C_2H_4Cl_2 \cdot 1.5\ Et_2O$, M_r = 3115.5, $d_{calcd.}$ = 1.242 gcm^{-3}, crystal dimension 0.2 × 0.2 × 0.1 mm^3, trigonal, space group *P*31*c*, *a* = *b* = 22.596(3), *c* = 18.842(4) Å, *V* = 8331(2) $Å^3$, *Z* = 2, *T* = 200 K, μ(Mo-K_α) = 2.928 mm^{-1}, *F*(000) = 3106. − Data collection: 2Θ = 4.68−51.88° in $-26 \le h \le 27$, $-20 \le k \le 27$, $-20 \le l \le 22$. 16498 measured reflections, of which 7922 were symmetry-independent and 7441 were observed with $I > 2\ \sigma(I)$. − Solution of the structure: An LP correction was applied with $R_{int.}$ = 0.0470. The applied absolute structural parameter was −0.012(9).[33] Parts of the host lattice are refined isotropically with a disorder (first order). The diethyl ether molecules are refined without hydrogen atoms at half-occupied positions. Maximum and minimum peaks in the final synthesis were 1.435 and −0.704 $eÅ^{-3}$. 13 geometrical restraints, 335 parameters, *R*1 = 0.0487, *wR*2 = 0.1437 (all data, $w = 1/[s^2(F_o^2) + [0.1019[(F_o^2 + 2\ F_c^2)/3]^2 + 8.6742[(F_o^2 + 2\ F_c^2)/3]]$), GOF = *S* = 1.093; residual electron density min./max. = −0.704/1.435 e $Å^{-3}$.[23]

Acknowledgments

Support of this research by the Deutsche Forschungsgemeinschaft and the Fonds der Chemischen Industrie is gratefully acknowledged. Degussa AG are thanked for supplying starting materials. We are also indebted to Priv.-Doz. Dr. H. A. Mayer and M. Steimann, Institut für Anorganische Chemie II, University of Tübingen, for helpful discussions regarding the interpretation of the NMR spectra and X-ray structural analyses, respectively. Dipl.-Chem A. Hagenbach, Institut für Anorganische Chemie I, University of Tübingen, is gratefully thanked for the determination of the cell constants.

[1] [1a] D. J. Cram, J. M. Cram, in *Container Molecules and Their Guests: Monographs in Supramolecular Chemistry* (Ed.: J. F. Stoddart), The Royal Society of Chemistry, Cambridge, **1994**. − [1b] B. J. Whitlock, H. W. Whitlock, *J. Am. Chem. Soc.* **1994**, *116*, 2301−2311. − [1c] B. Dietrich, P. Viout, J.-M. Lehn, *Macrocyclic Chemistry: Aspects of Organic and Inorganic Supramolecular Chemistry*, VCH, Weinheim, **1993**. − [1d] R. J. Pieters, F. Diederich, *J. Chem. Soc., Chem. Commun.* **1996**, 2255−2256. − [1e] C. Seel, F. Vögtle, *Angew. Chem.* **1992**, *104*, 542−563; *Angew. Chem. Int. Ed. Engl.* **1992**, *31*, 528−549.
[2] [2a] J. S. Moore, J. Zhang, *Angew. Chem.* **1992**, *104*, 873−874;

Angew. Chem. Int. Ed. Engl. **1992**, *31*, 922−923. − [2b] Z. Wu, S. Lee, J. S. Moore, *J. Am. Chem. Soc.* **1992**, *114*, 8730−8732. − [2c] F. Diederich, Y. Rubin, *Angew. Chem.* **1992**, *104*, 1123−1146; *Angew. Chem. Int. Ed. Engl.* **1992**, *31*, 1101−1124. − [2d] F. Diederich, *Nature* **1994**, *369*, 199−207. − [2e] R. W. Saalfrank, *Nature* **1996**, *383*, 124−125.

[3] [3a] F. Vögtle, *Cyclophane Chemistry*, Wiley, Chichester, **1993**. − [3b] J. Breitenbach, F. Ott, F. Vögtle, *Angew. Chem.* **1992**, *104*, 360−362; *Angew. Chem. Int. Ed. Engl.* **1992**, *31*, 307−309. − [3c] M. Nakazaki, K. Yamamoto, T. Toya, *J. Org. Chem.* **1980**, *45*, 2553−2554. − [3d] D. O′Krongly, S. R. Denmeade, M. Y. Chiang, R. Breslow, *J. Am. Chem. Soc.* **1985**, *107*, 5544−5545. − [3e] A. J. Hubert, M. Hubert, *Tetrahedron Lett.* **1966**, 5779−5782. − [3f] T. J. Seiders, K. K. Baldridge, J. S. Siegel, *J. Am. Chem. Soc.* **1996**, *118*, 2754−2755. − [3g] Y. Rubin, T. C. Parker, S. I. Khan, C. L. Holliman, S. W. KcElvany, *J. Am. Chem. Soc.* **1996**, *118*, 5308−5309.

[4] [4a] F. Diederich in *Cyclophanes: Monographs in Supramolecular Chemistry* (Ed.: J. F. Stoddart), The Royal Society of Chemistry, Cambridge, **1994**. − [4b] J.-M. Lehn, *Supramolecular Chemistry: Concepts and Perspectives*, VCH, Weinheim, **1995**. − [4c] F. Vögtle in *Cyclophan-Chemie* (Eds.: C. Elschenbroich, F. Hensel, H. Hopf), Teubner, Stuttgart, **1990**. − [4d] F. Vögtle in *Supramolekulare Chemie* (Eds.: C. Elschenbroich, F. Hensel, H. Hopf), Teubner, Stuttgart, **1992**.

[5] [5a] H. A. Mayer, W. C. Kaska, *Chem. Ber.* **1995**, *128*, 95−98. − [5b] E. J. Enemark, T. D. P. Stack, *Angew. Chem.* **1998**, *110*, 977−981; *Angew. Chem. Int. Ed. Engl.* **1998**, *37*, 932−935. − [5c] K. Worm, F. P. Schmidtchen, *Angew. Chem.* **1995**, *107*, 71−73; *Angew. Chem. Int. Ed. Engl.* **1995**, *34*, 65−66. − [5d] P. Jacopozzi, E. Dalcanale, *Angew. Chem.* **1997**, *109*, 665−667; *Angew. Chem. Int. Ed. Engl.* **1997**, *36*, 613−615. − [5e] J. S. Fleming, K. L. V. Mann, C.-A. Carraz, J. C. Jeffery, E. Psillakis, J. A. McCleverty, M. D. Ward, *Angew. Chem.* **1998**, *110*, 1315−1318; *Angew. Chem. Int. Ed. Engl.* **1998**, *37*, 1279−1281. − [5f] R. Vilar, D. M. P. Mingos, A. J. P. White, D. J. Williams, *Angew. Chem.* **1998**, *110*, 1323−1326; *Angew. Chem. Int. Ed. Engl.* **1998**, *37*, 1258−1261. − [5g] S. Roche, C. Haslam, H. Adams, S. L. Heath, J. A. Thomas, *J. Chem. Soc., Chem. Commun.* **1998**, 1681−1682. − [5h] C. Brückner, R. E. Powers, K. N. Raymond, *Angew. Chem.* **1998**, *110*, 1937−1940; *Angew. Chem. Int. Ed. Engl.* **1998**, *37*, 1837−1839. − [5i] D. L. Caulder, R. E. Powers, T. N. Parac, K. N. Raymond, *Angew. Chem.* **1998**, *110*, 1940−1943; *Angew. Chem. Int. Ed. Engl.* **1998**, *37*, 1840−1843.

[6] E. Lindner, W. Wassing, R. Fawzi, M. Steimann, *Angew. Chem.* **1994**, *106*, 363−365; *Angew. Chem. Int. Ed. Engl.* **1994**, *33*, 321−323.

[7] [7a] P. J. Stang, *Chem. Eur. J.* **1998**, *4*, 19−27. − [7b] M. Fujita, K. Ogura, *Coord. Chem. Rev.* **1996**, *148*, 249−264. − [7c] E. Lindner, M. W. Pitsch, R. Fawzi, M. Steimann, *Chem. Ber.* **1996**, *129*, 639−645. − [7d] E. Lindner, W. Wassing, M. W. Pitsch, R. Fawzi, M. Steimann, *Inorg. Chim. Acta* **1994**, *220*, 107−113. − [7e] E. E. Nifantyev, E. N. Rasadkina, L. K. Vasyanina, V. K. Belsky, A. I. Stash, *J. Organomet. Chem.* **1997**, *529*, 171−176. − [7f] J. R. Farrell, C. A. Mirkin, I. A. Guzei, L. M. Liable-Sands, A. L. Rheingold, *Angew. Chem.* **1998**, *110*, 484−487; *Angew. Chem. Int. Ed. Engl.* **1998**, *37*, 465−467.

[8] [8a] P. M. Van Calcar, M. M. Olmstead, A. L. Balch, *J. Chem. Soc., Chem. Commun.* **1996**, 2597−2598. − [8b] F.-Q. Liu, G. Harder, T. D. Tilley, *J. Am. Chem. Soc.* **1998**, *120*, 3271−3272.

[9] M. Fujita, S. Nagao, K. Ogura, *J. Am. Chem. Soc.* **1995**, *117*, 1649−1650.

[10] [10a] M. Fujita, D. Oguro, M. Miyazawa, H. Oka, K. Yamaguchi, K. Ogura, *Nature* **1995**, *378*, 469−471. − [10b] M. Fujita, S.-Y. Yu, T. Kusukawa, H. Funaki, K. Ogura, K. Yamaguchi, *Angew. Chem.* **1998**, *110*, 2192−2196; *Angew. Chem. Int. Ed. Engl.* **1998**, *37*, 2082−2085.

[11] C. M. Hartshorn, P. J. Steel, *J. Chem. Soc., Chem. Commun.* **1997**, 541−542.

[12] P. J. Stang, B. Olenyuk, D. C. Muddiman, R. D. Smith, *Organometallics* **1997**, *16*, 3094−3096.

[13] C. D. Beard, K. Baum, A. Grakauskas, *J. Org. Chem.* **1973**, *38*, 3673−3677.

[14] [14a] E. Lindner, E. Schauss, W. Hiller, R. Fawzi, *Angew. Chem.* **1984**, *96*, 727−728; *Angew. Chem. Int. Ed. Engl.* **1984**, *23*, 711−712. − [14b] E. Lindner, R.-M. Jansen, H. A. Mayer, *Angew. Chem.* **1986**, *98*, 1000−1001; *Angew. Chem. Int. Ed. Engl.* **1986**, *25*, 1008−1009. − [14c] E. Lindner, R.-M. Jansen, W. Hiller, R. Fawzi, *Chem. Ber.* **1989**, *122*, 1403−1409.

[15] F. Effenberger, W. Kurtz, *Chem. Ber.* **1973**, *106*, 511−524.

[16] J. Klein, A. Medlik, A. Y. Meyer, *Tetrahedron* **1976**, *32*, 51−56.

[17] M. J. Schweiger, U. Nagel, W. Beck, *J. Organomet. Chem.* **1988**, *355*, 289−296.

[18] E. Lindner, M. Pabel, K. Eichele, *J. Organomet. Chem.* **1990**, *386*, 187−194.

[19] C. J. Pedersen, *J. Am. Chem. Soc.* **1967**, *89*, 7017−7036.

[20] F. Diederich, *Angew. Chem.* **1988**, *100*, 372−396; *Angew. Chem. Int. Ed. Engl.* **1988**, *27*, 362, and references therein.

[21] [21a] L. Rossa, F. Vögtle in *Synthesis of Medio- and Macrocyclic Compounds by High Dilution Principle Techniques: Topics in Current Chemistry* (Ed.: F. Vögtle), Springer, Heidelberg, **1983**, vol. 113, *Cyclophanes I*, p. 1. − [21b] P. Knops, N. Sendhoff, H.-B. Mekelburger, F. Vögtle in *High Dilution Reactions − New Synthetic Applications: Topics in Current Chemistry* (Eds.: E. Weber, F. Vögtle), Springer, Heidelberg, **1992**, vol. 161, *Macrocycles*, p. 1.

[22] [22a] B. L. Shaw, *J. Organomet. Chem.* **1980**, *200*, 307−318. − [22b] X. Chi, A. J. Guerin, R. A. Haycock, C. A. Hunter, L. D. Sarson, *J. Chem. Soc., Chem. Commun.* **1995**, 2563−2565.

[23] Crystallographic data (excluding structural factors) for the structure reported in this paper has been deposited with the Cambridge Crystallographic Data Centre as supplementary publication no. CCDC-102873. Copies of the data can be obtained free of charge on application to CCDC, 12 Union Road. GB-Cambridge CB2 1EZ, UK [Fax: (internat.) code + 44-1223/336-033; E-mail: deposit@ccdc.cam.ac.uk].

[24] [24a] W. Schöniger, *Microchim. Acta* **1955**, 123−129. − [24b] W. Schöniger, *Microchim. Acta* **1956**, 869−876.

[25] G. Brunisholz, J. Michod, *Helv. Chim. Acta* **1954**, *37*, 598−602.

[26] H. Wagner, *Microchim. Acta* **1957**, 19.

[27] S. Meyer, Ph. D. Thesis, University of Tübingen, **1987**.

[28] T. Uchiyama, Y. Toshiyasu, Y. Nakamura, T. Miwa, S. Kawaguchi, *Bull. Chem. Soc. Jpn.* **1981**, *54*, 181−185.

[29] m: AA′MM′ pattern.

[30] m: AA′MM′XX′ pattern.

[31] m: AA′XX′ pattern.

[32] m: AXX′ pattern.

[33] H. D. Flack, *Acta Crystallogr. Sect A* **1983**, *39*, 876−881.

Received October 8, 1998
[I98342]

Structural Characterization and Magnetic Behaviour of the Ferro-Antiferromagnetic Alternating Manganese–Azido Chain $[Mn(3\text{-Et,4-Mepy})_2(\mu\text{-}N_3)_2]_n$ (3-Et,4-Mepy = 3-Ethyl-4-methylpyridine)

Morsy A. M. Abu-Youssef,[a] Albert Escuer,*[b] Mohamed A. S. Goher,*[c] Franz A. Mautner,[a] and Ramon Vicente*[b]

Keywords: Bridging ligands / Manganese / Azido bridge / Alternating chain / Magnetic properties

The ligands 3-ethyl-4-methylpyridine (3-Et,4-Mepy) and azide coordinate to Mn^{II} forming an alternating chain with the formula $[Mn(3\text{-Et,4-Mepy})_2(\mu\text{-}N_3)_2]_n$. This compound crystallizes in the space group $P-1$. The compound consists of chains of octahedrally coordinated manganese atoms alternately bridged by double end-to-end ($\mu_{1,3}$) and double end-on ($\mu_{1,1}$) azido bridges, which results in a structurally and magnetically alternating chain. The 3-ethyl-4-methylpyridine ligands are arranged *trans*, completing the six-fold coordination spheres of the manganese atoms. The Mn–Mn distances are distinctly different: Mn(1)–Mn(1A) = 5.149(3) Å (double end-to-end azido bridge) and Mn(1)–Mn(1B) = 3.402(2) Å (double end-on azido bridge). The magnetic properties of the compound, as studied in the temperature range 300–4 K, show bulk antiferromagnetic interaction. Fitting of the magnetic data by using an equation for alternating ferro-antiferromagnetic $S = 5/2$ 1-D systems gives the parameters $J_{AF} = -13.7(1)$ cm^{-1}, $J_F = 2.4(1)$ cm^{-1}, $g = 2.036(2)$.

The chemistry of the manganese(II)−(L)−azido-bridged system, L = N-aromatic ligand, affords habitually high-dimensional compounds: 3-D for L = pyridine (py)[1][2] and 2,2′-bipyrimidine (bipym),[3][4] 2-D for the substituted pyridines L = 3- and 4-acetylpyridine (3-Acpy[5] and 4-Acpy[6]), methyl- and ethyl isonicotinate (Meinc[7] and Etnic[2]), and 4-cyanopyridine (4-CNpy[5]), or 1-D for 2,2′-bipyridine,[8] 3-ethylpyridine, and 2-hydroxypyridine.[9] A 3-D network with a distorted perovskite structure has also been found for $[N(CH_3)_4][Mn(N_3)_3]$.[10] In contrast, only in the case of L = 2,2′:6′,2′′-terpyridine has a dinuclear compound been obtained.[11] The coordination mode of the azido bridge is commonly found to be $\mu_{1,3}$-N_3 (end-to-end, EE), although in some cases it is $\mu_{1,1}$-N_3 (end-on, EO), and even alternating 1-D or 2-D systems in which the two kinds of coordination mode coexist in the same compound have been found. No correlation has been identified between the properties of the ligand L and the coordination mode of the azido bridge, and from a synthetic point of view, the manganese(II)−azido system shows unpredictable behaviour, analogous to that observed for azido-bridged polynuclear copper(II) and nickel(II) systems. The magnetic behaviour of these compounds follows the same general trends as seen for copper and nickel(II) systems, i.e. end-to-end azido bridges lead to antiferromagnetic interaction, while end-on bridges give rise to ferromagnetic coupling. The main difference between these systems is the higher dimensionality shown by the manganese derivatives.

In continuation of our research on compounds of this kind, we report herein on a new system of the pyridine series, using L = 3-ethyl-4-methylpyridine to obtain the one-dimensional system $[Mn(3\text{-Et,4-Mepy})_2(\mu\text{-}N_3)_2]_n$ (**1**). This compound constitutes the second example of an alternating chain in which the manganese atoms are bridged alternately by two coplanar end-to-end and two end-on azido ligands, but is the first case with a *trans* arrangement of the EO and EE azido bridges. In the previously published alternating chain $[Mn(bipy)(\mu\text{-}N_3)_2]_n$, the EO and EE azido bridges have a *cis* arrangement.[8] The experimental magnetic susceptibility vs. T data for **1** have been fitted by using a recently published equation for $S = 5/2$ alternating F/AF-coupled 1-D systems.[8]

Results and Discussion

Infrared Spectra

The IR spectrum of the title complex $[Mn(3\text{-Et,4-Mepy})_2(N_3)_2]_n$ shows bands attributable to the 3-Et,4-Mepy ligand at the normal frequencies. In the 2000−2100 cm^{-1} region, the complex shows a very intense split band that can be assigned to the asymmetric stretching vibrations of the azide group [$\nu_{as}(N_3)$], centred at 2056 and 2080 cm^{-1}. In the region 1280−1360 cm^{-1}, no band was observed that could be attributed to the $\nu_s(N_3)$ mode, while the two bands at 2056 and 2080 cm^{-1} indicate the presence of two different symmetric and asymmetric azido groups. This was tentatively rationalized in terms of the coexistence of both μ(1,1)-EO and μ(1,3)-EE bridging azido groups, which was supported by the X-ray structural data. In the far infrared

[a] Institut für Physikalische und Theoretische Chemie, Technische Universität Graz,
A-8010 Graz, Austria
E-mail: Mautner.PTC.NAWI.TU-Graz@ptc.tu-graz.ac.at
[b] Departament de Química Inorgànica, Universitat de Barcelona, Diagonal 647, E-08028 Barcelona, Spain
E-mail: rvicente@kripto.qui.ub.es
[c] Chemistry Department, Faculty of Science, Kuwait University, P. O. Box 5969, Safat, 13060 Kuwait

 © WILEY-VCH Verlag GmbH, D-69451 Weinheim, 1999 1434−1948/99/0404−0687 $ 17.50+.50/0

region, one band attributable to the $\nu(Mn-N_3)$ mode around 310 cm^{-1} and two bands due to the $\nu[Mn-N(L)]$ mode around 254 and 230 cm^{-1} were observed.

Crystal Structure of $[Mn(3\text{-Et},4\text{-Mepy})_2(\mu\text{-}N_3)_2]_n$ (1)

The labelled diagram for **1** is shown in Figure 1. The structure consists of octahedrally coordinated manganese atoms, about which the coordination sites are occupied by two 3-ethyl-4-methylpyridine ligands in a *trans* arrangement and four coplanar azido ligands. Two azido groups act as end-to-end bridging ligands with a neighbouring manganese atom, while the other two act as end-on bridging ligands with another neighbouring manganese atom, giving a one-dimensional system with alternating $\mu_{1,3}$ and $\mu_{1,1}$ bridges extending along the *a* axis of the unit cell. The bond parameters relating to the end-on bridges are Mn(1)−N(21) = 2.209(2) Å, Mn(1)−N(21B) = 2.240(2) Å, N(21)−N(22)−N(23) = 178.2(4)°, Mn(1)−N(21)−

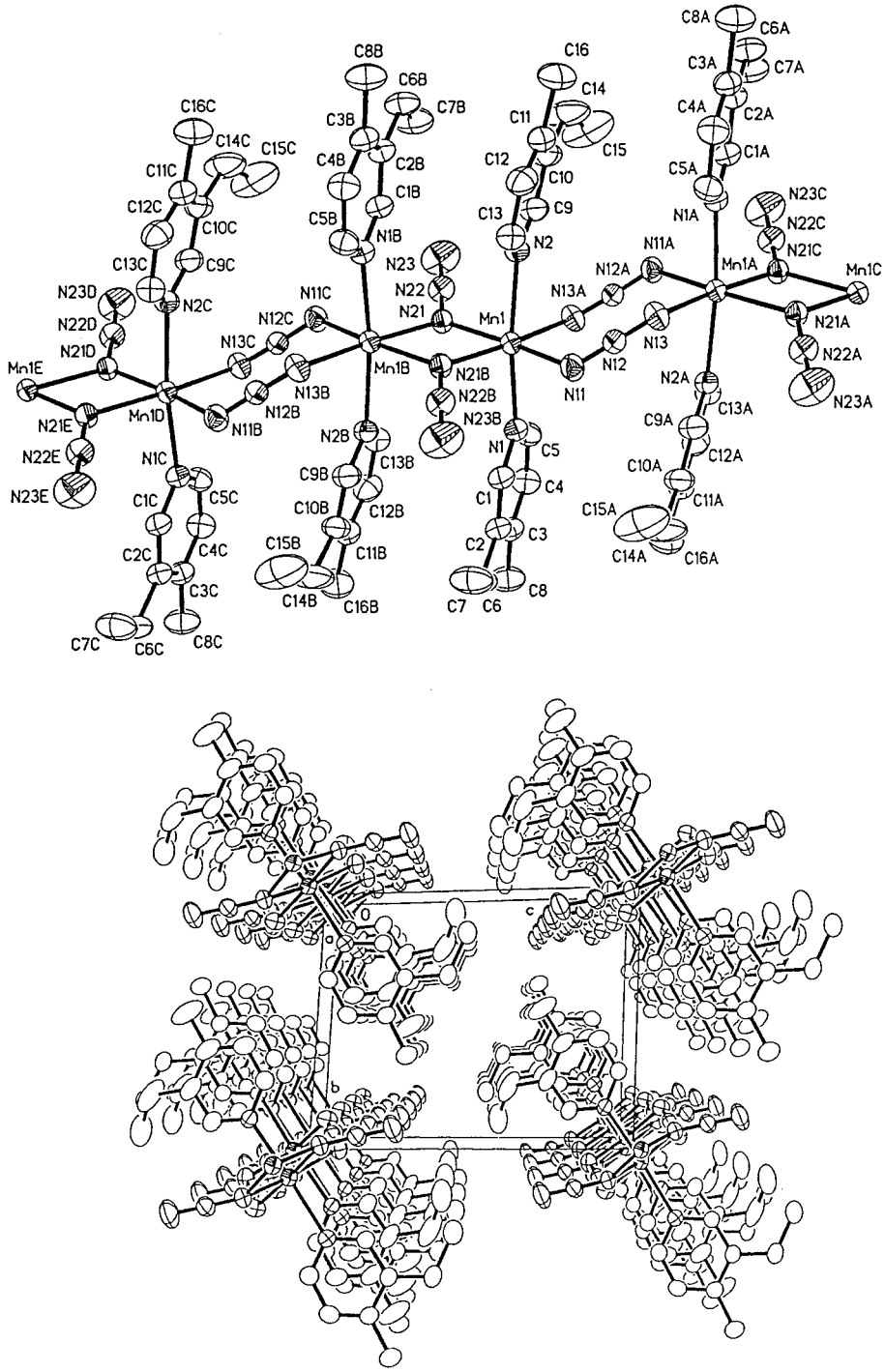
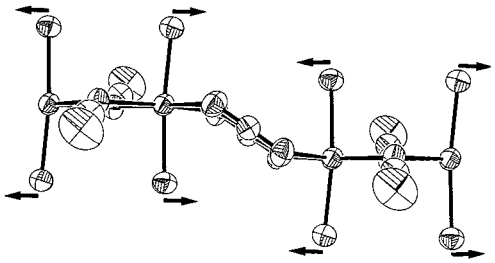


Figure 1. ORTEP drawing (thermal ellipsoids drawn at 40% probability) with atom labelling scheme and packing plot viewed along the *a* axis of the unit cell of $[Mn(3\text{-Et},4\text{-Mepy})_2(\mu\text{-}N_3)_2]_n$ (**1**)

Mn(1B) = 99.75(10)°, while those relating to the end-to-end bridges are Mn(1)−N(11) = 2.225(3) Å, Mn(1)−N(13A) = 2.256(3) Å, Mn(1)−N(11)−N(12) = 124.8(2) Å, Mn(1)−N(13A)−N(12A) = 123.2(2)°, N(11)−N(12)−N(13) = 177.9(3)°. The Mn(1)−Mn(1A) and Mn(1)−Mn(1B) distances amount to 5.149(3) Å and 3.402(2) Å, respectively. The degree of distortion of the $Mn_2(\mu_{1,3}\text{-}N_3)_2$ ring from planarity towards a chair form may be quantified by means of the acute angle δ between the normal to the planes defined by the six N atoms of the azido bridges and the corresponding N−Mn−N planes: δ in this case is 31.7(1)° [torsion Mn(1)−N(11)−N(12)−N(13)−Mn(1A) 51.2(2)°]. The neutral chains of **1** are well-isolated by the ligands, the minimum Mn−Mn interchain distance being 9.258(4) Å.

The alternation of $\mu_{1,3}$ and $\mu_{1,1}$ bridges along the *a* axis of the unit cell may be due to the effects of steric hindrances: In the $[Mn_2(\mu_{1,1}\text{-}N_3)_2(L_4)]$ unit the L rings are not oriented exactly perpendicular to the $[Mn_2(\mu_{1,1}\text{-}N_3)_2]$ mean plane, but are inclined out of this plane along the chain direction, resulting in an N(1)−Mn(1)−N(2) angle of 172.61(8)°.



For this reason, it is not possible to repeat the $[Mn_2(\mu_{1,1}\text{-}N_3)_2(L_4)]$ unit, which would necessitate short Mn−Mn distances. The structural solution to have a one-dimensional system is to add the $[Mn_2(\mu_{1,3}\text{-}N_3)_2(L_4)]$ unit, with longer Mn−Mn distances.

Magnetic Properties

The $\chi_M{\cdot}T$ product and the molar magnetic susceptibilities of $[Mn(3\text{-Et},4\text{-Mepy})_2(\mu\text{-}N_3)_2]_n$ (**1**) vs. *T* in the range 300−4 K are plotted in Figure 2. The overall behaviour of **1** corresponds to a bulk antiferromagnetically coupled system. The $\chi_M{\cdot}T$ value, which amounts to 3.75 $cm^3{\cdot}K{\cdot}mol^{-1}$ at 290 K, decreases on cooling and tends to zero at low temperatures. The χ_M vs. *T* plot shows an increase in χ_M from 1.29×10^{-2} $cm^3{\cdot}mol^{-1}$ at 290 K to a broad maximum between 60 and 20 K. On further cooling, this plot quickly tends to zero. The magnetic data were analysed by means of the expression recently published[8] by Cortés et al. for alternating ferro-antiferro one-dimensional *S* = 5/2 compounds, which was derived from the spin Hamiltonian:

$$H = -J_1\Sigma S_{2i}S_{2i+1} - J_2\Sigma S_{2i+1}S_{2i+2}$$

The best fit parameters obtained were $J_1 = -13.7(1)$ cm^{-1}, $J_2 = 2.4(1)$ cm^{-1} and $g = 2.036(2)$. No other local minima in the fitting process were found. J_1 and J_2 correspond to the double EE and the double EO superexchange pathways, respectively.

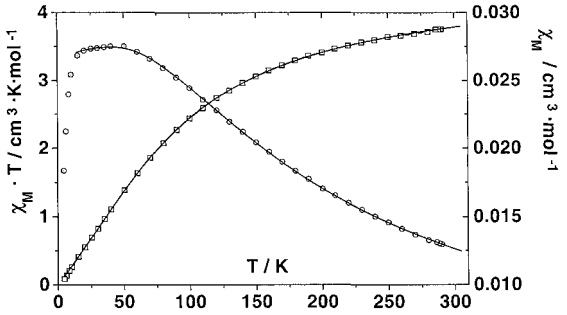


Figure 2. χ_M vs. *T* (○) and $\chi_M{\cdot}T$ vs *T* (□) plots for $[Mn(3\text{-Et},4\text{-Mepy})_2(\mu\text{-}N_3)_2]_n$ (**1**); the solid line shows the best fit theoretical curve

EPR spectra recorded on powdered samples at room temperature show an isotropic signal centred at $g = 2.020$ with a linewidth of 320 G. This signal is temperature-dependent; the spectrum at 4 K shows a signal centred at $g = 2.038$ with linewidth 541 G, as well as a weak signal at half-field. This linewidth is much larger than that of the sharp signals (linewidth 35 G at room temperature) recently reported for the related compounds $[Mn(pyOH)_2(\mu\text{-}N_3)_2]_n$ and $[Mn(3\text{-Etpy})_2(\mu\text{-}N_3)_2]_n$, where pyOH and 3-Etpy denote 2-hydroxypyridine and 3-ethylpyridine, respectively.[9]

This behaviour may be explained by considering the main factors[12] that influence the linewidth for an isotropic Heisenberg one-dimensional system, i.e. exchange narrowing, due to the superexchange interactions along the chain, and dipolar interactions, which induce broadening of the signal. Adequate characterization of these effects requires well-isolated chains in order to reduce the interchain interactions. This condition reduces the number of suitable systems and the well-known compound $[(CH_3)_4][MnCl_3]$, abbreviated as TMMC,[13] remains the standard reference compound 25 years after the first studies in this field. In the three $[Mn(R)_2(\mu\text{-}N_3)_2]_n$ complexes (R = 3-Et,4-Mepy; pyOH, and 3-Etpy), the chains are neutral and are well-isolated by the large pyridyl ligands (see Figure 1). Moreover, the interchain distances are slightly shorter than the 9.15 Å found in TMMC and compare well with the 7.60 Å reported for $Cs[MnBr_3]$[14] or the 7.5 Å reported for $[Mn(py)_2Cl_2]_n$.[15] The sharp signals reported for the pyOH and 3-ethyl derivatives may be attributed to exchange narrowing, taking into account the $-J$ values larger than 10 cm^{-1} and the negligible dipolar contribution (Mn···Mn distances larger than 5.4 Å in the EE bridges). In contrast, although $[Mn(3\text{-Et},4\text{-Mepy})_2(\mu\text{-}N_3)_2]_n$ has comparable superexchange interactions, it shows alternating Mn···Mn distances of 5.149 and 3.402 Å and thus the dipolar broadening mechanism becomes active in the Mn_2N_2 rings with double EO azide bridges. The same explanation may account for the large linewidth (close to 500 G) observed for the EPR signal of the alternating system $[Mn(bipy)(\mu\text{-}N_3)_2]_n$, which shows comparable superexchange parameters

J, interchain packing, and alternating Mn···Mn intrachain distances.[8]

Experimental Section

General: Infrared spectra (4000−400 cm^{-1}) were recorded using KBr pellets with a Nicolet 520 FT-IR spectrophotometer. Magnetic measurements were carried out with a DSM8 pendulum susceptometer, operating in the temperature range 300−4 K. The applied external magnetic field was 1.5 T. Diamagnetic corrections were estimated from Pascal tables. EPR spectra were recorded at X-band frequency with a Bruker ES200 spectrometer equipped with an Oxford liquid helium cryostat for variable-temperature work.

Synthesis of the Compound: The title complex $[Mn(3\text{-Et},4\text{-Mepy})_2(N_3)_2]_n$ was synthesized by mixing ca. 50 mL of a pure methanolic solution of manganese perchlorate hexahydrate (1.00 g, 2.7 mmol) and a solution of 0.61 g (ca. 5 mmol) of 3-ethyl-4-methylpyridine in 20 mL of methanol, with subsequent dropwise addition of a concentrated aqueous solution of sodium azide (0.65 g, 10 mmol). The solution became turbid and a gelatinous precipitate was produced, which was filtered off. By slow evaporation of the solvent from the clear filtrate, colourless transparent plates of the title complex, suitable for X-ray analysis, were formed within 6 d; yield: 0.60 g (ca. 65%). − $C_{16}H_{22}MnN_8$ (381.36): calcd. C 50.4, H 5.8, Mn 14.4, N 29.4; found C 50.6, H 5.9, Mn 14.3, N 29.2.

Table 1. Crystal data and structure refinement for $[Mn(3\text{-Et},4\text{-Mepy})_2(N_3)_2]_n$ (**1**)

Empirical formula	$C_{16}H_{22}MnN_8$
Formula mass	381.36
Crystal system	triclinic
Space group	$P-1$ (no. 2)
a [Å]	8.455(4)
b [Å]	9.778(3)
c [Å]	12.065(5)
α (°)	89.86(3)
β (°)	78.25(3)
γ (°)	75.08(3)
V [$Å^3$]	942.3(7)
Z	2
T [°C]	22(2)
λ(Mo-K_α) [Å]	0.71069
$d_{calcd.}$ [$g \cdot cm^{-3}$]	1.344
μ(Mo-K_α) [mm^{-1}]	0.716
max. transmission	1.000
min. transmission	0.395
max. peak in final diff. synthesis [$eÅ^{-3}$]	0.464
min. peak in final diff. synthesis [$eÅ^{-3}$]	−0.637
parameters refined	230
R[a]	0.0501
R^2w[b]	0.1243

[a] $R(F_o) = \Sigma||F_o|-|F_c||/\Sigma|F_o|$. − [b] $R_\omega(F_o)^2 = \{\Sigma[\omega[(F_o)^2 - (F_c)^2]^2]/\Sigma[\omega[(F_o)^2]^2]\}^{1/2}$.

Crystal Structure Determination and Refinement of the Structure: Single-crystal X-ray data for $[Mn(3\text{-Et},4\text{-Mepy})_2(N_3)_2]_n$ were collected with a modified STOE four-circle diffractometer. Crystal size: 0.60 × 0.50 × 0.24 mm. The crystallographic data, conditions maintained for the intensity data collection, and some features of the structure refinement are listed in Table 1. Graphite-monochromated Mo-K_α radiation (λ = 0.71069 Å) was used to collect the data set, employing the ω-scan technique. The accurate unit cell parameters were determined from automatic centering of 40 reflections (9.2° < θ < 14.9°) and refined by least-squares methods. 5167 reflections (4539 independent reflections, R_{int} = 0.0275) were collected in the range 2.76° < θ < 27.99°. An intensity decay of 12% for control reflections, measured after every set of 100 reflections, was observed during the data collection. Corrections were applied for Lorentz and polarization effects, for intensity decay, as well as for absorption, using the DIFABS[16] computer program. The structure was solved by direct methods using the SHELXS-86[17] program, and refined by full-matrix least-squares methods on F^2 using the SHELXL-93[18] program, as incorporated in the SHELXTL/PC V 5.03[19] program library, and the graphics program PLUTON.[20] All non-hydrogen atoms were refined anisotropically. The hydrogen atoms were geometrically fixed with the HFIX utility[19] (i.e.: hydrogen atoms riding with idealized geometrical values on their parent carbon atoms with fixed distances: CH = 0.93 Å, CH_2 = 0.97 Å and CH_3 = 0.96 Å; for each methyl group the torsion angle was set which maximizes the sum of the electron density at the three calculated hydrogen positions). Selected bond parameters are given in Table 2.

Atomic positional and thermal parameters, lists of bond lengths and angles, and F_o/F_c values are available as supplementary material from one of the authors (F. A. M.). Crystallographic data (excluding structure factors) for the structure reported in this paper have been deposited with the Cambridge Crystallographic Data Centre as supplementary publication No. CCDC-103250. Copies of the data can be obtained free of charge on application to CCDC,

Table 2. Selected bond lengths [Å] and angles [°]; symmetry codes: (a) $-x, -y, -z$; (b) $-x+1, -y, -z$

Mn(1)···Mn(1B)	3.402(2)	Mn(1)···Mn(1A)	5.149(3)
Mn(1)−N(21)	2.209(2)	Mn(1)−N(11)	2.225(3)
Mn(1)−N(21B)	2.240(2)	Mn(1)−N(13A)	2.256(3)
Mn(1)−N(1)	2.278(2)	Mn(1)−N(2)	2.305(2)
N(11)−N(12)	1.170(3)	N(12)−N(13)	1.166(3)
N(21)−N(22)	1.185(3)	N(22)−N(23)	1.152(4)
N(21)−Mn(1)−N(11)	168.61(9)	N(21)−Mn(1)−N(21B)	80.25(10)
N(11)−Mn(1)−N(21B)	88.77(9)	N(21)−Mn(1)−N(13A)	95.42(10)
N(11)−Mn(1)−N(13A)	95.47(10)	N(21b)−Mn(1)−N(13A)	175.42(9)
N(21)−Mn(1)−N(1)	92.60(9)	N(11)−Mn(1)−N(1)	91.37(10)
N(21B)−Mn(1)−N(1)	95.09(9)	N(13a)−Mn(1)−N(1)	86.58(9)
N(21)−Mn(1)−N(2)	90.59(9)	N(11)−Mn(1)−N(2)	86.75(10)
N(21B)−Mn(1)−N(2)	92.02(9)	N(13A)−Mn(1)−N(2)	86.49(9)
N(1)−Mn(1)−N(2)	172.61(8)	N(12)−N(11)−Mn(1)	124.8(2)
N(13)−N(12)−N(11)	177.9(3)	N(12)−N(13)−Mn(1A)	123.2(2)
N(22)−N(21)−Mn(1)	128.0(2)	N(22)−N(21)−Mn(1B)	125.8(2)
Mn(1)−N(21)−Mn(1B)	99.75(10)	N(23)−N(22)−N(21)	178.2(4)

12 Union Road, Cambridge CB2 1EZ, U.K. [Fax: (internat.) + 44-1223/336-033; E-mail: deposit@ccdc.cam.ac.uk].

Acknowledgments

This work was supported in part by the CICYT (Grant PB96/0163) and the OENB (Grant 6630). F. A. M. and M. A. M. A.-Y. thank Prof. C. Kratky and Dr. Belaj (University of Graz) for the loan of experimental equipment.

[1] M. A. S. Goher, F. A. Mautner, *Croat. Chem. Acta* **1990**, *63*, 559.
[2] A. Escuer, R. Vicente, M. A. S. Goher, F. A. Mautner, *Inorg. Chem.* **1996**, *35*, 6386.
[3] G. De Munno, M. Julve, G. Viau, F. Lloret, J. Faus, D. Viterbo, *Angew. Chem. Int. Ed. Engl.* **1996**, *35*, 1807.
[4] R. Cortés, L. Lezama, J. L. Pizarro, M. I. Arriortua, T. Rojo, *Angew. Chem. Int. Ed. Engl.* **1996**, *35*, 1810.
[5] A. Escuer, R. Vicente, F. A. Mautner, M. A. S. Goher, *Inorg. Chem.* **1997**, *36*, 3440.
[6] A. Escuer, R. Vicente, M. A. S. Goher, F. A. Mautner, *Inorg. Chem.* **1995**, *34*, 5707.
[7] A. Escuer, R. Vicente, M. A. S. Goher, F. A. Mautner, *J. Chem. Soc., Dalton Trans.* **1997**, 4431.
[8] R. Cortés, M. Drillon, X. Solans, L. Lezama, T. Rojo, *Inorg. Chem.* **1997**, *36*, 677.
[9] A. Escuer, R. Vicente, M. A. S. Goher, F. A. Mautner, *Inorg. Chem.* **1998**, *37*, 782.
[10] F. A. Mautner, R. Cortés, L. Lezama, T. Rojo, *Angew. Chem. Int. Ed. Engl.* **1996**, *35*, 78.
[11] R. Cortés, J. L. Pizarro, L. Lezama, M. I. Arriortua, T. Rojo, *Inorg. Chem.* **1994**, *33*, 2697.
[12] A. Bencini, D. Gatteschi, *Electron Paramagnetic Resonance of Exchange Coupled Systems*, Springer-Verlag, Berlin, Heidelberg, **1990**.
[13] A. Lagendijk, *Phys. Rev. B* **1978**, *18*, 1322, and references therein.
[14] H. Kalt, E. Siegel, N. Pauli, H. Mosebach, J. Wiese, A. Edgar, *J. Phys. C* **1983**, *16*, 6427.
[15] P. M. Richards, R. K. Quinn, B. Morosin, *J. Chem. Phys.* **1973**, *59*, 4474.
[16] N. Walker, D. Stuart, *Acta Crystallogr.* **1983**, *A39*, 158.
[17] G. M. Sheldrick, *SHELXS-86, Program for the Solution of Crystal Structures*, University of Göttingen, Germany, **1986**.
[18] G. M. Sheldrick, *SHELXL-93, Program for the Refinement of Crystal Structures*, University of Göttingen, Germany, **1993**.
[19] *SHELXTL 5.03 (PC version), Program Library for Structure Solution and Molecular Graphics*, Siemens Analytical Instruments Division, Madison, WI, **1995**.
[20] M. E. Fisher, *Am. J. Phys.* **1964**, *32*, 343.

Received October 12, 1998
[I98349]

Synthesis and Diels–Alder Reactions of Some New (Phthalocyanine)nickel Complexes

Bernd Hauschel,[a] Reiner Jung,[a] and Michael Hanack*[a]

Keywords: (Phthalocyanine)nickel complexes / Unsymmetrical phthalocyanines / Isobenzofurans / Diels–Alder reactions / Ladder-type molecules

The octasubstituted (phthalocyanine)nickel complexes **4a**,**b**, soluble in common organic solvents, bearing four dienophilic functionalities were synthesized from the corresponding phthalodinitriles **3a**,**b** and nickel(II) acetate. Reaction of **4a** with tetracyclone **5** led to the phthalocyanine–tetracyclone adduct **6** which is a precursor for an intermediate phthalocyanine **7** containing four isobenzofuran moieties. The capability of **7** to react as tetrakis(diene) was demonstrated by its reaction with naphthoquinone. Furthermore, the unsymmetrical phthalocyanines **13** and **16a**,**b**,**c** containing one dienophilic functionality were synthesized using a statistical approach. Their tetracyclone adducts **17**, **18a**,**b**,**c** can be used for the synthesis of ladder-type phthalocyanine dimers. The dimer **22** was synthesized from **18c** and *p*-benzoquinone via the isobenzofuran intermediate **19** and the benzoquinone adduct **21**. For dehydration experiments the naphthoquinone monoadduct **23** was synthesized from **18c**. Dehydration of **22** and **23** was carried out successfully with *p*-toluenesulfonic acid. The Diels–Alder reactions are discussed with respect to the occurring *exo*/*endo* ratio.

Introduction

We are involved in the synthesis of ladder-type oligomers and polymers consisting of metallomacrocycles (e. g. metallohemiporphyrazines and metallophthalocyanines) as repeating units.[1] Especially conjugated ladder polymers with phthalocyanine (Pc) subunits are expected to show − besides a high thermal and chemical resistance − remarkable properties like nonlinear optical behaviour and low band gaps.[2]

We already reported on the successful synthesis of ladder-type oligomers and polymers starting from hemiporphyrazine (Hp) building blocks,[3] whereby a Diels−Alder strategy[4] was used. Hp intermediates with isobenzofuran moieties (**2**) were generated from convenient precursors (**1**, compare Scheme 1) and used as bis(dienes) in repetitive Diels−Alder (DA) reactions.[3b,5] These diene moieties gave the best results regarding yields and the suppression of side reactions. In this paper, similar Pc intermediates are described.

Results and Discussion

In a previous work, we already reported the synthesis of unsubstituted PcM complexes bearing four diene or dienophilic functionalities (M = H_2, Ni, Zn).[6] Due to the poor solubility of these compounds, DA reactions with e.g. 2,3-dimethylbutadiene proceeded with unsatisfactory conversion rates. Therefore, we now attempted the synthesis of the tetrakis(dienophilic), octaalkoxy-substituted PcNi complexes **4a**,**b** (Scheme 2) showing an enhanced solubility in organic solvents. The reaction of the phthalodinitriles **3a,b**[7] in the presence of nickel(II) acetate and a catalytic amount of DBU in 1-butanol (**3a**) or *n*-hexanol (**3b**) at elevated temperatures furnished the PcNi complexes **4a**,**b** after several hours (24−36 h, the nucleophilic alkoxide ions generated from an *n*-alcohol and DBU may attack the phthalodinitriles **3a**,**b** and replace the alkoxy substituents; therefore, we chose the solvents in a way that the replacement led to identical molecules). Chromatographic work up on silica gel gave pure, deep green compounds in isolated yields of ca. 30%. **4a**,**b** proved to be well soluble in e.g. toluene or $CHCl_3$.

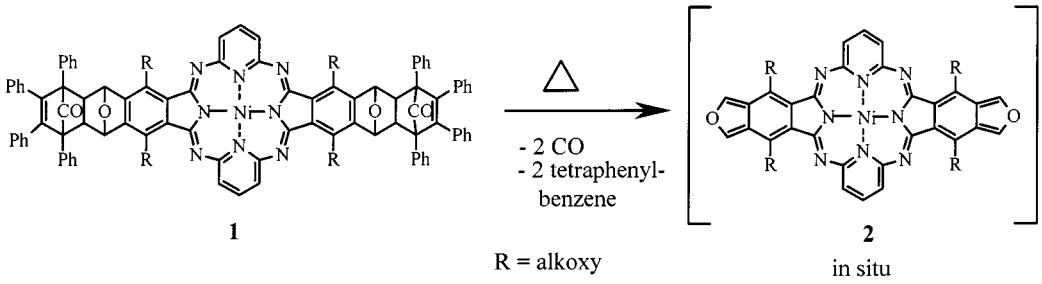
Attempts to synthesize similar octaalkyl-substituted PcNi (instead of octaalkoxy-substituted compounds) from 5,8-dialkyl-6,7-dicyano-1,4-dihydro-1,4-epoxynaphthalenes failed, probably due to the bigger steric interactions of the alkyl groups.

PcNi **4a,b** are unequivocally characterized by their NMR and FD-MS spectra (see Experimental Section). In the ^{1}H-NMR spectra of both compounds, only two slightly broadened singlets (at $\delta \approx 6.4$ and 7.3) appear besides the resonances of the aliphatic protons. These singlets are assigned to the two different kinds of protons on the oxo-brigded ring [**4a**: δ = 6.38 (2-H), 7.33 (1-H), **4b**: δ = 6.37 (2-H), 7.32 (1-H)].

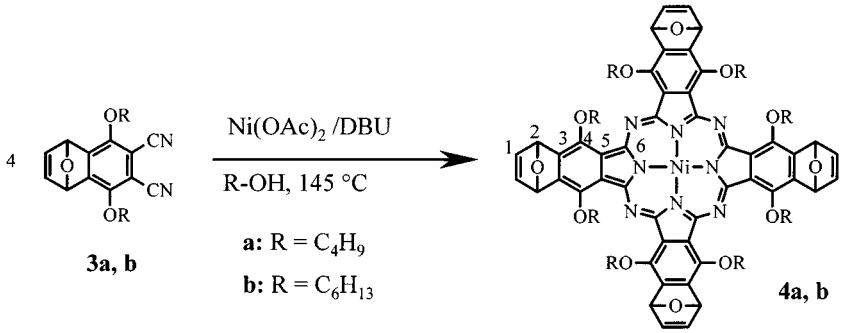
Due to the relative orientations of the epoxy bridges, the molecules **4a,b** can exist in four isomeric forms (C_{4v}, C_s, C_{2h}, D_{2d}). The NMR spectra do not allow the distinction between the single isomers. The separation of the mixture (e.g. by HPLC) was not furthermore pursued. Therefore, the relative amounts of the isomers in the mixture are not known.

[a] Institut für Organische Chemie, Universität Tübingen, Auf der Morgenstelle 18, D-72076 Tübingen, Germany
Fax: (internat.) + 49(0)7071/295244
E-mail: hanack@uni-tuebingen.de
WWW: http://www.uni-tuebingen.de/hanack/index.html

 © WILEY-VCH Verlag GmbH, D-69451 Weinheim, 1999 1434−1948/99/0404−0693 $ 17.50+.50/0



Scheme 1. Generation of the reactive isobenzofuran intermediate



Scheme 2. Synthesis of **4a,b** bearing four dienophilic groups

The UV/Vis spectra of the compounds **4a,b** (recorded from $CHCl_3$ solutions) do not show a remarkable influence of the side-chain length on the wavelength values of the electronic transitions. The $Q_{0\text{-}0}$ bands appear at 713 (**4a**) and 714 nm (**4b**), respectively. The $Q_{0\text{-}0}$ transition of the corresponding unsubstituted compound, namely [2,5,11,14,20,23,29,32-octahydro-2,5:11,14:20,23:29,32-tetraepoxynaphthalocyaninato]nickel(II) is found at 668 nm.[6] As expected, the introduction of eight auxochromic alkoxy substituents leads to a bathochromic shift of the Q band of ca. 45 nm. The comparison of the values of **4a,b** with the $Q_{0\text{-}0}$ transitions found for [1,4,8,11,15,18,22,25-octaalkoxyphthalocyaninato]nickel(II) complexes (which contain the same π-conjugated system as **4a,b**) shows a significant hypsochromic shift of ca. 30 nm [compare the $Q_{0\text{-}0}$ transition of the 1,4-substituted $(PentO)_8PcNi$ appearing at 742 nm[8]]. This shift seems to be caused by the electronic influence of the four epoxybenzo units attached to the phthalocyanine core.

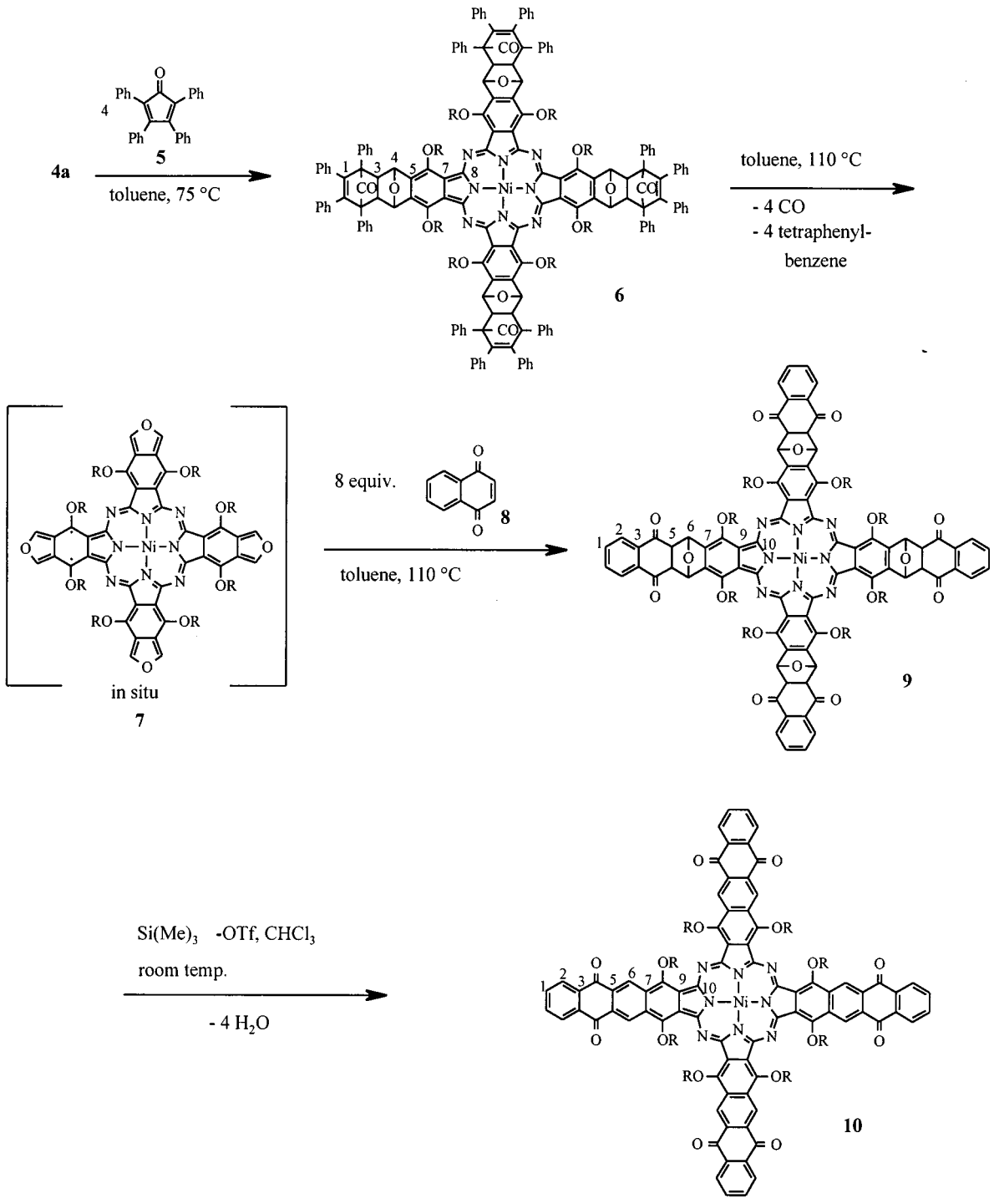
As already mentioned, the unsubstituted [2,5,11,14,20,23,29,32-octahydro-2,5:11,14:20,23:29,32-tetraepoxynaphthalocyaninato]nickel(II) complex underwent a DA reaction when heated with an excess of 2,3-dimethylbutadiene in toluene for several days.[6] However, this reaction proceeded with unsatisfactory conversion rates. The well-soluble compounds **4a,b** should give much better conversions when allowed to react with dienes.

In the next synthetic step, we therefore envisaged the addition of four molecules of 1,2,3,4-tetraphenylcyclopentadienone (tetracyclone, **5**) to the tetrafunctional PcNi **4a** (Scheme 3).[9] This was accomplished in a single reaction by stirring **4a** with a fourfold excess of **5** in toluene at 75°C over 48 h. Chromatographic workup (silica gel; *n*-hexane/ethyl acetate, 6:1) afforded the deep green compound **6** in 66% isolated yield. PcNi **6** is the precursor of the intermediate **7** exhibiting four isobenzofuran moieties.

The ability of **7** to react as a tetrafunctional diene was tested with excess naphthoquinone (**8**) as trapping dienophile (Scheme 3) in the following procedure: The precursor **6** and naphthoquinone (8 equiv.) were stirred in refluxing toluene for 24 h. Subsequent flash chromatography (*n*-hexane/ethyl acetate, 3:2) allowed the separation of 1,2,3,4-tetraphenylbenzene and of unreacted quinone as the first and second fraction. The third, deep green fraction proved to be the desired compound **9**. The PcNi **9** was obtained in a yield of 70%.

In previous work, exclusive *exo* orientation was observed during the DA addition of tetracyclone to 1,4-epoxynaphthalenes.[5a,b] Since the isomeric mixture of **4a** (vide infra) was used as starting material to prepare **6**, the tetracyclone adduct **6** is present as a mixture of at least four isomers. The NMR spectra of **6** are in agreement with exclusive *exo* addition, since two clearly separated resonances should appear for e.g. 3-H in the case of *endo* and *exo* addition. The resonances of 3-H and 4-H appear as signal groups of alleged singlets at $\delta = 3.49-3.66$ and at $6.44-6.50$. The appearance of several singlets arises from the magnetic non-equivalence of 3-H and 4-H even in a single all-*exo* isomer of **6** (with exception of the C_{4v} isomer). This non-equivalence and the presence of at least four isomers also complicates the ^{13}C-NMR spectrum (see Experimental Section).

The completeness of the tetracyclone addition is clearly demonstrated by the integration values obtained from the ^1H-NMR spectrum of **6** which are in excellent agreement with the expected values. Moreover, in the DEPT-135 spectrum of **6**, no signal is found downfield from $\delta = 131$. A



Scheme 3. Synthesis of the dehydrated naphthoquinone adduct **10**

remaining vinylic carbon signal (C-1 in structure **4a**) should appear at $\delta \approx 143$.

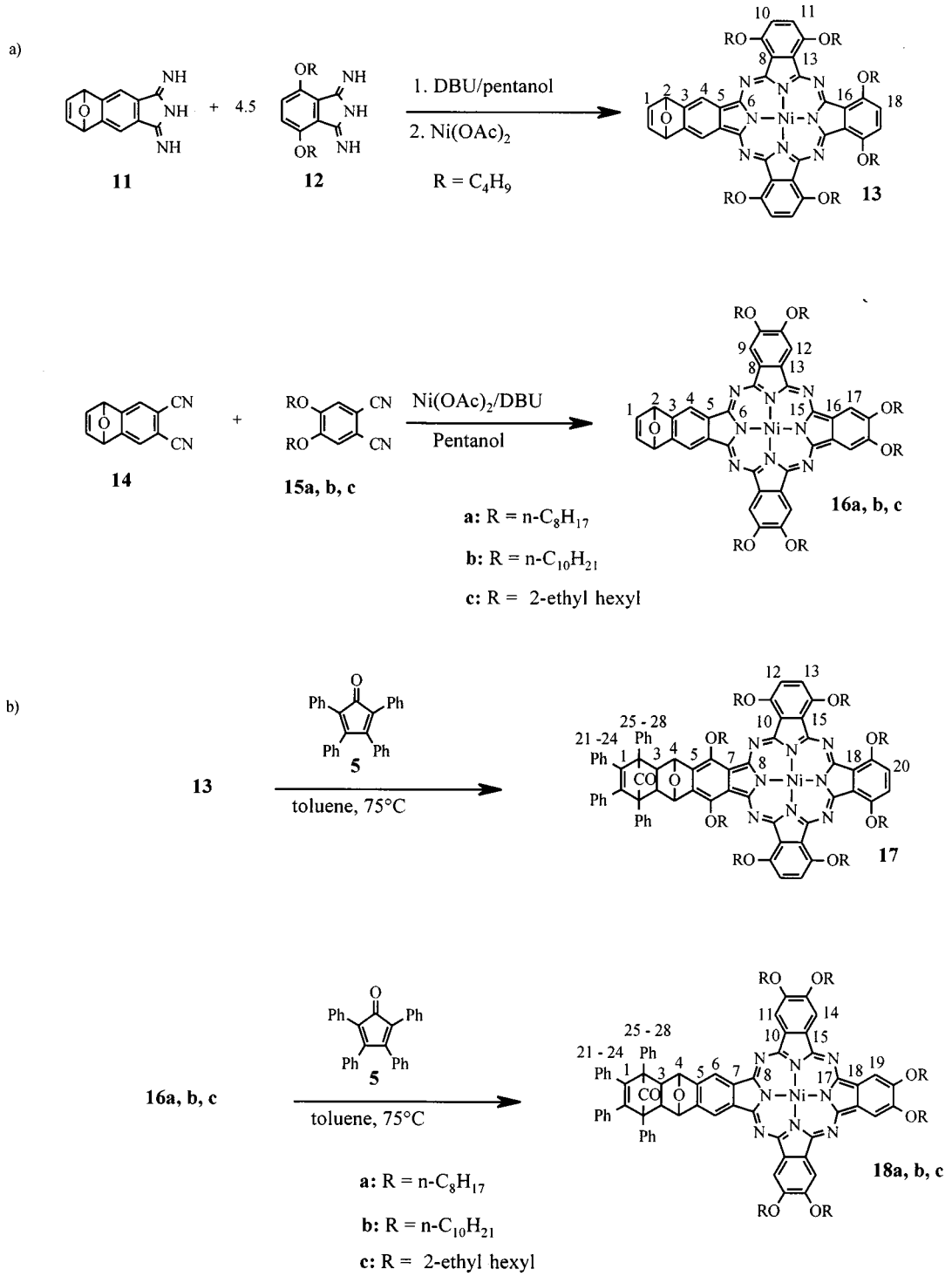
The Q-band transitions in the electronic spectrum of **6** ($CHCl_3$ solution) are bathochromically shifted compared to the "parent" compound **4a**. The $Q_{0\text{-}0}$ transition appears at 724 nm (**4a**: 713 nm, vide infra), thus indicating that the electronic influence of the epoxybenzo units on the Pc core decreases during the DA addition to the dienophilic double bonds in **4a**.

exo and *endo* attack was expected for the DA addition of naphthoquinone (**8**) to the isobenzofuran moieties of **7**.[3c,10] The fact that both orientations are present in compound **9** is reflected by two clearly separated broad signals for 5-H at $\delta = 3.51$ (*exo*) and 4.09 (*endo*) in the corresponding ^{1}H-NMR spectrum. The *exo*/*endo* assignments given in the Experimental Section are in agreement with the chemical shifts and with an additionally performed H,C-COSY experiment. Comparison of the integrals of the mentioned

5-H signals allowed the determination of the overall *exo*/*endo* ratio (*exo*/*endo* ≈ 2.5:1). Similar reactions of mono- and bifunctional hemiporphyrazine intermediates with *p*-benzoquinone proceeded with the same ratio.[3c]

The $Q_{0\text{-}0}$ transition in the electronic spectrum of compound **9** is found at 728 nm. In comparison to the "parent" molecule **4a**, the same tendency (bathochromic shift) as found for the above described DA adduct **6** occurs.

Full dehydration and therefore planarization of PcNi **9** was attempted next to obtain first informations about the behaviour of phthalocyanine–quinone adducts against dehydrating agents. Treatment with *p*-toluenesulfonic acid (toluene, reflux, 1 h) led to complete decomposition of **9**. The use of the Lewis acid trimethylsilyl triflate was more successful. When **9** was allowed to react with $SiMe_3OTf$ in dry $CHCl_3$ (room temp., 36 h), the reddish-brown naphtha-



Scheme 4. Synthesis of the unsymmetrical Pcs **13**, **16a–c** and their tetracyclone adducts **17**, **18a–c**

locyanine (Nc) **10** was formed (Scheme 3). **10** was isolated after quenching of the reaction and chromatographic workup (silica gel, toluene/ethyl acetate 8:1) in 12% yield. The low yield is due to partial decomposition of **10** during the reaction. The acid stability of substituted Ncs is generally lower than the one of Pcs. Overall 1,4-substitution on the Pc core additionally raises the lability to hydrolysing agents by causing a slight deviation from the perfect planarity of the macrocyclic plane. In air, compound **10** slowly decomposes over days.

Complete dehydration is clearly demonstrated by the absence of any residual signals from the starting compound **9** in the ^{1}H-NMR spectrum of **10**. A strongly downfield-shifted broad singlet at $\delta = 9.95$ is observed for 6-H. Characteristic of 1,6,10,15,19,24,28,33-octaalkoxy-substituted NcNi complexes, the $Q_{0\text{-}0}$ transition appears in the near IR region at 855 nm.

As described above, the overall substitution in the 1,4-positions on a Pc core decreases its hydrolytic stability. Therefore, the target molecules **13** and **16a,b,c** (having one DA functionality and a lower number of or even no 1,4-substituents) were chosen next to test DA building blocks with an increased hydrolytic stability (Scheme 4a). The synthesis of such AAAB-Pcs, composed of three subunits A and one subunit B, is possible by a statistical condensation of two differently substituted phthalodinitriles or diiminoisoindolines A and B,[11] whereby the desired compounds are formed besides other combinations. In order to obtain a relatively large amount of the AAAB-Pc, an excess of the starting compound A is generally used.

The 1,4-substituted PcNi **13** was obtained by the reaction of 1 equiv. of 5,8-dihydro-1,3-diimino-5,8-epoxybenz[*f*]isoindoline (**11**)[6] with 4.5 equiv. of 4,7-dibutoxy-1,3-diiminoisoindoline (**12**)[8][12] in refluxing *n*-pentanol and in the presence of catalytic amounts of DBU (72 h). Metallation was achieved by adding 1.2 equiv. of nickel(II) acetate to the reaction mixture and refluxing for further 6 h. The desired product **13** was separated from other Pcs formed by flash chromatography, whereby two subsequent separations with different eluents were performed (first column: $CHCl_3$/ethyl acetate, 2:1, **13** is contained in the 1st fraction; second column: toluene/ethyl acetate, 10:1, the pure blue-green compound **13** is eluted as the 2nd fraction in a yield of 9%).

The preparation of the 2,3-substituted PcNi **16a,b,c** was realized by the condensation reaction of 1 equiv. of 6,7-dicyano-1,4-dihydro-1,4-epoxynaphthalene (**14**)[6] with 8 equiv. of 1,2-dicyano-4,5-dioctyloxybenzene (**15a**), 1,2-dicyano-4,5-didecyloxybenzene (**15b**) and 1,2-dicyano-4,5-bis(2-ethylhexyloxy)benzene (**15c**),[13] respectively in *n*-pentanol at 145°C (18 h, catalytic amounts of DBU). To minimize the separation problems arising from the strong aggregation in a statistical mixture of 2,3-substituted PcNi molecules, we chose an 8-fold excess of the phthalodinitriles **15a,b,c** in order to obtain a product mixture mainly consisting of the AAAA-Pc besides the AAAB-Pcs **16a,b,c**. The blue-green compound **16a,b,c** was separated from other Pcs formed by flash chromatography starting with CH_2Cl_2 and later using CH_2Cl_2/ethyl acetate, 4:1 as the mobile phase (see Experimental Section). We obtained **16a,b** and **c** in average yields of 14%.

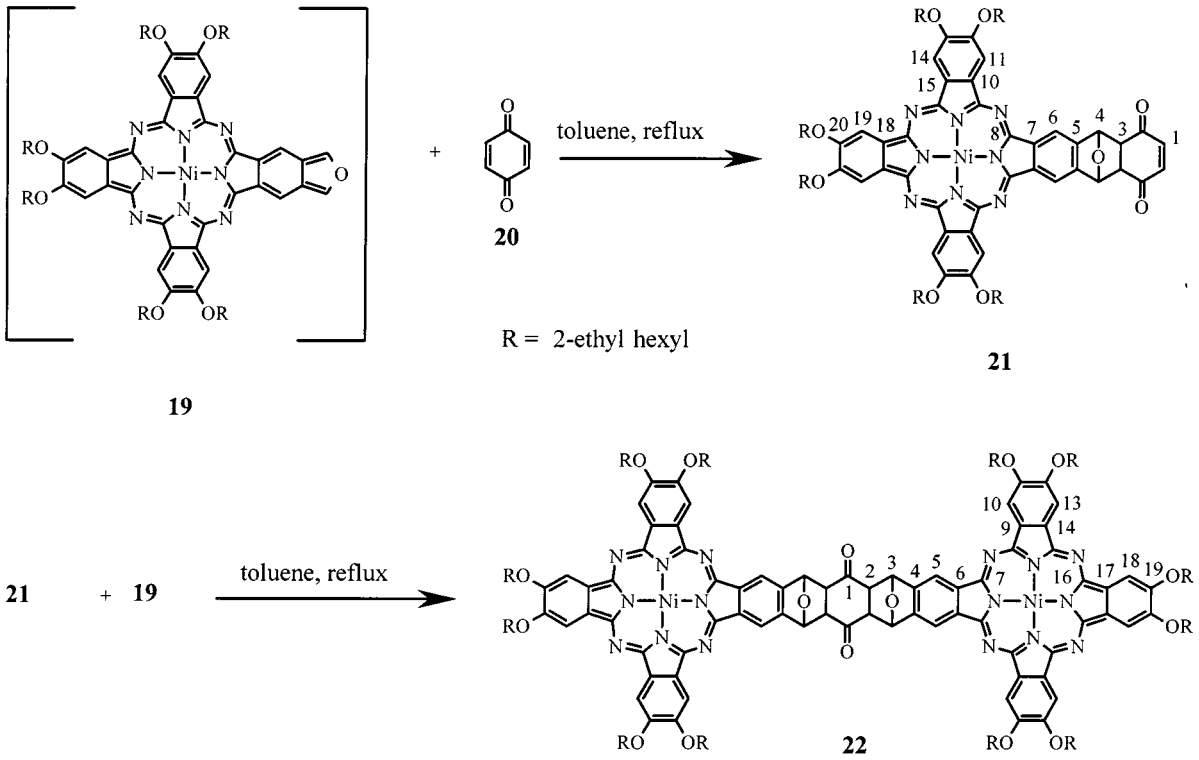
The hydrolytic stability of the PcNi dienophiles **13** and **16a** was tested by treating them with *p*-toluenesulfonic acid (200-fold excess) over a period of 1 h in a toluene solution (room temp.). **13** partially decomposed while **16a** showed no reaction at all (TLC control). The epoxy bridge in **13** and **16a** was not affected under these conditions.

The compounds **13** and **16a,b,c** could be converted to the corresponding PcNi–tetracyclone adducts **17**, **18a,b,c** in moderate to good yields (Scheme 4b). In a typical procedure, the corresponding PcNi (**13**, **16a,b,c**) was stirred with 1 equiv. of tetracyclone in toluene at 75°C (several days). In contrast to a similar addition reaction starting from hemiporphyrazines,[3b,14] the reaction could not be driven to completion within 7 days for **13** and **16a,b**. The isolated yields were 69% (**17**) and 55% (**18a,b**), respectively, whereas the reaction with HpNi complexes proceeded almost quantitatively within 24 h and gave isolated yields of ca. 90%.[3b,14] The hindered reactivity of the PcNi dienophiles **13** and **16a,b** during this DA addition may be due to aggregation phenomena in the corresponding reaction mixture. One possibility to suppress aggregation is the introduction of bulky or branched substituents on the Pc core.[15] Therefore, **16c** was expected to give better yields under identical reaction conditions. As expected, the reaction proceeded almost quantitatively and yields of 90% were obtained.

The purified compounds **13**, **16a,b,c**, **17** and **18a,b,c** were identified on the basis of their NMR and FD- or FAB-MS spectra (see Experimental Section). Characteristic for the epoxybenzo units in **13** and **16a,b,c** are three singlets in the ^{1}H-NMR spectra arising from 1-H, 2-H, and 4-H. In the case of compound **13**, these signals are sharp and appear at $\delta = 6.13$ (2-H), 7.24 (1-H) and 8.93 (4-H), while the stronger aggregation in $CDCl_3$ solutions of **16a,b,c** leads to broadened resonances. For **16a** these resonances appear at $\delta = 6.14$ (2-H), 7.23 (1-H) and 8.20 (4-H). All other NMR data are in agreement with the proposed structures.

By the addition of tetracyclone to the isolated double bonds in **13**, **16a,b,c**, the signals of the vinylic protons 1-H disappear and singlets for the methine protons 3-H are found at $\delta = 3.44$ (**17**) and 3.24 (**18a**), respectively. The appearance of singlets for 3-H, 4-H is in agreement with the expected *exo* orientation of the tetracyclone addition (vide infra). The *exo* orientation causes a dihedral angle between the two mentioned protons which is close to 90°. Therefore, a small coupling constant results.

The DA reaction of the isobenzofuran intermediate **19** (generated from **18c**) with *p*-benzoquinone **20** furnished the benzoquinone monoadduct **21** which (after removal of unreacted **20** by sublimation) was treated (without further purification) with a second equiv. of **19** to form the ladder-type phthalocyanine dimer **22** in a yield of 55%. **18a** was also treated with *p*-benzoquinone according to the same sequence, but the formed dimer could not be identified by spectroscopic means due to heavy aggregation (see below).



Scheme 5. Synthesis of Pc dimer **22**

A small amount of the benzoquinone adduct **21** was isolated and purified by flash chromatography (silica gel; CH_2Cl_2/ethyl acetate, 8:1). As described for compound **9**, *exo* and *endo* orientation is present in compound **21**. The ^{1}H-NMR spectrum shows two clearly separated broad signals for 3-H at δ = 3.24 (*exo*) and 3.88 (*endo*). The *exo*/*endo* assignments given in the Experimental Section are in agreement with the chemical shifts and comparison of the integrals of the mentioned 3-H signals allowed the determination of the overall *exo*/*endo* ratio (*exo*/*endo* ≈ 1:2).

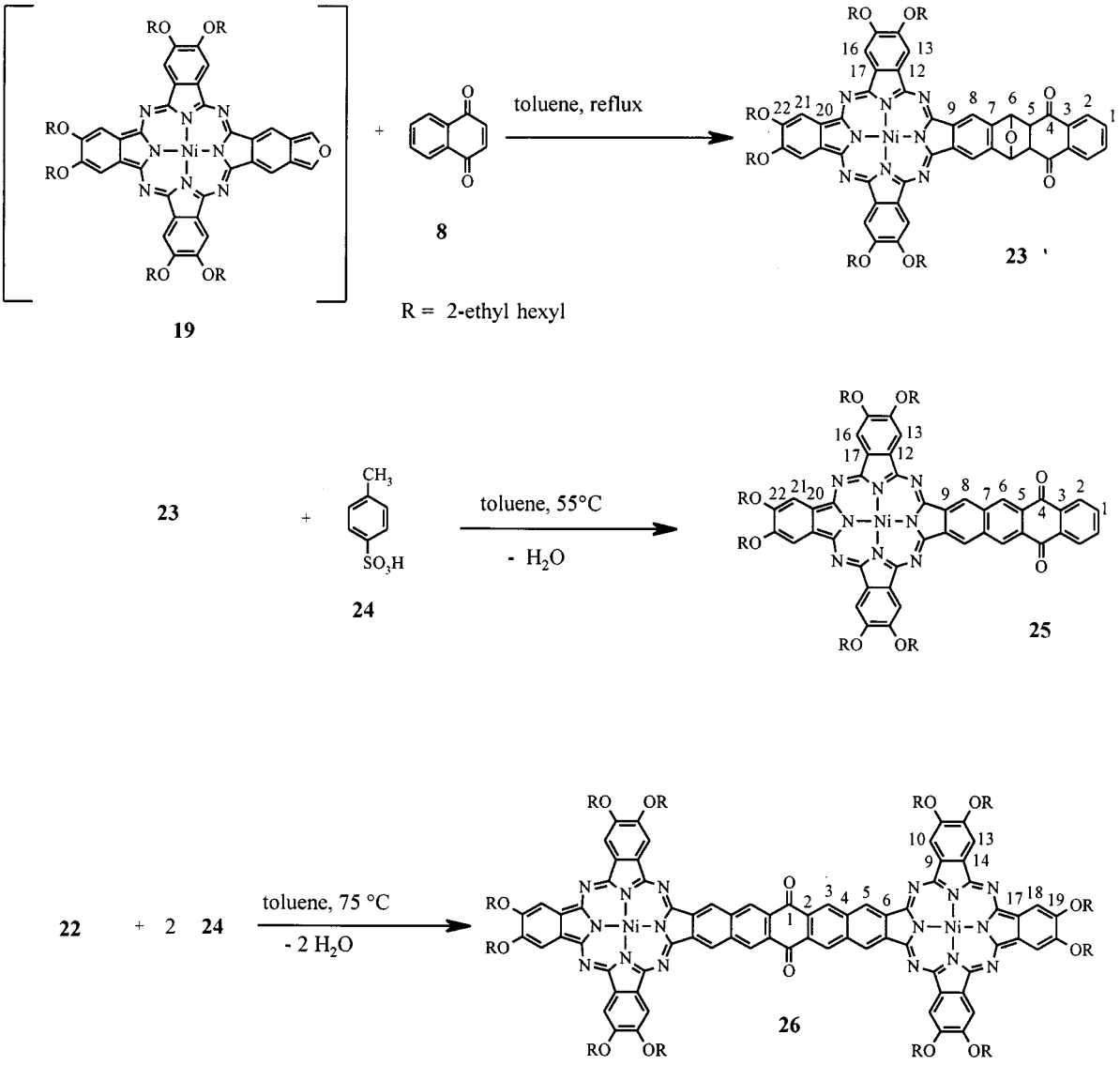
Due to aggregation phenomena and the fact that six isomers can be formed, the full spectroscopic characterization of the ladder-type PcNi dimer **22** was difficult. The resolution of the NMR spectra is only moderate, therefore a discussion of the *exo*/*endo* ratio is not possible. Yet all the signals found in the ^{1}H-NMR and the ^{13}C-NMR spectrum verify the proposed structure. The ^{1}H-NMR spectrum shows broad resonances for the methine proton 2-H at δ = 2.93, 3.48, and 3.74 and at δ = 6.11, 6.36, and 6.58 for 3-H. The corresponding carbon signals appear at δ = 53.7, 55.1, 55.3 (C-2) and at δ = 84.1, 85.1 (C-3), respectively. The IR spectrum shows the carbonyl band at 1701 cm^{-1}. If the DA addition of a second equiv. of isobenzofuran **19** had failed, the carbonyl band should still appear at 1676 cm^{-1} (**21**). The shift to higher wavelengths also indicates that the two carbonyl groups in the molecule are no longer conjugated.

In order to prepare a model compound for dehydration experiments we treated **18c** with a 7-equiv. excess of naphthoquinone (**8**, toluene, 110°C, 24 h,). The naphthoquinone monoadduct **23** was obtained in a yield of 70%. Again, the NMR spectra indicate *exo* and *endo* orientation. Two signals appear for 5-H at δ = 3.42 (*exo*), 4.14 (*endo*) and 6-H at 6.30 (*exo*), 6.38 (*endo*) The *exo* and *endo* isomers are formed in a ratio of 1:2.5 and can be separated by preparative TLC with CH_2Cl_2 as eluent. For further dehydration reactions the isomers were not separated because both isomers form the same product during the dehydration reaction.

Since **16a** proved to be stable against strong proton acids, **23** was expected to undergo acid-promoted dehydration easily to give the corresponding planarized and fully unsaturated naphthoquinone adduct **25** without decomposition.

By treating **23** with a 4-fold excess of *p*-toluenesulfonic acid (**24**) dehydration was carried out successfully and **25** was obtained in a yield of 85% after isolation by flash chromatography with CH_2Cl_2 as eluent. During the whole reaction time no decomposition was observed. Complete dehydration is clearly demonstrated by the absence of any residual signals from the methine proton 5-H in its ^{1}H-NMR spectrum.

A downfield-shifted singlet at δ = 8.17 is observed for 6-H. All NMR data are in agreement with the proposed structure and with an additionally performed H,C-COSY experiment. In the IR spectrum the carbonyl band has been shifted from 1680 cm^{-1} (**23**) to 1672 cm^{-1} in **25**. This shows an increased conjugation of the two carbonyl functions in the molecule. As expected the Q-band transitions in the electronic spectrum of **25** are bathochromically shifted compared to the precursor molecule **23**. The $Q_{0\text{-}0}$ transition appears at 708.5 nm (**23**: 668 nm).



Scheme 6. Synthesis of the dehydrated naphthoquinone adduct **25** and the fully unsaturated Pc dimer **26**

By an identical treatment of **22** with a 6-fold excess of toluenesulfonic acid (**24**) in toluene at 75°C the completely unsaturated dimer **26** was obtained in a yield of 68% after purification by flash chromatography with CH_2Cl_2 as eluent. Compared to the dehydration of **21** slightly higher reaction temperatures and longer reaction times were necessary to obtain optimized yields. During the reaction also the monodehydrated dimer was observed during TLC control. A small amount was isolated and identified by ^{1}H NMR. Further identification was not pursued.

The NMR spectra of **26** show that dehydration was successful although **26** has a strong tendency to form aggregates and the resolution of the ^{1}H-NMR spectrum is only moderate. The methine proton signals of **22** (2-H) have completely vanished and the 3-H signal now appears at δ = 8.1. Moreover, in the DEPT-135 spectrum no signal is found between δ = 40 and 60. A remaining methine carbon signal should appear at $\delta \approx 55$. In the IR spectrum the carbonyl band has been shifted to lower wavelengths (1695 cm^{-1}) compared with **23**. The Q transitions in the electronic spectrum of **26** are bathochromically shifted (730, 681 nm) compared to **22** (659, 628 nm).

Experimental Section

The following compounds were prepared as described in the literature: 5,8-dibutoxy-6,7-dicyano-1,4-dihydro-1,4-epoxynaphthalene (**3a**),[7] 6,7-dicyano-5,8-dihexyloxy-1,4-dihydro-1,4-epoxynaphthalene (**3b**),[7] 5,8-dihydro-1,3-diimino-5,8-epoxybenz[*f*]isoindoline (**11**),[6] 4,7-dibutoxy-1,3-diiminoisoindoline (**12**),[8][12] 6,7-dicyano-1,4-dihydro-1,4-epoxynaphthalene (**14**),[6] 1,2-dicyano-4,5-dioctyloxybenzene (**15a**), 1,2-dicyano-4,5-didecyloxybenzene (**15b**), 1,2-dicyano-4,5-bis(2-ethylhexyloxy)benzene (**15c**).[13] – FT IR: Bruker IFS 48. – UV/Vis: Shimadzu UV-2102 PC. – NMR: Bruker AC 250, Bruker ARX 250 (^{1}H: 250.1 MHz, ^{13}C: 62.9 MHz). – MS: Finnigan ISQ 70; Varian MAT 711A (modified by AMD Intectra). – Elemental analyses were performed with Carlo Erba Elemental Analyzer 1104, 1106. All chemical shifts are referenced to the signals of $CDCl_3$ (except for **16c**). All chromatographic sep-

arations (column chromatography or TLC) with "$CHCl_3$" as eluent or as part of the eluent were performed with $CHCl_3$ containing 1% of EtOH.

General Procedure for the Preparation of the PcNi 4a,b: The corresponding phthalodinitrile (**3a,b**), 1.2 equiv. of $Ni(OAc)_2 \cdot 4\ H_2O$ and a catalytic amount of DBU were suspended in the convenient *n*-alcohol (**3a**: *n*-butanol, **3b**: *n*-hexanol) under nitrogen. The mixture was then heated for several hours (**3a**: reflux, 36 h; **3b**: 145°C, 24 h). After cooling, the solvent was stripped from the butanol solution in a rotatory evaporator. The crude product was purified by column chromatography on silica gel. The hexanol solution was cooled down and poured into a mixture of $MeOH/H_2O$, 2:1. The precipitate was collected by centrifugation and washed several times with MeOH. The crude product was then dried and purified by column chromatography (silica gel). Both deep green solids were furthermore extracted with MeOH and dried in vacuo.

1,6,10,15,19,24,28,33-Octabutoxy-2,5,11,14,20,23,29,32-octahydro-2,5:11,14:20,23:29,32-tetraepoxynaphthalocyaninato]nickel(II) (4a): 550 mg (1.62 mmol) of **3a** and 121 mg (0.49 mmol) of $Ni(OAc)_2 \cdot 4\ H_2O$ were allowed to react in 30 ml of *n*-butanol according to the general procedure (36 h). Column chromatography was performed using *n*-hexane/ethyl acetate, 2:1 as eluent and afforded 172 mg (30%) of **4a**. R_f (SiO_2; toluene/ethyl acetate, 10:1) = 0.50. − IR (KBr): $\tilde{\nu}$ = 2957 cm^{-1}, 2928, 2858, 1591, 1518, 1493, 1466, 1362, 1288, 1246, 1178, 1124, 1111, 1076, 988, 870, 710. − UV/Vis ($CHCl_3$): λ_{max} = 713 nm, 642, 383, 338, 311. − ^1H NMR ($CDCl_3$): δ = 1.01 (t, *J* = 7.3 Hz, 24 H, CH_3), 1.51−1.66 (m, 16 H, CH_2), 1.89−2.02 (m, 16 H, CH_2), 4.72−5.03 (m, 16 H, OCH_2), 6.38 (s, 8 H, 2-H), 7.33 (s, 8 H, 1-H). − ^{13}C NMR ($CDCl_3$): δ = 14.1 (CH_3), 19.4 (CH_2), 32.6 (CH_2), 75.4 (OCH_2), 81.3 (C-2), 130.0 (C-5), 143.0 (C-1), 143.1, 144.9, 145.6 (C-3, C-4, C-6). − MS (FD); *m/z* (%): 1412.6 (100) [M^+]. − $C_{80}H_{88}N_8NiO_{12}$ (1412.3): calcd. C 68.04, H 6.28, N 7.93; found C 67.55, H 6.68, N 7.59.

[1,6,10,15,19,24,28,33-Octahexyloxy-2,5,11,14,20,23,29,32-octahydro-2,5:11,14:20,23:29,32-tetraepoxynaphthalocyaninato]-nickel(II) (4b): 107 mg (260 μmol) of **3b** and 20 mg (80 μmol) of $Ni(OAc)_2 \cdot 4\ H_2O$ were allowed to react for 24 h in 20 ml of *n*-hexanol according to the general procedure. Column chromatography was carried out with *n*-hexane/ethyl acetate, 4:1 as the mobile phase. R_f (SiO_2; toluene/ethyl acetate, 10:1) = 0.61. Yield: 34 mg (32%) of **4b**. − IR (KBr): $\tilde{\nu}$ = 2955 cm^{-1}, 2928, 2858, 1591, 1518, 1493, 1466, 1362, 1288, 1246, 1178, 1124, 1111, 1076, 988, 870, 710. − UV/Vis ($CHCl_3$): λ_{max} = 714 nm, 643, 385, 336, 313. − ^1H NMR ($CDCl_3$): δ = 0.89 (t, *J* = 6.7 Hz, 24 H, CH_3), 1.31−1.44 (m, 32 H, 2 × CH_2), 1.48−1.60 (m, 16 H, CH_2), 1.91−2.04 (m, 16 H, CH_2), 4.69−5.00 (m, 16 H, OCH_2), 6.37 (s, 8 H, 2-H), 7.32 (s, 8 H, 1-H). − ^{13}C NMR ($CDCl_3$): δ = 14.1 (CH_3), 22.7 (CH_2), 25.8 (CH_2), 30.4 (CH_2), 31.9 (CH_2), 75.7 (OCH_2), 81.3 (C-2), 130.0 (C-5), 143.0 (C-1), 143.1, 144.9, 145.6 (C-3, C-4, C-6). − MS (FD); *m/z* (%): 1636.1 (100) [M^+]. − $C_{96}H_{120}N_8NiO_{12}$ (1636.7): calcd. C 70.45, H 7.39, N 6.85; found C 71.75, H 7.41, N 7.50.

Tetrakis(tetracyclone) Adduct PcNi 6: 117 mg (82.8 μmol) of **4a** and 128 mg (332.9 μmol) of tetracyclone **5** were dissolved in 30 ml of toluene under nitrogen and stirred for 48 h at 75°C. After cooling and evaporation of the solvent, the raw product was purified using column chromatography (silica gel) with *n*-hexane/ethyl acetate, 6:1 (1st fraction: tetracyclone; 2nd fraction: **6**; 3rd fraction: incompletely converted products). After evaporating the solvent from the 2nd fraction, it was extracted several times with *n*-hexane to remove remaining traces of **5**. Drying in vacuo gave 162 mg (66%) of **6** as a deep green powder. R_f (SiO_2; *n*-hexane/ethyl acetate, 3:1) = 0.44. − IR (KBr): $\tilde{\nu}$ = 3057 cm^{-1}, 3028, 2957, 2932, 2872, 1778 (C=O), 1605, 1587, 1497, 1447, 1356, 1340, 1298, 1250, 1223, 1198, 1115, 1074, 1026, 982, 949, 897, 820, 752, 698. − UV/Vis ($CHCl_3$): λ_{max} = 724 nm, 651, 422 (sh), 360, 339, 306. − ^1H NMR ($CDCl_3$): δ = 0.96−1.11 (m, 24 H, CH_3), 1.59−1.88 (m, 16 H, CH_2), 2.05−2.44 (m, 16 H, CH_2), 3.49−3.66 (m, 8 H, 3-H), 4.57−5.57 (m, 16 H, OCH_2), 6.44−6.50 (m, 8 H, 4-H), 7.07 (br., 40 H, 10-H, 11-H, 12-H), 7.37−7.75 (m, 40 H, 14-H, 15-H, 16-H). − ^{13}C NMR ($CDCl_3$): δ = 14.1, 14.2 (CH_3), 19.4, 19.5 (CH_2), 32.5, 32.6 (CH_2), 46.9, 47.2 (C-3), 64.6 (C-2), 75.9 (OCH_2), 80.4 (C-4), 126.9, 127.7, 128.4, 129.74, 129.83, 129.95, 130.02 (C-10-12, C-14-16), 130.5 (C-7), 135.2, 135.27, 135.33, 135.6 (C-9, C-13), 138.8, 138.87, 138.90, 139.0 (C-1), 142.1, 142.2, 142.3, 142.5, 144.30, 144.34, 144.46, 144.52, 144.65, 144.74, 145.01, 145.07 (C-5, C-6, C-8), 196.6 (CO). − MS (FAB); *m/z* (%): 2949.0 (18) [M^+], 2538.7 (5) [M^+ − CO − $C_{30}H_{22}$], 2127.5 (5) [M^+ − 2 × CO − 2 × $C_{30}H_{22}$], 1717.9 (12) [M^+ − 3 × CO − 3 × $C_{30}H_{22}$], 1305.9 (90) [M^+ − 4 × CO − 4 × $C_{30}H_{22}$ − 1]. − $C_{196}H_{168}N_8NiO_{16}$ (2950.2): calcd. C 79.80, H 5.74, N 3.80; found C 79.10, H 5.92, N 4.07.

Tetrakis(naphthoquinone) Adduct PcNi 9: 155 mg (52.5 μmol) of **6** and 266 mg (1.68 mmol) of 1,4-naphthoquinone (**8**) were dissolved in 30 ml of toluene (under nitrogen) and heated under reflux for 24 h. The solvent was removed and the residue was separated by flash chromatography (*n*-hexane/ethyl acetate, 3:2), whereby 1,2,3,4-tetraphenylbenzene and unreacted naphthoquinone were eluted in front of the green fraction containing **9**. Drying in vacuo furnished 71 mg (70%) of **9** as a deep-green solid. R_f (SiO_2; *n*-hexane/ethyl acetate, 1:1) = 0.50. − IR (KBr): $\tilde{\nu}$ = 3071 cm^{-1}, 2959, 2934, 2872, 1682 (C=O), 1593, 1495, 1358, 1294, 1267, 1223, 1153, 1113, 989, 949, 750. − UV/Vis ($CHCl_3$): λ_{max} = 728 nm, 655, 425 (sh), 360, 308. − ^1H NMR ($CDCl_3$): δ = 1.02−1.13 [m, *exo*], 1.16−1.29 [m, *endo*] (24 H, CH_3), 1.58−1.95 (m, 16 H, CH_2), 2.07−2.25 (m, 16 H, CH_2), 3.46−3.56 [m, *exo*], 4.09 [br., *endo*] (8 H, 5-H), 4.30−5.50 (m, 16 H, OCH_2), 6.49 (m, 8 H, 6-H), 7.50−7.81 [m, *endo*, 1-H, 2-H], 7.85−7.89 [m, *exo*, 1-H], 8.26−8.30 [m, *exo*, 2-H] (16 H). − ^{13}C NMR ($CDCl_3$): δ = 14.2 (CH_3), 19.5 (CH_2), 32.3, 32.8 (CH_2), 50.8 [*endo*], 52.1 [*exo*] (C-5), 75.4, 75.8 (OCH_2), 82.4 [*endo*], 84.3 [*exo*] (C-6), 125.9 [br., *endo*], 127.5 [*exo*] (C-2), 129.8 [br.] (C-9), 132.6 [br., *endo*], 134.7 [*exo*] (C-1), 134.3, 135.7 (C-3), 139.1, 139.5 [br.] (C-7), 144.8 [br.], 145.0 [br.] (C-8, C-10), 193.4, 194.7 (CO). − MS (FAB); *m/z* (%): 1939.4 (55) [M^+], 1781.5 (35) [M^+ − $C_{10}H_6O_2$], 1623.3 (20) [M^+ − 2 × $C_{10}H_6O_2$], 1464.0 (30) [M^+ − 3 × $C_{10}H_6O_2$ − 1], 1307.4 (70) [M^+ − 4 × $C_{10}H_6O_2$]. − $C_{112}H_{104}N_8NiO_{20}$ (1940.7): calcd. C 69.31, H 5.40, N 5.77; found C 69.62, H 5.53, N 5.84.

Dehydrated Tetrakis(naphthoquinone) Adduct PcNi 10: 62 mg (31.9 μmol) of **9** was dissolved in 10 ml of freshly distilled, dry $CHCl_3$ in a nitrogen-purged vessel. 2 ml (11.1 mmol) of trimethylsilyl triflate was added by means of a syringe. The mixture, which turned immediately to a deep purple colour, was stirred for 36 h at room temp. Then 2 ml of NEt_3 was added before quenching the mixture dropwise with water. The organic layer was separated, washed two times with water, dried with $MgSO_4$ and the solvent was evaporated. Subsequent column chromatography (SiO_2; toluene/ethyl acetate, 8:1; R_f = 0.70) gave after drying in vacuo 7 mg (12%) of **10** as a reddish-brown powder. − IR (KBr): $\tilde{\nu}$ = 2959 cm^{-1}, 2932, 2872, 1671 (C=O), 1591, 1433, 1379, 1321, 1275, 1231, 1177, 1117, 978, 719. − UV/Vis (toluene): λ_{max} = 855 nm, 758, 484, 327. − ^1H NMR ($CDCl_3$): δ = 1.05 (t, 24 H, CH_3), 1.65−1.77 (m, 16 H, CH_2), 2.16−2.32 (m, 16 H, CH_2), 5.16 (t, J = 7.0 Hz, 16 H, OCH_2), 7.88−7.92 (m, 8 H, 1-H), 8.51−8.55 (m, 8 H, 2-H), 9.96 (s, br., 8 H, 6-H). − ^{13}C NMR, DEPT-135 ($CDCl_3$): δ = 14.1 (CH_3), 19.5 (CH_2), 32.6 (CH_2), 77.6 (OCH_2), 126.9, 127.7 (C-2, C-6), 134.3 (C-1). − MS (FD); *m/z* (%): 1868.0 (15) [M^+]. − $C_{112}H_{96}N_8NiO_{16}$

(1868.7): calcd. C 71.99, H 5.18, N 6.00; found C 68.08, H 5.27, N 5.58.

[1,4,8,11,15,18-Hexabutoxytribenzo[*b*,*g*,*l*]-23,26-dihydro-23,26-epoxynaphtho[*q*]porphyrazinato]nickel(II) (13): 300 mg (1.42 mmol) of the diiminoisoindoline **11** and 1.85 g (6.39 mmol) of the diiminoisoindoline **12** were suspended in 50 ml of *n*-pentanol (under nitrogen) and a catalytic amount of DBU was added. The mixture was kept under reflux for 72 h. 582 mg (2.34 mmol) of $Ni(OAc)_2 \cdot 4\ H_2O$ was added to the hot reaction mixture and it was heated for further 6 h. The mixture was allowed to cool down and poured into 200 ml of MeOH/H_2O, 3:1, whereby a green solid precipitated. This was collected by centrifugation and washed several times with MeOH. The crude statistical mixture was dried and separated using flash chromatography by doing two subsequent separations. The first column was performed with $CHCl_3$/ethyl acetate, 2:1 as the mobile phase. The desired PcNi **13** was contained in the 1st fraction. The second column was eluted with toluene/ethyl acetate, 10:1, whereby **13** was contained in the second blue-green fraction. After evaporation of the solvent, the residue was extracted several times with MeOH and dried in vacuo. Yield: 189 mg (9%) of **13**. R_f (SiO_2; $CHCl_3$/ethyl acetate, 3:2) = 0.63. − IR (KBr): $\tilde{\nu}$ = 2957 cm^{-1}, 2932, 2870, 1607, 1522, 1502, 1466, 1385, 1312, 1275, 1254, 1232, 1198, 1178, 1107, 1074, 926, 870, 852, 793, 760. − UV/Vis ($CHCl_3$): λ_{max} = 725 nm, 651, 448, 332, 305. − ^{1}H NMR ($CDCl_3$): δ = 1.06 (t, *J* = 7.4 Hz, 12 H, 4 CH_3), 1.30 (t, *J* = 7.3 Hz, 6 H, 2 CH_3), 1.54−1.70 (m, 8 H, 4 CH_2), 2.02−2.22 (m, 12 H, 6 CH_2), 2.29−2.40 (m, 4 H, 2 CH_2), 4.50−4.59 (m, 4 H, 2 OCH_2), 4.69−4.78 (m, 8 H, 4 OCH_2), 6.13 (s, 2 H, 2-H), 7.24 (s, 2 H, 1-H), 7.34 (m [AB], 4 H, 10-H, 11-H), 7.49 (s, 2 H, 18-H), 8.93 (s, 2 H, 4-H). − ^{13}C NMR ($CDCl_3$): δ = 14.1, 14.4 (CH_3), 19.4, 20.0 (CH_2), 31.5, 31.6, 32.4 (CH_2), 69.3, 71.2, 71.4 (OCH_2), 82.7 (C-2), 113.6 (C-4), 116.5, 117.0 (C-10, C-11, C-18), 125.8, 127.0, 127.5 (C-8, C-13, C-16), 136.1 (C-5), 143.0 (C-1), 145.37, 145.44, 145.9, 146.3 (C-3, C-9, C-12, C-17), 149.8, 150.0, 150.2, 150.5 (C-6, C-7, C-14, C-15). − MS (FD); *m*/*z* (%): 1068.3 (100) [M^+]. − $C_{60}H_{66}N_8NiO_7$ (1069.9): calcd. C 67.36, H 6.22, N 10.47; found C 68.51, H 6.60, N 10.66.

General Procedure for the Preparation of the PcNi 16a,b,c: 4.40 mmol of the corresponding phthalodinitrile **15a,b,c** (A), 0.55 mmol of the phthalodinitrile **14** and 1.49 mmol of $Ni(OAc)_2 \cdot 4\ H_2O$ were suspended in 50 ml of *n*-pentanol and a catalytic amount of DBU was added (under nitrogen). The mixture was heated to 145°C and stirred for 18 h. It was allowed to cool down and poured into 200 ml of MeOH. The formed precipitate was isolated using centrifugation and washed several times with MeOH. The raw mixture of PcNi complexes was separated by flash chromatography starting with CH_2Cl_2 as the mobile phase. After complete elution of the 1st fraction (AAAA-PcNi) a mixture of CH_2Cl_2/ethyl acetate, 4:1 was used as eluent to obtain **16a,b,c** as the 2nd fraction. The solvent was removed and the blue-green solid was extracted several times with acetone to achieve further purification. Drying in vacuo furnished average yields of 14% of **16a,b,c**.

[2,3,9,10,16,17-Hexaoctyloxytribenzo[*b*,*g*,*l*]-23,26-dihydro-23,26-epoxynaphtho[*q*]porphyrazinato]nickel(II) (16a): IR (KBr): $\tilde{\nu}$ = 2955 cm^{-1}, 2924, 2854, 1609, 1533, 1481, 1466, 1429, 1393, 1362, 1281, 1217, 1109, 849, 748. − UV/Vis ($CHCl_3$): λ_{max} = 671 nm, 604, 400, 328 (sh), 310, 288. − ^{1}H NMR ($CDCl_3$): δ = 1.00 (br., 18 H, CH_3), 1.30 (br., 12 H, 6 CH_2), 1.46 [br.], 1.56 [br.] (36 H, 18 CH_2), 1.81 (br., 12 H, 6 CH_2), 2.17 (br., 12 H, 6 CH_2), 4.37 [br.], 4.49 [br.] (12 H, OCH_2), 6.14 (s, br., 2 H, 2-H), 7.23 (s, br., 2 H, 1-H), 7.57, 7.67, 7.76 (3 s, br., 6 H, 9-H, 12-H, 17-H), 8.20 (s, br., 2 H, 4-H). − ^{13}C NMR ($CDCl_3$): δ = 14.1, 14.2 (CH_3), 22.9 (CH_2), 26.6 (CH_2), 29.6, 30.0 (3 × CH_2), 32.1 (CH_2), 69.3, 69.4 (OCH_2), 82.7 (C-2), 103.7, 103.8, 104.0 (C-9, C-12, C-17), 112.9 (C-4), 129.5, 129.7, 130.1 (C-8, C-13, C-16), 134.2 (C-5), 143.1 [br.], 144.0 [br.] (C-1, C-3, C-7, C-14, C-15), 148.3 (C-6), 150.9, 151.0, 151.1 (C-10, C-11, C-18). − MS (FD); *m*/*z* (%): 1404.1 (50) [M^+], 1291.9 (95) [$M^+ - C_8H_{16}$], 1180.0 (100) [$M^+ - 2 \times C_8H_{16}$]. − $C_{84}H_{114}N_8NiO_7$ (1406.6): calcd. C 71.73, H 8.17, N 7.97; found C 71.42, H 8.35, N 7.39.

[2,3,9,10,16,17-Hexadecyloxytribenzo[*b*,*g*,*l*]-23,26-dihydro-23,26-epoxynaphtho[*q*]porphyrazinato]nickel(II) (16b): IR (KBr) $\tilde{\nu}$ = 2924 cm^{-1}, 2853, 1647, 1607, 1531, 1481, 1466, 1429, 1389, 1360, 1279, 1215, 1140, 1108, 1070, 1059, 847, 750. − UV/Vis (CH_2Cl_2): λ_{max} = 667.5 nm, 611, 394. − ^{1}H NMR ($CDCl_3$): δ = 0.90, 1.29 (br., 36 H, CH_3), 1.43, 1.55 (br., 48 H, CH_2), 2.06 (m, 6 H, CH), 4.09 (br., 12 H, OCH_2), 6.14 (s, br., 2 H, 2-H), 7.16 (s, br., 2 H, 1-H), 7.32 (3 s, br., 6 H, 9-H, 12-H, 17-H), 8.16 (s, br., 2 H, 4-H). − ^{13}C NMR ($CDCl_3$): δ = 14.11, 14.18 (CH_3), 19.77, 22.69, 22.80, 23.43, 26.00, 26.61, 28.16, 29.37, 29.60, 29.93, 30.02, 31.64, 31.92, 32.09, 34.20 (CH_2), 68.91, 69.34, 69.49 (OCH_2), 82.64 (C-2), 103.75, 103.94, 106.44 (C-9, C-12, C-17), 112.98 (C-4), 129.71, 131.12, 132.53 (C-8, C-13, C-16), 134.35 (C-5), 143.14, 143.44, 144.23 (C-1, C-3, C-7, C-14, C-15), 148.0 (C-6), 150.70, 150.99 (br., C-10, C-11, C-18). − MS (FD); *m*/*z* (%): 1574.4 (100) [M^+], 1433 (65) [$M^+ - C_{10}H_{21}$]. − $C_{96}H_{138}N_8NiO_7$ (1574.9): calcd. C 73.15, H 8.83, N 7.11; found C 70.25, H 8.04, N 6.61.

[2,3,9,10,16,17-Hexakis(2-ethylhexyloxy)tribenzo[*b*,*g*,*l*]-23,26-dihydro-23,26-epoxynaphtho[*q*]porphyrazinato]nickel(II) (16c): IR (KBr) $\tilde{\nu}$ = 2958 cm^{-1}, 2926, 2872, 2858, 1607, 1531, 1460, 1427, 1381, 1360, 1277, 1217, 1197, 1105, 1068, 1058, 852, 750. − UV/Vis (CH_2Cl_2), λ_{max} = 665 nm, 601, 401, 309. − ^{1}H NMR (CD_2Cl_2): δ = 1.05, 1.18 (br., 36 H, CH_3), 1.52, 1.79 (br., 48 H, CH_2), 2.08 (br., 6 H, CH), 4.36 (br., 12 H, OCH_2), 6.24 (s, 2 H, 2-H), 7.36 (s, 2 H, 1-H), 8.23 (3 s, br., 6 H, 9-H, 12-H, 17-H), 8.80 (s, 2 H, 4-H). − ^{13}C NMR ($CDCl_3$): δ = 11.33, 11.54, 14.13, 14.25 (CH_3), 21.55, 23.10, 23.24, 23.94, 24.17, 29.24, 29.40, 29.45, 30.30, 30.68, 30.86 (CH_2), 39.68, 39.86 (CH), 71.79 (OCH_2), 82.69 (C-2), 103.84, 104.26, 104.50 (C-9, C-12, C-17), 113.44 (C-4), 130.48, 130.90 (br., C-8, C13, C-16), 135.06 (C-5), 143.22, 143.58, 144.73, 146.03 (C-1, C-3, C-7, C-14, C-15), 149.30 (C-6), 151.89, 152.11, 152.63 (C-10, C-11, C-18). − MS (FD); *m*/*z* (%): 1405.1 (100), [M^+], 1389 (10), 1293.0 (30) [$M^+ - C_8H_{16}$]. − $C_{84}H_{114}N_8NiO_7$ (1406.6): calcd. C 71.73, H 8.17, N 7.97; found C 70.40, H 7.96, N 7.68.

Mono(tetracyclone) Adduct PcNi 17: 62 mg (57.9 μmol) of **13** and 23 mg (59.8 μmol) of **5** were dissolved in 20 ml of toluene under nitrogen and stirred at 70−75°C (3−6 d; TLC control: SiO_2; CH_2Cl_2/ethyl acetate, 6:1). After cooling and evaporation of the solvent, the mixture was worked up by column chromatography on silica gel (toluene/ethyl acetate, 8:1; 1st fraction: tetracyclone; 2nd fraction: **17**). The solvent was removed from the second fraction, the residue extracted several times with *n*-hexane and then dried in vacuo. Yield: 58 mg (69%) of **17** as a blue-green solid. − R_f (SiO_2; toluene/ethyl acetate, 5:1): 0.71. − IR (KBr): $\tilde{\nu}$ = 3055 cm^{-1}, 2955, 2932, 2870, 1778 (C=O), 1605, 1501, 1466, 1447, 1385, 1310, 1273, 1223, 1200, 1090, 1072, 926, 760, 746, 697. − UV/Vis ($CHCl_3$): λ_{max} = 728 nm, 653, 452, 331, 304. − ^{1}H NMR ($CDCl_3$): δ = 1.06 (t, *J* = 7.3 Hz, 12 H, 4 CH_3), 1.36 (t, *J* = 7.4 Hz, 6 H, 2 CH_3), 1.57−1.71 (m, 8 H, 4 CH_2), 2.06−2.32 (m, 12 H, 6 CH_2), 2.44−2.55 (m, 4 H, 2 CH_2), 3.44 (s, 2 H, 3-H), 4.65−4.81 (m, 12 H, OCH_2), 6.25 (s, 2 H, 4-H), 7.06 (br., 10 H, 22-H, 23-H, 24-H), 7.32−7.61 (m, 16 H, 12-H, 13-H, 20-H, 26-H, 27-H, 28-H), 9.24 (s, 2 H, 6-H). − ^{13}C NMR ($CDCl_3$): δ = 14.1, 14.4 (CH_3), 19.4, 19.8 (CH_2), 31.5, 32.2 (CH_2), 47.2 (C-3), 64.6 (C-2), 69.2, 71.3 (OCH_2), 81.8 (C-4), 112.4 (C-6), 114.0, 116.8, 117.1 (C-12, C-13,

C-20), 125.9, 127.1, 127.5 (C-10, C-15, C-18), 126.9, 127.4, 127.6, 128.3, 129.7, 130.1 (C-22-24, C-26-28), 135.3, 135.5 (C-21, C-25), 137.3 (C-7), 138.9 (C-1), 145.2, 145.6, 146.2, 146.6, 147.7 (C-5, C-8, C-11, C-14, C-19), 150.2, 150.3, 150.5 (C-9, C-16, C-17), 196.4 (CO). − MS; *m/z* (%): FD: 1453.3 (100) [M^+]; FAB: 1043.3 (100) [$M^+ - C_{30}H_{22} - CO$]. − $C_{89}H_{86}N_8NiO_8$ (1454.4): calcd. C 73.50, H 5.96, N 7.70; found C 73.28, H 6.13, N 7.83.

General Procedure for the Preparation of the Mono(tetracyclone) Adducts 18a,b,c: 100 μmol of **16a,b,c** and 102 μmol of **5** were dissolved in 30 ml of toluene and stirred at 70−75°C (5−7 d; TLC control: SiO_2, $CHCl_3$). The solvent was evaporated and the residue was separated by flash chromatography (CH_2Cl_2; 1st fraction: tetracyclone; 2nd fraction: **18a,b,c**). Evaporation of the solvent and drying in vacuo gave average yields of 55% of **18a,b** and 90% of **18c** as a blue-green solid.

PcNi 18a: IR (KBr): $\tilde{\nu}$ = 2955 cm^{-1}, 2924, 2854, 1780 (C=O), 1607, 1531, 1481, 1464, 1429, 1393, 1362, 1279, 1236, 1202, 1109, 1092, 1065, 851, 750, 694. − UV/Vis ($CHCl_3$): λ_{max} = 672 nm, 605, 393, 327 (sh), 309, 289. − ^{1}H NMR ($CDCl_3$): δ = 0.96 (br., 18 H, CH_3), 1.41 (br., 24 H, 12 CH_2), 1.53 (br., 24 H, 12 CH_2), 1.78 (br., 12 H, 6 CH_2), 2.18 (br., 12 H, 6 CH_2), 3.24 (s, br., 2 H, 3-H), 4.46 [br.], 4.65 (br., 12 H, OCH_2), 6.20 (s, br., 2 H, 4-H), 7.13 (br., 10 H, 22-H, 23-H, 24-H), 7.33−7.60 (m, 10 H, 26-H, 27-H, 28-H), 8.08, 8.22, 8.27 (3 s, br., 6 H, 11-H, 14-H, 19-H), 8.75 (s, br., 2 H, 6-H). − ^{13}C NMR ($CDCl_3$): δ = 14.20, 14.22 (CH_3), 22.82, 22.85 (CH_2), 26.55, 26.59, 26.66 (CH_2), 29.57, 29.63, 29.66, 29.9, 30.0 (3 × CH_2), 32.06, 32.11 (CH_2), 46.9 (C-3), 64.5 (C-2), 69.3, 69.6 (OCH_2), 81.3 (C-4), 104.1, 104.3, 104.5 (C-11, C-14, C-19), 111.4 (C-6), 126.9, 127.4, 127.7, 128.3, 129.7, 130.1, 130.3, 130.5 (C-10, C-15, C-18, C-22-24, C-26-28), 135.36, 135.43 (C-21, C-25), 138.8 (C-1), 142.7, 143.9, 144.9, 145.2, 146.2 (C-5, C-6, C-8, C-9, C-16, C-17), 151.4, 151.6, 151.7 (C-12, C-13, C-20), 196.4 (CO). − MS (FAB); *m/z* (%): 1380.3 (15) [$M^+ - C_{30}H_{22} - CO$]. − $C_{113}H_{134}N_8NiO_8$ (1791.1): calcd. C 75.78, H 7.54, N 6.26; found C 75.67, H 8.04, N 6.39.

PcNi 18b: IR (KBr) $\tilde{\nu}$ = 2963 cm^{-1}, 2853, 1778 (ν_{CO}), 1607, 1481, 1464, 1429, 1391, 1360, 1263, 1213, 1199, 1103, 1022, 851, 800, 748, 694. − UV/Vis (CH_2Cl_2): λ_{max} = 669.5 nm, 605.5,388.5. − ^{1}H NMR ($CDCl_3$) δ = 0.91, 1.22 (br., 36 H, CH_3), 1.34, 1.54, 1.77 (br., 48 H, CH_2), 2.15 (br., 6 H, CH_2), 3.23(s, br., 2 H, 3-H), 4.48 (br., 12 H, OCH_2), 6.20 (s, 2 H, 4-H), 7.22 (br., 10 H, 22-H, 23-H, 24-H), 7.33−7.70 (br., 10 H, 26-H, 27-H, 28-H), 8.05, 8.15, 8.20 (3 s, br., 6 H, 11-H, 14-H, 19-H), 8.71 (s, br., 2 H, 6-H). − ^{13}C NMR ($CDCl_3$) δ = 14.24, 14.36 (CH_3), 22.88, 22.98, 23.75, 26.56, 26.61, 28.92, 29.54, 29.57, 29.69, 29.88, 29.90, 29.95, 30.37, 32.06 (CH_2), 46.96 (C-3), 64.59 (C-2), 68.16, 69.62 (OCH_2), 104.08, 104.35 (br., C-11,C-14, C-19), 111.80 (C-6), 126.92, 127.44, 127.73, 128.40, 129.78, 130.14, 130.54, 130.75 (C-10, C-15, C-18, C-22-24, C-26-28), 135.39, 135.46 (C-21, C-25), 138.82 (C-1), 145.13 (br., C-5, C-6, C-8, C-9, C-16, C-17), 151.43, 151,60, 151.70 (C-12, C-13, C-20), 196.50 (CO). − MS (FD); *m/z* (%): 1548.9 (100) [$M^+ - C_{30}H_{22} - CO$]. − $C_{125}H_{158}N_8NiO_8$ (1959.3): calcd. C 76.61, H 8.13, N 6.26; found C73.89, H7.42, N 4.37.

PcNi 18c: IR (KBr) $\tilde{\nu}$ = 2959 cm^{-1}, 2926, 2856, 1778 (ν_{CO}), 1605, 1481, 1462, 1427, 1391, 1358, 1275, 1263, 1234, 1215, 1202, 1105, 1061, 1026, 852, 802, 750, 696. − UV/Vis (CH_2Cl_2): $\lambda_{max\ =\ 6}$70 nm, 603, 391. − ^{1}H NMR (CD_2Cl_2) δ = 1.00 (br., 18 H, CH_3), 1.05 (br., 18 H, CH_3), 1.18 [br.],1.27 [br.], 1.52 [br.], 1.79 (48 H, CH_2), 2.06 (br., 6 H, CH), 3.39 (s, 2 H, 3-H), 4.35 (br., 12 H OCH_2), 6.33 (s, 2 H, 4-H), 7.20 (br., 10 H, 22-H, 23-H, 24-H), 7.40−7.68 (br., 10 H, 26-H, 27-H, 28-H), 8.07, 8.25, 8.41 (3 s, br., 6 H, 11-H, 14-H, 19-H), 9.12 (s, 2 H, 6-H). − ^{13}C NMR ($CDCl_3$) δ = 11.34, 11.52, 14.10, 14.25 (CH_3), 23.06, 23.24, 23.93, 29.16, 29.38, 30.68, 30.85 (CH_2), 39.63, 39.84 (CH), 47.10 (C-3), 64.61 (C-2), 68.16, 71.72 (OCH_2), 81.56 (C-4), 104.50, 104.57, 104.61 (C-11, C-14, C-19), 112.20 (C-6), 126.87, 127.51, 127.96, 128.01, 128.48, 129.31, 129.79, 130.10, 130.75(C-10, C-15, C-18, C-22-24, C-26-28), 135.37, 135.43,(C-21, C-25), 152.38, 154.47 [br.] (C-12, C-13, C-20), 196.63 (CO). − MS (FAB); *m/z* (%): 1790.5 (10) [M^+], 1380.0 (100) [$M^+ - C_{30}H_{22} - CO$]. − $C_{113}H_{134}N_8NiO_8$ (1791.1): calcd. C 75.78, H 7.54, N 6.26; found C 73.49, H 7.18, N 5.19.

PcNi 22 (Dimer): 90 mg (50.2 μmol) of **18c** and 23 mg (213 μmol) of *p*-benzoquinone (**20**) were dissolved in 30 ml of toluene (under nitrogen) and heated under reflux for 24 h. The solvent was evaporated and unreacted **20** was removed by sublimation (TLC control, CH_2Cl_2). Again 30 ml of toluene and 100 mg (55.2 μmol) of **18c** were added to the crude product **21** and the mixture was heated under reflux for 24 h. The solvent was removed and the residue was separated by flash chromatography starting with CH_2Cl_2 as eluent, whereby 1,2,3,4-tetraphenylbenzene was eluted in front of a green fraction containing unreacted **18c**. After complete elution of the 2nd fraction, CH_2Cl_2/ethyl acetate, 4:1 was used as eluent to obtain **22** as the 3rd fraction. The solvent was removed and the blue-green solid was extracted several times with acetone to achieve further purification. Drying in vacuo furnished 102 mg (55%) of **22**. − IR (KBr) $\tilde{\nu}$ = 2957 cm^{-1}, 2928, 1701, 1653, 1607, 1539, 1522, 1458, 1429, 1389, 1279, 1234, 1205, 1155, 1061, 1030, 1024, 972, 890, 845, 745. − UV/Vis (CH_2Cl_2): λ_{max} = 660 nm, 629, 440 (sh), 392, 288. − ^{1}H NMR ($CDCl_3$) δ = 0.96 (br., 36 H, CH_3), 1.13 (br., 36 H, CH_3), 1.20, 1.28, 1.38, 1.70 (br., 96 H, CH_2), 2.20 (br., 12 H, CH), 2.93, 3.48, 378 (br., 4 H, 2-H), 4.24, 4.32, 4.56, 4.75 (br., 24 H, OCH_2), 6.11, 6.36, 6.58 (br., 4 H, 3-H), 7.63, 7.96, 8.15, 8.24 (br., 12 H, 10-H, 13-H, 18-H), 8.78, 9.31 (br., 4 H, 5-H). − ^{13}C NMR ($CDCl_3$) δ = 10.6, 10.71, 14.2, 14.3, 14.9 (CH_3), 23.2, 24.0, 24.9, 29.4, 29.7, 30.8 (CH_2), 38.4, 38.8, 39.7, 40.4 (CH), 53.7, 55.1, 55.3 (C-2), 70.6, 71.0, 72.0 (OCH_2), 84.1, 85.1 (C-3), 102.5, 103.5, 103.7 103.9, 104.3 (C-10, C13, C-18), 112.3, 112.9 (C-5), 127.7, 129.7, 130.4 (C-6, C-9, C-14, C-17), 136.0, 141.6, 143.3, 143.7, 144.3, 145.0, 145.2, 145.8, (C-4, C-7, C-8, C-15, C-16), 150.6, 151.0 (C-11, C-12, C-19), 205.0 (C-1). − MS (FD); *m/z* (%): 1516.6 (20), 1380.3 (100) [M^+ (**19**)], 1271 (50). − $C_{170}H_{228}N_{16}Ni_2O_{16}$ (2869.1): calcd. C 71.17, H 8.01, N 7.80; found C 68.73, H 7.21, N 7.13.

Mono(*p*-benzoquinone) Adduct PcNi 21: IR (KBr) $\tilde{\nu}$ = 2957 cm^{-1}, 2926, 2856, 1734, 1676, 1653, 1607, 1533, 1481, 1387, 1277, 1221, 1200, 1105, 1061, 898, 857, 750. − UV/Vis (CH_2Cl_2): λ_{max} = 666 nm, 603, 390, 309, 288. − ^{1}H NMR ($CDCl_3$) δ = 0.97, 1.04, 1.11, 1.17 (br., 36 H, CH_3), 1.23, 1.50, 1.80, (br., 48 H, CH_2), 2.03, 2.06 (br., 6 H, CH), 3.24 [br., *exo*], 3.88 [d, br., *endo*] (2 H, 3-H), 4.43 (br., 12 H, OCH_2), 5.84 [br., *endo*], 6.98 [*exo*] (2 H, 1-H), 6.17 [*exo*], 6.28 [*endo*] (2 H, 4-H), 8.40, 8.51, 8.67, (br., 6 H, 11-H, 14-H, 19-H), 8.88, 9.07 (br., 2 H 6-H). − ^{13}C NMR ($CDCl_3$) δ = 11.5, 11.8, 14.2, 14.3 (CH_3), 23.2, 23.3, 24.1, 29.4, 29.7, 30.8, 31.0 (CH_2), 39.8, 40.0 (CH), 49.6 [*endo*], 51.6 [*exo*] (C-3), 71.9 ([br.] OCH_2), 82.9 [*endo*], 85.1 [*exo*] (C-4), 103.8, 104.7 ([br.] C-11, C-14, C-19), 112.2 [*exo*], 113.8 [*endo*] (C-6), 130.2, 131.0 (C-10, C-15, C-18), 135.8 (C-7), 139.4 (C-1), 141.9, 144.2, 145.9, 146.2 (C-5, C-8, C-16, C-17), 151.9, 152.1, 152.3 (12, 13, 20), 196.3 (C-2). − MS (FAB); *m/z* (%): 1488.7 (10) [M^+], 1380.7 (100) [$M^+ - C_6H_4O_2$], 1267.5 (60) [$M^+ - C_6H_4O_2 - C_8H_{17}$]. $C_{88}H_{116}N_8NiO_9$ (1488.6): calcd. C 71.0, H 7.85, N 7.52; found C 68.40, H 7.07, N 6.76.

Mono(naphthoquinone) Adduct PcNi 23: 395 mg (220 μmol) of **18c** and 300 mg (1.9 mmol) of 1,4-naphthoquinone (**8**) were dissolved in 50 ml of toluene (under nitrogen) and heated under reflux for 24 h. The solvent was removed and the residue was separated by

flash chromatography starting with CH_2Cl_2 as the mobile phase. After complete elution of the first two fractions (1,2,3,4-tetraphenylbenzene and unreacted naphthoquinone), a mixture of CH_2Cl_2/ethyl acetate, 4:1 was used as eluent to obtain **23** as the 3rd fraction. Drying in vacuo furnished 260 mg (76%) of **23** as a deep green solid. − IR (KBr) $\tilde{\nu}$ = 2957 cm^{-1}, 2926, 1680, 1605, 1531, 1481, 1460, 1429, 1389, 1381, 1360, 1294, 1277, 1103, 1061, 950, 900, 855, 755. − UV/Vis (CH_2Cl_2): λ_{max} = 668 nm, 603, 390.5, 309.5, 288.5. − ^{1}H NMR ($CDCl_3$) δ = 0.96, 1.06, 1.19, 1.22 (br., 36 H, CH_3), 1.52, 1.68, 1.78 (br., 48 H, CH_2), 2.09 (br., 6 H, CH), 3.42 [br., *exo*], 4.14 [br., *endo*] (2 H, 5-H), 4.39, 4.43, 4.49 (br., 12 H, OCH_2), 6.30 [br., *exo*], 6.38 [br., *endo*] (2 H, 6-H), 6.89 [br., *endo*] (1-H), 7.60 [br., *endo*] (2-H), 7.84 [br., *exo*] (1-H), 8.26 [br., *exo*] (2-H), 8.51, 8.61, 8.68 [br., *exo*] (13-H, 16-H, 21-H), 8.57, 8.65, 8.72 [br., *endo*] (13-H, 16-H, 21-H), 8.90 [br., *endo*] (8-H), 9.17 [br., *exo*] (8-H). − ^{13}C NMR ($CDCl_3$) δ = 11.3, 11.5, 11.6, 11.8, 14.1, 14.2, 14.3 (CH_3), 23.1, 23.2, 23.3, 24.0, 24.2, 29.2, 29.3, 29.7, 30.8, 31.0 (CH_2), 39.8, 40.1 (CH), 50.5 [*endo*], 52.4 [*exo*] (C-5), 68.5, 71.7, 72.0 (OCH_2), 83.3 [*endo*], 85.7 [*exo*] (C-6), 103.7, 104.0, 104.1, 104.6 (C-13, C-16, C-21), 111.31 [*exo*], 114.0 [*endo*] (C-8), 126.2, [*endo*], 127.3 [*exo*] (C-2), 130.1, 130.2, 130.3, 130.6, 130.8, 131.0 (C-9, C-12, C-17, C-20), 133.7 [*endo*], 134.4 [*exo*] (C-1),135.5 [*exo*], 135.7 [*endo*] (C-3), 142.4,142.5, 144.1 144.2, 144.8, 145.6, 145.7, 145.9 (C-7, C-10, C-11, C-18, C-19) 151.7, 151.9, 152.0, 152.3 (C-14, C-15, C-22)194.6 [*endo*], 195.1 [*exo*] (C-4). − MS (FD); *m/z* (%): 1380.5 (100) [$M^+ - C_{10}H_6O_2$]. − $C_{92}H_{118}N_8NiO_9$ (1538.6): calcd. C 71.82, H 7.73, N 7.28; found C 72.84, H 7.49, N 7.36.

Dehydrated Mono(naphthoquinone) Adduct PcNi 25: 42 mg (27.3 μmol) of **23** was dissolved in 40 ml of freshly distilled, dry toluene in a nitrogen-purged vessel and 17 mg (86 μmol) of *p*-toluenesulfonic acid (**24**) was added. The mixture was stirred for 1.5 h at 60°C. Then 1 ml of NEt_3 was added. After 15 min, the solvent was evaporated. Subsequent flash chromatography (SiO_2, CH_2Cl_2) gave after drying in vacuo 37 mg (87%) of **25** as an olive-green powder. − IR (KBr) $\tilde{\nu}$ = 2957 cm^{-1}, 2926, 1672, 1661, 1497, 1458, 1429, 1384, 1364, 1317, 1283, 1211, 1101, 1061, 1028, 966, 860, 756. − UV/Vis (CH_2Cl_2): λ_{max} = 708.5 nm, 680 (sh), 422, 329. − ^{1}H NMR ($CDCl_3$) δ = 1.02, 1.06, 1.08, 1.13, 1.20, 1.24 (br., 36 H, CH_3), 1.54, 1.61, 1.76, 1.88 (br., 48 H, CH_2), 2.06 (br., 6 H, CH), 4.03, 4.28, 4.41 (br., 12 H, OCH_2), 6.97 (br., 2 H, 1-H), 7.43 (br., 2 H, 2-H), 7.49 (s, 2 H, 13-H), 7.86 (s, 2 H, 8-H), 8.17, 8.21, 8.28 (br., 6 H, 6-H, 16-H, 21-H). − ^{13}C NMR ($CDCl_3$) δ = 11.5, 11.6, 14.2, 14.3, 14.4 (CH_3), 23.2, 23.3, 23.4, 23.9, 24.0, 29.3, 29.4, 30.6, 30.8 (CH_2), 39.5, 39.7, 39.9 (CH), 71.9 (OCH_2), 103.5, 103.8, 104.0 (C-13, C-16, C-21), 120.9 (C-8), 125.8 (C-2), 127.3 (C-9), 129.9 (C-6), 130.2 [br.] (C-12, C-17, C-20), 131.7 (C-1), 132.9 (C-3), 133.4 (C-5), 142.0 (C-7), 144.3, 144.7, 145.0 [br.] (C-10, C-11, C-18, C-19), 151.5, 151.7 [br.] (C-14, C-15, C-22), 180.4 (C-4). − MS (FAB); *m/z* (%): 1518.9 (100) [M^+], 1406.9 (40) [$M^+ - C_8H_{17}$]. − $C_{92}H_{116}N_8NiO_8$ (1520.6): calcd. C 72.68, H 7.69, N 7.37; found C 69.07, H 6.69, N 7.29.

Dehydrated Dimer PcNi 26: 32 mg (10.46 μmol) of **22** was dissolved in 30 ml of freshly distilled, dry toluene in a nitrogen-purged vessel and 25 mg (125 μmol) of *p*-toluenesulfonic acid (**24**) was added. The mixture was stirred for 4 h at 65°C. Then 1 ml of NEt_3 was added. After 15 min, the solvent was evaporated. Subsequent flash chromatography (SiO_2, CH_2Cl_2) gave after drying in vacuo 22 mg (68%) of **25** as an olive-green powder. − IR (KBr) $\tilde{\nu}$ = 2957 cm^{-1}, 2928, 1695, 1684, 1653, 1616, 1497, 1458, 1427, 1362, 1273, 1204, 1155. 1097, 1061, 991, 854, 750, 737. − UV/Vis (CH_2Cl_2): λ_{max} = 730 nm (sh), 681, 333, 287. − ^{1}H NMR ($CDCl_3$) δ = 0.91, 1.05, 1.15 (br., 72 H, CH_3), 1.40−2.0 (br., 96 H, CH_2), 2.0−2.3 (br., 12 H, CH), 4.54 (br., 24 H, OCH_2), 8.10, 8.50, 8.71, 8.92 (br., 20 H, 3-H, 5-H, 10-H, 13-H, 18-H). − ^{13}C NMR ($CDCl_3$) δ = 10.9, 11.4, 13.8, 14.1 (CH_3), 20.5, 22.7, 23.1, 23.6, 28.8, 29.3, 29.5, 30.2, 30.8 (CH_2), 39.0, 39.8 (CH), 71.7, 72.0 (OCH_2), 104.6 [br.] (C-10, C-13, C-18), 122.0 [br.] (C-5), 129.5−131.2 [br.] (C-2, C-3, C-9, C-14, C-17), 144.5−145.2 [br.] (C-4, C-6, C-7, C-8, C-15, C-16), 152.0, 152.7 (C-11, C-12, C-19), 199.3 (C-1). − MS (FAB); *m/z* (%): 2682.0 (10), 2412.1 (20), 2057.7 (10). − $C_{170}H_{224}N_{16}Ni_2O_{14}$ (2833.1): calcd. C 72.07, H 7.97, N 7.91; found C 69.42, H 7.28, N 7.36.

Acknowledgments

B. H. thanks the Stiftung Stipendien-Fonds des Verbandes der Chemischen Industrie for a Doktoranden-Stipendium.

[1] B. Hauschel, P. Stihler, M. Hanack, *Trends Polym. Sci.* **1996**, *4*, 348−354.
[2] P. Gomez-Romero, Y.-S. Lee, M. Kertesz, *Inorg. Chem.* **1988**, *27*, 3672−3675.
[3] [3a] M. Rack, M. Hanack, *Angew. Chem.* **1994**, *106*, 1712−1715; *Angew. Chem. Int. Ed. Engl.* **1994**, *33*, 1646−1648. − [3b] B. Hauschel, D. Ruff, M. Hanack, *J. Chem. Soc., Chem. Commun.* **1995**, 2449−2451. − [3c] B. Hauschel, P. Stihler, M. Hanack, *Synth. Met.* **1997**, *84*, 439−440.
[4] [4a] A.-D. Schlüter, *Adv. Mater.* **1991**, *3*, 282−291. − [4b] S. Wegener, K. Müllen, *Macromolecules* **1993**, *26*, 3037−3040.
[5] [5a] L. F. Fieser, M. J. Haddadin, *Can. J. Chem.* **1965**, *43*, 1599−1606. − [5b] J. Luo, H. Hart, *J. Org. Chem.* **1988**, *53*, 1341−1343. − [5c] B. Schlicke, H. Schirmer, A.-D. Schlüter, *Adv. Mater.* **1995**, *7*, 544−546.
[6] C. Feucht, T. Linßen, M. Hanack, *Chem. Ber.* **1994**, *127*, 113−117.
[7] M. Rack, B. Hauschel, M. Hanack, *Chem. Ber.* **1996**, *129*, 237−242.
[8] M. J. Cook, A. J. Dunn, S. D. Howe, A. J. Thomson, K. J. Harrison, *J. Chem. Soc., Perkin Trans. 1* **1988**, 2453−2458.
[9] M. Hanack, B. Hauschel, P. Stihler, M. Rack, T. Linßen, *Mat. Res. Soc. Symp. Proc.* **1996**, *413*, 465−470.
[10] K. Blatter, A.-D. Schlüter, *Chem. Ber.* **1989**, *122*, 1351−1356.
[11] [11a] N. B. McKeown, I. Chambrier, M. J. Cook, *J. Chem. Soc., Perkin Trans. 1* **1990**, 1169−1177. − [11b] T. G. Linssen, K. Dürr, M. Hanack, A. Hirsch, *J. Chem. Soc, Chem. Commun.* **1995**, 103−104. − [11c] T. G. Linßen, M. Hanack, *Chem. Ber.* **1994**, *127*, 2051−2057. − [11d] G. Schmid, M. Sommerauer, M. Geyer, M. Hanack in *Phthalocyanines: Properties and Applications*, vol. 4 (Eds.: C. C. Leznoff, A. B. P. Lever), VCH, New York, **1996**, p. 5.
[12] M. Rack, Ph. D. Thesis, Eberhard-Karls-Universität Tübingen, **1994**.
[13] M. Hanack, A. Gül, A. Hirsch, B. K. Mandal, L. R. Subramanian, E. Witke, *Mol. Cryst. Liq. Cryst.* **1990**, *187*, 365−382.
[14] P. Stihler, B. Hauschel, M. Hanack, *Chem. Ber.* **1997**, *130*, 801−806.
[15] S. Rodriguez-Morgade, M. Hanack, *Chem. Eur. J.* **1997**, *3*, 1042−1051.

Received August 28, 1997
[I97201]

Conformational Analysis of Seven-Membered Ring Chelates, 1

Conformations and Dynamic Behaviour of Rhodium Complexes with 1,4-Bis(diphenylphosphanyl)butane, DIOP and Its HO Analogue

Renat Kadyrov,*[a] Armin Börner,[a] and Rüdiger Selke[a]

Keywords: Conformation analysis / Molecular modelling / NMR spectroscopy / Seven-membered chelates / Rhodium / Ab initio calculations

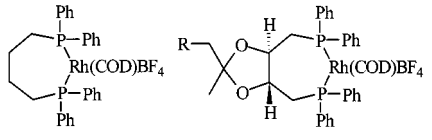
The temperature dependence of NMR spectra of $[(L)Rh(cod)]BF_4$ complexes with L = dppb (**1**), (*R*,*R*)-diop (**2**) and (*R*,*R*)-HO-diop (**3**) has been examined. Molecular mechanics and ab initio calculations on the [{1,4-bis(dimethylphosphanyl)butane}Rh^+(diolefin)] complex predict local energy minima for all twist-chair (TC_1, TC_2 = TC_7, TC_3 = TC_6, TC_4 = TC_5) and two boat (B_3 = B_6 and TB_1) conformations. Furthermore, ab initio calculations at the B3LYP/6-31G(d)/LANL2DZ level show that two minima are located in the wide-open region between the TC_7 and C_4 conformations. Relative B3LYP/6-31G(d) energies of the B_3, TC_1 and {C_4-TC_7} conformations are 0.0, 0.71 and 0.97–1.08 kcal mol^{-1}, respectively. Analysis of crystallographic data contained in the Cambridge Structural Database shows that the majority of structures are concentrated in the region {C_4-TC_7} and close to B_3. The symmetrical doublet in the ^{31}P-NMR spectra is assigned to the fast equilibrium {TC_7-C_4} ⇌ TC_1 ⇌ {C_5-TC_2}. The resonances of the other species are consistent with B_3 = B_6 geometry. A fused dioxolane ring forces the chelate in diop complexes to adopt the B_4 = B_5 conformation. For both types of ligand the chair-like conformation is enthalpically preferred at low temperatures ($\Delta H°$ = 0.45–0.46 kcal mol^{-1}), whereas the boat-shaped structure predominates at temperatures above 200 K ($\Delta S°$ = 0.9–1.3 cal K^{-1} mol^{-1}). Line-shape analysis provides a boat pseudorotation barrier for complex **1** of $\Delta G^{\neq}$ = 5.9 kcal mol^{-1} and for **2** $\Delta G^{\neq}$ = 5.3 kcal mol^{-1} at 184 K. The free energy of activation at this temperature for the boat–chair interconversion is $\Delta G^{\neq}$ = 8.6 kcal mol^{-1} for complex **1** and $\Delta G^{\neq}$ = 8.0 kcal mol^{-1} for complex **2**.

Introduction

Chelating bis(phosphane) ligands play a dominant role in metal-catalyzed stereoselective syntheses.[1] The relationship between catalyst conformation and the product configuration is well established. In general, the observed asymmetric induction is attributed to discriminatory interactions between substrate and bulky phosphane substituents adjusted by the chiral conformation of the chelate.[2] In particular, asymmetric hydrogenation catalyzed by cationic rhodium complexes containing chiral phenyl-substituted five-membered bis(phosphane) chelates is one of the most intensively investigated stereoselective reactions. The generally accepted basis for the enantioselectivity is the concept of pseudo axial−equatorial arrangement of the *P*-phenyl groups based on the "edge-to-face" model.[3] The configuration of the hydrogenation product is determined by the δ or the λ conformation of the five-membered ring.[4]

Complexes based on seven-membered bis(phosphane) chelates hydrogenate with higher reaction rates. The enhanced catalytic activity is associated with the high degree of conformational flexibility of the chelate ring. Only very few solution-NMR studies on seven-membered chelate conformations have been performed.[5] Although the crystallographic data show that these chelates may adopt some non-symmetrical conformations,[6] recent NMR results have been interpreted in terms of C_2-symmetrical geometries.[5a,7] Accordingly, idealized C_2-symmetrical twist-chair and twist-boat conformations were involved in mechanistic considerations on the origin of the stereoselectivity.[4b,8]

We examined the conformations and dynamic behaviour of seven-membered chelate rings of three complexes $[(L)Rh(cod]BF_4$ with L = 1,4-bis(diphenylphosphanyl)butane (**1**), (*R*,*R*)-diop (**2**) and (*R*,*R*)-HO-diop (**3**); cod = 1,5-*cis*-cyclooctadiene (Scheme 1).



1 (dppb) **2** R = H (diop) **3** R = OH (HO-diop)

Scheme 1

First, we calculated all basic conformations of the chelate ring by applying a simple MMX force field. The results of these calculations were used as input for ab initio calculations at the B3LYP/6-31G(d)/LANL2DZ level. X-ray data available from the Cambridge Structural Database were analyzed to verify the predicted favoured conformers. Low-temperature NMR spectroscopy was used to obtain infor-

[a] Institut für Organische Katalyseforschung an der Universität Rostock e.V.
Buchbinderstraße 5−6, D-18055 Rostock, Germany
Fax: (internat.) + 49(0)381/4669324
E-mail: renat.kadyrov@ifok.uni-rostock.de

 © WILEY-VCH Verlag GmbH, D-69451 Weinheim, 1999 1434−1948/99/0404−0705 $ 17.50+.50/0

mation about the conformers present in solution and their dynamic properties.

Results

Conformations of the Seven-Membered Chelate Rings — Computed versus Experimental Structures

Molecular mechanics calculations have been used to establish the main conformational features of cycloheptane and some seven-membered heterocycles.[9] Calculations based on empirically determined potential functions were also successfully applied to the solution of structural problems of the coordination chemistry[10] especially of square-planar transition-metal complexes.[11] Recently, some reports demonstrated the utility of the molecular modeling program PCMODEL for determining minimum-energy structures of a variety of flexible complexes.[12] For the following discussion we use the notation for conformations introduced by Hendrickson,[13] labelling the position of the metal as 1.

In order to reduce the independently varied parameters, we have involved the corresponding dimethylphosphanyl derivative in the calculations. The structure of [{1,4-bis(dimethylphosphanyl)butane}Rh^+(cod)] = [(dmpb) Rh^+(cod)] was constructed by use of PCMODEL 4.0 with the parameter set and interactions described in the Experimental Section. At first, we carried out a series of calculations to search all relative low-energy local minima. For identification the conformations were analyzed in terms of ring-puckering coordinates. These coordinates (q_2, q_3, ϕ, ψ) were calculated from the Cartesian coordinates according to the original Cremer−Pople method.[14] The puckering amplitudes q_i were replaced by the total puckering amplitude Q and the angle θ:

$$q_2 = Q \cos \theta$$
$$q_3 = Q \sin \theta$$

The angle θ specifies the relative contribution of boat- and chair-like conformations. The chair-twist-chair family has for cycloheptane a θ value of about 66°. Boat-twist-boat conformers are characterized by $\theta \approx 0°$.[15] The minimization procedures gave four different twist-chair conformations (TC_1, $TC_7 = TC_2$*, $TC_6 = TC_3$*, $TC_5 = TC_4$*) and two boat forms (TB_1 and distorted $B_3 = B_6$*), where $TC_7 = TC_2$* means that TC_2 is enantiomeric to TC_7. The calculated energies and geometries of conformers are summarized in Table 1. The twist-chair conformations are connected by a pseudorotation pathway as are the twist-boat conformations. Figures 1 and 2 display the energy profiles in the course of pseudorotation. The calculation of the energy variation along the pseudorotation pathways is detailed in the Appendix.

The geometries determined using MMX force fields for these conformers were used as starting points for the ab initio calculations of the [(dmpb) $Rh^+(C_2H_4)_2$]. For all six conformers, full geometry optimizations were done at the B3LYP/6-31G(d)/LANL2DZ level. The calculated energies and geometries of conformers are given in Table 1. These calculations also indicate the B_3 structure to be of lowest energy with the TC_1 structure only 0.71 kcal mol^{-1} higher in energy. Since the pseudorotation $TC_7 \rightleftharpoons C_4 \rightleftharpoons TC_1$ changes mainly the P−Rh torsion angle (see Appendix), it is expected that the behaviour of the potential energy curve in this region is affected by electronic interactions of the phosphane moiety with the metal centre. Therefore, we examined the potential energy surface along the TC_7 to TC_1 pseudorotation at the B3LYP/6-31G(d) level. At first, partial geometry optimization was performed for C_4 (at ϕ = 50°) conformation with fixed cyclic Rh−P torsion angle. Full optimization, in the next step, led to the additional minimum at ϕ = 30° (distorted C_4). Furthermore, the spline interpolation gave a nearly flat potential-energy curve for the $TC_7 \rightleftharpoons C_4 \rightleftharpoons TC_1 \rightleftharpoons C_5 \rightleftharpoons TC_2$ pseudorotation.

Table 1. Puckering coordinates[a] of optimized molecular geometries and calculated relative energies[b] for [(dmpb)Rh^+(cod)] at the MMX level and for [(dmpb) $Rh^+(C_2H_4)_2$] at the B3LYP/6-31G(d)/LANL2DZ level

Conformation	Method	Q	θ	ϕ	ψ	ΔE
Distorted B_3	MMX	1.51	9.1	29.1	10.5	0
	B3LYP	1.47	8.6	30.1	9.5	0
TB_1	MMX	1.15	11.1	90	90	5.69
	B3LYP	1.17	4.1	90	90	6.38
TC_7	MMX	1.19	49.5	13.2	49.2	2.22
	B3LYP	1.12	48.4	12.4	50.9	1.08
TC_1	MMX	0.97	53.5	90	90	2.27
	B3LYP	0.88	56.1	90	90	0.71
Distorted C_4	B3LYP	1.02	52.3	29.9	60.3	0.97
TC_6	MMX	1.08	38.9	−64.9	37.3	3.22
	B3LYP	1.21	45.5	-49.5	27.8	3.44
TC_5	MMX	1.03	43.2	-134.1	7.4	3.50
	B3LYP	1.00	31.5	-142.0	8.8	1.85

[a] Q in Å and θ, ϕ, ψ in°. − [b] In kcal mol^{-1}.

MMX and B3LYP calculations indicate that the most stable conformer is boat-shaped, and is represented in the energy hypersurface by a large well between canonical B_3 and TB_4 geometries. For clarity, we define this conformer as distorted B_3. The C_2-symmetrical TB_1 form, mostly mentioned in the literature, is 6.4 kcal mol^{-1} above. Pseudorotation $B_3 \rightleftharpoons B_6$ proceeds via B_1 and requires, according to the MMX molecular mechanics model, an activation energy of 5.5 kcal mol^{-1}. In the next family three low-energy chair forms, TC_7, distorted C_4 and TC_1, are separated by very low barriers. The barrier to the succeeding TC_6 at the molecular mechanics level is not as high as 3 kcal mol^{-1}, whereas TC_6 and TC_5 are separated by a barrier of approximately 7 kcal mol^{-1}. Therefore, conformation $TC_5 = TC_4$ should be distinguishable in the low-temperature NMR spectra from the fast equilibrium $TC_6 \rightleftharpoons TC_7 \rightleftharpoons TC_1 \rightleftharpoons TC_2 \rightleftharpoons TC_3$. Note that barrier calculations using the MMX model reflect exclusively steric and electrostatic influences of the inorganic unit of the molecule and give large deviations from those calculated by ab initio methods if substantial electronic interactions with the metal centre come into play.

We have analyzed the conformational preferences of the seven-membered chelate rings with 1,4-diphosphanylbutane fragments using crystallographic data collected in the Cambridge Structural Database (CSD).[16] There are 51 structures containing M(dpb) and M(diop) fragments, where M = transition metal of group VI−VIII and dpb = 1,4-diphosphanylbutane. Crystallographic data for these structures were saved in FDAT format and then the Cartesian coordinates of the chelating seven-membered ring were extracted. Puckering coordinates (Q, θ, ϕ, ψ) were calculated according to the procedure outlined above. 37 unique fragments present in the crystal structures are characterized by θ = 45−67° and can be identified as chair-like structures. Figure 1b displays scatter plots of phase angles ϕ, ψ for these fragments and projections of a pseudorotation map for the chair-twist-chair forms of cycloheptane. The majority of structures are concentrated in the region between two neighbouring cycloheptane conformations {C_4-TC_7} and only one of them exists in the TC_1 conformation.[28] The most obvious consequence is that the preferred chair-like conformation of the metal chelates with a diphosphanylbutane fragment located between the C_4 and TC_7 forms. Evidently, the shape of this conformation depends on the metal and nature of the co-ligands. Several structures were found in TC_5 and TC_6 conformations indicating the stabilization of these conformations in accordance with the theoretical calculations.

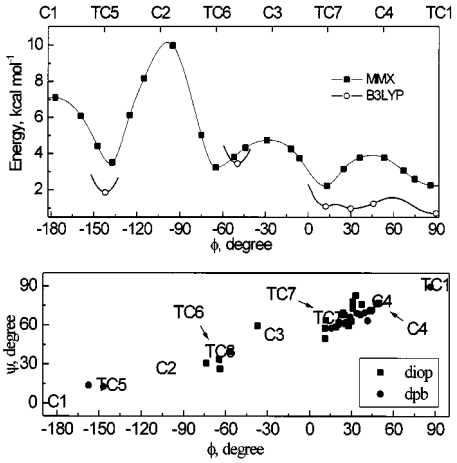


Figure 1. (a) (top) Relative MMX energy as a function of chair ⇌ twist-chair pseudorotation phase ϕ for [(dmpb)Rh^+(cod)] and relative energies of the B3LYP/6-31G(d)/LANL2DZ optimized geometries for [(dmpb) $Rh^+(C_2H_4)_2$]; (b) (bottom) scatter plot of pseudorotation phases ϕ, ψ for transition metal complexes bearing 1,4-diphosphanylbutane (●) or diop (■) fragments contained in CSD and projection of pseudorotation map for the chair ⇌ twist-chair forms of cycloheptane

The next 25 fragments are specified by θ = 3−11° and, therefore, may be assigned to the boat-like conformation. The structures on the scatter plot (Figure 2) are distributed in the regions of B_5−TB_6 conformations for the diop chelates and between B_3−TB_4 canonical forms for the chelates without rigid backbone. In this case, the calculations show satisfactory agreement with the structural information obtained by X-ray analysis. Since θ ≈ 0°, only ϕ defines the conformations in the boat family and the pseudorotation path is just a function of ϕ. Thus, one has to expect only one stable boat-shaped form for the seven-membered ring chelates, which can be represented as distorted B_3 for dpb. Although the twist-boat is more stable than the boat, introduction of the heteroatomic P−M−P fragments into the cycloheptane ring avoids some H/H bond eclipsing in the B_3 conformation. On the other hand, a large difference in the bond lengths forces the heterocyclic seven-membered ring out of its canonical boat and twist boat forms.

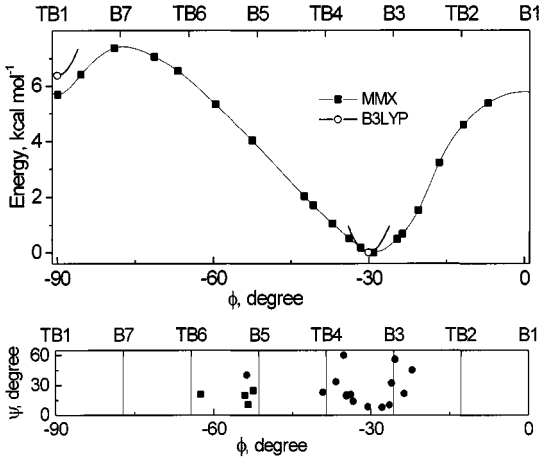


Figure 2. (a) (top) Relative MMX energy as a function of twist-boat ⇌ boat pseudorotation phase ϕ for [(dmpb)Rh^+(cod)] and relative energies of the B3LYP/6-31G(d)/LANL2DZ optimized geometries for [(dmpb) $Rh^+(C_2H_4)_2$]; (b) (bottom) scatter plot of pseudorotation phases ϕ, ψ for transition metal complexes bearing 1,4-diphosphanylbutane (●) , diop (■) fragments contained in CSD and projection of pseudorotation map for the twist-boat ⇌ boat forms of cycloheptane

Complexes bearing chiral diop-type ligands provide an interesting example of the *trans* fusion of a dioxolane ring to a seven-membered chelate ring. According to Hendrickson,[9a] *trans* fusion of cyclopentane to cycloheptane should be most favoured at either 2e-3e or 3e-4e of the twist chair that correspond to the 4e-5e-TC_6 and 4e-5e-TC_7 conformations in our definition. In fact, most structures examined by X-ray analysis reveal a 4e-5e-{C_4-TC_7} conformation and several structures were found in a 4e-5e-TC_6 conformation, as illustrated in Figure 1. The *trans* fusion across the 4−5 bond to the B_3 = B_6* conformation requires 4a-5e or 4e-5a orientation with a fusion angle of approximately 120° and, thus, would strain the system. On the contrary, the B_4 = B_5* conformation allows an energetically more favourable fusion at the 4e-5e position. This conformer is likely to be the most stable boat-shaped form of the diop chelates (Figure 2).

Variable-Temperature NMR Studies of Complexes

The Rh^I complexes with dppb (**1**), (*R*,*R*)-diop (**2**) and (*R*,*R*)-HO-diop (**3**) exhibit temperature-dependent NMR spectra. The sharp doublet in the $^{31}P\{^1H\}$-NMR spectrum of **2** in a mixture of $CHCl_2F/CD_2Cl_2$ (3:1) at 250 K (Figure 3) undergoes coalescence at approximately 188 K as the

sample is cooled. Two doublets separate below 179 K in a 1:0.45 intensity ratio, similar to those briefly described by Brown and Chaloner.[7]

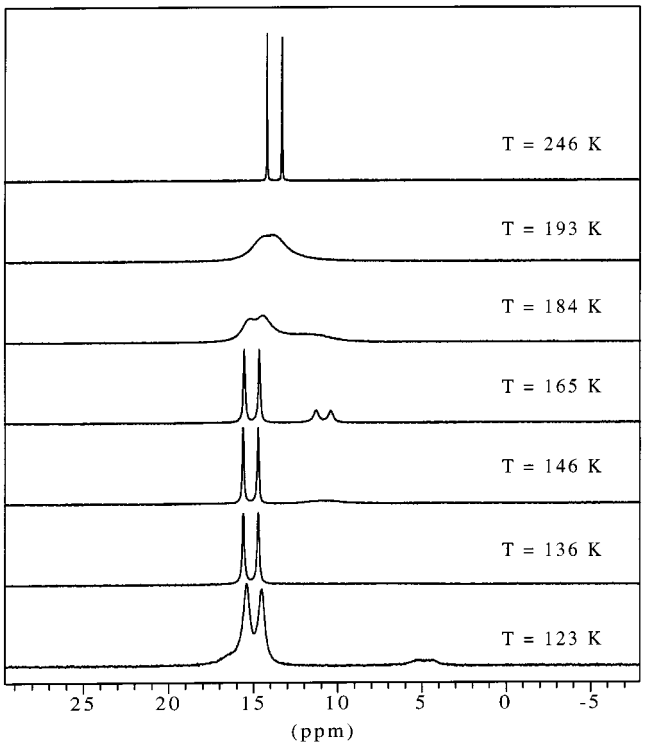


Figure 3. Variable-temperature $^{31}P\{^1H\}$-NMR spectra of complex **2** in $CD_2Cl_2/CHFCl_2$

While the downfield doublet at a chemical shift of δ = 14.7 due to the major isomer **A** sharpens as the temperature is lowered further, the upfield signals at δ = 10.5 of isomer **B** broaden and then separate below 123 K into two broad signals with Rh coupling at $\delta \approx 5.2$ and 15.9. The variable-temperature spectra of the complexes **1** and **3** show the same behaviour as for **2**, if one takes into account that the phosphorus atoms in **3** are diastereotopically not equivalent. The low-temperature ^{31}P-NMR data are included in Table 2. It is noteworthy that the resonances of the major species **A** in complex **1** are shifted to lower field compared to that in **2** and **3**. However, those of the minor species **B** in complex **1** exhibit significantly larger differences in chemical shifts than those in compounds **2** and **3**.

Structural Assignment of the Exchanging Sites in Solution

Detailed variable-temperature NMR studies of [(diop-4NMe$_2$)PtCl$_2$] confirmed that the species characterized at low temperature by a downfield phosphorus resonance has a rigid conformation with C_2 symmetry.[5a] The upfield signal broadens significantly as the temperature is lowered further. This indicates the flexibility of this species and that the C_2 symmetry is time-averaged.[5a] These results are in accordance with our observations of ^{31}P-NMR spectra of complexes **2** and **3**. Inspection of the X-ray data for [(HO-diop)Rh(cod)]BF$_4$ reveals two conformations for the seven-membered chelate in the solid state.[17] One of the ring conformations can be described as C_4 chair and the other as distorted B_5 boat (Figure 4).

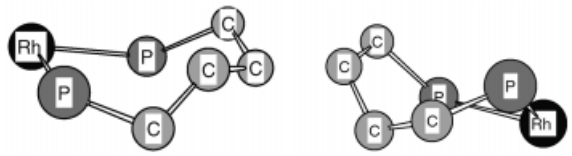


Figure 4. View of two chelate ring conformations as present in crystalline complex **3**: C_4 (left) and distorted B_5 (right)

Therefore, we assign the AMX pattern of the isomer **B** in the spectra of **2** and **3** at 123 K to the dissymmetric distorted B_5 structure which undergoes pseudorotation with an appreciable barrier to give a symmetrized doublet above 155 K. Note that the pseudorotation segment $C_5 \rightleftharpoons TC_1 \rightleftharpoons C_4$ connects two enantiomeric chair forms. According to the consideration in the first section this pseudorotation should be almost completely free. The symmetrical doublet at δ = 15 of the isomer **A** may be assigned to this fast equilibrium, because two phosphorus atoms remain equivalent just at very low temperatures. The dynamic phenomenon observed in the ^{31}P-NMR spectra between 210 K and 180 K is caused by the interconversion of two families of conformations. These assignments are consistent with recent solution-NMR investigations of similar compounds.[5a]

By analogy, it appears reasonable to assign the twist-chair conformation to the species **A** in the conformational equilibrium of the complex without a rigid backbone. The low-field shift of the **A** resonances in the case of complex **1** in comparison with those of complexes **2** and **3** is caused by other twist-chair conformations being appreciably popu-

Table 2. $^{31}P\{^1H\}$-NMR data of the complexes in $CD_2Cl_2/CHFCl_2$[a,b]

Complex	T [K]	P(**A**)	P_1(**B**)	P_2(**B**)
1	246		25.18 (J_{RhP} = 143.2)	
	124	27.84 (J_{RhP} = 141.6)	7.77 (J_{RhP} = 138)	39.57 (J_{RhP} = 146)
2	246		13.08 (J_{RhP} = 143.9)	
	126	14.95 (J_{RhP} = 143.8)	4.82 (J_{RhP} = 142)	16.37 (J_{RhP} = 142)
3	246		12.57 (J_{RhP} = 143.95)	
	135	14.17 (J_{RhP} = 143.0) 14.69 (J_{RhP} = 142.9) (J_{PP} = 39.0)	ca. 4−6	ca. 15−16

[a] Chemical shifts relative to H_3PO_4, coupling constants in Hz. − [b] J_{PP} could not be derived from the broad lines in the spectra.

lated in the fast conformational equilibrium. According to X-ray data the chelate ring in complex **1** has a B_3-shaped structure in the solid state.[18] Based on these data we assign the B_3-like conformer to the species **B** in solution. Evidently, this B_3-shaped moiety exhibits a much larger difference in chemical shifts than the B_5-like geometry.

Thermodynamic and Kinetic of Exchange

The equilibrium constants $K = [\mathbf{B}]/[\mathbf{A}]$ for the $\mathbf{A} \rightleftharpoons \mathbf{B}$ interconversion for the complexes **1** and **2** have been calculated at different temperatures by ^{31}P-NMR integration. The evaluated energy differences $\Delta G^\circ = -RT \ln K$ have been plotted against T giving a satisfactory linear least-squares fit (Figure 5). Linear-regression analysis of these data allows calculation of the enthalpy and entropy values which are shown in Table 3. The obtained values for ΔS° suggest that the boat-shaped conformation has a substantially higher entropy than the chair-like and is predominant at higher temperatures.

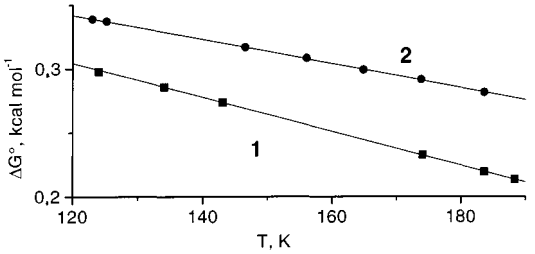


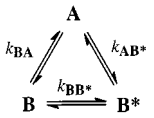
Figure 5. Plots of ΔG° vs. temperature obtained by $^{31}P\{^1H\}$-NMR integration for complexes **1** (■) and **2** (●)

Table 3. Thermodynamic and kinetic data for the complexes[a,b]

Complex	**1**	**2**
ΔG°_{AB}	0.22	0.28
ΔH°_{AB}	0.45 ± 0.02	0.46 ± 0.02
ΔS°_{AB}	1.3	0.9
$\Delta G^{\neq}_{AB}$	8.6	8.0
$\Delta H^{\neq}_{AB}$	8.4 ± 0.1	7.6 ± 0.2
$\Delta S^{\neq}_{AB}$	1.5 ± 1	3 ± 1
$\Delta G^{\neq}_{BB'}$	5.9	5.3
$\Delta H^{\neq}_{BB'}$	6.0 ± 0.1	5.9 ± 0.1
$\Delta S^{\neq}_{BB'}$	−1 ± 1	−3 ± 1

[a] ΔG and ΔH in kcal mol^{-1}, ΔS in cal mol^{-1} K^{-1}. – [b] All ΔG are given at 184 K.

By application of WIN-DYNAMICS,[19] spectra were simulated and iteratively fitted to the experimental spectra in order to evaluate the rate constants at various temperatures. The line-shape analysis was performed on the basis of the three-site exchange model (Scheme 2).



Scheme 2. Three-site exchange

The resulting rate constants as a function of the temperature were used to construct an Eyring plot (Figure 6). The activation parameters obtained from linear regression analysis are given in Table 3. The activation entropies are close to zero. The values of activation energy $\Delta G^{\neq}$ for complex **2** are lower than those found for complex **1**.

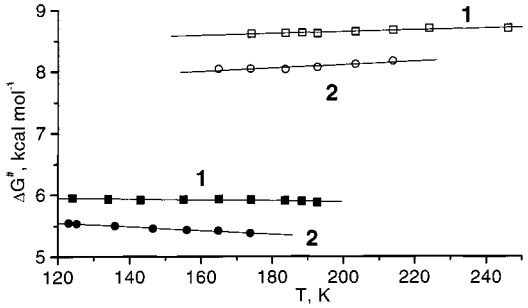


Figure 6. Eyring plots of $\Delta G^{\neq}$ vs. temperature from the kinetic data for compexes **1** (□, ■) and **2** (○, ●); the open symbols are the data for the $\mathbf{B} \rightleftharpoons \mathbf{A}$ exchange and the closed ones for the $\mathbf{B} \rightleftharpoons \mathbf{B}$ exchange

Discussion

NMR investigations by Brown and Chaloner[7] show the conformational flexibility of the seven-membered diop chelate ring. A dynamic equilibrium between at least two different basic conformers was manifested. Activation energies between 9.6 to 11.7 kcal mol^{-1} were obtained for Pt, Pd and Ni complexes at 220−250 K.[7][20] We have found activation energy values $\Delta G^{\neq}$ of the boat-to-chair interconversion of 8.6 kcal mol^{-1} in complex **1** and 8.0 kcal mol^{-1} in **2** at 184 K. These values are comparable with the barrier for chair-to-boat interconversion of about 8.5 kcal mol^{-1} in cycloheptane.[9c,21] The lower inversion barrier in the diop complex is in accordance with the diminished cyclohexane interconversion barrier by fusion with a cycloheptane ring and reflects increasing strain energy in the ground state.[22]

Nevertheless, the experimentally observed C_2 symmetry of the chair conformation is apparently time-averaged. The ab initio calculations show that part of a family of flexible conformers $TC_7 \rightleftharpoons C_4 \rightleftharpoons TC_1 \rightleftharpoons C_5 \rightleftharpoons TC_2$ form a large potential well with minima separated by very low barriers. This explains why X-ray studies show in most cases an unsymmetrical C_4 or TC_7 conformation,[6] but low-temperature NMR studies reveal C_2-symmetrical species. The pseudorotation in the boat family proceeds with higher activation energy. The observed barriers are 5.9 kcal mol^{-1} for **1** and 5.3 kcal mol^{-1} for **2**. These are much higher than calculated for cycloheptane (0.5 kcal mol^{-1}),[15] but are in surprisingly good accordance with that calculated using a simple MMX model for [(dmpb)Rh$^+$(cod)] (5.5 kcal mol^{-1}). Note that for diop-type chelates pseudorotation $B_4 \rightleftharpoons B_5$ proceeds via TB_1.

In fact, entropy favours the boat form, whereas the chair-like conformation is enthalpically stabilized and predominates at 124 K by only $\Delta G^\circ = 0.30$ kcal mol^{-1} in complex **1** and by $\Delta G^\circ = 0.34$ kcal mol^{-1} in **2**. Because of the coun-

tertrend of $\Delta H°$ and $\Delta S°$ there is a cross-over of the equilibrium constant K = [**B**]/[**A**] at about 180−200 K. Above that temperature the boat conformation is more stable. The relatively large magnitude of the entropy difference $\Delta S°$ = 0.9−1.3 cal K^{-1} mol^{-1} comes as somewhat of a surprise. On the other hand, the error in the $\Delta S°$ determination consists of the inaccuracy in temperature determination and the error of integration of the broadened lines in the NMR spectra at low temperatures. We could not ascertain the exact source of the error. Thus, the given values of ΔS should be taken with care.

We can conclude that seven-membered diphosphane chelates exist in two conformations, chair- and boat-like, with the position of equilibrium depending on the temperature. The $\{TC_2\text{-}C_5\}$ = $\{TC_7\text{-}C_4\}$ structure represents the enthalpically most stable conformation and undergoes pseudorotation readily. The other conformer has the distorted B_3 = B_6 geometry for dppb and distorted B_4 = B_5 arrangement for diop chelates. This moiety undergoes a conformational inversion with a higher barrier.

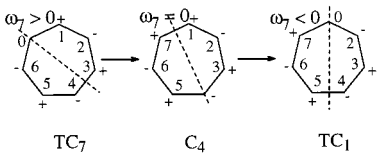
Experimental Section

General Remarks: All solvents were freeze-pump-thaw-degassed using a vacuum line and stored under argon. The diolefin complexes [(dppb)Rh(cod)]BF_4 and [(diop)Rh(cod)]BF_4 were prepared by standard methods from ligand and [(acac)Rh(cod)] by treatment with HBF_4.[23] The preparation of [(HO-diop)Rh(cod)]BF_4 has been previously described.[24] The NMR samples were prepared under an inert gas and the solvents were transferred under vacuum. The solution was degassed with one freeze-pump-thaw cycle and then the tube was sealed. − The NMR spectra were recorded with a Bruker ARX400 spectrometer. The ^{31}P chemical shifts are reported in δ units relative to H_3PO_4. The temperature of the NMR probe was calibrated using a methanol temperature standard and the low-temperature range by extrapolation of the difference in chemical shifts of CHF_2OH in ^1H-NMR spectra.

Molecular Mechanics Calculations: Except where noted, the molecular mechanics parameters were set to the PCMODEL[25] default values. The force field about the metal ion was designed so that the metal−ligand distances and the ligating atom−ligating atom interactions determined the shape of the coordination sphere. Default bending force constant for ideal P−Rh−P angle of 90° in a square-planar geometry was used. All other metal-dependent interactions were treated exactly as in a points-on-a-sphere approach.[26] This was accomplished by setting the L−Rh−L angle parameters, and L−Rh−L−A and Rh−L−A−B torsional parameters to zero.

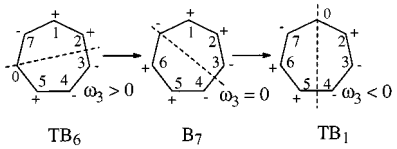
Ab Initio Calculations: All calculations were performed using the B3LYP hybrid functional. The full geometry optimizations have been carried out with LANL2DZ basis for rhodium, associated with the relativistic effective core potential, and the 6-31G(d) basis set for all other atoms. The calculations were performed with the program GAUSSIAN 94.[27]

Appendix: To calculate the energy along a pseudorotation path note that the sequence $TC_i \rightarrow C_{i-3} \rightarrow TC_{i+1}$ represents the elementary steps in the chair pseudorotation. Moreover, bond dihedral angles ω_i in one TC_i conformation change sign going on to the next TC_{i+1} conformation in the pseudorotation sequence as shown in Scheme 3.



Scheme 3. Sequence of the elementary steps in the chair pseudorotation

In addition, signs of the out-of-plane displacements (z coordinates) of each cyclic atom are drawn here for visual representation of conformation. The sequence $TB_i \rightarrow B_{i+1} \rightarrow TB_{i+2}$ constructs a pseudorotation in a boat family (Scheme 4).



Scheme 4. Sequence of the elementary steps in the boat pseudorotation

Therefore, each intermediate form between two twisted forms is unequivocally defined by a corresponding torsional angle. That is ω_i for the $TC_i \rightarrow TC_{i+1}$ movement and ω_{i+4} for the $TB_i \rightarrow TB_{i+2}$ conversion. Starting at the value of the initial twisted form the magnitude of ω was incremented (decremented) in 5° or 10° steps until the next twisted conformation was reached and the conformation of minimum energy was found for each given value of ω. The Cartesian coordinates of the optimized (by keeping ω constant) geometries were transformed into the puckering coordinates. The energies thus obtained for each value of ω were plotted against a phase angle ϕ and connected by an interpolation curve to give cuts of the energy surface along the pseudorotation tracks between two of each twisted forms. These cuts were combined in common plots for chair and boat pseudorotations, as shown in Figures 1 and 2.

Acknowledgments

The authors thank the Max-Planck-Gesellschaft, the BMBF (Förderkennzeichen 03D0053C5) and the Fonds der Chemischen Industrie for financial support, Dr. Shigehiro Yamaguchi for providing X-ray structure data and Dr. G. Stark for helpful discussions.

[1] H. Brunner, W. Zettlmeier *Handbook of Enantioselective Catalysis with Transition Metal Compounds*, vol. 2, Ligands − References, VCH Verlagsgesellschaft, Weinheim, **1993**, p. 359.

[2] [2a] M. D. Fryzuk, B. Bosnich, *J. Am. Chem. Soc*. **1978**, *100*, 5491−5494. − [2b] D. A. Slack, I. Greveling, M. C. Baird, *Inorg. Chem.* **1979**, *18*, 3125−3132. − [2c] P. A. MacNail, N. K. Roberts, B. Bosnich, *J. Am. Chem. Soc*. **1981**, *103*, 2273−2280. − [2d] B. Bosnich, N. K. Roberts *Adv. Chem. Ser.* **1982**, *196*, 337−354. − [2e] J. Bacos, I. Toth, B. Heil, G. Szalontai, L. Parkanyi, V. Fülöp, *J. Organomet. Chem.* **1989**, *370*, 263−276. − [2f] S. Sakuraba, T. Morimoto, K. Achiwa, *Tetrahedron: Asymmetry* **1991**, *2*, 597−600. − [2g] K. Angermund, W. Baumann, E. Dinjus, R. Fornika, H. Görls, M. Kessler, C. Krüger, W. Leitner, F. Lutz, *Chem. Eur. J.* **1997**, *3*, 755−764. − [2h] G. Zhu, P. Cao, Q. Jiang, X. Zhang, *J. Am. Chem. Soc*. **1997**, *119*, 1799−1800. − [2i] G. Trabesinger, A. Albinati, N. Feiken, R. W. Kunz, P. S. Pregosin, M. Tschoener, *J. Am. Chem. Soc*. **1997**, *119*, 6315−6323.

[3] [3a] W. S. Knowles, B. D. Vineyard, M. J. Sabacky, B. R. Stults in *Fundamental Research in Homogeneous Catalysis* (Ed.: M. Tsutsui), Plenum Press, New York, **1979**, pp. 537−547. − [3b] W. S. Knowles, *Acc. Chem. Res.* **1983**, *16*, 106−112. − [3c] J. D. Oliver, D. P. Riley, *Organometallics* **1983**, *2*, 1032−1038. − [3d] J. M. Brown, P. L. Evans, *Tetrahedron* **1988**, *44*, 4905−4916. − [3e] J. S. Giovannetti, C. M. Kelly, C. R. Landis, *J. Am. Chem. Soc*. **1993**, *115*, 4040−4057. − [3f] H. Brunner, A. Winter, J. Breu, *J. Organomet. Chem.* **1998**, *553*, 285−306.

[4] [4a] H. B. Kagan in *Comprehensive Organometallic Chemistry*, vol. 8 (Eds.: G. Wilkinson, F. G. A. Stone, E. W. Abel), Pergamon Press, Oxford, **1982**, pp. 463−498. − [4b] V. A. Pavlov, E. I. Klabunovskii, Yu. T. Struchkov, A. A. Voloboev, A. I. Yanovsky, *J. Mol. Catal.* **1988**, *44*, 217−243. − [4c] D. Seebach, D. A. Plattner, A. K. Beck, J. M. Wang, D. Hunziker, W. Petter, *Helv. Chim. Acta* **1992**, *75*, 2171−2209. − [4d] D. Seebach, E. Devaquet, A. Ernst, M. Hayakawa, F. N. M. Kühnle, W. B. Schweizer, B. Weber, *Helv. Chim. Acta* **1995**, *78*, 1636−1650. − [4e] N. M. Brunkan, P. S. White, M. R. Gagne, *Angew. Chem.* **1998**, *110*, 1615−1618; *Angew. Chem. Int. Ed.* **1998**, *37*, 1579−1582.

[5] [5a] I. Toth, B. Hanson, *Organometallics* **1993**, *12*, 1506−1513 and references therein. − [5b] K. Burgess, M. J. Ohlmeyer, K. H. Whitmire, *Organometallics* **1992**, *11*, 3588−3600. − [5c] M. Michalik, T. Freier, M. Schwarze, R. Selke, *Magn. Reson. Chem.* **1995**, *33*, 835−840.

[6] G. Balavoine, S. Brunie, H. B. Kagan, *J. Organomet. Chem*. **1980**, *187*, 125−139.

[7] J. M. Brown, P. A. Chaloner, *J. Am. Chem. Soc*. **1978**, *100*, 4307−4308.

[8] [8a] J. M. Brown, P. A. Chaloner, R. Glaser, S. Geresh, *Tetrahedron* **1980**, *36*, 815−825. − [8b] R. Selke M. Ohff, A. Riepe, *Tetrahedron* **1996**, *52*, 15079−15102.

[9] [9a] J. B. Hendrickson, *J. Am. Chem. Soc*. **1961**, *83*, 4537−4547. − [9b] J. B. Hendrickson, *J. Am. Chem. Soc*. **1967**, *89*, 7036−7046. − [9c] D. F. Bocian, H. L. Strauss, *J. Am. Chem. Soc*. **1977**, *99*, 2876−2882.

[10] [10a] G. R. Brubaker, D. W. Jonson, *Coord. Chem. Rev.* **1984**, *53*, 1−36. − [10b] B. P. Hay, *Coord. Chem. Rev.* **1993**, *126*, 177−236.

[11] V. S. Allured, C. M. Kelly, C. R. Landis, *J. Am. Chem. Soc*. **1991**, *113*, 1−12.

[12] [12a] L. H. Bryant, Jr., A. Lachgar, S. C. Jackels, *Inorg. Chem.* **1995**, *34*, 4230−4238. − [12b] I. Kovacs, M. C. Baird, *Organometallics* **1995**, *14*, 4084−4091 and references therein.

[13] J. B. Hendrickson, *J. Am. Chem. Soc*. **1967**, *89*, 7047−7061.

[14] D. Cremer, J. A. Pople, *J. Am. Chem. Soc*. **1975**, *97*, 1354−1358.

[15] D. F. Bocian, H. M. Pickett, T. C. Rounds, H. L. Strauss, *J. Am. Chem. Soc*. **1975**, *97*, 687−695.

[16] Cambridge Structural Database, Version 5.14, October 1997; see: F. H. Allen, O. Kennard, *Chemical Design Automation News* **1993**, *8*, 31−37.

[17] D. Heller, J. Holz, S. Borns, A. Spannenberg, R. Kempe, U. Schmidt, A. Börner, *Tetrahedron: Asymmetry* **1997**, *8*, 213−222.

[18] M. P. Anderson, L. H. Pignolet, *Inorg. Chem.* **1981**, *20*, 4101−4107.

[19] WIN-DYNAMICS 1.0 Release 951220, NMR Dynamic Spectra Simulation and Iteration, Bruker-Fanzen Analytik GmbH and K. Il'yasov, O. Nedopekin, Bremen, Germany.

[20] [20a] J. M. Brown, P. A. Chaloner, *J. Organomet. Chem*. **1981**, *217*, C2-C28. − [20b] E. M. Campi, P. S. Elmes, W. R. Jackson, R. J. Thomson, J. A. Weigold, *J. Organomet. Chem*. **1989**, *371*, 393−395.

[21] [21a] V. Elser, H. Strauss, *Chem. Phys. Lett*. **1983**, *96*, 276−278. − [21b] P. M. Ivanov, E. Osawa, *J. Comp. Chem*. **1984**, *5*, 307−313.

[22] [22a] W. B. Moniz, J. A. Dixon, *J. Am. Chem. Soc*. **1961**, *83*, 1671−1675. − [22b] N. −J. Schneider, N. Nguyen-Ba, *Org. Magn. Reson.* **1982**, *18*, 38−41.

[23] R. Selke, H. Pracejus, *J. Mol. Catal.* **1986**, *37*, 213−225.

[24] J. Holz, A. Börner, A. Kless, S. Borns, S. Trinkhaus, R. Selke, D. Heller, *Tetrahedron: Asymmetry* **1995**, *8*, 1973−1988.

[25] Available as PCMODEL 4.0 from Serena Software, Bloomington, USA; see: J. J. Gajewski, K. E. Gilbert, J. McKelvy, *Adv. Mol. Model*. **1990**, *2*, 65.

[26] B. P. Hay, J. R. Rustad, *J. Am. Chem. Soc*. **1994**, *116*, 6316−6326 and references therein.

[27] M. J. Frisch, G. W. Trucks, H. B. Schlegel, P. M. W. Gill, B. G. Johnson, M. A. Robb, J. R. Cheeseman, T. Keith, G. A. Petersson, J. A. Montgomery, K. Raghavachari, M. A. Al-Laham, V. G. Zakrzewski, J. V. Ortiz, J. B. Foresman, J. Cioslowski, B. B. Stefanov, A. Nanayakkara, M. Challacombe, C. Y. Peng, P. Y. Ayala, W. Chen, M. W. Wong, J. L. Andres, E. S. Replogle, R. Gomperts, R. L. Martin, D. J. Fox, J. S. Binkley, D. J. Defrees, J. Baker, J. P. Stewart, M. Head-Gordon, C. Gonzalez, and J. A. Pople, *Gaussian 94, Revision E.2*, Gaussian, Inc., Pittsburgh PA, **1995**.

[28] K. Tamao, K. Nakamura, S. Yamaguchi, M. Shiro, S. Saito, *Chem. Lett.* **1996**, 1007−1008.

Received August 4, 1998
[I98262]

Catalytic Transfer Hydrogenation of Ketones with $KHCr(CO)_5/HCO_2H/Et_3N$ Systems[+]

Jean-Jacques Brunet,*[a] Remi Chauvin,[a] and Pascale Leglaye[a]

Keywords: Chromates / Catalytic transfer hydrogenation / Hydrogenations / Reductions / α,β-Unsaturated ketones / Asymmetric synthesis

In the presence of a HCO_2H/Et_3N (1:1) mixture, $KHCr(CO)_5$ is an efficient catalyst precursor for the transfer hydrogenation of ketones in THF at room temperature. $KHCr(CO)_5$ is also a stoichiometric reagent for the selective reduction of the carbon–carbon double bond of α,β-unsaturated ketones.

Introduction

Main-group hydrides, such as the well-known boron and aluminium hydrides, are widely used in organic synthesis as reducing agents for a large range of functional groups and derivatives have been designed which exhibit very useful chemoselectivities.[1] These reagents must be used in stoichiometric quantities. In contrast, transition-metal hydrides are much less widely used, even though a large number of easily accessible derivatives are available. These compounds are interesting alternatives because of the possibility of using them in catalytic amounts in the presence of molecular hydrogen or of a hydrogen transfer agent.[2] As an extension of our work on carbonylhydridoferrates,[3,4] we recently became interested in the chromium series, and we developed a very easy and reproducible preparation of $K^+[HCr(CO)_5]^-$.[5]

The reactivity of $[PPN]^+[HCr(CO)_5]^-$ {$[PPN]^+$ = bis(triphenylphosphoranylidene)ammonium} has been previously investigated by Darensbourg et al.[6–8] This reagent has been shown to reduce selectively acid chlorides into aldehydes without further reduction to alcohols.[7] $[PPN]^+[HCr(CO)_5]^-$ itself is also inactive towards ketones, but becomes an efficient reducing agent in the presence of one equivalent of acetic acid (H^+ assistance and in situ protonolysis).[8]

Two catalytic systems involving carbonylchromates and molecular hydrogen have also been reported for the hydrogenation of ketones. Firstly, the system $Cr(CO)_6$/MeONa in methanol is active at 100–120°C under 100 bar of H_2.[9] Secondly, the complex $[PPN]^+[Cr(CO)_5(OAc)]^-$ is an active catalyst precursor for the hydrogenation of ketones in THF at 125°C under 40 bar of H_2.[10] In these catalytic reactions, $[HCr(CO)_5]^-$ is believed to be the active species.

To the best of our knowledge, no report has been published of the use of carbonylchromium complexes as catalyst precursors for the reduction of ketones by hydrogen transfer from easy-to-handle hydrogen donors.[11] Such reactions do not require the use of high-pressure reactors.

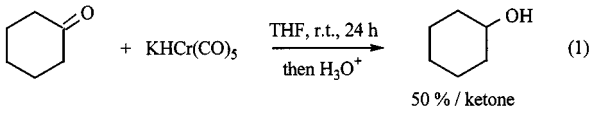
We report here that $K^+[HCr(CO)_5]^-$ (**1**) does react with ketones in THF at room temperature under *mild* conditions. Moreover, in the presence of the HCO_2H/Et_3N combination as a hydrogen transfer agent, *catalytic* reduction to the corresponding alcohols is achieved under atmospheric pressure at room temperature.

Results and Discussion

Stoichiometric Experiments

We have previously reported that $K^+[HFe(CO)_4]^-$ does not reduce normal ketones in the absence of a Brønstedt acid, either in THF or in methanol.[12] In contrast, we have now found that the chromium analogue **1** reacts with ketones to give the corresponding alcohol *in the absence of any Brønstedt acid*.

Treating cyclohexanone with **1** in THF at room temperature for 24 h resulted in 50% reduction (GC analysis) to cyclohexanol after hydrolysis of the reaction medium.



(1)

There is thus a significant difference in reactivity between $K^+[HCr(CO)_5]^-$ and $[PPN]^+[HCr(CO)_5]^-$ (vide supra). This phenomenon may be ascribed to K^+ assistance, as previously demonstrated for the hydrogenation of ketones with potassium hydrido(phosphane)ruthenate complexes.[13] From a more general point of view, and as previously observed for $[HFe(CO)_4]^-$,[4] the reactivity of $[HCr(CO)_5]^-$ seems to be strongly dependent on the associated cation, due to ion-pairing effects.[14] For example, it has been reported that $[PPN]^+[HCr(CO)_5]^-$ exchanges with MeOD (or D_2O) in THF at room temperature to give the corresponding deuteride $[PPN]^+[DCr(CO)_5]^-$[8] whereas $[Et_4N]^+[HCr(CO)_5]^-$ has been reported to react vigorously with MeOH at room temperature with H_2 evolution and formation of the dinuclear complex $[HCr_2(CO)_{10}]^-$[9] (however,

[+] Part of the thesis of P. L.

[a] Laboratoire de Chimie de Coordination du CNRS, UPR 8241, 205 route de Narbonne, F-31077 Toulouse Cedex 4, France
Fax: (internat.) + 33-5/61553003
E-mail: brunet@lcctoul.lcc-toulouse.fr

 © WILEY-VCH Verlag GmbH, D-69451 Weinheim, 1999 1434–1948/99/0404–0713 $ 17.50+.50/0

the reaction with 1-phenylethanol requires heating to 75°C). Similarly, we observed that, at room temperature, $K^+[HCr(CO)_5]^-$ slowly reacts with cyclohexanol in THF with formation of the dinuclear $[HCr_2(CO)_{10}]^-$ species.

If the reaction of **1** with cyclohexanone is conducted for longer reaction times (120 h), the reduction yield is not increased. After 24 h of reaction, ^{1}H-NMR analysis of the reaction medium (after evaporation of the solvent and redissolution in [D$_8$]THF) indicates that the starting complex **1** ($\delta_{CrH} = -7.05$) had been consumed and that the dinuclear hydrido anion $[HCr_2(CO)_{10}]^-$ ($\delta_{CrH} = -19.56$) is the only detectable hydride species. ^{13}C-NMR spectroscopy confirms the presence of $[HCr_2(CO)_{10}]^-$ ($\delta_{CO} = 222.4$ and 227.3) and suggests the presence of $[Cr_2(CO)_{10}]^{2-}$ ($\delta_{CO} = 243.8$ and 244.1).[15] The IR spectrum mainly exhibits the characteristic bands of $KHCr_2(CO)_{10}$ [2030 cm^{-1} (w), 1940 (vs) and 1882 (br.)], but also less intense bands at 2050 cm^{-1} (vw), 1919 (m), 1880 (br.) and 1766 (m) which may be ascribed to $[Cr_2(CO)_{10}]^{2-}$ or mixture of the latter with $[ROCr(CO)_5]^-$ (R = cyclohexyl) on the basis of literature data.[8][9] Unexpectedly, a ν_{OH} band corresponding to free cyclohexanol was also observed *before* hydrolysis of the reaction medium.

Control experiments indicated that the dinuclear hydride $KHCr_2(CO)_{10}$ reduces cyclohexanone in less than 5% yield after 72 h at room temperature in THF. It is thus reasonable to propose that **1** is the active species for the reduction. The first step of the reaction could occur by hydride transfer, generating an alkoxocarbonylchromate species (Equation 2).[9]

$$[HCr(CO)_5]^- + R^1R^2C{=}O \rightleftharpoons [R^1R^2CHOCr(CO)_5]^- \quad (2)$$

According to literature data, alkoxocarbonylchromates may further react with $[HCr(CO)_5]^-$, to give $[Cr_2(CO)_{10}]^{2-}$ (Equation 3)[9] and/or $[HCr_2(CO)_{10}]^-$ (Equation 4).[8]

$$[R^1R^2CHOCr(CO)_5]^- + [HCr(CO)_5]^- \longrightarrow R^1R^2CHOH + [Cr_2(CO)_{10}]^{2-} \quad (3)$$

$$[R^1R^2CHOCr(CO)_5]^- + [HCr(CO)_5]^- \longrightarrow [R^1R^2CHO]^- + [HCr_2(CO)_{10}]^{2-} \quad (4)$$

Quantitative conversion of the ketone thus requires another in situ evolution of the alkoxochromium complex, for example by protonation by HX (Equation 5) under conditions where $[HCr(CO)_5]^-$ does not decompose.

$$[R^1R^2CHOCr(CO)_5]^- + HX \longrightarrow R^1R^2CHOH + [XCr(CO)_5]^- \quad (5)$$

For a catalytic version, the carbonylhydridochromate $[HCr(CO)_5]^-$ has to be regenerated from $[XCr(CO)_5]^-$. This could be expected from the formato complex $[HCO_2Cr(CO)_5]^-$ which has been shown to undergo a rapid decarboxylation process according to Equation 6.[16]

$$[HCO_2Cr(CO)_5]^- \rightleftharpoons [HCr(CO)_5]^- + CO_2 \quad (6)$$

Formic acid itself cannot play the role of HX for the introduction of the formate moiety. Indeed, reaction of cyclohexanone with stoichiometric amounts of $KHCr(CO)_5$ in the presence of 1 equiv. of formic acid in THF resulted in less than 5% reduction to cyclohexanol after 24 h at room temperature (the same result was obtained by using acetic acid). These results are in contrast to the reported 95% yield reduction of cyclohexanone with $[PPN]^+[HCr(CO)_5]^-$/AcOH for 4 h in THF.[8] Both formic and acetic acids are too strong for the $KHCr(CO)_5$ base in THF, and preferentially lead to $KHCr_2(CO)_{10}$. However, when the strength of formic acid is moderated by the presence of triethylamine, the stoichiometric reduction of cyclohexanone (ketone/$KHCr(CO)_5$/HCO_2H/Et_3N in a 1:1:1:1 ratio) leads to a reduction yield of up to 65% after 24 h at room temperature. Using a 1:1:5:5 ratio of reagents resulted in a quantitative reduction to cyclohexanol after 6 h. By comparison, Noyori et al. recently reported the use of a different HCO_2H/Et_3N combination (5:2 azeotropic mixture[17]) for the ruthenium(II)-catalysed asymmetric transfer hydrogenation of ketones.[18]

Control experiments indicated that the formate ion alone [which could have been useful for displacing the unsaturated "Cr(CO)$_5$" moiety from the alkoxochromate, thus preventing $[HCr(CO)_5]^-$ consumption (Equations 3 and 4)] is not sufficient to promote the observed reactivity. Indeed, the association $KHCr(CO)_5/HCO_2K$ reduces cyclohexanone in the same yield than **1** alone (50%, 24 h at room temperature).

Catalytic Experiments

The system $KHCr(CO)_5/HCO_2H/Et_3N$ (1:5:5 ratio) was tested for the catalytic reduction of cyclohexanone. In the presence of stoichiometric amounts of HCO_2H/Et_3N as a hydrogen transfer agent, cyclohexanone is almost quantitatively (95%) reduced to cyclohexanol with 20% $KHCr(CO)_5$ after 24 h at room temperature in THF. Using lower amounts of **1** is also possible (10% $KHCr(CO)_5$: 83% yield after 24 h; 5% $KHCr(CO)_5$: 70% yield after 24 h) but complete conversion of cyclohexanone is achieved only after several days.

Performing the catalytic reaction at 0°C resulted in a decrease in reaction rate. However, if after 24 h at 0°C the temperature is raised to room temperature, the expected catalytic activity is restored. For reactions conducted at 60°C, the cyclohexanol yield is lower than 50% (24 h) and no longer evolves, suggesting that the catalytically active species have been destroyed competitively.

The above system was tested for the catalytic reduction of some representative ketones at room temperature (Table 1). For comparison, the experiments were stopped after 24 h.

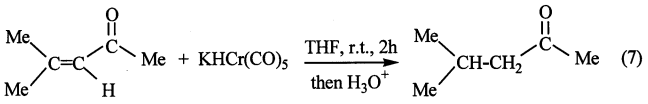
As expected from literature data on the reduction of ketones with hydridometallates,[8,9,19] cyclohexanones are more rapidly reduced than methyl ketones. In the case of 4-*tert*-butylcyclohexanone, the preponderant formation of the *trans* alcohol has previously been explained by the steric demand of the "$OCr(CO)_5$" group of the alkoxocarbonylchromate formed in the first step of the reaction (Equation 2).[9] This explanation also stands for the present system.

Table 1. Catalytic reduction of ketones with 20% $KHCr(CO)_5$ in the presence of HCO_2H/Et_3N[a,b]

	conversion (%)[c]	products[d] (yield%)[c]
2-hexanone	38	2-hexanol (38)
acetophenone	25	1-phenyl ethanol (25)
3-methyl-2-butanone	45	3-methyl-2-butanol (45)
cyclohexanone	95	cyclohexanol (95)
4-*tert*-butylcyclo-hexanone	80	4-*tert*-butylcyclohexanol (80)[e]
mesityl oxide	20	4-methyl-2-pentanone (20)

[a] Reactions conducted with 100 mg of $KHCr(CO)_5$ (0.43 mmol) in THF (10 mL) for 24 h at room temp. – [b] Ketone/$KHCr(CO)_5$/HCO_2H/Et_3N = 1:0.2:1:1. – [c] Determined by GC analysis with internal standards. – [d] Identified by GC retention times and GC-MS analysis. – [e] *cis*/*trans* ratio = 33:67.

The selective reduction of the carbon–carbon double bond of mesityl oxide to give 4-methyl-2-pentanone (Table 1) is noteworthy. This specificity of $KHCr(CO)_5$ has been confirmed by a stoichiometric experiment (*in the absence the HCO_2H/Et_3N combination*) leading to 4-methyl-2-pentanone in > 95% yield after 2 h at room temperature (Equation 7).



(7)

For this reaction, $KHCr(CO)_5$ is more reactive than $KHFe(CO)_4$ but exhibits the same chemoselectivity. Indeed, it has been shown that *under the same conditions*, $KHFe(CO)_4$ reduces mesityl oxide to give 4-methyl-2-pentanone in less than 25% yield after 24 h [literature data indicate that, in the presence of excess $Fe(CO)_5$, $NaHFe(CO)_4$ reduces mesityl oxide to 4-methyl-2-pentanone in 96% yield after 24 h *at 60°C* in MeOH[20]].

In control experiments, it has been shown that $KHCr_2(CO)_{10}$ (1 equiv.) also selectively reduces mesityl oxide under the conditions of Equation 7, but 4-methyl-2-pentanone was formed in less than 10% after 2 h. Thus, for this reaction, $KHCr(CO)_5$ is also much more reactive than $KHCr_2(CO)_{10}$. This order of reactivity between the mono- and dinuclear carbonylhydridochromates is in contrast to what has been reported in the iron series where $NaHFe_2(CO)_8$ is at least 26 times more reactive than mononuclear $NaHFe(CO)_4$ for the reduction of α,β-unsaturated ketones.[2,20,21]

Finally, exploratory experiments were conducted on a possible enantioselective catalytic system based on the chiral amine, quinine, instead of Et_3N. The system $KHCr(CO)_5$/(–)-quinine/HCO_2H (1:5:5 ratio.) reproducibly reacts with acetophenone (5 equiv.) in a catalytic manner to yield 1-phenylethanol in 45% yield and 10% ee (120 h in THF at room temperature).

Work is in progress to obtain a better mechanistic understanding of the observed reactivity of $KHCr(CO)_5$ (in particular, a catalytic cycle is to be sought) and to extend its use as reagent or catalyst in organic synthesis.

Experimental Section

General: All reactions were performed under argon using standard Schlenk tube techniques. THF was distilled under argon from Na/benzophenone. – NMR: Bruker AC 200 or AMX 400 apparatus. – IR: Perkin–Elmer 1725X FT-IR spectrometer with CaF_2 windows (0.5 mm). – GC: Hewlett–Packard HP 5890 apparatus equipped with a 30-m capillary Rt-β-DEXm chiral column. – GC MS: Hewlett–Packard HP 6890 apparatus (EC Wax, 30-m capillary column) equipped with an HP 5973 M ion detector. – $KHCr(CO)_5$[5] and $KHFe(CO)_4$[22] were prepared from the corresponding $Cr(CO)_6$ or $Fe(CO)_5$ and technical KOH, according to the reported procedures. $KHCr_2(CO)_{10}$ was prepared as follows. A solution of 86% KOH (0.290 g, 4.55 mmol) in 7.5 mL of absolute ethanol was added to 20mL of a CH_2Cl_2 solution of $Cr(CO)_6$ (0.500 g, 2.27 mmol). After stirring for 10 min, the solution was concentrated to 4 mL. Water (5 mL) was added and the solution stirred for 0.5 h at room temp. THF (2 × 10 mL) was added and each time concentrated to dryness to remove any trace of water. The resulting solid was dissolved in THF (20 mL), the solution filtered under argon, and concentrated to dryness to leave an orange solid (0.434 g, 90% yield). – IR (THF) $\tilde{\nu}$ = 2030 cm^{-1} (w), 1940 (s) and 1878 (vs). – ^1H NMR (CD_3CN, 200 MHz): δ = –19.56 (s).

Stoichiometric Reductions of Ketones: The general procedure is exemplified for the reduction of cyclohexanone. A solution of cyclohexanone (223 μL, 2.16 mmol) and nonane (138 mg, 1.08 mmol) in THF (10 mL) was cannulated to solid $KHCr(CO)_5$ (500 mg, 2.16 mmol). After stirring for 24 h at room temp., the solution was treated with 1 N HCl (10 mL) and diethyl ether (10 mL) was added. The aqueous phase was then extracted with diethyl ether (2 × 10 mL) and the ethereal phase analysed by GC. For complementary experiments (see text), additives (HCO_2H, AcOH, HCO_2K, or HCO_2H/Et_3N mixtures) were dissolved in the THF solution containing cyclohexanone before it was cannulated to solid $KHCr(CO)_5$.

Catalytic Reduction of Ketones: The general procedure is exemplified in the case of cyclohexanone. Triethylamine (300 μL, 2.16 mmol) and technical (95–97%) formic acid (82 μL, 2.16 mmol) were added to a solution of cyclohexanone (223 μL, 2.16 mmol) and nonane (138 mg, 1.08 mmol) in THF (10 mL). The resulting solution was then cannulated into a Schlenk flask containing solid $KHCr(CO)_5$ (100 mg, 0.43 mmol) and a stirring bar. The flask was closed with a glass stopper and the solution magnetically stirred at room temp. Aliquots (0.5 mL) were hydrolysed with dilute HCl (0.5 mL), extracted with diethyl ether (0.5 mL) and analysed by GC.

Acknowledgments

This work was supported by the Centre National de la Recherche Scientifique. The authors wish to thank L. Noé for GC-MS analyses.

[1] J. March, *Advanced Organic Chemistry*, 4th ed., Wiley-Interscience, New York, **1992**; J. Seyden-Penne, *Reduction by the Alumino- and Borohydrides in Organic Synthesis*, Verlag Chemie, New York, **1991**.

[2] J. P. Collman, L. S. Hegedus, J. R. Norton, R. G. Finke, *Principles and Applications of Organotransition Metal Chemistry*, 4th ed., University Science Books, Mill Valley, California, **1987**.

[3] J. J. Brunet, *Chem. Rev.* **1990**, *90,* 1041−1059.
[4] J. J. Brunet, R. Chauvin, O.Diallo, F. B. Kindela, P. Leglaye, D. Neibecker, *Coord. Chem. Rev.* **1998**, *178−180*, 331−351.
[5] J. J. Brunet, R. Chauvin, B. Donnadieu, P. Leglaye, D. Neibecker, *J. Organomet. Chem.* **1998**, *571*, 7−13.
[6] S. C. Kao, M. Y. Darensbourg, *Organometallics* **1984**, *3*, 646−647.
[7] S. C. Kao, P. L. Gaus, K. Youngdahl, M. Y. Darensbourg, *Organometallics* **1984**, *3*, 1601−1603.
[8] P. L. Gaus, S. C. Kao, K. Youngdahl, M. Y. Darensbourg, *J. Am. Chem. Soc.* **1985**, *107*, 2428−2434.
[9] L. Marko, Z. Nagy-Magos, *J. Organomet. Chem.* **1985**, *285*, 193−203.
[10] P. A. Tooley, C. Ovalles, S. C. Kao, D. J. Darensbourg, M. Y. Darensbourg, *J. Am. Chem. Soc.* **1986**, *108,* 5465−5470.
[11] N. Uematsu, A. Fujii, S. Hashigushi, T. Ikariya, R. Noyori, *J. Am. Chem. Soc.* **1996**, *118,* 4916−4917.
[12] J. J. Brunet, R. Chauvin, F. B. Kindela, D. Neibecker, *Tetrahedron. Lett.* **1994**, *47,* 8801−8804.
[13] R. A. Grey, G. P. Pez, A. Wallo, *J. Am. Chem. Soc.* **1981**, *103*, 7536−7542.
[14] S. C. Kao, M. Y. Darensbourg, W. Schenk, *Organometallics* **1984**, *3*, 871−876.
[15] D. H. Gibson, K. R. Phillips, F. U. Ahmed, *J. Organomet. Chem.* **1984**, *276*, 363−366.
[16] D. J. Darensbourg, A. Rokicki, *Organometallics* **1982**, *1*, 1685−1693.
[17] K. Wagner, *Angew. Chem. Int. Ed. Engl.* **1970**, *9*, 50−54; K. Narita, M. Sekiya, *Chem. Pharm. Bull.* **1977**, *25*, 135−140.
[18] A. Fujii, S. Hashigushi, N. Uematsu, T. Ikariya, R. Noyori, *J. Am. Chem. Soc.* **1996**, *118,* 2521−2522.
[19] K. Jothimony, S. Vanchesan, J. Kuriacose, *J. Mol. Catal.* **1985**, *32*, 11−16.
[20] R. Noyori, I. Uemeda, T. Ishigami, *J. Org. Chem.* **1972**, *37*, 1542−1545.
[21] J. P. Collman, R. G. Finke, P. L. Matlock, R. Wahren, R. G. Komoto, J. I. Brauman, *J. Am. Chem. Soc.* **1978**, *100,* 1119−1140.
[22] A. Baby, J. J. Brunet, F. B. Kindela, D. Neibecker, *Synth. Commun.* **1994**, *24,* 2827−2834.

Received October 26, 1998
[I98366]

Syntheses of $K[Co(tren)(NH_3)(SO_4)](S_4O_6)\cdot 2(H_2O)$ and of $[cis\text{-}\alpha\text{-}Co(trien)(NH_3)Cl](S_5O_6)$ – Compounds Produced by Hydrolytic Cleavage of Sulfur–Sulfur Bonds of the Tetrathionate Anion

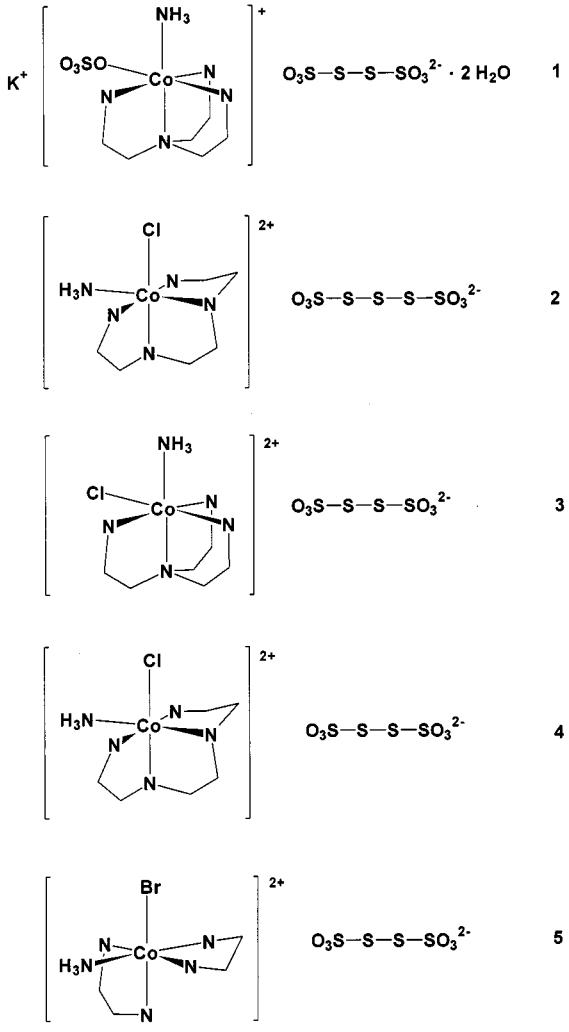
Hyungphil Chun[a] and Ivan Bernal*[a]

Keywords: Tetrathionates / Pentathionates / Sulfato ligands / Cobalt(III) complexes / *Thiobacillus ferrooxidans*

$K[Co(tren)(NH_3)(SO_4)](S_4O_6)\cdot 2(H_2O)$ (**1**) and $[cis\text{-}\alpha\text{-}Co(trien)(NH_3)Cl](S_5O_6)$ (**2**) have been prepared unexpectedly while attempting to obtain crystals suitable for X-ray diffraction of $[Co(tren)(NH_3)Cl](S_4O_6)$ (**3**) and of $[cis\text{-}Co(trien)(NH_3)Cl](S_4O_6)$ (**4**), respectively. **1** is derived from **3** by hydrolysis of the tetrathionate anion resulting in a sulfato moiety which displaces the chloro ligand from the coordination sphere of the metal center. **2** is derived from **4** by hydrolysis of the tetrathionate anion followed by reformation into pentathionate anion and H_2S, as described in previous chromatographic work by Steudel. Compounds **1** and **2** have been characterized by elemental analyses and by single-crystal X-ray diffraction studies.

Some time ago, we discovered that the compound $[cis\text{-}Co(en)_2(NH_3)Br](S_4O_6)$ (**5**) crystallizes as a conglomerate, as we had hoped.[1,2] (Conglomerate crystallization is the phenomenon whereby a racemic solution produces a mechanical mixture of enantiomorphically pure single crystals of both handedness.) By a crystal structure determination, we also demonstrated that the parent compound, $[cis\text{-}Co(en)_2(NH_3)Br]Br_2$, from which **5** was prepared was a racemate[2]. At the time, we argued that crystallization as a conglomerate was justified since both cation and anion are chiral, as one could expect for chiral recognition to occur giving rise to specificity and, indeed, that was the purpose of using the tetrathionate anion to begin with.[1] Interestingly, we found that the $S_4O_6^{2-}$ anion is hydrogen-bonded to the cations, via the SO_3 fragments, in exactly the same fashion as the $-SO_3$ of bromocamphorsulfonate when used as resolving agent for the same Co^{III} cation.[3,4] Finally, the sodium salt of the $S_4O_6^{2-}$ anion crystallizes as a conglomerate.[5]

At the time, we indicated[1] that we planned to examine a series of polythionates of the *cis*-amminehalo cations in order to establish whether the chirality of the countercation played a role in the selection of the crystallization pathway. In this report, we detail the results of our studies using tetrathionate with two different Co^{III} cations, results which produced novel and unexpected chemical products. Moreover, these results are in revealing and interesting agreement with the pioneering work of Steudel and associates,[6] who reached similar conclusions to ours using totally different sources of information.



Results and Discussion

As indicated by the results listed in Table 3, the structures are well behaved, that of **1** being a of a little higher quality than that of **2** caused by larger number of weak data present in the crystals of the latter substance and by a small amount of disorder present in C(6) of **2**; for details of the disorder, see below.

[a] Chemistry Department, University of Houston, Houston, Texas 77204-5641, USA

 © WILEY-VCH Verlag GmbH, D-69451 Weinheim, 1999 1434–1948/99/0404–0717 $ 17.50+.50/0

Upon solving the structures of the two compounds, we realized that marked changes from the expected compounds had occurred. This is evident from Figures 1, 2 (see also Tables 1, 2) which, to our great surprise, show the true molecular and stereochemical nature of the two compounds – a fact that was later verified by elemental analyses.

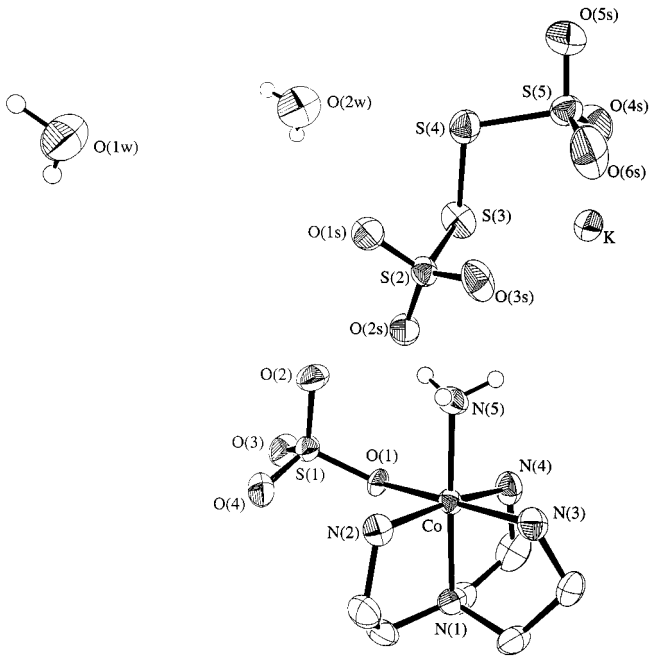


Figure 1. A view of the cations, anion and waters of crystallization of **1**; note the hydrogen bonds of the $-NH_3$ ligand to the oxygen atoms of S(2); those are the closest hydrogen bonds present in the molecule; also note the bonds between the potassium ion and the oxygen atoms of S(5)

Table 1. Selected bond lengths [Å] and angles [°] for **1**

Co–N(1)	1.955(3)	N(5)–Co–N(1)	177.6(2)
Co–N(2)	1.951(4)	N(2)–Co–N(4)	170.3(2)
Co–N(3)	1.924(4)	N(1)–Co–O(1)	91.75(13)
Co–N(4)	1.957(4)	N(2)–Co–O(1)	92.5(2)
Co–N(5)	1.952(4)	N(3)–Co–O(1)	175.1(2)
Co–O(1)	1.978(3)	N(4)–Co–O(1)	82.4(2)
S(1)–O(1)	1.540(3)	N(5)–Co–O(1)	90.6(2)
S(1)–O(2)	1.451(3)	N(2)–Co–N(1)	86.5(2)
S(1)–O(3)	1.468(3)	N(3)–Co–N(1)	86.3(2)
S(1)–O(4)	1.464(3)	N(4)–Co–N(1)	85.4(2)
S(2)–S(3)	2.109(2)	S(1)–O(1)–Co	129.5(2)
S(3)–S(4)	2.009(2)	S(2)–S(3)–S(4)	103.06(8)
S(4)–S(5)	2.121(2)	S(3)–S(4)–S(5)	104.68(8)
S(2)–O(1S)	1.448(3)	O(1S)–S(2)–S(3)	106.5(2)
S(2)–O(2S)	1.452(3)	O(2S)–S(2)–S(3)	99.2(2)
S(2)–O(3S)	1.438(3)	O(3S)–S(2)–S(3)	108.8(2)
S(5)–O(4S)	1.421(4)	O(4S)–S(5)–S(4)	106.4(2)
S(5)–O(5S)	1.435(4)	O(5S)–S(5)–S(4)	98.4(2)
S(5)–O(6S)	1.418(4)	O(6S)–S(5)–S(4)	107.8(2)
H(2N)–O(4)	2.111 (0.054)		
H(3N)–O(2W)_$1	1.988 (0.055)	$: 1 $-x$, $-y+1$, $-z+1$	
H(5N)–O(1W)_$1	2.192 (0.054)		
H(7N)–O(3)_$2	2.205 (0.072)	$: 2 $x-1$, y, z	
H(8N)–O(1S)_$1	2.277 (0.071)		
H(9N)–O(2)	2.268 (0.061)		
H(1W)–O(2S)_$4	1.826 (0.086)	$: 4 x, $y+1$, z	
H(3W)–O(5S)_$7	2.080 (0.035)	$: 7 $-x$, $-y+1$, $-z+2$	
H(4W)–O(5S)_$6	2.280 (0.070)	$: 6 $x+1$, y, z	

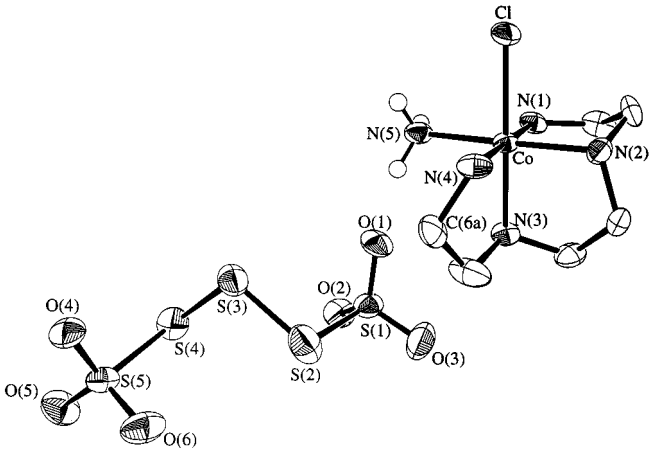


Figure 2. A view of the cation and anion of compound **2**; the anion is located at the position at which it forms the shortest hydrogen bonds to the cation, which are those with the $-NH_3$ hydrogen atoms; the carbon atom C(6a) is depicted as ordered in the position which poduces the lowest energy conformation of its ring, in this case λ

Table 2. Selected bond lengths [Å] and angles [°] for **2**

Co–N(1)	1.975(7)	N(5)–Co–N(2)	174.9(3)
Co–N(2)	1.958(7)	N(4)–Co–N(1)	179.1(3)
Co–N(3)	1.950(6)	N(3)–Co–Cl	174.2(2)
Co–N(4)	1.949(7)	N(1)–Co–Cl	90.6(2)
Co–N(5)	1.951(7)	N(2)–Co–Cl	91.7(2)
Co–Cl	2.266(2)	N(4)–Co–Cl	89.6(2)
C(5)–C(6A)	1.46(2)	N(5)–Co–Cl	88.4(2)
C(5)–C(6B)	1.44(2)	C(6A)–C(5)–N(3)	115.1(4)
C(6A)–N(4)	1.491(11)	C(6B)–C(5)–N(3)	111.1(9)
C(6B)–N(4)	1.51(2)	C(5)–C(6A)–N(4)	107.0(4)
S(1)–S(2)	2.102(4)	C(5)–C(6B)–N(4)	107.1(13)
S(2)–S(3)	2.053(4)	S(1)–S(2)–S(3)	98.7(2)
S(3)–S(4)	2.018(4)	S(2)–S(3)–S(4)	106.2(2)
S(4)–S(5)	2.122(3)	S(3)–S(4)–S(5)	100.4(2)
S(1)–O(1)	1.418(6)	O(1)–S(1)–S(2)	105.3(3)
S(1)–O(2)	1.444(6)	O(2)–S(1)–S(2)	105.5(4)
S(1)–O(3)	1.427(7)	O(3)–S(1)–S(2)	101.7(4)
S(5)–O(4)	1.434(6)	O(4)–S(5)–S(4)	105.8(3)
S(5)–O(5)	1.431(7)	O(5)–S(5)–S(4)	99.9(3)
S(5)–O(6)	1.441(6)	O(6)–S(5)–S(4)	106.2(3)
H(1C)–O(4)_$1	2.044(0.009)	$1: $x-1$, y, z	
H(1D)–O(6)_$2	2.191(0.010)	$2: $x-1$, $1/2-y$, $z-1/2$	
H(2C)–O(2)_$3	2.048(0.009)	$3: $2-x$, $y-1/2$, $1/2-z$	
H(5G)–O(1)	2.201(0.009)		
H(4C)–O(2)_$3	2.239(0.010)		

What those results demonstrate is that a $S-SO_3$ bond had been broken and that the terminal sulfur atom had been oxidized to S^{6+} creating a sulfato moiety. At the same time the chloro ligand, initially present in the Co^{III} substrate, has been eliminated and a sulfato ligand has replaced it using a single oxygen atom to coordinate the metal center. At a later time, the solubility limit of **1** was reached and crystals began to be deposited. A check of the literature revealed the following facts:

(a) the Cambridge Structural Database (CSD)[7] lists no mononuclear 3-d metal complex in the 3+ charge state containing a monodentate sulfato ligand. There are some 3-d metal complexes carrying such ligands; however, they are all 2+ complexes. Among them, the majority are Cu^{2+} complexes, some Zn^{2+} and three Co^{2+} examples. A large

number of sulfato complexes are known in which the ligand bridges two or more metal centers or acts as a bidentate ligand to a single metal center. We also examined the Inorganic Crystal Sturucture Database(ICSD)[8] which does not list a single example of a trivalent metal center bearing a monodentate sulfato ligand. These facts make compound **1** an interesting rarity.

(b) A check in the literature revealed the presence of a seminal paper by Steudel and colleagues[6] detailing their chromatographic separation experiments during the equilibration of polythionates in carefully controlled media. They reported detecting $S_nO_6^{2-}$ species, where $n = 2\ldots22$. Two equations of the equilibria they proposed are particularly relevant to the results we are reporting. They are:

$$S_4O_6^{2-} + H_2O \rightarrow HS_2SO_3^- + HSO_4^- \quad (1)$$

$$2\ HS_2SO_3^- \rightleftharpoons S_5O_6^{2-} + H_2S \quad (2)$$

All those species were detected in their chromatographic work and, now, we have trapped the sulfate as a ligand to the metal center in **1** and the pentathionate in Equation 2 is the counteranion to the metal center in compound **2**. Thus, the two studies are mutually reinforcing and it is specially pleasing that we were able to obtain the structures of the relevant moieties proposed by Steudel, et al.[6]

The Stereochemistry of 1 and 2

As shown in Figure 1, the cation of **1** consists of a Co^{III} cation surrounded by the four nitrogen atoms of the ligand tren [tris(2-aminoethyl)amine]. The ammine ligand is *trans* to the central nitrogen atom of tren (so-called *p*-mode of binding) and the sulfato ligand is *cis* to the ammine and bound to the metal center by a single oxygen atom. There are two waters of crystallization which are hydrogen-bonded to terminal $-NH_2$. The potassium cation is bonded to oxygen atoms of a terminal $-SO_3$ fragment of the tetrathionate anion (see Figure 4 for further details); finally, the $-SO_3$ fragment at the opposite end of the tetrathionate anion is hydrogen-bonded to the $-NH_3$ hydrogen atoms, as shown in Figure 1.

An interesting stereochemical result is that the S−O bond of the metal-bound sulfate is noticeably longer than those of the other three oxygen atoms which is to be expected since the bound oxygen atom is donating its electron density to the Co^{III} ion. The average value of the S−O distances in the tetrathionate anion is 1.435(4) Å which is significantly shorter than those in the bound sulfato ligand. Finally, the S−S distances within the tetrathionate differ in that the central S−S bond is significantly shorter than the outer two. This result is in close agreement with the values published earlier for compound **5**[1] where the central S−S bond was found to be 2.019(2) Å and the outer ones were 2.111(2) and 2.133(2) Å. The remaining stereochemistry of this molecule is normal and it does not require further comment. Its main importance is the fact that the postulated formation of the sulfate anion has been verified by the accident of trapping it into the cation of **1**.

The stereochemistry of **2** is shown in Figure 2 in which the trien (1,4,7,10-tetraazadecane) ligand is in the *cis*-α configuration. Figure 3 shows that C(6) is disordered (50:50) into its two alternate positions, making that ring either λ or δ, the former being the lowest energy conformation and it is the one shown in Figure 2.

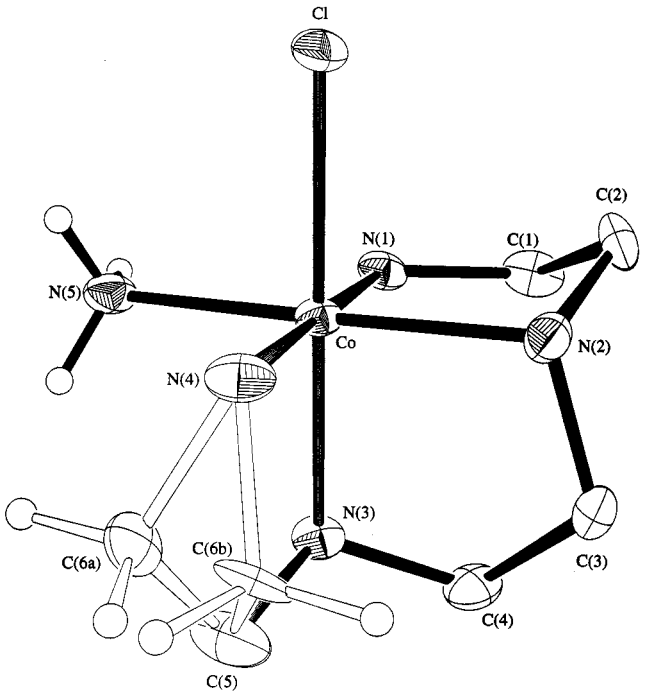


Figure 3. A view of the cation of **2** showing the disorder of the ring containing C(6)

This disorder contributes to the somewhat higher *R* factors listed in Table 3 since occupancy factors and anisotropic thermal parameters are correlated, as is widely known. Also, the partial disorder at C(6) is probably the result of steric hindrance with O(1) which is held in that position by hydrogen bonding to the $-NH_3$ hydrogen atoms, as is clear from Figures 2 and 5. The O(1)−C(6a) contact is 3.804 Å and the O(1)−H(6a2) is 3.282 Å while the hydrogen bond O(1)−H(5g) is 2.201 Å and these contacts are the likely source of the disorder we discovered. We also note that the $-NH_3$ hydrogen atoms were readily found in the structural analysis and were located at very reasonable positions indicating that the disorder problem is strictly localized at C(6). Figure 5 depicts the association of pentathionate anions with the cations in the crystal structure. Its S−O distances are fairly uniform, the longest being 1.444(6) Å and the shortest 1.418(6) Å, with an average of 1.433(7) Å. The small differences are probably due to differences in extents of hydrogen bonding of the two ends of the anion.

Mechanism of the Reactions Observed in 1 and 2

First, let us emphasize the fact that not every *cis*-amminehalo compound of a (polyamine)cobalt complex causes the fragmentation of the tetrathionate anion since we deter-

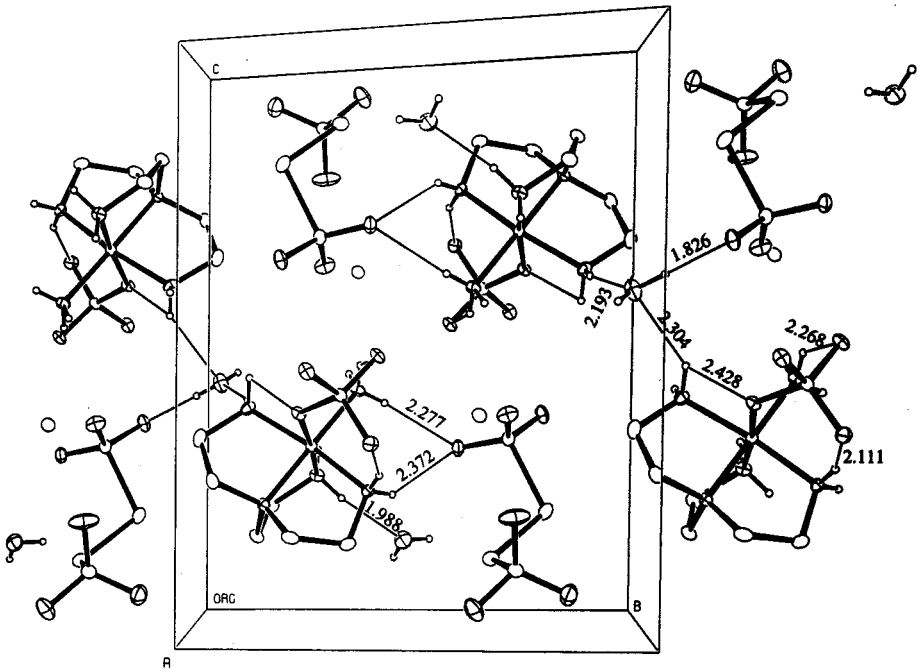


Figure 4. The packing of the ions and waters of crystallization of compound **1**; note the hydrogen bonds holding the pieces together; only the shortest ones are drawn (light lines) and their distances are given; the tetrathionate anions are bonded by a single oxygen atom to only two hydrogen atoms of a cation; in those cases of conglomerate crystallization (see ref.[1]) there were strong hydrogen bonds of the three oxygen atoms of one $-SO_3$ moiety to three hydrogen atoms of a *fac* face of its cation

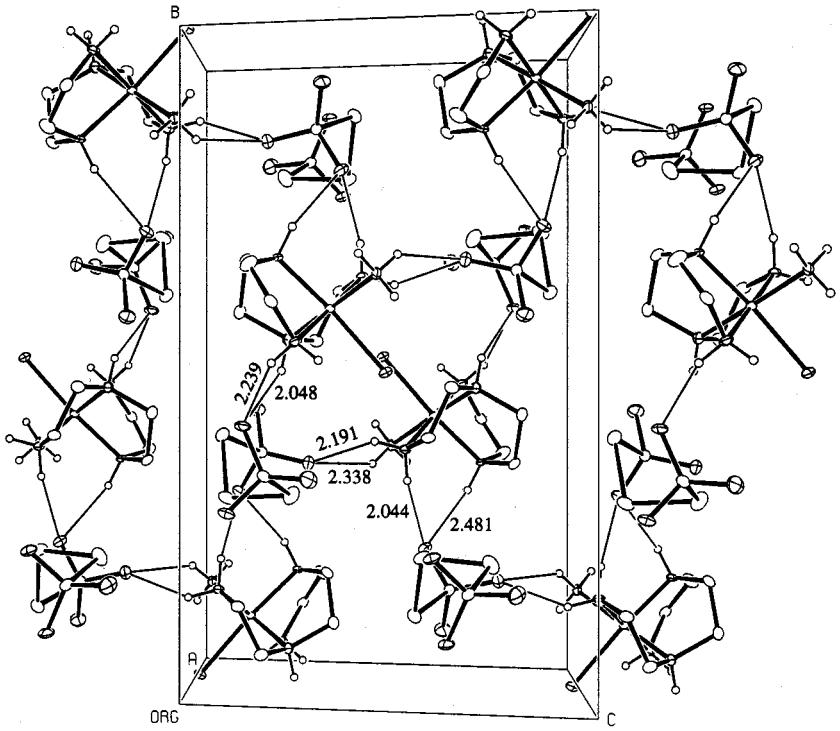


Figure 5. The packing of the ions of compound **2**; only the shortest hydrogen bonds are drawn (light lines) and their distances are given; note that the pentathionate anions are also bonded by two oxygen atoms to two hydrogen atoms of a pair of adjacent cations

mined[1] the crystal structure of [*cis*-Co(en)$_2$(NH$_3$)Br](S$_4$O$_6$) (**5**; conglomerate) and of pre-resolved (+)$_{589}$[*cis*-Λ(δλ)-Co(en)$_2$(NH$_3$)Br](S$_4$O$_6$) (**6**); we saw no evidence of the formation of either sulfate or of pentathionate with those compounds. These observations are the more interesting when viewed against the fact that the spectrochemical series classifies a chloro ligand as being stronger than a bromo ligand. Consequently, if sulfate were formed by cleavage of $S-SO_3$ in **5** and **6** it should more readily displace the bromo ligand from the coordination sphere of the cobalt center in

those cations; however, this is not the experimental result. Therefore, the suggestion is that only specific combinations of polythionates and *cis*-ammine(halo)cobalt cations are capable of giving rise to S−S cleavage reactions. As a matter of fact, we have recently determined the structure of [*cis*-$Co(en)_2(NH_3)Br](S_3O_6)$ and observed no evidence of S−S bond fragmentation, either.[9]

The $-NH_3$ ligands of **1** and **2** have remained bound to their cobalt centers and we note that in the latter the chloro ligand has also remained bound to its metal atom. This is a puzzling result in view of the fact that Equation 1 of the mechanism proposed by Steudel, et al.[6] requires the formation of $HS_2SO_3^- + HSO_4^-$ in order to use the former for the creation of the pentathionate found on **2**. This suggests that the first stage of the reaction (Equation 1; sulfate formation) happens without chloride elimination, concerted or otherwise. The suggestion is, then, that after the formation of the sulfate anion, the chloro ligand of **1** is replaced by a sulfato ligand which loses then its proton − an example of highly charged metal induction of proton elimination, as in the classical case of:

$$[M(H_2O)_6]^{3+} \rightarrow [M(H_2O)_5(OH)]^{2+} + H^+$$

We observed experimentally that such a process of halide elimination and sulfato substitution does not occur in the case of **2**. What could be the possible reason it does not do so?

First, we note that the chloro ligand in **1** is *trans* to a primary (terminal) $-NH_2$ ligand whereas in **2** it is *trans* to a secondary −NH− ligand, the latter being a better Lewis base; and, thus, a better σ donor to the metal center. It is fair to assume that in both compounds the chloro ligand is an equally good σ donor and π acceptor and is not the root of any differences in bonding. However, if more σ-electron density is donated to the metal center of **2**, one would expect a stronger (shorter) Co−Cl bond in the case of **2**. The structures of three different salts of $[Co(tren)(NH_3)Cl]^{2+}$ (the parent cation for **1**) were precisely determined by Buckingham et al.[10] who found Co−Cl bonds of 2.301(2), 2.288(2) and 2.291(4) Å. In compound **2**, the Co−Cl bond length is 2.266(2) Å, the difference from the average value of Buckingham′s results [2.293(3) Å] is 0.027 Å, which is greater than ca. 10 times the esds given. Thus, the difference is significant and may be the reason why the chloro ligand was not expelled by sulfato in the case of **2**.

The Connection with *Thiobacillus ferrooxidans* (*T. f.*)

It was pointed out by Steudel et al.[6] that *T. f.* is "a chemolithotrophic bacterium which participates in the sulfur cycle in nature and plays an important role in the bacterial leaching of mineral ores." Fe^{2+} is present in these bacterial cultures and the energy driving these systems is the oxidation of Fe^{2+} to Fe^{3+} and/or the oxidation of low-valent sulfur compounds to sulfate. Since we generated, and trapped, sulfate in the case of **1** and, presumably, we also formed sulfate in the case of **2** (see above arguments), our compounds may have some value as bio-inorganic models for such reactions, despite the fact that they are Co^{III} derivatives.

Experimental Section

Pure samples of $K_2S_4O_6$ and $Na_2S_4O_6·2H_2O$ were purchased from SIGMA Chemical Company. $[Co(tren)(NH_3)Cl]Cl(ClO_4)$ was prepared by a literature method[11] and $[Co(trien)(NH_3)Cl]Cl_2$ was prepared by the same method using trien instead of tren. The elemental analyses described were performed by Galbraith Laboratories.[12]

Synthesis of K[Co(tren)(NH_3)(OSO_3)](S_4O_6)·2(H_2O) (1): A solution of partially dissolved $[Co(tren)(NH_3)Cl]Cl(ClO_4)$ (1.46 g, 3.72 mmol) in 30mL of water was filtered and added slowly to 30 mL of an aqueous solution containing $K_2S_4O_6$ (1.35 g, 4.46 mmol). A small amount (35 mg) of single crystals suitable for X-ray diffraction study was obtained by liquid diffusion with acetone. − $C_6H_{25}CoKN_5O_{12}S_5$ (617.64): calcd. C 11.67, H 4.09, Co 9.54, N 11.34; found C 11.33, H 3.62, Co 9.26, N 11.06.

Synthesis of [*cis*-α-Co(trien)(NH_3)Cl](S_5O_6) (2): 1.0 g (3.21 mmol) of $[Co(trien)(NH_3)Cl]Cl_2$ was dissolved in 15 mL of water and was filtered directly into 10 mL of an aqueous solution of 1.0 g (3.27 mmol) of $Na_2S_4O_6·2H_2O$. Red crystalline products were formed and collected after 6 d (90 mg). − $C_6H_{21}ClCoN_5O_6S_5$ (513.96): calcd. C 14.02, H 4.12, N 13.63; found C 14.07, H 4.27, N 13.63.

Crystallography: Crystals of **1** and **2** were obtained directly from the reaction media and were mounted onto a goniometer head and

Table 3. Crystal data and structure refinement for K[Co(tren)-(NH_3)(OSO_3)](S_4O_6)·2(H_2O) (**1**) and [*cis*-α-Co(trien)(NH_3)Cl]-(S_5O_6) (**2**)

	1	**2**
Empirical formula	$C_6H_{25}CoKN_5O_{12}S_5$	$C_6H_{21}ClCoN_5O_6S_5$
Molecular mass	617.64	513.96
Crystal system	triclinic	monoclinic
Space group	$P-1$	$P2_1/c$
Z	2	4
a [Å]	7.260(3)	9.720(2)
b [Å]	11.202(4)	17.829(3)
c [Å]	13.914(7)	11.096(3)
α [°]	86.97(3)	90
β [°]	87.46(4)	104.16(2)
γ [°]	75.33(4)	90
V [Å^3]	1092.6(8)	1864.6(7)
D(calcd.) [g/cm^3]	1.877	1.831
μ [mm^{-1}]	1.518	1.657
Crystal size [mm]	0.66 × 0.44 × 0.41	0.14 × 0.25 × 0.58
2θ range [°]	4.00−48.00	4.00−50.00
Index ranges	±8, ±12, +15	±11, +21, +13
Collected reflections	3416	3438
Independent reflections	3416 (R_{int} = 0.0000)	3269 (R_{int} = 0.0550)
Obsd. with $I > 2\sigma(I)$	2912	1662
Data/restraints/ parameters	3416/2/371	3269/0/224
Goodness-of-fit on F^2	1.044	0.952
R_1 [$I > 2\sigma(I)$]	0.0378	0.0652
R_1 (all data)	0.0470	0.1444
Largest diff. peak/hole [e/Å^3]	1.716/−0.685	1.546/−0.671

transferred to an Enraf-Nonius CAD4 diffractometer. For both compounds the intensity data were collected with the Enraf-Nonius data-collection package for PC-driven diffractometers.[13] The crystals were centered with data in the range $14° \leq 2\theta \leq 36°$ and examination of the cell constants, systematic absences, and Niggli matrix[14] showed **1** to crystallize in the space group $P\bar{1}$ (no. 2) while **2** crystallizes in the space group $P2_1/c$ (no. 14). The intensity data were corrected for absorption using empirical curves derived from φ scans of suitable reflections. The solutions and refinements of the structures were carried out using SHELXS-86[15a] and SHELXL-93.[15b] The scattering curves were taken from Cromer and Waber's compilation.[16] During data collection three intensity and orientation standards were monitored and showed no significant deviations from the initial values. A summary of data collection and refinements for both compounds is given in Table 3. Selected bond lengths and angles for **1** and **2** are given in Tables 1 and 2, respectively. Crystallographic data (excluding structure factors) for the structures reported in this paper have been deposited with the Cambridge Crystallographic Data Centre as supplementary publication nos. CCDC-1018665 and -101866. Copies of the data can be obtained free of charge on application to CCDC, 12 Union Road, Cambridge CB2 1EZ, UK [Fax: int. code + 44-1223/336-033; E-mail: deposit@ccdc.cam.ac.uk].

Acknowledgments

We thank the Robert A. Welch Foundation for support of this research (Grant E-592 to I. B.) and for a fellowship granted to H. C.; I. B. also thanks the National Science Foundation for the funds used in purchasing the diffractometer.

[1] I. Bernal, J. Cetrullo, W. G. Jackson, *Inorg. Chem.* **1993**, *32*, 4098.
[2] I. Bernal, J. Cetrullo, W. G. Jackson, *J. Coord. Chem.* **1993**, *28*, 89.
[3] G. B. Kauffman, E. V. Linley, Jr., *Inorg. Synth*. **1976**, *8*, 198.
[4] M. Kuramoto, Y. Kushi, and. H. Yoneda, *Bull. Chem. Soc. Jpn.* **1978**, 51.
[5] P. C. Christides, P. J. Rentzeperis and C. A. Bolos, *Z. Kristallogr.* **1986**, *177*, 107.
[6] R. Steudel, G. Holdt, T. Göbel, W. Hazeu, *Angew. Chem. Int. Ed. Engl.* **1987**, *26*, 151.
[7] *Cambridge Structural Database* (version released April, 1998): F. H. Allen, J. E. Davies, J. J. Galloy, O. Johnson. O. Kennard, C. F. Macrae, E. M. Mitchell, G. F. Mitchell, J. M. Smith, D. G. Watson, *J. Chem. Info. Comp. Sci.* **1991**, *31*, 187.
[8] *Inorganic Crystal Structure Datebase*: M. Berndt, © FIZ Karlsruhe and Gmelin-Institut, **1990**, release 97/2.
[9] F. Somoza, H. Chun, I. Bernal, unpublished results.
[10] D. A. Buckingham, J. D. Edwards, J. M. McLaughlin, *Inorg. Chem.* **1982**, *21*, 2770.
[11] D. A. Buckingham, P. J. Creswell, A. M. Sargeson, *Inorg. Chem.* **1975**, *14*, 1485
[12] Galbraith Laboratories, Inc., P. O. Box 51610, Knoxville, TN 37950-1610, USA.
[13] CAD4 Version 5.0, Delft Instruments X-Ray Diffraction, P. O. Box 811, 2600 AV Delft, Netherlands.
[14] R. B. Roof, *A Theoretical Extension of the Reduced Cell Concept in Crystallography*, Report LA-4038, Los Alamos Scientific Laboratory, **1969**.
[15] [15a] G. M. Sheldrick, *Acta Crystallogr.* **1990**, *A46*, 467. – [15b] G. M. Sheldrick, *SHELXL-93*, University of Göttingen, Germany, **1993**.
[16] D. T. Cromer, J. T. Waber, *International Tables for X-Ray Crystallography*, vol. IV, Tables 2.2.8 and 2.3.1, respectively, for the scattering factor curves and the anomalous dispersion values, The Kynoch Press, Birmingham, England, **1975**.

Received June 19, 1998
[98193]

Crystal Structures of Oxalato and Oxamido Polyaminecobalt(III) Complexes Produced by Hydrolysis of Monooxamide

Hyungphil Chun,[a] Bobby J. Salinas,[a] and Ivan Bernal*[a]

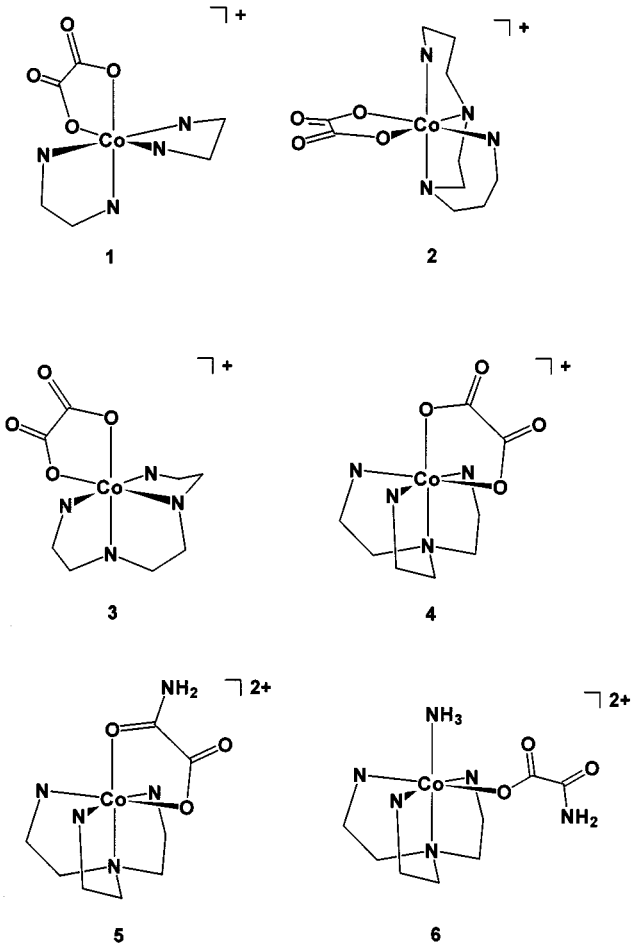
Keywords: Monooxamide / Amide hydrolysis / Cobalt(III)

The reactions of sodium monooxamide (H_2NCOCO_2Na) with *trans*-[Co(en)$_2$Cl$_2$]Cl, *trans*-[Co(3,2,3-tet)Cl$_2$]Cl (3,2,3-tet = 1,5,8,12-tetraazadodecane), *cis*-α-[Co(trien)Cl$_2$]Cl and [Co(tren)Cl$_2$]Cl result in the formation of [Co(en)$_2$(ox)]Cl · 4H_2O (**1**), *cis*-β-[Co(3,2,3-tet)(ox)]Cl· 4 H_2O (**2**), *cis*-α-[Co(trien)(ox)]Cl · 2 H_2O (**3**), and [Co(tren)(ox)](ClO_4) · 0.5 H_2O (**4**) respectively, implying a hydrolytic cleavage of the amide bond. [Co(tren)(*O*,*O*′-oxam)]Cl$_2$ · 2 H_2O (**5**) (oxam = $H_2NCOCO_2^-$) and *p*-[Co(tren)(NH_3)(*O*-oxam)]Cl$_2$ (**6**) have also been prepared in order to give mechanistic information for the hydrolysis of monooxamide. Crystal structures of the products are reported and possible pathways for the hydrolysis reactions are discussed.

Since we discovered[1] that compounds of composition [Co(en)$_2$(ox)]X · **n** H_2O (X = Cl^-, *n* = 4; X = Br^-, *n* = 1; X = I^-, *n* = 0) crystallize as conglomerates (conglomerate crystallization is a spontaneous resolution of a racemic solution by crystallization), we have decided to explore the effect of substituting the oxalato ligand with monooxamide ($H_2NCOCO_2^-$) in order to know whether it will displace *cis*- or *trans*-dichloro ligands of Co^{III} to act as a bidentate ligand as oxalate does, and whether additional hydrogen atoms of the NH_2 group will play a major role in their crystallization modes. Much to our surprise, the original purpose in designing this study has not been accomplished since the reaction products we isolated are not monooxamides; instead, they are oxalates obtained by the hydrolysis of the amide bond of the monooxamide anion.

Realizing that this hydrolysis occurs by dichlorocobalt(III) complexes with various types of multidentate polyamine ligands, such as (en)$_2$, 3,2,3-tet, or trien, we thought that we could obtain more detailed information about the hydrolysis of monooxamide including the reaction pathway if a Co^{III} compound with monodentate or bidentate monooxamide could be isolated and characterized unequivocally. *p*-[Co(tren)(NH_3)Cl]$^{2+}$ (the prefix *p*- denotes that the chloro ligand is *trans* to the primary nitrogen atom of the tren ligand) and [Co(tren)Cl$_2$]$^+$ ions were used for that purpose and *O*-bound monodentate and *O*,*O*′-bound bidentate monooxamidecobalt(III) complexes were obtained, respectively.

Although several studies describing the "catalytic" effects of Co^{III} complexes such as *cis*-[$CoN_4(OH_2)(OH)$]$^{2+}$, where N_4 is trien,[2] two ethylenediamines,[3] and tren,[4] and [Co(dien)X][5] (X = tripeptides) on the hydrolysis of amides and peptides have been reported, an amide hydrolysis has not previously been observed with *cis*- or *trans*-dihalo compounds of Co^{III} as in the case of **1**−**4**. Also the formation of oxamido compounds **5** and **6** is unique in that no trivalent transition metal compound containing monooxamide as a monodentate or bidentate ligand has been structurally characterized.



Scheme 1. Line-drawing formulas of the cations of compounds **1**−**6**

[a] Department of Chemistry, University of Houston, Houston, Texas 77204-5641, USA
Fax: (internat.) + 1-713/743-2709
E-mail: ibernal@uh.edu

 © WILEY-VCH Verlag GmbH, D-69451 Weinheim, 1999 1434−1948/99/0404−0723 $ 17.50+.50/0

Results and Discussion

In an attempt to probe the effect of exchanging monooxamide for oxalate ligands and recording its crystallization behavior we found that we had not prepared the desired $[Co(en)_2(O,O'\text{-oxam})]Cl_2$. Instead, we isolated the known conglomerate of oxalato compound **1** which suggests that the monooxamide anion had undergone hydrolysis at the amide bond. These results are reproducible and it makes no difference whether one uses the *cis* or *trans* isomer of the dichloro derivative. The structure of the resulting oxalato compound is identical with the published one[1] (see crystallography section).

In order to test the generality of the above observation, we treated the *trans*-$[Co(3,2,3\text{-tet})Cl_2]^+$ ion with sodium monooxamide, which resulted in the formation of the new compound **2**. Its structure (Figure 1) shows that the Co(3,2,3-tet) moiety displays the *cis*-β configuration and that the oxalato ligand faces an asymmetric surface in which one carbonyl group faces two chelate rings (a five- and a six-membered ring) and the other carbonyl group faces a single, six-membered ring, leading to two separate peaks for the carbonyl carbon atoms in the ^{13}C-NMR spectrum (see Experimental Section).

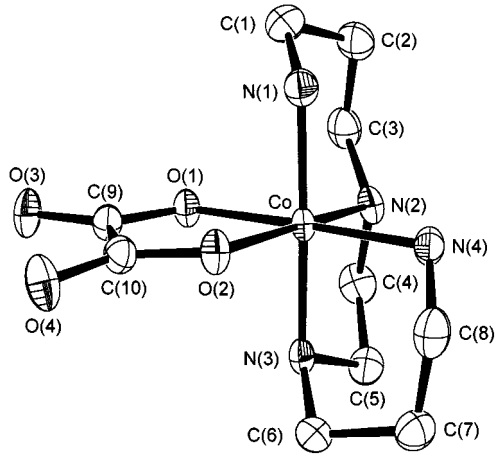


Figure 1. Structure of the cation of **2** drawn at 50% probability level; hydrogen atoms have been omitted for clarity; selected bond lengths and angles: Co−N(1) 1.968(2), Co−N(2) 1.959(2), Co−N(3) 1.961(2), Co−N(4) 1.963(2), Co−O(1) 1.912(2), Co−O(2) 1.921(2) Å; O(1)−Co−O(2) 85.21(7), O(1)−Co−N(2) 89.00(8), O(2)−Co−N(4) 91.86(8), O(1)−Co−N(4) 176.99(8), O(2)−Co−N(2) 173.44(8), N(1)−Co−N(3) 178.66(10)°

Compound **3** whose structure is shown in Figure 2 is the product of the reaction of the *cis*-α-$[Co(trien)Cl_2]^+$ ion with sodium monooxamide and indicates the generality of the reaction of *cis*- and *trans*-dichloropolyaminecobalt(III) with monooxamide.

Interestingly, a compound of composition $\{cis\text{-}\alpha\text{-}[Co(trien)(ox)]Cl\}_2 \cdot 9\ H_2O$ was prepared by rational methods and its structure has been reported by this group.[6] The only difference between the two is the number of waters of hydration, a phenomenon which seems to be common in coordination compounds as observed earlier and discussed in some detail.[7] It also would be interesting to note that

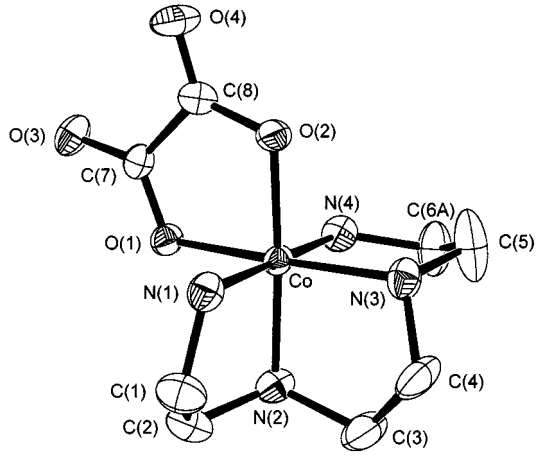


Figure 2. Structure of the cation of **3** drawn without hydrogen atoms; note that C(6) is disordered over two positions corresponding δ and λ conformations and only the former is shown; selected bond lengths and angles: Co−N(1) 1.958(3), Co−N(2) 1.940(3), Co−N(3) 1.943(3), Co−N(4) 1.949(3), Co−O(1) 1.908(2), Co−O(2) 1.906(2) Å; O(1)−Co−O(2) 85.60(10), O(1)−Co−N(2) 93.50(11), O(2)−Co−N(3) 93.80(11), O(1)−Co−N(3) 175.33(11), O(2)−Co−N(2) 174.93(11), N(1)−Co−N(4) 178.65(12)°

the crystal structure of the same compound as **3** but with *cis*-β configuration has been reported.[8]

Compound **4** whose crystal structure has not been reported was prepared by simple ligand displacement of chlorides with oxalate or by base hydrolysis of monooxamide with $[Co(tren)Cl_2]Cl$. As the structure of the cation shown in Figure 3 implies, only one peak is observed for the carbonyl carbon atoms in the ^{13}C-NMR spectrum. The crystallographic asymmetric unit of compound **4** contains two independent molecules and the two molecules are different only in that the five-membered chelate ring which is *trans* to the oxalato ligand has δ and λ conformations in Co(1a) and Co(1b) cations, respectively.

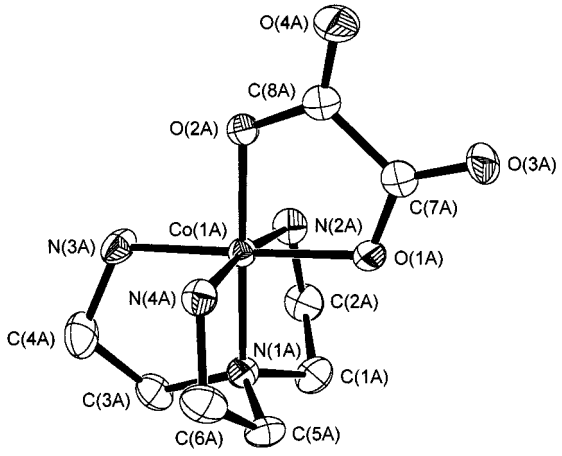


Figure 3. Structure of one of the two cations of **4**; the three chelate rings of tren ligand have (λδδ) conformation; the Co(1b) cation which is not shown here has (λλδ) conformation; selected bond lengths and angles: Co(1a)−N(1a) 1.936(4), Co(1a)−N(2a) 1.954(4), Co(1a)−N(3a) 1.938(4), Co(1a)−N(4a) 1.951(4), Co(1a)−O(1a) 1.925(3), Co(1a)−O(2a) 1.906(3) Å; O(1a)−Co(1a)−O(2a) 85.18(14), O(1a)−Co(1a)−N(1a) 94.2(2), O(2a)−Co(1a)−N(3a) 93.2(2), O(1a)−Co(1a)−N(3a) 177.9(2), O(2a)−Co(1a)−N(1a) 179.4(2), N(2a)−Co(1a)−N(4a) 171.9(2)°

When $[Co(tren)Cl_2]Cl$ was allowed to react with monooxamide in a neutral aqueous solution in a temperature range of 20−45°C, the hydrolysis does not occur and both chloro ligands are replaced by *O*,*O*′-bound monooxamide to give compound **5**. The structure of the cation is shown in Figure 4 and two separate peaks for the carbonyl carbon atoms are observed in the ^{13}C-NMR spectrum, as expected.

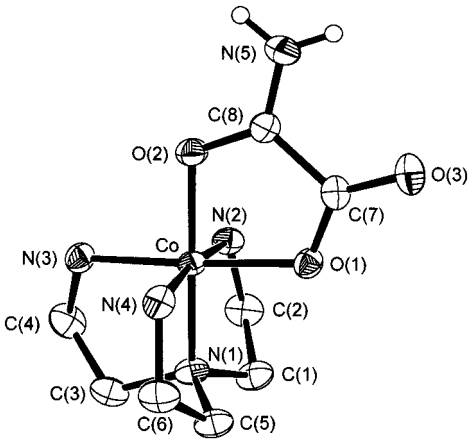


Figure 4. Structure of the cation of **5** showing the bidentate monooxamide ligand; hydrogen atoms of the tren ligand have been omitted for clarity; selected bond lengths and angles: Co−N(1) 1.918(3), Co−N(2) 1.957(3), Co−N(3) 1.931(3), Co−N(4) 1.957(3), Co−O(1) 1.929(2), Co−O(2) 1.917(3) C(8)−N(5) 1.299(5) Å; O(1)−Co−O(2) 85.00(11), O(1)−Co−N(1) 94.80(13), O(2)−Co−N(3) 92.51(13), O(1)−Co−N(3) 177.01(13), O(2)−Co−N(1) 179.63(12), N(2)−Co−N(4) 172.53(13)°

The Cambridge Structural Database[9] lists three transition metal compounds which contain bidentate *O*,*O*′-bound monooxamide ligands. They are of the structure type $[M(O,O'\text{-oxam})_2(H_2O)_x] \cdot n\ H_2O$ (M = Co^{2+}, $x = 2$, $n = 2$[10]; M = Zn^{2+}, $x = 2$, $n = 0$[11]; M = Cd^{2+}, $x = 4$, $n = 0$[12]). Note that all of them bore divalent metal cations.

Finally, the *p*-$[Co(tren)(NH_3)Cl]^{2+}$ ion was treated with monooxamide to give compound **6**. The structure of the cation (Figure 5) shows that only the chloro ligand has been replaced, as expected, by a monodentate *O*-bound monooxamide whose amide bond is still intact, which suggests that an unactivated amide bond of monooxamide would not easily be hydrolyzed, if at all.

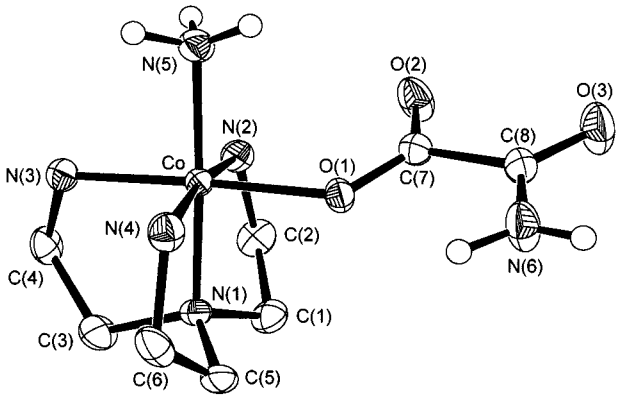
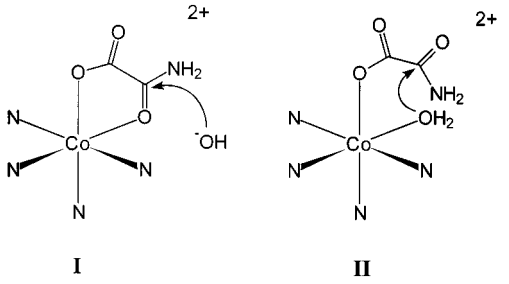


Figure 5. Structure of the cation of **6** showing the dangling NH_2 group of the monodentate monooxamide ligand; hydrogen atoms of the tren ligand have been omitted for clarity; selected bond lengths and angles: Co−N(1) 1.949(2), Co−N(2) 1.970(2), Co−N(3) 1.927(3), Co−N(4) 1.960(3), Co−O(1) 1.949(2), Co−N(5) 1.943(2) C(8)−N(6) 1.321(4) Å; O(1)−Co−N(2) 92.47(10), O(1)−Co−N(4) 83.24(10), O(1)−Co−N(5) 91.13(10), O(1)−Co−N(3) 175.53(10), N(5)−Co−N(1) 177.36(11), N(2)−Co−N(4) 171.19(11)°

As far as we know, a transition metal compound containing a monodentate monooxamide ligand has never been structurally characterized.

As reviewed earlier,[13] two reaction pathways, the so-called "direct activation" and "intramolecular attack", have been postulated for the hydrolysis of amide bonds by Co^{III} complexes. Although a detailed discussion concerning the hydrolysis mechanism can not be made without kinetic data obtained under pH-controlled condition, two key intermediates can be considered for this work according to the above concepts (Scheme 2).



Scheme 2. Key step for direct activation (**I**) and intramolecular attack (**II**)

Species **I** and **II** correspond to the direct activation and intramolecular attack, respectively. For compounds **1**−**3**, the possibility of hydrolysis through intermediate **I** can be excluded for the following reasons. First, relatively flexible binding modes of $(en)_2$, 3,2,3-tet, or trien coupled with labile chloro ligands would allow coordination of a solvent water molecule before monooxamide became a bidentate ligand. This is especially true for **1** and **2** which undergo *trans*/*cis* isomerization at raised temperature. Second, "neutral", deionized, solvent water used in this work was in fact slightly acidic (pH = 5.40) due to atmospheric CO_2, which makes the attack of HO^- ion to the amide carbon atom less likely to occur. The possibility of attack of solvent water to bidentate monooxamide can also be removed as the presence of compound **5** implies. Therefore, we cautiously adopt the intramolecular attack of a coordinated water molecule as the correct mechanism for the hydrolysis of monooxamide by Co^{III} complexes with configurationally versatile multidentate amine ligands.

The behavior of monooxamide with $[Co(tren)Cl_2]Cl$ also supports this argument. That is, when the multidentate amine ligand of a Co^{III} complex is configurationally rigid and chloro ligands are relatively stable with respect to the substitution by solvent water molecules, monooxamide coordinates as a bidentate ligand as in compound **5** and the hydrolysis of the amide bond does not occur. Once monooxamide is coordinated as a bidentate ligand, an additional source of HO^- ions is necessary in order to hydrolyze the amide bond.

In conclusion, monooxamide was found to be hydrolyzed by Co^{III} complexes containing various types of polyamine tetradentate ligands, such as $(en)_2$, 3,2,3-tet, trien, or tren to give their corresponding oxalato compounds **1**, **2**, **3**, and **4**, respectively. In compounds **1**, **2**, and **3**, intramolecular attack of coordinated water molecule is the likely pathway for the hydrolysis reactions. In compound **4**, the hydrolysis reaction seems to occur by attack of HO^- ions to the amide carbon atom of the bidentate monooxamide ligand. Compounds **5** and **6** are also important not only from their structural point of view, but also because of their implications in the hydrolysis mechanism.

Experimental Section

General: H_2NCOCO_2Na (Aldrich Chemical Company) and $(NH_4)_2C_2O_4 \cdot H_2O$ (Fisher Scientific Company) were used as received. *trans*-$[Co(en)_2Cl_2]Cl$,[14] *trans*-$[Co(3,2,3\text{-tet})Cl_2]Cl$,[15] *cis*-α-$[Co(trien)Cl_2]Cl \cdot 2\ H_2O$,[7] $[Co(tren)Cl_2]Cl$,[16] and *p*-$[Co(tren)(NH_3)Cl]Cl(ClO_4)$[17] were prepared using known methods. Elemental analyses were carried out by the Galbraith laboratories.[18] ^{13}C-NMR spectra were recorded with a GE QE-300 instrument using TMSPA as the internal standard.

$[Co(en)_2(ox)]Cl \cdot 4\ H_2O$ (1): 30 mL of an aqueous solution of 2.00 g (18 mmol) of H_2NCOCO_2Na was slowly added to a greenish solution of 4.08 g (14 mmol) of *trans*-$[Co(en)_2Cl_2]Cl$ in 30 mL of water. While heating the solution at 60°C, the color changed to purple and finally to red. When the volume was reduced to about 15 mL, it was allowed to stand at room temperature. After 10 d, red crystals were obtained which effloresce upon removal from the mother liquor. The compound was analyzed after drying to constant weight. − $C_6H_{16}ClCoN_4O_4$ (302.64): calcd. C 23.81, H 5.34, N 18.52; found C 22.55, H 5.59, N 17.90.

***cis*-β-[Co(3,2,3-tet)(ox)]Cl · 4 H_2O (2):** The same procedure as in the case of **1** was employed using *trans*-$[Co(3,2,3\text{-tet})Cl_2]Cl$. Red crystals were obtained after 10 d at room temperature. − $C_{10}H_{30}ClCoN_4O_8$ (428.76): calcd. C 28.01, H 7.07, N 13.07; found C 27.95, H 6.98, N 13.20. − ^{13}C NMR (300 MHz, D_2O): δ = 168.38 and 168.44 (2 C=O), 20.97, 26.01, 37.69, 38.22, 44.74, 47,49, 48.45, and 53.37 (8 CH_2).

***cis*-α-[Co(trien)(ox)]Cl · 2 H_2O (3):** The same procedure as in the case of **1** was used by treating equimolar amounts of *cis*-α-$[Co(trien)Cl_2]Cl \cdot 2\ H_2O$ and H_2NCOCO_2Na. Red crystals were collected after 3 weeks. − $C_8H_{22}ClCoN_4O_6$ (364.67): calcd. C 26.35, H 6.08, N 15.36; found C 25.80, H 6.08, N 15.46.

$[Co(tren)(ox)]ClO_4 \cdot 0.5\ H_2O$ (4): ***Warning: Metal amine perchlorates may be explosive!*** A solution of ammonium oxalate (0.46 g, 3.24 mmol) in 11 mL of water was added to a solution of $[Co(tren)Cl_2]Cl$ (1.00 g, 3.21 mmol) in 12 mL of water. The initially formed purple precipitate dissolved and the solution turned a clear red color after heating for 10 min; 0.40 g (3.27 mmol) of $NaClO_4$ was then added and the solution was filtered. Red crystals were formed upon standing and collected after 2 weeks (0.99 g, 77%). − $C_8H_{19}ClCoN_4O_{8.5}$ (401.65): calcd. C 23.92, H 4.77, N 13.95; found C 23.70, H 4.87, N 13.90. − ^{13}C NMR (300 MHz, D_2O):

Table 1. Summary of crystal data and structure refinement for oxalato compounds **2**, **3**, and **4**

	2	**3**	**4**
Empirical formula	$C_{10}H_{30}ClCoN_4O_8$	$C_8H_{22}ClCoN_4O_6$	$C_8H_{19}ClCoN_4O_{8.5}$
Molecular mass	428.76	364.68	401.65
T [K]		293(2)	
λ [Å]		0.71073	
Crystal system	Monoclinic	Triclinic	Triclinic
Space group	$P2_1/n$	$P\bar{1}$	$P\bar{1}$
a [Å]	8.186(2)	6.996(4)	11.1307(13)
b [Å]	15.508(7)	8.822(1)	11.508(2)
c [Å]	14.569(3)	12.537(2)	11.595(4)
α [°]	90	89.13(2)	97.45(2)
β [°]	102.53(1)	75.72(3)	90.609(12)
γ [°]	90	81.39(3)	97.955(12)
V [Å^3]	1805.6(9)	741.2(5)	1457.9(6)
Z	4	2	4
$D_{calcd.}$ [g/cm^3]	1.577	1.634	1.830
μ [mm^{-1}]	1.143	1.367	1.412
F(000)	904	380	828
Crystal size [mm]	0.53 × 0.34 × 0.29	0.49 × 0.17 × 0.16	0.50 × 0.30 × 0.26
θ range [°]	2 to 25	2 to 25	2 to 25
Index ranges (h, k, l)	±9, +18, +17	±8, ±10, +14	+13, ±13, ±13
Reflections collected	3387	2729	5392
independent (R_{int})	3163 (0.0212)	2597 (0.0247)	5107 (0.0634)
observed [I>2σ(I)]	2270	1844	3159
Absorption correction		ψ scan	
Transmission	0.9996−0.8779	0.9965−0.9382	0.9930−0.8425
Refinement method		Full-matrix least-squares on F^2	
Data/restraints/param.	3163/0/337	2597/0/208	5107/2/414
GOF on F^2	0.972	1.094	1.042
R indices[a] [$I > 2\sigma(I)$]	R_1 = 0.0266	R_1 = 0.0334	R_1 = 0.0480
	wR_2 = 0.0617	wR_2 = 0.0877	wR_2 = 0.1291
R indices (all data)	R_1 = 0.0543	R_1 = 0.0653	R_1 = 0.0995
	wR_2 = 0.0667	wR_2 = 0.0950	wR_2 = 0.1415
Largest diff. peak and hole [e/Å^3]	0.228 and −0.276	0.436 and −0.290	1.373 and −0.648

[a] $R_1 = \Sigma||F_o| - |F_c||/\Sigma|F_o|$, $wR_2 = [\Sigma w(F_o^2 - F_c^2)^2/\Sigma w(F_o^2)^2]^{1/2}$ and $w = 1/[\sigma^2F_o^2 + (a \cdot P)^2]$, where $P = (F_o^2 + 2\ F_c^2)/3$.

δ = 166.57 (2 C=O), 43.38, 44.12, 59.47, and 61.56 (6 CH_2). − The same product was obtained by adding 0.21 g (5.25 mmol) of NaOH to a solution containing 1.00 g (3.21 mmol) of [Co(tren)Cl_2]Cl and 0.36 g (3.24 mmol) of H_2NCOCO_2Na in 15 mL of water. The resulting dark red solution was filtered after stirring for 30 min; 0.4 g (3.27 mmol) of $NaClO_4$ was added to the solution after 5 d and the solution was filtered. The solution was filtered off frequently whenever a powdery precipitate was formed until red single-crystals suitable for X-ray diffraction study were obtained. The unit cell parameters [a = 11.1569(21), b = 11.5038(22), c = 11.5904(117) Å, α = 97.377(35), β = 90.782(31), γ = 97.974(14)°] and the Laue class of the unit cell were identical, within experimental error, with those of the compound prepared from ammonium oxalate, and therefore X-ray data were not collected. − calcd. C 23.92, H 4.77, N 13.95; found C 23.64, H 5.03, N 13.91.

[Co(tren)(O,O′-oxam)]Cl_2 · 2 H_2O (5): A mixture of 0.18 g (1.62 mmol) of H_2NCOCO_2Na in 3 mL and 0.50 g (1.61 mmol) of [Co(tren)Cl_2]Cl in 10 mL of water was stirred for 30 min at room temperature and then filtered. Red plate crystals were obtained upon standing and collected after 8 d (0.58 g, 90%). − $C_8H_{24}Cl_2CoN_5O_5$ (400.15): calcd. C 24.01, H 6.05, N 17.50; found C 22.75, H 5.68, N 16.21. Although duplicate analyses were carried out due to the disagreement between calculated and experimental results, all the experimental values were consistently smaller than calculated values. Because there is no doubt in the crystal structure and because the ratio of the number of each element to the other showed good agreement with calculated values, the apparent disagreement was ignored. − ^{13}C NMR (300 MHz, D_2O): δ = 166.53 [C(=O)O], 170.67 [C(=O)NH_2], 43.72, 44.13, 60.68, and 62.91 (6 CH_2). − In a separate experiment, the initial reaction mixture was warmed at 45°C for 30 min and then filtered. The purple solution turned red within 4 h. Red plate crystals were obtained upon standing and examined on a X-ray diffractometer to give the same unit cell parameters [a = 11.2172(45), b = 22.4952(76), c = 12.8525(120) Å, α = β = γ = 90°] and Laue symmetry as the compound obtained from the room-temperature reaction, and therefore X-ray data were not collected. − ^{13}C NMR (300 MHz, D_2O): δ = 166.50 [C(=O)O], 170.69 [C(=O)NH_2], 43.55, 43.96, 60.47, and 62.73 (6 CH_2).

***p*-[Co(tren)(NH_3)(O-oxam)]Cl_2 (6):** A partly dissolved solution containing 1.12 g (2.85 mmol) of *p*-[Co(tren)(NH_3)Cl]Cl(ClO_4) in 20 mL of water was directly filtered into a solution of H_2NCOCO_2Na (0.32 g, 2.88 mmol) in 10 mL of water. Small amounts of red crystals suitable for X-ray diffraction were obtained by liquid diffusion with acetone and collected after 10 d. − $C_8H_{23}Cl_2CoN_6O_3$ (381.15): calcd. C 25.21, H 6.09, N 22.05; found C 25.18, H 6.19, N 21.95.

Crystallography: For all six compounds the intensity data were collected with an Enraf-Nonius CAD4 diffractometer. Although the crystal of **1** was mounted inside a sealed capillary tube in order to prevent decay, it completely lost its crystallinity after collecting 1267 reflections with a total X-ray exposure time of 82387 s (22.87 h). The unit cell was orthorhombic with a = 6.340(3), b = 11.976(3), and c = 20.290(6). The limited data set showed only three systematic absences, $h \neq 2n$ for (h00), $k \neq 2n$ for (0k0) and $l \neq 2n$ for (00l), implying the unique space group $P2_12_12_1$ (no. 19). It was then noticed that the symmetry and unit cell dimensions agree with [Co(en)$_2$(ox)]Cl · 4 H_2O of ref.[1], which is orthorhombic, $P2_12_12_1$, a = 6.349(3), b = 11.969(4), and c = 20.311(5), and isotropic refinement of the structure using the atomic coordinates from the reference gave an R factor of 16% for 413 observed reflections [$I > 2\sigma(I)$]. For the compounds **2**−**6** routine procedures were used to collect data and solve the structures. Hydrogen atoms of **3**, **4**, and **5** were placed in their geometrically ideal positions with isotropic temperature factors 1.2 times of those of the attached non-hydrogen atoms. However, hydrogen atoms of water molecules and monooxamide ligand of those compounds along with all hydrogen atoms of **2** and **6** were located from difference maps and refined isotropically. SHELXS-86[19] and SHELXL-93[20] were used for solution and refinement, respectively. Parameters for data collection and structure refinements are summarized in Table 1 and 2. Crystallographic data (excluding structure factors) for the structures reported in this paper have been deposited with the Cambridge Crystallographic Data Centre[9] as supplementary publication no. CCDC-111984 to CCDC-111988.

Table 2. Summary of crystal data and structure refinement for oxamido compounds **5** and **6**

	5	**6**
rEmpirical formula	$C_8H_{24}Cl_2CoN_5O_5$	$C_8H_{23}Cl_2CoN_6O_3$
Molecular mass	400.15	381.15
T [K]	293(2)	
λ [Å]	0.71073	
Crystal system	Orthorhombic	Monoclinic
Space group	*Pbca*	$P2_1/c$
a [Å]	11.2213(9)	8.212(2)
b [Å]	22.502(2)	10.941(2)
c [Å]	12.913(2)	16.881(3)
β [°]	90	92.45(1)
V [Å^3]	3260.7(6)	1515.4(5)
Z	8	4
$D_{calcd.}$ [g/cm^3]	1.630	1.671
μ [mm^{-1}]	1.407	1.501
F(000)	1664	792
Crystal size [mm]	0.69 × 0.67 × 0.34	0.60 × 0.33 × 0.27
θ range [°]	2 to 25	2 to 25
Index ranges (h, k, l)	+13, +26, +15	±9, +12, +20
Reflections collected	2857	2745
iIndependent (R_{int})	2857 (0.0000)	2657 (0.0190)
observed [$I>2\sigma(I)$]	1678	1881
Absorption correction	ψ scan	
Transmission	0.9995−0.6583	0.9940−0.8514
Refinement method	Full-matrix least-squares on F^2	
Data/restraints/ parameters	2857/0/215	2657/0/273
GOF on F^2	0.958	1.014
R indices [$I > 2\sigma(I)$]	R_1 = 0.0347, wR_2 = 0.0876	R_1 = 0.0287, wR_2 = 0.0724
R indices (all data)	R_1 = 0.0913, wR_2 = 0.0996	R_1 = 0.0543, wR_2 = 0.0781
Extinction coefficient	0.0071(4)	−
Largest diff. peak and hole [e/Å^3]	0.429 and −0.436	0.421 and −0.371

Acknowledgments

We thank the Robert A. Welch Foundation for support of this research (Grant E-592 to I. B.) and for a fellowship granted to H. C. We appreciate the support B. J. S. received from the Center for Mexican-American Studies. Also, I. B. thanks the National Science Foundation for the funds used in purchasing the diffractometer.

[1] I. Bernal, J. Cetrullo, J. Myrczek, S. S. Massoud, *J. Coord. Chem.* **1993**, *30*, 29.
[2] [2a] J. P. Collman, D. A. Buckingham, *J. Amer. Chem. Soc.* **1963**, *85*, 3039. − [2b] D. A. Buckingham, J. P. Collman, D. A. R. Happer, L. Marzilli, *J. Amer. Chem. Soc.* **1966**, *85*, 1082.
[3] J. P. Collman, D. A. Buckingham, *Inorg. Chem.* **1967**, *6*, 1803.
[4] E. Kimura, S. Young, J. P. Collman, *Inorg. Chem.* **1970**, *9*, 1183.

[5] R. Gillard, D. A. Phipps, *J. Chem Soc., Chem. Commun.* **1970**, 800.
[6] I. Bernal, J. Cetrullo, J. Cai, *Trans. Met. Chem.* **1994**, *19*, 221.
[7] I. Bernal, *J. Coord. Chem.* **1987**, *15*, 337.
[8] E. C. Sheu, M. Shang, A. G. Lappin, *Inorg. Chem.* **1996**, *35*, 3031.
[9] Cambridge Crystallographic Data Centre, 12 Union Road, Cambridge, CB2 1EZ, UK.
[10] M. A. Pellinghelli, A. Tiripicchio, M.Tiripicchio Camellini, *Acta Crystallogr., Sect. B* **1972**, *28*, 998.
[11] A. Braibanti, M. A. Pellinghelli, A. Tiripicchio, M.Tiripicchio Camellini, *Acta Crystallogr., Sect.B* **1971**, *27*, 1240.
[12] S. Skoulika, A. Michaelides, A. Aubry, *Acta Crystallogr., Sect.C* **1988**, *44*, 931.
[13] P. A. Sutton, D. A. Buckingham, *Acc. Chem. Res.* **1987**, *20*, 364.
[14] J. C. Bailar, Jr., *Inorg. Synth.* **1946**, *2*, 222.
[15] I. Bernal, J. Cetrullo, J. Cai,, S. S. Massoud, *Struct. Chem*. **1995**, *6*, 99.
[16] D. A. Buckingham, J. D. Edwards, G. M. McLaughlin, *Inorg. Chem.* **1982**, *21*, 2770.
[17] D. A. Buckingham, P. J. Creswell, A. M. Sargeson, *Inorg. Chem.* **1975**, *14*, 1485.
[18] Galbraith Laboratories, Inc., P. O. Box 51610, Knoxville, TN 37950−1610, USA.
[19] G. M. Sheldrick, *Acta Crystallogr., Sect A* **1990**, *46*, 467.
[20] G. M. Sheldrick, *SHELXL-93, A program for crystal structure determination*, University of Göttingen, **1993**.

Received December 10, 1998
[I98422]

New Rare-Gas-Containing Neutral Molecules

Mika Pettersson,[a] Jan Lundell,[a] and Markku Räsänen*[a]

Keywords: Ab initio calculations / Matrix isolation / Rare-gas compounds / Solid-state chemistry / Photochemistry

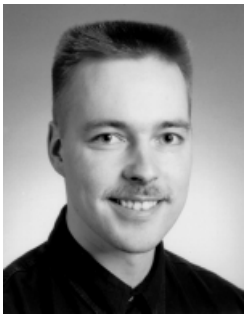
The synthesis of novel neutral rare-gas-containing molecules of type HXY, where X = Xe or Kr and Y is an electronegative atom or fragment, is discussed. The molecules are characterised experimentally by their vibrational spectra and computationally by extensive ab initio calculations. They are formed in low-temperature rare-gas solids from neutral reagents and their bonding consists of both covalent and ionic contributions. Our recent studies add to the previously known class of rare-gas chemical bonds in neutral ground-state molecules the new bonds Xe–H, Xe–I, Xe–Br, Xe–S, Kr–H, Kr–C, and Kr–Cl.

Introduction

The rare gases form one of the most abundant classes of constituents of our Universe. The beautiful octet rule led scientists to accept the nonreactivity of rare gases until 1933, when Linus Pauling suggested[1] from considerations of ionic radii of different elements that molecules like XeF_6 and KrF_6, and perhaps unstable compounds XeF_8 and H_4XeO_6, should be preparable. However, attempts to synthesize rare-gas-containing molecules were not successful at that time.[2]

It took about 30 years until the first rare-gas-containing chemical compound was found. Neil Bartlett reported[3a] first a solid compound with a structure $Xe^+[PtF_6]^-$, which was later shown to consist most probably of a mixture of $XeF^+PtF_6^-$ and $XeF^+Pt_2F_{11}^-$.[3b] The key idea for this discovery was the similar ionisation potentials of O_2 and Xe. Almost simultaneously independently of Bartletts results, Hoppe et al.[4] synthesized XeF_2, and slightly later, Claassen et al.[5] reported XeF_4. After these first findings a number of compounds, where Xe is bound to fluorine and/or oxygen, were characterised. The extent of rare-gas chemistry in its early stages accounted, in addition to the species

[a] Laboratory of Physical Chemistry,
P. O. Box 55, FIN-00014 University of Helsinki, Finland
E-mail: petters@csc.fi; lundell@csc.fi
markku.rasanen@helsinki.fi



Mika Pettersson (left, top), born in 1969, received his Ph.D. in 1998 from the laboratory of Physical Chemistry, University of Helsinki. The topic of his thesis was novel rare-gas compounds. At the moment he is continuing his investigations at the University of Helsinki. His research interests cover spectroscopy and computations on weakly bound and reactive species, photochemistry and IR-induced processes in low-temperature matrices.

Jan Lundell (left, bottom), born in 1966, received his Ph.D. in 1995 from the Laboratory of Physical Chemistry, University of Helsinki. After his Ph.D. he spent a postdoctoral year at the Fritz Haber Research Institute for Molecular Dynamics, The Hebrew University of Jerusalem with professor Robert B. Gerber. In 1996 he returned to University of Helsinki, where he is now as a postdoctoral researcher of the Academy of Finland. He focuses his interest on hydrogen-bonded complexes, weak chemical interactions, and photochemical processes of small molecules in low-temperature matrices.



Markku Räsänen (right), born in 1949, received his Ph.D. in 1983 from the Laboratory of Physical Chemistry, University of Helsinki. After this he spent a postdoctoral year at the AT&T Bell Laboratories, Murray Hill, NJ with professor Vladimir E. Bondybey. He was a senior researcher of the Academy of Finland and received in 1992 the position of Associate Professor in Physical Chemistry, University of Helsinki (the title was changed to Professor in 1998). His general interests are in spectroscopy (vibrational and time-resolved luminescence) and photochemistry of small impurity molecules in simple solids, e.g. rare gases at low temperatures. The light-induced processes of interest are bond dissociation with UV/Vis photons and conformational changes induced by vibrational excitations.



MICROREVIEWS: This feature introduces the readers to the authors' research through a concise overview of the selected topic. Reference to important work from others in the field is included.

 © WILEY-VCH Verlag GmbH, D-69451 Weinheim, 1999 1434–1948/99/0505–0729 $ 17.50+.50/0

mentioned above, for example molecules XeF_6, $XeOF_4$ and XeO_2F_2, $XeF_2 \cdot 2\,SbF_5$ and $XeF_6 \cdot AsF_5$ salts, and the XeF radical.[6−11] These species have been reviewed by several authors.[12−16] In addition, the theory of binding in the Xe compounds has been authoritatively reviewed by Coulson.[17]

These findings promoted an active search for the extent of chemical bonds between rare gases and other elements. In this search, carbon played an important role and the first reports on Xe−C bonds date in the early 1970s when the bond strength of CH_3Xe^+ was measured[18] (its value is 231.0 ± 10.5 kJ mol^{-1}[19]). Also, an unstable $FXeCF_3$[20] species has been suggested as a reaction intermediate and for $Xe(CF_3)_2$ a lifetime of ca. 30 min has been reported[21] even though the compound has not been characterised spectroscopically. A stable Xe−C-bonded molecule, pentafluorophenylxenon(II) fluoroborate, was found almost simultaneously by two groups in 1989.[22][23] After this, a number of novel organoxenonium compounds have been synthesized.[24][25]

Before the advent of Xe−C chemistry, some other elements were found to bond chemically to Xe. In an Xe matrix, Nelson and Pimentel[26] prepared $XeCl_2$ and also compound $FXeBF_2$ was reported.[27] In addition, in condensed phases xenon is found to form readily a dixenon cation (Xe_2^+).[28] The first Xe−N bond was found in fluoro-[imidobis(sulphuryl fluoride)]xenon, $FXeN(SO_2F)_2$.[29] After this, a number of xenon−nitrogen bonds were characterised in complex molecules.[30−38]

Chemistry related to the lighter rare gases is naturally much more sparse than that of Xe. The first reports dealt with fluorine−krypton compounds, molecules KrF_4[39] and KrF_2[40−42] being analogous to the fluorinated xenon compounds. Discoveries of Kr bonding to N and O have been done especially by the Schrobilgen group.[43−46]

The only serious candidate for Ar compounds, ArBeO, was prepared in low-temperature matrices by Thompson and Andrews.[47] The considerable spectral shifts suggested rather strong binding between Ar and BeO, and computational results give 0.29 eV for the interaction energy,[48] which is caused by induced dipole interactions. Various possible bonds between rare-gas atoms and other elements have been extensively studied theoretically by Frenking and Cremer.[49]

As referenced above, the early stages of rare-gas chemistry benefitted also of low-temparature matrix-isolation studies.[26,40,42,47] This method was originally developed for trapping unstable species and reaction intermediates at low temperatures.[50−52] The novel compounds described in this microreview have been up to now prepared in solid rare gases. In brief, the starting point for the preparation is the selection of a suitable hydrogen-containing precursor followed by photodissociative generation of hydrogen atoms and electronegative fragments and trapping them in the low-temperature solid for further reactions. The typically used precursors include hydrogen halides, HCN, H_2S etc. In solid rare gases, the photodissociation is often prevented by the strong cage effect.[53−58] However, the barrier for cage exit of hydrogen atoms during photodissociation in solid rare gases is relatively low, 1−2 eV[59][60], allowing photogeneration and isolation of H atoms. After preparation of the neutral reactants, hydrogen atoms are selectively mobilised by annealing the matrix at a suitable temperature (ca. 30 K for Kr and ca. 50 K for Xe). HXY-type rare-gas compounds (X = Kr or Xe; Y = Cl, Br, I, CN, ...) are then formed in a concerted reaction H + X + Y → HXY.

In this article we describe the solid-state synthesis of several HXY-type rare-gas molecules shown in Figure 1. It is to be noted that the present species *are not* van der Waals systems but truly chemically bound molecules. We give the spectral characteristics of these new compounds, describe their formation mechanism from neutral constituents as well as their stabilities. This review is based on original articles and a PhD Thesis during years 1995−1998.[61−67] Additionally, we connect ab initio results with the experimental data to aid the understanding of the bonding and charge distribution of the new molecules.

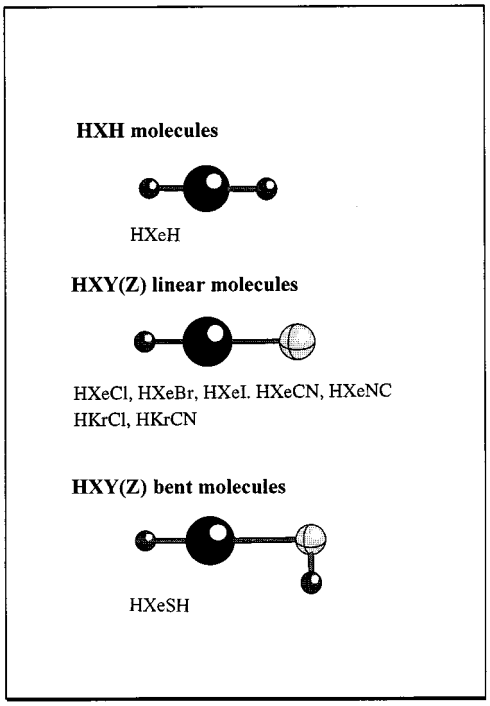


Figure 1. The HXH, HXY, and HXY(Z) molecules

Preparation of the HXY Molecules

In the following we describe shortly the solid-state experiments for preparing the new rare-gas-containing molecules. Solid rare gases (5−50 K) are used as the medium for synthesis and for spectroscopic identification of the formed species. The precursor molecules HY (hydrogen halides, HCN, H_2S, etc) are mixed with rare gases in the gas phase and isolated in a typical 1000-fold excess of the host atoms in a polycrystalline solid deposited onto an optically transparent substrate. The isolated species and their photoprod-

ucts can be monitored by measuring their infrared absorption spectra or by measuring the time-resolved luminescence spectra.

In order to promote the isolated precursor to photodissociative repulsive states different light sources can be used. The dissociation energies (D_0) of the hydrogen halides HCl, HBr, and HI are 4.43, 3.75, and 3.05 eV, respectively,[68] and various UV lamps work well for decomposing these precursors. For H_2S, photodissociation at 193 nm (ArF laser) is very efficient,[69] since the absorption maximum of the precursor is near this wavelength. Also HCN can be photodissociated at 193 nm in solid Kr and Xe even though the efficiency is low. Additionally, water, which is always present as an impurity, produces H atoms into the solid host upon 193 nm excitation.

Upon photolysis the IR absorptions of the precursor disappear and isolated H atoms and electronegative fragments Y are formed. This can be seen for instance from the appearance of the spin-orbit ($^2P_{1/2} \leftarrow {}^2P_{3/2}$) absorption at ca. 7600 and 3600 cm^{-1} for iodine and bromine atoms, respectively.[66] Both the H atoms and Y fragments are stable below the mobilisation temperature of hydrogen atoms (30−50 K). In very diluted matrices (M/A ratio > 1000), it is possible to convert a major part of the precursor molecules into hydrogen atoms and Y fragments. In more concentrated matrices, other processes like clusterization and photoinduced reactions of hydrogen atoms produce more complicated products and hydrogen molecules.[66,70]

The next step in the synthesis is the raising of the temperature to the point at which the photogenerated hydrogen atoms start to diffuse. In solid Xe, several separate experiments have shown that hydrogen atoms diffuse at around 45 K.[59,70−73] Randomly distributed hydrogen atoms diffuse until they find a Xe atom which has a fragment Y as a nearest neighbour. At this stage, these three fragments H, Xe, and Y react and form an HXY molecule. This process is described in Figure 2. Another possibility is a reaction of two hydrogen atoms with an Xe atom between them. This reaction produces xenon dihydride (HXeH) and it happens in any Xe matrix which contains hydrogen atoms. Most importantly, since HXY molecules are formed from H and Y which are too far from each other to be able to re-form the precursor HY, species HXY and HXeH are the major trapping sites for H atoms and Y fragments in solid rare gases after the mobilisation of hydrogen atoms.[67]

The formed HXY molecules are easily detected by IR spectroscopy since they have extremely intensive X−H stretching absorptions,[61,62,64,65] and the position of the stretching band is very characteristic for each Y. The Xe−H stretching bands of different HXeY molecules are presented in Figure 3. In addition to these absorptions, weaker bending absorptions can be detected for some of the compounds. Characteristic for HXeNC is also an intensive N−C stretching absorption. All vibrational bands of the HXY compounds observed thus far are collected in Table 1 including the deuterated compounds.

As can be seen from Table 1 and Figure 3, the position of the Xe−H stretching band (or more generally the X−H stretching band) changes considerably by varying the Y fragment. This property is rationalised in the following sections where the origin of the bonding is discussed. It will be shown that the position of the stretching band reflects both the Xe−H bond length as well as the charge distribution of the compounds. A striking example of this sensitivity of the ν_{Xe-H} absorption can be found by comparing the two isomers of HXeCN. For the more stable HXeCN the ν_{Xe-H} absorption is at 1624 cm^{-1} and it shifts +227

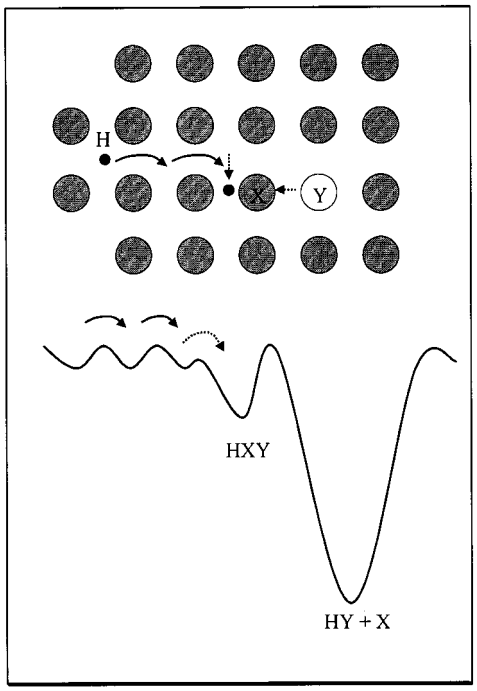


Figure 2. A schematic picture of the generation of the HXY (X = Kr, Xe; Y = Cl, Br, I, CN, ...) molecules in solid rare gases; the lower curve describes the potential energy

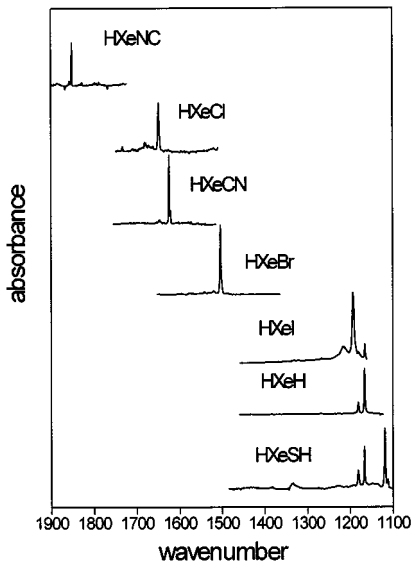


Figure 3. The Xe−H stretching absorptions of different HXeY compounds in solid Xe; note that the absorptions of HXeH at 1166 and 1181 cm^{-1} appear in the spectra of HXeI and HXeSH as well

cm^{-1} for HXeNC to 1851 cm^{-1}. This also measures the anisotropicity of the CN pseudohalogen.

The data in Table 1 also collects the observed overtones. At first it can be noted that HXeI, HXeBr, and HXeH show measurable intensity in the first overtone of Xe−H stretching vibration originating from anharmonic effects. Furthermore, this anharmonicity influences the fundamental wavenumber by several percent, which must be kept in mind while comparing the experimental and calculated (harmonic) wavenumbers.

Table 1. The observed IR absorptions [cm^{-1}] of different HXY(Z) compounds

Compound	ν[Xe−H(D)]	2ν[Xe−H(D)]	δ	2δ	ν(Y−Z)
HXeCl	1648				
DXeCl	1198				
HXeBr	1504	2869	489	965	
DXeBr	1100				
HXeI	1193	2190	450		
DXeI	893	1693			
HXeCN	1624				
DXeCN	1178				
HXeNC	1851				2044
DXeNC	1339				
HXeSH(D)	1119				
DXeSH(D)	833				
HXeH	1166, 1181	2003[a]	701		
HXeD	1093 ν(Xe−H) 753 ν(Xe−D)		621		
DXeD	846, 856		514		
HKrCl	1476		544	1070	
DKrCl	1106				
HKrCN	1497		618		
DKrCN	1109				

[a] Combination of symmetric and asymmetric Xe−H stretches or 2ν(Xe−H).

Mechanism of Formation

Before going into the details of bonding it is important to discuss the mechanism of formation of the rare-gas molecules. UV photolysis of halogen-doped rare gases may induce permanent charge separation as was shown by Fajardo and Apkarian,[74−76] which results in trapped ionic centers like X_2H^+, Y_2H^-, and X_n^+ (X = rare gas, Y = halogen).[77−80] Thus, thermal activation of the photolysed solids may also induce ionic reaction channels, which should not be neglected when considering the mechanism of formation of the HXY molecules. However, for HXeI we could experimentally show that the molecule originates from neutral atoms. The ν_{Xe-H} frequency of HXeI is 1193 cm^{-1}, $2\nu_{Xe-H}$ is 2190 cm^{-1}, and around energies $3\nu_{Xe-H} \approx$ 3000 cm^{-1} the molecule decomposes (see Figure 4). The HXeI photodissociation experiment[63] also yields the absorption profile for the $3\nu_{Xe-H}$ transition with an onset at 2950 cm^{-1} which can be taken as an approximate value for the D_0 dissociation energy of HXeI. After this IR decomposition the molecular form can be restored *quantitatively*. Important is that the quantitative restoration of the molecular form occurs at considerably lower temperatures than the global mobilisation of H atoms after initial UV photodissociation of the precursor. This means that the IR decomposition of HXeI produces atoms, which are in a dissociated form in close contact with each other and HXeI can be recovered by slight warming or even at the lowest temperatures by tunneling.[63] The low energy of the $3\nu_{Xe-H}$ infrared photons is not sufficient to produce ionic centers into the crystal and the only effect is bond breaking with the resulting neutral atoms being located at their van der Waals distances from each other. The final proof in favour of the formation of the HXeI molecule from neutral atoms was obtained by following the concentrations of HXeI and I atoms simultaneously by IR measurements. The increase of the spin-orbit absorption ($^2P_{1/2} \leftarrow {}^2P_{3/2}$) of I atoms[66] at 7457 cm^{-1} correlated with the decrease of HXeI and vice versa.[63]

In addition to this direct evidence on formation of HXeI from neutral atoms supporting information is available from Feldman and co-workers.[81,82] By combined infrared and ESR-spectroscopic studies on electron-irradiated hydrocarbon-containing Xe matrices these authors found that the decrease of hydrogen atoms correlated with the growth of HXeH. Also, addition of electron scavengers which enhanced the ion formation decreased the yield of xenon dihydride.[81,82] It can also be mentioned that these authors found indications of possible reactions of HXeH with hydrocarbons.

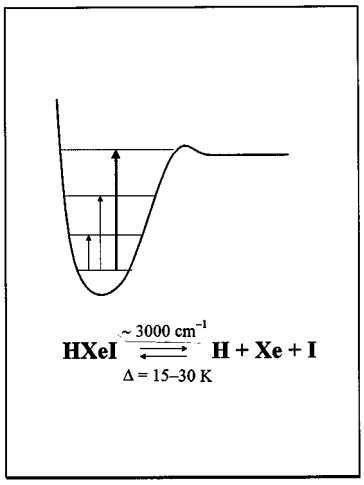


Figure 4. Photodissociation of the HXeI molecule with infrared light at ca. 3 μm

The result that the HXY compounds are formed from neutral atoms is very important because neither ions nor complex intermediates are needed to synthesize these molecules. Solid rare gases form an ideal environment for synthesis since one of the reactants is present as a solvent. Additionally, one needs only to find a suitable precursor molecule which can be photodissociated to hydrogen atoms and Y fragments. In most cases, hydrogen atoms can be selectively mobilised after photolysis, the Y fragments being immobile. This reduces the number of unwanted side reactions and only HXeH is a major "side product".

Considering the possible preparation of HXY in the gas phase, the major requirement appears to be the simultaneous production of H and X atoms, and the Y fragments. This can be achieved, for example, by microwave discharge. In preliminary attempts we have obtained HXeCl directly in the matrix by depositing a mixture of HCl and Xe through a discharge.[83] Unfortunately, it was impossible to determine whether HXeCl was produced in the gas phase or on the surface of the matrix. In any case, this positive result prompts for further gas-phase experiments.

A Simple Model for the Bonding

The origin of bonding in the HXY compounds can be understood on the basis of a simple ionic model. In this model, the HXY molecule is best described as an ion pair HX^+Y^-, which contains a covalently bound HX^+ interacting with Y^- mainly due to Coulombic attraction. This idea was presented by Last and George predicting the existence of HXe^+Cl^- in 1988 by their semiempirical DIIS method.[84] It is also interesting to note that the ionic $(HXe)^+$ and $(HKr)^+$ constituents of the new rare-gas molecules are isoelectronic with HI and HBr, respectively.

On the basis of this charge-transfer model it is informative to determine the main factors which affect the existence and stability of HXY. Figure 5 explains the model of HXY compounds in a simple manner. According to this model, HXY has ionic nature at the equilibrium structure which originates from the ionic $HX^+ + Y^-$ diabatic surface. However, when the bonds are stretched the system dissociates to the neutral H + X + Y limit due to the avoided crossing between the two diabatic surfaces. The ionization potential (*IP*) of X, electron affinity (*EA*) of Y and the dissociation energy (D_e) of XH^+ determine the energetics between the ionic and neutral limits. Low ionization potential of X and large electron affinity of Y are favourable with respect to the stability of HXY. The D_e values of XeH^+ and KrH^+ are about 4.05 and 4.8 eV, respectively.[85–88] These large values tend to bring the ionic limit low in energy and this explains partially the existence of the HXY compounds. Moreover, small Y^- fragments stabilise HXY more than the larger ones because they can approach closer to the HX^+ fragment and thus produce larger Coulombic stabilisation. Altogether, there is rather subtle balance between different factors affecting the energetics of HXY compounds and their properties depend strongly on Y as observed in experiments from the position of the X–H stretching band.

In terms of resonance structures, HXY should be described as a resonance hybrid between several possible structures from which the most important is HX^+Y^-. Other important structures are neutral H–X–Y and ionic H^-X^+Y. The ionic structures tend to stabilise the compound and the neutral structure destabilises it. HXeH is best described similarly as a resonance hybrid between HXe^+H^- and H^-Xe^+H.

The bonding of the HXeH molecule can be considered qualitatively within the Molecular Orbital (MO) theory also

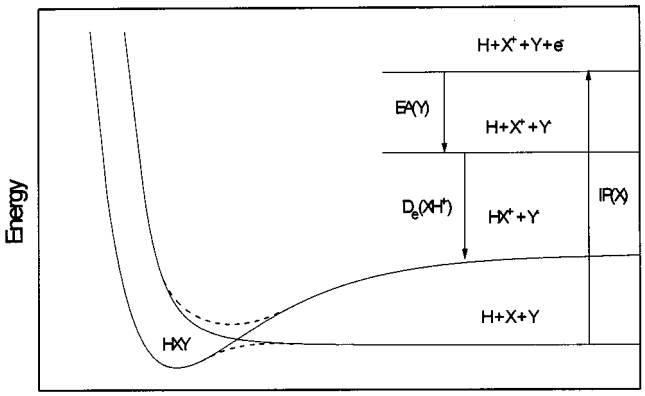


Figure 5. Schematic picture of the origin of bonding in the HXY molecules; the *x* axis describe the sum of the X–H and X–Y distances in a linear geometry

by a three-center four-electron model[12,17,89,90] in accordance to the fluorinated Xe compounds. The highest occupied orbital (σ_g) of HXeH is practically centered around the H atoms, being non-bonding.[90] The lowest σ_u molecular orbital, responsible for the covalent bonding, consists of a collinear set comprising one 5p orbital of Xe and the hydrogen 1s orbitals, being occupied by the two other electrons. Similar simple linear model should be valid also for other HXY molecules by replacing the other 1s hydrogenic orbital by the proper orbital of the Y fragment.

Computational Properties of the HXY Compounds

In order to understand the nature of bonding and spectral characteristics of the rare-gas molecules, ab initio methods have been applied extensively.[61,62,64,65,67,90] The computational results support strongly the bonding model presented above and they corroborate the experimental spectroscopic features as well as give insight to the stabilities of these molecules. The basis set and electron-correlation dependencies of the various properties are discussed separately in the following.

Selection of Computational Methods

From the computational point of view the HXY(Z) molecules are a challenging task. The ion-pair nature of these compounds, interaction of different neutral and ionic configurations, as well as relatively weak bonds and relativistic effects establish a test for the performance of the standard computational approaches. All-electron basis sets become unfeasibly large when rare-gas atoms are considered. Therefore, most of the studies on the HXY molecules have applied effective core potentials (ECP) to describe the rare-gas atoms while first- and second-row atoms are dealt with standard all-electron Gaussian-type basis sets. The use of ECPs diminishes the size of the calculation by the accounted number of electrons, for example, reducing the number of electrons in Xe from 54 to 8 or 18 in the valence

space. This enables also application of higher level correlation in the calculations. As an example, the calculated bond lengths and spectra of HXeH have been collected at various levels of theory in Table 2. Most of these calculations would not be feasible using all-electron basis sets on xenon.

Table 2. The calculated bond lengths [Å] compared with the calculated and experimentally observed vibrational frequencies [cm^{-1}] of linear HXeH

	r(H−Xe)	$\nu_1(\sigma_g)$	$\nu_2(\pi_u)$ [a]	$\nu_3(\sigma_u)$	Ref.
MP2/LANL1DZ	2.0193	1007	706	1221	[62]
MP2/LJ18[b]	1.8607	1559	876	1384	
Becke3-LYP/LJ18[b]	1.8789	1523	857	1334	
CCSD(T)/LJ18[c]	1.892	1281	777	1272	[90]
CCSD(T)/LJ18[c] + BSSE + SO	1.916	1216	773	1279	[90]
CCSD(T)/N8[d]	1.929	1028	735	1199	[90]
CCSD(T)/N8[d] + BSSE +SO	1.958	1018	708	1187	[90]
Experimental			701	1166/ 1181	[62]

[a] Doubly degenerate. − [b] 18-VE ECP basis on xenon and the 6−311++G(2d,2p) standard basis set on hydrogen. − [c] Modified 18-VE ECP basis on xenon and an aug-cc-pVTZ basis added with one f-function on hydrogen. − [d] Modified 8-VE ECP on xenon and an aug-cc-pVTZ+f basis on hydrogen.

Aiding the first observations of the HXY molecules HXeI, HXeBr, HXeCl, HKrCl, and HXeH the MP2/LANL1DZ level was used as the preliminary theoretical method.[61][62] This very inexpensive approach was observed to give a stable minimum for all the observed 5 molecules, whereas the HKrI and HKrBr molecules were unstable computationally and have, in fact, despite attempts, never been experimentally observed. The failure of the MP2/LANL1DZ calculations was that they predicted the HXY molecules to be energetically *above* the atomic dissociation limit. However, these calculations were able to predict the properties around the equilibrium structure reasonably well and the harmonic vibrational frequencies of the new HXY molecules were satisfactory. As can be seen in Table 2, the discrepancy between the MP2/LANL1DZ-calculated and the observed wavenumbers is quite small especially when taking into account the anharmonic effects. This is actually accidental as pointed out by Runeberg and co-workers.[90] These authors showed that increasing the level of correlation requires also a larger and more flexible basis set to work properly for the HXY molecules. Increasing only the basis set using the perturbation theory (MPn) shortens the Xe−H bond length thereby also increasing the harmonic vibrational frequency. If higher correlation levels are used the Xe−H bond length increases decreasing the harmonic frequencies. The most appropriate levels of theory seem to be the CCSD(T) and multireference-CI (MR-CI) levels when connected with extensive basis sets.[90] It must be noted, however, that even though the CCSD(T) theory, coupled with large basis sets and taking into account BSSE and spin-orbit effects, results in a qualitatively correct picture, it failed to reproduce a deep enough potential well to be consistent with the observed overtone/combination band of HXeH. Therefore, in most cases the low-level calculations are sufficient to help the interpretation of experimental data while obtaining an accurate potential energy surface is very demanding.

Computed Structures of the HXY Molecules

The observed new rare-gas molecules can roughly be divided into three groups: the centrosymmetric HXH molecule, the linear HXY(Z) molecules, and the bent HXYZ molecules (see Figure 1). In all of these cases, linear bonding around the rare-gas atom is found. The only new centrosymmetric molecule HXeH resembles its fluorine analog FXeF. Concerning the structures of these novel rare-gas molecules we have to rely on calculated values, experimental data being nonexistent so far. The calculated structural parameters, Mulliken charges and dipole moments of the various HXY(Z) molecules, are collected in Table 3. For comparison the experimental bond lengths of XeH^+ and KrH^+ are included.

It can be noted that the calculated parameters follow a general trend. The H−Xe bond length decreases with the increasing partial positive charge on xenon. The positive charge residing on xenon is largest (+0.88) for the HXeNC molecule resulting in the shortest H−Xe bond length (1.659 Å). This trend finally approaches the XeH^+ cation at the limit of complete ionic bonding. Similarly, in the Kr compounds the larger charge on Kr results in a shorter bond length converging towards the KrH^+ cation. It is also worth mentioning that these molecules have very large dipole moments due to the extent of charge separation.

To rationalize the difference of the HXY molecules from the van der Waals geometries of the constituents we can inspect the HXeI system. Figure 6 displays the molecular and van der Waals distances showing that chemical bond formation between the atoms results in more than two-fold decrease of the Xe−H distance and in almost 30% contraction of the Xe−I distance.

HXeSH is an interesting bent molecule representing the first example of an Xe−S bond. The Xe−S−H angle of ca. 91 degrees is very close to the angle of H_2S. Also the S−H bond length of HXeSH (calculated 1.334 Å) is almost the same as the experimental value for H_2S (1.336 Å).[91] Therefore it seems that the rare-gas atom is inserted into the covalent hydrogen−sulphur bond and has a negligible effect on the residing molecule. Also, for the linear HXeCN, HXeNC, and HKrCN molecules the rare-gas molecules restore the precursor structure, the novel molecules being linear and having C≡N bond lengths close to the HCN precursor.

Vibrational Spectra of the HXY Molecules

The Xe−H stretching motion is an essential part of the vibrational calculation of the HXY molecules. As discussed above, highly correlated calculations with large basis sets

Table 3. The computational properties of different HXY(Z) compounds at the MP2 level[a]; for comparison, values for KrH^+ and XeH^+ have been included

	r(H−X) [Å]	r(X−Y) [Å]	r(Y−Z) [Å]	q(H)	q(X)	q(Y)	q(Z)	μ [D]
HXeH	1.861			−0.344	0.688			0.0
HXeSH[b]	1.774	2.729	1.334	−0.226	0.671	−0.435	−0.009	4.458
HXeI	1.747	3.095		−0.178	0.645	−0.467		6.405
HXeCN	1.707	2.392	1.178	−0.203	0.847	−0.401	−0.242	7.432
HXeBr	1.694	2.837		−0.156	0.802	−0.647		7.331
HXeCl	1.685	2.663		−0.165	0.816	−0.651		7.246
HXeNC	1.659	2.342	1.187	−0.161	0.880	−0.424	−0.295	9.263
XeH^+[c]	1.596			+0.091	0.909			
HKrCN	1.466	2.349	1.177	−0.206	0.886	−0.488	−0.193	9.205
HKrCl	1.435	2.666		−0.178	0.887	−0.709		9.351
KrH^+[d]	1.382			+0.061	0.939			

[a] For Kr and Xe 18-VE ECPs and for I 17-VE ECP (denoted as LJ18, see ref.[93]) were used while the standard 6−311++G(2d,2p) basis set was applied for the first- and second-row atoms. − [b] This is the only bent molecule of the HXY(Z) molecules with the H−S−Xe angle being 91.02°. − [c] Experimental value 1.603 Å, ref.[94]. − [d] Experimental value 1.421 Å, ref.[85].

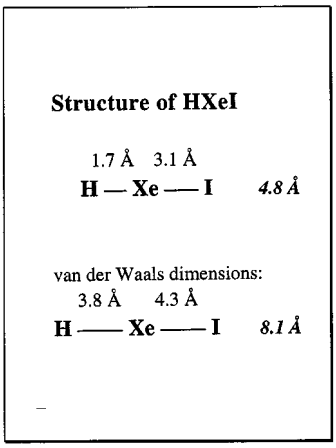


Figure 6. Structure of HXeI; the molecular bond lengths are taken from MP2/LJ18 calculations; the van der Waals dimensions are deduced from Xe−H[95] and Xe−I[96] pair potential minima

result in a good agreement with the experimental values.[90] This is especially important when the HXY molecule is relatively weakly bound, and the potential energy surface near the dissociation limit is not described accurately with modest computational methods like the perturbation theory. For instance, such examples are HKrCN[64] and HXeSH.[65] For HKrCN the MP2/LJ18-calculated Kr−H stretching wavenumber is 2011 cm^{-1}, while the largest correlation level, CCSD(T)/LJ18, gives a harmonic ν_{Kr-H} frequency of 1781 cm^{-1} for HKrCN, still being ca. 300 cm^{-1} above the experimental value of 1497 cm^{-1}.[64] As discussed previously, anharmonic effects explain partially the difference. In addition, the solid host red-shifts the observed wavenumber from its gas-phase value and the remaining discrepancy can mostly be attributed to the underestimated basis set used. For HXeSH the situation is similar: The MP2/LJ18 calculations predict the Xe−H stretching at 1521 cm^{-1}, while the CCSD(T)/LJ18 calculation reduces this value to 1148 cm^{-1}, the experimental value being 1119 cm^{-1}.

Increasing the size of the HXY molecules beyond three-atomics makes the use of state-of-art computational methods unfeasible. In the course of our work with the HXY-type molecules we have found that even the moderate MP2/LJ18 level gives reasonable qualitative results for structures, charge separation, and vibrational frequencies. In addition, the extreme intensities of the X−H stretching absorptions are well predicted. Therefore, we have collected the MP2/LJ18-calculated characteristic X−H bond lengths and vibrational frequencies, including IR intensities in Table 4 for comparison. Also the Becke3-LYP/LJ18-calculated values are included, since the DFT methods are becoming more attractive for larger molecular systems due to their computational efficiency.

The experimental Xe−H stretching wavenumbers shift to higher values when going from the HXeSH molecule to HXeNC. Even though the computational vibrational frequencies are generally overestimated the systematic trend among the present HXY molecules is correctly predicted as discussed in more details in ref.[67] Therefore, using a low-level, economical computational approach, quite useful approximations on the structures and especially on the ν_{X-H} wavenumbers and intensities of new HXY molecules can be done.

Energetics of the HXY Molecules

Even though the structure and vibrational frequencies appear to be reachable also with low-level computational methods, the energetics of the new HXY molecules is more challenging. As demonstrated in the simple bonding model derived earlier (see Figure 5), the HXY molecules possess both neutral (HXY) and ionic (HX^+Y^-) character. This means also that the closer the ionic surface lies to the neutral molecular surface, the larger interaction between the two surfaces is expected. The preliminary MP2/LANL1DZ calculations indicated that the H + X + Y atomic dissociation limit would be *below* the HXY molecular en-

Table 4. The calculated harmonic H−Xe stretching frequencies [cm^{-1}] of HXY(Z) molecules at the MP2 and Becke3-LYP levels; the numbers in the parentheses are the calculated intensities [km mol^{-1}], and the bond lengths are given in Å

	MP2/LJ18		Becke3-LYP/LJ18		Experimental
	r(H−Xe)	ν (I)	*r*(H−Xe)	ν (I)	ν
HXeSH	1.774	1523.1 (3100)	1.798	1556.5 (1800)	1119
HXeI	1.747	1514.8 (5500)	1.786	1559.9 (2200)	1193
HXeCN	1.707	1874.9 (1300)	1.740	1817.3 (800)	1624
HXeBr	1.694	1830.6 (2400)	1.747	1729.9 (1400)	1504
HXeCl	1.685	1904.6 (1700)	1.733	1799.0 (1000)	1648
HXeNC	1.659	2010.5 (500)	1.704	1935.8 (800)	1851
HKrCN	1.468	2010.6 (1700)	1.547	1738.0 (1400)	1497
HKrCl	1.435	2177.8 (2900)	1.543	1757.7 (1800)	1476

ergy[61][62] However, increasing the basis set *and* the correlation level the situation is reversed and the HXY configuration becomes *lower* in energy than the atomic dissociation limit. A dissociation energy of 0.32 eV was estimated for HXeH according to the dissociation limit Xe + 2 H.[90] This result was obtained at the CCSD(T) level, using a large 18-VE ECP basis for Xe and all-electron basis for hydrogen, and correcting the value for both BSSE and spin-orbit coupling effects. However, taking into account the observed overtone/combination transition at 2003 cm^{-1} and assuming this vibrational level to lie below the dissociation limit, and estimating the symmetric stretch wavenumber from the calculations (ca. 1100 cm^{-1}) we end up with a value of at least 0.48 eV for the experimental dissociation energy (D_e) of HXeH. The origin of the present discrepancy ($\geq$ 0.16 eV) between the calculated and experimental dissociation energies may be technical since also the stabilising role of the solid host has been estimated to be small (0.033 eV for quadrupole interaction of HXeH in Xe[90]).

For HXeI an experimental D_e value of about 0.42 eV has been deduced from IR pumping experiments.[63] These molecules together with HXeSH are the weakest bound of all the HXY molecules found up to now. They also have the lowest lying Xe−H stretching bands. The ν_{Xe-H} for HXeCl at 1648 cm^{-1} suggests a larger binding energy than for HXeH, HXeSH, and HXeI. Indeed, a preliminary high-level computational study at the CISD level estimates the binding energy of HXeCl to be 0.9 eV.[92] The computationally strongest bound molecule is HXeCN, which has a D_e of 1.43 eV[64] with respect to the dissociation limit H + Xe + CN. In general, the observed HXY molecules feature dissociation energies between 0.4 and 1.4 eV, and the corresponding fluorine compound HXeF is expected to be much more strongly bound but it has not yet been experimentally observed.

An additional interesting aspect of the calculation of the stabilization energy of the HXY molecules is that all calculations are performed for molecules in vacuo whereas the experimental evidence up to now is from low-temperature solid rare gases. This rises the question of the role of the rare gas lattice in stabilizing the HXY molecules. First, as found out in the IR pumping experiments on HXeI, the lattice traps the atomic fragments. Secondly, except HXeH, the HXY molecules possess strong dipole moments which could induce long-range interactions with the surrounding rare gases. Especially the xenon environment could be an important, additional stabilizing factor due to its large polarizability compared to argon and krypton. Anyhow, as was shown experimentally in ref.[61], HXeCl can be easily produced also in Kr surroundings and in this case the Xe−H stretch was shifted only by 16 cm^{-1} from its value in pure Xe. Corresponding shifts for HXeBr and HXeCN are 26 and 20 cm^{-1}, respectively,[61][64] indicating a relatively small environmental effect.

Conclusions

Rare-gas atoms X (Xe and Kr) are shown to react with a hydrogen atom and a neutral electronegative fragment Y in a concerted reaction to produce neutral ground-state HXY molecules. The very strong X−H stretching absorption is the most characteristic spectral feature of these molecules, its wavenumber reflecting sensitively the electron distribution in the HXY molecule. The present ab initio calculations show that the bonding comprises both covalent and ionic contributions. A bonding model based on avoided crossing of the neutral H + X + Y and ionic $(HX)^+ + Y^-$ surfaces is presented. This model is applicable for qualitative understanding of bonding in all of the new compounds: HXeI, HXeBr, HXeCl, HXeH, HXeCN, HXeNC, HXeSH, HKrCl, and HKrCN. At the present time these species are produced in solid rare gases by photodissociation of the HY precursor and thermal mobilisation of the fragments. The dissociation energies vary from 0.4 to over 1 eV, and warrant observation of these molecules also in the gas phase. Future computational studies will deepen our understanding in the bonding details as well as suggest the existence of further similar compounds.

Acknowledgments

Financial support from the Academy of Finland and the University of Helsinki are gratefully acknowledged.

[1] L. Pauling, *J. Am. Chem. Soc.* **1933**, *55*, 1895.
[2] [2a] H. Käding, N. Riehl, *Naturwiss.* **1933**, *21*, 479. – [2b] D. M. Yost, A. L. Kaye, *J. Am. Chem. Soc.* **1933**, *55*, 3890. – [2c] O. Ruff, W. Menzel, *Z. Anorg. Chem.* **1938**, *213*, 206. – [2d] A.v.

Antropoff, *Z. Angew. Chem.* **1933**, *46*, 23. – [2e] A.v. Antropoff, *Z. Anorg. Chem.* **1933**, *213*, 208.
[3] [3a] N. Bartlett, *Proc. Chem. Soc*. **1962**, 218. – [3b] F. O. Sladky, P. A. Bulliner, N. Bartlett, *J. Chem. Soc. A* **1969**, 2179.
[4] R. Hoppe, W. Dähne, H. Mattauch, K. H. Rödder, *Angew. Chem.* **1962**, *74*, 903.
[5] H. H. Claassen, H. Selig, J. G. Malm, *J. Am. Chem. Soc.* **1962**, *84*, 3593.
[6] F. O. Sladky, P. A. Bulliner, N. Bartlett, B. G. DeBoer, A. Zankin, *Chem. Comm.* **1968**, 1048.
[7] V. M. McRae, R. D. Peacock, D. R. Russell, *Chem. Comm.* **1969**, 62.
[8] J. H. Holloway, J. G. Knowles, *J. Chem. Soc. A* **1969**, 756.
[9] N. Bartlett, M. Gennis, D. D. Gibler, B. K. Morrell, A. Zalkin, *Inorg. Chem.* **1973**, *12*, 1717.
[10] D. E. McKee, C. J. Adams, N. Bartlett, *Inorg. Chem.* **1973**, *12*, 1722.
[11] J. R. Morten, W. E. Falconer, *J. Chem. Phys.* **1963**, *39*, 427.
[12] J. G. Malm, H. Selig, J. Jortner, S. A. Rice, *Chem. Rev.* **1965**, *65*, 199.
[13] N. Bartlett, F. O. Sladky in *Comprehensive Inorganic Chemistry*, Pergamon Press, New York, **1973**, vol. 3, pp. 213–330.
[14] E. Tommila, *Suom. Kemistil. A* **1963**, *36*, 209.
[15] K. Seppelt, D. Lentz, *Prog. Inorg. Chem.* **1982**, *29*, 167.
[16] J. H. Holloway, *J. Fluor. Chem.* **1986**, *33*, 149.
[17] C. A. Coulson, *J. Chem. Soc.* **1964**, 1442.
[18] D. Holtz, J. L. Beauchamp, *Science* **1971**, 1237. They reported the bond strength as 180 ± 33 kJ mol^{-1}.
[19] J. K. Hovey, T. B. McMahon, *J. Am. Chem. Soc.* **1986**, *108*, 528.
[20] M. Wechsberg, P. A. Bulliner, F. O. Sladky, R. Mews, N. Bartlett, *Inorg. Chem.* **1972**, *11*, 3063.
[21] L. J. Turbini, R. E. Aikman, R. J. Lagow, *J. Am. Chem. Soc.* **1979**, *101*, 5833.
[22] D. Naumann, W. Tyrra, *J. Chem. Soc., Chem. Commun.* **1989**, 47.
[23] H. J. Frohn, S. Jacobs, *J. Chem. Soc., Chem. Commun.* **1989**, 625.
[24] V. V. Zhdankin, P. J. Stang, N. S. Zefirov, *J. Chem. Soc., Chem. Commun.* **1992**, 578.
[25] D. Naumann, W. Tyrra, R. Gnann, D. Pfolk, T. Gilles, K. F. Tebbe, *Z. Anorg. Allg. Chem.* **1997**, *623*, 1821.
[26] L. Y. Nelson, G. C. Pimentel, *Inorg. Chem.* **1967**, *6*, 1758.
[27] C. T. Goetschel, K. R. Loos, *J. Am Chem. Soc.* **1972**, *94*, 3018.
[28] [28a] L. Stein, J. R. Norris, A. J. Down, A. Minihan, *J. Chem. Soc. Chem. Comm.* **1978**, 502. – [28b] T. Drews, K. Seppelt, *Angew. Chem. Int. Ed.* **1997**, *36*, 273.
[29] R. D. LeBlond, D. D. DesMarteau, *J. Chem. Soc., Chem. Commun.* **1974**, 555.
[30] D. D. DesMarteau, *J. Am. Chem. Soc.* **1978**, *100*, 6270.
[31] D. D. DesMarteau, R. D. LeBlond, S. F. Hossain, D. Nothe, *J. Am. Chem. Soc.* **1981**, *103*, 7734.
[32] A. A. A. Emara, G. J. Schrobilgen, *J. Chem. Soc., Chem. Commun.* **1987**, 1644.
[33] A. A. A. Emara, G. J. Schrobilgen, *J. Chem. Soc., Chem. Commun.* **1988**, 257.
[34] G. J. Schrobilgen, *J. Chem. Soc., Chem. Commun.* **1988**, 1506.
[35] J. Foropopoulos, Jr., D. D. DesMarteau, *J. Am. Chem. Soc.* **1982**, *104*, 4260.
[36] J. F. Sawyer, G. J. Schrobilgen, S. J. Sutherland, *Inorg. Chem.* **1982**, *21*, 4064.
[37] G. A. Schumacher, G. J. Schrobilgen, *Inorg. Chem.* **1983**, *22*, 2178.
[38] R. Faggiani, D. K. Kennepohl, C. J. L. Lock, G. J. Schrobilgen, *Inorg. Chem.* **1986**, *25*, 563.
[39] A. V. Grosse, A. D. Kirschenbaum, A. G. Streng, L. V. Streng, *Science* **1963**, *139*, 1047.
[40] J. J. Turner, G. C. Pimentel, *Science* **1963**, *140*, 975.
[41] D. R. MacKenzie, *Science* **1963**, *141*, 1171.
[42] W. F. Howard, L. Andrews, *J. Am. Chem. Soc.* **1974**, *96*, 7864.
[43] G. J. Schrobilgen, *J. Chem. Soc., Chem. Commun.* **1988**, 863.
[44] J. C. P. Sanders, G. J. Schrobilgen, *J. Chem. Soc., Chem. Commun.* **1989**, 1576.
[45] R. J. Gillespie, G. J. Schrobilgen, *Inorg. Chem.* **1976**, *15*, 22.
[46] G. J. Schrobilgen, *J. Chem. Soc., Chem. Commun.* **1988**, 1506.
[47] C. A. T. Thompson, L. Andrews, *J. Am. Chem. Soc.* **1994**, *116*, 423.
[48] A. Veldkamp, G. Frenking, *Chem. Phys. Lett.* **1994**, *226*, 11.
[49] G. Frenking, D. Cremer, in *Structure and Bonding*, *Noble Gas and High Temperature Chemistry* (Eds.: M. J. Clarke, J. B. Goodenough, J. A. Ibers, C. K. Jørgensen, D. M. P. Mingos, J. B. Neilands, G. A. Palmer, D. Reinen, P. J. Sadler, R. Weiss, R. J. P. Williams), Springer, Berlin, **1990**, p. 17–95.
[50] E. Whittle, D. A. Dows, G. C. Pimentel, *J. Chem. Phys.* **1954**, *22*, 1943.
[51] I. Norman, G. O. Porter, *Nature* **1954**, *174*, 508.
[52] H. Broida, J. R. Pellam, *Phys. Rev.* **1954**, *95*, 845.
[53] L. Andrews, G. C. Pimentel, *J. Chem. Phys.* **1967**, *47*, 3637.
[54] L. E. Brus, V. E. Bondybey, *Chem. Phys. Lett.* **1975**, *36*, 252.
[55] L. E. Brus, V. E. Bondybey, *J. Chem. Phys.* **1976**, *65*, 71.
[56] V. E. Bondybey, L. E. Brus, *J. Chem. Phys.* **1976**, *64*, 3724.
[57] V. E. Bondybey, L. E. Brus, *J. Chem. Phys.* **1975**, *62*, 620.
[58] V. E. Bondybey, C. Fletcher, *J. Chem. Phys.* **1976**, *64*, 3615.
[59] R. Schriever, M. Chergui, N. Schwentner, *J. Chem. Phys.* **1991**, *95*, 6124.
[60] K. H. Gödderz, N. Schwentner, M. Chergui, *J. Chem. Phys.* **1996**, *105*, 451.
[61] M. Pettersson, J. Lundell, M. Räsänen, *J. Chem. Phys.* **1995**, *102*, 6423.
[62] M. Pettersson, J. Lundell, M. Räsänen, *J. Chem. Phys.* **1995**, *103*, 205.
[63] M. Pettersson, J. Nieminen, L. Khriachtchev, M. Räsänen, *J. Chem. Phys.* **1997**, *107*, 8423.
[64] M. Pettersson, J. Lundell, L. Khriachtchev, M. Räsänen, *J. Chem. Phys.* **1998**, *109*, 618.
[65] M. Pettersson, J. Lundell, L. Khriachtchev, E. Isoniemi, M. Räsänen, *J. Am. Chem. Soc.* **1998**, 7979.
[66] M. Pettersson, J. Nieminen, *Chem. Phys. Lett.* **1997**, *283*, 1.
[67] M. Pettersson, Ph.D. Thesis, University of Helsinki, **1998**; available upon request from the author.
[68] H. Okabe, *Photochemistry of Small Molecules*, Wiley, New York, **1978**.
[69] L. Khriachtchev, M. Pettersson, E. Isoniemi, M. Räsänen, *J. Chem. Phys.* **1998**, *108*, 5747.
[70] D. LaBrake, E. T. Ryan, E. Weitz, *J. Chem. Phys.* **1995**, *102*, 4112.
[71] D. LaBrake, E. Weitz, *Chem. Phys. Lett.* **1993**, *211*, 430.
[72] J. Eberlein, M. Creutzburg, *J. Chem. Phys.* **1997**, *106*, 2118, and references therein.
[73] H. Muto, K. Nunome, M. Iwasaki, *J. Phys. Chem.* **1980**, *84*, 3402.
[74] M. E. Fajardo, V. A. Apkarian, *J. Chem. Phys.* **1986**, *85*, 5660.
[75] M. E. Fajardo, V. A. Apkarian, *J. Chem. Phys.* **1988**, *89*, 4102.
[76] M. E. Fajardo, V. A. Apkarian, *J. Chem. Phys.* **1988**, *89*, 4124.
[77] H. Kunttu, J. Seetula, M. Räsänen, V. A. Apkarian, *J. Chem. Phys.* **1992**, *96*, 5630.
[78] M. Räsänen, J. Seetula, H. Kunttu, *J. Chem. Phys.* **1993**, *98*, 3914.
[79] H. Kunttu, J. Seetula, *Chem. Phys.* **1994**, *189*, 273.
[80] T. F. Fridgen, J. M. Parnis, *J. Chem. Phys.* **1998**, *109*, 2155.
[81] V. I. Feldman, F. F. Sukhov, *Chem. Phys. Lett.* **1996**, *255*, 425.
[82] V. I. Feldman, F. F. Sukhov, A. Yu. Orlov, *Chem. Phys. Lett.* **1997**, *280*, 507.
[83] M. Pettersson, J. Nieminen, unpublished results.
[84] I. Last, T. F. George, *J. Chem. Phys.* **1988**, *89*, 3071.
[85] J. W. C. Johns, *J. Mol. Spectrosc.* **1984**, *106*, 124.
[86] H. E. Warner, W. T. Connor, R. C. Woods, *J. Chem. Phys.* **1984**, *81*, 5413.
[87] K. A. Peterson, R. H. Petrmichl, R. L. McClain, R. C. Woods, *J. Chem. Phys.* **1991**, *95*, 2352.
[88] R. Klein, P. Rosmus, *Z. Naturforsch.* **1984**, *39a*, 349.
[89] R. E. Rundle, *J. Am. Chem. Soc.* **1963**, *85*, 112.
[90] N. Runeberg, M. Seth, P. Pyykkö, *Chem. Phys. Lett.* **1995**, *246*, 239. N. Runeberg, Doctoral Dissertation, University of Helsinki, **1996**.
[91] W. C. Lane, T. H. Edwards, J. R. Gillis, E. S. Bonomo, F. J. Murcray, *J. Mol. Spectrosc.* **1982**, *95*, 365.
[92] M. Johansson, M. Hotokka, M. Pettersson, M. Räsänen, *Chem. Phys.*, accepted for publication.
[93] L. A. LaJohn, P. A. Christensen, R. B. Ross, T. Atashroo, W. C. Ermler, *J. Chem. Phys.* **1987**, *87*, 2812.
[94] S. A. Rogers, C. R. Brazier, P. F. Bernath, *J. Chem. Phys.* **1987**, *87*, 159.
[95] R. W. Bickes, Jr., B. Lantzsch, J. P. Toennies, K. Walaschewski, *Faraday Discuss. Chem. Soc.* **1973**, *55*, 167.
[96] P. Casavecchia, G. He, R. K. Sparks, Y. T. Lee, *J. Chem. Phys.* **1982**, *77*, 1878.

Received October 22, 1998
[I98370]

Synthesis and Hydrolysis of [Alkenyl(alkoxy)carbene]manganese Complexes: Evidence for a Transient Allylic Intermediate on the Way to α,β-Unsaturated Aldehydes

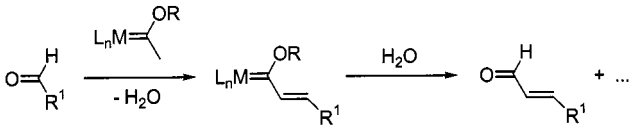
Carole Mongin,[a] Yannick Ortin,[a] Noël Lugan,*[a] and René Mathieu[a]

Keywords: Manganese / Carbenes / Hydrolyses / Aldehydes / Vinylogation

A variety of alkenylcarbene complexes [Cp′(CO)$_2$Mn=C(OEt)CH=CHR] (**3**) (Cp′ = η^5-MeC$_5$H$_4$) was obtained in a straightforward manner upon aldol condensation of [Cp′(CO)$_2$Mn=C(OEt)CH$_3$] (**1**) with aromatic and α,β-unsaturated aldehydes RC(H)O (**2**). The reaction is totally stereoselective, giving (*E*)- or (*all-E*)-alkenylcarbenes only. The protonation of **3** at low temperature followed by reaction with water affords the α,β-unsaturated aldehyde complexes [Cp′(CO)$_2$Mn(η^2-RCH=CHCHO] (**5**), from which the aldehydes RC(H)=C(H)C(H)O (**6**) were displaced by acetonitrile. The intermediate aldehyde complexes are shown to result from the hydrolysis of a transient cationic π-allyl species [Cp′(CO)$_2$Mn(η^3-RCHCHC(OEt)H]$^+$ ([**4**]$^+$) formed upon protonation of **3**.

Introduction

Alkenyl-alkoxy-substituted Fischer carbene complexes have been shown in some cases to release α,β-unsaturated aldehydes upon hydrolysis, with optimum efficiency at high pH values.[1,2] Though mechanistically clear under such conditions,[2b] the reaction has received little attention as a synthetic procedure. Yet, if we keep in mind that alkenyl-alkoxy-substituted Fischer carbenes can be obtained upon aldol condensation of alkyl(alkoxy)carbene complexes with aldehydes,[3,4] their hydrolysis can be regarded as part of a potential process for the homologation of aldehydes into α,β-unsaturated aldehydes (Scheme 1).

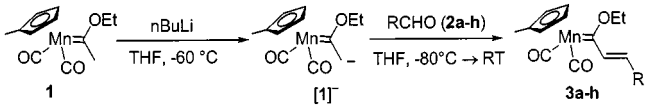


Scheme 1

The vinylogation of aldehydes is of special interest for the synthesis of molecular materials[5] and natural products.[6] Though several procedures derived from general olefination reactions have been devised,[7] the search for easy-to-handle, selective, and versatile reagents is still of current interest.[7e,8] As part of an ongoing effort to develop synthetically useful reactions employing cheap and readily available group-7 Fischer carbene complexes obtained from [Cp′Mn(CO)$_3$] (Cp′ = η^5-MeC$_5$H$_4$),[9] we were challenged to examine the scope of [Cp′(CO)$_2$Mn=C(OEt)CH$_3$] (**1**) for the above reaction. The present paper deals with the results of our investigation and provides insight into the mechanism of the hydrolysis of alkenyl-substituted Fischer carbene complexes under acidic conditions.[10]

Results and Discussion

The carbenemanganese anion [Cp′(CO)$_2$Mn=C(OEt)-CH$_2$]$^-$ ([**1**]$^-$), generated in situ by addition of *n*BuLi to a THF solution of [Cp′(CO)$_2$Mn=C(OEt)CH$_3$] (**1**) cooled at −60°C,[11] was treated at low temperature with one molar equivalent of various aromatic and α,β-unsaturated aldehydes RCHO (**2a**−**h**, Table 1). An aldol/elimination reaction subsequently occurred upon return to room temperature, giving the corresponding alkenyl(alkoxy)carbenes [Cp′(CO)$_2$Mn=C(OEt)CH=CHR] (**3a**−**h**) in valuable yields (Scheme 2, Table 1, entries 1−8).



Scheme 2. Aldol condensation of **1** with aldehydes **2a**−**h**

This sequence was reproduced with a dialdehyde, namely 1,1′-bis(formyl)ferrocene. Depending on the stoichiometry, the reaction could be directed toward either [{η^5-(Cp′(CO)$_2$Mn=C(OEt)CH=CHC$_5$H$_4$)}Fe{η^5-C$_5$H$_4$CHO}] (**3i$_1$**), or [{η^5-(Cp′(CO)$_2$Mn=C(OEt)CH=CHC$_5$H$_4$}$_2$Fe] (**3i$_2$**) (Scheme 3, Table 1, entries 9−10).

Complexes **3a**−**i** were characterized by ^{1}H-, ^{13}C-, and (when necessary) HMQC ^{1}H-^{13}C NMR analysis.[12] Their formation is totally stereoselective, giving (*E*) (for **3a**−**b**, **f**, **i**) or (*all-E*) (for **3c**−**e**, **g**−**h**) isomers only, as indicated by $^3J_{HH}$ coupling constants of ca. 15 Hz for the protons adjacent to the carbon−carbon double bonds.

In a first attempt to release α,β-unsaturated aldehydes from the above alkenyl(alkoxy)carbenes upon hydrolysis in

[a] Laboratoire de Chimie de Coordination du CNRS (UPR 8241), 205, route de Narbonne, F-31077 Toulouse Cedex 4, France
Fax: (internat.) + 33-5/61553003
E-mail: lugan@lcc-toulouse.fr

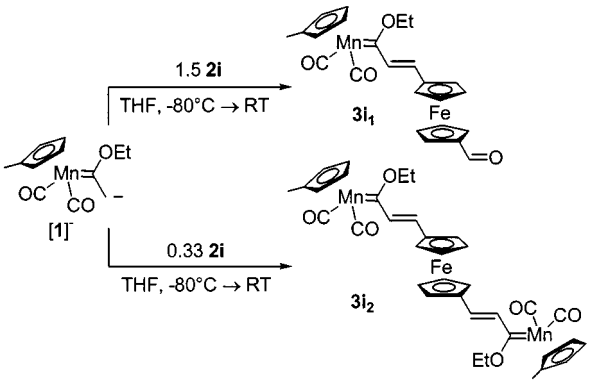
Supporting Information for this article is available on the WWW under http://www.wiley-vch.de/home/eurjic or from the author.

 © WILEY-VCH Verlag GmbH, D-69451 Weinheim, 1999 1434−1948/99/0505−0739 $ 17.50+.50/0

Table 1. Aldol condensation of **1** with aldehydes **2**, hydrolysis of **3**, and demetalation of the α,β-unsaturated aldehydes **6** (see Schemes 2−5)

Entry	Aldehyde RCHO (**2**)[a]	Product series	Yield (%)[f] **3**[g]	**5**[j]	**6**[k]
1	PhCHO	**a**	59	87	95
2	FcCHO	**b**	87	83	96
3	(*E*)-PhCH=CHCHO	**c**	65	88	92
4	(*E*)-MeCH=CHCHO	**d**	64	73	75
5	(*E*)-PhCH=C(Me)CHO	**e**	66	72	97
6	1,4-$Me_2NC_6H_4CHO$	**f**	85	72	97
7	(*E*)-FcCH=CHCHO[b]	**g**	77	72	97
8	(*E*,*E*)-PhCH=CHCH=CHCHO[c]	**h**	54	92	98
9	1,1′-diformylferrocene[d]	$\mathbf{i_1}$	86[h]	89	93
10	1,1′-diformylferrocene[e]	$\mathbf{i_2}$	71[i]	80	98

[a] 1 equiv. of **2** vs. [**1**]$^-$ was used, unless otherwise noted. − [b] Prepared from **2b** using **1** as a vinylogation reagent. − [c] Prepared from **2c** using **1** as a vinylogation reagent. − [d] 1.5 equiv. of **2i** vs. [**1**]$^-$ was used. − [e] 0.33 equiv. of **2i** vs. [**1**]$^-$ was used. − [f] Yields of isolated products. − [g] See Scheme 2. − [h] Based on [**1**]$^-$. − [i] Based on **2i**. − [j] See Scheme 4. − [k] See Scheme 5; except hitherto unkown $\mathbf{6i_1}$, which has been fully characterized,[12] the aldehydes were identified by comparison of their NMR spectra with literature data, or data recorded directly from authentic samples.



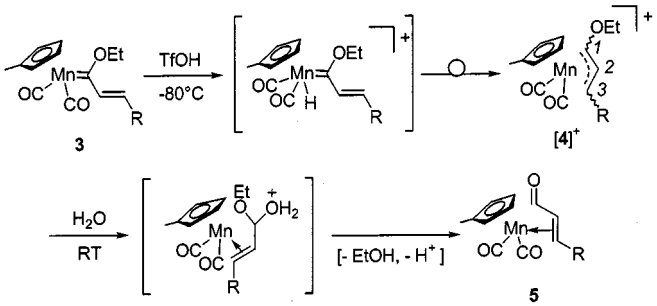
Scheme 3. Aldol condensation of **1** with 1,1′-diformylferrocene (**2i**)

basic conditions, **3c** was treated with urotropine in the presence of water according to a procedure Aumann et al. described for group-6 analogs.[1] No reaction was observed after 24 hours. This may be attributed to the insufficient electrophilic character of the carbene carbon atom that disfavors the required nucleophilic attack of hydroxide ions.[1,2b]

Keeping in mind that Fischer carbene complexes can be protolytically cleaved to form the corresponding aldehydes,[10] we next treated complexes **3** with one equivalent of TfOH at −80 °C in CH_2Cl_2 (but two equivalents in the case of **3f**[13] and in the case of the dialkenylcarbene $\mathbf{3i_2}$). An instantaneous reaction occurred, leading to a fairly stable species, whose IR spectra displayed two bands at ca. 2015 and 1970 cm^{-1} characteristic of $[Cp'(CO)_2MnLX]^+$-type complexes.[14,15] These were indeed identified as the π-allyl species $[Cp'(CO)_2Mn(\eta^3\text{-RCHCHC(OEt)H}]^+$ ([**4**]$^+$) on the basis of ^{1}H-, ^{13}C-, and HMQC ^{1}H-^{13}C NMR spectroscopy for [**4a**−**c**]$^+$.[12] In particular, the signals of the protons H^1, H^2, and H^3 within the π-allyl moiety (see Scheme 4) in [**4c**]$^+$ were observed at δ = 6.12, 5.55, and 3.41, respectively, in the ^{1}H dimension, and they correlate with the signals observed at δ = 138.1, 77.3, and 62.2 in the ^{13}C dimension. The proton H^1 clearly originates from TfOH, since the NMR spectrum of [D-**4c**]$^+$, generated from **3c** upon treatment with TfOD, does not show any resonance in the area around δ = 6.12. Within the $^{13}C\{^1H\}$-NMR sensitivity and resolution limits, the formation of [**4a**−**c**]$^+$ is quantitative and stereoselective. However, due to the systematic formation of paramagnetic impurities, their stereochemistry could not be determined by ^{1}H NMR.

When an excess of water was added to CH_2Cl_2 solutions of [**4a**−**i**]$^+$, IR monitoring showed the gradual disappearance of the bands due to [**4a**−**i**]$^+$ whereas three new bands grew at ca. 1965, 1905, and 1670 cm^{-1} indicative of the formation of the α,β-unsaturated aldehyde complexes $[Cp'(CO)_2Mn(\eta^2\text{-RCH=CHCHO})]$ (**5a**−**i**) (Scheme 3, Table 1).[16] The NMR data of **5a**−**i** clearly indicate that the α,β-unsaturated aldehyde ligand is coordinated in an η^2 fashion through the carbon−carbon double bond adjacent to the aldehyde function, and that the (*E*) or (*all-E*) arrangement of the alkenyl moieties in **3a**−**i** is maintained through their conversion into **5a**−**i**.[12] Finally, when [D-**4c**]$^+$ was treated with water, the deuterium label on C^1 was totally retained in the aldehyde function of $[Cp'(CO)_2Mn(\eta^2\text{-PhCH=CHCH=CDO})]$ [D-**5c**].[17]

The overall transformation of the alkenyl(alkoxy)carbene complexes **3** into the α,β-unsaturated aldehyde complexes **5** is depicted in Scheme 4.

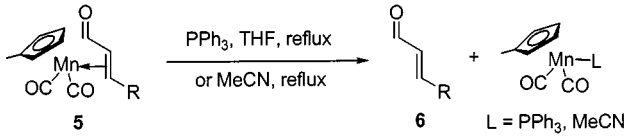


Scheme 4. Proposed mechanism for the formation of **5**

Though no intermediate hydride species could be observed, the context of chemistry and the results of previous studies on protonation reactions of electron-rich carbene complexes suggest that [**4**]$^+$ is likely to result from a protonation of **3** at the metal center followed by hydride migration to the carbene carbon atom,[18,19] and concomitant stabilization of the resulting 16e$^-$ species by coordination of the pendant alkenyl moiety.[20] Upon addition of water, hydrolysis of the highly electrophilic π-allyl ligand in [**4**]$^+$[15c] would then take place through initial nucleophilic addition of water (or hydroxide ions) at the carbon atom bearing the ethoxy group to give the final aldehyde complexes **5**.

Finally, the α,β-unsaturated aldehydes RCH=CHCHO (**6**, Table 1) could be released in nearly quantitative yields by displacement by triphenylphosphane in THF, or by

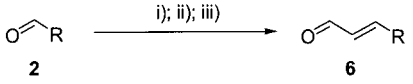
acetonitrile in neat acetonitrile, under refluxing conditions (Scheme 5).



5 6

Scheme 5. Demetalation of the α,β-unsaturated aldehydes **6**

Considering the satisfactory yields of the individual steps, as well as the efficient demetalation of the newly formed α,β-unsaturated aldehydes from the final complex, we logically became interested in a possible application of the above sequence to the vinylogation of aldehydes. A one-vessel procedure was thus developed (Scheme 6) giving the α,β-unsaturated aldehydes **6** in synthetically useful yields.



2 6

Scheme 6. Reagents and reaction conditions: i) $[\mathbf{1}]^-$, −78°C → 20°C, THF; ii) HCl (aq.), MeCN; iii) reflux

The best performances were recorded with formylferrocene (**2b**) and 4-(dimethylamino)benzaldehyde (**2f**) giving the corresponding vinylogated aldehydes **6b** and **6f** in 75%, and 68% yield, respectively. A practical limitation of the procedure is still the need of chromatographic workup to separate the newly formed aldehyde **6** from its precursor **2**.

In conclusion, whereas a recurrent problem with organometallic synthons is the difficulty to establish the mechanism of their participation in organic reactions, the carbenemanganese system disclosed here appears to be both synthetically useful and amenable to mechanistic studies due to the relative stability of the intermediates. In particular, we suggest that the mechanism established here for the hydrolysis of the (alkenylcarbene)manganese complexes under acidic conditions may serve as a model for parallel transformations occurring in related systems.[2b,10d]

Experimental Section

General Remarks: All synthetic manipulations were carried out using standard Schlenk techniques under dry N_2. THF used for the synthesis was distilled under N_2 from Na/benzophenone ketyl just before use. Other solvents were purified according to standard procedures, and stored under N_2. A liquid N_2/2-propanol slush bath was used to maintain samples at the desired low temperature. − Chromatographic separations were performed on alumina. − $[Cp'(CO)_2Mn{=}C(OEt)CH_3]$ (**1**) was prepared by modifications of literature procedures for related complexes.[21] 1,1′-Diformylferrocene (**2i**) was synthesized according to a published procedure.[22] − Solution-IR spectra were recorded with Perkin−Elmer 225 or Perkin−Elmer 983 spectrophotometers with 0.1-mm cells equipped with CaF_2 windows. − ^{1}H- and ^{13}C-NMR spectra were obtained with Bruker AC200, WM250, DPX300, or AMX400 spectrometers and were referenced to the residual signals of the solvents. − Mass spectra were recorded with a Nermag R10−10 mass spectrometer. − Microanalyses were performed with a Perkin−Elmer 2400 CHN analyzer.

1. Typical Procedure for the Synthesis of the Alkenyl(alkoxy)carbene Complexes $[Cp'(CO)_2Mn{=}C(OEt)CH{=}CHR]$ (3) as Illustrated for 3c [R = (*E*)-PhCH=CH]: The carbene anion $[\mathbf{1}]^-$ was generated in situ by addition of *n*BuLi (0.630 mL of a 1.6 M solution in hexanes, 1.1 mmol) to a solution of $[Cp'(CO)_2Mn{=}C(OEt)CH_3]$ (**1**, 0.260 g, 1.0 mmol) in THF (15 mL) at −60°C. After stirring for 20 min, the solution was cooled to −80°C and (*E*)-cinnamaldehyde (**2c**, 0.125 mL, 1.0 mmol) was added. The cooling bath was removed to allow the reaction medium to reach room temperature gradually. After stirring for an additional 1 h, the solvents were removed under vacuum. The brown oily residue was extracted with pentane (ca. 20 mL), and applied on top of an alumina column. Elution with pentane afforded a yellow band which was discarded. Elution with a diethyl ether/pentane (1:10) mixture gave a brown band containing $[Cp'(CO)_2Mn{=}C(OEt)CH{=}CHCH{=}CHPh]$ (**3c**), which was isolated as a brown solid after removal of the solvents under vacuum (0.245 mg, 0.65 mmol, 65% yield). − $C_{21}H_{21}MnO_3$ (376.33): calcd. C 67.02, H 5.58; found C 67.13, H 5.65. − Mp 94−96°C. − IR (ν_{CO}, THF): $\tilde{\nu}$ = 1940, 1876 cm^{-1}. − NMR ^{1}H (C_6D_6, 250 MHz, 298 K): δ = 7.27−7.09 (Ph), 7.00 (m, 1 H, H^2, J_{H2H3} = 15 Hz), 6.73 (m, 1 H, H^3, J_{H3H4} = 11 Hz), 6.63 (m, 2 H, H^4 and H^5, J_{H3H4} = 11 Hz, J_{H5H4} = 15 Hz), 4.82 (q, 2 H, OCH_2CH_3, J_{HH} = 7 Hz), 4.55−4.35 (m, 4 H, Me*Cp*), 1.71 (s, 3 H, *Me*Cp), 1.29 (t, 3 H, OCH_2CH_3). − NMR $^{13}C\{^1H\}$ (C_6D_6, 63 MHz, 298 K): δ = 316.1 (C^1), 233.9 (MnCO), 143.4 (C^2), 139.4 (C^5), 137.2−126.8 (Ph), 128.6 (C^3), 123.4 (C^4), 104.1, 87.7, 86.5 (Me*Cp*), 71.6 (OCH_2CH_3), 14.8 (OCH_2CH_3), 13.4 (*Me*Cp). − MS (EI); *m*/*z*: 376 [M$^+$].

2. In Situ Formation of the π-Allyl Complexes $Cp'(CO)_2Mn(\eta^3$-RCHC)C(OEt)H]$^+$ ([4][TfO]) as Illustrated for [4c][TfO] [R = (*E*)-PhCH=CH]: TfOH (0.018 mL, 0.2 mmol) was added to a solution of $[Cp'(CO)_2Mn{=}C(OEt)CH{=}CHCH{=}CHPh]$ (**3c**, 0.080 mg, 0.2 mmol) in CD_2Cl_2 (1 mL) at −80°C. The brown solution instantaneously turned red. The reaction mixture was allowed to reach room temperature, and the solution was filtered through a plug of celite directly into an NMR tube for analysis. Complex [D-**4c**][TfO] was generated in a similar manner from **3c** and TfOD. − IR (ν_{CO}, CH_2Cl_2): $\tilde{\nu}$ = 2010, 1970 cm^{-1}. − ^{1}H NMR (CD_2Cl_2, 300 MHz, 223 K): δ = 7.7−7.3 (m, 5 H, Ph), 7.2−6.7 (m, 2 H, H^4 and H^5), 6.12 [s (br.), 1 H, H^1], 5.55 [s (br.), 1 H, H^2], 5.3−4.9 (m, 4 H, Me*Cp*), 4.30 [s (br.), 2 H, OCH_2CH_3], 3.41 [s (br.), 1 H, H^3], 1.73 (s, 3 H, *Me*Cp), 1.29 [s (br.), 3 H, OCH_2CH_3]. − $^{13}C\{^1H\}$ NMR (CD_2Cl_2, 75 MHz, 223 K): δ = 227.5, 226.4 (MnCO), 138.1 (C^5), 132.2 (C^1), 134.8, 128.8, 128.4, 126.9 (Ph), 125.4 (C^4), 105.9, 90.9, 90.8, 89.5, 89.2 (Me*Cp*), 77.3 (C^2), 72.6 (OCH_2CH_3), 62.2 (C^3), 14.1 (OCH_2CH_3), 12.2 (*Me*Cp).

3. Typical Procedure for the Synthesis of the Aldehyde Complexes $[Cp'(CO)_2Mn(\eta^2$-RCH=CHCHO)] (5) as Illustrated for 5c [R = (*E*)-PhCH=CH]: TfOH (0.180 mL, 2.0 mmol) was added to a solution of $[Cp'(CO)_2Mn{=}C(OEt)CH{=}CHCH{=}CHPh]$ (**3c**, 0.750 g, 2.0 mmol) in dichloromethane (15 mL) at −80°C. The cooling bath was removed to allow the reaction medium to reach room temperature. An excess of water (5 mL) was added. After stirring for 30 min, the organic phase was separated and the volatiles were removed under vacuum. The brownish oily residue was purified by column chromatography on alumina. Elution with a diethyl ether/pentane (1:1) mixture gave a brown band, which was discarded. Elution with pure dichloromethane released $[Cp'(CO)_2Mn(\eta^2$-PhCH=CHCH=CHCHO) (**5c**), isolated as an orange solid after evaporation of the solvent (0.610 mg, 1.76 mmol, 88% yield). − $C_{19}H_{17}MnO_3$ (348.28): calcd. C 65.51, H 4.88; found C 65.68, H 4.81. − Mp 136°C (dec.). − IR (ν_{CO}, CH_2Cl_2): $\tilde{\nu}$ = 1965, 1904, 1675 cm^{-1}. − ^{1}H NMR (C_6D_6, 250 MHz, 298 K): δ = 8.32 (d, 1

H, H[1], J_{H1H2} = 7 Hz), 7.26−7.05 (Ph), 6.67 (d, 1 H, H[5], J_{H5H4} = 16 Hz), 5.55 (dd, 1 H, H[4], J_{H4H3} = 10 Hz), 3.83, 3.79, 3.75, 3.60 (m, 4 H, Me*Cp*), 4.05 [AB(X) pattern, 2 H, H[2] and H[3], J_{H2H3} = 11 Hz], 1.47 (s, 3 H, *Me*Cp). − $^{13}C\{^1H\}$ NMR (C_6D_6, 63 MHz, 298 K): δ = 233.0, 229.8 (MnCO), 192.2 (C[1]), 131.9 (C[5]), 131.8−125.0 (Ph), 129.9 (C[4]), 103.2, 86.2, 85.8, 85.5, 84.3 (Me*Cp*), 67.8 (C[3]), 60.5 (C[2]), 12.8 (*Me*Cp). − MS (EI); *m*/*z*: 348 [M^+].

4. Typical Procedure for the Demetallation of α,β-Unsaturated Aldehydes RCH=CHCHO (6) as Illustrated for (*E*,*E*)-PhCH=CHCH=CHCHO [6c (≡ 2h)]: Complex [Cp′$(CO)_2$Mn(η[2]-PhCH=CHCH=CHCHO)] (**5c**, 0.610 g, 1.76 mmol) was dissolved in degassed acetonitrile (15 mL) and then heated under reflux for 1 h. After cooling, acetonitrile was removed under vacuum. The oily yellow residue was chromatographed on an alumina column. Elution with a pentane/diethyl ether (1:1) mixture afforded a yellow band containing [Cp′$(CO)_2$Mn(NCMe)]. A second elution with pure diethyl ether afforded (*E*,*E*)-5-phenyl-2,4-pentadienal [**6c** (≡ **2h**)], which was isolated as a yellow solid (0.255 g, 1.62 mmol, 95% yield).

5. One-Vessel Vinylogation of Aldehydes as Illustrated for Formylferrocene (2b) To Give (3-Oxo-1-propenyl)ferrocene [6b (≡ 2g)]: The carbene anion [Cp′$(CO)_2$Mn=C(OEt)CH_2]$^-$ [**1**]$^-$ was generated in situ by addition of *n*BuLi (1.25 mL of a 1.6 M solution in hexanes, 2.0 mmol) to a solution of [Cp′$(CO)_2$Mn=C(OEt)CH_3] (**1**, 525 mg, 2.0 mmol) in THF (15 mL) at −60 °C in a two-necked flask fitted with a reflux condenser. After stirring for 20 min, the solution was cooled to −80°C and formylferrocene was added as a powder (430 mg, 2.0 mmol). The cooling bath was removed to allow the reaction medium to reach room temperature gradually, and the solution was stirred for an additional 1 h. THF was evaporated under vacuum and replaced by degassed acetonitrile (30 mL). Hydrochloric acid (0.330 mL of a 10 M solution in water) was added dropwise, and the mixture was heated under reflux for 1 h. After cooling, the volatiles were removed under vacuum. The oily residue was purified by column chromatography on alumina. Elution with a pentane/diethyl ether (1:1) mixture afforded a yellow band containing traces of [Cp′$(CO)_3$Mn], traces of **1**, and [Cp′$(CO)_2$Mn(NCMe)], which was discarded. A second elution with pure diethyl ether gave a purple band followed by an orange one. The first one contained (3-oxo-1-propenyl)ferrocene [**6b** (≡ **2g**)], isolated as a microcrystalline purple material (360 mg, 1.5 mmol, 75% yield), whereas the second one contained traces of unchanged formylferrocene.

Acknowledgments

We wish to thank the CNRS for financial support, the French Ministère de l'Education Nationale, de la Recherche et de la Technologie for a fellowship to C. M. and Y. O., and Dr. Guy Lavigne for helpful discussions.

[1] R. Aumann, P. Hinterding, C. Krüger, R. Goddard, *J. Organomet. Chem.* **1993**, *459*, 145.
[2] [2a] C. F. Bernasconi, *Chem. Soc. Rev.* **1997**, *26*, 299. − [2b] C. F. Bernasconi, F. X. Flores, K. W. Kittredge, *J. Am. Chem. Soc.* **1997**, *119*, 2103.
[3] [3a] C. P. Casey, R. A. Boggs, R. L. Anderson, *J. Am. Chem. Soc.* **1972**, *94*, 8947. − [3b] W. D. Wulff, S. R. Gilberson, *J. Am. Chem. Soc.* **1985**, *107*, 503. − [3c] R. Aumann, H. Heinen, *Chem. Ber.* **1987**, *120*, 537. − [3d] L. Lattuada, E. Licandro, S. Maiorana, A. Papagni, *J. Chem. Soc., Chem. Commun.* **1991**, 437. − [3e] H. Wang, R. P. Hsung, W. D. Wulff, *Tetrahedron Lett.* **1998**, *39*, 1849.
[4] C. S. Yi, G. L. Geoffroy, C. A. White, A. L. Rheingold, *J. Am. Chem. Soc.* **1993**, *115*, 3806.
[5] See for example: [5a] C. Andraud, T. Brotin, C. Garcia, F. Pellé, P. Goldner, B. Bigot, A. Collet, *J. Am. Chem. Soc.* **1994**, *116*, 2094. − [5b] T.-T. Nguyen, Y. Gouriou, M. Sallé, P. Frère, M. Jubault, A. Gorgues, L. Toupet, A. Riou, *Bull. Chem. Soc. Fr.* **1996**, *133*, 301.
[6] See for example: [6a] A. P. Kozikowski, P. J. Stein, *J. Org. Chem.* **1984**, *49*, 2301. − [6b] P. DeShong, J. M. Leginus, *J. Org. Chem.* **1984**, 3421. − [6c] H. Hopf, N. Krause, *Tetrahedron Lett.* **1986**, *27*, 6177.
[7] These include aldol condensation,[7a] Wittig-,[7b] Horner−Wadsworth−Emmons-,[7c] or Peterson-type[7d,7e] reactions, see for instance: [7a] G. Wittig, H. Reiff, *Angew. Chem., Int. Ed. Engl.* **1968**, *7*, 7. − [7b] B. Maryanoff, A. B. Reitz, *Chem. Rev.* **1989**, *89*, 863. − [7c] J. Boutagy, R. Thomas, *Chem. Rev.* **1974**, *74*, 87. − [7d] L. Duhamel, J. Gralak, B. Ngono, *J. Organomet. Chem.* **1989**, *363*, C4. − [7e] M. Bellassoued, A. Majidi, *J. Org. Chem.* **1993**, *58*, 2517.
[8] J. A. Cabezas, A. C. Oehlschlager, *Tetrahedron Lett.* **1995**, *36*, 5127.
[9] C. Mongin, N. Lugan, R. Mathieu, *Organometallics* **1997**, *16*, 3873.
[10] [10a] E. O. Fischer, S. Walz, G. Kreis, F. R. Kreissl, *Chem. Ber.* **1977**, **110**, 1651. − [10b] W. D. Wulff, D. C. Yang, *J. Am. Chem. Soc.* **1983**, *105*, 6726. − [10c] B. A. Anderson, W. D. Wulff, A. Rahm, *J. Am. Chem. Soc.* **1993**, *115*, 4602. − [10d] C. Baldoli, P. Hellier, E. Licandro, S. Maiorana, R. Manzotti, A. Papagni, *Tetrahedron Lett.* **1997**, *38*, 3769.
[11] C. Kelley, N. Lugan, M. R. Terry, G. L. Geoffroy, B. S. Haggerty, A. L. Rheingold, *J. Am. Chem. Soc.* **1992**, *114*, 6735.
[12] Complete spectroscopic data for all the new complexes are available as Supporting Information.
[13] The protonation of **3f** occurs first on the dimethylamino group to give [Cp′$(CO)_2$Mn=C(OEt)CH=CH_6C$_4$NHMe$_2$]$^+$ ([**3f**-H]$^+$).[12]
[14] B. V. Lokshin, A. G. Ginzburg, V. N. Setkina, D. N. Kursanov, I. B. Nemirovskaya, *J. Organomet. Chem.* **1972**, *37*, 347.
[15] [15a] V. V. Krivykh, O. V. Gusev, M. I. Rybinskaya, *Izv. Akad. Nauk. SSSR* **1983**, *3*, 644; *Chem. Abstr.* **1983**, *99*, 5761c. − [15b] A. M. Rosan, D. M. Romano, *Organometallics* **1990**, *9*, 1048. − [15c] G. R. Knox, P. L. Pauson, J. Rooney, *J. Organomet. Chem.* **1991**, *420*, 379.
[16] Complexes of a related type were obtained from *preformed* α,β-unsaturated aldehydes by substitution of labile ligands in [(η[5]-RC_5H_4)$(CO)_2$Mn(L)] (R = H, Me; L = THF, Et_2O, η[2]-cyclooctene) see: [16a] M. Giffard, E. Gentric, D. Touchard, P. Dixneuf, *J. Organomet. Chem.* **1977**, *129*, 371 − [16b] B. Buchman, A. Salzer, *J. Organomet. Chem.* **1985**, *295*, 63.
[17] ^{1}H-NMR spectra of D-**5c**, purified by crystallisation in Et_2O from the crude reaction mixture, do not show any signal in the area around δ = 8.5. However, we noticed that when D-**5c** is passed through an alumina column ca. 50% of the deuterium label is lost.
[18] [18a] G. R. Clark, S. V. Hoskins, T. C., Jones, W. R. Roper, *J. Chem. Rev.* **1988**, *88*, 1293. − [18b] H. Le Bozec, J.-L. Fillaut, P. H. Dixneuf, *J. Chem. Soc., Chem. Commun.* **1986**, 1182. − [18c] R. A. Michelin, R. Bertani, M. Mozzon, G. Bombieri, F. Benetollo, M. F. C. Guedes da Silva, A. J. L. Pombiero, *Organometallics* **1993**, *12*, 2372.
[19] [19a] V. A. Osborn, C. A. Parker, M. J. Winter, *J. Chem. Soc., Chem. Commun.* **1986**, 1185. − [19b] M. J. Winter, S. Woodward, *J. Organomet. Chem.* **1989**, *361*, C18. − [19c] H. Adams, N. A. Bailey, M. J. Winter, S. Woodward, *J. Organomet. Chem.* **1991**, *418*, C39. − [19d] J. E. Muir, A. Haynes, M. J. Winter, *J. Chem. Soc., Chem. Commun.* **1996**, 1765.
[20] [20a] While investigating the protonation of the group-7 carbene complex [Cp$(CO)_2$Re=C(H)$CH_2CH_2CHMe_2$] to form [Cp$(CO)_2$(Cl)ReCHC$H_2CH_2CHMe_2$] Casey et al. claimed a direct attack of H^+ at the carbene carbon atom since no intermediate hydride was detected.[20b] Thus, a direct protonation of the carbene carbon atom in **3** cannot be totally excluded. − [20b] C. P. Casey, P. C. Vosejpka, F. R. Askham, *J. Am. Chem. Soc.* **1990**, *112*, 3713.
[21] [21a] E. O. Fischer, A. Maasböl, *Chem. Ber.* **1967**, *100,* 2445. − [20b] R. Aumann, H. Heinen, *Chem. Ber.* **1988**, *121*, 1085.
[22] G. G. A. Balavoine, G. Doisneau, T. Fillebeen-Kahn, *J. Organomet. Chem.* **1992**, *412*, 381.

Received December 3, 1998
[I98410]

Synthesis and Homomolecular Metalation of Trialkylsilylphosphanides of Calcium and Barium

Matthias Westerhausen,*[a] Matthias H. Digeser,[a] Mathias Krofta,[a] Nils Wiberg,[a] Heinrich Nöth,[a][+] Jörg Knizek,[a][+] Werner Ponikwar,[a][+] and Thomas Seifert[a][+]

Keywords: Arsenic / Barium / Calcium / Metalations / NMR spectroscopy / Phosphorus

Metalation of triisopropylsilylphosphane with bis(tetrahydrofuran-*O*)calcium bis[bis(trimethylsilyl)amide] in tetrahydropyran (thp) in a molar ratio of 3:2 yields $(Me_3Si)_2NCa[\mu\text{-}P(H)Si\mathit{i}Pr_3]_3Ca(thp)_3$ (**1**) containing a trigonal-bipyramidal Ca_2P_3 core, the metal atoms occupying apical positions. Reaction of two equivalents of triisopropylsilylphosphane or -arsane with bis(tetrahydrofuran-*O*)barium bis[bis(trimethylsilyl)amide] in tetrahydrofuran gives the corresponding bis(phosphanide) **2** and bis(arsanide) **3**, compounds of the type $(thf)_3Ba[\mu\text{-}E(H)Si\mathit{i}Pr_3]Ba(thf)_2E(H)Si\mathit{i}Pr_3$ with E = P, As. The equimolar reaction of (tri-*tert*-butylsilyl)phosphane with $(thf)_2Ba[N(SiMe_3)_2]_2$ in toluene yields heteroleptic dimeric $(thf)_2Ba[N(SiMe_3)_2][P(H)Si\mathit{t}Bu_3]$ (**4**). Addition of a further equivalent of $H_2PSi\mathit{t}Bu_3$ leads to the formation of homoleptic $(thf)_nBa[P(H)Si\mathit{t}Bu_3]_2$ (**5**). Dissolution of the latter in aromatic hydrocarbons leads to the elimination of $H_2PSi\mathit{t}Bu_3$, yielding dimeric $(thf)Ba_3(PSi\mathit{t}Bu_3)_2[P(H)Si\mathit{t}Bu_3]_2$ (**6**). The inner core of **6** consists of the tetramer $(BaPSi\mathit{t}Bu_3)_4$ based on a Ba_4P_4 heterocubane unit, two opposite faces being capped with $(thf)Ba[P(H)Si\mathit{t}Bu_3]_2$ molecules.

Introduction

The bis(trialkylsilyl)amides and -phosphanides of the heavier alkaline earth metals calcium, strontium, and barium are gaining interest not only due to their unexpected solid-state and solution structures, but also due to their high reactivity.[1] Addition reactions of alkaline earth metal bis[bis(trimethylsilyl)amides] and the corresponding phosphanides with benzonitrile are followed by 1,3-trimethylsilyl group shifts, as is seen in the syntheses of the alkaline earth metal bis[*N*,*N*′-bis(trimethylsilyl)benzamidinates][2] and bis[1,3-bis(trimethylsilyl)-2-phenyl-1-aza-3-phosphapropenides].[3] Addition reactions of $M[P(SiMe_3)_2]_2$ (M = Ca, Sr, Ba) with diphenylbutadiyne yield the alkaline earth metal phospholides by a 1,3-trimethylsilyl group migration from the phosphorus to a carbon atom.[4]

Another type of reactivity stems from the pK_s values of compounds $HE(SiMe_3)_2$ (E = N, P). Metallations of substrates with more acidic hydrogen atoms such as alcohols,[1] thiols,[5] selenols,[1,6,7] and tellurols[7,8] are well known. The IR spectra of mono(trialkylsilyl)-substituted phosphanides such as tetrakis(tetrahydrofuran-*O*)calcium bis(triisopropylsilylphosphanide)[9] reveal a reduced force constant of the P−H bond compared with the corresponding bonds in the phosphanes $H_2PSi\mathit{i}Pr_3$ and $HP(Si\mathit{i}Pr_3)_2$.[9,10] This enhanced reactivity leads to slow decomposition of these compounds when they are dissolved in hydrocarbons such as toluene or benzene, but as yet we have been unable to determine the structures of the products thus formed. Because phosphanediides tend to be polymeric, insoluble, and poorly characterized materials, the synthesis of such compounds has remained a challenge and hence there are relatively few examples. Driess and co-workers prepared oxygen-centered Li_2O-containing oligomers[11] and R_3SiF adducts of a dimer[12] of dilithium triorganylsilylphosphanediide and -arsanediide. Monomeric bis[tris(trimethylsilyl)methylzinc] triisopropylsilylphosphanediide[13] displays a pyramidal coordination sphere at the phosphorus atom. Hexameric tin(II) triisopropylsilylphosphanediide crystallizes as a hexagonal Sn_6P_6 prism.[14]

The structures of dimeric alkaline earth metal bis(phosphanides) show an energetic minimum for the bicyclic derivatives $M(\mu\text{-}PH_2)_3MPH_2$ with M = Ca, Sr, and even for the tricyclic isomer $Ba(\mu\text{-}PH_2)_4Ba$, as shown by ab initio calculations.[1,9] The steric demand of the substituents at the phosphorus atom forces the adoption of a monocyclic dimeric structure, with two bridging and two terminally bonded phosphanide substituents.[15] The bicyclic nature of $(Me_3Si)_2NCa[\mu\text{-}P(H)Si\mathit{i}Pr_3]_3Ca(thf)_3$ has been deduced by NMR spectroscopy,[9] although we were unable to obtain single crystals to allow corroboration of this by an X-ray structure determination.

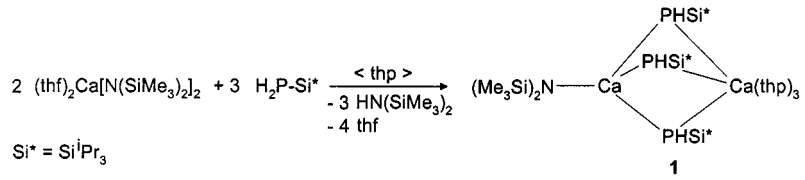
Results and Discussion

Synthesis

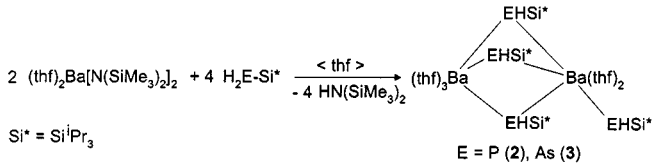
Metalation of triisopropylsilylphosphane with calcium bis[bis(trimethylsilyl)amide][16,17] in a 3:2 stoichiometric ratio in tetrahydropyran (thp) yields almost quantitatively bicyclic $(Me_3Si)_2NCa[\mu\text{-}P(H)Si\mathit{i}Pr_3]_3Ca(thp)_3$ (**1**). This compound exhibits somewhat surprising NMR data (vide infra).

[a] Institut für Anorganische Chemie der Ludwig-Maximilians-Universität,
Meiserstraße 1, D-80333 München, Germany
Fax: (internat.) + 49(0)89/5902-578
E-mail: maw@anorg.chemie.uni-muenchen.de
[+] X-ray structure determinations.

 © WILEY-VCH Verlag GmbH, D-69451 Weinheim, 1999 1434−1948/99/0505−0743 $ 17.50+.50/0



Scheme 1. Synthesis of **1**



Scheme 2. Synthesis of **2** and **3**

Barium bis[bis(trimethylsilyl)amide][16,18] metalates triisopropylsilylphosphane in thf to give the dimeric barium bis(triisopropylsilylphosphanide) **2** in a good yield. In contrast to the alkaline earth metal phosphanides characterized to date, **2** shows a monomer−dimer equilibrium in thf. Analogous investigations of a toluene solution were not possible since **2** undergoes immediate decomposition upon removal of the neutral coligand in vacuo or after dissolution in toluene. The corresponding arsanide H_2AsSi-iPr_3[19] displays a similar reactivity towards $(thf)_2Ba[N(SiMe_3)_2]_2$, the metalation resulting in the formation of barium bis(triisopropylsilylarsanide) **3**, although we were unable to obtain single crystals of this material. All these colorless compounds were found to be extremely air- and moisture-sensitive.

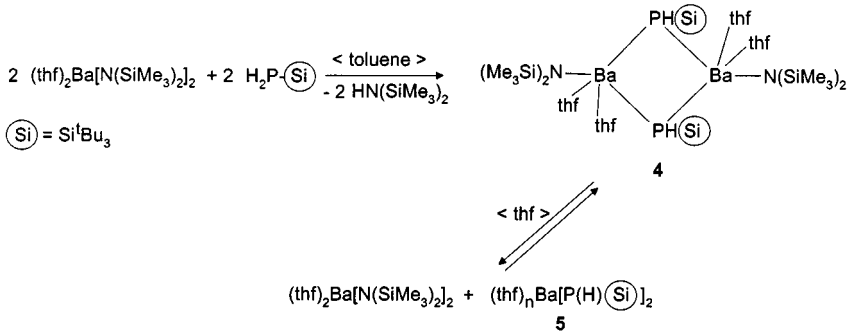
Compounds **1** and **2** decompose in toluene solution within a few days. The decomposition products show a 1:1 ratio of triisopropylsilylphosphanide and triisopropylsilylphosphanediide substituents, but all efforts to obtain a pure crystalline product were unsuccessful. Therefore, we metalated tri-*tert*-butylsilylphosphane[20] with barium bis[bis(trimethylsilyl)amide]. Reaction of equimolar amounts of $(thf)_2Ba[N(SiMe_3)_2]_2$ and $H_2PSitBu_3$ in toluene quantitatively affords heteroleptic dimeric bis(tetrahydrofuran-*O*)-barium bis(trimethylsilyl)amide tri-*tert*-butylsilylphosphanide (**4**), featuring a central Ba_2P_2 ring. Only the centrosymmetric isomer crystallizes from toluene, although numerous isomers were observed in solution. Assignment of the NMR data to specific isomers was not possible. Dissolution of **4** in thf leads to dismutation reactions and the formation of homoleptic derivatives, namely barium bis[bis(trimethylsilyl)amide] and barium bis(tri-*tert*-butylsilylphosphanide) **5**. Reaction of **4** with a further equivalent of $H_2PSitBu_3$ also quantitatively yields compound **5**, which decomposes with elimination of $H_2PSitBu_3$. Therefore, no monomer−dimer equilibrium could be investigated.

Decomposition of **5** yields colorless $\{(thf)Ba_3(\mu_4\text{-}PSitBu_3)_2[\mu_2\text{-}P(H)SitBu_3]_2\}_2$ (**6**) with a 1:1 molar ratio of $tBu_3SiP(H)^-$ and tBu_3SiP^{2-} anions. This complex can be regarded as a Ba_4P_4 heterocubane with two opposite sides capped by $(thf)Ba[P(H)SitBu_3]_2$ molecules, although the mechanism of its formation might well proceed via a polyhedron best described as a dimer of two pentagonal bipyramids with a common MP_2 face. Although heterocubane structures with heavier alkaline earth metals are only known for heterobimetallic tin(II)-containing molecules such as $[(thf)_3Ca]_2Sn_2(PSiMe_3)_4$[21] and $(toluene)BaSn_3(PSitBu_3)_4$,[22] the trigonal-bipyramidal M_2P_3 core seems to be more common.[1,21,23] Similar findings were published by Rabe et al.[24] in relation to the arylphosphanides of Rb (tetrameric, Rb_4P_4 heterocubane core) and Cs {dimeric, $Cs^+[Cs(\mu\text{-}PHR)_3Cs]^-$ with a trigonal Cs_2P_3 bipyramid}, whereas $NaP(H)SitBu_3$ crystallizes as a dimer with a central Na_2P_2 ring.[20c] The constitution of complex **6** was further proven by an X-ray structure determination (vide infra). Although the central Ba_6P_8 moiety is shielded by eight tri-*tert*-butylsilyl substituents, derivative **6** proved to be air- and moisture-sensitive.

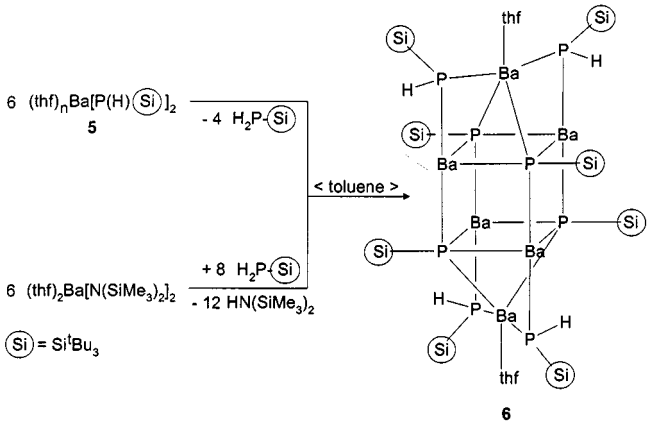
Metalations of $H_2PSiiPr_3$, $H_2AsSiiPr_3$, and $H_2PSitBu_3$ lead to shifts of the P−H stretching vibrations of approximately 70 cm^{-1} towards lower wavenumbers. The large reduction of the P−H force constant explains the increased reactivity with regard to the metalation reaction and accounts for the fact that compounds of the type $M[P(H)SiR_3]_2$ decompose so readily. In complex **6**, the remaining P−H fragments are shielded by the sterically demanding tri-*tert*-butylsilyl groups, which prevent further metalation, even in refluxing toluene.

NMR Spectroscopy

The ^{31}P-NMR spectrum of compound **1** (Figure 1) displays a coupling pattern of the AA′A′′XX′X′′ type with remarkably large $^2J(P,P)$ and $^3J(P,H)$ coupling constants of 92.3 and 11.7/2.1 Hz, respectively, which were verified by simulation. The $^1J(P,H)$ coupling constant of 186.1 Hz lies within the characteristic range. An explanation for these observations could be the close contact of the phosphanide anions due to the formation of the bicyclic Ca_2P_3 bipyramid. The barium complex **2** with a similar Ba_2P_3 core is dynamic in thf solution, with even the terminal and bridging substituents being indistinguishable by NMR. Only very broad signals with half-height widths between 15 (at



Scheme 3. Synthesis of **4** and dismutation reaction in thf



Scheme 4. Synthesis of **6**

−30°C, δ = −291.7) and 1060 Hz (at +50°C, δ = −280.2) are observed. Corresponding investigations of a toluene solution were not possible due to the decomposition of **2**. Similar results were obtained for **5**, which do not merit special comment.

In contrast to the NMR data of **1**, the ^2J(P,P) coupling constants of **6** are smaller than 3 Hz and are not resolved. With a ^1J(P,H) coupling constant of 149 Hz, however, the signal at δ = −222.9 can clearly be assigned to the phosphanide ligands. The tri-*tert*-butylsilylphosphanediide substituents show a remarkable low-field shift of δ = −25.0. This chemical shift may be explained by the rather high coordination number of five at the phosphorus atoms and might be taken as an indication that these molecules do not dissociate in solution.

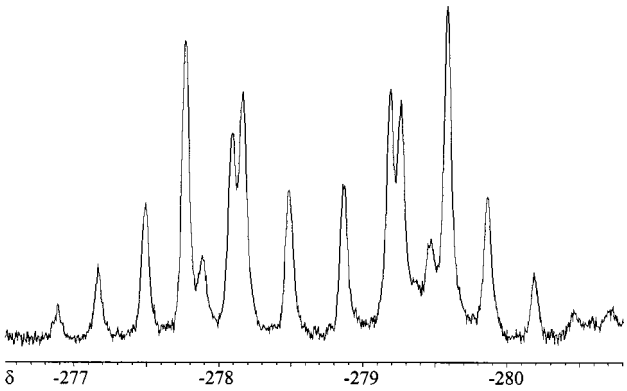


Figure 1. ^{31}P-NMR spectrum of $(Me_3Si)_2NCa[\mu\text{-}P(H)Si\textit{i}Pr_3]_3Ca(thp)_3$ (**1**) at δ = −278.68 ([D_8]toluene, 25°C, 109.365 MHz; coupling constants see text)

Molecular Structures

The molecular structure of **1**, showing the numbering scheme, is depicted in Figure 2. Ca1 is surrounded by three phosphorus atoms and an amide ligand in a distorted tetrahedral arrangement, whereas Ca2 has a coordination number of six and a distorted octahedral coordination sphere with a facial arrangement of the phosphorus and oxygen atoms. The thp coligands adopt chair conformations. The Ca2−O(*n*) distances are between 235 and 241 pm and thus lie within the characteristic range.[1]

The terminally bonded bis(trimethylsilyl)amide substituent exhibits a trigonal-planar coordination sphere at the nitrogen atom, the Ca1−N1 bond length of 228 pm matching the corresponding bond lengths in the calcium bis[bis(trimethylsilyl)amides].[1][25]

The triisopropylsilylphosphanide substituents occupy bridging positions. Due to the higher coordination number of Ca2, the Ca2−P(*n*) bonds (mean value 297.7 pm) are approximately 6 pm longer than the Ca1−P(*n*) bonds (mean distance 291.3 pm). These bond lengths are consistent with the Ca−P distances observed in other calcium bis-

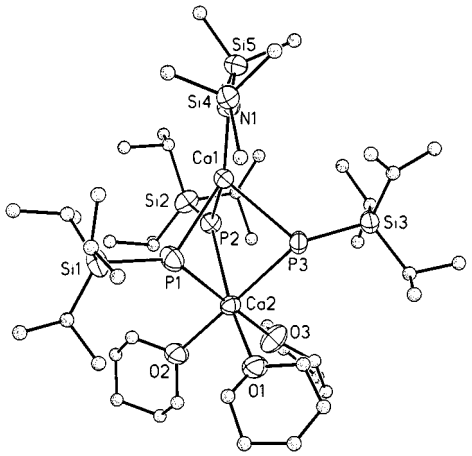


Figure 2. Molecular structure of **1**; C atoms are drawn with arbitrary radii and H atoms are omitted for clarity; the ellipsoids of the heavier atoms are drawn at a 40% probability level; selected bond lengths [pm] and angles [°]: Ca1−N1 228.1(9), Ca1−P1 290.9(4), Ca1−P2 294.7(4), Ca1−P3 288.2(3), Ca2−P1 297.8(4), Ca2−P2 298.3(3), Ca2−P3 297.1(4), Ca2−O1 240.7(8), Ca2−O2 240.1(7), Ca2−O3 235.0(9), P1−Si1 223.3(4), P2−Si2 221.8(4), P3−Si3 221.8(4), Ca1···Ca2 389.9(3); Ca1−P1−Ca2 83.0(1), Ca1−P1−Si1 128.8(2), Ca2−P1−Si1 139.3(2), Ca1−P2−Ca2 82.20(9), Ca1−P2−Si2 133.9(2), Ca2−P2−Si2 142.6(2), Ca1−P3−Ca2 83.51(9), Ca1−P3−Si3 123.0(2), Ca2−P3−Si3 138.8(2), P1−Ca1−P2 82.7(1), P1−Ca1−P3 81.8(1), P2−Ca1−P3 81.6(1), P1−Ca2−P2 80.9(1), P1−Ca2−P3 79.1(1), P2−Ca2−P3 79.57(9)

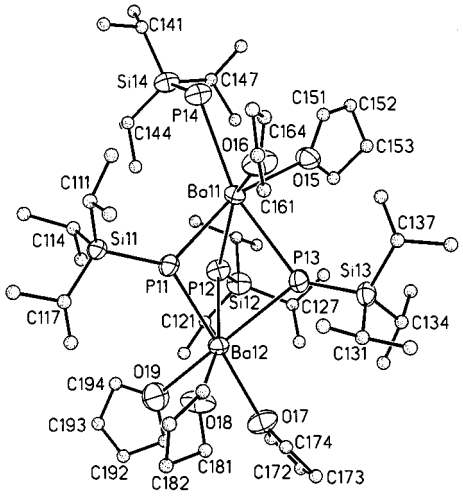


Figure 3. Molecular structure and numbering scheme of **2**; only one molecule is displayed; thermal ellipsoids represent a 40% probability level; C atoms are drawn with arbitrary radii and H atoms are omitted for clarity; selected bond lengths [pm] and angles [°]: Ba11−P11 330.6(2), Ba11−P12 330.1(2), Ba11−P13 333.5(2), Ba11−P14 328.5(3), Ba11−O15 273.8(6), Ba11−O16 272.9(6), Ba12−P11 324.7(2), Ba12−P12 323.9(2), Ba12−P13 321.5(2), Ba12−O17 274.7(6), Ba12−O18 273.9(6), Ba12−O19 274.0(7), P11−Si11 221.4(3), P12−Si12 221.0(3), P13−Si13 220.2(3), P14−Si14 219.3(3), Ba11···Ba12 461.03(9); Ba11−P11−Ba12 89.41(5), Ba11−P11−Si11 123.2(1), Ba12−P11−Si11 135.2(1), Ba11−P12−Ba12 89.64(5), Ba11−P12−Si12 137.9(1), Ba12−P12−Si12 121.0(1), Ba11−P13−Ba12 89.46(5), Ba11−P13−Si13 138.0(1), Ba12−P13−Si13 131.6(1), Ba11−P14−Si14 115.5(1), P11−Ba11−P12 77.60(6), P11−Ba11−P13 74.28(6), P12−Ba11−P13 72.41(6), P11−Ba12−P12 79.33(6), P11−Ba12−P13 76.69(6), P12−Ba12−P13 74.79(6)

(phosphanides).[1] The distortion of the tetrahedral environments of the phosphorus atoms is best illustrated by the angle sums at these centers, neglecting the hydrogen atoms [M, M′ = Ca1, Ca2, Si(*n*); ΣMP1M′ = 351.1°; ΣMP2M′ = 358.7°; ΣMP3M′ = 345.2°]. Compared to those in HP(Si*i*Pr$_3$)$_2$ (P−Si 226.5 pm[9]), the P(*n*)−Si(*n*) bonds are approximately 4 pm shorter due to the negative charge on the phosphorus atoms. Furthermore, the higher coordination number of four at the phosphorus atoms leads to elongated P−Si bonds compared with those in tetrakis(tetrahydrofuran-*O*)calcium bis[bis(trimethylsilyl)phosphanide] (P−Si 219 pm[21]) and tetrakis(tetrahydrofuran-*O*)bis(triisopropylsilylphosphanide) (P−Si 219.6 pm[9]). Moreover, the elongation of bond lengths within the ESi*i*Pr$_3$ fragment is a well-known consequence of the steric strain.[26]

Figure 3 shows the molecular structure and the numbering scheme of (thf)$_5$Ba$_2$[P(H)Si*i*Pr$_3$]$_4$ (**2**). The central moiety is a trigonal-bipyramidal Ba$_2$P$_3$ core with the barium atoms in apical positions. Both alkaline earth metal centers have a distorted octahedral coordination sphere. The asymmetric unit contains two virtually identical molecules with the barium atoms labelled Ba(*mn*), where *m* = 1 or 2 denotes the molecule number and *n* is a digit to distinguish between different atoms. Here, the discussion is limited to the molecule with *m* = 1.

Ba11 is bonded to four phosphanide anions and two thf molecules, whereas Ba12 is surrounded by three phosphanide substituents and three thf molecules. The Ba11−P(*n*) bond lengths vary over the narrow range of 331 ± 3 pm regardless of whether the phosphanide ligand is in a bridging or terminal position. The Ba12−P(*n*) distances have a mean value of 323.4 pm and are clearly smaller. These findings are consistent with an electrostatic viewpoint, where the size of the ions largely determines the intramolecular distances between the cations and anions, but not the coordination number at the phosphorus atoms. All the aforementioned Ba−P distances lie within the broad range of Ba−P values found in barium bis(phosphanides).[1]

As described for **1**, a flattening of the coordination spheres about the bridging phosphorus atoms is observed [M, M′ = Ba11, Ba12, Si(1*n*); ΣMP11M′ = 347.8°; ΣMP12M′ = 348.5°; ΣMP13M′ = 359.1°]. The smallest Ba−P(1*n*)−Si(1*n*) angle is realized within the terminal phosphanide substituent (*n* = 4), with a value of 115.5°. Due to the intramolecular strain, the Si*i*Pr$_3$ groups are pushed to the periphery of the molecule, thereby widening the Ba−P−Si angles and flattening the coordination spheres of the P atoms.

Figure 4 shows the molecular structure as well as the numbering scheme of dimeric heteroleptic **4**. The apostrophes indicate symmetry-related atoms. The bis(trimethylsilyl)amide ligand is in a terminal position, while the tri-*tert*-butylsilylphosphanide substituent adopts a bridging position. A coordination number of five at the alkaline earth metal center is achieved by the coordination of two thf coligands. In this case, we were able to locate the phosphorus-bonded hydrogen atoms. The Ba−N (260.1 pm) and Ba−P bond lengths (330 pm) have values in the expected

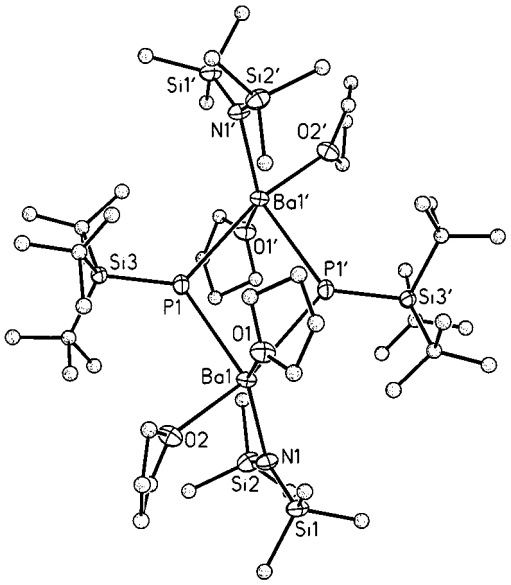


Figure 4. Molecular structure of **4**; thermal ellipsoids are drawn at a 40% probability level; C atoms are shown with arbitrary radii and H atoms are omitted for clarity; symmetry-related atoms ($-x + 1, -y, -z$) are marked with an apostrophe; selected bond lengths [pm] and angles [°]: Ba1−N1 260.1(2), Ba1−P1 330.27(7), Ba1−P1′ 329.25(7), Ba1−O1 275.4(2), Ba1−O2 278.9(2), N1−Si1 168.5(2), N1−Si2 167.5(2), P1−Si3 222.96(9); P1−Ba1−P1′ 73.25(2), Ba1−P1−Ba1′ 106.75(2), Ba1−P1−Si3 127.92(3), Ba1′−P1−Si3 124.45(3), Ba1−N1−Si1 117.6(1), Ba1−N1−Si2 115.3(1), Si1−N1−Si2 127.1(2)

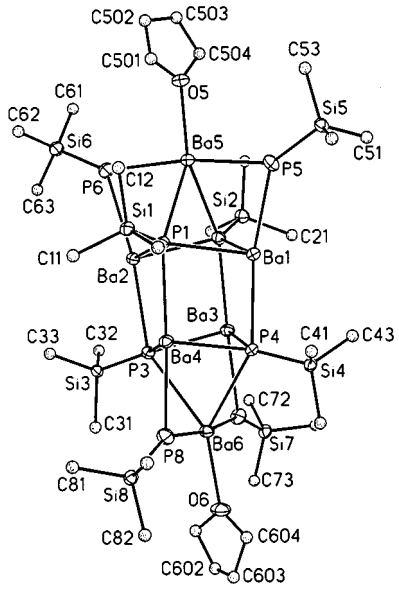


Figure 5. Molecular structure of **6**; the methyl groups of the Si*t*Bu$_3$ substituents and the H atoms are omitted for clarity; the remaining C atoms are shown with arbitrary radii; ellipsoids are drawn at a 40% probability level; selected bond lengths [pm] and angles [°]: see Table 1

ranges[1] and are essentially similar to those found in $\{(Me_3Si)_2NBa[\mu\text{-}P(SiMe_3)_2]\}_2$.[23] Neglecting H1, the coordination sphere about P1 is almost planar, having an angle sum of 359.1°.

Figure 5 displays the molecular structure and the numbering scheme of **6**. This molecule is built-up of four inner tri-*tert*-butylsilylphosphanediide ligands (P1 to P4) and four outer tri-*tert*-butylsilylphosphanide ligands (P5 to P8), held together by six barium atoms. The central Ba_6P_8 core is depicted in Figure 6 in a stereoscopic view. Whereas the phosphanide ligands contain quadruply coordinated phosphorus atoms, the inner P atoms are surrounded by four barium centers and one silicon atom. The Ba−P bond lengths are spread over a wide range from 311 to 347 pm (Table 1). The shortest Ba−P bond lengths are found within the four-membered rings Ba1−P1−Ba2−P2 and Ba3−P3−Ba4−P4. The Ba−P distances between these Ba_2P_2 cycles as well as the Ba−P values to the P(H)Si*t*Bu$_3$ substituents are significantly longer. All the barium atoms are bonded to four phosphorus atoms. Their coordination spheres are completed by the coordination of a thf molecule (Ba5 and Ba6) or by agostic interactions with *tert*-butyl groups (Ba1 to Ba4). The Ba−O bond lengths of 273 pm lie within the characteristic range.[1,18b] The close contacts between Ba5 and Ba6, respectively, and the neighboring metal centers are a consequence of the rather low coordination numbers of these barium atoms and the strong electrostatic attraction between the dianions and dications. The coordination polyhedra of Ba5 and Ba6 are trigonal-bipyramids with the phosphanide ligands in apical positions [P5−Ba5−P6 170.30(7)°, P7−Ba6−P8 172.73(7)°].

The angle sums ΣMPM′ at P5 (359.7°), P6 (359.7°), P7 (358.7°), and P8 (356.9°) indicate an almost planar environment at the phosphorus atoms. The hydrogen atoms at these P atoms were not located and due to the planar Ba_2PSi fragments the H atoms could be bonded on either side and several isomers are possible. However, the ^{31}P-NMR data show only one resonance for the PH groups. The P−Si bond lengths have values of approximately 222 pm, irrespective of whether mono- or dianions are considered. Due to shielding by the *tert*-butyl groups, the P−H moieties are not metalated by the still present barium bis[bis(trimethylsilyl)amide], not even at elevated temperatures such as in boiling toluene.

Conclusion

Metalations of H_2PSiR_3 (R = *i*Pr, *t*Bu) with bis(tetrahydrofuran-*O*)calcium and bis(tetrahydrofuran-*O*)barium bis[bis(trimethylsilyl)amide] yield the corresponding alkaline earth metal bis(trialkylsilylphosphanides) of the type $(L)_nM[P(H)SiR_3]_2$. These phosphanides show a weakening of the P−H bond compared to the phosphane and hence an increased reactivity. Consequently, these compounds react as metalating reagents and as metalation substrates. The elimination of H_2PSiR_3 yields a product of the type $(L)_nM[P(H)SiR_3]_2(PSiR_3)_2$. With R = *t*Bu, an X-ray structure determination has revealed a dimer of this formula unit. The central M_6P_8 core can be considered as two trigonal bipyramids with a common MP_2 face; this polyhedron dimerizes via the square-planar M_2P_2 plane.

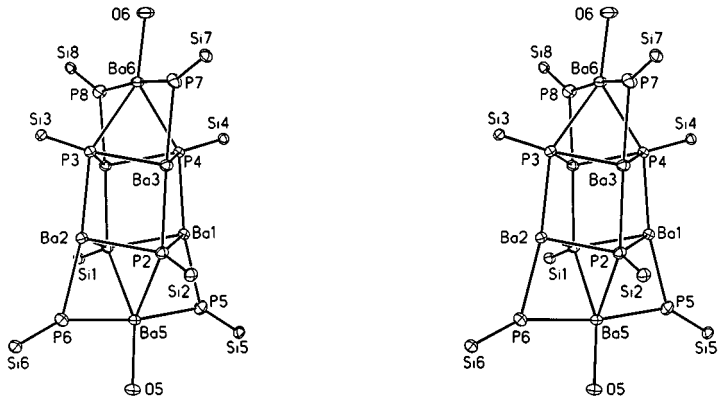
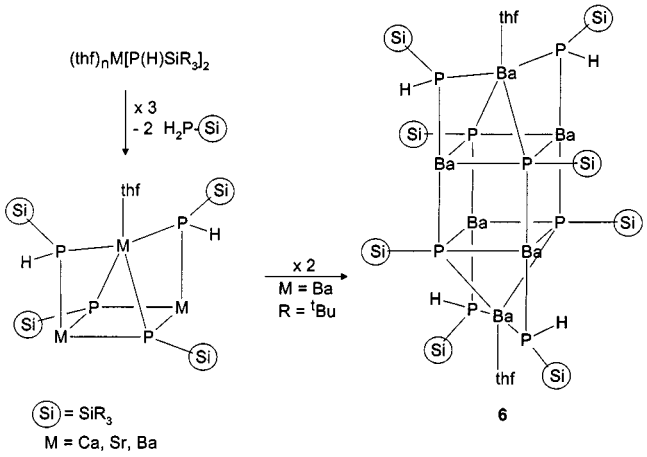


Figure 6. Stereoscopic view of the Ba_6P_8 polyhedron of **6**; the atoms are drawn at a 40% probability level

Table 1. Selected bond lengths [pm] and angles [°] of **6**

n	1	2	3	4	5	6	7	8
Ba1−P(*n*)	314.3(2)	311.1(2)		325.6(2)	313.8(2)			
Ba2−P(*n*)	313.6(2)	314.7(3)	331.6(2)			322.7(2)		
Ba3−P(*n*)		333.3(2)	314.2(2)	315.5(2)			324.6(2)	
Ba4−P(*n*)	328.7(2)		313.4(2)	316.2(2)				318.3(2)
Ba5−P(*n*)	337.7(2)	339.5(2)			327.1(3)	322.2(3)		
Ba6−P(*n*)			347.4(2)	331.5(2)			320.7(3)	323.9(3)
Ba(*n*)−O(*n*)					272.7(6)	272.7(6)		
P(*n*)−Si(*n*)	222.3(3)	221.9(3)	222.0(3)	222.4(3)	221.8(3)	222.2(4)	222.3(3)	222.1(3)
Ba1···Ba(*n*)		469.89(7)	436.82(7)	422.10(8)	402.58(5)			
Ba2···Ba(*n*)			432.71(8)	435.14(7)	405.77(5)			
Ba3···Ba(*n*)				475.78(7)		409.53(5)		
Ba4···Ba(*n*)						401.42(5)		
Ba1−P(*n*)−Si(*n*)	133.3(1)	134.0(1)		98.36(9)	137.6(1)			
Ba2−P(*n*)−Si(*n*)	129.8(1)	128.5(1)	99.55(9)			128.5(1)		
Ba3−P(*n*)−Si(*n*)		101.1(1)	129.2(1)	133.2(1)			124.4(1)	
Ba4−P(*n*)−Si(*n*)	98.46(9)		132.2(1)	129.1(1)				134.0(1)
Ba5−P(*n*)−Si(*n*)	111.71(9)	107.9(1)			144.3(1)	153.2(1)		
Ba6−P(*n*)−Si(*n*)			111.62(9)	109.72(9)			155.6(1)	145.5(1)



Scheme 5. Metalation of $H_2P - Si\mathit{i}Pr_3$ and formation of **6**

Experimental Section

General Remarks: All experiments and manipulations were carried out under argon or nitrogen that had been purified by passage through BTS catalyst and P_4O_{10}. Reactions were performed using standard Schlenk techniques and dried, thoroughly deoxygenated solvents. The starting materials $(thf)_2Ca[N(SiMe_3)_2]_2$,[16][17] $(thf)_2Ba[N(SiMe_3)_2]_2$,[16][18] $H_2PSi\mathit{i}Pr_3$,[9] and $H_2PSi\mathit{t}Bu_3$[20] were prepared according to literature procedures. − NMR spectra were recorded with Jeol GSX270 and EX400 spectrometers. − A Perkin-Elmer Paragon 1000 PC spectrophotometer was used to record the IR spectra; solid substances were examined as Nujol mulls between CsBr plates (vs very strong, s strong, m medium strong, w weak, vw very weak, sh shoulder). The frequencies in the region of the Nujol vibrations are not listed. − The low carbon values obtained in the elemental analyses can be attributed to carbide and carbonate formation, as well as to the loss of neutral coligands during handling and combustion of the compounds.

$(Me_3Si)_2NCa[\mu\text{-}P(H)Si\mathit{i}Pr_3]_3Ca(thp)_3$ (1): To 2.78 g of $(thf)_2Ca[N(SiMe_3)_2]_2$ (5.50 mmol), dissolved in 12 mL of thp, 1.33 mL of triisopropylsilylphosphane (8.25 mmol) was added at −60°C. After warming to room temp., this solution was stirred for a further 12 h. All volatiles were then removed at room temp. in vacuo. Addition of toluene and storage at −30°C led to the deposition of 0.93 g of crystalline **1** (0.87 mmol; 32%); dec. above 110°C. − NMR ([D_8]toluene, 30°C); ^{1}H: δ = −0.49 (m, PH), 0.50 (s, $SiMe_3$), 1.25 (m, CH), 1.31 (s, Me), 1.31, 1.39 and 3.77 (thp); $^{31}P\{^1H\}$: δ = −278.68; ^{31}P: δ = −278.63 [AA′A″XX′X″, simulation: ^1J(P,H) = 186.1(1) Hz, ^2J(P,P) = 92.3(1) Hz, ^3J(P,H′) = 11.7(6) Hz, ^3J(P,H″) = 2.1(6) Hz]. − IR: $\tilde{\nu}$ = 2274 m, 1462 s, 1442 m, 1384 w, 1379 w, 1362 w, 1357 w, 1328 vw, 1310 m, 1277 w, 1248 s, 1240 s, 1194 s, 1181 sh, 1125 sh, 1098 m, 1077 s, 1048 vs, 1033 vs, 1015 s, 992 s, 966 m, 931 m, 918 m, 881 vs, 865 s, 833 s, 820 s, 812 s, 767 m, 747 w, 708 sh, 683 sh, 664 sh, 652 s, 639 s, 626 m, 609 m,

584 s, 572 s, 563 s, 511 s, 474 m, 446 m, 429 w, 412 w, 381 w, 363 m. − $C_{33}H_{84}Ca_2NP_3Si_5$ (808.53, coligand-free complex): calcd. C 49.02, H 10.47, N 1.73; found C 47.60, H 9.85, N 1.63.

[*i*Pr$_3$Si(H)P](thf)$_2$Ba[μ-P(H)Si*i*Pr$_3$]$_3$Ba(thf)$_3$ (2): At −60°C, 1.36 mL of triisopropylsilylphosphane (6.08 mmol) was slowly added dropwise to a solution of 1.83 g of (thf)$_2$Ba[N(SiMe$_3$)$_2$]$_2$ (3.04 mmol) in 10 mL of thf. After completion of the addition, the solution was stirred for a further 48 h at room temp. and then concentrated to an oily residue. At −30°C, 1.24 g of colorless crystals of **2** (0.89 mmol; 59%) precipitated; m.p. 47°C. − NMR ([D$_8$]THF, 30°C); ^{1}H: δ = −1.97 [d, PH, ^1J(P,H) = 152.7 Hz], 0.91 (sept, CH), 1.02 [d, Me, ^3J(H,H) = 7.2 Hz], 1.76 and 3.62 (thf); ^{13}C{^{1}H}: δ = 15.03 [d, CH, ^2J(P,C) = 6.1 Hz], 19.62 (s, Me), 25.45 and 67.35 (thf); ^{29}Si{^{1}H}: δ = 27.19 [d, $|^1J$(P,Si) + ^3J(P,Si)| = 52.6 Hz]; ^{31}P{^{1}H}: δ = −287.76. − IR: $\tilde{\nu}$ = 2241 m, 1359 w, 1306 sh, 1293 vw, 1242 m, 1181 w, 1156 w, 1130 w, 1072 s, 1042 vs, 1012 m, 1005 sh, 989 s, 916 m, 882 vs, 843 sh, 747 vw, 698 w, 640 vs, 622 s, 586 s, 565 s, 512 s, 474 m, 445 w, 431 w, 416 w. − $C_{36}H_{88}Ba_2P_4Si_4$ (1031.90, coligand-free complex): calcd. C 41.90, H 8.60; found: C 39.21, H 8.03.

[*i*Pr$_3$Si(H)As](thf)$_2$Ba[μ-As(H)Si*i*Pr$_3$]$_3$Ba(thf)$_3$ (3): To a solution of 1.83 g of (thf)$_2$Ba[N(SiMe$_3$)$_2$]$_2$ (3.04 mmol) in 10 mL thf at −70°C, was slowly added 1.26 mL of triisopropylsilylarsane (6.08 mmol). Following the addition, the mixture was stirred for a further 48 h at room temp. Reduction to a volume of approximately 5 mL and storage at −30°C led to the deposition of waxy crystals of **3** (0.93 g, 0.69 mmol; 45%); m.p. 40°C. − NMR ([D$_8$]THF, 30°C); ^{1}H: δ = 0.27 (s, AsH), 0.95 (br., CH), 1.04 [Me, ^3J(H,H) = 6.8 Hz], 1.76 and 3.61 (thf); ^{13}C{^{1}H}: δ = 15.22 (CH), 19.87 (Me), 25.47 and 67.44 (thf); ^{29}Si{^{1}H}: δ = 32.25. − IR: $\tilde{\nu}$ = 2019 m, 1462 vs, 1382 sh, 1378 m, 1361 w, 1294 vw, 1250 m, 1226 sh, 1180 m, 1070 m, 1042 s, 1014 m, 1005 m, 989 s, 929 sh, 917 s, 882 vs, 842 m, 771 vw, 754 vw, 663 s, 648 s, 635 s, 603 sh, 586 sh, 573 s, 558 s, 503 s, 464 m, 444 sh, 425 vw, 385 w, 354 vw. − $C_{44}H_{104}As_4Ba_2O_2Si_4$ [1352.00, bis(thf) complex]: calcd. C 39.09, H 7.75; found C 39.09, H 7.32.

[(Me$_3$Si)$_2$N](thf)$_2$Ba[μ-P(H)Si*t*Bu$_3$]$_2$Ba(thf$_2$)[N(SiMe$_3$)$_2$] (4): A solution of 256 mg of tri-*tert*-butylsilylphosphane (1.1 mmol) in 5 mL of toluene was added dropwise to 663 mg of (thf)$_2$Ba[N(SiMe$_3$)$_2$]$_2$ (1.1 mmol), dissolved in 35 mL of toluene. After completion of the addition, the solution was reduced to a volume of a few mL. At 4°C, 607 mg of colorless cuboids of **4** (0.45 mmol; 82%) precipitated; m.p. 359°C (dec.). − NMR (30°C); ^{1}H ([D$_6$]benzene): δ = 0.32 (SiMe$_3$), 1.33 (*t*Bu), 1.36 and 3.58 (thf), PH signal not observed; ^{13}C{^{1}H} ([D$_6$]benzene): δ = 5.42 (SiMe$_3$), 24.05 (PSiC$_3$), 31.87 (Me$_{Bu}$), 24.98 and 68.61 (thf); ^{31}P ([D$_8$]toluene, three major isomers): δ = −220.1 [^1J(P,H) = 153 Hz], −229.1 [^1J(P,H) = 150 Hz], −233.5 [^1J(P,H) = 152 Hz]. − IR: $\tilde{\nu}$ = 2225 w, 1251 m, 1180 m, 1064 m, 1037 m, 1013 s, 932 s, 882 m, 842 s, 816 vs, 803 s, 757 vw, 729 vw, 694 vw, 664 vw, 594 m, 569 s, 511 s, 478 w, 456 m, 389 vw, 360 vw, 331 w. − $C_{44}H_{108}Ba_2N_2O_2P_2Si_6$ (1202.47): calcd. C 43.95, H 9.05, N 2.33; found C 43.93, H 7.97, N 2.12.

(thf)*n*Ba[P(H)Si*t*Bu$_3$]$_2$ (5): A solution of 558 mg of tri-*tert*-butylsilylphosphane (2.4 mmol) in 15 mL of toluene was slowly added dropwise to a solution of 723 mg of (thf)$_2$Ba[N(SiMe$_3$)$_2$]$_2$ (1.2 mmol) in 20 mL of toluene. After reduction to a volume of a few mL, the precipitate was dissolved by adding thf and characterized NMR-spectroscopically. − NMR ([D$_6$]benzene, 30°C); ^{1}H: δ = 1.24 (*t*Bu), 1.35 and 3.54 (thf), PH signal was not observed; ^{13}C{^{1}H}: δ = 24.00 (PSiC), 31.97 (Me), 25.49 and 67.46 (thf); ^{31}P: δ = −242.5 [^1J(P,H) = 147 Hz].

{(thf)Ba$_3$(μ$_4$-PSi*t*Bu3)$_2$[μ$_2$-P(H)Si*t*Bu$_3$]$_2$}$_2$ (6): 906 mg of (thf)$_2$Ba[N(SiMe$_3$)$_2$]$_2$ (1.5 mmol) and 466 mg of tri-*tert*-butylsilylphosphane (2.0 mmol) were dissolved in 23 mL of toluene and heated to 100°C for approximately 6 h. The solution turned dark brown. After cooling to room temp., the solid materials were removed and the solu-

Table 2. Crystallographic data of **1**, **2**, **4**, and **6**, as well as details of the structure solution and refinement procedures

Compound	**1**	**2**	**4**	**6**
Empirical formula	$C_{48}H_{111}Ca_2NO_3P_3Si_5$	$C_{56}H_{128}Ba_2O_5P_4Si_4$	$C_{52}H_{122}Ba_2N_2O_4P_2Si_6$	$C_{119}H_{250}Ba_6O_{2.25}P_8Si_8$
Molecular mass [g·mol^{-1}]	1063.90	1392.51	1344.68	3013.71
T [K]	183	183	173	173
Space group[28]	*Cc* (no. 9)	*P*−1 (no. 2)	*P*2$_1$/*c* (no. 14)	*P*2/*c* (no. 13)
a [pm]	1406.0(3)	1387.5(2)	1389.57(3)	3136.17(3)
b [pm]	2160.0(5)	2240.1(4)	1440.01(3)	1454.17(3)
c [pm]	2199.8(6)	2426.7(4)	1931.21(4)	3616.84(1)
α [°]	90	90.884(6)	90	90
β [°]	101.813(9)	90.865(7)	107.814(1)	103.275(1)
γ [°]	90	90.704(6)	90	90
V [nm^3]	6.539(3)	7.540(2)	3.6791(1)	16.0539(4)
Z	4	4	2	4
$d_{calcd.}$ [g·cm^3]	1.081	1.227	1.214	1.247
μ [mm^{-1}]	0.373	1.224	1.241	1.626
F(000)	2340	2928	1412	6200
Scan range [°]	1.75 < θ < 27.76	0.84 < θ < 29.52	1.54 < θ < 29.30	0.67 < θ < 29.41
Measured data	11050	44857	20540	90128
Unique data (R_{int})	8693 (0.0747)	24072 (0.0351)	6641 (0.0209)	30674 (0.0765)
Parameters	539	1142	386	1239
Restraints	15	94	0	0
wR_2[a] (all data, on F^2)	0.2254	0.1711	0.0704	0.1767
R_1[a] (all data)	0.1380	0.1008	0.0347	0.1370
Data with $I > 2\sigma(I)$	5560	14458	5876	14762
R_1 [$I > 2\sigma(I)$]	0.0865	0.0565	0.0283	0.0551
Goof s[b] on F^2	1.194	1.083	1.085	1.099
Residual density [e·nm^{-3}]	744, −438	816, −756	452, −661	1625, −687

[a] Definition of the *R* values: $R_1 = (\Sigma||F_o| - |F_c||)/\Sigma|F_o|$; $wR_2 = \{\Sigma[w(F_o^2 - F_c^2)^2]/\Sigma[w(F_o^2)^2]\}^{1/2}$ with $w^{-1} = \sigma^2(F_o^2) + (aP)^2$. − [b] $s = \{\Sigma[w(F_o^2 - F_c^2)^2]/(N_o - N_p)\}^{1/2}$.

tion was reduced to a volume of a few mL. At 4°C, 508 mg of light-brown crystals of **6** (0.19 mmol; 76%) precipitated; m.p. 378°C (dec.). – NMR (30°C); ^{1}H ([D$_6$]benzene): δ = 1.31 (PHSi*t*Bu$_3$), 1.53 (PSi*t*Bu$_3$), 1.36 and 3.56 (thf), PH signal was not observed; ^{13}C{^{1}H}: δ = 24.06 (PHSiC), 26.82 (PSiC), 31.83 (PHSiC*Me*$_3$), 33.90 (PSiC*Me*$_3$), 25.09 and 68.48 (thf); ^{31}P ([D$_8$]toluene): δ = −25.0 (s, PSi*t*Bu$_3$), −222.9 [d, PHSi*t*Bu$_3$, ^1J(P,H) = 149 Hz]. – IR: $\tilde{\nu}$ = 2234 w, 1251 m, 1180 m, 1064 m, 1037 m, 1013, 932 s, 881 m, 842 s, 816 vs, 803 s, 757 w, 729 vw, 694 vw, 685 vw, 664 vw, 594 m, 569 s, 511 vs, 478, 456 m, 389 vw, 360 vw, 331 vw. – $C_{96}H_{220}Ba_6P_8Si_8$ (2671.24): calcd. C 43.17, H 8.30; found C 43.15, H 7.31.

Structure Determinations:[27] Single crystals were covered with Nujol, sealed in thin-walled capillaries, mounted on a Siemens P4 diffractometer, and examined with graphite-monochromated Mo-K_α radiation (λ = 71.073 pm). A Siemens SMART-CCD area detector was used to monitor the reflections of **1**, **2**, **4**, and **6**. Crystallographic parameters and details of the data collection are summarized in Table 2.

All structures were solved by direct methods and refined with the software packages SHELXL-93 and SHELXL-97.[29] Neutral atom scattering factors were taken from Cromer and Mann,[30] and for the hydrogen atoms from Stewart et al.[31] The non-hydrogen atoms were refined anisotropically. The H atoms were considered as a riding model under restriction of ideal symmetry at the atoms to which they were attached. The disordering of *i*Pr groups in **1** and **2** is not shown in Figures 2 and 3. The methyl groups of the *t*Bu$_3$Si substituent of **4** show a two-site disorder. The structure of **6** contains two toluene molecules and a thf molecule between the barium phosphanide complexes. The carbon and oxygen atoms of these solvent molecules were refined isotropically.

Acknowledgments

We are grateful to the Deutsche Forschungsgemeinschaft, Bonn, and the Fonds der Chemischen Industrie, Frankfurt/Main, for the generous financial support. We would also like to thank Dr. H.-W. Lerner and Dr. K. Karaghiosoff for their helpful advice.

[1] [1a] M. Westerhausen, *Trends Organomet. Chem.* **1997**, *2*, 89–105. – [1b] M. Westerhausen, *Coord. Chem. Rev.* **1998**, *176*, 157–210.
[2] [2a] M. Westerhausen, W. Schwarz, *Z. Naturforsch.* **1992**, *47b*, 453–459. – [2b] M. Westerhausen, H.-D. Hausen, *Z. Anorg. Allg. Chem.* **1992**, *615*, 27–34. – [2c] M. Westerhausen, H.-D. Hausen, W. Schwarz, *Z. Anorg. Allg. Chem.* **1992**, *618*, 121–130. – [2d] M. Westerhausen, W. Schwarz, *Z. Anorg. Allg. Chem.* **1993**, *619*, 1455–1461.
[3] [3a] M. Westerhausen, M. H. Digeser, W. Schwarz, *Inorg. Chem.* **1997**, *36*, 521–527. – [3b] M. Westerhausen, M. H. Digeser, W. Schwarz, *Z. Anorg. Allg. Chem.* **1997**, *623*, 1237–1242.
[4] [4a] M. Westerhausen, M. H. Digeser, H. Nöth, T. Seifert, A. Pfitzner, *J. Am. Chem. Soc.* **1998**, *120*, 6722–6725. – [4b] M. Westerhausen, M. H. Digeser, H. Nöth, W. Ponikwar, T. Seifert, K. Polborn, *Inorg. Chem.*, in press.
[5] [5a] S. Chadwick, U. Englich, B. Noll, K. Ruhlandt-Senge, *Inorg. Chem.* **1998**, *37*, 4718–4725. – [5b] G. Kräuter, S. K. Sunny, W. S. Rees, *Polyhedron* **1998**, *17*, 391–395.
[6] K. Ruhlandt-Senge, K. Davis, S. Dalal, U. Englich, M. O. Senge, *Inorg. Chem.* **1995**, *34*, 2587–2592.
[7] D. E. Gindelberger, J. Arnold, *Inorg. Chem.* **1994**, *33*, 6293–6299.
[8] [8a] G. Becker, K. W. Klinkhammer, W. Schwarz, M. Westerhausen, T. Hildenbrand, *Z. Naturforsch.* **1992**, *47b*, 1225–1232. – [8b] D. E. Gindelberger, J. Arnold, *J. Am. Chem. Soc.* **1992**, *114*, 6242–6243.
[9] M. Westerhausen, R. Löw, W. Schwarz, *J. Organomet. Chem.* **1996**, *513*, 213–229.
[10] M. Driess, H. Pritzkow, *Z. Anorg. Allg. Chem.* **1996**, *622*, 1524–1530.
[11] M. Driess, H. Pritzkow, S. Martin, S. Rell, D. Fenske, G. Baum, *Angew. Chem.* **1996**, *108*, 1064–1066; *Angew. Chem. Int. Ed. Engl.* **1996**, *35*, 986–988.
[12] M. Driess, S. Rell, H. Pritzkow, R. Janoschek, *J. Chem. Soc., Chem. Commun.* **1996**, 305–306.
[13] M. Westerhausen, M. Wieneke, K. Doderer, W. Schwarz, *Z. Naturforsch.* **1996**, *51b*, 1439–1442.
[14] M. Driess, S. Martin, K. Merz, V. Pintchouk, H. Pritzkow, H. Grützmacher, M. Kaupp, *Angew. Chem.* **1997**, *109*, 1982–1985; *Angew. Chem. Int. Ed. Engl.* **1997**, *36*, 1894–1896.
[15] M. Westerhausen, G. Lang, W. Schwarz, *Chem. Ber.* **1996**, *129*, 1035–1040.
[16] [16a] M. Westerhausen, *Inorg. Chem.* **1991**, *30*, 96–101. – [16b] S. R. Drake, D. J. Otway, S. P. Perlepes, *Main Group Met. Chem.* **1991**, *14*, 243–256.
[17] [17a] P. B. Hitchcock, M. F. Lappert, G. A. Lawless, B. Royo, *J. Chem. Soc., Chem. Commun.* **1990**, 1141–1142. – [17b] P. S. Tanner, D. J. Burkey, T. P. Hanusa, *Polyhedron* **1995**, *14*, 331–333. – [17c] A. D. Frankland, M. F. Lappert, *J. Chem. Soc., Dalton Trans.* **1996**, 4151–4152.
[18] [18a] J. M. Boncella, C. J. Coston, J. K. Cammack, *Polyhedron* **1991**, *10*, 769–770. – [18b] B. A. Vaartstra, J. C. Huffman, W. E. Streib, K. G. Caulton, *Inorg. Chem.* **1991**, *30*, 121–125. – [18c] R. L. Kuhlmann, B. A. Vaartstra, K. G. Caulton, *Inorg. Synth.* **1997**, *31*, 8–10.
[19] M. Westerhausen, M. Wieneke, W. Schwarz, *J. Organomet. Chem.* **1999**, *572*, 249–257.
[20] [20a] N. Wiberg, H. Schuster, *Chem. Ber.* **1991**, *124*, 93–95. – [20b] N. Wiberg, A. Wörner, H.-W. Lerner, K. Karaghiosoff, D. Fenske, G. Baum, A. Dransfeld, P. v. R. Schleyer, *Eur. J. Inorg. Chem.* **1998**, 833–841; see also: [20c] N. Wiberg, *Coord. Chem. Rev.* **1997**, *163*, 217–252.
[21] M. Westerhausen, W. Schwarz, *Z. Anorg. Allg. Chem.* **1996**, *622*, 903–913.
[22] M. Westerhausen, M. Krofta, N. Wiberg, J. Knizek, H. Nöth, A. Pfitzner, *Z. Naturforsch.* **1998**, *53b*, 1489–1493.
[23] M. Westerhausen, H.-D. Hausen, W. Schwarz, *Z. Anorg. Allg. Chem.* **1995**, *621*, 877–888.
[24] G. W. Rabe, S. Kheradmandan, L. M. Liable-Sands, I. A. Guzei, A. L. Rheingold, *Angew. Chem.* **1998**, *110*, 1495–1497; *Angew. Chem. Int. Ed. Engl.* **1998**, *37*, 1404–1407; see also: J. D. Smith, *Angew. Chem.* **1998**, *110*, 2181–2183; *Angew. Chem. Int. Ed. Engl.* **1998**, *37*, 2071–2073.
[25] [25a] M. Westerhausen, W. Schwarz, *Z. Anorg. Allg. Chem.* **1991**, *604*, 127–140. – [25b] M. Westerhausen, M. Hartmann, N. Makropoulos, B. Wieneke, M. Wieneke, W. Schwarz, D. Stalke, *Z. Naturforsch.* **1998**, *53b*, 117–125.
[26] C. Rücker, *Chem. Rev.* **1995**, *95*, 1009–1064.
[27] Crystallographic data (excluding structure factors) for the structures of **1**, **2**, **4**, and **6** have been deposited with the Cambridge Crystallographic Data Centre as supplementary publication nos. CCDC-111475 for **1**, -111476 for **2**, -111477 for **4**, and -111478 for **6**. Copies of the data can be obtained on application to CCDC, 12 Union Road, Cambridge CB2 1EZ, U.K. [E-mail: deposit@ccdc.cam.ac.uk].
[28] T. Hahn (Ed.), *International Tables for Crystallography*, vol. A ("Space Group Symmetry"), 2nd ed., D. Reidel, Dordrecht, **1984**.
[29] G. M. Sheldrick, *SHELXL-93*, Universität Göttingen, **1993**; *SHELXL-97*, Universität Göttingen, **1997**.
[30] D. T. Cromer, J. B. Mann, *Acta Crystallogr.* **1968**, *24*, 321.
[31] R. F. Stewart, E. R. Davidson, W. T. Simpson, *J. Chem. Phys.* **1965**, *42*, 3175.

Received November 19, 1998
[I98397]

Organoamido- and Aryloxo-Lanthanoids, 19[+]

Synthesis and Structures of *cisoid* and *transoid* Bis(1,2-dimethoxyethane)bis(η²-pyrazolato)lanthanoid(II) Complexes

Glen B. Deacon,*[a] Ewan E. Delbridge,[a] Brian W. Skelton,[b] and Allan H. White[b]

Keywords: Lanthanide(II) complexes / Ytterbium / Europium / Samarium / Redox transmetallation / Thallium / Diphenylmercury

The complexes $[Yb(bind)_2(DME)_2]$, $[Yb(MePhpz)_2(DME)_2]$, $[Yb(azin)_2(DME)_2]$, and $[Eu(Ph_2pz)_2(DME)_2]$ (bindH = 4,5-dihydro-2*H*-benz[*g*]indazole; MePhpzH = 3-methyl-5-phenylpyrazole; azinH = 7-azaindole; Ph_2pzH = 3,5-diphenylpyrazole; DME = 1,2-dimethoxyethane) have been prepared by redox transmetallation between ytterbium or europium metal and the corresponding thallium(I) pyrazolate in tetrahydrofuran (THF) in the presence of mercury metal, followed by work up with DME. The thallium reagents were obtained by treatment of the appropriate pyrazole with thallium(I) ethoxide. Both $[Yb(Ph_2pz)_2(DME)_2]$ and $[Sm(Ph_2pz)_2(DME)_2]$ have been prepared by metathesis from $LnI_2(THF)_2$ and $K(Ph_2pz)$ in THF, whilst the former has also been obtained by redox transmetallation from $[Hg(Ph_2pz)_2]$ and ytterbium metal and by reaction of 3,5-diphenylpyrazole with $Yb(C_6F_5)_2$, and the latter from protolysis of $[Sm\{N(SiMe_3)_2\}_2(THF)_2]$ with Ph_2pzH, followed in each case by crystallisation of the crude product from DME. Europium(II) 3,5-di-*tert*-butylpyrazolate was synthesised by a redox transmetallation/ligand exchange reaction between europium metal chunks, diphenylmercury(II), and 3,5-di-*tert*-butylpyrazole (tBu_2pzH) in the presence of mercury metal in THF, and $[Eu(tBu_2pz)_2(DME)_2]$ was isolated on crystallisation of the crude product from DME. The X-ray crystal structures of $[Ln(L)_2(DME)_2]$ (Ln =Yb, L = bind or azin; Ln = Eu or Sm, L = Ph_2pz; Ln = Eu, L = tBu_2pz), each of a different crystallographic form, reveal eight-coordinate lanthanoid complexes with two η²-pyrazolate and two chelating DME ligands, but the structures differ in the relationship (*cisoid* or *transoid*) between the pyrazolate ligands. Thus cen–Ln–cen (cen = centre of the N–N bond) angles of 106.7° $[Yb(bind)_2(DME)_2]$ (**3a**), 141.4° $[Yb(azin)_2(DME)_2]$ (**3c**), 142.2° $[Eu(Ph_2pz)_2(DME)_2]$ (**4a**), 107.4° $[Eu(tBu_2pz)_2(DME)_2]$ (**4b**), and 102.1° $[Sm(Ph_2pz)_2(DME)_2]$ (**5**) are observed.

Introduction

Pyrazolate ligands have had an extensive role as bridging ligands particularly between d-block metals, and as chelating ligands, particularly to f-block metals.[2] This chemistry is now being enlivened by a range of new features, such as the first homoleptic η²-pyrazolates,[3a] the first η²-d block[3a,3b] and main-group[3c] pyrazolates, the use of pyrazolates in semiconductor doping,[3d] and new modes of pyrazolate coordination (μ-η²:η²[3e] and combined η² and μ-η¹:η¹[3f]). Recent investigations have provided synthetic routes to a range of lanthanoid(III) pyrazolates.[4–7] Structures of initially prepared compounds revealed cages and dimers with both bridging (μ-η¹:η¹) and chelating (η²) ligands.[4][5] However, lanthanoid(III) complexes of bulky 3,5-disubstituted pyrazolates $[Ln(R_2pz)_3(L)_n]$ (R = *t*Bu or Ph; L = tetrahydrofuran (THF), 1,2-dimethoxyethane (DME), or Ph_3PO; n = 1–3) are monomeric with exclusively η²-bonding.[6][7] Moreover, the preferred arrangements of the three η²-pyrazolate ligands, can induce unexpected coordination modes of the co-ligands, e.g. bridging DME ligands in $[Nd(tBu_2pz)_3(DME)]_\infty$, and novel unidentate DME in $[Er(Ph_2pz)_3(DME)_2]$.[7] Lanthanoid(II) pyrazolates appear less favoured since the redox transmetallation/ligand exchange reaction between Yb metal, $Hg(C_6F_5)_2$, and 3,5-di-*tert*-butylpyrazole yields $[Yb(tBu_2pz)_3(THF)_2]$ even when an excess of the highly reducing metal is used.[6a,6c] However, recently we have prepared the first lanthanoid(II) pyrazolate complex $[Yb(Ph_2pz)_2(DME)_2]$ by redox transmetallation between Yb metal and thallium(I) 3,5-diphenylpyrazolate, and also by redox transmetallation/ligand exchange between the lanthanoid element, $HgPh_2$, and 3,5-diphenylpyrazole.[8] Subsequently, use of 3,5-di-*tert*-butylpyrazole in the latter synthetic method and crystallisation of the product from petroleum ether gave $[Yb(tBu_2pz)_2(THF)]_2$, which contained the first example of a μ-η²:η²-bonded pyrazolate.[3e] We now report a detailed study of the synthesis and structures of a range of bis(1,2-dimethoxyethane)bis(pyrazolato)lanthanoid(II) complexes, as well as the preparation and structure of the closely related $[Yb(azin)_2(DME)_2]$ (azinH = 7-azaindole).

[a] Chemistry Department, Monash University,
Clayton, Victoria 3168, Australia
Fax: (internat.) + 61-3/9905-4597
E-mail: Glen.Deacon@sci.monash.edu.au
[b] The Department of Chemistry, The University of Western Australia,
Nedlands, Western Australia, 6907, Australia
Fax: (internat.) + 61-8/9380-1005

 © WILEY-VCH Verlag GmbH, D-69451 Weinheim, 1999 1434–1948/99/0505–0751 $ 17.50+.50/0

Results and Discussion

Synthesis

A key step in the route to lanthanoid(II) pyrazolates was the synthesis of the thallium(I) pyrazolates, Tl(bind) (**1a**) (bindH = 4,5-dihydro-2*H*-benz[*g*]indazole), Tl(MePhpz) (**1b**) (MePhpzH = 3-methyl-5-phenylpyrazole), Tl(azin) (**1c**), Tl(Ph_2pz)[8] (**1d**), and Tl($MePh_2pz$) (**1e**) ($MePh_2pzH$ = 4-methyl-3,5-diphenylpyrazole).

$$Tl(OEt) + R_2R'pzH \rightarrow Tl(R_2R'pz) + EtOH \quad (1)$$

However, Tl(tBu$_2$pz) could not be prepared by this method and appeared thermally unstable. Consistent with pyrazolate formation, no ν(NH) absorption was observed in the infrared spectra of the complexes, which were additionally characterized by parent ions in their mass spectra and/or satisfactory ^{1}H-NMR spectra. Another possible redox transmetallation reagent, mercury(II) 3,5-diphenylpyrazolate (**2a**), was prepared both by metathesis (Equation 2),

$$HgCl_2 + 2\ K(Ph_2pz) \rightarrow 2\ KCl + Hg(Ph_2pz)_2 \quad (2)$$

and by mercuration of diphenylpyrazole under alkaline conditions.

$$HgBr_4^{2-} + 2\ OH^- + 2\ Ph_2pzH \rightarrow Hg(Ph_2pz)_2 + 4\ Br^- + 2\ H_2O \quad (3)$$

The complex could not be obtained analytically pure, but the identity was clear from an MH^+ ion in the electrospray mass spectrum and the product was a viable source of $Yb(Ph_2pz)_2$ (below).

Several thallium(I) pyrazolates and Tl(azin) were found to undergo redox transmetallation with ytterbium and europium in tetrahydrofuran to give the corresponding divalent pyrazolates.

$$Ln + 2\ Tl(R_2pz) \rightarrow Ln(R_2pz)_2 + 2\ Tl\downarrow \quad (4)$$

Crystallisation of the crude products from DME gave the complexes [Yb(bind)$_2$(DME)$_2$] (**3a**), [Yb(MePhpz)$_2$(DME)$_2$] (**3b**), [Yb(azin)$_2$(DME)$_2$] (**3c**), and [Eu(Ph_2pz)$_2$(DME)$_2$] (**4a**). The reported [Yb(Ph_2pz)$_2$(DME)$_2$], previously prepared by Equation 4 and by redox transmetallation/ligand exchange from Yb metal, $HgPh_2$, and Ph_2pzH,[8] was prepared in modest to good yields by three further methods, viz. metathesis from ytterbium diiodide (Equation 5, Ln = Yb), redox transmetallation from impure Hg(Ph_2pz)$_2$ (Equation 6), and protolysis of bis(pentafluorophenyl)ytterbium(II) (Equation 7).

$$LnI_2 + 2\ K(Ph_2pz) \rightarrow Ln(Ph_2pz)_2 + 2\ KI \quad (5)$$

$$Yb + Hg(Ph_2pz)_2 \rightarrow Yb(Ph_2pz)_2 + Hg\downarrow \quad (6)$$

$$Yb(C_6F_5)_2 + 2\ Ph_2pzH \rightarrow Yb(Ph_2pz)_2 + 2\ C_6F_5H \quad (7)$$

Only, a short reaction time was needed for successful isolation of Yb(Ph_2pz)$_2$ from Equation 7, otherwise a black unidentified solid was obtained, similar to the unsuccessful outcome of an attempted synthesis by redox transmetallation/ligand exchange from Yb metal, Hg(C_6F_5)$_2$, and 3,5-diphenylpyrazole. Because of the failure to prepare Tl(tBu$_2$pz), an alternative to Equation 4 was needed for Eu(tBu$_2$pz)$_2$, and this was achieved by redox transmetallation/ligand exchange between europium metal, diphenylmercury, and 3,5-di-*tert*-butylpyrazole (Equation 8),

$$Eu + HgPh_2 + 2\ tBu_2pzH \rightarrow Eu(tBu_2pz)_2 + 2\ PhH + Hg\downarrow \quad (8)$$

followed by isolation as [Eu(tBu$_2$pz)$_2$(DME)$_2$] (**4b**). This synthetic method has previously been used for [Yb(Ph_2pz)$_2$(DME)$_2$] (**3d**)[8] and [Yb(tBu$_2$pz)$_2$(THF)]$_2$.[3e] Since an attempt to prepare Sm(Ph_2pz)$_2$ by Equation 4 yielded instead Sm(Ph_2pz)$_3$ (Equation 9),[8]

$$Sm + 3\ Tl(Ph_2pz) \rightarrow Sm(Ph_2pz)_3 + 3\ Tl\downarrow \quad (9)$$

two alternative approaches were used to give the divalent target compound, viz metathesis (Equation 5) (Ln = Sm), and protolysis of bis[bis(trimethylsilyl)amido]samarium(II) by 3,5-diphenylpyrazole.

$$Sm[N(SiMe_3)_2]_2 + 2\ Ph_2pzH \rightarrow Sm(Ph_2pz)_2 + 2\ HN(SiMe_3)_2 \quad (10)$$

After workup with DME a much higher yield of [Sm(Ph_2pz)$_2$(DME)$_2$] (**5**) was obtained by the former method.

Equation 4 opens the use of thallium-based redox transmetallation as a route to lanthanoid organoamides. Redox transmetallation with thallium(I) reagents was a source of only cyclopentadienyls[9] and phenolates,[10] prior to our preliminary report.[8] Mercury-based redox transmetallation (e.g. Equation 6) has previously been used for lanthanoid amides,[9c,11] whilst use of diphenylmercury in redox transmetallation/ligand exchange (e.g. Equation 8), is a recent development[11] by contrast with the extensive use of Hg(C_6F_5)$_2$.[9a−9c]

The different outcomes of the reactions of ytterbium and samarium with thallium 3,5-diphenylpyrazolate (Equation 4; Ln = Yb; R = Ph and Equation 9) are explicable by the observation (Experimental Section) that samarium metal does not reduce Sm(Ph_2pz)$_3$ whereas ytterbium metal reduces Yb(Ph_2pz)$_3$.

$$2\ Yb(Ph_2pz)_3 + Yb \rightarrow 3\ Yb(Ph_2pz)_2 \quad (11)$$

Formation of Yb(Ph_2pz)$_2$, rather than a trivalent complex from redox transmetallation/ligand exchange between ytterbium metal, diphenylmercury, and 3,5-diphenylpyrazole,[8] is guaranteed both by reduction (Equation 11), and also by the current finding that Yb(Ph_2pz)$_2$ does not undergo oxidation/ligand exchange with diphenylmercury and Ph_2pzH.

$$2\ Yb(Ph_2pz)_2 + HgPh_2 + 2\ Ph_2pzH \not\rightarrow 2\ Yb(Ph_2pz)_3 + 2\ PhH + Hg$$

This further illuminates the contrasting formation of Yb(tBu$_2$pz)$_3$ from synthesis with Hg(C_6F_5)$_2$[6a,6c] but Yb(t-Bu$_2$pz)$_2$ with $HgPh_2$.[3e] Synthetic consequences of the dif-

fering oxidising capacity of these mercurials have been previously observed in that $YbCp_2$ is converted by $Hg(C_6F_5)_2$ into $YbCp_2(C_6F_5)$, but is inert to diphenylmercury,[12a] and electrochemical reduction is more facile for $Hg(C_6F_5)_2$ than for $HgPh_2$.[12b,12c]

Despite the high air and moisture sensitivity of $[Ln(R_2pz)_2(DME)_2]$ complexes and $[Yb(azin)_2(DME)_2]$, all complexes were obtained with acceptable C, H, N, and Ln analyses. No ν(NH) absorptions were observed in the spectra, consistent with the formation of pyrazolatolanthanoid complexes. The ^{1}H-NMR spectra of the diamagnetic Yb^{II} complexes and of $[Sm(Ph_2pz)_2(DME)_2]$ were consistent with the proposed compositions, except for **3a** where the bind integrations were approximately half the expected intensity, and where all resonances, *especially* those of bind, were surprisingly broadened. This may be the source of the low integrations. A spectrum of a cooled solution showed the same features. No Yb^{III} impurities could be detected by electronic spectroscopy (Experimental Section), and the oxidation state is clear from spectroscopy, analysis and the X-ray crystallography. Not only was the ^{1}H-NMR spectrum of the paramagnetic Sm^{II} complex **5** clearly resolved and assigned (Experimental Section), but it was clearly distinguishable from that of the Sm^{III} analogue, $[Sm(Ph_2pz)_3(DME)_2]$.[8] The ^{171}Yb resonance of the azin complex **3c** (Experimental Section) was very close to that (δ = 480) of $[Yb(Ph_2pz)_2(DME)_2]$,[8] consistent with our view of the azin ligand as a pseudo-pyrazolate. It is also at lower frequencies than the ^{171}Yb chemical shift of seven-coordinate $[Yb(tBu_2pz)_2(THF)]_2$ (δ = 536).[3e] There is some evidence that a higher frequency shift accompanies a decrease in coordination number *in complexes with similar ligands*,[11][13] as in these examples, but **3c** and **3d** necessarily were examined in DME and $[Yb(tBu_2pz)_2(THF)]_2$ in PhMe. The visible/near-IR spectra of the complexes show moderately intense (for Ln complexes) features attributable to Ln→L charge transfer (Experimental Section). More notably near-infrared absorptions characteristic[14] of Yb^{III} and Sm^{III} were absent from the spectra of the Yb^{II} and Sm^{II} compounds.

X-ray Structure Determinations

Single-crystal X-ray structure determinations have been carried out for **3a**, **3c**, **4a**, **4b**, and **5**. No complexes, including the analogous **3d** of the preliminary report,[8] are isostructural, and all show crystallographically independent forms. These are displayed in Figures 1−6, attention being drawn to crystallographically significant features in the Figure captions and in the Experimental Section. Selected bond lengths and angles are in Tables 1 and 2. All $[Ln(R_2pz)_2(DME)_2]$ complexes have eight-coordinate monomeric structures with two chelating DME and two chelating (η^2)-pyrazolate or azin ligands. In each case the two nitrogen atoms bind nearly symmetrically to the metal centre such that the metal is approximately coplanar with the ligand plane (Figures 1−6). There are two different stereochemical types. Thus, the cen−Ln−cen angles (cen = centre of N−N bonds or, for azin, the centre of the N···N distance) (Table 3) are either in the range 101−108° (**3a**, **3d**, **4b**, **5**; Figures 1−4) giving a *cisoid* disposition of the pyrazolate ligands, or 141−143° (**3c**, **4a**; Figure 5, 6) giving a *transoid* array of Ph_2pz or azin ligands. A similar relationship is shown by the cen′−Ln−cen′ angles (cen′ = midpoint of the O···O distance) (Table 3), with **3a**, **4b**, **5**, and **3d** having values of 85−98° and a *cisoid* disposition of DME ligands. By contrast **3c** and **4a** have values of 138−143° respectively, arising from *transoid* DME ligands, where the four oxygen donor atoms are nearly coplanar. All single crystals were obtained from concentrated DME solutions, hence the difference in arrangement seen in the Ph_2pz complexes **3d**, **4a**, and **5**, and especially between the complexes of the adjacent metals Ln = Eu or Sm, is striking.

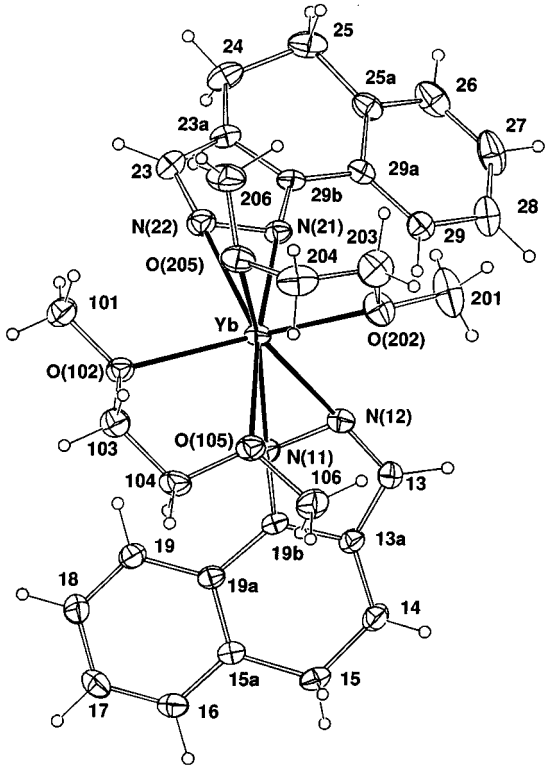


Figure 1. Molecular projection of $[Yb(bind)_2(DME)_2]$ (**3a**) down the quasi-*2* axis; no disorder is present

Amongst the *cis* complexes, **4b**, **5**, and **3d** differ from **3a** in that the $Ln(R_2pz)_2$ arrays have potential *mm* symmetry, one *m* bisecting the ligand and relating the two substituents. By contrast, the $Yb(bind)_2$ array in **3a** is disposed as approaching *2* symmetry. In the *transoid* complexes, **3c** and **4a**, the Ph_2pz and azin ligand pairs are closely coplanar with each other and with the metal atom. In the diphenylpyrazolate complexes **4a**, **5**, and **3d**, each pyrazolate ring is almost coplanar with its phenyl substituents, regardless of whether the Ph_2pz groups are *cisoid* or *transoid*.

In **3a**, one molecule devoid of crystallographic symmetry, and of any complicating factors such as different bind ligand orientations (possible by reversal of the inequivalent

Table 1. Metal atom environments in *cisoid* **5**, **4b** (molecules 1 and 2), **3d**, **3a**; connectivity to (*r* [Å]) or via the metal centre (angles [°]); * values are for the disordered/symmetry-related O component

Atom*	*r* [Å]	**5** N(11′) **4b(1)** N(112) **4b(2)** N(212) **3d** N(12) **3a** N(12)	N(21) N(121) N(221) N(21) N(21)	N(21′) N(122) N(222) N(22) N(22)	O(102) O(1102) O(2102) O(102) O(102)	O(105) O(1105) O(2105) O(105) O(105)	O(202) O(1202) O(2202) O(202) O(202)	O(205) O(1205) O(2205) O(205) O(205)
5 N(11)	2.556(3)	31.07(8)	105.47(8)	97.10(8)	91.1(1)	76.0(1)	118.7(1)	155.24(9)
4b(1) N(111)	2.53(1)	32.2(3)	112.8(3)	99.9(3)	92.3(3)	79.8(3)	123.4(3)	162.5(4)
4b(2) N(211)	2.51(1)	31.6(3)	110.7(3)	98.3(3)	94.9(3)	78.7(3)	124.1(4)	166.0(3)
3d N(11)	2.426(7)	32.7(2)	107.3(2)	95.5(2)	87.7(2)	91.2(2)	116.7(2)	174.7(2)
3a N(11)	2.465(3)	32.6(1)	101.5(1)	112.7(1)	91.80(9)	76.91(9)	112.9(1)	156.7(1)
5 N(11′)	(2.556(3))		(97.10(8))	(105.47(8))	121.4(1)*	87.6(1)*	89.8(1)*	(155.24(9))
4b(1) N(112)	2.527(9)		103.5(3)	108.3(3)	122.0(3)	85.6(3)	96.3(3)	158.4(3)
4b(2) N(212)	2.54(1)		101.9(3)	107.4(3)	123.3(3)	83.8(3)	97.5(4)	158.8(3)
3d N(12)	2.414(7)		96.4(2)	102.8(2)	119.7(2)	97.9(2)	86.8(2)	150.9(2)
3a N(12)	2.440(3)		90.6(1)	117.2(1)	123.5(1)	85.2(1)	83.7(1)	147.1(1)
5 N(21)	2.538(3)			30.99(1)	112.9(1)	173.0(1)	92.2(1)	97.1(1)
4b(1) N(121)	2.54(1)			31.4(3)	118.7(3)	167.1(3)	96.7(3)	81.1(3)
4b(2) N(221)	2.533(9)			32.3(3)	120.7(3)	169.6(3)	98.0(3)	79.5(3)
3d N(21)	2.430(7)			32.5(2)	116.8(2)	161.2(2)	91.0(2)	77.3(2)
3a N(21)	2.399(3)			33.1(1)	118.77(9)	174.3(1)	95.3(1)	101.8(1)
5 N(21′)	(2.538(3))				83.5(1)*	142.5(1)*	121.4(2)*	(97.1(1))
4b(1) N(122)	2.517(9)				92.2(3)	153.5(3)	125.6(4)	86.7(3)
4b(2) N(222)	2.511(9)				93.8(3)	154.0(3)	127.2(4)	85.3(3)
3d N(22)	2.424(7)				86.7(2)	151.2(2)	122.8(2)	87.1(2)
3a N(22)	2.459(3)				86.7(1)	152.6(1)	115.8(1)	87.1(1)
5 O(102)	2.720(7)					60.2(2)	134.8(2)	70.5(1)
4b(1) O(1102)	2.667(8)					61.4(3)	114.8(3)	71.2(4)
4b(2) O(2102)	2.693(8)					61.1(3)	110.4(3)	71.2(3)
3d O(102)	2.576(7)					65.6(2)	136.6(2)	87.9(2)
3a O(102)	2.519(3)					66.84(9)	133.26(9)	76.67(9)
5 O(105)	2.708(5)						93.0(2)	80.4(1)
4b(1) O(1105)	2.724(9)						72.9(3)	87.1(3)
4b(2) O(2105)	2.767(8)						72.4(3)	92.0(3)
3d O(105)	2.484(6)						77.8(2)	84.4(2)
3a O(105)	2.551(3)						80.5(1)	79.95(9)
5 O(202)	2.627(7)							69.5(1)
4b(1) O(1202)	2.69(1)							62.2(4)
4b(2) O(2202)	2.68(1)							61.5(4)
3d O(202)	2.502(6)							65.2(2)
3a O(202)	2.508(3)							65.1(1)
5 O(205)	2.551(4)							
4b(1) O(1205)	2.71(1)							
4b(2) O(2205)	2.73(1)							
3d O(205)	2.558(7)							
3a O(205)	2.577(3)							

N donor atoms), comprises the asymmetric unit. However, in **3c**, isomeric diversity arising from alternative azin orientations is manifested as disorder, although one of the four possible combinations is dominant, as is displayed in Figure 3a.

The pyrazolate and azin ligands are symmetrically coordinated with differences in Ln−N bond pairs ≤ 0.06 Å for all ligands and ≤ 0.03 Å for all but two. Even the largest differences, which, not surprisingly, are found for the unsymmetrical ligands bind and azin, are observed for only *one* ligand in each of **3a** and **3c**, respectively. Moreover, the maximum difference (0.06 Å) is less than those (0.07−0.10 Å) in some Ln^{III} complexes with Ph_2pz and tBu_2pz.[6b,7a] There is more asymmetry in the DME chelation with the largest pair of differences (0.10, 0.06 Å) in **3d** which has highly symmetrical Ph_2pz coordination, but different conformations of the (non-disordered) DME ligands. Further, no unusual asymmetry in the DME coordination is found in complexes of the unsymmetrical ligands bind and azin. In **3a**, the two DME ligands have different conformations whilst in **3c** they are the same. When appropriate allowance is made for the differences in the ionic radii of eight coordinate Eu^{2+}, Sm^{2+}, and Yb^{2+} [15], the <Ln−N> bond distances of all complexes are very similar with sole exception of **3c**, where <Yb−N> is ca. 0.13 Å longer than values for the other two Yb^{II} complexes, **3a** and **3d**. Given that the 7-azindolate ligand is not a pyrazolate, it would be unwise at this stage to attach too much significance to this difference, but it can be argued that azin has more steric stress in the immediate vicinity of the donor atoms than R_2pz ligands

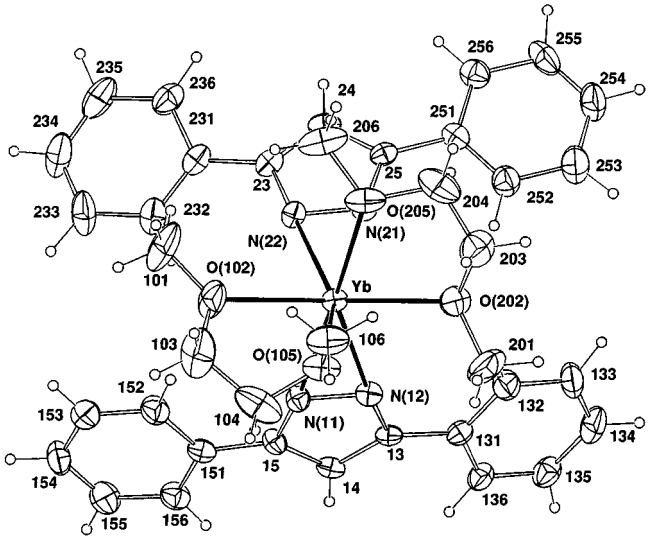


Figure 2. Molecular projection of $[Yb(Ph_2pz)_2(DME)_2]$ (**3d**) down the quasi-*2* axis; no disorder is present

and the "bite" is also larger. Greater uniformity is seen in ionic radius adjusted <Ln−O> values (despite greater individual variation than for Ln−N), with a slight deviation in <Eu−O> of **4b**, which is ca. 0.05 Å longer than for other complexes. This may be a consequence of the bulky *tert*-butyl substituents of the tBu_2pz ligand. For the azin complex **3c**, the Yb−O distances are similar to those of **3a** and **3d**, despite the longer Yb−N lengths. Comparison of bond lengths in *cisoid* and *transoid* Ph_2pz complexes **3d**, **5**, and **4a** reveals no significant differences after allowance for ionic radii differences. Subtraction of eight-coordinate Ln^{3+} radii[15] from <Ln−N> values gives a residue of 1.28−1.32 Å, for all complexes except for the anomalous **3c** (1.42 Å), and these are at the low end of the range, 1.26−1.38 Å, for $[Ln(R_2pz)_3L_n]$ (L = THF, n = 2 or 3; L = DME, n = 1 or 2) complexes.[6,7a] The uniqueness of the azin coordination is further illustrated by the subtraction value, which lies outside the normal pyrazolatolanthanoid range. Similar subtraction from <Ln−O> gives 1.38−1.40 Å with the exception of 1.45 Å for the tBu_2pz complex **4b**. Values for Ln^{III} complexes $[Ln(R_2pz)_3(THF)_n]$ (n = 2 or 3) cover the range 1.35−1.38 Å,[6] whilst $[Er(Ph_2pz)_3(\eta^2\text{-DME})(\eta^1\text{-DME})]$ gives 1.35 Å for the η^1-DME and 1.42 Å for the chelating DME.[7a] These subtraction residues suggest that the $[Ln(R_2pz)_2(DME)_2]$ structures are not greatly crowded, especially given that analogous values for Ln−O(THF) in crowded, bulky aryloxides lie in the range 1.49−1.59 Å.[10b,10c,16]

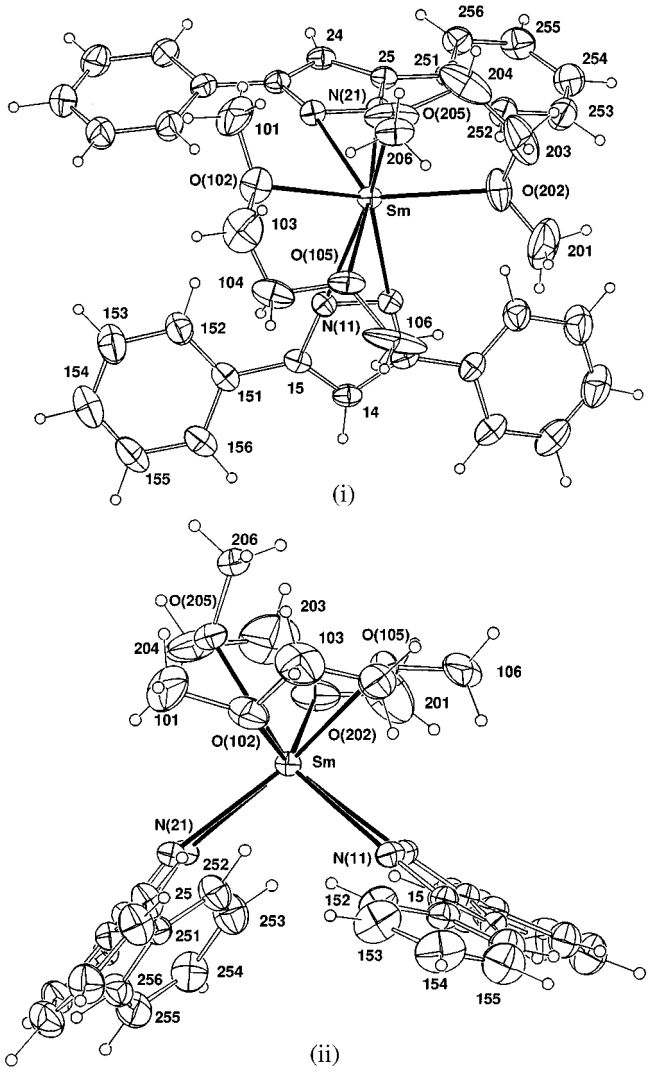


Figure 3. Molecular projections of $[Sm(Ph_2pz)_2(DME)_2]$ (**5**) (i) down and (ii) normal to the quasi-*2* axis; as modelled, the molecule lies disposed to either side of a crystallographic mirror plane, passing through samarium and the mid-points of the N−N bonds of the pyrazolate ligands, i.e. normal to and vertical in the page in (i) and in the plane of the page in (ii); the DME ligands are necessarily disordered to either side of that plane, the two components having different conformations, only one of each type being shown

Experimental Section

General: The compounds described here are extremely air- and moisture-sensitive and consequently all operations were carried out in an inert atmosphere (purified argon or nitrogen). Unless indicated otherwise, handling methods and solvent purification were as described previously.[17] Petroleum ether refers to the fraction boiling between 40 and 60°C. − IR data (4000−650 cm^{-1}) were obtained for Nujol mulls sandwiched between NaCl plates with a Perkin Elmer 1600 FTIR spectrometer. − Mass spectra were obtained with a VG Trio-1 GC mass spectrometer (Ln, Tl compounds) or a Micromass Platform Electrospray mass spectrometer $[Hg(Ph_2pz)_2]$. Each listed *m/z* value for metal-containing ions (where the metal has more than one isotope) is the most intense peak of a cluster with an isotope pattern in good agreement with the calculated pattern. − Room-temperature (20°C) NMR spectra were recorded with a Bruker AC 200 MHz (^1H, ^{13}C) or AM 300 MHz (^1H, ^{171}Yb) spectrometer. The chemical shift references were the residual solvent signals ([D_6]benzene: δ_H = 7.15, δ_C = 128.0; [D_8]THF: δ_H = 1.73, 3.58, δ_C = 25.3, 67.4; [D_8]toluene: δ_H = 2.09) or external $[Yb(C_5Me_5)_2(THF)_2]$ (0.15 M solution in THF) (^{171}Yb: δ = 0.0).[13] Degrees of substitution for ^{13}C nuclei were determined using $^1H/^{13}C$ *J*-modulation pulse sequences. [D_6]benzene (Cambridge Isotopes) was dried with sodium/potassium alloy and [D_8]THF (Cambridge Isotopes) was dried with CaH_2. The deuterated solvents were then vacuum-transferred to greaseless Schlenk tubes and stored under purified argon. − Lanthanoid analyses were by

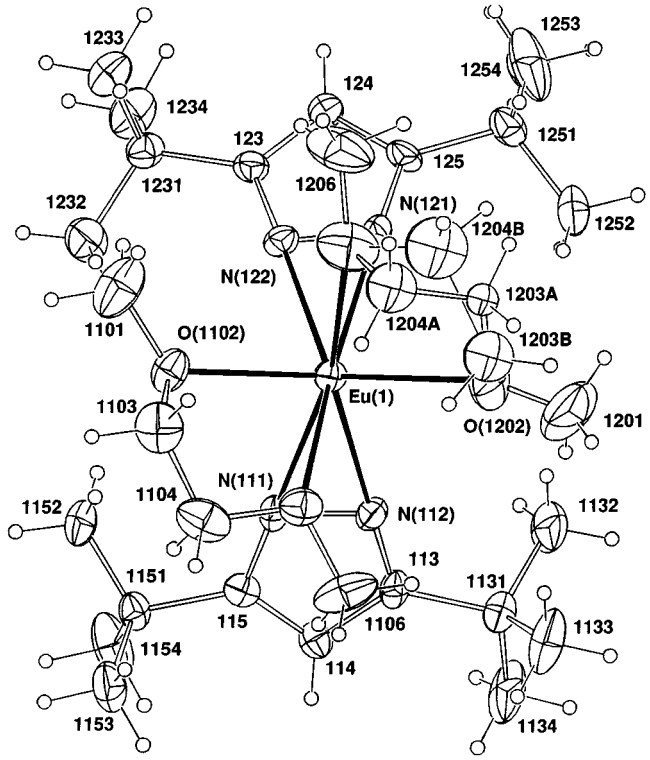


Figure 4. Molecular projection of $[Eu(tBu_2pz)_2(DME)_2]$ (**4b**) down the quasi-*2* axis (molecule 1 only is shown, molecule 2 being pseudo-symmetrically related and therefore similar); one of the DME ligands is disordered over two conformations, the two components of the relevant atoms of the CH_2CH_2 group being shown

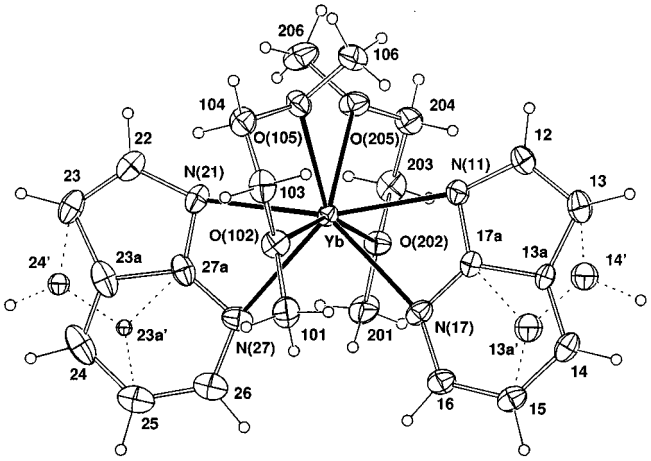


Figure 5. Molecular projection of $[Yb(azin)_2(DME)_2]$ (**3c**) normal to the the quasi-*2* axis; minor disordered azin components beeing shown

EDTA titration[18] with xylenol orange indicator of solutions prepared by digestion of accurately weighed samples in concentrated HNO_3/2% concentrated H_2SO_4 followed by dilution with water and buffering with hexamine. Thallium analyses were by potassium iodate titration[19] of solutions prepared by digestion of accurately weighed samples in concentrated HNO_3/2% concentrated H_2SO_4. Once the HNO_3 was removed by heating, the residue was treated with excess Na_2SO_3 to reduce Tl^{3+} to Tl^+, and the solution was boiled to expel excess SO_2. – Microanalysis samples were sealed in glass ampoules under purified argon and were determined either by the Campbell Microanalytical Service, University of Otago, New

Table 2. Metal atom environments in *transoid* **3c**, **4a** (molecules 1 and 2); connectivity to (*r* [Å]) or via the metal centre (angles [°])

Atom	*r* [Å]	**3c** N(11) **4a(1)** N(112) **4a(2)** N(212)	N(27) N(111′) N(211′)	N(21) N(112′) N(212′)	O(102) O(102) O(202)	O(105) O(105) O(205)	O(202) O(102′) O(202′)	O(205) O(105′) O(205′)
3c N(17) **4a(1)** N(111) **4a(2)** N(211)	2.569(6) 2.552(5) 2.554(6)	54.3(2) 31.0(2) 31.0(2)	87.6(2) 112.1(2) 111.7(2)	141.8(2) 141.4(2) 140.4(2)	83.4(2) 82.3(2) 80.9(2)	124.7(2) 123.1(2) 115.5(2)	80.3(2) 83.4(2) 84.2(2)	125.4(2) 107.6(2) 115.1(2)
3c N(11) **4a(1)** N(112) **4a(2)** N(212)	2.547(6) 2.582(4) 2.536(6)		141.7(2) (141.4(2)) (140.4(2))	163.9(2) 172.2(2) 171.1(2)	98.4(2) 80.5(2) 96.3(2)	85.3(2) 96.1(2) 99.8(2)	86.5(2) 97.8(2) 81.6(2)	81.4(2) 89.8(2) 87.0(2)
3c N(27) **4a(1)** N(111′) **4a(2)** N(211′)	2.596(6)			54.4(2) 31.0(2) 31.0(2)	77.7(2) 83.4(2) 84.2(2)	124.7(2) 107.6(2) 115.1(2)	83.7(2) 82.3(2) 80.9(2)	126.3(2) 123.1(2) 115.5(2)
3c N(21) **4a(1)** N(112′) **4a(2)** N(212′)	2.538(6)				85.1(2) (97.8(2)) (81.6(2))	82.0(2) (89.8(2)) (87.0(2))	96.7(2) (80.5(2)) (96.3(2))	85.6(2) (96.1(2)) (99.8(2))
3c O(102) **4a(1)** O(102) **4a(2)** O(202)	2.523(5) 2.637(6) 2.614(5)					65.2(2) 63.5(2) 62.9(2)	155.7(2) 154.4(2) 153.2(2)	138.8(2) 141.6(2) 143.9(2)
3c O(105) **4a(1)** O(105) **4a(2)** O(205)	2.565(5) 2.660(5) 2.684(5)						139.0(1) (141.6(2)) (143.9(2))	73.8(2) 80.9(2) 81.0(2)
3c O(202) **4a(1)** O(102′) **4a(2)** O(202′)	2.508(5)							65.3(1) (63.5(2)) (62.9(2))
3c O(205)	2.553(5)							

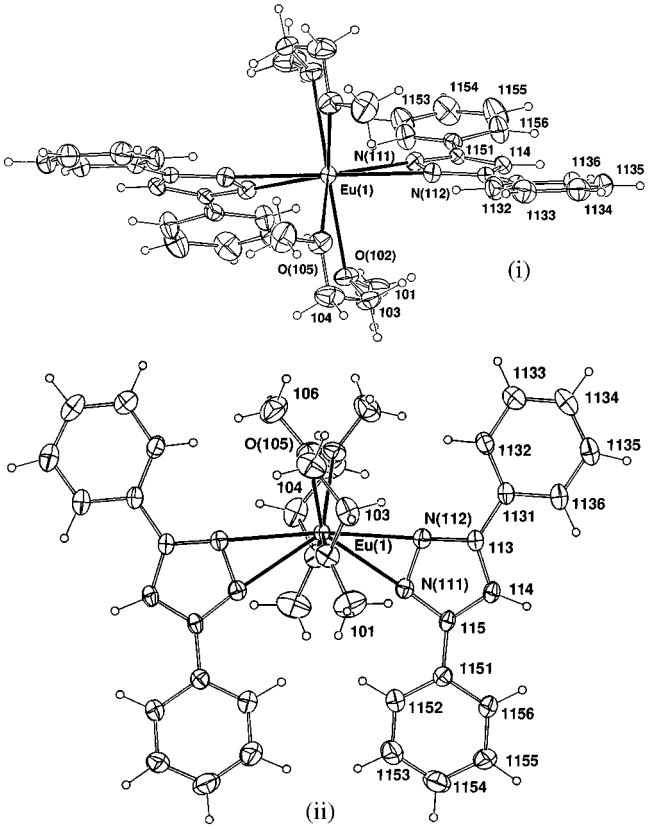
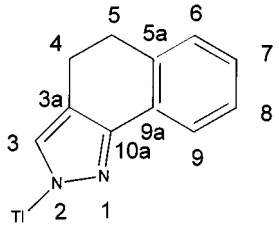


Figure 6. Molecular projections of $[Eu(Ph_2pz)_2(dme)_2]$ (**4a**) (i) down and (ii) normal to the quasi-*2* axis [molecule 1; in molecule 2, the ligand disposition, inclusive of DME conformations (ordered), is similar; each molecule is disposed about a crystallographic *2* axis]; note the quasi parallel pairs of ligand planes, indicative of dodecahedral stereochemistry about the metal centre

Zealand or by Chemical and Microanalytical Services Pty. Ltd, Belmont, Australia. − Lanthanoid elements as either powders or distilled metal ingots were obtained from Rhône-Poulenc. Thallium(I) ethoxide was purchased from Fluka or Merck and was filtered under argon to remove any thallium metal and stored at −20°C in the dark. 7-Azaindole and $HgPh_2$ were purchased from Aldrich. 4,5-Dihydro-2*H*-benz[*g*]indazole was synthesised by a reported method[20]. Other pyrazoles were synthesised[21] by treating the appropriate commercially available β-diketone with an equimolar amount of hydrazine hydrate in refluxing ethanol. These pyrazoles were then recrystallised from an acetone/petroleum ether mixture. Lanthanoid(II) diiodides[22], bis[bis(trimethylsilyl)amido]bis-(tetrahydrofuran)samarium(II),[23] bis(pentafluorophenyl)mercury-(II),[24] and bis(pentafluorophenyl)ytterbium(II)[24] were synthesised by the indicated reported method.

(4,5-Dihydro-2*H*-benz[*g*]indazolato)thallium(I) (1a): Thallium(I) ethoxide (0.35 mL, 1.25 g, 5.0 mmol) was added to a diethyl ether solution (30 mL) of 2*H*-benz[*g*]-4,5-dihydroindazole (0.85 g, 5.0 mmol) giving a white precipitate, which was filtered from solution and washed twice with petroleum ether (2 × 20 mL) yielding 1.62 g (87%) of a white crystalline solid. − IR: $\tilde{\nu}$ = 1608 cm^{-1} w, 1531 w, 1508 w, 1340 w, 1315 m, 1298 w, 1272 m, 1213 m, 1156 w, 1098 m, 1052 s, 1036 s, 1019 s, 1011 s, 960 s, 931 m, 887 m, 850 s, 762 vs, 732 s, 706 vs, 685 m, 659 w. − ^{1}H NMR (200 MHz, [D$_8$]THF): δ = 2.75 (t, 2 H, 4-H), 2.85 (t, 2 H, 5-H), 6.99−7.05 (m, 2 H, 6-H and 9-H), 7.15 (t, 1 H, 7-H), 7.44 (s, 1 H, 3-H), 7.62 (t, 1 H, 8-H). − ^{13}C{^{1}H} NMR (200 MHz, [D$_8$]THF): δ = 21.0 (C-4), 31.7 (C-5), 118.0 (C-3a), 123.0 (C-9), 126.5 (C-8), 127.2 (C-7), 128.9 (C-3 and C-6), 132.5 (C-9a), 137.3 (C-5a), 151.7 (C-10a). − MS (70 eV, EI); *m*/*z* (%): 374 (20) [(^{205}Tl)M$^+$], 205 (85) [^{205}Tl$^+$], 170 (100) [$C_{11}H_{10}N_2^+$]. − $C_{11}H_9N_2Tl$ (373.6): calcd. Tl 54.71; found Tl 55.26.



(3-Methyl-5-phenylpyrazolato)thallium(I) (1b): Thallium(I) ethoxide (0.35 mL, 1.25 g, 5.0 mmol) was added to a THF solution (30 mL) of 3-methyl-5-phenylpyrazole (0.79 g, 5.0 mmol) giving a pale yellow solution. The THF was removed under vacuum giving **3** as an off-white solid which was recrystallised from CH_2Cl_2 and petroleum ether [1.40 g (77%)]. − IR: $\tilde{\nu}$ = 1599 cm^{-1} m, 1292 w, 1261 m, 1154 vw, 1092 m, 1070 m, 1019 s, 962 m, 866 vw, 791 w, 759 vs, 716 s, 696 vs. − ^{1}H NMR (300 MHz, [D$_8$]THF): δ = 2.37 (s, 3 H, Me), 6.41 (s, 1 H, 4-H) 7.08−7.13 (m, 1 H, *p*-H), 7.17−7.23 (t, 2 H, *m*-H), 7.59 (d, 2 H, *o*-H). − MS (70 eV, EI); *m*/*z* (%): 362

Table 3. Diaza ligand centroid/other atom angles [°] (N_1, N_2 are the centroids of the pyrazolate ligands 1 and 2; O_1 and O_2 are the centres of the O···O vectors of the DME ligands 1 and 2)

Compound/molecule	**3c** *transoid*	**4a/1** *transoid*	**4a/2** *transoid*	**3a** *cisoid*	**3d** *cisoid*	**4b/1** *cisoid*	**4b/2** *cisoid*	**5** *cicoid*
N_1-Ln-N_2	$141._4$	$142._2$	$141._2$	$106._7$	$101._4$	$107._4$	$105._8$	$102._1$
$N_1-Ln-O(102)$	$91._0$	$81._1$	$88._5$	$107._6$	$103._7$	$107._2$	$109._3$	$106._3$
$N_1-Ln-O(105)$	$105._0$	$109._8$	$108._2$	$80._7$	$94._7$	$82._4$	$81._0$	$81._5$
$N_1-Ln-O(202)$	$82._6$	$90._7$	$82._6$	$98._5$	$101._8$	$110._1$	$111._0$	$104._3$
$N_1-Ln-O(205)$	$104._1$	$98._9$	$101._2$	$156._4$	$166._9$	$168._6$	$171._2$	$160._5$
N_1-Ln-O_1	$100._1$	$96._2$	$99._8$	$94._7$	$101._0$	$95._3$	$95._6$	$94._4$
N_2-Ln-O_2	$94._0$	$95._6$	$92._3$	$129._6$	$134._8$	$140._7$	$141._9$	$135._9$
$N_2-Ln-O(102)$	$80._3$	−	−	$102._6$	$101._8$	$105._7$	$107._5$	$98._2$
$N_2-Ln-O(105)$	$104._2$	−	−	$168._9$	$161._7$	$166._2$	$168._4$	$157._9$
$N_2-Ln-O(202)$	$90._2$	−	−	$106._1$	$106._9$	$111._2$	$112._7$	$106._9$
$N_2-Ln-O(205)$	$107._1$	−	−	$94._5$	$81._9$	$83._7$	$82._1$	$97._4$
N_2-Ln-O_1	$92._8$	−	−	$136._2$	$132._7$	$136._6$	$138._5$	$128._1$
N_2-Ln-O_2	$100._3$	−	−	$102._1$	$94._9$	$98._4$	$98._1$	$104._9$
O_1-Ln-O_2	$138._3$	$142._7$	$143._0$	$92._0$	$97._9$	$85._1$	$85._2$	$95._6$

(40) [(^{205}Tl)M$^+$], 205 (15) [^{205}Tl$^+$], 158 (15) [$C_{10}H_{10}N_2^+$]. − $C_{10}H_9N_2Tl$ (361.6): calcd. Tl 56.52; found Tl 56.84.

(7-Azaindolato)thallium(I) (1c): Thallium(I) ethoxide (2.56 mL, 9.01 g, 36.1 mmol) was added to an ether solution (30 mL) of 7-azaindole (4.26 g, 36.1 mmol) giving a white precipitate and a pale yellow solution. The white precipitate was filtered from solution and washed with petroleum ether (2 × 30 mL) giving **1c** [11.61 g (65%)]. − IR: $\tilde{\nu}$ = 1582 cm^{-1} w, 1534 w, 1333 w, 1278 m, 1257 w, 1150 m, 1092 m, 1044 w, 898 m, 798 s, 766 vs, 746 s, 721 vs, 622 m. − ^{1}H NMR (200 MHz, [D$_8$]THF): δ = 6.39 (s, 1 H, 3-H), 6.90 (dd, 1 H, 5-H) 7.30 (s, 1 H, 2-H), 7.87 (d, 1 H, 4-H), 8.05 (d, 1 H, 7-H). − $C_7H_5N_2Tl$ (321.5): calcd. Tl 63.57; found Tl 64.11.

(3,5-Diphenylpyrazolato)thallium(I) (1d): The preparation and properties have been given in a preliminary report.[8]

(4-Methyl-3,5-diphenylpyrazolato)thallium(I) (1e): Thallium(I) ethoxide (0.35 mL, 1.25 g, 5.0 mmol) was added to a THF solution (30 mL) of 4-methyl-3,5-diphenylpyrazole (1.17 g, 5.0 mmol) giving a deep yellow solution. This was reduced in volume to ca. 5 mL and petroleum ether was added causing deposition of **1e** as a white solid, which was filtered off and dried under vacuum [1.80 g (82%)]. − IR: $\tilde{\nu}$ = 1601 cm^{-1} m, 1528 w, 1516 w, 1292 w, 1248 w, 1225 w, 1145 w, 1117 s, 1070 s, 1011 s, 994 w, 966 w, 916 m, 847 w, 771 vs, 718 s, 700 vs. − ^{1}H NMR (300 MHz, [D$_8$]THF): δ = 2.26 (s, 3 H, CH_3), 7.20−7.26 (m, 2 H, *p*-H), 7.29−7.31 (m, 4 H, *m*-H), 7.44 (t, 4 H, *o*-H). − ^{13}C{^{1}H} NMR (400 MHz, [D$_8$]THF): δ = 12.2 (Me), 111.9 (C-4, pz), 127.2 (C-4, Ph), 129.1 (C-2,C-6 and C-3,C-5, Ph), 136.2 (C-1, Ph), 153.1 (C-3,C-5, pz). − MS (70 eV, EI); *m*/*z* (%): 438 (40) [(^{205}Tl)M$^+$], 234 (90) [$C_{16}H_{14}N_2^+$], 205 (15) [^{205}Tl$^+$], 130 (100) [$C_9H_8N^+$]. − $C_{16}H_{13}N_2Tl$ (437.7): calcd. C 43.90, H 2.99, N 6.40; found C 44.00, H 3.08, N 6.21.

Bis(3,5-diphenylpyrazolato)mercury(II) (2)

Method A: 3,5-Diphenylpyrazole (1.00 g, 4.5 mmol) was treated with a THF solution (30 mL) of potassium hydride (0.18 g, 4.5 mmol) at 0°C. Gas evolution was observed and a slightly pale yellow solution formed. $HgCl_2$ (0.62 g, 2.3 mmol) was added causing formation of a white precipitate. The reaction mixture was stirred for 1 h and then was treated with water. The precipitated mercurial **2** was filtered off, washed with water, ethanol, and ether, and then dried under vacuum for 30 min giving 1.10 g (76%) of impure **2** as a white powder. − IR: $\tilde{\nu}$ = 1604 cm^{-1} m, 1542 w, 1400 m, 1236 w, 1321 w, 1296 w, 1274 m, 1236 m, 1157 m, 1128 m, 1074 s, 1026 m, 1001 w, 986 m, 958 w, 914 m, 844 w, 800 w, 758 vs, 696 vs. − MS (electrospray); *m*/*z* (%): 641 (100) [(^{202}Hg)MH$^+$], 549 (100) [$^{202}HgC_{23}H_{15}N_4^+$], 467 (76) [$^{202}HgC_{17}H_{19}N_3^+$]. − $C_{30}H_{22}N_4Hg$ (639.1): calcd. C 56.38, H 3.47, N 8.77; found C 54.57, H 3.77, N, 8.07.

Method B: $HgBr_2$ (1.80 g, 5.0 mmol) and NaBr (2.05 g, 20 mmol) were dissolved in *t*BuOH (80 mL). 3,5-Diphenylpyrazole (2.20 g, 10 mmol) and NaOH (0.80 g, 20 mmol) were added and the reaction mixture was refluxed for 4 h. The cream-coloured solution was poured into distilled H_2O (150 mL) giving bis(3,5-diphenylpyrazolato)mercury as a cream precipitate which was filtered from the solution and dried under vacuum. The infrared spectrum of this compound was in good agreement with that of the product from Method A and a yield of > 90% was obtained.

Bis(2*H*-benz[*g*]-4,5-dihydroindazolato)bis(1,2-dimethoxyethane)-ytterbium(II) (3a): A mixture of ytterbium powder (0.69 g, 4.0 mmol) and (2*H*-benz[*g*]-4,5-dihydroindazolato)thallium(I) (0.74 g, 2.0 mmol) in THF (30 mL) was subjected to ultrasonication for 24 h. The resulting deep red solution with grey suspended solids was allowed to stand for several hours, when a filter cannula was employed to separate the red solution from the deposited grey solids. The THF was removed under vacuum yielding a red solid which was dissolved in DME (40 mL) and allowed to stand for several days at room temperature during which time 0.54 g (78%) of large red crystals formed. − IR: $\tilde{\nu}$ = 1605 cm^{-1} m, 1528 w, 1509 w, 1297 w, 1275 w, 1240 w, 1224 w, 1210 w, 1191 w, 1121 m, 1097 s, 1073 s, 1045 w, 1028 w, 1009 m, 977 m, 954 m, 943 m, 884 m, 855 s, 818 s, 766 vs, 734 m, 716 vs, 686 m, 673 m. − ^{1}H NMR (300 MHz, [D$_8$]THF): δ = 2.73 and 2.79 (br. d, overlapping signals, total integration 4 H, 4-H,5-H), 3.31 (br. s, 12 H, MeO, DME), 3.48 (br. s, 8 H, CH_2 DME), 7.00 (br. m, 3 H, 6-H,7-H,9-H), 7.55 (br. s, 1 H, 3-H), 7.85 (br. s, 1 H, 8-H). Integration of the indazolate protons showed approximately half the expected intensity. − Visible/near IR (THF): λ_{max} (ε): 430 (415) nm. − $C_{30}H_{38}N_4O_4Yb$ (691.7): calcd. C 52.09, H 5.54, N 8.10, Yb 25.02; found C 51.91, H 5.66, N 7.27, Yb 25.14.

Bis(1,2-dimethoxyethane)bis(3-methyl-5-phenylpyrazolato)-ytterbium(II) (3b): A mixture of ytterbium powder (1.73 g, 10.0 mmol), mercury metal (ca. 0.20 mL), and (3-methyl-5-phenylpyrazolato)thallium(I) (1.20 g, 2.31 mmol) in THF (30 mL) was subjected to ultrasonication for 48 h. The resulting deep red solution with grey suspended solids was allowed to stand for several hours until the suspension settled out. The reaction mixture was then filtered using a filter cannula. The filtrate was concentrated to dryness under vacuum yielding a red solid which was dissolved in DME which was subsequently removed under vacuum giving **3b** [0.48 g (62%)]. − IR: $\tilde{\nu}$ = 1602 cm^{-1} m, 1527 w, 1491 m, 1413 m, 1298 w, 1190 w, 1155 w, 1099 m, 1054 s, 1016 m, 964 m, 912 w, 888 m, 858 m, 762 vs, 712 m, 695 vs. − Visible/near IR (THF): λ_{max} (ε) = 389 nm (586). − ^{1}H NMR (300 MHz, [D$_8$]THF): δ = 2.22 (br. s, 6 H, 3-Me), 3.20 (s, 12 H, MeO DME), 3.36 (s, 8 H, CH_2 DME), 6.30 (br. s, 2 H, 4-H), 6.96 (br. s, 2 H, *p*-H), 7.14 (br. s, 4 H, *m*-H), 7.72 (br. s, 4 H, *o*-H). − $C_{28}H_{38}N_4O_4Yb$ (667.7): calcd. Yb 25.92; found Yb 25.82.

Bis(7-azaindolato)bis(1,2-dimethoxyethane)ytterbium(II) (3c): A mixture of ytterbium powder (1.73 g, 10.0 mmol), mercury metal (ca. 0.20 mL), and (7-azaindolato)thallium(I) (0.64 g, 2.0 mmol) in THF (30 mL) was subjected to ultrasonication for 16 h. The resulting deep red solution with grey suspended solids was allowed to stand for several hours until the suspension settled out. The reaction mixture was then filtered using a filter cannula. The filtrate was concentrated to dryness under vacuum yielding a red solid which was recrystallised from DME giving **3c** [0.41 g (70%)]. − IR: $\tilde{\nu}$ = 1581 cm^{-1} m, 1542 m, 1402 w, 1335 w, 1321 m, 1295 s, 1258 m, 1193 m, 1153 s, 1118 m, 1060 m, 1020 m, 984 m, 951 w, 907 w, 896 w, 857 vs, 795 s, 771 s, 744 s, 718 vs, 617 m, 598 m. − Visible/near IR (THF): λ_{max} (ε) = 480 nm (259). − ^{1}H NMR (300 MHz, [D$_6$]benzene): δ = 2.79 (s, 12 H, MeO DME), 2.83 (s, 8 H, CH_2 DME), 6.74 (m, 4 H, 2-H,5-H), 7.88 (s, 2 H, 2-H), 7.97 (m, 4 H, 4-H,7-H). − ^{171}Yb NMR (52.5 MHz, 0.04 M in DME): δ = 489 ($\Delta\nu_{1/2}$ = 54 Hz). − $C_{22}H_{30}N_4O_4Yb$ (587.6): calcd. C 44.97, H 5.15, N 9.54, Yb 29.45; found C 43.85, H 4.82, N 10.01, Yb 29.41.

Bis(1,2-dimethoxyethane)bis(3,5-diphenylpyrazolato)ytterbium(II) (3d)

Method A: A mixture of ytterbium powder (0.83 g, 4.8 mmol) and $Hg(Ph_2pz)_2$ (1.00 g, 2.4 mmol) in THF (30 mL) was subjected to ultrasonication for 6 d. The resulting deep red solution with grey suspended solids was allowed to stand for several hours, and was then filtered. The THF was removed under vacuum giving a deep red sticky solid which was recrystallised from DME affording 1.10 g (58%) of large red crystals. − IR: identical with that reported.[8] − $C_{38}H_{42}N_4O_4Yb$ (791.8): calcd. Yb 21.85; found Yb 22.28, 22.04.

Method B: $Yb(C_6F_5)_2$, generated in situ from ytterbium metal (1.73 g, 10.0 mmol) and $Hg(C_6F_5)_2$ (1.07 g, 2.0 mmol) was treated with 3,5-diphenylpyrazole (0.88 g, 4.0 mmol) in THF (30 mL). After stirring at room temerature for 15 min, the THF was removed and the red solid was recrystallised from DME [0.34 g, (22%)]. − IR and visible/near IR (THF): identical with those reported.[8]

Method C: 3,5-Diphenylpyrazole (0.59 g, 2.7 mmol) was treated with a THF solution (30 mL) of potassium hydride (0.11 g, 2.7 mmol) at 0°C. To the resulting solution $YbI_2(THF)_2$ (0.77 g, 1.35 mmol) was added causing an formation of a red solution and a white precipitate. After stirring for 12 h, removal of THF gave a sticky orange solid which was extracted with in toluene (80 mL) giving a red/brown solution and a white precipitate. After filtration, the toluene solution was concentrated to dryness giving a red solid which was recrystallised from DME [0.40 g (37%)]. − IR: identical with that reported.[8] − $C_{38}H_{42}N_4O_4Yb$ (791.8): calcd. Yb 21.85; found Yb 21.52.

Bis(1,2-dimethoxyethane)bis(3,5-diphenylpyrazolato)europium(II) (4a): A mixture of europium metal chunks (0.61 g, 4.0 mmol), mercury metal (ca. 0.20 mL) and (3,5-diphenylpyrazolato)thallium(I) (0.85 g, 2.0 mmol) in THF (30 mL) was subjected to ultrasonication for 48 h. The resulting deep yellow solution with grey suspended solids was allowed to stand for several hours. Filtration, and evaporation of the THF yielded a yellow solid, which was recrystallised from DME giving 0.69 g (90%) of **4a** as large yellow crystals. − IR: $\tilde{\nu}$ = 1602 cm^{-1} m, 1157 w, 1120 w, 1193 w, 1115 m, 1096 m, 1069 s, 1057 s, 1025 m, 1016 m, 980 m, 968 s, 907 w, 852 s, 832 w, 794 w, 770 m, 750 vs, 697 s, 682 s. − $C_{38}H_{42}EuN_4O_4$ (770.7): calcd. C 59.22, H 5.49, Eu 19.72, N 7.27; found C 59.06, H 5.67, Eu 19.68, N 7.59.

Bis(3,5-di-*tert*-butylpyrazolato)bis(1,2-dimethoxyethane)europium(II) (4b): A mixture of europium metal chunks (1.52 g, 10.0 mmol), mercury metal (ca. 0.20 mL), diphenylmercury(II) (0.98 g, 2.78 mmol) and 3,5-di-*tert*-butylpyrazole (1.00 g, 5.56 mmol) in THF (30 mL) was heated (60 °C) for 24 h. The resulting deep yellow solution with grey suspended solids was allowed to stand for several hours. Filtration, and evaporation of the THF yielded a yellow solid, which was recrystallised from DME giving 0.57 g (59%) of **4b** as large yellow crystals. − IR: $\tilde{\nu}$ = 1509 cm^{-1} m, 1404 w, 1354 m, 1318 w, 1248 s, 1218 m, 1195 m, 1158 w, 1123 m, 1103 m, 1078 s, 1032 m, 1010 s, 996 m, 860 vs, 769 vs, 722 vs. − Visible/near IR (THF): λ_{max} (ε) = 345 nm (477). − $C_{38}H_{42}EuN_4O_4$ (690.8): calcd. C 52.16, H 8.46, Eu 22.00, N 8.11; found C 51.28, H 8.39, Eu 22.02, N 8.88.

Bis(1,2-dimethoxyethane)bis(3,5-diphenylpyrazolato)samarium(II) (5)

Method A: 3,5-Diphenylpyrazole (0.27 g, 1.2 mmol) was treated with a THF solution (30 mL) of bis[bis(trimethylsilyl)-amido]bis(tetrahydrofuran)samarium(II) (0.38 g, 0.60 mmol). The resulting purple solution was stirred for 30 min, and the THF was then removed under vacuum yielding a purple solid which was washed twice with petroleum ether (2 × 30 mL). The purple solid was recrystallised from DME (30 mL) giving 0.12 g (25%) of **5** as dark purple crystals. − IR: $\tilde{\nu}$ = 1602 cm^{-1} m, 1509 w, 1243 w, 1220 w, 1156 w, 1121 w, 1101 m, 1073 s, 1026 m, 1014 w, 967 s, 913 w, 860 m, 849 m, 793 w, 758 vs, 697 s, 685 s. − Visible/near IR (THF) λ_{max} (ε): ca. 600 br. (900) nm. − ^1H NMR (300 MHz, [D_8]THF): δ = −11.76 (s, 2 H, H-4), 2.93 (d, 8 H, *o*-H), 3.48 (s, 12 H, MeO, DME), 3.54 (s, 8 H, CH_2, DME), 5.84 (t, 4 H, *p*-H), 6.73 (t, 8 H, *m*-H). − $C_{38}H_{42}N_4O_4Sm$ (769.2): calcd. C 59.34, H 5.50, N 7.28, Sm 19.55; found C 59.42, H 5.63, N 7.51, Sm 19.26.

Method B: $SmI_2(THF)_2$ (0.54 g, 1.0 mmol) was added to a THF solution (30 mL) of (3,5-diphenylpyrazolato)potassium(I) (2.0 mmol) (generated in situ as described above in the synthesis of **3d**) causing formation of a dark purple solution and a white precipitate. This reaction mixture was stirred for 12 h followed by removal of THF to give a sticky purple solid, which was extracted with toluene (30 mL) giving a red/brown solution and a white precipitate. The toluene solution was filtered and concentrated to dryness yielding dark purple **5** which was recrystallised from DME [0.48 g (62%)]. − IR: identical with that of the product from Method A. − $C_{38}H_{42}N_4O_4Sm$ (769.2): calcd. Sm 19.55; found Sm 19.90.

Reaction between 3d and $HgPh_2$ and Ph_2pzH: 3d (0.40 g, 0.50 mmol), $HgPh_2$ (0.89 g, 0.25 mmol) and Ph_2pzH (0.55 g, 0.25 mmol) were stirred in DME (30 mL) at room temperature for 2 d. The reaction mixture remained red and there were no signs of precipitated metal. A visible/near-IR spectrum of the reaction mixture was indentical to that reported[8] for **3d**.

Reaction between (1,2-Dimethoxyethane)tris(3,5-diphenylpyrazolato)ytterbium(III) and Ytterbium Metal: A mixture of (1,2-dimethoxyethane)tris(3,5-diphenylpyrazolato)ytterbium(III)[25] (0.46 g, 0.50 mmol), ytterbium metal (1.73 g, 10.0 mmol), and mercury metal (ca. 0.20 mL) in DME (30 mL) were subjected to ultrasonication for 24 h. The initially colourless solution turned deep red after sonication for 12 h. Separation of excess ytterbium and mercury followed by removal of DME yielded a red solid. Visible/near-IR and IR spectra were indentical with those reported[8] for **3d**.

Reaction between Bis(1,2-dimethoxyethane)tris(3,5-diphenylpyrazolato)samarium(III) and Samarium Metal: A mixture of bis(1,2-dimethoxyethane)tris(3,5-diphenylpyrazolato)samarium(III)[8] (0.99 g, 1.0 mmol), samarium metal (1.50 g, 10.0 mmol), and mercury metal (ca. 0.20 mL) in DME (30 mL) were subjected to ultrasonication for 2 d. The initially colourless solution remained colourless after sonication for 2d. A visible/near IR spectrum of the reaction mixture was indentical with that reported[8] for $[Sm(Ph_2pz)_3(DME)_2]$.

Attempted Reaction of Ytterbium Metal with $Hg(C_6F_5)_2$ and 3,5-Diphenylpyrazole: A mixture of ytterbium powder (1.73 g, 10.0 mmol), mercury metal (ca. 0.20 mL), bis(pentafluorophenyl)mercury(II) (0.53 g, 1.0 mmol), and 3,5-diphenylpyrazole (0.44 g, 2.0 mmol) in THF (40 mL) was stirred at room temperature for 4 d. On addition of THF an orange solution formed. This progressively darkened to a black solution over the course of the reaction. The resulting black solution with grey suspended solids was allowed to stand for several hours. Filtration and removal of THF under vacuum revealed a black solid which was insoluble in DME. The infrared spectrum of this black material was significantly different from that obtained for compound **3d**. − IR: $\tilde{\nu}$ = 1365 cm^{-1} m, 1303 w, 1246 m, 1193 m, 1112 br. s, 1028 m, 983 m, 940 m, 852 s, 763 vw, 723 vw.

Structure Determinations: Room-temperature single-counter/four-circle diffractometer data sets were measured on capillary-mounted specimens (2θ/θ-scan mode; graphite-monochromated radiation, λ = 0.7107_3 Å; $T \approx 295$ K), in most cases with symmetry equivalences, yielding N_{total} reflections, these being merged (R_{int} as specified) after absorption correction, yielding N (unique) data, N_o with $I > 2\sigma(I)$ being considered "observed" and used in the full-matrix least-squares refinement (n_v variables). Anisotropic thermal parameters were refined for the non-hydrogen atoms, (x, y, z, $U_{iso})_H$ being included constrained at estimated values. Conventional residuals R, R_w [statistical weights, derivative of $\sigma^2(I) = \sigma^2(I_{diff}) + 0.0004\ \sigma^4(I_{diff})$] on $|F|$ are quoted at convergence. Neutral atom complex scattering

factors were employed, the Xtal 3.4 program system[26] being used. Individual abnormalities, variations in procedure and idiosyncrasies are noted as "variata"; in no case was there difference-map evidence for occluded solvent, although ligand disorder was evident in some cases (see below). In Figures 1−6, 20% thermal ellipsoids are shown for the non-hydrogen atoms, hydrogen atoms having arbitrary radii of 0.1 Å. In the case of **5** and **4a** pairs of molecular projections (Figures 3 and 6) are shown and provide views (i) down the actual or putative *2* axis of the molecule, so as to display that symmetry, and (ii) normal to that axis. The latter is provided to display better (a) any difference in conformation among the pair of DME ligands, (b) any ligand disorder, (c) any tendency to dodecahedral coordination about the metal atom [the $(N_2)_2$ ligand pair comprising one of the two intersecting planes and the $(O_2)_2$ the other]. Crystallographic data (excluding structure factors and including torsion angles describing the DME conformations) for the structures reported in this paper have been deposited with the Cambridge Crystallographic Data Centre as supplementary publication nos. CCDC-101118 (**3d**)[8] and -109937−109941. Copies of the data can be obtained free of charge on application to CCDC, 12 Union Road, Cambridge CB2 1EZ, UK [Fax: int. code + 44-1223/336-033; E-mail: deposit@ccdc.cam.ac.uk].

Crystal/Refinement Data

3a [Yb(bind)$_2$(DME)$_2$]: $C_{30}H_{38}N_4O_4Yb$, M = 691.7. Monoclinic, space group $P2_1/c$ (C_{2h}^5, no. 14), a = 15.570(2), b = 23.434(5), c = 8.052(3) Å, β = 94.98(2)°, V = 2927 Å^3. $D_{calcd.}$ (Z = 4) = 1.570 g cm^{-3}; F(000) = 1392. μ_{Mo} = 32.4 cm^{-1}; specimen: 0.45 × 0.30 × 0.45 mm; $A^*_{min,max}$ = 2.28, 3.85 (analytical correction). $2\theta_{max}$ = 55°; N = 6476, N_o [$I > 3\sigma(I)$] = 4954; R = 0.026, R_w = 0.029; n_v = 333. $|\Delta\rho_{max}|$ = 1.13 e Å^{-3}.

3c [Yb(azin)$_2$(DME)$_2$]: $C_{22}H_{30}N_4O_4Yb$, M = 587.6. Orthorhombic, space group *Pbca* (D_{2h}^{15}, no. 61), a = 18.183(4), b = 16.567(6), c = 15.855(9) Å, V = 4776 Å^3. $D_{calcd.}$ (Z = 8) = 1.634 g cm^{-3}; F(000) = 2336. μ_{Mo} = 39.5 cm^{-1}; specimen: 0.12 × 0.40 × 0.45 mm; $A^*_{min,max}$ = 1.60, 4.2 (analytical correction). $2\theta_{max}$ = 55°; N_{total} = 11095, N = 5483 (R_{int} = 0.028), N_o = 3229; R = 0.034, R_w = 0.038; n_v = 299. $|\Delta\rho_{max}|$ = 0.80 e Å^{-3}.

Variata: Each azin ligand is capable of coordinating in two modes involving interchange of nitrogen atoms with various associated possibilities of isomerism; these modes are both observed for each ligand, C(4,4′) [Figure 5: C(14), C(14′) and C(24), C(24′) of the respective ligands] of each being the only constituent atoms sufficiently displaced from overlap to permit meaningful refinement of the alternate fragments. Site occupancies (x, 1 − x) for the two ligands refined to x = 0.83, 0.77(3), isotropic thermal parameter forms being used for the minor fragments.

[M(Ph$_2$pz)$_2$(DME)$_2$] (M = Yb, Eu, Sm): $C_{38}H_{42}MN_4O_4$.

[**3d (M = Yb)** has been recorded elsewhere;[8] a redeposition has been made, with atoms relabelled as shown in Figure 2, in conformity with present arrays, which conform to the quasi-*2* symmetry of the system.]

4a (M = Eu): **M** = 770.7. Monoclinic, space group $P2/c$ (C_{2h}^4, no. 13), a = 19.746(3), b = 12.635(2), c = 15.396(2) Å, β = 110.12(1), V = 3607 Å^3. $D_{calcd.}$ (Z = 4) = 1.419 g cm^{-3}; F(000) = 1572. μ_{Mo} = 17.8 cm^{-1}; specimen: 0.55 × 0.30 × 0.30 mm; $A^*_{min,max}$ = 1.50, 1.82 (gaussian correction). $2\theta_{max}$ = 50°; N = 6328, N_o = 4823; R = 0.046, R_w = 0.049; n_v = 427. $|\Delta\rho_{max}|$ = 0.85 e Å^{-3}.

5 (M = Sm): **M** = 769.1. Orthorhombic, space group *Pnma* (D_{2h}^{16}, no. 62), a = 7.9941(6), b = 24.263(3), c = 19.080(3) Å, V = 3701 Å^3. $D_{calcd.}$ (Z = 4) = 1.380 g cm^{-3}; F(000) = 1568. μ_{Mo} = 16.3 cm^{-1}; specimen: 0.25 × 0.35 × 0.55 mm; $A^*_{min,max}$ = 1.47, 1.72 (gaussian correction). $2\theta_{max}$ = 60°; N_{total} = 8395, N = 3650 (R_{int} = 0.029), N_o = 2240; R = 0.042, R_w = 0.037; n_v = 270. $|\Delta\rho_{max}|$ = 1.04 e Å^{-3}.

Variata: As modelled in the present space group, the DME moieties are disordered across the crystallographic mirror plane; meaningful refinement could not be achieved in a lower symmetry space group. An ordered component is shown in the Figures and Tables and has a crystallographic mirror plane passing through the metal atom and relating the two halves (including substituents) of each Ph$_2$pz ligand. Despite similar Ln sizes, the M = Eu, Sm adducts **4a**, **5** are not isomorphous with each other, or with the Yb adduct **3d**.

4b [Eu(*t*Bu$_2$pz)$_2$(DME)$_2$]: $C_{30}H_{58}EuN_4O_4$, M = 690.8. Triclinic, space group $P\bar{1}$ (C_i^1, no. 2), a = 22.791(4), b = 15.709(4), c = 10.289(3) Å, α = 89.38(2), β = 82.31(2), γ = 84.49(2)°, V = 3634 Å^3. $D_{calcd.}$ (Z = 4) = 1.263 g cm^{-3}; F(000) = 1444. μ_{Mo} = 17.6 cm^{-1}; specimen: 0.40 × 0.50 × 0.50 mm; $A^*_{min,max}$ = 1.60, 2.12 (gaussian correction). $2\theta_{max}$ = 50°; N_{total} = 19495, N = 12765 (R_{int} = 0.047), N_o [$I > 3\sigma(I)$] = 6027; R = 0.057, R_w = 0.064; n_v = 700. $|\Delta\rho_{max}|$ = 1.45 e Å^{-3}.

Variata: One of the DME groups is conformationally disordered in each molecule, discrete $(CH_2)_2$ carbon atoms being resolvable and refined (C thermal parameters isotropic) with site occupancies set at 0.5 after trial refinement. Crystal decomposition of 55% was evident during data collection (isotropic) and compensated by scaling.

Acknowledgments

We are grateful to the Australian Research Council for financial support and for the award of an Australian Postgraduate Award to E. E. D.

[1] G. B. Deacon, C. M. Forsyth, P. C. Junk, B. W. Skelton, A. H. White, *J. Chem. Soc., Dalton Trans.* **1998**, 1381−1388.
[2] [2a] S. Trofimenko, *Chem. Rev.* **1972**, *72*, 497−509. − [2b] S. Trofimenko, *Prog. Inorg. Chem.* **1986**, *34*, 115−210. − [2c] A. P. Sadimenko, S. S. Bassoon, *Coord. Chem. Rev.* **1996**, *147*, 247−297. − [2d] G. La Monica, G. A. Ardizzoia, *Prog. Inorg. Chem.* **1997**, *46*, 151−238. − [2e] J. E. Cosgriff, G. B. Deacon, *Angew. Chem.* **1998**, *110*, 298−299; *Angew. Chem. Int. Ed. Engl.* **1998**, *37*, 286−287.
[3] [3a] I. A. Guzei, A. G. Baboul, G. P. A. Yap, A. L. Rheingold, H. B. Schlegel, C. H. Winter, *J. Am. Chem. Soc.* **1997**, *119*, 2287−2288. − [3b] I. A. Guzei, G. P. A. Yap, C. H. Winter, *Inorg.Chem.* **1997**, *36*, 1738−1739. − [3c] D. Pfeiffer, M. J. Heeg, C. H. Winter, *Angew. Chem.* **1998**, *110*, 2674−2676; *Angew. Chem. Int. Ed. Engl.* **1998**, *37*, 2517−2519. − [3d] T. D. Culp, J. G. Cederberg, B. Bieg, T. F. Keuch, K. L. Bray, D. Pfeiffer, C. H. Winter, *J. Appl. Phys.* **1998**, *83*, 4918−4927. − [3e] G. B. Deacon, E. E. Delbridge, B. W. Skelton, A. H. White, *Angew. Chem.* **1998**, *110*, 2372−2373; *Angew. Chem. Int. Ed. Engl.* **1998**, *37*, 2251−2252. − [3f] C. Yélamos, M. J. Heeg, C. H. Winter, *Inorg. Chem.* **1998**, *37*, 3892−3894.
[4] H. Schumann, P. R. Lee, J. Loebel, *Angew. Chem.* **1989**, *101*, 1073−1074; *Angew. Chem. Int. Ed. Engl.* **1989**, *28*, 1033−1035.
[5] [5a] H. Schumann, J. Loebel, J. Pickardt, C. Qian, Z. Xie, *Organometallics* **1991**, *10*, 215−219. − [5b] G. B. Deacon, B. M. Gatehouse, S. Nickel, S. N. Platts, *Aust. J. Chem.* **1991**, *44*, 613−621.
[6] [6a] J. E. Cosgriff, G. B. Deacon, B. M. Gatehouse, H. Hemling, H. Schumann, *Angew. Chem.* **1993**, *105*, 906−907; *Angew. Chem. Int. Ed. Engl.* **1993**, *32*, 874−875. − [6b] J. E. Cosgriff, G. B. Deacon, B. M. Gatehouse, *Aust. J. Chem.* **1993**, *46*, 1881−1896. − [6c] J. E. Cosgriff, G. B. Deacon, B. M. Gatehouse, H. Hemling, H. Schumann, *Aust. J. Chem.* **1994**, *47*, 1223−1235.

[7] [7a] J. E. Cosgriff, G. B. Deacon, G. D. Fallon, B. M. Gatehouse, H. Schumann, R. Weimann, *Chem. Ber.* **1996**, *129*, 953−958. – [7b] J. E. Cosgriff, G. B. Deacon, B. M. Gatehouse, P. R. Lee, H. Schumann, *Z. Anorg. Allg. Chem.* **1996**, *622*, 1399−1403.

[8] G. B. Deacon, E. E. Delbridge, B. W. Skelton, A. H. White, *Eur. J. Inorg. Chem.* **1998**, 543−545.

[9] [9a] H. Schumann, J. A. Meese-Marktscheffel, L. Esser, *Chem. Rev.* **1995**, *95*, 865−986. – [9b] F. T. Edelmann, in *Comprehensive Organometallic Chemistry*, 2nd ed. (Eds.: G. Wilkinson, F. G. A. Stone, E. W. Abel), Pergamon, Oxford, **1995**, chapter 2. – [9c] M. N. Bochkarev, L. N. Zakharov, G. S. Kalinina, *Organoderivatives of Rare Earth Elements*, Kluwer Academic Press, Dordrecht, **1995**. – [9d] G. B. Deacon, G. N. Pain, T. D. Tuong, *Inorg. Synth.* **1990**, *28*, 291−297. – [9e] G. B. Deacon, A. J. Koplick, G. N. Pain, T. D. Tuong, in *Herrmann-Brauer, Synthetic Methods of Organometallic and Inorganic Chemistry*, 3rd ed. (Ed. W. A. Herrmann), G. Thieme, Stuttgart, **1997**, vol. 6, pp. 54−55, 86−87.

[10] [10a] G. B. Deacon, P. B. Hitchcock, S. A. Holmes, M. F. Lappert, P. MacKinnon, R. H. Newnham, *J. Chem. Soc., Chem. Comm.* **1989**, 935−937. – [10b] G. B. Deacon, T. Feng, S. Nickel, M. I. Ogden, A. H. White, *Aust. J. Chem.* **1992**, *45*, 671−683. – [10c] G. B. Deacon, T. Feng, P. MacKinnon, R. H. Newnham, S. Nickel, B. W. Skelton, A. H. White, *Aust. J. Chem.* **1993**, *46*, 387−399.

[11] G. B. Deacon, G. D. Fallon, C. M. Forsyth, H. Schumann, R. Weimann, *Chem. Ber.* **1997**, *130*, 409−415.

[12] [12a] G. B. Deacon, D. L. Wilkinson, *Inorg. Chim. Acta.* **1988**, *142*, 155−159. – [12b] K. P. Butin, A. N. Kashin, I. P. Beleskaya, L. S. German, V. R. Polishchuk, *J. Organomet. Chem.* **1970**, *25*, 11−16. – [12c] K. P. Butin, I. P. Beleskaya, A. N. Kashin, O. A. Reutov, *J. Organomet. Chem.* **1967**, *10*, 197−210.

[13] [13a] J. R. van den Hende, P. B. Hitchcock, S. A. Holmes, M. F. Lappert, *J. Chem. Soc., Dalton Trans.* **1995**, 1435−1440. – [13b] A. G. Avent, M. A. Edelman, M. F. Lappert, G. A. Lawless, *J. Am. Chem. Soc.* **1989**, *111*, 3423−3425.

[14] W. T. Carnell, in *The Absorption and Fluorescence Spectra of Rare Earth Ions in Solution* in *Handbook on the Physics and Chemistry of Rare Earths* (Eds.: K. A. Gschneidner, L. Eyring), North-Holland, Amsterdam, **1979**, vol. 3, chapter 24.

[15] R. D. Shannon, *Acta Crystallogr., Sect. A* **1976**, *32*, 751−767.

[16] G. B. Deacon, T. Feng, B. W. Skelton, A. H. White, *Aust. J. Chem.* **1995**, *48*, 741−756.

[17] G. B. Deacon, C. M. Forsyth, B. M. Gatehouse, A. Philosof, B. W. Skelton, A. H. White, P. A. White, *Aust. J. Chem.* **1997**, *50*, 959−970.

[18] J. L. Atwood, W. E. Hunter, A. L. Wayda, W. J. Evans, *Inorg. Chem.* **1981**, *20*, 4115−4119.

[19] G. H. Jeffery, J. Basset, J. Mendham, R. C. Denney, *Vogel's Textbook of Quantitative Chemical Analysis*, 5th ed., Longman Scientific & Technical, New York, **1989**, p. 404.

[20] A. L. Rheingold, R. L. Ostrander, B. S. Haggerty, S. Trofimenko, *Inorg. Chem.* **1994**, *33*, 3666−3676.

[21] [21a] B. Sjollema, *Justus Liebigs Ann. Chem*. **1894**, *279*, 248−257. – [21b] M. S. R. Murthy, E. V. Rao, *Indian Drugs* **1985**, *22*, 462−464 (*Chem. Abstr.* **1986**, *105*, 6443e).

[22] [22a] P. L. Watson, T. H. Tulip, I. Williams, *Organometallics* **1990**, *9*, 1999−2009. – [22b] J. L. Namy, P. Girard, H. B. Kagan, P. E. Caro, in *Herrmann-Brauer, Synthetic Methods of Organometallic and Inorganic Chemistry*, 3rd ed., (Ed.: W. A. Herrmann), G. Thieme, Stuttgart, **1997**, vol. 6, pp. 26−27.

[23] [23a] W. J. Evans, D. K. Drummond, H. Zhang, J. L. Atwood, *Inorg. Chem.* **1988**, *27*, 575−579. – [23b] W. J. Evans, D. K. Drummond, H. Zhang, J. L. Atwood, in *Herrmann-Brauer, Synthetic Methods of Organometallic and Inorganic Chemistry*, 3rd ed. (Ed.: W. A. Herrmann), G. Thieme, Stuttgart, **1997**, vol. 6, pp. 28−29.

[24] G. B. Deacon, J. E. Cosgriff, E. T. Lawrenz, C. M. Forsyth, D. L. Wilkinson, in *Herrmann-Brauer, Synthetic Methods of Organometallic and Inorganic Chemistry*, 3rd ed. (Ed.: W. A. Herrmann), G. Thieme, Stuttgart, **1997**, vol. 6, pp. 48−50.

[25] G. B. Deacon, E. E. Delbridge, B. W. Skelton, A. H. White, unpublished results.

[26] S. R. Hall, H. D. Flack, J. M. Stewart (Eds.), *The XTAL 3.2 Reference Manual*, Universities of Western Australia, Geneva and Maryland, **1992**.

Received November 17, 1998
[I98398]

1,3,5-Triphosphabicyclo[3.1.0]hexene-η^3,η^1-diyl Hafnium Complexes: Structure and Reactivity

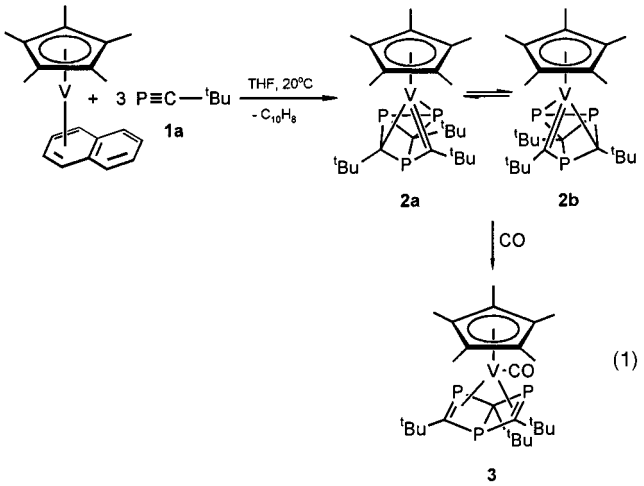
Paul Binger,*[a,b] Stefanie Stutzmann,[a] Jörg Stannek,[a] Klaus Günther,[b] Petra Phillips,[a] Richard Mynott,[a] Joachim Bruckmann,[a] and Carl Krüger[a]

Keywords: 1,3,5-Triphosphabicyclo[3.1.0]hexene-η^3,η^1-diyl hafnium complexes / 1,3,5-Triphosphabicyclo[3.1.0]hexene / 1,3,5-Triphosphacyclohexa-1,4-diene / Cyclotrimerization / Phosphaalkyne

It is shown that the $(P{\equiv}C{-}t\mathrm{Bu})_3$ ligand found in the hafnium complex (COT)Hf$(P{\equiv}C{-}t\mathrm{Bu})_3$ **5** (COT = cyclooctatetraene), which we reported recently,[3] is also present in the new hafnium complex **12**, prepared by reaction of hexachloroethane with complex **5** in pentane, as well as in its trimethylphosphane adduct **14**. The structures of complexes **12** and **14** have been determined by X-ray crystallography and that of **5** by comparing its ^{1}H-, ^{13}C-, and ^{31}P-NMR spectra with those of the complexes **12** and **14**. The organophosphorus ligand in all three complexes is a 2,4,6-tri-*tert*-butyl-1,3,5-triphosphabicyclo[3.1.0]hexene-η^3,η^1-diyl. Hydrolysis of complexes **5** and **12** with water gives the new phosphorus heterocycle **15**, whereas the new heterocycles **16** and **17** are formed in an approximately 1:1 mixture using either silica gel containing 2% H_2O or $Na_2SO_4 \cdot 10\ H_2O$.

Introduction

Although numerous reactions are known where phosphaalkynes (**1**), e.g. *tert*-butylphosphaalkyne (**1a**), are cyclodimerized in the coordination sphere of a transition metal, the corresponding cyclotrimerizations are rare.[1] Until recently, the only example reported where it has been established unambiguously that **1a** is cyclotrimerized is the reaction to give the stable vanadium complexes **2** and **3**.[2]



(1)

Recently, we succeeded in preparing an η^8-cyclooctatetraene hafnium$-(PC-t\mathrm{Bu})_3$ complex **5** from **1a** and η^8-cyclooctatetraene-η^4-butadiene hafnium **4a** in high yield. Subsequent reaction of **5** with hexachloroethane afforded the new cyclotrimer 2,4,6-tri-*tert*-butyl-1,3,5-triphosphabenzene **6** (Eq. 2a).[3] An extensive NMR study of complex **5** showed that the trimeric phosphaalkyne unit in this hafnium complex is not bonded to the metal as a triphosphabenzene **6**, even though this species is liberated in subsequent displacement reactions. However, the NMR experiments did not permit a full description of the bonding situation.[3]

Slight modification of the cyclooctatetraene ligand in complex **4** (introduction of trimethylsilyl substituents → **4b**) led to another hafnium$-(PC-t\mathrm{Bu})_3$ complex (**7**), in which a 7-hafna-1,3,5-triphosphanorbornadiene appears to be formed. Free 1,3,5-triphospha-Dewar-benzene **8** could be obtained by displacement of the $(PC-t\mathrm{Bu})_3$ unit from **7**[3] (Eq. 2b).

In the last few years, two transition metal complexes have been reported where a 1,3-diphosphabenzene[4] (**9**) and a 1,3,5-triphosphabenzene[5] (**10**) are incorporated as η^6-coordinated ligands. However, it would seem very unlikely that the η^6-phosphabenzene molybdenumdicarbonyl complex **11** published much earlier[6] does indeed have the claimed structure.[7]

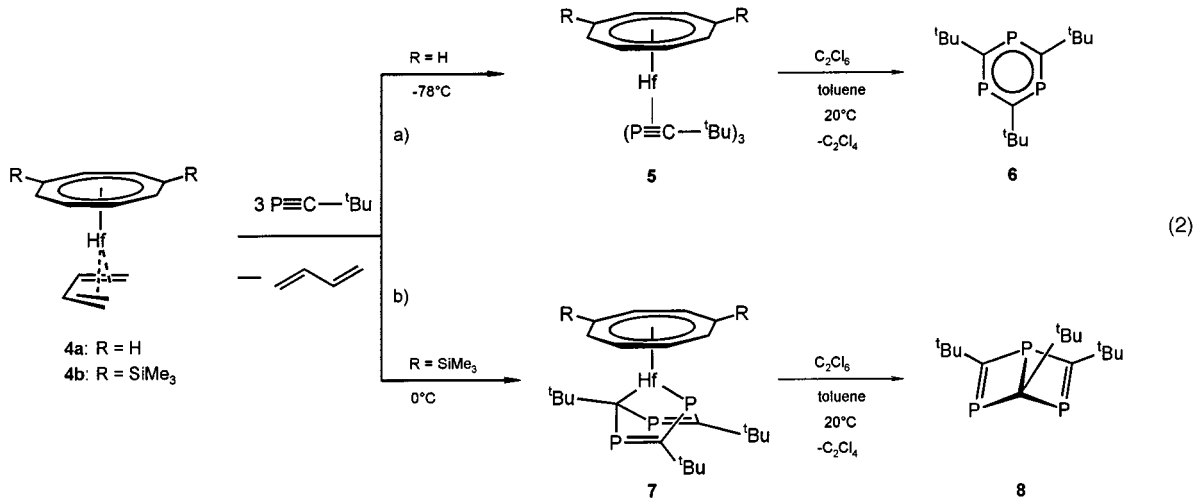
In this publication, we show that the $(P{\equiv}C-t\mathrm{Bu})_3$ ligand bonded to the hafnium in complex **5** as well as in the two new complexes **12** and **14** is a new type with a 1,3,5-triphosphabicyclo[3.1.0]hexene skeleton. This has been established by determining the structures of complexes **12** and **14** by X-ray crystallography. Supporting evidence comes from the observation that hydrolysis of complexes **5** and **12** yields the same phosphorus heterocycles **15**–**17**, indicating that the $(P{\equiv}C-t\mathrm{Bu})_3$ unit has the same structure in all three complexes **5**, **12**, and **14**.

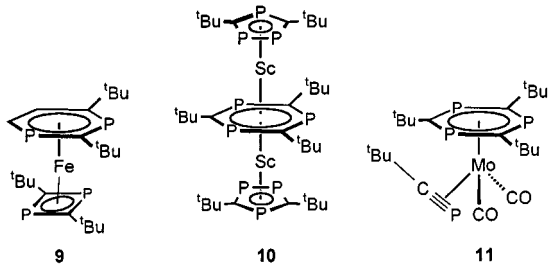
Results and Discussion

As described previously,[3] triphosphabenzene **6** can be generated from the hafnium complex **5** in 53% yield by a redox reaction with hexachloroethane (Eq. 2). The "(COT)-

[a] Max-Planck-Institut für Kohlenforschung, Kaiser-Wilhelm-Platz 1, D-45470 Mülheim a.d. Ruhr, Germany
[b] Present address: Fachbereich Chemie der Universität Kaiserslautern, Erwin-Schrödinger-Straße, D-67663 Kaiserslautern, Germany

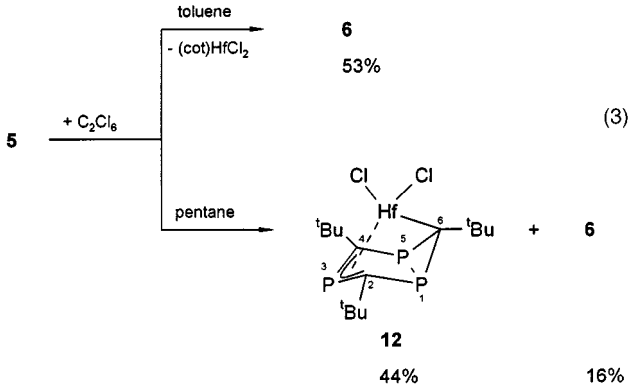
 © WILEY-VCH Verlag GmbH, D-69451 Weinheim, 1999 1434–1948/99/0505–0763 $ 17.50+.50/0





Scheme 1

hafnium(II)" fragment (COT = cyclooctatetraene) is oxidized to $(COT)HfCl_2$ and the hexachloroethane is reduced to tetrachloroethene. Unexpectedly, further studies revealed that the course of this reaction can be influenced by variation of the solvent. In our original experiments we had used toluene,[3] but replacing this by pentane led to an almost complete change in the reaction products. In the latter medium, the aforementioned redox reaction becomes merely a side reaction giving **6** only in ca. 16% yield, while the main product, 2,4,6-tri-*tert*-butyl-1,3,5-triphosphabicyclo[3.1.0]-hexene-η^3,η^1-diylhafnium dichloride **12** is formed in ca. 44% yield. The fate of the cyclooctatetraene ligand is unknown.



The new hafnium complex **12** is a red solid. Crystals suitable for X-ray analysis could be obtained from pentane at −20°C.

X-ray structural analysis of **12** revealed that it is dimeric in the solid state and contains a μ-Cl_2 bridge. Molecular weight measurements showed the complex to be monomeric in solution, e.g. in toluene. The $(PC-tBu)_3$ moiety in **12** possesses a hitherto unknown structure for this ligand: it is linked to the metal as a 1,3,5-triphosphabicyclo[3.1.0]hexenediyl via a C1−Hf σ-bond and an η^3-allyl bond (C6, C11, and P1). The bicyclic ligand adopts a chair conformation, with an interplanar angle P2−C1−P3 and C6−C11−P2−P3 of 77.9°; P1 is bent away from the metal by 24.1°. The P−C and P−P σ-bond lengths in the bicyclic system lie in the normal ranges,[8] e.g. P2−C1 = 1.924(6), P3−C1 = 1.893(6), P3−C6 = 1.950(6), P2−C11 = 1.851(6) Å. The η^3-allylic nature of the C6−P1−C11 moiety is evident from the typical bond lengths Hf−C6 = 2.442(6), Hf−C11 = 2.358(6), Hf−P1 = 2.727(2) Å and from the P−C distances P1−C6 = 1.729(6) and P1−C11 = 1.752(6), which lie between those known for P−C single and P−C double bonds.[8] Similar P−C distances have been found in η^3-P−C−C and η^3-C−P−C allylic complexes of cobalt,[9] nickel,[10] and molybdenum.[11] The Hf−C1 σ-bond is reflected in a short distance of 2.081(6) Å.

As mentioned above, the hafnium complex **12** is monomeric in solution and is therefore electronically and coordinatively unsaturated. Thus, it can be expected to react readily with electron-donating ligands such as isocyanides and phosphanes. Indeed, even at −78°C, complex **12** takes up one equivalent of *tert*-butyl isocyanides or trimethylphosphane to give the new hafnium complexes **13** and **14**, respectively. No further reactions, e.g. displacement of the $(PC-tBu)_3$ unit, are observed when these ligands are use in excess.

Both complexes were isolated as dark-red microcrystals. Only those of **14** proved to be stable at room temperature and both complexes were found to be unstable in solution above 0°C. The trimethylphosphane complex **14** dissociates into complex **12** and free trimethylphosphane, while the isonitrile complex **13** rearranges into a complex of unknown structure that gives rise to two new signals in the

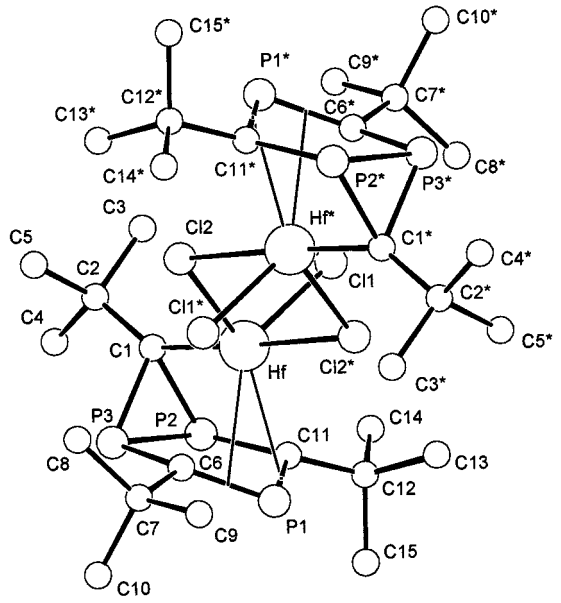
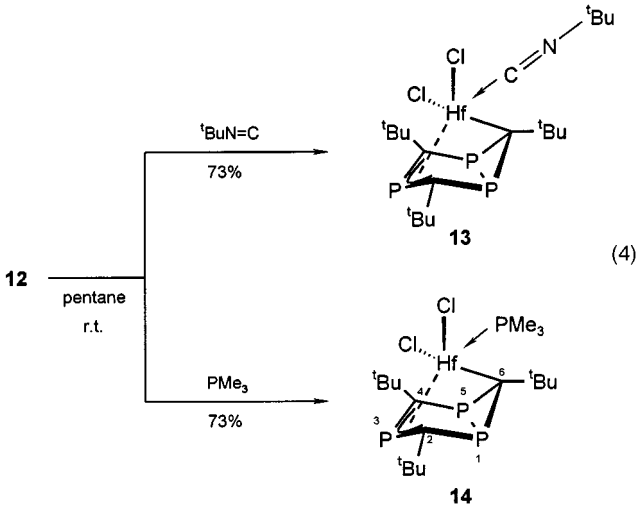


Figure 1. Molecular structure of **12**; selected bond lengths [Å] and angles [°]: Hf−Cl1 2.371(2), Hf−Cl2 2.489(1), Hf−P1 2.727(2), Hf−C6 2.442(6), Hf−C1 2.081(6), Hf−C11 2.358(6), P1−C6 1.729(6), P1−C11 1.752(6), P2−P3 2.213(2), P2−C1 1.924(6), P3−C1 1.893(6), P2−C11 1.851(6), P3−C6 1.950(6); P2−C1−P3 70.8(2), C1−P3−P2 55.2(2), C6−P3−P2 96.4(2), C6−P1−C11 98.9(3), P1−C6−P3 120.9(3)



(4)

^{31}P-NMR spectrum at δ = −163.8 and −100.4 in a 2:1 ratio.

X-ray analysis of crystals of **14**, obtained from pentane solution at −78°C, revealed that the complex is monomeric and contains a (PC−*t*Bu)$_3$ unit isostructural with that found in complex **12**. However, in view of the rather poor quality of the crystal structure analytical data, no further details will be discussed, neither here nor in the Experimental Section.

To gain insight into the structure of the [P_3C_3tBu$_3$] ligand of the complexes **5**, **12**, and **14** in solution, we examined their NMR spectra (^{1}H, ^{13}C, ^{31}P) in detail. In each case, the NMR spectra recorded at −30°C showed that a single complex of high symmetry was present. The similarity of the characteristic features of the spectra shows that the structure of the [P_3C_3tBu$_3$] ligand is the same in all three cases. For the three P and three C atoms of the [P_3C_3] unit, two signals are found in a 1:2 ratio in the ^{31}P- and ^{13}C-NMR spectra, respectively. In the ^{1}H-NMR spectra, two signals are observed in the same ratio due to the protons of the *tert*-butyl groups (see Table 1).

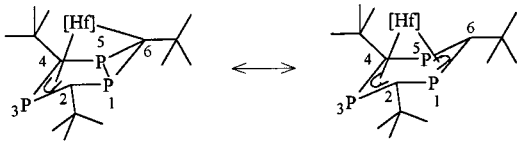
Although the ^{31}P-NMR spectra of the complexes are broadly similar, the positions of the signals differ somewhat depending on the nature of the other ligand bonded to the metal (e.g. **5**: δ = 357.1 and 17.3; **12**: δ = 410.2 and −45.6). Nevertheless, the P,P coupling constants remain almost unchanged (41.9−43.8 Hz). While the ^{13}C-chemical shifts of the three ring-carbon atoms of complexes **5**, **12**, and **14** differ considerably from compound to compound, the appearance of the multiplets and the magnitude of the coupling constants remains essentially the same.

For complex **12**, a detailed analysis of the ^{13}C multiplet at δ = 169.1 (C2 and C4) reveals that these carbon atoms constitute the X part of an AA′MX spin system (A, M = ^{31}P, X = ^{13}C). It consists of two AA′X subspectra, each of five signals, where the outer combination lines, just detectable above the noise, are split by $^1J_{P,C}$ = 73.4 Hz. Although an exact analysis is not possible, the spectrum allows adequately accurate estimates of $^1J_{P1,P5}$ (74 Hz), $^1J_{P3,C2}$ (73 Hz), $^1J_{P2,C2}$ (70 Hz), and $^3J_{P5,C2}$ (13 Hz) to be made. These values were confirmed by computer simulation. The interpretation of the magnitude of $J_{P1,P5}$ (74 Hz) is ambiguous: it appears to be rather small for a $^1J_{P,P}$ coupling, but large for a $^2J_{P,P}$ coupling (e.g. $^1J_{P,P}$ in complex **2a**, **b** = 219 Hz). On the basis of these NMR studies, we propose that the structure of the (P_3C_3tBu$_3$) ligand in complexes **5**, **12**, and **14** is best represented by the two canonical forms **a** and **b** (see Table 1).

Support for this interpretation of the NMR spectra is provided by the products of hydrolysis of complexes **5** and **12**. When the hafnium complex **5** is treated with an excess of water, the only metal-free reaction products obtained are the new bicyclic phosphorus heterocycle **15** (yield 55%) together with 10% of 1,3,5-triphosphabenzene **6**. Under milder and more controlled conditions, the addition of the second equivalent of water can be suppressed and the two new phosphorus heterocycles **16** and **17** are formed in almost equal amounts. Suitable reagents for this purpose are silica gel with a water content of 2% and the hydrate $Na_2SO_4 \cdot 10\ H_2O$. With these two reagents, both hafnium complexes **5** and **12** react to give 1,3,5-triphosphabicyclo[3.1.0]hex-2-ene **16** and 1,3,5-triphosphacyclohexa-1,4-diene **17** in yields of 83% and 90%, respectively. It is likely that **16** is an intermediate in the formation of **15** from complex **5**. The NMR spectra of **15**, **16**, and **17** indicate that only one isomer is formed in each case.

The structure determination of compounds **15**−**17** is based mainly upon their NMR data. The IR and mass spectra, as well as elemental analysis data support the proposed structures. The presence of a diphosphirane unit in compounds **15** and **16** is evident from the high field shifts of P1 and P5 [δ = −222.8 (s) in **15**; δ = −117.4 and −128.6

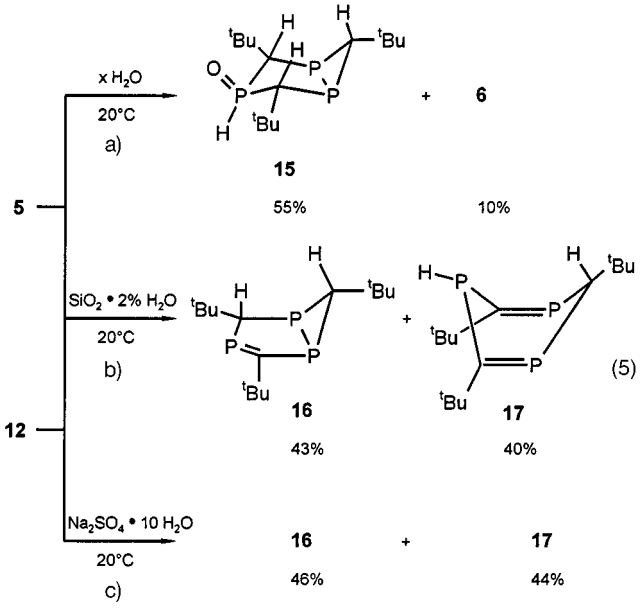
Table 1. Characteristic NMR data (^{1}H, ^{13}C, ^{31}P) of the [$P_3C_3tBu_3$] hafnium complexes **5**, **12**, and **14**



a b

	complex **5** [Hf] = (COT)Hf	complex **12** [Hf] = $HfCl_2$	complex **14** [Hf] = $HfCl_2(PMe_3)$
^{31}P NMR[a]	357.1 (t, $^2J_{P,P}$ = 43.8, P3) 17.3 (d, $^2J_{P,P}$ = 43.8, P1, P5)	410.2 (t, $^2J_{P,P}$ = 43.0, P3) −45.6 (d, $^2J_{P,P}$ = 43.0, P1, P5)	399.1 (dt, $^2J_{P,P}$ = 41.9, P3) 41.5 (dd, $^2J_{P,P}$ = 41.9, P1, P5)
^{1}H NMR[b]	0.81 (s, 9 H, *t*Bu at C6) 1.35 (s, 18 H, *t*Bu at C2, C4)	1.29 (s, 9 H, *t*Bu at C6) 1.42 (s, 18 H, *t*Bu at C2, C4)	1.49 (s, *t*Bu at C6) 1.41 (s, *t*Bu at C2, C4)
^{13}C NMR[c]	93.8 (t, $^1J_{C,P}$ = 59.4, C6) 139.3 (dt, $^1J_{C,P}$ = 74, 69.4, C2, C4)	176.3[d] (t, $^1J_{C,P}$ = 67.7, C6) 169.1[e] (dt, $^1J_{C,P}$ = 73.4, 83.0, C2, C4)	168.1 (br. m, C6) 165.1 (br. m, C2, C4)

[a] 162.0 MHz ([D_8]THF, −30°C, 85% H_3PO_4). − [b] 300 MHz ([D_8]THF, −30°C, TMS). − [c] 100.6 MHz ([D_8]THF, −30°C, TMS). − [d] A_2X spin system (A = ^{31}P, X = ^{13}C). − [e] AA′MX spin system (A,M = ^{31}P, X = ^{13}C).

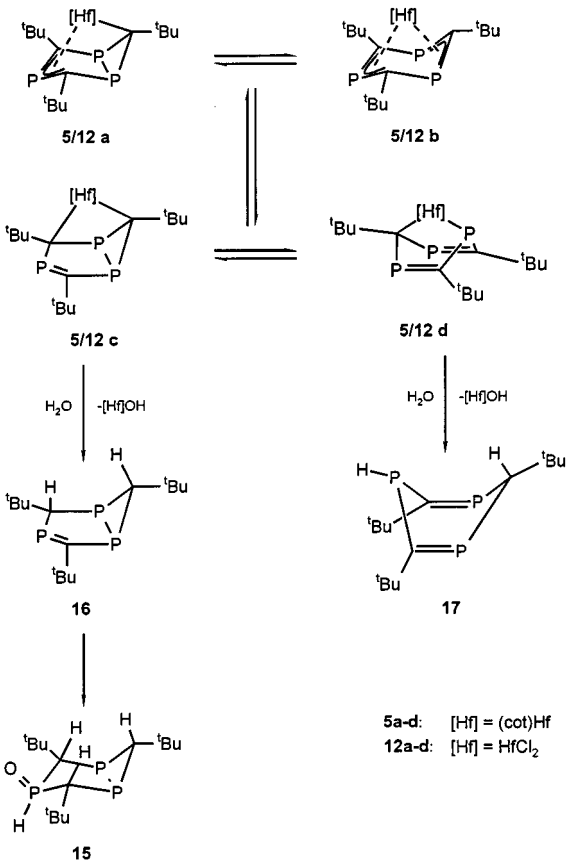


($^1J_{P,P}$ = 167.2 Hz) in **16**].[12] The proposed conformation of **15** shown in Eq. 5a is supported by the small magnitudes of the coupling constants between P1, P5 and 2-H and 4-H ($^3J_{P,H}$ = 3.5 Hz) and the high value of 16 Hz between P3 and 2,4-H, as well as by NOESY experiments. The presence of the PHO unit in **15** is indicated by its ^{31}P-NMR signal at δ = 39.4 with $^1J_{P,H}$ = 454.6 Hz and its IR absorptions at 2320 and 1183 cm^{-1}, which are typical for P−H and P=O bonds, respectively.[13] The small coupling constants between 4-H and the two adjacent P atoms reveal its *trans* orientation with respect to the lone pairs of these P atoms in compound **16**.[12] The high symmetry of 1,3,5-triphosphacyclohexa-1,4-diene **17** is reflected in its simple ^{31}P- and ^{13}C-NMR spectra, which feature only two sets of signals for the three P and C atoms of the six-membered ring and the three *tert*-butyl groups (^{31}P: δ = 241.3 and −24.9; ^{13}C: δ = 213.5 and 66.1) in a 2:1 ratio. The ^{1}H-, ^{13}C-, and ^{31}P-NMR chemical shifts are also consistent with the structure proposed for **17**. Analysis of the multiplets in the ^{13}C-NMR spectrum provides additional evidence for this structure. The signals attributable to C2, C4 and those of the *tert*-butyl groups linked to C2 and C4 all analyse as the X part of an AA′MX spin system (A, A′, M = ^{31}P, X = ^{13}C). The magnitude of the P1,P5 coupling constant, estimated as 10.5 Hz by simulation of the C2 multiplet, shows that P1 and P5 are not directly bonded.

The only difficulty in the interpretation of the ^{13}C-NMR spectrum of **17** was the finding that the signal of C6 at δ = 66.1 is a first-order triplet of doublets with a triplet splitting of $^1J_{P,C}$ = 51.5 Hz and a doublet splitting of $^3J_{P,C}$ = 42.2 Hz. While the value of $^1J_{P,C}$ is unremarkable, the magnitude of $^3J_{P,C}$ is unexpectedly large. In related organophosphorus compounds, a ^{31}P,^{13}C coupling constant of this order is more consistent with a one-bond coupling and we have not found any example of such a large coupling over three bonds in the literature. In order to show that P3 and C6 are not directly bonded and to confirm the connectivities in **17**, we determined the ^{13}C isotope shifts on the phosphorus chemical shifts. Analysis of the ^{13}C satellites in the ^{31}P-NMR spectrum showed that $^1\Delta^{31}P_1(^{13/12}C_6)$ amounts to −30.0 ppb, but that $^3\Delta^{31}P_3(^{13/12}C_6)$ is just −4.6 ppb. The latter is of a much smaller magnitude than is usually observed for $^1\Delta^{31}P(^{13/12}C)$ in similar compounds, confirming that P-3 and C-6 are not directly connected.[14] The observed ^{31}P,^{13}C and ^{31}P,^{1}H coupling constants are consistent with the electron pair on phosphorus and 6-H being *cis* to one another. The magnitude of ^3J(P-3,C-6) in compound **17** (42.2 Hz) is a further example illustrating the strong stereochemical dependence of $^3J(^{31}P,^{13}C)$[15,16] (for a full listing of NMR data, see Experimental Section).

As far as we are aware, the 1,3,5-triphosphabicyclo[3.1.0]hexane **15** and -hexene **16**, as well as the 1,3,5-triphosphacyclohexa-1,4-diene **17**, are the first examples of such phosphorus heterocycles to be reported. Their synthesis from the hafnium complexes **5** and **12** can be rationalized in terms of the hydrolysis of the two mesomeric forms **5c/12c** and **5d/12d**, which contain one P−M and one C−M σ-bond (see Scheme 2). In the presence of pure water, the

phosphorus heterocycle **16** adds a second equivalent of water to give compound **15**. In all these reactions, the hafnium part of the complexes **5** and **12** should be displaced as the corresponding hafnium dihydroxide, species that are known to be unstable.[17]



Scheme 2

In summary, we have determined the solid-state structures of the hafnium complexes **12** and **14** by X-ray analysis and have shown by extensive NMR studies and by hydrolysis of **5**, **12**, and **14** that all these hafnium complexes have the same structure in solution. By hydrolysis of **5** and **12** we have also been able to synthesize the new phosphorus heterocycles **15**, **16**, and **17**.

Experimental Section

General: All experiments were carried out under argon in anhydrous solvents. − MS: EI; Finnigan MAT 311 ADF. − ^{1}H- and ^{13}C-NMR: Bruker AC 200, AC 300, AMX 400, and DMX 600; chemical shifts were determined relative to solvent signals and converted to the TMS scale [$\delta(^1H)$ of C_6D_5H at 7.15; $\delta(^{13}C)$ of C_6D_6 at 128.0]. The ^{13}C multiplicities were confirmed by means of DEPT spectra. − ^{31}P-NMR: Bruker AC 200 (81.1 MHz) and AC 300 (121.5 MHz), external standard H_3PO_4. − Elemental analysis: Microanalytical laboratory, Dornis and Kolbe, Mülheim a.d. Ruhr. − Commercial chemicals: hexachloroethane, *tert*-butyl isocyanide (Aldrich); sodium sulfate decahydrate (Reininghaus). − (η^8-Cyclooctatetraene)(P≡C−*t*Bu)$_3$hafnium (**5**)[3] and trimethylphosphane[18] were prepared according to published procedures.

(2,4,6-Tri-*tert*-butyl-1,3,5-triphosphabicyclo[3.1.0]hexene-η^3,η^1-diyl)hafnium Dichloride (12): Hexachloroethane (230 mg, 0.97 mmol) was added to a suspension of the hafnium complex **5** (480 mg, 0.82 mmol) in pentane (10 mL). The reaction mixture was stirred at room temperature for 12 h, in the course of which the colour changed from green to red and a brown precipitate was formed. After filtration through Celite and washing the solid with pentane (2 × 3 mL), the filtrate was concentrated to a volume of ca. 4 mL and cooled to −78°C. Red-violet crystals of complex **12** (210 mg, 44%) precipitated, which were isolated by filtration. Triphosphabenzene **6** (40 mg, 16%) could be isolated from the filtrate by column chromatography. Complex **12**: m.p. 172°C (dec.). − ^{1}H and ^{31}P NMR: See Table 1. − ^{13}C{^{1}H} NMR (100.6 MHz, [D$_8$]THF, −30°C): δ = 176.3 (A_2X spin system, A = ^{31}P, X = ^{13}C, t, $^1J_{C,P}$ = 67.7 Hz, C-6), 169.1 (AA′MX spin system, AA′ = ^{31}P-1 and ^{31}P-5, M = ^{31}P-3, X = ^{13}C-2,4, $J_{M,X}$ = 73.4, $J_{A,A}$ = 73.7, $|J_{A,X}$ = 70|, $J_{A',X}$ = 13 Hz , values checked by simulation, C-2 and C-4), 42.8 [t, $^2J_{C,P}$ = 7.6 Hz, *C*(CH$_3$)$_3$ at C-6], 33.2 [C(*C*H$_3$)$_3$ at C-6], 41.8 [*C*(CH$_3$)$_3$ at C-2 and C-4], 36.4 [C(*C*H$_3$)$_3$ at C-2 and C-4]. − MS (EI, 70 eV); *m/z* (%): 550 (28) [M$^+$], 450 (17) [M − PC*t*Bu$^+$], 300 (12) [(PC*t*Bu)$_3^+$], 169 (31) [PC$_2$(*t*Bu)$_2^+$], 41 (100). − $C_{15}H_{27}P_3Cl_2Hf$ (549.7): calcd. C 32.78, H 4.95; found C 32.75, H 4.90.

***tert*-Butyl Isocyanide Adduct 13 of Complex 12:** *tert*-Butyl isocyanide (0.8 g, 9.6 mmol) was added to a cooled (−78°C) solution of the hafnium complex **12** (300 mg, 0.55 mmol) in pentane (5 mL) and the reaction mixture was stirred for 12 h. The solvent and excess isocyanide were then evaporated off at 0.5 bar and the residue was taken up in pentane (2 mL). At −78°C, dark-red microcrystals separated, which were collected by filtration and dried at −78°C and 0.5 bar to yield 150 mg (44%) of the isocyanide adduct **13**. Complex **13** was found to be unstable at room temperature and thus had to be stored at −78°C. − ^{1}H NMR (200.1 MHz, [D$_8$]toluene, 30°C): δ = 1.52 (s, 27 H, *t*Bu at C2, C4 and C6), 0.77 (s, *t*Bu at N). − ^{13}C{^{1}H} NMR (50.1 MHz, [D$_8$]toluene, 30°C): δ = 188.5−187.0 (br. m, C-2, C-4, C-6), 150.1 (m, C=N), 54.6 [br. s, *C*(CH$_3$) at N], 33.9 [dt, $J_{C,P}$ = 10.7 and 9.8 Hz, *C*(CH$_3$) at C-2, C-4 and C-6], 33.3 [t, $J_{C,P}$ = 7.9 Hz, C(*C*CH$_3$) at C-6], 30.3 [d, $J_{C,P}$ = 7.8 Hz, C(*C*H$_3$) at C-2 and C-4], 27.6 [s, C(*C*H$_3$) at N]. − ^{31}P NMR (81.1 MHz, [D$_8$]toluene, 30°C): δ = 315.1 (t, $J_{P,P}$ = 5.0 Hz, P-3), −24.1 (d, $J_{P,P}$ = 5.0 Hz, P-1 and P-5).

Trimethylphosphane Adduct 14 of Complex 12: Trimethylphosphane (0.1 mL, 0.8 g, 10.5 mmol) was added to a solution of the hafnium complex **12** (300 mg, 0.55 mmol) in pentane (5 mL), cooled to −78°C. After stirring for 2 h, all volatile components were removed at 0°C and 0.5 mbar and the red oily residue was redissolved in pentane (2 mL) at −10°C. At −78°C dark-red crystals of complex **14** (250 mg, 73%) suitable for X-ray analysis were obtained. The product was isolated by filtration and dried at 0.5 mbar. − ^{1}H and ^{31}P NMR: See Table 1. − ^{13}C{^{1}H} NMR (100.6 MHz, [D$_8$]THF, −30°C): δ = 168.1 (m, C-6), 165.1 (m, C-2 and C-4), 40.6 [t, $^2J_{P1,C}$ = $^2J_{P5,C}$ = 7.9 Hz, *C*(CH$_3$) at C-6], 40.1 [td, $^2J_{P3,C}$ = 16.6 Hz, $^2J_{P1,C}$ = $^3J_{P5,2}$ = 10.4 Hz, *C*(CH$_3$) at C-2 and C-4], 36.1 [s, C(*C*H$_3$) at C-2 and C-4], 32.4 [s, C(*C*H$_3$) at C-6], 13.0 [d, $^1J_{P,C}$ = 10.4 Hz, P(*C*H$_3$)$_3$].

2,4,6-Tri-*tert*-butyl-1,3,5-triphospha-3-oxobicyclo[3.1.0]hexane (15) from Hydrolysis of Hafnium Complex 5: To a green solution of complex **5** (300 mg, 0.51 mmol) in diethyl ether (5 mL) at 0°C was added water (1 mL, 5.56 mmol). After stirring for 10 h at room temperature, a brownish solid precipitated from the yellow solution. The precipitate was removed by filtration through Celite and all volatiles were distilled off from the filtrate at 20°C and 0.5 mbar.

Chromatographic separation of the solid residue on silica gel gave triphosphabenzene **6** (15 mg, 10%) as a first fraction on eluting with pentane, followed by compound **15** (90 mg, 55%) on eluting with THF. The latter was isolated by concentrating the THF fraction to 5 mL, adding pentane (5 mL), and cooling to −78°C, whereupon **15** precipitated as colourless needles; m.p. 198°C. − ^{1}H NMR ([D$_8$]THF, 400 MHz, 30°C): δ = 6.10 (dtt, $^1J_{P3,H}$ = 454.6 Hz, $^3J_{P1,H}$ = $^3J_{P5,H}$ = 2.0 Hz, $^3J_{2\,H,H}$ = $^3J_{4\,H,H}$ = 9.2 Hz, 3-H), 1.94 [t(d), $^2J_{P1,H}$ = $^2J_{P5,H}$ = 4.1 Hz, $^4J_{P3,H}$ ≈ 1.4 Hz, 6-H], 1.73 (dd/pseudo t, $^2J_{P3,H}$ = 16.0 Hz, $^2J_{P1,H}$ + $^3J_{P5,H}$ = 6.8 Hz, $^3J_{3\,H,H}$ = 9.2 Hz, 2-H and 4-H), 1.30 [s, 18 H, C(CH$_3$)$_3$ at C-2 and C-4], 0.94 [t, 9 H, $^4J_{P1,H}$ = $^4J_{P5,H}$ < 1 Hz, C(CH$_3$)$_3$ at C-6]. − ^{13}C NMR ([D$_8$]THF, 100.1 MHz, 30°C): δ = 51.1 [dtd(A$_2$MX), $^1J_{C,H}$ = 155, $^1J_{P1,C}$ = $^1J_{P5,C}$ = 47.3, $^3J_{P3,C}$ = 6.5 Hz, C-6], 47.3 [tdd(AA′MX), $^1J_{C,H}$ = 140, $^1J_{P3,H}$ = 54.9, $J_{P1,C}$ + $J_{P5,C}$ = 52.0 Hz, C-2 + C-4], 34.1 [dt(AA′MX), $J_{P1,C}$ + $J_{P5,C}$ = 17.6, $^2J_{P3,C}$ = 0.9 Hz, *C*(CH$_3$)$_3$ at C-2 and C-4], 33.5 [dt(A$_2$MX), $^2J_{P1,C}$ = $^2J_{P5,C}$ = 11.8, $^4J_{P3,C}$ = 6.0 Hz, *C*(CH$_3$)$_3$ at C-6], 30.3 [tq(A$_2$MX), $^1J_{C,H}$ = 126, $^3J_{P1,C}$ = $^3J_{P5,C}$ = 5.9 Hz, C(*C*H$_3$)$_3$ at C-6], 30.1 [dtt(AA′MX), $^1J_{C,H}$ = 126, $J_{P1,C}$ + $J_{P5,C}$ = 10.7, $^3J_{P3,C}$ = 5.6 Hz, C(*C*H$_3$)$_3$ at C-2 and C-4]. − ^{31}P NMR ([D$_8$]THF, 30°C, 81.1 MHz): δ = 39.4 (s, P-3), −222.8 (s, P-1 and P-5). − IR (KBr): $\tilde{\nu}$ = 2961 (*t*Bu), 2320 (P−H), 1393, 1363 (*t*Bu), 1138 cm^{-1} (P=O). − MS (EI, 70 eV): *m/z* (%): 320 (100) [M$^+$], 305 (47) [M − CH$_3^+$], 263 (72) [(M − *t*Bu$^+$], 251 (60), 57 (50) [*t*Bu$^+$]. − $C_{15}H_{31}OP_3$ (320.3): calcd. C 56.24, H 9.75; found C 56.18, H 9.68.

2,4,6-Tri-*tert*-butyl-1,3,5-triphosphabicyclo[3.1.0]hex-2-ene (16) and 2,4,6-Tri-*tert*-butyl-1,3,5-triphosphacyclohexa-1,4-diene (17): (a) By Hydrolysis of Hafnium Complex 5 with Hydrated Silica Gel: Silica gel (63−100 μm, Merck AG, dried at 150°C for 12 h and then deactivated with 2% water) was added to a suspension of complex **5** (300 mg, 0.55 mmol) in pentane (10 mL). Immediately, a colour change from green to yellow was observed. After stirring for 15 min, the reaction mixture was extracted with pentane. The combined extracts were concentrated to one-third of the original volume and crystallization at −78°C yielded **17** (60 mg, 40%) as a pale-yellow powder. Column chromatography (glass column, ∅ = 2 cm, 15 cm silica gel, argon pressure) of the mother liquor and evaporation of pentane from the appropriate fraction furnished **16** (67 mg, 43%) as a pale-yellow powder.

(b) By Hydrolysis of Hafnium Complex 12 with $Na_2SO_4 \cdot 10\ H_2O$: $Na_2SO_4 \cdot 10\ H_2O$ (156 mg, 1.10 mmol) was added to a solution of hafnium complex **12** (300 mg, 0.55 mmol) in diethyl ether (5 mL). After stirring the mixture for 12 h at room temperature, its colour changed from red-violet to yellow and a brownish precipitate was formed. Pentane (5 mL) was then added to complete the precipitation. The reaction mixture was filtered through Celite and compounds **16** and **17** were separated from the filtrate as described above. **16** (77 mg, 46%) and **17** (72 mg, 44%) were obtained as pale-yellow powders.

Compound 16: ^{1}H NMR (C$_6$D$_6$, 300.1 MHz, 30°C): δ = 2.92 (dd, $^2J_{P,H}$ = 4.2 and 1.1 Hz, 4-H), 2.57 (dd, ^2J = 9.3, 6.9 Hz, 6-H), 1.51 [d, $^4J_{P3,H}$ = 1.8 Hz, C(CH$_3$)$_3$ at C-2], 1.15 [s, C(CH$_3$)$_3$ at C-4], 0.95 [t, $^4J_{P,H}$ = 0.8 Hz, C(CH$_3$)$_3$ at C-6]. − ^{13}C{^{1}H} NMR (C$_6$D$_6$, 75.5 MHz, 30°C): δ = 230.8 (ddd, $^1J_{P3,C}$ = 74.5, $^1J_{P1,C}$ = 58.8, $^2J_{P5,C}$ = 2.5 Hz, C-2), 70.6 (t, $^1J_{P,C}$ = 53.0 Hz, C-6), 61.4 (ddd, $^1J_{P,C}$ = 48.5, 44.1, $^2J_{P,C}$ = 6.4 Hz, C-4), 43.1 [dd, $^2J_{P,C}$ = 20, 18 Hz, *C*(CH$_3$)$_3$ at C-2], 34.2 [dd, $^2J_{P,C}$ = 15.2, $^4J_{P,C}$ = 2.0 Hz, *C*(CH$_3$)$_3$ at C-6], 36.0 [dd, $J_{P,C}$ = 15.3, 2.8 Hz, *C*(CH$_3$)$_3$ at C-4], 33.6 [dd, $^3J_{P,C}$ = 14.6, 9.0 Hz, C(*C*H$_3$)$_3$ at C-2], 30.6 [t, $^3J_{P,C}$ = 5.5 Hz, C(*C*H$_3$)$_3$ at C-6], 30.0 [dd, $^3J_{P,C}$ = 10.5, 8.5 Hz, C(*C*H$_3$)$_3$ at C-4]. − ^{31}P NMR (C$_6$D$_6$, 121.5 MHz, 30°C): δ = 311.8 (dd, $^2J_{P1,P3}$ = 36.5, $^2J_{P3,P5}$ = 13.0 Hz, P-3), −117.4 (dd, $^1J_{P1,P5}$ = 167.2, $^2J_{P1,P3}$ = 36.5 Hz, P-1), −128.6 (dd, $^1J_{P1,P5}$ = 167.2, $^2J_{P3,P5}$ = 13.0 Hz, P-5). − MS (EI, 70 eV): *m/z* (%): 302 (96) [M$^+$], 245 (12) [M − *t*Bu$^+$], 231 (14), 175 (100) [M − CH*t*Bu$^+$], 162 (29), 131 (53) [P$_2$C*t*Bu$^+$], 113 (21), 100 (19) [PC*t*Bu$^+$], 69 (29), 57 (38) [*t*Bu$^+$]. − $C_{15}H_{29}P_3$ (302.3): calcd. C 59.60, H 9.67; found C 59.87, H 9.61.

Compound 17: ^{1}H NMR (C$_6$D$_6$, 400.1 MHz, 30°C): δ = 6.40 (dt, $^1J_{P,H}$ = 227.7, $^3J_{P,H}$ = 6.4 Hz, 3-H), 1.98 (dt, $^2J_{P,C}$ = 9.6 Hz, $^4J_{P,C}$ = 5.2 Hz, 6-H), 1.41 [s, C(CH$_3$)$_3$ at C-6], 1.35 [br. s, C(CH$_3$)$_3$ at C-2 and C-4]; structure established by NOESY. − ^{13}C{^{1}H} NMR (C$_6$D$_6$, 100.6 MHz, 30°C): δ = 213.5 (AA′MX spin system, $^1J_{P,C}$ = 40.8 and 50.0 Hz, C-2 and C-4), 66.1 (dt, $^1J_{P,C}$ = 51.5, $^3J_{P,C}$ = 42.2 Hz, C-6), 43.2 [AA′MX spin system, *J* not resolved, *C*(CH$_3$)$_3$ at C-2 and C-4], 34.2 [dt, $^2J_{P,C}$ = 15.3, $^4J_{P,C}$ = 2.5 Hz, *C*(CH$_3$)$_3$ at C-6], 32.7 [AA′MX spin system, $^3J_{P,C}$ = 14.1 and 3.5 Hz, $^5J_{P,C}$ = 0.8 Hz, C(*C*H$_3$)$_3$ at C-2 and C-4], 31.2 [td, $^3J_{P,C}$ = 9.5 Hz, $^5J_{P,C}$ = 0.9 Hz, C(*C*H$_3$)$_3$ at C-6]. − ^{31}P{^{1}H} NMR (C$_6$D$_6$, 162.0 and 243.0 MHz, 30°C): δ = 241.3 (t, $^2J_{P,P}$ = 5.5 Hz, P-1 and P-5), −249 (t, P-3). − IR (KBr): $\tilde{\nu}$ = 2957, 2898 (*t*Bu), 2329 cm^{-1} (P−H). − MS (EI, 70 eV): *m/z* (%): 302 (22) [M$^+$], 211 (11), 231 (5), 175 (23), 155 (21), 131 (22), 113 (7), 99 (100), 69 (33), 57 (84). − $C_{15}H_{29}P_3$ (302.3): calcd. C 59.60, H 9.67; found C 59.55, H 9.63.

X-ray Crystal Structure Analysis of 12:[19] Siemens SMART diffractometer (Mo-K_α radiation), T = 100 K; structure solution by heavy atom method (SHELXS-86[20]) and refinement by SHELXL-93;[21] monoclinic, space group *C*2/*c*; lattice constants a = 9.943(2), b = 18.315(4), c = 22.456(5) Å; β = 90.66(3)°, V = 4089.1(14) Å^3, Z = 8, μ(Mo-K_α) = 5.591 mm^{-1}, crystal size 0.46 × 0.39 × 0.21 mm, θ_{max} = 33.16°; 7591 independent reflections (R_{int} = 0.0680); 22971 measured reflections, of which 5300 were considered observed with $I > 2\sigma(I)$; empirical absorption correction; min./max. transmission 0.168/0.318; max./min. residual electronic density −5.883 and −3.151 e/Å^3 (less then 1 Å from Hf). 190 parameters [C, Cl, Hf, and P anisotropic; the positions of the H atoms were calculated for idealized distances (d_{C-H} = 0.980 Å)]; R_1 = 0.0590; wR^2 = 0.1340.

Acknowledgments

This work was supported by the Deutsche Forschungsgemeinschaft (Graduiertenkolleg "Phosphorchemie als Bindeglied verschiedener chemischer Disziplinen") and the Governement of Rheinland Pfalz (stipendium to K.G.)

[1] J. F. Nixon, *Chem. Rev.* **1988**, *88*, 1327−1362; M. Regitz, P. Binger, *Angew. Chem.* **1988**, *100*, 1541−1565; *Angew. Chem. Int. Ed. Engl.* **1988**, *27*, 1484−1508; P. Binger in *Multiple Bonds and Low Coordination in Phosphorus Chemistry* (Eds.: M. Regitz, O. J. Scherer), Thieme Verlag, **1990**, p. 90−107; J. F. Nixon, *Coord. Chem. Rev.* **1995**, *145*, 201−258; K. B. Dillon, F. Mathey, J. F. Nixon, *Phosphorus: The Carbon Copy*, Wiley, **1998**, p. 347−355.
[2] R. Milczarek, W. Rüsseler, P. Binger, K. Jonas, K. Angermund, C. Krüger, M. Regitz, *Angew. Chem.* **1987**, *99*, 957−958; *Angew. Chem. Int. Ed. Engl.* **1987**, *26*, 908−909.
[3] P. Binger, S. Leininger, J. Stannek, B. Gabor, R. Mynott, J. Bruckmann, C. Krüger, *Angew. Chem.* **1995**, *107*, 2411−2414; *Angew. Chem. Int. Ed. Engl.* **1995**, *34*, 2227−2230.
[4] D. Böhm, F. Knoch, S. Kummer, U. Schmidt, U. Zenneck, *Angew. Chem.* **1995**, *107*, 251−253; *Angew. Chem. Int. Ed. Engl.* **1995**, *34*, 198−201.
[5] P. L. Arnold, F. G. N. Cloke, P. B. Hitchcock, J. F. Nixon, *J. Am. Chem. Soc.* **1996**, *118*, 7630−7631.
[6] A. R. Barron, A. H. Cowley, *Angew. Chem.* **1987**, *99*, 956; *Angew. Chem. Int. Ed. Engl.* **1987**, *26*, 907−908.
[7] [7a] J. Haas, Diplomarbeit, Universität Bonn, **1988**. − [7b] P. Binger, J. Haas, J. Stannek, S. Stutzmann, C. Krüger, *Eur. J.*

Inorg. Chem. **1999**, 83−86. − [7c] M. Scheer, J. Krug, *Z. Anorg. Allg. Chem.* **1998**, *624*, 399−405.
[8] F. H. Allen, O. Kennard, D. G. Watson, L. Brammer, A. G. Orpen, R. Taylor, *J. Chem. Soc., Perkin Trans. 2* **1987**, 1.
[9] R. Appel, W. Schuhr, F. Knoch, *Angew. Chem.* **1985**, *97*, 421−422; *Angew. Chem. Int. Ed. Engl.* **1985**, *24*, 420−421; F. Mercier, C. Hugel-Legoff, L. Richard, F. Mathey, *J. Organomet. Chem.* **1990**, *389*, 389−397.
[10] R. Appel, W. Schuhr, F. Knoch, *J. Organomet. Chem.* **1987**, *319*, 345−350.
[11] C. Hugel-Legoff, F. Mercier, L. Richard, F. Mathey, *J. Organomet. Chem.* **1989**, *363*, 325−333.
[12] D. G. Gorenstein, D. O. Shah in *Phosphorus-NMR, Principles and Application* (Ed.: D. G. Gorenstein), Academic Press, **1984**, p. 549−591.
[13] L. C. Thomas, *Interpretation of the IR Spectra of Organophosphorus Compounds*, Heyden, London, **1974**.
[14] For the nomenclature of the isotope effect, see W. Gombler, *J. Am. Chem. Soc.* **1982**, *104*, 6616.
$^{j}\Delta^{k}X(^{llm}Y) = \delta_{X}(^{l}Y) - \delta_{X}(^{m}Y)$
where $^{j}\Delta$ is the isotope shift over *j* bonds observed for nucleus ^{k}X caused by the isotopes ^{l}Y and ^{m}Y (where *l* has the higher mass number). A shift to higher NMR frequency is positive.
[15] [15a] G. Heckmann, E. Fluck, *Magn. Res. Chem.* **1995**, *33*, 553. − [15b] W. Buchner, W. Ries, W. Malisch, *Magn. Res. Chem.* **1990**, *28*, 515. − [15c] Unpublished observations.
[16] R. Mynott, P. Phillips, manuscript in preparation for submission to *Magn. Res. Chem.*
[17] [17a] P. C. Wailes, R. S. P. Coutts, H. Weigold, *Organometallic Chemistry of Titanium, Zirconium and Hafnium*, Academic Press, New York, **1974**. − [17b] G. L. Hillhouse, J. E. Bercaw, *J. Am. Chem. Soc.* **1984**, *106*, 5472−5478 and references cited therein.
[18] W. Wolfsberger, H. Schmidbaur, *Synth. React. Inorg. Met.-Org. Chem.* **1974**, *4*, 149.
[19] Crystallographic data (excluding structure factors) for the structures reported in this paper have been deposited with the Cambridge Crystallographic Data Centre as supplementary publication no. CCDC-101625. Copies of the data can be obtained free of charge on application to The Director, CCDC, 12 Union Road, Cambridge CB2 1EZ, U.K. [Fax: (internat.) +44 (0)1223/ 336033; e-mail: deposit@chemcrys.cam.ac.uk].
[20] G. M. Sheldrick, *SHELXS-86*, *Program for Crystal Structure Solution*, Universität Göttingen, **1986**.
[21] G. M. Sheldrick, *SHELXL-93*, *Program for Crystal Structure Solution*, Universität Göttingen, **1993**.

Received December 2, 1998
[I98415]

Diazomethane Derivatives Bearing Dialkylaluminium or Dialkylgallium Substituents – The Isomeric Diazomethane and Nitrile Imine Structures Realized by the Different Coordination Behavior of Aluminium and Gallium

Werner Uhl,*[a] Frank Hannemann,[a] Wolfgang Saak,[a] and Rudolf Wartchow[b]

Keywords: Aluminium / Gallium / Diazo compounds / Dimerization / Coordination modes

Lithium trimethylsilyldiazomethanide $Li(SiMe_3)CN_2$ reacted with the dialkylaluminium or -gallium halides R_2AlCl and R_2GaBr [$R = CH(SiMe_3)_2$] by the elimination of lithium halide and the formation of the corresponding aluminium or gallium diazo compounds. As shown by a crystal structure determination, the gallium derivative **1** adopts the nitrile imine structure, in which the gallium atom is coordinated by the terminal nitrogen atom of the diazo group. The N–N–C–Si moiety is almost ideally linear with N–N and C–N bond lengths of 125.5 and 115.9 pm on average. In contrast, the diazomethane structure was formed with dialkylaluminium chloride, and the aluminium atom in **2** is attached to the carbon atom of diazomethane. The almost linear N–N–C group (174.1°) has N–N and N–C distances of 120.0 and 126.4 pm, respectively, inverse to that of the gallium derivative. The bonding situations can best be described by the resonance structures $R–C{\equiv}N^+–N^––GaR_2$ for **1** and $R_2Al–(R)C{=}N^+{=}N^–$ for **2**. The nitrile imine isomer of the aluminium compound could be detected by NMR spectroscopy as a by-product. Both compounds gave dimers in the solid state, a Ga_2N_2 four-membered heterocycle was formed of **1**, while an eight-membered $Al_2C_2N_4$ heterocycle resulted with **2**.

Diazomethane and its derivatives form a group of fascinating compounds due to their bonding situation and their singular chemical reactivity.[1] In many cases, they are used as a facile source of carbenes and for the synthesis of carbon−nitrogen heterocycles. As shown for the first time in 1933,[2] the methylene hydrogen atoms of diazomethane can be replaced by alkali metals, and those metalated diazomethane derivatives are very useful reagents for the syntheses of numerous diazomethane compounds containing main-group or transition-metal elements.[3−8] The lithiated compounds $Li–(H)CN_2$ and $Li–(Me_3Si)CN_2$ were theoretically investigated by the group of Boche.[8] By intramolecular rearrangements four isomeric structures are possible: $Li–(H)C{=}N^+{=}N^–$ (diazomethane), $C^–{\equiv}N^+–N(Li)H$ (*N*-isocyanoamine), $Li–C{\equiv}N^+–N^––H$ and $H–C{\equiv}N^+–N^––Li$ (nitrile imine), of which the second one was found to give the global minimum. The diazomethane formulation was intermediate, and both nitrile imine isomers were highest in energy. The energies of dimers were also calculated, and some aspects of their structures will be discussed below. Lithiated trimethylsilyldiazomethane was observed as a part of a complicated crystal structure by the same group.[8] Remarkably, it adopted the nitrile imine structure with the silyl group bound to the carbon atom and the lithium atom bound to the terminal nitrogen atom. The influence of the silyl group on the energy of the isomers could also be verified by theoretical calculations.[8] Previously, only one diazomethane compound of an element of the third main group was reported in literature, which has a tetracoordinated boron atom bound to the carbon atom of the CN_2 group.[6] The nitrile imine structure was found in two aluminium derivatives,[9] which have a phosphanyl group attached to the carbon atom and the terminal nitrogen atom coordinated by two alkylaluminium groups. We became interested in aluminium, gallium, or indium diazomethane derivatives for two reasons: (i) The nitrile imine molecular center is isosteric to an azido group. We recently succeeded in isolating a dialkylaluminium azide sterically highly shielded by bulky substituents, which formed a trimer with the unexpected head-to-tail coordination of the azido groups and a twelve-membered Al_3N_9 heterocycle.[10] Thus, we supposed that an unusual coordination behavior may be observed with the diazomethane derivatives, too. (ii) We hoped to use the reactivity of the diazomethane derivatives for the synthesis of novel organoaluminium or -gallium compounds. For instance, silylated diazomethane compounds inserted into the Al−Al bond of tetrakis[bis(trimethylsilyl)methyl]dialan(4), while a fragmentation reaction was observed with the corresponding gallium derivative.[11]

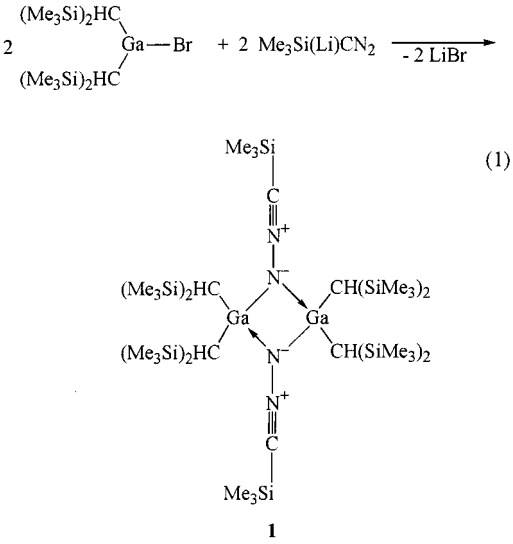
Reaction of Lithium Trimethylsilylmethyldiazomethanide with R_2AlCl and R_2GaBr [$R = CH(SiMe_3)_2$]

The reactive intermediate $Li–(Me_3Si)CN_2$ was obtained according to a literature procedure[3] by treating trimethylsilyldiazomethane with *n*-butyllithium at −100°C. The alkylgallium and -aluminium halides were added at this temperature, and the reaction mixtures were warmed slowly

[a] Fachbereich Chemie der Universität,
Postfach 2503, D-26111 Oldenburg, Germany
Fax: (internat.) + 49(0)441/798-3352
[b] Institut für Anorganische Chemie der Universität,
Callinstraße 9, D-30167 Hannover, Germany
Fax: (internat.) + 49(0)511/762-3006

 © WILEY-VCH Verlag GmbH, D-69451 Weinheim, 1999 1434−1948/99/0505−0771 $ 17.50+.50/0

to room temperature. Dialkylgallium bromide gave a mixture of compounds, from which the diazomethane product **1** was isolated in a yield of 38% (Equation 1). Compound **1** was identified by elemental analysis and a crystal structure determination (see below) as the nitrile imine isomer of diazomethane, in which the alkylgallium group is attached to the terminal nitrogen atom. The main component of the mother liquor was identified by NMR spectroscopy as the trialkylgallium derivative $Ga[CH(SiMe_3)_2]_3$,[12] which due to its high solubility in organic solvents could, however, not be isolated in a pure form. Three resonances were observed in the ^{1}H-NMR spectrum of **1**, which could be assigned to the methyl protons of the bis(trimethylsilyl)methyl groups, the protons of the $SiMe_3$ groups of diazomethane and the methine protons. The latter have a chemical shift of $\delta = -0.22$, which is just intermediate between the characteristic ranges of bis(trimethylsilyl)methyl compounds with coordination numbers of three and four at the central gallium atoms.[13–15] The IR spectrum showed an intensive absorption at 2120 cm^{-1}, which was attributed to the stretching vibration of the C–N group with a high π-bond order.[16] The molar mass of **1** cryoscopically determined in benzene is intermediate between those calculated of the monomer and the dimer, thus an equilibrium may exist between the monomeric and dimeric formula units, which is shifted in dilute solutions to the monomer.

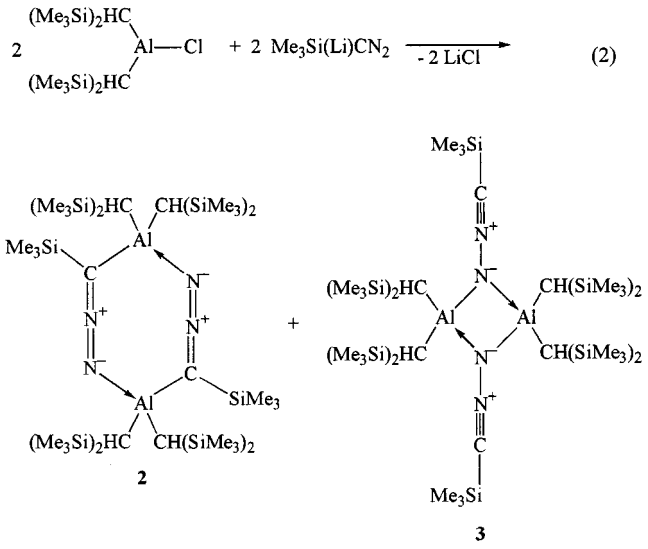


(1)

1

The reaction with dialkylaluminium chloride was different from that of the gallium analogue. Two compounds were formed. Only one could be isolated by recrystallization in a pure form (**2**): The second one (**3**) could be enriched by repeated recrystallization to a maximum concentration of only 70% besides **2** (Equation 2). The impure compound **3** crystallizes as colorless needles similar to **1** and has the resonances of the trimethylsilyl group attached to the carbon atom of diazomethane in the ^{1}H- and ^{13}C-NMR spectra at $\delta = 0.11$ and -0.8, respectively, which is similar to the chemical shifts observed for the corresponding group in **1**. In addition, two singlets are observed in each spectrum for the methine and methyl protons of the bis(trimethylsilyl)methyl group. Due to these strong similarities, we assume that compound **3** is the aluminium analogue of the gallium derivative **1** with the nitrile imine structure. Compound **2** was characterized by a crystal structure determination and has another constitution derived from the diazomethane isomer with the aluminium atom bound to the carbon atom of the CN_2 group. The compound is a dimer in the solid state (see below) and in solution, as shown by the cryoscopic determination of its molar mass in benzene. Due to the coordination of the central aluminium atom by two $CH(SiMe_3)_2$ groups and one carbon and one nitrogen atom of the diazomethane fragment, the trimethylsilyl groups become diastereotopic and, in contrast to **1** and **3**, give two resonances in the ^{1}H- and ^{13}C-NMR spectra. The protons of the N_2CSiMe_3 group shows a resonance at $\delta = 0.32$. It is shifted to lower field than the corresponding signals of **1** and **3**, which are part of the linear $Me_3Si-C\equiv N^+-N^-$ moieties. In the IR spectrum of **2**, three absorptions are observed between 2135 and 2220 cm^{-1}, which can be assigned to the stretching vibrations of both C=N=N groups of the heterocycle.[16] Remarkably, the ratio between both aluminium compounds in the mixture remains constant in solution, and no rearrangement by the 1,3 shift of the dialkylaluminium group to form a thermodynamically more favored product was observed even in hot benzene. Thus, the formation of the mixture may not be caused by the migration of alkylaluminium groups in any stage of the reaction, but may reflect the distribution of the lithiated diazomethane species in their complicated equilibrium in solution. With gallium, only the nitrile imine isomer was isolated in a low yield of 38%, and we observed the formation of the corresponding trialkylgallium derivative besides some further minor by-products. A diazomethane isomer similar to compound **2** could not be detected. This isomer may be formed as an intermediate, but possibly it is not stabilized by the formation of a strong dimer due to the lower Lewis acidity of gallium than of aluminium and decomposes by the release of nitrogen, for instance. A following redistribution reaction may yield GaR_3 as the main product. The lower stability of the gallium compounds due to the formation of only weak dimers is in agreement with the partial dissociation of **1** in benzene and its low decomposition point as discussed below.

Both products **1** and **2** were heated and irradiated with UV light, in order to investigate their stability and to prove their ability to lose nitrogen and to form carbene intermediates. Solutions in benzene can be stored at 60°C for many hours without any detectable secondary reaction. The crystals of compound **1** completely decomposed at temperatures as low as 117°C by the formation of a gaseous product, while the aluminium compound **2** was more stable and did not decompose below 200°C. But in each case the thermal decomposition yielded mixtures of many unknown products, from which none could be isolated in a pure form. A similar result was obtained upon irradiation of solutions with UV light, which led to the formation of oily residues with many unknown products.



Crystal Structures of 1 and 2

The molecular structure of compound **1** is depicted in Figure 1. The ligand derived from the starting diazomethane compound adopts the almost linear nitrile imine form, and with their terminal nitrogen atoms two of these ligands bridge two dialkylgallium fragments to yield a dimer with a Ga_2N_2 heterocycle. The geminal coordination of the terminal nitrogen atoms by two gallium atoms is similar to the situation in trimeric diisobutylaluminium nitrile imide[9] or to the structures of dialkylaluminium and -gallium azides,[17] which were derived from their IR-spectroscopic characterization. Further examples of a geminal bridging by azido groups could be verified by crystal structure determinations.[17] A different coordination was, however, found for the sterically highly shielded trimer of $[(Me_3Si)_2CH]_2AlN_3$, for which a 1,3 coordination of the azido group by the formation of a twelve-membered heterocycle was observed.[10] This unusual structure may be caused by the electrostatic repulsion between the positively charged aluminium atoms and a steric interaction between the bulky substituents. The electrostatic repulsion should be lower in the case of the more electronegative gallium. The formation of dimers with Al_2N_2 or Ga_2N_2 heterocycles comparable to compound **1** has not been observed before for this type of ambident ligands.

The angles N−N−C and N−C−Si in both independent molecules of **1** are on average 178.7° and 176.5°, respectively. The C−Si bonds to the terminal trimethylsilyl group of the ligand (184.5 pm on average) are not shorter than the expected value. The C−N bond lengths (115.9 pm) correspond to a normal C≡N triple bond[18], and the N−N bonds (125.5 pm on average) are a little longer than typical N=N double bonds,[19] which may indicate some π character of the bond or an electrostatic contribution to the N−N bond strength. These results are in excellent agreement with the theoretically obtained parameters of 114.6 and 127.8 pm for hydrogen-substituted nitrile imine or 114.6 and 121.4 pm for dimeric LiN_2CH with a central Li_2N_2 heterocycle.[8] They impressively confirm the formulation of compound **1** as a nitrile imine derivative with a main contribution of the resonance structure $R-C\equiv N^+-N^--GaR_2$, which gives a dimer by the interaction of a lone electron pair at the negatively charged nitrogen atom with a second gallium atom. The nitrogen atoms in the heterocycles have almost ideally planar surroundings, and the sum of the bond angles are between 358.6° and 360.0°. The heterocycles are slightly folded, and the angles between the normals of the planes GaN_2 are 12.3 and 12.1°. Similar to other compounds with a four-membered heterocycle like $R_4Ga_2(\mu\text{-}OH)_2$[14] or a $R_4Ga_2(\mu\text{-}F)_2$,[15] the most acute angles in the ring are observed at the gallium atoms (76.3°); the inner ring angles at the nitrogen atoms are 102.9°.

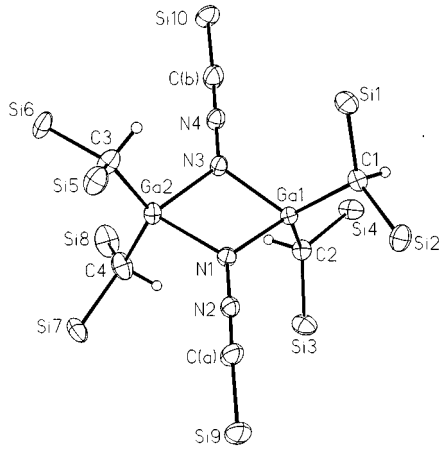


Figure 1. Molecular structure and numbering scheme of compound **1**; the thermal ellipsoids are drawn at the 40% probability level; methyl groups are omitted for clarity; only one of both independent molecules is shown; selected bond lengths [pm] and angles [°] (values of the second molecule in square brackets): Ga1−N1 200.7(3) [200.3(3)], Ga1−N3 202.5(3) [203.0(3)], Ga1−C1 200.5(4) [201.3(4)], Ga1−C2 202.2(4) [199.7(4)], Ga2−N1 202.9(3) [202.2(3)], Ga2−N3 202.6(3) [201.3(3)], Ga2−C3 200.0(4) [201.2(4)], Ga2−C4 201.9(4) [201.6(4)], N1−N2 126.0(4) [125.8(4)], N2−C(a) 115.3(5) [114.8(5)], N3−N4 124.2(4) [125.9(5)], N4−C(b) 117.2(5) [116.3(6)], C(a)−Si9 185.0(4) [185.7(4)], C(b)−Si10 183.5(4) [183.8(5)]; Ga1−N1−Ga2 103.0(1) [103.3(1)], Ga1−N3−Ga2 102.5(1) [102.7(1)], N1−Ga1−N3 76.7(1) [76.2(1)], N1−Ga2−N3 76.2(1) [76.2(1)], Ga1−N1−N2 128.5(3) [128.4(2)], Ga1−N3−N4 129.4(3) [126.4(3)], Ga2−N1−N2 127.1(2) [127.0(2)], Ga2−N3−N4 128.1(3) [129.5(3)], N1−N2−C(a) 178.4(4) [178.6(4)], N3−N4−C(b) 179.5(4) [178.3(4)], N2−C(a)−Si9 176.9(4) [175.8(4)], N4−C(b)−Si10 174.9(4) [178.4(5)]

The nitrile imine structure has been observed before in the complicated lithium compound $(LiN_2CSiMe_3)_6[LiC_2N_3(SiMe_3)_2]_2(Et_2O)_7$[8] and in two aluminium compounds, $(R_2PCN_2AliBu_2)_3$ and $[R_2PCN_2(AlCltBu_2)_2]^-$ (R = NMe_2).[9] While the nitrile imine fragments of the aluminium compounds have structural parameters similar to **1**, the C−N and N−N bonds are almost equally long in the lithium derivative. Furthermore, few nitrile imine derivatives of non-metals are known.[20] Their bond lengths and angles (C−N 117.2 pm and N−N 125.6 pm on average) resemble those observed for compound **1**. But their X−CN_2 groups with X the central atom of the terminal ligand deviate more significantly from linearity and show angles X−C−N between 137.3 and 165.1°.

Although compound **2** (Figure 2) also forms dimers in the solid state, a completely different structure is found, which is not derived from the nitrile imine, but from the diazomethane skeleton. The aluminium atom is bound to the diazomethane carbon atom, and an eight-membered centrosymmetric $Al_2C_2N_4$ heterocycle is formed by the interaction of the terminal diazomethane nitrogen atom with the aluminium atom of a second molecule. The Al−C bonds (Al−C3) within the ring have a length of 196.1(4) pm, which is in the range usually observed. The diazomethane group is almost linear with an angle C−N−N of 174.1°. The ratio of the C−N and N−N bond lengths in this group is inverted relative to those of **1**. The N−N bond is shorter than in **1** [120.0(6) pm] corresponding to an N=N double bond[19] and the C−N bond is longer [126.4(5) pm] indicating the formation of a C=N double bond.[18] Thus, the bonding in this part of the molecule is best described by the resonance structure $R_2Al-(R)C=N^+=N^-$. Usually, diazomethane[21] and its *C*-metalated, monomeric derivatives[5−7] show larger differences between their C−N and N−N bond lengths with longer C−N distances and very short N−N bonds, which are in the characteristic range of N≡N triple bonds. The exocyclic bond Si5−C3 [177.2(4) pm] is much shortened relative to the corresponding Si−C bond in compound **1** (184.5 pm), which may indicate some additional hyperconjugative interaction between the trimethylsilyl group and the carbon atom. The terminal nitrogen atom of the diazomethane group is coordinated to the aluminium atom of a second fragment with a long[22] Al−N distance of 208.4(6) pm. The angle Al−N1−N2 approaches linearity with 158.9°. All Al−C distances are, however, in the expected range. The eight-membered heterocycle is almost planar, and the largest deviation of an atom from the mean plane is observed for N2 with only 6.5 pm.

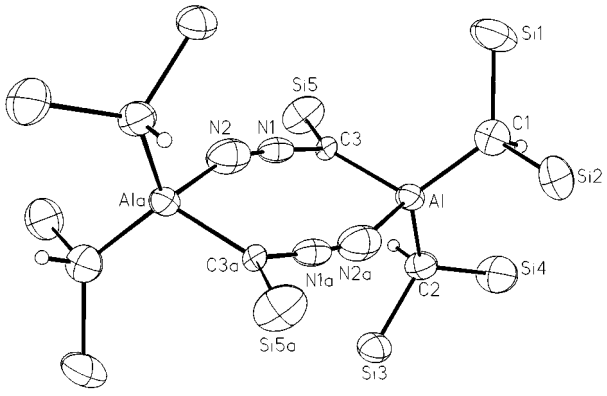


Figure 2. Molecular structure and numbering scheme of compound **2**; the thermal ellipsoids are drawn at the 40% probability level; methyl groups are omitted for clarity; selected bond lengths [pm] and angles [°]: Al−C3 196.1(4), Al−N2*a* 208.4(6), Al−C1 197.4(8) and 203.5(6) (disordered), Al−C2 198.8(5), C3−Si5 177.2(4), C3−N1 126.4(5), N1−N2 120.0(6); C3−Al−N2*a* 92.0(2), Al−C3−Si5 133.5(2), Al−C3−N1 113.7(3), N1−C3−Si5 112.2(3), C3−N1−N2 174.1(4), N1−N2−Al*a* 158.9(4); the atoms labeled *a* are generated by $-x + 2, -y, -z + 2$

Experimental Section

General: All procedures were carried out under purified argon in dried solvents (diisopropyl ether from Na/benzophenone, *n*-hexane and cyclopentane with $LiAlH_4$, pentafluorobenzene over molecular sieve). Bis[bis(trimethylsilyl)methyl]gallium bromide was synthesized as described in ref.[23] The corresponding aluminium chloride was obtained according to ref.[24] Commercially available solutions of trimethylsilyldiazomethane and *n*-butyllithium in *n*-hexane were used without further purification.

Synthesis of the Gallium Diazomethane Derivative 1: 0.9 mL (1.79 mmol) of a 2 M solution of trimethylsilyldiazomethane in hexane was diluted with 10 mL of hexane and cooled to −100°C. A cooled (−60°C) mixture of 1.12 mL (1.79 mmol) of a 1.6 M solution of *n*-butyllithium in hexane and 10 mL of the same solvent was added over a period of 10 min. After stirring for 15 min at −100°C, the lithium trimethylsilyldiazomethanide intermediate was treated with a cooled (−50 to −60°C) solution of 0.837 g (1.79 mmol) of $[(Me_3Si)_2CH]_2GaBr$ in 25 mL of hexane over a period of 20 min. The mixture was slowly warmed to room temperature and filtered. The solvent was removed in vacuo, and the residue was recrystallized twice from diisopropyl ether (20/−50°C). Yield 0.341 g (38%), colorless needles, which usually include small quantities of diisopropyl ether (less than 0.2 mol each monomeric formula unit of **1**), m.p. (argon, sealed capillary): 117°C (dec). − ^{1}H NMR (C_6D_6, 300 MHz): δ = 0.39 [36 H, $SiMe_3$ of $CH(SiMe_3)_2$], 0.15 (9 H, $SiMe_3$ of diazomethane), −0.22 (2 H, $GaCHSi_2$). − ^{13}C NMR (C_6D_6, 75.5 MHz): δ = 9.6 ($GaCSi_2$), 5.3 [$SiMe_3$ of $CH(SiMe_3)_2$], −0.3 ($SiMe_3$ of diazomethane); the carbon atom signal of the CN_2 group was not detected. − IR (CsBr, paraffin): $\tilde{\nu}$ = 2120 vs cm^{-1} νCN; 1464 vs, 1377 vs paraffin; 1335 vs, 1285 vs, 1248 vs δCH_3; 1169 vw, 1157 w, 1127 w, 1111 w diisopropyl ether; 1017 vs δCH; 963 m, 843 vs, 775 s, 758 s, 725 m ρCH_3(Si); 671 s ν_{as}SiC; 631 s ν_sSiC; 519 m, 478 vs, 405 m νGaC, νGaN; 347 vw δSiC. − $C_{18}H_{47}GaN_2Si_5$ (501.7 of the monomer): calcd. Ga 13.9, found Ga 14.1. − Mol. mass: 650 (cryoscopically in benzene).

Synthesis of the Aluminium Diazomethane Derivative 2: A cooled (−60 to −70°C) solution of *n*-butyllithium (2.07 mL, 1.6 M, 3.31 mmol) in hexane, diluted with 20 mL of same solvent, was added to a cooled (−100°C) mixture of 20 mL of hexane and 1.66 mL of a solution (2 M) of trimethylsilyldiazomethane in hexane (3.31 mmol) over a period of 40 min. The mixture was stirred at −100°C and treated with a cooled (−40 to −50°C) solution of 1.26 g (3.31 mmol) of $[(Me_3Si)_2CH]_2AlCl$ in 70 mL of hexane. The mixture was slowly warmed to room temperature and filtered. The solvent was removed in vacuo, and the residue was recrystallized from hexane (20/0°C) to isolate colorless crystals of compound **2**. Further fractions contain mixtures of **2** and the by-product **3**, which could not completely be separated even after repeated recrystallization. Yield: 0.32 g (21%). − M. p. (argon, sealed capillary): 200−204°C (dec.). − ^{1}H NMR (C_6D_6, 300 MHz): δ = 0.36 and 0.35 [each 36 H, $SiMe_3$ of $CH(SiMe_3)_2$], 0.32 (18 H, $SiMe_3$ of diazomethane), −0.90 (4 H, $AlCHSi_2$). − ^{13}C NMR (C_6D_6, 75.5 MHz): δ = 98.0 (C=N), 5.45 and 5.38 [$SiMe_3$ of $CH(SiMe_3)_2$], 3.0 ($AlCSi_2$), 0.7 ($SiMe_3$ of diazomethane). − IR (CsBr, paraffin): $\tilde{\nu}$ = 2220 m cm^{-1}, 2184 m, 2135 s νCNN; 1462 vs, 1377 vs paraffin; 1248 vs δCH_3; 1109 m, 1086 m; 1007 vs δCH; 959 w, 937 m, 843 vs, 775 s, 750 s, 727 s ρCH_3(Si); 671 s ν_{as}SiC; 638 w, 629 m, 613 w ν_sSiC; 505 s, 484 s, 455 s, 442 s νAlC, νAlN; 392 w, 382 w, 374 w, 361 w, 343 vw, 320 w δSiC. − $C_{36}H_{94}Al_2N_4Si_{10}$ (918.0): calcd. Al 5.9, found Al 5.9. − Mol. mass: 865 (cryoscopically in benzene).

Table 1. Crystal data, data-collection parameters and structure refinement for **1** and **2**[a]

	1	**2**
Formula	$C_{42}H_{95}F_5Ga_2N_4Si_{10}$	$C_{18}H_{47}AlN_2Si_5$
Crystal system	triclinic	monoclinic
Space group	$P-1$[25]	$P2_1/n$[25]
Z	4	4
T [K]	213(2)	300(2)
$d_{calcd.}$ [g/cm^3]	1.191	1.009
a [pm]	1507.1(1)	1156.8(1)
b [pm]	2260.6(2)	2151.3(2)
c [pm]	2305.1(1)	1235.2(1)
α [°]	116.272(8)	90
β [°]	105.664(8)	100.67(2)
γ [°]	96.402(8)	90
V [10^{-30} m^3]	6533.2(8)	3020.8(5)
μ [mm^{-1}]	0.994[b]	0.272
Crystal size [mm]	0.45 × 0.50 × 0.53	0.72 × 0.76 × 0.34
Diffractometer	Stoe-IPDS	
Radiation	Mo-K_α; graphite monochromator	
2Θ range [°]	$4.0 \le 2\Theta \le 52.1$	$4.0 \le 2\Theta \le 48.0$
Scan mode (number of exposures; Δφ)	267; 1.2°	180; 1.0°
Index ranges	$-18 \le h \le 18$ $-27 \le k \le 27$ $-28 \le l \le 28$	$-12 \le h \le 13$ $-24 \le k \le 24$ $-14 \le l \le 14$
Independent reflections	23924	4691
Reflections $F > 4\,\sigma(F)$	16842	3041
Parameters	1178	240
$R = \Sigma\|\|F_o\| - \|F_c\|\|/\Sigma\|F_o\|$; $[F > 4\,\sigma(F)]$[b]	0.045	0.071
$wR2 = \{\Sigma w(\|F_o\|^2 - \|F_c\|^2)^2/\Sigma w(F_o^2)^2\}^{1/2}$ (all data)	0.169	0.141
Max./min. residual electron density [10^{30} e/m^3]	1.06[c]/−0.75	0.61

[a]Programs: SHELXTL, SHELXL-93;[26] solutions by direct methods; full-matrix refinement with all independent structure factors. − [b]Numerical absorption correction. − [c]Near the solvent molecules.

NMR Characterization of 3: ^{1}H NMR (C_6D_6, 300 MHz, mixture with **2**): δ = 0.40 [72 H, $SiMe_3$ of $CH(SiMe_3)_2$], 0.11 ($SiMe_3$ of diazomethane), −0.73 (4 H, $AlCHSi_2$). − ^{13}C NMR (C_6D_6, 75.5 MHz): δ = 5.7 [$SiMe_3$ of $CH(SiMe_3)_2$], 4.9 ($AlCHSi_2$), −0.8 ($SiMe_3$ of diazomethane); the carbon atom signal of the diazomethane component could not be detected.

Crystal Structure Determinations: Single crystals of the compounds **1** and **2** were obtained by recrystallization from a mixture of pentafluorobenzene and cyclopentane (**1**) and from *n*-hexane (**2**). Crystal data and structure refinement parameters are given in Table 1.[27] The crystals of **1** include one molecule of pentafluorobenzene per formula unit. Two independent molecules were observed in the asymmetric unit, which have similar bond lengths and angles, but differ in the orientation of the bis(trimethylsilyl)methyl groups. Two trimethylsilyl groups (Si6 and Si7) showed a disorder, their atoms were isotropically refined by restrictions of bond lengths and angles with occupation factors of 0.75 and 0.25. The heterocycle of **2** is located on a crystallographic inversion center. One bis(trimethylsilyl)methyl group showed a disorder caused by different orientations of the methine C−H bond with a partial overlap of the atoms (Si1 and C11). All other atoms (C1, C12, C13) were isotropically refined with restrictions of bond lengths and angles using occupation factors of 0.52 and 0.48.

Acknowledgments

We are grateful to the Fonds der Chemischen Industrie for generous financial support.

[1] R. Huisgen, *Angew. Chem.* **1963**, *75*, 604−637 and 742−754; M. Jones, Jr., *Acc. Chem. Res.* **1974**, *7*, 415−421; W. Kirmse, *Carbene Chemistry*, Academic Press, New York, **1971**; R. A. Moss, M. Jones, *Reactive Intermediates − Carbenes*, John Wiley, New York, **1985**, p. 45.
[2] E. Müller, H. Disselhoff, *Naturwissenschaften* **1933**, *21*, 661.
[3] C. Charrier, N. Maigrot, L. Ricard, P. le Floch, F. Mathey, *Angew. Chem.* **1996**, *108*, 2282−2283; *Angew. Chem. Int. Ed. Engl.* **1996**, *35*, 2133−2134; T. Aoyama, S. Inoue, T. Shioiri, *Tetrahedron Lett.* **1984**, *25*, 433−436; D. Seyferth, T. C. Flood, *J. Organomet. Chem.* **1971**, *29*, C25−C28.
[4] E. Glozbach, J. Lorberth, *J. Organomet. Chem.* **1977**, *132*, 359−366; E. Glozbach, J. Lorberth, *J. Organomet. Chem.* **1980**, *191*, 371−379; A. Baceiredo, G. Bertrand, G. Sicard, *J. Am. Chem. Soc.* **1985**, *107*, 4781−4783; A. Baceiredo, A. Igau, G. Bertrand, M. J. Menu, Y. Dartiguenave, J. J. Bonnet, *J. Am. Chem. Soc.* **1986**, *108*, 7868−7869.
[5] C. Glidewell, G. M. Sheldrick, *J. Chem. Soc., Dalton Trans.* **1972**, 2409−2412; J. Lorberth, S.-H. Shin, H. Donath, S. Wocadlo, W. Massa, *J. Organomet. Chem.* **1991**, *407*, 167 -171; M. Birkhahn, E. Glozbach, W. Massa, J. Lorberth, *J. Organomet. Chem.* **1980**, *192*, 171−176; C. Glidewell, D. Lloyd, K. W. Lumbard, J. S. McKechnie, M. B. Hursthouse, R. L. Short, *J. Chem. Soc., Dalton Trans.* **1987**, 2981−2987; coordination compound: M. J. Menu, G. Crocco, M. Dartiguenave, Y. Dartiguenave, G. Bertrand, *J. Chem. Soc., Chem. Commun.* **1988**, 1598−1599.
[6] A. Ansorge, D. J. Brauer, H. Bürger, T. Hagen, G. Pawelke, *Angew. Chem.* **1993**, *105*, 429−430; *Angew. Chem. Int. Ed. Engl.* **1993**, *32*, 384−385.
[7] M. J. Menu, P. Desrosiers, M. Dartiguenave, Y. Dartiguenave, *Organometallics* **1987**, *6*, 1822−1824; E. Deydier, M.-J. Menu, M. Dartiguenave, Y. Dartiguenave, M. Simard, A. L. Beauchamp, J. C. Brewer, H. B. Gray, *Organometallics* **1996**, *15*, 1166−1175; S.-I. Murahashi, Y. Kitani, T. Uno, T. Hosokawa,

K. Miki, T. Yonezawa, N. Kasai, *Organometallics* **1986**, *5*, 356−365; S.-I. Murahashi, Y. Kitani, T. Hosokawa, K. Miki, N. Kasai, *J. Chem. Soc., Chem. Commun.* **1979**, 450−451.
[8] G. Boche, K. Harms, M. Marsch, F. Schubert, *Chem. Ber.* **1994**, *127*, 2193−2195; G. Boche, J. C. W. Lohrenz, F. Schubert, *Tetrahedron* **1994**, *50*, 5889−5902.
[9] N. Emig, F. P. Gabbai, H. Krautscheid, R. Réau, G. Bertrand, *Angew. Chem.* **1998**, *110*, 1037−1040; *Angew. Chem. Int. Ed. Engl.* **1998**, *37*, 989−992.
[10] W. Uhl, R. Gerding, S. Pohl, W. Saak, *Chem. Ber.* **1995**, *128*, 81−85.
[11] W. Uhl, F. Hannemann, *Eur. J. Inorg. Chem.* **1999**, 201−207.
[12] W. Uhl, M. Layh, T. Hildenbrand, *J. Organomet. Chem.* **1989**, *364*, 289−300.
[13] W. Uhl, I. Hahn, H. Reuter, *Chem. Ber.* **1996**, *129*, 1425−1428; W. Uhl, I. Hahn, R. Wartchow, *Chem. Ber.* **1997**, *130*, 417−420; W. Uhl, R. Graupner, I. Hahn, *Z. Anorg. Allg. Chem.* **1997**, *623*, 565−572; W. Uhl, R. Gerding, F. Hannemann, *Z. Anorg. Allg. Chem.* **1998**, *624*, 937−944.
[14] W. Uhl, I. Hahn, M. Koch, M. Layh, *Inorg. Chim. Acta* **1996**, *249*, 33−39.
[15] W. Uhl, R. Graupner, I. Hahn, T. Spies, W. Frank, *Eur. J. Inorg. Chem.* **1998**, 355−360.
[16] J. Weidlein, U. Müller, K. Dehnicke, *Schwingungsfrequenzen I − Hauptgruppenelemente*, Thieme Verlag, Stuttgart, **1981**.
[17] J. Müller, K. Dehnicke, *J. Organomet. Chem.* **1968**, *12*, 37−47; J. Müller, K. Dehnicke, *Z. Anorg. Allg. Chem.* **1966**, *348*, 261−272; V. Krieg, J. Weidlein, *Z. Anorg. Allg. Chem.* **1969**, *368*, 44−52; D. A. Atwood, R. A. Jones, A. H. Cowley, J. L. Atwood, S. G. Bott, *J. Organomet. Chem.* **1990**, *394*, C6−C8; J. McMurran, J. Kouvetakis, D. C. Nesbing, D. J. Smith, J. L. Hubbard, *J. Am. Chem. Soc.* **1998**, *120*, 5233−5237; R. A. Fischer, A. Miehr, E. Herdtweck, M. R. Mattner, O. Ambacher, T. Metzger, E. Born, S. Weinkauf, C. R. Pulham, S. Parsons, *Chem. Eur. J.* **1996**, *2*, 1353−1358.
[16] J. March, *Advanced Organic Chemistry*, 3rd ed., Wiley, **1985**, p. 19.
[17] A. F. Hollemann, E. Wiberg, N. Wiberg, *Lehrbuch der Anorganischen Chemie*, de Gruyter, Berlin, **1995**.
[20] R. Reau, G. Veneziani, F. Dahan, G. Bertrand, *Angew. Chem.* **1992**, *104*, 481−482; *Angew. Chem. Int. Ed. Engl.* **1992**, *31*, 439−440; M. Granier, A. Baceiredo, Y. Dartiguenave, M. Dartiguenave, M. J. Menu, G. Bertrand, *J. Am. Chem. Soc.* **1990**, *112*, 6277−6285; M. Granier, A. Baceiredo, G. Bertrand, V. Huch, M. Veith, *Inorg. Chem.* **1991**, *30*, 1161−1162; M.-P. Arthur, A. Baceiredo, J. Fischer, A. DeCian, G. Bertrand, *Synthesis* **1992**, 43−45; review: G. Bertrand, C. Wentrup, *Angew. Chem.* **1994**, *106*, 549−568; *Angew. Chem. Int. Ed. Engl.* **1994**, *33*, 527−546.
[21] A. P. Cox, L. F. Thomas, J. Sheridan, *Nature* **1958**, *181*, 1000−1001; related structures: D. J. Abraham, T. G. Cochran, R. D. Rosenstein, *J. Am. Chem. Soc.* **1971**, *93*, 6279−6281; G. B. Ansell, *J. Chem. Soc. B* **1969**, 729−733; H. Hope, K. T. Black, *Acta Crystallogr., Sect. B* **1972**, *28*, 3632−3634; A. F. Cameron, N. J. Hair, D. G. Morris, *J. Chem. Soc., Perkin Trans. 2* **1972**, 1331−1335.
[22] A. Haaland, in *Coordination Chemistry of Aluminum* (Ed.: G. H. Robinson), VCH, Weinheim, **1993**.
[23] W. Uhl, M. Layh, G. Becker, K. W. Klinkhammer, T. Hildenbrand, *Chem. Ber.* **1992**, *125*, 1547−1551.
[24] W. Uhl, *Z. Naturforsch., B.: Chem. Sci.* **1988**, *43*, 1113−1118.
[25] T. Hahn (Ed.), *International Tables for Crystallography, Space Group Symmetry*, Kluwer Academic Publishers, Dordrecht−Boston−London, **1989**, vol. A.
[26] *SHELXTL-Plus REL. 4.1*, Siemens Analytical X-RAY Instruments Inc., Madison, USA, **1990**; G. M. Sheldrick *SHELXL-93, Program for the Refinement of Structures*, Universität Göttingen, **1993**.
[27] The crystallographic data of **1** and **2** (excluding structure factors) were deposited with the Cambridge Crystallographic Data Centre as supplementary publication no. CCDC-103107 (**1**) and -103108 (**2**). Copies of the data can be obtained free of charge on application to CCDC, 12 Union Road, Cambridge CB2 1EZ, UK (Fax: int. code + 44-1223/336-033; E-mail: deposit@ccdc.cam.ac.uk).

Received October 15, 1998
[I98355]

Solid-State and Solution Structural Properties of Copper(I) Compounds with Bidentate Phosphane Ligands

Peter Comba,*[a] Charis Katsichtis,[a] Bernd Nuber,[a] and Hans Pritzkow[a]

Keywords: Copper / Phosphane / Solution structure / P ligands / NMR spectroscopy / Coordination chemistry

The copper(I) compounds $[Cu(dppe)_2]X$ [X = BF_4^-, I^-; dppe = 1,2-bis(diphenylphosphanyl)ethane], $[Cu(dppp)_2]X$ [X = BF_4^-, I^-; dppp = 1,3-bis(diphenylphosphanyl)propane], $[Cu_2(dppe)_3I_2]$, and $[Cu_2(dppe)_2I_2]$ have been prepared and their structural properties in solution and in the solid state have been determined. ^1H-, ^{13}C-, and ^{31}P-NMR spectra in solution [variable temperature and anion (I^-) concentrations] and analyses of solids (mass spectra, elemental analyses, and CPMAS ^{31}P-NMR spectra) are interpreted with equilibria in solution that involve two mono- and two dinuclear species. The structures of $[Cu(dppe)_2]ClO_4$, $[Cu(dppp)_2]BF_4$, and $[Cu_2(dppe)_3I_2] \cdot 2\ CHCl_3$ have been analyzed by X-ray crystallography. In all three structures the copper(I) center adopts a distorted tetrahedral geometry.

Introduction

Detailed structural studies and the understanding of solution equilibria and dynamics of copper(I) compounds of bidentate phosphanes are of importance due to their potential application as potent antitumor agents[1] and as free radical scavengers in industrial processes.[2][3] There are a number of published studies of solution equilibria and structures that involve copper(I) compounds with phosphane ligands with variable copper(I)-to-ligand ratios.[4] Similar equilibria have also been observed for silver(I) compounds of bidentate phosphane ligands.[5] Mononuclear[4e,4g,4i–4j,4l,4m,4p] and dinuclear phosphanecopper(I) compounds[4a–4d,4k,4n,4o,4q] with coordinated and bridging halide anions and with phosphane ligands in various coordination modes have been isolated and characterized. There is spectroscopic evidence that some of the structurally characterized solids lead to complex equilibria in solution. However, so far there is only relatively little thorough information on structures and dynamics in solution.[1,4f] Here we report our results from studies on the structural properties of copper(I) compounds of dppe and dppp in the solid state and in solution.

Results and Discussion

Syntheses and Properties of the Solids

Reaction of $[Cu(CH_3CN)_4]BF_4$ with dppe in CH_2Cl_2 in a 1:2 ratio yields $[Cu(dppe)_2]BF_4$ (**1**). $[Cu(dppe)_2]I$ (**2**), $[Cu_2(dppe)_3I_2]$ (**3**), and $[Cu_2(dppe)_2I_2]$ (**4**) are prepared under similar conditions from CuI and dppe in CH_2Cl_2 or $CHCl_3$ (1:2, 2:3, and 1:1 Cu^I-to-ligand ratios). Reaction of dppp with $[Cu(CH_3CN)_4]BF_4$ and CuI in a 2:1 ratio in CH_2Cl_2 yields the compounds $[Cu(dppp)_2]BF_4$ (**5**) and $[Cu(dppp)_2]I$ (**6**), respectively. X-ray quality crystals of **1** (as the perchlorate salt), **3** (with two disordered chloroform molecules in the lattice), and **5** were obtained by vapor diffusion of diethyl ether into a solution of the complexes in CH_2Cl_2 or $CHCl_3$. The solids were studied by X-ray diffractometry, mass spectrometry, elemental analysis, CPMAS ^{31}P-NMR and IR spectroscopy. ^1H, ^{13}C, and ^{31}P NMR was used to establish the solution structures of the compounds.

ORTEP[6] plots of the experimentally determined structures of $[Cu(dppe)_2]ClO_4$ (**1**), $[Cu_2(dppe)_3I_2]$ (**3**), and $[Cu(dppp)_2]BF_4$ (**5**) are presented in Figure 1, and selected structural parameters are given in Table 1. As expected, the copper(I) center adopts a distorted tetrahedral geometry in these structures. The copper(I)–phosphane distances are in the range expected from other known structures[4b,4e,4g,4r] but there is a rather large variation in the individual distances, also within each complex. The degree of distortion from tetrahedral geometry depends primarily on the chelate ring size (dppe vs. dppp), with bite angles of the five-membered chelate rings of approximately 90° and bite angles of the six-membered rings of approximately 98°, and this leads to a flattening of the tetrahedral chromophores (deviation of the angles θ in Table 1 from 90°). All chelate rings are puckered, and the six-membered rings have the expected chair conformations.

There is no crystal structural analysis of $[Cu_2(dppe)_2I_2]$ (**4**). The structural assignment given in Scheme 1 is based on the reported structures of $[Cu_2(dppf)_2I_2]$[7] [dppf: 1,1′-bis(diphenylphosphanylferrocene)] and $[Cu_2(PhPH_2)_4I_2]$[8] ($PhPH_2$: phenylphosphane). The signals in the CPMAS ^{31}P-NMR spectra of the copper(I) complexes are rather broad, due to distortion from tetrahedral symmetry, unresolved coupling to the copper nuclei, quadrupole interactions involving the copper centers and the presence of two isotopes (^{63}Cu, ^{65}Cu);[9] nevertheless, the observed spectra (see Table 2 for chemical shift data) are qualitatively in good agree-

[a] Anorganisch-Chemisches Institut der Universität,
Im Neuenheimer Feld 270, D-69120 Heidelberg, Germany,
Fax: (internat.) + 49(0)6221/546617
E-mail: comba@akcomba.oci.uni-heidelberg.de

 © WILEY-VCH Verlag GmbH, D-69451 Weinheim, 1999 1434–1948/99/0505–0777 $ 17.50+.50/0

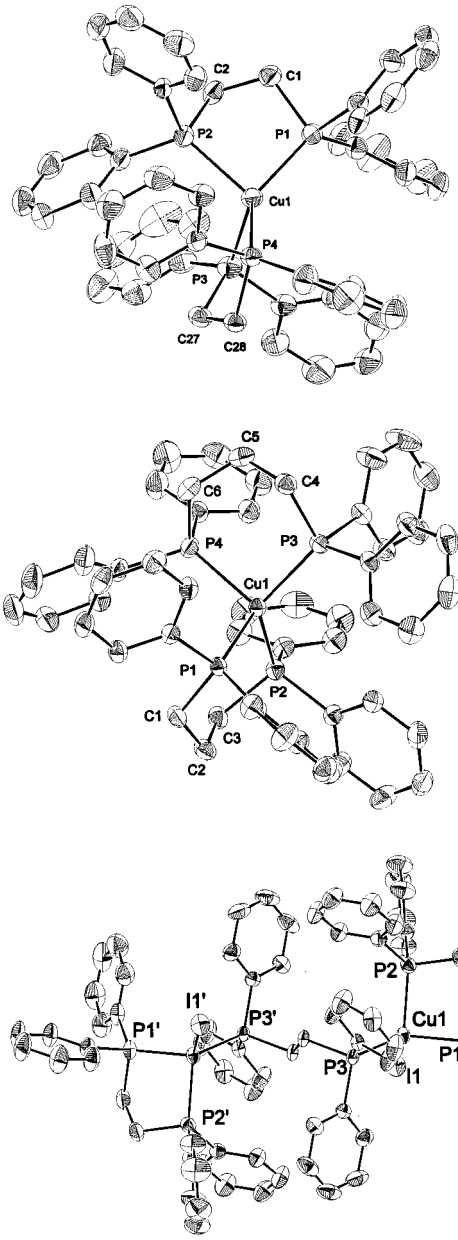
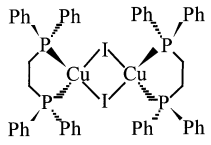


Figure 1. ORTEP[6] plots of the structures of the molecular cations of $[Cu(dppe)_2]ClO_4$ (**1**), $[Cu(dppp)_2]BF_4$ (**5**), and of the dinuclear compound $[Cu_2(dppe)_3I_2] \cdot 2\ CHCl_3$ (**3**)

ment with the X-ray structures of **1**, **3**, **5** (Figure 1), the putative structure of **4** (Scheme 1), published NMR data of $[CuP_4]^+$ and the structural assignments based on the solution NMR data (see below).



Scheme 1. Putative structure of $[Cu_2(dppe)_2I_2]$ (**4**) in solid state and in solution

Table 1. Selected structural parameters of $[Cu(dppe)_2]ClO_4$ (**1**), $[Cu(dppp)_2]BF_4$ (**5**), and $[Cu_2(dppe)_3I_2] \cdot 2\ CHCl_3$ (**3**)

Parameter	$[Cu(dppe)_2]ClO_4$	$[Cu(dppp)_2]BF_4$	$[Cu_2(dppe)_3I_2] \cdot 2\ CHCl_3$
Cu(1)−P(1)	2.259(2) Å	2.303(1) Å	2.315(2) Å
Cu(1)−P(2)	2.301(2) Å	2.298(1) Å	2.321(2) Å
Cu(1)−P(3)	2.300(2) Å	2.296(1) Å	2.273(2) Å
Cu(1)−P(4)	2.270(2) Å	2.317(1) Å	−
Cu(1)−I(1)	−	−	2.623(1) Å
P(1)−Cu(1)−P(2)	90.34(7)°	98.22(5)°	89.82(8)
P(1)−Cu(1)−P(3)	120.38(8)°	120.29(5)°	116.24(7)
P(2)−Cu(1)−P(3)	103.95(8)°	122.83(5)°	109.70(7)
P(3)−Cu(1)−P(4)	90.58(7)°	97.66(5)°	−
P(1)−Cu(1)−I(1)	−	−	113.88(6)
P(2)−Cu(1)−I(1)	−	−	116.29(6)
P(3)−Cu(1)−I(1)	−	−	109.79(5)
θ_1[a]	87.69°	81.44°	80.15°
θ_2[a]	74.43°	77.74°	76.79°

[a] Tetrahedral twist angles (tetrahedral, $\theta = 90°$; θ_2: planes involving the chelate rings).

Table 2. ^{1}H- and ^{31}P-NMR chemical shifts of Cu^I compounds of dppe and dppp

Compound	^{1}H NMR $\delta(CH_2)$ [ppm]	^{31}P NMR δ(P) [ppm]	CPMAS ^{31}P NMR δ(P) [ppm]
dppe	2.09	−12.47	−12.1
dppp	2.21; 1.58	−17.18; −17.26	−20.5; −24.4
$[Cu(dppe)_2]^+$	2.46	+7.5	+10.3
[Cu(dppe)(*P*-dppe)I]	−	−9.5	−
$[Cu_2(dppe)_3I_2]$	2.27	−5.0	−
$[Cu_2(dppe)_2I_2]$	2.56	−12.5	−20.0
$[Cu(dppp)_2]BF_4$	2.29; 1.62	−8.5	−10.1
$[Cu(dppp)_2]I$	2.28; 2.05; 1.64	−8.8; −17.5	−10.0

Equilibria in Solution

dppe Compounds

A broad signal at $\delta = 2.46$ is observed in the ^{1}H-NMR spectrum of $[Cu(dppe)_2]BF_4$ (**1**) in CD_2Cl_2. It is assigned to the methylene protons of the coordinated dppe ligands. The line broadening suggests unresolved ^{31}P-^{1}H coupling (relevant chemical shift data are assembled in Table 2). The ^{31}P-NMR spectrum of **1** in CD_2Cl_2 consists of a very broad signal centered at $\delta = +7.5$. It is assigned to the four phosphorus atoms coordinated to the copper(I) center. Lowering of the temperature leads to a significant decrease of $\Delta\nu_{1/2}$ (2500 Hz at 298 K vs. 250 Hz at 193 K) and a small upfield shift ($\Delta\delta \approx 0.9$) of this signal. This variation as a function of temperature is similar to that reported for $[Cu(dppey)_2]^+$[4p] [dppey = *cis*-bis(diphenylphosphanyl)-ethene] and consistent with the line shapes that have been calculated for fast quadrupolar relaxation[10] of a CuP_4 complex. No splitting is observed over the whole temperature range and the ^{31}P-NMR chemical shifts in the solid state and in solution are similar (Table 2). This suggests that only one species is present in solution, that is, the structure of **1** (see Figure 1) is conserved.

The high-field region of the ^{1}H-NMR spectrum of $[Cu(dppe)_2]I$ (**2**) is presented in Figure 2. There are three broad signals at $\delta = 2.56$, 2.46, and 2.26, the latter is split into two signals at $\delta = 2.27$ and 2.24. Three broad resonances at $\delta \approx +7.5$, -5, and -12.5 are observed in the ^{31}P-NMR spectrum of **2** (Figure 3a). The signals at $\delta = 2.46$ (^{1}H NMR) and +7.5 (^{31}P NMR) are due to the molecular cation observed in the solids of **1** and **2**, that is, to the structure that is conserved from the solid state; the other signals must be due to other species in solution, which is indicative of a chemical exchange process.

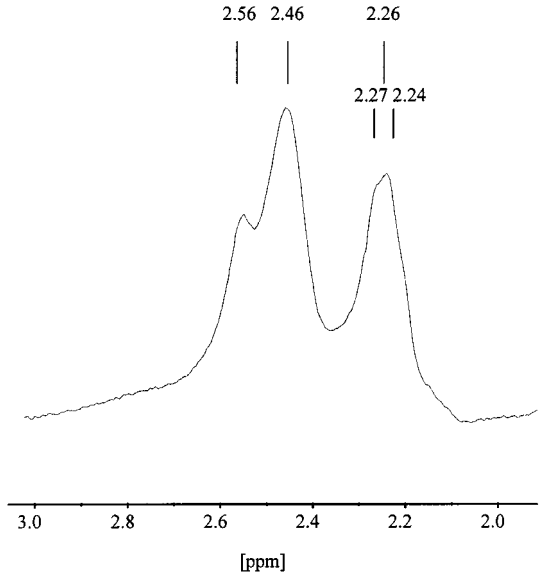


Figure 2. ^{1}H-NMR spectrum (200 MHz) of $[Cu(dppe)_2]I$ (**2**) (298 K; $CDCl_3$)

From variable-temperature ^{31}P-NMR spectra of **2** (Figure 3) it emerges that (i) there is a significant decrease in the line width and a small upfield shift of the signal at $\delta = +7.5$, assigned to $[Cu(dppe)_2]^+$ (see above); (ii) there is an additional multiplet at $\delta = -9.5$ which has maximum relative intensity around 240 K; (iii) at lower temperatures the relative intensity of the signal at $\delta = +7.5$ increases. The multiplet at $\delta = -9.5$ is tentatively assigned to a mononuclear intermediate with one bidentate and one monodentate dppe ligand, that is, a species that results from substitution of one phosphane donor by I^-. This is consistent with the chemical shift data (see below and Table 2), the concentration profile (relative intensities, see Figure 3 and above) and the NMR titration experiments (see below).

There is a broad signal at $\delta = 2.56$ in the ^{1}H-NMR spectrum of **4** (see Table 2). This is assigned to the methylene protons of the bidentate dppe ligands. A broad resonance at approximately $\delta = -12.5$ (close to that of the metal-free ligand) is observed in the corresponding ^{31}P-NMR spectrum. A similar observation was made in NMR studies of $[Cu_2(dppf)_2I_2]$, which was characterized by an X-ray crystal structure.[7] Addition of metal-free dppe to a solution of **4** in $CDCl_3$ leads to additional signals at $\delta = 2.27$ and -5 in the ^{1}H- and ^{31}P-NMR spectra, respectively (Figure 4). These new signals are tentatively assigned to a species with

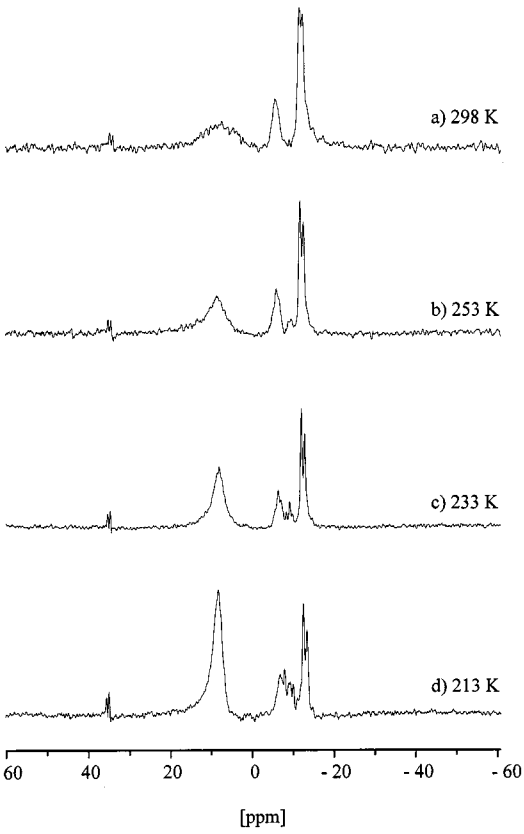
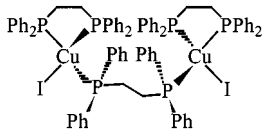


Figure 3. Temperature-dependent ^{31}P-NMR spectra (81 MHz) of $[Cu(dppe)_2]I$ (**2**) ($CDCl_3$; 85% H_3PO_4)

two chelated and one bridging phosphane ligand (Scheme 2). Further addition of dppe leads to decreasing intensity of the signal at $\delta = 2.56$ (^{1}H NMR), a sharpening of the signal at $\delta = -12.5$ (^{31}P NMR) and two additional signals at $\delta = 2.46$ (^{1}H NMR) and $\delta = +7.5$ (^{31}P NMR). That is, addition of dppe to $[Cu_2(dppe)_2I_2]$ produces $[Cu(dppe)_2]^+$ via $[Cu_2(dppe)_3I_2]$.



Scheme 2. Solution structure of $[Cu_2(dppe)_3I_2]$ based on ^{1}H- and ^{31}P-NMR spectroscopy

In a similar experiment ^{1}H- and ^{31}P-NMR spectra of $[Cu_2(dppe)_3I_2]$ (**3**) were measured in dependence of the concentration of added dppe. The two signals in the ^{1}H-NMR spectrum of **3** at $\delta = 2.46$ and 2.27 are assigned to the complexes $[Cu(dppe)_2]I$ and $[Cu_2(dppe)_3I_2]$, respectively. In the ^{31}P-NMR spectra there are signals at $\delta = +7.5$ and -5.0, respectively. Addition of excess dppe results in the disappearance of the resonances at $\delta = 2.27$ (^{1}H NMR) and -5.0 (^{31}P NMR). That is, as expected, the equilibrium is shifted towards $[Cu(dppe)_2]^+$. Hence, the signals at $\delta =$

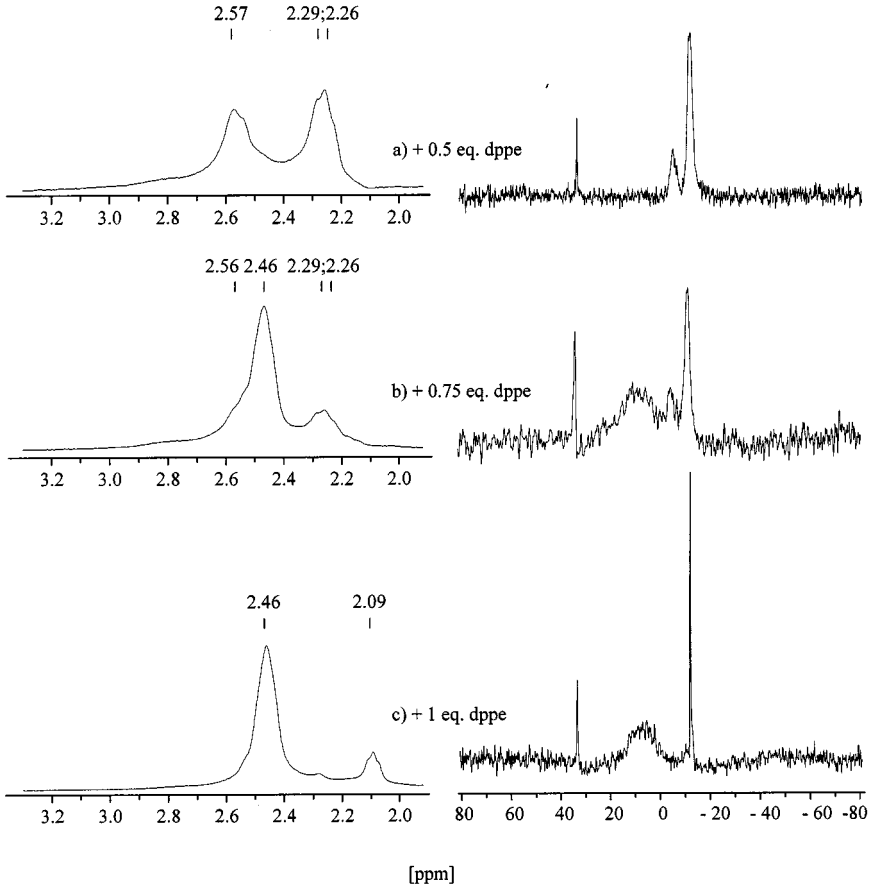


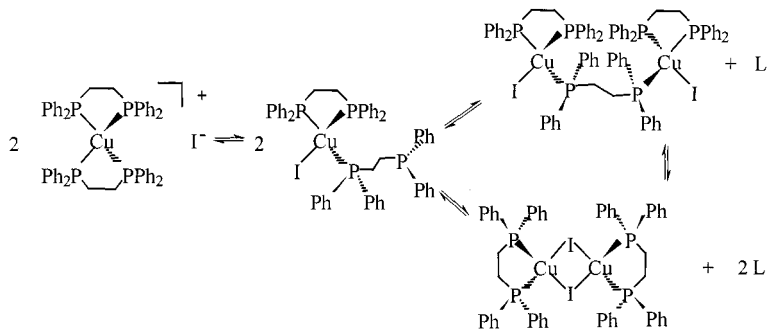
Figure 4. ^{1}H- and ^{31}P-NMR spectra (200 MHz, 81 MHz) of $[Cu_2(dppe)_2I_2]$ (**4**) with different concentrations of added ligand [$CDCl_3$; 298 K; a small amount of impurity at $\delta(^{31}P) \approx 33$ is due to phosphane oxide]

2.27 (^{1}H NMR) and −5.0 (^{31}P NMR) are assigned to the same compound, that is, to $[Cu_2(dppe)_3I_2]$.

The observations from temperature-dependent and ligand-concentration-dependent ^{1}H-NMR and ^{31}P-NMR data, and observations based on the solid-state samples are assembled in Scheme 3. The mononuclear compound $[Cu(dppe)_2]I$ is in equilibrium with the putative intermediate [Cu(dppe)(*P*-dppe)I], which only is observed at low temperature. Dissociation of one or two ligand molecules leads to the dinuclear compounds $[Cu_2(dppe)_3I_2]$ and $[Cu_2(dppe)_2I_2]$, respectively, which have been observed in the solid.

dppp Compounds

Two broad signals for $[Cu(dppp)_2]BF_4$ (**5**) with an intensity ratio of 2:1 are observed in the ^{1}H-NMR spectrum at $\delta = 2.29$ and 1.62 (methylene groups of the coordinated dppp ligands). A broad signal at $\delta = -8.5$ (upfield shift of approximately 8.7 ppm with respect to the metal-free ligand) is observed in the ^{31}P-NMR spectrum of **5** in CD_2Cl_2. This is assigned to the four coordinated phosphorus atoms. The ^{31}P-chemical shifts in the solid state and in solution are similar (see Table 2) and thus the structure of **5** (see Figure 1) is conserved in solution.



Scheme 3. Proposal for the solution equilibria of copper(I) compounds of dppe with two mono- and two dinuclear species

In the high-field region of the ^{1}H-NMR spectrum of $[Cu(dppp)_2]I$ (**6**) in CD_2Cl_2 there are multiplets at $\delta = 2.28$ and 1.64 and some signals of lower intensity at $\delta = 2.05$. The ^{31}P-NMR spectrum has a broad signal at $\delta = -8.80$ and a signal at -17.5. The low-intensity signals in the ^{1}H- and ^{31}P-NMR spectra of **6** suggest that chemical exchange processes, similar to those of $[Cu(dppe)_2]I$, take place. Unfortunately, the proximity of the ^{31}P-NMR signals, due to the smaller chemical shift of the six-membered ring bisphosphane compounds, makes an identification of intermediate compounds in the region between $\delta = -8$ and -17.5 difficult. Thus, a thorough investigation of the solution equilibrium was not appropriate.

The low-temperature ^{31}P-NMR spectrum of $[Cu(dppp)_2]BF_4$ (**5**) in CD_2Cl_2 (Figure 5) has features that are significantly different from those of $[Cu(dppe)_2]BF_4$ (**1**) (see Table 2). Below 213 K the signal at $\delta = -8.5$ splits into two signals ($\delta = -5.84$ and -10.36 at 193 K). The iodine salt **6** in CD_2Cl_2 leads to identical spectroscopic results; the signal at $\delta = -17.5$ (room temperature) disappears at low temperature (193 K). An interpretation of these observations emerges from temperature-dependent ^{1}H-NMR spectroscopy. The two signals at $\delta = 2.29$ and 1.62 (CD_2Cl_2, 298 K), assigned to the methylene protons of **5**, are split into five signals at $\delta = 2.85$, 2.53, 2.20, 1.47, and 0.88 (CD_2Cl_2, 193 K) with an intensity ratio of 1:1:2:1:1. The ^{13}C-NMR spectrum (CD_2Cl_2, 193 K) has three signals at $\delta = 26.97$, 25.91, and 16.62. These may be assigned to the three chemically and magnetically nonequivalent methylene groups of the six-membered ring in a frozen chair conformation. This is in agreement with the two signals in the ^{31}P-NMR spectrum, and these may be assigned to the two nonequivalent phosphorus atoms of the bidentate ligand. This interpretation is also supported by the [^{13}C-^{1}H] spectrum of **5** in CD_2Cl_2.

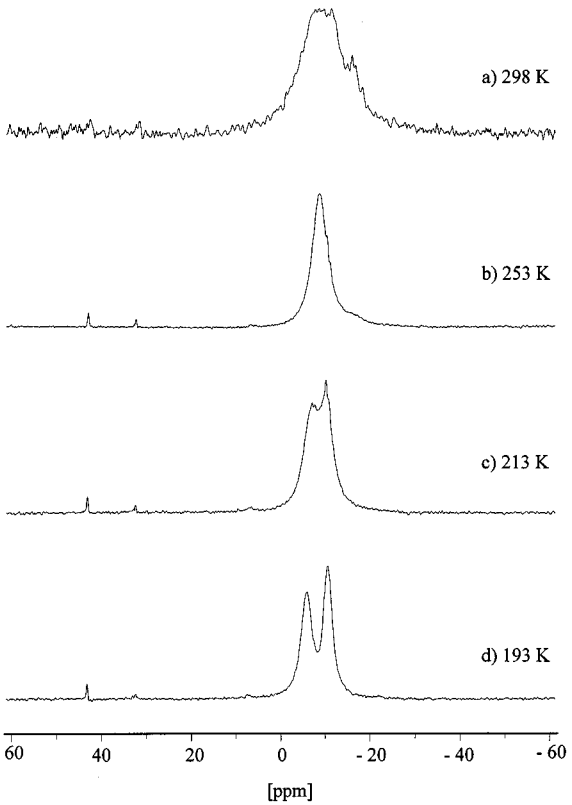


Figure 5. Temperature-dependent ^{31}P-NMR spectra (81 MHz) of $[Cu(dppp)_2]BF_4$ (**5**) (CD_2Cl_2; 85% H_3PO_4)

Experimental Section

Materials: 1,2-Bis(diphenylphosphanyl)ethane (dppe) and 1,3-bis(diphenylphosphanyl)propane (dppp) were purchased from Aldrich; CuI was obtained from Fluka and $Cu(BF_4)_2 \cdot x\ H_2O$ from ABCR Chemicals.

Measurements: ^{1}H-, ^{13}C-, and ^{31}P-NMR spectra at 200.13 or 300.13, 50.32 or 75.47, and 81.03 or 121.5 MHz, respectively, were measured with a Bruker AS 200 or a Bruker WH300 instrument with dichloromethane or chloroform as internal reference. H_3PO_4 (85%) was used as external reference for ^{31}P-NMR spectra. The ^{1}H-COSY and [^{13}C-^{1}H] spectra at 500.13 and 125.77 MHz were obtained with a Bruker Advance 500 instrument. − Infrared spectra (KBr pellets) were measured with a Perkin-Elmer 16PC FT-IR instrument. − Elemental analyses were obtained from the microanalytical laboratory of the chemical institutes of the University of Heidelberg. − Mass spectra (FAB or FD) were measured with a Finnigan 8400 (nitrobenzyl alcohol matrix) or a Jeol JMS-700 instrument.

Syntheses: All manipulations were carried out under Ar, using standard Schlenk techniques. CH_2Cl_2, $CHCl_3$, and diethyl ether were degassed by bubbling Ar through the solutions for 20 min. $[Cu(CH_3CN)_4]BF_4$ was prepared as reported in the literature.[11]

$[Cu(dppe)_2]BF_4 \cdot 0.5\ H_2O$ (1): $[Cu(CH_3CN)_4]BF_4$ (0.395 g, 1.26 mmol) was dissolved in CH_2Cl_2 (4 mL). The ligand dppe (1 g, 2.51 mmol) in CH_2Cl_2 (6 mL) was added (15 min) and the solution was stirred for 15 min at room temperature. After removing approximately 6 mL of the solvent and adding diethyl ether (10 mL), the solution was kept at −15°C over night. The resulting white precipitate was filtered off, recrystallized from methanol/water, and dried in vacuo. Yield (recrystallized): 0.63 g (0.66 mmol; 52%). − $C_{52}H_{48}BCuF_4P_4 \cdot 0.5\ H_2O$ (956.2): calcd. C 65.32, H 5.16, P 12.96; found C 65.43, H 5.13, P 13.03. − IR (KBr): $\tilde{\nu}$ [cm^{-1}] = 3050 (m, C_{ar}−H), 2918 (m, CH_2) 1482 (m, C_{ar}=C_{ar}), 1434 (s, P−Ph), 1054 (s, BF_4^-), 740, 694 (s, C_{ar}−H, 5 H neighboring). − MS (FAB); *m/z* (%): 859 (100) [M − BF_4], 646 (7) [M − BF_4 − $CH_2CH_2PPh_2$], 461 (98) [M − BF_4 − $CH_2CH_2PPh_2$ − PPh_2].

$[Cu(dppe)_2]I \cdot 0.5\ H_2O$ (2): A solution of dppe (1 g, 2.51 mmol) in $CHCl_3$ (6 mL) was slowly added to a suspension of CuI (0.239 g, 1.26 mmol) in $CHCl_3$ (2 mL). After stirring for 45 min, a pale yellow solution was obtained. The volume was reduced to 2 mL and diethyl ether was carefully added, until a white solid started to precipitate. After keeping at −15°C over night, the white precipitate was filtered off, recrystallized from methanol/water, and dried in vacuo. Yield (recrystallized): 0.43 g (0.43 mmol; 34%). − $C_{52}H_{48}CuIP_4 \cdot 0.5\ H_2O$ (996.3): calcd. C 62.69, H 4.96, P 12.44; found C 62.42, H 4.97, P 12.33. − IR (KBr): $\tilde{\nu}$ [cm^{-1}] = 3044 (m, C_{ar}−H), 2924 (m, CH_2) 1480 (m, C_{ar}=C_{ar}), 1432 (s, P−Ph), 740, 700 (s, C_{ar}−H, 5 H neighboring).

$[Cu_2(dppe)_3I_2]$ (3): A solution of dppe (1 g, 2.51 mmol) in CH_2Cl_2 (2 mL) was added to a suspension of CuI (0.319 g, 1.67 mmol) in CH_2Cl_2 (8 mL). The resulting colorless solution was stirred for 15 min, when a white solid started to precipitate. After storage at

Table 3. Crystallographic data for $[Cu(dppe)_2]ClO_4$ (**1**), $[Cu_2(dppe)_3I_2] \cdot 2\ CHCl_3$ (**3**), and $[Cu(dppp)_2]BF_4$ (**5**)[13]

Empirical formula	$C_{52}H_{48}ClCuO_4P_4$	$C_{80}H_{74}Cl_6Cu_2I_2P_6$	$C_{54}H_{52}BCuF_4P_4$
Formula mass	959.8	1814.9	975.3
Crystal dimensions [mm]	0.60 × 0.50 × 0.50	0.95 × 0.45 × 0.30	0.60 × 0.55 × 0.40
Crystal system	monoclinic	triclinic	monoclinic
a [Å]	12.169(3)	11.828(4)	17.432(3)
b [Å]	40.640(9)	12.341(7)	15.273(3)
c [Å]	19.738(5)	15.691(8)	18.209(4)
α [°]	90	77.03(5)	90
β [°]	97.25(2)	71.64(3)	99.86(2)
γ [°]	90	67.47(4)	90
V [$Å^{-3}$]	9683.3(40)	1993.8(17)	4776.3(16)
Space group	$P2_1/c$	$P-1$	$P2_1/c$
Z	8	2	4
Calcd. density [g cm^{-3}]	1.317	1.511	1.356
Absorption coeff. [mm^{-1}]	0.682	1.671	0.644
F(000)	3984	910	2024
θ range [°]	1.69−22.50	1.80−28.81	1.75−25.00
Radiation (λ [Å])	Mo-K_α (0.71073)	Mo-K_α (0.71073)	Mo-K_α (0.71073)
$R1$[a] [$I > 2\sigma(I)$]	0.062	0.072	0.061
$wR2$[b] (all data)	0.158	0.186	0.151
No. of reflections			
Measured	13116	10401	8702
Unique	12449 [R(int) = 0.032]	10400 [R(int) = 0.023]	8411 [R(int) = 0.060]
Obsd. [$I > 2\sigma(I)$]	8133	6652	6067
No. of variables	1150	444	782
Goodness of fit on F^2	1.131	1.057	1.063

[a] $R1 = \Sigma||F_o| - |F_c||/\Sigma|F_o|$. − [b] $wR2 = [(\Sigma w(|F_o| - |F_c|)^2/\Sigma wF_o^2)]^{1/2}$.

−15°C over night, the product was filtered off, recrystallized from methanol/water, and dried in vacuo. Yield (recrystallized): 0.8 g (0.51 mmol; 61%). − $C_{78}H_{72}Cu_2I_2P_6$ (1576.2): calcd. C 59.43, H 4.60, P 11.80; found C 59.72, H 4.77, P 11.63. − IR (KBr): $\tilde{\nu}$ [cm^{-1}] = 3046 (m, $C_{ar}-H$), 2902 (w, CH_2) 1482 (s, $C_{ar}=C_{ar}$), 1432 (s, P−Ph), 747, 705 (s, $C_{ar}-H$, 5 H neighboring). − MS (FD); *m/z* (%): 1449 (5) [M − I, $^{63/65}Cu$], 1051 (17) [M − I − $Ph_2PCH_2CH_2PPh_2$, $^{63/65}Cu$], 859 (100) [M − I − $Ph_2PCH_2CH_2PPh_2$ − CuI, $^{63/65}Cu$], 461 (5) [M − I − $Ph_2PCH_2CH_2PPh_2$ − CuI − $Ph_2PCH_2CH_2$ − PPh_2, $^{63/65}Cu$].

$[Cu_2(dppe)_2I_2] \cdot 0.2\ CH_2Cl_2$ (4): A suspension of CuI (0.239 g, 1.26 mmol) in CH_2Cl_2 (2 mL) was treated with a solution of dppe (0.5 g, 1.26 mmol) in CH_2Cl_2 (3 mL). After addition of $CHCl_3$ (5 mL) and stirring for 30 min at room temperature, diethyl ether was layered onto the colorless solution, which was kept over night at −15°C. The white precipitate was filtered off, washed with cold diethyl ether, and dried in vacuo. Yield: 0.85 g (0.72 mmol; 57%). − $C_{52}H_{48}Cu_2I_2P_4 \cdot 0.2\ CH_2Cl_2$ (1194.7): calcd. C 53.03, H 4.11, P 10.52; found C 51.94, H 4.06, P 10.22. − IR (KBr): $\tilde{\nu}$ [cm^{-1}] = 3043 (m, $C_{ar}-H$), 2924 (m, CH_2) 1481 (m, $C_{ar}=C_{ar}$), 1432 (s, P−Ph), 1096 (s, $C_{ar}=C_{ar}$), 739, 692 (s, $C_{ar}-H$, 5 H neighboring). − MS (FAB); *m/z* (%): 1051 (6) [M − I, $^{63/65}Cu$], 859 (100) [M − I − CuI], 653 (39) [M − I − $Ph_2PCH_2CH_2PPh_2$, $^{63/65}Cu$], 461 (70) [M − I − CuI − $Ph_2PCH_2CH_2PPh_2$].

$[Cu(dppp)_2]BF_4$ (5): A pale yellow solution of dppp (1 g, 2.43 mmol) in CH_2Cl_2 (5 mL) was slowly added to a solution of $[Cu(CH_3CN)_4]BF_4$ (0.382 g, 1.21 mmol) in CH_2Cl_2 (4 mL). After stirring for 15 min, the volume was reduced to 5 mL and diethyl ether was layered onto the solution. The resulting gum was solidified by scratching in ice-cold CH_2Cl_2, recrystallized from methanol/water, and dried in vacuo. Yield (recrystallized): 0.91 g, (0.93 mmol; 77%). − $C_{54}H_{52}BCuF_4P_4$ (975.3): calcd. C 66.50, H 5.37, P 12.70; found C 66.03, H 5.34, P 12.61. − IR (KBr): $\tilde{\nu}$ [cm^{-1}] = 3064 (m, $C_{ar}-H$), 2929 (m, CH_2) 1498 (m, $C_{ar}=C_{ar}$), 1439 (s, P−Ph), 1067 (s, BF_4^-), 746, 704 (s, $C_{ar}-H$, 5 H neighboring). − MS (FAB); *m/z* (%): 887 (51) [M − BF_4], 475 (100) [M − BF_4 − $Ph_2P(CH_2)_3PPh_2$].

$[Cu(dppp)_2]I \cdot 0.5\ H_2O$ (6): A white suspension of CuI (0.231 g, 1.21 mmol) in CH_2Cl_2 (2 mL) was added to a solution of dppp (1 g, 2.43 mmol) in CH_2Cl_2 (6 mL). After stirring for 15 min, a colorless solution was obtained. Addition of diethyl ether and storage at −15°C over night resulted in a white precipitate, which was filtered off, recrystallized from methanol/water, and dried in vacuo. Yield (recrystallized): 1.03 g (1.00 mmol; 83%). − $C_{54}H_{52}CuIP_4 \cdot 0.5\ H_2O$ (1824.3): calcd. C 63.32, H 5.21, P 12.09; found C 63.24, H 5.14, P 12.12. − IR (KBr): $\tilde{\nu}$ [cm^{-1}] = 3047 (m, $C_{ar}-H$), 2912 (m, CH_2) 1489 (m, $C_{ar}=C_{ar}$), 1439 (s, P−Ph), 746, 699 (s, $C_{ar}-H$, 5 H neighboring).

Structure Determinations: Intensity-measurement data were obtained with a Syntex R3 diffractometer, using Mo-K_α radiation and operating in the ω-scan mode at room temperature. Data were corrected for Lp and absorption effects (ψ scan). The structures were solved by direct methods (SHELXS 86[12a]) and refined by full-matrix least-squares methods based on F^2 (SHELXL 97[12b]), using anisotropic thermal parameters for all non-hydrogen atoms. Hydrogen atoms were placed in calculated positions, but their parameters were not refined. The $CHCl_3$ solvent molecules in $[Cu_2(dppe)_3I_2] \cdot 2\ CHCl_3$ and the BF_4^- anion in $[Cu(dppp)_2]BF_4$ are disordered. The crystallographic data for $[Cu(dppe)_2]ClO_4$, $[Cu_2(dppe)_3I_2] \cdot 2\ CHCl_3$ and $[Cu(dppp)_2]BF_4$ are summarized in Table 3.

Acknowledgments

We are grateful to Dr. Voelkel (BASF) for the CPMAS ^{31}P-NMR spectra, to Dr. Schilling for the HH- and CH-COSY spectra of $[Cu(dppp)_2]BF_4$ and to the BASF AG, Ludwigshafen, for financial support.

[1] [1a] S. J. Berners-Price, R. K. Johnson, C. K. Mirabelli, L. F. Faucette, F. L. McCabe, P. J. Sadler, *Inorg. Chem.* **1987**, *26*, 3383 − [1b] S. J. Berners-Price, C. Brevard, A. Pagelot, P. J. Sadler, *Inorg. Chem.* **1986**, *25*, 596.

[2] [2a] H. L. Finkbeiner, A. S. Hay, D. M. White, *Polymerization Processes* (Eds.: C. E. Schildknecht, I. Skeist), Wiley-Interscience, New York, **1977**, p. 537 – [2b] G. W. Parshall, *Homogeneous Catalysis*, Wiley-Interscience, New York, **1980**, p. 113 – [2c] P. M. Henry, *Adv. Organomet. Chem*. **1975**, *13*, 363 – [2d] E. W. Stern, *Catal. Rev.* **1968**, *1*, 74.

[3] [3a] M. Freiberg, D. Meyerstein, *J. Chem. Soc., Faraday Trans. 1* **1980**, *76*, 1825 – [3b] M. Freiberg, W. A. Mulac, K. H. Schmidt, D. Meyerstein, *J. Chem. Soc., Faraday Trans. 1* **1980**, *76*, 1838 – [3c] H. Cohen, D. Meyerstein, *Inorg. Chem.* **1986**, *25*, 1506 – [3d] S. Goldstein, G. Czapski, H. Cohen, D. Meyerstein, *Inorg. Chem.* **1992**, *31*, 2439 – [3e] N. Navon, G. Golub, H. Cohen, D. Meyerstein, *Organometallics* **1995**, *14*, 5670.

[4] [4a] V. G. Albano, P. L. Bellon, G. Ciani, M. Manassero, *J. Chem. Soc., Dalton Trans.* **1972**, 171 – [4b] V. G. Albano, P. L. Bellon, G. Ciani, *J. Chem. Soc., Dalton Trans.* **1972**, 1938 – [4c] A. Camus, G. Nardin, L. Randaccio, *Inorg. Chim. Acta* **1975**, *12*, 23 – [4d] P. G. Eller, G. J. Kubas, R. R. Ryan, *Inorg. Chem*. **1977**, *16*, 2454 – [4e] P. Leoni, M. Pasquali, C. A. Ghilardi, *J. Chem. Soc., Chem. Commun*. **1983**, 240 – [4f] D. J. Fife, W. M. Moore, K. W. Morse, *Inorg. Chem*. **1984**, *23*, 1684 – [4g] G. Doyle, K. A. Eriksen, D. Van Engen, *J. Am. Chem. Soc.* **1985**, *107*, 7914 – [4h] P. F. Barron, J. C. Dyason, P. Healy, L. M. Engelhardt, C. Pakawatchai, V. A. Patrick, A. H. White, *J. Chem. Soc., Dalton Trans.* **1987**, 1099 – [4i] S. J. Rettig, A. Storr, J. Trotter, *Can. J. Chem*. **1988**, *66*, 2194 – [4j] D. F. Dempsey, G. S. Girolami, *Organometallics* **1988**, *7*, 1208 – [4k] G. A. Bowmaker, A. Camus, P. C. Healy, B. W. Skelton, A. H. White, *Inorg. Chem*. **1989**, *28*, 3883 – [4l] G. A. Bowmaker, P. C. Healy, L. M. Engelhardt, J. D. Kildea, B. W. Skelton, A. H. White, *Aust. J. Chem*. **1990**, *43*, 1697 – [4m] D. J. Darensbourg, C. C. Chao, J. H. Reibenspies, C. J. Bischoff, *Inorg. Chem*. **1990**, *29*, 2153 – [4n] R. D. Hart, B. W. Skelton, A. H. White, *Aust. J. Chem*. **1991**, *44*, 919 – [4o] B. Mohr, E. E. Brooks, N. Rath, E. Deutsch, *Inorg. Chem*. **1991**, *30*, 4541 – [4p] S. J. Berners-Price, L. A. Colquhoun, P. C. Healy, K. A. Byriel, J. V. Hanna, *J. Chem. Soc., Dalton Trans.* **1992**, 3357 – [4q] G. A. Bowmaker, R. D. Hart, B. E. Jones, B. W. Skelton, A. H. White, *J. Chem. Soc., Dalton Trans.* **1995**, 3063 – [4r] S. Kitagawa, M. Kondo, S. Katawa, S. Wada, M. Maekawa, M. Munakata, *Inorg. Chem*. **1995**, *34*, 1455.

[5] S. J. Berners-Price, R. J. Brown, P. A. Harvey, P. C. Healey, G. A. Koutsantonis, *J. Chem. Soc., Dalton Trans.* **1998**, 1743.

[6] C. K. Johnson, *ORTEP, A Thermal Ellipsoid Plotting Program*, Oak Ridge National Laboratory, Tennessee, U.S.A., **1965**.

[7] S. P. Neo, Z. Y. Zhou, T. C. W. Mak, T. S. A. Hor, *J. Chem. Soc., Dalton Trans.* **1994**, 3451.

[8] R. J. Batchelor, T. Birchall, R. Faggiani, *Can. J. Chem*. **1985**, *63*, 928.

[9] E. M. Menger, W. S. Veeman, *J. Magn. Reson*. **1982**, *46*, 257.

[10] A. Marker, M. J. Gunter, *J. Magn. Reson*. **1982**, *47*, 118.

[11] G. J. Kubas, *Inorg. Synth*. **1979**, *19*, 90.

[12] [12a] G. M. Sheldrick, *SHELXS 86*, University of Göttingen, **1986** – [12b] G. M. Sheldrick, *SHELXL 97*, University of Göttingen, **1997**.

[13] Crystallographic data (excluding structure factors) for the structures reported in this paper have been deposited with the Cambridge Crystallographic Data Centre as supplementary publication nos. CCDC-114482 (**3**), -114483 (**1**), -114484 (**5**). Copies of the data can be obtained free of charge on application to CCDC, 12 Union Road, Cambridge CB2 1EZ, UK [Fax: int. code + 44-1223/336-033; E-mail: deposit@ccdc.cam.ac.uk].

Received November 30, 1998
[I98409]

Determination of the Se Atom Distribution in the Layered Compound $Nb_3(Se_{1-x}I_x)I_7$ by Scanning Tunneling Microscopy

Peter J. Schmidt,[a] Gerhard Thiele,*[a] and Myung-Hwan Whangbo*[b]

Keywords: Atom distribution / Mixed crystals / Scanning tunneling microscopy / Layered compounds

The layered compound $Nb_3(Se_{1-x}I_x)I_7$ is obtained when the I atoms at the face-capping sites of the layered compound Nb_3I_8 are replaced by Se atoms. The amount and distribution of the Se atoms in $Nb_3(Se_{1-x}I_x)I_7$ were examined by scanning tunneling microscopy. The analysis shows that the distribution of the Se atoms is completely random.

It is a challenging problem to study how chemical substitution or doping affect the structural and electronic properties of a material at the atomic level. A local-probe technique such as scanning tunneling microscopy (STM)[1][2] provides information about localized defects of a modified material, as demonstrated in a number of STM studies on layered compounds[3−6] and alloys.[7][8] Recently, a number of ternary compounds Nb_3YX_7 (X = halogen, Y = chalcogen) have been prepared.[9] As shown for $Nb_3S_{1-x}I_{7+x}$,[10] a wide range of mixed crystals between Nb_3X_8 and Nb_3YX_7 can be obtained. These compounds are related to the layered halides Nb_3X_8 (X = Cl, Br, I),[11] whose building block is an Nb_3X_{13} cluster (Figure 1a). Nb_3X_8 layers are obtained from these clusters upon sharing their outer octahedral edges (Figure 1b) in such a way that the two surfaces of an Nb_3X_8 layer are different: One surface (surface A) has the triangular face of each Nb_3 trimer capped by the X(4) atom, while the other surface (surface B) has the edges of each Nb_3 trimer capped by the X(1) atoms. The layers of Nb_3X_8 are stacked such that the interface between adjacent layers consists of either surface A or surface B (Figure 1c). Our single-crystal X-ray diffraction analysis of different $Nb_3Se_{1-x}I_{7+x}$ samples shows that only the face-capping site, i.e., I(4), is replaced by Se. When $0 < x < 1$, the face-capping sites of $Nb_3Se_{1-x}I_{7+x}$ are occupied by either I or Se so that each $Nb_3Se_{1-x}I_{7+x}$ layer consists of Nb_3I_{13} and Nb_3SeI_{12} clusters. In this paper, we demonstrate that the amount and distribution of the Se atoms in $Nb_3Se_{1-x}I_{7+x}$ can be determined by STM.

Typical STM images of $Nb_3Se_{1-x}I_{7+x}$ are divided into two groups, A and B, because the surface of the $Nb_3Se_{1-x}I_{7+x}$ sample mounted on the support can be either surface A or surface B. The STM images of group A show patterns of three bright and one less bright spots per unit cell (Figure 2a). This pattern can be readily seen by filtering the observed image by the two-dimensional fast Fourier transform procedure, as illustrated on the upper left part of Figure 2a. The STM images of group A exhibit image defects as dark spots that have the size of approximately one cluster unit. The STM images of group B show one bright spot for each unit cell, with varying degrees of brightness (Figure 2b). The STM images of group A and B recorded for $Nb_3Se_{1-x}I_{7+x}$ refer to the surfaces A and B, respectively. When the image defects are neglected, their unit cell patterns are similar in pattern to the partial density plots $\rho(r_0, E_f)$ calculated for surfaces A and B of Nb_3I_8, respectively.[12]

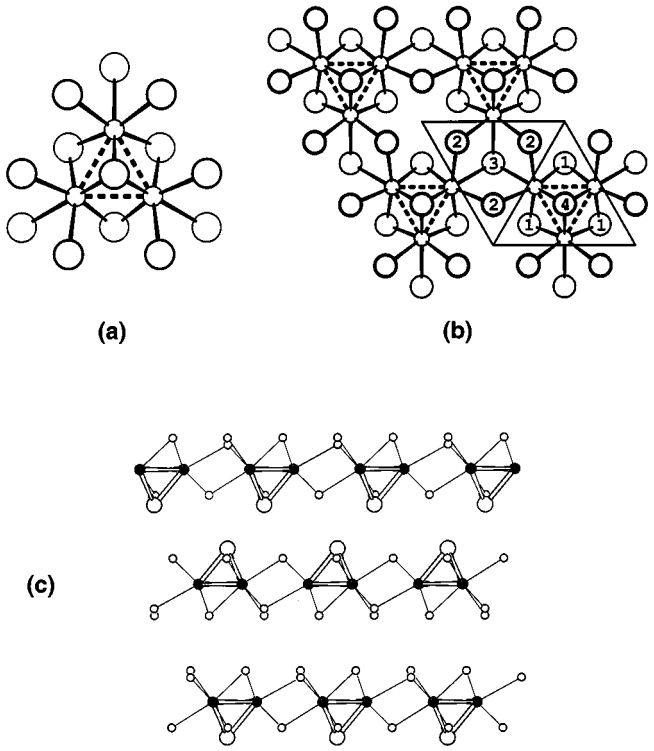


Figure 1. (a) Perspective view of an $[Nb_3X_{13}]^{5-}$ cluster, where the small and large circles represent Nb and X atoms, respectively; (b) top, (001) projection of a single Nb_3X_8 layer; the X(4) and X(1) atoms occupy the face- and edge-capping sites of each Nb_3 cluster, respectively; the X(2) atoms bridge two clusters, and the X(3) atoms connect three Nb_3 clusters; (c) schematic projection view of how the Nb_3X_8 layers stack in Nb_3I_8; the shaded circles represent the Nb atoms, the large open circles the X(4) atoms, and the small open circles all other X atoms

Figures 3a and 3c show representative STM images recorded for the surface B of $Nb_3Se_{0.24}I_{7.76}$. The image of Figure 3a was obtained with $I_{set\text{-}point}$ = 3.82 nA and V_{bias} =

[a] Institut für Anorganische und Analytische Chemie and Materialforschungszentrum (FMF), Albert-Ludwigs-Universität, Stefan-Meier-Strasse 21a, D-79104 Freiburg, Germany
[b] Department of Chemistry, North Carolina State University, Raleigh, North Carolina 27695-8204, USA

 © WILEY-VCH Verlag GmbH, D-69451 Weinheim, 1999 1434−1948/99/0505−0785 $ 17.50+.50/0

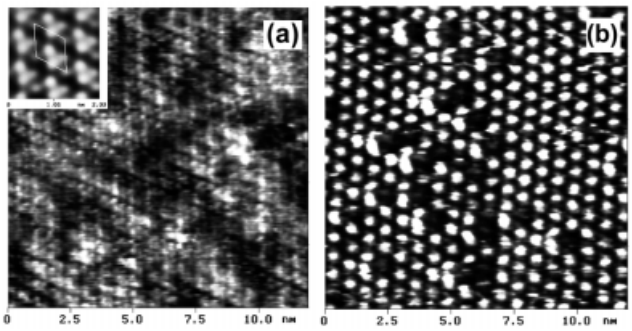


Figure 2. (a) STM current image of $Nb_3Se_{0.36}I_{7.64}$ ($V_{bias} = -164.8$ mV, $I_{set\text{-}point} = 19.89$ nA); (b) STM current image of $Nb_3Se_{0.09}I_{7.91}$ ($V_{bias} = -300$ mV, $I_{set\text{-}point} = 3.48$ nA)

-517.9 mV, and that of Figure 3c with $I_{set\text{-}point} = 15.98$ nA and $V_{bias} = -481.3$ mV. The tip-sample distance in contact-mode STM decreases with decreasing the resistance gap, $R_{gap} = |V_{bias}|/I_{set\text{-}point}$.[2d] Thus, the strength of the tip-sample repulsive interaction, and hence the extent of the sample indentation induced by the tip force, increases with decreasing R_{gap}.[2d] The values of R_{gap} used to obtain the STM images of Figures 3a and 3c are 135.6 and 30.12 MΩ, respectively, so that the tip-sample repulsive interaction leading to the STM image of Figure 3c was much stronger than that leading to the STM image of Figure 3a. To see how often the spot of any given contrast occurs in the STM image of Figure 3a, the contrast of each spot in this image was analyzed. The histogram of Figure 3b shows how many times (in relative number) the spot of a certain contrast occurs as a function of the contrast. The corresponding analysis carried out for the STM image of Figure 3c is summarized in Figure 3d. The bright and less bright spots are more clearly separated in Figure 3d than in Figure 3b. As will be shown below, the concentration ratio [Se]/[I(4)] in $Nb_3Se_{1-x}I_{7+x}$, which is given by $(1 - x)/x$, is equal to the number ratio of the dark spots to the bright spots in the STM images of group B. Thus, the difference between the Nb_3I_{13} and Nb_3SeI_{12} clusters in $Nb_3Se_{1-x}I_{7+x}$ is more clearly distinguished when the tip-sample force interaction is stronger. The reason for this observation will be discussed in our forthcoming paper.[13]

The above discussion shows that the content and distribution of Se in $Nb_3Se_{1-x}I_{7+x}$ can be detected by STM. To examine the nature of the Se atom distribution in $Nb_3Se_{1-x}I_{7+x}$, we analyzed the STM images recorded for the surface B of $Nb_3Se_{1-x}I_{7+x}$. It is easy to assign whether a given spot of the STM image is associated with the Nb_3I_{13} or the Nb_3SeI_{12} cluster; consequently, a given STM image can be converted into a digitized image consisting solely of bright and dark circles representing the Nb_3I_{13} and Nb_3SeI_{12} clusters, respectively. For instance, Figure 4 shows four digitized images obtained from the STM images determined on four different surface regions of $Nb_3Se_{0.24}I_{7.76}$. The amount of Se determined from the digitized images is in good agreement with that determined by wavelength-dispersive X-ray (WDX) analysis. In the digitized images,

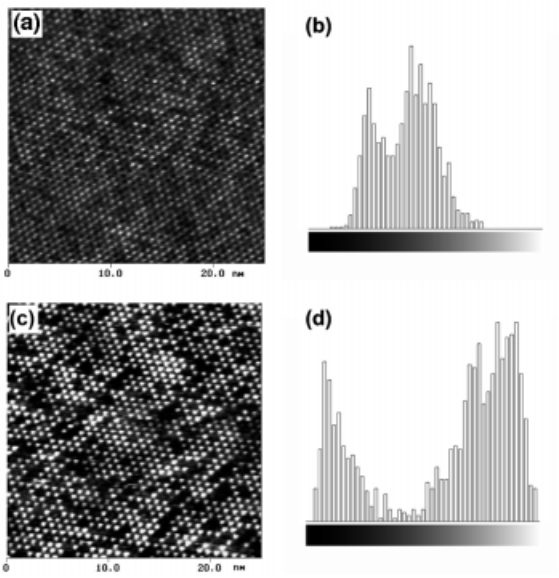


Figure 3. (a) STM current image recorded for surface B of $Nb_3Se_{0.24}I_{7.76}$ ($I_{set\text{-}point} = 3.82$ nA, $V_{bias} = -517.9$ mV); (b) histogram of how often the spot of any given contrast occurs in the STM image of (a); (c) STM current image recorded for surface B of $Nb_3Se_{0.24}I_{7.76}$ ($I_{set\text{-}point} = 15.98$ nA, $V_{bias} = -481.3$ mV); (d) histogram of how often the spot of any given contrast occurs in the STM image of (c); the images of (a) and (c) were obtained from the same sample surface, but the positions are not the same due to the thermal drift during the measurements; the contrast variations in (a) and (c) cover the same range and are proportional to ln I

bright and dark circles form a hexagonal lattice in which each circle is surrounded with six nearest neighbor circles.

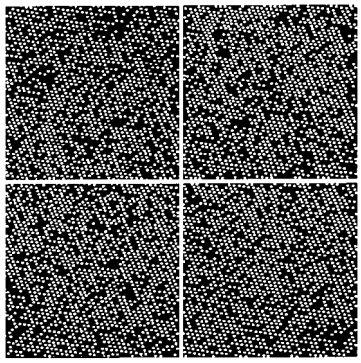


Figure 4. Digitized images derived from analyzing surface B STM images of $Nb_3Se_{0.24}I_{7.76}$ (30 nm × 30 nm); bright and dark spots refer to the Nb_3I_{13} and Nb_3SeI_{12} clusters, respectively

To determine if the distribution of the Se atoms is random, we examined each dark circle of the digitized image and counted how many of its nearest neighbor circles are dark circles. If the distribution of the Se atoms in $Nb_3Se_{1-x}I_{7+x}$ is truly random, then the probability $p(m)$ of finding $m = 0$, 1, 2, 3, 4, 5, or 6 dark circles as nearest neighbors of a given dark circle can be described by a binomial distribution (Equation 1)

$$p(m) = [6!/m!(6 - m)!](1 - x)^m(x)^{6-m} \quad (1)$$

The $p(m)$ values predicted by Equation 1 are compared with the experimental values determined by analyzing the

digitized images of $Nb_3Se_{0.24}I_{7.76}$ in Figure 5, which shows an excellent agreement between the theoretical and experimental $p(m)$ values. The same result is obtained with samples of different Se content. Thus, the distribution of the Se atoms in $Nb_3Se_{1-x}I_{7+x}$ is random.

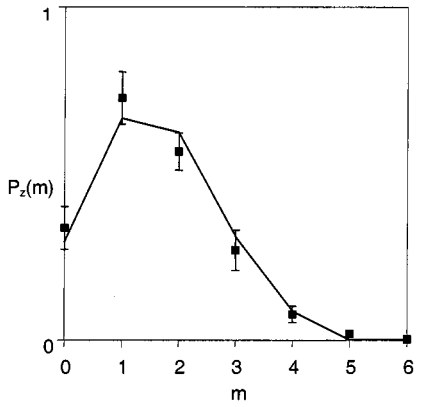


Figure 5. Comparison of the theoretical and experimental $p(m)$ values determined for the distribution of the Se atoms in $Nb_3Se_{0.24}I_{7.76}$

In summary, we determined the content and distribution of Se in $Nb_3Se_{1-x}I_{7+x}$ by carrying out STM experiments. Our work shows that the Nb_3I_{13} and Nb_3SeI_{12} clusters are distinguished by STM, and that the distribution of the Se atoms in $Nb_3Se_{1-x}I_{7+x}$ is random.

Experimental Section

Single crystals of $Nb_3Se_{1-x}I_{7+x}$ were obtained by heating mixtures of the elements in evacuated sealed silica tubes as described in ref.[11b] To avoid the twinning of crystals, the tubes were rapidly quenched at the end of reaction. Higher niobium iodides and niobium selenide iodides were separated from the desired product by sublimation before opening the tubes. The purity and homogeneity of the products were checked by powder X-ray diffraction. The structure and chemical composition of the products were determined by single-crystal X-ray diffraction analysis and by WDX analysis using β-Nb_3I_8 and LT-$NbSe_2I_2$[14] as standards. Samples of $Nb_3Se_{1-x}I_{7+x}$ were examined by STM, as described for Nb_3I_8 elsewhere.[12] Contact-mode STM measurements were carried out on freshly cleaved surfaces of the mounted crystal samples at ambient conditions using a commercial scanning probe microscope Nanoscope II (Digital Instruments, Inc.), mechanically sharpened Pt/Ir 70:30 tips for STM, and commercial cantilevers with Si_3N_4 probes for AFM.

Acknowledgments

The work at North Carolina State University was supported by the Office of Basic Energy Sciences, Division of Materials Sciences, U. S. Department of Energy, under Grant DE-FG05−86ER45259. The work at Freiburg University was financially supported by the Deutsche Forschungsgemeinschaft (DFG) and the Fonds der Chemischen Industrie.

[1] G. Binnig, H. Rohrer, C. Gerber, E. Weibel, *Phys. Rev. Lett.* **1982**, *49*, 57.
[2] [2a] R. Wiesendanger, H.-J. Güntherodt, *Scanning Tunneling Microscopy I, II and III*, Springer, Heidelberg, **1992** and **1993**. − [2b] C. J. Chen, *Introduction to Scanning Tunneling Microscopy*, Princeton University Press, Princeton, **1993**. − [2c] D. A. Bonnell, *Scanning Tunneling Microscopy and Spectroscopy*, VCH, New York, **1993**. − [2d] S. N. Magonov, M.-H. Whangbo, *Surface Analysis with STM and AFM*, VCH, Weinheim, **1996**.
[3] B. A. Parkinson, *J. Am. Chem. Soc.* **1990**, *112*, 1030.
[4] H. Dai, C. M. Lieber, *J. Phys. Chem.* **1993**, *97*, 2362.
[5] [5a] P. J. Schmidt, *Diploma Thesis*, Freiburg University, **1996**. − [5b] H. Hillebrecht, P. J. Schmidt, H. W. Rotter, G. Thiele, P. Zönnchen, H. Bengel, H.-J. Cantow, S. N. Magonov, M.-H. Whangbo, *J. Alloys Comp.* **1997**, *246*, 70.
[6] X. Lu, K. W. Hipps, X. D. Wang, U. Mazur, *J. Am. Chem. Soc.* **1996**, *118*, 7197.
[7] M. Schmid, H. Stadler, P. Varga, *Phys. Rev. Lett.* **1993**, *70*, 1441
[8] P. T. Wouda, B. E. Nieuwenhuys, M. Schmid, P. Varga, *Surf. Sci.* **1996**, *359*, 17
[9] [9a] S. Furuseth, W. Hönle, G. J. Miller, H. G. von Schnering, *9th International Conference on Solid Compounds of Transition Elements, Abstracts*, Royal Society of Chemistry, London, **1988**. − [9b] G. V. Khvorykh, A. V. Shevelkov, V. A. Dolgikh, B. A. Popovkin, *J. Solid State Chem.* **1995**, *120*, 311. − [9c] G. J. Miller, *J. Alloys Comp.* **1995**, *217*, 5. − [9d] G. J. Miller, *J. Alloys Comp.* **1995**, *229*, 93.
[10] [10a] C.-S. Lee, *M. Sc. Thesis*, Iowa State University, **1997**. − [10b] G. J. Miller, J. Lin, M. D. Smith, C. S. Lee, to be published.
[11] [11a] H. G. von Schnering, H. Wöhrle, H. Schäfer, *Naturwissenschaften* **1961**, *48*, 159. − [11b] A. Simon, H. G. von Schnering, *J. Less-Common Met.* **1966**, *11*, 31. − [11c] F. Hulliger, *Structural Chemistry of Layer-Type Phases* (Ed.: F. Lévy), Reidel, Dordrecht, The Netherlands, **1976**.
[12] S. N. Magonov, P. Zönnchen, H. W. Rotter, G. Thiele, H.-J. Cantow, J. Ren, M.-H. Whangbo, *J. Am. Chem. Soc.* **1993**, *115*, 2495.
[13] P. J. Schmidt, G. Thiele, H. -J. Cantow, J. Ren, M.-H. Whangbo, in preparation.
[14] J. Rijnsdorp, G. J. De Lange, G. A. Wiegers, *J. Solid State Chem.* **1979**, *30*, 365.

Received December 15, 1998
[I98432]

Nucleophilic Substitution Reactions with the 3-Borane-1,4,5-trimethylimidazol-2-ylidene Anion. – Unexpected Formation of an Imidazabole Isomer

Andreas Wacker,[a] Hans Pritzkow,[a] and Walter Siebert*[a]

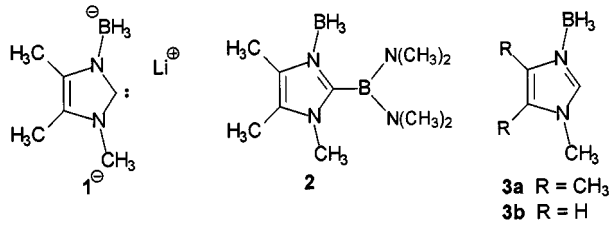
Dedicated to Prof. Bernt Krebs on the occasion of his 60th birthday

Keywords: Boranes / Carbenes / Heterocycles / Imidazoles / X-ray structures

The nucleophilic carbene 3-borane-1,4,5-trimethylimidazol-2-ylidene anion (**1**$^-$) reacts with the electrophiles CH_3I, $(CH_3)_3SiCl$, $(CH_3)_3SnCl$, and the bromodiazaboroline **7** to form the 2-substituted imidazoles **4**, **5**, **6**, and **8**. With triethylborane, the anionic carbene borane adduct **9**$^-$ is obtained. An unexpected result was achieved when chlorodimethoxyborane and $HBCl_2 \cdot S(CH_3)_2$ were used as electrophiles. In both cases only the imidazabole **14a** could be isolated. Imidazole **5**, the imidazole borane adduct **3a** and the imidazabole **14a** were characterized by X-ray structure analyses.

Introduction

Imidazol-2-ylidenes are stable carbenes which have attracted wide attention[1]. Recently, we described the synthesis and characterization of the first anionic imidazol-2-ylidene, the 3-borane-1,4,5-trimethylimidazol-2-ylidene anion (**1**$^-$),[2] and showed that it reacts with bis(dimethylamino)chloroborane to form **2**. We now report further details on the reactivity of **1**$^-$ towards various electrophiles.

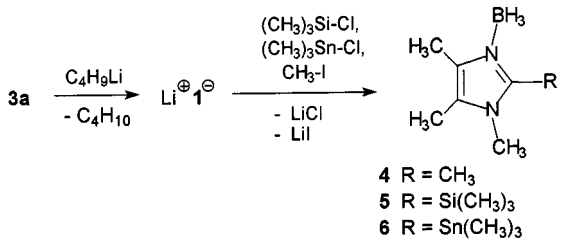


Results and Discussion

Formation of Substituted Imidazoles

The anion **1**$^-$ reacts with iodomethane, chlorotrimethylsilane and -stannane to give the expected 2-substituted imidazoles (Scheme 1). The products **4**, **5**, and **6** are obtained as air-stable compounds.

The reaction of **1**$^-$ with iodomethane results in the formation of 3-borane-1,2,4,5-tetramethylimidazole (**4**), which was first prepared[3] from 1,2,4,5-tetramethylimidazole and $BH_3 \cdot SMe_2$. The donor-acceptor compound is isoelectronic with the pentamethylimidazolium ion[3]. **4** is separated from LiI by sublimation which, however, lowers the yield com-



Scheme 1

pared with that of **5** and **6**. In the ^{1}H-NMR spectrum the signal for the methyl group in 2-position is found at δ = 2.45 which is 0.33 ppm at low-field compared with the shift for the CH_3 substituents in 4- and 5-position. The ^{13}C-NMR spectrum shows the expected high-field shift of the C2 carbon atom from δ = 191.3 in **1** to δ = 142.3. In the ^{11}B-NMR spectrum a 1:3:3:1 quartet is observed at δ = −22.4, [^1J(BH) = 82 Hz].

The analogous reaction of **1**$^-$ with chlorotrimethylsilane leads to 3-borane-1,4,5-trimethyl-2-(trimethylsilyl)imidazole (**5**) in quantitative yield. Its NMR data are similar to those of **4**. The trimethylsilyl group shows a resonance in the ^{1}H-NMR spectrum at δ = 0.52 and in the ^{13}C-NMR spectrum at δ = 1.7. As in **4**, the C2 carbon atom again experiences a high-field shift to δ = 146.9 and the ^{11}B-NMR signal is found as a quartet at δ = −19.7. **5** is an isomer of the 1-borane-2,4,5-trimethyl-3-trimethylsilylimidazole adduct (δ^{11}B = −21.8)[3].

Analogously, 3-borane-1,4,5-trimethyl-2-(trimethylstannyl)imidazole (**6**) is quantitatively synthesized from **1**$^-$ and chlorotrimethylstannane. The NMR spectra of **6** are nearly identical with those of **5**: The trimethylstannyl group is found in the ^{1}H-NMR spectrum at δ = 0.49 and in the ^{13}C-NMR spectrum at δ = −5.1. The signal for the C2 carbon atom appears at δ = 151.5 which is five ppm low-field com-

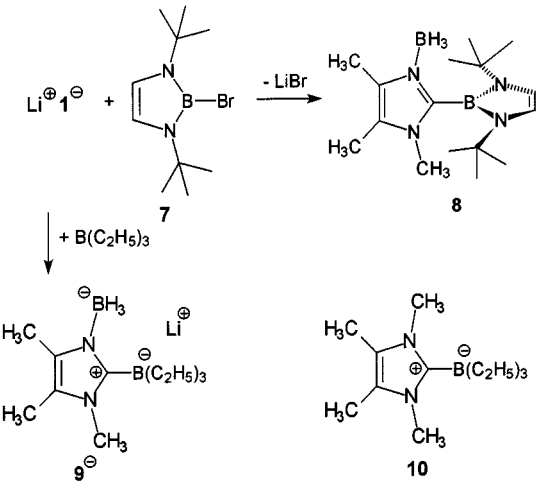
[a] Anorganisch-Chemisches Institut der Universität,
Im Neuenheimer Feld 270, D-69120 Heidelberg, Germany
Fax: (internat.) + 49(0)6221/54-5609
E-mail: ci5@ix.urz.uni-heidelberg.de

 © WILEY-VCH Verlag GmbH, D-69451 Weinheim, 1999 1434–1948/99/0505–0789 $ 17.50+.50/0

pared to that of **5**. In the ^{11}B-NMR spectrum the signal appears at $\delta = -19.9$.

2-Bromo-1,3-di(*tert*-butyl)-1,3,2-diazaboroline (**7**) reacts with the anion $\mathbf{1}^-$ to give **8** (Scheme 2) which is characterized by NMR and mass spectroscopy. The ^{1}H-NMR spectrum shows three singlets for the methyl groups of the imidazole ring at $\delta = 2.14$, 2.20, and 3.38. The signals for the diazaboroline substituent are found at $\delta = 1.18$ (*tert*-butyl) and 6.46 (C-H). The appearance of only two singlets indicates that the C_2N_2B-ring is orientated perpendicular to the imidazole plane, due to the steric hindrance of the *tert*-butyl substituents. As expected, all signals are shifted to higher field compared with those of a cationic carbene borane adduct, obtained from **7** and 1,3-dimethyl-imidazol-2-ylidene[4].

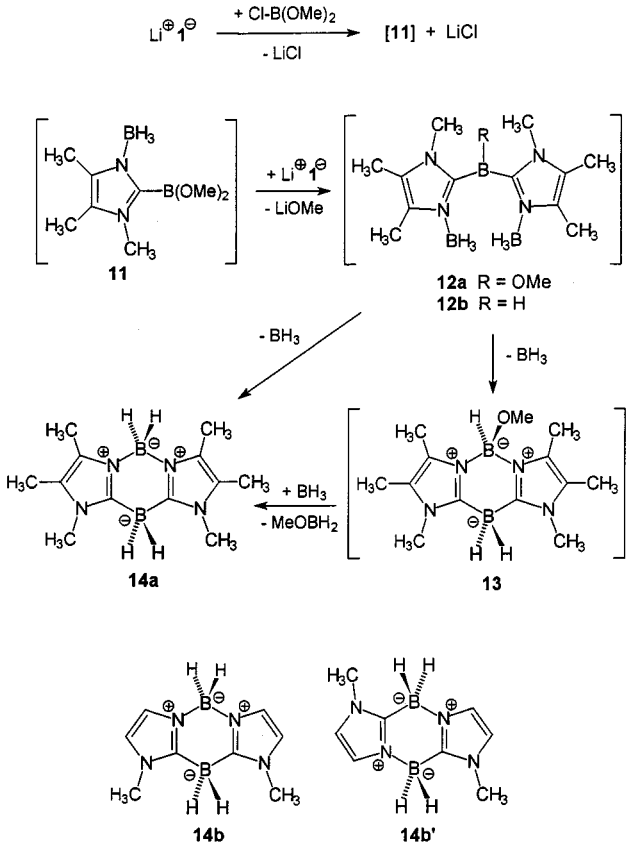
The ^{13}C-NMR spectrum shows the signals for the diazaboroline ring at $\delta = 31.0$, 53.1, and 114.7 and five more at $\delta = 8.6$, 10.1, 32.8, 123.9, and 132.0 belonging to the imidazole. The C2 atom is not observed. In the ^{11}B-NMR spectrum two signals at $\delta = 19.1$ (C-BN_2) and -20.1 (N-BH_3) are found.



Scheme 2

Reaction of 1^- with Boranes

When $\mathbf{1}^-$ is treated with the Lewis acid triethylborane, the anionic borane adduct $\mathbf{9}^-$ is obtained (Scheme 2). Neutral carbene-borane adducts of 1,3-dialkyl-imidazol-2-ylidenes and BH_3 or BF_3 are already known[5] as well as 1,3,4,5-tetramethyl-2-(triethylborane)imidazoline (**10**), which was recently prepared by a different route[2]. $\mathbf{9}^-$ and **10** are isoelectronic, a formal substitution of CH_3 in **10** by BH_3^- leads to $\mathbf{9}^-$. In its ^{1}H-NMR spectrum the signals for the B-C_2H_5 substituents are found as a broad multiplet ($\delta = 1.1-1.3$) and for the methyl groups at $\delta = 1.68$, 2.24, and 3.55. In the ^{13}C-NMR spectrum the B-C_2H_5 substituents show resonance at $\delta = 12.6$ (CH_3) and 16 (CH_2) of which the latter signal is broadened. The C2 carbon atom in $\mathbf{9}^-$ ($\delta = 175$) exhibits a different chemical shift compared with those of **4**, **5**, and **6**. – As expected, $\mathbf{9}^-$ shows two signals



Scheme 3

in the ^{11}B-NMR spectrum at $\delta = -12.5$ (C-BEt_3) and -21.6 (N-BH_3).

An interesting observation was made, when $\mathbf{1}^-$ was treated with chlorodimethoxyborane. In analogy to the formation of **4**–**6**, and **8**, we expected to find the dimethoxyboryl-substituted imidazole **11** but to our surprise, the only product that could be isolated was the imidazabole **14a** (Scheme 3). It is likely that in the first step **11** is formed, however, it then reacts with additional $\mathbf{1}^-$ to give **12a**. Obviously, ring closure to **13a** occurs with elimination of BH_3 and migration of H^- to the B–R group The methoxy group in **13a** is exchanged for hydrogen to give **14a** and [$(CH_3O)BH_2$] of which the latter was not identified.

To study the influence of boranes on the formation of **14a** the anion $\mathbf{1}^-$ was treated with $BH_3 \cdot$ thf. In the reaction mixture **14a** could be identified in the ^{11}B-NMR spectrum besides other signals that were not assigned. When $\mathbf{1}^-$ was treated with $HBCl_2 \cdot S(CH_3)_3$ in a ratio of 2:1, **14a** was obtained in 48% yield (calculated for $\mathbf{1}^-$). With a 3:1 ratio, the yield increased to 66%. These findings indicate that BH_3, set free in the ring closure process, participates in the reaction with $\mathbf{1}^-$ to give **14a**.

The structure of **14a** follows from the NMR and MS data. The two triplets in the ^{11}B-NMR spectrum at $\delta = -10$ (C_2BH_2) and -32 (N_2BH_2) clearly show that **14a** has been formed. In the ^{1}H-NMR spectrum three signals appear at $\delta = 2.10$, 2.17, and 3.49 and in the ^{13}C-NMR spectrum at $\delta = 9.2$, 10.3, and 31.9. The signals for the ring

carbon atoms are observed at δ = 123.6 and 127.3, that of the C2 atom was not found.

14a is isomeric to the imidazabole **14b′** which was obtained by Contreras, Wrackmeyer et al. in the thermolysis reaction of **3b**[6]. During their investigations they could isolate both isomers **14b** and **14b′**. We did not observe the formation of **14a′**. Thus, a change of the substituents at the boron atom by choosing chlorodimethoxyborane instead of a chlorodiaminoborane leads to a completely different reaction pathway in which the substituted imidazoles **11** and **12b** are postulated intermediates. Different reaction conditions like changing the order in which the starting materials are added as well as carrying out the reaction at elevated temperature have no influence on product formation.

X-ray Structure Analyses of 3a, 5, and 14a

Figure 1 shows the structure of planar **3a**. The B6−N1 distance of **3a** [1.584(3) Å] is similar to that of the trimethylsilyl derivative **5**. Single crystals of **5** were grown from a toluene/hexane solution and the structure is depicted in Figure 2. Comparism of **5** with the carbene anion **1**$^-$ and the imidazole borane adduct **3a** (Figure 1) shows that the structural parameters lie between those of **1**$^-$ and **3a**.

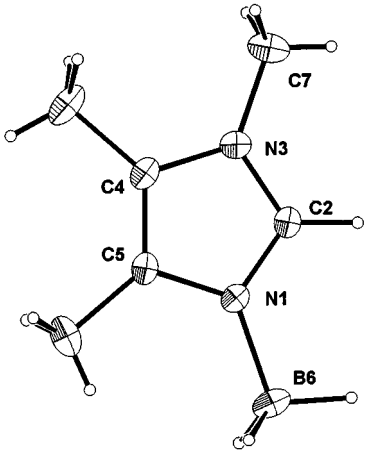


Figure 1. Structure of **3a** in the crystal; bond lenghts and angles are listed in Table 1

Imidazol-2-ylidenes characteristically have smaller N−C−N and larger C−N−C angles than imidazoles. Their C2−N1/2 bonds are equal in contrast to that of imidazole molecules which show single and double bond character[1−3]. In the case of **5**, the following observations are made: First, the C2−N1/2 distances with 1.348(3) and 1.367(3) Å exhibit bond length alternations as in imidazole molecules and they are shorter in comparison with those in **1**$^-$ but are still longer than in **3a** (Table 1). Second, the N−C−N angle of 106.6° has increased compared with that of **1**$^-$ but is still considerably smaller than that of **3a**. The third characteristic structural pattern, the C−N−C angles also show the same tendency: With 109.1° and 109.7° they lie between those found for **1**$^-$ and **3a**. A similar trend is observed in the ^{13}C-NMR shifts of the C2 atoms which

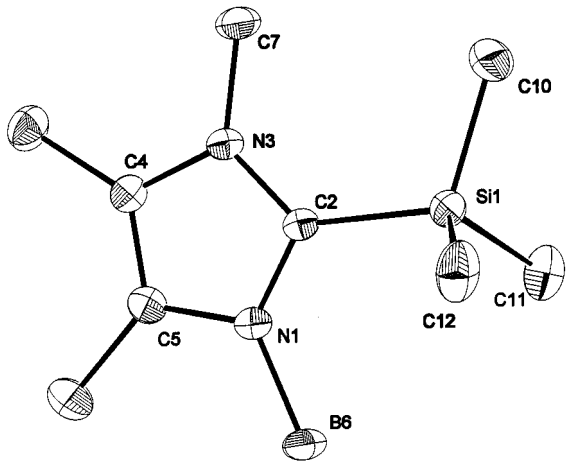


Figure 2. Structure of **5** in the crystal; bond lenghts and angles are listed in Table 1

Table 1. Selected bond lengths [Å] and angles [°] in Li$^+$ **1**$^-$, **3a**, and **5**

	Li$^+$ **1**$^-$ [2]	**5**	**3a**
N1−C2	1.373(3)	1.348(3)	1.320(2)
N3−C2	1.368(3)	1.367(3)	1.335(2)
N1−C5	1.398(3)	1.379(3)	1.386(2)
N3−C4	1.393(3)	1.385(3)	1.381(2)
C4−C5	1.355(3)	1.356(3)	1.358(3)
N1−B6	1.572(3)	1.588(3)	1.584(3)
N3−C7	1.463(3)	1.463(3)	1.461(3)
C2−Si1		1.913(2)	
N1−C2−N3	104.0(2)	106.6(2)	110.4(1)
C2−N1−C5	110.3(2)	109.1(2)	107.2(1)
C2−N3−C4	112.2(2)	109.7(2)	107.7(1)
N3−C4−C5	105.7(2)	106.2(2)	106.7(2)
N1−C5−C4	107.9(2)	108.4(2)	107.8(2)

move to higher field [δ = 191.3 (**1**$^-$), 146.9 (**5**), and 135.7 (**3a**)].

The structure of **14a** is shown in Figure 3. Single crystals were obtained from a $CDCl_3$ solution. The molecule is disordered, the structure found is a superposition of two orientations, created by a rotation around the axis through C4 and C4′. Therefore all other positions in the ring are occupied partly by nitrogen and carbon. The distances found are mean values, and the chemically different boron atoms cannot be distinguished. The result of the structure analysis

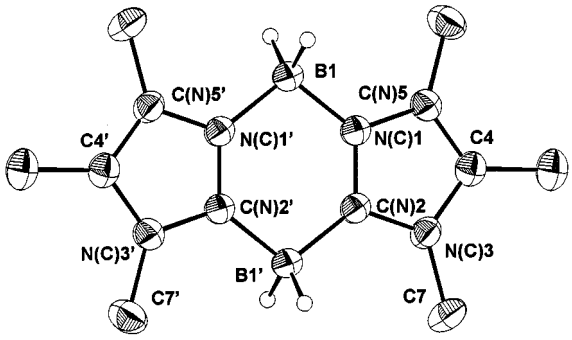


Figure 3. Structure of **14a** in the crystal

does not allow to distinguish **14a** from **14a′** (the analog of **14b′**) in contrast to the ^{11}B-NMR spectrum. A discussion of the angles and distances is therefore not meaningful.

Conclusion

The nucleophilic carbene union $\mathbf{1}^-$ obtained by deprotonation of the imidazole borane adduct **3a** reacts with electrophiles to form the 2-substituted imidazoles **4**, **5**, **6**, and **8**, which are confirmed by NMR and MS data and X-ray structure analyses for **3a** and **5**. With the Lewis acid BEt_3 the carbene addduct $\mathbf{9}^-$ is formed. Surprisingly, the reaction of $\mathbf{1}^-$ with $ClB(OMe)_2$, BH_3, or with $HBCl_2 \cdot SMe_2$ leads to the tricyclic imidazabole **14a**. In the crystal the molecule **14a** is disordered by superposition of two orientations. However, the ^{11}B-NMR spectrum of **14a** proves the presence of one C_2BH_2 and one N_2BH_2 group in the molecule.

Experimental Section

General: The reactions were carried out under dry argon, using standard Schlenk techniques. Solvents were dried, distilled, and saturated with nitrogen. Glassware was dried with a heat-gun in high-vacuum. − ^{1}H-, ^{13}C-, ^{11}B-NMR: Bruker AC 200 or AC 300 spectrometer, NMR references are $(CH_3)_4Si$ and $BF_3 \cdot Et_2O$. − Mass spectra were obtained with a Finnigan MAT 8200 plus spectrometer using EI technique. − Melting points (uncorrected) were obtained with a Büchi apparatus, using a capillary which was filled under argon and sealed. − 3-Borane-1,4,5-trimethylimidazole (**3a**)[2], chlorotrimethylstannane[7a] and 2-bromo-1,3-di(*tert*-butyl)-1,3,2-diazaboroline[7b] were prepared according to literature procedures.

General Procedure for the Preparation of the 2-Substituted Imidazoles 4, 5, and 6: To a suspension of **3a** [0.49 g (4.0 mmol) for **4**; 1.02 g (8.2 mmol) for **5** and 0.87 g (7.0 mmol) for **6**] in 30 mL of thf the equimolar amount of *n*-butyllithium (2.5 N in hexane) was added dropwise at −40°C. The mixture was allowed to warm to room temp. and was stirred for 1 h. Then the corresponding electrophiles [0.75 g (5.3 mmol) of iodomethane; 0.98 g (9.0 mmol) of chlorotrimethylsilane; 1.40 g (7.0 mmol) of chlorotrimethylstannane)] were added at −40°C, the solution again warmed to room temp. and stirred for 1 h. The solvent was removed in vacuo and the white precipitate (**4**) sublimed in vacuo (120−160°C, 10^{-2}−10^{-3} Torr). **5** and **6** were dissolved in toluene and LiCl was separated by filtration. The solution contained the pure product which was isolated by evaporating the solvent or by crystallization from a toluene/hexane solution.

3-Borane-1,2,4,5-tetramethylimidazole (4): Yield: 0.32 g (58%) white powder, m.p.: 140−160°C (decomp.). − ^{1}H NMR (300.1 MHz, $CDCl_3$): δ = 2.08, 2.14 (2s, 6 H, C-CH_3), 2.45 (s, 3 H, C-CH_3), 3.42 (s, 3 H, N-CH_3). − ^{13}C NMR (75.5 MHz, $CDCl_3$): δ = δ = 8.6 (C-*C*H$_3$), 10.5 (C-*C*H$_3$), 11.2 (C-*C*H$_3$), 30.7 (N-CH$_3$), 122.4, 129.5 (C=*C*-N), 142.3 (N=C-N). − ^{11}B NMR (64.2 MHz, C_6D_6): δ = −22.4 (q, $^1J_{B\text{-}H}$ = 82 Hz). − $C_7H_{15}BN_2$ (138.0): calcd. C 60.91, H 10.95, N 20.29; found. C 60.46, H 10.82, N 20.24.

3-Borane-1,4,5-trimethyl-2-trimethylsilylimidazole (5): Yield: 1.48 g (92%) white powder, m.p.: 115−120°C. − ^{1}H NMR (300.1 MHz, $CDCl_3$): δ = 0.52 [s, 9 H, $Si(CH_3)_3$], 2.12, 2.20 (2s, 6 H, C-CH_3), 3.58 (s, 3 H, N-CH_3). − ^{13}C NMR (50.3 MHz, C_6D_6): δ = 1.7 (Si-CH_3), 8.4, 10.7 (C-*C*H$_3$), 32.3 (N-CH$_3$), 126.1, 133.4 (C=*C*-N), 146.9 (N=C-N). − ^{11}B NMR (64.2 MHz, C_6D_6): δ = −19.7 (q, $^1J_{B\text{-}H}$ = 93 Hz). − $C_9H_{21}BN_2Si$ (196.2): calcd. C 55.10, H 10.78, N 14.27; found. C 55.18, H 10.86, N 14.02.

3-Borane-1,4,5-trimethyl-2-trimethylstannylimidazole (6): Yield: 1.91 g (95%) colorless crystals, m.p. 110−115°C. − ^{1}H NMR (200.1 MHz, $CDCl_3$): δ = 0.49 [s, 9 H, $Sn(CH_3)_3$, $^2J_{Sn\text{-}H}$ = 29 Hz],

Table 2. Crystal data and structure refinement for **3a**, **5**, and **14a**

	3a	**5**	**14a**
Empirical formula	$C_6H_{13}BN_2$	$C_9H_{21}BN_2Si$	$C_{12}H_{22}B_2N_4$
Formula weight	124.0	196.2	244.0
Crystal system	orthorhombic	monoclinic	triclinic
Space group	*Pmnb*	$P2_1/c$	$P\bar{1}$
Unit cell			
a [Å]	7.053(4)	8.510(4)	6.491(5)
b [Å]	8.537(4)	24.530(12)	7.465(7)
c [Å]	13.273(7)	12.351(6)	8.448(6)
α [deg]	90	90	101.41(7)
β [deg]	90	102.7(1)	111.45(6)
γ [deg]	90	90	107.12(9)
Volume [Å^3]	799.2(7)	2515(2)	342.0(5)
Z	4	8	1
Calc. density [g/cm^3]	1.03	1.034	1.19
Adsorp.coeff. [mm^{-1}]	0.06	0.15	0.07
F(000)	272	864	132
Crystal size [mm]	0.30 × 0.34 × 0.80	0.45 × 0.80 × 0.80	0.10 × 0.35 × 0.50
Θ-range [deg]	30	25	25
Index-ranges	0/+9, 0/+12, 0/+18	−10/+9, 0/+29, 0/14	−7/+6, −8/+8, 0/+10
No. of reflections			
unique	1255	4426	1175
observed [I>2σ(I)]	865	3459	1061
Transmission	0.92 − 1.00	0.94 − 1.00	0.91 − 1.00
Parameters	68	273	99
Final R indices			
*R*1 [$I > 2\sigma(I)$]	0.050	0.045	0.041
*wR*2	0.181	0.127	0.111
Largest diff.peak / hole[e/Å^3]	0.20 / −0.18	0.37 / −0.24	0.28 / −0.15

2.10, 2.16 (2s, 6 H, C-CH_3), 3.53 (s, 3 H, N-CH_3). – ^{13}C NMR (50.3 MHz, C_6D_6): δ = −5.1 (s, Sn-CH_3, $^1J_{Sn-C}$ = 380 Hz), 8.8, 10.4 (C-*C*H_3), 33.2 (N-CH_3), 126.3, 132.5 (C=*C*-N), 151.5 (N=C-N). – ^{11}B NMR (64.2 MHz, C_6D_6): δ = −19.9 (q, $^1J_{B-H}$ = 87 Hz). – $C_9H_{21}BN_2Sn$ (286.8): calcd. C 37.69, H 7.38, N 9.76; found. C 37.77, H 7.21, N 9.88.

2-(1-Borane-3,4,5-trimethylimidazolyl)-1,3-di(*tert*-butyl)-1,3,2-diazaboroline (8): To a suspension of 310 mg (2.5 mmol) of **3a** in 25 mL of thf 1.0 mL of *n*-butyllithium (2.5 N in hexane) were added dropwise at −40°C. The mixture was allowed to warm to room temp. and stirred for 1 h. Then a solution of 650 mg (2.5 mmol) of 2-bromo-1,3-(*tert*-butyl)-1,3,2-diazaboroline in 5 mL of thf was added at −78°C. During warming to room temp. the solution became orange colored and was then stirred for 1 h. The solvent was removed in vacuo, the white precipitate dissolved in toluene and LiBr was separated by filtration. After adding hexane to the solution at −30°C the product precipitates. Yield: 170 mg (32%) white powder, sensitive to air and moisture. – ^{1}H NMR (200.1 MHz, $CDCl_3$): δ = 1.18 [s, 18 H, C(CH_3)$_3$], 2.14, 2.20 (2s, 6 H, C-CH_3), 3.38 (s, 3 H, N-CH_3), 6.46 (s, 2 H, C-H). – ^{13}C NMR (50.3 MHz, $CDCl_3$): δ = 8.6, 10.1 (C-*C*H_3), 31.0 [N-C(*C*H_3)$_3$], 32.8 (N-CH_3), 53.1[N-*C*(CH_3)$_3$], 114.7 (C-H), 123.9, 132.0 (C=*C*-N), C2 (imidazole) not observed. – ^{11}B NMR (64.2 MHz, C_6D_6): δ = 19.1 (N-B-N), −20.1 (BH_3). – EI-MS; *m/z* (%) = 302 [M^+] (25), 245 [M^+ − C(CH_3)$_3$] (26), 123 [$C_6H_{12}BN_2^+$] (100).

Lithium 3-Borane-1,4,5-trimethyl-2-(triethylborane)imidazoline (Li^+ 9^-): To a suspension of 500 mg (4.0 mmol) of **3a** in 25 mL of thf 1.65 mL of *n*-butyllithium (2.5 N in hexane) were added dropwise at −40°C. The mixture was allowed to warm to room temp. and stirred for 1 h. Then 390 mg (4.0 mmol) of triethylborane were added at 0°C, then warmed to room temp. and stirred for 1 h. The solvent was removed in vacuo, leaving the product as a yellow oil. Yield: 1.58 g [96% for Li(thf)$_3^+$ 9^-], sensitive to air and moisture. – ^{1}H NMR (200.1 MHz, C_6D_6): δ = 1.1−1.3 (m, 15 H, C_2H_5), 1.4−1.5 (m, 12 H, thf), 1.68, 2.24 (2s, 6 H, C-CH_3), 3.5−3.6 (m, 15 H, N-CH_3 + thf). – ^{13}C NMR (50.3 MHz, C_6D_6): δ = 9.2, 12.6 (C-*C*H_3), 12.6 (CH_2-*C*H_3), 16 (br., *C*$H_2$$CH_3$), 25.5 (thf), 33.1 (N-$CH_3$), 68.4 (thf), 121.8, 128.1 (C=*C*-N), 175 (br., N-C=N). – ^{11}B NMR (64.2 MHz, C_6D_6): δ = −12.5 (C-BEt_3), −21.6 (br., N-BH_3).

Imidazabole 14a: To a suspension of 500 mg (4.0 mmol) of **3a** in 20 mL of thf 1.7 mL of *n*-butyllithium (2.5 N in hexane) were added dropwise at −40°C. The mixture was allowed to warm to room temp. and stirred for 1 h. Then 450 mg (4.2 mmol) of chlorodi(methoxy)borane were added at −70°C, the solution was warmed to room temp. and stirred for 1 h. The solvent was removed in vacuo. The white precipitate was dissolved in toluene and LiCl was separated by filtration. **14a** was allowed to crystallize from a toluene/hexane solution at −30°C. Yield: 200 mg (54%) white, air-stable solid, m.p. > 270°C. – ^{1}H NMR (200.1 MHz, $CDCl_3$): δ = 2.10 (s, 6 H, C-CH_3), 2.17 (s, 6 H, C-CH_3), 3.49 (s, 6 H, N-CH_3). – ^{13}C NMR (50.3 MHz, $CDCl_3$): δ = 9.2, 10.3 (C-*C*H_3), 31.9 (N-CH_3), 123.6, 127.3 (C=*C*-N), 163 (br., N=C-N). – ^{11}B NMR (64.2 MHz, $CDCl_3$): δ = −10.0 (t, C_2-BH_2, $^1J_{B-H}$ = 100 Hz), −31.4 (t, N_2-BH_2, $^1J_{B-H}$ = 87 Hz). – EI-MS: *m/z* (%) 243 (100) [M^+ − H].

Formation of 14a from 1^- and $HBCl_2 \cdot S(CH_3)_2$: To a suspension of 1.00 g (8.1 mmol) [1.05 g (8.5 mmol)] of **3a** in 30 mL of thf 3.5 mL [3.4 mL] of *n*-butyllithium (2.5 N in hexane) were added dropwise at −40°C. The mixture was allowed to warm to room temp. and stirred for 1 h. Then 600 mg (4.2 mmol) [390 mg (2.7 mmol)] of $HBCl_2 \cdot S(CH_3)_2$ were added at −78°C and the solution was allowed to warm to room temp. After stirring for 1 h, the solvent was removed in vacuo and the white precipitate dissolved in toluene. LiCl was separated by filtration. The solvent was evaporated, the residue dissolved in chloroform and allowed to crystallize at −30°C. Yield: 470 mg (48%) [680 mg (66%)] white, air-stable **14a** (analytical data see above).

Crystal Structure Determinations of 3a, 5, and 14a: Crystal data and details of the structure determinations are listed in Table 2. Unique sets of intensity data were collected at −70°C (**5**, **14a**) and at 23°C (**3a**) with a 4-circle diffractometer (Mo-*K*α-radiation λ = 0.71073 Å, graphite monochromator, ω-scan). Empirical absorption corrections (ψ-scans) were applied. The structures were solved by direct methods [SHELXS86][8] and refined by least-squares methods based on F^2 with all measured reflections [SHELXL97][9]. All non-hydrogen atoms were refined anisotropically. The structure of **14a** is disordered. A refinement in $P\bar{1}$ did not converge and gave no reasonable result.

Crystallographic data (excluding structure factors) for the structures reported in this paper have been deposited with the Cambridge Crystallograhpic Data Center as supplementary publication no. CCDC 102759 (**3a**), 102760 (**5**), 102761 (**14a**). Copies of the data can be obtained free of charge on application to the Director, CCDC, 12 Union Road, Cambridge CB2 1EZ, UK (fax: int. code +44(1223) 336-001; e-mail: deposit@ccdc.cam.ac.uk.

Acknowledgments

This work was supported by Deutsche Forschungsgemeinschaft (SFB 247) and Fonds der Chemischen Industrie.

[1] [1a] A.J. Arduengo, R.L. Harlow, M. Kline, *J. Am. Chem. Soc.* **1991**, *113*, 361−363. – [1b] A.J. Arduengo, H.V. Rasika Dias, R.L. Harlow, M. Kline, *J. Am. Chem. Soc.* **1992**, *114*, 5530−5534. – [1c] N. Kuhn, T. Kratz, D. Bläser, R. Boese, *Chem. Ber.* **1995**, *128*, 245−250. – [1d] M. Regitz, *Angew. Chem. Int. Ed. Engl.* **1996**, *35*, 725−728, *Angew. Chem.* **1996**, *108*, 791−794. – [1e] W.A. Herrmann, C. Köcher, *Angew. Chem.* **1997**, *109*, 2256−2282; *Angew. Chem. Int. Ed. Engl.* **1997**, *36*, 2162−2187.
[2] A. Wacker, H. Pritzkow, W. Siebert, *Eur. J. Inorg. Chem.* **1998**, 843−849.
[3] N. Kuhn, G. Henkel, J. Kreutzberg, *Z. Naturforsch.* **1991**, *46b*, 1706−1712.
[4] L. Weber, E. Dobbert, H.-G. Stammler, B. Neumann, R. Boese, D. Bläser, *Chem. Ber./Recueil* **1997**, *130*, 705−710.
[5] N. Kuhn, G. Henkel, T. Kratz, J. Kreutzberg, R. Boese, A.H. Maulitz, *Chem. Ber.* **1993**, *126*, 2041−2045.
[6] I. I. Padilla-Martinez, F. J. Martinez-Mastinez, A. López-Sandoval, K. I. Girón-Castillo, A. Brito, and R. Contreras *Eur.. J. Inorg. Chem.* **1998**, 1547−1553.
Note added in proof (February 17, 1999): New imidazabole derivatives are reported by: I. I. Padilla-Martinez, F. J. Martinez-Martinez, A. López-Sandoral, K. I. Girón-Castillo, A. Brito, R. Contreras, *Eur. J. Inorg. Chem.* **1988**, 1547−1553.
[7] [7a] Gmelin, *Handbuch der Anorg. Chemie, Sn-organische Verbindungen*, Teil 5, S. 63 (**1978**). – [7b] G. Schmid, J. Schulze, *Chem. Ber.* **1977**, *116*, 2744−2749.
[8] G. M. Sheldrick, *SHELXS86*, Univ. Göttingen, **1986**.
[9] G. M. Sheldrick, *SHELXS97*, Univ. Göttingen, **1997**.

Received August 28, 1998
[I98295]

Syntheses, Stereochemistry, and Dynamic Behavior of Chiral Zwitterionic (Ammoniomethyl)bis[glycolato(2–)-O^1,O^2]silicates

Reinhold Tacke,*[a] Rüdiger Bertermann,[a] Andreas Biller,[a] Olaf Dannappel,[a] Melanie Pülm,[a] and Reiner Willeke[a]

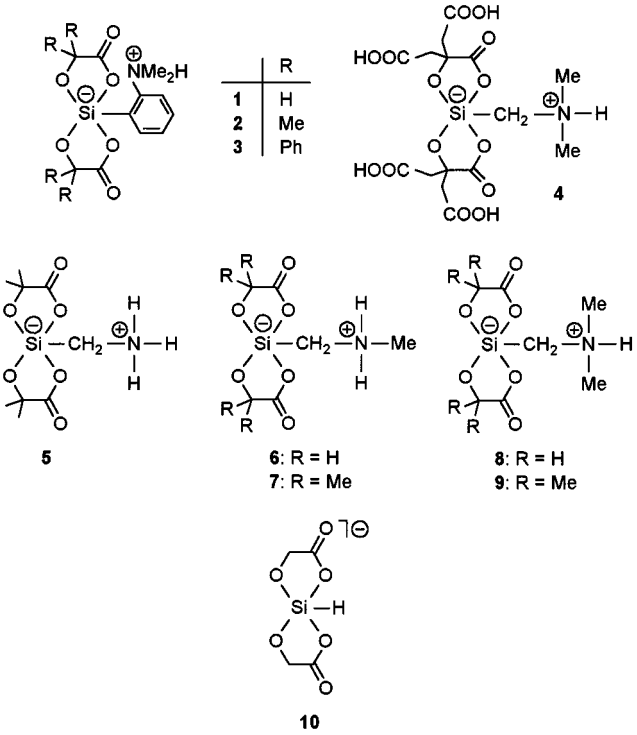
Dedicated to Professor Bernt Krebs on the occasion of his 60th birthday

Keywords: Ab initio studies / Chirality / Pentacoordinate silicon / Stereochemistry / Zwitterionic λ^5*Si*-silicates

The syntheses of the zwitterionic (molecular) spirocyclic λ^5*Si*-silicates **5**–**9** are described. These chiral compounds contain a pentacoordinate (formally negatively charged) silicon atom and a tetracoordinate (formally positively charged) nitrogen atom. The stereochemistry and dynamic behavior of **5**–**9** were investigated. For this purpose, compounds **5**–**9** were studied by solution-state NMR spectroscopy (^{1}H, ^{13}C, ^{29}Si; including VT ^{1}H-NMR studies of **9**) and solid-state NMR spectroscopy (^{13}C CP/MAS, ^{29}Si CP/MAS). In addition, compounds **5**·H_2O, **7**, **8**, **9**·H_2O, and **9**·2CH_3CN were structurally characterized by single-crystal X-ray diffraction, and ab initio investigations of the zwitterion **8** and the related anionic model species **10** were carried out.

Introduction

The study of compounds with higher coordinate silicon atoms currently represents one of the main areas of research in silicon chemistry.[1] In context with our systematic investigations on zwitterionic λ^5*Si*-silicates,[1f,1h,1i,2] we have recently reported on the syntheses and crystal structure analyses of the spirocyclic compounds **1**−**3**[2e] and **4**·H_2O[2g]. These molecular pentacoordinate silicon compounds each contain two identical bidentate diolato(2−) ligands that derive from α-hydroxycarboxylic acids. λ^5*Si*-silicates of this particular formula type offer a variety of interesting stereochemical features. In this paper, the results of experimental and theoretical studies concerning the stereochemistry and dynamic behavior of such compounds are described. We report here on the syntheses and characterization of the zwitterionic λ^5*Si*-silicates **5**−**9**, including (i) the crystal structure analyses of **5**·H_2O, **7**, **8**, **9**·H_2O, and **9**·2CH_3CN, (ii) VT ^{1}H-NMR studies of **9**, and (iii) ab initio investigations of **8** and **10**.[3]



Results and Discussion

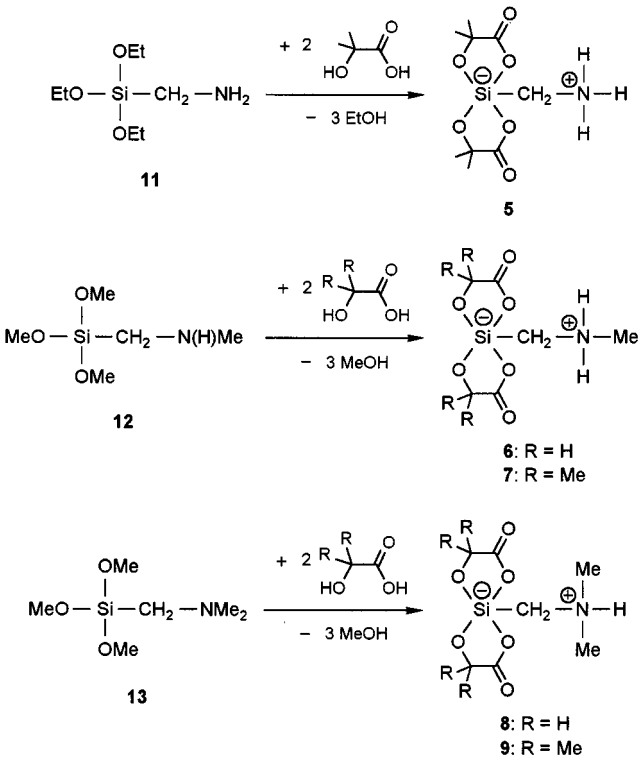
Syntheses

The zwitterionic λ^5*Si*-silicates **5**−**9** were prepared according to Scheme 1, starting from the trialkoxy(aminomethyl)silanes $(EtO)_3SiCH_2NH_2$ (**11**), $(MeO)_3SiCH_2N(H)Me$ (**12**), and $(MeO)_3SiCH_2NMe_2$ (**13**). Compounds **8** and **9** were synthesized alternatively according to Scheme 2 and 3, starting from the dialkoxy(phenyl)(aminomethyl)silane $Ph(MeO)_2SiCH_2NMe_2$ (**14**) and from the (ammoniomethyl)tetrafluorosilicate $F_4SiCH_2NMe_2H$ (**15**), respectively.

Following the strategy described for the synthesis of **1**−**4**,[2e,2g] compounds **5**−**9** were prepared according to *method a* by reaction of the respective silanes **11**−**13** with two mol equivalents of glycolic acid and 2-methyllactic acid, respectively (Scheme 1). The reactions were performed in acetonitrile at room temperature and the products **5**−**9** were formed spontaneously in precipitation reactions. Com-

[a] Institut für Anorganische Chemie, Universität Würzburg
Am Hubland, D-97074 Würzburg, Germany
Fax: (internat.) +49(0)931/888-4609
E-mail: r.tacke@mail.uni-wuerzburg.de

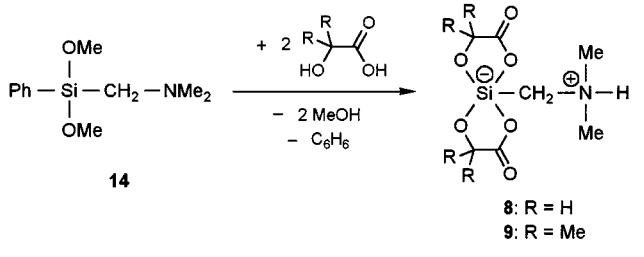
 © WILEY-VCH Verlag GmbH, D-69451 Weinheim, 1999 1434−1948/99/0505−0795 $ 17.50+.50/0



Scheme 1. Syntheses of compounds **5**−**9** according to *method a*

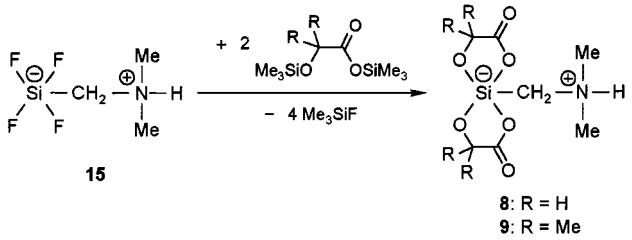
pounds **6**−**9** were isolated, after recrystallization from acetonitrile and drying in vacuo, as colorless crystalline solids (yields: **6**, 77%; **7**, 73%; **8**, 88%; **9**, 79%), whereas compound **5** was obtained as the crystalline hydrate **5**·H_2O (recrystallization from water; yield 78%). Recrystallization of **9** from water also yielded the corresponding hydrate **9**·H_2O which was isolated in almost quantitative yield as a colorless crystalline solid.

Compounds **8** and **9** were synthesized alternatively according to *method b* by reaction of the silane **14** with two mol equivalents of glycolic acid and 2-methyllactic acid, respectively, in acetonitrile at room temperature (Scheme 2). As these syntheses involve a relatively slow Si−C cleavage reaction as rate-determining step, product formation (first crystals formed after several hours) was significantly slower than that observed for *method a*. The syntheses according to *method b* generally yielded directly well-crystallized products which did not need further purification by recrystallization (yields after drying in vacuo: **8**, 98%; **9**, 88%). Crystals of **9**·$2CH_3CN$ (no drying in vacuo) were isolated directly from the reaction mixture.



Scheme 2. Syntheses of compounds **8** and **9** according to *method b*

The third strategy *(method c)* for the preparation of compounds **8** and **9** is based on the reaction of the zwitterionic λ^5*Si*-tetrafluorosilicate **15** with two mol equivalents of $Me_3SiOCH_2C(O)OSiMe_3$ (**16**) and $Me_3SiOCMe_2C(O)OSiMe_3$ (**17**), respectively (Scheme 3). These syntheses were also carried out in acetonitrile at room temperature (first crystals formed after ca. 30 minutes) and the products **8** and **9** were isolated, after recrystallization from acetonitrile and drying in vacuo, as colorless crystalline solids (yields: **8**, 91%; **9**, 79%).



Scheme 3. Syntheses of compounds **8** and **9** according to *method c*

Because of their zwitterionic nature, the high-melting compounds **5**·H_2O, **6**−**9**, **9**·H_2O, and **9**·$2CH_3CN$ are almost insoluble in unpolar organic solvents and also exhibit a very poor solubility in most polar organic solvents. The identity of **5**·H_2O, **6**−**9**, and **9**·H_2O was established by elemental analyses (C, H, N) and solution-state (^1H, ^{13}C, ^{29}Si) and solid-state (^{13}C and ^{29}Si CP/MAS) NMR studies. In addition, the zwitterions **6**−**9** were characterized by mass-spectrometric investigations (FAB MS). Furthermore, crystal structure analyses of compounds **5**·H_2O, **7**, **8**, **9**·H_2O, and **9**·$2CH_3CN$ were performed.

Crystal Structure Analyses

Compounds **5**·H_2O, **7**, **8**, **9**·H_2O, and **9**·$2CH_3CN$ were structurally characterized by single-crystal X-ray diffraction. The structures of the chiral zwitterions **5** and **7**−**9** in the crystal are depicted in Figures 1−5. In all cases the crystals were found to be built up by pairs of Λ- and Δ-enantiomers. The crystal data and the experimental parameters used for these experiments are summarized in Table 6; selected interatomic distances and angles are listed in Table 1.

The *Si*-coordination polyhedra of the zwitterions **5** and **7**−**9** can be described as somewhat distorted trigonal bipyramids, in which each of the axial positions is occupied by the carboxylate oxygen atoms (transition trigonal bipyramid → square pyramid: **5**·H_2O, 4.4%; **7**, 5.4%; **8**, 14.6%; **9**·H_2O, 8.9%; **9**·$2CH_3CN$, 5.1%; pivot atom C1).[4] In all structures the axial Si−O distances [1.7930(12)−1.822(2) Å] are significantly longer than the equatorial ones [1.656(2)−1.6764(8) Å]. The Si−C distances amount to 1.883(2)−1.896(2) Å. Generally, the structural data obtained for the *Si*-coordination polyhedra of the zwitterions **5** and **7**−**9** are very similar to those calculated for **8** and **10** (see ab initio Studies).

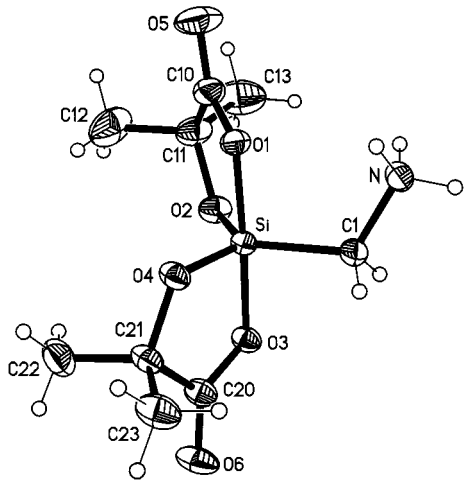


Figure 1. Molecular structure of **5** in the crystal of **5**·H_2O (probability level of displacement ellipsoids 50%), showing the atomic numbering scheme

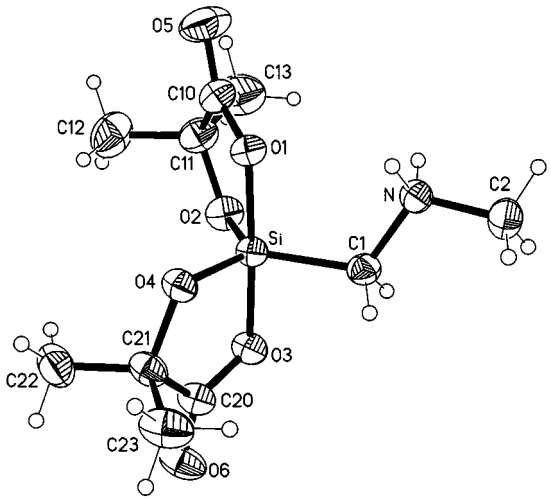


Figure 2. Molecular structure of **7** in the crystal (probability level of displacement ellipsoids 50%), showing the atomic numbering scheme

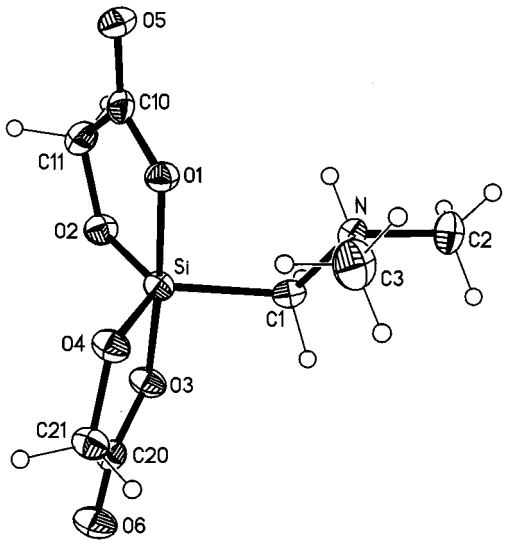


Figure 3. Molecular structure of **8** in the crystal (probability level of displacement ellipsoids 50%), showing the atomic numbering scheme

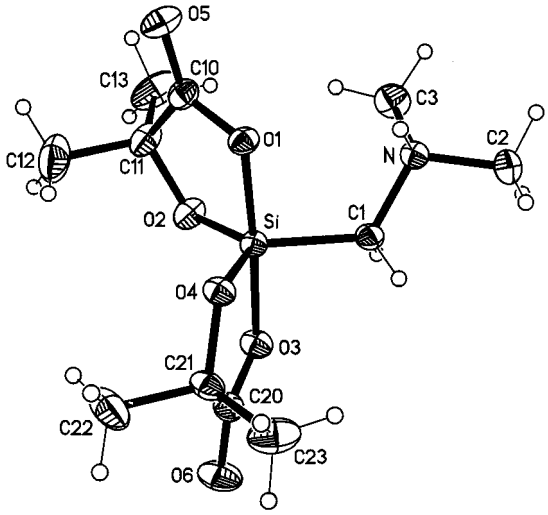


Figure 4. Molecular structure of **9** in the crystal of **9**·H_2O (probability level of displacement ellipsoids 50%), showing the atomic numbering scheme

As would be expected from the presence of the potential NH donor functions and potential oxygen acceptor atoms, intra- and intermolecular N−H···O hydrogen bonds between the zwitterions exist in the crystal of **5**·H_2O, **7**, **8**, **9**·H_2O, and **9**·2CH_3CN. For the hydrates additional intermolecular O−H···O (**5**·H_2O, **9**·H_2O) and N−H···O (**5**·H_2O) hydrogen bonds between the water molecules and the zwitterions were observed. Based on the relevant geometric data, the existence of the hydrogen bonds listed in Table 2 can be assumed.

A bifurcate hydrogen bond [N−H···O1 (intra), N−H···O5 (inter)] leads to the formation of centrosymmetric dimers in the crystal of **8** (Figure 6). These dimers are built up by pairs of enantiomers. The crystal lattices of all the other compounds are characterized by a more complex hydrogen bonding system (Table 2). Although **5**·H_2O, **7**, **9**·H_2O, and **9**·2CH_3CN differ significantly in their hydrogen bonding network, there is at least one common structural feature: in all cases trifurcate hydrogen bonds were observed, each consisting of an intramolecular N−H···O1 interaction and intermolecular N−H···O1 and N−H···O4 interactions.

ab initio Studies

The structure and dynamic behavior of the title compounds were investigated by quantum-chemical methods. For this purpose, computational studies of the anionic model species **10** and the zwitterion **8** were performed. The computational methods used are described in the Experimental Section.

As demonstrated for the model species bis[glycolato(2−)-O^1,O^2]hydridosilicate(1−) (**10**), five different idealized geometries (**10a**−**10e**, Figure 7) have to be considered for the

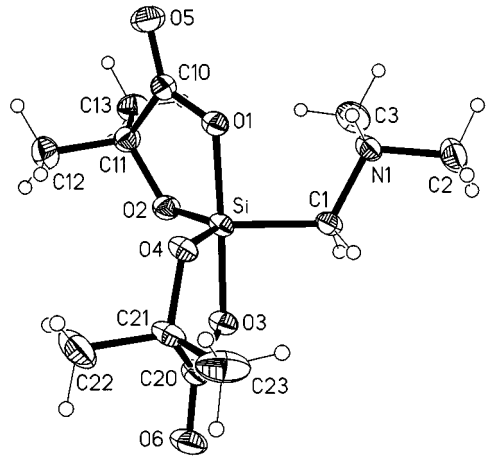


Figure 5. Molecular structure of **9** in the crystal of **9**·2CH_3CN (probability level of displacement ellipsoids 50%), showing the atomic numbering scheme

Table 1. Selected interatomic distances [Å] and angles [°] for **5**·H_2O, **7**, **8**, **9**·H_2O, and **9**·2CH_3CN

	5·H_2O	**7**	**8**	**9**·H_2O	**9**·2CH_3CN
Si–O1	1.7943(12)	1.7941(14)	1.822(2)	1.8003(8)	1.8060(12)
Si–O2	1.6623(12)	1.656(2)	1.666(2)	1.6636(8)	1.6656(12)
Si–O3	1.7974(12)	1.8132(14)	1.795(2)	1.8029(8)	1.7930(12)
Si–O4	1.6601(12)	1.6733(14)	1.656(2)	1.6764(8)	1.6751(13)
Si–C1	1.883(2)	1.889(2)	1.893(2)	1.8915(11)	1.896(2)
O1–Si–O2	89.13(6)	89.92(6)	88.50(7)	89.45(4)	89.03(6)
O1–Si–O3	177.17(5)	176.98(5)	175.46(7)	176.06(4)	177.51(6)
O1–Si–O4	89.05(6)	89.20(7)	89.37(7)	88.28(4)	88.59(6)
O1–Si–C1	93.52(6)	94.33(7)	93.96(8)	95.43(4)	93.92(6)
O2–Si–O3	89.94(6)	89.08(6)	87.74(7)	89.58(4)	90.63(6)
O2–Si–O4	120.30(6)	120.59(7)	125.51(8)	122.20(4)	120.98(6)
O2–Si–C1	121.84(7)	121.91(8)	119.93(9)	120.82(5)	122.26(7)
O3–Si–O4	89.11(5)	88.85(6)	90.74(7)	89.01(4)	89.47(6)
O3–Si–C1	89.25(6)	88.62(7)	90.13(8)	88.34(4)	88.34(6)
O4–Si–C1	117.83(7)	117.38(8)	114.54(9)	116.88(5)	116.74(7)

title compounds. For energetic reasons, trigonal bipyramids with the hydrogen (carbon) atom in an axial site and square pyramids with the hydrogen (carbon) atom in a basal position can be excluded. The trigonal-bipyramidal isomers **10a**–**10c** and the square-pyramidal species **10d** are chiral and therefore exist as pairs of Λ- and Δ-enantiomers, whereas the square-pyramidal species **10e** is achiral. Calculations of the vibrational frequencies for **10a**–**10e** have demonstrated that only the isomers **10a**–**10c** represent local minima, the isomer **10a** being the energetically most favorable one (for selected geometric parameters of **10a**–**10e**, see Table 3).[5] This result is in agreement with the experimentally established crystal structures of **5**·H_2O, **7**, **8**, **9**·H_2O, and **9**·2CH_3CN, indicating that the trigonal-bipyramidal geometry, with the carboxylate oxygen atoms in the axial sites, is indeed the energetically most favorable one. Based on this particular structure, geometry optimizations at the SCF/SVP level were carried out for the zwitterionic λ^5*Si*-silicate **8** (Figure 8).[6] As can be seen from Table 4, the calculated interatomic distances and angles for the *Si*O_4C framework of **8** are in good agreement with the experimentally established values for **5**·H_2O, **7**, **8**, **9**·H_2O, and **9**·2CH_3CN.

These results suggest that the energetically preferred trigonal-bipyramidal *Si*-coordination polyhedra of **5**–**9**, with the carboxylate oxygen atoms in the axial sites, also play the major role in solution, all compounds being expected to exist as pairs of enantiomers. As demonstrated for the model species **10**, an intramolecular isomerization of the antipodes of **5**–**9** should be possible leading to an inversion of absolute configuration of their chiral trigonal-bipyramidal λ^5*Si*-silicate skeletons (Figure 9). According to the results of ab initio studies, the enantiomers Λ-**10a** and Δ-**10a** can be converted into each other along the reaction coordinate Λ-**10a** ⇌ **10**$^{\ddagger 2}$ ⇌ Δ-**10c** ⇌ **10**$^{\ddagger 3}$ ⇌ Λ-**10b** ⇌ **10**$^{\ddagger 1}$ ⇌ Δ-**10b** ⇌ **10**$^{\ddagger 3'}$ ⇌ Λ-**10c** ⇌ **10**$^{\ddagger 2'}$ ⇌ Δ-**10a** (**10**$^{\ddagger 1}$ = **10e**; the pairs **10**$^{\ddagger 2}$/**10**$^{\ddagger 2'}$ and **10**$^{\ddagger 3}$/**10**$^{\ddagger 3'}$ are antipodes) (Figure 9).[7,8] The square-pyramidal species **10**$^{\ddagger 1}$ and the trigonal-bipyramidal species **10**$^{\ddagger 2}$ and **10**$^{\ddagger 3}$ are transition states in this isomerization process.[9] Their relative energies amount to 31.4 kJ mol^{-1} (**10**$^{\ddagger 1}$), 47.1 kJ mol^{-1} (**10**$^{\ddagger 2}$), and 70.8 kJ mol^{-1} (**10**$^{\ddagger 3}$). The hydrogen atoms in these transition states occupy an apical (**10**$^{\ddagger 1}$), equatorial (**10**$^{\ddagger 2}$), or axial (**10**$^{\ddagger 3}$) position (for selected geometric data, see Table 3). The conversions Λ-**10b** ⇌ **10**$^{\ddagger 1}$ ⇌ Δ-**10b** and the conversions Λ-**10a** ⇌ **10**$^{\ddagger 2}$ ⇌ Δ-**10c** (Δ-**10a** ⇌ **10**$^{\ddagger 2'}$ ⇌ Λ-**10c**) can be described in terms of a Berry-type mechanism, with the hydrogen atom as the pivot ligand. In contrast, the conversions Δ-**10c** ⇌ **10**$^{\ddagger 3}$ ⇌ Λ-**10b** (Λ-**10c** ⇌ **10**$^{\ddagger 3'}$ ⇌ Δ-**10b**) differ significantly from a Berry-type mechanism, the transition state being characterized by a distorted trigonal-bipyramidal *Si*-coordination polyhedron with the hydrogen atom in an axial position. As the structure of this transition state is rather twisted [one of the diolato(2–) ligands occupies two equatorial positions], the term "twist mechanism" is suggested for this particular intramolecular isomerization process. The calculated relative energy of the corresponding transition state **10**$^{\ddagger 3}$ (70.8 kJ mol^{-1}) is in good agreement with the experimentally established energy barrier for the isomerization process Λ-**9** ⇌ Δ-**9** (see VT ^{1}H-NMR Studies of **9**).

NMR Studies of 5·H_2O, 6–9, and 9·H_2O

Compounds **5**·H_2O, **6**–**9**, and **9**·H_2O were studied by ^{1}H, ^{13}C, and ^{29}Si solution-state NMR experiments (solvent [D_6]DMSO) and by ^{13}C and ^{29}Si CP/MAS solid-state NMR experiments.[10] All these investigations were performed at room temperature (for VT ^{1}H-NMR studies of **9**, see next chapter).

The isotropic ^{29}Si chemical shifts obtained in the CP/MAS NMR studies of **5**·H_2O, **6**–**9**, and **9**·H_2O (Table 5) clearly characterize the ^{29}Si resonances as arising from pentacoordinate silicon atoms. In the case of **5**·H_2O, **7**, **8**, **9**·H_2O, and **9**·2CH_3CN, pentacoordination of silicon was established independently by single-crystal X-ray diffraction (see Crystal Structure Analyses). As the ^{29}Si chemical shifts obtained in the solid-state NMR experiments are very simi-

Table 2. Hydrogen-bonding geometries for **5**·H_2O, **7**, **8**, **9**·H_2O, and **9**·2CH_3CN in the crystal

	Donor−H···Acceptor	D−H [Å]	H···A [Å]	D···A [Å]	D−H···A [°]
5·H_2O[a]	N−H1···O1	0.87(2)	2.39(3)	2.744(2)	104.8(18)
	N−H1···O1′	0.87(2)	2.55(2)	3.151(2)	127(2)
	N−H1···O4′	0.87(2)	2.04(2)	2.866(2)	157(2)
	N−H2···O1W	0.95(3)	1.79(3)	2.730(3)	172(2)
	N−H3···O6′	0.90(2)	2.02(2)	2.805(2)	144(2)
	O1W−H1W···O5	0.80(4)	1.97(4)	2.754(3)	167(3)
	O1W−H2W···O2	0.83(4)	2.09(4)	2.894(3)	164(4)
7[b]	N−H2···O1	0.89(2)	2.39(2)	2.786(3)	107.6(16)
	N−H2···O1′	0.89(2)	2.48(2)	3.109(3)	128.1(17)
	N−H2···O4′	0.89(2)	2.08(2)	2.901(3)	152.6(19)
	N−H1···O6′	0.945(19)	1.946(19)	2.809(3)	150.9(17)
8[c]	N−H···O1	0.89(2)	2.38(2)	2.790(2)	108.6(17)
	N−H···O5′	0.89(2)	2.05(2)	2.830(3)	146(2)
9·H_2O[d]	N−H···O1	0.871(15)	2.450(14)	2.8685(12)	110.1(11)
	N−H···O1′	0.871(15)	2.416(15)	3.0640(12)	131.6(12)
	N−H···O4′	0.871(15)	2.126(15)	2.9373(12)	154.7(13)
	O1W−H1···O6	0.92(3)	1.96(3)	2.8695(15)	168(2)
	O1W−H2···O6	0.82(2)	2.10(2)	2.9204(16)	173(3)
9·2CH_3CN[e]	N−H···O1	0.89(2)	2.36(2)	2.8115(19)	111.2(16)
	N−H···O1′	0.89(2)	2.43(2)	3.058(2)	128.0(16)
	N−H···O4′	0.89(2)	2.14(2)	2.949(2)	150.7(18)

[a] O1···H1···O1′ = 80.5(7)°, O1···H1···O4′ = 97.1(10)°, O1′···H1···O4′ = 62.6(6)°. − [b] O1···H2···O1′ = 81.8(7)°, O1···H2···O4′ = 98.2(8)°, O1′···H2···O4′ = 63.8(6)°. − [c] O1···H···O5′ = 90.6(8)°. − [d] O1···H···O1′ = 77.9(4)°, O1···H···O4′ = 91.6(5)°, O1′···H···O4′ = 64.1(4)°. − [e] O1···H···O1′ = 79.8(6)°, O1···H···O4′ = 96.8(8)°, O1′···H···O4′ = 64.0(6)°.

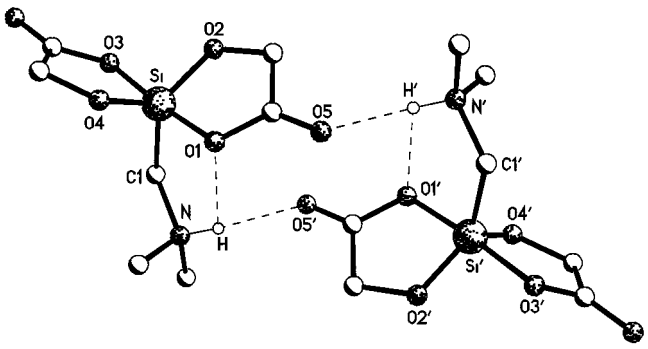


Figure 6. Structure of the centrosymmetric dimer in the crystal of **8**. The hydrogen atoms (except for N*H*) are omitted for clarity

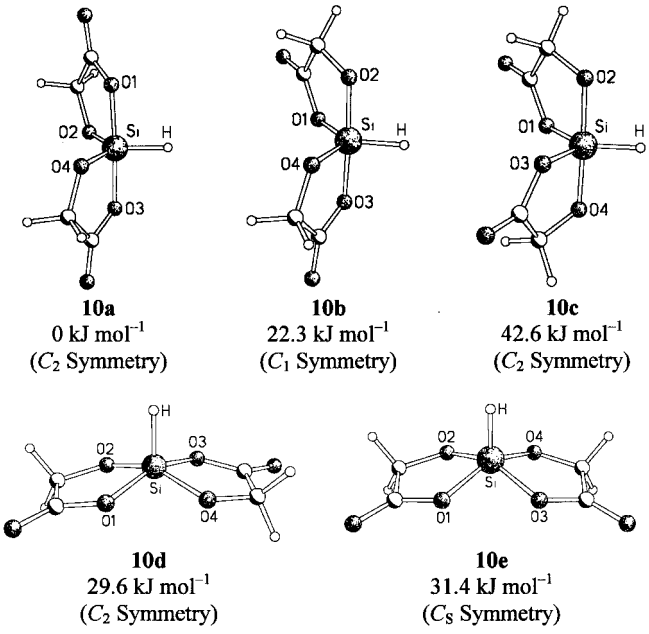


Figure 7. Calculated structures and relative energies of the isomers **10a**−**10e** as obtained by SCF/SVP geometry optimizations

lar to those obtained for the zwitterions **5**−**9** in [D_6]DMSO ($\Delta\delta^{29}Si \leq 2.1$; Table 5), it is concluded that pentacoordination of silicon is also present in solution. In addition, the ^1H chemical shifts observed for the NH protons [δ^1H = 7.2 (**5**·H_2O), 7.9 (**6**), 7.8 (**7**), 8.3 (**8**), 8.4 (**9**, **9**·H_2O)] clearly indicate the presence of ammonium groups in solution. Furthermore, the ^{13}C CP/MAS NMR data of **5**·H_2O, **6**−**9**, and **9**·H_2O are very similar to those obtained for these compounds in solution. Thus, the NMR experiments unequivocally demonstrate that the zwitterions **5**−**9** also exist in [D_6]DMSO.

The solution-state NMR data of the zwitterions **5**−**9** are compatible with the presence of one particular species (such as the trigonal-bipyramidal isomer, with the carboxylate oxygen atoms in the axial positions) or with a rapid low-energy interconversion of different isomers (in this context, see ab initio Studies). As the trigonal-bipyramidal structure, with the carboxylate oxygen atoms in the axial sites, is the energetically most favorable one, it is likely to assume that this particular species is also dominant in solution. The chiral nature of the respective λ^5*Si*-silicate frameworks of **5**−**9** is reflected by the diastereotopism observed for the $SiCH_2N$ (**5**−**9**; AB systems) and $OC(CH_3)_2C$ protons (**5**, **7**, **9**; two separated singlets for the two methyl groups), indicating that the Λ- and Δ-enantiomers of **5**−**9** are configurationally

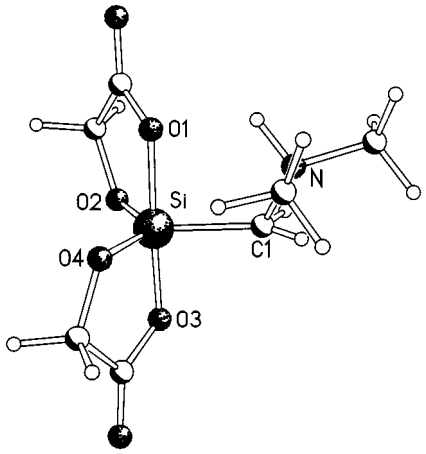


Figure 8. Calculated structure (local minimum) of **8** as obtained by SCF/SVP geometry optimizations

Table 3. Calculated interatomic distances [Å] and angles [°] for the isomers **10a**−**10e** and the transition states $\mathbf{10}^{\neq 1}$−$\mathbf{10}^{\neq 3}$ as obtained by SCF/SVP geometry optimizations[a]

	10a	**10b**	**10c**	**10d**	**10e**	$\mathbf{10}^{\neq 2}$	$\mathbf{10}^{\neq 3}$
Si−O1	1.799	1.724	1.732	1.771	1.770	1.735	1.720
Si−O2	1.666	1.722	1.727	1.690	1.697	1.727	1.682
Si−O3	1.799	1.813	1.732	1.771	1.770	1.735	1.852
Si−O4	1.666	1.670	1.727	1.690	1.697	1.727	1.678
Si−H	1.464	1.466	1.469	1.472	1.467	1.470	1.486
O1−Si−O2	87.7	87.8	87.3	87.0	86.4	86.9	94.0
O1−Si−O3	176.8	87.7	111.4	157.0	84.1	124.9	88.7
O1−Si−O4	90.7	117.2	91.5	87.5	151.1	89.0	126.2
O1−Si−H	91.6	121.3	124.3	101.5	102.0	117.6	97.7
O2−Si−O3	90.7	175.4	91.5	87.5	151.1	89.0	87.9
O2−Si−O4	120.4	94.2	177.7	152.0	89.0	171.0	138.6
O2−Si−H	119.8	93.5	91.1	104.0	106.7	94.5	96.3
O3−Si−O4	87.7	87.0	87.3	87.0	86.4	86.9	83.9
O3−Si−H	91.6	89.6	124.3	101.5	102.0	117.6	172.0
O4−Si−H	119.8	121.2	91.1	104.0	106.7	94.5	88.5

[a] The isomer **10e** and the transition state $\mathbf{10}^{\neq 1}$ are identical.

stable on the NMR time scale at room temperature. As demonstrated by VT ^{1}H-NMR studies of **9**, the interconversion of the Λ- and Δ-enantiomer is characterized by an energy barrier of 76(1) kJ mol^{-1} ([D$_6$]DMSO), 75(1) kJ mol^{-1} (CD_3CN), and 82(2) kJ mol^{-1} ($CDCl_3$) (see next chapter).

VT ^{1}H-NMR Studies of 9

Compound **9** was studied by solution-state ^{1}H-NMR spectroscopy at 300.1 MHz in the temperature range of 21−118°C ([D$_6$]DMSO), 22−94°C (CD_3CN), and 24−83°C ($CDCl_3$). The concentrations of **9** were 2.5 mmol L^{-1}, 25 mmol L^{-1}, and 250 mmol L^{-1} ([D$_6$]DMSO), 5.0 mmol L^{-1} (CD_3CN), and 2.0 mmol L^{-1} ($CDCl_3$). For all solutions studied, two separated singlets for the diastereotopic methyl groups of the 2-methyllactato(2−) ligands were observed at room temperature, indicating that Λ-**9** and Δ-**9** are configurationally stable on the NMR time scale under these conditions. Upon heating coalescence was observed, indicating a dynamic behavior of the enantiomers of **9** in solution. The temperature dependence of the ^{1}H-NMR spectra of **9** is characterized by complete reversibility (see Figure 10).

For all solutions of **9** in [D$_6$]DMSO (c = 2.5−250 mmol L^{-1}) coalescence was observed at 76°C. The calculated energy barrier (line-shape analysis) for the Λ/Δ-interconversion of the enantiomers of **9** amounts to $\Delta G^{\neq}$ = 76(1) kJ mol^{-1} and is independent on the concentration. The activation free enthalpy is similar in CD_3CN [$\Delta G^{\neq}$ = 75(1) kJ mol^{-1}] and somewhat higher in $CDCl_3$ [$\Delta G^{\neq}$ = 82(2) kJ mol^{-1}]. The coalescence temperature in CD_3CN was 66°C. As coalescence in $CDCl_3$ could not be observed below the boiling point of the solvent, the respective coalescence temperature could not be established directly in these experiments and therefore had to be determined by simulations (calculated coalescence temperature ca. 90°C).

As the coalescence temperature does not depend on the concentration (studies with **9** in [D$_6$]DMSO; c = 2.5−250 mmol L^{-1}), first-order kinetics for the Λ/Δ-isomerization can be assumed suggesting an intramolecular process. This is in accordance with the results obtained by the ab initio

Table 4. Selected calculated interatomic distances [Å] and angles [°] for **8** and the differences between these data and the corresponding experimental values[a] for **5**·H_2O, **7**, **8**, **9**·H_2O, and **9**·2CH_3CN

	8	Δ(**8**/**5**·H_2O)	Δ(**8**/**7**)	Δ(**8**/**8**)	Δ(**8**/**9**·H_2O)	Δ(**8**/**9**·2CH_3CN)
Si−O1	1.810	+0.016	+0.016	−0.012	+0.010	+0.004
Si−O2	1.649	−0.013	−0.007	−0.017	−0.015	−0.017
Si−O3	1.746	−0.051	−0.067	−0.049	−0.057	−0.047
Si−O4	1.653	−0.007	−0.020	−0.003	−0.023	−0.022
Si−C1	1.939	+0.056	+0.050	+0.046	+0.048	+0.043
O1−Si−O2	87.0	−2.1	−2.9	−1.5	−2.5	−2.0
O1−Si−O3	177.7	+0.5	+0.7	+2.2	+1.6	+0.2
O1−Si−O4	92.0	+3.0	+2.8	+2.6	+3.7	+3.4
O1−Si−C1	87.7	−5.8	−6.6	−6.3	−7.7	−6.2
O2−Si−O3	93.1	+3.2	+4.0	+5.4	+3.5	+2.5
O2−Si−O4	122.8	+2.5	+2.2	−2.7	+0.6	+1.8
O2−Si−C1	121.0	−0.8	−0.9	+1.1	+0.2	−1.3
O3−Si−O4	89.8	+0.7	+1.0	−0.9	+0.8	+0.3
O3−Si−C1	90.3	+1.1	+1.7	+0.2	+2.0	+2.0
O4−Si−C1	116.1	−1.7	−1.3	+1.6	−0.8	−0.6

[a] Experimental data taken from Table 2.

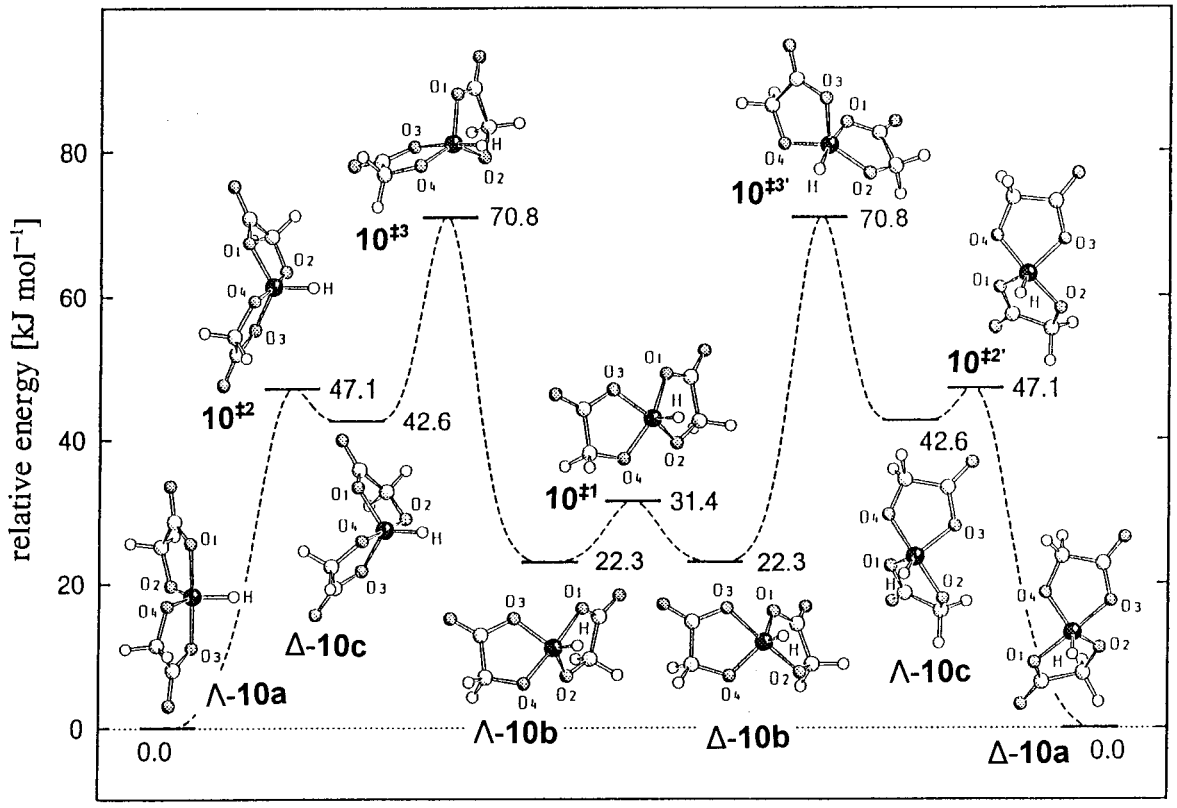


Figure 9. Calculated intramolecular reaction path for the isomerization of **10a** (Λ-**10a** ⇌ Δ-**10a**), showing the structures and relative energies of the local minima **10a**−**10c** and of the transition states $\mathbf{10}^{\ddagger 1}$ (= **10e**), $\mathbf{10}^{\ddagger 2}$ ($\mathbf{10}^{\ddagger 2'}$), and $\mathbf{10}^{\ddagger 3}$ ($\mathbf{10}^{\ddagger 3'}$)

Table 5. ^{29}Si-NMR data for **5**·H_2O, **6**−**9**, and **9**·H_2O in solution ([D_6]DMSO) and in the crystal (chemical shifts in ppm; spectra recorded at room temperature)

Compound	δ(solution)	δ(crystal)[a]
5·H_2O	−98.0	−96.4
6	−89.2	−88.7
7	−99.2	−98.1
8	−90.3	−88.6
9	−100.5	−100.9, −100.1
9·H_2O	−100.5	−98.4

[a] Isotropic chemical shifts obtained by ^{29}Si CP/MAS NMR experiments.

studies with the model species **10** (calculated energy barrier for the intramolecular Λ/Δ-isomerization: 70.8 kJ mol^{-1}).

Conclusions

The chiral title compounds exist as pairs of Λ- and Δ-enantiomers in the solid state and in solution. The trigonal-bipyramidal structure of the respective λ^5*Si*-silicate skeletons, with the carboxylate oxygen atoms in the axial sites, is the energetically most stable one. The Λ- and Δ-enantiomers of the zwitterionic λ^5*Si*-silicates **5**−**9** are configurationally stable in solution on the NMR time scale (organic solvents, room temperature) and undergo an intramolecular

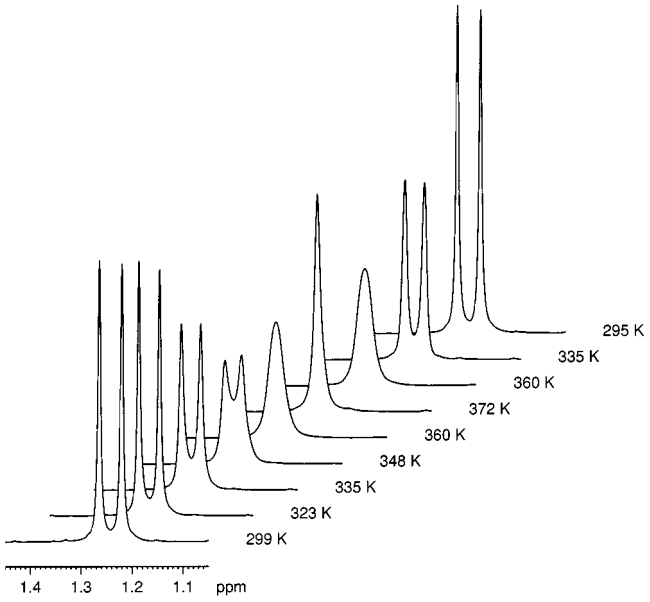


Figure 10. Temperature dependence of the ^{1}H-NMR signals for the two diastereotopic methyl groups of the 2-methyllactato(2−) ligands of **9** (solution in [D_6]DMSO; c = 250 mmol L^{-1}, 300.1 MHz) upon heating from 299 K to 372 K and subsequent cooling to 295 K

Λ/Δ-isomerization with an activation free enthalpy of ca. 75−80 kJ mol^{-1} (experimentally established for **9**; calculated energy barrier for **10**: 70.8 kJ mol^{-1}).

Experimental Section

General Procedures: All syntheses were carried out under dry nitrogen. The organic solvents used were dried and purified according to standard procedures and stored under nitrogen. − Melting points were determined with a Leitz Biomed microscope equipped with a heater (Leitz, Model M 350). − The ^{1}H, ^{13}C, and ^{29}Si solution-state NMR spectra were recorded at room temperature on a Bruker DRX-300 NMR spectrometer (^{1}H, 300.1 MHz; ^{13}C, 75.5 MHz; ^{29}Si, 59.6 MHz). $CDCl_3$, CD_3CN, C_6D_6, and [D$_6$]DMSO were used as solvents. Chemical shifts (ppm) were determined relative to internal $CHCl_3$ (^{1}H, δ = 7.24; $CDCl_3$), CHD_2CN (^{1}H, δ = 1.94; CD_3CN), C_6HD_5 (^{1}H, δ = 7.28; C_6D_6), C_6D_6 (^{13}C, δ = 128.0; C_6D_6), [D$_5$]DMSO (^{1}H, δ = 2.50; [D$_6$]DMSO), [D$_6$]DMSO (^{13}C, δ = 39.43; [D$_6$]DMSO), and external TMS (^{29}Si, δ = 0; C_6D_6, [D$_6$]DMSO). Assignment of the ^{13}C-NMR data was supported by DEPT 135 experiments. ^{13}C and ^{29}Si CP/MAS NMR spectra were recorded at room temperature on a Bruker DSX-400 NMR spectrometer with bottom layer rotors of ZrO_2 (diameter 7 mm) containing ca. 20−300 mg of sample [^{13}C, 100.6 MHz; ^{29}Si, 79.5 MHz; TMS as external standard (δ = 0); spinning rate 5000 Hz; contact time 5 ms; 90° ^{1}H transmitter pulse length 4.0 μs; repetition time 5 s (^{13}C) or 4 s (^{29}Si)]. − Mass spectra were obtained with a Finnigan MAT-8430 mass spectrometer (FAB MS; 3-nitrobenzyl alcohol as liquid matrix, xenon as FAB source) or a Trio-1000 mass spectrometer (ThermoQuest; EI MS, 70 eV). The selected *m*/*z* values given refer to the isotopes ^{1}H, ^{12}C, ^{14}N, ^{16}O, and ^{28}Si. − Elemental analyses were determined by Beller, Mikroanalytisches Laboratorium (Göttingen, Germany).

(Ammoniomethyl)bis[2-methyllactato(2−)-*O*^{1},*O*^{2}]silicate Hydrate (5·H$_2$O): A solution of **11** (967 mg, 5.00 mmol) in acetonitrile (2.5 mL) was added dropwise at room temperature within 2 min to a solution of 2-methyllactic acid (1.04 g, 9.99 mmol) in acetonitrile (22.5 mL). The reaction mixture was stirred for 1 min and then kept undisturbed at room temperature for 24 h (formation of a precipitate ca. 8 min after combining the reactants). The precipitate (compound **5**, crude product) was filtered off, washed with cold acetonitrile (3 × 5 mL), dissolved in water (40 mL), and the solution then kept undisturbed at room temperature for 6 d (slow evaporation of the water). Compound **5**·H$_2$O was isolated in 78% yield (1.10 g) as a colorless crystalline product. Mp 264°C. − ^{1}H NMR ([D$_6$]DMSO, 300.1 MHz): δ = 1.21 (s, 6 H, CCH_3), 1.25 (s, 6 H, CCH_3), 2.01 and 2.19 (AB system, J_{AB} = −16.0 Hz, 2 H, $SiCH_2N$), 3.33 (s, 2 H, H_2O), 7.2 (broad s, 3 H, NH_3). − $^{13}C\{^{1}H\}$ NMR ([D$_6$]DMSO, 75.5 MHz): δ = 26.8 (CCH_3), 27.6 (CCH_3), 28.1 ($SiCH_2N$), 73.7 (OCC_3), 178.5 (C=O). − ^{13}C CP/MAS NMR (36854 transients): δ = 24.7 and 27.3 (CCH_3, $SiCH_2N$), 76.3 (OCC_3), 180.7 (C=O), 182.5 (C=O). − $^{29}Si\{^{1}H\}$ NMR ([D$_6$]DMSO, 59.6 MHz): δ = −98.0. − ^{29}Si CP/MAS NMR (13168 transients): δ = −96.4. − $C_9H_{19}NO_7Si$ (281.3): calcd C 38.42, H 6.81, N 4.98; found C 38.7, H 6.6, N 4.9.

Bis[glycolato(2−)-*O*^{1},*O*^{2}][(methylammonio)methyl]silicate (6): The synthesis was carried out analogously to that of compound **5** by combining a solution of **12** (826 mg, 5.00 mmol) in acetonitrile (2.5 mL) with a solution of glycolic acid (761 mg, 10.0 mmol) in acetonitrile (22.5 mL) (spontaneous formation of a precipitate after combining the reactants). Compound **6** was isolated in 77% yield (852 mg) as a colorless crystalline product. Mp 165°C. − ^{1}H NMR ([D$_6$]DMSO, 300.1 MHz): δ = 2.27 and 2.32 (AB system, J_{AB} = −15.7 Hz, 2 H, $SiCH_2N$), 2.46 (s, 3 H, NCH_3), 3.92 (s, 4 H, OCH_2C), 7.9 (broad s, 2 H, NH_2). − $^{13}C\{^{1}H\}$ NMR ([D$_6$]DMSO, 75.5 MHz): δ = 36.1 (NCH_3), 39.0 ($SiCH_2N$), 62.8 (OCH_2C), 174.0 (C=O). − ^{13}C CP/MAS NMR (3540 transients): δ = 37.2, 38.4, 39.5, and 41.3 (NCH_3, $SiCH_2N$), 62.6 (OCH_2C), 63.3 (OCH_2C), 64.1 (OCH_2C), 174.5 (C=O), 179.2 (C=O), 180.5 (C=O). − $^{29}Si\{^{1}H\}$ NMR ([D$_6$]DMSO, 59.6 MHz): δ = −89.2. − ^{29}Si CP/MAS NMR (215 transients): δ = −88.7. − FAB MS (positive ions): *m*/*z* (%) = 222 (32) [*M* + H$^+$], 154 (100) [matrix]. − $C_6H_{11}NO_6Si$ (221.2): calcd C 32.57, H 5.01, N 6.33; found C 32.5, H 5.2, N 6.2.

[(Methylammonio)methyl]bis[2-methyllactato(2−)-*O*^{1},*O*^{2}]silicate (7): The synthesis was carried out analogously to that of compound **5** by combining a solution of **12** (826 mg, 5.00 mmol) in acetonitrile (2.5 mL) with a solution of 2-methyllactic acid (1.04 g, 9.99 mmol) in acetonitrile (22.5 mL) (spontaneous formation of a precipitate after combining the reactants). Compound **7** was isolated in 73% yield (1.01 g) as a colorless crystalline product. Mp 310°C (dec.) − ^{1}H NMR ([D$_6$]DMSO, 300.1 MHz): δ = 1.21 (s, 6 H, CCH_3), 1.26 (s, 6 H, CCH_3), 2.18 and 2.39 (AB system, J_{AB} = −15.9 Hz, 2 H, $SiCH_2N$), 2.47 (s, 3 H, NCH_3), 7.8 (broad s, 2 H, NH_2). − $^{13}C\{^{1}H\}$ NMR ([D$_6$]DMSO, 75.5 MHz): δ = 26.7 (CCH_3), 27.6 (CCH_3), 36.2 (NCH_3), 39.2 ($SiCH_2N$), 73.8 (OCC_3), 178.4 (C=O). − ^{13}C CP/MAS NMR (109 transients): δ = 25.4 (CCH_3), 27.2 (CCH_3), 27.8 (CCH_3), 28.4 (CCH_3), 38.7 (NCH_3), 41.4 ($SiCH_2N$), 75.3 (OCC_3), 76.6 (OCC_3), 179.6 (C=O), 183.7 (C=O). − $^{29}Si\{^{1}H\}$ NMR ([D$_6$]DMSO, 59.6 MHz): δ = −99.2. − ^{29}Si CP/MAS NMR (293 transients): δ = −98.1. − FAB MS (positive ions): *m*/*z* (%) = 278 (30) [*M* + H$^+$], 154 (100) [matrix]. − $C_{10}H_{19}NO_6Si$ (277.3): calcd C 43.31, H 6.90, N 5.05; found C 43.4, H 6.9, N 5.1.

[(Dimethylammonio)methyl]bis[glycolato(2−)-*O*^{1},*O*^{2}]silicate (8): *Method a:* The synthesis was carried out analogously to that of compound **5** by combining a solution of **13** (896 mg, 5.00 mmol) in acetonitrile (2.5 mL) with a solution of glycolic acid (761 mg, 10.0 mmol) in acetonitrile (22.5 mL) (spontaneous formation of a precipitate after combining the reactants). Compound **8** was isolated in 88% yield (1.04 g) as a colorless crystalline product. Mp 221°C (dec). − ^{1}H NMR ([D$_6$]DMSO, 300.1 MHz): δ = 2.51 and 2.63 (AB system, J_{AB} = −15.9 Hz, 2 H, $SiCH_2N$), 2.73 (s, 6 H, NCH_3), 3.94 (s, 4 H, OCH_2C), 8.3 (broad s, 1 H, NH). − $^{13}C\{^{1}H\}$ NMR ([D$_6$]DMSO, 75.5 MHz): δ = 45.8 (NCH_3), 49.3 ($SiCH_2N$), 62.7 (OCH_2C), 173.9 (C=O). − ^{13}C CP/MAS NMR (1437 transients): δ = 44.3 (NCH_3), 49.0 (NCH_3), 50.8 ($SiCH_2N$), 64.0 (OCH_2C), 64.9 (OCH_2C), 176.6 (C=O), 179.9 (C=O). − $^{29}Si\{^{1}H\}$ NMR ([D$_6$]DMSO, 59.6 MHz): δ = −90.3. − ^{29}Si CP/MAS NMR (20 transients): δ = −88.6. − FAB MS (positive ions): *m*/*z* (%) = 236 (39) [*M* + H$^+$], 154 (100) [matrix]. − $C_7H_{13}NO_6Si$ (235.3): calcd C 35.74, H 5.57, N 5.95; found C 35.2, H 5.6, N 6.1.

Method b: A solution of **14** (1.13 g, 5.01 mmol) in acetonitrile (2.5 mL) was added at room temperature to a solution of glycolic acid (761 mg, 10.0 mmol) in acetonitrile (22.5 mL). The reaction mixture was stirred for 1 min and then kept undisturbed at room temperature for 7 d (formation of a precipitate ca. 18 h after combining the reactants). The precipitate was isolated by filtration, washed with cold acetonitrile (3 × 5 mL), and then dried in vacuo (0.01 Torr, 20°C, 12 h) to give 1.15 g (yield 98%) of colorless crystals. Mp 221°C (dec). − $C_7H_{13}NO_6Si$ (235.3): calcd C 35.74, H 5.57, N 5.95; found C 35.7, H 5.6, N 6.3. For spectroscopic data, see above.

Method c: **16** (1.36 g, 6.17 mmol) was added to a stirred solution of **15** (502 mg, 3.08 mmol) in acetonitrile (20 mL) (formation of a precipitate ca. 20 min after combining the reactants) and the reaction mixture stirred at room temperature for 24 h. The precipitate was filtered off and recrystallized from acetonitrile. The product was isolated by filtration and then dried in vacuo (0.01 Torr, 20°C, 4 h) to give 658 mg (yield 91%) of colorless crystals. Mp 221°C

(dec). – $C_7H_{13}NO_6Si$ (235.3): calcd C 35.74, H 5.57, N 5.95; found C 35.8, H 5.4, N 6.1. For spectroscopic data, see above.

[(Dimethylammonio)methyl]bis[2-methyllactato(2–)-*O*¹,*O*²]silicate (**9**): *Method a:* The synthesis was carried out analogously to that of compound **5** by combining a solution of **13** (896 mg, 5.00 mmol) in acetonitrile (2.5 mL) with a solution of 2-methyllactic acid (1.04 g, 9.99 mmol) in acetonitrile (22.5 mL) (spontaneous formation of a precipitate after combining the reactants). Compound **9** was isolated in 79% yield (1.15 g) as a colorless crystalline product. Mp 242°C. – ^{1}H NMR ([D$_6$]DMSO, 300.1 MHz): δ = 1.21 (s, 6 H, CCH_3), 1.26 (s, 6 H, CCH_3), 2.46 and 2.66 (AB system, J_{AB} = −15.9 Hz, 2 H, $SiCH_2N$), 2.75 (s, 6 H, NCH_3), 8.4 (broad s, 1 H, NH). – ^{13}C{^{1}H} NMR ([D$_6$]DMSO, 75.5 MHz): δ = 26.6 (C*C*H$_3$), 27.5 (C*C*H$_3$), 46.4 (NCH_3), 50.2 ($SiCH_2N$), 73.7 (O*C*C$_3$), 178.3 (C=O). – ^{13}C CP/MAS NMR (912 transients): δ = 24.8–29.7 (C*C*H$_3$), 47.4 (NCH_3), 48.6 (NCH_3), 51.5 ($SiCH_2N$), 52.2 ($SiCH_2N$), 75.7 (O*C*C$_3$), 76.2 (O*C*C$_3$), 177.1 (C=O), 177.7 (C=O), 178.4 (C=O), 182.0 (C=O). – ^{29}Si{^{1}H} NMR ([D$_6$]DMSO, 59.6 MHz): δ = −100.5. – ^{29}Si CP/MAS NMR (54 transients): δ = −100.9, −100.1. – FAB MS (positive ions): *m*/*z* (%) = 292 (100) [*M* + H$^+$]. – $C_{11}H_{21}NO_6Si$ (291.4): calcd C 45.34, H 7.26, N 4.81; found C 45.9, H 7.3, N 4.9.

Method b: The synthesis was carried out analogously to that of **8** *(method b)* by combining a solution of **14** (1.13 g, 5.01 mmol) in acetonitrile (2.5 mL) with a solution of 2-methyllactic acid (1.04 g, 9.99 mmol) in acetonitrile (22.5 mL) (first crystals formed ca. 40 h after combining the reactants). Compound **9** was isolated in 88% yield (1.28 g) as a colorless crystalline product. Mp 242°C. – $C_{11}H_{21}NO_6Si$ (291.4): calcd C 45.34, H 7.26, N 4.81; found C 45.1, H 7.4, N 4.9. For spectroscopic data, see above.

Method c: The synthesis was carried out analogously to that of **8** *(method c)* by combining a solution of **17** (2.51 g, 10.1 mmol) with a solution of **15** (770 mg, 4.72 mmol) in acetonitrile (20 mL) (formation of a precipitate ca. 30 min after combining the reactants). Compound **9** was isolated in 79% yield (1.09 g) as a colorless crystalline product. Mp 242°C. – $C_{11}H_{21}NO_6Si$ (291.4): calcd C 45.34, H 7.26, N 4.81; found C 45.3, H 7.1, N 4.8. For spectroscopic data, see above.

[(Dimethylammonio)methyl]bis[2-methyllactato(2–)-*O*¹,*O*²]silicate Hydrate (**9**·H_2O): Compound **9** (291 mg, 999 μmol) was dissolved in water (10 mL) and the solution kept undisturbed at room temperature for 6 d (slow evaporation of the water). Compound **9**·H_2O was isolated in 99% yield (306 mg) as a colorless crystalline product. Mp 276°C. – ^{1}H NMR ([D$_6$]DMSO, 300.1 MHz): the NMR data were identical with those of **9**, with an additional resonance signal at δ = 3.33 (s, 2 H, H_2O). – ^{13}C{^{1}H} NMR ([D$_6$]DMSO, 75.5 MHz): the NMR data were identical with those of **9**. – ^{13}C CP/MAS NMR (204 transients): δ = 26.2 (C*C*H$_3$), 27.0 (C*C*H$_3$), 28.5 (C*C*H$_3$), 30.4 (C*C*H$_3$), 47.3 (NCH_3), 49.3 (NCH_3), 51.1 ($SiCH_2N$), 75.8 (O*C*C$_3$), 76.3 (O*C*C$_3$), 181.4 (C=O). – ^{29}Si{^{1}H} NMR ([D$_6$]DMSO, 59.6 MHz): the NMR data were identical with those of **9**. – ^{29}Si CP/MAS NMR (200 transients): δ = −98.4 – $C_{11}H_{23}NO_7Si$ (309.4): calcd C 42.70, H 7.49, N 4.53; found C 42.4, H 7.4, N 4.4.

[(Dimethylammonio)methyl]bis[2-methyllactato(2–)-*O*¹,*O*²]silicate–Diacetonitrile (**9**·2CH_3CN): The synthesis was carried out analogously to that of **9** *(method b)*, except for the isolation by filtration and drying of the crystals formed. The crystal used for the X-ray diffraction study was taken directly from the reaction mixture. Attempts to characterize the bulk material after filtration and careful drying gave unsatisfactory results due to the loss of acetonitrile. Drying in vacuo at room temperature resulted in a complete loss of acetonitrile.

(Aminomethyl)triethoxysilane (**11**): Synthesis according to ref.[11]

Trimethoxy[(methylamino)methyl]silane (**12**): A mixture of (chloromethyl)trimethoxysilane (synthesis according to ref.[12]) (17.1 g, 100 mmol) and methylamine (15.5 g, 499 mmol) was heated in an autoclave at 120°C/20 bar for 16 h. After the reaction mixture was cooled to room temperature, the excess methylamine was evaporated and *n*-pentane (100 mL) added to the residue. The resulting precipitate was filtered off and the solvent removed from the filtrate under reduced pressure. The oily residue was distilled in vacuo over a Vigreux column to give 7.60 g (yield 46%) of a colorless liquid. Bp 40°C/6 Torr. – ^{1}H NMR (C_6D_6, 300.1 MHz): δ = 0.8 (broad s, 1 H, NH), 2.27 (s, 2 H, $SiCH_2N$), 2.38 (s, 3 H, NCH_3), 3.60 (s, 9 H, OCH_3). – ^{13}C{^{1}H} NMR (C_6D_6, 75.5 MHz): δ = 36.4 ($SiCH_2N$), 41.0 (NCH_3), 50.5 (OCH_3). – ^{29}Si{^{1}H} NMR (C_6D_6, 59.6 MHz): δ = −47.7. – EI MS: *m*/*z* (%) = 165 (14) [*M*$^+$], 121 (22) [*M*$^+$ – $CH_2N(H)CH_3$], 44 (100) [CH_2=N(H)CH_3^+]. – $C_5H_{15}NO_3Si$ (165.3): calcd C 36.34, H 9.15, N 8.48; found C 36.1, H 8.9, N 8.1.

[(Dimethylamino)methyl]trimethoxysilane (**13**): Synthesis according to ref.[2a]

[(Dimethylamino)methyl]dimethoxy(phenyl)silane (**14**): The synthesis was carried out analogously to that of **12** by treating (chloromethyl)dimethoxy(phenyl)silane (synthesis according to ref.[12]) (12.3 g, 56.8 mmol) with an excess of dimethylamine (6.92 g, 153 mmol). Compound **14** was isolated in 81% yield (10.4 g) as a colorless liquid. Bp 115°C/6 Torr. – ^{1}H NMR (C_6D_6, 300.1 MHz): δ = 2.31 (s, 2 H, $SiCH_2N$), 2.31 (s, 6 H, NCH_3), 3.61 (s, 6 H, OCH_3), 7.3–7.4 and 7.9–8.1 (m, 5 H, SiC_6H_5). – ^{13}C{^{1}H} NMR (C_6D_6, 75.5 MHz): δ = 47.7 ($SiCH_2N$), 49.7 (NCH_3), 50.5 (OCH_3), 128.1 (C-3/C-5, SiC_6H_5), 130.4 (C-4, SiC_6H_5), 133.7 (C-1, SiC_6H_5), 134.9 (C-2/C-6, SiC_6H_5). – ^{29}Si{^{1}H} (C_6D_6, 59.6 MHz): δ = −23.1. – EI MS: *m*/*z* (%) = 225 (2) [*M*$^+$], 210 (6) [*M*$^+$ – CH_3], 167 (8) [*M*$^+$ – $CH_2N(CH_3)_2$] 58 (100) [CH_2=N$(CH_3)_2^+$]. – $C_{11}H_{19}NO_2Si$ (225.4): calcd C 58.63, H 8.50, N 6.22; found C 59.0, H 8.6, N 6.0.

[(Dimethylammonio)methyl]tetrafluorosilicate (**15**): Synthesis according to ref.[2k]

(Trimethylsilyloxy)acetic Acid Trimethylsilyl Ester (**16**): Synthesis according to ref.[13]

2-Methyl-2-(trimethylsilyloxy)propionic Acid Trimethylsilyl Ester (**17**): Synthesis according to ref.[14]

Crystal Structure Analyses: Suitable single crystals of **5**·H_2O and **9**·H_2O were obtained by crystallization of **5** and **9** from water (slow evaporation of the solvent at room temperature), single crystals of **7** and **8** were obtained by crystallization from acetonitrile (slow cooling of a boiling saturated solution to room temperature). A suitable single crystal of **9**·2CH_3CN was isolated directly from the reaction mixture (synthesis according to *method b*). The crystals were mounted on a glass fiber and then transferred to the cold gas stream of the diffractometer [**5**·H_2O, **9**·H_2O: Syntex-R3 diffractometer; **7**: Stoe STADI-4 diffractometer; **8**: Enraf-Nonius CAD4 diffractometer; **9**·2CH_3CN: Stoe IPDS; monochromated Mo-*Kα* radiation (λ = 0.71073 Å)]. For compound **7** a semiempirical absorption correction (ψ scans) was applied. All structures were solved by direct methods.[15] All non-hydrogen atoms were refined anisotropically.[16] For the structures of **7**, **8**, **9**·H_2O, and **9**·2CH_3CN a riding model was employed in the refinement of the CH hydrogen atom positions; for the structure of **5**·H_2O the CH hydrogen atoms were localized in difference Fourier syntheses and

Table 6. Crystal data and experimental parameters for the crystal structure analyses of **5**·H_2O, **7**, **8**, **9**·H_2O, and **9**·$2CH_3CN$

Compound	**5**·H_2O	**7**	**8**	**9**·H_2O	**9**·$2CH_3CN$
empirical formula	$C_9H_{19}NO_7Si$	$C_{10}H_{19}NO_6Si$	$C_7H_{13}NO_6Si$	$C_{11}H_{23}NO_7Si$	$C_{15}H_{27}N_3O_6Si$
formula mass [g mol^{-1}]	281.34	277.35	235.27	309.39	373.49
collection T [K]	203(2)	203(2)	173(2)	203(2)	173(2)
λ(Mo Kα) [Å]	0.71073	0.71073	0.71073	0.71073	0.71073
crystal system	monoclinic	monoclinic	orthorhombic	monoclinic	orthorhombic
space group (no.)	$P2_1/c$ (14)	$P2_1/c$ (14)	*Pbca* (61)	$P2_1/c$ (14)	*Pbca* (61)
a [Å]	9.050(3)	8.943(5)	7.7606(9)	9.0530(11)	13.207(3)
b [Å]	12.917(4)	12.993(9)	12.734(3)	12.286(2)	14.367(3)
c [Å]	13.122(4)	13.111(9)	20.372(7)	13.927(2)	21.097(4)
β [deg]	106.56(2)	106.92(5)	90	96.526(12)	90
V [Å^3]	1470.3(8)	1458(2)	2013.3(8)	1539.0(4)	4003.1(14)
Z	4	4	8	4	8
D(calcd) [g cm^{-3}]	1.271	1.264	1.552	1.335	1.239
μ [mm^{-1}]	0.183	0.179	0.244	0.181	0.151
F(000)	600	592	992	664	1600
crystal dimens [mm]	0.4×0.4×0.2	0.6×0.3×0.3	0.7×0.5×0.4	0.8×0.6×0.6	0.3×0.3×0.2
2θ range [deg]	5.66−60.00	4.52−54.00	4.00−49.94	4.44−58.02	4.62−49.52
index ranges	$-12 \le h \le 12$, $-18 \le k \le 18$, $-18 \le l \le 18$	$0 \le h \le 11$, $0 \le k \le 16$, $-16 \le l \le 16$	$-2 \le h \le 9$, $0 \le k \le 15$, $-24 \le l \le 24$	$-12 \le h \le 12$, $-11 \le k \le 16$, $0 \le l \le 19$	$-15 \le h \le 15$, $-14 \le k \le 16$, $-22 \le l \le 24$
no. of coll reflns	16726	3160	4018	4422	12253
no. of indep reflns	4288	2961	1766	4091	3416
R_{int}	0.0570	0.0317	0.0278	0.0212	0.0789
no. of reflns used	4288	2961	1766	4091	3416
no. of parameters	239	177	143	200	238
S[a]	1.045	1.049	1.036	1.046	0.907
weight params a/b[b]	0.0540/0.4089	0.0845/0.1256	0.0353/0.9794	0.0415/0.4621	0.0661/0
$R1$[c] [$I > 2\sigma(I)$]	0.0462	0.0401	0.0330	0.0296	0.0431
$wR2$[d] (all data)	0.1138	0.1188	0.0802	0.0847	0.1094
extinction coefficient	−	0.005(2)	0.0019(5)	0.0213(13)	−
max/min res electron density [e Å^{-3}]	+0.552/−0.580	+0.442/−0.402	+0.254/−0.323	+0.357/−0.261	+0.264/−0.381

[a] $S = \{\Sigma[w(F_o^2 - F_c^2)^2] / (n - p)\}^{0.5}$; n = no. of reflections; p = no. of parameters. − [b] $w^{-1} = \sigma^2(F_o^2) + (aP)^2 + bP$, with $P = (F_o^2 + 2F_c^2) / 3$. − [c] $R1 = \Sigma||F_o| - |F_c|| / \Sigma|F_o|$. − [d] $wR2 = \{\Sigma[w(F_o^2 - F_c^2)^2] / \Sigma[w(F_o^2)^2]\}^{0.5}$.

refined freely. In all cases, the positions of the NH and OH hydrogen atoms were localized in difference Fourier syntheses and refined freely.

Crystallographic data (excluding structure factors) for the structures reported in this paper have been deposited with the Cambridge Crystallographic Data Centre as supplementary publication no. CCDC-101620 (**5**·H_2O), CCDC-101621 (**7**), CCDC-101622 (**8**), CCDC-101623 (**9**·H_2O), and CCDC-101624 (**9**·$2CH_3CN$). Copies of the data can be obtained free of charge on application to CCDC, 12 Union Road, Cambridge CB2 1EZ, UK [fax: (+44) 1223/336-033; e-mail: deposit@ccdc.cam.ac.uk].

Computational Methods: Geometry optimizations at the SCF/SVP level for the anionic model species **10** and the zwitterion **8** were performed using the TURBOMOLE program system.[17] Stationary geometries and transition states were characterized as local minima (zero imaginary frequencies) and saddle points (one imaginary frequency), respectively, by calculation of the vibrational frequencies. The energies given for **10** include the single point MP2 energy (SVP basis set) and the zero point vibrational energy.

VT ^{1}H-NMR Studies of 9: The experiments were carried out analogously to the standard ^{1}H-NMR measurements using a Bruker DRX-300 NMR spectrometer. [D_6]DMSO, CD_3CN, and $CDCl_3$ were used as solvents. The thermocouple used with the probe was calibrated for high temperatures according to ref.[18] using a 80% solution of 1,2-ethanediol in [D_6]DMSO. Spectra were recorded in the temperature range of 21−118°C ([D_6]DMSO), 22−94°C (CD_3CN), and 24−83°C ($CDCl_3$). The time required for temperature equilibration was 15 min. The data obtained were fitted and simulated by using the Bruker software program WinDyna 1.0b (line-shape analysis). From the simulated spectra the coalescence temperatures T_C and the exchange rates k_C at the coalescence points were extracted and the respective values for the activation free enthalpy $\Delta G^{\neq}$ for the exchange process were calculated by using the Eyring equation:

$$\Delta G^{\neq} = 19.14\ T_C\ [10.32 + \log(T_C/k_C)]\ [\text{J mol}^{-1}]$$[19]

Acknowledgments

We thank the Deutsche Forschungsgemeinschaft and the Fonds der Chemischen Industrie for financial support, and the Bayer AG (Leverkusen and Wuppertal, Germany) and Merck KGaA (Darmstadt, Germany) for various gifts of chemicals. In addition, the authors would like to thank Prof. Dr. R. Ahlrichs and Dr. M. Häser (†) for helpful discussions in context with the ab initio studies.

[1] Reviews and proceedings dealing with pentacoordinate silicon compounds: [1a] S. N. Tandura, M. G. Voronkov, N. V. Alekseev, *Top. Curr. Chem.* **1986**, *131*, 99−189. − [1b] W. S. Sheldrick, in *The Chemistry of Organic Silicon Compounds, Part 1* (Eds.: S. Patai, Z. Rappoport), Wiley, Chichester, **1989**, pp. 227−303. − [1c] R. J. P. Corriu, J. C. Young, in *The Chemistry of Organic Silicon Compounds, Part 2* (Eds.: S. Patai, Z. Rappoport), Wiley, Chichester, **1989**, pp. 1241−1288. − [1d] R. R. Holmes, *Chem. Rev.* **1990**, *90*, 17−31. − [1e] C. Chuit, R. J. P. Corriu, C. Reye, J. C. Young, *Chem. Rev.* **1993**, *93*, 1371−1448. − [1f] R. Tacke, J. Becht, A. Lopez-Mras, J. Sperlich, *J. Organomet. Chem.* **1993**,

446, 1−8. − [1g] C. Y. Wong, J. D. Woollins, *Coord. Chem. Rev.* **1994**, *130*, 175−241. − [1h] R. Tacke, O. Dannappel, M. Mühleisen, in *Organosilicon Chemistry II − From Molecules to Materials* (Eds.: N. Auner, J. Weis), VCH, Weinheim, **1996**, pp. 427−446. − [1i] R. Tacke, O. Dannappel, in *Tailor-made Silicon-Oxygen Compounds − From Molecules to Materials* (Eds.: R. Corriu, P. Jutzi), Vieweg, Braunschweig/Wiesbaden, **1996**, pp. 75−86. − [1j] E. Lukevics, O. A. Pudova, *Chem. Heterocycl. Compd.* **1996**, *353*, 1605−1646. − [1k] R. R. Holmes, *Chem. Rev.* **1996**, *96*, 927−950. − [1l] D. Kost, I. Kalikhman, in *The Chemistry of Organic Silicon Compounds, Part 2, Vol. 2* (Eds.: S. Patai, Z. Rappoport), Wiley, Chichester, **1998**, pp. 1339−1445.

[2] [2a] R. Tacke, A. Lopez-Mras, J. Sperlich, C. Strohmann, W. F. Kuhs, G. Mattern, A. Sebald, *Chem. Ber.* **1993**, *126*, 851−861. − [2b] R. Tacke, A. Lopez-Mras, W. S. Sheldrick, A. Sebald, *Z. Anorg. Allg. Chem.* **1993**, *619*, 347−358. − [2c] R. Tacke, J. Becht, A. Lopez-Mras, W. S. Sheldrick, A. Sebald, *Inorg. Chem.* **1993**, *32*, 2761−2766. − [2d] J. Sperlich, J. Becht, M. Mühleisen, S. A. Wagner, G. Mattern, R. Tacke, *Z. Naturforsch. B* **1993**, *48*, 1693−1706. − [2e] R. Tacke, A. Lopez-Mras, P. G. Jones, *Organometallics* **1994**, *13*, 1617−1623. − [2f] R. Tacke, M. Mühleisen, P. G. Jones, *Angew. Chem.* **1994**, *106*, 1250−1252; *Angew. Chem., Int. Ed. Engl.* **1994**, *33*, 1186−1188. − [2g] M. Mühleisen, R. Tacke, *Chem. Ber.* **1994**, *127*, 1615−1617. − [2h] M. Mühleisen, R. Tacke, *Organometallics* **1994**, *13*, 3740−3742. − [2i] R. Tacke, M. Mühleisen, *Inorg. Chem.* **1994**, *33*, 4191−4193. − [2j] R. Tacke, M. Mühleisen, A. Lopez-Mras, W. S. Sheldrick, *Z. Anorg. Allg. Chem.* **1995**, *621*, 779−788. − [2k] R. Tacke, J. Becht, O. Dannappel, R. Ahlrichs, U. Schneider, W. S. Sheldrick, J. Hahn, F. Kiesgen, *Organometallics* **1996**, *15*, 2060−2077. − [2l] R. Tacke, J. Heermann, M. Pülm, *Organometallics* **1997**, *16*, 5648−5652. − [2m] M. Pülm, R. Tacke, *Organometallics* **1997**, *16*, 5664−5668. − [2n] B. Pfrommer, R. Tacke, *Eur. J. Inorg. Chem.* **1998**, 415−418. − [2o] R. Tacke, J. Heermann, M. Pülm, I. Richter, *Organometallics* **1998**, *17*, 1663−1668. − [2p] R. Tacke, B. Pfrommer, K. Lunkenheimer, R. Hirte, *Organometallics* **1998**, *17*, 3670−3676. − [2q] R. Tacke, J. Heermann, M. Pülm, E. Gottfried, *Monatsh. Chem.* **1999**, *130*, 99−107.

[3] Some preliminary results have already been published in conference proceedings.[1h,1i]

[4] [4a] E. L. Muetterties, L. J. Guggenberger, *J. Am. Chem. Soc.* **1974**, *96*, 1748−1756. − [4b] R. R. Holmes, J. A. Deiters, *J. Am. Chem. Soc.* **1977**, *99*, 3318−3326. − [4c] The degree of distortion was calculated by using the dihedral angle method described in ref.[4a,4b] (all nine dihedral angles and the values for the reference geometry of the ideal square pyramid given in ref.[4a] were considered for this calculation).

[5] Calculated energies (SCF + single point MP2 + E(vib0) energies [Hartree]): **10a**, −893.70429 (C_2 symmetry); **10b**, −893.69580 (C_1 symmetry); **10c**, −893.68806 (C_2 symmetry); **10d**, −893.69303 (C_2 symmetry); **10e**, −893.69233 (C_S symmetry).

[6] Calculated SCF energy [Hartree]: **8**, −1064.66653.

[7] As the equipotential surface around the local minimum **10c** is quite flat and the energy difference between **10c** and the transition state $\mathbf{10}^{\pm 2}$ is rather small, further calculations with a larger basis set have to be performed in order to differentiate more precisely between the relative energies of **10c** and $\mathbf{10}^{\pm 2}$.

[8] The calculated transition state **10d** is not needed to realize the Λ/Δ-isomerization according to Figure 9.

[9] Calculated energies (SCF + single point MP2 + E(vib0) energies [Hartree]): $\mathbf{10}^{\pm 1}$, −893.69233 (C_S symmetry); $\mathbf{10}^{\pm 2}$, −893.68635 (C_2 symmetry); $\mathbf{10}^{\pm 3}$, −893.67732 (C_1 symmetry).

[10] ^{29}Si CP/MAS NMR experiments with **9**·2CH_3CN gave unsatisfactory results (loss of CH_3CN in the course of the experiments).

[11] J. E. Noll, J. L. Speier, B. F. Daubert, *J. Am. Chem. Soc.* **1951**, *73*, 3867−3871.

[12] R. Tacke, J. Pikies, H. Linoh, R. Rohr-Aehle, S. Gönne, *Liebigs Ann. Chem.* **1987**, 51−57.

[13] [13a] A. Wissner, *Tetrahedron Lett.* **1978**, 2749−2752. − [13b] A. Wissner, *J. Org. Chem.* **1979**, *44*, 4617−4622.

[14] G. Schwarz, H. Alberts, H. R. Kricheldorf, *Liebigs Ann. Chem.* **1981**, 1257−1270.

[15] G. M. Sheldrick, SHELXS-96, University of Göttingen, Germany, **1996**; G. M. Sheldrick, *Acta Crystallogr., Sect. A* **1990**, *46*, 467−473.

[16] G. M. Sheldrick, SHELXL-96, University of Göttingen, Germany, **1996**.

[17] Program system TURBOMOLE: R. Ahlrichs, M. Bär, M. Häser, H. Horn, C. Kömel, *Chem. Phys. Lett.* **1989**, *162*, 165−169. Optimized SVP basis sets used (in this context, see ref.[2k]): Si, (10s7p1d)/[4s3p1d]; C, N, and O, (7s4p1d)/[3s2p1d]; H, (4s1p)/[2s1p].

[18] S. Braun, H.-O. Kalinowski, S. Berger, *100 and More Basic NMR Experiments*, VCH, Weinheim, **1996**, pp. 115−117.

[19] U. Weber, H. Thiele, *NMR Spectroscopy: Modern Spectral Analysis*, Wiley-VCH, Weinheim, **1998**, pp. 339−361.

Received October 12, 1998
[I98350]

New Chiral Zwitterionic λ^5*Si*-Silicates with an SiO_5 or SiO_4C Framework: Syntheses, Crystal Structures, and Properties

Reinhold Tacke,*[a] Brigitte Pfrommer,[a] Melanie Pülm,[a] and Rüdiger Bertermann[a]

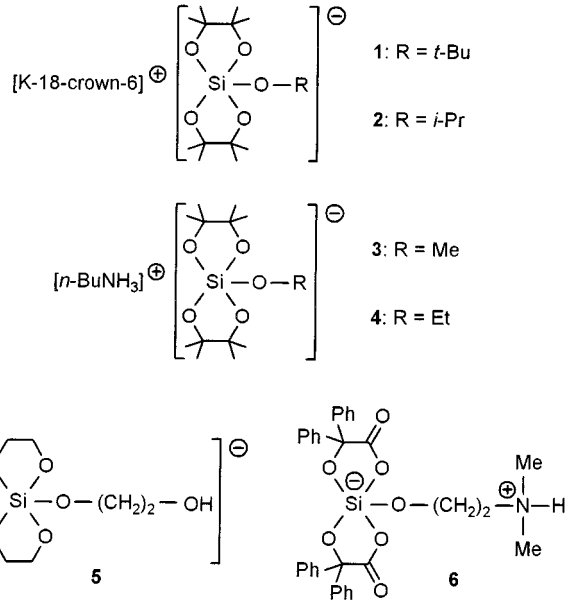
Dedicated to Professor Helmut Werner on the occasion of his 65th birthday

Keywords: Ab initio studies / Chirality / Pentacoordinate silicon / Stereochemistry / Zwitterionic λ^5*Si*-silicates

The syntheses of the zwitterionic (molecular) spirocyclic λ^5*Si*-silicates **7** and **8** (SiO_5 skeletons) and **10**–**12** (SiO_4C skeletons) are described. These chiral compounds contain a pentacoordinate (formally negatively charged) silicon atom and a tetracoordinate (formally positively charged) nitrogen atom. The pairs **7**/**11** and **8**/**12** are isoelectronic O/CH_2 analogues and **10**–**12** represent a series of homologous compounds containing different alkylene spacers that connect the *ate* and *onium* center of these zwitterions. Compound **7**, **8**, and **10**–**12** were studied by single-crystal X-ray diffraction, solution-state (^{1}H, ^{13}C, ^{29}Si) and solid-state (^{29}Si CP/MAS) NMR spectroscopy, and VT ^{1}H-NMR spectroscopy. The experimental investigations were completed by ab initio studies of the related anionic λ^5*Si*-silicate **13**.

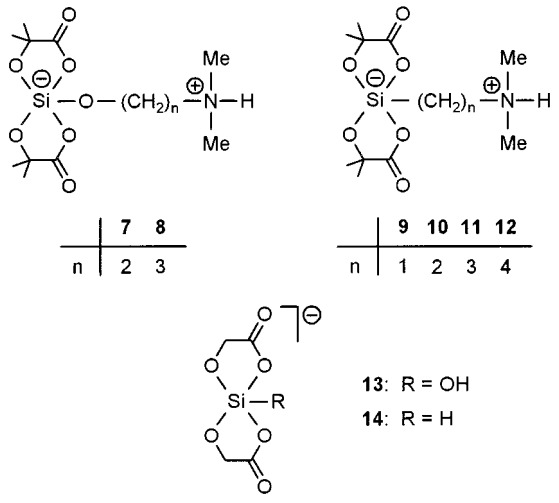
Introduction

Numerous pentacoordinate silicon compounds have been described in the literature over the past thirty years.[1] Surprisingly, only a few examples with an SiO_5 skeleton have been reported. To the best of our knowledge, the ionic λ^5*Si*-silicates **1**,[2a] **2**,[2b] **3**·MeOH,[2a] **4**,[2a] and **5**[2c] as well as the zwitterionic λ^5*Si*-silicate **6**·DMF[2d] are the only examples of this particular type of compound that have been structurally characterized by single-crystal X-ray diffraction.[2]



The spirocyclic anions of **1**−**5** contain two bidentate ligands of the ethane-1,2-diolato(2−) type, whereas the spirocyclic zwitterion **6** contains two bidentate benzilato(2−)-O^1,O^2 ligands.

Here we report on the syntheses, crystal structure analyses, and properties of two further zwitterionic λ^5*Si*-silicates with an SiO_5 framework, compounds **7** and **8**.[3] These spirocyclic zwitterions contain two bidentate 2-methyllactato(2−)-O^1,O^2 ligands. In addition, the syntheses, crystal structures, and properties of the related zwitterionic λ^5*Si*-silicates **10**−**12** (SiO_4C skeletons) are described.[3] The zwitterions **11** and **12** formally derive from compounds **7** and **8** by replacement of an oxygen atom by a methylene group. Furthermore, the zwitterions **10**−**12** can be regarded as homologs of compound **9** which has recently been described in the literature.[4] The zwitterionic λ^5*Si*-silicates **9**−**12** differ in their alkylene spacers that connect the *ate* and *onium* centers of these molecules. The experimental investigations



[a] Institut für Anorganische Chemie, Universität Würzburg
Am Hubland, D-97074 Würzburg, Germany
Fax: (internat.) +49(0)931/888-4609
E-mail: r.tacke@mail.uni-wuerzburg.de

 © WILEY-VCH Verlag GmbH, D-69451 Weinheim, 1999 1434−1948/99/0505−0807 $ 17.50+.50/0

concerning compounds **7** and **8** (SiO_5 skeletons) were completed by ab initio studies of the related anionic λ^5*Si*-silicate **13** (for ab initio investigations of the anion **14**, see ref.[4]).

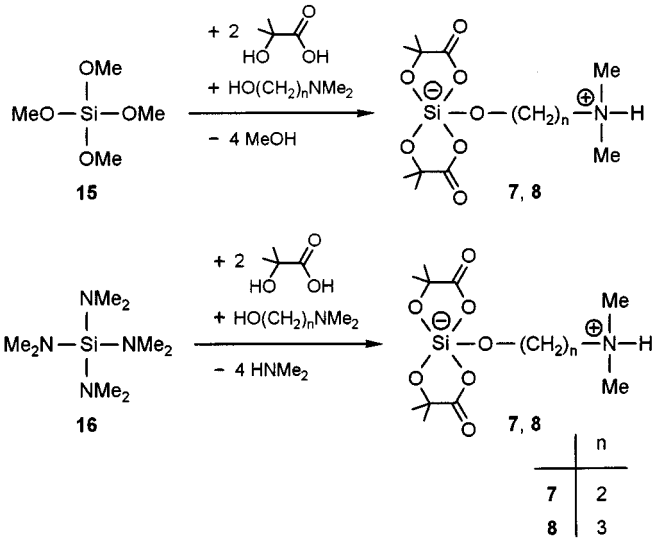
The main goal of the experimental and computational studies presented here was to contribute to the chemistry of pentacoordinate silicon compounds with an SiO_5 framework. These investigations were carried out with a special emphasis on the comparison of the structures and properties of the O/CH_2 analogues **7/11** and **8/12**. A further concern was to study the influence of the alkylene spacer on the structures and properties of the homologs **9**−**12**.

Results and Discussion

Syntheses

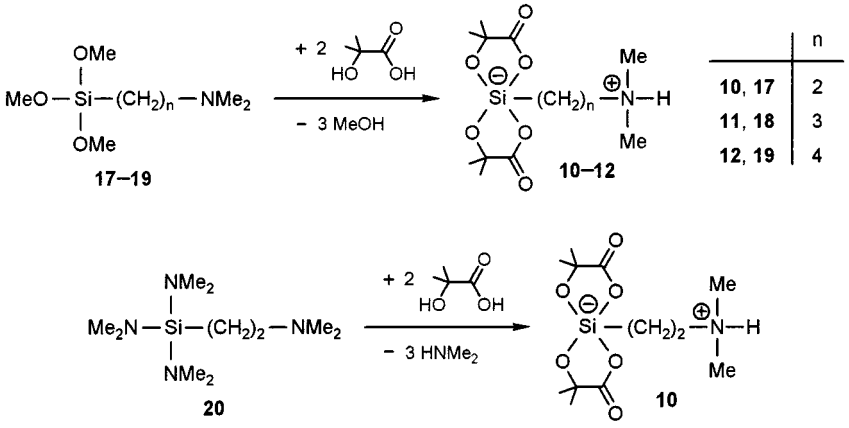
The zwitterionic λ^5*Si*-silicates **7** and **8** were prepared according to Scheme 1 using two different synthetic methods each. The first method implies reaction of tetramethoxysilane (**15**) with two mol equivalents of 2-methyllactic acid and one mol equivalent of 2-(dimethylamino)ethanol and 3-(dimethylamino)propanol, respectively. The reactions were carried out in boiling acetonitrile and the resulting methanol, along with part of the solvent, was removed by distillation. After the reaction mixtures were cooled to room temperature, the products precipitated. Compounds **7** and **8** were isolated, after recrystallization from acetonitrile, in 73% (**7**) and 71% yield (**8**). The second method is based on treatment of tetrakis(dimethylamino)silane[5] (**16**) with one mol equivalent of the respective aminoalcohol, followed by treatment with two mol equivalents of 2-methyllactic acid. The syntheses were again carried out in boiling acetonitrile and compounds **7** and **8** were isolated, after recrystallization from acetonitrile, in 62% (**7**) and 53% yield (**8**).

The zwitterionic λ^5*Si*-silicates **10**−**12** were synthesized according to Scheme 2 by reaction of the respective [(dimethylamino)alkyl]trimethoxysilanes **17**−**19** with 2-methyllactic acid (molar ratio 1:2) in acetonitrile at room temperature. Compounds **10**−**12** were isolated, after recrystallization from acetonitrile, in 78% (**10**), 88% (**11**), and 90% yield (**12**). Alternatively, compound **10** was synthesized according to Scheme 2 by treatment of tris(dimethylamino)[2-(dimethylamino)ethyl]silane[6] (**20**) with two mol equivalents of 2-methyllactic acid in acetonitrile and isolated, after recrystallization from acetonitrile, in 82% yield.

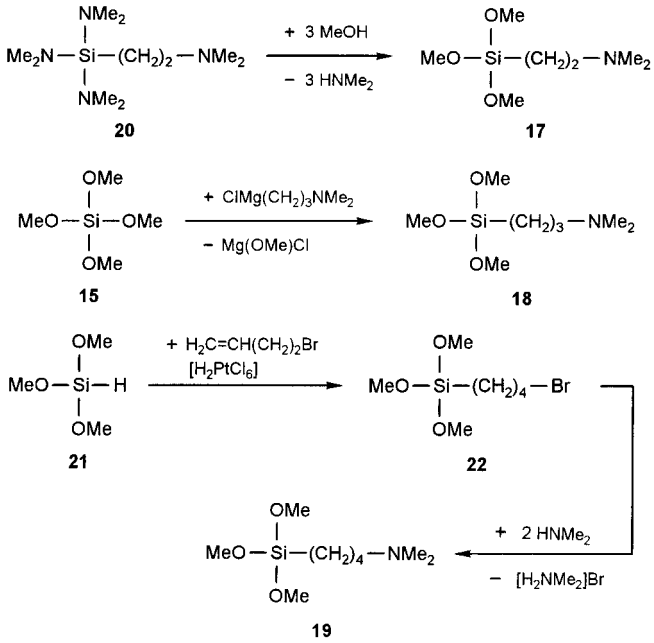


Scheme 1. Syntheses of compounds **7** and **8**

The [(dimethylamino)alkyl]trimethoxysilanes **17**−**19** used for the syntheses of **10**−**12** were prepared according to Scheme 3. [2-(Dimethylamino)ethyl]trimethoxysilane (**17**) was synthesized by methanolysis of the corresponding tris(dimethylamino)silane **20** (yield 84%). [3-(Dimethylamino)propyl]trimethoxysilane (**18**) was obtained by reaction of tetramethoxysilane (**15**) with 3-(dimethylamino)prop-1-ylmagnesium chloride in tetrahydrofuran (yield 71%). [4-(Dimethylamino)butyl]trimethoxysilane (**19**) was prepared by a two-step synthesis starting from trimethoxysilane (**21**). Hydrosilylation of 4-bromo-1-butene with **21** in an autoclave (H_2PtCl_6 as catalyst) gave (4-bromobutyl)trimethoxysilane (**22**) (yield 71%) which upon reaction with dimethylamine in an autoclave yielded the corresponding [4-(dimethylamino)butyl]silane **19** (yield 82%). The silanes **17**−**19** and **22** were isolated as colorless liquids. Their identity was established by elemental analyses, NMR studies (^{1}H, ^{13}C, ^{29}Si), and mass-spectrometric investigations (EI MS).



Scheme 2. Syntheses of compounds **10**−**12**



Scheme 3. Syntheses of compounds **17**−**19**

The title compounds **7**, **8**, and **10**−**12** are colorless crystalline solids with melting points in the temperature range between 162°C (**10**) and 298°C (**12**, dec). They are almost insoluble in nonpolar organic solvents and also exhibit a poor solubility in polar organic solvents. The identity of **7**, **8**, and **10**−**12** was established by elemental analyses (C, H, N), solution-state (^{1}H, ^{13}C, ^{29}Si) and solid-state (^{29}Si CP/MAS) NMR studies, and mass-spectrometric investigations (FAB MS). In addition, all compounds were studied by VT ^{1}H-NMR experiments and were structurally characterized by single-crystal X-ray diffraction. All these studies unequivocally established the zwitterionic structure of **7**, **8**, and **10**−**12** in the solid state and in solution.

Crystal Structure Analyses

Compounds **7**, **8**, and **10**−**12** were studied by single-crystal X-ray diffraction. They crystallize in the space group $P2_1/n$ (**11**), $P2_1/c$ (**7**, **8**, **12**), or $P\bar{1}$ (**10**). All crystals are built up by pairs of Λ- and Δ-enantiomers. There are two crystallographically independent zwitterions each in the crystal lattice of **8**, **10**, and **12**. The structures of compounds **7**, **8**, and **10**−**12** in the crystal are depicted in Figures 1−5. The crystal data and the experimental parameters used for these experiments are summarized in Table 7. Selected interatomic distances and angles are listed in Tables 1 and 2. For reasons of comparison, the respective data for compound **9**·H_2O[4] are included in Table 2.

The coordination polyhedra around the silicon atoms of **7**, **8**, and **10**−**12** can be described as distorted trigonal bipyramids, each bidentate 2-methyllactato(2−)-O^1,O^2 ligand spanning one axial (O1, O3) and one equatorial site (O2, O4). In all compounds, the axial sites are occupied by the carboxylate oxygen atoms. In terms of the Berry pseudorotation coordinate, the geometry of the coordination polyhedra is displaced by 6.1% (**7**), 19.4% (**8**, *molecule A*), 19.2% (**8**, *molecule B*), 32.6% (**10**, *molecule A*), 10.2% (**10**, *molecule B*), 9.2% (**11**), 17.2% (**12**, *molecule A*), and 19.6% (**12**, *molecule B*).[7] The atoms O5 (O5′) and C1 (C1′), respectively, are the pivot atoms that best fit to the Berry pseudorotation coordinate. For compound **9**·H_2O a similar structure was determined, the Berry distortion amounting to 8.9%.[4]

The axial Si−O distances in the SiO_5 skeletons of **7** and **8** [1.773(2)−1.810(2) Å] are significantly longer than the

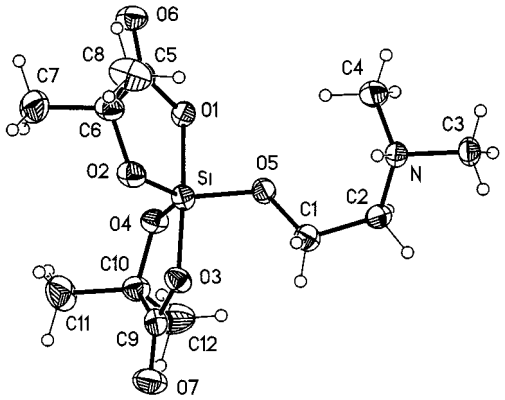


Figure 1. Molecular structure of **7** (probability level of displacement ellipsoids 50%), showing the atomic numbering scheme

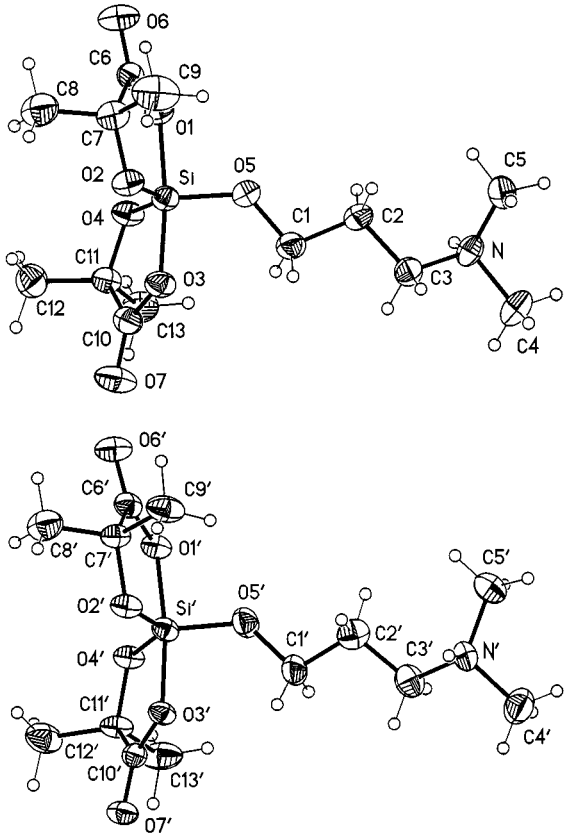


Figure 2. Molecular structures of the two crystallographically independent zwitterions (*molecule A*, above; *molecule B*, below) in the crystal of **8** (probability level of displacement ellipsoids 50%), showing the atomic numbering scheme

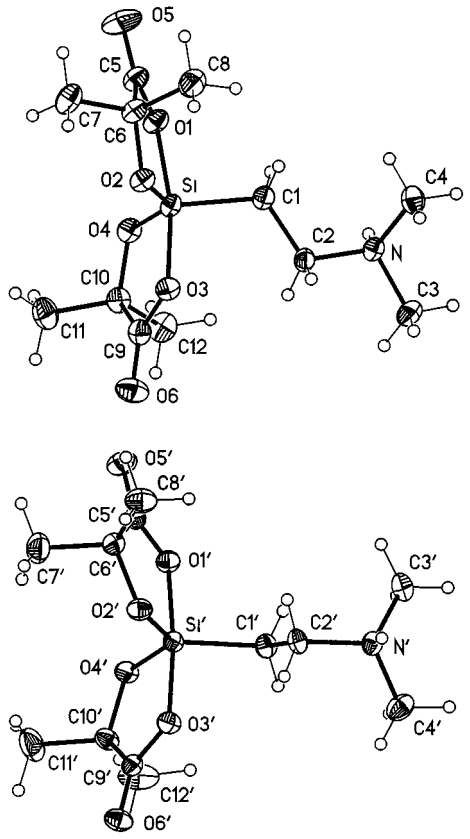


Figure 3. Molecular structures of the two crystallographically independent zwitterions (*molecule A*, above; *molecule B*, below) in the crystal of **10** (probability level of displacement ellipsoids 50%), showing the atomic numbering scheme

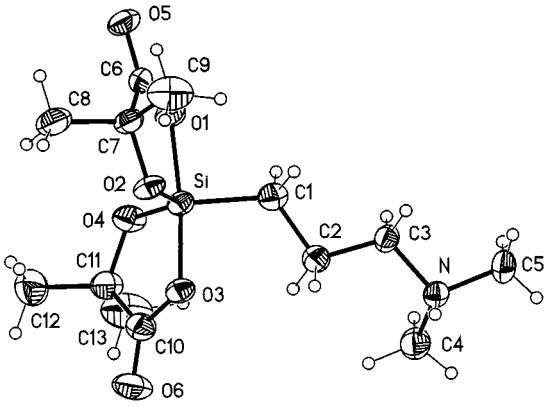


Figure 4. Molecular structure of **11** (probability level of displacement ellipsoids 50%), showing the atomic numbering scheme

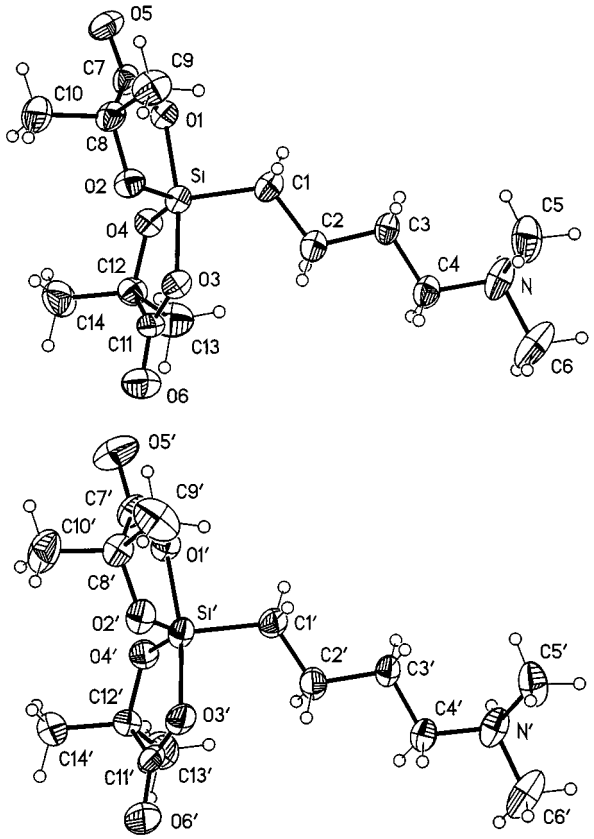


Figure 5. Molecular structures of the two crystallographically independent zwitterions (*molecule A*, above; *molecule B*, below) in the crystal of **12** (probability level of displacement ellipsoids 50%), showing the atomic numbering scheme

Table 1. Selected interatomic distances [Å] and angles [°] for **7** and **8**

	7	**8**	
		molecule A	*molecule B*
Si−O1	1.798(2)	1.804(2)	1.785(2)
Si−O2	1.659(2)	1.665(2)	1.662(2)
Si−O3	1.773(2)	1.785(2)	1.810(2)
Si−O4	1.653(2)	1.660(2)	1.668(2)
Si−O5	1.643(2)	1.633(2)	1.634(2)
O1−Si−O2	88.68(8)	88.41(11)	89.40(12)
O1−Si−O3	176.83(8)	172.68(12)	172.02(12)
O1−Si−O4	88.61(8)	87.50(11)	87.92(11)
O1−Si−O5	88.03(8)	90.81(11)	91.24(12)
O2−Si−O3	89.82(8)	88.14(11)	86.97(12)
O2−Si−O4	121.01(9)	125.98(13)	125.36(13)
O2−Si−O5	119.97(9)	116.63(13)	117.58(13)
O3−Si−O4	89.77(8)	89.32(11)	88.39(11)
O3−Si−O5	95.14(8)	96.50(12)	96.74(11)
O4−Si−O5	118.80(9)	117.26(13)	117.03(13)

equatorial ones [1.633(2)−1.668(2) Å]. The same holds true for the axial [1.786(3)−1.841(3) Å] and equatorial Si−O distances [1.663(3)−1.685(3) Å] in the *Si*O_4C frameworks of **10**−**12**. Generally, in the case of those oxygen atoms that are involved as acceptor atoms in N−H···O hydrogen bonds (see below), significantly elongated Si−O distances were observed. The Si−C distances for **10**−**12** are very similar [1.868(4)−1.884(2) Å]. Both replacement of oxygen atoms by methylene groups (**7** → **11**; **8** → **12**) and elongation of the $SiO(CH_2)_nN$ and $Si(CH_2)_nN$ chains (**7** → **8**; **9** → **10** → **11** → **12**) do not affect the geometry of the *Si*-coordination polyhedra in a systematic manner. It rather appears that the distortion of the trigonal-bipyramidal coordination polyhedra of the title compounds is mainly influenced by the crystal packing, including hydrogen-bonding interactions between the zwitterions (see below). This is best reflected by the quite different Berry distortions observed for the two crystallographically independent zwitterions in the crystal of **10** (*molecule A*, 32.6%; *molecule B*, 10.2%).

Table 2. Selected interatomic distances [Å] and angles [°] for **9**·H_2O and **10**−**12**

	9·H_2O[a]	**10**		**11**	**12**	
		molecule A	*molecule B*		*molecule A*	*molecule B*
Si−O1	1.8003(8)	1.8334(12)	1.8004(12)	1.832(2)	1.841(3)	1.836(4)
Si−O2	1.6636(8)	1.6669(12)	1.6670(13)	1.672(2)	1.663(3)	1.665(4)
Si−O3	1.8029(8)	1.7907(12)	1.8371(12)	1.804(2)	1.786(3)	1.810(4)
Si−O4	1.6764(8)	1.6771(13)	1.6687(11)	1.670(2)	1.685(3)	1.671(3)
Si−C1	1.8915(11)	1.884(2)	1.884(2)	1.871(4)	1.874(4)	1.868(4)
O1−Si−O2	89.45(4)	87.55(6)	89.22(6)	87.71(10)	87.8(2)	87.9(2)
O1−Si−O3	176.06(4)	168.64(6)	173.70(5)	173.40(11)	170.1(2)	169.82(14)
O1−Si−O4	88.28(4)	85.66(6)	88.49(6)	87.26(9)	86.3(2)	86.3(2)
O1−Si−C1	95.43(4)	92.89(7)	94.40(7)	90.46(13)	92.9(2)	93.9(2)
O2−Si−O3	89.58(4)	88.58(5)	88.27(6)	89.29(10)	88.0(2)	87.4(2)
O2−Si−O4	122.20(4)	130.22(6)	121.50(6)	120.52(12)	122.9(2)	124.0(2)
O2−Si−C1	120.82(5)	114.38(7)	118.74(7)	120.61(14)	118.5(2)	118.7(2)
O3−Si−O4	89.01(4)	88.70(6)	87.90(6)	89.21(10)	88.5(2)	88.9(2)
O3−Si−C1	88.34(4)	98.43(7)	91.87(7)	96.14(13)	97.0(2)	96.3(2)
O4−Si−C1	116.88(5)	115.18(7)	119.72(7)	118.7(2)	118.5(2)	117.2(2)

[a] Data taken from ref.[4]

As expected from the presence of their potential NH donor functions and potential oxygen acceptor atoms, all title compounds form N−H···O hydrogen bonds in the crystal. The relevant geometric data for the respective hydrogen-bonding systems are summarized in Table 3.

Table 3. Geometric data for the N−H···O hydrogen bonds in the crystal of **7**, **8**, and **10**−**12**

compd	N−H···O	N···O [Å]	N−H [Å]	H···O [Å]	N−H···O [°]
7[a]	N−H···O1	3.041(3)	0.90(3)	2.48(3)	120(2)
	N−H···O6	2.803(3)	0.90(3)	1.90(3)	178(3)
8[b]	N−H···O1	3.021(4)	0.97(3)	2.24(3)	137(3)
	N−H···O6	2.895(4)	0.97(3)	1.98(3)	157(3)
	N′−H′···O3′	3.246(4)	0.98(3)	2.55(4)	129(3)
	N′−H′···O7′	2.787(4)	0.98(3)	1.82(3)	169(3)
10[c]	N−H···O1	2.8934(18)	0.86(2)	2.08(2)	157(2)
	N−H···O4	3.2833(18)	0.86(2)	2.58(2)	139(2)
	N′−H′···O3′	3.147(2)	0.91(2)	2.60(2)	119.3(18)
	N′−H′···O6′	2.8146(18)	0.91(2)	1.90(2)	176(2)
11[d]	N−H···O1	2.956(3)	0.86(4)	2.30(4)	133(3)
	N−H···O5	3.015(3)	0.86(4)	2.17(4)	167(3)
12[e]	N−H···O1	2.841(6)	1.00(7)	1.88(7)	162(6)
	N−H···O4	3.270(6)	1.00(7)	2.52(7)	132(5)
	N′−H′···O1′	2.847(6)	0.89(6)	1.98(6)	163(4)

[a] O1···H···O6, 59.0(7)°. − [b] O1···H···O6, 62.9(10)°; O3′···H′···O7′, 58.4(10)°. − [c] O1···H···O4, 60.4(6)°; O3′···H′···O6′, 56.8(6)°. − [d] O1···H···O5, 59.4(10)°. − [e] O1···H···O4, 65(2)°.

For compounds **7**, **8**, and **11**, intermolecular bifurcate N−H···O/O hydrogen bonds were observed leading to the formation of infinite chains in the crystal. These chains each are built up by zwitterions with the same (**7**, **8**) or alternating (**11**) absolute configuration. In the case of compound **8**, these chains each contain crystallographically identical molecules. In the crystal of **10** and **12**, centrosymmetric dimers were observed containing zwitterions with opposite absolute configuration. These dimers are built up by intermolecular bifurcate N−H···O/O hydrogen bonds (**10**, *molecules A* and *B*; **12**, *molecule A*) or intermolecular non-furcate N−H···O hydrogen bonds (**12**, *molecule B*). Both axial (**7**, **8**, **10**−**12**) and equatorial oxygen atoms (**10**, **12**) in the *Si*-coordination polyhedra were found to act as acceptor atoms in the above-mentioned hydrogen-bonding systems. In all cases, these intermolecular N−H···O interactions lead to a significant elongation of the respective Si−O distances compared to those of the chemically equivalent SiO moieties that are not involved in hydrogen bonding. Interestingly, the equatorial O5 oxygen atoms of **7** and **8** do not participate in any hydrogen bonding.

NMR Studies

Compounds **7**, **8**, and **10**−**12** were studied by ^{29}Si CP/MAS NMR experiments in the solid state and by ^{1}H-, ^{13}C-, and ^{29}Si-NMR experiments in solution ([D_6]DMSO). All these investigations were performed at room temperature (for VT ^{1}H-NMR studies, see next chapter).

The isotropic ^{29}Si-NMR chemical shifts obtained in the solid-state NMR studies (Table 4) clearly characterize these ^{29}Si resonances as arising from pentacoordinate silicon atoms. For compounds **8** and **10** separated resonance signals for the two crystallographically independent molecules were detected. Replacement of an oxygen ligand atom by a methylene group in **7** (→ **11**) and **8** (→ **12**) leads to a significant change in the isotropic ^{29}Si chemical shift by 24.9 ppm and 27.3 ppm, respectively. In contrast, the length of the spacers between the *ate* and *onium* centers of the zwitterions (comparison of **7**/**8** and **9**/**10**/**11**/**12**) does not significantly affect the ^{29}Si chemical shift.

As the isotropic ^{29}Si chemical shifts for **7**, **8**, and **10**−**12** are very similar to those observed for these compounds in solution [maximum deviation 4.1 ppm (**10**)] (Table 4), it is concluded that pentacoordination is present in solution as well. In addition, the ^{1}H chemical shifts observed for the NCH_3 (δ = 2.71 to 2.78) and NH moieties (δ = 8.7 to 9.2) clearly indicate the presence of ammonium groups in solution. Thus, the NMR experiments unequivocally demonstrate that the zwitterions **7**, **8**, and **10**−**12** also exist in solution.

Table 4. ^{29}Si NMR data for **7**−**12** in the crystal and in solution[a]

compound	δ^{29}Si (crystal)[b]	δ^{29}Si (solution)[c]
7	−115.4	−111.6
8	−115.2/−116.2	−114.8
9[d]	−98.4	−100.5
10	−89.5/−95.2	−93.6
11	−90.5	−90.3
12	−88.4	−89.4

[a] Spectra recorded at room temperature. − [b] Isotropic chemical shifts, ppm values. − [c] Chemical shifts obtained in [D$_6$]DMSO, ppm values. − [d] ^{29}Si CP/MAS NMR studies were performed with **9**·H$_2$O[4].

In all cases the solution-state NMR data are compatible with the presence of one particular species or with a rapid low-energy interconversion of different isomers (in this context, see ab initio Studies). The results of both the crystal structure analyses and the ab initio studies suggest that the trigonal-bipyramidal structure, with the carboxylate oxygen atoms in the axial positions (the energetically most stable structure), dominates in solution. The diastereotopism observed for the two methyl groups of the 2-methyllactato(2−) ligands (two separated singlets in the ^{1}H- and ^{13}C{^{1}H}-NMR spectra) is in accordance with the chiral nature of the respective λ^5*Si*-silicate skeletons of **7**, **8**, and **10**−**12**. In addition, the NMR data obtained indicate that the Λ- and Δ-enantiomers of these species are configurationally stable on the NMR time scale at room temperature.

VT ^{1}H-NMR Studies

Compounds **7**, **8**, and **10**−**12** were investigated by VT ^{1}H-NMR studies at 300.1 MHz in the temperature ranges of 27−116°C (**7**, **10**), 27−124°C (**8**), and 27−128°C (**11**, **12**) (solvent [D$_6$]DMSO). For all solutions studied two separated singlets for the diastereotopic methyl groups of the 2-methyllactato(2−) ligands were observed, indicating that the respective Λ- and Δ-enantiomers of these λ^5*Si*-silicates are configurationally stable on the NMR time scale under these conditions. Upon heating coalescence of the two singlets was observed in all cases, the temperature dependence of the ^{1}H-NMR spectra being completely reversible on subsequent cooling. These results can be interpreted in terms of an intramolecular isomerization process that leads to a conversion of the respective Λ- and Δ-enantiomers into each other (in this context, see ref.[4]). As determined by line-shape analyses, the activation free enthalpies for this process amount to 79.7(4) kJ mol^{-1} (**7**) to 89(2) kJ mol^{-1} (**12**) (Table 5). According to these results, both the O/CH$_2$ exchange (**7** → **11**; **8** → **12**) and the elongation of the SiO(CH$_2$)$_n$N and Si(CH$_2$)$_n$N chains (**7** → **8**; **9** → **10** → **11** → **12**) lead to an increase of the respective $\Delta G^{\neq}$ values for the Λ/Δ-isomerization. The experimentally established activation free enthalpies are comparable with the respective energy barriers calculated for the anionic model species

Table 5. Activation free enthalpies $\Delta G^{\neq}$ for the Λ/Δ-isomerization of **7**−**12** in [D$_6$]DMSO as determined by VT ^{1}H-NMR spectroscopy

compound	$\Delta G^{\neq}$ [kJ mol^{-1}]	compound	$\Delta G^{\neq}$ [kJ mol^{-1}]
7	79.7(4)	**10**	84.6(4)
8	84.6(6)	**11**	88.5(7)
9[a]	76(1)	**12**	89(2)

[a] Data taken from ref.[4]

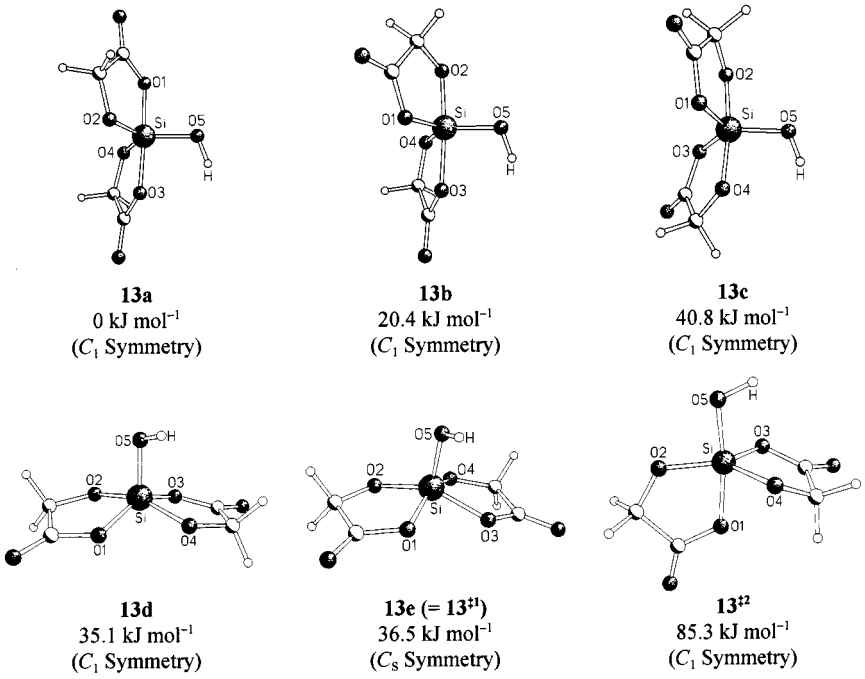


Figure 6. Calculated structures and relative energies of the local minima **13a**−**13c** and the transition states **13d**, **13e** (= 13$^{\neq 1}$), and **13**$^{\neq 2}$

13 (85.3 kJ mol^{-1}; see next chapter) and **14** (70.8 kJ mol^{-1}; see ref.[4]).

ab initio Studies

The structure and dynamic behavior of compounds **7** and **8** (SiO_5 skeletons) were studied by quantum-chemical methods using the anionic λ^5*Si*-silicate bis[glycolato(2−)-O^1,O^2]hydroxosilicate(1−) (**13**) as a model species. The computational methods used are described in the Experimental Section.

Five different idealized geometries (**13a**−**13e**, Figure 6) for the anion **13** were considered in this study. For energetic reasons, trigonal bipyramids with the hydroxo ligand in an axial site and square pyramids with the hydroxo group in a basal position were excluded. Calculations of the vibrational frequencies demonstrated that the chiral trigonal-bipyramidal isomers **13a**−**13c** represent local minima, whereas the square-pyramidal species **13d** (chiral) and **13e** (**13**$^{\neq 1}$) (achiral) are transition states (for selected geometric parameters of **13a**−**13e**, see Table 6).[8] Isomer **13a**, with the two carboxylate oxygen atoms in the axial sites, was found to be the energetically most favorable one. This is in agreement with the experimentally established crystal structures of **7** and **8**.

Table 6. Calculated interatomic distances [Å] and angles [°] for the local minima **13a**−**13c** and the transition states **13d**, **13e** (= **13**$^{\neq 1}$), and **13**$^{\neq 2}$ as obtained by SCF/SVP geometry optimizations

	13a	**13b**	**13c**	**13d**	**13e**	**13**$^{\neq 2}$
Si−O1	1.772	1.720	1.731	1.764	1.771	1.873
Si−O2	1.664	1.704	1.701	1.687	1.687	1.661
Si−O3	1.812	1.826	1.731	1.759	1.771	1.726
Si−O4	1.665	1.666	1.735	1.704	1.687	1.676
Si−O5	1.650	1.651	1.654	1.653	1.654	1.673
O1−Si−O2	88.6	88.6	87.6	86.8	86.7	83.8
O1−Si−O3	177.0	87.0	124.0	146.2	83.7	86.2
O1−Si−O4	91.0	120.5	89.4	86.3	151.3	88.1
O1−Si−O5	92.0	117.1	115.8	105.8	101.4	172.7
O2−Si−O3	90.3	174.6	88.8	86.6	151.3	130.7
O2−Si−O4	119.9	93.2	171.9	156.2	89.1	134.1
O2−Si−O5	119.0	95.0	94.8	102.1	107.0	89.2
O3−Si−O4	87.2	86.3	86.7	86.5	86.7	93.5
O3−Si−O5	91.0	89.8	120.2	108.0	101.4	97.0
O4−Si−O5	121.1	122.0	93.2	101.7	107.0	98.3

As shown by further ab initio studies, the enantiomers Λ-**13a** and Δ-**13a** can be converted into each other by an intramolecular isomerization process along the reaction path Λ-**13a** ⇌ Δ-**13c** ⇌ **13**$^{\neq 2}$ ⇌ Λ-**13b** ⇌ **13**$^{\neq 1}$ ⇌ Δ-**13b** ⇌ **13**$^{\neq 2'}$ ⇌ Λ-**13c** ⇌ Δ-**13a** (**13**$^{\neq 1}$ and **13e** are identical; **13**$^{\neq 2'}$ is the antipode of **13**$^{\neq 2}$) (Figure 7).[9−11] The structure of the trigonal-bipyramidal transition state **13**$^{\neq 2}$ is also depicted in Figure 6. The hydroxo groups in the transition states occupy an apical (**13**$^{\neq 1}$) or axial position (**13**$^{\neq 2}$). The species **13**$^{\neq 1}$ can be regarded as a transition state of a Berry-type conversion (OH as pivot ligand), whereas **13**$^{\neq 2}$ (**13**$^{\neq 2'}$) represents the transition state of a "twist-type" mechanism (in this context, see ref.[4]). The highest relative energy was calculated for **13**$^{\neq 2}$ (**13**$^{\neq 2'}$) (85.3 kJ mol^{-1}), the energy being very similar to the experimentally established activation free enthalpies for the isomerization processes Λ-**7** ⇌ Δ-**7** and Λ-**8** ⇌ Δ-**8** (see VT ^{1}H-NMR Studies).

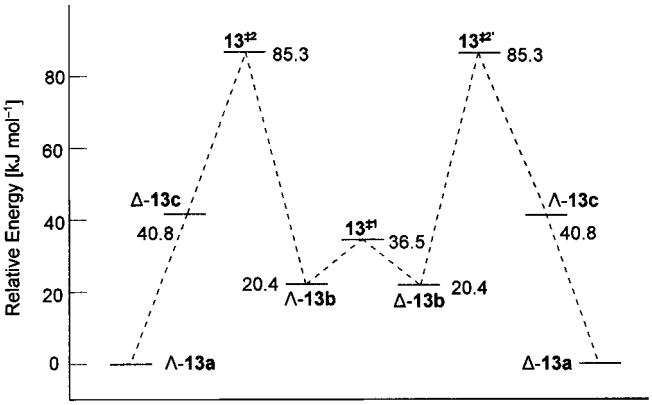


Figure 7. Calculated intramolecular reaction path for the isomerization of **13a** (Λ-**13a** ⇌ Δ-**13a**), showing the relative energies of the local minima **13a**−**13c** and of the transition states **13**$^{\neq 1}$ (= **13e**) and **13**$^{\neq 2}$ (**13**$^{\neq 2'}$)

Experimental Section

General: All syntheses were carried out under dry nitrogen. The organic solvents used were dried and purified according to standard procedures and stored under nitrogen. − Melting points were determined with a Büchi Melting Point apparatus, type B-540. − The ^{1}H, ^{13}C, and ^{29}Si solution-state NMR spectra were recorded at room temperature on a Bruker DRX-300 NMR spectrometer (^{1}H, 300.1 MHz; ^{13}C, 75.5 MHz; ^{29}Si, 59.6 MHz). $CDCl_3$ and [D_6]DMSO were used as solvents. Chemical shifts (ppm) were determined relative to internal $CHCl_3$ (^{1}H, δ = 7.24; $CDCl_3$), $CDCl_3$ (^{13}C, δ = 77.0; $CDCl_3$), [D_5]DMSO (^{1}H, δ = 2.49; [D_6]DMSO), [D_6]DMSO (^{13}C, δ = 39.5; [D_6]DMSO), and external TMS (^{29}Si, δ = 0; $CDCl_3$, [D_6]DMSO). Assignment of the ^{13}C-NMR data was supported by DEPT 135 experiments. ^{29}Si CP/MAS NMR spectra were recorded at room temperature on a Bruker DSX-400 NMR spectrometer with bottom layer rotors of ZrO_2 (diameter 7 mm), containing ca. 200 mg of sample [79.5 MHz, TMS as external standard (δ = 0), spinning rate 5000 Hz, contact time 5 ms, 90° ^{1}H transmitter pulse length 3.6 μs, repetition time 4 s]. − Mass spectra were obtained with a Finnigan MAT-8200 or Finnigan MAT-8430 mass spectrometer (FAB MS, 3-nitrobenzyl alcohol as liquid matrix, xenon as FAB source) and with a Trio-1000 mass spectrometer (ThermoQuest; EI MS, 70 eV). The selected *m*/*z* values given refer to the isotopes ^{1}H, ^{12}C, ^{14}N, ^{16}O, ^{28}Si, and ^{79}Br. − Compounds **15** and **21** were purchased from Aldrich, **16**[5] and **20**[6] were prepared as described in the literature.

[2-(Dimethylammonio)ethoxy]bis[2-methyllactato(2−)-*O*^{1},*O*^{2}]silicate (7) and [3-(Dimethylammonio)propoxy]bis[2-methyllactato(2−)-*O*^{1},*O*^{2}]silicate (8):

Preparation from 15: A solution of **15** (2.04 g, 13.4 mmol) in acetonitrile (20 mL) was added dropwise within 10 min to a stirred boiling solution of 2-methyllactic acid (2.79 g, 26.8 mmol) and the respective aminoalcohol (13.4 mmol) in acetonitrile (35 mL). Subsequently, part of the solvent (30−40 mL) was removed by distillation (760 Torr) and the residue allowed to cool to room temperature (formation of a precipitate after ca. 6 h). The precipitate was filtered off, recrystallized from acetonitrile (slow cooling of a saturated boiling solution to room temperature), and dried in vacuo

(0.01 Torr, 6 h) to give a colorless crystalline product [**7**, 3.14 g (yield 73%); **8**, 3.21 g (yield 71%)].

Preparation from 16: A solution of the respective aminoalcohol (4.80 mmol) in acetonitrile (30 mL) was added within 30 min to a boiling solution of **16** (981 mg, 4.80 mmol) in acetonitrile (50 mL). Subsequently, a solution of 2-methyllactic acid (999 mg, 9.60 mmol) in acetonitrile (50 mL) was added dropwise to this mixture within 2 h and part of the solvent was removed slowly by distillation at the same time. The distillation was continued for a further 2 h until ca. 80 mL of the solvent were removed. The reaction mixture was then kept at 20°C for 24 h (**7**) or at −20°C for 72 h (**8**), and the resulting precipitate was filtered off and dried in vacuo (0.01 Torr, 6 h) to give a colorless crystalline product [**7**, 950 mg (yield 62%); **8**, 860 mg (yield 53%)].

Data for 7: Mp 243°C (dec). − ^{1}H NMR ([D$_6$]DMSO): δ = 1.17 (s, 6 H, CCH$_3$), 1.20 (s, 6 H, CCH$_3$), 2.78 (s, 6 H, NCH$_3$), 3.12−3.14 (m, 2 H, CCH$_2$N), 3.70−3.87 (m, 2 H, CCH$_2$O), 9.2 (broad s, 1 H, NH). − ^{13}C{^{1}H} NMR ([D$_6$]DMSO): δ = 27.2 (C*C*H$_3$), 27.5 (C*C*H$_3$), 42.8 (NCH$_3$), 57.9 and 58.2 (C*C*H$_2$N, O*C*H$_2$C), 73.5 (O*C*C$_3$), 178.4 (C=O). − ^{29}Si{^{1}H} NMR ([D$_6$]DMSO): δ = −111.6. − ^{29}Si CP/MAS NMR (359 transients): δ = −115.4. − FAB MS (positive ions): *m*/*z* 322 (1) [*M* + H$^+$], 90 (100) [HO(CH$_2$)$_2$NH(CH$_3$)$_2^+$]. − FAB MS (negative ions): *m*/*z* 320 (1) [*M* − H$^+$], 249 (100) [{OCMe$_2$C(O)O}$_2$SiOH$^-$]. − $C_{12}H_{23}NO_7Si$ (321.4): calcd C 44.84, H 7.21, N 4.36; found C 44.5, H 7.3, N 4.4.

Data for 8: Mp 162 (dec). − ^{1}H NMR ([D$_6$]DMSO): δ = 1.16 (s, 6 H, CCH$_3$), 1.19 (s, 6 H, CCH$_3$), 1.72−1.79 (m, 2 H, CCH$_2$C), 2.76 (s, 6 H, NCH$_3$), 3.04−3.08 (m, 2 H, CCH$_2$N), 3.45−3.64 (m, 2 H, CCH$_2$O), 9.1 (broad s, 1 H, NH). − ^{13}C{^{1}H} NMR ([D$_6$]DMSO): δ = 27.2 (C*C*H$_2$C), 27.2 (C*C*H$_3$), 27.3 (C*C*H$_3$), 42.4 (NCH$_3$), 55.0 and 59.7 (C*C*H$_2$N, O*C*H$_2$C), 73.2 (O*C*C$_3$), 178.9 (C=O). − ^{29}Si{^{1}H} NMR ([D$_6$]DMSO): δ = −114.8. − ^{29}Si CP/MAS NMR (1661 transients): δ = −115.2, −116.2. − FAB MS (positive ions): *m*/*z* 336 (1) [*M* + H$^+$], 104 (100) [HO(CH$_2$)$_3$NH(CH$_3$)$_2^+$]. − FAB MS (negative ions): *m*/*z* 334 (1) [*M* − H$^+$], 249 (100) [{OCMe$_2$C(O)O}$_2$SiOH$^-$]. − $C_{13}H_{25}NO_7Si$ (335.4): calcd C 46.55, H 7.51, N 4.18; found C 46.7, H 7.5, N 4.3.

[2-(Dimethylammonio)ethyl]bis[2-methyllactato(2−)-*O*^{1},*O*^{2}]silicate (**10**):

Preparation from 17: Compound **17** (622 mg, 3.22 mmol) was added to a stirred solution of 2-methyllactic acid (671 mg, 6.44 mmol) in acetonitrile (10 mL) and the reaction mixture kept at room temperature for 4 h. After part of the solvent (ca. 6 mL) was removed by distillation (760 Torr), the boiling solution was cooled slowly to room temperature (formation of a crystalline solid after ca. 3 h). After 24 h the precipitate was filtered off, recrystallized from acetonitrile (slow cooling of a saturated boiling solution to room temperature), and dried in vacuo (0.02 Torr, 6 h) to give 770 mg (yield 78%) of a colorless crystalline product.

Preparation from 20: A solution of **20** (2.00 g, 8.60 mmol) in acetonitrile (30 mL) was added to a stirred solution of 2-methyllactic acid (1.79 g, 17.2 mmol) in acetonitrile (40 mL) and the reaction mixture kept at room temperature for 4 h. After part of the solvent (ca. 40 mL) was removed by distillation (760 Torr), the boiling solution was cooled slowly to room temperature (formation of a crystalline solid after ca. 2 h). After 24 h the precipitate was filtered off, recrystallized from acetonitrile (cooling of a saturated boiling solution to room temperature), and dried in vacuo (0.02 Torr, 6 h) to give 2.15 g (yield 82%) of a colorless crystalline product.

Data for 10: Mp 287°C. − ^{1}H NMR ([D$_6$]DMSO): δ = 0.81−0.98 (m, 2 H, SiCH$_2$C), 1.17 (s, 6 H, CCH$_3$), 1.20 (s, 6 H, CCH$_3$), 2.71 (s, 6 H, NCH$_3$), 2.84−3.04 (m, 2 H, CCH$_2$N), 8.7 (broad s, 1 H, NH). − ^{13}C{^{1}H} NMR ([D$_6$]DMSO): δ = 14.4 (Si*C*H$_2$C), 27.1 (C*C*H$_3$), 27.7 (C*C*H$_3$), 41.2 (NCH$_3$), 55.8 (C*C*H$_2$N), 73.3 (O*C*C$_3$), 178.7 (C=O). − ^{29}Si{^{1}H} NMR ([D$_6$]DMSO): δ = −93.6. − ^{29}Si CP/MAS NMR (109 transients): δ = −89.5, −95.2. − FAB MS (positive ions): *m*/*z* 306 (100) [*M* + H$^+$]. − FAB MS (negative ions): *m*/*z* 304 (100) [*M* − H$^+$]. − $C_{12}H_{23}NO_6Si$ (305.4): calcd C 47.19, H 7.59, N 4.59; found C 46.8, H 7.6, N 4.6.

[3-(Dimethylammonio)propyl]bis[2-methyllactato(2−)-*O*^{1},*O*^{2}]silicate (**11**) **and [4-(Dimethylammonio)butyl]bis[2-methyllactato(2−)-*O*^{1},*O*^{2}]silicate** (**12**): The respective silane (**18**, **19**; 7.62 mmol) was added dropwise within 2 min to a stirred solution of 2-methyllactic acid (1.58 g, 15.2 mmol) in acetonitrile (40 mL) (formation of a precipitate after ca. 10 min). After 48 h the precipitate was filtered off, recrystallized from acetonitrile (slow cooling of a saturated boiling solution to room temperature), and dried in vacuo (0.02 Torr, 6 h) to give a colorless crystalline product [**11**, 2.13 g (yield 88%); **12**, 2.15 (yield 90%)].

Data for 11: Mp 292°C (dec). − ^{1}H NMR ([D$_6$]DMSO): δ = 0.42−0.47 (m, 2 H, SiCH$_2$C), 1.16 (s, 6 H, CCH$_3$), 1.18 (s, 6 H, CCH$_3$), 1.50−1.61 (m, 2 H, CCH$_2$C), 2.71 (s, 6 H, NCH$_3$), 2.90−3.00 (m, 2 H, CCH$_2$N), 9.0 (broad s, 1 H, NH). − ^{13}C{^{1}H} NMR ([D$_6$]DMSO): δ = 15.0 (Si*C*H$_2$C), 20.1 (C*C*H$_2$C), 27.1 (C*C*H$_3$), 27.8 (C*C*H$_3$), 42.2 (NCH$_3$), 59.7 (C*C*H$_2$N), 73.2 (O*C*C$_3$), 178.9 (C=O). − ^{29}Si{^{1}H} NMR ([D$_6$]DMSO): δ = −90.3. − ^{29}Si CP/MAS NMR (253 transients): δ = −90.5. − FAB MS (positive ions): *m*/*z* 320 (100) [*M* + H$^+$]. − FAB MS (negative ions): *m*/*z* 318 (100) [*M* − H$^+$]. − $C_{13}H_{25}NO_6Si$ (319.4): calcd C 48.88, H 7.89, N 4.38; found C 48.8, H 7.7, N 4.4.

Data for 12: Mp 298°C (dec). − ^{1}H NMR ([D$_6$]DMSO): δ = 0.44−0.55 (m, 2 H, SiCH$_2$C), 1.15 (s, 6 H, CCH$_3$), 1.16 (s, 6 H, CCH$_3$), 1.21−1.31 (m, 2 H, SiCCH$_2$C), 1.50−1.61 (m, 2 H, CCH$_2$CN), 2.72 (s, 6 H, NCH$_3$), 2.95−3.00 (m, 2 H, CCH$_2$N), 9.1 (broad s, 1 H, NH). − ^{13}C{^{1}H} NMR ([D$_6$]DMSO): δ = 18.3 (Si*C*H$_2$C), 21.9 (C*C*H$_2$C), 27.2 (C*C*H$_3$), 27.3 (C*C*H$_2$C), 27.9 (C*C*H$_3$), 42.2 (NCH$_3$), 56.8 (C*C*H$_2$N), 73.1 (O*C*C$_3$), 179.0 (C=O). − ^{29}Si{^{1}H} NMR ([D$_6$]DMSO): δ = −89.4. − ^{29}Si CP/MAS NMR (97 transients): δ = −88.4. − FAB MS (positive ions): *m*/*z* 334 (100) [*M* + H$^+$]. − FAB MS (negative ions): *m*/*z* 332 (100) [*M* − H$^+$]. − $C_{14}H_{27}NO_6Si$ (333.5): calcd C 50.43, H 8.16, N 4.20; found C 50.1, H 8.1, N 4.2.

[2-(Dimethylamino)ethyl]trimethoxysilane (**17**): Compound **20** (17.2 g, 74.0 mmol) was added dropwise at 0°C within 20 min to a stirred solution of methanol (14.2 g, 443 mmol). The solution was warmed to room temperature within 30 min and then heated under reflux for 1 h. The volatile components of the reaction mixture were removed under reduced pressure (ca. 100 Torr), and the residue was distilled over a Vigreux column to give 12.0 g (yield 84%) of a colorless liquid. Bp 162°C/760 Torr. − ^{1}H NMR (CDCl$_3$): δ = 0.46−0.52 (m, 2 H, SiCH$_2$C), 2.03 (s, 6 H, NCH$_3$), 2.19−2.24 (m, 2 H, CCH$_2$N), 3.39 (s, 9 H, OCH$_3$). − ^{13}C{^{1}H} NMR (CDCl$_3$): δ = 8.6 (Si*C*H$_2$C), 44.8 (OCH$_3$), 50.5 (NCH$_3$), 53.7 (C*C*H$_2$N). − ^{29}Si{^{1}H} NMR (CDCl$_3$): δ = −42.4. − EI MS: *m*/*z* 193 (24) [*M*$^+$], 162 (4) [*M*$^+$ − OCH$_3$], 121 (51) [*M*$^+$ − (CH$_2$)$_2$N(CH$_3$)$_2$], 58 (100) [H$_2$C=N(CH$_3$)$_2^+$]. − $C_7H_{19}NO_3Si$ (193.3): calcd C 43.49, H 9.91, N 7.25; found C 43.7, H 10.0, N 7.2.

[3-(Dimethylamino)propyl]trimethoxysilane (**18**): A Grignard reagent, prepared from 1-chloro-3-(dimethylamino)propane (24.3 g, 200 mmol) and magnesium (5.10 g, 210 mmol) in THF (150 mL), was added dropwise at 0°C within 1 h to a solution of **15** (25.9 g, 170 mmol) in THF (160 mL). The mixture was heated under reflux for 4 h and then stirred at room temperature for a further 18 h.

Table 7. Crystal data and experimental parameters for the crystal structure analyses of **7**, **8**, and **10**−**12**

compound	**7**	**8**	**10**	**11**	**12**
empirical formula	$C_{12}H_{23}NO_7Si$	$C_{13}H_{25}NO_7Si$	$C_{12}H_{23}NO_6Si$	$C_{13}H_{25}NO_6Si$	$C_{14}H_{27}NO_6Si$
formula mass [g mol^{-1}]	321.40	335.43	305.40	319.43	333.46
collection T [K]	173(2)	173(2)	173(2)	173(2)	173(2)
λ(Mo-$K\alpha$) [Å]	0.71073	0.71073	0.71073	0.71073	0.71073
cryst syst	monoclinic	monoclinic	triclinic	monoclinic	monoclinic
space group (no.)	$P2_1/c$ (14)	$P2_1/c$ (14)	$P\bar{1}$ (2)	$P2_1/n$ (14)	$P2_1/c$ (14)
a [Å]	6.611(2)	16.307(4)	11.151(2)	8.232(2)	10.4880(12)
b [Å]	18.633(4)	11.553(2)	11.659(2)	16.583(3)	24.640(3)
c [Å]	14.328(4)	19.072(5)	13.969(3)	13.133(3)	14.1119(13)
α [deg]	90	90	85.31(3)	90	90
β [deg]	103.04(3)	106.53(6)	76.50(3)	99.89(3)	95.908(13)
γ [deg]	90	90	62.07(3)	90	90
V [Å^3]	1719.6(8)	3444.4(14)	1559.4(5)	1766.0(6)	3627.4(7)
Z	4	8	4	4	8
D(calcd) [g cm^{-3}]	1.241	1.294	1.301	1.201	1.221
μ [mm^{-1}]	0.165	0.168	0.174	0.156	0.155
F(000)	688	1440	656	688	1440
cryst dimens [mm]	0.4×0.3×0.2	0.4×0.4×0.2	0.8×0.6×0.3	0.4×0.3×0.2	0.5×0.02×0.01
2θ range [deg]	5.26−45.98	4.18−46.52	4.24−52.24	4.92−46.52	4.40−46.62
index ranges	$-7 \le h \le 3$, $0 \le k \le 20$, $-15 \le l \le 15$	$-18 \le h \le 17$, $0 \le k \le 12$, $0 \le l \le 21$	$-13 \le h \le 13$, $-14 \le k \le 14$, $-17 \le l \le 17$	$-8 \le h \le 8$, $-18 \le k \le 18$, $-14 \le l \le 14$	$-7 \le h \le 11$, $-27 \le k \le 27$, $-15 \le l \le 13$
no. of coll reflns	3792	4943	14753	12204	10717
no. of indep reflns	2392	4943	5664	2426	4726
R_{int}	0.0247	−	0.0592	0.0980	0.0756
no. of reflns used	2392	4943	5664	2426	4726
no. of params	200	418	545	290	417
S[a]	1.015	1.015	1.015	0.918	0.865
weight params a/b[b]	0.0372/0.2836	0.0345/2.7399	0.0464/0.3261	0.0672/0	0.0894/0
$R1$[c] [$I > 2\sigma(I)$]	0.0374	0.0491	0.0373	0.0448	0.0585
$wR2$[d] (all data)	0.0839	0.1043	0.0861	0.1104	0.1566
extinction coeff	−	0.0018(2)	−	−	−
max/min res electron dens [e Å^{-3}]	+0.163/−0.233	+0.453/−0.257	+0.314/−0.224	+0.492/−0.331	+1.447/−0.303

[a] $S = \{\Sigma[w(F_o^2 - F_c^2)^2] / (n - p)\}^{0.5}$; n = no. of reflections; p = no. of parameters. − [b] $w^{-1} = \sigma^2(F_o^2) + (aP)^2 + bP$, with $P = (F_o^2 + 2F_c^2)/3$. − [c] $R1 = \Sigma||F_o| - |F_c|| / \Sigma|F_o|$. − [d] $wR2 = \{\Sigma[w(F_o^2 - F_c^2)^2] / \Sigma[w(F_o^2)^2]\}^{0.5}$.

The precipitate was filtered off, the solvent removed under reduced pressure, and the residue distilled in vacuo to give 24.9 g (yield 71%) of a colorless liquid. Bp 42°C/0.05 Torr. − ^{1}H NMR ($CDCl_3$): δ = 0.46−0.52 (m, 2 H, $SiCH_2C$), 1.37−1.48 (m, 2 H, CCH_2C), 2.07 (s, 6 H, NCH_3), 2.08−2.13 (m, 2 H, CCH_2N), 3.42 (s, 9 H, OCH_3). − $^{13}C\{^1H\}$ NMR ($CDCl_3$): δ = 6.9 ($SiCH_2C$), 21.0 (CCH_2C), 45.7 (OCH_3), 50.7 (NCH_3), 62.9 (CCH_2N). − $^{29}Si\{^1H\}$ NMR ($CDCl_3$): δ = −41.5. − EI MS: *m*/*z* 207 (16) [M^+], 176 (6) [$M^+ - OCH_3$], 121 (51) [$M^+ - (CH_2)_3N(CH_3)_2$], 58 (100) [$H_2C{=}N(CH_3)_2^+$]. − $C_8H_{21}NO_3Si$ (207.3): calcd C 46.34, H 10.21, N 6.76; found C 46.3, H 10.2, N 6.8.

[4-(Dimethylamino)butyl]trimethoxysilane (**19**): A mixture of **22** (4.00 g, 15.6 mmol) and dimethylamine (2.16 g, 47.9 mmol) was heated in an autoclave at 60°C/10 bar for 4 h. After the mixture was cooled to room temperature, the excess amine was evaporated and *n*-pentane (25 ml) added to the residue. The precipitate was filtered off, the solvent removed under reduced pressure, and the residue distilled in vacuo to give 2.83 g (yield 82%) of a colorless liquid. Bp 92°C/11 Torr. − ^{1}H NMR ($CDCl_3$): δ = 0.54−0.60 (m, 2 H, $SiCH_2C$), 1.30−1.44 (m, 4 H, CCH_2C), 2.11 (s, 6 H, NCH_3), 2.12−2.17 (m, 2 H, CCH_2N), 3.47 (s, 9 H, OCH_3). − $^{13}C\{^1H\}$ NMR ($CDCl_3$): δ = 9.5 ($SiCH_2C$), 21.0 (CCH_2C), 31.5 (CCH_2C), 45.9 (OCH_3), 50.8 (NCH_3), 59.9 (CCH_2N). − $^{29}Si\{^1H\}$ NMR ($CDCl_3$): δ = −41.8. − EI MS: *m*/*z* 221 (15) [M^+], 190 (2) [$M^+ - OCH_3$], 121 (34) [$M^+ - (CH_2)_4N(CH_3)_2$], 58 (100) [$H_2C{=}N(CH_3)_2^+$]. − $C_9H_{23}NO_3Si$ (221.4): calcd C 48.83, H 10.47, N 6.33; found C 48.7, H 10.5, N 6.3.

(4-Bromobutyl)trimethoxysilane (**22**): A mixture of 4-bromo-1-butene (5.00 g, 37.0 mmol), **21** (6.78 g, 55.5 mmol), hexachloroplatinic acid hexahydrate (20 mg, 39 μmol), and 2-propanol (0.2 mL) was heated in an autoclave at 140°C/2 bar for 8 h. After the mixture was cooled to room temperature, the solid particles were removed by filtration, and the filtrate was distilled in vacuo to give 6.72 g (yield 71%) of a colorless liquid. Bp 49°C/2 Torr. − ^{1}H NMR ($CDCl_3$): δ = 0.52−0.58 (m, 2 H, $SiCH_2C$), 1.39−1.53 (m, 2 H, CCH_2C), 1.72−1.83 (m, 2 H, CCH_2C), 3.29−3.33 (m, 2 H, CCH_2Br), 3.48 (s, 9 H, OCH_3). − $^{13}C\{^1H\}$ NMR ($CDCl_3$): δ = 11.2 ($SiCH_2C$), 21.6 (CCH_2C), 33.7 (CCH_2C), 36.1 (CCH_2Br), 50.7 (OCH_3). − $^{29}Si\{^1H\}$ NMR ($CDCl_3$): δ = −42.2. − EI MS: *m*/*z* 256 (1) [M^+], 121 (100) [$M^+ - C_4H_8Br$]. − $C_7H_{17}BrO_3Si$ (257.2): calcd C 32.69, H 6.66; found C 32.2, H 6.7.

Crystal Structure Analyses: Suitable single crystals of **7**, **8**, and **10**−**12** were obtained by crystallization from acetonitrile (slow cooling of saturated boiling solutions to room temperature). The crystals were mounted in inert oil (RS 3000, Riedel-de Haën) on a glass fiber and then transferred to the cold gas stream of the diffractometer [**7**, **8**: Enraf-Nonius CAD4; **10**−**12**: Stoe IPDS; graphite-monochromated Mo-$K\alpha$ radiation (λ = 0.71073 Å)]. The structures were solved by direct methods.[12] All non-hydrogen atoms were refined anisotropically.[13] The positions of the NH hydrogen atoms were localized in difference Fourier syntheses and refined freely (**8**: with one distance restraint). The CH hydrogen atoms were refined freely (**10**, **11**) or a riding model was employed in the refinement of the CH hydrogen atom positions (**7**, **8**, and

12). The maximum residual electron density of 1.447 e $Å^{-3}$ in the crystal of **12** corresponds to a single peak which could be refined to a (hydrogen bonded) oxygen atom (occupation 0.3), but neither the ^{1}H-NMR data nor the elemental analyses confirm any content of water in the crystal of **12** (second residual electron density peak: 0.21 e $Å^{-3}$).

Crystallographic data (excluding structure factors) for the structures reported in this paper have been deposited with the Cambridge Crystallographic Data Centre as supplementary publication no. CCDC-102600 (**7**), CCDC-102601 (**8**), CCDC-102602 (**10**), CCDC-102603 (**11**), and CCDC-102604 (**12**). Copies of the data can be obtained free of charge on application to CCDC, 12 Union Road, Cambridge CB2 1EZ, UK [fax: (+44) 1223/ 336-033; e-mail: deposit@ccdc.cam.ac.uk].

VT ^{1}H-NMR Studies: The experiments were carried out analogously to the standard ^{1}H-NMR measurements using a Bruker DRX-300 spectrometer. [D_6]DMSO was used as solvent. The thermocouple used with the probe was calibrated for high temperatures according to ref.[14] using a 80% solution of 1,2-ethanediol in [D_6]DMSO. Spectra were recorded in the temperature ranges of 27−116°C (**7**, **10**), 27−124°C (**8**), and 27−128°C (**11**, **12**). The time required for temperature equilibration was 15 min. The data obtained were fitted and simulated by using the Bruker software program WinDyna 1.0b (line-shape analysis). From the simulated spectra the coalescence temperatures T_C and the exchange rates k_C at the coalescence points were extracted, and the respective values for the activation free enthalpy $\Delta G^{\neq}$ for the exchange process were calculated by using the Eyring equation: $\Delta G^{\neq} = 19.14 \cdot T_C \cdot [10.32 + \log (T_C/k_C)]$ [J mol^{-1}].[15]

Computational Methods: Geometry optimizations at the SCF/SVP level for the anionic model species **13** were performed using the TURBOMOLE program system.[16] Stationary geometries and transition states were characterized as local minima (zero imaginary frequencies) and saddle points (one imaginary frequency), respectively, by calculation of the vibrational frequencies. The energies given for **13** include the single point MP2 energy (SVP basis set) and the zero point vibrational energy.

Acknowledgments

We thank the Deutsche Forschungsgemeinschaft and the Fonds der Chemischen Industrie for financial support and the Bayer AG (Leverkusen and Wuppertal-Elberfeld, Germany) and Merck KGaA (Darmstadt, Germany) for various gifts of chemicals.

[1] Reviews and proceedings dealing with pentacoordinate silicon compounds: [1a] S. N. Tandura, M. G. Voronkov, N. V. Alekseev, *Top. Curr. Chem.* **1986**, *131*, 99−189. − [1b] W. S. Sheldrick, in *The Chemistry of Organic Silicon Compounds, Part 1* (Eds.: S. Patai, Z. Rappoport), Wiley, Chichester, **1989**, pp. 227−303. − [1c] R. R. Holmes, *Chem. Rev.* **1990**, *90*, 17−31. − [1d] C. Chuit, R. J. P. Corriu, C. Reye, J. C. Young, *Chem. Rev.* **1993**, *93*, 1371−1448. − [1e] R. Tacke, J. Becht, A. Lopez-Mras, J. Sperlich, *J. Organomet. Chem.* **1993**, *446*, 1−8. − [1f] C. Y. Wong, J. D. Woollins, *Coord. Chem. Rev.* **1994**, *130*, 175−241. − [1g] R. Tacke, J. Becht, O. Dannappel, M. Kropfgans, A. Lopez-Mras, M. Mühleisen, J. Sperlich, in *Progress in Organosilicon Chemistry* (Eds.: B. Marciniec, J. Chojnowski), Gordon and Breach Publishers, Amsterdam, **1995**, pp. 55−68. − [1h] R. Tacke, O. Dannappel, M. Mühleisen, in *Organosilicon Chemistry II − From Molecules to Materials* (Eds.: N. Auner, J. Weis), VCH, Weinheim, **1996**, pp. 427−446. − [1i] R. Tacke, O. Dannappel, in *Tailor-made Silicon-Oxygen Compounds − From Molecules to Materials* (Eds.: R. Corriu, P. Jutzi), Vieweg, Braunschweig/ Wiesbaden, **1996**, pp. 75−86. − [1j] E. Lukevics, O. A. Pudova, *Chem. Heterocycl. Compd.* **1996**, *353*, 1605−1646. − [1k] R. R. Holmes, *Chem. Rev.* **1996**, *96*, 927−950. − [1l] D. Kost, I. Kalikhman, in *The Chemistry of Organic Silicon Compounds, Part 2, Vol. 2* (Eds.: Z. Rappoport, Y. Apeloig), Wiley, Chichester, **1998**, pp. 1339−1445.

[2] Publications dealing with pentacoordinate silicon compounds with an SiO_5 skeleton that have been structurally characterized by single-crystal X-ray diffraction: [2a] R. R. Holmes, R. O. Day, J. S. Payne, *Phosphorus, Sulfur, Silicon* **1989**, *42*, 1−13. − [2b] K. C. Kumara Swamy, V. Chandrasekhar, J. J. Harland, J. M. Holmes, R. O. Day, R. R. Holmes, *J. Am. Chem. Soc.* **1990**, *112*, 2341−2348. − [2c] R. M. Laine, K. Y. Blohowiak, T. R. Robinson, M. L. Hoppe, P. Nardi, J. Kampf, J. Uhm, *Nature* **1991**, *353*, 642−644. − [2d] R. Tacke, M. Mühleisen, *Inorg. Chem.* **1994**, *33*, 4191−4193. − [2e] Added at proofs: W. Donhärl, I. Elhofer, P. Wiede, U. Schubert, *J. Chem. Soc., Dalton Trans.* **1998**, 2445−2446.

[3] Some preliminary results have been presented at the 4th Munich Silicon Days (April 7−8, **1998**).

[4] R. Tacke, R. Bertermann, A. Biller, O. Dannappel, M. Pülm, R. Willeke, *Eur. J. Inorg. Chem.* **1999**, 795−805.

[5] [5a] E. W. Abel, R. P. Bush, *J. Organomet. Chem.* **1965**, *3*, 245−252. − [5b] G. Kannengiesser, F. Damm, *Bull. Soc. Chim. Fr.* **1967**, 2492−2495.

[6] B. Pfrommer, R. Tacke, *Eur. J. Inorg. Chem.* **1998**, 415−418.

[7] [7a] E. L. Muetterties, L. J. Guggenberger, *J. Am. Chem. Soc.* **1974**, *96*, 1748−1756. − [7b] R. R. Holmes, J. A. Deiters, *J. Am. Chem. Soc.* **1977**, *99*, 3318−3326. − [7c] The degree of distortion was calculated by using the dihedral angle method described in ref.[7a,7b] All nine dihedral angles and the values for the reference geometry of the ideal square pyramid given in ref.[7a] were considered for this calculation.

[8] Calculated energies (SCF + single point MP2 + E(vib0) energies [Hartree]): **13a**, −968.7280119 (C_1 symmetry); **13b**, −968.7202435 (C_1 symmetry); **13c**, −968.7124818 (C_1 symmetry); **13d**, −968.7145996 (C_1 symmetry); **13e**, −968.7141209 (C_S symmetry).

[9] Calculated energy (SCF + single point MP2 + E(vib0) energies [Hartree]): $\mathbf{13}^{\neq 2}$, −968.6955135 (C_1 symmetry).

[10] As the equipotential surface around the local minimum **13c** is quite flat, further calculations with a larger basis set have to be performed to determine the Berry-type transition state which is expected to connect the two minima **13a** and **13c**. In the case of the anionic model species **14**, a related transition state could be found (see ref.[4]).

[11] The caclulated transition state **13d** is not needed to realize the Λ/Δ-isomerization according to Figure 7.

[12] G. M. Sheldrick, SHELXS-97, University of Göttingen, Germany, **1997**; G. M. Sheldrick, *Acta Crystallogr., Sect. A* **1990**, *46*, 467−473.

[13] G. M. Sheldrick, SHELXL-97, University of Göttingen, Germany, **1997**.

[14] S. Braun, H.-O. Kalinowski, S. Berger, *100 and More Basic NMR Experiments*, VCH, Weinheim, **1996**, pp. 115−117.

[15] U. Weber, H. Thiele, *NMR Spectroscopy: Modern Spectral Analysis*, Wiley-VCH, Weinheim, **1998**, pp. 339−361.

[16] Program system TURBOMOLE: R. Ahlrichs, M. Bär, M. Häser, H. Horn, C. Kömel, *Chem. Phys. Lett.* **1989**, *162*, 165−169. Optimized SVP basis sets used (in this context, see also: R. Tacke, J. Becht, O. Dannappel, R. Ahlrichs, U. Schneider, W. S. Sheldrick, J. Hahn, F. Kiesgen, *Organometallics* **1996**, *15*, 2060−2077): Si, (10s7p1d)/[4s3p1d]; C, N, and O, (7s4p1d)/[3s2p1d]; H, (4s1p)/[2s1p].

Received October 12, 1998
[I98351]

Contributions to the Chemistry of Boron, 244[+] Preparation and Structural Characterization of Lithium Silylborates

Wolfgang Lippert,[a] Heinrich Nöth,*[a] Werner Ponikwar,[a][§] and Thomas Seifert[a][§]

Dedicated to Prof. Dr. P. Jutzi on the occasion of his 60th birthday

Keywords: Lithium (triphenylsilyl)trihydridoborate / Lithium (*tert*-butyldiphenylsilyl)trihydridoborate / Lithium tris(trimethylsilyl)methylborate / Lithium tetrakis(trimethylsilyl)borate / X-ray structure analysis

Borane triethylamine reacts with lithium triphenylsilanide or lithium *tert*-butyldiphenylsilanide with formation of lithium (triphenylsilyl)trihydridoborate or lithium (*tert*-butyldiphenylsilyl)trihydridoborate. Complexation of the lithium cation with various ligands allows the isolation of compounds **1**, **2a**, and **2b**. Trimethoxyborane reacts with lithium trimethylsilanide to form lithium tetrakis(trimethylsilyl)borate **3** and lithium tris(trimethylsilyl)methylborate **4**. Mixed single crystals of **3** and **4** show an unexpected coordination of the lithium cation due to the lack of any supporting donor molecule. All silylborates exhibit short Si–B bond lengths compared to tricoordinated silylboranes.

Introduction

In 1961, Seyferth et al. described the preparation of the first tetracoordinated borate containing a silicon−boron bond.[2] The addition of triphenylborane to lithium triphenylsilanide leads to the formation of lithium (triphenylsilyl)triphenylborate. In 1982, we reported the synthesis of (trimethylsilyl)borates from alkoxyboranes and trimethylsilyllithium.[3] Although aryl-/alkylsilylborates have been known for some time, as yet no data concerning their molecular structures are available. In 1993, Schmidbaur et al. described the crystal structure of tricyclohexylphosphane-(trimethylsilyl)borane.[4] Nevertheless, to the best of our knowledge, the structures of anionic silylborates have not yet been determined.

Due to their use in organic synthesis, research is ongoing in the field of hydridoborates.[5] This field could be extended by the preparation of silylhydridoborates, which may possess electronic and/or reducing properties different from those of the known and well-investigated alkyl-/arylhydridoborates.[6]

The present report deals with the preparation of new silylhydridoborates, as well as of known (trimethylsilyl)borates. Their molecular structures have been determined by means of X-ray diffraction analysis.

Results and Discussion

One might envisage the most straightforward pathway to monosilyltrihydridoborates as being the addition of BH_3 to alkali metal silanides, $MSiR_3$, with $BH_3 \cdot THF$ as the source of borane, as shown in Eq. 1. However, reactions of $BH_3 \cdot THF$ with various lithium silanides invariably lead to only small amounts (10−20%) of compounds $Li(H_3BSiR_3)$, as shown by ^{11}B-NMR spectroscopy. The main product is $LiBH_4$, which is formed according to Eq. 2. Separation of $Li(H_3BSiR_3)$ from $LiBH_4$ by fractional crystallization has proved impossible.

In order to prevent rapid hydride transfer from $Li(H_3SiBR_3)$ to BH_3, a less reactive BH_3 source was necessary, a requirement that was met by $BH_3 \cdot NEt_3$. In this case, heating the THF solution under reflux was necessary to complete the reaction (Eq. 3) within a few hours. Under these conditions, the formation of $LiBH_4$ could not be completely suppressed. A silylhydridoborate was, however, the main species generated.

$$LiSiR_3 + H_3B{\cdot}THF \xrightarrow{THF} Li(H_3BSiR_3){\cdot}n\,THF \quad (1)$$

$$Li(H_3BSiR_3) + H_3B{\cdot}THF \longrightarrow LiBH_4 + H_2BSiR_3 \quad (2)$$

$$LiSiR_3 + H_3B{\cdot}NEt_3 \xrightarrow[RF]{THF} Li(H_3BSiR_3) + NEt_3 \quad (3)$$

Scheme 1

The triorganylsilyltrihydridoborates **1** and **2** were separated from $LiBH_4$ by crystallization. Compound **2a** was isolated as a THF solvate, while addition of nitrogen-containing ligands to the hexane solution resulted in compounds **1** and **2b**. It is interesting to note that NEt_3 clearly does not coordinate to Li, because **2a** crystallizes from a hexane solution containing NEt_3.

The monosilyltrihydridoborates could not be isolated in the absence of a supporting ligand. In contrast, the tetrasilylborate $LiB(SiMe_3)_4$ (**3**) is known to exist as a ligand-free

[+] Part 243: Ref.[1]

[a] Institute of Inorganic Chemistry, University of Munich, Meiserstraße 1, D-80333 München, Germany
Fax: (internat.) + 49(0)89/5902-451
E-mail: Noeth@anorg.chemie.uni-muenchen.de

[§] X-ray diffraction studies.

 © WILEY-VCH Verlag GmbH, D-69451 Weinheim, 1999 1434−1948/99/0505−0817 $ 17.50+.50/0

compound. It was obtained as described in the literature[3] (Eq. 4). In addition to **3**, $LiMeB(SiMe_3)_3$ (**4**) was formed in approximately 10% yield (^{11}B NMR). Compound **4** is accessible directly from $LiSiMe_3$ and $MeB(OMe)_2$.[3]

$(Ph_3SiBH_3)Li \cdot 3\ TMEDA$ **1**

$(^tBuPh_2SiBH_3)Li \cdot 3\ THF$ **2a**

$(^tBuPh_2SiBH_3)Li \cdot PMDTA$ **2b**

$[(Me_3Si)_4B]Li$ **3**

$[(Me_3Si)_3BMe]Li$ **4**

Scheme 2

$$4\ LiSiMe_3 + B(OMe)_3 \longrightarrow [(Me_3Si)_4B]Li + 3\ LiOMe \quad (4)$$

$$[(Me_3Si)_4B]Li \longrightarrow [(Me_3Si)_3BMe]Li + "SiMe_2" \quad (5)$$

Scheme 3

The 10% contamination of **3** by **4** can be removed by crystallization from hexane. However, a hexane solution of pure **3** shows the presence of **4** after storage for several weeks. Therefore, we suggest that compound **4** is formed according to Eq. 5.

It was of interest to compare the structures of these compounds with those of **1** and **2**.

NMR and IR Spectra

The ^{11}B-NMR spectra of the monosilyltrihydridoborates, recorded in C_6D_6 solution, are almost identical. The chemical shifts δ span the narrow range from δ = −42.5 to −43.8. This is the same region as found for the the ^{11}B resonance of $LiBH_4$ (THF solution, δ = −41.6).[7] A 1:3:3:1 quartet is seen in the proton-coupled ^{11}B-NMR spectra of the silyltrihydridoborates with $^1J(^{11}B,^1H)$ = 78−79 Hz, while $LiBH_4$ is characterized by a quintet with $^1J(^{11}B,^1H)$ = 82.4 Hz.[7] The main differences between the various silyltrihydridoborates lie in the linewidths, which are 22 Hz for **1**, 41 Hz for **2a**, and 20 Hz for **2b**. No $^{29}Si^{11}B$ coupling could be observed, nor any ^{29}Si signal was observed in the ^{29}Si-NMR spectrum. We attribute this to the same relaxation process as that which is operative in CB units, where the ^{13}C resonance is not usually observable due to strong quadrupolar line broadening.

The quartet structures of the ^{11}B-NMR signals suggest that all the hydrogen atoms bonded to the boron atom are magnetically and chemically equivalent, in spite of the fact that this is not the case in the solid state (vide infra). Therefore, free rotation of the BH_3 group about the B−Si bond occurs in solution.

In contrast, the IR spectra of **2a** and **2b** are quite different. **2a** shows two strong BH_3 stretching bands at 2284 and 2257 cm^{-1}, while for **2b** three bands are observed [at 2335 (m), 2266 (vs), and 2237 (s) cm^{-1}]. The two strong bands for **2a** and **2b** are consistent with local C_{3V} symmetry, while the band at 2335 cm^{-1} observed for **2b** most probably results from an overtone of the $\delta(BH_3)$ absorption found at 1167 cm^{-1} (2 × 1167 cm^{-1} = 2334 cm^{-1}). Although the anionic parts of **2a** and **2b** are, at least formally, identical, there is a 20 cm^{-1} difference in the position of the BH_3 stretching bands. We attribute this to the influence of the differently coordinated Li cation.

Molecular Structures in the Solid State

Single crystals of **1**, **2a**, and **2b** were obtained, which allowed the determination of their molecular structures in the solid state. These are depicted in Figures 1−3, and relevant molecular parameters are summarized in Table 1.

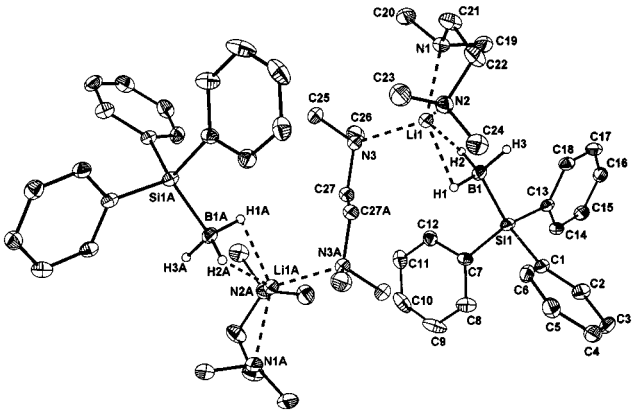


Figure 1. Molecular structure of the TMEDA adduct of lithium (triphenylsilyl)trihydridoborate **1** in the crystal. Thermal ellipsoids are drawn at a 25% probability level; hydrogen atoms (except those on boron) are omitted for the sake of clarity

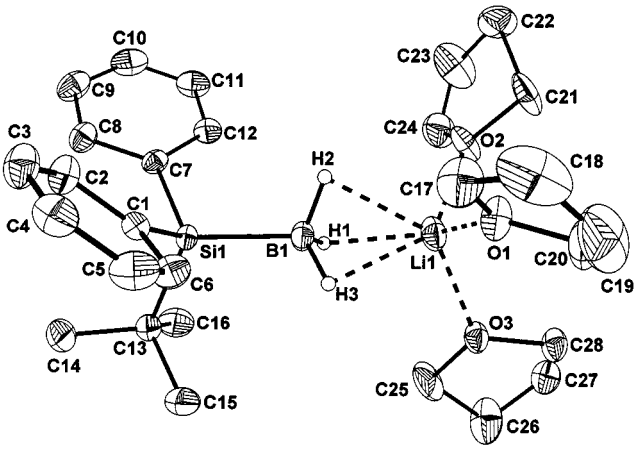


Figure 2. Molecular structure of the THF adduct of lithium (*tert*-butyldiphenylsilyl)trihydridoborate **2a** in the crystal. Thermal ellipsoids are drawn at a 25% probability level; hydrogen atoms (except those on boron) are omitted for the sake of clarity

Lithium (triphenylsilyl)trihydridoborate **1** crystallizes with 1.5 TMEDA ligands per molecule and can be described by the formula $[(Ph_3SiBH_3)Li \cdot TMEDA]_2 \cdot$

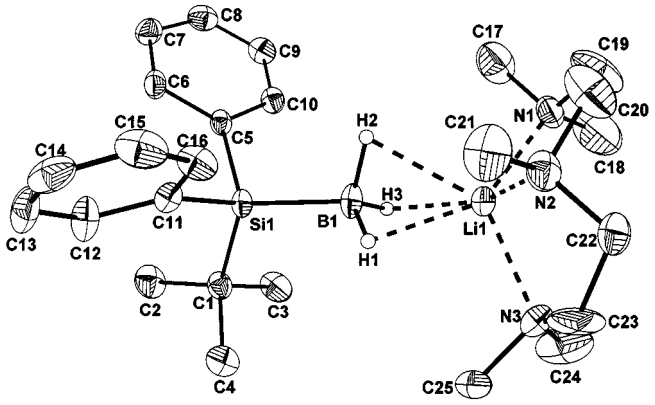


Figure 3. Molecular structure of the PMDTA adduct of lithium (*tert*-butyldiphenylsilyl)trihydridoborate **2b** in the crystal. Thermal ellipsoids are drawn at a 25% probability level; hydrogen atoms (except those on boron) are omitted for the sake of clarity; only one position of the disordered PMDTA ligand is shown

Table 1. Selected bond lengths [Å] and bond angles [°] of compounds **1**, **2a**, and **2b**; estimated standard deviations are given in parentheses

bond lengths	**1**	**2a**	**2b**
B1−Si1	1.984(5)	1.989(2)	1.993(5)
B1−Li1	2.337(8)	2.255(4)	2.252(8)
B1−Li1a	2.337(8)	−	−
Si1−C_{Ph}	1.901(4)	1.906(2)	1.899(4)
		1.907(2)	1.909(4)
Si1−C_{tBu}	−	1.925(2)	1.926(5)
B1−H1	1.07	1.13	1.02
B1−H2	1.13	1.14	1.03
B1−H3	1.15	1.13	1.19
Li1−H1	2.07	2.21	2.09
Li1−H2	2.24	2.13	2.25
Li1−H3	−	2.07	1.97
bond angles			
C_{tBu}−Si1−B1	−	112.9(1)	113.3(2)
C_{Ph}−Si1−B1	111.8(2)	110.5(1)	111.7(2)
	112.7(2)	110.7(1)	110.0(2)
	112.4(2)		
C_{tBu}−S1−C_{Ph}	−	107.1(1)	106.7.(2)
		105.6(1)	109.8(2)
C_{Ph}−Si1−C_{Ph}	106.1(2)	109.8(1)	105.0(2)
	106.3(2)		
	107.2(2)		
Si1−B1−Li1	165.2(3)	175.2(2)	176.2(4)

TMEDA. There is one chelating ligand per Li atom, while the third TMEDA molecule binds to the two centers via one N atom each. Moreover, each Li coordinates to two hydrogen atoms of the BH_3 units, making the lithium pentacoordinated. Thus, the $SiBH_3$ unit acts as a $\mu_2{}^1$ ligand with B−H distances of 1.07(3) (H1) and 1.13(3) Å (H2). The molecule has a center of inversion at the midpoint of the C27−C27a bond.

Lithium (*tert*-butyldiphenylsilyl)trihydridoborate · tris(tetrahydrofuran), **2a**, is present as a monomer in the crystal (see Figure 2).[8] In contrast to compound **1**, the Li center in **2a** is hexacoordinated, in this case by three oxygen atoms and three hydrogen atoms. In **2a**, all hydrides of the BH_3 unit are involved in Li−H bonding, with the BH_3 group acting as a $\mu_3{}^1$ ligand. As compound **2b** is also present as a monomeric molecular species (or contact ion pair) in the solid state, it is apparent that the change from oxygen coligands (in **2a**) to nitrogen (in **2b**) has no influence on the molecular structure of **2** in the solid state. The B−H atom distances span a range from 1.02 to 1.19(3) Å.

According to Edelstein et al.,[9] the B−M distance is a function of the bonding mode of the $BH_4{}^-$ ligand, this distance decreasing as we move along the series M···H−BH_3, M···$(H)_2BH_2$, M···$(H)_3BH$, in other words when the BH_4 group acts as a $\mu_1{}^1$, $\mu_2{}^1$, or $\mu_3{}^1$ donor. For geometrical reasons, this of course also holds for $RBH_3{}^-$ groups.

Thus, it can be seen that when the $R_3SiBH_3{}^-$ group acts as a $\mu_2{}^1$ ligand (in compound of type **1**), the Li···B atom distance is 2.377(8) or 2.49(1) Å, whereas in **2a** and **2b**, with $\mu_3{}^1$-R_3SiBH_3 groups, this distance is as short as 2.255(4) or 2.252(8) Å. No influence of the coligands (oxygen in **2a**, nitrogen in **2b**) on the B···Li atom distance was observed. Owing to the different coordination of the Li atom in **1** compared with that in **2a** and **2b**, different Si−B−Li bonding angles are found. While **2a** [175.2(2)°] and **2b** [176.2(4)°] show an almost linear array of the Li, B, and Si atoms, an Si−B−Li angle of 165.2(3)° is found for compound **1**. Irrespective of the degree of association and the different BH_3···Li interactions, the B−Si bond lengths in **1**, **2a**, and **2b** are equal within the margin of the standard deviation, leading to an average Si−B bond length of 1.988 Å. This distance is significantly shorter than the Si−B bond length found in $(c\text{-}C_6H_{11})_3P \cdot H_2BSiMe_3$ [2.007(4) Å[4]]. Surprisingly, the Si−B distances in **1**, **2a**, and **2b** are even shorter than those in trivalent silylboranes,[10] where bond lengths between 2.038 and 2.127 Å have been found. This is a remarkable observation because bond lengths of a certain ligand generally increase with increasing coordination number of the central atom; in this case the B−Si bond length to a tetracoordinated boron atom would be expected to be longer than that to a tricoordinated boron species, but in fact the reverse is found. The shortest B−Si bond length found to date is 1.926(2) Å, observed in the three-membered heterocycle 1-(*tert*-butyl)-3-(diisopropylamino)-2,2-(dimesityl)azasilaboriridine.[11]

Single crystals of the trimethylsilylborates **3** and **4** could not be obtained. However, when these compounds were mixed in a 1:1 ratio, single crystals containing **3** and **4** in this ratio were obtained from hexane solution. Figure 4 shows the molecular structure of **3** and Figure 5 the structure of **4**. The packing of the two species in the unit cell is depicted in Figure 6. Selected structural parameters are summarized in Table 2.

As can be seen in Figure 4, the Li atom of compound **3** resides in a cleft formed by three methyl groups bonded to three different Si atoms, and this imposes an almost C_3 point group symmetry on the molecule. It is particularly surprising that the B−Si bond lengths in **3** are nevertheless all equal [B1 to Si1: 2.025(2), to Si2: 2.027(2), to Si3: 2.025(2), to Si4: 2.025(2) Å], in spite of the fact that the $Si(3)Me_3$ group is not involved in the interaction with Li1.

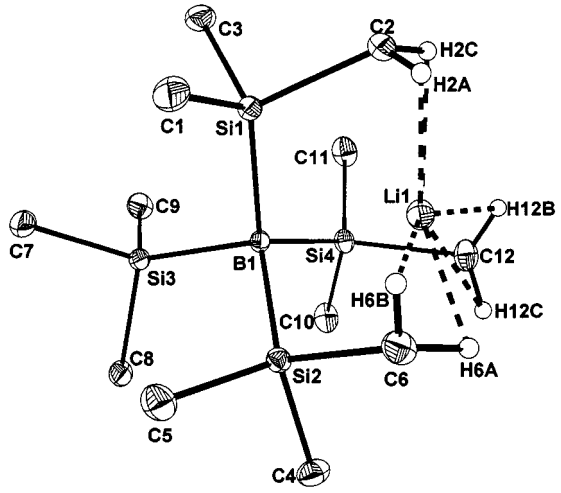


Figure 4. Molecular structure of lithium tetrakis(trimethylsilyl)borate **3** in the crystal. Thermal ellipsoids are drawn at a 25% probability level; hydrogen atoms (except those which show contact to Li) are omitted for the sake of clarity

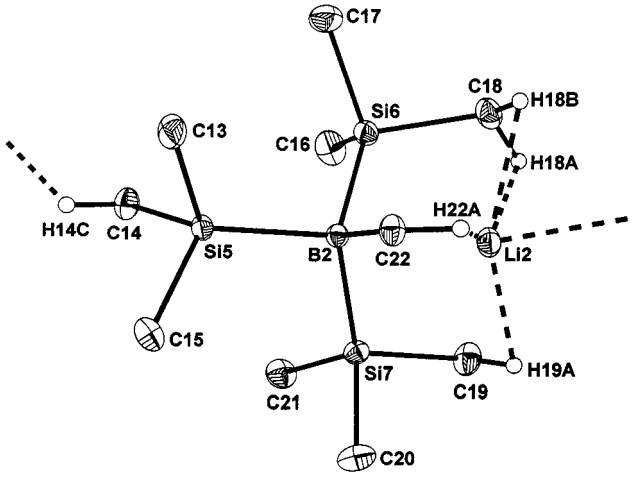


Figure 5. Molecular structure of lithium methyl tris(trimethylsilyl)borate **4** in the crystal. Thermal ellipsoids are drawn at a 25% probability level; hydrogen atoms (except those which show contact to Li) are omitted for the sake of clarity

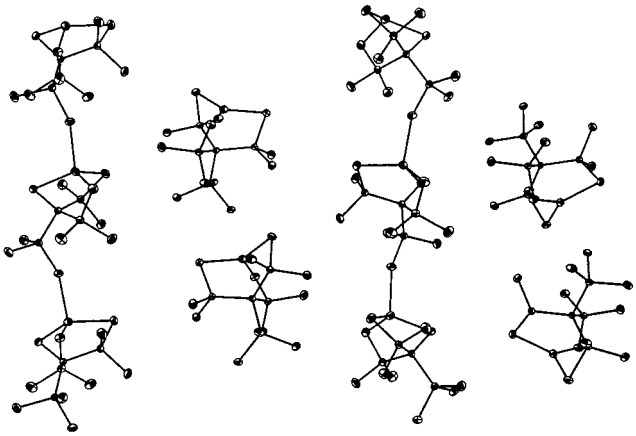


Figure 6. Arrangement of **3** and **4** in the crystal

Table 2. Selected bond lengths [Å] and bond angles [°] of compounds **3** and **4**; estimated standard deviations are given in parentheses

bond lengths	**3**	**4**
aver. $Si_{Li}-B$	2.025	2.032
Si−B	2.025(2)	2.017(2)
aver. $Si-C_{Li}$	1.917	1.920
aver. Si−C	1.884	1.881
B−Li	2.387(4)	2.276(4)
$Li\cdots H-C_B$	1.87	–
aver. $Li\cdots H-C_{Si}$	2.19	2.17
bond angles		
Si−B−Li	178.9(1)	173.2(1)
aver. $Si_{Li}-B-Si$	105.6	107.2
aver. $Si_{Li}-B-Si_{Li}$	113.0	113.2

The angle Si3−B1···Li1 is 178.9(1)°. Moreover, the Si−B1−Si angles of the silyl groups orientated towards Li1 are on average 113.0°, while the average of angles Si3−B1−Si is 105.6°. This demonstrates that the Li···H interaction (average Li···H distance 2.17 Å) leads to a widening of the tetrahedral angle.

Lithium methyl tris(trimethylsilyl)borate **4** exhibits an unsymmetrical structure in the solid state. The Li atom is in contact with a total of five hydrogen atoms, four of which are from the same anionic species, while the fifth is from a neighbouring anion. Therefore, the molecules of **4** are associated so as to form a chain structure. Li2−H distances are on average 2.19 Å for the hydrogen atoms of $SiMe_3$ groups, but are as short as 1.87 Å for the contacts with the hydrogens of the BMe group.

In contrast to the structure of the silylborate **3**, two different B−Si bond lengths are found in compound **4**. The Si5−B2 bond measures 2.017(2) Å and is therefore shorter than the Si6−B2 and Si7−B2 bonds [2.034(2), 2.030(2) Å]. Hydrogen atoms of the $Si(6)Me_3$ and $Si(7)Me_3$ groups coordinate intramolecularly to the Li2 center. The Si6−B2−Si7 bond angle is 113.2(1)°, i.e. 3.6° larger than the ideal tetrahedral angle. This deviation, together with the longer Si−C bonds to the $SiMe_3$ groups of Si6 and Si7, indicates that there should be more negative charge on these silyl groups than on that of Si5, and that "hyperconjugation" leads to bond lengthening. Indeed, the Si−C bond lengths of the methyl groups involved in CH···Li interactions are longer [Si6−C18, Si7−C19: 1.920(2) Å] than all the other Si−C distances (average: 1.881 Å). The fact that Li2 is not located between three $SiMe_3$ groups indicates that BCLi "hyperconjugation" is preferred to BSiLi "hyperconjugation". This is also reflected in a rather long BC bond length of 1.679(3) Å, compared with BC bonds of between 1.621(5) and 1.642(4) Å in $LiBMe_4$.[12] In this molecule the Li−B atom distance is 2.541(5) Å, in contrast to **4** where it is only 2.276(4) Å, which is even shorter than that in compound **3** [B1···Li1: 2.387(4) Å].

The packing of the molecules **3** and **4** in the lattice is depicted in Figure 6. There are only van der Waals' contacts

between hydrogen atoms. The chains of molecule **4** are oriented along the *b* axis.

As has been reported previously,[3] all hydrogen atoms of the tetrakis(trimethylsilyl)borate are equivalent on the NMR timescale. The molecule is thus fluxional, and the same holds true for compound **4**. While it can readily be seen from the crystal structures of **3** and **4** that these compounds will be present as molecules in solution, the process that leads to fluxionality is still unknown. We assume that this does not occur by a dissociative process, but rather by a simultaneous movement of the Li centers with rotation of the $SiMe_3$ groups about the B−Si bonds.

Conclusion

Lithium silyltrihydridoborates $Li(R_3SiBH_3)$ are accessible by reacting lithium silanides with $BH_3 \cdot NEt_3$. In contrast to the reaction of lithium organyls with $H_3B \cdot NMe_3$,[13] no deprotonation at the organyl groups of the amine occurs. Depending on the coligand (THF, TMEDA, PMDTA), either bridged dimeric or monomeric molecules are formed. Two different kinds of hydride bridges B−H···Li are observed, corresponding to $\mu_2{}^1$- and $\mu_3{}^1$-BH_3R groups, which are responsible for the association. In contrast, $LiB(SiMe_3)_4$ is monomeric in the solid state, with the Li center "buried" in a cleft between three $SiMe_3$ groups. There are six C−H···Li interactions. Only minor distortion of the $B(SiMe_3)_4{}^-$ anion occurs, the most notable feature being the lengthening of the Si−C bonds when H atoms are involved in C−H···Li interactions. This can be explained in terms of "hyperconjugation". $LiMeB(SiMe_3)_3$ is less symmetrical than **3** because the BMe group is involved in bonding to Li. B−C bond lengthening, which exceeds that observed for $LiBMe_4$, indicates that BCLi "hyperconjugation" is more pronounced than SiCLi "hyperconjugation".

The structures of **3** and **4** are unique for main group organometallic compounds and it would be interesting to compare them with the structures of $LiB(t\mathrm{Bu})_4$ and $LiMeB(t\mathrm{Bu})_3$. However, $LiB(t\mathrm{Bu})_4$ is unstable and decomposes readily with loss of isobutene to give $LiHB(t\mathrm{Bu})_3$, while $LiMeB(t\mathrm{Bu})_3$ ($d^{11}B = -10.4$) has only been observed in THF solution,[14] and has yet to be isolated and characterized, other than by NMR.

Experimental Section

General Remarks: All experiments were performed under anhydrous conditions under N_2 or Ar using Schlenk techniques. All reagents were purified prior to use either by distillation or crystallization. The reactions were monitored by using a Bruker WP 200 PFT NMR spectrometer equipped with a multinuclear probe. − $BH_3 \cdot THF$ was prepared from $NaBH_4$ in diglyme and BF_3; the diborane released was dissolved in pure THF. $BH_3 \cdot NEt_3$ was prepared by adding an equimolar amount of NEt_3 to a solution of $BH_3 \cdot THF$. Lithium silanides were obtained by standard literature procedures.[15] − Elemental analyses, using a Heraeus MX instrument, were performed at the microanalytical laboratory of the Institute. A systematic lack of 1−2% carbon in the analyses is due to the formation of SiC and BC. − IR: Perkin-Elmer FT spectrometer. − NMR: Bruker WP 200 PFT, JEOL GSX 270, and JEOL EX 400 instruments; internal TMS ($^{1\ H,\ 13}C$), external $BF_3{\cdot}OEt_2$ (^{11}B) as standards.

Bis[lithium (triphenylsilyl)trihydridoborate] · Tris(tetramethylethylenediamine) (1): A THF solution (30 mL) of freshly prepared triphenylsilyllithium (10 mmol)[15] was added dropwise to a stirred solution of $BH_3 \cdot NEt_3$ (10 mmol) in THF (20 mL) at −30°C. In the course of the addition, the deep-green colour of the lithium silanide changed to reddish-brown. The mixture was allowed to warm to ambient temperature over a period of 4 h, and was then heated under reflux for 48 h, which resulted in a colourless solution. According to NMR analysis of this solution, $LiBH_4$ and the silyltrihydridoborate **1** were present in a ratio of 1:17. All volatiles were then removed in vacuo, leaving a white powder. **1** was separated from $LiBH_4$ by washing the powder with hexane (3× 30 mL). An attempted crystallization from hexane solution was unsuccessful, a 100% excess of TMEDA (20 mmol) was added. At −20°C, **1** precipitated within 2 weeks as colourless crystals, which were suitable for X-ray diffraction analysis. Yield: 2.90 g (3.2 mmol, 64%), m.p. 110−114°C (decomp.). − $C_{54}H_{84}B_2Li_2N_6Si_2$ (908.97): calcd. C 71.35, H 9.31, N 9.25; found C 70.44, H 8.96, N 8.94. − ^{11}B NMR (64 MHz, C_6D_6): δ = −42.6 [q, ^1J(B,H) = 78 Hz, $h_{1/2}$ = 34 Hz]. − ^1H NMR (400 MHz, C_6D_6): δ = 7.93 (m, Si−C_6H_5), 7.57 (m, Si−C_6H_5), 7.24 (m, Si−C_6H_5), 7.11 (m, Si−C_6H_5), 2.02 (br. s, 12 H, N−CH_2−), 1.98 (br. s, 36 H, N−CH_3), 0.00 [br. q, ^1J(B,H) = 78 Hz]. − ^{13}C NMR (100 MHz, C_6D_6): δ = 136.7 (arom. C_i), 136.2 (arom. C_o), 130.1 (arom. C_p), 128.4 (arom. C_m), 51.6 (N−CH_2−), 46.1 (N−CH_3).

Lithium [(*tert*-Butyldiphenylsilyl)trihydridoborate] · Tris(tetrahydrofuran) (2a): A THF solution (30 mL) of freshly prepared *tert*-butyldiphenylsilyllithium (10 mmol) was added dropwise to a stirred solution of $BH_3 \cdot NEt_3$ (10 mmol) in THF (20 mL) at −30°C. In the course of the addition, the dark-brown colour of the lithium silanide became lighter, but did not disappear entirely. The mixture was allowed to warm to ambient temperature over a period of 4 h, and was then heated under reflux for 48 h, which resulted in a colourless but cloudy solution. According to NMR analysis of this solution, $LiBH_4$ and the silyltrihydridoborate were present in a ratio of 1:9. The volatiles were then removed in vacuo, leaving a white powder. **2a** was separated from $LiBH_4$ by washing the powder with hexane (3× 30 mL). At −20°C, **2a** precipitated from the hexane solution within 2 weeks as colourless crystals, which were suitable for X-ray diffraction analysis. Yield: 2.7 g (5.7 mmol, 57%), m.p. 98−101°C (decomp.). − $C_{28}H_{46}BLiO_3Si$ (476.49): calcd. C 70.58, H 9.73; found C 69.28, H 9.53. − ^{11}B NMR (64 MHz, C_6D_6): δ = −43.8 [q, ^1J(B,H) = 78 Hz, $h_{1/2}$ = 41 Hz]. − ^1H NMR (400 MHz, C_6D_6): δ = 8.11 (m, Si−C_6H_5), 7.31 (m, Si−C_6H_5), 3.52 (m, 12 H, THF: −O−CH_2−), 1.47 [s, 9 H, Si−C(CH_3)$_3$], 1.33 (m, 12 H, THF: −O−CH_2−CH_2−), −0.09 [q, ^1J(B,H) = 78 Hz, 3 H, BH_3]. − ^{13}C NMR (100 MHz, C_6D_6): δ = 137.0 (arom. C_o), 136.1 (arom. C_i), 127.2 (arom. C_p), 127.0 (arom. C_m), 68.3 (O−CH_2−CH_2), 29.5 [Si−C(CH_3)$_3$], 27.7 [Si−C(CH_3)$_3$], 25.4 (O−CH_2−CH_2−). − IR (Nujol): $\tilde{\nu}$ = 2284.3 (br. vs), 2257.2 (br. vs), 1962.4 (vw), 1946.4 (vw), 1483.6 (m), 1467.6 (m), 1459.2 (m), 1425.6 (vs), 1383.0 (m), 1370.0 (w), 1356.1 (m), 1341.6 (w), 1305.3 (w), 1293.8 (w), 1258.4 (m), 1182.2 (m), 1096.1 (vs), 1049.2 (vs), 1010.2 (m), 998.8 (w), 988.8 (vw), 935.2 (w), 916.7 (m), 894.3 (s), 820.8 (s), 738.3 (s), 731.6 (s), 702.5 (vs), 687.7 (s), 636.7 (s), 617.6 (m), 571.8 (m), 490.8 (s), 482.8 (s), 448.3 (m), 397.6 (w), 373.4 (w), 330.8 (w), 323.6 (w), 306.9 (w), 293.5 (m), 250.4 (vw).

Lithium [(*tert*-Butyldiphenylsilyl)trihydridoborate] · Pentamethyldiethylenetriamine (**2b**): A stoichiometric amount of PMDTA was added to a solution of **2a** in hexane. From the resulting solution, colorless crystals grew at −20°C within 7 days; m.p. 106−108°C (decomp.). − $C_{25}H_{45}BLiN_3Si$ (433.48): calcd. C 69.27, H 10.46, N 9.69; found C 68.43, H 9.98, N 8.97. − ^{11}B NMR (64 MHz, C_6D_6): δ = −43.8 [q, ^1J(B,H) = 79 Hz, $h_{1/2}$ = 20 Hz]. − ^{1}H NMR (400 MHz, C_6D_6): δ = 8.27 (m, Si−C_6H_5), 7.35 (m, Si−C_6H_5), 2.00 (br. s, 8 H, −N−CH_2−CH_2−), 1.87 (br. s, 16 H, N−CH_3), 1.54 [s, 9 H, Si−C(CH_3)$_3$], −0.10 [q, 3 H, ^1J(B,H) = 79 Hz, BH_3]. − ^{13}C NMR (100 MHz, C_6D_6): δ = 137.4 (arom. C_o), 136.3 (arom. C_i), 126.9 (arom. C_m), 126.8 (arom. C_p), 57.1 (N−CH$_2$−), 45.9 (N−CH$_3$), 29.9 [Si−C(CH$_3$)$_3$], 28.1 [Si−C(CH$_3$)$_3$]. − IR (Nujol): $\tilde{\nu}$ = 2335.4 (br. m), 2266.4 (br. ss), 2237.5 (br. s), 2008.4 (vw), 1956.5 (vw), 1882.8 (vw), 1826.5 (vw), 1770.2 (vw), 1653.2 (vw), 1588.3 (vw), 1484 (m), 1470.7 (vs), 1463.9 (vs), 1454.9 (vs), 1425.1 (vs), 1410.3 (w), 1390.0 (w), 1379.9 (w), 1361.4 (m), 1351.9 (m), 1324.0 (vw), 1299.3 (m), 1289.1 (m), 1250.4 (w), 1214.8 (vw), 1167.5 (m), 1151.5 (m), 1106.7 (vs), 1094.1 (vs), 1065.0 (m), 1055.7 (m), 1035.6 (s), 1030.1 (s), 1017.7 (m), 999.02 (w), 983.9 (m), 935.0 (m), 897.5 (w), 856.8 (vw), 818.7 (m), 788.3 (w), 773.1 (w), 738.6 (s), 703.7 (vs), 689.3 (s), 645.6 (m), 620.7 (m), 605.5 (vw), 597.9 (vw), 571.6 (m), 509.0 (vw), 482.4 (s), 433.6 (m), 404.9 (w), 3992.2 (w), 343.9 (vw), 316.0 (vw).

Lithium Tetrakis(trimethylsilyl)borate (**3**) and **Lithium Tris(trimethylsilyl)methylborate** (**4**) were prepared as described in the literature.[3]

X-ray Structure Determinations: Single crystals of compounds **1**, **2a**, **2b**, **3**, and **4** were obtained from hexane solutions at −20°C. The selected crystals were covered with perfluoroether oil, mounted on a glass fibre, placed on the goniometer head of the diffractometer, and cooled to −90°C under a flow of N_2. Preliminary dimensions of the unit cells were calculated from the reflections collected at four different settings of the crystal by recording 15 frames each with a CCD area detector. Data collection was performed with a 10 s exposure time per frame by rotating the crystal by 0.3° in φ at two different χ settings. The data from 1350 frames were reduced using the program SAINT[16] and the structures were solved by direct methods using the XS and SHELX97 programs for structure solution and refinement. The structure of compound **2b** showed disorder of one $NC_2H_4NMe_2$ bridge of the PMDTA coligand with an SOF of 0.5. Refinement of this disorder needed restraints in bond length for N−C and C−C distances. Atoms C17, C18, C20, C22, C22a, C24a, and C25a were refined with isotropic thermal parameters. All other non-hydrogen atoms were refined anisotropically, and the positions of hydrogens as found by difference Fourier maps were refined freely. Relevant data are presented in Table 3.

Crystallographic data (excluding structure factors) have been deposited with the Cambridge Crystallographic Data Centre as supplementary publication nos. CCDC 105281−105284. Copies of the data can be obtained free of charge on application to CCDC, 12 Union Road, Cambridge CB2 1EZ, U.K. [Fax: (internat.) +44 (0)1223/ 336033; E-mail: deposit@ccdc.cam.ac.uk].

Acknowledgments

We gratefully acknowledge the support of the Deutsche Forschungsgemeinschaft (Schwerpunktprogramm: Polyhedra of Main Group Elements), the Fonds der Chemischen Industrie, and

Table 3. Selected crystallographic data for the structures of **1**, **2a**, **2b**, **3**, and **4** and data referring to data collection and structure refinement

	1	**2a**	**2b**	**3**, **4**
Empirical formula	$C_{27}H_{42}BLiN_3Si$	$C_{28}H_{46}BLiO_3Si$	$C_{25}H_{45}BLiN_3Si$	$C_{22}H_{66}B_2Li_2Si_7$
Mol. mass	454.48	476.49	433.48	562.88
Crystal size [mm]	0.05 × 0.10 × 0.20	0.40 × 0.40 × 0.40	0.10 × 0.10 × 0.20	0.2 × 0.3 × 0.3
Crystal system	Triclinic	Monoclinic	Triclinic	Orthorhombic
Space group	*P*-1	*P*2(1)/*c*	*P*-1	*Pbca*
a [Å]	11.3191(1)	12.073	10.3485(3)	17.439(5)
b [Å]	11.3967(3)	13.5337(1)	11.9161(2)	15.528(5)
c [Å]	12.4007(5)	19.1765(2)	12.3191(3)	28.02(1)
α [°]	93.292(2)	90	90.908(1)	90
β [°]	90.514(1)	107.519(1)	111.653(1)	90
γ [°]	113.966(1)	90	94.406(1)	90
V [Å^3]	1458.45(7)	2987.94(4)	1406.14(6)	7588(4)
Z	2	4	2	8
ρ_{calcd} [Mg/m^3]	1.035	1.059	1.024	0.985
μ [mm^{-1}]	0.098	0.103	0.099	0.262
F(000)	494	1040	476	2496
Index range	$-13 \le h \le 13$ $-14 \le k \le 14$ $-8 \le l \le 16$	$-15 \le h \le 15$ $-17 \le k \le 11$ $-23 \le l \le 23$	$-13 \le h \le 10$ $-14 \le k \le 15$ $-15 \le l \le 15$	$-18 \le h \le 18$ $-20 \le k \le 20$ $-34 \le l \le 34$
2θ [°]	58.02	58.24	57.60	55.72
T [K]	193	193	193	183(3)
Refl. collected	8508	16426	8029	40823
Refl. unique	4564	5432	4383	7484
Refl. observed (4σ)	2672	4140	3153	5617
R (int.)	0.0664	0.0276	0.0257	0.0501
No. of variables	322	414	348	562
Weighting scheme[a]	0.0394/0.9659	0.0489/1.4893	0.1398/2.3485	0.0319/2.7715
GooF	1.072	1.065	1.038	1.066
Final *R* (4σ)	0.0669	0.0570	0.0964	0.0364
Final *wR*2	0.1208	0.1289	0.2555	0.0714
Larg. res. peak	0.283 [e/Å^3]	0.240	0.718 [e/Å^3]	0.298 [e/Å^3]

[a] $w^{-1} = \sigma^2F_o^2 + (xP)^2 + yP$; $P = (F_o^2 + 2F_c^2)/3$.

Chemetall GmbH. Moreover, we thank Prof. Dr. B. Singaram, University of Santa Cruz, California, for stimulating discussions.

[1] H. Hommer, H. Nöth, W. Ponikwar, *Eur. J. Inorg. Chem.* **1998**, 1519−1528.
[2] D. Seyferth, G. Raab, S. O. Grim, *J. Org. Chem.* **1961**, *26*, 3034−3045.
[3] W. Biffar, H. Nöth, *Chem. Ber.* **1982**, *115*, 934−945.
[4] H. Schmidbaur, A. Blumenthal, P. Bissinger, *J. Organomet. Chem.* **1993**, *462*, 107−110.
[5] H. Nöth, S. Thomas, M. Schmidt, *Chem. Ber.* **1996**, *129*, 451−458; H. H. Giese, H. Nöth, H. Schwenk, S. Thomas, *Eur. J. Inorg. Chem.* **1998**, 941−949; D. Stalke, *J. Organomet. Chem.* **1997**, *542*, 25−28; T. A. Antsychkina, G. G. Sadikor, M. A. Porai-Koshits, V. N. Konoplev, T. A. Silina, A. S. Sizareva, *Koord. Khim.* **1994**, *20*, 277−284; T. A. Antsychkina, G. G. Sadikor, M. A. Porai-Koshits, V. N. Konoplev, T. A. Silina, A. S. Sizareva, *Koord. Khim.* **1994**, *20*, 274−276; N. Maltseva, Y. N. Shevchenko, A. I. Golovanova, *Russ. J. Inorg. Chem.* **1987**, *32*, 1038−1039; D. R. Amaskong, W. Clegg, H. M. Colquhoun, J. A. Daniels, R. E. Mulvey, I. R. Stephenson, K. Wade, *J. Chem. Soc., Chem. Commun.* **1987**, 630−632.
[6] B. Singaram, E. T. Cole, H. C. Brown, *Organometallics* **1984**, *3*, 774−777; B. Singaram, E. T. Cole, H. C. Brown, *Organometallics* **1984**, *3*, 1520−1523.
[7] H. Nöth, B. Wrackmeyer, *NMR Spectroscopy of Boron Compounds, NMR Principles and Progress*, vol. 14 (Eds.: R. Diehl, E. Fluck, R. Kosfeld), Springer Publishers, Heidelberg, New York, **1973**.
[8] Also isolated and characterized by X-ray structure determination was $[(t\mathrm{BuPh_2Si})\mathrm{BH_3} \cdot \mathrm{Li(thf)_2}]_2$. This compound was obtained in an experiment similar to that described for the preparation of **2a**. Its $\mathrm{SiBH_3}$ group acts as a $\mu_2{}^1$, $\mu_1{}^1$-ligand, bridging two Li units, which are pentacoordinated by two O atoms and 3 H atoms (of the THF molecules and two $\mathrm{BH_4}$ units). However, the crystal quality was less than satisfactory since refinement could not be improved beyond $R1 = 10.31$. Furthermore, solution was only possible in the triclinic space proup $P1$bar, whereas the unit cell dimensions showed the presence of a monoclinic crystal system. Crystal data are: $a = 12.2823(6)$, $b = 13.4825(6)$, $c = 15.4181(7)$ Å, $\alpha = 89.996(2)$, $\beta = 86.881(1)$, $\gamma = 89.984(1)°$, $Z = 2$. The data of the structure refinement have also been deposited with the CCDC.
[9] N. Edelstein, *Inorg. Chem.* **1981**, *20*, 197−299.
[10] W. Lippert, H. Nöth, in preparation, to be submitted to *Eur. J. Inorg. Chem.*
[11] P. Paetzold, D. Hahnfeld, U. Englert, W. Wojnowski, B. Dreczewski, Z. Pawelec, L. Walz, *Chem. Ber.* **1992**, *125*, 1073−1078.
[12] W. E. Rhine, G. Stucky, S. W. Peterson, *J. Am. Chem. Soc.* **1975**, *97*, 6401−6405.
[13] W. Biffar, H. Nöth, D. Sedlak, *Organometallics* **1983**, *2*, 579−585.
[14] W. Biffar, Dissertation, University of Munich, **1981**.
[15] H. Gilman, D. J. Peterson, D. Wittenberg, *Chem. Ind.* **1958**, 1479−1480.
[16] *SHELXTL*, Version 5, Siemens X-ray Analytical Instruments, **1994**.

Received: October 30, 1998
[I98374]

Facile Preparation of Mono- and Bis(tin)-Substituted Niobocenes with Functionalized Stannyl Ligands: The Search for Non-Classical Interligand Interactions

Georgii I. Nikonov,*[a] Lyudmila G. Kuzmina,[b] Jörg Lorberth,[c] and Judith A. K. Howard[d]

Keywords: Niobium / Tin / Hydrides / Group 5 / Group 14

The reaction of niobocene trihydride [Cp_2NbH_3] with one equivalent of an alkyl- or aryltin halide X_nSnR_{4-n} (n = 1, 2) leads to products of the displacement of hydride by tin, i.e. [$Cp_2NbH_2(SnX_{3-n}R_n)$] [R = Me, n = 3 (**1**); R = Me, X = Cl, n = 2 (**3**); R = Ph, n = 3 (**4**); R = Ph, X = Cl, n = 2 (**5**); R = Et, X = Br, n = 2 (**6**)]. Use of an excess of the tin reagent results in a halodealkylation exchange reaction at the tin atom bound to the metal center. Reaction of the mono(silyl) complexes [$Cp_2NbH_2(SiXMe_2)$] (X = Cl, Ph) with organotin halides X_nSnR_{4-n} gives products of the displacement of silicon by tin, whereas the bis(silyl) complex [$Cp_2NbH(SiPhMe_2)_2$] does not undergo this reaction. The bis(tin)-substituted niobocene [$Cp_2NbH(SnMe_3)_2$] has been prepared by the reaction of [$Cp_2NbH_2(SnMe_3)$] with the tin amide Me_3SnNMe_2 under thermal conditions, as well as by the literature method of thermolysis of [$Cp_2NbH(\eta^2\text{-}C_2H_3Ph)$] in the presence of Me_3SnH. Reaction of [$Cp_2NbH(SnMe_3)_2$] with two equivalents of Cl_2SnMe_2 affords the bis(tin)-substituted complex [$Cp_2NbH(SnClMe_2)_2$] (**9**). The possible presence of non-classical hypervalent H···Sn–Cl interactions in this compound has been assessed by means of X-ray structure analysis. The structural data for **9** are in accord with an essentially classical description as a tin-substituted dihydride complex without significant Sn···H interactions.

Introduction

We have been studying the chemistry of trisubstituted Group-5 metallocene complexes bearing hydride and main-group element ligands in the bisecting plane of the metallocene moiety.[1–3] Initially, we focused on the development of convenient synthetic approaches to compounds of this class. These efforts resulted in the introduction of the insertion/deprotonation method based on the interaction of metallocene trihydrides [Cp_2MH_3] (M = Nb, Ta) with Group-15 halides XER_2 (E = P, As, Sb, Bi; X = Cl, Br).[1] This method provides easy access to dihydrides of the general formula [$Cp_2MH_2(ER_2)$]. A very similar approach, namely main-group element displacement of hydride, has recently been used by ourselves in the preparation of a plumbio-substituted niobocene,[2] and previously by Bulychev et al. in the preparation of a tin-substituted tantalocene.[4]

In this paper, we report an extension of these studies to the syntheses of mono- and bis(tin)-substituted niobocenes. Our interest in compounds of this type was intensified following our recent discovery of non-classical H···Si–Cl interligand interactions in the related silicon-substituted niobocene complexes [$Cp_2NbYH(SiR_2X)$] (Y = H, SiR_2X) bearing functionalized silyl ligands SiR_2X.[2] Thus, we were interested in finding analogous H···Sn–Cl interactions in the present systems. The main-group element displacement of hydride and halodealkylation exchange approaches reported herein provide a convenient entry to the chemistry of tin-substituted metallocenes bearing functionalized stannyl substituents SnX_nR_{3-n} (X = Cl, Br; R = Et, Me; n = 1, 2).

[a] Chemistry Department, Moscow State University, Vorob′evy Gory, 119899 Moscow, Russia
Fax: (internat.) + 7-095/932-8846
E-mail: nikonov@org.chem.msu.su
[b] Institute of General and Inorganic Chemistry, RAS, Leninsky Prosp. 31, 117907 Moscow, Russia
[c] Fachbereich Chemie, Philipps-Universität Marburg, Hans-Meerwein-Strasse, D-35032 Marburg, Germany
[d] Chemistry Department, University of Durham, South Road, Durham DH1 3LE, U.K.

Results and Discussion

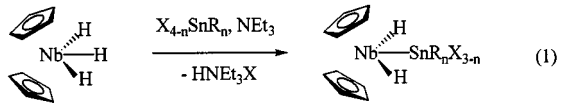
Mono(tin)-Substituted Complexes

The first tin-substituted niobocene hydrides [$Cp_2NbH_2(SnMe_3)$] (**1**) and [$Cp_2NbH(SnMe_3)_2$] (**2**), were prepared by Green et al. by means of oxidative addition of $HSnMe_3$ to the 16-electron intermediates [Cp_2NbH] and [$Cp_2NbCH_2CH_2Ph$], which were generated in situ from [Cp_2NbH_3] and the styrene complex [$Cp_2NbH(\eta^2\text{-}C_2H_3Ph)$], respectively.[5] This approach cannot, however, be applied to the syntheses of complexes bearing functionalized stannyl ligands since the parent compounds $XSnR_2H$ are not easily accessible. Green et al. also reported a metathetical reaction leading to **1**, between the anionic complex [Cp_2NbH_2]Li and $ClSnMe_3$, although this reaction proceeds under reducing conditions, thus restricting the use of functionalized tin reagents.[5] In 1986, Bulychev et al. showed that Cl_3SnMe and Cl_2SnMe_2 react with the d^0 complex [Cp_2TaH_3] to give [$Cp_2TaH_2(Cl_nSnMe_{3-n})$] ($n$ = 1, 2), whereas $ClSnMe_3$ does not undergo such a reaction.[4] The highest yields were observed when these reactions were carried out in the presence of an amine, which served to consume the generated HCl. These findings prompted this study of the analogous niobocene chemistry.

[Cp_2NbH_3] reacts readily with one equivalent of a tin halide X_nSnR_{4-n} (n = 1, 2) in diethyl ether in the presence of

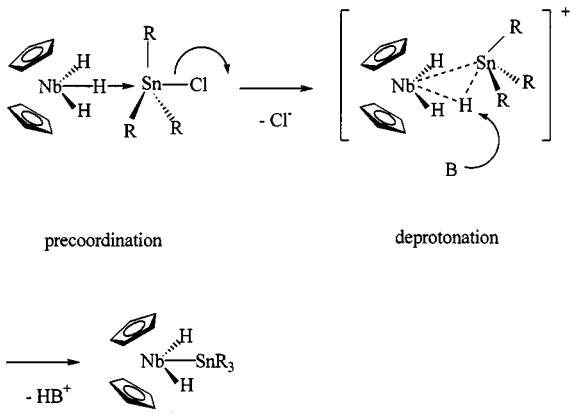
 © WILEY-VCH Verlag GmbH, D-69451 Weinheim, 1999 1434–1948/99/0505–0825 $ 17.50+.50/0

NEt_3, to give the mono(tin)-substituted complexes $[Cp_2NbH_2(SnX_{3-n}R_n)]$ [R = Me, n = 3 (**1**); R = Me, X = Cl, n = 2 (**3**); R = Ph, n = 3 (**4**); R = Ph, X = Cl, n = 2 (**5**); R = Et, X = Br, n = 2 (**6**)] (Equation 1). The reactions commence immediately after the reactants are mixed and result in the formation of a flocculent precipitate of $ClH{\cdot}NEt_3$. The mixtures were left to stir overnight to ensure completion of the reactions. Complexes **1**, **3**–**6** could easily be isolated (after filtration and removal of the solvent) and were obtained as pale-yellow, air-sensitive, crystalline materials. The products seemingly showed indefinite thermal stability, as is also the case for the related plumbyl-substituted complex $[Cp_2NbH_2(PbMe_3)]$.[2] In contrast, the related Group-15 substituted complexes $[Cp_2NbH_2(EPh_2)]$ (E = Sb, Bi) exhibit little thermal stability and $Cp_2NbH_2(BiPh_2)$ is also very light-sensitive. Complexes **1**, **3**–**6** were characterized by NMR and IR spectroscopy. Their ^{1}H-NMR spectra are in accord with the formation of only one isomer, specifically that having a centrally positioned tin substituent and lateral hydride ligands. In contrast, the mono(silyl) complex $[Cp_2NbH_2(SiClMe_2)]$ exists in two isomeric forms, one of which, with a lateral silyl group, exhibits non-classical bonding between the hydride and silicon ligands.[3]



X	Cl	Cl	Cl	Cl	Br
R	Me	Me	Ph	Ph	Et
n	3	2	3	2	2
	1	**3**	**4**	**5**	**6**

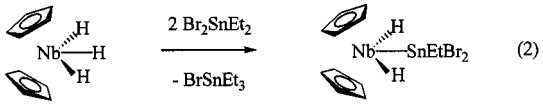
The mechanism of the reaction according to Equation 1 is intriguing. The d^0 complex $[Cp_2NbH_3]$ lacks a metal-centered lone pair of electrons, hence conventional nucleophilic substitution of halide at the tin center is not possible. Although the reaction is carried out in the presence of an amine to consume the HCl released, the amine cannot effect deprotonation of $[Cp_2NbH_3]$ to give a metallocene anion $[Cp_2NbH_2]^-$ amenable to a substitution reaction. It has long been shown by Tebbe that $[Cp_2NbH_3]$ is a basic, rather than an acidic hydride compound.[6] In fact, it can only be deprotonated by bases as strong as BuLi. Moreover, it has been shown that alkyltin halides react with $[Cp_2TaH_3]$ even in the absence of an amine, the yield being decreased as a result of subsequent reactions of the product with the generated HCl.[7] The absence of intermediate $[Cp_2NbH_2]^-$ in the reaction of Equation 1 was further supported by the results of an attempted reaction of $[Cp_2NbH_3]$ with D_2O in the presence of NEt_3. No deuterium incorporation was observed by NMR spectroscopy after stirring the mixture overnight. Therefore, the reaction of $[Cp_2NbH_3]$ with an alkyltin halide must occur through a direct interaction of a basic Nb–H bond with the tin reagent. The most likely mechanism is similar to that proposed by Pasynskii et al. for the reaction of $[Cp_2NbH(CO)]$ with tin halides.[8] It involves coordination of the Sn–Cl bond along the M–H polar bond forming a hydride-bridged bimetallic adduct and a five-coordinated tin center. Proton abstraction and halide dissociation complete the reaction (Scheme 1). At present, it is not clear as to whether dissociation of a halide precedes (this possibility is shown in Scheme 1) or follows the proton abstraction. More detailed studies are required to elucidate this matter.



Scheme 1

Preparation of compound **1** according to Equation 1 has apparent advantages over the reported procedures[5] since it allows for easy isolation of the product and requires only one step rather than two, starting from $[Cp_2NbH_3]$. Moreover, it provides an easy access to complexes with functionalized tin ligands. In order to carry out this reaction successfully, it is necessary to use strictly one equivalent of the tin halide, since excess X_nSnR_{4-n} effects a facile halodealkylation exchange reaction. For example, reaction of Cp_2NbH_3 with two equivalents of $ClSnMe_3$ gives a mixture of **1** and **3**. Similarly, addition of $ClSnMe_3$ to **1** results in the slow replacement of Me by Cl in **1** to give **3**, a process that could be monitored by NMR spectroscopy over a period of several days. In contrast, reaction of **1** with the more electrophilic Cl_2SnMe_2, leading to complex **3** and $ClSnMe_3$, reached completion in the course of overnight monitoring. Analogously, reaction of $[Cp_2NbH_3]$ with two equivalents of Br_2SnEt_2 furnished the dibrominated complex $Cp_2NbH_2(SnBr_2Et)$ (**7**) in high yield (Equation 2). Halodealkylation exchange reactions between transition metal tin complexes and tin halides have previously been observed in some tin-substituted molybdenocenes[9] and tungstenocenes.[10] Moreover, some silyl-substituted molybdenocene compounds have been shown to undergo intramolecular halodealkylation exchange between their coordinated silyl groups.[11] In comparison, in the non-transition metal chemistry of tin, and even more so in the case of silicon, analogous group interchange requires elevated temperatures. Apparently, it is coordination to the transition metal center that facilitates the exchange reaction, probably as a result of weakening of the Sn–C bond of the coordinated stannyl moiety. Bulychev showed that coordination of a stannyl group to a transition metal center effects rehybridization of the tin center,[9][12] in accordance with Bent's rule.[13] Thus, more tin s-orbital character contributes to

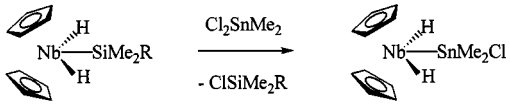
bonding with the metal center and consequently more tin p-orbital character is left for bonding with the alkyl substituents. This also means that the Sn−C bonds become more polar. The increase in p-orbital character also causes lengthening of the Sn−C bonds, which should decrease steric strain in the transition state for exchange. The observation that treatment of $[Cp_2Nb(CO)(SnPh_3)]$ with HCl leads to the formation of $[Cp_2Nb(CO)(SnCl_3)]$[8] rather than to cleavage of the Sn−Nb bond is a further manifestation of the rehybridization effect.



(2)

Tin-for-Silicon Exchange

We were interested in employing the hydride by tin displacement reaction for the preparation of mixed silicon/tin-substituted niobocenes of the formula $[Cp_2NbH(SiR'_3)(SnR_3)]$. No compounds of this type have hitherto been prepared. However, we found that the action of $X_{4-n}SnR_n$ on the mono(silyl) complexes $[Cp_2NbH_2(SiPhMe_2)]$ and $[Cp_2NbH_2(SiClMe_2)]$ led to quantitative yields of the corresponding mono(tin) compounds $[Cp_2NbH_2(SnX_{3-n}R_n)]$ (Equation 3). Addition of Cl_2SnMe_2 to the bis(silyl) complex $[Cp_2NbH(SiPhMe_2)_2]$ resulted in no reaction. In the latter case, the central hydride ligand is seemingly sterically too hindered by the silyl ligands to allow interaction with the tin halide. Two mechanisms can, in principle, be invoked to account for the above tin-for-silicon exchange. One implies a direct attack of the tin halide on the metal−silicon bond, while the second involves interaction of X_nSnR_{4-n} with the lateral hydride ligand as discussed above, with subsequent attack of the released halide anion X^- on the silicon substituent, as shown in Scheme 2. We favour the latter possibility, since it necessitates a less hindered transition state. The driving force for this exchange reaction seems to be the formation of a stable Si−Cl bond.

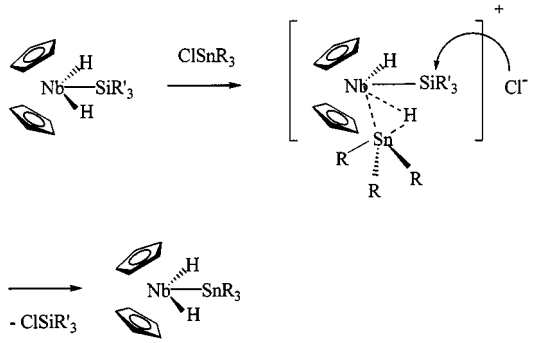


(3)

R = Ph, Cl

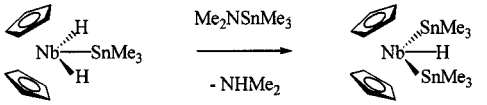
Bis(tin)-Substituted Complexes

The bis(tin)-substituted niobocene $[Cp_2NbH(SnMe_3)_2]$ (**2**) has been prepared by Green et al. by oxidative addition of $HSnMe_3$ to the olefin hydride complex $[Cp_2NbH(\eta^2\text{-}C_2H_3Ph)]$.[5] Reaction of $[Cp_2NbH(SnMe_3)]K \cdot$ (18-crown-6) with $ClSnMe_3$ has also been reported to give **2**.[14] In contrast, we have found the anionic mono(tin)-substituted



Scheme 2

complex $[Cp_2NbH(SnMe_3)]Li \cdot$ (15-crown-5) (**8**) to be incapable of serving as a precursor for bis(tin) derivatives. Attempted reaction of Cl_2SnMe_2 with **8** resulted in a complex mixture of products. The potassium salt appears to have a weakly bound cation and therefore a more nucleophilic metallocene anion, whereas the lack of selectivity in the latter reaction can be explained in terms of effective competition between the metathetical reaction and the facile halodealkylation. This presumably leads to a mixture of mono- and bis(tin)-substituted complexes with variable numbers of alkyl and halogen groups on each tin atom. Also, as mentioned above, due to the facile halodealkylation at the tin center, the hydride-by-tin displacement reaction cannot be employed for the synthesis of bis(tin) derivatives starting from the mono(tin)-substituted compounds. As an alternative approach to complex **2**, we studied Lappert's amine elimination reaction.[15] This method involves interaction of a metal hydride with a tin amide $R_2NSnR'_3$ and requires elevated temperatures (ca. 80−100°C). Lappert et al. used this reaction to prepare $[Cp_2TaH_2(SnMe_3)]$ from $[Cp_2TaH_3]$ and Me_2NSnMe_3, whereas an analogous reaction with $[Cp_2NbH_3]$ led to bis(niobocene) owing to the low thermal stability of niobocene trihydride.[5] By heating a mixture of complex **1** with Me_2NSnMe_3 at 85°C for 8 h, we obtained **2** as the main reaction product (Equation 4).

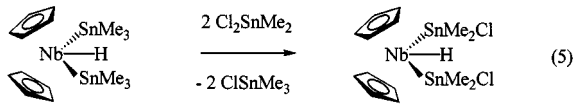


(4)

1 **2**

Complex **2** was used as a starting material for the synthesis of the functionalized bis(tin)-substituted complex $[Cp_2NbH(SnClMe_2)_2]$ (**9**) by the chlorodemethylation exchange reaction. Thus, overnight stirring of a mixture of two equivalents of Cl_2SnMe_2 with one equivalent of **2** led to complex **9** in high yield (Equation 5). The product was characterized by spectroscopic methods and X-ray diffraction analysis.

As the mono(tin)-substituted niobocenes have centrally positioned tin ligands, they were considered unlikely to show any significant interligand Sn−H interactions.[3c] In contrast, the bis(tin) complex **9** is a structural analogue of the non-classical bis(silyl) complex $[Cp_2NbH-$



(5)

2 9

$(SiClMe_2)_2]$,[3a] and therefore might be expected to show analogous non-classical bonding between Sn and the hydride ligands. To clarify this matter, an X-ray structural investigation of **9** was undertaken. Structures of four tin-substituted niobocenes[5][8] and of one tin-substituted tantalocene[7] have previously been reported, but only one of these, namely the anionic complex $[Cp_2Nb(SnMe_3)_2]^-$, has two tin ligands bound at the metal center.[5a] Crystals of **9** suitable for X-ray analysis were grown from diethyl ether solution. The crystal structure was found to contain two independent molecules of **9** per unit cell. The molecular structure of one of these is shown in Figure 1. Selected bond lengths and angles are given in Table 1. It is noteworthy that in both independent molecules the hydride ligands could be localized from the difference map and refined to the realistic Nb−H distances of 1.76(6) and 1.80(5) Å, in spite of the presence of three heavy atoms. In a neutron diffraction study of $[Cp_2NbH(SiClMe_2)_2]$, the hydride was found at a distance of 1.813 Å from the niobium,[16] while the Nb−H bond lengths in $[Cp_2NbH_3]$, determined by accurate NMR relaxation studies, were found to fall in the range 1.78−1.80 Å.[17] However, the two molecules of **9** are different in that in one of them the hydride is symmetrically positioned in the bisecting plane of the niobocene moiety, while in the second it is shifted closer to one of the tin centers resulting in a short contact of 2.13 Å. An analogous short Sn−H contact of 2.16(4) Å found in the compound $[Cp'Mn(CO)_2HSnPh_3]$ was taken as an indication of complexation of the $H-SnR_3$ bond.[18] Apart from this, the geometries of the four tin centers in the two molecules of **9** are very similar, which rules out any speculation about Sn−H non-classical bonding in the asymmetric structure of **9**. Thus, the observed Nb−Sn σ-bond lengths lie in the range 2.8015−2.8114(6) Å, while the Sn−Cl bonds fall in the range 2.448−2.479(1) Å, but no systematic trends in these parameters are in evidence. Both the Nb−Sn and Sn−Cl bonds are somewhat shorter in the second molecule than the corresponding bonds in the first, which can be attributed to crystal packing effects. This observation suggests that the coordination environments about the tin atoms are very soft. In comparison, the Nb−Sn bond lengths in other tin derivatives of niobocene, bearing SnR_3 (R = alkyl, aryl) ligands, are found in the range 2.817−2.862(1) Å,[5][8] whereas in the trichlorotin derivative $[Cp_2Nb(CO)(SnCl_3)]$[8] a shorter Nb−Sn bond length of 2.764(1) Å is observed due to the electron-withdrawing effect of the chloro substituents. The most compelling evidence in favour of a classical description of **9** and the absence of significant Sn−H interaction is provided by the large values of 109.7(2)° and 108.87(2)° for the Sn−Nb−Sn bond angles in the two independent molecules. In the non-classical complex $[Cp_2NbH(SiClMe_2)_2]$, a noticeably smaller Si−Nb−Si bond angle of 105.57(4)° is found, which reflects the attraction of the lateral Si atoms to the central hydride.[3a] The former values are close to the Si−M−Si bond angles of 110.81(5)° and 109.90(7)° found in the classical complexes $[Cp_2NbH(SiPhMe_2)_2]$[3c] and $[Cp_2TaH(SiHMe_2)_2]$,[19] respectively.

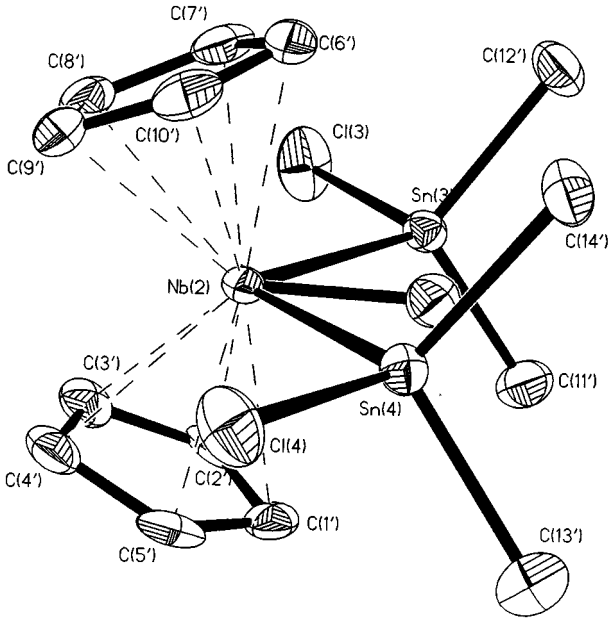


Figure 1. Molecular structure of **9**; hydrogen atoms other than hydride are omitted for the sake of clarity

Conclusions

We have shown herein that reaction of niobocene trihydride with alkyltin halides gives the products of direct displacement of hydride by tin, and thus represents an effective method for the synthesis of niobocene dihydride complexes substituted by functionalized tin ligands. Moreover, we have found that the use of an excess of the tin halide effects a halodealkylation exchange reaction at the coordinated tin center, thus giving products with a larger number of halide substituents at the tin atom. In comparison with the corresponding chemistry in uncoordinated-to-metal tin compounds, this reaction is remarkably facile. This approach has been exploited synthetically in the preparation of the bis(tin)-substituted complex $[Cp_2NbH(SnClMe_2)_2]$ (**9**) from $[Cp_2NbH(SnMe_3)_2]$. At present, it would seem that this halodealkylation exchange reaction represents the only feasible route for preparing compound **9**. Reaction of tin halides with silyl hydride derivatives of niobocene proceeds only for the mono(silyl) dihydride substituted compounds and affords the products of displacement of silicon by tin. Thus, a synthetic approach to the elusive mixed tin/silicon complexes of the formula $[Cp_2NbH(SnR_3)(SiR'_3)]$ has still to be developed. Finally, an X-ray structure determination of compound **9** did not reveal any significant non-classical Sn−H interligand interaction. The reason for this appears

Table 1. Selected bond lengths [Å] and angles [°] for **9**

		lengths	
Nb(1)−Sn(1)	2.8062(5)	Nb(2)−Sn(4)	2.8015(5)
Nb(1)−Sn(2)	2.8114(6)	Nb(2)−Sn(3)	2.8072(5)
Nb(1)−H(1)	1.76(6)	Nb(2)−H(2)	1.80(5)
Sn(1)−C(11)	2.143(6)	Sn(3)−C(11′)	2.144(6)
Sn(1)−C(12)	2.156(6)	Sn(3)−C(12′)	2.151(6)
Sn(1)−Cl(1)	2.4787(14)	Sn(3)−Cl(3)	2.4475(14)
Sn(2)−C(14)	2.141(7)	Sn(4)−C(13′)	2.149(6)
Sn(2)−C(13)	2.146(7)	Sn(4)−C(14′)	2.157(5)
Sn(2)−Cl(2)	2.4781(14)	Sn(4)−Cl(4)	2.4704(13)
Sn(2)−H(1)	2.13(6)		
		angles	
Sn(1)−Nb(1)−Sn(2)	109.675(17)	Sn(4)−Nb(2)−Sn(3)	108.865(17)
Sn(1)−Nb(1)−H(1)	60.5(18)	Sn(4)−Nb(2)−H(2)	54.6(15)
Sn(2)−Nb(1)−H(1)	49.1(18)	Sn(3)−Nb(2)−H(2)	54.3(15)
C(11)−Sn(1)−C(12)	106.8(3)	C(11′)−Sn(3)−C(12′)	106.9(3)
C(11)−Sn(1)−Cl(1)	96.4(2)	C(11′)−Sn(3)−Cl(3)	100.4(2)
C(12)−Sn(1)−Cl(1)	96.89(19)	C(12′)−Sn(3)−Cl(3)	97.2(2)
C(11)−Sn(1)−Nb(1)	122.5(2)	C(11′)−Sn(3)−Nb(2)	118.96(19)
C(12)−Sn(1)−Nb(1)	119.92(16)	C(12′)−Sn(3)−Nb(2)	120.45(19)
Cl(1)−Sn(1)−Nb(1)	108.49(4)	Cl(3)−Sn(3)−Nb(2)	108.77(4)
C(14)−Sn(2)−C(13)	108.1(3)	C(13′)−Sn(4)−C(14′)	105.7(3)
C(14)−Sn(2)−Cl(2)	96.8(2)	C(13′)−Sn(4)−Cl(4)	98.22(19)
C(13)−Sn(2)−Cl(2)	100.8(2)	C(14′)−Sn(4)−Cl(4)	98.65(17)
C(14)−Sn(2)−Nb(1)	121.5(2)	C(13′)−Sn(4)−Nb(2)	120.66(19)
C(13)−Sn(2)−Nb(1)	118.6(2)	C(14′)−Sn(4)−Nb(2)	116.42(18)
Cl(2)−Sn(2)−Nb(1)	106.37(4)	Cl(4)−Sn(4)−Nb(2)	113.62(4)
Cl(2)−Sn(2)−H(1)	145.0(15)		

to be the long Nb−Sn bond length, which leads to only minor overlap between the Nb−H bonding and Sn−Cl antibonding orbitals, and therefore precludes the transfer of electron density from the former to the latter.

Experimental Section

General: All manipulations were carried out using conventional Schlenk techniques. − Solvents were dried with sodium or sodium benzophenone ketyl. − NMR: Varian VXR-400 spectrometer (^{1}H: 400 MHz; ^{13}C: 100.4 MHz). − IR: Perkin-Elmer 1600 FT-IR spectrometer. − Tin halides were purchased from Merck. − [Cp_2NbH_3] was prepared by the modified procedure reported in an earlier publication.[1a] Compounds **1** and **2** have been reported previously.[5]

Preparation of $Cp_2NbH_2(SnMe_3)$ (1): 0.502 g (2.22 mmol) of [Cp_2NbH_3] and 0.442 g (2.22 mmol) of Me_3SnCl were mixed in 70 mL of diethyl ether, and then 3 mL of NEt_3 was added. The mixture was stirred overnight, then filtered, and the residue was washed with 50 mL of diethyl ether. All volatiles were then removed in vacuo from the combined filtrate and washings to leave a light-beige powder. Yield: 0.730 g (1.88 mmol, 85%). NMR data are as reported in the literature.[5b]

Preparation of $Cp_2NbH_2(SnMe_2Cl)$ (3). − Method a: The preparation was carried out analogously to that of **1**, to afford **3** in 80% yield.

Method b: [$Cp_2NbH_2SnMe_3$] (0.502 g, 1.72 mmol) and Me_2SnCl_2 (0.386 g, 1.72 mmol) were mixed in 20 mL of diethyl ether, and then 2 mL of NEt_3 was added. The resulting mixture was stirred for 2 d. The solvent was then removed in vacuo and the residue was extracted with toluene. The solution was filtered and all volatiles were removed in vacuo to leave rose-pink crystals. Yield: 0.233 g (0.54 mmol, 32%).

Method c: 0.142 g (1.34 mmol) of [$Cp_2NbH_2SiMe_3$] was added to a solution of 0.098 g (0.45 mmol) of Me_2SnCl_2 in 2 mL of NEt_3 and 10 mL of diethyl ether. The resulting mixture was left overnight, then filtered, and the residue was extracted with 10 mL of diethyl ether. All volatiles were removed in vacuo from the combined fractions, to leave a pale-pink substance. Yield: 0.184 g (0.45 mmol, 100%).

Method d: 0.483 g (0.45 mmol) of [$Cp_2NbH_2SiMe_2Ph$] was added to 0.295 g (1.34 mmol) of Me_2SnCl_2 and 3 mL of NEt_3 in 40 mL of diethyl ether. A bright-red colour soon developed. The mixture was left overnight, whereupon a light-lilac solution was obtained. This solution was filtered, and the residue was extracted with 4× 40 mL of diethyl ether. All volatiles were removed in vacuo from the combined fractions to leave a lilac-coloured substance. Yield: 0.540 g. NMR spectra showed the product to be a mixture of $Cp_2NbH_2SnMe_2Cl$ and $ClSiMe_2Ph$.

Analytically pure material, prepared by Method b, was obtained by recrystallization from diethyl ether. − ^{1}H NMR ([D_6]benzene): δ = 4.82 (s, 10 H, Cp), 1.05 [s + d, ^2J(Sn−H) = 31.6 Hz, 6 H, CH_3], −4.79 [s + 2d, ^2J(Sn−H) = 254.5 and 239.2 Hz, 2 H, Nb−H]. − ^{13}C NMR ([D_6]benzene): δ = 87.4 (s, Cp), 18.0 (s, Me). − $C_{12}H_{18}ClNbSn$ (409.34): calcd. C 35.21, H 4.43; found C 34.95, H 4.01.

Preparation of $Cp_2NbH_2(SnPh_3)$ (4): 0.335 g (1.48 mmol) of [Cp_2NbH_3] and 0.571 g (1.48 mmol) of Ph_3SnCl were mixed in 15 mL of toluene, and then 1 mL of NEt_3 was added. The resulting mixture was stirred overnight, then filtered, and the residue was washed with 15 mL of diethyl ether. All volatiles were removed in vacuo from the combined fractions to leave a white powder. Yield: 0.800 g (1.33 mmol, 90%). − IR (Nujol): $\tilde{\nu}$ = 1682 cm^{-1} (Nb−H). − ^{1}H NMR ([D_6]benzene): δ = 7.98 [d, J(H−H) = 7.6 Hz, 6 H, Ph], 7.32 [t, J(H−H) = 7.4 Hz, 6 H, Ph], 7.22 [t, J(H−H) = 7.4 Hz, 3 H, Ph], 4.48 (s, 10 H, Cp), −4.28 [s + d, ^2J(Sn−H) = 180.8

Hz, 2 H, Nb−H]. − ^{13}C NMR ([D$_6$]benzene): δ = 137.3 (s, Ph), 128.7 (s, Ph), 128.6 (s, Ph), 127.4 (s, Ph), 86.8 (s, Cp). − $C_{28}H_{27}NbSn$ (575.14): calcd. C 58.47, H 4.73; found C 58.58, H 4.96.

Preparation of $Cp_2NbH_2(SnClPh_2)$ (5): 0.448 g (1.98 mmol) of [Cp_2NbH_3] and 0.681 g (1.48 mmol) of Ph_2SnCl_2 were mixed in 15 mL of diethyl ether, and then 1 mL of NEt_3 was added. The resulting mixture was stirred overnight. The supernatant solution was then decanted and the residue was extracted with 5 × 10 mL of toluene. All volatiles were removed in vacuo from the combined toluene fractions to leave a white crystalline material. Yield: 0.388 g (0.727 mmol, 37%). − IR (Nujol): $\tilde{\nu}$ = 1682 cm^{-1} (Nb−H). − ^{1}H NMR ([D$_6$]benzene): δ = 8.60 [d, J(H−H) = 6.8 Hz, 4 H, Ph], 7.32 [t, J(H−H) = 7.6 Hz, 4 H, Ph], 7.18 (t, J_{H-H} = 7.2 Hz, 2 H, Ph), 4.52 (s, 10 H, Cp), −4.18 [s + 2d, J(Sn−H) = 131 Hz and ^2J(Sn−H) = 125 Hz, 2 H, Nb−H]. − ^{13}C NMR ([D$_6$]benzene): δ = 152.8, 135.5, 128.6, 128.3 (s, Ph), 87.7 (s, Cp). − $C_{22}H_{22}ClNbSn$ (533.49): calcd. C 49.53, H 4.16; found C 49.51, H 4.88.

Preparation of $Cp_2NbH_2(SnEt_2Br)$ (6): 3 mL of NEt_3 was added to 0.730 g (3.23 mmol) of [Cp_2NbH_3] in 40 mL of diethyl ether. Then, 1.087 g (3.23 mmol) of Et_2SnBr_2 in 10 mL of diethyl ether was added, resulting in the immediate deposition of white flakes. The mixture was stirred overnight, then filtered, and the residue was washed with 10 mL of diethyl ether. All volatiles were removed in vacuo from the combined fractions to leave a light-yellow powder. Yield: 1.148 g (2.38 mmol, 74%). − IR (Nujol): $\tilde{\nu}$ = 1682 cm^{-1} (Nb−H). − ^{1}H NMR ([D$_6$]benzene): δ = 4.57 (s, 10 H, Cp), 1.56 [t, ^3J(H−H) = 7.8 Hz, 6 H, CH_3], 1.35 (m, 4 H, CH_2), −4.61 [s + d, ^2J(Sn−H) = 247.7 Hz, 2 H, Nb−H]. − ^{13}C NMR ([D$_6$]benzene): δ = 87.2 (s, Cp), 17.3 (s, CH_3), 11.8 (s, CH_2). − $C_{14}H_{22}BrNbSn$ (481.85): calcd. C 34.90, H 4.60; found C 34.54, H 4.37.

Preparation of $Cp_2NbH_2(SnEtBr_2)$ (7): 4 mL of NEt_3 was added to 0.292 g (0.606 mmol) of $Cp_2NbH_2(SnEt_2Br)$ in 25 mL of diethyl ether. Then, 0.204 g (0.606 mmol) of Et_2SnBr_2 was added, resulting in the immediate deposition of white flakes. The mixture was stirred overnight, then filtered, and the residue was washed with 25 mL of diethyl ether. All volatiles were removed in vacuo from the combined fractions to leave a light-yellow powder, which was recrystallized from cold diethyl ether. NMR spectra revealed the product to be **7** contaminated by a minor impurity; complete removal of this impurity could not be achieved. Yield: 0.210 g. − IR (Nujol): $\tilde{\nu}$ = 1728.2 cm^{-1} (Nb−H). − ^{1}H NMR ([D$_6$]benzene): δ = 4.67 (s, 10 H, Cp), 1.52 [t, ^3J(H−H) = 7.8 Hz, 6 H, CH_3], 1.38 (m, 4 H, CH_2), −4.60 [s + d, ^2J(Sn−H) = 247.4 Hz, 2 H, Nb−H]. − ^{13}C NMR ([D$_6$]benzene): δ = 87.33 (s, Cp), 17.46 (s, CH_3), 11.74 (s, CH_2).

Preparation of $Cp_2NbH(SnMe_3)_2$ (2). − Method a: Preparation from [$Cp_2NbH(C_2H_3Ph)$] in 82% yield according to the literature method.[5b]

Method b: A mixture of 0.381 g (0.98 mmol) of [$Cp_2NbH_2(SnMe_3)$] and 0.204 g (0.98 mmol) of Me_3SnNMe_2 in 10 mL of toluene was heated at 85°C for 8 h. All volatiles were then removed in vacuo and the residue was extracted with 20 mL of diethyl ether. Removal of the solvent left 0.250 g (0.45 mmol, 46%) of a brown substance. The obtained product was found to be contaminated by minor amounts of impurities. NMR data are as reported in the literature.[5b]

Preparation of $Cp_2NbH(SnClMe_2)_2$ (8): 0.652 g (2.97 mmol) of Me_2SnCl_2 was added to a suspension of 0.819 g (1.48 mmol) of [$Cp_2NbH(SnMe_3)_2$] in 50 mL of diethyl ether and the resulting mixture was stirred overnight. The supernatant solution was then decanted and the residue was extracted with 30 mL of diethyl ether. All volatiles were removed in vacuo from the combined fractions to leave 0.777 g of a white crystalline substance. This material was washed with 15 mL of petroleum ether to ensure complete removal of Me_3SnCl and then recrystallized from diethyl ether. Yield: 0.547 g (0.92 mmol, 62%). − IR (Nujol): $\tilde{\nu}$ = 1664 cm^{-1} (Nb−H). − ^{1}H NMR ([D$_6$]benzene): δ = 4.58 [s + d, J(Sn−H) = 4.5 Hz, 10 H, Cp], 0.52 [s + d, ^2J(Sn−H) = 35.8 Hz, 12 H, Me], −4.78 [s + d, ^2J(Sn−H) = 280.0 Hz, 1 H, Nb−H]. − ^{13}C NMR ([D$_6$]benzene): δ = 88.0 (s, Cp), 5.2 (s, Me). − $C_{14}H_{23}Cl_2NbSn_2$ (592.77): calcd. C 28.38, H 3.91; found C 28.01, H 3.77.

Crystal Structure Determination of 9: Colourless crystals of **9** were grown from diethyl ether solution. A crystal of **9** of dimensions 0.22 × 0.16 × 0.12 mm was covered with oil and mounted at 150(2) K on a Siemens three-circle diffractometer equipped with an area CCD detector (SMART system). Crystal data: M_r = 592.77; monoclinic, space group $P2(1)/n$; a = 17.0123(3) Å, b = 8.31860(10) Å, c = 27.76540(10), β = 96.82°, Z = 8, V = 3901.48(8) Å^3, $d_{calcd.}$ = 2.018 gcm^{-3}. Data collection: 2θ range from 1.34° to 26.50°, *hkl* range −19 to 21, −10 to 8, −34 to 31; 25550 measured reflections, of which 8085 were considered as unique [R(int) = 0.0527]; analytical absorbtion correction based on Ψ scans (μ = 3.380 mm^{-1}, T_{max} = 0.6872, T_{min} = 0.5235). The structure amplitudes for the 8085 independent reflections were obtained after the usual Lorentz and polarization corrections. The structure was solved by direct methods[20] and refined by full-matrix least-squares procedures[21] against F^2. Only the reflections with $F_o^2 > 2\sigma F_o^2$ were used in the refinements (6371). Hydrogen atoms were found from the difference map and were refined isotropically. In the final cycles of the refinement, all non-hydrogen atoms were refined with anisotropic temperature parameters. $R1$ = 0.0351 and $wR2$ = 0.0553 (only observed reflections), and $R1$ = 0.0574 and $wR2$ = 0.0598 (all data); 528 parameters, $GooF$ = 1.121. The largest peak in the final difference Fourier map had an electron density of 0.704 e·Å^{-3}, while the lowest hole had a value of −0.764 e·Å^{-3}. The location and magnitude of the residual electron density was of no chemical significance. Further details of the crystal structure investigation may be obtained from the Cambridge Crystallographic Data Centre on quoting the depository number (CCDC-105593), the names of the authors, and the full journal citation.

Acknowledgments

Support of this research by the Russian Fund for Basic Research is gratefully acknowledged.

[1] [1a] G. I. Nikonov, D. A. Lemenovskii, J. Lorberth, *Organometallics* **1994**, *13*, 3127. − [1b] G. I. Nikonov, L. G. Kuzmina, P. Mountford, D. A. Lemenovskii, *Organometallics* **1995**, *14*, 3588. − [1c] G. I. Nikonov, L. G. Kuzmina, Yu. K. Grishin, D. A. Lemenovskii, N. B. Kazennova, *J. Organomet. Chem.* **1997**, *547*, 183. − [1d] G. I. Nikonov, K. Harms, J. Lorberth, D. A. Lemenovskii, *Inorg. Chem.* **1995**, *34*, 2461. − [1e] G. I. Nikonov, A. J. Blake, J. Lorberth, D. A. Lemenovskii, S. Wocadlo, *J. Organomet. Chem.* **1997**, *547*, 235. − [1f] G. I. Nikonov, D. A. Lemenovskii, J. Lorberth, *Polyhedron* **1996**, *15*, 1565. − [1g] G. I. Nikonov, L. G. Kuzmina, J. A. K. Howard, *Organometallics* **1997**, *16*, 3723.

[2] G. I. Nikonov, E. V. Avtomonov, W. Massa, *Chem. Ber.* **1997**, *130*, 1629.

[3] [3a] G. I. Nikonov, L. G. Kuzmina, D. A. Lemenovskii, V. V. Kotov, *J. Am. Chem. Soc.* **1995**, *117*, 10133. − [3b] G. I. Nikonov, L. G. Kuzmina, D. A. Lemenovskii, V. V. Kotov, *J. Am. Chem. Soc.* **1996**, *118*, 6333 [corr.]. − [3c] G. I. Nikonov, S. F.

Vyboishchikov, L. G. Kuzmina, D. A. Lemenovskii, J. A. K. Howard, *Chem. Eur. J.*, accepted.
[4] T. M. Arkhireeva, B. M. Bulychev, A. N. Protsky, G . L. Soloveichik, V. K. Bel′sky, *J. Organomet. Chem*. **1986**, *317*, 33.
[5] [5a] M. L. H. Green, A. K. Hughes, P. Mountford, *J. Chem. Soc., Dalton Trans.* **1991**, 1699. – [5b] M. L. H. Green, A. K. Hughes, P. Mountford, *J. Chem. Soc., Dalton Trans.* **1991**, 1407.
[6] F. N. Tebbe, *J. Am. Chem. Soc.* **1973**, *96*, 5412.
[7] T. M. Arkhireeva, B. M. Bulychev, A. N. Protsky, G. L. Soloveichik, V. K. Bel′sky, *Koord. Khimiia* **1987**, *13*, 986.
[8] V. V. Skripkin, O. G. Volkov, A. A. Pasynskii, A. S. Antyshkina, L. M. Dikareva, V. N. Ostikova, M. A. Porai-Koshits, S. L. Davydova, S. G. Sakharov, *J. Organomet.Chem*. **1984**, *263*, 345.
[9] A. N. Protsky, B. M. Bulychev, G. L. Soloveichik, V. K. Bel′sky, *Inorg. Chim. Acta* **1986**, *115*, 121.
[10] M. L. H. Green, A. K. J. Hughes, *J. Organomet. Chem*. **1996**, *506*, 221.
[11] [11a] D. C. Pestana, T. S. Koloski, D. H. Berry, *Organometallics* **1994**, *13*, 4173. – [11b] L. K. Figge, P. J. Carroll, D.H. Berry, *Organometallics* **1996**, *15*, 209.
[12] V. K. Bel′sky, A. N. Protsky, B. M. Bulychev, G. L. Soloveichik, *Doklady AN SSSR, Chem.* **1986**, *287*, 857; *Chem. Abstr.* **1987**, *106*, 50365a.
[13] H. A. Bent, *Chem. Rev.* **1961**, *61*, 275.
[14] A. K. Hughes, Ph. D. Thesis, Oxford University, **1990**.
[15] D. H. Harris, S. A. Keppie, M. F. Lappert, *J. Chem. Soc., Dalton Trans.* **1973**, 1653.
[16] M. Leech, J. A. K. Howard, L. G. Kuzmina, G. I. Nikonov, manuscript in preparation.
[17] V. I. Bakhmutov, E. V. Vorontsov, G. I. Nikonov, D. A. Lemenovskii, *Inorg. Chem.* **1998**, *37*, 279.
[18] U. Schubert, E. Kunz, B. Harkers, J. Willnecker, J. Meyer, *J. Am. Chem. Soc.* **1989**, *111*, 2572.
[19] Q. Jiang, P. J. Carroll, D. H. Berry, *Organometallics* **1991**, *10*, 3648.
[20] G. M. Sheldrick, "SHELXS-86, Program for Crystal Structure Solution", *Acta Crystallogr.* **1990**, *146*, 467.
[21] G. M. Sheldrick, *SHELXTL-96, Program for Crystal Structure Refinement*, Universität Göttingen, **1996**.

Received November 3, 1998
[I98377]

Lead(II) and Bismuth(III) Complexes with Macrocyclic Ligands

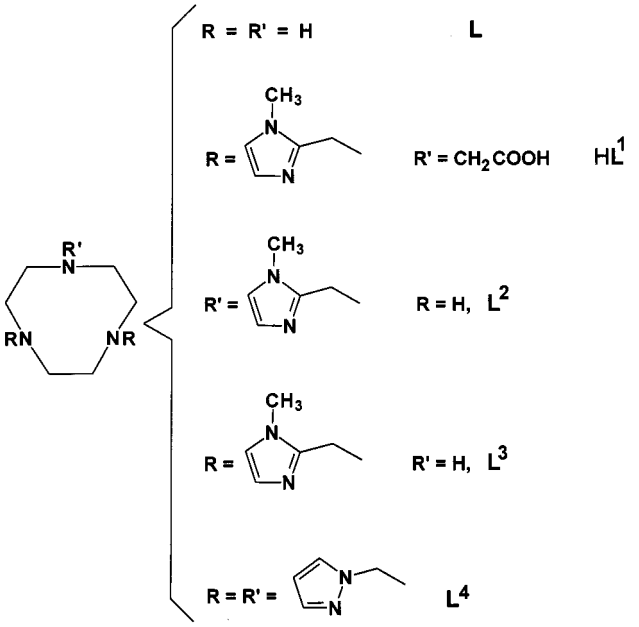
Massimo Di Vaira,[a] Fabrizio Mani,*[a] and Piero Stoppioni[a]

Keywords: Lead / Bismuth / Coordination chemistry / Macrocyclic ligands / Tetraphenylborate–lead(II) interaction

The preparation and X-ray characterization of a Pb^{2+} and a Bi^{3+} complex formed with macrocyclic ligands are reported. In the dimeric complex $[\{Pb(CH_3COO)\mathbf{L}BPh_4\}_2]$, where **L** is 1,4,7-triazacyclononane, the metal atoms are chelated by **L** and bridged by an acetate group; moreover, each of the metal atoms is at contact distance from a tetraphenylborate phenyl group, which completes the coordination. The unsymmetrically derivatized macrocycle 1-carboxymethyl-4,7-bis(1-methylimidazol-2-ylmethyl)-1,4,7-triazacyclononane ((AUTHOR: Substituents are alphabetized: c before m!)), $\mathbf{HL^1}$, in its deprotonated ($\mathbf{L^1}$, anionic) form gives the complex of formula $BiCl\mathbf{L^1}BPh_4$ with Bi^{3+}, which contains $[BiCl\mathbf{L^1}]_2^{2+}$ dimeric cations with eight-coodinated Bi^{3+} and bridging acetate groups within the dimer.

Lead is a persistent and ubiquitous toxic metal, and soil contamination by lead is widespread owing to several industrial activities, mainly battery making and recycling, oil refining, and paint manufacturing.[1] Amongst the techniques for lead-contaminated soil remediation that are being investigated, the removal of the contaminant by chelation is apparently the environmentally most sound.[2]

Within the field of the coordination chemistry of lead(II) we are interested in the synthesis and characterization of its complexes with functionalized macrocycles. In the course of these studies we have found that lead(II) coordinated to 1,4,7-triazacyclononane bearing one, two, or three appended groups ($\mathbf{L^2}$, $\mathbf{L^3}$, $\mathbf{L^4}$) (Scheme 1) further interacts in an η^6-C_6H_5 fashion with a phenyl group of a BPh_4^- anion.[3][4] These results show that the contact interaction of BPh_4^- with lead(II), although unprecedented, is not fortuitous as long as functionalized macrocycles of the above nature are employed. With the aim of further investigating the conditions that make the BPh_4^- interaction with a metal ion feasible, we have prepared a lead(II) complex with the unsubstituted macrocycle 1,4,7-triazacyclononane **L** in the presence of $NaBPh_4$. In the course of investigations into an analogous trend in bismuth(III) complexes we have prepared a Bi^{3+} complex of the unsymmetrically substituted 1,4,7-triazacyclononane $\mathbf{HL^1}$ ligand (Scheme 1). Bismuth(III) is isoelectronic with lead(II) and possesses a similar electronegativity value, but has a smaller ionic radius than lead(II): 103 pm and 119 pm for six-coordinate species.[5] Bismuth and its compounds are regarded as less toxic than lead and have been widely used in traditional medicine.[6] More recently, compounds of bismuth(III) have gained considerable importance because of their potential applications in therapy of cancer[7] (^{212}Bi radioactive isotope) and gastric ulcers,[8] as well as in the technology of high-temperature superconductors.[9] For all these reasons the coordination chemistry of lead(II) and bismuth(III) has attracted increasing attention in recent years, particularly in the search for chelating ligands that may function as efficient metal-sequestring agents (Pb^{2+})[10] and for possible applications in biomedical science (Bi^{3+}).[11–13]



Scheme 1. Ligands referred to in the text

We report here the syntheses and X-ray structural characterizations of the two complexes $[Pb(CH_3COO)\mathbf{L}BPh_4]$ (**1**) (**L** = 1,4,7-triazacyclononane) and $[BiCl\mathbf{L^1}BPh_4]$ (**2**) [$\mathbf{L^1}$ is the deprotonated form of the compound 1-carboxymethyl-4,7-bis(1-methylimidazol-2-ylmethyl)-1,4,7-triazacyclononane, $\mathbf{HL^1}$].

Results and Discussion

The reaction of lead(II) acetate with the cyclic triamine 1,4,7-triazacyclononane **L** and $NaBPh_4$ in MeOH/MeCN solution produces colourless crystals of a compound with the formula $Pb(CH_3COO)\mathbf{L}BPh_4$ (**1**) where a BPh_4^- anion has replaced an acetate anion of the starting $Pb(CH_3COO)_2 \cdot 3\,H_2O$ salt. Two lead(II) complexes formed

[a] Dipartimento di Chimica, Università di Firenze, Via Maragliano 77, I-50144 Florence, Italy

 © WILEY-VCH Verlag GmbH, D-69451 Weinheim, 1999 1434–1948/99/0505–0833 $ 17.50+.50/0

by the **L** macrocycle, Pb**L**$(ClO_4)_2$ and Pb**L**$(NO_3)_2$, have been described previously[14] and their X-ray structural characterizations have shown that, in addition to the **L** macrocycle, both anions are coordinated to lead(II) in each complex, giving rise to highly irregular coordination polyhedra. In order to establish the possible role of the BPh_4^- anion in the coordination of the metal atom in complex **1**, the structure of the compound has been determined. Partly for comparison purposes $BiCl_3$ (Bi^{3+} is isoelectronic with Pb^{2+}) was allowed to react with the macrocycles, shown in Scheme 1, in the presence of $NaBPh_4$. A crystalline product was obtained only when the unsymmetrically functionalized macrocycle 1-carboxymethyl-4,7-bis(1-methylimidazol-2-ylmethyl)-1,4,7-triazacyclononane (**HL^1**) containing an appended acetate group in addition to methylimidazoles, was employed. The complex obtained had the formula Bi**Cl**$\mathbf{L^1}BPh_4$ (**2**) (**L^1** is the anionic form of the **HL^1** ligand) and its crystal structure was determined by X-ray diffraction. The affinity of bismuth(III) for nitrogen donors is considered to be significant and, in particular, larger than that of lead(II).[12][15] In agreement with this, in the formation of **2** most bonds within the $BiCl_3$ reactant are broken and the available coordination sites about the metal centre are occupied by the donor atoms of the macrocyclic ligand, which are predominantly nitrogen atoms. On the other hand, when ligands with uncharged oxygen donors, such as the 4,5,6-donor crown ether, are employed,[13] the $BiCl_3$ unit is found to remain intact and neutral complexes are obtained with non-coordinated oxygen atoms.

The structure of complex **1** consists of $[Pb(CH_3COO)\mathbf{L}BPh_4]_2$ dimers where the monometal fractions, related by a twofold symmetry axis, are joined by an acetate anion in a disordered orientation (Figure 1). Each lead(II) atom is coordinated by the three nitrogen atoms of the macrocycle and by three oxygen atoms from the acetate groups, which have fractional occupancies. In addition, the lead(II) atom is approached at contact distance by a tetraphenylborate phenyl group in a similar fashion to that previously detected for lead(II) complexes formed by the **L** macrocycle bearing various substituents.[3][4] The distance of 3.37(1) Å between the metal atom and the phenyl centroid is within the range (3.06−3.44 Å) of the distances previously found. Each of the acetate anions in the dimer is randomly distributed between two positions related by the symmetry axis. As detailed in the Experimental Section, all fractions of the acetate anions have been assigned a population parameter of 0.5. As a consequence of this, and also given the fact that the position of the bridging (fractional) oxygen atom [O(1)] almost coincides with that of its symmetry-related fraction, the lead(II) atom is surrounded by an oxygen site having full occupancy [O(1) + O(1)′; symmetry operation $1 - x$, y, $1/2 - z$] and by two half-occupied sites [O(2) and O(3)]. The acetate group in the bridging position is also chelating the metal atom through O(1) and O(2), whereas the other group is essentially non-chelating, since its O(4) atom lies at a considerably longer distance from the metal centre than the coordinating O(3) atom (Table 1). In agreement with the arrangement found for the four structures previously investigated, which exhibit a close approach of a phenyl group to the metal atom,[3][4] one macrocycle nitrogen, N(1) in **1**, lies almost *trans* to the phenyl ring while the other two N and the fractional O donors are approximately arranged in a plane almost perpendicular to the N(1)−ring centroid direction. As described previously,[3][4] the metal atom is displaced from that plane in the direction of the phenyl group. The Pb−N distances formed by the unsubstituted triazamacrocycle (mean value 2.50 Å) are shorter than those formed by the macrocycle nitrogen atoms when **L** be-

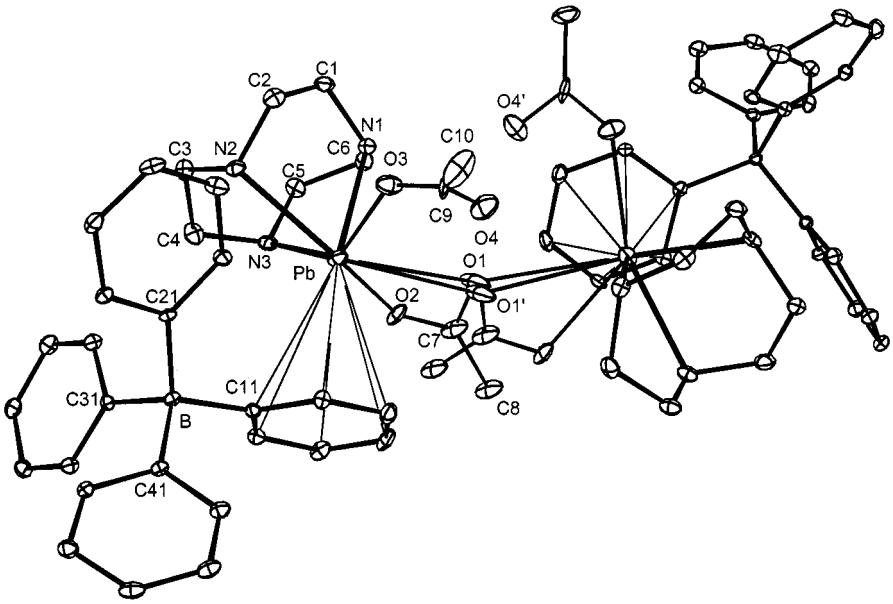


Figure 1. A view of the $[Pb(CH_3COO)\mathbf{L}BPh_4]_2$ dimer in the structure of **1**, showing the atom numbering scheme; all atoms of the acetate groups have a population parameter of 0.5; hydrogen atoms are not shown and only the *ipso*-carbon atoms of phenyl rings are labeled for clarity; primed atoms are related to the corresponding unprimed ones through a twofold symmetry axis

ars substituents (2.52−2.81 Å, range of individual values),[3][4] but are longer than the distances (mean 2.43 Å) found for the two lead(II) complexes formed by the same **L** macrocycle and the coligands with limited space demands ClO_4^- and NO_3^-.[14] The Pb−O distances are in the range of those found for carboxylate complexes.[16]

Table 1. Selected bond lengths [Å] and angles [°] for compound **1**[a−c]

Pb−N(1)	2.423(8)	Pb−O(1)′[b]	2.92(4)
Pb−N(2)	2.558(7)	Pb−O(2)	2.46(1)
Pb−N(3)	2.509(8)	Pb−O(3)	2.60(1)
Pb−O(1)[b]	2.86(4)	Pb···O(4)	3.37(2)
N(1)−Pb−N(2)	70.0(3)	O(2)−Pb−N(1)	86.8(4)
N(1)−Pb−N(3)	70.0(3)	O(2)−Pb−N(2)	137.4(4)
N(2)−Pb−N(3)	68.5(3)	O(2)−Pb−N(3)	70.2(4)
O(1)−Pb−O(2)	38.4(5)	O(3)−Pb−N(1)	79.5(4)
O(1)−Pb−N(1)	76.6(1.3)	O(3)−Pb−N(2)	80.1(4)
O(1)−Pb−N(2)	146.5(1.3)	O(3)−Pb−N(3)	141.8(4)
O(1)−Pb−N(3)	101.3(1.2)	Pb−O(1)−Pb′	149.1(4)

[a] All of the oxygen sites, belonging to the acetate anions, have 0.5 occupancy. Primed atoms are related to the corresponding unprimed ones by a twofold symmetry axis. − [b] The O(1) and O(1)′ sites are almost coincident and together provide one full-occupancy donor atom site in the coordination sphere of each metal atom. − [c] The Pb···C contact distances with the phenyl group carbon atoms are in the range 3.54−3.79 Å.

In agreement with previous results,[3][4] extended Hückel calculations[17][18] on suitable model systems for **1** have shown that the lead(II) lone pair, forming the HOMO of the metal fragment, is neatly oriented away from the region of the "normally" coordinating ligands toward the centre of the phenyl group. This result is practically unaffected by changes to the model aimed at mimicking the partial acetate anion occupancies. Calculations of this type do not account for charge effects and provide rather indirect evidence for the polarization effects that are expected to contribute significantly to the attractive interaction. On the other hand, such calculations stress the repulsive contribution originating from the interaction between the lone pair and the bonding system of the phenyl group. That repulsive contribution is minimized if the lone pair points toward the centre of the phenyl group, as has been shown to occur by the calculations for all five cases investigated. Although the lead(II)/phenyl group interaction under discussion should be considered as a van der Waals interaction augmenting the non-specific ionic component, its surprisingly high strength is revealed by the fact that it appears to be one of the factors that control the packing in the solid state for the compounds in which it has been detected.

Although, in principle, the type of interaction with the tetraphenylborate anion discussed above might be expected to also occur in the bismuth compound **2**, it was found not to be present in that case, probably due to lower extension of the bismuth(III) lone pair compared to that of lead(II) and to the greater importance of ionic interactions in the structure of the bismuth complex. The structure consists of centrosymmetric dimeric $[BiCl\mathbf{L^1}]_2^{2+}$ cations and isolated BPh_4^- anions. Each metal atom is eight-coordinated by the three macrocycle nitrogen atoms and the two methylimidazole nitrogen atoms of the $\mathbf{L^1}$ ligand, by two carboxylate oxygen atoms from different ligands and by the chlorine atom (Figure 2). Each carboxylate group is bridging within the

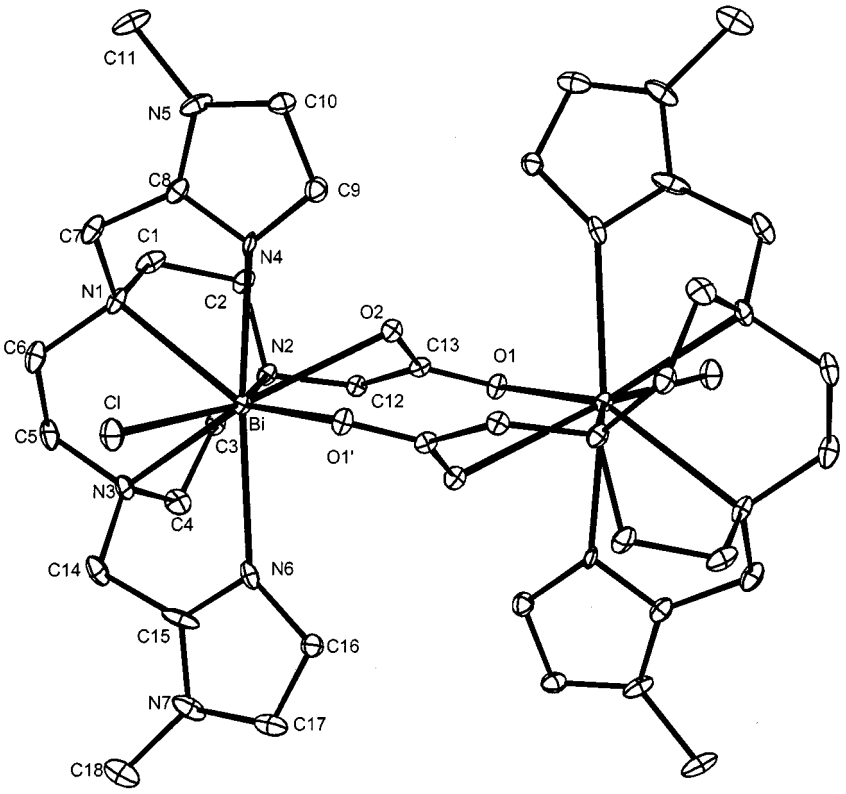


Figure 2. A view of the centrosymmetric $[BiCl\mathbf{L^1}]_2^{2+}$ cation in the structure of **2**; atom O1′ is related to O1 through the inversion centre

dimer, with its two oxygen atoms linked to the different metal atoms. There are five donor atoms [N(1), N(3), N(4), N(6), and O(1)′, symmetry operation $-x, -y, -z$] lying approximately in a plane that also contains the metal atom, with the largest deviations from the plane being < 0.4 Å. The chlorine atom and the midpoint of the two remaining donor atoms N(2) and O(2) define a direction perpendicular to the above plane. Although close comparisons between the present structures are not possible, it is worth noting that the mean value of the distances to the metal centre formed by the macrocycle nitrogen atoms is larger in **2** by 0.22 Å in comparison to **1**, whereas that of the metal−oxygen distances is smaller by 0.14 Å in **2**. These features may again reveal the effect of substituents on the macrocyclic ring, discussed above for the metal−nitrogen interactions in lead(II) compounds, but they may also be due to a higher preference of bismuth(III) for bonds having appreciable ionic character, compared to lead(II). The conformation attained by the $\mathbf{L^1}$ ligand in the bismuth(III) complex differs from the more regular arrangement, approaching threefold symmetry, found for the same ligand in monometal complexes of first-transition-row metal ions.[19] On the other hand, it is not too dissimilar from the arrangement of the pyrazole-trisubstituted macrocycle in the lead(II) complex $Pb\mathbf{L^4}(BPh_4)_2$, where a BPh_4^- phenyl group makes a close approach to the metal atom.[4] By means of extended Hückel calculations on a model of the monometal fraction of the bismuth(III) complex where the environment of the metal atom was schematized in the usual ways,[3][4] with the coordination geometry accurately reproduced, it was verified that the HOMO of the complex essentially consists of the unhybridized metal s orbital, and therefore is without specific directional properties.

Table 2. Selected bond lengths [Å] and angles [°] for compound **2**

Bi−N(1)	2.63(1)	Bi−N(6)	2.54(1)
Bi−N(2)	2.72(1)	Bi−Cl	2.619(4)
Bi−N(3)	2.80(1)	Bi−O(1)′[a]	2.412(8)
Bi−N(4)	2.45(1)	Bi−O(2)	2.601(9)
N(1)−Bi−N(2)	69.0(3)	Cl−Bi−N(1)	81.1(3)
N(1)−Bi−N(3)	65.1(3)	Cl−Bi−N(2)	143.3(2)
N(2)−Bi−N(3)	63.9(3)	Cl−Bi−N(3)	84.7(3)
N(1)−Bi−N(4)	65.5(3)	Cl−Bi−N(4)	88.0(3)
N(3)−Bi−N(6)	62.6(3)	Cl−Bi−N(6)	85.3(3)
N(4)−Bi−N(6)	164.6(3)	Cl−Bi−O(1)′[a]	81.2(2)
O(1)′−Bi−O(2)[a]	75.9(3)	Cl−Bi−O(2)	150.3(2)

[a] The O(1)′ atom is related to O(1) by the inversion centre.

Experimental Section

All reagents were reagent grade. Commercial solvents, when required in the synthetic procedures, were dried according to standard methods and distilled just before use. Hydrated lead(II) acetate (Baker), anhydrous bismuth(III) chloride (Acros), and sodium tetraphenylborate (Baker) were used as received. **L**[20] and $\mathbf{HL^1}$[19] were prepared using procedures reported previously. General experimental methods and measuring techniques were as reported in ref.[19]

$Pb(CH_3COO)LBPh_4$ (1): The salt $Pb(CH_3COO)_2 \cdot 3\,H_2O$ (0.379 g, 1.00 mmol), dissolved in MeOH (20 mL), and a solution of **L** (0.129 g, 1.00 mmol) in MeCN (20 mL) were mixed together at reflux temperature with stirring. Sodium tetraphenylborate (0.684 g, 2.00 mmol) in MeCN (10 mL) was subsequently added to the above mixture and the resulting solution was concentrated nearly to dryness. The residue was redissolved in MeOH and, after addition of EtOH and concentration to a small volume at room temperature, colourless crystals of the complex were obtained. The crystals used for X-ray analysis were obtained by concentration at room temperature of a dilute acetonitrile solution of **1**. − $C_{32}H_{38}BN_3O_2Pb$ (714.65): calcd. C 53.8, H 5.36, N 5.88, found C 53.3, H 5.56, N 5.59. − IR (KBr): $\nu_{asym}(COO^-) = 1590\ cm^{-1}$.

$BiClL^1BPh_4$ (2): $NaBPh_4$ (0.684 g, 2.00 mmol), dissolved in Me_2CO (20 mL), was added with stirring to a boiling solution of anhydrous $BiCl_3$ (0.315 g, 1.00 mmol) and $\mathbf{HL^1}$ (0.376 g, 1.00 mmol) in MeOH (35 mL). On concentrating the resulting solution to a small volume, colourless crystals of **2** were obtained. Recrystallization of the complex from boiling MeCN gave crystals suitable for X-ray diffraction. − $C_{42}H_{48}BBiClN_7O_2$ (938.11): calcd. C 53.8, H 5.16, N 10.5, found C 53.1, H 5.22, N 10.2. − IR (KBr): $\nu_{asym}(COO^-) = 1580\ cm^{-1}$.

Crystal-Structure Analyses: X-ray diffraction data for both compounds were collected at room temperature with an Enraf Nonius CAD4 diffractometer with graphite-monochromated Mo-K_α radiation (λ = 0.71069 Å). Crystal data and details about structure refinements are given in Table 3. Empirical absorption corrections (ψ scans) were applied. The structures were solved by direct methods[21] and heavy-atom procedures.[22] In the structure of **1**, both acetate anions are distributed over two positions related by the twofold symmetry axis. The two images of the anion in bridging position [atoms O(1)−C(8)] overlap substantially (therefore they cannot exceed the population parameter value 0.5), whereas those of the other anion [O(3)−C(10)] lie apart and may not be mutually exclus-

Table 3. Crystal data, data collection and structure refinement for compounds **1** and **2**

Formula	$C_{32}H_{38}BN_3O_2Pb$ (**1**)	$C_{42}H_{48}BBiClN_7O_2$ (**2**)
M	714.65	938.11
Crystal system	monoclinic	triclinic
Space group	*C*2/*c* (No. 15)	$P\bar{1}$ (No. 2)
a [Å]	33.708(8)	11.454(9)
b [Å]	10.640(2)	13.851(7)
c [Å]	17.748(3)	14.111(5)
α [°]	90	105.31(4)
β [°]	105.70(2)	94.29(5)
γ [°]	90	103.33(5)
V [Å^3]	6128(2)	2079(2)
Z	8	2
$D_{calcd.}$ [g cm^{-3}]	1.549	1.499
Crystal size [mm]	0.20 × 0.35 × 0.50	0.20 × 0.40 × 0.60
μ [mm^{-1}]	5.54	4.35
Collection range [°]	$5 \le 2\theta \le 50$	$5 \le 2\theta \le 50$
Collected refl.	5612	8278
Independent refl.	5377	7287
Obsd. with $I > 2\sigma(I)$	3274	5581
R(int.)	0.037	0.059
No. of parameters	394	489
No. of restraints	18	0
Goodness of fit	1.027	1.096
*R*1 (4)	0.046	0.063
*R*1 (all data)	0.103	0.098
*wR*2	0.134	0.202
Largest res. peak and hole [e/Å]	0.84 and −0.96	2.61 and −1.12

ive, the shortest contact between the two images being O(4)···O(4)′ = 2.55 Å. The possibility that the O(1)−C(8) sites might have an occupancy < 0.5 with the complementary value for the sites O(3)−C(10) could be excluded on the basis of the results (*R* values, thermal parameters values) of test refinements; then, all acetate fractions were assigned the population parameter 0.5. In the final refinement cycles, on F_o^2, all non-hydrogen atoms were refined anisotropically and H atoms were refined using a riding model. Crystallographic data (excluding structure factors) for the structures reported in this paper have been deposited with the Cambridge Crystallographic Data Centre as supplementary publications no. CCDC-106167 (**1**) and -106169 (**2**). Copies of the data can be obtained free of charge on application to CCDC, 12 Union Road, Cambridge CB2 1EZ, UK [Fax: + 44-1223/336-033, E-mail: deposit@ccdc.cam.ac.uk].

Acknowledgments

We acknowledge financial support by the Italian Ministero dell′Università e della Ricerca Scientifica e Tecnologica.

[1] M. J. Hynes, B. Jonson, *Chem. Soc. Rev.* **1997**, *26*, 133; J. M. Ratcliffe, *Lead in Man and Environment*, Wiley, New York, **1981**; G. G. S. Holmgren, M. W. Meyer, R. L. Chaney, R. B. Daniels, *J. Environ. Qual.* **1993**, *22*, 335; S. Krishnamurthy, *Environ. Prog.* **1992**, *11*, 256.
[2] G. C. Rampley, K. L. Ogden, *Environ. Sci. Technol.* **1998**, *32*, 987; B. E. Reed, P. C. Carriere, R. Moore, *J. Environ. Eng.* **1996**, *122*, 48; K. Abu-Dari, F. E. Hahn, K. N. Raymond, *J. Am. Chem. Soc.* **1990**, *112*, 1519.
[3] M. Di Vaira, F. Mani, P. Stoppioni, *J. Chem. Soc., Dalton Trans.* **1998**, 3209.
[4] M. Di Vaira, M. Guerra, F. Mani, P. Stoppioni, *J. Chem. Soc., Dalton Trans.* **1996**, 1173.
[5] N. N. Greenwood, A. Earnshaw, *Chemistry of the Elements*, Pergamon Press, Oxford, **1984**, pp. 430, 642.
[6] *Comprehensive Coordination Chemistry* (Eds.: G. Wilkinson, R. D. Gillard, J. A. McCleverty), Pergamon, London, **1987**, vol. 3, p. 292.
[7] M. D. Manhart, *Rev. Infect. Dis.* **1990**, *12*, S11; R. W. Kozak, T. A. Waldmann, R. W. Atcher, O. A. Gansow, *Trends Biotechnol.* **1985**, *4*, 259.
[8] G. F. Baxter, *Chem. Br.* **1992**, *28*, 445.
[9] A. W. Sleight, *Science* **1990**, *247*, 656.
[10] D. L. Reger, J. E. Collins, A. L. Rheingold, L. M. Liable-Sands, G. P. A. Yap, *Inorg. Chem.* **1997**, *36*, 345; J. Parr, A. T. Ross, A. M. Z. Slawin, *J. Chem. Soc., Dalton Trans.* **1996**, 1509; A. Andres, A. Bencini, A. Carachalios, A. Bianchi, P. Dapporto, E. Garcia-España, P. Paoletti, P. Paoli, *J. Chem. Soc., Dalton Trans.* **1993**, 3507; K. Abu-Dari, T. B. Karpishin, K. N. Raymond, *Inorg. Chem.* **1993**, *32*, 3052; D. L. Reger, M. F. Huff, A. L. Rheingold, B. S. Haggerty, *J. Am. Chem. Soc.* **1992**, *114*, 579.
[11] J. A. Parkinson, H. Sun, P. J. Sadler, *J. Chem. Soc., Chem. Commun.* **1998**, 881; R. Luckay, I. Cukrowski, J. Mashishi, J. H. Reibenspies, A. H. Bond, R. D. Rogers, R. D. Hancock, *J. Chem. Soc., Dalton Trans.* **1997**, 901; E. Asato, K. Katsura, M. Mikuriya, U. Turpeinen, I. Mutikainen, J. Reedijk, *Inorg. Chem.* **1995**, *34*, 2447; S. P. Summers, K. A. Abboud, S. R. Farrah, G. J. Palenik, *Inorg. Chem.* **1994**, *33*, 88; E. Asato, W. L. Driessen, R. A. G. de Graaff, F. B. Hulsbergen, J. Reedijk, *Inorg. Chem.* **1991**, *30*, 4210.
[12] R. D. Hancock, I. Cukrowski, J. Baloyi, J. Mashishi, *J. Chem. Soc., Dalton Trans.* **1993**, 2895.
[13] R. D. Rogers, A. H. Bond, S. Aguinaga, *J. Am. Chem. Soc.* **1992**, *114*, 2960.
[14] K. Wieghardt, M. Kleine-Boymann, B. Nuber, J. Weiss, L. Zsolnai, G. Huttner, *Inorg. Chem.* **1986**, *25*, 1647.
[15] I. Cukrowski, F. Marsicano, R. D. Hancock, T. T. Tshetlo, W. A. L. van Otterlo, *Polyhedron* **1995**, *14*, 1661.
[16] Ref.[4] and refs. cited therein.
[17] R. Hoffman, *Angew. Chem. Int. Ed. Engl.* **1990**, *67*, 399.
[18] *CACAO*: C. Mealli, D. M. Proserpio, *J. Chem. Educ.* **1990**, *13*, 2429.
[19] M. Di Vaira, F. Mani, P. Stoppioni, *Inorg. Chim. Acta* **1998**, *273*, 151.
[20] T. J. Atkins, J. E. Richman, W. F. Oettle, *Org. Synth.* **1978**, *58*, 86; K. Wieghardt, W. Schmid, B. Nuber, J. Weiss, *Chem. Ber.* **1978**, *112*, 2220.
[21] *SIR92*: A. Altomare, M. C. Burla, M. Camalli, G. Cascarano, C. Giacovazzo, A. Guagliardi, G. Polidori, *J. Appl. Crystallogr.* **1994**, *27*, 435.
[22] G. M. Sheldrick, *SHELXL 93, Program for Crystal Structure Refinement*, University of Göttingen, **1993**.

Received November 3, 1998
[I98379]

Synthesis and Crystal Structure of $[Re_2Br_4(Te_2)(TeBr)_2(TeBr_2)_2]$, a Dinuclear Complex with Te_2^{2-}, $TeBr^-$, and $TeBr_2$ Ligands

Johannes Beck*[a] and Klaus Müller-Buschbaum[a]

Keywords: Rhenium / Tellurium / Bromine compounds / Dinuclear rhenium complex / Crystal structure

The reaction of $ReBr_4$, Te and $TeBr_4$ in $SiBr_4$ as solvent in a sealed glass ampoule at 150 °C yields black crystals of $Re_2Te_6Br_{10}$. As the X-ray crystal structure determination shows [monoclinic, $P2_1$, $Z = 2$, $a = 1127.5(1)$, $b = 861.85(9)$, $c = 1231.0(2)$pm, $\beta = 105.47(9)°$], the structure consists of discrete dinuclear complexes. A Re–Re dumb-bell with d(Re–Re) = 279.9 pm is coordinated by a μ-Te_2 group and two μ-TeBr groups. Additionally, each Re atom is coordinated to two terminal bromine atoms and a $TeBr_2$ ligand leading to the formula $[Re_2Br_4(Te_2)(TeBr)_2(TeBr_2)_2]$. $Re_2Te_6Br_{10}$ is one of only a few compounds known in the ternary system Re/Te/Br.

Introduction

In lower oxidation states rhenium is known to form dinuclear complexes with multiple Re−Re bonds as well as a large variety of clusters.[1] Among the rhenium chalcogenide halides hexanuclear octahedral cluster compounds are predominant,[2] but trinuclear triangular clusters like $Re_3E_7X_7$ (E = S, Se; X = Cl, Br)[3−5] and tetranuclear clusters like $Re_4S_4Te_4$[6] or $[Re_4(\mu_3\text{-}Te)_4(TeBr_2)_4Br_8]$ with a Re_4Te_4 heterocubane core[7] are known, too.

In the ternary system Re/Te/Br only very few compounds are known so far. Two examples of hexanuclear clusters were reported, $[Re_6Te_8(TeBr_2)_6]Br_2$[8], $Re_6Te_4Br_{10}$,[9] and the above-mentioned tetranuclear complex $[Re_4(\mu_3\text{-}Te)_4(TeBr_2)_4Br_8]$. Recently, we discovered that $ReCl_4$, Te and $TeCl_4$ yield $Te_8[ReCl_6]$.[10] We extended our synthetic attempts to the reactions of $ReBr_4$ with elemental chalcogen and its tetrabromides. Here we report the synthesis and crystal structure of a new dinuclear complex containing unusual ligands.

Results and Discussion

Synthesis

The reaction of $ReCl_4$, Te and $TeCl_4$ leads to $Te_8[ReCl_6]$ and is carried out in a sealed, evacuated ampoule at 230°C under the conditions of the chemical vapor transport.[10] All attempts to obtain polycation-containing compounds starting from $ReBr_4$, Te and $TeBr_4$ failed. The only crystalline material which could be identified was Re_3Br_9.[11][12] The use of $SiBr_4$ as solvent allowed a moderate reaction temperature of 150°C and proved to be successful for the synthesis of a ternary compound. Within two weeks black cuboid crystals of $Re_2Te_6Br_{10}$ were deposited from the solution besides silvery crystals of tellurium.

$$4\ ReBr_4 + 11\ Te + TeBr_4 \xrightarrow{SiBr_4} 2\ Re_2Te_6Br_{10}$$

An excess of tellurium was found to be necessary for the formation of the ternary phase. In other solvents like $SnBr_4$ or S_2Br_2, $Re_2Te_6Br_{10}$ was not obtainable.

Crystal Structure

The crystal structure is built of discrete molecular complexes with the formula $Re_2Te_6Br_{10}$ (Figure 1). Central unit is an Re−Re dumb-bell coordinated by a Te_2 group and two TeBr groups, bridging both Re atoms. Additionally, each Re atom has two terminal Br ligands. The coordination sphere is completed by two $TeBr_2$ molecules, bound to each Re atom. The Re−Re distance is 279.9(2) pm which represents a weak bond. In Re^{III} halides containing an Re_3 triangle with a formal Re−Re double bond, distances between 245 and 250 pm are observed.[11][13] However, the Re−Re distance in $Re_2Te_6Br_{10}$ is in good agreement with $[Re_4Te_4(TeBr_2)_4Br_8]$, for which 277.4 pm and 283.1 pm were found.[7] The angles Re−Te−Re are all in the range from 61.9 to 64.2° and thus notably acute. In the complex $[(\mu\text{-}Te)\{Cp^*Re(CO)_2\}_2]$, which contains a comparable Re−Te−Re unit, this angle is 71.8° and the Re−Re distance 314 pm.[14] Apparently, steric hindrance and the requirements for orbital overlap in the Re−Te−Re units are limiting factors for the Re−Re distances. All Re−Te bonds in $Re_2Te_6Br_{10}$ are in the narrow range from 261.7(2) to 273.5(2) pm. The Te(3)−Te(4) distance in the Te_2 group is 268.7(4) pm, slightly shorter than a Te−Te single bond of 275 pm, but comparable to other compounds containing Te_2 groups, e.g. $Nb_2Te_2X_6$ (X = Br, I) with 267.0 and 268.5 pm.[15] The distance Te(2)−Te(5) is 324.9(3) pm, indicating only a very weak interaction and the absence of a second Te_2 group. Two Br atoms are bound to Te(2) and Te(5) with Te−Br distances of 260.9(4) and 264.5(5) pm. Thus, $Re_2Te_6Br_{10}$ contains two TeBr groups, a type of ligand

[a] Institut für Anorganische und Analytische Chemie der Justus-Liebig-Universität,
Heinrich-Buff-Ring 58, D-35392 Gießen, Germany
Fax: (internat.) + 49(0)641/99-34109
E-mail: johannes.beck@anorg.chemie.uni-giessen.de

 © WILEY-VCH Verlag GmbH, D-69451 Weinheim, 1999 1434−1948/99/0505−0839 $ 17.50+.50/0

which so far has been only observed in $Mo_4Te_7Br_8$, and as the analogous TeCl groups in $Mo_4Te_7Cl_8$.[16]

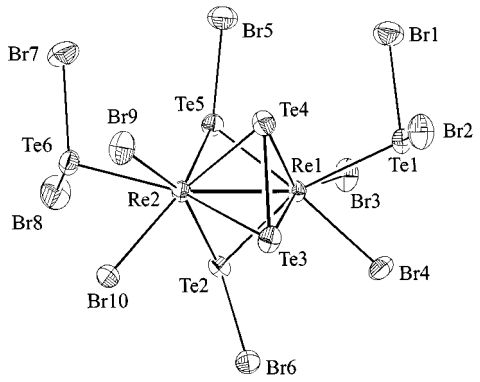


Figure 1. The structure of the molecular complex $[Re_2Br_4(Te_2)(TeBr)_2(TeBr_2)_2]$; thermal ellipsoids are drawn at a 50% probability level[27]

$TeBr_2$ is unstable in the solid state,[17] but can be stabilized by coordination, which was already shown in the structures of $[Re_4(\mu_3\text{-}Te)_4(TeBr_2)_4Br_8]$[7] and $[Re_6Te_8(TeBr_2)_6]Br_2$.[8] With mean Te−Br bond lengths of 252.6 pm and Br−Te−Br angles of 96.7° the conformation of the coordinated $TeBr_2$ molecules in the structure of $Re_2Te_6Br_{10}$ is quite similar to that in the gas phase (251 pm and 98°).[18]

Together with the two terminal Br ligands each Re atom is sevenfold coordinated in a piano-stool fashion. The bonding in the complex can be rationalized by an ionic formula. Counting the terminal bromine ligands as Br^-, the Te_2 groups as Te_2^{2-}, the TeBr groups as $TeBr^-$ and thus analogous to a hypochlorite ion, and the $TeBr_2$ ligands as neutral molecules, one obtains the ionic formula $[(Re^{4+})_2(Br^-)_4(Te_2^{2-})(TeBr^-)_2(TeBr_2)_2]$. This formula is consistent with the assumption of a bonding Re−Re interaction. The presence of Re^{4+} has also been suggested for the heterocubane cluster $[Re_4Te_4(TeBr_2)_4Br_8]$. The mean Re−Br bond lengths between the central atom and the terminal bromide ligands generally are very sensitive to changes in the oxidation state of the central atom. Figure 2 shows the arrangement of the molecules in the unit cell.

Molybdenum and tungsten form a class of dinuclear chalcohalide complexes of the general formula $M_2E_6X_{10}$ (M = Mo, W; E = S, Se, Te; X = Cl, Br).[19][20] Although the formula is analogous to $Re_2Te_6Br_{10}$, these complexes are not isostructural. Mo and W compounds contain two E_2^{2-} groups, three terminal halide ligands for each metal atom and two EX_2 molecules connected with the metal atoms through the chalcogen atoms, but no TeX^- groups. Therefore, the ionic formula is $[(M^{5+})_2(X^-)_6(E_2^{2-})_2(EX_2)_2]$. The significant difference between this family of complexes and $Re_2Te_6Br_{10}$ lies in the function of two halide ligands. In the Mo and W complexes they act as terminal ligands bound to the metal atoms resulting in a coordination number of eight for Mo/W, while in $Re_2Te_6Br_{10}$ they are bound to the Te atoms of a "former" Te_2 group with the consequence of loss of the Te−Te bond and the formation of the unusual $TeBr^-$ ligands.

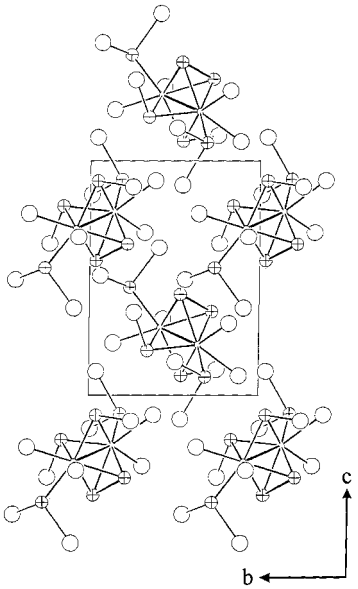


Figure 2. The unit cell of $[Re_2Br_4(Te_2)(TeBr)_2(TeBr_2)_2]$ in a view along the *a* axis showing the noncentrosymmetry of the structure; rhenium atoms are shown as small, bromine atoms as large white circles, tellurium atoms as cross-hatched circles

Experimental Section

General: Tellurium (Alfa Chemicals) was sublimed before use, $TeBr_4$ was prepared from the elements,[21] using bromine (Riedel-

Table 1. Crystal data, details of the diffraction data collection and structure analysis for $Re_2Te_6Br_{10}$

Formula	$Re_2Te_6Br_{10}$
Molecular mass [g mol^{-1}]	1937.1
Crystal system	monoclinic
Space group	$P2_1$
a [pm]	1127.5(1)
b [pm]	861.95(9)
c [pm]	1231.0(2)
β [°]	105.47(9)
Z	2
Density (calculated) [g cm^{-3}]	5.58
μ (Mo-K_α) [cm^{-1}]	325.4
Temperature [K]	293(2)
Scan range (2 θ) [°]	3.3, 52.1
hkl range	−13 to 13, −10 to 10, −15 to 15
Measured reflections	7204
Reflections without overlap with second twin individual	4176
Unique reflections	2525
Data for refinement	2525
Parameters refined	163
Flack parameter	0.037(20)
ρ[a]; max./min. [e pm^{-3} 10^{-6}]	+3.51/−2.30
$R(\|F\|)$[b]	0.065
$R(\|F\|)$[b]; $I > 2\,\sigma(I)$	0.063
$wR(F^2)$[c]	0.167

[a] Largest final difference hole and peak. − [b] $R(|F|) = (\Sigma||F_o| - |F_c||)/\Sigma|F_o|$. − [c] $wR(F^2) = \{\Sigma[w(F_o^2 - F_c^2)^2]/\Sigma[w(F_o^2)]\}$.

Table 2. Selected distances [pm] and angles [°] between atoms of $[Re_2Br_4(Te_2)(TeBr)_2(TeBr_2)_2]$

Atoms	Distance [pm]	Atoms	Distance [pm]	Atoms	Distance [pm]	Atoms	Distance [pm]
Re1−Re2	279.9(2)	Re1−Te2	262.4(3)	Re1−Te5	264.7(3)	Re1−Te4	267.3(3)
Re1−Te1	270.0(3)	Re1−Te3	273.5(2)	Re2−Te5	261.7(2)	Re2−Te2	264.5(3)
Re2−Te4	269.1(3)	Re2−Te3	271.1(3)	Re2−Te6	271.7(3)	Re1−Br3	261.3(4)
Re1−Br4	262.4(4)	Re2−Br10	261.4(4)	Re2−Br9	263.0(4)	Te1−Br1	251.9(5)
Te1−Br2	254.3(5)	Te1−Br3	292.4(5)	Te6−Br7	251.7(5)	Te6−Br8	252.6(6)
Te6−Br10	293.1(4)	Te2−Br6	260.9(4)	Te5−Br5	264.5(5)	Te3−Te4	268.7(4)
Te2−Te5	324.9(3)	Te4−Te5	330.3(3)	Te2−Te3	353.8(4)		

Atoms	Angles [°]	Atoms	Angles [°]	Atoms	Angles [°]
Re2−Re1−Te2	58.27(6)	Re2−Re1−Te3	58.65(6)	Re2−Re1−Te4	57.36(6)
Re2−Re1−Te5	58.85(7)	Re1−Re2−Te2	57.56(6)	Re1−Re2−Te3	59.49(6)
Re1−Re2−Te4	58.24(7)	Re1−Re2−Te5	58.40(6)	Te3−Re1−Te4	59.57(8)
Te3−Re2−Te4	59.66(9)	Re1−Te2−Re2	64.16(7)	Re1−Te3−Re2	61.87(6)
Re1−Te4−Re2	62.91(7)	Re1−Te5−Re2	64.23(6)		

de Haën) dried with P_4O_{10}. BBr_3 (Riedel-de Haën) was used as received, $ReCl_5$ prepared from the elements, using Re (Riedel-de Haën), purified with H_2 at 1000°C, and chlorine gas dried with H_2SO_4. $ReBr_4$ was prepared from $ReCl_5$ and BBr_3.[22] $SiBr_4$ (Aldrich) was distilled prior to use. All compounds were handled in an argon glovebox or by standard vacuum techniques.

Synthesis of $[Re_2Br_4(Te_2)(TeBr)_2(TeBr_2)_2]$: The reaction of $ReBr_4$, Te and $TeBr_4$ was carried out in an evacuated glass ampoule of 14 mm diameter and 13 cm length. The ampoule was loaded with 250 mg of the solid starting materials in a glovebox, $SiBr_4$ was added under a flow of argon. The molar ratio of all starting materials was $ReBr_4/Te/TeBr_4/SiBr_4$ = 2:13:1:40. The solids showed only little solubility in the solvent. Within 14 d black crystals of $[Re_2Br_4(Te_2)(TeBr)_2(TeBr_2)_2]$ were formed at 150°C. Yields were generally low and no increase was observed on prolonged heating or at higher temperatures. The solvent was decanted and the crystals were dried in vacuo. Crystals of $[Re_2Br_4(Te_2)(TeBr)_2(TeBr_2)_2]$ are weakly moisture-sensitive. They decompose in moist air within several hours under evolution of HBr.

Crystal Structure Determination: Crystals of $[Re_2Br_4(Te_2)(TeBr)_2(TeBr_2)_2]$ were sealed in glass capillaries under argon. The crystal finally chosen for the data collection had dimensions of 0.32 × 0.24 × 0.06 mm. Preliminary precession photographs showed a systematic twinning of all crystals examined with a twofold axis along the diagonal of the reciprocal $a-c$ plane as the twin element. The crystal system was determined to be monoclinic with the Laue group $2/m$. The systematic extinction $0k0$ only present for $k = 2n$ led to the spacegroups $P2_1/m$ and $P2_1$ of which the noncentrosymmetric group was confirmed by the structure analysis. Data were collected with a STOE Image Plate diffractometer using graphite monochromized radiation. The reflections of the two individuals were indexed separately with the aid of the programm RECIPE.[23] Overlapping reflex intensities were excluded from the data sets. A structure model was obtained by direct methods[24] and refined against F^2 by full-matrix least squares with anisotropic displacement parameters for all atoms and both sets of data.[25] A numerical absorption correction was applied,[26] although this is principially problematic for twinned crystals. Crystallographic data and details on the structure analysis are given in Table 1, selected distances and angles in Table 2. Further crystal structure data have been deposited at the Fachinformationszentrum Karlsruhe, D-76344 Eggenstein-Leopoldshafen, Germany. Inquiries should be accompanied by the depository number CSD-410190.

Acknowledgments

The financial support by the Deutsche Forschungsgemeinschaft and the Fonds der Chemischen Industrie is gratefully acknowledged.

[1] G. Rhoushias, *Chem. Rev.* **1974**, *74*, 521−566.
[2] L. Leduc, A. Perrin, M. Sergent, *Mater. Lett.* **1985**, *3*, 209−215.
[3] N. I. Timoshchenko, V. L. Kolesnichenko, S. V. Volkov, Y. L. Slovokhotov, Y. T. Struchkov, *Koord. Khim.* **1990**, *16*, 1062−1066; *Chem. Abstr.* **1991**, *114*, 16504a.
[4] L. A. Aslanov, S. V. Volkov, V. L. Kolesnichenko, T. B. Mischanuk, V. B. Rybakov, N. I. Timoshchenko, *Ukr. Khim.* **1991**, *57*, 675−680; *Chem. Abstr.* **1992**, *116*, 74881y.
[5] J. Beck, K. Müller-Buschbaum, *Z. Kristallogr. Suppl.* **1998**, *15*, 48 (Proceedings of the DGK Meeting, Karlsruhe, **1998**).
[6] V. E. Fedorov, Yu. V. Mironov, V. P. Fedin, Yu. I. Mironov, H. Imoto, T. Saito, *Acta Crystallogr.* **1996**, *C52*, 1065−1067.
[7] E. Schulz-Lang, U. Abram, J. Strähle, *Z. Anorg. Allg. Chem.* **1996**, *622*, 251−253.
[8] Yu. V. Mironov, M. A. Pell, J. A. Ibers, *Inorg. Chem.* **1996**, *35*, 2709−2710.
[9] S. S. Yarovoi, Yu. I. Mironov, Yu. V. Mironov, A. V. Virovets, V. E. Fedorov, *Mater. Res. Bull.* **1997**, *32*, 1271−1277.
[10] J. Beck, K. Müller-Buschbaum, *Z. Anorg. Allg. Chem.* **1997**, *623*, 409−413.
[11] B. Jung, H. Erhardt, G. Meyer, *Z. Anorg. Allg. Chem.* **1991**, *603*, 49−56.
[12] L. A. Aslanov, S. V. Volkov, V. L. Kolesnichenko, V. B. Rybakov, N. I. Timoshchenko, *Ukr. Khim. Zh.* **1992**, *58*, 279−281; *Chem. Abstr.* **1992**, *117*, 39134f.
[13] M. Irmler, G. Meyer, *Z. Anorg. Allg. Chem.* **1987**, *552*, 81−89.
[14] W. A. Hermann, C. Hecht, E. Herdtweck, H.-J. Kneuper, *Angew. Chem.* **1987**, *99*, 158−160; *Angew. Chem. Int. Ed. Engl.* **1987**, *26*, 132.
[15] H. F. Franzen, W. Hönle, H. G. v. Schnering, *Z. Anorg. Allg. Chem.* **1983**, *497*, 13−20.
[16] J. Beck, *Angew. Chem.* **1994**, *106*, 172−182; *Angew. Chem. Int. Ed. Engl.* **1994**, *33*, 172; *J. Solid State Chem.* **1996**, *125*, 165−170.
[17] R. Kniep, A. Rabenau, *Top. Curr. Chem.* **1983**, *111*, 145.
[18] M. T. Rodgers, R. A. Spurr, *J. Amer. Chem. Soc.* **1947**, *69*, 2102−2103.
[19] S. V. Volkov, V. L. Kolesnichenko, N. I. Timoshchenko, *Koord. Khim.* **1988**, *17*, 367−372; *Chem. Abstr.* **1988**, *108*, 229969u.
[20] T. Schlörb, Ph. D. Thesis, University of Giessen, **1997**; F. Wolf, Ph. D. Thesis, University of Giessen, **1997**; J. Wetterau, Ph. D. Thesis, University of Giessen, **1998**; publication in preparation.
[21] G. Brauer, *Handbuch der Präparativen Anorganischen Chemie*, F. Enke Verlag, Stuttgart, **1981**.
[22] H. Müller, R. Waschinski, *Inorg. Nucl. Chem. Lett.* **1972**, *8*, 413−415.

[23] *RECIPE/TWIN, STOE IPDS Software Packet*, STOE et Cie., Darmstadt, Germany, **1996**.
[24] G. M. Sheldrick, *SHELXS86, Program for Crystal Structure Solution*, University of Göttingen, Germany, **1986**.
[25] G. M. Sheldrick, *SHELXL93, Program for Crystal Structure Refinement*, University of Göttingen, Germany, **1993**.
[26] W. Herrendorf, H. Bärnighausen, *HABITUS, Program for the Optimization of the Crystal Shape of Numerical Absorption Correction*, University of Karlsruhe, Germany, **1993**.
[27] C. K. Johnson, *ORTEP, Program for the Graphical Representation of Crystal Structures*, Oak Ridge National Laboratory, Tennesse, **1965**; modified version of K. B. Plötz, M. Rath, M. Scheikowski, University of Kiel, Germany, **1994**.

Received November 9, 1998
[I98384]

Metallocenes of Nb and Ta with η^2-Se_2H, SeH, and Se Ligands – Crystal Structures of $[Cp'_2Ta(SeH)H_2]$ and $[Cp'_2Ta(=Se)H{\cdot}W(CO)_5]$ ($Cp' = tBuC_5H_4$)

Henri Brunner,[a] Marek M. Kubicki,[b] Jean-Claude Leblanc,[b] Walter Meier,[a] Claude Moïse,[b] André Sadorge,[b] Bernhard Stubenhofer,[a] Joachim Wachter,*[a] and Robert Wanninger[a]

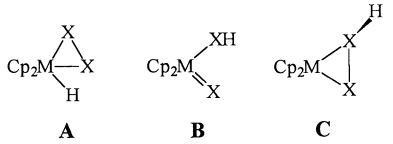
Keywords: Metallocenes / Hydroselenide ligands / Selenium / Se coordination chemistry

The reactions of $[Cp^{\#}_2NbBH_4]$ (**1**) [$Cp^{\#} = C_5Me_5$ (Cp^*) or C_5Me_4Et] and $[Cp'_2TaH_3]$ ($Cp' = tBuC_5H_4$) with elemental selenium give complexes of the general composition $[Cp_2MSe_2H]$. These exist in three isomeric forms, **A–C**, depending on the metal and the chalcogen. $[Cp^{\#}_2NbSe_2H]$ (**2**) incorporates the novel η^2-Se_2H ligand (**C**), which is labile when exposed to light. Solutions of **2**(Cp^*) can be converted into $[Cp^*_2NbSe_2H]$ (**3**), which exists in two isomeric forms **A** or **B**, along with $[Cp^*_2NbSe_3H]$ (**4**) and $[Cp^*_2NbO_2H]$ (**5**). $[Cp'_2Ta(\eta^2\text{-}Se_2)H]$ (**6**) is the only isomer found for the Ta system. Se abstraction by means of $P(OEt)_3$ gives $[Cp'_2Ta(=Se)H]$ (**7**). Complex **7** can be reduced with Na/Hg and subsequently hydrolysed to give $[Cp'_2Ta(SeH)H_2]$ (**8**), which has also been observed during the formation of **6**. Coordination of $[W(CO)_5THF]$ at the Se lone pair of **7** affords the heterobimetallic complex **9**. All compounds have been characterized by means of ^1H- and, in some cases, ^{77}Se-NMR spectroscopy. Products **8** and **9** have also been subjected to X-ray diffraction analysis.

Introduction

Metallocenes of the early transition metals are excellent reagents for the stabilization of chalcogenido ligands.[1] However, only a few comparative studies have been carried out, in which the coordination behavior of various chalcogens has been studied at a specific transition metal.[2] Compounds of the class $[Cp_2MX_2H]$ (Cp = any substituted cyclopentadienyl) are predominant in Nb and Ta chalcogen chemistry. They occur as isomers **A**−**C**, where the form adopted depends on the combination of substituted cyclopentadienyl ligands [$Cp' = tBuC_5H_4$; $Cp^{\#} = C_5Me_5$ (Cp^*) or C_5Me_4Et] with the appropriate metals (M = Nb, Ta) and chalcogens (X = S, Se, Te). Examples existing as isomeric form **A** are $[Cp^{\#}_2NbS_2H]$,[3] $[Cp'_2TaS_2H]$,[3] and $[Cp^*_2TaX_2H]$ (X = S,[4] Se,[5] Te[6]). The chemistry of this isomeric form is characterized by the nucleophilic behavior of the free electron pairs of the dichalcogenido ligands, which can ultimately lead to the formation of polymetallic compounds.[7] Another feature is the photolytic rupture of its X−X bond, giving isomers of type **B** (M = Nb, Ta: X = S;[8] M = Ta: X = Se[5]). Only one example (M = Nb: X = Te) corresponding to isomer form **C** has been reported, which involves a chiral X atom: $[Cp^{\#}_2Nb(\eta^2\text{-}Te_2H)]$ serves as a reagent for the transfer of Te^0[9] or Te^{2-} ligands[10] to other organometallic complexes.

Whereas peralkylated tantalocene compounds of type **A** are well established for X = S, Se, and Te, the corresponding niobocene selenides are not known. Therefore, we decided to investigate the reactions of $[Cp^{\#}_2NbBH_4]$ and of $[Cp'_2TaH_3]$ with elemental selenium. The latter was employed because sulfido compounds containing the Cp'_2Ta fragment exhibit striking relationships in their chemical behavior when compared to sulfido compounds involving the $Cp^{\#}_2Nb$ fragment.[11]



A **B** **C**

Scheme 1. Isomeric forms of Cp_2MX_2H (M = Nb, Ta; X = S, Se, Te)

Results

The $Cp^{\#}_2Nb$/Se System

Reaction of $[Cp^{\#}_2NbBH_4]$ **1** with 2.3 equivalents of red selenium in the dark at ambient temperature gives the green compounds **2** in 85−89% yields (Equation 1). The reaction of **1** with grey Se requires a temperature of at least 40°C. FD mass spectra and elemental analyses of the products indicate their composition to be $[Cp^{\#}_2NbSe_2H]$. The ^1H-NMR spectra of compounds **2** invariably exhibit a high-field resonance at $\delta = -0.90$, surrounded by ^{77}Se satellites. ^{77}Se-NMR spectra feature resonances at $\delta = -210$ and 230, respectively, the latter exhibiting a $^{77}Se-^1H$ coupling of 34 Hz. The absence of a highly deshielded resonance rules out the presence of double-bonded Se.[5][12] The ^1H-NMR spectrum of $[(C_5Me_4Et)_2Nb(Se_2H)]$ (Figure 1) features a

[a] Institut für Anorganische Chemie, Universität Regensburg, D-93040 Regensburg, Germany
[b] Laboratoire de Synthèse et d'Electrosynthèse Organométalliques (URA 1685), Université de Bourgogne, F-21100 Dijon, France

 © WILEY-VCH Verlag GmbH, D-69451 Weinheim, 1999 1434−1948/99/0505−0843 $ 17.50+.50/0

multiplet attributable to the CH_2 protons. A similar NMR pattern has been observed for $[(C_5Me_4Et)_2Nb(\eta^2\text{-}Te_2H)]$, the structure of which has been determined by X-ray crystallography.[9] On this basis, compounds **2** are assigned the isomeric form **C**.

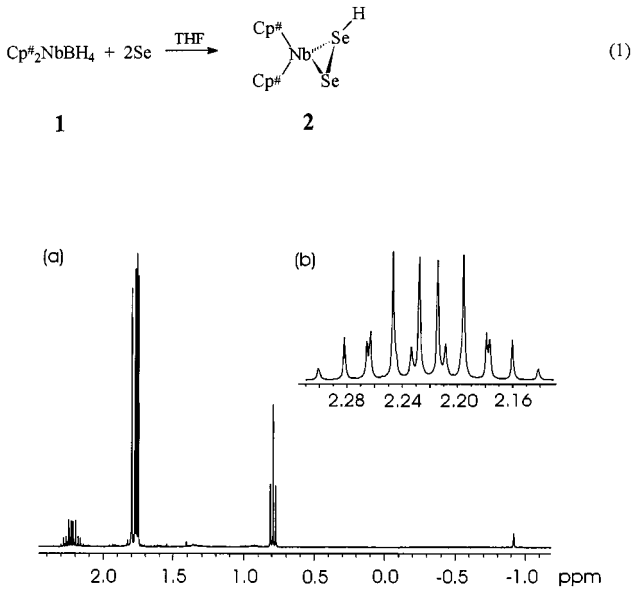


Figure 1. ^{1}H-NMR spectrum (400 MHz, C_6D_6) of $[(C_5Me_4Et)_2Nb(\eta^2\text{-}Se_2H)]$ (Figure 1a) and CH_2 resonances of the C_5Me_4Et ligands (· 5; Figure 1b)

The green solutions of **2** slowly become orange when exposed to light. This process was studied by ^{1}H-NMR spectroscopy in the case of **2**(Cp*) in C_6D_6 solution. The signals at $\delta = 1.73$ (CH_3) and $\delta = -0.89$ (SeH) disappear as new signals develop (Figure 2), the latter being attributable to the compounds $[Cp^*_2NbSe_2H]$ (**3**), $[Cp^*_2NbSe_3H]$ (**4**), and $[Cp^*_2NbO_2H]$ (**5**) (Equation 2). The products were identified, after partial chromatographic separation, on the basis of their mass-spectrometric and ^{1}H-NMR-spectroscopic data, following irradiation of a solution of **2**(Cp*) on a preparative scale. Separation into discrete compounds could not be achieved, and consequently there is some scatter in the C,H elemental analysis data for **3** and **4**. In the ^{1}H-NMR spectrum of **3**, the "hydride" resonance is flanked by two pairs of ^{77}Se satellites (Figure 2b). A structural assignment to one of the two isomers **A** or **B** (Scheme 1) is not yet possible because the low solubility of **3** does not allow a ^{77}Se-NMR spectrum of sufficient quality to be recorded. IR spectra are of little use in assigning the isomeric form as the only significant absorptions are those of the ν(C−H) vibrations of the $Cp^{\#}$ rings. Irradiation of the C_5Me_4Et derivative of **2** proceeds in a similar manner, but separation into discrete complexes proved even more difficult, thus preventing clear assignments of signals in the NMR spectra. Although an unambiguous assignment of the structures of **3** and **4** is not yet possible, further support for the proposed isomeric forms is provided by the thermolysis of $[Cp^*_2NbS_2H]$. Here, isomer **A** is converted to isomer **B** in the formation of $[Cp^*_2NbS_3H]$, and both structures have been confirmed by X-ray studies.[3][8]

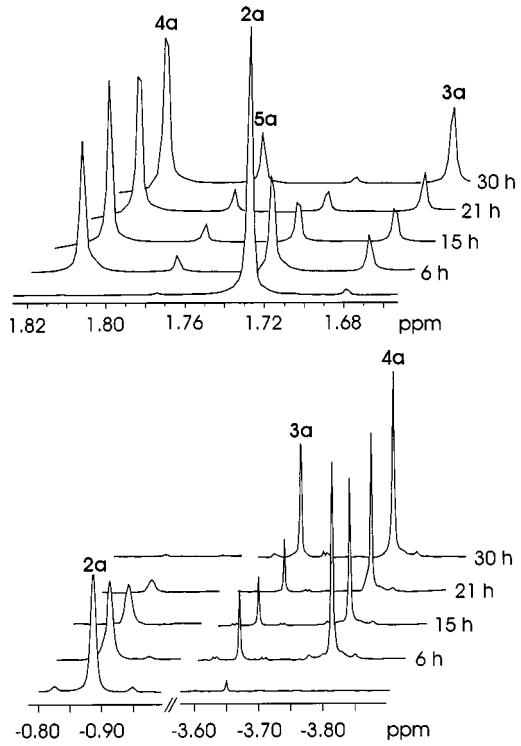
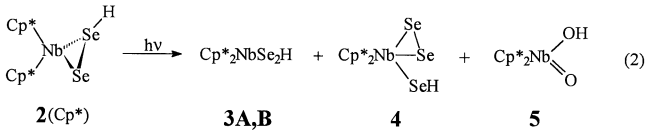


Figure 2. ^{1}H-NMR investigation of the isomerization of $[Cp^*_2Nb(\eta^2\text{-}Se_2H)]$ [**2**(Cp*)] during irradiation (400 MHz, C_6D_6); methyl resonances of the Cp* ligands of **2**(Cp*), $[Cp^*_2NbSe_2H]$ (**3**), $[Cp^*_2Nb(Se_2)SeH]$ (**4**), and $[Cp^*_2Nb(O)OH]$ (**5**) (see text; Figure 2a); high-field region (· 20; Figure 2b)

The formation of **5** may be rationalized in terms of the substitution of selenide ligands by traces of oxygen. In a control experiment, a solution of **2**(Cp*) produced bright-yellow $[Cp^*_2NbO_2H]$ (**5**) along with red selenium when exposed to air. Complex **5** belongs to the class of oxoniobocenes of the type $[Cp^*_2Nb(=O)R]$ (R = H, Cl, OCH_3, etc.).[13]



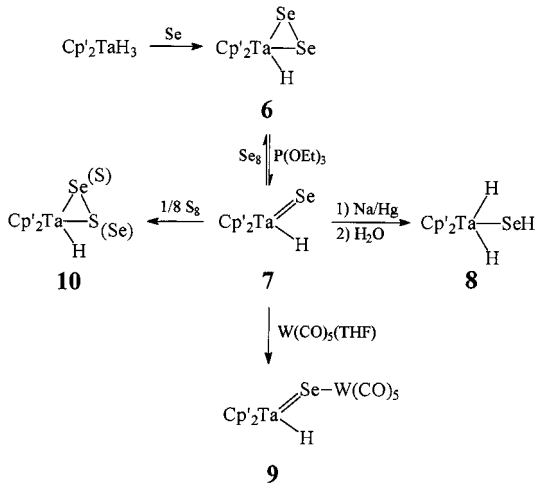
(2)

The Cp'_2Ta/Se System

Stirring of a toluene solution of $[Cp'_2TaH_3]$ with an excess of grey selenium (12 h, 25°C) leads to the formation of the red complex $[Cp'_2TaSe_2H]$ (**6**) (Scheme 2). The isomeric form **A** can be proposed on the basis of spectroscopic data. The IR spectrum of **6** shows an absorption at 1710 cm^{-1} characteristic of ν(Ta−H), and the ^{1}H-NMR spectrum exhibits a singlet at $\delta = 1.11$ for the TaH proton and a set of four resonances ($\delta = 3.81$, 4.21, 4.34, and 6.15) due to the cyclopentadienyl protons. Two resonances ($\delta = -251$ and −571) are observed for the two non-equivalent chalcogen atoms in the ^{77}Se-NMR spectrum. In contrast to the anal-

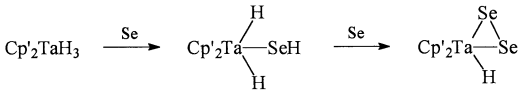
ogous $[Cp^*_2Ta(\eta^2\text{-}Se_2)H]$,[5] no $^{77}Se-^1H$ coupling is observed.

Treatment of a toluene solution of **6** with triethyl phosphite (4 h, reflux) leads to formation of the monoselenido complex $[Cp'_2Ta(=Se)H]$ (**7**). The ^{77}Se-NMR spectrum of **7** exhibits a deshielded signal at $\delta = 2303$, which is typical for doubly bonded Se.[5][12] The signal at $\delta = 7.52$ in the ^{1}H-NMR spectrum, attributable to the TaH group, is suggestive of a protic rather than a hydridic nature of the hydrogen ligand.[14] $[Cp'_2Ta(\eta^2\text{-}Se_2)H]$ (**6**) is regenerated upon addition of an excess of Se_8 to solutions of **7** (Scheme 2).



Scheme 2

Like the related tantalocene sulfide,[14][15] the Ta=Se bond in **7** can be expected to exhibit an interesting reaction potential. Thus, when a pale-blue THF solution of **7** is treated with sodium amalgam and then with a few drops of water, rapid decolouration of the reaction mixture occurs, from which the white complex **8** can subsequently be isolated. Analytical data for **8** are consistent with the composition $[Cp'_2TaSeH_3]$. In this context, it is of interest that the FD mass spectrum of **8** features the parent ion peak, whereas that of its precursor **7** shows only the peak of **6**, which is richer in Se. The ^{1}H-NMR spectrum of **8** exhibits two multiplets at $\delta = 4.91$ and $\delta = 4.37$ for the Cp protons, and a singlet at $\delta = 1.29$ for the *t*Bu group. This is in accord with the presence of two equivalent cyclopentadienyl rings. The "hydride" resonances appear as a doublet at $\delta = 2.43$ and a triplet at $\delta = -4.86$ (ratio 2:1). The ^{77}Se-NMR spectrum shows a triplet at $\delta = -570$ with $^2J(^{77}Se-^1H) = 23$ Hz. The same coupling is found for the doublet, whereas the aforementioned high-field triplet does not exhibit any SeH coupling, even upon irradiation of the doublet. The high-field resonance disappears in D_2O as $[Cp'_2Ta(SeD)H_2]$ is formed. As in the case of the related $[Cp'_2Ta(SD)H_2]$, which shows a similar spectrum,[16] no evidence for Ta–D bond formation could be detected. This is in contrast to the exchange process hydrochalcogenido vs. hydrido ligands observed by Bergman et al. in the case of $[Cp^*_2Ti(SH)H]$.[17] Complex **8** is also observed in the course of formation of **6**, so that it may be considered as the first relatively stable intermediate product in the activation of elemental selenium by $[Cp'_2TaH_3]$ (Equation 3).



8 **6** (3)

In order to gain further insight into the structure of **8**, a single-crystal X-ray analysis was carried out. This revealed the typical bent metallocene structure (Figure 3), with the Se atom located in the plane defined by the centers of the Cp ligands and the Ta atom. The final difference Fourier map exhibits several positive peaks close (< 1.5 Å) to the Ta and Se atoms. However, none of them could be refined as a bona fide hydrogen atom. Thus, even though we were unable to locate the hydrogen atoms, the overall metallocene geometry[18] of **8**, together with a long Ta–Se bond of 2.646(1) Å {some 0.3 Å longer than the Ta=Se bond in $[Cp^*_2Ta(=Se)H]$[5]}, are clearly indicative of the presence of a hydroselenide ligand. Complex **8** is one of the few examples containing this ligand.[5][19]

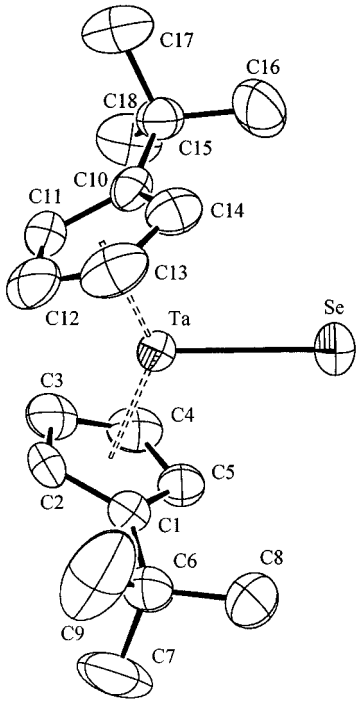


Figure 3. Molecular structure (ORTEP drawing at 50% probability level) of $[Cp'_2TaH_2SeH]$ (**8**); selected bond lengths [A] and angles [°]: Ta–Se 2.646(1), Ta–Cp1 2.09, Ta–Cp2 2.08 (Cp1 and Cp2 are the centers of the rings C1–C5 and C10–C14, respectively); Cp1–Ta–Cp2 136.9; the H atoms attached to Ta and Se could not be localized

The selenido complex **7** reacts with $[W(CO)_5(THF)]$ to afford the brown, heterobimetallic compound **9** in 65% yield (Scheme 2). This complex has been characterized by both spectroscopic and crystallographic measurements. The IR spectrum of **9** exhibits the typical absorption pattern for the coordinated $W(CO)_5$ moiety and the ^{1}H-NMR spectrum features one signal for the *t*Bu protons. The molecular

structure of **9** is shown in Figure 4. It may be classified as being of the pseudotetrahedral metallocene-type,[18] with the Se atom located 0.86 Å from the central Cp−Ta−Cp plane (cf. the "in-plane" position of Se in the structure of **8**). The Ta−Se distance [2.422(2) Å] is only slightly longer than that of other Ta=Se bonds.[5][20] The orientation of the $W(CO)_5$ group towards one of the Cp rings in the solid state should be of no relevance in solution. As in the related $[Cp'_2Ta(S)H \cdot W(CO)_5]$, a low barrier to rotation about the metal−selenium bond may be expected.[15]

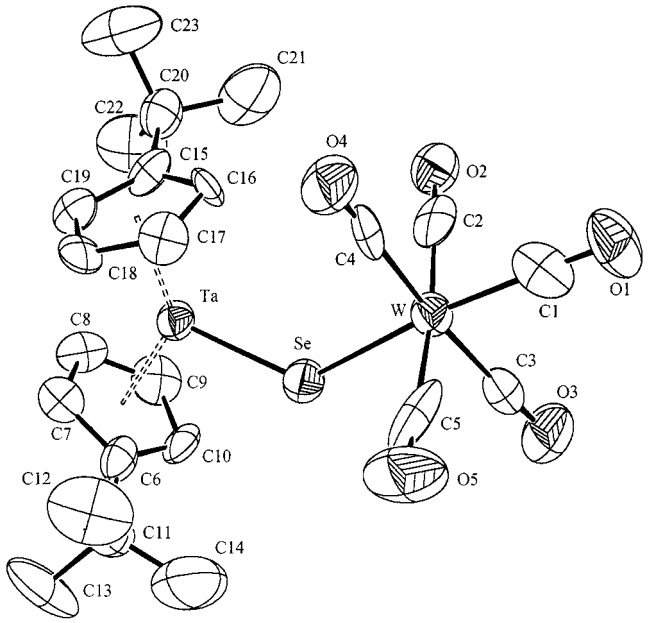


Figure 4. Molecular structure (ORTEP drawing at 50% probability level) of $[Cp'_2TaSeH{\cdot}W(CO)_5]$ (**9**); selected bond lengths [Å] and angles [°]: Ta−Se 2.422(4), Ta−Cp1 2.09, Ta−Cp2 2.09 (Cp1 and Cp2 are the centers of the rings C6−C10 and C15−C19, respectively), W−Se 2.672(2); Ta−Se−W 130.92(8), Cp1−Ta−Cp2 134.8; the H atom attached to Ta could not be localized

Another aspect of the reactivity of **7** is illustrated by its behavior towards S_8. When a toluene solution of **7** is treated with an excess of elemental sulfur, there is an immediate colour change from blue to dark-brown. After chromatographic work-up, a brown band is obtained, which consists mainly of the mixed complex $[Cp'_2Ta(SeS)H]$ (**10**), as established by mass spectrometry. The ^{1}H-NMR spectrum shows the presence of two isomers, arising from different orientations of the (η^2-SeS) ligands, besides ca. 10% of $[Cp'_2Ta(\eta^2\text{-}S_2)H]$.[3] Unfortunately, full chromatographic separation could not be achieved, precluding the analytical characterization of these isomers. However, dechalcogenation of the mixture with $P(OEt)_3$ appears to be chemoselective, since it affords exclusively $[Cp'_2Ta(=S)H]$[3] along with $Se=P(OEt)_3$. The same reactivity is observed in the cross-reaction when $[Cp'_2Ta(=S)H]$ is exposed to an excess of Se_8.

Conclusions

Transition metal complexes with hydroselenido ligands are still rare. In this paper, we have reported the facile syntheses of two different ligand types containing Se−H bonds. The results show that $Cp^{\#}{}_2Nb$ fragments play a particular role in the activation of elemental selenium as opposed to other chalcogens. Like its Te congener $[Cp^{\#}{}_2Nb(Te_2H)]$, which has already been successfully employed in the synthesis of telluride clusters,[9][10] the novel hydroselenido ligand in **2** merits attention as a potential source of reactive Se. On the other hand, the ligand arrangements in complexes **3** and **4** show similarities to niobocene−sulfide chemistry. The Se coordination chemistry induced by the Cp'_2Ta fragment closely resembles that observed for the systems Cp'_2Ta/S_8 and Cp^*_2Ta/X (X = Se, Te). The crucial difference is the stabilization of the dihydrido−hydroselenido complex **8** as an intermediate product during activation of elemental selenium. Another complex typical of tantalocene−selenium chemistry is **7**, for which a series of novel reactions have been described.

Experimental Section

General: All procedures were carried out under N_2 using dry solvents. − Elemental analyses (C,H) were performed at the Mikroanalytisches Laboratorium, Universität Regensburg. − IR spectra were obtained with a Perkin−Elmer 580 B instrument. − Molecular masses were determined by field desorption (FD) mass spectrometry (toluene solutions) using a Finnigan MAT 95 instrument. − ^{1}H- and ^{77}Se-NMR (standard: external Me_2Se) spectra were recorded with Bruker AC 200, WM 250, and WM 400 instruments. − $[(C_5Me_5)_2NbBH_4]$,[21] $[(C_5Me_4Et)_2NbBH_4]$,[22] and $[Cp'_2TaH_3]$[23] were prepared according to literature procedures. − ***Note:*** Work should be carried out in a well-ventilated fume hood because of the possible evolution of H_2Se.

Preparation of $[Cp^{\#}{}_2NbSe_2H]$ (2): It was essential that all operations were carried out in the absence of light. A mixture of 1.50 mmol of **1**, 373 mg (4.7 mmol) of red amorphous selenium,[24] and 70 mL of THF was stirred for 20 h at room temperature. After evaporation of the solvent, chromatography of the residue on SiO_2 (column 25 cm, Ø 5 cm) gave upon elution with toluene a green band containing $[Cp^{\#}{}_2NbSe_2H]$ (**2**) in 85−89% yield. − **2**: $C_{20}H_{31}NbSe_2$ (522.3): calcd. C 45.99, H 5.98; found C 45.71, H 6.01. − Mol. mass 519.1 (FD-MS, ^{78}Se). − ^{1}H NMR (400 MHz, C_6D_6): δ = 1.72 (s, 30 H, CH_3), −0.90 [s, 1 H, SeH, ^1J(H−Se) = 33.9 Hz]. − ^{77}Se NMR (76 MHz, C_6D_6): δ = 236.7 [d, 1 Se, ^1J(Se−H) = 34 Hz], −209.0 (s, 1 Se). − $C_{22}H_{35}NbSe_2$ (550.3): calcd. C 48.01, H 6.41; found C 48.00, H 6.40. − Mol. mass 547.0 (FD-MS, ^{78}Se). − ^{1}H NMR (400 MHz, C_6D_6): δ = 1.74 (s, 6 H, CH_3), 1.76 (s, 6 H, CH_3), 1.77 (s, 6 H, CH_3), 1.78 (s, 6 H, CH_3), 0.86 (t, 6 H, CH_3), 2.22 (m, 4 H, CH_2), −0.92 [s, 1 H, SeH, ^1J(H−Se) = 34.4 Hz]. − ^{77}Se NMR (76 MHz, C_6D_6): δ = 223.2 [d, 1 Se, ^1J(Se−H) = 33.6 Hz], −217.4 (s, 1 Se).

Irradiation of $[Cp^*_2NbSe_2H]$ [2(Cp*)]: A green solution of 1.5 g (2.87 mmol) of **2**(Cp*) in 150 mL of toluene was stirred for 7 d at room temperature and exposed to daylight. During this time the colour slowly changed to brown-orange. After evaporation of the solvent, the brown residue was dissolved in 20 mL of toluene and then chromatographed on SiO_2 (column 25 cm, Ø 5 cm). Elution with toluene/pentane (2:1) gave a broad yellow band containing 80 mg of product. Further elution with toluene/pentane (3:1) gave two very broad bands containing 420 and 850 mg, respectively. On the basis of mass-spectrometric and ^{1}H-NMR investigations, the

first band was found to consist of 68% [Cp*$_2$NbSe$_2$H] (**3**), 8% [Cp*$_2$NbSe$_3$H] (**4**), and 13% [Cp*$_2$NbO$_2$H] (**5**). The second band was shown to contain these compounds in a ratio of 21:68:9, while the third band consisted almost exclusively of **5**, which exhibited the same properties as an independently prepared sample (see below). − **3**: $C_{20}H_{31}NbSe_2$ (522.3): Mol. mass 519.1 (FD-MS, ^{78}Se). − ^{1}H NMR (400 MHz, C_6D_6): δ = 1.67 (s, 30 H, CH_3), −3.67 [s, 1 H, J(H−Se) = 20.9, 25.5 Hz]. − **4**: $C_{20}H_{31}NbSe_3$ (601.3): Mol. mass 598.1 (FD-MS, ^{78}Se). − ^{1}H NMR (400 MHz, C_6D_6): δ = 1.82 (s, 30 H, CH_3), −3.84 [s, 1 H, SeH, ^1J(H−Se) = 21.2 Hz].

Reaction of [Cp*$_2$NbSe$_2$H] [2(Cp*)] with Air: A solution of 300 mg (0.575 mmol) of **2**(Cp*) in 100 mL of THF was stirred for 12 h in the dark in an open flask. After filtration of the precipitated amorphous selenium, the solvent was evaporated from the yellow filtrate to give 200 mg (88% yield) of a pale-yellow powder. Recrystallization from toluene/pentane (1:2) gave analytically pure **5**. − **5**: $C_{20}H_{31}NbO_2$ (396.0): calcd. C 60.61, H 7.83; found C 60.12, H 7.71. − Mol. mass 396.0 (FD-MS). − IR (KBr): $\tilde{\nu}$ = 3470 cm^{-1} m [ν(OH)], 843 cm^{-1} s [ν(Nb=O)]. − ^{1}H NMR (250 MHz, C_6D_6): δ = 1.77 (s, 30 H, CH_3), 2.11 (s, 1 H, OH).

Synthesis of [Cp′$_2$TaSe$_2$H] (6): A mixture of 100 mg (0.23 mmol) of [Cp′$_2$TaH$_3$], 100 mg (1.26 mmol) of grey selenium, and 10 mL of toluene was stirred for 18 h at 25°C (when red selenium was used, the reaction was complete within 3 h). The solvent was subsequently removed in vacuo and the dark residue was purified by chromatography on SiO_2 (column 12 cm, Ø 2.5 cm). Elution with toluene/THF gave a red band containing 67 mg (49% yield) of **6**. Recrystallization from toluene/pentane gave red crystals. − **6**: $C_{18}H_{27}TaSe_2$ (582.3): calcd. C 37.13, H 4.67; found C 36.84, H 4.77. − Mol. mass 580.0 (FD-MS, ^{78}Se). − IR (CsI): $\tilde{\nu}$ = 1710 cm^{-1} w [ν(Ta−H)]. − ^{1}H NMR (200 MHz, C_6D_6): δ = 1.11 (s, 1 H, TaH), 1.23 (s, 18 H, CH_3), 3.81 (m, 2 H, C_5H_4R), 4.21 (m, 2 H, C_5H_4R), 4.34 (m, 2 H, C_5H_4R), 6.15 (m, 2 H, C_5H_4R). − {^{1}H}^{77}Se NMR (95 MHz, C_6D_6): δ = −251, −571.

Synthesis of [Cp′$_2$TaSeH] (7): A solution of 90 mg (0.15 mmol) of **6** and 0.5 mL (excess) of P(OEt)$_3$ in 12 mL of toluene was refluxed for 4 h. After cooling, the solvent was removed under reduced pressure and the residual solid was washed with pentane. After drying in vacuo, 55 mg (70% yield) of crude **7** was obtained as a blue solid. Recrystallization from toluene/pentane gave an analytically pure sample, the FD-MS spectrum of which showed exclusively the more Se-rich peak of the precursor **6**. − **7**: $C_{18}H_{27}TaSe$ (503.3): calcd. C 42.95, H 5.41; found C 42.69, H 5.47. − IR (CsI): $\tilde{\nu}$ = 1862 cm^{-1} w [ν(Ta−H)]. − ^{1}H NMR (200 MHz, C_6D_6): δ = 1.29 (s, 18 H, CH_3), 4.76 (m, 2 H, C_5H_4R), 5.10 (m, 2 H, C_5H_4R), 5.42 (m, 2 H, C_5H_4R), 5.82 (m, 2 H, C_5H_4R), 7.52 (s, 1 H, TaH). − {^{1}H}^{77}Se NMR (95 MHz, C_6D_6): δ = 2303.

Synthesis of [Cp′$_2$Ta(H)$_2$SeH] (8): A solution of 70 mg (0.14 mmol) of **7** in 8 mL of THF was stirred with excess sodium amalgam for 20 min and then 3−4 drops of water were added. After decantation of the organic layer and washing of the amalgam residue with THF, the solvent was evaporated to leave crude **8** as a white solid (53 mg, 75% yield). Recrystallization from toluene/pentane gave white needles. − **8**: $C_{18}H_{29}TaSe$ (505.3): calcd. C 42.78, H 5.78; found C 42.83, H 5.71. − Mol. mass 504.2 (FD-MS, ^{78}Se). − ^{1}H NMR (200 MHz, C_6D_6): δ = −4.86 [t, 1 H, SeH, ^3J(H−H) = 8.3 Hz], 1.29 (s, 18 H, CH_3), 2.43 [d, 2 H, TaH, ^3J(H−H) = 8.3 Hz, ^2J(Se−H) = 22.6 Hz], 4.37 (m, 4 H, C_5H_4R), 4.91 (m, 4 H, C_5H_4R) [^1J(Se−H) not observed]. − {^{1}H}^{77}Se NMR (95 MHz, C_6D_6): δ = −570 [t, 1 Se, ^2J(Se−H) = 23 Hz].

Synthesis of [Cp′$_2$TaSeH · W(CO)$_5$] (9): A mixture of 90 mg (0.18 mmol) of **7**, 0.22 mmol of [W(CO)$_5$(THF)], and 15 mL of THF was stirred at room temperature for 30 min. After evaporation of the solvent, the residue was chromatographed on SiO_2 (column 10 cm, Ø 2.5 cm). Eluting with toluene, a red-brown band was obtained, which was found to contain 100 mg (65% yield) of **9**. Recrystallization from toluene/pentane gave dark-brown crystals. − **9**: $C_{23}H_{27}O_5SeTaW$ (827.2): calcd. C 33.40, H 3.29; found C 33.77, H 3.27. − Mol. mass 828 (FD-MS; calcd. 828.0 for $C_{23}H_{27}TaO_5{}^{78}Se^{184}W$). − IR (THF): $\tilde{\nu}$ = 2061 s, 1928 s, 1918 sh, 1894 m cm^{-1} [ν(CO)]. − ^{1}H NMR (200 MHz, C_6D_6): δ = 1.06 (s, 18 H, CH_3), 4.32 (m, 2 H, C_5H_4R), 4.81 (m, 2 H, C_5H_4R), 5.43 (m, 2 H, C_5H_4R), 5.81 (m, 2 H, C_5H_4R), 7.36 (s, 1 H, TaH).

Synthesis of [Cp′$_2$TaSeSH] (10): To a solution of 60 mg (0.12 mmol) of **7** in 10 mL of toluene, 5 equiv. of sulfur were added. The mixture was stirred for 5 min. The solvent was then evaporated and the residual brown solid was chromatographed on SiO_2 (column 10 cm, Ø 2.5 cm). Eluting with toluene/THF (9:1), a brown band was obtained, which was found to contain **10** as a mixture of two isomers and an inseparable small amount (15%) of [Cp′$_2$TaS$_2$H] (overall yield 65%). − **10**: $C_{18}H_{27}TaSSe$ (536.1): Mol. mass 536.1 (FD-MS). − ^{1}H NMR (200 MHz, C_6D_6): Major isomer (60%): δ = 1.23 (s, 18 H, CH_3), 2.28 (s, 1 H, TaH), 3.86 (m, 2 H, C_5H_4R), 4.37 (m, 2 H, C_5H_4R), 4.43 (m, 2 H, C_5H_4R), 5.91 (m, 2 H, C_5H_4R). − Minor isomer (40%): δ = 1.24 (s, 18 H, CH_3), 1.52 (s, 1 H, TaH), 3.92 (m, 2 H, C_5H_4R), 4.37 (m, 4 H, C_5H_4R), 6.15 (m, 2 H, C_5H_4R).

X-ray Structure Determinations[25] of Complexes 8 and 9. − [Cp′$_2$Ta(H)$_2$SeH] (8): Yellow prisms (0.4 × 0.3 × 0.2 mm), monoclinic $P2_1/n$ (no. 14); cell: a = 8.036(1), b = 18.255(2), c = 12.666(2) Å, β = 97.77(1)°; V = 1840.9 Å^3, Z = 4; $d_{calcd.}$ = 1.823 gcm^{-3}; absorption correction (ψ scan): 73.64/99.86. Linear absorption μ = 79.38 cm^{-1}; F(000) = 976. Enraf-Nonius CAD4 diffractometer; Mo-K_α radiation, graphite monochromator, 3240 unique observed reflections; 2603 independent reflections [$I > 2\sigma(I)$]. Structure solution by means of direct methods and subsequent Fourier syntheses using the SHELX97 package. Refinement on F^2 with 181 variables; R = 0.036, wR = 0.093, GoF = 1.039; residual electron density (max./min.): 1.23 (close to the Ta atom)/−1.74 e/Å^3. − **[Cp′$_2$TaSeH·W(CO)$_5$]** (9): Red-brown plates (0.15 × 0.10 × 0.05 mm), monoclinic $P2_1/n$ (no. 14); cell: a = 13.321(2), b = 18.418(4), c = 12.792(3) Å, β = 116.39(2)°; V = 2600.3 Å^3, Z = 4; $d_{calcd.}$ = 2.113 gcm^{-3}; absorption correction (ψ scan): 71.98/99.80. Linear absorption μ = 100.53 cm^{-1}; F(000) = 1544. Enraf-Nonius CAD4 diffractometer; Mo-K_α radiation, graphite monochromator, 5505 unique observed reflections; 2212 independent reflections [$I > 2\sigma(I)$]. Structure solution by means of direct methods and subsequent Fourier syntheses using the SHELX97 package. Refinement on F^2; number of variables = 280; R = 0.056, wR = 0.098, GoF = 0.952; residual electron density (max./min.): 1.99 (close to the Ta atom)/−2.04 e/Å^3.

Acknowledgments

We are grateful to the Deutsche Forschungsgemeinschaft (grant Wa 485/2−3) for support of parts of this work.

[1] Recent reviews may be found in: M. Draganjac, T. B. Rauchfuss, *Angew. Chem. Int. Ed. Engl.* **1985**, *24*, 742; J. Wachter, *Angew. Chem. Int. Ed. Engl.* **1989**, *28*, 1613; P. Royo, E. Ryan in *Metallocenes* (Eds.: A. Togni, R. L. Halterman), Wiley-VCH, **1998**, vol. 1, p. 378−401.

[2] G. Erker, T. Mühlenbernd, R. Benn, A. Rufinska, G. Tainturier, B. Gautheron, *Organometallics* **1985**, *5*, 1023; G. Tainturier, M. Fakim, B. Gautheron, *J. Organomet. Chem.* **1989**, *373*, 193; W.

Howard, G. Parkin, *J. Am. Chem. Soc.* **1994**, *116*, 606; W. A. Howard, G. Parkin, A. L. Rheingold, *Polyhedron* **1995**, *14*, 25; W. A. Howard, T. M. Truka, M. Waters, G. Parkin, *J. Organomet. Chem.* **1997**, *528*, 95.
[3] H.-J. Bach, H. Brunner, J. Wachter, M. M. Kubicki, J.-C. Leblanc, C. Moise, F. Volpato, B. Nuber, M. L. Ziegler, *Organometallics* **1992**, *11*, 1403.
[4] H. Brunner, J. Wachter, G. Gehart, J.-C. Leblanc, C. Moise, *Organometallics* **1996**, *15*, 1327.
[5] J. H. Shin, G. Parkin, *Organometallics* **1995**, *14*, 1104.
[6] J. H. Shin, G. Parkin, *Organometallics* **1994**, *13*, 2147.
[7] H. Brunner, G. Gehart, J.-C. Leblanc, C. Moise, B. Nuber, B. Stubenhofer, F. Volpato, J. Wachter, *J. Organomet. Chem.* **1996**, *517*, 47; H. Brunner, M. M. Kubicki, G. Gehart, E. Lehrl, D. Lucas, W. Meier, Y. Mugnier, B. Nuber, B. Stubenhofer, J. Wachter, *J. Organomet. Chem.* **1996**, *510*, 291; O. Blacque, H. Brunner, M. M. Kubicki, D. Lucas, W. Meier, Y. Mugnier, B. Nuber, B. Stubenhofer, J. Wachter, *J. Organomet. Chem.* **1998**, *564*, 71.
[8] H. Brunner, G. Gehart, W. Meier, J. Wachter, B. Nuber, *J. Organomet. Chem.* **1993**, *454*, 117.
[9] O. Blacque, H. Brunner, M. M. Kubicki, B. Nuber, B. Stubenhofer, J. Wachter, B. Wrackmeyer, *Angew. Chem. Int. Ed. Engl.* **1997**, *36*, 352.
[10] B. Stubenhofer, Thesis, Universität Regensburg, **1997**; H. Brunner, D. Lucas, W. Meier, Y. Mugnier, B. Nuber, B. Stubenhofer, J. Wachter, R. Wanninger, M. Zabel, manuscript in preparation.
[11] J.-C. Leblanc, C. Moise, F. Volpato, H. Brunner, G. Gehart, J. Wachter, B. Nuber, *J. Organomet. Chem.* **1995**, *485*, 237.
[12] D. Rabinovich, G. Parkin, *Inorg. Chem.* **1994**, *33*, 2313.
[13] H. Brunner, J.-C. Leblanc, D. Lucas, W. Meier, C. Moise, Y. Mugnier, B. Nuber, S. Rigny, A. Sadorge, J. Wachter, *J. Organomet. Chem.* **1998**, *566*, 203.
[14] H. Brunner, M. M. Kubicki, J.-C. Leblanc, C. Moise, F. Volpato, J. Wachter, *J. Chem. Soc., Chem. Commun.* **1993**, 851.
[15] H. Brunner, S. Challet, M. M. Kubicki, J.-C. Leblanc, C. Moise, F. Volpato, J. Wachter, *Organometallics* **1995**, *14*, 3623.
[16] A. Sadorge, P. Sauvageot, J.-C. Leblanc, C. Moise, *C. R. Acad. Sci. Paris, Série IIb* **1997**, *325*, 593; S. Challet, O. Blacque, G. Gehart, M. M. Kubicki, J.-C. Leblanc, C. Moise, H. Brunner, J. Wachter, *New J. Chem.* **1997**, *21*, 903.
[17] Z. K. Sweeny, J. L. Polse, R. A. Andersen, R. G. Bergman, M. G. Kubinec, *J. Am. Chem. Soc.* **1997**, *119*, 4543.
[18] J. W. Lauher, R. Hoffmann, *J. Am. Chem. Soc.* **1976**, *98*, 1729.
[19] M. Schmidt, G. G. Hoffmann, *Angew. Chem. Int. Ed. Engl.* **1978**, *17*, 598; I. M. Blacklaws, E. A. V. Ebsworth, D. W. H. Rankin, H. E. Robertson, *J. Chem. Soc., Dalton Trans.* **1978**, 753; F. Bottomley, T.-T. Chin, G. O. Egharevba, L. M. Kane, D. A. Pataki, P. S. White, *Organometallics* **1988**, *7*, 1214.
[20] V. Christou, J. Arnold, *Angew. Chem. Int. Ed. Engl.* **1993**, *32*, 1450.
[21] R. A. Bell, S. A. Cohen, N. M. Doherty, R. S. Threlkel, J. E. Bercaw, *Organometallics* **1986**, *5*, 972.
[22] H. Brunner, G. Gehart, W. Meier, J. Wachter, B. Wrackmeyer, B. Nuber, M. L. Ziegler, *J. Organomet. Chem.* **1992**, *436*, 313.
[23] M. L. H. Green, B. Jousseaume, *J. Organomet. Chem.* **1980**, *193*, 339.
[24] F. Fehér in *Handbuch der Präparativen Anorganischen Chemie* (Ed.: G. Brauer), Enke Verlag, Stuttgart, **1975**, vol. I, p. 411.
[25] Crystallographic data for **8** and **9** (excluding structure factors) have been deposited with the Cambridge Crystallographic Data Centre as supplementary publication nos. CCDC-104027 and -104028. Copies of the data can be obtained free of charge on application to CCDC, 12 Union Road, Cambridge CB2 1EZ, U.K. [Fax: (internat.) + 44-1223/336-033; E-mail: deposit@ccdc.cam.ac.uk].

Received November 10, 1998
[I98387]

Synthesis and X-ray Structure Determination of *tert*-Butylhydrazinium Azide and *N,N,N*-Trimethylhydrazinium Azide

Tassilo Habereder,[a][+] Anton Hammerl,[a] Gerhard Holl,[b] Thomas M. Klapötke,*[a] Jörg Knizek,[a][+] and Heinrich Nöth[a][+]

Keywords: Azides / Hydrazinium azide / Hydrazine / Nitrogen compounds

tert-Butylhydrazinium azide $[t\mathrm{BuNH_2NH_2}]^+[\mathrm{N_3}]^-$ (**1**) was prepared in a high yield reaction from *tert*-butylhydrazine and HN_3. *N,N,N*-Trimethylhydrazinium azide $[NH_2N(CH_3)_3]^+[N_3]^-$ (**2**) was prepared from the reaction of silver azide with *N,N,N*-trimethylhydraziniumiodide. Both were characterized by X-ray structural analysis, IR, Raman, and multinuclear (^{1}H, ^{13}C, ^{14}N) NMR spectroscopy.

Introduction

Hydrazinium azide, first reported by Curtius in 1891,[1a] is a powerful explosive that produces only nitrogen, hydrogen, and ammonia after explosion.[1b]

During the last 8 years, significant advances have been made in the area of inorganic azides, as indicated by the number of recent reviews covering various aspects of the subject.[2a–c] In contrast to the chemistry of many hydrazinium salts, which has been extensively explored in the last 30 years,[3][4] detailed studies into the chemistry of ionic hydrazinium azides have only recently come to fruition.[5a,b] We have recently become interested in the preparation of hydrazinium azides and their possible application as high-energy-density materials (*HEDM*) for military use.[6][7] The low melting point and the high volatility of hydrazine azide prevent its use. In order to increase the melting point and to decrease the volatility, organic substituents were attached to hydrazine. The first attempt in this direction was the synthesis of *N,N*-dimethylhydrazinium azide,[8] which proved to be more volatile than hydrazinium azide. The goal for the current research was to find a hydrazinium azide derivative that has a higher melting point and is less volatile than hydrazinium azide.

Results and Discussion

Anhydrous *tert*-butylhydrazine reacts at 0°C with a solution of hydrazoic acid in ether to form *tert*-butylhydrazinium azide **1** (Equation 1). Hydrazoic acid must be used in excess to prevent the formation of an adduct of **1** with *tert*-butylhydrazine.

$$t\mathrm{BuNHNH_2} + \mathrm{HN_3} \xrightarrow{\mathrm{Et_2O}} [t\mathrm{BuNH_2NH_2}]^+[\mathrm{N_3}]^- \quad (1)$$

The vibrational spectra show the characteristic absorptions of an ionic azide at 2037 cm^{-1} (ν_{as}, IR) and 1340 cm^{-1} (ν_s, Raman). The ^{1}H-NMR spectrum contains a broad signal at $\delta = 7.26$, which is characteristic for a hydrazinium ion. The ^{14}N-NMR spectrum shows two signals at $\delta = -134$ and -277, corresponding to the terminal azide nitrogen atom and the the central azide nitrogen atom respectively. No ^{14}N-NMR resonance was detected for the hydrazinium ion. This effect is observed with other ammonia and hydrazine compounds.[9]

Crystals of **1** are orthorhombic with space group P_{bcm} and $Z = 4$ molecules in the unit cell. The bond lengths and angles of the *tert*-butylhydrazinium ion, as indicated in Figure 1, are in accordance with the bond lengths and angles of known compounds.[10][11] The N–C bond length is in compliance with the literature data for this kind of molecule. The bond length is with 1.52 Å slightly longer than the N–C bond length of primary carbon atoms due to the bulky substituent. The bond length and angles of the azide ion are also in agreement with the literature data.[12] As can be seen in Figure 1, the azide anions are linked to the hydrazinium ions through hydrogen bonding between the terminal azide nitrogens and both nitrogen atoms of the *tert*-butylhydrazinium ion. In total there are four hydrogen bonds per azide anion (two per terminalazide nitrogen). One terminal azide nitrogen is connected through each of ist to hydrogen bonds to the protonated nitrogen atom of the hydrazinium ion. These two bonds have a length of 1.91 Å. The other terminal azide nitrogen is analogously connected to the non-protonated nitrogen of the *tert*-butylhydrazinium ion. These two bonds are longer, with a length of 2.25 Å.

This results in a highly symmetric crystal structure. The azide ions form layers, which are sandwiched between two different layers of hydrazinium ions.

[+] Crystal structure analysis.
[a] Institute of Inorganic Chemistry, University of Munich, Butenandtstraße 5–13 (Haus D), D-81377 München, Germany
Fax: (internat.) + 49(0)89/2180-7492
E-mail: tmk@cup.uni-muenchen.de
[b] Wehrwissenschaftliches Institut für Werk-, Explosiv- und Betriebsstoffe, D-53913 Swisstal, Germany

 © WILEY-VCH Verlag GmbH, D-69451 Weinheim, 1999 1434–1948/99/0505–0849 $ 17.50+.50/0

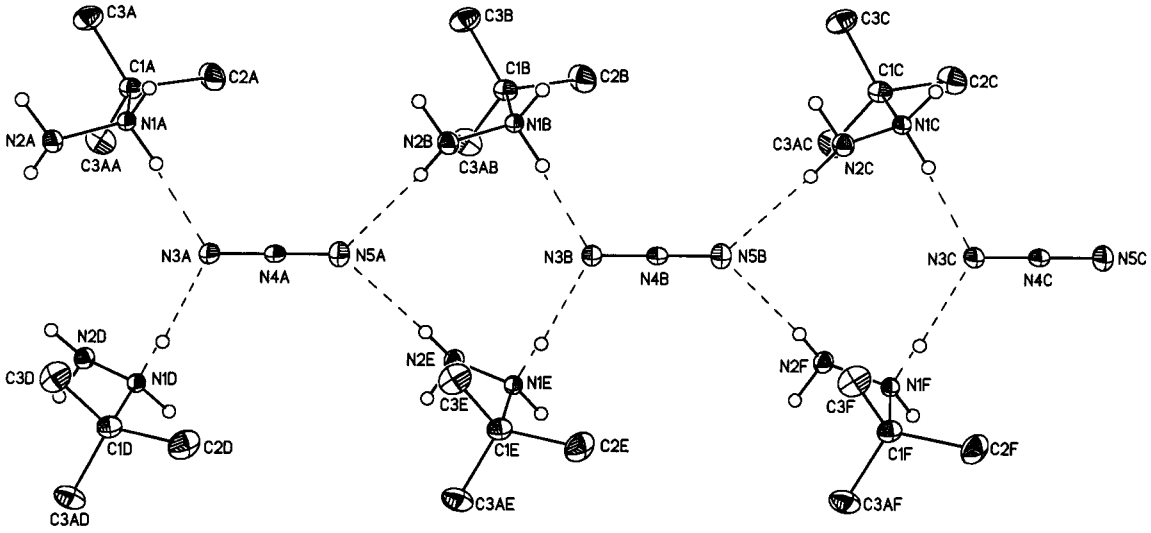


Figure 1. Molecular structure and hydrogen bonds of **1** as ORTEP plot (thermal ellipsoids represent 25% probability); selected bond lengths [Å] and angles [°] of **1**: N(1)−N(2) 1.441(2), N(1)−C(1) 1.522(2), C(1)−C(3/3A) 1.514(2), C(1)−C(2) 1.529(2), N(2)−N(1)−C(1) 107.9(7), N(1)−C(1)−C(2) 104.14(1), C(3/3A)−C(1)−N(1) 108.44(8), C(3/3A)−C(1)−C(2) 111.57(9), N(5)−N(4)−N(3) 180.0.

Synthesis of 2

N,N,N-Trimethylhydrazinium azide **2** is prepared via an ion exchange reaction with silver azide in aqueus solution. After removal of byproducts and water, **2** crystallizes from methanol.

$$[(CH_3)_3NNH_2]^+[I]^- + AgN_3 \xrightarrow[-\ AgI]{H_2O} [(CH_3)_3NNH_2]^+[N_3]^- \quad (2)$$

As mentioned for **1**, the vibrational spectra show the typical azide absorptions at 2055 cm^{-1} (ν_{as}, IR) and 1327 cm^{-1} (ν_s, Raman). The region around 3200 cm^{-1}, where NH vibrations typically occur, is different from *N,N,N*-trimethylhydrazinium iodide. Otherwise the vibrational spectra, ^{1}H-NMR and ^{13}C-NMR spectra are in agreement with the iodide.[13] The ^{14}N-NMR spectrum shows two signals for the azide ion at $\delta = -133$ (*N*N*N*) and −278 (N*N*N). The two signals of the hydrazinium ion give a very broad signal at $\delta = -306$. The compound has a melting point of 174°C and is not volatile. **2** is also very hygroscopic.

Crystal Structure of 2

Bond lengths and angles of **2** are similar to *N,N,N*-trimethylhydrazinium chloride.[14] The major difference is in the structure of the hydrogen bonds between the hydrazinium and the azide ions, explaining the different NH-vibrational bands in the vibrational spectra. The azide ion has four hydrogen bonds to adjacent hydrazinium ions. Each terminal azide nitrogen atom has two short hydrogen bonds to two hydrazinium ions of two different layers (2.20 Å and 2.17 Å). Another hydrazinium ion has two very long

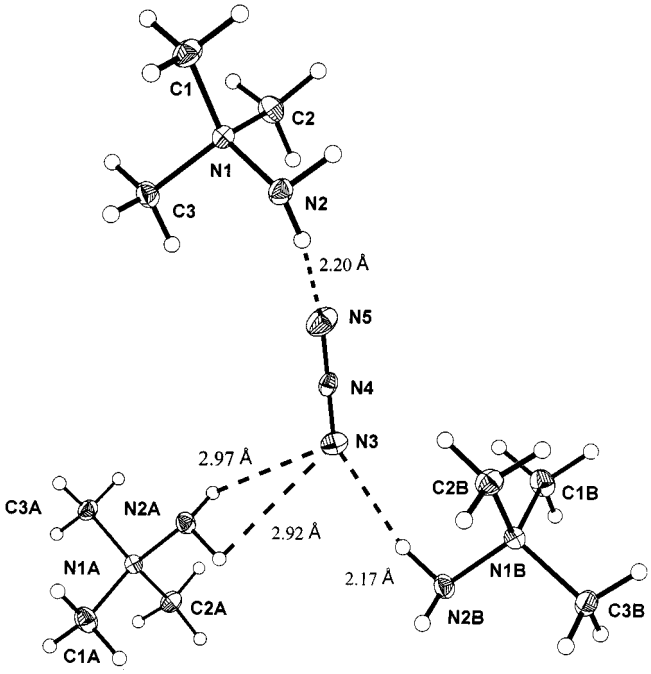


Figure 2. Molecular structure and atom numbering scheme of **2** as ORTEP plot (thermal ellipsoids represent 25% probability); selected bond lengths [Å] and angles [°] of **2**: N(1)−N(2) 1.459(1), N(1)−C(1) 1.489(2), N(1)−C(2) 1.497(2), N(1)−C(3) 1.493(2), N(3)−N(4) 1.180(2), N(4)−N(5) 1.163(2), N(2)−N(1)−C(1) 107.16(9), N(2)−N(1)−C(2) 109.4(1), N(2)−N(1)−C(3) 107.14(9), C(1)−N(1)−C(3) 109.8(1), C(1)−N(1)−C(2) 110.2(1), C(3)−N(1)−C(2) 109.4(1), N(5)−N(4)−N(3) 179.9(1).

hydrogen bonds of 2.92 Å and 2.97 Å to the terminal azide nitrogen atom that has the shorter bond length of 2.17 Å.

Tetraethylphosphonium azide lacks hydrogen bonds.[15] Therefore, there are only alternating layers of phosphonium and azide ions. In **2** there are also alternating layers of hydrazinium and azide ions. In contrast to tetraethylphos-

phonium azide the layer of the hydrazinium ions is ordered due to the hydrogen bonds.

Conclusion

The volatility of hydrazine azide can be reduced by attaching organic substituents to the hydrazine. The melting point of such substituted hydrazinium azides also rises. **1** and **2** have very symmetric crystal structures. In both compounds, hydrogen bridges are an important factor. Substance **2** is very hygroscopic, preventing its use for commercial purposes. Substance **1** does not show hygroscopicity, but has yet to be tested for its explosive properties

Experimental Section

General Remarks: ***CAUTION:*** Silver azide, hydrazoic acid, and compounds **1** and **2** are explosives. Safety equipment like leather gloves, face-shield, and ear plugs is recommended. The synthesis of **1** was carried out using standard schlenk-line techniques under dry nitrogen. Diethyl ether was purified by destillation over Na/benzophenone, methanol by destillation over Na. The destillates were stored under nitrogen. − *tert*-Butylhydrazine was prepared by the reaction of potassium hydroxide with *tert*-buylhydrazine dihydrochloride (Aldrich), *N,N,N*-Trimethylhydrazinium iodide was prepared by literature methods.[15] − NMR: Jeol EX 400 (^{1}H (400 MHz), ^{13}C (100 MHz): chemical shifts refer to $\delta_{TMS} = 0.00$; ^{14}N (28.6 MHz): external standard CH_3NO_2). − IR: Nicolet 520 FT-IR (as KBr pellets). − Raman: Perkin−Elmer FTIR-2000 spektrometer (Nd-Yag Laser: 1064 nm, Laser power: 100 mW, scattering angle: 90°). − CHN analysis: Elementar Vario EL analysator. − Melting points: Büchi B450.

***tert*-Butylhydrazinium Azide (1):** 45 mL of a 2 M solution of hydrazoic acid in ether were slowly added to 4.0 g (55 mmol) of anhydrous *tert*-butylhydrazine. A white precipitate was isolated and purified by sublimation at 10^{-3} Torr. Recrystallization from methanol yielded colorless prisms. Yield: 5.3 g (90%); m.p. 137°C. − IR (cm^{-1}): $\tilde{\nu}$ = 3428 w, 3319 m, 3194 w, 2981 w, 2828 vw, 2784 vw, 2696 vw, 2696 vw, 2506 w, 2037 s (ν_{as} N_3^-), 1605 m, 1490 w, 1469w, 1455 w, 1398 m, 1378 m, 1337 w, 1288 vw, 1254 vw, 1200 vw, 1121 m, 1031 w, 947 w, 924 w, 840 w, 728 w, 651 w and 639 vw (ν and δN_3^-), 619 vw, 518 w, 467 w, 356 w, 325 w. − Raman (cm^{-1}): $\tilde{\nu}$ = 3321 w, 3213 w, 2986 m, 2928 m, 2748 vw,2503 vw, 1509 vw, 1494 vw, 1460 w, 1340 s(ν_s N_3^-), 1289 w, 1223 w, 1120 w, 941.0 vw, 924 vw, 851 vw, 735 m, 652 vw, 517 m, 474 w, 365 w, 241 vw, 115 s. − ^{1}H NMR ([D6]DMSO): δ = 1.15 (s, 9 H, CH_3), 7.26 (s, 4 H, NH). − ^{13}C NMR ([D_6]DMSO): δ = 23.9 (CH_3), 57.4 (C quat.). − ^{14}N NMR ([D_6]DMSO): δ = −134 (*N*NN), −277 (N*N*N). − $C_4H_{13}N_5$ (131.18): calcd. C 36.62, H 9.99, N 53.39; found C 36.35, H 10.38, N 54.03.

***N,N,N*-Trimethylhydrazinium Azide (2):** Silver azide was prepared by adding a solution of 7.94 g (53.3 mmol) of silver nitrate in 50 mL of water to a solution of 3.46 g (53.3 mmol) of sodium azide in 50 mL of water. Silver azide was filtered off and washed with water. The wet product was introduced to a solution of 4.12 g (20.3 mmol) *N,N,N*-trimethylhydrazinium iodide. Yellow silver iodide precipitated immediately. The reaction mixture was stirred over night, silver iodide was filtered off, and the water removed under vacuum. The crude product was washed with CH_2Cl_2 and recrystallized from methanol yielding 1.96 g (81%) of colorless needles. m.p. 174°C. − IR (cm^{-1}): $\tilde{\nu}$ = 3409 vw, 3358 m, 3316 vw, 3287 m, 3213 m, 3113 m, 2946 w, 2849 w, 2055 s, (ν_{as} N_3^-), 1632 s, 1485 s, 1467 m, 1450 w, 1397 m, 1292 m, 1159 m, 1068 w, 954 s, 922 m, 749 m, 504 m, 459 m. − Raman (cm^{-1}): $\tilde{\nu}$ = 3268 vw, 3140 w, 3034 m, 2952 m, 2876 vw, 1465 m, 1399 vw, 1327 s (ν_s N_3^-), 1246 m, 944 w, 913 w, 749 m, 465 w, 390 vw, 106 s. − ^{1}H NMR ([D_6]DMSO): δ = 3.25 (s, 9 H, CH_3), 6.21 (s, 2 H, NH). − ^{13}C NMR ([D_6]DMSO): δ = 57.1 (CH_3). − ^{14}N NMR ([D_6]DMSO): δ = −133 (*N*NN), −278 (N*N*N), −306 ($H_2NN(CH_3)_3$). − $C_3H_{11}N_5$ (117.15): calcd. C 30.76, H 9.46, N 59.78; found C 29.64, H 8.85, N 57.81.

Crystal Structure Determinations: Crystals of each compound were mounted on a glass fibre with a small amount of perflourether oil. Data was collected at 193 K on a Siemens P4 diffractometer, equipped with a Siemens CCD area detector with graphite monochromated Mo-K_α radiation (λ = 0.71073 Å). The structure was solved by direct methods (SHELXL 93 and 97).

Table 1. Crystallographic data and data related to data aquisition and refinement for compounds **1** and **2**

Compound	**1**	**2**
Empirical formula	$C_4H_{13}N_5$	$C_3H_{11}N_5$
Molecular mass	131.19	117.17
Cryst. size [mm]	0.20×0.30×0.30	0.20×0.20×0.30
Cryst. system	Orthorhombic	Orthorhombic
Space group	*Pbcm*	*Pbca*
a [Å]	6.9234(1)	10.9689(1)
b [Å]	12.1203(3)	10.5082(3)
c [Å]	9.5133(3)	11.0937(2)
V, [Å^3]	798.30(3)	1278.70(4)
Z	4	8
ρ(calcd.), [mg/m^3]	1.092	1.217
μ [mm^{-1}]	0.076	0.087
F(000)	288	512
Index range	$-8 \le h \le 8$	$-13 \le h \le 14$
	$-15 \le k \le 15$	$-13 \le k \le 9$
	$-9 \le l \le 12$	$-14 \le l \le 13$
2 θ [°]	57.70	58.58
Temp. [K]	183(2)	193
Refl. collected	4320	6762
Refl. unique	903	1339
Refl. observed (4σ)	737	1066
R (int.)	0.0212	0.0345
No. Variables	77	78
Weighting scheme[a] x/y	/	0.0534/0.2582
GOOF	1.042	1.100
Final *R*(4σ)	0.0346	0.0408
Final *wR*2	0.0927	0.1014
Larg. res. Peak [e/Å^3]	0.180	0.156

[a] $w^{-1} = \sigma^2 F_o^2 + (xP)^2 + yP$; $P = (F_o^2 + 2F_c^2)/3$.

Further information on the crystal-structure determinations has been entered in the Cambridge Crystallographic Data Centre as supplementary publication no. CCDC 106145/106146 and may be obtained from CCDC, 12 Union Road, Cambridge CB2 1EZ, U.K. [Fax: (internat.) + 44-1223/336033; E-mail: deposit@ccdc.cam.ac.uk].

[1] [1a] T. Curtius, *Chem. Ber.* **1891**, *24*, 3341. − [1b] E. P. Kirpichev, A. P. Alekseev, Yu. I. Rubtsov, G. B. Manelis, *Russian Journal of Phys. Chem.* **1973**, *47*, 1654.
[2] [2a] I. C. Tornieporth-Oetting, T. M. Klapötke, *Angew. Chem.* **1995**, *107*, 509; *Angew. Chem. Int. Ed. Engl.* **1995**, *34*, 511. − [2b] T. M. Klapötke, *Chem. Ber.* **1997**, *130*, 443. − [2c] I. C. Tornieporth-Oetting, T. M. Klapötke, *Combustion Efficiency and Air Quality* (Eds.: I. Hargittai, T. Vidoczy), p. 51, Plenum Press, New York, **1995**.

[3] K. Jones, *Comprehensive Inorganic Chemistry* (Eds.: J. C. Bailar, H. J. Emeleus, R. Nyholm, A. F. Trotman-Dickenson), vol. 2, p. 250. Pergamon Press, Oxford, **1973**.
[4] H. W. Schiessl, *Aldrichim. Acta* **1980**, *13*, 33.
[5] [5a] H. Holfter, T. M. Klapötke, A. Schulz, *Eur. J. Solid State Chem.* **1996**, 33, 855. – [5b] T. M. Klapötke, P. S. White, I. C. Tornieporth-Oetting, *Polyhedron* **1996**, *15*, 2579.
[6] H. Holfter, T. M. Klapötke, A. Schulz, *Propellants, Explos., Pyrotech.* **1997**, *22*, 1.
[7] W.-H. Walther, T. M. Klapötke, G. Holl, *29th Annual Conference of ICT* **1998**, P134, Fraunhofer Institut für Chemische Technologie (ICT), Karlsruhe.
[8] T. M. Klapötke, H. Nöth, H. Schwenk-Kircher, W.-H. Walther, *Polyhedron*, in press.
[9] M. Witanowski, L. Stefaniak, G. A. Web, *Annual Reports on NMR Spektroscopy*, Academic Press, San Diego, **1993**, p. 25.
[10] L. M. Trefonas, J. Couvillion, *Acta Crystallogr.* **1963**, *16*, 576.
[11] P. A. Carpy, J.-M. Leger, J.-C. Colleter, *Acta Crystallogr. Sect. B* **1980**, *36*, 2837–2840.
[12] T. M. Klapötke, I. C. Tornieporth-Oetting, *Nichtmetallchemie,* p. 263, VCH Verlagsgesellschaft, Weinheim, **1994**.
[13] U. Anthoni, *Acta Chem. Scand.* **1970**, *24*, 959–984.
[14] T. J. Giordano, G. J. Palenik, H. H. Sisler, *Inorg. Chem.* **1976**, *15*, 751.
[15] R. Goesl, A. Meuwsen, *Chem. Ber.* **1953**, *92*, 2521–2529.

Received November 13, 1998
[I98393]

Tri- and Tetranuclear Mixed-Metal Clusters Containing Alkyne Ligands: Synthesis and Structure of $[Ru_3Ir(CO)_{11}(RCCR')]^-$, $[Ru_2Ir(CO)_9(RCCR')]^-$, and $[HRu_2Ir(CO)_9(RCCR')]$

Vincent Ferrand,[a] Georg Süss-Fink,*[a] Antonia Neels,[a] and Helen Stoeckli-Evans[a]

Keywords: Cluster compounds / Ruthenium / Iridium / Alkynes / Butterfly structures

The tetrahedral cluster anion $[Ru_3Ir(CO)_{13}]^-$ (**1**) reacts with internal alkynes RC≡CR′ to afford the alkyne derivatives $[Ru_3Ir(CO)_{11}(RCCR')]^-$ (**2**: R = R′ = Ph; **3**: R = R′ = Et; **4**: R = Ph; R′ = Me; **5**: R = R′ = Me) which have a butterfly arrangement of the Ru_3Ir skeleton in which the alkyne is coordinated in a μ_4-η^2 fashion. Under CO pressure they undergo fragmentation to give the trinuclear cluster anions $[Ru_2Ir(CO)_9(RCCR')]^-$ (**6**: R = R′ = Ph; **7**: R = R′ = Et; **8**: R = Ph; R′ = Me; **9**: R = R′ = Me), in which the alkyne ligand is coordinated in a μ_3-η^2 parallel fashion. Protonation of these trinuclear anions leads to the formation of the corresponding neutral hydrido clusters $[HRu_2Ir(CO)_9(RC{\equiv}CR')]$ (**10**: R = R′ = Ph; **11**: R = R′ = Et; **12**: R = Ph; R′ = Me; **13**: R = R′ = Me). The protonation of the butterfly anions **2** and **3**, however, gives rise to the formation of the neutral tetrahedral clusters $[HRu_3Ir(CO)_{11}(RCCR')]$ (**14**: R = R′ = Ph and **15**: R = R′ = Et), respectively. The analogous clusters $[HRu_3Ir(CO)_{11}(PhCCCH_3)]$ (**16**) and $[HRu_3Ir(CO)_{11}(CH_3CCCH_3)]$ (**17**) are only accessible from the reaction of the neutral cluster $[HRu_3Ir(CO)_{13}]$ with the corresponding alkynes. The complexes **2**, **4**, **5**, **6**, **10**, **12** and **15** are characterised by X-ray structure analysis.

Introduction

The chemistry of mixed-metal clusters of transition metals has been studied in great detail in recent years,[1][2] stimulated by their possible catalytic potential and the combination of different metals in the same complex.[3a,3b] The mixed-metal cluster $Pt_3Ru_6(CO)_{20}(\mu_3\text{-}PhC_2Ph)(\mu_3\text{-}H)(\mu\text{-}H)$ has been shown by R. D. Adams et al. to be an very active catalyst for the hydrogenation of alkynes[3c−3e]. Tetranuclear clusters with the butterfly structure[4][5] have received much attention, due to their intermediary position between tetrahedral and square-planar clusters. They have been also considered as a model for chemisorption of small molecules,[6] and they have been studied as intermediates in homogeneous catalytic processes.[4,7,8] Both, metal atoms and ligands can vary widely in butterfly-type clusters, which determines, on the one hand, the structural properties of the butterfly framework and, on the other hand, the chemistry of the coordinated ligands.[4]

In a recent publication,[8] we have described the reactivity of the neutral tetrahedral cluster $[HRu_3Ir(CO)_{13}]$[9] towards alkynes and its catalytic potential in hydrogenation reactions. We now report the reaction of its precursor, the cluster anion $[Ru_3Ir(CO)_{13}]^-$[9] with internal alkynes, which affords anionic alkyne clusters of the type $[Ru_3Ir(CO)_{11}(RCCR')]^-$, and we also report on the reactivity of the latter anions towards CO and H^+.

[a] Institut de Chimie, Université de Neuchâtel,
Avenue de Bellevaux 51, CH-2000 Neuchâtel, Switzerland
Fax: (internat.) + 41-32/718-2400
E-mail: Georg.Suess-Fink@ch.unine.ch

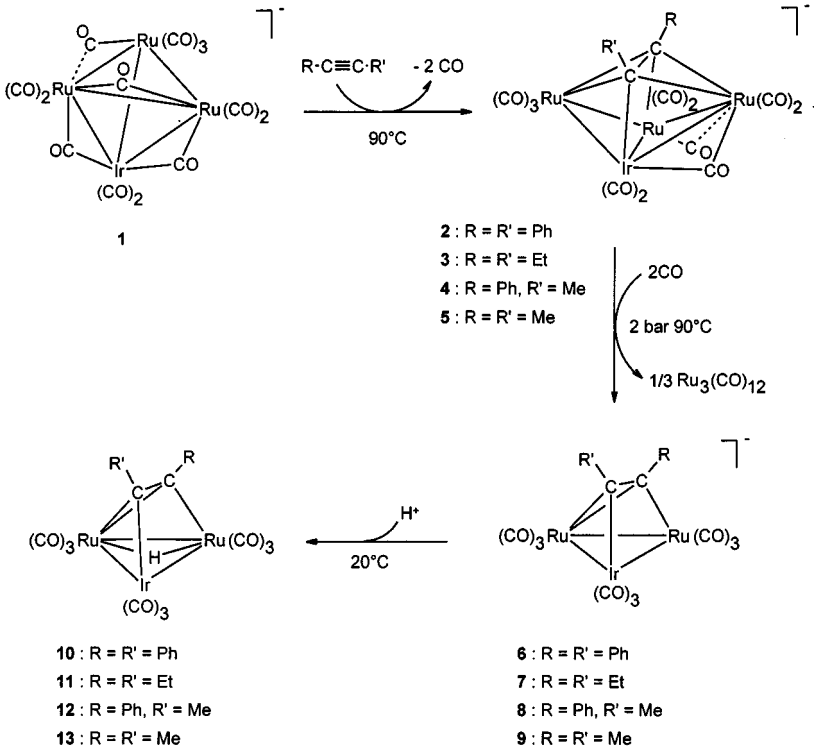
Results and Discussion

Synthesis of the Cluster Anions $[Ru_3Ir(CO)_{11}(RCCR')]^-$ (2−5)

The thermal reaction of the tetrahedral cluster anion $[Ru_3Ir(CO)_{13}]^-$ (**1**) with the internal alkynes diphenylacetylene, 3-hexyne, 1-phenyl-1-propyne, or 2-butyne yields, at 90 °C in CH_2Cl_2 solution (pressure Schlenk tube), the alkyne derivatives $[Ru_3Ir(CO)_{11}(RCCR')]^-$ (**2**: R = R′ = Ph; **3**: R = R′ = Et; **4**: R = Ph; R′ = Me; **5**: R = R′ = Me) (Scheme 1). These anions can be isolated as the bis(triphenylphosphoranylidene)ammonium salts from a mixture of diethyl ether and hexane (**2**, **4**, and **5**), or from a mixture of ethanol and pentane (**3**). Complexes **2**, **4**, and **5** gave suitable crystals for X-ray structure analysis.

The infrared spectra of all the compounds display the same absorption pattern in the ν_{co} region, indicating the presence of terminal as well as bridging CO ligands (Table 1). The ^{1}H-NMR spectra of **2**−**5** are complicated by the multiplets of the $[N(PPh_3)_2]^+$ cation; for **2** and **4**, the resonances of the phenyl protons of the alkyne ligands overlap with the signals of the cation. In the case of **4** (containing an unsymmetrical alkyne ligand), only one singlet at δ = 2.82 is observed for the methyl group, indicating the presence of only one isomer. In the case of **3** and **5** (containing a symmetrical alkyne ligand), the two alkyl substituents on the alkyne are nonequivalent, suggesting the alkyne ligand to be coordinated in a nonsymmetrical fashion to the Ru_3Ir framework (Table 1). This is confirmed by the X-ray structure analysis of the bis(triphenylphosphoranylidene)ammonium salts of **2**, **4**, and **5**.

 © WILEY-VCH Verlag GmbH, D-69451 Weinheim, 1999 1434−1948/99/0505−0853 $ 17.50+.50/0



Scheme 1. Synthetic routes to clusters **2**−**13**

Molecular Structures of $[Ru_3Ir(CO)_{11}(RCCR')]^-$ (2, 4, and 5)

Suitable crystals of **2**, **4**, and **5** {$[N(PPh_3)_2]^+$ salts} were grown at room temperature from a mixture of diethyl ether and hexane. The molecular structures of the anions **2**, **4**, and **5** are depicted in Figures 1, 2, and 3, respectively. Selected bond lengths and angles of complexes **2**, **4**, and **5** are summarized in Tables 2, 3, and 4, respectively. The crystal structures consist of discrete $[N(PPh_3)_2]^+$ cations and $[Ru_3Ir(CO)_{11}(RCCR')]^-$ anions showing normal intermolecular contacts between the atoms of the ions. The cluster anions **2**, **4**, and **5** have the same overall structure: The four metal atoms form a butterfly skeleton where the iridium atom occupies a hinge position, whereas in the known cobalt analogue $[Ru_3Co(CO)_{11}(PhCCPh)]^-$,[10] obtained by reaction of $[Ru_3Co(CO)_{13}]^-$ with diphenylacetylene, the cobalt atom occupies a wingtip position. In other mixed-metal clusters anions with the butterfly core structure, such as $[Ru_3M(CO)_{10}Cp(CH_3CCCH_3)]^-$ (M = W, Mo)[11] and $[Co_3Ru(CO)_{10}(PhCCPh)]^-$,[12a] the single metal atom M always occupies a hinge position as found in **2**, **4**, and **5**.

All metal−metal distances in **2**, **4**, and **5** are different (Tables 2, 3, 4), but in the expected range for Ru−Ru and Ru−Ir single bonds.[4,8,9] In the three clusters, the coordination of the eleven carbonyl ligands is the same: While nine carbonyl groups are terminal, one CO ligand [C(6)O(6) in **2**, C(20)O(20) in **4**, C(10)O(10) in **5**] is bridging the Ir−Ru(3) edge, one CO ligand [C(10)O(10) in **2**, C(14)O(14) in **4**, C(15)O(15) in **5**] being coordinated to Ru(2) is semi-

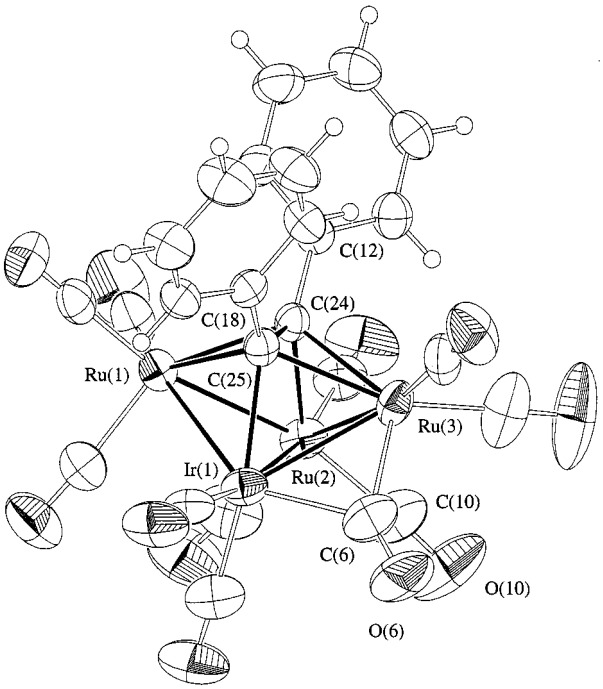


Figure 1. ORTEP plot of $[IrRu_3(CO)_{11}(\mu_4\text{-}\eta^2\text{-}C_2Ph_2)]^-$ (anion **2**); thermal ellipsoids are drawn at 50% of propability

bridging to Ru(3) as indicated by the distances carbon−Ru(2) [**2**: C(10)−Ru(2) = 1.903(7) Å; **4**: C(14)−Ru(2) = 1.896(3) Å; **5**: C(15)−Ru(2) = 1.903(6) Å] and the carbon−Ru(3) [**2**: C(10)−Ru(3) = 2.8893(3) Å; **4**:

Table 1. IR and NMR data of the complexes **2**−**17**

Complexes	ν_{CO} [cm^{-1}][a]	δ (^1H) [ppm][b−d]
$[N(PPh_3)_2][Ru_3Ir(CO)_{11}(PhCCPh)]$ (**2**)	2055(m), 2009(vs), 1988(s), 1960(sh), 1913(w), 1801(w)	7.70−6.80 (C_6H_5, m)
$[N(PPh_3)_2][Ru_3Ir(CO)_{11}(EtCCEt)]$ (**3**)	2052(m), 2002(vs), 1983(s), 1962(sh), 1937(m), 1913(w), 1794(w)	7.70−7.40 (C_6H_5, m); 2.68 ($CH_3CH_2CCCH_2CH_3$, q $^3J_{HH}$ 7.4 Hz); 2.61 ($CH_3CH_2CCCH_2CH_3$, q $^3J_{HH}$ 7.4 Hz); 0.94 ($CH_3CH_2CCCH_2CH_3$, t $^3J_{HH}$ 7.4 Hz); 0.90 ($CH_3CH_2CCCH_2CH_3$, t $^3J_{HH}$ 7.4 Hz)
$[N(PPh_3)_2][Ru_3Ir(CO)_{11}(PhCCMe)]$ (**4**)	2055(m), 2007(vs), 1986(s), 1963(sh), 1936(m), 1909(w), 1799(w)	7.70−7.39 (C_6H_5, m); 2.82 (CH_3CCPh, s)
$[N(PPh_3)_2][Ru_3Ir(CO)_{11}(MeCCMe)]$ (**5**)	2054(m), 2004(vs), 1984(s), 1959(sh), 1934(m), 1906(w), 1800(w)	7.70−7.42 (C_6H_5, m); 3.14 (CH_3CCCH_3, s); 2.91 (CH_3CCCH_3, s)
$[N(PPh_3)_2][Ru_2Ir(CO)_9(PhCCPh)]$ (**6**)	2054(m), 2011(s), 1998(vs), 1980(s), 1940(m)	6.60−7.70 (C_6H_5, m)
$[N(PPh_3)_2][Ru_2Ir(CO)_9(EtCCEt)]$ (**7**)	2048(w), 2002(s), 1992(vs), 1971(m), 1932(w)	7.70−7.20 (C_6H_5, m); 3.41 ($CH_{3c}CH_aH_bCCCH_{a'}H_{b'}CH_{3c'}$, dq $^3J_{HaHc}$ 7.2 Hz, $^2J_{HaHb}$ 13.3 Hz); 2.74 ($CH_{3c}CH_aH_bCCCH_{a'}H_{b'}CH_{3c'}$, dq $^3J_{Ha'Hc'}$ 7.3 Hz, $^2J_{Ha'Hb'}$ 13.0 Hz); 2.10 ($CH_{3c}CH_aH_bCCCH_{a'}H_{b'}CH_{3c'}$, dq $^3J_{HbHc}$ 7.2 Hz, $^2J_{HaHb}$ 13.3 Hz); 1.97 ($CH_{3c}CH_aH_bCCCH_{a'}H_{b'}CH_{3c'}$, dq $^3J_{Hb'Hc'}$ 7.3 Hz, $^2J_{Ha'Hb'}$ 13.0 Hz);1.14 ($CH_{3c}CH_aH_bCCCH_{a'}H_{b'}CH_{3c'}$, t $^3J_{HH}$ 7.3 Hz); 1.07 ($CH_{3c}CH_aH_bCCCH_{a'}H_{b'}CH_{3c'}$, t $^3J_{HH}$ 7.3 Hz);
$[N(PPh_3)_2][Ru_2Ir(CO)_9(PhCCMe)]$ (**8**)	2052(w), 2007(s), 1996(vs), 1976(m), 1938(w)	7.70−6.90 (C_6H_5, m); 2.64 (CH_3CCPh, s(isomer 1)); 2.30 (CH_3CCPh, s(isomer 2))
$[N(PPh_3)_2][Ru_2Ir(CO)_9(MeCCMe)]$ (**9**)	2049(w), 2002(s), 1993(vs), 1971(m), 1934(w)	7.71−7.35 (C_6H_5, m); 2.70 (CH_3CCCH_3, s); 2.40 (CH_3CCCH_3, s)
$[HRu_2Ir(CO)_9(PhCCPh)]$ (**10**)	2101(w), 2072(vs), 2061(s), 2034(s), 2022(m), 2016(m), 2005(w)	7.20−6.80 (C_6H_5, m); −15.07 (Ru*H*Ru, s)
$[HRu_2Ir(CO)_9(EtCCEt)]$ (**11**)	2099(w), 2069(s), 2057(s), 2030(vs), 2018(m), 2008(m), 1990(w)	2.93 ($CH_3CH_2CCCH_2CH_3$, q $^3J_{HH}$ 7.4 Hz); 2.42 ($CH_3CH_2CCCH_2$ CH_3, q $^3J_{HH}$ 7.4 Hz); 1.34 ($CH_3CH_2CCCH_2CH_3$, t $^3J_{HH}$ 7.4 Hz); 1.20 ($CH_3CH_2CCCH_2CH_3$, t $^3J_{HH}$ 7.4 Hz); −15.39 (Ru*H*Ru, s)
$[HRu_2Ir(CO)_9(PhCCMe)]$ (**12**)	2100(w), 2071(vs), 2060(s), 2032(s), 2021(m), 2003(m), 1994(w)	7.20−6.90 (C_6H_5, m); 2.80 (CH_3CCPh, s); −15.27 (Ru*H*Ru, s)
$[HRu_2Ir(CO)_9(MeCCMe)]$ (**13**)	2099(w), 2069(vs), 2057(s), 2030(vs), 2018(m), 2008(m), 1991(w)	2.83 (CH_3CCCH_3, s); 2.37 (CH_3CCCH_3, s); −15.31 (Ru*H*Ru, s)
$[HRu_3Ir(CO)_{11}(PhCCPh)]$ (**14**)	2095(w), 2071(s), 2053(s), 2037(vs), 2012(m), 1994(m), 1842(w)	7.30−7.00 (C_6H_5, m); −18.88 (Ru*H*Ru, s)
$[HRu_3Ir(CO)_{11}(EtCCEt)]$ (**15**)	2095(w), 2070(s), 2051(s), 2034(vs), 2010(m), 1991(m), 1840(w)	2.98 ($CH_3CH_aH_bCCCH_{a'}H_{b'}CH_3$, dq $^3J_{HH}$ 7.3 Hz, $^2J_{HH}$ 15.0 Hz); 2.74 ($CH_3CH_aH_bCCCH_{a'}H_{b'}CH_3$, dq $^3J_{HH}$ 7.3 Hz, $^2J_{HH}$ 15.0 Hz); 1.28 ($CH_3CH_aH_bCCCH_{a'}H_{b'}CH_3$, t $^3J_{HH}$ 7.3 Hz); −19.10 (Ru*H*Ru, s)
$[HRu_3Ir(CO)_{11}(PhCCMe)]$ (**16**)	2093(w), 2065(s), 2048(s), 2032(vs), 2006(m), 1989(m), 1842(w)	7.50−7.20 (C_6H_5, m); 2.80 (CH_3, s) −18.88 (Ru*H*Ru, s)
$[HRu_3Ir(CO)_{11}(MeCCMe)]$ (**17**)	2094(w), 2068(s), 2049(s), 2033(vs), 2009(m), 1988(m), 1844(w)	2.72 (CH_3, s); −18.98 (Ru*H*Ru, s)

[a] Recorded in ether (**2**−**5**), CH_2Cl_2 (**6**−**9**, **14**−**17**), hexane (**10**−**12**, **13**). − [b] Measured in $CDCl_3$ solution at 294 K at 200 MHz (**2**, **4**−**6**, **9**, **10**, **12**−**15**, **17**). − [c] Measured in $CDCl_3$ solution at 294 K at 400 MHz (**3**, **7**, **8**, **11**, **16**). − [d] Measured in $CDCl_3$ solution at 215 K at 400 MHz (**7**, **8**).

C(14)−Ru(3) = 2.8115(3) Å; **5**: C(15)−Ru(3) = 2.8613(7) Å]. The angles C(10)−Ru(2)−Ru(3) = 73.7(2)° (**2**), C(14)−Ru(2)−Ru(3) = 71.86(10)° (**4**), C(15)−Ru(2)−Ru(3) = 73.00(19)° (**5**) are found to be similar to the angle observed in the cluster anion $[FeRu_3(CO)_{12}NO]^-$ [13] for a semibridging CO group.[14] These findings are comfirmed by the infrared spectra of **2**−**5** which exhibit a ν_{co} absorption around 1920 cm^{-1}.

The alkyne ligand in **2**, **4**, and **5** is coordinated to the Ru_3Ir metal core in a μ_4-η^2 fashion. One of the carbon atoms is σ-bonded to Ir, whereas the second one is σ-bonded to Ru(2), both carbon atoms being π-bonded to Ru(1) and Ru(3). This observation is confirmed by the ^1H-NMR spectra of **3** and **5** which display two different chemical shifts for the two ethyl or methyl substituents, respectively. The carbon−carbon bond is closer to Ru(1) than to Ru(3) in the three clusters, the torsion angle between the carbon−carbon backbone and the Ir(1)−Ru(2) edge is close to 0° [**2**: 0.0°(18); **4**: −0.04(11); **5**: 0.3°(2)] indicating that these two bonds are almost parallel.

With an electron count of 60e, **2**, **4**, and **5** are electron-deficient, since an M_4 butterfly cluster consistent with the noble-gas rule would require 62 electrons. However, considering **2**, **4**, and **5** as octahedral Ru_3IrC_2 clusters, an electron count of 60e is consistent with Wade's rules which predict a *closo* structure.[15]

Synthesis of $[Ru_2Ir(CO)_9(RCCR')]^-$ (6−9)

The cluster anions $[Ru_3Ir(CO)_{11}(RCCR')]^-$ (**2**: R = R′ = Ph; **3**: R = R′ = Et; **4**: R = Ph; R′ = Me; **5**: R = R′ = Me) undergo fragmentation of the metal core under CO pressure (2 bar) at 90 °C to give the trinuclear alkyne cluster anions $[Ru_2Ir(CO)_{11}(RCCR')]^-$ (Scheme 1). They can be isolated as the bis(triphenylphosphoranylidene)ammonium salts from a mixture of CH_2Cl_2 and diethyl ether (**6**) or from ethanol and pentane (**7**−**9**). The loss of metal fragments from a cluster has already been observed;[16][17] for example the cluster anion $[RuCo_3(CO)_{10}(\mu_4\text{-}\eta^2\text{-}C_2Ph_2)]^-$ can release a "Co(CO)" fragment to give the trinuclear complex $[RuCo_2(CO)_9(\mu_3\text{-}\eta^2\text{-}C_2Ph_2)]$ in which the alkyne adopts a parallel coordination.[12][18]

The infrared spectra of **6**−**9** exhibit in the carbonyl region absorptions of only terminal CO ligands (Table 1). The room-temperature ^1H-NMR spectrum of **8** reveals, in addition to the signals of the $[N(PPh_3)_2]^+$ cation, two singlets for the methyl group of the MeCCPh ligand in a ratio of

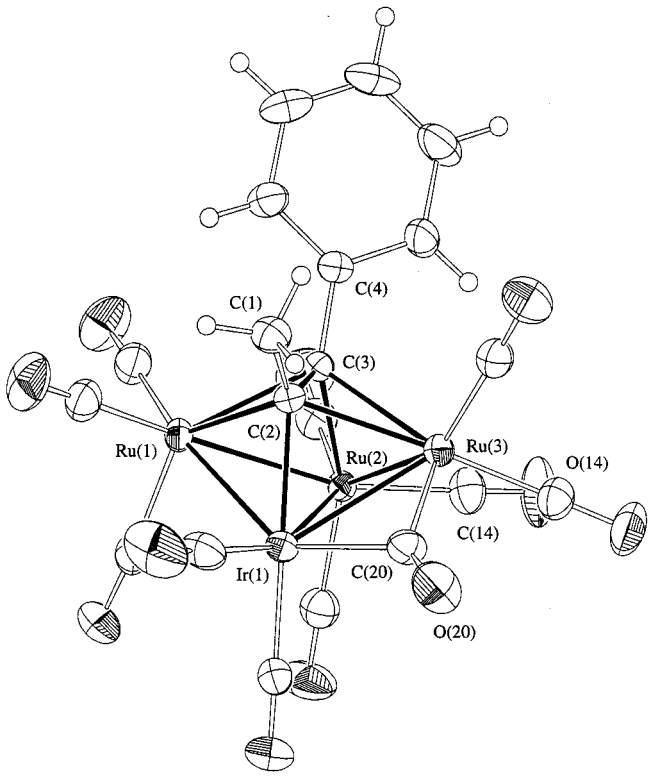


Figure 2. ORTEP plot of $[IrRu_3(CO)_{11}(\mu_4\text{-}\eta^2\text{-}PhCCMe)]^-$ (anion **4**); thermal ellipsoids are drawn at 50% of propability

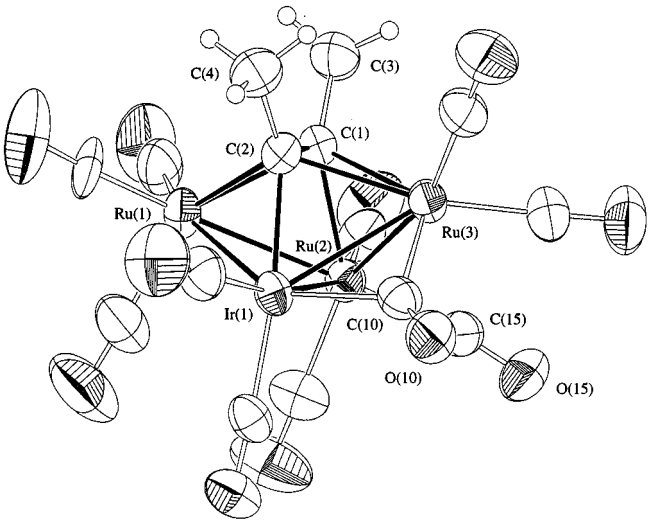


Figure 3. ORTEP plot of $[IrRu_3(CO)_{11}(\mu_4\text{-}\eta^2\text{-}C_2Me_2)]^-$ (anion **5**); thermal ellipsoids are drawn at 50% of propability

45:55. This ratio does not change down to −58 °C ($CDCl_3$), suggesting the presence of two isomers.[19−22] In the case of $[Ru_2Ir(CO)_9(MeCCMe)]^-$ (**9**), two singlets for the methyl substituents are observed in a ratio of 1:1, because the chemical environment of each CCH_3 moiety is different. The spectrum of $[Ru_2Ir(CO)_9(EtCCEt)]^-$ (**7**) is more complicated, presenting a temperature dependence of the signals of the ethyl substituents: At room temperature, four broad signals for the hydrogen atoms of the methylene groups are observed, resulting in four well-resolved multiplets at −58 °C, in a ratio of 1:1:1:1. In a selective decoupling experiment by irradiating at the resonances of the methyl proton, the four methylene multiplets resolve into four doublets with a coupling constant of 13 Hz, showing the protons of each methylene group to be diastereotopic (Table 1).[20,22a,22c,23a]

Table 2. Selected bond lengths [Å], bond angles [°], and torsion angles [°] for the anion **2**; estimated standard deviations in parentheses

Ir(1)−Ru(1)	2.7223(5)	Ru(3)−C(25)	2.298(4)
Ir(1)−Ru(3)	2.7235(6)	Ru(3)−C(24)	2.335(4)
Ir(1)−Ru(2)	2.7756(5)	Ru(3)−C(6)	1.993(6)
Ir(1)−C(6)	2.133(7)	C(24)−C(25)−C(18)	126.1(4)
Ir(1)−C(25)	2.188(4)	C(25)−C(24)−C(12)	127.1(4)
Ru(1)−Ru(2)	2.7357(6)	O(6)−C(6)−Ir(1)	134.9(6)
Ru(1)−C(25)	2.242(4)	O(6)−C(6)−Ru(3)	142.5(6)
Ru(1)−C(24)	2.258(5)	C(10)−Ru(2)−Ru(3)	73.7(2)
C(24)−C(25)	1.443(6)	O(10)−C(10)−Ru(2)	173.6(7)
		C(25)−Ir(1)−-Ru(2)−C(24)	0.00(18)

Table 3. Selected bond lengths [Å], bond angles [°], and torsion angles [°] for the anion **4**; estimated standard deviations in parentheses

Ir(1)−Ru(1)	2.7025(4)	Ru(3)−C(2)	2.338(3)
Ir(1)−Ru(3)	2.7018(4)	Ru(3)−C(3)	2.375(3)
Ir(1)−Ru(2)	2.8690(4)	Ru(3)−C(20)	1.977(3)
Ir(1)−C(20)	2.105(3)	C(1)−C(2)−C(3)	124.8(2)
Ir(1)−C(2)	2.132(3)	C(2)−C(3)−C(4)	123.5(2)
Ru(1)−Ru(2)	2.7158(5)	O(20)−C(20)−Ir(1)	135.5(3)
Ru(1)−C(2)	2.282(3)	O(20)−C(20)−Ru(3)	141.6(3)
Ru(1)−C(3)	2.297(3)	C(14)−Ru(2)−Ru(3)	71.86(10)
Ru(2)−Ru(3)	2.7483(5)	O(14)−C(14)−Ru(2)	167.4(3)
Ru(2)−C(14)	1.896(3)	C(3)−Ru(2)−Ir(1)−C(2)	0.04(11)
Ru(2)−C(3)	2.151(3)	C(2)−C(3)	1.429(4)

Table 4. Selected bond lengths [Å], bond angles [°], and torsion angles [°] for the anion **5**; estimated standard deviations in parentheses

Ir(1)−Ru(1)	2.7044(7)	Ru(3)−C(1)	2.356(6)
Ir(1)−Ru(3)	2.7182(7)	Ru(3)−C(2)	2.321(5)
Ir(1)−Ru(2)	2.8000(8)	Ru(3)−C(10)	2.012(6)
Ir(1)−C(10)	2.125(6)	C(3)−C(1)−C(2)	123.7(5)
Ir(1)−C(2)	2.150(6)	C(1)−C(2)−C(4)	124.3(5)
Ru(1)−Ru(2)	2.7114(9)	O(10)−C(10)−Ir(1)	136.1(5)
Ru(1)−C(1)	2.272(5)	O(10)−C(10)−Ru(3)	141.8(5)
Ru(1)−C(2)	2.242(6)	C(15)−Ru(2)−Ru(3)	73.00(19)
Ru(2)−Ru(3)	2.7647(8)	O(15)−C(15)−Ru(2)	170.5(6)
Ru(2)−C(1)	2.154(6)	C(2)−Ir(1)−Ru(2)−C(1)	0.3(2)
Ru(2)−C(15)	1.903(6)	C(1)−C(2)	1.406(8)

Molecular Structure of $[Ru_2Ir(CO)_9(PhCCPh)]^-$(6)

The molecular structure of **6** was confirmed by a single-crystal X-ray structure analysis of the bis(triphenylphosphoranylidene)ammonium salt. Suitable crystals were obtained by slow diffusion of diethyl ether into a concentrated dichloromethane solution at room temperature. The molecular structure of the anion is depicted in Figure 4. Selected bond lengths and angles are presented in Table 5. The crystal structure consists of discrete $[N(PPh_3)_2]^+$ cations and

$[Ru_2Ir(CO)_9(PhCCPh)]^-$ anions showing normal intermolecular contacts between the atoms of the ions. The ruthenium and iridium atoms of the cluster anion form a closed triangle in which all the metal−metal distances are different but within the range of Ru−Ru and Ir−Ru single bonds (Table 5). Each metal atom is bonded to three terminal CO groups.

Table 5. Selected bond lengths [Å], bond angles [°], and torsion angles [°] for the anion **6**; estimated standard deviations in parentheses

Ir(1)−Ru(1)	2.7120(8)	Ru(2)−C(1)	2.096(8)
Ir(1)−Ru(2)	2.7952(10)	Ru(2)−C(1)	2.096(8)
Ir(1)−C(2)	2.117(8)	C(1)−C(2)	1.363(11)
Ru(1)−Ru(2)	2.7084(11)	C(1)−C(2)−C(3)	125.4(7)
Ru(1)−C(1)	2.260(8)	C(2)−C(1)−C(9)	123.5(7)
Ru(1)−C(2)	2.246(8)	C(9)−C(1)−C(2)−C(3)	−9.8(13)

The alkyne ligand is coordinated in a classical μ_3-η^2 fashion over the metal triangle[18] as observed in $[Co_2Ru(CO)_9(C_2Ph_2)]$[12] The C(1)−C(2) backbone is almost parallel to the Ir(1)−Ru(2) edge [C(2)−Ir(1)−Ru(2)−C(1) 1.2(3)°]. The carbon atoms C(1) and C(2) are σ-coordinated to Ir(1) and Ru(2), respectively, and are both π-bonded to Ru(1).

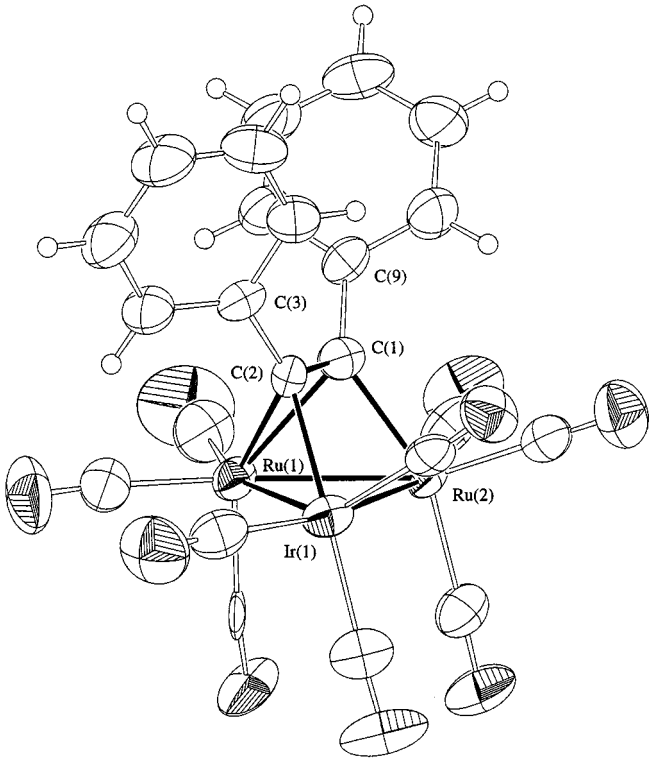


Figure 4. ORTEP plot of $[IrRu_2(CO)_9(\mu_3\text{-}\eta^2\text{-}C_2Ph_2)]^-$ (anion **6**); thermal ellipsoids are drawn at 50% of propability

The carbon−carbon bond is shorter in **6** [C(1)−C(2) 1.363(11) Å] than in **2** [C(24)−C(25) 1.443(6) Å]. This is due to the coordination of the alkyne to only three metal atoms in **6** with respect to **2** where it is coordinated to four metal atoms. The carbon−carbon bond length in **6** [C(1)−C(2) 1.363(11) Å] compares well with that in $[Co_2Ru(CO)_9(C_2Ph_2)]$ (C−C 1.370(3) Å)[12] and related complexes in which the C−C bond length varies from 1.33 to 1.47 Å.[18] Clusters **6**−**9** have the expected electron count of 48e for trinuclear clusters which obey the noble gas rule.

Synthesis of $[HRu_2Ir(CO)_9(RCCR')]$ (10−13)

The reaction of the anions $[Ru_2Ir(CO)_9(RCCR')]^-$ (**6**−**9**) with an excess of $HBF_4 \cdot OEt_2$ at room temperature leads to the formation of the neutral hydrido clusters $[HRu_2Ir(CO)_9(RCCR')]$ (**10**: R = R′ = Ph; **11**: R = R′ = Et; **12**: R = Ph; R′ = Me; **13**: R = R′ = Me), which can be isolated by chromatographic methods and recrystallized from hexane at −18 °C (Scheme 1).

The infrared spectra of **10**−**13** display an almost identical ν_{co} absorption pattern in the region of terminal carbonyl ligands (Table 1). The ^{1}H-NMR spectra of **10**−**13** indicate, in addition to the signals of the alkyne substituents, the resonance of a bridging hydrido ligand at around δ = −15 (Table 1). In all cases, only one isomer is observed. For $[HRu_2Ir(CO)_9(EtCCEt)]$ (**11**) and $[HRu_2Ir(CO)_9(MeCCMe)]$ (**13**), the two ethyl or methyl groups are found to be nonequivalent.

Molecular Structure of $[HRu_2Ir(CO)_9(RCCR')]$ (10, 12)

Suitable crystals of $[HRu_2Ir(CO)_9(PhCCPh)]$ (**10**) and $[HRu_2Ir(CO)_9(PhCCMe)]$ (**12**) have been obtained from a concentrated hexane solution at −18 °C. The molecular structure of **10** is depicted in Figure 5 and that of **12** in Figure 6. Selected bond lengths and angles are presented in Tables 6 and 7. The crystal-structure analysis of **10** reveals two independent molecules per asymmetric unit of the unit cell, which have the same constitution, but differ slightly in bond lengths and angles.

The two clusters **10** and **12** have the same overall structure, showing the same carbonyl and alkyne coordination. The three metal atoms form a closed triangle. Each metal atom is bonded to three terminal CO groups. In both complexes the longer Ru(1)−Ru(2) distance [**10**: 2.7965(10); **12**: 2.7943(7) Å] suggests the presence of the hydrido bridge across this edge.

The alkyne ligand is coordinated in a μ_3-η^2 fashion over the Ru_2Ir framework as also found in cluster **6**. All carbon−carbon and carbon−metal distances compare well with those in other $M_3(\mu_3\text{-}\eta^2\text{-}RCCR')$ complexes.[18] The neutral complexes $[HRu_2Ir(CO)_9(RCCR')]$ (**10**−**13**) have, as the anions **6**−**9**, the expected electron count of 48e.

Reaction of $[Ru_3Ir(CO)_{11}(RCCR')]^-$ with $HBF_4 \cdot OEt_2$

Protonation of the anions $[Ru_3Ir(CO)_{11}(RCCR')]^-$ gives different results depending on the nature of the coordinated alkyne ligand. For R = R′ = Ph (**14**) or R = R′ = Et (**15**), the neutral hydrido complexes $[HRu_3Ir(CO)_{11}(PhCCPh)]$

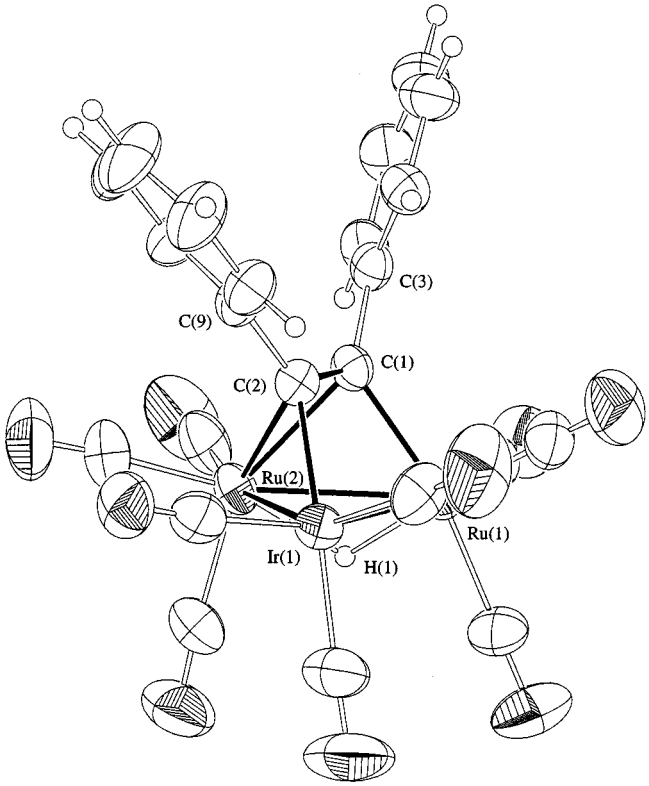


Figure 5. ORTEP plot of $[HIrRu_2(CO)_9(\mu_3\text{-}\eta^2\text{-}C_2Ph_2)]$ **10**; thermal ellipsoids are drawn at 50% of propability

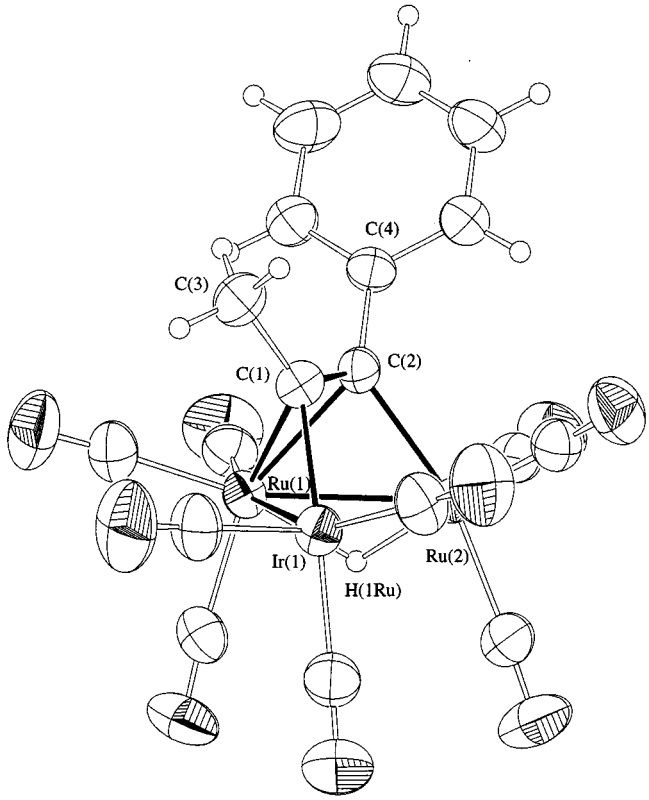


Figure 6. ORTEP plot of $[HIrRu_2(CO)_9(\mu_3\text{-}\eta^2\text{-}PhCCMe)]$ **12**; thermal ellipsoids are drawn at 50% of propability

Table 6. Selected bond lengths [Å], bond angles [°], and torsion angles [°] for **10**; estimated standard deviations in parentheses

Molecule A		Molecule B	
Ir(1)−Ru(2)	2.6901(7)	Ir(2)−Ru(4)	2.6936(9)
Ir(1)−Ru(1)	2.7523(8)	Ir(2)−Ru(3)	2.7517(8)
Ir(1)−C(2)	2.076(6)	Ir(2)−C(25)	2.080(6)
Ru(1)−Ru(2)	2.7965(10)	Ru(3)−C(24)	2.119(7)
Ru(1)−C(1)	2.113(7)	Ru(3)−Ru(4)	2.7938(9)
Ru(1)−H(1)	1.77(11)	Ru(3)−H(2)	1.63(11)
Ru(2)−C(1)	2.295(6)	Ru(4)−C(25)	2.310(6)
Ru(2)−C(2)	2.307(6)	Ru(4)−C(24)	2.325(7)
Ru(2)−H(1)	1.85(11)	Ru(4)−H(2)	1.91(11)
C(1)−C(2)	1.374(9)	C(24)−C(25)	1.375(9)
C(2)−C(1)−C(3)	123.9(6)	C(25)−C(24)−C(26)	124.4(6)
C(1)−C(2)−C(9)	125.0(6)	C(24)−C(25)−C(32)	124.9(6)
C(3)−C(1)−C(2)−C(9)	8.7(10)	C(26)−C(24)−C(25)−C(32)	−6.5(10)

Table 7. Selected bond lengths [Å], bond angles [°], and torsion angles [°] for **12**; estimated standard deviations in parentheses

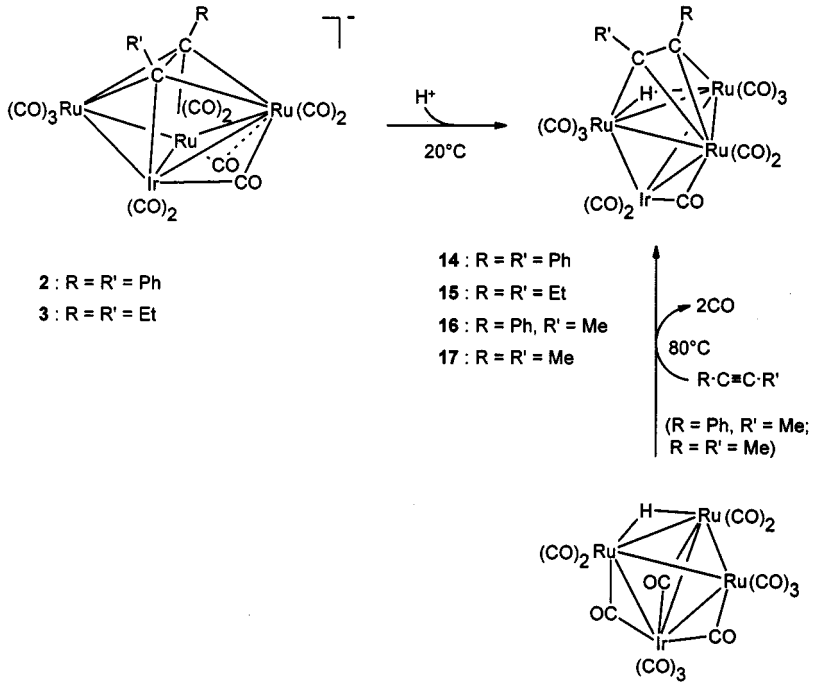
Ir(1)−Ru(1)	2.6924(6)	Ru(2)−C(2)	2.111(6)
Ir(1)−Ru(2)	2.7578(5)	Ru(2)−H(1Ru)	1.78(7)
Ir(1)−C(1)	2.074(6)	C(1)−C(2)	1.372(9)
Ru(1)−Ru(2)	2.7943(7)	C(2)−C(1)−C(3)	123.9(6)
Ru(1)−C(2)	2.285(6)	C(1)−C(2)−C(4)	124.4(5)
Ru(1)−C(1)	2.318(6)	C(3)−C(1)−C(2)−C(4)	−0.3(10)
Ru(1)−H(1Ru)	1.81(7)		

(**14**) and $[HRu_3Ir(CO)_{11}(EtCCEt)]$ (**15**) are formed (Scheme 2). When R or R′ is a methyl group, the reaction does not afford the neutral hydrido complex, but leads to an unidentified green decomposition product. The expected clusters $[HRu_3Ir(CO)_{11}(PhCCMe)]$ (**16**) and $[HRu_3Ir(CO)_{11}$-(MeCCMe)] (**17**) are, however, accessible from the reaction of the neutral hydrido cluster $[HRu_3Ir(CO)_{13}]$ with the corresponding alkyne (Scheme 2). Clusters **14** and **17** have already been reported[8] and they are included here for the sake of completeness.

The infrared spectra of **14**−**17** display in the ν_{co} region the same absorption pattern: Five bands are assigned to terminal CO ligands and one absorption around 1840 cm^{-1} corresponds to a bridging CO group (Table 1). In the ^{1}H-NMR spectra of **14**−**17**, the hydrido ligand resonates as a singlet around $\delta = -19$. In **15** the ethyl substituents of the alkyne ligand are found to be equivalent, but the two hydrogen atoms of the methylene groups are diastereotopic (Table 1). The molecular structure of **15** is confirmed by a single-crystal X-ray structure analysis.

Molecular Structure of $[HRu_3Ir(CO)_{11}(EtCCEt)]$ (15)

Suitable crystals of **15** were grown at −18 °C in hexane. The molecular structure of **15** is depicted in Figure 7. Selected bond lengths and angles of **15** are listed in Table 8. The complex **15** has the same overall structure as found in **14** and **17**,[8] showing the same carbonyl, alkyne and hydride coordination pattern.



Scheme 2. Synthetic routes to clusters **14**−**17**

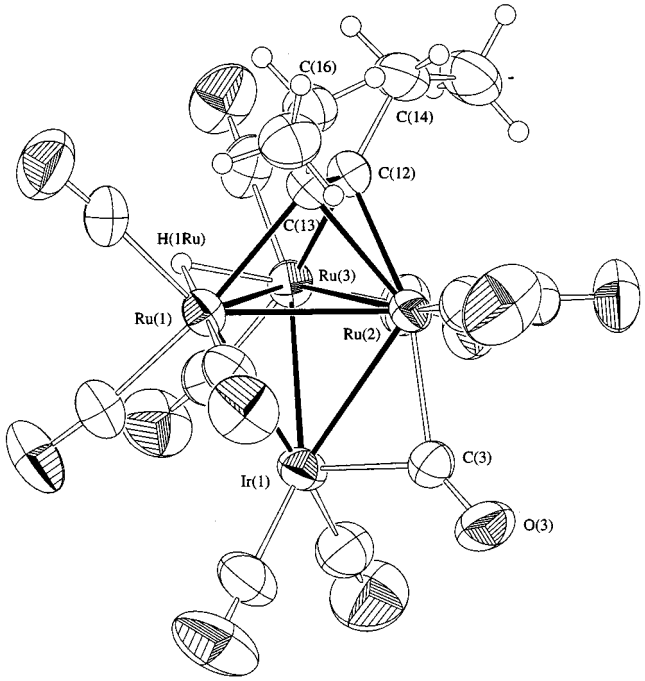


Figure 7. ORTEP plot of $[HIrRu_3(CO)_{11}(\mu_3\text{-}\eta^2\text{-}C_2Et_2)]$ **15**; thermal ellipsoids are drawn at 50% of propability

The four metal atoms form a tetrahedron in which the Ru−Ir distances vary from 2.7228(11) to 2.7833(8) Å and the Ru−Ru distances from 2.7981(10) to 2.8514(9) Å, in accordance with metal−metal single bonds.[8] The cluster **15** presents, as expected for a tetrahedral arrangement, an electron count of 60 e. The short distance Ru(2)−Ir [2.7228(11) Å] is due to the bridging carbonyl ligand over this edge. The base of the tetrahedron is composed of three ruthenium atoms. The longer Ru(1)−Ru(3) distance [2.8514(9) Å] suggests the presence of the hydrido bridge across this edge. Two of the three ruthenium atoms are bonded to three terminal CO groups, whereas Ru(2) and Ir are bonded to two terminal CO groups and share the bridging CO ligand. The alkyne is coordinated in a μ_3-η^2-bonding mode over the Ru_3 face of the tetrahedron. Due to the coordination of the alkyne group to the metal core, the carbon−carbon bond is lengthened [C(12)−C(13) 1.395(11) Å], but is in the range observed in **14**, **17**,[8] and other clusters such as $HCpWOs_3[\mu_3\text{-}\eta^2\text{-}C_2(Tol)_2]$.[24][25]

Table 8. Selected bond lengths [Å], bond angles [°], and torsion angles [°] for **15**; estimated standard deviations in parentheses

Ir(1)−Ru(1)	2.7727(9)	Ru(2)−C(12)	2.183(7)
Ir(1)−Ru(2)	2.7228(11)	Ru(2)−C(13)	2.168(7)
Ir(1)−Ru(3)	2.7833(8)	Ru(3)−C(12)	2.149(8)
Ru(1)−Ru(2)	2.7981(10)	Ru(3)−H(1Ru)	1.75(6)
Ru(1)−Ru(3)	2.8514(9)	C(12)−C(13)	1.395(11)
Ru(1)−C(13)	2.154(7)	C(13)−C(12)−C(14)	121.7(7)
Ru(1)−H(1Ru)	1.81(6)	C(12)−C(13)−C(16)	122.7(7)
Ru(2)−Ru(3)	2.8110(9)	C(14)−C(12)−C(13)−C(16)	0.4(11)

Conclusions

The Ru_3Ir framework shows a great fexibility with respect to the coordination of alkyne ligands: The tetrahedral metal skeleton in $[Ru_3Ir(CO)_{13}]^-$ (**1**) opens up upon coordination of an alkyne ligand to give a butterfly framework in $[Ru_3Ir(CO)_{11}(RCCR)]^-$ (**2**−**5**). Protonation of the butterfly clusters **2** and **3** leads, with closure of the Ru−Ru bond, back to a tetrahedral metal skeleton in the neutral clusters $[HRu_3Ir(CO)_{11}(RCCR')]$ (**14**−**15**). The second important

feature is the fragmentation of the tetranuclear anions in $[Ru_3Ir(CO)_{11}(RCCR)]^-$ (**2**−**5**) under CO pressure to give the trinuclear anions $[Ru_2Ir(CO)_9(RCCR)]^-$ (**6**−**9**). In a comparison of the 3-hexyne complexes, it is interesting to note that in the case of **3** and **11**, the two protons of the two different CH_2 groups of the 3-hexyne ligand are equivalent, whereas in **7** and **15** they are nonequivalent (diastereotopic). In the case of the tetranuclear cluster $[Ru_3Ir(CO)_{11}(EtCCEt)]^-$ (**3**) the averaging of the methylene protons may be explained by a carbonyl fluxionality involving the bridging and semi-bridging carbonyl ligands which could brigde equally well to both wingtip ruthenium atoms. In the case of the trinuclear cluster $[HRu_2Ir(CO)_9(EtCCEt)]$ (**11**), the μ_3-alkyne ligand itself might be fluxional on the trinuclear metal core, as observed in $[H_2Ru_3(CO)_9(EtCCEt)]$,[22a] $[Co_2Ru(CO)_9(EtCCEt)]$,[19] $[FeCo_2(CO)_9(EtCCEt)]$,[21] $[CpNiCoM(CO)_6(EtCCEt)]$ (M = Fe, Ru, Os),[23a] $[H_2Os_3(CO)_9(C_9H_6)]$.[23b]

Experimental Section

General: All reactions were carried out under pure nitrogen with standard Schlenk techniques. Solvents were destilled with appropriate drying agents, deoxygenated, and nitrogen-saturated prior to use.[26] − Preparative thin-layer chromatography was performed using 20 cm × 20 cm plates coated with Fluka silica gel G. The starting complexes $[Ru_3Ir(CO)_{13}]^-$ and $[HRu_3Ir(CO)_{13}]$ were prepared according to a published method.[9] − Diphenylacetylene was purchased from Fluka; 3-hexyne, 1-phenyl-1-propyne, and 2-butyne were purchased from Aldrich and used as recieved. − NMR spectra were recorded with a Varian Gemini 200 BB or a Bruker AMX 400 spectrometer, using the resonance of the residual protons of the deuterated solvents as reference. − Infrared spectra were recorded with a Perkin−Elmer 1720X FT IR spectrometer. − Micro-analyses were carried out by the Mikroelementaranalytisches Laboratorium of the ETH Zürich, Switzerland.

Preparations

$[N(PPh_3)_2][Ru_3Ir(CO)_{11}(RCCR')]$ (Anions 2−5): A solution of $[N(PPh_3)_2][Ru_3Ir(CO)_{13}]$ (anion **1**) (100 mg, $7.15\bullet10^{-2}$ mmol) in CH_2Cl_2 (30 mL) was stirred with an excess of RC≡CR′ (**2**: 38 mg, $21.46\bullet10^{-2}$ mmol; **3**: 24 μL, $21.46\bullet10^{-2}$ mmol; **4**: 27 μL, $21.46\bullet10^{-2}$ mmol; **5**: 17 μL, $21.46\bullet10^{-2}$ mmol) at 90 °C in a pressure Schlenk tube. During the reaction the pressure was released once. The reaction was followed by infrared spectroscopy; after 2.5 h, the IR spectrum in the ν_{CO} region indicated the complete desappearance of the starting complex **1**. Then the solvent was evaporated and the red-orange oil was washed three times with 10 mL of hexane to remove the excess of the unreacted alkyne. The residue was dissolved in 20 mL of Et_2O, and the solution was filtered. Dark-red air-stable crystals of the $[N(PPh_3)_2]^+$ salts of **2**, **4**, **5** were obtained by slow evaporation (room temperature) of a diethyl ether/hexane solution. The crystals were dried in vacuo. − **2**: Yield 92 mg (85%). − $C_{61}H_{40}IrNO_{11}P_2Ru_3$ (1520.36): calcd. C 48.19, H 2.65, N 0.92; found C 48.32, H 2.58, N 0.93. − **4**: Yield 83 mg (80%). − $C_{56}H_{38}O_{11}NP_2Ru_3Ir$ (1458.28): calcd. C 46.12, H 2.63, N 0.96, found C 45.94, H 2.37, N 1.00. − **5**: Yield 75 mg (75%). − $C_{51}H_{36}O_{11}NP_2Ru_3Ir$ (1396.22): calcd. C 43.87, H 2.60, N 1.00; found C 43.77, H 2.45, N 1.01. − For **3**, a different method of crystallisation was used. The filtered diethyl ether solution containing **3** was concentrated to dryness, the residue was dissolved in 10 mL of ethanol, followed by the dropwise addition of pentane until the solution became cloudy. Then the solution was cooled to −18 °C for a few days giving the $[N(PPh_3)_2]^+$ salt of **3** as dark-violet needles. The crystals were dried in vacuo. − **3**: Yield 76 mg (75%). − $C_{53}H_{40}IrNO_{11}P_2Ru_3 \bullet H_2O$ (1424.28): calcd. C 44.13, H 2.93, N 0.97; found C 43.96, H 2.76, N 1.02.

$[N(PPh_3)_2][Ru_2Ir(CO)_9(PhCCPh)]$ (Anion 6): A solution containing $[N(PPh_3)_2]$ $[Ru_3Ir(CO)_{11}(PhCCPh)]$ (anion **2**), prepared from 0.0715 mmol of **1** as described above, in Et_2O (20 mL) was placed in a pressure Schlenk tube and stirred at room temperature for 20 h under a pressure of 2 bar of CO. The colour changed from red-orange to wine-red, then to orange with precipitation of the $[N(PPh_3)_2]^+$ salt of **6** as a yellow powder. The precipitate was filtered off, washed with Et_2O (3 × 10 mL) and crystallised at room temperature by slow diffusion of Et_2O into a CH_2Cl_2 solution. The yellow crystals were dried in vacuo. **6**: Yield (with respect to **1**): 73 mg (75%). − $C_{59}H_{40}IrNO_9P_2Ru_2$ (1363.27): calcd. C 51.98, H 2.99, N 1.03; found C 51.68, H 2.99, N 1.04.

$[N(PPh_3)_2][Ru_2Ir(CO)_9(RCCR')]$ (Anions 7, 8, 9): A solution containing $[N(PPh_3)_2][Ru_3Ir(CO)_{11}(RCCR')]$ (**3**: R = R′ = Et; **4**: R = Ph; R′ = Me; **5**: R = R′ = Me), prepared from 0.0715 mmol of **1** as described above, in CH_2Cl_2 (25ml) was placed in a pressure Schlenk tube and stirred at 90 °C for 45 min under a pressure of 2 bar of CO. The colour changed, from red-orange to wine-red, then to orange. After removal of the solvent, the orange residue was washed with hexane (3 × 10 ml) to remove $Ru_3(CO)_{12}$ formed during the reaction. The remaining orange oil was dried and dissolved in 5−10 mL of ethanol, followed by the addition of pentane until the solution became cloudy. In the case of **8** no pentane was added. Then the solution was cooled to −18 °C for a few days which gave the $[N(PPh_3)_2]^+$ salt of **7** as yellow-orange crystals and the $[N(PPh_3)_2]^+$ salts of **8** and **9** precipitated as a yellow-brown powder. The solids were dried in vacuo. − **7**: Yield (with respect to **1**): 51 mg (56%). − $C_{51}H_{40}IrNO_9P_2Ru_2 \bullet 2.5\ H_2O$ (1267.19): calcd. C 46.65, H 3.42, N 1.06; found C 46.42, H 3.02, N 1.11. − **8**: Yield (with respect to **1**): 56 mg (60%). − $C_{54}H_{38}IrNO_9P_2Ru_2$ (1301.20): calcd. C 49.85, H 2.94, N 1.08; found C 49.66, H 3.16, N 1.16. − **9**: Yield (with respect to **1**): 49 mg (55%). − $C_{49}H_{36}IrNO_9P_2Ru_2$ (1239.13): calcd. C 47.50, H 2.93, N 1.13; found C 47.24, H 3.13, N 1.19.

$[HRu_2Ir(CO)_9(RCCR')]$ (10−13): To a solution of $[N(PPh_3)_2]$-$[Ru_2Ir(CO)_9(RCCR')]$ (anions **6**: R = R′ = Ph; **7**: R = R′ = Et; **8**: R = Ph; R′ = Me; **9**: R = R′ = Me) (0.0370 mmol) in CH_2Cl_2 (30 mL) a slight excess of $HBF_4 \bullet OEt_2$ (54%, 60 μL) was added under stirring. After 30 min, the solvent was evaporated, and the residue was dissolved in the minimum quantity of CH_2Cl_2. The solution was separated by thin-layer chromatography with a mixture of CH_2Cl_2 and hexane (1:6) as eluent. The yellow band containing the product was extracted with CH_2Cl_2, followed by concentration to dryness. The resulting yellow oil was dissolved in hexane and cooled to −18 °C to give yellow crystals of **10**−**13**. The crystals were dried in vacuo. − **10**: Yield 21 mg (68%). − $C_{23}H_{11}IrO_9Ru_2$ (825.69): calcd. C 33.46, H 1.34; found C 33.48, H 1.32. − **11**: Yield 18 mg (66%). − $C_{15}H_{11}IrO_9Ru_2$ (729.61): calcd. C 24.69, H 1.52; found C 24.51, H 1.54. − **12**: Yield 17 mg (60%). − $C_{18}H_9IrO_9Ru_2$ (763.62): calcd. C 28.31, H 1.19; found C 28.40, H 1.24. − **13**: Yield 16 mg (62%). − $C_{13}H_7IrO_9Ru_2$ (701.55): calcd. C 22.26, H 1.01; found C 22.12, H 1.04.

$[HRu_3Ir(CO)_{11}(RCCR')]$ (14−15): To a solution of $[N(PPh_3)_2]$-$[Ru_3Ir(CO)_{11}(RCCR')]$ (**2**: R = R′ = Ph; **3**: R = R′ = Et), prepared from 0.0715 mmol of $[N(PPh_3)_2]$**1** as described above, in 20 mL of Et_2O was added a slight excess of $HBF_4 \bullet OEt_2$ (54%,

Table 9. Crystallographic data and refinement details for compounds **2**, **4**, **5**, and **6**

	2	**4**	**5**	**6**
Formula	$C_{61}H_{40}O_{11}NP_2IrRu_3$ 0.25 C_6H_{14}	$C_{56}H_{38}O_{11}NP_2IrRu_3$	$C_{51}H_{36}O_{11}NP_2IrRu_3$	$C_{59}H_{40}O_9NP_2IrRu_3$
M	1520.42	1458.22	1396.16	1363.20
Crystal system	Triclinic	Triclinic	Triclinic	Triclinic
Space group	$P-1$	$P-1$	$P-1$	$P-1$
a [Å]	10.1350(8)	9.2769(10)	10.678(2)	10.5124(11)
b [Å]	15.5218(13)	16.7823(16)	15.741(4)	15.545(3)
c [Å]	19.8838(17)	17.2250(17)	15.705(3)	17.830(3)
α [°]	98.652(10)	88.034(12)	102.672(19)	100.04(2)
β [°]	99.163(10)	84.463(12)	91.363(12)	101.543(14)
γ [°]	94.583(10)	80.982(12)	103.730(13)	101.551(19)
V [Å^3]	3035.6(4)	2635.7(5)	2493.7(9)	2726.3(8)
Z	2	2	2	2
Crystal size [mm]	0.38 × 0.15 × 0.11	0.50 × 0.50 × 0.30	0.65 × 0.58 × 0.53	0.57 × 0.27 × 0.27
Colour	Dark-red	Black	Black	Yellow
D_c [g cm^{-3}]	1.687	1.837	1.859	1.661
μ [mm^{-1}]	3.028	3.482	3.675	3.097
Transmission factors: min/max	–	0.479/0.832	0.3979/0.6612	0.3427/0.3917
F(000)	1505	1416	1352	1336
θ limits [°]	2.13–25.88	2.38–25.88	2.10–25.48	2.01–25.49
hkl ranges	−12 to 11, −19 to 18, −24 to 24	−11 to 11, −20 to 20, −20 to 21	−12 to 12, −19 to 18, 0 to 19	−12 to 12, −18 to 18, 0 to 21
Reflections measured	23865	20460	9251	10126
Independent reflections	10950	9406	9251	10126
Observed reflections	7930	8994	8542	8153
$R1$ [$I > 2\sigma(I)$]/$R1$ (all data)[a]	0.0316/0.0483	0.0226/0.0240	0.0371/0.0433	0.0551/0.0778
$wR2$ [$I > 2\sigma(I)$]/$wR2$ (all data)[b]	0.0739/0.0783	0.0567/0.0576	0.1004/0.1107	0.1184/0.1334
Goodness of fit on F^2[c]	0.882	1.065	1.379	1.169
Maximum δ/σ	0.002	0.002	0.061	0.019
Largest diff. peak and hole [e Å^3]	1.070/−1.829	1.342/−1.125	1.580/−1.373	1.749/−1.457

[a] $R1 = \Sigma||F_o| - |F_c||/\Sigma|F_o|$. – [b] $wR2 = [\Sigma w(F_o^2 - F_c^2)^2/\Sigma w(F_o)^4]^{1/2}$. – [c] $S = [\Sigma w(F_o^2 - F_c^2)^2/(n - p)]^{1/2}$ (n: number of reflections; p: number of parameters).

Table 10. Crystallographic data and refinement details for compounds **10**, **12**, and **15**

	10	**12**	**15**
Formula	$C_{23}H_{11}O_9IrRu_2$	$C_{18}H_9O_9IrRu_2$	$C_{17}H_{11}O_{11}IrRu_3$
M	825.66	763.59	886.67
Crystal system	Triclinic	Triclinic	Triclinic
Space group	$P-1$	$P-1$	$P-1$
a [Å]	10.927(2)	9.1281(5)	8.0650(14)
b [Å]	14.480(3)	9.9456(6)	9.4766(13)
c [Å]	16.793(2)	12.6212(14)	16.423(4)
α [°]	70.080(13)	96.966(9)	96.392(19)
β [°]	85.071(17)	108.833(9)	101.47(2)
γ [°]	86.106(19)	96.349(7)	109.063(14)
V [Å^3]	2486.8(8)	1062.70(15)	1141.4(4)
Z	4	2	2
Crystal size [mm]	0.57 × 0.57 × 0.42	0.68 × 0.34 × 0.34	0.95 × 0.65 × 0.36
Colour	Yellow	Yellow	Red-orange
D_c [g cm^{-3}]	2.205	2.386	2.580
μ [mm^{-1}]	6.586	7.695	7.811
Transmission factors: min/max	0.0474/0.0845	0.0671/0.1236	0.0137/0.0460
F(000)	1544	708	820
θ limits [°]	2.20–25.47	2.09–25.48	2.32–25.46
hkl ranges	−13 to 13, −16 to 17, 0 to 20	−11 to 10, −12 to 11, 0 to 15	−9 to 9, −11 to 11, 0 to 19
Reflections measured	9223	3941	4324
Independent reflections	9223	3941	4234
Observed reflections	8141	3774	4134
$R1$ [$I > 2\sigma(I)$]/$R1$ (all data)[a]	0.0360/0.0441	0.0290/0.0309	0.0365/0.0387
$wR2$ [$I > 2\sigma(I)$]/$wR2$ (all data)[b]	0.0870/0.0920	0.0833/0.0849	0.1071/0.1127
Goodness of fit on F^2[c]	1.258	1.292	1.280
Maximum δ/σ	0.004	0.001	0.001
Largest diff. peak and hole [e Å^3]	0.916/−0.876	1.237/−0.987	1.831/−1.445

[a] $R1 = \Sigma||F_o| - |F_c||/\Sigma|F_o|$. – [b] $wR2 = [\Sigma w(F_o^2 - F_c^2)^2/\Sigma w(F_o)^4]^{1/2}$. – [c] $S = [\Sigma w(F_o^2 - F_c^2)^2/(n - p)]^{1/2}$ (n: number of reflections; p: number of parameters).

60 μL). After 30 min at room temperature, the white precipitate was filtered off, washed twice with 10 mL of Et_2O and then discarded. The solution was concentrated, the residue dissolved in CH_2Cl_2 (2 mL) and submitted to thin-layer chromatography (silica gel, CH_2Cl_2/hexane, 1:3). The product was extracted from the orange main band with CH_2Cl_2 and crystallised from hexane at

−18 °C. The orange air-stable crystals were dried in vacuo. − **14**: Yield (starting from **1**) 36 mg (51%). − **15**: Yield (starting from **1**) 29 mg (45%) − $C_{17}H_{11}IrO_{11}Ru_3$ (886.69): calcd. C 23.02, H 1.25; found C 23.21, H 1.30.

[$HRu_3Ir(CO)_{11}$(PhCCMe)] (16): A solution of [$HRu_3Ir(CO)_{13}$][9] (83 mg, 0.096 mmol) and PhC≡CMe (18 μL, 0.145 mmol) in hexane (30 mL) was stirred at 80−85 °C in a pressure Schlenk tube. During the reaction, the pressure was released once. After 1 h, the solution changed colour from red to orange. After removal of the solvent, the dark orange residue was dissolved in 5 ml of CH_2Cl_2 and submitted to thin-layer chromatography (silica gel, CH_2Cl_2/hexane, 1:3). From the orange main band, **16** was extracted with CH_2Cl_2 and crystallised from hexane at −18 °C. The orange air-stable crystals were dried in vacuo. − **16**: Yield 27 mg (31%) − $C_{20}H_9IrO_{11}Ru_3$ (920.71): calcd. C 26.09, H 0.99; found, C 26.02, H 0.99.

X-ray Structure Analyses: Single crystals of **2**, **4**, **5, 6**, **10**, **12**, and **15** were obtained as described under Preparations. Selected crystallographic data for the complexes are summarised in Tables 9 and 10, and selected bond lengths and bond angles are listed in Tables 2−8. Single-crystal X-ray diffraction data of the $[N(PPh_3)_2]^+$ salts of **2** and **4** were collected at room temperature and −50 °C, respectively with a Stoe Imaging Plate Diffractometer System (Stoe & Cie, 1995) equipped with a one-circle goniometer and a graphite monochromator. 200 exposures (3 min per exposure) were obtained at an image-plate distance of 70 mm with $0° < \phi < 200°$ and with the crystal oscillating through 1° in φ. The $[N(PPh_3)_2]^+$ salts of **5** and **6** and complexes **10**, **12**, and **15** were measured at room temperature with a Stoe-Siemens AED2 four-circle diffractometer using Mo-K_α graphite-monochromated radiation (λ = 0.71073 Å; ω-2θ scans). The structures of the $[N(PPh_3)_2]^+$ salts of **2**, **4**, **5**, **6**, and that of complex **15** were solved by direct methods, whereas those of **10** and **12** were solved by Patterson methods using the program SHELXS-97.[27] All the structures were refined by full-matrix least squares on F^2 with SHELXL-97.[28] The salt $[N(PPh_3)_2]$**2** crystallises with a quarter of a disordered molecule of hexane. The five carbon atoms C62A, C62B, C63A, C63B, and C64 were refined isotropically using the SHELXL-97 default parameters. In compounds $[N(PPh_3)_2]$**5** and $[N(PPh_3)_2]$**6** one of the carbonyl ligands is found to be disordered and has been split into C6A-O6A and C6B-O6B (anion **5**), C21A-O21A and C21B-O21B (anion **6**), respectively, with an occupancy of a half for each atom. The position of the hydride ligands in **10**, **12**, and **15** were located from Fourier difference maps and refined isotropically, while the remaining hydrogen atoms of the methyl, ethyl or phenyl substituents were included in calculated positions and treated as riding atoms with SHELXL-97 default parameters. For $[N(PPh_3)_2]$**4**, an empirical absorption correction was applied using DIFABS[29] and for $[N(PPh_3)_2]$**5**, $[N(PPh_3)_2]$**6**, **10** **12**, **15** it was based on ψ scans.[30] The Figures were drawn with ORTEP[31] (thermal ellipsoids, 50% probability level). Complete tables of bond lengths and angles and lists of thermal parameters have been deposited with the Cambridge Crystallographic Data Centre, 12 Union Road, Cambridge CB2 1EZ, UK. Copies of the data can be obtained free of charge on application to CCDC, 12 Union Road, Cambridge CB2 1EZ, UK [Fax: int. code + 44-1223/336-033; E-mail: deposit@ccdc.cam.ac.uk], on quoting the deposition numbers CCDC-111752−111758.

Acknowledgments

We thank the Fonds National Suisse de la Recherche Scientifique for financial support of this work. A generous loan of ruthenium(III) chloride hydrate from the Johnson Matthey Research Centre is gratefully acknowledged.

[1] R. D. Adams, in *Comprehensive Organometallic Chemistry 2* (Eds.: E. W. Abel, F. G. A. Stone, G. Wilkinson), Elsevier, Oxford, **1995**, vol. 10, p. 1.
[2] Y. Chi, D. K. Hwang, in *Comprehensive Organometallic Chemistry 2* (Eds.: E. W. Abel, F. G. A. Stone, G. Wilkinson), Elsevier, Oxford, **1995**, vol. 10, p. 85.
[3] [3a] P. Braunstein, J. Rosé, in *Comprehensive Organometallic Chemistry 2* (Eds.: E. W. Abel, F. G. A. Stone, G. Wilkinson), Elsevier, Oxford, **1995**, vol. 10, p. 351. − [3b] For a general review see: *Catalysis by Di- and Polynuclear Metal Cluster Complexes* (Eds.: R. D. Adams, F. A. Cotton), Wiley-VCH, Chichester, **1998**. − [3c] R. D. Adams, T. S. Barnard, Z. Li, W. Wu, J. H. Yamamoto, *J. Am. Chem. Soc.* **1994**, 116, 9103. − [3d] R. D. Adams, T. S. Barnard, *Organometallics* **1998**, 17, 2567. − [3e] R. D. Adams, T. S. Barnard, *Organometallics* **1998**, *17*, 2885.
[4] E. Sappa, A. Tiripicchio, A. J. Carty, G. E. Toogood, *Prog. Inorg. Chem.* **1987**, *35*, 437 and references therein.
[5] P. R. Raithby, M. J. Rosales, *Adv. Inorg. Chem. Radiochem.* **1985**, *29*, 169.
[6] E. L. Muetterties, T. N. Rhodin, E. Band, C. F. Brucker, W. R. Pretzer, *Chem. Rev.* **1979**, *79*, 91.
[7] A. Fusi, R. Ugo, R. Psaro, P. Braunstein, J. Dehand, *J. Mol. Catal.* **1982**, *16*, 217.
[8] V. Ferrand, G. Süss-Fink, A. Neels, H. Stoeckli-Evans, *J. Chem. Soc., Dalton Trans.* **1998**, 3825.
[9] G. Süss-Fink, S. Haak, V. Ferrand, A. Neels, H. Stoeckli-Evans, *J. Chem. Soc., Dalton Trans.* **1997**, 3861.
[10] O. Benali-Baitich, J. C. Daran, Y. Jeannin, *J. Organomet. Chem.* **1988**, *344*, 393.
[11] M. Cazanoue, N. Lugan, J. J. Bonnet, R. Mathieu, *Organometallics* **1988**, *7*, 2480.
[12] [12a] P. Braunstein, J. Rosé, *J. Organomet. Chem.* **1983**, *252*, C101. − [12b] E. Roland, H. Vahrenkamp, *Organometallics* **1983**, *2*, 1048.
[13] D. E. Fjare, W. L. Gladfelter, *J. Am. Chem. Soc.* **1984**, *106*, 4799.
[14] R. H. Crabtree, M. Lavin, *Inorg. Chem.* **1986**, *25*, 805.
[15] K. Wade, *Adv. Inorg. Chem. Radiochem.* **1976**, *18*, 1.
[16] J. C. Wang, Y. Chi, S.-M. Peng, G.-H. Lee, S.-G. Shyu, F.-H. Tu, *J. Organomet. Chem.* **1994**, *481*, 143.
[17] M. Bergamo, T. Beringhelli, G. Dalfonso, P. Mercandelli, M. Moret, A. Sironi, *Organometallics* **1997**, *19*, 4129.
[18] S. Deabate, R. Gordiano, E. Sappa, *J. Cluster Sci.* **1997**, *8*, 407.
[19] E. Roland, W. Bernhardt, H. Vahrenkamp, *Chem. Ber.* **1985**, *118*, 2858.
[20] S. Aime, R. Gobetto, L. Milone, D. Osella, L. Violano, A. J. Arce, Y. De Sanctis, *Organometallics* **1991**, *10*, 2854.
[21] D. Boccardo, M. Botta, R. Gobetto, D. Osella, A. Tiripicchio, M. Tiripicchio-Camellini, *J. Chem. Soc., Dalton Trans.* **1988**, 1249.
[22] [22a] J. Evans, G. Mc Nulty, *J. Chem. Soc., Dalton Trans.* **1981**, 2017. − [22b] D. Boccardo, M. Botta, R. Gobetto, D. Osella, A. Tiripicchio, M. Tiripicchio-Camellini, *J. Chem. Soc., Dalton Trans.* **1988**, 1249. − [22c] M. A. Gallop, B. F. G. Johnson, R. Khattar, J. Lewis, P. Raithby, *J. Organomet. Chem.* **1990**, *386*, 121.
[23] [23a] F. W. B. Einstein, K. G Tyers, A. S. Tracey, D. Sutton, *Inorg. Chem.* **1986**, *25*, 1631. − [23b] A. J. Deemings, *J. Organomet. Chem.* **1978**, *150*, 123.
[24] J. T. Park, J. R. Shapley, M. Rowen Churchill, C. Bueno, *J. Am. Chem. Soc.* **1983**, *105*, 6182.
[25] J. T. Park, J. R. Shapley, C. Bueno, J. W. Ziller, M. Rowen Churchill, *Organometallics* **1988**, *7*, 2307.
[26] D. D. Perrin, W. L. F. Armarego, *Purification of Laboratory Chemicals*, 3rd ed., Pergamon Press, Oxford, **1988**.
[27] G. M. Sheldrick, *Acta Crystallogr., Sect. A* **1990**, 46, 467.
[28] G. M. Sheldrick, *SHELXL-97, Program for crystal structure refinement*, University of Göttingen, Germany, **1997**.
[29] N. Walker, D. Stuart, *Acta Crystallogr., Sect. A* **1990**, *46*, 158.
[30] A. C. T. North, D. C. Phillips, F. C. Mathews, *Acta Crystallogr., Sect. A* **1968**, *24*, 351.
[31] C. K. Johnson, *ORTEP*, Oak Ridge National Laboratory, Oak Ridge, TN, modified for PC by L. Zsolnai, H. Pritzkow, University of Heidelberg, Germany, **1994**.

Received November 30, 1998
[I98407]

Preparation and Structural Investigations of $(dippNSiMe_3Si)_2(Cp^*Ti)_2(NH)_6$ (dipp = 2,6-$iPr_2C_6H_3$), $[dippNSiMe_3Si(NH_2)NH]_3$ and $[dippNSiMe_3Ge(NH_2)NH]_3$

Karsten Wraage,[a] Hans-Georg Schmidt,[a] Mathias Noltemeyer,[a] and Herbert W. Roesky*[a]

Dedicated to Professor John P. Fackler on the occasion of his 65th birthday

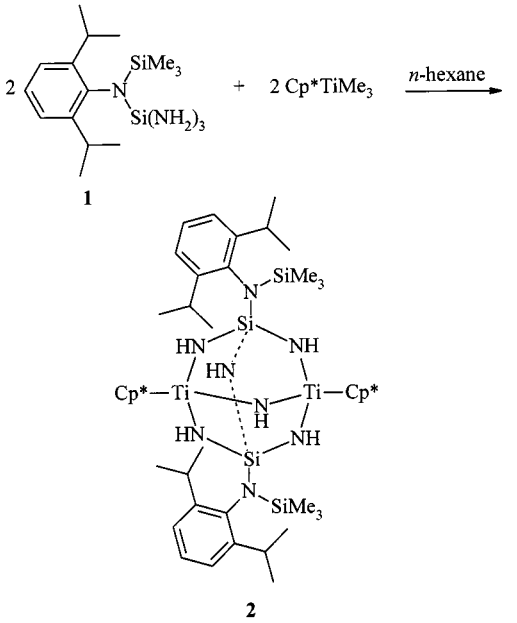
Keywords: Germanium / Nitrogen / Silicon / Titanium

The reaction of $dippNSiMe_3Si(NH_2)_3$ (**1**) (dipp = 2,6-$iPr_2C_6H_3$) with Cp^*TiMe_3 ($Cp^* = C_5Me_5$) and Me_3SnCl yields the new heterocyclic adamantane $(dippNSiMe_3Si)_2(Cp^*Ti)_2(NH)_6$ (**2**) containing the $Si_2Ti_2(NH)_6$ core and the silicon–nitrogen six-membered ring compound $[dippNSiMe_3Si(NH_2)NH]_3$ (**4**). $[dippNSiMe_3Ge(NH_2)_2]_2NH$ (**5**) reacts with $AlMe_3$ to give the germanium–nitrogen six-membered ring compound $[dippNSiMe_3Ge(NH_2)NH]_3$ (**6**). The compounds **2**, **4** and **6** have been structurally characterized by single-crystal X-ray structural analysis.

Introduction

Beyond the investigation of silanetriols as building blocks for new catalysts, the reactions of the isoelectronic triaminosilanes with organometallic precursors are of broad interest for materials research.[1][2] In 1995 we described the reaction of $dippNSiMe_3Si(NH_2)_3$ (**1**) with Cp^*TiMe_3 to yield a silicon−nitrogen−titanium four-membered ring system. Furthermore, we reported on the reaction of **1** and Me_3SnCl forming a compound with a monosubstituted nitrogen−tin bond. Moreover, in 1997 we published reactions of triaminosilanes with alumazene and $AlMe_3$. The reaction with alumazene forms a compound with an adamantane-like core.[3−5] Consequently, in 1998 we synthesized and published the first germanium compound containing more than one terminal amino group.[6]

Herein, we describe the reactions of $dippNSiMe_3Si(NH_2)_3$ with Cp^*TiMe_3 and Me_3SnCl under more drastic conditions and the reaction of $[dippNSiMe_3Ge(NH_2)_2]_2NH$ (**5**) with $AlMe_3$.



(1)

Scheme 1. Synthesis of compound **2**

Results and Discussion

Synthesis and Spectra

$dippNSiMe_3Si(NH_2)_3$ (**1**), prepared from $dippNSiMe_3SiCl_3$ and ammonia, reacts with Cp^*TiMe_3 in *n*-hexane under reflux with evolution of methane gas (Scheme 1) to give $(dippNSiMe_3Si)_2(Cp^*Ti)_2(NH)_6$ (**2**).

Compound **2** was characterized by mass spectrometry, NMR-spectral studies and by single-crystal X-ray diffraction. The proton-NMR spectrum of **2** shows a multiplet (δ = 7.19) due to the aromatic protons of the dipp-ligand. Resonances at δ = 4.05, 3.70 and 1.25 can be attributed to the methylene and methyl protons of the *i*Pr group, respectively. The signal of the methyl protons of the Cp* ligand appear as a singlet (δ = 1.91). The signal of the N−H protons is found at δ = 0.67, and the signals of the methyl protons of the $SiMe_3$ groups are observed at δ = 0.27 and 0.21. Thus, it is clear that the two $SiMe_3$ groups are in slightly different environments, and in solution the rigid structure is maintained.

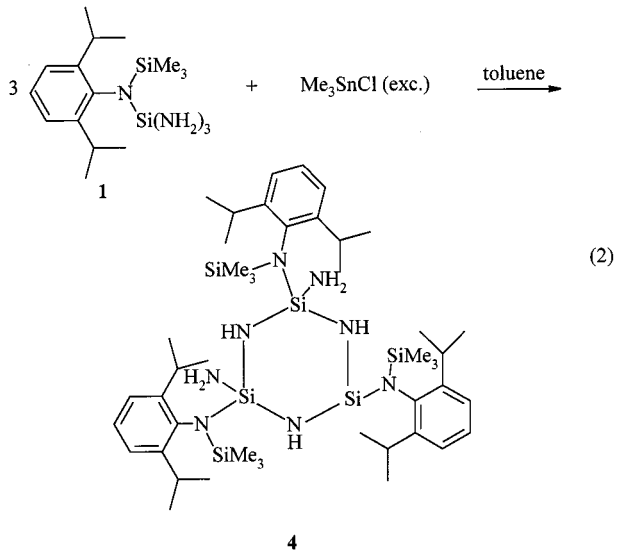
The mass spectrum of the compound shows the molecular ion peak $[M^+]$ at *m*/*z* 1009 and a signal at *m*/*z* 994 due to the fragment $[M^+ - CH_3]$.

[a] Institut für Anorganische Chemie der Universität Göttingen, Tammannstrasse 4, D-37077, Göttingen, Germany
Fax: (internat.) + 49(0)551/393373

 © WILEY-VCH Verlag GmbH, D-69451 Weinheim, 1999 1434−1948/99/0505−0863 $ 17.50+.50/0

Recently, we reported that compound **1** reacts with Me_3SnCl under smooth conditions to yield the monosubstituted derivative $dippNSiMe_3Si(NH_2)_2NHSnMe_3$ (**3**).[3] However, we were interested to obtain the fully substituted compound $dippNSiMe_3Si(NHSnMe_3)_3$.

Therefore we treated **1** with Me_3SnCl in toluene under reflux for 6 h and subsequent workup afforded compound $[dippNSiMe_3Si(NH_2)NH]_3$ (**4**) instead (Scheme 2).



(2)

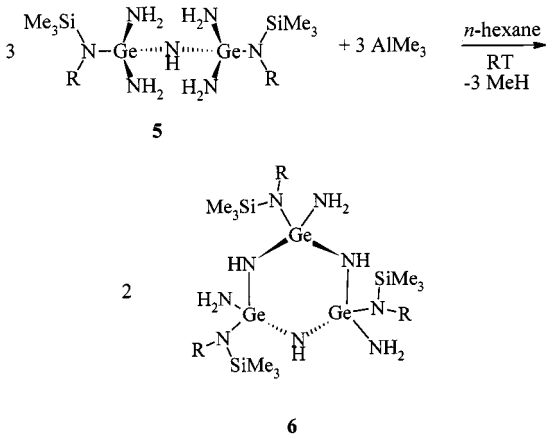
Scheme 2. Synthesis of compound **4**

Compound **4** was characterized by elemental analysis, NMR spectroscopy, mass spectrometry, and by single-crystal X-ray diffraction. The proton-NMR spectrum of **4** shows a multiplet (δ = 7.10) due to the aromatic protons of the dipp ligand. Resonances at δ = 3.67 and 1.31 can be attributed to the methylene and methyl protons of the *i*Pr group, respectively. The signals of N−H protons and unreacted NH_2 protons are found at δ = 0.65 and 0.75, and the signals of the methyl protons of the $SiMe_3$ groups are observed at δ = 0.12, 0.10 and 0.06.

The IR spectrum of **4** shows three absorptions ($\tilde{\nu}$ = 3401, 3486 and 3152 cm^{-1}), which are due to the N−H stretching frequencies. The mass spectrum of **4** exhibits an intense peak at *m/z* 906 [$M^+ - NH_2$].

The reaction to give compound **4** can be described as an "acid-catalyzed" condensation reaction. The intermediate **3** we had previously isolated and characterized is a product of the reaction of an amino group that functions as a Lewis base and the tin atom of Me_3SnCl as a Lewis acid. Finally, the cleavage of tin−chlorine and N−H bond takes place yielding HCl.[3] The condensation reaction occurred three times under evolution of ammonia. Due to steric reasons only the molecule containing the six-membered ring is formed.

$[dippNSiMe_3Ge(NH_2)_2]_2NH$ (**5**), prepared from $dippNSiMe_3GeBr_3$ and ammonia, reacts with $AlMe_3$ in *n*-hexane at room temperature with evolution of methane gas (Scheme 3) to yield $[dippNSiMe_3Ge(NH_2)NH]_3$ (**6**). So far we were not able to characterize any other by-products.



(3)

Scheme 3. Synthesis of compound **6**; R = dipp

Compound **6** was characterized by elemental analysis, NMR spectroscopy, mass spectrometry, and single-crystal X-ray diffraction analysis. The proton-NMR spectrum of **6** exhibits a multiplet (δ = 7.04) due to the aromatic protons of the dipp ligands. Resonances at δ = 3.60, 1.25 and 1.20 can be attributed to the methylene and methyl groups of the *i*Pr group, respectively. The signals of the N−H protons are found at δ = 0.70 and 0.65. The integration ratio of the intensities of the two N−H resonances is 1:2. We assign the signal at δ = 0.70 to the protons of the bridging N−H group. In the silicon-NMR spectrum we observed one signal (δ = 4.8) associated with the $SiMe_3$ group.

The IR spectrum of **6** shows three bands ($\tilde{\nu}$ = 3309, 3386, 3619 cm^{-1}) due the N−H stretching frequencies. The mass spectrum of **6** exhibits an intense peak at *m/z* 1040 [M^+ − Me].

X-ray Structures of 2, 4 and 6

The structure of compound **2** was determined by single-crystal X-ray structural analysis. Compound **2** crystallizes in the space group $P2_1/n$. The structure can be described as a distorted heterocyclic adamantane (Figure 1). The centroid distance of Ti−Cp* is 206 pm and the angles involving this distance are in the range of 116 to 119°. The dipp ligands and Cp* ligands are in staggered positions.

The titanium−nitrogen bond lengths are in the range of 189.9−196.4 pm and are comparable to those of the Ti−N_2−Si four-membered ring, and the average Si−N bond length (171.9−175 pm) is comparable to that in **1** (169−172 pm).[3]

The N−Ti−N angles (99.7−101.0°) are somewhat smaller than the tetrahedral bond angles, but the N−Si−N bond angles (106.1−109.9°) are in the range of a regular tetrahedron.

The central unit of the structure of **4** can be described as a six-membered ring consisting of alternating silicon and nitrogen atoms (Figure 2).

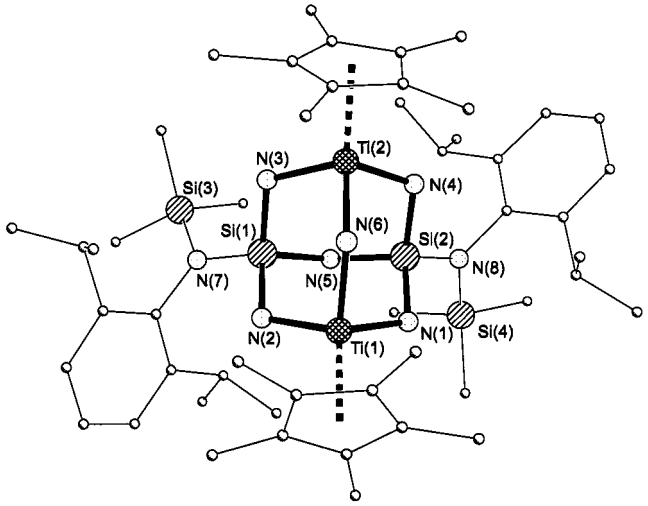


Figure 1. Crystal structure of **2**

Table 1. Selected bond lengths [pm] and angles [°] of compound **2**.

Ti(1)−N(6)	189.9(4)	Ti(1)−N(2)	192.3(4)
Ti(1)−N(1)	195.7(4)	Ti(2)−N(4)	193.3(4)
Ti(2)−N(3)	196.4(4)	Ti(2)−N(6)	191.3(4)
Si(1)−N(2)	171.9(4)	Si(1)−N(3)	172.2(4)
Si(1)−N(5)	175.0(4)	Si(2)−N(4)	172.4(4)
Si(2)−N(1)	171.7(4)	Si(2)−N(5)	174.2(4)
N(6)−Ti(1)−N(2)	101.1(2)	N(6)−Ti(1)−N(1)	99.7(2)
N(2)−Ti(1)−N(1)	100.1(2)	N(6)−Ti(1)−Ti(2)	29.12(11)
N(2)−Ti(1)−Ti(2)	82.54(11)	N(1)−Ti(1)−Ti(2)	81.11(11)
N(6)−Ti(2)−N(4)	100.9(2)	N(6)−Ti(2)−N(3)	100.6(2)
N(4)−Ti(2)−N(3)	101.0(2)	N(6)−Ti(2)−Si(2)	83.44(12)
N(4)−Ti(2)−Si(2)	29.52(11)	N(3)−Ti(2)−Si(2)	81.00(12)
N(6)−Ti(2)−Ti(1)	28.89(11)	N(4)−Ti(2)−Ti(1)	83.07(11)
N(3)−Ti(2)−Ti(1)	81.87(11)	Si(2)−Ti(2)−Ti(1)	58.68(3)
N(2)−Si(1)−N(3)	109.3(2)	N(2)−Si(1)−N(5)	108.3(2)
N(3)−Si(1)−N(5)	106.4(2)	N(1)−Si(2)−N(4)	108.8(2)
N(1)−Si(2)−N(5)	106.1(2)	N(4)−Si(2)−N(5)	109.9(2)
N(1)−Si(2)−Ti(2)	91.33(13)	N(4)−Si(2)−Ti(2)	33.54(12)
N(5)−Si(2)−Ti(2)	88.68(13)	Si(2)−N(1)−Ti(1)	119.0(2)
Si(1)−N(2)−Ti(1)	118.5(2)	Si(1)−N(3)−Ti(2)	118.1(2)
Si(2)−N(4)−Ti(2)	116.9(2)	Si(2)−N(5)−Si(1)	117.3(2)
Ti(1)−N(6)−Ti(2)	122.0(2)		

Compound **4** crystallizes in the space group $P-1$. The silicon−nitrogen bond lengths within the ring are of nearly equal size (170 pm), and they are comparable to those in the starting material dippNSiMe$_3$Si(NH$_2$)$_3$ (average 171 pm). The bond angles N−Si−N (in the range of 102.63−104.46°) and Si−N−Si (in the range of 131.53−134.79°) are part of a distorted six-membered ring.

The atoms Si(1, 2, 3) and N(1, 3) are forming a plane while N(2) is out of the plane (61.57 pm), giving an envelope conformation.

The central unit of the structure of compound **6** is analogous to that of **4** (Figure 3).

Compound **6** crystallizes in the space group $P-1$. The Ge−N bond lengths in the ring are in the range of 181.9−182.8 pm. They are comparable to those described by George et al. in the six-membered ring of [(*t*BuS)$_2$Ge(NH)]$_3$.[7] The N−Ge−N bond angles are nearly 104° and the Ge−N−Ge angles (in the range of 124.8−127.6°) are part of a distorted (GeN)$_3$ six-membered ring system.

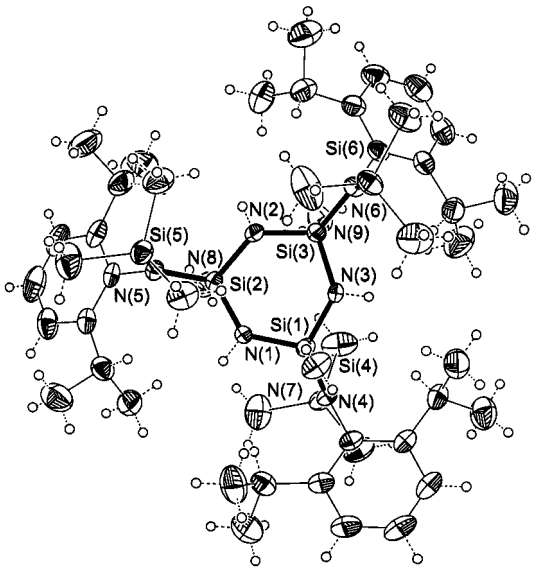


Figure 2. Crystal structure of **4**

Table 2. Selected bond lengths [pm] and angles [°] of compound **4**

Si(1)−N(1)	170.5(2)	Si(1)−N(3)	170.3(2)
Si(2)−N(1)	170.3(2)	Si(2)−N(2)	170.6(2)
Si(3)−N(2)	171.1(2)	Si(3)−N(3)	170.5(2)
N(3)−Si(1)−N(1)	103.95(9)	N(1)−Si(2)−N(2)	104.46(9)
N(3)−Si(3)−N(2)	102.63(9)	Si(1)−N(3)−Si(3)	134.79(11)
Si(2)−N(1)−Si(1)	131.53(12)	Si(2)−N(2)−Si(3)	124.04(11)

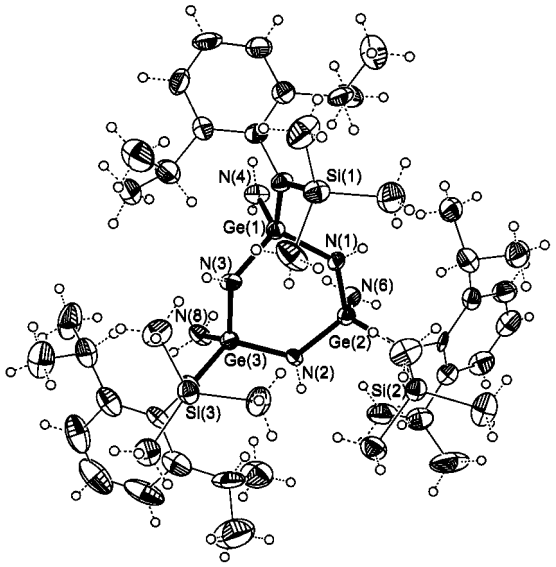


Figure 3. Crystal structure of **6**

The atoms Ge(1, 2) and N(2, 3) are forming a plane while Ge(3) and N(1) are out of the plane (19.2 and −19.2 pm), giving a chair conformation.

Conclusion

In summary, we have shown that silicon and germanium compounds containing terminal NH$_2$ groups are interesting

Table 3. Selected bond lengths [pm] and angles [°] of compound **6**

Ge(1)−N(1)	181.9(7)	Ge(1)−N(3)	182.8(8)
Ge(1)−N(4)	183.2(9)	Ge(2)−N(2)	182.4(8)
Ge(2)−N(6)	181.8(9)	Ge(3)−N(2)	182.4(8)
Ge(2)−N(1)	182.7(7)	Ge(3)−N(8)	182.1(9)
Ge(3)−N(3)	180.7(7)	N(1)−Ge(1)−N(3)	104.0(3)
N(2)−Ge(2)−N(1)	104.7(4)	N(2)−Ge(3)−N(3)	104.4(4)
Ge(1)−N(1)−Ge(2)	124.8(5)	Ge(1)−N(3)−Ge(3)	127.6(4)
Ge(2)−N(2)−Ge(3)	127.3(4)		

starting materials for preparing new inorganic ring systems with functional groups. A marked difference in reactivity has been observed while Cp*$TiMe_3$ yields the $Si_2Ti_2(NH)_6$ adamantane core, the main-group reagents Me_3SnCl and $AlMe_3$ lead to six-membered $(SiN)_3$ and $(GeN)_3$ condensation products.

Experimental Section

General: Due to the water and air sensitivity of the compounds, oxygen and moisture were excluded during all procedures. ^{1}H-NMR data were recorded with a Bruker AM 200 FT NMR spectrometer, IR data were recorded with a BIO RAD Digilab FTS 7 spectrometer and mass data with a Finnigan MAT 95 and a Varian MAT CH5 spectrometer. Elemental analyses were performed by the analytical laboratory of the institute. The starting materials dippNSiMe_3Si$(NH_2)_3$ and Cp*$TiMe_3$ were prepared by literature methods.[3][8] Me_3SnCl and dippNH_2 were commercially available.

Synthesis of 2: To a solution of 0.46 g (2 mmol) of Cp*$TiMe_3$, in *n*-hexane (8 ml), was added dropwise a solution of 0.65 g (2 mmol) of **1**, dissolved in 6 mL of *n*-hexane, at room temperature while stirring. The reaction mixture was warmed up to 69°C until the gas evolution ceased (3 h). The solvent was removed in vacuo and recrystallization of **2** from *n*-hexane (5 mL) afforded single crystals of **2**; yield 0.8 g (79%) (m.p. 260°C). −$C_{50}H_{88}N_8Si_4Ti_2$ (1008.71): calcd. C 61.39, H 9.38; found C 61.81, H 9.48. − IR (Nujol): $\tilde{\nu}$ = 3365 cm^{-1}, 3409, 3481 (N−H). − ^{1}H NMR (200 MHz, C_6D_6): δ = 0.21 [s, 9 H, Si(CH_3)$_3$], 0.27 [s, 9 H, Si(CH_3)$_3$], 0.67 (s, 6 H, NH), 1.25 [m, 24 H, CH(CH_3)$_2$], 1.91 (s, 30 H, CH_3, Cp*), 3.70 [sept, 2 H, CH(CH$_3$)$_2$], 4.05 [sept, 2 H, CH(CH$_3$)$_2$], 7.19 (m, 6 H, aromatic H). − ^{29}Si NMR (49 MHz, C_6D_6): δ = −38.7 (*Si*NH), 3.1 (*Si*Me_3). − MS (EI); *m*/*z* (%): 1009 (100) [M$^+$].

Synthesis of 4: 0.65 g (2 mmol) of **1** and 1.19 g (6 mmol) of Me_3SnCl were dissolved in 20 mL of toluene. Then the reaction mixture was warmed up to 111°C for 6 h. Removal of solvent and Me_3SnCl in vacuo afforded a white solid and recrystallization of the crude product from *n*-hexane (3 mL) gave colorless single crystals of **4**; yield 0.48 g (78%) (m.p. 260°C). − $C_{45}H_{87}N_9Si_6$ (922.07): calcd. N 13.68, Si 18.28; found N 12.65, Si 18.14. − IR (Nujol): $\tilde{\nu}$ = 3401 cm^{-1}, 3486, 3152 (N−H). − ^{1}H NMR (200 MHz, $CDCl_3$): δ = 0.06 [s, 9 H Si(CH_3)$_3$], 0.10 [s, 9 H Si(CH_3)$_3$], 0.12 [s, 9 H Si(CH_3)$_3$], 0.65 [s, 3 H, Si(NH)NH$_2$], 0.75 [s, 6 H, Si(NH)NH_2], 1.31 [m, 36 H, CH(CH_3)$_2$], 3.67 [m, 6 H, CH(CH$_3$)$_2$], 7.10 (m, 9 H, aromatic H). − ^{29}Si NMR (49 MHz, $CDCl_3$): δ −43.1 [*Si*(NH)NH$_2$], −41.4 [*Si*(NH)NH$_2$], −39.8 [*Si*(NH)NH$_2$], 4.2 (*Si*Me_3), 4.7 (*Si*Me_3), 5.3 (*Si*Me_3). − MS (EI); *m*/*z* (%): 906 (80) [M$^+$ − NH$_2$], 905 (100) [M$^+$ − NH$_2$ − H].

Synthesis of 6: To a solution of 0.62 g (2 mmol) of **5** in *n*-hexane (10 mL) was added dropwise 0.53 mL of a solution of $AlMe_3$ in *n*-hexane (1.6 M) at room temperature. After 2 h, the evolution of methane ceased. Subsequently, the solvent was removed in vacuo and the colorless solid recrystallized from *n*-hexane/trichloromethane (1:1) to give single crystals of **6**; yield 0.6 g (67%) (m.p. 177°C). − $C_{45}H_{87}Ge_3N_9Si_3$ (1055.64): calcd. H 8.24, Ge 20.63; found H 7.94, Ge 19.63. − IR (KBr): $\tilde{\nu}$ = 3309 cm^{-1}, 3386, 3619 (N−H). − ^{1}H NMR (200 MHz, C_6D_6): δ = 0.21 [s, 27 H, Si(CH_3)$_3$], 0.65 [s, 6 H, Ge(NH_2)NH], 0.70 [s, 3 H, Ge(NH$_2$)NH], 1.20 [d, 18 H, CH(CH_3)$_2$], 1.25 [d, 18 H, CH(CH_3)$_2$], 3.60 [sept, 6 H, CH(CH$_3$)$_2$], 7.04 (m, 9 H, aromatic H). − ^{29}Si NMR (49 MHz, C_6D_6): δ = 4.8 (*Si*Me_3). − MS (EI); *m*/*z* (%): 73 (90) [$SiMe_3$], 1040 (100) [M$^+$ − Me].

Crystal Structure Determination of Compounds 2, 4 and 6: Data collection and processing: Intensity data were collected using the ω-2θ scan method at 153(2) K for **2**, 193(2) K for **4** and 150(2) K for **6** with a Siemens AED2 four-circle diffractometer using graphite-monochromated Mo-K_α radiation (λ = 71.073 pm) and according to the Learnt-Profile Method.[9] Of the 11865 reflections measured of compound **2** (3.51° ≤ θ ≤ 22.56°) 8424 were unique (merging R = 0.0468), of the 12450 reflections measured of compound **4** (3.51° ≤ θ ≤ 22.55°) 7708 were unique (merging R = 0.0238) and of the 16520 reflections measured of compound **6** (3.52° ≤ θ ≤ 25.04°) 11734 were unique (merging R = 0.1137). All of the reflections were used in the refinement. − X-ray crystallographic study: The structures were solved by direct methods (SHELXS-90)[9] and refined against F^2 by means of the full-matrix least-squares technique using SHELXL 93 and SHELXL 97.[10][11] The weighting schemes were $w^{-1} = \sigma^2(F_o^2) + (0.080 \cdot P)^2 + 18.55 \cdot P$ for **2**, $w^{-1} = \sigma^2(F_o^2) + (0.040 \cdot P)^2 + 1.95 \cdot P$ for **4** and $w^{-1} = \sigma^2(F_o^2) + (0.20 \cdot P)^2 + 0 \cdot P$ for **6** with $P = (F_o^2 + 2F_c^2)/3$ were applied in the final cycles of refinement. The converged residuals were $R1$ = 0.0791 for reflections with $I > 2\sigma(I)$, and $wR2$ = 0.1798 for all data of **2**, the converged residuals were $R1$ = 0.0791 for reflections with $I > 2\sigma(I)$, and $wR2$ = 0.0.0909 for all data of **4** and the converged residuals were $R1$ = 0.1066 for reflections with $I > 2\sigma(I)$, and $wR2$ = 0.2625 for all data of **6**. A final Fourier difference map showed the largest peak and hole 904 and −520 e nm^{-3} for **2**, 331 and −358 e nm^{-3} for **4** and 218.3 and 142.2 e nm^{-3} for **6**. All non-hydrogen atoms were refined anisotropically. All the hydrogen atoms were located in positions riding on the corresponding C atoms.

Acknowledgments

This work was financially supported by the Deutsche Forschungsgemeinschaft.

[1] R. Murugavel, A.Voigt, M. G.Walawalkar, H. W. Roesky, *Chem. Rev.* **1996**, *96*, 2205.
[2] R. Murugavel, V. Chandrasekhar, H. W. Roesky, *Acc. Chem. Res.* **1996**, *29*, 183.
[3] K. Wraage, A. Künzel, M. Noltemeyer, H.-G. Schmidt, H.W. Roesky, *Angew. Chem.* **1995**, 107, 2954; *Angew. Chem. Int. Ed. Engl.* **1995**, *34*, 2645.
[4] C. Rennekamp, A. Gouzyr, A. Klemp, H.W. Roesky, C. Brönneke, J. Kärcher, R. Herbst-Irmer, *Angew. Chem.* **1997**, *109*, 413; *Angew. Chem. Int. Ed. Engl.* **1997**, *36*, 404.
[5] H. Wessel, C. Rennekamp, D.-S. Waeszada, H.W. Roesky, M.L. Montero, I. Uson, *Organometallics* **1997**, *16*, 3243.
[6] K. Wraage, L. Lameyer, D.Stalke, H. W. Roesky, *Angew. Chem.* **1998**, accepted.
[7] C. George, A. P. Purdy, *Acta Crystallogr., Sect. C* **1996**, *52*, 2489.
[8] M. Mena, P. Royo, R. Serrano, M.A. Pellinghelli, A. Tiripicchio, *Organometallics* **1989**, *8*, 476.
[9] G.M. Sheldrick, *Acta Crystallogr., Sect. A* **1990**, *46*, 467.
[10] G.M. Sheldrick, *SHELXL-93*, University of Göttingen, Germany, **1993**.

[11] G. M. Sheldrick, Universität Göttingen, **1997**.
[12] Further details of the crystal structure investigations are available on request from the Cambridge Crystallographic Data Centre (CCDC), 12 Union Road, Cambridge CB2 1EZ, UK on quoting the depository numbers CCDC-111763 for **2**, -111764 for **4** and -111765 for **6**, the names of the authors, and the journal citation (Fax: int. code + 44-1223/336−033; E-mail: deposit@ccdc.cam.ac.uk).

Received December 7, 1998
[I98418]

Synthesis of $(RSn)_4X_6$ Adamantanes (X = O, S, Se) in Liquid Ammonia and in the Two-Phase System Liquid Ammonia/THF

Karsten Wraage,[a] Thomas Pape,[a] Regine Herbst-Irmer,[a] Mathias Noltemeyer,[a] Hans-G. Schmidt,[a] and Herbert W. Roesky*[a]

Dedicated to Professor Dietmar Seyferth on the occasion of his 70th birthday

Keywords: Adamantane / Liquid ammonia / Oxygen / Sulfur and selenium / Tin

The reactions of $trisSnBr_3$ (**1**) [tris = $(Me_3Si)_3C$] and nBuSnCl$_3$ with Na_2X (X = O, S, Se) yield the heterocyclic adamantanes **2**–**6**. The reaction of **1** with Na_2O is carried out in liquid ammonia under normal pressure at –78 °C to give $(trisSn)_4O_6$ (**2**). However, the reaction of **1** with Na_2S and Na_2Se under pressure at room temperature results in the formation of $(trisSn)_4S_6$ (**3**) and $(trisSn)_4Se_6$ (**4**). nBuSnCl$_3$ reacts with Na_2S and Na_2Se in liquid ammonia at –33 °C under normal pressure to give $(n\text{BuSn})_4S_6$ (**5**) and $(n\text{BuSn})_4Se_6$ (**6**), respectively.

Introduction

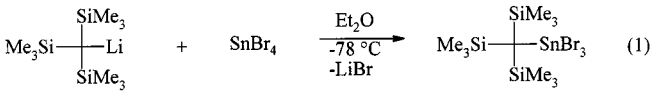
Compounds of the type $(RE)_4X_6$ (E = Si, Ge, Sn; X = S, Se) with an adamantane or a double-decker structure have been reported.[1–3] Unno et al. described the synthesis of $(RE)_4X_6$ compounds (E = Si and Ge; X = S and Se), with a double-decker structure, which afforded the corresponding adamantane upon heating.[1] Another contribution by Berwe and Haas dealt with the reaction of $RSnCl_3$ with $Na_2S \cdot 9\,H_2O$ and $Me_3SiSSiMe_3$, where a heterocyclic adamantane $(RSn)_4S_6$ was reported to be the major product.[2]

Herein the synthesis of the hitherto unknown $trisSnBr_3$ (**1**) [tris = $(Me_3Si)_3C$] and a general method for the preparation of $(RSn)_4X_6$ [R = tris; X = O (**2**), S (**3**), Se (**4**); R = nBu; X = S (**5**), Se (**6**)] are reported.

Results and Discussion

Synthesis and Spectra

$trisSnBr_3$ (**1**) is easily obtained by the treatment of tin tetrabromide with tris(trimethylsilyl)methyllithium in diethyl ether (Equation 1).[4] Compound **1** is a colorless, sublimable crystalline solid, whereas n-butyltin trichloride is a liquid.

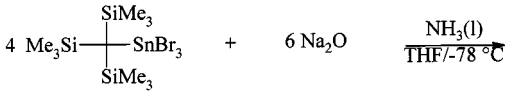


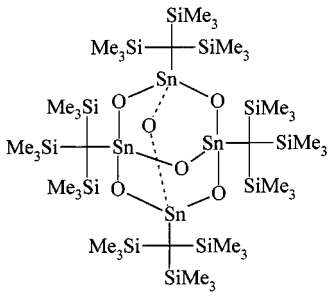
(1)

1

Compound **1** was characterized by mass spectrometry and NMR-spectral studies. The ^{1}H-NMR spectrum of **1** gives a singlet at δ = 0.32 for the protons of the methyl groups of the tris ligand, and ^{119}Sn- and ^{29}Si-NMR spectra also show singlets (at δ = −237.4 and 1.8, respectively). The mass spectrum exhibits a peak at m/z 575 [M^+ − Me]. The spectral data and elemental analysis confirm the composition of the compound to be $C_{10}H_{27}Br_3Si_3Sn$ (**1**).

Compound **1** reacts with Na_2X (X = O, S, Se) in liquid ammonia to give $(RSn)_4X_6$ [R = tris; X = O (**2**), S (**3**), Se (**4**)]. While Na_2O reacts with **1** at − 78 °C under normal pressure in liquid ammonia, Na_2S and Na_2Se, generated in situ in liquid ammonia at −78 °C, react under pressure in liquid ammonia (Equations 2 and 3). The formation of Na_2S and Na_2Se in situ is indicated by a color change of the reaction medium from blue to yellow and red, respectively.





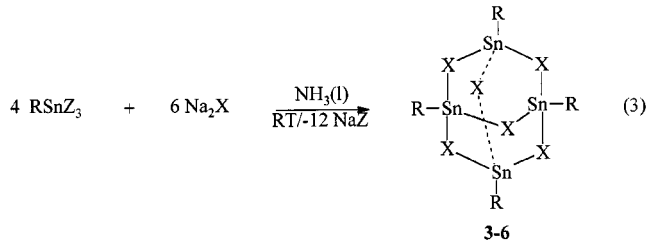
(2)

2

The proton-NMR spectrum of $(trisSn)_4O_6$ (**2**) shows four singlets (δ = 0.13, 0.24, 0.28, 0.51), as does the ^{29}Si-NMR spectrum (δ = −1.0, −0.42, −0.27, −0.17), which indicates that the tris groups are not equivalent. However, the four tin atoms are equivalent and the compound gives only one ^{119}Sn resonance (δ = 94.3). The mass spectrum exhibits the molecular ion peak at m/z (%) 1496 (100) [M^+].

[a] Institut für Anorganische Chemie der Universität Göttingen, Tammannstraße 4, D-37077 Göttingen, Germany
Fax: (internat.) + 49(0)551/393373
E-mail: hroesky@gwdg.de

 © WILEY-VCH Verlag GmbH, D-69451 Weinheim, 1999 1434–1948/99/0505–0869 $ 17.50+.50/0



(3)

R = tris, *n*-Bu Z = Cl, Br X = S, Se

Compounds $(trisSn)_4S_6$ (**3**) and $(trisSn)_4Se_6$ (**4**) were characterized by elemental analysis, multinuclear NMR spectra and mass spectrometry. Unlike in the case of **2**, the ^{1}H-NMR spectra of both compounds **3** and **4** show singlets at $\delta = 0.22$ and 0.20, respectively. Similarly, the ^{29}Si-NMR spectra of **3** and **4** give singlets at $\delta = 4.5$. This indicates that in both compounds the tris ligands are equivalent, unlike in the case of **2**. The ^{119}Sn-NMR spectrum of **3** shows a singlet ($\delta = 72.8$) which is downfield shifted compared to that of **1** ($\delta = -237.4$) due to the formation of the heterocyclic adamantane. It should be pointed out that ^{119}Sn- and ^{77}Se-NMR spectra could not be recorded in the case of **4** due to its instability in solution. Compound **4** decomposed with the formation of selenium. The same behavior was observed for the corresponding tellurium derivative.

The mass spectrum of **3** exhibits two intense peaks (*m*/*z* 1594 [M^+], 1579 [$M^+ - CH_3$]). However, no molecular ion peak [M^+] could be observed for compound **4**, instead a peak at *m*/*z* (%) 1645 (100) [M^+ − tris] was observed.

Similar to **1**, *n*BuSnCl$_3$ reacts with Na_2S and Na_2Se in liquid ammonia at refluxing temp. (−33°C) to give $(n\text{BuSn})_4S_6$ (**5**) and $(n\text{BuSn})_4Se_6$ (**6**), respectively.

Compounds **5** and **6** were characterized by elemental analysis, mass spectrometry and multinuclear NMR-spectral studies. The ^{1}H-NMR spectra of **5** and **6** give a typical spectral pattern due to the *n*butyl group. The ^{119}Sn-NMR spectra of **5** and **6** show singlets at $\delta = 144$ and −22, respectively. This difference in resonances is due to the difference in electronegativities of S and Se. The ^{77}Se-NMR spectrum of **6** exhibits a singlet at $\delta = -169.9$. Thus, the NMR-spectral studies agree well with the proposed adamantane structure. The mass spectrum of **5** shows a peak at *m*/*z* (%) 839 (70) [M^+ − *n*-butyl]. **6** is characterized in the gas phase by two peaks: first the molecular ion peak at *m*/*z* (%) 1177 (20) and second the fragment at *m*/*z* (%) 1120 (90) [M^+ − *n*-butyl].

In all cases we were unable to detect the coupling constants of ^{117}Sn/^{119}Sn, ^{119}Sn/^{77}Se and ^{119}Sn/^{29}Si.

X-ray Structures of 2 and 3

The structure of **2** (see Figure 1) shows a highly symmetric, regular adamantane core (point group *T*) consisting of tin and oxygen atoms. This geometry is defined by a threefold axis through the Sn−C bond and three equivalent twofold axes through two opposite O atoms, so that only 1/12 of the whole molecule exists in the asymmetric unit. Due to this symmetry, each of the Sn atoms shows a distorted tetrahedral geometry with three equivalent bridging oxygen atoms and a terminal tris(trimethylsilyl)methyl group heading away from the core. All Sn−O bond lengths are equal [196.8(1) pm], as well as the Sn−C bond lengths [213.4(3) pm] and the corresponding bond angles [O−Sn−O 103.8(1)°, O−Sn−C 114.7(1)°]. Two solvent molecules of benzene exist close to the special position 1/4, 1/4, 0 and appear to rotate freely.

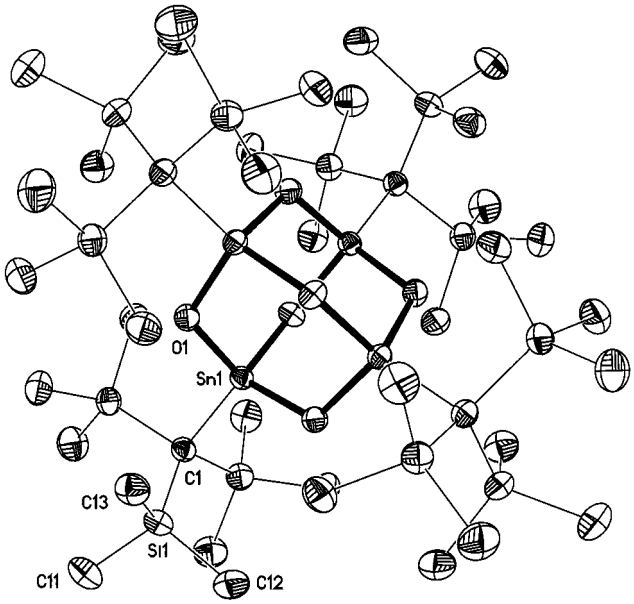


Figure 1. Crystal structure of **2**

3 (see Figure 2) is isomorphous with **2** but the O atoms are replaced by S. This substitution leads to longer bonds in the adamantane core [Sn−S 240.8(3) pm] and a longer Sn−C bond [223(2) pm] in **3**, causing the terminal tris(trimethylsilyl)methyl group to be disordered. Because of this

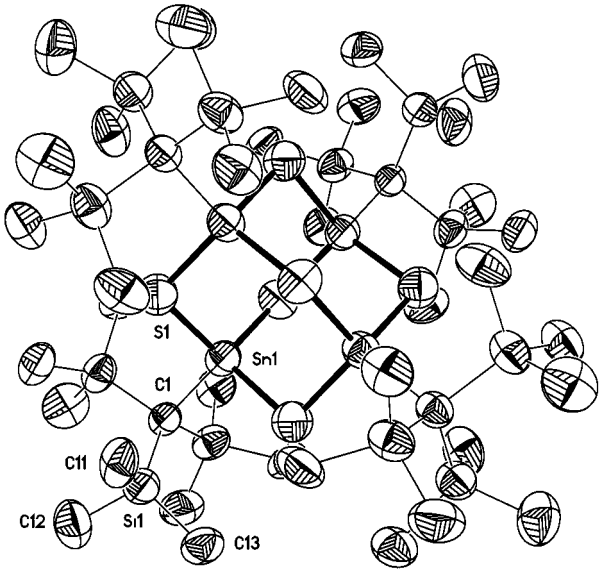


Figure 2. Crystal structure of **3**

disorder a mirror plane is added to the symmetry of the data, the space group is *Fd*−3*m* instead of *Fd*−3 as in **2**.

Conclusion

In summary, we have shown that tin adamantanes containing the chalcogens oxygen, sulfur and selenium are easily accessible using liquid ammonia as a reaction media. The structure of $(trisSn)_4O_6$ has been shown to have the most regular adamantane core of this series

Experimental Section

General: All reactions were carried out under dry nitrogen using Schlenk techniques and a drybox. Solvents were dried and distilled under nitrogen prior to use. − ^{1}H NMR (200 MHz): Bruker AM 200. − ^{29}Si NMR (49.7 MHz), ^{119}Sn NMR (93.3 MHz), ^{77}Se NMR (47.7 MHz): Bruker AC 250 NMR, tetramethylsilane, tetramethyltin and dimethylselenium, respectively, as external standards. − MS: Bruker AM 200 MS, Bruker MSL 400 MS . − M.p.: Bühler SPA-1. − The starting materials trisLi[4] and Na_2X (X = S, Se)[5] were prepared by literature methods. Tin tetrabromide and *n*-butyltin trichloride were commercially available.

Synthesis of 1: A solution of $(trisLi)_2 \cdot 4$ THF (4.4 g, 5.7 mmol, dissolved in 40 mL of diethyl ether) was added dropwise to a solution of $SnBr_4$ (5.0 g, 11.4 mmol, dissolved in 30 mL of diethyl ether) at −78°C while stirring. The reaction mixture was allowed to warm up to room temp., and the residue was dissolved in 50 mL of *n*-hexane and the precipitate of lithium bromide filtered off. 50% of the solvent was removed in vacuo. Recrystallization of the crude product at −30°C afforded 6.0 g (89%) of a colorless crystalline solid (sublimation at 155°C). − ^{1}H NMR (200 MHz, C_6D_6): δ = 0.32 {s, 27 H, $C[Si(CH_3)_3]_3$}. − ^{29}Si NMR (49.7 MHz, C_6D_6): δ = 1.8 [$C(SiMe_3)_3$]. − ^{119}Sn NMR (93.3 MHz, C_6D_6): δ = −237.4 ($trisSnBr_3$). − MS (EI); *m*/*z* (%): 575 (100) [M^+ − Me].

Synthesis of 2: Na_2O (0.093 g, 1.5 mmol) was suspended in 30 g of liquid ammonia at −78°C. **1** (0.59 g, 1 mmol) was dissolved in 20 mL of THF and added dropwise to the suspension of Na_2O while stirring. The reaction mixture was cooled at −78°C for 6 h and then warmed up slowly to room temp. THF was removed in vacuo. The remaining solid was dissolved in 50 mL of *n*-hexane, the precipitate of sodium bromide filtered off and the filtrate concentrated in vacuo. The residue was a white solid (0.28 g, 80%). Recrystallization from benzene resulted in colorless single crystals (m.p. > 250°C). − $C_{40}H_{108}Si_{12}Sn_4O_6$ (1398.38): calcd. C 32.11, H 7.71; found C 31.9, H 7.7. − ^{1}H NMR (200 MHz, C_6D_6): δ = 0.13 {s, 27 H, $C[Si(CH_3)_3]_3$}, 0.24 {s, 27 H, $C[Si(CH_3)_3]_3$}, 0.28 {s, 27 H, $C[Si(CH_3)_3]_3$}, 0.51 {s, 27 H, $C[Si(CH_3)_3]_3$}. − ^{29}Si NMR (49.7 MHz, C_6D_6): δ = −1.0 ($SiMe_3$), −0.42 ($SiMe_3$), −0.27 ($SiMe_3$), −0.17 ($SiMe_3$). − ^{119}Sn NMR (93.3 MHz, C_6D_6): δ = 94.3 (Sn_{ad}) (ad = adamantane). − MS (EI); *m*/*z* (%): 1496 (100) [M^+], 1481 (75) [M^+ − Me].

Synthesis of 3: Sulfur (0.096 g, 3 mmol) was suspended in liquid ammonia in a glass autoclave at −78°C. Sodium (0.138 g, 6 mmol) was added to the suspension while stirring. The stirring was continued until the color changed from blue to yellow. Solid **1** (1.18 g, 2 mmol) was added to the stirred suspension of sodium sulfide, and the glass autoclave was closed. The reaction mixture was allowed to warm up to room temp. After 25 min, the color of the reaction mixture changed from yellow to green. After 24 h, the autoclave was opened and the liquid ammonia vaporized. Subsequently, the residue was dissolved in 20 mL of toluene, the sodium bromide filtered off and the filtrate concentrated in vacuo. Recrystallization from benzene afforded 0.6 g (75%) of yellow crystals (decomp. 168°C). − $C_{40}H_{108}S_6Si_{12}Sn_4$ (1593.56): calcd. C 30.15, H 6.78, S 12.07, Si 21.15; found C 31.3, H 7.1, S 11.8., Si 21.3. − ^{1}H NMR (200 MHz, C_6D_6): δ = 0.22 {s, 108 H, 4 $C[Si(CH_3)_3]_3$}. − ^{29}Si NMR (49.7 MHz, C_6D_6): δ = 4.5 ($SiMe_3$). − ^{119}Sn NMR(93.3 MHz, C_6D_6): δ = 72.8 (Sn_{ad}). − MS (EI); *m*/*z* (%): 1579 (100) [M^+ − Me], 1594 (45) [M^+].

Syntheses of 4: Compound **4** was synthesized in an analogous manner to that of **3**. The reaction and isolation afforded 0.38 g (81%) of a yellow/red powder (decomp. 195−205°C). − $C_{40}H_{108}Se_6Si_{12}Sn_4$ (1874.92): calcd. C 25.62, H 5.81; found C 26.0, H 5.7. − ^{1}H NMR (200 MHz, $CDCl_3$): δ = 0.20 {s, 108 H, $C[Si(CH_3)_3]_3$}. − ^{29}Si NMR (49.7 MHz, $CDCl_3$): δ = 4.5 ($SiMe_3$). − MS (EI); *m*/*z* (%): 1645 (100) [M^+ − tris].

Synthesis of 5: Sulfur (0.144 g, 4.5 mmol) was suspended in 40 g of liquid ammonia in a 100-mL Schlenk flask at −78°C. Sodium (0.207 g, 9 mmol) was slowly added to this mixture. The reaction mixture was stirred until it became yellow. nBuSnCl_3 (0.847 g, 3 mmol) was then added to the suspension which was then allowed to warm up to −33°C and refluxed in liquid ammonia for 2 h. The liquid ammonia vaporized overnight. The residue was dissolved in 20 mL of *n*-hexane, the precipitate of sodium chloride filtered off and the filtrate concentrated in vacuo, yielding 0.3 g (45%) of a yellow powder (decomp. 130°C). − $C_{16}H_{36}S_6Sn_4$ (895.7): calcd. C 21.46, H 4.05, S 21.48; found C 20.9, H 4.2, S 22.3. − ^{1}H NMR (200 MHz, $CDCl_3$): δ = 0.85−0.95 (t, 12 H, CH_3CH_2-$CH_2CH_2Sn_{ad}$), 1.35−1.50 (m, 8 H, $CH_3CH_2CH_2CH_2Sn_{ad}$), 1.70−1.80 (m, 16 H, $CH_3CH_2CH_2CH_2Sn_{ad}$). − ^{119}Sn NMR (93.3 MHz, $CDCl_3$): δ = 144 (Sn_{ad}). − MS (EI); *m*/*z* (%): 839 (70) [M^+ − nBu], 655 (100) [M^+ − nBu − Sn − 2 S].

Synthesis of 6: Selenium (0.355 g, 4.5 mmol) was suspended in 40 g of liquid ammonia in a 100-mL Schlenk flask at −78°C. Sodium (0.207 g, 9 mmol) was added slowly to this mixture while stirring, until the solution became red. Finally, *n*-butyltin trichloride (0.847 g, 3 mmol) was added. After warming up to −33°C, the mixture was refluxed for 5 h. The liquid ammonia was vaporized overnight. The residue was dissolved in 20 mL of *n*-hexane, the precipitated sodium chloride filtered off and the solvent removed in vacuo to yield 0.6 g (68%) of a yellow powder (decomp. 118°C). − $C_{16}H_{36}Se_6Sn_4$ (1177.06): calcd. Sn 40.34; found Sn 40.5. − ^{1}H NMR (200 MHz, $CDCl_3$): δ = 0.90−1.00 (t, 12 H, 4 CH_3-$CH_2CH_2CH_2Sn_{ad}$), 1.35−1.55 (sext, 8 H, 4 $CH_3CH_2CH_2CH_2Sn_{ad}$), 1.65−1.80 (quint, 8 H, 4 $CH_3CH_2CH_2CH_2Sn_{ad}$), 1.90−1.98 (t, 8 H, 4 $CH_3CH_2CH_2CH_2Sn_{ad}$). − ^{119}Sn NMR (93 MHz, $CDCl_3$): δ = −22 (Sn_{ad}). − ^{77}Se NMR (47 MHz, $CDCl_3$): δ = −165.5 (Sn_{ad}-$Se_{1.5ad}$). − MS (EI); *m*/*z* (%): 1120.4 (90) [M^+ − nBu], 1177 (20) [M^+].

X-ray Crystallographic Study:[6] Crystals were grown by cooling a saturated solution of benzene (**2**) or benzene/trichloromethane (**3**) to 8°C and then mounted on a glass fiber in a rapidly cooled perfluoro polyether.[7] − Crystal data for **2**: $C_{40}H_{108}O_6Si_{12}Sn_4$ + 3 C_6H_6, M = 1731.43, space group *Fd*−3, a = 2541.2(3) pm, V = 16.41(10) nm^3, Z = 8, $\rho_{calcd.}$ = 1.402 g cm^{-3}, data collection: Stoe-Siemens-Huber four-circle diffractometer, coupled to a Siemens CCD area detector, graphite-monochromated Mo-K_α radiation, crystal size 0.5 × 0.4 × 0.4 mm, all measurements at 133(2) K, φ- and ω-collecting mode, 4.5° ≤ 2θ ≤ 59.5°, 92370 reflections measured, 1940 unique (R_{int} = 0.0270), 1795 with $I > 2\sigma(I)$, 1.419 mm^{-1} absorption coefficient, semi-empirical absorption correction from

Table 1. Selected bond lengths [pm] and angles [°] of **2**; symmetry transformations for equivalent atoms are indicated

Sn(1)−O(1)	196.8(1)
Sn(1)−C(1)	213.4(3)
Si(1)−C(1)	190.8(1)
O(1)−Sn(1)−O(1)[a]	103.8(1)
O(1)−Sn(1)−C(1)	114.7(1)
Sn(1)−O(1)−Sn(1)[b]	120.0(1)
Si(1)[c]−C(1)−Si(1)	112.9(1)
Si(1)[c]−C(1)−Sn(1)	105.8(1)

[a] $-x + 3/4, -y + 3/4, z$. − [b] $-x + 5/4, y, -z + 1/4$. − [c] $x - 1/2, -y + 3/4, -z + 1/4$.

Table 2. Selected bond lengths [pm] and angles [°] of **3**; symmetry transformations for equivalent atoms are indicated

Sn(1)−C(1)	223(2)
Sn(1)−S(1)	240.8(3)
C(1)−Si(1)	191.2(7)
C(1)−Sn(1)−S(1)	108.1(1)
S(1)[a]−Sn(1)−S(1)	110.8(1)
Sn(1)−S(1)−Sn(1)[b]	106.7(2)
Si(1)−C(1)−Si(1)[a]	112.3(5)
Si(1)−C(1)−Sn(1)	106.5(6)

[a] $-x + 3/4, -y + 1/4, z + 1/2$. − [b] $-x + 5/4, y + 0, -z + 1/4$.

equivalents (0.5373−0.6007 transmission factors). Data/restraints/parameters: 1940/181/124, final $R1 = 0.0265$ for $I > 2\sigma(I)$ and $wR2 = 0.0635$ for all data $\{R1 = \Sigma||F_o| - |F_c||/\Sigma|F_o|$, $wR2 = [\Sigma w(F_o^2 - F_c^2)^2/\Sigma w(F_o^2)^2]^{1/2}$, $w^{-1} = \sigma^2(F_o)^2 + (0.0180{\cdot}P)^2 + 79.5121{\cdot}P$, $P = [F_o^2 + 2F_c^2]/3\}$, largest peak and hole in final diff. map = 642 and −745 e nm^{-3}. − Crystal data for **3**: $C_{40}H_{108}S_6Si_{12}Sn_4 + 1.57\ C_6H_6 + 0.43\ CHCl_3$, $M = 1767.39$, space group $Fd{-}3m$, $a = 2554.1(3)$ pm, $V = 16.66(10)$ nm^3, $Z = 8$, $\rho_{calcd.} = 1.409$ g cm^{-3}, data collection: Stoe-Siemens-AED2 four-circle diffractometer, graphite-monochromated Mo-K_α radiation, crystal size 0.5 × 0.4 × 0.4 mm, all measurements at 150(2) K, learnt-profile method, $7.8° \le 2\theta \le 49.3°$, 6642 reflections measured, 713 unique ($R_{int} = 0.1007$), 544 with $I > 2\sigma(I)$, data/restraints/parameters: 713/33/76, final $R1 = 0.0673$ for $I > 2\sigma(I)$ and $wR2 = 0.2304$ for all data, $w^{-1} = \sigma^2(F_o)^2 + (0.1268{\cdot}P)^2 + 304.6513{\cdot}P$, largest peak and hole in final diff. map = 1260 and −1049 e nm^{-3}. − Structural analysis and refinement: Both structures (see Tables 1 and 2) were solved by direct methods using SHELXS-97[8] and refined against F^2 on all data by full-matrix least squares with SHELXL-97.[9] All non-hydrogen atoms except those of the solvent molecules were refined anisotropically. Hydrogen atom positions were calculated from idealized geometries and refined using a riding model. In **2** solvent benzene molecules close to the special position 1/4, 1/4, 0 could not be resolved properly, and were refined using strong restraints on geometry and displacement parameters. Special position constraints were suppressed. In **3** the electron density for the solvent showed an even more disordered site than in **2** so that the solvent molecules were refined as a rigid benzene molecule and a strongly restrained trichloromethane molecule. The two molecules share the same position, the sum of their occupation factors is 1. Since this model does not describe the true situation very well the difference electron density is comparitively high. The severe disorder in structure **3** leads to a significantly worse refinement compared to structure **2**.

Acknowledgments

This work was financially supported by the Deutsche Forschungsgemeinschaft.

[1] M. Unno, Y. Kawai, H. Shioyama, H. Matsumoto, *Organometallics* **1997**, *16*, 4428−4434.
[2] H. Berwe, A. Haas, *Chem. Ber.* **1987**, *120*,1175−1182.
[3] W. Ando, T. Kadowaki, Y. Kabe, M. Ishii, *Angew. Chem.* **1992**, *104*, 84−85; *Angew. Chem. Int. Ed. Engl.* **1992**, *31*, 59.
[4] S. S. Dua, C. Eaborn, D. A. R. Happer, S. P. Hopper, K. D. Safa, D. R. M. Walton, *J. Organomet. Chem.* **1979**, *178*, 75−82.
[5] E. Zintl, A. Harder, B. Dauth, *Z. Elektrochem.* **1934**, *40*, 588−593.
[6] Further details of the crystal structure investigations are available on request from the Cambridge Crystallographic Data Centre (CCDC), 12 Union Road, Cambridge CB2 1EZ, UK on quoting the depository numbers CCDC-111980 for **2** and -111981 for **3**, the names of the authors, and the journal citation [Fax: int. code + 44-1223/336-033; E-mail: deposit@ccdc.cam.ac.uk].
[7] J. Kottke, D. Stalke, *J. Appl. Crystallogr.* **1993**, *26*, 615.
[8] G. M. Sheldrick, *SHELXS-97, Programm zur Strukturlösung*, Universität Göttingen, **1997**.
[9] G. M. Sheldrick, *SHELXL-97, Programm für die Kristallstrukturverfeinerung*, Universität Göttingen, **1997**.

Received December 7, 1998
[I98419]

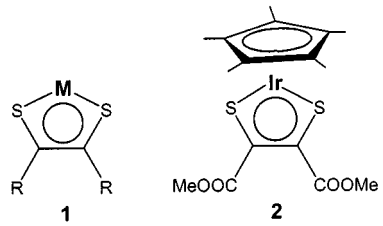
The NMR-Spectroscopic and X-ray Crystal-Structural Characterization of Two Cp*Ir Halfsandwich Complexes Containing the 1,2-Dicarba-*closo*-dodecaborane-1,2-diselenolato Ligand

Max Herberhold,*[a] Guo-Xin Jin,[b] Hong Yan,[a] Wolfgang Milius,[a] and Bernd Wrackmeyer*[a]

Keywords: Iridium / Selenium / Diselenolenes / Carboranes / X-ray crystal structure analysis / NMR spectroscopy

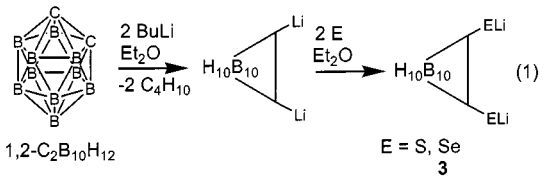
The reaction of $[Cp^*IrCl_2]_2$ with dilithium 1,2-*ortho*-carborane-1,2-diselenolate **3** leads to the green 16-electron diselenolene complex $[Cp^*Ir\{Se_2C_2(B_{10}H_{10})\}]$ (**4**) which takes up two-electron ligands such as trimethylphosphane to give the 18-electron diselenolate derivative $[Cp^*Ir(PMe_3)\{Se_2C_2(B_{10}H_{10})\}]$ (**5**). The molecular structures of **4** and **5** were determined by X-ray crystal structure analysis. The ^{77}Se-nuclear shielding in **4** is lower by almost 500 ppm relative to that in **5**.

The bonding in metallacyclic 16-electron dithiolene complexes of type **1** is a matter of debate.[1] In this context, we have recently reported[2] the X-ray crystal structure analysis of the 1,2-bis(methoxycarbonyl)dithiolene complex **2** in which **M** is the (pentamethylcyclopentadienyl)iridium moiety (Cp*Ir). In order to obtain further structural and spectroscopic information, we have now combined the Cp*Ir half-sandwich fragment with the *ortho*-carboranediselenolate ligand $[H_{10}B_{10}C_2Se_2]^{2-}$ (**3**). Direct structural evidence is expected to correlate in particular with the ^{77}Se-NMR data.

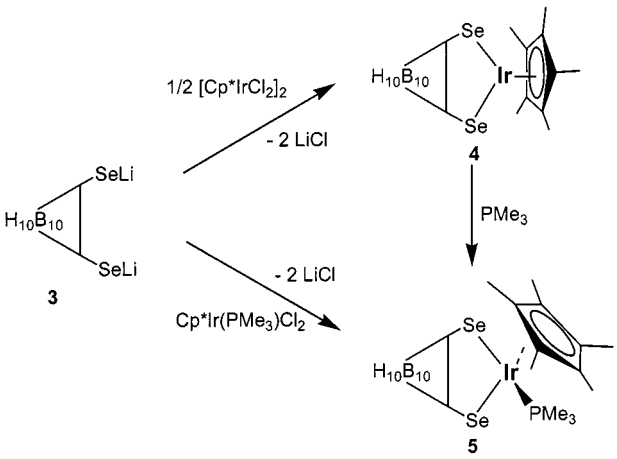


1 **2**

Although complexes containing the *ortho*-carboranedithiolate ligand chelated to Mo,[3] Re,[3] Co,[4] Ni,[4] Pd,[3] Pt,[5] and Au[6] have been prepared starting from the dithiol $H_{10}B_{10}C_2(SH)_2$, the analogous or related diselenolate compounds have not been described. We prepared both *ortho*-carboranedithiolate and -diselenolate complexes from the dilithium dichalcogenates $H_{10}B_{10}C_2(ELi)_2$ [E = S, Se (**3**)] which were obtained in situ by insertion of either sulfur or selenium (1:2) into the dilithiated *ortho*-carborane intermediate (Equation 1).



As shown in Scheme 1, the dilithium *o*-carboranediselenolate **3** reacts with $[(Cp^*IrCl_2)_2]$ to give the green diselenolene complex **4**, and with $[Cp^*IrCl_2(PMe_3)]$ the yellow diselenolate complex **5**. Compound **4** takes up two-electron ligands L such as L = CO, CN*t*Bu, phosphanes and pyridines. However, attempts to remove PMe_3 from **5** using sulfur were not successful.



Scheme 1

The molecular structures of both **4** and **5** in the crystal were determined by X-ray crystal structure analyses (Figures 1 and 2). The molecule of **4** corresponds to point group symmetry C_{2v} with two perpendicular mirror planes. Addition of PMe_3 to form the 18-electron complex **5** leads to

[a] Laboratorium für Anorganische Chemie der Universität Bayreuth,
D-95440 Bayreuth, Germany
Fax: (internat.) + 49(0)921/55-2157
E-mail: Max.Herberhold@uni-bayreuth.de
[b] Changchun Institute of Applied Chemistry, Chinese Academy of Sciences,
Changchun 130022, P. R. China

 © WILEY-VCH Verlag GmbH, D-69451 Weinheim, 1999 1434–1948/99/0505–0873 $ 17.50+.50/0

C_s symmetry with only one mirror plane left. The iridadiselenolene heterocycle in **4** (which is coplanar with the centers of both the Cp* ring and the *ortho*-dicarbadodecaborane cluster) is bent in **5** with a dihedral angle at the Se···Se vector of 156.1°. Apparently, the ligand L = PMe_3 destroys the pseudoaromatic $IrSe_2C_2$ system in **4**. This is particularly evident from the fact that on going from **4** to **5**, the C(1)−C(2) bond length increases [from 161.2(9) to 165.0(10) pm], the Ir−Se bond lengths grow significantly [from 237.0 (av.) to 247.0 (av.) pm], while the Se−Ir−Se angle decreases [from 93.65(3) to 90.2(1)°]. Compared to **4**, the trimethylphosphane adduct **5** is an ordinary diselenolate chelate complex.

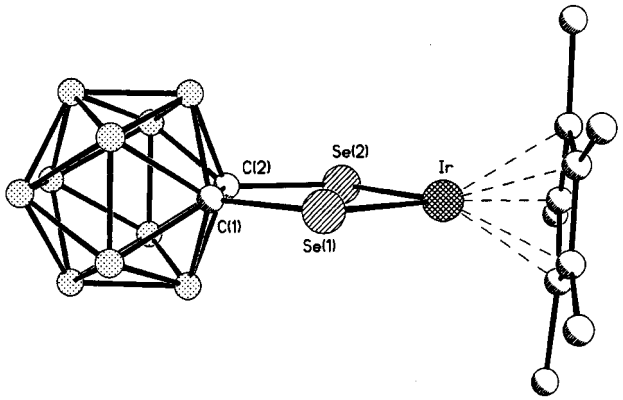


Figure 1. Molecular structure of [Cp*Ir($Se_2C_2B_{10}H_{10}$)] (**4**); selected bond lengths [pm] and angles [°]: Ir−Se(1) 237.53(9), Ir−Se(2) 236.56(9), Se(1)−C(1) 194.1(7), Se(2)−C(2) 193.7(7), C(1)−C(2) 161.2(9), Ir−Z(Cp*) 179.4; Se(1)−Ir−Se(2) 93.65(3), Ir−Se(1)−C(1) 104.6(2), Ir−Se(2)−C(2) 105.0(2), Se(1)−C(1)−C(2) 118.5(5), Se(2)−C(2)−C(1) 118.3(5); dihedral angle Se(1)IrSe(2)/Se(1)C(1)C(2)Se(2) 180°

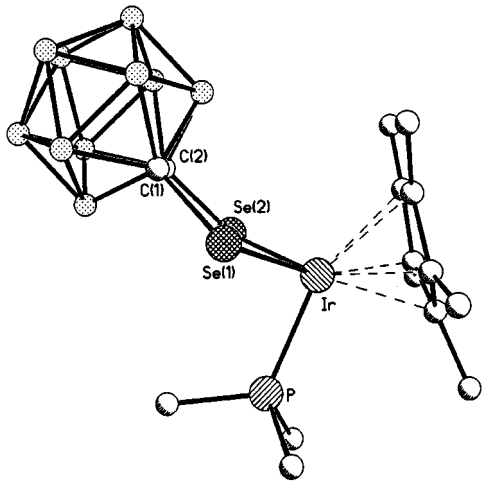


Figure 2. Molecular structure of [Cp*Ir($Se_2C_2B_{10}H_{10}$)(PMe_3)] (**5**); selected bond lengths [pm] and angles [°]: Ir−Se(1) 247.3(1), Ir−Se(2) 246.6(2), Ir−P 227.3(2), Se(1)−C(1) 194.9(6), Se(2)−C(2) 195.2(6), C(1)−C(2) 165.0(10), Ir−Z(Cp*) 188.7. Se(1)−Ir−Se(2) 90.2(1), Se(1)−Ir−P 89.1(1), Se(2)−Ir−P 89.1(1), Ir−Se(1)−C(1) 103.1(2), Ir−Se(2)−C(1) 103.9(2), Se(1)−C(1)−C(2) 119.0(4), Se(2)−C(2)−C(1) 117.6(4); dihedral angle Se(1)IrSe(2)/Se(1)C(1)C(2)Se(2) 156.1°

The ^{1}H-, ^{11}B-, ^{13}C-, ^{31}P-, and ^{77}Se-NMR data (Table 1) of **4** and **5** in solution are in complete agreement with their solid-state structures. In the case of **4**, the C_{2v} symmetry requires four ^{11}B-NMR signals in the intensity ratio of 2:4:2:2, as observed in the 180.5-MHz ^{11}B-NMR spectrum, whereas the C_s symmetry of **5** should give rise to seven ^{11}B-NMR signals in the ratio of 1:1:2:2:1:1:2, of which six are observed. The range of the δ^{11}B-NMR data is similar to that of other 1,2-substituted derivatives of 1,2-$C_2B_{10}H_{12}$.[7] There is only one ^{13}C(carborane) signal each for **4** and **5**, as expected, the one of **4** being shifted by 6.8 ppm to lower field relative to that of **5**. The structural changes between **4** and **5** are most strikingly reflected by the ^{77}Se-nuclear deshielding of almost 500 ppm in the 16-electron complex **4** relative to the 18-electron complex **5**. Such a deshielding is typical of ^{77}Se nuclei becoming part of a heteroaromatic system.[8] This effect can be traced to magnetic field induced mixing of electronic ground and energetically low-lying excited states present in such heterocycles. The complexes **4** and **5** are the first examples to compare the influence of electronic structure on ^{77}Se-nuclear shielding in closely related transition metal diselenolene complexes. A similar comparison has been carried out between titanocene diselenolene metallacycles (also 16-electron complexes) and non-cyclic derivatives.[9] However, in these cases the metallacycles are non-planar and the differences in ^{77}Se-nuclear shielding are rather small.

Experimental Section

The starting complexes [{Cp*$IrCl_2$}$_2$][10] and [Cp*Ir(PMe_3)Cl_2][11] were prepared according to established procedures; the *ortho*-carborane 1,2-$C_2B_{10}H_{12}$ is commercially available. − NMR measurements: Bruker ARX 250 and DRX 500 spectrometers; chemical shifts are given relative to $CHCl_3/CDCl_3$ (δ^1H = 7.24; δ^{13}C = 77.0), external Et_2O-BF_3 [δ^{11}B = 0 for Ξ(^{11}B) = 32.083971 MHz], external 85% aqueous H_3PO_4 [δ^{31}P = 0 for Ξ(^{31}P) = 40.480747 MHz], external Me_2Se [δ^{77}Se = 0 for Ξ(^{77}Se) = 19.071523 MHz]. − Mass spectra: VARIAN MAT CH7, EI MS (70 eV), direct inlet. − IR spectra: Perkin−Elmer 983 G.

Dilithium 1,2-Dicarba-*closo*-dodecaborane-1,2-diselenolate (3): A solution of 1,2-$C_2B_{10}H_{12}$ (0.29 g; 2 mmol) in Et_2O (40 mL) was lithiated by addition of 2.75 mL of 1.6 M butyllithium (4.4 mmol) in hexane. Addition of selenium (0.32 g; 4 mmol) gave a yellow solution of $H_{10}B_{10}C_2(SeLi)_2$ (**3**) in quantitative yield.

Pentamethylcyclopentadienyl-(1,2-dicarba-*closo*-dodecaborane-1,2-diselenolato)iridium ([Cp*Ir{$Se_2C_2(B_{10}H_{10})$}], 4): A solution of **3** (1 mmol) in Et_2O (60 mL) was added to a solution of [{Cp*$IrCl_2$}$_2$] (0.40 g; 0.5 mmol) in THF (60 mL). The colour of the Et_2O/THF solution changed gradually from red to dark green. After 24 h of stirring at ambient temperature, the solvents were evaporated under reduced pressure and the residue chromatographed on silica. Elution with CH_2Cl_2/hexane (5:1) gave a dark green zone which contained 0.57 g (91%) of **4**. Dark green prismatic crystals were grown from CH_2Cl_2/hexane/THF solvent mixtures. − IR (CsI): $\tilde{\nu}$ = 2586 cm^{-1}, ν(B−H). − EI MS (70 eV); *m/z* (%): 628 (100) [M^+], 484 (38) [$M^+ - C_2B_{10}H_{12}$], 143 (100) [$C_2B_{10}H_{11}^+$].

(1,2-Dicarba-*closo*-dodecaborane-1,2-diselenolato)(pentamethylcyclopentadienyl)(trimethylphosphane)iridium ([Cp*Ir{Se_2C_2-($B_{10}H_{10}$)}(PMe_3)], 5): Trimethylphosphane (0.10 g, 1.32 mmol) was added to the green solution of **4** (0.30 g; 0.48 mmol) in CH_2Cl_2

Table 1. NMR-spectroscopic data[a] of **4** and **5**

	[Cp*Ir($Se_2C_2B_{10}H_{10}$)] (**4**)	[Cp*Ir($Se_2C_2B_{10}H_{10}$)(PMe_3)] (**5**)
δ^1H	1.83 s Cp*	1.80 (2.1) d Cp*, 1.71 (10.5) d Me_3P
$\delta^{11}B$[b]	−6.0, −7.1, −7.5, −8.4 [ratio 2:4:2:2]	−2.4, −4.2, −6.2, −8.0/−8.4, −10.7 [ratio 1:1:2:4:2]
$\delta^{13}C$	10.6, 90.7 Cp*; 72.8 $C_2B_{10}H_{10}$	9.4 (1.1), 97.0 (3.2) Cp*; 66.1 (3.5) $C_2B_{10}H_{10}$;17.5 (43.3) Me_3P
$\delta^{31}P$	–	−29.3
$\delta^{77}Se$	855.5	363.4 (38.0)[c]

[a] Measured from diluted solutions in $CDCl_3$ at 20 ± 1°C; coupling constants $J(^{31}P,X)$ (X = ^1H, ^{13}C, ^{77}Se), ± 0.5 Hz, are given in parentheses. – [b] The number of boron atoms corresponding to the signals is given in square brackets. – [c] The $\delta^{77}Se$ value depends only slightly on the nature of L in [Cp*Ir($Se_2C_2B_{10}H_{10}$)(L)], e.g. 342.7 (L = CO), 360.0 (L = CN*t*Bu).

(60 mL). The colour turned yellow immediately. The solvent was evaporated, the residue washed with hexane and recrystallized from CH_2Cl_2/hexane mixtures to give 0.31 g (93%) of orange-yellow crystals of **5**. – IR (CsI): $\tilde{\nu}$ = 2580 cm^{-1}, ν(B–H). – EI MS (70 eV); *m*/*z* (%): 620 (43) [$M^+ - PMe_3$], 549 (100) [$M^+ - PMe_3Se$].

X-ray Crystal Structure Analyses of 4 and 5:[12] The intensity data of both compounds were collected with a Siemens P4 diffractometer using Mo-K_α radiation (λ = 71.073 pm, graphite-monochromated). The stability of the primary beam was controlled by monitoring three check reflections every 100 reflections.

4: $C_{12}H_{25}B_{10}IrSe_2$; M_r = 627.6; ρ = 1.954 g cm^{-3}; black prism of the dimensions 0.12 × 0.15 × 0.20 mm, monoclinic space group $P2_1/c$, with lattice parameters a = 1478.30(17), b = 1105.57(13), c = 1483.0(2) pm, β = 117.990(9)° and Z = 4; unit cell volume $V = 2140.3(5) \cdot 10^6$ pm^3, absorption coefficient μ = 9.633 mm^{-1}. Data collection: Intensity data of 5977 reflections in the range 3° ≤ 2ϑ ≤ 55° have been measured in the ω-scan mode (measuring temperature 296 K); 4868 (R_{int} = 0.033) reflections were unique and assigned to be observed; the data were Lorentz-, polarization-, and absorption-corrected (ψ-scans, min./max. transmission 0.2796/0.4392). Structure solution and refinement: Direct methods (Siemens SHELXTL PLUS v5.01); refinement (against F_o^2) with 222 parameters converged at $R1$ = 0.0412 and $wR2$ = 0.0961 [$I \geq 2\sigma(I)$]; max./min. residual electron density was 1.09/−1.34 10^{-6} e pm^{-3}.

5: $C_{15}H_{34}B_{10}PIrSe_2$ (CH_2Cl_2); M_r = 703.6; ρ = 1.729 g cm^{-3}; orange prism with dimensions 0.20 × 0.15 × 0.12 mm, monoclinic space group $C2/c$ with the lattice parameters a = 24.886(5), b = 17.636(4), c = 14.734(3) pm, β = 123.27(3)°, and Z = 8, V = 5407(2) 10^6 pm^3, absorption coefficient μ = 7.693 mm^{-1}. Data collection: Intensity data of 7222 reflections in the range 3° ≤ 2 ϑ ≤ 55° have been measured in the ω-scan mode, 6144 reflections were unique (R_{int} = 0.03) and 5482 were assigned to be observed [$F_o \geq 2\sigma(F_o)$]; the data were corrected for Lorentz, polarization, and absorption effects (ψ-scans, min./max. transmission 0.4145/0.9647). Structure solution and refinement: Direct methods (Siemens SHELXTL PLUS v4.2), refinement (against F_o) with 277 parameters converged at R = 0.0383/wR = 0.0325 [$w^{-1} = \sigma^2(F_o)$]; max./min. residual electron density was $1.22/-2.03 \cdot 10^6$ e · pm^{-3}.

Acknowledgments

Financial support by the Deutsche Forschungsgemeinschaft and the Fonds der Chemischen Industrie is gratefully acknowledged. G.-X. J. thanks the Max-Planck-Gesellschaft for a fellowship in the German-Chinese Exchange Program (1998).

[1] U. T. Mueller-Westerhoff, B. Vance, "Dithiolenes and Related Species" in *Comprehensive Coordination Chemistry* (Eds. R. D. Gillard, J. A. McCleverty, G. Wilkinson), Pergamon, Oxford, **1987**, vol. 2, ch. 16.5, p. 595–631.
[2] G.-X. Jin, M. Herberhold, A. L. Rheingold, *New. J. Chem.* **1998**, *22*, 1035–1036.
[3] J. D. McKinney, H. Chen, T. A. Hamor, K. Paxton, C. J. Jones, *J. Chem. Soc., Dalton Trans.* **1998**, 2163–2168.
[4] H. D. Smith, Jr., M. A. Robinson, S. Papetti, *Inorg. Chem.* **1967**, *6*, 1014–1018.
[5] K. Base, M. W. Grinstaff, *Inorg. Chem*. **1998**, *37*, 1432–1433.
[6] [6a] O. Crespo, M. C. Gimeno, P. G. Jones, B. Ahrens, A. Laguna, *Inorg. Chem.* **1997**, *36*, 495–500. – [6b] O. Crespo, M. C. Gimeno, D. G. Jones, A. Laguna, *J. Organomet. Chem.* **1997**, *547*, 89–95.
[7] [7a] A. R. Siedle, *Annu. Rep. NMR Spectrosc.* **1988**, *20*, 205–314. – [7b] F. Teixidor, R. W. Rudolph, *J. Organomet. Chem.* **1983**, *241*, 301–312.
[8] [8a] I. Johannsen, H. Eggert, *J. Am. Chem. Soc.* **1984**, *106*, 1240–1243. – [8b] H. Poleschner, R. Radeglia, H. Meyer, *Org. Magn. Reson.* **1984**, *22*, 480–485. – [8c] H. Poleschner, R. Radeglia, J. Fuchs, *J. Organomet. Chem.* **1992**, *427*, 213–230. – [8d] B. Olk, R.-M. Olk, *Z. Anorg. Allg. Chem.* **1991**, *600*, 89–93. – [8e] R. A. Fischer, H.-J. Kneuper, W. A. Herrmann, *J. Organomet. Chem.* **1987**, *330*, 365–376.
[9] [9a] T. Klapötke, *Spectrochim. Acta* **1988**, *44A*, 461–462. – [9b] T. M. Klapötke, M. Broschag, *Compilation of Reported* ^{77}Se NMR Chemical Shifts, Wiley, Chichester, **1996**.
[10] C. White, A. Yates, P. M. Maitlis, *Inorg. Synth.* **1992**, *29*, 228–230.
[11] K. Isobe, P. M. Bailey, P. M. Maitlis, *J. Chem. Soc., Dalton Trans.* **1981**, 2003–2008.
[12] Crystallographic data (excluding structure factors) for the structures reported in this paper have been deposited with the Cambridge Crystallographic Data Centre as supplementary publication no. CCDC-112292 (**5**) and -112293 (**4**). Copies of the data can be obtained free of charge on application to CCDC, 12 Union Road, Cambridge CB2 1EZ, UK [Fax: (internat.) + 44-1223/336-033; E-mail: deposit@ccdc.cam.ac.uk].

Received December 10, 1998
[I98423]

Spin State and Ligand Dissociation in [$CpCoL_2$] Complexes (L = PH_3, $H_2C{=}CH_2$): A Computational Study

Rinaldo Poli*[a] and Kevin M. Smith[a]

Keywords: Cobalt / Density functional calculations / Electronic structure / Ligand effects / Spin state

The relative energies of [CpCoL] compounds (L = PH_3, $H_2C{=}CH_2$) were calculated at the DFT/B3LYP level of theory. The triplet spin state was found to be favored over the singlet by between 33.0 and 21.0 kcal mol^{-1} for both fixed and optimized geometries. The basis set size was found to be important for the energy calculations, particularly when the energetics of ligand dissociation was examined. The role of the triplet spin state in facilitating the ligand dissociation process is discussed.

Introduction

The role of spin-state changes in the reactivity of [$CpCoL_2$] species remains under dispute. Several kinetic, spectroscopic, and theoretical studies have investigated this issue. Bergman et. al. examined the mechanism of phosphane substitution in [$CpCo(PPh_3)_2$] in order to determine whether interconversion between singlet and triplet species resulted in an activation barrier for the dissociative pathway. The first step in the ligand-replacement reaction was found to be the rapid, reversible formation of [$CpCo(PPh_3)$].[1] Extended Hückel molecular orbital theory calculations by Hofmann and Padmanabhan suggested that, although linear d^8 [CpML] compounds are symmetry-required to have a triplet ground spin state, a "bent" geometry for [$CpCo(PPh_3)$] (i.e. Cp−Co−P angle < 180°) might allow the substitution reaction to proceed via the singlet spin surface, thereby accounting for the observed lack of a "spin-flip barrier".[2] Later studies by Bergman, Moore, and co-workers demonstrated that photogenerated [CpCo(CO)] and [Cp*Co(CO)] did not form adducts with alkanes or noble gases, although these unsaturated species did react very rapidly with CO.[3] Using a variety of computational techniques including density functional theory (DFT), Siegbahn calculated that [CpCo(CO)] possesses a triplet ground spin state, and attributed the difference in reactivity of the 16-electron species with alkanes and CO to the varying ability of the incoming ligand to induce triplet-to-singlet spin crossover.[4] In contrast, Brookhart et. al. have recently reported C−H activation reactions of [Cp*Co(η^2-$H_2C{=}CHSiMe_3$)$_2$] that proceed by oxidative addition of benzene or aldehydes to unsaturated [Cp*Co(η^2-$H_2C{=}CHSiMe_3$)].[5]

As part of an ongoing investigation of spin state and reactivity,[6] we have recently used DFT techniques to examine how ligands can affect the relative energy of the singlet and triplet states (ΔE_{S-T}) of 16-electron [CpM(NO)]-containing complexes of Cr, Mo, and W.[7] Ultrafast IR studies have implicated triplet [$CpMn(CO)_2$] in the photolysis of [$CpMn(CO)_3$] in Et_3SiH.[8] Spin-state changes have also been proposed to play a critical role in the reactivity of cytochrome P450.[9] The computational study described in this paper was performed to address the following questions: (1) What is the ground spin state of *bent* [CpCoL] species (L = PH_3, $H_2C{=}CH_2$)? (2) Is ΔE_{S-T} substantially altered for [CpCoL] species by variation of L? (3) Can the observed C−H bond-activation reactivity of [Cp*Co(η^2-$H_2C{=}CHSiMe_3$)] be attributed to a difference in ground spin state compared to triplet [CpCo(CO)]?

Results and Discussion

Calculated Geometries and Energies

The saturated [$CpCoL_2$] (L = PH_3, $H_2C{=}CH_2$) complexes were studied with DFT using the three-parameter form of the Becke, Lee, Yang, and Parr functional (B3LYP)[10] and two basis sets, following the methodology recently developed by Siegbahn and co-workers.[11] The geometries were optimized without constraints (C_1 symmetry) with the LanL2DZ basis set;[12] the structural parameters for both complexes are listed in Table 1. Since energy calculations are more sensitive to basis set size than geometry optimizations,[13] the energies of the LanL2DZ structures were also calculated with the larger 6-311+G(2d,2p) basis set.

Table 1. Optimized geometries for [$CpCo(PH_3)_2$] and [$CpCo(C_2H_4)_2$][a]

Parameter[b]	[$CpCo(PH_3)_2$]	[$CpCo(C_2H_4)_2$]
CNT−Co	1.800	1.837
Co−X	2.231	1.950
	2.235	1.939
CNT−Co−X	131.44	130.45
	130.69	130.26
X−Co−X	97.87	99.28

[a] Bond lengths in Å and angles in °. − [b] CNT = center of gravity of the Cp ring, X = P for [$CpCo(PH_3)_2$] or center of C−C bond for [$CpCo(C_2H_4)_2$].

[a] Laboratoire de Synthèse et d'Electrosynthèse Organométalliques, Faculté des Sciences "Gabriel", Université de Bourgogne, 6 Boulevard Gabriel, F-21100 Dijon, France
Fax: (internat.) + 33-3/80396098
E-mail: Rinaldo.Poli@u-bourgogne.fr

 © WILEY-VCH Verlag GmbH, D-69451 Weinheim, 1999 1434−1948/99/0505−0877 $ 17.50+.50/0

The bond lengths obtained for the optimized $[CpCoL_2]$ geometries are marginally longer than those reported for the solid-state molecular structures of $[CpCo(PEt_3)_2]$[14b] and $[Cp^*Co(\eta^2\text{-}H_2C{=}CHSiMe_3)_2]$.[5c] For instance, the average calculated Co−C(Cp) bond lengths are 0.09 Å longer than those found experimentally, and the theoretical Co−L(average) distances are 0.015 Å and 0.035 Å longer than those found in the corresponding X-ray molecular structures for the phosphane and alkene complexes, respectively. The alkene orientation of $[CpCo(\eta^2\text{-}H_2C{=}CH_2)_2]$ corresponds to the alignment observed experimentally, namely parallel with the Cp plane.[5] The calculated alkene C−C bond lengths in $[CpCo(\eta^2\text{-}H_2C{=}CH_2)_2]$ (1.417 and 1.414 Å) are almost identical to those reported for $[Cp^*Co(\eta^2\text{-}H_2C{=}CHSiMe_3)_2]$ (1.414 and 1.404 Å). The slight distortions in C−C bond lengths in the Cp ligand also correspond well with those previously discussed for related $[CpCoL_2]$ derivatives.[14]

As noted in the introduction, Hofmann and Padmanabhan have previously suggested that ligand dissociation from d^8 $[CpML_2]$ complexes may remain on the singlet spin hypersurface if the unsaturated [CpML] intermediate adopts a bent geometry.[2] To test this hypothesis, the energies of bent [CpCoL] compounds were calculated in both singlet and triplet spin states, using the optimized $[CpCoL_2]$ geometries with one L group removed and leaving the other structural parameters unchanged. For both $[CpCo(PH_3)]$ and $[CpCo(\eta^2\text{-}H_2C{=}CH_2)]$ in this bent conformation (Cp−Co−L < 132°), the triplet state is greatly favored over the singlet. The value of ΔE_{S-T} decreases only slightly when the larger basis set is employed, from −31.0 to −28.1 kcal mol^{-1} for the phosphane system and from −25.9 to −23.9 kcal mol^{-1} for the alkene system. Overall, only a minor difference in ΔE_{S-T} is observed upon changing the L group in [CpCoL].

Analogous results are obtained when the [CpCoL] geometries are optimized using B3LYP/LanL2DZ. Optimized triplet $[CpCo(PH_3)]$ was found to be 33.0 kcal mol^{-1} more stable using the LanL2DZ basis set, and 27.1 kcal mol^{-1} more stable at the B3LYP/6-311+G(2p,2d) level. For the alkene system, triplet $[CpCo(\eta^2\text{-}H_2C{=}CH_2)]$ was calculated to be 26.5 kcal mol^{-1} more stable than the singlet at the B3LYP/LanL2DZ level, and 21.0 kcal mol^{-1} more stable using the larger basis set. By comparison, Siegbahn's B3LYP calculation of [CpCo(CO)] gave a ΔE_{S-T} value of −27.8 kcal mol^{-1}, which falls between the results obtained here for the phosphane and alkene derivatives.[4] The structural parameters of the B3LYP/LanL2DZ optimized [CpCoL] geometries are listed in Table 2, and the relative energies are illustrated in Figure 1.

An indication of the energetics of the ligand dissociation process can be attained by comparing the energy of $[CpCoL_2]$ complexes with the sum of the energies of optimized [CpCoL] and the free L ligand, as shown in Table 3. For these relative energies, the difference between the values obtained with the two different basis sets is pronounced. In fact, at the B3LYP/LanL2DZ level, $[CpCo(PH_3)_2]$ is calculated to be 4.3 kcal mol^{-1} less stable than triplet $[CpCo(PH_3)]$ and free PH_3, contrary to experimental observations. This erroneous result is presumably due to the previously observed correlation between basis set size and bond strength.[4] Thus, while the relative energies calculated with the small basis set are skewed in favor of the dissociated species, employing the larger 6-311+G(2d,2p) basis set results in the saturated complex being 7.3 kcal mol^{-1} more stable, in accord with experimental studies of the $[CpCo(PPh_3)_2]$ system.[1]

Table 2. Optimized geometries for $[CpCo(PH_3)]$ and $[CpCo(C_2H_4)]$[a]

Parameter[b]	$[CpCo(PH_3)]$	$[CpCo(C_2H_4)]$
CNT−Co	1.782 (1.881)	1.793 (1.958)
Co−X	2.241 (2.325)	1.851 (1.932)
CNT−Co−X	140.92 (140.43)	148.32 (149.09)

[a] Singlet bond lengths in Å and angles in °, with triplet parameters indicated in parentheses. − [b] CNT = center of gravity of the Cp ring, X = P for $[CpCo(PH_3)_2]$ or center of C−C bond for $[CpCo(C_2H_4)_2]$.

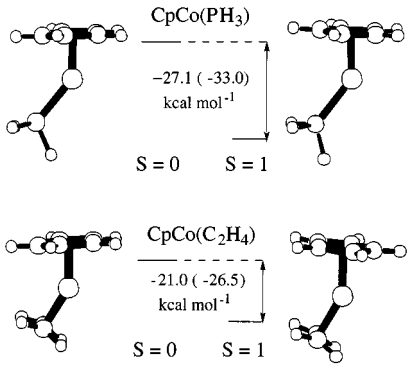


Figure 1. Relative energies of singlet and triplet $[CpCo(PH_3)]$ and $[CpCo(C_2H_4)]$; ΔE_{S-T} calculated at the B3LYP/6-311+G(2d,2p) level of theory, with B3LYP/LanL2DZ values indicated in parentheses

Table 3. Relative energies of $[CpCoL_2]$ and [CpCoL] + L[a]

	$[CpCo(PH_3)]$	$[CpCo(C_2H_4)]$
Singlet	−34.4 (−28.8)	−24.6 (−25.1)
Triplet	−7.3 (+4.3)	−3.6 (+1.4)

[a] ΔE (in kcal mol^{-1}) calculated at the B3LYP/6-311+G(2d,2p) level of theory, with B3LYP/LanL2DZ values indicated in parentheses.

Implications for Reactivity

It has been previously proposed that the lack of a high activation barrier for ligand exchange reactions in d^8 $[CpML_2]$ compounds might be due to the bent geometry of

unsaturated [CpML] species, which allows the singlet spin state to be maintained thoughout the dissociative substitution process.[15] Although extended Hückel molecular orbital calculations did not permit the relative energies of the singlet and triplet [CpML] species to be ascertained, Hofmann and co-workers recognized that this possibility was more likely for Rh and Ir than for Co.[2] Our results at the DFT/B3LYP level indicate that even in the bent conformation, the triplet spin state is considerably lower in energy for [$CpCo(PH_3)$] and [$CpCo(\eta^2\text{-}H_2C{=}CH_2)$] than the corresponding singlet electronic configuration.

It should be observed that the crossover from the singlet to the triplet surface upon phosphane dissociation from [$CpCo(PPh_3)_2$] will in fact lower the enthalpic barrier to the phosphane exchange process if the crossing point is located below the singlet [$CpCo(PPh_3)$] species. A change in spin state would only translate into an entropic contribution to the activation free energy. Thus, the facile phosphane exchange process observed for [$CpCo(PPh_3)_2$] is in fact quite nicely rationalized by the large energetic stabilization of the [$CpCo(PPh_3)$] intermediate upon changing the spin state, accompanied by a low-energy crossing point and lack of a "spin-flip barrier".[16]

Differences in ground spin state between [CpCo(CO)] and the heavier Rh and Ir congeners were utilized by Siegbahn to explain the experimentally observed differences in alkane binding and C−H bond activation reactivity of these species.[4] With this precedent, it seemed conceivable that the H/D exchange reactivity with C_6D_6 and the aldehyde C−H activation reactions observed by Brookhart and co-workers might be attributable to a low-lying or ground singlet spin state for [$Cp^*Co(\eta^2\text{-}H_2C{=}CHSiMe_3)$] intermediates.[5] Although the present study indicates that ΔE_{S-T} is *slightly* more favorable for the singlet alkene species than for the analogous phosphane system, the triplet state is still the ground state by over 20 kcal mol^{-1} for [$CpCo(\eta^2\text{-}H_2C{=}CH_2)$]. However, it has previously been shown that photogenerated [CpCo(CO)] *does* form a solvated complex with benzene[17] and forms alkene adducts at diffusion-limited rates.[17][18] Therefore, it is possible that the discrepancy in reactivity between [$Cp^*Co(CO)$] and [$Cp^*Co(\eta^2\text{-}H_2C{=}CHSiMe_3)$] is due to substrate effects; i.e. that the aromatic C_6D_6 solvent or the C=O bond of the aldehyde may help to facilitate the spin state change from triplet to singlet in the 16-electron alkene intermediate, whereas alkanes do not induce this process for [$Cp^*Co(CO)$]. MP2 calculations have indicated that a similar difference in the ability of the incoming ligand to induce spin-crossover was responsible for the experimentally observed variation between the rate of addition of CO and N_2 to triplet $Cp^*MoCl(PMe_3)_2$.[19]

Conclusion

The triplet spin state is calculated to be much more stable than the singlet state for [CpCoL] species, even in "bent" structures derived directly from the saturated [$CpCoL_2$] precursors. Varying the ligand in [CpCoL] exerts only a minor influence on the energy difference between singlet and triplet species: our present results for the PH_3 and $H_2C{=}CH_2$ systems lie on either side of the ΔE_{S-T} value obtained by Siegbahn for the CO complex. The C−H bond activation reactions reported for [$Cp^*Co(\eta^2\text{-}H_2C{=}CHSiMe_3)$] may thus be attributable to substrate effects rather than to a difference in ground spin state of the unsaturated intermediate. The comparatively high energy of the singlet [CpCoL] complexes suggest that the ligand dissociation process from [$CpCoL_2$] may be facilitated by spin crossover to the lower energy triplet species. Although the ΔE_{S-T} values are relatively basis-set-independent, the energies of the [CpCoL] species relative to the saturated [$CpCoL_2$] complexes shows a marked dependence on the size of the basis set used.

Experimental Section

General Remarks: All calculations were performed with GAUSSIAN 94[20] using an SGI Origin 200 workstation. The geometries of the [$CpCoL_2$] and [CpCoL] species and the free L ligands were optimized using B3LYP,[10] a DFT type of calculation, employing the LanL2DZ basis set. The LanL2DZ basis set includes both Dunning and Hay's D95 sets for H and C and the core potential sets of Hay and Wadt for the heavy atoms.[12] Electrons outside the core were all those for H and C, the 3s and 3p electrons for P, and the 3s, 3p, 3d, and 4s electrons for Co. All geometries were optimized at the B3LYP/LanL2DZ level without constraints, with the exception of triplet $CpCo(PH_3)$, which failed to achieve geometric convergence despite several attempts from various initial geometries. At the suggestion of a reviewer, the complex was optimized with imposed C_s symmetry starting from both possible orientations of the Cp ligand. Convergence was attained in both cases, and the configuration with the unique C−H group opposite to the P was found to be slightly less stable than the other conformation, with an energy difference of less than 0.1 kcal mol^{-1}. The fixed, bent [CpCoL] geometries were obtained from the [$CpCoL_2$] structures by removing one L ligand and keeping all other parameters unchanged. The B3LYP energy calculations were performed separately with both the LanL2DZ basis set and the larger 6-311+G(2d,2p) basis set, which has two sets of polarization functions on all atoms including two f sets on Co, and also diffuse functions.[11]

The mean value of the first-order electronic wavefunction, which is not an exact eigenstate of S^2 for unrestricted calculations on the triplet systems, was considered suitable for unambiguous identification of the spin state. Spin contamination was carefully monitored and the value of $<S^2>$ for the unrestricted B3LYP (UB3LYP) calculations on the triplet [CpCoL] species using the 6-311+G(2d,2p) basis set (LanL2DZ results shown in parentheses) [L = bent PH_3, 2.0261 (2.0228); optimized PH_3, 2.0234 (2.0205); bent $H_2C{=}CH_2$, 2.0499 (2.0463); optimized $H_2C{=}CH_2$, 2.0531 (2.0484)] indicated minor spin contamination. The energies shown in the Results and Discussion section correspond to UB3LYP calculations for the triplet [CpCoL] compounds, and to restricted B3LYP calculations for the singlet [CpCoL] and [$CpCoL_2$] complexes.[21]

Acknowledgments

R. P. thanks the Région Bourgogne for supporting this research, and K. M. S. thanks the European Commission for a TMR Marie Curie Postdoctoral Fellowship.

[1] A. H. Janowicz, H. E. Bryndza, R. G. Bergman, *J. Am. Chem. Soc.* **1981**, *103*, 1516−1518.
[2] P. Hofmann, M. Padmanabhan, *Organometallics* **1983**, *2*, 1273−1284.
[3] A. A. Bengali, R. G. Bergman, C. B. Moore, *J. Am. Chem. Soc.* **1995**, *117*, 3879−3880.
[4] P. E. M. Siegbahn, *J. Am. Chem. Soc.* **1996**, *118*, 1487−1496.
[5] [5a] C. P. Lenges, M. Brookhart, B. E. Grant, *J. Organomet. Chem.* **1997**, *528*, 199−203. − [5b] C. P. Lenges, M. Brookhart, *J. Am. Chem. Soc.* **1997**, *119*, 3165−3166. − [5c] C. P. Lenges, P. S. White, M. Brookhart, *J. Am. Chem. Soc.* **1998**, *120*, 6965−6979.
[6] [6a] R. Poli, *Chem. Rev.* **1996**, *96*, 2135−2204. − [6b] R. Poli, *Acc. Chem. Res.* **1997**, *30*, 494−501.
[7] [7a] P. Legzdins, W. S. McNeil, K. M. Smith, R. Poli, *Organometallics* **1998**, *17*, 615−622. − [7b] K. M. Smith, R. Poli, P. Legzdins, *Chem. Commun.* **1998**, 1903−1904.
[8] H. Yang, M. C. Asplund, K. T. Kotz, M. J. Wilkens, H. Frei, C. B. Harris, *J. Am. Chem. Soc.* **1998**, *120*, 10154−10165.
[9] [9a] S. Shaik, M. Filatov, D. Schröder, H. Schwartz, *Chem. Eur. J.* **1998**, *4*, 193−199. − [9b] P. H. Toy, M. Newcomb, P. F. Hollenberg, *J. Am. Chem. Soc.* **1998**, *120*, 7719−7729.
[10] A. D. Becke, *J. Chem. Phys.* **1993**, *98*, 5648−5652.
[11] [11a] P. E. M. Siegbahn, R. H. Crabtree, *J. Am. Chem. Soc.* **1997**, *119*, 3103−3113. − [11b] M. R. A. Blomberg, P. E. M. Siegbahn, S. Styring, G. T. Babcock, B. Akermark, P. Korall, *J. Am. Chem. Soc.* **1997**, *119*, 8285−8292. − [11c] M. Pavlov, P. E. M. Siegbahn, M. R. A. Blomberg, R. H. Crabtree, *J. Am. Chem. Soc.* **1998**, *120*, 548−555. − [11d] P. E. M. Siegbahn, J. Westerberg, M. Svensson, R. H. Crabtree, *J. Chem. Phys. B* **1998**, *102*, 1615−1625. − [11e] M. R. A. Blomberg, P. E. M. Siegbahn, G. T. Babcock, *J. Am. Chem. Soc.* **1998**, *120*, 8812−8824.
[12] [12a] P. J. Hay, W. R. Wadt, *J. Chem. Phys.* **1985**, *82*, 270−283. − [12b] W. R. Wadt, P. J. Hay, *J. Chem. Phys.* **1985**, *82*, 284−298. − [12c] P. J. Hay, W. R. Wadt, *J. Chem. Phys.* **1985**, *82*, 299−310.
[13] P. E. M. Siegbahn, *Adv. Chem. Phys.* **1996**, *93*, 333−387.
[14] [14a] L. R. Byers, L. F. Dahl, *Inorg. Chem.* **1980**, *19*, 277−284. − [14b] R. L. Harlow, R. J. McKinney, J. F. Whitney, *Organometallics* **1983**, *2*, 1839−1842. − [14c] J. W. Chambers, A. J. Baskar, S. G. Bott, J. L. Atwood, M. D. Rausch, *Organometallics* **1986**, *5*, 1635−1641. − [14d] M. Y. Antipin, Y. T. Struchkov, A. N. Chernega, M. F. Meidine, J. F. Nixon, *J. Organomet. Chem.* **1992**, *436*, 79−82.
[15] For a detailed analysis of the orbital mixing and energetic changes that accompany variation of the Cp−M−L angle, see ref.[2]
[16] J. L. Detrich, O. M. Reinaud, A. L. Rheingold, K. H. Theopold, *J. Am. Chem. Soc.* **1995**, *117*, 11745−11748.
[17] E. P. Wasserman, R. G. Bergman, C. B. Moore, *J. Am. Chem. Soc.* **1988**, *110*, 6076−6084.
[18] T. P. Dougherty, E. J. Heilweil, *J. Chem. Phys.* **1994**, *100*, 4006−4009.
[19] D. W. Keogh, R. Poli, *J. Am. Chem. Soc.* **1997**, *119*, 2516−2523.
[20] M. J. Frisch, G. W. Trucks, H. B. Schlegel, P. M. W. Gill, B. G. Johnson, M. A. Robb, J. R. Cheesman, T. A. Kieth, G. A. Petersson, J. A. Montgomery, K. Raghavarchi, M. A. Al-Laham, V. G. Zakrzewski, J. V. Ortiz, J. B. Foreman, J. Cioslowski, B. B. Stefanov, A. Nanayakkara, M. Challacombe, C. Y. Peng, P. Y. Ayalla, W. Chen, M. W. Wong, J. L. Andres, E. S. Replogle, R. Gomperts, R. L. Martin, D. J. Fox, J. S. Binkley, D. J. Defrees, J. Baker, J. P. Stewart, M. Head-Gordon, C. Gonzales, J. A. Pople, *Gaussian 94, Revision E.1*, Gaussian Inc., Pittsburgh, PA, **1995**.
[21] Note added in proof (March 4, 1999): Recent calculations at the B3LYP/LanL2DZ level indicate that the $CpM(Ph_3)$ (M = Rh, Ir) congeners also possess ground triplet spin states, with $\Delta E_{S\text{-}T} = -13.2$ and -16.9 kcal mol^{-1}, respectively: M.-D. Su, S.-Y. Chu, *Chem. Eur. J.* **1999**, *5*, 198−207.

Received December 17, 1998
[I98435]

Synthesis, Structure and Properties of a Mixed Mononuclear/Dinuclear Iron(II) Spin-Crossover Compound with the Ligand 4-(*p*-Tolyl)-1,2,4-triazole

Jeroen J. A. Kolnaar,[a] Martine I. de Heer,[a] Huub Kooijman,[b] Anthony L. Spek,[b] Georg Schmitt,[c] Vadim Ksenofontov,[c] Philipp Gütlich,[c] Jaap G. Haasnoot,*[a] and Jan Reedijk[a]

Keywords: Iron(II) / Spin crossover / Pentanuclear assembly / Triazole ligand / Structure elucidation

A new iron(II) compound with the formula $[Fe_2(L)_5(NCS)_4]_2$-$[Fe(L)_2(NCS)_2(H_2O)_2]$ (**I**) [where L = 4-(*p*-tolyl)-1,2,4-triazole] has been synthesized and subjected to X-ray structure determination. Compound **I** crystallizes in the triclinic space group *P*–1 (no. 2) with a = 14.5785(11), b = 16.1253(11), c = 16.1963(8) Å, α = 80.930(5), β = 85.796(5), γ = 78.132(6)°, V = 3676.2(4) Å^3. The structure refinement converged to $wR2$ = 0.172, R_F = 0.084. The structure was found to consist of two types of iron-containing structural units, a mononuclear unit and a dinuclear one. The mononuclear unit has a crystallographic inversion centre, and is coordinated by two *N*CS anions, two triazole N1 nitrogen atoms, and two water molecules, each hydrogen-bonded to one of the two dinuclear units. The dinuclear units consist of two iron(II) ions bridged by three triazole ligands in a 1,2-fashion. The coordination spheres of both iron ions are completed by two *N*CS anions and one monodentate triazole ligand. The monodentate triazole ligands are connected through the non-coordinating N atom to the mononuclear iron unit by hydrogen bonds from its coordinated water molecule. Magnetic susceptibility measurements indicate a spin transition (ST) only for the iron ions in the dinuclear units, centred at around $T_{1/2}$ = 111 K. The transition takes place within a relatively narrow T range. The mononuclear iron ion remains in the high-spin (HS) state even at very low temperature, yielding a ratio of 4:1 for the ST and HS iron ions. Temperature-dependent Mössbauer spectroscopy confirms these results.

Introduction

In the research on iron(II) compounds with a spin transition[1] (hereafter abbreviated as ST), the compounds with 4-substituted 1,2,4-triazoles have a special place. The variety of structural types and the physical properties of these compounds have been a topic of research for over 15 years. The structures characterized to date vary from mononuclear to trinuclear compounds with two triple bridges,[2–4] but one-, two-, and three-dimensional polynuclear compounds have also been found with various bridging triazole ligands.[5–7] Here, we focus on the linear structures obtained with 4-R-1,2,4-triazoles.

The variety of structural and physical properties leads to questions about the influences of variables such as the ligand substituents, the nature of the anion, and the metal-to-ligand ratio on the transition temperature, the form of the transition curve and the structure.[7] The substituents used to date have included primary and secondary alkyl and (substituted) phenyl groups.

The anions used in earlier research have varied from coordinating, e.g. NCS^- and $NCSe^-$, to non-coordinating, e.g. BF_4^-, ClO_4^- and triflate.[2–4] The effect of non-coordinating anions on the structure of the resulting compounds is usually restricted to effects related to hydrogen bonding. In an earlier paper, it was stated that the influence of non-coordinated anions is much more pronounced than the influence of the substituent used, although steric effects of the substituent can play an important role in the ST behaviour.[4] The effect of coordinating anions on the structure of divalent transition metal compounds with 1,2,4-triazole ligands is to block coordination sites. Therefore, coordinated anions limit the number of coordinated triazoles to four per metal core. For 1,2,4-triazoles having only two possible coordination sites, this leads to dinuclear units either with three bridging triazoles and one monodentate triazole per metal core,[8] or with NCS anions linking the dinuclear unit, yielding a polynuclear structure.[9] Because of this more pronounced influence on the structure, the influence on the ST behaviour can be expected to be rather large as well. It is, however, difficult to compare the influence of coordinated anions to the influence of non-coordinated anions, because of the difference in structural properties.

We now wish to report a new triazole compound, in which the mononuclear moiety shows no ST, whereas the dinuclear part shows a clear ST. The ligand used in this study is 4-(*p*-tolyl)-1,2,4-triazole, which has not previously been used in this context.

[a] Leiden Institute of Chemistry, Gorlaeus Laboratories, Leiden University,
P. O. Box 9502, NL-2300 RA Leiden, The Netherlands
E-mail: Haasnoot@chem.leidenuniv.nl
[b] Bijvoet Centre for Biomolecular Research, Crystal and Structural Chemistry, Utrecht University,
Padualaan 8, NL-3584 CH Utrecht, The Netherlands
[c] Institut für Anorganische und Analytische Chemie, Universität Mainz,
Staudingerweg 9, D-55099 Mainz, Germany

 © WILEY-VCH Verlag GmbH, D-69451 Weinheim, 1999 1434–1948/99/0505–0881 $ 17.50+.50/0

Results and Discussion

Structural Description of I

The structure was found to consist of two types of iron-containing structural units, i.e. a mononuclear unit (Figure 1) on a crystallographic inversion centre, hydrogen-bonded by two coordinated water molecules to two dinuclear units (Figures 2 and 3).

The mononuclear unit situated on a crystallographic inversion centre consists of an Fe^{II} ion, coordinated by two thiocyanate nitrogen atoms (N65) at a distance of 2.094(10) Å, two monodentate tolyl-triazole N1 atoms at 2.194(9) Å, and two water oxygen atoms (O1) at 2.185(9) Å, in an octahedral environment. The NCS anion is non-linear with the N65−C65−S5 angle 173.7(12)°; the angle of coordination to iron Fe3−N65−C65 is also non-linear being 168.8(10)°. An iron(II) centre with this chromophore of relatively weak ligand field strength can be expected to be in a high-spin (HS) state without an ST. The Fe−ligand distances are consistent with an HS state at room temperature.

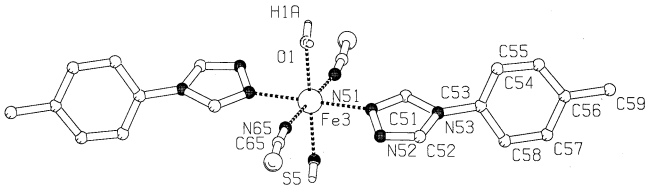


Figure 1. Structure of the mononuclear unit $Fe(L)_2(H_2O)_2(NCS)_2$ in **I**; non-water H atoms are omitted for clarity

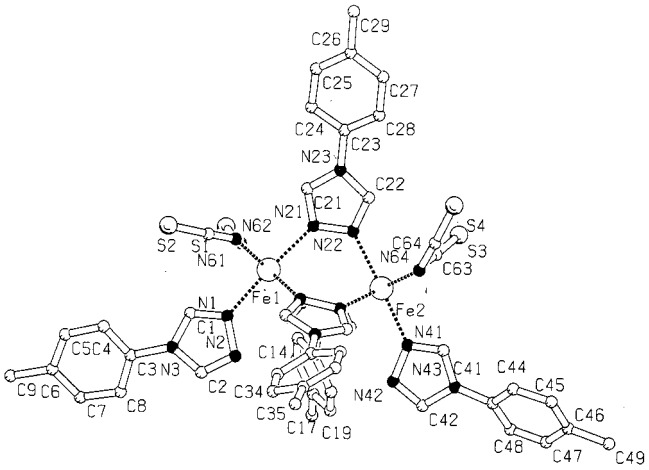


Figure 2. Structure of the dinuclear unit $[Fe_2(L)_5(NCS)_4]$ in **I**; H atoms are omitted for clarity

The unit cell also contains two dinuclear units. Both units consist of two iron ions linked by three 1,2-triazole bridges with Fe−N distances ranging from 2.151(8) Å to 2.223(8) Å, typical for an HS iron ion bound by triazole. The coordination spheres of both iron ions are completed by two thiocyanate N atoms at 2.092(9) to 2.188(9) Å, and a monodentate tolyl-triazole ligand at 2.152(8) and 2.173(8) Å, yielding a distorted octahedral N6 chromophore, which is known to produce ST compounds.

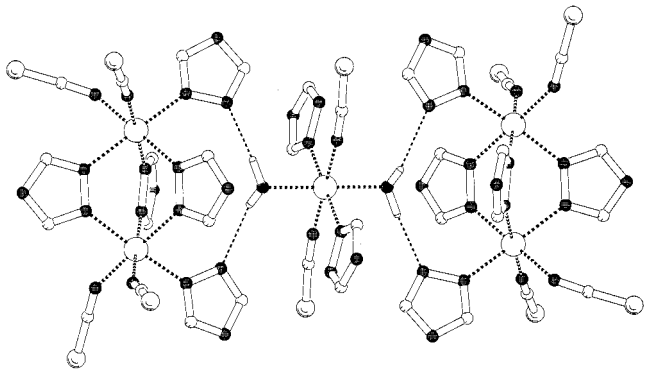


Figure 3. Pentanuclear assembly $[Fe_2(L)_5(NCS)_4]_2[Fe(L)_2(NCS)_2(H_2O)_2]$ (**I**), non-water H atoms and tolyl C atoms are omitted for clarity

Dinuclear units with this structure, M_2(1,2,4-triazole)$_5$(NCS)$_4$ (with M = divalent first-row transition metal ion), are known from the literature.[8][10] However, in these structures the monodentate triazoles are coordinated *trans* with respect to the metal−metal axis rather than *cis*, as is observed in the present structure. The *cis* configuration is clearly stabilized by a hydrogen-bonding network, which involves the water molecules coordinated by the mononuclear iron core. These water molecules form hydrogen bonds to the non-coordinated N atoms of the monodentate triazoles from the dinuclear unit (Table 1). The overall structure can thus be described as a pentanuclear unit, consisting of two dinuclear units linked by a mononuclear unit.

The overall structure contains four iron ions that might exhibit a temperature-induced ST, and one iron ion which is expected to be in an HS state at all temperatures.

Magnetic Measurements

At 290 K, χT was found to be 3.6 cm^3 K mol^{-1}, indicating all iron ions to be present in the HS state, as would be expected from the structure determination. On lowering the temperature, this value decreased only slightly, e.g. to 3.5 cm^3 K mol^{-1} at 150 K. On lowering the temperature still further, the sample showed a sharp drop in magnetization in the temperature range from 130 to 90 K. The $T_{1/2}$ was estimated to be 111 K. At 80 K, χT was found to be 0.7 cm^3 K mol^{-1} per iron ion, in agreement with one of the five iron ions being in an HS state and the other 4 being in low-spin (LS) state at low temperatures. This is in good agreement with the observed structure. Thus, a quantitative spin-state conversion $^5T_2 \rightarrow {}^1A_1$ occurs in 80% of all the iron(II) ions. This is shown clearly in Figure 4, where the fraction of HS molecules, derived from the magnetic measurements, is plotted as a function of temperature, $\gamma_{HS}(T)$. The conversion curves merge into a plateau at $\gamma_{HS} = 0.2$ at low temperatures, reflecting the expected 20% fraction of the iron ions, i.e. those localized in the centre of the pentanuclear assembly, that remain in the HS state at all temperatures. The compound did not show any variation of behaviour on cooling or heating, which is also apparent from

Table 1. Hydrogen bond geometries for **I**

	D···A [Å]	D−H [Å]	H···A [Å]	D−H···A [°]
O(1)−H(1A)···N(2) [1 − *x*,1 − *y*,−*z*]	3.031(13)	0.72(12)	2.36(13)	157(13)
O(1)−H(1B)···N(42) [1 − *x*,1 − *y*,−*z*]	3.128(13)	0.99(11)	2.15(11)	172(9)

Figure 4, where the transition curves for the cooling and heating directions are identical. No hysteresis is observed within the limits of experimental error.

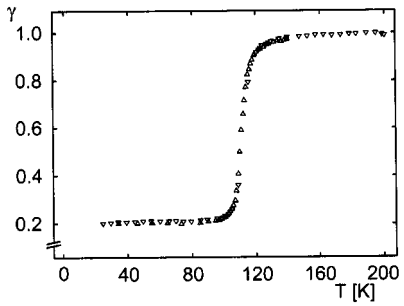


Figure 4. Molar fraction of the iron(II) HS molecules, γ_{HS}, in compound **I** as function of temperature; the conversion curves in cooling direction (▽) and heating direction (Δ) match perfectly

Mössbauer Spectroscopy

Mössbauer spectra of **I** were obtained in a temperature range between 80 K and 293 K. Figure 5 shows a selection of spectra recorded between 80 K and 200 K. At temperatures below $T_{1/2}$, the spectrum observed is indicative of two types of iron cores; at 80 K one core is in an LS state, as indicated by the apparent strong singlet absorption. The central core is in an HS state, yielding the doublet absorption (outer two signals) typical for an HS iron(II) complex denoted as HS^c. The ratio of the two states is 1 HS for every 4 LS cores, as one would expect from both the structural and magnetic data. Accordingly, one would expect a 1:4 intensity ratio (ratio of area fractions) of the LS and HS resonances in the low-temperature Mössbauer spectra. Inspecting the data of the relative area *A* (%) for the respective signals in Table 2, however, one notices that the HS area fraction at 80 K, for instance, is about 10% smaller than the expected value to match the 1:4 ratio. This discrepancy is due to the fact that the Lamb−Mössbauer factor of the LS state[11−13] differs from the HS state. The data collected in Table 2 are the results of the fitting procedure that included the thickness correction for the Mössbauer absorber.

The spectra obtained from the ST region show a clear transition from the LS state to two additional HS states; the new HS states HS1 and HS2 relate to the four iron(II) ions in the two dinuclear fragments. They are best fitted by two doublets with the same intensity and slightly different quadrupole splitting (see Table 2). This behaviour might be explained by the difference in the coordination spheres of the iron ions in the two dinuclear units. The intensity increase of the new HS quadrupole doublets is in line with the disappearance of the LS state. No change is observed in the central HS quadrupole doublet HS^c other than a normal temperature-dependent change in the splitting energy arising from the known temperature dependence of the valence electron contribution on the electric field gradient. At 200 K and above, broadened Mössbauer spectra were observed, which could satisfactorily be deconvoluted into three iron(II) HS doublets with intensity ratios of 2:2:1 at all temperatures as expected from the crystal structure. As an example, the spectrum measured at 200 K is depicted in Figure 6, together with the calculated subspectra of the three HS doublets derived from the fitting procedure.

Conclusion

The work described herein represents an important new example of the versatility of the 4-substituted 1,2,4-triazole ligand system. The new type of structural assembly is of interest from several points of view. Though the subunits of the assembly, especially the dinuclear unit, are not uncommon, and the hydrogen bonding through a non-coordinated triazole N atom has been described previously,[8] the re-

Table 2. Parameters of Mössbauer spectra at different temperatures: partial areas (%), isomer shift (I. S.) and quadrupole splitting (Q. S.)

	HS1				HS2				HS^c				LS				Impurity			
T K	%	I. S. mm/s	Q. S. mm/s	Γ mm/s	%	I. S. mm/s	Q. S. mm/s	Γ mm/s	%	I. S. mm/s	Q. S. mm/s	Γ mm/s	%	I. S. mm/s	Q. S. mm/s	Γ mm/s	%	I. S. mm/s	Q. S. mm/s	Γ mm/s
200	38.21.019	2.75	0.13	38.20.990	2.36	0.13	19.1	1.034	2.91	0.13	–	–	–	–	4.5	0.107	0.31	0.15
180	38.41.031	2.82	0.13	38.41.003	2.44	0.13	19.2	1.044	2.98	0.13	–	–	–	–	4.0	0.107	0.31	0.15
160	38.61.035	2.90	0.13	38.61.016	2.51	0.13	19.3	1.065	3.04	0.13	–	–	–	–	3.5	0.107	0.31	0.15
140	38.61.026	2.58	0.13	38.61.033	2.96	0.13	19.8	1.097	3.10	0.13	2.0	0.390	0.14	0.13	1.0	0.107	0.31	0.15
120	34.91.037	2.63	0.12	34.91.043	3.01	0.12	20.0	1.114	3.21	0.15	10.0	0.390	0.14	0.13	0.2	0.107	0.31	0.15
110	14.71.040	2.69	0.18	14.71.048	3.08	0.14	19.9	1.132	3.36	0.16	50.7	0.398	0.14	0.13	–	–	–	–
100	3.51.040	3.09	0.14	3.51.038	2.91	0.15	16.9	1.130	3.47	0.14	76.7	0.398	0.14	0.13	–	–	–	–
80	0.91.040	3.13	0.12	0.91.038	3.11	0.18	17.6	1.143	3.51	0.15	80.6	0.400	0.13	0.14	–	–	–	–

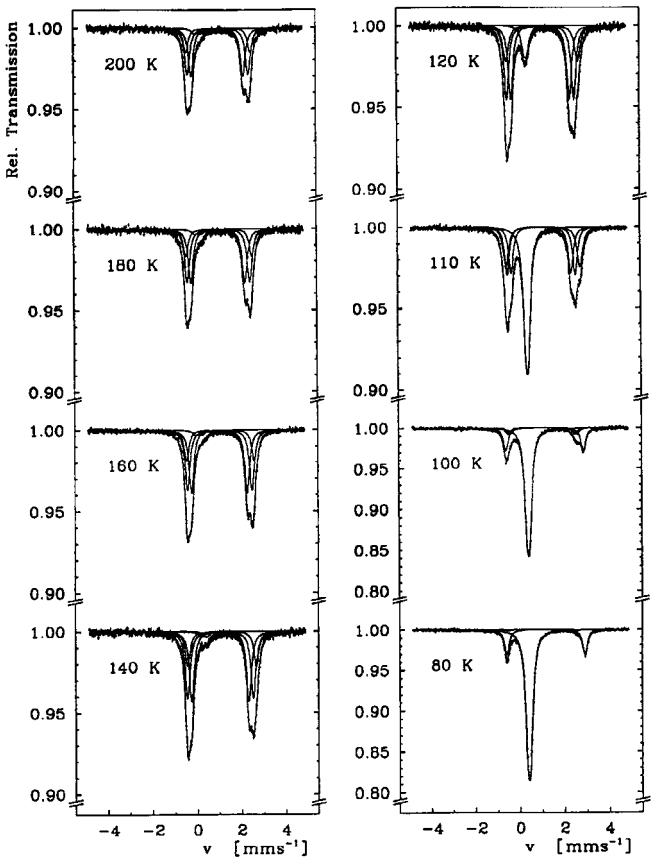


Figure 5. Selected Mössbauer spectra of compound **I** as function of temperature

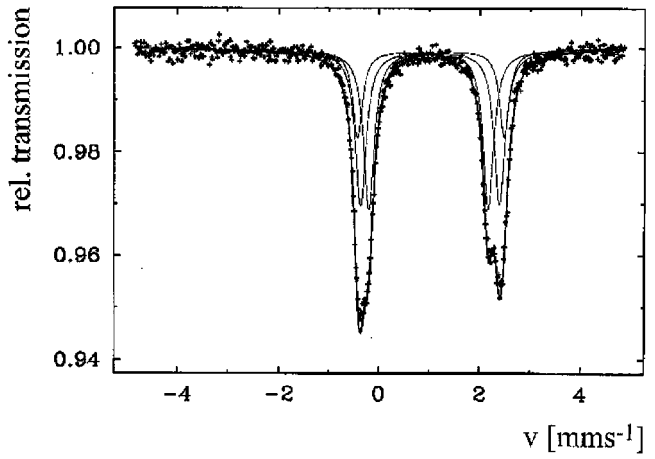


Figure 6. Mössbauer spectrum of compound **I** measured at 200 K; the broadened doublet is composed of three iron(II) HS doublets with intensity ratios of 2:2:1; the two with equal intensity relate to the four iron ions in the dinuclear units; the doublet with lowest intensity but largest splitting energy arises from the central iron(II) ion, which remains in the HS state at all temperatures

sulting species is a quite unique pentanuclear assembly, with two dinuclear units hydrogen-bonded to a mononuclear unit. The iron ion in the bridging, mononuclear unit remains in an HS state throughout the temperature range from 20 to 300 K, and does not show any variation in its Mössbauer spectra other than the normal temperature-dependent variation. On the other hand, a spin transition is observed, which is attributed to the iron ions in the dinuclear units. The Mössbauer spectra show two doublets for the iron ions with a spin transition; the slight differences in the splitting energy might be explained by the slight differences in the coordination spheres of these iron ions. This difference is mainly due to a difference in the metal−ligand bond lengths in the dinuclear unit. Though the iron ions seem to be slightly different, this has no observable influence on the spin transition temperature ($T_{1/2}$), as this is observed at a sharp T of 111 K.

Experimental Section

Preparation of I: The ligand 4-(*p*-tolyl)-1,2,4-triazole (L) was prepared according to a modified literature procedure.[14] $[Fe_2(L)_5(NCS)_4]_2[Fe(L)_2(NCS)_2(H_2O)_2]\ H_2O$ (**I**) was synthesized by adding a solution of 2.5 mmol of L in 25 mL of hot water to a solution of 1 mmol of FeCl2·2H2O and 2 mmol of NH_4NCS in 25 mL of hot water. Crystals appeared upon slow cooling to room temperature; single crystals suitable for X-ray diffraction structure determination were collected from this solution. − $C_{118}H_{114}Fe_5N_{46}O_3S_{10}$ (2824.5): calcd. C 50.18, H 4.07, N 22.81, S 11.35, Fe 9.89; found C 50.21, H 4.05, N 22.93, S 10.72, Fe 9.10.

Crystal Structure Determination of I: A block-shaped crystal of approximate dimensions 0.2 × 0.3 × 0.3 mm, suitable for X-ray structure determination, was sealed in a Lindemann glass capillary and transferred to an Enraf-Nonius CAD4-T diffractometer on a rotating anode. Accurate unit cell parameters and an orientation matrix were obtained from a least-squares fitting of the setting angles of 25 well-centred reflections (SET 4[15]) in the range 8.42° < θ < 15.11°. The unit cell parameters were checked for the presence of higher lattice symmetry.[16] Crystal data and details of the data collection are presented in Table 1. Data were collected at ambient temperature in ω/2 scan mode, with scan angle Δω = 0.82 + 0.35 tan θ°. Total data of 10732 reflections were collected, 10102 of which were independent. Data were corrected for L_P effects and for 1% instability in the three periodically measured reference reflections (2 0 4, 4 2 0, −3 1 2) during 37 h of X-ray exposure time, but not for absorption. The structure was solved by automated Patterson methods and subsequent difference Fourier techniques (DIRDIF-92[17]). Refinement on F^2 was carried out using full-matrix least-squares techniques (SHELXL-93[18]); no observance criterion was applied during refinement. Hydrogen atoms, except the water hydrogen atoms [H(1A) and H(1B)], were included in the refinement in calculated positions, riding on their carrier atoms. The coordinates of the water hydrogen atoms were allowed to refine freely. The methyl hydrogen atoms were refined as a rigid group, allowing for rotation about the C−C bond. At this stage of the refinement, a difference Fourier map revealed a number of residual density peaks (approx. height 1.5 e Å^{-3}) in a channel running parallel to the *b* axis and located at $x = 1/2$, $z = 0$, with a volume of 491.9 Å^3. No discrete solvent model could be refined. The BYPASS procedure,[19] as implemented in the program PLATON,[20] was used to take this electron density into account. A total number of 123 electrons was found in the channel, which is probably occupied by water. All non-hydrogen atoms were refined with anisotropic thermal parameters. The hydrogen atoms were included in the refinement with fixed isotropic thermal parameters related to the value of the equivalent isotropic displacement parameter of the carrier atom by a factor of 1.5 for the methyl and water hydrogen

atoms, and of 1.2 for the aromatic hydrogen atoms. Convergence was reached at $wR2 = 0.172$, $w^{-1} = \sigma^2(F^2) + (0.0574P)^2$, where $P = [\mathrm{Max}(F_o^2,0) + 2F_c^2]/3$, $R_F = 0.084$ for 3501 $F_o > 4\,\sigma\,(F_o)$, $S = 0.84$ for 829 parameters. The residual density was in the range -0.48 to 0.42 e Å^{-3}. The relatively high R values and the rather high U_1/U_3 ratios for some atoms are related to the weak scattering that is most probably a consequence of the disorder in the solvent-filled channels. Selected bond lengths and angles are given in Table 4. Neutral atom scattering factors and anomalous dispersion corrections were taken from the International Tables for Crystallography.[21] Geometrical calculations and illustrations were performed with PLATON. All calculations were performed with a DEC5000 cluster. Crystallographic data (excluding structure factors) for the structure reported in this paper have been deposited with the Cambridge Crystallographic Data Centre as supplementary publication no CCDC-100926. Copies of the data can be obtained free of charge on application to CCDC, 12 Union Road, Cambridge CB2 1EZ, U.K. [Fax: (internat.) + 44-1223/336033; E-mail: deposit@ccdc.cam.ac.uk].

Table 3. Crystallographic data for **I**

Empirical formula	$C_{118}H_{112}N_{46}Fe_5O_2S_{10}$ [a]
Molecular mass	2806.39[a]
Space group	$P-1$
a [Å]	14.5785(11)
b [Å]	16.1253(11)
c [Å]	16.1963(8)
α [°]	80.930(5)
β [°]	85.796(5)
γ [°]	78.132(6)
V [Å^3]	3676.2(4)
Z	1
$\rho_{calcd.}$ [g cm^{-3}]	1.2677(1)[a]
μ (Mo-K_α) [cm^{-1}]	6.8[a]
R_F[b]	0.084
$wR2$[c]	0.172
S	0.84
λ [Å]	0.71073 (Mo-K_α, graphite monochromator)

[a] Without disordered solvent contribution. – [b] $R_F = \Sigma||F_o| - |F_c||/\Sigma|F_o|$. – [c] $wR2 = \{\Sigma[w(F_o^2 - F_c^2)^2]/\Sigma[w(F_o^2)^2]\}^{1/2}$.

Table 4. Selected bond lengths [Å] and angles [°] for **I**

(a) Distances [Å]			
Fe(1)–N(1)	2.152(8)	Fe(2)–N(32)	2.193(8)
Fe(1)–N(11)	2.202(9)	Fe(2)–N(41)	2.173(8)
Fe(1)–N(21)	2.180(8)	Fe(2)–N(63)	2.092(9)
Fe(1)–N(31)	2.195(8)	Fe(2)–N(64)	2.148(9)
Fe(1)–N(61)	2.100(10)	Fe(3)–O(1)	2.185(9)
Fe(1)–N(62)	2.188(9)	Fe(3)–N(51)	2.194(9)
Fe(2)–N(12)	2.151(8)	Fe(3)–N(65)	2.094(10)
Fe(2)–N(22)	2.223(8)		
(b) Angles [°]			
N(1)–Fe(1)–N(11)	88.8(3)	N(12)–Fe(2)–N(22)	93.3(3)
N(1)–Fe(1)–N(21)	173.6(3)	N(12)–Fe(2)–N(32)	87.9(3)
N(1)–Fe(1)–N(31)	87.2(3)	N(12)–Fe(2)–N(41)	89.5(3)
N(1)–Fe(1)–N(61)	93.2(4)	N(12)–Fe(2)–N(63)	90.2(3)
N(1)–Fe(1)–N(62)	89.9(4)	N(12)–Fe(2)–N(64)	176.6(3)
Fe(1)–N(61)–C(61)	154.1(9)	Fe(2)–N(63)–C(63)	172.0(9)
Fe(1)–N(62)–C(62)	152.6(9)	Fe(2)–N(64)–C(64)	142.7(8)
O(1)–Fe(3)–N(51)	90.0(3)	N(51)–Fe(3)–N(65)	89.9(4)
O(1)–Fe(3)–N(65)	88.2(4)	Fe(3)–N(65)–C(65)	168.8(10)

Magnetic Properties: The magnetic susceptibility of **I** was measured over the temperature range 4.2–300 K with a fully automated Manics DSM-8 susceptometer equipped with a TBT continuous-flow cryostat and a Drusch EAF 16 NC electromagnet, operating at ca. 1.4 T, and over the temperature range 20–200 K with a FONER-type magnometer (PAR 155) equipped with a Cryovac continuous-flow cryostat and a Bruker electromagnet, operating at 1 T. Data were corrected for magnetization of the sample holder and for diamagnetic contributions, which were estimated from the Pascal constants.

Mössbauer Spectra: These were measured with a ^{57}Co(Rh) source using a constant acceleration spectrometer in a cryostat with exchange gas. The obtained spectra of polycrystalline samples were fitted with Lorentzian-shaped lines using a non-linear iterative minimization routine (MOSFUN).

Acknowledgments

Financial support by the European Community, allowing regular exchange of preliminary results with several European colleagues under contract ERBCHRXCT920080, is gratefully acknowledged. The work described herein has been supported by the Leiden University Study Group WFMO (Werkgroep Fundamenteel Onderzoek Materialen), and also in part by the Netherlands Foundation of Chemical Research (SON) with financial aid from the Netherlands Organization for Scientific Research (NWO) to A. L. S.

[1] [1a] H. A. Goodwin, *Coord. Chem. Rev.* **1976**, *18*, 293. – [1b] P. Gütlich, *Struct. Bonding (Berlin)* **1981**, *44*, 83. – [1c] E. König, G. Ritter, K. Kulshreshtha, *Chem. Rev.* **1985**, *85*, 219. – [1d] J. K. Beattie, *Adv. Inorg. Chem.* **1988**, *32*, 1. – [1e] H. Toftlund, *Coord. Chem. Rev.* **1989**, *94*, 67. – [1f] P. Gütlich, A. Hauser, *Coord. Chem. Rev.* **1990**, *97*, 1. – [1g] O. Kahn, J. Kröber, C. Jay, *Adv. Mater.* **1992**, *4*, 718. – [1h] P. Gütlich, A. Hauser, H. Spiering, *Angew. Chem. Int. Ed. Engl.* **1994**, *33*, 2024.

[2] M. Thomann, O. Kahn, J. Guilhem, F. Varret, *Inorg. Chem.* **1994**, *33,* 6029.

[3] G. Vos, R. A. G. de Graaff, J. G. Haasnoot, A. M. van der Kraan, P. de Vaal, J. Reedijk, *Inorg. Chem.* **1984**, *23,* 2905.

[4] J. J. A. Kolnaar, G. van Dijk, H. Kooijman, A. L. Spek, V. Ksenofontov, P. Gütlich, J. G. Haasnoot, J. Reedijk, *Inorg. Chem.* **1997**, *36*, 2433.

[5] [5a] J. P. Martin, J. Zarembowitch, A. Bousseksou, A. Dworkin, J. G. Haasnoot, F. Varret, *Inorg. Chem.* **1994**, *33*, 6325. – [5b] W. Vreugdenhil, J. H. van Diemen, R. A. G. de Graaff, J. G. Haasnoot, J. Reedijk, A. M. van der Kraan, O. Kahn, J. Zarembowitch, *Polyhedron* **1990**, *9*, 2971.

[6] [6a] J. Kröber, J. P. Audière, R. Claude, E. Codjovi, O. Kahn, J. G. Haasnoot, F. Grolière, C. Jay, A. Bousseksou, J. Linarès, F. Varret, A. Gonthier-Vassal, *Chem. Mater.* **1994**, *6*, 1404. – [6b] J. Kröber, E. Codjovi, O. Kahn, F. Grolière, C. Jay, *J. Am. Chem. Soc.* **1993**, *115*, 9810. – [6c] N. V. Bausk, S. B. Erenburg, L. N. Mazalov, L. G. Lavrenova, V. N. Ikorskii, *J. Struct. Chem.* **1994**, *35*, 509. – [6d] L. G. Lavrenova, N. G. Yudina, V. N. Ikorskii, V. A. Varnek, I. M. Oglezneva, S. V. Larionov, *Polyhedron* **1995**, *14*, 1333. – [6e] K. H. Sugiyarto, H. A. Goodwin, *Aust. J. Chem* **1994**, *47*, 263. – [6f] V. A. Varnek, L. G. Lavrenova, *J. Struct. Chem.* **1994**, *35*, 842. – [6g] A. Michalowicz, J. Moscovici, B. Ducourant, D. Cracco, O. Kahn, *Chem. Mater.* **1995**, *7*, 1833.

[7] J. G. Haasnoot in ″Magnetism: A Supramolecular Function“ (Ed.: O. Kahn), NATO Advanced Study Institute Series, vol. C 484, Kluwer Acad. Publ., Dordrecht, The Netherlands, **1996**, p. 299.

[8] D. W. Engelfriet, G. C. Verschoor, W. den Brinker, *Acta. Crystallogr.* **1980**, *B36*, 1554.

[9] G. Vos, Ph.D. Thesis, Leiden University, **1983**, p. 120.

[10] D. W. Engelfriet, G. C. Verschoor, W. J. Vermin, *Acta Crystallogr.* **1979**, *35B*, 2927.

[11]] J. Jung, Ph. D. Thesis, D77, Johannes Gutenberg-Universität Mainz, **1995**.

[12] J. Jung, H. Spiering, Z. Yu, P. Gütlich, *Hyperfine Interact.* **1995**, *95*, 107
[13] J. Jung, H. Spiering, P. Gütlich, *Nuovo Cimento* **1995**, *50*, 879.
[14] C. Ainsworth, N. R. Easton, M. Livezey, D. E. Morrison, W. R. Gibson, *J. Med. Pharm. Chem.* **1962**, *5*, 383.
[15] J. L. de Boer, A. J. M. Duisenberg, *Acta Crystallogr.* **1984**, *A40*, C410.
[16] A. L. Spek, *J. Appl. Crystallogr.* **1988**, *21,* 578.
[17] P. T. Beurskens, G. Admiraal, G. Beurskens, W. P. Bosman, S. García-Granda, R. O. Gould, J. M. M. Smits, C. Smykalla, *The DIRDIF program system*, Technical report of the Crystallography Laboratory, University of Nijmegen, The Netherlands, **1992**.
[18] G. M. Sheldrick, *SHELXL-93, Program for crystal structure refinement*, University of Göttingen, Germany, **1993**.
[19] P. van der Sluis, A. L. Spek, *Acta Crystallogr.* **1990**, *A46*, 194.
[20] A. L. Spek, *Acta Crystallogr.* **1990**, *A46,* C34.
[21] A. J. C. Wilson (Ed.), *International Tables for Crystallography*, vol. C, Kluwer Academic Publishers, Dordrecht, The Netherlands, **1992**.

Received May 5, 1998
[98132]

Intramolecular Donor-Assisted Cyclization of Organotin Compounds

Michael Mehring,[a] Christian Löw,[a] Markus Schürmann,[a] and Klaus Jurkschat*[a]

Dedicated to Professor Bernt Krebs on the occasion of his 60th birthday

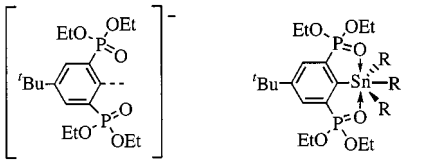
Keywords: Tin / Phosphorus / Intramolecular coordination / O ligands / Heterocycles

New intramolecularly coordinated organotin compounds containing the monoanionic O,C,O-coordinating ligand {4-*tert*-Bu-2,6-$[P(O)(OEt)_2]_2C_6H_2\}^-$ have been synthesized by substitution reactions starting from organotin halides. In view of the enhanced reactivity of the intramolecularly coordinated compounds {4-*tert*-Bu-2,6-$[P(O)(OEt)_2]_2C_6H_2\}SnR_2R'$ (**2**, R = Ph, R′ = CH_2SiMe_3; **3**, R = R′ = Ph; **6**, R = R′ = Cl), cationic tin species are suggested to occur as intermediates in the formation of the heterocyclic compounds [1(Sn),3(P)-$Ph_2SnOP(O)(OEt)$-5-*tert*-Bu-7-$P(O)(OEt)_2]C_6H_2$ (**8**), [1(Sn),3(P)-$Ph(Me_3SiCH_2)SnOP(O)(OEt)$-5-*tert*-Bu-7-$P(O)(OEt)_2]$-$C_6H_2$ (**15**), and {[1(Sn),3(P)-$Cl_2SnOP(O)(OEt)$-5-*tert*-Bu-7-$P(O)(OEt)]C_6H_2\}_2$ (**16**). The latter compounds are formed by intramolecular cyclizations of pentacoordinate cationic tin species under elimination of ethyl halide. Furthermore, the synthesis of [1(Sn),3(P)-$Ph_2SnOP(O)(OH)$-5-*tert*-Bu-7-$P(O)$-$(OH)_2]C_6H_2$ (**13**) is described. Reaction of **8** with an excess of Me_3SiBr leads to the unexpected formation of {2-$[P(O)(OEt)(OSiMe_3)]$-4-*tert*-Bu-6-$[P(O)(OEt)_2]C_6H_2\}SnPhBr_2$ (**9**) as a result of an O–Sn bond cleavage initiated by Me_3SiBr and subsequent reaction of the intermediate with further Me_3SiBr under Sn–C bond cleavage. The high donor capacity and the rigidity of the new ligand {4-*tert*-Bu-2,6-$[P(O)(OEt)_2]_2C_6H_2\}^-$ are demonstrated by X-ray diffraction analyses of the tetraorganotin compound **2** and the monoorganotin trichloride **6**. Furthermore, the molecular structures of the 2,3,1-oxaphosphastannoles **8** and **16** are discussed.

Introduction

Penta- and hexacoordinate compounds of the heavier group 14 elements Sn[1] and Si[2] have been extensively studied during the last few decades. The great interest in inter- and intramolecularly coordinated silicon and tin compounds stems from their enhanced reactivity,[1a-d][2a-c][3] their stereochemical non-rigidity,[1a][1c][2a-c][2k][4] and their biological activity.[5] In particular, the use of ligands with intramolecular donor sites has led to the stabilization of highly reactive compounds such as silylenes[6] and stannylenes,[7] as well as organosilicon-[8] and organotin cations.[9] We have recently reported the novel anionic O,C,O-coordinating ligand $\{4\text{-}tert\text{-Bu-2,6-}[P(O)(OEt)_2]_2C_6H_2\}^-$ (**A**) and have demonstrated its potential in the synthesis of intramolecularly coordinated organotin[1b] and organosilicon[2p] compounds of type **B**. The rigidity of the ligand frame of **A**, coupled with the high donor capacity of its P=O groups, make this compound an eminent pincer ligand for the stabilization of cationic as well as of low-valent group 14 organoelement compounds.

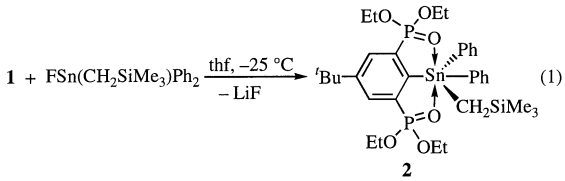
In this paper, we describe our attempts to synthesize organotin cations starting from intramolecularly coordinated organotin compounds of type **B**. However, as a result of an unexpected intramolecular donor-assisted cyclization reaction, we obtained pentacoordinate 2,3,1-benzoxaphosphastannole derivatives rather than the corresponding tin cations. Furthermore, a new intramolecularly stabilized tin(II) compound, the synthesis and reactivity of which will be described in detail in a forthcoming paper, is shown to serve as a precursor in the synthesis of a novel hexacoordinate monoorganotin trichloride. The latter can also be converted into a 2,3,1-benzoxaphosphastannole.



Results and Discussion

Intramolecularly Coordinated Organotin Compounds

The intramolecularly coordinated tetraorganotin compound $\{4\text{-}tert\text{-Bu-2,6-}[P(O)(OEt)_2]_2C_6H_2\}SnPh_2(CH_2SiMe_3)$ (**2**) has been prepared in moderate yield by the reaction of $\{4\text{-}tert\text{-Bu-2,6-}[P(O)(OEt)_2]_2C_6H_2\}Li$ (**1**) with $FSnPh_2(CH_2SiMe_3)$[10] (eq. 1).

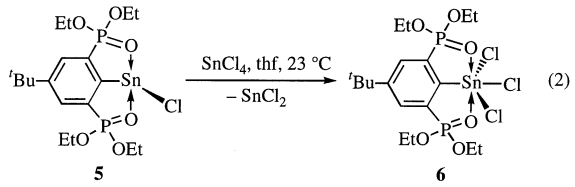


(1)

[a] Lehrstuhl für Anorganische Chemie II der Universität Dortmund,
D-44221 Dortmund, Germany
Fax: (internat.) +49(0)231/755-3797
E-mail: kjur@platon.chemie.uni-dortmund.de

 © WILEY-VCH Verlag GmbH, D-69451 Weinheim, 1999 1434–1948/99/0505–0887 $ 17.50+.50/0

The structurally related tetraorganotin compound of type **B** {4-*tert*-Bu-2,6-[P(O)(OEt)$_2$]$_2$C$_6$H$_2$}SnPh$_3$ (**3**), as well as the hexacoordinate diorganotin compound of type **B** {4-*tert*-Bu-2,6-[P(O)(OEt)$_2$]$_2$C$_6$H$_2$}SnPhCl$_2$ (**4**) were prepared as described previously.[1b] The monoorganotin trichloride {4-*tert*-Bu-2,6-[P(O)(OEt)$_2$]$_2$C$_6$H$_2$}SnCl$_3$ (**6**) was synthesized by a simple redox process between $SnCl_4$ and the heteroleptic stannylene {4-*tert*-Bu-2,6-[P(O)(OEt)$_2$]$_2$C$_6$H$_2$}-SnCl (**5**)[11] (eq. 2). It is worth noting that the homoleptic stannylene $(C_5Me_5)_2Sn$ undergoes a similar redox reaction with $SnCl_4$ to give $(C_5Me_5)_2SnCl_2$ and $SnCl_2$.[12]



5 **6** (2)

Selected NMR data for **2**−**6** are listed in Table 1. The ^{119}Sn- and ^{31}P-NMR spectra show that weak O−Sn contacts are present in **2** and **3**, whereas strong intramolecular coordination is observed in the halogen-containing compounds **4** and **6**. In comparison with tetracoordinate $Ph_3SnCH_2SiMe_3$ [$\delta(^{119}Sn) = -88.6$],[13a] the ^{119}Sn-NMR data of **2** [$\delta(^{119}Sn) = -127.5$, $J(^{119}Sn-^{31}P) = 38$ Hz] indicate a coordination number greater than four at the tin atom.[13b] Moreover, the ^{31}P-NMR chemical shift of **2** [$\delta(^{31}P) = 23.0$, $J(^{31}P-^{119}Sn) = 37$ Hz] is shifted to higher frequency than that of the phosphonate precursor 5-*tert*-Bu-1,3-[P(O)(OEt)$_2$]$_2$C$_6$H$_3$ [$\delta(^{31}P) = 18.2$].[1b] These data indicate the tin atom in **2** to be [4+2]-coordinated, in solution as well as in the solid state, by four carbons and two weak O−Sn interactions, as has previously been reported for the tetraorganotin compound **3** and its silicon analogue.[1b,2p] The formal exchange of the phenyl groups in **3** by chlorine leads to a tin center of higher Lewis acidity and thus to a remarkably stronger O−Sn interaction, as shown by the ^{119}Sn-NMR chemical shifts of the dichlorotin derivative **4** [$\delta(^{119}Sn) = -424.8$, $J(^{119}Sn-^{31}P) = 91$ Hz] and the trichlorotin derivative **6** [$\delta(^{119}Sn) = -528.8$, $J(^{119}Sn-^{31}P) = 281$ Hz]. Although some intramolecularly coordinated monoorganotin trichlorides have been characterized by X-ray crystallography,[14] to the best of our knowledge there have not been any reports of hexacoordinate monoorganotin trichlorides containing a pincer ligand. The heptacoordinate tris(2,6-dimethoxyphenyl)methyltin trichloride,[14f] the molecular structure of which is best described as a tricapped tetrahedron, shows a ^{119}Sn-NMR chemical shift of $\delta(^{119}Sn) = -344$, i.e at a significantly higher frequency than that of the O,C,O-coordinated compound **6** [$\delta(^{119}Sn) = -528.8$]. This difference in the chemical shifts highlights the high donor capacity of the new O,C,O-coordinating ligand in **6** and suggests that the O−Sn interaction in the latter is stronger than that in tris(2,6-dimethoxyphenyl)methyltin trichloride.[14f]

Intramolecularly Coordinated Organotin Heterocycles

Previously, we reported the syntheses of {4-*tert*-Bu-2,6-[P(O)(OEt)$_2$]$_2$C$_6$H$_2$}SnPhX$_2$ (**4**, X = Cl; **7**, X = Br) by reaction of **3** with two molar equivalents of HCl and bromine, respectively. The ^{119}Sn-NMR spectra of the crude reaction mixtures showed, besides the signals at $\delta(^{119}Sn) = -442.8$ and $\delta(^{119}Sn) = -432.3$ attributable to the major products **4** and **7**, respectively, one signal of low intensity (5%) at about $\delta(^{119}Sn) = -224$. This minor signal could be attributed to compound **8** (Scheme 1), which is formed as a by-product. Surprisingly, attempted synthesis of the corresponding diorganotin diiodide (X = I) by reaction of **3** with two molar equivalents of iodine was unsuccessful. Instead, compound **3** reacts with one molar equivalent of iodine to give the novel intramolecularly coordinated 2,3,1-benzoxaphosphastannole **8** in high yield. The preparation and characterization of a similar class of heterocyclic compounds has been reported previously; starting from R$_2$Sn(H)(CH$_2$)$_2$P(H)Ph (R = alkyl) and sulfur, 1-thio-1,2,5-thiaphosphastannolanes were produced.[15a,b] Compound **8** is obtained as a colorless, crystalline solid and is readily soluble in common organic solvents such as CH_2Cl_2, $CHCl_3$, Et_2O, and thf.

The ^{119}Sn-NMR spectrum of **8** shows an ABB′-type resonance at $\delta(^{119}Sn) = -224$ [$J(^{119}Sn-^{31}P) = 19$, 23 Hz]. In the ^{31}P-NMR spectrum, two signals with equal integrals are observed at $\delta(^{31}P) = 17.3$ ($W_{1/2} = 20$ Hz) and $\delta(^{31}P) = 28.6$ [$J(^{31}P-^{119}Sn) = 19$ Hz], which are characteristic of a non-coordinating P(O)(OR)$_2$ moiety and a strongly coordinating P(O)(OR)$_2$ group, respectively.[1b][15c,d] Furthermore, both the ^{1}H- and the ^{13}C-NMR spectra confirm the presence of three distinct ethoxy groups in the molecule.

The formation of the 2,3,1-benzoxaphosphastannole **8** can be formally rationalized as shown in Scheme 1. In a first step, the triphenyltin derivative **3** reacts with one molar equivalent of HCl or X$_2$ (X = Br, I) to give the intermediate cation **8a**, which is best described by the two resonance structures shown in Scheme 1. The existence of donor-stabilized triorganotin cations is well established[15e-t] and recently we succeeded in isolating and fully characterizing {4-*tert*-Bu-2,6-[P(O)(O*iso*-Pr)$_2$]$_2$C$_6$H$_2$}SnPh$_2^+$ PF$_6^-$,[15u] a related derivative of **8a**.

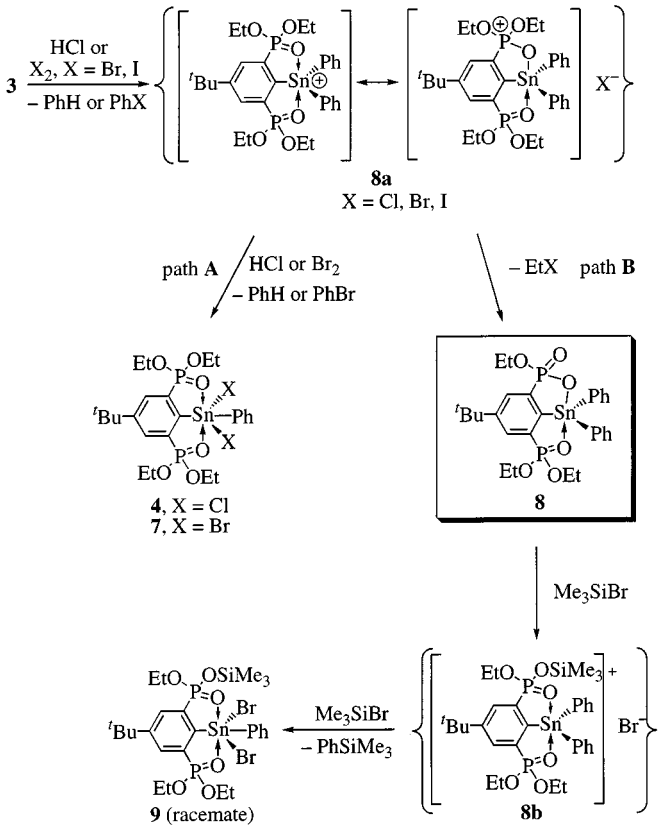
Depending on the lifetime of **8a**, which is determined by the nucleophilicity of the anion X$^-$, it either reacts with a second molar equivalent of HCl or Br$_2$ to give **4** or **7**, respectively (path **A**), or else nucleophilic attack of X$^-$ (X = Cl, Br, I) at the POEt function leads to the 2,3,1-benzoxaphosphastannole **8** (path **B**). The latter reaction path is dominant when X = I, whereas path **A** dominates when X = Cl, Br.

The reaction of phosphonates with excess Me_3SiBr usually leads to complete transesterification.[16] However, reaction of the 2,3,1-benzoxaphosphastannole **8** with an excess

Table 1. Selected ^{31}P- and ^{119}Sn-NMR data[a] of **2**–**9**, **13**, **16a**, 5-*tert*-Bu-1,3-$[P(O)(OEt)_2]_2C_6H_3$,[1b] $Ph_3SnCH_2SiMe_3$,[13] Ph_2SnCl_2,[34] $PhSnCl_3$,[34] and $\{[2,6\text{-}(MeO)_2C_6H_3]C\}_3SnCl_3$[14f]

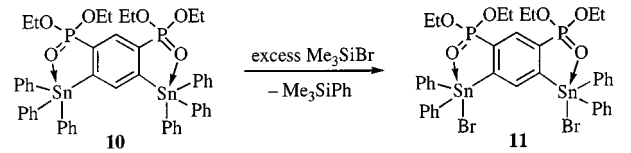
Compound[b]	$\delta(^{31}P)$ [$J(^{31}P-^{119}Sn)$]	$\delta(^{119}Sn)$ [$J(^{119}Sn-^{31}P)$]
R-H	18.2	
R-$SnPh_3$ (**3**)	20.7 [37]	−186.1 (t) [38]
R-$Sn(CH_2SiMe_3)Ph_2$ (**2**)	23.0 [37]	−127.5 (t) [38]
$Me_3SiCH_2SnPh_3$		−88
Ph_2SnCl_2		−33
R-$SnPhCl_2$ (**4**)	27.1 [89]	−424.8 (t) [91]
R-$SnPhBr_2$ (**7**)	26.7 [87]	−432.3 (t) [87]
R′-$SnPhBr_2$ (**9**)[c]	17.3 [103], 26.7 [97]	−439.6 (t) [100]
$PhSnCl_3$		−63
$\{[2,6\text{-}(MeO)_2C_6H_3]CH\}SnCl_3$		−344
R-$SnCl_3$ (**6**)	24.4 [288]	−528.8 (t) [281]
R-SnCl (**5**)	39.1 [113]	−99.7 (t) [116]
heterocycle **8**	17.3 [n.o.][d], 28.6 [19]	−223.6 (dd) [19, 23]
heterocycle **13**	20.3 [n.o.][d], 20.4 [n.o.][d]	−239.9 [70]
heterocycle **16a**	11.9 (d)[e] [137], 25.2 (d)[e] [335]	−547.9 (ddd) [139, 320, 336]

[a] Coupling constants J are given in Hz and chemical shifts δ in ppm. – [b] **R** = {4-*tert*-Bu-2,6-$[P(O)(OEt)_2]_2C_6H_2$}. – [c] **R′** = {4-*tert*-Bu-2-$[P(O)(OEt)_2]$-6-$[P(O)(OEt)(OSiMe_3)]C_6H_2$}. – [d] Not observed. – [e] $^4J(^{31}P-^{31}P)$ = 6.6 Hz.



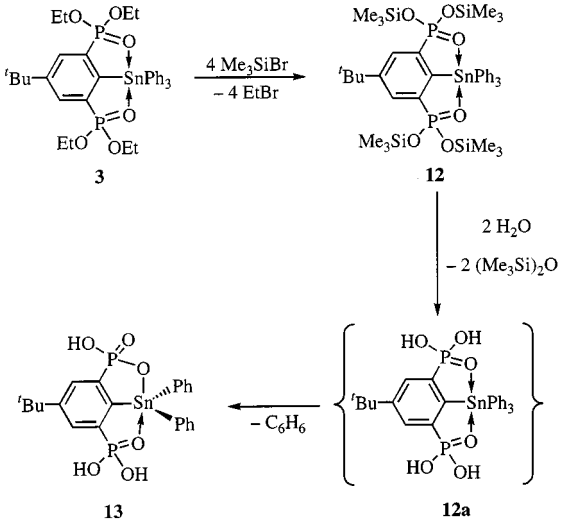
Scheme 1. Synthesis of compounds **4** and **7**–**9**

of Me_3SiBr gave the intramolecularly hexacoordinated diorganotin dibromide **9**, with only one ethoxy group being substituted by a trimethylsiloxy group (Scheme 1). This unusual reactivity is the result of an O–Sn bond cleavage in **8** by attack of Me_3SiBr, which gives the cationic tin species **8b** as an intermediate product. Subsequently, the intermediate **8b** reacts with further Me_3SiBr, which reacts here as an HBr equivalent leading to Sn–C bond cleavage, to provide the diorganotin dibromide **9**. In the ^{31}P-NMR spectrum of the crude reaction mixture, besides the signals due to **9** at $\delta(^{31}P)$ = 17.3 [$J(^{31}P-^{119}Sn)$ = 103 Hz] and $\delta(^{31}P)$ = 26.7 [$J(^{31}P-^{119}Sn)$ = 97 Hz], two minor signals (5%) with equal integrals are seen at $\delta(^{31}P)$ = 19.3 ($W_{1/2}$ = 20 Hz) and $\delta(^{31}P)$ = 29.6 ($W_{1/2}$ = 20 Hz). We tentatively attribute the latter two signals to a heterocyclic compound related to **8**, but attempts to isolate this species were unsuccessful. Evidently, the strong intramolecular O–Sn coordination in the intramolecularly coordinated cation **8b** activates the tin–carbon bonds, thereby facilitating the almost quantitative formation of the hexacoordinate diorganotin dibromide **9**. The O–Sn interactions in the reaction product **9** prevent the latter from undergoing further transesterification at the POEt function upon exposure to excess Me_3SiBr. Similar reactivity was observed when 2,4-bis(diethoxyphosphonyl)-1,5-bis(triphenylstannyl)benzene (**10**)[1b] was treated with an excess of Me_3SiBr (Scheme 2). Instead of a transesterification, substitution of phenyl by bromine was observed as a result of the strong intramolecular coordination. The reaction product, 2,4-bis(diethoxyphosphonyl)-1,5-bis(bromodiphenylstannyl)benzene (**11**) has previously been prepared by reaction of **10** with bromine and has been fully characterized.[1b] Similar reactions of Me_3SnCH_2-$CHX[P(O)(OiPr)_2]$ [X = $P(O)Ph_2$, P(O)(O*i*Pr)Ph, $P(O)(OiPr)_2$, C(O)Ph, C(O)O*i*Pr] with excess Me_3SiBr require higher temperatures, which, in turn, favour redistributions as side reactions.[16b] The intramolecularly coordinated compounds **8** and **10**, however, react even at low temperatures to give predominantly the intramolecularly coordinated organotin bromides **9** and **11**, respectively.



Scheme 2. Bromination of the intramolecularly coordinated tetraorganotin compound **10** with Me_3SiBr

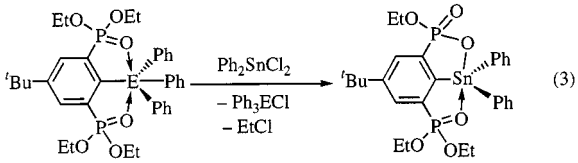
Previous investigations[1b] have shown that in the [4+2]-coordinated compound **3** the intramolecular O−Sn interactions are weaker than those in **10**. Consequently, and in contrast to the situation with **8** and **10**, the *in situ* reaction of **3** with Me_3SiBr proceeds with complete transesterification to give the silylphosphonate **12** (Scheme 3), which has been characterized by ^{31}P-, ^{29}Si-, and ^{119}Sn-NMR. The ^{119}Sn-NMR chemical shifts of the silylphosphonate **12** [$\delta(^{119}Sn) = -188.4$] and of the starting material **3** [$\delta(^{119}Sn) = -186.1$] are very similar, indicating comparable O−Sn coordination strengths in the two compounds. Subsequent reaction of **12** with water afforded the 2,3,1-benzoxaphosphastannole **13** and benzene (Scheme 3). The intermediate free acid **12a** could not be isolated. Richter and Weichmann have shown that the hydrolysis of silylphosphonates and silylphosphinates of 2,2-functionally disubstituted organotin compounds gives the corresponding stannylmethylated phosphonic and phosphinic acids, respectively, which undergo similar intramolecular cyclizations.[16b]



3 **12** **13** **12a**

Scheme 3. Transesterification and intramolecular cyclization of **3**

Recently, van Koten et al.[1d] have shown that $\{(Me_3Sn)_2$-1,4-$[C_6(CH_2NMe_2)_4$-2,3,5,6$]\}$ and $Me_3Sn[C_6H_3$-$(CH_2NMe_2)_2$-2,6] react with Me_3SnCl to give the pentacoordinate species $\{[Me_2Sn]_2$-1,4-$[C_6(CH_2NMe_2)_4$-2,3,5,6$]\}^{2+}$ $[(Me_3SnCl_2)^-]_2$ and $\{Me_2Sn[C_6H_3(CH_2NMe_2)_2$-2,6$]\}^+$ $(Me_3SnCl_2)^-$, respectively. In order to investigate whether compound **3** could be directly transformed into its cationic derivative or into the 2,3,1-benzoxaphosphastannole **8** by this method, the tetraorganotin compound **3** and Ph_2SnCl_2 were heated in refluxing toluene for 4 h. ^{119}Sn-NMR analysis of the reaction mixture showed that the heterocycle **8** was formed as the major product (eq. 3). Additional broad resonances were seen at $\delta(^{119}Sn) = -125$ (9%), −243 (24%), and −284 (28%), which were not assigned. Moreover, reaction of the intramolecularly coordinated tetraorganosilicon compound $\{4$-*tert*-Bu-2,6-$[P(O)(OEt)_2]_2C_6H_2\}SiPh_3$ (**14**)[2p] with Ph_2SnCl_2, which was performed under the same reaction conditions, also gave the 2,3,1-benzoxaphosphastannole **8** as the major product (eq. 3). This result can be explained in terms of $Si-C^{aryl}$ bond cleavage and subsequent insertion of a Ph_2SnCl moiety to give the organotin cation **8a** (X = Cl), followed by intramolecular cyclization with elimination of EtCl.

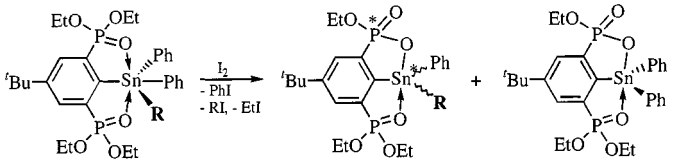


(3)

3, E = Sn
14, E = Si

8

Having established that the reaction of the intramolecularly coordinated tetraorganotin compound **3** with one molar equivalent of iodine gives the 2,3,1-benzoxaphosphastannole **8**, we decided to check whether it would be possible to prepare diastereomeric 2,3,1-benzoxaphosphastannoles starting from the tetraorganotin compound **2**. Reaction of **2** with iodine (Scheme 4) gave 78% of the two diastereomers of 2,3,1-benzoxaphosphastannole **15** in a ratio of 1:0.8, together with 22% of the 2,3,1-benzoxaphosphastannole **8**, as a result of $Sn-C^{phenyl}$ and $Sn-C^{alkyl}$ bond cleavage, respectively. In contrast, reaction of triphenyl(trimethylsilylmethyl)tin with iodine resulted in exclusive cleavage of the $Sn-C^{phenyl}$ bond. Due to the intramolecular O,C,O-coordination in **2**, the Sn−C bond cleavage does not simply follow the expected order of phenyl > alkyl as is well documented for tetraorganotin compounds.[17] A similar reversed order of bond cleavage has previously been reported by Weichmann[18] and by Jousseaume[19] for related compounds.



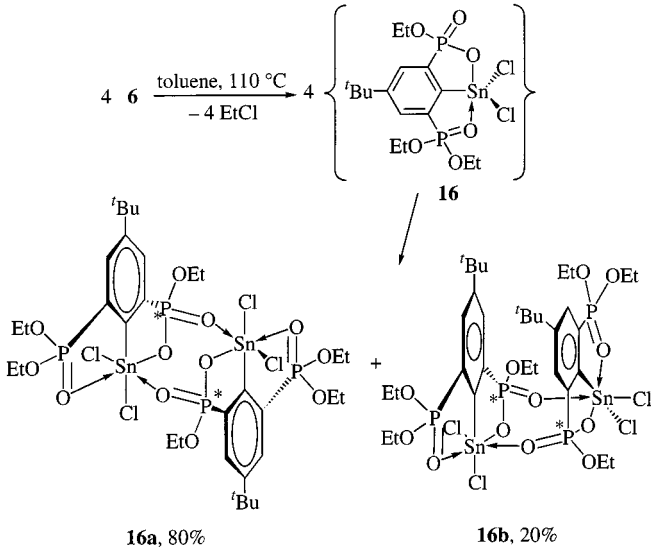
2 **15** (2 diastereomers, 1:0.8) **8**

R = CH_2SiMe_3 78% 22%

Scheme 4. Reaction of intramolecularly coordinated **2** with iodine

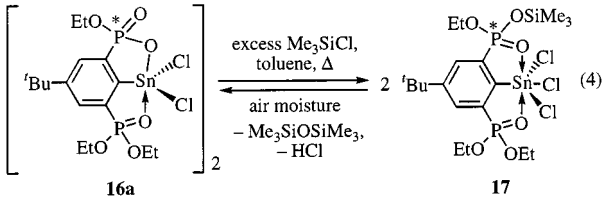
The ease with which the heterocycle **8** is formed suggests that the hexacoordinate monoorganotin trichloride **6** should also undergo intramolecular cyclization to provide a dichloro-substituted 2,3,1-benzoxaphosphastannole. Indeed, this reaction occurred simply by heating **6** in refluxing toluene for several hours. As a result of intermolecular O−Sn coordination, the dichloro-substituted 2,3,1-benzoxaphosphastannole **16** formed by this reaction dimerizes to give a diastereomeric mixture of **16a** (80%) and **16b** (20%), as was apparent from the observation of four ^{31}P-NMR signals at $\delta = 11.95$ [$J(^{31}P-^{119/117}Sn) = 316/301$ Hz, $J(^{31}P-^{119/117}Sn) = 137/125$ Hz] (**16a**), $\delta = 13.12$ [$J(^{31}P-^{119/117}Sn) = 304$ Hz] (**16b**), $\delta = 25.17$ [$J(^{31}P-^{119/117}Sn) = 334/320$ Hz] (**16a**), and $\delta = 25.14$ [$J(^{31}P-^{119/117}Sn) =$

324 Hz] (**16b**), in an integral ratio of 4:1:4:1 (Scheme 5). The diastereomer **16a** could be separated by recrystallization from toluene/chloroform in 65% yield. Its molecular structure is discussed below.



Scheme 5. Intramolecular cyclization of the monoorganotin trichloride **6**

Given that the reaction of the 2,3,1-benzoxaphosphastannole **8** with Me_3SiBr led to a ring-opening, we investigated the reaction of dimeric **16a** with Me_3SiCl (eq. 4). This led to a racemic mixture of the organotin trichloride **17**. Compound **17** proved to be moisture-sensitive and after stirring for 5 days at room temperature the monosilylphosphonate had been hydrolyzed to give almost quantitatively the starting material **16a** (eq. 4) by loss of HCl and $(Me_3Si)_2O$.



This reversible transesterification of **16a** to provide **17** was investigated by ^{31}P-NMR spectroscopic analysis of a sample that had been exposed to atmospheric moisture (Figure 1). The reaction of **17** with water to give **16a** was shown to be diastereoselective; there was no indication of the presence of any **16b**.

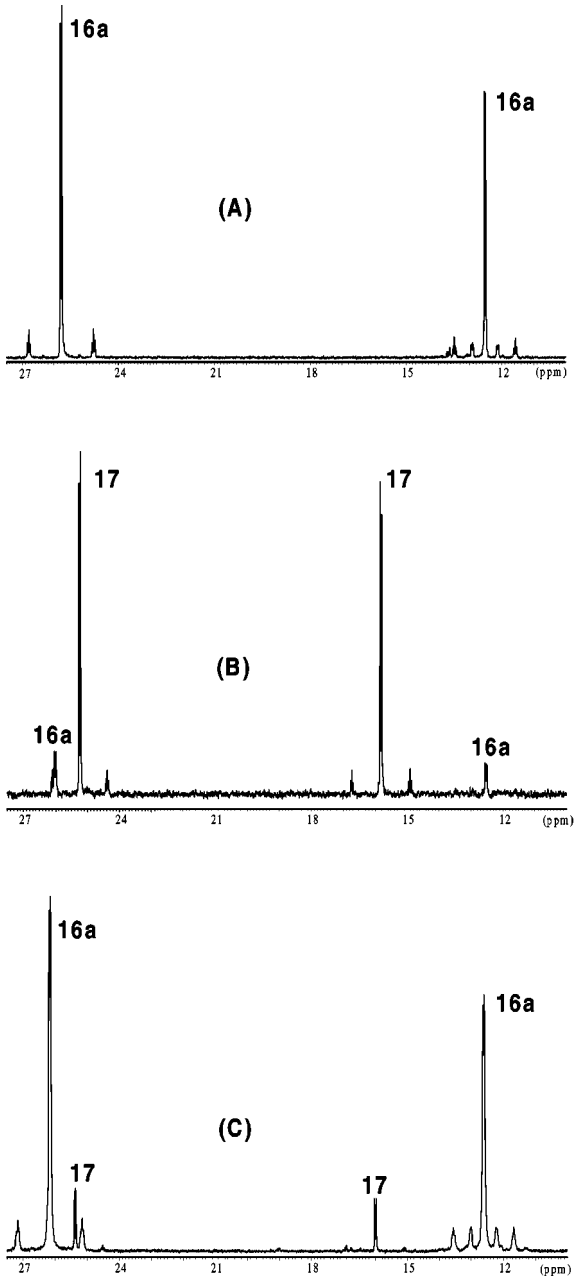


Figure 1. ^{31}P-NMR spectra in $CDCl_3$/toluene of the reversible transesterification of **16a** to **17**; (A) spectrum of a solution of **16a**, (B) spectrum after addition of Me_3SiCl, (C) spectrum after 5 d exposure of the sample to air

Molecular Structures of 2, 6, 8, and 16a

The molecular structures of compounds **2**, **6**, **8**, and **16a** are shown in Figures 2–5 and relevant crystallographic parameters are listed in Table 2. Selected bond lengths and bond angles are collected in Tables 3–5.

In compound **2**, the tetrahedral geometry of the tin atom is markedly distorted and the C–Sn–C angles are found in the range between 95.1(1)° and 122.7(1)°. As has previously been reported for the tetraorganotin compound **3**[1b] and 1-Ph_3Sn-2,4,6-$(CF_3)_3C_6H_2$,[14f] the Sn(1)–C(1) bond lengths of 2.184(3) Å is longer than the Sn–C^{aryl} bond lengths Sn(1)–C(11) [2.155(3) Å] and Sn(1)–C(21) [2.161(3) Å] as a result of the steric repulsion of the rigid ligand frame. In the molecular structure of **2**, two oxygen–tin contacts of 3.108(2) Å and 2.939(2) Å are found for Sn(1)–O(1) and Sn(1)–O(2), respectively, which are significantly shorter than the sum of the van der Waals′ radii of tin and oxygen

(3.700 Å).[20] The overall coordination geometry at the tin center is thus 4+2.

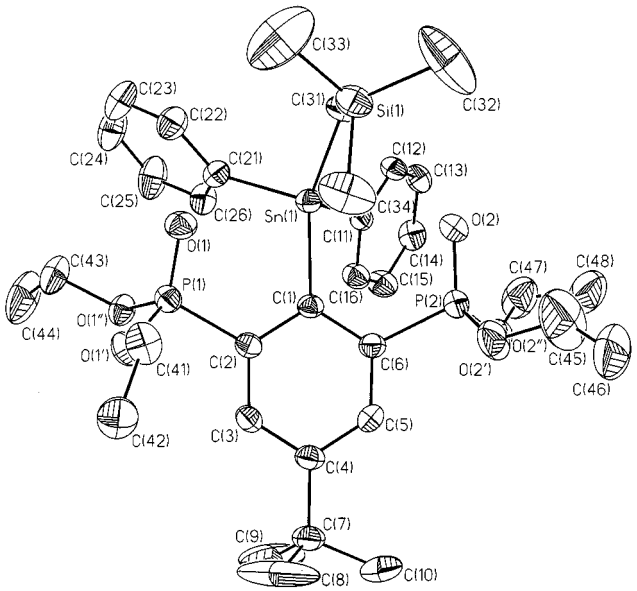


Figure 2. General view (SHELXTL-PLUS) of a molecule of **2** showing 30% probability displacement ellipsoids and the atom numbering scheme

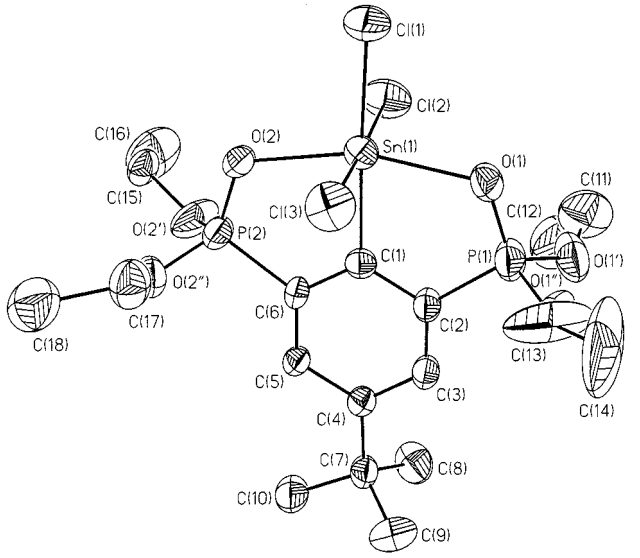


Figure 3. General view (SHELXTL-PLUS) of a molecule of **6** showing 30% probability displacement ellipsoids and the atom numbering scheme

In contrast to compound **2**, strong intramolecular O−Sn contacts are found in the monoorganotin trichloride **6**, in which the tin center adopts a distorted octahedral coordination geometry. The degree of distortion is reflected in *cis*-angles ranging from 80.4(1)° to 91.8(1)° and *trans*-angles of 177.8(1)°, 177.20(5)°, and 161.1(1)° for C(1)−Sn(1)−Cl(1), Cl(2)−Sn(1)−Cl(3), and O(1)−Sn(1)−O(2), respectively. In the previously reported {4-*tert*-Bu-2,6-$[P(O)(OEt)_2]_2$-C_6H_2}$SnPhCl_2$ (**4**),[1b] the same large deviation of the O−Sn−O angle [161.1(2)°] was found as a result of the rigid ligand frame. The intramolecular bond lengths O(1)−Sn(1) and O(2)−Sn(1) amount to 2.225(3) Å and 2.221(3) Å, respectively, and thus are slightly longer than the intermolecular O−Sn interactions reported for hexacoordinate monoorganotin trichlorides such as $RSnCl_3 \cdot 2\,HMPA$ (R = Ph,[21] Et,[22] Me;[23] O−Sn 2.124−2.180 Å), $RSnCl_3 \cdot 2\,DMF$ (R = *i*Pr,[24] Me;[25] O−Sn 2.150−2.22 Å), $EtSnCl_3 \cdot 2\,Ph_3PO$ (O−Sn 2.175 Å),[22] and $(Cl_3Sn)_2CH_2 \cdot 4\,DMSO$ (O−Sn 2.109 Å).[26] In the case of the intramolecularly hexacoordinated compound $CH_3OOCCH_2CH(COOCH_3)CH_2SnCl_3$[14h] and the heptacoordinate $[2,6\text{-}(MeO)_2C_6H_4]_3CHSnCl_3$,[14f] weak O−Sn interactions of 2.460−2.640 Å have been observed, whereas in the molecular structures of $CH_2{=}CHCH_2OC(O)CH_2CH_2SnCl_3 \cdot Ph_3PO$[14e] and BuOC(O)-$CH(CH_3)CH_2SnCl_3 \cdot Ph_3PO$,[14c] weak intramolecular O−Sn interactions of 2.413 and 2.356 Å have been found, along with strongly coordinated Ph_3PO ligands with O−Sn distances of 2.188 and 2.191 Å.

It is worth noting that in spite of a substantial difference in the Lewis acidities of the monoorganotin trichloride **6** and the diorganotin dichloride **4** [O−Sn 2.203/2.278 Å],[1b] the O−Sn contacts in the two compounds are still similar, which can be attributed to the rigidity of the ligand frame in compounds of type **B**. In contrast, for intermolecularly coordinated compounds, the O−Sn interaction depends strongly on the number of chlorine atoms bonded to tin, as demonstrated by the following two pairs of complexes: $Et_2SnCl_2 \cdot 2\,Ph_3PO$ (O−Sn 2.36/2.258 Å)[27] *vs.* $EtSnCl_3 \cdot 2\,Ph_3PO$ (O−Sn 2.175 Å)[2] and $Me_2SnCl_2 \cdot 2\,HMPA$ (O−Sn 2.231 Å)[28] *vs.* $MeSnCl_3 \cdot 2\,HMPA$ (O−Sn 2.175 Å).[23] The IR spectrum of **6** is indicative of strong P=O−Sn interactions, featuring a ν(P=O) band at 1170 cm^{-1}.

The 2,3,1-benzoxaphosphastannole **8** is characterized by a slightly distorted trigonal-bipyramidal tin center, with O(1) and O(2′) occupying axial and C(1), C(11), and C(21) occupying equatorial positions. The O(1)−Sn(1)−O(2′) angle amounts to 160.2(2)°, which is very close to the O−Sn−O angle in **6**. The configuration at tin in the molecular structure of **8** can be classified as being located on the tetrahedral−trigonal bipyramidal path.[29] The position on this path is given by the difference of the sums of the equatorial and axial angles [$\Delta\Sigma(\theta)$], which amounts to 90° for the ideal trigonal bipyramid, 0° for the ideal tetrahedron, and 77.7° for compound **8**. The displacement of the tin atom from the trigonal plane defined by C(1), C(11), and C(21) amounts to 0.136 Å in the direction of O(2′). Compared with the dative O−Sn bond lengths in **6**, the dative O−Sn interaction of 2.396(4) Å in **8** is slightly longer, but is nevertheless comparable to the O−Sn bond distance found in the structurally related [2-(diphenylphosphanyl)-phenyl]dimethyltin chloride [O−Sn 2.357 Å].[30] In the crystal lattice of **8**, a polymeric chain structure is observed as a result of the incorporation of water molecules, with each water molecule linking two 2,3,1-benzoxaphosphastannoles via O(1)···H−O(3)−H···O(2′) interactions. The IR spectrum of compound **8** shows two ν(P=O) absorptions at 1172 cm^{-1} and 1242 cm^{-1}, which correspond to the P(1)−O(1) and P(2)−O(2) bond distances of 1.488(4) and

1.463(6) Å, respectively, and which unambiguously demonstrate the simultaneous presence of both a strongly coordinating and a non-coordinating phosphonyl group. The slight decrease in the ν(P=O) of the non-coordinating P=O group in comparison with a "free" arylphosphonyl group[1b] can be attributed to weak hydrogen-bonding interactions.

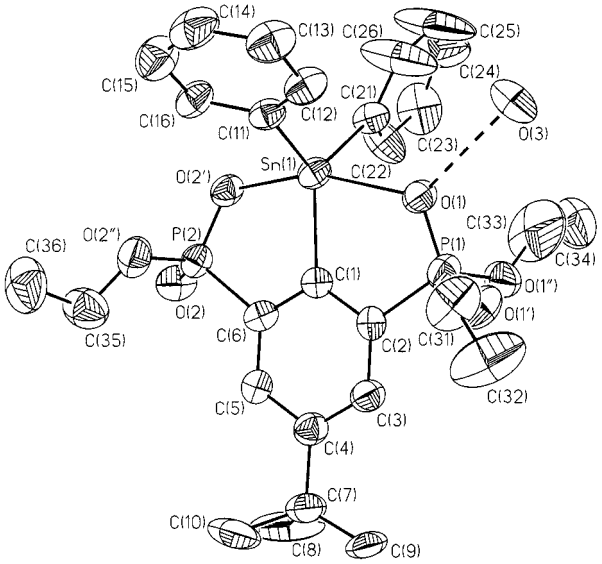


Figure 4. General view (SHELXTL-PLUS) of a molecule of **8** showing 30% probability displacement ellipsoids and the atom numbering scheme (symmetry transformations used to generate equivalent atoms: $a = -x + 0.5, -y + 0.5, -z + 0.5$)

As a result of both intermolecular and intramolecular O−Sn interactions, the tin centers in the dimeric 2,3,1-benzoxaphosphastannole **16a** adopt a distorted octahedral coordination geometry, with *cis*-angles ranging from 81.7(1)° to 97.97(7)°, and *trans*-angles of 172.8(1)°, 173.98(8)°, and 161.78(9)° for C(1)−Sn(1)−Cl(2), Cl(1)−Sn(1)−O(2a), and O(1)−Sn(1)−O(2′), respectively. In comparison with the corresponding O−Sn bond lengths in the monomeric 2,3,1-benzoxaphosphastannole **8**, the O−Sn bond lengths in **16a** are shortened. The dative bond O(1)−Sn(1) in **16a** amounts to 2.204(3) Å. The almost equal O(2′)−Sn(1) and O(2a)−Sn(1) bond lengths of 2.147(3) Å and 2.140(3) Å, respectively, are even shorter and lie in the typical range for O−Sn single bonds (2.15 Å),[31] showing that the phosphonyl group acts as a bidentate bridging ligand. Since the Lewis acidity of the tin atom in **16a** is greater than that of the tin atom in **8**, the former displays a distorted octahedral coordination as a result of dimerization. A similar control of coordination chemistry at tin has previously been reported for compounds of the type $MeXYSnCH_2C(Z)[P(O)(OiPr)_2]_2$ (X, Y = Me, Cl, Br; Z = H, Me). With X = Cl, Y = Me, and Z = H, a five-coordinate compound[15d] was observed, bearing a coordinated and a non-coordinated phosphonyl group. An increase in the Lewis acidity (X = Br, Y = Cl, Z = H)[32] led to the formation of a six-coordinate tin center, with two intramolecular O−Sn contacts. Intra- as well as intermolecular O−Sn coordination has been observed in a dimeric hexacoordinate compound by increasing the steric hindrance (X = Y = Br, Z = Me).[33]

The results of the IR spectroscopic measurements are in agreement with the X-ray data. The ν(P=O) band for the datively bonded phosphonyl group is found at 1168 cm^{-1}. Furthermore, a strong absorption at 1139 cm^{-1} can be assigned to the bidentate bridging phosphonyl group.

Conclusion

We have demonstrated the utility of the new O,C,O-coordinating ligand $\{4\text{-}tert\text{-Bu-2,6-}[P(O)(OEt)_2]_2C_6H_2\}^-$ in the synthesis of various intramolecularly coordinated organotin compounds. As a result of the high donor capacity of intramolecularly coordinating phosphonyl groups, the 2,3,1-benzoxaphosphastannole **8** and the tetraorganotin compound **10** react with Me_3SiBr under Sn−C rather than P−O bond cleavage. The high donor capacity and the rigidity of the ligand skeleton make the O,C,O-coordinating ligand $\{4\text{-}tert\text{-Bu-2,6-}[P(O)(OEt)_2]_2C_6H_2\}^-$ an eminently suitable substituent for the intramolecular donor-stabilization of highly reactive compounds.

Experimental Section

General: All manipulations were performed under an inert atmosphere of argon using standard Schlenk and vacuum line techniques. Solvents were distilled from the appropriate desiccants prior to use. Literature procedures were used to prepare $\{4\text{-}tert\text{-Bu-2,6-}[P(O)(OEt)_2]_2C_6H_2\}Li$ (**1**),[1b] $FSnPh_2(CH_2SiMe_3)$,[10] $\{4\text{-}tert\text{-Bu-2,6-}[P(O)(OEt)_2]_2C_6H_2\}SnPh_3$ (**3**),[1b] $\{4\text{-}tert\text{-Bu-2,6-}[P(O)(OEt)_2]_2C_6H_2\}SnPhCl_2$ (**4**),[1b] $\{4\text{-}tert\text{-Bu-2,6-}[P(O)(OEt)_2]_2C_6H_2\}SnCl$ (**5**),[11] $Ph_3SnCH_2SiMe_3$,[10] $\{4\text{-}tert\text{-Bu-2,6-}[P(O)(OEt)_2]_2C_6H_2\}SnPhBr_2$ (**7**),[1b] $1,5\text{-}[P(O)(OEt)_2]_2\text{-}2,4\text{-}(Ph_3Sn)_2C_6H_2$ (**10**),[1b] and $\{4\text{-}tert\text{-Bu-2,6-}[P(O)(OEt)_2]_2C_6H_2\}SiPh_3$ (**14**).[2p] − IR spectra were obtained using a Bruker FT-IR IFS 113v spectrometer. − ^{119}Sn-, ^{29}Si-, ^{13}C-, ^{1}H-, and ^{31}P-NMR spectra were recorded on Bruker DRX 400 and DPX 300 spectrometers. Chemical shifts δ are given in ppm and were referenced against Me_4Sn (^{119}Sn), Me_4Si (^{1}H, ^{13}C, ^{29}Si), and 85% H_3PO_4 (^{31}P).

{[2,6-Bis(diethoxyphosphonyl)-4-*tert*-butyl]phenyl}diphenyl(trimethylsilylmethyl)tin (2): To a solution of $FSnPh_2(CH_2SiMe_3)$ (1.66 g, 4.37 mmol) in 100 mL thf at −25°C, $\{4\text{-}tert\text{-Bu-2,6-}[P(O)(OEt)_2]_2C_6H_2\}Li$ (**1**) (1.80 g, 4.37 mmol) was added in small portions. After stirring for 20 h at room temp., the solid material formed was removed by filtration. The filtrate was concentrated to dryness in vacuo and the residue was recrystallized from ethanol to give 1.30 g (39%) of **2** as colorless crystals; m.p. 133°C. − ^{1}H NMR (400.13 MHz, C_6D_6): δ = 0.36 (s, 9 H, Me_3Si), 0.95 (t, 12 H, CH_3), 1.15 (s, 9 H, CH_3), 1.29 [s, $^{2}J(^{1}H-^{119}Sn)$ = 86 Hz, 2 H, CH_2Sn], 3.44−3.54 (complex pattern, 4 H, CH_2), 3.74−3.84 (complex pattern, 4 H, CH_2), 7.12−7.30 (complex pattern, 6 H, H^{Ph}), 8.12 [d, $^{3}J(^{1}H-^{119}Sn)$ = 49 Hz, 4 H, H^{Ph}], 8.60 (complex pattern, 2 H, H^{Ph}). − $^{13}C\{^{1}H\}$ NMR (100.63 MHz, $CDCl_3$): δ = 1.1 [s, $^{1}J(^{13}C-^{119/117}Sn)$ = 341/323 Hz, 1 C, CH_2Sn], 1.7 [s, $^{3}J(^{13}C-^{119}Sn)$ = 18 Hz, $^{1}J(^{13}C-^{29}Si)$ = 50 Hz, 3 C, Me_3Si], 15.98 [d, $^{3}J(^{13}C-^{31}P)$ = 4 Hz, 2 C, CH_3], 16.01 [d, $^{3}J(^{13}C-^{31}P)$ = 4 Hz, 2 C, CH_3], 30.9 (s, 3 C, CCH_3), 34.6 (s, 1 C, CCH_3), 61.55

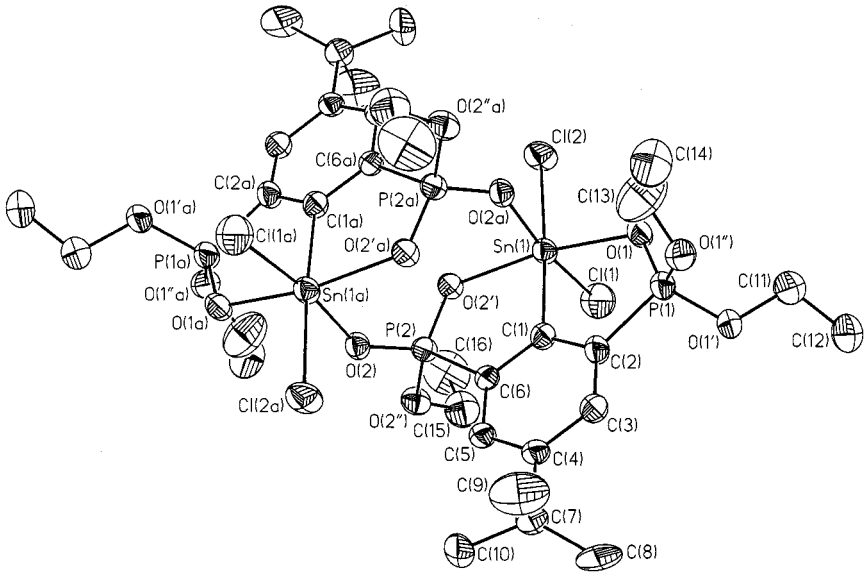


Figure 5. General view (SHELXTL-PLUS) of a molecule of **16a** showing 30% probability displacement ellipsoids and the atom numbering scheme (symmetry transformations used to generate equivalent atoms: $a = -x, -y, -z$)

[$^2J(^{13}C-^{31}P)$ = 3 Hz, 2 C, CH_2], 61.58 [$^2J(^{13}C-^{31}P)$ = 3 Hz, 2 C, CH_2], 126.9 (s, 2 C, C^{para}), 127.2 [s, $^3J(^{13}C-^{119}Sn)$ = 54 Hz, 4 C, C^{meta}], 133.1 (AA′BB′ pattern, 2 C, $C^{3,5}$), 136.9 [s, $^2J(^{13}C-^{119}Sn)$ = 36 Hz, 4 C, C^{ortho}], 137.3 [dd, $^1J(^{13}C-^{31}P)$ = 193 Hz, $^3J(^{13}C-^{31}P)$ = 20 Hz, 2 C, $C^{2,6}$], 147.5 [s, $^1J(^{13}C-^{119/117}Sn)$ = 554/530 Hz, 2 C, C^{ipso}], 150.2 [t, $^3J(^{13}C-^{31}P)$ = 13 Hz, 1 C, C^4], 153.9 [t, $^2J(^{13}C-^{31}P)$ = 23 Hz, 1 C, C^1]. – $^{119}Sn\{^1H\}$ NMR (111.91 MHz, $CDCl_3$): δ = −127.5 [t, $J(^{119}Sn-^{31}P)$ = 38 Hz]. – $^{31}P\{^1H\}$ NMR (121.49 MHz, $CDCl_3$): δ = 23.0 [$J(^{31}P-^{119}Sn)$ = 37 Hz]. – $^{29}Si\{^1H\}$ NMR (59.63 MHz, $CDCl_3$): δ = 5.0. – IR (KBr): $\tilde{\nu}$ = 1242 cm^{-1} (P=O). – $C_{34}H_{52}O_6P_2SiSn$ (765.55): calcd. C 53.34, H 6.84; found C 53.55, H 7.15.

{[2,6-Bis(diethoxyphosphonyl)-4-*tert*-butyl]phenyl}tin Trichloride (6): To a solution of {4-*tert*-Bu-2,6-$[P(O)(OEt)_2]_2C_6H_2$}SnCl (**5**) (2.00 g, 3.5 mmol) in 50 mL thf at room temp., $SnCl_4(thf)_2$ (1.20 g, 3.5 mmol) was added in small portions. After stirring the reaction mixture for 2 h, the solvent was evaporated in vacuo. The residue was suspended in 40 mL chloroform and after filtration the solvent was evaporated in vacuo. This procedure was repeated three times, eventually leading to the isolation of 1.3 g (58%) of **4** as colorless crystals; m.p. > 350°C. Crystals suitable for X-ray crystallography were grown from $CDCl_3$. – ^1H NMR (400.13 MHz, $CDCl_3$): δ = 1.36 (t, 12 H, CH_3), 1.37 (s, 9 H, CH_3), 3.93–4.00 (complex pattern, 4 H, CH_2), 4.41–4.50 (complex pattern, 4 H, CH_2), 7.96 (AA′BB′ pattern, 2 H, H^{Ph}). – $^{13}C\{^1H\}$ NMR (100.63 MHz, $CDCl_3$): δ = 15.5 (s, 4 C, CH_3), 30.6 (s, 3 C, CCH_3), 35.0 (s, 1 C, CCH_3), 65.4 (s, 4 C, CH_2), 123.1 [dd, $^1J(^{13}C-^{31}P)$ = 184 Hz, $^3J(^{13}C-^{31}P)$ = 17 Hz, 2 C, $C^{2,6}$], 131.2 (AA′BB′ pattern, 2 C, $C^{3,5}$), 154.4 [t, $^3J(^{13}C-^{31}P)$ = 12 Hz, 1 C, C^4], 173.1 [t, $^2J(^{13}C-^{31}P)$ = 17 Hz, 1 C, C^1]. – $^{119}Sn\{^1H\}$ NMR (149.18 MHz, $CDCl_3$): δ = −522.9 [t, $J(^{119}Sn-^{31}P)$ = 286 Hz]. – $^{31}P\{^1H\}$ NMR (161.98 MHz, $CDCl_3$): δ = 28.0 [$J(^{31}P-^{119/117}Sn)$ = 287/273 Hz]. – IR (KBr): $\tilde{\nu}$ = 1170 cm^{-1} (P=O). – $C_{18}H_{31}Cl_3O_6P_2Sn$ (630.48): calcd. C 34.29, H 4.95, Cl 16.87; found C 34.32, H 5.06, Cl 16.82.

5-*tert*-Butyl-7-diethoxyphosphonyl-3-ethoxy-3-oxo-1,1-diphenyl-2,3,1-benzoxaphosphastannole (8). – Method A: To a solution of {4-*tert*-Bu-2,6-$[P(O)(OEt)_2]_2C_6H_2$}$SnPh_3$ (**3**) (254 mg, 0.34 mmol) in 8 mL CH_2Cl_2 at 0°C, 4.15 mL of a bromine solution (0.08 mol/L in CH_2Cl_2) was added dropwise. The reaction mixture was stirred for 24 h at room temp., the solvent was then removed in vacuo, and the residue was recrystallized from hexane/diethyl ether to give 203 mg (93%) of **8** as colorless crystals; m.p. 166–168°C.

Method B: To a solution of {4-*tert*-Bu-2,6-$[P(O)(OEt)_2]_2$-C_6H_2}$SnPh_3$ (**3**) (232 mg, 0.31 mmol) in 5 mL CH_2Cl_2 at room temp., iodine (78 mg, 0.31 mmol) was added in small portions. The reaction mixture was stirred for 36 h at room temp., the solvent was then removed in vacuo, and the residue was recrystallized from hexane/diethyl ether to give 187 mg (89%) of **8** as colorless crystals; m.p. 167–168°C. – ^1H NMR (400.13 MHz, $CDCl_3$): δ = 1.13 (t, 3 H, CH_3), 1.25 (t, 3 H, CH_3), 1.28 (t, 3 H, CH_3), 1.34 (s, 9 H, CH_3), 3.73–4.14 (complex pattern, 6 H, CH_2), 7.34–7.37 (complex pattern, 6 H, H^{Ph}), 7.74–7.92 (complex pattern, 5 H, H^{Ph}), 8.25 (d, 1 H, H^{Ph}). – $^{13}C\{^1H\}$ NMR (100.63 MHz, $CDCl_3$): δ = 15.9 [d, $^3J(^{13}C-^{31}P)$ = 6 Hz, 1 C, CH_3], 16.0 [d, $^3J(^{13}C-^{31}P)$ = 6 Hz, 1 C, CH_3], 16.6 [d, $^3J(^{13}C-^{31}P)$ = 7 Hz, 1 C, CH_3], 31.1 (s, 3 C, CCH_3), 35.2 (s, 1 C, CCH_3), 61.0 [d, $^2J(^{13}C-^{31}P)$ = 6 Hz, 1 C, CH_2], 64.0 [d, $^2J(^{13}C-^{31}P)$ = 6 Hz, 1 C, CH_2], 64.1 [d, $^2J(^{13}C-^{31}P)$ = 6 Hz, 1 C, CH_2], 128.5 [s, $^3J(^{13}C-^{119}Sn)$ = 74 Hz, 4 C, C^{meta}], 128.9/132.1 [dd/dd, $^2J(^{13}C-^{31}P)$ = 14 Hz/$^2J(^{13}C-^{31}P)$ = 12 Hz, $^4J(^{13}C-^{31}P)$ = 3 Hz/$^4J(^{13}C-^{31}P)$ = 4 Hz, 2 C, $C^{3,5}$], 129.0/140.4 [dd/dd, $^1J(^{13}C-^{31}P)$ = 184 Hz/$^1J(^{13}C-^{31}P)$ = 180 Hz, $^3J(^{13}C-^{31}P)$ = 16 Hz/$^3J(^{13}C-^{31}P)$ = 16 Hz, 2 C, $C^{2,6}$], 129.8 [s, $^3J(^{13}C-^{119}Sn)$ = 16 Hz, 1 C, C^{para}], 129.9 [s, $^4J(^{13}C-^{119}Sn)$ = 16 Hz, 1 C, $C^{para'}$], 135.7 [s, $^2J(^{13}C-^{119}Sn)$ = 51 Hz, 2 C, C^{ortho}], 136.0 [s, $^2J(^{13}C-^{119}Sn)$ = 52 Hz, 2 C, $C^{ortho'}$], 138.2 [t, $J(^{13}C-^{31}P)$ = 4 Hz, 1 C, C^{ipso}], 138.8 [t, $J(^{13}C-^{31}P)$ = 3 Hz, 1 C, $C^{ipso'}$], 153.3 [t, $^2J(^{13}C-^{31}P)$ = 18 Hz, 1 C, C^1], 154.9 [t, $^3J(^{13}C-^{31}P)$ = 12 Hz, 1 C, C^4]. – $^{119}Sn\{^1H\}$ NMR (111.91 MHz, $CDCl_3$): δ = −223.6 [dd, $J(^{119}Sn-^{31}P)$ = 19/23 Hz]. – $^{31}P\{^1H\}$ NMR (121.49 MHz, $CDCl_3$): δ = 17.3, 28.6 [$J(^{31}P-^{119}Sn)$ = 19 Hz]. – IR (KBr): $\tilde{\nu}$ = 1172, 1242 cm^{-1} (P=O). – $C_{28}H_{36}O_6P_2Sn$ (649.27): calcd. C 51.80, H 5.58; found C 51.60, H 5.75.

{[4-*tert*-Butyl-6-diethoxyphosphonyl-2-ethoxy(trimethylsiloxy)-phosphonyl]phenyl}phenyltin Dibromide (9): To a solution of **8** (190 mg, 0.29 mmol) in 2.5 mL CH_2Cl_2 at −30°C was added Me_3SiBr (0.15 mL, 1.16 mmol). After stirring the reaction mixture for 20 min. at room temp., the solvent was evaporated, the residue was washed three times with 2 mL hexane, and dried in vacuo to give

115 mg (49%) of **9** as a colorless solid; m.p. 133°C. – ^{1}H NMR (400.13 MHz, $CDCl_3$): δ = 0.40 (s, 9 H, $SiMe_3$), 1.28 (t, 3 H, CH_3), 1.32 (t, 3 H, CH_3), 1.33 (t, 3 H, CH_3), 1.38 (s, 9 H, CH_3), 4.13–4.54 (complex pattern, 6 H, CH_2), 7.33–7.41 (complex pattern, 3 H, H^{Ph}), 7.92 [d, $^3J(^1H-^{31}P)$ = 13 Hz, 1 H, H^{Ph}], 7.94 [d, $^3J(^1H-^{31}P)$ = 14 Hz, 1 H, H^{Ph}], 8.14 [d, $^3J(^1H-^{119}Sn)$ = 142 Hz, 2 H, H^{Ph}]. – $^{13}C\{^1H\}$ NMR (100.63 MHz, $CDCl_3$): δ = 1.2 (s, 3 C, $SiMe_3$), 16.13 [d, $^3J(^{13}C-^{31}P)$ = 4 Hz, 1 C, CH_3], 16.17 [d, $^3J(^{13}C-^{31}P)$ = 4 Hz, 1 C, CH_3], 16.19 [d, $^3J(^{13}C-^{31}P)$ = 4 Hz, 1 C, CH_3], 31.2 (s, 3 C, CCH_3), 35.3 (s, 1 C, CCH_3), 65.22 [d, $^2J(^{13}C-^{31}P)$ = 4 Hz, 1 C, CH_2], 65.58 [d, $^2J(^{13}C-^{31}P)$ = 5 Hz, 1 C, CH_2], 65.67 [d, $^2J(^{13}C-^{31}P)$ = 5 Hz, 1 C, CH_2], 123.9 [dd, $^1J(^{13}C-^{31}P)$ = 183 Hz, $^3J(^{13}C-^{31}P)$ = 18 Hz, 1 C, C^2], 125.8 [dd, $^1J(^{13}C-^{31}P)$ = 191 Hz, $^3J(^{13}C-^{31}P)$ = 18 Hz, 1 C, C^6], 128.1 [s, $^3J(^{13}C-^{119/117}Sn)$ = 144/138 Hz, 2 C, C^{meta}], 129.6 [s, $^4J(^{13}C-^{119}Sn)$ = 27 Hz, 1 C, C^{para}], 131.3 [t, $J(^{13}C-^{31}P)$ = 3 Hz, 2 C, $C^{3,5}$], 133.9 [s, $^2J(^{13}C-^{119}Sn)$ = 87 Hz, 2 C, C^{ortho}], 149.4 [s, $J(^{13}C-^{31}P)$ = 5 Hz, 1 C, C^{ipso}], 153.5 [t, $^3J(^{13}C-^{31}P)$ = 13 Hz, 1 C, C^4], 172.8 [t, $^2J(^{13}C-^{31}P)$ = 18 Hz, 1 C, C^1]. – $^{119}Sn\{^1H\}$ NMR (149.18 MHz, $CDCl_3$): δ = −439.6 [t, $J(^{119}Sn-^{31}P)$ = 100 Hz]. – $^{31}P\{^1H\}$ NMR (161.98 MHz, $CDCl_3$): δ = 17.3 [$J(^{31}P-^{119/117}Sn)$ = 103/98 Hz, $^4J(^{31}P-^{31}P)$ = 7 Hz], 26.7 [$J(^{31}P-^{119/117}Sn)$ = 97/93 Hz, $^4J(^{31}P-^{31}P)$ = 7 Hz]. – IR (KBr): $\tilde{\nu}$ = 1173 cm^{-1} (P=O). – $C_{25}H_{40}Br_2O_6P_2SiSn$ (805.17): calcd. C 37.29, H 5.00; found C 36.70, H 5.20.

1,5-Bis(bromodiphenylstannyl)-2,4-bis(diethoxyphosphonyl)benzene (11): To a solution of 1,5-$[P(O)(OEt)_2]_2$-2,4-$(Ph_3Sn)_2C_6H_2$ (**10**) (139 mg, 0.13 mmol) in 2.5 mL CH_2Cl_2 at −50°C was added Me_3SiBr (0.15 mL, 1.16 mmol). The reaction mixture was allowed to warm to room temp., the solvent was evaporated in vacuo, and the residue was washed three times with 2 mL hexane to give 93 mg (67%) of **11** as colorless solid; m.p. 230–231°C (Lit. 231–233°C)[1b]. – $^{119}Sn\{^1H\}$ NMR (149.18 MHz, $CDCl_3$): δ = −180.7 (AA′XX′ pattern). – $^{31}P\{^1H\}$ NMR (161.98 MHz, $CDCl_3$): δ = 25.8 [$J(^{31}P-^{119}Sn)$ = 34 Hz, $^5J(^{31}P-^{119}Sn)$ = 15 Hz].

5-*tert*-Butyl-3-hydroxy-3-oxo-1,1-diphenyl-7-phosphono-2,3,1-benzoxaphosphastannole (13): To a solution of {4-*tert*-Bu-2,6-$[P(O)(OEt)_2]_2C_6H_2$}$SnPh_3$ (**3**) (100 mg, 0.13 mmol) in 0.5 mL $CDCl_3$ at −30°C, Me_3SiBr (0.10 mL, 0.77 mmol) was added dropwise. The reaction mixture was allowed to warm to room temp., whereupon ^{119}Sn-, ^{31}P-, and ^{29}Si-NMR spectra were recorded, which indicated the formation of {4-*tert*-Bu-2,6-$[P(O)(OSiMe_3)_2]_2C_6H_2$}$SnPh_3$ (**12**) ($^{119}Sn\{^1H\}$ NMR (149.18 MHz, $CDCl_3$): δ = −188.4. – $^{31}P\{^1H\}$ NMR (161.98 MHz, $CDCl_3$): δ = −2.82 [$J(^{31}P-^{119}Sn)$ = 40 Hz]. – $^{29}Si\{^1H\}$ NMR (79.49 MHz, $CDCl_3$): δ = 20.1). After distilling off the solvent, the residue was redissolved in 2 mL acetone, water (0.15 mL) was added, and the solution was stirred for 2 h at room temperature. The solvent was then removed in vacuo and the residue was washed three times with 2 mL hexane to give 41 mg (57%) of **13** as a colorless solid; m.p. 280°C (dec.). – ^{1}H NMR (400.13 MHz, [D_6]-acetone): δ = 1.46 (s, 9 H, CH_3), 7.29–7.34 (complex pattern, 6 H, H^{Ph}), 7.80–8.00 (complex pattern, 4 H, H^{Ph}), 8.06–8.08 (complex pattern, 2 H, H^{Ph}). – $^{119}Sn\{^1H\}$ NMR (149.18 MHz, [D_6]acetone): δ = −239.9 [t, $J(^{119}Sn-^{31}P)$ = 70 Hz]. – $^{31}P\{^1H\}$ NMR (161.98 MHz, [D_6]acetone): δ = 20.3, 20.4. – IR (KBr): $\tilde{\nu}$ = 1173 cm^{-1} (P=O), 3400 cm^{-1} (br, O–H). – $C_{22}H_{24}O_6P_2Sn$ (565.11): calcd. C 46.76, H 4.28; found C 46.55, H 4.65.

Reaction of {4-*tert*-Bu-2,6-$[P(O)(OEt)_2]_2C_6H_2$}$SnPh_3$ (3) with Ph_2SnCl_2: To a solution of **3** (150 mg, 0.20 mmol) in 4 mL toluene was added Ph_2SnCl_2 (69 mg, 0.20 mmol) and the reaction mixture was heated under reflux for 5 h. The solvent was then removed in vacuo, the residue was redissolved in 0.5 mL $CDCl_3$ and the ^{119}Sn-NMR spectrum of this solution was recorded. – $^{119}Sn\{^1H\}$ NMR (149.18 MHz, $CDCl_3$): δ = −125, −221 [t, $J(^{119}Sn-^{31}P)$ = 19 Hz], −243 (br.), −284 (br.); integral ratio 0.6:2.6:1.6:1.9.

Reaction of {4-*tert*-Bu-2,6-$[P(O)(OEt)_2]_2$-C_6H_2}$SiPh_3$ (15) with Ph_2SnCl_2: To a solution of **14** (60 mg, 0.090 mmol) in 5 mL toluene was added Ph_2SnCl_2 (31 mg, 0.090 mmol) and the reaction mixture was heated under reflux for 24 h. The solvent was then removed in vacuo, the residue was redissolved in 0.5 mL $CDCl_3$, and the ^{119}Sn-NMR spectrum of this solution was recorded. – $^{119}Sn\{^1H\}$ NMR (149.18 MHz, $CDCl_3$): δ = −223 [t, $J(^{119}Sn-^{31}P)$ = 19 Hz], −236 (br.), −258 (br.); integral ratio 1.0:0.3:0.6.

Reaction of {[2,6-Bis(diethoxyphosphonyl)-4-*tert*-butyl]phenyl}-diphenyl(trimethylsilylmethyl)tin (2) with Iodine: To a solution of **2** (250 mg, 0.33 mmol) in 5 mL CH_2Cl_2 was added iodine (83 mg, 0.33 mmol). The reaction mixture was stirred at room temp. for 24 h, then the solvent was removed in vacuo, the residue was redissolved in 0.5 mL of $CDCl_3$, and the ^{119}Sn-NMR spectrum of this solution recorded. – $^{119}Sn\{^1H\}$ NMR (149.18 MHz, $CDCl_3$): δ = −138.3 ($W_{1/2}$ = 21 Hz), −139.2 ($W_{1/2}$ = 23 Hz), −224.1 ($W_{1/2}$ = 58 Hz); integral ratio 1:0.8:0.5.

Bis[5-*tert*-butyl-1,1-dichloro-7-diethoxyphosphonyl-3-ethoxy-3-oxo-2,3,1-benzoxaphosphastannole] (16): A solution of **6** (500 mg, 0.79 mmol) in 25 mL toluene was heated under reflux for 16 h. After removing the solid material formed by filtration, the solvent was removed in vacuo and the residue was redissolved in $CDCl_3$. The ^{31}P-NMR spectrum of this solution was recorded, which indicated formation of the two diastereomers **16a** and **16b**. – $^{31}P\{^1H\}$ NMR (161.98 MHz, toluene/D_2O-cap.): **16a**: δ = 11.95 [d, $^4J(^{31}P-^{31}P)$ = 6.8 Hz, $J(^{31}P-^{119/117}Sn)$ = 316/301 Hz, $J(^{31}P-^{119/117}Sn)$ = 137/125 Hz], 25.17 [d, $^4J(^{31}P-^{31}P)$ = 6.6 Hz, $J(^{31}P-^{119/117}Sn)$ = 334/320 Hz]. – **16b**: δ = 13.12 [d, $^4J(^{31}P-^{31}P)$ = 7.8 Hz, $J(^{31}P-^{119/117}Sn)$ = 304 Hz], 25.14 [d, $^4J(^{31}P-^{31}P)$ = 7.0 Hz, $J(^{31}P-^{119/117}Sn)$ = 324 Hz]. The $CDCl_3$ was removed in vacuo and the residue was recrystallized from toluene/$CHCl_3$ to give 290 mg (65%) of the diastereomer **16a** as colorless crystals; m.p. > 350°C. – ^{1}H NMR (400.13 MHz, $CDCl_3$): δ = 1.04 (t, 6 H, CH_3), 1.30 (t, 12 H, CH_3), 1.34 (s, 18 H, CH_3), 3.68–3.78 (complex pattern, 2 H, CH_2), 3.92–4.02 (complex pattern, 2 H, CH_2), 4.09–4.23 (complex pattern, 4 H, CH_2), 4.27–4.41 (complex pattern, 4 H, CH_2), 7.77–7.91 [d, $^3J(^1H-^{31}P)$ = 13.4 Hz, $^4J(^1H-^{119}Sn)$ = 41.8 Hz, 2 H, H^{Ph}], 8.12–8.26 [d, $^3J(^1H-^{31}P)$ = 13.6 Hz, $^4J(^1H-^{119}Sn)$ = 41.0 Hz, 2 H, H^{Ph}]. – $^{13}C\{^1H\}$ NMR (100.63 MHz, $CDCl_3$): δ = 15.1 (m, 6 C, CH_3), 30.3 (s, 6 C, CCH_3), 34.6 (s, 2 C, CCH_3), 62.2 [d, $^2J(^{13}C-^{31}P)$ = 5 Hz, 2 C, CH_2], 64.5 [d, $^2J(^{13}C-^{31}P)$ = 5 Hz, 2 C, CH_2], 64.7 [d, $^2J(^{13}C-^{31}P)$ = 5 Hz, 2 C, CH_2], 122.6 [dd, $^1J(^{13}C-^{31}P)$ = 181 Hz, $^3J(^{13}C-^{31}P)$ = 16 Hz, 2 C, C^2], 128.6 [dd, $^2J(^{13}C-^{31}P)$ = 12 Hz, $^4J(^{13}C-^{31}P)$ = 3 Hz, 2 C, C^5], 129.5 [dd, $^1J(^{13}C-^{31}P)$ = 176 Hz, $^3J(^{13}C-^{31}P)$ = 16 Hz, 2 C, C^6], 132.7 [dd, $^2J(^{13}C-^{31}P)$ = 12 Hz, $^4J(^{13}C-^{31}P)$ = 3 Hz, 2 C, C^3], 154.1 [dd, $^3J(^{13}C-^{31}P)$ = 13 Hz, 2 C, C^4], 167.4 [dd, $^2J(^{13}C-^{31}P)$ = 17 Hz, $^2J(^{13}C-^{31}P)$ = 16 Hz, 2 C, C^1]. – $^{119}Sn\{^1H\}$ NMR (149.18 MHz, $CDCl_3$): δ = −547.9 [ddd, $^2J(^{119}Sn-^{31}P)$ = 139 Hz, $J(^{119}Sn-^{31}P)$ = 320 Hz, $J(^{119}Sn-^{31}P)$ = 336 Hz]. – $^{31}P\{^1H\}$ NMR (161.98 MHz, $CDCl_3$): δ = 11.9 [d, $^4J(^{31}P-^{31}P)$ = 6.6 Hz, $J(^{31}P-^{119/117}Sn)$ = 316/302 Hz, $J(^{31}P-^{119/117}Sn)$ = 137/122 Hz], 25.2 [d, $^4J(^{31}P-^{31}P)$ = 6.6 Hz, $J(^{31}P-^{119/117}Sn)$ = 335/321 Hz]. – IR (KBr): $\tilde{\nu}$ = 1168, 1139 cm^{-1} (P=O). – $C_{32}H_{52}Cl_4O_{12}P_4Sn_2$ (1131.93): calcd. C 33.96, H 4.63; found C 33.55, H 4.79.

Crystallography: Intensity data for the colorless crystals were collected on a Nonius Kappa CCD diffractometer using graphite-monochromated Mo-K_α (λ = 0.71069 Å) radiation at 293 K. The

Table 2. Crystallographic data for **2**, **6**, **8**, and **16a**

	2	**6**	**8**	**16a**
formula	$C_{34}H_{52}O_6P_2SiSn$	$C_{18}H_{31}O_6P_2Cl_3Sn \cdot 0.5\ C_7H_8$	$C_{28}H_{36}O_6P_2Sn \cdot 0.5\ H_2O$	$C_{32}H_{52}Cl_4O_{12}P_4Sn_2$
form. wt.	765.48	676.47	658.22	1131.80
cryst. syst.	triclinic	orthorhombic	monoclinic	monoclinic
cryst. size, mm	0.20 × 0.15 × 0.15	0.30 × 0.15 × 0.15	0.20 × 0.05 × 0.03	0.40 × 0.15 × 0.15
space group	$P\bar{1}$	*Pbcn*	$P2_1/n$	$P2_1/n$
a, Å	11.464(1)	15.640(1)	12.453(1)	10.268(1)
b, Å	21.736(1)	19.706(1)	14.598(1)	11.253(1)
c, Å	14.134(1)	19.346(1)	17.316(1)	20.563(1)
α, °	72.633(1)	90	90	90
β, °	85.610(1)	90	92.934(1)	101.902(1)
γ, °	85.232(1)	90	90	90
V, Å^3	1959.8(3)	5962.5(6)	3143.7(4)	2324.9(3)
Z	2	8	4	2
ρ_{calcd}, Mg/m^3	1.297	1.507	1.391	1.617
μ, mm^{-1}	0.802	1.265	0.953	1.494
F(000)	796	2744	1348	1136
θ range, deg	2.73 to 28.76	4.14 to 25.01	3.24 to 21.17	3.54 to 25.69
index ranges	$-15 \le h \le 15$	$-16 \le h \le 16$	$-12 \le h \le 12$	$-12 \le h \le 12$
	$-17 \le k \le 17$	$-23 \le k \le 23$	$-13 \le k \le 13$	$-13 \le k \le 13$
	$-18 \le l \le 19$	$-23 \le l \le 23$	$-17 \le l \le 17$	$-21 \le l \le 21$
no. of reflns. colld.	22983	77474	13616	31787
completeness to θ_{max}	89.4	95.9	83.9	93.4
no. of indep. reflns./R_{int}	9111/0.042	5038/0.048	2907/0.066	4125/0.047
no. of reflns. obsd. with [$I > 2\sigma(I)$]	4843	2427	1717	2430
no. of refined params.	407	347	372	291
GooF (F^2)	0.859	0.831	0.884	0.895
*R*1 (*F*) [$I > 2\sigma(I)$]	0.0422	0.0381	0.0390	0.0331
*wR*2 (F^2) (all data)	0.0908	0.0807	0.0817	0.0700
$(\Delta/\sigma)_{max}$	0.001	0.001	< 0.001	< 0.001
Largest diff. peak/hole, e/Å^3	0.483/−0.370	0.350/−0.352	0.280/−0.202	0.306/−0.321

Table 3. Selected interatomic distances (Å) and angles (deg) for **2** and **6**

	2 X = C(11); Y = C(21); Z = C(31)	**6** X = Cl(1); Y = Cl(2); Z = Cl(3)
Sn(1)−C(1)	2.184(3)	2.132(4)
Sn(1)−X	2.155(3)	2.332(1)
Sn(1)−Y	2.161(3)	2.434(1)
Sn(1)−Z	2.144(3)	2.422(1)
Sn(1)−O(1)	3.108(2)	2.225(3)
Sn(1)−O(2)	2.939(2)	2.221(3)
P(1)−O(1)	1.456(2)	1.493(3)
P(2)−O(2)	1.452(2)	1.499(3)
C(1)−Sn(1)−X	100.0(1)	177.8(1)
C(1)−Sn(1)−Y	114.9(1)	90.9(1)
C(1)−Sn(1)−Z	122.7(1)	91.8(1)
X−Sn(1)−Y	95.1(1)	88.49(5)
X−Sn(1)−Z	114.2(1)	88.91(6)
Y−Sn(1)−Z	106.6(1)	177.20(5)
C(1)−Sn(1)−O(1)	68.63(9)	80.4(1)
C(1)−Sn(1)−O(2)	73.4(1)	80.7(1)
X−Sn(1)−O(1)	153.1(1)	97.48(8)
X−Sn(1)−O(2)	74.6(1)	101.39(8)
Y−Sn(1)−O(1)	70.1(1)	90.44(9)
Y−Sn(1)−O(2)	168.1(1)	89.69(8)
Z−Sn(1)−O(1)	91.9(1)	90.93(8)
Z−Sn(1)−O(2)	73.5(1)	89.81(8)
O(1)−Sn(1)−O(2)	121.70(7)	161.1(1)
C(2)−P(1)−O(1)	112.5(1)	107.8(2)
C(6)−P(2)−O(2)	114.4(2)	108.7(2)
P(1)−O(1)−Sn(1)	96.7(1)	117.6(2)
P(2)−O(2)−Sn(1)	102.6(1)	116.3(1)

Table 4. Selected interatomic distances (Å) and angles (deg) for **8**

Sn(1)−C(1)	2.110(6)	P(1)−O(1)	1.488(4)
Sn(1)−C(11)	2.100(8)	P(2)−O(2)	1.463(6)
Sn(1)−C(21)	2.078(9)	P(2)−O(2′)	1.524(5)
Sn(1)−O(1)	2.396(4)	O(1)−O(3)	2.84(1)
Sn(1)−O(2′)	2.124(4)	O(3)−O(2a)	2.76(1)
C(1)−Sn(1)−C(11)	120.7(3)	C(21)−Sn(1)−O(2′)	99.7(3)
C(1)−Sn(1)−C(21)	121.7(3)	O(1)−Sn(1)−O(2′)	160.2(2)
C(11)−Sn(1)−C(21)	116.3(4)	O(1)−P(1)−C(2)	108.8(3)
C(1)−Sn(1)−O(1)	77.6(2)	O(2′)−P(2)−C(6)	103.3(3)
C(1)−Sn(1)−O(2′)	82.7(2)	P(1)−O(1)−Sn(1)	113.3(2)
C(11)−Sn(1)−O(1)	91.8(3)	P(2)−O(2′)−Sn(1)	119.1(2)
C(11)−Sn(1)−O(2′)	99.2(3)	O(1)−O(3)−O(2a)	111.9(3)
C(21)−Sn(1)−O(1)	89.9(3)		

a = $-x + 0.5, y + 0.5, -z + 0.5$.

data collection covered almost the whole sphere of reciprocal space with 360 frames by ω-rotation (Δ/ω = 1°) at two times, 10 s (**2**), 20 s (**6**, **16a**), and 75 s (**8**), per frame. The crystal-to-detector distance was 2.7 cm (**2**, **6**, **16a**) and 2.9 cm (**8**). Crystal decay was monitored by repeating the initial frames at the end of the data collection. The data were not corrected for absorption effects. On analyzing the duplicate reflections, no indication of any decay was found. The structure was solved by direct methods SHELXS-97[35] (Sheldrick, 1990) and successive difference Fourier syntheses. Refinement employed full-matrix least-squares methods SHELXL-97[36] (Sheldrick, 1997). The H atoms were placed in geometrically calculated positions and refined with common isotropic temperature factors for alkyl and aryl H atoms [C−H$^{prim.}$ 0.96 Å, C−H$^{sec.}$ 0.97 Å, C−H^{aryl} 0.93 Å; U_{iso} 0.139(3) (**2**), 0.166(5) (**6**), 0.189(9) (**9**), 0.131(5) Å^2 (**16a**)]. The occupancy (s.o.f.) of the water molecule O(3) in **8** was found to be 0.5. Disordered groups were found in **2** [OEt group C46 and C46′ (s.o.f. 0.5)], in **6** [OEt groups C11, C13, C14, C15, C17, C11′, C13′, C14′, C15′, C17′ (s.o.f. 0.5)], in **8** [*t*-Bu group C8,

Table 5. Selected interatomic distances (Å) and angles (deg) for **16a**

Sn(1)−C(1)	2.122(4)	P(1)−O(1′)	1.560(3)
Sn(1)−Cl(1)	2.399(1)	P(1)−O(1′′)	1.549(3)
Sn(1)−Cl(2)	2.321(1)	P(1)−C(2)	1.780(4)
Sn(1)−O(1)	2.204(3)	P(2)−O(2)	1.502(3)
Sn(1)−O(2′)	2.147(3)	P(2)−O(2′)	1.529(3)
Sn(1)−O(2a)	2.140(3)	P(2)−O(2′′)	1.565(3)
P(1)−O(1)	1.501(3)	P(2)−C(6)	1.803(4)
C(1)−Sn(1)−Cl(1)	96.2(1)	O(1)−P(1)−O(1′′)	113.01(17)
C(1)−Sn(1)−Cl(2)	172.8(1)	O(1)−P(1)−O(1′)	114.33(18)
C(1)−Sn(1)−O(1)	81.2(1)	O(1′′)−P(1)−O(1′)	104.28(18)
C(1)−Sn(1)−O(2a)	88.8(1)	O(1)−P(1)−C(2)	108.25(17)
C(1)−Sn(1)−O(2′)	81.7(1)	O(1′′)−P(1)−C(2)	110.6(2)
Cl(1)−Sn(1)−O(2a)	173.98(8)	O(1′)−P(1)−C(2)	106.19(18)
Cl(1)−Sn(1)−Cl(2)	90.97(5)	O(2)−P(2)−O(2′)	115.83(14)
Cl(1)−Sn(1)−O(1)	91.65(9)	O(2)−P(2)−O(2′′)	104.01(16)
Cl(1)−Sn(1)−O(2′)	96.36(8)	O(2′)−P(2)−O(2′′)	111.40(16)
O(1)−Sn(1)−O(2′)	161.78(9)	O(2)−P(2)−C(6)	111.20(17)
O(1)−Sn(1)−O(2a)	84.2(1)	O(2′)−P(2)−C(6)	105.19(16)
O(1)−Sn(1)−Cl(2)	98.23(7)	O(2′′)−P(2)−C(6)	109.21(16)
Cl(2)−Sn(1)−O(2a)	84.06(7)	P(1)−O(1)−Sn(1)	116.9(2)
Cl(2)−Sn(1)−O(2′)	97.97(7)	P(2)−O(2)−Sn(1a)	138.0(2)
O(2a)−Sn(1)−O(2′)	89.6(1)	P(2)−O(2′)−Sn(1)	119.0(1)

a = $-x$, $-y$, $-z$.

C9, C10, C8′, C9′, C10′ (s.o.f. 0.5)], and in **16a** [*t*-Bu group C8, C9, C10, C8′, C9′, C10′; OEt group C14, C14′, (s.o.f. 0.5)]. Atomic scattering factors for neutral atoms and real and imaginary dispersion terms were taken from *International Tables for X-ray Crystallography.*[37] The figures were created by SHELXTL-Plus[38] (Sheldrick, 1991). Crystallographic data are given in Table 2; selected bond distances and angles for **2** and **6** in Table 3, for **8** and Table 4, and for **16a** and Table 5. Crystallographic data for the structures reported in this paper have been deposited with the Cambridge Crystallographic Data Centre as supplementary publications nos. CCDC-102841 (**8**), CCDC-102842 (**2**), CCDC-102843 (**6**), and CCDC-102844 (**16a**). Copies of the data can be obtained free of charge on application to CCDC, 12 Union Road, Cambridge CB2 1EZ, U.K. [Fax: (internat.) + 44-1223/336033; E-mail: deposit@ccdc.cam.ac.uk].

Acknowledgements

We gratefully acknowledge support of this work by the Deutsche Forschungsgemeinschaft and the Fonds der Chemischen Industrie.

[1] [1a] J. T. B. H. Jastrzebski, G. van Koten, *Adv. Organomet. Chem.* **1993**, *35*, 241−294 and references therein. − [1b] M. Mehring, M. Schürmann, K. Jurkschat, *Organometallics* **1998**, *17*, 1227−1237 and references therein. − [1c] N. Pieper, C. Klaus-Mrestani, M. Schürmann, K. Jurkschat, M. Biesemans, I. Verbruggen, J. C. Martins, R. Willem, *Organometallics* **1997**, *16*, 1043−1053. − [1d] P. Steenwinkel, J. T. B. H. Jastrzebski, B.-J. Deelman, D. M. Grove, H. Koojman, N. Veldman, W. J. J. Smeets, A. L. Spek, G. van Koten, *Organometallics* **1997**, *16*, 5486−5498. − [1e] D. Dakternieks, K. Jurkschat, R. Tozer, J. Hook, E. R. T. Tiekink, *Organometallics* **1997**, *16*, 3696−3706. − [1f] M. Beuter, U. Kolb, A. Zickgraf, E. Bräu, M. Bletz, M. Dräger, *Polyhedron* **1997**, *16*, 4005−4015. − [1g] U. Kolb, M. Dräger, M. Dargatz, K. Jurkschat, *Organometallics* **1995**, *14*, 2827−2834. − [1h] T. P. Lockhart, F. Davidson, *Organometallics* **1987**, *6*, 2471−2478. − [1i] T. P. Lockhart, J. C. Calabrese, F. Davidson, *Organometallics* **1987**, *6*, 2479−2483. − [1j] F. Huber, H. Preut, E. Hoffmann, M. Gielen, *Acta Cryst.* **1989**, *C45*, 51−54. − [1k] M. Suzuki, I.-H. Son, R. Noyori, H. Masuda, *Organometallics* **1990**, *9*, 3043−3053.

[2] [2a] R. J. P. Corriu, J. C. Young, Hypervalent Silicon Compounds, in *The Chemistry of Organic Silicon Compounds* (Eds.: S. Patai, Z. Rappoport), Wiley, New York, **1989**, 1241−1288. − [2b] C. Chuit, R. J. P. Corriu, C. Reyé, J. C. Young, *Chem. Rev.* **1993**, *93*, 1371−1448. − [2c] R. R. Holmes, *Chem. Rev.* **1996**, *96*, 927−950. − [2d] S. N. Tandura, N. V. Alekseev, M. G. Voronkov, *Top. Curr. Chem.* **1986**, *131*, 99−189. − [2e] F. H. Carré, R. J. P. Corriu, G. F. Lanneau, P. Merle, F. Soulairol, J. Yao, *Organometallics* **1997**, *16*, 3878−3888. − [2f] F. Carré, C. Chuit, R. J. P. Corriu, A. Mehdi, C. Reyé, *Angew. Chem.* **1994**, *106*, 1152−1154; *Angew. Chem. Int. Ed. Engl.* **1994**, *33*, 1097. − [2g] F. Carré, C. Chuit, R. J. P. Corriu, A. Fanta, A. Mehdi, C. Reyé, *Organometallics* **1995**, *14*, 194−198. − [2h] W. Ziche, B. Ziemer, P. John, J. Weis, N. Auner, *J. Organomet. Chem.* **1996**, *521*, 29−31. − [2i] N. Auner, R. Probst, F. Hahn, E. Herdtweck, *J. Organomet. Chem.* **1993**, *459*, 25−41. − [2j] M. Tasaka, M. Hirotsu, M. Kojima, S. Utsuno, Y. Yoshikawa, *Inorg. Chem.* **1996**, *35*, 6981−6986. − [2k] I. Kalikhman, S. Krivonos, D. Stalke, T. Kottke, D. Kost, *Organometallics* **1997**, *16*, 3255−3257. − [2l] M. Weinmann, A. Gehrig, B. Schiemenz, G. Huttner, B. Nuber, G. Rheinwald, H. Lang, *J. Organomet. Chem.* **1998**, *563*, 61−72. − [2m] V. Gevorgyan, L. Borisova, A. Vyater, V. Ryabova, E. Lukevics, *J. Organomet. Chem.* **1997**, *548*, 149−155. − [2n] A. Kawachi, Y. Tanaka, K. Tamao, *Organometallics* **1997**, *16*, 5102−5107. − [2o] A. Mix, U. H. Berlekamp, H.-G. Stammler, B. Neumann, P. Jutzi, *J. Organomet. Chem.* **1996**, *521*, 177−183. − [2p] K. Jurkschat, C. Mügge, J. Schmidt, A. Tzschach, *J. Organomet. Chem.* **1985**, *287*, C1−C4. − [2q] M. Mehring, M. Schürmann, K. Jurkschat, *Main Group Metal Chem.* **1998**, *21*, 635−646 and references therein.

[3] [3a] E. Vedejs, A. R. Haight, W. O. Moss, *J. Am. Chem. Soc.* **1992**, *114*, 6556−6558. − [3b] J. M. Brown, M. Pearson, J. T. B. H. Jastrzebski, G. van Koten, *J. Chem. Soc., Chem. Commun.* **1992**, 1440−1441.

[4] [4a] R. Colton, D. Dakternieks, *Inorg. Chim. Acta* **1985**, *102*, L17−L18. − [4b] R. Colton, D. Dakternieks, *Inorg. Chim. Acta* **1988**, *148*, 31−36. − [4c] M. Gielen, *Top. Curr. Chem.* **1982**, *104*, 57−105. − [4d] R. J. P. Corriu, C. Guerin, *Adv. Organomet. Chem.* **1982**, *20*, 265−311. − [4e] C. Brelière, R. J. P. Corriu, G. Royo, J. Zwecker, *Organometallics* **1989**, *8*, 1834−1836. − [4f] C. Brelière, F. Carré, R. J. P. Corriu, W. E. Douglas, M. Poirier, G. Royo, M. W. C. Man, *Organometallics*, **1992**, *11*, 1586−1593. − [4g] F. Carré, C. Chuit, R. J. P. Corriu, A. Mehdi, C. Reyé, *Organometallics* **1995**, *14*, 2754−2759.

[5] [5a] A. J. Crowe in *Metal Complexes in Cancer Chemotherapy* (Ed.: B. K. Keppler), VCH, Weinheim, **1993**, 369−379. − [5b] M. Gielen, P. Lelieveld, D. de Vos, R. Willem in *Metal Complexes in Cancer Chemotherapy* (Ed.: B. K. Keppler), VCH, Weinheim, **1993,** 381−390. − [5c] M. Gielen, P. Lelieveld, D. de Vos, R. Willem, Metal-Based Drugs, in *Metal-Based Antitumor Drugs* (Ed.: M. Gielen), Freund Publishing House, Tel Aviv, **1992**, Vol. 2, 29−54. − [5d] R. Tacke, H. Linoh, Bioorganosilicon Chemistry in *The Chemistry of Organic Silicon Compounds* (Eds.: S. Patai, Z. Rappoport), Wiley-Interscience, New York, **1989**, 1143−1206. − [5e] E. Lukevics, L. Ignatovich, *Appl. Organomet. Chem.* **1992**, *6*, 113−126.

[6] For examples see: [6a] R. J. P. Corriu, G. Lanneau, C. Priou, F. Soulairol, N. Auner, R. Probst, R. Conlin, C. Tan, *J. Organomet. Chem.* **1994**, *466*, 55−68. − [6b] K. Tamao, K. Nagata, M. Asahara, A. Kawachi, Y. Ito, M. Shiro, *J. Am. Chem. Soc.* **1995**, *117*, 11592−11593. − [6c] J. Belzner, U. Dehnert, H. Ihmels, M. Hübner, P. Müller, I. Usón, *Chem. Eur. J.* **1998**, *4*, 852−863. − [6d] H. Handwerker, M. Paul, J. Blümel, C. Zybill, *Angew. Chem.* **1993**, *105*, 1375−1377; *Angew. Chem. Int. Ed. Engl.* **1993**, *32*, 1313. − [6e] R. J. P. Corriu, G. Lanneau, C. Priou, *Angew. Chem.* **1991**, *103*, 1153−1155; *Angew. Chem. Int. Ed. Engl.* **1991**, *30*, 1130. − [6f] R. J. P. Corriu, G. F. Lanneau, B. P. S. Chauhan, *Organometallics* **1993**, *12*, 2001−2003.

[7] For examples see: [7a] H.-P. Abicht, K. Jurkschat, A. Tzschach, K. Peters, E.-M. Peters, H. G. von Schnering, *J. Organomet. Chem.* **1987**, *326*, 357−368. − [7b] K. Jurkschat, H.-P. Abicht, A. Tzschach, B. Mahieu, *J. Organomet. Chem.* **1986**, *309*, C47−C50. − [7c] K. Angermund, K. Jonas, C. Krüger, J. L. Latten, Y.-H. Tsay, *J. Organomet. Chem.* **1988**, *353*, 17−25. − [7d] J. T. B. H. Jastrzebski, P. A. van der Schaaf, J. Boersma, G. van Koten, M. C. Zoutberg, D. Heijdenrijk, *Organometallics* **1989**, *8*, 1373−1375. − [7e] L. M. Engelhardt, B. S. Jolly, M. F. Lappert, C. L. Raston, A. H. White, *J. Chem. Soc., Chem. Commun.* **1988**, 336−338. − [7f] W.-P. Leung, W.-H. Kwok, L.-H. Weng, L. T. C. Law, Z. Y. Zhou, T. C. W. Mak, *J. Chem. Soc., Dalton Trans.* **1997**, 4301−4305. − [7g] C. Drost, P. B. Hitchcock, M. F. Lappert, L. J.-M. Pierssens, *J. Chem. Soc., Chem.*

Commun. **1997**, 1141−1142. − [7h] C. J. Cardin, D. J. Cardin, S. P. Constantine, M. G. B. Drew, H. Rashid, M. A. Convery, D. Fenske, *J. Chem. Soc., Dalton Trans.* **1998**, 2749−2753.

[8] [8a] V. A. Benin, J. C. Martin, M. R. Willcott, *Tetrahedron Lett.* **1994**, *35*, 2133−2136. − [8b] M. Chauhan, C. Chuit, R. J. P. Corriu, A. Mehdi, C. Reyé, *Organometallics* **1996**, *15*, 4326−4333. − [8c] J. Belzner, *Angew. Chem.* **1997**, *109*, 1331−1334; *Angew. Chem. Int. Ed. Engl.* **1997**, *36*, 1277−1280. − [8d] C.-H. Ottosson, D. Cremer, *Organometallics* **1996**, *15*, 5309−5309. − [8e] C. Chuit, R. J. P. Corriu, A. Mehdi, C. Reyé, *Angew. Chem.* **1993**, *105*, 1372−1375; *Angew. Chem. Int. Ed. Engl.* **1993**, *32*, 1311. − [8f] F. Carré, M. Chauhan, C. Chuit, R. J. P. Corriu, C. Reyé, *J. Organomet. Chem.* **1997**, *540*, 175−183.

[9] G. van Koten, J. T. B. H. Jastrzebski, J. G. Noltes, A. L. Spek, J. C. Schoone, *J. Organomet. Chem.* **1978**, *148*, 233−245.

[10] $Ph_2(Me_3SiCH_2)SnF$ was prepared in a similar manner to $Ph_2FSn(CH_2)_2SnPh_2F$ (D. Dakternieks, K. Jurkschat, H. Zhu, E. R. T. Tiekink, *Organometallics* **1995**, *14*, 2512−2521) starting from $Ph_3SnCH_2SiMe_3$ (S. Papetti, H. W. Post, *J. Org. Chem.* **1957**, *22*, 526−528) and was isolated as a colorless solid that gave a correct elemental analysis.

[11] The synthesis, characterization, and reactivity of the heteroleptic stannylene {4-*tert*-Bu-2,6-$[P(O)(OEt)_2]_2C_6H_2$}SnCl will be reported in a forthcoming paper.

[12] P. Jutzi, F. Kohl, *J. Organomet. Chem.* **1979**, *164*, 141−152.

[13] [13a] M. Mehring, K. Jurkschat, unpublished results. − [13b] J. T. B. H. Jastrzebski, D. M. Grove, J. Boersma, G. van Koten, J.-M. Ernsting, *Magn. Reson. Chem.* **1991**, *29*, 25−30.

[14] [14a] R. A. Howie, E. S. Paterson, J. L. Wardell, J. W. Burley, *J. Organomet. Chem.* **1983**, *259*, 71−78. − [14b] P. G. Harrison, T. J. King, M. A. Healy, *J. Organomet. Chem.* **1979**, *182*, 17−36. − [14c] R. A. Howie, E. S. Paterson, J. L. Wardell, J. W. Burley, *J. Organomet. Chem.* **1986**, *304*, 301−308. − [14d] W. Clegg, C. M. J. Grievson, K. Wade, *J. Chem. Soc., Chem. Commun.* **1987**, 969−970. − [14e] M. Gielen, H. Pan, E. R. T. Tiekink, *Bull. Soc. Chim. Belg.* **1993**, *102*, 447−453. − [14f] S. Dostal, S. J. Stoudt, P. Fanwick, W. F. Sereatan, B. Kahr, J. E. Jackson, *Organometallics* **1993**, *12*, 2284−2291. − [14g] B. Fitzsimmons, D. G. Othen, H. M. M. Shearer, K. Wade, G. Whitehead, *J. Chem. Soc., Chem. Commun.* **1977**, 215−216. − [14h] O.-S. Jung, J. H. Jeong, Y. S. Sohn, *J. Organomet. Chem.* **1990**, *397*, 17−20. − [14i] A. Hayashi, M. Yamaguchi, M. Hirama, C. Kabuto, M. Ueno, *Chem. Lett.* **1993**, 1881−1884.

[15] [15a] H. Weichmann, J. Meunier-Piret, M. van Meerssche, *J. Organomet. Chem.* **1986**, *309*, 273−282. − [15b] C. Mügge, H. Weichmann, A. Zschunke, *J. Organomet. Chem.* **1980**, *192*, 41−46. − [15c] U. Kolb, M. Dräger, E. Fischer, K. Jurkschat, *J. Organomet. Chem.* **1992**, *423*, 339−350. − [15d] F. Richter, M. Dargatz, H. Hartung, D. Schollmeyer, H. Weichmann, *J. Organomet. Chem.* **1996**, *514*, 233−241. − [15e] A. G. Davies, J. P. Goddard, M. B. Hursthouse, N. P. C. Walker, *J. Chem. Soc., Chem. Commun.* **1983**, 597−598. − [15f] D. Britton, Y. M. Chow, *Acta Cryst.* **1983**, *39C*, 1539−1540. − [15g] W. A. Nugent, R. J. McKinney, R. L. Harlow, *Organometallics* **1984**, *3*, 1315−1318. − [15h] N. W. Kong, C. Wie, V. G. K. Das, R. J. Butcher, *J. Organomet. Chem.* 1989**,** *361***,** 53−61. − [15i] E. G. Perevalova, M. D. Reshetova, P. N. Ostapchuk, Yu. L. Slovokhotov, Yu. T. Struchkov, F. M. Spiridonov, A. V. Kisin, I. G. Yukhno, *Metalloorg. Khim.* **1990**, *3*, 100. − [15j] R. E. Marsh, *Acta Cryst.* **1997**, *53B*, 317−322. − [15k] A. Blaschette, I. Hippel, J. Krahl, E. Wieland, P. G. Jones, A. Sebald, *J. Organomet. Chem.* **1992**, *437*, 279−297. − [15l] I. Lange, J. Krahl, P. G. Jones, A. Blaschette, *J. Organomet. Chem.* **1994**, *474*, 97−106. − [15m] G. van Koten, J. T. B. H. Jastrzebski, J. G. Noltes, J. C. Schoone, *J. Organomet. Chem.* **1978**, *148*, 233−245. − [15n] C. Pettinari, F. Marchetti, M. Pellei, A. Cingolani, L. Barba, A. Cassetta, *J. Organomet. Chem.* **1996**, *515*, 119−130. − [15o] L. A. Aslanov, V. M. Attiya, A. B. Permin, V. S. Petrosyan, *Zh. Strukt. Khim.* **1977**, *18*, 1113. − [15q] L. R. Sita, I. Kinoshita, S. P. Lee, *Organometallics* **1990**, *9*, 1644−1650. − [15r] B. Wrackmeyer, S. Kundler, W. Milius, R. Boese, *Chem. Ber.* **1994**, *127*, 333−342. − [15s] M. M. Amini, M. J. Heeg, R. W. Taylor, J. J. Zuckerman, S. W. Ng, *Main Group Met. Chem.* **1993**, *16*, 415−418. − [15t] I. Lange, D. Henschel, A. Wirth, J. Krahl, A. Blaschette, P. G. Jones, *J. Organomet. Chem.* **1995**, *503*, 155−170. − [15u] M. Mehring, M. Schürmann, C. Löw, K. Jurkschat, to be published.

[16] [16a] C. E. McKenna, M. T. Higa, N. H. Cheung, M. C. McKenna, *Tetrahedron Lett.* **1977**, 155−158. − [16b] F. Richter, H. Weichmann, *J. Organomet. Chem.* **1994**, *466*, 77−87. − [16c] R. W. Deemie, J. C. Fettinger, D. A. Knight, *J. Organomet. Chem.* **1997**, *538*, 257−259. − [16d] H. Gross, C. Böck, B. Costisella, J. Gloede, *J. prakt. Chem.* **1978**, *320*, 344−350.

[17] J. L. Wardell in *Chemistry of Tin* (Ed.: P. J. Smith), 2nd ed., Blackie, London, **1998**, 121−137.

[18] H. Weichmann, B. Rensch, *Z. anorg. allg. Chem.* **1983**, *503*, 106−114.

[19] B. Jousseaume, P. Villeneuve, *J. Chem. Soc., Chem. Commun.* **1987**, 513−514.

[20] A. Bondi, *J. Phys. Chem.* **1964**, *68*, 441−451.

[21] A. V. Yatsenko, S. V. Medvedev, L. A. Aslanov, *Zh. Strukt. Khim.* **1992**, *33*, 126−131.

[22] A. I. Tursina, L. A. Aslanov, S. V. Medvedev, A. V. Yatsenko, *Koord. Khim.* **1985**, *11*, 417.

[23] L. A. Aslanov, V. M. Ionov, V. M. Attiya, A. B. Permin, V. S. Petrosyan, *Zh. Strukt. Khim.* **1977**, *18*, 1103−1112.

[24] H. Reuter, H. Puff, *J. Organomet. Chem.* **1992**, *424*, 23−31.

[25] L. A. Aslanov, V. M. Ionov, V. M. Attiya, A. B. Permin, V. S. Petrosyan, *Zh. Strukt. Khim.* **1978**, *19*, 315−318.

[26] T. J. Karol, J. P. Hutchinson, J. R. Hyde, H. G. Kuivila, J. A. Zubieta, *Organometallics* **1983**, *2*, 106−114.

[27] A. I. Tursina, L. A. Aslanov, V. V. Chernyshev, S. V. Medvedev, A. V. Yatsenko, *Koord. Khim.* **1985**, *11*, 1420.

[28] A. L. Rheingold, S. W. Ng, J. J. Zuckerman, *Inorg. Chim. Acta* **1984**, *86*, 179−183.

[29] [29a] U. Kolb, M. Beuter, M. Dräger, *Inorg. Chem.* **1994**, *33*, 4522−4530. − [29b] U. Kolb, M. Beuter, M. Gerner, M. Dräger, *Organometallics* **1994**, *13*, 4413−4425. − [29c] U. Kolb, M. Dräger, B. Jousseaume, *Organometallics* **1991**, *10*, 2737−2742.

[30] H. Hartung, D. Petrick, C. Schmoll, H. Weichmann, *Z. anorg. allg. Chem.* **1987**, *550*, 140−148.

[31] P. G. Harrison in *Chemistry of Tin* (Ed.: P. G. Harrison), Blackie, London, **1989**, 10.

[32] S. Freitag, R. Herbst-Irmer, F. U. Richter, H. Weichmann, *Acta Cryst.* **1994**, *C50*, 1588−1590.

[33] H. Hartung, A. Krug, F. Richter, H. Weichmann, *Z. anorg. allg. Chem.* **1993**, *619*, 859−864.

[34] B. Wrackmeyer in *Ann. Rep. NMR Spectroscopy* (Ed.: G. A. Webb), Academic Press, London, **1985**, Vol. 16, 73−186.

[35] G. M. Sheldrick, *Acta Cryst.* **1990**, *A46*, 467−473.

[36] G. M. Sheldrick, University of Göttingen, **1997**.

[37] *International Tables for Crystallography*, Kluwer Academic Publishers, Dordrecht, **1992**, Vol. C.

[38] G. M. Sheldrick, SHELXTL-PLUS Release 4.1, Siemens Analytical X-ray Instruments Inc., **1991**.

Received October 26, 1998
[I98369]

Multistep Reversible Redox Systems, LXVII[+]

2,5-Disubstituted *N,N′*-Dicyanobenzoquinonediimines (DCNQIs): Charge-Transfer Complexes and Radical-Anion Salts and Copper Salts with Ligand Alloys: Syntheses, Structures and Conductivities

Siegfried Hünig,*[a] Martina Kemmer,[a] Hubert Meixner,[a][2] Klaus Sinzger,[a][2] Hermann Wenner,[a] Thomas Bauer,[b][++] Ekkehart Tillmanns,[b][++] Franz Rudolf Lux,[c] Michael Hollstein,[c] Hans-Georg Groß,[d] Uwe Langohr,[d] Hans-Peter Werner,[d] Jost Ulrich von Schütz,[d] and Hans-Christoph Wolf[d]

Keywords: Conducting materials / Charge-transfer complexes / Radical-anion salts / Alloyed ligands / Crystal structures

The new members of the series of 2,5-disubstituted DCNQIs, **1d** (Cl/OMe), **1e** (Br/OMe), **1j** (Cl/I), **1k** (Br/I), **1l** (I/I), form conducting charge-transfer complexes with TTF (tetrathiofulvalene) which are comparable to known DCNQI/TTFs. From these DCNQIs highly conducting radical-anion salts [2-X, 5-Y-DCNQI]$_2$M (M = Li, Na, K, NH_4, Tl, Rb, Ag, Cu) can also be prepared either from the DCNQIs and MI (not AgI), on a metal wire (Ag, Cu), or by electrocrystallization (M = Tl, Ag,Cu). For better crystals a method using periodical switching between reduction and partial oxidation has been developed. With CF_3 (large, strongly electron-attracting) as the substituent in DCNQIs **1m** (OMe/CF_3) and **1n** (Me/CF_3), conducting TTF complexes remain whereas only **1n** yields an insulating copper salt. DCNQI–Cu salts with high conductivities are obtained with alloys containing two or three different DCNQIs. The temperature-dependent conductivities of DCNQI–M salts (other than copper) are similar to those of metal-like semiconductors. All new DCNQI–Cu salts are metallic [M] down to low temperatures, except [**1d** (Cl/OMe)]$_2$Cu which undergoes a sharp phase transition to an insulating state[M → I]. By variation of the ligands or their ratios in conducting alloys of DCNQI–Cu salts temperature-dependent conductivities can be tuned from M → I to M. In addition, alloying three ligands produced for the first time a radical salt with temperature-independent conductivity from 5 to 300 K. Most remarkably, alloys of the type [(2,5-Me$_2$DCNQI)$_m$] Cu/[{2,5-(CD$_3$)$_2$-DCNQI}$_n$]$_2$Cu which exhibit a sharp M → I phase transition on further cooling reenter the conducting state by an I → M transition, with changes of ca. 10^8 Scm^{-1} both ways. For the first time in the field of organic metals crystal structures of DCNQI–copper salts have been determined by X-ray powder diffraction methods and refined by Rietveld analysis. Unit cell data, coordination angles and distances of the π planes are in excellent agreement with the single-crystal X-ray data. However, bond lengths and angles of the ligands are to be less accurate. This powder method proves to be most valuable if only microcrystalline material is available.

The discovery of electrical conducting solids based on tetrathiofulvalene (TTF)[1−3] has triggered an avalanche of research for new suitable materials up to the present. The interest has been focussed both on the understanding of this unusual phenomenon and on tailoring compounds for practical applications.[4]

Although the basic requirements for conductivity of low molecular organic solids are now clear a more detailed understanding of the interplay of molecular geometry, crystal structure and conductivity (together with its temperature dependence) was hampered by the differing crystal lattices of the various materials. This situation changed with the discovery of (substituted) *N,N*-dicyanoquinoneimines (DCNQIs).[5] Especially radical-anion salts of 2,5-disubstituted DCNQIs prefer all the same space group $I4_1/a$ (or a closely related one) and therefore allow a comparison of their properties.

Thus very subtle substituent effects are translated in minor variations of the basic crystal lattice with definite changes in temperature-dependent conductivities, allowing a much more detailed understanding of this interplay.[6]

We therefore set out to explore the limit of this generalization in the papers of this series.

In a preceding paper we described a variety of new 2,5-disubstituted DCNQIs, together with their redox properties.[8] We now conclude our research activities in this field by posing the following questions arising from the already accumulated experience:

(1) Will the additional examples of 2,5-disubstituted DCNQIs presented here produce charge-transfer complexes

[+] Part LXVI: Ref.[1]

[a] Institut für Organische Chemie der Universität Würzburg, Am Hubland, D-97074 Würzburg
[b] Institut für Mineralogie und Kristallstrukturlehre der Universität Würzburg, Am Hubland, D-97074 Würzburg
[c] Institut für Radiochemie der TU München, Walther-Meissner-Str. 3, D-85748 Garching
[d] 3. Physikalisches Institut der Universität Stuttgart, Pfaffenwaldring 57, D-70569 Stuttgart
[++] New address: Institut für Mineralogie und Kristallographie, Althanstraße 14, A-1090 Wien

Supporting information for this article is available on the WWW under http://www.wiley-vch.de/home/eurjic or from the author.

 © WILEY-VCH Verlag GmbH, D-69451 Weinheim, 1999 1434−1948/99/0505−0899 $ 17.50+.50/0

and radical-anion salts with properties similar to those already described, especially in the presence of the large and strongly electron-attracting CF_3 substituent?

(2) Can the growth of single crystals by electrocrystallization be improved by rhythmic reversal of the current flow?

(3) Which variations are tolerated for ligand alloying in DCNQI−Cu salts with two different 2,5-disubstituted DCNQIs (ratio and pattern)?

(4) Will the temperature-dependent conductivities of those alloyed copper salts mimic those of the two single copper salts or will new properties arise, especially with respect to phase transitions?

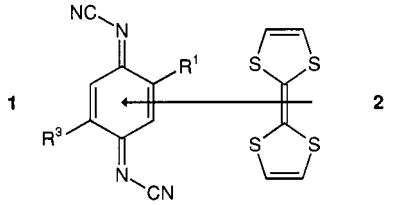
(5) Which structural data for DCNQI−Cu salts can safely be derived from powder-diffraction data refined by Rietveld analysis (so far rarely applied to organic solids) compared to single-crystal X-ray data?

The following sections concentrate mainly on answering these questions.

Charge-Transfer Complexes of DCNQIs 1a−n with TTF

As with other 2,5-disubstituted DCNQI[9] derivatives, **1a−n** immediately form black microcrystalline charge-transfer complexes on mixing their solutions in acetonitrile or dichloromethane with those of TTF (**2**). The stoichiometry in all the examples listed in Table 1 was found to be 1:1.

Table 1. Charge-transfer complexes 1:1 from DCNQIs (**1**) and TTF (**2**) together with their powder conductivities σ [Scm^{-1}]



1	R^1	R^3	Yield (%)	m.p. [°C][b]	σ [$S\,cm^{-1}$]	Ref.
a	OMe	OMe	60	199	5×10^{-2}	[c]
b	Me	OMe	54	118	2×10^{-2}	[c]
c	Me	Me	52	114	$< 10^{-7}$	[c]
d	Cl	OMe	93	155	3×10^{-2}	[d]
e	Br	OMe	75	160	3×10^{-2}	[d]
f	I	OMe	74	122	2×10^{-2}	[d]
g	Cl	Me	98	144	2×10^{-1}	[c]
h	Br	Me	87	129	6×10^{-1}	[c]
i	I	Me	75	144	3×10^{-2}	[c]
j[a]	Cl	I	77	125	1×10^{-3}	[d]
k[a]	Br	I	78	127	2×10^{-2}	[d]
l[a]	I	I	83	152	2×10^{-3}	[d]
m	OMe	CF_3	95	212	1×10^{-3}	[d]
n	Me	CF_3	90	198	1×10^{-2}	[d]

[a] Physical data of the DCNQIs, see ref.[9] − [b] Determined by DTA. − [c] Ref.[10] − [d] This paper.

The rather high powder conductivities (10^{-1}−10^{-3} Scm^{-1}) of the new complexes correlate well with those of the complexes already reported.[9] Together with their total absorption in the infrared these data point to segregated stacks of two components. However, this arrangement is kinetically controlled since, e.g. growing single crystals of **1a·2**, **1h·2**, and **1i·2** affords insulating charge-transfer complexes with mixed stacks.[10] It is remarkable that despite the wide range of redox potentials of the DCNQIs from $E_2 = 0.15$ V of **1a** (OMe/OMe) to $E_2 = 0.63$ V of **1l** (I/I) charge-transfer complexes with TTF can be obtained, even with the same stoichiometry. However, for $E_2 = 0.83$ V, the potential of the DCNQI with R^3, $R^5 = CF_3$,[8] no charge-transfer complex with TTF could be isolated, probably due to total electron transfer to the acceptor (see ref.[11][13]). If solubilities allow, hot acetonitrile is to be preferred to dichloromethane for high-potential DCNQIs.[11−13]

In accord with $E_2 = +0.53$ V for **1m** (R^1 = OMe, R^3 = CF_3) and $E_2 = +0.55$ V for **1n** (R^1 = Me, R^3 = CF_3) both donors yield 1:1 complexes with TTF of normal conductivities. Slight deviations from the ideal 1:1 stoichiometry may either be interpreted as due to experimental errors in the combustion analysis or defective crystal growth.[13] Obviously, the rather large diameter of the CF_3 group (5.2 to 5.6 Å) does not interfere with the close packing of the π planes in the acceptor stacks, a prerequisite for conductivity. The CF_3 groups of neighbouring molecules are probably interlocked like cog wheels, similar to the acceptor itself,[8] thereby diminishing their actual size.

Radical-Anion Salts $[DCNQI]_2M$ with Monovalent Cations

Quionoid acceptors such as DCNQIs can generally be transformed into their radical-anion salts by three methods.

Preparation from Metal Iodides

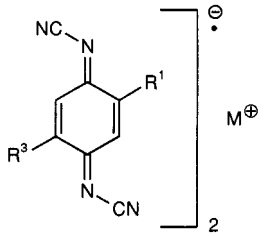
The use of metal iodides as electron donors and their subsequent successful application to TCNQs has already been described by Melby.[17] Consequently, iodides have also been employed for various DNCQIs.[18] We now describe further radical-anion salts of the stoichiometry $[2\text{-X,5-Y-DCNQI}]_2M$ with M = Li, Na, K, NH_4, Rb and Cu produced by this method. Without special precautions the black salts are formed as microcrystalline powders (Table 2).

This simple and quick method is applicable to a remarkably broad variety of 2,5-substituted DCNQIs as well as to different metal ions. With one exception (**1n·**Rb) all salts display powder conductivities up to 1 to 10^{-3} Scm^{-3} from which single-crystal conductivities up to 1000^{-1} Scm^{-1} can be expected (vide infra).

Preparation from Metal Wire

DCNQI radical-anion salts of copper and silver can be most easily prepared from DCNQIs and the corresponding

Table 2. Microcrystalline radical-anion salts $\mathbf{1}_2$M from DCNQIs **1** and metal or ammonium iodides; yields (%), melting points (m.p. [°C]) by DTA and powder conductivities σ [S cm^{-1}]



	R^1	R^3	M	Yield (%)	m.p. [°C]	σ [S cm^{-1}]
a	OMe	OMe	Li[a]	88	211	7×10^{-2}
			Na[b]	35	198	2×10^{-3}
			K	94	170	2×10^{-2}
			NH_4	dec.	–	–
			Rb	58	170	1×10^{-4}
			Cs	[c]	–	–
			Cu	67	243	2×10^{-2}
b	Me	OMe	Li[d]	73	64[e]	[f]
			Na	100	140	3×10^{-3}
			K	[g]	–	–
			NH_4	dec	–	–
			Rb	70	90	3×10^{-3}
			Cu[h]	82	166	4×10^{-2}
c	Me	Me	Li[b]	100	192	–
			Na[b]	88	176	–
			K[b]	96	176	–
			NH_4	44	129	1×10^{-1}
			Rb[b]	69	160	–
			Cs	[i]	–	–
			Cu[j]	100	201	0.4
d	Cl	Me	Li[a]	56	76[d]	1.0
			Cu	96	180	2×10^{-2}
e	Br	OMe	Li[f]	–	–	–
			Cu	98	176	2×10^{-2}
f	I	OMe	Cu	47	n.d.	4×10^{-2}
h	Br	Me	NH_4	85	134	2×10^{-2}
i	I	Me	NH_4	77	134	4×10^{-2}
j	Cl	I	Cu	72	150	3×10^{-2}
k	Br	I	Cu	74	164	2×10^{-2}
l	I	I	Cu	91	164	2×10^{-2}
m	OMe	CF_3	Cu	[f]	–	–
n	Me	CF_3	Cu	62	n.d.	1×10^{-3}

[a] Contains 1 H_2O. – [b] Ref.[14–16,18] – [c] **1a** reisolated. – [d] Contains 1.8 H_2O. – [e] Decomposition. – [f] Varying data. – [g] Green solution. – [h] Ref.[18] – [i] Blue solution. – [j] Ref.[6]

metal wire in acetonitrile yielding very often single crystals of good quality.[12]

For the variety of DCNQIs described in the previous paper[8] this method has already been discussed.[14] For comparison of their conductivities with radical salts obtained by the other methods, some earlier results are also included here (Table 3).

Conductivities of these salts agree completely with those of samples prepared from metal wire and by electrocrystallization, as is to be expected from earlier results, thereby confirming the same structural features.[12]

Preparation by Electrocrystallization

The most widely used technique of electrocrystallization was also applied to a variety of DCNQIs listed in Table 4.

Table 3. Radical-anion salts $(DCNQI)_2$M(Cu, Ag) grown in acetonitrile on a metal wire in solutions of the DCNQIs **1** and $CuBr_2$ or $AgNO_3$, respectively, and their single-crystal (s) or powder (p) conductivities [S cm^{-1}]

	DCNQI **1** R^1/R^3	M	Yield (%)	Needles [mm]	σ [S cm^{-1}]
1a	OMe/OMe	Cu[a]	48	1	(p) 0.1
1b	Me/OMe	Cu[a]	70	10	(p) 0.1
1c	Me/Me	Ag	98	8	(p) 6×10^{-2}
1d	Cl/OMe	Cu	68	5	(s) 500
1e	Br/OMe	Cu	87	25	(s) 500
1h	Br/Me	Ag	98	15	(s) 22
1i	I/Me	Ag	85	10	(p) 2×10^{-2}
1j	Cl/I	Cu	–	fur	–
		Ag	60	3	(p) 3×10^{-3}
1k	Br/I	Cu	87	4	(p) 1×10^{-2}
		Ag	51	3	(p) 6×10^{-3}
1l	I/I	Cu	–	fur	(p) 2×10^{-2}

[a] Ref.[19]

Besides some new, highly conducting DCNQI copper salts (**1b**, **1d**, **1e**, **1f**), radical-anion salts with cations rubidium (**1a**), thallium (**1c**[20], **1h**, **1i**), and silver (**1k**) could also be prepared.

Table 4. Radical-anion salts $(DCNQI)_2$M by electrolysis of DCNQIs **1** in acetonitrile in the presence of A = ($RbClO_4$), B = (CF_3CO_2Tl), C = [$Cu(CH_3CN)_4ClO_4$], D = ($AgNO_3$). Current I = 9–10 μA (A, C, D), 20–30 μA (B): Yields, lengths of the crystal needles and single-crystal (s) and powder (p) conductivities [S cm^{-1}]

DCNQI **1** R^1/R^3	M	A, B C, D	Yield (%)	Needles [mm]	σ [S cm^{-1}]
1a OMe/OMe	Rb	A	29	3[a][f]	(p) 1×10^{-4}
	Cu	C	20	15	(s) 700[c]
1b Me/OMe	Cu	C	23	15[b]	(s) 80
1c Me/Me	Tl	B	48	6	(s) 50[d]
1d Cl/OMe	Cu	C	34	5	(s) 500
1e Br/OMe	Cu	C	39	7	(s) 500
1f I/OMe	Cu	C	8	3[b][f]	(p) 4×10^{-2}
1h Br/Me	Tl	B	22	3	–
1i I/Me	Tl	B	28	3[b]	–
1j Cl/I	Cu	C	29	10[b]	(s) 70[e]
1k Br/I	Cu	C	50	8	(s) 500
	Ag	D	21	2	–
1l I/I	Cu	C	45	15[b]	(s) 70[e]

[a] Cubes. – [b] Bushels of very thin needles. – [c] Ref.[19] – [d] Ref.[20] – [e] Microwave measurements. – [f] Current switching 70:30 s^{-1}, see this paper.

The rather low conductivities of 70 Scm^{-1} measured for $(\mathbf{1f})_2$Cu and $(\mathbf{1l})_2$Cu compared to 500 Scm^{-1} for $(\mathbf{1k})_2$Cu are probably due to the microwave techniques which had to be used for these very thin needles. Evaluations by this method are based on the exact dimensions of the sample which could not be determined in our material with sufficient accuracy.[21]

Sometimes, even electrocrystallization yields only microcrystalline material, in spite of the systematic variation of solvent, supporting electrolyte, concentration, temperature, and density of the current. In this situation, rhythmic reversal of the current flow in the electrochemical cell (see circuit diagram, Figure 13) may be helpful. This procedure is based

on the common fact that small crystals dissolve faster than large ones due to their more extended surface. From a microcrystalline material at the electrode, the smallest particles should therefore dissolve faster on reversing the current flow for a certain time. In this way, on normal current flow, new material should be deposited on the larger crystals which finally grow at the cost of the smaller ones. Indeed, single crystals of good quality were easily obtained for [2,5-$(MeO)_2$DCNQI]$_2$Cu, (**1b**)$_2$Cu and [2-I,5-(MeO)DCNQI]$_2$-Cu, (**1f**)$_2$Cu by current switching 70:30/s.

This method, disclosed here for the first time, may be advisable also for other types of electrocrystallizations.

Tables 2−4 clearly demonstrate that whenever solid DCNQI radical salts are obtained electric conductivity is

Table 5. Copper salts from two different 2,5-disubstituted DCNQIs (**1**) (1:1); single crystals grown on a copper wire in acetonitrile containing $CuBr_2$ during 2−4 d

No.	**1**	DCNQIs R^1/R^3 (*m*)	Yield Cu salt (%)	*m*/*n*[a]	m.p.[b] [C°]	σ[c] [S cm^{-1}]	C calcd. found	H	N	Cu
1	**a**	OMe/OMe	99	1.0:1.0	185	(s) 220	51.77	3.43	24.16	13.70
	c	Me/Me					51.84	3.51	23.91	14.10
2	**a**	OMe/OMe	86	0.6:1.4	183	(s) 220	41.21	2.20	20.68	
	c	Br/Me					41.55	2.08	20.44	
3	**a**	OMe/OMe	76	0.7:1.3	185	(s) 180	37.79	2.07	18.81	
	c	I/Me					38.04	1.99	18.81	
4	**b**	Me/OMe	48	0.8:1.2	173	(s) 40	54.01	3.63	25.20	14.29
	c	Me/Me					53.72	3.60	25.41	13.66
5	**b**	Me/OMe	41	1.0:1.0	170	2×10^{-1}	44.29	2.56	21.85	
	h	Br/Me					44.29	2.44	21.89	
6	**b**	Me/OMe	98	1.2:0.8	195	(s) 260	42.65	2.54	20.73	11.75
	i	I/Me					42.50	2.41	20.89	11.30
7	**b**	Me/OMe	50	1.4:0.6	175	4×10^{-1}	33.15	1.23	17.99	
	p	Br/Br					33.30	1.36	17.53	
8	**c**	Me/Me	96	1.2:0.8	173	(s) 180	45.93	2.71	22.38	
	e	Br/OMe					45.79	2.50	22.41	
9	**c**	Me/Me	93	0.9:1.1	191	3×10^{-1}	49.95	2.82	24.66	13.99
	g	Cl/Me					50.14	2.95	24.14	14.23
10	**c**	Me/Me	92	1.1:0.9[d]	197	2×10^{-1}	46.78	2.79	22.86	11.74
	h	Br/Me					46.82	2.58	22.76	12.96
11	**c**	Me/Me	90	1.0:1.0	192	2×10^{-1}	41.96	2.42	20.61	11.68
	i	I/Me					42.48	2.52	20.76	11.89
12	**c**	Me/Me	94	1.0:1.0	191	(s) 130	45.73	2.14	23.71	13.44
	o	Cl/Cl					45.48	2.05	23.11	13.57
13	**c**	Me/Me	85	1.1:0.9	180	3×10^{-1}	42.97	2.10	22.03	
	q	Cl/Br					42.97	1.93	22.29	
14	**c**	Me/Me	82	1.0:1.0	187	−	38.49	1.80	19.96	
	p	Br/Br					38.06	1.60	19.86	
15	**e**	Br/OMe	61	0.2:1.8	192	2×10^{-1}	38.27	1.79	19.84	
	h	Br/Me					38.33	1.71	19.97	
16	**g**	Cl/Me	99	1.0:1.0	187	2×10^{-1}	41.79	1.95	21.66	
	h	Br/Me					41.76	1.90	21.90	
17	**g**	Cl/Me	95	0.5:1.5	191	(s) 340	41.69	1.95	21.62	
	i	I/Me					42.05	1.89	21.62	
18	**g**	Cl/Me	75	0.8:1.2	183	(s) 230	40.58	1.30	22.54	
	o	Cl/Cl					40.43	1.39	21.80	
19	**g**	Cl/Me	97	1.0:1.0	172	−	37.97	1.31	20.85	
	q	Cl/Br					38.04	1.41	20.40	
20	**g**	Cl/Me	41	1.1:0.9	188	2×10^{-1}	35.96	1.29	19.62	
	p	Br/Br					35.96	1.28	19.02	
21	**h**	Br/Me	85	1.0:1.0[e]	185	1×10^{-1}	35.51	1.66	18.41	
	i	I/Me					35.41	1.81	18.28	
22	**h**	Br/Me	84	1.0:1.0	174	1×10^{-1}	37.97	1.31	20.84	
	o	Cl/Cl					38.13	1.32	20.56	
23	**h**	Br/Me	88	1.0:1.0	175	2×10^{-1}	35.07	1.21	19.25	
	q	Cl/Br					35.48	1.34	18.99	
24	**h**	Br/Me	83	1.0:1.0	180	2×10^{-1}	32.58	1.13	17.89	
	p	Br/Br					32.55	1.19	17.39	
25	**i**	I/Me	89	1.0:1.0	176	(s) 280	34.92	1.21	19.17	
	o	Cl/Cl					36.28	1.26	19.29	
26	**i**	I/Me	80	1.3:1.7	175	(s) 110	31.17	1.21	16.79	
	p	Br/Br					30.92	0.98	17.07	
27	**a**	OMe/OMe	81	0.6	186	(s) 70	44.26	2.93	20.89	
	c	Me/Me		0.8			43.95	2.61	21.36	
	i	I/Me		0.6						

[a] Calculated from elemental analysis. − [b] By DTA. − [c] (s) single crystal, otherwise powder. − [d] 7 d; neutron activation: A/B = 0.90:1.10, calcd. Br = 17.46, Cu = 12.62; found Br = 17.75, Cu = 12.32. − [e] Neutron activation A/B = 1.15:0.85, calcd. Br = 15.27, Cu = 10.56; found Br = 15.15, Cu = 10.61.

observed also. As well two large substituents of opposite electronic properties (OMe/OMe or I/I) are tolerated as two substituents strongly differing in size with equal (e.g. MeO/Me or Cl/I) or opposite electronic effects (Cl/OMe or I/Me). This great variability fortunately is connected especially with copper as gegenion (metallic conductivity[6][7]). By contrast, thallium[20] yielded a solid radical salt with **1c** (Me/Me) only. Conductivity data from crystal powder (p) are much less reliable than those obtained from single crystals (s) [cf. **1a**Cu: 0.1 Scm^{-1} (p), 700 Scm^{-1} (s)[19] vs. **1b**Cu: 0.1 Scm^{-1} (p), 80 Scm^{-1} (s)]. The accuracy of powder data suffer both from the method of measurement (compression between two electrodes) and the variable surface properties of the microcrystals.

Ligand Alloys in Copper Salts of 2,5-Disubstituted DCNQIs

As demonstrated earlier[15,16,22–27] and in this paper (vide infra), radical-anion salts of the general type [2-X,5-Y-DCNQI]$_2$Cu all crystallize in the highly symmetrical space group $I4_1/a$ in spite of the strong variation of the substituents and redox potentials of the DCNQI ligands. One group of these salts shows metallic conductivity down to low temperatures (M), whilst others possess a phase transition to an insulating state at various temperatures (M → I).

Because of the great variability in the 2,5-substituent pattern, two or even three different 2,5-disubstituted DCNQIs may form an alloy of ligands in the stacks of DCNQI−Cu salts. A study of the properties of these alloys could lead to a better understanding of the substituent dependence of electric conductivity and the temperature of phase transitions.[28]

For the preparation of the mixed DCNQI−Cu salts, a copper wire was immersed into a solution of different DCNQIs (1:1 and 10:1:1) in acetonitrile in the presence of copper(II) bromide. In this way, 26 binary and one ternary salt were isolated (Table 5).

In most cases the ratios of the components in the mixed DCNQI−Cu salts are close to those in the starting solution, namely 1:1. These ratios are calculated from the elemental analyses which are also given in Table 5. Their accuracy should not be overestimated, as can be judged from two examples where comparison with probably more precise results from neutron activation analysis (NAA) (Br, Cu, vide infra) was possible. In entry 10 the ratio 1.1:0.9 is reversed to 0.9:1.1 by NAA. Similarly in entry 21 the ratio 1.0:1.0 changes to 1.15:0.85 by NAA.

The 1:1 ratio of the two different DCNQI ligands was only expected for combinations with similar redox potentials. However, they are obviously not important for the composition of the alloys, as can be exemplified by entry 14. Although E_2 = +0.21 V of 2,5-Me_2DCNQI[30] and E_2 = +0.62 V of 2,5-Br_2DCNQI[29] differ by as much as 400 mV the copper salt contains the ligands in a ratio of 1:1, whereas a large excess of 2,5-Br_2DCNQI is to be expected. The different rates of crystal growth and solubility, which are well known from the single component salts (see Tables 3 and 4), probably outweigh the differences in reducibility. This rationalization is in line with the exceptional ratios 1.4:0.6 (entry 2), 1.8:0.2 (entry 15), and 0.5:1.5 (entry 17) where the faster growing component is the preferred one. On this basis, however, the ratio 0.6:1.4 (entry 7) should be reversed.

Electrochemical generation of DCNQI−Cu alloys was used for three different pairs of DCNQIs with varying ratios of the two acceptors. The intention was to create a series of different alloys from the same pair of DCNQIs. This was indeed possible, as can be judged from Table 6, e.g. from 2,5-Me_2DCNQI (**1c**) and 2-Br,5-MeDCNQI (**1h**) ten different mixed copper salts were obtained with ligand ratios from 1.95:0.5 to 0.10:1.9 (Table 1 of the supporting information comprises 22 entries). The ratios were again calculated from the elemental analyses. In samples which contained a bromine substituent, however, the crystals were irradiated with a neutron source and the amount of bromine and copper determined from the half life of their radioactive isotopes (NAA). The percentage of the bromine-substituted ligand can be calculated from the constant stoichiometry [DCNQI]$_2$Cu. In eleven alloys the ratio of the two ligands could be calculated in both ways. These ratios agree reasonably well, the NAA data (± 0.2%) being more reliable. The ratio of the ligands in different alloys reflects the ratio of the corresponding DCNQIs in solution but not in a linear way, as demonstrated in Figure 1.

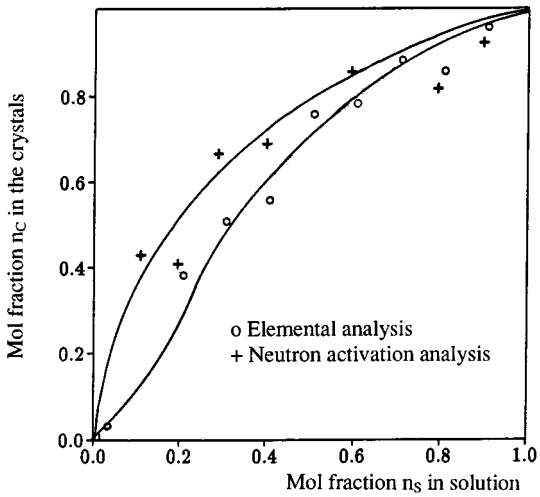


Figure 1. Correlation of the mol fractions of the products [(2,5-Me_2DCNQI)$_m$(2-Br,5-MeDCNQI)$_n$]Cu (n_C) with those of the corresponding DCNQIs in the solution for electrocrystallization (n_S)

This correlation agrees well with that of a similar investigation on the same system.[31]

The DCNQI−Cu salts generated both electrochemically and at a copper wire represent alloys with statistically distributed ligands and not crystals with domains of the two DCNQIs or even crystal mixtures of the individual salts. This conclusion can be drawn from the following results:[32] (a) Different crystals of the same mixed salt produce identical mass spectra with the same pattern; (b) in X-ray powder diagrams (vide infra) of the system [(2-Cl,5-

MeDCNQI)$_m$(2-I,-5-MeDCNQI)$_n$]$_2$Cu reflections appear which do not occur in the copper salts of the two components; the rather broad reflections, however, point to strong disorder in the crystal structure; (c) temperature-dependent single-crystal conductivities of two halves of a needle from [(2,5-Me$_2$DCNQI)$_{1.57}$(2-I,5-MeDCNQI)$_{0.43}$]Cu are identical. The existence of large domains of the two ligands is therefore improbable.

All isolated alloys have in common a total absorption between 4000 and 600 cm^{-1} indicating a high powder conductivity of > 0.2 Scm^{-1}.

Deuterated DCNQIs in Alloys of Copper Salts

In 2,5-Me$_2$DCNQI (**1c** ≡ **1c**·H$_8$) the two methyl groups can be replaced by trideuteriomethyl groups, yielding 2,5-(CD$_3$)$_2$DCNQI (**1c**·D$_6$).[3] Since (**1c**·D$_6$)$_c$Cu displays an unprecedented giant secondary isotope effect in its temperature-dependent conductivity ($\Delta\sigma = 10^8$ Scm^{-1})[29][32] the behaviour of alloys of [**1c**·H$_8$]$_2$Cu and [**1c**·D$_6$]$_2$Cu was of special interest. Mixtures of **1c**·H$_8$ and **1c**·D$_6$ in ratios from 90:10 to 10:90 (10% intervals) were therefore employed in order to grow the corresponding copper salts by electrocrystallization. Because of the extremely small differences between the two ligands the composition of the alloys {(2,5-Me$_2$DCNQI)$_m$[2,5-(CD$_3$)$_2$DCNQI]$_n$}$_2$Cu are assumed to represent the ratio of the two acceptors in solution. These alloys of DCNQI copper salts very often display a pattern of temperature-dependent conductivity which cannot be achieved by employing the corresponding salts containing only one of DCNQI ligands of the alloy (vide infra).

Temperature-Dependent Conductivity of DCNQI Radical-Anion Salts

Most valuable information can be drawn from the temperature dependence of conductivity, especially concerning semi- or metallic conduction and phase transitions. The following background has to be presented here because otherwise the very special effects observed with alloyed DCNQI copper salts could not be appreciated.

Non-Copper Salts

Silver and alkali salts of 2,5-disubstituted DCNQIs so far known have already been demonstrated to behave as "metal-like semiconductors"[35] of low dimensionality.[12,25,27,36] On cooling, the conductivity of solids of this type remains nearly constant, but finally they become insulators at very low temperatures (4-K$_f$ transition,[37] Peierls distortion[38]). The existence of an additional 2-K$_f$ transition (spin-Peierls transformation[39]) between ca. 80 and 100 K can be deduced from their high-resolution IR spectra

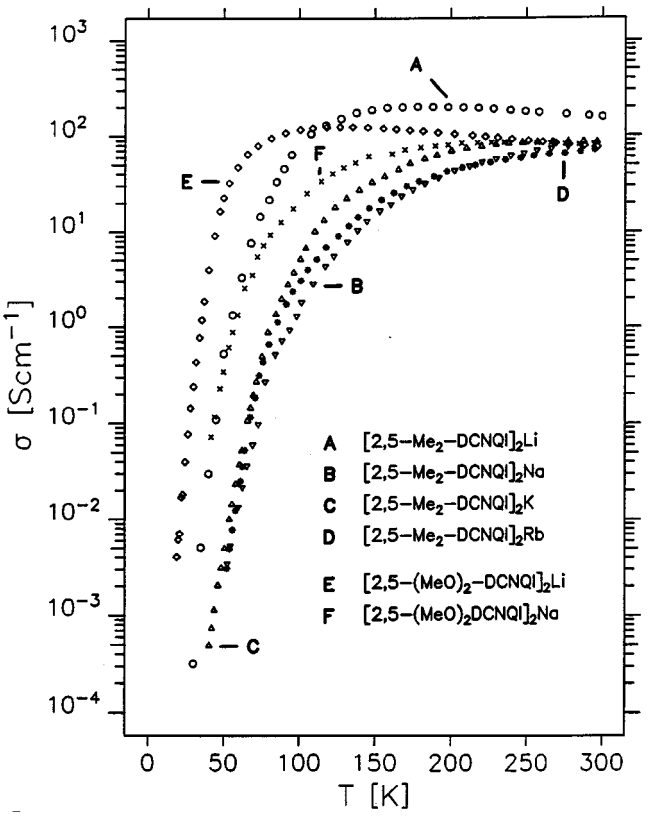


Figure 2. Temperature-dependent single-crystal conductivities of [2,5-Me$_2$DCNQI]$_2$M (M = Li, Na, K, Rb) and [2,5-(MeO)$_2$DCNQI]$_2$M (M = Li, Na)

but is not observed as a change in conductivity.[40] Figure 2 shows the temperature-dependent conductivity of various alkali metals with two sets of DCNQI ligands under identical conditions.[41]

Starting from similar conductivities (ca. 80−180 Scm^{-1}) at ambient temperature their turn to lower conductivity strongly depends on the size of the alkali ion: Rb > K > Na >> Li. In the case of [2,5-Me$_2$DCNQI]$_2$Li a slight increase in conductivity is even observed down to ca. 150 K. However, the larger and more strongly donating methoxy groups extend the range of high conductivity down to even lower temperatures. The lowest temperature for high conductivity so far observed for a non-copper DCNQI salt has been determined to be ca. 70 K for [2,5-(MeO)$_2$-DCNQI]$_2$Li.[41]

The temperature-dependent conductivity of the thallium salt [2,5-Me$_2$DCNQI]$_2$Tl has already been extensively discussed.[20] The temperature/conductivity pattern resembles that of the potassium salt in Figure 2 and that of the corresponding silver salt.[42] Although in the thallium salt the Tl−N≡C− distances are normal (sum of the van der Waals radii 309 pm) this compound is the only one (apart from the DCNQI−Cu salts) which displays a definite knight shift[43] of the $^{205}Tl^+$ ion. Therefore the s orbitals of the thallium ions must become polarized onto the DCNQI stacks.[20]

Copper Salts[6]

All DCNQI copper salts are three-dimensional metallic conductors with $\sigma = 100-1000\ Scm^{-1}$ at ambient temperature. At lower temperatures, however, they split into two groups: group M (metallic conductivity down to lowest temperatures without phase transition as shown in Figure 3), group M → I [on cooling metallic conductivity breaks down between 210 and 160 K at a sharp phase transition (Peierls transformation)[38] to an insulating state (Figure 4)]. Four-point wiring of the very thin needles of [2-I,5-MeODCNQI]$_2$Cu was not possible, although since the ESR signal is totally broadened down to 0.4 K, this salt must definitely belong to group M (Figure 3).

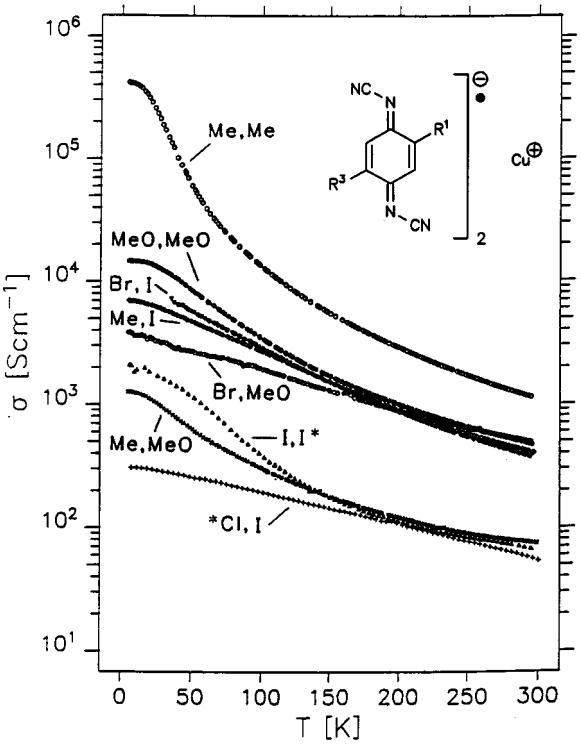


Figure 3. Temperature-dependent conductivities of DCNQI−Cu salts (group M)

The substituent dependence of this different behaviour, as well as the substituent-dependent temperature of the phase transitions, has been thoroughly discussed.[6,8,33] [2,5-Me$_2$DCNQI]$_2$Cu displays the highest conductivity (500000 Scm^{-1}) at 0.4 K, but is a borderline case of group M; under pressure[44] or on deuteration[33,34] it switches to group M → I (vide infra).

Temperature-Dependent Conductivity of Alloys of DCNQI−Cu Salts

As already discussed, most alloys of copper salts with two or three different DCNQI ligands display high metallic conductivities (see Table 5). Compared to the situation pictured in Figures 3 and 4 conductivity/temperature correlations of the following alloys are therefore of special interest: (1) all ligands from group M; (2) one ligand group from M, the other from group M → I; (3) all ligands from group M → I at constant and varying ratios of acceptors.

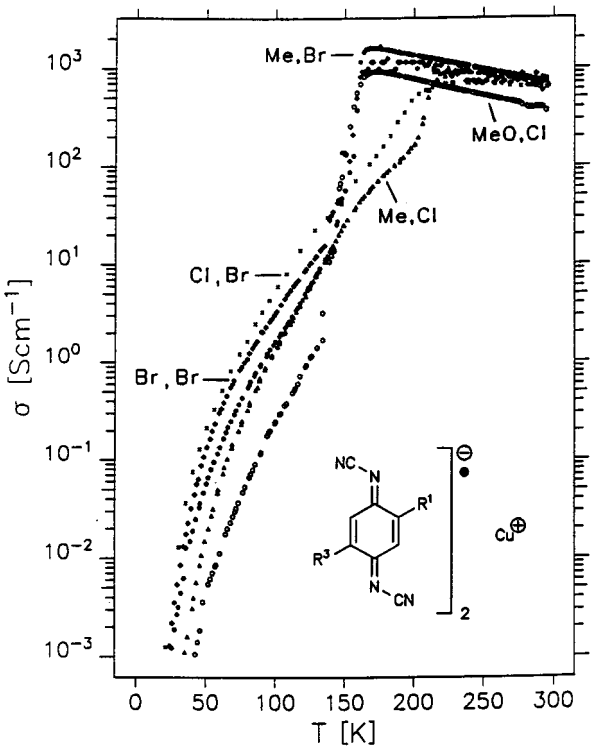
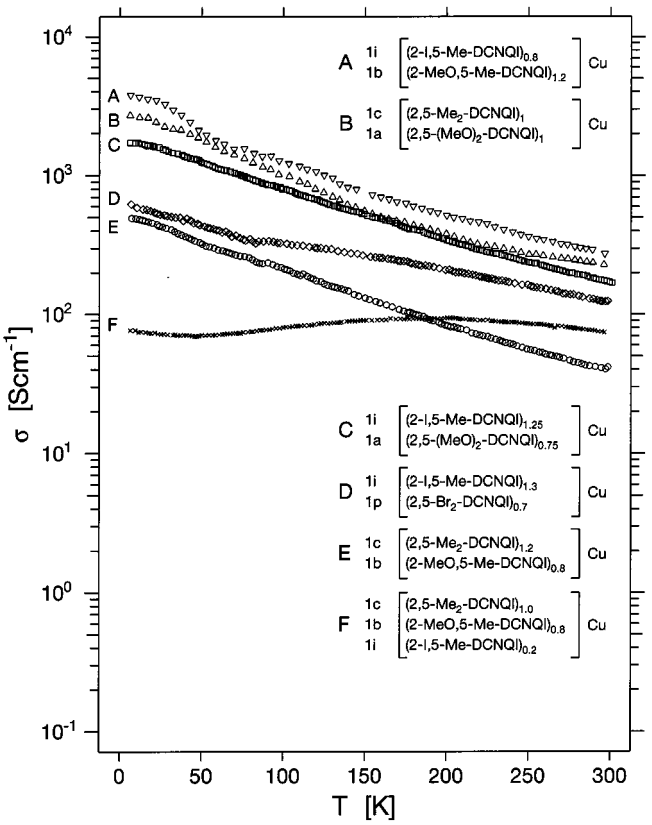


Figure 4. Temperature-dependent conductivities of DCNQI−Cu salts (group M → I)

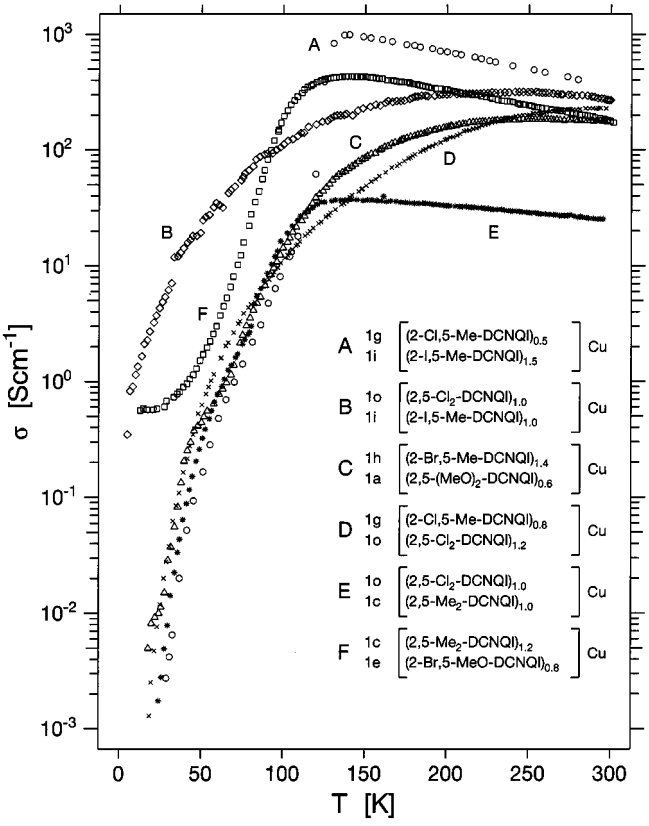
For alloys grown on a copper wire from solutions of the acceptors in acetonitrile with ratios close to 1:1 (Table 5) temperature-dependent conductivities were registered and are collected in Figures 5 and 6. In Figure 5 the similarity of the ascending slopes of curves A−E is remarkable. Curves A and C show a pattern which is expected from that of the pure DCNQI−Cu salts of Figure 3. In the case of curves B and E the strong increase in conductivity of [2,5-Me$_2$DCNQI]$_2$Cu (Figure 3) is suppressed in its alloys. Curve D represents the first case in which the M → I transition of one component ([2,5-Br$_2$DCNQI]$_2$Cu, Figure 4) is suppressed by alloying it with a group-M partner. The slight dip at ca. 80 K may reflect the suppressed M → I transition.

Another surprise comes from curve F which marks the *nearly constant conductivity over a range of 5−300 K (!)* of this ternary alloy. From the metallic behaviour of all three single components (Figure 3) an increase of conductivity as in curves A−E of Figure 5 was at least anticipated. This unprecedented behaviour demonstrates *the high potential of ligand alloying by producing temperature-independent conducting materials.*

The alloys listed in Figure 6 (except D) all belong to group M → I, albeit with strongly differing phase transitions. Curves B, C, and D resemble those for metal-like semiconductors (Figure 4). This behaviour cannot be simply connected to the fact that these alloys contain a group-M and a group-M → I ligand (A, B, C and E); only alloys



Figures 5. Temperature-dependent conductivities of alloys [2-X,5-Y-DCNQI]$_m$(2-W,5-Z-DCNQI)$_n$−Cu grown from the acceptors on a copper wire; for m and n see Table 5; group-M alloys



Figures 6. Temperature-dependent conductivities of alloys [2-X,5-Y-DCNQI]$_m$(2-W,5-Z-DCNQI)$_n$−Cu grown from the acceptors on a copper wire; for m and n see Table 5; group-M → I alloys

A and E suffer from a sharp phase transition. In addition, *the binary alloy formed from two group-M → I ligands (D) with sharp phase transitions (Figure 4) has lost this feature completely.*

The shape of curve F was not expected at all because both ligands of the alloy belong to group M (Figure 3). Obviously the borderline ligand 2,5-Me$_2$DCNQI cannot keep its group-M properties. The levelling off of curve F at < 30 K is unusual and may be connected to the reentry phenomenon of [2,5-Me$_2$DCNQI]$_2$Cu observed under pressure[28] or by alloying with its deuterated counterpart[33][34] (vide infra).

An alloy composed of the borderline group-M salt and a typical group-M → I salt, [(2,5-Me$_2$DCNQI)$_m$(2-Br,5-MeDCNQI)$_n$]$_2$Cu was also investigated (Figure 7). With the small fraction n = 0.025 (curve B) the metallic behaviour is principally retained (m = 0.975). However, the inflection between 100 and 50 K marks a phase transition which is reversed at lower temperatures ("reentrance phenomenon", vide infra). However, for n = 0.37 (curve C) at ca. 90 K a sharp M → I transition occurs typical for n = 1 (curve F, M → I at ca. 170 K) but at much lower temperatures (ca. 90 K). Interestingly, with n = 0.63 and n = 0.88 (curves D and E) this sharp phase transition disappears and a pattern is observed which resembles that of metal-like semiconductors. Independent investigations of the same alloyed DCNQI copper salt[23] are consistent with these results.

The last series of alloys studied comprised one "normal" group-M acceptor and one group-M → I acceptor [(2-I,5-MeDCNQI)$_m$(2-Br,5-MeDCNQI)$_n$]$_2$Cu (Figure 8).

In this alloy the type of metallic conductivity observed for m = 1 (n = 0, curve A) is preserved for n = 0.42 (curve B) and even for n = 0.60 (curve C) although the latter shows signs of a phase transformation. With a slightly higher concentration of the group-M → I component, n = 0.69 (curve D), a sharp phase transition occurs at ca. 110 K which keeps its pattern but moves closer to that of pure n = 1 (curve G) with n = 0.83 and n = 0.92 (curves E and F).

The rather low sensitivity of [2-I,5-MeDCNQI]$_2$Cu to doping with a second partner results from the disorder in the crystal lattice caused by the large iodine and the small methyl substituents. The bromine substituents in 2-Br,5-MeDCNQI may possibly just occupy the positions of the iodine substituent in the first ligand.

Temperature-Dependent Conductivities in Deuterated [2,5-Me$_2$DCNQI]$_2$Cu Alloys

The most remarkable effects observed for some of these alloys have already been discussed in detail.[33,45,46] For comparison with the alloys described above some features

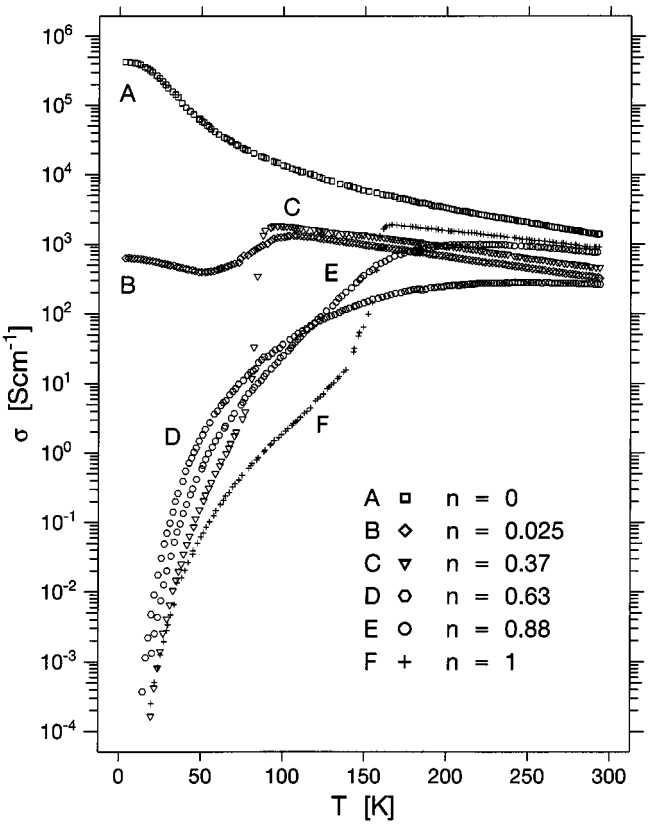


Figure 7. Temperature-dependent conductivities of alloys [(2,5-Me_2DCNQI)$_m$(2-Br,5-MeDCNQI)$_n$]$_2$Cu

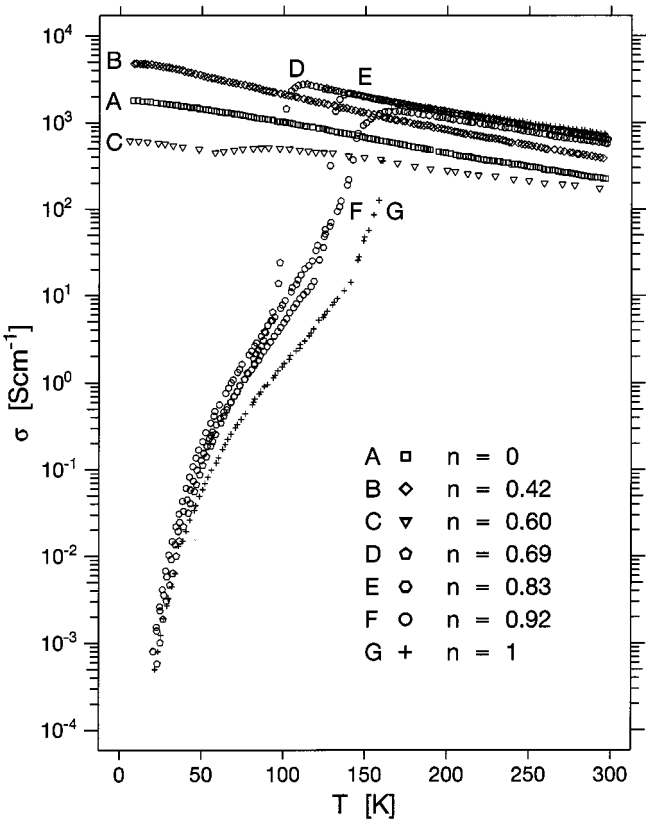


Figure 8. Temperature-dependent conductivities of alloys [(2-I,5-MeDCNQI)$_m$(2-Br,5-MeDCNQI)$_n$]Cu

of {(2,5-Me_2DCNQI)$_m$[2,5-$(CD_3)_2$DCNQI]$_n$}Cu alloys ("H_8/D_6") should be also be addressed here.

As seen in Figure 9, the metallic behaviour of "H_8" at temperatures down to 0.4 K is lost in "D_8". In this case, a sharp phase transition is observed at 73 K, where the conductivity drops by the order of 10^7-10^9.

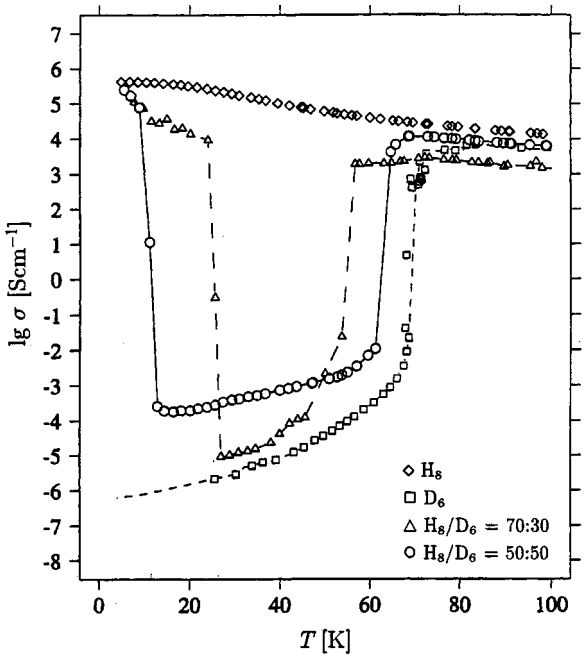


Figure 9. Temperature-dependent conductivities of [2,5-Me_2DCNQI]$_2$Cu (H_8) and [2,5-CD_3DCNQI]$_2$Cu (D_6) together with their alloys

On cooling, alloys with H_8/D_6 = 70:30 and 50:50 show similar conductivities and phase transitions. However, at lower temperatures (25 K and 12 K, respectively) reentrance into the starting phase occurs with complete regeneration of the high conductivities. This process is connected to a strong hysteresis as shown for H_8/D_6 = 70:30 in Figure 10a. Using this phenomenon a very sensitive pressure/light-triggered switch can be designed.[46] Outside the highly conducting state the extremely broad ESR signal narrows sufficiently to become visible (Figure 10b and c).

All the results presented in this section clearly demonstrate that alloying DCNQI copper salts provides a powerful tool for manipulating the temperature dependence of conductivity within an unprecedented broad range.

Crystal Structures of DCNQI Metal Salts

All published structures of DCNQI salts with monovalent cations exist in the same 2:1 stoichiometry. The space group in which the salts crystallize depends entirely on the cation and not on the substituent (Scheme 1) and may be either $I4_1/a$ or the closely related space group $P4/n$ and $C2/c$ (or $I2/a$, respectively).

The structures of all radical-anion salts listed in Tables 2–4 also fit completely into this scheme. Some of these structures have already been published.

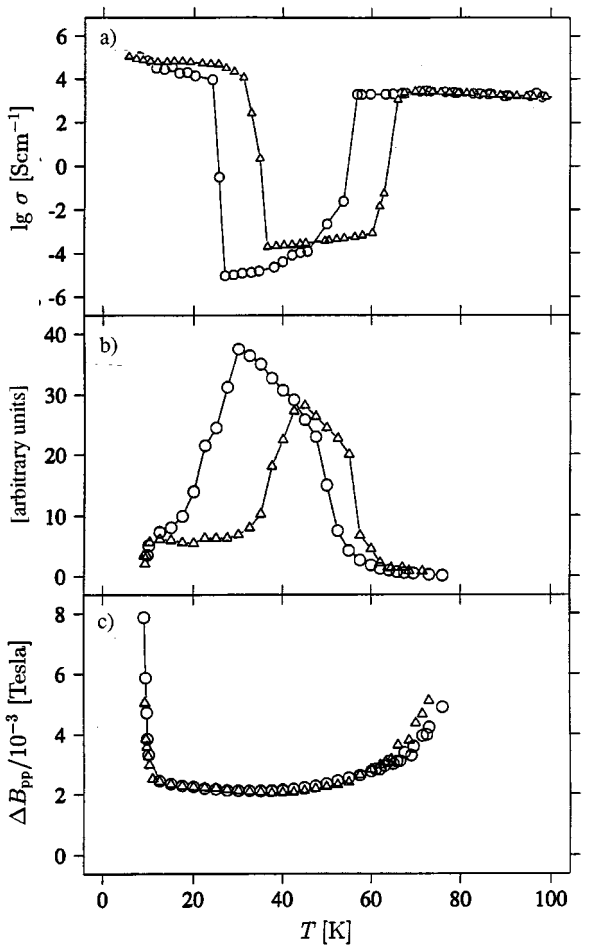
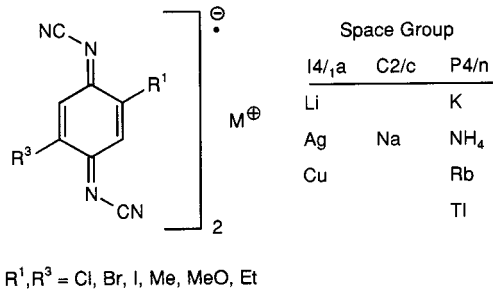


Figure 10. Alloy "H_8/D_6" = 70:30; temperature dependence of a) conductivity, b) ESR intensity, c) ESR line width; O = cooling; Δ = warming



Scheme 1. Space groups for radical-anion salts [2-X,5-Y-DCNQI]$_2$M

Thallium(+1) salts resemble both silver and potassium salts. Due to the large ionic radius of this cation (K^+ = 133 pm, Tl^+ = 147 pm) the radical-anion salts (**1c**)$_2$Tl, (**1h**)$_2$Tl and (**1i**)$_2$Tl (Table 4) adopt space group *P4/n*. The special features of [2,5-Me_2DCNQI]$_2$Tl [(**1c**)$_2$Tl] have already been discussed.[20] Its structural data will be included here only for comparison with the isomophic structure of [2,5-(MeO)$_2$DCNQI]$_2$Rb[48] of the same space group and with [2-Br,5-IDCNQI]$_2$Cu[48] of type $I4_1/a$ (Scheme 2).

Scheme 2 reveals the close relationship between the two space groups. The very similar bond lengths within the DCNQI ligands are especially remarkable, in spite of their different substituent pattern in these three examples.

The coordination angle α = 122.5° in the *c* direction of the somewhat flattened tetrahedron in [2-Br,5-IDCNQI]$_2$Cu is below the limiting angle for phase transition and therefore guarantees metallic conductivity down to low temperatures.[33] The lengths of the four N−Cu bonds are equal (198.7 pm) whereas the cubic coordination in the rubidium− and thallium−DCNQIs involves two sets with four DCNQIs of different M−NC bond lengths (Rb: 303.3 and 310.9 ppm; Tl: 293.8 and 318.1 ppm).

The ligands are arranged in skewed stacks with the favourable "ring-over-bond" arrangement that is typical for these radical-anion salts and which provides maximum π-orbital overlap for electron transfer. As is seen in Figure 11, even the bent methoxy groups in [2,5-(MeO)$_2$DCNQI]$_2$Rb are coplanar with the π system.

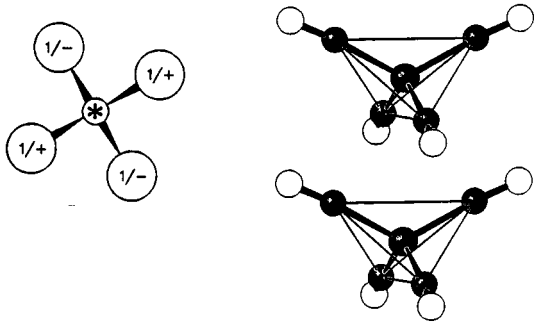
A Comparison of Structural Information from X-ray Single-Crystal and Powder-Diffraction Data

Although DCQNI−metal salts can easily be prepared as microcystalline solids, suitable crystals for single-crystal X-ray analysis cannot, so far, be obtained for all salts. Structural information from X-ray powder diagrams would therefore be most welcome. In 1967, H. M. Rietveld derived a mathematical procedure for successfully refining crystal structures from neutron powder-diffraction data.[47] This method, which in the beginning was mostly employed for metal or inorganic crystals with small unit cells, has now been extended to X-ray diffraction data of not only inorganic but also organic compounds. T. Bauer[48] was one of the first to compare systematically crystal-structure refinements of organic compounds based on X-ray single-crystal and powder-diffraction data. These results are reported in this paper.

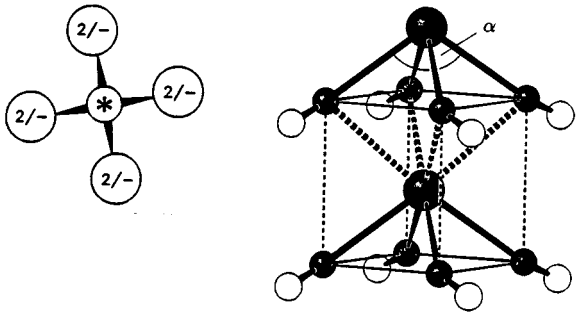
Since DCNQI radical-anion salts crystallize as isotypic compounds in space group $I4_1/a$ or related groups they represent good examples for a Rietveld treatment even though the highly ordered microcrystals can give rise to preferred orientation in the powder sample, an effect which has to be reduced by special sample preparation or corrected for during refinement. To test the reliability of this simple method, the corresponding single-crystal X-ray data of nine of these DCNQI copper salts were used as standards for comparison. Relevant parameters of single-crystal data and their deviations measured by powder diffraction are given in Table 6 (the data themselves are collected in Tables 2 and 3 of the Supporting Information).

Entries 1−5 clearly demonstrate that the cell parameters, as well as the angles around the coordination centers (Cu), and also the distances between the π planes are obtained

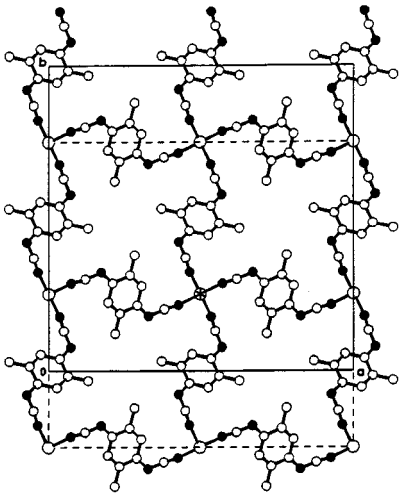
$I4_1/a$
Distorted tetrahedral coordination at M.....N ≡ C–R



$P4/_n$
Cubic coordination with two different M.....N ≡ C–R distances

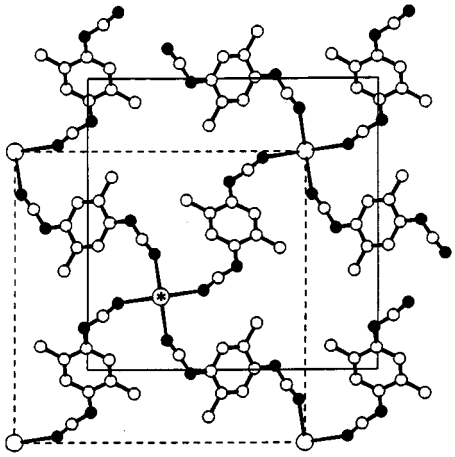


$I4_1/a$
KZ = 4, M = Cu, Li, Ag

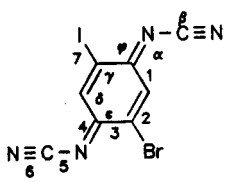


a,b-projection

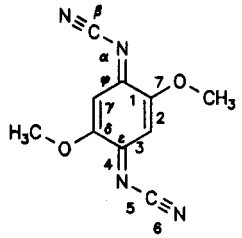
$P4/n$
KZ = 8, M = K, Rb, Tl



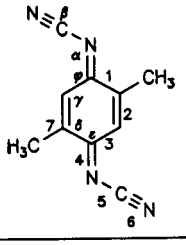
a,b-projection along c [001]



[2-Br,5-I-DCNQI]$_2$Cu	
Bond Length [pm]	Angle [°]
1 = 144.6(5)	α = 120.6(4)
2 = 135.0(6)	β = 173.0(5)
3 = 143.3(6)	γ = 120.8(4)
4 = 132.3(6)	δ = 118.0(4)
5 = 132.7(5)	ε = 121.7(3)
6 = 116.0(5)	φ = 117.5(4)
7 = 200.8(4)	



[2,5-(MeO)$_2$-DCNQI]$_2$Rb	
Bond Length [pm]	Angle [°]
1 = 142.6(3)	α = 120.1(2)
2 = 135.4(3)	β = 172.4(3)
3 = 146.2(3)	γ = 120.4(2)
4 = 132.6(3)	δ = 121.3(2)
5 = 131.7(3)	ε = 121.3(2)
6 = 115.0(4)	φ = 117.6(2)
7 = 134.0(3)	



[2,5-Me$_2$-DCNQI]$_2$Tl	
Bond Length [pm]	Angle [°]
1 = 144.1(7)	α = 121.7(4)
2 = 135.2(7)	β = 172.0(6)
3 = 144.6(7)	γ = 116.8(4)
4 = 132.6(6)	δ = 118.6(4)
5 = 132.1(8)	ε = 121.7(5)
6 = 115.0(7)	φ = 119.8(5)
7 = 149.9(8)	

Scheme 2. Structural arrangements of radical-anion salts [2-X,5-Y-DCNQI]$_2$M in space groups $I4_1/a$ and $P4/n$ and typical parameters of the ligands

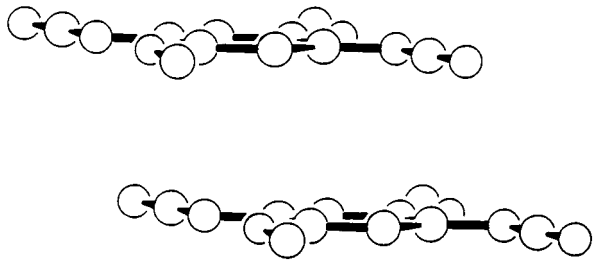


Figure 11. Side view of two ligands in the stacks of [(2,5-Me_2DCNQI)DCNQI]$_2$Br

Table 6. Precision of powder-diffraction data after Rietveld analysis compared to single-crystal X-ray data (± 0.3 to 1.0 pm, ± 0.4 to 0.8°) for radical-anion copper salts from **1a**, **1c**, **1g**, **1h**, **1i**, **1k**, **1l**, **1o**, **1p**; unit-cell data (space group $I4_1/a$) and coordination geometries (entries 1−5); bond lengths (BL) and angles of the DCNQI ligands (entries 6−14)

	Range of data from single crystals	Maximal deviation by powder data
1	*a* axis 2162−2252 pm	−3 to + 1 pm
2	*c* axis 381−411 pm	−0.3 to 0.2 pm
3	∠ α 126−138°	−0.5 to 0.5°
4	∠ θ 155−178°	−0.4 to +0.3°[a]
5	$d_{\phi\text{-}\phi}$ 314−321 pm	0 to +3 pm
6	$d_{CN\text{-}Cu}$ 196−198 pm	−10 to 5 pm
7	BLa 138−145 pm	−2 to 10 pm[b]
8	Blb 133−135 pm	−5 to 7 pm
9	Blc 143−145 pm	−11 to +9 pm
10	Bld 133−134 pm	−5 to 8 pm
11	Ble 130−132 pm	−9 to + 12 pm
12	Blf 115−116 pm	−10 to 12 pm
13	∠ β CNC 120−121°	−9° to +6°
14	∠ NCN 171°	−14 to 0 pm

[a] Only for **10**: +10°. − [b] Only for **1**: +28 pm.

from powder diffraction with excellent accuracy. Compared to single-crystal data they stay well within the range of error.

However, the powder data connected to the ligand (various bond lengths and angles, entries 6−14) are much less accurate. They are still useful to picture the geometry around the ligand but not precise enough to compare the rather subtle effects of the 2,5-substituents in DCNQIs.

The same situation was found for various non copper salts (M = Li, Na, K, Rb, Tl, Ag; details see Table 4 of Supporting Information).

In Table 7 unit-cell data from powder diffraction are listed for those DCNQI radical salts where single crystals were not available. They have to be considered as highly reliable and therefore can be discussed safely like the corresponding data by single-crystal X-ray analysis.

Since further improvements in powder-diffraction techniques and evaluation of data have been already achieved in the meantime, this method is expected to gain increasing importance for organic microcrystalline solids.

Conclusions

The broad range of investigations on DCNQI derivatives presented in this paper reports on our concluding efforts in this field. Backed by the experiences gained in the last 12 years we succeeded to answer the questions from which we started in this paper in the following way.

1. In addition to the already successfully tested substituent pattern in 2-X,5-Y-DCNQIs the new substituent pairs in **1d** (Cl/OMe), **1e** (Br/OMe), **1f** (I/OMe), **1j** (Cl/I), **1k** (Br/I), **1l** (I/I) all form CT complexes with TTF ($\sigma \approx 10^{-1}-10^{-3}$ Scm^{-1}, cf. Table 1) despite the strong increase in size of the halogen substituent. Even one CF_3 group is tolerated [**1m** (OMe/CF_3); **1n** (Me/CF_3)] despite its size and strong electron attraction.

The new anion radical salts all exhibit the stoichiometry [2-X,5-Y-DCNQI]$_2$M with M = Li, Na, K, NH_4, Rb, Tl, Cu, and Ag prepared by proved methods. With respect to the CF_3 substituent only with **1n** (Me/CF_3) a copper salt deposited. Powder conductivities similar to former ones were found in the usual range ($10^{-1}-10^{-3}$ Scm^{-1}).

2. In some cases the quality of single crystals prepared by electrocrystallization could be improved by partly rhythmic reversal of the redox process. This new method may be of general importance.

3. Much effort was devoted to prepare alloyed DCNQI radical copper salts from two or three differing ligands. The ratio of the DCNQIs in solution is connected to that in the solid radical salt in a nonlinear way (Figure 1). The composition of the alloy surprisingly is hardly determined by the redox potentials of the two DCNQIs but rather by their velocity to form solid radical salts. Since their high conductivities at ambient temperature resemble those of the corresponding DCNQI copper salts with only one type of ligand, the important space group $I4_1/a$ obviously is preserved. These experiments clearly demonstrate that a wealth of alloyed DCNQI copper salts can be designed. This variation offers an approach to organic metals with rather unexpected and partly unprecedent patterns of temperature-dependent conductivity (vide infra).

4. Investigation of the temperature-dependent conductivities of various alloyed DCNQI copper salts produced rermarkable, unexpected effects. Instead of duplicating the pattern of the single components incorporated into the alloys, new patterns evolved: Metal insulation phase transitions may be induced, excluded or shifted to a different temperature range. Most remarkably even a temperature-independent conductivity between 5 and 300 K can be achieved (Figure 5). On the other hand the alloyed copper salt from 2,5-Me_2DCNQI and its deuterated counterpart

Table. 7. Unit-cell data of various salts [2-X, 5-Y-DCNQI]$_2$M observed from powder-diffraction data refined by Rietveld analysis

DCNQI	R^1/R^3	M	Space group	*a* axis [pm]	*c* axis [pm]	PC−PDF[49]
1a	OMe/OMe	Na	$I2/a$[a]	2422.9(5) b = 379.8(1)	2280.1(3) β = 91.2(1)°	41−1885
1b	Me/OMe	Rb	$P4/n$	1668.3(2)	383.50(8)	41−1783
1c	Me/Me	Li	$I4_1/a$	2183.4(4)	385.3(1)[b]	40−1624
	Me/Me	NH_4	$P4/n$	1634.9(2)	385.14(9)	41−1784
	Me/Me	Rb	$P4/n$	1611.9(6)	382.78(4)	40−1987
1h	Me/Br	Li	$I4_1/a$	2190.6(2)	387.00(6)	40−1979
1i	I/Me	Li	$I4_1/a$	2294.7(1)	395.0(1)	40−1990

[a] Different but symmetrically equivalent setting of the unit cell see ref.[27] − [b] Structure not refined.

on cooling undergoes sharp phase transition with loss of conductivity of 10^7 to 10^8 Scm^{-1} which is restored at even lower temperatures (Figure 9). Because a rather broad hysteresis between heating and cooling is involved this phenomenon can be exploited for a very sensitive pressure/light-triggered switch (Figure 10).

These two extreme patterns qualify ligand alloying of DCNQI copper salts as a powerful tool for the design of highly conducting materials with a definite temperature profile.

5. Radical-anion salts of the type [2-X,5-Y-DCNQI]$_2$M with X,Y = MeO, Me, Cl, Br, I and M^+ = Li, Na, K, NH_4, Rb, C, M, Ag, Cu prefer the space group $I4_1/a$ or a closely related one. Therefore only in this type of organic metals relations between the individual electric properties and very subtle changes of the crystal lattice can be evaluated, provided single crystals for X-ray analysis are at hand. Since often only microcrystalline material is available extension to the evaluation of powder diagrams by the so-called Rietveld analysis is most welcome. This method, so far not employed to organic metals, yields excellent cell data of various DCNQI copper salts but less precise values for the geometries of the ligands.

Experimental Section

General: Melting points of the DCNQI/TTF complexes and the DCNQI radical-anion salts could not be determined with a Kofler microscope but had to be determined by differential thermoanalysis (DTA, Du Pont de Nemours Thermal Analyser TA 990). − IR spectra: Perkin Elmer 1420 and Nicolet 5 DXC FT-IR spectrometer. − Conductivities of microcrystalline solids were measured in a quartz capillary by compressing the powder with the two electrodes until the first cracks were seen. Single crystals were measured by the standard 4-point method. Solvents were purified and dried according to standard methods. Data from crystal-structure analyses: see Tables 8 and 9.

Neutron-Activation Analysis of Bromine and Copper (Table 6): The copper and bromine contents of the substances were determined by neutron-activation analysis (NAA). As reference nuclides ^{64}Cu ($t_{1/2}$ = 12.700 h) was used for copper and ^{82}Br ($t_{1/2}$ = 35.34 h) for bromine. Samples and standards were packed in quartz ampoules (Suprasil AN, Heraeus Quarzschmelze GmbH, Hanau) which had been cleaned before use. The sample mass per analysis was between 0.5 and 4 mg. Copper standard: copper(II) oxide granulated for analysis (E. Merck, Darmstadt), weighed in quantities betweeen 1.6 and 4.5 mg. Bromine standard: 50 μL of a $KBrO_3$ solution with p_{Br} = 2.664 g/l (Fixanal®, Riedel-de Haen, Seelze) was dried in a quartz ampoule (desiccator) → m_{Br} = 133.2 μg. Of the sealed ampoules, sets consisting of three samples, including a copper standard and a bromine standard were packed in aluminium foil and irradiated in the Forschungsreaktor München at xxx_{th} $Ø_{th}$ = 1.3 × 10^{13} $cm^{-2}s^{-1}$. Irradiation time = 15 min. After a waiting time (t_w) between 30 and 50 h the samples and standards were measured in the ampoules which had been cleaned outside.[50] − Counting equipment: 130-cm^3 intrinsic coaxial Ge detector, 1.9 keV resolution and 27% relative efficiency (both for the 1332.47-keV γ-line of ^{60}Co), main amplifier Silena model 7611, ADC Silena model 7423 UHS, memory buffer module Silena 7329−16K, personal computer AT/03/CO. For the evaluation of the γ spectra, emulation software mmb3 (Silena) was used. The ampoules were positioned with their axis parallel to the detector surface at a distance of 20 to 50 cm. The counting time was usually 2 h.

As a reference line for ^{64}Cu in most cases the 511-keV line was used (annihilation radiation of β^+ of ^{64}Cu). The 1345.9-keV γ-line (I_{rel} = 0.6%) was taken as the reference line if the 1368.6-keV γ-line of ^{24}Na was detected because ^{24}Na causes 511-keV radiation, too (a consequence of the pair production of the ^{24}Na γ-rays of 1368.6 keV and of 2754.1 keV). In addition, a contribution to the 511-keV line was taken into consideration by the pair ^{80m}Br (I.T.) ^{80}Br which is generated in parallel with ^{82}Br from bromine by neutron irradiation. ^{80}Br emits β^+ (2.6%). Its $t_{1/2}$ is only 17.6 min, but the $t_{1/2}$ of ^{80}Br is 4.2 h. Estimations by both calculation and measurement of bromine standards showed that after the above-mentioned t_w a contribution to the 511-keV line caused by ^{80}Br was either not detectable or negligibly small. For ^{82}Br its 776.49-keV γ-line (I_{rel} = 83%) was used as a reference.

DCNQI/TTF Complexes. − General Procedure 1 (GP1): Under nitrogen a concentrated solution of TTF in MeCN or dichloromethane (DCM) was added dropwise to a concentrated solution of the DCNQI in MeCN (20−80°C) or DCM. From the dark green to black solution the black microcrystalline charge-transfer complex separated within 1 min to 10 h. After cooling (0 to 10°C) of the mixture overnight, the solid was separated, washed with solvent and pentane and dried over silica gel (see Table 1).

2-Chloro-*N*,*N*′-dicyano-5-methoxy-1,4-benzoquinonediimine/Tetrathiafulvalene (1:1, 1d/TTF): TTF (30.4 mg, 100 μmol) in MeCN (1 mL); **1d** (22.1 mg, 100 μmol) in MeCN (3 mL, 60°). **1d**/TTF (37.0 mg, 93%), m.p. 155°C.− IR (KBr): $\tilde{\nu}$ = 4000−600 cm^{-1} total absorption. − $C_{15}H_9ClN_4OS_4$ (424.7): calcd. C 42.42, H 2.14, N 13.30; found C 40.33, H 2.05, N 12.27.

2-Bromo-*N*,*N*′-dicyano-5-methoxy-1,4-benzoquinone/Tetrathiafulvalene (1:1; 1e/TTF): TTF (40.8 mg, 200 μmol) in MeCN (2 mL);

Table 8. Single-crystal X-ray data

Compound	[**1a**]$_2$Rb[48]	[**1c**]$_2$Tl[20]	[**1k**]$_2$Cu[48]
Empirical formula	$C_{20}H_{16}N_8O_4Rb$	$C_{20}H_{16}N_8Tl$	$C_{16}H_4Br_2CuI_2N_8$
Molecular mass	517.87	572.77	785.43
a [pm]	1697.9(4)	1604.3(3)	2165.3(6)
c [pm]	384.0(2)	380.9(1)	402.3(2)
V [pm^3]	1107(1) × 10^6	980(1) × 10^6	1886(1) × 10^6
Z	2	2	4
d(calcd.) [g cm^{-3}]	1.55	1.94	2.77
Space group	*P*4/*n*	*P*4/*n*	*I*4$_1$/*a*
Diffractometer	Nonius	CAD-4	CAD-4
Radiation		Mo-K$_\alpha$	
Monochromator		graphite	
Crystal size [mm]	0.09 × 0.12 × 0.9	0.03 × 0.03 × 0.11	0.03 × 0.05 × 0.9
Data collection mode		ω-2 θ	
θ range [°]	1−25	1−20	2−30
Reciprocal lattice segment	$h = 0 \rightarrow 20$ $k = 0 \rightarrow 20$ $l = 0 \rightarrow 4$	$h = 0 \rightarrow 14$ $k = -14 \rightarrow 14$ $l = 0 \rightarrow 4$	$h = 0 \rightarrow 30$ $k = 0 \rightarrow 30$ $l = -5 \rightarrow 5$
No. refl. measd.	1050	933	2692
No. unique refl.	979	456	1371
No. refl. $F_o^2 > 2\sigma(F_o^2)$	907	430	1186
μ [mm^{-1}]	2.22	8.94	8.65
Absorption correction		Ψ scan	
Solution by		Patterson method	
Method of refinement	full-matrix least-squares, H atoms isotropic		
Data-to-parameter ratio	9.9	5.4	16.9
R, R_w	0.031, 0.041	0.012, 0.014	0.039, 0.044
Weighting scheme		$w = 4_o F_o^2/\sigma^2(F_o^2)$	
Largest difference peak	0.6 e/Å^3	0.2 e/Å^3	1.5 e/Å^3
Largest difference hole	0.2 e/Å^3	0.2 e/Å	0.4 e/Å^3
Program used		SHELX76	

1e (53.0 mmg, 200 μmol) in MeCN (6 mL, 60°C). **1e**/TTF (70.0 mg, 75%), m.p. 160°C. − IR (KBr): $\tilde{\nu}$ = 4000−600 cm^{-1} total absorption. − $C_{15}H_9BrN_4OS_4$ (469.4): calcd. C 38.38, H 1.94, N 11.94; found C 38.51, H 1.85, N 11.97.

***N*,*N*′-Dicyano-2-iodo-5-methoxy-1,4-benzoquinonediimine/Tetrathiafulvalene (1:1; 1f/ TTF):** TTF (40.8 mg, 200 μmol) in MeCN (15 mL); **1f** (62.0 mg, 200 μmol) in MeCN (5 mL, 80°C). **1f**/TTF (77 mg, 74%), m.p. 122°C (dec.). − IR (KBr): $\tilde{\nu}$ = 4000−600 cm^{-1} total absorption. − $C_{15}H_{19}IN_4OS_4$ (516.4): calcd. C 34.89, H 1.76, N 10.85; found C 35.02, H 1.73, N 10.85.

2-Chloro-*N*,*N*′-dicyano-5-iodo-1,4-benzoquinonediimine/Tetrathiafulvalene (1:1; 1j/TTF): TTF (20.4 mg, 100 μmol) in DCM (1 mL); **1j** (31.6 mg, 100 μmol) in DCM (10 mL). **1j**/TTF (40.0 mg, 77%), m.p. 125°C. − IR (KBr): $\tilde{\nu}$ = 2110 cm^{-1}. − $C_{14}H_6ClIN_4S_4$ (520.6): calcd. C 32.30, H 1.16, N 10.76; found C 32.05, H 1.16, N 10.66.

2-Bromo-*N*,*N*′-dicyano-5-iodo-1,4-benzoquinonediimine/Tetrathiafulvalene (1:1; 1k/TTF): TTF (20.4 mg, 100 μmol) in DCM (1 mL); **1k** (36.1 mg, 100 μmol) in DCM (10 mL). **1k** (44.0 mg, 78%), m.p. 127°C (dec.). − IR (KBr): $\tilde{\nu}$ = 2110 cm^{-1}. − $C_{14}H_6BrIN_4S_4$ (565.0): calcd. C 29.74, H 1.07, N 9.92; found C 29.18, H 0.74, N 9.60.

***N*,*N*′-Dicyano-2,5-diiodo-1,4-benzoquinonediimine/Tetrathiafulvalene (1:1; 1j/TTF):** TTF (20.4 mg, 100 μmol) in DCM (1 mL); **1l** (41.0 mg, 100 μmol) in DCM (20 mL). **1l**/TTF (51.0 mg, 83%), m.p. 152°C (dec.). − IR (KBr): $\tilde{\nu}$ = 2080 cm^{-1}. − $C_{14}H_6I_2N_4S_4$ (612.3): calcd. C 27.46, H 0.99, N 9.15; found C 27.72, H 0.97, N 9.45.

***N*,*N*′-Dicyano-2-methoxy-5-trifluoromethyl-1,4-benzoquinonediimine/Tetrathiafulvalene (1:1; 1m/TTF):** TTF (48.0 mg, 200 μmol) in MeCN (1 mL); **1m** (51.0 mg, 200 μmol) in MeCN (4 mL). **1m**/TTF (93.2 mg, 98%), m.p. 126°C. − IR (KBr): $\tilde{\nu}$ = 2100 cm^{-1}. − $C_{16}H_9F_3N_4OS_4$ (458.5): calcd. C 41.91, H 1.99, N 12.22, S 27.96; found C 41.79, H 2.26, N 11.92, S 26.85.

***N*,*N*′-Dicyano-2-methyl-5-trifluoromethyl-1,4-benzoquinonediimine/Tetrathiafulvalene (1:1; 1n/TTF):** TTF (40.8 mg, 200 μmol) in MeCN (4 mL); **1n** (48.0 mg, 200 μmol) in MeCN (3 mL). **1n**/TTF (80.0 mg, 90%). − $C_{10}H_9F_3N_4S_4$ (442.5): calcd. C 43.43, H 2.05, N 12.66, S 28.98; found C 42.53, H 2.08, N 11.60, S 31.02.

DCNQI Radical-anion Salts from Iodides. − General Procedure 2 (GP2): Under nitrogen a concentrated, degassed and filtered solution of the metal (ammonium) iodide in MeCN was added to a concentrated solution (20−80°C) of the DCNQI in MeCN. The black microcrystalline salt deposited from the dark solution. After cooling, the solid was separated, washed with MeCN and pentane and dried over silica gel (see Table 2).

Bis(*N*,*N*′-dicyano-2,5-dimethoxy-1,4-benzoquinonediimine)lithium [(1a)$_2$Li]: 1a (43.2 mg, 200 μmol) in MeCN (4 mL, 50°C); lithium iodide (54 mg, 400 mmol) in MeCN (2 mL). (**1a**)$_2$Li·H$_2$O (40.0 mg, 88%), m.p. 211°C (dec.). − IR (KBr): $\tilde{\nu}$ = 3400 cm^{-1} (O−H), 2135 (C≡N). − $[C_{10}H_8N_4O_2]_2Li \cdot H_2O$ (457.4): calcd. C 52.52, H 3.97, N 24.50; found C 52.54, H 3.53, N 24.59.

Bis(*N*,*N*′-dicyano-2,5-dimethoxy-1,4-benzoquinonediimine)-potassium [(1a)$_2$K]: 1a (21.6 mg, 100 μmol) in MeCN (2 mL, 80°C); potassium iodide (33 mg, 200 mmol) in MeCN (5 mL). (**1a**)$_2$K (44.0 mg, 94%), m.p. 170°C (dec.). − IR (KBr): $\tilde{\nu}$ = 2150 cm^{-1} (C≡N). − $[C_{10}H_8N_4O_2]_2K$ (471.5): calcd. C 50.51, H 3.40, N 23.57; found C 50.72, H 3.07, N 24.01.

Bis(*N*,*N*′-dicyano-2,5-dimethoxy-1,4-benzoquinonediimine)rubidium [(1a)$_2$Rb]: 1a (21.6 mg, 100 μmol) in MeCN (2 mL, 80°C); rubid-

Table 9. X-ray powder diffraction: experimental parameters and crystallographic data of the DCNQI copper salts obtained by X-ray powder diffraction and Rietveld analysis; all compounds crystallize in space group $I4_1/a$ with $Z = 4$; wavelengths used were $\lambda_1 = 154.056$ pm and $\lambda_2 = 154.439$ pm[48]

Compound	[DMeDCNQI]$_2$-Cu	[Me,ClDCNQI]$_2$-Cu	[Me,BrDCNQI]$_2$-Cu	[Me,IDCNQI]$_2$-Cu	[DClDCNQI]$_2$-Cu	[Cl,JDCNQI]$_2$-Cu
Empirical formula	$C_{20}H_{16}CuN_8$	$C_{18}H_{10}Cl_2CuN_8$	$C_{18}H_{10}Br_2CuN_8$	$C_{18}H_{10}CuI_2N_8$	$C_{16}H_4Cl_4CuN_8$	$C_{16}H_4Cl_2CuI_2N_8$
a [pm]	2162.8(1)	2168.5(1)	2169.5(2)	2170.7(2)	2164.9(1)	2170.3(1)
c [pm]	388.49(4)	383.49(3)	387.59(4)	398.87(3)	381.69(3)	396.77(3)
V [pm$^3 \cdot 10^6$]	1817	1803	1824	1880	1789	1869
$d_{calcd.}$ [g/cm^3]	1.58	1.74	2.05	2.32	1.91	2.48
Sample holder[a]	G1.	G1.	Q.	Q.,M.	G2.	G1.
Step width (2θ) [°]	0.03	0.03	0.03	0.03	0.03	0.03
2 θ range [°]	6.5−102	6−102	7−102	8−95	6−100	7−100
No. observations	3183	3200	3167	2900	3133	3100
No. reflections	487	485	489	425	464	481
No. profile parameters	9	9	9	9	9	9
No. structure parameters	31	34	28	23	26	26
$R_{wp} = [\Sigma w_i(y_{oi} - 1/C \cdot y_{ci})^2/\Sigma w_i y_{oi}^2]^{1/2}$ (%)[b]	15.4	10.6	7.6	6.1	8.4	8.1
$R_p' = [\Sigma(y_{oi} - 1/C \cdot y_{ci})^2/\Sigma(y_{oi} - y_{bi})]$ (%) [b]	19.6	18.6	18.8	27.2	19.5	21.9
$R_B = \Sigma\lvert I_{oi} - 1/C \cdot I_{ci}\rvert\Sigma I_{oi}$ (%)[b]	6.3	5.1	6.0	10.4	5.7	7.6
$R_e = [(N - P)/\Sigma w_i y_{oi}]^{1/2}$ (%)[b]	1.6	1.6	2.3	5.5	2.2	3.5
Isotropic displacement parameters refined	yes	yes	partly	no	no	no

Compound	[Me,MeODCNQI]$_2$Cu	[DMeODCNQI]$_2$Cu	DBrDCNQI]$_2$Cu	[DIDCNQI]$_2$Cu	[I,BrDCNQI]$_2$Cu
Empirical formula	$C_{20}H_{16}CuN_8O_2$	$C_{20}H_{16}CuN_8O_4$	$C_{16}H_4Br_4CuN_8$	$C_{16}H_4CuI_4N_8$	$C_{16}H_4Br_2CuI_2N_8$
a [pm]	2219.2(1)	2251.5(1)	2162.5(1)	2172.0(6)	2168.3(1)
c [pm]	387.13(2)	384.35(2)	390.71(2)	411.20(2)	402.50(2)
V [pm$^3 \cdot 10^6$]	1907	1948	1827	1944	1892
$d_{calcd.}$ [g/cm^3]	1.62	1.69	2.52	3.01	2.76
Sample holder[a]	G1., M.	G2.	Q.	Q.,M.	Q.
Step width (2θ) [°]	0.02	0.03	0.03	0.03	0.03
2 θ range [°]	6−90	6−95	7−100	7.5−114	6−100
No. observations	4176	2967	3100	3550	3133
No. reflections	392	452	474	658	487
No. profile parameters	9	9	9	9	9
No. structure parameters	29	26	31	23	26
$R_{wp} = [\Sigma w_i(y_{oi} - 1/C \cdot y_{ci})^2/\Sigma w_i y_{oi}^2]^{1/2}$ (%)[b]	6.2	7.2	9.1	6.7	10.3
$R_p' = [\Sigma(y_{oi} - 1/C \cdot y_{ci})^2/\Sigma(y_{oi} - y_{bi})]$ (%)[b]	22.3	23.9	15.3	22.2	16.3
$R_B = \Sigma\lvert I_{oi} - 1/C \cdot I_{ci}\rvert\Sigma I_{oi}$ (%)[b]	6.1	8.3	5.6	9.6	4.7
$R_e = [(N - P)/\Sigma w_i y_{oi}]^{1/2}$ (%)[b]	2.5	3.3	1.9	3.8	2.5
Isotropic displacement parameters refined	no	no	yes	no	no

[a] G1.: glass sample holder with a diameter of 22 mm and a depth of 0.25 mm; Q.: quartz sample holder with a diameter of 20 mm and a depth of 0.05 mm; G2.: glass sample holder with a diameter of 25 mm and a depth of 0.05 mm; M.: mixture with glass powder to decrease effects of preferred orientation. − [b] C: scale factor; y_o,y_c,y_b: observed, calculated and background profile intensities; I_o,I_c : observed and calculated integrated intensities; N: number of statistically independent observations; P: number of variable least-squares parameters; w: weight $= 1/y_o$

ium iodide (31.9 mg, 150 μmol) in MeCN (5 mL, 12 h room temp.). (**1a**)$_2$Rb (15.0 mg, 58%), m.p. 170°C (dec.). − IR (KBr): $\tilde{\nu}$ = 2140 cm^{-1} (C≡N). − $[C_{10}H_8N_4O_2]_2$Rb (517.9): calcd. C 46.38, H 3.12, N 21.64; found C 46.60, H 2.95, N 20.95.

Bis(*N*,*N*′-dicyano-2-methoxy-5-methyl-1,4-benzoquinonediimine)lithium [(1b)$_2$Li · 1.8 H$_2$O]: 1b (40.0 mg, 200 μmol) in MeCN (3 mL); lithium iodide (54 mg, 400 μmol) in MeCN (2 mL, −20°C, 12 h). (**1b**)$_2$Li · 1.8 H$_2$O (32.0 mg, 73%), m.p. 64°C (dec.). − IR (KBr): $\tilde{\nu}$ = 3400 cm^{-1} (O−H), 2110 (C≡N). − After 3 d a brown amorphous powder was formed by decomposition. − $[C_{10}H_8N_4O]_2$Li · 1.8 H$_2$O (430.9): calcd. C 54.62, H 4.46, N 25.48; found C 54.64, H 3.50, N 27.50.

Bis(*N*,*N*′-dicyano-2-methoxy-5-methyl-1,4-benzoquinonediimine)sodium [(1b)$_2$Na]: 1b (40.0 mg, 200 μmol) in MeCN (3 mL); sodium iodide (60 mg, 400 mmol) in MeCN (3 mL, 50 → 20°C, 12 h). (**1b**)$_2$Na (42.0 mg, 100%), m.p. 138°C (dec.). − IR (KBr): $\tilde{\nu}$ = 2140 cm^{-1} (C≡N). − $[C_{10}H_8N_4O]_2$Na (423.4): calcd. C 56.73, H 3.80, N 26.46; found C 56.31, H 3.79, N 25.95.

Bis(*N*,*N*′-dicyano-2-methoxy-5-methyl-1,4-benzoquinonediimine)rubidium [(1b)$_2$Rb]: 1b (20.0 mg, 100 μmol) in MeCN (2 mL, 50°C), rubidium iodide (32 mg, 150 μmol) in MeCN (5 mL, −35°C, 12 h). (**1b**)$_2$Rb (17.0 mg, 70%), m.p. 90°C (dec.). − IR (KBr): $\tilde{\nu}$ = 2145 cm^{-1} (C≡N). − $[C_{10}H_8N_4O]_2$Rb (485.9): calcd. C 49.43, H 3.33, N 23.07; found C 48.98, H 3.00, N 22.23.

Bis(*N*,*N*′-dicyano-2,5-dimethyl-1,4-benzoquinonediimine)ammonium [(1c)$_2$NH$_4$]: 1c (55.3 mg, 300 μmol) in MeCN (5 mL, 60°C); ammonium iodide (73 mg, 500 μmol) in MeCN (10 mL, 60 → 20°C). (**1c**)$_2$NH$_4$ (35.0 mg, 40%), m.p. 129°C (dec.). − IR (KBr): $\tilde{\nu}$ = 2135

cm^{-1} (C≡N). − $[C_{10}H_8N_4]_2NH_4$ (386.4): calcd. C 62.15, H 5.23, N 32.62; found C 61.81, H 5.30, N 32.75.

Bis(2-chloro-*N*,*N*′-dicyano-5-methoxy-1,4-benzoquinonediimine)lithium [(1d)$_2$Li·H$_2$O]: 1d (44.2 mg, 200 μmol) in MeCN (8 mL); lithium iodide (50 mg, 300 μmol) in MeCN (2 mL, 20 → 0°C, 10 min). (**1d**)$_2$Li·H$_2$O (26.0 mg, 56%), m.p. 76°C (dec.). − IR (KBr): ṽ = 3400 cm^{-1} (O−H), 2240, 2150 (C≡N). − After 4 d, a brown amorphous powder had formed by decomposition. − $[C_9H_5N_4ClO]_2Li·H_2O$ (466.2): calcd. C 46.37, H 2.60, N 24.04; found C 46.89, H 3.34, N 23.71.

Bis(2-chloro-*N*,*N*′-dicyano-5-methoxy-1,4-benzoquinonediimine)copper [(1d)$_2$Cu]: 1d (44.1 mg, 200 μmol) in MeCN (8 mL, 50°C); copper(I) iodide (59 mg, 300 μmol) in MeCN (4 mL). (**1d**)$_2$Cu (48.0 mg, 96%), m.p. 180°C (dec.). − IR (KBr): ṽ = 4000−600 cm^{-1}, total absorption. − $[C_9H_5N_4ClO]_2Cu$ (504.8): calcd. C 42.85, H 2.00, N 22.20; found C 42.73, H 1.97, N 22.34.

Bis(2-bromo-*N*,*N*′-dicyano-5-methoxy-1,4-benzoquinonediimine)copper [(1e)$_2$Cu]: 1e (26.5 mg, 100 μmol) in MeCN (6 mL, 60°C); copper(I) iodide (29 mg, 150 μmol) in MeCN (5 mL, → 0°C). (**1e**)$_2$Cu (29.0 mg, 98%), m.p. 176°C (dec.). − IR (KBr): ṽ = 4000−600 cm^{-1}, total absorption. − $[C_9H_5N_4BrO]_2Cu$ (593.8): calcd. C 36.41, H 1.70, N 18.88; found C 36.31, H 1.58, N 18.69.

Bis(*N*,*N*′-dicyano-2-iodo-5-methoxy-1,4-benzoquinone)copper [(1f)$_2$Cu]: 1f (57 mg, 300 μmol) in MeCN (3 mL); copper(I) iodide in MeCN (3 mL). (**1f**)$_2$Cu (65.0 mg, 47%). − IR (KBr): ṽ = 4000−600 cm^{-1}, total absorption. − $C_{18}H_{10}CuI_2N_8O_2$ (687.7): calcd. C 31.44, H 1.47, N 16.29; found C 30.60, H 1.37, N 15.81.

Bis(2-bromo-*N*,*N*′-dicyano-5-methyl-1,4-benzoquinonediimine)-ammonium [(1h)$_2$NH$_4$]: 1h (99.6 mg, 400 μmol) in MeCN (5 mL, 60°C); ammonium iodide (87 mg, 600 μmol) in MeCN (10 mL, → 0°C). (**1h**)$_2$NH$_4$ (87.0 mg, 85%), m.p. 134°C (dec.). − IR (KBr): ṽ = 2145 cm^{-1} (C≡N). − $[C_9H_5N_4Br]_2NH_4$ (516.2): C 41.88, H 2.74, N 24.43; found C 41.52, H 2.64, N 23.57.

Bis(*N*,*N*′-dicyano-2-iodo-5-methyl-1,4-benzoquinonediimine)-ammonium [(1i)$_2$NH$_4$]: 1i (119 mg, 400 μmol) in MeCN (6 mL, 60°C); ammonium iodide (87 mg, 600 μmol) in MeCN (10 mL; → 10°C, 1 h). (**1e**)$_2$Cu (93.0 mg, 77%), m.p. 134°C (dec.). − IR (KBr): ṽ = 2140 cm^{-1} (C≡N). − $[C_9H_5N_4I]_2NH_4$ (610.2): calcd. C 35.43, H 2.31, N 20.66; found C 35.85, H 2.44, N 19.85.

Bis(2-chloro-*N*,*N*′-dicyano-5-iodo-1,4-benzoquinonediimine)copper [(1j)$_2$Cu]: 1j (63.3 mg, 200 μmol) in MeCN (10 mL); copper(I) iodide (59 mg, 300 μmol) in MeCN (4 mL, → 10°C). (**1j**)$_2$Cu (50.0 mg, 72%), m.p. 150°C (dec.). − IR (KBr): ṽ = 4000−600 cm^{-1}, total absorption. − $[C_8H_2N_4ClI]_2Cu$ (696.5): C 27.59, H 0.58, N 16.08, found: C 27.78, H 0.77, N 16.11.

Bis(2-bromo-*N*,*N*′-dicyano-5-iodo-1,4-benzoquinonediimine)copper [(1k)$_2$Cu]: 1k (90.3 mg, 250 μmol) in MeCN (25 mL); copper(I) iodide (66.5 mg, 350 μmol) in MeCN (5 mL). (**1k**)$_2$Cu (72.0 mg, 74%), m.p. 164°C (dec.). − IR (KBr): ṽ = 4000−600 cm^{-1}, total absorption. − $[C_8H_2N_4BrI]_2Cu$ (785.4): calcd. C 24.46, H 0.51, N 14.27; found C 24.27, H 0.50, N 14.32.

Bis(*N*,*N*′-dicyano-2,5-diiodo-1,4-benzoquinonediimine)copper [(1l)$_2$Cu]: 1l (40.8 mg, 100 μmol) in MeCN (25 mL, 60°C); copper(I) iodide (38 mg, 200 μmol) in MeCN (5 mL, → 20°C). (**1l**)$_2$Cu (40.0 mg, 91%), m.p. 164°C (dec.). − IR (KBr): ṽ = 4000−600 cm^{-1}, total absorption. − $[C_8H_2N_4I_2]_2Cu$ (879.4): calcd. C 21.85, H 0.50, N 12.74; found C 21.49, H 0.59, N 12.41.

Bis(*N*,*N*′-dicyano-2-methyl-5-trifluoromethyl-1,4-benzoquinonediimine)copper [(1n)$_2$Cu]: **1n** (72 mg, 300 μmol) in MeCN (4 mL); copper(I) iodide (38 mg, 200 μmol) in MeCN (2 mL). (**1n**)$_2$Cu (50.0 mg, 62%). − IR (KBr): ṽ = 4000−600 cm^{-1}, total absorption. − $C_{20}H_{10}CuF_6N_8$ (539.9): calcd. C 44.49, H 1.87, N 20.76; found C 44.05, H 2.00, N 21.02. − (**1n**)$_2$Cu was obtained only with the given stoichiometry of the components. The usual ratio **1n**/CuI = 300:450 yielded a different black amorphous compound with a 7:5 stoichiometry, a distinct IR spectrum and $\sigma_p = 2 \times 10^{-7}$ Scm^{-1}, m.p. 168°C (dec.). − IR (KBr): ṽ = 2130 cm^{-1} (C≡N), 1580 (C=N). − $C_{70}H_{35}Cu_5F_{21}N_{28}$ (1984.9): calcd. C 42.36, H 1.78, N 19.76; found C 41.82, H 2.23, N 20.05.

DCNQI Radical-Anion Salts Grown on Silver or Copper Wires. − General Procedure 3 (GP3): A silver wire (diameter 0.3 mm) was flattened, polished and treated with toluene and acetonitrile. This wire was immersed 1−2 cm deep into a degassed solution of silver nitrate (100 μmol) and DCNQI **1** (100 μmol) in 8 mL of acetonitrile. After 3−10 d, the solution became colourless and from the silver wire black, shiny needles (1−20 mm) were harvested, washed with MeCN and pentane and dried over silica gel. The same procedure was followed with a copper wire (diameter = 1 mm, cleaned with 2 M HCl/3% H_2O_2, polished and treated with MeCN. The MeCN solution (10 mL) contained DCNQI **1** (100 μmol) and copper(II) bromide (100 μmol). Analytical data are collected in Table 10, and yields and conductivities in Table 3.

Table 10. Analytical data for DCNQI salts grown on a silver and copper wire

No.	m.p. [°C]	ṽ(C≡N) [$^{-1}$]	Elemental analysis[a] C	H	N
(**1c**)$_2$Ag	173	2165	50.43	3.39	23.53
			49.75	3.30	22.87
(**1d**)$_2$Cu	180	[b]	42.82	2.00	22.20
			43.04	1.99	22.48
(**1e**)$_2$Cu	154	[b]	36.41	1.70	18.86
			36.25	1.65	18.54
(**1h**)$_2$Ag	162	2140	35.75	1.67	18.49
			34.89	1.28	17.74
(**1i**)$_2$Ag	159	2170	30.88	1.44	16.01
		2140	31.40	1.32	15.92
(**1j**)$_2$Ag	148	2170	25.93	0.54	15.18
		2130	26.07	0.69	15.33
(**1k**)$_2$Cu	175	2110	24.46	0.51	14.17
			24.71	0.58	13.85
(**1k**)$_2$Ag	163	2140	23.16	0.49	13.51
			23.44	0.56	15.31

[a] Calculated (above), found (below). − [b] IR (KBr): total absorption between 4000−600 cm^{-1}.

Radical-Anion Salts (DCNQI)$_2$M by Electrocrystallization. − General Procedure 4 (GP4): Three- (C3)[51] or two- (C2) -compartment[52] cells were used with a Pt cathode (either plates, 2 cm^2 or rods, diameter = 1 mm, *l* = 5 mm, ca. 0.17 cm^2) for different current densities. Anodes were rods from platinum or glassy carbon (Fa. Sigri). Electrolysis was run at constant current in degassed acetonitrile under argon (C3 = 60 mL, C2 = 80 mL) containing *x* μmol of DCNQI **1** and *y* μmol of supporting electrolyte [A = $RbClO_4$; B = CF_3CO_2Tl; C = $Cu(CH_3CN)_4ClO_4$; D = $AgNO_3$]. The radical salts which deposited in black shiny (thin) needles were harvested before all the DCNQI had been reduced, washed with MeCN and pentane and dried (see Table 4). Periodical switching between reduction and partial oxidation was performed with a home-made apparatus (B. Brunner) according to a circuit diagram given in the Supporting Information.

(1a)$_2$Cu: 1a (130 mg, 600 μmol), C (229 mg, 700 μmol), C2; 9 μA; Pt rod (53 μA cm^{-2}), switching 7:3/s, 5°C, 264 h. (**1a**)$_2$Cu (29.0 mg, 20%), m.p. 220°C (dec.). − IR (KBr): ṽ = 4000−600 cm^{-1}, total

absorption. − $[C_{10}H_8N_4O_2]_2Cu$ (495.9): calcd. C 48.43, H 3.26, N 22.60; found C 48.44, H 3.22, N 23.05.

(1a)$_2$Rb: 1a (43.2 mg, 200 μmol), A (185 mg, 1.0 mmol), C3; 5 μA; Pt plate (2.5 μA cm^{-2}), −18°C, 117 h. (**1a**)$_2$Rb (15.2 mg, 29%), m.p. 167°C (dec.). − IR (KBr): $\tilde{\nu}$ = 2140 cm^{-1}, 2090 (C≡N). − $[C_{10}H_8N_4O_2]_2Cu$ (517.9): calcd. C 46.38, H 3.12; N 21.64; found C 46.24, H 3.14, N 21.38.

(1b)$_2$Cu: 1b (120 mg, 600 μmol), C (229 mg, 700 μmol), C3; 9 μA; Pt rod (53 μA cm^{-2}), 22°C, 97 h. (**1b**)$_2$Cu (32.0 mg, 23%), m.p. 158°C (dec.). − IR (KBr): $\tilde{\nu}$ = 4000−600 cm^{-1}, total absorption. − $[C_{10}H_8N_4O]_2Cu$ (463.9): calcd. C 51.77, H 3.48, N 24.16; found C 51.61, H 3.67, N 23.81.

(1c)$_2$Tl: 1c (36.8 mg, 200 μmol), B (64 mg, 200 μmol), C2; 30 μA, Pt plate (15 μA cm^{-2}); −18°C, 72 h. (**1c**)$_2$Tl (27.1 mg, 48%), m.p. 161°C (dec.). − IR (KBr): $\tilde{\nu}$ = 2120 cm^{-1}, 2080 (C≡N). − $[C_{10}H_8N_4]_2Tl$ (572.7): calcd. C 41.93, H 2.82, N 19.57; found C 41.84, H 2.78, N 19.64.

(1d)$_2$Cu: 1d (44.1 mg, 200 μmol), C (98 mg, 300 μmol); C2; 10 μA, Pt rod (59 μA cm^{-2}); 20°C, 72 h. (**1d**)$_2$Cu (17.1 mg, 34%), m.p. 180°C (dec.). − IR (KBr): $\tilde{\nu}$ = 4000−600 cm^{-1}, total absorption. − $[C_9H_5N_4ClO]_2Cu$ (504.8): calcd. C 42.82, H 2.00, N 22.20; found C 42.75, H 1.92, N 21.79.

(1e)$_2$Cu: 1e (53.0 mg, 200 μmol), C (98 mg, 300 μmol); C2; 10 μA, Pt rod (59 μA cm^{-2}); 20°C, 72 h. (**1e**)$_2$Cu (23.1 mg, 39%), m.p. 196°C (dec.). − IR (KBr): $\tilde{\nu}$ = 4000−600 cm^{-1}, total absorption. − $[C_9H_5N_4BrO]_2Cu$ (563.7): calcd. C 36.41, H 1.70, N 18.88; found C 36.48, H 1.72, N 18.77.

(1f)$_2$Cu: 1f (94 mg, 300 μmol), C (195 mg, 600 μmol); C2; 9 μA, Pt rod (53 μA cm^{-2}), switching 7:3/s, 20°C, 14 d. (**1f**)$_2$Cu (10.0 mg, 8%) − IR (KBr): $\tilde{\nu}$ = 4000−600 cm^{-1}, total absorption. − $C_{18}H_{10}CuI_2N_8O_2$ (687.7): calcd. C 31.44, H 1.47, N 16.29; found C 30.60, H 1.37, N 15.81.

(1h)$_2$Tl: 1h (74.4 mg, 300 μmol), B (95 mg, 300 μmol); C2; 20 μA, Pt plate (10 μA cm^{-1}), −18°C, 44 h. (**1h**)$_2$Tl (15.1 mg, 22%), m.p. 106°C (decomposition within 4 d). − IR (KBr): $\tilde{\nu}$ = 2130 cm^{-1}, 2090 (C≡N). − $[C_9H_5N_4Br]_2Tl$ (702.5): calcd. C 31.05, H 1.30, N 15.60; found C 30.77, H 1.44, N 15.95.

(1i)$_2$Tl: 1i (59.2 mg, 200 μmol), B (95 mg, 300 μmol); C2; 25 μA, Pt plate (12.5 μA cm^{-2}), −18°C, 44 h. (**1h**)$_2$Tl (15.1 mg, 22%), m.p. 111°C (dec.).− IR (KBr): $\tilde{\nu}$ = 2090 cm^{-1} (C≡N). − $[C_9H_5N_4I]_2Tl$ (976.5): calcd. C 27.14, H 1.27, N 14.07; found C 27.13, H 1.30, N 14.08.

(1j)$_2$Cu: 1j (95.0 mg, 300 μmol), C (98 mg, 300 μmol); C2; 9 μA, Pt rod (53 μA cm^{-2}), 20°C, 72 h. (**1j**)$_2$Cu (30.0 mg, 29%), m.p. 209°C (dec.).− IR (KBr): $\tilde{\nu}$ = 4000−600 cm^{-1}, total absorption. − $[C_8H_2N_4ClI]_2Cu$ (696.5): calcd. C 27.59, H 0.58, N 16.09; found C 28.08, H 0.72, N 16.01.

(1k)$_2$Cu: 1k (108 mg, 300 μmol), C (147 mg, 450 μmol); C2; 9 μA, Pt rod (53 μA cm^{-2}), 20°C, 144 h. (**1h**)$_2$Cu (59.0 mg, 50%), m.p. 228°C (dec.). − IR (KBr): $\tilde{\nu}$ = 4000−600 cm^{-1}, total absorption. − $[C_8H_2N_4BrI]_2Cu$ (785.4): calcd. C 24.47, H 0.51, N 14.27; found C 24.71, H 0.66, N 13.82.

(1k)$_2$Ag: 1k (36.1 mg, 100 μmol), D (34 mg, 200 μmol); C3; 10 μA, Pt plate (5 μA cm^{-2}), −25°C, 153 h. (**1k**)$_2$Ag (17.1 mg, 21%), m.p. 164°C (dec.). − IR (KBr): $\tilde{\nu}$ = 2180 cm^{-1}, 2140 (C≡N). − $[C_8H_2N_4BrI]Ag$ (829.8): calcd. C 23.16, H 0.49, N 13.51; found C 23.77, H 0.62, N 13.58.

(1l)$_2$Cu: 1l (81.6 mg, 200 μmol), C (98 mg, 300 μmol),; C2, 9 μA, Pt rod (53 μA cm^{-2}), 20°C, 135 h. (**1l**)$_2$Cu (39.0mg, 45%), m.p. 201°C (dec.). − IR (KBr): $\tilde{\nu}$ = 4000−600 cm^{-1}, total absorption. − $[C_8H_2N_4I_2]_2Cu$ (879.4): calcd. C 21.85, H 0.46, N 12.74; found C 22.01, H 0.32, N 12.51.

DCNQI Radical-Anion Copper Salts Grown from Two Different DCNQIs on a Copper Wire: Two different DCNQIs **1** (100 μmol each) and copper(II) bromide (150 μmol) were dissolved in acetonitrile (25 mL) saturated with argon. According to GP3 (vide supra) a copper wire was immersed and after 3−5 d the dark needles (1−20 mm) which had formed were harvested. All specimens showed total absorption in their IR spectra between 4000−600 cm^{-1}. For details see Table 5.

DCNQI Radical-Anion Copper Salts with different DCNQI Ligands by Electrocrystallization: Following GP4 (vide supra) a pair of DCNQIs was applied in various ratios. The harvested needles (5−20 mm long, diameter 5−15 μm) appeared similar to those grown from one DCNQI only and showed total absorption in their IR spectra between 4000−600 cm^{-1}. For details see Table 6.

Acknowledgments

Financial support by the Fonds der Chemischen Industrie, Frankfurt/Main and the BASF AG, Ludwigshafen/Rhein together with generous donations of chemicals are gratefully acknowledged.

[1] Part LXVI: M. Hemmerling, S. Hünig, M. Kemmer, K. Peters, *Eur. J. Org. Chem*. **1998**, 1989−1996.
[2] H. Meixner, Ph.D. Thesis, University of Würzburg, **1991**; K. Sinzger, Ph.D. Thesis, University of Würzburg, **1995**.
[1] F. Wudl, D. Wobschall, E. J. Hufnagel, *J. Am. Chem. Soc.* **1972**, *94*, 670.
[2] J. Ferraris, D. O. Cowan, V. Walatka, Jr., J. H. Perlstein, *J. Am. Chem. Soc.* **1973**, *95*, 948.
[3] L. B. Coleman, M. J. Cohen, D. J. Sandman, F. G. Yamagishi, A. F. Garito, A. J. Heeger, *Solid State Commun.* **1973**, *12*, 1125.
[4] Cf.: J. M. Williams, J. R. Ferraro, R. J. Thorn, K. D. Carlson, U. Geiser, H. H. Wang, A. M. Kini, M.-H. Whangbo, *Organic Conductors (Including Fullerenes). Synthesis, Structure, Properties and Theory*, Prentice Hall, Englewood Cliffs, NJ, **1992**, p. 115.
[5] A. Aumüller, P. Erk, S. Hünig, G. Klebe, J. U. von Schütz, H.-P. Werner, *Angew. Chem.* **1986**, *98*, 760−761; *Angew. Chem. Int. Ed. Engl.* **1986**, *25*, 740−741.
[6] Review: S. Hünig, *J. Mater. Chem.* **1995**, *5*, 1469−1479.
[7] Cf. also: N. Martin, J. L. Segura, C. Seoane, *J. Mater. Chem.* **1997**, *7*, 1661−1676.
[8] Part LXIII: S. Hünig, R. Bau, M. Kemmer, T. Metzenthin, K. Peters, K. Sinzger, J. Gulbis, *Eur. J. Org. Chem.* **1998**, 335−348.
[9] A. Aumüller, P. Erk, S. Hünig, H. Meixner, J. U. von Schütz, H.-P. Werner, *Liebigs Ann. Chem.* **1987**, 997−1006.
[10] P. Erk, S. Hünig, G. Klebe, M. Krebs, J. U. von Schütz, *Chem. Ber.* **1991**, 2005−2011.
[11] A. Aumüller, Ph.D. Thesis, University of Würzburg, **1985**.
[12] P. Erk, S. Hünig, H. Meixner, J. U. von Schütz, H.-P. Werner, *Liebigs Ann. Chem.* **1988**, 157−159.
[13] R. C. Wheland, J. L. Gillson, *J. Am. Chem. Soc.* **1976**, *98*, 3916−3925.
[14] A. Aumüller, P. Erk, H. Meixner, S. Hünig, J. U. von Schütz, H.-J. Gross, U. Langohr, H.-P. Werner, H. C. Wolf, C. Burschka, G. Klebe, K. Peters, H. G. von Schnering, *Synth. Met.* **1988**, *27*, B 181−188.
[15] R. Kato, H. Kobayashi, A. Kobayashi, T. Mori, H. Inokuchi, *Chem. Lett.* **1987**, 1579−1582.
[16] H. Kobayashi, R. Kato, A. Kobayashi, T. Mori, H. Inokuchi, *Solid State Commun.* **1988**, *65*, 1351−1354.
[17] L. R. Melby, *Can. J. Chem.* **1965**, *43*, 1448.
[18] P. Erk, Ph.D. Thesis, University of Würzburg, **1989**.
[19] A. Kobayashi, T. Mori, H. Inokuchi, R. Kato, *Synth. Met.* **1988**, *27*, B275−280.
[20] S. Hünig, H. Meixner, T. Metzenthin, U. Langohr, H. U. von Schütz, H. C. Wolf, E. Tillmanns, *Adv. Mater.* **1990**, *2*, 361−363.

[21] H. W. Helberg, personal communication, March **1991**.
[22] [22a] S. Hünig, *Pure Appl. Chem.* **1990**, *62*, 395−406. − [22b] S. Hünig, P. Erk, *Adv. Mater.* **1991**, *3*, 225−236.
[23] P. Erk, H. Meixner, T. Metzenthin, S. Hünig, U. Langohr, J.-U. von Schütz, H.-P. Werner, H. C. Wolf, R. Burkert, G. Schaumburg, H. W. Helberg, *Adv. Mater.* **1991**, *3*, 311−315.
[24] R. Kato, H. Kobayashi, A. Kobayashi, *J. Am. Chem. Soc.* **1989**, *111*, 5224−5232.
[25] A. Aumüller, P. Erk. S. Hünig, J. U. von Schütz, H.-P. Werner, H. C. Wolf, G. Klebe, *Mol. Cryst. Liq. Cryst. Inc. Nonlin. Opt.* **1988**, *156*, 215−221.
[26] T. Bauer, E. Tillmanns, S. Hünig, H. Meixner, T. Metzenthin, U. Langohr, H. Rieder, J. U. von Schütz, H. C. Wolf, *Acta Crystallogr.* **1991**, *A46*, C362.
[27] R. Kato, H. Kobayashi, A. Koboyashi, T. Mori, H. Inokuchi, *Synth. Met.* **1988**, *27*, B263−B268.
[28] Preliminary publication: H. J. Gross, U. Langohr, J. U. von Schütz, H.-P. Werner, H. C. Wolf, S. Tomic, D. Jérome, P. Erk, S. Hünig, H. Meixner, *J. Phys. (Paris)* **1989**, *50*, 2347−2355; P. Erk, S. Hünig, H. J. Gross, U. Langohr, H. Meixner, H.-P. Werner, J. U. von Schütz, H. C. Wolf, *Angew. Chem.* **1989**, *101*, 1297−1298; *Angew. Chem. Int. Ed. Engl.* **1989**, *28*, 1245−1246.
[29] A. Aumüller, S. Hünig, *Liebigs Ann. Chem.* **1986**, 165−176.
[30] A. Aumüller, P. Erk, S. Hünig, H. Meixner, J. U. von Schütz, H.-P. Werner, *Liebigs Ann. Chem.* **1987**, 997−1006.
[31] A. Kobayashi, R. Kato, H. Kobayashi, *Synth. Met.* **1991**, *42*, 1769−1774; A. Kobayashi, R. Kato, H. Kobayashi, *Chem. Lett.* **1989**, 1843−1646.
[32] See also ref.[28]
[33] K. Sinzger, S. Hünig, M. Jopp, D. Bauer, W. Bietsch, J. U. von Schütz, H. C. Wolf, R. K. Kremer, T. Metzenthin, R. Bau, S. I. Khan, A. Lindbaum, C. L. Lengauer, E. Tillmanns, *J. Am. Chem. Soc.* **1993**, *115*, 7696−7705.
[34] S. Hünig, K. Sinzger, M. Jopp, D. Bauer, W. Bietsch, J. U. von Schütz, *Angew. Chem.* **1992**, *104*, 896−899; *Angew. Chem. Int. Ed. Engl.* **1992**, *31*, 859−862.
[35] [35a] A. J. Epstein, E. M. Conwell, *Solid State Commun.* **1977**, *24*, 627−630. − [35b] J. S. Miller, A. J. Epstein, *Angew. Chem.* **1987**, *99*, 332−339; *Angew. Chem. Int. Ed. Engl.* **1987**, *26*, 287.
[36] S. Hünig, P. Erk, E. Günther, H. Meixner, T. Metzenthin, J. U. von Schütz, M. Bair, H.-J. Gross, U. Langohr, S. Söderholm, H.-P. Werner, H. C. Wolf, E. Tillmanns, *Synth. Met.* **1991**, *42*, 1781−1788.
[37] R. Moret, P. Erk, S. Hünig, J. U. von Schütz, *J. Phys. (Paris)* **1988**, *49*, 1925−1931.
[38] R. E. Peierls, *Quantum Theory of Solids*, Oxford University Press, Oxford, **1955**, p. 108.
[39] H.-P. Werner, J. U .von Schütz, H. C. Wolf, R. K. Kremer, M. Gehrke, A. Aumüller, P. Erk, S. Hünig, *Solid State Commun.* **1989**, *69*, 1127−1130.
[40] R. Bozio, C. Pecile, *Spectroscopy of Advanced Materials* (Eds.: R. J. H. Clark, R. E. Hester), John Wiley, Chichester, **1990**; M. Meneghetti, G. Lunardi, R. Bozio, C. Pecile, *Synth. Met.* **1991**, *42*, 1775−1780.
[41] Earlier measurements: $[2,5\text{-}Me_2DCNQI]_2M$; M = Li: J. U. von Schütz, M. Bair, H.-P. Werner, H. C. Wolf, A. Aumüller, P. Erk, S. Hünig, in *Organic and Inorganic Low Dimensional Crystalline Materials* (Eds.: P. Delhaes, M. Drillon), Plenum Press, Oxford, **1987**; R. Kato, H. Kobayashi, A. Kobayashi, T. Mori, H. Inokuchi, *Synth. Met.* **1988**, *27*, B263−B268; R. Kato, H. Kobayashi, A. Kobayashi, *Chem. Lett.* **1987**, 1579−1582; Na, K: M. Helmle, J. Reiner, U. Rempel, M. Mehring, J. U. von Schütz, P. Erk, S. Hünig, H. Meixner, *Synth. Met.* **1991**, *42*, 1763−1768; Rb: D. Schmeißer, P. Bätz, W. Göpel, W. Jaegermann, C. Pettenkofer, H. Wachtel, A. Jimenez-Gonzales, J. U. von Schütz, H. C. Wolf, J. Taborski, V. Wüstenhagen, E. Umbach, P. Erk, S. Hünig, H. Meixner, *Ber. Bunsenges. Phys. Chem.* **1991**, *95*, 1442−1443.
[42] S. Hünig, P. Erk, *Adv. Mater.* **1991**, *3*, 225−236.
[43] J. C. Carter, L. H. Benett, D. H. Kahan, "Metallic Shift in NMR", *Progress in Material Science*, vol. 20, part I, Pergamon Press, Oxford, **1977**.
[44] S. Tomic, D. Jérome, A. Aumüller, P. Erk, S. Hünig, J. U. von Schütz, *J. Phys. C: Solid State Phys.* **1982**, *21*, L203−207. S. Tomic, D. Jérome, A. Aumüller, P. Erk, S. Hünig, J. U. von Schütz, *Synth. Met.* **1988**, *27*, B281.
[45] D. Bauer, J. U. von Schütz, H. C. Wolf, S. Hünig, K. Sinzger, R. K. Kremer, *Adv. Mater.* **1993**, *5*, no. 11, 829−834.
[46] D. Gómez, J. U. von Schütz, H. C. Wolf, S. Hünig, *J. Phys. I* **1996**, *6*, 1655−1671.
[47] [47a] H. M. Rietveld, *Acta Crystallogr.* **1967**, *22*, 151−152. − [47b] H. M. Rietveld, *J. Appl. Crystallogr.* **1969**, *2*, 65−71.
[48] Th. Bauer, M.Sc. Thesis, University of Würzburg, **1990**.
[49] Powder Diffraction File, International Centre for Diffraction Data, Newtown, Newtown Square, PA, USA, **1996**.
[50] F. Lux, S. Trebert Haeberlin, W. Erhardt, *Fresenius Z. Anal. Chem.* **1986**, *323*, 833.
[51] D. Jérome, personal communication to P. Erk, **1989**.
[52] M. L. Kaplan, *J. Cryst. Growth* **1976**, *33*, 161−164; D. Schweitzer, personal communication to A. Aumüller, **1984**.

Received July 27, 1998
[I98247]

Effects of Halides and Related Ligands on Reactions of Carbonylruthenium Complexes (Ru^0–Ru^{II})

Guy Lavigne[a]

Dedicated to Herbert D. Kaesz on the ocassion of his 66th birthday

Keywords: Halides / Homogeneous catalysis / Organometallics / Ruthenium

While the primary motivation of fundamental studies on carbonylhalotriruthenium complexes was to understand the promoter effect of halides on certain ruthenium-based catalytic systems of industrial relevance, such complexes have gained significance in their own right due to their remarkable ability to provide low-activation energy pathways for the coordination of organic substrates. Limitations inherent to the fragility of these prototypes led to the design and development of a related family of more sophisticated derivatives where an aminopyridyl group serves as an alternate *hemilabile* ancillary ligand. Studies of their reactivity have revealed the possibility of achieving a number of stoichiometric or moderately catalytic "cluster-mediated" transformations of organic substrates under very mild conditions. Yet, the viability of these systems is still limited to a narrow low-energy domain. By contrast, halotriruthenium derivatives are still seen to function as catalyst precursors under the actual conditions of certain catalytic reactions where they act as sources of ruthenium(II) halide complexes that become the active components of the system. The second part of the review focuses on novel aspects of their fascinating chemistry.

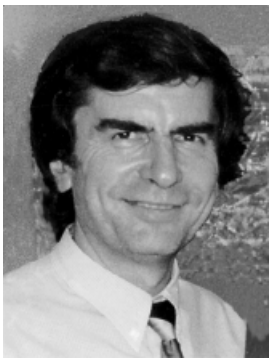
Introduction

The association of carbonylruthenium complexes with halides has long been known to produce remarkably efficient catalyst precursors. Historically, Dombek and Knifton were the first to draw attention on the effects of these "magic" mixtures in two fascinating series of independent reports revealing, respectively, that *enhanced selectivity* in the syngas conversion into ethylene glycol could be achieved in the homogeneous phase with an $Ru_3(CO)_{12}$/iodide system,[1] or by ruthenium "melt" catalysis, where a bromide salt acts both as solvent and co-catalyst.[2] Two anionic species, $[Ru_3(\mu\text{-}H)(CO)_{11}]^-$ and $[Ru(CO)_3X_3]^-$, both directly generated in situ under CO/H_2, were found to be essential for optimum activity.

The CO hydrogenation leading to glycol was proposed to begin with the formation of a formyl species by *intermolecular hydride transfer* from $[Ru_3(\mu\text{-}H)(CO)_{11}]^-$ (or, more probably from $[HRu(CO)_4]^-$ generated in situ)[3] to one of the electrophilic carbonyl groups of the haloruthenium(II) complex.

At that time, however, and even though interesting model studies were done with other metals,[4] the proposed halo(hydroxyalkyl)ruthenium(II) intermediates on the way to glycol remained elusive and were even thought to be too short-lived for proper detection, which may no longer be true on the basis of recent observations (vide infra).

[a] Laboratoire de Chimie de Coordination du CNRS,
205 route de Narbonne, F-31077 Toulouse Cedex, France
Fax: (intenat.) + 33-5/61553003
E-mail: lavigne@lcc-toulouse.fr



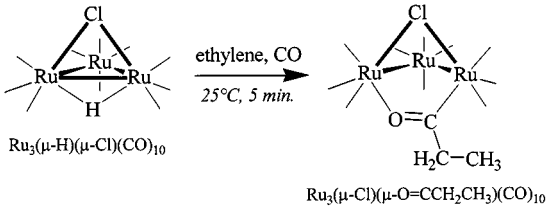
Guy Lavigne was born in Toulouse in 1947. He obtained his Ph.D. ("Doctorat d'Etat des Sciences") from the University of Paris VI under the supervision of Professor Yves Jeannin. In 1979, he joined the group of Professor Jean-Jacques Bonnet at the "Laboratoire de Chimie de Coordination du CNRS" (LCC). After post-doctoral studies at UCLA with Professor Herbert D. Kaesz in 1984, he returned to Toulouse at the LCC/CNRS where he was appointed Research Director in 1988. His research deals with the fundamental aspects of metal-mediated carbon–carbon bond-forming reactions and their application to homogeneous catalysis.

MICROREVIEWS: This feature introduces the readers to the authors' research through a concise overview of the selected topic. Reference to important work from others in the field is included.

 © WILEY-VCH Verlag GmbH, D-69451 Weinheim, 1999 1434–1948/99/0606–0917 $ 17.50+.50/0

These and related[5] pioneering observations paved the way to a dramatic development of research on Ru-based syngas reactions,[2b] with notable modifications including the use of different promoters such as onium chloride salts and weak acids[6] or even benzimidazoles.[7] The mixture of $[HRu_3(CO)_{11}]^-$ and $[Ru(CO)_3X_3]^-$ (X = Br or I) was later found to be active for various related reactions[8] including, in particular, the oxonation of olefins[9] and their alkoxycarbonylation.[10] Besides, Cenini and co-workers published an interesting phosgene-free process for the carbonylation of aromatic nitro compounds to carbamates, again using mixtures of $Ru_3(CO)_{12}$ and halide salts.[11]

While examining the chemical behavior of the same complexes within a much lower energy domain, Kaesz and co-workers discovered at the same time that the presence of a halide in the ligand shell of a carbonylruthenium cluster results in the regioselective incorporation of phosphane ligands[12] or organic substrates[13] under unprecedented mild conditions. A spectacular report[13] included a reaction between the halide-containing species $Ru_3(\mu\text{-H})(\mu\text{-Cl})(CO)_{10}$ and ethylene/CO mixtures (5 atm), giving the propionyl complex $Ru_3\{\mu\text{-C(O)CH}_2\text{CH}_3\}(\mu\text{-Cl})(CO)_{10}$ within minutes at 25°C (Scheme 1), thus nicely modeling a key step in olefin hydroformylation, a reaction independently found to be catalyzed by $[Ru_3(\mu\text{-H})(CO)_{11}]^-$.[14]



$Ru_3(\mu\text{-H})(\mu\text{-Cl})(CO)_{10}$

$Ru_3(\mu\text{-Cl})(\mu\text{-O=CCH}_2\text{CH}_3)(CO)_{10}$

Scheme 1. Facile activation of ethylene by a carbonylchlorohydridotriruthenium complex

In attempts to devise an anion route to the above halohydridotriruthenium derivative, Kaesz and Lavigne discovered that $Ru_3(CO)_{12}$ reacts spontaneously at 25°C with onium salts of halides or pseudohalides *in the absence of ion pairing* to give hitherto unknown adducts of the type $[Ru_3(CO)_{12-n}(X)]^-$ (n = 0−3) exhibiting remarkably *enhanced substitutional lability*.[15] These *"activated"* species primarily drew attention while appearing as the first formed intermediates on the way to Dombek's catalysts (vide supra). In fact, as explained below in the first part of this review, these and related complexes were further shown to be of specific interest as synthetic tools for a number of stoichiometric or moderately catalytic *cluster-mediated* transformations of organic substrates occurring on a laboratory scale *under very mild conditions*[16] but having no direct relevance to the applied reactions mentioned above.

A renewal of interest for ruthenium/halide systems emerged in 1989 with Keim's report[17] that carbonylruthenium chloride clusters were catalyst precursors for the hydroesterification of ethylene with methyl formate, originally disclosed by Sneeden et al.[18] The reaction was later shown by Petit and co-workers to be much more efficiently catalyzed by the multi-component Ru/iodide/DMF system.[19]

Based on what we knew at that time, carbonylhaloruthenium clusters appeared to us unlikely to survive under the reported experimental conditions. We were thus challenged to re-investigate the hydroesterification reaction with the aim of tracing the transformation of Ru_3/halide precursors toward the formation of the active species. Studies in collaboration with Kalck and co-workers led us to observe that the aforementioned anionic mononuclear carbonylruthenium(II) halide species $[Ru(CO)_3X_3]^-$ was again implied, and could even be used alone as a catalyst precursor.[20] A literature survey indicated that, in spite of the newly established implication of carbonylhaloruthenium(II) complexes as catalyst precursors in a growing number of C−C bond-forming reactions,[21] the present state of knowledge of their reactivity rests essentially on early pioneering studies.[22] Thus, a new research project was undertaken with the aim of filling the gap between the basic knowledge on these compounds and their applied reactions. The first results of our new investigation are summarized in the second part of this review.

I. Chemistry of "Anion-Promoted" Ruthenium Cluster Complexes Under Mild Conditions

I.1 Catalysis of CO Displacement by Phosphanes in $Ru_3(CO)_{12}$ in the Presence of Anionic Nucleophiles

In 1984, we made the intriguing observation that addition of catalytic amounts of $[(PPh_3)_2N]Cl$ to a THF solution containing a mixture of $Ru_3(CO)_{12}$ and triphenylphosphane, results in the rapid formation of the monosubstituted derivative $Ru_3(CO)_{11}(PPh_3)$ at 25°C[15] (Equation 1).

$$Ru_3(CO)_{12} + PR_3 \xrightarrow[\text{THF, 25°C}]{\text{onium salt of Nu}^-\text{* (catalytic amounts)}} Ru_3(CO)_{11}(PR_3) + CO \quad (1)$$

(*) Nu^- = (i) CN^-, CH_3COO^-, F^-, Cl^-, Br^-, or I^-;
or, (ii) $[BHR_3]^-$ or $[HRu(CO)_4]^-$

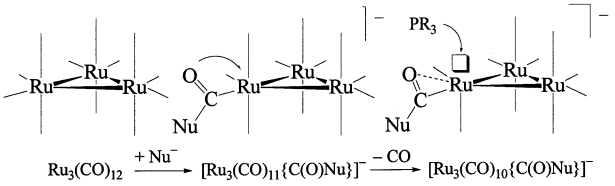
Whereas the thermally induced substitution (ca. 2 h, 90°C) was known to give only the "thermodynamic" trisubstituted derivative $Ru_3(CO)_9(PPh_3)_3$,[23] catalysis by the salt under highly dissociating conditions (i.e. in the absence of ion pairing) appeared as a valuable means to *selectively* trap the kinetic substitution product. The system was rapidly extended to a range of nucleophilic anions [see Equation 1, catalysts type (i)] whose relative efficiencies were established on the basis of a preliminary kinetic study revealing a zero-order rate dependence on $[Ru_3(CO)_{12}]$. The effect of these ions was interpreted in terms of the enhanced substitutional lability of the methoxycarbonyl adducts $[Ru_3\{\eta^1\text{-C(O)OMe}\}(CO)_{11}]^-$ established by Ford[24] in stoichiometric reactions with phosphanes (see Equations 2−3)[25] or molecular hydrogen (sequence of Equations 2 and 4),[26] and independently applied to ^{13}CO enrichment by Darensbourg.[27]

$$Ru_3(CO)_{12} + OCH_3^- \rightarrow [Ru_3(CO)_{11}\{C(O)OCH_3\}]^- \quad (2)$$

$$[Ru_3(CO)_{11}\{C(O)OCH_3\}]^- + PR_3 \rightarrow Ru_3(CO)_{11}PR_3 + CO + OCH_3^- \quad (3)$$

$$[Ru_3(CO)_{11}\{C(O)OCH_3\}]^- + H_2 \rightarrow Ru_3(\mu\text{-}H)(CO)_{11}]^- + HC(O)OCH_3 \quad (4)$$

It was suggested[15b] (Scheme 2) that CO labilization by the oxygen atom of a transient nucleophile-CO adduct "C(O)Nu" would allow the phosphane to reach the metal center. The increased basicity brought by this incoming ligand would then cause a reduction of the δ^+ character of the carbon atom, thereby facilitating the expulsion of the nucleophilic anion Nu^- and its intermolecular transfer to a neighboring cluster for the propagation of the effect.



Scheme 2. Proposed pathway for anion-promoted CO labilization (the square box denotes a vacant coordination site)

While reasoning that the simplest nucleophilic anion H^- is likely to give the same type of transient adduct $[Ru_3\{\eta^1\text{-}C(O)H\}(CO)_{11}]^-$ (or $[Ru_3\{H\}(CO)_{12}]^-$), we were able to show that catalysis of CO displacement by phosphanes into $Ru_3(CO)_{12}$ can also be efficiently carried out by *intermolecular hydride transfer*, using simple hydridic reagents like potassium tri-*sec*-butylhydroborate (K-Selectride) or $[HRu(CO)_4]^-$ as catalysts [Equation 1, catalyst type (ii)].[28] The latter procedure, exceeding the performance of the sodium benzophenone ketyl catalyst proposed earlier by Bruce,[29] is of high practical synthetic utility since "super hydrides" are found in any chemical laboratory. Significantly, the catalytic substitution can also be initiated by adding few crystals of $[PPN][Ru_3(\mu\text{-}H)(CO)_{11}]$ to a THF solution of $Ru_3(CO)_{12}$ and phosphane under CO.[28] In that case, however, an induction period is required for the latter anion to generate the actual hydride transfer agent $[Ru_3\{\eta^1\text{-}C(O)H\}(CO)_{11}]^-$ (or $[Ru_3\{H\}(CO)_{12}]^-$[30]). The mechanism proposed at that time for the formation of such adducts[28] found further support in the results of a more recent kinetic study reported by Shore,[30c] indicating that $^{13}CO/^{12}CO$ exchange in $[Ru_3(\mu\text{-}H)(CO)_{11}]^-$ is governed by competition between two parallel pathways, namely, a dissociative pathway (zero-order in anion and zero-order in CO) and an associative step (first-order in anion and first-order in CO), the latter becoming increasingly significant with increasing concentration of ^{13}CO. Thus, just like in the water gas shift reaction[30] [and also like in the hydride transfer occurring in the glycol synthesis (vide supra)], the preceding substitution reaction is governed by an associative step.

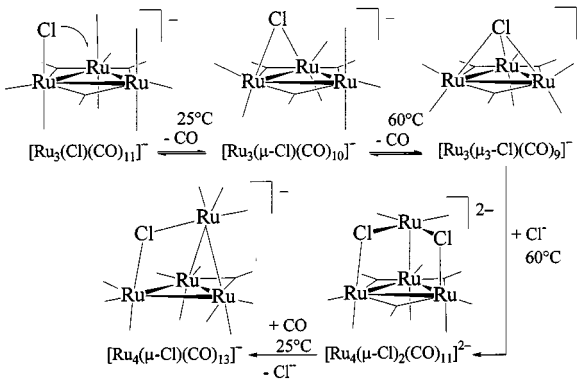
For anionic nucleophiles such as halides and pseudohalides, the nature of the initial site of attack proposed in Scheme 2 cannot be ascertained since the first formed adducts are very short-lived. Competitive nucleophilic attack at CO and at the metal center was reasonably suggested by Ford on the basis of a thorough kinetic study.[31]

I.2 Intramolecular Halide-Promoted CO Labilization and Its Application to the Controlled Activation of Unsaturated Substrates

Whereas the primary adducts discussed above are involved in the catalysis of phosphane substitution, we will now see that the subsequent anionic derivatives $[Ru_3(Cl)(CO)_{12-n}]^-$ ($n = 1-3$) are of synthetic utility when the incoming ligands are unsaturated organic substrates.

I.2.1 Equilibria within Ru_3/Halide Systems

The complete elucidation of the precise nature of these halide adducts rests on the concerted efforts of several groups.[15,20,32–35] Though Scheme 3 displays all equilibria appearing within the $Ru_3(CO)_{12}$/chloride system, the present paragraph deals only with the first three adducts $[Ru_3(Cl)(CO)_{12-n}]^-$ ($n = 1-3$), whereas further re-arrangement to tetranuclear species occurring under specific conditions will be discussed in section II.1.



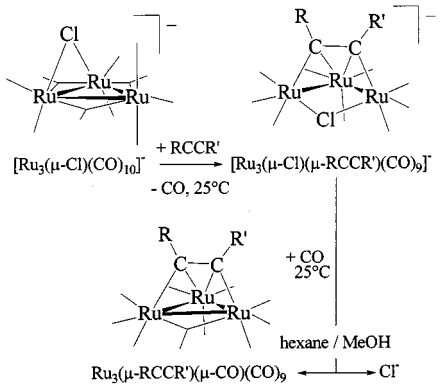
Scheme 3. Equilibria within Ru_3/halide systems

In the first observable adduct, $[Ru_3(Cl)(CO)_{11}]^-$ (readily obtained at 25°C), the halide ligand occupies an axial coordination site onto the metal triangle.[33] It then slowly labilizes one vicinal CO at 25°C while moving into an edge-bridging position to yield $[Ru_3(\mu\text{-}Cl)(CO)_{10}]^-$. Finally, it may still use one more electron pair to coordinate in a face-bridging position with concomitant CO labilization to form $[Ru_3(\mu_3\text{-}Cl)(CO)_9]^-$. However, this requires the assistance of thermal activation (60°C) and a stream of inert gas to evacuate the released CO.[34]

I.2.2 Activation of Alkynes under Ambient Conditions

Opening of the halogen bridge in $[Ru_3(\mu\text{-}Cl)(CO)_{10}]^-$ or $[Ru_3(\mu_3\text{-}Cl)(CO)_9]^-$ provides a low-activation-energy path for the reaction of these complexes with alkynes at 25°C, giving only one species $[Ru_3(\mu\text{-}Cl)(\mu\text{-}RCCR)(CO)_9]^-$ in quantitative yield within few minutes (Scheme 4).[34][36]

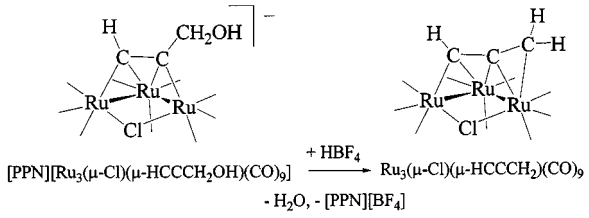
The kinetics of this reaction were investigated by Basolo.[37] The halide ligand appears to be so lightly coordinated to the metal core in the latter anionic species that its displacement by a CO ligand can be readily catalyzed by a



Scheme 4. Halide-promoted reaction of alkynes with $Ru_3(CO)_{12}$

protic solvent like methanol. Hence, if a biphasic hexane/methanol solvent mixture is used, the neutral complex $Ru_3(\mu\text{-RCCR})(\mu\text{-CO})(CO)_9$ transfers itself to the hexane phase, from which it can be recovered pure without chromatographic workup.[34][36] The latter complex is the kinetic product of the reaction between $Ru_3(CO)_{12}$ and alkynes, and is not observable under thermal activation.[38]

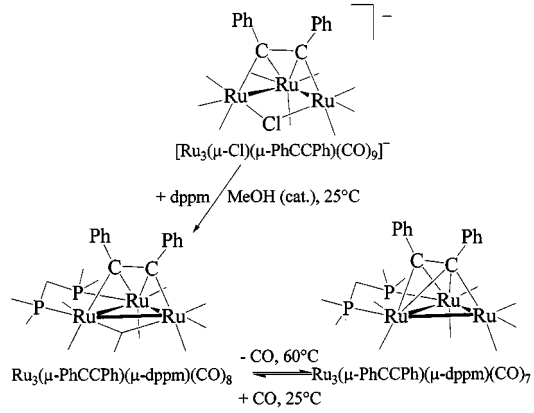
Slight modifications of the above synthetic strategy allowed the preparation of various alkyne-, alkynyl-[34][36] or allenyltriruthenium[39] complexes. For example, the new allenyl complex $Ru_3(\mu\text{-Cl})(\mu\text{-HCCCH}_2)(CO)_9$ was readily obtained within a few minutes by reaction of the anionic chlorotriruthenium complex with propargylic alcohol followed by proton-induced dehydration of the cluster-bound ligand (Scheme 5).[39]



Scheme 5. Facile dehydration of a cluster-bound alkynol

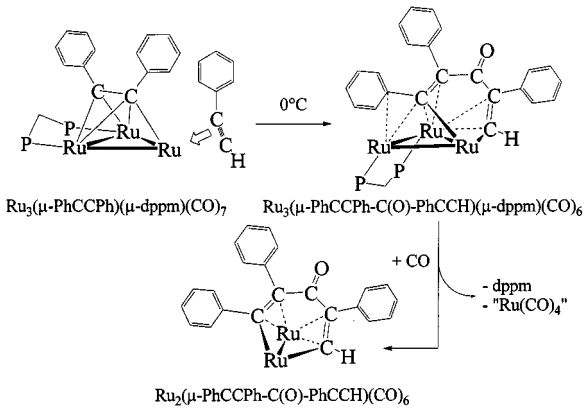
Significantly, the first and still unique prototype of unsaturated 46e$^-$-alkynetriruthenium complex, $Ru_3(\mu_3\text{-}\eta^2\text{-PhCCPh})(\mu\text{-dppm})(CO)_7$, was also prepared from the anionic alkynedecacarbonylchlorotriruthenium derivative by methanol-induced halide abstraction in the presence of dppm according to the sequence shown in Scheme 6.[40]

While the synthetic utility of the halide appeared obvious in light of the above reactions, we rapidly faced a new problem while attempting to achieve a full transformation of the "activated" alkyne directed toward the liberation of an oligomeric substrate. This is illustrated in Scheme 7.[41] We first made the encouraging observation that the cluster-bound alkyne ligand in the triruthenium complex $Ru_3(\mu\text{-PhCCPh})(\mu\text{-dppm})(CO)_7$ could be readily engaged in C−C bond formation with an incoming phenylacetylene molecule within minutes at 0°C, giving the coordinatively unsaturated "fly-over"-type complex $Ru_3[\mu\text{-PhCCPh}-C(O)-PhCCH](\mu\text{-dppm})(CO)_6$ where the dialkenyl ketone fragment



Scheme 6. Synthesis of the first prototype of an unsaturated alkyne-triruthenium cluster complex and observation of a "windshield-wiper" motion of the alkyne ligand onto the metal triangle

HC=CPh−C(O)−PhC=CPh appeared as the result of an intramolecular alkyne/CO/alkyne coupling.[41] Bearing in mind the existence of a patented process for the synthesis of hydroquinone using $Ru_3(CO)_{12}$ as a catalyst precursor,[42] we treated the newly formed derivative with CO, hoping to release a cyclic ketone or a quinone. However, this resulted in successive losses of the supporting dppm ligand and of one metal center, ending with the formation of a stable dimetallic fly-over species. It was thus becoming clear that the elimination of the free organic molecule (probable under forcing conditions, but not observed under those of our experiment) would take place only from a low-nuclearity fragment after complete degradation of the cluster (see Scheme 7, ancillary ligands omitted for clarity).



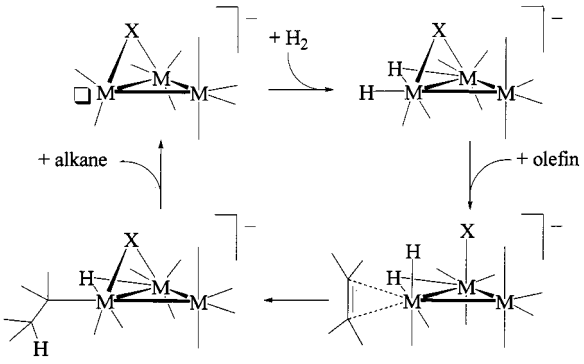
Scheme 7. Intramolecular akyne/CO/alkyne coupling

A modification of our strategy was thus required in order to observe full transformations of organic substrates on the metal core (see section I.3).

I.2.3 Activation of Olefins

In 1986, Gladfelter and co-workers reported that olefins can be readily hydrogenated at ambient temperature in the presence of the isocyanatotriruthenium cluster complex $[Ru_3(NCO)(CO)_{10}]^-$,[43] another member of the growing family of "anion-promoted" triruthenium clusters.[16] The

system was understood in terms of the ability of the pseudohalide $X^- = NCO^-$ to function reversibly as a one- or three-electron donor, thereby helping to maintain similar relative energies of the intermediates. The catalytic reaction observed with ruthenium was modeled with osmium (Scheme 8) for which the alkyl intermediate was intercepted, using succinoyl anhydride as the olefin.[44]

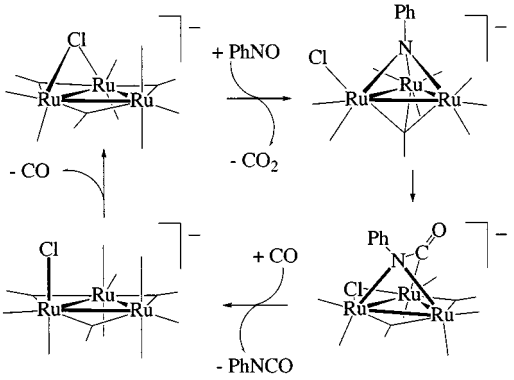


Scheme 8. Mechanism of the anion-promoted olefin hydrogenation proposed by Gladfelter and co-workers; the square box appearing in the scheme denotes a vacant coordination site on the metal center

A limitation of the system for $X^- = Cl^-$ appeared to be the facile reductive elimination of HCl from the anionic halohydrido intermediate, giving the anion $[HRu_3(CO)_{11}]^-$, a pathway related to the one shown in Equation 4.

I.2.4 Carbonylation of Nitrosobenzene

In connection with the above-mentioned discovery by Cenini et al. of a promoter effect of halides on the ruthenium-catalyzed synthesis of carbamates from aromatic nitro compounds,[11] Geoffroy and co-workers were able to show that the lightly coordinated halide in $[Ru_3(\mu\text{-}Cl)(CO)_{10}]^-$ can be engaged in bridge-opening/closing reactions assisting both the coordination of nitrosobenzene prior to NO bond cleavage and the carbonylation of the incipient nitrene intermediate to give phenyl isocyanate (Scheme 9).[45]



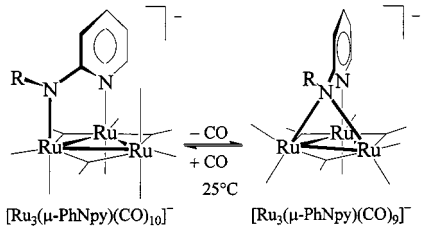
Scheme 9. Mechanism of the anion-promoted conversion of nitrosobenzene into isocyanate, as proposed by Geoffroy and co-workers

However, given that such a transformation occurs only under very mild conditions, there is no evidence for its value as a model for the effective carbonylation of aromatic nitro compounds, which is known to take place only under more forcing conditions.

I.3 Effects of Related Nitrogen-Based Hemilabile Ancillary Ligands

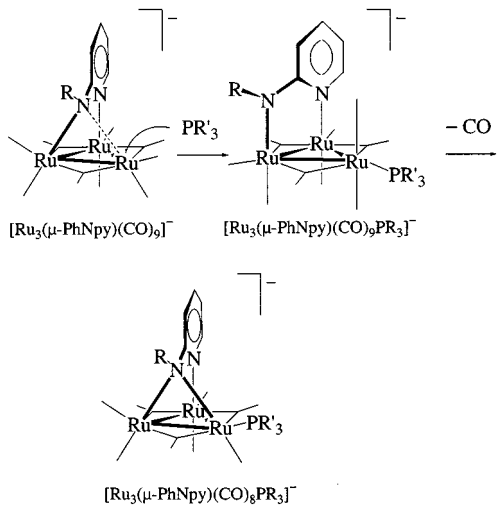
I.3.1 The Basic Concept

Since the adventitious loss of the halide from the above triruthenium species appeared as an undesirable dead end in several cases, we were led to devise a related family of "activated" cluster complexes incorporating aminopyridyl groups as alternate *hemilabile* ancillary ligands. As shown in Scheme 10, whereas the pyridyl group functions as an anchor, the amido group can adopt terminal or bridging coordination modes quite analogous to those occurring with halides (see Scheme 3).[46]



Scheme 10. Reversible CO uptake by a triruthenium cluster incorporating an aminopyridyl group as hemi-labile ancillary ligand

An advantage of aminopyridyl ligands is the possibility to tune their nucleophilicity by modifying the nature of the R group. Second-order kinetics were observed by Basolo for the reactions of anionic (aminopyridyl)triruthenium complexes with phosphanes.[47] The results were consistent with a mechanistic scheme in which nucleophilic attack by the phosphane gives an adduct bearing the amido ligand in



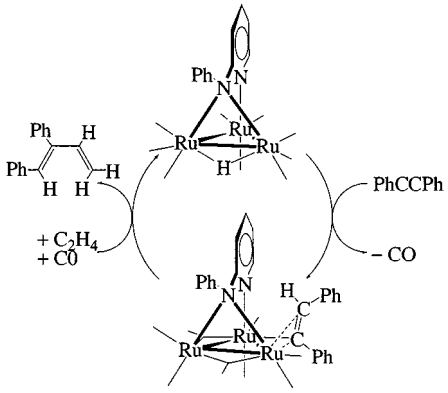
Scheme 11. Isolation of a phosphane adduct on the way to the substituted derivative

terminal position. After isomerization of such an intermediate, further reformation of the amido bridge through intramolecular nucleophilic attack with concomitant CO expulsion leads to the substituted derivative. The energy barrier for the latter step is dependent on the nucleophilicity of the amido group. Thus, whereas the intermediate adduct is trappable with R = Ph, the reaction proceeds directly to the substituted derivative when R = Me.

I.3.2 Activation of Alkynes and Vinyl-Group Transfer Reactions

The hemilabile behavior demonstrated for the above anionic species was suggested to account for the high reactivity of the corresponding protonated complexes $Ru_3(\mu\text{-}H)(\mu\text{-}RNpy)(CO)_9$ whose reactions with phosphanes proved to be too fast, even at −40 °C, to be amenable to kinetic studies.

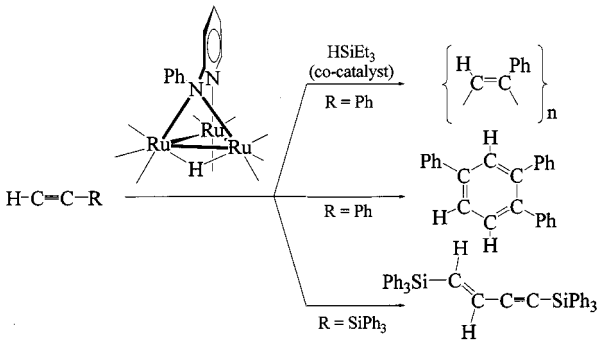
In 1990, we made the original observation that the anilinopyridyl complex $Ru_3(\mu\text{-}H)(\mu\text{-}PhNpy)(CO)_9$ is prone to activate alkynes selectively via the alkenyl intermediate $Ru_3(\mu\text{-}H)(\mu\text{-}PhNpy)(PhC{=}CHPh)(CO)_8$ and to promote the catalytic hydrogenation of diphenylacetylene as well as its stoichiometric hydrovinylation.[46] Whereas the kinetics and mechanism of the former reaction were subsequently investigated in detail by the group of Cabeza and Riera,[48] we became more interested in the second type of transformation which involved C−C bond formation (Scheme 12).



Scheme 12. Cluster-mediated hydrovinylation of diphenylacetylene

The co-dimerization leading to 1,2-diphenyl-1,3-butadiene was understood in terms of an insertion of ethylene into a ruthenium−alkenyl bond followed by β-elimination, a mechanism similar to the one established by Knox for a parallel reaction occurring at a diruthenium center.[49]

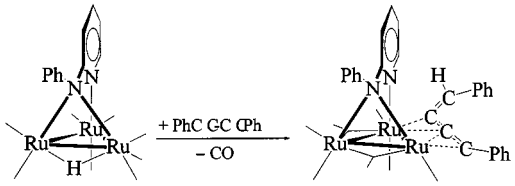
With more reactive 1-alkynes (and in the absence of alkene), multiple alkyne insertions were observed. Curiously, whereas ruthenium is not known to be an efficient alkyne polymerization catalyst, the regioselective polymerization of phenylacetylene to the *cis*-polyphenylacetylene was found to take place within few minutes at room temperature in the presence of the hydrido species $Ru_3(\mu\text{-}H)(\mu\text{-}PhNpy)(CO)_9$ and of triethylsilane (as a co-catalyst) (Scheme 13).[50] By contrast, trimerization was observed in the absence of silane.



Scheme 13. Oligomerization of terminal alkynes in the presence of the (anilinopyridyl)hydridotriruthenium complex as catalyst precursor

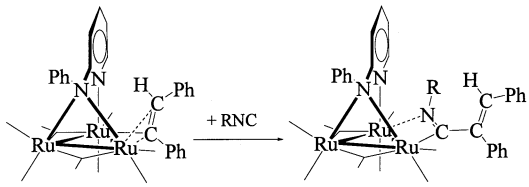
Though polymerization of phenylacetylene under hydrosilylation conditions has been also observed in a few instances with other metals,[51] the promoter effect of the silane as a co-catalyst remains unclear.

With triphenylsilylacetylene as the incoming substrate (and in the absence of silane), a rapid but poorly catalytic dimerization was observed (see Scheme 13), leading selectively to the (*E*)-1,4-bis(triphenylsilyl)but-1-en-3-yne, obtained pure as beautiful crystals appearing on the walls of the glassware. Here again, no intermediates could be detected and our approach to the mechanism had to rely on model studies. First, in order to test the mechanistic possibility of a vinylidene/acetylide coupling,[52] which should have generated a transient butenynyl intermediate,[53] we treated the hydrido complex with a preformed diyne whose insertion into the Ru−H bond was likely to give such an intermediate. Though a butenynyl complex was effectively isolated (Scheme 14),[54] it could not be regarded as a plau'sible intermediate since it was not possible to promote its reductive elimination as an enyne in the presence of an incoming alkyne.



Scheme 14. Activation of a diyne by insertion into an Ru−H bond and formation of a butenynyl ligand

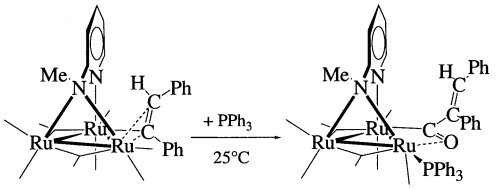
Though not firmly established, the alternate possibility of an alkenyl/acetylide coupling was preferred in light of the parallel observation of a facile alkenyl-group transfer from the alkenyl complex to the α-carbon atom of an incoming isocyanide (Scheme 15).[50][54]



Scheme 15. Alkenyl/isocyanide coupling giving an azabutadienyl ligand

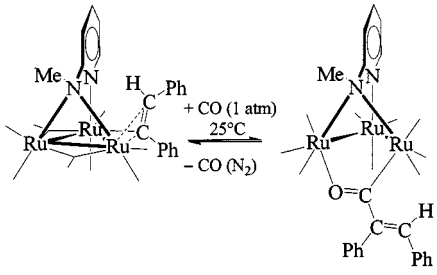
Here, the incorporation of the isocyanide ligand onto the $48e^-$ species occurs at 25°C by an associative pathway consistent with a mechanistic scheme where the transient opening of the amido bridge (or another weak bond, vide infra) assists the incorporation of the ligand, whereas its subsequent reformation triggers C−C bond formation, in exact parallel with reactions observed earlier with halides and related ancillary ligands.

With the aim of verifying the generality of such a working hypothesis, we treated our alkenyl complex with triphenylphosphane and effectively observed that the incorporation of this ligand also caused migratory CO insertion of the alkenyl group (Scheme 16).



Scheme 16. Phosphane-induced migratory CO insertion of an alkenyl group

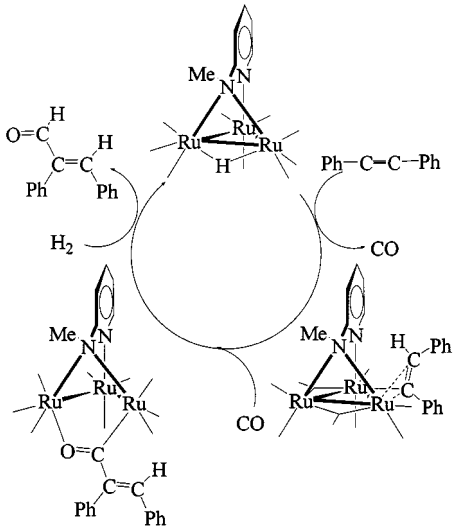
Though obtained within few minutes under very mild conditions, the resulting propenoyl complex proved to be the thermodynamic product of the reaction.[55] Evidence for the existence of a kinetic intermediate was obtained from additional experiments[55] including a preliminary kinetic study carried out by Basolo.[56] Further work indicated that, of course, CO gas itself is readily incorporated and promotes the same migratory insertion. Though the corresponding adduct is stable only under CO, we succeeded in crystallizing it under such conditions (Scheme 17).[50][55]



Scheme 17. CO-induced migratory CO insertion of an alkenyl group

Significantly, *two* carbonyl ligands were incorporated without a detectable intermediate. The fact that an open $50e^-$ cluster was obtained (rather than a closed $48e^-$ species bearing a terminal amido group) raised recurrent questions about the nature of the initial elusive adduct formed upon ligand addition to the alkenyl cluster complex. Indeed, let us remind ourselves that there are three types of weak bonds in this complex whose rupture is plausible: (i) the Ru−N bonds of the amido bridge, (ii) the π interaction between the alkenyl group and the cluster and (iii) the metal−metal bonds. Thus, hypotheses regarding the rupture of any of such bonds may be equally reasonable due to the probable similar magnitude of their respective enthalpies. However, we believe that a more realistic scheme involves *a global expansion of the structure by lengthening of several of these bonds without localized rupture*,[55] as independently demonstrated for another ligand-bridged triruthenium cluster complex.[57] Another notable feature, highlighted by the previous equilibrium, is the ease with which the propenoyl group migrates at the periphery of the cluster.

Following the isolation of the propenoyl adduct, we succeeded in releasing α-phenylcinnamaldehyde upon treatment with CO/H_2 mixtures under very mild conditions. The propenoyl complex could then be tied to a catalytic cycle for the hydroformylation of diphenylacetylene (Scheme 18).[55]



Scheme 18. Catalytic cycle for the hydroformylation of diphenylacetylene showing the isolated intermediates

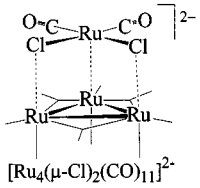
Though the reaction could cycle catalytically, the viability of the system under non-optimized conditions was affected by a competitive CO insertion into the Ru−N bond of the methylaminopyridyl group, ending with the formation of an inactive carboxamido complex of lower nuclearity.

II. Aspects of the Chemistry of Carbonylhaloruthenium(II) Complexes

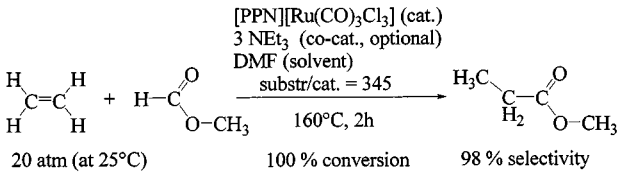
II.1 Evolution of $Ru_3(CO)_{12}$/Halide Mixtures under the Conditions of a Typical Hydroesterification Reaction

Studies reported in this section were undertaken in collaboration with Kalck and co-workers. Philippe Kalck was interested in the use of methyl formate as a valuable feedstock in organic synthesis. The "direct" addition of this substrate to olefins for the production of esters appeared to be a challenging reaction[58] that had been shown by Keim[17] to be catalyzed by $Ru_3(CO)_{12}$ alone or (albeit less efficiently) by the anion $[Ru_3(\mu\text{-}Cl)(CO)_{10}]^-$. A preliminary screening of the above-mentioned series of anionic triruthenium complexes incorporating halides, anilinopyridyl or alkoxypyridyl groups led us to focus on the $Ru_3(CO)_{12}$/[PPN]Cl system, which proved to be highly efficient pro-

vided that an amide-type solvent like DMF was used. During the course of preliminary experiments aimed at determining the optimum Ru/Cl ratio, we noted that the $[Ru_3(\mu\text{-}Cl)(CO)_9]^-$ reacts cleanly with an excess of halide at 60°C to give the novel unsaturated dianionic species $[PPN]_2[Ru_4(\mu\text{-}Cl)_2(CO)_{11}]$ already shown in Scheme 3.[20][59] Strikingly, its structure, of an unprecedented type, gave the image of a mononuclear Ru^{II} complex "$Ru(CO)_2Cl_2$" supported on an anionic triruthenium unit "$[Ru_3(CO)_9]^{2-}$".

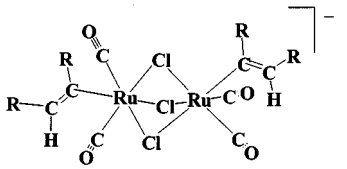


Intuitively, the liberation of such a fragment under catalytic conditions was thus conceivable. In fact, the above dianionic cluster species could be used alone as a catalyst precursor, just like other haloruthenium cluster complexes of the same series shown in Scheme 3. After overnight catalytic experiments, the principal species recovered in the reactor was the well-known carbido cluster $[Ru_6(C)(CO)_{16}]^{2-}$. Remembering that this inactive product had been previously detected by Dombek[1] at the end of syngas reactions using Ru/halide mixtures as catalyst precursors (vide supra), we reasoned that the active species in both systems might be the same. Then, different catalytic runs using $[PPN][HRu_3(CO)_{11}]^-$ and $[PPN][Ru(CO)_3X_3]$ (X = Cl, I) either separately, or as mixtures, led us to conclude that under the conditions of our hydroesterification reaction, the best precursor was $[PPN][Ru(CO)_3Cl_3]$ "alone".[59] It was thus appearing that the active species (still elusive) could be generated from either Ru^0 or Ru^{II} precursors. With $[PPN][Ru(CO)_3Cl_3]$, the reaction started without an induction period and proved to be very efficient (Scheme 19).



Scheme 19. Experimental conditions and performances of the catalytic hydroesterification reaction

A DMF complex $[PPN][Ru(CO)_2Cl_3(DMF)]$ appeared to be readily formed by decarbonylation of the above precursor. Interestingly, three closely related alkyl complexes $[PPN][Ru_2(\mu\text{-}Cl)_3(CO)_4RR']$ (R = Et or Me; R′ = Et or Me) were subsequently intercepted in the reactor by quenching the catalytic reaction as the system reached its optimum activity.[60] It was shown that, under the reaction conditions, the alkyl moieties were derived principally from ethylene (by insertion into an Ru−H bond) but also from the alkyl formate [by cleavage of the O−C(sp^3) bond]. Effectively, at that time, the only way to exclusively obtain the dimeric ethyl complex in a pure form proved to be the catalyzed addition of *ethyl* formate to ethylene.



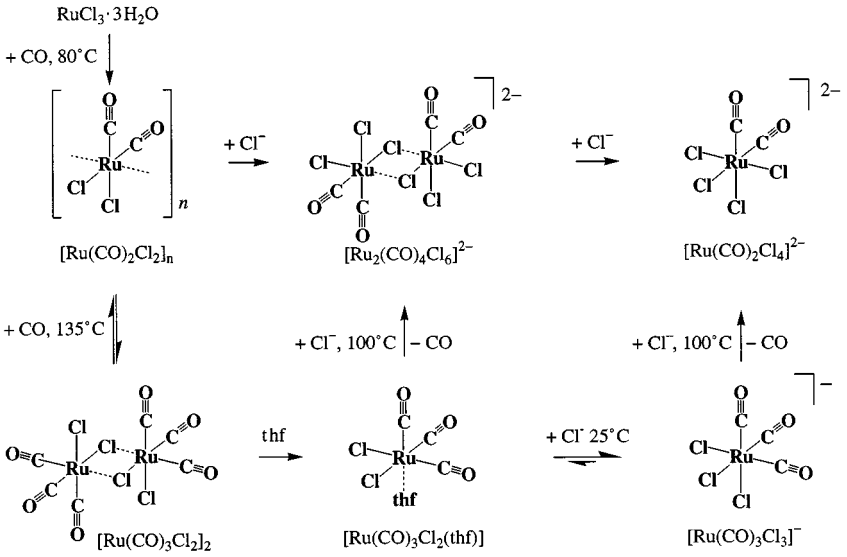
It was amazing to realize that a catalytic run performed in 1997 led to the discovery of the existence of a simple yet hitherto unknown species, some thirty years after its antecedent $[PPN][Ru(CO)_3Cl_3]$(!). Clearly, this revealed that the reactivity of carbonylchlororuthenium(II) species toward unsaturated organic substrates had not been examined in detail, or, at least needed to be revisited.

II.2 Pioneering Observations on Carbonylhaloruthenium(II) Complexes

The present state of knowledge of the chemistry of carbonylchlororuthenium(II) complexes rests on the important pioneering discoveries made in the 1960s and 1970s by several groups[22] amongst which we recognize names that have marked the development of this field: Chatt,[61] Halpern and James,[62] Bruce and Stone,[63] Braca,[64] Calderazzo,[65] Johnson and Lewis,[66] Collmann and Roper,[67] and Wilkinson.[68]

Equilibria involving the principal binary carbonylchloro derivatives are shown in Scheme 20. Chatt[61] was the first to observe that bubbling CO through a solution of $RuCl_3 \cdot 3\,H_2O$ at 85°C gives a red solution containing a structurally ill-defined polymeric complex $[Ru(CO)_2Cl_2]_n$. Prolonged treatment with CO at 120−140°C[63] gives the 16e⁻ tricarbonyl unit "$Ru(CO)_3Cl_2$", which spontaneously stabilizes itself by forming halide bridges to give $[Ru(CO)_3Cl_2]_2$.[69] Since the reverse decarbonylation is also operative at high temperature, a mixture of $[Ru(CO)_2Cl_2]_n$ and $[Ru(CO)_3Cl_2]_2$, known as the "yellow solution",[70] is generally obtained. The only way to drive the equilibrium toward the more CO-rich derivative is thus to pursue the carbonylation at room temperature.[59] As originally reported by Bruce and Stone,[63] splitting of the dimer $[Ru(CO)_3Cl_2]_2$ by a donor solvent like THF gives the nice crystalline complex $Ru(CO)_3Cl_2(thf)$ from which THF may be subsequently displaced by a halide anion to give the anionic species $[Ru(CO)_3Cl_3]^-$.

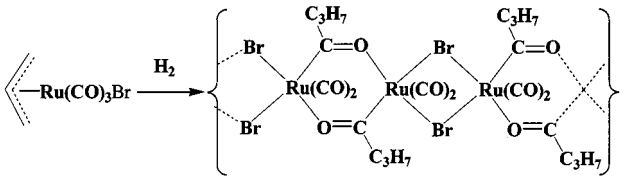
In fact, the complexes shown in Scheme 20 represent the principal possibilities to stabilize the 14e⁻ fragment "$Ru(CO)_2Cl_2$" by using all possible combinations of CO and Cl^- ligands. For a long time, these complexes were mainly regarded as intermediates for the preparation of more elaborate species.[22] For example, ruthenium chemists have long been using the above-mentioned "yellow solution" for the preparation of $Ru_3(CO)_{12}$ (by reduction with CO in the presence of zinc as a halide acceptor),[70] whereas fascinat-



Scheme 20. Interconversion between the principal known carbonylhaloruthenium(II) complexes

ing new complexes are still made nowadays by treatment of $[Ru(CO)_2Cl_2]_n$ with sophisticated phosphanes.[71]

In the early work of Pino et al.[72] we find a rare example of a carbonylhaloruthenium(II) complex bearing a hydrocarbon fragment as the only additional ligand. This is the allyl species $Ru(C_3H_5)(CO)_3Br$, prepared by oxidative addition of allyl bromide to $Ru_3(CO)_{12}$. Such a compound was shown to act as a catalyst precursor for olefin hydrogenation and isomerization,[64c] whereas its reaction with hydrogen gave a structurally ill-defined polymeric acyl species resulting from a hydrogenation of the allyl moiety followed by migratory CO insertion.[64c]

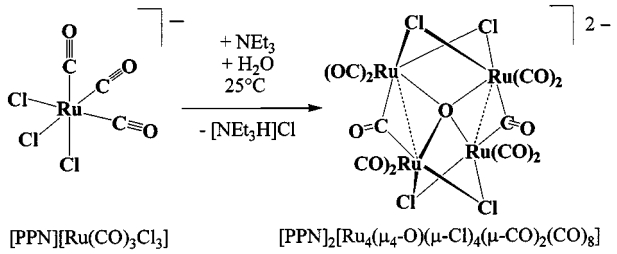


Further treatment of the latter with CO/methanol led to the stoichiometric formation of esters, thus prefigurating the possibility to achieve hydroesterification reactions.

II.3 New Findings in the Footsteps of the Pioneers

II.3.1 Facile Activation of Water

In attempts to trace the evolution of $[PPN][Ru(CO)_3Cl_3]$ under the conditions of a typical hydroesterification reaction, it was noted that treatment of this complex with triethylamine (the optional co-catalyst) resulted in *halide displacement rather than CO substitution*.[73] This provided an indication that the *neutral* fragment "$Ru(CO)_3Cl_2$" might be the reacting entity, whereas the weakly coordinated halide anion could be regarded as a lightly stabilizing ligand for the neutral unit. Furthermore, with wet triethylamine, the known[20] oxo complex $[PPN]_2[Ru_4(\mu_4\text{-}O)(\mu\text{-}Cl)_4(\mu\text{-}CO)_2(CO)_8]$ was obtained,[74] which was indicative of a facile activation of water accompanied by reductive elimination of HCl, trapped as $[NEt_3H]Cl$.



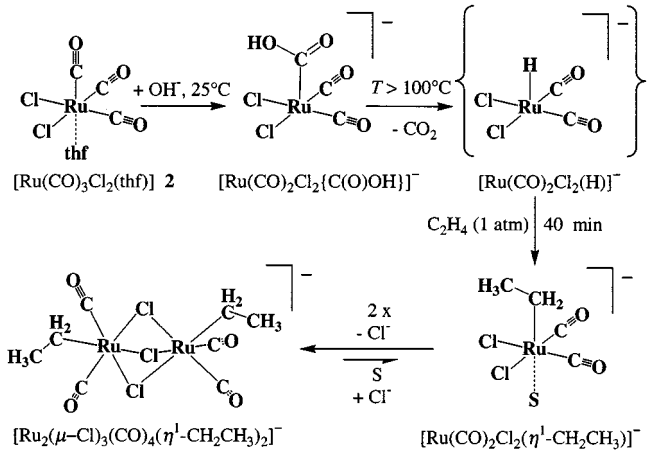
Scheme 21. Facile activation of water by a carbonylchlororuthenium(II) complex with formation of an oxoruthenium(II) species

Though not fully understood, the reaction was thought to involve initial attack of OH^- ions at the carbon atom of a coordinated CO ligand.

II.3.2 A Simple Route to "Unprotected" Alkyl and Alkenyl Complexes

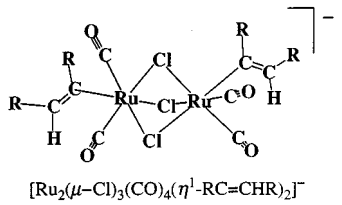
An obvious analogy of the preceding reaction with the basic principle of the water gas shift[24] led us to attempt the generation of a transient hydrido species by treatment of the neutral complex $[Ru(CO)_3Cl_2(thf)]$ with KOH and to examine its ability to insert olefins and, by extension, any unsaturated organic substrate. The logical sequence we envisaged (Scheme 22) effectively allowed a clean preparation of the anionic ethyl complex $[Ru_2(\mu\text{-}Cl)_3(CO)_4(CH_2CH_3)_2]^-$ in a one-pot procedure requiring no ethylene pressure.[75]

Subsequently, it was not a problem to extend the reaction to the case of alkynes and to observe in such cases a parallel



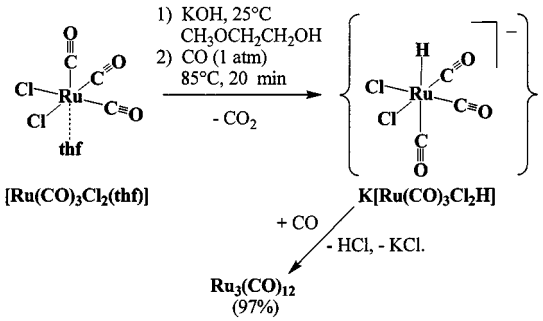
Scheme 22. Proposed mechanism for the formation of the isolated alkyl complex

cis insertion leading to the corresponding isostructural alkenyl derivative $[Ru_2(\mu\text{-}Cl)_3(CO)_4(RC{=}CHR)_2]^-$.[75]



II.3.3 Facile Interconversion $Ru^{II}-Ru^0$

A (naive) tentative attempt to intercept the transient hydrido species, generated in the preceding reaction by decarboxylation of the intermediate hydroxycarbonyl species in the presence of CO (and in the *absence* of any unsaturated substrate), led us to observe the formation of $Ru_3(CO)_{12}$ in quantitative yield(!).

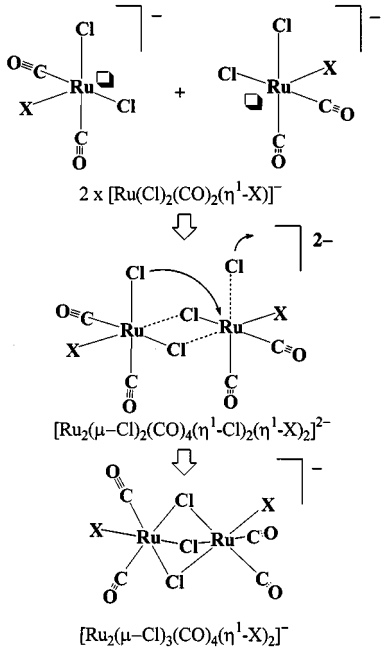


Scheme 23. A facile reduction of Ru^{II} to Ru^0

Apart from the interest in the procedure on account of its performance and of the established possibility to run the reaction directly from commercial $RuCl_3$,[75] an important extension of this finding was to establish that an extremely facile reduction of carbonylhaloruthenium(II) precursors to Ru^0 intermediates can take place by reductive elimination of HCl as soon as traces of water are present. This may have relevance to various catalytic systems involving carbonylhalo derivatives.[76]

II.3.4 A New Binary Carbonylchlororuthenium(II) Species

An intriguing point in the sequence shown in Scheme 22 was the fact that dimerization of the monoanionic alkyl intermediate $[Ru(CO)_2Cl_2(\eta^1\text{-}X)]^-$ (X = R) (observable only in a donor solvent like DMF) gave a monoanionic dimer $[Ru_2(CO)_4(\mu\text{-}Cl)_3(\eta^1\text{-}X)_2]^-$ (by loss of a halide ion, see Scheme 24) rather than the expected dianionic dimer "$[Ru_2(CO)_4(\mu\text{-}Cl)_2(Cl)_2(\eta^1\text{-}X)_2]^{2-}$" (X = R), which might have been isostructural with the known "allchloro" (X = Cl) analog $[Ru_2(CO)_4(\mu\text{-}Cl)_2(Cl)_4]^{2-}$shown in Scheme 20.



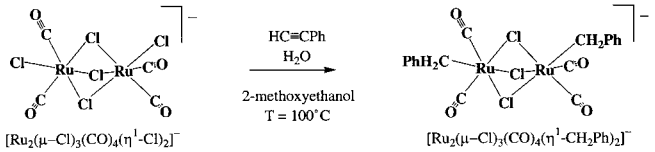
Scheme 24. Aggregation of unsaturated 16-e^- haloruthenium fragments and formation of a face-sharing bi-octahedral species (FSBO); the square box appearing in the scheme denotes a vacant coordination site on the metal center

Conversely, the fact that the hypothetical allchloro anion $[Ru_2(CO)_4(\mu\text{-}Cl)_3(\eta^1Cl)_2]^-$ had never been intercepted was also intriguing. In fact, we found that such a compound does exist, and can be simply prepared by thermal decarbonylation of $[Ru(CO)_3Cl_2(thf)]$ in the presence of the appropriate amount of halide (1/2 equiv. per Ru unit).[75] It can be regarded as the simplest association of two neutral units "$Ru(CO)_2Cl_2$" that are lightly stabilized by a weakly coordinating halide.

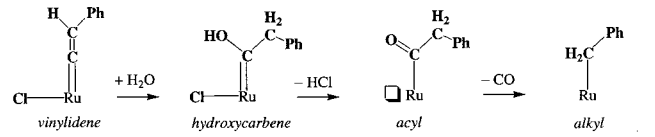
II.3.5 A Simple Route to Vinylidenes

The simple "non-hydridic" complex $[(PPh_3)_2N][Ru_2(\mu\text{-}Cl)_3(CO)_4(\eta^1\text{-}Cl)_2]$ allows the facile activation of alkynes to give *vinylidenes*.[75] To date, the latter intermediates have not yet been intercepted. Yet, we do observe *the product of their*

clean hydration involving C−C bond activation. Typically, activation of phenylacetylene gives the benzyl derivative $[Ru_2(CO)_4(\mu\text{-}Cl)_3(\eta^1\text{-}CH_2Ph)_2]^-$ (Scheme 25). The mechanism we propose for such a reaction is fully consistent with the one previously established by Bruce,[77] Bianchini[78] and Esteruelas.[79] In the present case, a transient opening of the halide bridge is believed to provide the vacant site required for alkyne activation, whereas its closure assists the final CO loss.



Proposed mechanistic pathway:



Scheme 25. Activation of the C−C triple bond of a terminal alkyne by hydration of the transient vinylidene; the square box appearing in the scheme denotes a vacant coordination site on the metal center

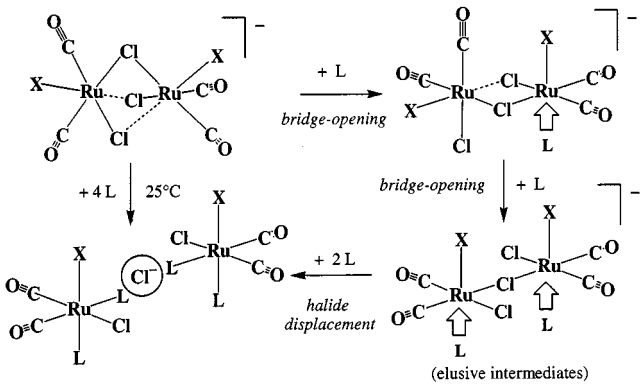
Interestingly, related ruthenium(II) halide complexes have been recently shown by Wakatsuki[80] to catalyze the hydration of alkynes to produce aldehydes and ketones. Unobserved carbenoid species have also been recently postulated as key intermediates in the construction of polycyclic ring systems from enynes involving $[Ru(CO)_3Cl_2]_2$ as a catalyst precursor.[21a]

II.3.6 Aspects of the Reactivity of FSBO (Face-Sharing Bi-Octahedral) Complexes

While the aggregation of carbonylhaloruthenium(II) species is understood to be a means for the unsaturated organometallic fragments to relieve their unsaturation, the reverse reaction, namely, a transient opening of halide bridges, constitutes the main pathway for substrate activation, as illustrated by the preceding reaction (Scheme 25).

A notable structural feature is that the Ru−Cl bridge bonds that are *trans* to the sigma donor (alkyl, alkenyl) are significantly longer than those *trans* to CO. This suggests the possibility of a selective opening of these bonds through a sequence (Scheme 26) that is reminiscent of the one proposed by Cotton and Poli for related FSBO species.[81]

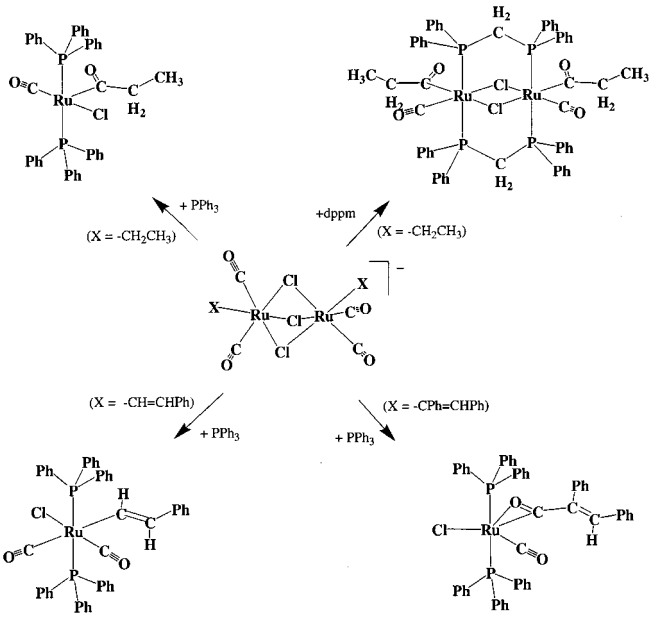
Thus, the masked unsaturation of these aggregates also allows the facile formation of adducts with a variety of donor ligands, ultimately leading to more elaborate complexes. With L = phosphanes, a rearrangement occurs within the coordination sphere of the final mononuclear species to give the *trans*-P isomer only. If X is an alkyl group, the phosphane also induces migratory CO insertion, giving the



Scheme 26. General scheme for the reaction of face-sharing bi-octahedral species with nucleophiles

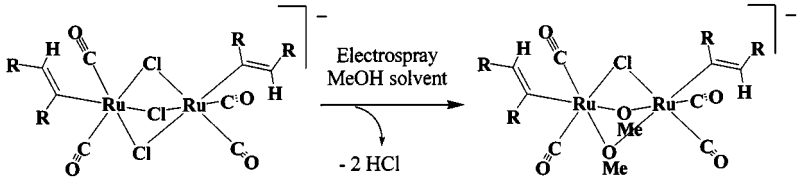
$16e^-$-acyl species $[Ru\{C(O)R\}(PR_3)_2(CO)Cl]$ (Scheme 27).[60]

If X is an alkenyl group, whether it migrates or not depends on the nature of the starting alkyne. As shown in Scheme 27, we have been able to obtain the alkenyl complex $[Ru(CH{=}CHPh)(PPh_3)_2(CO)_2Cl]$ from phenylacetylene, and the propenoyl complex $[Ru\{\eta^2C(O){-}PhC{=}CHPh\}(PPh_3)_2(CO)Cl]$ from diphenylacetylene, and to determine their respective structures.[82] It is noteworthy that the same complexes were originally prepared by Ros[83] from $RuH(CO)Cl(PR_3)_2$. The chemistry of these and related derivatives is currently being investigated by Werner[84a,b], Esteruelas[84] and Caulton.[85] With our procedure, retention of the dinuclear structure is possible by using a bridging ligand like bis(diphenylphosphanyl)methane, as exemplified by the facile synthesis of the dimeric acyl complex $[Ru_2(\mu\text{-}Cl)_2\{C(O)CH_2CH_3\}_2(\mu\text{-dppm})_2(CO)_2]$ (Scheme 27).[86] We are currently exploring the reactivity of the dimers $[Ru_2(\mu\text{-}Cl)_3(CO)_4(\eta^1\text{-}X)_2]$ with a variety of other ancillary ligands and substrates.



Scheme 27. Facile reactions of alkyl- and alkenylcarbonylchloro complexes with phosphanes

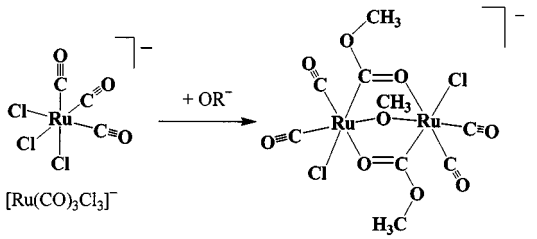
Another aspect of their reactivity is the facile replacement of halides by methoxide ions, which we have observed in some instances. For example, during the course of electrospray mass-spectral analyses of crystals of the dimeric alkenyl complex $[(PPh_3)_2N][Ru_2(\mu\text{-}Cl)_3(CO)_4(\eta^1\text{-}PhC{=}CHPh)_2]$ (whose structure had been ascertained by X-ray diffraction) we observed the ion $[Ru_2(\mu\text{-}Cl)(\mu\text{-}OMe)_2(CO)_4(\eta^1\text{-}PhC{=}CHPh)_2]^-$ when methanol was used as a solvent for the introduction of the samples (Scheme 28).



Scheme 28. Facile replacement of halides by methoxide ligands under the experimental conditions of electrospray mass spectrometry

We are currently exploring various possibilities to induce a systematic replacement of halides by other ancillary ligands through activation of hydrogen−element bonds, starting from compounds like thiols, imidazoles, aldehydes, etc. A full replacement of halides by methoxide ions has been reported by Süss-Fink in related methoxycarbonyl complexes.[87]

Finally we wish to conclude this section by specifying that groups other than the halides may participate in the formation of bridges between the Ru^{II} centers. Typically, in the treatment of $[PPN][Ru(CO)_3Cl_3]$ by methoxide ions, Süss-Fink isolated a complex which probably results from a transformation of the unobserved primary adduct (which we believe is $[PPN][Ru\{C(O)OMe\}(CO)_2Cl_2]$). Once again, a monoanionic aggregate (rather than a dianionic species) is obtained after loss of a halide ion. Interestingly, the new compound bears *terminal* halides and *bridging* methoxycarbonyl groups (Scheme 29).[87]



Scheme 29. Formation of methoxycarbonyl bridges rather than halide bridges in the stabilization of unsaturated carbonylhalo(methoxycarbonyl)ruthenium(II) fragments

Of course, we cannot exclude the same type of aggregation when the hydroxycarbonyl adduct we have observed (Scheme 22) is generated in a noncoordinating solvent. In that case, the whole sequence of Scheme 22 would proceed entirely through dimeric units.

Conclusion

A tantalizing observation about carbonylruthenium clusters incorporating halides or related hard bases as *hemilabile* ancillary ligands is that, in spite of their fascinating reactivity, their ability to catalyze substrate transformations with retention of the polymetallic structure is effective only under very mild conditions that are still too close to those liable to cause their degradation. An illustration of this can be found in our recent report of a *cluster-mediated* hydroformylation of diphenylacetylene.

Significantly, we now find that simple carbonylhaloruthenium(II) derivatives, easily generated from carbonylruthenium (Ru^0)/halide mixtures or by direct carbonylation of $RuCl_3$, are prone to react with olefins or alkynes in the presence of a simple source of hydride to give trappable *alkyl* or *alkenyl* complexes, whereas transient *vinylidene* species are formed from alkynes in the absence of a hydride source. These unsaturated complexes tend to relieve their unsaturation by forming aggregates whose dissociation may in turn release reactive organometallic fragments. Thus, we believe such complexes will provide realistic models for elementary transformations occurring in applied catalysis involving Ru/halide mixtures. An interplay between Ru^{II} and Ru^0 species may be expected in these multicomponent systems, due to the facile and reversible reductive elimination of HCl. Further work aimed at understanding such processes is in progress.

Acknowledgments

The author wishes to express his gratitude to all colleagues and coworkers who have made an important contribution to the research work summarized here, and, in particular, Herbert D. Kaesz, Noël Lugan, Jean-Jacques Bonnet, Philippe Kalck, Fred Basolo, Jean-Yves Saillard and Jean-François Halet. Financial support from the CNRS is also gratefully acknowledged.

[1] [1a] B. D. Dombek, *J. Am. Chem. Soc.* **1981**, *103*, 6508. – [1b] B. D. Dombek, *J. Organomet. Chem.* **1983**, *250*, 467. – [1c] B. D. Dombek, *J. Organomet. Chem.* **1989**, *372*, 151 and references therein.

[2] [2a] J. F. Knifton, *J. Am. Chem. Soc.* **1981**, *103*, 3959. – [2b] J. F. Knifton in *Aspects of Homogeneous Catalysis* (Ed.: R. Ugo), Reidel, Dordrecht, **1988**, vol 6, p. 1 and references therein.

[3] [3a] B. D. Dombek, A. M. Harrison, *J. Am. Chem. Soc.* **1983**, *105*, 2485. – [3b] M. Tanaka, T. Sakakura, T. Hayashi, T.-A. Kobayashi, *Chem. Lett.* **1986**, 39.

[4] [4a] C. P. Casey, S. M. Neumann, *J. Am. Chem. Soc.* **1978**, *100*, 2544. – [4b] W. Tam, G.-Y. Lin, W.-K. Wong, W. A. Kiel, V. K. Wong, J. A. Gladysz, *J. Am. Chem. Soc.* **1982**, *104*, 141.

[5] [5a] G. Braca, G. Sbrana, G. Valentini, G. Andrich, G. Gregorio, *J. Am. Chem. Soc.* **1978**, *100*, 6238. – [5b] A. M. Raspolli Galletti, G. Braca, G. Sbrana, F. Marchetti, *J. Mol. Catal.* **1985**, *32*, 291. – [5c] G. Braca, A. M. Raspolli Galletti, G. Sbrana, F. Zanni, *J. Mol. Catal.* **1986**, *34*, 183. – [5d] G. Braca, A. M. Raspolli Galleti, G. Sbrana, E. Trabuco, *J. Mol. Catal.* **1989**, *55*, 184. – [5e] G. Braca, A. M. Raspolli Galletti, G. Sbrana, *J. Organomet. Chem.* **1991**, *417*, 41.

[6] [6a] S.-I. Yoshida, S. Mori, H. Kinoshita, Y. Watanabe, *J. Mol. Catal.* **1987**, *42*, 215. – [6b] H. Ono, K. Fujiwara, M. Hashimoto, H. Watanabe, K. Yoshida, *J. Mol. Catal.* **1990**, *58*, 289.
[7] Y. Kiso, K. Saeki, *J. Organomet. Chem.* **1986**, *309*, C26.
[8] [8a] K.-I. Tominaga, Y. Sasaki, M. Kawai, T. Watanabe, M. Saito, *J. Chem. Soc., Chem. Commun.* **1993**, 629. – [8b] K.-I. Tominaga, Y. Sasaki, T. Watanabe, M. Saito, *Bull. Chem. Soc. Jpn.* **1995**, *68*, 2837.
[9] [9a] J. F. Knifton, *J. Mol. Catal.* **1987**, *43*, 65. – [9b] J. F. Knifton, *J. Mol. Catal.* **1988**, *47*, 99.
[10] M. Hidai, Y. Koyasu, K. Chikanari, Y. Uchida, *J. Mol. Catal.* **1987**, *40*, 243.
[11] [11a] S. Cenini, M. Pizzotti, C. Crotti, F. Porta, G. La Monica, *J. Chem. Soc., Chem. Commun.* **1984**, 1286. – [11b] S. Cenini, C. Crotti, M. Pizzotti, F. Porta, *J. Org. Chem.* **1988**, *53*, 1243. – [11c] S. Cenini, M. Pizzotti, C. Crotti in *Aspects of Homogeneous Catalysis* (Ed.: R. Ugo), Reidel, Dordrecht, **1988**, vol. 6, p. 59 and references therein.
[12] C. E. Kampe, H. D. Kaesz, *Inorg. Chem.* **1984**, *23,* 4646.
[13] C. E. Kampe, N. M. Boag, H. D. Kaesz, *J. Am. Chem. Soc.* **1983**, *105*, 2896.
[14] [14a] G. Süss-Fink, G. Hermann, *J. Chem. Soc., Chem. Commun.* **1985**, 735. – [14b] K. Langenbahn, K.Bernauer, G. Süss-Fink, *J. Organomet. Chem.* **1989**, *379*, 165.
[15] [15a] G. Lavigne, H. D. Kaesz, *J. Am. Chem. Soc.* **1984**, *106*, 4647. – [15b] G. Lavigne, H. D. Kaesz in *Metal Clusters in Catalysis* (Eds.: B. C. Gates, L. Guczi, H. Knözinger), Elsevier, Amsterdam, The Netherlands, **1986**, p. 43.
[16] [16a] G. Lavigne in *The Chemistry of Metal Clusters* (Eds.: D. F. Shriver, H. D. Kaesz, R. D. Adams), VCH Publishers, Weinheim, Germany, **1990**, p. 201. – [16b] G. Lavigne, B. de Bonneval in *Catalysis by Di- and Polynuclear Metal Cluster Complexes* (Eds.: R. D. Adams, F. A. Cotton) Wiley-VCH Inc., Weinheim, Germany, **1998**, p. 39.
[17] W. Keim, J. Becker, *J. Mol. Catal.* **1989**, *54*, 95.
[18] P. Isnard, B. Denise, R. P. A. Sneeden, J. M. Cognion, P. Durual, *J. Organomet. Chem.* **1983**, *256*, 135.
[19] C. Legrand, Y. Castanet, A. Mortreux, F. Petit (Atochem), *Eur. Pat. Appl.* 449693A, **1991**; *Chem. Abstr.* **1991,** *115*, 231708.
[20] G. Lavigne, N. Lugan, P. Kalck, J.-M. Soulié, O. Lerouge, J.-Y. Saillard, J.-F. Halet, *J. Am. Chem. Soc.* **1992**, *114*, 10669.
[21] [21a] N. Chatani, K. Kataoka, S. Murai, N. Furukawa, Y. Seki, *J. Am. Chem. Soc.* **1998**, *120*, 9104. – [21b] N. Chatani, T. Morimoto, T. Muto, S. Murai, *J. Am. Chem. Soc.* **1994**, *116*, 6049–6050. – [21c] T. Naota, H. Takaya, S.-I. Murahashi, *Chem. Rev.* **1998**, *98*, 2599–2660.
[22] [22a] M. I. Bruce in *Comprehensive Organometallic Chemistry* (Eds.: E. W. Abel, F. G. A. Stone, G. Wilkinson), Elsevier, Oxford, **1982**, vol. IV, p. 661 and references therein. – [22b] See also *Comprehensive Organometallic Chemistry II* (Eds.: E. W. Abel, F. G. A. Stone, G. Wilkinson) Pergamon Elsevier, Oxford, **1996**, vol. IV.
[23] N. Brodie, A. Poë, V. Sekhar, *J. Chem. Soc., Chem. Commun.* **1985**, 1090.
[24] For a review on nucleophilic activation of CO, see P. C. Ford, A. Rokicki, *Adv. Organomet. Chem.* **1988**, *28*, 139.
[25] M. Anstock, D. Taube, D. C. Gross, P. C. Ford, *J. Am. Chem. Soc.* **1984**, *106*, 3696.
[26] D. J. Taube, A. Rokicki, M. Anstock, P. C. Ford, *Inorg. Chem.* **1987**, *26*, 526.
[27] D. J. Darensbourg, R. L. Gray, M. Pala, *Organometallics* **1984**, *3*, 1928.
[28] G. Lavigne, N. Lugan, J.-J. Bonnet, *Inorg. Chem.* **1987**, *26*, 2347.
[29] M. I. Bruce, B. K. Nicholson, M. L. Williams, *Inorg. Synth.* **1989**, *26*, 271.
[30] [30a] J. C. Briker, C. C. Nagel, A. A. Bhattacharyya, S. G. Shore, *J. Am. Chem. Soc.* **1985**, *107*, 377. – [30b] M. W. Payne, D. L. Leussing, S. G. Shore, *J. Am. Chem. Soc.* **1987**, *109*, 617. – [30c] M. W. Payne, D. L. Leussing, S. G. Shore, *Organometallics* **1991**, *10*, 574.
[31] J. Lillis, A. Rokicki, T. Chin, P. C. Ford, *Inorg. Chem.* **1993**, *32*, 5040.
[32] S.-H. Han, G. L. Geoffroy, B. D. Dombek, A. L. Rheingold, *Inorg. Chem.* **1988**, *27*, 4355.
[33] T. Chin-Choy, W. T. Harrison, G. D. Stucky, N. Keder, P. C. Ford, *Inorg. Chem.* **1989**, *28*, 2028.
[34] S. Rivomanana, G. Lavigne, N. Lugan, J.-J. Bonnet, *Organometallics* **1991**, *10*, 2285.
[35] N. Lugan, G. Lavigne, J.-M. Soulié, P. Kalck, J.-Y. Saillard, J.-F. Halet, *Organometallics* **1995**, *14*, 1713.
[36] S. Rivomanana, G. Lavigne, N. Lugan, J.-J. Bonnet, R. Yanez, R. Mathieu, *J. Am. Chem. Soc.* **1989**, *111*, 8959.
[37] J.-K. Shen, F. Basolo, *Gazz. Chim. Ital.* **1994**, *124*, 439.
[38] [38a] E. Sappa, A. Tiripicchio, P. Braunstein, *Chem. Rev.* **1983**, *83*, 203. – [38b] E. Sappa, *J. Cluster Sci.* **1994**, *5*, 211.
[39] G. Lavigne, unpublished observations
[40] S. Rivomanana, G. Lavigne, N. Lugan, J.-J. Bonnet, *Inorg. Chem.* **1991**, *30*, 4110.
[41] S. Rivomanana, C. Mongin, G. Lavigne, *Organometallics* **1996**, *15*, 1195.
[42] [42a] P. Pino, *Chem. Ind.* **1968**, *49*, 1732. – [42b] Lonza, A. G. (P. Pino, F. Piacenti, M. Bianchi), DE 1.767.398, **1968/1977**; *Chem. Abstr.* **1970**, *72*, 78667. – [42c] Lonza Ltd., GB 1,119,520, **1968**; DE-OS 1,930,431, **1970**; *Chem. Abstr.* **1968**, *69*, 96232.
[43] J. L. Zuffa, M. L. Blohm, W. L. Gladfelter, *J. Am. Chem. Soc.* **1986**, *108*, 552.
[44] J. L. Zuffa, W. L. Gladfelter, *J. Am. Chem. Soc.* **1986**, *108*, 4669.
[45] [45a] S.-H. Han, G. L. Geoffroy, A. L. Rheingold, *Inorg. Chem.* **1987**, *26*, 3426. – [45b] S.-H. Han, J.-S. Song, P. D. Macklin, T. Nguyen, G. L. Geoffroy, A. L. Rheingold, *Organometallics* **1989**, *8*, 2127. – [45c] D. L. Ramage, G. L. Geoffroy, A. L. Rheingold, B. S. Haggerty, *Organometallics* **1992**, *11*, 1242. – [45d] E. D. Morrison, G. L. Geoffroy, *J. Am. Chem. Soc.* **1985**, *107*, 3541.
[46] [46a] N. Lugan, F. Laurent, G. Lavigne, T. P. Newcomb, E. W. Liimatta, J.-J. Bonnet, *J. Am. Chem. Soc.* **1990**, *112*, 8607. – [46b] N. Lugan, F. Laurent, G. Lavigne, J.-J. Bonnet *Organometallics* **1992**, *11*, 1351.
[47] J. K. Shen, F. Basolo, P. Nombel, N. Lugan, G. Lavigne, *Inorg. Chem.* **1996**, *35*, 755.
[48] For a review, see J. A. Cabeza, J. M. Fernandez-Colinas, A. Llamazares, *Synlett* **1995**, 579.
[49] G. C. Bruce, S. A. R. Knox, A. J. Philips, *J. Chem. Soc., Chem. Commun.* **1990**, 716.
[50] P. Nombel, N. Lugan, F. Mulla, G. Lavigne, *Organometallics* **1994**, *13*, 4673.
[51] Y. Goldberg, H. Alper, *J. Chem. Soc., Chem. Commun.* **1994**, 1209.
[52] [52a] Y. Wakatsuki, H. Yamazaki, N. Kumegawa, T. Satoh, J. Y. Satoh, *J. Am. Chem. Soc.* **1991**, *113*, 9604. – [52b] M. Shäfer, N. Mahr, J. Wolf, H. Werner, *Angew. Chem. Int. Ed. Engl.* **1993**, *32*, 1315. – [52c] C. Bianchini, P. Frediani, D. Masi, M. Peruzzini, F. Zanobini, *Organometallics* **1994**, *13*, 4616.
[53] H. Matsuzaka, Y. Takagi, Y. Ishii, M. Nishio, M. Hidai, *Organometallics* **1995**, *14*, 2153.
[54] [54a] P. Nombel, Thèse de L′Université Paul Sabatier (No. 2253), **1996**. – [54b] P. Nombel, N. Lugan, G. Lavigne, manuscripts in preparation.
[55] P. Nombel, N. Lugan, B. Donnadieu, G. Lavigne, *Organometallics* **1999**, *18*, 187.
[56] J. K. Shen, F. Basolo, personal communication.
[57] N. Lugan, P. L. Fabre, D. de Montauzon, G. Lavigne, J.-J. Bonnet, J.-Y. Saillard, J. F. Halet, *Inorg. Chem.* **1994**, *33*, 434.
[58] [58a] J. S. Lee, J. S. Kim, Y.G. Kim, *Appl. Catal.* **1990**, *57*, 1. – [58b] W. Leitner, *Angew. Chem. Int. Ed. Engl.* **1995**, *34*, 2207.
[59] N. Lugan, G. Lavigne, J.-M. Soulié, S. Fabre, P. Kalck, J.-Y. Saillard, J. F. Halet, *Organometallics* **1995**, 14, 1713.
[60] S. Fabre, P. Kalck, G. Lavigne, *Angew. Chem. Int. Ed. Engl.* **1997**, *36*, 1092.
[61] J. Chatt, B. L. Shaw, A. E. Field, *J. Chem. Soc.* **1964**, 3466.
[62] J. Halpern, B. R. James, L. W. Kemp, *J. Am. Chem. Soc.* **1966**, *88*, 5142.
[63] M. I. Bruce, F. G. A. Stone, *J. Chem. Soc. A* **1967**, 1238.
[64] [64a] G. Braca, G. Sbrana, P. Pino, E. Benedetti, *Chim. Ind. (Milan)* **1967**, *49*, 1381. – [64b] H. Benedetti, G. Braca, G. Sbrana, F. Sauvetti, H. Grassi, *J. Organomet. Chem.* **1972**, 37, 361. – [64c] G. Sbrana, G. Braca, E. Benedetti, *J. Chem. Soc., Dalton Trans.* **1975**, 754.
[65] F. Calderazzo, F. L′Eplattenier, *Inorg. Chem.* **1967**, *6*, 1220.
[66] B. F. G. Johnson, R. D. Johnston, J. Lewis, *J. Chem. Soc. A* **1969**, 792.
[67] J. P. Collmann, W. R. Roper, *J. Am. Chem. Soc.* **1965**, *87*, 4008.
[68] [68a] S. D. Robinson, G. Wilkinson, *J. Chem. Soc. A* **1966**, 300. – [68b] J. V. Kingston, J. W. S. Jameson, G. Wilkinson, *J. Inorg. Nucl. Chem.* **1967**, *29*, 133.
[69] P. Teulon, J. Rozière, *J. Organomet. Chem.* **1981**, *214*, 391.
[70] A. Mantovani, S. Cenini, *Inorg. Synth.* **1976**, *16*, 46.

[71] C. Wieser-Jeunesse, D. Matt, A. de Cian, *Angew. Chem. Int. Ed. Engl.* **1998**, *37*, 2861.
[72] G. Sbrana, G. Braca, F. Piacenti, P. Pino, *J. Organomet. Chem.* **1968**, *13*, 240.
[73] C. Andres, G. Lavigne, unpublished results.
[74] S. Fabre, Thèse de Doctorat de L′Université Paul Sabatier, **1996**.
[75] M. Faure, L. Maurette, G. Lavigne, *Angew. Chem. Int. Ed. Engl.* **1999**, *38*, 518.
[76] V. V. Grushin, *Acc. Chem. Res.* **1993**, *26*, 279.
[77] M. I. Bruce, A. G. Swincer, *Aust. J. Chem.* **1980**, *33*, 1471.
[78] C. Bianchini, J. A. Casares, M. Peruzzini, A. Romerosa, F. Zanobini, *J. Am. Chem. Soc.* **1996**, *118*, 4585−4594 and references therein.
[79] M. L. Buil, M. A. Esteruelas, A. M. Lopez, E. Onate, *Organometallics* **1997**, *16*, 3169−3177.
[80] M. Tokunaga, Y. Wakatsuki, *Angew. Chem. Int. Ed. Engl.* **1998**, *37*, 2867.
[81] [81a] F. A. Cotton, J. L. Eglin, S.-J. Kang, *J. Am. Chem. Soc.* **1992**, *114*, 4015. – [81b] R. Poli, J. C. Gordon, *J. Am. Chem. Soc.* **1992**, *114*, 6723.
[82] M. Faure, G. Lavigne, in preparation.
[83] [83a] M. R. Torres, A. Perales, H. Loumrhari, J. Ros, *J. Organomet. Chem.* **1990**, *384*, C61. – [83b] H. Loumrhari, J. Ros, M. R. Torres, A. Santos, A. M. Echavarren, *J. Organomet. Chem.* **1991**, *411*, 255.
[84] [84a] M. A. Esteruelas, H. Werner, *J. Organomet. Chem.* **1986**, *303*, 221. – [84b] H. Werner, M. A. Esteruelas, H. Otto, *Organometallics* **1986**, *5*, 2295. – [84c] C. Bohanna, M. A. Esteruelas, F. J. Lahoz, E. Onate, L. A. Oro, *Organometallics* **1995**, *14*, 4685. – [84d] M. A. Esteruelas, F. J. Lahoz, E. Onate, L. A. Oro, C. Valero, B. Zeier, *J. Am. Chem. Soc.* **1995**, *117*, 7935. – [84e] M. A. Esteruelas, F. Liu, E. Onate, E. Sola, B. Zeier, *Organometallics* **1997**, *16*, 2919.
[85] D. Huang, K. Folting, K. G. Caulton, *Inorg. Chem.* **1996**, *35*, 7035.
[86] C. Andres, G. Lavigne, in preparation.
[87] G. Süss-Fink, J. M. Soulié, G. Rheinwald, H. Stoeckli-Evans, Y. Sasaki, *Organometallics* **1996**, *15*, 3416.

Received December 15, 1998
[I98436]

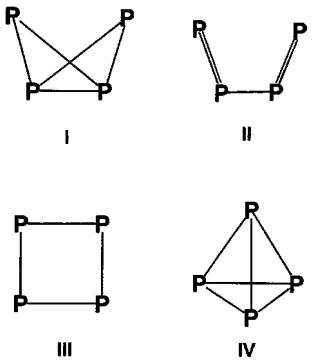
Synthesis and Characterisation of *tetrahedro*-Tetraphosphorus Complexes of Rhenium – Evidence for the First Bridging Complex of White Phosphorus

Maurizio Peruzzini,*[a] Lorenza Marvelli,[b] Antonio Romerosa,[c] Roberto Rossi,[b] Francesco Vizza,[a] and Fabrizio Zanobini[a]

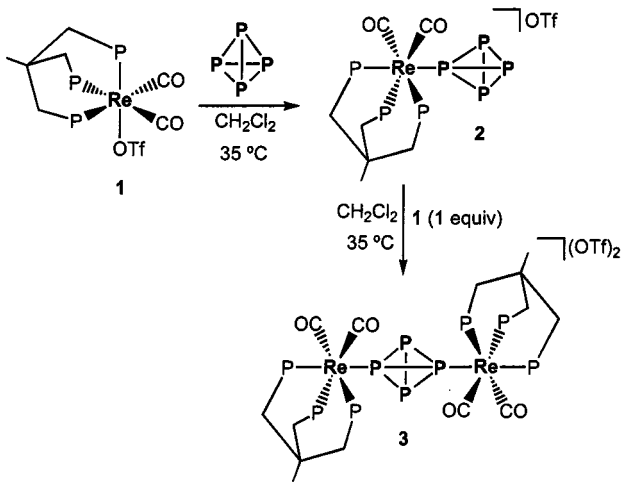
Keywords: Phosphorus / Rhenium / ^{31}P-NMR spectroscopy / Tripodal polyphosphanes

Reaction of white phosphorus with [(triphos)Re(CO)$_2$(OTf)] (**1**) in dichloromethane affords the new tetraphosphorus complex [(triphos)Re(CO)$_2$(η^1-P$_4$)](OTf) (**2**) [triphos = MeC(CH$_2$PPh$_2$)$_3$; OTf = OSO$_2$CF$_3$]. Compound **2** reacts with a second equivalent of **1** to give the binuclear complex [{(triphos)Re(CO)$_2$}$_2$(μ,η^1,η^1-P$_4$)](OTf)$_2$ (**3**) in which a *tetrahedro*-P$_4$ ligand behaves as tethering unit between two [(triphos)Re(CO)$_2$]$^+$ moieties. Complexes **2** and **3** represent the first soluble metal complexes of the tetraphosphorus molecule where the P$_4$ ligand has not undergone any major modification.

The reaction of transition-metal complexes with white phosphorus has been extensively studied and has resulted in a large variety of P$_x$ ligands (x < 15) which are often unpredictable.[1] In most instance, the integrity of the P$_4$ molecule is not retained in the final complex and extensive fragmentation and aggregation processes take place.[1][2] In some cases the four atoms of the P$_4$ ligand are incorporated into the coordination polyhedron of the resulting metal complex affording derivatives containing the tetraphosphabicyclobutane[2d,3] (**I**) or the tetraphosphabutadiene[3f,4] (**II**) units. Complexes containing the *cyclo*-P$_4$ (**III**) moiety are also known.[3f,5] In contrast, there are still very few compounds featuring an intact P$_4$ molecule in the form of a simple mono-*hapto*-P$_4$ (**IV**) ligand although this coordination mode would mimic the initial interaction of white phosphorus with the metal species.



To the best of our knowledge, η^1-tetrahedral P$_4$ complexes remain limited to the [(NP$_3$)M(η^1-P$_4$)] derivatives [M = Ni, Pd; NP$_3$ = N(CH$_2$CH$_2$PPh$_2$)$_3$] described in the late 1970s by Sacconi et al.[6,9] The nickel complex was authenticated by X-ray crystallography which confirmed the presence of a tetrahedral Ni^0 complex with one coordination position taken by one of the four P atoms of an intact P$_4$ molecule.[6a] Unfortunately, these complexes are quite insoluble in common organic solvents thus *preventing any characterisation of the tetraphosphorus ligand in solution and any investigation of the reactivity of the coordinated P$_4$* molecule. Despite synthetic efforts, related complexes have not yet been described in the literature.[1] Now, in this report, we detail the synthesis and the spectroscopic characterisation of the first examples of soluble mono- and dinuclear tetraphosphorus metal complexes for which the η^1-coordination mode of the P$_4$ molecule has been confirmed by ^{31}P-NMR spectroscopy.[7]



Scheme 1. Reaction of [(triphos)Re(CO)$_2$(OTf)] with white phosphorus

Reaction of a dichloromethane solution of the weakly coordinated triflate complex [(triphos)Re(CO)$_2$(OTf)][8] (**1**) [triphos = 1,1,1-tris(diphenylphosphanylmethyl)ethane)] with a small excess of white phosphorus at ca. 35°C under nitrogen (Scheme 1), affords, after addition of ethanol/*n*-

[a] Istituto per lo Studio della Stereochimica ed Energetica dei Composti di Coordinazione, ISSECC, CNR,
Via J. Nardi 39, I-50132 Firenze, Italy
Fax: (internat.) + 39-055/247-8366
E-mail: peruz@cacao.issecc.fi.cnr.it
[b] Dipartimento di Chimica, Università di Ferrara,
Via L. Borsari 46, I-44100 Ferrara, Italy
[c] Departamento de Quimica, Universidad de Almeria,
E-04071 Almeria, Spain

 © WILEY-VCH Verlag GmbH, D-69451 Weinheim, 1999 1434–1948/99/0606–0931 $ 17.50+.50/0

hexane and fast concentration under nitrogen, mustard-coloured microcrystals of [(triphos)Re(CO)$_2$(η^1-P$_4$)](OTf) (**2**) in good yield. Once thus obtained, **2** is slightly air-sensitive and can be manipulated in the air and maintained at room temperature without noticeable decomposition for a few hours. When dissolved in various solvents (dichloromethane, thf, chloroform), **2** is air- and moisture-sensitive and quickly decomposes to an orange uncharacterised solid. **2** exhibits a particularly informative $^{31}P\{^1H\}$-NMR spectrum consisting of a temperature-invariant AB_2MX_3 spin system featuring strong couplings between the nuclei P_M and P_X ($^1J_{PMPX}$ = 235.7 Hz) and P_A and P_M ($^2J_{PAPM}$ = 204.7 Hz). The magnitude of the latter coupling diagnoses the *trans* disposition between one of the triphos P atoms and the unique Re-bonded P atom of the *tetrahedro*-tetraphosphorus ligand. The invariance of the ^{31}P-NMR spectrum indicates that no dynamic process is exchanging the four atoms of the P$_4$ ligand and points to the existence of a P$_4$ moiety freely rotating around the P$_A$−Re−P$_M$ axis. This causes the magnetic equivalence of the basal P atoms of the P$_4$ tetrahedron whose signal appears as a doublet at δ = −488.9 in the high-field region of the spectrum [see trace (a) in Figure 1]. Noticeably, the two sets of resonances of the P$_4$ ligand are slightly deshielded upon coordination by ca. 38.0 ppm (P$_X$) and ca. 136.4 ppm (P$_M$, δ = −390.52) when compared with the free molecule of white phosphorus (δ = −526.9). These relatively small coordination chemical shifts [Δ = δ(P$_{M/Xcoord}$) − δ(P$_{4free}$)] suggest that, upon coordination to the (triphos)rhenium moiety, only a minor perturbation of the electron density of the P$_4$ tetrahedron has occurred.

In keeping with these observations, the "distal" P$_3$-face unit of the *tetrahedro*-P$_4$ ligand is still endowed with reactivity towards unsaturated transition metal complexes and electrophiles and we envisage the generation of several new polynuclear compounds and P$_4$-functionalisation products from **2**. We are currently exploring this interesting area and preliminary tests confirm our hypothesis.

As an example, when a dichloromethane solution of **2** is treated with a small excess of **1**, coordination of a second [(triphos)Re(CO)$_2$]$^+$ moiety to the P$_4$ ligand takes place and the dinuclear complex [{(triphos)Re(CO)$_2$}$_2$(μ,η^1,η^1-P$_4$)](OTf)$_2$ (**3**) may be isolated as air-stable pale yellow microcrystals after workup (yield 90%). On the basis of the spectroscopic data, **3** is assigned a bimetallic structure where two [(triphos)Re(CO)$_2$]$^+$ fragments are held together by a tethering P$_4$ unit which behaves as a bridging μ,η^1,η^1 ligand. The formation of a dimeric compound is witnessed by the drastic modification of the high-field part of the $^{31}P\{^1H\}$-NMR spectrum which, on moving from **2** to **3**, transforms into an AA′B$_2$B′$_2$MM′X$_2$ spin system [see trace (b) in Figure 1]. Interestingly, upon coordination of the second [(triphos)Re(CO)$_2$]$^+$ unit, a more relevant downfield shift of the signals of the metallated P atoms takes place while the resonance ascribable to the uncoordinated P$_2$ atoms moves slightly downfield. To the best of our knowledge, this kind of coordination mode for a *tetrahedro*-P$_4$ molecule is unprecedented in the rich chemistry of main-group−transition-metal compounds.[1]

Investigations are continuing in our laboratories with the focus on the reactivity of the soluble P$_4$ ligand in **2** and **3**

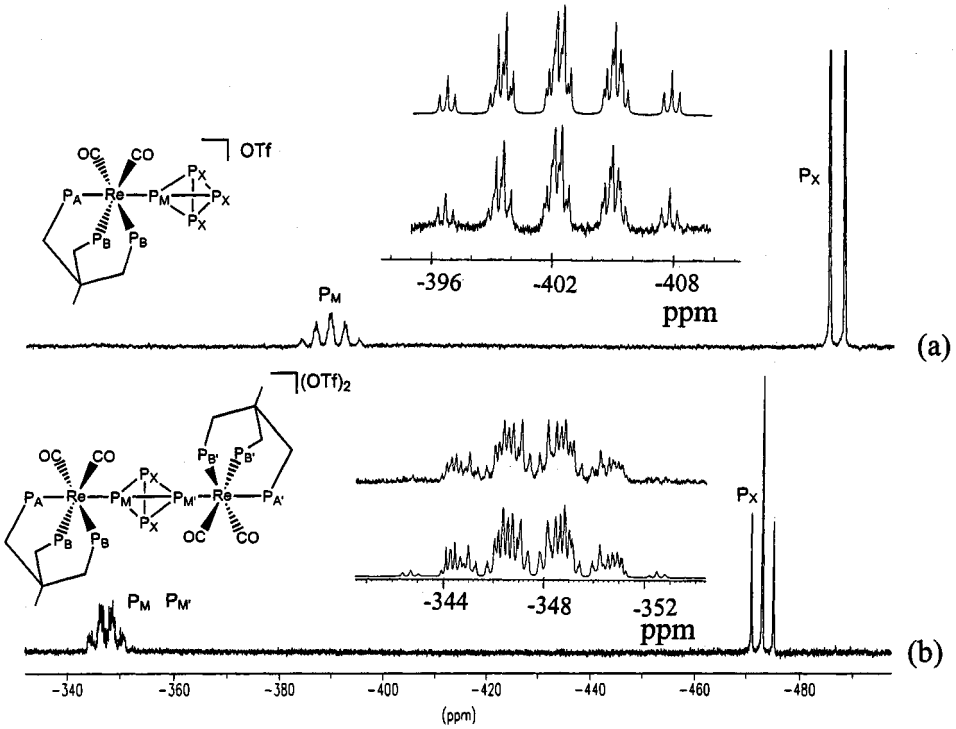


Figure 1. $^{31}P\{^1H\}$-NMR spectra of **2** (trace a) and **3** (trace b) in the high-field region (81.01 MHz, CD_2Cl_2, 298 K, 85% H_3PO_4 reference); the insets show the computed and experimental multiplets of the metallated P atom of the P$_4$ ligand in the two complexes.

as well as on the possible transferability of naked P atoms to inorganic and organic molecules.

Experimental Section

General Information: Dichloromethane was purified by distillation under nitrogen from P_2O_5. Complex **1** was prepared as described in the literature.[8] – ^{1}H- and ^{31}P{^{1}H}-NMR spectra were recorded with a Bruker AC200 or Bruker AVANCE DRX 500 spectrometers operating at 200.13 or 500.13 MHz (^{1}H) and 81.01 or 202.45 MHz (^{31}P), respectively. Peak positions are relative to tetramethylsilane (^{1}H) or 85% H_3PO_4 with downfield values taken as positive (^{31}P). The ^{31}P,^{31}P-2D COSY NMR experiments were conducted with an AVANCE DRX 500 Bruker spectrometer in the absolute magnitude mode using a 90° pulse after the incremental delay. – Elemental analyses (C, H) were performed using a Carlo Erba model 1106 elemental analyzer.

Complex 2: A dichloromethane solution (20 mL) of **1** (0.50 g, 0.49 mmol) was treated at ca. 35°C with a small excess of white phosphorus (0.08 g, 0.64 mmol) under nitrogen. Addition of ethanol/*n*-hexane (10 mL, 1:2 v/v) and concentration of the resulting solution under a brisk current of nitrogen, gave mustard-coloured microcrystals of **2** which were filtered under nitrogen and washed with ethanol (2 × 3 mL) and light petroleum ether (2 × 5 mL). Yield 76%. – IR (nujol mull): $\tilde{\nu}_{CO}$ = 1967 vs, 1912 vs; $\tilde{\nu}_{OTf}$ = 1265 s cm^{-1}. – ^{1}H NMR (CD_2Cl_2, 200.13 MHz): δ = 7.80–6.95 (30 H, m, phenyl protons), 2.70–2.40 (6 H, m, PCH_2), 1.58 (3 H, q, $^4J_{HP}$ = 2.8 Hz, CH_3). – ^{31}P{^{1}H} NMR (CD_2Cl_2, 81.01 MHz): AB_2MX_3 spin system; δ = –7.31 (1 P, dtq, $^2J_{PAPM}$ = 204.7 Hz, $^2J_{PAPB}$ = 23.7 Hz, $^3J_{PAPX}$ = 5.2 Hz, P_A), –14.59, (2 P, dd, $^2J_{PBPM}$ = 31.4 Hz, P_B), –390.52 (1 P, qdt, $^2J_{PMPX}$ = 235.7 Hz, P_M), –488.90 (3 P, dd, P_X); the assignments were confirmed by ^{31}P,^{31}P-COSY 2D-NMR spectroscopy and by computer simulation of the spectra. – FABMS; *m/z*: 867 [$M^+ - P_4$]; 839, 811 [$M^+ - P_4 - n$CO; *n* = 1–2]. – $C_{44}H_{39}F_3O_5P_7ReS$ (1139.87): calcd. C 46.36, H 3.45; found C 46.1, H 3.4.

Complex 3: Into a Schlenk flask, containing a dichloromethane solution (20 mL) of **2** (0.25 g, 0.22 mmol), a small excess of **1** (0.25 g, 0.25 mmol) was added under nitrogen as a solid in small portions. The solution was slowly heated at 35°C for 15 min and then 10 mL of an ethanol/*n*-hexane mixture (1:2 v/v) was added. Workup as described above for **2** afforded pale yellow microcrystals of **3** which were collected in the air and washed with ethanol (2 × 3 mL) and light petroleum ether (2 × 5 mL). Yield 90%. – IR (nujol mull): $\tilde{\nu}_{CO}$ = 1958 vs, 1919 vs; $\tilde{\nu}_{OTf}$ = 1267 s cm^{-1}. – ^{1}H NMR (CD_2Cl_2, 200.13 MHz): δ = 7.75–6.80 (60 H, m, phenyl protons), 2.90–2.50 (6 H, m, PCH_2), 1.72 (3 H, q, $^4J_{HP}$ = 2.9 Hz, CH_3). – ^{31}P{^{1}H} NMR (CD_2Cl_2, 81.01 MHz): δ = $AA'B_2B'_2MM'X_2$ spin system; –9.18 (2 P, m, $^2J_{PAPB}$ and $^2J_{PA'PB'}$ = 23.5 Hz, $^2J_{PAPM}$ and $^2J_{PA'PM'}$ = 201.0 Hz, $^3J_{PAPX}$ and $^3J_{PA'PX'}$ = 5.0 Hz, P_A and $P_{A'}$), –15.03 (4 P, m, $^2J_{PBPM}$ and $^2J_{PB'PM'}$ = 28.2 Hz, P_B and $P_{B'}$), –347.61 (2 P, m, $^1J_{PMPX}$ and $^1J_{PM'PX'}$ = 168.8 Hz, $^1J_{PMPM'}$ = 182.4 Hz, P_M and $P_{M'}$), –473.37 (2 P, td, P_X). – $C_{88}H_{78}F_6O_{10}P_{10}Re_2S_2$ (2155.84): calcd. C 49.03, H 3.65; found C 48.8, H 3.5.

Acknowledgments

This work was supported by the European Commission (INCO Copernicus Project ERBIC15CT960746). Thanks are expressed to Dr. José Antonio Ramirez (Valencia, Spain) and Dr. Andrea Meli (ISSECC CNR) for the simulation of the ^{31}P-NMR spectra.

[1] Reviews: [1a] M. Di Vaira, M. Peruzzini, P. Stoppioni, *Polyhedron* **1987**, *6*, 351. – [1b] O. J. Scherer, *Comments Inorg. Chem.* **1987**, *6*, 1. – [1c] O. J. Scherer, *Angew. Chem. Int. Ed. Engl.* **1990**, *29*, 1104. – [1d] M. Scheer, E. Harrmann, *Z. Chem.* **1990**, *29*, 41. – [1e] O. J. Scherer in *Multiple Bonds and Low Coordination in Phosphorus Chemistry* (Eds.: M. Regitz, O. J. Scherer), Thieme, Stuttgart, Germany, **1990**, chapter 3. – [1f] K. H. Whitmire, *Adv. Organomet. Chem.* **1998**, *42*, 2.

[2] Few examples of P_4-functionalization reactions have been reported, see: [2a] E. Hey, M. F. Lappert J. L. Atwood, S. G. Bott, *Chem. Commun.* **1987**, 597. – [2b] M. B. Power, A. R. Barron, *Angew. Chem. Int. Ed. Engl.* **1991**, *30*, 1353. – [2c] J. C. Green, M. L. H. Green, G. E. Morris, *Chem. Commun.* **1974**, 212. – [2d] M. Peruzzini, J. A. Ramirez, F. Vizza, *Angew. Chem. Int. Ed. Engl.* **1998**, *37*, 2257.

[3] [3a] A. P. Ginsberg, W. E. Lindsell, K. J. McCullough, C. P. Sprinkle, A. J. Welch, *J. Am. Chem. Soc.* **1986**, *108*, 403. – [3b] W. E. Lindsell *Chem. Commun.* **1982**, 1422. – [3c] O. J. Scherer, M. Swarowsky, G. Wolmershauser, *Organometallics* **1989**, *8*, 841. – [3d] M. Scheer, U. Becker, E. Matern, *Chem. Ber.* **1996**, *129*, 721. – [3e] M. Scheer, M. Dargatz, A. Rufinska, *J. Organomet. Chem.* **1992**, *440*, 327. – [3f] O. J. Scherer, G. Schwarz, G. Wolmershäuser, *Z. Anorg. Allg. Chem.* **1996**, *622*, 951.

[4] O. J. Scherer, M. Swarowsky, H. Swarowsky,, G. Wolmershäuser, *Angew. Chem. Int. Ed. Engl.* **1988**, *27*, 694.

[5] [5a] O. J. Scherer, J. Vondung, G. Wolmershäuser, *Angew. Chem. Int. Ed. Engl.* **1989**, *28*, 1355. – [5b] M. Scheer, E. Herrmann, J. Sieler, M. Oehme, *Angew. Chem. Int. Ed. Engl.* **1991**, *30*, 969. – [5c] M. Scheer, U. Becker, J. C. Huffman, M. H. Chisholm, *J. Organomet. Chem.* **1993**, *461*, C1.

[6] [6a] P. Dapporto, S. Midollini, L. Sacconi, *Angew. Chem. Int. Ed. Engl.* **1979**, *12*, 469. – [6b] P. Dapporto, L. Sacconi, P. Stoppioni, F. Zanobini, *Inorg. Chem.* **1981**, *20*, 3834.

[7] Severe problems of crystal twinning have so far frustrated all our attempts to provide structural data for the new phosphorus complexes confirming whether the η^1 and the μ,η^1,η^1 structures of **2** and **3** in solution are also maintained in the solid state.

[8] P. Bergamini, F. Fabrizi DeBiani, L. Marvelli, N. Mascellani, M. Peruzzini, R. Rossi, P. Zanello, *New J. Chem.* **1999**, 207.

[9] ***Note added in proof*** (March 25, 1999): After submission of this paper a report describing the complex $[W(CO)_3(PCy_3)_2(P_4)]$ appeared: T. Gröer, G. Baum, G. M. Scheer, *Organometallics* **1998**, *17*, 5916.

Received December 17, 1998
[I98437]

Structural, Spectroscopic, Magnetic and Thermal Properties in the $[SrM(C_3H_2O_4)_2(H_2O)_5] \cdot 2\ H_2O$ (M = Mn, Fe, Co, Ni) System: Precursors of $SrMO_{3-x}$ Mixed Oxides

Izaskun Gil de Muro,[a] Maite Insausti,[a] Luis Lezama,[a] José L. Pizarro,[b] Maria I. Arriortua,[b] and Teófilo Rojo*[a]

Keywords: Malonate / Mixed oxides / Crystal structure / Thermochemistry / Magnetic properties

The $[SrM(C_3H_2O_4)_2(H_2O)_7]$ (M = Mn, Fe, Co, Ni) compounds have been prepared and characterised by chemical analysis and X-ray diffraction. The crystal structure of $[SrCo(C_3H_2O_4)_2(H_2O)_5] \cdot 2\ H_2O$ has been solved [monoclinic, $P2_1/c$, $Z = 4$, $a = 6.880(1)$, $b = 14.360(2)$, $c = 15.800(2)$ Å. $\beta = 101.69(1)°$]. The compound exhibits a three-dimensional chain/snake structure consisting of $-CoO_6-[SrO_7]_\infty-CoO_6-$ repeating units parallel to the [0 1 1] and [0 –1 1] directions. UV/Vis data are consistent with the cations being in a high-spin octahedral symmetry. Magnetic measurements show antiferromagnetic interactions for all compounds with approximate θ values of –0.5 K, except for the cobalt compound (–24.5 K) where the decrease of the $\chi_m T$ curve can also be attributed to the spin-orbit coupling. Thermal analyses performed in air and under nitrogen show three consecutive steps: dehydration, ligand pyrolysis, and inorganic residue evolution. Thermal treatments in tubular furnaces were performed in order to obtain pure $SrMO_{3-x}$ phases. In all cases the oxides are nonstoichiometric and oxygen-deficient with structures related to that of perovskite. Lower temperatures and reaction times than those given in the literature have been used when using the ceramic method. These "soft" treatments gave rise to homogeneous particles of small grain size.

Introduction

Since the discovery of high-temperature superconducting oxides, much interest has been paid to the 3d transition metal oxides. In particular, the electronic states of the perovskite-type oxides have been extensively investigated from the standpoint of 3d band filling,[1−3] those that have transition metal ions such as Mn^{4+}, Fe^{4+}, Co^{4+}, Ni^{3+}, or Cu^{3+} in unusually high oxidation states, as well as mixed valence states, being those most studied.

The physical properties of these kinds of oxides depend greatly upon the oxidation state and the location of the cation at either tetrahedral or octahedral sites. The electronic and magnetic properties of the $SrFeO_{3-x}$ system vary a great deal with the oxidation state of the iron ions, ranging from the antiferromagnetic insulator oxide $SrFeO_{2.5}$, a brown millerite-type structure, to the antiferromagnetic metallic compound $SrFeO_3$, with cubic perovskite structure.[4] The $SrMnO_{3-x}$ phase becomes increasingly anion-deficient in air with increasing temperature.[5] For this reason the physical properties related to the crystal structures have been studied.[6] In the case of the cobalt oxides, the named cobaltites have attracted special attention due to their application as low-cost fuel-cell electrodes.[7]

In addition to the oxidation state, the physical properties also depend on either the final particle size or the preparative methods used to obtain the materials. In the last few years, "soft" chemical routes have often been employed to prepare advanced ceramic powders, as an alternative method to the conventional ceramic method. The solid solution precursor technique used for the preparation of fine oxide materials at low temperatures in this way has frequently been reported.[8] This method is quite advantageous, due to the excellent stoichiometry and low impurity content of the final phases.[9]

We are interested in the study of organometallic compounds with carboxylates, as well as their use as precursor materials for obtaining mixed oxides.[10] The chemistry of transition metal complexes involving malonate as a bridging ligand has been investigated due to a wide variety of physical properties,[11] the results concerning magnetic properties of 1D, 2D, and 3D systems being of special interest.[12]

Recently, a series of metal malonate complexes has been reported.[13] In this paper, the synthesis and characterisation of the $[SrM(C_3H_2O_4)_2(H_2O)_7]$ (M = Mn, Fe, Co, Ni) compounds is presented. Hereafter, these complexes will be denoted as SrMn, SrFe, SrCo, and SrNi, respectively. Spectroscopic and magnetic studies have been performed on these compounds. In order to obtain information concerning the formation of pure mixed oxides from the organometallic precursors, a detailed thermal study has been carried out.

[a] Departamento de Química Inorgánica, Facultad de Ciencias. Universidad del País Vasco,
Apdo. 644, E-48080 Bilbao, Spain
[b] Departamento de Mineralogía-Petrología, Facultad de Ciencias. Universidad del País Vasco,
Apdo. 644, E-48080 Bilbao, Spain
Fax: (internat.) + 34-94/464-8500
E-mail: qiproapt@lg.ehu.es

 © WILEY-VCH Verlag GmbH, D-69451 Weinheim, 1999 1434−1948/99/0606−0935 $ 17.50+.50/0

Results and Discussion

The synthesis of the complexes was performed as described in the Experimental Section. Crystal structure analyses were performed for the $[SrCo(C_3H_2O_4)_2(H_2O)_7]$ complex. Crystal data and details of the structure determination are summarized in Table 1. Bond lengths and angles for non-hydrogen atoms are given in Table 2.

Table 1. Data collection and structure refinement for the $[SrCo(C_3H_2O_4)_2(H_2O)_5] \cdot 2\ H_2O$ compound

Molecular Formula	$C_6H_{18}CoO_{15}Sr$
a [Å]	6.880(1)
b [Å]	14.360(2)
c [Å]	15.800(2)
β	101.69(1)°
V [Å^3]	1528.6(4)
Z	4
Molecular mass [g]	476.75
Space group	$P2_1/c$
T [°C]	293(2)
$\rho_{obsd.}$ [g cm^{-3}]	2.07(6)
$\rho_{calcd.}$ [g cm^{-3}]	2.054
μ [mm^{-1}]	4.651
λ [Å]	0.71070
$R(F_o)$[a]	0.0427
$R_w(F_o^2)$[b]	0.0967

[a] $R_1(F_o) = [\Sigma||F_o| - |F_c||/\Sigma|F_o|]$. — [b] $wR_2(F_o^2) = \{\Sigma[w(F_o^2 - F_c^2)^2]/\Sigma[w(F_o^2)^2]\}^{1/2}$

The asymmetric unit consists of diaquobis(malonato)cobaltate(II) anions linked to strontium ions and two water molecules of crystallization, O(6w) and O(7w) (see Figure 1). The cobalt(II) centres adopt an octahedral coordination pattern. The polyhedron is formed by the four carboxylate groups from the two malonate ions and the O(1w) and O(2w) water molecules, which are located in the axial plane. The O(1), O(5), O(3), and O(7) atoms are coplanar at average distances of 2.06 Å. The O−Co−O angles are close to 90°, in good agreement with those observed for other related compounds.[13][14] The cobalt atom is raised by 0.016(1) Å above the square plane in the direction of O(2w). The distortion around the cobalt(II) ion has been calculated by quantification of the Muetterties and Guggenberger description.[15] The value obtained, $\Delta = 0.04$, is indicative of a quite regular octahedron.

The strontium ions are surrounded by nine oxygen atoms, five of them belonging to three malonate groups, and four water molecules, O(3w), O(3w)^3, O(4w), O(5w), forming an irregular polyhedron. The average Sr−O distance is 2.67 Å. The strontium polyhedra are linked between them along the [1 0 0] direction via two different common edges, O(8)^1−O(8)^2 and O(3w)−O(3w)^3, due to the presence of an inversion centre at the middle point of these edges [at x = 0 and 1/2, for O(8)^1−O(8)^2 and O(3w)−O(3w)^3, respectively]. The Sr−O(8)−Sr and Sr−O(3w)−Sr angles are both 113.9(2)°. These $[SrO_7]_\infty$ chains, running along the [100] direction, are linked between them by corner-sharing CoO_6 distorted octahedra, where O(1) and O(7) oxygens are the common corners. These connections form new "perpendicular" chains parallel to [0 1 1] and [0 −1 1] directions

Table 2. Selected bond lengths [Å] and angles [°] for the $[SrCo(C_3H_2O_4)_2(H_2O)_5] \cdot 2\ H_2O$ compound; symmetry transformations used to generate equivalent atoms: (1): $-x + 1$, $y - 1/2$, $-z + 1/2$; (2): x, $-y + 1/2$, $z + 1/2$; (3): $-x$, $-y$, $-z + 1$; (4): $-x + 1$, $-y$, $-z + 1$; (5): x, $-y + 1/2$, $z - 1/2$; (6): $-x + 1$, $y + 1/2$, $-z + 1/2$

Sr−O(8)^1	2.583(4)	O(2)−C(1)	1.249(7)
Sr−O(2)	2.595(4)	O(3)−C(3)	1.261(7)
Sr−O(4w)	2.596(4)	O(4)−C(3)	1.238(7)
Sr−O(5w)	2.599(4)	O(5)−C(4)	1.259(7)
Sr−O(3w)	2.665(4)	O(6)−C(4)	1.243(7)
Sr−O(8)^2	2.675(4)	O(7)−C(6)	1.252(7)
Sr−O(7)^2	2.737(4)	O(8)−C(6)	1.246(7)
Sr−O(3w)^3	2.752(4)	O(8)−Sr^6	2.583(4)
Sr−O(1)	2.847(4)	O(8)−Sr^5	2.675(4)
Co−O(3)	2.047(5)	C(1)−C(2)	1.504(9)
Co−O(5)	2.050(4)	C(2)−C(3)	1.493(9)
Co−O(1)	2.068(4)	C(2)−H(21)	0.97
Co−O(7)	2.091(4)	C(2)−H(22)	0.97
Co−O(1w)	2.096(5)	C(4)−C(5)	1.514(8)
Co−O(2w)	2.128(4)	C(5)−C(6)	1.519(8)
O(1)−C(1)	1.250(7)	C(5)−H(51)	0.97
		C(5)−H(52)	0.97
O(8)1−Sr−	91.42(14)	O(2)−Sr−O(8)^2	148.71(14)
O(2)−Sr−O(4w)	93.44(14)	O(2)−Sr−O(1)	47.05(12)
O(2)−Sr−O(5w)	119.17(13)	O(4w)−Sr−O(1)	67.85(13)
O(2)−Sr−O(3w)	76.86(13)	O(4w)−Sr−O(3w)	136.36(14)
O(3)−Co−O(5)	178.7(2)	O(3)−Co−O(1)	88.9(2)
O(5)−Co−O(1)	91.9(2)	O(3)−Co−O(2w)	88.9(2)
O(1)−Co−O(1w)	91.4(2)	O(1)−Co−O(7)	179.1(2)
O(1)−Co−O(2w)	92.9(2)	O(1w)−Co−O(2w)	175.0(2)
Sr−O(3 W)−Sr^3	113.9(2)	C(1)−O(1)−Co	127.9(4)
C(6)−O(7)−Co	126.0(3)	C(1)−O(1)−Sr	88.7(3)
C(6)−O(7)−Sr^5	93.2(3)	Co−O(1)−Sr	143.4(2)
Co−O(7)−Sr^5	140.6(2)	C(1)−O(2)−Sr	100.7(4)
C(6)−O(8)−Sr^6	149.2(4)	C(3)−O(3)−Co	130.4(4)
C(6)−O(8)−Sr^5	96.3(3)	C(4)−O(5)−Co	127.5(4)
Sr^6−O(8)−Sr^5	113.87(14)	O(4)−C(3)−O(3)	123.4(6)
O(2)−C(1)−O(1)	121.9(5)	O(4)−C(3)−O(3)	123.4(6)
C(3)−C(2)−C(1)	125.2(6)	O(6)−C(4)−O(5)	122.5(6)
O(8)−C(6)−O(7)	122.7(5)	C(4)−C(5)−C(6)	118.6(5)
H(21)−C(2)−H(22)	106.3	H(51)−C(5)−H(52)	107.1

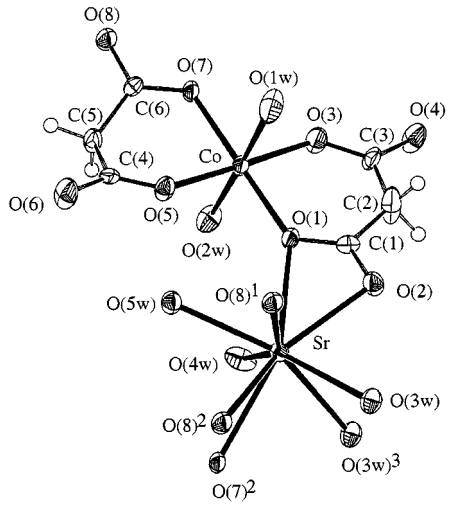


Figure 1. View of the coordination polyhedra for strontium and cobalt ions with atom numbering for the $[SrCo(C_3H_2O_4)_2(H_2O)_5] \cdot 2\ H_2O$ compound

formed by $-CoO_6-[SrO_7]_\infty-CoO_6-$ units, as can be seen in Figure 2. In these chains, the Co···Co^2 direct distance is 7.908(2) Å and the exchange distance through the O(1)−Sr−O(7)^2 atoms is 9.74 Å. In this way, the structure

could be described as a three dimensional package of strontium dimers linked through CoO_6 polyhedra. (1: $1 - x$, $y - 1/2$, $1/2 - z$; 2: x, $1/2 - y$, $1/2 + z$; 3: $-x$, $-y$, $1 - z$).

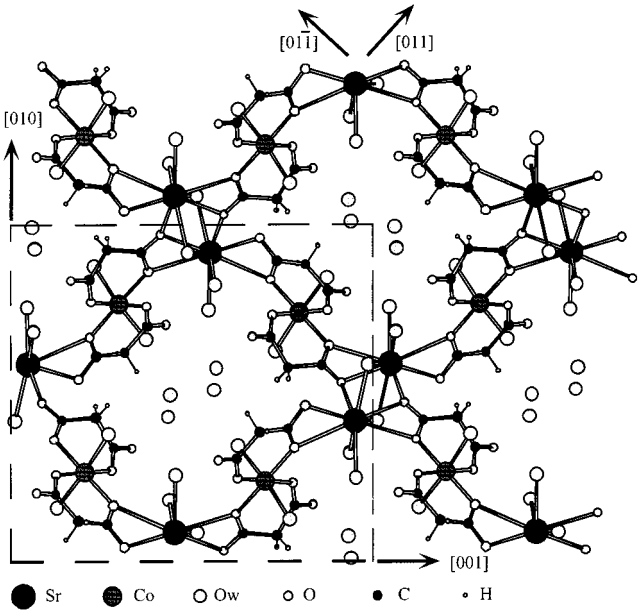


Figure 2. A perspective view of the $[SrCo(C_3H_2O_4)_2(H_2O)_5] \cdot 2\,H_2O$ compound in the *bc* plane

In the malonate ligands, the dihedral angle between the planes O(5)−C(4)−O(6) and O(7)−C(6)−O(8) is 143.8(7)° and between O(4)−C(3)−O(3) and O(1)−C(1)−O(2) it is 9.4(5)°. The chelated malonate ring formed by the O(5)−C(4)−C(5)−C(6)−O(7) atoms has an envelope conformation in which only the methylene group is significantly displaced from the ring plane, while the other ring formed by the O(3)−C(3)−C(2)−C(1)−O(1) atoms is quite planar. The difference in the C(3)−C(2)−C(1), 125.2(6)° and C(4)−C(5)−C(6), 118.6(5)° angles could be explained on the basis of these linkages and the conformation of the ligands. In both malonate ions, the average C−O distances and O−C−O angles are 1.25 Å and 122.6°, respectively. All the oxygen atoms belonging to the malonate ligand are bonded to one or two metal ions, except the O(4) and O(6) atoms which are uncoordinated.

In the crystal structure, extensive hydrogen bonds involving the carboxyl groups and water molecules could be described by acceptor-donor distances of ca. 3 Å. However, the difficulty in locating the water hydrogen atoms prevents us from predicting this kind of bonding in the structure.

For the SrMn, SrFe, and SrNi phases, high-quality crystals were not obtained. X-ray diffraction patterns of the microcrystalline products were performed in the 2θ range of 5−70°. Indexation of the diffraction profile and refinement of the cell parameters were made by FULLPROF (pattern-matching analysis)[16] on the basis of the space group, $P2_1/c$, and the cell parameters found for the SrCo phase. The calculated values are given in Table 3. Taking into account these results, the four phases can be considered to be isostructural.

Table 3. Crystallographic data for the $[SrM(C_3H_2O_4)_2(H_2O)_5] \cdot 2\,H_2O$ (M = Mn, Fe, Ni, Co) compounds

Compound	SrMn	SrFe	SrNi	SrCo
a [Å]	6.9517(3)	6.9105(3)	6.8762(5)	6.880(1)
b [Å]	14.5678(7)	14.4758(7)	14.296(1)	14.360(2)
c [Å]	15.7760(6)	15.7808(8)	15.889(1)	15.800(2)
β [°]	102.31(2)	102.03(3)	101.36(4)	101.69(1)
V [Å^3]	1560.9	1543.9	1531.3	1528.6(4)
Space group	$P2_1/c$	$P2_1/c$	$P2_1/c$	$P2_1/c$
Z	4	4	4	4

The IR spectra of the compounds show a strong broad absorption band in the region 3100−3600 cm^{-1}, corresponding to the stretching vibration of the hydroxy groups, ν(O−H), of the water molecules. The presence of a band at around 1580 cm^{-1} is attributed to the stretching vibration of the carbonyl group linked to the metal ions. This band appears together with the antisymmetric $\upsilon_a(COO^-)$ vibration. The bands corresponding to the symmetric $\upsilon_s(COO^-)$ vibration are localised in the 1380−1452 cm^{-1} range. The relative positions of these two bands, $\Delta = \upsilon_a(COO^-) - \upsilon_s(COO^-)$, are lower than those corresponding to the free malonic acid. This fact indicates that the coordination of the ligands to the metal ions could be through the formation of a chelate, giving rise to an electronic delocalization in the carboxylate group.[17] The presence of a shoulder at around 1700 cm^{-1} in the IR spectra could be attributed to the existence of C=O groups, which are not linked to any metal ions as was observed in the crystal structure of the SrCo compound. Nevertheless, the appearance of a broad band in this region, probably due to the presence of hydrogen bonds between the water molecules and the carboxylate groups, hampers the localization of free carboxylate groups in the IR spectra. Finally, the band observed for all compounds in the 1100−1300 cm^{-1} range corresponds to the bending vibration of the carbonyl group, δ(C=O).

Reflectance spectra were recorded for the $[SrM(C_3H_2O_4)_2(H_2O)_7]$ (M = Fe, Co, Ni) compounds. For the nickel phase the bands that appear at frequencies $\tilde{\nu}_1$ = 8930, $\tilde{\nu}_2$ = 13513 and $\tilde{\nu}_3$ = 26315 cm^{-1} have been assigned to the three allowed transitions $^3A_{2g} \rightarrow {}^3T_{2g}$, $^3T_{1g}$ (F) and $^3T_{1g}$(P). The spin-forbidden transitions $^3A_{2g} \rightarrow {}^1E_g$ and $^1T_{2g}$ were also observed $\tilde{\nu}_4$ = 15570 and $\tilde{\nu}_5$ = 21500 cm^{-1}, respectively. The Dq and Racah parameters, calculated by fitting the experimental frequencies to an energy level diagram for octahedral d^8 systems are: Dq = 893 cm^{-1}, B = 957 cm^{-1} and C = 4264 cm^{-1}, values usually found for octahedrally coordinated Ni^{II} compounds.[18] In the case of the $[SrCo(C_3H_2O_4)_2(H_2O)_7]$ compound, the positions of the bands are in the range usually found for Co^{II} ions in octahedral geometries, $\tilde{\nu}_1$ = 8550, $\tilde{\nu}_2$ = 16670 and $\tilde{\nu}_3$ = 20200 cm^{-1} which have been assigned to the $^4T_{1g} \rightarrow {}^4T_{2g}(F)$, $^4A_{2g}$ (F) and $^4T_{1g}(P)$ transitions. The Dq = 966 cm^{-1} and B = 851 cm^{-1} values confirm the octahedral geometry. For the

iron compound the band corresponding to the $^5T_{2g} \rightarrow {}^5E_g$ transition is split into two, due to the Jahn−Teller distortion of the ^5E_g energy level. From the position of these bands, 11235 and 6875 cm^{-1}, a value of $(8/3)d\sigma = 4360$ cm^{-1} was calculated. This fact is indicative of the presence of a slight distortion around the metal ion in this compound.

The X-band EPR spectra of polycrystalline samples of the $[SrM(C_3H_2O_4)_2(H_2O)_7]$ (M = Mn, Co) compounds have been performed in the temperature range 4.2−300 K. The spectra at 4 K are shown in Figure 3. In the case of the manganese phase broad and isotropic signals appear at room temp., and these signals are narrower at low temperatures. The corresponding g_{iso} parameter at 4 K has a value of 2.00, in good accordance with that corresponding to the Mn^{II} ions in octahedral geometry. The spectrum of the cobalt phase shows the strong anisotropy of the g factor. The signal presents a very broad linewidth due to the spin-orbit coupling which hampers the determination of good g values for this compound.

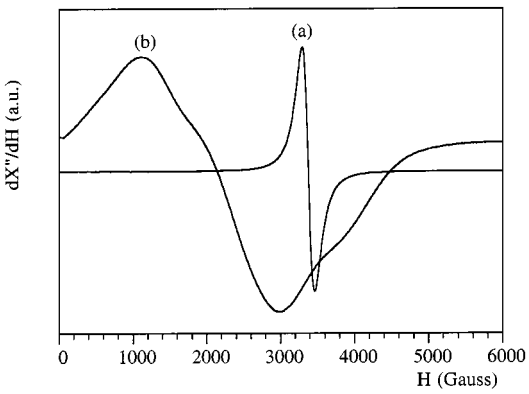


Figure 3. Powdered X-band ESR spectra for the $[SrM(C_3H_2O_4)_2(H_2O)_5] \cdot 2\,H_2O$ compounds at 4 K (a) M = Mn, (b) M = Co

Susceptibility magnetic measurements of the $[SrM(C_3H_2O_4)_2(H_2O)_7]$ (M = Mn, Co, Fe, Ni) compounds were carried out in the temperature range of 1.8−300 K. A similar magnetic behaviour was observed for the SrFe, SrNi, and SrMn phases. The $\chi_m{}^{-1}$ and $\chi_m T$ vs T curves for the Mn^{II} compound is represented in Figure 4a. The $\chi_m{}^{-1}$ vs T curves for these compounds show a Curie−Weiss behaviour in the range 5−300 K with negative intercepts of −0.68 K (SrFe), −0.36 K (SrNi), and −1.8 K (SrMn). These negative θ values and the overall appearance of the $\chi_m T$ vs T curves are indicative of the presence of antiferromagnetic interactions. The values for the Curie constants are 3.65, 1.18, and 4.36 cm^3 K/mol, respectively. The $\chi_m T$ products are practically temperature-independent for $T >$ 50 K, reaching values of 2.45 (SrFe), 1.12 (SrNi), 3.7 (SrMn) cm^3 K/mol when cooling from this temperature to 4.2 K. Taking into account the crystallographic description, the magnetic behaviour could be described on the basis of either a Heisenberg square-planar system or a 3D network. Nevertheless, in all cases the best least-squares fit leads to J/k values less than 1 K.

For the SrCo compound the high-temperature data ($T >$ 60 K) were also fitted to a Curie−Weiss law with θ = −24.5 K and $Cm = 3.77$ cm^3 $Kmol^{-1}$ of metal ion (Figure 4b). The continuous decrease in the $\chi_m T$ curve must be ascribed to the antiferromagnetic exchange interactions, together with the effect of the spin-orbit coupling ($\lambda = -170$ cm^{-1} for the free Co^{2+} ion),[19] which leads to an effective spin $S = 1/2$ for the system at low temperatures ($T <$ 30 K). This effect is qualitatively similar to those of the antiferromagnetic interactions, making difficult to distinguish between the contributions of these two effects on the whole magnetic behaviour of this compound.

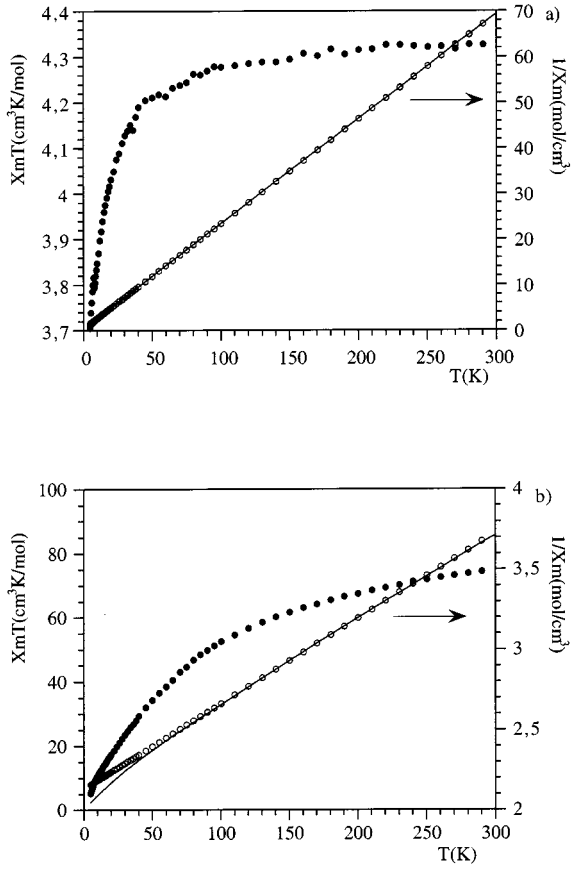


Figure 4. Thermal variations of the magnetic susceptibility ($\chi_m{}^{-1}$) and ($\chi_m T$) for $[SrM(C_3H_2O_4)_2(H_2O)_5] \cdot 2\,H_2O$ compounds a) M = Mn, b) M = Co

Thermal treatments in air and under nitrogen were performed for all compounds. The TG curves are shown in Figure 5. The decomposition steps can be explained as three consecutive processes: namely dehydration, ligand pyrolysis, and evolution of the inorganic residue. The dehydration process occurs in the 70−190°C range, and it is in good accordance with the loss of the seven water molecules present in the complexes. This process seems to take place in only one step, except for the SrNi compound. However, this fact does not allow the presence of different water molecules to be deduced, as was previously observed from the structural data. After a period of stability, ligand pyrolysis occurs at around 350°C. As can be expected, and considering the nature of the cations coordinated to the malonate

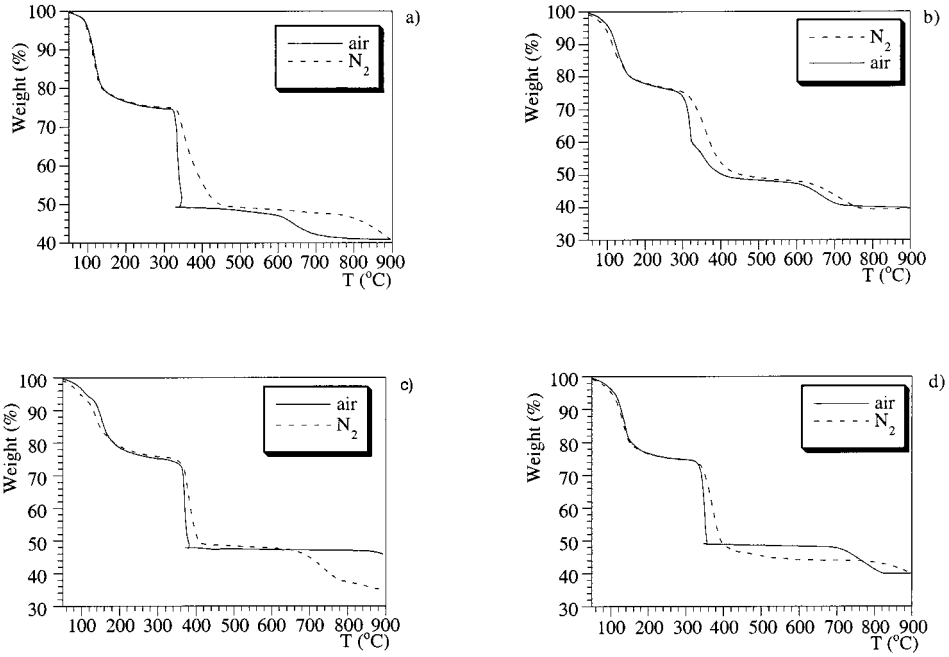


Figure 5. TGA curves for the $[SrM(C_3H_2O_4)_2(H_2O)_5] \cdot 2\,H_2O$ compounds, a) M = Mn, b) M = Fe, c) M = Ni, d) M = Co, in air (−) and under nitrogen (- - -)

ligand,[20] the weight loss is in good accordance with the formation of the products obtained from its decarboxylation, such as the corresponding transition metal oxide and $SrCO_3$. This fact can be attributed to the very high stability of the alkaline-earth metal carbonates. This step remains stable until temperatures above 650°C, when carbonates undergo decomposition to yield mixed oxides. In fact, it is in this process where some differences have been observed between the treatments in air and under nitrogen. The formation of mixed oxides is obviously favoured in air. In this way, the $SrMnO_{3-x}$, $SrCoO_{2.52}$, and $SrFeO_{3-x}$ oxides have been identified by X-ray diffraction as pure phases.[21] However, in the case of the nickel compound, the final residue is formed by the mixture of NiO and $SrCO_3$. The decomposition processes under nitrogen gave rise to a mixture of phases (carbonates, metal oxides, mixed oxides) in all compounds.

In order to improve the above results and to obtain more information about the mixed oxides, thermal treatments in tubular furnaces were performed in air and under nitrogen. In this case, the malonate precursors were fired at 400°C for 12 h. to remove the organic part, followed by treatments at higher temperatures. The resulting products were characterised by IR, X-ray powder diffraction (Figure 6) and differential thermal analysis (DTA).

The metallic ions exhibit mixed valence state in all compounds obtained. In order to propose a chemical formula for all the oxides the oxidation states for the different cations have been determined by a titration method. The samples were dissolved under nitrogen in a solution of HCl, which reacts with metals in the formal +3 and +4 oxidation state. The evolving gas is collected in a solution of KI and after that, titrated with thiosulfate.[22]

The thermal decomposition of the manganese organometallic precursor at 650°C for 10 h gave rise to the non-stoichiometric $SrMnO_{3-x}$ oxide.[23] This product exhibits a dark brown color. The results of the titration analysis are consistent with the formula $SrMnO_{2.95}$. The X-ray diffraction pattern of this phase has been indexed on the basis of an orthorhombic cell with parameters a = 9.437(3), b = 5.453(2) and c = 9.083(4) Å (Figure 6). It is important to note the difference observed between this oxide and that reported in the literature which was obtained from the ceramic method. This latter compound is stoichiometric and crystallises in the hexagonal system. The presence of mixed valence Mn^{3+}/Mn^{4+}, together with a distortion to an orthorhombic symmetry, appears at temperatures above 1035°C. This fact can be due to the creation of oxygen vacancies in the compound.[24] The cell parameters of this non-stoichiometric oxide are similar to those given for $SrMnO_{2.95}$ which was obtained by using the organometallic method. Taking into account these results, and with the aim of confirming the presence of a mixed valence in the last phase, we performed further IR and ESR experiments. The IR spectrum shows two broad bands at around 600 cm^{-1} and 400cm^{-1} (Figure 7a), which could be assigned to the ν_3 stretching vibration corresponding to the $Mn^{3+}-O$ and $Mn^{4+}-O$ bonds, respectively, as usually appears in perovskites with mixed valences.[25] The split of the bands is indicative of a lowering in the symmetry of the manganese environment, probably due to the presence of oxygen vacancies in the surrounding of these ions.

The ESR spectra of this oxide at different temperatures are given in Figure 8a. As can be observed, an isotropic signal appears at room temp. with an ΔHpp value of 960 G. The intensity of the signal decreases with decreasing

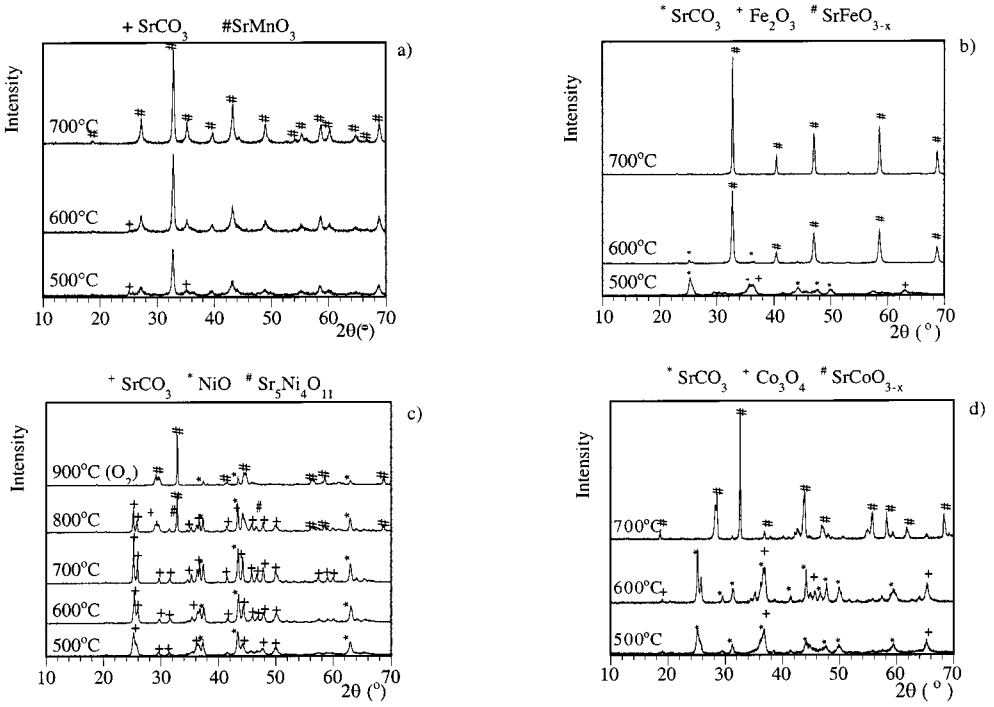


Figure 6. X-ray diffraction patterns of the phases obtained at different temperatures from the $[SrM(C_3H_2O_4)_2(H_2O)_5] \cdot 2\,H_2O$ precursors, a) M = Mn, b) M = Fe, c) M = Ni, d) M = Co

temp., being undetectable at temperatures less than 250 K. These results are characteristic of compounds with antiferromagnetic interactions. Taking into account that the ESR spectra of Mn^{4+} ions show a very broad signal, the results obtained for this phase can be explained as due to the presence of a small amount of Mn^{3+} ions in the compound. These results are in good agreement with those obtained from chemical analyses.

From the decomposition of the $[SrFe(C_3H_2O_4)_2(H_2O)_5] \cdot 2\,H_2O$ phase, the $SrFeO_{2.86}$ oxide[26] was obtained at 650°C for 10 h. The oxygen content was deduced from titration. The X-ray diffraction pattern (Figure 6) has been indexed on the basis of a tetragonal unit cell, *P*4*mm*, with parameters $a = 3.853(4)$ and $c = 3.861(2)$ Å. In order to observe the presence of non-stoichiometry in this phase, ATD measurements under argon were carried out up to 1100°C. An endothermic peak was observed at around 620°C, which would correspond to the reduction of the phase giving rise to the $SrFeO_{2.5}$ stoichiometric oxide. When cooling this sample to room temp. an ordered brown millerite-like structure is obtained. This ordered phase undergoes a reversible transition to the disordered cubic structure at 840°C. These results are in good agreement with those given in the literature for this phase.[27] In order to study the presence of a mixed valence state for the transition metal, IR spectra and ESR measurements in the $SrFeO_{2.86}$ oxide were carried out. As can be seen in the IR spectrum (Figure 7b), no absorption band was observed in the range 600−400 cm^{-1}, as would be expected for a perovskite with mixed valence Fe^{3+}/Fe^{4+}. This result can be explained on the basis of a short range hopping between the Fe^{3+}/Fe^{4+} positions.[27] The ESR spectrum shows an isotropic signal with a *g* value of 2.006 (Figure 8b). This result, together with the value of 620 G for the linewidth, confirms the presence of mixed valence Fe^{3+}/Fe^{4+} in this phase.

The decomposition of the $[SrNi(C_3H_2O_4)_2(H_2O)_5] \cdot 2\,H_2O$ precursor at low temperatures (500−700°C) yielded a mixture of $SrCO_3$ and NiO. The $Sr_5Ni_4O_{11}$ mixed oxide was obtained only after thermal treatments up to 800°C;[28] however, the presence of NiO appears as an impurity phase in the final product (Figure 6). Further attempts to oxidise the total amount of Ni^{II} were unsuccessful.

Thermal treatments of the $[SrCo(C_3H_2O_4)_2(H_2O)_5] \cdot 2\,H_2O$ compound at 700°C for 10 h., gave rise to the formation of the $SrCoO_{2.56}$ phase. Several days at 1100°C were necessary to obtain the mixed oxide from the ceramic method.[29] The X-ray diffraction pattern of the $SrCoO_{2.56}$ phase shows the presence of peaks related to the 2H-Perovskite-type structure. However, not all the diffraction peaks were indexed with this kind of structure. The diffraction patterns do not undergo any significant changes when the compounds are obtained from different thermal treatments under both oxygen and nitrogen. The chemical analysis indicates the presence of a small amount of Co^{IV} in the sample. In order to corroborate this result, further spectroscopic and magnetic measurements were carried out. The IR spectrum shows the characteristic bands at 600 and 400 cm^{-1} (see Figure 7c), corresponding to the ν_3 stretching vibration of $Co^{3+}-O$ and $Co^{4+}-O$ bonds, respectively. Magnetic measurements on this $SrCoO_{2.56}$ oxide were carried out in the temperature range of 1.8−300 K. The thermal evolution of the $\chi_m T$ and χ_m^{-1} is shown in Figure 9.

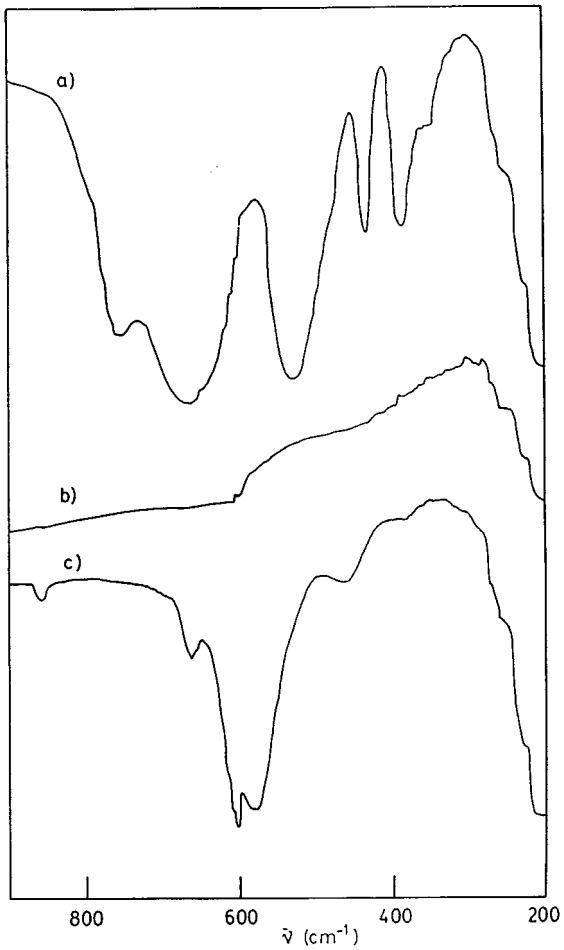


Figure 7. IR spectra of the a) $SrMnO_{2.95}$ b) $SrFeO_{2.86}$, and c) $SrCoO_{2.55}$ oxides

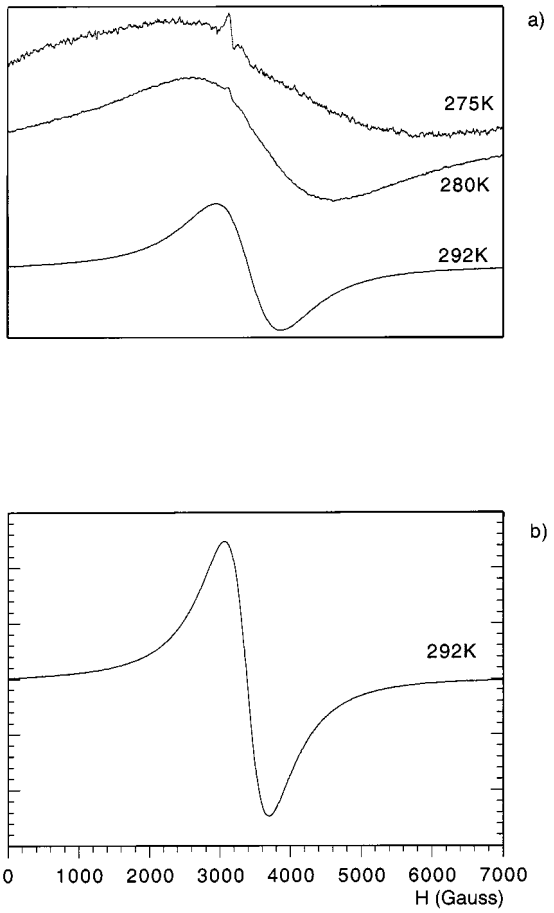


Figure 8. X-band ESR spectra for the a) $SrMnO_{2.95}$ and b) $SrFeO_{2.86}$ phases

The continual decrease observed in the $\chi_m T$ vs T curve is indicative of the presence of an antiferromagnetic ordering, with a Neel temperature value at around 25 K. It is to note an increase of the $\chi_m{}^{-1}$ values at low temperatures, which can be explained as due to the presence of a small amount of Co^{IV}, hampering the total compensation of the Co^{III} spin moments.

A scanning electron microscopic photograph of one of the oxide pellets is shown in Figure 10. In all cases, powders consisting of small homogeneous particles were observed, due to the use of soft synthesis methods. The $SrFeO_{2.86}$ oxide was obtained at the lowest temp., 650°C, and particles with a very small size (diameter less than 0.3 μm) have been favoured.

The more the temperature increases, the higher the size of the grains. Furthermore, particles with a prismatic form have been observed for the $SrCoO_{2.55}$ compound.

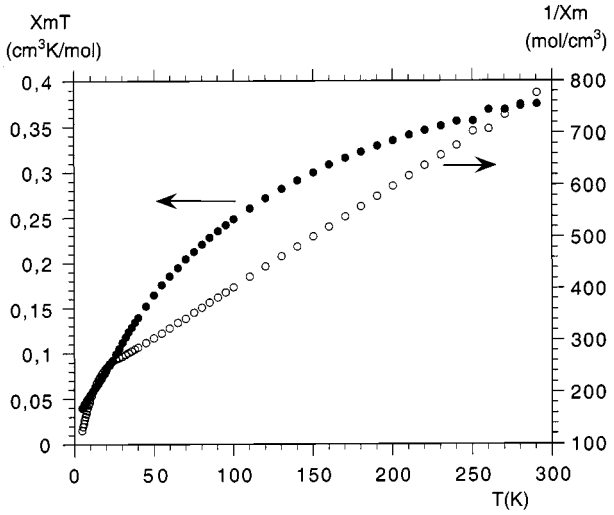


Figure 9. Thermal variation of the χ^{-1} and $\chi_m T$ product for the $SrCoO_{2.55}$ compound

Conclusions

With the aim of obtaining $SrMO_{3-x}$ oxides using soft synthesis routes, four isostructural complexes with the formula $[SrM(C_3H_2O_4)_2(H_2O)_7]$ (M = Mn, Fe, Co, Ni) have been synthesised and characterised. The structure of $[SrCo(C_3H_2O_4)_2(H_2O)_5] \cdot 2\,H_2O$ consists of a 3D network of metal ions coordinated by malonate ligand bridges. The cobalt(II) centres adopt an octahedral coordination while the strontium ions are surrounded by nine oxygen atoms. Magnetic measurements indicate the presence of weak anti-

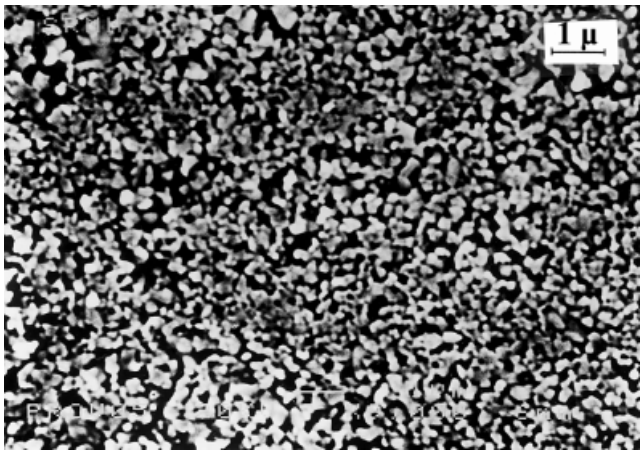


Figure 10. SEM photograph of the $SrMnO_{2.95}$ oxide

ferromagnetic interactions in all compounds. For the cobalt compound, the effect of a spin-orbit coupling must also be considered when discussing the magnetic behaviour. The decomposition steps of the metallo-organic phases, as well as the temperatures in which the evolution of the inorganic residue occurs, were deduced from the TGA studies. This information was utilised in order to perform the thermal treatments, in tubular furnaces, with the aim of obtaining mixed oxides. Depending on the reaction conditions (temperature, reaction time, atmosphere employed, etc.) control of the stoichiometry of these mixed oxides has been achieved. In this way, the oxides with stoichiometry $SrFeO_{2.86}$, $SrCoO_{2.56}$, and $SrMnO_{2.95}$ were synthesised at 600, 700, and 650°C, respectively. The appearance of Co^{IV} in $SrCoO_{2.56}$ and the presence of Mn^{III} in the $SrMnO_{2.95}$ phase is of note. This last oxide was obtained as a stoichiometric phase when synthesised using ceramic methods. The use of soft synthesis methods have also afforded homogeneous and small size particles of oxides, which have been visualised by scanning electron microscopy. In conclusion, it has been shown that from a metallo-organic precursor non-stoichiometric mixed oxides have been obtained at much lower temperatures and reaction times than those employed using the ceramic method

Experimental Section

General: IR: Mattson FTIR 1000 spectrophotometer between 400−4000 cm^{-1}, KBr disks. − Diffuse reflectance spectra: Cary 2415 spectrometer in the range 5000−45000 cm^{-1}, room temp. − Thermogravimetric measurements: Perkin−Elmer System-7 DSC-TGA, crucibles containing 20 mg of sample were heated at 5°/min under dry nitrogen and in air. − DTA: Setaran atd 92 equipment under argon. − Powder X-ray diffraction: Philips X-PERT diffractometer with Cu-$K_{\alpha 1}$ radiation, data were collected by scanning in the range 5° < 2θ < 120° with increments of 0.02°(2θ). − Magnetic susceptibilities and field dependences of magnetization (up to 7 Tesla): Quantum Design MPMS-7 Squid magnetometer, temperature range 1.8−300 K. − ESR: Bruker ESP300 spectrometer, equipped with a standard Oxford low-temperature device operating at X and Q bands, magnetic field was measured with a Bruker bnm 200 gaussmeter, and the frequency was determined with a Hewlett−Packard 5352B microwave frequency counter. Nickel(II) chloride, iron(II) chloride, sodium carbonate, and malonic acid were purchased from Aldrich Co. Strontium chloride was purchased from Merck and cobalt(II) and manganese(II) chlorides from Fluka. All of them were used without further purification.

Preparation of the Compounds: The corresponding chloride of the transition metal (3.0 mmol) was added to an aq. solution of 6.0 mmol (0.624 g) of malonic acid, neutralized with sodium carbonate. The reaction mixture was stirred without heating for about 1 h, and then an equimolar amount of strontium chloride added. The addition of ethanol (3 mL) afforded polycrystalline powders of all phases. In the case of the iron compound a closed system with nitrogen was employed. For the cobalt compound, pale pink crystals in the form of needles were collected after leaving the remaining solution for some days. The compounds were washed with water and acetone, and dried over P_2O_5. The crystals were of good quality for X-ray single-crystal studies. Attempts to obtain single crystals for the other compounds have been unsuccessful. Elemental analysis, together with Inductively Coupled Plasma measurements, were carried out in order to determine the C, H, and metal contents. − $C_6H_{18}MnO_{15}Sr$ (472.75): calcd. C 15.24, H 3.84, Mn 11.62, Sr 18.54; found C 14.94, H 3.21, Mn 11.51, Sr 17.91. − $C_6H_{18}FeO_{15}Sr$ (473.65): calcd. C 15.22, H 3.83, Fe 11.79, Sr 18.50; found C 14.93, H 3.52, Fe 11.52, Sr 19.00. − $C_6H_{18}CoO_{15}Sr$ (476.75): calcd. C 15.12, H 3.81, Co 12.36, Sr 18.38; found C 15.34, H 3.49, Co 12.11, Sr 18.47. − $C_6H_{18}NiO_{15}Sr$ (476.51): calcd. C 15.12, H 3.81, Ni 12.32, Sr 18.39; found C 15.40, H 3.59, Ni 12.86, Sr 17.62.

X-ray Crystal.Structural Determination of $[SrCo(C_3H_2O_4)_2(H_2O)_7]$: Pale pink crystals of $C_6H_{18}SrCoO_{15}$ were sealed in a glass capillary and used for data collection. Preliminary cell dimensions were calculated by Weissenberg photographs. Diffraction experiments were performed with a crystal of dimensions 0.6 × 0.1 × 0.05 mm using an Enraf-Nonius CAD4 automatic diffractometer with graphite-monochromatized Mo-K_α radiation (λ = 0.7107 Å) and the ω-scan technique. Orientation matrix and lattice parameters were determined by least-squares refinement of the diffraction data from 25 machine-centred high-angle reflections in the range 10° < 2θ < 26°. Intensities and angular positions of two standard reflections were measured every 2 h, and these showed neither decrease nor misalignment during data collection. The observed systematic extinctions were consistent with the space group $P2_1/c$. Lorentz and polarization corrections and an empirical absorption correction using XABS2 program were applied to the data.[30] The structure was solved by Patterson interpretation using the program Shelxs86.[31] It was then refined by full-matrix methods based on F^2, using Shelx93.[32] Non-hydrogen atomic scattering factors were taken from International Tables for X-ray Crystallography[33] and anisotropic thermal parameters were assigned. Difference Fourier synthesis did not allow the location of H atoms. Therefore, the hydrogen atoms of the malonate groups were calculated and isotropic thermal parameters were assigned. The final difference Fourier map showed no peaks higher than 0.70 or lower than −0.83 e $Å^{-3}$. The geometric calculations were performed with Parst[34] and Bondla[35] and molecular illustration were drawn with Platon94[36] and Atoms.[37] Crystallographic data (excluding structure factors) for the structure reported in this paper have been deposited with the Cambridge Crystallographic Data Centre as supplementary publication no. CCDC-106908. Copies of the data can be obtained free of charge on application to CCDC, 12 Union Road, Cambridge CB2 1EZ, UK [Fax: int. code + 44-1223/336-033; E-mail: deposit@ccdc.cam.ac.uk].

Acknowledgments

This work has been carried out with the financial support of the Ministerio de Educación y Ciencia (DGICYT PB94−0469 Grant) which we gratefully acknowledge. I. G. M. thanks the Spanish Government for a Doctoral Fellowship.

[1] A. Fujimori, *J. Phys. Chem. Solids* **1992**, *53*, 1595.
[2] [2a] M. Abbate, F. M. F. de Groot, J. C. Fuggle, A. Fujimori, O. Strebel, F. Lopez, M. Domke, G. Kaindl, G. A. Sawatzky, M. Takano, Y. Takeda, H. Eisaki, S. Uchida, *Phys. Rev. B* **1992-II**, 4511. − [2b] T. Arima, Y. Tokura, J. B. Torrance, *Phys. Rev. B: Condens. Matter* **1993-I**, *48*, 17006.
[3] K. Kumagai, T. Suzuki, Y. Taguchi, Y. Okada, Y. Fujishima, Y. Tokura, *Phys. Rev. B* **1993-II**, *48*, 7636.
[4] S. Nakamura, S. Iida, *Jpn. J. Appl. Phys.* **1995**, *34,* L291.
[5] T. Negas, R. S. Roth, *J. Solid State Chem.* **1970**, *1*, 409.
[6] K. J. Lee, E. Iguchi, *J. Solid State Chem*. **1995**, *114*, 242.
[7] [7a] D. W. Meadowcraft, *Nature* **1970**, *226*, 847. − [7b] M. R. Tarasevich, B. F. Efremev, in *Electrodes of Conductive Metallic Oxides* (Ed.: S. Trasatti), Elsevier, New York, **1980**, p. 221.
[8] K. C. Patil, *Bull. Mater. Sci.* **1993**, *16*, 533.
[9] B. N. Sivasankar, S. Govindarajan, *Mater. Res. Bull.* **1996**, *31*, 47.
[10] [10a] M. Insausti, R. Cortés, M. I. Arriortua, T. Rojo, E. H. Bocanegra, *Solid States Ionics* **1993**, *63−65*, 351. − [10b] M. Insausti, J. L. Pizarro, L. Lezama, R. Cortés, E. H. Bocanegra, M. I. Arriortua, T. Rojo, *Chem. Mater.* **1994**, *6*, 707. − [10c] J. García-Jaca, J. I. R. Larramendi, M. Insausti, M. I. Arriortua, T. Rojo, *J. Mater. Chem.* **1995**, *5*, 1995.
[11] [11a] N. J. Ray, B. J. Hathaway, *Acta Crystallogr*. **1982**, *B38*, 770. − [11b] D. Chattopadhyay, S. K. Chattopadhyay, P. R. Lowe, C. H. Schwalbe, S. K. Mazumder, A. Rana, S. Ghosh, *J. Chem Soc., Dalton Trans.* **1993**, 913.
[12] S. M. Saadeh, L. T. Kathleen, J. W. Kampf, W. E. Hatfield, V. L. Pecoraro, *Inorg. Chem*. **1993**, *32*, 3034.
[13] I. Gil de Muro, F. A. Mautner, M. Insausti, L. Lezama, M. I. Arriortua, T. Rojo, *Inorg. Chem*. **1998**, *37,* 3243.
[14] D. Chattopadhyay, S. K. Chattopadhyay, P. R. Lowe, C. H. Schwalbe, S. K. Mazumder, A. Rana, S. Ghosh, *J. Chem. Soc., Dalton Trans.* **1993**, 913.
[15] E. L. Muetterties, L. Guggenberger, *J. Am. Chem. Soc.* **1974**, *96*, 1748.
[16] FULLPROF, J. Rodriguez-Carvajal, *Physica, B* **1992**, *192*, 55.
[17] K. Nakamoto, *Infrared Spectra of Inorganic and Coordination Compounds*, 4th ed., John Wiley & Sons, New York, **1986**.
[18] A. B. P. Lever, *Inorganic Electronic Spectroscopy*, Elsevier Science, Amsterdan, **1984**.
[19] T. M. Dunn, *Trans. Faraday Soc*. **1961**, *57*, 1441.
[20] M. Insausti, I. Gil de Muro, L. Lorente, T. Rojo, E. H. Bocanegra, M. I. Arriortua, *Thermochim. Acta* **1996**, *287*, 81.
[21] *Powder Diffraction File*, Cards Nos. 25-900, 40-1018, 33-678, Joint Committe on Powder Diffraction Standards, Swarthmore, PA, **1984**.
[22] B. E. Gushee, L. Katz, R. Ward, *J. Am. Chem. Soc.* **1957**, *79*, 5601
[23] *Powder Diffraction File*, Card No. 25-900, Joint Committe on Powder Diffraction Standards, Swarthmore, PA, **1984**.
[24] [24a] T. Negas, R. S. Roth, *J. Solid State Chem.* **1970**, *1*, 409. − [24b] P. D. Battle, T. C. Gibb, C. W. Jones, *J. Solid State Chem.* **1988**, *74*, 60. − [24c] K. J. Lee, E. Iguchi, *J. Solid State Chem*. **1995**, *114*, 242.
[25] [25a] R. P. S. M. Lobo, F. Grevais, *Solid State Commun.* **1996**, *98*, 61. − [25b] M. A. Subramanian, *J. Solid State Chem*. **1994**, 111, 134.
[26] *Powder Diffraction File*, Card No. 33-678, Joint Committe on Powder Diffraction Standards, Swarthmore, PA, **1984**.
[27] L. Fournès, Y. Patin, G. Grenier, G. Demazeau, M. Pouchard, *Solid State Commun.* **1987**, *62*, 239.
[28] J. Lee, G. F. Holland, *J. Solid State Chem.* **1991**, *93*, 267.
[29] J. C. Grenier, L. Fournès, M. Pouchard, P. Hagenmuller, *Mat. Res. Bull*. **1986**, *21*, 441.
[30] S. Parkin, B. Moezzi, H. Hope *J. Appl. Crystallogr.* **1995**, *28*, 53.
[31] G. M. Sheldrick *Acta Crystallogr*. **1990**, *A46*, 467.
[32] G. M. Sheldrick, *SHELX93, Program for the Refinement of Crystal Structures*, University of Göttingen, Germany, **1993**.
[33] *International Tables for X-ray Crystallography*, vol. IV, Kynoch Press, Birmingham, U. K., **1974**, p. 72−98.
[34] M. Nardelli. PARST, *Comp. Chem.* **1983**, *7*, 95−98.
[35] J. M. Stewat (Ed.), *The X-ray System, Technical Report TR-446 of the Computer Science Center*, University of Maryland, College Park, Maryland, **1976**.
[36] A. L. Spek, *PLATON94, Program for the Automated Analysis of Molecular Geometry*, **1994**.
[37] E. Dowty, *ATOMS, A Computer Program for Displaying Atomic Structures*, version 2.0, Kingsport, TN, **1993**.

Received November 9, 1998
[I98388]

Cobalt Complexes with 1,3-Bis(trimethylsilyl)cyclopentadienyl and Substituent-Free P_n Ligands

Otto J. Scherer,*[a] Thomas Völmecke,[a] and Gotthelf Wolmershäuser[a][+]

Keywords: Phosphorus / P_n / $C_5H_3(SiMe_3)_2$ ligands / Cobalt / Coordination chemistry / Crystallography

The thermal or photochemical reaction of $[Cp''Co(CO)_2]$ (**1**) [Cp'' = $C_5H_3(SiMe_3)_2$-1,3] with white phosphorus (P_4) gives $[\{Cp''Co\}_2(P_5–P_5)\{CoCp''\}_2]$ (**2**) and $[\{Cp''Co\}_3P_4(\mu\text{-}CO)]$ (**3**) as well as $[\{Cp''Co\}_2(\mu\text{-}\eta^2\text{:}\eta^2\text{-}P_2)_2]$ (**4**). Cobalt complexes **2**, **3**, and **4** have been characterized by an X-ray crystal-structure determination.

Introduction

In the chemistry of transition-metal complexes with substituent-free ("naked") P_n ligands the choice of the additional Cp^R ligands plays an important role.[1] Illustrative examples are the reactions of $[\{Cp^R(OC)_2Fe\}_2](Fe–Fe)$ with white phosphorus (P_4).

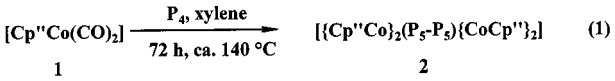
Starting with $Cp^R = C_5H_5$ the cothermolysis gives the tetranuclear cluster $[\{CpFe\}_4(P_2)_2]$ with a triangulated dodecahedral Fe_4P_4 skeleton.[2] In the case of $Cp^R = C_5H_2tBu_3$-1,2,4 the complex $[\{Cp^R(OC)_2Fe\}_2(\mu\text{-}\eta^1\text{:}\eta^1\text{-}P_4)]$, a molecule with a P_4 butterfly framework was synthesized.[3] Finally, the use of $Cp^R = C_5Me_5$ gave for the first time $[Cp^*Fe(\eta^5\text{-}P_5)]$, a sandwich complex with a *cyclo*-P_5^- ligand, the all-phosphorus analogue of the cyclopentadienide ion $C_5H_5^-$.[4]

The photochemical route, realized for $Cp^R = C_5H_4Me$ or $C_5H_3tBu_2$-1,3 (Cp''), affords $[Cp^R{}_4Fe_4(CO)_6P_8]$ with an open-edged P_8 cuneane geometry[5] and all five members of the series $[Cp''{}_2Fe_2P_4(CO)_{4-n}]$ (n = 0–4) with different P_4 ligands.[6]

The experiences of the last decade have shown that especially highly alkylated Cp^R ligands are very useful in the coordinative stabilization of different P_n ligands. Interestingly, to the best of our knowledge, until now transition-metal complexes with trimethylsilyl-substituted Cp^R ligands are unknown as starting materials in P_n chemistry.

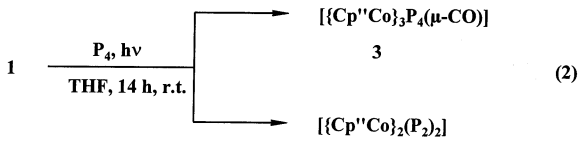
Thermal and Photochemical Reaction of $[Cp''Co(CO)_2]$ [1, Cp'' = $C_5H_3(SiMe_3)_2$-1,3] with White Phosphorus (P_4)

According to Equation 1 the cothermolysis of $[Cp''Co(CO)_2]$ (**1**) and P_4 (Co/P ≈ 1:7) affords exclusively the tetranuclear cobalt complex **2** with a P_{10} ligand in the unusually high yield of 87%.



Cp'' = $C_5H_3(SiMe_3)_2$-1,3

For a stoichiometry of Co/P ≈ 1:2 the photochemical alternative gives 30 % of **3** and 10 % of **4** (Equation 2) besides traces of **2**.



Cp'' = $C_5H_3(SiMe_3)_2$-1,3

The air-sensitive olive-green (**2**), dark-red (**3**), or black-purple (**4**) complexes are sparingly to well soluble in *n*-hexane and dissolve readily in toluene or dichloromethane.

NMR- and IR-Spectroscopic Investigations

The ^{1}H-, ^{31}P-NMR data of the complexes **2**, **3**, and **4** as well as $\tilde{\nu}$(CO) of **3** are compiled in Table 1.

The ^{1}H-NMR spectrum of **2** (measured at 340 K) affords 11 signals with relative integrals 2:2:2:2:2:1:1:18:18:18:18 in agreement with a local symmetric environment for each Cp'' ligand. In the ^{31}P-NMR spectrum of **2** (340 K) the P_{10} skeleton (Figure 1) consists of an ABCC′DD′EE′FF′ spin system. A comparison of the $^1J(P_AP_B)$ coupling constants of the P_2 bridge in **2** (−205 Hz) and **5** (−95 Hz)[7] suggests deviation of the lone pairs in the "bridge" P1–P1′ from an antiperiplanar position for complex **2**.

The Schakal plot shows that each $C_5H_3(SiMe_3)_2$-1,3 ligand of **2** is locked between two adjacent ligands.

Comparing the spectroscopic data of **3** and **7**[8] the following discrepancies were found: In contrast to the "remarkable high-field shift" discussed for **7**[8] (δ = −398.6) for the P atom surrounded by three cobalt atoms, a value of δ = 487.8 (Table 1) was measured for **3**. A redetermination of the ^{31}P-NMR spectrum of **7** gives instead of the

[+] Crystal-structure analyses.

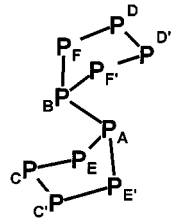
[a] Fachbereich Chemie der Universität Kaiserslautern, Erwin-Schrödinger-Straße, D-67663 Kaiserslautern, Germany

 © WILEY-VCH Verlag GmbH, D-69451 Weinheim, 1999 1434–1948/99/0606–0945 $ 17.50+.50/0

Table 1. ^{1}H-, ^{31}P-NMR, and $\tilde{\nu}$(CO) data of the complexes **2**, **3**, and **4**

Cp′′ = $C_5H_3(SiMe_3)_2$-1,3	[{Cp′′Co}$_4$P$_{10}$] (**2**)	[{Cp′′Co}$_3$P$_4$(CO)] (**3**)	[{Cp′′Co}$_2$(P$_2$)$_2$] (**4**)
	5.66 (s, 2 H)	5.89 (s, br, 2 H)	4.54 (s, br, 4 H)
	5.52 (s, 2 H)	5.77 (s, br, 1 H)	4.36 (s, br, 2 H)
	5.17 (s, 2 H)	5.05 (s, br, 6 H)	0.47 (s, 36 H)
^{1}H NMR[a]	5.02 (s, 2 H)	0.49 (s, 18 H)	
δ [ppm]	4.90 (s, 2 H)	0.45 (s, 18 H)	
	4.68 (s, 1 H)	0.32 (s, 18 H)	
	4.66 (s, 1 H)		
	0.70 (s, 18 H)		
	0.68 (s, 18 H)		
	0.36 (s, 18 H)		
	0.35 (s, 18 H)		
Spin system	ABCC′DD′EE′FF′	AM_2X	A_4
	269.6 (m, 1 P, P_A)	487.8 (t, 1 P, P_A)	−36.3 (s)
	268.7 (m, 1 P, P_B)	239.7 (dd, 2 P, P_M)	
^{31}P NMR[b]	74.4 (pdd, 2 P, P_C)	22.0 (t, 1 P, P_X)	
δ [ppm]	70.7 (pdd, 2 P, P_D)		
	−137.2 (m, 2 P, P_E)		
	−139.6 (m, 2 P, P_F)		
	$^1J_{AB}$ = −205, $^1J_{AE}$ = −311	J_{AM} = 43	
	$^2J_{AD}$ = 33	$^1J_{MX}$ = −364	
^nJ [Hz]	$^1J_{BF}$ = −307, $^2J_{BC}$ = 6		
	$^1J_{CE}$ = −359, $^2J_{CC'}$ = 79		
	$^1J_{DF}$ = −358, $^2J_{DD'}$ = 75		
	$^2J_{CE'}$ = 34, $^2J_{DF'}$ = 46		
$\tilde{\nu}$(CO) [cm^{-1}][c]		1808 (s)	

[a] 400 MHz: **2**: 340 K; **3/4**: 298 K. − [b] 162 MHz: **2**: 340 K; **3/4**: 298 K (C_6D_6, 85% H_3PO_4 ext.). − [c] 298 K, THF.



[{Cp''Co}$_2$(P$_5$-P$_5$){CoCp''}$_2$] (2)

ABCC'DD'EE'FF'-spin system

Figure 1. Spin system of complex **2**

[{Cp'''Co}$_2$(P$_5$-P$_3$){CoCp'''}]

5

Cp''' = $C_5H_2Bu^t_3$-1,2,4

[{Cp''Rh}$_2$(P$_5$-P$_5$){RhCp''}$_2$]

6

Cp'' = $C_5H_3Bu^t_2$-1,3

reported[8] δ = −398.6 the expected low-field shift (δ = 413.8). The other ^{31}P-NMR signals (**7**: δ = 227.5, 9.9) are in agreement with the published data.[8] Going from **7** to **3** all ^{31}P-NMR signals are shifted down-field in the bis(trimethylsilyl)cyclopentadienyl derivative **3** (cf. Table 1).

[{Cp''Co}$_3$P$_4$(μ-CO)]

7

Cp'' = $C_5H_3Bu^t_2$-1,3

The redetermination of $\tilde{\nu}$(CO) in **7** gives 1793 cm^{-1} instead of the published 1934 cm^{-1}.[8] This value is in accordance with 1808 cm^{-1} measured for **3**. Both bands are in the region expected for a μ-CO ligand (cf. Figure 5).

X-ray Crystal-Structure Determinations of the Complexes 2, 3, and 4

Compound 2

The most interesting structural aspect of complex **2** is its Co_4P_{10} skeleton (Figure 2).

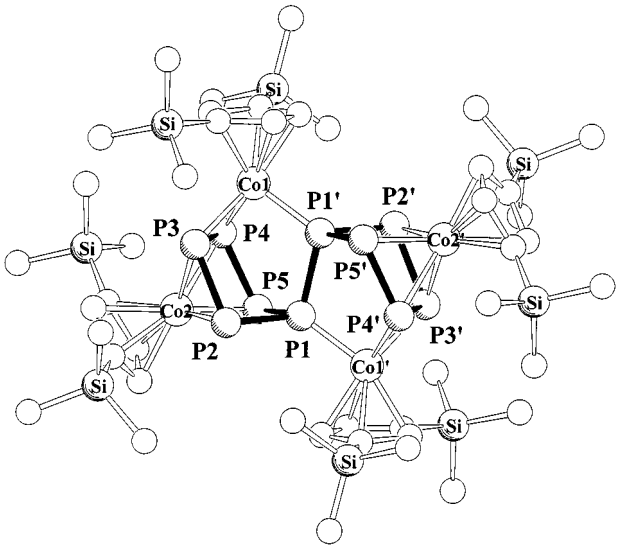


Figure 2. Selected bond lengths [Å] and angles [°]: P1−P1′ 2.1793(18), P2−P1 2.1948(14), P2−P3 2.1573(14), P3−P4 2.4743(15), P4−P5 2.1573(14), P5−P1 2.1985(14), Co1−P1′ 2.1311(11), Co1−P3 2.2405(11), Co1−P4 2.2446(11), Co2−P2 2.3108(12), Co2−P5 2.3196(12), Co2−P3 2.3355(11), Co2−P4 2.3753(11), Co1−Cp′′(centr.) 1.72, Co2−Cp′′(centr.) 1.72; P1′−Co1−P3 93.95(4), P1′−Co1−P4 93.44(4), P3−Co1−P4 66.96(4), Co1−P1′−P1 111.43(6), P2−P1−P1′ 100.11(7), P2−P1−P5 90.82(5), P5−P1−P1′ 101.18(6)

The P_{10} framework can be derived formally from the P_{10} dihydrofulvalene **A** (Figure 3) where the two 4π systems bind to Co2(2′) giving 18e⁻ per cobalt atom. This electron count can also be obtained for Co1(1′) taking into account the lone pair on P1(1′) and the bond(s) P3(3′)−P4(4′) (2.47 Å, Figure 2) which is reasonably close to the longest known 2c2e⁻-P−P bonds. For the side-on coordinated white phosphorus (P_4) in $[(Ph_3P)_2Rh(Cl)(\eta^2\text{-}P_4)]$ this edge is elongated from 2.21 Å (P_4 itself) to 2.46 Å.[9] Interestingly, for the analogous Rh_4P_{10} compound **6** a distinctly longer P···P bond (open edged) of 2.62 Å was found.[10] All the other P−P bond lengths of the P_{10} ligand in the complexes **2** and **6** are comparable [two shorter P2−P3, P4−P5: 2.16/2.15 Å (**2**/**6**); two longer: 2.20/2.19 Å (**2**/**6**)].

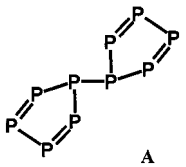


Figure 3. Hypothetic P_{10} dihydrofulvalem

Alternatively, the Co_4P_{10} framework of **2** can also be derived from Li_3P_7 (Figure 4, **B**), a well-known molecule in polyphosphide chemistry.[11]

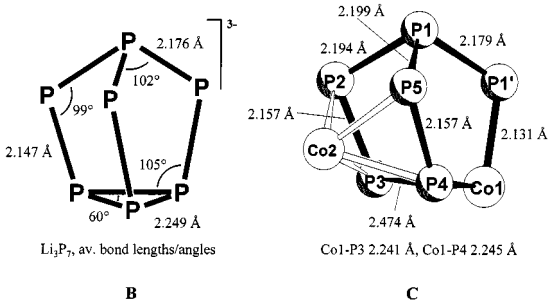


Figure 4. Comparison of P_7^{3-} with the Co_2P_6 cage of **2**

Formally, **C** (Figure 4) can be derived from **B** by replacing one basal P atom by the Co1Cp′′ fragment and capping the four-electron donor P2,3,4,5 unit by the Co2Cp′′ unit. Electron count and *d*(P1′−Co1) are in favour of a multiple-bond character.

The connection of two Co_2P_6 subunits **C** with a common edge (P1−P1′) formally gives the Co_4P_{10} skeleton of compound **2** (Figure 2). The biggest difference in bond lengths between **B** and **C** occurs, as one would expect, in the basal triangle P3,P4,Co1 (P3−P4 2.47 Å).

A further interesting parallel is realized with complexes **8**,[12] synthesized by Eichhorn's group.

$$[(\eta^4\text{-}P_7)\{M(CO)_3\}]^{3-},\quad M = Cr, Mo, W$$

8

Its carbonylation affords $[(\eta^2\text{-}P_7)W(CO)_4]^{3-}$ (**9**) where the norbornadiene-type geometry of the P_7 ligand in **8** has changed to the nortricyclane-like structure of **9** ($\eta^4 \rightarrow \eta^2$-$P_7$).[12b]

The polycyclic P_{10} core of the paramagnetic complex $[\{Cp(CO)_2Cr\}_5P_{10}]$ (**10**) consists of a P_7 norbornane with a P_2 bridge and a terminal P atom.[13]

Compound 3

Bond lengths and angles of the trinuclear cobalt complex **3** (Figure 5) differ only slightly from the values of the analogous complex **7** with $C_5H_3tBu_2$-1,3 ligands.[8]

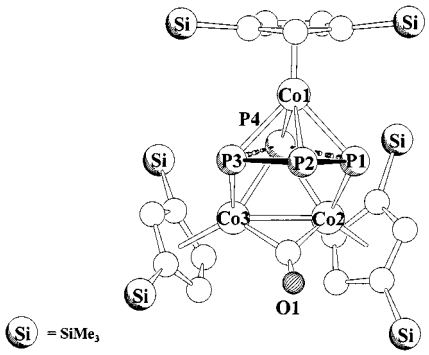


Figure 5. Selected bond lengths [Å] and angles [°]: P1−P2 2.1609(10), P2−P3 2.1585(9), P3···P4 2.5237(9), P4···P1 2.4879(8), Co2−Co3 2.4485(5), Co1−P1 2.3099(6), Co1−P2 2.2706(7), Co1−P3 2.3207(7), Co1−P4 2.2711(7), Co2−P1 2.2714(7), Co2−P4 2.2483(6), Co3−P3 2.2787(7), Co3−P4 2.2290(7), Co1−Cp′′(centr.) 1.73, Co2−Cp′′(centr.) 1.75, Co3−Cp′′(centr.) 1.74, P1−P4−P3 78.93(3), P2−P1−P4 93.02(3), P2−P3−P4 92.09(3), P3−P2−P1 95.03(4), Co2−P4−Co3 66.30(2)

A small kite-like distortion of a *cyclo*-P_4 ligand was realized for the first time in $[\{Cp^*(OC)_2Nb\}(\eta^4\text{-}P_4)]$ (**11**), Cp′′ = $C_5H_3tBu_2$-1,3.[14] Interestingly, a much stronger distortion was found for **3** and **7**. For both complexes the P···P bonds to P4 coordinating to three $CoCp^R$ fragments are distinctly longer [average of **3**: 2.50; **7**: 2.503(2) Å]. EHT calculations on **7** are in agreement with a weak P···P bonding[8] {c.f. the 2c1e⁻ P···P bond length of 2.634(3) Å in the P_4 rectangle of the diradical $[R_2N-CP_2]_2^{\bullet\bullet}$ (R = *i*Pr)[15]}.

In contrast to the planar P_4 ligand of **7** the P4 atom in **3** lies 0.34 Å above the P1,P2,P3 plane (Figure 5). The missing mirror plane in compound **3** leads to small differences in bond lengths and angles relative to those in **7** (the mean values of both compounds are nearly identical).

According to the electron-counting rules[16] of Wade and Mingos complex **3** belongs to an *arachno* cluster with (*n* + 3) = 10 SEPs (skeleton electron pairs). Its framework can formally be derived from a *closo* tricapped trigonal prism by successive elimination of two vertices.

Compound 4

The bond lengths and angles of complex **4** (Figure 6) are very similar to those of the X-ray-crystallographically characterized derivatives $[\{Cp^*Co\}_2(\mu\text{-}\eta^2\text{:}\eta^2\text{-}P_2)_2]$ (**12**)[17] and $[\{Cp'''Co\}_2(\mu\text{-}\eta^2\text{:}\eta^2\text{-}P_2)]$ (**13**) (Cp′′′ = $C_5H_2tBu_3$-1,2,4).[18]

For the side-on coordinated 4e⁻ donor P_2, which is isoelectronic and isolobal with acetylene (|P≡P| ⟶

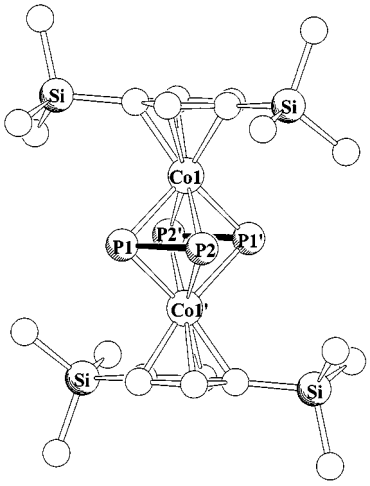


Figure 6. Selected bond lengths [Å] and angles [°]: P1−P2 2.0538(15), P1···P2′ 2.7131(14), Co1−P1 2.3069(10), Co1−P1′ 2.3162(10), Co1−P2 2.3050(10), Co1−P2′ 2.3164(10), Co1−Cp′′-(centr.) 1.70, Co1···Co1′ 3.127; P1−P2−P1′ 90.04(4), P2−P1−P2′ 89.96(4)

HC≡CH), *d*(P−P) lies in the range of 2.054 (**4**), 2.053 (**12**), and 2.052 Å (**13**) which is typical for P−P double bonds.[1] The long P···P edges of the rectangular $(P_2)_2$ ligands have nonbonding distances of 2.713, 2.705 (mean value), and 2.663 Å, *d*(Co−P) ranges from 2.311 to 2.305 and 2.308 Å, respectively. Such small differences also exist for Co···Co (3.127, Figure 6) (**12**: 3.102; **13**: 3.164 Å). For all three complexes the least-squares plane defined by the two μ-η^2:η^2-P_2 units and the planes of the two Cp^R rings differ only slightly (2°, 1°, and 2°) from a parallel arrangement.

Experimental Section

All experiments were carried out under argon in anhydrous solvents. − NMR: Bruker AMX 400, ^{1}H NMR (400.13 MHz), ^{31}P NMR (161.98 MHz). − The ^{31}P-NMR spectra of **2** was simulated with PERCH.[20] IR spectra were recorded with an FT-IR spectrometer Perkin−Elmer 16 PC. − UV irradiation: 150-W Hg high-pressure lamp, TQ 150, Heraeus Quarzlampen GmbH, Hanau. − [Cp′′Co(CO)$_2$] (**1**) [Cp′′ = $C_5H_3(SiMe_3)_2$] was synthesized from [$Co_2(CO)_8$] and Cp′′H in analogy to ref.[19]

Cothermolysis of [Cp′′Co(CO)$_2$] (1) and White Phosphorus (P_4): 1.72 g (5.3 mmol) of **1** and 1.2 g (9.7 mmol) of P_4 were heated to reflux in 50 mL of xylene for 72 h. After evaporation of the solvent under oil-pump vacuum (0 → 35°C), the residue was dissolved in ca. 20 mL of dichloromethane, and ca. 5 g of neutral Al_2O_3 (activity grade II) was added. The solvent was evaporated under oil-pump vacuum from the mixture until the residue was free-flowing. It was placed on top of a column (2 × 15 cm) filled with neutral Al_2O_3 and petroleum ether. A mixture of petroleum ether/diethyl ether (40:1) eluted [{Cp′′Co}$_2$(P_5−P_5){CoCp′′}$_2$] (**2**); yield 1.7 g (87 %) of olive-green crystals. − $C_{50}H_{98}Co_4P_{10}Si_8$ (1469.4): calcd. C 40.86, H 6.72; found C 40.34; H 6.77.

Cophotolysis of 1 and P_4: 1.13 g (3.5 mmol) of **1** and 0.19 g (1.5 mmol) of P_4 were irradiated (150-W Hg high-pressure lamp) for 14 h in 100 mL tetrahydrofuran until the ν̃(CO) bands of **1** had disappeared and a new one at 1808 cm^{-1} had emerged. Column chromatography as described for complex **2** gave with the same mixture of solvents as first fraction 115 mg (10 %) of purple [{Cp′′Co}$_2$(P_2)$_2$] (**4**) followed by 330 mg (30 %) of red-brown [{Cp′′Co}$_3$$P_4$(CO)] (**3**). − **3**: $C_{34}H_{63}Co_3OP_4Si_6$ (957.1): calcd. C 42.66, H 6.63; found C 40.05, H 6.65. − **4**: $C_{22}H_{42}Co_2P_4Si_4$ (660.7): calcd. C 39.99, H 6.41; found C 27.19 (incomplete combustion), H 5.87.

Single-Crystal X-ray Structure Determination: See also Table 2. Crystallographic data (excluding structure factors) for the struc-

Table **2**. Crystallographic data for complexes **2**, **3**, and **4**[a]

Cp′′ = $C_5H_3(SiMe_3)_2$-1,3	[{Cp′′Co}$_4$$P_{10}$] (**2**)	[{Cp′′Co}$_3$$P_4$(CO)] (**3**)	[{Cp′′Co}$_2$(P_2)$_2$] (**4**)
formula	$C_{50}H_{98}Co_4P_{10}Si_8$	$C_{34}H_{63}Co_3OP_4Si_6$	$C_{22}H_{42}Co_2P_4Si_4$
M_r	1469.4	957.1	660.7
crystal size [mm]	0.51 × 0.30 × 0.22	0.40 × 0.20 × 0.12	0.64 × 0.29 × 0.14
crystal system	triclinic	monoclinic	triclinic
space group	$P\bar{1}$	$P2_1/n$	$P\bar{1}$
a [Å]	10.9820(10)	17.7233(15)	6.5930(10)
b [Å]	14.117(2)	12.3106(6)	11.297(2)
c [Å]	14.6760(10)	23.9381(18)	11.981(3)
α [°]	109.180(10)	90	79.42(2)
β [°]	102.050(10)	111.286(9)	79.08(2)
γ [°]	109.890(10)	90	78.95(2)
V [Å^3]	1884.6(3)	4866.6(6)	849.9(3)
Z	1	4	1
T [K]	293	293	293
$d_{calcd.}$ [g cm^{-3}]	1.295	1.306	1.291
μ [mm^{-1}]	1.234	1.314	1.315
2Θ range [°]	2.05−25.00	2.43−27.50	2.74−27.50
measured refl.	7676	60076	4905
independent refl.	6341	11105	3897
refined parameters	339	451	152
*R*1 ($I \geq 2\sigma I$)	0.0410	0.0285	0.0409
*wR*2 (all data)	0.0997	0.0538	0.1144
residual electron density [e·Å^{-3}]	0.519/−0.255	0.318/−0.235	0.619/−0.514
diffractometer	Siemens P4	Stoe IPDS	Siemens P4

[a] Structure solution by Direct Methods SHELXL-97, SIR 92; refinement: full-matrix least-squares methods against F^2.

tures reported in this paper have been deposited with the Cambridge Crystallographic Data Centre as supplementary publication no. CCDC-115135 (**2**), -115137 (**3**), -115136 (**4**). Copies of the data can be obtained free of charge on application to CCDC, 12 Union Road, Cambridge CB2 1EZ, UK [Fax: int. code + 44-1223/336-033; E-mail: deposit@ccdc.cam.ac.uk].

Acknowledgments

This work was supported by the Fonds der Chemischen Industrie and the Graduiertenkolleg: "Phosphorus Chemistry as a Link between Different Chemical Disciplines".

[1] O. J. Scherer, *Angew. Chem.* **1990**, *102*, 1137−1155; *Angew. Chem. Int. Ed. Engl.* **1990**, *29*, 1104−1122.
[2] O. J. Scherer, G. Kemény, G. Wolmershäuser, *Chem. Ber.* **1995**, *128*, 1145−1148.
[3] O. J. Scherer, T. Hilt, G. Wolmershäuser, *Organometallics* **1998**, *17*, 4110−4112.
[4] O. J. Scherer, T. Brück, *Angew. Chem.* **1987**, *99*, 59; *Angew. Chem. Int. Ed. Engl.* **1987**, *26*, 59.
[5] M. E. Barr, B. R. Adams, R. R. Weller, L. F. Dahl, *J. Am. Chem. Soc.* **1991**, *113*, 3052−3060.
[6] O. J. Scherer, G. Schwarz, G. Wolmershäuser, *Z. Anorg. Allg. Chem.* **1996**, *622*, 951−957.
[7] O. J. Scherer, G. Berg, G. Wolmershäuser, *Chem. Ber.* **1996**, *129*, 53−58.
[8] M. Scheer, U. Becker, M. H. Chisholm, J. C. Huffman, F. Lemoigno, O. Eisenstein, *Inorg. Chem.* **1995**, *34*, 3117−3119.
[9] A. P. Ginsberg, W. E. Lindsell, K. J. McCullough, C. R. Sprinkle, A. J. Welch, *J. Am. Chem. Soc.* **1986**, *108*, 403−416.
[10] O. J. Scherer, B. Höbel, G. Wolmershäuser, Angew. Chem. **1992**, *104*, 1042−1043; *Angew. Chem. Int. Ed. Engl.* **1992**, *31*, 1027−1028.
[11] Reviews: H.-G. von Schnering, W. Hönle, *Chem. Rev.* **1988**, *88*, 243−273; M. Baudler, K. Glinka, *Chem. Rev.* **1993**, *93*, 1623−1667; **1994**, *94*, 1273−1297.
[12] [12a] S. Charles, B. W. Eichhorn, A. L. Rheingold, S. G. Bott; *J. Am. Chem. Soc.* **1994**, *116*, 8077−8086. − [12b] S. Charles, J. C. Fettinger, B. W. Eichhorn, *Inorg. Chem.* **1996**, *35*, 1540−1548.
[13] L. Y. Goh, R. C. S. Wong, E. Sinn, *J. Chem. Soc., Chem. Commun.* **1990**, 1484−1485; L. Y. Goh, R. C. S. Wong, E. Sinn, *Organometallics* **1993**, *12*, 888−894.
[14] O. J. Scherer, J. Vondung, G. Wolmershäuser, *Angew. Chem.* **1989**, *101*, 1395−1397; *Angew. Chem. Int. Ed. Engl.* **1989**, *28*, 1355−1357.
[15] Y. Canac, D. Bourissou, A. Baceiredo, H. Gornitzka, W. W. Schoeller, G. Bertrand, *Science* **1998**, *279*, 2080−2082.
[16] K. Wade, *Adv. Inorg. Chem. Radiochem.* **1976**, *18*, 1−66; D. M. P. Mingos, R. L. Johnston, *Struct. Bond.* **1987**, *68*, 29−87.
[17] M. E. Barr, L. F. Dahl, *Organometallics* **1991**, *10*, 3991−3996.
[18] O. J. Scherer, G. Berg, G. Wolmershäuser, *Chem. Ber.* **1995**, *128*, 635−639.
[19] S. A. Frith, J. L. Spencer, *Inorg. Synth.* **1985**, *23*, 15−21.
[20] R. Laatikainen, M. Niemitz, J. Sundelin, T. Hassinen, Program package *PERCH*, version 1/96, University of Kuopio, Finland, **1996**.

Received December 28, 1998
[I98452]

Vinylidene Transition-Metal Complexes, 50[+] Carbynehydrido- and Vinylidenehydridoosmium Complexes with $Os(PCy_3)_2$ as a Molecular Unit

Helmut Werner,*[a] Stefan Jung,[a] Birgit Weberndörfer,[a] and Justin Wolf[a]

Dedicated to Professor Christoph Elschenbroich on the occasion of his 60th birthday

Keywords: Osmium / Alkynes / Carbyne complexes / Hydrido complexes / Vinylidene complexes

The reaction of $OsCl_3 \cdot 2H_2O$ with PCy_3 leads under reducing conditions either to $[OsH_6(PCy_3)_2]$ (**1**) or $[OsH_2Cl_2(PCy_3)_2]$ (**2**). Treatment of **2** with terminal alkynes HC≡CR (R = Ph, $SiMe_3$) affords the carbynehydrido complexes $[OsHCl_2(\equiv CCH_2R)(PCy_3)_2]$ (**4**, **5**), of which **5** (R = $SiMe_3$) is easily converted with traces of water into $[OsHCl_2(\equiv CCH_3)(PCy_3)_2]$ (**6**). Compound **4** (R = Ph) reacts with NaOMe to yield the vinylidenehydridoosmium(II) complex $[OsHCl(=C=CHPh)(PCy_3)_2]$ (**7**) which upon treatment with HBF_4/OEt_2 gives the five-coordinate cationic species $[OsHCl(\equiv CCH_2Ph)(PCy_3)_2]BF_4$ (**8**). The reaction of $[OsH_3Cl(PCy_3)_2]$ (**9**) with $HC\equiv CC(CH_3)_2Cl$ affords a mixture of $[OsHCl_2(\equiv CCH{=}CMe_2)(PCy_3)_2]$ (**10**) and $[OsCl_2(H_2)(=CHCH{=}CMe_2)(PCy_3)_2]$ (**11**). Compound **11** is quite labile and by elimination of H_2 gives **10**. The molecular structure of **10** has been determined by X-ray crystallography.

In the course of our continuous studies on the synthesis and reactivity of vinylidenemetal complexes with d^6- and d^8-metal centers,[1] we recently reported that the reaction of the ruthenium(IV) compound $[RuH_2Cl_2(P\textit{i}Pr_3)_2]$ with terminal alkynes HC≡CR led, depending on the conditions, to the formation not only of the expected vinylidene complexes $[RuCl_2(=C=CHR)(P\textit{i}Pr_3)_2]$ but also of the related carbene derivatives $[RuCl_2(=CHCH_2R)(P\textit{i}Pr_3)_2]$.[2] Since compounds of this type, in particular with PCy_3 instead of $P\textit{i}Pr_3$ as P-donor ligand, proved to be excellent catalysts for olefin metathesis (including RCM and ROMP),[3] we became interested in studying the formation of carbene complexes $[RuCl_2(=CHCH_2R)(PR'_3)_2]$ from Ru-containing precursors and HC≡CR in more detail. As a consequence we developed a convenient and very efficient one-pot synthesis of compounds $[RuCl_2(=CHCH_2R)(PCy_3)_2]$ (R = H, Ph) from ruthenium trichloride, PCy_3, Mg, H_2, water, and terminal alkynes as starting materials.[4] The principal advantage of this method is that it avoids expensive precursors such as $[RuCl_2(PPh_3)_3]$,[5] $[Ru(\eta^4\text{-}C_8H_{12})(\eta^6\text{-}C_8H_{10})]$,[6] or $[RuH_2(H_2)_2(PCy_3)_2]$,[7] and uses alkynes instead of cyclopropenes, diazoalkanes, vinyl chlorides, or propargylic chlorides as carbene sources.

The aim of the present work was to find out whether the osmium counterparts to the Grubbs-type carbeneruthenium complexes are equally accessible and if so, what their catalytic activity is. Here we report that the preparative routes which for ruthenium give the five-coordinate compounds $[RuCl_2(=CHR)(PCy_3)_2]$ afford the isomeric carbynehydrido complexes $[OsHCl_2(\equiv CR)(PCy_3)_2]$ in good yields in the case of osmium. While these six-coordinate compounds are quite stable and inert towards olefins, the five-coordinate cationic complex $[OsHCl(\equiv CCH_2Ph)(PCy_3)_2]BF_4$ is catalytically active and catalyzes the ring-opening metathesis polymerization (ROMP) of cyclopentene.

Results and Discussion

Dihydrido- and Polyhydridoosmium Complexes

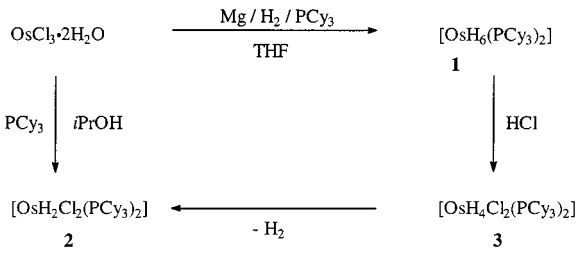
Under the conditions under which $RuCl_3 \cdot 3\,H_2O$ is converted into the hydrido(dihydrogen) complex $[RuHCl(H_2)(PCy_3)_2]$,[4] the reaction of $OsCl_3 \cdot 2\,H_2O$ with activated Mg and PCy_3 under H_2 takes a different course. After the suspension in THF was stirred for 4 h at 65°C, a mixture of products was formed in which, besides two unknown compounds, the dihydridoosmium(IV) complex **2** (Scheme 1) could be identified by ^{1}H- and ^{31}P-NMR spectroscopy. The trihydrido derivative $[OsH_3Cl(PCy_3)_2]$, the generation of which was anticipated in analogy to that of $[RuHCl(H_2)(PCy_3)_2]$, could not be detected. If the reaction mixture formed from $OsCl_3 \cdot 2\,H_2O$ was continuously stirred under H_2 at 85°C for 19 h, an off-white solid precipitated from which upon extraction with CH_2Cl_2 the hexahydrido complex $[OsH_6(PCy_3)_2]$ (**1**) was isolated. The preparation of this compound was previously reported by Halpern et al.[8] who treated $(NH_4)_2[OsCl_6]$ with PCy_3 and $NaBH_4$ in the presence of ethanol. The new synthetic route described here is more efficient and has the advantage of

[+] Part 49: J. Gil-Rubio, B. Weberndörfer, H. Werner, *J. Chem. Soc., Dalton Trans.*, submitted.

[a] Institut für Anorganische Chemie der Universität Würzburg, Am Hubland, D-97074 Würzburg, Germany

 © WILEY-VCH Verlag GmbH, D-69451 Weinheim, 1999 1434–1948/99/0606–0951 $ 17.50+.50/0

the starting material $OsCl_3 \cdot 2\,H_2O$ instead of the more expensive $(NH_4)_2[OsCl_6]$.



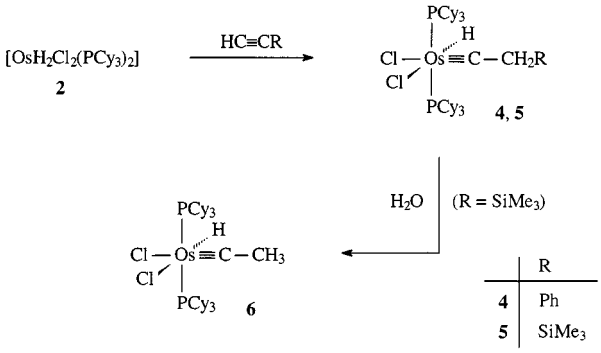
Scheme 1

The above-mentioned dihydridoosmium(IV) complex $[OsH_2Cl_2(PCy_3)_2]$ (**2**) is accessible from $OsCl_3 \cdot 2\,H_2O$ and PCy_3 in 2-propanol under reflux conditions. The same procedure had already been applied in our laboratory to afford the related species $[OsH_2Cl_2(L)_2]$ with L = P*i*Pr$_3$ and P*t*Bu$_2$Me, which represented the first examples of hexacoordinate osmium(IV) dihydrides.[9] Compound **2** was also obtained in almost quantitative yield on treatment of **1** with gaseous HCl in hexane. The most typical spectroscopic features of **2** (which is a red-brown, moderately air-sensitive solid) is the singlet for the two phosphane ligands in the ^{31}P-NMR spectrum at $\delta = 33.6$ and the triplet for the OsH_2 protons in the ^{1}H-NMR spectrum at $\delta = -15.68$. Based on the analogy of these spectroscopic data to those of $[OsH_2Cl_2(P\mathit{i}Pr_3)_2]$, we assume that the structure of **2** is similar to that of the bis(triisopropylphosphane) derivative, which is best described as a square antiprism with two missing vertexes.[9]

The reaction of **1** with hydrogen chloride deserves a special comment. If a slow stream of HCl is passed through a suspension of **1** in hexane, almost instantaneously a flocculent white precipitate is formed which, after the reaction mixture is stirred for 10−15 min, is converted into the red-brown compound **2**. When the treatment of the starting material with HCl is stopped after ca. 30 s and the flocculent precipitate separated from the solution, we observed that the color of the off-white solid changed to brown. The ^{31}P-NMR spectrum of the freshly isolated intermediate displayed, besides the signals of **1** and **2** at $\delta = 45.0$ and 33.6, a third singlet at $\delta = 13.1$, which we tentatively assign to the dichlorotetrahydridoosmium(VI) complex **3** (Scheme 1). The ^{1}H-NMR spectrum of the crude product supports this proposal since it shows in the high-field region a signal at $\delta = -10.16$ which due to P-H coupling is split into a triplet. Recently, Berke et al. reported the preparation of the corresponding triisopropylphosphane derivative $[OsH_4Cl_2(P\mathit{i}Pr_3)_2]$, the ^{1}H-NMR spectrum of which displays a resonance at $\delta = -10.55$ with a ^2J(PH) coupling constant of 10.1 Hz.[10] We note that even if the ^{1}H-NMR spectrum of the intermediate is measured in CD_2Cl_2 at −78°C, a slow evolution of gas (H_2) takes place accompanied by the conversion of compound **3** to the more stable dichlorodihydridoosmium(IV) complex **2**.

Carbyne- and Vinylideneosmium Complexes

We recently reported that the ruthenium counterpart of compound **2** with the composition $[RuH_2Cl_2(PCy_3)_2]$, which was prepared by Chaudret et al. from $[RuH_2(H_2)_2(PCy_3)_2]$ and aqueous HCl in ether[11] and independently by us from $[RuHCl(H_2)(PCy_3)_2]$,[12] reacts with phenylacetylene to give the five-coordinate vinylidene complex $[RuCl_2(=C=CHPh)(PCy_3)_2]$.[12] In contrast, treatment of **2** with three equivalents of HC≡CPh in hexane at 60°C affords instead of $[OsCl_2(=C=CHPh)(PCy_3)_2]$ the six-coordinate carbynehydrido compound **4** in 63% yield of isolated product. The analogous reaction of **2** with HC≡CSiMe$_3$ leads to a mixture of two products **5** and **6**, of which the first is by far the most dominant species (Scheme 2). The ^{31}P-NMR spectrum of the freshly isolated yellow solid displays a rather strong singlet at $\delta = 11.2$ and a weaker resonance at $\delta = 10.8$, which we assign to compounds **5** and **6**, respectively. In the hydride region of the ^{1}H-NMR spectrum of the mixture of **5** and **6** two triplets appear, the chemical shifts and the P-H coupling constants of which are only slightly different. Compound **5** containing the CH_2SiMe_3-substituted carbyne is completely converted into **6** upon addition of two drops of H_2O to a solution in CD_2Cl_2. Therefore, we assume that the small quantities of the carbyne complex **6** formed in the reaction of **2** with HC≡CSiMe$_3$ in hexane originate from traces of water in the reaction system. Besides the hydride resonance in the ^{1}H-NMR spectrum, a characteristic spectroscopic feature for **5** and **6** is the signal of the carbyne carbon atom in the ^{13}C-NMR spectrum which appears at $\delta = 267.6$ (**5**) and 265.5 (**6**), respectively. The corresponding resonance for **4** is observed at $\delta = 265.8$.

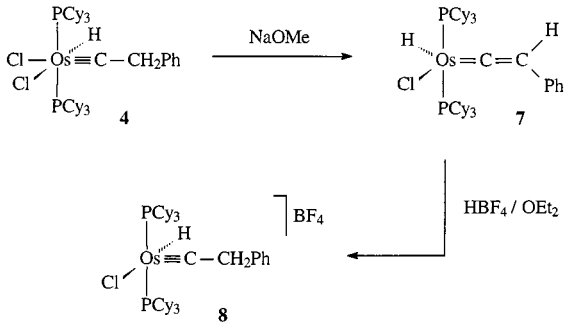


Scheme 2

With regard to the mechanism of formation of **4** and **5**, we assume that the starting material **2**, containing a metal center with a 16-electron configuration, generates in the initial step of the reaction a 1:1 adduct with the alkyne. It is conceivable that this seven-coordinate species is in equilibrium with the (dihydrogen)osmium(II) compound $[OsCl_2(H_2)(HC{\equiv}CR)(PCy_3)_2]$, which could first rearrange to the isomeric vinylidene derivative $[OsCl_2(H_2)(=C=CHR)(PCy_3)_2]$ and finally by intramolecular hydrogen transfer to $[OsHCl_2(\equiv CCH_2R)(PCy_3)_2]$. A similar reaction scheme has been proposed by Esteruelas and Oro et al.,

who prepared analogous carbynehydridoosmium complexes with two triisopropylphosphane ligands from $[OsH_2Cl_2(PiPr_3)_2]$ and HC≡CR.[13] A different synthetic route leading to $[OsHCl_2(\equiv CCH_2R)(PiPr_3)_2]$ was most recently reported by Caulton and co-workers, who used instead of 1-alkynes the corresponding alkenes CH_2=CHR as starting materials.[14] There is ample precedence for this water-assisted conversion of **5** into **6**, as we[15] as well as others[13a,16] observed that upon treatment of various low-valent transition-metal compounds with silylated alkynes or diynes in the presence of traces of H_2O or HX, metal complexes with C−H instead of C−SiR_3 bonds are formed.

The six-coordinate carbynehydrido complex **4** reacts with NaOMe in THF to give the five-coordinate vinylidenehydridoosmium(II) compound **7** in 87% isolated yield. The related bis(triisopropylphosphane) complex had been prepared on a similar route.[13b] The ^{1}H-NMR spectrum of **7** (which is a deep green, moderately air-sensitive solid) exhibits in the high-field region a triplet at δ = −16.38 which is typical for species of this type.[12][13] The presence of the vinylidene ligand is indicated by the ^{13}C-NMR resonances at δ = 282.8 and 107.3, which are assigned to the α- and β-carbon atoms of the Os=C=CHR chain. Since the ^{31}P-NMR spectrum of **7** displays a singlet at δ = 26.6, we assume, in agreement with theoretical studies by Eisenstein, Caulton et al.[17], that for the five-coordinate hydridovinylidene compound a distorted trigonal-bipyramidal geometry is most likely.

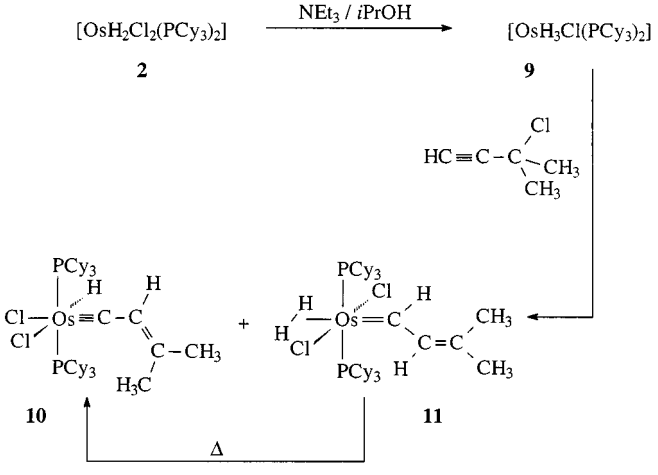


Scheme 3

The reactivity of compound **7** resembles that of the ruthenium counterpart $[RuHCl(=C=CH_2)(PCy_3)_2]$.[18] If HBF_4 is used as the substrate, the attack of the proton does not occur at the metal but at the β-carbon atom of the Os=C=CHPh unit and thus converts the vinylidene into a carbyne ligand (Scheme 3). In contrast to $[RuHCl(\equiv CCH_3)(OEt_2)(PCy_3)_2]BF_4$, which is rather labile and decomposes in CH_2Cl_2 at room temperature within 20−30 min,[18] the osmium complex **8** is considerably more stable. In the solid state, it can be stored under argon at 25°C for days, and in solution (CD_2Cl_2) at −18°C it does not decompose within 24 h.

The elemental analysis as well as the ^{1}H-NMR spectrum confirm that in **8**, unlike in $[RuHCl(\equiv CCH_3)(S)(PCy_3)_2]^+$ (S = OEt_2, OH_2)[18] and $[OsHCl(\equiv CCH_2Ph)(OH_2)(PiPr_3)_2]^+$,[13b] the open coordination site is not occupied by a solvent molecule. By taking the molecular structure of compound **10** (see below) and of the cationic carbyne complex $[OsH\{\equiv CCH=C(CH_3)_2\}(\kappa^2\text{-}O_2CCH_3)(PiPr_3)_2]^+$ into consideration,[19] we assume that in **8** the coordination around the metal center corresponds to that of a square pyramid with the carbyne moiety in the apical position. In agreement with this proposal, the ^{1}H-NMR spectrum of **8** displays a resonance for the hydrido ligand at δ = −8.75 and the ^{13}C-NMR spectrum exhibits a signal for the carbyne carbon atom at δ = 279.6, the latter of which is split into a triplet due to P-C coupling. For the related bis(triisopropylphosphane) complex $[OsHCl(\equiv CCH_2Ph)(PiPr_3)_2]^+$, which was most recently isolated by Spivak and Caulton with $[\{3,5\text{-}(CF_3)_2C_6H_3\}_4B]^-$ as the anion, the chemical shifts for the hydride and the carbyne carbon resonances are δ = −9.84 and 282.6, respectively.[20]

The synthesis of neutral six-coordinate carbynehydridoosmium(II) compounds is also possible by using propargylic chlorides instead of 1-alkynes such as HC≡CPh or $HC\equiv CSiMe_3$ as substrates. In this case, the starting material **2** was first converted into $[OsH_3Cl(PCy_3)_2]$ (**9**), which was obtained from **2** and 2-propanol in the presence of NEt_3 as a brown-yellow air-sensitive solid in almost quantitative yield (Scheme 4). The counterparts of **9** with $PiPr_3$ and $PtBu_2Me$ as phosphane ligands were recently prepared along a similar route.[17][21] Each of the three compounds of the general composition $[OsH_3Cl(PR_3)_2]$ is fluxional in solution. The ^{1}H-NMR spectrum of **9** (in CD_2Cl_2) displays a broad singlet at δ = −19.22 at 25°C, which upon cooling the solution to 0°C is split into a triplet. Below −23°C, a new broadening of the hydride signal is observed which, however, is not resolved even at −60°C. Caulton and coworkers reported that the spectrum of $[OsH_3Cl(PiPr_3)_2]$ shows AB_2 patterns in the hydride region below −80°C.[21a]



Scheme 4

The reaction of **9** with 3-chloro-3-methylbut-1-yne in dichloromethane at −40°C gives a mixture of two products. The more labile component is the carbene(dihydrogen) derivative **11** (see Scheme 4), which could not be separated from the mixture and was therefore characterized by ^{1}H-

and ^{13}C-NMR spectroscopy. Compound **11** reacts upon warming to 25°C to afford the carbynehydrido complex **10**, which was isolated as a pale brownish solid in 53% yield. The most typical spectroscopic features in the ^{1}H-NMR spectrum for **10** are, besides the resonances for the hydrido ligand and the carbyne carbon atom, the signals for the =CH proton at δ = 4.39 and for the inequivalent =CMe_2 methyl protons at δ = 2.01 and 1.50. The resonances for the =CH and =*C*Me_2 carbon nuclei appear in the ^{13}C-NMR spectrum at δ = 135.9 and 162.1.

The result of the X-ray crystal structure analysis of **10** is shown in Figure 1. The coordination geometry around the osmium center can be described as a distorted octahedron with the two phosphane ligands in the apical positions. The carbyne unit is disposed *trans* to one of the two chlorides. Both the C1−Os−Cl2 and P1−Os−P2 axes are slightly bent, the bond angle P1−Os−P2 [167.95(3)°] in **10** being somewhat larger than in the non-hydride-containing derivative [$OsCl_2$(≡CCH=CPh_2)(κ^1-*P*-*i*$Pr_2PCH_2CO_2Me$)-{κ^2-*P*,*O*-*i*$Pr_2PCH_2C(O)O$}] [165.0(1)°], which was recently prepared in our laboratory.[22] The Os−C1 distance in **10** [1.715(4) Å] is nearly identical to that in the above-mentioned carbyne complex [1.72(1) Å][22] as well as in the triisopropylphosphane derivative [$OsHCl_2$(≡CCH_2Ph)-(P*i*Pr_3)$_2$] [1.711(4) Å].[13a] There is, however, a significant difference between the Os−C bond length in **10** and in [OsCl(≡CC_6H_4Me-4)(CO)(PPh_3)$_2$] [1.78(2) Å][23] which could be explained by the different oxidation state and coordination number of the two compounds. The C1−C2 and C2−C3 bond lengths in **10** are in the expected range and this is true also for the Os−P distances.

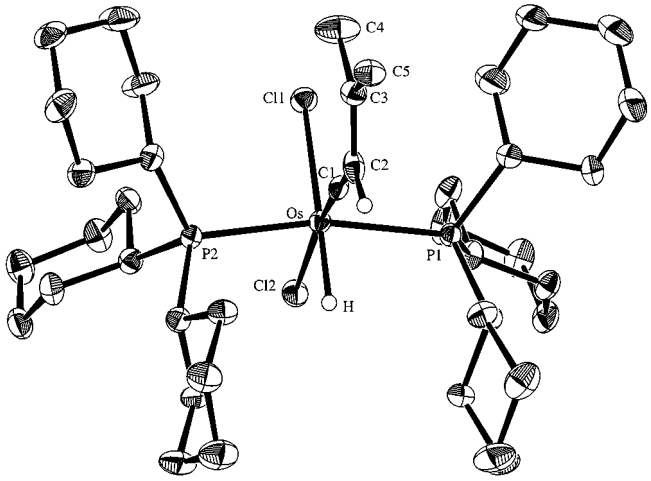


Figure 1. Molecular structure (ORTEP plot) of **10**;[a] the carbon atoms of the cyclohexyl rings are reduced in size for clarity; selected bond lengths [Å] and angles [°]: Os−C1 1.715(4), Os−P1 2.417(1), Os−P2 2.422(1), Os−Cl1 2.515(1), Os−Cl2 2.488(1), C1−C2 1.434(5), C2−C3 1.364(5), C3−C4 1.480(6), C3−C5 1.490(5); P1−Os−P2 167.95(3), P1−Os−C1 90.9(1), P1−Os−Cl1 95.42(3), P1−Os−Cl2 88.24(3), P2−Os−C1 91.0(1), P2−Os−Cl1 95.87(3), P2−Os−Cl2 87.76(3), C1−Os−Cl1 101.0(1), C1−Os−Cl2 170.0(1), Cl1−Os−Cl2 89.02(4), Os−C1−C2 174.4(3), C1−C2−C3 120.6(4), C2−C3−C4 124.1(4), C2−C3−C5 119.5(3), C4−C3−C5 116.3(3)

Catalytic Studies

It was recently found in our laboratory[18] that the cationic carbynehydridoruthenium complexes [RuHCl-(≡CCH_3)(S)(PCy_3)$_2$]BF_4 (S = OEt_2, OH_2) are highly efficient catalysts for olefin metathesis. They are not only more active than the Grubbs compound [$RuCl_2$(=CHPh)(PCy_3)$_2$] in the ring-opening metathesis polymerization (ROMP) of cyclooctene but, even more remarkably, they also catalyze the cross-olefin metathesis of cyclopentene with methyl acrylate. By this novel route, a homologous series of multiply unsaturated esters is formed. For the neutral carbyneruthenium complexes [RuCl(≡CR)(CO)-(PPh_3)$_2$], prepared by Roper et al.,[24] a similar catalytic activity is unkown.[25]

According to these results, it is not surprising that under standard conditions[5e] neither **4** nor **10** is catalytically active in ROMP of cyclopentene. However, the cationic species **8** reacts rather smoothly in CH_2Cl_2 with this olefin. After 24 h at room temperature, a highly viscous material was generated from which, after it was dissolved in $CHCl_3$ and the solution poured into methanol, a white powder could be obtained in about 40% yield. The comparison of the ^{1}H- and ^{13}C-NMR data of the polymer with those reported in the literature[25] revealed that 77% of the double bonds are *trans*-configured. The turnover frequency was determined as 154.2 h^{-1} at 25°C. To the best of our knowledge, compound **8** is the first well-defined osmium complex which catalyzes ROMP of cyclopentene.[25] We note that $OsCl_3 \cdot x\ H_2O$, an adduct of osmium chloride and cycloocta-1,5-diene,[26] and also OsO_4[25] were found to be catalytically active in olefin metathesis but as far as we know not in ROMP of cyclopentene.

Experimental Section

All operations were carried out under argon with Schlenk techniques. The alkynes and PCy_3 were commercial products from Strem and ABCR. − NMR: Bruker AC 200 and AMX 400 [vt = virtual triplet; $N = {}^1J(PC) + {}^3J(PC)$]. − Melting points determined by DTA.

1. Preparation of [$OsH_6(PCy_3)_2$] (1): To a slurry of 0.5 g (20.6 mmol) of magnesium turnings, which were activated with 0.50 mL of 1,2-$C_2H_4Cl_2$, in 25 mL of THF was added stepwise 2.23 g (7.80 mmol) of PCy_3 and 557 mg (1.70 mmol) of $OsCl_3 \cdot 2\ H_2O$. The reaction mixture was heated under vigorous stirring under H_2 (1 bar) for 90 min at 65°C and then for 19 h at 85°C. After the mixture was cooled to room temperature, the solution was separated from the solid (mainly Mg) and the solvent was removed in vacuo. The residue was dissolved in 30 mL of CH_2Cl_2 and 10 mL of H_2O. The organic layer was separated, concentrated to dryness in vacuo, and the residue washed twice with 15-mL portions of 2-propanol and dried. The remaining white solid was identified as **1** by comparison of the ^{1}H- and ^{31}P-NMR data with those reported in the literature;[8] yield 742 mg (58%).

2. Preparation of [$OsH_2Cl_2(PCy_3)_2$] (2): a) A suspension of 611 mg (1.87 mmol) of $OsCl_3 \cdot 2\ H_2O$ in 2 mL of 2-propanol was treated with a solution of 2.76 g (9.85 mmol) of PCy_3 in 20 mL of 2-propanol and then heated for 24 h under reflux. After the reaction mix-

ture was cooled to room temperature, a red-brown solid precipitated. The solid was separated from the mother liquor, washed twice with 10-mL portions of methanol (0°C), twice with 10-mL portions of ether (0°C) and dried in vacuo; yield 1.21 g (79%). – **b)** A slow stream of dry HCl was passed through a suspension of 86 mg (0.11 mmol) of **1** in 8 mL of hexane for 30 s at room temperature. A dark brown solution was formed from which, after it had been stirred for 10 min, a red-brown solid precipitated. The mother liquor was separated and the residue was washed with 5 mL of hexane and dried; yield 90 mg (96%); m.p. 94°C. – ^{1}H NMR (400 MHz, C_6D_6): δ = 2.28–1.15 (m, 66 H, C_6H_{11}), –15.68 [t, *J*(PH) = 35.1 Hz, 2 H, OsH_2]. – ^{13}C NMR (100.6 MHz, C_6D_6): δ = 39.9 [d, *J*(PC) = 30.5 Hz, *ipso*-C of C_6H_{11}], 30.0 (s, *m*-C of C_6H_{11}), 27.8 [d, *J*(PC) = 10.2 Hz, *o*-C of C_6H_{11}], 26.9 (s, *p*-C of C_6H_{11}). – ^{31}P NMR (162.0 MHz, C_6D_6): δ = 33.6 (s). – $C_{36}H_{68}Cl_2OsP_2$ (824.0): calcd. C 52.48, H 8.32; found C 52.26, H 8.24.

3. Preparation of [$OsHCl_2$(≡CCH_2Ph)(PCy_3)$_2$] (4): A suspension of 393 mg (0.48 mmol) of **2** in 18 mL of hexane was treated with 156 μL (1.42 mmol) of phenylacetylene and stirred for 24 h at 60°C. A pale brownish solid precipitated. After the reaction mixture was cooled to room temperature, the mother liquor was separated, the solid residue was washed twice with 5-mL portions of hexane and dried; yield 282 mg (63%); m.p. 129°C. – ^{1}H NMR (400 MHz, CD_2Cl_2): δ = 7.45–7.25 (m, 5 H, C_6H_5), 2.61 (s, 2 H, CH_2Ph), 2.33–1.04 (m, 66 H, C_6H_{11}), –6.64 [t, *J*(PH) = 16.8 Hz, 1 H, OsH]. – ^{13}C NMR (100.6 MHz, CD_2Cl_2): δ = 265.8 [t, *J*(PC) = 11.5 Hz, Os≡C], 129.5, 129.1, 128.8, 128.1 (all s, C_6H_5), 56.9 (s, *C*H_2Ph), 36.8 (br. s, *ipso*-C of C_6H_{11}), 29.9, 29.4 (both s, *m*-C of C_6H_{11}), 27.9 (br. s, *o*-C of C_6H_{11}), 27.0 (s, *p*-C of C_6H_{11}). – ^{31}P NMR (162.0 MHz, CD_2Cl_2): δ = 8.8 [s, *J*(OsP) = 169.6 Hz]. – $C_{44}H_{74}Cl_2OsP_2$ (926.1): calcd. C 57.06, H 8.05; found C 56.58, H 7.97.

4. Preparation of [$OsHCl_2$(≡CCH_2SiMe_3)(PCy_3)$_2$] (5): A suspension of 307 mg (0.37 mmol) of **2** in 15 mL of hexane was treated with 156 μL (1.10 mmol) of HC≡$CSiMe_3$ and stirred for 6 h at 60°C. A yellow solid precipitated which was isolated as described for **4**; yield 178 mg. The NMR spectra of the isolated product indicated that besides **5** also small amounts of **6** were already formed. Typical data for **5**: ^{1}H NMR (400 MHz, CD_2Cl_2): δ = 0.06 (s, $SiMe_3$), –7.64 [t, *J*(PH) = 17.6 Hz, OsH]. – ^{13}C NMR (100.6 MHz, CD_2Cl_2): δ = 267.6 (br. s, Os≡C), 30.5 (s, CH_2). – ^{31}P NMR (162.0 MHz, CD_2Cl_2): δ = 11.2 (s).

5. Preparation of [$OsHCl_2$(≡CCH_3)(PCy_3)$_2$] (6): A suspension of 220 mg (0.27 mmol) of **2** in 15 mL of hexane was treated with 112 μL (0.79 mmol) of HC≡$CSiMe_3$ and a few drops of water and then stirred for 24 h at 60°C. A pale brownish solid precipitated, which was isolated as described for **4**; yield 136 mg (60%); m.p. 152°C. – ^{1}H NMR (400 MHz, CD_2Cl_2): δ = 2.40–1.30 (m, 66 H, C_6H_{11}), 0.94 (s, 3 H, CH_3), –7.31 [t, *J*(PH) = 16.8 Hz, 1 H, OsH]. – ^{13}C NMR (100.6 MHz, CD_2Cl_2): δ = 265.5 [t, *J*(PC) = 11.5 Hz, Os≡C], 38.6 (s, CH_3), 35.7 (br. s, *ipso*-C of C_6H_{11}), 29.9, 29.5 (both s, *m*-C of C_6H_{11}), 28.1, 27.9 (both vt, *N* = 10.2 Hz, *o*-C of C_6H_{11}), 27.1 (s, *p*-C of C_6H_{11}). – ^{31}P NMR (162.0 MHz, CD_2Cl_2): δ = 10.8 [s, *J*(OsP) = 167.9 Hz]. – $C_{38}H_{70}Cl_2OsP_2$ (850.0): calcd. C 53.69, H 8.30; found C 53.62, H 8.38.

6. Preparation of [OsHCl(=C=CHPh)(PCy_3)$_2$] (7): A suspension of 208 mg (0.23 mmol) of **4** in 35 mL of THF was treated with 14.6 mg (0.27 mmol) of NaOMe and stirred for 2 h at room temperature. After the solvent was removed, the residue was extracted with 20 mL of toluene. The extract was concentrated to dryness in vacuo, and the remaining green solid was washed with small quantities of toluene and pentane (both 0°C) and dried; yield 163 mg (87%); m.p. 131°C. – ^{1}H NMR (400 MHz, C_6D_6): δ = 7.56–6.78 (m, 5 H, C_6H_5), 2.66 (br. s, 1 H, =C*H*Ph), 2.21–1.18 (m, 66 H, C_6H_{11}), –16.38 [t, *J*(PH) = 13.0 Hz, 1 H, OsH]. – ^{13}C NMR (100.6 MHz, C_6D_6): δ = 284.1 [t, *J*(PC) = 9.5 Hz, Os=C], 128.3, 128.1, 123.4, 122.8 (all s, C_6H_5), 108.6 (s, Os=C=*C*), 36.1 (vt, *N* = 22.9 Hz, *ipso*-C of C_6H_{11}), 30.9, 30.6 (both s, *m*-C of C_6H_{11}), 28.1, 27.9 (both vt, *N* = 10.2 Hz, *o*-C of C_6H_{11}), 26.9 (s, *p*-C of C_6H_{11}). – ^{31}P NMR (162.0 MHz, C_6D_6): δ = 26.6 [s, *J*(OsP) = 181.4 Hz]. – $C_{44}H_{73}ClOsP_2$ (889.7): calcd. C 59.40, H 8.27; found C 59.07, H 7.87.

7. Preparation of [OsHCl(≡CCH_2Ph)(PCy_3)$_2$]BF_4 (8): A solution of 244 mg (0.27 mmol) of **7** in 40 mL of toluene was treated dropwise with 2 mL of a 1.4 M solution (2.8 mmol) of HBF_4 in ether. A rapid change of color from deep green to brown-yellow took place. After the reaction mixture had been stirred for 10 min at room temperatuere, a pale brownish solid precipitated which was separated from the mother liquor, washed twice with 8-mL portions of toluene and dried; yield 112 mg (43%); m.p. 134°C (dec.). – ^{1}H NMR (400 MHz, CD_2Cl_2): δ = 7.36–7.05 (m, 5 H, C_6H_5), 3.01 (s, 2 H, CH_2), 2.39–1.17 (m, 66 H, C_6H_{11}), –8.75 (br. s, 1 H, OsH). – ^{13}C NMR (100.6 MHz, CD_2Cl_2): δ = 279.6 [t, *J*(PC) = 10.8 Hz, Os≡C], 130.1, 129.2, 129.0, (all s, C_6H_5), 57.1 (s, CH_2), 36.3 (vt, *N* = 25.4 Hz, *ipso*-C of C_6H_{11}), 30.6, 30.1 (both s, *m*-C of C_6H_{11}), 27.6, 27.4 (both vt, *N* = 10.2 Hz, *o*-C of C_6H_{11}), 26.3 (s, *p*-C of C_6H_{11}). – ^{31}P NMR (162.0 MHz, CD_2Cl_2): δ = 46.3 (br. s). – $C_{44}H_{74}BClF_4OsP_2$ (977.5): calcd. C 54.07, H 7.63; found C 53.61, H 7.77.

8. Preparation of [OsH_3Cl(PCy_3)$_2$] (9): A suspension of 89 mg (0.11 mmol) of **2** in 5 mL of 2-propanol was treated with 38 μL (0.27 mmol) of NEt_3 and stirred for 2 h at room temperature. A change of color from red-brown to brown-yellow occurred. The solvent was removed in vacuo and the residue was dissolved in 10 mL of benzene. The solution was filtered and the filtrate was concentrated to dryness in vacuo. The remaining brown-yellow solid was repeatedly washed with methanol and dried; yield 75 mg (86%); m.p. 40°C (dec.). – ^{1}H NMR (400 MHz, C_6D_6, 25°C): δ = 2.31–1.15 (m, 66 H, C_6H_{11}), –19.22 (br. s, 3 H, OsH_3). – ^{1}H NMR (200 MHz, CD_2Cl_2, 0°C): δ = 2.10–1.21 (m, 66 H, C_6H_{11}), –19.74 [t, *J*(PH) = 11.5 Hz, 3 H, OsH_3]. – ^{13}C NMR (100.6 MHz, C_6D_6, 25°C): δ = 37.4 (vt, *N* = 23.4 Hz, *ipso*-C of C_6H_{11}), 31.0 (s, *m*-C of C_6H_{11}), 28.0 (vt, *N* = 10.2 Hz, *o*-C of C_6H_{11}), 27.0 (s, *p*-C of C_6H_{11}). – ^{31}P NMR (162.0 MHz, C_6D_6, 25°C): δ = 41.8 (s). – ^{31}P NMR (81.0 MHz, CD_2Cl_2, 0°C): δ = 41.8 (s). – $C_{36}H_{69}ClOsP_2$ (789.5): calcd. C 54.77, H 8.81; found C 55.22, H 8.64.

9. Reaction of Compound 9 with 3-Chloro-3-methylbut-1-yne: A solution of 57 mg (0.07 mmol) of **9** in 0.5 mL of CD_2Cl_2 was treated at –40°C in an NMR tube with 8.5 μL (0.18 mmol) of HC≡$CC(CH_3)_2Cl$. The NMR spectra of the solution indicated the formation of a mixture of **10** and **11** which could not be separated by fractional crystallization. Therefore, the more labile component **11** was characterized by NMR spectroscopy. Typical data for **11**: ^{1}H NMR (400 MHz, CD_2Cl_2, –70°C): δ = 16.88 [d, *J*(HH) = 12.7 Hz, 1 H, Os=CH], 7.03 [d, *J*(HH) = 12.7 Hz, 1 H, C*H*=CMe_2], 2.95–0.77 (m, 72 H, C_6H_{11} and CH_3], –7.52 [br. s, 2 H, $Os(H_2)$]. – ^{13}C NMR (100.6 MHz, CD_2Cl_2, –70°C): δ = 254.9 (br. s, Os=C). – ^{31}P NMR (162.0 MHz, CD_2Cl_2, –70°C): δ = –1.1 (br. s). – ^{31}P NMR (81.0 MHz, CD_2Cl_2, –40°C): δ = 1.2 (s).

10. Preparation of [$OsHCl_2$(≡CCH=CMe_2)(PCy_3)$_2$] (10): The solution, obtained from **9** and HC≡$CC(CH_3)_2Cl$ as described above, was stirred after warming for 1 h at room temperature. The solvent was removed, the remaining pale brownish solid was washed with

2 mL of hexane and dried; yield 34 mg (53%); m.p. 122°C. – ^{1}H NMR (400 MHz, CD_2Cl_2): δ = 4.39 (s, 1 H, C*H*=CMe$_2$), 2.36–1.15 (m, 66 H, C_6H_{11}), 2.01 (s, 3 H, $CH_{3\ trans}$ to =CH), 1.50 (s, 3 H, $CH_{3\ cis}$ to =CH), −7.17 [t, *J*(PH) = 17.6 Hz, 1 H, OsH]. – ^{13}C NMR (100.6 MHz, CD_2Cl_2): δ = 256.0 [t, *J*(PC) = 11.4 Hz, Os≡C], 162.1 (s, =*C*Me$_2$), 135.9 (s, =CH), 36.5 (br. vt, *N* = 11.4 Hz, *ipso*-C of C_6H_{11}), 29.6, 29.3 (both s, *m*-C of C_6H_{11}), 28.2, 28.0 (both vt, *N* = 5.1 Hz, *o*-C of C_6H_{11}), 27.1 (s, *p*-C of C_6H_{11}), 26.4, 23.6 (both s, CH_3). – ^{31}P NMR (162.0 MHz, CD_2Cl_2): δ = 8.2 [s, *J*(OsP) = 169.6 Hz]. – $C_{41}H_{74}Cl_2OsP_2$ (890.1): calcd. C 55.33, H 8.38; found C 55.16, H 8.16.

11. ROMP of Cyclopentene with Compound 8 as Catalyst: A solution of 30 mg (0.03 mmol) of **8** in 1 mL of CH_2Cl_2 was treated with 10 mL (0.11 mol) of cyclopentene and stirred for 24 h at room temperature. The highly viscous reaction mixture was dissolved in 40 mL of $CHCl_3$ and the solution was poured into 100 mL of methanol. The white material was filtered and, after it was dried in vacuo, characterized by ^{1}H- and ^{13}C-NMR spectroscopy. The comparison of the NMR data with those reported in the literature[25] revealed a *trans*/*cis* ratio of the configuration at the double bonds of 77:23; yield 4.19 g.

12. Determination of the X-ray Crystal Structure of 10:[27] Single crystals of **10** were grown from CH_2Cl_2. Crystal data (from 5000 reflections, 4.26° < Θ < 54.06°): monoclinic; space group *I*2/*a* (No. 15); *a* = 25.655(5), *b* = 9.527(2), *c* = 39.988(8) Å, β = 107.26(3)°; *V* = 9333(3) Å^3; *Z* = 8; $d_{calcd.}$ = 1.448 gcm^{-3}; μ(Mo-K_α) = 3.115 mm^{-1}; crystal size 0.13 × 0.12 × 0.10 mm; STOE (IPDS), Mo-K_α radiation (0.71073 Å), graphite monochromator; *T* = 173(2) K; ψ-scans, max. 2Θ = 54.06°; 82743 reflections measured, 10147 independent ($R_{int.}$ = 0.0303), 7230 with $I > 2\sigma(I)$. Intensity data were corrected for Lorentz and polarization effects. The structure was solved by direct methods (SHELXS-86).[28] Atomic coordinates and the anisotropic thermal parameters of non-hydrogen atoms were refined by full-matrix least squares on F^2 (SHELXL-93).[29] The positions of all hydrogen atoms, except of metal-bound H, were calculated according to ideal geometry and refined by using the riding method. The position of H could be located in a final difference Fourier synthesis and was refined with fixed U_{eq}. The asymmetric unit includes one and a half molecules of CH_2Cl_2 which were refined anisotropically. Two alternative positions for CH_2Cl_2 consisting of C91, Cl5, and Cl6 were found and refined with the occupancy factors 0.54:0.46 with restraints. Conventional *R* = 0.0313 [for 7230 reflections with $I > 2\sigma(I)$], and weighted wR_2 = 0.0682 for all 10137 located reflections; reflection/parameter ratio 21.12; residual electron density +2.401/−1.213 eÅ^{-3}.

Acknowledgments

This work was supported by the Deutsche Forschungsgemeinschaft (SFB 347) and the Fonds der Chemischen Industrie. We thank Dr. W. Buchner and Mrs. M.-L. Schäfer for NMR spectra, and Mrs. R. Schedl and Mr. C. P. Kneis for elemental analyses and DTA measurements. Generous support by the BASF AG and the Degussa AG (gifts of chemicals) is also gratefully acknowledged.

[1] [1a] H. Werner, *Nachr. Chem. Tech. Lab.* **1992**, *40*, 435–444. – [1b] H. Werner, *J. Organomet. Chem.* **1994**, *475*, 45–55.
[2] C. Grünwald, O. Gevert, J. Wolf, P. González-Herrero, H. Werner, *Organometallics* **1996**, *15*, 1960–1962.
[3] [3a] R. H. Grubbs, S. J. Miller, G. C. Fu, *Acc. Chem. Res.* **1995**, *28*, 446–452. – [3b] M. Schuster, S. Blechert, *Angew. Chem.* **1997**, *109*, 2124–2144; *Angew. Chem. Int. Ed. Engl.* **1997**, *36*, 2036–2055. – [3c] A. S. K. Hashmi, *J. Prakt. Chem.* **1997**, *339*, 195–199. – [3d] A. Fürstner, *Top. Catal.* **1997**, *4*, 285–299.
[4] J. Wolf, W. Stüer, C. Grünwald, H. Werner, P. Schwab, M. Schulz, *Angew. Chem.* **1998**, *110*, 1165–1167; *Angew. Chem. Int. Ed. Engl.* **1998**, *37*, 1124–1126.
[5] [5a] S. T. Nguyen, L. K. Johnson, R. H. Grubbs, *J. Am. Chem. Soc.* **1992**, *114*, 3974–3975. – [5b] G. C. Fu, S. T. Nguyen, R. H. Grubbs, *J. Am. Chem. Soc.* **1993**, *115*, 9856–9857. – [5c] S. T. Nguyen, R. H. Grubbs, J. W. Ziller, *J. Am. Chem. Soc.* **1993**, *115*, 9858–9859. – [5d] P. Schwab, M. B. France, J. W. Ziller, R. H. Grubbs, *Angew. Chem.* **1995**, *107*, 2179–2181; *Angew. Chem. Int. Ed. Engl.* **1995**, *34*, 2039–2041. – [5e] P. Schwab, R. H. Grubbs, J. W. Ziller, *J. Am. Chem. Soc.* **1996**, *118*, 100–110. – [5f] D. M. Lynn, S. Kanaoka, R. H. Grubbs, *J. Am. Chem. Soc.* **1996**, *118*, 784–790.
[6] T. R. Belderrain, R. H. Grubbs, *Organometallics* **1997**, *16*, 4001–4003.
[7] [7a] M. L. Christ, S. Sabo-Etienne, B. Chaudret, *Organometallics* **1994**, *13*, 3800–3804. – [7b] M. Oliván, K. G. Caulton, *J. Chem. Soc., Chem. Commun.* **1997**, 1733–1734.
[8] P. J. Desrosiers, L. Cai, Z. Lin, R. Richards, J. Halpern, *J. Am. Chem. Soc.* **1991**, *113*, 4173–4184.
[9] [9a] M. Aracama, M. A. Esteruelas, F. J. Lahoz, J. A. Lopez, U. Meyer, L. A. Oro, H. Werner, *Inorg. Chem.* **1991**, *30*, 288–293. – [9b] U. Meyer, Dissertation, Universität Würzburg, **1988**.
[10] D. G. Gusev, V. F. Kuznetsov, I. L. Eremenko, H. Berke, *J. Am. Chem. Soc.* **1993**, *115*, 5831–5832.
[11] V. Rodriguez, S. Sabo-Etienne, B. Chaudret, J. Thoburn, S. Ulrich, H.-H. Limbach, J. Eckert, J.-C. Barthelat, K. Hussein, C. J. Marsden, *Inorg. Chem.* **1998**, *37*, 3475–3485.
[12] J. Wolf, W. Stüer, C. Grünwald, O. Gevert, M. Laubender, H. Werner, *Eur. J. Inorg. Chem.* **1998**, 1827–1834.
[13] [13a] J. Espuelas, M. A. Esteruelas, F. J. Lahoz, L. A. Oro, N. Ruiz, *J. Am. Chem. Soc.* **1993**, *115*, 4683–4689. – [13b] M. Bourgault, A. Castillo, M. A. Esteruelas, E. Oñate, N. Ruiz, *Organometallics* **1997**, *16*, 636–645.
[14] G. J. Spivak, J. N. Coalter, M. Oliván, O. Eisenstein, K. G. Caulton, *Organometallics* **1998**, *17*, 999–1001.
[15] [15a] A. Höhn, H. Otto, M. Dziallas, H. Werner, *J. Chem. Soc., Chem. Commun.* **1987**, 852–854. – [15b] A. Höhn, H. Werner, *J. Organomet. Chem.* **1990**, *382*, 255–272. – [15c] W. Knaup, H. Werner, *J. Organomet. Chem.* **1991**, *411*, 471–489. – [15d] T. Rappert, O. Nürnberg, H. Werner, *Organometallics* **1993**, *12*, 1359–1364. – [15e] H. Werner, D. Schneider, M. Schulz, *J. Organomet. Chem.* **1993**, *451*, 175–182. – [15f] H. Werner, M. Baum, D. Schneider, B. Windmüller, *Organometallics* **1994**, *13*, 1089–1097. – [15g] H. Werner, R. W. Lass, O. Gevert, J. Wolf, *Organometallics* **1997**, *16*, 4077–4088.
[16] [16a] Y. Kawata, M. Sato, *Organometallics* **1997**, *16*, 1093–1096; and references therein. – [16b] M. I. Bruce, G. A. Koutsantonis, *Aust. J. Chem.* **1991**, *44*, 207–217. – [16c] C. Bianchini, A. Marchi, L. Marvelli, M. Peruzzini, A. Romerosa, R. Rossi, *Organometallics* **1996**, *15*, 3804–3816.
[17] M. Oliván, E. Clot, O. Eisenstein, K. G. Caulton, *Organometallics* **1998**, *17*, 897–901.
[18] W. Stüer, J. Wolf, H. Werner, P. Schwab, M. Schulz, *Angew. Chem.* **1998**, *110*, 3603–3606; *Angew. Chem. Int. Ed. Engl.* **1998**, *37*, 3421–3423.
[19] P. Crochet, M. A. Esteruelas, A. M. López, M.-P. Martinez, M. Oliván, E. Oñate, N. Ruiz, *Organometallics* **1998**, *17*, 4500–4509.
[20] G. J. Spivak, K. G. Caulton, *Organometallics* **1998**, *17*, 5260–5266.
[21] [21a] D. Gusev, R. Kuhlman, G. Sini, O. Eisenstein, K. G. Caulton, *J. Am. Chem. Soc.* **1994**, *116*, 2685–2686. – [21b] R. H. Kuhlman, E. Clot, C. Leforestier, W. E. Streib, O. Eisenstein, K. G. Caulton, *J. Am. Chem. Soc.* **1997**, *119*, 10153–10169.
[22] [22a] B. Weber, P. Steinert, B. Windmüller, J. Wolf, H. Werner, *J. Chem. Soc., Chem. Commun.* **1994**, 2595–2596. – [22b] B. Weber, Dissertation, Universität Würzburg, **1995**.
[23] [23a] G. R. Clark, K. Marsden, W. R. Roper, L. J. Wright, *J. Am. Chem. Soc.* **1980**, *102*, 6570–6571. – [23b] W. R. Roper, *J. Organomet. Chem.* **1986**, *300*, 167–190.
[24] M. A. Gallop, W. R. Roper, *Adv. Organomet. Chem.* **1986**, *25*, 121–198.
[25] K. J. Ivin, J. C. Mol, *Olefin Metathesis and Metathesis Polymerization*, Academic Press, London **1997**.
[26] D. T. Laverty, J. J. Rooney, A. Stewart, *J. Catal.* **1976**, *45*, 110–113.

[27] Crystallographic data (excluding structure factors) for the structures reported in this paper have been deposited with the Cambridge Crystallographic Data Centre as supplementary publication no. CCDC-114480. Copies of the data can be obtained free of charge on application to CCDC, 12 Union Road, Cambridge CB2 1EZ, UK (Fax: internat. +44-1223/336-033; E-mail: deposit@ccdc.cam.ac.uk).

[28] G. M. Sheldrick, *Acta Crystallogr., Sect. A* **1990**, *46*, 467.

[29] G. M. Sheldrick, *A program for crystal structure refinement*, University of Göttingen, **1993**.

Received February 16, 1999
[I99053]

Synthesis and X-ray Structures of New Mononuclear and Dinuclear Diimine Complexes of Late Transition Metals

Timo V. Laine,*[a] Martti Klinga,[a] and Markku Leskelä[a]

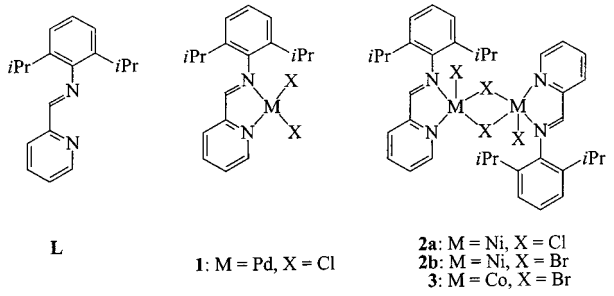
Keywords: Nickel / Palladium / Cobalt / N ligands / Crystal structures

Synthesis of new palladium(II) (**1**), nickel(II) (**2a** and **2b**), and cobalt(II) (**3**) complexes bearing the unsymmetrical, bidentate nitrogen ligand 2,6-bis(1-methylethyl)-*N*-(2-pyridinylmethylene)phenylamine (**L**) is described. The solid-state structures of **1**, **2a**, and **2b** have been determined by single-crystal X-ray diffraction. The Pd^{II} compound exists in the monomeric form whereas the nickel complexes were observed as centrosymmetric dimers with slightly distorted square-pyramidal coordination sphere around each nickel center.

Introduction

During the past 15 years extensive research effort from academic and industrial laboratories has been devoted to the development of transition-metal-catalyzed polymerization processes.[1] As a result the polyolefin industry has since the early 1990s had the option to transfer from mixture-type systems of the classical Ziegler−Natta technology to more sophisticated single-site catalysts, such as group-4 metallocenes,[2] in which well-defined active centers and catalyst structures enable tailoring of polymer properties by modifying the catalyst precursor itself.[3] Some signs of the next prospective catalyst generation are already emerging:[1] The disclosure by the group of Brookhart in 1995 that they produced high molecular weight polyethylene for the first time with late transition metal complexes[4] has revived the investigation of late transition metal compounds as potential catalyst precursors.[5] Prior reports of the use of group-10 metals exist,[6] but these systems suffer from the highly competitive chain-termination step and produce only short-chain oligomers of up to 40 carbon atoms.[7] Therefore, very little utilization had been found for such systems leaving the nickel-catalyzed oligomerization of ethylene in the Shell Higher Olefin Process (SHOP)[8] as the sole industrial-scale application. This disadvantage was, however, overcome by the use of nickel(II) and palladium(II) complexes bearing sterically demanding 1,4-diazabutadiene ligands,[4] in which bulky aryl groups of the ligand protect the active center by blocking the axial coordination sites thus enhancing chain growth and disfavoring termination processes.[9] Depending on the ligand substitution pattern and process parameters these catalysts can produce a wide variety of products ranging from linear high-density material to highly branched, amorphous polyethylene[4,10] or even short-chain oligomers.[11] Also different types of ethylene copolymers incorporating polar comonomers, such as alkyl acrylates, can be manufactured.[12] Due to the demonstrated versatility and industrial potential[13] a comprehensive patent application covering the syntheses of numerous diazabutadiene-type transition-metal compounds and their use as polymerization catalysts has been filed.[14]

According to recent reports the group of applicable catalyst precursor metals is extending rapidly to cover other, more scarcely utilized transition metals as well. In addition to group-10 metal compounds[4,10,15] some five-coordinate iron(II) and cobalt(II) complexes bearing triimine-type ligands have demonstrated suitability as active ethylene polymerization catalysts after activation with alkylaluminum compounds.[16] Also the first examples of homogeneous chromium(III) catalysts have been published recently.[17] Reported studies, however, have mainly involved symmetrical ligands with two electronically or sterically equivalent imine nitrogen atoms.[5] In this article we present the synthesis and characterization of novel group-9 and -10 metal complexes containing the unsymmetrical, bidentate ligand 2,6-bis(1-methylethyl)-*N*-(2-pyridinylmethylene)phenylamine (**L**).



Scheme 1

Results and Discussion

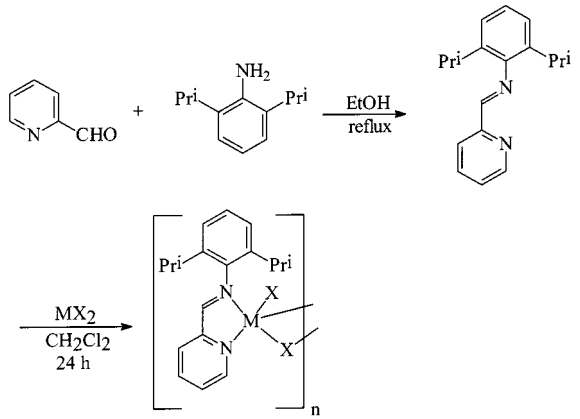
Synthetic Aspects

The ligand **L** is prepared by a facile one-step condensation of 2-pyridinecarboxaldehyde and 2,6-bis(1-methylethyl)phenylamine, as shown in Scheme 2, yielding pale yellow, crystalline material after purification and recrystalliza-

[a] Laboratory of Inorganic Chemistry, Department of Chemistry, P. O. Box 55, FIN-00014 University of Helsinki, Finland
Fax: (internat.) + 358-9/1914-0198
E-mail: timo.laine@helsinki.fi

 © WILEY-VCH Verlag GmbH, D-69451 Weinheim, 1999 1434−1948/99/0606−0959 $ 17.50+.50/0

tion from pentane. Due to the limited solubility of anhydrous late transition metal halides in organic solvents only in the case of cobalt the subsequent complex formation step could be performed by a direct reaction of the ligand with the metal halide. Otherwise, solvent-adduct-based precursor compounds were needed (the adduct was 1,2-dimethoxyethane and 1,5-cyclooctadiene for nickel and palladium, respectively). Complexation products were isolated as yellow (**1**), orange (**2a**), orange-red (**2b**), or deep brown (**3**) powders in good yields (70−96%). All compounds gave satisfactory distribution patterns in elemental analysis.



1: M = Pd; X = Cl; n = 1
2a: M = Ni, X = Cl; n = 2
2b: M = Ni, X = Br; n = 2
3: M = Co, X = Br; n = 2

Scheme 2. Synthesis of compounds **1**−**3**

Analysis of the palladium compound **1** by ^{1}H-NMR spectroscopy reveals certain changes in chemical shifts. First of all, the sharp doublet signal from the isopropyl methyl groups of the free ligand at $\delta = 1.17$ has been split into two smaller doublets at $\delta = 1.03$ and $\delta = 1.43$ after complexation. This may be explained by the blocking effect of the chloride ions attached to the palladium center. While in the free ligand the aryl group can rotate unobstructed around the carbon−nitrogen bond, the chloride positioned *cis* to the imine nitrogen atom restricts this movement and subjects the inner methyl groups to some degree of deshielding resulting in the observed separation of peaks. Another distinctive consequence of complex formation is the movement of certain signals in the spectrum. Protons situated in the *ortho* and *para* positions in the aromatic ring systems as well as the proton of the imine carbon atom are especially affected with chemical shifts transferred downfield by 0.30−0.51 ppm. Measurements of the ^{1}H-NMR spectra for the nickel and cobalt complexes (**2a**, **2b**, and **3**) failed apparently as a result from the interfering effect caused by the associated metal center.

Treating the nickel compounds with methylaluminoxane (MAO) provides quite effective catalysts for ethylene polymerization, while the cobalt complex shows nearly negligible activity. In nickel-catalyzed reactions the activities and polymer molecular weights depend on the polymerization temperature: Lowering the temperature to 0 °C leads to an increase in molecular weights by an order of magnitude at the expense of declining catalytic activity.[18] The MAO-activated palladium compound could not be utilized for the polymerization of ethylene but it proved to be highly active with cyclic monomers, such as norbornene.[19] In order to take full advantage of the potential provided by these systems our current work is concentrating on the effects of different ligand substitution patterns on the polymerization behavior of these compounds.

X-ray Crystallography

Crystallization from acetone (for **1**) or a mixture of acetone and pentane (2:1 for **2a**, 1:1 for **2b**) yielded deep orange crystals suitable for structural analysis. The crystal data, together with the data collection and structure refinement parameters are presented in Table 2. Selected bond lengths and angles are given in Table 1. In each compound the solid-state structures are stabilized only by van der Waals forces between the molecules.

The palladium compound **1** crystallizes in the monomeric form with two chlorine atoms (Cl1 and Cl2) and two nitrogen atoms (N1 and N8) of the bidentate ligand forming the expected square-planar coordination sphere around the palladium center (see Figure 1). The palladium atom is situated exactly in the coordination plane N1−N8−Cl2−Cl1 (0.029 Å above the calculated plane) as the average off-plane deviation is 0.053 Å. The narrow N1−Pd−N8 angle 80.08(11)° resulting from the relatively small bite size of the ligand, however, distorts the square structure in a similar fashion as observed in other pyridylimine[20] or bipyridine[21,22] complexes of palladium, but without any coordination plane distortion out of the ligand plane.[22a] In fact, the significant bond lengths and angles in complex **1** resemble the ones reported for the structure of the C_2-symmetric dichloro(2,2′-bipyridine)palladium(II),[21] which indicates electronic similarity of the two nitrogen coordination sites. The variation between the ligand nitrogen atoms, therefore, originates from the difference in steric environment of the two binding sites: The phenyl ring of the imino side arm adopts a position almost perpendicular to the metal coordination plane with the phenyl−coordination plane angle 86.84(8)° and, thus, shields the metal center from one side.

The nickel complexes **2a** and **2b**, in turn, crystallize as centrosymmetric dimers in which each nickel atom is coordinated to two ligand nitrogen atoms (N1 and N8) as two bridging halogen atoms (Cl1 and Cl1a in **2a**, Br1 and Br1a in **2b**) connect the two metal centers. A terminal halide ion (Cl2 and Br2 in **2a** and **2b**, respectively) completes the square-pyramidal coordination sphere. The intramolecular nickel−nickel distance of the chloro complex **2a** is slightly shorter [3.475(1) Å] than recently reported for other nitrogen-ligand-containing nickel(II) dimers,[23c] which is also reflected in a sharper Ni−Cl−Ni angle. Dimeric structures are commonly known for dichloronickel(II) complexes of this type,[23] while similar bipyridine-based dibromonickel-

Table 1. Selected bond lengths [Å] and angles [°] for **1**, **2a**, and **2b**

1		**2a**		**2b**	
Bond lengths					
Pd−N1	2.028(3)	Ni−N1	2.039(2)	Ni−N1	2.050(9)
Pd−N8	2.022(3)	Ni−N8	2.095(2)	Ni−N8	2.099(9)
Pd−Cl1	2.2809(11)	Ni−Cl1	2.3965(8)	Ni−Br1	2.533(2)
Pd−Cl2	2.2768(10)	Ni−Cl1a$^{\#}$	2.3366(8)	Ni−Br1a*	2.459(2)
C6−C7	1.457(5)	Ni−Cl2	2.2729(9)	Ni−Br2	2.411(2)
C7−N8	1.279(4)	C6−C7	1.463(4)	C6−C7	1.455(16)
N8−C9	1.448(4)	C7−N8	1.278(3)	C7−N8	1.282(14)
		N8−C9	1.440(3)	N8−C9	1.423(14)
Bond angles					
N1−Pd−N8	80.08(11)	N1−Ni−N8	79.37(9)	N1−Ni−N8	79.9(4)
N1−Pd−Cl1	94.33(9)	N1−Ni−Cl1	91.08(6)	N1−Ni−Br1	91.5(2)
N1−Pd−Cl2	174.51(9)	N1−Ni−Cl1a$^{\#}$	161.14(6)	N1−Ni−Br1a*	160.1(3)
N8−Pd−Cl1	172.85(8)	N1−Ni−Cl2	94.00(6)	N1−Ni−Br2	95.0(3)
N8−Pd−Cl2	94.64(8)	N8−Ni−Cl1	148.86(6)	N8−Ni−Br1	153.2(3)
Cl1−Pd−Cl2	91.05(4)	Cl1−Ni−Cl1a$^{\#}$	85.53(3)	Br1−Ni−Br1a*	85.84(7)
		Ni−Cl1−Nia$^{\#}$	94.47(3)	Ni−Br1−Nia*	94.16(7)

Symmetry transformations used to generate equivalent atoms: $^{\#}$ $-x, -y, -z+1$; * $-x, -y+2, -z+2$.

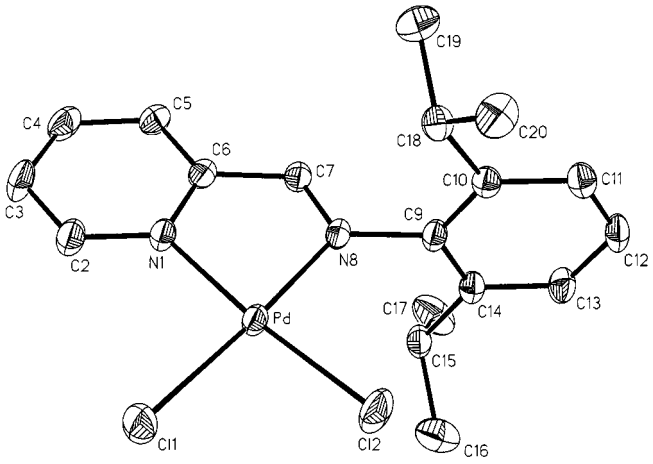


Figure 1. Crystal structure of complex **1** showing the labeling scheme; displacement ellipsoids are drawn at the 40% probability level; hydrogen atoms are omitted for clarity

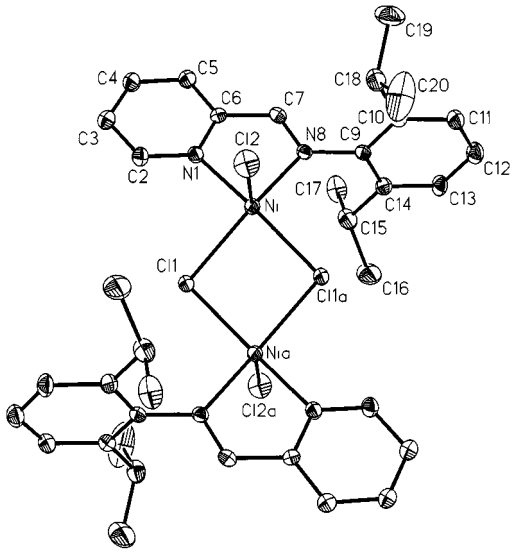


Figure 2. Molecular structure of compound **2a** with the labeling scheme

(II) compounds may exhibit monomeric complexes if additional steric bulk is introduced.[23a]

As with complex **1** also in the case of the nickel analogs the narrow nitrogen−nickel−nitrogen angle [79.37(9)° in **2a** and 79.9(4)° in **2b**] slightly deforms the basal square structure. The effect from dimerization contributes to further structural distortion leading to unequal nickel−nitrogen and nickel−halogen bond lengths: The shorter nickel−halogen bond of the bridge (Ni−Cl1 and Ni−Br1) corresponds to a similarly shorter Ni−N bond (the bond to the imino nitrogen atom N8) situated in the *trans* position. The axial chlorine atom Cl2 or bromine atom Br2, however, has the shortest bond length of all three nickel−halogen bonds.

Another common structural feature between the palladium and nickel complexes is the lack of double-bond delocalization in all three compounds. Relative to other bonds in the imino bridge [values ranging from 1.423(14) to 1.463(4) Å] the C=N double bond (C7−N8) is still the shortest [1.279(4), 1.278(3), and 1.282(14) Å for **1**, **2a**, and **2b**, respectively] even after complexation.

Besides in coordination geometry the nickel compounds differ from their palladium analog in the nature of the coordination plane. In **1** the coordination plane exhibits only slight puckering while more severe puckering was observed in the nickel compounds with average deviations of 0.119 Å for **2a** and 0.071 Å for **2b**, although the calculated value of **2b** is quite close to the average deviation in the palladium complex **1**. Also the palladium atom, as described earlier, is situated in the middle of the coordination plane whereas in the nickel complexes the metal center is elevated from the plane by 0.475(1) and 0.456(4) Å in **2a** and **2b**, respectively.

Analysis of the cobalt coordination sphere in compound **3** revealed a dimeric structure in which one terminal and two bridging bromine atoms as well as two ligand nitrogen

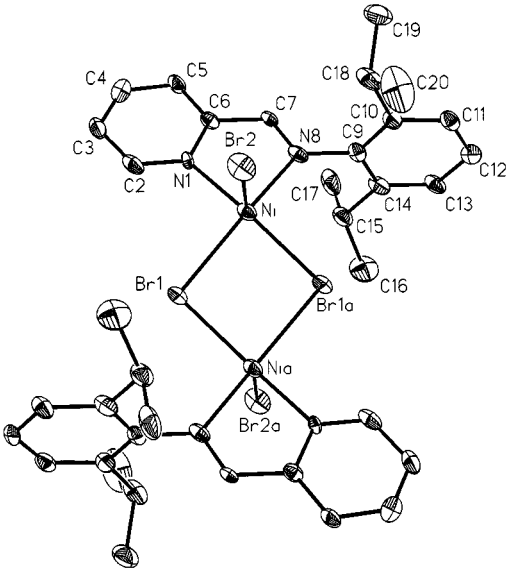


Figure 3. Molecular structure of complex **2b**

atoms create square-based pyramids around each five-coordinate metal center.[24]

Experimental Section

General: All complex preparations were performed under argon with standard Schlenk techniques. Acetone was dried by storing under argon with $CaSO_4$ granules, other solvents by refluxing with a drying agent (P_2O_5 for dichloromethane and sodium/benzophenone for the non-halogenated solvents) and distillation under argon. Dichloro(1,5-cyclooctadiene)palladium(II)[25] [(COD)$PdCl_2$] as well as dichloro(1,2-dimethoxyethane)nickel(II) [(DME)$NiCl_2$] and dibromo(1,2-dimethoxyethane)nickel(II) [(DME)$NiBr_2$][26] were prepared according to the literature. Anhydrous $CoBr_2$ (Aldrich, 99%), 2-pyridinecarboxaldehyde (Merck, 98%), and 2,6-bis(1-methylethyl)phenylamine (Aldrich, 90%) were used as received. − ^{1}H NMR: Varian Gemini 200 spectrometer (200 MHz); $CDCl_3$ or [D_6]acetone as solvent, TMS as internal standard. − EI MS: Finnigen SSQ 7000 spectrometer (70 eV); direct inlet probe. − Elemental analyses were carried out at the University of Ulm, Germany, except for the bromine content determination of complex **3**, which was performed by gravimetric analysis at the University of Helsinki.

2,6-Bis(1-methylethyl)-*N*-(2-pyridinylmethylene)phenylamine (L): The ligand was synthesized by modifying the literature procedure[27] reported for the analogous 2,6-dimethyl compound. Ethanol (100 mL), 2,6-bis(1-methylethyl)phenylamine (15.76 g, 80.0 mmol), and 2-pyridinecarboxaldehyde (8.57 g, 80.0 mmol) were combined and refluxed for 20 min. The solvent was removed and the residue was vacuum-distilled followed by chromatography on basic alumina with pentane/ethyl acetate (3:1) as eluent. Recrystallization from pentane yielded pale yellow crystals, 14.36 g (67%). − ^{1}H NMR ($CDCl_3$): δ = 1.17 (d, 12 H, H_{Me}), 2.97 (m, 2 H, C*H*Me_2), 7.16 (m, 3 H, H_{arom}), 7.42 (m, 1 H, $H_{pyridine,5}$), 7.86 (t, 1 H, $H_{pyridine,4}$), 8.27 (d, 1 H, $H_{pyridine,3}$), 8.31 (s, 1 H, C*H*=N), 8.73 (d, 1 H, $H_{pyridine,6}$). − $C_{18}H_{22}N_2$ (266.39): calcd. C 81.16, H 8.32, N 10.52; found C 81.01, H 8.37, N 10.39.

Dichloro[2,6-bis(1-methylethyl)-*N*-(2-pyridinylmethylene)-phenylamine]palladium(II) (1): The ligand **L** (0.76 g, 2.87 mmol) was dissolved in 10 mL of dichloromethane and added to a solution of [(COD)$PdCl_2$] (0.80 g, 2.80 mmol in 40 mL of CH_2Cl_2). Stirring was continued for 24 h at ambient temperature at which time precipitation occurred. The precipitated yellow powder was collected by filtration, washed with diethyl ether (2 × 20 mL) and dried in vacuo; yield 1.07 g (96%). − ^{1}H NMR ([D_6]acetone): δ = 1.03 (d, 6 H, H_{Me}), 1.43 (d, 6 H, H_{Me}), 3.27 (m, 2 H, C*H*Me_2), 7.12 (m, 3 H, H_{arom}), 7.93 (m, 1 H, $H_{pyridine,5}$), 8.22 (d, 1 H, $H_{pyridine,3}$), 8.36 (t, 1 H, $H_{pyridine,4}$), 8.69 (s, 1 H, C*H*=N), 9.18 (d, 1 H, $H_{pyridine,6}$). − $C_{18}H_{22}Cl_2PdN_2$ (443.71): calcd. C 48.73, H 5.00, N 6.31; found C 48.29, H 5.05, N 6.19.

Di-μ-chlorodichlorobis[2,6-bis(1-methylethyl)-*N*-(2-pyridinylmethylene)phenylamine]dinickel(II) (2a): To a suspension of [(DME)$NiCl_2$] (1.86 g, 8.45 mmol) in 40 mL of dichloromethane was added the yellow ligand solution (2.34 g, 8.77 mmol in 15 mL of CH_2Cl_2). After stirring the brown reaction mixture for 24 h at room temperature, the solvent was evaporated and the resulting solid material was washed with pentane (3 × 20 mL) and dried in vacuo yielding complex **2a** as orange powder, 2.65 g (79%). − $C_{36}H_{44}Cl_4N_4Ni_2$ (791.97): calcd. C 54.60, H 5.60, N 7.07; found C 54.61, H 5.94, N 6.68.

Di-μ-bromodibromobis[2,6-bis(1-methylethyl)-*N*-(2-pyridinylmethylene)phenylamine]dinickel(II) (2b): Analogously to the preparation of **2a**, complex **2b** was prepared from [(DME)$NiBr_2$] (0.40 g, 1.30 mmol) and **L** (0.36 g, 4.89 mmol) in CH_2Cl_2. The orange-red powder was collected by filtration, washed with pentane (3 × 10 mL) and vacuum-dried; yield 0.44 g (70%). − $C_{36}H_{44}Br_4N_4Ni_2$ (969.77): calcd. C 44.59, H 4.57, N 5.78; found C 44.10, H 4.59, N 5.68.

Di-μ-bromodibromobis[2,6-bis(1-methylethyl)-*N*-(2-pyridinylmethylene)phenylamine]dicobalt(II) (3): Anhydrous $CoBr_2$ (0.55 g, 2.52 mmol) was dissolved in 10 mL of acetone and combined with the ligand solution (0.68 g, 2.55 mmol in 10 mL of acetone). The resulting green-brown solution was stirred for 24 h at room temperature. After solvent evaporation, the residue was washed with hexane (3 × 10 mL) and vacuum-dried. The complex was obtained as brown powder, 1.02 g (83%). − EI MS (70 eV); *m*/*z*: 483, 485, 487 [1/2 M^+]; 404, 406 [1/2 M^+ − Br]; 323 [1/2 M^+ − 2 Br]. − $C_{36}H_{44}Br_4Co_2N_4$ (970.25): calcd. C 44.57, H 4.57, Br 32.94, N 5.77; found C 44.54, H 4.75, Br 32.61, N 5.62.

Crystal-Structure Determinations: The crystals were mounted to a glass fiber with the oil drop method.[28] Crystal data obtained with the ω−2θ scan mode were collected on an automated four-circle Rigaku AFC-7S diffractometer using graphite-monochromatized Mo-K_α radiation (λ = 0.71073 Å) at 193 K. Three standard reflections were monitored after every 200 intensity scans. The intensities were corrected for Lorentz and polarization effects. For all compounds ψ-scans were used for absorption correction.[29] Data sets were compressed to reflection files with TEXSAN Single Crystal Structure Analysis Software.[30] The structures were solved with SHELXTL PC 4.1 program package[31] using direct methods while further refinement with full-matrix least squares on F^2 was carried out with SHELXL-93[32] (for **2a**) or SHELXL-97[33] (for **1** and **2b**). All non-hydrogen atoms were refined anisotropically. Hydrogen atoms were introduced in calculated positions (riding model) with 1.2 times the displacement factors of the host carbon atoms. Crystallographic data (excluding structure factors) for the structures reported in this paper have been deposited with the Cambridge Crystallographic Data Centre as supplementary publications no. CCDC-103369 (for **1**), -103368 (for **2a**), and -103370 (for **2b**). Copies of the data can be obtained on application to CCDC, 12 Union

Table 2. Crystallographic data for complexes **1**, **2a**, and **2b**

	1	**2a**	**2b**
Empirical formula	$C_{18}H_{22}Cl_2N_2Pd$	$C_{36}H_{44}Cl_4N_4Ni_2$	$C_{36}H_{44}Br_4N_4Ni_2$
Formula weight	443.71	791.97	969.77
Crystal color and form	Yellow, prismatic	Orange, prismatic	Orange-brown, prismatic
Crystal system	Monoclinic	Monoclinic	Monoclinic
Space group	$P2_1/c$ (no. 14)	$P2_1/n$ (no. 14)	$P2_1/n$ (no.14)
a [Å]	10.035(2)	9.817(6)	9.885(6)
b [Å]	12.523(3)	14.602(5)	14.515(7)
c [Å]	14.853(3)	13.833(6)	14.127(7)
β [°]	94.70(3)	109.13(4)	106.82(4)
V [Å^3]	1860.3(7)	1873.4(7)	1940.2(18)
Z	4	2	2
$D_{calcd.}$ [Mg/m^3]	1.584	1.404	1.660
Absorption coefficient [mm^{-1}]	1.285	1.321	5.119
F(000)	896	824	968
Crystal size [mm]	0.25 × 0.15 × 0.15	0.25 × 0.25 × 0.25	0.15 × 0.15 × 0.10
Scan mode	ω−2θ	ω−2θ	ω−2θ
θ_{max} [°]	25.00	26.49	25.00
Number of collected reflections	3298	4506	2955
Number of independent reflections	3119	3395	2802
Number of parameters	234	234	212
Goodness-of-fit on F^2	1.066	1.061	1.029
Final R indices [$I > 2\sigma(I)$]	$R = 0.0322$, $wR = 0.0761$	$R = 0.0360$, $wR = 0.0922$	$R = 0.0761$, $wR = 0.1647$
R indices (all data)	$R = 0.0371$, $wR = 0.0779$	$R = 0.0431$, $wR = 0.0955$	$R = 0.1273$, $wR = 0.1848$
Largest differential peak and hole [e/Å^3]	0.539 and −0.981	0.637 and −0.856	0.991 and −0.979

Road, Cambridge CB2 1EZ, UK (Fax: + 44-1223/336-033; E-mail: deposit@ccdc.cam.ac.uk).

Acknowledgments

Financial support from the Academy of Finland and the Technology Development Center of Finland (TEKES) is gratefully acknowledged. The authors wish to thank Dr. Ulf Dietrich and Ms. Alexandra Abele (University of Ulm, Germany) for arranging the EA and MS measurements.

[1] A. A. Montagna, R. M. Burkhart, A. H. Dekmezian, *Chemtech* **1997**, *27*(12), 26−31.
[2] For recent reviews on metallocenes, see: [2a] H. H. Brintzinger, D. Fischer, R. Mülhaupt, B. Rieger, R. M. Waymouth, *Angew. Chem. Int. Ed. Engl.* **1995**, *34*, 1143−1170. − [2b] W. Kaminsky, *Macromol. Chem. Phys.* **1996**, *197*, 3907−3945. − [2c] M. Bochmann, *J. Chem. Soc., Dalton Trans.* **1996**, 255−270. − [2d] W. Kaminsky, M. Arndt, *Adv. Polym. Sci.* **1997**, *127*, 143−187.
[3] A. M. Thayer, *Chem. Eng. News* **1995**, *73*(37), 15−20.
[4] L. K. Johnson, C. M. Killian, M. Brookhart, *J. Am. Chem. Soc.* **1995**, *117*, 6414−6415.
[5] [5a] A. S. Abu-Surrah, B. Rieger, *Angew. Chem. Int. Ed. Engl.* **1996**, *35*, 2475−2477. − [5b] W. A. Herrmann, B. Cornils, *Angew. Chem. Int. Ed. Engl.* **1997**, *36*, 1048−1067.
[6] A. M. al-Jarallah, J. A. Anabtawi, M. A. B. Siddiqui, A. M. Aitani, A. W. al-Sa′doun, *Catal. Today* **1992**, *14*, 42−121 and references therein.
[7] [7a] W. Keim, A. Behr, M. Röper in *Comprehensive Organometallic Chemistry* (Eds.: G. Wilkinson, F. G. A. Stone, E. W. Abel), vol. 8, Pergamon Press, Oxford, **1982**, chapter 56.2. − [7b] P. W. Jolly in *Comprehensive Organometallic Chemistry* (Eds.: G. Wilkinson, F. G. A. Stone, E. W. Abel), vol. 8, Pergamon Press, Oxford, **1982**, chapter 52.2.
[8] G. R. Lappin, L. H. Nemec, J. D. Sauer, J. D. Wagner in *Kirk-Othmer Encyclopedia of Chemical Technology*, (Eds.: J. I. Kroschwitz, M. Howe-Grant), vol. 17, 4th ed., John Wiley & Sons, New York, **1996**, p. 848−850.
[9] For recent theoretical studies, see: [9a] D. G. Musaev, R. D. J. Froese, M. Svensson, K. Morokuma, *J. Am. Chem. Soc.* **1997**, *119*, 367−374. − [9b] L. Deng, P. Margl, T. Ziegler, *J. Am. Chem. Soc.* **1997**, *119*, 1094−1100. − [9c] D. G. Musaev, M. Svensson, K. Morokuma, S. Strömberg, K. Zetterberg, P. E. M. Siegbahn, *Organometallics* **1997**, *16*, 1933−1945. − [9d] L. Deng, T. K. Woo, L. Cavallo, P. M. Margl, T. Ziegler, *J. Am. Chem. Soc.* **1997**, *119*, 6177−6186. − [9e] S. Strömberg, K. Zetterberg, P. E. M. Siegbahn, *J. Chem. Soc., Dalton Trans.* **1997**, 4147−4152. − [9f] D. G. Musaev, R. D. J. Froese, K. Morokuma, *New J. Chem.* **1997**, *21*, 1269−1282. − [9g] R. D. J. Froese, D. G. Musaev, K. Morokuma, *J. Am. Chem. Soc.* **1998**, *120*, 1581−1587. − [9h] D. G. Musaev, R. D. J. Froese, K. Morokuma, *Organometallics* **1998**, *17*, 1850−1860.
[10] D. Pappalardo, M. Mazzeo, C. Pellecchia, *Macromol. Rapid Commun.* **1997**, *18*, 1017−1023.
[11] C. M. Killian, L. K. Johnson, M. Brookhart, *Organometallics* **1997**, *16*, 2005−2007.
[12] L. K. Johnson, S. Mecking, M. Brookhart, *J. Am. Chem. Soc.* **1996**, *118*, 267−268.
[13] J. Haggin, *Chem. Eng. News* **1996**, *74*(6), 6−7.
[14] L. K. Johnson, C. M. Killian, S. D. Arthur, J. Feldman, E. F. McCord, S. J. McLain, K. A. Kreutzer, M. A. Bennett, E. B. Coughlin, S. D. Ittel, A. Parthasarathy, D. J. Tempel, M. S. Brookhart, *PCT Int. Appl. 96/23010*, **1996**.
[15] R. F. de Souza, R. S. Mauler, L. C. Simon, F. F. Nunes, D. V. S. Vescia, A. Cavagnolli, *Macromol. Rapid Commun.* **1997**, *18*, 795−800.
[16] [16a] B. L. Small, M. Brookhart, A. M. A. Bennett, *J. Am. Chem. Soc.*, **1998**, *120*, 4049−4050. − [16b] G. J. P. Britovsek, V. C. Gibson, B. S. Kimberley, P. J. Maddox, S. J. McTavish, G. S. Solan, A. J. P. White, D. J. Williams, *Chem. Commun.* **1998**, 849−850.
[17] V. C. Gibson, P. J. Maddox, C. Newton, C. Redshaw, G. A. Solan, A. J. P. White, D. J. Williams, *Chem. Commun.* **1998**, 1651−1652.
[18] For details of polymerization results with compounds **2a**, **2b**, and **3**, see: T. V. Laine, K. Lappalainen, J. Liimatta, E. Aitola, B. Löfgren, M. Leskelä, *Macromol. Rapid Commun.*, submitted.
[19] T. V. Laine, K. Lappalainen, M. Klinga, E. Aitola, M. Leskelä, manuscript in preparation.
[20] R. E. Rülke, J. G. P. Delis, A. M. Groot, C. J. Elsevier, P. W. N. M. van Leeuwen, K. Vrieze, K. Goubitz, H. Schenk, *J. Organomet. Chem.* **1996**, *508*, 109−120.
[21] [21a] M. Maekawa, M. Munakata, S. Kitagawa, M. Nakamura, *Anal. Sci.* **1991**, *7*, 521−522. − [21b] A. J. Canty, B. W. Skelton, P. R. Traill, A. H. White, *Aust. J. Chem.* **1992**, *45*, 417−422.
[22] [22a] G. R. Newkome, F. R. Fronczek, V. K. Gupta, W. E. Puckett, D. C. Pantaleo, G. E. Kiefer, *J. Am. Chem. Soc.* **1982**, *104*, 1782−1783. − [22b] F. R. Fronczek, I. Kahwa, S. Lu, G. R. Newkome, M. A. Ollino, W. D. Pitts, A. Sittattrakul, J. Wang, S. F. Watkins, *Acta Crystallogr.* **1988**, *C44*, 933−934. − [22c] P.

D. Beer, N. C. Fletcher, M. G. B. Drew, T. J. Wear, *Polyhedron* **1997**, *16*, 815−823.
[23] [23a] R. J. Butcher, E. Sinn, *Inorg. Chem.* **1977**, *16*, 2334−2343. − [23b] J. C. Jansen, H. van Koningsveld, J. A. C. van Ooijen, J. Reedijk, *Inorg. Chem.* **1980**, *19*, 170−174. − [23c] G. A. van Albada, J. J. A. Kolnaar, W. J. J. Smeets, A. L. Spek, J. Reedijk, *Eur. J. Inorg. Chem.* **1998**, 1337−1341.
[24] Red-brown prismatic crystals were obtained from the acetone solution of **3** by slow evaporation of the solvent over several months. Single-crystal X-ray structure determination was performed using the same apparatus and methods as with the other compounds reported in this paper: $C_{36}H_{44}Br_4Co_2N_4$, monoclinic, space group $P2_1/a$, a = 14.324(3), b = 10.277(2), c = 38.656(8) Å, β = 90.20(3)°, V = 5690(13) Å^3, Z = 6, $\rho_{calcd.}$ = 1.699 Mg m^{-3}, μ = 5.12 mm^{-1}; 4901 unique reflections (R_{int} = 0.0607), S = 1.219; R = 0.1564, wR = 0.2960 for $I > 2\sigma(I)$. Due to low data quality a comprehensive structural analysis could not be carried out.
[25] D. Drew, J. R. Doyle, *Inorg. Synth.* **1972**, *13*, 47−55.
[26] L. G. L. Ward, *Inorg. Synth.* **1972**, *12*, 154−164.
[27] G. Schmauss, P. Barth, *Z. Naturforsch.* **1970**, *25b*, 789−798.
[28] T. Kottke, D. Stalke, *J. Appl. Crystallogr.* **1993**, *26*, 615−619.
[29] A. C. T. North, D. C. Phillips, F. S. Mathews, *Acta Crystallogr.* **1968**, *A24*, 351−359.
[30] *TEXSAN: Single Crystal Structure Analysis Software, Version 1.6*, Molecular Structure Corporation, The Woodlands, TX, **1993**.
[31] G. M. Sheldrick, *SHELXTL PC Release 4.1*, Siemens Analytical X-Ray Instruments Inc., Madison, WI, **1990**.
[32] G. M. Sheldrick, *SHELXL-93, Program for the Refinement of Crystal Structures*, University of Göttingen, Germany, **1993**.
[33] G. M. Sheldrick, *SHELXL-97, Program for the Refinement of Crystal Structures*, University of Göttingen, Germany, **1997**.

Received October 22, 1998
[I98364]

Synthesis, Structural Characteristics and Biological Activities of Complexes of Zn^{II}, Cd^{II}, Hg^{II}, Pd^{II}, and Pt^{II} with 2-Acetylpyridine 4-Methylthiosemicarbazone

Elena Bermejo,[a] Rosa Carballo,[b] Alfonso Castiñeiras,*[a] Ricardo Domínguez,[a] Anthony E. Liberta,[d] Cäcilia Maichle-Mössmer,[c] Michelle M. Salberg,[d] and Douglas X. West[d]

Keywords: 2-Acetylpyridine 4-methylthiosemicarbazone / Palladium / Platinum / Group-12 metal(II) complexes

Reaction of 2-acetylpyridine 4-methylthiosemicarbazone (H4ML) with halides of zinc(II), cadmium(II), and mercury(II) afforded complexes of the form $[M(H4ML)X_2]$ [M = Zn^{II} (**1**–**3**), Cd^{II} (**4**–**6**) or Hg^{II} (**7**–**9**); X = Cl, Br, or I]. Reaction of H4ML with K_2PdCl_4 and K_2PtCl_4 gave compounds of the form [M(4ML)Cl] [M = Pd^{II} (**10**) or Pt^{II} (**11**)]. In all the new compounds, which were characterized by elemental analyses, conductance measurements, and electronic, IR and ^{1}H- and ^{13}C-NMR spectroscopy, and by ^{113}Cd-, ^{195}Pt-, or ^{199}Hg-NMR spectroscopy when relevant, the ligand is N,N,S-tridentate, coordinating to the metal centre through its pyridine and azomethine nitrogen atoms and its thiocarbonyl sulfur atom, as was confirmed by X-ray diffraction studies in the cases of **4** · 2 DMSO, **5** · 2 DMSO, **6** · 2 DMSO, **7** · 2 DMSO, **10**, and **11**. In in-vitro assays, only $[Zn(H4ML)Cl_2]$ and $[Zn(H4ML)Br_2]$ showed some sign of antifungal activity against *Aspergillus niger* or *Paecilomyces variotii*.

Introduction

It has been known for some time that thiosemicarbazones have a wide range of actual or potential medical applications as antiviral,[1] antitumoral,[2] antimalarial,[3] antifungal,[4] and antibacterial[5] agents. Their mechanism of action is still controversial in many respects, but it is known that heterocyclic thiosemicarbazones act by inhibiting ribonucleotide reductase, a key enzyme in the biosynthesis of DNA precursors.[6] This effect is probably due to the thiosemicarbazone's binding to the metallic centre of the enzyme as an N,N,S-tridentate ligand, and interest in the coordination chemistry of these compounds has grown accordingly. Most work in this area has concerned coordination to transition metals;[7−13] nontransition metals have received relatively little attention.[14−16] In this article we describe the synthesis, structural characteristics and antifungal activity of complexes of zinc(II), cadmium(II), mercury(II), palladium(II), and platinum(II) with a heterocyclic thiosemicarbazone derived from 2-acetylpyridine 4-methylthiosemicarbazone (H4ML).

[a] Universidad de Santiago de Compostela, Departamento de Química Inorgánica, Facultad de Farmacia,
Campus Universitario Sur, E-15706 Santiago de Compostela, Spain
E-mail: qiac01@usc.es
[b] Universidad de Vigo, Departamento de Química Inorgánica, Lagoas-Marcosende, E-36200 Vigo, Spain
[c] Institut für Anorganische Chemie der Universität Tübingen, Auf der Morgenstelle 18, D-72076 Tübingen, Germany
[d] Department of Chemistry, Illinois State University, Normal, IL 61790-4160, USA
Supporting information for this article is available on the WWW under http://www.wiley-vch.de/home/eurjic or from the author.

Results and Discussion

The condensation of 2-acetylpyridine with 4-methylthiosemicarbazide affords 2-acetylpyridine 4-methylthiosemicarbazone (H4ML). H4ML is a powerful ligand able to form coordination compounds of the types $[M(H4ML)X_2]$ (M = Zn^{II}, Cd^{II}, or Hg^{II} and X = Cl, Br, or I) and [M(4ML)X] (M = Pd^{II} or Pt^{II}, X = Cl). The ligand and its complexes are stable in air. The complexes are pale yellow or orange solids that are moderately soluble in common organic solvents. Their molar conductance values of 6.27−13.97 ohm^{-1} cm^2 mol^{-1} in DMF solution indicate nonelectrolytic behaviour. Their melting points and analytical data are listed in Table 1.

Molecular Structures

Figure 1 shows that in the solid state H4ML adopts an (*E*) conformation (for the nomenclature of the conformations of thiosemicarbazones derived from 2-formyl- and 2-acetylpyridine, see refs.[17][18]). This places the C(5)−N bond of the pyridine ring *trans* to the azomethine bond. Selected bond lengths and bond angles of H4ML are listed in Table 2. The N−N distance, 1.381(4) Å, is similar to those found in related thiosemicarbazones.[19] In particular, it is shorter than the accepted length of single N−N bonds (1.44 Å) which is compatible with the notion that charge delocalization extends throughout the molecule, affecting the thiosemicarbazone chain as well as the ring. Likewise, as in other thiosemicarbazones,[20] the partial double-bond nature of the C−S bond is shown by a length [1.675(4) Å] between those of single and double bonds (1.82 and 1.56 Å, respectively)[21] and partial double bonding is similarly

 © WILEY-VCH Verlag GmbH, D-69451 Weinheim, 1999 1434−1948/99/0606−0965 $ 17.50+.50/0

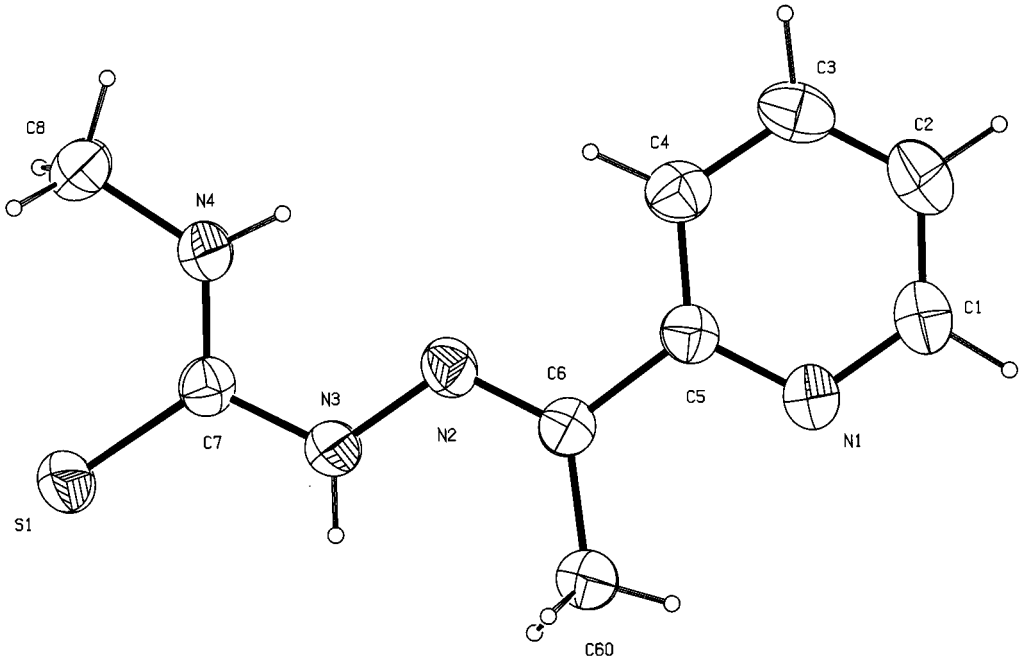


Figure 1. Molecular structure of H4ML and numbering scheme

shown by the lengths of C(7)−N(3), C(7)−N(4) and, in particular, the azomethine bond [length 1.284(4) Å]. There is an intramolecular hydrogen bond between the terminal thioamide hydrogen atom and the azomethine nitrogen atom [N(4)−H(40)−N(2): 1.02(5), 2.17(4), 2.68(3) Å, 105(3)°].

The $[M(H4ML)X_2]$ complexes for which crystals suitable for X-ray diffraction were obtained are **4** · 2 DMSO, **5** · 2 DMSO, **6** · 2 DMSO, and **7** · 2 DMSO; selected bond lengths and bond angles of the ligand in these complexes are listed in Table 2 and those involving the metal atom in Table 3. Figures 2−5 show the molecular structures. The crystals of all these compounds include two molecules of DMSO per molecule of complex, and **5** · 2 DMSO, **6** · 2 DMSO, and **7** · 2 DMSO are mutually isotypic.[22] In all these complexes H4ML is a neutral N,N,S-tridentate ligand, coordinating through its pyridine and azomethine nitrogen atoms and its thiocarbonyl sulfur atom to a metal atom whose coordination number is made up to five by bonds with the two halogen atoms. The values of 0.05−0.11 obtained for τ[23](Table 4) show that, in spite of the large deviations of both α and β from 180°, the coordination

Table 1. Analytical[a] data and some properties of the H4ML complexes

Compound	Complex	Colour	Yield (%)	Analysis (%) C	H	N	M.p. [°C]
1	$[Zn(H4ML)Cl_2]$	yellow	60	31.5 (31.4)	4.3 (3.5)	16.1 (16.3)	> 300
2	$[Zn(H4ML)Br_2]$	yellow	63	25.0 (24.9)	2.7 (2.8)	13.0 (12.9)	280[b]
3	$[Zn(H4ML)I_2]$	yellow	73	20.8 (20.5)	2.3 (2.8)	10.6 (10.6)	287
4	$[Cd(H4ML)Cl_2]$	yellow	67	27.1 (27.6)	2.7 (3.0)	13.8 (14.3)	296
5	$[Cd(H4ML)Br_2]$	yellow	77	22.8 (22.5)	2.5 (2.5)	11.4 (11.7)	291
6	$[Cd(H4ML)I_2]$	yellow	71	18.8 (18.8)	1.9 (2.1)	9.5 (9.8)	270[b]
7	$[Hg(H4ML)Cl_2]$	yellow	80	23.1 (22.5)	2.5 (2.5)	11.7 (11.7)	165
8	$[Hg(H4ML)Br_2]$	yellow	67	18.4) (19.0)	1.3 (2.1)	9.8) (9.9)	> 300
9	$[Hg(H4ML)I_2]$	orange	68	15.9 (16.3)	1.1 (1.8)	8.5 (8.5)	206[b]
10	[Pd(4ML)Cl]	yellow	78	29.6 (30.9)	2.9 (3.4)	15.0 (16.0)	> 300
11	[Pt(4ML)Cl]	orange	74	24.5 (24.6)	2.4 (2.7)	12.1 (12.8)	> 300

[a] Calculated values are given in parentheses. − [b] Temperature of decomposition.

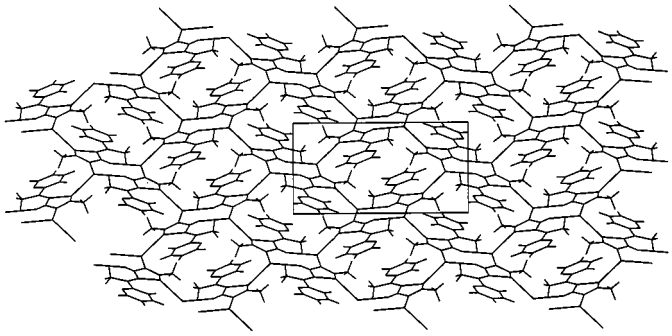


Figure 2. Crystal packing of H4ML viewed perpendicularly to the *a* axis; intermolecular hydrogen bonding parameters: N(3)−H(30)−S(1^{i}), 0.84(3), 2.80(3), 3.594(2) A, 158(3)° ($i = 1 - x$, $1 - y$, $-z$); N(4)−H(40)−S(1^{ii}), 0.84(3), 2.86(3), 3.510(2) A, 136(2)° ($ii = 1 - x$, $1/2 + y$, $1/2 - z$)

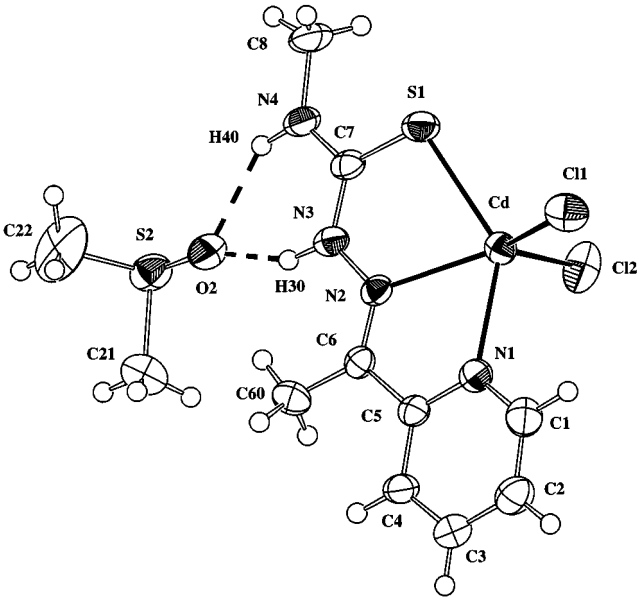


Figure 3. Molecular structure of the cadmium complex **4** · 2 DMSO, showing the hydrogen bonding

polyhedron around the metal atom is in all cases more nearly a tetragonal pyramid with halogen X(2) at its apex than a trigonal bipyramid; distorsion towards a trigonal bipyramid with N(2) and X(1) at its poles increases with the size of the halogen and with the size of the metal. The Cd−S distances (Table 3) are within the usual range for cadmium coordinated to thiocarbonyl[16][24] or thiolato[25] sulfur atoms. The distances between the cadmium atom and the pyridine and azomethine nitrogen atoms are also unexceptional,[16][24] but it may be noted that the Cd−N(azomethine) bond is in all three cases the weaker, whereas the reverse is the case in **10** and **11** (see below) and in $[Cd(HL')Cl_2] \cdot H_2O$ (HL′ = pyridine-2-carbaldehyde thiosemicarbazone).[16] In **7** · 2 DMSO the Hg−S, Hg−N(pyridine), and Hg−Cl distances are all similar to those found in other complexes of mercury(II) halides with ligands coordinating through carbonyl sulfur and pyridine nitrogen atoms,[26][27] but the Hg−N(azomethine) bond, longer than Hg−S, is very weak.

In the isotypic compounds **10** and **11** (Figures 6 and 7), in which the ligand is deprotonated, the metal centre again coordinates to the pyridine and azomethine nitrogen atoms and the thiolato sulfur atom, but has just one halogen ligand. The four donor atoms are almost coplanar, and the metal atom itself lies just 0.01 Å from the least-squares plane through the four, but distorsion of the plane tetragon appears in the S−M−N(1) and N(2)−M−Cl angles [165.7(2)° and 178.4(2)° respectively in **10**, 166.0(5)° and 177.4(5)° in **11**]. Comparison of the M−N(1) and M−N(2) distances [2.051(4) versus 1.950(3) Å in the Pd complex, 2.029(14) versus 1.969(16) Å in the Pt complex] shows that the bond with the azomethine nitrogen atom is the stronger, doubtless due to the greater basicity of this nitrogen atom and, possibly, the *trans* effect. The M−S and M−Cl distances are similar to those found in other complexes in which Pd and Pt coordinate to S[13][28] or Cl.[29] The delocalization of the charge originated by deprotonation at N(3) is apparent upon comparison of the thiosemicarbazone bond lengths in the complexes and the free ligand (Table 2): In the complexes N(3)−C(7) is shorter and C(7)−S is longer than in free H4ML, showing that, as in similar complexes,[18] bond order is increased in the former

Table 2. Selected bond lengths [Å] and angles [°] of H4ML and the complexes[a]

	H4ML	**4** · 2 DMSO	**5** · 2 DMSO	**6** · 2 DMSO	**7** · 2 DMSO	**10**	**11**
C(6)−N(2)	1.286(3)	1.295(6)	1.25(1)	1.28(2)	1.27(1)	1.297(4)	1.273(13)
N(2)−N(3)	1.372(3)	1.357(5)	1.346(9)	1.38(2)	1.37(1)	1.373(3)	1.365(13)
N(3)−C(7)	1.366(3)	1.370(6)	1.38(1)	1.36(1)	1.34(1)	1.320(4)	1.328(15)
C(7)−S(1)	1.680(2)	1.695(5)	1.69(1)	1.696(8)	1.691(9)	1.755(3)	1.755(13)
C(7)−N4)	1.326(3)	1.320(6)	1.36(1)	1.33(1)	1.35(1)	1.336(4)	1.306(14)
N(1)−C(5)−C(4)	122.2(2)	122.0(4)	121(2)	122.6(8)	122.9(9)	120.5(3)	120.0(12)
C(4)−C(5)−C(6)	122.5(2)	121.2(4)	123.0(9)	120.4(7)	122.1(8)	123.9(3)	124.5(12)
N(1)−C(5)−C(6)	115.3(2)	116.9(4)	115.5(9)	117.1(7)	116.7(9)	115.5(3)	115.4(12)
C(5)−C(6)−N(2)	115.8(2)	115.1(4)	116.1(9)	114.0(6)	113.0(8)	114.2(3)	114.6(12)
C(6)−N(2)−N(3)	118.3(2)	120.0(4)	119.4(8)	119.8(6)	120.3(7)	118.9(3)	120.2(11)
N(2)−N(3)−C(7)	119.0(2)	119.2(4)	116.9(7)	118.9(6)	118.2(7)	112.0(3)	113.7(10)
N(3)−C(7)−S(1)	119.8(2)	123.3(4)	125.8(9)	124.0(7)	126.5(8)	125.5(2)	124.1(10)
N(3)−C(7)−N(4)	116.3(2)	114.9(5)	113.9(8)	113.5(7)	114.2(8)	117.6(3)	118.6(12)
S(1)−C(7)−N(4)	124.0(2)	121.7(3)	120.2(8)	122.5(7)	119.2(7)	116.9(3)	117.2(10)

[a] Estimated standard deviations in units of the least significant figures given in each case are quoted in parentheses.

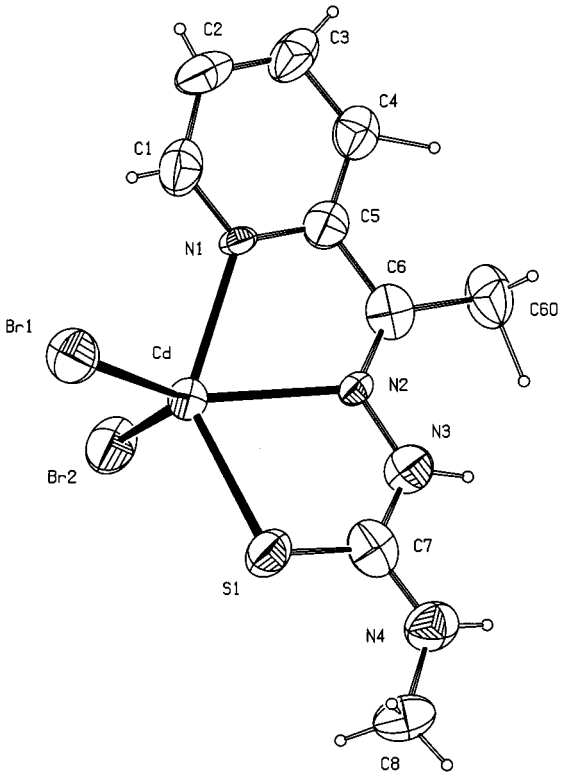


Figure 4. Molecular structure of the cadmium complex **5**

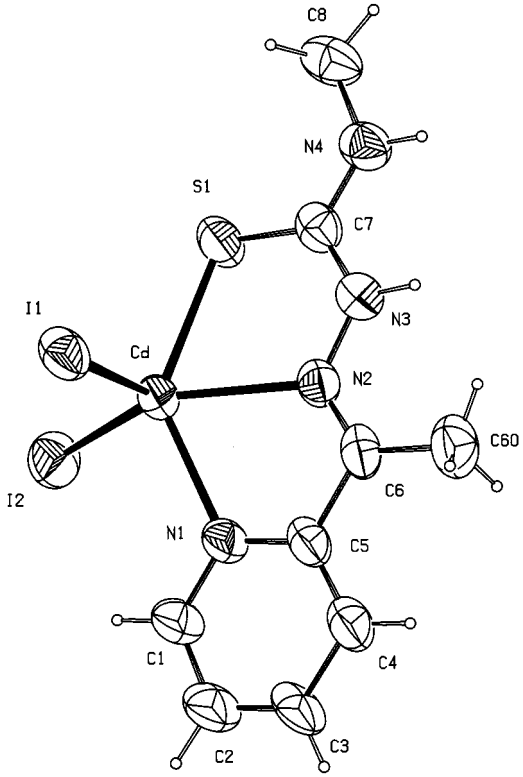


Figure 5. Molecular structure of the cadmium complex **6**

case and decreased in the latter. The stability of the complex is no doubt increased by the rigidity of the planar tricyclic system formed by the pyridine ring and the two five-membered chelation rings.

Electronic Spectra

The electronic spectra of the palladium(II) and platinum(II) complexes were recorded in DMF/MeCN solutions. The positions of the absorption bands were not significantly different from those observed in the solid-state diffuse-reflectance spectra indicating that these complexes underwent no electronic or geometric changes upon dissolution.

The absorption bands of the Pd^{II} complex, with maxima at $\tilde{\nu}$ = 21,692, 24,096, and 27,100 cm^{-1}, may be assigned to spin-allowed *d-d* transitions corresponding to the one-electron transitions $^1A_{1g} \rightarrow {}^1A_{2g}$, $^1A_{1g} \rightarrow {}^1B_{1g}$ and $^1A_{1g} \rightarrow {}^1E_g$. Similarly, the Pt^{II} complex displayed an absorption spectrum with maxima at $\tilde{\nu}$ = 22,124, 25,126−25,707, and 26,882 cm^{-1} attributed to these same transitions. These wavenumbers are comparable to those observed previously

Table 3. Coordinating bond lengths [Å] and angles [°] of the complexes[a]

	4 · 2 DMSO	**5** · 2 DMSO	**6** · 2 DMSO	**7** · 2 DMSO	**10**	**11**
M−X(1)	2.450(1)	2.574(1)	2.761(1)	2.460(3)	2.310(1)	2.304(3)
M−X(2)	2.432(2)	2.575(1)	2.758(1)	2.476(5)	−	−
M−S(1)	2.596(1)	2.581(4)	2.588(3)	2.561(4)	2.256(1)	2.256(3)
M−N(1)	2.345(4)	2.348(9)	2.351(7)	2.423(8)	2.056(3)	2.023(9)
M−N(2)	2.405(4)	2.408(8)	2.414(6)	2.532(7)	1.955(2)	1.961(10)
N(1)−M−X(1)	96.7(2)	95.4(2)	97.6(9)	93.3(2)	98.05(8)	97.2(3)
N(1)−M−X(2)	102.2(2)	101.8(2)	100.3(8)	96.0(3)	−	−
N(1)−M−N(2)	67.8(1)	67.3(4)	66.8(2)	63.2(3)	80.57(11)	80.6(4)
N(2)−M−X(1)	139.8(1)	139.9(2)	139.9(2)	138.7(2)	178.34(8)	177.7(3)
N(2)−M−X(2)	103.8(1)	102.0(2)	101.5(6)	100.1(2)	−	−
X(1)−M−X(2)	115.69(5)	117.30(5)	117.94(2)	116.6(1)	−	−
S(1)−M−X(1)	101.92(5)	102.01(8)	100.38(6)	108.9(1)	96.23(4)	96.85(12)
S(1)−M−X(2)	106.01(5)	105.82(7)	106.44(5)	109.6(1)	−	−
S(1)−M−N(1)	136.7(1)	135.3(3)	135.2(4)	132.4(2)	165.72(8)	165.9(3)
S(1)−M−N(2)	72.8(1)	73.0(2)	72.9(5)	72.9(2)	85.16(8)	85.4(3)

[a] Estimated standard deviations in units of the least significant figures given in each case are quoted in parentheses.

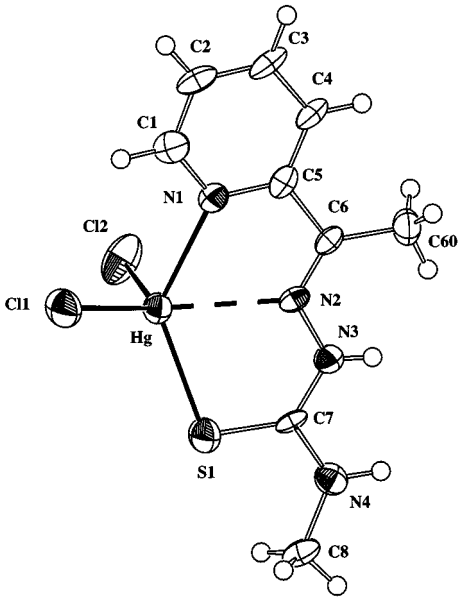


Figure 6. Molecular structure of the mercury complex **7** [the weaker Hg−N(azomethine) interaction is shown by the dashed line]

Table 4. Deviation from tetragonal-pyramidal coordination in the compounds **4**− **7**

Compound	β(N−M−X)	α(S−M−N)	β − α	τ = (β − α)/60
4 · 2 DMSO	139.8	136.7	3.1	0.05
5 · 2 DMSO	139.9	135.3	4.6	0.08
6 · 2 DMSO	140.1	135.2	4.9	0.08
7 · 2 DMSO	138.7	132.4	6.3	0.11
bpt[a]	120.0	180.0	60.0	1.00
t-p[b]	180.0	180.0	0.0	0.00

[a] Trigonal bipyramid. − [b] Tetragonal pyramid.

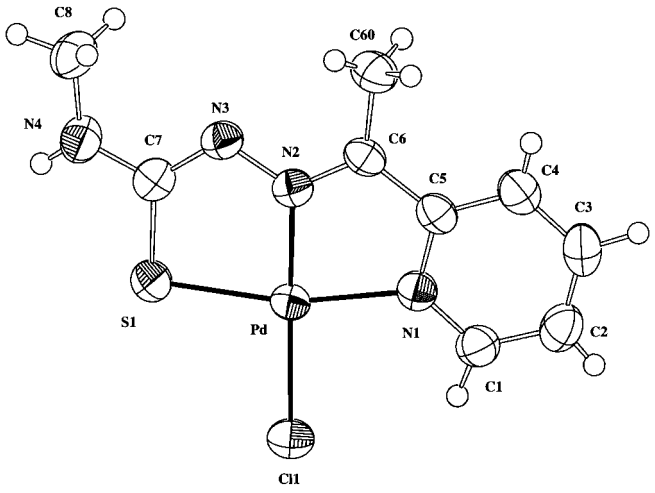


Figure 7. Molecular structure of the palladium complex **10**

for square-planar palladium and platinum complexes involving similar donor atoms. In the UV region, the strong absorptions above 28,000 cm^{-1} may be charge-transfer bands[30] or intraligand bands.

Infrared Spectra

The chief IR bands of free H4ML[31] and the complexes are listed and assigned in the Supporting Information. Most of the ligand bands shift to higher frequencies upon complexation. In particular, the shifts in ν(C=N) and ν(N−N) are evidence of coordination through the azomethine nitrogen atom[32][33], while coordination through the pyridine nitrogen atom is shown by the shift to higher frequencies of the ν(CN) + ν(CC) (1539 cm^{-1}), α(CCC) (626 cm^{-1}), and φ(CC) (403 cm^{-1}) ring vibrations.[34] The shifts to lower frequencies of ν(CS) at 833 cm^{-1} in the free ligand[31] and, in the Zn, Cd, and Hg complexes, ν(NH), are the result of coordination through the thiocarbonyl sulfur atom[35] and the nitrogen atom bound to N(3).[36] The spectra of the Pd and Pt complexes, in which the ligand is deprotonated, show only one strong band instead of two in the ν(NH) region. Deprotonation results in the frequency of this remaining band increasing (rather than decreasing, as it does in the Zn, Cd, and Hg complexes), and enhances the shifts of other bands affected by complexation. In particular, the shift of about 160 cm^{-1} in ν(CS), as against about 120 cm^{-1} in the Zn, Cd, and Hg compounds, shows the ligand to be closer to a thiolato form in the Pd and Pt compounds than in the others.

In the 500−100 cm^{-1} region, the one or two strong bands whose frequencies increase in the order I complex < Br complex < Cl complex for a given metal and in the order Hg complex < Cd complex < Zn complex for a given halogen (Table 5) are attributed to metal-halogen stretching vibrations, in keeping with which the resulting values of ν(M−Br)/ν(M−Cl) (av. 0.70) and ν(M−I)/ν(M−Cl) (av. 0.63) (see Supporting Information) are similar to previously reported values.[26,27,37] The less intense band observed in the range 300−280 cm^{-1} in the Zn, Cd, and Hg compounds and around 360 cm^{-1} in the Pd and Pt compounds is attributable to ν(M−S), and those appearing in the ranges 350−330 and 330−310 cm^{-1} or at 500 and 490 cm^{-1} to ν(M−N) vibrations.[38] In the Pd and Pt compounds this latter pair are very close together; in the others it is probably the higher frequency band that corresponds to the pyridine nitrogen atom, the M−N(1) distances being slightly shorter than the M−N(2) distances in the crystals of **7** · 2 DMSO and all the Cd complexes.

^{1}H-NMR Spectra

The ^{1}H-NMR signals of H4ML and the complexes are listed in the Supporting Information. The nonappearance of the N(3)H signal (at δ = 10.34 in the free ligand), in the spectra of **10** and **11** shows that in these complexes the ligand remains deprotonated in DMSO solution. The deshielding of N(4)H in these compounds is probably due to withdrawal of charge from N(4) as the result of an increase in charge delocalization upon complexation through the thiocarbonyl sulfur atom; the shielding of the N(4) methyl protons is attributable to the same mechanism. The H(1) signal shifts upfield in the Pd complex because coordination

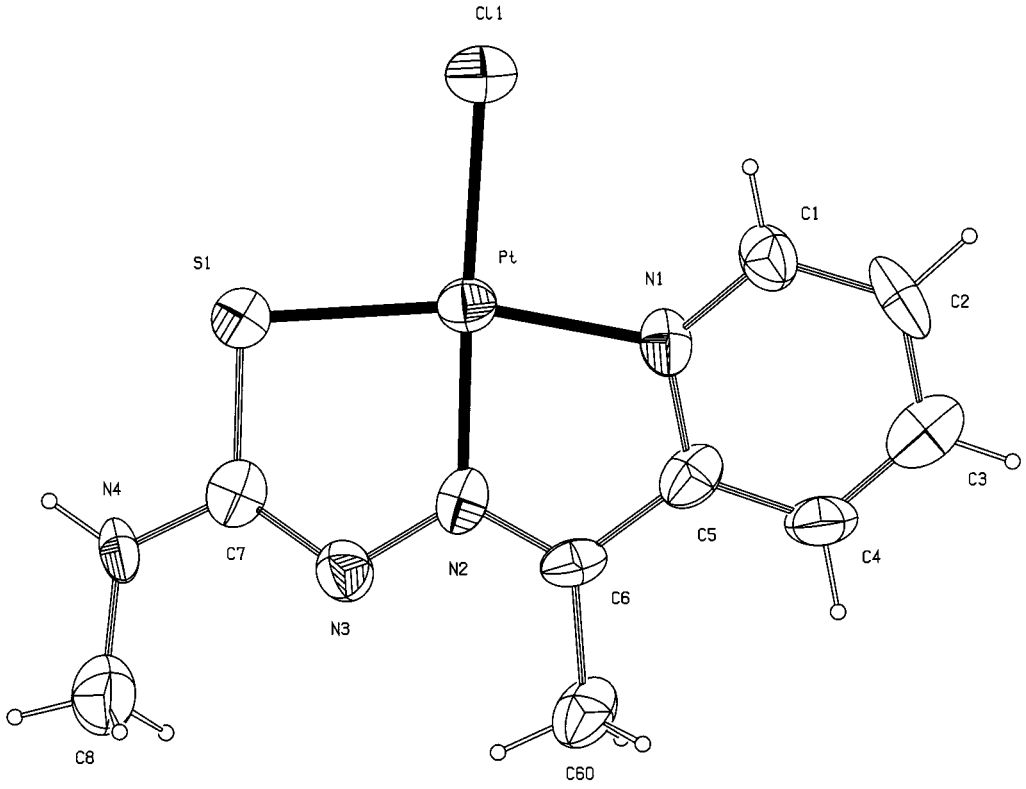


Figure 8. Molecular structure of the platinum complex **11**

through the pyridine nitrogen atom prevents H(1) from being deshielded, as it is in the free ligand, as the result of the anisotropy of the C(6)=N(2) bond and the proximity of the nitrogen atom with sp^2 hybridization.[39] In the Pt complex, on the other hand, the H(1) signal shifts downfield (as in the complex of Pt^{II} with 1-phenyl-2-formylpyridine thiosemicarbazone[40]), possibly due to the replacement of the chloride ion *trans* to the azomethine nitrogen atom by a DMSO molecule. In the $[M(H4ML)X_2]$ complexes the persistence of the N(3)H signal shows that this proton is retained in DMSO solution. The downfield shifts of the N(3)H and N(4)H signals, which increase in the order Cd < Zn < Hg, are attributable to coordination through the azomethine nitrogen atom and thiocarbonyl sulfur atom, respectively, and/or to the formation of hydrogen bonds between N(3)H [and to a much lesser extent N(4)H] and DMSO.

^{13}C-NMR Spectra

The ^{13}C-NMR signals of H4ML and all the complexes except **4**, for which we were unable to obtain a spectrum of adequate quality, are listed in the Supporting Information. The deshielding of C(7) and C(8) in the [M(4ML)Cl] complexes is attributable to a combination of the inductive effect of the metal and the move towards the thiol form induced by complexation. The simultaneous shift of the C(6) signal to higher field and that of C(60) to lower field is in consonance with coordination through the azomethine nitrogen atom in these compounds, whereas coordination through the pyridine nitrogen atom is pointed to by the behaviour of the pyridine carbon signals [shielding of the *ortho*-carbon atoms C(1) and C(5), deshielding of the others], which is qualitatively similar to their behaviour in the pyridinium ion[41] and in the protonated form of other thiosemicarbazones derived from 2-acetylpyridine.[40] In the $[M(H4ML)X_2]$ complexes C(8) (δ = 31.27) is deshielded (except in **1** and **2**) but C(7) (δ = 179.24) is shielded (although **1** is again an exception); the greatest shielding is shown in the complexes of the "*soft*" metal Hg. The other carbon signals exhibit more or less the same pattern in $[M(H4ML)X_2]$ as in [M(4ML)Cl], although the pyridine carbon shifts are generally less marked.

^{113}Cd-, ^{195}Pt and ^{199}Hg-NMR Spectra

The ^{113}Cd-NMR spectra of the Cd compounds show a single signal at δ = 363.7, 345.7, or 279.8 for the Cl, Br, and I derivatives, respectively. The nuclide is thus less shielded than in the corresponding halide CdX_2 in DMSO,[42] especially in the case of the Cl derivative. The progressive increase in shielding upon replacement of Cl by Br and of Br by I is in keeping with the decreasing electronegativity of the halogen, and the observed chemical shifts are within what may be expected for pentacoordinate halide complexes.[43]

Of the mercury compounds, only **7** was sufficiently soluble for ^{199}Hg-NMR spectroscopy. The spectrum obtained exhibits a single signal at δ = −1092.4, which is compatible with pentacoordination to the extent that it shows the nu-

Table 5. Diameters [mm] of growth inhibition zones in in-vitro antifungal activity assays (6.0 indicates no inhibition)

Concentration [μg mL^{-1}]	200	400	600	1000	1600
Aspergillus niger					
H4ML	6.0	9.8	12.2	16.2	17.5
1	6.0	6.0	15.5	–	–
NYSTATIN	9.0	10.7	12.8	17.3	19.2
Paecilomyces variotii					
H4ML	6.0	8.3	10.0	14.4	17.7
1	6.0	6.0	6.0	10.6	–
2	6.0	6.0	6.0	10.2	–
NYSTATIN	12.8	14.5	16.5	25.2	26.0

clide to be more shielded than is usual in tetrahedral complexes of the form HgL_2Cl_2.[44]

The Pt^{II} complex give rise to single, relatively sharp ^{195}Pt resonance at $\delta = -3092$. This supports the idea that the coordination mode of of the platinum(II) complex in solution is similar to that observed in the solid state; there is probably no exchange of the Cl^- ion for another donor.[40]

Biological Results

H4ML and the complexes were assayed in vitro for antifungal activity against the pathogens *Aspergillus niger* and *Paecilomyces variotii* (for previous data for H4ML see ref.[45]). Table 5 lists the results obtained with the compounds that at some concentration inhibited fungal growth, together with those obtained with the currently prescribed drug nystatin. Only the zinc complexes displayed some activity: At a concentration of 600 μg·mL^{-1} **1** inhibited *A. niger* rather more than either H4ML or nystatin, and at a concentration of 1000 μg·mL^{-1} both **1** and **2** inhibited *P. variotii*, though considerably less than nystatin did.

Experimental Section

General: All commercial reagents were Aldrich, Merck, or Ventron reagent-grade products. – Elemental analysis was performed with a Carlo Erba 1108 analyser. – Melting points were determined with a Büchi apparatus. – Infrared spectra were recorded with a Mattson Instruments Cygnus 100 FTIR spectrometer using KBr discs for spectra run from 4000 to 400 cm^{-1} and polyethylene-sandwiched Nujol mulls for the range 500–100 cm^{-1}. – UV/Vis spectra and reflectance spectra were recorded with a Shimadzu UV-3101PC spectrophotometer. – ^{1}H- and ^{13}C-NMR spectra were run with a Bruker WM-300 using DMSO as internal reference; chemical shifts are referred to TMS. ^{113}Cd-, ^{195}Pt-, and ^{199}Hg-NMR spectra were run with a Bruker WM-250 using DMSO solutions of about 10^{-2} M, and are referred to 0.1 M $Cd(ClO_4)_2$, H_2PtCl_6, and $HgMe_2$, respectively.

2-Acetylpyridine 4-Methylthiosemicarbazone (H4ML): H4ML was synthesized using the general procedure by Klayman et al.[3][46] for condensation of amines with aldehydes or ketones. To an aqueous solution of 4-methylthiosemicarbazide heated to 60 °C was slowly added a solution of an equimolecular amount of 2-acetylpyridine in ethanol. The reaction mixture was refluxed for 2 h, and upon cooling afforded a whitish crystalline solid which was filtered off and recrystallized from warm ethanol. After storage at low temperature, the remaining recrystallization solution afforded crystals suitable for study by X-ray diffraction. Yield 98%, m.p. 176 °C. – $C_9H_{12}N_4S$ (208): calcd. C 51.8, , H 5.8, N 27.0; found C 51.8, H 6.2, N 26.7.

Preparation of the Complexes: Complexes of the form $[M(H4ML)X_2]$ (M = Zn^{II}, Cd^{II}, Hg^{II}; X = Cl, Br, I) (**1**–**9**) were obtained by treating H4ML with the corresponding metal salts in a 1:1 molar ratio in ethanol. After prolonged stirring (about 1 week) at room temperature, the reaction mixture afforded solids (generally microcrystalline) that were filtered off, washed with ethanol, and vacuum-dried. In the cases of the cadmium complexes and $[Hg(H4ML)Cl_2]$ it was possible to obtain single crystals by redissolving the solids in DMSO and slowly evaporating the sol-

Table 6. Crystal and structure refinement data for H4ML and the complexes **4**–**7**, **10**, and **11**

Compound	H4ML	**4** · 2 DMSO	**5** · 2 DMSO	**6** · 2 DMSO	**7** · 2 DMSO	**10**	**11**
Empirical formula	$C_9H_{12}N_4S$	$C_{13}H_{24}CdCl_2N_4O_2S_3$	$C_{13}H_{24}Br_2CdN_4O_2S_3$	$C_{13}H_{24}CdI_2N_4O_2S_3$	$C_{13}H_{24}Cl_2HgN_4O_2S_3$	$C_9H_{11}ClN_4PdS$	$C_9H_{11}ClN_4PtS$
Formula weight	208.29	547.88	636.78	730.78	636.06	349.13	437.82
Crystal size [mm]	0.30×0.25×0.15	0.75×0.10×0.10	0.50×0.40×0.30	0.50×0.40×0.30	0.30×0.15×0.10	0.35×0.10×0.05	0.30×0.20×0.15
Crystal shape	prism	prism	prism	prism	prism	plate	prism
Crystal system	monoclinic	monoclinic	triclinic	triclinic	triclinic	monoclinic	monoclinic
Space group	$P2_1/c$ (No 14)	$P2_1/c$ (No 14)	$P-1$ (No. 2)	$P-1$ (No 2)	$P-1$ (No 2)	$P2_1/n$ (No 14)	$P2_1/n$ (No 14)
a [Å]	8.813(2)	9.535(1)	8.939(4)	9.428(3)	8.605(1)	7.764(2)	7.695(3)
b [Å]	7.720(1)	10.217(1)	10.156(5)	10.484(5)	10.109(1)	16.660(2)	16.778(3)
c [Å]	15.580(3)	22.893(2)	13.597(5)	13.699(4)	13.375(1)	9.302(3)	9.340(4)
α [°]	90	90	96.21(3)	93.72(2)	97.07(1)	90	90
β [°]	106.11(1)	90.23(2)	107.74(2)	109.51(3)	104.16(1)	93.87(2)	94.17(1)
γ [°]	90	90	102.18(3)	104.70(3)	100.61(1)	90	90
V [Å^3]	1018.4(3)	2230.1(4)	1129.3(9)	1217.8(9)	1091.5(2)	1200.5(5)	1202.7(7)
Z	4	4	2	2	2	4	4
$D_{calcd.}$ [Mg/m^3]	1.358	1.632	1.872	1.994	1.935	1.932	2.418
F(000)	440	1104	624	696	616	688	816
θ range	3.09–28.93	3.00–33.00	2.00–27.00	3.00–31.00	3.00–33.00	3.29–28.92	3.27–28.89
Temperature [K]	293(2)	223(2)	213(2)	223	223(2)	293(2)	293(2)
h_{min}/h_{max}	0/11	−14/14	−1/11	−13/13	0/13	0/10	0/10
k_{min}/k_{max}	0/10	0/15	−12/12	−2/15	−15/15	0/22	0/22
l_{min}/l_{max}	−21/21	0/35	−17/17	−19/19	−20/20	−12/12	−12/12
μ [mm^{-1}]	0.283	1.51	2..40	1.85	7.85	1.919	12.040
Max./min. transmissions	0.9587/0.9198	1.003/0.553	1.206/0.717	1.319/0.698	1.197/0.744	0.830/0.474	0.804/0.418
Refl. collected/unique	2838/2676 [R_{int} = 0.038]	9763/7973 [R_{int} = 0.024]	5885/3959 [R_{int} = 0.026]	9540/5784 [R_{int} = 0.017]	4453/3531 [R_{int} = 0.032]	3369/3157 [R_{int} = 0.019]	3372/3157 [R_{int} = 0.070]
Data/parameters	2676/175	4702/238	2503/230	4946/227	3234/227	3157/189	3157/147
Final R	0.051	0.044	0.048	0.048	0.041	0.031	0.057
Final $wR2$	0.108	0.047	0.053	0.052	0.050	0.057	0.081
GOOF	1.013	1.042	0.987	1.012	2.493	1.027	0.986
Max. Δρ [eÅ^{-3}]	0.244	0.927	1.05	1.842	2.402	0.384	1.210

vent. − For [Pd(4ML)Cl] and [Pt(4ML)Cl] (**10** and **11**) the metal salts were dissolved in water and the reaction mixture was refluxed for 1 h. Evaporation of the solvent from the filtered reaction mixture at room temperature gave monocrystals suitable for study by X-ray diffraction.

X-ray Crystallography: Crystals of H4ML, **4**−**7**, **10**, and **11** suitable for X-ray diffraction were mounted on glass fibres and transferred to an Enraf Nonius CAD4 diffractometer. Accurate unit-cell parameters and an orientation matrix were determined by least-squares refinement of the setting angles of a set of well-centred reflections (SET4)[47] in the θ range 6.1−11.7 (H4ML), 9.0−13.0 (**4**), 4.6−12.0 (**5**), 5.7−13.2 (**6**), 7.3−14.9 (**7**), 6.1−13.3 (**10**), and 4.9−13.0° (**11**). Reduced cell calculations did not indicate higher lattice symmetry.[48] Crystal data and details of the data collection and refinement are given in Table 6. Data were corrected for Lp effects and for observed linear decay of the reference reflections. An empirical absorption correction (DIFABS)[49] was applied for all compounds. The structures were solved by automated Patterson or direct methods and subsequent difference Fourier techniques (SHELX86)[50] and refined on F (SDP/VAX)[51] or F^2 (SHELXL97).[52] Hydrogen atoms were included in the refinement in calculated positions riding on their carrier atoms. In two structures, a DMSO molecule proved to be disordered and a disorder model consisting of two (**4**) or three (**5**) alternative sites was included in the refinement; the occupation factors for **4** were 0.75 [S(31)] and 0.25 [S(32)] and for **5** were 0.40, [S(31)], 0.40, [S(32)], and 0.20 [S(33)]. Neutral atom scattering factors and anomalous dispersion corrections were taken from the International Tables for X-ray Crystallography.[53] Geometrical calculations and illustrations were performed or generated with the SHELXL97,[52] ZORTEP,[54] and PLATON98[55] packages. Crystallographic data for the structures reported in this paper (excluding structure factors) have been deposited with the Cambridge Crystallographic Data Centre as supplementary publication nos. CCDC-106651 and -106653 to -106658. Copies of the data can be obtained free of charge on application to CCDC, 12 Union Road, Cambridge CB2 1EZ, UK (Fax: + 44-1223/336-033; E-mail: deposit@ccdc.cam.ac.uk).

[1] J. C. Logan, M. P. Fox, J. H. Morgan, C. J. Pfau, *J. Gen. Virol.* **1975**, *28*, 271.
[2] E. J. Blanz, Jr., F. A. French, *Cancer Res.* **1968**, *28*, 2419.
[3] D. L. Klayman, F. J. Bartosevich, T. S. Griffin, C. J. Mason, J. P. Scovill, *J. Med. Chem.* **1979**, **22**, 855.
[4] S. P. Mittal, S. K. Sharma, R. V. Singh, J. P. Tandon, *Curr. Sci.* **1981**, *50*, 483.
[5] A. S. Dobeck, D. L. Klayman, E. J. Dickson, Jr., J. P. Scovill, E. C. Tramont, *Antimicrob. Agents Chemother.* **1980**, *18*, 27.
[6] F. A. French, E. J. Blanz, Jr., J. R. Amaral, D. A. French, *J. Med. Chem.* **1970**, *13*, 1117.
[7] E. S. Raper, *Coord. Chem. Rev.* **1985**, *61*, 115.
[8] D. X. West, S. B. Padhye, P. B. Sonawane, *Structure and Bonding* **1991**, *76*, 4.
[9] M. C. Rodríguez-Argüelles, M. B. Ferrari, G. G. Fava, C. Pelizzi, P. Tarasconi, R. Albertini, P. P. Dall′Aglio, P. Lunghi, S. Pinelli, *J. Inorg. Biochem.* **1995**, *58*, 157.
[10] J. S. Casas, M. S. García-Tasende, C. Maichle-Mössmer, M. C. Rodriguez-Argüelles, A. Sánchez, J. Sordo, A. Vázquez-López, S. Pinelli, P. Lunghi, R. Albertini, *J. Inorg. Biochem.* **1996**, *62*, 41.
[11] M. B. Ferrari, G. G. Fava, G. Tarasconi, R. Albertini, S. Pinelli, R. Starcich, *J. Inorg. Biochem.* **1994**, *53*, 13.
[12] R. Alonso, E. Bermejo, A. Castiñeiras, T. Pérez, R. Carballo, *Z. Anorg. All. Chem.* **1997**, *623*, 881.
[13] D. Kovala-Demertzi, A. Domopoulou, M. A. Demertzis, J. Valdés-Martínez, S. Hernández-Ortega, G. Espinosa-Pérez, D. X. West, M. M. Salberg, G. A. Bain, P. D. Bloom, *Polyhedron* **1996**, *15*, 2587.
[14] J. S. Casas, M. V. Castaño, M. C. Argüelles, A. Sánchez, J. Sordo, *J. Chem. Soc., Dalton Trans.* **1993**, 1253.
[15] J. S. Casas, E. E. Castellano, A. Macías, M. C. Argüelles, A. Sánchez, J. Sordo, *J. Chem. Soc., Dalton Trans.* **1993**, 755.
[16] J. S. Casas, M. V. Castaño, M. S. García-Tasende, I. Martínez-Santamarta, J. Sordo, E. E. Castellano, J. Zukerman-Spechtor, *J. Chem. Res.* **1992**, 324.
[17] [17a] D. X. West, B. L. Mokijewski, H. Gebremedhin, T. J. Romack, *Transition Met. Chem.* **1992**, *17*, 384. − [17b] D. X. West, G. A. Bain, R. J. Butcher, J. P. Jasinski, Y. Li, R. Y. Pozdniakiv, J. Valdés-Martínez, R. A. Toscano, S. Hernández-Ortega, *Polyhedron* **1996**, *15*, 665.
[18] D. Kovala-Demertzi, A. Domopoulov, M. A. Demertzis, C. P. Raptopoulov, A. Terzis, *Polyhedron* **1994**, *13*, 1917.
[19] J. Palenik, D. F. Reudle, W. S. Carter, *Acta Crystallogr.. Sect. B* **1974**, *30*, 2390.
[20] R. Restivo, G. J. Lapenik, *Acta Crystallogr., Sect. B* **1970**, *26*, 1397.
[21] L. E. Sutton, *Tables of Interatomic Distances and Configuration in Molecules and Ions* (Supplement), The Chemical Society, London, **1965**.
[22] There is an isostructural form of **4** · 2 DMSO with unit cell dimensions: a = 8.813(2), b = 10.003(4), c = 13.343(7) Å, α = 96.56(2), β = 104.57(2), and γ = 101.16(1)°, isotypic with **5** · 2 DMSO, **6** · 2 DMSO, and **7** · 2 DMSO.
[23] A. W. Addinson, T. N. Rao, J. Reedijk, J. van Rijn, G. C. Verschoor, *J. Chem. Soc., Dalton Trans.* **1984**, 1349.
[24] A. G. Orpen, L. Brammer, F. H. Allen, O. Kennard, D. G. Waston, R. Taylor, *J. Chem. Soc., Dalton Trans.* **1989**, 51.
[25] R. Castro, M. L. Durán, J. A. García-Vázquez, J. Romero, A. Sousa, A. Castiñeiras, W. Hiller, J. Strähle, *Z. Naturforsch.* **1992**, *47b*, 1067.
[26] R. Carballo, A. Castiñeiras, M. C. G. Conde, W. Hiller, *Polyhedron* **1993**, *12*, 1655.
[27] A. Castiñeiras, G. Díaz, F. Florencio, S. García-Blanco, S. García-Carrera, *Z. Anorg. Allg. Chem.* **1988**, *567*, 101.
[28] H. B. Bürgi, J. D. Dunitz (Eds.), *Structure Correlation*, vol. 2, VCH, Weinheim, **1994**.
[29] G. R. Giesbrecht, G. S. Hanan, G. E. Kilkham, S. J. Loeb, *Inorg. Chem.* **1992**, *31*, 3291.
[30] A. B. P. Lever, *Inorganic Electronic Spectroscopy*, Elsevier, Amsterdam, **1986**.
[31] D. X. West, N. C. Lewis, *Transition Met. Chem.* **1987**, *12*, 365.
[32] D. X. West, J. P. Scovill, J. V. Silverton, A. Bavoso, *Transition Met. Chem.* **1986**, *11*, 123.
[33] [33a] B. V. Agarvala, S. Himgorani, V. Puri, C. L. Khetrapal, G. A. Naganagowda, *Transition Met. Chem.* **1992**, *19*, 25. − [33b] M. J. M. Campbell, *Coord. Chem. Rev.* **1975**, *15*, 279. − [33c] R. Mukkanti, K. B. Pandeya, R. P. Singh, *Synth. React. Inorg. Met.-Org. Chem.* **1985**, *15*, 613.
[34] [34a] N. S. Gill, H. J. Kingdon, *Aust. J. Chem.* **1966**, *19*, 2197. − [34b] C. Airoldi, A. S. Gonçalves, *J. Inorg. Nucl. Chem.* **1978**, *40*, 1817.
[35] A. Castiñeiras, A. Arquero, J. R. Masaguer, *Transition Met. Chem.* **1984**, *9*, 429.
[36] J. V. Quagliano, G. F. Svatos, C. Curran, *Anal. Chem.* **1959**, *26*, 429.
[37] [37a] R. J. H. Clark, C. S. Williams, *Inorg. Chem.* **1965**, *4*, 350. − [37b] G. B. Deacon, J. H. S. Green, D. J. Harrison, *Spectrochim. Acta* **1968**, *24A*, 1921. − [37c] A. Arquero, J. R. Masaguer, A. Castiñeiras, *Z. Anorg. Allg. Chem.* **1994**, *531*, 183. − [37d] A. Castiñeiras, C. F. Vidal, R. Bastida, A. Macías, W. Hiller, *Polyhedron* **1988**, *7*, 2503.
[38] [38a] K. Nakamoto, *Infrared and Raman Spectra of Inorganic and Coordination Compounds*, 4th ed., Wiley, New York, **1986**. − [38b] J. Weidlein, U. Müller, K. Dehnicke, *Schwingungsfrequenzen II*, Thieme Verlag, Stuttgart, **1986**.
[39] I. Antonini, F. Claudi, P. Franchetti, M. Grifantini, S. Martelli, *J. Med. Chem.* **1977**, *20*, 447.
[40] K. R. Koch, *J. Coord. Chem.* **1991**, *22*, 289.
[41] R. J. Pugmire, D. M. Grant, *J. Am. Chem. Soc.* **1968**, *90*, 687.
[42] T. Drakenberg, N.-O. Björk, R. Portanova, *J. Phys. Chem.* **1978**, *82*, 2423.
[43] J. J. H. Ackerman, T. Vorr, V. J. Bartuska, G. E. Maciel, *J. Am. Chem. Soc.* **1979**, *101*, 341.
[44] A. A. Isab, H. P. Perzanowski, *J. Coord. Chem.* **1990**, *21*, 247.

[45] D. X. West, C. S. Carlson, A. C. Whyte, A. E. Liberta, *Transition Met. Chem.* **1990**, *15*, 43.
[46] [46a] D. L. Klayman, J. P. Scovill, J. F. Bartosevich, C. J. Mason, *J. Med. Chem.* **1979**, *22*, 1367. – [46b] J. P. Scovill, D. L. Klayman, C. F. Franchino, *J. Med. Chem.* **1982**, *25*, 1261. – [46c] D. L. Klayman, J. P. Scovill, J. F. Bartosevich, J. Bruce, *J. Med. Chem.* **1983**, *26*, 35. – [46d] J. P. Scovill, D. L. Klayman, C. Lambros, G. E. Childs, J. D. Notsch, *J. Med. Chem.* **1984**, *27*, 87.
[47] J. L. de Boer, A. J. M. Duisenberg, *Acta Crystallogr., Sect. A* **1984**, *40*, 410.
[48] A. L. Spek, *J. Appl. Crystallogr.* **1988**, *21*, 578.
[49] N. Walker, D. Stuart, *Acta Crystallogr., Sect. A* **1983**, *39*, 158.
[50] G. M. Sheldrick, *SHELXS86*, Universität Göttingen, **1986**.
[51] B. A. Frenz and Associates Inc. & Enraf-Nonius, *SPD/VAX Structure Determination Package*, V. 2.2, College Station, Texas, USA, **1986**,
[52] G. M. Sheldrick, *SHELXL97*, Universität Göttingen, **1997**.
[53] A. J. C. Wilson, *International Tables for Crystallography*, vol. C, Kluwer Academic Publishers, Dordrecht, The Netherlands, **1992**.
[54] L. Zsolnai, *ZORTEP*, Universität Heidelberg, **1997**.
[55] A. L. Spek, *Acta Crystallogr., Sect. A* **1990**, *46*, C34.

Received November 5, 1998
[I98381]

$EuPdIn_2$, $YbPdIn_2$, and $YbAuIn_2$: Syntheses, Structures, and Properties of New Intermetallic Compounds with Ordered Re_3B-Type Structure

Yaroslav V. Galadzhun,[a] Rolf-Dieter Hoffmann,[a] Gunter Kotzyba,[a] Bernd Künnen,[a] and Rainer Pöttgen*[a]

Keywords: Europium / Ytterbium / Indium / Intermetallic compounds / Ferromagnetism

The new compounds $EuPdIn_2$ (**1**), $YbPdIn_2$ (**2**), and $YbAuIn_2$ (**3**) have been synthesized by high-frequency melting of the elements in sealed tantalum tubes and subsequent annealing at about 900 K. Their crystal structures have been determined by single-crystal X-ray diffraction techniques. Compounds **1**, **2**, and **3** crystallize with the $MgCuAl_2$-type structure (space group *Cmcm*), a ternary ordered version of the Re_3B type. Structural elements in these compounds are transition metal centered trigonal prisms made up of the rare earth and indium atoms. The transition metal (T) and indium atoms form a three-dimensionally infinite $[TIn_2]$ polyanionic network in which the large rare earth metal atoms occupy one-dimensional pentagonal tubes. A semiempirical band structure calculation on **1** reveals a non-vanishing density-of-states (DOS) at the Fermi level. The strongest bonding interactions are found for the In–In and Pd–In contacts; the Eu–Pd and Eu–In interactions are much weaker. Magnetic investigations indicate divalent character of the ytterbium atoms in **2**, showing negative susceptibilities below room temperature. Compound **1** exhibits Curie–Weiss behavior above 50 K with an experimental magnetic moment of 7.8(1) μ_B, thus indicating divalent europium. Ferromagnetic ordering was observed at T_C = 14.5(5) K, with a saturation moment of 6.8(1) μ_B/Eu at 5.5 T and 4 K, as determined from magnetization measurements. Compounds **1** and **2** are found to be metallic conductors.

Introduction

The ternary systems rare earth (RE)/transition metal (T)/indium have been extensively studied in the course of phase analytical investigations and crystal structure determinations.[1][2] The structures of a multitude of ternary compounds of this type are governed by two- or three-dimensionally infinite polyanions made up of the transition metal and indium atoms. The rare earth metal atoms, as the most electropositive component, are located within cavities or channels of the $[T_xIn_y]$ networks.

Investigations to date have mainly been focused on compounds with trivalent rare earth metal atoms, whereas relatively little information is available on compounds with alkaline earth metals, europium, or ytterbium as the electropositive component. A reason for this is most certainly the more complicated synthesis conditions required for the latter systems.

Most of the compounds $RE_xT_yIn_z$ with trivalent rare earth metals are easily accessible by means of arc-melting of the elemental components. However, due to the low boiling temperatures of the alkaline earth metals, europium, and ytterbium, such a synthetic approach employing arc-melting techniques would invariably result in large weight losses due to evaporation of these volatile metals. We have now succeeded in overcoming these experimental difficulties by modifying the synthesis conditions: (i) alkaline earth compounds such as CaAuIn[3] can be prepared in a quantitative manner by reacting the elements in glassy carbon crucibles in a novel, water-cooled sample chamber in a high-frequency furnace[3]; (ii) compounds with europium and ytterbium as the electropositive component are best prepared by high-frequency melting of the elements in sealed tantalum containers in a water-cooled quartz glass apparatus. The latter technique was first employed in syntheses of the stannides YbPtSn and $Yb_2Pt_3Sn_5$.[4] We have now extended these syntheses to indium compounds and have succeeded in preparing the new compounds $EuPdIn_2$, $YbPdIn_2$, and $YbAuIn_2$ reported herein. The present paper also deals with structure determinations and an analysis of the chemical bonding in these systems, as well as a detailed investigation of their physical properties.

Results and Discussion

Crystal Structures and Chemical Bonding of $EuPdIn_2$, $YbPdIn_2$, and $YbAuIn_2$

The new intermetallic compounds **1**, **2**, and **3** each adopt the $MgCuAl_2$-type structure,[5] a ternary ordered version of the Re_3B type.[6] As a representative example, a projection of the $EuPdIn_2$ structure is presented in Figure 1. From a geometrical point of view, the indium and europium atoms in **1** form slightly distorted trigonal prisms (every other prism is shifted by half the translation period *a*), and these prisms have palladium atoms at their centers.

The Pd−In distances (Table 1) of 277 and 284 pm in **1** agree well with the sum of Pauling single bond radii of 278 pm.[7] Similar distances have also been observed in the distorted tetrahedral [PdIn] polyanion in equiatomic EuPdIn (282 and 283 pm).[8] Due to the twofold higher indium con-

[a] Anorganisch-Chemisches Institut, Universität Münster, Wilhelm-Klemm-Straße 8, D-48149 Münster, Germany
E-mail: pottgen@uni-muenster.de

 © WILEY-VCH Verlag GmbH, D-69451 Weinheim, 1999 1434−1948/99/0606−0975 $ 17.50+.50/0

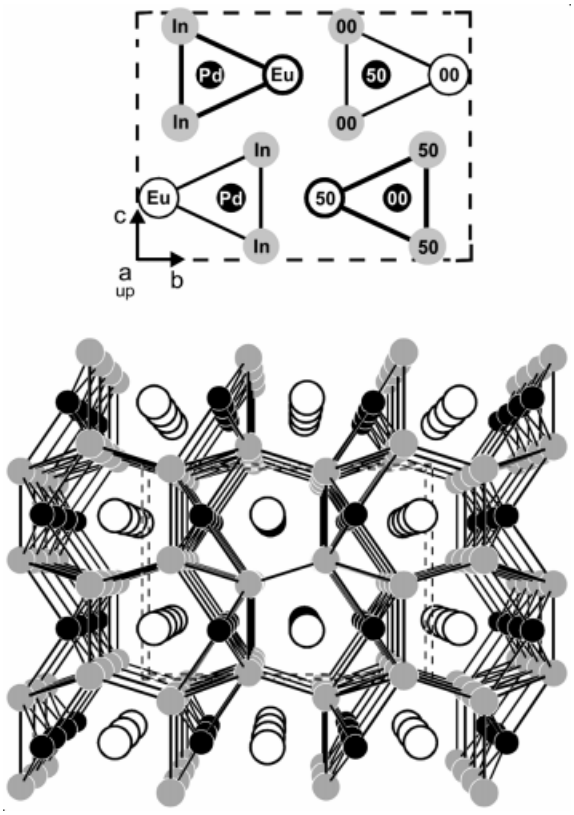


Figure 1. Projection (upper part) of the crystal structure of $EuPdIn_2$ onto the *yz* plane, emphasizing the topological arrangement of palladium-centered trigonal prisms made up of europium and indium atoms (black filled, open, and grey filled circles, respectively). The height of the atoms is given in the upper part in hundredths. In the lower part, a perspective view of the same orientation is depicted, showing an outline of the polyanionic network of palladium and indium atoms

tent, **1** has a higher degree of linkage of indium atoms, four contacts at 308 (1×) and 324 pm (3×), as compared to EuPdIn, which has one contact at 326 pm. The indium atoms together with the palladium atoms form a three-dimensionally infinite $[PdIn_2]$ polyanion, in which the europium atoms occupy distorted pentagonal channels as outlined in Figure 1. Nevertheless, there are still quite short Eu−Pd (297 and 323 pm) and Eu−In (341 pm) contacts, indicating a weak linkage of the europium atoms to the pentagonal channels. This rough assessment of the chemical bonding in **1**, made by considering only the interatomic distances, is nicely supported by the results of an extended Hückel calculation, which is discussed in detail below.

The density-of-states (DOS) for **1** is presented in Figure 2. In the DOS, the palladium contribution extends mainly from −10 eV to −8 eV, while the indium contributions extend over the whole valence region. The non-vanishing DOS at the Fermi level is in agreement with the metallic behavior discussed below. A Mulliken population analysis reveals the net charges Eu: +1.78, Pd: −1.16, In: −0.31, with the palladium atoms as the most electronegative component of **1**, in good agreement with Pearsons′ absolute electronegativities[9] of 4.45 and 3.10 eV for palladium and indium, respectively. Unfortunately, no value for the absolute electronegativity of europium is listed by Pearson.[9] Since europium exhibits chemical behavior similar to that of the alkaline earth metals calcium (χ = 2.2 eV) and strontium (χ = 2.0 eV), we assume a comparably low χ value for this rare earth element.

Table 1. Interatomic distances (pm) in the structures of $EuPdIn_2$, $YbPdIn_2$, and $YbAuIn_2$; all distances of the first coordination sphere are listed; standard deviations are all 0.2 pm or less

	$EuPdIn_2$			$YbPdIn_2$			$YbAuIn_2$		
Eu:	1	Pd	296.9	Yb:	1	Pd	292.8	Yb:	1	Au	308.5
	2	Pd	323.2		2	Pd	314.6		2	Au	323.6
	2	In	304.5		4	In	334.2		4	In	328.2
	4	In	341.2		2	In	336.0		2	In	345.7
	4	In	353.5		4	In	346.3		4	In	355.1
	2	Eu	414.9		2	Yb	413.2		2	Au	404.7
	2	Pd	425.0		2	Pd	420.1		2	Yb	411.2
	2	Eu	453.6		2	Yb	444.3		2	Yb	455.9
Pd:	2	In	277.4	Pd:	2	In	276.1	Au:	2	In	281.2
	4	In	283.7		4	In	280.5		4	In	285.0
	1	Eu	296.9		1	Yb	292.8		1	Yb	308.5
	2	Eu	323.2		2	Yb	314.6		2	Yb	323.6
	2	Eu	425.0		2	Yb	420.1		2	Yb	404.7
In:	1	Pd	277.4	In:	1	Pd	276.1	In:	1	Au	281.2
	2	Pd	283.7		2	Pd	280.5		2	Au	285.0
	1	In	307.7		1	In	307.0		1	In	300.7
	2	In	323.6		1	In	308.3		1	In	301.0
	1	In	323.9		2	In	322.6		2	Yb	328.2
	1	Eu	340.5		2	Yb	334.2		2	In	344.9
	2	Eu	341.2		1	Yb	336.0		1	Yb	345.7
	2	Eu	353.5		2	Yb	346.3		2	Yb	355.1

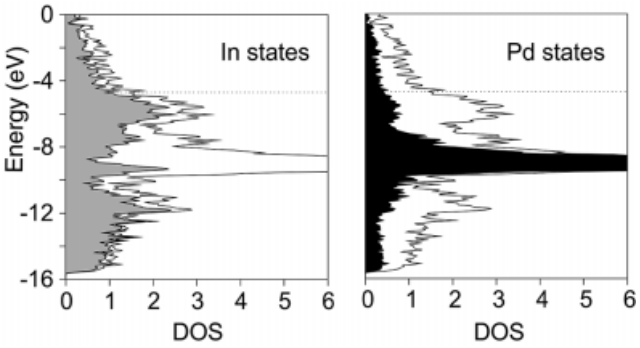


Figure 2. Density-of-states (DOS) for $EuPdIn_2$ with the indium and palladium contributions emphasized in grey and black, respectively; the Fermi level E_F is drawn as a dotted line

The In−In distances in **1** are all shorter than in the tetragonal body-centered structure of elemental indium (a = 325.2 pm, c = 494.7 pm[10]), where each indium atom has four nearest neighbors at 325.2 pm and eight further neighbors at 337.7 pm. The strong bonding character of the In−In contacts in **1** is reflected by the highest overlap population (OP) of +0.522 (Figure 3). The close Pd−In contacts (277−284 pm) also show a significant overlap population of +0.390.

In contrast, the Eu−Pd (OP +0.022) and Eu−In (OP +0.039) overlap populations are much smaller, in agreement with our description in terms of a polyanionic $[PdIn_2]$ network. Bonding between the palladium and indium atoms within the network is much stronger than the interactions of the europium atoms in the distorted pentagonal

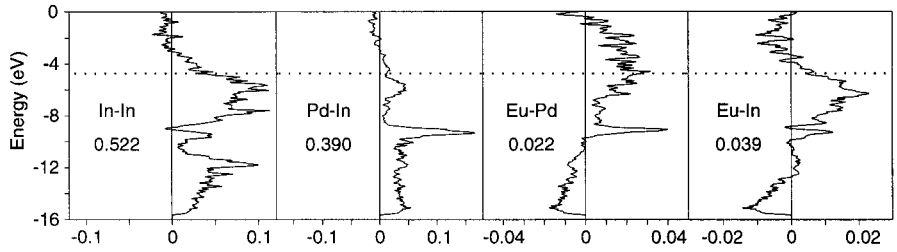


Figure 3. Chemical bonding from semiempirical crystal orbital overlap populations (COOP) for various bonding contributions in $EuPdIn_2$; the numbers represent the integrated values of the overlap population per bond, integrated up to the Fermi level (dotted line)

channels with the network. Chemical bonding in isotypic **2** and **3** is most likely analogous to that in **1**, with the palladium and gold atoms carrying most of the negative charge.

Magnetic Properties

The magnetic susceptibility of **2** as a function of temperature is plotted in Figure 4. Over the whole temperature range investigated the susceptibility of **2** is negative and has a value of $-6.2(2)\cdot10^{-9}$ m^3/mol at room temperature. At first sight, these findings appear to suggest diamagnetism. This, however, would seem to be at variance with the metallic behavior discussed below. In fact, the core diamagnetism of **2** dominates compared to the much weaker Pauli contribution of the conduction electrons, thus resulting in slightly negative susceptibilities. Similar magnetic behavior has recently been observed for the indium-rich binary compounds TIn_3 (T = Co, Ru, Rh, Ir)[11][12] and the isotypic calcium compounds $CaTIn_2$ (T = Pd, Pt, Au).[13] A reasonable correction for the core diamagnetism, however, is difficult to perform, since no reliable increments for ytterbium, palladium, and indium are available in the literature. Rough estimates for the diamagnetic contributions in TIn_3 (T = Co, Rh, Ir) and $CaAuIn_2$ are reported in ref.[12] and ref.[13]

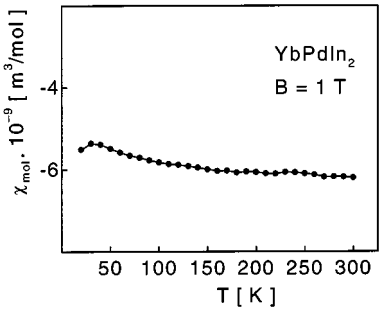


Figure 4. Temperature dependence of the magnetic susceptibility of **2**, measured at a magnetic flux density of 1 T

Compound **1** shows Curie−Weiss behavior above 50 K (Figure 5). An evaluation of the data above 50 K resulted in an experimental magnetic moment of 7.8(1) μ_B/Eu and a paramagnetic Curie temperature of $\theta = 22(1)$ K. Ferromagnetic ordering of the europium atoms was detected at low temperatures (Figure 6). The precise Curie temperature of $T_C = 14.5(5)$ K was determined from the derivative $d\chi/dT$ of a kink-point measurement (inset of Figure 6) at a magnetic flux density of 0.002 T. The derivative additionally revealed a further feature at 12.5(2) K, probably due to a very small impurity of EuPdIn,[8] which has a Néel temperature of 13.0 K.[8][14] Nevertheless, our Guinier powder pattern revealed a single-phase material. The magnetization curve at 50 K (Figure 7) was linear, as expected for a paramagnet. At 4 K, we observed a strong increase of the magnetization, even at very low field strengths. The magnetization curve tends to saturation at just 1 T and shows only a small hysteresis with negligible coercitivity and remanent magnetization. On the basis of these features, **1** can clearly be classified as a soft ferromagnet. At the highest obtainable magnetic field of 5.5 T, the saturation magnetization amounts to $\mu_{SM(exp)} = 6.8(1)$ μ_B/Eu, in good agreement with the maximum possible value of $\mu_{SM(calcd)} = 7.0$ μ_B/Eu, indicating an almost fully parallel spin alignment.

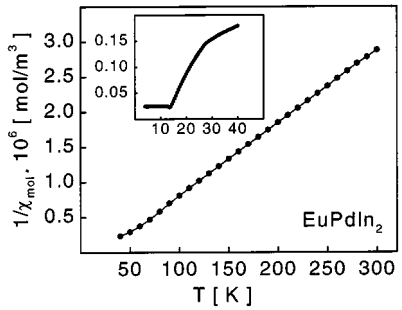


Figure 5. Temperature dependence of the reciprocal susceptibility of **1** determined at a magnetic flux density of 2 T; the low-temperature behaviour is shown in the inset

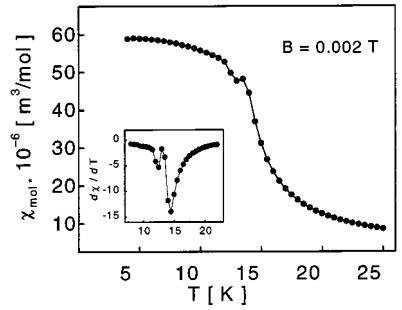


Figure 6. Low-temperature susceptibility (field-cooling mode) of **1** at 0.002 T (kink-point measurement). The inset shows the derivative $d\chi/dT$, which has a sharp peak at $T_C = 14.5(2)$ K. The second anomaly at 12.5(5) K is most likely due to a minor impurity of metamagnetic EuPdIn, which becomes magnetically ordered at 13.0 K[8][14]

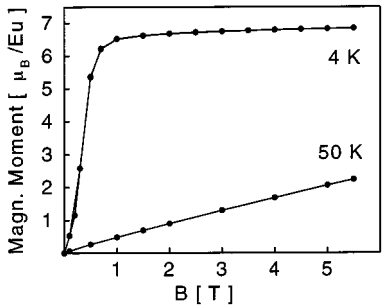


Figure 7. Magnetic moment vs. external magnetic flux density, B_{ext}, of **1** at 50 and 4 K

Electrical Conductivity

The temperature dependences of the specific resistivities of **1** and **2** are plotted in Figure 8. The specific resistivities of both compounds decrease with decreasing temperature, as is of course typical for metallic conduction. At room temperature, the values amount to 34 ± 5 μΩcm for **1** and 27 ± 5 μΩcm for **2**, indicating that both compounds are relatively good metallic conductors. The large margins of error account for the different values obtained with a series of samples. At about 4 K, the specific resistivities of **1** and **2** fall to 68% and 59% of their room temperature values, respectively. While no anomaly can be detected in the temperature dependence of ρ in the case of **2**, a very small drop is seen for **1** at the Curie temperature. This most likely results from a freezing of spin-disorder scattering below T_C.

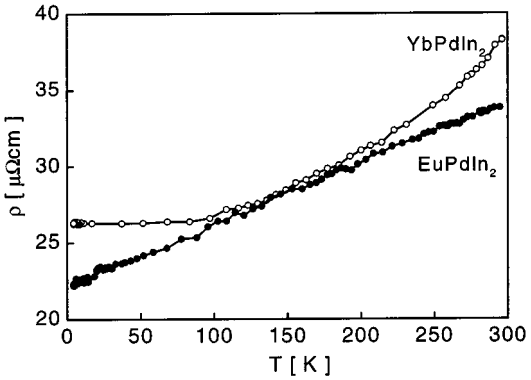


Figure 8. Temperature dependence of the specific resistivities of **1** and **2**

Experimental Section

Syntheses: Starting materials were europium ingots (Johnson Matthey), ytterbium rods (Kelpin), palladium powder (Degussa), gold wire (Degussa, ∅ 1 mm), and indium "teardrops" (Johnson Matthey), all with stated purities in excess of 99.9%. The moisture-sensitive ingots of europium and ytterbium were stored in vacuo prior to carrying out the reactions. The elemental components were mixed in the ideal 1:1:2 atomic ratio and sealed in tantalum tubes under an argon pressure of about 800 mbar. The argon was purified by passage over silica gel, molecular sieves, and titanium sponge (900 K). The tantalum tubes were then annealed in a novel, water-cooled sample chamber[4] in a high-frequency furnace (Kontron, Roto-Melt). In a first step, the tubes were heated with the maximum power output of the high-frequency generator. The occurrence of the strongly exothermic reactions was evident from a heat flash that lasted for about two seconds. The annealing temperature was then lowered to about 1000−1100 K for one minute and then raised to the maximum possible once more. Subsequently, the tubes were annealed for 30 min at about 800−900 K. The reactions resulted in polycrystalline products, which could easily be separated from the tantalum tubes. No tantalum contamination could be detected by EDX analyses. While **1** and **2** were obtained as single-phase products, **3** was accompanied by very small amounts of YbAuIn[15] (Fe_2P type) and elemental indium. Products **1**, **2**, and **3** are grey in compact form, while single crystals are silvery with a metallic lustre. Powders and compact pieces of these intermetallic compounds are stable in air; no deterioration was observed over a period of several weeks.

X-ray Investigations: Guinier powder patterns of all samples were recorded with Cu-$K_{\alpha 1}$ radiation using α-quartz (a = 491.30 pm, c = 540.46 pm) as an internal standard. The indexing of the patterns was facilitated by comparison of the observed patterns with calculated ones,[16] taking the atomic positions from the structure refinements. Single-crystal intensity data were collected at room temperature using a four-circle diffractometer (Enraf-Nonius, CAD4) with graphite-monochromated Mo-K_α radiation (λ = 71.073 pm) and a scintillation counter with pulse height discrimination. The scans were taken in the ω−2θ mode. Absorption corrections were applied on the basis of Ψ-scan data. Single crystals of **1**, **2**, and **3** were isolated from the samples by mechanical fragmentation. Buerger precession photographs of the three compounds (reciprocal layers *hk*0 and 0*kl*) showed C-centered orthorhombic lattices with symmetry *mmm*. The systematic extinctions (*hkl* only observed for $h + k = 2n$; 0*kl* only with $k = 2n$) led to the space groups *Cmcm* (No. 63) and $Cmc2_1$ (No. 36), of which the centrosymmetric group was found to be the correct one during the structure refinements. All relevant crystallographic data and experimental details are listed in Table 2.

The starting atomic parameters were obtained by direct methods using an automatic interpretation as implemented in SHELXS-86.[17] The structures were subsequently refined with anisotropic displacement parameters for all atoms using SHELXL-97 (full-matrix least-squares on F^2).[18] Final difference Fourier syntheses were flat and revealed no significant residual peaks. The results of the refinements are summarized in Table 2. Atomic coordinates and interatomic distances are listed in Tables 3 and 1, respectively. Further details of the crystal structure determinations may be obtained from the Fachinformationszentrum Karlsruhe, D-76344 Eggenstein-Leopoldshafen (Germany), by quoting the registry numbers CSD-410438 ($EuPdIn_2$), CSD-410437 ($YbPdIn_2$), and CSD-410436 ($YbAuIn_2$).

Electronic Structure Calculations: Semiempirical band structure calculations were based on an extended Hückel Hamiltonian,[19][20] where off-site Hamiltonian matrix elements were evaluated according to the weighted Wolfsberg−Helmholz formula,[21] minimizing counter-intuitive orbital mixing. The extended Hückel parameters used for the calculations were taken from refs.[22][23] (ξ orbital exponents in parentheses): Eu 6s −4.663 eV (1.345) and Eu 6p −3.403 eV (1.231); Pd 5s −9.224 eV (1.658), Pd 5p −3.279 eV (1.182), and Pd 4d −8.985 eV, ξ_1 = 3.746, c_1 = 0.815, ξ_2 = 1.501, c_2 = 0.338; In 5s −10.79 eV (2.02) and In 6p −5.35 eV (1.47). The eigenvalue problem was solved in reciprocal space at 144 k points within the irreducible wedge of the Brillouin zone by using the YAEHMOP code.[24]

Table 2. Crystal data, details of the data collections, and structure refinements of $EuPdIn_2$ (**1**), $YbPdIn_2$ (**2**), and $YbAuIn_2$ (**3**) (all with space group *Cmcm* and $Z = 4$)

Empirical formula	$EuPdIn_2$	$YbPdIn_2$	$YbAuIn_2$
Molar mass	488.0 g/mol	509.08 g/mol	599.65 g/mol
Lattice constants	$a = 453.6(1)$ pm	$a = 444.3(1)$ pm	$a = 455.9(2)$ pm
(Guinier data)	$b = 1054.3(3)$ pm	$b = 1031.2(2)$ pm	$b = 1076.4(3)$ pm
	$c = 785.3(2)$ pm	$c = 779.9(2)$ pm	$c = 755.2(2)$ pm
	$V = 0.3756(2)$ nm^3	$V = 0.3573(2)$ nm^3	$V = 0.3706(2)$ nm^3
Calculated density	8.63 g/cm^3	9.46 g/cm^3	10.75 g/cm^3
Crystal size	$25 \times 40 \times 50$ μm^3	$40 \times 40 \times 100$ μm^3	$5 \times 40 \times 80$ μm^3
Absorption correction	Ψ-scan, ellipsoidal	Ψ-scan, ellipsoidal	Ψ-scan, laminar (100)
Transmission ratio (max./min.)	1.40	1.56	6.56
Absorption coefficient	33.0 mm^{-1}	43.3 mm^{-1}	76.5 mm^{-1}
$F(000)$	828	856	988
θ range for data colln.	2° to 40°	2° to 36°	2° to 33°
Range in *hkl*	$0 < h < 8$, ±18, ±14	$0 < h < 7$, ±16, ±12	±6, ±16, $-2 < l < 11$
Total no. of reflns.	2502	1815	1626
Independent reflns.	673 ($R_{int} = 0.0326$)	492 ($R_{int} = 0.0574$)	382 ($R_{int} = 0.0316$)
Reflns. with $I > 2\sigma(I)$	602 ($R_{sigma} = 0.0216$)	441 ($R_{sigma} = 0.0361$)	365 ($R_{sigma} = 0.0193$)
Data/restraints/params.	673/0/16	492/0/16	382/0/16
Goodness-of-fit on F^2	1.123	1.177	1.132
Final R indices [$I > 2\sigma(I)$]	$R1 = 0.0197$	$R1 = 0.0200$	$R1 = 0.0412$
R indices (all data)	$R1 = 0.0255$, $wR2 = 0.0429$	$R1 = 0.0237$, $wR2 = 0.0469$	$R1 = 0.0428$, $wR2 = 0.1288$
Extinction coefficient	0.0022(1)	0.0138(4)	0.0036(7)
Largest diff. peak and hole	1.58 and −2.64 e/Å^3	2.38 and −2.14 e/Å^3	5.53 and −6.04 e/Å^3

Table 3. Atomic coordinates and isotropic displacement parameters (pm^2) for $EuPdIn_2$ (**1**), $YbPdIn_2$ (**2**), and $YbAuIn_2$ (**3**) (each of space group *Cmcm*; standard deviations are given in parentheses)

Atom	Wyckoff site	X	Y	Z	U_{eq}[a]
$EuPdIn_2$					
Eu	4*c*	0	0.06363(3)	1/4	111(1)
Pd	4*c*	0	0.78202(4)	1/4	100(1)
In	8*f*	0	0.35177(2)	0.05411(3)	101(1)
$YbPdIn_2$					
Yb	4*c*	0	0.06623(3)	1/4	116(1)
Pd	4*c*	0	0.78227(5)	1/4	100(1)
In	8*f*	0	0.35604(3)	0.05319(4)	100(1)
$YbAuIn_2$					
Yb	4*c*	0	0.07562(8)	1/4	121(4)
Au	4*c*	0	0.78901(8)	1/4	109(4)
In	8*f*	0	0.3648(1)	0.0509(1)	107(4)

[a] U_{eq} is defined as one-third of the trace of the orthogonalized U_{ij} tensor.

Physical Measurements

Magnetic Data: The magnetic susceptibilities of polycrystalline pieces of **1** and **2** were determined with an MPMS SQUID magnetometer (Quantum Design, Inc.) in the temperature range 4.2−300 K, with magnetic flux densities of up to 5.5 T.

Electrical Conductivity: The specific resistivities of **1** and **2** were measured on small irregular shaped blocks using a conventional four-probe technique over the temperature range 4.2−300 K. Cooling and heating curves were identical within the error limits and were reproducible for different samples.

Acknowledgments

We thank Prof. Wolfgang Jeitschko for his interest and support of this work. We are also indebted to Dipl.-Ing. Ute C. Rodewald for the single-crystal data collections, to Klaus Wagner for the EDX analyses, and to Dr. Wolfgang Gerhartz (Degussa AG) for generous gifts of palladium powder and gold wire. Ya. V. G. is indebted to the DAAD for a research stipend. This work was financially supported by the Deutsche Forschungsgemeinschaft (Po573/1-2) and the Fonds der Chemischen Industrie.

[1] *Pearson's Handbook of Crystallographic Data for Intermetallic Phases* (Eds.: P. Villars, L. D. Calvert), American Society for Metals, Materials Park, OH 44073, Second Edition, **1991**.
[2] Ya. M. Kalychak, *J. Alloys Compds.* **1997**, *262−263*, 341.
[3] D. Kußmann, R.-D. Hoffmann, R. Pöttgen, *Z. Anorg. Allg. Chem.* **1998**, 624, 1727.
[4] R. Pöttgen, A. Lang, R.-D. Hoffmann, R. Müllmann, B. D. Mosel, B. Künnen, G. Kotzyba, *Z. Kristallogr.* **1999**, *214*, 143.
[5] H. Perlitz, A. Westgren, *Ark. Kemi, Mineral. Geol.* **1943**, *16B*, 1.
[6] B. Aronsson, M. Bäckman, S. Rundqvist, *Acta Chem. Scand.* **1960**, *14*, 1001.
[7] L. Pauling, *The Nature of the Chemical Bond and the Structure of Molecules and Crystals*, Cornell University Press, **1960**.
[8] R. Pöttgen, *J. Mater. Chem.* **1996**, *6*, 63.
[9] R. G. Pearson, *Inorg. Chem.* **1988**, *27*, 734.
[10] J. Donohue, *The Structures of the Elements*, Wiley, New York, **1974**.
[11] R. Pöttgen, *J. Alloys Compds.* **1995**, *226*, 59.
[12] R. Pöttgen, R.-D. Hoffmann, G. Kotzyba, *Z. Anorg. Allg. Chem.* **1998**, *624*, 244.
[13] R.-D. Hoffmann, R. Pöttgen, G. A. Landrum, R. Dronskowski, B. Künnen, G. Kotzyba, *Z. Anorg. Allg. Chem.*, in press.
[14] T. Ito, S. Nishigori, I. Hirimitsu, M. Kurisu, *J. Magn. Magn. Mater.* **1998**, *177−181*, 1079.
[15] R. Pöttgen, J. Grin, *Z. Kristallogr.* **1997**, *Suppl. 12*, 136.
[16] K. Yvon, W. Jeitschko, E. Parthé, *J. Appl. Crystallogr.* **1977**, *10*, 73.
[17] G. M. Sheldrick, *SHELXS*-86, *Program for the Solution of Crystal Structures*, University of Göttingen, Germany, **1986**.
[18] G. M. Sheldrick, *SHELXL-97*, *Program for the Refinement of Crystal Structures*, University of Göttingen, Germany, **1997**.
[19] R. Hoffmann, *J. Chem. Phys.* **1963**, *39*, 1397.
[20] R. Hoffmann, *Solids and Surfaces: A Chemist's View of Bonding in Extended Structures*, VCH, Weinheim, New York, **1988**.
[21] J. H. Ammeter, H.-B. Bürgi, J. C. Thibeault, R. Hoffmann, *J. Am. Chem. Soc.* **1978**, *100*, 3686.
[22] J. P. Desclaux, *At. Data Nucl. Data Tables* **1973**, *12*, 311.
[23] P. Pyykkö, L. L. Lohr, Jr., *Inorg. Chem.* **1981**, *20*, 1950.
[24] G. A. Landrum, YAEHMOP (*Yet Another Extended Hückel Molecular Orbital Package*), Version 2.0, **1997**; available at: http://overlap.chem.cornell.edu:8080/yaehmop.html

Received November 16, 1998
[I98394]

A Molecular Mechanics Force Field for Alkylcobaloximes, a Model of Vitamin B_{12} Coenzyme – Implications of Steric and Electronic Factors in the Co–C Bond Cleavage

Silvano Geremia,[a] Mario Calligaris,[a] and Lucio Randaccio*[a]

Keywords: Cobaloximes / Vitamin B_{12} / Semiempirical calculations / Force field / Conformation analysis / Cone angles / Crystal structure

Molecular mechanics force field constants have been derived for alkylcobaloximes, (alkyl)Co(DH)$_2$L (DH = monoanion of dimethylglyoxime and L = planar N-donor ligand), implementing the AMBER force field. Atomic charges have been calculated by the semiempirical ZINDO/1 method. Stretching and bending constants have been calculated by the Badger and Halgren equations, with the introduction of simple functions for the description of the electronic influence of the axial ligands on the coordination geometry. 26 parameters have been optimized, by the Simplex method, to fit 4523 bond lengths and angles of 52 alkylcobaloxime accurate crystal structures. In spite of the oversimplification of the adopted method for the description of the electronic effects, this approach provides a good description of the metal coordination geometries. The root-mean-square deviations of the calculated bond lengths and angles from the experimental values average to 0.023 Å and 1.4°, respectively. The molecular mechanics results are discussed in terms of the steric properties of the axial ligands and correlated with their calculated cone angles. The force field has been used to analyse some conformational features of these compounds, such as the influence of the rotation of the axial ligands on their coordination geometry. The calculated energy for the Co–N rotational barrier agrees well with the experimetal ones derived from dynamic and saturation ^{1}H-NMR spectroscopy in (alkyl)Co(DH)$_2$(2-NH$_2$-py). In order to have more experimental data for this analysis, the crystal structures of two new cobaloximes, (CH$_2$Cl)Co(DH)$_2$L with L = py, **1**, and 1-Me-Im, **2**) have been determined. The results of a conformational analysis on ribosyl-imidazole derivatives, taken as a suitable vitamin B_{12} coenzyme model, suggest that the 1-Me-imidazole-like ligands have a significantly greater rotation freedom with respect to the benzimidazole-like ones, but cause similar stretchings of the Co–C bond, and a significantly less stretching of the Co–N one. Implications for the recent findings on the binding mode of the coenzyme B_{12} in the enzyme active site are discussed.

Introduction

For many years, simple organometallic octahedral Co^{III} complexes have been proposed as vitamin B_{12} coenzyme models and a great amount of work on these systems has been performed in solution and in the solid state. Such extensive studies have provided a foundation for understanding the behaviour of the more complex vitamin B_{12} system.[1] The structurally accurate characterization of numerous complexes, RCo(chel)L, with several alkyl groups, R, and neutral Lewis bases, L, with chel = (DH)$_2$ (cobaloximes), (DO)(DOH)pn (Costa model), salen, saloph,[2] has supplied an enormous amount of data,[1b,1c,3] which has allowed in-depth analysis of the variations in geometry of the R−Co−L fragment, on the basis of the electronic and steric properties of the R and L groups[4] as well as rationalization of the relationships between solution behaviour and structure.[4−6]

It was deduced that, irrespective of the identity of the L and chel ligands (including corrin), the influence of R on the geometry of the R−Co−L fragment is evidenced by a lengthening of the Co−L bond by up to 0.15 Å as the σ-donating ability of R increases (electronic *trans* influence) and by a lengthening of the Co−C bond by up to 0.20 Å as the bulk (steric *cis* influence) and the σ-donating ability of R increase.[4b] Recently, a statistical analysis,[4b] based on the Principal Component Analysis (PCA), of the variation with R of several experimental properties of alkylcobaloximes has suggested that the geometry of the axial fragment may be described fairly well by introducing three parameters, t_1, t_2, and t_3. Parameters t_1 and t_2 reflect the electronic and steric properties of R, respectively, whereas t_3 is related to the Co−CH$_2$−X angular deformation. It was found that the Co−C distances are a linear combination of the three parameters, whereas the axial Co−N distance is a linear function of only t_1.[4b]

The influence of the bulk of L on the Co−L (steric *cis* influence) and on the Co−C (steric *trans* influence) distances has been structurally detected,[7] the latter being particularly pronounced when R has a large bulk.[8] Analogously, the Co−C bond dissociation energies (BDE) decrease with the increase in bulk of the phosphane in the two series RCo(DH)$_2$PR$_3$ when R = CH(Me)Ph and CH$_2$Ph.[9] Structural evidence of the electronic influence of L on the Co−C bond is not so apparent.[10] On the other hand, Halpern has found that the Co−C BDE increases with the increase of the p*K*a of 4-substituted pyridines in the series

[a] Dipartimento di Scienze Chimiche, Università di Trieste, I-34127 Trieste, Italy

Supporting information for this article is available on the WWW under http://www.wiley-vch.de/home/eurjic or from the author.

 © WILEY-VCH Verlag GmbH, D-69451 Weinheim, 1999 1434−1948/99/0606−0981 $ 17.50+.50/0

[CH(Me)Ph]Co(DH)$_2$(4-X-py).[11] However, a large deviation from the BDE trend was detected when L = 2-NH$_2$-py,[12a] due to the steric interaction of 2-NH$_2$-py with the equatorial moiety, which induces a lengthening of the axial Co−N bond by about 0.1 Å with respect to the analogous py derivative.[12b] The Co−L bond is significantly influenced by the nature of chel (*cis* influence), while the Co−C bond is essentially unaffected,[1c] although, very recently, it has been reported that the Co−C bonds in (DO)(DOH)pn complexes are slightly longer (0.01−0.03 Å) than in cobaloximes.[6] Finally, it has been observed that the geometry of the Co(DH)$_2$ moiety is not affected by the nature of the axial ligands.[1b,1c]

All these studies have given qualitative evidence of many properties of the Co coordination sphere in cobaloximes, which in many respects parallel those apparent in the vitamin B$_{12}$ system.[1][13] Thus, as illustrated above, many chemical properties of cobaloximes and cobalamins, which are related to the metal coordination, involve steric influences. The first step in the catalytic cycle of the B$_{12}$-dependent isomerases is believed to be the homolytic cleavage of the Co−C bond and steric effects, acting in several ways, have been suggested to be responsible of the Co−C bond labilization.[13][14] The task of quantifying steric interactions is not a simple one, although arguments invoking steric effects are intuitively appealing. Questions such as this should, in principle, be amenable to investigation by molecular mechanics (MM) methods, which have been proved to be a useful approach to investigate the structure and reactivity of coordination compounds.[15−17] The combined application of X-ray crystallography and MM methods to the study of structural and conformational properties of metallo-organic systems represents a useful approach, and development and parametrization of suitable force fields are receiving increasing attention.[18−21] Many reports which give force fields for Co^{III} compounds with N-donor ligands are available.[16] However, only recently have force field parameters for cobalamins been proposed, based on the structures of six derivatives,[19a] and for cobaloximes, on the basis of a large number of structures.[19b] The last force field parameters for the Co−C bond and the Co−C−C angle have been transferred to the cobalamins, showing that the previously reached conclusions[19a] remained essentially unchanged.[19b] However, all these force fields, which we can call "conventional", do not take into account the influence of electronic effects (e.g. *trans* influence) on the molecular geometry. An attempt to face this problem has been proposed by Rappé et al.,[19c] with the introduction of empirical fractional bond orders, in their Universal Force Field (UFF). However, this correction is introduced a posteriori to improve the agreement between the calculated and the experimental distances. This approach does not allow reproduction of the observed continuous variation of the axial bond lengths when the bulk and the σ-donating ability of the axial ligands are varied, as it occurs in RCo(DH)$_2$L.[22][23]

Recently, a new method for the optimization of force-field parameters, fitting experimental bond lengths and angles, and using empirical functions for the calculation of stretching and bending constants, has been described.[24] The present paper describes the derivation of force-field parameters for alkylcobaloximes, applying the above method, implemented with the introduction of a specific function, based on a fundamental parameter, which is assumed to take into account a priori the influence of the electronic factors on the coordination bond lengths and angles. Such an "unconventional" force field should permit the quantification of the intramolecular steric interactions contributing to the conformational properties. This should also allow a clear distinction of the origin (steric or electronic) of the observed structural deformations induced by the change of the axial ligands, such as the axial bond elongation, the orientation of the axial ligands with respect to the equatorial one and deformations in the equatorial moiety. In fact, there are many questions still open which are directly linked with the problem of the Co−C labilization.

The force-field parameters have been optimized to reproduce the X-ray structures of the 52 alkylcobaloximes, containing planar N-donor ligands, listed in Table 1. These include two new cobaloximes, (CH$_2$Cl)Co(DH)$_2$L, with L = py (**1**) and 1-MeIm (**2**), whose crystal structure have been determined in order to obtain further experimental data useful for the study of the influence of the orientation of L upon the Co−C and Co−N bond lengths. Finally, the biochemical implications of the MM calculations in the vitamin B$_{12}$ coenzyme model are discussed.

Results and Discussion

Methods

The AMBER force field[25] has been selected, in view of its successful application to other coordination compounds,[17][24] and the possibility of extension to the vitamin B$_{12}$ system. As known, in AMBER, the molecular strain energy, E, is given by the sum of deformation terms for bond lengths (d), bond angles (θ), and dihedral angles (ψ) (including improper torsion angles which model out-of-plane displacements), together with the van der Waals and electrostatic contributions:

$$E = \Sigma_b k^d(d - d^\circ)^2 + \Sigma_a k^\theta(\theta - \theta^\circ)^2 + \Sigma_d\{V_n/2[1 + \cos(n\psi - \psi_o)]\} + \Sigma_{ij}(a_{ij}/r_{ij}^{12} - b_{ij}/r_{ij}^{6} + q_iq_j/Dr_{ij})$$

with $a_{ij} = (\varepsilon_i\varepsilon_j)^{1/2}\ (r_i^* + r_j^*)^{12}$ and $b_{ij} = 2(\varepsilon_i\varepsilon_j)^{1/2}(r_i^* + r_j^*)^6$, where r^* and ε are the van der Waals radii and the energy well depth, respectively, for two atoms of the same type, q is the atomic charge and D the dielectric constant.

Although the oxime bridge hydrogen atoms are found either symmetrically positioned between the oxygen atoms or bonded to one oxygen atom, we have assumed that the bridge hydrogen atoms are fixed to lie on the median of the O···O segment (Figure 1). The H atom is bonded to both O atoms in order to avoid large tetrahedral distortions of

Table 1. The axial ligands of the 52 $RCo(DH)_2L$ complexes, whose structural data[a] were used in the FF minimization; the solidus separates the two axial ligands R and L[b]

1. adamantyl/1-Me-Im	27. $NC(CH_2)_2$/3-Et-py	14. $NC(CH_2)_3$/1,2-Me_2-Im	40. $ClCH_2$/1-Me-Im
2. adamantyl/1,5,6-Me_3-Bzm	28. $NC(CH_2)_2$/3-Me-py	15. Me/1,2-Me_2-Im	41. $ClCH_2$/py
3. adamantyl/4-Me_2N-py	29. $NC(CH_2)_2$/3-NC-py	16. Me/1-Me-Im	42. $(NCCH_2)(NC)CH$/1,5,6-Me_3-Bzm
4. *c*-C_6H_{11}/1,5,6-Me_3-Bzm	30. $PhCH_2$/py	17. Me/Im	43. F_3CCH_2/4-NC-py
5. *i*Pr/1,2-Me_2-Im	31. $(EtO_2C)_2(Me)CCH_2$/py	18. Me/1,5,6-Me_3-Bzm	44. Cl(NC)CH/py
6. *i*Pr/1,5,6-Me_3-Bzm	32. NC(Me)CH/4-Me-py	19. Me/py	45. Cl_2CH/1,5,6-Me_3-Bzm
7. *i*Pr/py	33. NC(Me)CH/py	20. Me/6-Cl-purine	46. Cl_2CH/py
8. *i*Pr/2-NH_2-py	34. NC(Me)CH/4-NC-py	21. $NC(CH_2)_2$/4-NH_2-py	47. O_2NCH_2/1,2-Me_2-Im
9. $(Me_3C)_3CH_2$/py	35. $(MeO_2C)(Me)CH$/py	22. $NC(CH_2)_2$/1-Me-Im	48. O_2NCH_2/1,5,6-Me_3-Bzm
10. Et/4-[(MeO)C=NH]-py	36. $(MeO_2C)(Me)CH$/4-Cl-py	23. $NC(CH_2)_2$/4-Et-py	49. O_2NCH_2/py
11. Et/1,5,6-Me_3-Bzm	37. $(MeO_2C)(Me)CH$/4-NC-py	24. $NC(CH_2)_2$/4-Me-py	50. F_3C/py
12. Et/py	38. $NCCH_2$/1,2-Me_2-Im	25. $NC(CH_2)_2$/py	51. $Cl_2(NC)C$/1,2-Me_2-Im
13. ribosyl[c]/py	39. $NCCH_2$/py	26. $NC(CH_2)_2$/3-NH_2-py	52. $(F_3C)_3CF$/py

[a] Structural data are taken from the Cambridge Structural Data Files, except those of 40 (**1**) and 41 (**2**) reported in the present work. – [b] Im = imidazole, Bzm = benzimidazole. – [c] ribosyl = 5-deoxy-β-D-ribofuranos-5-yl.

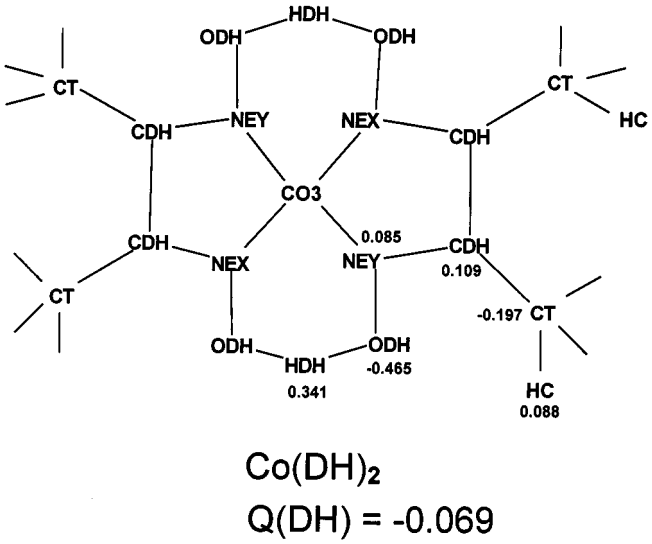


Figure 1. Atom types and charges for the equatorial $Co(DH)_2$ moiety

the equatorial moiety. Atom types are given in Figures 1 and the Supporting Information.

Energy calculations have been performed with a Pentium-200 PC, using the HYPERCHEM 4.5 molecular modeling package.[26] The Polak–Ribiere version of the conjugate gradient method was used in all energy minimizations, until the convergence criterion of 0.001 kcal mol^{-1} $Å^{-1}$ was reached.

As previously reported,[24] the potential constants for all $i-j$ bonds were calculated from Badger's rule,[27] $k^d_{ij} = [(A_{ij} - D_{ij})/(d^\circ_{ij} - D_{ij})]^3$, using the parameters proposed by Herschbach and Laurie;[28] while potential constants for the $i-j-k$ bond angles were calculated from the Halgren's equation:[29] $k^\theta_{ijk} = 1.75\ Z_iC_jZ_k\ (d_{ij} + d_{ik})^{-1}\ (\theta^\circ_{ijk})^{-2}$ $\exp[-2(d_{ij} - d_{jk})^2/(d_{ij} + d_{ik})^2]$. This approach allows automatic variation of the stretching and bending constants as a function of the reference bond lengths (d°_{ij}) and angles (θ°_{ijk}). For cobalt, two different C values (*cis* and *trans* bonds) and one Z value were assumed. Force-field constants, reported in Table 2, were optimized by an iterative procedure, in which the sum of the squares of the differences (Δ) between observed and calculated values were reduced upon variation of the parameters.[30] The observables are the bond lengths and angles of 52 accurate (crystallographic R index < 0.08) crystal structures of alkylcobaloximes (Table 1). Weights were assigned to the experimental data on the basis of the average estimated errors, $w = 1/\sigma^2$. Since several of the starting structures were taken from CSD (version 1997), where individual errors for bond lengths and angles are not reported, these were evaluated for each structure from the average differences among chemically equivalent parameters of the $Co(DH)_2$ moiety, $\bar{\sigma}$. In order to take into account the different accuracy in the atom location, related to the different electron density, the $\bar{\sigma}$ values were weighted on the basis of the atomic numbers Z, according to the equation $\sigma_w = [\Sigma(\bar{\sigma} \cdot Z \cdot n)]/\Sigma n$, where Z is the sum of atomic numbers of the atoms involved in the bond length or angle and n is the number of chemically equivalent parameters. In this calculation summations were extended over the different types of bond lengths or bond angles. The two σ_w values, for distances and angles, respectively, were used to calculate individual estimated errors as $\sigma = \sigma_w/Z$. The σ values obtained by this procedure well agree with the available experimental values, therefore providing a useful way to evaluate σ values for CSD data.

As for the previously reported Ru–sulfoxide complexes,[24] the optimization procedure was performed by adopting the Simplex method, in view of the non-linear nature of the equations and the facility of introducing restraints in the minimization.[31] Convergence was controlled by a goodness-of-fit (GOF) parameter defined as $[\Sigma w\Delta^2/(n_{obs} - n_p)]^{1/2}$, where n_{obs} = number of observables and n_p = number of parameters. Convergence was reached when the absolute relative difference between the lowest and the highest GOF values was less than 0.0001. During the preliminary refinement a marked discrepancy between the observed and calculated axial Co–N distance was found for the 2-NH_2-py derivative, together with relatively high differences between the axial Co–N–C bond angles. Change of the aminic group hydrogen atom type from H to H1 yielded a remarkable improvement, so that H1 was taken as the atom type for hydrogen atoms attached to nitrogen atoms. Torsional barriers around C–C and C–N bonds were calcu-

Table 2. Optimized force field constants (a [Å], b [Å/e], C, Z, ε [kcal mol^{-1}], r^* [Å], d° [Å], θ° [°], D), and related stretching and bending constants (k^d [kcal mol^{-1} Å^{-2}], k^θ [kcal mol^{-1} rad^{-2}])

a_{Co-C}		1.959
b_{Co-C}		0.17
a_{Co-N}		1.997
b_{Co-N}		0.30
C_{CO3}[a]		0.52
C_{CO3}[b]		3.23
Z_{CO3}		1.15
ε_{CO3}		0.502
r^*_{CO3}		1.691
D		7.8
Stretching constants	k[d]	d°
CO3−NER[c]	94.9	1.997
CDH−CDH	325.1	1.424
CDH−NER[c]	607.5	1.284
ODH−NER[c]	457.3	1.344
ODH−HDH	198.9	1.269
Bending constants	k^θ	θ°
CO3−NER−ODH[c]	61.6	123.8
CO3−NER−CDH[c]	48.5	124.6
CDH−CDH−NER[c]	76.4	117.8
CT−CDH−NER[c]	70.8	120.2
CO3−NAZ−C[d]	50.6	122.0
CO3−CAZ−F	61.4	110.6
CO3−CAZ−C[e]	55.4	111.7
CO3−CAZ−CL	60.4	111.6
CO3−CAZ−N	63.7	108.3
CL−CAZ−CL	74.3	110.1
F−CAZ−F	97.8	102.9

[a] For θ° = 90°. − [b] For θ° = 180°. − [c] R = X, Y. − [d] C = CA, CK, CQ; k^θ = 50.4 for CB and 50.5 for CW. − [e] C = C, CT; k^θ = 55.5 for CA and 55.7 for C1.

lated as in AMBER.[25] Barriers around coordination bonds were not considered.[32]

The observed bond lengths and, particularly, the coordination bond angles can be slightly modified by packing effects, which can force the molecule into a strained conformation. In order to simulate crystal packing effects, the torsional angles around single bonds and involving non-H atoms were constrained by a 16 kcal mol^{-1} energy barrier in the energy minimization to maintain the crystal structure conformation.

For the electrostatic contribution, atomic charges were calculated by the semi-empirical ZINDO/1 method, included in HYPERCHEM 4.5.[26] Charges of chemically equivalent atoms were averaged over the same ligands. The cobalt atom charges assured the electroneutrality of the complexes. Atom types and charges for the $Co(DH)_2$ moiety are shown in Figure 1, while for the R and L groups they are given in the Supporting Information, together with total charges, Q. The *vacuum* value (D = 1) was initially assumed for the dielectric constant. However, this value was refined since the inclusion of the dielectric constant in the optimization process ensures the proper scaling of the electrostatic contribution. The final value of 7.8 is consistent with the fact that we are considering solid-state and not gas-phase structures.

Since the Co−C and Co−N axial bonds are significantly influenced by the electronic nature of R,[1][4] the force-field parameter optimization procedure was carried out in two steps. In the first step, electronic effects were neglected, therby producing approximate parameters for the functions involving the equatorial ligand atoms, together with "average" d° values for the axial Co−C and Co−N bonds. At convergence (d°_{Co-C} = 1.964, d°_{Co-N} = 2.007 Å), the goodness of fit was quite reasonable: GOF = 3.48 for 4523 observables and 24 variables. However, as expected, the differences between observed and calculated Co−C and Co−N axial distances were rather high (see Table 3). In fact, in this step (constant d° values for Co−C and Co−N distances) the calculated axial distances can only reflect the steric contribution and not the electronic one. Thus, the differences (δ) between the calculated and observed axial distances should be related to the σ-donating ability of the R group. As a measure of the latter, the total electrostatic charge of R, Q, was taken. The validity of this choice is supported by the fairly good linear relationship (r = 0.91, n = 21) between Q and the available values of EP, which have previously been shown to provide an experimental measure of the electron-donating ability of R.[4a] In fact, the δ values for the Co−C and Co−N distances correlate well with Q, the correlation coefficients being 0.83 and 0.94, respectively.

Table 3. Average differences, <Δ>, between observed and calculated bond lengths [Å] and angles [°], together with rms values and number of observations, n, after the first and second step of the force field parameter optimization process; X, Y, Z represent generic non-metal atoms

Distances	n	first step <Δ>	rms	second step <Δ>	rms
Co−N equatorial	208	0.004	0.010	0.004	0.009
Co−N axial	52	−0.014	0.028	0.008	0.016
Co−C axial	52	−0.016	0.032	−0.003	0.020
X−Y equatorial	728	−0.009	0.017	−0.008	0.017
X−Y axial	592	−0.016	0.031	−0.016	0.031
All distances	1632	−0.010	0.024	−0.009	0.023
Angles					
Co−N−X equatorial	416	−0.1	0.6	−0.1	0.6
Co−C(N)−X axial	177	0.1	1.8	−0.1	1.8
X−Co−Y	780	−0.2	1.4	−0.2	1.3
All angles	2891	−0.1	1.4	−0.1	1.4

In order to take into account the different electronic effect of the R groups on the Co−C and Co−N axial distances,[1][4] in the second optimization step, the d° values of the Co−C and Co−N bonds were assumed to be a linear function of Q, according to Equations 1 and 2.

$$d^\circ_{Co-C} = a_{Co-C} + b_{Co-C}Q \quad (1)$$

$$d^\circ_{Co-N} = a_{Co-N} + b_{Co-N}Q \quad (2)$$

The coefficients of Equations 1 and 2 were optimized, together with all the other force-field parameters. At convergence, the GOF value reduced to 3.30 for n_{obs} = 4523 and n_p = 26.

Final values of the refined parameters are reported in Table 2, together with the calculated stretching and bending

constants. All force-field constants are reported in the Supporting Information.

The potential energy for the isolated molecules ($D = 7.8$) were explored using local Excel© Macro functions, which allow the minimization of the strain energy as the conformation of the molecule is varied through rotation around the axial Co−N bond, ψ. The torsional angle was varied in 5° steps from −180° to 180°, introducing a constraint of 1000 kcal mol^{-1}. The zero value of ψ was taken at the point where the plane of L bisects the oxime bridge. The minimum energy conformer was finally minimized using a convergence gradient of 0.001 kcal mol^{-1} $Å^{-1}$.

Cone angles for the axial ligands were calculated according to the Immirzi′s algorithm,[33] as modified in ref.[21], using the atom coordinates of the 52 energy minimized structures. The van der Waals radii used for the ligand atoms were those given by Bondi,[34] assigning a zero value to the metal-coordinated atoms. The solid cone angle Ω and the corresponding Tolman′s angle Θ were calculated at distances corresponding to the Co−C and Co−N d° values of Equations 1 and 2 and averaged for each axial ligand. The Ω and Θ values are given in Table 4 together with the d°(R) and d°(L) values.

X-ray Diffraction Analysis of Compounds 1 and 2

The ORTEP drawings with the atom numbering scheme for **1** and **2** are given in Figures 2 and 3, respectively. The schemes apply to both the crystallographically independent molecules A and B. The molecules A and B of **1** are very similar, while in **2** they display different orientations of both the axial groups with respect to the equatorial ligand, which cause a slight, but significant, difference in the Co−N axial distance and in the Co−C−Cl bond angles. In **1** the torsional angles around the Co−N(py) bond (ψ) and the Co−C bond (φ) are 4° and 74° in A, and 3° and 72° in B, respectively. On the other hand, in **2** the corresponding angles are 49° and −47° in A, and 38° and −105° in B.

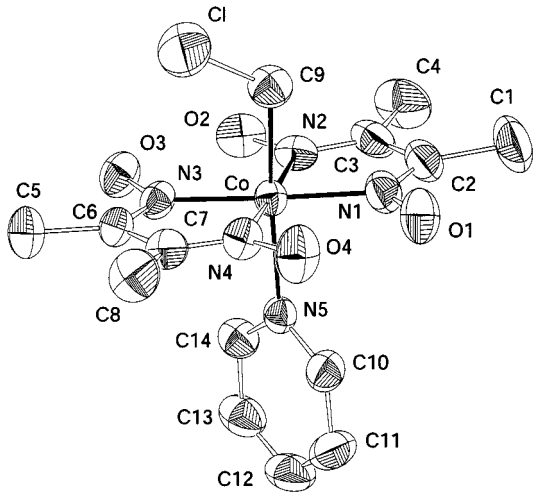


Figure 2. ORTEP drawing (50% thermal ellipsoids) of **1** together with he atom numbering scheme

It is of interest to compare the 1-Me-Im orientation in A and B with those found in other derivatives with R = Me, CH_2CH_2CN, and adamantyl. In the last derivative, the 1-Me-Im plane nearly bisects the oxime bridge ($\psi \approx 0°$), whereas in the others it approximately crosses the equatorial five-membered rings ($\psi \approx 90°$).[1c] This comparison indicates that there is significant conformational freedom for rotation around the Co−N(1-Me-Im) bond when R has a relatively small bulk. Conversely, the rotation is hindered in the case of very bulky R groups such as adamantyl, which imposes the bending of the equatorial moiety towards the *trans* N ligand and, consequently, forces the latter into the orientation with $\psi \approx 0°$. Such confor-

Table 4. d°(R) [Å], d°(L) [Å], Ω [ster rad] and Θ [°] values for R and L ligands

R	d°(R)	d°(L)	Ω	Θ	L	Ω	Θ
Me	1.960	1.999	1.85	90.3	Im	1.99	93.9
CH_2Cl	1.943	1.969	2.18	98.4	1-Me-Im	1.99	93.9
$NCCH_2$	1.944	1.970	2.21	99.2	py	2.24	100.0
Et	1.966	2.010	2.29	101.0	1,5,6-Me_3-Bzm	2.28	100.8
$NC(CH_2)_3$	1.961	2.001	2.30	101.3	1,2-Me_2Im	2.40	103.8
F_3C	1.924	1.936	2.33	102.0	6-Cl-purine	2.68	110.0
O_2NCH_2	1.925	1.937	2.38	103.3	2-NH_2-py	2.87	114.2
$NC(CH_2)_2$	1.958	1.996	2.41	103.8			
Cl_2CH	1.927	1.940	2.52	106.5			
F_3CCH_2	1.938	1.960	2.53	106.7			
Cl(NC)CH	1.931	1.948	2.55	107.1			
$PhCH_2$	1.957	1.993	2.61	108.4			
NC(Me)CH	1.951	1.984	2.66	109.6			
$(NCCH_2)(NC)CH$	1.942	1.967	2.67	109.9			
ribosyl	1.963	2.003	2.69	110.3			
*i*Pr	1.971	2.017	2.75	111.5			
c-C_6H_{11}	1.972	2.020	2.79	112.4			
$(MeO_2C)(Me)CH$	1.947	1.975	2.88	114.3			
$Cl_2(NC)C$	1.911	1.913	2.90	114.8			
$(Me_3C)_3CH_2$	1.968	2.013	3.00	116.9			
$(EtO_2C)_2(Me)CCH_2$	1.956	1.991	3.31	123.4			
adamantyl	1.975	2.026	3.32	123.7			
$(F_3C)_3CF$	1.906	1.903	3.49	127.2			

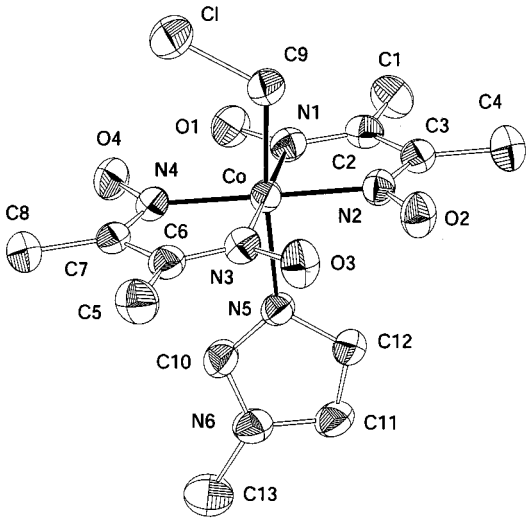


Figure 3. ORTEP drawing (50% thermal ellipsoids) of **2** together with he atom numbering scheme

mational freedom is typical of Im and 1-Me-Im ligands, since in all the structurally characterized alkylcobaloximes containing planar N ligands − such as 1,5,6-Me_3-Bzm, 1,2-Me_2-Im and py − only the orientation with $\psi \approx 0°$ is found, regardless of the bulk of the R group.[1c]

Validation of the Force Field

The consistency of the force field can be evaluated from the average values of the differences (<Δ>) between observed and calculated bond lengths and angles and their root-mean-square deviations, rms = $[(\Sigma\Delta^2)/n]^{1/2}$. Deviation from zero of the average values gives a measure of the asymmetry of the Δ distribution or indicates the presence of systematic errors, while rms gives a measure of the spread of the Δ values and hence of the fit between calculated and experimental structures. The agreement between observed and calculated values appears to be quite satisfactory, especially after the second optimization step, as shown in Table 3. Inspection of Table 3 reveals a marked reduction of both the <Δ> and rms values after the second parameter optimization step only for the axial Co−C and Co−N distances, while for the other bond lengths and angles no significant improvement in <Δ> and rms values is apparent. In fact, only the axial distances are strongly affected by electronic factors, which are not taken into account in the model used in the first step. This improvement supports the assumption that the electronic factors, introduced in the second optimization step, are related to the overall charge Q of the alkyl group according to Equations 1 and 2. The axial Co−C and Co−N distances are fairly well reproduced, as shown in Figure 4, where the observed values are plotted against those calculated for the 52 cobaloximes.

In order to evidence the improvement on the axial distances derived from the introduction of the electronic factor, the experimental values are compared in Table 5 with those calculated after the first and the second step, for the

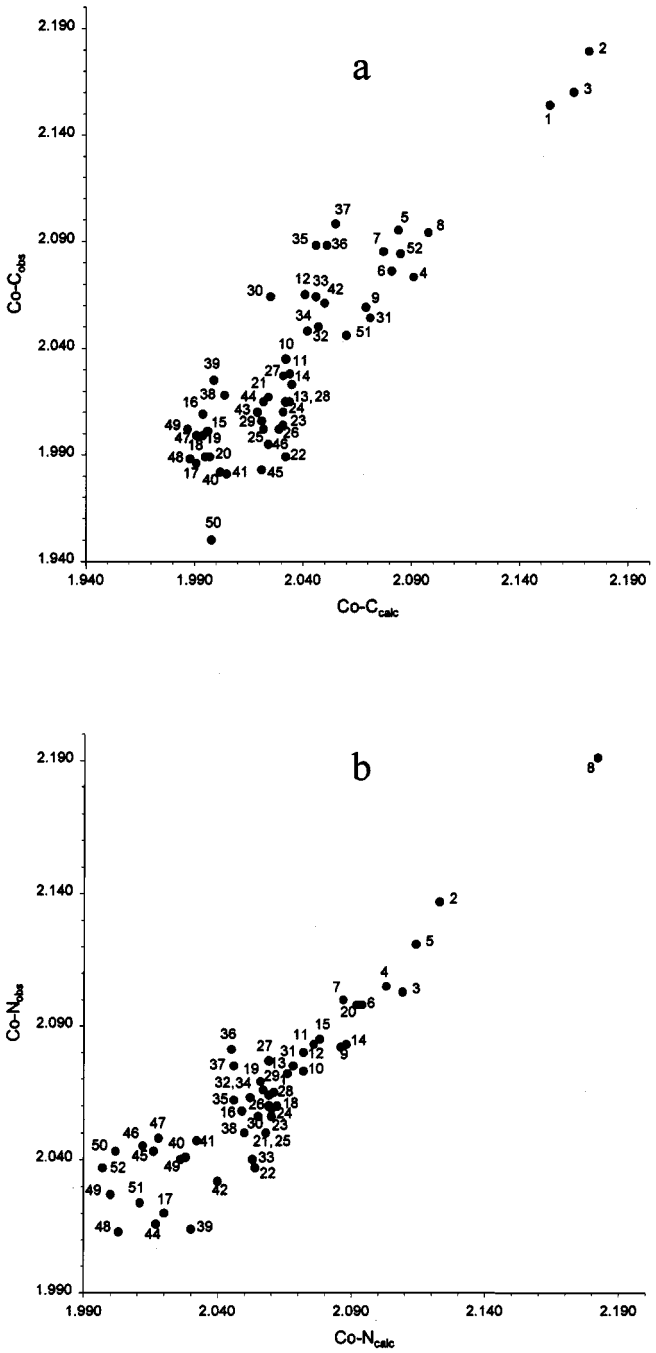


Figure 4. Plot of the observed vs. calculated Co−C (a) and Co−N (b) axial distances

series $RCo(DH)_2$(1,2-Me_2Im), having R with significantly different bulk and σ-donating ability and a relatively bulky N-donor ligand. It is also apparent that the introduction of the electronic factor well reproduces the shortening of both the Co−C and Co−N bonds when R is an electron-withdrawing group such as CCl_2CN, in agreement with the PCA results.[4b]

The geometry of the Co−R grouping is characterized by experimental Co−C(sp^3)−X angles which span a rather wide range, from 113.7° to 130.3°, and increase with the increasing of the bulk of X. This variation is well repro-

Table 5. Observed and calculated Co−C and Co−N bond lengths [Å] for $RCo(DH)_2(1,2\text{-}Me_2Im)$, after the first and second step of the present force field parameter optimization process

R		obs	step 2	step 1
CCl_2CN	Co−C	2.046	2.060	2.115
	Co−N	2.024	2.011	2.108
CH_2NO_2	Co−C	1.999	1.991	2.030
	Co−N	2.048	2.018	2.090
CH_2CN	Co−C	2.018	2.004	2.031
	Co−N	2.050	2.050	2.090
CH_2CH_2CN	Co−C	2.023	2.035	2.038
	Co−N	2.083	2.088	2.094
Me	Co−C	2.001	1.996	1.999
	Co−N	2.085	2.078	2.086
*i*Pr	Co−C	2.095	2.084	2.079
	Co−N	2.121	2.114	2.103

duced by the present force field, with just a few exceptions (see below). However, the differences between observed and calculated values appear quite acceptable if we consider that experimental values may be affected by several errors. For example, diffraction data quality (crystal quality), thermal motion effects or local static disorder, and residual packing and electronic effects.[25] In fact, for only two out of the nine $(NCCH_2CH_2)Co(DH)_2L$ derivatives considered are large differences between the observed and calculated Co−C−C angle detected when L = py[4a] (6.5°) and 1-MeIm[35] (11.2°), whereas for the other derivatives the differences do not exceed 1.9°. The two structures were accurately refined to $R = 0.042$,[4a,35] but inspection of atomic parameters shows that the thermal B factors of the C-β atom in both cases are anomalously high (by about a factor of three) relative to those of the other atoms, indicating a significant statistical occupancy disorder of that atom. Finally, the largest disagreement in the axial bond lengths is observed in the complexes containing COOMe and halogens bonded to the C-α atom (Figure 4).

Besides the general agreement between the observed and calculated structures, the validity of the present force field is further illustrated by its ability to reproduce the angular deformations around the metal center (Table 3), even using the same unstrained values of 90° or 180° for metal coordination angles. In particular, the experimental values for the equatorial N−Co−N angles average to 98.7° on the side of the oxime bridge and to 81.3° on the other side. The calculated values average to 98.5° and 81.5°, respectively. Furthermore, the remarkable angular deformations of the two Co−N(sp^2)−C angles for the coordinated lopsided ligands 1,5,6-Me_3-Bzm, 1,2-Me_2-Im, 2-NH_2-py, and 6-Cl-purine are very well reproduced, even using the same unstrained value for all the Co−N−C angles (122.0°). In fact, in these derivatives, the experimental values of the two angles differ significantly, with average values of 133.5/120.7°, 133.4/121.6°, 129.7/115.6°, and 125.9/120.6°, respectively, whereas the corresponding calculated values are 132.9/121.8°, 131.5/122.8°, 125.5/117.2°, and 125.2/120.2°.

Finally, it is of interest to compare the results of this force field for $(CN)(CH_2CN)CHCo(DH)_2$(1,5,6-Me_3Bzm) with those obtained by UFF[19c] for the same structure (Table 6). The Δ differences between observed and calculated values are similar for the Co−C distance, while the Co−N bond length, which undergoes a strong *trans* influence, is much better reproduced by the present force field.

Table 6. Differences, Δ [Å], between observed and calculated Co−C, Co−N(ax), and Co−N(eq) bond lengths for $(EtO_2C)_2$-(Me)$CCH_2Co(DH)_2$(py), obtained after the first and second step of the present force field parameter optimization process and after UFF calculations

Δ	step 1	step 2	UFF
Co−C	−0.027	−0.017	−0.023
Co−N(ax)	0.009	0.006	0.047[a]
Co−N(eq)	0.002	0.006	−0.043

[a] Assumed bond order, 1/2.

Cone Angles

According to the proposed model, the difference, δ, between the observed Co−L and Co−R axial distances and the corresponding $d°$(Co−R) and $d°$(Co−L) values should give the lengthening due to steric effects. Therefore, the δ values were expected to correlate with the bulkiness of the axial ligands, as measured by their cone angles. In fact, as shown in Figure 5, fairly good linear relationships are found, supporting the hypothesis that the steric and electronic contribution to the bond length can be considered approximately additive.

Conformational Analysis

For $MeCo(DH)_2L$ derivatives (L = Im, py, 1,5,6-Me_3-Bzm, 1,2-Me_2-Im, 6-Cl-purine, and 2-NH_2-py) the variation of the strain energy with ψ, scaled to its minimum value, is shown in Figure 6a in the range from −180° to +180°. All the curves have similar shapes with the lowest minimum at ψ = 0° and a rather broad, but structured, higher energy region around ψ = 90° ± 32°, which is particularly apparent for lopsided ligands. The latter region is characterized by two maxima and one minimum in between, with small energy differences (< 1.5 kcal mol^{-1}), for all the ligands, except 2-NH_2-py, where three maxima and two minima are observed (Figure 6a). However, the rotational energy barrier, E_{rot}, significantly increases from L = Im ($E_{rot} \approx 2$ kcal mol^{-1}), to L = py, 1,2-Im, 1,5,6-Me_3-Bzm ($E_{rot} \approx 4$ kcal mol^{-1}) up to L = 2-NH_2-py ($E_{rot} \approx 10$ kcal mol^{-1}). The variation in the axial Co−N distance with ψ, given in Figure 6b, follows a similar trend, showing that the shortest distances occur at ψ = 0° and the longest ones around ψ = 90°, for all the L ligands, with differences, Δd, which increase from L = Im ($\Delta d = 0.02$ Å), to L = 2-NH_2-py ($\Delta d = 0.05$ Å).

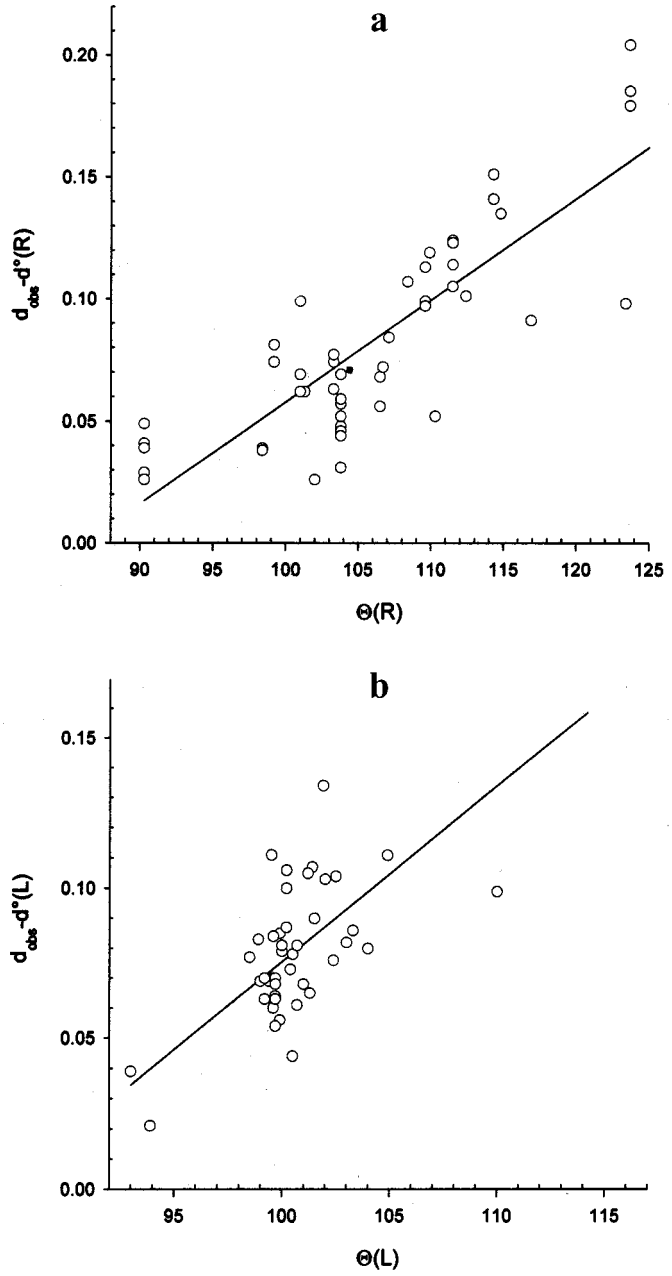


Figure 5. Plot of the differences $d(\text{obs})_{\text{Co-R}} - d°(\text{R})$ (a) and $d(\text{obs})_{\text{Co-L}} - d°(\text{L})$ (b) vs. Tolman's cone angles Θ(R) and Θ(L), respectively

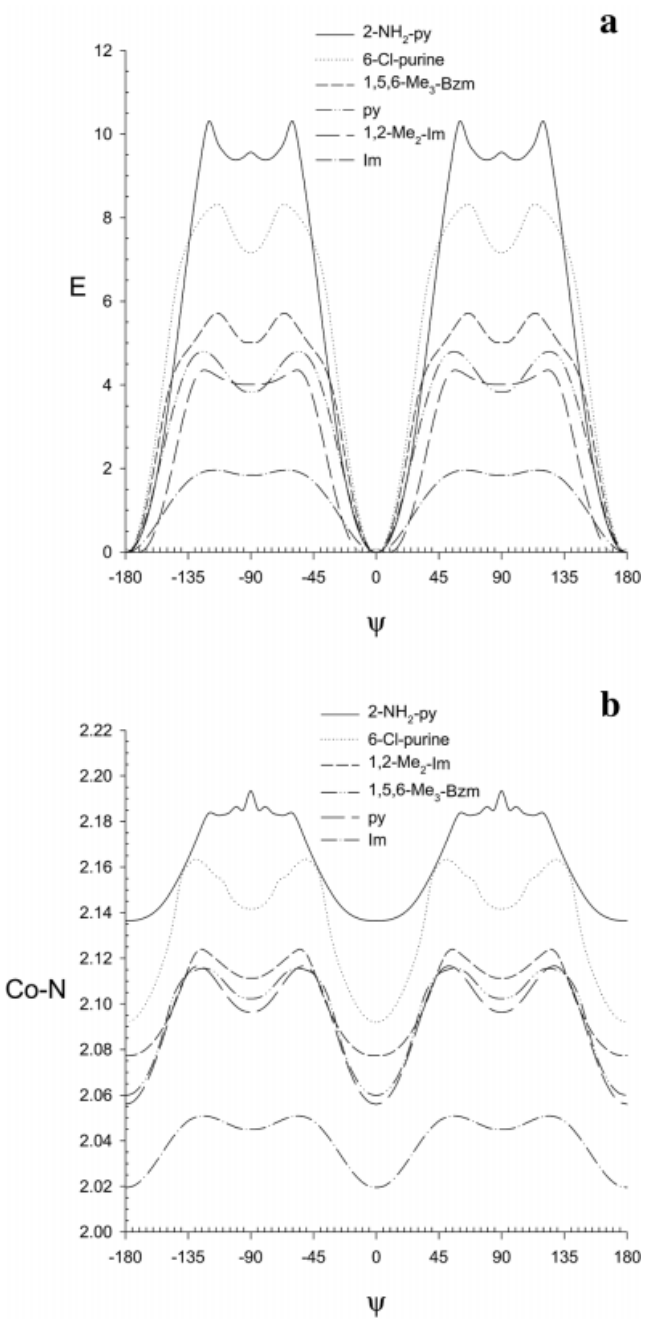


Figure 6. Plot of the strain energy (a) and of the Co−N axial distance (b) vs. ψ for different L ligands

Axial Co−N Distances

The fairly linear trend between the $d°$(Co−N) values and the experimental axial distances in complexes with the same L ligand suggests that these distances are essentially influenced by the σ-donating ability of the R groups. However, the present calculations indicate that the bulk (Figure 5b) and the orientation (Figure 6b) of the planar L ligand influence the axial Co−L bond length, as previously suggested.[1b] Since in the present model the electronic influence of R on the Co−L distance is taken into account by $d°$(Co−L), the difference between the experimental values and $d°$, δ(Co−L) = d(Co−L) − $d°$(Co−L), should represent the contribution to the distance ascribable to the bulk and orientation effects. Within this assumption, δ(Co−L) should correlate with the calculated cone angles of the L ligands, Θ(L), having the same orientation. In fact, a good correlation is found, as shown in Figure 5b for all the cobaloximes in which the L orientation nearly corresponds to $\psi \approx 0°$, i.e. in all the examined cobaloximes, with the exclusion of most of those having L = 1-Me-Im or Im. The vertical spread in Figure 5b could be related to the steric *trans* influence on the Co−L bond due to the R groups, which are able to induce an appreciable bending of the equatorial moiety towards L, displacing the latter and

lengthening the *trans* Co−L bond.[7] Thus, when L = 1,5,6-Me_3-Bzm, δ(Co−N) is 0.061 Å for R = Me and 0.111 Å for R = adamantyl, and the bending angles between the two DH units are 4.7° and −6.1°, respectively (the negative sign indicates bending towards L). The energy profiles, reported in Figure 6a for the different L ligands, clearly show that the rotation around the Co−N axial bond is significantly less hindered when L = Im, where the rotational barrier is about 2 kcal mol^{-1}, while this increases to 4 and 10 kcal mol^{-1} going from py to 2-NH_2-py. This is the reason why only for cobaloximes containing the Im (or 1-Me-Im) ligand are different orientations of L observed in the crystal, as evidenced above in the section Description and Discussion of the Structures. In fact, in $RCo(DH)_2$(1-Me-Im), ψ = 66° when R = Me, ψ = 67° when R = CH_2CH_2CN, and ψ = 38 and 49° when R = CH_2Cl. It is very likely that in these structures crystal forces are strong enough to stabilize different orientations, overwhelming the rotation energy barriers. Conversely, with the other L ligands having higher torsional barriers only the orientation with ψ ≈ 0° is found in the solid state.[1b] Inspection of Figure 6b, in which the trend of the Co−N distance vs. ψ is shown, indicates also that the lengthening of the latter distance increases significantly for the same non-zero ψ value in the order Im ≈ 1-Me-Im < py ≈ 1,5,6-Me_3Bzm ≈ 1,2-Me-Im < 6-Cl-purine < 2-NH_2-py. Finally, it is worthwhile noting that for L = 2-NH_2-py, the barrier height between ψ = 0° and ψ = 90° is about 10 kcal mol^{-1}, a value very close to the activation energies (9.2−13.1 kcal mol^{-1}) for rotation about the axial Co−N bond as derived from dynamic and saturation ^{1}H-NMR spectroscopy for the $RCo(DH)_2$(2-NH_2-py) complexes [R = *i*Pr, Et, neopentyl, CH_2Br, $CH_2C(Me)(CO_2Et)_2$, CH_2CN, and CH_2NO_2].[36] The two limit orientations, ψ = 0° and ψ = 90°, are generally distinguished as A and B, respectively.[1c,6,23] These observations lead to the suggestion that the L orientation is principally determined by steric factors (crystal packing forces in 1-Me-Im derivatives, and intramolecular forces in the other L-containing derivatives) more than to electronic ones.[1c,3a,36]

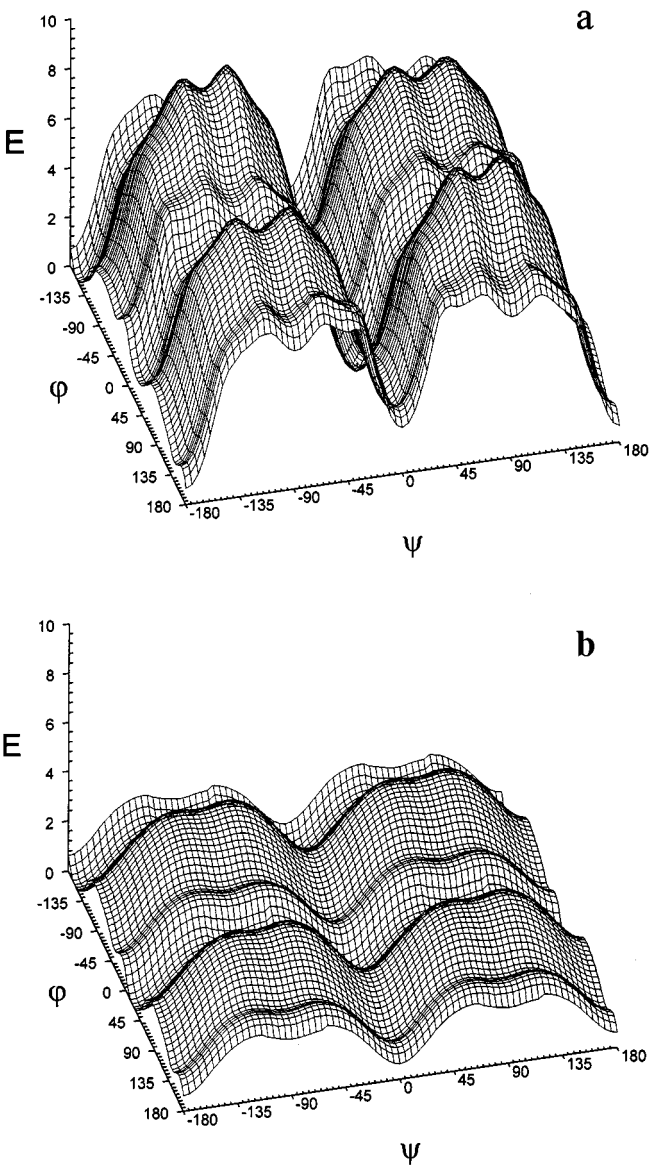


Figure 7. Plot of the strain energy vs. ψ for (ribosyl)$Co(DH)_2$(1,5,6-Me_3-Bzm) (a) and (ribosyl)$Co(DH)_2$(Im) (b)

Axial Co−C Distances

Unlike the Co−N distances, the experimental Co−C distances do not correlate with the $d°$(Co−C) values and, therefore, are significantly influenced by both the bulk (steric *cis* influence) and the σ-donating ability (electronic *trans* influence) of the R groups.[7] Therefore, the difference, δ(Co−R) between the experimental Co−R distances and $d°$(Co−R), is a measure of the contribution of the steric strain to the distance due to the bulk of R, and should correlate with the calculated cone angles of R, Θ(R). In fact, a good linear relationship is shown in Figure 5a. However, the vertical spread suggests some influence of the bulk of the *trans* N ligand on the Co−R bond, particularly when R is a bulky ligand, although some other secondary effects influencing the Co−C distance should be taken into account particularly for lopsided R ligands (vide infra). Thus, the calculated Co−adamantyl distances are 2.161 (exp. 2.154) Å and 2.182 (exp. 2.179) Å when L is 1-Me-Im and 1,3,5-Me_3-Bzm, respectively. A more enhanced effect (steric *trans* influence) was observed in adamantylcobaloximes for larger variations in the bulk of L.[8] In fact, Co−adamantyl distances of 2.129(3) and 2.217(7) Å were found when L = H_2O and PPh_2Et, respectively, whereas for the Me analogues the Co−Me distances were 1.990(5) and 2.026(6) Å, respectively. These results agree with the previous PCA analysis, where the Co−C distances are a linear combination of the three parameters, t_1, t_2, and t_3, whereas the axial Co−N distance is a linear function of only t_1.[4b] However, since the t_3 parameter is not easily functionalized, it has not been included in the force field and so the Co−C distance cannot be reproduced well as the Co−N one (Table 3).

Biological Implication

The recent X-ray crystal structure determination of the coenzyme B_{12} dependent methylmalonyl-CoA mutase[37] has promoted several studies about the benzimidazole base-off, protein histidine base-on forms of adenosylcobalamin (adoCbl).[38] In order to make a contribution to the investigation of the role of the cobalt-bound axial bases, we have carried out a conformational analysis on (ribosyl)-$Co(DH)_2L$ complexes with ribosyl = 5-deoxy-β-D-ribofuranos-5-yl and L = 1,5,6-Me_3-Bzm and Im, which are assumed to be acceptable models for the adenosyl base-on benzimidazole and adenosyl base-on histidine species. This allows the study of the geometrical variations induced in the axial fragment upon rotation around the Co−N(ψ) and Co−C(φ) bonds. The three-dimensional plot of the strain energy as a function of ψ and φ for L = 1,5,6-Me_3-Bzm is given in Figure 7a. As expected, it is characterized by steep high potential barriers (ca. 10 kcal mol^{-1}) at $\psi \approx 90°$ and 270°, over the minima at $\psi \approx 0°$ and 180°, indicating that the benzimidazole base is restricted by intramolecular forces to an orientation nearly bisecting the oxime bridges. The energy variation with φ is smoother, with a barrier of about 2−3 kcal mol^{-1}. The corresponding plot for L = Im is given in Figure 7b. It is similar to that of Figure 7a, but characterized by significantly lower energy barriers, in spite of the axial Co−N distances, which are on average shorter than those in the benzimidazole case (Table 7). The geometrical parameters of the N−Co−CH_2X fragment, at the highest and lowest energies, are compared in Table 7. This comparison indicates that the conformational strain causes a similar lengthening of the Co−C bonds in the two compounds, but a more marked increase of the Co−N bond length in the benzimidazole derivative. This situation should be even more enhanced when the equatorial ligand is corrin, whose "sentinel" side groups hinder more strongly the rotation around the Co−N axial bond. Thus, it can be concluded that histidine-like bases can rotate about the Co−N bond much more freely than benzimidazole-like ligands, but still significantly stretch the axial Co−N and Co−C bonds. This leads to the suggestion that histidine-like bases can bind to Co more easily than benzimidazole at ψ values which would require axial bond stretchings (vide infra), possibly because of geometrical protein−coenzyme binding demands. These stretchings would contribute both electronically[1a,39] and sterically[1b,1c] to enhance the Co−C homolysis, specially after the entrance of the substrate in the active site. It is kown that the enhancement of the homolysis rate of about 13 orders of magnitude for adoCbl in the enzyme with respect to the free coenzyme is for 5−6 orders of magnitude attributed to the substrate entrance in the active site.[40] Inspection of the structural results in the methylmalonyl-coenzymeA mutase[37] reveals that in addition to the long Co−N(histidine) bond of 2.50 Å, the angles Co−N−C are 130° and 116°. Although of low accuracy, these data indicate that the protein conformation requirements impose on the "symmetric" histidine imidazole an asymmetric coordination to Co (as in lopsided ligands) with a lengthening of the Co−N bond. The possible consequences upon the Co−C bond stability may be derived from earlier structural and BDE results, obtained for cobaloximes. In fact, comparison of the structures of *i*PrCo$(DH)_2$Py and *i*PrCo$(DH)_2$(2-NH_2-py) reveals an abnormally long axial bond of 2.194(4) Å in the latter compared with that of 2.094(2) Å for the py analogue, associated with a strong asymmetry in the Co−N−C angles, which are 115.7(3) and 129.7(4)° (on the side of NH_2).[12b] These angles are essentially equal and close to 120° in the py derivative. However, only a slight increase of 0.01 Å is observed in the Co−*i*Pr distance in the 2-NH_2-py complex. Correspondingly, Halpern et al.[12a] have found that the homolytic Co−C BDE in [Ph(Me)CH]Co$(DH)_2$L is of 17 and 20 kcalmol^{-1} for L = 2-NH_2-py and py, respectively. An opposite trend should be expected from the lower p*K*a of the latter ligand (5.2 vs 6.7). If these findings in models, possibly more enhanced, apply to the coenzyme in the active site, it may be concluded that histidine-like ligands are, both sterically and electronically, more suitable than benzimidazole-like ones to respond to the changes induced on the Co coordination geometry favouring homolysis. The fact that substitution of benzimidazole by imidazole gives more thermal Co−C bond heterolysis in cobinamides[38], a cobalamin-like system, does not contrast with such a hypothesis, since the steric requirements for hystidine-like ligands, due to the binding to the protein, are not fulfilled in the free cobinamide. In fact, The two Co−N−C angles are essentially equal to 127° in Co-β-cyanoimidazolylcobamide, but, as well known, they are significantly different in CNCbl (123.3° and 133.0°).[41] On the other hand, FT Raman spectroscopy measurements in methylcorrinoids[42] showed that the Co−Me stretching frequency (about 505 cm^{-1}) was only minimally affected by replacement of the benzymidazole by the imidazole moiety. However, these results are obtaind in the isolated cobalamin, in which the imidazole is symmetrically coordinated, in contrast to the asymmetric coordination of the hystidine within the enzyme.[37]

Table 7. Coordination bond lengths [Å] and angles [°] for the minimum and maximum energy conformers, of (ribosyl)$Co(DH)_2$L, with L = Im (ΔE = 4.1 kcal mol^{-1}) and 1,5,6-Me_3-Bzm (ΔE = 9.4 kcal mol^{-1})

	L = Im	L = 1,5,6-Me_3-Bzm		
	minimum	maximum	minimum	maximum
Co−N	2.026	2.061	2.068	2.130
Co−C	2.024	2.046	2.031	2.061
Co−C−C	116.5	119.4	116.4	121.1
Co−N−C	127.3	126.9	123.3	121.1
	126.7	127.9	131.0	134.2
N−Co−C	178.1	178.0	179.3	176.4

Conclusion

To our knowledge, this work represents the first example of derivation of a self-consistent force field for organomet-

Table 8. Crystal data and structure refinement for **1** and **2**

	1	**2**
Empirical formula	$C_{14}H_{21}ClCoN_5O_4$	$C_{13}H_{22}ClCoN_6O_4$
Formula weight	417.74	420.74
Temperature [K]	293(2)	293(2)
Wavelength [Å]	0.71073	0.71073
Crystal system	triclinic	triclinic
Space group	$P-1$	$P-1$
a [Å]	10.569(5)	8.840(1)
b [Å]	13.114(9)	14.629(2)
c [Å]	15.032(7)	14.865(2)
α [°]	108.34(3)	75.04(1)
β [°]	108.01(2)	83.14(1)
γ [°]	96.23(3)	76.58(1)
V [Å^3]	1831(4)	1802.9(5)
Z	4	4
Density (calcd.) [Mg/m^3]	1.516	1.550
Absorption coeff. [mm^{-1}]	1.11	1.13
F(000)	864	872
Crystal size [mm]	0.2 × 0.3 × 0.3	0.2 × 0.5 × 0.6
θ range for data collection [°]	2 to 28	2 to 26
Index ranges, h k l	−13/13, −17/16, 0/18	−10/10, −17/18, 0/18
Reflections collected	9074	7338
Independent reflections $I > 3\sigma(I)$	4187	4811
R(int)	0.021	0.018
Data/parameters	4187/452	4811/452
Goodness-of-fit on F^2	1.52	1.11
R [$I > 3\sigma(I)$]	0.047	0.034
wR [$I > 3\sigma(I)$]	0.048	0.035
Extinction coeff.	–	$2 \cdot 10^{-7}$
Largest diff. peak [eÅ^{-3}]	0.59 and −0.35	0.20 and −0.13

allic complexes which takes into account, in a simple but general way, the electronic *trans* influence.

The present results show that, even if the correlation between the electronic and steric properties of the axial ligands[4b,43] is neglected, the metal coordination geometry in cobaloximes is well reproduced. The force field could be also applied to the more complex cobalamins, as well as to other vitamin B_{12} coenzyme models, when MM calculations are used to gain insight into the factors affecting the Co−C cleavage. The present calculations suggest that a change from conformation A to B, stretches essentially the Co−N bond. Since the lengthening of this bond decreases the BDE of the *trans* Co−C bond[12a] it can be inferred that the Co−C bond is weaker in conformation B. This is supported by near-IR FT-Raman measurements which indicate that in methyl derivatives of similar vitamin B_{12} models, the Co−Me stretching frequencies (504−506 cm^{-1}) are higher by about 6 cm^{-1} in complexes having an orientation close to A.[44]

Finally, the conformational analysis, based on the proposed force field, allows the rationalization of the different structural behaviour of the imidazole- and benzimidazole-like ligands in cobaloximes.

Experimental Section

X-ray Diffraction: Compound **1**: $C_{14}H_{21}ClCoN_5O_4$, M = 417.74, triclinic, space group $P\bar{1}$, a = 10.569(5) Å, b = 13.114(9) Å, c = 15.032(7) Å, α = 108.34(3)°, β = 108.01(2)°, γ = 96.23(3)°, V = 1831(4) Å^3, Z = 4, D_c = 1.516 g/cm^3, μ(Mo-K_α) = 1.11 mm^{-1}, final R, wR, and S are 0.047, 0.048, and 1.52 for 452 parameters and 4187 unique observed reflections with $I > 3\sigma(I)$. − Compound **2**: $C_{13}H_{22}ClCoN_6O_4$, M = 420.74, triclinic, space group $P\bar{1}$, a = 8.840(1) Å, b = 14.629(2) Å, c = 14.865(2) Å, α = 75.04(1)°, β = 83.14(1)°, γ = 76.58(1)°, V = 1802.9(5) Å^3, Z = 4, D_c = 1.550 g/cm^3, μ(Mo-K_α) = 1.13 mm^{-1}, final R, wR, and S are 0.034, 0.035, and 1.11 for 452 parameters and 4811 unique observed reflections with $I > 3\sigma(I)$. Data were collected at 293 K using an Enraf Nonius CAD4 single-crystal diffractometer with the Mo-K_α radiation (λ = 0.71073 Å). The structures were solved by the heavy-atom method. Refinement was carried out by full-matrix least squares of F^2 using the Molen package. Crystallographic data (excluding structure factors) reported in this paper have been deposited at the Cambridge Crystallographic Data Centre and allocated the deposition numbers CCDC-109437 and -109438. Copies of the data can be obtained free of charge on application to CCDC, 12 Union Road, Cambridge CB2 1IZ (Fax: + 44-1223/336-033; E-mail: deposit@ccdc.cam.ac.uk).

Acknowledgments

This work has been supported by the Ministero della Ricerca Scientifica e Tecnologica (Rome) and by the Consiglio Nazionale delle Ricerche (Rome).

[1] [1a] J. Halpern, *Science* **1985**, *227*, 869−875. − [1b] N. Bresciani-Pahor, M. Forcolin, L. G. Marzilli, L. Randaccio, M. F. Summers, J. P. Toscano, *Coord. Chem. Rev.* **1985**, *63*, 1−125. − [1c] L. Randaccio, N. Bresciani-Pahor, E. Zangrando, L. G. Marzilli, *Chem. Soc. Rev.* **1989**, *18*, 225−250.

[2] DH = monoanion of dimethylglyoxime, (DO)(DOH)pn = N^2,$N^{2\prime}$-propanedyilbis(2,3-butanedione 2-imine 3-oxime), salen = dianion of N,N'-disalicylidene−ethylendiamine, saloph = dianion of N,N'-disalicylidene−o-phenylenediamine

[3] [3a] N. Bresciani-Pahor, L. Randaccio, E. Zangrando, *Inorg. Chim. Acta* **1990**, *168*, 115−121; P. J. Toscano, H. Brand, S.

Geremia, L. Randaccio, E. Zangrando, *Organometallics* **1991**, *10*, 713−720 and references therein; C. Tavagnacco, G. Balducci, G. Costa, K. Taschler, W. von Philipsborn, *Helv.Chim. Acta* **1990**, *73*, 1469−1479; A. Sekine, Y. Ohashi, *Bull. Chem. Soc. Jpn.* **1991**, *64*, 2183−2187. − [3b] A. Gerli, M. Sabat, L. G. Marzilli, *J. Am. Chem. Soc*. **1992**, *114*, 6711−6718; L. G. Marzilli, A. Gerli, A. M. Calafat, *Inorg. Chem*. **1992**, *31*, 4617−4627; J. P. Charland, E. Zangrando, N. Bresciani-Pahor, L. Randaccio, L. G. Marzilli, *Inorg. Chem*. **1993**, *32*, 4256−4267; R. Dreos, G. Tauzher, S. Vuano, F. Asaro, G. Pellizer, G. Nardin, L. Randaccio, S. Geremia, *J. Organomet. Chem*. **1995**, *505*, 135−138; R. Dreos, G. Tauzher, D. H. Trendafilova, G. Nardin, L. Randaccio, *Inorg. Chem*. **1996**, *35*, 2715−2716; S. M. Polson, L. Hansen, L. G. Marzilli, *Inorg. Chem*. **1997**, *36*, 307−313; S. Geremia, L. Randaccio, E. Zangrando, *Gazz. Chim. Ital*. **1992**, *122*, 229−232.

[4] [4a] E. Zangrando, N. Bresciani-Pahor, L. Randaccio, J. P. Charland, L. G. Marzilli, *Organometallics* **1986**, *5*, 1938−1944. − [4b] L. Randaccio, S. Geremia, E. Zangrando, C. Ebert, *Inorg. Chem*. **1994**, *33*, 4641−4650 and references therein. − [4c] D. J. A. De Ridder, E. Zangrando, H. B. Burgi, *J. Mol. Struct*. **1996**, *374*, 63−83.

[5] D. Datta, G. T. Sharma, *J. Chem. Soc. Dalton Trans.* **1989**, 115−118; N. Bresciani-Pahor, S. Geremia, C. Lopez, L. Randaccio, *Inorg. Chem*. **1990**, *29*, 1043−1049; K. L. Brown, S. Satyanarayana, *J. Am. Chem. Soc*. **1992**, *114*, 5674−5684; S. Hirota, S. M. Polson, J. M. Puckett, Jr., S. J. Moore, M., B. Mitchell, L. G. Marzilli, *Inorg. Chem*. **1996**, *35*, 5646−5653 and references therein.

[6] S. M. Polson, R. Cini, C. Pifferi, L. G. Marzilli, *Inorg. Chem.* **1997**, *36*, 314−322.

[7] N. Bresciani-Pahor, L. Randaccio, P. J. Toscano, A. C. Sandercock, L. G. Marzilli, *J. Chem. Soc. Dalton Trans.* **1982**, 129−134.

[8] S. Geremia, L. Randaccio, E. Zangrando, L. Antolini, *J. Organomet. Chem*. **1992**, *425*, 131−139.

[9] F. T. T. Ng, G. L. Rempel, J. Halpern, *Inorg. Chim. Acta* **1983**, *77*, L165-L166.

[10] N. Bresciani Pahor, S. Geremia, E. Zangrando, A. Raeto Raselli, *Inorg. Chim. Acta* **1989**, *162*, 205−209.

[11] F. T. T. Ng, G. L. Rempel, J. Halpern, *J. Am. Chem. Soc*. **1982**, *104*, 621−623.

[12] [12a] F. T. T. Ng, G. L. Rempel, C. Mancuso, J. Halpern, *Organometallics* **1990**, *9*, 2762−2772. − [12b] M. F. Summers, P. J. Toscano, N. Bresciani Pahor, G. Nardin, L. Randaccio, L. G. Marzilli, *J. Am. Chem. Soc*. **1983**, *105*, 6259−6263.

[13] L. G Marzilli in *Bioinorganic Catalysis* (Ed.: J. Reedijk), Marcel Dekker, New York, USA, **1993**, p. 227; C. Krakty, G. Färber, K. Gruber, K. Wilson, Z. Dauter, H. Nolting, R. Konrat, B. Kräutler, *J. Am. Chem. Soc*. **1995**, *117*, 4654−4670.

[14] J. M. Pratt, *Chem. Soc. Rev.* **1985**, *14*, 161−170; M. K. Geno, J. Halpern, *J. Am. Chem. Soc*. **1987**, *109*, 1238−1239; T. Toraya, A. Ishida, *Biochemistry* **1988**, *27*, 7677−7681; L. G. Marzilli, M. F. Summers, N. Bresciani Pahor, E. Zangrando, J. P. Charland, L. J Randaccio,. *Am. Chem. Soc*. **1985**, *107*, 6880−6888; L. Randaccio, N. Bresciani Pahor, E. Zangrando, *Recl. Trav. Chim. Pays-Bas* **1987**, *106*, 343.

[15] R. D. Hanckock, *Prog. Inorg. Chem*. **1989**, *37*, 187−291.

[16] B. P. Hay, *Coord. Chem. Rev.* **1993**, *126*, 177−236 and references therein.

[17] M. Zimmer, *Chem. Rev.* **1995**, *95*, 2629−2649.

[18] O., Q. Munro, H. M. Marques, P. G. Debrunner, K. Maharao, W. R. Scheidt, *J. Am. Chem. Soc*. **1995**, *117*, 935−954 and references therein.

[19] [19a] H. M. Marques, K. L. Brown, *J. Mol. Struct. (Theochem)* **1995**, *340*, 97−124; H. M. Marques, K. L. Brown, *Polyhedron* **1996**, *15*, 2187−2197. − [19b] H. M. Marques, C. Warden, M. Honye, M. S. Shongwe, K. L. Brown, *Inorg. Chem.* **1998**, *37*, 2578−2579. − [19c] A. K. Rappé, C. J. Casewit, K. S. Colwell, Goddard, III; W. M. Skiff, *J. Am. Chem. Soc*. **1992**, *114*, 1024−1035; A. K. Rappé, K. S. Colwell, C. J Casewit, *Inorg. Chem*. **1993**, *32*, 3438−3450.

[20] P. V. Bernhard, P. Comba, *Inorg. Chem*. **1992**, *31*, 2638−2651.

[21] M. Calligaris, P. Faleschini, F. Todone, E. Alessio, S Geremia,. *J. Chem. Soc., Dalton Trans.* **1995**, 1653−1661.

[22] L. M. Hansen, P. N. V. Pavan Kumar, D. S. Marynick, *Inorg. Chem*. **1994**, *33*, 728−735. These calculations confirmed that the steric properties of the R and L ligands, but not their σ-donating ability, influence the Co−C bond. However, this study was limited to alkylcobaloximes without any electron-withdrawing R ligand.

[23] N. Bresciani Pahor, L. Randaccio, E. Zangrando, *Inorg. Chim. Acta* **1990**, *168*, 115−121; W. O. Parker, Jr., E. Zangrando, P. A. Marzilli, L. Randaccio, L. G. Marzilli, *Inorg. Chem*. **1988**, *27*, 2170−2180.

[24] S. Geremia, M. Calligaris, *J. Chem. Soc., Dalton Trans.* **1997**, 1541−1547; S. Geremia, L. Vicentini, M. Calligaris, *Inorg. Chem.* **1998**, *37*, 4094−4103.

[25] W. D. Cornell, P. Cieplak, I. R. Bayly, I. R. Gould, K. M. J. Merz, D. M. Ferguson, D. C. Spellmeyer, T. Fox, J. W. Calwell, P. A. Kollman, *J. Am. Chem. Soc*. 1**995**, *117*, 5179−5197.

[26] HYPERCHEM, Hypercube, Inc., Waterloo, Ontario, **1994**.

[27] R. M. Badger, *J. Chem. Phys.* **1934**, *2*, 128−131.

[28] D. R. Herschbach, V. W. Laurie, *J. Chem. Phys.* **1961**, *35*, 458−463.

[29] T. A. Halgren, *J. Mol. Struct. (Theochem.)* **1988**, *163*, 431; *J. Am. Chem Soc.* **1990**, *112*, 4710−4723.

[30] O. Ermer, *Struct. Bonding (Berlin)* **1976**, *27*, 161−211.

[31] P. C. Jurs, *Computer software applications in chemistry*, Wiley, New York, **1996**.

[32] G. R. Brubaker, D. W. Johnson, *Coord. Chem. Rev.* **1984**, *53*, 1−36.

[33] A. Immirzi, A. Musco, *Inorg. Chim. Acta* **1977**, *25*, L41−L42.

[34] A. Bondi, *J. Phys. Chem.* **1964**, *68*, 441−451.

[35] N. Bresciani Pahor, W. M. Attia, S. Geremia, L. Randaccio, C. Lopez, *Acta Crystallogr.* **1989**, *C45*, 561−566.

[36] L. G. Marzilli, M. F. Summers, E. Zangrando, N. Bresciani Pahor, L. Randaccio, *J. Am. Chem. Soc*. **1986**, *108*, 4830−4838.

[37] F. Mancia, N. H. Keep, A. Nakagawa, P. F. Leadlay, S. McSweeney, B. Rasmussen, P. Böscke, O. Diat, P. R. Evans, *Structure* **1996**, *4*, 339−350.

[38] J. M. Sirovatka, R. G. Finke, *J. Am. Chem. Soc.* **1997**, *119*, 3057−3067.

[39] L. G. Marzilli, M. F. Summers, N. Bresciani Pahor, E. Zangrando, J. P. Charland, L. Randaccio, *J. Am. Chem. Soc*. **1985**, *107*, 6880−6888; C. Mealli, M. Sabat, L. G. Marzilli, *J. Am. Chem. Soc*. **1987**, *109*, 1593−1594.

[40] J. M. Pratt, in *Metal Ions in Biological Systems* (Eds.: H. Sigel, A. Sigel), Marcell Dekker, New York, **1993**, p. 229 and references therein.

[41] B. Kräutler, R. Konrat, E. Stupperich, G. Färber, K. Gruber, C. Kratky, *Inorg. Chem*. **1994**, *33*, 4128−4139. However, it should be noted that in the imidazolylcyanocobalamin, in which an imidazole residue replaces the dimethylbenzimidazole one, the Co−N axial distance is very short [1.978(9) A].

[42] J. M. Puckett, Jr., M. B. Mitchell, S. Hirota, L. G. Marzilli, *Inorg. Chem.* **1996**, *35*, 4656−4662.

[43] S. H. Unger, L. Hausch, *Prog. Phys. Org. Chem*. **1976**, *12*, 91.

[44] S. Hirota, S. M. Polson, J. M. Puckett, Jr., S. J. Moore, M. B. Mitchell, L. G. Marzilli, *Inorg. Chem.* **1996**, *35*, 5646−5653.

Received November 19, 1998
[I98399]

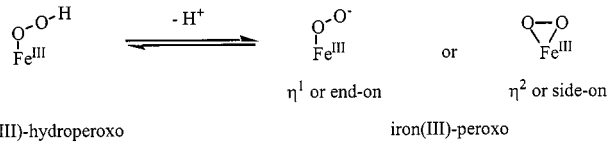
Characterization of a Nonheme Mononuclear Peroxoiron(III) Intermediate by UV/Vis and EPR Spectroscopy and Mass Spectrometry

Ariane Jalila Simaan,[a] Frédéric Banse,[a] Pierre Mialane,[a] Alain Boussac,[b] Sun Un,[b] Taraneh Kargar-Grisel,[c] Guy Bouchoux,[c] and Jean-Jacques Girerd*[a]

Keywords: Peroxo complexes / Iron / Nonheme iron / Iron / EPR spectroscopy / Mass spectrometry / UV/Vis spectroscopy

Some nonheme hydroperoxoiron(III) species have been recently characterized by several groups. The reported examples were obtained by adding H_2O_2 in excess to an Fe^{II} complex with a neutral polypyridine ligand. We show here that on deprotonation, the purple low-spin hydroperoxoiron(III) complex $[L^5Fe^{III}OOH]^{2+}$ [L^5 = *N*-methyl-*N*,*N*′,*N*′-tris(2-pyridylmethyl)ethane-1,2-diamine] gives a blue high-spin species which we characterized as the η^2-peroxoiron(III) species $[L^5Fe^{III}O_2]^+$. It seems that with such an auxiliary ligand, the hydroperoxo group is acidic in contrast with its basicity when it is coordinated to a heme group.

Several nonheme hydroperoxoiron(III) complexes have been recently prepared[1−6] as models of "Activated Bleomycin" which was demonstrated to contain an $Fe^{III}OOH$ unit.[7] A hydroperoxoiron(III) intermediate has also been postulated as an active oxidant in a cytochrome P450 mutant[8][9] and in heme oxygenase.[10] A peroxo intermediate has been detected by Benson et al.[11] and Vaz et al.[12] in cytochrome P450 mutants in which the protonation of the distal oxygen atom of the peroxo group is inhibited. Peroxoiron(III) species have been observed several times in heme models,[13−15] but only once in a nonheme model system.[16] In these models an η^2-coordination mode was suggested based on spectroscopic studies.



Scheme 1

We show here that, by deprotonation of the hydroperoxoiron(III) species, prepared with the pentadentate ligand L^5 [*N*-methyl-*N*,*N*′,*N*′-tris(2-pyridylmethyl)ethane-1,2-diamine],[3][6] a peroxoiron(III) species is obtained. EPR spectroscopy suggests a side-on coordination mode for the peroxo group.

[a] Laboratoire de Chimie Inorganique, UMR CNRS 8613, Université Paris-Sud, F-91405 Orsay, France
[b] Section de Bioenergétique, URA CNRS 2096, CEA Saclay, F-91191 Gif-sur-Yvette, France
[c] Laboratoire des Mécanismes Réactionnels, UMR CNRS 7651, Ecole Polytechnique, F-91128 Palaiseau, France

The synthesis and spectroscopic characteristics of $[L^5Fe^{II}Cl]PF_6$ have been reported by Bernal et al.[3] In MeOH, an excess of H_2O_2 (100 equiv.) leads to the purple species $[L^5Fe^{III}OOH]^{2+}$.[3][6] It exhibits a UV/Vis spectrum with an intense band at λ_{max} = 537 nm (ε = 1000 $M^{-1}\cdot cm^{-1}$) and an EPR spectrum typical for a low-spin Fe^{III} species (g_2 = 2.19, g_2 = 2.12, g_3 = 1.95). We have synthesized the analogous $[L^5Fe^{II}Cl]Cl$ complex and observed the same intermediate in the presence of H_2O_2 which we have also detected by mass spectrometry at *m*/*z* 218.[6]

Upon adding a base to a purple methanol solution of $[L^5Fe^{III}OOH]^{2+}$, a blue color appeared and was stable for about 15 minutes at room temperature. Figure 1 shows the UV/Vis spectra recorded at 0 °C before and after addition of 5 equiv. (based on Fe) of triethylamine. The band at 537 nm disappeared and a new band appeared at 740 nm (ε = 500 $M^{-1}\cdot cm^{-1}$). This blue species has also been obtained with other bases (NaOH, 2,6-dimethylpyridine). Depending on the pK_a, different amounts of base were needed to complete the reaction. To obtain the maximum absorbance of the band at 740 nm, 3 equiv. of NaOH, 5 equiv. of NEt_3 or 50 equiv. of 2,6-dimethylpyridine were necessary. Because of its steric hindrance 2,6-dimethylpyridine cannot coordinate to the iron center, confirming that the blue adduct is obtained by deprotonation of $[L^5Fe^{III}OOH]^{2+}$.

The same blue species has also been characterized at 10 K by EPR spectroscopy as shown in Figure 2. Spectra recorded at various temperatures ranging from 4 K to 30 K are typical for high-spin Fe^{III}. The analysis of the set of spectra led to the conclusion that two different species were present. One of them has an E/D = 0.29 with the resonances at g = 9.3 and g = 4.3 arising from the lower and middle Kramers doublet of a nearly rhombic complex.[17] The other has an E/D = 0.08 with the resonances at g = 7.5 and 5.9 arising from the upper Kramers doublet and the middle one with $D < 0$.[18] The decrease in intensity of

 © WILEY-VCH Verlag GmbH, D-69451 Weinheim, 1999 1434−1948/99/0606−0993 $ 17.50+.50/0

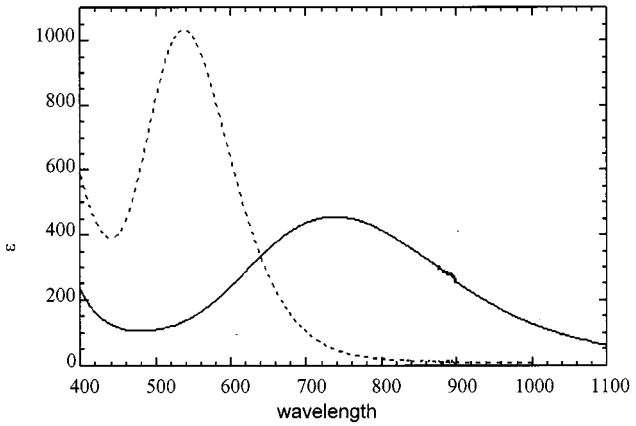


Figure 1. UV/Vis spectra at 0°C of $[L^5Fe^{III}OOH]^{2+}$ (1 mM in MeOH, 100 equiv. of H_2O_2) before (- - -) and after addition of 5 equiv. of NEt_3 (−); the bands at 537 nm and 740 nm are attributed to LMCT transitions respectively in $[L^5Fe^{III}OOH]^{2+}$ and $[L^5Fe^{III}O_2]^+$; ε in $M^{-1}\cdot cm^{-1}$, wavelength in nm

the UV/Vis band at 740 nm was followed at room temperature as a function of time while EPR spectra were recorded at 10 K on several aliquots sampled at known times and quickly frozen in liquid nitrogen. During the course of the experiment, the resonances at $g = 7.5$ and $g = 5.9$ decreased in intensity while that at $g = 4.3$ increased. The $E/D = 0.08$ species corresponds to the blue intermediate and that at $E/D = 0.29$ to a Fe^{III} degradation product.

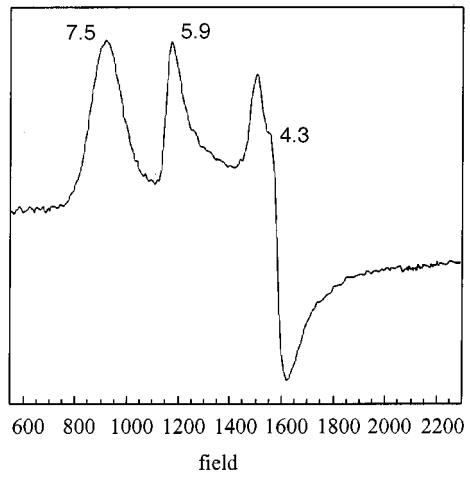


Figure 2. EPR spectrum of $[L^5Fe^{III}OOH]^{2+}$ + 5 NEt_3 recorded at 10 K; the resonances at $\delta = 7.5$ and 5.9 are attributed to the quasi-axial high-spin $[L^5Fe^{III}O_2]^+$ species and the resonances at $\delta \approx 4.3$ to a rhombic high-spin Fe^{III} degradation product; field in gauss

Electrospray ionization mass spectra of methanol solutions of [L5FeCl]Cl treated with H_2O_2 and either NaOH or triethylamine were identical. Both spectra exhibit a peak at *m/z* 435 (Figure 3) which can be attributed to $[L^5Fe^{III}O_2]^+$. This assignment is supported by the theoretical isotopic pattern shown in Figure 3 and corroborates the fact that the hydroperoxoiron group is acidic enough to yield a per-

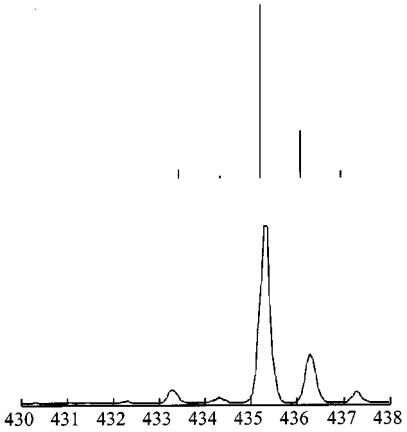
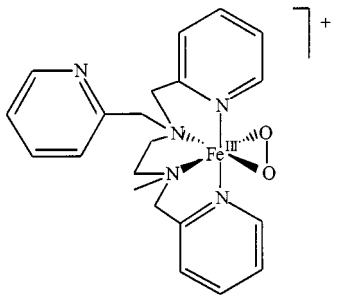


Figure 3. Electrospray-ionization mass-spectroscopic features (*m/z* values) of $[L^5Fe^{III}O_2]^+$ at *m/z* 435; theoretical isotope patterns are represented by bars above the peak cluster

oxoiron species in the presence of a base. We propose that the blue species is the high-spin Fe^{III} species $[L^5Fe^{III}O_2]^+$.

By analogy with $[L^5Fe^{III}OOH]^{2+}$, one expects an η^1-peroxo complex $[L^5Fe^{III}O_2]^+$, in which L^5 is pentacoordinated, to be low spin. The blue species must thus contain a peroxo group linked in an η^2-mode. Moreover the EPR spectrum of $[L^5Fe^{III}O_2]^+$ is very similar to those of two high-spin iron(III) species with two *cis*-chloro groups: $[(bispicMe_2en)Fe^{III}Cl_2]^+$[19][20] and $[(bispicBz_2en)Fe^{III}Cl_2]^+$.[21] We thus suggest that $[L^5Fe^{III}O_2]^+$ has the structure represented in Scheme 2.



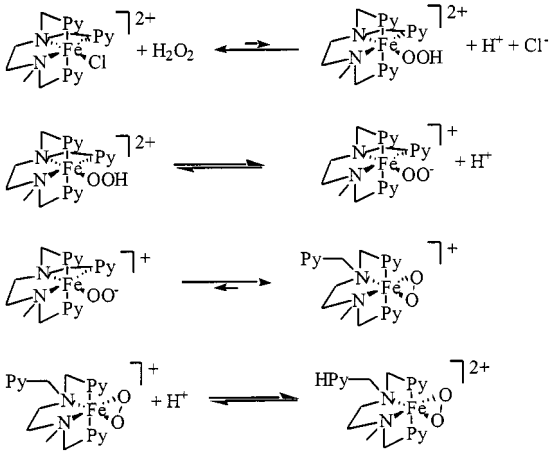
Scheme 2

In this complex, the pentadentate ligand L^5 acts as a tetradentate one as already reported by Nivorozhkin et al.[22] for $[L^5ClFe^{III}OFe^{III}ClL^5]^{2+}$. Raman spectroscopy experiments have been performed to observe a peroxidic vibrational signal but the adduct appeared to degrade when irradiated as already described for a similar compound.[2]

The deprotonation of $[L^5Fe^{III}OOH]^{2+}$ has also been studied with a smaller amount of base ($NEt_3/Fe < 5$ or $NaOH/Fe < 3$) by UV/Vis spectroscopy at 2 °C. Under these experimental conditions, the blue species was not formed quantitatively, and moreover it disappeared slowly while the $[L^5Fe^{III}OOH]^{2+}$ species reappeared, but without attaining its original concentration. This slow and incomplete reappearance of $[L^5Fe^{III}OOH]^{2+}$ was attributed to a slow increase in proton concentration due to the sluggish formation of $Fe^{III}-O-Fe^{III}$ decomposition products fol-

lowing the condensation reaction according to Equation 1. The experimental observations reported here can be summarized by the reactions shown in Scheme 3.

$$2\ Fe^{III}(OH_2) \rightarrow Fe^{III}-O-Fe^{III} + H_2O + 2\ H^+ \quad (1)$$



Scheme 3

During the first step, a chloro group of $[L^5Fe^{III}Cl]^{2+}$ is replaced by a hydroperoxo group. As this reaction needs an excess of H_2O_2, the reverse reaction is assumed to be predominant. The second step is the acid-base equilibrium between $[L^5Fe^{III}OOH]^{2+}$ and its deprotonated η^1-form. The next reaction leads to the blue $[L^5Fe^{III}O_2]^+$ adduct after coordination of the peroxo group in an η^2-fashion and decoordination of a pyridine group. This reaction must be rapid and favorable since we did not detect a low-spin species such as η^1-$[L^5Fe^{III}O_2]^+$. The protonation of the pendant pyridine moiety is certainly possible. However, this cannot compete since pyridine is a weak base.

In conclusion, our study reports the formation and spectroscopic characterization of a new nonheme mononuclear iron(III) complex with an η^2-peroxo and a nonoxygenated ligand. In the model presented here, as in other examples of artificial peroxoiron(III) units, the η^2-coordination mode is found, which must correspond to a profound trend for this unit. Proteins as cytochrome P450 may stabilize the intrinsically unstable η^1-coordination either by hydrogen bonding with amino acid groups in the distal side or, as proposed recently by Selke and Valentine,[23] by the axial cysteine ligand that may act as a switch that opens the side-on bound peroxo. Our study shows also that the deprotonation of the hydroperoxoiron(III) is thermodynamically easy and may be easier than with heme or bleomycin systems since we are able to produce the peroxo species in the presence of water while the peroxo species of cytochrome P450, for example, is protonated by a water molecule.[24] The acidity or basicity of the hydroperoxo group must be a function of the auxiliary ligand: Negatively charged ligands like hemes must favor basicity and neutral ligands acidity. It is clear that the enhancement of basicity in the case of hemes is crucial for the subsequent formation of the active ferryl species.

Experimental Section

General: All manipulations were carried out by using standard Schlenk techniques. Starting materials were purchased from Acros. Solvents were purchased from Merck and were used without further purification. − UV/Vis: Varian Cary 5E equipped with a temperature controller was used. − MS: Quattro II (Micromass, Manchester, UK) triple quadrupole electrospray mass spectrometer. Typical optimized values for the source parameters were: capillary 2.94 kV, counterelectrode 0.4 kV, source temperature 80 °C, RF lens 0.7 V, skimmer lens offset 5 V, cone voltage 25 V. − EPR: X-band Bruker ER 200 E and 300 spectrometers were used. Low-temperature experiments were performed using an Oxford Instruments continuous-flow liquid-helium cryostat and a temperature-control system. − Syntheses of L^5 and $[L^5FeCl]PF_6$: The ligand and the complex were prepared as described in the literature.[3]

Synthesis of the Complex $[L^5FeCl]Cl$: A solution of 200 mg (1 mmol) of $FeCl_2 \cdot 4\ H_2O$ in 10 mL of THF was added to a solution of L^5 (1 mmol) in 10 mL of THF. A yellow powder precipitated and was collected by filtration (yield 50%). − ESI MS; *m/z*: 438 ($[L^5FeCl]^+$). − $C_{21}H_{25}Cl_2FeN_5 \cdot 2.5\ H_2O$ (519.2): calcd. C 48.58, H 5.82, N 13.49; found C 48.67, H 5.16, N 12.93. − UV/Vis: $\lambda_{max} = 385$ nm ($\varepsilon = 1750\ м^{-1} \cdot cm^{-1}$).

[1] R. J. Guajardo, S. E. Hudson, S. J. Brown, P. K. Mascharak, *J. Am. Chem. Soc.* **1993**, *115*, 7971−7977.
[2] M. Lubben, A. Meetsma, E. C. Wilkinson, B. Feringa, L. Que, Jr., *Angew. Chem. Int. Ed. Engl.* **1995**, *34*, 1512−1514.
[3] I. Bernal, I. M. Jensen, K. B. Jensen, C. J. McKenzie, H. Toftlund, J.-P. Tuchagues, *J. Chem. Soc. Dalton Trans.* **1995**, 3667−3675.
[4] C. Kim, K. Chen, J. Kim, L. Que, Jr., *J. Am. Chem. Soc.* **1997**, *119*, 5964−5965.
[5] M. E. de Vries, R. M. La Crois, G. Roelfes, H. Kooijman, A. L. Spek, R. Hage, B. L. Feringa, *Chem. Commun.* **1997**, 1549−1550.
[6] P. Mialane, A. Nivorojkine, G. Pratviel, L. Azéma, M. Slany, F. Godde, J. Simaan, F. Banse, J. Sainton, O. Horner, J. Guilhem, L. Tchertanov, B. Meunier, J.-J. Girerd, *Inorg. Chem.*, submitted.
[7] J. W Sam, X.-J. Tang, J. Peisach, *J. Am. Chem. Soc.* **1994**, *116*, 5250−5256.
[8] P. H. Toy, M. Newcomb, M. J. Coon, A. D. N. Vaz, *J. Am. Chem. Soc.* **1998**, *120*, 9718−9719.
[9] A. D. N. Vaz, D. F. McGuinnity, M. J. Coon, *Proc. Nat. Acad. Sci. USA* **1998**, *95*, 3555−3560.
[10] P. R. Ortiz de Montellano, *Acc. Chem. Res.* **1998**, *31*, 543−549.
[11] D. E. Benson, K. S. Suslick, S. G. Sligar, *Biochemistry* **1997**, *36*, 5104−5107.
[12] A. D. N. Vaz, S. J. Pernecky, G. M. Raner, M. J. Coon, *Proc. Nat. Acad. Sci. USA* **1996**, *93*, 4644−4648.
[13] E. McCandlish, A. R. Miksztal, M. Nappa, A. Q. Sprenger, J. S. Valentine, J. D. Stong, T. G. Spiro, *J. Am. Chem. Soc.* **1980**, *102*, 4268−4271.
[14] J. N. Burstyn, J. A. Roe, A. R. Miksztal, B. A. Shaevitz, G. Lang G., J. S. Valentine, *J. Am. Chem. Soc.* **1988**, *110*, 1382−1388.
[15] P. Friant, J. Goulon, J. Fisher, L. Ricard, M. Schappacher, R. Weiss, M. Momenteau, *New J. Chem.* **1985**, *9*, 33−40.
[16] S. Ahmad, J. D. McCallum, A. K. Shiemke, E. H. Appelman, T. M. Loehr, J. S. Loehr, *Inorg. Chem.* **1988**, *27*, 2230−2233.
[17] The resonance at $g = 9.3$ is detected only at 4.0 K.
[18] As explained by R. Aasa, T. Vännegard, *J. Magn. Reson.* **1975**, *9*, 308−315, the intensity of the spectrum was multiplied by the temperature. The new spectrum so obtained presents also a peak at $g = 7.5$. The area under this peak decreased with the temperature. Care was taken to avoid saturation conditions.
[19] Abbreviations: bispicBz_2en: *N,N′*-dibenzyl-*N,N′*-bis(2-pyridylmethyl)ethane-1,2-diamine; bispicMe_2en: *N,N′*-dimethyl-*N,N′*-bis(2-pyridylmethyl)ethane-1,2-diamine.

[20] R. Hazell, K. B. Jensen, C. J. McKenzie, H. Toftlund, *J. Chem. Soc., Dalton Trans.* **1995**, 707−717.
[21] S. Poussereau, J. Simaan, G. Blondin, C. Philouze, L. Tchertanov, J.-J. Girerd, unpublished results.
[22] A. L. Nivorozhkin, E. Anxolabéhère-Mallart, P. Mialane, R. Davydov, J. Guilhem, M. Cesario, J. P. Audière J. J. Girerd, S. Styring, L. Schussler, J. L. Seris, *Inorg. Chem.* **1997**, *36*, 846.
[23] M. Selke, J. S. Valentine, *J. Am. Chem. Soc.* **1998**, *120*, 2652−2653.
[24] M. Vidakovic, S. G. Sligar, H. Li, T. L. Poulos, *Biochemistry* **1998**, *37*, 9211−9219.

Received November 25, 1998
[O98405]

Syntheses and Crystal Structures of $(Pr_4N)_2Re_4Q_4(CH_3CONH)_2Cl_8$ (Q = S, Se) – Conversion of Solvent CH_3CN into the Acetamido Ligand

Yuri V. Mironov[a][+]

Keywords: Rhenium / Clusters / Solid-state structures

The first two Re_4 chalcogenide halide clusters $(Pr_4N)_2Re_4Q_4(CH_3CONH)_2Cl_8$ (Q = S, Se) with ionic molecular structures have been synthesized by treatment of neutral molecular clusters $Re_4Q_4Cl_8(TeCl_2)_4$ (Q = S, Se) with Pr_4NCl in refluxing CH_3CN. During the reaction acetonitrile solvent molecules are converted into acetamido ligands, coordinated as dinucleating ligands to Re–Re bonds.

Introduction

Rhenium chalcogenide halide cluster compounds have been studied extensively in recent years, the majority of which contain Re_6 octahedra.[1−4] Recently, the first examples of Re_4 tetrahedra chalcogenide halide clusters of general formula $Re_4Q_4X_8(TeX_2)_4$ with Q = S, Se, Te and X = Cl, Br[5,6] have been prepared. These are neutral molecular compounds that are insoluble in organic solvents and water.

Here we describe two new Re_4 chalcogenide halide clusters with ionic structures $(Pr_4N)_2Re_4Q_4(CH_3CONH)_2Cl_8$ (Q = S, Se). The only known ionic examples of this class of compound are $[Re_4S_4(\mu\text{-}S_3)_6]^{4-}$[7,8] and $[Re_4Q_4(CN)_{12}]^{4-}$[9−11]. We have now successfully extended this work to allow the isolation of the first clusters with terminal chloride ligands. To our surprise the characterised compounds also included bridging acetamido ligands, which are presumably formed by reaction of CH_3CN solvent molecules with H_2O in the metal coordination sphere.

Results

Treatment of molecular clusters $Re_4Q_4Cl_8(TeCl_2)_4$ (Q = S, Se) with Pr_4NCl in refluxing CH_3CN leads to formation of the soluble ionic complexes $(Pr_4N)_2Re_4Q_4(CH_3CONH)_2Cl_8$ (Q = S, Se).

During the reaction acetonitrile solvent molecules are converted into acetamido $(CH_3CONH)^-$ ligands, coordinated as bridging ligands to Re−Re bonds. In total we observe an exchange of four $TeCl_2$ neutral ligands by two acetamido ligands $(CH_3CONH)^-$.

The structures of both compounds $(Pr_4N)_2Re_4S_4(CH_3CONH)_2Cl_8$ (**1**) and $(Pr_4N)_2Re_4Se_4(CH_3CONH)_2Cl_8$ (**2**) were determined by single-crystal X-ray analysis. The view of the cluster anion **2** is shown in Figure 1. Compounds **1** and **2** are isostructural and possess crystallographic $\bar{3}$ symmetry. Each contains an Re_4Q_4 cubane-like core formed from a nearly regular Re_4 tetrahedron with two slightly shorter Re−Re distances, resulting from the coordination of acetamido ligands to these bonds. Distances are similar [2.656(1) (**1**) and 2.695(1) Å (**2**)] for these acetamido-bridged Re−Re bonds and in the ranges 2.754(2)−2.760(1) (**1**) and 2.813(2)−2.821(1) Å (**2**) for the remaining Re−Re bonds. Each Re atom is further ligated by two terminal chloro ligands [Re−Cl distances are in range 2.395(5)−2.413(5) for **1** and 2.419(6)−2.438(6) Å for **2**] and by an oxygen or nitrogen atom of a bridging acetamido ligand, with Re−O and Re−N distances of 2.13(1) and 2.12(2) Å in **1** and 2.14(1) and 2.10(2) Å in **2**.

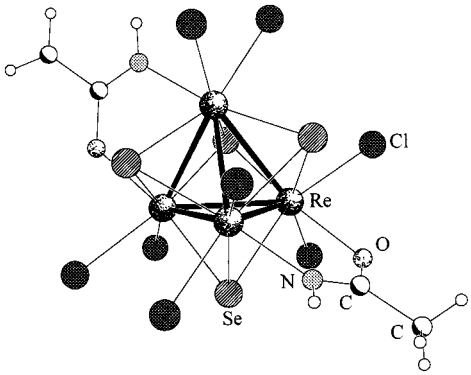


Figure 1. Structure of $[Re_4Q_4(CH_3CONH)_2Cl_8]^{2+}$ [Q = S (**1**), Se (**2**)] cation; selected bond lengths [Å] and angles [°]: **1**: Re1−Re2 2.656(1), Re1−Re1a 2.754(2), Re1−Re2a 2.760(1), Re−S in range 2.301(4)−2.340(5), Re1−O 2.128(12), Re1−N 2.122(15), Re2−Re1−Re1a 61.33(2), Re2−Re1−Re2a 61.10(3), Re1a−Re1−Re2a 57.58(2), Re1−Re2−Re2a 61.32(3), Re1−Re2−Re1a 61.10(3), Re2a−Re2−Re1a 57.57(2), C−O−Re1 122.2(12), C−N−Re2 123.5(13) N−C−O 125(2); **2**: Re1−Re2 2.695(1), Re1−Re1a 2.813(2), Re1−Re2a 2.821(1), Re−Se in range 2.419(2)−2.452(2), Re1−O 2.138(14), Re1−N 2.095(17), Re2−Re1−Re1a 61.57(3), Re2−Re1−Re2a 61.29(4), Re1a−Re1−Re2a 57.16(3), Re1−Re2−Re2a 61.56(3), Re1−Re2−Re1a 61.28(3), Re2a−Re2−Re1a 57.15(3), C−O−Re1 121(2), C−N−Re2 125(2) N−C−O 126(2)

An interesting feature of these syntheses is the conversion of the solvent molecules (CH_3CN) into acetamido ligands. Conversion of acetonitrile into acetamide in the metal coordination sphere is well known for Pt complexes and takes

[a] Lehrstuhl für Analytische Chemie, Ruhr-Universität Bochum, D-44780 Bochum, Germany
[+] On leave from Institute of Inorganic Chemistry of RAS, Novosibirsk, Russia.

 © WILEY-VCH Verlag GmbH, D-69451 Weinheim, 1999 1434−1948/99/0606−0997 $ 17.50+.50/0

place in alkaline solution.[12,13] A similar conversion into the one discussed in the present work has recently been described for the reaction of K_2PtCl_6 with *cyclo*-$(CH_3AsO)_n$ in a sealed tube at 100 °C, with further coordination taking place to a Pt−As bond.[14] In the present work, formation of the acetamido ligand has been observed at a lower temperature and normal pressure.

In the title compounds the C−O and C−N distances of 1.27(2) and 1.29(2) Å in the (CH_3CONH) units of **1** and 1.32(3) and 1.26(3) Å (**2**) are close to each other and similar to the values found for Pt complexes.[14] The determination of the positions of O and N atoms was made by comparison of the corresponding isotropic temperature factors and by the localisation of an H atom at the appropriate site for an amide nitrogen atom in a difference Fourier synthesis. The mechanism of formation of the acetamido ligands may be proposed to involve initial N coordination of a solvent CH_3CN molecule to an Re atom to afford the intermediate compound $(Pr_4N)_2Re_4Q_4(CH_3CN)_2Cl_{10}$. Subsequent nucleophilic attack on the C atom of the C≡N bond by an oxygen atom of water followed by deprotonation (giving HCl) and coordination of this O atom to the neighbouring Re atom, generates **1** and **2**. The formation of these clusters is not observed when the reactions are performed in carefully dried CH_3CN under argon.

The presence of the acetamido ligands in **1** and **2** is confirmed by spectroscopic studies. In the IR spectra of these two complexes the N−H stretching vibrations occur at 3384 (**1**) and 3381 cm^{-1} (**2**) as very sharp lines. Two bands at 1542 and 1521 (**1**) and 1540 and 1517 cm^{-1} (**2**) correspond to C=O vibrations of acetamido ligands. In ^{1}H-NMR spectra δ(NH) = 7.23 (**1**) and 7.07 (**2**); δ(CH_3) = 2.39 (**1**) and 2.47 (**2**). The resonances exhibit an integral ratio of 1:3.

Experimental Section

All manipulations were performed in air. $Re_4Q_4Te_4Cl_{16}$ (Q = S, Se) were obtained as described before.[5] − ^{1}H NMR: Bruker AM 400 FT-NMR. − FTIR: Perkin−Elmer 1760X. − Elemental analyses: Elemental Analyser system Vario E1.

$(Pr_4N)_2Re_4S_4(CH_3CONH)_2Cl_8$ (1): $Re_4S_4Te_4Cl_{16}$ (195 mg, 0.1 mmol) was refluxed in 20 mL of CH_3CN with Pr_4NCl (222 mg, 1 mmol) for 1 h. The final solution was filtered and the filtrate concentrated in air at room temperature. The solid product was then redissolved in 5 mL of CH_3CN, and recrystallised from the system CH_3CN/toluene to afford brown-red crystals of **1** which were filtered, washed with methanol and ether, and then dried. Yield 90 mg (55%). − $C_{28}H_{64}Cl_8N_4O_2Re_4S_4$ (1645.47): calcd. C 20.4, H 3.9, N 3.4, S 7.8; found C 20.1, H 3.9, N 3.3, S 7.6. − IR (KBr): $\tilde{\nu}$ = 3390 (m), 2969 (m), 2878 (w), 1541 (m), 1522 (m), 1460 (s), 1195 (m), 1034 (w), 970 (m), 751 (w), 704 (m), 670 (m), 588 (w). − ^{1}H NMR (CD_3CN): δ = 0.921−0.96 (m, CH_3), 1.60−1.70 (m, CH_2), 3.03−3.07 (m, CH_2) (Pr_4N); δ = 2.39 (CH_3), 7.23 (NH) (CH_3CONH).

$(Pr_4N)_2Re_4Se_4(CH_3CONH)_2Cl_8$ (2): 120 mg (66%) of **2** was obtained from $Re_4Se_4Te_4Cl_{16}$ (214 mg, 0.1 mmol) and Pr_4NCl (222 mg, 1 mmol) as described for **1**. − $C_{28}H_{64}Cl_8N_4O_2Re_4Se_4$ (1833.07): calcd. C 18.4, H 3.5, N 3.1; found C 18.3, H 3.6, N 3.1. − FAB MS; *m/z* (%): 1652 (20) $[M - (Pr_4N)]^-$, 1463 (20) $[M - 2\,(Pr_4N)]^-$, 732 (10) $[M - 2\,(Pr_4N)]^{2-}$, 1428 (100) $[M - 2\,(Pr_4N) - Cl]^-$, 1389 (50) $[M - 2\,(Pr_4N) - 2\,Cl]^-$, 1289 (26) $[M - 2\,(Pr_4N) - 5\,Cl]^-$, 1253 (32) $[M - 2\,(Pr_4N) - 6\,Cl]^-$, 1219 (37) $[M - 2\,(Pr_4N) - 7\,Cl]^-$. − IR (KBr): $\tilde{\nu}$ = 3385 (m), 2967 (m), 2876 (w), 1539 (m), 1517 (m), 1456(s), 1186 (m), 1037 (w), 968 (m), 750 (w), 700 (m), 668 (m), 586 (w). − ^{1}H NMR (CD_3CN): δ = 0.91−0.95 (m, CH_3), 1.59−1.69 (m, CH_2), 3.02−3.06 (m, CH_2) (Pr_4N); δ = 2.48 (CH_3), 7.07 (NH) (CH_3CONH).

X-ray Structural Analyses: Siemens P4 difractometer, graphite monochromator, Mo-K_α radiation (λ = 0.71073 Å), SHELXS-86[15] for structure solution by direct methods and SHELXL-93[16] for refinement by full-matrix least squares. Semi-empirical absorption corrections were applied to the intensity data by use of ψ scans. Hydrogen atoms were included at calculated position.[17]

1: $(Pr_4N)_2Re_4S_4(CH_3CONH)_2Cl_8$, M = 1645.47, trigonal, space group $P3_221$, $a = b$ = 12.670(3), c = 26.09(1) Å, V = 3627(2) Å^3, Z = 3, $D_{calcd.}$ = 2.260 g cm^{-3}, μ = 10.63 mm^{-1}. Crystal size 0.43 × 0.38 × 0.25 mm; ω-scan, scan range: 2θ ≤ 55.02° ($0 \le h \le 16$, $-16 \le k \le 0$, $0 \le l \le 33$), 3313 symmetry-independent reflection from 5515 collected (R_{int} = 0.0772), max./min. transmission: 0.627, 0.289; 229 parameters refined; R = 0.052 [$I > 2\sigma(I)$], wR_2 = 0.127 [all reflections], S = 0.826; $\Delta\rho_{max}$ = 1.79 eÅ^{-3}, $\Delta\rho_{min}$ = −2.78 eÅ^{-3}.

2: $(Pr_4N)_2Re_4Se_4(CH_3CONH)_2Cl_8$, M = 1833.07, trigonal, space group $P3_221$, $a = b$ = 12.726(1), c = 26.534(5) Å, V = 3721.6( ) Å^3, Z = 3, $D_{calcd.}$ = 2.454 g cm^{-3}, μ = 13.12 mm^{-1}. Crystal size 0.2 × 0.2 × 0.12 mm; ω-scan, scan range: 2θ ≤ 55.02° ($0 \le h \le 16$, $-14 \le k \le 14$, $0 \le l \le 34$), 3743 symmetry independent reflection from 5721 collected (R_{int} = 0.0540), max./min. transmission: 0.570, 0.307; 224 parameters refined; R = 0.063 [$I > 2\sigma(I)$], wR_2 = 0.149 [all reflections], S = 1.025; $\Delta\rho_{max}$ = 1.56 eÅ^{-3}, $\Delta\rho_{min}$ = −1.14 eÅ^{-3}.

Acknowlegments

I am grateful to the Alexander von Humboldt foundation for a fellowship and to Prof. W. S. Sheldrick for helpful discussions.

[1] J. R. Long, A. S. Williamson, R. H. Holm, *Angew. Chem. Int. Ed. Engl.* **1995**, *34*, 226−229.
[2] S. Uriel, K. Boubekeur, P. Batail, J. Orduna, E. Canadell, *Inorg. Chem.* **1995**, *34*, 5307−5313.
[3] Y. V. Mironov, M. A. Pell, J. A. Ibers, *Inorg. Chem.* **1996**, *35*, 2709−2710.
[4] Y. V. Mironov, M. A. Pell, J. A. Ibers, *Angew. Chem. Int. Ed. Engl.* **1996, 35,** 2854−2856.
[5] Y. V. Mironov, T. E. Albrecht-Schmitt, J. A. Ibers, *Inorg. Chem.* **1997**, *36*, 944−946.
[6] E. S. Lang, U. Abram, J. Strähle, *Z. Anorg. Allg. Chem.* **1996**, *622*, 251−253.
[7] A. Müller, E. Krickemeyer, H. Bögge, *Angew. Chem. Int. Ed. Engl.* **1986**, *25*, 272−273.
[8] A. Müller, E. Krickemeyer, H. Bögge, *Z. Anorg. Allg. Chem.* **1987**, *554*, 61−78.
[9] M. Laing, P. M. Kiernan, W. P. Griffith, *J. Chem. Soc., Chem. Commun.* **1977**, 221−222.
[10] V. P. Fedin, M. R. J. Elsegood, W. Clegg, A. G. Sykes, *Polyhedron* **1996**, *15*, 485−488.
[11] Y. V. Mironov, T. E. Albrecht-Schmitt, J. A. Ibers, *Z. Kristallogr., New Cryst. Struct.* **1997**, *212*, 308.
[12] A. Erxleben, I. Mutikainen, B. Lippert, *J. Chem. Soc. Dalton Trans.* **1994**, 3667−3675.
[13] F. D. Rochon, P. C. Kong, R. Melanson, *Inorg. Chem.* **1990**, *29*, 1352−1356.

[14] I. M. Müller, W. S. Sheldrick, *Eur. J. Inorg. Chem.* **1998**, 1999–2004.
[15] G. M. Sheldrick, SHELXS-86, *Acta Crystallogr., Sect. A* **1990**, *46*, 467.
[16] G. M. Sheldrick, *SHELXL-93*, Universität Göttingen, **1993**.
[17] Crystallographic data (excluding structure factors) for the structures reported in this paper have been deposited with the Cambridge Crystallographic Data Centre. Copies of the data (deposition numbers CCDC-112135 and -112136) may be obtained free of charge on application to the Director, CCDC, 12 Union Road, Cambridge CB2 1EZ, UK (Fax: int. code + 44-1223/336-033, E-mail: deposit@ccdc. cam.ac.uk).

Received December 11, 1998
[I98426]

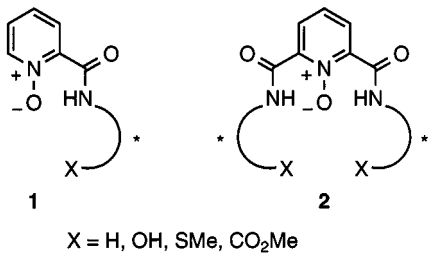
Novel Chiral Pyridine *N*-Oxide Ligands and Their Application in the Enantioselective Catalytic Reduction of Ketones and the Addition of Diethylzinc to Aldehydes

Volker Derdau,[a] Sabine Laschat,*[a] Eike Hupe,[a] Wilfried A. König,[b] Ina Dix,[a] and Peter G. Jones[c]

Keywords: Pyridine *N*-oxide / Pyridine / Asymmetric catalysis / Amino acids / Amino alcohols

Starting from picolinic acids **3** and **4**, the amino acid-derived 2-aminoacylpyridine *N*-oxides **1a**,**c**–**e** and 2,6-bis(aminoacyl)pyridine *N*-oxides **2b**–**e** can be prepared in two steps by the coupling of picolinic acid *N*-oxides **5** and **6** under Appel conditions with the corresponding L-amino acid ester or (1*R*,2*S*)-norephedrine. Compounds **1** and **2** were used as chiral ligands in two different asymmetric catalyses. In the catalytic addition of diethylzinc to benzaldehyde **11**, low enantioselectivities (2–29% *ee*) were obtained regardless of the amino acid moiety. However, the corresponding 2,6-bis(aminoacyl)pyridines **7** and **8** led to increased *ee* values (55% *ee*). In the catalytic reduction of ketones **9a**–**c** to alcohols **10a**–**c** low enantioselectivities were observed for alanine-, valine-, and leucine-derived *N*-oxides **1a**,**c** and **2b**,**c**. An increase of selectivity was observed for bis-methionine ligand **2d** (32–38% *ee*) relative to that of mono-methionine ligand **1d** (7–16% *ee*). However, mono-norephedrine ligand **1e** (≤ 64% *ee*) and the corresponding bis-norephedrine ligand **2e** (≤ 51% *ee*) displayed the highest selectivities. The influence of the *N*-oxide moiety on the enantioselectivity was demonstrated by the observation that 2,6-bis(aminoacyl)pyridines **7** and **8** gave much lower selectivities than the corresponding pyridine *N*-oxides **2d** and **e**.

Chiral pyridines and especially 2,6-diacylpyridines have been used extensively as ligands in asymmetric catalysis.[1][2] It was also found that metallomicelles containing diacylpyridine moieties show a prominent catalytic ability to mimic hydrolytic metallo enzymes.[3] In contrast, pyridine *N*-oxides have been used mainly in achiral form for rate enhancement of transition metal catalyzed processes.[4] They were employed only in few cases as ligands,[5] e.g. for the thione−thiol rearrangement[6] or as chiral NMR solvating agents.[7] This is surprising for several reasons. First, the amine *N*-oxide acts as a strong electron donor, which provides a suitable electronic environment for a central metal ion.[8] Second, attachment of chiral substituents to the pyridine *N*-oxide is easily achieved with a 2,6-diacylpyridine precursor and a chiral amine. Because of the wide variety of chiral amines derived from natural products, it should therefore be possible to tune the stereochemical environment of the ligand as desired. In particular, 2,6-bis(aminoacyl)pyridine *N*-oxides might even be used for asymmetric transformations as chiral ligands in the absence of any metal ion, because of their marked ability to form hydrogen bonds.[9] Therefore we decided to prepare mono- and disubstituted pyridine *N*-oxides **1**and **2** (Scheme 1). For evaluation of the enantioselectivity of the ligands **1** and **2** two different asymmetric catalyses were chosen, viz. the catalytic reduction of ketones with $BH_3 \bullet SMe_2$[10] and the addition of diethylzinc to aldehydes.[11] In order to enhance the chelating abilities and hopefully the enantioselectivity, chiral amines derived from amino acids bearing additional donor groups X were employed, because previous work by O′Neil et al. has shown that amine *N*-oxides derived from tertiary amines could be successfully used for the enantioselective reduction of ketones.[12] The authors reported increased selectivities for those amine *N*-oxides bearing donor groups such as hydroxy or pyridine. The following manuscript describes the synthesis of the novel ligands **1** and **2** and their application in asymmetric catalysis.



Scheme 1

Two different synthetic approaches towards pyridine *N*-oxides **1** and **2** are conceivable. Starting from picolinic acids **3** and **4**, either the amides may be formed first followed by subsequent oxidation, or alternatively **3** and **4** are oxidized to the corresponding *N*-oxides **5** and **6** and then coupled with chiral amines to give **1** and **2** (Scheme 2). Preliminary

[a] Institut für Organische Chemie, Technische Universität Braunschweig,
Hagenring 30, D-38106 Braunschweig, Germany
Fax (internat.): ++49 (0)531/ 391 5388
[b] Institut für Organische Chemie, Universität Hamburg,
Martin-Luther-King-Platz 6, D-20146 Hamburg, Germany
Fax (internat.): ++49 (0)40/ 4123 4325
[c] Institut für Anorganische und Analytische Chemie, Technische Universität Braunschweig,
Hagenring 30, D-38106 Braunschweig, Germany
Fax (internat.): ++49 (0)531/ 391 5387

 © WILEY-VCH Verlag GmbH, D-69451 Weinheim, 1999 1434−1948/99/0606−1001 $ 17.50+.50/0

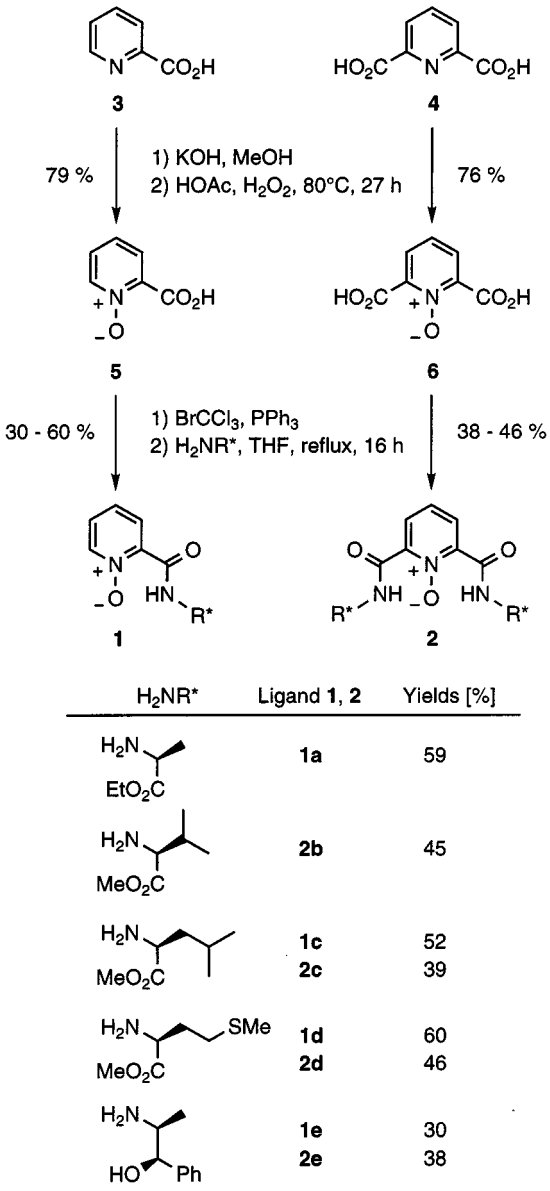
experiments showed that oxidation of aminoacylpyridines proceeded rather sluggishly even under forcing conditions. This was particularly true for the disubstituted derivative, presumably as a result of the steric hindrance of the carbonyl oxygens around the pyridine nitrogen. A similar observation was recently reported by Sharpless when he attempted to prepare methyl picolinate *N*-oxide with bis(trimethylsilyl)peroxide in the presence of catalytic amounts of perrhenic acid.[13]

We therefore turned our attention to the second strategy. Following a procedure by Profft and Steinke,[14] 2-picolinic acid **3** was converted into the corresponding potassium carboxylate, which was further oxidized with hydrogen peroxide in HOAc to give *N*-oxide **5** in 79% yield. Analogous reaction of 2,6-dipicolinic acid **4** gave *N*-oxide **6** in 76% yield.[15] Unfortunately, facile racemization of the amino acids prevented the use of acid chlorides for amide formation. In addition, application of milder coupling agents such as *N,N'*-dicyclohexylcarbodiimide[16] gave only low conversions to **1** and **2**. Next, we tried a method of Hruby[17] employing bromotrichloromethane/triphenylphosphane for activation of the carboxylic acids **5** and **6**, which gave the desired amides **1** and **2** upon addition of a chiral amine in moderate yields. The following amines were used: *L*-alanine ethyl ester, L-valine methyl ester, L-leucine methyl ester, L-methionine methyl ester, and (1*R*,2*S*)-norephedrine.

In case of the bis-methionine pyridine *N*-oxide **2d**, an X-ray crystal structure could be obtained, which is shown in Figure 1.[18] In the solid state compound **2d** displays exact C_2 symmetry, whereby the amino acid moieties are oriented in such a way that the *N*-oxide is stabilized via two intramolecular hydrogen bonds. The absolute configuration was confirmed on the basis of anomalous scattering by sulfur.

For comparison, the corresponding 2,6-bis(aminoacyl)-pyridines **7** and **8** were prepared by converting **4** to the 2,6-diacyl chloride and subsequent treatment with methionine methyl ester or norephedrine,[2b] respectively (Scheme 3).

Chiral pyridine *N*-oxides **1** and **2** and pyridines **7** and **8** were used as ligands in the catalytic reduction of ketones **9a**–**c** with $BH_3 \cdot SMe_2$ (Scheme 5).[19] In a typical experiment 5 mol-% of ligand **1**, **2**, **7**, or **8** were sufficient to achieve complete conversion of **9** within 5 min.[20] After workup the corresponding alcohols **10** were obtained in 97–99% yield. Concerning the reduction of acetophenone **9a** and propiophenone **9b**, the results in Table 1 show that both mono- and disubstituted pyridine *N*-oxides **1a**,**c** and **2b**,**c** derived from alkyl-substituted amino acids such as alanine, leucine or valine gave only low enantioselectivities (7–17% *ee*). This outcome is in good agreement with previous results by Grundon et al.[21]. The authors observed 17–20% *ee* for the reduction of **9a** with amino acid ester borane complexes derived from leucine, phenylalanine, or valine. In contrast, ligands derived from methionine or norephedrine displayed a different behavior. Whereas the monosubstituted ligands **1d**,**e** again resulted in low *ee* values (7–21% *ee*), a significant increase of the enantioselectivity was observed for the corresponding disubstituted ligands **2d**,**e** (31–38% *ee*). When methionine- and norephedrine-derived diacylpyridines **7** and **8** were used for the reduction of acetophenone **9a** instead of the corresponding *N*-oxides **2d**,**e** the enantioselectivity dropped to 4 and 14% *ee*, respectively. This clearly demonstrates the influence of the *N*-oxide moiety. Using 2-chloroacetophenone **9c** gave slightly increased enantioselectivities over those of the other ketones **9a**,**b**. Again bis-methionine ligand **2d** produced a much higher enantiomeric excess (37% *ee*) than monomethionine ligand **1d** (16% *ee*). The only exceptions to the general trend were the norephedrine-derived ligands **1e**, **2e**. Contrary to the previously mentioned cases, mono-norephedrine ligand **1e** gave alcohol **10c** in 64% *ee*, compared to 51% *ee* for the disubstituted ligand **2e**. As shown in Scheme 4, the major enantiomers of the product alcohols **10a**–**c** have the same absolute configuration. It should be noted however that, because of the priority rules of the CIP system, alcohols **10a**,**b** are (*R*) configured, whereas alcohol



H_2NR^*	Ligand **1**, **2**	Yields [%]
H_2N, EtO_2C	**1a**	59
H_2N, MeO_2C	**2b**	45
H_2N, MeO_2C	**1c**	52
	2c	39
H_2N, SMe, MeO_2C	**1d**	60
	2d	46
H_2N, HO, Ph	**1e**	30
	2e	38

Scheme 2

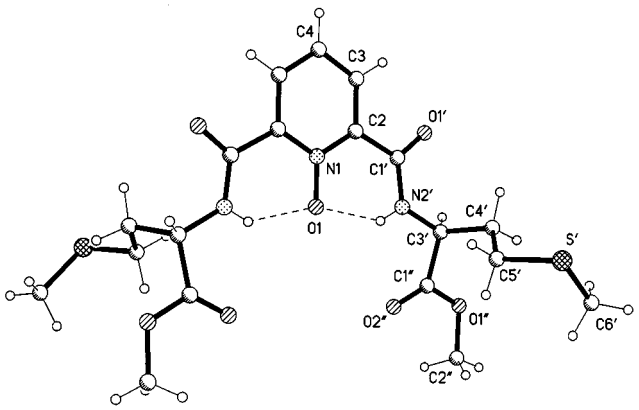
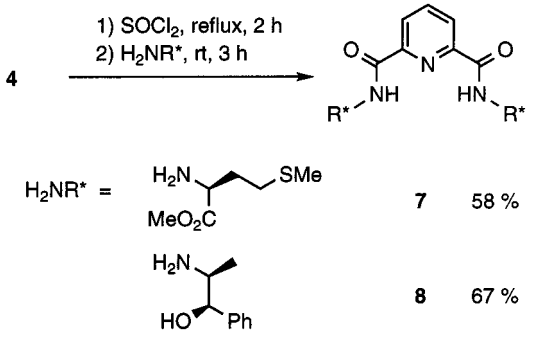
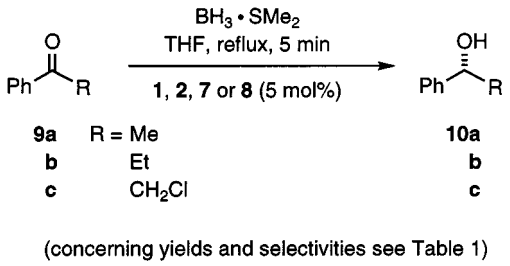


Figure 1. X-ray crystal structure of bis-methionine ligand **2d**. Selected bond lengths [pm] and angles [°]: O(1)−N(1) 131.3(3), N(1)−C(2) 137.0(2), C(1′)−C(2) 151.6(3), N(2′)−C(1′) 133.6(3), O(1′)−C(1′) 122.8(2), N(2′)−C(3′) 144.7(2), N(2′)−H 75(2), H−O(1) 199(2), N(2′)−O(1) 259.9(2), O(1)−N(1)−C(2) 99.83(10), N(1)−C(2)−C(1′) 123.19(18), N(2′)−C(1′)−C(2) 118.66(18), C(1′)−N(2′)−C(3′) 120.29(18), N(2′)−H−O(1) 139(2).



Scheme 3

10c is (*S*) configured. O′Neil reported 68 and 96% *ee* for alcohols (*R*)-**10a** and (*S*)-**10c**, respectively, when using chiral prolinol *N*-oxides.[12] In his ligands the presence of a tertiary alcohol and a pyridyl moiety seemed to be essential for achieving high enantioselectivities.



Scheme 4

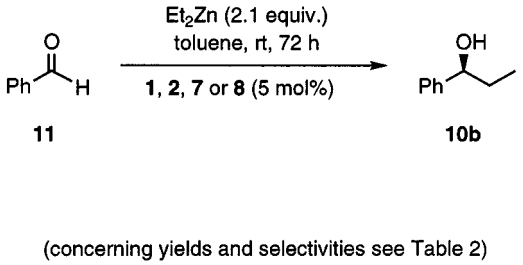
Next, pyridine *N*-oxides **1** and **2** were tested in the asymmetric addition of diethylzinc to aldehydes (Scheme 5). According to a procedure by Chelucci[22] *N*-oxides **1** and **2** were treated with diethylzinc at 0° C, followed by addition of benzaldehyde **11**. After 72 h at room temperature the mixture was worked up to give 1-phenylpropanol **10b** in moderate to high yields depending on the ligand (Table 2). Higher yields were generally observed with disubstituted ligands **2b**−**e**. Both mono- and disubstituted ligands **1a**,**c** and

Table 1. Yields and enantiomeric excesses of alcohols **10** via reduction of ketones **9** with $BH_3 \cdot SMe_2$ in the presence of chiral ligands **1**, **2**, **7**, or **8**[a,b]

Ligand	**10a** (R = Me) Yield [%]	% *ee*	Alcohols**10b** (R = Et) Yield [%]	% *ee*	**10c** (R = CH_2Cl) Yield [%]	% *ee*
1a	99	7	98	8	99	20
1c	99	11	99	17	97	21
1d	99	7	99	12	99	16
1e	99	20	98	21	99	64
2b	97	9	98	9	99	21
2c	99	10	99	16	99	33
2d	99	32	99	38	99	37
2e	99	31	99	33	98	51
10	99	4	---	---	---	---
11	99	14	---	---	---	---

[a] Reaction conditions: **9** (1 equiv.), $BH_3 \cdot SMe_2$ (1 equiv.), ligand **1**, **2**, **7**, or **8** (0.05 equiv.), THF, reflux, 5 min. Yields refer to isolated product. − [b] Enantiomeric excesses were determined by capillary GC of the crude products using a chiral stationary phase. Depending on the substituent R, the major enantiomer of **10** has the following absolute configuration: (*R*)-**10a** (R = Me), (*R*)-**10b** (R = Et), (*S*)-**10c** (R = CH_2Cl). For details see Experimental Section.

2b,**c** derived from alanine, valine, or leucine gave only low enantioselectivities (7−16% *ee*). An increase of selectivity and yield was discovered for bis-methionine ligand **2d** (92%, 29% *ee*) relative to that of mono-methionine ligand **1d** (37%, 2% *ee*). Surprisingly low selectivities were obtained for the norephedrine ligands (**1e**: 9% *ee*, **2e**: 8% *ee*). However, much higher enantioselectivities of **10b** could be accomplished by using 2,6-bis(aminoacyl)pyridines **7** and **8** (55 and 56% *ee*, respectively). Except for the reaction catalyzed by *N*-oxide **2e**, the absolute configuration of the major enantiomer of **10b** was assigned (*S*).



Scheme 5

From these results several conclusions can be drawn. It seems reasonable to assume that concerning the enantioselective reduction of ketones **9** proceeds by in situ complexation of boron by the oxygen atom of the *N*-oxide.[23] This stabilization is enhanced by the presence of additional donor groups such as thiomethyl (**1d**, **2d**) or hydroxy (**1e**, **2e**).[24] Thus a boronate species with a stereochemically defined environment is formed, which coordinates the prochiral ketone, so that attack of the hydride occurs preferentially from the *Si*-face (for **12a**,**b**) or *Re*-face (for **12c**). In particular, bis-methionine *N*-oxide **2d** and norephedrine *N*-oxides **1e** and **2e** are superior to the corresponding 2,6-bis(aminoacyl)pyridines **7** and **8** and seem to be good candidates for designing further novel ligands for the catalytic

Table 2. Yields and enantiomeric excesses of 1-phenylpropanol **10b** (R = Et) via addition of diethylzinc to benzaldehyde **11** in the presence of chiral ligands **1**, **2**, **7**, or **8**[a,b]

Ligand	**10b** Yield [%]	% *ee*	Configuration
1a	52	16	(*S*)
1c	37	12	(*S*)
1d	37	2	(*S*)
1e	71	9	(*S*)
2b	71	11	(*S*)
2c	88	7	(*S*)
2d	92	29	(*S*)
2e	88	8	(*R*)
10	66	55	(*S*)
11	56	56	(*S*)

[a] Reaction conditions: 1) Et_2Zn (2.2 equiv.), ligand **1**, **2**, **7**, or **8** (0.05 equiv.), THF, 0°C to room temp., 20 min; 2) **11** (1.0 equiv.), rt, 72 h . Yields refer to isolated product. − [b] Enantiomeric excesses were determined by capillary GC of the crude products using a chiral stationary phase. For details see Experimental Section.

asymmetric reduction of ketones. Work towards this end is currently in progress. In contrast, 2,6-bis(aminoacyl)pyridine ligands **7** and **8** are much better suited to the diethylzinc addition than the corresponding pyridine *N*-oxides **1** and **2**. This reaction is probably highly dependent on the presence of a β-amino alcohol function in the catalytic species in order to achieve high enantioselectivities

Experimental Section

General: All reactions were carried out under nitrogen with standard Schlenk techniques. Solvents were dried and deoxygenated by standard procedures. − Analytical TLC was performed on precoated Merck Si 254 F plates (0.25 mm thickness) and the products were visualized by UV detection. Flash chromatography[25] was carried out with Merck silica gel 60 (230−400 mesh). − NMR spectra: Bruker AC 200 P (^{1}H: 200 MHz, ^{13}C: 50 MHz), Bruker AM 400 (^{1}H: 400 MHz, ^{13}C: 100 MHz). Multiplets in ^{13}C-NMR spectra were assigned with the aid of DEPT experiments. − Optical rotations (1-dm cells, 1-mL capacity, room temp.): Perkin−Elmer Model 241 polarimeter. − Melting points: Rheometric Scientific DSC SP, heating and cooling rate: 10 K min^{-1}. − IR: Nicolet 5DXC FT-IR spectrometer. − MS: Finnigan Model MAT 8430 (EI). − For determination of enantiomeric excesses of **10a**,**b** a Carlo Erba Instruments GC (column 1) coupled with a Carlo Erba Instruments GC (column 2) was used. Column 1: Macherey−Nagel DD-wax capillary column (ID 0.25 mm, length 30 m), column 2: Macherey−Nagel Hydrodex β-3P capillary column (ID 0.25 mm, length 25 m). For determination of enantiomeric excesses of **10c** a GC with heptakis(6-*O*-*tert*-butyldimethylsilyl-2,3-di-*O*-methyl)-β-cyclodextrine as chiral stationary phase (50% in polysiloxane OV 1701, w/w, column length 10 m)[26] was used. − (1′*R*,2′*S*)-2,6-Bis[2-(1-hydroxy-1-phenyl)propylaminocarbonyl]-pyridine (**8**) was prepared according to ref.[2b] The absolute configuration was determined by comparison with authentic samples.

Picolinic Acid *N*-Oxide (5): To an ice-cooled solution of picolinic acid **3** (25.0 g, 0.20 mol) in MeOH (140 mL) was added KOH (11.4 g, 0.20 mol). The solvent was removed in vacuo and the remaining solid was dissolved in HOAc (120 mL). Then H_2O_2 (24 mL, 30% aqueous solution) was added and the mixture was heated at 80°C for 3 h. Additional H_2O_2 (20 mL, 30% aqueous solution) was added and the mixture was stirred at 90°C for 24 h. After removal of the solvent in vacuo, the residue was dissolved in H_2O (10 mL) and the pH adjusted to 1 by addition of conc. HCl. The precipitate was filtered and washed with ice-cold H_2O (100 mL) to give 21.9 g (0.16 mol, 79%) of a colorless solid: mp. 162°C. − ^{1}H NMR (200 MHz, NaOD): δ = 7.45 (d, *J* = 6.1 Hz, 1 H, 6-H), 6.93 (dd, *J* = 7.0/8.2 Hz, 1 H, 5-H), 6.69−6.65 (m, 2 H, 4-H, 3-H). − ^{13}C NMR (50 MHz, NaOD): δ = 168.1 (CO), 147.6 (C-2), 139.6 (C-6), 132.4, 126.5, 124.4 (C-3, C-4, C-5). − MS (EI) *m*/*z* (%): 139 (42) [M$^+$], 95 (67), 78 (100), 63 (8), 51 (23). $C_6H_5NO_3$ (139.11): calcd. C 51.80, H 3.62, N 10.07; found C 51.68, H 3.76, N 10.08.

Dipicolinic Acid *N*-Oxide (6): Following the procedure described for **5** but using dipicolinic acid **4** (16.7 g, 0.10 mol) 13.9 g (76.0 mmol, 76%) of a colorless solid were obtained: mp. 171°C. − ^{1}H NMR (400 MHz, $CDCl_3$): δ = 14.67−14.59 (br, 2 H, COOH), 8.74 (d, *J* = 8.0 Hz, 2 H, 3-H), 7.99 (t, *J* = 8.0 Hz, 1 H, 4-H). − ^{13}C NMR (100 MHz, $CDCl_3$): δ = 158.3 (COOH), 138.2 (C-2), 133.7 (C-3), 132.5 (C-4). − MS (EI) *m*/*z* (%): 183 (22) [M$^+$], 139 (100), 122 (78), 106 (18), 94 (30), 78 (41), 63 (8), 51 (34). − $C_7H_5NO_5$ (183.02): calcd. C 45.91, H 2.75, N 7.65; found C 46.02, H 2.94, N 7.53.

General Procedure for the Preparation of Pyridine *N*-Oxides (1, 2): To a solution of triphenylphosphane (1.05 g, 4.00 mmol), picolinic acid *N*-oxides **5** or **6** (4.00 mmol), and bromotrichloromethane (0.79 g, 4.00 mmol) in THF (20 mL) was added amine (8.00 mmol in case of **5** or 16.0 mmol in case of **6**), and the resulting mixture was refluxed for 16 h. After cooling to room temperature, the precipitate was removed by filtration. The solvent was removed in vacuo and the crude product was purified by flash chromatography.

(2′*S*)-2-[(1-Ethoxycarbonyl)ethylaminocarbonyl]pyridine *N*-Oxide (1a): Flash chromatography on SiO_2 (hexanes/$CHCl_3$/2-propanol, 8:3:1) gave 560 mg (2.35 mmol, 59%) of a yellow oil; $[\alpha]_D^{22}$ = 0.3 (*c* = 1.00, $CHCl_3$). − IR (KBr): ṽ = 1740 cm^{-1}, 1669, 1530. − ^{1}H NMR (400 MHz, $CDCl_3$): δ = 11.71 (d, *J* = 5.4 Hz, 1 H, NH), 8.40 (dd, *J* = 2.5/7.9 Hz, 1 H, 3-H), 8.27 (dd, *J* = 1.0/6.4 Hz, 1 H, 6-H), 7.46 (ddd, *J* = 1.0/6.4/7.4 Hz, 1 H, 4-H), 7.42 (ddd, *J* = 2.5/7.9/7.4 Hz, 1 H, 5-H), 4.77 (dd, *J* = 5.4/7.2 Hz, 1 H, 2′-H), 4.25 (q, *J* = 7.3 Hz, 2 H, OCH_2CH_3), 1.55 (d, *J* = 7.2 Hz, 3 H, 3′-H), 1.30 (t, *J* = 7.3 Hz, 3 H, OCH_2CH_3). − ^{13}C NMR (100 MHz, $CDCl_3$): δ = 172.0 (COO), 159.2 (CONH), 140.5 (C-6), 140.3 (C-2), 128.8 (C-3), 127.4 (C-5), 126.9 (C-4), 61.4 (OCH_2CH_3), 48.8 (C-2′), 18.0 (OCH_2CH_3), 14.0 (C-3′). − MS (EI) *m*/*z* (%): 239 (100) [M$^+$ + 1], 223 (11), 165 (32), 160 (5), 141 (6), 122 (6). − $C_{11}H_{14}N_2O_4$ (238.24): calcd. C 55.46, H 5.92, N 11.76; found C 54.90, H 6.03, N 11.52.

(2′*S*)-2-[(1-Methoxycarbonyl-3-methyl)butylaminocarbonyl]pyridine *N*-Oxide (1c): Flash chromatography on SiO_2 (hexanes/$CHCl_3$/2-propanol, 8:3:1) gave 550 mg (2.07 mmol, 52%) of a yellow oil; $[\alpha]_D^{22}$ = 4.3 (*c* = 1.00, $CHCl_3$). − IR (KBr): ṽ = 1747 cm^{-1}, 1673, 1538. − ^{1}H NMR (400 MHz, $CDCl_3$): δ = 11.65 (d, *J* = 7.7 Hz, 1 H, NH), 8.41 (dd, *J* = 2.4/7.7 Hz, 1 H, 3-H), 8.27 (dd, *J* = 1.5/6.4 Hz, 1 H, 6-H), 7.48 (ddd, *J* = 1.5/7.7/7.4 Hz, 1 H, 4-H), 7.42 (ddd, *J* = 2.4/6.4/7.4 Hz, 1 H, 5-H), 4.79−4.76 (m, 1 H, 2′-H), 3.75 (s, 3 H, OCH_3), 1.82−1.76 (m, 3 H, 3′-H, 4′-H), 0.99 (d, *J* = 2.9 Hz, 3 H), 0.97 (d, *J* = 3.0 Hz, 3 H, 5′-H). − ^{13}C NMR (100 MHz, $CDCl_3$): δ = 172.5 (COO), 159.5 (CONH), 140.5 (C-6), 140.3 (C-2), 128.9 (C-3), 127.4 (C-5), 127.0 (C-4), 52.3 (OCH_3), 51.5 (C-1′), 40.9 (C-2′), 25.0 (C-3′), 22.8, 21.7 (C-4′, C-5′). − MS (CI) *m*/*z* (%): 267 (100) [M$^+$ + 1], 259 (24), 234 (38), 207 (8), 146

(12), 86 (4). − $C_{11}H_{14}N_2O_4$ (266.30): calcd. C 58.64, H 6.81, N 10.52; found C 58.62, H 7.18, N 10.39.

(2′*S*)-2-[(1-Methoxycarbonyl-3-thiomethyl)propylaminocarbonyl]pyridine *N*-Oxide (1d): Flash chromatography on SiO_2 ($CHCl_3$/hexanes/2-propanol, 3:8:1) gave 550 mg (2.07 mmol, 52%) of a yellow solid; mp. 78°C; $[\alpha]_D^{22}$ = 8.6 (*c* = 1.00, $CHCl_3$). − IR (KBr): $\tilde{\nu}$ = 1741 cm^{-1}, 1663, 1527. − ^1H NMR (400 MHz, $CDCl_3$): δ = 11.81 (d, *J* = 6.9 Hz, 1 H, NH), 8.42 (dd, *J* = 2.3/6.9 Hz, 1 H, 3-H), 8.29 (dd, *J* = 1.3/6.3 Hz, 1 H, 6-H), 7.49 (ddd, *J* = 1.3/6.9/7.7 Hz, 1 H, 4-H), 7.42 (ddd, *J* = 2.3/6.3/7.7 Hz, 1 H, 5-H), 4.92 (ddd, *J* = 6.9/7.7/7.8 Hz, 1 H, 2′-H), 3.77 (s, 3 H, OCH_3), 2.63 (t, *J* = 7.4 Hz, 2 H, 4′-H), 2.30−2.12 (m, 2 H, 3′-H), 2.11 (s, 3 H, SCH_3). − ^{13}C NMR (100 MHz, $CDCl_3$): δ = 171.5 (COO), 159.6 (CONH), 140.5 (C-6), 140.1 (C-2), 128.9 (C-3), 127.5 (C-5), 127.0 (C-4), 52.5 (OCH_3), 52.0 (C-2′), 31.5, 30.1 (C-3′, C-4′), 15.4 (SCH_3). − MS (CI) *m/z* (%):285 (100) [M^+ + 1], 269 (4). − $C_{12}H_{16}N_2O_4S$ (284.33): calcd. C 50.69, H 5.67, N 9.85, S 11.28; found C 50.20, H 5.67, N 9.62, S 11.42.

(1′*R*,2′*S*)-2-[2-(1-Hydroxy-1-phenyl)propylaminocarbonyl]pyridine *N*-Oxide (1e): Flash chromatography on SiO_2 ($CHCl_3$/hexanes/MeOH, 9:3:1) gave 332 mg (1.22 mmol, 30%) of a yellow oil; $[\alpha]_D^{22}$= −10.1 (*c* = 1.00, $CHCl_3$). − IR (KBr): $\tilde{\nu}$ = 1664 cm^{-1}, 1655, 1534. − ^1H NMR (400 MHz, $CDCl_3$): δ = 11.45 (d, *J* = 7.4 Hz, 1 H, NH), 8.44 (dd, *J* = 2.2/8.0 Hz, 1 H, 3-H), 8.22 (dd, *J* = 0.9/6.4 Hz, 1 H, 6-H), 7.69 (ddd, *J* = 0.9/8.0/8.4 Hz, 1 H, 4-H), 7.57 (ddd, *J* = 2.2/6.4/8.4 Hz, 1 H, 5-H), 7.48−7.25 (m, 5 H, 2′′-H, 3′′-H, 4′′-H, 5′′-H, 6′′-H), 5.01 (d, *J* = 3.3 Hz, 1 H, 1′-H), 4.51 (m, 1 H, 2′-H), 4.13−4.09 (br, 1 H, OH), 1.17 (d, *J* = 6.9 Hz, 3 H, 3′-H). − ^{13}C NMR (100 MHz, $CDCl_3$): δ = 159.4 (CO), 141.2 (C-2), 140.5 (C-6), 132.1, 131.9 (C-1′, C-4′), 128.8 (C-3), 128.5, 128.3 (C-2′, C-3′, C-5′, C-6′), 128.1 (C-5), 127.2 (C-4), 75.7 (C-1′), 51.7 (C-2′), 14.0 (C-3′). − MS (CI) *m/z* (%): 273 (100) [M^+ + 1], 257 (58), 239 (4), 195 (2), 149 (6). − $C_{15}H_{16}N_2O_3$ (272.30): calcd. C 66.16, H 5.92, N 10.29; found C 66.20, H 5.91, N 10.49.

(2′*S*)-2,6-Bis[(1-methoxycarbonyl-2-methyl)propylaminocarbonyl]pyridine *N*-Oxide (2b): Flash chromatography on SiO_2 (hexanes/$CHCl_3$/2-propanol, 10:1:1) gave 368 mg (0.90 mmol, 45%) of a colorless oil; $[\alpha]_D^{22}$ = 53.9 (*c* = 1.00, $CHCl_3$). − IR (KBr): $\tilde{\nu}$ = 1744 cm^{-1}, 1680, 1522. − ^1H NMR (400 MHz, $CDCl_3$): δ = 11.15 (d, *J* = 7.8 Hz, 2 H, NH), 8.57 (d, *J* = 7.9 Hz, 2 H, 3-H), 7.63 (t, *J* = 7.9 Hz, 1 H, 4-H), 4.71 (dd, *J* = 7.8/5.0 Hz, 2 H, 2′-H), 3.79 (s, 6 H, OCH_3), 2.39 (dd, *J* = 5.0/2.1 Hz, 2 H, 3′-H), 1.08 (d, *J* = 2.1 Hz, 6 H), 1.06 (d, *J* = 2.1 Hz, 6 H, 4′-H). − ^{13}C NMR (100 MHz, $CDCl_3$): δ = 171.6 (COO), 159.3 (CONH), 141.1 (C-2), 131.4 (C-3), 127.7 (C-4), 58.4 (OCH_3), 52.1 (C-2′), 30.9 (C-3′), 19.2, 18.0 (C-4′). − MS (CI) *m/z* (%): 409 (2) [M^+], 392 (92), 391 (100) [$M^+ - H_2O$]. − $C_{19}H_{28}N_3O_7$ [M^+ + H]: calcd. 410.1927, found 410.1912 (MS).

(2′*S*)-2,6-Bis[(1-methoxycarbonyl-3-methyl)butylaminocarbonyl]pyridine *N*-Oxide (2c): Flash chromatography on SiO_2 (hexanes/$CHCl_3$/2-propanol, 8:3:1) gave 340 mg (0.78 mmol, 39%) of a yellow oil; $[\alpha]_D^{22}$ = 5.2 (*c* = 1.00, $CHCl_3$). − IR (KBr): $\tilde{\nu}$ = 1747 cm^{-1}, 1677, 1522. − ^1H NMR (400 MHz, $CDCl_3$): δ = 10.97 (d, *J* = 7.9 Hz, 2 H, NH), 8.57 (d, *J* = 8.0 Hz, 2 H, 3-H), 7.60 (t, *J* = 8.0 Hz, 1 H, 4-H), 4.84−4.79 (m, 2 H, 2′-H), 3.77 (s, 6 H, OCH_3), 1.80−1.76 (m, 6 H, 3′-H, 4′-H), 1.01−0.99 (m, 12 H, 5′-H). − ^{13}C NMR (100 MHz, $CDCl_3$): δ = 172.7 (COO), 159.2 (CONH), 141.1 (C-2), 131.5 (C-3), 127.6 (C-4), 52.4 (OCH_3), 51.6 (C-2′), 41.1 (C-3′), 25.0 (C-4′), 22.8, 21.8 (5′-H). − MS (CI) *m/z* (%): 455 (21) [M^+ + NH_4], 438 (100) [M^+ + 1], 420 (18), 378 (34), 318 (4), 279 (16). − $C_{21}H_{31}N_3O_7$ (437.49): calcd. C 57.65, H 7.14, N 9.60; found C 57.94, H 7.19, N 8.99.

(2′*S*)-2,6-Bis[(1-methoxycarbonyl-3-thiomethyl)propylaminocarbonyl]pyridine *N*-Oxide (2d): Flash chromatography on SiO_2 (hexanes/acetone, 3:2) gave 431 mg (0.91 mmol, 46%) of a yellow solid; mp. 49°C; $[\alpha]_D^{22}$ = −5.0 (*c* = 1.00, $CHCl_3$). − IR (KBr): $\tilde{\nu}$ = 1744 cm^{-1}, 1676, 1524. − ^1H NMR (400 MHz, $CDCl_3$): δ = 11.11 (d, *J* = 7.5 Hz, 2 H, NH), 8.58 (d, *J* = 8.0 Hz, 2 H, 3-H), 7.62 (t, *J* = 8.0 Hz, 1 H, 4-H), 4.98 (ddd, *J* = 7.5/7.7/7.8 Hz, 2 H, 2′-H), 3.81 (s, 6 H, OCH_3), 2.65 (t, *J* = 7.5 Hz, 4 H, 4′-H), 2.36−2.28 (m, 2 H, 3′-H_a), 2.23−2.09 (m, 2 H, 3′-H_b), 2.14 (s, 6 H, SCH_3). − ^{13}C NMR (100 MHz, $CDCl_3$): δ = 171.7 (COO), 159.2 (CONH), 141.1 (C-2), 131.6 (C-3), 127.8 (C-4), 52.7 (OCH_3), 52.2 (C-2′), 31.5, 30.2 (C-3′, C-4′), 15.5 (SCH_3). − MS (CI) *m/z* (%): 491 (38) [M^+ + NH_4], 474 (100) [M^+ + 1], 458 (40). − $C_{19}H_{27}N_3O_7S_2$ (473.56): calcd. C 48.19, H 5.75, N 8.87, S 13.54; found C 48.14, H 5.75, N 8.70, S 13.63. − X-Ray structure analysis of **2d**: $C_{19}H_{27}N_3O_7S_2$, M_r = 473.56, crystal size 0.90 × 0.42 × 0.16 mm, monoclinic, space group *C*2, *a* = 2388.9(5) pm, *b* = 925.7(2) pm, *c* = 520.27(10) pm, β = 98.720(15)°, *V* = 1.1372(4) nm^3, $\rho_{calcd.}$ = 1.383 Mg m^{-3}, *T* = 173(2) K, *Z* = 2, λ = 71.073 pm. Siemens P4 diffractometer, 2883 reflections collected to 2θ 55°, 2603 independent reflections, 148 refined parameters, *R*1 = 0.0338, *wR*2 = 0.0771. The absolute configuration was confirmed crystallographically: χ = 0.15(8). Programs used: SHELXL-93. See ref.[18]

(1′*R*,2′*S*)-2,6-Bis[2-(1-hydroxy-1-phenyl)propylaminocarbonyl]pyridine *N*-Oxide (2e): Flash chromatography on SiO_2 ($CHCl_3$/hexanes/MeOH, 9:6:1) gave 341 mg (0.76 mmol, 38%) of a colorless solid; mp. 53°C; $[\alpha]_D^{22}$ = 11.5 (*c* = 1.00, $CHCl_3$). − IR (KBr): $\tilde{\nu}$ = 1668 cm^{-1}, 1514. − ^1H NMR (400 MHz, $CDCl_3$): δ = 10.81 (d, *J* = 7.9 Hz, 2 H, NH), 8.51 (d, *J* = 7.9 Hz, 2 H, 3-H), 7.56 (t, *J* = 7.9 Hz, 1 H, 4-H), 7.42 (d, *J* = 6.9 Hz, 4 H, 2′′-H), 7.36 (dd, *J* = 6.9/5.9 Hz, 4 H, 3′′-H), 7.29 (t, *J* = 5.9 Hz, 2 H, 4′′-H), 5.04 (s, 2 H, OH), 4.51 (ddd, *J* = 2.9/7.9/6.9 Hz, 2 H, 2′-H), 3.25 (d, *J* = 2.9 Hz, 2 H, 1′-H), 1.17 (d, *J* = 6.9 Hz, 6 H, 3′-H). − ^{13}C NMR (100 MHz, $CDCl_3$): δ = 159.2 (CONH), 141.3 (C-2), 140.7 (C-1′′), 131.1 (C-3), 128.2, 127.7, 127.6 (C-4), 126.2 (C-2′′, C-3′′, C-4′′, C-5′′, C-6′′), 75.7 (C-1′), 51.9 (C-2′), 14.1 (C-3′). − MS (CI) *m/z* (%): 450 (100) [M^+ + 1], 432 (28), 425 (54), 343 (26), 279 (60), 195 (50). − $C_{25}H_{27}N_3O_5$ (449.51): calcd. C 66.80, H 6.05, N 9.35; found C 66.39, H 6.33, N 9.58.

(2′*S*)-2,6-Bis[(1-methoxycarbonyl-3-thiomethyl)propylaminocarbonyl]pyridine (8): A mixture of dipicolinic acid **4** (140 mg, 0.75 mmol) and thionyl chloride (8.15 g, 5 mL, 70.0 mmol) was refluxed for 2 h. After removal of the remaining thionyl chloride in vacuo, the residue was dissolved in CH_2Cl_2 (5 mL) and added dropwise to an ice-cooled solution of L-methionine methyl ester (262 mg, 1.60 mmol) in CH_2Cl_2 (5 mL). The mixture was stirred for 3 h at room temperature and then hydrolyzed with 1 N NaOH (10 mL). The layers were separated and the aqueous layer was extracted with CH_2Cl_2 (2× 20 mL). After drying the combined organic layers with $MgSO_4$ and evaporating the solvent in vacuo, the crude product was purified by flash chromatography on SiO_2 (ether) to give 230 mg (0.50 mmol, 67%) of a yellow oil; $[\alpha]_D^{22}$ = −8.0 (*c* = 1.00, $CHCl_3$). − IR (film): $\tilde{\nu}$ = 1744 cm^{-1},1679, 1526. − ^1H NMR (400 MHz, $CDCl_3$): δ = 8.62 (d, *J* = 7.9 Hz, 2 H, NH), 8.36 (d, *J* = 7.9 Hz, 2 H, 3-H), 8.06 (t, *J* = 7.9 Hz, 1 H, 4-H), 4.97 (ddd, *J* = 7.9/7.4/5.4 Hz, 1 H, 2′-H), 3.80 (s, 6 H, OCH_3), 2.67 (t, *J* = 7.4 Hz, 2 H, 4′-H), 2.34−2.29 (m, 1 H, 3′-H_a), 2.25−2.18 (m, 1 H, 3′-H_b), 2.14 (s, 6 H, SCH_3). − ^{13}C NMR (100 MHz, $CDCl_3$): δ = 172.0 (COO), 163.2 (CONH), 148.2 (C-2), 139.0 (C-4), 125.3 (C-3), 52.6 (OCH_3), 51.9 (C-2′), 31.1, 30.2

(C-3′, C-4′), 15.4 (SCH_3). − MS (EI) *m/z* (%): 457 (26) [M^+], 398 (20), 383 (100), 351 (24), 328 (21), 268 (45), 252 (12), 220 (13), 194 (25), 162 (26), 134 (10), 124 (11), 106 (17), 78 (13), 61 (31). − $C_{19}H_{27}N_3O_6S_2$: calcd. 457.1341, found 457.1335 (MS).

General Procedure for the Reduction of Ketones (9a−c) to Alcohols (10a−c): To a solution of pyridine *N*-oxide **1**, **2** or pyridine **7**, **8** (0.05 mmol) in THF (5 mL) was added $BH_3 \bullet SMe_2$ (0.5 mL, 0.10 mmol of a 2 M solution in THF) and the resulting mixture was refluxed for 5 min. Then ketone **9** (1.00 mmol) in THF (1.0 mL) was added dropwise and the mixture was refluxed for 5 min.[20] After cooling to room temperature the mixture was hydrolyzed by addition of H_2O (3 mL) and the aqueous layer was extracted with CH_2Cl_2 (3× 30 mL). The combined organic layers were dried with $MgSO_4$, evaporated in vacuo and the crude products **10a**,**b** and **10c** were analyzed by capillary GC-GC and capillary GC respectively, using chiral stationary phases.

1-Phenylethanol (10a): Temperature program: 170°C isothermal for 3 min, then with 5°C min^{-1} up to 200°C (column 1), 100°C isothermal for 20 min, then with 1°C min^{-1} up to 160°C (column 2). *(R)-Isomer:* R_t = 15.25 min. *(S)-Isomer:* R_t = 15.88 min.

1-Phenylpropanol (10b): Temperature program: 170°C isothermal for 3 min, then with 5°C min^{-1} up to 200°C (column 1), 100°C isothermal for 5 min, then with 1°C min^{-1} up to 160°C (column 2). *(R)-Isomer:* R_t = 24.55 min. *(S)-Isomer:* R_t = 25.19 min.

2-Chloro-1-phenylethanol (10c): Temperature: 100°C isothermal. *(S)-Isomer:* R_t = 9.18 min. *(R)-Isomer:* R_t = 11.25 min.

General Procedure for the Addition of Diethylzinc to Benzaldehyde (11): Diethylzinc (2.2 mL, 2.20 mmol of a 1 M solution in hexane) was added dropwise over 5 min at 0°C to a solution of pyridine *N*-oxide **1** or **2** (0.05 mmol) and the resulting mixture was stirred for 20 min at room temperature and then cooled to 0°C. Then benzaldehyde **11** (106 mg, 1.00 mmol) was added dropwise and the mixture was stirred for 72 h at room temperature. After hydrolysis with H_2SO_4 (5 mL, 10% aqueous solution), the mixture was extracted with Et_2O (3× 30 mL), washed with sat. $NaHCO_3$ (30 mL), and dried with $MgSO_4$. After removal of the solvent in vacuo the crude product **10b** was analyzed by capillary GC using chiral stationary phases as described above.

Acknowledgements

Generous financial support by the Deutsche Forschungsgemeinschaft (Gerhard-Hess Prize for S. L.) and the Fonds der Chemischen Industrie is gratefully acknowledged. We would like to thank Bernd Bonnländer for his help with enantio-differentiating gas chromatography.

[1] Review: G. Chelucci, *Gazz. Chim. Ital.* **1992**, *122*, 89−98.
[2] Recent examples: [2a] Q. Yu, T. E. Baroni, L. Liable-Sands, A. L. Rheingold, A. S. Borovnik, *Tetrahedron Lett.* **1998**, *39*, 6831−6834. [2b] I. W. Davies, L. Gerena, N. Lu, R. D. Larsen, P. J. Reider, *J. Org. Chem.* **1996**, *61*, 9629−9630. [2c] H. Nishiyama, M. Kondo, T. Nakamura, K. Itoh, *Organometallics* **1991**, *10*, 500−508. [2d] . A. Evans, J. A. Murry, M. C. Kozlowski, *J. Am. Chem. Soc.* **1996**, *118*, 5814−5815. [2e] D. A. Evans, J. A. Murry, P. von Matt, R. D. Nororos, S. J. Miller, *Angew. Chem.* **1995**, *113*, 864−867; *Angew. Chem. Int. Ed. Engl.* **1995**, *34*, 798−801. [2f] G. Chelucci, V. Caria, A. Saba, *J. Mol. Catal. A: Chem.* **1998**, *130*, 51−55. [2g] G. Sekar, A. DattaGupta, V. K. Singh, *J. Org. Chem.* **1998**, *63*, 2961−2967. [2h] T. Constantieux, J. M. Brunel, A. Labande, G. Buono, *Synlett* **1998**, 49−50. [2i] J.-M. Brunel, T. Constantieux, A. Labande, F. Lubatti, G. Buono, *Tetrahedron Lett.* **1997**, *38*, 5971−5974. [2j] P. C. Hellier, J. S. Bradshaw, J. J. Young, X. X. Zhang, R. M. Reed, *J. Org. Chem.* **1996**, *61*, 7270−7275. [2k] H. Kotsuki, Y. Nakagawa, N. Moriya, H. Tateishi, M. Ochi, T. Suzuki, K. Isobe, *Tetrahedron Asym.* **1995**, *6*, 1165−1174. [2l] A. Bacchi, G. Chelucci, G. Pelizzi, C. Solinas, *J. Chem. Crystallogr.* **1994**, *24*, 659−663. [2m] K. Stingl, J. Martens, *Liebigs Ann. Chem.* **1994**, 485−490. [2n] C. Bolm, M. Ewald, M. Felder, *Chem. Ber.* **1992**, *125*, 1205−1215. [2o] C. Bolm, *Tetrahedron Asym.* **1991**, *2*, 701−704. [2p] J. Uenishi, T. Hiraoka, S. Hata, K. Nishiwaki, O. Yonemitsu, K. Nakamura, H. Tsukube, *J. Org. Chem.* **1998**, *63*, 2481−2487. [2q] Y. Habata, J. S. Bradshaw, X. X. Zhang, R. M. Izatt, *J. Am. Chem. Soc.* **1997**, *119*, 7145−7146. [2r] G. Chelucci, *Tetrahedron Asym.* **1995**, *6*, 811−826. [2s] M. A. Cabras, G. Chelucci, G. Giacomelli, F. Soccolini, *Gazz. Chim. Ital.* **1994**, *124*, 23−25. [2t] C. Bolm, G. Schlingloff, K. Harms, *Chem. Ber.* **1992**, *125*, 1191−1203. [2u] B. Schmidt, D. K. Ehlert, *Tetrahedron Lett.* **1998**, *39*, 3999−4002.
[3] [3a] J. You, X. Yu, X. Li, Q. Yan, R. Xie, *Tetrahedron Asym.* **1998**, *9*, 1197−1203. [3b] S. Kumar, V. Bhalla, H. Singh, *Tetrahedron* **1998**, *54*, 5575−5586.
[4] [4a] M. Palucki, G. J. Mc Cormick, E. N. Jacobsen, *Tetrahedron Lett.* **1995**, *36*, 5457−5460. [4b] E. G. Samsel, K. Srinivasan, J. K. Kochi, *J. Am. Chem. Soc.* **1985**, *107*, 7606−7617. [4c] N. S. Finney, P. J. Pospisil, S. Chang, M. Palucki, R. G. Konsler, K. B. Hansen, E. N. Jacobsen, *Angew. Chem.* **1991**, *109*, 1798−1801; *Angew. Chem. Int. Ed. Engl.* **1991**, *30*, 477−515. [4d] A. Berkessel, M. Frauenkron, *J. Chem. Soc. Perkin Trans. I* **1997**, 2265−2266. [4e] D. L. Hughes, G. B. Smith, J. Liu, G. C. Dezeny, C. H. Senanayake, R. D. Larsen, T. R. Verhoeven, P. J. Reider, *J. Org. Chem.* **1997**, *62*, 2222−2229.
[5] Chiral amine *N*-oxides derived from alkaloids have been used as chiral promoters in a few cases: [5a] T. Petrowitsch, P. Eilbracht, *Synlett* **1997**, 287−288. [5b] V. Derdau, S. Laschat, P. G. Jones, *Heterocycles* **1998**, *48*, 1445−1453. [5c] W. J. Kerr, G. G. Kirk, D. Middlemiss, *Synlett* **1995**, 1085−1086.
[6] M. B. Diana, M. Marchetti, G. Melloni, *Tetrahedron Asym.* **1995**, *6*, 1175−1176.
[7] M. Nakajima, Y. Sasaki, M. Shiro, S. Hashimoto, *Tetrahedron Asym.* **1997**, *8* 341−344.
[8] [8a] A. Albini, *Synthesis* **1993**, 263−277. [8b] N. M. Karayannis, L. L. Pytlewski, C. M. Mikulski, *Coord. Chem. Rev.* **1973**, *11*, 93−159. [8c] R. H. Holm, *Chem. Rev.* **1987**, *87*, 1401−1449. [8d] M. Antolovich, D. J. Philips, A. D. Rae, *J. Chem. Soc. Chem. Commun.* **1984**, 582−583. [8e] M. Antolovich, D. J. Philips, A. D. Rae, *Inorg. Chim. Acta* **1995**, *230*, 139−144.
[9] Y. Hamuro, S. J. Geib, A. D. Hamilton, *J. Am. Chem. Soc.* **1996**, *118*, 7529−7541.
[10] Reviews: [10a] E. J. Corey, C. J. Helal, *Angew. Chem.* **1998**, *110*, 2092−2118; *Angew. Chem. Int. Ed. Engl.* **1998**, *37*, 1986−2012. [10b] L. Deloux, M. Screbnik, *Chem. Rev.* **1993**, *93*, 763−784. [10c] V. K. Singh, *Synthesis* **1992**, *7*, 605−617. [10d] S. Wallbaum, J. Martens, *Tetrahedron Asym.* **1992**, *3*, 1475−1504.
[11] Reviews: [11a] K. Soai, S. Niwa, *Chem. Rev.* **1992**, *92*, 833−856. [11b] R. Noyori, M. Kitamura, *Angew. Chem.* **1991**, *103*, 34−55; *Angew. Chem. Int. Ed. Engl.* **1991**, *30*, 49−70.
[12] I. A. O′Neil, C. D. Turner, S. B. Kalindjian, *Synlett* **1997**, 777−780.
[13] C. Coperet, H. Adolfsson, J. P. Chiang, A. K. Yudin, K. B. Sharpless, *Tetrahedron Lett.* **1998**, *39*, 761−764.
[14] E. Profft, W. Steinke, *J. prakt. Chem.* **1961**, *13*, 59−75.
[15] R. P. Thummel, S. Chirayil, C. Hery, J.-L. Lim, T.-L. Wang, *J. Org. Chem.* **1993**, *58*, 1666−1671.
[16] J. C. Sheehan, G. P. Hess, *J. Am. Chem. Soc.* **1955**, *77*, 1067−1068.
[17] L. E. Barstow, V. J. Hruby, *J. Org. Chem.* **1971**, *36*, 1305−1306.
[18] Crystallographic data for structure **2d** have been deposited with the Cambridge Crystallographic Data Centre as supplementary publication no. CCDC−112394. Copies of the data can be obtained free of charge on application to CCDC, 12 Union Road, Cambridge CB2 1EZ, UK [Fax: (internat.) + 44-1223/336-033; E-mail: deposit@ccdc.cam.ac.uk].
[19] M. P. Gamble, J. R. Studley, M. Wills, *Tetrahedron Lett.* **1996**, *37*, 2853−2856.
[20] In order to test the effect of the temperature on the reaction rate and enantioselectivity, acetophenone **9a** was treated with borane dimethylsulfide (1 equiv.) and ligand **2e** (5 mol-%) in THF at various temperatures. For example, phenylethanol **10a** was obtained in 90% yield albeit with very low enantioselectivity (5% *ee*) after 3 h at room temp. When the reduction was

performed at subambient temperatures, the rate decreased and the product was obtained in racemic form.
[21] M. F. Grundon, D. G. McCleery, J. W. Wilson, *Tetrahedron Lett.* **1976**, *4*, 295−296.
[22] G. Chelucci, D. Berta, D. Fabbri, G. A. Pinna, A. Saba, F. Ulgheri, *Tetrahedron Asym.* **1998**, *9*, 1933−1940.
[23] B. B. Lohray, V. Bushan, in *Organic Synthesis Highlights III*, (Eds.: J. Mulzer, H. Waldmann), Wiley-VCH, Weinheim, **1998**, p. 44−50.
[24] For the use of cysteine-derived bis-β-amino alcohols in borane reduction and dialkylzinc addition see: M. Kossenjans, J. Martens, *Tetrahedron Asym.* **1998**, *9*, 1409−1417.
[25] W. C. Still, M. Kahn, A. Mitra, *J. Org. Chem.* **1978**, *43*, 2923−2925.
[26] C. Wolf, W. A. König, C. Roussel, *Liebigs Ann. Chem.* **1995**, 781−786.

Received December 18, 1998
[I98442]

Thermochemical Study of Reduction and Oxidation Reactions of Molybdovanadophosphoric Heteropolyacids in Aqueous Solutions

E. G. Zhizhina,*[a] V. F. Odyakov,[a] and K. I. Matveev[a]

Keywords: Heteropolyacids / Molybdovanadophosphates / Hydrazine hydrate / Reduction / Oxidations / Thermochemistry

Differential enthalpies of reduction, $-\Delta_r H_{4j}$, have been found at 343 K for 0.2 m aqueous heteropolyacids $H_{3+x}PV_xMo_{12-x}O_{40}$ (HPA-x, where $1 \le x \le 6$) and their salts by hydrazine hydrate (HH). The $-\Delta_r H_{4j}$ values depend on x and m, where $m = [V^{IV}]/[\text{HPA-x}]$. At $m \approx 0$, the initial $-\Delta_r H_{4j}$ value is 436 ± 14 kJ mol^{-1} HH for all HPA-x. For HPA-x with $3 \le x \le 6$, the curves $-\Delta_r H_{4j} = f(m_j)$ have maxima associated with formation and reduction of the outer-sphere cation $V^{V}V^{IV}O_3^{3+}$. A similar maximum is observed on reduction of 0.1 M VO_2ClO_4 in 4 m $HClO_4$. No maxima are observed for the reduction of HPA-1, HPA-2, and salts of HPA-3. For HPA-3 salts, $-\Delta_r H_{4j} = f(m_j)$ depends primarily on the pH of the salt solution, rather than on the nature of the cation. Reduction and oxidation of HPA-x and their salts are reversible reactions. In HPA-x solutions, VO_2^+ in the outer sphere is reduced first, and V^V in the inner coordination sphere of the heteropoly anion is reduced next. Differential enthalpies for the oxidation of the reduced HPA-x by dioxygen ($-\Delta_r H_{2j}$) have been calculated. The sequence of the oxidation of different V^{IV} forms in the reduced H_mHPA-x solutions is the reverse of that for the reduction of the V^V forms in the initial HPA-x solutions.

Introduction

The aqueous solutions of heteropolyacids $H_{3+x}PV_xMo_{12-x}O_{40}$ (HPA-x, $1 \le x \le 6$) of the Keggin structure and their acidic salts with cations such as $M_bH_{3+x-bz}PV_xMo_{12-x}O_{40}$ (where z is the cation charge and b is the number of cation atoms), are widely used as homogeneous oxidation catalysts, for example, in reactions[1][2] such as the oxidation of ethylene to acetaldehyde,[3] C_3-C_8 olefins to ketones,[4][5] CO to CO_2,[6] and H_2S to sulfur.[7] Substituted phenols and hydroxynaphthalenes are selectively oxidized in the presence of these catalysts to *p*-quinones.[8][9] The compounds HPA-x are very promising catalysts for oxidation of many other substrates.

In oxidation catalysis, the ability of HPA-x to perform reversible reductions[10][11] is used. Thus, the oxidation of substrates (Su) by reaction according to Equation 1 is followed by the reduction of HPA-x to H_mHPA-x, where H_mHPA-x = $H_{3+x+m}PV_m^{IV}V_{x-m}^{V}Mo_{12-x}O_{40}$ [where m is the number of vanadium(IV) atoms]. The reduced forms, H_mHPA-x, are oxidized further by dioxygen (reaction according to Equation 2) regenerating the initial HPA-x forms. Thus, reduction and oxidation of HPA-x/H_mHPA-x correspond to the valence transition $V^V \rightarrow V^{IV}$ and back. The substrate oxidation is, therefore, a combined catalytic process.

$$\text{Su} + H_2O + {}^2/_m\ \text{HPA-}x \rightarrow \text{SuO} + {}^2/_m\ H_m\text{HPA-}x \quad (1)$$

$${}^4/_m\ H_m\text{HPA-}x + O_2 \rightarrow {}^4/_m\ \text{HPA-}x + 2\ H_2O \quad (2)$$

$$2\ \text{Su} + O_2 \xrightarrow{\text{HPA-}x} 2\ \text{SuO} \quad (3)$$

[a] Boreskov Institute of Catalysis,
Prospekt Akademika Lavrentieva 5, Novosibirsk, 630090, Russia
Fax: (internat.) + 7-3832/343056
E-mail: matv@catalysis.nsk.su

It is very important to exclude any direct contact between the oxidized substrate and dioxygen, as the latter can form explosive mixtures with gaseous substrates (e.g. C_2H_4). This precaution is also necessary if dioxygen initiates some side reactions. In this case, stages (1) and (2) must be performed in separate reactors.[12]

It is necessary to know the heat effects and enthalpies of each stage, such as $\Delta_r H_1 = -q_1/n_{Su}$ and $\Delta_r H_2 = -q_2/n_{O_2}$ where n is the number of moles and the heats, q and q_2 are the enthalpies of reactions (1) and (2), $\Delta_r H_1$ and $\Delta_r H_2$, respectively.

The enthalpy of reaction (3) is readily found as the difference between standard (tabled) enthalpies of the product and the substrate formation (SuO and Su): $\Delta_r H_3 = \Delta_f H_{SuO} - \Delta_f H_{Su}$. However, the enthalpies of stages (1) and (2) are still unknown, since there is no reliable information in the literature on the enthalpies of HPA-x reduction and oxidation.

Reaction (2) is common for oxidation processes of type (3). However, direct measurements of its heat effects are hindered, because its rate changes by three powers of ten.[13] To calculate the heat effects of reactions (1) and (2), the difference of enthalpies $\Delta_f H_{H_mHPA\text{-}x} - \Delta_f H_{HPA\text{-}x}$ must be known; this difference can be found experimentally using a model reaction. The most reliable and accurate data for $\Delta_r H_2$ were obtained indirectly by measuring the heats of reaction for the oxidation of hydrazine hydrate (HH) by heteropolyacid to release gaseous N_2,[14] that is, heats q_4 of reaction (4).

$$N_2H_4 \cdot H_2O + {}^4/_m\ \text{HPA-}x \rightarrow N_2 \uparrow + {}^4/_m H_m\text{HPA-}x + H_2O \quad (4)$$

If $\Delta_r H_4$ for reaction (4) and $\Delta_r H_5$ for reaction (5) are known, one can readily calculate $\Delta_r H_2$ by Equation (6).

$$N_2H_4 \cdot H_2O + O_2 \rightarrow N_2 + 3\ H_2O \quad (5)$$

 © WILEY-VCH Verlag GmbH, D-69451 Weinheim, 1999 1434–1948/99/0606–1009 $ 17.50+.50/0

$$\Delta_r H_2 = \Delta_r H_5 - \Delta_r H_4 \quad (6)$$

The enthalpies of reactions (1) and (2) for various HPA-x compounds are also significant for steering of catalytic activity of HPA-x ions in these reactions.

The initial (oxidized) forms of HPA-x dissociate reversibly eliminating cation VO_2^+ by reaction (7) due to the acidity of HPA-x itself.[15][16] In turn, the reduced H_mHPA-x forms ($m = x$) eliminate the cation VO^{2+} even more easily by reaction (8),[17][18] resulting in an increase of pH in the course of reduction of HPA-x solutions.[9]

$$(13-x)PV_xMo_{12-x}O_{40}^{(3+x)-} + 27\ H^+ \overset{K_{ox}}{\rightleftharpoons} (12-x)PV_{x-1}Mo_{13-x}O_{40}^{(2+x)-} + 12\ VO_2^+ + H_3PO_4 + 12\ H_2O \quad (7)$$

$$(13-m)PV^{IV}{}_mMo_{12-m}O_{40}^{(3+2m)-} + 51\ H^+ \overset{K_{rel}}{\rightleftharpoons} (12-m)PV^{IV}{}_{m-1}Mo_{13-m}O_{40}^{(1+2m)-} + 12\ VO^{2+} + H_3PO_4 + 24\ H_2O \quad (8)$$

Therefore, the enthalpies $\Delta_r H_1$,and $\Delta_r H_4$ depend on $m = [V^{IV}]/[HPA\text{-}x]$, which is the degree of HPA-x reduction.[17] They also depend on the solvent nature which influences the degree of HPA-x or H_mHPA-x dissociation in reactions (7) and (8).

The only thermochemical study of reaction (4)[14] was performed using HPA-x solutions with a high concentration of SO_4^{2-} anions, which essentially affected the results. The SO_4^{2-} anion forms complexes with both VO_2^+[19] and VO^{2+}.[20][21] Enthalpies of formation for the sulfate complexes are different, and they depend differently on solution pH. In turn, the pH of HPA-x solutions depends on the degree of HPA-x reduction (see Figure 5 in ref.[9]). These features enhance the complexity of the composition of HPA-x solutions,[14] and somehow affect the enthalpy values. In addition, some heat losses caused by scattering were not taken into account,[14] because the heats were measured at room temperature (299 K), when reaction (4) proceeded very slowly (up to 80 min).

Results and Discussion

Here and later, we use index j for the interpolated values of m_j and $\Delta_r H_{4j}$. The same values without an index refer to the reference data.

Reduction of VO_2ClO_4 Solutions by Hydrazine Hydrate

Solutions of VO_2ClO_4 (0.1 M) in $HClO_4$ have a simple composition. They are reduced by hydrazine hydrate (HH) by reaction (9).

$$4\ VO_2^+\ (aq.) + N_2H_4\ (aq.) + 4\ H^+\ (aq.) \rightarrow 4\ VO^{2+}\ (aq.) + N_2\uparrow + 4\ H_2O \quad (9)$$

The calculation of the enthalpy for reaction (9) from the enthalpies of formation $\Delta_f H$ for each component (data from ref.[22]) gives: $-\Delta_r H_9 = 524.8$ kJ mol^{-1} HH. However, experimental $-\Delta_r H_{9j}$ values were often not constant, and changed with α_j, where $\alpha = [VO^{2+}]/([VO^{2+}] + [VO_2^+])$ is the fraction of vanadium reduced to VO^{2+} (aq.) (Figure 1).

When $[HClO_4] = 1$ M, $-\Delta_r H_9$ does not depend on α and is equal to 435 ± 6 kJ mol^{-1} HH (Figure 1, curve 1). When $[HClO_4] = 4$ M, there is a sharp maximum $-\Delta_r H_{9j} = f(\alpha_j)$ (Figure 1, curve 2), which reaches ca. 660 kJ mol^{-1} HH at $[VO_2^+] \approx [VO^{2+}]$. We attribute this maximum to formation of a cation with mixed valences of vanadium by reaction (10).

$$VO_2^+(aq.) + VO^{2+}(aq.) \rightleftharpoons V^VV^{IV}O_3^{3+}\ (aq.) \quad (10)$$

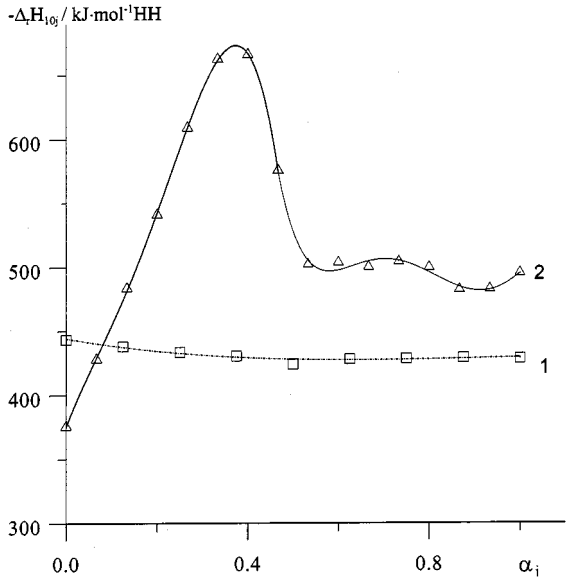


Figure 1. Differential enthalpies for reaction (9) vs. fraction of vanadium reduced to VO^{2+} (aq.) for 0.1 M solutions of VO_2ClO_4: 1: $[HClO_4] = 1$ M; 2: $[HClO_4] = 4$ M

The formation of such a cation was also observed by spectrophotometry in ≥ 3 M H_2SO_4 or $HClO_4$,[23][24] but not in 1 M $HClO_4$.[24] The composition of this cation with mixed valences of vanadium is likely to be $V^V{}_2V^{IV}O_4^{6+}$ rather than $V^VV^{IV}O_3^{3+}$.[23][24] Such a composition is more consistent with the influence of acidity on $V^V{}_2V^{IV}O_4^{6+}$ formation, and the position of the maximum in curve 2 (Figure 1).

$$2\ VO_2^+\ (aq.) + VO^{2+}\ (aq.) + 2\ H^+ \rightleftharpoons V^V{}_2\ V^{IV}O_4^{6+}\ (aq.) + H_2O \quad (10a)$$

Reduction of Aqueous $H_{3+x}PV_xMo_{12-x}O_{40}$ Solutions by Hydrazine Hydrate

For $x = 1$, ^{31}P- and ^{51}V-NMR spectra of HPA-1 solution show the presence of only one heteropoly anion $PVMo_{11}O_{40}^{4-}$.[25] For $x > 1$, these spectra show that solutions of average composition $PV_xMo_{12-x}O_{40}^{(3+x)-}$ actually contain the complex equilibrium mixtures of different indi-

vidual heteropoly anions $PV_yMo_{12-y}O_{40}^{(3+y)-}$, where $y = x, x \pm 1, x \pm 2$, etc.,[25][26] including their isomers.[27] These solutions also contain equilibrium concentrations of VO_2^+ cation, and $H_zPO_4^{(3-z)-}$ anions.[21] The heat evolution coincided at times with the nitrogen liberation. The absence of any heat effects after complete dinitrogen liberation indicates that the equilibration between different heteropoly anions is faster than any interaction of these anions with HH.

The cations VO_2^+ in HPA-x solutions are considered to exist as outer-sphere complexes with $PV_yMo_{12-y}O_{40}^{(3+y)-}$ anions (see below). According to ^{51}V-NMR spectroscopy,[28] an outer-sphere complex of VO_2^+ and HPA-2 is formed from HPA-2 and $Na_6V_{10}O_{28}$ in a of solution water + acetic acid. Thus, reduction of HPA-x solutions in reaction (4) is more complicated than that of VO_2^+ (aq.) in reaction (9).

The relationships $-\Delta_rH_{4j} = f(m_j)$ for reduction of different HPA-x or their salts depend on the number x. On reduction of HPA-1 and HPA-2, $-\Delta_rH_{4j}$ values decrease gradually with an increase of m_j (Figure 2, curves 1 and 2). This decrease is especially sharp when m_j is close to x. The initial $-\Delta_rH_{4j}$ values (at $m_j \leq 0.5$) are 431 ± 11, and 440 ± 14 kJ mol^{-1} HH for HPA-1 and HPA-2, respectively. Note that these values are very close to $-\Delta_rH_{9j} = 435 \pm 6$ kJ mol^{-1} HH for reduction of 0.1 M VO_2ClO_4 in 1 M $HClO_4$. At $m_j > x$, HPA-1 reduces further, indicating a valence transition of Mo^{VI} to Mo^{V} (see Figure 2, curve 1) . Such an over-reduction of HPA-1 was also observed by potentiometry.[18][29]

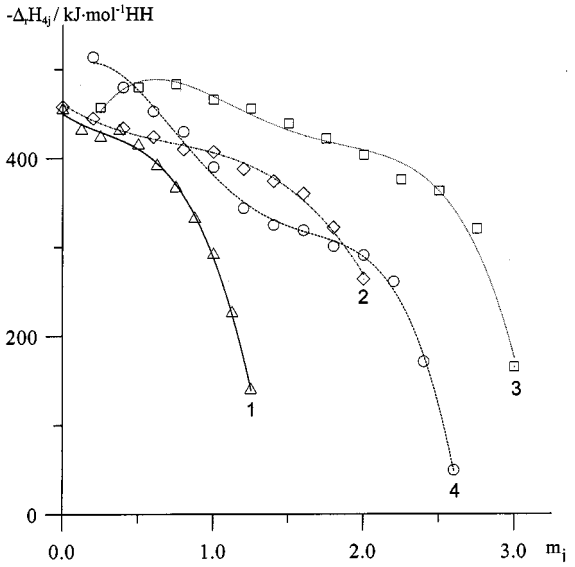


Figure 2. Differential enthalpies for reaction (4) vs. degree of reduction of various HPA-x and salts of HPA-3 in 0.2 M aqueous solutions: 1: $H_4PVMo_{11}O_{40}$; 2: $H_5PV_2Mo_{10}O_{40}$; 3: $H_6PV_3Mo_9O_{40}$; 4: $MgH_4PV_3Mo_9O_{40}$, $Na_2H_4PV_3Mo_9O_{40}$, and $K_2H_4PV_3Mo_9O_{40}$

For HPA-x with $x \geq 3$, the relationships $-\Delta_rH_{4j} = f(m_j)$ have a maximum (Figures 2 and 3), when $-\Delta_rH_{4j}$ values increase slightly at first (as m_j values are low) and then decrease. The higher the value of x (the number of vanadium atoms in HPA-x), the greater the shift of maximum $-\Delta_rH_{4j}$ to the region of high m_j values. Thus, the maximum occurs at $m_j \approx 0.65$ for HPA-3 (Figure 2, curve 3), and at $m_j \approx 1.2$ for HPA-4 and HPA-6 (Figure 3). For the latter solutions, there is a region of m_j after the maximum of $-\Delta_rH_{4j}$, where $-\Delta_rH_{4j}$ values practically do not change and reach 300 ± 7 kJ mol^{-1} HH. This region with a roughly constant $-\Delta_rH_{4j}$ occurs at ca. $2.5 \leq m_j \leq 3.5$, and ca. $3 \leq m_j \leq 5.8$ for HPA-4, and HPA-6, respectively.

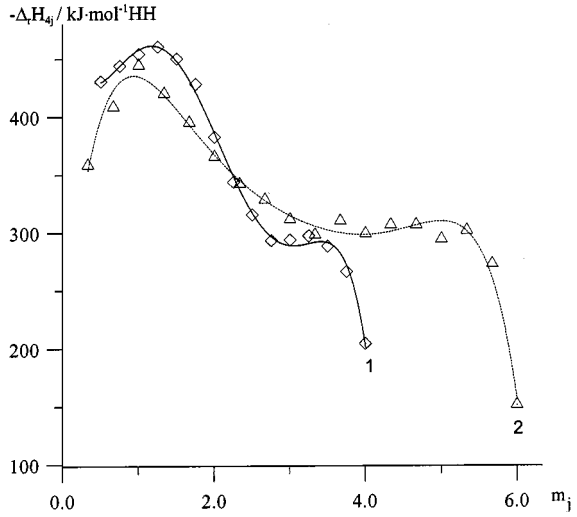


Figure 3. Differential enthalpies for reaction (4) vs. degree of reduction of HPA-x in 0.2 M aqueous solutions: 1: $H_7PV_4Mo_8O_{40}$; 2: $H_9PV_6Mo_6O_{40}$

For HPA-x solutions regenerated with dioxygen or H_2O_2, $-\Delta_rH_{4j} = f(m_j)$ relationships agree with those for fresh HPA-x solutions. Therefore, the composition and properties of HPA-x solutions are completely reversible.

For 0.2 M solutions of salts $M^I{}_2H_4PMo_9V_3O_{40}$ with cation $M^I = Na^+$, K^+, or 1/2 Mg^{2+}, the relationships $-\Delta_rH_{4j} = f(m_j)$ do not depend on the cation nature (Figure 2, curve 4). The $-\Delta_rH_{4j}$ values for these salts are lower than for HPA-3 itself (Figure 2, curve 3). This difference is associated with higher values of $pH_j = \varphi(m_j)$ for HPA-3 salts as compared with HPA-3 itself. Thus, the pH_0 of 0.2 M HPA-3 is ca. 0.4, whereas the pH_0 of each 0.2 M twice-substituted salt of HPA-3 is ca. 0.6.

Table 1. Dependence of m_j and Δ_rH_{4j} on the pH_j value for 0.2 M solutions of HPA-3 and its magnesium salt; index a refers to the acid, index s refers to the salt

0.2 M solution	pH_j	Interpolated values m_{ja} or m_{js}	$-\Delta_rH_{4j}$ [kJ mol^{-1} HH]
$H_6PMo_9V_3O_{40}$	0.8	1.65	429
$MgH_4PMo_9V_3O_{40}$		0.75	435
$H_6PMo_9V_3O_{40}$	1.0	2.14	391
$MgH_4PMo_9V_3O_{40}$		1.06	381

As m increases, the pH values of different HPA-x or their salts solutions increase too.[9] That is, $pH = \varphi(m)$. We chose m_{ja} values for HPA-3 itself, and m_{js} values for HPA-3 salts

in order to obtain the same pH_j values for their solutions (see Table 1). It is proved that $-\Delta_r H_{4j}$ values are very similar, when pH_j are identical. Thus, relationships $-\Delta_r H_{4j} = f(m_j)$ for HPA-x salts depend primarily on the pH of HPA-x salt solution rather than on the nature of cation M.

For partially reduced 0.2 M solutions of HPA-x, the pH values are limited within $0.4 \leq pH \leq 1.5$.[9] At these pH values, cation VO_2^+ (aq.) is readily hydrolyzed to acid $H_2V_{12}O_{31}\cdot xH_2O$,[30] whose solubility is 0.047 g at V L^{-1} in 0.2 M $HClO_4$.[31] According to ^{51}V-NMR spectroscopy, the equilibrium concentration of VO_2^+ is about 0.1 M, 0.16 M, and 0.4 M in 0.2 M solution of HPA-3, HPA-4, and HPA-6, respectively.[26] Such a concentration is much higher than the equilibrium concentration of VO_2^+ in the absence of heteropoly anions and other complexing agents. Therefore, VO_2^+ is not free in HPA-x solutions. It evidently forms outer-sphere complexes with heteropoly anions. Thus, the solvated large heteropoly anion (> 1.3 nm in size[32]) is considered as an acidic particle with weakly bound less acidic cations VO_2^+ and VO^{2+}. (Their sizes do not exceed 0.3 nm.[33])

Reaction (10) between cations VO_2^+ and VO^{2+} can proceed either in 4 M $HClO_4$ or likely in the outer coordination sphere of HPA-x with $3 \leq x \leq 6$. This follows from the similarity of the position of the maxima in curves $-\Delta_r H_{9j} = f(\alpha_j)$ (Figure 1), and $-\Delta_r H_{4j} = f(m_j)$ (Figures 2 and 3). However, the maxima in curves $-\Delta_r H_{4j} = f(m_j)$ are less sharp than in curve $-\Delta_r H_{9j} = f(\alpha_j)$. It seems that the enthalpy of reaction (10) in the outer coordination sphere of the heteropoly anion is probably less than in $HClO_4$ solution.

For 0.2 M HPA-1, HPA-2, and salts of HPA-3 solutions, there are no maxima in the $-\Delta_r H_{4j} = f(m_j)$ curves. This is associated with a low equilibrium concentration of VO_2^+ in these solutions. The ^{51}V-NMR spectra indicate that the VO_2^+ concentration is zero, < 0.01 M, and about 0.1 M in 0.2 M solution of HPA-1, HPA-2, and HPA-3, respectively.[26] The equilibrium concentration of VO_2^+ in solutions of HPA-x salts decreases with increasing pH.[34] Therefore, it is lower for solutions of HPA-3 salts than for those of HPA-3 itself. This explains the absence of maximum $-\Delta_r H_{4j} = f(m_j)$ on the reduction of HPA-3 salts solutions.

Values of $-\Delta_r H_4$ for solutions of VO_2HSO_4 and HPA-x in sulfate medium were found per 1 mole of HPA-x.[14] We recalculated them per 1 mole of HH, and found that they ranged from 679 to 879 kJ mol^{-1} HH. Rather high values of $-\Delta_r H_4$ for sulfate medium probably indicate, that complexes of SO_4^{2-} with VO^{2+}[20][21] are much stronger than with VO_2^+.[19]

The run of curves $-\Delta_r H_{4j} = f(m_j)$ for $H_{3+x}PV_xMo_{12-x}O_{40}$ solutions shows a definite sequence of reduction of different forms of vanadium(V) in these solutions. At lower m_j, the outer-sphere cation VO_2^+ is likely to be reduced first ($-\Delta_r H_{4j}$ = 431 ± 14 kJ mol^{-1} HH). For HPA-2, this quasi-free cation is reduced at $m_j \leq 0.5$. Note that the normal oxidation potential of VO_2^+ (aq.)/VO^{2+} (aq.) couple (1.00 V[22]) is higher than that of molybdovanadophosphates (from 0.68 to 0.715 V[29]). For HPA-x with $3 \leq x \leq 6$, it is reduced in the region of initial and maximal values of $-\Delta_r H_{4j}$. Vanadium(V) in the structure (inner sphere) of heteropoly anions $PV_yMo_{12-y}O_{40}^{(3+y)-}$ is reduced next. In this case, there is a region of curves $-\Delta_r H_{4j} = f(m_j)$ with a relatively small inclination (for HPA-2 and HPA-3) or relatively constant $-\Delta_r H_{4j}$ = 300 ± 7 kJ mol^{-1} HH (for HPA-4 and HPA-6). Figure 3 illustrates that this region has a longer length for HPA-6 than for HPA-4. We assume that the $H_{3+x+m}PV^{IV}{}_mV^V{}_{x-m}Mo_{12-x}O_{40}$ formed dissociates to eliminate vanadium(IV) as a quasi-free cation VO^{2+} [see Equation (8)]. Thus, the concentration of VO^{2+} in the outer sphere of heteropoly anions becomes higher than the initial concentration of VO_2^+ in the same sphere. (For HPA-2 solutions, this is also shown in ref.[35]) At the last stage, when m_j values are rather close to x, $-\Delta_r H_{4j}$ drops. In this stage, vanadium(V) in the structure of heteropoly anion is reduced without elimination of the cation VO^{2+}.

Oxidation of $H_{3+x+m}PV^{IV}{}_mV^V{}_{x-m}Mo_{12-x}O_{40}$ Solutions by Dioxygen

The calculated relationships $-\Delta_r H_{2j} = f(m_j)$ for oxidation of 0.2 M solutions of $H_{3+x+m}PV^{IV}{}_mV^V{}_{x-m}Mo_{12-x}O_{40}$ (H_mHPA-x) by dioxygen are shown in Figure 4. It follows from Equation (6) that changes in $-\Delta_r H_{2j}$ are always contrary to changes in $-\Delta_r H_{4j}$. For lower H_mHPA-x (x = 1, 2), the values of $-\Delta_r H_{2j}$ gradually decrease with decreasing m_j. For H_mHPA-x with $3 \leq x \leq 6$, they go through a minimum. For H_mHPA-x with x = 4 or 6, there is a region with relatively constant $-\Delta_r H_{2j}$ values (306 ± 7 kJ mol^{-1} O_2) at a rather high m_j (Figure 4). This region for oxidation of H_mHPA-x is similar to that for reduction of HPA-x (see Figure 3).

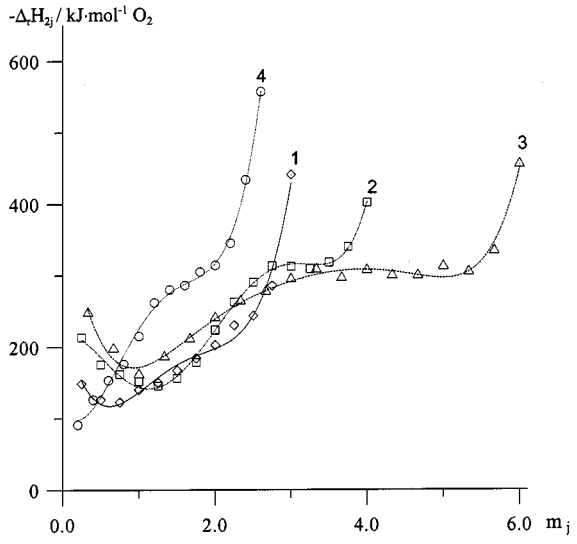


Figure 4. Differential enthalpies for reaction (2) vs. degree of reduction of HPA-x in 0.2 M aqueous solutions: 1: $H_{6+m}PV^{IV}{}_mV^V{}_{3-m}Mo_9O_{40}$; 2: $H_{7+m}PV^{IV}{}_mV^V{}_{4-m}Mo_8O_{40}$; 3: $H_{9+m}PV^{IV}{}_mV^V{}_{6-m}Mo_6O_{40}$; 4: $MgH_{5+m}PV^{IV}{}_mV^V{}_{4-m}Mo_8O_{40}$, $Na_2H_{5+m}PV^{IV}{}_mV^V{}_{4-m}Mo_8O_{40}$, and $K_2H_{5+m}PV^{IV}{}_mV^V{}_{4-m}Mo_8O_{40}$

We found earlier that the rates of reaction (2) decreased with decreasing m_j.[13] This means that changes in $-\Delta_r H_{2j}$ follow the changes in the rates of reaction (2).

The sequence of oxidation of different vanadium (IV) forms in $H_{3+x+m}PV^{IV}{}_mV^V{}_{x-m}Mo_{12-x}O_{40}$ solutions is evidently the reverse of the sequence of reduction of different vanadium (V) forms in $H_{3+x}PV_xMo_{12-x}O_{40}$ solutions. At the highest values of m_j, vanadium(IV) in the structure of anions $PV^{IV}{}_mV^V{}_{y-m}Mo_{12-y}O_{40}{}^{(3+x+m)-}$ is oxidized with high enthalpies $-\Delta_r H_{2j}$, which gradually decrease. Subsequently, at the middle values of m_j, the outer-sphere VO^{2+}, weakly bound with heteropoly anion $H_mHPA\text{-}x$, is oxidized to vanadium(V) which enters the structure of the heteropoly anion. (Outer-sphere complexes of the cation VO^{2+} with heteropoly anions are likely to be formed, for example, in dehydration of hydrated VO^{2+} salts of $H_4SiW_{12}O_{40}$ or $H_3PMo_{12}O_{40}$ at 423 to 523 K.[36]) Such regions are observed for HPA-x with $2 \leq x \leq 6$. At the lowest m_j, the outer sphere VO^{2+} is oxidized to $VO_2{}^+$ with the lowest $-\Delta_r H_{2j}$ values (from 120 to 180 kJ mol^{-1} O_2) remaining in the outer sphere. Cations $VO_2{}^+$ and VO^{2+} in the outer sphere of the heteropoly anion can probably interact reversibly with each other to yield mixed valence cations.

Thus, the thermochemical study of the $H_{3+x}PV_xMo_{12-x}O_{40}$ reduction and the $H_{3+x+m}PV^{IV}{}_mV^V{}_{x-m}Mo_{12-x}O_{40}$ oxidation in aqueous solutions proves that the composition of heteropoly anions changes reversibly in the course of reactions (1) and (2).[11] In these conversions, the cations $VO_2{}^+$ and VO^{2+} participate and can also interact in the outer coordination sphere of the heteropoly anion.

Experimental Section

We used HPA-x solutions containing no foreign anions which could act as complexing agents. Reaction (4) was carried out at 343 ± 0.1 K for 5 to 15 min. Under these conditions, the effect of uncontrolled factors on measuring data was minimal.

For preparing 0.2 M aqueous solutions of $H_{3+x}PV_xMo_{12-x}O_{40}$ (HPA-x, $1 \leq x \leq 6$), the reaction of H_3PO_4 and MoO_3 with an aqueous solution of $H_6V_{10}O_{28}$ was used.[26] The initial pH value of the HPA-x solutions (hereafter designated as pH_0) ranged from 0.35 to 0.4. For preparing 0.2 M solutions of HPA-3 salts of $M^I{}_2H_4PMo_9V_3O_{40}$ composition, metal carbonates were dissolved in the 0.2 M solution of HPA-3. Values of the pH of prepared solutions (HPA-x and their salts) were measured using a digital ionometer I-130.

For preparing 0.1 M solutions of VO_2ClO_4 in $HClO_4$, V_2O_5 was dissolved in cold 5% H_2O_2;[37] the solutions of the peroxyvanadium compounds produced were decomposed to yield O_2 and $H_6V_{10}O_{28}$,[37] which was transformed to VO_2ClO_4 using the calculated amount of $HClO_4$. An analogous 0.2 M solution of VO_2ClO_4 in 1 M $HClO_4$ could not be prepared either by our method or by the direct dissolution of V_2O_5 in $HClO_4$.[38] Hydrazine hydrate (of analytical grade purity) was used as a ca. 10 M aqueous solution, whose precise concentration was determined by iodometry.[39]

Our experiments were carried out in a thermostated Thiane-Calvet glass reactor-calorimeter[40] (150 mL in volume), equipped with a stirrer. The reactor was adapted to studies of liquid-phase reactions. The high sensitivity of the calorimeter was provided by two sensors (thermocouple batteries) connected towards each other. The sensors measured the temperature difference between the inner reactor part and the outer thermostated water and the sensor signals were then magnified and registered by an integrator. The heat released in the reactor was proportional to the temperature difference and the duration of heat liberation, recorded by the integrator. The gas space of the reactor was connected to a thermostated burette for measuring the volume of released dinitrogen. The proportionality coefficient K between the released heat q_{4i} and a number of heat pulses k_i on the integrator was found by a current calibration of the reactor-calorimeter. One pulse of the integrator corresponded to 0.0335 J. The average error of the q_{4i} measurements was within ± 2%. The volume of dinitrogen released, V_{gi}, was recalculated to the number of moles n_{gi}.

Each solution under study (HPA-x or VO_2ClO_4) was tested in 3−5 runs in dinitrogen, q_{4i} and V_{gi} being measured. During a run, 7−12 small portions of HH solution (thoroughly agitated) were injected through a rubber membrane into the reactor, containing 100 mL of the solution being under study. This permitted a stepwise increase of m_i, allowing calculation of differential enthalpies $-\Delta_r H_{4i}$ per mole of HH, which depend on the instantaneous m_i. We used fresh solutions of HPA-x as well as those reoxidized by dioxygen or H_2O_2. Since the heat of dilution of ca. 10 M HH solution is below 8.6 kJ mol^{-1},[41] it does not exceed the errors of our measurements and we therefore did not take it into account.

All heat effects were observed only in the course of dinitrogen liberation. The number of moles of released nitrogen, n_{gi}, was equal to that of introduced HH with an accuracy of ± 1%. This proves that vanadium(V) in the HPA-x solution was reduced stoichiometrically by Equation (4a), and any side conversions of HH did not occur.

$$4\,[V^V]_{HPA\text{-}x} + N_2H_4{\cdot}H_2O \rightarrow 4\,[V^{IV}]_{H_mHPA\text{-}x} + 4\,H^+ + H_2O + N_2\uparrow \quad (4a)$$

When the reactor contained $n_L = C_LV_L$ moles of HPA-x, the degree of reduction of HPA-x increased to $m_i = m_{i-1} + 4\,n_{gi}/n_L$ after the ith injection of HH. The measured differential heats, $q_{4i} = K{\cdot}k_i$ were related to the average degree of HPA-x reduction $m_i = 0.5\,(m_{i-1} + m_i)$. The enthalpy of reaction (4a) was calculated in all cases for 1 mole of dinitrogen (HH, respectively): $\Delta_r H_{4i} = -q_{4i}/n_{gi}$.

The sum of reactions (4) and (2) corresponds to reaction (5). At 343 K, the enthalpy of this reaction, $\Delta_r H_5$, was calculated from the standard formation enthalpies of H_2O and $N_2H_4{\cdot}H_2O$,[22] and is approximately equal to 606 kJ·mol^{-1} (Equation 11).

$$\Delta_r H_2 = -606 - \Delta_r H_4 \quad (11)$$

The m_i and corresponding $\Delta_r H_{4i}$ and $\Delta_r H_{2i}$ values were calculated using a special computer program. To interpolate $\Delta_r H_{4i} \rightarrow \Delta_r H_{4j}$ and $\Delta_r H_{2i} \rightarrow \Delta_r H_{2j}$, we used the standard programs for uniformly distributed m_j, followed by averaging for several runs. The interpolation errors were below ± 2.5%. The total error for $\Delta_r H_{4j}$ and $\Delta_r H_{2j}$ did not exceed ± 4.5%.

Acknowledgments

The authors thank Dr. Yu. D. Pankratiev for assistance in experiments, and Dr. R. I. Maksimovskaya for a discussion about the composition of HPA-x solutions.

[1] R. J. J. Jansen, H. M. van Veldhuisen, M. A. Schwegler, H. van Bekkum, *Recl. Trav. Chim. Pays-Bas* **1994**, *113*, 115−135.
[2] I. V. Kozhevnikov, *Chem. Rev.* **1998**, *98*, 171−198.
[3] K. I. Matveev, E. G. Zhizhina, N. B. Shitova, L. I. Kuznetsova, *Kinetika i Kataliz* **1977**, *18*, 380−386; *Chem. Abstr.* **1977**, *87*, 22002a.
[4] V. F. Odyakov, K. I. Matveev, N. L. Litvinenko, *Issledovanie svoistv i primenenie geteropolikislot v katalize,* Institute of Catalysis, Novosibirsk, **1978**, p. 233−240; *Chem. Abstr.* **1979**, *91*, 19842b.
[5] F. A. Chernyshkova, D. V. Mushenko, G. N. Gvozdovskii, L. N. Romanova, V. F. Odyakov, K. I. Matveev, V. I. Fedorova, ref.[4], p. 229−232; *Chem. Abstr.* **1979**, *91*, 4391f.
[6] E. G. Zhizhina, L. I. Kuznetsova, R. I. Maksimovskaya, S. N. Pavlova, K. I. Matveev, *J. Mol. Catal.* **1986**, *38*, 345−353.
[7] K. I. Matveev, L. I. Rachkovskaya, I. V. Kozhevnikov, ref.[4], p. 220−223; *Chem. Abstr.* **1979**, *90*, 142593c.
[8] O. A. Kholdeeva, A. V. Golovin, I. V. Kozhevnikov, *React. Kinet. Catal. Lett.* 1992, *46*, 107−113.
[9] K. I. Matveev, V. F. Odyakov, E. G. Zhizhina. *J. Mol. Catal., A: Chem.* **1996**, *114*, 151−160.
[10] K. I. Matveev, ref.[4], p. 3−17; *Chem. Abstr.* **1979**, *90*, 142594d.
[11] K. I. Matveev, I. V. Kozhevnikov, *Kinetika i Kataliz* **1980**, *21*, 1189−1198; *Chem. Abstr.* **1981**, *94*, 29616g.
[12] R. Jira, W. Blau, D. Grimm, *Hydrocarbon Process.* **1976**, *55*, 97−100.
[13] Patent 1584200, USSR, *Izobreteniya N* **1994**, *22*, 196; *Chem. Abstr.* **1995**, *123*, 285237a.
[14] E. N. Yurchenko, L. G. Matvienko, L. I. Kuznetsova, Yu. D. Pankratiev, K. I. Matveev, *React. Kinet. Catal. Lett.* **1976**, *4*, 405−411.
[15] P. Souchay, F. Chauveau, P. Courtin, *Bull. Soc. Chim. Fr.* **1968**, 2384−2389.
[16] L. G. Detusheva, E. N. Yurchenko, *Koord. Khim.* **1990**, *16*, 930−934; *Chem. Abstr.* **1990**, *113*, 121647b.
[17] L. I. Kuznetsova, E. N. Yurchenko, R. I. Maksimovskaya, K. I. Matveev, *Koord. Khim.* **1976**, *2*, 67−70; *Chem. Abstr.* **1976**, *84*, 112446r.
[18] V. F. Odyakov, E. G. Zhizhina, K. I. Matveev, *Zh. Neorg. Khim.*, to be published.
[19] A. P. Filippov, I. V. Härsing, *Zh. Neorg. Khim.* **1978**, *23*, 1523−1528; *Chem. Abstr.* **1978**, *89*, 66247e.
[20] H. Strehlow, H. Wendt, *Inorg. Chem*. **1963**, *2*, 6−10.
[21] A. A. Ivakin, E. M. Voronova, *Zh. Neorg. Khim.* **1973**, *18*, 1809−1812; *Chem. Abstr.* **1973**, *79*, 108728p.
[22] *Standard Potentials in Aqueous Solution* (Eds.: A. J. Bard, R. Parsons, J. Jordan), Marcel Dekker, New York and Basel, **1985**.
[23] A. P. Filippov, I. Härsing, E. Kirjanen, I. Kirjanen, *Izv. Akad. Nauk Estonskoi SSR, Ser. Khim.* **1981**, *30*, 235−241; *Chem. Abstr.* **1981**, *95*, 139622j.
[24] P. Blanc, C. Madic, J. P. Launay, *Inorg. Chem.* **1982**, *21*, 2923−2928.
[25] R. I. Maksimovskaya, M. A. Fedotov, V. M. Mastikhin, L. I. Kuznetsova, K. I. Matveev, *Dokl. Akad. Nauk SSSR* **1978**, *240*, 117−120; *Chem. Abstr.* **1978**, *89*, 31722d.
[26] V. F. Odyakov, E. G. Zhizhina, R. I. Maksimovskaya, K. I. Matveev, *Kinet. Catal.* **1995**, *36*, 733−738.
[27] L. Pettersson, I. Andersson, A.Selling, J. H. Grate, *Inorg. Chem.* **1994**, *33*, 982−993.
[28] O. A. Kholdeeva, R. I. Maksimovskaya, *Zh. Neorg. Khim.* **1992**, *37*, 1349−1354; *Chem. Abstr.* **1992**, *117*, 225202b.
[29] V. F. Odyakov, L. I. Kuznetsova, K. I. Matveev, *Zh. Neorg. Khim.* **1978**, *23*, 457−460; *Chem. Abstr.* **1978**, *88*, 128246u.
[30] R. N. Pletnev, A. A. Ivakin, V. V. Gorshkov, A. K. Chirkov, *Dokl. Akad. Nauk SSSR* **1975**, *224*, 106−108; *Chem. Abstr.* **1976**, *84*, 10669y.
[31] A. A. Ivakin, A. P. Yatsenko, N. S. Matveeva, *Zh. Neorg. Khim.* **1976**, *21*, 1335−1340; *Chem. Abstr.* **1976**, *85*, 37775n.
[32] Y. Sasaki, *Nippon Kesshogaku Kaishi (J. Crystallogr. Soc. Jpn.)* **1975**, *17*, 127−144.
[33] P. Kirkegaard, J. M. Longo, *Acta Chem. Scand.* **1965**, *19*, 1906−1914.
[34] V. F. Odyakov, E. G. Zhizhina, R. I. Maksimovskaya, K. I. Matveev, *Zh. Neorg. Khim.* **1998**, *43*, 1451−1455.
[35] L. Pettersson, *Polyoxometalates: From Platonic Solids to Anti-Retroviral Activity* (Eds.: M. T. Pope, A. Müller), Kluwer, Dordrecht, **1994**, p. 27−40.
[36] E. Cadot, C. Marchal, M. Furnier, A. Tézé, G. Hervé, ref.[35], p. 315−326.
[37] K. F. Jahr, F. Preuss, *Chem. Ber.* **1965**, *98*, 3297−3303.
[38] M. J. La Salle, J. W. Cobble, *J. Phys. Chem.* **1955**, *59*, 519−524.
[39] J. Čihalík, *Potenciometrie*, ČSAV, Praha, **1961**, p. 512.
[40] E. Calvet, H. Prat, *Microcalorimétrie*, Masson et Cie, Paris, **1956**.
[41] N. V. Korovin, *Gidrazin*, Khimiya, Moscow, **1980**, p. 25.

Received July 10, 1998
[I98225]

Synthesis and ^{1}H-, ^{15}N-, ^{31}P-, ^{183}W-Multinuclear Magnetic Resonance Study of the Cyclotriphosphazenes $[N_3P_3(dobp)_2(OC_5H_4N\text{-}4)_2]$ and $[N_3P_3(dobp)(OC_5H_4N\text{-}4)_4]$ and Their $W(CO)_5$ Complexes (dobp = 2,2′-dioxybiphenyl)

Gabino A. Carriedo,*[a] Francisco J. García Alonso,[a] José L. García,[a] Rodrigo J. Carbajo,[a] and Fernando López Ortiz*[b]

Keywords: Cyclotriphosphazenes / Oxypyridine / Carbonyltungsten compounds / NMR spectroscopy / Heterocycles

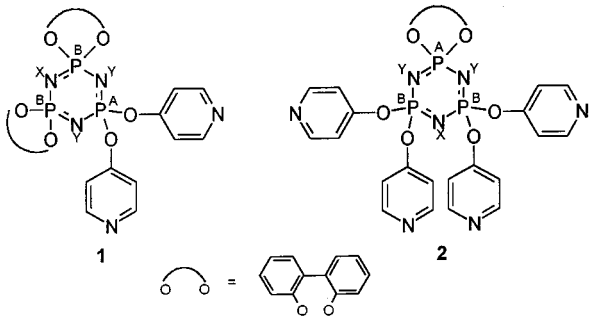
The reactions of $[N_3P_3(dobp)_2Cl_2]$ and $[N_3P_3(dobp)Cl_4]$ with a mixture of HOC_5H_4N-4 and K_2CO_3 in acetone give the cyclotriphosphazenes $[N_3P_3(dobp)_2(OC_5H_4N\text{-}4)_2]$ and $[N_3P_3(dobp)(OC_5H_4N\text{-}4)_4]$, respectively. These compounds react with $[W(MeOH)(CO)_5]$ in methanol to give mixtures of the polymetallic complexes $[N_3P_3(dobp)_2(OC_5H_4N\text{-}4)_2\{W(CO)_5\}_x]$ (x = 1, 2) and $[N_3P_3(dobp)(OC_5H_4N\text{-}4)_4\{W(CO)_5\}_x]$ (x = 1–4), which are unstable in solution, slowly undergoing loss of the pentacarbonyl moiety. A complete characterization by multinuclear ^{1}H, ^{15}N, ^{31}P, ^{183}W magnetic resonance has revealed that the complexation of the N atom of one 4-oxypyridine ligand by the $W(CO)_5$ fragment has a measurable effect on other parts of the phosphazene molecule very far away from the coordination site. The changes observed in $\delta^{183}W$ have been used to identify the components in mixtures of compounds incorporating different numbers of tungsten atoms in the molecule. The characterization of less sensitive nuclei has been accomplished by means of indirect detection methods.

Introduction

Polyphosphazenes bearing aryloxy side groups are materials with interesting properties. For example, they exhibit fire-retardant properties,[1] have high refractive indices,[2] and might find application in non-linear optics,[3] as ferroelectric materials,[4] as liquid crystals,[5] or as photoactive materials.[6] In all applications, their properties depend on the substituents linked to the aryloxy rings. One way of modifying the phenoxy moiety would be the introduction of a nitrogen atom into the ring. The resulting polymers would then contain pyridine side groups with N-donor sites available for metal complexation,[7] opening new possibilities for modifying their properties. The key aspect of this chemistry can be envisaged as being the incorporation of transition metals into the structure of the polymer.

At a macromolecular level, the evaluation of structural effects induced by the side groups bonded to phosphorus is difficult. However, a reasonable starting point would be to focus on small model compounds suitable for NMR-spectroscopic characterization. This strategy is well documented with cyclotriphosphazenes as model molecules,[8] although the number of cyclotriphosphazenes complexed to transition metals through the side groups remains relatively few.[9][10] Recently, we reported the synthesis of several carbonylmanganese complexes of cyclic phosphazenes bearing either nitrile or pyridine ligands.[11] In principle, the incorporated transition metal atom might have constituted a probe for assessing structural and bonding effects of the coordination, in view of the high sensitivity of such nuclei to subtle electronic and steric effects in the molecule.[12] However, ^{55}Mn is a quadrupolar nucleus (I = 5/2) with a medium-sized quadrupole moment ($Q = 0.55 \times 10^{-28}$ m^2). Consequently, very broad signals can be expected,[13] which would be useless for the measurement of small changes in the nuclear shielding. On the contrary, ^{183}W would give the characteristic sharp signals of a spin 1/2 nucleus, albeit with the difficulty presented by its low sensitivity. Fortunately, this drawback can easily be overcome through the use of indirect detection methods.[14] In fact, ^{183}W is one of the most extensively studied transition metal nuclei.[12a,15]

In this article, we describe the multinuclear magnetic resonance characterization of the cyclotriphosphazenes **1** and **2** (Scheme 1), as well as that of their pentacarbonyltungsten complexes **3**–**11**, formed by adding variable amounts of the labile complex $[W(MeOH)(CO)_5]$ in methanolic solution. The study extends to the nuclei ^{1}H, ^{15}N, ^{31}P, and ^{183}W.



Scheme 1. Starting cyclotriphosphazenes

[a] Departamento de Química Orgánica e Inorgánica, Facultad de Química, Universidad de Oviedo,
C/ Julián Clavería s/n, E-33071 Oviedo, Spain
[b] Universidad de Almería, Área de Química Orgánica,
Cañada de San Urbano s/n, E-04120 Almería, Spain

 © WILEY-VCH Verlag GmbH, D-69451 Weinheim, 1999 1434–1948/99/0606–1015 $ 17.50+.50/0

Results

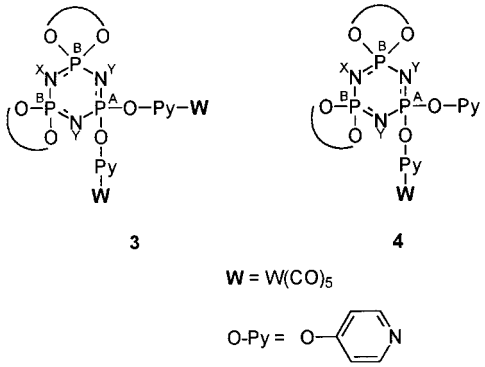
The phosphazenes bearing oxypyridine groups $[N_3P_3(dobp)_2(OC_5H_4N\text{-}4)_2]$ (**1**) and $[N_3P_3(dobp)(OC_5H_4N\text{-}4)_4]$ (**2**) were prepared from the corresponding chlorophosphazenes and HOC_5H_4N-4 with K_2CO_3 in acetone, following the general method published previously.[16]

The NMR spectra of **1** and **2** are relatively simple and the relevant ^1H, ^{31}P, and ^{15}N data are collected in Table 1. For the discussion below we will focus on the protons *ortho* to the nitrogen atom of the pyridine ring (hereafter denoted H^o), since these are subject to the largest shielding modifications upon coordination of tungsten. Their signals appear at $\delta = 8.65$ and $\delta = 8.55$ in compounds **1** and **2**, respectively {cf. $\delta H^o = 7.68$ in 4-hydroxypyridine and $\delta H^o = 8.5$ in $[N_3P_3(OC_5H_4N\text{-}4)_6]$[11]}.

The ^{15}N chemical shifts of **1** and **2** lie within the expected range for nitrogen atoms incorporated into cyclotriphosphazene[17][18] or pyridine rings.[19] The nitrogen atoms of the phosphazene could be straightforwardly identified through their correlations in the 2D $^{31}P,^{15}N\{^1H\}$-HMQC spectra. The phosphorus nucleus labelled A shows a cross-peak with only one nitrogen atom, while that labelled B correlates with the two heterotopic nitrogen nuclei of the ring. The $^1J(^{31}P,^{15}N)$ coupling constants were measured from the ^{15}N satellites in the ^{31}P-NMR spectra obtained by performing the $^{31}P,^{15}N\{^1H\}$-HMQC pulse sequence in the 1D mode.

Addition of phosphazene **1** to a solution of two equivalents of $[W(MeOH)(CO)_5]$ in methanol resulted in a mixture of the bi- and monometallic complexes $[N_3P_3(dobp)_2(OC_5H_4N\text{-}4)_2\{W(CO)_5\}_x]$, $x = 2$ (**3**), $x = 1$ (**4**) (Scheme 2), containing a slightly variable amount of unreacted **1**, depending on the isolation procedure used. Increasing the amount of the pentacarbonyltungsten reagent gave mixtures richer in **3**, but a very large excess had to be used in order to generate exclusively this bimetallic complex. Moreover, the ^1H- and ^{31}P-NMR spectra showed that the latter, as well as the mixtures, continuously lose $W(CO)_5$ in solution (ca. 8% per month), a process which is much slower in the solid state as monitored by NMR measurements on freshly prepared samples from different stocks of tungsten complexes. By monitoring the relative intensities of the signals of the *ortho* protons of the three species, it could be concluded that the step from **3** to **4** is slightly faster than that from **4** to **1**. The assignment of the signals to the complexes **4** and **3** was based on the variation of their intensities with the $W(CO)_5$ content in the mixtures.

Taking compound **1** as a reference, coordination at one of the pyridine rings in compound **4** leads to a deshielding of 0.16 ppm of the protons *ortho* to the nitrogen atom. This shift increases to 0.20 ppm in **3**, where both pyridine rings are coordinated to tungsten (Table 1). The signal due to the *ortho* protons of the uncoordinated pyridine of **4** is practically unaffected. A similar trend is observed in the ^{31}P-NMR signals: P_A is deshielded by 0.06 ppm in **4** and by 0.09 ppm in **3**. Interestingly, P_B seems to be more sensitive to the coordination to $W(CO)_5$ than P_A and is shifted to lower δ values rather than being deshielded: $\Delta\delta(P_B) = -0.55$ and -1.01 ppm for **4** and **3**, respectively. Substituent effects in excess of 1 ppm on phosphorus shielding transmitted through phenoxy groups have previously been observed for aryl phosphates.[20]



Scheme 2. Tungsten complexes of cyclotriphosphazene **1**

The successive coordination of pyridine substituents to tungsten also has a measurable effect on the nitrogen atom of the phosphazene ring: N_Y is deshielded by 0.6 ppm in **4** and by 1.5 ppm in **3**. Unfortunately, the intensity of the N_X signal is too low to allow its discernment above the noise. Obviously, the largest $\delta^{15}N$ variation is observed for the pyridine nitrogen atom, which is shielded by about 75 ppm upon coordination to the tungsten atom. The 5.5 ppm shielding shown by the ^{15}N of the free pyridine in **4** is, however, also noteworthy. Similar substituent effects have previously been reported for fluorinated monophosphazenes.[21]

Considering the high sensitivity of transition metal nuclei to very small electronic modifications in their environment, the shielding effect in the present case should also be detectable on the tungsten atom. Indeed, in the $^1H,^{183}W$-HMQC correlation spectrum, the chemical shift of **3** is deshielded by 4 ppm compared to that of **4**, which represents a relatively large shift for an interaction between two apparently distant groups (Table 1).

The spectra of the mixtures of **3** and **4** obtained in various independent experiments showed the presence of small amounts (not reproducible, but never exceeding 5 mol-%) of another species **5** with $\delta^{183}W = -2728$. However, all attempts to characterize this contaminant were unsuccessful.

Like **1**, the phosphazene **2** reacted with $[W(MeOH)(CO)_5]$ in methanol to give mixtures of the polymetallic complexes $[N_3P_3(dobp)(OC_5H_4N\text{-}4)_4\{W(CO)_5\}_x]$, $x = 4$ (**6**), $x = 3$ (**7**), $x = 2$ (**8**, **9**, **10**), $x = 1$ (**11**) (Scheme 3). Thus, upon addition of 4.4 equivalents of the pentacarbonyltungsten reagent to **2**, two major products **6** and **7** (> 97%) were formed in a relative ratio of 85:15, as measured from the integrals of H_{meta} in the ^1H-NMR spectrum. For the mixture, the spectral region corresponding to the H^o protons ($\delta = 8.5-9.0$, Figure 1) features only one intense multiplet at $\delta = 8.85$ attributable to **6**, while at least three signals at $\delta = 8.65$, 8.76 and 8.82 of equal relative intensity

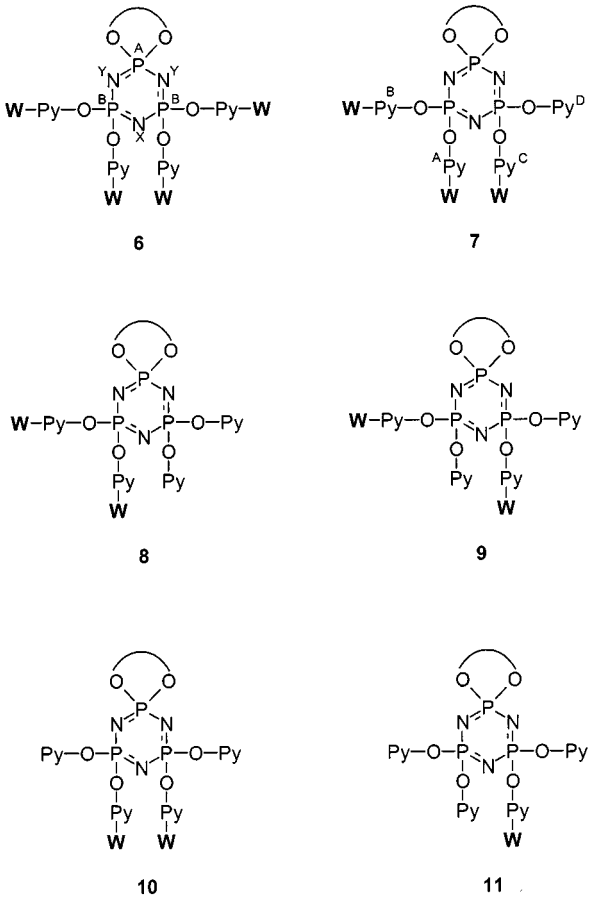
Table 1. NMR data for compounds **1**−**11** (δ in ppm, *J* in Hz)

	δ^1H^o Coord.	δ^1H^o Non-coord.	$\delta^{31}P_A$	$\delta^{31}P_B$	$^2J_{PA,PB}$	$\delta^{15}N$ pyridine Coord.	$\delta^{15}N$ pyridine Non-coord.	δ^{15} Ncycle X	δ^{15} Ncycle Y	$\delta^{183}W$
1		8.65	9.09	25.13	95.7		−76.3	−312.4[a]	−307.9	
2		8.55	23.89	8.19	95.3		−74.5	−306.8[b]	−310.5	
3	8.85		9.18	24.12	96.2	−150.8			−306.4	−2707
4	8.81	8.69	9.15	24.58	95.9	−151.8	−81.8		−307.3	−2711
6	8.85		21.90	7.04	92.9	−147.9				−2696
7	8.85 (A)	8.65 (D)	22.41	7.42	92.9	−149.0				−2699
	8.82 (C)					−149.8				−2701
	8.76 (B)					−148.2				−2699
8	8.78		22.94[c]	7.85	94.5					−2700
9	8.76		22.45	7.52	94.0					−2703
10	8.82		22.45	7.52	94.0					−2703
11	8.75		23.41	8.06	94.5					−2706

[a] $^1J_{PBNX}$ = 11.7; $^1J_{PANY}$ = 7.4; $^1J_{PBNY}$ = 4.7. − [b] $^1J_{PBNX}$ = 5.7; $^1J_{PANY}$ = 11.6; $^1J_{PBNY}$ = 3.5. − [c] Calculated values have been approximated to an AB_2 spin system.

are observed for **7**. The excess of $[W(MeOH)(CO)_5]$ used implies that **6** must be the tetracoordinated $W(CO)_5$ complex of **2**, and consequently **7** must be its tricoordinated tungsten derivative. Furthermore, on the basis of a statistical distribution of tungsten on the pyridine nitrogen atoms of **2**, the two additional multiplets at δ = 8.59 and δ = 8.63 of very low intensity (< 3%) may be assigned to the corresponding bimetallic complexes **8**−**10**. Considering the low intensity of the dicoordinated complexes, the monometallic species **11** would not be detectable. The assignment of the ^{31}P-NMR spectra of compounds **7**−**10** was accomplished through titration experiments using different ratios of **2**/$[W(MeOH)(CO)_5]$ (1:1; 1:2; 1:3; 1:4.4). The spectra are summarized in Table 1. As expected, the increase in the tungsten content has a shielding effect on each of the phosphorus nuclei in the phosphazene ring (cf. **4** and **3**). However, the ^{31}P nucleus bonded to the biphenoxy substituent again shows the greatest upfield shift. Due to the similarity of **9** and **10**, there is some overlapping of their ^{31}P signals. Significantly, the ^{31}P nuclei in compound **8** are seen to be deshielded compared to those in **9** and **10**.

Compound **7** contains four different pyridine rings. However, only three signals with an intensity ratio of 1:1:1 are observed for the H^o protons. The fourth multiplet is overlapped by the signal of the H^o protons of **6**, as revealed by the integrals of the multiplet at δ = 8.85 and of the signal due to the *meta* protons of the pyridine rings. This overlap indicates that both types of protons are found in the same environment. By comparison with the H^o signals of **3** and **4**, the most deshielded protons of **7** can be assigned as H^o(A) (Scheme 3), while the most shielded multiplet of **7** should be attributable to H^o of the pyridine molecule not coordinated to tungsten H^o(D). The assignment of H^o(B) and H^o(C) poses some difficulties because the nuclear shielding of these protons will be determined by a combination of the electronic effects induced by the coordination of the nitrogen atom to $W(CO)_5$ and the diamagnetic anisotropy of the neighbouring rings, the latter depending on the orientation of the interacting groups (cf., for example, the crystal structure of the hexasubstituted phosphazene $[N_3P_3(OC_5H_4N\text{-}4)_6]$, where one of the three 4-oxypyridines



Scheme 3. Tungsten complexes of cyclotriphosphazene **2**

on one side of the N_3P_3 plane is oriented almost perpendicular to the other two).

These difficulties could be overcome by analysing the ^{183}W-NMR data obtained from the ^{1}H,^{183}W-HMQC correlation spectrum of the mixture of **6** and **7**. This spectrum featurs seven signals, which are labelled **I**−**VII** in Figure 2: $\delta^{183}W$ = −2696 (**I**), −2699 (**II**, **III**), −2700 (**IV**), −2701 (**V**), −2703 (**VI**, **VII**). The ^{183}W chemical shift variations observed between **3** and **4** suggest that $\delta^{183}W$ values are not subject to neighbouring anisotropy effects, but are deter-

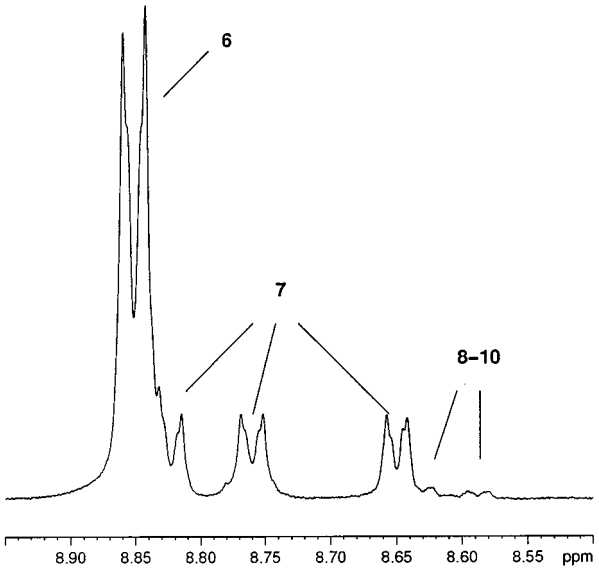


Figure 1. H^o region of the ^{1}H-NMR spectrum of a mixture of **2** with excess [W(MeOH)(CO)$_5$]

mined by the number of W(CO)$_5$ moieties coordinated to the substituents on a given phosphorus atom: the greater the number, the larger the ^{183}W chemical shift. Accordingly, the cross-peak **I** in the ^{1}H,^{183}W-HMQC spectrum of **6** and **7** can be assigned to the tungsten signal of **6**. Following the same reasoning, the two cross-peaks at $\delta^{183}W = -2699$ with the protons at $\delta = 8.85$ and 8.76 (**II**, **III**) can be ascribed to the long-range coupling of H^o(A) and H^o(B) of **7** with W_A and W_B, respectively. Since H^o(A) has been previously assigned to the multiplet at $\delta = 8.85$, it follows that H^o(B) resonates at $\delta = 8.76$. By a process of elimination, H^o(C) must be responsible for the multiplet at $\delta = 8.82$, which correlates with the most shielded ^{183}W of **7** at $\delta = -2701$ (**V**) [i.e. the tungsten bonded to the moiety with the lower W(CO)$_5$ content]. Additionally, the signal at $\delta = 8.65$ can be confirmed as being due to H^o(D), in view of the lack of any correlation with the tungsten atom. The shielding differences between H^o(B) and H^o(C) can be ascribed to differences in the diamagnetic anisotropy effect produced by the adjacent rings on the same side of the phosphazene plane. Upon rotation of the pyridine rings, H^o(B) would temporarily be oriented in a perpendicular arrangement in relation to an unperturbed pyridine and therefore would experience the full shielding effect of the ring current induced by its six π electrons. On the other hand, H^o(C) would, under these circumstances, experience a smaller ring current effect as these protons would be faced by a pyridine coordinated to tungsten, part of the electronic density of which will be involved in bonding to the transition metal.

Cross-peaks **IV**, **VI**, and **VII** in the $^{1\,H,183}$W-HMQC spectrum may be attributed to correlations with the H^o protons in the three possible dicoordinated W(CO)$_5$ complexes **8**–**10**. Applying the same assignment criteria as discussed for **7**, it can be concluded that the most deshielded signal **IV** arises from the two equivalent ^{183}W nuclei of **8**, "pendant" from the same phosphorus atom. The corresponding

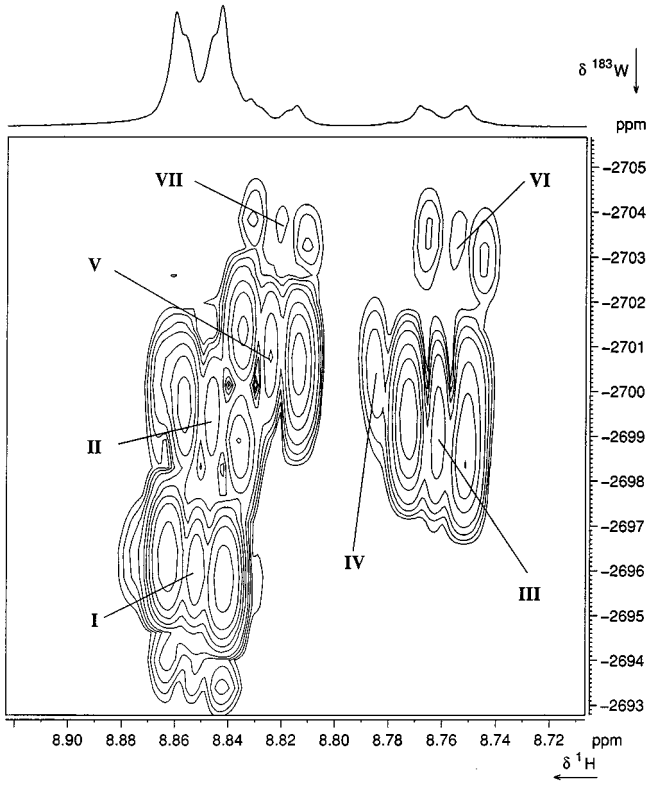


Figure 2. ^{1}H,^{183}W HMQC of a mixture of **2** and [W(MeOH)(CO)$_5$] in a ratio of 1:4.4

H^o protons appear at $\delta = 8.78$ and this signal is partially overlapped by that of H^o(B) of **7**. The two remaining cross-peaks **VI** and **VII** originate from tungsten nuclei bonded to pyridine substituents on different phosphorus atoms. Focusing on the H^o protons of the pyridine ring coordinated to W(CO)$_5$, it can be concluded that the neighbourhood, and therefore the diamagnetic anisotropic effect, of these protons in **9** is very similar to that of H^o(B) in **7**, while the analogous protons in **10** resemble H^o(C) in **7**. On the basis of these observations, the ^{1}H signals at $\delta = 8.76$ and 8.82 can be assigned to **9** and **10**, respectively. Finally, the signals at $\delta = 8.59$ and 8.63 can be assigned to two of the three types of H^o protons of the pyridines not bonded to the metal center. The unobserved third signal is most probably overlapped by the multiplet at $\delta = 8.76$ due to the proton H^o(D) of **7**.

To our surprise, the ^{1}H,^{15}N-HMQC spectrum was much less informative. The signal-to-noise ratio achieved was rather poor and only the H^o protons of the pyridines coordinated to the metal center in **6** and **7** showed correlations with ^{15}N. The data obtained are collected in Table 1. Once the identity of the H^o protons had been established, the assignment of the corresponding ^{15}N signals was trivial. Significantly, the ^{15}N chemical shifts vary in the same way as the δ^{183}W values and by a similar order of magnitude (see Table 1). On the other hand, the solubility of the complexes proved to be too low to allow measurement of ^{15}N data for the nitrogen atoms of the cyclotriphosphazene through phosphorus detection.

The above assignments are supported by the NMR data obtained by performing the reaction in a 1:3 ratio. The ^1H spectrum shows a strong overlap between multiplets in the region corresponding to the H^o protons. The high intensity of the signal at $\delta = 8.75$ indicates that it is attributable to the monometallic species **11**. The ^{31}P spectrum features a large number of lines of different intensity arising from the AB_2-like multiplets produced by the various components of the mixture.

On the contrary, the $^1H,^{183}W$-HMQC spectrum of the mixture is much easier to interpret and supports the assignments given above (Figure 3). Now, the signals of W_A in **7** and of the tungsten atom in **8** are slightly shifted to higher field ($\Delta\delta \approx 0.5$ ppm). However, the important point is that a new correlation is observed between a ^1H multiplet at $\delta = 8.75$ and a tungsten signal at $\delta = -2706$, which must correspond to the monometallic complex **11**. This confirms that $\delta^{183}W$ in the series of complexes studied here decreases on decreasing the amount of $W(CO)_5$ in the molecule.

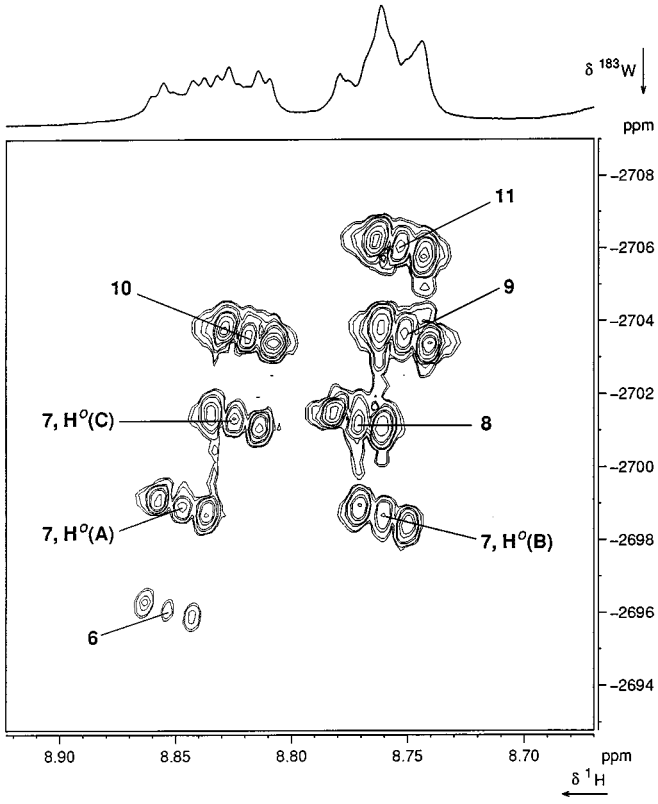


Figure 3. $^1H,^{183}W$ HMQC of a mixture of **2** and $[W(MeOH)(CO)_5]$ in a ratio of 1:3

Conclusions

The multinuclear magnetic resonance study performed on the two model cyclotriphosphazenes and their $W(CO)_5$ complexes has revealed that complexation can be monitored through several nuclei of the molecule. The δ^1H variations can be explained in terms of a mixture of charge polarization and anisotropic effects, which are difficult to predict. Moreover, the ^1H-NMR spectra of the polymetallic complexes show strongly overlapped signals, which render this nucleus of low diagnostic value for identification purposes. However, the high sensitivity of transition metal nuclei to small electronic changes in their coordination spheres has allowed the use of ^{183}W NMR in assigning all the components of the complex mixtures of compounds incorporating different amounts of tungsten, as well as positional isomers, with ^{183}W chemical shift differences in the range of 1−4 ppm. $\delta^{183}W$ values have been found to decrease on increasing the number of tungsten atoms in the molecule, and screening of the ^{15}N nuclei of the pyridine rings bonded to the metal center has revealed the same trend.

Experimental Section

General: All reactions were carried out under dry nitrogen. K_2CO_3 was dried at 140°C prior to use. The acetone used as solvent was predistilled from $KMnO_4$, and distilled twice from anhydrous $CaSO_4$. Methanol was distilled from CaH_2. Petroleum ether refers to the fraction boiling in the range 60−65°C. Hexachlorocyclotriphosphazene $[N_3P_3Cl_6]$ (Fluka) was purified by recrystallization from hot petroleum ether and dried in vacuo. The starting phosphazenes $[N_3P_3(dobp)Cl_4]$ and $[N_3P_3(dobp)_2Cl_2]$ were prepared as described elsewhere.[22] The complex $[W(MeOH)(CO)_5]$ was obtained as described in the literature.[23] − Elemental analyses: Perkin−Elmer 2400. − IR: Perkin−Elmer FT 1720-X, Paragon 1000 (KBr pellets). − NMR: Bruker AMX 400; spectra were referenced to tetramethylsilane for ^1H, neat $MeNO_2$ for ^{15}N, 85% H_3PO_4 for ^{31}P, and Na_2WO_4 for ^{183}W. The spectral parameters for the $^{31}P,^{15}N\{^1H\}$-HMQC[17] and $^1H,^{183}W$-HMQC[24] experiments have been described previously. Linear prediction of the 2D spectra using standard Bruker software was employed. Samples were prepared in $CDCl_3$ and the spectra were measured at 303 K. In view of the very small shifts in δ that we aimed to detect, experiments were performed several times with different samples in order to minimize systematic errors arising from concentration and temperature variations.

$[N_3P_3(dobp)_2(OC_5H_4N\text{-}4)_2]$ (1): A mixture of $[N_3P_3(dobp)_2Cl_2]$ (0.304 g, 0.53 mmol), HOC_5H_4N-4 (0.122 g, 1.28 mmol) and K_2CO_3 (2.0 g, 14.5 mmol) in acetone (50 mL) was refluxed for 3 h. The volatiles were then removed in vacuo and the residual solid was washed with water (3 × 80 mL) and extracted with CH_2Cl_2 (3 × 50 mL). The organic phase was dried over anhydrous Na_2SO_4, filtered, and the solvent was evaporated in vacuo. The product was recrystallized from CH_2Cl_2/petroleum ether to give **1** as a very pale yellow crystalline solid. Yield 0.25 g (67%). − $C_{42}H_{24}N_5O_6P_3$ (786.9): calcd. C 59.1, H 3.50, N 10.1; found C 58.4, H 3.60, N 9.82.

$[N_3P_3(dobp)(OC_5H_4N\text{-}4)_4]$ (2): A mixture of $[N_3P_3(dobp)Cl_4]$ (0.461 g, 1 mmol), HOC_5H_4N-4 (0.456 g, 4.8 mmol) and K_2CO_3 (2.0 g, 14.5 mmol) in acetone (50 mL) was refluxed for 6 h. The volatiles were then removed in vacuo and the residual solid was washed with water (3 × 80 mL) and extracted with CH_2Cl_2 (3 × 50 mL). The organic phase was dried with anhydrous Na_2SO_4, filtered, and the solvent was evaporated in vacuo. The product was recrystallized from CH_2Cl_2/petroleum ether to give **2** as a very pale yellow crystalline solid. Yield 0.52 g (75%). − $C_{36}H_{24}N_7O_6P_3$ (742.9): calcd. C 55.3, H 3.48, N 14.1; found C 55.0, H 3.35, N 13.9.

Preparation of the Mixture of Complexes $[N_3P_3(dobp)_2(OC_5H_4N\text{-}4)_2\{W(CO)_5\}_x]$, $x = 1$ (4), $x = 2$ (3): A water-cooled solution of $[W(CO)_6]$ (0.104 g, 0.296 mmol) in methanol (18 mL) was ir-

radiated with UV light until the disappearance of the IR band at 1977 cm^{-1} (ca. 1 h). The resulting orange solution (IR bands at 2075 w, 1932 s, and 1887 m, br. cm^{-1}) was then added to a solution of the phosphazene $[N_3P_3(dobp)_2(OC_5H_4N\text{-}4)_2]$ (**1**) (0.100 g, 0.145 mmol) in CH_2Cl_2 (20 mL) and the mixture was stirred at room temperature until the disappearance of the IR band at 1887 cm^{-1} (ca. 4 h). The volatiles were then removed in vacuo and the residue was washed with petroleum ether (2 × 30 mL) to leave a yellow solid. Yield 0.12 g. Variation of the proportions of the carbonyltungsten and the phosphazene resulted in mixtures of different composition. − IR (KBr pellet): $\tilde{\nu}$ = 2072 w cm^{-1}, 1975 w, 1918 s, br. (CO).

Preparation of the Mixture of Complexes $[N_3P_3(dobp)(OC_5H_4N\text{-}4)_4\{W(CO)_5\}_x]$, x = 1 (11), x = 2 (8, 9, 10), x = 3 (7), x = 4 (6): A water-cooled solution of $[W(CO)_6]$ (0.208 g, 0.591 mmol) in methanol (24 mL) was irradiated with UV light until the disappearance of the IR band at 1977 cm^{-1} (ca. 1 h). The resulting orange solution (IR bands at 2075 w, 1932 s, and 1887 m, br. cm^{-1}) was then added to a solution of the phosphazene $[N_3P_3(dobp)(OC_5H_4N\text{-}4)_4]$ (**2**) (0.092 g, 0.133 mmol) in CH_2Cl_2 (24 mL) and the mixture was stirred at room temperature until the disappearance of the IR band at 1887 cm^{-1} (ca. 13 h). The volatiles were then removed in vacuo and the residue was washed with petroleum ether (2 × 30 mL) to leave a yellow-brown solid. Yield 0.10 g. Variation of the proportions of the carbonyltungsten and the phosphazene resulted in mixtures of different composition. − IR (KBr pellet): $\tilde{\nu}$ = 2073 w cm^{-1}, 1975 sh, 1910 s, br. (CO).

Acknowledgments

Financial support by the Spanish Dirección General de Investigación Científica y Técnica (Projects PB93-1005 and PB94-1346) is gratefully acknowledged. R. J. C. thanks the Ministerio de Educación y Cultura for a predoctoral grant. The Servicio de RMN of the Universidad de Oviedo and the Universidad de Almería are acknowledged for allocating measuring time to this project.

[1] P. J. Lieu, J. H. Magill, Y. C. Alarie, *J. Fire Flammability* **1980**, *11*, 167−183.
[2] M. A. Olshavsky, H. R. Allcock, *Macromolecules* **1995**, *28*, 6188−6197.
[3] A. A. Dembek, C. Kim, H. R. Allcock, R. L. S. Devine, Y. Shi, W. H. Steier, C. W. Spangler, *Macromolecules* **1991**, *24*, 1000−1010.
[4] A. A. Dembek, C. Kim, H. R. Allcock, R. L. S. Devine, Y. Shi, W. H. Steier, C. W. Spangler, *Chem. Mater.* **1991**, *3*, 1120−1132.
[5] [5a] R. E. Singler, R. A. Willingham, R. W. Lenz, A. Furukawa, H. Finkermann, *Macromolecules* **1987**, *20*, 1727−1728. − [5b] H. R. Allcock, C. Kim, *Macromolecules* **1991**, *24*, 2846−2851.
[6] P. Bortolus, M. Gleria, *J. Inorg. Organomet. Polym.* **1994**, *4*, 1−236, and references cited therein.
[7] U. Diefenbach, M. Kretschmann, Ö. Çavdarci, *Phosphorus Sulfur Silicon* **1994**, *93*−*94*, 415−416.
[8] [8a] H. R. Allcock, S. Al-Shali, D. C. Ngo, K. N. Vissler, M. Parvez, *J. Chem. Soc., Dalton Trans.* **1995**, 3521−3532. − [8b] H. R. Allcock, S. Al-Shali, D. C. Ngo, K. N. Vissler, M. Parvez, *J. Chem. Soc., Dalton Trans.* **1996**, 3549−3559.
[9] [9a] S. S. Krishnamurthy, M. Woods, *Ann. Rep. NMR Spectrosc.* **1987**, *19*, 175−320. − [9b] V. Chandrasekhar, K. R. Justin Thomas, *Appl. Organomet. Chem.* **1993**, *7*, 1−31. − [9c] S. S. Krishnamurthy, *Phosphorus Sulfur Silicon* **1994**, *87*, 101−111. − [9d] L. Weber, *Coord. Chem. Rev.* **1997**, *158*, 1−67.
[10] G. A. Carriedo, L. Fernández-Catuxo, F. J. García Alonso, P. Gómez-Elipe, *J. Organomet. Chem.* **1995**, *503*, 59−67.
[11] G. A. Carriedo, P. Gómez-Elipe, F. J. García Alonso, L. Fernández-Catuxo, M. R. Díaz, S. García-Granda, *J. Organomet. Chem.* **1995**, *498*, 207−212.
[12] [12a] B. E. Mann, *Ann. Rep. NMR Spectrosc.* **1991**, *23*, 141−207. − [12b] D. Rehder, *Coord. Chem. Rev.* **1991**, *110*, 161−210. − [12c] D. White, N. J. Coville, *Adv. Organomet. Chem.* **1994**, *36*, 95−158.
[13] P. S. Pregosin, in *Transition Metal Nuclear Magnetic Resonance* (Ed.: P. S. Pregosin), Elsevier, Amsterdam, **1991**, pp. 91.
[14] [14a] R. Benn, A. Rufinska, *Magn. Reson. Chem.* **1988**, *26*, 895−902. − [14b] S. Berger, T. Fäcke, R. Wagner, *Magn. Reson. Chem.* **1996**, *34*, 4−13. − [14c] F. López-Ortiz, R. J. Carbajo, *Curr. Org. Chem.* **1998**, *2*, 97−130.
[15] [15a] M. Minelli, J. H. Enemark, *Coord. Chem. Rev.* **1985**, *68*, 169−278. − [15b] C. Brevard, R. Thouvenot, in *Transition Metal Nuclear Magnetic Resonance* (Ed.: P. S. Pregosin), Elsevier, Amsterdam, **1991**, pp. 82.
[16] G. A. Carriedo, L. Fernández-Catuxo, F. J. García-Alonso, P. Gómez-Elipe, P. A. González, G. Sánchez, *J. Appl. Polym. Sci.* **1996**, *59*, 1879−1885.
[17] E. Peláez-Arango, F. J. García-Alonso, G. A. Carriedo, F. López-Ortiz, *J. Magn. Reson. A* **1996**, *121*, 154−159.
[18] [18a] B. Thomas, G. Grossmann, *Russ. Chem. Rev.* **1986**, *55*, 622−637. − [18b] F. López-Ortiz, E. Peláez-Arango, P. Gómez-Elipe, *J. Magn. Reson. A* **1996**, *119*, 247−251.
[19] M. Witanowski, L. Stefaniak, G. A. Webb, *Ann. Rep. NMR Spectrosc.* **1986**, *18*, 1−737.
[20] S. Berger, S. Braun, H. O. Kalinowski, in *NMR-Spektroskopie von Nichtmetallen;* ^{31}P-NMR-Spektroskopie, George Thieme Verlag, Stuttgart, **1993**.
[21] S. Yolles, J. H. R. Woodland, *J. Organomet. Chem.* **1975**, *93*, 297−308.
[22] G. A. Carriedo, L. Fernández-Catuxo, F. J. García-Alonso, P. Gómez-Elipe, P. A. González, *Macromolecules* **1996**, *29*, 5320−5325.
[23] D. J. Darenbourg, C. J. Bishoff, J. H. Reibenspies, *Inorg. Chem.* **1991**, *30*, 1144−1147.
[24] R. J. Carbajo, L. Zhang, F. López-Ortiz, *Magn. Reson. Chem.* **1998**, *36*, 807−814.

Received August 8, 1998
[I98255]

Syntheses and Characterization by NMR Spectroscopy and X-ray Diffraction of Complexes Derived from Metals of Groups 2 and 13 and the Ligand Bis(3,5-di-*tert*-butyl-1-hydroxy-2-phenyl)amine

Carlos Camacho-Camacho,[a] Gabriel Merino,[b] Francisco Javier Martínez-Martínez,[c] Heinrich Nöth,[d] and Rosalinda Contreras*[b]

Keywords: Alkaline earth metals / Group-13 metals / Coordination chemistry / Bis(3,5-di-*tert*-butyl-1-hydroxy-2-phenyl)amine ligand / Nonacoordinated strontium compound

Reaction of 3,5-di-*tert*-butylcatechol and aqueous ammonia with boron, aluminum, gallium, or strontium chloride, or with calcium or barium acetate produce, under oxidizing conditions, neutral complexes of stoichiometric formulae ML (M = BCl), ML_2, [M = Al (**2**), Ga (**3**), Ca (**4**), and Ba (**5**)], and ML_3H [M = Sr (**6**)] [L = different oxidation states of bis(3,5-di-*tert*-butyl-1-hydroxy-2-phenyl)amine]. The structures of **1** and **4**–**6** were established by ^1H- and ^{13}C-NMR spectroscopy and of **2**, **3**, and **6** by X-ray diffraction. The coordination compound ClBL (**1**) was obtained by transmetallation of ZnL_2 with BCl_3. It is a tetracyclic compound with tetracoordinated boron and nitrogen atoms, the ligand being in the reduced form, bis(hydroxyphenyl)amine. The paramagnetic complexes **2** and **3** crystallized in the triclinic system and are hexacoordinated with two orthogonal planar ligands bonded to the metal atoms. The ligands appear in two different oxidation states: one as the monoanion and another as a radical dianion. Based on their X-ray diffraction molecular structures, it is deduced that both ligands have similar structures, confirming electronic delocalization and fast interconversion of their oxidation states. Ca and Ba complexes are diamagnetic and hexacoordinated, both ligands being monoanions The strontium complex crystallized in the monoclinic system, the metal atom is nonacoordinated, having two ligands as monoanions, and a third one is a neutral protonated diquinone. Its structure is a distorted helix with three paddles in a C_3 geometry and its unexpected diamagnetic behaviour is due to the presence of a reduced protonated ligand.

Introduction

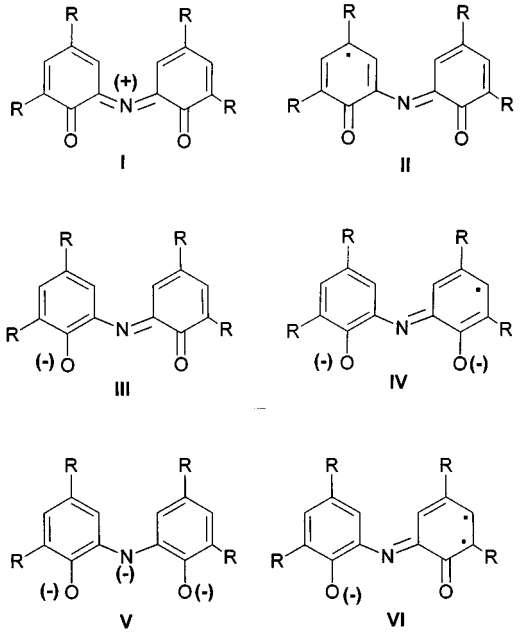
We are interested in developing the heterocyclic chemistry of main-group elements and bis(hydroxyphenyl)amines.[1−7] These heterocycles are particularly stable and are suitable models for structural and spectroscopic investigation. The preparation of some organometallic heterocycles bearing a bis(hydroxyphenyl)amine ligand has already been reported.[2,6,8−10] A relevant property of the bis(hydroxyphenyl)amine molecules is that they allow the stabilisation of uncommon species such as some which contain pentacoordinated phosphorus atoms.[1,2,4]

The template synthesis with 3,5-di-*tert*-butylcatechol and metals in the presence of ammonia lead to metallic hexacoordinated complexes bearing two ligands formed by the condensation of two catechol molecules to one nitrogen atom.[11] The complexes have two planar, tridentate ligands. The analogous transition-metal complexes of general formula ML_2 have been the subject of extensive research work[11−19] and several X-ray diffraction structures have been reported.[12−18] Theoretically, several different stable oxidation states could exist for this ligand, ranging in charge from 0 to −3 (Scheme 1). It is surprising that only the monoanion (**III**) and the radical dianion (**IV**) have been found in the previously reported complexes. The oxidation state of the ligand depends on the nature of the metals: With metals in oxidation state II both ligands appear as monoanion (**III**), while for metals in oxidation state III one ligand is a monoanion (**III**) and the other is a radical dianion (**IV**), and in metals in oxidation state IV both are radical dianions (**IV**).

The reports in the literature have focused on complexes formed with two different oxidation forms of the ligand, **III** and **IV**. Detailed magnetic and electrochemical studies of these compounds have been performed.[11−21] The magnetic studies indicate that there is a strong ferromagnetic coupling between the ligands through the empty metal orbitals. It was proposed that they are valence tautomers with an intramolecular electronic tautomeric equilibrium due to electronic transfer between the ligand and the metal.[21] In addition, it was found by electrochemical studies that the complexes can suffer one-electron oxidation or one-electron reduction, both processes occurring at the ligand-based orbitals.[20]

[a] Departamento de Sistemas Biológicos, Universidad Autónoma Metropolitana-Xochimilco,
Calzada del Hueso 1100, Col. Villa Quietud, México 04960 D.F.
[b] Departamento de Química, Centro de Investigación y de Estudios Avanzados del Instituto Politécnico Nacional,
Apartado Postal 14-740, México 07000 D.F.
Fax: (internat.) + 52-5/747-7113
E-mail: rcontrer@mail.cinvestav.mx
[c] Departamento de Química, Unidad Profesional Interdisciplinaria de Biotecnología del Instituto Politécnico Nacional,
Av. Acueducto s/n. Barrio la Laguna Ticomán, México 07340 D. F.
[d] Institute of Inorganic Chemistry, University of Munich,
Meiserstr, 1, D-80333 München, Germany

 © WILEY-VCH Verlag GmbH, D-69451 Weinheim, 1999 1434−1948/99/0606−1021 $ 17.50+.50/0



Scheme 1. Oxidation states of the bis(3,5-di-*tert*-butyl-1-hydroxy-2-phenyl)amine ligand

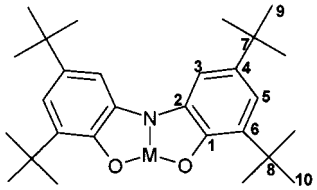
The versatile behaviour of this ligand guarantees the interest of further studies on these compounds. Relatively little effort has been directed toward synthesising and studying the reactivity of the bis(hydroxyphenyl)amines and main-group and alkaline-earth metals. Therefore we have investigated the complexes derived from bis(3,5-di-*tert*-butyl-1-hydroxy-2-phenyl)amine and boron (**1**), aluminium (**2**), gallium (**3**), calcium (**4**), barium (**5**), and strontium (**6**). During the preparation of this manuscript the synthesis and a magnetic investigation for the aluminium derivative has been reported;[21] the crystal structure for this compound is presented in this study.

Results and Discussion

Compound **1** has been synthesized by BCl_3 transmetallation of ZnL_2. Complexes **2**–**6** have been prepared directly by reaction of 3,5-di-*tert*-butylcatechol and the metallic chloride or acetate in the presence of ammonia. All are dark solids.

Compounds **1** and **4**–**6** are diamagnetic and their ^{1}H-NMR spectra are similar (Table 1). The ^{13}C-NMR spectra of the complexes **1** and **4**–**6** (Table 2) show six resonances in the aromatic domain indicating that the phenyl rings in each complex are equivalent. The chemical shift of atom C-1 in compound **1** is $\delta = 153.9$, characteristic of a phenoxy group. In contrast, the chemical shift for this atom in compounds **4**–**6** ($\delta = 176-180$) is consistent with quinone character. The chemical shift for the ^{11}B-NMR resonance ($\delta = +14.9$) of compound **1** indicates that the boron atom is tetrahedral and coordinated to the nitrogen atom. ^{1}H- and ^{13}C-NMR data, the mass spectrum and the elemental analysis indicate that the boron atom is bonded to one chlorine atom and to one reduced ligand **V**. Its structure is depicted in Scheme 2.

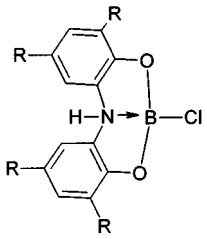
Table 1. ^{1}H-NMR chemical shift data of complexes **1** and **4**–**6** (in C_6D_6); the numbering of the atoms is shown in the figure



Compound	3-H	5-H	9-H (*t*Bu)	10-H (*t*Bu)
1	7.21	6.95	1.34	1.28
4	7.05	6.89	1.20	1.08
5	7.08	6.91	1.22	1.11
6	7.26	6.75	1.37	1.24

Table 2. ^{13}C-NMR chemical-shift data of complexes **1**, and **4**–**6** (in C_6D_6)

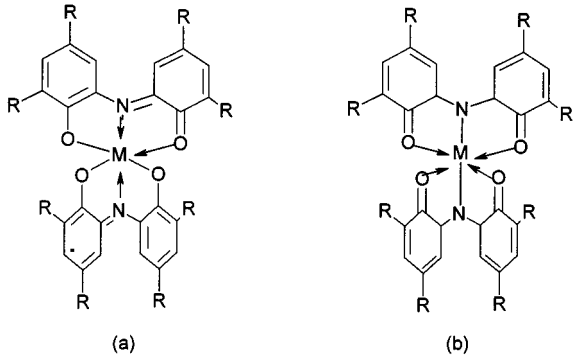
Compound	C-1	C-2	C-3	C-4	C-5
1	153.9	130.9	116.3	140.6	123.5
4	176.8	142.7	117.4	144.3	130.7
5	176.0	142.8	117.5	144.4	130.7
6	178.6	142.0	116.5	144.0	130.2
	C-6	C-7	C-8	C-9	C-10
1	135.3	34.6	31.7	34.4	29.2
4	142.8	35.21	30.43	34.73	29.43
5	143.5	35.1	30.3	34.7	29.5
6	142.8	34.7	29.4	34.1	28.7



Scheme 2. Proposed structure for compound **1**

Complexes **2** and **3** were found to crystallize from CH_2Cl_2/ethanol. Crystals of **2** and **3** are triclinic, space group $P-1$. Selected bond length and angles are listed in Table 3 and the molecular structures are depicted in Figures 1–3. The neutral complexes **2** and **3** show oxygen atoms occupying the equatorial sites of an octahedron, with two tridentate ligands, the four cycles of each ligand lying almost in the same plane. The MO_4N_2 coordination spheres show only slight distortions in bond angles at the equatorial atoms. Thus, angles for compound **2** are O2–Al–O4 91.0(2), O2–Al–O3 91.5(2), O1–Al–O4 92.3(2), O1–Al–O3 89.6(2)°, and those for compound **3** are O1–Ga–O4 92.7(1), O1–Ga–O3 91.5(1), O2–Ga–O4 89.8(1), O2–Ga–O3 91.52(14)°, while the angles between the atoms N–M–O show deviations from ideal octahedral geometry (Tables 3, 4). The nitrogen atoms are in *trans* po-

sitions [N1−Al−N2 176.8(3) and N1−Ga−N2 176.7(1)°]. The M−O bond lengths are identical, for compound **2** the average Al−O bond length is 1.877(5) Å and for compound **3** the average Ga−O bond length is 1.959(3) Å, similar to the Ga−O bonds reported for other hexacoordinated gallium compound [1.96(1) Å].[8] The Al−N and Ga−N bond lengths differ slightly [Al−N1 1.982(5), Al−N2 1.976(5), Ga−N1 2.014(3), Ga−N2 2.025(3) Å]. It is proposed[21] that the Al and Co^{III} compounds are formed by the bonding of two ligands in two different oxidation states, ligand **III** and ligand **IV** (Schemes 1 and 3). The C−O bond lengths in **2** and **3** are similar (1.29 Å) and indicate a double-bond character; the C−N bond lengths are also similar and their lengths are in between a double and a single bond (1.35 Å). The pattern of carbon−carbon bond lengths in **2** and **3** shows that the bonds C3−C4 and C5−C6 are consistently shorter than the other C−C bonds. We could not distinguish, based on bond lengths, two different structures of the ligands that could be attributed to different oxidation states. This could mean that the ligands become similar by the electronic delocalization and fast interconversion of the oxidation states between them as has been proposed for other compounds.[21]



Scheme 3. (a) Proposed structure for compounds **2** and **3**; (b) proposed structure for compounds **4** and **5**

From the NMR data and elemental analysis, it is deduced that compounds **4** and **5** derived from calcium and barium are bonded to two monoanionic ligands **III** in a hexacoordinated array analogous to that of aluminium and gallium complexes.

Compound **6** crystallizes from CH_2Cl_2/ethanol monoclinic in space group $P2(1)/c$, and its X-ray structure is shown in Figures 3−4. The complex presents a new coordination behaviour because three ligands are bonded to a metal centre, resulting in a nonacoordinate strontium atom. The nine bond lengths between the strontium and the ligands are normal coordination bonds with Sr−O bonds varying from 2.47 to 2.71 Å, whereas the Sr−N bonds vary from 2.67 to 2.77 Å. The strontium bond lengths are in accord with another nonacoordinated compound [strontium bis(thiocyanate)−hexaethylene glycol].[22] The structure of the molecule can be best described as a helix of three paddles of distorted C_3 geometry. If the different oxidation states of the ligand are considered the compound must be formed by two ligands in the monoanion oxidation state

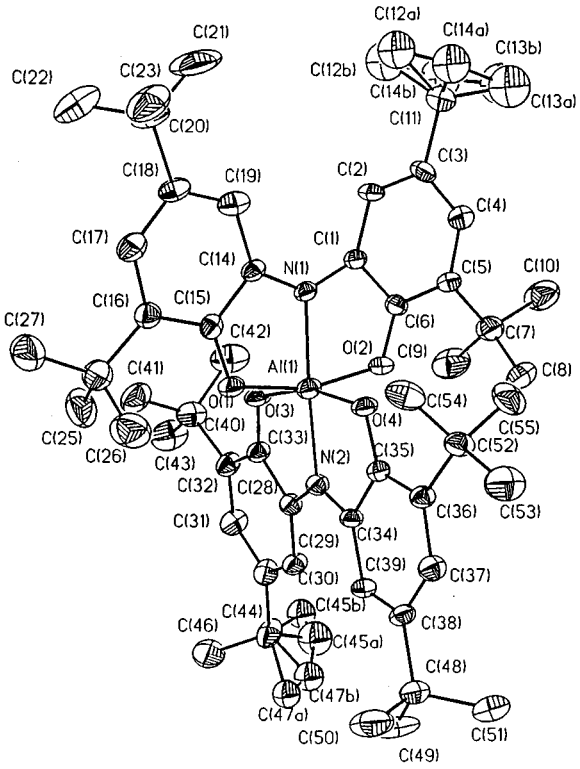


Figure 1. Molecular structure of $C_{56}H_{80}AlN_2O_4$ (**2**); thermal ellipsoids represent a 30% probability

Table 3. Selected bond lengths [Å] and angles [°] for compound **2**

Bond lengths [Å]			
Al−O1	1.874(5)	Al−O2	1.871(5)
Al−O3	1.885(5)	Al−O4	1.879(5)
Al−N1	1.981(5)	Al−N2	1.975(5)
O1−C1	1.292(7)	O2−C7	1.289(7)
O3−C13	1.288(8)	O4−C19	1.300(7)
N1−C2	1.351(8)	N1−C8	1.352(8)
N2−C20	1.345(8)	N2−C14	1.352(8)
C1−C6	1.426(9)	C1−C2	1.440(9)
C13−C18	1.427(9)	C13−C14	1.443(9)
C2−C3	1.413(9)	C3−C4	1.364(9)
C14−C15	1.419(9)	C15−C16	1.355(9)
C4−C5	1.40(1)	C5−C6	1.372(9)
C16−C17	1.42(1)	C17−C18	1.365(9)
C7−C12	1.405(9)	C7−C8	1.464(9)
C19−C24	1.419(9)	C19−C20	1.446(9)
C8−C9	1.409(9)	C9−C10	1.351(9)
C20−C21	1.415(9)	C21−C22	1.351(8)
C10−C11	1.42(1)	C11−C12	1.368(9)
C22−C23	1.424(9)	C23−C24	1.367(9)
Bond angles [°]			
O2−Al−O1	164.2(2)	O2−Al−O4	91.0(2)
O1−Al−O4	92.3(2)	O2−Al−O3	91.5(2)
O1−Al−O3	89.6(2)	O4−Al−O3	163.8(2)
O2−Al−N2	96.1(2)	O1−Al−N2	99.7(2)
O4−Al−N2	81.7(3)	O3−Al−N2	82.1(3)
O2−Al−N1	82.2(3)	O1−Al−N1	82.2(3)
O4−Al−N1	95.7(2)	O3−Al−N1	100.5(2)
N2−Al−N1	176.9(3)		

(**III**) plus a neutral radical (**II**). This description would not, however, correspond to a diamagnetic compound. Looking carefully at the X-ray diffraction structure the presence of

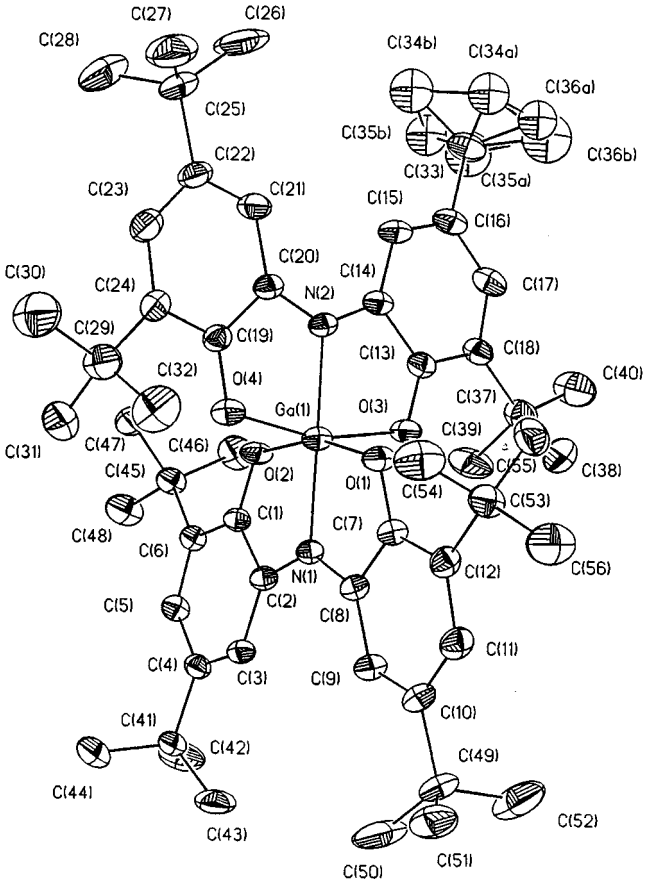
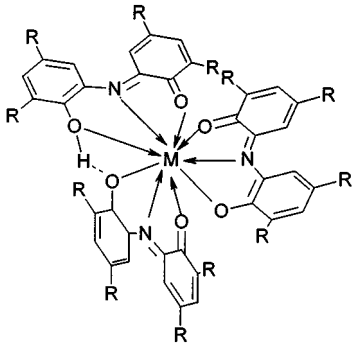


Figure 2. Molecular structure of $C_{56}H_{80}GaN_2O_4$ (**3**); thermal ellipsoids represent a 30% probability

Table 4. Selected bond lengths [Å] and angles [°] for compound **3**

Bond lengths [Å]			
Ga−O1	1.967(3)	Ga−O2	1.965(3)
Ga−O3	1.952(3)	Ga−O4	1.954(3)
Ga−N1	2.015(3)	Ga−N2	2.024(3)
O1−C7	1.294(5)	O2−C1	1.291(5)
O3−C13	1.299(5)	O4−C19	1.291(5)
N1−C2	1.351(5)	N1−C8	1.357(5)
N2−C20	1.3486)	N2−C14	1.354(6)
C1−C6	1.427(6)	C1−C2	1.4556)
C13−C18	1.4236)	C13−C14	1.456(6)
C2−C3	1.417(6)	C3−C4	1.356(6)
C14−C15	1.418(6)	C15−C16	1.360(7)
C4−C5	1.423(6)	C5−C6	1.360(6)
C16−C17	1.4107)	C17−C18	1.368(7)
C7−C12	1.431(6)	C7−C8	1.445(6)
C19−C24	1.425(7)	C19−C20	1.449(6)
C8−C9	1.410(6)	C9−C10	1.353(6)
C20−C21	1.423(6)	C21−C22	1.362(7)
C10−C11	1.424(7)	C11−C12	1.367(6)
C22−C23	1.407(7)	C23−C24	1.3657)
Bond angles [°]			
O2−Ga−O1	161.9(1)	O2−Ga−O4	92.8(1)
O1−Ga−O4	89.8(1)	O2−Ga−O3	91.5(1)
O1−Ga−O3	91.6(1)	O4−Ga−O3	162.3(1)
O2−Ga−N2	96.0(1)	O1−Ga−N2	102.1(1)
O4−Ga−N2	81.0(1)	O3−Ga−N2	81.4(1)
O2−Ga−N1	80.9(1)	O1−Ga−N1	81.0(1)
O4−Ga−N1	100.2(1)	O3−Ga−N1	97.4(1)
N2−Ga−N1	176.7(1)		

a hydrogen atom sitting between the oxygen atoms O4 and O5 was discovered (bond lengths: O4−H 1.341 Å, O5−H 1.148 Å, bond angle O4−H−O5 174.1°) and the position of this hydrogen atom was freely refined (x, y, z; H_{iso} = 0.0897). Thus, the third ligand was in fact a new reduced neutral form of the ligand (Scheme 4). In each ligand, the four carbon and nitrogen atoms are found in a plane. If only these atoms are considered the structure resembles a helix formed with three bidentate chelates in a hexacoordinated array (Figure 4). If the oxygen atoms are examined, they lie slightly out of the plane for each ligand and they are folded in a *trans* orientation. Examination of the bond lengths shows that the two ligands bonded to the hydrogen atom are similar with one short C−O bond length (1.23−1.26 Å) and a longer C−O one (1.33 Å, Table 5). The other ligand has two short C−O bonds (1.26 Å). The point group of **6** is not perfectly C_3 because of the presence of the hydrogen atom, the bond lengths of the atoms bonded to the strontium atom are different. The presence of the hydrogen bonding between atoms O4 and O5 makes the angle O4−Sr−O5 narrower [54.6(1)°] than the other two similar angles O2−Sr−O3 [90.03(1)°] and O6−Sr−O1 [87.7(1)°]. One of the ligands presents shorter distances [Sr−O1 2.475(2), Sr−O2 2.476(2) Å] than the other two [Sr−O3 2.569(2), Sr−O4 2.686(2) Å and Sr−O5 2.719(2), Sr−O6 2.575(2) Å]. The aromatic rings in each ligand are twisted due to the steric effect of the *tert*-butyl groups and the helical structure.



Scheme 4. Proposed structure for compound **6**

Conclusions

The X-ray diffraction of complexes of Al and Ga show that they are isostructural and that the ligands in these compounds also have similar structures, confirming the electronic delocalization and fast interconversion of the oxidation state of the ligands (**III** → **IV**). Hexacoordinated complexes are also proposed for the diamagnetic complexes of Ba and Ca. The strontium compound is the first example with a nonacoordinated metal atom for the complexes with bis(3,5-di-*tert*-butyl-1-hydroxy-2-phenyl)amine as ligand. The compound has three tridentate ligands in a distorted helix of three paddles, with a geometry close to C_3. The diamagnetic behaviour results from the presence of a new

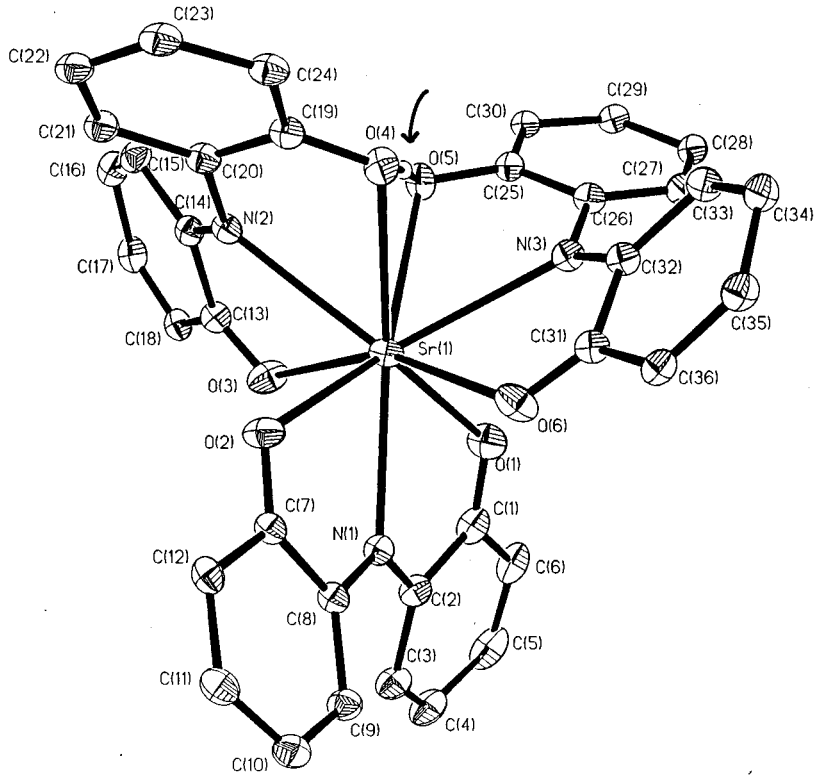


Figure 3. Molecular structure of $C_{84}H_{120}SrN_3O_6$ (**6**); the *tert*-butyl groups are not shown and the arrow marks the position of the hydrogen atom bonded to O4 and O5; thermal ellipsoids represent a 25% probability

oxidation state of the ligand that transforms the neutral radical oxidation state **II** (Scheme 1) into a diamagnetic neutral one.

Experimental Section

General Remarks: All solvents were freshly distilled and dried before use according to established procedures. − Melting points were measured with a Gallenkamp apparatus and are uncorrected. − The IR spectra were taken in KBr discs using a Perkin Elmer 16F PC IR spectrometer. − All the NMR spectra were obtained on a JEOL GXS-270 and JEOL-400 spectrometers in $CDCl_3$ solution. ^1H- and ^{13}C-NMR spectra were measured with TMS as the internal reference. − Elemental analyses were performed with a Fisons Instrument EA 1108 elemental analyzer CHNS-O. − Mass spectra were obtained with a Hewlett-Packard HP 5989A. − The X-ray

Table 5. Selected bond lengths [Å] and angles [°] for compound **6**

Bonds lengths [Å]							
Sr−O1	2.475(2)	Sr−O2	2.476(2)	Sr−O3	2.569(2)	Sr−O4	2.686(2)
Sr−O5	2.719(2)	Sr−O6	2.575(2)	Sr−N1	2.667(2)	Sr−N2	2.762(2)
Sr−N3	2.771(2)	O1−C1	1.258(4)	O2−C7	1.262(3)	O3−C13	1.231(3)
O4−C19	1.332(4)	O5−C25	1.337(3)	O6−C31	1.231(3)	N1−C2	1.342(4)
N1−C8	1.345(3)	N2−C20	1.394(3)	N2−C14	1.302(3)	N3−C26	1.397(3)
N3−C32	1.295(3)	C1−C6	1.457(4)	C1−C2	1.471(4)	C2−C3	1.434(4)
C3−C4	1.355(4)	C4−C5	1.436(5)	C5−C6	1.359(5)	C7−C8	1.466(4)
C8−C9	1.429(4)	C9−C10	1.359(4	C10−C11	1.431(4)	C11−C12	1.369(4)
C7−C12	1.450(4)	C13−C14	1.505(4)	C14−C15	1.449(4)	C15−C16	1.354(4)
C16−C17	1.455(4)	C17−C18	1.347(4)	C13−C18	1.472(4)	C19−C20	1.418(4)
C20−C21	1.406(4)	C21−C22	1.383(4)	C22−C23	1.408(4)	C23−C24	1.385(4)
C19−C24	1.420(4)	C25−C26	1.415(4)	C26−C27	1.401(4)	C27−C28	1.385(4)
C28−C29	1.412(4)	C29−C30	1.386(4)	C30−C25	1.417(4)	C31−C32	1.504(4)
C32−C33	1.444(4)	C33−C34	1.352(4)	C34−C35	1.463(4)	C35−C36	1.346(4)
C31−C36	1.467(4)						
Bond angles [°]							
O1−Sr−O2	124.6(1)	O2−Sr−O4	93.7(1)	O1−Sr−O4	139.0(1)	O2−Sr−O3	90.3(1)
O1−Sr−O3	81.0(1)	O4−Sr−O3	115.8(1)	O2−Sr−O6	80.4(1)	O1−Sr−O6	87.7(1)
O3−Sr−O6	157.7(1)	O2−Sr−O5	140.2(1)	O6−Sr−O5	115.4(1)	O1−Sr−O5	93.6(1)
O4−Sr−O5	54.6(1)	O3−Sr−O5	84.6(1)	O6−Sr−O4	85.2(1)	O2−Sr−N1	62.2(1)
O1−Sr−N1	62.5(1)	O2−Sr−N2	79.8(1)	O1−Sr−N2	134.5(1)	O2−Sr−N3	133.8(1)
O1−Sr−N3	77.8(1)	O4−Sr−N1	150.8(1)	O3−Sr−N1	82.7(1)	O4−Sr−N2	58.7(1)
O3−Sr−N2	59.2(1)	O4−Sr−N3	64.1(1)	O3−Sr−N3	135.4(1)	O6−Sr−N1	75.1(1)
O5−Sr−N1	154.3(1)	O6−Sr−N2	137.1(1)	O5−Sr−N2	63.7(1)	O6−Sr−N3	58.9(1)
O5−Sr−N3	58.5(1)	N1−Sr−N2	125.9(1)	N2−Sr−N3	114.5(1)	N1−Sr−N3	119.6(1)

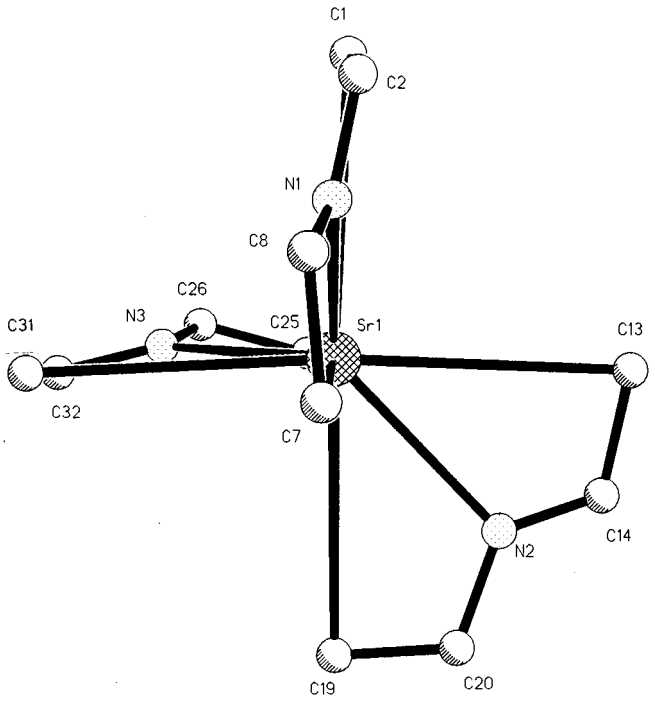


Figure 4. The core structure of the strontium complex **6** showing a helix of three paddles, the four carbon and nitrogen atoms being coplanar

diffraction studies of the gallium and aluminium compounds were performed with an Enraf-Nonius CAD4 diffractometer [λ(Mo-K_α) = 0.71073 Å, monochromator: graphite, T = 293(2) K, ω−2θ scan]. Cell parameters were determined by least-squares refinement of diffractometer angles for 24 automatically centred reflections. The X-ray diffraction study of the strontium compound **6** was performed with a Siemens P4 instrument equipped with a CCD area detector and a low-temperature device LTP2. The unit cell was determined from the data for 75 frames and data collection was performed in the hemisphere mode with Δφ = 0−3°, 10 s/frame exposures. Data reduction used the program SAINT. The structures were solved by direct methods (SHELXL-86). The experimental parameters are listed in Table 6. Atom H of compound **6** was found in the difference Fourier and refined freely including U_i. Crystallographic data (excluding structure factors) for the structures reported in this paper have been deposited with the Cambridge Crystallographic Data Centre as supplementary publication no. CCDC-114655 to -114657. Copies of the data can be obtained free of charge on application to CCDC, 12 Union Road, Cambridge CB2 1EZ, UK [Fax: int. code + 44-1223/336-033; E-mail: deposit@ccdc.cam.ac.uk].

[Bis(3,5-di-*tert*-butyl-2-hydroxy-2-phenyl)amine]boron Chloride (1): A solution of 0.50 g (0.54 mmol) of Zn[3,5-di-*tert*-butyl-1,2-quinone (3,5-di-*tert*-butyl-2-hydroxy-1-phenyl)imine]$_2$[11] in 20 mL of dry benzene was treated dropwise at room temperature and under vigorous stirring with BCl3·DMS (96 mg, 0.54 mmol). Additional stirring for 5 h afforded a suspension. The $ZnCl_2$ formed was filtered and the solvents were removed at reduced pressure to leave a violet powder. The powder was washed with hexane to obtain 0.156 g of **1** (63%). − ^{11}B NMR: δ = +14.9. − IR (KBr): $\tilde{\nu}$ = 2960 cm^{-1}, 1458, 1420, 1364, 1202, 1036, 876, 670 and 474. − MS; *m*/*z*: 469 [M$^+$] (calcd. 469). − $C_{28}H_{41}BClNO_2$ (469.81): calcd. C 71.05, H 2.98, N 8.79; found C 71.05, H 2.51, N 8.35.

Aluminium Complex 2: A solution of 1.33 g (6.0 mmol) of 3,5-di-*tert*-butylcatechol in 30 mL of 95% ethanol was added to a solution of 0.36 g (1.5 mmol) of aluminium chloride hexahydrate in 15 mL of 95% ethanol. After the addition of 2 mL of 25% aqueous ammonia and stirring for 5 h, the solution became dark green. After 3 d, the crystalline product was filtered and washed with 5 mL of water and 3 mL of ethanol and dried under vacuum. Recrystallization from $CHCl_3$ yielded pure **2**, m.p. 240°C (1.17 g, 90%). − IR

Table 6. Crystallographic data for the complexes **2**, **3**, and **6**; disorder of the *tert*-butyl groups was found for the aluminium and gallium compounds

Compound	**2**	**3**	**6**
Empirical formula	$C_{56}H_{80}AlN_2O_4$	$C_{56}H_{80}GaN_2O_4$	$C_{84}H_{120}N_30_6Sr$
Molecular mass	872.20	914.94	1355.45
Space group	$P-1$	$P-1$	$P2(1)/c$
Crystal size [mm^3]	0.3 × 0.2 × 0.2	0.3 × 0.2 × 0.1	0.2 × 0.2 × 0.2
a [Å]	11.446(2)	11.592(2)	13.4814(1)
b [Å]	12.314(2)	12.323(2)	28.1594(4)
c [Å]	20.777(4)	20.737(2)	22.7799(1)
α [°]	90.08(3)	89.43(3)	90
β [°]	105.03(3)	105.73(3)	104.9270(1)
γ [°]	104.18(3)	104.27(3)	90
V [Å]	2735.5(8)	2758.1(8)	8356.07
Z	2	2	4
Linear abs. coeff. [mm^{-1}]	0.080	0.541	0.694
D_c [g ml^{-3}]	1.059	1.102	1.077
2θ limits [°]	5.14 to 36.24	4.40−50.26	2.90−58.88
Octants collected	−10, 9; −10, 10; 0, 18	−13, 13; −14, 0; −24, 24	−15, 17;−35, 35;−29, 29
No. of data collected	3976	10251	48989
No. of unique data collected	3820(R_{int} = 0.0164)	9756 (R_{int} = 0.0354)	15425(R_{int} = 0.0488)
No. of unique data used	2838 [$F > 4\sigma(F)$]	5478 [$F > 4\sigma(F)$]	10708 [$F > 4\sigma(F)$]
Intensity variation (σ)	> 4	> 4	> 4
R	0.0620	0.0582	0.0530
Rw	0.1512	0.1538	0.0916
Goodness of fit	1.120	1.036	1.113
No. of variables	568	568	847
$\Delta\rho_{min}$ [e A^{-1}]	−0.364	−0.555	−0.338
$\Delta\rho_{max}$ [e A^{-1}]	0.454	0.908	0.525

(KBr): $\tilde{\nu}$ = 2956 cm^{-1}, 2868, 1576, 1560, 1526, 1490, 1424, 1392, 1362, 1244, 1162, 1092, 970, 904, 858 and 736. − $C_{56}H_{80}AlN_2O_4$ (872.06): calcd. C 77.11, H 9.25, N 3.21; found C 77.16, H 9.22, N 3.21.

Gallium, Calcium, Barium, and Strontium Complexes 3−6: A similar procedure as for compound **2** was applied. − **3**: dark crystals obtained from CH_2Cl_2/ethanol. m.p. > 300°C (85% yield). − $C_{56}H_{80}GaN_2O_4$ (914.81): calcd.C 73.44, H 8.81, N 3.06; found C 73.16, H 8.98, N 3.08. − **4**: dark powder, m.p. 230°C (78% yield). − IR (KBr): $\tilde{\nu}$ = 2958 cm^{-1}, 2870, 1550, 1526, 1478, 1458, 1394, 1360, 1294, 1174, 1096, 994, 932, 860 and 732. − $C_{56}H_{80}CaN_2O_4$ (885.16): calcd. C 75.97, H 9.11, N 3.16; found C 76.01, H 9.13, N 3.22. − **5**: dark blue powder, m.p. 138°C (70% yield). − IR (KBr): $\tilde{\nu}$ = 2960 cm^{-1}, 2868, 1544, 1520, 1478, 1456, 1398, 1360, 1274, 1180, 1098, 994, 932, 864 and 732. − $C_{56}H_{80}BaN_2O_4 \cdot H_2O$ (1000.38): calcd. C 67.26, H 8.26, N 2.80; found C 67.27, H 8.21, N 2.85. − **6**: dark blue crystals m.p. 186°C (75% yield). − IR (KBr): $\tilde{\nu}$ = 2958 cm^{-1}, 2858, 1542, 1522, 1478, 1458, 1394, 1360, 1282, 1180, 1096, 994, 932, 896 and 732. − $C_{84}H_{120}SrN_3O_6 \cdot CH_2Cl_2$ (1440.16): calcd. C 70.88, H 8.53, N 2.92; found C 70.75, H 8.71, N 2.92.

Acknowledgments

Financial support from Conacyt-Mexico is acknowledged. We thank M. A. Leiva-Ramirez for performing the X-ray diffraction studies of compounds **2** and **3**.

[1] R. Contreras, A. Murillo, G. Uribe, A. Klaébé. *Heterocycles* **1985**, *23*, 2187−2192.
[2] N. Farfán, P. Joseph-Nathan, L.M. Chiquete, R. Contreras, *J. Organometal. Chem*. **1988**, *348*, 149−156.
[3] M. A. Paz-Sandoval, C. Fernández-Vincent, G. Uribe, R. Contreras, A. Klaébé, *Polyhedron* **1988**, *7*, 679−684.
[4] R. Contreras, A. Murillo, P. Joseph-Nathan, *Phosphorus Sulfur Silicon* **1990**, *47*, 215−224.
[5] A. Murillo, L. M. Chiquete, P. Joseph-Nathan, R. Contreras, *Phosphorus Sulfur Silicon* **1990**, *53*, 87−101.
[6] C. Camacho-Camacho, H. Tlahuext, H. Nöth, R. Contreras, *Heteroatom Chem*. **1997**, *9*, 321−326.
[7] C. Camacho-Camacho, F.J. Martínez-Martínez, M.J. Rosales-Hoz, R. Contreras, *Phosphorus Sulfur and Silicon* **1994**, *91*, 189−203.
[8] H. B. Stegmann, K. Scheffler, *Chem. Ber.* **1970**, *103*, 1279−1285.
[9] H. B. Stegmann, K. B. Ulmschneider, K. Scheffler, *J. Organomet. Chem.* **1974**, *72*, 41−58.
[10] K. Ohkata, T. Yano, T. Kuwati, K. Akiba, *Chem. Lett*. **1990**, 1721−1724.
[11] A. Y. Girgis, A. L. Balch, *Inorg. Chem*. **1975**, *14*, 2724−2727.
[12] C. G. Pierpont, S. K. Larsen, S. R. Boone, *Pure Appl. Chem.* **1988**, 1331−1336.
[13] S. K. Larsen, C. G. Pierpont, *J. Am. Chem. Soc*. **1988**, *110*, 1827−1832.
[14] C. L. Simpson, S. R. Boone, C. G. Pierpont, *Inorg. Chem.* **1996**, *35*, 3519−3524.
[15] A. Caneschi, A. Dei, D. Gatteschi, *J. Chem. Soc., Chem Commun*. **1992**, 630−631.
[16] B. R. McGarvey, A. Ozarowski, Z. Tian, D. G. Tuck, *Can. J. Chem*. **1995**, *73*, 1213−1222.
[17] S. Bruni, A. Caneschi, F. Cariati, C. Delfs, A. Dei and D. Gatteschi, *J. Am. Chem. Soc*. **1994**, *116*, 1388−1394.
[18] G. Speier, J. Csihony, A. M. Whalen, C. G. Pierpont, *Inorg. Chem.* **1996**, *35*, 3519−3524.
[19] G. Swarnabala, M. V. Rajasekharan, S. Padhye, *Chem. Phys. Lett.* **1997**, *267*, 539−544.
[2o] B. G. Maiya, Y. Deng, K. M. Kadish, *J. Chem. Soc., Dalton Trans.* **1990**, 3571−3576.
[21] A. Caneschi, A. Cornia, A. Dei, *Inorg. Chem*. **1998**, *37*, 3419−3421.
[22] I. Yamaguchi, K. Miki, N. Yasuoka, N. Kasai, *Bull. Chem. Soc. Jpn.* **1982**, *55*, 1372−1375.

Received October 5, 1998
[I98338]

Steric Promotion of Aromatic C–H Bond Activation in Primary Benzylamines

Valery V. Dunina,*[a] Lyudmila G. Kuz'mina,[b] Marina Yu. Kazakova,[a] Ol'ga N. Gorunova,[a] Yury K. Grishin,[a] and Elena I. Kazakova[c]

Keywords: Palladium / Primary benzylamines / NMR spectroscopy / Structure elucidation / Conformation analysis

ortho-Palladation of a sterically crowded primary benzylamine, α-phenylneopentylamine, was accomplished in a moderate yield of 50% in the reaction with the weakest of palladation agents (Li_2PdCl_4) under very mild conditions, due to a steric promotion of an aromatic C–H bond activation. The structure of dimer **1a** thus formed and the palladacycle conformation were established on the basis of ^{1}H-NMR spectroscopy of its mononuclear derivatives with [D_5]pyridine (**3a**) and triphenylphosphane (**4a**), and an X-ray investigation of the latter.

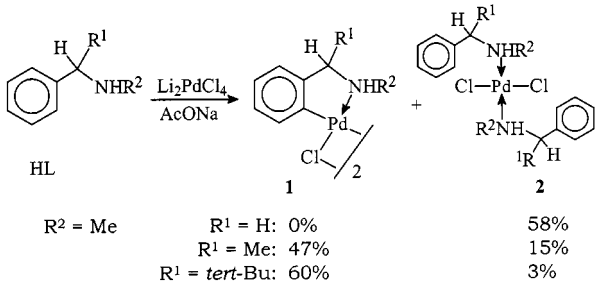
Introduction

Widening the scope of direct intramolecular palladation reactions is of great importance for further development of regioselective palladium-mediated organic synthesis.[1][2] In particular, cyclometallated derivatives of primary amines seem to be especially promising synthons for the heterocyclization processes based on a combined use of the C−Pd and N−H bond reactivities.[3−5] However, after initial unsuccessful attempts with the use of tetrachloropalladate,[6] the direct *ortho*-palladation reactions of these substrates proved to be elusive.

Several recent findings have made an important contribution towards a solution to this problem: (i) the use of palladation agents of higher electrophilicity; and (ii) the realization of the necessity for creating a coordination vacancy at a metal centre. The first point includes a substitution of palladium acetate for commonly used tetrachloropalladate salts.[7−11] The second goal may be simply achieved by keeping the palladium/ligand ratio equal to 1:1. It results in the formation of binuclear coordination complexes as reaction intermediates capable of dissociating easily to form two unsaturated tricoordinated species of high reactivity.[8][10] At this stage, a polar solvent may facilitate the dissociative formation of the coordination vacancy that is required for a subsequent C−H bond activation. In principle, all these problems may be solved simultaneously by utilizing the methodology involving a halide abstraction from the intermediate bis(amine) complexes [$Pd(HL)_2Hal_2$] by the action of soluble Ag^+ salts.[12][13]

Despite numerous publications dealing with the direct cyclopalladation of primary benzylamines, the possibility of steric promotion of this process still remains unexplored. The pioneer work of Lewis and co-workers[14] cannot be considered as conclusive enough because this publication does not contain any spectral evidence that the isolated (triphenylmethylamine)palladium complexes have a cyclopalladated structure.

Our investigation of the direct *ortho*-palladation of secondary arylalkylamines[15−19] has revealed a phenomenon of a remarkable steric facilitation of this process. The reaction of Li_2PdCl_4 with a series of *N*-methylbenzylamines was found to be dependent on the volume of substituent R^1 (R^1 = H, Me, *t*Bu) in the α-benzylic position.



Scheme 1. Steric promotion of aromatic C−H bond activation in secondary benzylamines

Thus, the reaction with α-nonsubstituted *N*-methylbenzylamine stops at the stage of the simple coordination complex of type **2**;[15] α-Me-substituted amine forms *ortho*-palladated dimer of type **1** only in refluxing methanol in moderate yield of 47%.[15] In contrast, α-*t*Bu-substituted analogue undergoes the cyclopalladation reactions even at room temperature in excellent yield of 86%.[18][20] Moreover, activation of sp^3 C−H bond (26%) becomes possible in the case of the latter sterically crowded benzylamine in competition with sp^2 C−H bond activation (60%) to give two possible regioisomers in a ca. 1:3 ratio.[20]

These findings gave an impetus for studying a similar steric effect in the C−H bond activation of primary benzylamines. The role of solvents, particularly acetone, in these processes is also of interest. Another task is the inves-

[a] Department of Chemistry, M. V. Lomonosov Moscow State University,
119899, V-234, Vrob′yovy Gory, Moscow, Russia
Fax: (internat.) + 7-095/932-8846
E-mail: dunina@org.chem.msu.su
[b] N. S. Kurnakov Institute of General and Inorganic Chemistry, Leninsky Prospect, 31, 117907, Moscow, Russia
[c] Department of Chemistry and Biology, Syktyvkar State University,
167005, Petrozavodskaya Street, 120, Syktyvkar, Komi Republik, Russia

Supporting information for this article is available on the WWW under http://www.wiley-vch.de/home/eurjic or from the author.

 © WILEY-VCH Verlag GmbH, D-69451 Weinheim, 1999 1434−1948/99/0606−1029 $ 17.50+.50/0

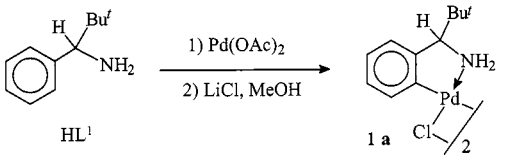
tigation of conformational features of the five-membered palladacycles containing a primary amino group using ^{1}H-NMR and X-ray studies. These characteristics seem to be especially important for utilization of the new kind of palladacycles in the processes of chiral recognition (for example, see ref.[21]).

Results and Discussion

Cyclopalladation Reactions

To estimate the role of steric effects in the processes of the intramolecular C−H bond activation in primary benzylamines, we have chosen α-phenylneopentylamine (HL^1) bearing a bulky *tert*-butyl group in the α-benzylic position as the most suitable ligand. In accordance with recent information regarding the cyclometalation mechanisms,[22−24] the equimolar ligand/Pd ratio was kept under all conditions to facilitate the formation of the free coordination vacancy after the first stage of the ligand-to-palladium *N*-coordination.

Firstly, a study of the HL^1 *ortho*-palladation was carried out using palladium(II) acetate, one of the most efficient reagents due to its high electrophilicity.



Conditions for 1) and yields: benzene, r.t., 24h - 43%
acetone, 50°C, 50h - 68%
MeOH, 50°C, 1.5 h - 68%
MeOH, r.t., 24h - 71%

Scheme 2. Influence of conditions on the *ortho*-palladation of the primary amine HL^1 with palladium(II) acetate

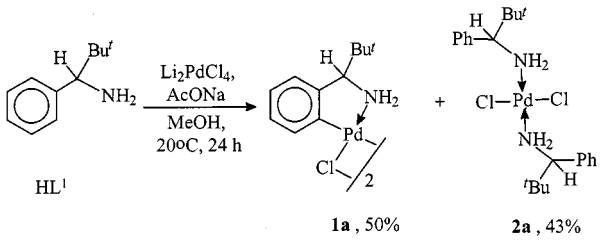
The reaction performed in benzene at room temperature afforded (after standard AcO^-/Cl^- metathesis and chromatographic purification) the desired dimeric chloro-bridged *ortho*-palladated complex **1a** in a 43% yield. In comparison, the α-methyl-substituted μ-bromo analogue was obtained previously under similar conditions in a yield of only 17% after one day, or in the same yield (43%) after three days.[9] Both enantiomers of the corresponding μ-chloro dimer were prepared by Fuchita in higher yields of 57−63% by means of a two-step procedure (including the isolation of the intermediate μ-acetato dimer) only after heating at 50°C for a long period of time.[11]

The yield of dimeric complex **1a** was increased to 68% by carrying out the same reaction in acetone at higher temperature (50°C); however, this procedure requires ca. 50 hours of heating. The best results were achieved when the reaction was performed in methanol; dimer **1a** was isolated in a yield of nearly 70% after heating for 1.5 hours at 50°C or after stirring for 24 hours at room temperature. In comparison, the formation of the α-Me-substituted analogue in a 50−70% yield required heating at 60°C for four hours.[21]

The results obtained in this series of *ortho*-palladation reactions with palladium(II) acetate make it evident that polar solvents have some advantages over the non-polar ones. It may be a consequence of their strong solvating effect that assists in the generation of the reactive three-coordinate intermediate of the [(HL)Pd(OAc)$_2$(Solv)]-type[8] required for subsequent C−H bond activation. Solvent basicity may also be important at the stage of C−H bond activation.[24]

The first successes in the palladation of primary benzylamines were achieved with the use of acetone as solvent.[8,11,13] Such a choice seems to be a rather strange one when the possibility of a metal-assisted interaction between the carbonyl and NH_2 groups is considered. Precedents for the C=N bond formation[25] and cleavage[26−28] at the palladium matrix are known. These transformations may allow the reaction to go through *ortho*-palladation of the more reactive short-lived ketimine intermediate. This route may result in the facilitation of the whole process. However, contrary to expectations, the use of acetone as solvent in the palladation of the amine HL^1 did not provide any advantages over the use of methanol; moreover, in this case, more vigorous conditions or increased reaction times are required. This observation allowed for the exclusion of the *ortho*-palladation route via intermediate ketimine ligand formation (at least for HL^1).

The results obtained when using the weak palladation agent Li_2PdCl_4 may be considered as the most convincing evidence for the steric promotion of the C−H bond activation: dimer **1a** was isolated in a 50% yield in the reaction performed in MeOH in the presence of sodium acetate excess at room temperature.



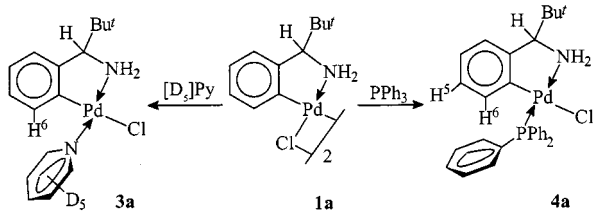
Scheme 3. *ortho*-Palladation of primary amine HL^1 using tetrachloropalladate

Under these conditions a simple coordination complex *trans*-[Pd(HL^1)$_2$Cl$_2$] (**2a**) was isolated in a yield of ca. 43% (based on the ligand) as a side product. Its 1:2 stoichiometry differs from the starting Pd/HL^1 ratio of 1:1 and may be explained by a partial Pd^{II} reduction. Under the same conditions, primary α-methylbenzylamine forms only a coordination compound of type **2**, which tends to decompose at increased temperatures.[15] The formation of complex **2a** occurs without any diastereoselectivity: a mixture of nearly equal amounts of (*R**,*R**)- and (*S*,*R*)-diastereomers was isolated in the reaction of racemic HL^1 with Li_2PdCl_4. One of these diastereomers may be separated by crystallization.

We believe that two main factors determine the easier *ortho*-palladation of the sterically hindered ligands (includ-

ing amine HL^1): (i) a large effective volume of the ligand must increase an internal energy of the intermediate binuclear coordination compounds due to a set of unfavourable non-bonding interactions,[29] thus stimulating an intermediate dissociation to form reactive three-coordinate species; (ii) the same steric effect must result in a weakening of the Pd−N bond in the coordination intermediate,[30] to make the palladium(II) centre more electrophilic. Both effects essentially facilitate the C−H bond activation.

For the subsequent spectral and structural investigations of the new dimeric complex **1a**, its mononuclear derivative with [D_5]pyridine (**3a**) was generated in situ, and an adduct with PPh_3 (**4a**) was prepared by a standard μ-chloro bridge cleavage.



Scheme 4. Mononuclear derivatives of the *ortho*-palladated primary amine HL^1

The identity of the samples of dimer **1a** prepared under all afore-mentioned conditions was confirmed by their melting points, TLC of complex **1a** and the ^{1}H-NMR spectra of its mononuclear derivatives **3a** and **4a**.

Structure of Complexes 1a−4a in Solution

The *ortho*-palladated structure of complexes **1a**, **3a** and **4a** was confirmed by the IR and ^{1}H-NMR spectra (Table 1) using a comparison with the spectral data for simple coordination compound **2a**. An assignment of their ^{1}H-NMR spectra was based on homonuclear spin-spin decoupling experiments and NOE differential spectroscopy.[31]

The IR spectrum of dimer **1a** contains a single intense absorption of the aromatic C−H bonds out-of-plane deformation at 740 cm^{-1}[18,19,32,33] compared to two bands found in the IR spectra of the free starting amine HL^1 and coordination complex **2a** (720, 785 and 705, 750 cm^{-1}, respectively). The ^{1}H-NMR spectra of mononuclear adducts **3a** and **4a** reveal only four well-resolved single-proton resonances of the *ortho*-phenylene group in the aromatic field (δ = 6.0−7.0), compared to two complicated multiplets of *ortho* (δ = 7.00, 4 H) and *meta* and *para* protons (δ = 7.27, 6 H) further downfield in the case of coordination complex **2a**.

The nine-proton singlet of the *t*Bu group (δ = 1.23−1.30 for adducts **3a** and **4a**) unambiguously supports the suggestion that the palladation site is the *ortho*-position of benzylamine Ph ring. Both the diastereotopic nonequivalence (Δδ = 0.3−2.7 ppm) and the coordination shift values (Δδ = 1.7−4.5 ppm) observed for the two NH_2 protons in the complexes **2a**−**4a** confirm the *Pd*-coordination of the primary amino group. Thus, the η^1-*N*-coordination of the HL^1 ligand in complex **2a** and η^2-*C*,*N*-binding of the $(L^1)^-$ ligand in adducts **3a**, **4a** and also in starting dimer **1a** are evident enough.

The assignment of the signals of the aromatic palladacycle protons is important not only for the confirmation of the *ortho*-palladated structure and the geometric configuration of these and related complexes, but also for the utilization of the palladacycle as an internal reference in the estimation of the stereochemistry of *Pd*-bonded chiral ligands.[34−39]

Unfortunately, most publications devoted to the *ortho*-palladation of primary benzylamines either disregard any

Table 1. ^{1}H-NMR-spectroscopic data for ligand HL^1 and its palladium complexes **2**−**4**[a]

	Side chain protons				Aromatic protons [b]			
	tBu, 9 H	α-C*H*, 1 H	N*H*^{1}, 1 H	N*H*^{2}, 1 H	*H*^{6}, 1 H	*H*^{5}, 1 H	*H*^{4}, 1 H	*H*^{3}, 1 H
HL^1	0.91 (s)	3.69 (s)	1.40 (br. s., 2 H)		7.21−7.32 (m, 5 H)			
2a[c]	0.83 (s)	3.73 (dd, $^3J_{HCNH^1}$ = 11.2, $^3J_{HCNH^2}$ = 3.1)	3.11 (br. tr, $^2J_{HNH}$ = 11.0, $^3J_{HNCH}$ = 11.2)	3.81 (br. d, $^2J_{HNH}$ = 11.0, $^3J_{HNCH}$ = 3.1)	7.00 (m, 2 H, *ortho*-H), 7.27 (m, 3 H, *meta*- and *para*-H)			
3a	1.23 (s)	3.96 (d, $^3J_{HCNH}$ = 5.7)	3.16 (br. d, $^2J_{HNH}$ = 10.7)	5.89 (br. m, $^3J_{HCNH}$ = 5.7, $^2J_{HNH}$ = 10.7)	6.04 (A-part, $^3J_{5,6}$ = 7.7, $^4J_{4,6}$ = 1.2)	6.75 (B-part, $^3J_{4,5}$ = 7.4, $^4J_{3,5}$ = 1.4)	6.98 (C-part, $^3J_{3,4}$ = 7.6, $^4J_{4,6}$ = 1.2)	7.01 (D-part, $^3J_{3,4}$ = 7.6, $^4J_{3,5}$ = 1.4)
4a[d]	1.30 (s)	4.06 (dd, $^3J_{HCNH}$ = 5.8, $^4J_{HP}$ = 6.5)	3.73 (br. dd, $^2J_{HNH}$ = 10.6, $^3J_{HNP}$ = 3.1)	4.01 (br. m, $^2J_{HNH}$ = 10.6, $^3J_{HNCH}$ = 5.8, $^3J_{HNP}$ = 5.0)	6.39 (A-part, $^3J_{5,6}$ = 7.7, $^4J_{4,6}$ = 1.3, J_{HP} = 6.0	6.44 (B-part, $^3J_{4,5}$ = 7.4, $^4J_{3,5}$ = 1.5, J_{HP} = 0.5)	6.83 (C-part, $^3J_{3,4}$ = 7.4, $^4J_{3,5}$ = 1.3)	7.00 (D-part, $^3J_{3,4}$ = 7.7, $^4J_{3,5}$ = 1.5)
4a[e,f]	1.28 (s)	4.07 (dd, $^3J_{HCNH}$ = 6.0, $^4J_{HP}$ = 7.0)	3.58 (br. d, $^2J_{HNH}$ = 10.6, $^3J_{HNP} \leq$ 1.0)	5.18 (br. m, $^2J_{HNH}$ = 10.6, $^3J_{HNCH}$ = 6.0, $^3J_{HNP}$ = 4.0)	6.31 (m, 2 H, H^5 + H^6)		6.78 (m)	6.95 (m)

[a] Spectra recorded at 400 MHz in $CDCl_3$ (except where noted), δ in ppm relative to TMS as internal standard, *J* in Hz. − [b] ABCD system in the case of **3a**, ABCDX system (X = ^{31}P) for **4a**. − [c] Spectrum of individual (*R*,*R*)* diastereomer. − [d] Signals of PPh_3 protons ($CDCl_3$): δ = 7.36 (m, 6 H, *meta*-H), 7.42 (m, 3 H, *para*-H), 7.73 (m, 6 H, $^3J_{HP}$ 11.1, *ortho*-H). − [e] Spectrum was recorded in [D_6]acetone/$CDCl_3$, 10:1. − [f] Signals of PPh_3 protons: δ = 7.35 (m, 6 H, *meta*-H), 7.42 (m, 3 H, *para*-H), 7.70 (m, 6 H, $^3J_{HP}$ 11.2, *ortho*-H), 1.95 (s, 3 H, MeCN).

assignments of the aromatic protons[9,13,21] or do so only in part.[11] Moreover, several attempts to assign these signals for phosphane adducts[8][10] gave a result which strongly disagreed with the usual trends reported for the related derivatives of secondary[7,18,19,40,41] and tertiary [33,42−44] benzylamines. This disagreement includes three points: (i) the most downfield signal was assigned to the H^6 proton (nearest to the metallation site); (ii) as a result, the long-range constant $^5J_{HP}$ of a very high value was ascribed to the H^3 proton that is far remote from the ^{31}P nucleus; (iii) at the same time, the corresponding constant for the H^6 proton is lacking despite its proximity to the ^{31}P nucleus being closer than the sum of their van der Waals radii of 3.0 Å[45] (for example, 2.78 Å was found by the X-ray study of a related complex[46]).

Such a large discrepancy between the spectral characteristics of palladacycles for derivatives of primary benzylamines on the one hand, and those of secondary and tertiary amines on the other, forced us to provide unambiguous support for our version of assignment on the basis of the NOE differential spectra of the phosphane adduct **4a**.

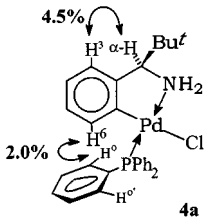


Figure 1. Selected $^1H\{^1H\}$ NOEs for the phosphane adduct **4a** in $CDCl_3$

The irradiation of the low-field H^3 proton of the palladated phenylene ring (δ = 7.00 for the **4a** in $CDCl_3$) results in an enhancement of ca. 4.5% of the signal for the α-benzylic methine proton nearest to H^3 (see Figure 1); when the *ortho*-protons of the PPh groups were irradiated (δ = 7.73, identified on the basis of the constant value of $^3J_{HP}$ = 11.1 Hz) the only observed interligand response was that of the H^6 proton (δ = 6.39, ca. 2%). Hence, a downfield position of the H^3 signal and an upfield location of the H^6 resonance of the palladated phenylene group are evident.

Thus, in the ^1H-NMR spectra of the arylphosphane adducts of *ortho*-palladated primary benzylamines, the sequence of the signals of the phenylene H^6-H^3 protons remains the same as in the case of their analogues derived from secondary and tertiary amines, namely, from high field (H^6) to low field (H^3). This tendency, as well as the detection of the J_{HP} constant for the H^6 proton, may be used for the reliable estimation of the geometric configuration and for the solution of stereochemical problems by means of NOE technique (cf. ref.[39,47,48]) using palladacycles as an internal reference.

A *trans*(C,Cl) geometry of the mononuclear derivatives of dimer **1a** seems to be evident enough from the high field position of the signals of the H^6 proton (**3a**) or the H^6 and H^5 protons (**4a**) of the palladated phenylene moiety, caused by the influence of anisotropy of the pyridine or *P*-phenyl rings, respectively. The large high-field value of the H^6 resonance in the ^1H-NMR spectrum of adduct **3a** (δ = 6.04) may be considered as an indication of the nearly orthogonal mutual arrangement of the pyridine and palladated phenylene rings.[49]

In the case of phosphane derivative **4a**, the signal of the H^6 proton appears at δ = 6.39, with the constant J_{HP} = 6.0 Hz, which is in close agreement with the values previously reported for related derivatives of primary aralkylamines (J_{HP} = 5.5−6.4 Hz).[50][51] For the more distant aromatic H^5 proton, this value decreases to J_{HP} = 0.5 Hz; it can only be detected by means of an NMR-spectrum simulation.

The conformation of the palladacycle formed by primary benzylamine HL^1 could be estimated by means of the analysis of the $HC^{\alpha}-NH$, $HC^{\alpha}-^{31}P$ and $HN-^{31}P$ spin-spin coupling constants. A strong dependence of the efficiency of the interaction between the protons of palladacycle and the ^{31}P nucleus of *Pd*-bonded phosphane ligands on the extent of their planarity may be expected from general considerations.[52][53]

A distinction in the assignments of two NH protons (NH^{eq} and NH^{ax}) is not a simple problem. In most reported ^1H-NMR spectra of *ortho*-palladated primary aralkylamines, these resonances were described as broad multiplets[8,13,21,51] or broad singlets[9][11] without their assignments. In the spectrum of pyridine adduct **3a** recorded in $CDCl_3$, the diastereotopic NH_2 proton signals appear as a broad apparent singlet (Δν > 20 Hz) and a broad doublet at δ = 5.89 and 3.14, respectively, with a typical geminal coupling constant of $^2J_{NH\text{-}NH} \approx 11$ Hz (cf. ref.[51,54,55]).

Homonuclear decoupling of adduct **3a** showed that a broad downfield signal at δ = 5.89 originates from the NH proton interacting with the α-methine proton ($^3J_{HCNH}$ = 5.7 Hz). In the case of phosphane adduct **4a**, the signals of NH protons are additionally complicated due to their spin-spin coupling with the ^{31}P nucleus. In the ^1H-NMR spectrum of **4a** measured in a $[D_6]$acetone/$CDCl_3$ mixture, two NH proton signals appear as a broad multiplet at δ = 5.19 ($^3J_{HNP}$ = 4.0 Hz, $^3J_{HCNH}$ = 6.0 Hz) and a doublet at δ = 3.58 ($^3J_{HNP} \leq 1.0$ Hz) with a geminal coupling constant of $^2J_{HNH}$ = 10.6 Hz.

Under these conditions, the α-methine proton of **4a** appears as a doublet of doublets at δ = 4.13 with the $^3J_{HCNH}$ and $^4J_{HCP}$ constants of 6.0 and 7.0 Hz, respectively. Both of these constants seem to be extremely useful for conformational analysis. The dependence of ^1H-^{31}P spin-spin coupling on the position of the α-CH proton (*pseudo*-axial or *pseudo*-equatorial) becomes evident from the spectral pattern for α-nonsubstituted palladacycles. Only one of the diastereotopic protons of the α-CH_2 group in phosphane adducts of *ortho*-palladated secondary[7][19] and tertiary benzylamines[56] shows a coupling with the ^{31}P nucleus ($^4J_{HCP}$ = 2.0−4.2). The average constant value of $^4J_{HCP}$ = 2.8 Hz reported for the two equivalent (on NMR time scale) α-benzylic protons in the more flexible α,*N*-nonsubstituted palladacycles,[50] may be used as a middle point for the conformation estimates. The $^4J_{HCP}$ = 6−8 Hz reported

for the strictly planar aldimine palladacycles may serve as the upper boundary point.[21][57]

The values of the $^4J_{HCP}$ constant for the α-methine proton ranging within 6.5−7.0 Hz in the ^{1}H-NMR spectra of complex **4a** are close to the above-mentioned upper limit. It may serve as an indication of its *pseudo*-equatorial position which is in agreement with the prediction of a *pseudo*-axial position of a bulky α-*t*Bu group. A comparison of these characteristics with those for the related derivatives of secondary[18][41] and tertiary α-*tert*-butylbenzylamines[44] ($^4J_{HCP}$ = 5.4−6.1 Hz) allows for a suggestion that a steric interaction between the α-*t*Bu substituent and the aromatic H^3 proton is the main factor controlling the palladacycle conformation. The role of the *N*-substituents seems not to be very significant in this case, in contrast with the assumption made previously.[58][59]

Unfortunately, no information could be found regarding the $^4J_{HCP}$ constant for the α-methine proton of related α-Me-substituted palladacycles based on primary arylalkylamines; usually this signal was described as a multiplet,[8][13] or a broad multiplet.[9][21] If the signal of the α-methine proton for the *ortho*-palladated derivative of primary α-(1-naphthyl)ethylamine is really a pure quadruplet as was reported,[51] the value of this constant must be equal to zero. Hence, the palladacycle must adopt the conformation with the α-Me group in an equatorial position, which contradicts the data ($^4J_{HCP}$ = 5.8-6.3 Hz) reported for related derivatives of the corresponding tertiary amine containing η^1-*P*-bonded phosphane ligands.[60−63]

A valuable additional source of stereochemical information is the HN−C^{α}H coupling. Newman projections along the N−C^{α}H bond for two possible conformations of the palladacycle, λ(*S*) and δ(*S*) (Figure 2), were constructed with regard to the real values of the torsion angles taken from the X-ray study of adduct **4a** (see the next section).



λ(*S*) δ(*S*)

Figure 2. Newman projections of (*S*)-palladacycle along the N−C(α) bond for two possible conformations, λ(*S*) and δ(*S*)

The most important dihedral angles between the C^α−H and the *pseudo*-axial and *pseudo*-equatorial N−H bonds for the λ(*S*) conformation are equal to ca. 31° and −88°, respectively, in the crystal of **4a**. As a result, an observable $^3J_{HCNH}$ constant can be predicted only for one of the two NH protons, namely NH^{ax}, if the same λ(*S*) conformation remains in solution. This particular situation takes place in the case of adducts **3a** and **4a**: $^3J_{HCNH}$ = 5.6−6.0 Hz was found for only one downfield resonance of the NH proton.

In contrast, in the case of the hypothetical δ(*S*) conformation of the palladacycle, the dihedral angles between the C^α−H and axial and equatorial N−H bonds should be nearly equal to one another from the point of view of the Carplus−Conroy equation[64] (ca. −30° and −150°, respectively). Hence, nearly equal values of the $^3J_{HCNH}$ constant are expected for both of the NH protons of the primary amino group. Moreover, the C^α−H bond in this conformation should be oriented nearly orthogonally to the mean coordination plane, and the $^4J_{HCP}$ constant for this proton should be approximately zero (cf. ref.[52,53,65]).

All these arguments allow for the exclusion of the δ(*S*) conformation of palladacycle in **3a** and **4a** from the consideration. It should be noted that the opposite (and incorrect) conclusion can be made from the analysis of "classic" Newman projections constructed without regard for the palladacycle flattening (with all dihedral angles equal to 60°): nearly equal $^3J_{HCNH}$ constant values have to be predicted for both NH protons in the λ(*S*) conformation and different values only for the δ(*S*) skew-envelope. The difference in the predicted values of the $^3J_{HCNH}$ constant may serve as a basis of the reliable criteria for identification of the axial and equatorial NH protons in the palladacycles derived from primary and secondary benzylamines.

As additional support for the axial position of the *t*Bu group in the palladacycle of λ(*S*) or δ(*R*) conformation, the downfield shift of its signal compared to the free ligand HL^1 should be mentioned (Δδ = 0.4−0.5 ppm for the complexes **3a** and **4a**). Commonly, such an effect is considered as a consequence of the metal anisotropy influence.[66][67] In the case of **3a** and **4a** complexes, the actual shift calculated for one proton must be essentially higher (Δδ up to 4 ppm) if one keeps in mind that each of the nine protons of the *t*Bu group spends nearly one ninth of all time in the proximity to the metal centre. Such a high shift may serve as an indirect indication for a weak *t*Bu···Pd agostic interaction.[66−69]

All these data support our statement that the palladacycles of dimer **1a** and its mononuclear derivatives **3a** and **4a** exist in solutions predominantly in the λ(*S*) or δ(*R*) conformation with the equatorial α-CH proton and the axial *t*Bu group. This result is important for further practical use of this new chiral matrix, because the conformational rigidity of palladacycles enhances their ability for chiral recognition.[36,52,53,63,70,71]

The relation between the $^3J_{HNP}$ constants for the two N−H protons of the primary amino group is difficult to predict. Taking into account the similar dihedral angles H^{ax}−N−Pd−P and H^{eq}−N−Pd−P, found for adduct **4a** in the crystal (110.7° and −130.9°, respectively), it is conceivable to suggest that both NH protons may reveal a spin-spin coupling with the ^{31}P nucleus. A little more efficient interaction may be expected for the *pseudo*-equatorial NH proton. However, the ^{1}H-NMR spectrum of **4a** reveals the reverse relation, namely, $^3J_{HNP}$ = 4.0−5.0 and 1.0−3.1 Hz for the NH^{ax} and NH^{eq} protons, respectively. Examples of equal[37,38,62,72] and substantially different[36,60,62,73] values of the $^4J_{HP}$ constant for NMe groups may be found among the spectra of phosphane complexes with the *ortho*-palladated *N*,*N*-dimethyl-α-(1-naphthyl)ethylamine, despite a high conformational stability of this palladacycle. This ob-

servation made the J_{HP} values for NH_2 and NMe_2 groups less suitable for the conformation analysis.

The structure of coordination complex **2a** can shed some light on the nature of the steric promotion of *ortho*-palladation reactions. Its ^{1}H-NMR spectrum indicates a restricted rotameric mobility of η^1-*N*-coordinated ligand HL[1]. A large difference between $^3J_{HCNH}$ constant values for two NH protons (11.2 and 3.1 Hz) pointed to the φ^3 or φ^5 conformation of *Pd*-bonded amine, with *transoid* orientation of one of the NH protons relative to the α-methine one. For the alternative φ^1 rotamer, nearly equal and low values of $^3J_{HCNH}$ constant may be predicted[64] from the Newman projections (Figure 3).

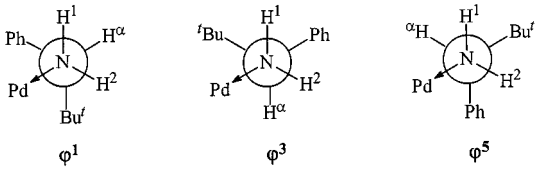


Figure 3. Newman projections of *Pd*-coordinated (*S*)-α-phenylneopentylamine along the N−C(α) bond for three main rotamers, φ^1, φ^3 and φ^5

The absence of deshielding effects (caused by the metal anisotropy[66−69]) for the *t*Bu protons in the spectra of complex **2a** (δ = 0.83 is close to δ = 0.91 for the free ligand HL[1]) allows for the differentiation between φ^3 and φ^5 rotameric forms in favour of the latter, where the *t*Bu group is far remote from the palladium centre.

Therefore, at the stage of monodentate *N*-coordination, the bulky HL[1] ligand adopts predominantly the φ^5 conformation with the Ph ring disposed in proximity to the metal centre (cf. ref.[74][75]). This conformation seems to be the most suitable starting state for the subsequent *ortho*-palladation. In contrast, monodentate *N*-coordination of the related α-Me-substituted primary benzylamine in the framework of binuclear μ-acetato coordination complex occurs in the φ^3 conformation with remote *transoid* position of the Ph ring with respect to the palladium centre.[10] Such a difference in the starting rotameric states of *N*-coordinated α-*t*Bu- and α-Me-substituted primary benzylamines may contribute to some extent to the steric promotion of the C−H bond activation in the former instance.

X-ray Structure Investigation of Phosphane Derivative 4a

Suitable crystals of triphenylphosphane adduct **4a** were grown from a dichloromethane/acetonitrile mixture. The molecular structure of the complex is presented in Figures 4 and 5; selected bond lengths and angles are given in Tables 2 and 3, respectively.

Only two other triphenylphosphane adducts of *ortho*-palladated primary benzylamines have been previously characterized structurally, namely, that of the α-Me-substituted analogue (*R*)-**4b**[13] and of the 2-phenylglycine methyl ester derivative (*R*)-**4c**.[11] The related derivative of 2-phenylethylamine containing a six-membered palladacycle was also studied by X-ray diffraction.[10]

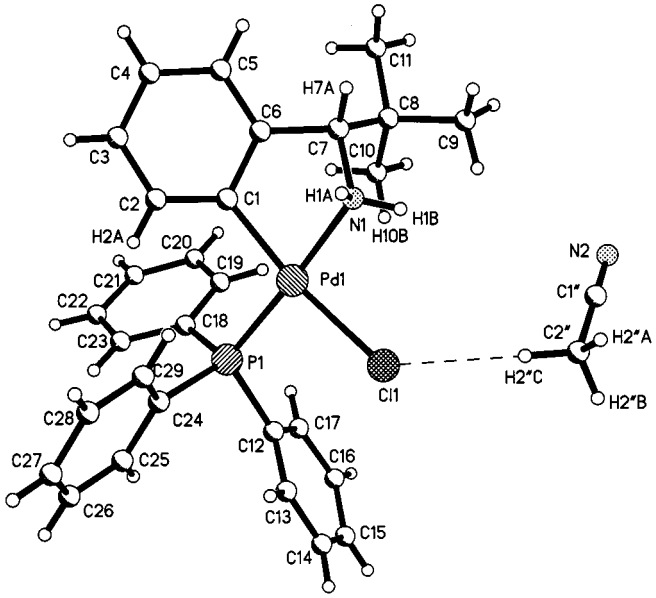


Figure 4. Molecular structure of the acetonitrile solvate of phosphane adduct **4a**

Table 2. Bond lengths [Å] for [2-(1-amino-2,2-dimethylpropyl)phenyl-*C*,*N*]chloro(triphenylphosphane)palladium(II)·MeCN solvate **4a**

Pd(1)−C(1)	2.006(4)	C(12)−C(13)	1.381(6)
Pd(1)−N(1)	2.087(4)	C(13)−C(14)	1.379(7)
Pd(1)−P(1)	2.256(2)	C(14)−C(15)	1.356(8)
Pd(1)−Cl(1)	2.3996(14)	C(15)−C(16)	1.370(8)
P(1)−C(24)	1.817(5)	C(16)−C(17)	1.382(8)
P(1)−C(12)	1.827(4)	C(18)−C(19)	1.383(6)
P(1)−C(18)	1.826(5)	C(18)−C(23)	1.391(6)
N(1)−C(7)	1.496(5)	C(19)−C(20)	1.376(7)
C(1)−C(2)	1.385(6)	C(20)−C(21)	1.365(9)
C(1)−C(6)	1.423(6)	C(21)−C(22)	1.372(9)
C(2)−C(3)	1.395(6)	C(22)−C(23)	1.403(8)
C(3)−C(4)	1.369(7)	C(24)−C(29)	1.379(6)
C(4)−C(5)	1.384(7)	C(24)−C(25)	1.390(6)
C(5)−C(6)	1.387(6)	C(25)−C(26)	1.376(7)
C(6)−C(7)	1.510(6)	C(26)−C(27)	1.371(8)
C(7)−C(8)	1.544(6)	C(27)−C(28)	1.374(8)
C(8)−C(11)	1.526(7)	C(28)−C(29)	1.390(7)
C(8)−C(10)	1.531(7)	N(2)−C(1″)	1.129(11)
C(8)−C(9)	1.537(7)	C(1″)−C(2″)	1.448(11)
C(12)−C(17)	1.377(7)		

Complex **4a** exists in the crystal as a racemate; the unit cell contains two centrosymmetrically related enantiomers of the mononuclear complex and two solvate molecules of acetonitrile (Figure 4). *ortho*-Palladated structure of adduct

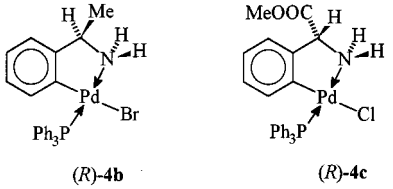


Table 3. Bond angles [°] for [2-(1-amino-2,2-dimethylpropyl)phenyl-*C*,*N*]chloro(triphenylphosphane)palladium(II)·MeCN solvate **4a**

C(1)−Pd(1)−N(1)	80.6(2)	C(11)−C(8)−C(7)	109.0(4)
C(1)−Pd(1)−P(1)	96.00(13)	C(10)−C(8)−C(7)	112.0(4)
N(1)−Pd(1)−P(1)	176.38(11)	C(9)−C(8)−C(7)	109.4(4)
C(1)−Pd(1)−Cl(1)	169.37(12)	C(17)−C(12)−C(13)	117.4(4)
N(1)−Pd(1)−Cl(1)	89.04(11)	C(17)−C(12)−P(1)	122.2(4)
P(1)−Pd(1)−Cl(1)	94.39(5)	C(13)−C(12)−P(1)	120.4(3)
C(24)−P(1)−C(12)	103.4(2)	C(14)−C(13)−C(12)	121.4(5)
C(24)−P(1)−C(18)	107.2(2)	C(15)−C(14)−C(13)	120.2(5)
C(12)−P(1)−C(18)	103.0(2)	C(14)−C(15)−C(16)	119.7(5)
C(24)−P(1)−Pd(1)	111.8(2)	C(15)−C(16)−C(17)	120.0(6)
C(12)−P(1)−Pd(1)	115.42(14)	C(16)−C(17)−C(12)	121.2(5)
C(18)−P(1)−Pd(1)	114.9(2)	C(19)−C(18)−C(23)	118.6(4)
C(7)−N(1)−Pd(1)	110.5(3)	C(19)−C(18)−P(1)	118.3(3)
C(2)−C(1)−C(6)	117.1(4)	C(23)−C(18)−P(1)	123.1(4)
C(2)−C(1)−Pd(1)	129.7(3)	C(20)−C(19)−C(18)	121.9(5)
C(6)−C(1)−Pd(1)	112.9(3)	C(21)−C(20)−C(19)	119.4(6)
C(1)−C(2)−C(3)	122.3(4)	C(22)−C(21)−C(20)	120.4(5)
C(4)−C(3)−C(2)	119.9(5)	C(21)−C(22)−C(23)	120.6(5)
C(3)−C(4)−C(5)	119.5(5)	C(18)−C(23)−C(22)	119.0(5)
C(4)−C(5)−C(6)	121.4(4)	C(29)−C(24)−C(25)	118.6(4)
C(5)−C(6)−C(1)	119.8(4)	C(29)−C(24)−P(1)	119.5(4)
C(5)−C(6)−C(7)	121.9(4)	C(25)−C(24)−P(1)	121.7(4)
C(1)−C(6)−C(7)	118.2(4)	C(26)−C(25)−C(24)	121.0(5)
N(1)−C(7)−C(6)	105.1(3)	C(27)−C(26)−C(25)	120.0(5)
N(1)−C(7)−C(8)	112.3(4)	C(26)−C(27)−C(28)	119.8(5)
C(6)−C(7)−C(8)	117.0(4)	C(27)−C(28)−C(29)	120.5(5)
C(11)−C(8)−C(10)	108.6(5)	C(24)−C(29)−C(28)	120.0(5)
C(11)−C(8)−C(9)	107.9(5)	N(2)−C(1″)−C(2″)	178.3(11)
C(10)−C(8)−C(9)	109.8(5)		

4a (and, therefore, that of starting dimer **1a**) is supported. The complex has a *trans*(C,Cl) geometry, expected from the spectral data. The Pd−C and Pd−N bond lengths [2.006(4) and 2.087(4) Å, respectively] are similar to those reported for other derivatives of primary benzylamines (2.019 and 2.092−2.089 Å for **4b** and **4c**, respectively).[10,11,13] The shorter value of the Pd−N bond in the structures of complexes **4a−c**, compared to that reported for the related derivatives of tertiary benzylamines [for example, 2.19(1) Å for *N*-isopropyl-*N*,α-dimethylbenzylamine analogue[46]] may serve as reliable evidence in favour of a tighter coordination of the primary amino group with the palladium centre.

The palladium atom in complexes **4a** and **4b** has nearly square-planar coordination with a slight tetrahedral distortion: the dihedral angles between the planes (CPdN) and (PPdHal) fall within the range 2.7−7.8°.

The palladacycle conformation in adduct **4a** may be described as a distorted envelope with the nitrogen atom displaced from the plane ($PdC^1C^6C^7$) of the remaining four atoms by −0.5999 Å as compared to −0.5113 and 0.399 Å for **4b** and **4c**, respectively. As a measure of a palladacycle twisting, the value of the dihedral angle between the phenylene ring of the benzylaminate ligand (C_6H_4) and the mean coordination plane (PdC^1HalNP) may be used. The values equal to 20.0 and 15.5° for **4a** and **4b**, respectively, indicate a more puckered conformation of the α-*t*Bu-substituted palladacycle.

The stereochemistry of palladacycle conformation is in agreement with the ^{1}H-NMR data in solutions, namely, λ for the (*S*), and δ for the (*R*) enantiomer. The bulky α-*t*Bu substituent assumes a position close to the axial one and the α-methine proton is arranged nearly equatorially: C^7-C^8 and C^7-H^{7a} bonds form angles of 168.4° (an adjacent angle 11.6°) and 66.9°, respectively, with the normal to the mean coordination plane.

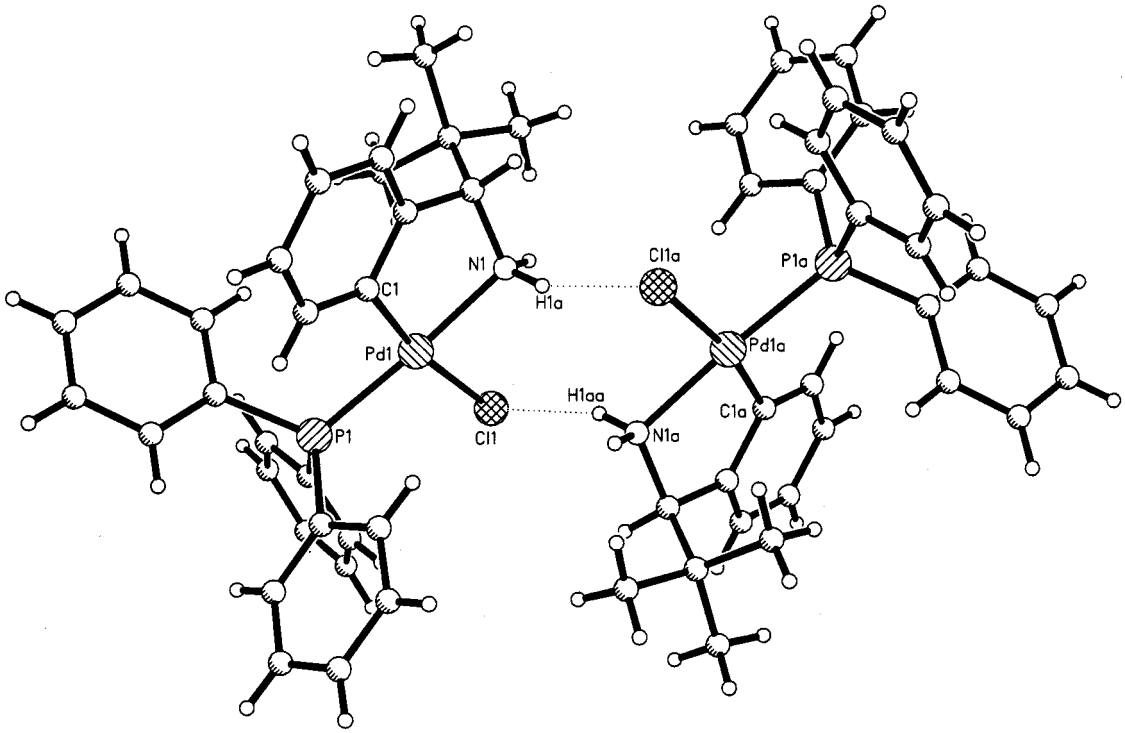


Figure 5. The mutual arrangement of two H-bonded (N−H···Cl) centrosymmetrically related enantiomers of phosphane adduct **4a** in the crystal

It is probable that a weak agostic interaction between one of the Me groups of the *t*Bu substituent with the palladium centre contributes to some extent to a stabilization of this conformation: the $H^{10b}\cdots Pd$ distance is 2.802 Å, which is less than the sum of the van der Waals radii for these atoms (3.1 Å[45]). It is noteworthy that similar secondary interactions were previously observed in the structures of *ortho*-palladated derivatives of α-*tert*-butyl-*N*,*N*-dimethylbenzylamine, namely, of a dimer (2.91−2.92 Å[76]) and its mononuclear derivative with pyridine (2.74−2.85 Å[20]).

The presence of the primary amino group in the palladacycle of **4a** results in a specific packing of molecules in the crystal, based on the hydrogen bonds of the type N−H···Cl (see Figure 5). Two enantiomers of the racemic complex are bonded in a centrosymmetric dimer by means of two rather strong hydrogen bonds, with the $NH^{1a}\cdots Cl^{1a}$ distances being equal to 2.416 Å, which is essentially less than the sum of the van der Waals radii for these atoms (3.3 Å[45]). The similar NH···Br hydrogen bonds (2.46 Å) were also found in the structure of α-Me-substituted analogue **4b**.[13]

In the crystal, the solvate acetonitrile is bonded with the coordinated chlorine atom by means of a hydrogen bond involving a methyl hydrogen atom (see Figure 4): The $CH^{2''f}\cdots Cl^{1}$ distance of 2.672 Å is also less than the sum of the van der Waals radii for these atoms (3.3 Å[45]).

Conclusions

The possibility of a steric promotion of the aromatic C−H bond activation in primary benzylamines bearing only one bulky α-substituent was shown. *ortho*-Palladation of α-phenylneopentylamine may be achieved under very mild conditions, using Li_2PdCl_4 in methanol at room temperature.

To the best of our knowledge, this work is the first presentation of the completely interpreted ^{1}H-NMR spectra of *ortho*-palladated primary benzylamine. It allows for establishing that the palladacycle formed adopts the λ(*S*) or δ(*R*) conformation with an axially oriented α-*t*Bu group both in the crystal and in solution. It seems reasonable to propose that such stereochemistry is dictated by unfavourable interactions between a bulky equatorial α-substituent and the neighbouring phenylene proton in alternative δ(*S*) or λ(*R*) conformations. The conformational stability of a new palladacycle shows a promising utility in a homochiral state as a matrix for the diverse processes of chiral recognition.

Experimental Section

General: ^{1}H- and ^{31}P-NMR spectra were recorded with a Varian VXR-400 spectrometer operating at the frequencies 400 and 161.9 MHz for ^{1}H and ^{31}P nuclei, respectively. The measurements were carried out at ambient temperature in $CDCl_3$ solutions (unless otherwise indicated). The proton chemical shifts are reported in parts per million relative to TMS as internal standard; the ^{31}P chemical shifts are given relative to H_3PO_4 as an external reference. The assignment of signals was performed on the basis of homonuclear decoupling, NOE experiments and spectral simulation. − IR spectra were recorded with a UR-250 spectrometer.

Solvents: Acetonitrile was distilled under argon from P_2O_5 and then from K_2CO_3; benzene, hexane and ether were dried with the appropriate drying agents and then distilled under argon from Na; anhydrous MeOH was prepared by distillation from MgOMe; dichloromethane was passed through a short Al_2O_3 column and distilled under argon; CCl_4 was refluxed in the presence of P_2O_5 and distilled; acetone of highest purity, and [D_1]chloroform (from Aldrich) were used as received; [D_5]pyridine was dried with 4-Å molecular sieves and distilled from KOH.

Reagents: Sodium acetate trihydrate was dehydrated by heating at 400°C; triphenylphosphane was purified by twofold recrystallization from a benzene/hexane mixture; hydroxylamine hydrochloride was used as received; lithium tetrachloropalladate was prepared according to a published procedure[6] and carefully dried in vacuo (3 Torr) over P_2O_5; palladium(II) acetate was purchased from Aldrich and used as received.

Starting Compounds: *tert*-Butyl phenyl ketone oxime was prepared by heating of pivalophenone[77] (12.80 g, 79 mmol) with hydroxylamine hydrochloride (6.05 g, 87 mmol) in the presence of $AcONa\cdot 3H_2O$ (11.8 g, 87 mmol) in aqueous methanol according to a published procedure;[78] after recrystallization from EtOH, the oxime was isolated in an 88% yield (17.93 g); m.p. 163−164°C. − ^{1}H NMR ($CDCl_3$): δ = 1.15 (s, 9 H, *t*Bu), 7.12 (dd, $^3J_{HH}$ = 7.9 Hz, $^4J_{HH}$ = 1.5 Hz, 2 H, *ortho-H* of Ph group), 7.33−7.45 (m, 3 H, *meta-H* and *para-H* of Ph group), 9.25 (br. s, 1 H, O*H*).

Racemic α-*tert*-Butylbenzylamine (HL^1) was prepared by reduction of *tert*-butyl phenyl ketone oxime (16.68 g, 0.094 mmol) under conditions previously described[79] in a yield of 72% (11.06 g, 0.068 mmol); b.p. 108−109°C/18 Torr; ^{1}H NMR ($CDCl_3$): δ = 0.91 (s, 9 H, *t*Bu), 1.40 (br. s, 2 H, NH_2), 3.69 (s, 1 H, α-C*H*), 7.21−7.32 (m, 5 H, Ph).

Synthesis of Cyclopalladated Compounds: All reactions were performed under argon in anhydrous solvents. Reactions were monitored by means of TLC on Silufol plates using an ether/heptane (5:1) mixture as eluent (unless otherwise indicated). In the case of μ-acetato complex formation, its conversion into the μ-chloro analogue by AcO^-/Cl^- metathesis (by treatment of a test probe of reaction mixture with LiCl solution in MeOH) was undertaken before spotting on the TLC plate. Dimeric complexes obtained were purified (unless otherwise indicated) using flash chromatography on a "dry" column[80][81] (Silpearl, *d* = 2.5 cm, *h* = 3.5 cm) with the eluents' polarity increasing (ether/heptane mixtures in the ratios from 1:10 up to 10:1 and then pure ether).

Di-μ-chlorobis[2-{1-amino-2,2-dimethylpropyl}phenyl-*C*,*N*]-dipalladium (II) (1a)

1. *ortho*-Palladation with Palladium(II) Acetate: i) Palladium acetate (0.206 g, 0.918 mmol) was added to racemic α-*tert*-butylbenzylamine HL^1 (0.150 g, 0.919 mmol) in methanol (5 mL) and the reaction mixture was stirred for 24 h at room temp. A solution of lithium chloride (0.190 g, 4.48 mmol) in methanol (3 mL) was added and the mixture was stirred for 2 h and then filtered. The residue was washed with methanol, combined with the mother liquor, concentrated in vacuo, and redissolved in dichloromethane (10 mL). The solution formed was washed with water to remove inorganic components, dried with sodium sulfate and concentrated to a volume of 2−3 mL. Flash column chromatography gave the coordination complex **2a** (from the first fraction) as a pale yellow microcrystalline solid in a yield of 19% (0.0443 g, 0.088 mmol) after

recrystallization from a dichloromethane/hexane mixture. From the second fraction, the μ-Cl dimer **1a** was isolated as a lime-yellow amorphous powder in a yield of 70% (0.195 g, 0.321 mmol) after precipitation from benzene by hexane.

For dimer **1a**: m.p. 217−219°C (dec). − R_f = 0.54. − IR (nujol): $\tilde{\nu}$ = 3213, 3308 cm^{-1} [ν(NH_2)]; 740 cm^{-1} [δ(CH_{ar})]. − ^{1}H NMR ($CDCl_3$, isomeric mixture): δ = 1.14 (br. s, 9 H, *t*Bu), 2.87 and 4.03 (br. s, 2 H, N*H*$_2$), 3.62 and 3.66 (s, 1 H, α-C*H*), 6.72 (br. s, 1 H, C_6H_4), 6.89 (m, 2 H, C_6H_4), 7.19 (br. s, 1 H, C_6H_4). − $C_{22}H_{32}Cl_2N_2Pd_2$ (608.26): calcd. C 43.44, H 5.30, N 4.23; found C 43.85, H 5.29, N 4.61.

For coordination complex **2a**: m.p. 171−173°C, R_f = 0.92.

ii) The same reaction of palladium acetate (0.225 g, 1.00 mmol) and amine HL[1] (0.163 g, 1.0 mmol) conducted in methanol (5 mL) at 50°C required 1.5 h for completion. After the treatment of the reaction mixture as described above [i)] it afforded the dimer **1a** in a 68% yield (0.207 g, 0.340 mmol); m.p. 217−219°C (dec), R_f = 0.54 (ether/heptane, 5:1); R_f = 0.44 (benzene/acetone, 7:1). − $C_{22}H_{32}Cl_2N_2Pd_2$: calcd. C 43.44, H 5.30, N 4.23; found C 43.40, H 5.35, N 4.27. − Under these conditions the coordination complex **2a** was formed in trace quantities.

iii) In a similar way, the reaction of palladium acetate (0.281 g, 1.25 mmol) and amine HL[1] (0.204 g, 1.25 mmol) was performed in acetone (10 mL). After heating at 50°C for 50 h and treatment of the reaction mixture as described above [i)], dimer **1a** was isolated in a yield of 68% (0.258 g, 0.424 mmol); m.p. 219−221°C (dec), R_f = 0.54.

iv) The interaction of palladium acetate (0.212 g, 0.944 mmol) and ligand HL[1] (0.154 g, 0.943 mmol) in benzene (7 mL) at room temp. afforded, after the stirring for 24 h and the treatment of reaction mixture as described above [i)] the dimer **1a** in a 43% yield (0.123 g, 0.202 mmol); m.p. 217−219°C (dec), R_f = 0.54. Under these conditions the coordination complex **2a** was isolated in a 41% yield (0.097 g, 0.193 mmol): m.p. 172−173°C, R_f = 0.92.

2. *ortho*-Palladation with Lithium Tetrachloropalladate(II): Racemic α-*tert*-butylbenzylamine (0.150 g, 0.919 mmol) in methanol (20 mL) was added to a mixture of lithium tetrachloropalladate (0.255 g, 0.973 mmol) and excess of sodium acetate (0.232 g, 2.83 mmol) in methanol (20 mL). The reaction mixture was stirred at room temp. for 23 h; after overnight storage, it was filtered and the residue was washed with methanol and then dichloromethane. The combined organic solutions were concentrated in vacuo and redissolved in dichloromethane (10 mL). Chromatographic separation using a dry column (Silpearl, d = 2.5 cm, h = 5 cm, ether/hexane from 1:10 up to 10:1 and then pure ether) and recrystallization as described above [i)] gave dimer **1a** as a limon−yellow amorphous powder in a yield of 50% (0.140 g, 0.230 mmol) from the second fraction. The mixture of diastereomeric coordination complexes (*R*,*R*)*/(*R*,*S*)-**2a** in an approximately 1:1 ratio (^{1}H-NMR data) was isolated from the first fraction in a 43% yield based on the ligand (0.100 g, 0.198 mmol); one of diastereomers was separated from this mixture by recrystallization from benzene/hexane and then from dichloromethane/hexane in a yield of 12% (0.0286 g, 0.057 mmol) as a pale yellow microcrystalline solid.

For **1a**: m.p. 217−219°C (dec), R_f = 0.54. − $C_{22}H_{32}Cl_2N_2Pd_2$ (608.26): calcd. C 43.44, H 5.30, N 4.23; found C 43.51, H 5.55, N 4.36.

For (*R*,*R*)*-**2a**: m.p. 171−173°C, R_f = 0.92. − IR (nujol): $\tilde{\nu}$ = 3310, 3230 cm^{-1} [br., ν(NH_2)], 750, 790 [δ(CH_{ar})]; (CCl_4): $\tilde{\nu}$ = 3310, 3233 cm^{-1} [br., ν(NH_2)]. − For ^{1}H-NMR data of the individual diastereomer **2a** see Table 1. − $C_{22}H_{34}Cl_2N_2Pd$ (503.85): calcd. C 52.44, H 6.80, N 5.56; found C 52.73, H 6.73, N 5.76.

^{1}H NMR of mixture of diastereomers (*R*,*R*)*/(*R*,*S*)-**2a** ($CDCl_3$): δ = 0.81 (s, 18 H, *t*Bu), 0.82 (s, 18 H, *t*Bu), 3.15 (br. t, 2 H, N*H*), 3.19 (br. t, 2 H, N*H*), 3.67 (br. m, 4 H, N*H*), 3.74 (m, 4 H, α-C*H*), 7.04 (m, 8 H, *ortho*-*H* of Ph groups), 7.26 (m, 12 H, *meta*- and *para*-*H* of Ph groups).

[2-{1-Amino-2,2-dimethylpropyl}phenyl-*C*,*N*]chloro([D$_5$pyridine)]-palladium(II) (3a) was generated in situ by the addition of 2−3 drops of [D_5]pyridine to a solution of dimer **1a** in $CDCl_3$ in an NMR tube. For ^{1}H-NMR data of complex **3a** see Table 1.

[2-{1-Amino-2,2-dimethylpropyl}phenyl-*C*,*N*]chloro(triphenylphosphane)palladium (II) (4a) was prepared by treatment of dimeric complex **1a** (0.100 g, 0.164 mmol) with triphenylphosphane (0.086 g, 0.33 mmol) in benzene (15 mL). The reaction mixture was stirred for 40 min at room temp. and concentrated to dryness. Recrystallization from dichloromethane/hexane and then from dichloromethane/acetonitrile afforded the mononuclear adduct **4a** in

Table 4. Crystal data, data collection, structure solution and refinement parameters for [2-(1-amino-2,2-dimethylpropyl)phenyl-*C*,*N*]chloro(triphenylphosphane)palladium(II)·MeCN solvate **4a**

Empirical formula	$C_{31}H_{34}ClN_2PPd$
Formula weight	607.42
Colour, habit	Light yellow, prism
Crystal size [mm]	0.09 × 0.12 × 0.45
Crystal system	triclinic
Space group	$P\bar{1}$
Unit cell dimensions:	
a [Å]	10.112(2)
b [Å]	12.245(2)
c [Å]	12.939(3)
α [°]	90.88(3)
β [°]	111.45(3)
γ [°]	101.40(3)
V [Å^3]	1455.0(5)
Z	2
Density (calcd.) [g/cm^3]	1.386
Absorption coefficient [mm^{-1}]	0.806
F(000)	624
Diffractometer	Enraf−Nonius CAD-4
T [K]	293
Radiation λ [Å]	graphite-monochromated Mo-K_α (0.71073)
Scan mode	ω/2θ
Scan width [°]	1.2 + 0.35 tan(θ)
Min/max scan rate [°/min]	2/8
θ range [°]	2.22−24.97
Index ranges	$-12 \le h \le 11$, $-14 \le k \le 14$, $0 \le l \le 15$
Reflections collected	4696
Independent reflections	4486 [R(int) = 0.0326]
Absorption correction	empirical (Ψ scan)
Min. and max. transmission	0.7365 and 0.9643
Decay correction	none
Solution method	direct methods (SHELX-86)
Refinement method	full-matrix least-squares on F^2 (SHELXL-93)
Hydrogen treatment	all H atoms found in Fourier synthesis and refined using riding model
Data/restraints/parameters	4486/0/330
Goodness of fit on F^2	0.996
Final R indices [$I > 2\sigma(I)$]	R_1 = 0.0351, wR_2 = 0.0850
R indices (all data)	R_1 = 0.0654, wR_2 = 0.0941
Extinction coefficient	0.0000(5)
Largest diff. peak and hole [e × Å^{-3}]	0.583 and −0.682

a 79% yield (0.147 g, 0.260 mmol) as a colourless microcrystalline MeCN solvate, m.p. 208−209°C, R_f = 0.30 (Silufol, benzene/acetone, 7:1). − IR (CCl_4): $\tilde{\nu}$ = 3238 cm^{-1} (br.), 3260, 3302 cm^{-1} [$\nu(NH_2)$]. − For ^{1}H-NMR data of complex **4a** see Table 1. − $^{31}P\{^1H\}$ NMR (CH_2Cl_2): δ = 41.57 (s). − $C_{29}H_{31}ClNPPd \cdot C_2H_3N$ (607.47): calcd. C 61.29, H 5.64, N 4.61; found C 60.82, H 5.70, N 4.24.

X-ray Crystallography for Complex 4a: Details of the X-ray experiment are given in Table 5. The experimental data were collected with an ENRAF Nonius CAD4 diffractometer using graphite-monochomatized Mo-K_α radiation. Experimental reflections were corrected for Lorentz and polarization effects. The hydrogen atoms were found from a difference Fourier synthesis and included in the refinement using the "riding model" with B_{iso} equal to $1.5B_{eq}$ of the parent atom. The structure was refined in the anisotropic approximation for the non-hydrogen atoms. A solvent molecule of acetonitrile was found during the structure solution, which forms a hydrogen bond with the coordinated chloride ligand of the main complex. The structure was solved and refined using the SHELXS-86[82] and SHELXL-93[83] software. Crystallographic data (excluding structure factors) for the structure reported in this paper have been deposited with the Cambridge Crystallographic Data Centre as supplementary publication no. CCDC-104570. Copies of the data can be obtained free of charge on application to CCDC, 12 Union Road, Cambridge CB2 1EZ, UK [Fax: int. code + 44-1223/336-033; E-mail: deposit@ccdc.cam.ac.uk].

Acknowledgments

This work was supported in part by the Russian Foundation for Basic Research (grant 95-03-09227).

[1] M. Pfeffer, *Pure Appl. Chem*. **1992**, *64*, 335.
[2] A. D. Ryabov, *Synthesis* **1985**, 233−252.
[3] J. Chengebroyen, M. Pfeffer, C. Sirlin, *Tetrahedron Lett*. **1996**, *37*, 7263−7266.
[4] J. Vicente, J.-A. Abad, A. D. Frankland, M.-C. Ramirez de Arellano, *J. Chem. Soc., Chem. Commun*. **1997**, 959−960.
[5] J. F. Hartwig, *Synlett* **1997**, 329−340.
[6] A. C. Cope, E. C. Friedrich, *J. Am. Chem. Soc*. **1968**, *90*, 909−913.
[7] Y. Fuchita, H. Tsuchiya, A. Miyafuji, *Inorg. Chim. Acta* **1995**, *233*, 91−96.
[8] J. Vicente, I. Saura-Liamas, M. G. Palin, P. G. Jones, *J. Chem. Soc., Dalton Trans*. **1995**, 2535−2539.
[9] J. Albert, J. Granell, A. Luque, J. Minguez, R. Moragas, M. Font-Bardia, X. Solans, *J. Organomet. Chem*. **1996**, *522*, 87−95.
[10] J. Vicente, I. Saura-Liamas, M. G. Palin, P. G. Jones, M. C. R. de Arellano, *Organometallics* **1997**, *16*, 826−833.
[11] Y. Fuchita, K. Yoshinaga, Y. Ikeda, J. Kinoshita-Kawashima, *J. Chem. Soc., Dalton Trans*. **1997**, 2495−2499.
[12] A. Avshu, R. D. O′Sullivan, A. W. Parkins, *J. Chem. Soc., Dalton Trans*. **1983**, 1619−1624.
[13] J. Vicente, I. Saura-Liamas, P. G. Jones, *J. Chem. Soc., Dalton Trans*. **1993**, 3619−3624.
[14] B. N. Cockburn, D. V. Howe, T. Keating, B. F. G. Johnson, J. Lewis, *J. Chem. Soc., Dalton Trans*. **1973**, 404−410.
[15] V. V. Dunina, O. A Zalevskaya, V. M. Potapov, *J. Gen. Chem. USSR* (*Engl. Transl.*) **1984**, *54*, 389−397.
[16] V. V. Dunina, O. A Zalevskaya, I. P. Smolyakova, V. M. Potapov, *J. Gen. Chem. USSR* (*Engl. Transl.*) **1986**, *56*, 674−684.
[17] L. G. Kuz′mina, O. Yu. Burtseva, M. A. Porai-Koshitz, V. V. Dunina, O. A. Zalevskaya, V. M. Potapov, *J. Gen. Chem. USSR* (*Engl. Transl.*) **1989**, *59*, 2525−2534.
[18] V. V. Dunina, N. S. Gulyukina, E. B. Golovan′, I. Yu. Nalimova, A. A. Koksharova, I. P. Beletskaya, *Organomet. Chem. USSR* (*Engl. Transl.*) **1993**, *6*, 36−46.
[19] V. V. Dunina, N. S. Gulyukina, I. V. Byakova, Yu. F. Oprunenko, I. P. Beletskaya, *Russ. J. Org. Chem*. (*Engl. Transl.*) **1994**, *30*, 1497−1506.
[20] V. V. Dunina, L. G. Kuz′mina, E. B. Golovan′, O. N. Gorunova, Yu. K. Grishin, *J. Organomet. Chem*., to be submitted.
[21] J. Albert, J. Granell, J. Minguez, G. Muller, D. Sainz, P. Valegra, *Organometallics* **1997**, *16*, 3561−3564.
[22] A. D. Ryabov, *Chem. Rev*. **1990**, *90*, 403−424.
[23] A. J. Canty, G. van Koten, *Acc. Chem. Res*. **1995**, *28*, 406−413.
[24] T. Yagyu, S.-i. Aizawa, Sh. Funahashi, *Bull. Chem. Soc. Jpn*. **1998**, *71*, 619−629.
[25] J. Dehand, M. Pfeffer, *C. R. Acad. Sci. Paris, Ser. C* **1975**, *281*, 363−366.
[26] H. Onoue, J. Moritani, *J. Organomet. Chem*. **1972**, *43*, 431−436.
[27] I. Jardine, F. J. McQuillin, *Tetrahedron Lett*. **1972**, 459−461.
[28] A. G. J. Ligtenbard, E. K. van den Beuken, A. Meetsma, N. Veldman, W. J. J. Smeets, A. L. Spek, B. L. Feringa, *J. Chem. Soc., Dalton Trans*. **1998**, 263−270.
[29] V. V. Dunina, O. A. Zalevskaya, V. M. Potapov, *Russ. Chem. Rev*. (*Engl. Transl.*) **1988**, *57*, 434−473 and refs. therein.
[30] A. L. Seligson, W. C. Trogler, *J. Am. Chem. Soc*. **1991**, *113*, 2520−2527.
[31] J. K. M. Sanders, J. D. Mersh, *Progr. NMR Spectrosc*. **1982**, *15*, 353−400.
[32] L. J. Bellami, *The Infrared Spectra of Complex Molecules*, J. Wiley, London, New York, **1963**, chapter 5.
[33] V. V. Dunina, V. P. Kislyi, N. S. Gulyukina, Yu. K. Grishin, I. P. Beletskaya, *Organomet. Chem. USSR* (*Engl. Transl.*) **1992**, *5*, 1297−1305.
[34] C. E. Barclay, G. Deeble, R. J. Doyle, Sh. A. Elix, G. Salem, T. L. Jones, S. B. Wild, A. C. Willis, *J. Chem. Soc., Dalton Trans*. **1995**, 57−65.
[35] R. J. Doyle, G. Salem, A. C. Willis, *J. Chem. Soc., Dalton Trans*. **1997**, 2713−2723.
[36] D. G. Allen, G. M. McLaughlin, G. B. Robertson, W. L. Steffen, G. Salem, S. B. Wild, *Inorg. Chem*. **1982**, *21*, 1007−1014.
[37] G. Salem, S. B. Wild, *Inorg. Chem*. **1983**, *22*, 4049−4054.
[38] J. W. L. Martin, J. A. L. Palmer, S. B. Wild, *Inorg. Chem*. **1984**, *23*, 2664−2668.
[39] Q. Jiang, H. Ruegger, L. M. Venanzi, *J. Organomet. Chem*. **1995**, *488*, 233−240.
[40] Y. Fuchita, H. Tsuchiya, *Inorg. Chim. Acta* **1993**, *209*, 229−230.
[41] V. V. Dunina, E. B. Golovan′, N. S. Gulyukina, A. V. Buyevich, *Tetrahedron: Asymmetry* **1995**, *6*, 2731−2746.
[42] V. V. Dunina, E. B. Golovan′, V. V. Pedchenko, A. A. Borisenko, I. P. Beletskaya, *Organomet. Chem. USSR* (*Engl. Transl.*) **1992**, *5*, 1121−1129.
[43] V. V. Dunina, E. B. Golovan′, *Tetrahedron: Asymmetry* **1995**, *6*, 2747−2754.
[44] V. V. Dunina, M. Yu. Kazakova, Yu. K. Grishin, O. R. Malyshev, and E. I. Kazakova, *Russ. Chem. Bull*. (*Engl. Transl.*) **1997**, N7, 1375−1384.
[45] A. Bondi, *J. Phys. Chem*. **1964**, *68*, 441−451.
[46] L. G. Kuz′mina, Yu. T. Struchkov, O. A. Zalevskaya, V. V. Dunina, V. M. Potapov, *J. Gen. Chem. USSR* (*Engl. Transl.*) **1987**, *57*, 2499−2507.
[47] B.-H. Aw, S. Selvaratnam, P.-H. Leung, N. H. Rees, W. McFarlane, *Tetrahedron: Asymmetry* **1996**, *7*, 1753−1762.
[48] P.-H. Leung, S. Selvaratnam, C. R. Cheng, K. F. Mok, N. H. Rees, W. McFarlane, *J. Chem. Soc., Chem. Commun*. **1997**, 751−752.
[49] A. J. Deeming, I. P. Rothwell, M. B. Hursthouse, L. New, *J. Chem. Soc., Dalton Trans*. **1978**, 1490−1496.
[50] P. W. Clark, S. F. Dyke, *J. Organomet. Chem*. **1985**, *281*, 389−396.
[51] J. Albert, J. M. Cadena, J. Granell, *Tetrahedron: Asymmetry* **1997**, *8*, 991−994.
[52] N. W. Alcock, J. M. Brown, D. I. Hulmes, *Tetrahedron: Asymmetry* **1993**, *4*, 743−756.
[53] N. W. Alcock, D. I. Hulmes, J. M. Brown, *J. Chem. Soc., Chem. Commun*. **1995**, 395−397.
[54] R. Annunziata, S. Cenini, F. Demartin, G. Palmisano, S. Tollari, *J. Organomet. Chem*. **1995**, *496*, C1−C3.
[55] V. V. Dunina, L. G. Kuz′mina, A. G. Parfyonov, Yu. K. Grishin, *Tetrahedron: Asymmetry* **1998**, *9*, 1917−1921.
[56] K. Tani, H. Tashiro, M. Yoshida, Ts. Yamagata, *J. Organomet. Chem*. **1994**, *469*, 229−236.
[57] P. W. Clark, S. F. Dyke, *J. Organomet. Chem*. **1984**, *276*, 421−430.

[58] S. Y. M. Chooi, M. K. Tan, P.-H. Leung, K. F. Mok, *Inorg. Chem*. **1994**, *33*, 3096−3103.
[59] S. Y. M. Chooi, T. S. A. Hor, P.-H. Leung, K. F. Mok, *Inorg. Chem*. **1992**, *31*, 1494−1500.
[60] P.-H. Leung, A. C. Willis, S. B. Wild, *Inorg. Chem*. **1992**, *31*, 1406−1410.
[61] M. Pabel, A. C. Willis, S. B. Wild, *Inorg. Chem*. **1996**, *35*, 1244−1249.
[62] S. Y. M. Chooi, S.-Y. Siah, P.-H. Leung, K. F. Mok, *Inorg. Chem*. **1993**, *32*, 4812−4818.
[63] D. C. R. Hockless, P. A. Gugger, P.-H. Leung, R. C. Mayadunne, M. Pabel, S. B. Wild, *Tetrahedron* **1997**, *53*, 4083−4094.
[64] H. Gunter, *NMR Spectroscopy − Basic Principles, Concepts, and Applications in Chemistry*, John Wiley, Chichester, **1995**, p. 115.
[65] H. Jendralla, Ch. H. Li, E. Paulus, *Tetrahedron: Asymmetry* **1994**, *5*, 1297−1320.
[66] W. Lesueur, E. Solari, C. Floriani, A. Chiesi-Villa, C. Rizzoli, *Inorg. Chem*. **1997**, *36*, 3354−3362.
[67] M.-C. Lagunas, R. A. Gossage, W. J. J. Smeets, A. L. Spek, G. van Koten, *Eur. J. Inorg. Chem.* **1998**, 163−168.
[68] M. Brookhart, M. L. H. Green, *J. Organomet. Chem*. **1983**, *250*, 395−408.
[69] T. C. Jones, A. J. Nielson, C. E. Rickard, *Aust. J. Chem*. **1984**, *37*, 2179−2192.
[70] J.-M. Valk, T. D. W. Claridge, J. M. Brown, *Tetrahedron: Asymmetry* **1995**, *6*, 2597−2610.
[71] G. Chelucci, M. A. Cabras, A. Saba, A. Sechi, *Tetrahedron: Asymmetry* **1996**, *7*, 1027−1032.
[72] H. Doucet, J. M. Brown, *Tetrahedron: Asymmetry* **1997**, *8*, 3775−3784.
[73] S. Gladiali, S. Pulacchini, D. Fabbri, M. Manassero, M. Sansoni, *Tetrahedron: Asymmetry* **1998**, *9*, 391−395.
[74] V. V. Dunina, O. A. Zalevskaya, I. P. Smolyakova, V. M. Potapov, L. G. Kuz′mina, Yu. T. Struchkov, L. N. Reshetova, *J. Gen. Chem. USSR* (*Engl. Transl.*) **1986**, *56*, 1164−1175.
[75] L. G. Kuz′mina, Yu. T. Struchkov, V. V. Dunina, O. A. Zalevskaya, V. M. Potapov, *J. Gen. Chem. USSR* (*Engl. Transl.*) **1987**, *57*, 599−609.
[76] V. V. Dunina, L. G. Kuz′mina, M. Yu. Kazakova, Yu. K. Grishin, Yu. A. Veits, E. I. Kazakova, *Tetrahedron: Asymmetry* **1997**, *8*, 2537−2545.
[77] J. H. Ford, C. D. Thompson, C. S. Marvel, *J. Am. Chem. Soc*. **1935**, *57*, 2619−2623.
[78] G. A. Tsatsas, *Ann. Chim., Ser. 12* **1946**, *1*, 342−394.
[79] P. Billon, *Ann. Chim., Ser. 10* **1927**, *7*, 314−384.
[80] J. T. Sharp, I. Gosney, A. G. Rowley, *Practical Organic Chemistry − A student handbook of techniques*, London − New York, Chapman and Hall, **1989**, chapter 4.2.2d.
[81] L. M. Harwood, *Aldrichim. Acta* **1985**, *18*, 25.
[82] G. M. Sheldrick, *Acta Crystallogr*. **1990**, *A46*, 467.
[83] G. M. Sheldrick, *SHELXL-93 − Program for the Refinement of Crystal Structures*, University of Göttingen, Germany, **1993**.

Received October 27, 1998
[I98367]

Synthesis and Reactivity of Bis(phospholyl)neodymium(III) and -samarium(III) Chlorides and Alkyl Derivatives

François Nief,*[a] Philippe Riant,[a] Louis Ricard,[a] Pascale Desmurs,[b] and Denise Baudry-Barbier[b]

Keywords: Organolanthanide / Neodymium / Samarium / Phospholyl / Hydrides / Lanthanides

The reaction of 2,3,4,5-tetramethylphospholylpotassium [C_4Me_4PK] with [$LnCl_3(THF)_x$] (Ln = Nd, Sm) in a 2:1 ratio gave unsolvated ate complexes of the formula [$(C_4Me_4P)_2LnCl_2K$]. Crystallisation of the samarium complex from ether afforded a polymeric ether solvate: {[(η^5-C_4Me_4P)Sm(μ_3-Cl)$_2$(μ:η^5,η^1-C_4Me_4P)K(Et_2O)]$_\infty$}, which was characterised by X-ray crystallography. Reaction of [$(C_4Me_4P)_2LnCl_2K$] with [$LiCH(SiMe_3)_2$] in toluene gave the alkyl complexes [$(C_4Me_4P)_2LnCH(SiMe_3)_2$]; these complexes were most efficiently prepared from [$LnCl_3(THF)_x$], [KC_4Me_4P] and [$LiCH(SiMe_3)_2$] in a one-pot procedure. Reaction of [$(C_4Me_4P)_2LnCH(SiMe_3)_2$] with molecular hydrogen gave [$(C_4Me_4P)_2NdH$], when Ln = Nd, whereas, when Ln = Sm, reduction occurred and the already known [$(C_4Me_4P)_2Sm$] was isolated instead.

Introduction

Bis(cyclopentadienyl) and substituted bis(cyclopentadienyl) complexes of trivalent lanthanides are interesting because of their structural and mechanistic properties, and also for their catalytic potential.[1] Modification of the parent cyclopentadienyl ligands has been achieved by the introduction of various types of substituents, e.g. those with bulky,[2] chiral and/or bridging properties.[3] A heterocyclopentadienyl ligand such as the 2,3,4,5-tetramethylphospholyl ligand (C_4Me_4P) has been used successfully as an alternative to the cyclopentadienyl ligand in organolanthanide and organoactinide chemistry.[1a] The C_4Me_4P ligand is interesting because it can be considered as relatively bulky, with steric properties resembling that of the ubiquitous C_5Me_5 ligand (in fact very close to that of the tetramethylcyclopentadienyl ligand[4]), while it is much less electron-rich than polyalkylated cyclopentadienyl ligands, and its electronic properties are similar to those of the unsubstituted Cp ring.[5] The authors have described previously (in a communication) the interaction of the C_4Me_4P ligand with the halides of yttrium and lutetium and the synthesis of the ate complexes [$(C_4Me_4P)_2LnCl_2Li(solv.)_2$],[6] and wish to extend these results to the synthesis of bis(tetramethylphospholyl) complexes of samarium and neodymium, because of the more interesting potential of bis(cyclopentadienyl) complexes of the larger Nd^{III} and Sm^{III} ions in catalysis. While catalytic tests on the title compounds are underway, this paper reports on the synthetic part of the work concerning the synthesis of bis(tetramethylphospholyl)neodymium and -samarium chlorides and alkyl derivatives, and the synthesis of a bis(phospholyl)neodymium hydride.

[a] Laboratoire Hétéroéléments et Coordination, CNRS UMR 7653, DCPH, Ecole Polytechnique,
F-91128 Palaiseau, France
Fax: (internat.) + 33-1/69333990
E-mail: nief@mars.polytechnique.fr
[b] Laboratoire de Synthèse et Electrosynthèse Organométalliques, CNRS UMR 5632, Université de Bourgogne,
B. P. 138, F-21004 Dijon, France

Results

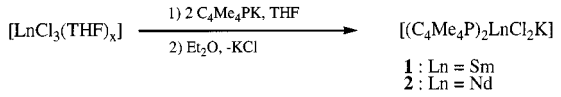
Synthesis of [$(C_4Me_4P)_2SmCl_2K$] (1) and [$(C_4Me_4P)_2NdCl_2K$] (2)

The preparation of [$(C_4Me_4P)_2LnCl_2Li(solv.)_2$] involved the reaction of anhydrous [YCl_3] or [$LuCl_3$] with two equiv. of [C_4Me_4PLi] prepared in situ. Due to the previous development of the use of the potassium salt [C_4Me_4PK],[7] which can be isolated and purified by recrystallization, the reaction of two equiv. of [C_4Me_4PK] with one equiv. of anhydrous [$SmCl_3$] or [$NdCl_3$] in THF was tried initially. No reaction was found to occur even after refluxing overnight: No colour change took place, and examination of the reaction mixture by ^{31}P NMR only showed the [C_4Me_4PK] resonance.

However, when THF-solvated [$LnCl_3(THF)_x$] was substituted for anhydrous [$LnCl_3$], the reaction with two equiv. of [C_4Me_4PK] started immediately (at room temp.), as indicated by a colour change to orange (Ln = Sm) or blue (Ln = Nd), and was completed within 1 h. After evaporation of the solvent, extraction of the residue with ether and drying under vacuum, light orange (Ln = Sm) or light blue (Ln = Nd) powders were obtained in fair to good yield. These products were assigned the formulas of unsolvated ate complexes [$(C_4Me_4P)_2SmCl_2K$] (**1**) and [$(C_4Me_4P)_2NdCl_2K$] (**2**), respectively, on the following grounds: (a) ^{31}P- and ^1H-NMR spectra of the isolated products displayed coordination shifts of the methyl and phosphorus resonances indicating that coordination of the C_4Me_4P ligand around Nd and Sm had indeed occurred, (b) only very small traces of ether or THF were present according to the ^1H-NMR spectra of either the Nd or Sm

 © WILEY-VCH Verlag GmbH, D-69451 Weinheim, 1999 1434–1948/99/0606–1041 $ 17.50+.50/0

complexes in [D$_8$]THF, (c) elemental analyses were not compatible with the possibility of neutral complexes such as {[(C$_4$Me$_4$P)$_2$LnCl]$_x$} but were in agreement with the formulae given above for **1** and **2** (Scheme 1).



Scheme 1. Synthesis of the complexes **1** and **2**

[LaCl$_3$(THF)$_x$] also reacted with [C$_4$Me$_4$PK] but the isolated product, presumably [(C$_4$Me$_4$P)$_2$LaCl$_2$K], was obtained in very low yield because the ether extraction procedure worked poorly for the very insoluble La compound.

Crystal Structure of {[(η^5-C$_4$Me$_4$P)Sm(μ_3-Cl)$_2$(μ:η^5,η^1-C$_4$Me$_4$P)K(Et$_2$O)]$_\infty$} (3)

In order to gain more insight into the structure of the aforementioned ate complexes X-ray analysis of the crystal structure was carried out. Recrystallization of **1** from diethyl ether gave crystals that were suitable for X-ray analysis. It appears that **1** picked up one diethyl ether molecule in the process, which ended up coordinated to the potassium ion in the crystal, and that the analyzed structure was that of **3**: {[(η^5-C$_4$Me$_4$P)Sm(μ_3-Cl)$_2$(μ:η^5,η^1-C$_4$Me$_4$P)K(Et$_2$O)]$_\infty$}. X-ray details are listed in Table 1, selected bond lengths and angles are collected in Table 2 while ORTEP plots of the asymmetric unit of **3** and of four such repeating units are shown in Figures 1 and 2, respectively. The structure of **3** closely resembles that of [{(η^5-C$_5$Me$_5$)$_2$Ce(μ_3-Cl)$_2$K(THF)}$_\infty$] previously described by Evans:[8] In both cases it is the triply bridging chlorine atoms (between the Ln and K atoms) that are responsible for the polymeric chain that links the organolanthanide residues. However, there are two differences between the structures of **3** and of Evans' cerium complex: (a) in Evans' complex, which is noncentrosymmetric, the (C$_5$Me$_5$)$_2$CeCl$_2$K(THF) unit repeats itself by a glide plane along the axis of the polymeric chain, whereas in **3**, which is centrosymmetric, the (C$_4$Me$_4$P)$_2$SmCl$_2$K(Et$_2$O) units are related by inversion centres on the axis of the chain; (b) in **3** the potassium atom is six-coordinate because of additional bonding with the phosphorus lone pair on one of the C$_4$Me$_4$P ligands.

Bond lengths and angles of **3** are listed in Table 2. The Sm−Cl bonds (2.66 and 2.67 Å) are unusually short for a triply bridging chlorine atom bonded to Sm (usually 2.76−2.92 Å).[9] Interestingly, Evans had also noted short Ce−Cl bonds for the triply bridging chlorine atoms in {[(η^5-C$_5$Me$_5$)$_2$Ce(μ_3-Cl)$_2$K(THF)]$_\infty$}. The Sm−P bonds are similar to that of other phospholylsamarium(III) complexes.[10] The K−P2 distance is within the recorded bond length-limits (towards the high end, however),[11] denoting K−P electrostatic interaction. The K−O bond length is significantly longer (0.1 Å) than in other K−OEt$_2$ solvates.[12]

Table 1. Table of X-ray data for **3**

Empirical formula	$C_{20}H_{33}Cl_2KOP_2Sm$
Crystal description and size [mm]	orange plate, 0.22 × 0.20 × 0.07
Space group	monoclinic, $P2_1/n$ (no. 14)
a [nm]	1.6145(2)
b [nm]	0.8661(1)
c [nm]	1.8883(2)
β [°]	101.55(2)
V [nm^3]	2.587(1)
Z	4
$d_{calcd.}$ [g·cm^{-3}]	1.570
F(000)	1224
Radiation	Mo-K_α (λ = 71.073 pm)
μ [mm^{-1}]	2.778
Temperature [K]	123 ± 0.1
Max. 2θ [°]	60
No. of unique reflections	7514
Reflections included	4755 [$F_o^2 > 3\sigma(F_o^2)$]
Corrections	Lorentz polarisation, absorption (ψ-scans), min. 0.743, max. 1.000
R	0.039
R_w	0.047
G.O.F.	1.008
convergence, largest shift/error	0.00
Minimisation function	$w(\|F_o\| - \|F_c\|)^2$, $w = 4F^2/\sigma^2(F^2)$
Least-squares weights	$4F_o^2/\sigma^2(F_o^2)$, $\sigma^2(F^2) = \sigma^2(I) + (pF^2)^2$
Instrument instability factor, p	0.06
Largest peak in final diff. map	1.87(16) eÅ^{-3}
Largest hole in final diff. map	−0.32(16) eÅ^{-3}

Table 2. Selected bond lengths [pm] and angles [°] for **3**

Sm−Cl1	266.2(1)	K−P2	346.8(2)
Sm−Cl2	267.1(1)	K−O	282.7(4)
Sm−P1	290.5(2)	P−C(av.)	176.0(7)
Sm−P2	292.6(1)		
Sm−C(av.)	278(2)	Cl1−Sm−Cl2	90.55(4)
Cl1−K	318.8(2)	Cl1−K−Cl2	70.89(4)
Cl2−K	334.4(2)	Cnt−Sm−Cnt[a]	131.6

[a] Cnt denotes the centroid of the phospholyl ligand.

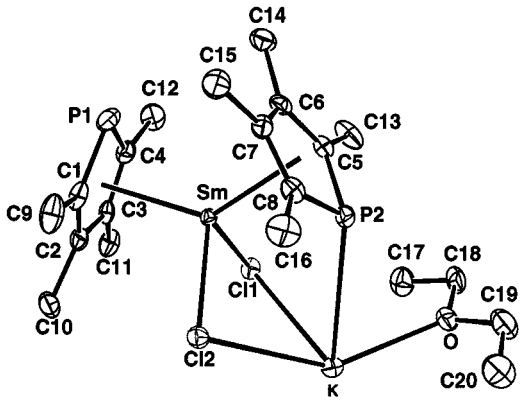


Figure 1. ORTEP plot of **3** (asymmetric unit) together with the numbering scheme used; ellipsoids are scaled to enclose 50% of the electronic density

Synthesis of [(C$_4$Me$_4$P)$_2$SmCH(SiMe$_3$)$_2$] (4) and [(C$_4$Me$_4$P)$_2$NdCH(SiMe$_3$)$_2$] (5)

Alkyl compounds of organolanthanides are the precursors of organolanthanide hydrides by hydrogenolysis of the lanthanide−carbon σ-bond. [Bis(trimethylsilyl)methyl]lan-

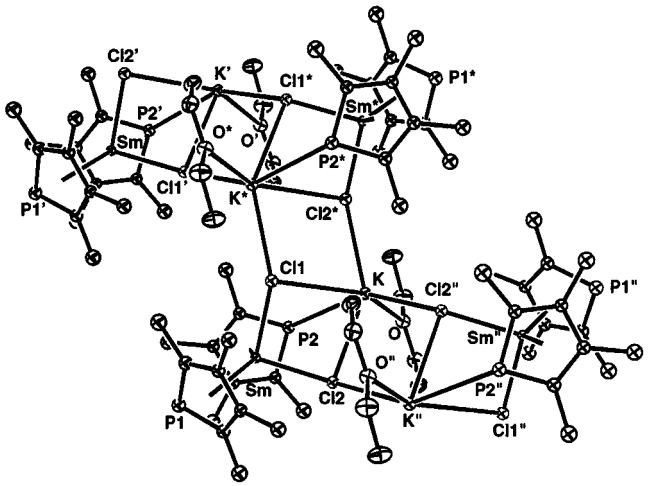
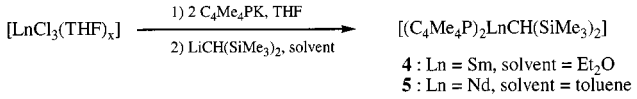


Figure 2. ORTEP plot of **3** (four repeating units); ellipsoids are scaled to enclose 50% of the electronic density

thanide complexes are often used because they are usually hydrocarbon-soluble unsolvated compounds that can be straightforwardly obtained by reaction of organolanthanide halides with $[LiCH(SiMe_3)_2]$.[2g,2i] Initially, small-scale experiments established that reaction of **1** and **2** with $[LiCH(SiMe_3)_2]$ did produce the desired alkyl complexes $[(C_4Me_4P)_2SmCH(SiMe_3)_2]$ (**4**) and $[(C_4Me_4P)_2NdCH(SiMe_3)_2]$ (**5**). However, the overall yields were not especially good and we found that **4** and **5** were best prepared by a one-pot reaction: The crude products from the reaction of $[LnCl_3(THF)_x]$ with $[C_4Me_4PK]$ reacted smoothly with $[LiCH(SiMe_3)_2]$ to give **4** and **5** in fair to good yields. The main advantage was in avoiding the long extraction procedure necessary to isolate pure **1** and **2** (Scheme 2).



Scheme 2. One-pot synthesis of alkyl complexes **4** and **5**

$[(C_4Me_4P)_2LaCH(SiMe_3)_2]$ was also obtained by the same procedure, but the yields were very low and inconsistent. The NMR properties of **4** and **5** are similar to that of their C_5Me_5 analogues:[2g] The steric bulk of the $(C_4Me_4P)_2Ln$ moiety impedes free rotation of the alkyl ligand around the Ln−C σ-bond so that the two C_4Me_4P rings are anisochronous. Thus, **4** and **5** each show four proton signals for the α-, β-, α′- and β′-methyl groups and two phosphorus resonances.

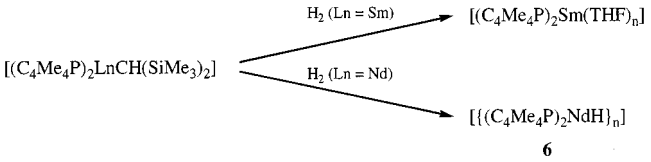
Reaction of $[(C_4Me_4P)_2LnCH(SiMe_3)_2]$ with H_2 (Ln = Sm, Nd) and the Synthesis of $[\{(C_4Me_4P)_2NdH\}_n]$ (6)

Exposure of a benzene solution of **4** to dihydrogen resulted in the formation of a dark black product which gradually separated from solution. ^1H NMR of the reaction mixture indicated the presence of bis(trimethylsilyl)-methane. The black product was characterised as $[(C_4Me_4P)_2Sm(THF)_n]$ on the basis of the known high-field position of its ^{31}P resonance in THF solution (δ = −540).[13] Thus, presumably hydrogenolysis of the Sm−C bond occurred, but the hydride $[(C_4Me_4P)_2SmH]$ is unstable and decomposes by disproportionation into $[(C_4Me_4P)_2Sm]$ and H_2.

Hydrogenolysis of **5** under 1 atm of dihydrogen was then attempted in C_6D_6 (NMR experiment) and in pentane (preparative experiment). In the NMR experiment, formation of bis(trimethylsilyl)methane was evident from the ^1H-NMR data of the yellow solution while new resonances (α- and β-methyl groups on the C_4Me_4P ligand) appeared at δ = +17.8 and δ = −17.8; the phosphorus resonance was shifted to δ = 551. Exposure of this reaction mixture to THF vapour caused a colour change to green and a shift in the phosphorus resonance to δ = 377.

In the preparative experiment, a yellow precipitate was isolated, having an elemental analysis compatible with the composition $(C_4Me_4P)_2NdH$. However, this precipitate was sparingly soluble in C_6D_6, and the proton spectrum was complex; exposition of the NMR tube to THF vapour resulted in complete dissolution into a green solution and the appearance of a phosphorus resonance at δ = 377. The yellow precipitate was also soluble in C_4D_8O ($[D_8]$THF) and the proton spectrum displayed resonances at δ = 11.7 and δ = 1.14.

These experiments were interpreted as follows: In the NMR-tube experiment, the new peaks at δ = +17.8 and −17.8 (^1H) and 551 (^{31}P) are attributed to $\{[(C_4Me_4P)_2NdH]_n\}$ (**6**); upon exposure to THF vapour, a shift in the ^{31}P-NMR spectrum and colour change to green are presumably due to the formation of $[(C_4Me_4P)_2NdH(THF)]$. In the preparative experiment **6** was also formed. After precipitation from pentane, it was obtained in a sparingly soluble oligomeric form which converted into $[(C_4Me_4P)_2NdH(THF)]$ upon exposure to THF. The proton spectrum in C_4D_8O shows the resonances of the α- and β-methyl groupss of the C_4Me_4P ligand in $[(C_4Me_4P)_2NdH([D_8]THF)]$ (Scheme 3).



Scheme 3. Reaction of the alkyl complexes **4** and **5** with dihydrogen

Discussion

The reaction of $[C_4Me_4PK]$ with early lanthanide chlorides gives ate complexes containing the $[(C_4Me_4P)_2LnCl_2K]$ unit. The crystal structures of **3** $\{[(\eta^5\text{-}C_5Me_4P)_2Sm(\mu_3\text{-}Cl)_2K(Et_2O)]_\infty\}$ and of its analog $\{[(\eta^5\text{-}C_5Me_5)_2Ce(\mu_3\text{-}Cl)_2K(THF)]_\infty\}$ are closely related to one another. However, the vacuum-dried ate complexes $[(C_4Me_4P)_2LnCl_2K]$ isolated with the phospholyl ligand are

desolvated, in contrast with those isolated with the C_5Me_5 ligand; the neutral complex $\{[(C_5Me_5)_2CeCl]_n\}$ was obtained upon heating $[(C_5Me_5)_2CeCl_2K(THF)]$ under vacuum.[8] It is to be noted that the K−O(ether) bond in **3** is one of the longest recorded; a weakness of the K−O bond might thus account for the ease of desolvation in the case of the bis-(phospholyl) ate complexes.

The one-pot reaction leading to **4** and **5** gives yields comparable to those obtained for the methods used in the preparation of other [bis(trimethylsilyl)methyl]lanthanide complexes, e.g. the analog $[(C_5Me_5)_2LnCH(SiMe_3)_2]$. Like these analogs, the alkyl complexes **4** and **5** are unsolvated, pentane-soluble crystalline powders. Whereas $[(C_5Me_5)_2SmCH(SiMe_3)_2]$ gives the hydride $\{[(C_5Me_5)_2SmH]_2\}$ in the presence of dihydrogen, the reaction of **4** with dihydrogen is different because in this case $[(C_4Me_4P)_2Sm]$ was isolated. The reduction of alkylsamarium(III) to Sm^{II} in the presence of H_2 is unprecedented. It is known in actinide chemistry that the uranium(IV) dihydride $[(C_5Me_5)_2UH_2]$ is unstable and disproportionates into the uranium(III) hydride $\{[(C_5Me_5)_2UH]_n\}$ and H_2, whereas $[(C_5Me_5)_2ThH_2]$ is stable.[14] Likewise, it has been reported that $[(C_4Me_4P)_2UH_2]$ was not detected when $[(C_4Me_4P)_2UR_2]$ (R = CH_3, CH_2SiMe_3) was exposed to dihydrogen; $[(C_4Me_4P)_3U]$ was obtained under these conditions.[15] Although the mechanistic pathway for the reduction to Sm^{II} is unknown, a samarium(III) hydride might be less stabilised with respect to reduction by the relatively poor π-donating C_4Me_4P ligand than by the electron-rich C_5Me_5 ligand.

Similarly to $[(C_5Me_5)_2NdCH(SiMe_3)_2]$, the reaction of **5** with dihydrogen gives the hydride $\{[(C_4Me_4P)_2NdH]_n\}$ (**6**). However, when isolated in pentane, this compound is in a sparingly soluble oligomeric form.

Experimental Section

General: All isolated compounds are air- and moisture-sensitive and were handled in rigourously inert-atmosphere conditions, on a vacuum line, or under argon in a glovebox (Braun Labmaster 130) with H_2O, O_2 < 1 ppm. $[C_4Me_4PK]$[7] was recrystallised from DME/THF. $[LiCH(SiMe_3)_2]$[16] was purified by extraction and crystallisation from hexane. Anhydrous lanthanide trichlorides were used as received from the suppliers and transformed into $[LnCl_3(THF)_x]$[17] according to known procedures. All solvents were dried by vacuum transfer from sodium/benzophenone. − NMR: 200 MHz for ^1H and 80 MHz for ^{31}P. − Elemental analyses: CHN analyser at the Université de Dijon.

General Procedure for the Synthesis of $[(C_4Me_4P)_2LnCl_2K]$: In a glovebox, a mixture of $[LnCl_3(THF)_x]$ (1 equiv.) and $[C_4Me_4PK]$ (2 equiv.) was placed in a vessel fitted to a swivel Schlenk filter. The filter assembly was then taken out of the glovebox, attached to a vacuum line through a vacuum PTFE stopcock and evacuated. THF (20 mL) was then transferred in vacuo onto the solids and the assembly was isolated from the vacuum by closing the stopcock.. The reaction mixture immediately became orange (Ln = Sm) or blue (Ln = Nd). After stirring at room temp. for 1 h, the solution was concentrated to dryness and diethyl ether (20 mL) was transferred in vacuo onto the residue. The filter assembly was then rotated and the solid residue continuously extracted on the frit with warm diethyl ether by placing the receiving flask in a water bath at about 40°C, whereupon the product precipitated from the diethyl ether solution. The extraction usually took 1−2 d (Ln = Sm) and 4−5 d (Ln = Nd). The swivel filter was then rotated back into its original position and the product filtered, rinsed with cold diethyl ether and dried under vacuum overnight. The filter assembly was then returned to the glovebox and the product collected and weighed.

Isolation of $[(C_4Me_4P)_2SmCl_2K]$ (1): 340 mg (0.63 mmol, 63%) of **1** was isolated from $[SmCl_3(THF)_3]$ (474 mg, 1 mmol) and $[C_4Me_4PK]$ (356 mg, 2 mmol). − ^1H NMR ($[D_8]$THF): δ = 0.87 (s, 12 H), 1.98 (s, 12 H). − ^{31}P NMR: δ = 49.7. − $C_{16}H_{24}Cl_2KP_2Sm$ (538.68): calcd. C 35.68, H 4.49; found C 34.81, H 4.49.

Isolation of $[(C_4Me_4P)_2NdCl_2K]$ (2): 0.680 g (1.28 mmol, 57%) of **2** was isolated from $[NdCl_3(THF)_{1.5}]$ (800 mg, 2.23 mmol) and $[C_4Me_4PK]$ (0.800 g, 4.49 mmol). − ^1H NMR ($[D_8]$THF):δ = 0.66 (s, 12 H), 13.03 (s, 12 H). − ^{31}P NMR: δ = 459. − $C_{16}H_{24}Cl_2KNdP_2$ (532.56): calcd. C 36.09, H 4.54; found C 35.74, H 4.65.

Synthesis of $[(C_4Me_4P)_2SmCH(SiMe_3)_2]$ (4) (One-Pot Procedure): THF (20 mL) was condensed onto a mixture of $SmCl_3(THF)_3$ (474 mg, 1 mmol) and $[C_4Me_4PK]$ (356 mg, 2 mmol). After 1 h at room temp., the solvent was evaporated to dryness in vacuo. Solid $[LiCH(SiMe_3)_2]$ (166 mg, 1 mmol) was added to the residue and 20 mL of diethyl ether condensed onto the mixture. After 2.5 h, the reddish/brown reaction mixture was concentrated to dryness and extracted into 20 mL of hexane. The reaction mixture was concentrated to a small volume whereupon a precipitate appeared, which was filtered and rinsed with cold hexane, leaving **4** as an orange/brown powder (310 mg, 0.53 mmol, 53%) that was recrystallised from hexane. − ^1H NMR (C_6D_6): δ = −4.46 (s, 18 H), −3.02 (s, 6 H), −2.60 (s, 6 H), 2.70 (s, 6 H), 3.11 (s, 6 H), 20.31 (s, 1 H). − ^{31}PNMR: δ = 43.4 (s), 46.7 (s). − $C_{23}H_{43}P_2Si_2Sm$ (588.07): calcd. C 46.98, H 7.37; found C 46.32, H 7.68.

Synthesis of $[(C_4Me_4P)_2NdCH(SiMe_3)_2]$ (5) (One-Pot Procedure): THF (20 mL) was condensed onto a mixture of $[NdCl_3(THF)_{1.5}]$ (490 mg, 1.37 mmol) and $[C_4Me_4PK]$ (490 mg, 2.75 mmol). After 1 h at room temp., the solvent was evaporated to dryness in vacuo. Solid $[LiCH(SiMe_3)_2]$ (0.225 g, 1.35 mmol) was added to the residue and 20 mL of toluene was condensed onto the mixture. After 2.5 h, the green reaction mixture was concentrated to dryness and extracted into 20 mL of pentane. The reaction mixture was concentrated to a small volume whereupon a precipitate appeared, which was filtered and rinsed with cold pentane, leaving **5** as a forest-green powder (0.530 g, 0.91 mmol, 67%) that was recrystallised in pentane. − ^1H NMR (C_6D_6): δ = −11.71 (s, 18 H), −10.55 (s, 6 H), −8.01 (s, 6 H), 12.96 (s, 6 H), 13.34 (s, 6 H), 91.52 (br. s, 1 H). − ^{31}P NMR: δ = 456 (s), 501 (s). − $C_{23}H_{43}NdP_2Si_2$ (581.95): calcd. C 47.47, H 7.45; found C 47.11, H 7.40.

Reaction of $[(C_4Me_4P)_2SmCH(SiMe_3)_2]$ (4) with H_2: Dihydrogen gas was admitted to a solution of **4** (5 mg) in C_6D_6 at 0°C. The reaction mixture immediately turned dark brown and a black precipitate appeared. While $CH_2(SiMe_3)_2$ was present in the C_6D_6 solution, a ^{31}P-NMR spectrum of the black precipitate in THF showed a signal at δ = −540, characteristic of $[(C_4Me_4P)_2Sm(THF)_x]$.

Reaction of $[(C_4Me_4P)_2NdCH(SiMe_3)_2]$ (4) with H_2 (NMR Scale): An NMR tube containing a solution of $[(C_4Me_4P)_2NdCH(SiMe_3)_2]$ (6 mg, 0.01 mmol) in C_6D_6 (0.5 mL) was exposed to 1 atm of dihydrogen gas. An immediate colour change from green to yellow was

observed, $CH_2(SiMe_3)_2$ was detected in the solution, and new signals appeared that were attributed to $\{[(C_4Me_4P)_2NdH]_n\}$ (**6**). – ^{1}H NMR: δ = −17.8 (s, 12 H), 17.8 (s, 12 H); H−Nd signal was not detected. – ^{31}P NMR: δ = 551. – Exposure of the tube to THF vapour caused a colour change to green and a shift in the ^{31}P spectrum to δ = 347.

Synthesis of $[\{(C_4Me_4P)_2NdH\}_n]$ (6): Dihydrogen gas was admitted to a solution of **5** (80 mg, 0.14 mmol) in pentane at 0°C. The reaction mixture turned yellow and a precipitate appeared. This precipitate was filtered, rinsed with pentane and **6** was isolated as a yellow powder (50 mg, 0.12 mmol, 85%). – NMR (C_6D_6): no interpretable spectrum (see text). – ^{31}P NMR (THF):δ = 377. – $C_{16}H_{25}NdP_2$ (423.56): calcd. C 45.37, H 5.95; found C 45.40, H 5.70.

X-ray Crystallographic Study of 3: Crystals of **3**, $C_{20}H_{33}Cl_2KOP_2Sm$ (611.79), were grown at room temp. from a diethyl ether solution of the compound. Data were collected with an Enraf-Nonius CAD4 diffractometer. The compound crystallised in the centrosymmetric space group $P2_1/n$ (no. 14). The crystal structure was solved by direct methods (SIR) and refined using the Enraf-Nonius MOLEN software package. Anisotropic temperature factors were assigned to all non-hydrogen atoms, while hydrogen atoms were included as fixed contributions to the structure factor. A non-Poisson weighting scheme was applied with a *p* factor equal to 0.06. The final agreement factors were $R = 0.039$, $R_w = 0.047$, G.O.F. = 1.01. Crystallographic data (excluding structure factors) for the structure reported in this paper have been deposited with the Cambridge Crystallographic Data Centre as supplementary publication no. CCDC-106502. Copies of the data can be obtained free of charge on application to CCDC, 12 Union road, Cambridge CB2 1EZ [Fax: (internat.) + 44-1223/336-033; E-mail: deposit@ccdc.cam.ac.uk].

Acknowledgments

The authors wish to thank CNRS, Ecole Polytechnique and Université de Dijon for financial support of this work.

[1] [1a] F. T. Edelmann in *Comprehensive Organometallic Chemistry II* (Eds.: E.W. Abel, F. G. A. Stone), vol.4 (Scandium, Yttrium, Lanthanides, Actinides and Titanium group), Pergamon Press, Oxford, New York, Tokyo, **1995**, p. 11. – [1b] H. Schumann, J. A. Meese-Marktscheffel, L. Esser, *Chem. Rev.* **1995**, *95*, 865. – [1c] C.J. Schavieren, *Adv. Organomet. Chem.* **1995**, *36*, 283.

[2] [2a] P. L. Watson, J. F. Whitney, R. L. Halow, *Inorg. Chem.* **1981**, *20*, 3271. – [2b] M. F. Lappert, A. Singh, J. L. Atwood, W. E. Hunter, *J. Chem. Soc., Chem. Commun.* **1981**, 1181. – [2c] W. J. Evans, I. Bloom, W. E. Hunter, J. L. Atwood, *J. Am. Chem. Soc.* **1983**, *105*, 1401. – [2d] J. M. Boncella, T. D. Tilley, R. A. Andersen, *J. Chem. Soc., Chem. Commun.* **1983**, 69. – [2e] M. F. Lappert, A. Singh, J. L. Atwood, W. E. Hunter, H. −M. Zhang, *J. Chem. Soc., Chem. Commun.* **1983**, 69. – [2f] W. J. Evans, I. Bloom, W. E. Hunter, J. L. Atwood, *Organometallics* **1985**, *4*, 112. – [2g] G. Jeske, H. Lauke, H. Mauermann, P. N. Swepston, H. Schumann, T. J. Marks, *J. Am. Chem. Soc.* **1985**, *107*, 8091. – [2h] M. D. Rausch, K. J. Moriarty, J. L. Atwood, J. A. Weeks, W. E. Hunter, *Organometallics* **1986**, *5*, 1281. – [2i] H. J. Heeres, J. Renkema, M. Booij, A. Meetsma, J. Teuben, *Organometallics* **1988**, *7*, 2495. – [2j] A. Recknagel, D. Stalke, H. W. Roesky, F. T. Edelmann, *Angew. Chem. Int. Ed. Engl.* **1989**, *28*, 445. – [2k] M. Yasuda, Y. Yamamoto, K. Yokota, A. Nakamura, *Chem. Lett.* **1989**, 1309. – [2l] H. J. Heeres, A. Meetsma, J. Teuben, *Angew. Chem. Int. Ed. Engl.* **1990**, *29*, 420. – [2m] W. J. Evans, T. A. Ulibarri, J. W. Ziller, *J. Am. Chem. Soc.* **1990**, *112*, 2314. – [2n] A. Recknagel, M. Noltemeyer, U. Pieper, H. −G. Schmidt, F. T. Edelmann, *J. Organomet. Chem.* **1991**, *411*, 347. – [2o] A. Recknagel, F. Knossel, H. Gornitzka, M. Noltemeyer, F. T. Edelmann, *J. Organomet. Chem.* **1991**, *417*, 363. – [2p] K. −H. Thiele, A. Scholtz, J. Scholtz, U. Bohme, R. Kempe, J. Sieler, *Z. Naturforsch., B* **1993**, *48*, 1753. – [2q] W. J. Evans, R. A. Keyer, J. W. Ziller, *Organometallics* **1993**, *12*, 2618. – [2r] H. Schumann, E. C. E. Rosenthal, G. Kociok-Kohn, G. A. Molander, J. Winterfeld, *J. Organomet. Chem.* **1995**, *496*, 233. – [2s] Y. K. Gun′ko, P. B. Hitchcock, M. F. Lappert, *J. Organomet. Chem.* **1995**, *499*, 213. – [2t] D. J. Schwartz, R. A. Andersen, *Organometallics* **1995**, *14*, 4308. – [2u] N. S. Radu, T. D. Tilley, A. L. Rheingold, *J. Organomet. Chem.* **1996**, *516*, 41. – [2v] W. J. Evans, K. J. Forrestal, J. W. Ziller, *J. Am. Chem. Soc.* **1998**, *120*, 9273.

[3] [3a] G. Jeske, L. E. Schock, P. N. Swepston, H. Schumann, T. J. Marks, *J. Am. Chem. Soc.* **1985**, *107*, 8103. – [3b] N. Hock, W. Oroschin, G. Paolucci, R. D. Fischer, *Angew. Chem. Int. Ed. Engl.* **1986**, *25*, 738. – [3c] D. Stern, M. Sabat, T. J. Marks, *J. Am. Chem. Soc.* **1990**, *112*, 9558. – [3d] H. Schumann, L. Esser, J. Loebl, A. Dietrich, D. Van der Helm, X. Ji, *Organometallics* **1991**, *10*, 2585. – [3e] V. P. Conticello, L. Brard, M. A. Giardello, Y. Tsuji, M. Sabat, C. L. Stern, T. J. Marks, *J. Am. Chem. Soc.* **1992**, *114*, 2761. – [3f] V. P. Conticello, L. Brard, M. A. Giardello, Y. Tsuji, M. Sabat, C. L. Stern, T. J. Marks, *J. Am. Chem. Soc.* **1992**, *114*, 2761. – [3g] K. Quiao, R. D. Fischer, *J. Organomet. Chem.* **1993**, *456*, 185. – [3h] J. R. Van den Ende, P. B. Hitchcock, M. F. Lappert, T. A. Nile, *J. Organomet. Chem.* **1994**, *472*, 79. – [3i] J. Graper, R. D. Fischer, R. D. Paolucci, *J. Organomet. Chem.* **1994**, *471*, 87. – [3j] H. Schumann, M. Glanz, H. Hemling, *Chem. Ber.* **1994**, *127*, 2363. – [3k] M. A. Giardello, V. P. Conticello, L. Brard, M. Sabat, A. L. Rheingold, C. L. Stern, T. J. Marks, *J. Am. Chem. Soc.* **1994**, *116*, 10212. – [3l] C.M. Haar, C. L. Stern, T. J. Marks, *Organometallics* **1996**, *15*, 1765. – [3m] H. Schumann, M. Glanz, E. C. Rosenthal, H. Hemling, *Z. Anorg. Allg. Chem.* **1996**, *622*, 1865. – [3n] A. Recknagel, F. T. Edelmann, *Angew. Chem. Int. Ed. Engl.* **1991**, *30*, 693.

[4] [4a] P. Gradoz, C. Boisson, D. Baudry, M. Lance, M. Nierlich, J. Vigner, M. Ephritikhine, *J. Chem. Soc., Chem. Commun.* **1992**, 1720. – [4b] F. G. N. Cloke, S. A. Hawkes, P. B. Hitchcock, P. Scott, *Organometallics* **1994**, *13*, 2895.

[5] P. Gradoz, D. Baudry, M. Ephritikhine, M. Lance, M. Nierlich, J. Vigner, *J. Organomet. Chem.* **1994**, *466*, 107.

[6] F. Nief, F. Mathey, *J. Chem. Soc., Chem. Commun.* **1989**, 800.

[7] P. Gradoz, D. Baudry, M. Ephritikhine, F. Nief, F. Mathey, *J. Chem. Soc., Dalton Trans.* **1992**, 1720.

[8] W. J. Evans, J. M. Olofson, H. Zhang, J. L. Atwood, *Organometallics* **1988**, *7*, 629.

[9] [9a] C. Sun, G. Wei, Z. Jin, W. Chen, *J. Organomet. Chem.* **1993**, *453*, 61. – [9b] R. K. Minhas, Y. Ma, J. −I. Song, S. Gambarotta, *Inorg. Chem.* **1996**, *35*, 1866.

[10] H. −J. Gosink, F. Nief, L. Ricard and F. Mathey, *Inorg. Chem.* **1995**, *34*, 1306.

[11] [11a] M. Andrianarison, D. Stalke, U. Klingebiel, *Chem. Ber.* **1990**, *71*, 123. – [11b] M. C. Fermin, J. Ho, D. W. Stephan, *Organometallics* **1995**, *14*, 4247.

[12] [12a] H. Bock, C. Nather, K. Ruppert, *J. Chem. Soc., Chem. Commun.* **1992**, 765. – [12b] V. Jordan, U. Behrens, F. Olbrich, E. Weiss, *J. Organomet. Chem.* **1996**, *517*, 81. – [12c] W. J. Grisby, P. P. Power, *J. Am. Chem. Soc.* **1996**, *118*, 7981.

[13] F. Nief and F. Mathey, *Synlett* **1991**, 745.

[14] P. J. Fagan, J. M. Manriquez, E. A. Maata, A. M. Seyam, T. J. Marks, *J. Am. Chem. Soc.* **1981**, *103*, 6650.

[15] P. Gradoz, Thesis, Université de Paris XI ORSAY, **1993**, p. 66.

[16] P. J. Davidson, D. H. Harris, M. F. Lappert, *J. Chem. Soc., Dalton Trans.* **1976**, 2268.

[17] K. Rossmanith, *Monatsh. Chem.* **1969**, *100*, 1484.

Received November 5, 1998
[I98380]

Catalytic Formation of Carbon–Carbon Bonds by Activation of Carbon–Hydrogen Bonds

Yannick Guari,[a] Sylviane Sabo-Etienne,[a] and Bruno Chaudret*[a]

Keywords: Homogeneous catalysis / C–H activation / Carbon–carbon coupling

The direct functionalization of C–H bonds by formation of a C–C bond is an interesting and important alternative to coupling reactions involving halide derivatives. These reactions are complex but during the past few years a number of new systems have been developed which display promising scope. This microreview will briefly mention the different mechanisms leading to C–H activation and describe the new systems leading to the catalytic formation of carbon–carbon bonds.

Introduction

Much research has been devoted during the past 20 years to the activation of the carbon−hydrogen bond,[1] whether it concerns intermolecular (Equations 1−3)[1a−1k] or intramolecular (cyclometallation, Equation 4) activation.[1l−1q] The first process is of special interest for the functionalisation of hydrocarbons, whereas the second one is of importance for the synthesis of fine chemicals where the production of by-products is minimized. A great deal of knowledge has been gained on the process of C−H bond activation and three main mechanisms identified, namely oxidative addition,[2] σ-bond metathesis,[3] and electrophilic

[a] Laboratoire de Chimie de Coordination CNRS,
205 route de Narbonne, F-31077 Toulouse Cedex, France
E-mail: Chaudret@lcc-toulouse.fr



Yannick Guari (left, top) was born in Castelnaudary, France, in 1971. He studied chemistry at the Université Paul Sabatier in Toulouse, France, where he graduated. He then joined the group of Bruno Chaudret to work in the field of dihydrogen complexes and received his doctoral degree in 1998. He is now a postdoctoral fellow at the Universiteit van Amsterdam, The Netherlands, with Prof. Piet W. N. M. van Leeuwen. His current interest concerns palladium-catalysed carbon−nitrogen bond formation.



Sylviane Sabo-Etienne (right) was born in 1956 in Tarbes (France). She studied at the Université Paul Sabatier, Toulouse, and obtained her "Thèse de Troisième Cycle" in 1980 working under the supervision of Prof. Danièle Gervais. She then entered the CNRS in 1980 and obtained her "Doctorat d'Etat" in 1984. In 1985 she went to the Université de Bretagne Occidentale in Brest, to work with Prof. Hervé des Abbayes. After a year working with Prof. Maurice Brookhart (Chapel Hill, USA) she returned to the Laboratoire de Chimie de Coordination where she is currently "Directrice de Recherche". Her research interests concern the chemistry and spectroscopic properties of polyhydride, dihydrogen, silane, and more generally σ-bond complexes, with particular focus on catalytic applications.

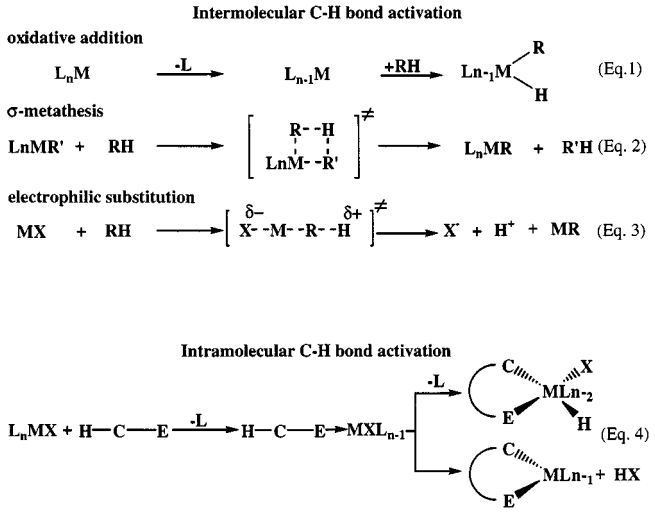


Bruno Chaudret (left bottom) was born in 1953 in Ferolles (France). He received his degree from the "Ecole Nationale Supérieure de Chimie de Paris" in 1975, his Ph.D. from Imperial College of Science and Technology, London, working under the direction of Prof. Sir Geoffrey Wilkinson in 1977 and his "Doctorat d'Etat" from the Université Paul Sabatier, Toulouse, working under the direction of Prof. René Poilblanc in 1979. He entered the CNRS in 1977 and was promoted to the position of "Directeur de Recherche" in 1988. His research interests concern the chemistry and spectroscopic properties of polyhydride, dihydrogen and more generally σ-bond complexes and their application in catalysis and for C−H activation as well as the synthesis, chemistry, and physical properties of nanoparticles of metals, alloys, and oxides.

MICROREVIEWS: This feature introduces the readers to the authors' research through a concise overview of the selected topic. Reference to important work from others in the field is included.

 © WILEY-VCH Verlag GmbH, D-69451 Weinheim, 1999 1434−1948/99/0707−1047 $ 17.50+.50/0

substitution,[4] all of which have been substantiated by stoichiometric studies.



However, despite this intense research activity, the number of catalytic processes including C−H bond activation as an elementary step have remained limited. This microreview will focus on the catalytic activation of cabon−hydrogen bonds leading to the formation of new carbon−carbon bonds. This will omit some very promising systems, such as that involving Pt(bipym) complexes recently described by Periana et al.[5] We will also omit the MERCAT process developed by Crabtree et al.[6] This is probably the most powerful system used to date to create new carbon−carbon and carbon−heteroatom bonds from alkanes, but it involves a mechanism based on electron transfer, and has recently been reviewed by Crabtree.

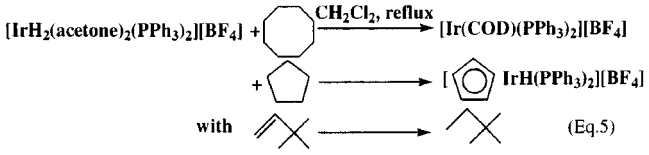
After the activation of a carbon−hydrogen bond, a new metal−carbon bond is generated. The new species has several possible pathways to react further: i) reductive elimination of an alkane in the case of an oxidative addition process; ii) β-elimination of the alkyl group to give an alkene; iii) insertion of small molecules into the metal−carbon bond leading to new functionalities. The first process is non-productive, we will consider only the latter two processes in the following review, and include the dehydrogenation processes as they formally generate a new carbon−carbon bond.

1. Alkane Dehydrogenation

With a Hydrogen Acceptor

Hydrocarbon dehydrogenation has been known in heterogeneous catalysis since 1937;[7] however, only recently have homogeneous systems been developed.

Alkane dehydrogenation could, in principle, be performed by good hydrogenation catalysts but this reaction is energetically unfavourable ($\Delta H \approx 30$ kcal·mol^{-1}). In order to circumvent this problem, Crabtree has employed a hydrogen acceptor, 3,3-dimethylbut-1-ene (*tert*-butylethylene), which is bulky enough to coordinate weakly to the transition metal centre, and which also shows a high enthalpy of hydrogenation. By using $[IrH_2(acetone)_2(PPh_3)_2][BF_4]$,[8] only stoichiometric reactions were observed (Equation 5).



However, catalytic dehydrogenation of cyclooctane to cyclooctene was achieved at 150°C using $IrH_2(CF_3CO_2)$-$[P(p\text{-}F-C_6H_4)_3]_2$ with a total turnover number of 16.[9] A similar system was developed by Felkin, Ephritikhine, and Baudry with polyhydrides such as $ReH_7(PR_3)_2$, $IrH_5(PR_3)_2$, and $RuH_4(PR_3)_3$ as catalysts.[10] At 150°C turnover numbers reaching 70 were obtained for the best systems.

The reaction path is proposed to involve a mechanism which is the reverse to that of alkene hydrogenation,[11] and which also involves highly coordinatively unsaturated intermediates (see Figure 1).[10]

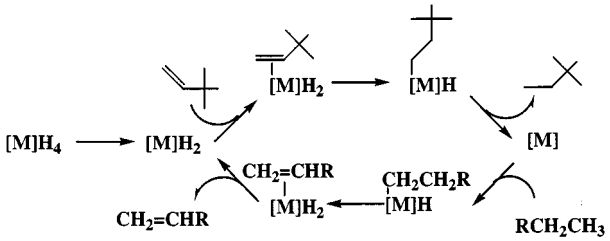


Figure 1. Proposed catalytic cycle for the dehydrogenation of saturated hydrocarbons

The first significant improvement was brought about by Goldman who performed the dehydrogenation reaction with $RhCl(CO)(PMe_3)_2$ as a catalyst and under a dihydrogen pressure of 69 bars. This system allows very high turnover numbers (1000) to be reached under mild conditions (60°C), but the problem is the necessary consumption of 6−8 mol of norbornene (used as hydrogen acceptor) per mol of dehydrogenated hydrocarbon. A number of linear and cyclic alkanes could be dehydrogenated in this way.[12]

More recently, Jensen et al. found that the complex $IrH_2[C_6H_3(CH_2PtBu_2)_2\text{-}2,6]$ (very stable even at high temperatures) could dehydrogenate cyclooctane to cyclooctene at 200°C in the presence of *tert*-butylethylene with a turnover frequency of 12 min^{-1}.[13] The thermal stability of this compound results from the use of the "pincer" ligand $C_6H_3(CH_2PtBu_2)_2\text{-}2,6$. Furthermore this system is able to dehydrogenate ethylbenzene or ethylcyclohexane to styrene, tetrahydrofuran to dihydrofuran,[14] cyclohexane to cyclohexene and benzene and decalin to octahydronaphthalene, tetrahydronaphthalene, and eventually naphthalene.[15] These reactions are slower than the dehydrogenation of cyclooctane. It is, however, remarkable that the formation of arenes does not poison the system.

Without a Hydrogen Acceptor

Whilst the interest of these systems is not in doubt, the presence of hydrogen acceptors make them unpractical. Therefore, several authors have looked for photocatalytic systems which avoid the use of hydrogen acceptors. Crabtree has shown that $IrH_2(CF_3CO_2)(PCy_3)_2$ is able to dehydrogenate cyclooctane to cyclooctene under UV irradiation with a turnover number of 7 at 25°C.[9] In this system, dehydrogenation of linear alkanes leads to a mixture of alkenes. Catalytic dehydrogenation of hexane, heptane, and octane has been carried out by Saito[16] using $RhCl(CO)(PR_3)_2$ (R = Me, Et, Ph), and Tanaka[17] using $RhCl(CO)(PMe_3)_2$. The reactions of Saito are carried out between 60 and 92°C and display a moderate variation in rate as a function of temperature, but no such variation as a function of the nature of the alkane substrate. The activity of the catalyst decreases in the order $PMe_3 > PEt_3 > PPh_3$. Tanaka's experiments were carried out under photolytic conditions and concern hexane as well as cycloalkanes such as cyclohexane and cyclooctane. In the case of hexane, 155 turnovers were obtained after 27 h, leading to (*E*)-/(*Z*)-2-hexene.

In all cases, the mechanism is proposed to involve β-elimination from an alkyl hydrido complex produced by oxidative addition of alkane to a coordinatively unsaturated species.

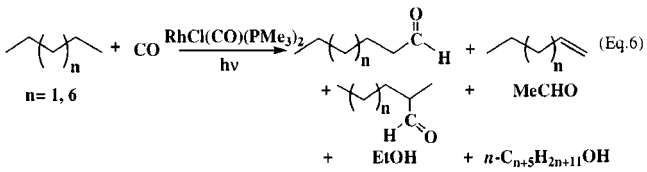
The best system was again found in 1997 by Goldman and Jensen, and involves the dehydrogenation of cyclodecane at 201°C under refluxing conditions leading to 360 turnovers after 24 h. The system is much less active for dehydrogenation of cyclooctane in a sealed tube at 200°C, thus suggesting the need for reflux.[18]

2. Formation of Carbon−Carbon Bonds

2.1 Insertion of Carbon Monoxide

The insertion of carbon monoxide into a carbon−hydrogen bond being thermodynamically unfavourable, all processes are photoassisted. Eisenberg was the first to show that square-planar iridium and rhodium complexes are able to catalytically insert carbon monoxide into a C−H bond of benzene when exposed to light (λ > 366 nm).[19] The complexes used were IrH(CO)(dppe), IrBr(CO)(dppe), $IrCl(CO)(PPh_3)_2$, and $RhCl(CO)(PPh_3)_2$ which gave rise to 2 catalytic cycles. A kinetic study carried out in the latter case shows that initial rates increase under reduced CO pressures, whereas larger turnover numbers were obtained under a high CO pressure.[19]

A similar but more efficient system was developed by Tanaka al. Using $RhCl(CO)(PMe_3)_2$, it was possible to catalytically carbonylate benzene itself or benzene monosubstituted by methyl, methoxy, chloro, or cyano groups with efficiencies reaching that of 65 turnovers.[20] This system can be extended to the carbonylation of saturated hydrocarbons. In this case, products of both carbonylation and dehydrogenation are obtained, those involving the initial activation of the terminal methyl groups being the most abundant (Equation 6).[20b,21]

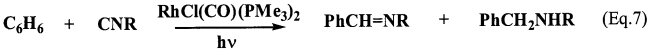


The mechanism of this reaction was studied at wavelengths shorter than 320 nm by Goldman et al.[22] Under these conditions, the authors propose that the first step is the oxidative addition of a benzene C−H bond to a photoexcited catalyst, and not photoextrusion of a ligand (CO or PR_3). Field et al. have prepared $RhHCl(Ph)(CO)(PMe_3)_2$ (2 isomers: *cis*-HCl and *trans*-HCl) by irradiation of $RhCl(CO)(PMe_3)_2$ in a benzene/tetrahydrofuran mixture at low temperatures in the absence of added CO.[23] Kinetic activation parameters (ΔH^{+} and ΔS^{+}) for the interconversion of both isomers are in agreement with those obtained by Goldman, and strongly suggest the intermediacy of a photoactive intermediate such as $RhHCl(Ph)(CO)(PMe_3)_2$ in benzene photocarbonylation. Finally, Eisenberg has also shown that d^8-ruthenium complexes accomodating carbonyl and phosphane ligands are also active for the photocarbonylation of benzene.[24]

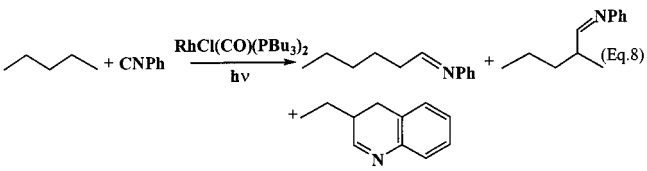
Sen and co-workers have studied electrophilic systems for the functionalization of alkanes.[1r] Whereas most systems concern the oxidation of alkanes, the reaction of $RhCl_3 \cdot 3\,H_2O$ with methane, dioxygen, and carbon monoxide in a mixture of C_3F_7COOH, $(CF_3)_2CHOH$, and D_2O produces methanol and acetic acid at 80°C with high efficiency. The proposed mechanism involves insertion of CO into a rhodium−methyl bond.[4k,4l] This direct formation of acetic acid is a promising method of activating methane.

2.2 Isocyanide Insertion

Insertion reactions of isocyanide groups (RNC, R = Ph, Me, *t*Bu, *p*-tolyl), a ligand formally similar to the carbonyl ligand, into a C−H bond of benzene have been carried out by Tanaka et al. using $RhCl(CO)(PMe_3)_2$. The reaction needs to be photoassisted and leads mainly to aldimines (Equation 7).[25]

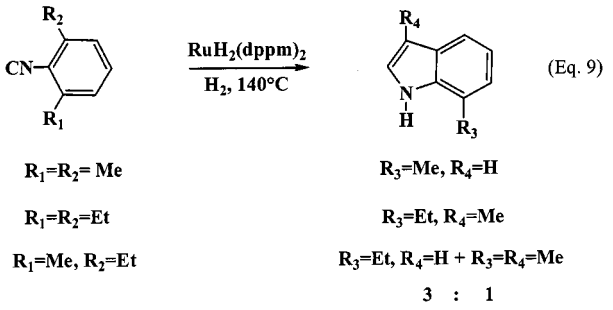


In the case of linear alkanes, $RhCl(CO)(PBu_3)_2$ was used and the reaction was found to be only stoichiometric (Equation 8).



A similar reaction had been previously described by Jones et al. who showed that isocyanide insertion into the C−H bond of benzene could be catalysed at room temp. by $Fe(CNR)_3(PMe_3)_2$ (R = Me, *t*Bu, CH_2CMe, Ph, 2,6-xylyl) under UV light.[26] This reaction does not work for alkanes such as pentane or cyclohexane. The same reaction is possible using $RhCl(CNR')(PR_3)_2$ (R = Me, Et, *i*Pr and R′ = neopentyl, 2,6-xylyl, Me) as a catalyst, leading to 7.7 turnovers after 16 h in the best case (R = *i*Pr et R′ = neopentyl) but again no insertion of isocyanides into the C−H bond of alkanes was observed using this system.[27]

$RuH(naphthyl)(dmpe)_2$,[28] the first complex to be shown to activate C−H bonds of aryl and activated aliphatic C−H bonds, was reinvestigated by Jones for the synthesis of indoles from bulky isocyanides. 2,6-Xylyl isocyanide reacts at 60°C with $RuH(naphthyl)(dmpe)_2$ for 24 h in toluene to give *trans*-$RuH[2\text{-}(7\text{-methylindole})](dmpe)_2$ which isomerizes at 100°C to *cis*-$RuH[2\text{-}(7\text{-methylindole})](dmpe)_2$. The latter eliminates 7-methylindole at 140°C under 0.66 bar H_2 to yield $RuH_2(dmpe)_2$. The mechanism involves initial intramolecular C−H activation of a methyl substituent of the xylyl group attached to the isocyanide moiety. Using $RuH_2(dmpe)_2$, 3.6 turnovers could be obtained at 140°C (Equation 9).



2.3 Alkene and Alkyne Insertion into Unsupported Carbon−Hydrogen Bonds

The insertion of alkynes into C−H bonds of benzene, *n*-hexane, cyclohexane, or diethyl ether can be achieved with $RhCl(CO)(PMe_3)_2$ in the presence of UV light. However, the reaction is less efficient than carbon monoxide or isocyanide insertion, and only 6 turnovers were obtained in the best case.[29] In addition to insertion products, the reaction in the case of benzene leads to dimers and trimers of acetylenes as well as biphenyl. The latter product, and other biaryls, can be obtained directly from the photolysis of arenes in the presence of $RhCl(CO)(PMe_3)_2$.[30] Cyclohexane, *n*-hexane, and diethyl ether react in the same way with phenylacetylene to give the corresponding α-substituted styrenes with a good regioselectivity but in low yield (from 19%/Rh for cyclohexane to 77%/Rh for *n*-hexane) and with the formation of several by-products.[29]

Some thermal systems involving insertion of unsaturated molecules into C−H bonds of benzene have been known for a long time. Thus, Hong et al. have shown that insertion of alkynes (RC≡CR′; R = Ph, Me, R′ = Ph; R = R′ = *p*-MeC_6H_4),[31] heterocumulenes,[32] aryl isocyanates (RN=C=O; R = Ph, *p*-MeC_6H_4, *p*-ClC_6H_4, α-$C_{10}H_7$),[32] ethylene,[33] monosubstituted ethylene (CH_2=CHCOR; R = OMe, OH, NMe_2, NMePh, Me),[34] disubstituted ethylene (RCH=CHR′; R = Me, Ph, CO_2Me, R′ = CO_2Me;[34] CH_2=CRR′; R = Me, R′ = CO_2Me)[34] and cyclic alkenes[34] into the C−H bonds of benzene, arenes (PhR; R = Me, OMe, F; Figure 2) or furans ($C_4H_3R''O$; R″ = H, Me, $MeCO_2$, MeCO, CHO; Figure 3) could be achieved at 220°C with $Rh_4(CO)_{12}$ as catalyst and under a pressure of CO. A maximum turnover number of 360 was obtained in the case of the addition of CH_2=$CHCO_2Me$ to benzene under 29 bars of CO. The reaction is favoured by the presence of electron-withdrawing substituents leading the authors to propose initial attack of a nucleophilic low-valent rhodium cluster onto the substrate C−H bond, followed by C−H bond cleavage and alkyne or isocyanate insertion. The CO pressure would be necessary to regenerate the active catalytic species. In some cases, secondary products can be formed, such as indenones in the case of the reaction between acetylenes and benzene, which result from CO insertion.

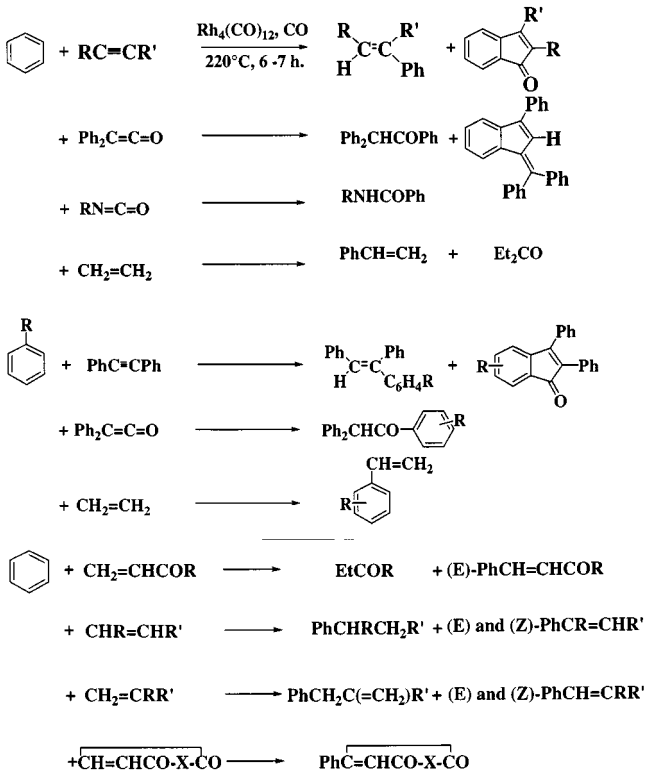


Figure 2. Carbon−carbon bond formation between arenes and unsaturated hydrocarbons catalysed by $Rh_4(CO)_{12}$

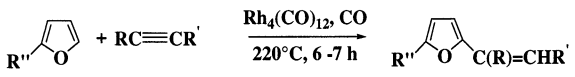
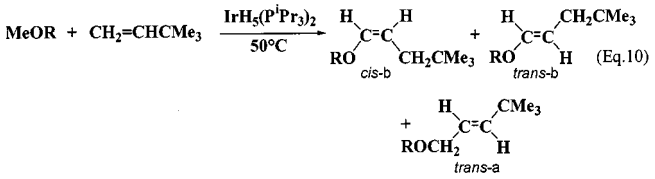


Figure 3. Carbon−carbon bond formation between furan and unsaturated hydrocarbons catalysed by $Rh_4(CO)_{12}$

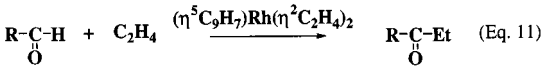
An interesting coupling reaction between a C−H bond of methyl ethers (MeOR; R = CH_2CH_2OMe, C_6H_{11},

$C_6H_{10}Me$) and 3,3-dimethylbut-1-ene has been reported by Lin, Ma, and Lu with $IrH_5(PiPr_3)_2$ as the catalyst.[35] The reaction produces olefins and enol esters with a maximum turnover number of 12 after 24 h at 50°C (Equation 10).



The mechanism of this reaction involves the formation of an unsaturated 14-electron intermediate, similar to that proposed by Felkin et al. for alkane dehydrogenation, which is able to insert into the activated C−H bond of the methyl ether. The absence of β-hydrogen allows the coupling reaction to occur. This reaction is followed by a rapid isomerisation of the olefin formed.

Finally, the coupling reaction between aldehydes and olefins involves the activation of a particular C−H bond. Milstein et al. have shown that $[(\eta^5C_9H_7)Rh(\eta^2C_2H_4)_2]$ catalyses the insertion of ethylene at 100°C under 69 bars into the C−H bond of aldehydes RC(O)H (R = Ph, *p*-$CF_3C_6H_4$, *p*-MeC_6H_4) with a turnover frequency of 4 h^{-1}(Equation 11).[36]



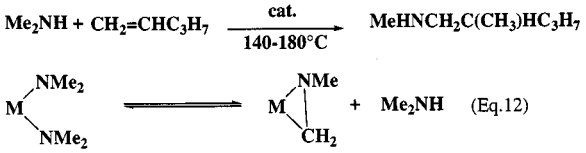
The reaction presumably proceeds by initial activation of the aldehyde C−H bond, as in the decarbonylation reactions of aldehydes catalysed by numerous transition metal complexes. It is, however, interesting to note that no decarbonylation product has been observed in this case.

2.4 Alkene and Alkyne Insertion into Potentially Chelating Systems

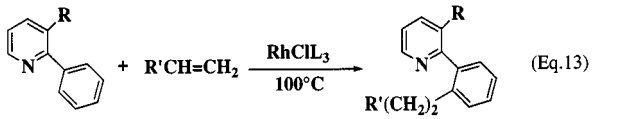
It has been shown in section 2.3 that most systems involving direct C−C coupling through C−H activation were relatively inefficient. It is, however, known from literature on organometallics that the activation of a C−H bond linked to a functional group (phosphane, amine, ketone, ...), thus maintaining it in close proximity to a metal centre, is much easier. This led several authors to investigate the functionalization of cyclometallated hydrocarbons. Lewis and Smith[37] have described the insertion of ethylene into the ruthenium−carbon bond of an *ortho*-metallated phosphite group. However, catalytic reactions were developed for systems containing a nitrogen or oxygen donor group as chelating assistant of the insertion reaction into the C−H bond.

Nitrogen Donor Chelating Assistants

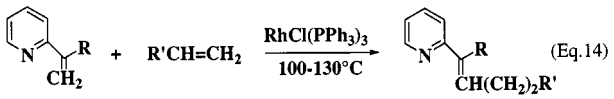
A catalytic amination reaction of olefines has been described by Nugent et al.[38] which does not involve, as expected, the formation of a C−N bond, but the formation of a C−C bond. The catalysts are amido transition metal complexes. The proposed mechanism involves the intermediacy of a metallacycle and the insertion of the olefin into the M−C bond (Equation 12).



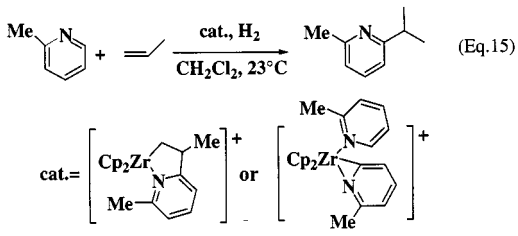
Recently, Lim, Kim, and Bang have described the catalytic alkylation of the phenyl ring of 2-phenylpyridine and 3-methyl-2-phenylpyridine in the *ortho* position relative to pyridine. Several olefins were used, namely R′CH=CH_2 [R′ = $Me(CH_2)_2$, $Me(CH_2)_3$, $Me(CH_2)_5$, $Me_3C(CH_2)_2$, $Si(OEt)_3$, $Si(OMe)_3$], in the presence of the catalyst $RhCl(PPh_3)_3$ leading at 100°C to 10 turnovers in 22 h for the best system (Equation 13).[39]



The intermediacy of an *ortho*-metallated hydridorhodium complex has been postulated. The reaction has been extended to carbon−carbon coupling reactions of substituted 2-vinylpyridines *o*-RC(=CH_2)−C_6H_4N (R = Me, Ph) with the olefins R′CH=CH_2 previously mentioned.[40] This reaction leads to 10 turnovers at 100−130°C (in the best case) in the presence of the same rhodium catalyst (Equation 14).



More unexpectedly, chelating assistance by the pyridine nitrogen atom is also involved in the functionalisation of *ortho* C−H bonds in pyridine. Jordan et al. have first described the alkylation of pyridines in *ortho* position relative to the nitrogen atom. The reaction occurs under H_2 at 23°C in the presence of cationic zirconium complexes, leading to up to 40 turnovers (Equation 15).[41]



The mechanism involves the initial formation of $[Cp_2Zr(\eta^2\text{-6-methylpyrid-2-yl})(THF)]^+$ from $[Cp_2ZrMe(THF)]^+$ through a σ-bond metathesis process. In this system intermediates were isolated and demonstrated to be ac-

tive in the catalytic coupling of 2-methylpyridine with propene (see Figure 4).

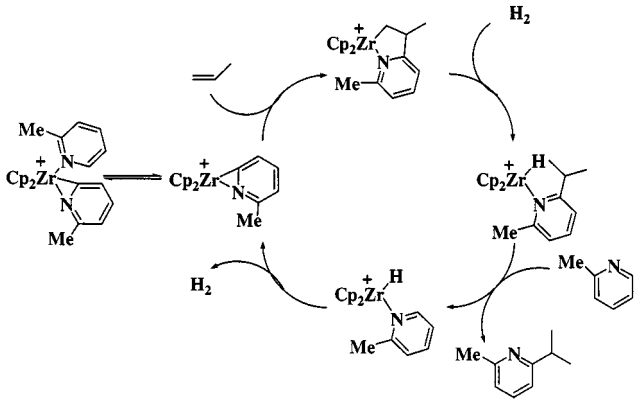
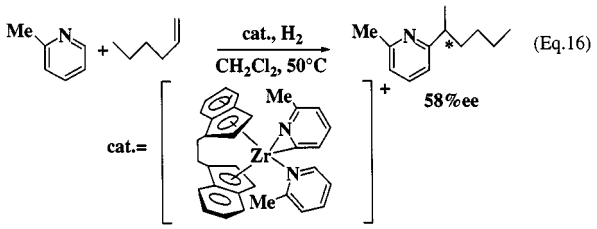
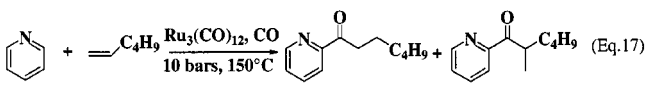


Figure 4. Reaction mechanism of coupling between 2-methylpyridine and propene catalysed by zirconium complexes

Recently, this reaction was extended to the regio- and stereoselective insertion of olefins into a methylpyridine C−H bond using chiral catalysts such as [$^{ch}Cp_2Zr(\eta^2$-pyrid-2-yl)]$^+$ [$^{ch}Cp_2$ = ethylenebis(indenyl) (EBI) or ethylenebis-(tetrahydroindenyl) (EBTHI)].[42] The catalytic activity of the chiral complexes is 10 times lower, but at 50°C, in the presence of H_2, [(*S*,*S*)-(EBTHI)Zr(η^2-6-methylpyrid-2-yl)(2-methylpyridine)]$^+$, generated in situ from (*S*,*S*)(EBTHI)$ZrMe_2$, [$HNBu_3$][BPh_4], and 2-methylpyridine, catalyses the addition of 1-hexene to 2-methylpyridine to give (*R*)-2-methyl-6-(2-hexyl)pyridine with a 58% enantiomeric excess (Equation 16).

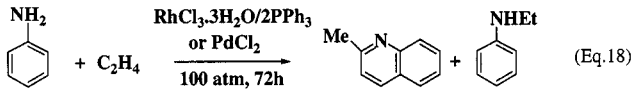


Moore et al. have shown that it is possible to insert two different molecules, namely carbon monoxide and olefins (R′CH=CH_2; R′ = H, C_4H_9, $C_{18}H_{37}$, Me_3C), into the C−H bond of pyridine in the *ortho* position relative to the nitrogen atom.[43] The reaction occurs at 150°C, under 10 bars of CO and leads to a turnover frequency of up to 300 h^{-1} when using 3,3-dimethyl-1-butene. The reaction can be extended to quinolines and to the use of cyclic alkenes but does not work for tri- and tetrasubstituted olefines. The authors present evidence for the implication of a trinuclear catalyst based on kinetic data and the absence of reactivity of photolytically generated mononuclear species (Equation 17).



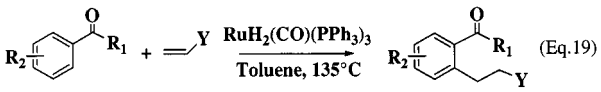
A very similar system was used by Murai for the acylation of substituted imidazoles. The reaction is carried out under relatively harsh conditions (160°C, 20 bars of CO) and leads to a limited yield of coupling products; up to 23 turnovers in the best case.[44]

Finally, during attempts to catalyse olefin amination, Diamonds and co-workers observed a new cyclization reaction leading to the formation of 2-methylquinoline. The reaction conditions are severe (200°C, 101 bars, 72 h) and the yields modest (30 turnovers for the formation of *N*-ethylaniline and 10 turnovers for 2-methylquinoline), but this reaction represents the first catalytic synthesis of heterocycles and is thought to involve intermediate species containing *ortho*-metallated aniline (Equation 18).[45]



Oxygen Donor Chelating Assistants

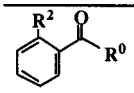
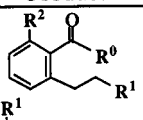
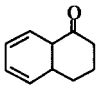
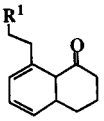
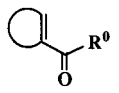
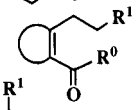
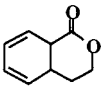
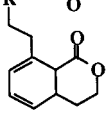
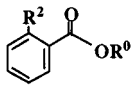
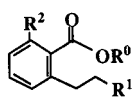
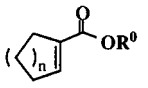
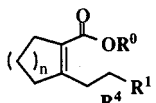
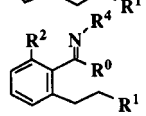
Perhaps the most interesting and promising system for the functionalization of aromatic hydrocarbons in α-position relative to a functional group has been described by Murai and co-workers.[46−48] Initially, Murai (1993) described the alkylation of aromatic ketones using ruthenium catalysts, namely $RuH_2(CO)(PPh_3)_3$ (the most efficient example), $Ru(H)_2(PPh_3)_4$, $Ru(CO)_2(PPh_3)_3$, and $Ru(CO)_3(PPh_3)_2$.[46−48] The reaction was carried out in vigourously refluxing toluene, a temperature of 135°C being indicated by the authors, and led to ca. 50 turnovers of coupling product in the best case (Equation 19).



The scope of the reaction has proven to be fairly general. Thus, similar alkylation reactions were observed for acylbenzene derivatives,[46−48] α-tetralones,[49] α,β-enones,[50] lactones,[51] aromatic and heteroaromatic esters,[51] cyclic esters,[52] and aromatic imines[52] using substituted olefins[46−48,50−52] and alkynes.[49] Table 1 summarizes some of the reactions studied by Murai′s group. This system has since then been extended by Weber et al. to the copolymerization of acetophenone with α,ω-dienes[53] as well as to the modification of unsaturated polymers,[54] whereas Woodgate used this system for alkylating hydroxyacetophenone and extended it to the functionalization of aromatic diterpenoids.[55]

The mechanism proposed by Murai involves the formation of a 16-electron ruthenium(0) intermediate produced by hydrogenation of the incoming olefin. The formation of triethoxyethylsilane (0.036 mmol) has been observed when $RuH_2(CO)(PPh_3)_3$ (0.04 mmol) was treated with 3 equiv. of triethoxyvinylsilane at 135°C for 1 min. The ruthenium complex was not identified. Addition of acetophenone (0.08 mmol), at 135°C and within 1 min, leads to the coupling product. An *ortho*-metallated intermediate, "RuH[*o*-C_6H_4−C(O)R]", is proposed (see Figure 5). Similar com-

Table 1. Some substrates used in Murai's reaction for coupling with an olefin $CH_2=CHR^1$

Substrate	Product	Reference
		46, 47, 48
		46, 48
		50
		51
		51
		57
		52

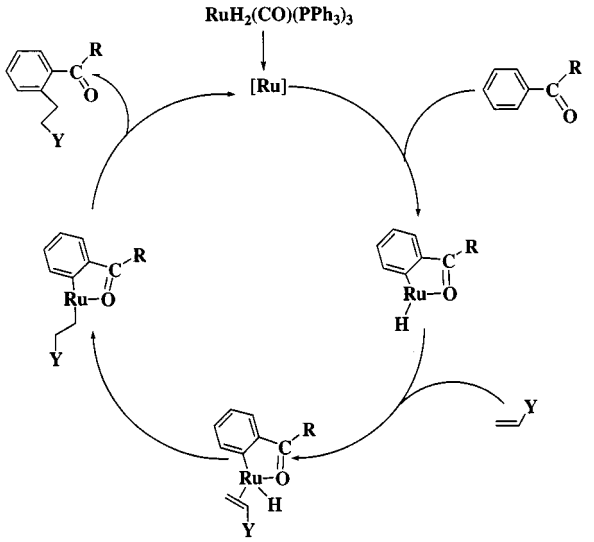


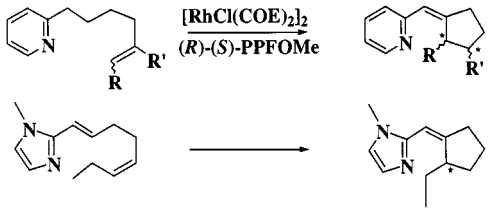
Figure 5. Mechanism proposed for Murai's reaction

plexes have been known since their first preparation by Cole-Hamilton and Wilkinson.[56] Hydrogen migration and carbon−carbon coupling would lead to the organic product and regenerate the active species [Ru].[46−52]

Trost et al. have studied the coupling of olefins with α-unsaturated esters catalysed by $RuH_2(CO)(PPh_3)_3$.[57] The catalytic activity is similar to that observed by Murai and the reaction is inhibited by the presence of a CO pressure or when carried out in a closed system, hence suggesting the need for CO to be eliminated for the reaction to proceed. The authors propose an active species "$RuS(PPh_3)_3$" stabilized by interaction with the solvent S.[57]

Weber et al. have recently mentioned the isolation of $[Ru\{MeC(O)C_6H_4CH=CH_2\}(CO)(PPh_3)_2]$ through the reaction of *o*-acetylstyrene with $[RuH_2(CO)(PPh_3)_3]$ in the presence of styrene at 120°C.[58] Such a complex could be a model for a late intermediate in the catalytic alkylation cycle and catalyses the copolymerisation of acetophenone and 1,3-divinyltetramethyldisiloxane.

More recently, Murai et al. have extended their study to the intramolecular asymetric coupling of substituted 1-(2-pyridyl)-1,5-dienes (Equations 20 and 21) or substituted 1-(1-methyl-2-imidazolyl)-1,5-dienes using a different catalytic system: $[RhCl(COE)_2]_2$ in the presence of alkyl (*R*)-1-[(*S*)-2-(diphenylphosphanyl)ferrocenyl] ether {alkyl = Me [(*R*)-(*S*)-PPFOMe], Et}.[59] The reaction proceeds at 25°C giving rise to 2 turnovers after 20 h and an enantiomeric excess of 78%. Up to 15 turnovers can be obtained at 120°C within 1 h but the enantiomeric excess decreases to 71%.



In our group, we have recently prepared a series of hydrido dihydrogen complexes containing *ortho*-metallated ligands (see Figure 6). For example, the reaction of 2-phenylpyridine leads to a new complex displaying interesting spectroscopic properties.[60a] These complexes are reminiscent of the intermediates proposed by Murai. This led us to attempt the same reaction with acetophenone and benzophenone. Hydrido dihydrogen complexes containing *ortho*-metallated aromatic ketones can thus be synthesized. These complexes further react with CO to give carbonyl hydrido complexes corresponding to precursors in Murai's cycle. The bis(dihydrogen) complex $[Ru(H)_2(H_2)_2(PCy_3)_2]$[60b] and the complexes containing *ortho*-metallated aromatic ketones were tested as catalysts for Murai's reaction in order to validate the catalytic cycle and define the role of CO. The reactions were carried out at room temp. in the presence of ethylene (20 bars). A catalytic reaction was observed when using $[RuH_2(H_2)_2(PCy_3)_2]$ or $[RuH(H_2)[OC(R)C_6H_4]-(PCy_3)_2]$ (R = Me, Ph) leading to the alkylation of the phenyl group in the *ortho* position of the ketone substituent. 10 turnovers are obtained under these conditions for the alkylation of acetophenone after 20 h, and 20 turnovers in the alkylation of benzophenone (see Figure 7). In the latter case, the reaction produces almost exclusively the dialkylated product. However, when using the carbonyl hydrido complexes $[RuH(CO)\{OC(R)C_6H_4\}(PCy_3)_2]$ (R = Me, Ph) no reaction was observed, even upon heating the solution. This suggests that the need for a high temperature in Murai's reaction is due to the necessity to eliminate CO from the coordination sphere of the ruthenium centre.

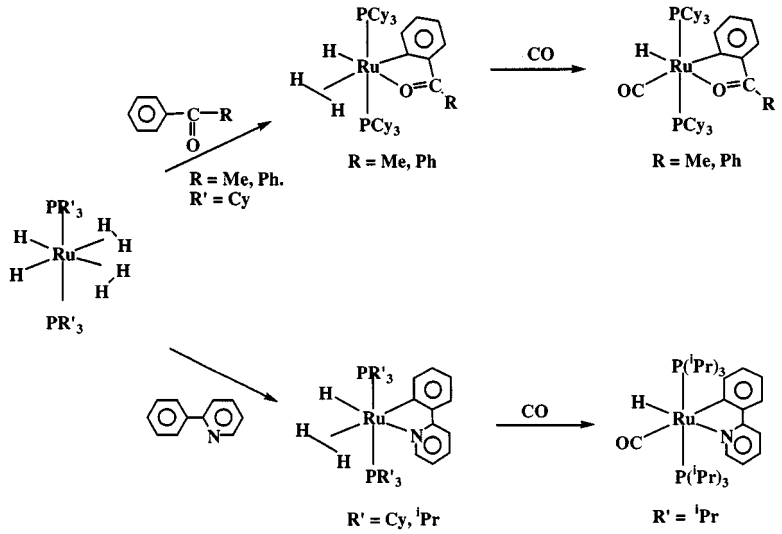


Figure 6. Synthesis of hydrido(dihydrogen)ruthenium complexes containing *ortho*-metallated ligands

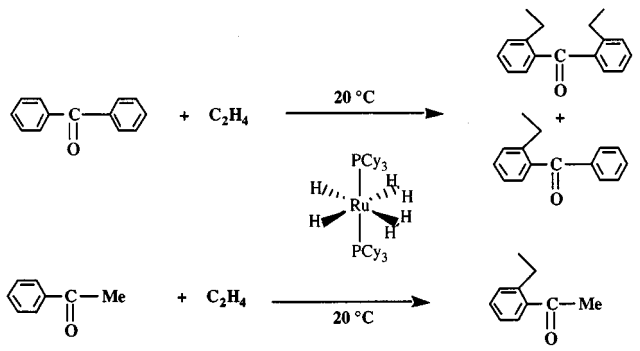


Figure 7. Alkylation reactions catalysed at room temp. by $RuH_2(H_2)_2(PCy_3)_2$

Conclusion

In conclusion, in this microreview we have briefly presented some of the latest results concerning the functionalization of C−H bonds through the formation of C−C bonds. If the alkane dehydrogenation is still difficult and requires harsh conditions, the catalytic insertion of alkenes into aromatic C−H bonds seems to be one of the most promising reactions regarding synthetic applications, especially if these reactions can be carried out under mild conditions (at room temperature for example). The development of such reactions would then avoid the by-products of conventional routes, salts in particular, and this research could therefore lead to new "environmentally friendly" processes.

[1] Selected reviews: [1a] D. E. Webster, *Adv. Organomet. Chem.* **1977**, *15*, 147. – [1b] R. H. Crabtree, *Chem. Rev.* **1985**, *85*, 245. – [1c] A. E. Shilov in *The activation of saturated hydrocarbons by transition metal complexes*, Reidel, Dordrecht, **1984**. – [1d] A. Sen, *Acc. Chem. Res.* **1988**, *21*, 421. – [1e] I. P. Rothwell, *Polyhedron* **1985**, *2*, 177. – [1f] R. G. Bergman, *Acc. Chem. Res.* **1995**, *28*, 154. – [1g] G. W. Parshall, *Acc. Chem. Res.* **1975**, *8*, 113. – [1h] E. L. Muetterties, *Chem. Soc. Rev.* **1983**, *12*, 283. – [1i] G. W. Parshall, *Acc. Chem. Res.* **1970**, *3*, 139. – [1j] C. L. Hill in *Activation and functionalization of alkanes*, Wiley Interscience, New York, **1989**. – [1k] A. E. Shilov, G. B. Shul′pin, *Chem. Rev.* **1997**, *97*, 2879. – [1l] M. I. Bruce, *Angew. Chem. Int. Ed. Engl.* **1977**, *16*, 73. – [1m] E. C. Constable, *Polyhedron* **1984**, *3*, 1037. – [1n] J. Dehand, M. Pfeffer, *Pure Appl. Chem.* **1992**, *3*, 335. – [1o] A. E. Ryabov, *Chem. Rev.* **1990**, *90*, 403. – [1p] M. Brookhart, M. L. H. Green, *J. Organomet. Chem.* **1983**, *250*, 395. – [1q] B. M. Trost, *Angew. Chem. Int. Ed. Engl.* **1995**, *34*, 259. – [1r] A. Sen, *Acc. Chem. Res.* **1998**, *31*, 550.

[2] [2a] A. M. Janowicz, R. G. Bergman, *J. Am. Chem. Soc.* **1982**, *104*, 352. – [2b] A. M. Janowicz, R. G. Bergman, *J. Am. Chem. Soc.* **1983**, *105*, 3929. – [2c] R. A. Periana, R. G. Bergman, *Organometallics* **1984**, *3*, 508. – [2d] R. G. Bergman, *Science* **1984**, *223*, 902. – [2e] R. G. Bergman, *Chem. Eng. News.* **1983**, *61*, 33. – [2f] J. K. Hoyano, W. A. G. Graham, *J. Am. Chem. Soc.* **1982**, *104*, 3723. – [2g] J. K. Hoyano, A. D. McMaster, W. A. G. Graham, *J. Am. Chem. Soc.* **1983**, *105*, 7190. – [2h] W. D. Jones, F. J. Feher, *Organometallics* **1983**, *2*, 686. – [2i] W. D. Jones, F. J. Feher, *J. Am. Chem. Soc.* **1984**, *106*, 1650.

[3] [3a] P. L. J. Watson, *J. Chem. Soc., Chem. Commun.* **1983**, 276. – [3b] P. L. Watson, *J. Am. Chem. Soc.* **1983**, *105*, 6491. – [3c] P. L. Watson, G. W. Parshall, *Acc. Chem. Res.* **1985**, *18*, 51. – [3d] M. E. Thompson, J. E. Bercaw, *Pure Appl. Chem.* **1984**, *56*, 1. – [3e] M. E. Thompson, S. M. Baxter, R. Bulls, B. J. Burger, M. C. Nolan, B. D. Santarsiero, W. P. Schaefer, J. E. Bercaw, *J. Am. Chem. Soc.* **1987**, *109*, 203. – [3f] C. M. Fendrick, T. J. Marks, *J. Am. Chem. Soc.* **1984**, *106*, 2214. – [3g] C. M. Fendrick, T. J. Marks, *J. Am. Chem. Soc.* **1986**, *108*, 425. – [3h] F. Quignard, C. Lecuyer, A. Choplin, D. Olivier, J. M. Basset, *J. Mol. Catal.* **1992**, *74*, 353.

[4] [4a] N. F. Gol'dschleger, M. B. Tyabin, A. E. Shilov, A. A. Shteinman, *Zh. Fiz. Khim.* **1969**, *43*, 2174; *Chem. Abstr.* **1969**, *71*, 105782a. – [4b] R. J. Hodges, J. L. Garnett, *J. Phys. Chem.* **1968**, *72*, 1673. – [4c] N. F. Gol'dschleger, V. Es'kova, A. E. Shilov, A. A. Shteinman, *Zh. Fiz. Khim.* **1972**, *46*, 785; *Chem. Abstr.* **1972**, *77*, 87715y. – [4d] J. A. Labinger, A. M. Herring, J. E. Bercaw, *J. Am. Chem Soc.* **1990**, *112*, 5628. – [4e] G. A. Luinstra, J. A. Labinger, J. E. Bercaw, *J. Am. Chem. Soc.* **1993**, *115*, 3004. – [4f] J. A. Labinger, A. M. Herring, K. D. Lyon, G. A. Luinstra, J. E. Bercaw, *Organometallics* **1993**, *12*, 895. – [4g] G. A. Luinstra, L. Wang, S. S. Stahl, J. A. Labinger, J. E. Bercaw, *Organometallics* **1994**, *13*, 755. – [4h] P. E. Siegbahn, R. H. Crabtree, *J. Am. Chem. Soc.* **1996**, *118*, 4442. – [4i] V. V. Zamashchikov, V. G. Popov, E. S. Rudakov, *Kinet. Katal.* **1994**, *35*, 372; *Chem. Abstr.* **1994**, *121*, 109224. – [4j] S. S. Stahl, J. Labinger, J. E. Bercaw, *J. Am. Chem. Soc.* **1996**, *118*, 5961. – [4k] M. Lin, A. Sen, *Nature* **1994**, *368*, 613. – [4l] M. Lin, T. E. Hogan, A. Sen, *J. Am. Chem. Soc.* **1996**, *118*, 4574.

[5] R.A. Periana, D. J. Taube, S. Gamble, H. Taube, T. Satoh, H. Fuji, *Science* **1998**, *280*.

[6] R. H. Crabtree *Pure Appl. Chem.* **1995**, *67*, 39.

[7] R. P. Linstead, F. Millidge, S. L. S. Thomas, A. L. Walpole, *J. Chem. Soc.* **1937**, 1146.

[8] R. H. Crabtree, J. M. Mihelcic, J. M. Quirck, *J. Am. Chem. Soc.* **1979**, *101*, 7738.

[9] M. J. Burk, R. H. Crabtree, D. V. McGrath, *J. Chem. Soc., Chem. Commun*. **1985**, 1829.
[10] [10a] D. Baudry, M. Ephritikhine, H. Felkin *J. Chem. Soc., Chem. Commun*. **1980**, 1243. – [10b] D. Baudry, M. Ephritikhine, H. Felkin, R. Holmes-Smith *J. Chem. Soc., Chem. Commun*. **1983**, 788. – [10c] H. Felkin, T. Fillebeen-Khan, Y. Gault, R. Holmes-Smith, J. Zakrzewski, *Tetrahedron Lett*. **1984**, *25*, 1279.
[11] R. H. Crabtree, M. F. Mellea, J. M. Mihelcic, J. M. Quirck, *J. Am. Chem. Soc*. **1982**, *104*, 107.
[12] [12a] J. A. Maguire, A. S. Goldman, *J. Am. Chem. Soc*. **1991**, *113*, 6706. – [12b] J. A. Maguire, A. Petrillo, A. S. Goldman, *J. Am. Chem. Soc*. **1992**, *114*, 9492.
[13] M. Gupta, C. Hagen, R. J. Flesher, W. Kaska, C. M. Jensen, *J. Chem. Soc., Chem. Commun*. **1996**, 2083.
[14] M. Gupta, W. C. Kaska, C. M. Jensen *J. Chem. Soc., Chem. Commun*. **1997**, 461.
[15] M. Gupta, C. Hagen, W. C. Kaska, R. E. Cramer, C. M. Jensen *J. Am. Chem. Soc*. **1997**, *119*, 840.
[16] K. Nomura, Y. Saito, *J. Chem. Soc., Chem. Commun*. **1988**, 161.
[17] T. Sakakura, T. Sodeyama, M. Tokunaga, M. Tanaka, *Chem. Lett*. **1988**, 263.
[18] W.-W. Xu, P. Rosini, M. Gupta, C. M. Jensen, W. C. Kaska, K. Krogh-Jepersen, A. S. Goldman, *J. Chem. Soc., Chem. Commun*. **1997**, 461.
[19] [19a] B. J. Fischer, R. Eisenberg, *Organometallics* **1983**, *2*, 764. – [19b] A. J. Kunin, R. Eisenberg, *J. Am. Chem. Soc*. **1986**, *108*, 535. – [19c] A. J. Kunin, R. Eisenberg, *Organometallics* **1988**, *7*, 2124.
[20] [20a] M. Tanaka, *Chemtech* **1989**, 59. – [20b] T. Sakakura, T. Sodeyama, K. Sasaki, K. Wada, M. Tanaka, *J. Am. Chem. Soc*. **1990**, *112*, 7221.
[21] T. Sakakura, M. Tanaka, *J. Chem. Soc., Chem. Commun*. **1987**, 758.
[22] G. P. Rosini, W. T. Boese, A. S. Goldman, *J. Am. Chem. Soc*. **1994**, *116*, 9498.
[23] S. E. Boyd, L. D. Field, M. G. Partridge, *J. Am. Chem. Soc*. **1994**, *116*, 9492.
[24] E. M. Gordon, R. Eisenberg, *J. Mol. Catal*. **1988**, *45*, 57.
[25] M. Tanaka, T. Sakakura, Y. Tokunaga, T. Sodeyama, *Chem. Lett*. **1987**, 2373.
[26] W. D. Jones, G. P. Foster, J. M. Putinas, *J. Am. Chem. Soc*. **1987**, *109*, 5047.
[27] W. D. Jones, E. T. Hessell, *Organometallics* **1990**, *9*, 718.
[28] [28a] W. D. Jones, W. P. Kosar, *J. Am. Chem. Soc*. **1986**, *108*, 5640. – [28b] G. C. Hsu, W. P. Kosar, W. D. Jones, *Organometallics* **1994**, *113*, 385.
[29] Y. Tokunaga, T. Sakakura, M. Tanaka, *J. Mol. Catal*. **1989**, *56*, 305.
[30] T. Sakakura, T. Sodeyama, Y. Tokunaga, M. Tanaka, *Chem. Lett*. **1987**, 2211.
[31] [31a] P. Hong, B-R. Cho, Y. Yamazaki, *Chem. Lett*. **1980**, 507. – [31b] P. Hong, B-R. Cho, H. Yamazaki, *Chem. Lett*. **1979**, 339. – [32] P. Hong, H. Yamazaki, K. Sonogashia, N. Hagihara, *Chem. Lett*. **1978**, 535.
[33] P. Hong, H. Yamazaki, *Chem. Lett*. **1979**, 1335.
[34] P. Hong, H. Yamazaki, *J. Mol. Catal*. **1984**, *26*, 297.
[35] X. Lin, D. Ma, X. Lu, *Tetrahedron Lett*. **1987**, *28*, 3249.
[36] T. B. Marder, D. C. Roe, D. Milstein, *Organometallics* **1988**, *7*, 1451.
[37] L. N. Lewis, J. F. Smith, *J. Am. Chem. Soc*. **1986**, *108*, 2728.
[38] W. A. Nugent, D. W. Ovenall, S. J. Holmes, *Organometallics* **1983**, *2*, 161.
[39] Y.-G. Lim, Y. H. Kim, J.-B. Kang, *J. Chem. Soc., Chem. Commun*. **1994**, 2267.
[40] Y.-G. Lim, J.-B. Kang, Y. H. Kim, *J. Chem. Soc., Chem. Commun*. **1996**, 585.
[41] R. F. Jordan, D. F. Taylor, *J. Am. Chem. Soc*. **1989**, *111*, 778.
[42] [42a] S. Rodewald, R. F. Jordan, *J. Am. Chem. Soc*. **1994**, *116*, 4491. – [42b] S.Dagorne, S. Rodewald, R. F. Jordan, *Organometallics* **1997**, *16*, 5541.
[43] E. J. Moore, W. E. Pretzer, T. J. O′connell, J. Harris, L. LaBounty, L. Chou, S. S. Grimmer, *J. Am. Chem. Soc*. **1992**, *114*, 5888.
[44] N. Chatani, T. Fukuyama, F. Kakiuchi, S. Murai, *J. Am. Chem. Soc*. **1996**, *118*, 493.
[45] S. E. Diamonds, A. Szalkiewicz, F. Marès, *J. Am. Chem. Soc*. **1979**, *101*, 490.
[46] S. Murai, F. Kakiuchi, S. Sekine, Y. Tanaka, A. Kamatani, M. Sonoda, W. Chatani, *Nature* **1993**, *366*, 529.
[47] S. Murai, F. Kakiuchi, S. Sekine, Y. Tanaka, A. Kamatani, M. Sonoda, N. Chatani, *Pure Appl. Chem*. **1994**, *66*, 1527.
[48] F. Kakiuchi, S. Sekine, Y. Tanaka, A. Kamatani, M. Sonoda, N. Chatani, S. Murai, *Bull. Chem. Soc. Jpn*. **1995**, 61.
[49] F. Kakiuchi, Y. Yamamoto, N. Chatani, S. Murai, *Chem. Lett*. **1995**, 681.
[50] F. Kakiuchi, Y. Tanaka, T. Sato, N. Chatani, S. Murai, *Chem. Lett*. **1995**, 679.
[51] M. Sonoda, F. Kakiuchi, A. Kamatani, N. Chatani, S. Murai, *Chem. Lett*. **1996**, 113.
[52] F. Kakiuchi, Y. Tanaka, T. Sato, N. Chatani, S. Murai, *Chem. Lett*. **1996**, 111.
[53] [53a]. Guo, W. P. Weber, *Polymer Bull*. **1994**, *32*, 525. – [53b] H. Guo, M. A. Tapssak, W. P. Weber, *Macromolecules* **1995**, *28*, 4717.
[54] H. Guo, M. A. Tapsak, W. P. Weber, *Polymer Bull*. **1994**, *33*, 417.
[55] P. W. E. Harris, P. D. Woodgate, *J. Organomet. Chem*. **1997**, *530*, 211.
[56] D. J. Cole-Hamilton, G. Wilkinson, *Nouv. J. Chim.* **1977**, *1*, 14.
[57] B. M. Trost, K. Imi, I. W. Davies, *J. Am. Chem. Soc*. **1995**, *117*, 5371.
[58] P. Lu, J. Paulasaari, K. Jin, R. Bau, W. P. Weber, *Organometallics* **1998**, *17*, 584.
[59] N. Fujii, K. Fumitoshi, A. Yamada, S. Murai, *Chem. Lett*. **1997**, 425.
[60] [60a] Y. Guari, S. Sabo-Etienne, B. Chaudret, *J. Am. Chem. Soc*. **1998**, *120*, 4228. – [60b] S. Saba-Etienne, B. Chaudret, *Coord. Chem. Rev.* **1998**, *178–180*, 381.

Received December 17, 1998
[I98434]

Cycloisomerization of Alkynols at Transition Metal Templates

Bernd Weyershausen[a] and Karl Heinz Dötz*[a]

Keywords: Alkynols / Isomerizations / Oxacycloalkylidene complexes / Vinylidene complexes / Transition metal templates

The metal-assisted cycloisomerization of ω-alkynols to oxacycloalkylidene complexes is reviewed. A variety of low-valent coordinatively unsaturated transition metal templates from group 6 to 10 mediate the cyclization of ω-butynols, -pentynols, and -hexynols to give the corresponding oxacycloalkylidene complexes. In some cases kinetic hydroxyalkylvinylidene complex intermediates can be isolated and characterized.

Introduction

Carbene ligands coordinated to a transition metal center play an important role in both stoichiometric reactions directed towards organic synthesis,[1] and in catalytic processes such as olefin metathesis.[2] Recently, stable nucleophilic carbenes have received a great deal of attention.[3] Their ligand properties resemble those of the well-established phosphane ligands; thus, they may serve as "spectator" ligands in transition metal complexes, which have been successfully applied to olefin metathesis,[4] hydroformylation, and Heck-type reactions.[5] Electrophilic carbenes can be stabilized by coordination to low-valent transition metals; this type of complexes, developed by E. O. Fischer in the 1960s and 1970s,[6] has been increasingly used in stoichiometric C−C bond formation. They undergo ligand-centered reactions which are assisted by a carbonylmetal electron-acceptor fragment; moreover, the metal fragment may serve as a template which activates unsaturated ligands for cycloaddition reactions.[1c,1e,7]

This review deals with the cycloisomerization of alkynols at coordinatively unsaturated transition metal templates of group 6 to 10 metals affording cyclic electrophilic carbene complexes. Although the most versatile route to acyclic Fischer-type carbene complexes is still based on the two-step addition of a nucleophile and an electrophile across the C−O bond in carbonylmetal compounds,[8] the most

[a] Kekulé-Institut für Organische Chemie und Biochemie, Gerhard-Domagk-Straße 1, D-53121 Bonn, Germany
Fax: (internat.) + 49(0)228/735813
E-mail: doetz@uni-bonn.de



Bernd Weyershausen studied chemistry at the University of Bonn. After the diploma thesis with Prof. J. Barluenga at the University of Oviedo (Spain) he started his Ph. D. thesis under the supervision of Prof. K. H. Dötz at the University of Bonn and received his Ph. D. degree there in 1998. Currently, he is working as a postdoctoral fellow in the group of Prof. K. C. Nicolaou at The Scripps Research Institute in La Jolla (USA) supported by a Feodor Lynen Fellowship.

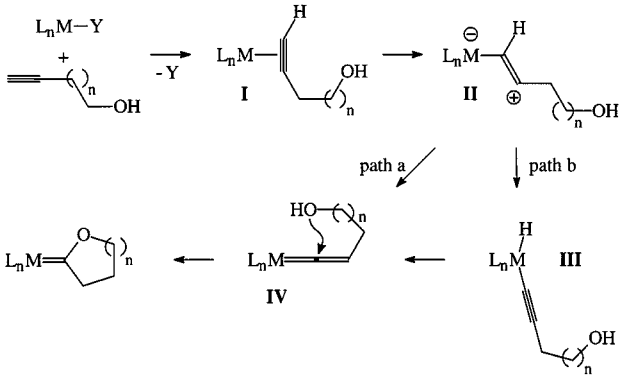
Karl Heinz Dötz was born in 1943 and began his chemical education at the Technical University of Munich where he received his Ph. D. with Professor E. O. Fischer. He then moved towards the borderline between Inorganic and Organic Chemistry, focussed during his habilitation on the organic chemistry of metal carbenes which he applied to novel metal-assisted cycloaddition patterns. In 1986 he became Professor of Organometallic Chemistry at the University of Marburg. In 1992 he was lucky to choose among a few offers, and finally joined the University of Bonn where he was appointed Professor of Organic Chemistry and Co-Director of the Kekulé Institute. He holds visiting appointments in Princeton and Paris, and is a recipient of the Victor Grignard−Georg Wittig Lectureship. His research interests concentrate on organometallic template reactions, stereoselective synthesis, asymmetric catalysis and on carbohydrate chemistry.



MICROREVIEWS: This feature introduces the readers to the authors' research through a concise overview of the selected topic. Reference to important work from others in the field is included.

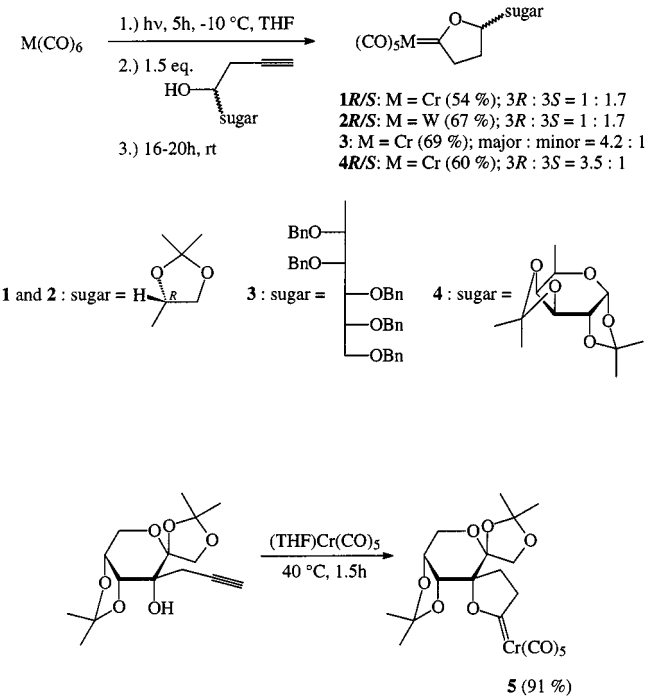
 © WILEY-VCH Verlag GmbH, D-69451 Weinheim, 1999 1434−1948/99/0707−1057 $ 17.50+.50/0

common approach to cyclic Fischer-type carbene complexes is the metal-assisted cyclization of alkynols at low-valent metal templates.[9] Heteroatom-containing cyclic carbene transition metal complexes have also been prepared via ω-haloacyl-,[10] carbamoyl-, alkoxycarbonyl-, or imidometal intermediates,[11] and through the ring opening of epoxides by deprotonated Fischer-type carbene complexes followed by elimination of lithium methoxide upon intramolecular cyclization of the γ-lithium alkoxide substituted complex intermediate.[12] Even direct activation of tetrahydrofuran and other cyclic ethers by $TpIr^{III}$ complexes[13] has been observed with formation of Fischer-type carbene derivatives.[14] Another route is based on the addition of alcohol nucleophiles to vinylidene species accessible from the isomerization of terminal alkynes at a late transition metal center. This strategy, initiated by Chisholm and Clark,[15] has been extended to alkynols which have been treated with a series of group 6 to 10 metals. The formation of the cyclic carbene ligands from ω-alkynols can be rationalized in terms of a vinylidene complex intermediate **IV** which undergoes an intramolecular nucleophilic attack of the hydroxy function at the α-carbon atom of the vinylidene complex (Scheme 1). Experiments using a series of different metal systems have demonstrated that vinylidene complexes can be generated from terminal alkynes by 1,2-hydride migration.[16] These reactions are supposed to involve an initial η^2-alkyne complex **I** which rearranges to its η^1 isomer **II**. The 1,2-hydride shift may occur either directly to the β-carbon atom (path a) or by oxidative addition to a σ-alkynyl(hydrido) species **III** (path b). Whereas calculations favour a direct hydrogen transfer,[17] the oxidative addition pathway is established by experimental evidence.[18]



Scheme 1. Mechanism of the cycloisomerisation of ω-alkynols at metal templates

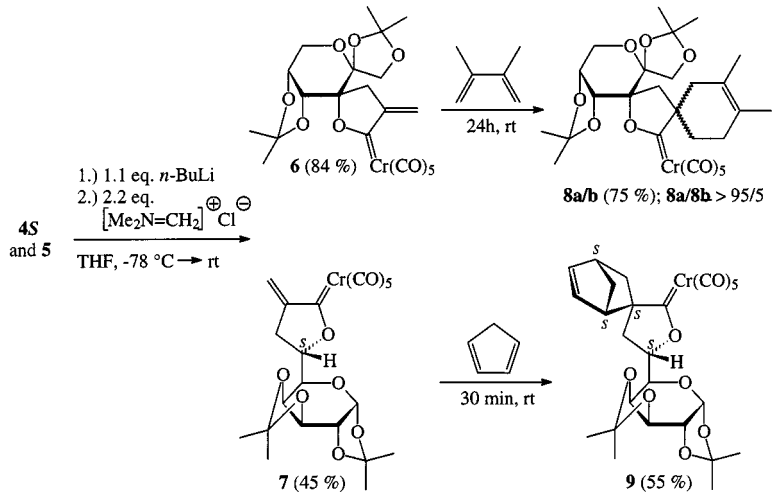
actions.[1c,1e,7] Recently, the authors have started a program aimed at the synthesis of carbohydrate-functionalized oxacycloalkylidene complexes[20] in order to exploit the chiral information provided by the carbohydrate moiety in stereoselective reactions, and to evaluate their potential in the synthesis of natural products and biologically active compounds. As the cycloisomerization of alkynols at coordinatively unsaturated group 6 metals[9] is the most common approach to oxacyclocarbene complexes, interest is focused on the preparation of carbohydrate-derived alkynols and their cyclization at a solvent-stabilized pentacarbonylchromium or -tungsten template. In general, butynols are easily accessible by addition of propargylic organometals to carbonyl compounds.[21] In this case, however, the reagent of choice turned out to be allenylmagnesium bromide[22] which at low temperature undergoes clean γ-addition to the carbonyl functionality of carbohydrate-based aldehydes and ketones to give the desired butynols in yields up to 90%. Carbohydrate-derived aldehydes afford mixtures of diastereomeric butynols, whereas the allenylmagnesium bromide adds with complete diastereoselectivity to carbohydrate-derived ketones. As the diasteromeric butynols are difficult to separate using chromatographic techniques, they were treated as a mixture of diastereomers with pentacarbonyl(tetrahydrofuran)chromium(0) or -tungsten(0) generated by UV irradiation of the corresponding hexacarbonylmetal in tetrahydrofuran at −10°C. The separation of the resulting mixtures of diastereomeric carbene complexes was readily achieved by column chromatography and afforded pure diastereomers of various acyclic[23] and spirocyclic[24] carbohydrate-functionalized 2-oxacyclopentylidene complexes; some examples are shown in Scheme 2.



(Oxacycloalkylidene)chromium, -molybdenum, and -tungsten Complexes

Cyclic Fischer-type metal carbene complexes are valuable tools in organic synthesis.[1] Carbene complexes with group 6 metals are especially synthetically useful reagents, and their synthetic potential is based on both the pronounced α-CH acidity[19] within the alkyl side chain, and on either metal-centered or carbene ligand-centered cycloaddition re-

Scheme 2. Synthesis of carbohydrate-functionalized 2-oxacyclopentylidene complexes



Scheme 3. Diastereoselective Diels–Alder reaction with α-*exo*-methylene-functionalized 2-oxacyclopentylidene complexes

The absolute configuration of the major diastereomers **1*S*** and **2*S*** has been determined by single-crystal X-ray analysis to be (3*S*,4′*R*).[25] In the case of the complex **4** the absolute configuration at C-3 of the minor diastereomer has been determined by single-crystal X-ray analysis of the Diels–Alder product **9** (Scheme 3) to be (3*S*).[26] In general the cycloisomerization of butynols at a tungsten template requires shorter reaction times and gives higher yields of the corresponding carbene complex, indicating that the tungsten template is more reactive than the chromium analogue. Following the procedure reported by Maiorana et al.[27] the carbohydrate-functionalized 2-oxacyclopentylidene complexes could be converted into their α-*exo*-methylene derivatives which serve as potent dienophiles in diastereoselective Diels–Alder reactions (Scheme 3).[20,25,26]

In contrast to the Diels–Alder reaction with 2,3-dimethylbutadiene, the stereoselective addition of cyclopentadiene to the α-*exo*-methylene double bond of complex **7** requires a differentiation not only between *si*- and *re*-side attack, but also between *exo* and *endo* addition. If we take into consideration the absolute stereochemistry at C-3 of complex **7** the diene is expected to add to the α-*exo*-methylene double bond from the top face (*si* side) due to the sterical hindrance of the bottom face (*re* side) caused by the carbohydrate moiety. A single-crystal X-ray analysis of **9** revealed that, due to the steric requirements of the bulky pentacarbonylchromium fragment resulting from the fixed *s-cis* conformation of the (vinylcarbene)metal dienophile **7**, the stereochemical outcome is in accord with an *exo* approach of the diene to the sterically less hindered face (*si* side) of the dienophile (Figure 1).[26][28]

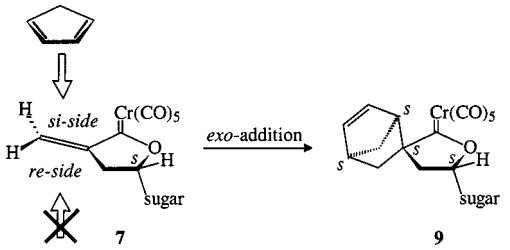
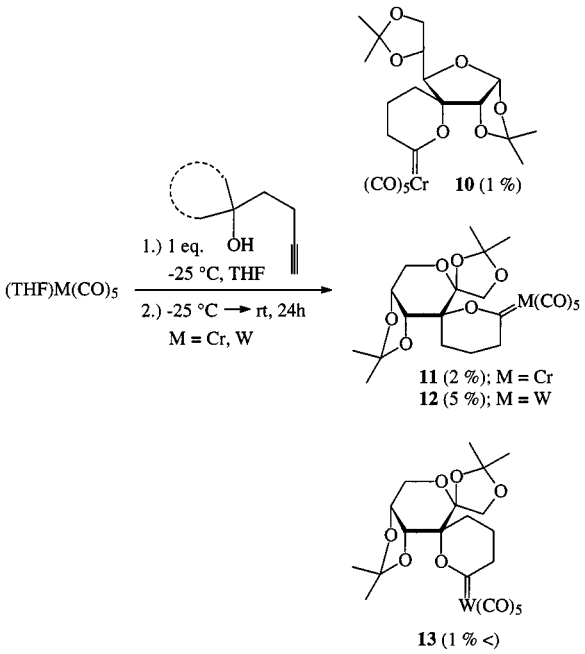


Figure 1. Stereopreference for the addition of the diene to the α-*exo*-methylene double bond

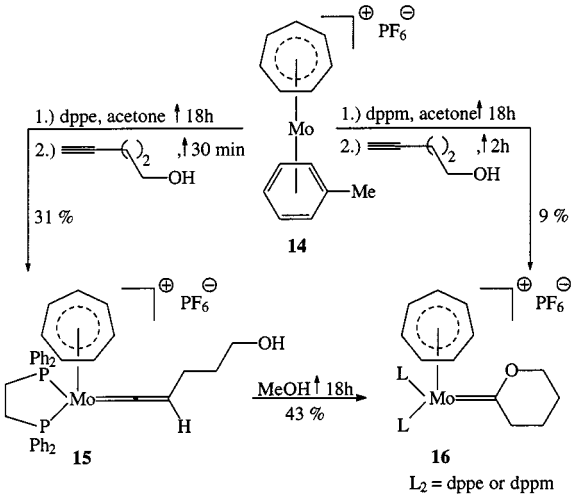
In order to evaluate the potential of this methodology for the synthesis of spirocyclic carbohydrate-derived 2-oxacyclohexylidene complexes the metal-assisted cycloisomerization of suitable carbohydrate-based ω-pentynol precursors was addressed.[29] (Scheme 4). Although in general the cycloisomerization of ω-pentynols gives lower yields compared with the cyclization of ω-butynols, the yields obtained for complexes **10**–**13** were below expectations. This



Scheme 4. Carbohydrate-derived spirocyclic 2-oxacyclohexylidene complexes

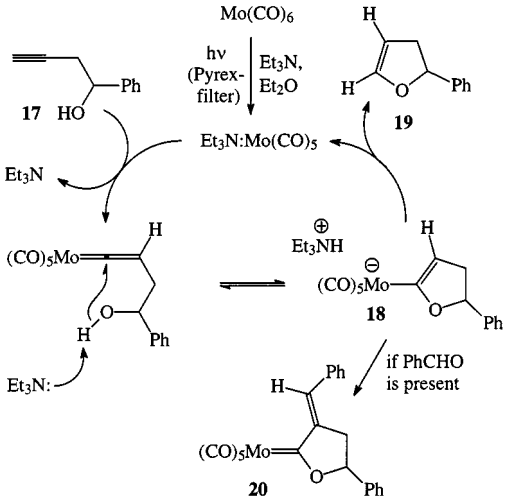
outcome might be rationalized in terms of a slower intramolecular nucleophilic attack of the ω-pentynol hydroxy group at the α-carbon atom of the vinylidene complex inter-

mediate, as a result of a higher flexibility of the hydroxyalkyl substituent combined with a lower thermal stability of the vinylidene complex intermediate. It is noteworthy that in contrast to the reaction of the psicose-based butynol with pentacarbonyl(tetrahydrofuran)chromium(0) affording the complex **5**, the analogous reaction with the psicose-based pentynol resulted in neither isolation of the desired 2-oxacyclohexylidene complex nor in its in situ identification by IR spectroscopy. The more reactive tungsten template allowed the formation of the psicose-derived spirocyclic oxacycloalkylidene complex **13**, as monitored spectroscopically by IR as a decrease in the intensity of the $A_1{}^1$ band of pentacarbonyl(tetrahydrofuran)tungsten(0) at 2074 cm^{-1} along with an increased intensity of the $A_1{}^1$ band of 2-oxacyclohexylidene complex **13** at 2068 cm^{-1}; after 24 h, a small amount of **13** was isolated by column chromatography. Attempts to heat the reaction mixture up to 40°C did not improve the yield, but resulted in decomposition of the solvent-stabilized tungsten template without formation of **13**. So far, there are only a few examples of 2-oxacyclohexylidene group 6 metal complexes which have been prepared by cycloisomerization of the corresponding pentynol.[30][31] The successful isolation and characterization of the hydroxyalkylvinylidene complex **15** suggest that the length and the flexibility of the alkyl chain of the vinylidene complex intermediate as well as the ligands[32] coordinated to the metal template play an important role in the subsequent cyclization[29] (Scheme 5).



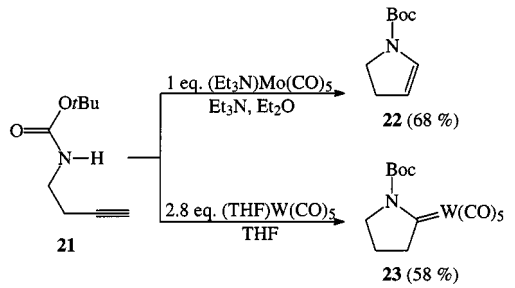
Scheme 5. Isolation and subsequent cyclization of the hydroxyvinylidene intermediate **14**

It has been previously suggested that the formation of oxacycloalkylidene complexes from ω-alkynols proceeds by intramolecular cyclization of a hydroxyalkylvinylidene intermediates.[9b,24c,33] The molybdenum sandwich **14** is able to cycloisomerize ω-pentynol in the presence of DPPM to give the oxacyclohexylidene complex **16** in poor yield.[34] If DPPM is replaced by DPPE the hydroxyalkylvinylidene complex **15** was isolated, which could be converted into **16** in refluxing methanol for 18 h. McDonald et al. reported on a modestly catalytic cycloisomerization of ω-butynols[35] to 2,3-dihydrofurans, and of epoxyalkynes[36] to furans. The pentacarbonylmolybdenum template required for these transformations is best generated by photolysis of hexacarbonylmolybdenum in a mixture of diethyl ether and triethylamine. The mechanism proposed for the cycloisomerization of alkynol **17** to 2,3-dihydrofuran **19** (89% optimized yield using 26 mol-% hexacarbonylmolybdenum) is shown in Scheme 6.



Scheme 6. Proposed mechanism for the catalytic alkynol cycloisomerization

The role of the carbenemolybdenum anion **18** as an intermediate in the catalytic cycle was supported by isolation of the apparent aldol condensation−dehydration[12b,37] product **20**, obtained from the reaction of **17** with $(Et_3N)Mo(CO)_5$ in the presence of benzaldehyde. The metal-promoted cycloisomerization methodology has also been extended to *N*-protected alkynylamines and 2-alkynylanilines.[38] For example, the reaction of *N*-BOC-aminobutyne **21** with 1 equiv. of $(Et_3N)Mo(CO)_5$ in a mixture of triethylamine and diethyl ether as solvent afforded a yield of 68% of 2,3-dihydropyrrole **22**; similarly, azacycloalkylidene complex **23** was formed in a yield of 58% upon the reaction of **21** with 2.8 equiv. of pentacarbonyl(tetrahydrofuran)tungsten(0) (Scheme 7).

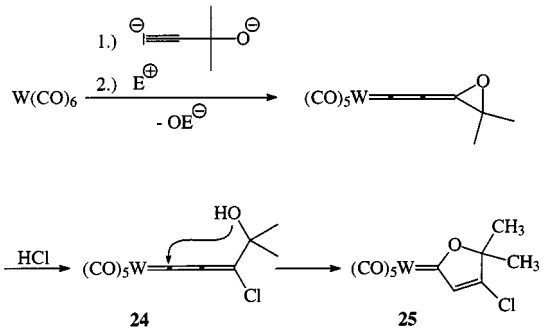


Scheme 7. Cycloisomerization of alkynylamide **21**

This route provides a complementary access to azacycloalkylidene complexes. Their synthesis, so far, has been reported from γ-lactams requiring $K_2[M(CO)_5]$ as a troublesome organometal nucleophile,[39] or from 2-oxacyclopentylidene complexes by aminolysis to give an open-

chain (γ-hydroxyalkyl)aminocarbene complex, which may subsequently undergo nucleophilic cyclization under Mitsunobu conditions[40] to afford 2-azacyclopentylidene complexes.[23][41] The pentacarbonylmolybdenum-catalyzed cycloisomerization is also compatible with alkynyl-substituted carbon nucleophiles such as diethyl 2-(3-butyn-1-yl)-malonate, giving the corresponding cyclopentene derivatives.[42]

Whereas great attention has been paid to 2-oxacycloalkylidene complexes bearing a saturated carbon skeleton, less effort has focused on their endocyclic α,β-unsaturated analogues. The first example of this type of compound was prepared by Berke et al.[43] who studied the reaction of 1,1-dimethylpropynolate with hexacarbonyltungsten. Deoxygenation and subsequent hydrochlorination of the acyltungstate have been suggested in order to generate a hydroxyallenylidene intermediate **24**, which undergoes cyclization to give the 2-oxacyclopentenylidene complex **25** (Scheme 8). Subsequently, complementary routes to endocyclic α,β-unsaturated oxacycloalkylidene complexes have been reported,[37b,44] including classic elimination reactions[12d] or addition of alkyl radicals, generated from epoxides and $(Cp_2TiCl)_2$, to alkynylalkoxycarbene complexes.[31a]



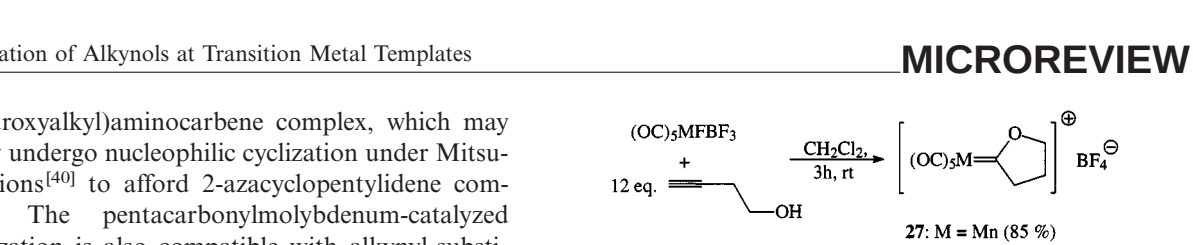
Scheme 8. Synthesis of 2-oxacyclopentenylidene complex **25**

The alkynol cycloisomerization at group 6 metal templates has been successfully applied to the synthesis of natural products and bioactive compounds[30c,30e,45] such as stavudin (d4T)[46] or (±)-andirolactone.[47]

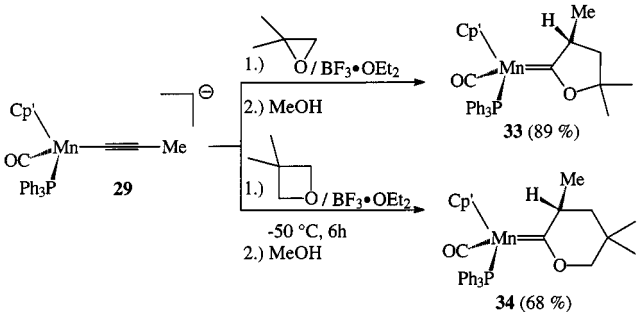
(Oxacycloalkylidene)manganese and -rhenium Complexes

Based on the isoelectronic relation of pentacarbonyl compounds of group 6 and cationic pentacarbonyl compounds of group 7 metal templates, Beck and co-workers[48] extended the alkynol cycloisomerization to cations $[(OC)_5M]^+$ (M = Mn, Re) stabilized by the weakly coordinating tetrafluoroborate ligand. $(OC)_5MFBF_3$ complexes (M = Mn, Re) react with excess 3-butyn-1-ol in dichloromethane to give excellent yields of the cationic 2-oxacyclopentylidene complexes **27** and **28** (Scheme 9).

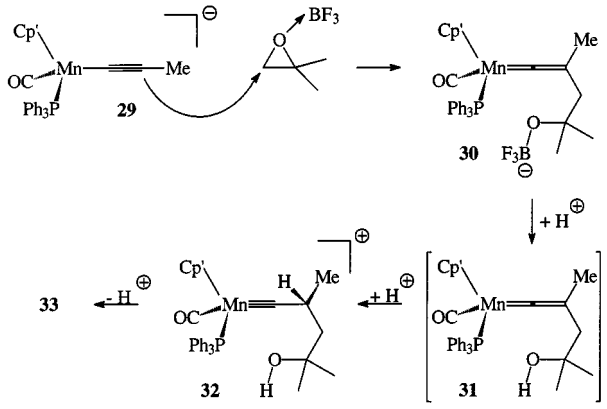
Chiral oxacycloalkylidene complexes can be obtained by ring expansion of oxiranes and oxetanes by the highly nucleophilic anionic alkynyl complex $[(\eta^5\text{-}C_5H_4Me)(OC)(Ph_3P)MnC{\equiv}CMe]^-$ (**29**).[49] Activation of the strained 2,2-dimethyloxirane and 3,3-dimethyloxetane by boron trifluoride–diethyl ether allows for the addition of the organometallic alkynyl nucleophile to afford, after protonation with methanol, the chiral (oxacycloalkylidene)-manganese complexes **33** and **34** in good to very good yields (Scheme 10). The NMR data of the oxycylopentylidene complex **33** indicated the formation of a single pair (*RR*/*SS* or *RS*/*SR*) of diastereomers, implying that the configuration at the metal center efficiently controls the configuration at the chiral ring-carbon atom of the cyclic carbene ligand. Single-crystal X-ray analysis established an (*RS*/*SR*) configuration, placing the methyl substituent and the bulky triphenylphosphane ligand on opposite sides of the (oxacyclopentylidene)metal fragment, as anticipated on the basis of steric arguments. The mechanism proposed for the formation of **33** is shown in Scheme 11.



Scheme 9. Cationic 2-oxacyclopentylidene complexes of manganese and rhenium



Scheme 10. Synthesis of the chiral (oxacycloalkylidene)manganese complexes



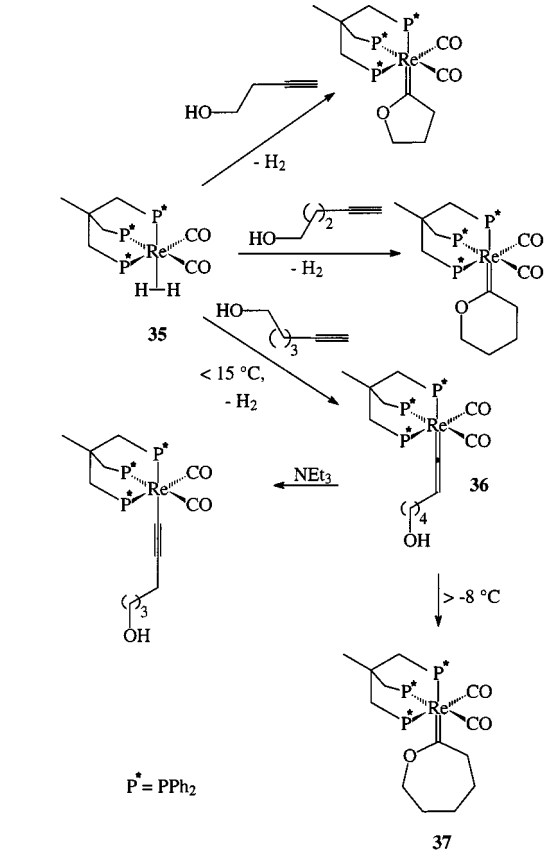
Scheme 11. Proposed mechanism for the formation of **33**

The first step likely involves a Lewis acid assisted ring opening of the epoxide by the nucleophilic attack of **29** to form the anionic vinylidene complex **30**, which represents

another variety of hydroxyalkylvinylidene intermediates, as previously proposed for the cycloisomerization of alkynols at coordinatively unsaturated metal templates. The complex **30** eluded isolation, but its formation was supported by monitoring the reaction by IR; after 10 min, IR absorption bands appeared in the regions characteristic of similar vinylidene complexes prepared by Geoffroy and co-workers[49] [$\tilde{\nu}_{CO}$ = 1886 cm^{-1}, $\tilde{\nu}_{C=C}$ = 1636 cm^{-1}]. Based on the observation of a carbonyl IR absorption band at 1998 cm^{-1}, indicative of a carbynemanganese cation[49][50] and detected in solution after the addition of methanol, the authors favour a stepwise double protonation of **30**, at the oxygen and the β-carbon atoms to form the cationic carbyne complex **32**, over a direct cyclization of the hydroxyalkylvinylidene intermediate **31**. Finally, the hydroxy group is supposed to add to the carbyne carbon atom with concomitant deprotonation to give **33**. It should be noted that the formation of oxacyclopentylidene complex **33** also occurs slowly and with lower yield in the absence of the Lewis acid, whereas for the ring expansion of 3,3-dimethyloxetane the presence of $F_3B \cdot OEt_2$ is crucial.

The mechanism of the oxacycloalkylidene formation was addressed in a very recent comparative study on the reaction of a comparable rhenium template $[\{MeC(CH_2PPh_2)_3\}Re(CO)_2]^+$[51] with a series of ω-alkynols bearing different numbers of CH_2 spacers between the alkynyl and hydroxy functionalities. Previous experiments revealed that the intramolecular addition of the hydroxy group to the α-carbon atom of the hydroxyalkylvinylidene complex is disfavoured with increasing length of the alkyl chain separating the alkynyl and hydroxy moieties.[29,32,49] Consequently, the activation of 5-hexyn-1-ol at a coordinatively unsaturated metal template results in the formation of stable hydroxybutylvinylidene complexes[52] rather than that of the corresponding 2-oxacycloheptylidene isomer. For instance, Bianchini and co-workers succeeded in the interception and charactization of the kinetic (hydroxybutylvinylidene)rhenium intermediate **36**, which they could further convert into the thermodynamically more stable 2-oxacycloheptylidene complex **37** (Scheme 12).[51]

NMR monitoring of the reaction of the dihydrogen complex **35** with a series of ω-alkynols in the temperature range from −50°C to 20°C established the vinylidenerhenium complex **36** as an intermediate in the cycloisomerization of 5-hexyn-1-ol to the thermodynamically stable 2-oxacycloheptylidene complex **37**. In contrast, no homologous intermediate could be detected in the reactions with ω-butynol and ω-pentynol. The hydroxybutylvinylidene complex **36** is stable in solution below −10°C, which allows its unambiguous characterization in solution and its isolation in the solid state. However, it is slowly converted into the 2-oxacycloheptylidene isomer **37** at increasing temperature, and the conversion is fast at room temp. Fischer-type carbene complexes bearing a 2-oxacycloheptylidene ligand are extremely rare compounds. To the best of the authors knowledge, only one other example of the activation of ω-hexynol at a transition metal template, leading to the 2-oxacycloheptylidene complex **38** (Figure 2), has been mentioned in the literature as a footnote without further details.[53] Two other examples of 2-oxacycloheptylidene complexes have been described. The dinuclear dimanganese complex **39** was prepared by reaction of the pentacarbonylmetalate $K[Mn(CO)_5]$ with α,ω-bistriflatopentane,[54] whilst the γ,δ-unsaturated (2-oxacycloheptylidene)chromium complex **40** was synthesized by ring-closure metathesis of the [allyloxy(butenyl)carbene]metal precursor (Figure 2).[55]



Scheme 12. Reaction of $[(triphos)Re(CO)_2]^+$ template with ω-alkynols

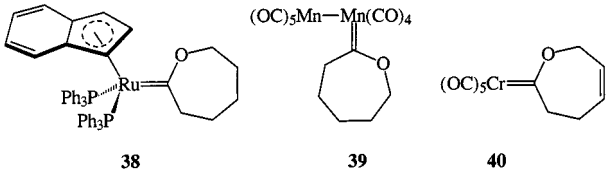
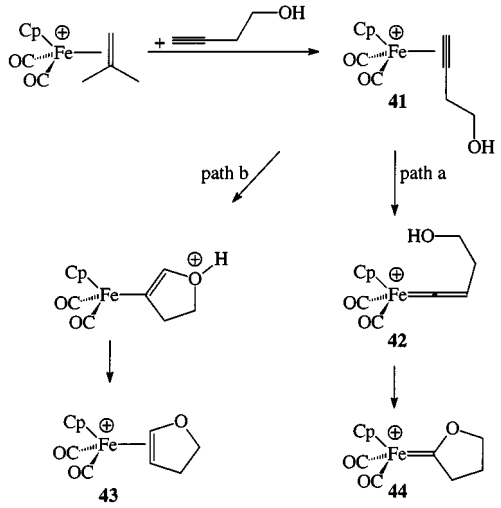


Figure 2. Oxacyclohept(en)ylidene complexes

(Oxacycloalkylidene)iron, -ruthenium, and -osmium Complexes

The reaction of 3-butyn-1-ol with the dicarbonyl(η^5-cyclopentadienyl)iron cation led to a 1:1 mixture of two compounds which, after careful separation by fractional crystallization, were identified as η^2-2,3-dihydrofuran complex **43** and 2-oxacyclopentylidene complex **44** (Scheme

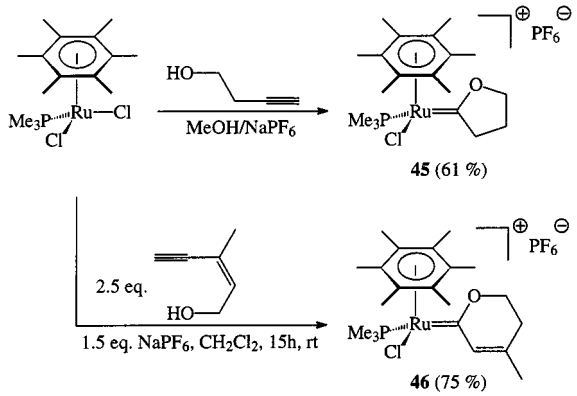
13).[56] Interestingly, the anticipated η^2-alkyne complex intermediate **41** does not only rearrange to the vinylidene complex **42** (path a) as expected, but is also able to undergo direct nucleophilic attack of the hydroxy function at C-4 of the coordinated 3-butyn-1-ol (path b) leading to an η^1-2,3-dihydrofuran-4-yl complex intermediate, which finally undergoes a σ,π rearrangement to give **43**. A chiral metal analogue of **44**, the carbonyl(η^5-cyclopentadienyl)(2-oxacyclopentylidene)(triphenylphosphane)iron(II) cation, was applied to the stereoselective synthesis of 2,2-dialkylbutyrolactones.[57]



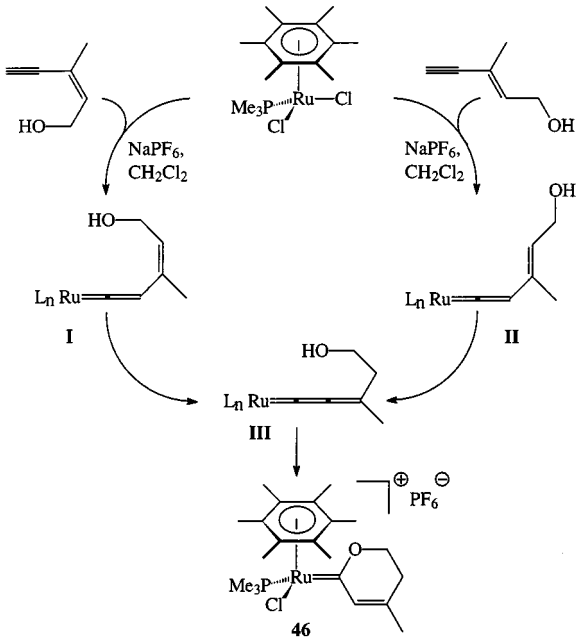
Scheme 13. Competitive pathways for the reaction of 3-butyn-1-ol with $[Cp(OC)_2Fe]^+$

Chiral (oxacycloalkylidene)ruthenium complexes such as **45** are accessible from hexamethylbenzene(trimethylphosphane)ruthenium(II) dichloride and 3-butyn-1-ol (Scheme 14).[58] An extension of the cycloisomerization strategy from simple ω-alkynols to enynols resulted in the synthesis of α,β-unsaturated 2-oxacyclohexylidene complexes,[59] e.g. **46** (Scheme 14).[60] Remarkably, both the (*Z*)- and (*E*)-enynol isomer are activated by the ruthenium template to afford the same α,β-unsaturated 2-oxacyclohexenylidene complex **46**. Obviously, the cycloisomerization does not result from an intramolecular nucleophilic attack of the hydroxy group at the α-carbon atom of vinylidene complex **II** (Scheme 15). Previous results[61] rather suggest the subsequent formation of an allenylidene intermediate **III**[62] involving a 1,3-H migration from the β-carbon atom of **II** to C-4. Thus, the stereochemical information present in the enynol precursor is lost, and the activation of both (*Z*) and (*E*) isomers is expected to lead to the same allenylidene intermediate **III** which, upon intramolecular addition of the hydroxy group to the α-carbon atom, finally produces the α,β-unsaturated cyclic carbene complex **46**. Other (2-oxacyclopentylidene)ruthenium(II) complexes have also been described in the literature.[63]

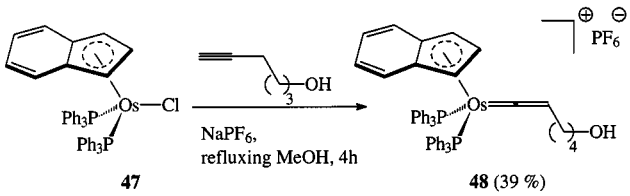
The electron-rich osmium template, provided by (η^5-indenyl)bis(triphenylphosphane)osmium(II) chloride (**47**), also effects the activation of ω-alkynols to metal-coordinated vinylidene compounds.[52b] Whereas ω-butynol and ω-pentynol undergo in situ cycloisomerization to give cycloalkylidene complexes,[64] the activation of ω-hexynol stops at the hydroxybutylvinylidene complex stage **48** (Scheme 16). The stability of **48** reflects the typical increased stability of osmium derivatives compared with their ruthenium analogues,[52b] as demonstrated for the cycloisomerization of ω-hexynol with the ruthenium analogue of **47**.



Scheme 14. (Oxacycloalkylidene)ruthenium complexes **45** and **46**



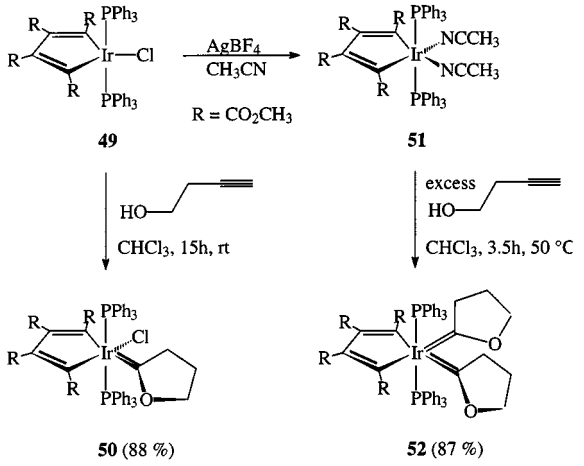
Scheme 15. Proposed mechanism for the formation of **46** from both (*Z*)- and (*E*)-enynol



Scheme 16. Synthesis of (hydroxybutylvinylidene)osmium complex **48**

Oxacycloalkylidene Complexes of Group 9 and 10 Metals

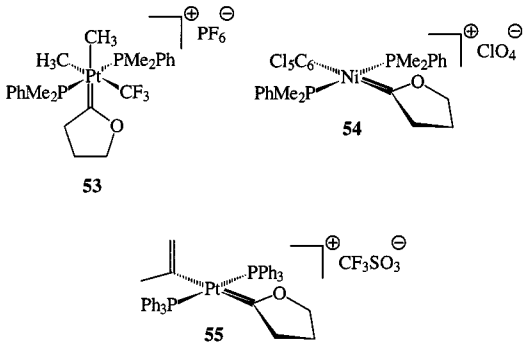
Octahedral (oxacycloalkylidene)iridium(III) complexes were among the first examples of alkynol cycloisomerization products.[65] More recently, the excellent leaving-group properties of triflate ligands have been exploited in the synthesis of square planar (2-oxacyclopentylidene)rhodium and -iridium(II) complexes.[66] The cycloisomerization of alkynols is compatible with the presence of additional metal−carbon σ-bonds. Activation of 3-butyn-1-ol at room temperature by the iridacycle **49** afforded the oxacyclopentylidene complex **50** which represents the first isolable example of a metallacyclic carbene complex (Scheme 17).[67] The metallacyclic template **51**, bearing two labile leaving group type ligands, undergoes a high-yield double cycloisomerization to give the bis(oxacyclopentylidene) complex **52**, which is remarkably stable towards carbene dimerization.[68] The crucial role of the metal template is evident from the comparison of the iridacyclopentadiene **49** with a similar rhodium analogue. The rhodacyclopentadiene did not induce the cycloisomerization of 3-butyn-1-ol; instead, alkyne insertion into the metallacyclic rhodium−carbon bond occurred, followed by reductive elimination to give an aromatic six-membered ring.[67b,69]



Scheme 17. Metallacycle−carbene and −bis(carbene) complexes

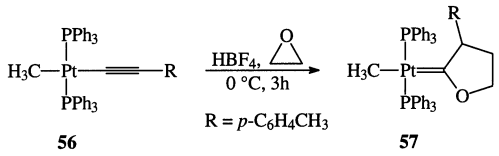
The cationic platinum(IV) complex **53**[15c] was the first example of a carbene ligand coordinated to a metal center in an oxidation state higher than two. Other (oxacycloalkylidene)nickel[70] and -platinum[65][71] complexes, such as **54** and **55**, bearing a metal(II) center have been synthesized by cycloisomerization of 3-butyn-1-ol (Scheme 18).

A complementary route to (2-oxacyclopentylidene)platinum complexes is based on the ring opening of oxiranes by alkynylplatinum(II) complexes assisted by HBF_4 (Scheme 19).[72] Two possible mechanisms, both of which so far lack experimental support, have been suggested for this reaction: The first involves protonation of the alkynyl complex **56**, generating a reactive vinylidene intermediate which may undergo nucleophilic addition of the oxirane oxygen atom at the α-carbon atom. Oxirane opening and subsequent re-



Scheme 18. (Oxacycloalkylidene)nickel and -platinum complexes

cyclization afford the oxacycloalkylidene complex **57**. The second proposal relies on initial protonation of the oxirane followed by β-carbon atom attack of the alkynyl complex **56**, to give a reactive hydroxyethylvinyl intermediate. Final intramolecular cyclization results in the formation of the (oxacycloalklidene)metal complex.



Scheme 19. (Oxacyclopentylidene)platinum complex **57** by ring opening of oxirane

Conclusions

The cycloisomerization of 1,ω-alkynols at transition metal templates provides a general and straightforward approach to oxacycloalkylidene complexes. Recently, this methodology has been successfully extended to alkynylamines and alkynyl-substituted carbon nucleophiles leading to azacycloalkylidene complexes and 2,3-dihydropyrroles, respectively, as well as cyclopentenes. In some cases, hydroxyalkylvinylidene complex intermediates could be intercepted and characterized, supporting the mechanism suggested earlier. In particular, oxacycloalkylidene complexes of group 6 metals have been developed to provide valuable reagents in organic synthesis. The multifunctionality of Fischer-type oxacycloalkylidene complexes may be exploited in subsequent addition reactions of nucleophiles,[23] as well as in metal-[44f,73] or ligand-centered[25,28,44g] cycloaddition reactions aiming at targets both in organometallic and organic chemistry.

Acknowledgments

Financial support of the research carried out in the authors' laboratory provided by the Deutsche Forschungsgemeinschaft (SFB 260 and 334), and the Fonds der Chemischen Industrie and the Ministry of Science and Research NRW is gratefully acknowledged.

[1] For reviews see: [1a] K. H. Dötz, H. Fischer, P. Hofmann, F. R. Kreissl, U. Schubert, K. Weiss, *Transition Metal Carbene Complexes*, Verlag Chemie, Weinheim, **1983**. – [1b] K. H. Dötz, *Angew. Chem.* **1984**, *96*, 573–594; *Angew. Chem. Int. Ed. Engl.* **1984**, *23*, 587–608. – [1c] W. D. Wulff in *Comprehensive Organic Synthesis* (Eds.: B. M. Trost, I. Fleming, L. A. Paquette), Pergamon Press, Oxford, **1991**, vol. 5, p. 1065–1113. – [1d] M. J. Winter in *Comprehensive Organometallic Chemistry II* (Eds.: E. W. Abel, F. G. A. Stone, G. Wilkinson), Pergamon Press, Oxford, **1995**, vol. 5, p. 155–214. – [1e] W. D. Wulff in *Comprehensive Organometallic Chemistry II* (Eds.: E. W. Abel, F. G. A. Stone, G. Wilkinson), Pergamon Press, Oxford, **1995**, vol. 12, p. 469–547. – [1f] L. S. Hegedus in *Comprehensive Organometallic Chemistry II* (Eds.: E. W. Abel, F. G. A. Stone, G. Wilkinson), Pergamon Press, Oxford, **1995**, vol. 12, p. 549–576. – [1g] D. F. Harvey, D. M. Sigano, *Chem. Rev.* **1996**, *96*, 271–288. – [1h] A. de Meijere, *Pure Appl. Chem.* **1996**, *68*, 61–72. – [1i] J. Barluenga, *Pure Appl. Chem.* **1996**, *68*, 543–552. – [1j] L. S. Hegedus, *Tetrahedron* **1997**, *53*, 4105–4128.

[2] For recent reviews see: [2a] R. R. Schrock, *Acc. Chem. Res.* **1990**, *23*, 158–165. – [2b] R. H. Grubbs, S. H. Pine in *Comprehensive Organic Synthesis* (Eds.: B. M. Trost, I. Fleming, L. A. Paquette), Pergamon Press, Oxford, **1991**, vol. 5, p. 1115–1127. – [2c] R. R. Schrock, *Pure Appl. Chem.* **1994**, *66*, 1447–1454. – [2d] M. Schuster, S. Blechert, *Angew. Chem.* **1997**, *109*, 2124–2144; *Angew. Chem. Int. Ed. Engl.* **1997**, *36*, 2036–2055. – [2e] R. H. Grubbs, S. Chang, *Tetrahedron* **1998**, *54*, 4413–4450.

[3] [3a] M. Regitz, *Angew. Chem.* **1996**, *108*, 791–794; *Angew. Chem. Int. Ed. Engl.* **1996**, *35*, 725–728. – [3b] Review: W. A. Herrmann, C. Köcher, *Angew. Chem.* **1997**, *109*, 2256–2282; *Angew. Chem. Int. Ed. Engl.* **1997**, *36*, 2162–2187.

[4] T. Weskamp, W. C. Schattenmann, M. Spiegler, W. A. Herrmann, *Angew. Chem.* **1998**, *110*, 2631–2633; *Angew. Chem. Int. Ed. Engl.* **1998**, *37*, 2490–2493.

[5] W. A. Herrmann, M. Elison, J. Fischer, C. Köcher, G. R. J. Artus, *Angew. Chem.* **1995**, *107*, 2602–2605; *Angew. Chem. Int. Ed. Engl.* **1995**, *34*, 2371–2374.

[6] E. O. Fischer, *Adv. Organomet. Chem.* **1976**, *14*, 1–32.

[7] [7a] H. W. Frühauf, *Chem. Rev.* **1997**, *97*, 523–596. – [7b] K. H. Dötz, P. Tomuschat, *J. Chem. Soc., Chem. Rev.*, in print.

[8] E. O. Fischer, A. Maasböl, *Angew. Chem.* **1964**, *76*, 645–646; *Angew. Chem. Int. Ed. Engl.* **1964**, *3*, 580–581.

[9] [9a] A. Parlier, H. Rudler, *J. Chem. Soc., Chem. Commun.* **1986**, 514–515. – [9b] K. H. Dötz, W. Sturm, H. G. Alt, *Organometallics* **1987**, *6*, 1424–1427.

[10] [10a] M. F. Semmelhack, G. L. Lee, *Organometallics* **1987**, *6*, 1839–1844. – [10b] F. A. Cotton, C. M. Lukehart, *J. Am. Chem. Soc.* **1973**, *95*, 3552–3564. – [10c] C. H. Game, M. Green, J. R. Moss, F. G. A. Stone, *J. Chem. Soc., Dalton Trans.* **1974**, 351–357.

[11] [11a] R. B. King, *J. Am. Chem. Soc.* **1963**, *85*, 1922. – [11b] C. P. Casey, R. L. Anderson, *J. Am. Chem. Soc.* **1971**, *93*, 3554–3555. – [11c] R. A. Michelin, L. Zanotto, D. Braga, P. Sabatino, R. J. Angelici, *Inorg. Chem.* **1988**, *27*, 93–99.

[12] [12a] C. P. Casey, R. L. Anderson, *J. Organomet. Chem.* **1974**, *73*, C28– C30. – [12b] C. P. Casey, W. R. Brunsvold, *J. Organomet. Chem.* **1975**, *102*, 175–183. – [12c] C. P. Casey, W. R. Brunsvold, D. M. Scheck, *Inorg. Chem.* **1977**, *16*, 3059–3063. – [12d] L. Lattuada, E. Licandro, S. Maiorana, H. Molinari, A. Papagni, *Organometallics* **1991**, *10*, 807–812. – [12e] C. Baldoli, L. Lattuada, E. Licandro, S. Maiorana, A. Papagni, *Organometallics* **1993**, *12*, 2994–3000.

[13] Tp = $HB(3,5\text{-dimethylpyrazole})_3$.

[14] [14a] O. Boutry, E. Gutiérrez, A. Monge, M. C. Nicasio, P. J. Pérez, E. Carmona, *J. Am. Chem. Soc.* **1992**, *114*, 7288–7290. – [14b] E. Gutiérrez-Puebla, A. Monge, M. C. Nicasio, P. J. Pérez, M. P. Poveda, E. Carmona, *Chem. Eur. J.* **1998**, *4*, 2225–2236.

[15] [15a] M. H. Chisholm, H. C. Clark, *J. Chem. Soc., Chem. Commun.* **1970**, 763. – [15b] M. H. Chisholm, H. C. Clark, *Inorg. Chem.* **1971**, *10*, 1711–1716.– [15c] M. H. Chisholm, H. C. Clark, *J. Am. Chem. Soc.* **1972**, *94*, 1532–1539. – [15d] M. H. Chisholm, H. C. Clark, *Acc. Chem. Res.* **1973**, *6*, 202–209.

[16] [16a] M. I. Bruce, A. G. Swincer, *Adv. Organomet. Chem.* **1983**, *22*, 59–128. – [16b] R. M. Bullock, *J. Chem. Soc., Chem. Commun.* **1989**, 165–167. – [16c] M. I. Bruce, *Chem. Rev.* **1991**, *91*, 197–257.

[17] J. Silvestre, R. Hoffmann, *Helv. Chim. Acta* **1985**, *68*, 1461–1506.

[18] J. Wolf, H. Werner, O. Serhadli, M. L. Ziegler, *Angew. Chem.* **1983**, 95, 428–429; *Angew. Chem. Int. Ed. Engl.* **1983**, *22*, 414–415.

[19] [19a] C. G. Kreiter, *Angew. Chem.* **1968**, 80, 402; *Angew. Chem. Int. Ed. Engl.* **1968**, *7*, 390. – [19b] C. P. Casey, W. R. Brunsvold, *J. Organomet. Chem.* **1976**, *118*, 309–323.

[20] Review on carbohydrate-modified carbenemetal complexes: K. H. Dötz, R. Ehlenz, *Chem. Eur. J.* **1997**, *3*, 1751–1756; and references cited therein.

[21] H. Yamamoto in *Comprehensive Organic Synthesis* (Eds.: B. M. Trost, I. Fleming, C. H. Heathcock), Pergamon Press, Oxford, **1991**, vol. 2, p. 81–98.

[22] L. Brandsma, H. Verkruijsse, *Preparative Polar Organometallic Chemistry I*, Springer, Berlin, **1987**, p. 63.

[23] R. Ehlenz, O. Neuß, M. Teckenbrock, K. H. Dötz, *Tetrahedron* **1997**, *53*, 5143–5158.

[24] [24a] O. Neuß, Dissertation, Universität Bonn, **1997**. – [24b] K. H. Dötz, O. Neuß, *Synlett* **1996**, 995–996. For non-carbohydrate-functionalized spirocyclic 2-oxacyclopentylidene complexes see: [24c] P. Quayle, S. Rahman, E. L. M. Ward, J. Herbert, *Tetrahedron Lett.* **1994**, *35*, 3801–3804. – [24d] B. Schmidt, P. Kocienski, G. Reid, *Tetrahedron* **1996**, *52*, 1617–1630.

[25] B. Weyershausen, M. Nieger, K. H. Dötz, *Organometallics* **1997**, *16*, 1602–1607.

[26] B. Weyershausen, M. Nieger, K. H. Dötz *J. Org. Chem.*, accepted for publication.

[27] L. Lattuada, E. Licandro, S. Maiorana, A. Papagni, *Gazz. Chim. Ital.* **1993**, *123*, 31–33.

[28] Recently Barluenga et al. reported on a similar *exo*-selective Diels–Alder reaction: J. Barluenga, F. Aznar, S. Barluenga, S. García-Granda, C. Alvarez-Rúa, *Synlett* **1997**, 1040–1042; for references concerning *exo*-selective Diels–Alder reactions see therein.

[29] B. Weyershausen, M. Nieger, H. Hupfer, K. H. Dötz, to be submitted for publication.

[30] [30a] F. E. McDonald, J. L. Bowman, *Tetrahedron Lett.* **1996**, *37*, 4675–4678. – [30b] R. L. Beddoes, R. W. Grime, Z. I. Hussain, M. W. Whiteley, *J. Chem. Soc., Dalton Trans.* **1996**, 3893–3895. – [30c] F. E. McDonald, H. Y. H. Zhu, *Tetrahedron* **1997**, *53*, 11061–11068. – [30d] K.-W. Liang, W.-T. Li, S.-M. Peng, S.-L. Wang, R.-S. Liu, *J. Am. Chem. Soc.* **1997**, *119*, 4404–4412. – [30e] J. L. Bowman, F. E. McDonald, *J. Org. Chem.* **1998**, *63*, 3680–3682.

[31] For the synthesis of 2-oxacyclohexylidene complexes of group 6 metals by other methodologies than metal-assisted alkynol cycloisomerization see: [31a] C. A. Merlic, D. Xu, *J. Am. Chem. Soc.* **1991**, *113*, 9855–9856. – [31b] S. Aoki, T. Fujimura, E. Nakamura, *J. Am. Chem. Soc.* **1992**, *114*, 2985–2990 and ref.[10b]

[32] The formation of carbene complexes from the vinylidene precursors $[(\eta^5\text{-}C_9H_7)L_2Ru{=}C{=}CHR]^+$ and simple alcohols depending on the ligand sphere (L_2 = DPPM, DPPM, 2 PPh_3) was recently examined: M. P. Gamasa, J. Gimeno, B. M. Martín-Vaca, J. Borge, S. García-Granda, E. Perez-Carreño, *Organometallics* **1994**, 13, 4045–4057.

[33] M. I. Bruce, A. G. Swincer, B. J. Thomas, R. C. Wallis, *Aust. J. Chem.* **1980**, *33*, 2605–2613.

[34] R. L. Beddoes, R. W. Grime, Z. I. Hussain, M. W. Whiteley, *J. Chem. Soc., Dalton Trans.* **1996**, 3893–3895.

[35] F. E. McDonald, C. C. Connolly, M. M. Gleason, T. B. Towne, K. D. Treiber, *J. Org. Chem.* **1993**, *58*, 6952–6953.

[36] F. E. McDonald, C. C. Schultz, *J. Am. Chem. Soc.* **1994**, *116*, 9363–9364.

[37] [37a] W. D. Wulff, S. R. Gilbertson, *J. Am. Chem. Soc.* **1985**, *107*, 503–505. – [37b] R. Aumann, H. Heinen, *Chem. Ber.* **1987**, *120*, 537–540.– [37c] W. D. Wulff, B. A. Anderson, A. J. Toole, *J. Am. Chem. Soc.* **1989**, *111*, 5485–5487.

[38] F. E. McDonald, A. K. Chatterjee, *Tetrahedron Lett.* **1997**, *38*, 7687–7690.

[39] M. A. Schwindt, J. R. Miller, L. S. Hegedus, *J. Organomet. Chem.* **1991**, *413*, 143–153.

[40] [40a] O. Mitsunobu, M. Wada, T. J. Sano, *J. Am. Chem. Soc.* **1972**, *94*, 679–680. – [40b] O. Mitsunobu, *Synthesis* **1981**, 1–28.

[41] K. H. Dötz, W.-C. Haase, M. Klumpe, M. Nieger, *J. Chem. Soc., Chem. Commun.* **1997**, 1217–1218

[42] F. E. McDonald, T. C. Olson, *Tetrahedron Lett.* **1997**, *38*, 7691–7692.

[43] H. Berke, P. Härter, G. Huttner, J. v. Seyerl, *J. Organomet. Chem.* **1981**, *219*, 317−327.
[44] [44a] F. Camps, J. M. Moretó, S. Ricart, J. M. Viñas, E. Molins, C. Miravitlles, *J. Chem. Soc., Chem. Commun.* **1989**, 1560−1562. − [44b] S. L. B. Wang, W. D. Wulff, *J. Am. Chem. Soc.* **1990**, *112*, 4450−4452. − [44c] K. L. Faron, W. D. Wulff, *J. Am. Chem. Soc.* **1990**, *112*, 6419−6420. − [44d] F. Camps, L. Jordi, J. M. Moretó, S. Ricart, *J. Organomet. Chem.* **1992**, *436*, 189−198. − [44e] L. Jordi, J. M. Moretó, S. Ricart, J. M. Viñas, *J. Organomet. Chem.* **1993**, *444*, C28−C30. − [44f] F. Stein, M. Duetsch, M. Noltemeyer, A. de Meijere, *Synlett* **1993**, 486−488. − [44g] J. Christoffers, K. H. Dötz, *Chem. Ber.* **1994**, *128*, 157−161. − [44h] E. Licandro, S. Maiorana, A. Papagni, A. Zanotti-Gerosa, F. Cariati, S. Bruni, A. Chiesi Villa, *Inorg. Chim. Acta* **1994**, *220*, 233−247. − [44i] L. Jordi, F. Camps, S. Ricart, J. M. Viñas, J. M. Moretó, M. Mejias, E. Molins, *J. Organomet. Chem.* **1995**, *494*, 53−64.
[45] [45a] P. Quayle, S. Rahman, J. Herbert, *Tetrahedron Lett.* **1995**, *36*, 8087−8088. − [45b] F. E. McDonald, M. M. Gleason, *J. Am. Chem. Soc.* **1996**, *118*, 6648−6659.
[46] F. E. McDonald, M. M. Gleason, *Angew. Chem.* **1995**, *107*, 356−358; *Angew. Chem., Int. Ed. Engl.* **1995**, *34*, 350−352.
[47] P. Quayle, E. L. M. Ward, *Tetrahedron Lett.* **1994**, *35*, 8883−8884.
[48] E. Fritsch, T. Kerscher, K. Polborn, W. Beck, *J. Organomet. Chem.* **1993**, *460*, C25−C27.
[49] C. Kelley, N. Lugan, M. R. Terry, G. L. Geoffroy, B. S. Haggerty, A. L. Rheingold, *J. Am. Chem. Soc.* **1992**, *114*, 6735−6749.
[50] [50a] E. O. Fischer, G. Besl, *Z. Naturforsch.* **1979**, *34B*, 1186−1189. − [50b] E. O. Fischer, E. W. Meineke, F. R. Kreissl, *Chem. Ber.* **1977**, *110*, 1140−1147.
[51] C. Bianchini,A. Marchi, N. Mantovanti, L. Marvelli, D. Masi, M. Peruzzini, R. Rossi, *Eur. J. Inorg. Chem.* **1998**, 211−219.
[52] [52a] H. Werner, T. Rappert, *Chem. Ber.* **1992**, *126*, 669−678. − [52b] M. P. Gamasa, J. Gimeno, M. Gonzalez-Cueva, E. Lastra, *J. Chem. Soc., Dalton Trans.* **1996**, 2547−2551.
[53] See citation 8 in ref.[52b] and citation 17 in ref.[51]
[54] E. Lindner, M. Pabel, R. Fawzi, H. A. Mayer, K. Wurst, *J. Organomet. Chem.* **1992**, *435*, 109−121.
[55] J. Sültemeyer, M. Nieger, K. H. Dötz, publication in preparation.
[56] D. F. Marten, *J. Chem. Soc., Chem. Comm.* **1980**, 341−342.
[57] P. L. Curtis, S. G. Davies, *J. Chem. Soc., Chem. Commun.* **1984**, 747−748.
[58] H. Le Bozec, K. Ouzzine, P. H. Dixneuf, *Organometallics* **1991**, *10*, 2768−2772.
[59] A ruthenium(II) complex containing a saturated 2-oxacyclohexylidene ligand has earlier been described; see ref.[33]
[60] N. Ruiz, D. Péron, P. H. Dixneuf, *Organometallics* **1995**, *14*, 1095−1097.
[61] D. Devanne, P. H. Dixneuf, *J. Chem. Soc., Chem. Commun.* **1990**, 641−643.
[61] For a general review on ruthenium complexes bearing vinylidene and cumulene ligands see: S. G. Davies, J. P. McNally, A. J. Smallridge, *Adv. Organomet. Chem.* **1990**, *30*, 1−76.
[63] [63a] H. Werner, A. Stark, P. Steinert, C. Grünwald, J. Wolf, *Chem. Ber.* **1995**, *128*, 49−62. − [63b] W.-H. Leung, E. Y. Y. Chan, I. D. Williams, W.-T. Wong, *Organometallics* **1997**, *16*, 3234−3240. − [63c] L. P. Barthel-Rosa, K. Maitra, J. Fischer, J. H. Nelson, *Organometallics* **1997**, *16*, 1714−1723.
[64] [64a] The synthesis of benzeneosmium(II) complexes bearing oxacycloalkylidene and vinyl ether ligands have been reported by Werner and co-workers: H. Werner, W. Knaup, M. Schulz, *Chem. Ber.* **1991**, *124*, 1121−1125. − [64b] The isolation of a (dihydrogen)(oxacyclopentylidene)(tetraammine)osmium complex upon reduction of $[Os^{III}(NH_3)_4(CF_3SO_3)_3]$ with Zn/Hg has been described: Z.-W. Li, H. Taube, *J. Am. Chem. Soc.* **1994**, *116*, 11584−11585.
[65] H. C. Clark, L. E. Manzer, *J. Organomet. Chem.* **1973**, *47*, C17−C20.
[66] P. J. Stang, Y.-H. Huang, *J. Organomet. Chem.* **1992**, *431*, 247−254.
[67] [67a] J. M. O'Connor, L. Pu, A. L. Rheingold, *J. Am. Chem. Soc.* **1987**, *109*, 7578−7579. − [67b] J. M. O′Connor, L. Pu, A. L. Rheingold, *J. Am. Chem. Soc.* **1990**, *112*, 6232−6247.
[68] Bis(carbene) complexes remain highly illusive species. For references on bis(ylidene) complexes, see also: [68a] J. Barluenga, F. Aznar, B. Weyershausen, S. García-Granda, E. Martín, *J. Chem. Soc., Chem. Commun.* **1996**, 2455−2456. − [68b] C. P. Casey, R. L. Anderson, *J. Chem. Soc., Chem. Comm.* **1975**, 895−896.
[69] [69a] E. Müller, *Synthesis* **1974**, 761. − [69b] K. P. C. Vollhardt, *Acc. Chem. Res.* **1977**, *10*, 1. − [69c] K. P. C. Vollhardt, *Angew. Chem., Int. Ed. Engl.* **1984**, *23*, 539.
[70] K. Oguro, M. Wada, R. Okawara, *J. Organomet. Chem.* **1978**, *159*, 417−429.
[71] R. J. Hinkle, P. J. Stang, A. M. Arif, *Organometallics* **1993**, *12*, 3510−3516.
[72] R. A. Michelin, M. Mozzon, B. Vialetto, R. Bertani, F. Benetollo, G. Bombieri, R. J. Angelici, *Organometallics* **1996**, *15*, 4096−4099.
[73] (α-*exo*-Alkylidene)(2-oxacycloalkylidene)chromium complexes have been photo-activated for benzannulation leading to 2,3-dihydro-5-benzofuranol and chroman-6-ol skeletons: [73a] B. Weyershausen, K. H. Dötz, *Eur. J. Org. Chem.* **1998**, 1739−1742. − [73b] B. Weyershausen, K. H. Dötz, *Synlett*, accepted for publication.

Received January 26, 1999
[I99025]

A Square-Planar Dinickel(II) Complex with a Noninnocent Dinucleating Oxamate Ligand: Evidence for a Ligand Radical Species

Ally Aukauloo,*[a] Xavier Ottenwaelder,[a] Rafael Ruiz,[a][+] Sandrine Poussereau,[a] Yu Pei,[a] Yves Journaux,*[a] Paul Fleurat,[b] Francois Volatron,[b] Beatriz Cervera,[c] M. Carmen Muñoz[d]

Keywords: Amides / Nickel / Polynuclear complexes / Radicals / Redox chemistry

The new bimetallic nickel(II) compound $(PPh_4)_4[Ni_2(\mathbf{2})]\cdot 6H_2O$ (**3**), where H_8[**2**] stands for *N*,*N*′,*N*″,*N*‴-1,2,4,5-benzenetetrayltetrakis(oxamic acid), has been synthesized and its crystal structure determined by single-crystal X-ray diffraction. The structure of **3** consists of $[Ni_2(\eta^4{:}\eta^4\text{-}\mathbf{2})]^{4-}$ anions, tetraphenylphosphonium cations, and water molecules. Facile one-electron oxidation of the square-planar diamagnetic dinickel(II) complex $[Ni_2(\eta^4{:}\eta^4\text{-}\mathbf{2})]^{4-}$ generates the metallo-radical species $[Ni_2(\eta^4{:}\eta^4\text{-}\mathbf{2}^{\cdot+})]^{3-}$ with characteristic *intra*-ligand π-cation radical transitions in the visible region (475–550 nm) as well as a typical quasi-isotropic EPR signal at $g \approx 2.0$.

Interest in the chemistry of metal coordination compounds with organic ligands of a radical nature (radical ligands) is rapidly increasing in several areas ranging from bioinorganic chemistry to solid-state physics.[1][2] Radical ligand complexes are currently being studied as biomimetic catalysts, because experimental evidence is accumulating about the involvement of organic radical species in the active sites of diverse metalloproteins.[3][4] Likewise, mixed materials incorporating organic radicals coordinated to metal ions have been extensively investigated with the aim of generating molecular-based magnets.[5][6] The development of these new classes of compounds relies on the firm understanding of factors that influence the ligand′s innocence or noninnocence in describing of the electronic structure of metal complexes. This plays a pivotal role in the coordination chemistry field in connection with the formal oxidation state assignment of the metal centre and, particularly, in high-valent transition metal complexes where the coordinated ligand contains an extended delocalized system.[7]

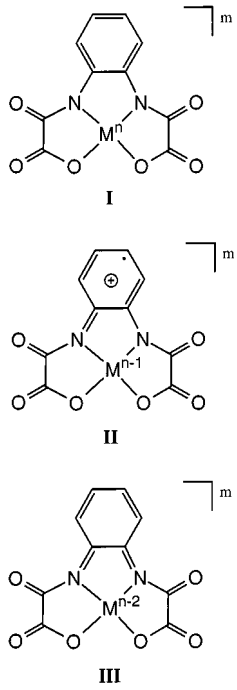
Recently, we have shown that substituted oxamato ligands like H_4[**1**],[8] the parent acid of the tetraanionic polychelating ligand *N*,*N*′-1,2-phenylenebis(oxamate), can stabilize unusual high oxidation states of first-row transition metal ions, ranging from manganese to copper.[8–11] We have found that the resulting square-planar four-coordinated copper(II) and nickel(II) complexes, $[M(\mathbf{1})]^{2-}$, oxidise at relatively low potentials, i.e. 0.41 and 0.60 V vs. SCE, respectively[10][11] (CH_3CN, 25 °C, 0.1 mol·dm^{-3} NBu_4PF_6). For the nickel complex, however, a second electron can be removed but at a higher potential (1.10 V vs. SCE). Since this particular ligand H_4[**1**] contains a benzenediamido-N unit with potential π-noninnocent character, these oxidation processes may involve the metal ion as well as the ligand. Thus, the electronic distribution in a given oxidised complex can be described by any one of the three redox isomers depicted in Scheme 1, for which the formal oxidation states of the metal centre are different (resonance forms **I** to **III**). Our observations clearly indicate that, at least the one-electron-oxidised species, $[M(\mathbf{1})]^{-}$ (M = Cu, Ni), are genuine copper(III) and nickel(III) complexes of form **I**.[10][11] Metal-radical ligand species (form **II**) can be ruled out as might be expected on the basis of the strong σ field of the tetradentate planar ligand (high σ-donor capacity of the amido-N group[12–15]).

Hence, in the scope of our continuous research in this field we have extended our studies to the related ligand H_8[**2**], the parent acid of the ligand *N*,*N*′,*N*″,*N*‴-1,2,4,5-benzenetetrayltetrakis(oxamate) (Scheme 2). Potentially, this dinucleating ligand possesses a noninnocent character, as its mononucleating counterpart, because the benzenetetraamido-N fragment is also a putative oxidation site.[16] We report herein the synthesis, general physical and structural characterisation together with the electrochemical properties of the tetraphenylphosphonium salt of the dinickel(II) complex of formula $(PPh_4)_4[Ni_2(\mathbf{2})]\cdot 6\,H_2O$ (**3**), as well as a preliminary ab initio theoretical study of its electronic structure.

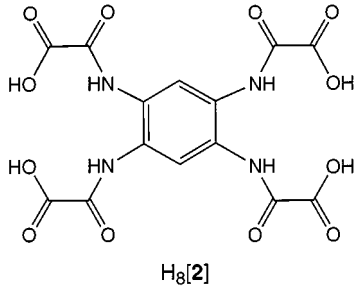
The ^{1}H-NMR spectrum of **3** shows a sharp singlet corresponding to the two magnetically equivalent phenylene protons of the ligand at δ = 8.35, along with the signals from the aromatic protons of the PPh_4^+ cations located in the region δ = 7.7–8.0. The sharpness of these NMR peaks, as well as the small shift of 0.50 ppm for the benzene proton

[a] Laboratoire de Chimie Inorganique, UMR CNRS 8613, Université de Paris-Sud,
F-91405 Orsay, France
Fax: (internat.) + 33-1/69157436
E-mail: jour@icmo.u-psud.fr
[b] Laboratoire de Chimie Théorique, ESA CNRS Q8077, Université de Paris-Sud,
F-91405 Orsay, France
[c] Departament de Química Inorgànica, Universitat de València,
E-46100 Burjassot (València), Spain
[d] Departamento de Física Aplicada, Universidad Politécnica de València,
E-46071 València, Spain
[+] Present address: Departament de Química Inorgànica de la Universitat de València.

 © WILEY-VCH Verlag GmbH, D-69451 Weinheim, 1999 1434–1948/99/0707–1067 $ 17.50+.50/0



Scheme 1. Resonance structures of the metal complexes with the noninnocent *N*,*N*′-1,2-phenylenebis(oxamato) ligand



Scheme 2. *N*,*N*′,*N*′′,*N*′′′-1,2,4,5-Benzenetetrayltetrakis(oxamic acid)

signal relative to that of the free ligand Et_4H_4[**2**] (δ = 7.85) are indicative of a diamagnetic nickel(II) complex. That is to say, the Ni^{II} ion is in a square-planar coordination geometry (low-spin d^8-electronic configuration for Ni^{II}). This spectroscopic observation was further confirmed by a single-crystal X-ray structure analysis.

The structure of **3** includes centrosymmetric dinuclear nickel(II) complex anions, $[Ni_2(\mathbf{2})]^{4-}$ (Figure 1), tetraphenylphosphonium cations and water molecules of crystallisation. As expected, the coordination environment of each nickel atom is essentially square-planar, formed by two deprotonated amide-N and two carboxylate-O atoms of the bis-tetradentate chelating ligand [largest deviations from the plane of the four donor atoms are 0.002(1) Å with the metal ion 0.018(1) Å out of the mean basal plane]. The average Ni−N and Ni−O bond lengths (1.82 and 1.89 Å, respectively) are identical to those found for the monomeric nickel(II) complex $(PPh_4)_2$[Ni(**1**)],[11] but significantly shorter than those of the copper(II) complex, $(PPh_4)_2$[Cu(**1**)] (1.91 and 1.95 Å, respectively).[10b] The entire ligand skeleton is nearly planar [maximum deviation from the mean molecular plane of 0.264(2) Å for O(5)] (Figure 1, top). All the bond lengths are identical, within the 3σ criterion, to those of the related mononucleating ligand in the isostructural complexes $(PPh_4)_2$[Cu(**1**)][10b] and $(PPh_4)_2$[Ni(**1**)].[11] The observed C−C *intra*-ring benzene distances in **3** are almost equivalent and are intermediate between those of single and double bonds (average 1.40 Å), whereas the C−N bond lengths between the benzene ring and the amide nitrogen atoms are characteristic of single bonds (average 1.42 Å), thereby reflecting complete π delocalisation mainly within the benzene ring.

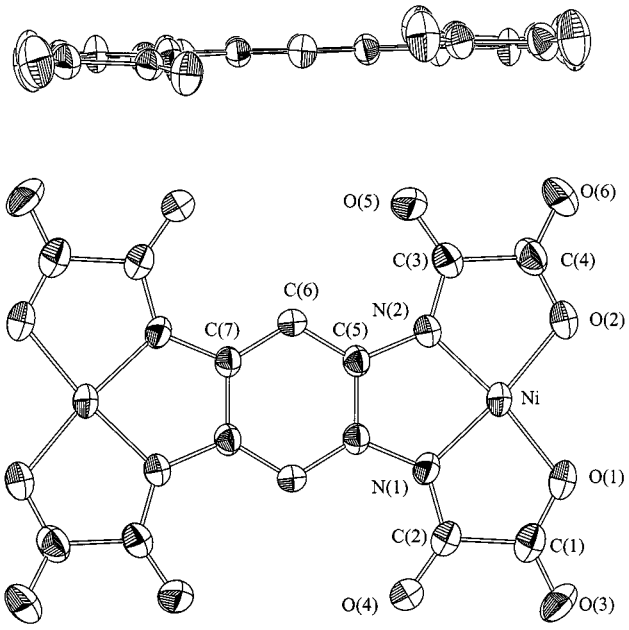


Figure 1. Perspective views of the anionic dinuclear unit of **3** with the atom-numbering scheme; thermal ellipsoids are drawn at the 30% probability level (hydrogen atoms have been omitted for clarity); selected bond lengths [Å] and angles [°] with standard deviations in parentheses: Ni−N(1) 1.822(2), Ni−N(2) 1.823(2), Ni−O(1) 1.879(2), Ni−O(2) 1.889(2); N(1)−Ni−N(2) 86.36(10), N(1)−Ni−O(1) 86.76(10), N(1)−Ni−O(2) 172.74(10), N(2)−Ni−O(1) 173.06(10), N(2)−Ni−O(2) 86.47(10), O(1)−Ni−O(2) 100.39(10)

The cyclic voltammogram of **3** in dry acetonitrile shows two well-separated one-electron reversible oxidation waves at the remarkably low potentials of 0.05 and 0.40 V vs. SCE (25 °C, 0.1 mol·dm^{-3} NBu_4PF_6). The one-electron nature of both waves was confirmed by coulometric measurements. A comparison of the potentials of the $[Ni_2(\mathbf{2})]^{3-/4-}$ and $[Ni_2(\mathbf{2})]^{2-/3-}$ redox couples with that of $[Ni(\mathbf{1})]^{-/2-}$ (0.60 V vs. SCE), where both ligands have the same set of donor atoms, reveals that both oxidised dinuclear complexes $[Ni_2(\mathbf{2})]^{3-}$ and $[Ni_2(\mathbf{2})]^{2-}$ are much more easily accessible than the corresponding mononuclear complex $[Ni(\mathbf{1})]^{-}$. A survey on the kinetic stability of the oxidised species obtained after bulk electrolysis of **3** in dry acetonitrile (−40 °C, 0.2 mol·dm^{-3} NBu_4PF_6, 0.24 and 0.60 V vs. SCE, respectively), indicates that the complex $[Ni_2(\mathbf{2})]^{3-}$ is stable over several days under nitrogen at room temperature. However, the doubly oxidised species, $[Ni_2(\mathbf{2})]^{2-}$, rapidly de-

composes under these same conditions, being stable only on the time-scale of the cyclic voltammetry measurement. Preliminary electrochemical studies by combined UV/Vis and EPR techniques have been carried out in order to determine the nature of the chemically stable one-electron-oxidised species of **3**.

The electronic absorption spectrum of the orange complex **3** in acetonitrile [Figure 2, curve (a)] consists of two intense asymmetric bands in the UV region centred at 425 and 370 nm, corresponding to the π-π* *intra*-ligand charge transfer. A third, less intense band appears in the visible region at 560 nm, which corresponds to a d−d transition of a low-spin d^8-Ni^{II} ion.[17] The most remarkable feature of the spectrum of the electrochemically generated red complex $[Ni_2(\mathbf{2})]^{3-}$ is the appearance of new absorption bands on the high- and low-energy side of the visible region [Figure 2, curve (b)]. The first group of transitions are formed by two rather sharp and intense bands located at 555 and 515 nm, along with additional bands at 540 (sh), 500 (sh), and 475 nm. All these bands, which are not present in the spectrum of the nickel(III) complex $[Ni(\mathbf{1})]^-$, are similar in both shape and intensities to those observed for the "Wurster′s Blue" salts containing the 1,4-bis(dimethylamino)-benzene radical cation.[16] The absorption intensities and energies of these bands are dependent on the substitution pattern on the benzene ring. This observation can therefore be assigned to a ligand-centred one-electron oxidation process of **3** rather than the nickel centre. Accordingly, the second group of bands in the Vis/NIR region comprising one broad, intense band at 1230 nm with two distinct shoulders at 1030 and 900 nm probably originates from metal-to-ligand charge-transfer (MLCT) transitions. The presence of this rather low-energy MLCT transition on the spectrum of $[Ni_2(\mathbf{2})]^{3-}$ at 1230 nm (8130 cm^{-1}) indicates that there is a relatively small energy separation between the ground and excited states (corresponding to the two opposed situations where the locus of oxidation is the ligand and the metal ion, respectively). Consequently, a small portion of mixing can occur between both electronic states.

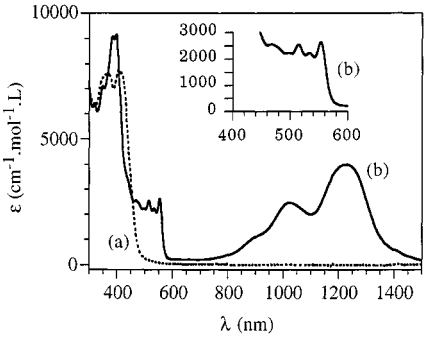
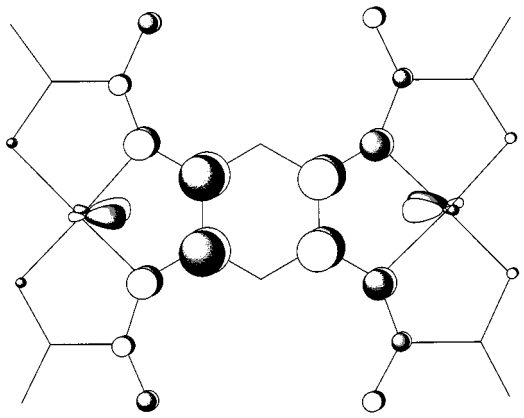


Figure 2. Electronic absorption spectra in acetonitrile solution of the dinickel(II) complex $[Ni_2(\mathbf{2})]^{4-}$ (a) and the electrochemically generated complex $[Ni_2(\mathbf{2})]^{3-}$(b)

Theoretical calculations have been performed on both dinuclear ($[Ni_2(\mathbf{2})]^{4-}$) and mononuclear ($[Ni(\mathbf{1})]^{2-}$) species at the DFT-B3LYP level with the Gaussian 94 package.[18−20] Preliminary calculations have been carried out on unsubstituted, 1,2-diamido- and 1,2,4,5-tetraamidobenzene molecules. The HOMO is of π-type in both cases and rises in energy from −6.7 (benzene) to −6.0 (diamide) and to −5.6 eV (tetraamide). These calculations indicate, as expected, that the π-donating ability of the ligand is enhanced with the number of amide substituents.

The electronic structure of $Na_4[Ni_2(\mathbf{2})]$[19] shows that the HOMO is essentially located on the organic moiety of the complex. Coefficients of the d orbital are small (about 0.03) whereas those of the p orbitals on the ligand atoms are considerably larger (0.10−0.16). The HOMO is strongly polarised on the benzene ring and results from the antibonding combination of the tetraamidobenzene HOMO with the d_{xz} of the nickel atoms as illustrated in Scheme 3. Due to the high energy of the ligand orbital, the contribution from the metallic moiety in this combination is very weak. Similar calculations on the mononickel complex $Na_2[Ni(\mathbf{1})]$ give rather different results and show that the three highest molecular orbitals are mainly of d character.



Scheme 3. Shape of the HOMO of $[Ni_2(\mathbf{2})]^{4-}$ moiety

The EPR spectrum at 4.4 K of the electrochemically generated complex $[Ni_2(\mathbf{2})]^{3-}$ exhibits an almost unique and narrow resonance band *g* close to 2.0 having a linewidth of only 50 G [Figure 3, curve (a)], typical of an isotropic radical species. This observation further supports the hypothesis of ligand rather than metal oxidation. Once again, this is in clear contrast with the observed EPR spectrum of the nickel(III) complex $[Ni(\mathbf{1})]^-$, where a nearly axial signal with apparent *g* at 2.230 and 2.006 is observed [Figure 3, curve (b)]. In that case, the large anisotropy and the average *g* value of 2.155 for $[Ni(\mathbf{1})]^-$ unambiguously indicate that the oxidation is located on the metal centre. Moreover, the fact that $g_\perp > g_{||} \approx 2.0$ clearly establishes a d_{z^2}-electronic ground-state configuration for the Ni^{III} ion.[14b,15b] However, the situation for $[Ni_2(\mathbf{2})]^{3-}$ is somewhat more complicated; actually, the EPR signal is slightly anisotropic with $g_1 = 2.037$, $g_2 = 2.012$ and $g_3 = 1.998$. The result can primarily be interpreted as an $Ni^{II}{}_2$ complex containing a ligand-based π-cation radical; this feeble anisotropy observed on the EPR signal being due to the partial delocalisation of the unpaired electron onto the d_π-type orbitals of the nickel centres.

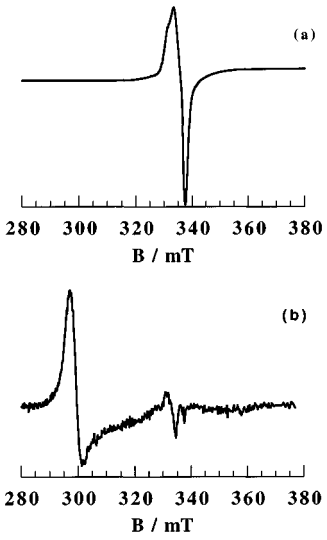


Figure 3. X-band EPR spectrum in frozen acetonitrile solution of the electrochemically generated complex $[Ni_2(\mathbf{2})]^{3-}$ (a) compared to that of complex $[Ni(\mathbf{1})]^{-}$ (b) at 4.4 K

In summary, compound **3** represents an interesting example of radical-ligand bimetallic complex precursor when oxidised to the π-cation radical species. In one, we have shown that the dinucleating ligand provides a ready locus of oxidation due to its larger π-electron donor properties than those of the mononucleating ligand analogue. Secondly, it also shifts the oxidation potentials of the metal ions to values beyond those of the aromatic π system because of its smaller σ-electron donor properties,[17] thus precluding metal oxidation. Substitution of diamagnetic nickel(II) ions by paramagnetic ones, such as copper(II), is a promising strategy to electrochemically control the magnetic exchange coupling in dimetallic complexes.[21] On the other hand, it may always be expected that these dinickel and dicopper complexes readily bind additional paramagnetic ions to the terminal carbonyl oxygen atoms giving oxamato-bridged polymetallic compounds, as is the case for the mononuclear analogues.

Experimental Section

Synthesis of H_8[2]: The proligand H_8[**2**] resulted from the condensation of 1,2,4,5-tetraaminobenzene and ethyl oxalyl chloride in *N*,*N*-dimethylformamide under inert atmosphere, and it was isolated as its tetraethyl ester derivative Et_4H_4[**2**]: To a solution of 1,2,4,5-tetraaminobenzene tetrahydrochloride (2.84 g, 10 mmol) in DMF (250 mL) was added ethyldiisopropylamine (14 mL, 80 mmol). This solution was then added dropwise, by using a dropping funnel, to ethyl oxalyl chloride (4.7 mL, 40 mmol). The resulting mixture was stirred for 1.5 h at 50°C and the solvent removed in a rotatory evaporator. The remaining oil was dissolved in a minimum amount of methanol and treated with diethyl ether to give a white solid, which was collected by filtration and dried under vacuum (3.76 g, 70%). − ^{1}H NMR ([D$_6$]DMSO): δ = 1.29 (t, 12 H, CH_3), 4.24 (q, 8 H, CH_2O), 7.82 (s, 2 H, *p*-H of $C_6H_2N_4$), 10.45 (s, 4 H, NH). − IR (KBr): $\tilde{\nu}$ = 3280 cm^{-1} (NH), 1770, 1743, and 1702 cm^{-1} (C=O). − $C_{22}H_{26}N_4O_{12}$ (538): calcd. C 49.07, H 4.87, N 10.40; found C 49.24, H 5.26, N 10.21.

Synthesis of 3: The sodium salt of the dinickel(II) complex was obtained by reaction of the tetraethyl ester Et_4H_4[**2**] with Ni^{2+} in basic aqueous media: To a suspension of Et_4H_4[**2**] (1.1 g, 2.0 mmol) in water (50 mL) was added an aqueous solution (10 mL) of NaOH (0.68 g, 17 mmol). After stirring for 15 min at room temperature until complete dissolution, an aqueous solution (25 mL) of $Ni(NO_3)_2 \cdot 6\,H_2O$ (1.16 g, 4.0 mmol) was added dropwise. The orange solid that formed was collected by filtration, washed with ethanol and air-dried (90%). Then, the tetraphenylphosphonium salt of complex **3** was obtained by metathesis of the sodium salt through the intermediacy of the silver salt: To a suspension of $Na_4[Ni_2(\mathbf{2})]$ (0.95 g, 1.5 mmol) in water (100 mL) was added an excess of $AgNO_3$ (1.36 g, 8 mmol). After 30 min of stirring, the orange solid was collected by filtration, washed with water and ethanol, and air-dried (1.3 g, 90%). To a suspension of $Ag_4[Ni_2(\mathbf{2})]$ (0.97 g, 1 mmol) in water (25 mL) was added a solution of PPh_4Cl (1.5 g, 4 mmol), dissolved in a minimum amount of water (10 mL). A white precipitate of AgCl formed and was removed by filtration after 15 min of stirring. Well-shaped large crystals of **3** suitable for X-ray diffraction were obtained from slow concentration of the mother liquor. − ^{1}H NMR ([D$_6$]DMSO): δ = 8.35 (s, 2 H, *p*-H of $C_6H_2N_4$), 7.71−8.10 (m, 80 H, C_6H_5 of PPh_4^+). − IR (KBr): $\tilde{\nu}$ = 1661 and 1617 cm^{-1} (C=O). − $C_{110}H_{82}Ni_2P_4N_4O_{12} \cdot 6\,H_2O$ (2001): calcd. C 65.96, H 4.70, N 2.80; found C 65.90, H 4.64, N 2.88.

X-ray Crystallographic Study of 3:[23] Crystal data: $C_{55}H_{47}NiP_2N_2O_9$, *FW* = 1000.6, triclinic, space group *P*−1, *a* = 13.558(1) Å, *b* = 13.799(2) Å, *c* = 14.604(1) Å, α = 78.43(1)°, β = 73.01(1)°, γ = 67.33(1)°, *V* = 2399.1(5) Å^3, *d* = 1.385 g cm^{-3}, *Z* = 2. − Data collection: Enraf-Nonius CAD-4 diffractometer, Mo-K_α radiation, λ = 0.71073 Å, graphite monochromator, 293 K, ω-2θ, Lorentz and polarization effects and absorption correction, μ = 0.532 mm^{-1}, 2.0° ≤ θ ≤ 22.5°, crystal size 0.1 × 0.1 × 0.1 mm. 6280 unique reflections, and 6259 assumed as observed with $I > 2\sigma(I)$. − Structural analysis and refinement: standard Patterson methods with subsequent full-matrix least-squares method refinement on F^2, SHELX93.[24] The hydrogen atoms were located from a difference synthesis and refined with an overall isotropic thermal parameter. Refinement of 811 variables with anisotropic thermal parameters for all nonhydrogen atoms gave R = 0.035 and R_w = 0.079 with S = 1.029.

Acknowledgments

This work was supported by the CNRS (France) and the DGICYT (Spain) through project PB94−1002. B. Cervera thanks the Conselleria de Educació i Ciència de la Generalitat Valenciana (Spain) for a grant.

[1] Recent reviews: [1a] J. Stubbe, W. A. Van der Donk, *Chem. Rev.* **1998**, *98*, 705−762, and references therein. − [1b] M. Sono, M. P. Roach, E. D. Coulter, J. H. Dawson, *Chem. Rev.* **1996**, *96*, 2841−2887. − [1c] L. Que, Jr., R. Y. N. Ho, *Chem. Rev.* **1996**, *96*, 2607−2624.

[2] Recent reviews: [2a] J. S. Miller, A. J. Epstein, *Chem. Commun.* **1998**, 1319−1325, and references therein. − [2b] H. Iwamura, K. Inoue, N Koga, *New J. Chem.* **1998**, 201−210. − [2c] A. Caneschi, D. Gatteschi, P. Rey *Prog. Inorg. Chem.* **1991**, *39*, 331−429.

[3] Y. Wang, J. L. DuBois, B. Hedman, K. O. Hodgson, T. D. P. Stack, *Science* **1998**, *279*, 537−540.

[4] [4a] D. D. Cox, L. Que, Jr., *J. Am. Chem. Soc.* **1988**, *110*, 8085−8092. − [4b] H. G. Jang, D. D. Cox, L. Que, Jr., *J. Am. Chem. Soc.* **1991**, *113*, 9200−9204. − [4c] W. O. Koch, H. J. Krüger, *Angew. Chem.* **1995**, *107*, 2928−2931; *Angew. Chem. Int. Ed. Engl.* **1995**, *34*, 2671−2674.

[5] K. Inoue, H. Iwamura, *J. Am. Chem. Soc.* **1994**, *116*, 3173−3174.
[6] [6a] J. M. Manriquez, G. T. Yee, R. S. McLean, A. J. Epstein, J. S. Miller, *Science* **1991**, *252*, 1415−1417. − [6b] J. Zhang, J. Ensling, V. Ksenofontov, P. Gütlich, A. J. Epstein, J. S. Miller, *Angew. Chem.* **1998**, *110*, 676−679; *Angew. Chem. Int. Ed. Engl.* **1998**, *37*, 657−660.
[7] [7a] T. J. Collins, R. P. Powell, C. Slebodnick, E. S. Uffelman, *J. Am. Chem. Soc.* **1991**, *113*, 8419−8425. − [7b] M. J. Bartos, C. Kidwell, K. E. Kauffmann, S. W. Gordon-Wylie, T. J. Collins, G. C. Clark, E. Münck, S. T. Weintraub, *Angew. Chem.* **1995**, *107*, 1345−1348; *Angew. Chem. Int. Ed. Engl.* **1995**, *34*, 1216−1219.
[8] [8a] R. Ruiz, A. Aukauloo, Y. Journaux, A. L. Roselló, I. Fernández, J. R. Pedro, B. Cervera, I. Castro, M. C. Muñoz, *Chem. Commun*. **1998**, 989−990. − [8b] R. Ruiz, M. Traianidis, A. Aukauloo, Y. Journaux, I. Fernández, J. R. Pedro, B. Cervera, I. Castro, M. C. Muñoz, *Chem. Commun.* **1997**, 2283−2284.
[9] [9a] J. Estrada, I. Fernández, J. R. Pedro, X. Ottenwaelder, R. Ruiz, Y. Journaux, *Tetrahedron Lett*. **1997**, *38*, 2377−2380. − [9b] I. Fernández, J. R. Pedro, A. L. Roselló, R. Ruiz, X. Ottenwaelder, Y. Journaux, *Tetrahedron Lett*. **1998, 39**, 2869−2872.
[10] [10a] R. Ruiz, C. Surville-Barland, A. Aukauloo, E. Anxolabehere-Mallart, Y. Journaux, J. Cano, M. C. Muñoz, *J. Chem. Soc., Dalton Trans.* **1997**, 745−751. − [10b] B. Cervera, J. L. Sanz, M. J. Ibañez, G. Vila, F. Lloret, M. Julve, R. Ruiz, X. Ottenwaelder, A. Aukauloo, S. Poussereau, Y. Journaux, M. C. Muñoz, *J. Chem. Soc., Dalton Trans.* **1998**, 781−790.
[11] R. Ruiz, X. Ottenwaelder, A. Aukauloo, S. Poussereau, Y. Journaux, B. Cervera, M. C. Muñoz, manuscript in preparation.
[12] [12a] F. P. Bossu, D. W. Margerum, *J. Am. Chem. Soc.* **1976**, *98*, 4003−4013. − [12b] F. P. Bossu, K. L. Chellapa, D. W. Margerum, *J. Am. Chem. Soc.* **1977**, *99*, 2195−2203.
[13] L. Fabbrizzi, A. Perotti, A. Poggi, *Inorg. Chem.* **1983**, *22,* 1411−1412.
[14] [14a] F. C. Anson, T. J. Collins, T. G. Richmond, B. D. Santarsiero, J. E. Toth, B. G. R. T. Treco, *J. Am. Chem. Soc.* **1987**, *109*, 2974−2979. − [14b] T. J. Collins, T. R. Nichols, E. S. Uffelman, *J. Am. Chem. Soc.* **1991**, *113*, 4708−4709.
[15] [15a] J. Hanss, H. J. Krüger, *Angew. Chem.* **1996**, *108*, 2989−2991; *Angew. Chem. Int. Ed. Engl.* **1996**, *35*, 2827−2830. − [15b] J. Hanss, H. J. Krüger, *Angew. Chem.* **1998**, *110*, 366−369; *Angew. Chem. Int. Ed. Engl.* **1998**, *37*, 360−363.
[16] L. Michaelis, M. P. Schubert, S. Granick, *J. Am. Chem. Soc*. **1939**, *61*, 1981−1992.
[17] The electronic absorption spectrum of the nickel(II) complex $(PPh_4)_2$[Ni(**1**)] in acetonitrile shows a similar pattern to that of **3**, consisting of an intense band in the UV region located at 350 nm and a less intense band in the visible region at 420 nm. The significant red shift observed in the visible d−d absorption maximum of the orange dinickel complex $[Ni_2(\mathbf{2})]^{4-}$ related to the yellow nickel complex $[Ni(\mathbf{1})]^{2-}$, in spite of the presence of the same chromophor NiN_2O_2, clearly indicates the weaker ligand field associated with the ligand $[\mathbf{2}]^{8-}$ than with $[\mathbf{1}]^{4-}$. Likewise, the *intra*-ligand UV bands in the spectrum of $[Ni_2(\mathbf{2})]^{4-}$ corresponding to intraligand π-π* transitions within the aromatic benzene ring are also red-shifted with respect to the analogous band in $[Ni(\mathbf{1})]^{2-}$. The higher aromaticity of the 1,2,4,5-tetrasubstituted benzene ring of $[\mathbf{2}]^{8-}$ than of the 1,2,-disubstituted benzene ring of $[\mathbf{1}]^{4-}$ is presumably responsible for this bathochromic effect. These differences in the spectroscopic properties between the dinuclear nickel(II) complex and the mononuclear analogue already announce their dramatically different electrochemical behaviour.
[18] A. D. Becke, *J. Chem. Phys.* **1993**, *98*, 5648. C. Lee, W. Yang, R. G. Parr, *Phys. Rev.* **1988**, *B37*, 785.
[19] M. J. Frisch, G. W. Trucks, H. B. Schlegel, P. M. W. Gill, B. G. Johnson, M. A. Robb, J. R. Cheeseman, T. Keith, G. A. Petersson, J. A. Montgomery, K. Raghavachari, M. A. Al-Laham, V. G. Zakrzewski, J. V. Ortiz, J. B. Foresman, J. Cioslowski, B. B. Stefanov, A. Nanayakkara, M. Challacombe, C. Y. Peng, P. Y. Ayala, W. Chen, M. W. Wong, J. L. Andres, E. S. Replogle, R. Gomperts, R. L. Martin, D. J. Fox, J. S. Binkley, D. J. Defrees, J. Baker, J. P. Stewart, M. Head-Gordon, C. Gonzalez, J. A. Pople, *Gaussian 94, Revision E.1*, Gaussian, Inc., Pittsburgh, PA, **1995**. In the calculations, the metal ions and the ligand have been explicitly taken into account. The PPh_4^+ counterions have been replaced by Na^+ cations and are located at the phosphorus site of PPh_4^+ cations. Furthermore, the geometry used has been taken from the one determined by X-ray crystallography. We have used the 6-31G* basis set for the ligands atoms. The nickel basis set is that determined by Wachters supplemented with f-polarization function. The sodium cations have been taken as point charges (no vacant orbital on the atom), the core electrons being described by an effective core potential. This procedure, which explicitly takes into account a repulsion potential, avoids too strong orbital polarizations towards the point charges.
[20] A. J. H. Wachters, *J. Chem. Phys.* **1970**, *66*, 1033. This set has been supplemented with two functions to describe the 4p orbitals (those optimized by Wachters multiplied by 1.5), a diffuse d function and f-polarization function.
[21] S. W. Gordon-Wylie, B. L. Claus, C. P. Horwitz, Y. Leychkis, J. M. Workman, A. J. Marzec, G. R. Clark, C. E. F. Rickard, B. J. Conklin, S. Sellers, G. T.Yee, T. J. Collins *Chem. Eur. J.* **1998**, *11*, 2173−2181.
[22] [22a] C. Surville-Barland, R. Ruiz, A. Aukauloo, Y. Journaux, I. Castro, B. Cervera, M. Julve, F. LLoret, F. Sapiña, *Inorg. Chim. Acta* **1998**, *278*, 159−169. − [22b] R. Ruiz, C. Surville-Barland, Y. Journaux, J. C. Colin, I. Castro, B. Cervera, M. Julve, F. LLoret, F. Sapiña, *Chem. Mater.* **1997**, *9*, 201−209.
[23] Crystallographic data (excluding structure factors) for the structure reported in this paper have been deposited with the Cambridge Crystallographic Data Centre as supplementary publication no. CCDC-102916. Copies of the data can be obtained free of charge on application to CCDC, 12 Union Road, Cambridge CB21EZ, UK [Fax: + 44-1223/336-033; E-mail: deposit@ccdc.cam.ac.uk].
[24] G. M. Sheldrick, *SHELXL93, Program for the Refinement of Crystal Structures*, University of Göttingen, DFR, **1993**.

Received December 21, 1998
[I98449]

Fast Palladium Catalyzed Arylation of Alkenes Using Bulky Monodentate Phosphorus Ligands

Gino P. F. van Strijdonck,[a] Maarten D. K. Boele,[a] Paul C. J. Kamer,[a] Johannes G. de Vries,*[b] and Piet W. N. M. van Leeuwen*[a]

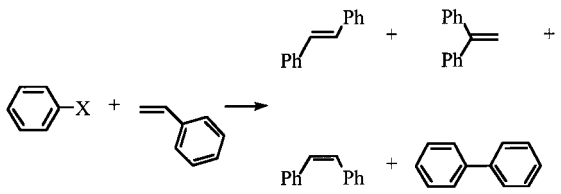
Keywords: C–C coupling / Homogeneous catalysis / Kinetics / Palladium / Phosphorus amidite

Complex **1b** shows an unprecedented high activity in the Heck reaction. Kinetic studies show that in this system not the oxidative addition but the alkene coordination/migratory insertion is the rate determining step.

The palladium-catalyzed arylation of alkenes, also known as the Heck reaction, has proven to be a versatile method for the formation of carbon−carbon bonds.[1] The Heck reaction is compatible with a broad range of substituents, but it also suffers from severe drawbacks which often preclude industrial use.[2] Even though some progress has been reported towards catalyst performance,[3] there is still a need for better catalysts.

Ligand effects[4] have been studied extensively for many metal catalyzed reactions. In the Heck reaction mainly phosphanes have been used. In a limited amount of papers the use of 1,10-phenanthroline derivatives has been reported[5] and recently phosphites were used.[6] Pfaltz and co-workers have reported on the use of mixed phosphane oxazoline ligands in an enantioselective Heck reaction.[7] Phosphorus amidites form a unique class of ligands, which have proven their usefulness in catalysis.[8] Their electronic properties are in between those of phosphanes and phosphites. As part of our studies on ligand effects, we decided to study the effect of phosphorus amidites and phosphites in the Heck reaction.

As a model reaction to study the effect of electronic and steric properties of the ligands on the Heck reaction we have chosen the reaction of iodobenzene with styrene in acetonitrile and triethylamine as a base.



Scheme 1. Heck reaction of styrene with phenyl halides

The use of 1 mol-% of $Pd(dba)_2$ and 2 equivalents of phosphorus amidite **1b** (80°C) resulted in the very fast formation of mainly *trans*-stilbene, the Heck product (Scheme 1). In a series of ligands with approximately the same steric bulk the order of activity was found to be: phosphorus amidites (**1**) > phosphites (**3**) > phosphanes (**2**). Within a series of phosphorus amidite ligands with increasing steric bulk, ligand **1b** gave the fastest catalysis. In the phosphane and phosphite series a similar trend was observed, viz. **b** > **a** > **c** (see Table 1). When more equivalents of ligands are used, the activity drops, except for **1b**. Addition of more equivalents of this ligand does not affect the activity. Using the more bulky ligands **c**, relatively more of the *cis* product and less *trans*-stilbene was found with increasing L/Pd ratio.

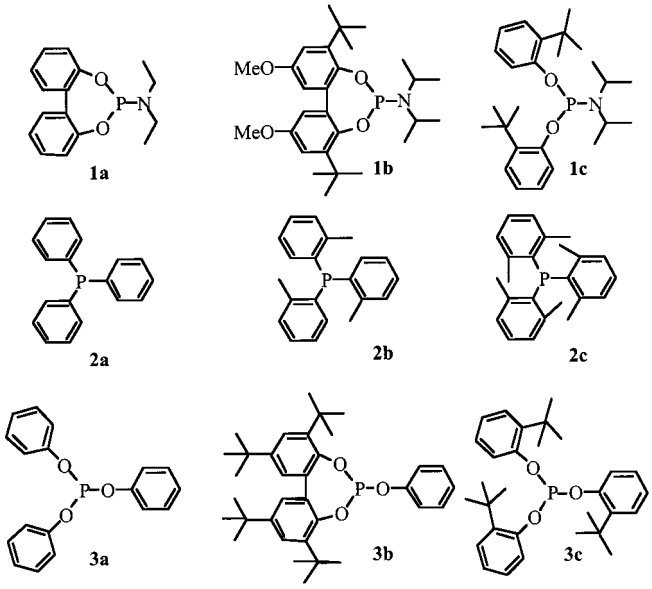


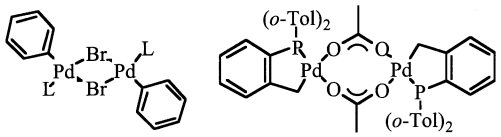
Figure 1. Monodentate ligands

The use of $Pd(dba)_2$ without an additional ligand resulted in a low conversion and the formation of palladium black. The same was observed using $Pd(OAc)_2$ without additional ligand.

Recently, Beller and co-workers reported on cyclometallated palladium complexes as efficient catalysts for Heck

[a] Institute for Molecular Chemistry, Department of Inorganic Chemistry, University of Amsterdam,
Nieuwe Achtergracht 166, NL-1018 WV Amsterdam, The Netherlands
Fax: (internat.) +31-20/525-6456
E-mail: PWNM@anorg.chem.uva.nl
[b] DSM Research, Dept. Fine Chemicals,
P.O. Box 18, NL-6160 MD Geleen, The Netherlands

 © WILEY-VCH Verlag GmbH, D-69451 Weinheim, 1999 1434−1948/99/0707−1073 $ 17.50+.50/0



4a: L=2b
4b: L=1b

5

Figure 2. Pd^{II} compounds

reactions.[3d] Palladacycle **5**, however, was not very active in the reaction of iodobenzene with styrene in acetonitrile and triethylamine as a base. Probably the formation of the active species[3f] is slow under the conditions employed.

Table 1. Heck reaction of iodobenzene and styrene[a]

Catalyst	Conversion[b] [%]	Selectivity[c] *trans*-stilbene [%]	*cis*-stilbene [%]	1,1-diphenyl-ethylene [%]
$Pd(OAc)_2$	5	90	1	9
$Pd(dba)_2$	7	90	1	9
$Pd(dba)_2$/**1a**	18	90	1	9
$Pd(dba)_2$/**1b**	100	90	1	9
$Pd(dba)_2$/**1c**	6	88	1	11
$Pd(dba)_2$/**2a**	6	90	1	9
$Pd(dba)_2$/**2b**	12	90	1	9
$Pd(dba)_2$/**2c**	1	89	1	10
$Pd(dba)_2$/**3a**	8	90	1	9
$Pd(dba)_2$/**3b**	48	90	1	9
$Pd(dba)_2$/**3c**	6	85	1	14
5	8	90	1	9

[a] Conditions: see Experimental Section. – [b] Based on iodobenzene, measured after 45 minutes. – [c] Less than 1% biphenyl was formed.

Phosphorus amidite **1b** gave the most active catalyst. To obtain further details of the catalytic cycle, we performed a kinetic study. To avoid interference of equilibria between the pre-catalyst and the intermediates involved in the catalytic cycle[9], we prepared compound **4b** and compared its catalytic behavior with that of tris(*o*-tolyl)phosphane-coordinated complex **4a** in the reaction of iodobenzene with styrene. Osmometric molecular mass determination in dichloromethane showed that compound **4b** exists as a dimer. A broad signal at $\delta = 118.3$ in the ^{31}P-NMR spectrum is indicative of a fast equilibrium between the *cis* and the *trans* isomers[10]. After cooling the solution to 240 K we observed two sharp peaks at $\delta = 119.8$ and 117.5 in a 4:3 ratio. The major product is probably the *trans* product. In acetonitrile, only one sharp singlet was observed at $\delta = 122.3$ in a temperature range of 255–335 K.

The rate of the reaction between iodobenzene and styrene catalyzed by palladium complexes **4** was independent of the concentration of iodobenzene (0.10–2.0 M) and the concentration of triethylamine (0.16–2.5 M). Figure 3 shows a linear dependence of the initial turn over frequency (TOF_{ini}) on the styrene concentration (0–4.0 M). The reaction rate increases linearly with the square root of the palladium concentration (0–4.0 mM; see Figure 4). Using palladium concentrations below 4.0 mM and conversions up to 70% no formation of palladium black was observed.

The rate of the Heck reaction shows a large dependence on the solvent and the alkene used. In acetonitrile, the reaction of iodobenzene with styrene (1 M), catalyzed with 0.125 mol-% complex **4b** (0.25% Pd) gave 50% conversion after 2 h. In DMF, the conversion after 2 h. was 75%. In *N*-methyl pyrrolidinone (NMP) the reaction was even faster: within 45 minutes the reaction was completed. Reaction of iodobenzene with *n*-butylacrylate, in NMP at 80°C with 0.125 mol-% complex **4b**, was completed within 6 minutes. This reaction was more than 99% selective towards the *trans* coupled product. With this system we do not only have an extremely fast but also a stable catalyst and a very high turn-over number (> 500 000) has been obtained.

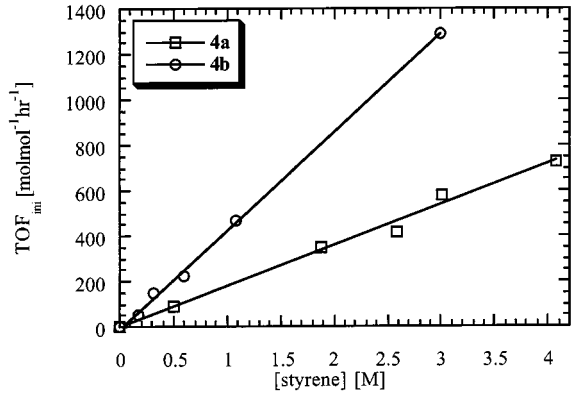


Figure 3. Plot of TOF_{ini} versus [styrene] for the reaction of iodobenzene with styrene in CH_3CN at 65°C catalyzed with complexes **4** (TOF_{ini} is the amount of products formed per mol Pd per hour after 5 min)

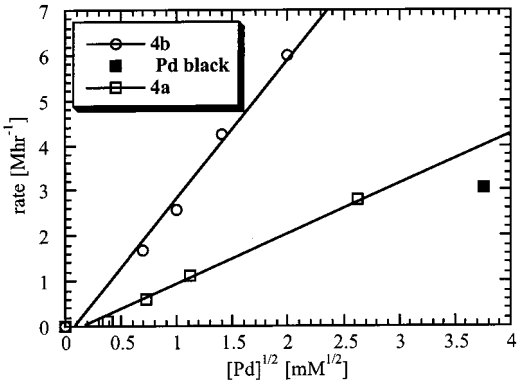


Figure 4. Plot of the rate versus $[Pd]^{1/2}$ for the reaction of iodobenzene with styrene in CH_3CN at 65°C catalyzed with complexes **4** (rate = *d*[products]/*d*t, measured after 5 min)

The unique kinetic observations are rationalized in terms of the catalytic cycle shown in Figure 5. In this cycle oxidative addition of an aryl halide to [PdL] gives a Pd^{II} compound which is in fast equilibrium with its dimer. The monomer forms a complex with the alkene. Next, the migratory insertion of this alkene takes place. After β-hydrogen elimination and reductive elimination of HX, the intermediate palladium(0) species with one ligand per palladium is obtained again.

Studies on phosphapalladacycles in the Heck reaction[3f,11] suggest that a monophosphane palladium(0) species, [R_3P-Pd], is a crucial intermediate of the cycle. This species is presumed to undergo fast oxidative addition of aryl halides followed by a dimerization giving the known compound **4a**.[10] Molecular weight determinations indicated that also complex **4b** exists as a dimer.

After alkene coordination and subsequent insertion of the alkene, the reaction is assumed to follow the widely accepted[12] pathway shown in Figure 5.

This proposed cycle is consistent with the kinetic data. Kinetic studies on the use of diphosphane ligands in the palladium catalyzed reaction of iodobenzene with styrene showed that the oxidative addition is one of the slower steps of the catalytic cycle. Since in the case of the bulky monodentate ligands the rate is independent of the concentration of iodobenzene the oxidative addition is not the turn over limiting step in these systems. This is quite surprising since phosphorus amidites render palladium less electron rich than phosphanes. The reaction rate is linearly dependent on the square root of the palladium concentration and first order in styrene concentration. This means that in this system either the alkene complexation or the migratory insertion must be the turn over limiting step. This step proceeds faster for complex **4b** than for complex **4a**.[13]

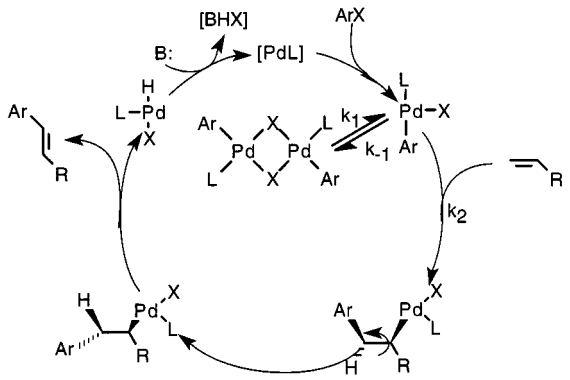


Figure 5. Postulated catalytic cycle for the Heck reaction; if we assume that $k_{-1} >> k_1 >> k_2$[alkene], then the rate = $k_2K^{1/2}$[alkene][Pd]$^{1/2}$; $K = k_1/k_{-1}$

The subtle combination of electronic and steric properties of ligand **1b** results in a highly active catalyst for the Heck reaction. The ligand is sufficiently bulky to provide complexes having a Pd:P ratio of 1:1. A bulkier ligand, however, retards the reaction. The relatively small phosphorus amidite **1a** forms a palladium compound with two ligands under the reaction conditions as can be concluded from the NMR data.[14] This also decreases the activity of the catalyst.

In summary, the use of a bulky phosphorus amidite as ligand in the palladium-catalyzed arylation of alkenes resulted in an extremely active catalyst system. From kinetic studies we conclude that, under the reaction conditions employed, not the oxidative addition, but the coordination or insertion of the alkene is the rate-determining step in this reaction. Further exploration of the scope of the reaction and the implications of the unprecedented kinetics are in progress.

Experimental Section

The ligands were prepared as described in the literature.[8a][15]

Complex **4a** was prepared as described by Hartwig.[11b] Complex **4b** was prepared in an analogous way in 81% yield. – $C_{68}H_{94}Br_2N_2O_4Pd_2$: calcd. C 54.38, H 6.31, N 1.86; found C 54.86, H 6.38, N 1.69. – $^{31}P\{^1H\}$ NMR (121 MHz, $CDCl_3$, 25°C, H_3PO_4): δ = 118.3 (s). – ^1H NMR (300 MHz, $CDCl_3$, 25°C, TMS): δ = 1.23 (s, 12 H, CH_3), 1.25 (s, 12 H, CH_3), 1.41 (s, 36 H, *t*Bu), 3.81 (s, 12 H, CH_3O), 4.45 (m, 4 H, CH), 6.62 (m, 10 H, ArH), 6.81 (m, 4 H, ArH), 6.94 (m, 4 H, ArH). – $^{13}C\{^1H\}$ NMR (78 MHz, $CDCl_3$, 25°C, TMS): δ = 25.0 (CH_3), 31.7 (*t*Bu), 35.6 (C), 49.9 [d, ^2J(C,P) = 18 Hz, CH], 50.0 (CH), 55.4 (CH_3O), 113.2 (ArH), 114.5 (ArH), 117.1 (Ar), 122.7 (ArH), 126.7 (ArH), 131.3 (Ar), 135.2 (ArH), 141.9 (Ar), 143.0 [d, ^2J(C,P) = 14 Hz, Ar], 155 (Ar).

Catalysis with in situ Prepared Catalysts: Under a dinitrogen atmosphere, a Schlenk vessel, fitted with a septum, was charged with $Pd(dba)_2$ (26.1 mg, 0.05 mmol) and ligand (0.1 mmol). Subsequently, 5 mL of freshly distilled acetonitrile (CaH_2), 250 μL of decane (1.28 mmol) as internal standard, 550 μL of iodobenzene (4.9 mmol) and 650 μL of styrene (5.5 mmol) were injected. The Schlenk vessel was heated to 80°C and 750 mL of triethylamine (5.4 mmol) was added. The reactions were monitored by gas chromatography (DB1 column).

Kinetic Studies: Under a dinitrogen atmosphere, a Schlenk vessel, fitted with a septum, was charged with complex **4**. Subsequently, freshly distilled acetonitrile (to a total volume of 10 mL), 500 μL of decane (2.56 mmol) as internal standard, iodobenzene, and styrene were injected. The Schlenk vessel was heated to 65°C and triethylamine was added (t = 0). The reactions were monitored by gas chromatography (DB1 column).

Catalysis with Complex 4a: Under a dinitrogen atmosphere, a Schlenk vessel, fitted with a septum, was charged with complex **4a** (9.4 mg, 0.00625 mmol). Subsequently, 5 mL of freshly distilled solvent, 250 μL of decane (1.28 mmol) as internal standard, 550 μL of iodobenzene (4.9 mmol) and alkene (5.5 mmol) were injected. The Schlenk vessel was heated to 80°C and 750 mL of triethylamine (5.4 mmol) was added. The reactions were monitored by gas chromatography (DB1 column).

[1] [1a] R. F. Heck, *Acc. Chem. Res.* **1979**, *12*, 146–151. – [1b] R. F. Heck, *Org. React.* **1982**, *27*, 345–390. – [1c] A. de Meijere, F. E. Meyer, *Angew. Chem. Int. Ed. Engl.* **1994**, *33*, 2379–2411; *Angew. Chem.* **1994**, *106*, 2473–2506. – [1d] W. Cabri, I. Candiani, *Acc. Chem. Res.* **1995**, *28*, 2–7. – [1e] T. Jeffrey, *Tetrahedron* **1996**, *52*, 10113–10130.

[2] M. S. Stephan, A. J. J. M. Teunissen, G. K. M. Verzijl, J. G. de Vries, *Angew. Chem. Int. Ed.* **1998**, *37*, 662–663; *Angew. Chem.* **1998**, *110*, 668–690.

[3] [3a] Y. Ben-David, M. Portnoy, M. Gozin, D. Milstein, *Organometallics* **1992**, *11*, 1995–1996. – [3b] M. Portnoy, Y. Ben-David, D. Milstein, *Organometallics* **1993**, *12*, 4734–4735. – [3c] M. Portnoy, Y. Ben-David, I. Rousso, D. Milstein, *Organometallics* **1994**, *13*, 3465–3479. – [3d] W. A. Herrmann, C. Brossmer, K. Öfele, C.-P. Reisinger, T. H. Riermeier, M. Beller, H. Fischer, *Angew. Chem. Int. Ed.* **1995**, *34*, 1844–1847; *Angew. Chem.* **1995**, *107*, 1989–1992. – [3e] W. A. Herrmann, C. Brossmer, C.-P. Reisinger, T. H. Riermeier, K. Öfele, M. Beller, *Chem. Eur. J.* **1997**, *3*, 1357–1364. – [3f] M. Beller, T. H. Riermeier, *Eur. J. Inorg. Chem.* **1998**, 29–35. – [3g] M. Ohff, A. Ohff, M. van der Boom, D. Milstein, *J. Am. Chem. Soc.* **1997**,

119, 11687−1688. − [3h] M. R. Reetz, G. Lohmer, R. Schwickardi, *Angew. Chem. Int. Ed.* **1998**, *37*, 481−483; *Angew. Chem.* **1998**, *110*, 492−495.

[4] The Tolman parameters θ and χ are commonly used as a measure for the ligand parameters. C. A. Tolman, *Chem. Rev.* **1977**, *77*, 313−348.

[5] [5a] W. Cabri, I. Candiani, A. Bedeschi, R. Santi, *J. Org. Chem.* **1993**, *58*, 7421−77427. − [5b] K. H. Ang, S, Bräse, A. G. Steinig, F. E. Meyer, A. Lleboria, K. Voigt, A. de Meijere, *Tetrahedron* **1996**, *52*, 11503−11528. − [5c] D. Grotjahn, X. Zhang, *J. Mol. Catal. A: Chem.* **1997**, *116*, 99−107.

[6] [6a] M. Beller, A. Zapf, *Synlett.* **1998**, 792−793. − [6b] D. A Albisson, R. B. Bedford, S. E. Lawrence, P. N. Scully, *J. Chem. Soc., Chem. Commun.* **1998**, 2095−2096.

[7] O. Loiseleur, M. Hayahashi, N. Schmees, A. Pfaltz, *Synthesis*, **1997**, 1338−1345.

[8] [8a] A. van Rooy, D. Burgers, P. C. J. Kamer, P. W. N. M. van Leeuwen, *Recl. Trav. Chim. Pays-Bas* **1996**, *115*, 492−498. − [8b] A. H. M. de Vries, A. Meetsma, B. L. Feringa, *Angew. Chem. Int. Ed. Engl.* **1996**, *35*, 2374−2376; *Angew. Chem.* **1996**, *108*, 2526−2528. − [8c] B. L. Feringa, M. Pineski, L. A. Arnold, R. Imbor, A. H. M. de Vries, *Angew. Chem. Int. Ed. Engl.* **1997**, *36*, 2620−2623; *Angew. Chem.* **1997**, *109*, 2733−2736.

[9] It has been shown that dba retards the oxidative addition: C. Amatore, G. Broeker, A. Jutand, F. Khalil, *J. Am. Chem. Soc.* **1997**, *119*, 5176−5185.

[10]]10a] V. V. Grushin, H. Alper, *Organometallics* **1993**, *12*, 1890−1901. − [10b] F. Paul, J. Patt, J. F. Hartwig, *Organometallics* **1995**, *14*, 3037−3039.

[11] J. Louie, J. Hartwig, *Angew. Chem. Int. Ed. Engl.* **1996**, *35*, 2359−2361; *Angew. Chem.* **1996**, *108*, 2531−2533.

[12] [12a] Recently Shaw proposed an alternative mechanism involving Pd^{II}/Pd^{IV}: B. L. Shaw, *New. J. Chem.* **1998,** 77−79. − [12b] B. L. Shaw, S. D. Perera, E. A. Staley, *J. Chem. Soc., Chem. Commun.* **1998**, 1361−1362.

[13] When the more electron withdrawing phosphites are used it seems that the oxidative addition at palladium becomes rate limiting.

[14] Reaction of $Pd(dba)_2$ with various amounts of **2a** showed in the ^{31}P-NMR spectrum a singlet for the free ligand and two doublets [δ = 161.9 and δ = 163.9; ^2J(P,P) = 84 Hz], assigned to $L_2Pd(dba)$.

[15] A. van Rooy, E. N. Orij, P. C. J. Kamer, P. W. N. M. van Leeuwen, *Organometallics* **1995**, *14*, 34−43.

Received January 15, 1999
[99010]

How the Organic Moiety Drives the Coordination Chemistry of Metal Phosphonates: The First Enantiomerically Pure Zinc Phosphonate

Florence Fredoueil,[a] Michel Evain,[b] Martine Bujoli-Doeuff,[b] and Bruno Bujoli*[a]

Keywords: Zinc / Phosphonate complexes / Chirality / P ligands

The first enantiomerically pure metallophosphonate, (*R*)-$Zn[O_3PCH_2P(O)(CH_3)(C_6H_5)]\cdot H_2O$ has been prepared. The layered arrangement in this compound is drastically different from that observed in the racemic series; this observation gives clear evidence of the critical role played by the organic moiety that fully drives the coordination chemistry of phosphonic acids with transition metals.

Metal phosphonate chemistry is undergoing rapid expansion, with applications in various areas such as ion exchange, catalysis, sensors, proton conductors, magnetism, or photochemically active materials.[1] Furthermore, an attractive feature is their potential for supramolecular assembly, provided that the structure of the phosphonate framework can be finely tuned by the suitable design of the RPO_3H_2 phosphonic acid precursor. For that purpose, it is essential to know, for a given metal, the role played by the organic moiety R attached to the phosphorus atom [via its shape, its rigidity, and the number and nature of its functional groups], on the structure and dimensionality of the resulting metal phosphonates. In this context, we have recently reported the coordination chemistry of phosphonic acids bearing functionalities of various bulks, showing that a control of the dimensionality of zinc phosphonates could be achieved.[2] Another aspect that has never been studied is the possibility to get enantiomerically pure phosphonate networks using chiral precursors. In this paper, we report the synthesis and structural characterization of the first enantiomerically pure metal phosphonate: (*R*)-$Zn[O_3PCH_2P(O)(CH_3)(C_6H_5)]\cdot H_2O$ (compound **A**), based on mixed phosphonic acid−phosphane oxide chiral building blocks.

The phosphonic acid $H_2O_3PCH_2P(O)(CH_3)(C_6H_5)$ racemate was prepared as previously described[2c] and the optical resolution was performed using quinine to give a 1:1 complex [quinine:$H_2O_3PCH_2P(O)(CH_3)(C_6H_5)\cdot 2\,H_2O$] in 81% yield (based on one of the enantiomer). The complex was treated with two equivalents of aqueous sodium hydroxide, and after extraction with dichloromethane to remove quinine, the pure enantiomeric (*R*)-form of the acid was quantitatively recovered by evaporation of the aqueous phase ($[\alpha]_D^{20} = -18$ (*c* = 1.0 in 1 M HCl)); reaction with zinc nitrate in water, under neutral-pH conditions, then yielded compound **A** in 85% yield. To ensure that all the crystals of the preparation corresponded to the same enantiomeric form, the specific rotation of compound **A** (after dissolution in 1 M HCl) was measured and found to be identical to that of the isolated resolved phosphonic acid precursor.

The structure consists of layers (*ab* plane; Figure 1) in which the zinc atoms are tetrahedrally coordinated with three oxygen atoms from the phosphonate groups [Zn−O: 1.891(6)−1.918(7) Å] and one oxygen atom from the phosphane oxide moiety [Zn−O: 1.993(5) Å]. In each layer, the zinc atoms are arranged in 12-membered rings, constructed by corner-sharing of alternating ZnO_4 and PO_3C tetrahedra. The phenyl groups are oriented toward the interlayer space, with a basal spacing (*c*/2 = 12.65 Å) shorter than the usual 15−16 Å value observed for layered metal phenylphosphonates, due to a close-packing of the sheets caused by the interdigitation of the aromatic rings from neighbouring slabs (Figure 2). The lattice water molecules are present

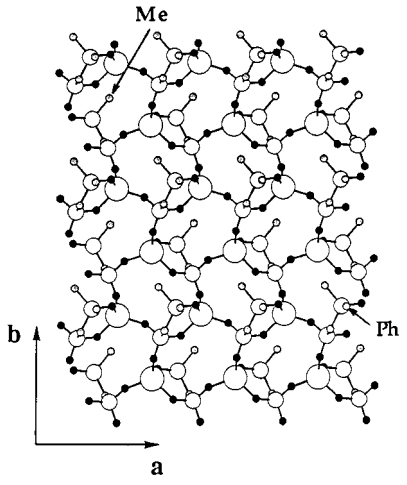


Figure 1. Schematic representation of a (*R*)-[$Zn(O_3PCH_2P(O)(CH_3)(C_6H_5)]\cdot H_2O$ layer viewed down the *c* axis. The water molecule O(5) and the carbon atoms that are not directly bonded to the phosphorus atoms have been omitted for clarity (Me = methyl, Ph = phenyl)

[a] Laboratoire de Synthèse Organique, UMR CNRS 6513, BP 92208, 2 Rue de la Houssinière 44322 Nantes Cedex 03, France
[b] Institut des Matériaux de Nantes, UMR CNRS 6502, BP 92208, 2 Rue de la Houssinière, 44322 Nantes Cedex 03, France
Fax: (internat.) 33-2/ 5112 5412
Email: bujoli@chimie.univ-nantes.fr

 © WILEY-VCH Verlag GmbH, D-69451 Weinheim, 1999 1434−1948/99/0707−1077 $ 17.50+.50/0

between the layers, presumably weakly hydrogen-bonded to phosphonate oxygen atoms [dO(H_2O)−O(phosphonate) = 3.06(1), 3.17(1), and 3.34(1) Å], thus explaining the low temperature (55°C) at which the dehydration takes place.

One important feature of this compound is the configuration of the phosphorus atom of the phosphane oxide that was unambiguously determined to be (*R*) (see Figure 2). Moreover, in a previous study, we had prepared from the phosphonic acid racemic precursor, in similar pH conditions, a layered zinc phosphonate (**B**) of composition $Zn[O_3PCH_2P(O)(CH_3)(C_6H_5)] \cdot 0.67\ H_2O$, in which the phosphane oxide is similarly bonded to zinc. It is important to note that the metal−PO_3 arrangement within the layers in this latter product (Figure 3) is different from that described for **A**; for example we can notice the presence of 16-membered rings forming at their junction smaller rings (see detail in Figure 3), in which the $O_3PCH_2P(O)(CH_3)(C_6H_5)$ units are arranged in pairs of opposite configurations, leading to a racemic zinc phosphonate. This observation clearly demonstrates that the inorganic framework has to adapt itself even to the presence of chiral atoms on the organic backbone, according to its racemic or optically pure character.

In summary, this study nicely gives an additional evidence for the critical role played by the organic moiety that fully drives the coordination chemistry of phosphonic acids with transition metals. Furthermore, when the chiral organic precursor is enatiomerically pure, no racemization occurs during the preparation of the corresponding metal phosphonate, leading to an enantiomerically pure product.

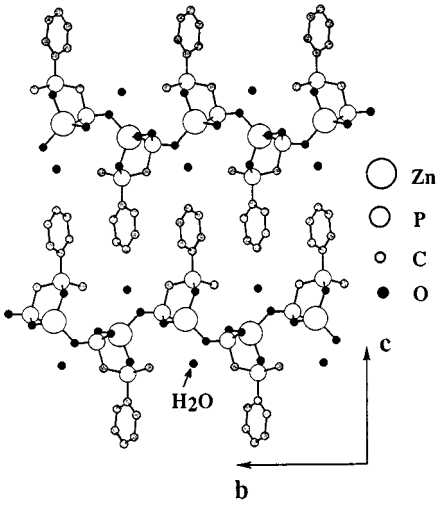


Figure 2. Schematic representation of (*R*)-$Zn[O_3PCH_2P(O)(CH_3)(C_6H_5)] \cdot H_2O$ (**A**) as seen perpendicular to the *a* axis; the (*R*)-configuration of the phosphorus atom of the phosphane oxide is clearly apparent

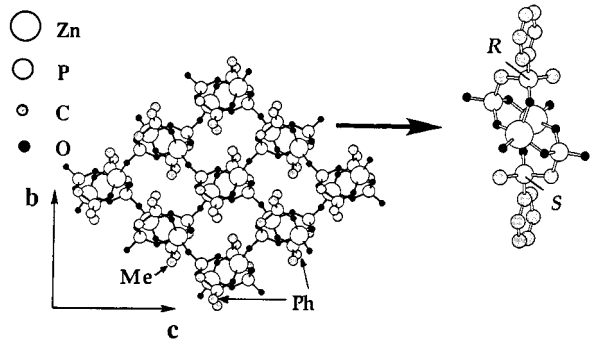


Figure 3. Schematic representation of a (*R*/*S*)-$Zn[O_3PCH_2P(O)(CH_3)(C_6H_5)] \cdot 0.67\ H_2O$ (**B**) layer as seen perpendicular to the *a* axis, according to ref.[2c] The water molecule O(5) and the carbon atoms that are not directly bonded to the phosphorus atoms have been omitted for clarity (Me = methyl, Ph = phenyl). A detail of the structure showing the pairs of $O_3PCH_2P(O)(CH_3)(C_6H_5)$ blocks of opposite configuration (*R*) and (*S*) is given.

Experimental Section

Synthesis of (*R*)-$Zn[O_3PCH_2P(O)(CH_3)(C_6H_5)] \cdot H_2O$ (A): A solution of 500 mg of racemic $H_2O_3PCH_2P(O)(CH_3)(C_6H_5)$ [2.13 mmol] in 30 mL of hot ethanol was added to a solution of 1.039 g of quinine [3.2 mmol] in 15 mL of ethanol. The mixture was allowed to stand for 5 days at room temperature, after which the crystals that gradually appeared were isolated by filtration, corresponding to a 1:1 dihydrate complex (81% yield. Elemental analysis: found: P 9.97, C 56.29, H 6.76, N 4.72; calcd. for $C_{28}P_2O_8N_2H_{40}$: P 10.42, C 56.56, H 6.78, N 4.71. $[\alpha]_D^{20} = -153$ (c = 1.0 in 1 M HCl). The complex (150 mg) was then suspended in 45 mL of water; 2 equivalents of sodium hydroxide were then added and the mixture was stirred for 1 hour. The reaction medium was then extracted 2 times with dichloromethane, allowing to recover quinine in the organic phase. The pure enantiomeric (*R*)-form of the acid was then quantitatively recovered by evaporation of the aqueous phase ($[\alpha]_D^{20} = -18$ (c = 1.0 in 1 M HCl)). The same result was obtained using cinchonidine as the resolving agent. Then a mixture of zinc nitrate (0.3 mmol) and the resolved phosphonic acid described above (0.2 mmol) in 20 mL water was placed in the PTFE cell of an autoclave, that was sealed and kept at 110°C in a drying oven for 3 days. Compound **A** was obtained as white crystals, used for the X-ray structure determination, in 85% yield.

Structure Determination: Data were collected from a single crystal (0.2 × 0.04 × 0.006 mm) on an STOE image plate system (ω scan, $\sin(\theta)/\lambda \leq 0.57$) and a Nonius CAD-4F diffractometer (ω/2θ scan, $\sin(\theta)/\lambda \leq 0.68$) at room temperature. After the usual Lorentz-polarization and decay (< 2%) corrections, the 8233 reflections from the IPDS and the 4234 reflections from the CAD4 were merged based upon the intensities of 218 common reflections with $I/\sigma(I) > 10$. Since the data set was consistent with the $P2_12_12_1$ space group, the reflections were then averaged according to the point group 222 (internal (*R*) value of 7.5%). Data processing and structure refinements were carried out with the JANA98 program.[3] Direct methods (using SHELXTL V5.0 package)[4] revealed the positions of all Zn and P and some C and O atoms. Subsequent full-matrix, least-squares refinements on *F* followed by difference Fourier syntheses revealed the position of the remaining O and C atoms. All hydrogen atoms were refined, but those of the water molecule were placed at their theoretical positions. The CH_3 group was refined as a rigid body. The refinement of the zinc, phosphorus, oxygen, and carbon atoms with independent anisotropic displacement parameters (ADP) converged with $R/wR = 0.0309/0.0312$ for 1071 independent reflections with $I/\sigma(I) > 3$ and 148 parameters. The hydrogen ADPs were restrained to those of the atom the hydrogen atom was attached to.

Crystal data: $ZnP_2O_4C_8H_{10} \cdot H_2O$; orthorhombic $P2_12_12_1$; a = 5.5378(11), b = 8.4143(12), c = 25.270(8) Å, V = 1177.5(5) Å^3

from the centering of 25 high angle reflections (CAD4) and monochromated Mo-K-$L_{2,3}$ radiation; $Z = 4$; $M = 315.5$; $\rho_{calcd.} = 1.779\ g.cm^{-3}$; $\mu = 23.5\ cm^{-1}$; residual electron density [−0.49, +0.39] e/Å^3. The absolute configuration was determined by refining the inversion twin ratio. Crystallographic data (excluding structure factors) for the structure reported in this paper have been deposited with the Cambridge Crystallographic Data Centre as supplementary publication no. CCDC-112086. Copies of the data can be obtained free of charge on application to CCDC, 12 Union Road, Cambridge CB2 1EZ, UK [fax: (+44) 1223/ 336-033; E-mail: deposit@ccdc.cam.ac.uk].

[1] For a recent review see: A. Clearfield in *Progress in Inorganic Chemistry, Vol. 47*, (Ed.: K. D. Karlin), John Wiley & Sons, Inc., New York, **1998**, pp. 371−510.
[2] [2a] S. Drumel, P. Janvier, P. Barboux, M. Bujoli-Doeuff, B. Bujoli, *Inorg. Chem* **1995**, *34*, 148−156. − [2b] S. Drumel, P. Janvier, D. Deniaud, B. Bujoli, *J. Chem. Soc., Chem. Commun* **1995**, 1051−1052. − [2c] F. Fredoueil, V. Pénicaud, M. Bujoli-Doeuff, B. Bujoli, *Inorg. Chem* **1997**, *36*, 4702−4706.
[3] V. Petricek, M. Dusek, *JANA98*: *Programs for modulated and composite crystals*, Institute of Physics, Praha, Czech Republic, **1998**.
[4] G. M. Sheldrick, *SHELXTL V5.0*, Analytical X-ray Instruments Inc., Madison, WI, USA, **1995**.

Received March 4, 1999
[I99086]

Formation of Anionic $PdX_3(PPh_3)^-$ Complexes by Reaction of Halide Ions with $PdX_2(PPh_3)_2$

Christian Amatore,*[a] Anny Jutand,*[a] and Loïc Mottier[a]

Keywords: Palladium / Anionic complexes / Phosphane substitution

Halide ions react with $PdX_2(PPh_3)_2$ (X = Cl, Br, I) complexes in an equilibrated reaction in which the phosphane ligand is substituted by the halide X^- to form anionic complexes $PdX_3(PPh_3)^-$ in THF and DMF. The equilibrium constants have been determined by cyclic voltammetry.

Introduction

It has been established that halide ions are good ligands for palladium(0) complexes.[1−3] The best way to investigate the effect of halide ions on the structure and reactivity of palladium(0) complexes in oxidative addition with aryl halides[2−5] was to generate them by electrochemical reduction of $PdX_2(PPh_3)_2$ in the presence of various amounts of halides X^- (X = Cl,[2][3] Br,[3] I[3]) in THF. However, during the course of these reactions, it was observed that the reduction peak of $PdX_2(PPh_3)_2$ was affected by the presence of added X^- so that its usual single bielectronic reduction peak became split into two peaks whose relative currents depended on the halide concentration: the higher the concentration of X^-, the higher the second reduction peak current relative to the first one.[2][3] This phenomenon was first discarded and tentatively interpreted as the formation of an intermediate palladium(I) complex by reduction of the palladium(II) complex. Its stabilization by halide ions as an anionic 18-electron dimer e.g. $[Pd^I(PPh_3)_2X_2]_2^{2-}$ would indeed make it less easily reduced than $Pd^{II}X_2(PPh_3)_2$, thus giving rise to the second reduction peak.[2][3]

However, careful investigation of this reaction led us now to reconsider our first tentative hypothesis and to establish that reactions of halides X^- with $PdX_2(PPh_3)_2$ result in substitution of one phosphane ligand with formation of an anionic $PdX_3(PPh_3)^-$ species; this palladium(II) complex is more difficult to reduce. In other words, the two peaks represent the reduction of two different palladium(II) complexes.[6]

Results and Discussion

Evidence of the Formation of $PdX_3(PPh_3)^-$ Complexes by Reaction of X^- and $PdX_2(PPh_3)_2$ by ^{31}P-NMR Spectroscopy in THF and DMF

The ^{31}P-NMR spectra of $PdCl_2(PPh_3)_2$ (3 mmol dm^{-3}) in THF exhibited a single signal at δ = 23.80. Two new signals appeared in the presence of 120 equivalents of nBu_4NCl (Figure 1): one signal at δ = −5.27 characteristic of the phosphane PPh_3 and a second one at δ = 27.42 assigned to the anionic species $PdCl_3(PPh_3)^-$ by comparison with an authentic sample of $[PdCl_3(PPh_3)^-, nBu_4N^+]$.[7]

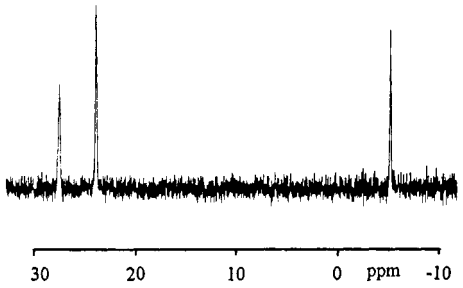


Figure 1. ^{31}P-NMR spectrum (162 MHz) of a solution of $PdCl_2(PPh_3)_2$ (3 mmol·dm^{-3}) and nBu_4NCl (360 mmol dm^{-3}) in 3 mL of THF and 0.2 mL of [D_6]acetone with H_3PO_4 as an external reference

The signal of $PdCl_2(PPh_3)_2$ was still present even in the presence of a large excess of chloride ions suggesting that Cl^- substituted one phosphane from $PdCl_2(PPh_3)_2$ through an equilibrated reaction (Equation 1).

$$Pd^{II}Cl_2(PPh_3)_2 + Cl^- \rightleftharpoons Pd^{II}Cl_3(PPh_3)^- + PPh_3 \quad (1)$$

The dynamic of this equilibrium is relatively slow compared to the time-scale of the NMR experiment since three distinct narrow signals were observed for $PdCl_2(PPh_3)_2$, $PdCl_3(PPh_3)^-$, and PPh_3 (Figure 1). Similar equilibria have been observed using ^{31}P-NMR spectroscopy by treating nBu_4NBr with $PdBr_2(PPh_3)_2$ and nBu_4NI with $PdI_2(PPh_3)_2$ in THF (Equation 2, Table 1).

$$Pd^{II}X_2(PPh_3)_2 + X^- \rightleftharpoons Pd^{II}X_3(PPh_3)^- + PPh_3 \qquad K_X \quad (2)$$

X = Cl, Br, I

In DMF, in the absence of any added halide ions, the ^{31}P-NMR spectra of $PdCl_2(PPh_3)_2$ exhibited three signals. The major signal at δ = 24.4 is assigned to $PdCl_2(PPh_3)_2$. The two other minor (10%) but of same magnitude signals are assigned to PPh_3 (δ = −5.54) and to the dimer

[a] Ecole Normale Supérieure, Département de Chimie, CNRS URA 1679,
24 Rue Lhomond, F-75231 Paris Cedex 5, France
Fax: (internat.) + 33-1/44323325
E-mail: Amatore@ens.fr
Anny.Jutand@ens.fr

 © WILEY-VCH Verlag GmbH, D-69451 Weinheim, 1999 1434−1948/99/0707−1081 $ 17.50+.50/0

Table 1. ^{31}P-NMR signals and reduction peak potentials of palladium(II) complexes involved in the equilibrium $PdX_2(PPh_3)_2 + X^- \rightleftharpoons PdX_3(PPh_3)^- + PPh_3$, with nBu_4N^+ as the countercation

X		Cl	Br	I	Cl	Br	I
		δ[a]	δ[a]	δ[a]	E^p [V][b]	E^p [V][b]	E^p [V][b]
$PdX_2(PPh_3)_2$	THF	23.80	22.57	13.34	−1.040	−0.830	−0.725
$PdX_2(PPh_3)_2$	DMF	24.36	22.86	13.35	−1.015		
$PdX_3(PPh_3)^-$	THF	27.42	29.3	30.70	−1.255	−1.075	−1.025
$PdX_3(PPh_3)^-$	DMF	28.12			−1.370		

[a]162 MHz versus H_3PO_4 as external standard. − [b] Volt versus SCE at a gold disk electrode at 0.2 V s^{-1} at 25 °C.

$Pd_2Cl_4(PPh_3)_2$ (δ = 33.54) by comparison with authentic samples.[9] These results suggest that the equilibrium according to Equation 3[10] operates in DMF and not in THF and is frozen on the time-scale of ^{31}P-NMR spectroscopy.

$$2\ PdCl_2(PPh_3)_2 \rightleftharpoons Pd_2Cl_4(PPh_3)_2 + 2\ PPh_3 \quad (3)$$

In DMF, the ^{31}P-NMR spectra of $PdBr_2(PPh_3)_2$ also exhibited three signals. However, the signal at δ = 25.47, assigned to the dimer $Pd_2Br_4(PPh_3)_2$, was detected at traces level compared to that of $PdBr_2(PPh_3)_2$ at δ = 22.86. A solution of $PdI_2(PPh_3)_2$ exhibited a single signal at δ = 13.40 in DMF suggesting that the dimer $Pd_2I_4(PPh_3)_2$ was not formed.

Determination of the Equilibrium Constant K_X by Cyclic Voltammetry in THF and DMF

As recalled in the introduction, progressive addition of nBu_4NCl to a solution of $PdCl_2(PPh_3)_2$ (1.5 mmol·dm^{-3} in THF containing nBu_4NBF_4 0.3 mol·dm^{-3}) provoked a split of its bielectronic reduction peak R_1 at $E^p = -1.04$ V versus SCE into two reduction peaks, R_1 and R_2 at $E^p = -1.25$ V versus SCE (Figure 2a).[2][3]

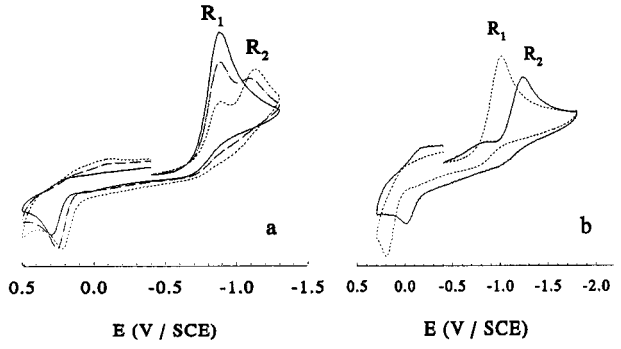


Figure 2. Cyclic voltammetry performed in THF (containing nBu_4NBF_4, 0.3 mol·dm^{-3}) at a steady gold disk electrode (i.d. = 0.5 mm) with a scan rate of 2 V s^{-1}, at 25 °C: (a) $PdCl_2(PPh_3)_2$ (1.5 mmol·dm^{-3}) in the presence of 0 (——), 14 (− − −), 85 (····) equivalents of nBu_4NCl; (b) [$PdCl_3(PPh_3)^-$, nBu_4N^+] (0.8 mmol·dm^{-3}): alone (——); in the presence of 10 equivalents of PPh_3 (····)

From the ^{31}P-NMR investigation reported above, it can be inferred that the second reduction peak is not relevant to the reduction of intermediate palladium(I) complexes as earlier proposed[2][3] but to the reduction of the anionic divalent complex $Pd^{II}Cl_3(PPh_3)^-$. This assumption has been confirmed by the cyclic voltammetry of an authentic sample of [$PdCl_3(PPh_3)^-$, nBu_4N^+][7] performed in THF which exhibited the unique reduction peak R_2 (Figure 2b). Moreover, when 10 equivalents of PPh_3 were added to $PdCl_3(PPh_3)^-$, the reduction peak R_2 of $PdCl_3(PPh_3)^-$ disappeared and was replaced by the reduction peak R_1 of $PdCl_2(PPh_3)_2$ (Figure 2b), evidencing the backward reaction of equilibrium 2 (X = Cl).

$$\underset{R_1}{PdX_2(PPh_3)_2} + X^- \rightleftharpoons \underset{R_2}{PdX_3(PPh_3)^-} + PPh_3 \quad (2)$$

The formation of anionic species was also observed by performing cyclic voltammetry on mixtures of nBu_4NBr and $PdBr_2(PPh_3)_2$, as well as on mixtures of nBu_4NI and $PdI_2(PPh_3)_2$ in THF. The reduction peak potentials of the neutral and anionic complexes are collected in Table 1.

From ^{31}P-NMR spectroscopy, the equilibrium according to Equation 2 was found to be slow compared to the time-scale of the NMR experiment. In cyclic voltammetry, the reduction of $PdX_2(PPh_3)_2$ at R_1 is governed by a CE mechanism.[11] If the equilibrium according to Equation 2 is fast compared to the time-scale of the cyclic voltammetry, reduction of $PdX_2(PPh_3)_2$ at R_1 should result in a shift of the equilibrium to its left-hand side by the continuous consumption of $PdX_2(PPh_3)_2$ due to its reduction in the diffusion layer. A dynamic concentration should be measured which becomes larger as the scan rate is reduced. If not, thermodynamic equilibrium concentrations can be determined. The ratio $r = i/i_0$ [i: reduction peak current at R_1 of $PdCl_2(PPh_3)_2$ in the presence of 100 equivalents of nBu_4NCl; i_0: same current but in the absence of added nBu_4NCl] was then plotted versus the logarithm of the scan rate (Figure 3a).

This ratio clearly does not depend on the scan rate which means that within the time-scale of the cyclic voltammetry investigated here ($0.2 < v < 20$ V s^{-1}), equilibrium 2 is frozen, so that the thermodynamic concentration of $PdCl_2(PPh_3)_2$ in the equilibrium can be determined by the ratio $r = i/i_0 = [PdCl_2(PPh_3)_2]_{equil}/[PdCl_2(PPh_3)_2]_0$. This allows the determination of the equilibrium constant K_{Cl}. In the present case, the dynamics of equilibrium 2 are not accessible because it would require scan rates much lower than 0.2 V s^{-1}, which could not be used since diffusion processes would be contaminated by convection.

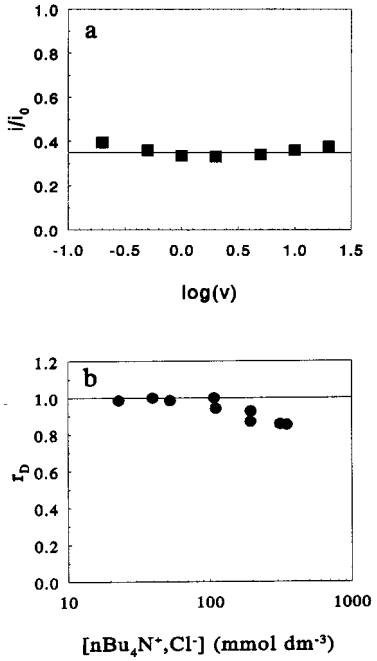


Figure 3. (a) Variation of the ratio $r = i/i_0$ versus the logarithm of the scan rate (v in $V{\cdot}s^{-1}$); i: reduction peak current at R_1 of $PdCl_2(PPh_3)_2$, 1.5 $mmol{\cdot}dm^{-3}$ in THF (containing nBu_4NBF_4, 0.3 $mol{\cdot}dm^{-3}$) in the presence of 100 equivalents of nBu_4NCl; i_0: same current but in the absence of added nBu_4NCl at 20 °C; the reduction peak currents were measured at steady gold disk electrodes (i.d. = 0.5 mm for $v < 5$ $V{\cdot}s^{-1}$ and i.d. = 0.125 mm for $v > 5$ $V{\cdot}s^{-1}$); (b) variation of the ratio $r_D = i/i_0$ versus the logarithm of the concentration of nBu_4NCl; i: reduction peak current at R_1 of $PdCl_2(PPh_3)_2$, 1.5 $mmol{\cdot}dm^{-3}$ in THF (containing nBu_4NBF_4, 0.3 $mol{\cdot}dm^{-3}$) in the presence of n equivalents of nBu_4NCl and 10 equivalents of PPh_3; i_0: same current but in the absence of added nBu_4NCl; the reduction peak currents were measured at a steady gold disk electrode (i.d. = 0.5 mm) with a scan rate of 0.2 $V{\cdot}s^{-1}$ at 20 °C

$$PdX_2(PPh_3)_2 + X^- \rightleftharpoons PdX_3(PPh_3)^- + PPh_3 \quad K_X \qquad (2)$$

at t = 0	C_0	nC_0	0	0
at equil.	rC_0	$(n-1+r)C_0 \approx nC_0$	$C_0(1-r)$	$C_0(1-r)$

$$K_X = \frac{[PdX_3L^-][L]}{[PdX_2L_2][X^-]} = \frac{(1-r)^2}{n\times r} \quad \text{where } n = [X^-]_0/[PdX_2(PPh_3)_2]_0$$

From this expression one obtains

$$r^2 - 2r(1 + nK_X/2) + 1 = 0$$

so that

$$r = 1 + nK_X/2 - \{(nK_X/2)^2 + nK_X\}^{1/2} \qquad (4)$$

The ratio $r = i/i_0$ was measured for various amounts of X^- [n equivalents/Pd^{II}] at a given scan rate. Plotting the experimental value of r versus log n at a given rate constant and comparison with the theoretical curve should allow the determination of K_X. However, this calculation is based on the fact that the reduction peak current i at R_1 is proportional to the concentration of the species $PdX_2(PPh_3)_2$ which is in fact true if the diffusion coefficient D of $PdX_2(PPh_3)_2$ ($i \propto D^{1/2}$)[12] does not vary with the experimental conditions i.e. when the concentration of nBu_4NX and consequently the ionic strength increases. This has been checked by performing cyclic voltammetry of $PdX_2(PPh_3)_2$ for X = Cl, Br, I, in the presence of various amounts of nBu_4NX but with a large excess of PPh_3 (10 equivalents), so that the equilibrium according to Equation 2 was completely shifted to its left-hand side and consequently only the reduction peak R_1 of $PdX_2(PPh_3)_2$ was observed. Under these conditions, the reduction peak current i of $PdX_2(PPh_3)_2$, at a constant scan rate, was found to vary with the concentration of nBu_4NX (X = Cl, Br). This is illustrated in Figure 3b where the ratio $r_D = i/i_0$ [i: reduction peak current at R_1 of $PdCl_2(PPh_3)_2$ in the presence of n equivalents of nBu_4NCl and 10 equivalents of PPh_3; i_0: same current but in the absence of added nBu_4NCl] was plotted versus log [nBu_4NCl]. The ratio r_D differs from unity at high chloride concentrations. This suggests that the diffusion coefficient of $PdCl_2(PPh_3)_2$ is not constant but decreases upon increasing the concentration of chloride ions because of the higher and higher viscosity of the solution. Consequently, the equilibrium constant K_X was determined as explained above but by plotting the ratio $i/(i_0 \times r_D)$ instead of i/i_0 versus log n (Figure 4). The values of the equilibrium constant K_X (X = Cl, Br, I) are collected in Table 2.

Table 2. Equilibrium constant K_X for the equilibrium $PdX_2(PPh_3)_2 + X^- \rightleftharpoons PdX_3(PPh_3)^- + PPh_3$, with nBu_4N^+ as the countercation at 25 °C

X		Cl	Br	I
$10^{+3}K_X$	THF	10 (±1)	0.9 (±0.1)	1.7 (±0.3)
$10^{+3}K_X$	DMF	2 (±1)	n.d.	n.d.

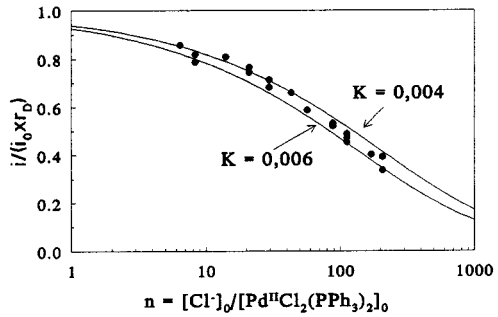


Figure 4. Determination of the equilibrium constant K_{Cl} (see Equations 2 and 4) in THF at 20 °C; plot of $i/(i_0 \times r_D)$ versus the logarithm of n (equivalents of nBu_4NCl); i: reduction peak current at R_1 of $PdCl_2(PPh_3)_2$, 1.5 $mmol{\cdot}dm^{-3}$ in THF (containing nBu_4NBF_4, 0.3 $mol{\cdot}dm^{-3}$) in the presence of various amounts of nBu_4NCl; i_0: same current but in the absence of added nBu_4NCl; the reduction peak currents were measured at a steady gold disk electrode (i.d. = 0.5 mm) with a scan rate of 0.2 $V{\cdot}s^{-1}$; for the definition of r_D see caption of Figure 3b; the solid lines are the theoretical predictions according to Equation 4

The equilibrium constant K_{Cl} has been determined at different temperatures in THF. The equilibrium according to Equation 2 favors production of the anionic species at higher temperatures. The Arrhenius plot of $\ln K_{Cl}$ versus $1/T$ (Figure 5) allows the determination of the activation par-

ameters from the slope and intercept, so that $\Delta H^0 = 20$ kJ mol^{-1} and $\Delta S^0 = -20$ J K^{-1}.

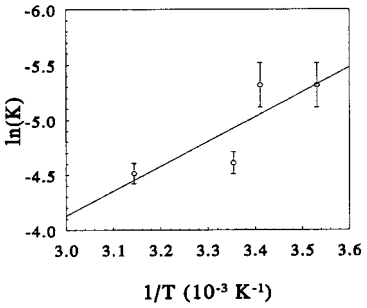


Figure 5. Arrhenius plot for the equilibrium $PdCl_2(PPh_3)_2 + Cl^- \rightleftharpoons PdCl_3(PPh_3)^- + PPh_3$ (with nBu$_4$N as counter-cation) in THF containing nBu$_4$NBF$_4$ (0.3 mol·dm^{-3}); variation of ln K_{Cl} versus $1/T$

The small value of ΔS^0 is indicative of a reaction in which there is no variation of the numbers of species in solution.

Miscellaneous Reactions

All reactions investigated above concern the substitution of the phosphane ligand by the same halide X^- as those present in $PdX_2(PPh_3)_2$. Reactions are more complicated when different halides are considered. For example: when 30 equivalents of nBu$_4$NI were added to a solution of $PdCl_2(PPh_3)_2$ (2.4 mmol·dm^{-3}) in THF, PPh_3 was detected in the ^{31}P-NMR spectrum as a narrow signal indicative of the substitution of the phosphane ligand by one iodide ion which generates anionic species: $PdCl_2I(PPh_3)^-$.

$$PdCl_2(PPh_3)_2 + I^- \rightarrow PdCl_2I(PPh_3)^- + PPh_3 \quad (5)$$

However, this complex could not be characterized since an unresolved broad signal was present at $\delta = 17.5$ suggesting that scrambling reactions occurred by equilibria such as in Equation 6 and/or 7.

$$PdCl_2I(PPh_3)^- + PPh_3 \rightleftharpoons PdICl(PPh_3)_2 + Cl^- \quad (6)$$

$$PdCl_2(PPh_3)_2 + I^- \rightleftharpoons PdICl(PPh_3)_2 + Cl^- \quad (7)$$

Under these conditions, several neutral or anionic complexes may be formed: $PdICl(PPh_3)_2$, $PdI_2(PPh_3)_2$, $PdCl_2I(PPh_3)^-$, $PdClI_2(PPh_3)^-$, $PdI_3(PPh_3)^-$ involved in different and simultaneous equilibria, responsible for the unresolved broad signal observed in the ^{31}P-NMR spectrum.

Discussion and Conclusion

Halide ions can substitute a phosphane ligand in $PdX_2(PPh_3)_2$ complexes to afford anionic species $PdX_3(PPh_3)^-$ by an equilibrium. Similar anionic $NiCl_3(PR_3)^-$ (R = isopropyl) complexes have been reported to be formed by phosphane substitution[13] while $PtCl_3(PR_3)^-$ complexes are usually synthesized by allowing chloride ions to react with phosphane-deficient dimeric complexes, $Pt_2Cl_4(PR_3)_2$.[14] However, $PdX_2(PPh_3)_2$ remains the more stable complex in THF and DMF for moderate halide ion concentrations. The phosphane substitution is easier for chloride ions which reveals the higher nucleophilic affinity of Cl^- for the palladium(II) center than that of Br^- or I^-. This can be understood as an interaction between "hard" Lewis acids and bases. The substitution of the phosphane by the chloride is more efficient in THF than in DMF probably due to the lower capacity of THF relative to DMF to solvate chloride ions compared to the larger anionic species PdX_3L^-.

Conversely, we have reported that the affinity of Cl^- for palladium(0) centers is less than that of Br^- or I^- which can be rationalized as an interaction between "soft" centers.[3] Those results evidence the ability of halide ions to coordinate both palladium(0) and palladium(II) complexes and thus probably to influence further reactions involving such complexes. We have already reported the consequences of the ligation of palladium(0) complexes by halide[3–5] or acetate ions[5][15] on the mechanism of palladium-catalyzed reactions. Although palladium(II) dihalide complexes are less involved as promoters of catalytic reactions than palladium(0) complexes, arylpalladium(II) halide complexes are postulated to be crucial intermediates in palladium(0)-catalyzed reactions involving aryl halides. Reactions of halide ions X'^- with $ArPdX(PPh_3)_2$ complexes do not result in a substitution of one phosphane ligand but rather substitution of the halide X^- to form neutral $ArPdX'(PPh_3)_2$ complexes.[16] In fact, we have established that $ArPdX(PPh_3)_2$ complexes are not reactive intermediates in cross-coupling[3][5] or Heck[5][15] reactions and the effect of chloride or acetate anions on the course of these reactions is to produce new anionic or neutral complexes such as $ArPdX(Cl)(PPh_3)_2^-$, $ArPdX(OAc)(PPh_3)_2^-$, $ArPd(OAc)(PPh_3)_2$ where the two phosphane ligands remain attached to the palladium(II) center

Experimental Section

General: ^{31}P-NMR spectra were recorded with a Bruker W 400 spectrometer (162 MHz) with H_3PO_4 as an external reference. Cyclic voltammetry was performed with a home-made potentiostat and a waveform generator Tacussel GSTP4 or EGG. The cyclic voltammograms were recorded with a Nicolet 301 oscilloscope.

Chemicals: DMF was distilled from calcium hydride under vacuum and kept under argon. Commercial nBu$_4$NCl, nBu$_4$NBr, nBu$_4$NI (Acros) were used after crystallisation. They were melted and dried under vacuum. $PdCl_2(PPh_3)_2$, $PdBr_2(PPh_3)_2$, $PdI_2(PPh_3)_2$, was prepared according to described procedures.[17]

Electrochemical Set Up and Electrochemical Procedure for Cyclic Voltammetry: Experiments were carried out in a three-electrode cell connected to a Schlenk line. The counter electrode was a platinum wire of ca. 1 cm^2 apparent surface area; the reference was a saturated calomel electrode (Tacussel) separated from the solution by a bridge filled with 3 mL of THF or DMF containing nBu$_4$NBF$_4$ (0.3 mol·dm^{-3}).

General Procedure: 12 mL of THF or DMF containing nBu$_4$NBF$_4$ (0.3 mol·dm^{-3}) was poured into the cell followed by $PdCl_2(PPh_3)_2$

(16.8 mg, 0.024 mmol) and various amounts of nBu$_4$NCl. Cyclic voltammetry was performed at steady gold disk electrodes with various scan rates.

[1] E. I. Negishi, T. Takahashi, K. Akiyoshi, *J. Chem. Soc., Chem. Commun.* **1986**, 1338−1339.
[2] C. Amatore, M. Azzabi, A. Jutand, *J. Organomet. Chem.* **1989**, *363*, C41−C45.
[3] C. Amatore, M. Azzabi, A. Jutand, *J. Am. Chem. Soc.* **1991**, *113*, 1670−1677.
[4] C. Amatore, A. Jutand, A. Suarez, *J. Am. Chem. Soc.* **1993**, *115*, 9531−9541.
[5] For a review see: C. Amatore, A. Jutand, *J. Organomet. Chem.* **1999**, *573*, 254−278.
[6] L. Mottier, part of Ph.D. thesis, University Paris VII, **1995**.
[7] [$PdCl_3(PPh_3)^-$, nBu$_4$N$^+$] has been synthesized independently by treating $Pd_2Cl_4(PPh_3)_2$ with two equivalents of nBu$_4$NCl, in THF according to a reported procedure:[8] $Pd_2Cl_4(PPh_3)_2 + 2\ Cl^- \rightarrow 2\ PdCl_3(PPh_3)^-$. It was characterized by its ^{31}P-NMR spectrum at $\delta = 27.42$ similar to the signal of the complex formed in Equation 1.
[8] R. J. Goodfellow, P. L. Goggin, D. A. Duddell, *J. Chem. Soc. A* **1968**, 504−506.
[9] J. Chatt, L. M. Venanzi, *J. Chem. Soc.* **1957**, 2351−2356.
[10] R. Bardi, A. M. Piazzesi, A. Del Pra, G. Cavinato, L. Toniolo, *Inorg. Chim. Acta* **1983**, *75*, 15−19.
[11] A. J. Bard, L. R. Faulkner, *Electrochemical Methods*, Wiley, New York, **1980**, p. p. 443−449.
[12] A. J. Bard, L. R. Faulkner, *Electrochemical Methods*, Wiley, New York, **1980**, p. 213−248.
[13] [13a] G. G. Eberhardt, W. P. Griffin, *J. Catal.* **1970**, *16*, 245−253. − [13b] Y. Chauvin, unpublished results, personal communication, **1996**.
[14] P. L. Goggin, R. J. Goodfellow, S. R. Haddock, B. F. Taylor, I. R. H. Marshall, *J. Chem. Soc., Dalton Trans.* **1976**, 459−467.
[15] C. Amatore, E. Carré, A. Jutand, M. A. M′Barki, G. Meyer, *Organometallics* **1995**, *14*, 5605−5614.
[16] M. C. Pilon, V. V. Grushin, *Organometallics* **1998**, *17*, 1774−1781.
[17] F. R. Hartley, *Organomet. Chem. Rev., Sect. A* **1970**, *6*, 119.

Received January 7, 1999
[I99007]

Structural Studies of Novel Siloxysilsesquioxanes

Norbert Auner,*[a] Burkhard Ziemer,[b] Bernhard Herrschaft,[a] Wolfgang Ziche,[c] Peter John,[c] and Johann Weis[c]

Dedicated to Prof. Dr. Peter Jutzi on the occasion of his 60th birthday

Keywords: Silsesquioxanes / MALDI-TOF / DSC / Structure elucidations / Thermochemistry / Mass spectrometry

Five silsesquioxanes $(RSiO_{3/2})_{2n}$ with R = siloxy and n = 4, 5 have been investigated by X-ray crystallography, MALDI-TOF mass spectrometry, and differential scanning calorimetry (DSC).

Silicon and silicon-containing compounds have found widespread use in modern technology; this field includes purely inorganic materials (e.g. for electronics) as well as organosilicon polymers.[1] Especially interesting are globular oligosilsesquioxanes $(RSiO_{3/2})_{2n}$ (n = 3, 4, 5, ...), also called spherosiloxanes due to their shape,[2] in which the Si−O core is trigonal-prismatic (n = 3), cubic (n = 4), or pentagonal-prismatic (n = 5). These are widely used in fields ranging from optical fibres to cosmetics.[3−5] Generally, silsesquioxanes may be best described as an interface between the purely inorganic silicates and carbosilanes composed of a rigid silicate core and chemically useful peripheral organic functionalities. Thus, silsesquioxanes serve as precursors for novel organosilicon polymers,[6] organolithiated macromolecular materials,[7][8] and porous hybrid inorganic-organic materials.[9] By virtue of the fact that they are both rigid and polyfunctional, they serve as suitable cores for the formation of three-dimensional dendrimers[10] and liquid crystals.[11] Furthermore, they are useful as templates for the preparation of polymeric and ceramic materials by sol-gel techniques.[12] Their derivatization with organometallic functionalities leads to precursors for catalyst preparation (e.g. cobalt carbide nanoparticles in a silicaceous matrix[13]) or to materials that are useful in electrochemical devices.[14]

The hydrido species $(HSiO_{3/2})_{2n}$ may be employed for the deposition of SiO_2 films in material technology,[15][16] and is widely used as a starting compound for the synthesis of substituted silsesquioxanes.[12][17] The silsesquioxanes also serve as model compounds for the study and understanding of the properties of zeolites and silicates.[18] While crystal structures have been reported for hydrido siloxanes[19] and organosilsesquioxanes,[20] not much is known about siloxy-functionalized silsesquioxanes (or silyl silicates),[21−25] although the pioneering work of Lentz[26] and Hoebbel[27] dates back to the 1960s.

In this paper, we report the crystal structures of five basic siloxysilsesquioxanes (R = $OSiMe_3$, $OSiMe_2H$, $OSiMe_2Vi$ for n = 4, and R = $OSiMe_3$, $OSiMe_2H$ for n = 5). Discrepancies between the structures obtained and the results of ^{29}Si-MAS-NMR studies are clarified by investigation of the thermal behaviour of the cage compounds by DSC. Their suitability as siloxane mass standards for MALDI-TOF mass spectrometry is tested. The siloxysilsesquioxane $[(M_3Q)DQ]_8$, **6** [R = $OSiMe_2(OSiMe_3)$, n = 4], for which no crystal structure could be obtained, was also included in this part of the study.

Molecular Structures

The common structural feature of the present eight-membered cyclic compounds $Si_8O_{20}R_8$ is a heterocubane anion in which the silicon atoms are placed at the corners of a cube, each one bearing a terminal oxygen atom. Twofold bridging oxygen atoms are positioned at each edge of the cube, leading to the coordination formula $[(SiO_{1/1}O_{3/2})^{1-}]_8 = [Si_8O_{20}]^{8-}$ for the core. Eight silyl groups, specifically $SiMe_3$ in **1** $[M_8Q_8]$, $SiMe_2H$ in **2** $[M^H{}_8Q_8]$, and $SiMe_2Vi$ in **3** $[M^V{}_8Q_8]$, are attached to the terminal oxygen atoms, resulting in electrically neutral molecules. Relative to the $[Si_8O_{20}]^{8-}$ anion in Ekanite, $ThKCaNa[Si_8O_{20}]$[28], the Si−O distances in compounds **1**−**3** are slightly longer and the bond angles at the bridging oxygen atoms have slightly smaller values. This clearly stems from the coordinative requirements in Ekanite, which are essentially dominated by the geometrical constraints imposed by the cations. In **1**−**3**, these are replaced by bulky SiR_3 substituents with a comparably high steric demand, hence the molecular units are no longer linked together by electrostatic cation interactions, but only by weak dispersion interactions caused by the relatively non-polar silyl groups.

[a] Institut für Anorganische Chemie, Johann Wolfgang Goethe Universität,
Marie-Curie-Strasse 11, D-60439 Frankfurt/M., Germany
Fax: (internat.) + 49(0)69/798-29188
E-mail: auner@chemie.uni-frankfurt.de
[b] Institut für Anorganische und Allgemeine Chemie, Humboldt-Universität zu Berlin,
Hessische Strasse 1−2, D-10115 Berlin, Germany
Fax: (internat.) + 49(0)30/2093-6966
E-mail: burkhard=ziemer@chemie.hu-berlin.de
[c] Wacker Chemie GmbH,
Johannes-Hess-Strasse 24, D-84489 Burghausen, Germany

 © WILEY-VCH Verlag GmbH, D-69451 Weinheim, 1999 1434−1948/99/0707−1087 $ 17.50+.50/0

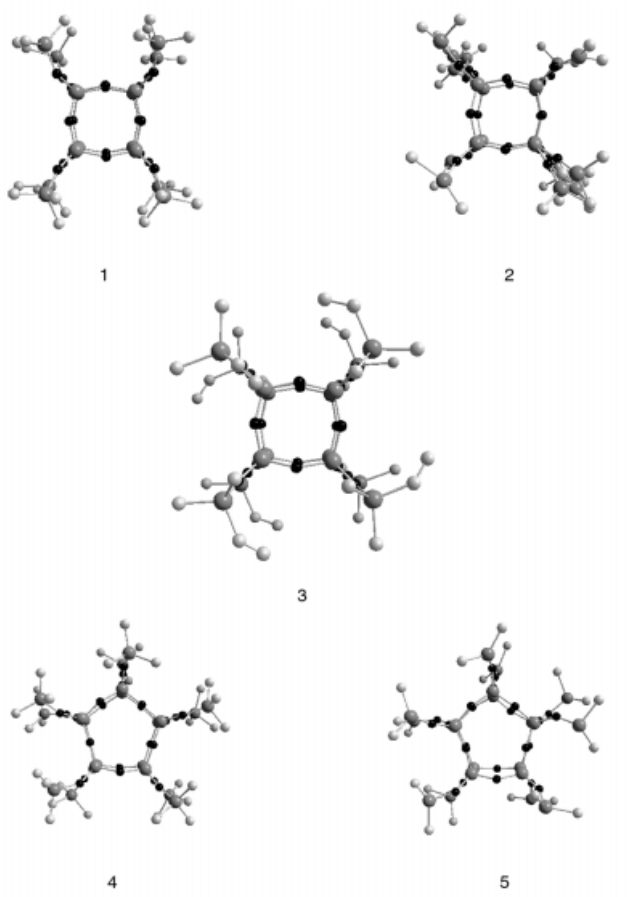


Figure 1. Molecular structures of compounds **1**−**5**

The molecular core of the silsesquioxanes $Si_{10}O_{25}R_{10}$, derived from $[Si_{10}O_{25}]^{10-}$ anions, formally results from the insertion of an $[O(SiO_{1/2}O_{1/1})_2]^{2-} = [Si_2O_5]^{2-}$ unit into a pseudo-cubic $[Si_8O_{20}]^{8-}$ anion, leading to a pentagonal-prismatic anion $[(SiO_{1/1}O_{3/2})^{1-}]_{10} = [Si_{10}O_{25}]^{10-}$. Isolated anions of this type have not been observed in the solid state, but they do occur as building blocks in zeolites (pentasil units in ZSM-5 and ZSM-11)[29]. The novel cyclic silicates $Si_{10}O_{25}R_{10}$ (**4**, R = $SiMe_3$, $M_{10}Q_{10}$; **5**, R = $SiMe_2H$, $M^H{}_{10}Q_{10}$) may be regarded as model compounds of the anions $[Si_{10}O_{25}]^{10-}$ characterized as their silyl-substituted molecular entities. The geometrical features are similar to those discussed for $Si_8O_{20}R_8$. The molecular structures of

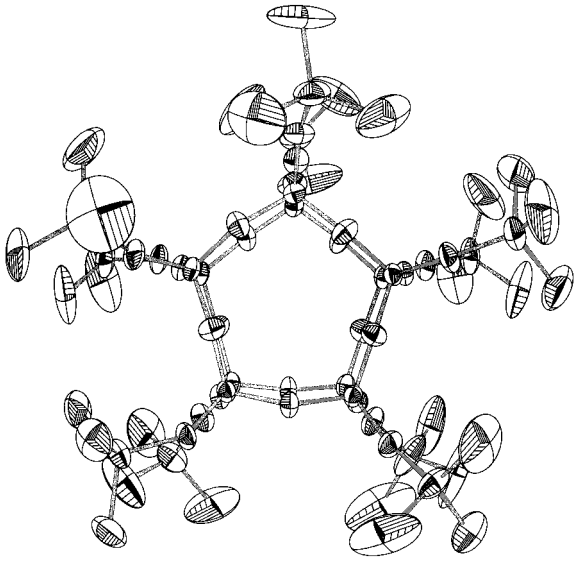


Figure 2. Molecular structure of **4** showing 15% probability atomic displacement ellipsoids

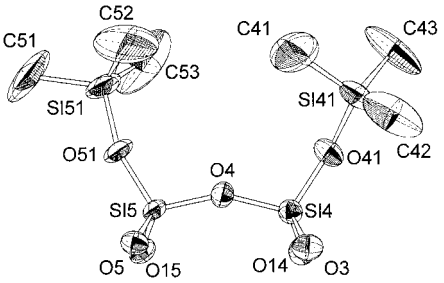


Figure 3. Part of the molecular structure in **5** showing 30% probability atomic displacement ellipsoids

the silsesquioxanes **1**−**5** have been determined by single-crystal X-ray diffraction and are shown in Figure 1.

Results and Discussion

As can be seen from Table 1, no unusual interatomic distances or bond angles were detected.[30] As expected, the accuracies of the Si−O and Si−C bond-length determinations are higher for the low-temperature structure analysis and decrease considerably on going from the inner to

Table 1. Variations of bond lengths [Å] and bond angles [°] in molecules **1**−**5** [bond parameters of atoms on split sites are omitted; cage (c) and ligand (l) are distinguished]

	1 T = 295 K	**2** 200 K	**3** 200 K	**4** 295 K	**5** 200 K
$Si-O_c$	1.585−1.616(9)	1.599−1.607(5)	1.597−1.608(3)	1.574−1.609(8)	1.585−1.613(6)
$Si-O_{c/l}$	1.581−1.583(9)	1.585−1.627(7)	1.580−1.606(3)	1.549−1.600(9)	1.568−1.594(6)
$O-Si_l$	1.582−1.587(9)	**not reliable for**	1.594−1.606(3)	1.542−1.610(9)	1.526−1.630(7)
$Si-C_l$	1.66−1.86(3)	**split sites**	1.74−1.99(1)	1.70−1.89(4)	1.62−1.86(2)
$O-Si-O_c$	108.1−110.3(5)	108.9−110.1(2)	108.9−110.1(2)	108.3−110.7(5)	108.1−111.0(4)
$Si-O-Si_c$	147.2−150.5(6)	148.1−148.3(3)	148.1−148.3(3)	149.3−157.9(6)	142.2−156.0(4)
$Si-O-Si_l$	147.8−156.1(7)	159.1−159.1(4)	152.6−153.7(2)	144.8−172.4(8)	141.3−172.4(6)
$O-Si-C_l$	105−114(1)	**not reliable for**	106.0−112.1(3)	105−113(1)	108.8−122.5(7)
$C-Si-C_l$	98−126(2)	**split sites**	107.8−114.1(4)	97−110(2)	110.2−123.7(8)

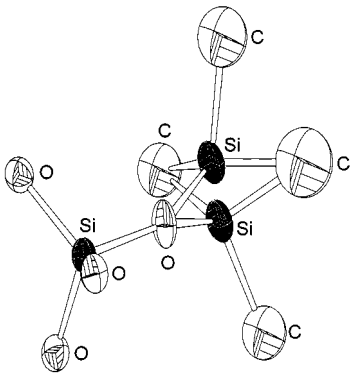


Figure 4. Disorder of $OSiMe_3$ groups in **1** (15% probability, hydrogen atoms omitted for clarity)

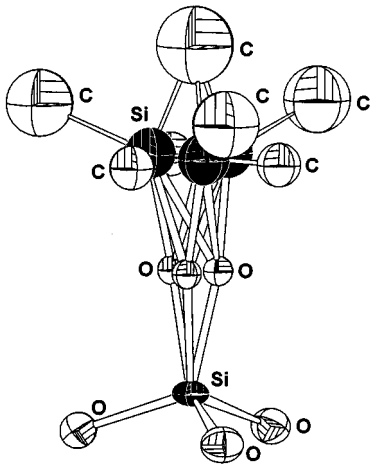


Figure 5. Superposition structure of **2** about the threefold axis; detail of disordered $OSiMe_3$ groups: "ice-cream cone motif"

the outer sphere within each molecule. This disorder may be explained either in terms of an intense thermal motion of the atoms at room temperature, which is frozen on cooling, or, alternatively, by considering closely neighbouring but slightly different atom positions partially occupied by almost fixed atoms at low temperature.

As mentioned above, these experimental findings may be attributed to a decrease in the rigidity of the core owing to the replacement of metal cations, or in this particular case – following the syntheses of silsesquioxanes **1**–**5** given in the Experimental Section – of ammonium cations $[NR_4]^+$ ($R = CH_3$, C_4H_9), by organosilyl groups. All five structures are characterized by unusually large anisotropic displacement parameters. Figure 2 shows the ellipsoids for **4**, which

Table 2. Crystal data, details of data collection and structure refinement for cubes **1**, **2**, **3**, and compounds **4** and **5**

	1	**2**	**3**	**4**	**5**
Empirical formula	$C_{24}H_{72}O_{20}Si_{16}$	$C_{16}H_{56}O_{20}Si_{16}$	$C_{32}H_{72}O_{20}Si_{16}$	$C_{30}H_{90}O_{25}Si_{20}$	$C_{20}H_{70}O_{25}Si_{20}$
M_r	1130.40	1018.16	1226.48	1413.00	1272.7
Crystal system	triclinic	trigonal-rhombohedral	triclinic	monoclinic	monoclinic
Space group	$P-1$ (2)	$R-3$ (148)	$P-1$ (2)	$P21/a$ (14)	$P21/c$ (14)
Crystal size [mm]	0.42, 0.38, 0.22	0.39, 0.23, 0.19	0.62, 0.31, 0.23	1.00, 0.63, 0.12	0.40, 0.38, 0.23
a [Å]	11.046(3)	16.103(3)	11.098(3)	12.636(12)	19.101(4)
b [Å]	11.104(2)	16.103(3)	11.126(3)	44.455(13)	15.029(3)
c [Å]	13.554(2)	17.349(4)	15.006(4)	15.462(4)	22.148(4)
α [°]	77.68(3)		70.15(2)		
β [°]	82.08(4)		71.04(2)	111.90(3)	100.81(2)
γ [°]	84.04(4)		83.59(3)		
V [Å^3]	1603.9(6)	3896(1)	1648.3(8)	8058(8)	6248(2)
$\rho_{calcd.}$ [gcm^{-3}]	1.170	1.302	1.236	1.165	1.354
Z	1	3	1	4	4
$F(000)$ [e]	600	1608	648	3000	2680
μ(Mo-K_α) [mm^{-1}]	0.323	0.395	0.317	0.321	0.41
Data collection					
Diffractometer	STOE Stadi4	STOE Ipds	STOE Ipds	STOE Stadi4	STOE Ipds
Radiation		Mo-K_α, 0.71071 Å graphite monochromator			
T [K]	295(2)	200(2)	200(2)	295(2)	200(2)
Scan mode	2θ/ω = 1.0	φ oscillat.	φ oscillat.	2θ/ω = 0.5	φ oscillat.
hkl range	± 10/10/± 13	± 19/± 19/± 21	± 13/± 13/± 18	± 11/42/± 14	± 21/±17/± 25
Measured refl.	4764	11081	16119	12278	39351
Unique refl. ($> 2\ \sigma_I$)	2982	1714	6010	7480	9731
R_{int}	0.0499	0.0511	0.0508	0.0700	0.0594
Used refl.	2978	1714	6008	7026	9729
Absorption correction	no	no	no	empirical	no
T_{min}/T_{max}	–/–	–/–	–/–	0.8879/0.9995	–/–
Refinement					
Refined parameters	262	93	297	677	586
H atoms (found/calcd.)	0/72	0/56	0/72	0/90	0/70
$R1$[a] [$F_o > 4\ \sigma(F_o)$]	0.1153 (2186 refl.)	0.1008 (761 refl.)	0.0563 (4365 refl.)	0.0809 (4307 refl.)	0.0971 (5393 refl.)
$wR2$[b] (all)	0.2725	0.3032	0.1741	0.3013	0.2747
GooF (all)	1.180	0.961	1.069	1.342	1.070
Weighting par. a, b[c]	0.0830/8.776	0.1884/0.000	0.0902/0.789	0.0650/42.497	0.1040/46.046
ρ_{final}(max/min) [eÅ^{-3}]	0.468/–0.271	0.489/–0.815	0.450/–0.294	0.411/–0.455	2.16/–1.38

[a] $R1 = \Sigma||F_o| - |F_c||/\Sigma|F_o|$. – [b] $wR2 = [\Sigma w(F_o^2 - F_c^2)^2/\Sigma w(F_o^2)^2]^{1/2}$. – [c] $w = 1/[\sigma^2(F_o^2) + (a\,P)^2 + b\,P]$; $P = (F_o^2 + 2\,F_c^2)/3$.

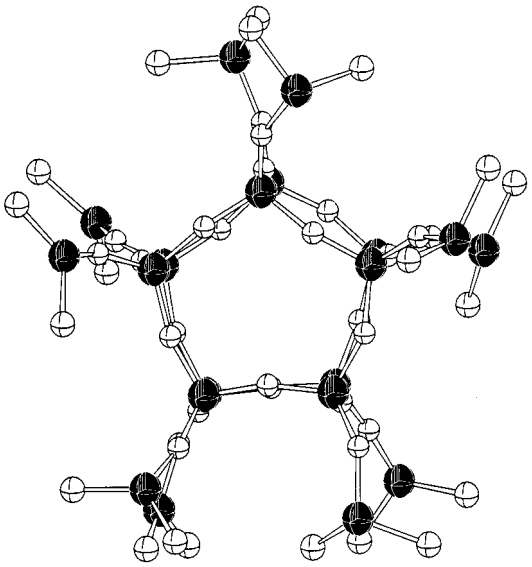


Figure 6. Model structure of **5** with twenty crystallographically independent silicon sites at 200 K

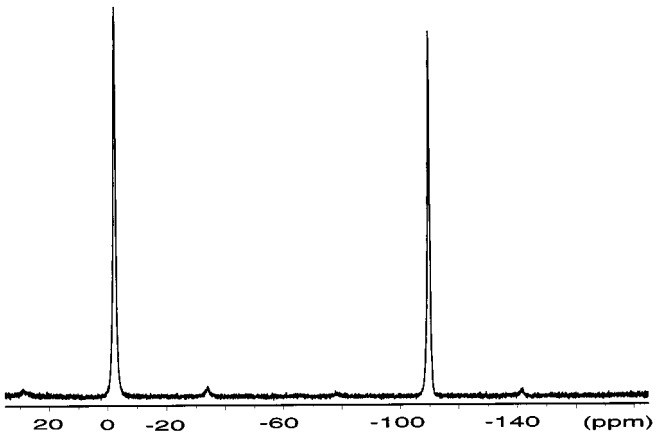


Figure 7. ^{29}Si-MAS-NMR spectrum (spinning rate 2000 Hz) of **5** at 293 K, showing two signals for two sets of ten magnetically equivalent silicon atoms

are seen to increase markedly on going from the inner to the outer part of the molecule.

Unusually large anisotropic displacement parameters U_{ij} with $U_3/U_1 > 10$ were found for two peripheral C atoms in **1**, for thirteen C atoms in **4**, and for two C atoms and two ligand Si atoms in **5**. Figure 3 shows a detail of a part of **5** containing one such ligand (Si51, C51, and C52). However, the same figure reveals that the neighbouring ligand (Si41, C41, and C42) does not exhibit unusually large anisotropic displacement parameters.

This indicates atom site disorder, which is individually different for the various ligands and, therefore, cannot be a consequence of a rigid body motion of the whole molecule.

The $OSiMe_3$ groups in **1** are found to be disordered (Figure 4); this may explain why other researchers did not succeed in determining an accurate molecular structure.[21]

The highest degree of disorder in all the crystal structures reported in this paper was observed for compound **2**. Here, a split-atom model had to be introduced in order to permit refinement of the atomic positions of all the ligands. Figure 5 shows the superposition structure of **2** about the threefold axis, with each atom site one-third occupied for reasons of symmetry. The ligands at the other corners of the cube are also strongly disordered, but are not subject to any symmetry constraints.

Inspection of the data in Table 2 reveals that **1** and **4** have significantly lower densities than the other silsesquioxanes **2**, **3**, and **5**. In contrast to the other compounds, **1** and **4** have exclusively methyl groups as their outer ligands, which may be a reason for their loose crystal packings.

From the crystal-structure analysis of **5**, it can be seen that at temperatures as low as 200 K (measuring temperature) the whole molecule can be regarded as an asymmetrical unit, with ten crystallographically independent silicon sites making up the core subunit (Figure 6). Notably, in the solid-state ^{29}Si-MAS-NMR spectrum (Figure 7) of the

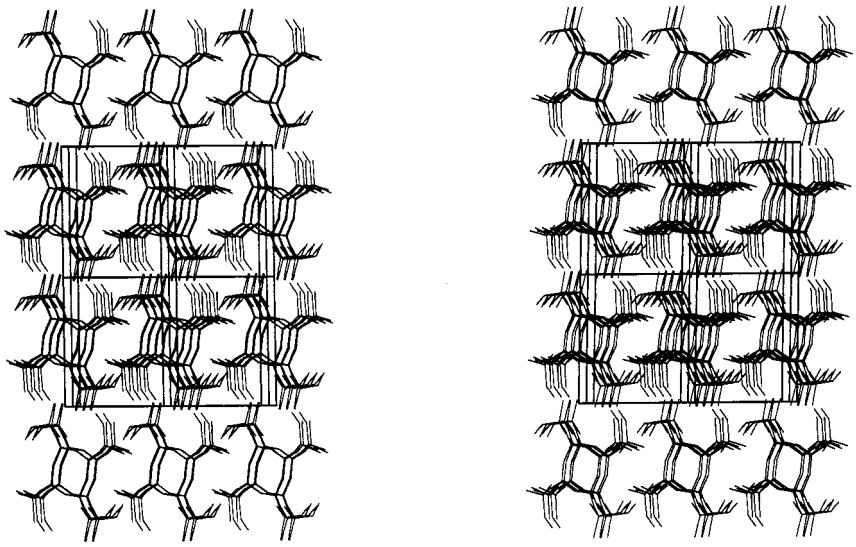


Figure 8. Ordering of **3** in the lattice by interlocking of the vinyl groups; slightly skewed stereo view along the *c* axis

Table 3. Results of DSC measurements

	Measurement details and observations[a]	T [°C]	ΔH [Jg^{-1}] −: endothermic +: exothermic	Interpretation
1	Closed pan, no weight loss	198.8	−6.9	phase transition
		295.4	−2.3	m.p.
		−118.2	endothermic	phase transition
2	Open pan, 49% weight loss	260.3	−15.9	m.p.
	Repetition with same sample, 89% weight loss	>220		m.p. after partial decomposition
	Closed pan, no weight loss	183.9	+4.6	reaction
	TGA, onset of sublimation at 177°C	259.2	−16.7	m.p.
	Closed pan, −140 to +30°C, no weight loss	−117.9	endothermic	phase transition
3	Closed pan, no weight loss	125 (br.)	−4.1	phase transition
		161.8 (br.)	+8.2	reaction
		257.3	−8.7	m.p.
	Repetition with same sample	73.0	−3.3	phase transition
		249.1 and ca. 256	−5.7	m.p.s after partial decomposition
	Open pan, 11% weight loss	125.5	−4.0	phase transition
		253.8	−8.1	m.p.
	Repetition with same sample, 10% weight loss	74.2	−1.3	phase transition
		122.0	−1.9	phase transition
		250.3	−6.4	m.p.
	Closed pan, −140 to +30°C, no weight loss	−45.2	endothermic	phase transition
		−100.0	endothermic	phase transition
4	Closed pan, no weight loss	119.4	−10.0	phase transition
		252.6	−3.2	phase transition
		262.0	−0.7	m.p.
		269.1	+3.3	reaction
	Repetition with same sample	116.8	−9.6	phase transition
		251.4	−3.1	phase transition
		262.0	−1.4	m.p.
		−83.3	endothermic	phase transition
5	Closed pan, no weight loss	83.4	−2.9	phase transition
		135.8	−5.6	m.p.
		143.2	+8.8	reaction
	Repetition with same sample	98.7 (br.)	−3.0	m.p. after partial decomposition
	Open pan, 12% weight loss	83.5	−2.9	phase transition
		135.8	−7.9	m.p.
	Repetition with same sample, 4.7% weight loss	−	−	no phase transition, m.p. or reaction
	Open pan, −100 to +30°C, no weight loss	−60.7	5.0	phase transition
		−44.9	10.6	phase transition
	Closed pan, −140 to +30 °C, no weight loss	24.2	endothermic	phase transition
		−53.3	endothermic	phase transition
		−69.5	endothermic	phase transition
6	Open pan, 100% weight loss at 600°C	144.2	−1.5	phase transition
		232.9	−1.2	phase transition
		> 330−540	−32.9	sublimation
	Open pan, 1.8% weight loss up to 300°C	124.3	−4.0	phase transition
		254.8	−8.1	phase transition
	Closed pan, no weight loss up to 375°C	95.0	endothermic	phase transition
		144.3	endothermic	phase transition
		230.9	endothermic	phase transition
	Closed pan, −140 to +30 °C, no weight loss	18.8	endothermic	phase transition
		−75.5	endothermic	phase transition

[a] Weight loss in open-pan measurements due to sublimation of the compound; measurement up to 300 °C with a 10 °C min^{-1} heating rate.

sample, only two rather than twenty signals appear at ambient temperature, one for the siloxy groups and one upfield-shifted signal for the carbosiloxy groups, indicating the magnetic equivalence of the individual silicon atoms within the two sets of silicon sites.[31]

A better ordering and relative orientation of the silsesquioxanes is achieved by the introduction of vinyl groups into the peripheral silyl substituents at the Si−O core, as exemplified by the crystal structure analysis of **3**. A stereo plot illustrates the interlocking of the vinyl groups (Figure 8).

The findings of (i) the disorder in **1** and **2**, and (ii) the discrepancy between the results of the ^{29}Si-MAS-NMR-spectrometric investigations and of the X-ray analysis of **5** prompted us to measure the DSC curves of the siloxysilsesquioxanes. The results are summarized in Table 3.

Compound **5** shows low-temperature phase transitions (Figure 9). Thus, the differences between the ^{29}Si-MAS-

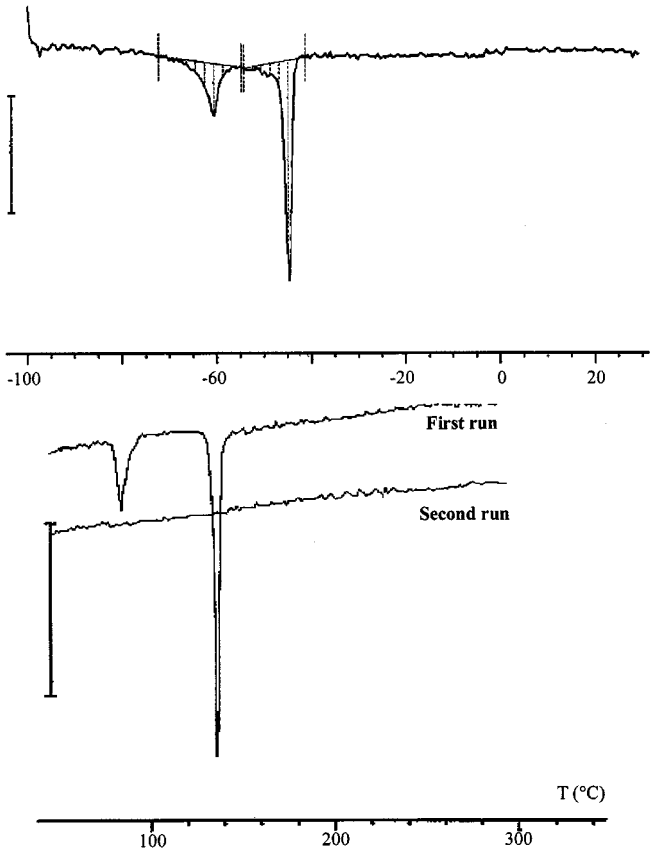


Figure 9. DSC traces of **5** from −100°C to 30°C (vertical bar 0.1 Wg^{-1}; 2°C min^{-1}) and from 30°C to 300°C (top trace; 10°C min^{-1}), repetition with same sample (bottom trace; vertical bar 0.2 Wg^{-1})

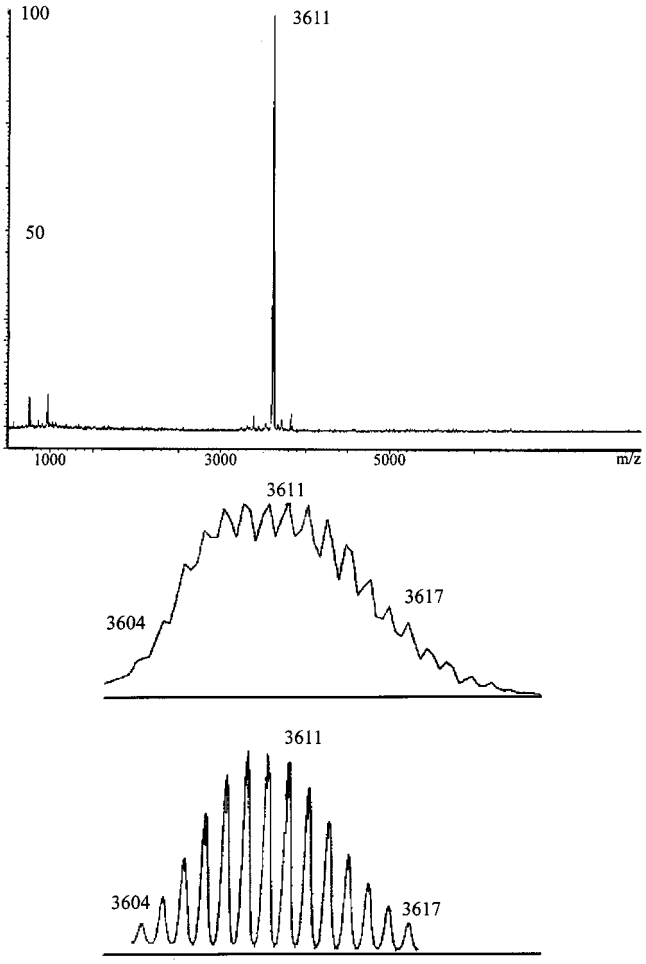


Figure 10. MALDI-TOF mass spectrum of $[(M_3Q)DQ]_8$ (**6**) at *m/z* = 3611; insert shows measured and calculated spectrum from *m/z* = 3604 to 3620

NMR results and the X-ray crystallography analysis are understandable: While at low temperatures a highly asymmetric modification is stable, at room temperature a much more symmetric arrangement is energetically favoured. Another interesting feature is the low melting point of **5**, which is more than 100°C lower than those of the other studied silsesquioxanes.

Silsesquioxanes bearing peripheral reactive groups undergo reaction when heated. In particular, **5** reacts completely to form an amorphous glass, which no longer shows any prominent peaks in a subsequent DSC run. ^{29}Si-NMR studies on a sample heated to 220°C under exclusion of air for 4 h show the formation of $HSiO_{3/2}$ and $Me_2SiO_{2/2}$ groups.

X-ray powder-diffraction experiments were utilized to investigate the nature of two-phase transitions in **1** and **5**.

The diffraction pattern of **1** breaks down at 200°C. This temperature is in good accord with the phase transition at 199°C detected by DSC. Simultaneously, **1** begins to decompose and/or to sublime. This behaviour may be explained in terms of the well-known Hedvall effect.[32] The diffraction pattern of **5** changes at 80°C (upwards) and reversibly at 40°C (downwards). The high-temperature modification obtained shows a sharp diffraction pattern on the Guinier photograph, but despite this it could not be indexed for a unit-cell determination. A single crystal of **5** heated to 90°C on a STOE IPDS diffractometer crumbled to a powder, indicating that no topotactic relationship exists between the low- and high-temperature modification.

In addition to structural investigations, compounds **1**−**5** were also characterized by mass-spectrometric methods. Simultaneously, the applicability of the siloxysilsequioxanes as mass standards for **M**atrix-**A**ssisted **L**aser **D**esorption **I**onisation/**T**ime **o**f **F**light (MALDI-TOF) mass spectrometry was investigated (Table 4). Despite the expected high stabilities of the siloxanes, fragmentation and reaction with matrix components was found in some cases. **1** and **2** were found to be contaminated by Q_6M_6[33]; the H-siloxanes reacted with the acidic matrix and showed quite extensive decomposition and fragmentation under the experimental conditions. The excellent result for **3** is not surprising in view of the well-known coordination of carbon−carbon multiple bonds to silver ions. Quite astonishing, however, is the clean spectrum of **6** (Figure 10).[34]

Experimental Section

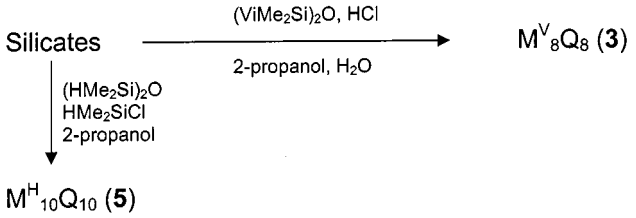
General: Compounds **1**−**6** were prepared according to known literature procedures[35] by treating freshly precipitated silicic acid

Table 4. Results of MALDI-TOF mass spectrometry

Compound	Fragmentation[a]	Molecular ion[a]
1 Q_8M_8	771 (85%): Q_6M_6 − Me_3Si; 1165 (100%): Q_8M_8 − $SiMe_2CH_2$	1237 (77%)
2 $M^H{}_8Q_8$	1253 (100%): $M^H{}_8Q_8$ − H + O-octyl; 3 others below 20%, "noise" ca. 5%	1125 (37%)
3 $M^V{}_8Q_8$		1333 (100%)
4 $Q_{10}M_{10}$	771 (22%) Q_6M_6 − Me_3Si; 1743 (100%): ?	1520 (59%)
5 $M^H{}_{10}Q_{10}$	1539 (44%): Si−O−Si in $M^H{}_{10}Q_{10}$ cleaved and substituted by two Me_3Si−O groups; fragments distributed from 1000 to 1700, max. 12%	1379 (100%)
6 $[(M_3Q)DQ]_8$		3611 (100%)

[a] Ag^+ adducts.

with tetramethylammonium hydroxide to form the cyclic octasilicate $[(NMe_4)^+]_8[Si_8O_{20}]$. From the condensation reaction of $Si(OEt)_4$ with tetrabutylammonium hydroxide/H_2O, the decasilicates were obtained. Subsequent treatment of these silicates with mixtures of the corresponding disiloxanes and chlorosilanes or HCl in 2-propanol solution, furnished the octasiloxy- or decasiloxy-substituted silsesquioxanes **1**−**6** in good yields. The representative syntheses of compounds **3** and **5** are depicted in Scheme 1.



Scheme 1. Syntheses of siloxysilsesquioxanes

The crystalline products thus obtained were recrystallized from CH_2Cl_2/CH_3CN (1:1) by slow evaporation of the solvents at 25°C. Purities were checked by ^{1}H-, ^{13}C-, and ^{29}Si-NMR spectroscopy in $CDCl_3$ solution.

MALDI-TOF: 10 mg of the sample was dissolved in 1 mL of THF. The matrix solution was made up from 10 mg of 2-nitrophenyl octyl ether in 1 mL of acetone, to which 10 μL of 0.1% trifluoroacetic acid had been added. To assist the ionization, a 0.01 M solution of silver trifluoroacetate in acetone was used. The thin-layer technique was used for sample preparation: 0.5-μL aliquots of the matrix, silver salt, and sample solutions were successively applied. The spectra thus showed the silver adducts. External calibration was carried out with a peptide mixture (substance P and insulin). The mass accuracy was ±1 Da; the masses were rounded to integral numbers.

DSC and TGA measurements were carried out using a Netzsch STA 429 apparatus.

IR and Raman spectra correspond to literature data.[36] Vibrations due to the siloxane framework are assigned as follows (vibrations of organic functional groups are omitted). − IR: 1252−1257 cm^{-1} (s, δ_s Si−CH_3), 1074−1098 (vs, ν_{as} Si−O−Si), 755, 844, 868 (s, δ_s Me−Si−O in **1**, **4**, and **6**), 772, 838 (s, δ_s Me−Si−O in **2** and **5**), 621 (m), 559−522 (several s, ν_s Si−O−Si), 901 (s, δ O−Si−H in **2** and **5**). − Raman: Strongest bands at 2902−2912 cm^{-1} (vs, ν CH_3) and 2963−2971 (s, ν CH_3), and at 608−652 (vs, ν_s Si−O−Si); other bands: 1410−1412 (w, δ C−H), 692 (w, ν_s Si−O−Si), several below 420 (w to m, δ O−Si−O); 3057, 1597, 1274, 786 attributable to −CH=CH_2 in **3**; 474 (ν_s Si−O−Si) in **6**.

Crystal-Structure Determination: Single crystals of compounds **1** and **4** were examined with a four-circle diffractometer (STOE; STADI4) at room temperature in air. Single crystals of compounds **2**, **3**, and **5** were examined with a one-circle diffractometer equipped with an imaging plate area detector (STOE; IPDS) at 200 K under nitrogen. Intensity data were corrected for Lorentz and polarization effects and in the case of **4** an absorption correction had to be applied (ψ-scan technique[37]) since a crystal of rather anisotropic habit was used for the data collection. The structures were solved by direct methods[38] and refined by full-matrix least-squares techniques against F^2.[39] The thermal motion of all non-hydrogen atoms, better described in terms of atomic displacement parameters (adp′s) in the present structures, was treated anisotropically. All hydrogen atoms were calculated in idealized positions and allowed to ride on their corresponding carbon atoms. Their isotropic thermal parameters were set at 1.2 times that of the adjacent C atom. Crystallographic data (excluding structure factors) for the crystal structures reported in this paper have been deposited with the Cambridge Crystallographic Data Centre as supplementary publication no. CCDC-101329. Copies of the data can be obtained free of charge on application to CCDC, 12 Union Road, Cambridge CB2 1EZ, U.K. [Fax: (internat.) + 44-1223/336-033; E-mail: deposit@ccdc.cam.ac.uk]. High-temperature X-ray diffraction on powders of **1** and **5**, representing structure types M_8Q_8 and $M_{10}Q_{10}$, respectively, were carried out with a Nonius Guinier-Lenné camera. The powders were prepared on a platinum gauze and heated to temperatures below their melting points in air or under nitrogen.

[1] [1a] *Inorganic Polymers* (Eds.: J. E. Mark, H. R. Allcock, R. West), Prentice Hall, New York, **1992**. − [1b] *Silicon-Based Polymer Science, A Comprehensive Resource* (Eds.: J. M. Zeigler, F. W. G. Fearon), Advances in Chemistry Series 224, American Chemical Society, Washington, **1990**. − [1c] D. A. Loy, K. J. Shea, *Chem. Rev.* **1995**, *95*, 1431. − [1d] *Organosilicon Chemistry II − From Molecules to Materials* (Eds.: N. Auner, J. Weis), VCH, Weinheim, **1996**. − [1e] *Organosilicon Chemistry III − From Molecules to Materials* (Eds.: N. Auner, J. Weis), Wiley-VCH, Weinheim, **1997**.
[2] M. G. Voronkov, V. I. Lavrent′yev, *Top. Curr. Chem.* **1982**, *102*, 199.
[3] G. Calzaferri, *Proc. Tailor-Made Silicon-Oxygen Compounds, Mol. Mater.*, Bielefeld, Sept. 3−5, 1995, **1996**, 149.
[4] H. Bürgy, G. Calzaferri, D. Herren, A. Zhdanov, *Chimia* **1991**, *45*, 3.
[5] R. H. Baney, M. Itoh, A. Sakakibara, T. Suzuki, *Chem. Rev.* **1995**, *95*, 1409.
[6] D. Hoebbel, I. Pitsch, D. Z. Heidemann, *Z. Anorg. Allg. Chem.* **1991**, *592*, 207.
[7] P. A. Agaskar, *J. Am. Chem. Soc.* **1989**, *111*, 6858.
[8] P. A. Agaskar, *Inorg. Chem.* **1990**, *29*, 1603.
[9] P. G. Harrison, R. Kannengiesser, *J. Chem. Soc., Chem. Commun.* **1996**, 415.
[10] A. R. Bassindale, T. E. Gentle, *J. Mater. Chem.* **1993**, *3*, 1319.
[11] F. H. Kreuzer, R. Maurer, P. Spes, *Macromol. Chem., Macromol. Symp.* **1991**, *50*, 215.
[12] V. W. Day, W. G. Klemperer, V. V. Mainz, D. M. Millar, *J. Am. Chem. Soc.* **1985**, *107*, 8262.

[13] P. G. Harrison, R. Kannengiesser, *J. Chem. Soc., Chem. Commun.* **1995**, 2065.
[14] M. Morán, C. M. Casado, L. Cuadrado, J. Losada, *Organometallics* **1993**, *12*, 4327.
[15] S. B. Desu, C. H. Peng, T. Shi, P. A. Agaskar, *J. Electrochem. Soc.* **1992**, *139*, 2682.
[16] M. D. Nyman, S. B. Desu, C. H. Peng, *Chem. Mater.* **1993**, *5*, 1636.
[17] [17a] H. Bürgy, G. Calzaferri, *Helv. Chim. Acta* **1990**, *73*, 698. – [17b] D. Herren, H. Bürgy, G. Calzaferri, *Helv. Chim. Acta* **1991**, *74*, 24. – [17c] G. Calzaferri, D. Herren, R. Imhof, *Helv. Chim. Acta* **1991**, *74*, 1278. – [17d] G. Calzaferri, R. Imhof, *J. Chem. Soc., Dalton Trans.* **1992**, 3391. – [17e] G. Calzaferri, I. Imhof, K. W. Törnroos, *J. Chem. Soc., Dalton Trans.* **1993**, 3741. – [17f] C. Marcolli, R. Imhof, G. Calzaferri, *Microchim. Acta* **1997**, Suppl. 14. – [17g] B. J. Hendan, H. C. Marsmann, *J. Organomet. Chem.* **1995**, *483*, 33. – [17h] U. Dittmar, B. J. Hendan, U. Flörke, H. C. Marsmann, *J. Organomet. Chem.* **1995**, *489*, 185.
[18] [18a] G. Calzaferri, R. Hoffmann, *J. Chem. Soc., Dalton Trans.* **1991**, 917. – [18b] M. Bärtsch, P. Bornhauser, G. Calzaferri, R. Imhof, *J. Phys. Chem.* **1994**, *98*, 2817. – [18c] J. A. W. Harkless, D. K. Stillinger, F. H. Stillinger, *J. Phys. Chem.* **1996**, *100*, 1098. – [18d] V. A. Ermoshin, K. S. Smirnov, D. Bougeard, *Chem. Phys.* **1996**, *202*, 53. – [18e] A. J. M. de Man, J. Sauer, *J. Phys. Chem.* **1996**, *100*, 5025. – [18f] A. M. Bieniok, H.-B. Bürgi, *J. Phys. Chem.* **1994**, *98*, 10735. – [18g] F. J. Feher, D. A. Newman, J. F. Walzer, *J. Am. Chem. Soc.* **1989**, *111*, 1741.
[19] $(HSiO_{3/2})_8$: [19a] T. P. E. Auf der Heyde, H.-B. Bürgi, H. Bürgy, K. W. Törnroos, *Chimia* **1991**, *45*, 38. – [19b] K. W. Törnroos, *Acta Crystallogr.* **1994**, *C50*, 1646. – [19c] $(HSiO_{3/2})_{10}$: H.-B. Bürgi, K. W. Törnroos, G. Calzaferri, H. Bürgy, *Inorg. Chem.* **1993**, *32*, 4914. – [19d] $(HSiO_{3/2})_{12}$: K. W. Törnroos, H.-B. Bürgi, G. Calzaferri, H. Bürgy, *Acta Crystallogr.* **1995**, *B51*, 155. – $(HSiO_{3/2})_{14}$: See ref.[16]
[20] See, for example: [20a] R = Me, *n* = 10: I. A. Baidina, N. V. Podberezskaya, S. V. Borisov, V. I. Alexeev, T. N. Matynova, A. N. Kanev, *Zh. Strukt. Khim.* **1980**, *21*, 125; *Chem. Abstr.* **1980**, *93*, 177686z. – [20b] R = (2-dimethylamino)phenyl, *n* = 8: R. Tacke, A. Lopez-Mras, W. S. Sheldrick, A. Sebald, *Z. Anorg. Allg. Chem.* **1993**, *619*, 347.
[21] For R = $OSiMe_3$ no entries are found in the Cambridge Crystallographic Database. Two papers, however, report X-ray structures[22]; an ORTEP representation is found in ref.[23], but no further crystallographic details. For R = $OSiMe_3$ and *n* = 3 a structure is reported in ref.[24] For R = $OSiMe_3$ and *n* = 5 the cell constants and space group have been determined.[25] For R = $OSiMe_2H$, *n* = 4, an X-ray structure analysis was reported during the reviewing process of the present paper.[40]
[22] [22a] Y. I. Smolin, F. Shepeler, R. Pomes, *Khim. Silik. Oksidov* **1982**, 68; *Chem. Abstr.* **1982**, *97*, 118501r. – [22b] R. P. Hernández, Y. I. Smolin, Y. F. Shepelev, *Rev. Cient. Univ. Oriente, Cienc. Nat. Mat.* **1977**, *1*, 17.
[23] R. Sasamori, Y. Okaue, T. Isobe, Y. Matsuda, *Science* **1994**, *265*, 1691.
[24] D. Hoebbel, G. Engelhardt, A. Samoson, K. Újszászy, Y. I. Smolin, *Z. Anorg. Allg. Chem.* **1987**, *552*, 236.
[25] D. Hoebbel, W. Wieker, P. Franke, A. Otto, *Z. Anorg. Allg. Chem.* **1975**, *488*, 35.
[26] C. W. Lentz, *Inorg. Chem.* **1964**, *3*, 574.
[27] D. Hoebbel, W. Wieker, *Z. Anorg. Allg. Chem.* **1971**, *38*, 43.
[28] U. I. Moke′eva, N. I. Golovastikov, *Dokl. Akad. Nauk SSSR* **1966**, *167*, 1131; *Chem. Abstr.* **1966**, *65*, 6429d.
[29] C. N. R. Rao, J. Gopalakrishnan, *New Directions in Solid-State Chemistry*, Cambridge Solid-State Science Series, Cambridge University Press, Cambridge, New York, Melbourne, **1986**, p. 40, and literature cited therein.
[30] *International Tables for Crystallography* **1995**, vol. C, Table 9.5.1.1.
[31] M. Backer, A.-R. Grimmer, N. Auner, P. John, J. Weis, *Solid State Nucl. Magn. Reson.* **1997**, *9*, 241. Low-temperature MAS-NMR studies are currently being carried out.
[32] J. A. Hedvall, L. Leffler, *Z. Anorg. Allg. Chem.* **1937**, *234*, 235; and in: K. Hauffe, *Reaktionen in und an festen Stoffen*, Springer-Verlag, Berlin, Göttingen, Heidelberg, **1955**.
[33] Obviously, MALDI-TOF is quite sensitive to Q_6M_6 contamination as the compound was not found in ^{29}Si- and ^{1}H-NMR spectra.
[34] Unfortunalety, no single crystals could be obtained for **6**, a waxy solid. MALDI-TOF-MS and ^{29}Si-MAS-NMR, however, proved to be valuable analytical tools for the structural analysis of this compound.
[35] [35a] C. Freyer, J. Wolferseder, U. Peetz (Wacker Chemie GmbH), EP 0 624 591 A1, **1994**. – [35b] R. Weidner, N. Zeller, B. Deubzer, V. Frey (Wacker Chemie GmbH), EP 0 367 222 B1, **1989**; *Chem. Abstr.* **1990**, *113*, 11645m. – [35c] R. Weidner, N. Zeller, B. Deubzer, V. Frey (Wacker Chemie GmbH), DE 3837397 A1, **1988**; *Chem. Abstr.* **1990**, *113*, 116465m.
[36] C. Marcolli, P. Lainé, R. Bühler, G. Calzaferri, J. Tomkinson, *J. Phys. Chem.* **1997**, *101*, 1171.
[37] A. C. T. North, D. C. Phillips, F. S. Mathews, *Acta Crystallogr.* **1968**, *A24*, 351−359.
[38] G. M. Sheldrick, *Acta Crystallogr.* **1990**, *A46*, 467.
[39] G. M. Sheldrick, *Program for Crystal Structure Refinement*, Universität Göttingen, Germany, **1993**.
[40] A. Provatas, M. Luft, J. C. Mu, A. H. White, J. G. Matisons, B. W. Skelton, *J. Organomet. Chem.* **1998**, *565*, 159.

[I98330]

Silaheterocycles, 35[+]

Carbon=Carbon Hydrogenation of Silicon-Functionalized Silaheterocycles

Norbert Auner,*[a] Hans-Uwe Steinberger,[b] and Bernhard Herrschaft[a]

Dedicated to Prof. Dr. Drs. h.c. Hans Bock on the occasion of his 70th birthday

Keywords: Silanorbornenes / Silanorbornanes / Silicon-functionalized olefins / Silacyclobutanes / Hydrogenations / Heterocycles

Catalytic hydrogenation of olefins containing functionalized silicon groups affords the saturated products in good yields. Chloro and alkoxy substituents at the silicon atom remain unaffected and, in the case of heterocyclic compounds, the cyclic or bicyclic moieties remain intact. The 2-silanorbornanes **4**, **5**, and **6** were synthesized from the corresponding 2-silanorbornenes **1**, **2**, and **3**, and organosilanes **13** and **14** possessing the cyclopentyl group, were prepared from the cyclopentenyl-substituted precursors **10** and **12**. The 3-vinyl-substituted silacyclobutanes **15**, **17**, and **18** were also hydrogenated in a simple apparatus with diethyl ether or THF as solvent, and Pd/C as a recoverable catalyst system. A basic organosilicon compound, trichloro(vinyl)silane, is hydrogenated in a nearly quantitative yield to form the saturated trichloro(ethyl)silane; this emphasizes the general applicability of this method.

Introduction

Vinylsilanes are of great importance in organosilicon chemistry both for academic research and industrial applications.[2] This class of compounds[3] is available by large-scale processes (such as the cleveage of disilanes by vinylic chlorides,[4] the hydrosilylation of conjugated dienes or acetylenic derivatives,[5] and the thermal condensation of chlorohydridosilanes with vinylic chlorides[6]) and it′s members are commonly used as starting materials for the production of silicon-based polymers, the hydrosilylation reaction being widely used to crosslink silicon and carbon moieties.[2] Particularly in polymerization reactions, the defunctionalization of vinyl groups, directly attached to silicon centers or bound to carbon atoms in the polymeric backbone, is of importance in controlling the molecular mass or in preventing polymerization taking place. In this respect the hydrogenation of the vinylic unit could be a valuable method, but the reaction has to be very selective, forming the corresponding saturated derivatives in high yield, even in the presence of other functional groups, such as chlorine or alkoxy, at the silicon atom. In general, the direct synthesis of chloro(ethyl)silanes results in a complex mixture of differently substituted products with low yields.[7] Using catalysts for the hydrogenation of vinylsilanes the application is restricted to nonhalogenated derivatives, since the catalyst (e.g. Adam′s platinum or Raney′s nickel[8]) can affect the chlorine function or can be deactivated. Only Dunogues has reported on an efficient method using nickel chloride/triethylsilane as a catalyst,[9] but this method does not seem very practical for large-scale syntheses.[10] This paper reports on a synthetic route to transform unsaturated carbon−carbon moieties of organosilicon compounds into their corresponding saturated derivatives by use of Pd/C as a catalyst for a heterogeneous catalytic hydrogenation. This combination is well known to be cheap, easily available, and most effective in organic chemistry.[11] For these very basic studies we synthesized a series of silyl-functionalized silaheterocycles as model compounds containing both endo- or exocyclic vinyl subunits.[12] Carrying out the hydrogenation reactions, the chloro and alkoxy functionalities at the silicon atom and the cyclic carbon skeletons are preserved.

Results and Discussion

The hydrogenation of carbon−carbon doubly bonded moieties is technologically a very important reaction[13] and requires the activation of molecular hydrogen and/or the unsaturated substrates by catalysts.[14] Heterogeneous hydrogenation uses Ni, Pd, Pt, and Rh metals supported on activated carbon, silica, aluminium oxides, and barium sulfate as catalysts.[15]

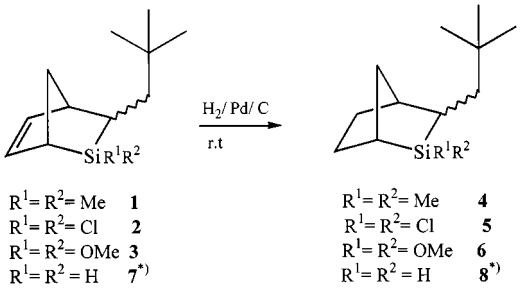
For the hydrogenation of a series of silaheterocycles Pd/C was used as a catalyst at room temperature in ether or THF as solvent. Starting from the 2-silanorbornenes **1**, and **2** (which were synthesized by the reaction of chlorodimethyl-(vinyl)silane,[16] trichloro(vinyl)silane,[17] and *tert*-butyllithium in the presence of cyclopentadiene) and from **3**, which

[+] Part 34: Ref.[1]

[a] Institut für Anorganische Chemie, Johann-Wolfgang-Goethe-Universität,
Marie-Curie-Str. 11, D-60439 Frankfurt am Main, Germany
Fax: (internat.) + 49(0)69/798-29188
E-mail: Auner@chemie.uni-frankfurt.de
[b] Institut für Anorganische und Allgemeine Chemie, Humboldt-Universität zu Berlin,
Hessische Strasse 1−2, D-10115 Berlin, Germany

 © WILEY-VCH Verlag GmbH, D-69451 Weinheim, 1999 1434−1948/99/0707−1095 $ 17.50+.50/0

is easily available from **2** by a substitution reaction,[18] the corresponding 2-silanorbornanes are accessible in a yield of about 90% (after distillation) (see Scheme 1). The products were fully characterized by NMR and MS methods. In order to facilitate the NMR-spectroscopic assignments a semipreparative gas-chromatographic separation of the *exo*/*endo* diastereoisomers **4** was carried out (see Experimental Section).



$R^1 = R^2 = Me$ **1**
$R^1 = R^2 = Cl$ **2**
$R^1 = R^2 = OMe$ **3**
$R^1 = R^2 = H$ **7***)

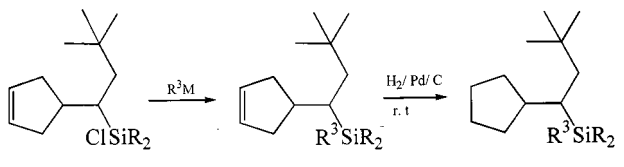
$R^1 = R^2 = Me$ **4**
$R^1 = R^2 = Cl$ **5**
$R^1 = R^2 = OMe$ **6**
$R^1 = R^2 = H$ **8***)

Scheme 1. Synthesis of silanorbornanes from silanorbornenes; *) formation of polymeric products from hydrosilylation

Surprisingly, hydrogenation of the *Si*-dihydro-substituted silanorbornene (**7**), which is available from **2** and $LiAlH_4$,[17] failed. Instead hydrosilylation took place, giving polymeric products, which have not been characterized in detail. Alternatively, the parent dihydro-substituted silanorbornane **8** can be synthesized from **5** by the use of $LiAlH_4$ as a reducing agent.

The hydrogenation reactions described in Scheme 1 provide another route for the synthesis of 2-silanorbornane skeletons: These bicyclic compounds are also available from both, the intramolecular hydrosilylation reaction of cyclopentenyl-substituted silanes $C_5H_7CH(HSiR_2)CH_2tBu$[18] and the reaction of the latter with catalytic amounts of trityl tetrakis(pentafluorophenyl)borate via the intermediacy of a silanorbornyl cation.[19][20] Furthermore, a carbon-functionalized 2-silanorbornane is easily available from silanorbornene **2** by the addition of hydrogen chloride to the carbon−carbon double bond.[18]

In contrast to compound **2**, the 2-silanorbornenes **1** and **3** do not add hydrogen chloride, but an allylic cleavage gives the cyclopentenyl-substituted chloro(organo)silanes **9**, and **11**.[18] The organo-substituted derivatives **10** and **12** were synthesized by the reactions of the chlorosilane precursors **9** and **11**, respectively, with fluorenyllithium and a 1-naphthyl Grignard reagent (see Scheme 2). After recrystallisation of **10** from ether/pentane (1:5), suitable single crystals were obtained for X-ray crystal analysis.



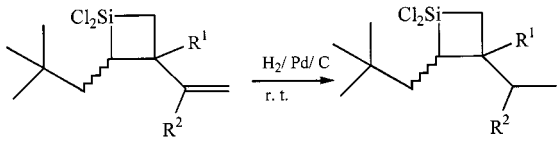
R= Me **9**
R= OMe **11**

R= Me, R^3= fluorenyl **10, 13**
R= OMe, R^3= 1- naphthyl **12, 14**

Scheme 2. Synthesis of cyclopentane-substituted organosilanes

Notably, the hydrogenation of the cyclopentenyl derivatives **10** and **12** gives the corresponding cyclopentane-substituted compounds **13** and **14** in high yields (**13**: 88%; **14**: 82%).

In order to prove the utility of the hydrogenation reaction for exocyclic vinyl groups, 1,1-dichloro-3-vinyl-1-silacyclobutanes **15**, **17**, and **18** were chosen as model compounds. These compounds are easily prepared by the reaction of trichloro(vinyl)silane, Li*t*Bu, and isoprene (**17**, **18** isomeric mixture) or 2,3-dimethylbutadiene (**15**).[21] The corresponding 3-ethyl-substituted derivatives **16**, and an isomeric product mixture of **19** and **20** were exclusively obtained from the catalyst-supported reaction at room temperature and were isolated in high yields (ca 75%) after distillation. The four-membered ring moieties remain stable and the same is true for the dichlorosilyl functionality (see Scheme 3).



$R^1 = R^2 = Me$ **15**
$R^1 = Me, R^2 = H$ **17**
$R^1 = H, R^2 = Me$ **18**

$R^1 = R^2 = Me$ **16**
$R^1 = Me, R^2 = H$ **19**
$R^1 = H, R^2 = Me$ **20**

Scheme 3. Synthesis of 3-ethyl-substituted silacyclobutanes from vinyl-substituted precursors

Molecular Structure of 10

The crude slightly yellow crystalline organosilane **10** was recrystallized from an *n*-pentane/ether (5:1) mixture; a single crystal was used for X-ray diffraction analysis. In the solid state **10** forms a 1:1 inclusion compound with acetaldehyde, which was obviously introduced by an impurity within the solvents used for recrystallization (see Figure 2). No exceptionally short intermolecular distances indicating the presence of strong intermolecular interactions between silane **10** and the solvent molecule are observed. The packing of the silane and the disordered solvent molecules in the crystal structure is as close as possible and no further potentially solvent accessible cavities are left. The silicon atom is tetrahedrally surrounded by four carbon atoms of two methyl groups, the 5-fluorenyl, and the (3-cyclopentenyl)-3,3-dimethylbutyl substituent. Although sterically demanding ligands are present in the molecule, the bond angle C14−Si−C15 (113.26°) beween the methyl groups is the largest one at the silicon center. The mean distance $Si-C_{Me}$ is slightly shorter (187 pm) than the $Si-C_{fluorenyl}$ and the $Si-C_{butyl}$ bond length (191 pm) (see Figure 1). The fluorenyl ligand is mutually planar within the accuracy achieved and the observed range for the C−C bond lengths is characteristic for aromatic hydrocarbons in the solid state. The cyclopentenyl substituent adopts an envelope conformation with a carbon−carbon bond length of 130.4 pm. Due to the packing in the crystal structure the orientation of the *tert*-butyl group is ideally staggered with respect to

the C22−C23 bond (torsion angles: 61.8°, 63.3°, and 179.8°).

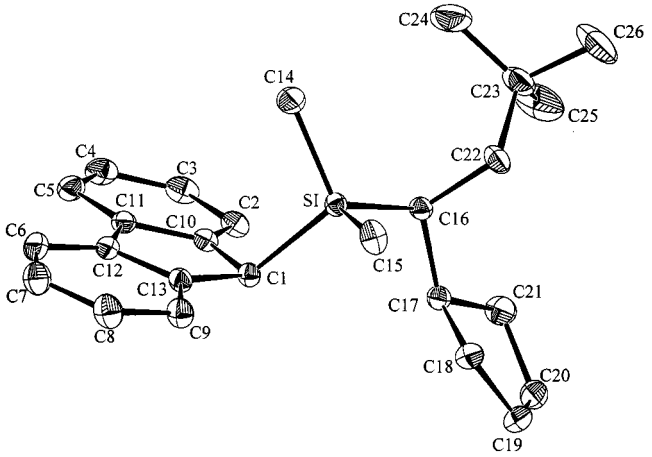


Figure 1. DIAMOND[22] drawing (30% envelopes) of 3-(3-cyclopentenyl)-2-fluorenyl-2,5,5-trimethyl-2-silahexane (**10**): Si−C1 191.41(14) pm, Si−C14 186.74(16), Si−C15 187.82(19), Si−C16 190.25(14); C14−Si−C15 106.85(9)°, C14−Si−C16 113.28(7), C15−Si−C16 111.16(7), C14−Si−C1 107.05(7), C15−Si−C1 109.78(7), C16−Si−C1 108.60(6)

Conclusion

The Pd/C-catalyzed hydrogenation of endo- and exocyclic carbon−carbon doubly bonded moieties occurs under mild conditions, e.g. one atmosphere of hydrogen pressure and at room temperature, in nearly quantitative yields. Functional groups at the silicon atom, e.g. chlorine, alkoxy, or aryl substituents are preserved, as well as the mono- or bicyclic carbosilane skeletons. No side products can be detected, the yields for the hydrogenated compounds given in Table 1 in the Experimental Section are those after distillation.

To prove the whole range of applicability and to show the limitations of the discussed synthetic method, an industrially (economically) important chloro(vinyl)silane was used as a starting compound for hydrogenation: Within 24 h trichloro(vinyl)silane was completely converted into the corresponding ethylsilane, $Cl_3SiCH_2CH_3$. From this finding we conclude that the reaction may be widely used for the synthesis of chloro(ethyl)silanes from their vinyl-substituted precursors. However, the method does not work when the C=C bond is strongly shielded by sterically demanding substituents. Thus, treating 1,1-dichloro-2,3-diphenyl-4-neopentyl-1-silacyclobutene,[23] under comparable conditions, no hydrogenation occurs to form a silacyclobutane; the silacyclobutene is completely recovered from the reaction mixture. Further studies to expand this method using different vinylsilanes and a variety of functional groups at the silicon atom are currently being carried out in our laboratories.

Experimental Section

General Remarks: All manipulations were performed under purified argon using standard Schlenk techniques. Solvents were dried by refluxing under nitrogen with the appropriate drying agent and were distilled prior before use. $CDCl_3$ was dried with molecular sieves, while [D_6]benzene was dried with potassium/sodium and distilled prior to NMR sample preparation. − NMR spectra: Bruker AM 300 (^{29}Si), DPX 300 (^{1}H, ^{13}C) and AMX 600 (^{1}H, ^{13}C), ^{1}H- and ^{13}C-NMR chemical shifts (δ) were internally referenced [δ(C*H*Cl_3) = 7.24, δ(*C*DCl_3) = 77.00, δ(C_6D_5*H*) = 7.15, δ(C_6D_6) = 128.00], ^{29}Si-NMR shifts were externally referenced to TMS. − GC/MS: Chrompack CP 9000 (capillary column CP-SIL/5CB-MS, diameter 0.25 mm, 12.5 m length) coupled with a Finnigan MAT Ion Trap Detector 800 (electron impact, space current 3000 μA, ionisation energy 70 eV, ion-source temperature 250°C), for chemical ionisation methanol was used. − Elemental analyses: Microanalytical Laboratory of the Department of Chemistry, Humboldt-University, Berlin. Trichloro(vinyl)- and chlorodimethyl(vinyl)-silane were distilled from sodium carbonate prior before use. *tert*-Butyllithium was used as a 1.7 M solution in pentane. All other chemicals were used as purchased by Aldrich and Fluka.

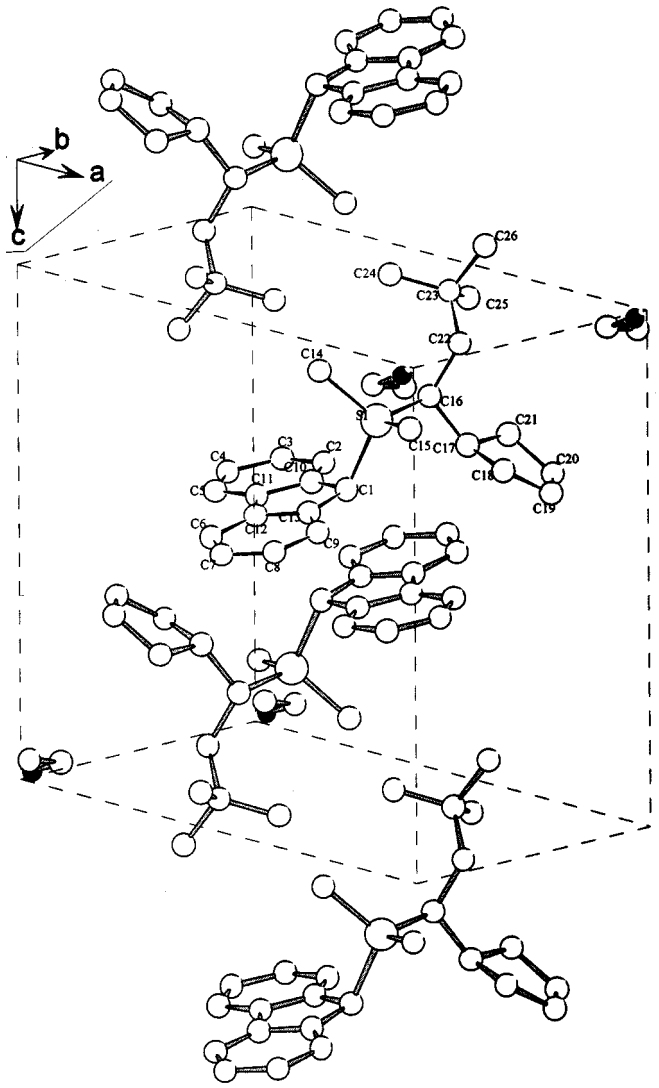


Figure 2. DIAMOND[22] representation of the crystal structure viewed along [100] showing the inclusion of acetaldehyde molecules

Hydrogenation Apparatus: A suitable reaction flask was connected to a set of two dropping funnels by a small glass tube. The two dropping funnels themselves were connected with a flexible tube

Table 1. Preparative details of the hydrogenation reactions

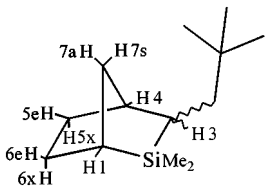
Starting compound	Amount [g; mmol]	Pd/C [mol-%]	Solvent; amount [mL]	Product	Reaction time [h]	Yield [g;%]	Boiling point [°C/10^{-2} mbar]
1	1.4; 6.72	3.50	THF; 20	**4**	16	1.3; 92	62
2	3.6; 14.52	1.62	ether; 30	**5**	24	3.0; 82	58
3	5.2; 21.67	1.08	ether; 50	**6**	16	4.1; 79	55
10	2.3; 6.23	3.77	ether; 30	**13**	16	2.0; 88	oil[a]
12	1.9; 5.41	4.34	THF; 30	**14**	16	1.7; 82	oil[a]
15	4.3; 16.21	1.45	ether; 30	**16**	48	3.2; 73	73
17 + **18**	10.2; 40.80	0.58	THF; 50	**19** + **20**	24	7.7; 75	98

[a] A highly viscous residue, b.p. not determined.

and filled with silicone oil as sealing fluid. Then the oil in the first dropping funnel was displaced by hydrogen. The volume was marked before the tap of the reaction flask was opened. During the hydrogenation reaction the amount of hydrogen consumed was monitored as change in volume. For a sketch of the hydrogenation apparatus described see ref.[24]

General Reaction Procedure: The carbon−carbon unsaturated silaheterocycles or the vinylsilanes were placed in the reaction flask of the hydrogenation apparatus described and dissolved in THF or diethyl ether. 250 mg of Pd/C (10% on activated carbon) were added. Then the reaction mixture was stirred and allowed to react with hydrogen for 16 h. The volume of gas consumed indicated the end of the reaction. The catalyst Pd/C was filtered off, the solvent removed under reduced pressure, and the products distilled for purification at 10^{-2} mbar (Table 1).

For a semipreparative gas-chromatographic separation of the *exo*-/*endo*-3-neopentyl diastereomers **4** a packed column (10% OV 101 on 80−100 mesh Chromosorb W, HO, DMCS) was used in a Chromatron gas chromatograph. The column temperature was 110°C (isotherm) and the flow rate was set to 3.6 L H_2/h. A heat conductivity cell (Chromatron) was used for detection. The purity of the separation had been checked with a capillary gas chromatogaph and was detected to be 98.5% (2,2-dimethyl-*exo*-3-neopentyl-2-silabicyclo[2.2.1]silaheptane) and 98.7% (2,2-dimethyl-*endo*-3-neopentyl-2-silabicyclo[2.2.1]silaheptane). For the assignment of the NMR-chemical shifts of the silanorbornanes **4**−**6** and **8** the atoms are numbered as shown by the formula in Scheme 4.



Scheme 4. Numbering scheme for **4**−**6** and **8**

2,2-Dimethyl-*exo*-3-neopentyl-2-silabicyclo[2.2.1]silaheptane (*exo*-4): ^{1}H NMR (600 MHz, $CDCl_3$): δ = 0.07 (s, 3 H, $SiCH_{3\ endo}$), 0.13 (s, 3 H, $SiCH_{3\ exo}$), 0.45 (m, 1 H, 3-H), 0.95 [s, 9 H, $C(CH_3)_3$], 1.21 (dddd, $^2J_{5x/5e}$ = 12.2 Hz, $^3J_{5x/6e}$ = 6.0 Hz, $^3J_{5x/6x}$ = 8.3 Hz, $^4J_{5x/7s}$ = 1.8 Hz, 1 H, 5x-H), 1.25 (dd, $^2J_{HH}$ = 13.8 Hz, $^3J_{HH}$ = 4.6 Hz, 1 H, CH_aH_btBu), 1.26 (m, 1 H, 1-H), 1.47 (dddd, $^2J_{7a/7s}$ = 10.8 Hz, $^3J_{7a/1}$ = 2.8 Hz, $^3J_{7a/4}$ = 2.8 Hz, $^4J_{7a/3}$ = 2.9 Hz, 1 H, 7a-H), 1.50 (dd, $^2J_{HH}$ = 13.8 Hz, $^3J_{HH}$ = 6.8 Hz, 1 H, CH_aH_btBu), 1.60 (d, br., $^2J_{HH}$ = 10.8 Hz, 1 H, 7s-H), 1.63 (m, 1 H, 6x-H), 1.68 (dddd, $^2J_{6e/6x}$ = 12.0 Hz, $^3J_{6e/1}$ = 5.9 Hz, $^3J_{6e/5e}$ = 12.0 Hz, $^3J_{6e/5x}$ = 6.0 Hz, 1 H, 6e-H), 1.78 (dddd, $^2J_{5e/5x}$ = 12.2 Hz, $^3J_{5e/6e}$ = 12.0 Hz, $^3J_{5e/6x}$/$^3J_{5e/4}$ = 6.0, 4.0 Hz, 1 H, 5e-H), 2.15 (s, br., 1 H, 4-H). − ^{13}C NMR (75.40 MHz, $CDCl_3$): δ = 47.11 (C-4), 46.28 (C-8), 36.36 (C-7), 31.51 (C-9), 31.53 (C-5), 23.85 (C-6), 29.76 (C-10), 29.35 (C-1), 24.23 C-3), −4.21 [$SiCH_3$ (*exo*)], −4.35 [$SiCH_3$ (*endo*)]. − ^{29}Si NMR (59.25 MHz, $CDCl_3$): δ = 10.20. − MS (70 eV); *m*/*z* (%): 210 (0) [M^+], 153 (74.73) [$M^+ - t$Bu], 125 (98.91), 59 (100), 57 (33.15) [tBu$^+$].

2,2-Dimethyl-*endo*-3-neopentyl-2-silabicyclo[2.2.1]silaheptane (*endo*-4): ^{1}H NMR (600 MHz, $CDCl_3$): δ = 0.06 (s, 3 H, $SiCH_{3\ endo}$), 0.10 (s, 3 H, $SiCH_{3\ exo}$), 0.84 (m, 1 H, 3-H), 0.95 [s, 9 H, $C(CH_3)_3$], 1.29 (dd, $^2J_{HH}$ = 13.6 Hz, $^3J_{HH}$ = 4.0 Hz, 1 H, CH_aH_btBu), 1.29 (m, 1 H, 1-H), 1.42 (m, 2 H, 5e-H and 5x-H), 1.45 (dd, $^2J_{HH}$ = 13.6 Hz, $^3J_{HH}$ = 8.5 Hz, 1 H, CH_aH_btBu), 1.48 (d, br., $^2J_{7s/7a}$ = 10.8 Hz, 1 H, 7s-H), 1.57 (m, 1 H, 6x-H), 1.58 (m, 1 H, 7a-H), 1.68 (dddd, $^2J_{6e/6x}$ = 12.1 Hz, $^3J_{6e/1}$ = 5.9 Hz, $^3J_{6e/5e}$ = 12.0 Hz, $^3J_{6e/5x}$ = 6.0 Hz, 1 H, 6e-H). − ^{13}C NMR (75.40 MHz, $CDCl_3$): δ = 44.81 (C-4), 42.05 (C-8), 38.65 (C-7), 31.22 (C-9), 29.90 (C-10), 27.07 (C-3), 25.57 (C-1), 24.66, 23.94 (C-5/C-6), −1.82 [$SiCH_3$ (*exo*)], −6.25 [$SiCH_3$ (*endo*)]. − ^{29}Si NMR (59.25 MHz, $CDCl_3$): δ = 17.47. − MS (70 eV); *m*/*z* (%): 210 (0) [M^+], 153 (73.73) [$M^+ - t$Bu], 125 (95.47), 59 (100), 57 (31.73) [tBu$^+$].

***exolendo*-4:** $C_{13}H_{26}Si$ (210.18): calcd. C 74.22, H 12.47; found C 73.99, H 12.41.

2,2-Dichloro-*exo*-3-neopentyl-2-silabicyclo[2.2.1]silaheptane (*exo*-5): ^{1}H NMR (300 MHz, $CDCl_3$): δ = 0.86 (m, 1 H, 3-H), 0.92 (s, 9 H, CH_2tBu), 1.17 (dd, 1 H, $^2J_{HH}$ = 13.6 Hz, $^3J_{HH}$ = 6.8 Hz, CH_aH_btBu), 1.29 (m, 1 H, 5x-H), 1.52 (m, 1 H, 7s-H), 1.69 (m, 1 H, 1-H), 1.69−1.81 (m, 2 H, 6x-H, 6e-H), 1.72 (m, 1 H, 7a-H), 1.73 (dd, 1 H, $^2J_{HH}$ = 13.6 Hz, $^3J_{HH}$ = 7.9 Hz, CH_aH_btBu), 1.80 (m, 1 H, 5e-H), 2.21 (s, br., 1 H, 4-H). − ^{13}C NMR (75.40 MHz, $CDCl_3$): δ = 46.15 (C-4), 44.52 (C-8), 34.85 (C-3), 34.11 (C-7), 30.93 (C-9), 30.30 (C-5), 21.97 (C-6), 29.28 (C-10), 28.53 (C-1), 21.97 (C-6). − ^{29}Si NMR (59.25 MHz, $CDCl_3$): δ = 40.60. − MS (70 eV); *m*/*z* (%): 240 (0) [M^+], 193 (30.33), 195 (19.78), 197 (3.96) [$M^+ - t$Bu] ($SiCl_2$ isotopic pattern), 67 (38.46) [$C_5H_7^+$], 57 (100) [tBu$^+$].

2,2-Dichloro-*endo*-3-neopentyl-2-silabicyclo[2.2.1]silaheptane (*endo*-5): ^{1}H NMR (300 MHz, $CDCl_3$): δ = 0.91 (s, 9 H, CH_2tBu), 1.20 (dd, 1 H, $^2J_{HH}$ = 13.9 Hz, $^3J_{HH}$ = 6.8 Hz, CH_aH_btBu), 1.30 (m, 1 H, 3-H), 1.47 (m, 1 H), 1.62 (dd, 1 H, $^2J_{HH}$ = 13.9 Hz, $^3J_{HH}$ = 8.4 Hz, CH_aH_btBu), 1.68−1.81 (m, 3 H), 1.71−1.74 (m, 2 H, 7s-H, 7a-H), 1.74 (m, 1 H, 1-H), 2.44 (s, br., 1 H, 4-H). − ^{13}C NMR (75.40 MHz, $CDCl_3$): δ = 43.57 (C-4), 40.43 (C-8), 36.35 (C-7), 32.79 (C-3), 30.66 (C-9), 23.23, 22.72 (C-5/C-6), 29.94 (C-1), 29.28 (C-10). − ^{29}Si NMR (59.25 MHz, $CDCl_3$): δ = 37.57. − MS (70 eV); *m*/*z* (%): 240 (0) [M^+], 193 (37.14), 195 (28.12), 197 (3.98) [$M^+ - t$Bu] ($SiCl_2$ isotopic pattern), 67 (50.66) [$C_5H_7^+$], 57 (100) [tBu$^+$].

***exolendo*-5:** $C_{11}H_{20}Cl_2Si$ (250.07): calcd. C 52.58, H 8.02, Cl 28.22; found C 51.61, H 8.08, Cl 28.94.

2,2-Dimethoxy-*exo*-3-neopentyl-2-silabicyclo[2.2.1]silaheptane (*exo*-6): ^{1}H NMR (300 MHz, $CDCl_3$): δ = 0.39 (m, 1 H, 3-H), 0.78 (s, 9 H, CH_2tBu), 1.01 (dd, $^2J_{HH}$ = 13.6 Hz, $^3J_{HH}$ = 4.5 Hz, 1 H, CH_aH_btBu), 1.21 (m, 1 H, 5x-H), 1.25 (m, 1 H, 1-H), 1.30 (m, 1 H, 7-H), 1.31−1.67 (m, 2 H, 6x-H, 6e-H), 1.54 (m, 1 H, 7-H), 1.56 (dd, $^2J_{HH}$ = 13.6 Hz, $^3J_{HH}$ = 4.9 Hz, 1 H, CH_aH_btBu), 1.65 (m, 1 H, 5e-H), 2.01 (s, br., 1 H, 4-H), 3.43 (s, 3 H, $SiOCH_3$), 3.44 (s, 3 H, $SiOCH_3$). − ^{13}C NMR (75.40 MHz, $CDCl_3$): δ = 51.27 ($SiOCH_3$), 50.77 ($SiOCH_3$), 45.41 (C-4), 43.60 (C-8), 34.80 (C-7), 31.23 (C-9), 30.53 (C-5), 29.33 (C-10), 27.99 (C-3), 21.83 (C-6), 19.14 (C-1). − ^{29}Si NMR (59.45 MHz, $CDCl_3$): δ = 4.55. − MS (70 eV); *m/z* (%): 242 (7.60) [M^+], 210 (13.90) [$M^+ - CH_3OH$], 185 (68.40) [$M^+ - t$Bu], 157 (100), 91 (40.30), 57 (16.55) [tBu$^+$].

2,2-Dimethoxy-*endo*-3-neopentyl-2-silabicyclo[2.2.1]silaheptane (*endo*-6): ^{1}H NMR (300 MHz, $CDCl_3$): δ = 0.78 (s, 9 H, CH_2tBu), 0.89 (m, 1 H, 3-H), 1.11 (dd, $^2J_{HH}$ = 13.6 Hz, $^3J_{HH}$ = 4.8 Hz, 1 H, CH_aH_btBu), 1.31−1.67 (m, 5 H, 5x-H, 5e-H, 6x-H, 6e-H, 1-H), 1.41 (dd, $^2J_{HH}$ = 13.6 Hz, $^3J_{HH}$ = 7.5 Hz, 1 H, CH_aH_btBu), 1.46 (m, 2 H, 7a-H, 7s-H) 2.27 (s, br., 1 H, 4-H), 3.43 (s, 3 H, $SiOCH_3$), 3.44 (s, 3 H, $SiOCH_3$). − ^{13}C NMR (75.40 MHz, $CDCl_3$): δ = 50.98 ($SiOCH_3$), 50.67 ($SiOCH_3$), 42.43 (C-4), 40.13 (C-8), 37.24 (C-7), 31.00 (C-9), 29.46 (C-10), 26.09 (C-1), 22.61, 23.49 (C-5/C-6). − ^{29}Si NMR (59.25 MHz, $CDCl_3$): δ = 0.34. − MS (70 eV); *m/z* (%): 242 (5.84) [M^+], 210 (15.00) [$M^+ - OCH_3$], 185 (84.52) [$M^+ - t$Bu], 157 (100), 91 (54.32), 57 (19.09) [tBu$^+$].

***exolendo*-6:** $C_{13}H_{26}SiO_2$ (242.45): calcd. C 64.41, H 10.81; found C 64.28, H 10.91.

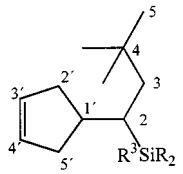
Synthesis of *exolendo*-3-Neopentyl-2-silabicyclo[2.2.1]silaheptane (*exolendo*-8): 1.61 g (42.34 mmol) of $LiAlH_4$ and 80 mL of diethyl ether were placed in a flask. The suspension was cooled to 0°C and 5.32 g (21.17 mmol) of **5** added dropwise. The reaction mixture was heated under reflux for 5 h. The solvent was removed by evaporation in vacuo. The product was then extracted with 60 mL of *n*-pentane, excess lithium alanate filtered off, and washed with pentane (2 × 10−15 mL). After removing the solvent, the mixture was distilled at 10^{-2} mbar to give 3.40 g of **8** (88%). The product is a colourless, viscous liquid; b.p. 67°C/10^{-2} mbar.

***exo*-8:** ^{1}H NMR (300 MHz, $CDCl_3$): δ = 0.77 (m, 1 H, 3-H), 0.90 (s, 9 H, CH_2tBu), 1.15 (m, 1 H, 5x-H), 1.57 (m, 1 H, 1-H), 1.41 (m, 1 H, 7a-H), 1.41 (dd, $^2J_{HH}$ = 13.9 Hz, $^3J_{HH}$ = 3.7 Hz, 1 H, CH_aH_btBu), 1.45 (m, 1 H, 6x-H), 1.46 (dd, $^2J_{HH}$ = 13.9 Hz, $^3J_{HH}$ = 5.5 Hz, 1 H, CH_aH_btBu), 1.49 (m, 1 H, 7s-H), 1.64 (m, 1 H, 6e-H), 1.65 (m, 1 H, 5e-H), 2.16 (s, br., 4-H), 3.36 [dm, $^2J_{HH}$ = 11.9 Hz, 1 H, SiH (*exo*)], 3.78 [dm, $^2J_{HH}$ = 11.9 Hz, 1 H, SiH (*endo*)]. − ^{13}C NMR (75.40 MHz, $CDCl_3$): δ = 49.02 (C-8), 45.44 (C-4), 35.88 (C-7), 31.87 (C-9), 31.11 (C-5), 29.77 (C-10), 24.74 (C-6), 24.32 (C-1), 20.98 (C-3). − ^{29}Si NMR (59.25 MHz, $CDCl_3$): δ = −10.23 ($^1J_{SiH}$ = 203 Hz). − MS (70 eV); *m/z* (%): 181 (3.16) [M^+ − H], 125 (38.14) [$M^+ - t$Bu], 97 (100), 57 (23.00) [tBu$^+$].

***endo*-8:** ^{1}H NMR (300 MHz, $CDCl_3$): δ = 0.90 (s, 9 H, CH_2tBu), 1.16 (m, 1 H, 3-H), 1.36 (dd, $^2J_{HH}$ = 13.2 Hz, $^3J_{HH}$ = 3.2 Hz, 1 H, CH_aH_btBu), 1.37 (m, 1 H, 7-H), 1.40 (m, 1 H, 5x-H), 1.47 (m, 1 H, 6x-H), 1.48 (dd, $^2J_{HH}$ = 13.2 Hz, $^3J_{HH}$ = 5.2 Hz, 1 H, CH_aH_btBu), 1.52 (m, 1 H, 5e-H), 1.53 (m, 1 H, 1-H), 1.73 (m, 1 H, 6e-H), 2.36 (s, br., 4-H), 3.36 (dm, $^2J_{HH}$ = 11.9 Hz, 1 H, SiH), 3.88 (dm, $^2J_{HH}$ = 11.9 Hz, SiH). − ^{13}C NMR (75.40 MHz, $CDCl_3$): δ = 44.20 (C-8), 43.44 (C-4), 39.19 (C-7), 31.32 (C-9), 29.77 (C-10), 26.51 (C-6), 23.91 (C-5), 22.75 (C-3), 22.01 (C-1). − ^{29}Si NMR (59.25 MHz, $CDCl_3$): δ = −16.03 ($^1J_{SiH}$ = 206 Hz). − MS (70 eV); *m/z* (%): 181 (3.21) [M^+ − H], 125 (40.00) [$M^+ - t$Bu], 97 (100), 67 (17.01) [C_5H_7+], 57 (26.26) [tBu$^+$].

***exolendo*-8:** $C_{11}H_{22}Si$ (182.15): calcd. C 72.44, H 12.16; found C 72.55, H 12.65.

Synthesis of 3-(3-Cyclopentenyl)-2-fluorenyl-2,5,5-trimethyl-2-silahexane (10): Fluorenyllithium was synthesized by the dropwise addition of 7.8 mL *n*BuLi (1.7 M in hexane) to a solution of 2.12 g (12.77 mmol) of fluorene in 40 mL of *n*-pentane and 10 mL of diethyl ether at 0°C. The yellow precipitate was stirred vigorously for 1 h and then 2.12 g (12.77 mmol) of **9** was added slowly. After stirring for 1 h, the solution was filtered off from LiCl. The solvent was removed in vacuo and **10** was isolated as a crude (slightly yellow) crystalline solid. After recrystallisation from pentane/ether (5:1), a white solid was obtained [yield: 3.01 g (63%)]; m.p. 57°C. For the assignment of the NMR chemical shifts in **10** the atoms are numbered as expressed by the formula in Scheme 5. − ^{1}H NMR ($CDCl_3$): δ = −0.12 (s, 3 H, $SiCH_3$); 0.07 (s, 3 H, $SiCH_3$); 0.96 (s, 9 H, CH_2tBu), 1.21−1.52 (m, 3 H, CH_2tBu and C*H*−Si), 2.24−2.38 [m, 2 H, CH_2 (cyclopentenyl)], 2.42−2.58 [m, 2 H, CH_2 (cyclopentenyl)], 2.77 [m, 1 H, CH (cyclopentenyl)], 4.11 [s, br., 1 H, aliphatic CH group (fluorenyl)], 5.82 (s, br., 2 H, 2 CH olefin.), 7.43−7.46 (m, 4 H, 4 aromatic CH groups), 7.68 (m, 2 H, aromat.), 7.96 (m, 2 H, aromat.). − ^{13}C NMR (75.40 MHz, $CDCl_3$): δ = 130.78 (C-3′), 130.78 (C-4′), 41.90 (C-1′), 41.25 (C-4), 40.71 [C-7′′ (fluorenyl)], 38.29, 38.21 (C-2′/C-5′), 31.67 (C-5), 30.53 (C-6), 23.11 (C-3), −3.01, 3.01 (C-1/$SiCH_3$). − **10** has 12 diastereotopic aromatic carbon atoms, their ^{13}C-chemical shifts are: δ = 146.26, 146.01, 140.84, 140.79 (4 C_q, fluorenyl), 126.06 (CH intensity 2), 125.40 (CH intensity 2), 120.06 (CH intensity 2), 124.33, 124.26 (in total 8 aromatic CH groups). − ^{29}Si NMR (59.25 MHz, $CDCl_3$): δ = 8.27. − MS(CI); *m/z* (%): 375 (0) [(M + 1)$^+$], 358 (31.00) [$M^+ - CH_4$], 209 (100) [$M^+ - C_{13}H_9$ (fluorenyl)], 165 (22.54) [$C_{13}H_9^+$ (fluorenyl)], 194 (8.19) [$M^+ - CH_3 - C_{13}H_9$], 223 (27.26) [$SiMe_2$fluorenyl$^+$]. − $C_{26}H_{34}Si$ (374.644): calcd. C 83.36, H 9.15; found C 80.94, H 10.25.



Scheme 5. Numbering scheme of **10** and **12**

X-ray Structure Determination of 10: The single crystal was mounted on the glass fibre tip, glued with silicone grease (Wacker AG, FRG), and transfered to the goniometer. The crystal was cooled to 180 K (Oxford Cryo Stream, UK) for all subsequent manipulations. The data collection was performed by means of a four-circle diffractometer (Stoe Stadi4, Darmstadt, FRG) equipped with a fine focus sealed X-ray tube (Mo-K_α radiation, 50 kV, 35 mA), a graphite monochromator and an eulerian cradle. The initial lattice constants were determined by indexing 16 accurately centered, independant reflections (15° < 2Θ < 25°). The initial orientation matrix was refined by centering 32 strong reflections measured at large angles in 2Θ (35° < 2Θ < 45°). To obtain accurately scaled raw intensities, the intensity data collection (3° < 2Θ < 60°) was monitored by the repeated (every 12 h) measurement of three medium strong control reflections taken from the strong reflection set found. 7403 reflections were collected and corrected for Lorentz and polarisation effects. To refine the lattice constants 13 large angle reflections (45° < 2Θ < 49°) were recentered to estimate the final lattice constants. The atom form factors[25] were implemented in the used program system. The crystal structure was solved by Direct Methods (SHELXS86).[26] After two cycles of difference

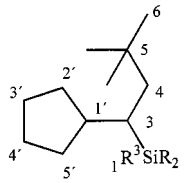
Fourier syntheses and subsequent full-matrix least-squares refinement (SHELXL93)[27] the structure model was complete. All non-hydrogen atoms were assigned as anisotropic, no absortion or extinction correction was done. 20 reflections seemed to be disturbed by a strong extinction and were therefore excluded from the refinement calculations. Hydrogen atoms were calculated in their ideal positions and allowed to ride on their pivot atom. Further details of the crystal structure analysis are given in Table 2. Crystallographic data (excluding structural factors) for the structure reported in this paper have been deposited with the Cambridge Crystallographic Data Centre as supplementary publication no. CCDC-103265. Copies of the data can be obtained free of charge on application to CCDC, 12 Union Road, Cambridge CB2 1EZ, U.K. [Fax: (internat.) + 44-1223/336-033; E-mail: deposit@ccdc.cam.ac.uk].

Table 2. Crystal data and structure refinement of **10**

Empirical formula	$C_{27.39}H_{36.77}O_{0.69}Si$
Molecular mass	405.09
Temperature [K]	180(2)
Wavelength [pm]	71.069
Space group	$P-1$ (no. 2)
Unit cell dimensions	a = 1018.0(2) pm, α = 88.63(3)° b = 1064.3(7) pm, β = 77.180(10)° c = 1276.6(2) pm, γ = 71.22(3)°
Volume [nm^3]	1.2752(9)
Z	2
Density (calcd.) [Mg/m^3]	1.055
Absorption coefficient [mm^{-1}]	0.105
F(000)	441
Crystal size [mm^3]	0.80 × 0.40 × 0.04
Φ range for data collection [°]	1.64 to 29.97
Index ranges	$-13 \le h \le 14$, $-14 \le k \le 14$, $0 \le l \le 17$
Reflections collected	7374
Independent reflections	7374 [R(int) = 0.0000]
Completeness to Φ = 29.97°	99.4%
Refinement method	Full-matrix least squares on F^2
Data/restraints/parameters	7374/0/285
Goodness-of-fit on F^2	1.021
Final R indices [$I > 2\sigma(I)$]	$R1$ = 0.0575, $wR2$ = 0.1616
R indices (all data)	$R1$ = 0.0672, $wR2$ = 0.1728
Largest diff. peak and hole [eÅ^{-3}]	0.725 and −0.578

Synthesis of 2-(3-Cyclopentenyl)-1,1-dimethoxy-4,4-dimethyl-1-naphthyl-1-silapentane (12): 570 mg (13.10 mmol, 30% excess) of magnesium and 150 mL of diethyl ether were placed into a 250-mL 3-necked flask with a dropping funnel and a reflux condenser. 4.94 mL (13.10 mmol, 30% excess) of 1-bromonaphthalene was added dropwise. The mixture was refluxed for 3 h. After cooling to room temperature, 3.04 g (10.08 mmol) of **11** was slowly added. The reaction mixture was then refluxed for 2 h. The solvent was removed in vacuo, the residue dissolved in 50 mL of pentane, and the magnesium salts were filtered off and extracted with pentane (2 × 15 mL). After removing the solvent, **12** (2.30 g) was isolated as a slightly yellow viscous oil (57%). For the assignment of the NMR chemical shifts the atoms are numbered as expressed by the formula in Scheme 5. − ^{1}H NMR (300 MHz, $CDCl_3$): δ = 1.03 (s, 9 H, CH_2tBu), 1.07−1.25 (m, 1 H, CHSi), 1.58 (dd, $^2J_{HH}$ = 14.1 Hz, $^3J_{HH}$ = 5.1 Hz, 1 H, CH_aH$_b$tBu), 2.10 (dd, $^2J_{HH}$ = 14.1 Hz, $^3J_{HH}$ = 4.9 Hz, 1 H, CH$_a$$H_b$tBu), 2.40−2.46 [m, 2 H, CH_2 (cyclopentenyl)], 2.52−2.57 [m, 2 H, CH_2 (cyclopentenyl)], 2.74−2.84 [m, 1 H, CH (cyclopentenyl)], 3.81 (s, 3 H, $SiOCH_3$), 3.82 (s, 3 H, $SiOCH_3$), 5.78−5.80 (m, 2 H, 2 CH olefin.), 7.61−7.73 (m, 3 H, aromat.), 7.97−8.05 (m, 2 H, aromat.), 8.18−8.25 (d, $^3J_{HH}$ = 6.8 Hz, 1 H, aromat.), 8.61 (d, $^3J_{HH}$ = 8.4 Hz, 1 H, aromat.). − ^{13}C NMR (75.40 MHz, $CDCl_3$): δ = 130.71 (C-3′), 130.64 (C-4′), 51.37 ($SiOCH_3$), 51.02 ($SiOCH_3$), 40.41 (C-1′), 40.28 (C-3), 38.29 (C-2′), 37.86 (C-5′), 30.66 (C-4), 30.11 (C-5), 25.98 (C-2). − **12** contains 10 diastereotopic aromatic carbon atoms, their ^{13}C chemical shifts are: 137.37, 133.27, 132.49 (3 C_q); 136.30, 130.81, 129.12, 128.28, 126.27, 125.62, 125.29 (7 CH aromatic). − ^{29}Si NMR (59.25 MHz, $CDCl_3$): δ = −18.61. − MS (70 eV); *m/z* (%): 368 (2.65) [M^+], 337 (7.63) [$M^+ - OCH_3$], 241 (100) [$M^+ - C_{10}H_7$ (naphthyl)], 217 (18.80) [$Si(OCH_3)_2$naphthyl$^+$], 67 (6.25) [$C_5H_7^+$], 57 (26.16) [tBu$^+$]. − $C_{23}H_{32}SiO_2$ (368.59): calcd. C 74.95, H 8.75; found C 74.78, H 8.69.

3-Cyclopentyl-2-fluorenyl-2,5,5-trimethyl-2-silahexane (13): For the assignment of the NMR chemial shifts in **13** the atoms are numbered as expressed by the formula in Scheme 6. − ^{1}H NMR (300 MHz, $CDCl_3$): δ = −0.42 (s, 3 H, $SiCH_3$), −0.06 (s, 3 H, $SiCH_3$), 0.80 (s, 9 H, CH_2tBu), 0.84−0.86 (m, 2 H), 1.10−1.33 (m, 5 H), 1.37−1.75 (m, 4 H), 1.97−2.03 [m, 1 H, CH (cyclopentyl)], 4.02 (s, 1 H, fluorenyl−CH), 7.27−7.35 (m, 4 H, aromatic), 7.54 (dm, J_{HH} = 6.8 Hz, 2 H, aromatic), 7.84 (dm, J_{HH} = 7.8 Hz, 2 H, aromatic). − ^{13}C NMR (75.40 MHz, $CDCl_3$): δ = 43.98 (fluorenyl−CH), 41.64 (C-1′), 40.83 (C-4), 32.60, 31.14 (C-2′/C-5′), 31.49 (C-5), 29.73 (C-6), 25.10, 24.48 (C-3′/C-4′), 21.89 (C-3), −3.26 ($SiCH_3$), −3.74 ($SiCH_3$). − Aromatic ^{13}C shifts: 146.16, 145.96, 140.70, 140.63 (4 C_q), 125.89 (intensity 2), 125.17 (intensity 2), 124.22, 124.17, 119.83 (intensity 2) (in total 8 CH aromatic). − ^{29}Si NMR (59.25 MHz, $CDCl_3$): δ = 8.43. − MS (70 eV); *m/z* (%): 376 (0) [M^+], 211 (26.05) [$M^+ - C_{13}H_9$ (fluorenyl)], 165 (33.33) [$C_{13}H_9^+$ (fluorenyl)], 73 (100), 67 (12.01) [$C_5H_7^+$], 59 (61.00), 57 (56.01) [tBu$^+$]. − $C_{26}H_{36}Si$ (376.66): calcd. C 82.91, H 9.63; found C 83.07, H 9.72.

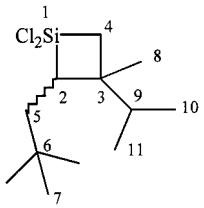


Scheme 6. Numbering scheme of **13** and **14**

2-Cyclopentyl-1,1-dimethoxy-4,4-dimethyl-1-naphthylsilapentane (14): For the assignment of the NMR chemial shifts in **14** the atoms are numbered as expressed by the formula in Scheme 6. − ^{1}H NMR (300 MHz, $CDCl_3$): δ = 0.94 (s, 9 H, CH_2tBu), 1.02−1.08 (m, 1 H, CHSi), 1.28−1.68 (m, 6 H), 1.82−1.83 [m, 2 H, CH_2 (cyclopentyl)], 2.01−2.29 [m, 3 H, CH_2 and CH (cyclopentyl)], 3.73 (s, 3 H, $SiOCH_3$), 3.75 (s, 3 H, $SiOCH_3$), 7.49−7.66 (m, 3 H, aromat.), 7.87−7.95 (2 H, aromat.), 8.14−8.16 (d, $^3J_{HH}$ = 7.4 Hz, 1 H, aromat.), 8.55 (d, $^3J_{HH}$ = 8.1 Hz, 1 H, aromat.). − ^{13}C NMR (75.40 MHz, $CDCl_3$): δ = 50.73 ($SiOCH_3$), 50.31 ($SiOCH_3$), 42.82 (C-1′), 40.07 (C-3), 32.37, 31.17 (C-2′/C-5′), 31.53 (C-4), 29.49 (C-5), 25.00, 24.99 (C-3′/C-4′), 24.99 (C-2). − Aromatic ^{13}C shifts: 136.97, 133.13, 132.21 (3 C_q aromatic), 135.74, 130.26, 128.58, 127.74, 125.89, 125.08, 124.75 (in total 7 aromatic CH groups). − ^{29}Si NMR (59.25 MHz, $CDCl_3$): δ = −21.71. − MS (CI); *m/z* (%): 371 (1.81) [(M + 1)$^+$], 339 (75.81) [$M^+ - OCH_3$], 243 (100) [$M^+ - C_{10}H_7$ (naphthyl)], 128 (12.24) [$C_{10}H_8^+$], 57 (22.22) [tBu$^+$]. − $C_{23}H_{34}SiO_2$ (370.61): calcd. C 74.54, H 9.25; found C 74.39, H 9.13.

(*E*)-1,1-Dichloro-3-isopropyl-3-methyl-2-neopentyl-1-silacyclobutane (*E*-16): For the assignment of the NMR chemical shifts in **16** the atoms are numbered as expressed by the formula in Scheme 7. − ^{1}H NMR (300 MHz, $CDCl_3$): δ = 0.86−0.90 (m, 6 H, 10-H and 11-H), 0.91 [s, 9 H, C(CH_3)$_3$], 0.99 (s, 3 H, 8-H), 1.33 (dd, $^2J_{HH}$ =

13.2 Hz, $^3J_{HH}$ = 2.6 Hz, 1 H, CH_aH$_b$*t*Bu), 1.54 (m, 1 H, 4-H), 1.60 (dd, $^2J_{HH}$ = 13.2 Hz, $^3J_{HH}$ = 12.8 Hz, 1 H, CH$_a$$H_b$*t*Bu), 1.64 (m, 1 H, 9-H), 1.76 (m, 1 H, 4-H), 1.96 (dd, $^3J_{HH}$ = 12.8 Hz, $^3J_{HH}$ = 2.6 Hz, 1 H, 2-H). − ^{13}C NMR (75.40 MHz, $CDCl_3$): δ = 46.37 (C-2), 42.60 (C-6), 40.87 (C-3), 40.40 (C-9), 38.50 (C-4), 30.53 (C-10), 29.51 (C-11), 28.73 (C-4), 17.77 (C-7), 17.95 (C-8). − ^{29}Si NMR (59.25 MHz, $CDCl_3$): δ = 19.65.



Scheme 7. Numbering scheme of **16**, **19**, and **20**

(*Z*)-1,1-Dichloro-3-isopropyl-3-methyl-2-neopentyl-1-silacyclobutane (*Z*-16): ^{1}H NMR (300 MHz, $CDCl_3$): δ = 0.86−0.90 (m, 6 H, 10-H and 11-H), 0.90 [s, 9 H, C(CH_3)$_3$], 1.18 (s, 3 H, 8-H), 1.34 (m, 1 H, 9-H), 1.46 (dd, $^2J_{HH}$ = 13.6 Hz, $^3J_{HH}$ = 2.3 Hz, 1 H, CH_aH$_b$*t*Bu), 1.57 (m, 1 H, 4-H), 1.61(dd, $^2J_{HH}$ = 13.6 Hz, $^3J_{HH}$ = 12.6 Hz, 1 H, CH$_a$$H_b$*t*Bu), 1.88 (m, 1 H, 2-H), 2.14 (m, 1 H, 4-H). − ^{13}C NMR (75.40 MHz, $CDCl_3$): δ = 49.53 (C-2), 41.43 (C-3), 38.23 (C-9), 36.26 (C-4), 32.92 (C-6), 30.60 (C-10), 29.45 (C-11), 27.40 (C-5), 18.86 (C-8), 18.70 (C-7). − ^{29}Si NMR (59.25 MHz, $CDCl_3$): δ = 19.35. − MS (70 eV) of (***E*/*Z*)-16**; *m*/*z* (%): 266 (4.65), 268 (3.37), 270 (0.71) [M^+] (isotopic pattern $SiCl_2$), 251 (1.17), 253 (1.27) [$M^+ - CH_3$] (isotopic pattern $SiCl_2$), 235 (0.56) [M^+ − Cl], 209 (9.35)/211 (7.34) [M^+ − *t*Bu] (isotopic pattern $SiCl_2$). − $C_{12}H_{24}Cl_2Si$ (267.32): calcd. C 53.92, H 9.05, Cl 26.53; found C 53.95, H 10.29, Cl 26.04.

(*E*)-1,1-Dichloro-3-ethyl-3-methyl-2-neopentyl-1-silacyclobutane (*E*-19): Numbering of atoms in *E*-**19** see Scheme 7, 11 = H. − ^{1}H NMR (300 MHz, $CDCl_3$): δ = 0.84−0.89 (m, 3 H, 10-H), 0.91 [s, 9 H, C(CH_3)$_3$], 1.16 (s, 3 H, 8-H), 1.24 (dd, $^2J_{HH}$ = 13.2 Hz, $^3J_{HH}$ = 3.0 Hz, 1 H, CH_aH$_b$*t*Bu), 1.46 (m, 1 H, 9-H), 1.55 (m, 1 H, 4-H), 1.59 (m, 1 H, 9-H), 1.66 (dd, $^2J_{HH}$ = 13.2 Hz, $^3J_{HH}$ = 12.1 Hz, 1 H, CH$_a$$H_b$*t*Bu), 1.92 (m, 1 H, 4-H), 1.94 (dd, $^3J_{HH}$ = 12.1 Hz, $^3J_{HH}$ = 3.0 Hz, 1 H, 2-H). − ^{13}C NMR (75.40 MHz, $CDCl_3$): δ = 50.65 (C-2), 39.64 (C-8), 38.48 (C-3), 38.33 (C-4), 30.22 (C-9), 29.53 (C-10), 28.86 (C-5), 28.82 (C-6), 8.41 (C-7). − ^{29}Si NMR (59.25 MHz, $CDCl_3$): δ = 18.88.

(*Z*)-1,1-Dichloro-3-ethyl-3-methyl-2-neopentyl-1-silacyclobutane (*Z*-19): Numbering of atoms in *Z*-**19** see Scheme 7, 11 = H. − ^{1}H NMR (300 MHz, $CDCl_3$): δ = 0.84−0.89 (m, 3 H, 10-H), 0.91 [s, 9 H, C(CH_3)$_3$], 1.07 (s, 3 H, 8-H), 1.28 (dd, $^2J_{HH}$ = 13.4 Hz, $^3J_{HH}$ = 3.0 Hz, 1 H, CH_aH$_b$*t*Bu), 1.44 (m, 1 H, 9-H), 1.52 (m, 1 H, 4-H), 1.60 (m, 1 H, 9-H), 1.62 (dd, $^2J_{HH}$ = 13.4 Hz, $^3J_{HH}$ = 12.6 Hz, 1 H, CH$_a$$H_b$*t*Bu), 1.88 (dd, $^3J_{HH}$ = 12.6 Hz, $^3J_{HH}$ = 3.0 Hz, 1 H, 2-H), 1.92 (m, 1 H, 4-H). − ^{13}C NMR (75.40 MHz, $CDCl_3$): δ = 47.17 (C-2), 38.95 (C-8), 37.95 (C-3), 37.77 (C-4), 35.43 (C-6), 30.22 (C-9), 29.53 (C-10), 22.33 (C-5), 9.10 (C-7). − ^{29}Si NMR (59.25 MHz, $CDCl_3$): δ = 18.12. − Mass spectra and elemental analysis of ***E*/*Z*-19** together with ***E*/*Z*-20**. The isomeric mixture could not be seperated by distillation.

(*E*/*Z*)-1,1-Dichloro-3-isopropyl-2-neopentyl-1-silacyclobutane (*E*/*Z*-20): A detailed interpretation of the ^{1}H-NMR spectra was avoided because of small signal intensities and complex superpositions of NMR signals.

(E)-1,1-Dichloro-3-isopropyl-2-neopentyl-1-silacyclobutane (*E*-20): Numbering of atoms in *E*-**20** see Scheme 7, 8 = H. − ^{13}C NMR (75.40 MHz, $CDCl_3$): δ = 43.74 (C-9), 42.09 (C-2), 41.98 (C-3), 30.62 (C-10), 29.46 (C-11), 27.33 (C-4), 22.33 (C-6), 21.04 (C-7), 19.03 (C-5). − ^{29}Si NMR (59.25 MHz, $CDCl_3$): δ = 16.13.

(*Z*)-1,1-Dichloro-3-isopropyl-2-neopentyl-1-silacyclobutane (*Z*-20): Numbering of atoms in *Z*-**20** see Scheme 7, 8 = H. − ^{13}C NMR (75.40 MHz, $CDCl_3$): δ = 42.85 (C-9), 41.98 (C-2), 40.78 (C-3), 31.97 (C-4), 30.38 (C-10), 29.46 (C-11), 21.28 (C-6), 20.26 (C-7), 19.45 (C-5). − ^{29}Si NMR (59.25 MHz, $CDCl_3$): δ = 17.07. − MS (70 eV) of **19** and **20**; *m*/*z* (%): 252 (3.58), 254 (2.59), 256 (0.58) [M^+] (isotope pattern of $SiCl_2$), 237 (0.91), 239 (0.96) [$M^+ - CH_3$] (isotope pattern of $SiCl_2$), 217 (0.35) [M^+ − Cl], 195 (7.11), 197 (5.66) [M^+ − *t*Bu]. − Elemental analysis of **19** and **20**; $C_{11}H_{22}Cl_2Si$ (253.29): calcd. C 52.16, H 8.75, Cl 27.99; found C 52.44, H 9.85, Cl 26.35.

Acknowledgments

We thank the Wacker-Chemie GmbH and Chemetall GmbH for gifts of chlorosilanes and alkyllithium compounds; we are grateful to the Dow Corning Corp. for financial support.

[1] B. Goetze, B. Herrschaft, N. Auner, *Chem. Eur. J.* **1997**, *3*, 948.
[2] A. Tomanek, *Silicones and Industry*, Wacker-Chemie GmbH, Munich, 7/**1991**, Carl Hauser Verlag, Munich, **1991**; *Silicone, Chemie und Technologie*, Vulkan-Verlag, Essen, **1989**.
[3] For the synthesis of various ethylsilanes by ethylation of halosilanes using appropriate organometallics, mainly Grignard reagents, see: R. N. Lewis, *J. Am. Chem. Soc.* **1947**, *69*, 717; M. F. Shostakovskii, D. A. Kochkin, I. A. Shikhiev, V. M. Vlassov, *Zh. Obshch. Khim.* **1955**, *25*, 622 (*Chem. Abstr.* **1956**, *50*, 3270b; L. H. Sommer, F. C. Whitmore, *J. Am. Chem. Soc*. **1946**, *68*, 485; V. F. Mironov, V. V. Nepomnina, *Izv. Akad. Nauk SSSR, Otd. Khim. Nauk* **1959**, 1231 (*Chem. Abstr.* **1960**, *54*, 1268e); G. V. Golodnikov, G. N. Koroleva, *Zh. Obshch. Khim*. **1961**, *31*, 3738 (*Chem. Abstr.* **1962**, *57*, 8601d).
[4] H. Matsumato, S. Nagashima, T. Kato, Y. Nagai, *Angew. Chem.* **1978**, *90*, 288, *Angew. Chem. Int. Ed. Engl*. **1978**, *17*, 279; R. Calas, J. Dunoguès, G. Deleris, N. Duffaut, *J. Organomet. Chem*. **1982**, 225, 117.
[5] E. Lukevics, Z. V. Belyakova, M. G. Pomorentseva, M. G. Voronkov, *J. Organomet. Chem. Libr*. **1977**, *5*, 1.
[6] A. D. Petrov, B. F. Mironov, V. A. Ponomarenko, E. A. Chernyshev, *Synthesis of Organosilicon Monomers*, Heywood & Co., Ltd., London, **1964**.
[7] That is why the reaction of silicon, alkyl chloride and copper as catalyst is almost restricted to the production of chloro(methyl)silanes: R. J. H. Voorhoeve, *Organohalosilanes, Precursors to Silicones*, Elsevier, New York, **1967**; A. G. MacDiarmid, *Organometallic Compounds of the Group IV Elements*, M. Dekker, Inc., New York, **1972**, vol. 2 ("The Bond to Halogenes and Halogenoids", part 1).
[8] V. Bazant, V. Chvalovský, J. Rauthouský, *Organosilicon Compounds*, Academic Press, New York, **1965**, vol. 1.
[9] J. P. Picard, J. Dunogues, A. Elyusufi, M. Lefort, *Synth. Commun*. **1984**, *14*, 95.
[10] For the hydrogenation of 0.1 mol of vinylsilane 0.04 mol of triethylsilane, $7.7 \cdot 10^{-3}$ mol of dry nickel chloride and 2.5 L of hydrogen are required. Especially with respect to the amount of Et_3SiH, this hydrogenation method does not seem practicable for large-scale syntheses. Furthermore, $NiCl_2$ might affect the carbon skeletons of silaheterocycles.
[11] H. Beyer, W. Walter, *Lehrbuch der Organischen Chemie*, S. Hirzel Verlag, Stuttgart, **1991**.
[12] N. Auner, "Neopentylsilenes − Laboratory Curiosities or useful Building Blocks for the Synthesis of Silaheterocycles" in *Organosilicon Chemistry − From Molecules to Materials* (Eds.: N. Auner, J. Weis), VCH Verlag, Weinheim, **1994**, pp. 103.
[13] For example see: Fat hardening, catalytical high pressure hydrogenation, the Fischer-Tropsch-Process (coal liquefaction) [H. Anderson, *The Fischer-Tropsch Synthesis*, Academic Press, Orlando, **1984**].

[14] G. R. Pearson, *Acc. Chem. Res.* **1971**, *4*, 152; G. R. Pearson, *Trans. Am. Crystallogr. Assoc*. **1978**, *14*, 89.
[15] For a summary see: F. Zarea, *Chem. Rev.* **1995**, *95*, 2651.
[16] P. R. Jones, T. F. O. Lim, R. A. Pierce, *J. Am. Chem. Soc*. **1980**, *102*, 4970.
[17] N. Auner, *J. Organomet. Chem*. **1988**, *353*, 257.
[18] H.-U. Steinberger, N. Auner, *Z. Naturforsch*. **1994**, *49b*, 1743.
[19] H.-U. Steinberger, T. Müller, N. Auner, in preparation.
[20] H.-U. Steinberger, T. Müller, N. Auner, C. Maerker, P.v.R. Schleyer, *Angew. Chem*. **1997 109**, 667; *Angew. Chem. Int. Ed. Engl.* **1997**, 36 , 626.
[21] N. Sewald, W. Ziche, A.Wolff, N. Auner, *Organometallics* **1993**, *12*, 4123.
[22] *Visuelles Informationssystem für Kristallstruktur*: Prof. Dr. G. Bergerhoff, Gerhard-Domagk-Str., D-53121 Bonn.
[23] N. Auner, C. Seidenschwarz, E. Herdtweck, *Angew. Chem*. **1991**, *103*, 1172; *Angew. Chem. Int. Ed. Engl*. **1991**, *30*, 1151; N. Auner, C.-R. Heikenwälder, C. Wagner, *Organometallics* **1993**, *12*, 4135.
[24] H.-U. Steinberger, N. Auner, "Catalytic Carbon−Carbon Hydrogenation of Silicon-Functionalized Olefins" in *Organosilicon Chemistry III − From Molecules to Materials* (Eds.: N. Auner, J. Weis), VCH Verlag, Weinheim, **1998**, pp. 113.
[25] *International Tables for Crystallography*, vol.C, Table 4.2.6.8, Table 6.1.1.4, Kluwer Academic Publishers, Dordrecht, Boston, London, **1993**.
[26] G.M. Sheldrick in *Crystallographic Computing 3* (Eds.: G. M. Sheldrick, C. Krüger, R. Goddard), Oxford University Press, Oxford, **1985**, p. 175.
[27] G.M. Sheldrick, *SHELXL93, A Program for the Refinement of Crystal Structures*, Universität Göttingen, Germany, **1993**.

Received October 6, 1998
[I98341]

Gold(I) Complexes with Amine Ligands, 4[+]

The Role of N–H···Cl Hydrogen Bonds in Gold(I) Complexes with Aliphatic Amine Ligands

Birte Ahrens,[a] Peter G. Jones,*[a] and Axel K. Fischer[b]

Keywords: Amines / Aurophilicity / Gold / Hydrogen bonds

Various gold(I) complexes of aliphatic amines have been prepared by the reaction of chloro(tetrahydrothiophene)-gold(I) with the respective amines. The stability of these complexes can be attributed partly to the formation of hydrogen bonds involving the N–H functions, and partly to aurophilic interactions. Analysis of these secondary contacts suggests an inverse correlation between lengths of aurophilic interactions and hydrogen bonds.

Introduction

Amine complexes of gold(I) have been little studied and are generally regarded as relatively unstable; this has been rationalized in terms of incompatibility of the soft metal centre with the hard nitrogen donor. Exceptions are furnished by complexes also involving a phosphane or similar ligand as a stabilising influence.[1] From previous studies of systems with solely amine or halide ligands only three structure types are known: (i) $[L_2Au^+][AuCl_2^-]$ (e.g. L = pyridine, 3-methylpyridine),[2][3] (ii) $[L_2Au^+]Cl^-$ (e.g. L = 4-hydroxymethyl-1,5-dimethylimidazole),[4] (iii) [LAuCl] (e.g. L = 2-methylpyridine, piperidine).[3][5] For the imine L = diphenylmethanimine, structures of type (i) and (iii) are known.[6] Type (ii) is also represented by the ammine complex $[(NH_3)_2Au^+]Br^-$.[7]

We have begun a more systematic study of gold(I) complexes with aliphatic amine ligands, generally bearing an N−H function, and have recently reported the structure of $[(pyrrolidine)_4Au_3Cl_3]$,[8] where structure types (ii) and (iii) were present in the same crystal.

Stabilising influences in gold(I) complexes tend to be provided by formally non-bonding Au···Au contacts (aurophilic interactions);[9] the role of hydrogen bonds is of course limited to those systems where suitable functional groups are available, but they have been shown to stabilise e.g. iminegold(I) complexes.[10] In $[(pyrrolidine)_4Au_3Cl_3]$ the Au···Au contacts were long and thus presumably weak [3.2041(7), 3.5834(4) Å],[8] whereas hydrogen bonds were more significant [N···Cl 3.179(6), 3.284(6) Å]. In [(piperidine)AuCl][5] similar Au···Au contacts were observed [Au···Au 3.301(5) Å], but hydrogen bonding was not commented upon, although it is in fact present in the form of bifurcated three-centre hydrogen bonds (Figure 1; N···Cl 3.346, 3.358 Å).

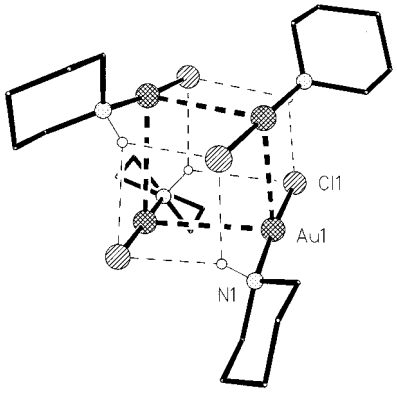


Figure 1. Chloro(piperidine)gold(I),[5] monomeric units related by a $\bar{4}$ axis; only the asymmetric unit is numbered; atom radii are arbitrary; dashed lines represent hydrogen bonds (thin) and aurophilic interactions (thick); carbon-bound hydrogen atoms are omitted for clarity

Here we report the synthesis of gold(I) complexes with the amine ligands piperidine {the complexes [(piperidine)AuCl], $[(piperidine)_2Au^+]Cl^-$, and $[(piperidine)_2Au^+]PF_6^-$ had been previously synthesised by us},[5] 2,2,6,6-tetramethylpiperidine, 4-methylpiperidine, morpholine, piperazine, pyrrolidine, diethylamine, dicyclohexylamine, cyclohexylamine, benzylamine, 1-phenylethylamine, and 3-iodobenzylamine; all complexes were obtained from (tht)AuCl (tht = tetrahydrothiophene) and the corresponding amine. With pyrrolidine, morpholine, cyclohexylamine, and benzylamine, complexes of empirical formula L_2AuCl were obtained; with the other ligands complexes of empirical formula LAuCl. For L = piperidine formerly only crystals of the loosely associated tetramer $(LAuCl)_4$ were obtained;[5] in contrast, we have only been able to obtain crystals of the ionic type $[L_2Au^+]Cl^-$. For L = pyrrolidine, we have now shown that the previously reported $L_4Au_3Cl_3$[8] is a by-product; the main product is $[L_2Au^+]Cl^-$.

No evidence was found for an ionic nature of the complexes in solution: all complexes behave as non-conductors

[+] Part 3: Ref.[11]

[a] Institut für Anorganische und Analytische Chemie, Technische Universität Braunschweig,
Postfach 3329, D-38023 Braunschweig, Germany
E-mail: jones@xray36.anchem.nat.tu-bs.de
[b] Chemisches Institut, Otto von Guericke Universität Magdeburg, Universitätsplatz 2, D-39106 Magdeburg, Germany

 © WILEY-VCH Verlag GmbH, D-69451 Weinheim, 1999 1434−1948/99/0707−1103 $ 17.50+.50/0

in acetone solution (Λ_c < 25 cm^2 Ω^{-1} mol^{-1}; c.f. Λ_c = 140 cm^2 Ω^{-1} mol^{-1} in the case of 1:1 electrolytes such as PPN^+Cl^-), implying that for all aminegold(I) complexes the molecular structure LAuCl is the more stable in solution. Even complexes L_2AuCl were essentially non-conducting, implying some equilibrium involving the uncharged species [LAuCl] in solution.

We have crystallographically characterised complexes of empirical formula LAuCl (L = 2,2,6,6-tetramethylpiperidine: **1**; dicyclohexylamine: **2**), both molecular in nature, and L_2AuCl (L = piperidine: **3**; pyrrolidine: **4**; and cyclohexylamine: **5**). For the latter complexes the ionic structure type (i), $[L_2Au^+]Cl^-$, was found for all three structures. Because no structure is known of a molecular aminegold(I) complex with empirical formula L_2AuX (i.e. where gold would be three-coordinate, with two amine ligands L), we assume an ionic composition for all aminegold(I) complexes of this empirical formula.

Because both types of structure, [LAuCl] and $[L_2Au^+]Cl^-$, have been observed for L = piperidine, it might be concluded that the energetic difference between both types cannot be large. Similar conclusions were drawn from the reactions of (tht)AuCl with methylpyridines,[3] and from ab initio calculations for various spatial associations of complexes with formula $[L_2Au^+][AuCl_2^-]$.[11]

Treatment of the new gold(I) complexes [LAuCl] (L = dicyclohexylamine) or $[L_2Au^+]Cl^-$ (L = piperidine or cyclohexylamine) with $AgSbF_6$ and excess L led in all cases to ionic complexes $[L_2Au^+]SbF_6^-$ (**13**, **14**, and **15**). Complex **13** was crystallographically characterised.

In all the new complexes hydrogen bonding is important in the solid state (Table 1), and for the ionic compounds appears more important than aurophilic interactions (see below). All complexes are less stable in solution than in the solid state. This could be attributed to a change in hydrogen bonding in solution, where the N−H protons are involved in hydrogen bonds to solvent molecules (in ^{1}H-NMR experiments broad signals for the N−H protons were observed, but no variation for the chemical shift). The low solubility of complexes with NH_2 functional groups could also be attributed to hydrogen bonding.

Molecular Structures

We have reported the structure of **2** in a preliminary communication.[12] The structure of **1** (Figure 2) is similar to that of **2** (Figure 3). Both complexes crystallise as loose molecular dimers $(LAuCl)_2$ and display ring motifs. In **1** and **2** only one crystallographically independent hydrogen bond is present, and therefore the ring motifs can be described by the graph set[13] $N_1 = R_2^2(8)$ at unitary level.

The dimers in **1** and **2** have inversion symmetry, making the N−Au−Cl axes antiparallel. Additionally, the molecule of **1** has crystallographic mirror symmetry, with N, Au, Cl, and C3 in the mirror plane. The gold atom in **1** is linearly coordinated [N−Au−Cl 177.21(9)°]. The Au−N and Au−Cl bond lengths of 2.088(3) and 2.2693(10) Å are

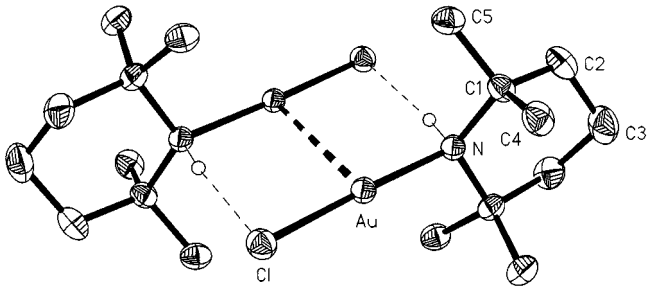


Figure 2. Chloro(2,2,6,6-tetramethylpiperidine)gold(I), **1**, monomeric units related by inversion symmetry; only the asymmetric unit is numbered; thermal ellipsoids are shown with 50% probability; hydrogen radii are arbitrary; dashed lines represent hydrogen bonds (thin) and aurophilic interactions (thick); carbon-bound hydrogen atoms are omitted for clarity

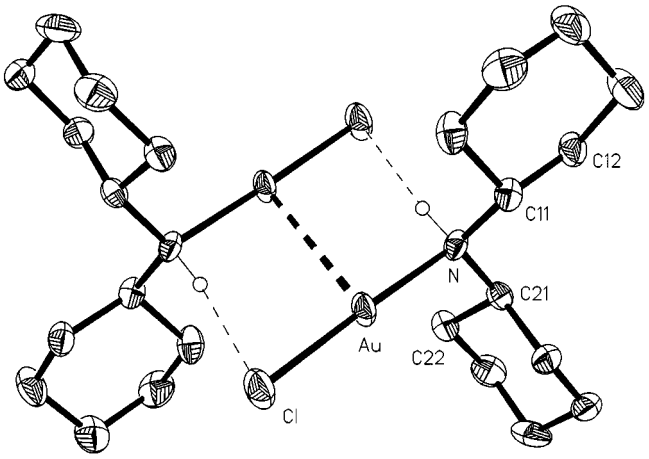


Figure 3. Chloro(dicyclohexylamine)gold(I), **2**, monomeric units related by inversion symmetry; only the asymmetric unit is numbered; thermal ellipsoids are shown with 50% probability; hydrogen radii are arbitrary; dashed lines represent hydrogen bonds (thin) and aurophilic interactions (thick); carbon-bound hydrogen atoms are omitted for clarity

longer than those in (piperidine)AuCl [2.068(18), 2.256(8) Å][5] but similar to those in **2** [2.077(7), 2.266(2) Å]. The dimers of **1** display aurophilic interaction and hydrogen bonding [Table 1; Au···Au 3.2792(4), N···Cl 3.417(3) Å], comparable to those in **2** [3.2676(14), 3.391(8) Å] and (piperidine)AuCl [3.301(5), 3.346 and 3.580 Å].[5]

Ionic Structures

We have reported the structure of **3** in a preliminary communication.[12] In **3** two crystallographically independent hydrogen bonds are involved in the ring motif (Table 1, Figure 4), which can be described by the graph set $N_2 = R_4^2(12)$ at binary level. In **3** the gold atom is linearly coordinated [N1−Au−N2 179.0(3)°]. The N−Au bond lengths of 2.050(6) and 2.055(6) Å are similar to those of 2.068(18) in (piperidine)AuCl.[5] Thus it can be assumed that the *trans* influence of amine and chloro groups is similar.

The hydrogen bonds (Table 1) in the ionic compound **3** are shorter [N···Cl 3.108(6), 3.122(7) Å] and the Au···Au distance in **3** of 4.085(2) Å is remarkably longer than in

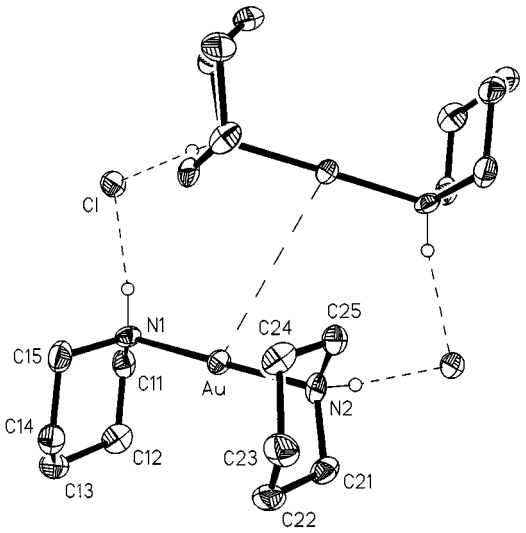


Figure 4. Bis(piperidine)gold(I) chloride, **3**, monomeric units related by a twofold axis; only the asymmetric unit is numbered; thermal ellipsoids are shown with 50% probability; hydrogen radii are arbitrary; dashed lines represent hydrogen bonds and aurophilic interactions; carbon-bound hydrogen atoms are omitted for clarity

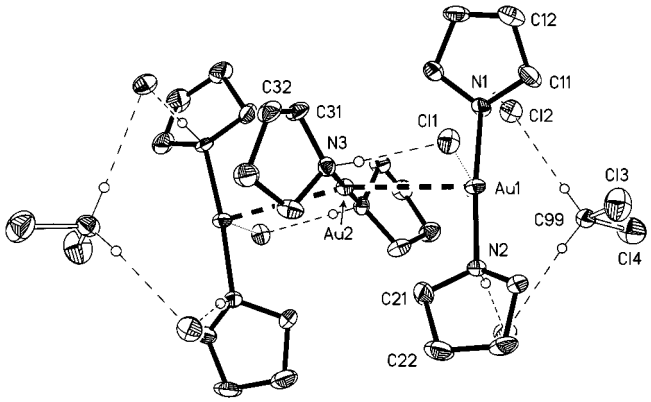


Figure 5. Bis(pyrrolidine)gold(I) chloride (dichloromethane solvate), **4**; only the asymmetric unit is numbered; thermal ellipsoids are shown with 50% probability; hydrogen radii are arbitrary; dashed lines represent hydrogen bonds (thin) and aurophilic interactions (thick), dotted lines Au···Cl interactions; carbon-bound hydrogen atoms are omitted for clarity

(piperidine)AuCl,[5] **1** and **2**. Gold−gold distances within the range of 2.50 to 4.00 Å have been considered as aurophilic interactions.[14] Thus the gold-gold interaction in **3** must be extremely weak.

Compounds **4** and **5** both crystallise as dichloromethane solvates $[(L_2AuCl)_3 \cdot (CH_2Cl_2)_2]$ with chain and layer structures. In **4** the L_2Au^+ cations (with L = pyrrolidine) form trimers about a twofold axis, with Au2 on this axis and Cl1 on an inversion centre (Figure 5). Both gold atoms of the asymmetric unit are linearly coordinated [N−Au−N 175.0(3), 179.6(4)°]. The Au−N bond lengths Au1−N1 of 2.055(7), Au1−N2 of 2.052(6), and Au2−N3 of 2.052(5) Å are slightly longer than those in $(pyrrolidine)_4Au_3Cl_3$ of 2.042(6) and 2.048(6) Å.[8] The gold atoms of the trimers in **4** display aurophilic interactions [Au1···Au2 3.2790(7) Å]. The N−Au−N axes within these dimers are nearly perpendicular to each other, with torsion angles of 87.3(3) and −93.2(3)° (N1−Au1···Au2−N3, N2−Au1···Au2−N3, respectively). The hydrogen atom at N3 is involved in a hydrogen bond to Cl1 [N3···Cl1 3.311(5) Å; Table 1]. This hydrogen bond connects the trimers to form chains parallel to (0 0 1) [descriptor $C_2^1(6)$; Figure 6], which are additionally stabilised by short Au···Cl contacts [Au1···Cl1 3.176(1) Å]. The hydrogen atoms at N1 and N2 are involved in hydrogen bonds to Cl2 [N1···Cl2 3.149(7), N2···Cl2′ 3186(7) Å; Table 1]. These hydrogen bonds connect the chains to form layers perpendicular to (0 0 1), with descriptor $C_2^1(6)$ at binary level (Figure 7). The dichloromethane molecules lie within these layers. They show non-conventional hydrogen bonding to the chloride anion Cl2 [C···Cl 3.625 Å (mean)]. One of the chlorine atoms of the dichloromethane molecules is involved in a weak contact to one of the gold atoms [Au1···Cl3 3.635(3) Å], the other chlorine atom displays a Cl···Cl contact to the symmetry-equivalent atom of the next dichloromethane moiety [Cl4···Cl4′ 3.547(5) Å; operator $1 - x, 1 - y, -z$]. The secondary contacts of the dichloromethane molecules result in a honeycomb-like pattern within the layers perpendicular to (0 0 1) (Figure 7). These contacts presumably have a stabilising influence on

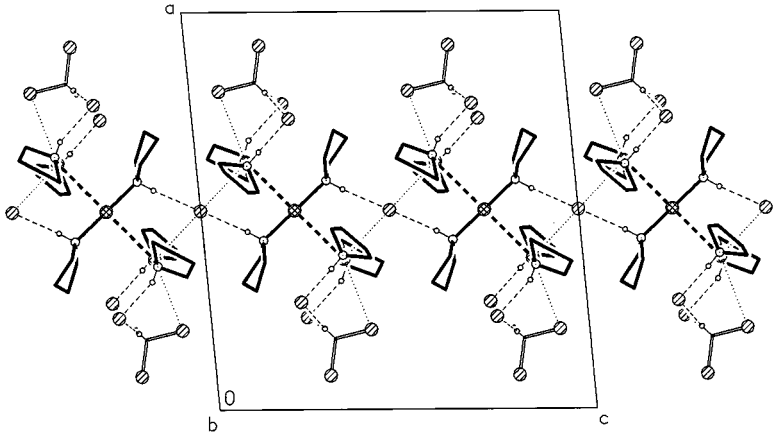


Figure 6. Bis(pyrrolidine)gold(I) chloride (dichloromethane solvate), **4**, chain structure parallel to (0 0 1); atom radii are arbitrary; dashed lines represent hydrogen bonds (thin) and aurophilic interactions (thick), dotted lines Au···Cl interactions; carbon-bound hydrogen atoms, except for CH_2Cl_2, are omitted for clarity

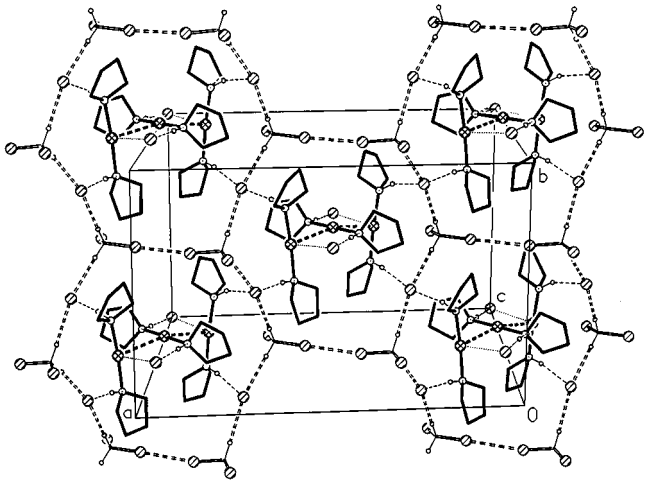


Figure 7. Bis(pyrrolidine)gold(I) chloride (dichloromethane solvate), **4**, layer structure perpendicular to (0 0 1); atom radii are arbitrary; dashed lines represent hydrogen bonds (thin) and aurophilic interactions (thick), dotted lines Au···Cl^- interactions; Au···dichloromethane interactions are not shown; double dashed lines represent secondary interactions of the dichloromethane molecules; carbon-bound hydrogen atoms, except for CH_2Cl_2, are omitted for clarity.

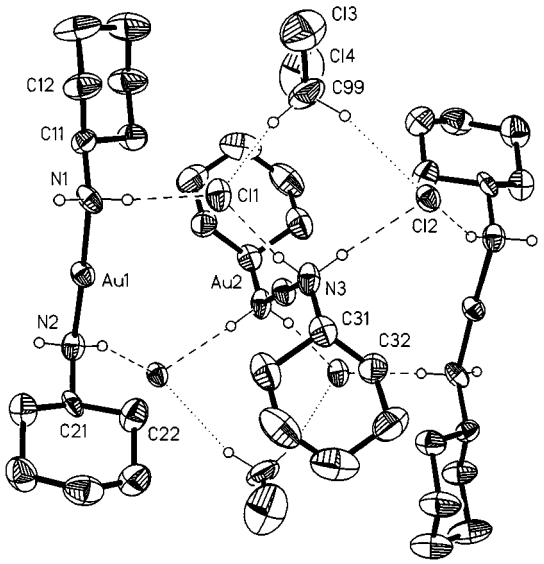


Figure 8. Bis(cyclohexylamine)gold(I) chloride (dichloromethane solvate), **5**, asymmetric unit with numbering scheme; thermal ellipsoids are shown with 50% probability; hydrogen radii are arbitrary; dashed lines represent N−H hydrogen bonds, dotted lines C−H hydrogen bonds; carbon-bound hydrogen atoms, except for CH_2Cl_2, are omitted for clarity

the structure, in addition to that of the N−H···Cl hydrogen bonds discussed above.

In **5** the L_2Au^+ cations (with L = cyclohexylamine) also form trimeric units (Figure 8), here with inversion symmetry (Au2 and Cl2 lie on inversion centres). The gold atoms are linearly coordinated [N1−Au1−N2 177.6(4), N3−Au2−N3′ 180° (by symmetry)]. The Au−N bond lengths Au1−N1 of 2.036(9), Au1−N2 of 2.047(9) and Au2−N3 of 2.051(8) Å are similar to those in (pyrrolidine)$_4Au_3Cl_3$ or **2** [2.042(6)−2.055(7) Å].[8] No aurophilic interactions are observed, the shortest Au···Au distance being 4.740(1) Å. The cations are connected to form layers parallel to the *xy* plane via N−H···Cl hydrogen bonds (Figure 9, Table 1), with N···Cl contacts between 3.230(9) and 3.343(9) Å, resulting in a pattern of ring motifs. These rings are associated with descriptors from graph sets at higher levels: $R_4^2(8)$ (binary and ternary), $R_4^2(12)$ (ternary). Every dichloromethane molecule is involved in two non-conventional hydrogen bonds [C99···Cl1 3.576(15), C99···Cl2 3.641(13) Å]. Cl1 is the acceptor atom for one, Cl2 (because of the inversion centre) for two of these hydrogen bonds. The dichloromethane molecules are thus positioned alternately above and below the layer (Figure 8).

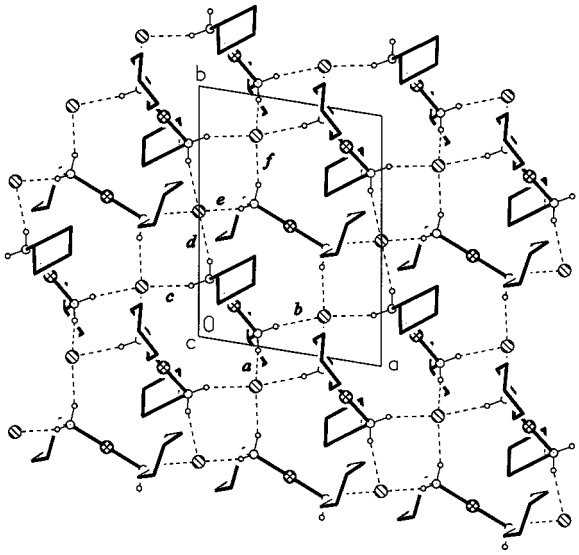


Figure 9. Bis(cyclohexylamine)gold(I) chloride (dichloromethane solvate), **5**, layer structure; atom radii are arbitrary; dashed lines represent hydrogen bonds (Table 1); dichloromethane molecules and carbon-bound hydrogen atoms are omitted for clarity

Anion Exchange

By preparing the compound bis(dicyclohexylamine)-gold(I) hexafluoroantimonate, **13** (Figure 10), it was shown that it is possible to obtain L_2Au^+ cations even with this bulky ligand.

The gold atom in **13** is linearly coordinated [N1−Au−N2 179.1(2)°]. The Au−N bond lengths of 2.085(6) and 2.069(6) Å are similar to those in **2** [2.077(7) Å], consistent with our previous observation on *trans* influences (see above). The hydrogen atoms of the amine groups are involved in long hydrogen bonds to fluorine atoms of two hexafluoroantimonate anions [N···F 2.975(8), 3.268(9) Å; Table 1], thereby forming chains [graph set $N_2 = C_2^2(8)$].

Conclusions

Many complexes of gold(I) with aliphatic amines are stable, in contrast to the generally held view based on the

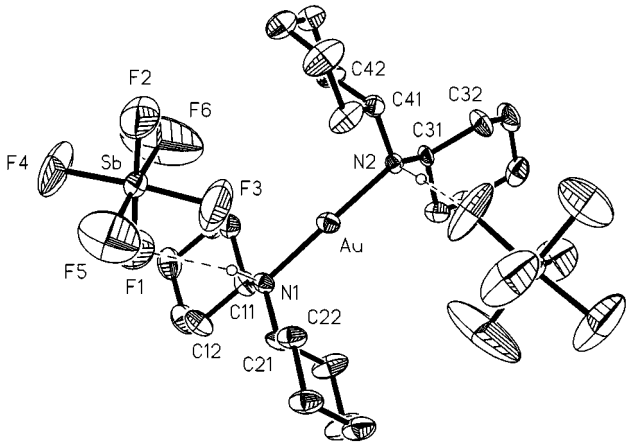


Figure 10. Bis(cyclohexylamine)gold(I) hexafluoroantimonate, **13**, asymmetric unit with numbering scheme; thermal ellipsoids are shown with 50% probability; hydrogen radii are arbitrary; dashed lines represent hydrogen bonds

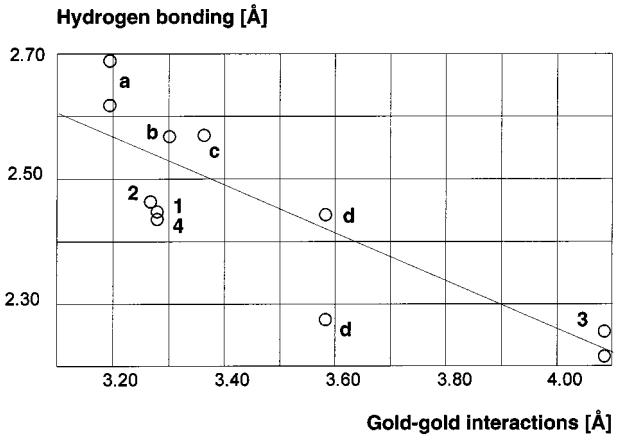


Figure 11. Plot of hydrogen bonding against aurophilic interactions for aminegold(I) complexes; the correlation coefficient is −0.842; a: $[(Ph_2C{=}NH)_2Au^+][AuCl_2^-]$;[6] b: [(piperidine)AuCl];[5] c: $[(Ph_2C{=}NH)AuCl]$;[6] d: $[(pyrrolidine)_4Au_3Cl_3]$[8]

incompatibility of hard ligands with soft metal centres. The stability results in part from the formation of hydrogen bonds involving the N−H functions. In ionic complexes of empirical formula L_2AuCl, hydrogen bonds appear to be more important than in complexes of empirical formula LAuCl; this may be attributable to the positive charge of the gold moiety in the former. Aurophilic interactions appear to have greater influence in complexes of empirical formula LAuCl. By combining data for similar structures (obtained from a search in the CSD database)[15] with our results, we found a tendency that shorter hydrogen bonds are accompanied by longer aurophilic interactions and vice versa (Figure 11). In the complexes with L = pyrrolidine ($L_4Au_3Cl_3$,[8] **4**) hydrogen bonds and aurophilic interactions appear to be necessary to stabilise the complexes, which, surprisingly for complexes with charged gold moieties, display short aurophilic interactions.

Previous difficulties in preparing aminegold(I) complexes may have been caused by (i) the insolubility of many products, (ii) the tendency to form mixtures of complexes (e.g. for pyrrolidine) and/or by-products such as amine hydrochlorides or hemihydrochlorides[16] or (iii) the use of unsuitable amines (e.g. tertiary amines, where we could not obtain stable complexes, presumably because of the lack of hydrogen bonding).

Anions with more functional groups for hydrogen bonding (e.g. disulfonylamine anions) are expected to render a stabilising contribution to aminegold(I) complexes. It may

Table 1. Hydrogen bonds and unitary graph sets (N_1)

Compound	Bond	H···A [Å][a]	H···A [Å][b]	D···A [Å][c]	D-H···A [°]	N_1
1	N−H···Cl^{ii}	2.45(5)	2.40	3.417(3)	174(4)	$R_2^2(8)$
2	N−H···Cl^{vi}	2.46(4)	2.39	3.391(8)	167(8)	$R_2^2(8)$
3	N1−H1···Cl1	2.26(4)	2.16	3.122(7)	158(7)	D
3	N2−H2···Cl1^{i}	2.21(3)	2.10	3.108(6)	172(9)	D
4	N1−H1···Cl2	2.35(7)	2.24	3.149(7)	149(9)	D
4	N2−H2···Cl2^{iii}	2.32(5)	2.18	3.186(7)	171(7)	D
4	N3−H3···Cl1	2.44(4)	2.29	3.311(5)	175(5)	$C_2^1(6)$
4	C99−H99A···Cl2^{iv}	2.63	2.55	3.625(9)	179	D
4	C99−H99B···Cl2^{v}	2.64	2.55	3.625(8)	174	D
5	N1−H1A···Cl1^{vii} *(a)*	2.36	2.26	3.256(9)	166	D
5	N1−H1B···Cl1 *(b)*	2.35	2.25	3.264(10)	171	D
5	N2−H2A···Cl1^{viii} (c)	2.45	2.36	3.297(9)	154	D
5	N2−H2B···Cl2^{viii} *(d)*	2.47	2.37	3.343(9)	159	$D_2^1(3)$
5	N3−H3A···Cl2 *(e)*	2.34	2.25	3.230(9)	161	$C_2^1(6)$
5	N3−H3B···Cl1 *(f)*	2.34	2.25	3.241(9)	165	$D_2^2(7)$
5	C99−H99A···Cl1	2.73	2.66	3.576(15)	144	D
5	C99−H99B···Cl2	2.69	2.60	3.641(13)	162	$D_2^1(3)$
13	N1−H1···F1	2.37	2.28	3.268(9)	163	D
13	N2−H2···F4^{ix}	2.06	1.97	2.975(8)	168	D

[a] Hydrogen bonds without standard deviation were included using a riding model. − [b] Distances were normalised with C−H 1.08, N−H 1.02 Å.[18] − [c] Cf. van der Waals radii: N 1.55, Cl 1.75, H 1.20, C 1.70, F 1.47 Å.[19] − Operators: i: 2 − *x*, *y*, 1.5 − *z*; ii: 1 − *x*, 1 − *y*, 1 − *z*; iii: 1.5 − *x*, 0.5+*y*, 0.5 − *z*; iv: *x* − 0.5, *y* − 0.5, *z*; v: 1 − *x*, *y*, 0.5 − *z*; vi: −*x*, 1 − *y*, 1 − *z*; vii: 1 − *x*, *y*, 1 − *z*; viii: 1+*x*, *y*, *z*; ix: *x* − 0.5, 1.5 − *y*, *z* − 0.5.

Table 2. Crystallographic data

Compound	**1**	**2**	**3**	**4**	**5**	**13**
Formula	$C_9H_{19}AuClN$	$C_{12}H_{23}AuClN$	$C_{10}H_{22}AuClN_2$	$C_{8.67}H_{19.33}AuCl_{2.33}N_2$	$C_{12.67}H_{27.33}AuCl_{2.33}N_2$	$C_{24}H_{46}AuF_6N_2Sb$
M_r	373.67	413.73	402.71	431.28	487.38	795.34
Crystal habit	Colourless tablet	Colourless prism	Colourless prism	Colourless prism	Colourless plate	Colourless prism
Crystal size [mm]	0.30 × 0.10 × 0.08	0.36 × 0.19 × 0.11	0.20 × 0.15 × 0.11	0.20 × 0.20 × 0.10	0.70 × 0.10 × 0.02	0.54 × 0.27 × 0.19
Crystal system	Orthorhombic	Triclinic	Monoclinic	Monoclinic	Triclinic	Monoclinic
Space group	*Pnnm*	$P\bar{1}$	*C*2/*c*	*C*2/*c*	$P\bar{1}$	$P2_1/n$
Cell dimensions						
a [Å]	10.6298(10)	8.306(3)	21.346(5)	18.859(3)	9.2497(12)	9.880(2)
b [Å]	10.2047(10)	8.978(2)	6.480(2)	11.963(2)	12.0358(15)	19.208(4)
c [Å]	10.5774(10)	10.132(3)	19.630(5)	17.890(2)	12.2298(16)	15.402(4)
α [°]	90	68.24(2)	90	90	100.042(9)	90
β [°]	90	85.17(3)	111.54(3)	95.45(2)	108.767(11)	98.40(2)
γ [°]	90	77.71(3)	90	90	95.455(13)	90
V [Å^3]	1147.37(19)	685.7(3)	2525.8(13)	4018.0(10)	1355.0(3)	2891.6(11)
Z	4	2	8	12	3	4
D_x [Mg m^{-3}]	2.163	2.004	2.118	2.139	1.792	1.827
μ [mm^{-1}]	13.008	10.894	11.829	11.418	8.476	6.055
F(000)	2448	396	1536	704	708	1552
T [°C]	−100	−100	−130	−100	−100	−130
$2\theta_{max}$ [°]	50	50	50	56.6	50	50
Transmission	0.34−0.99	0.65−0.94	0.53−0.68	0.54−1.00	0.59−0.98	0.61−0.97
No. of reflections						
Measured	3720	2402	3568	7330	4604	5837
Independent	3532	2336	2228	1506	4566	5076
R_{int}	0.045	0.039	0.036	0.030	0.023	0.028
Parameters	203	139	135	67	247	307
Restraints	33	1	2	0	45	263
*WR*2(F^2, all refl.)	0.051	0.088	0.067	0.034	0.110	0.108
*R*1[$F>2\sigma(F)$]	0.031	0.036	0.030	0.017	0.046	0.044
S	0.834	0.989	1.053	1.105	0.895	1.016
Max. Δ.σ	0.002	< 0.001	< 0.001	0.002	0.001	< 0.001
Max. Δρ [eÅ^{-3}]	1.143	3.322	1.178	0.762	1.903	2.172

Table 3. Selected bond lengths and angles [Å,°] for **1**

Au−N	2.088(3)	Au−Cl	2.2693(10)
Au−Au^{ii}	3.2792(4)	N−C(1)	1.528(3)
N−Au−Cl	177.21(9)	N−Au−Au^{ii}	82.30(9)
Cl−Au−Au^{ii}	100.49(3)	C(1)^{x}−N−C(1)	118.9(3)
C(1)−N−Au	112.25(16)		

Operators: ii: 1 − *x*, 1 − *y*, 1 − *z*; x: *x*, *y*, 1 − *z*.

Table 4. Selected bond lengths and angles [Å,°] for **2**

Au−N	2.077(7)	Au−Cl	2.266(2)
Au−Au^{vi}	3.2676(14)	N−C(11)	1.505(11)
N−C(21)	1.505(11)		
N−Au−Cl	177.7(2)	N−Au−Au^{vi}	80.8(2)
Cl−Au−Au^{vi}	101.50(7)	C(11)−N−C(21)	115.1(6)
C(11)−N−Au	113.4(5)	C(21)−N−Au	111.1(5)

Operator: vi: −*x*, 1−*y*, 1−*z*.

be possible to stabilise the less robust amine complexes such as **7** and $[(RNH_2)_2Au^+]$ (R = Me, Et, *t*Bu)[7] with such counter-ions. This influence will be discussed in a forthcoming paper of this series.

Table 5. Selected bond lengths and angles [Å,°] for **3**

Au−N(1)	2.050(6)	Au−N(2)	2.055(6)
N(1)−C(11)	1.493(10)	N(1)−C(15)	1.521(10)
N(2)−C(21)	1.483(10)	N(2)−C(25)	1.502(10)
N(1)−Au−N(2)	179.0(3)	C(11)−N(1)−C(15)	109.9(6)
C(11)−N(1)−Au	116.0(5)	C(15)−N(1)−Au	111.4(5)
C(21)−N(2)−C(25)	110.3(6)	C(21)−N(2)−Au	114.2(5)
C(25)−N(2)−Au	113.5(5)		

Table 6. Selected bond lengths and angles [Å,°] for **4**

Au(1)−N(2)	2.052(6)	Au(1)−N(1)	2.055(7)
Au(1)−Au(2)	3.2790(7)	N(1)−C(14)	1.492(10)
N(1)−C(11)	1.516(9)	N(2)−C(21)	1.466(10)
N(2)−C(24)	1.485(9)	Au(2)−N(3)	2.052(5)
Au(2)−Au(1)^{v}	3.2790(7)	N(3)−C(31)	1.485(9)
N(3)−C(34)	1.508(9)	C(99)−Cl(3)	1.755(7)
C(99)−Cl(4)	1.761(8)		
N(2)−Au(1)−N(1)	175.0(3)	N(2)−Au(1)−Au(2)	93.49(19)
N(1)−Au(1)−Au(2)	91.49(17)	C(14)−N(1)−C(11)	104.4(6)
C(14)−N(1)−Au(1)	116.9(5)	C(11)−N(1)−Au(1)	112.6(5)
C(21)−N(2)−C(24)	102.8(6)	C(21)−N(2)−Au(1)	117.7(5)
C(24)−N(2)−Au(1)	115.3(5)	N(3)−Au(2)−N(3)^{v}	179.6(4)
N(3)−Au(2)−Au(1)^{v}	91.29(14)	N(3)−Au(2)−Au(1)	88.65(14)
Au(1)^{v}−Au(2)−Au(1)	164.762(17)	C(31)−N(3)−C(34)	104.9(5)
C(31)−N(3)−Au(2)	115.4(4)	C(34)−N(3)−Au(2)	116.3(4)
Cl(3)−C(99)−Cl(4)	110.6(4)		

Operator: v: 1 − *x*, *y*, 0.5 − *z*.

Table 7. Selected bond lengths and angles [Å, °] for **5**

Au(1)−N(1)	2.036(9)	Au(1)−N(2)	2.048(9)
Au(2)−N(3)	2.051(8)	N(1)−C(11)	1.492(14)
N(2)−C(21)	1.470(14)	N(3)−C(31)	1.459(15)
C(99)−Cl(3)	1.742(15)	C(99)−Cl(4)	1.746(14)
N(1)−Au(1)−N(2)	177.6(4)	N(3)^{ii}−Au(2)−N(3)	180.0
C(11)−N(1)−Au(1)	117.2(7)	C(21)−N(2)−Au(1)	117.3(7)
C(31)−N(3)−Au(2)	119.9(7)	Cl(3)−C(99)−Cl(4)	112.3(8)

Operator ii: $1 - x$, $1 - y$, $1 - z$.

Table 8. Selected bond lengths and angles [Å, °] for **13**

Au−N(2)	2.070(6)	Au−N(1)	2.085(6)
Au−F(3)	3.460(9)	Au−F(4)^{ix}	3.981(7)
N(1)−C(21)	1.501(10)	N(1)−C(11)	1.502(9)
N(2)−C(31)	1.505(9)	N(2)−C(41)	1.526(9)
N(2)−Au−N(1)	179.1(2)	N(2)−Au−F(3)	111.7(2)
N(1)−Au−F(3)	68.6(2)	N(2)−Au−F(4)^{ix}	46.8(2)
N(1)−Au−F(4)^{ix}	132.5(2)	F(3)−Au−F(4)^{ix}	96.46(18)
C(21)−N(1)−C(11)	115.9(6)	C(21)−N(1)−Au	111.4(5)
C(11)−N(1)−Au	112.0(4)	C(31)−N(2)−C(41)	114.1(6)
C(31)−N(2)−Au	113.5(4)	C(41)−N(2)−Au	111.6(4)
Sb−F(3)−Au	129.6(5)		

Operator: ix: $x - 0.5$, $1.5 - y$, $z - 0.5$.

Experimental Section

General: NMR spectra were measured with a Bruker AC 200 spectrometer in $CDCl_3$ solution with TMS as internal standard (if not otherwise stated). Frequencies: 200.1 MHz (^{1}H), 50.3 MHz (^{13}C). − Mass spectra were recorded with a Finnigan MAT 8430. − Conductivities were measured with a WTW LF 530 (LTA 1 electrode) conductometer. − All reactions were carried out with exclusion of light at room temperature. − All aminegold(I) complexes with liquid amines were prepared as follows: (tht)AuCl (tht = tetrahydrothiophene) (160 mg, 0.5 mmol) was dissolved in neat amine (5 mL). The solution was stirred for 1 h with exclusion of light at room temperature; a white precipitate formed. Light petroleum ether was added and after cooling for 1 h at −18 °C the precipitate was filtered off and recrystallised from dichloromethane/light petroleum ether. Except for **5** (see below) crystals were obtained by diffusion of light petroleum ether into dichloromethane solution. − All complexes with SbF_6^- anions were prepared as follows: [LAuCl] or [L_2Au^+]Cl^- (0.5 mmol) was dissolved in a solution of 5 mL of dichloromethane and 1 mL of amine (L) and $AgSbF_6$ (344 mg, 1 mmol) was added. The suspension was stirred for 1 h with exclusion of light at room temperature. The AgCl precipitate was filtered off through a layer of $MgSO_4$. Light petroleum ether was added to the solution and after cooling overnight at −18 °C colourless, light-sensitive crystals were obtained.

Chloro(2,2,6,6-tetramethypiperidine)gold(I) (1): Yield 53%, dec. >122 °C. − ^{1}H NMR: δ = 1.44 (s, 6 H, CH_3), 1.48 (m, 2 H, β-CH_2), 1.57 (s, 6 H, CH_3), 1.65 (m, 2 H, γ-CH_2), 1.76 (m, 2 H, β-CH_2), 4.6 (br., NH). − ^{13}C NMR: δ = 17.12, (γ-CH_2), 28.14, (CH_3), 37.26, (β-CH_2), 59.27 (α-CH_2) (classified by C-H correlation). − EI MS; *m/z* (%): 126 (100) [M − CH_3 − AuCl], 141 (2) [M − AuCl]. − Conductivity: Λ_c = 8 cm^2 Ω $^{-1}$ mol^{-1}. − $C_9H_{19}AuClN$ (373.68): calcd. C 28.93, H 5.12, N 3.75; found C 28.85, H 5.08, N 3.51.

Chloro(dicyclohexylamine)gold(I) (2): Yield 75%, dec. > 114 °C. − ^{1}H NMR: δ = 1.26−1.84 (16 H, CH_2), 2.12, 2.40 [m, 4 H, 2-, 2′-CH_2 (eq.)], 2.99 (m, 2 H, CH). − ^{13}C NMR: δ = 25.05 (3-C), 35.50 (4-C), 34.82 (2-C), 58.73 (1-C). − EI MS; *m/z* (%): 181 (16) [M − Au − Cl]. − $C_{12}H_{23}AuClN$ (413.74): calcd. C 34.84, H 5.60, N 3.39; found C 34.86, H 5.55, N 3.34.

Bis(piperidine)gold(I) Chloride (3): Yield 91%, dec. > 86 °C. − ^{1}H NMR: δ = 1.73 (m, 4 H, β-CH_2), 3.25 (m, 4 H, α-CH_2). − ^{13}C NMR: δ = 23.41 (β-CH_2), 26.52 (γ-CH_2), 53.50 (α-CH_2). − EI MS; *m/z* (%): 84 (100) [M − Au − Cl − H]. − Conductivity: Λ_c = 24 cm^2 Ω^{-1} mol^{-1}. − $C_{10}H_{22}AuClN_2$ (402.72): calcd. C 29.82, H 5.51, N 6.96; found C 29.34, H 5.35, N 7.06.

Bis(pyrrolidine)gold(I) Chloride (4): Yield 85%, dec. at room temperature. − ^{1}H NMR: δ = 1.90 (br., 4 H, β-CH_2); 3.00 (br., 2 H), 3.54 (br., 2 H) (α-CH_2). − ^{13}C NMR: δ = 23.62 (β-CH_2); 52.54 (α-CH_2). − FAB MS (pos.); *m/z* (%): 72 (100) [K − $C_4H_8NAu]^+$. − $C_8H_{18}AuClN_2 \cdot 0.67\ CH_2Cl_2$ (431.20): calcd. C 24.15, H 4.52, N 6.50; found C 23.95, H 4.67, N 7.05; the elemental analysis is affected by co-crystallised dichloromethane, which could not be removed even after prolonged pumping. − (Pyrrolidine)$_4Au_3Cl_3$[8] was obtained as a by-product of this reaction.

Bis(cyclohexylamine)gold(I) Chloride (5): Crystals were obtained by diffusion of cyclohexylamine into a solution of (tht)AuCl in dichloromethane. Yield 75%, dec. > 114 °C. − ^{1}H NMR: δ = 1.16 (m, 12 H, CH_2, ax.); 1.77 (m, 10 H, CH_2, eq.); 2.62 (m, 2 H, CH); 4.5 (br., NH_2). − ^{13}C NMR: δ = 26.95 (3-C); 31.06 (4-C); 35.54 (2-C); 55.69 (1-C). − EI MS; *m/z* (%): 99 (19) [M − $C_6H_{13}NAuCl$]. − $C_{12}H_{26}AuClN_2$ (430.77): calcd. C 33.46, H 6.08, N 6.50; found C 33.57, H 6.07, N 6.52.

Chloro(4-methylpiperidine)gold(I) (6): Yield 55%, dec. > 67 °C. − ^{1}H NMR: δ = 0.87 (d, 3 H, CH_3), 0.93 (d, 3 H, CH_3), 1.28 (m, 1 H, β-CH_2), 1.45 (br., 1 H, γ-CH), 1.63 (m, 1 H, γ-CH), 1.67 (m, 3 H, β-CH_2), 3.01 (m, 2 H, α-CH_2), 3.36 (m, 1 H, α-CH_2), 3.52 (m, 1 H, α-CH_2), 5.5 (br., NH) (classified by C-H correlation). − ^{13}C NMR: δ = 21.60, 21.65 (CH_3); 29.93, 30.14 (γ-CH); 34.17, 35.26 (β-CH_2); 52.28, 53.72 (α-CH_2) [doubling of signals is due to two conformers (*cis* and *trans*)]. − EI MS; *m/z* (%): 98 (100) [M − AuCl − H]. − Conductivity: Λ_c = 21 cm^2 Ω^{-1} mol^{-1}. − $C_6H_{13}AuClN$ (331.60): calcd. C 21.73, H 3.95, N 4.22; found C 23.99, H 4.27, N 4.34.

Bis(morpholine)gold(I) Chloride (7): Yield 76%, dec. > 72 °C. This compound was not stable enough to obtain NMR spectra. − EI MS; *m/z* (%): 87 (100) [M − $C_4H_9NOAuCl$]. − Conductivity: Λ_c = 22 cm^2 Ω^{-1} mol^{-1}. − $C_8H_{18}AuClN_2O_2$ (406.66): calcd. C 23.63, H 4.46, N 6.89; found C 23.41, H 4.42, N 7.49.

Chloro(piperazine)gold(I) (8): (tht)AuCl (160 mg, 0.5 mmol) was dissolved in a solution of piperazine in ethanol (10 mL, 50% excess of piperazine). The suspension was stirred for 1 h with exclusion of light at room temperature. Diethyl ether was added and after cooling for 1 h at −18 °C the white precipitate was filtered off and recrystallised from dichloromethane/light petroleum ether. Yield 75%, dec. > 109 °C. − ^{1}H NMR: δ = 2.94 (m, 8 H, CH_2). − EI MS; *m/z* (%): 86 (66) [M − AuCl]. − $C_4H_{10}AuClN_2$ (318.56): calcd. C 15.08, H 3.16, N 8.79; found C 15.54, H 3.28, N 8.94. − This compound was not soluble enough to obtain crystals.

Chloro(diethylamine)gold(I) (9): Yield 95%, dec. at room temperature. − ^{1}H NMR: δ = 1.39 (br., 6 H, CH_3), 3.02 (br., 4 H, CH_2), 4.9 (br., NH). − EI MS; *m/z* (%): 73 (34) [M − AuCl]. − $C_4H_{11}AuClN$ (305.56): calcd. C 15.72, H 3.63, N 4.58; found C 15.68, H 3.69, N 4.63. − This compound was not stable enough to obtain crystals.

Bis(benzylamine)gold(I) Chloride (10): Yield 82%, dec. > 149 °C. This compound was not soluble enough for NMR measurements.

− EI MS; *m/z* (%): 107 (65) [M − C_7H_9NAuCl]. − $C_{14}H_{18}AuClN_2$ (446.73): calcd. C 37.64, H 4.06, N 6.27; found C 37.91, H 4.05, N 6.33. − This compound was not soluble enough to obtain crystals.

Chloro(1-phenylethylamine)gold(I) (11): Yield 46%, dec. > 123°C. − ^{1}H NMR: δ = 1.38, 1.41 (s, 3 H, CH_3), 4.12 (dd, 1 H, CH), 7.35 (m, 2 H, Ph). − EI MS; *m/z* (%): 106 (100) [M − CH_3 − AuCl], 121 (2) [M − AuCl]). − $C_8H_{11}AuClN$ (353.60): calcd. C 27.17, H 3.14, N 3.96; found C 27.36, H 3.09, N 3.77. − This compound was not soluble enough to obtain crystals.

Chloro(3-iodobenzylamine)gold(I) (12): Yield 49%, dec. > 119°C. − ^{1}H NMR ([D_6]DMSO): δ = 3.96 (m, 2 H, CH_2), 7.18 (m, 1 H, *m*-Ph), 7.44 (m, 1 H, *p*-Ph), 7.67 (m, 1 H, o^6-Ph), 7.84 (m, 1 H, o^2-Ph), 5.8 (br., NH_2). − EI MS; *m/z* (%): 106 (100) [M − I − AuCl]), 233 (32) [M − AuCl]). − $C_7H_8AuClNI$ (465.47): calcd. C 18.06, H 1.73, N 3.01, Cl 7.62; found C 17.74, H 1.68, N 2.87, Cl 7.64. − This compound was not soluble enough to obtain crystals.

Bis(dicyclohexylamine)gold(I) Hexafluoroantimonate (13): Yield 59%, dec. > 112°C. − ^{1}H NMR ([D_6]acetone): δ = 1.07−2.98 (40 H, CH_2); 3.25 (m, 4 H, CH); 5.3 (br., NH). − FAB MS (pos.); *m/z* (%): 559 (100) $[K]^+$. − $C_{24}H_{46}AuF_6N_2Sb$ (795.35): calcd. C 36.24, H 5.83, N 3.52; found C 36.12, H 5.82, N 3.44.

Bis(piperidine)gold(I) Hexafluoroantimonate (14): Yield 30%, dec. > 173°C. − ^{1}H NMR: δ = 1.75 (m, 6 H, β-, γ-CH_2), 3.24 (m, 4 H, α-CH_2), 4.4 (br., NH). − FAB MS (pos.); *m/z* (%): 86 (18) [K − $C_5H_{10}NAu]^+$, 282 (2) [K − $C_5H_{11}N]^+$, 367 (100) $[K]^+$. − $C_{10}H_{22}AuF_6N_2Sb$ (603.01): calcd. C 19.92, H 3.68, N 4.65; found C 19.81, H 3.70, N 4.59.

Bis(cyclohexylamine)gold(I) Hexafluoroantimonate (15): Yield 23%, dec. > 74°C. − ^{1}H NMR ([D_6]acetone): δ = 1.16−2.28 (20 H, CH_2), 3.81 (m, 2 H, CH), 5.5 (br., NH). − FAB MS (pos.); *m/z* (%): 100 (100) [K − $C_6H_{12}NAu]^+$, 395 (42) $[K]^+$. − $C_{12}H_{26}AuF_6N_2Sb \cdot 0.5\ C_6H_{13}N$ (680.65): calcd. C 26.47, H 4.81, N 5.14; found C 27.72, H 5.39, N 5.10; the elemental analysis is affected by co-crystallised excess cyclohexylamine, which could not be removed even after prolonged pumping.

X-ray Structure Determinations: Crystal data: Table 2. − Data collection and reduction: The crystals were mounted in inert oil on a glass fibre. Data were measured using Mo-K_α radiation (λ = 0.71073 Å) with a Stoe STADI4 (**3**, **13**), Siemens P4 diffractometer (**2**, **4**, **5**) or a Siemens Smart area detector (**1**), each fitted with an LT-2 low-temperature attachment. Semi-empirical absorption corrections were based on psi-scans (XEMP) (**2**, **3**, **4**, **5**, **13**) or on multiple scans (SADABS) (**1**). Structures were solved by direct (**2**, **3**) or Patterson (**1**, **4**, **5**, **13**) methods and subjected to full-matrix least-squares refinement on F^2 (program SHELXL-97).[17] All non-hydrogen atoms were refined anisotropically. Hydrogen atoms were included using a riding model except for those bonded to nitrogen atoms in **1**, **2**, **3** and **4**, which were refined "freely", in **1**, **2** and **4** with restrained N−H bond lengths. − Crystallographic data (excluding structure factors) have been deposited with the Cambridge Crystallographic Data Centre under the numbers CCDC-440/051 (**2**, **3**),[12] CCDC-113728 (**1**), CCDC-113729 (**4**), CCDC-113730 (**5**) and CCDC-113731 (**13**). Copies may be obtained without charge from: CCDC, Union Road, Cambridge CB2 1EZ, UK [Fax: internat. + 44-1223/336-033; E-mail: deposit@ccdc.cam.ac.uk].

Acknoledgments

We thank the Fonds der Chemischen Industrie (Frankfurt) for financial support and Mr. A. Weinkauf for technical assistance.

[1] W. Schneider, A. Bauer, A. Schier, H. Schmidbaur, *Chem. Ber.* **1997**, *130*, 1417−1422.
[2] H. N. Adams, W. Hiller, J. Strähle, *Z. Anorg. Allg. Chem.* **1982**, *485*, 81−91.
[3] P. G. Jones, B. Ahrens, *Z. Naturforsch.* **1998**, *53b*, 653−662.
[4] C. J. L. Lock, Z. Wang, *Acta Crystallogr.* **1993**, *C49*, 1330−1333.
[5] J. J. Guy, P. G. Jones, M. J. Mays, G. M. Sheldrick, *J. Chem. Soc., Dalton Trans.* **1977**, 8−10.
[6] W. Schneider, A. Bauer, H. Schmidbaur, *J. Chem. Soc., Dalton Trans.* **1997**, 415−420.
[7] D. M. P. Mingos, J. Yau, S. Menzer, D. J. Williams, *J. Chem. Soc., Dalton Trans.* **1995**, 319−320.
[8] P. G. Jones, B. Ahrens, *Chem. Ber.* **1997**, *130*, 1813−1814.
[9] [9a] H. Schmidbaur, *Gold Bull.* **1990**, *23*, 11−21. − [9b] H. Schmidbaur, *Chem. Soc. Rev.* **1995**, 391−400.
[10] J. Vicente, M.-T. Chicote, M.-D. Abrisqueta, R. Guerrero, P. G. Jones, *Angew. Chem.* **1997**, *109*, 1252−1254; *Angew. Chem. Int. Ed. Engl.* **1997**, *36*, 1203−1205.
[11] P. Pyykkö, W. Schneider, A. Bauer, A. Bayler, H. Schmidbaur, *Chem. Commun.* **1997**, 1111−1112.
[12] P. G. Jones, B. Ahrens, *New J. Chem.* **1998**, 1041−1042.
[13] J. Bernstein, R. E. Davis, L. Shimoni, N.-L. Chang, *Angew. Chem.* **1995**, *107*, 1689−1708; *Angew. Chem. Int. Ed. Engl.* **1995**, *34*, 1545−1554.
[14] S. S. Pathaneni, G. R. Desiraju, *J. Chem. Soc., Dalton Trans.* **1993**, 319−322.
[15] F. H. Allen, O. Kennard, *Chem. Des. Autom. News* **1993**, *8*, 31−37.
[16] P. G. Jones, B. Ahrens, *Eur. J. Org. Chem.* **1998**, 1687−1688.
[17] G. M. Sheldrick, *SHELXL-97*, *Program for crystal structure refinement*, University of Göttingen, **1997**.
[18] T. Steiner, *Acta Crystallogr.* **1998**, *B54*, 456−463.
[19] A. Bondi, *J. Phys. Chem.* **1964**, *68*, 441−451.

Received January 25, 1999
[I99024]

Group-4 Metallocene Cation Complexes of Oligopeptides: Reaction of $[Cp_2ZrCH_3(THF)^+BPh_4^-]$ with Boc-Protected Di- and Tripeptide Esters

Jörg Wonnemann,[a] Markus Oberhoff,[a] Gerhard Erker,*[a] Roland Fröhlich,[a] and Klaus Bergander[a]

Keywords: Bioorganometallic chemistry / Zirconocene complexes / Metallocene cations / Group-4 metallocene peptide complexes

The dipeptide derivatives Boc-Gly-Val-OMe (**2**) and Boc-Ala-Val-OMe (**3**) selectively add the methylzirconocene cation **1** to the carbonyl oxygen atom of the *N*-terminal amino acid residue (κ-C^4=O coordination) upon treatment with $[Cp_2ZrCH_3(THF)^+BPh_4^-]$ in dichloromethane at low temperature (< 0 °C) to generate the complexes **2-I** and **3-I**, respectively. Above 0 °C methane is eliminated to give the stable chelate peptide metallocene cation complexes **2-A** and **3-A**, respectively, both featuring a combined C^1=O/N2/C^4=O coordination to the zirconium center. Complex **3-A** was characterized by X-ray diffraction. The analogous tripeptide derivatives Boc-Gly-Val-Val-OMe (**6**), Boc-Ala-Ala-Val-OMe (**7**), Boc-Ala-Val-Val-OMe (**8**), and Boc-Val-Val-Gly-OMe (**9**) all form analogous κ-C^4=O $Cp_2ZrCH_3^+$ cation adducts (**6–9**)-**I** under kinetic control and after subsequent loss of CH_4 C^1=O/N2/C^4=O chelate complexes (**6–9**)-**A** under thermodynamic control, both involving selective bonding of the organometallic cation to the terminal amino acid residue of the respective peptide derivatives. Thermolysis of the primary adduct **7-I** (> 0 °C) resulted in methane elimination and formation of a mixture of the isomers **7-B** and **7-A** (isolated in a 3:4 ratio). According to the detailed NMR analysis **7-A** shows the favored chelate coordination at the *N*-terminus involving C^1=O/N2/C^4=O bonding, whereas the cation complex **7-B** exhibits a similar chelate structure at the internal Ala moiety, characterized by C^4=O/N5/C^7=O coordination to the zirconium center. Similarly, methane liberation from **8-I** and **9-I** gave mixtures of the respective cationic chelate complex isomers **8-A/8-C** (2:3) and **9-A/9-C** (1:1), respectively. The (**8**,**9**)-**A** isomers have the zirconium ion bonded at the *N*-terminus, whereas (**8**,**9**)-**C** exhibit the Cp_2Zr^+ unit at the *C*-terminus of the peptide chain, involving the ester carbonyl group in forming the chelate framework (C^7=O/N8/C^{10}=O coordination). The (**6–9**)-**A** isomers are thermodynamically favored. The cation complexes **7-B**, **8-C**, **9-C** rearrange to the **A**-type isomers upon prolonged standing at temperatures > 0 °C in dichloromethane solution.

Introduction

Principles and many details of the important interaction of metal ion systems with typical biomolecules have been recognized due to a large number of investigations in the field of bioinorganic chemistry. Bioorganometallic chemistry is a much less mature discipline.[1] It tries to combine favorably the characteristic features of typical biomolecules, such as amino acids, oligopeptides, heterocyclic nucleobases, oligonucleotides etc., with those of organometallic building blocks in order to generate e.g. new reagents for organic synthesis or precursors of novel active and selective catalyst systems, but also to study the response of the "natural" bio-related systems to interactions with rather "unnatural" organometallic metal/ligand combinations and arrangements.[2] A major problem in bioorganometallic chemistry is to find suitable conditions that allow to combine the usually rather hydrophilic biomolecules with the in part extremely hydrophobic world of many organometallic systems and to keep their mutual adducts and reaction products stable. It is very likely that many useful applications will follow once this has been achieved for a sufficient number of bioorganometallic systems.[3]

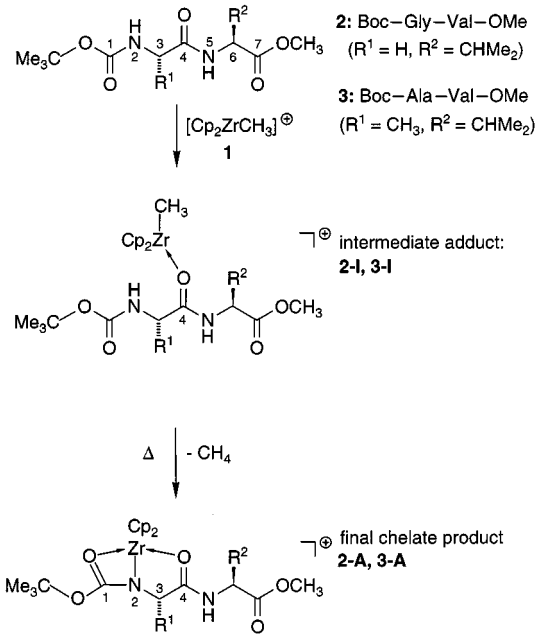
The methylzirconocene cation ($[Cp_2ZrCH_3^+]$, **1**) is a sensitive, very electrophilic organometallic fragment that has found important use in homogeneous metallocene Ziegler catalysis.[4] We have used this species as a typical model system to investigate the modes of interaction of a very reactive, extremely hydrophobic organometallic building block derived from an oxophilic transition metal from the left side of the periodic table with peptide derivatives, as typical examples of biomolecule-related substrates. This has led to the disclosure of interesting coordination behavior and subsequent reactions of this metallocene-derived reagent with such multifunctional and polar substrates. A series of typical examples is described in this article.

Results and Discussion

As the organometallic starting material the ligand-stabilized $[Cp_2ZrCH_3(THF)^+BPh_4^-]$ methylzirconocene cation **1a** was used in this study.[4a] The coordinated tetrahydrofuran is readily exchanged for other donor ligands under very mild conditions. The cation complex **1a** was treated with a variety of *N*-*tert*-butoxycarbonyl-(i.e. Boc-)protected oligopeptide esters. Here the outcome of the reactions with two

[a] Organisch-Chemisches Institut der Universität Münster, Corrensstraße 40, D-48149 Münster, Germany
Fax: (internat.) + 49(0)251/833-6503
E-mail: erker@uni-muenster.de

 © WILEY-VCH Verlag GmbH, D-69451 Weinheim, 1999 1434–1948/99/0707–1111 $ 17.50+.50/0



Scheme 1. Reaction of **1** with dipeptide derivatives

Table 1. Selected ^{1}H-NMR chemical shifts of the [$Cp_2ZrCH_3^+$] (**1**) plus dipeptide (**2**, **3**) reaction products (atom numbering as in Scheme 1)[a]

Compound	CMe_3	2-H[b]	3-H	5-H[b]	6-H	OCH_3	$ZrCH_3$
2	1.40	5.86	3.78	7.16	4.46	3.69	–
2-I	1.43	7.69	3.63	7.45	4.35	3.80	0.48
2-A	1.52	–	3.54	7.36	4.33	3.77	–
3	1.41	5.00	4.15	6.65	4.49	3.70	–
3-I[c]	1.42	5.30	3.65	8.60	3.85	3.78	0.54
3-A	1.56	–	4.39	[d]	4.39	3.83	–

[a] In CD_2Cl_2, chemical shifts in ppm, δ scale, 258 K. – [b] N-H signals, see Scheme 1. – [c] At 223 K. – [d] Not located.

selected dipeptide and a series of four tripeptide methyl esters will be described.[5]

The reaction of **1a** with the dipeptide ester Boc-Gly-Val-OMe (**2**) shall serve as an example to illustrate a typical reaction series. Upon mixing the two components in a 1:1 stoichiometry at −15°C in [D_2]dichloromethane an instantaneous reaction was observed by NMR to take place. THF is liberated from "Jordan's cation" ([$Cp_2ZrCH_3(THF)^+$]) and the reactive $Cp_2ZrCH_3^+$ cation takes up a dipeptide ester as a ligand. A combination of various NMR techniques (for details see the Experimental Section) has allowed for a complete spectroscopic characterization of this rapidly formed primary product as the [$Cp_2Zr(CH_3)$(Boc-Gly-Val-OMe)$^+$] coordination complex **2-I** (see Scheme 1). As it is evident from the compilation of the ^{1}H- and ^{13}C-NMR data (Tables 1 and 2), compound **2-I** still contains all the intact components of both the subunits [Cp_2Zr-CH_3^+] (**1**) and Boc-Gly-Val-OMe (**2**): The zirconium-bonded [Zr]-CH_3 group is still there and both NH functionalities are intact. From the ^{13}C-NMR comparison between **2** and **2-I** (see Table 2) it is deduced that complex formation has apparently occurred by coordination of the glycine-derived amido carbonyl group to the zirconium center. The pronounced shifting of the respective O=C^4 ^{13}C-NMR resonance from δ = 170.1 to δ = 179.1 strongly indicates the newly formed (Gly)amido−Zr bond as the essential structural feature of the primary [(Boc-Gly-Val-OMe)·**1**] adduct. All the other ^{13}C-NMR resonances are essentially unaffected.

Table 2. Selected ^{13}C-NMR data of the peptide derivatives **2**, **3**, and their reaction products with the methylzirconocene cation (atom numbering as in Scheme 1)[a]

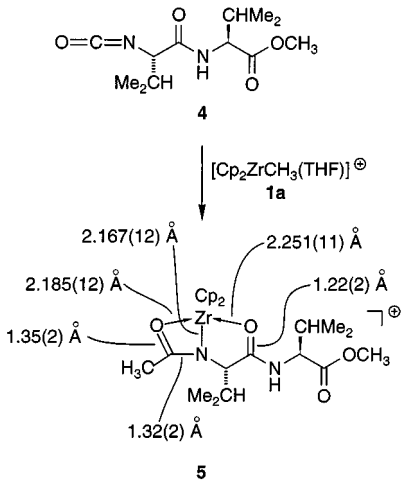
Compound	*C*Me_3	C-1	C-3	C-4	C-6	C-7	OCH_3	$ZrCH_3$
2	79.9	156.2	44.1	170.1	57.0	172.7	52.5	–
2-I	81.1	155.3	44.1	179.1	58.4	168.4	53.0	33.0
2-A	85.5	156.6	50.0	179.1	60.3	170.0	53.1	–
3[b]	79.7	155.4	51.8	172.7	56.9	172.0	49.8	–
3-I	81.6	155.0	51.8	182.5	58.8	168.8	[c]	33.4
3-A	86.3	156.5	57.3	182.2	60.2	170.3	[c]	–

[a] In CD_2Cl_2 at 258 K, chemical shifts in ppm, δ scale. – [b] In $CDCl_3$. – [c] Hidden under solvent signal.

Complex **2-I** is a reactive intermediate. At temperatures above 0°C it reacts further. Methane is formed[6] and the final product **2-A** is obtained. The stable complex **2-A** was synthesized by treatment of **1a** with Boc-Gly-Val-OMe in dichloromethane (0°C to room temperature for a few hours) on a preparative scale and isolated in 96% yield. Both the ^{1}H- and the ^{13}C-NMR spectra show that the [Zr]-CH_3 group is no longer present. It has been utilized for selectively abstracting the N*H* proton[6b] of the Gly part of the peptide ligand systems. Consequently, the former 2-H resonance of the peptide chain is not observed in the ^{1}H-NMR spectrum of the product **2-A** (see Table 1 and Scheme 1). The pronounced shift of the amido O=C^4 ^{13}C-NMR resonance to a larger δ value for **2-A** relative to the free peptide ligand **2** (Δδ = +9.0 ppm) strongly indicates the coordination of this amido group to the zirconium center.[7]

A more detailed picture of the coordination behavior of the mono-deprotonated peptide ligand to the remaining Cp_2Zr unit in the cation complex **2-A** is hard to obtain from the NMR-spectroscopic analysis alone, but − as we will see later − can be derived quite confidently in a combination of the spectroscopic features with the result of an X-ray crystal structure analysis.

We had recently characterized a related (peptide)zirconocene tetraphenylborate salt by X-ray diffraction.[3b] The complex **5** was prepared by treatment of **1a** with the isocyanate **4** of the dipeptide H-Val-Val-OMe.[8] The Zr−CH_3 group had added to the heterocumulene to form the cationic bis-chelate complex **5**. It was shown by X-ray diffraction that the zirconium center was bonded to the *N*-terminal Val-nitrogen atom and to the oxygen atoms of both adjacent C=O groups, i.e. the *N*-acetyl carbonyl group and the C=O group of the *N*-terminal Val moiety (see Scheme 2).



Scheme 2. Formation and structural parameters of **5**

Treatment of Boc-Ala-Val-OMe (**3**) with **1a** at low temperature (−15°C) in CD_2Cl_2 gave the adduct **3-I** (see Scheme 1 and Tables 1 and 2). The NMR analysis also indicates the selective coordination of the $Cp_2ZrCH_3^+$ cation to the amido carbonyl group of the *N*-terminal amino acid building block (i.e. formation of $C^4{=}O{-}$[Zr] of the Ala moiety). Warming to room temperature again leads to a rapid reaction that results in (Ala)N^2-H deprotonation with liberation of methane and the selective formation of the cationic chelate complex **3-A**. Diffusion of pentane vapor into a solution in bromobenzene gave single crystals of **3-A** for an X-ray crystal structure analysis. This structure suffers from the presence of a small nonidentified molecule (probably water). Therefore, we will not discuss the structure in detail. But the X-ray analysis is of a sufficient quality to characterize the overall structural arrangement of **3-A** as being of the same type as **5**. Thus, complex **3-A** is again of a bis-chelate type and exhibits a metallabicyclic central framework around the zirconium center. In this, the amido carbonyl group of the *N*-terminal Ala unit strongly coordinates to the zirconium ion − this was already deduced from the strong deshielding effect[3b] in the ^{13}C-NMR spectrum (C4 coordination shift **3** → **3-A** $\Delta\delta = +10$ ppm, see Table 2). In addition, the *N*-Boc carbonyl group also coordinates strongly to the zirconium ion (see Figure 1). This feature did not show up in the ^{13}C-NMR analysis, which is probably due to a compensation effect (the $C^1{=}O$ bond becomes weaker upon coordination, but at the same time the C1=N2 bond becomes stronger). But a close inspection of the ^{13}C-NMR data (see Table 2) shows that the chelate coordination (i.e. the transformation of **3-I** → **3-A**) results in a pronounced and characteristic shift of the Boc-*C*Me_3 ^{13}C-NMR resonance to larger δ values ($\Delta\delta = +4.7$ ppm for **3-A**, +5.4 for **2-A**). We thus conclude, that the thermodynamically favored final products **2-A** and **3-A** are both characterized by a doubly chelating coordination of the Boc−amido unit and the internal amido moiety of the *N*-terminal amino acid building block of the dipeptide derivatives as depicted in Scheme 1. This follows from the combined NMR/X-ray analysis. This typical coordination mode does not lead to any significant shifting of the $C^1{=}O$ ^{13}C-NMR signal, but can readily be recognized by the resulting pronounced ^{13}C-NMR coordination shifts of the Boc-*C*Me_3 and the $C^4{=}O$ resonances.

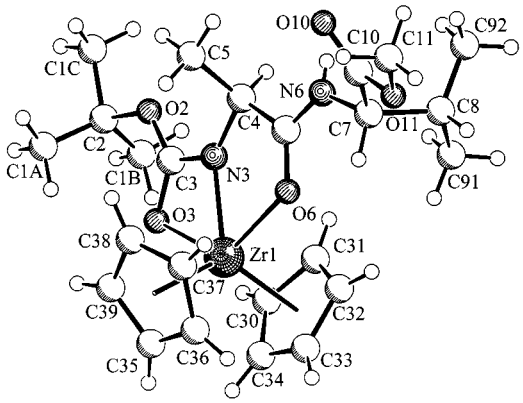
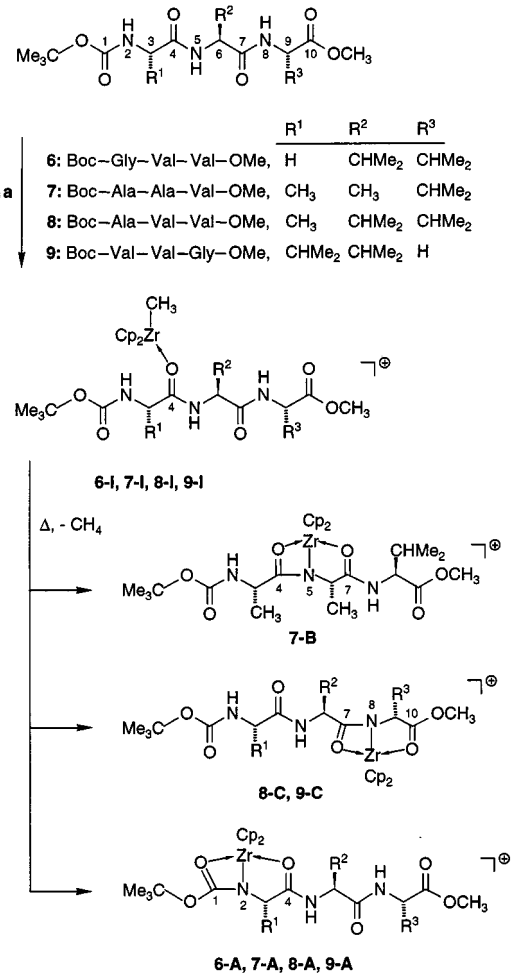


Figure 1. A view of the molecular structure of the product **3-A** (cation only, with unsystematical atom numbering scheme) as determined by X-ray diffraction

We next treated "Jordan's cation" (**1a**) with the tripeptide derivative Boc-Gly-Val-Val-OMe (**6**).[9] There is a clean and selective adduct formation observed at −15°C in [D_2]dichloromethane. The product contains the intact $Cp_2Zr{-}CH_3^+$ unit coordinated to the tripeptide framework. This is evident from the observation of the NMR signals of a pair of diastereotopic Cp ligands at the zirconium center and the presence of a [Zr]$-CH_3$ group. From the characteristic coordination shift of the carbonyl carbon atom C4 in the ^{13}C-NMR spectrum ($\Delta\delta = +7.8$ ppm) attachment of the methylzirconocene cation to the $C^4{=}O$ amido carbonyl group of the *N*-terminal Gly moiety of **6** is indicated. Since there are no other significant NMR changes we must assume that the **1a** + **6** reaction has resulted in a simple adduct formation to give the cationic complex **6-I** (see Scheme 3, with BPh_4^- anion).

Warming of the intermediate **6-I** above 0°C again leads to methane evolution. In this case also a single thermodynamically favored product (**6-A**) is obtained, that was also prepared and isolated on a preparative scale. The ^{1}H-NMR spectrum (see Table 3) shows that the N*H* proton of the Gly section of the tripeptide has been abstracted by the [Zr]$-CH_3$ group to give methane. The adjacent amido carbonyl group ($C^4{=}O$) is involved in the chelate complex formation. This is evident by the shifting of the ^{13}C-NMR signals of carbon atoms C4 ($\Delta\delta = +7.7$ ppm) and C3 ($\Delta\delta = +6.2$ ppm) for the **6** → **6-A** transformation. Again, we must assume that the $C^1{=}O$ amido carbonyl group adjacent to the directly bonded nitrogen atom N2 is involved and used for constructing the typical second chelate "arm" of the overall metallabicyclic framework. This is evident from the characteristic shifting of the *C*Me_3 ^{13}C NMR signal of the Boc group ($\Delta\delta = +5.9$ ppm), whereas the corresponding C1 resonance remains completely unaffected from the **6** → **6-A** transformation, probably due to the typical compensation effect discussed above and in the literature.[3b] Thus, treatment of the tripeptide derivative **6** with $Cp_2ZrCH_3^+$



Scheme 3. Reactions of **1a** with tripeptide derivatives

Table 3. Selected ^{1}H-NMR data of the reaction products of **1a** with the peptide derivatives **6** and **7** (atom numbering as in Scheme 3)[a]

Compound	CMe_3	2-H[b]	3-H	5-H[b]	6-H	8-H[b]	9-H	OCH_3	$ZrCH_3$
6	1.38	6.14	3.86	7.84	4.45	7.72	4.54	3.68	–
6-I	1.43	7.78	3.71	6.66	4.16	6.41	4.46	3.76	0.50
6-A	1.57	–	4.21	6.78	4.45	9.13	4.49	3.78	–
7	1.38	5.80	4.26	7.53	4.68	7.59	4.46	3.69	–
7-I	1.44	5.54	3.78	8.67	3.82	9.17	3.93	3.79	0.54
7-B	1.55	5.26	3.88	–	4.99	8.31	4.48	3.82	–
7-A	1.54	–	4.41	8.13	4.33	6.32	4.49	3.74	–

[a] In CD_2Cl_2 at 258 K, chemical shifts in ppm, δ scale. – [b] N-H resonances.

from **1a** leads to a selective kinetically controlled adduct formation at the *N*-terminal Gly amido group followed by thermally induced methane elimination to give a single cationic metallocene/peptide chelate complex (**6-A**) where the zirconium center is bonded to the C^1=O, N2, and C^4=O groups (see Scheme 3).

The reaction between Boc-Ala-Ala-Val-OMe (**7**) with **1a** is slightly more complicated. At low temperature, the adduct [Boc-Ala-Ala-Val-OMe · $ZrCp_2CH_3^+$] (**7-I**) is formed selectively. Unfortunately, this is the only case where we

Table 4. Selected ^{13}C-NMR data of the **1a** + **6/7** reaction products (atom numbering as given in Scheme 3)[a]

Compound	CMe_3	C-1[b]	C-3	C-4[b]	C-6	C-7[b]	C-9	C-10[b]	OCH_3	$ZrCH_3$
6	79.6	156.2	43.9	170.1	57.3	172.6	58.5	172.2	52.4	–
6-I	81.5	156.1	44.8	177.9	58.1	171.3	60.0	171.7	52.2	32.4
6-A	85.5	156.2	50.1	177.8	60.1	169.7	58.1	171.5	52.7	–
7	79.6	155.5	49.9	173.1	48.8	172.4	57.2	172.6	52.3	–
7-I	81.8	156.8	51.9	[c]	50.7	[c]	59.7	169.6	53.3	33.6
7-B	80.6	155.4	47.8	181.0	57.0	179.0	59.7	170.4	53.3	–
7-A	85.5	156.0	56.8	180.8	50.7	170.0	57.8	171.8	52.7	–

[a] In CD_2Cl_2 at 258 K, chemical shifts in ppm, δ scale. – [b] Carbonyl carbon signals. – [c] Not located.

were not able to locate two of the ^{13}C-NMR carbonyl resonances, but from the overall spectral characteristics it is quite obvious that again the typical Zr coordination to the amide oxygen atom of the *N*-terminal amino acid residue (here: Ala) has taken place (see Tables 3 and 4).

Raising the temperature again results in consumption of the reactive intermediate **7-I** with formation of CH_4. However, in this case a mixture of two bis-chelate complexes is obtained. These were formed in a ratio of **7-B**/**7-A** ≈ 3:4 under the specific conditions used for their synthesis on a preparative scale (see the Experimental Section for details). Complex **7-A** exhibits the typical spectroscopic features (see Tables 3 and 4) that identifies it as an example of the *N*-terminal chelate peptide/zirconocene cation complex type. Analogously, as in the "**A**-type" cation examples discussed above, the double framework is formed by attaching the C^1=O/N2/C^4=O subunits to the central Cp_2Zr moiety.

Complex **7-B** is of a similar type, only that the C^4=O/N5/C^7=O groups are here involved in the coordination to the zirconium center. The ^{1}H-NMR spectra show that in this case it is the 5-H amido hydrogen atom that is lost upon thermally induced methane formation. In addition, pronounced ^{13}C-NMR shift differences have resulted in the **7** → **7-B** transformation at the carbonyl carbon atoms C4 (Δδ = +7.7 ppm) and C7 (Δδ = +6.6 ppm) as well as the adjacent Ala-*C*HMe carbon atom C6 (Δδ = +8.2 ppm).

The *N*-terminal chelate cation complex **7-A** seems to be the thermodynamically favored product. During ca. two weeks at 0°C in CD_2Cl_2 the by-product **7-B** has almost completely disappeared and has been transformed into the more stable peptide–group-4 metallocene cation system **7-A**.

A similar situation was found when the peptide derivatives Boc-Ala-Val-Val-OMe (**8**) or Boc-Val-Val-Gly-OMe (**9**) were treated with **1a**. In each case a single $Cp_2ZrCH_3^+$ adduct was formed at low temperature (–15°C). Coordination at the C^4=O carbonyl oxygen atom of the *N*-terminal amino acid moiety was evident from the NMR analysis (see Tables 5 and 6). The thus formed primary product **8-I** eliminated methane at temperatures > 0°C to form a mixture of the new cationic chelate complex **8-C** (see Scheme 3) in addition to **8-A** (obtained in a 2:3 ratio on a preparative scale). In the case of **8-C** the C^7=O/N8 amido

Table 5. Selected ^{1}H-NMR data of the **1a** + **8/9** reaction products (atom numbering as given in Scheme 3)[a]

Compound	CMe_3	2-H[b]	3-H	5-H[b]	6-H	8-H[b]	9-H	OCH_3	$ZrCH_3$
8	1.38	6.04	4.40	7.79	4.52	7.60	4.47	3.68	–
8-I	1.44	5.29	4.08	8.36	4.50	7.62	4.43	3.71	0.59
8-C	1.54	5.25	4.00	8.10	4.51	–	5.12	3.75	–
8-A	1.40	–	4.51	8.64	4.50	6.42	4.37	3.82	–
9	1.38	5.62	3.98	7.23	4.36	7.62	3.98	3.67	–
9-I	1.44	5.27	3.97	6.78	3.78	[c]	3.82	3.79	0.55
9-C	1.55	5.82	4.17	7.89	3.77	–	3.84	3.71	–
9-A	1.48	–	4.37	7.46	3.67	7.59	3.20	3.74	–

[a] In CD_2Cl_2 at 258 K, chemical shifts in ppm, δ scale. – [b] N-H signals. – [c] Not observed.

Table 6. Selected ^{13}C-NMR data of the **1a** + **8/9** reaction products (atom numbering as given in Scheme 3)[a]

Compound	CMe_3	C-1[b]	C-3	C-4[b]	C-6	C-7[b]	C-9	C-10[b]	OCH_3	$ZrCH_3$
8	79.5	156.6	49.9	173.3	57.1	171.9	58.7	172.5	52.3	–
8-I	82.1	156.7	53.1	176.3	59.7	167.4	60.1	169.7	52.1	33.8
8-C	80.9	155.9	46.9	171.5	59.9	180.8	66.8	179.8	57.9	
8-A	85.5	156.7	58.5	181.5	60.0	169.1	57.1	170.1	52.7	–
9	79.9	156.2	60.4	172.1	58.2	171.8	41.0	170.2	52.3	–
9-I	82.7	155.4	61.9	178.2	58.8	167.3	42.3	166.6	50.6	33.4
9-C	80.9	155.6	66.5	169.5	57.5	179.3	41.3	180.6	52.6	–
9-A	85.9	157.2	66.8	180.8	59.9	168.5	42.5	167.7	52.8	–

[a] In CD_2Cl_2 at 258 K, chemical shifts in ppm, δ scale. – [b] Carbonyl signals.

group of the *C*-terminal Val moiety and C^{10}=O of the terminal ester group have formed the chelate coordination to the zirconium center [^{13}C-NMR shift differences of the **8** → **8-C** transformation: Δδ = +8.9 ppm (C7), +7.3 (C10), +8.1 (C9)].

Similarly, the selectively formed addition product **9-I** (C^4=O coordinated to zirconium, see Scheme 3 and Tables 5 and 6) is transformed to a ca. 1:1 mixture of **9-C** and **9-A** upon heating (with loss of CH_4). Again the product **9-C** exhibits C^7=O/N8/C^{10}=O chelate coordination to zirconium [Δδ = +7.5 ppm (C7), +10.4 (C10)] whereas complex **9-A** is again characterized by the presence of the *N*-terminal C^1=O/N2/C^4=O chelate. Both the complexes **8-C** and **9-C** do not represent the most stable structures on their respective hypersurfaces. They both convert completely to their thermodynamically favored isomers **8-A** and **9-A**, respectively, upon standing for prolonged time at temperatures > 0°C.

We conclude that complexes between the electrophilic methylzirconocene cation and *N*- and *C*-protected di- and tripeptides can readily be generated. In the series investigated these are formed with a very high selectivity – in all the cases characterized here the [$Cp_2ZrCH_3^+$] attachment takes place exclusively at the amido carbonyl oxygen function of the *N*-terminal amino acid moiety, i.e. adjacent to the Boc-protective group. We assume that this position is sterically the least shielded, and that the regioselective formation of the adduct complexes (**2**, **3**, **6**–**9**)-**I** under kinetic control is probably governed by steric effects. Very stable chelate complexes (**2**, **3**, **6**–**9**)-**A** are obtained from these intermediates by thermally induced methane elimination. Overall, an analogous regiochemical preference for the *N*-terminal amino acid coordination (here with involvement of the C^1=O group of the Boc-protective group) is observed for this product formation under thermodynamic control. Other regioisomers (**7-B**, **8-C**, **9-C**) that have been observed on the way to these final chelate products may again be less favored because of steric interference. For this series of peptide derivative/$Cp_2ZrCH_3^+$ reactions we have shown that a group-4 metal complex fragment can rather readily and even selectively be attached to peptide frameworks. The resulting complexes are rather stable and they can be prepared on a preparative scale. This might open new ways to use peptide derivatives as stereochemically active and well-defined ligand systems in less protected early transition metal complexes that may have an interesting potential especially in asymmetric catalysis. Such developments are actively being pursued in our laboratory.

Experimental Section

General Remarks: Reactions involving organometallic compounds were carried out under argon in a glove box or using Schlenk type glassware. Solvents (including deuterated solvents) were dried and distilled under argon prior to use. – NMR experiments were performed on a Varian Unity Plus 600 spectrometer at 258 K (^{1}H: 600 MHz, ^{13}C: 150 MHz). Assignments in ^{1}H- and ^{13}C-NMR spectra were confirmed by GCOSY, 1D-TOCSY, GHSQC, and GHMBC experiments.[10] Atom numbering as given in Schemes 1 and 3. – IR spectra were acquired with a Nicolet 5 DXC Fourier transform IR spectrometer. – Melting points were obtained by differential scanning calorimetry (DSC 2010, TA Instruments), elemental analyses were determined with a Foss-Heraeus CHN-Rapid elemental analyzer. – The organometallic reagent [$Cp_2ZrCH_3(THF)^+BPh_4^-$] (**1a**),[4a] the oligopeptides and Boc-protected di- and tripeptide esters were prepared according to literature procedures.[9][11]

General Procedures. – Preparation of Protected Dipeptide Esters (A): A typical run was as follows: To a stirred and ice-cooled solution of the Boc-protected amino acid (20 mmol) in chloroform (30 mL) dicyclohexylcarbodiimide (4.13 g, 20 mmol) was added. After 30 min, the mixture was combined with a mixture of the amino acid methyl ester hydrochloride (20 mmol) and triethylamine (2.02 g, 2.72 mL, 20 mmol) in chloroform (30 mL). The combined phases were stirred in an ice bath for 3 h and then kept overnight; then a few drops of acetic acid were added. The mixture was stirred for 15 min and filtered. The filtrate was washed successively with water, a 10 % citric acid solution, a 5 % sodium hydrogen carbonate solution, and water. The solution was dried with magnesium sulfate; solvent was then removed in vacuo. Separation from remaining dicyclohexyl urea was achieved by solving the dipeptide ester product in ethyl acetate and filtering off the insoluble urea. The ethyl acetate was removed in vacuo to yield the analytically pure dipeptide derivative as a white solid.

Preparation of Protected Tripeptide Esters (B): A typical run was as follows: To an ice-cooled solution of the *C*-deprotected Boc-dipeptide (10 mmol) in chloroform (20 mL) hydroxybenztriazol

(1.54 g, 10 mmol) and dicyclohexylcarbodiimide (2.06 g, 10 mmol) were added. After 30 min, the mixture was combined with a mixture of the amino acid methyl ester hydrochloride (10 mmol) and triethylamine (1.01 g, 1.39 mL, 10 mmol) in chloroform (30 mL). The combined phases were stirred in an ice bath for 3 h and then kept overnight. A few drops of acetic acid were added. The mixture was then stirred for 15 min and filtered. The filtrate was washed successively with water, a 10% citric acid solution, a 5% sodium hydrogen carbonate solution, and water. The solution was dried with magnesium sulfate and solvent was then removed in vacuo. Separation from remaining dicyclohexyl urea was done by dissolving the dipeptide in ethyl acetate and filtering off the insoluble urea. Further purification was by chromatography on a silica-gel column using an ethyl acetate/petroleum ether/ether solvent mixture as eluent.

Preparation of the Metal Peptide Complexes (C): A solution of the protected dipeptide or tripeptide ester (2.0 mmol) in dichloromethane (5 mL) was combined with a solution of Jordan′s cation (2.0 mmol) in dichloromethane (10 mL) at 0 °C. The mixture was stirred for 3 h and then warmed to room temperature. The solvent was removed in vacuo, the residue washed with toluene and pentane to yield the analytically pure metal peptide complex as a white solid.

Preparation of the Metal Peptide Complexes (NMR Experiment) (D): A solution of the protected dipeptide or tripeptide ester (63.8 μmol) in [D_2]dichloromethane (0.4 mL) was combined with a solution of Jordan′s cation (63.8 μmol) in [D_2]dichloromethane (0.4 mL) at −15°C.

Preparation of Boc-Gly-Val-OMe (2): *N-tert*-Butoxycarbonylglycine (3.50 g, 20.0 mmol) and valine methyl ester hydrochloride (3.35 g, 20 mmol) were treated according to procedure A to yield the dipeptide Boc-Gly-Val-OMe (5.25 g, 91%) as an oil. − IR (KBr): $\tilde{\nu}$ = 3326 (s, NH), 2971 (m), 2932 (m), 2878 (w), 1744 (m), 1683 (s), 1664 (vs), 1525 (s), 1366 (w), 1169 (m), 864 (m), 737 (w) cm^{-1}. − ^{1}H NMR (CD_2Cl_2, 599.8 MHz): δ = 7.16 (br., 1 H, 5-H), 5.86 (br., 1 H, 2-H), 4.46 (dd, ^3J = 9.0 Hz, ^3J = 5.2 Hz, 1 H, 6-H), 3.78 (m, 2 H, 3- and 3′-H), 3.69 (s, 3 H, 7-OCH_3), 2.17 [m, 1 H, 6-CH(CH_3)$_2$], 1.40 [s, 9 H, 1-OC(CH_3)$_3$], 0.88 and 0.84 [2 d, 2 ^3J = 7.4 Hz, 2× 3 H, 6-CH(CH_3)$_2$]. − ^{13}C NMR (CD_2Cl_2, 150.8 MHz): δ = 172.7 (C-7), 170.1 (C-4), 156.2 (C-1), 79.9 [1-OC(CH_3)$_3$], 57.0 (C-6), 52.5 (7-OCH_3), 44.1 (C-3), 31.3 [6-CH(CH_3)$_2$], 28.1 [1-OC(CH$_3$)$_3$], 19.0 and 17.6 [6-CH(CH$_3$)$_2$].

Reaction of Boc-Gly-Val-OMe (2) with [$Cp_2ZrCH_3(THF)^+BPh_4^-$] (1a). − Formation of 2-I: Boc-Gly-Val-OMe (18.4 mg, 63.8 μmol) and **1a** (40.0 mg, 63.8 μmol) were treated according to procedure D to generate **2-I**. − ^{1}H NMR (CD_2Cl_2, 599.8 MHz): δ = 7.69 (br., 1 H, 2-H), 7.45 (br., 1 H, 5-H), 6.24 and 6.20 (2 s, 2 × 5 H, Cp- and Cp′-H), 4.35 (br., 1 H, 6-H), 3.80 (s, 3 H, 7-OCH_3), 3.63 (m, 2 H, 3- and 3′-H), 2.10 [m, 1 H, 6-CH(CH_3)$_3$], 1.43 [s, 9 H, 1-OC(CH_3)$_3$], 0.87 and 0.84 [2 d, 2 ^3J = 6.7 Hz, 2 × 3 H, 6-CH(CH_3)$_2$], 0.48 (s, 1 H, Zr-CH_3), [BPh_4]$^-$: 7.45 (m, 8 H, *o*-H), 7.10 (m, 8 H, *m*-H), 6.93 (m, 4 H, *p*-H); THF: δ = 3.72 (m, 4 H, α-H), 1.81 (m, 4 H, β-H). − ^{13}C NMR (CD_2Cl_2, 150.8 MHz): δ = 179.1 (C-4), 168.4 (C-7), 155.3 (C-1), 113.2 and 113.1 (Cp C and Cp′ C), 81.1 [1-OC(CH_3)$_3$], 58.4 (C-6), 53.0 (7-OCH_3), 44.1 (C-3), 33.0 (Zr-CH$_3$), 31.0 [6-CH(CH_3)$_2$], 27.4 [1-OC(CH$_3$)$_3$], 18.1 and 16.8 [6-CH(CH$_3$)$_2$]; [BPh_4]$^-$: δ = 163.8 (q, $^1J_{CB}$ = 49 Hz, *i-C*), 135.3 (*o*-C), 125.7 (*m*-C), 121.7 (*p*-C); THF: δ = 67.9 (α-C), 25.2 (β-C).

Reaction of 2 with 1a. − Formation of 2-A: Boc-Gly-Val-OMe (**2**, 0.58 g, 2.0 mmol) and **1a** (1.25 g, 2 mmol) were treated according to procedure C to yield the metal peptide complex **2-A** (1.59 g, 96 %) as a white solid; m.p. 51 °C (decomp). − $[\alpha]_D$ = −25 (*c* = 0.10, CH_2Cl_2). − $C_{47}H_{53}BN_2O_5Zr$ (828.0): calcd. C 68.18, H 6.45, N 3.38; found C 68.24, H 6.74, N 3.30. − IR (KBr): $\tilde{\nu}$ = 3377 (s, NH), 3045 (m), 2965 (s), 1743 (s), 1684 (s), 1591 (s), 1431 (s), 1155 (m), 797 (vs), 703 (s) cm^{-1}. − ^{1}H NMR (CD_2Cl_2, 599.8 MHz): δ = 7.36 (br., 1 H, 5-H), 6.19 and 6.16 (2 s, 2 × 5 H, Cp- and Cp′-H), 4.33 (dd, ^3J = 8.3 Hz, ^3J = 5.2 Hz, 1 H, 6-H), 3.77 (s, 3 H, 7-OCH_3), 3.54 (m, 2 H, 3- and 3′-H), 2.17 [m, 1 H, 6-CH(CH_3)$_2$], 1.52 [s, 9 H, 1-OC(CH_3)$_3$], 0.96 and 0.94 [2 d, 2 ^3J = 6.9 Hz, 2 × 3 H, 6-CH(CH_3)$_2$]; [BPh_4]$^-$: δ = 7.37 (m, 8 H, *o*-H), 7.07 (m, 8 H, *m*-H), 6.92 (m, 4 H, *p*-H). − ^{13}C NMR (CD_2Cl_2, 150.8 MHz): δ = 179.1 (C-4), 170.0 (C-7), 156.6 (C-1), 115.1 and 115.0 (Cp C and Cp′ C), 85.5 [1-OC(CH_3)$_3$], 60.3 (C-6), 53.1 (7-OCH$_3$), 50.0 (C-3), 31.0 [6-CH(CH_3)$_2$], 28.7 [1-OC(CH_3)$_3$], 19.1 and 18.3 [CH(CH$_3$)$_2$]; [BPh_4]$^-$: δ = 164.6 (q, $^1J_{CB}$ = 49 Hz, *i-C*), 135.7 (*o*-C), 126.0 (*m*-C), 122.2 (*p*-C).

Preparation of Boc-Ala-Val-OMe (3): *N-tert*-Butoxycarbonylalanine (3.78 g, 20 mmol) and valine methyl ester hydrochloride (3.35 g, 20 mmol) were treated according to procedure A to yield the dipeptide **3** (5.25 g, 89 %) as a white solid; m.p. 66 °C. − $[\alpha]_D$ = −28 (*c* = 0.10, CH_2Cl_2). − IR (KBr): $\tilde{\nu}$ = 3318 (s, NH), 2971 (m), 2935 (m), 2878 (w), 1744 (m), 1727 (m), 1662 (vs), 1522 (s), 1366 (w), 1169 (m), 860 (m) cm^{-1}. − ^{1}H NMR (CD_2Cl_2, 599.8 MHz): δ = 6.82 (d, ^3J = 8.8 Hz, 1 H, 5-H), 5.17 (d, ^3J = 7.1 Hz, 1 H, 2-H), 4.44 (dd, ^3J = 8.8 Hz, ^3J = 4.9 Hz, 1 H, 6-H), 4.13 (m, 1 H, 3-H), 3.68 (s, 3 H, 7-OCH_3), 2.13 [m, 1 H, 6-CH(CH_3)$_2$], 1.40 [s, 9 H, 1-OC(CH_3)$_3$], 1.28 (d, ^3J = 7.1 Hz, 3 H, 3-CH_3), 0.87 and 0.84 [2 d, 2 ^3J = 6.8 Hz, 2 × 3 H, 6-CH(CH_3)$_2$]. − ^{13}C NMR (CD_2Cl_2, 150.8 MHz): δ = 172.5 and 172.3 (C-4 and C-7), 155.3 (C-1), 79.9 [1-OC(CH_3)$_3$], 56.8 (C-6), 52.3 (C-3), 50.0 (7-OCH$_3$), 31.2 [6-CH(CH_3)$_2$], 28.0 [1-OC(CH$_3$)$_3$], 18.8 (3-CH$_3$), 17.5 and 17.3 [6-CH(CH$_3$)$_2$].

Generation of the Intermediate Adduct 3-I: Boc-Ala-Val-OMe (**3**, 19.3 mg, 63.8 μmol) and **1a** (40.0 mg, 63.8 μmol) were treated according to procedure D to give **3-I**. − ^{1}H NMR (CD_2Cl_2, 599.8 MHz): δ = 7.48 (d, ^3J = 7.8 Hz, 1 H, 5-H), 6.32 and 6.28 (2 s, 2 × 5 H, Cp- and Cp′-H), 5.08 (br., 1 H, 2-H), 4.85 (m, 1 H, 6-H), 3.81 (s, 3 H, 7-OCH_3), 3.61 (m, 1 H, 3-H), 2.14 [m, 1 H, 6-CH(CH_3)$_2$], 1.47 [s, 9 H, 1-OC(CH_3)$_3$], 1.05 (d, ^3J = 7.1 Hz, 1 H, 3-CH_3), 0.92 [pst, ^3J = 7.0 Hz, 2 × 3 H, 6-CH(CH_3)$_2$], 0.59 (s, 1 H, Zr-CH_3); [BPh_4]$^-$: δ = 7.36 (m, 8 H, *o*-H), 7.08 (m, 8 H, *m*-H), 6.93 (m, 4 H, *p*-H); THF: 3.73 (m, 4 H, α-H), 1.86 (m, 4 H, β-H). − ^{13}C NMR (CD_2Cl_2, 150.8 MHz): δ = 182.9 (C-4), 168.9 (C-7), 155.4 (C-1), 113.9 and 113.8 (Cp C and Cp′ C), 82.1 [1-OC(CH_3)$_3$], 59.1 (C-6), 53.5 (7-OCH$_3$), 52.3 (C-3), 33.9 (Zr-CH$_3$), 31.3 [6-CH(CH_3)$_2$], 27.8 [1-OC(CH$_3$)$_3$], 18.7 and 17.7 [6-CH(CH$_3$)$_2$], 16.5 (3-CH$_3$); [BPh_4]$^-$: δ = 163.9 (q, $^1J_{CB}$ = 49 Hz, *i-C*), 135.9 (*o*-C), 125.9 (*m*-C), 122.0 (*p*-C); THF: δ = 67.9 (α-C), 25.6 (β-C).

Preparation of the Chelate Product 3-A: Boc-Ala-Val-OMe (**3**, 0.61 g, 2.0 mmol) and **1a** (1.25 g, 2 mmol) were treated according to procedure C to yield the metal peptide complex **3-A** (1.57 g, 1.9 mmol, 95 %) as a white solid; m.p. 44 °C (decomp). − $[\alpha]_D$ = −14 (*c* = 0.10, CH_2Cl_2). − $C_{47}H_{53}BN_2O_5Zr$ (828.0): calcd. C 68.47, H 6.58, N 3.33; found C 67.32, H 6.58, N 3.29. − IR (KBr): $\tilde{\nu}$ = 3340 (w, NH), 3055 (m), 2981 (s), 1744 (s), 1597 (s), 1551 (s), 1438 (s), 1370 (m), 1150 (s), 812 (s), 733 (s), 704 (vs) cm^{-1}. − ^{1}H NMR (CD_2Cl_2, 599.8 MHz): δ = 7.88 (d, ^3J = 8.1 Hz, 1 H, 5-H), 6.21 and 6.20 (2 s, 2 × 5 H, Cp- and Cp′-H), 4.45 (dd, ^3J = 8.3 Hz, ^3J = 5.0 Hz, 1 H, 6-H), 4.42 (q, ^3J = 6.8 Hz, 1 H, 3-H), 3.82 (s, 3 H, 7-OCH_3), 2.25 [m, 1 H, 6-CH(CH_3)$_2$], 1.55 [s, 9 H, 1-OC(CH_3)$_3$], 1.47 (d, ^3J = 6.8 Hz, 3 H, 3-CH_3), 1.01 and 0.96 [2 d, 2 ^3J = 6.9 Hz, 2 × 3 H, 6-CH(CH_3)$_2$]; [BPh_4]$^-$: δ = 7.35 (m, 8 H, *o*-

H), 7.08 (m, 8 H, *m*-H), 6.93 (m, 4 H, *p*-H). − ^{13}C NMR (CD_2Cl_2, 150.8 MHz): δ = 181.7 (C-4), 170.4 (C-7), 155.9 (C-1), 114.7 and 114.6 (Cp C and Cp′ C) 85.6 [1-O*C*$(CH_3)_3$], 59.6 (C-6), 56.7 (C-3), 53.2 (7-OCH_3), 30.9 [6-*C*H$(CH_3)_2$], 28.4 [1-OC(*C*$H_3)_3$], 19.0 and 18.4 [6-CH(C$H_3)_2$], 17.7 (3-*C*H_3); $[BPh_4]^-$: δ = 163.9 (q, $^1J_{CB}$ = 49 Hz, *i*-C), 135.9 (*o*-C), 125.8 (*m*-C), 122.0 (*p*-C).

X-ray Crystal Structure Analysis of 3-A: Formula $C_{48}H_{55}BN_2O_5Zr \cdot 1/2\ H_2O$, M = 849.97, colorless crystal, 0.60 × 0.30 × 0.20 mm, a = 14.468(2), b = 19.939(2), c = 33.232(2) Å, V = 9586.7(17) Å^3, $\rho_{calcd.}$ = 1.178 g cm^{-3}, F(000) = 3568 e, μ = 2.74 cm^{-1}, empirical absorption correction via φ scan data (0.853 ≤ T ≤ 0.947), Z = 8, orthorhombic, space group $P2_12_12_1$ (No. 19), λ = 0.71073 Å, T = 223 K, ω scans, 8838 reflections collected (+h, +k, +l), [(sinθ)/λ] = 0.59 Å^{-1}, 8837 independent and 3416 observed reflections [$I \geq 2\ \sigma(I)$], 895 refined parameters, R = 0.079, wR^2 = 0.204, max. residual electron density 0.71 (−0.61) e Å^{-3}, Flack parameter 0.05(11), Cp rings and phenyl groups refined as rigid groups, hydrogen atoms at N6 and N26 from difference Fourier, others calculated and all refined as riding atoms. Data set was collected with an Enraf Nonius MACH3 diffractometer. Programs used: data reduction MolEN, structure solution SHELXS-86, structure refinement SHELXL-97, graphics SCHAKAL-92. Crystallographic data (excluding structure factors) for the structures reported in this paper have been deposited with the Cambridge Crystallographic Data Centre as supplementary publication no. CCDC-114803. Copies of the data can be obtained free of charge on application to CCDC, 12 Union Road, Cambridge CB2 1EZ, UK [Fax: int. code + 44-1223/336-033, E-mail: deposit@ccdc.cam.ac.uk].

Preparation of Boc-Gly-Val-Val-OMe 6: (*N-tert*-Butoxycarbonylglycyl)valine (2.74 g, 10.0 mmol) and valine methyl ester hydrochloride (1.68 g, 10 mmol) were treated according to procedure B to yield the tripeptide Boc-Gly-Val-Val-OMe (**6**, 2.91 g, 75 %) as a white solid; m.p. 215 °C. − $[\alpha]_D$ = −14 (c = 0.10, CH_2Cl_2). − $C_{18}H_{33}N_3O_6$ (387.5): calcd. C 55.80, H 8.58, N 10.84; found C 55.36, H 8.60, N 10.52. − IR (KBr): ṽ = 3311 (s, NH), 2967 (m), 2936 (m), 2877 (w), 1747 (m), 1723 (m), 1648 (vs), 1545 (s), 1367 (w), 1162 (m), 864 (m), 786 (m) cm^{-1}. − ^{1}H NMR (CD_2Cl_2, 599.8 MHz): δ = 7.84 (d, 1 H, ^3J = 8.5 Hz, 5-H), 7.72 (d, 1 H, ^3J = 8.6 Hz, 8-H), 6.14 (br. s, 1 H, 2-H), 4.54 (dd, ^3J = 8.6 Hz, ^3J = 5.4 Hz, 1 H, 9-H), 4.45 (dd, ^3J = 8.5 Hz, ^3J = 5.7 Hz, 1 H, 6-H), 3.86 (m, 2 H, 3- and 3′-H), 3.68 (s, 3 H, 10-OCH_3), 2.11 [m, 1 H, 6-C*H*$(CH_3)_2$], 1.98 [m, 1 H, 9-C*H*$(CH_3)_2$], 1.38 [s, 9 H, 1-OC(C$H_3)_3$], 0.90 and 0.88 [2 d, 2 ^3J = 6.8 Hz, 2 × 3 H, 9-CH(C$H_3)_2$], 0.86 and 0.83 [2 d, 2 ^3J = 6.8 Hz, 6 H, 6-CH(C$H_3)_2$]. − ^{13}C NMR (CD_2Cl_2, 150.8 MHz): δ = 172.6 (C-7), 172.2 (C-10), 170.0 (C-4), 156.2 (C-1), 79.6 [1-O*C*$(CH_3)_3$], 58.5 (C-9), 57.3 (C-6), 52.4 (10-O*C*H$_3$), 43.9 (C-3), 31.6 [6-*C*H$(CH_3)_2$], 31.0 [9-*C*H$(CH_3)_2$], 28.3 [1-OC(*C*$H_3)_3$], 19.1 and 19.0 [9-CH(*C*$H_3)_2$], 18.6 and 17.8 [6-*C*H$(CH_3)_2$].

Generation of the Intermediate Adduct 6-I: Boc-Gly-Val-Val-OMe (**6**, 24.7 mg, 63.8 μmol) and **1a** (40.0 mg, 63.8 μmol) were treated according to procedure D to give **6-I**. − ^{1}H NMR (CD_2Cl_2, 599.8 MHz): δ = 7.78 (br., 1 H, 2-H), 6.66 (br., 1 H, 5-H), 6.41 (br., 1 H, 8-H), 6.26 and 6.20 (2 s, 2 × 5 H, Cp- and Cp′-H), 4.46 (br., 1 H, 9-H), 4.16 (br., 1 H, 6-H), 3.71 (m, 2 H, 3- and 3′-H), 3.76 (s, 3 H, 10-OCH_3), 2.25 [m, 1 H, 9-C*H*$(CH_3)_2$], 1.98 [m, 1 H, 6-C*H*$(CH_3)_2$], 1.43 [s, 9 H, 1-OC(C$H_3)_3$], 0.99 and 0.95 [2 d, 2 ^3J = 7.0 Hz, 6 H, 9-CH(C$H_3)_2$], 0.89 and 0.88 [2 d, 2 ^3J = 7.0 Hz, 2 × 3 H, 6-CH(C$H_3)_2$], 0.50 (s, 3 H, Zr-CH_3); $[BPh_4]^-$: δ = 7.43 (m, 8 H, *o*-H), 7.10 (m, 8 H, *m*-H), 6.94 (m, 4 H, *p*-H); THF: 3.72 (m, 4 H, α-H), 1.85 (m, 4 H, β-H). − ^{13}C NMR (CD_2Cl_2, 150.8 MHz): δ = 177.9 (C-4), 171.7 (C-10), 171.3 (C-7), 156.1 (C-1), 114.8 and 113.7 (Cp C and Cp′ C), 81.5 [1-O*C*$(CH_3)_3$], 60.0 (C-9), 58.1 (C-6), 52.2 (10-O*C*H$_3$), 44.8 (C-3), 32.4 (Zr-*C*H$_3$), 31.8 [6-*C*H$(CH_3)_2$], 30.2 [9-*C*H$(CH_3)_2$], 27.8 [1-OC(*C*$H_3)_3$], 18.9 and 18.6 [6-CH(C$H_3)_2$], 17.8 and 17.2 [9-CH(C$H_3)_2$]; $[BPh_4]^-$: δ = 163.9 (q, $^1J_{CB}$ = 49 Hz, *i*-*C*), 135.7 (*o*-C), 126.0 (*m*-C), 122.1 (*p*-C); THF: δ = 68.0 (α-C), 25.7 (β-C).

Preparation of the Chelate Product 6-A: Boc-Gly-Val-Val-OMe (**6**, 0.78 g, 2.0 mmol) and **1a** (1.25 g, 2 mmol) were treated according to procedure C to yield the metal peptide complex **6-A** (1.59 g, 97 %) as a white solid; m.p. 67 °C (decomp). − $[\alpha]_D$ = −59 (c = 0.10, CH_2Cl_2). − $C_{52}H_{62}BN_3O_6Zr$ (927.1): calcd. C 67.37, H 6.74, N 4.53; found C 67.13, H 6.69, N 4.42. − IR (KBr): ṽ = 3292 (s, NH), 3269 (m), 2966 (m), 2966 (s), 2877 (w), 1743 (m), 1652 (vs), 1591 (s), 1543 (s), 1240 (s), 1159 (m), 869 (m), 789 (m) cm^{-1}. − ^{1}H NMR (CD_2Cl_2, 599.8 MHz): δ = 9.13 (br., 1 H, 8-H), 6.78 (br., 1 H, 5-H), 6.25 and 6.19 (2 s, 2 × 5 H, Cp- and Cp′-H), 4.49 (dd, ^3J = 8.2 Hz, ^3J = 4.9 Hz, 1 H, 9-H), 4.45 (dd, ^3J = 8.8 Hz, ^3J = 6.0 Hz, 1 H, 6-H), 4.21 (AB, ^2J = 18.7 Hz, 2 H, 3- and 3′-H), 3.78 (s, 3 H, 10-OCH_3), 2.26 [m, 1 H, 9-C*H*$(CH_3)_2$], 2.13 [m, 1 H, 6-C*H*$(CH_3)_2$], 1.57 [s, 9 H, 1-OC(C$H_3)_3$], 1.07 and 0.99 [2 d, 2 ^3J = 7.0 Hz, 6 H, 6-CH(C$H_3)_2$], 1.02 and 1.00 [2 d, 2 ^3J = 7.0 Hz, 2 × 3 H, 9-CH(C$H_3)_2$]; $[BPh_4]^-$: δ = 7.41 (m, 8 H, *o*-H), 7.10 (m, 8 H, *m*-H), 6.96 (m, 4 H, *p*-H). − ^{13}C NMR (CD_2Cl_2, 150.8 MHz): δ = 177.8 (C-4), 171.5 (C-10), 169.7 (C-7), 156.2 (C-1), 114.8 and 114.7 (Cp C and Cp′ C), 85.5 [1-O*C*$(CH_3)_3$], 60.1 (C-6), 58.1 (C-9), 52.7 (10-O*C*H$_3$), 50.1 (C-3), 32.3 [6-*C*H$(CH_3)_2$], 30.8 [9-*C*H$(CH_3)_2$], 28.4 [1-OC(*C*$H_3)_3$], 19.1 and 19.0 [6-CH(*C*$H_3)_2$], 18.0 and 17.9 [9-CH(*C*$H_3)_2$]; $[BPh_4]^-$: δ = 164.0 (q, $^1J_{CB}$ = 49 Hz, *i*-*C*), 135.8 (*o*-C), 125.8 (*m*-C), 121.9 (*p*-C).

Preparation of Boc-Ala-Ala-Val-OMe (7): (*N-tert*-Butoxycarbonylalanyl)alanine (2.60 g, 10.0 mmol) and valine methyl ester hydrochloride (1.68 g, 10 mmol) were treated according to procedure B to yield the tripeptide Boc-Ala-Ala-Val-OMe **7** (2.58 g, 69 %) as a white solid material; m.p. 146 °C. − $[\alpha]_D$ = −61 (c = 0.10, CH_2Cl_2). − $C_{17}H_{31}N_3O_6$ (373.4): calcd. 54.68, H 8.37, N 11.25; found C 54.68, H 8.41, N 10.90. − IR (KBr): ṽ = 3382 (s, NH), 3308 (s, NH), 2978 (s), 2934 (m), 2878 (w), 1738 (m), 1706 (m), 1638 (vs), 1535 (s), 1347 (w), 1166 (m), 865 (m), 789 (w) cm^{-1}. − ^{1}H NMR (CD_2Cl_2, 599.8 MHz): δ = 7.59 (d, ^3J = 8.6 Hz, 1 H, 8-H), 7.53 (d, ^3J = 7.2 Hz, 1 H, 5-H), 5.80 (d, ^3J = 7.2 Hz, 1 H, 2-H), 4.68 (m, 1 H, 6-H), 4.46 (dd, ^3J = 8.6 Hz, ^3J = 5.2 Hz, 1 H, 9-H), 4.26 (m, 1 H, 3-H), 3.69 (s, 3 H, 10-OCH_3), 2.11 [m, 1 H, 9-C*H*$(CH_3)_2$], 1.38 [s, 9 H, 1-OC(C$H_3)_3$], 1.31 (d, ^3J = 7.0 Hz, 3 H, 6-CH_3), 1.27 (d, ^3J = 7.0 Hz, 3 H, 3-CH_3), 0.87 and 0.84 [2 d, 2 ^3J = 6.8 Hz, 2 × 3 H, 9-CH(C$H_3)_2$]. − ^{13}C NMR (CD_2Cl_2, 150.8 MHz): δ = 173.1 (C-4), 172.6 (C-10), 172.4 (C-7), 155.5 (C-1), 79.6 [1-O*C*$(CH_3)_3$], 57.2 (C-9), 52.3 (10-O*C*H$_3$), 49.9 (C-3), 48.8 (C-6), 31.2 [9-*C*H$(CH_3)_2$], 28.1 [1-OC(*C*$H_3)_3$], 18.9 (6-*C*H$_3$), 18.8 (3-*C*H$_3$), 18.4 and 17.7 [9-CH(*C*$H_3)_2$].

Generation of the Intermediate Adduct 7-I: Boc-Ala-Ala-Val-OMe (**7**, 23.8 mg, 63.8 μmol) and **1a** (40.0 mg, 63.8 μmol) were treated according to procedure D to give **7-I**. − ^{1}H NMR (CD_2Cl_2, 599.8 MHz): δ = 9.17 (br., 1 H, 8-H), 8.67 (br., 1 H, 5-H), 6.33 and 6.30 (2 s, 2 × 5 H, Cp- and Cp′-H), 5.54 (br., 1 H, 2-H), 3.92 (br., 1 H, 9-H), 3.82 (br., 1 H, 6-H), 3.79 (s, 3 H, 10-OCH_3), 3.78 (br., 1 H, 3-H), 2.24 [m, 1 H, 9-C*H*$(CH_3)_2$], 1.44 [s, 9 H, 1-OC(C$H_3)_3$], 1.24 (d, ^3J = 6.9 Hz, 3 H, 6-CH_3), 1.18 (d, ^3J = 7.2 Hz, 3 H, 3-CH_3), 0.92 and 0.90 [2 d, 2 ^3J = 6.7 Hz, 2 × 3 H, 9-CH(C$H_3)_2$], 0.54 (s, 3 H, Zr-CH_3); $[BPh_4]^-$: 7.32 (m, 8 H, *o*-H), 7.07 (m, 8 H, *m*-H), 6.92 (m, 4 H, *p*-H); THF: δ = 3.71 (m, 4 H, α-H), 1.84 (m, 4 H, β-H). − ^{13}C NMR (CD_2Cl_2, 150.8 MHz): δ = 169.6 (C-10), 156.8 (C-1), 113.9 and 113.8 (Cp C and Cp′ C), 81.8

[1-O*C*(CH_3)$_3$], 59.7 (C-9), 53.3 (10-O*C*H_3), 51.9 (C-3), 50.7 (C-6), 33.6 (Zr-*C*H_3), 30.3 [9-*C*H(CH_3)$_2$], 27.9 [1-OC(*C*H_3)$_3$], 19.0 (6-*C*H_3), 18.4 (3-*C*H_3), 17.1 and 16.8 [9-CH(*C*H_3)$_2$]; [BPh_4]$^-$: δ = 163.8 (q, $^1J_{CB}$ = 49 Hz, *i-C*), 135.8 (*o*-C), 126.0 (*m*-C), 122.0 (*p*-C); THF: δ = 68.0 (α-C), 25.7 (β-C). The resonance signals of C-7 and C-11 were not observed.

Preparation of the Chelate Products 7-A/B: Boc-Ala-Ala-Val-OMe (**7**, 0.75 g, 2.0 mmol) and **1a** (1.25 g, 2 mmol) were treated according to procedure C to yield a mixture of the two isomeric metal peptide complexes **7-A** and **7-B** (1.75 g, 96 %) in a 4:3 ratio as a white solid; m.p. 59 °C. (decomp). − $[\alpha]_D$ = −43 (*c* = 0.10, CH_2Cl_2). − $C_{51}H_{60}BN_3O_6Zr$ (913.1): calcd. C 67.09, H 6.62, N 4.60; found C 66.39, H 6.91, N 4.45. − IR (KBr): ṽ = 3295 (s, NH), 3054 (s), 2985 (m), 2964 (m), 1744 (m), 1690 (m), 1609 (m), 1264 (s), 1157 (m), 858 (m), 785 (m) cm^{-1}. − Isomer **7-A**: ^{1}H NMR (CD_2Cl_2, 599.8 MHz): δ = 8.13 (d, ^3J = 5.6 Hz, 1 H, 5-H), 6.32 (br., 1 H, 8-H), 6.21 and 6.19 (2 s, 2 × 5 H, Cp- and Cp′H), 4.49 (dd, ^3J = 7.0 Hz, ^3J = 4.8 Hz, 1 H, 9-H), 4.41 (q, ^3J = 7.1 Hz, 1 H, 3-H), 4.33 (m, 1 H, 6-H), 3.74 (s, 3 H, 10-OC*H*$_3$), 2.20 [m, 1 H, 9-C*H*(CH_3)$_2$], 1.54 [s, 9 H, 1-OC(C*H*$_3$)$_3$], 1.44 (d, ^3J = 7.1 Hz, 3 H, 3-C*H*$_3$), 1.29 (d, ^3J = 7.1 Hz, 3 H, 6-C*H*$_3$), 0.97 and 0.93 [2 d, 2 ^3J = 6.8 Hz, 2 × 3 H, 9-CH(C*H*$_3$)$_2$]; [BPh_4]$^-$: δ = 7.34 (m, 8 H, *o*-H), 7.07 (m, 8 H, *m*-H), 6.92 (m, 4 H, *p*-H). − ^{13}C NMR (CD_2Cl_2, 150.8 MHz): δ = 180.8 (C-4), 171.8 (C-10), 170.0 (C-7), 156.0 (C-1), 114.7 and 114.6 (Cp C and Cp′ C), 85.5 [1-OC(*C*H_3)$_3$], 57.8 (C-9), 56.8 (C-3), 52.7 (10-O*C*H_3), 50.8 (C-6), 31.1 [9-*C*H(CH_3)$_2$], 28.4 [1-OC(*C*H_3)$_3$], 21.0, 19.0, 18.9, 18.8, 18.5, 17.8, 17.7, and 15.8 [9-CH(*C*H_3)$_2$ of both isomers]; [BPh_4]$^-$: δ = 163.9 (q, $^1J_{CB}$ = 49 Hz, *i-C*), 135.9 (*o*-C), 125.9 (*m*-C), 121.9 (*p*-C). − Isomer **7-B**: ^{1}H NMR (CD_2Cl_2, 599.8 MHz): δ = 8.31 (d, ^3J = 8.4 Hz, 1 H, 8-H), 6.24 and 6.19 (2 s, 2 × 5 H, Cp- and Cp′-H), 5.26 (d, ^3J = 5.5 Hz, 1 H, 2-H), 4.99 (q, ^3J = 7.1 Hz, 1 H, 6-H), 4.48 (dd, ^3J = 8.4 Hz, ^3J = 5.0 Hz, 1 H, 9-H), 3.88 (m, 1 H, 3-H), 3.82 (s, 3 H, 10-OC*H*$_3$), 2.29 [m, 1 H, 9-C*H*(CH_3)$_2$], 1.55 [s, 9 H, 1-OC(C*H*$_3$)$_3$], 1.51 (d, ^3J = 7.1 Hz, 3 H, 6-C*H*$_3$), 1.27 (d, ^3J = 7.1 Hz, 3 H, 3-C*H*$_3$), 1.04 and 0.99 [2 d, 2 ^3J = 6.9 Hz, 2 × 3 H, 9-CH(C*H*$_3$)$_2$]; [BPh_4]$^-$: δ = 7.34 (m, 8 H, *o*-H), 7.07 (m, 8 H, *m*-H), 6.92 (m, 4 H, *p*-H). − ^{13}C NMR (CD_2Cl_2, 150.8 MHz): δ = 181.0 (C-4), 179.0 (C-7), 170.4 (C-10), 155.4 (C-1), 115.0 and 114.8 (Cp C and Cp′ C), 80.6 [1-O*C*(CH_3)$_3$], 59.7 (C-9), 57.0 (C-6), 53.3 (10-O*C*H_3), 47.8 (C-3), 30.9 [9-*C*H(CH_3)$_2$], 28.1 [1-OC(*C*H_3)$_3$], 21.0, 19.0, 18.9, 18.8, 18.5, 17.8, 17.7, and 15.8 [9-CH(*C*H_3)$_2$ of both isomers]; [BPh_4]$^-$: δ = 163.9 (q, $^1J_{CB}$ = 49 Hz, *i-C*), 135.9 (*o*-C), 125.9 (*m*-C), 121.9 (*p*-C). − Upon standing at 0 °C for two weeks isomer **7-B** rearranged quantitatively to form isomer **7-A**.

Preparation of Boc-Ala-Val-Val-OMe (8): (*N-tert*-Butoxycarbonylalanyl)valine (2.88 g, 10.0 mmol) and valine methyl ester hydrochloride (1.68 g, 10 mmol) were treated according to procedure B to yield the tripeptide Boc-Ala-Val-Val-OMe (**8**, 2.73 g, 68 %) as a white solid; m.p. 214 °C. − $[\alpha]_D$ = −66 (*c* = 0.10, CH_2Cl_2). − IR (KBr): ṽ = 3325 (m, NH), 2967 (m), 2933 (m), 1745 (m), 1696 (m), 1648 (s), 1541 (s), 1169 (m), 834 (m), 711 (s) cm^{-1}. − ^{1}H NMR (CD_2Cl_2, 599.8 MHz): δ = 7.79 (d, ^3J = 8.7 Hz, 1 H, 5-H), 7.60 (d, ^3J = 8.7 Hz, 1 H, 8-H), 6.04 (d, ^3J = 8.3 Hz, 1 H, 2-H), 4.52 (dd, ^3J = 8.7 Hz, ^3J = 5.6 Hz, 1 H, 6-H), 4.47 (pst, ^3J = 8.7 Hz, 1 H, 9-H), 4.40 (m, 1 H, 3-H), 3.68 (s, 3 H, 10-OC*H*$_3$), 2.13 [m, 2 H, 6-C*H*(CH_3)$_2$], 1.99 [m, 2 H, 9-C*H*(CH_3)$_2$], 1.38 [s, 9 H, 1-OC(C*H*$_3$)$_3$], 1.22 (d, ^3J = 7.0 Hz, 3 H, 3-C*H*$_3$), 0.91 and 0.89 [m, 12 H, 9-CH(C*H*$_3$)$_2$], 0.86 and 0.82 [m, 12 H, 6-CH(C*H*$_3$)$_2$]. − ^{13}C NMR (CD_2Cl_2, 150.8 MHz): δ = 173.3 (C-4), 172.5 (C-10), 171.9 (C-7), 156.6 (C-1), 79.5 [1-O*C*(CH_3)$_3$], 58.7/58.6 (C-9), 57.1/57.0 (C-6), 52.3 (10-O*C*H_3), 49.9 (C-3), 31.3/31.1 [6-*C*H(CH_3)$_2$], 31.1/31.0 [9-*C*H(CH_3)$_2$], 28.3 [1-OC(*C*H_3)$_3$], 19.1 and 19.0 [6-CH(*C*H_3)$_2$], 18.6 and 17.8 [9-CH(*C*H_3)$_2$], 18.5 (3-*C*H_3).

Generation of the Intermediate Adduct 8-I: Boc-Ala-Val-Val-OMe (**8**, 25.6 mg, 63.8 μmol) and **1a** (40.0 mg, 63.8 μmol) were treated according to procedure D to give **8-I**. − ^{1}H NMR (CD_2Cl_2, 599.8 MHz): δ = 8.36 (br. s, 1 H, 5-H), 7.62 (d, ^3J = 7.3 Hz, 1 H, 8-H), 6.33 and 6.32 (2 s, 2 × 5 H, Cp- and Cp′-H), 5.29 (br. s, 1 H, 2-H), 4.50 (dd, ^3J = 8.6 Hz, ^3J = 4.5 Hz, 1 H, 6-H), 4.43 (m, 1 H, 9-H), 4.08 (br. s, 1 H, 3-H), 3.80 (s, 3 H, 10-OC*H*$_3$), 2.28 [m, 1 H, 9-C*H*(CH_3)$_2$], 2.01 [m, 1 H, 6-C*H*(CH_3)$_2$], 1.44 [s, 9 H, 1-OC(C*H*$_3$)$_3$], 1.27 (d, ^3J = 7.2 Hz, 3 H, 3-C*H*$_3$), 1.01 and 0.97 [2 d, 2 ^3J = 6.8 Hz, 2 × 3 H, 9-CH(C*H*$_3$)$_2$], 0.97 and 0.92 [2 d, 2 ^3J = 6.2 Hz, 2 × 3 H, 6-CH(C*H*$_3$)$_2$], 0.59 (s, 3 H, Zr-C*H*$_3$); [BPh_4]$^-$: δ = 7.34 (m, 8 H, *o*-H), 7.07 (m, 8 H, *m*-H), 6.92 (m, 4 H, *p*-H); THF: δ = 3.74 (m, 4 H, α-H), 1.86 (m, 4 H, β-H). − ^{13}C NMR (CD_2Cl_2, 150.8 MHz): δ = 176.3 (C-4), 169.7 (C-10) 167.4 (C-7), 156.7 (C-1), 113.9 and 113.8 (Cp C and Cp′ C), 82.1 [1-O*C*(CH_3)$_3$], 60.1 (C-9), 59.7 (C-6), 53.1 (C-3), 52.1 (10-O*C*H_3), 33.8 (Zr-*C*H_3), 33.1 [6-*C*H(CH_3)$_2$], 32.4 [9-*C*H(CH_3)$_2$], 27.9 [1-OC(*C*H_3)$_3$], 19.3 and 19.0 [6-CH(*C*H_3)$_2$], 18.6 and 17.1 [9-CH(*C*H_3)$_2$], 18.1 (3-*C*H_3); [BPh_4]$^-$: δ = 163.9 (q, $^1J_{CB}$ = 49 Hz, *i-C*), 135.9 (*o*-C), 125.9 (*m*-C), 122.0 (*p*-C); THF: δ = 67.9 (α-C), 25.7 (β-C).

Preparation of the Chelate Products 8-A/C: Boc-Ala-Val-Val-OMe (**8**, 0.80 g, 2.0 mmol) and **1a** (1.25 g, 2 mmol) were treated according to procedure C to yield the isomeric metal peptide complexes **8-A** and **8-C** (1.75 g, 93 %) in a ratio of 3:2 as a white solid; m.p. 56 °C (decomp). − $[\alpha]_D$ = −29 (*c* = 0.10, CH_2Cl_2). − $C_{53}H_{64}BN_3O_6Zr$ (941.0): calcd. C 67.64, H 6.85, N 4.46; found C 66.04, H 6.85, N 4.22. − IR (KBr): ṽ = 3296 (s, NH), 3069 (m), 2969 (s), 1743 (m), 1660 (s), 1612 (m), 1546 (s), 1433 (s), 1249 (s), 1171 (m), 806 (s), 709 (vs) cm^{-1}. − **Isomer 8-A:** ^{1}H NMR (CD_2Cl_2, 599.8 MHz): δ = 8.64 (br. s, 1 H, 5-H), 6.42 (br. d, ^3J = 7.5 Hz, 1 H, 8-H), 6.29 and 6.10 (2 s, 2 × 5 H, Cp- and Cp′-H), 4.51 (q, ^3J = 5.5 Hz, 1 H, 3-H), 4.37 (m, 1 H, 9-H), 4.50 (dd, ^3J = 8.0 Hz, ^3J = 5.3 Hz, 1 H, 6-H), 3.82 (s, 3 H, 10-OC*H*$_3$), 2.31 [m, 1 H, 9-C*H*(CH_3)$_2$], 2.21 [m, 1 H, 6-C*H*(CH_3)$_2$], 1.40 [s, 9 H, 1-OC(C*H*$_3$)$_3$], 1.42 (d, ^3J = 5.5 Hz, 3 H, 3-C*H*$_3$), 1.10 and 1.09 [2 d, 2 ^3J = 6.9 Hz, 2 × 3 H, 9-CH(C*H*$_3$)$_2$], 1.04 and 1.03 [2 d, 2 ^3J = 7.0 Hz, 2 × 3 H, 6-CH(C*H*$_3$)$_2$]; [BPh_4]$^-$: δ = 7.34 (m, 8 H, *o*-H), 7.07 (m, 8 H, *m*-H), 6.92 (m, 4 H, *p*-H). − ^{13}C NMR (CD_2Cl_2, 150.8 MHz): δ = 181.5 (C-4), 170.1 (C-10), 169.1 (C-7), 156.7 (C-1), 114.8 and 114.6 (Cp C and Cp′ C), 85.5 [1-O*C*(CH_3)$_3$], 60.0 (C-6), 58.5 (C-3), 57.1 (C-9), 52.7 (10-O*C*H_3), 33.1 [6-*C*H(CH_3)$_2$], 30.9 [9-*C*H(CH_3)$_2$], 28.4 [1-OC(*C*H_3)$_3$], 19.2 (3-*C*H_3), 18.8 and 18.7 [6-CH(*C*H_3)$_2$], 18.0 and 17.8 [9-CH(*C*H_3)$_2$]; [BPh_4]$^-$: δ = 164.0 (q, $^1J_{CB}$ = 49 Hz, *i-C*), 135.8 (*o*-C), 125.9 (*m*-C), 121.9 (*p*-C). − **Isomer 8-C:** ^{1}H NMR (CD_2Cl_2, 599.8 MHz): δ = 8.10 (d, ^3J = 7.5 Hz, 1 H, 5-H), 6.22 and 6.21 (2 s, 2 × 5 H, Cp- and Cp′-H), 5.25 (d, ^3J = 6.0 Hz, 1 H, 2-H), 5.12 (d, ^3J = 6.0 Hz, 1 H, 9-H), 4.48 (m, 1 H, 6-H), 4.01 (m, 1 H, 3-H), 3.76 (s, 3 H, 10-OC*H*$_3$), 2.22 [m, 1 H, 9-C*H*(CH_3)$_2$], 2.19 [m, 1 H, 6-C*H*(CH_3)$_2$], 1.54 [s, 9 H, 1-OC(C*H*$_3$)$_3$], 1.31 (d, ^3J = 7.0 Hz, 3 H, 3-C*H*$_3$), 1.08 and 1.06 [2 d, 2 ^3J = 6.9 Hz, 2 × 3 H, 6-CH(C*H*$_3$)$_2$], 0.97 and 0.94 [2 d, 2 ^3J = 6.8 Hz, 2 × 3 H, 9-CH(C*H*$_3$)$_2$]; [BPh_4]$^-$: δ = 7.34 (m, 8 H, *o*-H), 7.07 (m, 8 H, *m*-H), 6.92 (m, 4 H, *p*-H). − ^{13}C NMR (CD_2Cl_2, 150.8 MHz): δ = 180.8 (C-7), 179.8 (C-10), 171.5 (C-4), 155.9 (C-1), 115.3 and 115.0 (Cp C and Cp′ C), 80.9 [1-O*C*(CH_3)$_3$], 66.8 (C-9), 59.9 (C-6), 57.9 (10-O*C*H_3), 46.9 (C-3), 30.7 [9-*C*H(CH_3)$_2$], 34.6 [6-*C*H(CH_3)$_2$], 28.1 [1-OC(*C*H_3)$_3$], 19.0 and 18.9 [6-CH(*C*H_3)$_2$], 18.7 and 17.6 [9-CH(*C*H_3)$_2$], 17.9 (3-*C*H_3); [BPh_4]$^-$: δ = 164.0 (q, $^1J_{CB}$ = 49 Hz, *i-C*), 135.8 (*o*-C), 125.9 (*m*-C), 121.9 (*p*-C). Isomer **8-C** rearranges upon standing at 25 °C for 4 d to form isomer **8-A** quantitatively.

Preparation of Boc-Val-Val-Gly-OMe (9): (*N-tert*-Butoxycarbonyl-valyl)valine (3.17 g, 10.0 mmol) and glycine methyl ester hydrochloride (1.26 g, 10 mmol) were treated according to procedure B to yield the tripeptide Boc-Val-Val-Gly-OMe (**9**, 2.76 g, 74 %) as a white solid; m.p. 176°C. − $[\alpha]_D = -35$ (c = 0.10, CH_2Cl_2). − $C_{18}H_{33}N_3O_6$ (373.5): calcd. C 55.80, H 8.58, N 10.84; found C 55.81, H 8.61, N 10.63. − IR (KBr): $\tilde{\nu}$ = 3295 (vs, NH), 2967 (s, NH), 2933 (m), 1759 (m), 1695 (s), 1640 (vs), 1554 (s), 1526 (s), 1393 (w), 1365 (w), 1209 (s), 1179 (m), 781 (s) cm^{-1}. − ^1H NMR (CD_2Cl_2, 599.8 MHz): δ = 7.62 (br., 1 H, 8-H), 7.23 (d, ^3J = 8.9 Hz, 1 H, 5-H), 5.62 (d, ^3J = 6.6 Hz, 1 H, 2-H), 4.36 (dd, ^3J = 8.9 Hz, ^3J = 6.8 Hz, 1 H, 6-H), 3.98 (m, 2 H, 9- and 9′-H), 3.98 (m, 1 H, 3-H), 3.67 (s, 3 H, 10-OCH_3), 2.15 [m, 1 H, 6-CH(CH$_3$)$_2$], 2.05 [dsept, ^3J = 6.9 Hz, ^3J = 6.8 Hz, 1 H, 3-CH(CH$_3$)$_2$], 1.38 [s, 9 H, 1-OC(CH_3)$_3$], 0.95−0.94, [m, 4 × 3 H, 3- and 6-CH(CH_3)$_2$]. − ^{13}C NMR (CD_2Cl_2, 150.8 MHz): δ = 172.1 (C-4), 171.8 (C-7), 170.2 (C-10), 156.2 (C-1), 79.9 [1-OC(CH$_3$)$_3$], 60.4 (C-3), 58.2 (C-6), 52.3 (10-OCH$_3$), 41.0 (C-9), 30.5 [3-CH(CH$_3$)$_2$], 30.4 [6-CH(CH$_3$)$_2$], 28.0 [1-OC(CH$_3$)$_3$], 19.1 and 19.0 [6-CH(CH$_3$)$_2$], 17.9 and 17.6 [3-CH(CH$_3$)$_2$].

Generation of the Intermediate Adduct 9-I: Boc-Val-Val-Gly-OMe (**9**, 24.7 mg, 63.8 μmol) and 40.0 mg (63.8 μmol) of **1a** were treated according to procedure D to give **9-I**. − ^1H NMR (CD_2Cl_2, 599.8 MHz): δ = 6.78 (br., 1 H, 5-H), 6.30 and 6.29 (2 s, 2 × 5 H, Cp- and Cp′-H), 5.27 (br. s, 1 H, 2-H), 3.97 (dd, ^3J = 6.2 Hz, ^3J = 3.6 Hz, 1 H, 3-H), 3.82 (ABX, ^2J = 17.8 Hz, 2 H, 9- and 9′-H), 3.79 (s, 10-OCH_3), 3.78 (dd, ^3J = 4.4 Hz, ^3J = 2.5 Hz, 1 H, 3-H), 2.14 [m, 1 H, 6-CH(CH$_3$)$_2$], 2.04 [m, 1 H, 3-CH(CH$_3$)$_2$], 1.44 [s, 9 H, 1-OC(CH_3)$_3$], 1.05 and 1.03 [2 d, 2 ^3J = 7.0 Hz, 2 × 3 H, 3-CH(CH_3)$_2$], 0.98 and 0.97 [2 d, 2 ^3J = 7.2 Hz, 2 × 3 H, 6-CH(CH_3)$_2$], 0.55 (s, 3 H, Zr-CH_3); [BPh$_4$]$^-$: δ = 7.35 (m, 8 H, *o*-H), 7.07 (m, 8 H, *m*-H), 6.92 (m, 4 H, *p*-H); THF: δ = 3.70 (m, 4 H, α-H), 1.84 (m, 4 H, β-H), the 8-H resonance was not observed. − ^{13}C NMR (CD_2Cl_2, 150.8 MHz): δ = 178.2 (C-4), 167.3 (C-7), 166.6 (C-10), 155.4 (C-1), 113.8 and 113.7 (Cp C and Cp′ C), 82.7 [1-OC(CH$_3$)$_3$], 61.9 (C-3), 58.8 (C-6), 50.6 (10-OCH$_3$), 42.3 (C-9), 33.4 (Zr-CH$_3$), 33.1 [3-CH(CH$_3$)$_2$], 29.5 [6-CH(CH$_3$)$_2$], 27.9 [1-OC(CH$_3$)$_3$], 19.7 and 19.1 [6-CH(CH$_3$)$_2$], 17.7 and 15.6 [3-CH(CH$_3$)$_2$]; [BPh$_4$]$^-$: δ = 164.0 (q, $^1J_{CB}$ = 49 Hz, *i-C*), 135.8 (*o*-C), 126.2 (*m*-C), 122.3 (*p*-C); THF: δ = 68.0 (α-C), 25.7 (β-C).

Preparation of the Chelate Products 9-A/C: Boc-Val-Val-Gly-OMe (**9**, 0.78 g, 2.0 mmol) and **1a** (1.25 g, 2 mmol) were treated according to procedure C to yield the two isomeric metal peptide complexes **9-A** and **9-C** (1.72 g, 93 %) in a 1:1 ratio as a white solid; m.p. 61 °C (decomp). − $[\alpha]_D = -44$ (c = 0.10, CH_2Cl_2). − $C_{52}H_{62}N_3O_6Zr$ (927.1): calcd. C 67.37, H 6.74, N 4.53; found C 66.54; H 6.99; N 4.42. − IR (KBr): $\tilde{\nu}$ = 3293 (s, NH), 3269 (m), 2963 (m), 2934 (w), 1760 (m), 1677 (m), 1611 (s), 1544 (s), 1262 (s), 1016 (m), 799 (vs) cm^{-1}. − **Isomer 9-A:** ^1H NMR (CD_2Cl_2, 599.8 MHz): δ = 7.59 (br., 1 H, 8-H), 7.46 (br., 1 H, 5-H), 6.23 and 6.04 (2 s, 2 × 5 H, Cp- and Cp′-H), 4.37 (d, ^3J = 3.0 Hz, 1 H, 3-H), 3.74 (s, 3 H, 10-OCH_3), 3.67 (hidden by the THF resonance signal, 1 H, 6-H), 3.20 (ABX, ^2J = 17.5 Hz, 2 H, 9- and 9′-H), 2.17 [m, 1 H, 3-CH(CH$_3$)$_2$], 1.93 [m, 1 H, 6-CH(CH$_3$)$_2$], 1.48 [s, 9 H, 1-OC(CH_3)$_3$], 1.07−0.93 [m, 4 × 3 H, 3- and 6-CH(CH_3)$_2$]; [BPh$_4$]$^-$: δ = 7.37 (m, 8 H, *o*-H), 7.08 (m, 8 H, *m*-H), 6.93 (m, 4 H, *p*-H). − ^{13}C NMR (CD_2Cl_2, 150.8 MHz): δ = 180.8 (C-4), 168.5 (C-7), 167.7 (C-10), 157.2 (C-1), 115.3 and 114.9 (Cp C and Cp′ C), 85.9 [1-OC(CH$_3$)$_3$], 66.8 (C-3), 59.9 (C-6), 52.8 (10-OCH$_3$), 42.5 (C-9), 34.8 [3-CH(CH$_3$)$_2$], 29.3 [6-CH(CH$_3$)$_2$], 28.4 [1-OC(CH$_3$)$_3$], 18.8 [6-CH(CH$_3$)$_2$], 18.6 and 18.2 [3-CH(CH$_3$)$_2$]; [BPh$_4$]$^-$: δ = 164.0 (q, $^1J_{CB}$ = 49 Hz, *i-C*), 135.8 (*o*-C), 126.2 (*m*-C), 122.3 (*p*-C). − **Isomer 9-C:** ^1H NMR (CD_2Cl_2, 599.8 MHz): δ = 7.89 (br., 1 H, 5-H), 6.30 and 6.17 (2 s, 2 × 5 H, Cp- and Cp′-H), 5.82 (br., 1 H, 2-H), 4.17 (dd, ^3J = 8.4 Hz, ^3J = 5.9 Hz, 1 H, 3-H), 3.84 (AB, ^2J = 17.0 Hz, 2 H, 9- and 9′-H), 3.77 (m, 1 H, 6-H), 3.71 (s, 3 H, 10-OCH_3), 2.01 [m, 1 H, 3-CH(CH$_3$)$_2$], 1.95 [m, 1 H, 6-CH(CH$_3$)$_2$], 1.55 [s, 9 H, 1-OC(CH_3)$_3$], 1.07−0.93 [m, 4 × 3 H, 3- and 6-CH(CH_3)$_2$]; [BPh$_4$]$^-$: δ = 7.37 (m, 8 H, *o*-H), 7.08 (m, 8 H, *m*-H), 6.93 (m, 4 H, *p*-H). − ^{13}C NMR (CD_2Cl_2, 150.8 MHz): δ = 180.6 (C-10), 179.3 (C-7), 169.5 (C-4), 155.6 (C-1), 114.8 and 114.4 (Cp C and Cp′ C), 80.9 [1-OC(CH$_3$)$_3$], 66.5 (C-6), 57.5 (C-3), 52.6 (10-OCH$_3$), 41.3 (C-9), 34.8 [3-CH(CH$_3$)$_2$], 31.6 [6-CH(CH$_3$)$_2$], 28.2 [1-OC(CH$_3$)$_3$], 20.5 and 19.7 [6-CH(CH$_3$)$_2$], 17.8 and 16.8 [3-CH(CH$_3$)$_2$]; [BPh$_4$]$^-$: δ = 164.0 (q, $^1J_{CB}$ = 49 Hz, *i-C*), 135.8 (*o*-C), 126.2 (*m*-C), 122.3 (*p*-C). Isomer **9-C** rearranges upon standing at 0 °C for one month to form isomer **9-A** quantitatively.

Acknowledgments

Financial support from the Fonds der Chemischen Industrie, the Bundesminister für Bildung, Wissenschaft, Forschung und Technologie (BMBF), and the Deutsche Forschungsgemeinschaft is gratefully acknowledged.

[1] Review: K. Severin, R. Bergs, W. Beck, *Angew. Chem.* **1998**, *110*, 1723; *Angew. Chem. Int. Ed. Engl.* **1998**, *37*, 1634.

[2] See for example: P. Köpf-Meier, H. Köpf, *Chem. Rev.* **1987**, *87*, 1137. I. Haiduc, C. Silvestru, *Coord. Chem. Rev.* **1990**, *99*, 253. H. Sun, H. Li, R. A. Weir, P. J. Sadler, *Angew. Chem.* **1998**, *110*, 1622; *Angew. Chem. Int. Ed. Engl.* **1998**, *37*, 1577, and references cited in these articles.

[3] [3a] M. Oberhoff, L. Duda, J. Karl, R. Mohr, G. Erker, R. Fröhlich, M. Grehl, *Organometallics* **1996**, *15*, 4005 and references cited therein. − [3b] M. Oberhoff, G. Erker, R. Fröhlich, *Chem. Eur. J.* **1997**, *3*, 1521.

[4] [4a] R. F. Jordan, W. E. Dasher, S. F. Echols, *J. Am. Chem. Soc.* **1986**, *108*, 1718. R. F. Jordan, C. S. Bajgur, R. Willet, B. Scott, *J. Am. Chem. Soc.* **1986**, *108*, 7410. S. L. Borkowsky, R. F. Jordan, G. D. Hinch, *Organometallics* **1991**, *10*, 1268. − [4b] Review: R. F. Jordan, *Adv. Organomet. Chem.* **1991**, *32*, 325.

[5] For other representative examples of group-4 metal complexes with amino acid or peptide derivatives see e.g.: C. J. Cardin, A. Roy, *Inorg. Chim. Acta* **1985**, *107*, L33. A. Schäfer, E. Karl, L. Zsolnai, G. Huttner, H.-H. Brintzinger, *J. Organomet. Chem.* **1987**, *328*, 87. J. Recht, B. I. Cohen, A. S. Goldman, J. Kohn, *Tetrahedron Lett.* **1990**, *31*, 7281. T. M. Klapötke, H. Köpf, I. C. Tornipoerth-Oetting, P. S. White, *Angew. Chem.* **1994**, *106*, 1587; *Angew. Chem. Int. Ed. Engl.* **1994**, *33*, 1518; *Organometallics* **1994**, *13*, 3628. I. C. Tornipoerth-Oetting, P. S. White, *Organometallics* **1995**, *14*, 1632. K. Severin, W. Beck, G. Trojandt, K. Polborn, W. Steglich, *Angew. Chem.* **1995**, *107*, 1570; *Angew. Chem. Int. Ed. Engl.* **1995**, *34*, 1449. D. A. Gately, J. R. Norton, *J. Am. Chem. Soc.* **1996**, *118*, 3479.

[6] For related methane elimination reactions see e.g.: [6a] A. Bertuleit, C. Fritze, G. Erker, R. Fröhlich, *Organometallics* **1997**, *16*, 2891. − [6b] J. M. Meyer, C. J. Curtis, J. E. Bercaw, *J. Am. Chem. Soc.* **1983**, *115*, 2651. S. L. Buchwald, B. T. Watson, M. W. Wannamaker, C. Dewan, *J. Am. Chem. Soc.* **1989**, *111*, 4486. N. Coles, M. C. J. Harris, R. J. Whitby, J. Blagg, *Organometallics* **1994**, *13*, 190. − [6c] B. Temme, G. Erker, *J. Organomet. Chem.* **1995**, *488*, 177. D. Röttger, G. Erker, R. Fröhlich, S. Kotila, *J. Organomet. Chem.* **1996**, *518*, 17. A. D. Horton, *Organometallics* **1996**, *15*, 2675.

[7] For other examples of amidate (and amidinate) ligands at Zr see: [7a] G. Erker, K. Berg, *J. Organomet. Chem.* **1984**, *263*, 37. S. Gambarotta, S. Strogolo, C. Floriani, A. Chiesi-Villa, C. Guastini, *J. Am. Chem. Soc.* **1985**, *107*, 6278; *Inorg. Chem.* **1985**, *24*, 654. M. Vivanco, J. Ruiz, C. Floriani, A. Chiesi-Villa, C. Rizzoli, *Organometallics* **1993**, *12*, 1794. − [7b] R. Duchateau, A. Meetsma, H. J. Teuben, *Organometallics* **1996**, *15*, 1565. R. Duchateau, C. T. van Wee, A. Meetsma, P. T. van Duijnen, H. J. Teuben, *Organometallics* **1996**, *15*, 2279. R. Kempe, S. Brenner, P. Arndt, *Organometallics* **1996**, *15*, 1071. D. Walther, R. Fischer, M. Friedrich, P. Gebhardt, H. Görls, *Chem. Ber.*

1996, *129*, 1389. A. Littke, N. Sleiman, C. Bensimon, D. S. Richeson, G. P. A. Yap, S. J. Brown, *Organometallics* **1998**, *17*, 446. J. R. Hagadorn, J. Arnold, *Angew. Chem.* **1998**, *110*, 1813; *Angew. Chem. Int. Ed. Engl*. **1998**, *37*, 1729.

[8] Prepared by treatment of the amino acid or peptide ester with trichloromethyl chloroformate ("phosgene dimer"): S. Goldschmidt, M. Wick, *Justus Liebigs Ann. Chem*. **1952**, *575*, 217. Y. Iwakura, K. Uno, S. Kang, *J. Org. Chem*. **1965**, *30*, 1158. H. Jeschkeit, G. Losse, K. Neubert, *Chem. Ber*. **1966**, *99*, 2803. J. S. Nowick, N. A. Powell, T. M. Nguyen, G. Noronha, *J. Org. Chem*. **1992**, *57*, 7364.

[9] The oligopeptide derivatives were prepared by conventional methods: M. Bodanszky, *Peptide Chemistry*, Springer, Berlin, **1993**. M. Bodanszky, A. Bodanszky, *The Practice of Peptide Synthesis*, Springer, Berlin, **1994**. L. A. Carpino, M. Beyermann, H. Wenschuh, M. Bienert, *Acc. Chem. Res.* **1996**, *29*, 268, and references cited in these articles.

[10] S. Braun, H. Kalinowski, S. Berger, *100 and More Basic NMR Experiments*, VCH, Weinheim, **1996**, and references cited therein.

[11] [11a] Y. Ariyoshi, *Bull. Chem. Soc. Jpn*. **1984**, *57*, 3197. – [11b] J. C. Sheehan, G. P. Hess, *J. Am. Chem. Soc.* **1955**, *77*, 1067. R. König. W. Geiger, *Chem. Ber*. **1970**, *103*, 788, 2024, 2034.

Received February 19, 1999
[I99058]

Anti-Markonikov Reactions, 6[+]

Rhodium-Catalyzed Amination of Vinylpyridines: Hydroamination versus Oxidative Amination

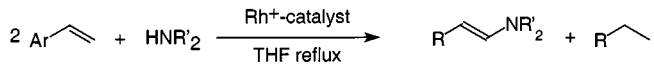
Matthias Beller,*[a,b] Harald Trauthwein,[b] Martin Eichberger,[†] Claudia Breindl,[b] and Thomas E. Müller[b]

Keywords: Coordination chemistry / Rhodium / Aminations / Hydroaminations / Oxidative aminations / Vinylpyridines

Cationic rhodium complexes catalyze the amination of 2- and 4-vinylpyridine with secondary amines. Depending on the substrate and the reaction conditions either oxidative amination to yield the corresponding enamines **1a−8a** or hydroamination to give 2-aminoethylpyridines **1b−8b** occurs. In all cases products with anti-Markovnikov regioselectivity are obtained. For mechanistic studies novel cationic complexes of rhodium(I)-containing cyclooctadiene and vinylpyridine **12** as well as complexes containing cyclooctadiene, vinylpyridine, and morpholine **13** were prepared and characterized by NMR spectroscopy and X-ray diffraction analysis.

Introduction

The construction of carbon−nitrogen bonds by using transition metal catalysts, especially for the synthesis of amines, has become an area of intensive research. Catalytic aminations of olefins[2] to selectively give primary, secondary, or tertiary amines are particularly interesting because of the atom efficiency of the process and the availability of feedstocks. One of the few examples is the newly developed intermolecular oxidative amination of aromatic olefins to give enamines.[3] Interestingly, this reaction yields the anti-Markovnikov products in a highly selective manner (Scheme 1).



Ar = aryl; R' = aryl, alkyl

Scheme 1. Anti-Markovnikov oxidative amination of styrene

This amination process allows the conversion of simple monoamines, such as piperidine and diethylamine, into the corresponding ω-enamines in good yields by employing cationic (phosphane)rhodium complexes as catalysts. An additional equivalent of the aromatic olefin is concurrently reduced to ethylbenzene. For the first time the transition-metal-catalyzed hydroamination of styrene is possible in an anti-Markovnikov manner with amines, such as morpholine, that contain a hemilabile second coordination site.[1]

In connection with mechanistic studies to understand the features that control whether hydroamination or oxidative amination of olefins occurs, we became interested in the reaction of vinylpyridines. Additional interest in these reactions results from the fact that 2-(2′-aminoethyl)pyridines are used as building blocks for pharmaceuticals and fine chemicals for hydrometallurgy.[4]

In contrast to styrene, 2- and 4-vinylpyridine are Michael systems, i.e. the double bond is in conjugation with an electron-withdrawing group. This activation favors the anti-Markovnikov hydroamination of 2- and 4-vinylpyridine. However, in contrast to acrylamide or acrylnitrile, which react quantitatively with amines without a catalyst even under mild conditions, 2- and 4-vinylpyridine react only sluggishly without a catalyst due to the weaker electron-withdrawing effect of the pyridine ring.

The hydroamination of vinylpyridines was first reported in the late 1940s.[5] Typically, the hydroamination of vinylpyridines is catalyzed by either acid or base.[6] For example, Matusko et al. obtained good results with vinylpyridines by employing a mixture of methanol and acetic acid.[7] However, some amines, like pyrrolidine, are not basic enough to react under these conditions. Successful amination of 2-vinylpyridine occurs when the reaction is performed with the addition of catalytic sodium metal in order to generate the more nucleophilic amide.[8] Surprisingly, the use of transition metal catalysts in the amination of vinylpyridines is rare.[9]

In this report we present for the first time various amination reactions of 2- and 4-vinylpyridines using cationic rhodium catalysts. Depending on the reaction conditions, varying amounts of hydroamination and oxidative amination products are obtained. In order to understand the mechanistic background, new cationic rhodium complexes that contain 2-vinylpyridine as a ligand have been isolated and characterized by X-ray crystallography. These complexes are shown to be important intermediates in the catalytic hydroamination of vinylpyridines.

[+] Part 5: Ref.[1]

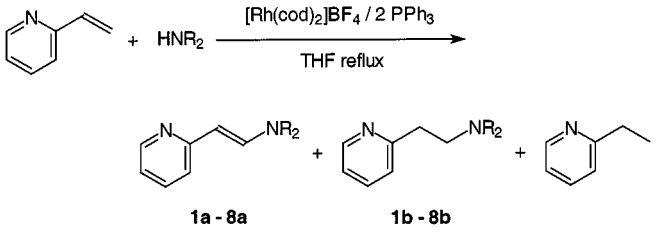
[a] Institut für Organische Katalyseforschung (IfOK) an der Universität Rostock e.V.,
Buchbinderstraße 5−6, D-18055 Rostock, Germany
[b] Anorganisch-chemisches Institut, Technische Universität München,
Lichtenbergstraße 4, D-85747 Garching, Germany
[†] Deceased 1997.

 © WILEY-VCH Verlag GmbH, D-69451 Weinheim, 1999 1434−1948/99/0707−1121 $ 17.50+.50/0

Results and Discussion

Catalytic Amination of 2- and 4-Vinylpyridine

Cationic (phosphane)rhodium complexes such as $[Rh(cod)_2]BF_4/2\ PPh_3$ are the only known class of active transition metal catalysts for the intermolecular anti-Markovnikov amination and hydroamination of styrenes.[2] In order to investigate how these catalysts effect the amination of a more activated olefin the reaction of 2-vinylpyridine with piperidine was chosen for initial studies (Scheme 2). Under the typical reaction conditions of the oxidative amination of styrene (THF reflux, 2.5 mol-% $[Rh(cod)_2]BF_4$/ 2 PPh_3, 20 h) three products are obtained. The major product, *N*-[2-(2′-pyridyl)ethyl]piperidine (**2b**), resulting from a hydroamination reaction, was isolated in 53% yield. Also, for the first time an intermolecular oxidative amination of 2-vinylpyridine was achieved giving *N*-[2-(2′-pyridyl)ethenyl]piperidine (**2a**) in 47% yield. A second equivalent of 2-vinylpyridine is concurrently reduced to 2-ethylpyridine, which was isolated in 42% yield. All yields are based on piperidine.



Scheme 2. Rhodium-catalyzed amination of 2-vinylpyridine

As expected, all amination reactions occur exclusively with anti-Markovnikov regioselectivity. This is explained by the strong polarization of the vinyl group by the pyridine ring. When the reaction is performed under identical conditions without a catalyst the hydroamination product *N*-[2-(2′-pyridyl)ethyl]piperidine is obtained in only 3% yield. Hence, both the hydroamination and the oxidative amination are catalyzed by the cationic rhodium catalyst.

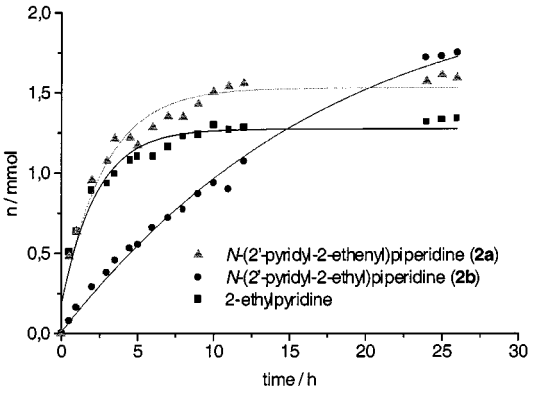


Figure 1. Time/concentration diagram for the reaction of 2-vinylpyridine and piperidine

In a further catalysis experiment the reaction of piperidine with 2-vinylpyridine to form the different amination products was followed with time. As depicted in Figure 1 it is evident that enamine and ethylpyridine are formed mainly during the first hours. After about 10 h, no further enamine formation is observed. In contrast, only a small amount of aminoalkylpyridine is formed at the beginning of the reaction, but the rate of its formation remains nearly constant until all piperidine is consumed. Similar to the oxidative amination of styrene, the enamine formation is probably catalyzed by cationic rhodium species that contain monodentate phosphane ligands. During the course of the reaction the rhodium catalyst is deactivated, either by loss of its cationic character or by the formation of chelate complexes with the products behaving as bidentate ligands. Independent of the oxidative amination process, the formation of the alkylamine proceeds by a different mechanism. In order to gain further insight into the different reaction pathways and to evaluate the critical reaction parameters for both oxidative amination and hydroamination we varied the catalyst system and the reaction conditions (Table 1).

The oxidative amination proceeds best with THF as the solvent (entries 1, 6). The catalyst is also active in toluene, although the formation of alkylamine is increased (entry 2). The dipolar aprotic solvent dimethylacetamide (DMAC) completely inhibits the enamine formation and lowers the yield of alkylamine (entry 3). By reducing the amount of catalyst from 2.5 mol-% to 1 mol-% (entry 1 vs. 4) it is shown that the oxidative amination is more sensitive than the hydroamination to the concentration of the cationic catalyst. This is a good indication that the hydroamination reaction is catalyzed by various rhodium species, while the oxidative amination is catalyzed by a discrete cationic (phosphane)rhodium complex. Further support for this assumption comes from the fact that the presence of phosphane is a prerequisite for enamine formation (entry 5). In the presence of $[Rh(cod)_2]BF_4$ without triphenylphosphane, only hydroamination occurs to give *N*-[2-(2′-pyridyl)ethyl]-piperidine (**2b**) in high yields (97%). By lowering the ratio of vinylpyridine to piperidine to 2:1 the oxidative amination becomes the major reaction pathway and *N*-[2-(2′-pyridyl)ethenyl]piperidine (**2a**) is isolated in 82% yield (entry 6). The different influence of the olefin/amine ratio on the oxidative amination of styrenes and 2-vinylpyridines can be explained by the different coordination ability of styrene and 2-vinylpyridine. 2-Vinylpyridine is able to coordinate to the rhodium center through the pyridine-nitrogen atom, which is not possible for styrene. The coordination of the nitrogen atom of pyridine activates the olefinic bond in 2-vinylpyridine for a nucleophilic attack of the amine, which enhances hydroamination but has no effect on the oxidative amination. In contrast, we assume that the oxidative amination proceeds by an amine-activation mechanism. A lower concentration of 2-vinylpyridine would favor the coordination of the amine to the rhodium center, which facilitates N−H activation.

In order to investigate the influence of pK_a, steric and electronic parameters of the amines on the amination reaction, we tested different aliphatic amines R_2NH, such as piperazines, which have an additional functional group (Table 2).

Table 1. Rhodium-catalyzed reaction of 2-vinylpyridine and piperidine[a]

Entry	Olefin/Amine	Catalyst (mol-%)	Solvent, reaction time	Amine product (%)	Enamine (%)	Ethylpyridine (%)	Amine product/Enamine
1	4:1	$[Rh(cod)_2]BF_4$/2 PPh_3 (2.5)	THF, reflux, 20 h	53	47	42	1.1
2	4:1	$[Rh(cod)_2]BF_4$/2 PPh_3 (2.5)	Toluene, reflux, 20 h	61	30	24	2.0
3	4:1	$[Rh(cod)_2]BF_4$/2 PPh_3 (2.5)	DMAC, 140 °C, 20 h	44	< 0.1	21	–
4	4:1	$[Rh(cod)_2]BF_4$/2 PPh_3 (1.0)	THF, reflux, 20 h	47	8	7	5.9
5	4:1	$[Rh(cod)_2]BF_4$ (2.5)	THF, reflux, 20 h	97	2	2	48.5
6	2:1	$[Rh(cod)_2]BF_4$/2 PPh_3 (2.5)	THF reflux, 20 h	16	82	46	0.2

[a] The yield was determined by GC with hexadecane as internal standard and is referred to amine.

Table 2. Rhodium-catalyzed amination of 2-vinylpyridine with aliphatic amines[a]

Entry	Amine (pK_a)[23]	Enamine (%)	Amine product[b] (%)	Ethylpyridine (%)	Amine product/Enamine
1	Pyrrolidine (11.27)	54 [**1a**]	21 (3) [**1b**]	56	0.4
2	Piperidine (11.02)	47 [**2a**]	53 (8) [**2b**]	42	1.1
3	Hexahydroazepine	30 [**3a**]	29 (< 1) [**3b**]	25	1.0
4	Morpholine (8.33)	2 [**4a**]	98 (5) [**4b**]	2	49
5	Thiomorpholine	< 1	98 (26) [**5b**]	< 1	> 99
6	Piperazine (9.83)	[c]	[c]	[c]	–
7	*N*-Methylpiperazine	20 [**7a**]	62 (6) [**7b**]	23	3.1
8	*N*-Phenylpiperazine	8 [**8a**]	91 (10) [**8b**]	6	11.4
9a–c	HNR_2, R = Et (10.49), *i*Pr, *n*Bu	< 1	< 1	< 1	–
10	*n*-Butylamine	< 1	< 1	< 1	–

[a] 2-Vinylpyridine/amine = 4:1, 2.5 mol-% $[Rh(cod)_2]BF_4$/2 PPh_3 referred to amine, THF reflux, 20 h. The yield was determined by GC with hexadecane as internal standard and is referred to amine. – [b] The results of the uncatalyzed reaction under the same conditions as the rhodium-catalyzed reaction are shown in parentheses. – [c] The reaction of piperazine is shown in Scheme 3.

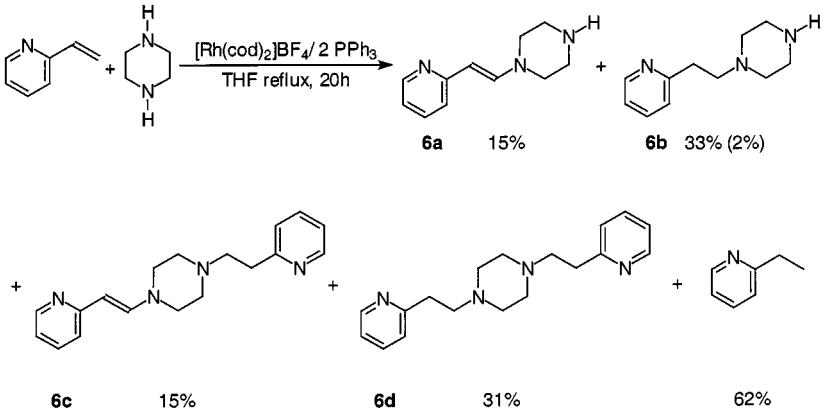
The reactions were performed in refluxing THF for 20 h. In all cases only the 2-(2′-aminoethyl)pyridine derivatives were detected as hydroamination products due to the polarization of the double bond. The yields, which were obtained without a catalyst, are given in brackets. Apart from thiomorpholine the amines reacted only to a slight extent (< 10%) without a catalyst. Also, no oxidative amination was observed, i.e. neither the corresponding enamine nor ethylpyridine was formed. Comparing the ring size of the amine applied (pyrrolidine, piperidine, and hexahydroazepine) it is evident that the yield of the oxidative amination product decreases with increased ring size of the amine, with pyrrolidine providing the highest yield in enamine. Bifunctional amines predominantly led to hydroamination reactions. It is likely that the conformation favored by the chelating effect infers the β-H-elimination step that is required for oxidative amination. Interestingly, enamine formation was observed to some extent with all three piperazine derivatives. This is in contrast to the rhodium-catalyzed amination of styrene and piperazine derivatives. In the latter reaction chelating amines inhibit the reaction, which is caused by the formation of insoluble (piperazine)rhodium complexes.[10] Thus, we assume that the amination of 2-vinylpyridine proceeds by activation of the 2-vinylpyridine.

Piperazine, which has two reactive N–H groups, leads to the formation of five different products (Scheme 3). Apart from 2-ethylpyridine, mono- and dialkylated piperazines **6a–d** were obtained in a ratio of 2.2:1:2.1:1.

The ratio of hydroamination products **6b** and **6d** to enamines **6a** and **6c** is approximately 2:1. Surprisingly, no product with two enamine groups was detected. Hence, it is assumed that the dialkylated products are formed mainly by a consecutive reaction of *N*-[2-(2′-pyridyl)ethyl]piperazine. This might be due to the better coordination ability of *N*-[2-(2′-pyridyl)ethyl]piperazine (**6b**) in comparison to *N*-[2-(2′-pyridyl)ethenyl]piperazine (**6a**).

In addition to aliphatic amines, we tested aromatic amines (aniline, pyrrole) as well as amides (acetamide) in the rhodium-catalyzed amination of 2-vinylpyridines. Unfortunately, these substrates did not react in either a hydroamination or in an oxidative reaction. We explain this behavior as being due to the lower pK_a value of these substrates compared to that of 2-vinylpyridine [pK_a(pyridine) = 5.2]. Due to the lower nucleophilicity, hydroamination does not occur even after activation of vinylpyridine. Oxidative amination is not observed because the formation of (amine)rhodium complexes is unfavorable. Hence, N–H activation by the rhodium center is not possible.

Next, we studied the reaction of 4-vinylpyridine with three amines (Table 3). None of the amines reacted with 4-vinylpyridine in the absence of a rhodium catalyst. In the presence of the catalyst system $[Rh(cod)_2]BF_4$/2 PPh_3 all



Scheme 3. Reaction of 2-vinylpyridine and piperazine; the yields obtained without catalyst are given in parentheses

Table 3. Rhodium-catalyzed amination of 4-vinylpyridine with aliphatic amines[a]

Entry	Amine	Enamine (%)	Pyridylamine (%)	Ethylpyridine (%)
1	Piperidine	< 1	57 [**9**]	< 1
2	Hexahydroazepine	< 1	21 [**10**]	< 1
3	Morpholine	< 1	54 [**11**]	< 1

[a] 4-Vinylpyridine/amine = 4:1, 2.5 mol-% $[Rh(cod)_2]BF_4$/2 PPh_3 referred to amine, THF reflux, 20 h. The yield is referred to amine and was determined by GC with hexadecane as internal standard.

amines employed gave only the terminal hydroamination products **9**, **10**, **11**. Oxidative amination was not observed. It is evident that for oxidative amination to occur both the nitrogen atom of the pyridine ring and the vinyl group have to be in steric proximity to the rhodium center.

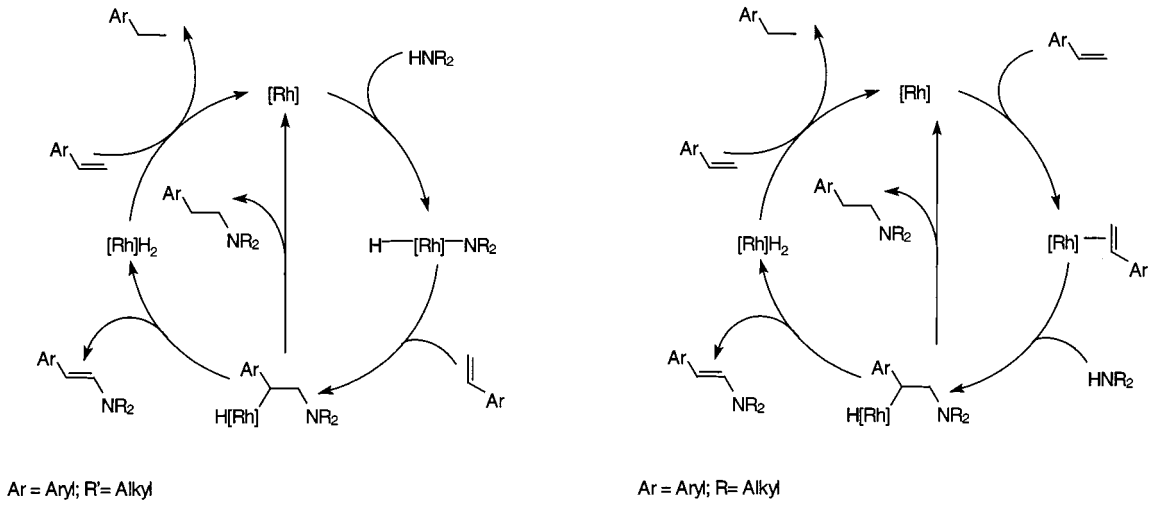
Mechanistic Studies − Cationic Rhodium Complexes with 2-Vinylpyridine as Ligand

Amination of olefins can take place either by activation of the olefin or by activation of the amine N−H bond.[11] In general, non-functionalized olefins become susceptible towards nucleophiles upon complexation to an electrophilic metal center. Addition of a nucleophile to the metal-bound olefin and protolysis yields the corresponding product and the catalyst. Alternatively, β-hydride elimination results in the formation of imines or enamines. It is important to note that catalytic activation of olefins in the presence of amines is difficult to achieve due to the strong binding of amines to electrophilic metal centers. One possible amine activation pathway involves oxidative addition of an amine to an unsaturated metal center in a low oxidation state. The resulting amido hydrido complex may insert an olefin into the metal−nitrogen bond yielding an aminoalkyl hydrido complex. Subsequent reductive elimination of the amine produced regenerates the catalyst. Alternatively, β-hydride elimination can take place to give enamines and dihydridometal complexes.

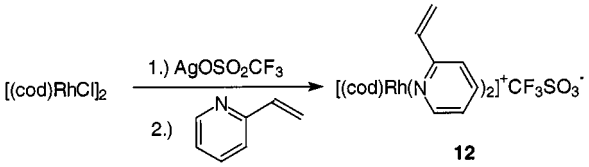
In contrast to other olefins, vinylpyridines can be activated by cationic rhodium complexes either by coordination of the double bond, the heteroaromatic ring or by coordination of the nitrogen atom. As suggested above, the mode of coordination of the vinylpyridine is of fundamental importance for explaining the various results obtained in the amination of 2- and 4-vinylpyridine. Therefore, we investigated the coordination chemistry of cationic rhodium complexes with amines and 2-vinylpyridine as ligands.

In contrast to the organometallic chemistry of cationic rhodium complexes with secondary amines that has been described recently,[10] rhodium complexes with 2-vinylpyridine as a ligand have not been studied in detail. Denise and Pannetier described the synthesis of $[Rh(cod)(2\text{-vinylpyridine})_2]PF_6$ by treatment of $[Rh(cod)Cl]_2$ with 2-vinylpyridine and $NaPF_6$.[12] However, no detailed characterization by NMR and X-ray studies of this complex has been performed. Therefore, we synthesized $[Rh(cod)(2\text{-vinylpyridine})_2]OSO_2CF_3$ (**12**) by combining $[Rh(cod)Cl]_2$ and $AgOSO_2CF_3$ followed by addition of 2-vinylpyridine.

At room temperature the ^{1}H-NMR spectrum (Figure 2) of **12** shows several broad resonances indicating fluxionality in the molecule. The signals at $\delta = 8.9$ and 8.7 are assigned to 6-H in the pyridine ring and the internal proton of the olefin, respectively. The other signals in the olefinic and aromatic region of the ^{1}H-NMR spectrum are sharper and are ascribed to 4-H ($\delta = 7.66$), 3-H ($\delta = 7.55$), and 5-H ($\delta = 7.32$). The terminal olefinic protons of the vinyl group show resonances at $\delta = 6.05$. Clearly, the protons that are adjacent to the rhodium center have broader signals compared to the protons that are further away from the metal center. The resonances of both the olefinic protons at $\delta = 4.0$ and the two sets of aliphatic protons of the cod ligand at $\delta = 2.7$ and 2.0 are very broad at room temperature, which is most likely caused by free rotation of the 2-vinylpyridine. Upon cooling **12** to −60°C the broad signals in the ^{1}H-NMR spectrum sharpen to give clearly distinguishable signals. It is interesting to note that the resonances of the olefins show a vicinal and geminal coupling of $J = 11$



Scheme 4. Catalytic cycles for the amination of aromatic olefins by (a) amine activation and (b) olefin activation



Scheme 5. Synthesis of the cationic complex [Rh(cod)(2-vinylpyridine)$_2$]CF_3SO_3 (**12**)

and 17 Hz, respectively. The signals of the cod protons, which appear as three sharp pseudo-doublets, can be used as a probe for the conformation of **12**. Due to steric reasons, both vinyl groups should be opposite to each other.

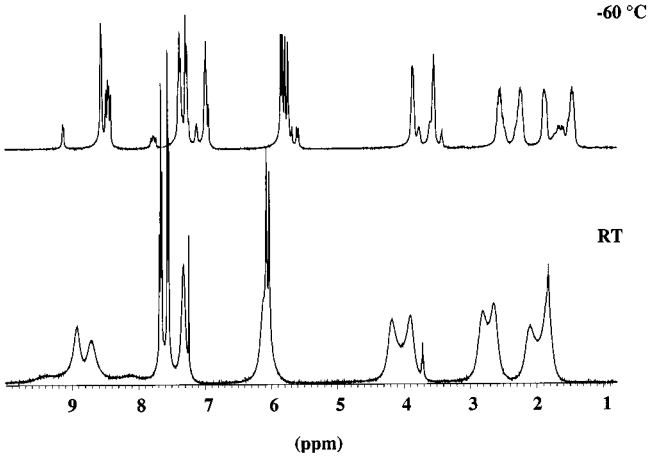


Figure 2. ^{1}H-NMR spectrum of [Rh(cod)(2-vinylpyridine)$_2$]CF_3SO_3 at room temperature and at −60°C in $CDCl_3$

The ^{13}C-NMR spectrum supports this conformational analysis. At room temperature the resonances of the olefinic carbon atoms of the cod ligand are very broad. However, at −60°C two doublets appear, due to the Rh-C coupling ($J_{Rh\text{-}C}$ = 12.6 and 11.7 Hz). This confirms that the olefinic carbon atoms are not identical. Also, there is no interaction between the vinyl group of the 2-vinylpyridine and the rhodium center, as no Rh-C coupling was detected here.

In both the ^{1}H-NMR and the ^{13}C-NMR spectra a second set of patterns (5% intensity) appears upon lowering the temperature. We tentatively ascribe this minor pattern to a rhodium species with pyridine rings, where both vinylic groups are pointing in the same direction.

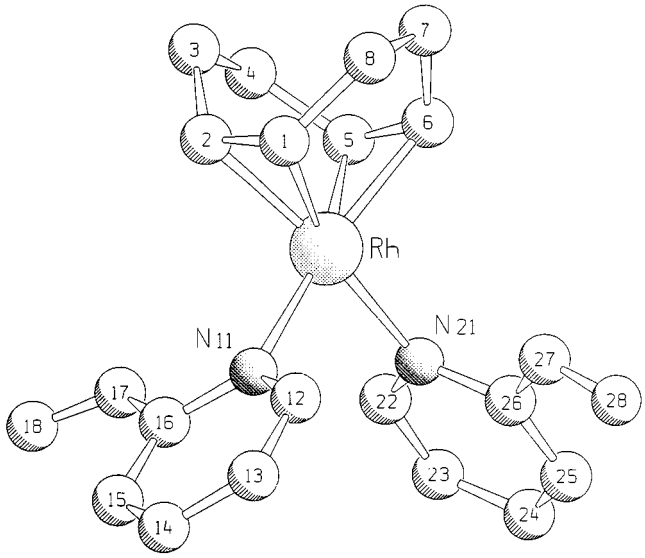


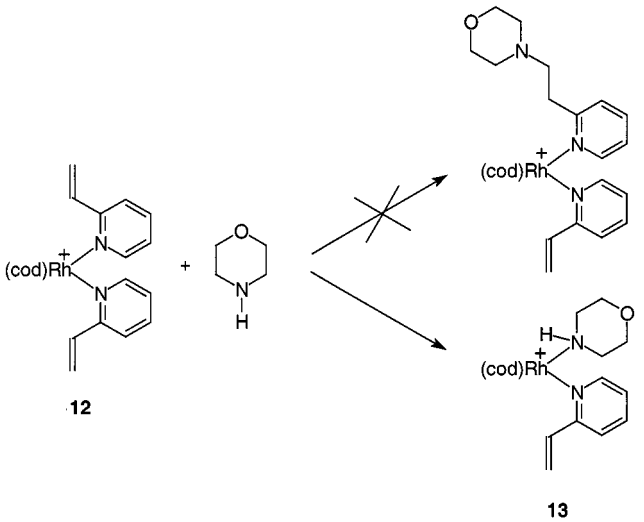
Figure 3. The molecular structure of [Rh(cod)(2-vinylpyridine)$_2$]$^+$

Crystals of **12** were obtained by slowly adding diethyl ether to a dichloromethane solution of **12**. The X-ray analysis (Table 4) is in agreement with the conformation discussed on the basis of the NMR studies. The rhodium center is in an approximately square-planar coordination sphere. The lengths of the rhodium−amine bonds [Rh−N11 = 2.129(2) Å and Rh−N21 = 2.118(3) Å] and the distances from rhodium to the centers X1 and X2 of the cod double bonds C1−C2 and C5−C6 (Rh−X1 = 2.019 Å, Rh−X2 = 2.018 Å) are within the typical range. The angles X1−Rh−X2 (87.6°) and N11−Rh−N21 [89.2(1)°] are close to right angles. The coordination sphere is distorted tetraedric. Associated distances from a mean plane contain-

Table 4. Selected bond lengths [Å] and angles [°] of [Rh(cod)(2-vinylpyridine)$_2$]CF_3SO_3 (**12**)

Rh−N(11)	2.129 (2)	Rh−N(21)	2.118 (3)
Rh−C(1)	2.122 (4)	Rh−C(2)	2.139 (3)
Rh−C(5)	2.121 (3)	Rh−C(6)	2.143 (3)
C(1)−C(2)	1.385 (5)	C(5)−C(6)	1.386 (6)
C(17)−C(18)	1.303 (6)	C(27)−C(28)	1.308 (6)
N(11)−Rh−C(2)	92.42 (11)	N(11)−Rh−C(6)	163.90 (13)
N(21)−Rh−C(1)	157.70 (13)	N(21)−Rh−C(2)	164.34 (13)
N(21)−Rh−C(5)	91.04 (14)	N(21)−Rh−C(6)	92.74 (14)
N(11)−Rh−N(21)	89.23 (10)	N(11)−C(16)−C(17)	117.4 (3
N(21)−C(26)−C(27)	117.2 (3)	C(1)−Rh−C(2)	37.93 (14)
C(1)−Rh−C(5)	97.9 (2)	C(1)−Rh−C(6)	82.2 (2)
C(1)−Rh−N(11)	89.94 (12)	C(2)−Rh−C(5)	81.7 (2)
C(2)−Rh−C(6)	90.0 (2)	C(5)−Rh−C(6)	37.9 (2)
C(5)−Rh−N(11)	158.06 (13)		

ing the rhodium atom are X1 +0.057 Å, X2 −0.061 Å, N21 +0.053 Å and N11 −0.057 Å. The 2-vinylpyridine ligands are arranged perpendicular to the coordination plane (82.1°, 89.2°), so that both ring systems are also perpendicular to each other (88.2°). The vinylic groups are on opposite sides of the coordination plane and are slightly twisted against the parent aromatic ring (5.9° and 13.6° for the vinyl group defined by C16, C17, C18 and C26, C27, C28, respectively). There is no coordinative interaction of the vinylic group in the two 2-vinylpyridine ligands with the rhodium center. This is confirmed by a shorter vinylic double bond [C17−C18 = 1.303(6) Å, C27−C28 = 1.308(6) Å] compared to the double bonds in the cod ligand [C1−C2 = 1.385(5) Å, C5−C6 = 1.386(6) Å].



Scheme 6. Reaction of [Rh(cod)(2-vinylpyridine)$_2$]CF_3SO_3 (**12**) with morpholine

Cationic rhodium complexes containing an amine as well as a 2-vinylpyridine ligand are likely intermediates in the catalytic cycle of the amination of 2-vinylpyridine. In order to gain more insight into this system we studied the stoichiometric reaction of [Rh(cod)(2-vinylpyridine)$_2$]CF_3SO_3 (**12**) with 2 equivalents of morpholine. The reaction led to [Rh(cod)(morpholine)(2-vinylpyridine)]CF_3SO_3 (**13**), which was formed in 84% yield (Scheme 6). This is confirmed by mass spectrometry and elemental analysis as well as by IR spectroscopy, where a strong N−H frequency at 3215 cm^{-1} is observed. Interestingly, there is no indication for an attack of the amine on the activated vinyl group of the 2-vinylpyridine.

The ease of formation of the (morpholine)(2-vinylpyridine)rhodium complexes suggests that these complexes are precursors for the intermediates in the catalytic cycle.

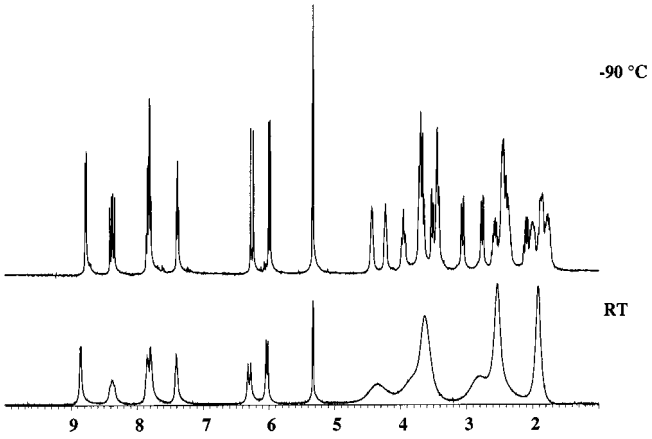


Figure 4. ^{1}H-NMR spectrum of [Rh(cod)(morpholine)(2-vinylpyridine)]CF_3SO_3 (**13**) at room temperature and at −90°C in CD_2Cl_2

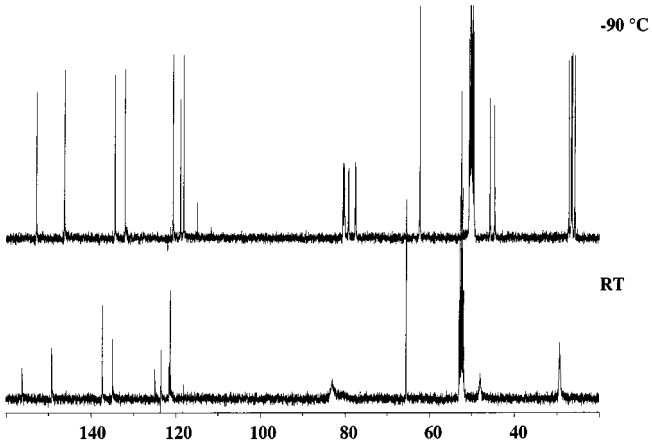


Figure 5. ^{13}C-NMR spectrum of [Rh(cod)(morpholine)(2-vinylpyridine)]CF_3SO_3 (**13**) at room temperature and −90°C in $CDCl_3$

The ^{1}H- and ^{13}C-NMR spectra of [Rh(cod)(morpholine)(2-vinylpyridine)]CF_3SO_3 (**13**) are depicted in Figures 4 and 5, respectively. The signals in the ^{1}H-NMR spectrum at room temperature are broad, especially in the aliphatic region. ^{1}H-NMR analysis at −90°C shows sharper signals, which indicates the existence of a preferential conformation. The splitting of the resonances reveals interesting details about the preferred low-temperature conformation. The multiplets at δ = 3.67 and 3.43 are assigned to the olefinic cod protons as well as the protons of the morpholine protons adjacent to the oxygen atom. There is also a splitting of the resonance of the methylene group of the morpholine ligand adjacent to the nitrogen atom with signals observed at δ = 3.05 and 2.75.

The ^{13}C-NMR spectrum shows similar behavior. The olefinic and the aliphatic cod resonances are very broad at room temperature, but at −90°C the broad olefinic signal at δ = 82.9 is split into four doublets, while the broad aliphatic signal at δ = 29.3 is split into four singlets. Information about the conformation of the morpholine ligand can be obtained from the ^{13}C-NMR spectrum at −90°C. The signal of the methylene group adjacent to the oxygen atom is a singlet, whereas the resonance of the methylene group adjacent to the nitrogen atom is a doublet. The latter methylene groups seem to be influenced by the 2-vinylpyridine ring, whereas the methylene groups adjacent to the oxygen atom in the morpholine ligand are too far away from the pyridine ring for the resonance to be split. Complex **13** was also characterised by X-ray crystallography. The molecular structure of **13** is shown in Figure 6 and selected bond lengths and angles are summarized in Table 5.

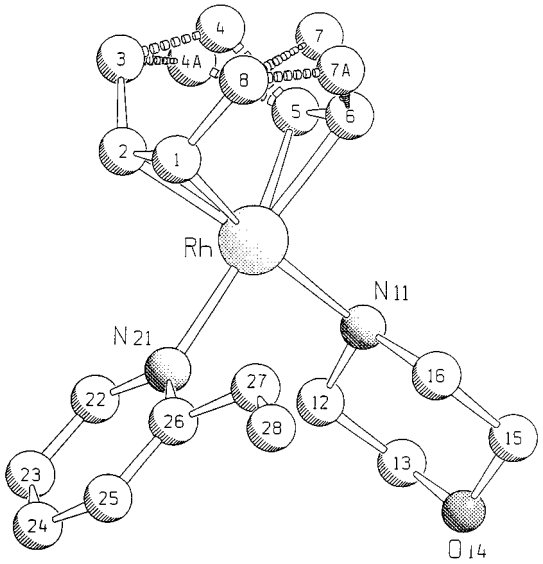


Figure 6. The molecular structure of [Rh(cod)(morpholine)-(2-vinylpyridine)]$^{+}CF_3SO_3^{-}$

Table 5. Selected bond lengths [Å] and angles [°] of [Rh(cod)(morpholine)(2-vinylpyridine)]CF_3SO_3 (**13**)

Rh−C(1)	2.132(3)	Rh−C(2)	2.139(3)
Rh−C(5)	2.123(3)	Rh−C(6)	2.111(3)
Rh−N(11)	2.155(2)	Rh−N(21)	2.129(3)
C(1)−C(2)	1.360(5)	C(5)−C(6)	1.360(6)
C(27)−C(28)	1.310(6)		
C(1)−Rh−C(2)	37.12(14)	C(1)−Rh−C(5)	94.4(2)
C(1)−Rh−C(6)	82.26(14)	C(1)−Rh−N(11)	162.78(13)
C(2)−Rh−C(5)	81.01(13)	C(2)−Rh−C(6)	92.33(14)
C(2)−Rh−N(11)	160.00(12)	C(5)−Rh−C(6)	37.5(2)
C(5)−Rh−N(11)	90.60(12)	C(5)−Rh−N(21)	157.1(2)
C(6)−Rh−N(11)	91.89(12)	C(6)−Rh−N(21)	165.0(2)
C(12)−N(11)−Rh	115.0(2)	C(16)−N(11)−Rh	112.7(2)
C(16)−N(11)−C(12)	109.5(2)	N(21)−Rh−C(1)	90.46(12)
N(21)−Rh−C(2)	89.65(11)	N(21)−Rh−N(11)	91.30(9)
N(21)−C(26)−C(27)	115.3(3)		

The rhodium center is coordinated in a square-planar fashion with the bond lengths Rh−N11 = 2.155(2) Å and Rh−N21 = 2.129(3) Å, as expected for cationic amine−-rhodium bonds.[10] The bond lengths from rhodium to the centers X1 and X2 of the two double bonds C1−C2 and C5−C6 associated with the cod ligand are 2.023 Å and 2.007 Å, respectively. Each ligand around the rhodium center is arranged nearly perpendicular to the two neighbors with X1−Rh−X2 = 87.4°, X2−Rh−N11 = 91.3°, N11−Rh−N21 = 91.3(1)° and N21−Rh−X1 = 89.9°. There is a slight pyramidal distortion, which can be seen by positive distances for each of the coordinating atoms from a plane through the rhodium center (X1 +0.022 Å, X2 +0.075 Å, N11 +0.027 Å and N21 +0.073 Å). The 2-vinylpyridine is arranged nearly perpendicular (87.8°) to the coordination plane. The vinyl group is twisted by 1.7° against the aromatic ring of the 2-vinylpyridine. The double bond of the vinyl group is significantly shorter than the double bonds of the cod ligand [C27−C28 = 1.310(6) Å vs. C1−C2 = 1.360(5) Å, C5−C6 = 1.360(6) Å]. This is in agreement with an elongation of the C1−C2 and C5−C6 bonds caused by their coordination to the rhodium center. There is no coordinative interaction of the rhodium center with the vinyl group in 2-vinylpyridine. The proton of the amine forms a hydrogen bond with the tosylate [H11···O1 = 2.27 Å, N11−H11 = 0.83(2) Å, N11−H11···O1 = 160.3°] and there is a C−H···O hydrogen bond between the aromatic ring and the oxygen atom of the morpholine ligand in a neighboring molecule (H24···O14 = 2.33 Å, C24−H24 = 0.93 Å, C24−H24···O14 = 159.0°).[13]

Table 6. Examples for complexes containing vinylpyridine as ligand; the lengths of the vinylic C−C bond, its distance from the metal center and the twist of the vinyl group against the pyridine ring are given

Complex	*d*(CC) [Å]	*d*(MX) [Å]	α [°]	Ref.
12	1.303(6)	n. b.	5.9	
	1.308(6)	n. b.	13.6	
13	1.310(6)	n. b.	1.7	
$[Cu_2(\mu\text{-vpy})_2(vpy)_2](ClO_4)_2$	1.307(23)	n. b.	10.0	[24a]
	1.368(17)	1.917	2.4	
	1.358(16)	1.903	5.7	
	1.319(23)	n. b.	14.9	
$[Cu(vpy)Cl]_\infty$	1.380(7)	1.940	1.9	[24b]
	1.378(7)	1.984	7.8	
$[Cu(vpy)I]_\infty$	1.29(2)	n. b.	10.0	[24b]
$[Ni(PPh_3)(vpy)]_2$	1.414(5)	1.848	9.9	[24c]
	1.433(5)	1.854	9.6	
$[Os_3(\mu\text{-H})_2(CO)_9(\mu\text{-CH-}\eta^2\text{-vpy})]$	1.43(2)	2.068	17.0	[24d]
$[Os_3(\mu\text{-H})_2(CO)_9(\mu_3\text{-C-vpy})]$	1.39(2)	n. b.	28.2	[24d]

X = center of the vinylic C−C bond, vpy = 2-vinylpyridine, n. b. = non bonded.

The X-ray structures of complexes **12** and **13** reveal that in the solid state there is no binding interaction of the rhodium center with the vinyl group in 2-vinylpyridine. The consequence of this are relatively short C−C bond lengths in the vinyl groups, a fact that is in agreement with other late transition metal complexes containing the 2-vinylpyridine ligand (Table 6). The dimeric $[Cu_2(\mu\text{-vpy})_2(vpy)_2](ClO_4)_2$ (vpy = 2-vinylpyridine) incorporates two copper

centers bridged by two vinylpyridine molecules with each of the copper atoms coordinating one further vinylpyridine molecule in a monodentate fashion through the nitrogen atom. The C−C bonds of the two vinyl groups coordinated to the copper center [1.368(17) Å, 1.358(16) Å] are slightly longer compared to non-coordinated vinyl groups [1.307(23) Å, 1.319(23) Å]. Similar vinylic C−C bond lengths are observed in the complexes $[Cu(vpy)Cl]_\infty$ and $[Ni(PPh_3)(vpy)]_2$ [1.380(7) Å, 1.378(7) and 1.414(5) Å, 1.433(5) Å, respectively], which contain the vinylpyridine in a bridging fashion, whereas the vinylpyridine ligand in the complex $[Cu(vpy)I]_\infty$ is bound only through the nitrogen atom that is associated with a shorter vinylic C−C bond [1.29(2) Å]. Other examples are the complexes $[Os_3(\mu\text{-}H)_2(CO)_9(\mu\text{-}CH\text{-}\eta^2\text{-}vpy)]$ and $[Os_3(\mu\text{-}H)_2(CO)_9(\mu_3\text{-}C\text{-}vpy)]$. In these complexes the nitrogen atom of the vinylpyridine moiety is bound to a methylidyne and methylidene bridge connecting three or two osmium atoms, respectively. The vinyl group in the former complex is coordinated to the metal center, whereas it is not coordinated in the second complex. This is associated with slightly longer C−C bond lengths in the first complex [1.43(2) Å] compared to the latter complex [1.39(2) Å].

The comparison with these data confirms that in **12** and **13** there is no binding interaction of the rhodium center with the vinyl group in 2-vinylpyridine. Hence, the activation of 2-vinylpyridine in the presence of cationic rhodium complexes towards hydroamination most likely proceeds by a coordination of the rhodium center to the pyridine nitrogen atom, which leads to a decrease in the electron density of the vinyl group. Clearly, oxidative amination that takes place in the presence of additional phosphane ligands must take place by a different mechanism. Unfortunately, all efforts to isolate or characterize an (amine)(phosphane)(vinylpyridine)rhodium complex turned out to be unsuccessful. Further work in this direction is in progress.

Conclusion

For the first time the oxidative amination of 2-vinylpyridine is described. In the presence of cationic (phosphane)rhodium complexes both oxidative amination as well as hydroamination occurs to yield products with anti-Markovnikov regiochemistry. Interestingly, the ratio of enamine to alkylamine is strongly influenced by the solvent, the phosphane and the ratio of olefin to amine. It is assumed that the hydroamination is initiated by an activation of the 2-vinylpyridine through coordination of the pyridine nitrogen atom to the rhodium center. In contrast, oxidative amination proceeds by a different mechanism. While cyclic amines that do not contain additional heteroatoms give good yields of the corresponding enamines, hydroamination dominates in the case of bidentate amines such as morpholine. Hydroamination of 4-vinylpyridine is achieved under surprisingly mild conditions.

A possible intermediate for the catalyst formation, $[Rh(cod)(2\text{-vinylpyridine})_2]CF_3SO_3$ (**12**) was synthesized and completely characterized. **12** reacts selectively with morpholine to give $[Rh(cod)(morpholine)(2\text{-vinylpyridine})]CF_3SO_3$ (**13**), which is a likely intermediate in the catalytic cycle.

Experimental Section

Materials and Methods: All reactions of air- and/or water-sensitive compounds were performed using standard high-vacuum or Schlenk techniques. All solvents were dried and distilled prior to use according to standard procedures. Amines were distilled from CaH_2, silver salts and other chemicals were purchased from Fluka or Aldrich and used as received. $[Rh(cod)Cl]_2$[14] and $[Rh(cod)_2]BF_4$[15] were prepared as described in the appropriate reference.

Physical and Analytical Methods: ^{1}H- and ^{13}C-NMR spectra were recorded with a Bruker AT 360 and referenced in ppm relative to tetramethylsilane. − Infrared spectra were obtained with a Perkin−Elmer 1600 spectrometer. − Mass-spectrometric analysis was performed with a Finnigan MAT 311A by the Fast Atom Bombardment (FAB) method. − Elemental analyses were performed by the Microanalytical Laboratory of the Technische Universität München. − GC analyses were conducted with a Hewlett−Packard 6890 instrument using an HP-1 capillary column. Yields were determined against hexadecane as an internal standard. GC/MS analyses were conducted with a Hewlett-Packard 5890 with 70-eV electron impact ionization (detector: HP 5970 B).

Reaction of 2-Vinylpyridine with Pyrrolidine: 45 mg of $[Rh(cod)_2]BF_4$ (0.11 mmol) and 58 mg of PPh_3 (0.22 mmol) were mixed in 10 mL of THF. Subsequently, 0.37 mL of pyrrolidine (4.40 mmol) and 1.90 mL of 2-vinylpyridine (17.6 mmol) were added at room temperature. The reaction was heated to reflux for 20 h before being cooled to room temperature. The yield of (*E*)-*N*-[2-(2-pyridyl)ethenyl]pyrrolidine (**1a**) was determined by gas chromatography with hexadecane as an internal standard. − In order to isolate a more stable derivative of (*E*)-*N*-[2-(2-pyridyl)ethenyl]-pyrrolidine (**1a**) , 0.5 g of Pd/C (5%) was added to the crude reaction and the mixture was stirred for 48 h under H_2 at a pressure of 1 atm. After filtration, the solvent was removed by evaporation. The residue was dissolved in 20 mL of dichloromethane and extracted three times with 5% HCl. The combined aqueous phases were neutralized by adding NaOH until pH = 9 was reached and the product was extracted three times with dichloromethane. The combined organic layers were dried with $MgSO_4$ and the solvent was distilled off. *N*-[2-(2-Pyridyl)ethyl]pyrrolidine (**1b**) was obtained after column chromatography (chloroform/methanol, 50:1) in 75% yield.

(*E*)-*N*-[2-(2-Pyridyl)ethenyl]pyrrolidine (1a): GC yield: 54%. − MS; *m/z*: 174 [M^+], 145 [$M^+ - C_2H_3$], 131 [$M^+ - C_3H_7$], 118 [$M^+ - C_3H_7N$], 105 [$C_5H_4N{-}C_2H_5^+$].

***N*-[2-(2-Pyridyl)ethyl]pyrrolidine (1b):** GC yield (before hydrogenation): 54%; GC yield (after hydrogenation): 75%. − MS; *m/z*: 176 [M^+], 106 [$C_5H_4N{-}C_2H_4^+$], 84 [$(C_5H_{10})NCH_2^+$]. − ^{1}H NMR (360 MHz, 25°C, $CDCl_3$): δ = 8.50 [d, ^3J(H,H) = 5.6 Hz, 1 H, 6-H], 7.57 [dt, ^3J(H,H) = 7.8 Hz, ^4J(H,H) = 4.8 Hz, 1 H, 4-H], 7.14 [d, ^3J(H,H) = 7.8 Hz, 1 H, 3-H], 7.08 (m, 1 H, 5-H), 3.04 (m, 2 H, Py−CH_2−CH_2−N), 2.87 (m, 2 H, Py−CH_2), 2.61 (m, 4 H, N−CH_2), 1.79 [q, ^3J(H,H) = 3.2 Hz, 4 H, N−CH_2−CH_2]. −^{13}C{^{1}H} NMR (91 MHz, 25°C, $CDCl_3$): δ = 160.2 (C-2), 149.2 (C-6), 136.2 (C-4), 123.1 (C-3), 121.2 (C-5), 56.0 (Py−C−*C*), 54.1

(*C*−N), 35.7 (Py−*C*), 22.5 (N−C−*C*). − MS; *m*/*z*: 176 [M^+], 106 [$C_5H_4N-C_2H_4^+$], 84 [$(C_5H_{10})NCH_2^+$].

Reaction of 2-Vinylpyridine with Piperidine: In a procedure analogous to the synthesis of **1**, 0.44 mL of piperidine (4.40 mmol) and 1.90 mL of 2-vinylpyridine (17.6 mmol) in 10 mL of THF were treated in the presence of 45 mg of $[Rh(cod)_2]BF_4$ (0.11 mmol) and 58 mg of PPh_3 (0.22 mmol).

(*E*)-*N*-[2-(2-Pyridyl)ethenyl]piperidine (2a): GC yield: 47%. − MS; *m*/*z*: 188 [M^+], 159 [$M^+ - C_2H_5$], 131 [$M^+ - C_3H_7N$], 118 [$M^+ - C_4H_8N$], 106 [$C_5H_4N-C_2H_5^+$].

***N*-[2-(2-Pyridyl)ethyl]piperidine (2b):** GC yield (before hydrogenation): 53%; GC yield (after hydrogenation): > 99.9%; isolated yield: 86% (718 mg). − ^{1}H NMR (360 MHz, 25°C, $CDCl_3$): δ = 8.47 [d, ^3J(H,H) = 4.8 Hz, 1 H, 6-H], 7.54 [dt, ^3J(H,H) = 7.9 Hz, ^4J(H,H) = 4.8 Hz, 1 H, 4-H], 7.14 [d, ^3J(H,H) = 7.9 Hz, 1 H, 3-H], 7.05 (m, 1 H, 5-H), 2.96 (m, 2 H, Py−CH_2−CH_2−N), 2.68 (m, 2 H, Py−CH_2), 2.44 (m, 4 H, CH_2−N), 1.56 (m, 4 H, N−CH_2−CH_2), 1.40 (m, 2 H, N−CH_2−CH_2−CH_2). − $^{13}C\{^1H\}$ NMR (91 MHz, 25°C, $CDCl_3$): δ = 160.6 (C-2), 149.1 (C-6), 136.2 (C-4), 123.1 (C-3), 120.9 (C-5), 59.2 (Py−C−*C*), 54.4 (*C*−N), 35.7 (Py−*C*), 25.9 (N−C−*C*), 24.3 (N−C−C−*C*). − MS; *m*/*z*: 190 [M^+], 106 [$C_5H_4N-C_2H_4^+$], 98 [$(C_5H_{10})NCH_2^+$].

Reaction of 2-Vinylpyridine with Hexahydroazepine: In a procedure analogous to the synthesis of **1**, 0.50 mL of hexahydroazepine (4.40 mmol) and 1.90 mL of 2-vinylpyridine (17.6 mmol) in 10 mL of THF were treated in the presence of 45 mg of $[Rh(cod)_2]BF_4$ (0.11 mmol) and 58 mg of PPh_3 (0.22 mmol).

(*E*)-*N*-[2-(2-Pyridyl)ethenyl]hexahydroazepine (3a): GC yield: 30%. − MS; *m*/*z*: 202 [M^+], 187 [$M^+ - CH_3$], 173 [$M^+ - C_2H_5$], 145 [$M^+ - C_4H_9$], 131 [$M^+ - C_5H_{11}$], 117 [$M^+ - C_6H_{13}$], 106 [$M^+ - C_6H_{13}N$].

***N*-[2-(2-Pyridyl)ethyl]hexahydroazepine (3b):** GC yield (before hydrogenation): 30%; GC yield (after hydrogenation): 59%; isolated yield: 36% (323 mg). − ^{1}H NMR (360 MHz, 25°C, $CDCl_3$): δ = 8.37 [d, ^3J(H,H) = 5.6 Hz, 1 H, 6-H], 7.56 [t, ^3J(H,H) = 8.8 Hz, 4-H], 7.16 (m, 1 H, 3-H), 7.07 (m, 1 H, 5-H), 2.94 [t, ^3J(H,H) = 4.7 Hz, 4 H, CH_2−N−Py], 2.75 (m, 4 H, Py−CH_2−CH_2), 1.64 (m, 8 H, CH_2−CH_2−CH_2−N). − $^{13}C\{^1H\}$ NMR (91 MHz, 25°C, $CDCl_3$): δ = 160.4 (C-2), 149.0 (C-6), 136.0 (C-4), 123.0 (C-3), 120.9 (C-5), 58.0 (Py−C−*C*), 54.6 (*C*−N−Et), 35.9 (Py−*C*), 27.6 (C−*C*−C−N), 26.8 (*C*−C−C−N). − MS; *m*/*z*: 204 [M^+], 112 [$C_6H_{12}NCH_2$].

Reaction of 2-Vinylpyridine with Morpholine: In a procedure analogous to the synthesis of **1**, 0.38 mL of morpholine (4.40 mmol) and 1.90 mL of 2-vinylpyridine (17.6 mmol) in 10 mL of THF were treated in the presence of 45 mg of $[Rh(cod)_2]BF_4$ (0.11 mmol) and 58 mg of PPh_3 (0.22 mmol).

(*E*)-*N*-[2-(2-Pyridyl)ethenyl]morpholine (4a): GC yield: 2%. − MS; *m*/*z*: 190 [M^+], 159 [$M^+ - CH_3O$], 131 [$M^+ - C_3H_7O$], 118 [$M^+ - C_4H_8O$], 105 [$C_5H_4N-C_2H_4^+$].

***N*-[2-(2-Pyridyl)ethyl]morpholine (4b):** GC yield (before hydrogenation): 98%; GC yield (after hydrogenation): > 99.9%; isolated yield: 81% (684 mg). − ^{1}H NMR (360 MHz, 25°C, $CDCl_3$): δ = 8.50 [d, ^3J(H,H) = 4.8 Hz, 1 H, 6-H], 7.55 [dt, ^3J(H,H) = 7.8 Hz, ^3J(H,H) = 4.8 Hz, 1 H, 4-H], 7.19 [d, ^3J(H,H) = 7.8 Hz, 1 H, 3-H], 7.08 (m, 1 H, 5-H), 3.66 [t, ^3J(H,H) = 4.5 Hz, 4 H, CH_2−O], 2.98 (m, 2 H, Py−CH_2−CH_2−N), 2.75 (m, 2 H, Py−CH_2−CH_2−N), 2.50 [t, ^3J(H,H) = 4.5 Hz, 4 H, CH_2−N]. − $^{13}C\{^1H\}$ NMR (91 MHz, 25°C, $CDCl_3$): δ = 159.8 (C-2), 148.8 (C-6), 135.8 (C-4), 122.7 (C-3), 120.7 (C-5), 66.4 (CH_2−O), 58.2 (Py−C−*C*), 53.2 (CH_2−N), 35.1 (Py−*C*). − MS; *m*/*z* = 192 [M − H^+], 132, 106 [$C_5H_4N-C_2H_4^+$], 100 [$CH_2{=}N(CH_2)_4O^+$].

Reaction of 2-Vinylpyridine with Thiomorpholine: In a procedure analogous to the synthesis of **1**, 0.44 mL of thiomorpholine (4.40 mmol) and 1.90 mL of 2-vinylpyridine (17.6 mmol) in 10 mL of THF were treated in the presence of 45 mg of $[Rh(cod)_2]BF_4$ (0.11 mmol) and 58 mg of PPh_3 (0.22 mmol). **5** was purified by column chromatography (hexane/ethyl acetate/NEt_3, 1:1:0.01).

***N*-[2-(2-Pyridyl)ethyl]thiomorpholine (5):** GC yield: 98%; isolated yield: 41% (375 mg). − ^{1}H NMR (360 MHz, 25°C, $CDCl_3$): δ = 8.37 [d, ^3J(H,H) = 5.9 Hz, 1 H, 6-H], 7.46 [dt, ^3J(H,H) = 7.6 Hz, ^4J(H,H) = 1.7 Hz, 1 H, 4-H], 7.06 (m, 1 H, 3-H), 6.96 (m, 1 H, 5-H), 2.84 [t, ^3J(H,H) = 4.7 Hz, 4 H, S−CH_2−CH_2−N−Py], 2.75 (m, 4 H, Py−CH_2−CH_2), 2.79 [t, ^3J(H,H) = 4.7 Hz, 4 H, CH_2−S]. − $^{13}C\{^1H\}$ NMR (91 MHz, 25°C, $CDCl_3$): δ = 160.1 (C-2), 149.0 (C-6), 136.1 (C-4), 123.0 (C-3), 121.0 (C-5), 58.8 (Py−C−*C*−N), 54.6 (CH_2−N), 35.2 (Py−CH_2−CH_2−N), 17.8 (CH_2−S). − MS; *m*/*z*: 208 [M^+], 175 [M^+ − SH], 116 [$S(C_4H_8)NCH_2^+$].

Reaction of 2-Vinylpyridine with Piperazine: In a procedure analogous to the synthesis of **1**, 0.38 g of piperazine (4.40 mmol) and 1.90 mL of 2-vinylpyridine (17.6 mmol) in 10 mL of THF were treated in the presence of 45 mg of $[Rh(cod)_2]BF_4$ (0.11 mmol) and 58 mg of PPh_3 (0.22 mmol).

***N*-[2-(2-Pyridyl)ethyl]piperazine (6a):** GC yield (before hydrogenation): 33%; GC yield (after hydrogenation): 48%. − ^{1}H NMR (360 MHz, 25°C, $CDCl_3$): δ = 8.26 [d, ^3J(H,H) = 4.0 Hz, 1 H, 6-H], 7.34 [dt, ^3J(H,H) = 7.8 Hz, ^4J(H,H) = 1.8 Hz, 1 H, 4-H], 6.92 [d, ^3J(H,H) = 7.8 Hz, 1 H, 3-H], 6.86 (m, 1 H, 5-H), 2.74 (m, 2 H, Py−CH_2), 2.54 (m, 2 H, Py−CH_2−CH_2), 2.39 (m, 8 H, CH_2−N). − $^{13}C\{^1H\}$ NMR (91 MHz, 25°C, $CDCl_3$): δ = 159.8 (C-2), 149.0 (C-6), 136.1 (C-4), 123.0 (C-3), 121.0 (C-5), 58.1 (Py−C−*C*), 51.6 (*C*−N−C−C−Py), 44.1 (*C*−NH), 35.2 (Py−*C*). − MS; *m*/*z*: 191 [M^+], 149 [$M^+ - C_2H_4N$], 106 [$C_5H_4N-C_2H_4^+$], 99 [$HNC_4H_8NCH_2^+$].

(*E*)-*N*-[2-(2-Pyridyl)ethenyl]piperazine (6b): GC yield: 15%. − MS; *m*/*z*: 189 [M^+], 147 [$M^+ - C_2H_4N$], 133 [$M^+ - C_3H_6N$], 106 [$C_5H_4N-C_2H_4^+$].

Bis{*N*,*N*′-[2-(2-pyridyl)ethyl]}piperazine (6c): GC yield (before hydrogenation): 31%; GC yield (after hydrogenation): 46%. − ^{1}H NMR (360 MHz, 25°C, $CDCl_3$): δ = 8.48 [d, ^3J(H,H) = 5.9 Hz, 2 H, 6-H], 7.56 [dt, ^3J(H,H) = 11.4 Hz, ^4J(H,H) = 1.7 Hz, 2 H, 4-H], 7.15 [d, ^3J(H,H) = 11.4 Hz, 2 H, 3-H], 7.06 (m, 2 H, 5-H), 2.84 [t, ^3J(H,H) = 4.7 Hz, 4 H, Py−CH_2], 2.75 (m, 4 H, Py−CH_2−CH_2), 2.79 [t, ^3J(H,H) = 4.7 Hz, 8 H, CH_2−N]. − $^{13}C\{^1H\}$ NMR (91 MHz, 25°C, $CDCl_3$): δ = 159.9 (C-2), 149.2 (C-6), 136.3 (C-4), 123.2 (C-3), 121.2 (C-5), 58.0 (Py−C−*C*), 57.3 (*C*−N−C−C−Py), 35.4 (Py−*C*).

***(E)*-*N*-[2-(2-Pyridyl)ethenyl]-*N*′-[2-(2-pyridyl)ethyl]piperazine (6d):** GC yield: 15%. − MS; *m*/*z*: 294 [M^+], 279 [$M^+ - CH_3$], 189 [$M^+ - C_5H_4N-C_2H_4$], 161, 133, 106 [$C_5H_4N-C_2H_4^+$].

Reaction of 2-Vinylpyridine with *N*-Methylpiperazine: In a procedure analogous to the synthesis of **1**, 0.49 mL of *N*-methylpiperazine (4.40 mmol) and 1.90 mL of 2-vinylpyridine (17.6 mmol) in 10 mL of THF were treated in the presence of 45 mg of $[Rh(cod)_2]BF_4$ (0.11 mmol) and 58 mg of PPh_3 (0.22 mmol).

(*E*)-*N*-[2-(2-Pyridyl)ethenyl]-*N*′-methylpiperazine (7a): GC yield: 20%. − MS; *m*/*z*: 203 [M^+], 188 [$M^+ - CH_3$], 159 [$M^+ - C_2H_6N$], 131 [$M^+ - C_4H_{10}N$], 118, 106 [$C_5H_4N-C_2H_4^+$].

***N*-[2-(2-Pyridyl)ethyl]-*N*′-methylpiperazine (7b):** GC yield (before hydrogenation): 62%; GC yield (after hydrogenation): 82%; isolated

yield: 65% (586 mg). – ^{1}H NMR (360 MHz, 25°C, $CDCl_3$): δ = 8.42 [d, ^3J(H,H) = 5.8 Hz, 1 H, 6-H], 7.50 (m, 1 H, 4-H), 7.08 (m, 1 H, 3-H), 7.00 (m, 1 H, 5-H), 2.94 (m, 2 H, Py−CH_2−CH_2), 2.70 (m, 2 H, Py−CH_2), 2.54 (s, br., 4 H, N−CH_2), 2.48 (s, br., 4 H, N−CH_2), 2.21 (s, 3 H, N−CH_3). – ^{13}C{^{1}H} NMR (91 MHz, 25°C, $CDCl_3$): δ = 160.2 (C-2), 149.1 (C-6), 136.2 (C-4), 123.0 (C-3), 121.0 (C-5), 58.2 (Py−C−*C*), 54.9 (*C*H_2−N), 52.9 (*C*H_2−N), 45.9 (N−*C*H_3), 35.7 (Py−*C*). – MS; *m*/*z*: 205 [M^+], 161 [M^+ − C_2H_6N], 149 [M^+ − C_3H_6N], 135 [M^+ − C_4H_8N], 106 [C_5H_4N−$C_2H_4^+$].

Reaction of 2-Vinylpyridine with *N*′-Phenylpiperazine: In a procedure analogous to the synthesis of **1**, 0.67 mL of *N*-phenylpiperazine (4.40 mmol) and 1.90 mL of 2-vinylpyridine (17.6 mmol) in 10 mL of THF were treated in the presence of 45 mg of $[Rh(cod)_2]BF_4$ (0.11 mmol) and 58 mg of PPh_3 (0.22 mmol).

(*E*)-*N*-[2-(2-Pyridyl)ethenyl]-*N*′-phenylpiperazine (8a): GC yield: 8%. – MS; *m*/*z*: 265 [M^+], 207 [M^+ − C_3H_8N], 160 [M^+ − C_5H_4N−C_2H_3], 120 [C_5H_4N−$C_2H_4N^+$], 104 [C_5H_4N−$C_2H_2^+$].

***N*-[2-(2-Pyridyl)ethyl]-*N*′-phenylpiperazine (8b):** GC yield (before hydrogenation): 91%; GC yield (after hydrogenation): 99%; isolated yield: 88% (1033 mg). – ^{1}H NMR (360 MHz, 25°C, $CDCl_3$): δ = 8.52 [d, ^3J(H,H) = 5.9 Hz, 1 H, 6-H], 7.60 [dt, ^3J(H,H) = 7.7 Hz, ^4J(H,H) = 1.7 Hz, 1 H, 4-H], 7.26 (m, 3 H, 3-H, *H*-8), 7.12 (m, 1 H, *H*-10), 6.99 (m, 3 H, 5-H, *H*-9), 3.28 [t, ^3J(H,H) = 4.7 Hz, 4 H, CH_2−N], 3.10 (m, 2 H, Py−CH_2−CH_2), 2.94 (m, 2 H, Py−CH_2), 2.79 [t, ^3J(H,H) = 4.7 Hz, 4 H, CH_2−N]. – ^{13}C{^{1}H} NMR (91 MHz, 25°C, $CDCl_3$): δ = 160.2 (C-2), 151.2 (C-7), 149.1 (C-6), 136.3 (C-4), 129.0 (C-9), 123.2 (C-3), 121.2 (C-5), 119.7 (C-10), 116.0 (C-8), 58.3 (Py−C−*C*), 53.1 (*C*−N), 52.9 (*C*−N), 35.7 (Py−*C*). – MS; *m*/*z*: 267 [M^+], 175 [C_6H_5−N($C_4H_8NCH_2$)$^+$], 161 [C_6H_5−N(C_4H_8N)$^+$], 148 [C_5H_4N−$C_2H_4N(CH_2)_2^+$], 135 [C_5H_4N−$C_2H_4NCH_3^+$], 120 [C_5H_4N−$C_2H_4N^+$], 106 [C_5H_4N−$C_2H_4^+$].

Reaction of 4-Vinylpyridine with Piperidine: In a procedure analogous to the synthesis of **1**, 0.44 mL of piperidine (4.40 mmol) and 1.90 mL of 4-vinylpyridine (17.6 mmol) in 10 mL of THF were treated in the presence of 45 mg of $[Rh(cod)_2]BF_4$ (0.11 mmol) and 58 mg of PPh_3 (0.22 mmol).

***N*-[2-(4-Pyridyl)ethyl]piperidine (9):** GC yield: 57%; isolated yield: 36% (301 mg). – ^{1}H NMR (360 MHz, 25°C, $CDCl_3$): δ = 8.34 [d, ^3J(H,H) = 4.9 Hz, 2 H, *H*-2], 7.01 [d, ^3J(H,H) = 4.9 Hz, 2 H, 3-H], 2.65 (m, 2 H, Py−CH_2−CH_2−N), 2.44 (m, 2 H, Py−CH_2−CH_2−N), 2.37 (m, 4 H, N−CH_2), 1.47 (m, 4 H, N−CH_2−CH_2), 1.31 (m, 2 H, N−CH_2−CH_2−CH_2). – ^{13}C{^{1}H} NMR (91 MHz, 25°C, $CDCl_3$): δ = 149.6 (C-2), 149.6 (C-4), 124.1 (C-3), 59.8 (Py−C−*C*−N), 54.4 (*C*−N), 32.9 (Py−*C*), 25.9 (N−C−*C*), 24.3 (N−C−C−*C*). – MS; *m*/*z*: 190 [M − H^+], 105 [C_5H_4N−$C_2H_3^+$], 98 [CH_2=N$(CH_2)_5^+$].

Reaction of 4-Vinylpyridine with Hexahydroazepine: In a procedure analogous to the synthesis of **1**, 0.50 mL of hexahydroazepine (4.40 mmol) and 1.90 mL of 4-vinylpyridine (17.6 mmol) in 10 mL of THF were treated in the presence of 45 mg of $[Rh(cod)_2]BF_4$ (0.11 mmol) and 58 mg of PPh_3 (0.22 mmol).

***N*-[2-(4-Pyridyl)ethyl]hexahydroazepine (10):** GC yield: 21%; isolated yield: 13% (116 mg). – ^{1}H NMR (360 MHz, 25°C, $CDCl_3$): δ = 8.40 [d, ^3J(H,H) = 4.9 Hz, 2 H, *H*-2], 7.05 [d, ^3J(H,H) = 4.9 Hz, 2 H, 3-H], 2.71 (m, 8 H, Py−CH_2−CH_2−N−CH_2), 1.17 (m, 8 H, N−CH_2−CH_2−CH_2). – ^{13}C{^{1}H} NMR (91 MHz, 25°C, $CDCl_3$): δ = 149.7 (C-2), 149.6 (C-4), 124.3 (C-3), 58.9 (Py−C−*C*−N), 54.4 (*C*−N), 33.4 (Py−*C*), 27.9 (N−C−*C*), 27.0 (N−C−C−*C*). – MS; *m*/*z*: 203 [M^+], 112 [$C_6H_{12}NCH_2^+$].

Reaction of 4-Vinylpyridine with Morpholine: In a procedure analogous to the synthesis of **1**, 0.38 mL of morpholine (4.40 mmol) and 1.90 mL of 4-vinylpyridine (17.6 mmol) in 10 mL of THF were treated in the presence of 45 mg of $[Rh(cod)_2]BF_4$ (0.11 mmol) and 58 mg of PPh_3 (0.22 mmol).

***N*-[2-(4-Pyridyl)ethyl]morpholine (11):** GC yield: 54%; isolated yield: 44% (37 mg). – ^{1}H NMR (360 MHz, 25°C, $CDCl_3$): δ = 8.28 [d, ^3J(H,H) = 4.5 Hz, 2 H, *H*-2], 7.01 [d, ^3J(H,H) = 4.5 Hz, 2 H, 3-H], 3.60 [t, ^3J(H,H) = 4.4 Hz, 4 H, CH_2−O], 2.67 (m, 2 H, Py−CH_2−CH_2), 2.51 (m, 2 H, Py−CH_2), 2.40 [t, ^3J(H,H) = 4.4 Hz, 4 H, CH_2N]. – ^{13}C{^{1}H} NMR (91 MHz, 25°C, $CDCl_3$): δ = 149.5 (C-2), 149.1 (C-4), 124.0 (C-3), 66.7 (*C*−O), 59.1 (Py−C−*C*), 53.4 (*C*−N), 32.4 (Py−*C*). – MS; *m*/*z*: 192 [M − H^+], 132, 106 [C_5H_4N−$C_2H_4^+$], 100 [CH_2=N$(CH_2)_4O^+$].

[(1,2,5,6-η)-1,5-Cyclooctadiene]bis[*N*-(2-vinylpyridine)]rhodium(I) Tetrafluoroborate (12): 100 mg of $[Rh(cod)Cl]_2$ (0.20 mmol) and 80 mg of $AgBF_4$ (0.41 mmol) were dissolved in 2 mL of THF and the solution was stirred for 10 min. After filtering off the AgCl precipitate, the orange solution was cooled to 0°C and 94 mg of 2-vinylpyridine (0.90 mmol) was added. After stirring the reaction mixture for several minutes, a yellow precipitate was obtained. After filtration, the crude product was washed three times with 1 mL of THF and three times with pentane. Drying in vacuo furnished 154 mg of **12** (76%). – ^{1}H NMR (400 MHz, $CDCl_3$, 20°C): δ = 8.92 (s, br., 1 H, 6-H), 8.71 (s, br., 1 H, *H*-7), 7.66 [t, ^3J(H,H) = 7.9 Hz, 1 H, 4-H], 7.55 [d, ^3J(H,H) = 7.9 Hz, 1 H, 3-H], 7.32 (s, 1 H, 5-H), 6.05 [d, br., ^3J(H,H) = 17.6 Hz, 2 H, *H*-8], 4.17 [s, br., 2 H, C*H* (cod)], 3.90 [s, br., 2 H, C*H* (cod)], 2.81 [s, br., 2 H, CH_2 (cod)], 2.64 [s, br., 2 H, CH_2 (cod)], 2.10 [s, br., 2 H, CH_2 (cod)], 1.84 [s, br., 2 H, CH_2 (cod)]. – ^{13}C NMR (100 MHz, $CDCl_3$, 20°C): δ = 157.1 (C-2), 151.0 (C-6), 138.2 (C-8), 135.7 (C-4), 124.4 (C-5), 123.0 (C-7), 121.8 (C-3), 85.4 [*C*H (cod)], 83.9 [C*H* (cod)], 31.5 [CH_2 (cod)], 29.6 [CH_2 (cod)]. – At −60°C, in both the ^{1}H-NMR and the ^{13}C-NMR spectra, a second set of weak resonances (w) appears, which has only 1/10 of the intensity of the main one (ss): ^{1}H NMR (400 MHz, $CDCl_3$, −60°C): δ = 9.43 (w, m, 1 H), 8.92 [ss, d, ^3J(H,H) = 4.4 Hz, 1 H, 6-H], 8.74 [ss, dd, ^3J(H,H) = 11.0 Hz, ^3J(H,H) = 17.0 Hz, 1 H, *H*-7], 8.08 [w, dd, ^3J(H,H) = 11.0 Hz, ^3J(H,H) = 17.0 Hz], 7.66 [ss, t, ^3J(H,H) = 7.9 Hz, 1 H, 4-H], 7.55 [ss, d, ^3J(H,H) = 8.0 Hz, 1 H, 3-H], 7.42 (w, m, 1 H), 7.28 (ss, m, 1 H, 5-H), 6.09 [ss, dd, br., ^3J(H,H) = 17.6 Hz, ^3J(H,H) = 11.0 Hz, 2 H, *H*-8], 6.00 (w, m, 1 H), 5.89 [w, d, ^3J(H,H) = 11.0 Hz], 4.16 [ss, m, 2 H, C*H* (cod)], 4.06 (w, s, 1 H), 3.93 (w, s, 1 H), 3.83 [ss, m, 2 H, C*H* (cod)], 2.84 [ss, m, 2 H, CH_2 (cod)], 2.64 [ss, m, br., 2 H, CH_2 (cod)], 2.17 [ss, m, 2 H, CH_2 (cod)], 1.97 (w, m, 1 H), 1.82 (w, m, 1 H), 1.84 [ss, br., 2 H, CH_2 (cod)]. – ^{13}C NMR (100 MHz, $CDCl_3$, −60°C): δ = 157.1 (ss, C-2), 156.0 (w, C-2), 151.1 (ss, C-6), 150.6 (w, C-6), 138.4 (ss, C-8), 138.1 (w, C-8), 136.5 (w, C-4), 135.6 (ss, C-4), 124.7 (w, C-5), 124.5 (ss, C-5), 123.5 (ss, C-7), 122.3 (w, C-7), 122.0 (ss, C-3), 121.6 (w, C-3), 88.2 [w, d, ^1J(C,Rh) = 11.7 Hz, *C*H (cod)], 85.2 [ss, d, ^1J(C,Rh) = 11.7 Hz, *C*H (cod)], 84.9 [ss, d, ^1J(C,Rh) = 11.7 Hz, C*H* (cod)], 81.2 [w, d, ^1J(C,Rh) = 11.7 Hz, C*H* (cod)], 32.1 [ss, CH_2 (cod)], 30.6 [w, CH_2 (cod)], 30.4 [w, CH_2 (cod)], 29.1 [ss, CH_2 (cod)]. – $C_{22}H_{26}BF_4N_2Rh$ (508.17): calcd. C 52.0, H 5.2, N 5.5; found C 51.8, H 5.3, N 5.4.

Crystal Data and Structure Refinement of 12: Crystals were grown by slow diffusion of Et_2O into a solution of [Rh(cod)(2-vinylpyridine)$_2$]CF_3SO_3 in CH_2Cl_2. A yellow crystal of dimensions 0.35 × 0.30 × 0.17 mm was mounted by the Lindeman technique. Cell constants were determined by least-squares refinement of 5000 reflections in the intervall 16.8° < 2Θ < 49.8° with the program

CELL.[16] Crystal data: monoclinic $P2_1/n$; a = 11.3081(7) Å, b = 17.0699(6) Å, c = 12.2946(7) Å, β = 90.911(6)°; V = 2372.9(2) Å^3; formula unit = $C_{23}H_{26}F_3N_2O_3RhS$ with Z = 4; FW = 570.43; F(000) = 1160; μ(Mo-K_α) = 8.59 cm^{-1}; λ(Mo-K_α) = 0.71069 Å; $\rho_{calcd.}$ = 1.597 g cm^{-3}. Preliminary examination and data collection were carried out with an imaging-plate diffraction system (IPDS; STOE & Cie) equipped with a rotating anode (NONIUS FR591; 50 kV; 80 mA) and graphite monochromator. The data were collected at 293(2) K with an exposure time of 5.0 min per image (rotation scan modus from φ = 0.0° to 300° with Δφ = 1°). 24641 reflections were collected (2.05° < Θ < 24.6°). Final full-matrix least-squares refinement (on F^2) based on 3760 unique reflections of which 3753 were used converged with 452 variable parameters and 15 restraints. Non-hydrogen atoms were refined anisotropically, hydrogen atoms were refined isotropically with U(H) = 1.2 U_{eq}(parent atom). $R1$ = 0.0300, for $F^2 > 2\ \sigma(F^2)$; $wR2$ = 0.0770;[17] Goof(F^2) = 0.953; $\Delta\rho_{max}$ = 0.56, $\Delta\rho_{min}$ = −0.42 e$^-$ Å^{-3}. The data analysis and the drawing were made using the programs STRUX-V,[18] SIR-92,[19] SHELXL-93,[20] and SCHAKAL-97.[21]

[(1,2,5,6-η)-1,5-Cyclooctadiene](*N*-morpholine)[*N*-(2-vinylpyridine)]-rhodium(I) Trifluoromethylsulfonate (13): 100 mg of [Rh(cod)(2-vinylpyridine)$_2$]CF_3SO_3 (0.18 mmol) was dissolved in 1 mL of THF. 16 mg of morpholine was added to the yellow solution. Immediately a yellow precipitate was obtained, which was filtered off and washed three times with 1 mL of THF and 1 mL of pentane. After drying in vacuo, 83 mg (84%) of **13** was obtained. − ^{1}H NMR (400 MHz, CD_2Cl_2, 20°C): δ = 8.85 (s, 1 H, 6-H), 8.38 (s, br., 1 H, *H*-7), 7.48 [d, ^3J(H,H) = 6.5 Hz, 1 H, 4-H], 7.80 (s, 1 H, 3-H), 7.41 (s, 1 H, 5-H), 6.29 [d, ^3J(H,H) = 17.0 Hz, 1 H, *H*-8 (*trans*)], 6.03 [d, ^3J(H,H) = 11.0 Hz, 1 H, *H*-8 (*cis*)], 4.34 [s, br., 2 H, C*H* (cod)], 3.63 [s, br., 7 H, C*H* (cod), N−*H*, CH_2−O], 2.79 (s, br., 2 H, N−CH_2), 2.53 [s, br., 6 H, CH_2 (cod), N−CH_2], 1.9 [s, br., 4 H, CH_2 (cod)]. − ^{13}C NMR (100 MHz, $CDCl_3$, 20°C): δ = 156.2 (C-2), 149.2 (C-6), 137.3 (C-8), 134.9 (C-4), 124.9 (C-5), 123.5 (C-7), 121.3 (C-3), 82.9 [C*H* (cod)], 65.5 (*C*−O), 48.0 (*C*−N), 29.3 [CH_2 (cod)]. − IR (KBr): $\tilde{\nu}$ = 3215 cm^{-1} s, 2941 m, 2987 m, 1601 m, 1480 s, 1444 m, 1272 ss, 1263 ss, 1249 ss, 1153 ss, 1029 ss, 880 s. − MS; (FAB) *m/z*: 316 [M$^+$ − morpholine]. − $C_{19}H_{28}BF_4N_2ORh$ (552.41): calcd. C 44.9, H 5.2, N 4.8; found C 44.9, H 4.7, N 5.2.

Crystal Data and Structure Refinement of 13: Crystals were grown by slow diffusion of Et_2O into a solution of [Rh(cod)(morpholine)(2-vinylpyridine)]CF_3SO_3 in CH_2Cl_2. A yellow crystal of dimensions 0.25 × 0.27 × 0.1 mm was mounted by the Lindeman technique. Cell constants were determined by least-squares refinement of 1998 reflections in the intervall 27.3° < 2Θ < 51.7° with the program CELL. Crystal data: triclinic $P-1$; a = 9.7085(2), b = 10.7786(2), c = 12.6294(2) Å, α = 76.3538(14)°, β = 72.1748(14)°, γ = 65.7518(11)°; V = 1137.86(4) Å^3; empirical formula $C_{20}H_{28}F_3N_2O_4RhS$, Z = 2; FW = 552.41; F(000) = 564; μ(Mo-K_α) = 8.95 cm^{-1}; λ(Mo-K_α) = 0.71073 Å; $\rho_{calcd.}$ = 1.612 g cm^{-3}. Preliminary examination and data collection were carried out with a Kappa-CCD equipped with a rotating anode (NONIUS FR591; 50 kV; 80 mA) and graphite monochromator. The data were collected at 293(2) K with an exposure time of 20 s per image (detector−image 30 mm, rotation-scan modus from φ = 0.0° to 360° with Δφ = 1°). 15058 reflections were collected (4.60° < Θ < 26.35°). Final full-matrix least-squares refinement (on F^2) based on 3917 unique reflections converged with 367 variable parameters and 28 restraints. Non-hydrogen atoms were refined anisotropically, hydrogen atoms were refined isotropically with U(H) = 1.2 U_{eq}(parent atom) using a riding model. The R factor is slightly increased due to disorder in the cod ligand (C4 and C7), the 2-vinylpyridine and the tosylate. $R1$ = 0.0281, for $F^2 > 2\ \sigma(F^2)$; $wR2$ = 0.0701;[17] Goof(F^2) = 1.035; $\Delta\rho_{max}$ = 0.40, $\Delta\rho_{min}$ = −0.50 e$^-$ Å^{-3}. The data analysis and the drawing were made using the programs STRUX-V,[18] SIR-92,[19] SHELXL-93,[20] and SCHAKAL-97.[21]

Acknowledgments

We thank Dr. E. Herdtweck and Dr. W. Scherer (TU München) for performing the X-ray analyses. Prof. B. Hanson (Virginia Tech) is thanked for helpful comments on this manuscript. H. T. thanks the Fonds der Chemischen Industrie for a fellowship and T. E. M. for a Liebig-Stipendium. Financial support (Be 1931−3/1) from the Deutsche Forschungsgemeinschaft (DFG) and loans of precious metals by the Degussa AG and the Hoechst AG are gratefully acknowledged.

[1] M. Beller, H. Trauthwein, M. Eichberger, C. Breindl, T. E. Müller, O. Thiel, J. Herwig, *Chem. Eur. J.* **1999**, *5*, 1306.
[2] For a recent review see: T. E. Müller, M. Beller, *Chem. Rev.* **1998**, *98*, 675. − [2a] D. R. Coulson (Du Pont), US 3.758.586, **1973**; *Chem. Abstr.* **1973**, *79*, 125808g. − [2b] D. R. Coulson, *Tetrahedron Lett.* **1971**, 429. − [2c] L. S. Hegedus, *Angew. Chem.* **1988**, *100*, 1147; *Angew. Chem. Int. Ed. Engl.* **1988**, *27*, 1113. − [2d] A. L. Casalnuovo, J. L. Calabrese, D. Milstein, *J. Am. Chem. Soc.* **1988**, *110*, 6738. − [2e] D. Steinborn, B. Thies, I. Wagner, R. Taube, *Z. Chem.* **1989**, *29*, 333. − [2f] M. R. Gagné, T. J. Marks, *J. Am. Chem. Soc.* **1989**, *111*, 4108. − [2g] D. Selent, D. Scharfenberg-Pfeiffer, G. Reck, R. Taube, *J. Organomet. Chem.* **1991**, *415*, 417. − [2h] M. R. Gagné, C. L. Stern, T. J. Marks, *J. Am. Chem. Soc.* **1992**, *114*, 275. − [2i] J.-J. Brunet, D. Neibecker, K. Philippot, *Tetrahedron Lett.* **1993**, *34*, 3877. − [2j] R. C. Larock, T. R. Hightower, L. A. Hasvold, K. P. Peterson, *J. Org. Chem.* **1996**, *61*, 3584. − [2k] Y. Li, T. J. Marks, *J. Am. Chem. Soc.* **1996**, *118*, 707. − [2l] Y. Li, T. J. Marks, *J. Am. Chem. Soc.* **1996**, *118*, 9295. − [2m] Y. W. Li, T. J. Marks, *Organometallics* **1996**, *15*, 10212. − [2n] C. Hahn, J. Sieler, R. Taube, *Chem. Ber.* **1997**, *130*, 939. − [2o] R. Dorta, P. Egli, F. Zürchner, A. Togni, *J. Am. Chem. Soc.* **1997**, *119*, 10857. − [2p] C. Hahn, A. Vitagliano, F. Giordano, R. Taube, *Organometallics* **1998**, *17*, 2060.
[3] [3a] M. Beller, M. Eichberger, H. Trauthwein, *Angew. Chem.* **1997**, *109*, 2306; *Angew. Chem. Int. Ed. Engl.* **1997**, *36*, 2225. − [3b] M. Beller, M. Eichberger, H. Trauthwein, *Catalysis of Organic Reactions* (Ed.: F. Herkes), Marcel Dekker, **1998**.
[4] [4a] G. Roscher, F. Hofmann, K. A. Adey, W. Jeblick, H.-J. Klimisch in *Ullmann's Enzyclopädie der Technischen Chemie*, vol. 23, 4th ed. (Ed.: W. Gerhartz), VCH, Weinheim, **1983**, p. 612. − [4b] P. C. Jain, V. Kapoor, N. Anand, A. Ahmad, G. Patnaik, *J. Med. Chem.* **1967**, *10*, 812.
[5] W. Doering, R. A. N. Weil, *J. Am. Chem. Soc.* **1947**, *69*, 2461.
[6] [6a] E. Profft, *J. Prakt. Chem.* **1956**, *4*, 19. − [6b] A. P. Phillips, *J. Am. Chem. Soc.* **1956**, *78*, 4441. − [6c] G. Magnus, R. Levine, *J. Am. Chem. Soc.* **1956**, *78*, 4127.
[7] A. J. Matusko, A. Taurins, *Can. J. Chem.* **1954**, *32*, 538.
[8] H. E. Reich, R. Levine, *J. Am. Chem. Soc.* **1955**, *77*, 4913.
[9] M. I. Druzin, A. K. Valkova, A. B. Pashkov, I. V. Zaitseva, N. V. Bogdanova, L. D. Pertsov, S. F. Kalinkin, B. M. Kuindzhi, U.S.S.R. 215,997, **1968**; *Chem. Abstr.* **1968**, *69*, P52016d.
[10] M. Beller, H. Trauthwein, M. Eichberger, C. Breindl, T. E. Müller, A. Zapf, *J. Organomet. Chem.* **1998**, *566*, 277.
[11] [11a] M. S. Driver, J. F. Hartwig, *J. Am. Chem. Soc.* **1996**, *118*, 4206. − [11b] P. Diversi, L. Ermini, G. Ingrosso, A. Lucherini, C. Pinzino, L. Saramora, *J. Organomet. Chem.* **1995**, *494*, C1. − [11c] M. Schulz, D. Milstein, *J. Chem. Soc., Chem. Commun.* **1993**, 318. − [11d] A. L. Seligson, R. L. Cowan, W. C. Trogler, *Inorg. Chem.* **1991**, *30*, 3371. − [11e] M. D. Fryzuk, C. D. Montgomery, *Coord. Chem. Rev.* **1989**, *95*, 1.
[12] B. Denise, G. Pannetier, *J. Organomet. Chem.* **1978**, *161*, 171.
[13] H. S. Rzepa, M. H. Smith, M. L. Webb, *J. Chem. Soc., Perkin Trans. 2* **1994**, 703; P. N. Jagg, P. F. Kelly, H. S. Rzepa, D. J. Williams, J. D. Woolins, W. Wylie, *J. Chem. Soc., Chem. Commun.* **1991**, 942.
[14] G. Giordano, R. H. Crabtree, *Inorg. Synth.* **1979**, *19*, 218.

[15] R. R. Schrock, J. A. Osborn, *J. Am. Chem. Soc.* **1971**, *93*, 3089.
[16] *IPDS Operating System*, Version 2.7, STOE & Cie. GmbH, Darmstadt, Deutschland, **1996**.
[17] $R1 = \Sigma(||F_o| - |F_c||)/\Sigma|F_o|$); $wR2 = \{\Sigma[w(F_o^2 - F_c^2)^2]/\Sigma[w(F_o^2)^2]\}^{1/2}$.
[18] G. Artus, W. Scherer, T. Priermeier, E. Herdtweck, *STRUX-V, A Program System to Handle X-ray Data*, TU München, Germany, **1994**.
[19] A. Altomare, G. Cascarano, C. Giacovazzo, A. Guagliardi, M. C. Burla, G. Polidori, M. Camalli, *SIR-92*, University of Bari, Italy, **1992**.
[20] G. M. Sheldrick, *SHELXL-93, Program for the Refinement of Crystal Structures* (Ed.: G. M. Sheldrick), University of Göttingen, Germany, **1993**.
[21] E. Keller, *SCHAKAL-97*, Albert-Ludwigs-Universität Freiburg, Germany, **1997**.

Received November 10, 1998
[I98386]

Derivative Chemistry of $[Ru_2(\mu\text{-bdt})(CO)_6]$, a Binuclear Ruthenium(I) Carbonyl Complex Containing a Bridging Benzene-1,2-dithiolate Ligand

Javier A. Cabeza,*[a] M. Angeles Martínez-García,[a] Víctor Riera,[a] Diego Ardura,[b] Santiago García-Granda,[b] and Juan F. Van der Maelen[b]

Keywords: Ruthenium / Thiolate ligands / Dithiolate ligands / Substitution reactions / Electrophilic additions

The known dithiolate-bridged ruthenium(I) complex $[Ru_2(\mu\text{-bdt})(CO)_6]$ (**1**) (bdt = benzene-1,2-dithiolate) has been prepared in fair yield (55%) by the sequential treatment of $RuCl_3{\cdot}nH_2O$ with carbon monoxide, benzene-1,2-dithiol and zinc in a one-pot reaction. Complex **1** reacts readily with monodentate phosphanes to give, stepwise, the penta- and tetracarbonyl derivatives $[Ru_2(\mu\text{-bdt})(CO)_{6-n}(PR_3)_n]$ (n = 1, 2; R = Ph, Cy, *i*Pr). However, the reaction of **1** with one equivalent of bis(diphenylphosphanyl)methane (dppm) affords a mixture of complex **1** and the disubstituted derivative $[Ru_2(\mu\text{-bdt})(CO)_4(\eta^1\text{-dppm})_2]$, in which the dppm ligands are monodentate. This mixture is subsequently transformed into a polymeric material of formula $[\{Ru_2(\mu\text{-bdt})(CO)_4\}(\mu\text{-dppm})]_n$, which consists of binuclear $\{Ru_2(\mu\text{-bdt})(CO)_4\}$ units linked to each other by bridging dppm ligands. The use of two equivalents of dppm leads to $[Ru_2(\mu\text{-bdt})(CO)_4(\eta^1\text{-dppm})_2]$ in quantitative yield. The X-ray diffraction structure of $[Ru_2(\mu\text{-bdt})(CO)_4(P\textit{i}Pr_3)_2]$ (**3c**) confirms that the phosphane ligands are located in axial positions, *cis* to both sulfur atoms, and that the Ru–Ru distance is short [2.6753(7) Å]. A comparative study of the reactivity of complexes **1** and **3c** with the electrophiles H^+, $[Au(PPh_3)]^+$, and $HgCl_2$ has allowed the isolation of the derivatives $[Ru_2(\mu\text{-H})(\mu\text{-bdt})(CO)_{6-n}(P\textit{i}Pr_3)_n][BF_4]$ (n = 0, 2), $[Ru_2Au(\mu\text{-bdt})(CO)_{6-n}(P\textit{i}Pr_3)_n(PPh_3)][BF_4]$ (n = 0, 2) and $[Ru_2HgCl_2(\mu\text{-bdt})(CO)_{6-n}(P\textit{i}Pr_3)_n]$ (n = 0, 2), respectively.

Introduction

Over the past few years, several authors have reported general high-yield routes to binuclear ruthenium(I) tetracarbonyl complexes containing two bridging alkyl- or arylthiolate ligands of the type $[Ru_2(\mu\text{-SR})_2(CO)_4(PR_3)_2]$[1–4]. However, the closely related hexacarbonyl compounds $[Ru_2(\mu\text{-SR})_2(CO)_6]$, although known for many years, have so far been prepared in low yields[5–11], their derivative chemistry being virtually unexplored.

We now report a new synthesis of the hexacarbonyl complex $[Ru_2(\mu\text{-bdt})(CO)_6]$ (**1**) (bdt = benzene-1,2-dithiolate), starting from readily accessible starting materials ($RuCl_3 \cdot n\ H_2O$, benzene-1,2-dithiol, carbon monoxide, and zinc), in a fair yield (50–60%), following a simple one-pot reaction which can be carried out on milligram or gram scales.

Such a convenient synthetic procedure, in addition to the fact that the doubly bridging attachment of the bdt ligand to the metal atoms in complex **1** rules out the complication of having *syn* and *anti* isomers, which do exist in bis(monothiolate)-bridged complexes[4], makes complex **1** an excellent candidate for reactivity studies. We report herein its reactivity with some nucleophilic and electrophilic reagents. This type of reactivity study has not been previously reported on hexacarbonyl thiolate-bridged diruthenium(I) complexes, probably as a consequence of the lack of a convenient synthetic route to such compounds.

[a] Departamento de Química Orgánica e Inorgánica,
[b] Departamento de Química Física y Analítica, Universidad de Oviedo,
E-33071 Oviedo, Spain
Fax: (internat.) + 34-985/103446
E-mail: jac@sauron.quimica.uniovi.es

Results and Discussion

Synthesis of Complex 1

The reaction of carbon monoxide with $RuCl_3 \cdot n\ H_2O$ in 2-methoxyethanol at reflux temperature gives a yellow solution. Treatment of this solution with benzene-1,2-dithiol and granular zinc as reducing agent has allowed the isolation of the hexacarbonyl complex **1** in 55% yield. This complex has previously been prepared in lower yield (35%) by treating $[Ru_3(CO)_{12}]$ with benzene-1,2-dithiol in toluene at reflux temperature[11].

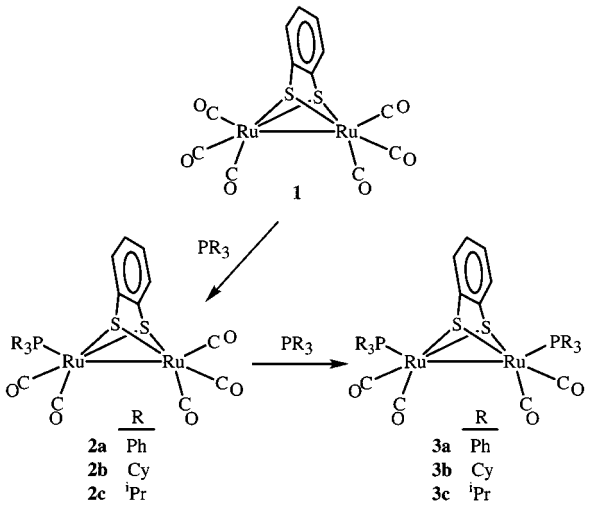
An analogous synthetic method has previously been used to prepare other complexes containing ligand-bridged $Ru(CO)_3$ units, such as $[Ru_2(\mu\text{-pz})_2(CO)_6]$ (Hpz = pyrazole)[12] and $[Ru_3(\mu\text{-}PPh_2)_3(CO)_9]Cl$[13]. It is well known that the yellow solution formed by treating $RuCl_3 \cdot n\ H_2O$ with carbon monoxide in 2-methoxy- or 2-ethoxyethanol is a useful precursor for the synthesis of mononuclear ruthenium(II) compounds[14] and for the low-pressure preparation of $[Ru_3(CO)_{12}]$[15]; however, not until recently was the colorless ruthenium(II) dimer $[Ru_2Cl_2(\mu\text{-Cl})_2(CO)_6]$ described as the major component of that yellow solution[16].

Reactions of Complex 1 with Monodentate Phosphane Ligands

Addition of one equivalent of a monodentate phosphane ligand to a room temperature THF solution of compound

 © WILEY-VCH Verlag GmbH, D-69451 Weinheim, 1999 1434–1948/99/0707–1133 $ 17.50+.50/0

1 led to the quantitative (IR) formation of monosubstituted derivatives of the type $[Ru_2(\mu\text{-bdt})(CO)_5(PR_3)]$ (**2a**: R = Ph; **2b**: R = Cy; **2c**: R = *i*Pr). The three compounds have very similar IR spectra in the carbonyl stretching region (Table 1), as expected for compounds having analogous structures. The structure depicted in Scheme 1 for these compounds, in which the phosphane ligand is in a position *cis* to both sulfur atoms, has been unequivocaly inferred from their ^{1}H-NMR spectra, which show the aromatic protons of the bridging bdt ligand as two multiplets corresponding to an AA′MM′ spin system; therefore, the phosphorus atom of the phosphane ligand is in a mirror plane that cuts the bdt ligand into two identical halves (C_s symmetry).



Scheme 1. Reactivity of complex **1** with monophosphanes

Table 1. Selected IR and NMR data

Comp	ν(CO)[a] [cm^{-1}]	δ(^{31}P{^{1}H})[b] [ppm]
2a	2064 (s), 2009 (vs), 1985 (m), 1948 (w)[c]	40.6 (s)
2b	2059 (s), 2001 (vs), 1979 (m), 1937 (w)[c]	56.6 (s)
2c	2061 (s), 2002 (vs), 1981 (m), 1938 (w)[c]	64.2 (s)
3a	2013 (vs), 1978 (m), 1948 (s)[c]	37.4 (s)
3b	2002 (vs), 1986 (m), 1934 (s)[c]	48.7 (s)
3c	2007 (vs), 1964 (m), 1935 (s)[c]	57.8 (s)
4	2011 (vs), 1975 (m), 1945 (s)[c]	25.7 (m), −24.9 (m)
5	1997 (vs), 1967 (m), 1938 (s)[d]	
6b	2068 (vs), 2050 (m), 2010 (s)[c]	63.7(s)
7a	2097 (vs), 2055 (s), 2040 (m)[c]	64.8 (s)
7b	2020 (w), 2002 (m), 1962 (vs)[c]	59.5 (d)[e], 57.2 (t)[e]
8a	2119 (vs), 2069 (s), 2008 (w), 1985 (w)[f]	
8b	2049 (m), 2034 (m), 1995 (s)[c]	59.4 (s)

[a] Abbreviations for IR data: s = strong, m = medium, w = weak, v = very. − [b] In $CDCl_3$; abbreviations for NMR data: s = singlet, d = doublet, t = triplet, m = multiplet. − [c] In CH_2Cl_2. − [d] In Nujol mull. − [e] $J_{P\text{-}P}$ = 32.0 Hz. − [f] In acetone.

Addition of at least two equivalents of a monodentate phosphane ligand to a room temperature THF solution of compound **1** led to the immediate formation of monosubstituted derivatives. The incorporation of a second phosphane ligand into the complexes required a higher temperature (THF under reflux), leading to the compounds $[Ru_2(\mu\text{-bdt})(CO)_4(PR_3)_2]$ (**3a**: R = Ph; **3b**: R = Cy; **3c**: R = *i*Pr). The structure of C_{2v} symmetry shown in Scheme 1 for these compounds is validated by their IR [three ν(CO) absorptions] and NMR spectroscopic data (an AA′MM′ spin system accompanied by the signals corresponding to the phosphane ligand in the ^{1}H-NMR spectrum and one singlet in the ^{31}P{^{1}H}-NMR spectrum), which are compatible with the existence in the compounds of two perpendicular mirror planes.

It has been reported that the binuclear ruthenium(I) complex $[Ru_2(\mu\text{-dan})(CO)_6]$ (H_2dan = 1,8-diaminonaphthalene), which is structurally related to **1** but has an *N*-donor instead of an *S*-donor bridging ligand, undegoes a rapid substitution of two CO ligands by phosphane ligands at room temperature[17]. This has been associated with a strong *cis* labilization effect of the hard *N*-donor bridging ligand[18]. The fact that the second substitution of CO by a phosphane ligand in **1** is slow indicates that the bdt ligand is not as strong *cis* labilizer as the dan ligand, probably due to the softer character of the *S*-donor ligand.

Compounds **3a**, **3b**, and **3c** could also be prepared in fair yields (43−73%) in one-pot reactions starting from $RuCl_3 \cdot n\,H_2O$, in an analogous procedure as that described above for compound **1** but carrying out the final step in the presence of the appropriate phosphane ligand. While this work was in progress, Shiu et al. reported an alternative synthesis of compound **3a** by treating the cationic binuclear compound $[Ru_2(CO)_4(PPh_3)_2(MeCN)_4][BF_4]_2$ with benzene-1,2-dithiol in the presence of triethyl amine[3].

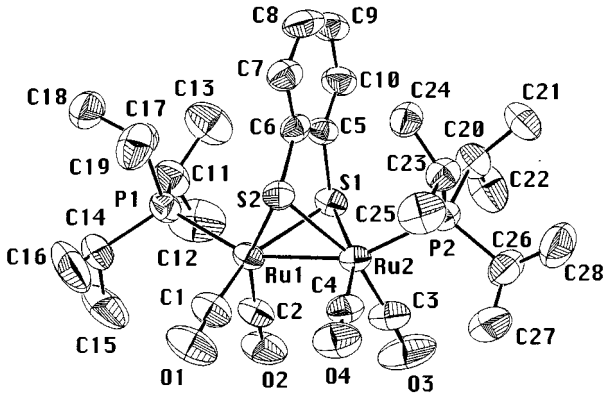


Figure 1. Molecular structure of complex **3c**. Thermal ellipsoids are drawn at 50% probability level

Compound **3c** has been characterized by X-ray diffraction methods (Figure 1). Relevant bond lengths and angles are given in Table 2. Overall, the structure reminds those of many other diruthenium(I) complexes containing bridging ligands[2−4,11,18,19]. The most interesting feature is that the Ru−Ru distance [2.6753(7) Å] is comparable to that found in the unsubstituted complex **1** [2.650(2) Å][11] and also to those found in related complexes containing other thiolate bridging ligands[2−4]. These data indicate that the metal−metal distance in diruthenium(I) compounds containing bridging ligands is little affected by the nature of the terminal ligands. However, such a distance is indeed affected

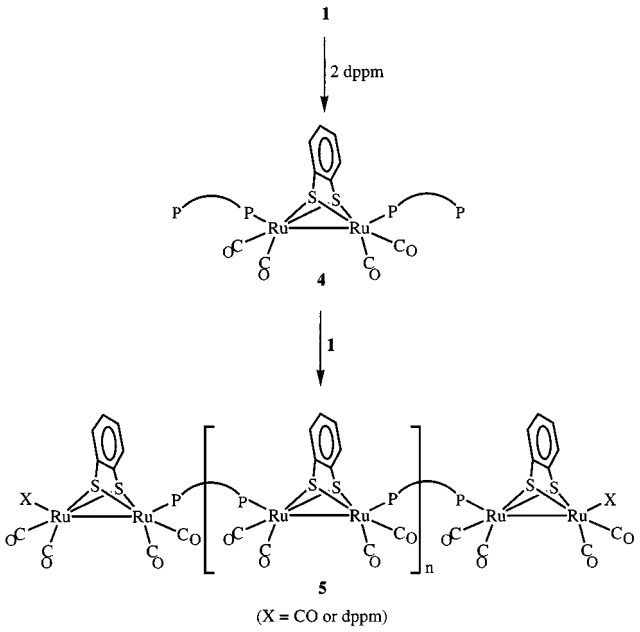
by the nature of the bridging ligands, since the shorter Ru−Ru distance found in the complex $[Ru_2(\mu\text{-dab})(CO)_4(PPh_3)_2]$ (H_2dab = 1,2-diaminobenzene), 2.558(1) Å[19], which is analogous to **3a** but has *N*-donor instead of *S*-donor atoms, can be associated to the smaller size of bridgehead nitrogen atom.

Table 2. Selected structural parameters in complex **3c**

Bond Lengths [Å]		*Bond Angles* [°]	
Ru(1)−Ru(2)	2.6753(7)	C(1)−Ru(1)−C(2)	89.4(3)
Ru(1)−S(1)	2.430(2)	C(1)−Ru(1)−S(1)	155.8(3)
Ru(1)−S(2)	2.428(2)	C(1)−Ru(1)−S(2)	93.2(2)
Ru(2)−S(1)	2.428(2)	C(2)−Ru(1)−S(1)	91.4(2)
Ru(2)−S(2)	2.434(2)	C(2)−Ru(1)−S(2)	157.1(2)
Ru(1)−P(1)	2.411(2)	S(1)−Ru(1)−Ru(2)	56.54(4)
Ru(2)−P(2)	2.400(2)	S(2)−Ru(1)−Ru(2)	56.73(4)
Ru(1)−C(1)	1.868(8)	S(1)−Ru(1)−S(2)	77.20(6)
Ru(1)−C(2)	1.862(7)	P(1)−Ru(1)−Ru(2)	153.30(4)
Ru(2)−C(3)	1.865(7)	P(1)−Ru(1)−S(1)	104.18(6)
Ru(2)−C(4)	1.858(9)		

Reactions of Complex 1 with the Bidentate Ligand dppm

Treatment a THF solution of compound **1** with bis(diphenylphosphanyl)methane (dppm), in a 1:1 mol ratio, readily resulted (30 min, room temperature) in the formation of the disubstituted derivative $[Ru_2(\mu\text{-bdt})(CO)_4(\eta^1\text{-dppm})_2]$ (**4**), while half the initial amount of the starting complex **1** remained (IR identification). After stirring for 4 h, a yellow solid began to precipitate from the solution. After 3 days the precipitate was copious and the liquid phase was nearly colorless. This solid, subsequently identified as the polymer $[\{Ru_2(\mu\text{-bdt})(CO)_4\}(\mu\text{-dppm})]_n$ (**5**), is insoluble in all common solvents. Compound **4** can be prepared in high yield by treating **1** with dppm in a 1:2 mol ratio.



Scheme 2. Reactivity of complex **1** with dppm

The structure shown in Scheme 2 for complex **4** is substantiated by its analytical and spectroscopic data. In particular, its $^{31}P\{^1H\}$-NMR spectrum, which consists of two multiplets at δ = 25.7 and −24.9 (AA′XX′ spin system), indicates that the two dppm ligands are symmetry-related and that they are coordinated in a monodentate mode. The ν(CO) region of its IR spectrum is comparable to those of compounds **3a**, **3b**, and **3c** (Table 1), indicating a similar arrangement of the carbonyl ligands (C_{2v} symmetry). Analogous spectral data have previously been reported for the related diruthenium(I) complexes $[Ru_2(\mu\text{-dan})(CO)_4(\eta^1\text{-dppm})_2]$[17] and $[Ru_2(\mu\text{-MeCO}_2)_2(CO)_4(\eta^1\text{-dppm})_2]$[20], which contain *N*- and *O*-donor bridging ligands, respectively.

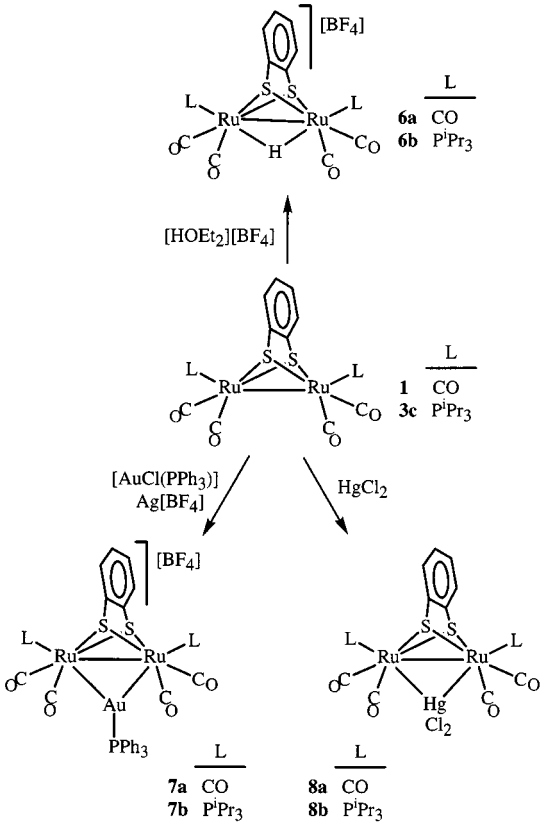
Due to its insolubility, compound **5** could only be characterized by microanalysis and IR spectroscopy. Nevertheless, we think that its structure is likely to be that depicted in Scheme 2, because the available data indicate that there is only one dppm ligand per $\{Ru_2(\mu\text{-bdt})(CO)_4\}$ unit (CHN microanalysis) and that the local C_{2v} symmetry of the $\{Ru_2(\mu\text{-bdt})(CO)_4\}$ unit is maintained in the polymer since three ν(CO) absorptions are observed in the IR spectrum (Table 1). It has been reported that the compounds $[\{Ru_2(\mu\text{-dan})(CO)_4\}(\mu\text{-dppm})]_n$[17] and $[\{Ru_2(\mu\text{-MeCO}_2)_2(CO)_4\}(\mu\text{-dppm})]_n$[20] also have a polymeric nature, in which the dppm ligands linking the corresponding dimetallic units. However, the iodide-bridged compound $[Ru_2(\mu\text{-I})_2(CO)_4(\mu\text{-dppm})]$ is not polymeric and the dppm ligand spans the same metal atoms as the iodide bridges[21].

Reactions of Compounds 1 and 3c with Electrophilic Reagents

The availability of both the hexacarbonyl compound **1** and the phosphane-substituted tetracarbonyl derivative **3c** allowed us to carry out a comparative study of their reactions with electrophilic reagents. Among the phosphane-substituted tetracarbonyl derivatives prepared from complex **1**, we decided to use **3c** for the reactivity studies because it contains the most basic phosphane ligand. Such a reactivity study would help us to determine whether or not the nucleophilic character of the dithiolate-bridged ruthenium(I) dimers is affected by the nature of the axial ligands. Furthermore, such a study, coupled to previous ones carried out with related complexes having *N*-donor bridging ligands[17,22,23], would also shed light on the effect that the nature of the bridging ligand has on the nucleophilic character of this class of ligand-bridged ruthenium(I) dimers.

Both compounds, **1** and **3c**, could be protonated with an excess of $[HOEt_2][BF_4]$ in dichloromethane solvent to give the cationic derivatives $[Ru_2(\mu\text{-H})(\mu\text{-bdt})(CO)_{6-n}(P\textit{i}Pr_3)_n][BF_4]$ (**6a**: $n = 0$; **6b**: $n = 2$). Compound **6a** was unstable in solution and it undergoes spontaneous deprotonation in the absence of an excess of acid, even in solvents of low basicity such as dichloromethane or chloroform, to reform the neutral precursor **1**[11]. However, the substituted derivative **6b**

is stable as far as deprotonation in solution is concerned. Curiously, it has been reported that the behavior of $[Ru_2(\mu\text{-dan})(CO)_6]$[17] and $[Ru_2(\mu\text{-dan})(CO)_4(P\textit{i}Pr_3)_2]$[22] in protonation reactions is comparable to that observed for complexes **1** and **3c**.



Scheme 3. Reactions of compounds **1** and **3c** with electrophilic reagents

Compounds **1** and **3c** reacted with $[AuCl(PPh_3)]$ in the presence of $Ag[BF_4]$ to give AgCl and the cationic trinuclear derivatives $[Ru_2Au(\mu\text{-bdt})(CO)_{6-n}(P\textit{i}Pr_3)_n(PPh_3)][BF_4]$ (**7a**: $n = 0$; **7b**: $n = 2$). In related reactions, treatment of **1** and **3c** with mercury(II) chloride resulted in the formation of the corresponding adducts $[Ru_2HgCl_2(\mu\text{-bdt})(CO)_{6-n}(P\textit{i}Pr_3)_n]$ (**8a**: $n = 0$; **8b**: $n = 2$). Their IR spectra display the ν(CO) absorptions shifted to higher wavenumbers than those of the corresponding starting materials (Table 1), confirming a decrease of electron density at the ruthenium atoms. The $^{31}P\{^1H\}$-NMR spectra of the tetracarbonyl derivatives **7b** and **8b** indicate that both compounds have equivalent $P\textit{i}Pr_3$ ligands since that of **7b** consists of an AX_2 spin system and that of **8b** is just a singlet, supporting the structures depicted in Scheme 3. It has been reported that the diamido-bridged compound $[Ru_2(\mu\text{-dan})(CO)_6]$ is not basic enough to react with the metallic electrophiles $[Au(PPh_3)]^+$ and $HgCl_2$[17]; however, they do react with the disubstituted derivative $[Ru_2(\mu\text{-dan})(CO)_4(P\textit{i}Pr_3)_2]$ to give the corresponding adducts[22][23]. The related compound $[Ru_2(\mu\text{-dab})(CO)_4(PPh_3)_2]$ also reacts with electrophilic metallic fragments to give stable adducts[24].

All these data indicate that, in ligand-bridged diruthenium(I) carbonyl complexes, the basicity of the metal atoms is greatly affected by the nature of both the terminal and the bridging ligands. It was known that compounds having terminal phosphane ligands are more basic than their unsubstituted carbonyl precursors[22][23], but the results commented above experimentally demonstrate that complexes containing thiolate bridging ligands are more basic than their amido-bridged relatives. These results have also been confirmed by simple theoretical calculations at the extended Hückel level, which have shown that (a) the HOMOs of this kind of binuclear ligand-bridged ruthenium(I) complexes are of bonding character between the metal atoms, (b) that their composition is based mainly of orbitals belonging to the metal atoms[11][25] and (c) that the positive charges beared by the metal atoms in $[Ru_2(\mu\text{-dan})(CO)_6]$ and $[Ru_2(\mu\text{-bdt})(CO)_6]$ are higher than those beared by the substituted derivatives $[Ru_2(\mu\text{-dan})(CO)_4(PH_3)_2]$ and $[Ru_2(\mu\text{-bdt})(CO)_4(PH_3)_2]$. These charges are expected to be inversely related to the basicity of the metal atoms in the complexes (the higher the charge, the less basic the metal atom), thus supporting the experimental reactivity results.

Experimental Section

General: Solvents were dried with sodium diphenyl ketyl (THF, diethyl ether, hydrocarbons), molecular sieves (2-methoxyethanol) or CaH_2 (dichloromethane) and distilled under nitrogen prior to use. − Unless otherwise stated, the reactions were carried out under nitrogen at room temperature by Schlenk-vacuum line techniques, and were routinely monitored by solution IR spectroscopy (carbonyl stretching region). − The compounds **6a**[11] and $[AuCl(PPh_3)]$[26] were prepared as described in the literature, $RuCl_3 \cdot n\,H_2O$ was purchased from Pressure Chemicals, all other reagents were purchased from Aldrich. − IR: Perkin−Elmer FT 1720-X. − NMR: Bruker AC-200 and AC−300, 23°C, $SiMe_4$ (internal, for ^1H) or 85% H_3PO_4 (external, for ^{31}P) as standards (δ = 0 ppm). − Microanalyses were obtained from the University of Oviedo Analytical Service.

One-Pot Synthesis of 1 from $RuCl_3 \cdot n\,H_2O$: Carbon monoxide was bubbled through a solution of $RuCl_3 \cdot n\,H_2O$ (500 mg, 2.054 mmol) in 2-methoxyethanol (30 mL) at reflux temperature until the color changed to pale yellow (ca. 3 h). The addition of H_2bdt (130 μL, 1.130 mmol) was followed by addition of granular zinc (ca. 1 g). Maintaining the bubbling of carbon monoxide, the mixture was stirred at reflux temperature for 2 h to give an orange precipitate. After cooling to room temperature, the mixture was poured into a beaker containing water (500 mL). The tan precipitate was filtered through a celite pad. The solid was washed with water (3× 5 mL), dried by passing air through the filter and extracted from the filter with dichloromethane. The extracts were concentrated to ca. 2 mL and the concentrate introduced into a chromatography column (2.5 × 10 cm) packed with neutral alumina (activity I) in hexane. After the column was washed with hexane, dichloromethane eluted a yellow band which afforded compound **1** as a yellow solid. − Yield: 270 mg (55%). − Its analytical and spectroscopic data matched those reported in the literature[11].

Preparation of 2a, 2b, 2c, 3a, 3b, and 3c by Reaction of Compound 1 with Monodentate Phosphane Ligands: The appropriate amount

of the corresponding phosphane ligand was added to a solution of compound **1** in THF (10 mL). After being stirred at the appropriate temperature, the solvent was removed under reduced pressure and the residue was washed with hexane (2× 2 mL) and dried under vacuum to give the product as a yellow solid.

2a: Reagents: 42 mg (0.082 mmol) of **1** and 22 mg (0.083 mmol) of PPh_3. − Reaction time: 3 h at room temperature. − Yield: 50 mg (81%). − $C_{29}H_{19}O_5PRu_2S_2$: calcd: C 46.77, H 2.57; found: C 46.54, H 2.55. − ^{1}H NMR ($CDCl_3$): δ = 7.44−7.22 (m, 15 H), 6.61 (m, 2 H), 6.24 (m, 2 H).

2b: Reagents: 80 mg (0.156 mmol) of **1**, 44 mg (0.156 mmol) of PCy_3. − Reaction time: 3 h at room temperature. − Yield: 80 mg (67%). − $C_{29}H_{37}O_5PRu_2S_2$: calcd: C 44.66, H 4.89; found: C 44.86, H 5.01. − ^{1}H NMR ($CDCl_3$): δ = 7.13 (m, 2 H), 6.60 (m, 2 H), 2.30−1.10 (m, 33 H).

2c: Reagents: 50 mg (0.098 mmol) of **1**, 18.4 μL (0.098 mmol) of P*i*Pr$_3$. − Reaction time: 10 min at room temperature. − Yield: 55 mg (78%). − $C_{20}H_{25}O_5PRu_2S_2$: calcd: C 37.38, H 3.92; found: C 37.02, H 3.94. − ^{1}H NMR ($CDCl_3$): δ = 7.11 (m, 2 H), 6.57 (m, 2 H), 2.10 (m, 3 H), 1.22 (m, 18 H).

3a: Reagents: 30 mg (0.059 mmol) of **1**, 33 mg (0.124 mmol) of PPh_3. − Reaction time: 20 min at reflux temperature. − Yield: 40 mg (70%). − $C_{46}H_{34}O_4P_2Ru_2S_2$: calcd: C 56.44, H 3.75; found: C 56.41, H 3.75. − ^{1}H NMR ($CDCl_3$): δ = 7.42−7.29 (m, 30 H), 6.06 (m, 2 H), 5.85 (m, 2 H).

3b: Reagents: 30 mg (0.059 mmol) of **1**, 33 mg (0.117 mmol) of PCy_3. − Reaction time: 40 min at reflux temperature. − Yield: 45 mg (78%). − $C_{46}H_{70}O_4P_2Ru_2S_2$: calcd: C 56.32, H 7.19; found: C 56.10, H 7.15. − ^{1}H NMR ($CDCl_3$): δ = 7.06 (m, 2 H), 6.54 (m, 2 H), 1.52−1.17 (m, 66 H).

3c: Reagents: 50 mg (0.098 mmol) of **1**, 46 μL (0.245 mmol) of P*i*Pr$_3$. − Reaction time: 25 min at reflux temperature. − Yield: 60 mg (79%). − $C_{28}H_{46}O_4P_2Ru_2S_2$: calcd: C 43.40, H 5.98; found: C 42.98, H 5.71. − ^{1}H NMR ($CDCl_3$): δ = 7.02 (m, 2 H), 6.47 (m, 2 H), 2.07 (m, 6 H), 1.22 (m, 36 H).

One-pot Synthesis of 3a, 3b, and 3c from $RuCl_3 \cdot n\,H_2O$: Carbon monoxide was bubbled through a solution of $RuCl_3 \cdot n\,H_2O$ (500 mg, 2.054 mmol) in 2-methoxyethanol (30 mL) at reflux temperature until the color changed to pale yellow (ca. 3 h). The addition of H_2bdt (130 μL, 1.130 mmol) was followed by addition of granular zinc (ca. 1 g). Maintaining the bubbling of carbon monoxide, the mixture was stirred at reflux temperature for 15 min to give an orange precipitate. After adding the appropriate amount of the corresponding phosphane ligand (2.060 mmol), the mixture was cooled to room temperature under nitrogen and was stirred for 3 h. The suspension was filtered through a celite pad. The liquid phase was discarded off and the solid was extracted from the filter with dichloromethane. The extract was evaporated to dryness and the residue was washed with diethyl ether (2 × 3 mL) to give the corresponding product as a yellow solid. − Yields: 48% (**3a**), 43% (**3b**), and 73% (**3c**).

Preparation of 4: Solid dppm (75.3 mg, 0.196 mmol) was added to a solution of complex **1** (50 mg, 0.098 mmol) in THF (25 mL). The solution was stirred for 5.5 h and the solvent was removed under reduced pressure. The residue was washed with diethyl ether (2× 2 mL) and dried under vacuum to give complex **4** as a yellow solid. − Yield 90 mg (75%). − $C_{60}H_{48}O_4P_4Ru_2S_2$: calcd: C 58.74, H 4.05; found: C 58.92, H 3.95. − ^{1}H NMR ($CDCl_3$): δ = 7.1−7.3 (m, 40 H), 6.16 (m, 4 H) 2.96 (m, 4 H).

Preparation of 5: Solid dppm (37.6 mg, 0.098 mmol) was added to a solution of complex **1** (50 mg, 0.098 mmol) in THF (25 mL). After stirring for 30 min, the IR spectrum showed a ca. 50% mixture of complexes **1** and **4**. After 4 h, a yellow solid began to precipitate. The mixture was stirred for 3 days, when the precipitate was copious and the liquid phase was nearly colorless. The liquid was decanted off and the solid was washed with THF (2 × 5 mL) and dried under vacuum. − Yield 90 mg (75%). − $C_{35}H_{26}O_4P_2Ru_2S_2$: calcd: C 50.12, H 3.12; found: C 49.38, H 3.02.

Preparation of 6b: An excess of $[HOEt_2][BF_4]$ (4 drops from a pasteur pipette) was added to a solution of complex **1** (100 mg, 0.129 mmol) in dichloromethane (10 mL). The color of the solution changed from yellow to very pale yellow. The solvent was removed under reduced pressure and the oily residue was washed with diethyl ether (3 × 2 mL) to give complex **6b** as a white powder. − Yield 89 mg (80%). − $C_{28}H_{47}BF_4O_4P_2Ru_2S_2$: calcd: C 38.98, H 5.49; found: C 38.29, H 5.78. − ^{1}H NMR (CD_2Cl_2): δ = 7.24 (m, 2 H), 6.83 (m, 2 H), 2.20 (m, 6 H), 1.3 (m, 36 H), −16.16 (t, $J_{H\text{-}P}$ = 29.5 Hz, 1 H).

Preparation of 7a and 7b: Solid $Ag[BF_4]$ was added to a THF solution (15 mL) containing $[AuCl(PPh_3)]$ and the appropriate ruthenium starting complex. A white precipitate of AgCl was immediately formed. The mixture was stirred for 30 min and the solvent was removed under reduced pressure. The residue was extracted with dichloromethane (3 × 5 mL) and the filtered solution was evaporated to dryness. The yellow solid was washed with diethyl ether (2 × 3 mL) and dried under vacuum.

7a: Reagents: 20 mg (0.039 mmol) of **1**, 19.3 mg (0.039 mmol) of $[AuCl(PPh_3)]$, 7.6 mg (0.039 mmol) of $Ag[BF_4]$. − Yield: 29 mg (73%). − $C_{30}H_{19}AuBF_4O_6Ru_2S_2$: calcd: C 35.14, H 1.87; found: C 34.89, H 1.98. − ^{1}H NMR ($CDCl_3$): δ = 7.6−7.3. (m, 17 H), 6.88 (m, 2 H).

7b: Reagents: 50 mg (0.064 mmol) of **3c**, 31.7 mg (0.064 mmol) of $[AuCl(PPh_3)]$, 13 mg (0.064 mmol) of $Ag[BF_4]$. − Yield: 60 mg (72%). − $C_{46}H_{61}AuBF_4O_4P_2Ru_2S_2$: calcd: C 42.83, H 4.77; found: C 42.91, H 4.83. − ^{1}H NMR ($CDCl_3$): δ = 7.57 (m, 15 H), 7.15 (m, 2 H), 6.78 (m, 2 H), 2.23 (m, 6 H), 1.72 (m, 36 H).

Preparation of 8a and 8b: Solid $HgCl_2$ was added to a solution of the appropriate ruthenium starting complex in THF (15 mL). The solution was stirred for 30 min to give a yellow solid (**8a**) or a yellow solution (**8b**). The solvent was removed under reduced pressure and the solid yellow residue was washed with diethyl ether (2 × 3 mL) and dried under vacuum.

8a: Reagents: 30 mg (0.059 mmol) of **1**, 16 mg (0.059 mmol) of $HgCl_2$. − Yield: 30 mg (65%). − $C_{12}H_4Cl_2HgO_6Ru_2S_2$: calcd: C 18.43, H 0.52; found: C 18.41, H 0.75. − ^{1}H NMR ([D$_6$]acetone): δ = 7.44 (m, 2 H), 6.92 (m, 2 H).

8b: Reagents: 50 mg (0.064 mmol) of **3c**, 17.5 mg (0.064 mmol) of $HgCl_2$. − Yield: 40 mg (60%). − $C_{28}H_{46}Cl_2HgO_4P_2Ru_2S_2$: calcd: C 32.14, H 4.43; found: C 31.83, H 4.36. − ^{1}H NMR ($CDCl_3$): δ = 7.19 (m, 2 H), 6.77 (m, 2 H), 2.21 (m, 6 H), 1.3 (m, 36 H).

Crystal Structure Determination of 3c: Crystal data and details of the structure determination are listed in Table 3. The unit cell dimensions were determined from the angular settings of 25 reflections with 15° < Θ < 20°. The orthorhombic space group $P2_1nb$ was determined from systematic absences and confirmed by the structure determination. The intensity was checked throughout data collection by monitoring three standard reflections every 60 min. Final drift correction factors were between 1.00 and 1.01. Profile analysis[27] was performed on all reflections. A semiempirical absorption correction was applied, using ψ scans[28] (correction factors were in the range 0.973 to 1.000). No doubly measured

reflections were obtained. Lorentz and polarization corrections were applied and data were reduced to $|F_o|^2$ values.

Table 3. Crystallographic and refinement data for complex **3c**

formula	$C_{28}H_{46}O_4P_2Ru_2S_2$
fw	774.85
cryst syst	orthorhombic
space group	$P2_1nb$
a, b, c [A]	11.503(1), 26.781(3), 11.023(2)
V [Å^3]	3395.9(9)
Z	4
F(000)	1584
D_{calcd} [g/cm^3]	1.516
absorption correction	ψ-scans
μ [mm^{-1}]	1.136
cryst size [mm]	0.33 × 0.33 × 0.33
radiation (λ [A])	Mo-K_α (0.71073)
diffractometer	Enraf-Nonius CAD4
monochromator	graphite
temp [K]	293 (2)
scan method	ω−2θ
min/max h, k, l	0 /13, 0/31, 0/13
θ range [°]	1.52 to 24.97
data set	3137
unique data	3137
data with $I>2\sigma(I)$	2633
restraints, parameters	1, 383
$R(F)_{I>2\sigma(I)}$[a]	0.0281
$R_w(F^2)_{\text{all data}}$[b]	0.0733
GOF[c]	1.027
Δ/σ	0.001
max, min Δρ [e/Å^3]	0.339, −0.409

[a] $R(F) = \Sigma||F_o| - |F_c||/\Sigma|F_o|$. − [b] $R_w(F^2) = [\Sigma w(F_o^2 - F_c^2)^2/\Sigma w(F_o^2)^2]^{1/2}$, period − [c] Goodness of fit (GOF) = $[\Sigma w(F_o^2 - F_c^2)^2/(N - P)]^{1/2}$.

The structure was solved by Patterson interpretation using the program DIRDIF92[29]. An isotropic least-squares refinement, using a local version of SHELX[30], was followed by an empirical absorption correction[31] (maximum and minimum correction factors 1.547 and 0.698, respectively). Full-matrix anisotropic least-squares refinement over F^2, using the program SHELXL92[32], followed by a difference Fourier synthesis allowed the location of all the hydrogen atoms. Positional parameters and anisotropic thermal parameters of the non-hydrogen atoms were refined. All hydrogen atoms were refined isotropically, constraining the bond angles but with free distances to their parent atoms. The thermal parameter used for the aliphatic hydrogen atoms was differerent from that used for the aromatic hydrogen atoms. The function minimized was $\Sigma w(|F_o|^2 - |F_c|^2)^2$, $w = 1/[\sigma^2(F_o^2) + (0.0462{\cdot}P)^2]$, with $\sigma(F_o)$ from counting statistics and $P = (F_o^2 + 2F_c^2)/3$. Atomic scattering factors were taken from the literature[33]. The plot in Figure 1 was made with the EUCLID package[34]. Geometrical calculations were made with PARST[35]. All computations were performed on an Alpha AXP3000 workstation.

Crystallographic data (excluding structure factors) for compound **3c** have been deposited with the Cambridge Crystallographic Data Centre as supplementary publication no. CCDC-109933. Copies of the data can be obtained free of charge on application to CCDC, 12 Union Road, Cambridge CB2 1EZ, UK [fax: +44 (1223) 336033, E-mail: deposit@ccdc.cam.ac.uk, www: http://www.ccdc.cam.ac.uk].

EHMO Calculations: Theoretical MO calculations were carried out at the extended Hückel level[36], using the CACAO program[37]. The geometrical parameters used were based on X-ray diffraction data, averaging the appropriate distances and angles in order to obtain ideal C_{2v} symmetry. The orbital parameters used in the calculations were those used in previous works[11].

Acknowledgments

Financial support from the Dirección General de Enseñanza Superior (Grants PB95−1042 and PB96−0558) is gratefully acknowledged.

[1] P. L. Andreu, J. A. Cabeza, V. Riera, F. Robert, Y. Jeannin, *J. Organomet. Chem.* **1989**, *372*, C15.
[2] J. Soler, J. Ros, M. R. Carrasco, A. Ruiz, A. Alvarez-Larena, J. F. Piniella, *Inorg. Chem.* **1995**, *34*, 6211.
[3] K. B. Shiu, C. H. Li, T. J. Chan, S. M. Peng, M. C. Cheng, F. L. Liao, M. Y. Chiang, *Organometallics* **1995**, *14*, 524.
[4] K. B. Shiu, S. L. Wang, F. L. Liao, M. Y. Chiang, S. M. Peng, G. H. Lee, J. C. Wang, L. S. Liou, *Organometallics* **1998**, *17*, 1790.
[5] B. F. G. Johnson, D. R. Johnston, P. L. Josty, J. Lewis, I. G. Williams, *Nature* **1967**, *213*, 901.
[6] G. R. Crooks, B. F. G. Johnson, J. Lewis, I. G. Williams, *J. Chem. Soc. A* **1969**, 797.
[7] E. Sappa, O. Gambino, G. Cetini, *J. Organomet. Chem.* **1971**, *30*, 67.
[8] G. Cetini, O. Gambino, E. Sappa, M. Valle, *J. Organomet. Chem.* **1972**, *35*, 375.
[9] R. D. Adams, J. H. Yamamoto, *Organometallics* **1995**, *14*, 3704.
[10] R. D. Adams, J. H. Yamamoto, *J. Cluster Sci.* **1996**, *7*, 643.
[11] J. A. Cabeza, M. A. Martínez-García, V. Riera, D. Ardura, S. García-Granda, *Organometallics* **1998**, *17*, 1471.
[12] [12a] J. A. Cabeza, C. Landázuri, L. A. Oro, A. Tiripicchio, M. Tiripicchio-Camellini, *J. Organomet. Chem.* **1987**, *322*, C16. − [12b] J. A. Cabeza, C. Landázuri, L. A. Oro, D. Belletti, A. Tiripicchio, M. Tiripicchio-Camellini, *J. Chem. Soc., Dalton Trans.* **1989**, 1093.
[13] J. A. Cabeza, F. J. Lahoz, A. Martín, *Organometallics* **1992**, *11*, 2754.
[14] E. A. Seddon, K. R. Seddon, *The Chemistry of Ruthenium*, Elsevier, Amsterdam, **1984**, chapter 9.
[15] A. Mantovani, S. Cenini, *Inorg. Synth.* **1976**, *16*, 47.
[16] N. Lugan, G. Lavigne, J. M. Soulié, S. Fabre, P. Kalck, J. Y. Saillard, J. F. Halet, *Organometallics* **1995**, *14*, 1712.
[17] J. A. Cabeza, J. M. Fernández-Colinas, V. Riera, M. A. Pellinghelli, A. Tiripicchio, *J. Chem. Soc., Dalton Trans.* **1991**, 371.
[18] J. A. Cabeza, J. M. Fernández-Colinas, *Coord. Chem. Rev.* **1993**, *126*, 319.
[19] S. García-Granda, R. Obeso-Rosete, J. M. Rubio, A. Anillo, *Acta Crystallogr.* **1990**, *C46*, 2043.
[20] S. J. Sherlock, M. Cowie, E. Singleton, M. M. de V. Steyn, *Organometallics* **1988**, *7*, 1663.
[21] A. Colombie, G. Lavigne, J. J. Bonnet, *J. Chem. Soc., Dalton Trans.* **1986**, 899.
[22] J. A. Cabeza, J. M. Fernández-Colinas, V. Riera, S. García-Granda, J. F. Van der Maelen, *Inorg. Chim. Acta* **1991**, *185*, 187.
[23] J. A. Cabeza, J. M. Fernández-Colinas, S. García-Granda, V. Riera, J. F. Van der Maelen, *Inorg. Chem.* **1992**, *31*, 1233.
[24] A. Anillo, J. A. Cabeza, R. Obeso-Rosete, V. Riera, *J. Organomet. Chem.* **1990**, *393*, 423.
[25] See also the theoretical studies described in: [25a] C. Mealli, A. Ienco, A. Anillo, S. García-Granda, R. Obeso-Rosete, *Inorg. Chem.* **1997**, *26*, 3724. − [25b] C. Mealli, A. Ienco, A. Anillo, S. García-Granda, R. Obeso-Rosete, *J. Chem. Soc., Dalton Trans.* **1997**, 1441.
[26] R. Usón, A. Laguna, M. Laguna, *Inorg. Synth.* **1989**, *26*, 85.
[27] [27a] M. S. Lehman, F. K. Larsen, *Acta Crystallogr.* **1974**, *A30*, 580. − [27b] D. F. Grant, E. J. Gabe, *J. Appl. Crystallogr.* **1978**, *11*, 114.
[28] A. C. T. North, D. C. Phillips, F. S. Mathews, *Acta Crystallogr.* **1968**, *A24*, 351.
[29] P. T. Beurskens, G. Admiraal, G. Beurskens, W. P. Bosman, S. García-Granda, R. O. Gould, J. M. M. Smits, C. Smykalla, *The DIRDIF92 Program System*, University of Nijmegen, Nijmegen, The Netherlands, **1992**.
[30] J. F. Van der Maelen, Ph. D. Thesis, University of Oviedo, Oviedo, Spain, **1991**.

[31] S. Parkin, B. Moezzi, H. Hope, *J. Appl. Crystallogr.* **1995**, *28*, 53.
[32] G. M. Sheldrick, in *Crystallographic Computing 6*, (Eds.: H. D. Flack, L. Párkányi, K. Simon), International Union of Crystallography and Oxford University Press, Oxford, U. K., **1993**, p. 111.
[33] *International Tables for Crystallography*; vol. C, Kynoch Press, Birmingham, U. K., **1992** (present distributor: Kluwer Acad. Publ., Dordrecht, The Netherlands).
[34] A. L. Spek, in *Computational Crystallography* (Ed.: D. Sayre), Clarendon Press, Oxford, U. K., **1982**, p. 528.
[35] M. Nardelli, *Comput. Chem.* **1983**, *7*, 95.
[36] [36a] R. Hoffmann, W. N. Lipscomb, *J. Chem. Phys.* **1962**, *36*, 2179. – [36b] R. Hoffmann, W. N. Lipscomb, *J. Chem. Phys.* **1962**, *36*, 3489. – R. Hoffmann, *J. Chem. Phys.* **1963**, *39*, 1379.
[37] C. Mealli, D. M. Proserpio, *J. Chem. Ed.* **1990**, *67*, 399.

Received December 4, 1998
[I98416]

Ruthenium Tris(pyrazolyl)borate Complexes, 12[+] Cross Coupling of Acetylenes with Olefins – Formation of η^3-Butadienyl and η^2-Butadiene Complexes via a Metallacyclobutane Intermediate

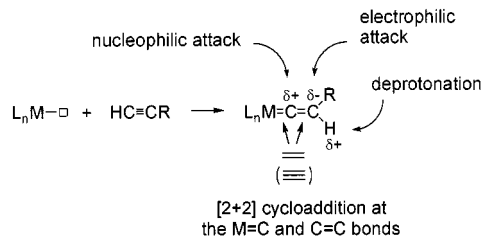
Christian Slugovc,[a] Kurt Mereiter,[b] Roland Schmid,[a] and Karl Kirchner,*[a]

Keywords: C–C coupling / Metallacycles / Metallacyclobutane / Ruthenium / Tripodal ligands / Vinylidene complexes

Selective coupling of olefins and terminal acetylenes is shown to be effected in the coordination sphere of Ru^{II} by the successive intermediacy of vinylidene and ruthenacyclobutane complexes. Subsequent deprotonation of one of the β-hydrogen atoms of the latter by NaOEt yields η^3-butadienyl complexes, while in the presence of Cl^- rearrangement takes place to give neutral η^2-butadiene complexes by a β-hydrogen elimination/reductive elimination sequence. [Ru(tp)(COD)Cl] and [Ru(tp){η^3-(*P,C,C*)-$Ph_2PCH{=}CHC(Ph){=}CH_2$}Cl] were the starting materials which were treated with HC≡CR (R = Ph, C_6H_9, ferrocenyl, CH_2Ph, *n*Bu). The η^3-butadienyl complexes are nucleophilic at the enynyl carbon atom reacting readily with the electrophiles H^+ and I_2 to give the corresponding η^2-butadienyl complexes. X-ray structures of representative products are given.

Introduction

The transition metal mediated transformation of acetylenic substrates is an important process in applied (organometallic) chemistry.[1] Particularly reactive are terminal alkynes which form, when exposed to a transition metal center, vinylidene complexes. This class of compounds exhibits a wide range of reactivity as illustrated in Scheme 1 including migratory insertions of alkyl, aryl, vinyl, alkynyl, and hydride ligands onto the electrophilic α-carbon atom of the vinylidene moiety.[2]



Scheme 1. Formation and common modes of reaction of vinylidene complexes

A rather rare example of C−C bond formation within a vinylidene complex is the cycloaddition of alkynes and olefins to the M=C bond giving metallacyclobutene and metallacyclobutane intermediates, respectively, which then polymerize through ring opening.[3] Although the underlying process is characteristic of early transition metals, we report here a facile C−C coupling reaction between olefins and terminal acetylenes proceeding via a ruthenacyclobutane[4] intermediate which finally converts into either η^3-butadienyl or η^2-butadiene complexes depending on the reaction conditions.[2c,5] In addition, we demonstrate that η^3-butadienyl complexes are nucleophilic at the enynyl carbon atom and react with electrophiles to give the corresponding functionalized η^2-butadiene complexes. A preliminary account of this work has already been published.[6]

Results and Discussion

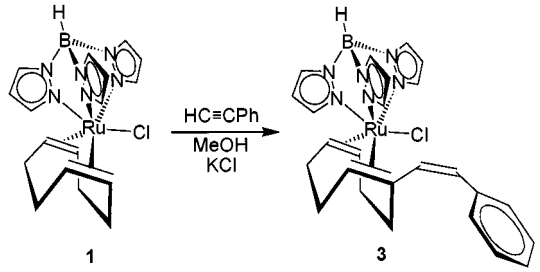
In an attempt to prepare the cationic vinylidene complex $[Ru(tp)(COD)(=C=CHPh)]^+$ (tp = hydrido(trispyrazolyl)-borate, COD = 1,5 cyclooctadiene), [Ru(tp)(COD)Cl] (**1**) has been treated with HC≡CPh in boiling MeOH. A polar medium has been chosen to allow for better ionization of the chloride to facilitate the opening of a coordination site. We[7] and others[8] have already shown that protic solvents favor cationic vinylidene complexes. However, no such complex was formed and basically unchanged **1** was obtained, together with polymeric materials[9] and a small amount of a new complex identified as [Ru(tp){(1,2-η;5,6-η)-1-[(*Z*)-3-phenyl-1-ethenyl]cyclooctadiene}Cl] (**3**). In the presence of excess KCl (6 equiv.) the formation of polymeric compounds is largely suppressed to afford **3**, isolated in 74% yield (Scheme 2). Characterization of **3** was by a combination of elemental analysis, and ^{1}H- and $^{13}C\{^1H\}$-NMR spectroscopy. Characteristic solution ^{1}H-NMR-spectroscopic data for **3** include two doublets at δ = 6.82 and 6.58 with a coupling constant $^3J_{HH}$ = 11.7 Hz, consistent with a (*Z*) arrangement of the double bond. All other resonances are unremarkable. The structural identity of **3** was unequivocally proven by X-ray crystallography. The result is depicted in Figure 1 with selected bond lengths and angles reported in the caption. The overall structure of **3** is similar

[+] Part 11: C. Slugovc, K. Mauthner, M. Kacetl, K. Mereiter, R. Schmid, K. Kirchner, *Chem. Eur. J.* **1998**, *4*, 2043.

[a] Institute of Inorganic Chemistry, Vienna University of Technology,
Getreidemarkt 9/153, A-1060 Vienna, Austria
Fax: (internat.) + 43-1/58801-15399
E-mail: kkirch@mail.zserv.tuwien.ac.at
[b] Institute of Mineralogy, Crystallography, and Structural Chemistry, Vienna University of Technology,
Getreidemarkt 9/171, A-1060 Vienna, Austria

 © WILEY-VCH Verlag GmbH, D-69451 Weinheim, 1999 1434−1948/99/0707−1141 $ 17.50+.50/0

to that of Ru(tp)(COD)Br and related complexes containing the $[Ru(tp)(COD)]^+$ fragment.[10]



Scheme 2. Reaction of **1** with HC≡CPh in the presence of excess KCl

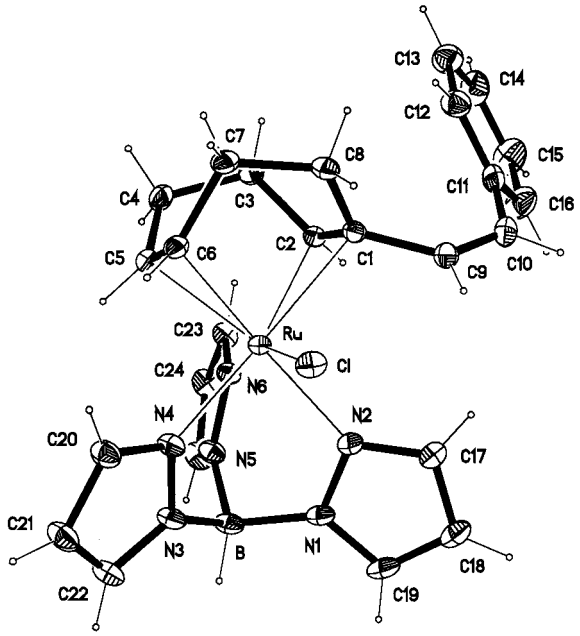
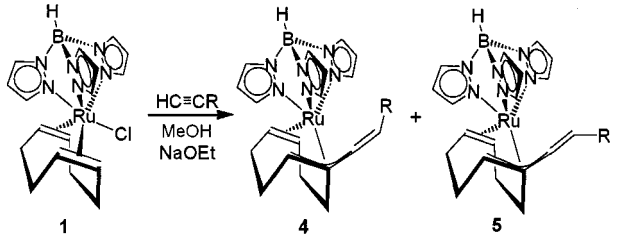


Figure 1. Structural view of **3**; selected bond lengths [Å] and angles [°]: Ru−N(2) 2.163(1), Ru−N(4) 2.121(1), Ru−N(6) 2.166(1), Ru−C(1) 2.311(2), Ru−C(2) 2.243(2), Ru−C(5) 2.226(2), Ru−C(6) 2.219(2), Ru−Cl 2.427(1), C(1)−C(2) 1.385(2), C(5)−C(6) 1.384(2), C(9)−C(10) 1.335(3); N(6)−Ru−Cl 159.9(1), N(4)−Ru−N(2) 87.3(1), N(4)−Ru−N(6) 86.2(1), N(2)−Ru−N(6) 79.7(1)

It is interesting to note that only the (*Z*) isomer is formed in which the −CH=CHPh substituent points towards the chloride ligand. Complex **3** did not undergo a further coupling reaction with HC≡CPh (to give a COD ligand containing two −CH=CHPh substituents). It is interesting that under the same reaction conditions (and even after prolonged heating and extended reaction times) internal acetylenes such as PhC≡CPh and MeOOCC≡CCOOMe did not undergo an oxidative coupling. Instead, unchanged **1** was largely recovered together with about 15% of the known hydride complex [Ru(tp)(COD)H].[11]

In order to establish whether [Ru(tp)(COD)H] is an intermediate on the pathway to **3**, [Ru(tp)(COD)H] (in place of **1**) was treated with HC≡CPh under otherwise the same conditions. However, no **3** but small amounts (< 20%) of the new compound η^3-butadienyl complex [Ru(tp){(5,6-η;η^3)-2-[(*E*)-2-phenyl-1-ethenylidene]-5-cyclooctenyl}] (**5a**) (vide infra) were obtained, in addition to polyacetylenes as the main products. Likewise, internal alkynes, such as PhC≡CPh do not react with **1** and [Ru(tp)(COD)H] is apparently not a precursor to **3**. Accordingly, the formation of **5a** can be interpretated that under basic conditions ([Ru(tp)(COD)H] may act as a base) a different course of reaction is followed. Treatment of Ru(tp)(COD)Cl (**1**)[10] with terminal acetylenes HC≡CR (R = Ph, C_6H_9, ferrocenyl, CH_2Ph, *n*Bu) in MeOH in the presence of NaOEt (1 equiv., 65°C, 24 h) afforded the η^3-butadienyl complexes **4a**−**e** and **5a**−**e** in high yields (Table 1). Characterization of **4** and **5** was again by elemental analysis, and ^{1}H- and $^{13}C\{^1H\}$-NMR spectroscopy. The solution ^{1}H-NMR spectra for **4** include a singlet between δ = 5.9 and 6.9 assigned to the terminal (*E*)-butadienyl proton, while in the corresponding (*Z*)-butadienyl fragment there is a slight upfield shift of the terminal proton giving rise to a signal between δ = 4.7 and 5.9. In the $^{13}C\{^1H\}$-NMR spectrum, the enynyl carbon atoms exhibit a characteristic resonance at δ = 171−181. All other resonances are unremarkable.

Table 1. Conversion and product distribution of the reaction of **1** with terminal acetylenes



			products[a]	
entry	R	% conversion[a]	% Z	% E
1	Ph	100	**4a** 98	
2	C_6H_9	100	**4b** 24	**5b** 76
3	ferrocenyl	100		**5c** 97
4	CH_2Ph	97	**4d** 94	**5d** 6
5	*n*-Bu	93	**4e** 66	**5e** 33

[a] Conversions and product distributions have been determined by ^{1}H NMR spectroscopy

It may be emphasized that **4a** appears to be the first (η^3-butadienyl)ruthenium complex with tp as a co-ligand. The molecular structure determined by X-ray crystallography is shown in Figure 2, with selected bond lengths and angles given in the caption. The most notable feature is the distorted *s-trans* structure of the butadienyl moiety. Since the two allyl carbon atoms, C(1), C(2), are noticeably further from the Ru center [Ru−C(1) = 2.153(3) Å, Ru−C(2) = 2.154(3) Å] than the enynyl carbon atom C(9) [Ru−C(9) = 2.038(3) Å], a major resonance contribution from the vinyl alkene structure is indicated. Furthermore, the relatively uniform bond lengths for the three allyl carbon atoms point to a substantial π-electron delocalization [C(1)−C(2) =

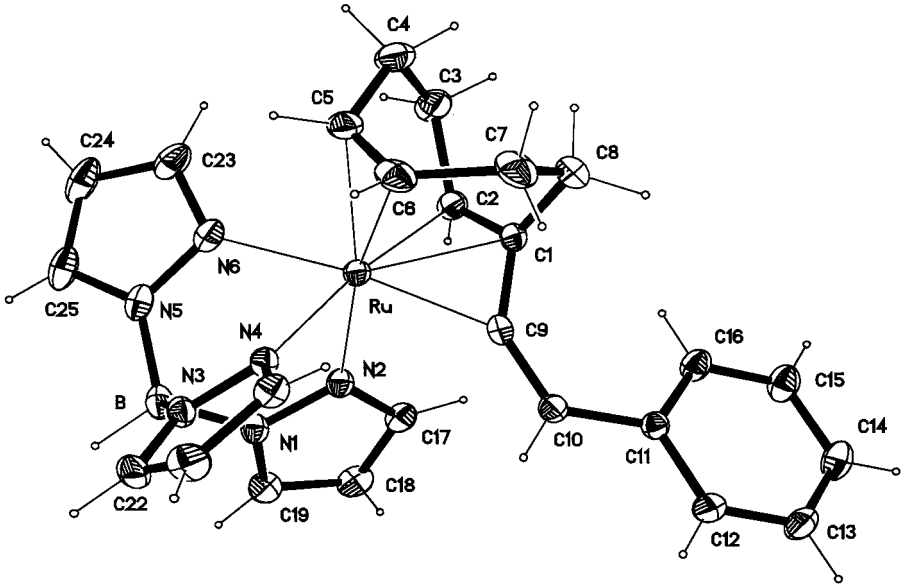
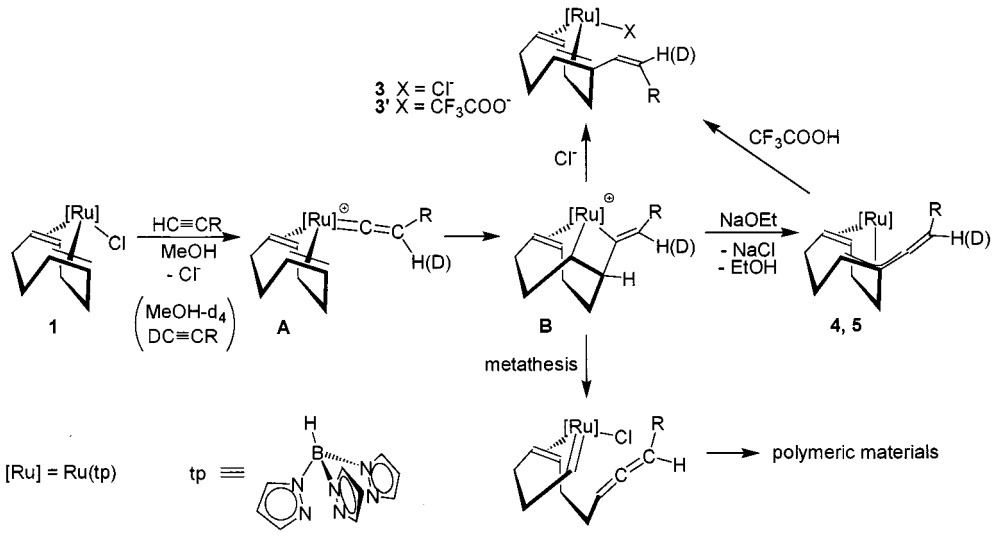


Figure 2. Structural view of **4a**; selected bond lengths [Å] and angles [°]: Ru−N(2) 2.149(2), Ru−N(4) 2.158(2), Ru−N(6) 2.223(2), Ru−C(1) 2.153(3), Ru−C(2) 2.154(3), Ru−C(9) 2.038(3), Ru−C(5) 2.184(3), Ru−C(6) 2.218(3), C(1)−C(9) 1.418(4), C(1)−C(2) 1.425(4), C(9)−C(10) 1.328(4), C(5)−C(6) 1.386(5); C(9)−Ru−N(2) 80.4(1), C(9)−Ru−C(1) 39.4(1), N(2)−Ru−C(1) 101.1(1), C(9)−Ru−C(2) 71.6(1), N(2)−Ru−C(2) 90.5(1), C(1)−Ru−C(2) 38.7(1), C(9)−Ru−N(4) 103.0(1), C(9)−Ru−N(6) 160.1(1)

1.425(4) Å, C(2)−C(9) = 1.418(4) Å].[2c,5] The Ru−N(tp) bond lengths are within the usual range.[10][12]

The reaction mechanism shown in Scheme 3 represents our final working hypothesis providing the formation of the η^2-butadiene complexes **3**, the η^3-butadienyl products **4** and **5**, and polymeric materials. For the first step, the formation of the cationic vinylidene complex **A** by a 1,2-hydrogen shift is a now well-established process.[13] Prerequisite for this process is the availiability of a vacant coordination site. In this context, it has to be noted that the chloride ligand in **1** is easily replacable by Br^- and CN^- on treatment with KBr and KCN in MeOH at elevated temperatures indicating that the Cl^- ligand is substitutionally labile under these conditions.[14] Attempts to prepare **A** by treating **1** with 1 equiv. of $AgCF_3SO_3$ and HC≡CPh in CH_2Cl_2 failed.[10] The metallacyclobutane complex **B** is subsequently formed by a [2+2] cycloaddition, followed by deprotonation of one of the β-hydrogen atoms of **B**, yielding the stable η^3-butadienyl complex. The following observations may be taken to support this mechanism. (i) The occurrence of a vinylidene intermediate could be verified by a labeling experiment. Thus, the η^3-butadienyl product **[D$_1$]4a** of the reaction of deuterium-labeled phenylacetylene DC≡CPh and **1** contain deuterium bound exclusively at the olefinic carbon atom of the butadienyl moiety (Scheme 3). On the other hand, the η^3-butadienyl complex **4a** did not incorporate deuterium to give **[D$_1$]4a** under reflux in [D$_4$]MeOH in the presence of NaOEt.



Scheme 3. Vinylidene mechanism

(ii) In the absence of base only polyacetylenes[9] were obtained with decomposition of the Ru complex to intractable materials. (iii) When in place of NaOEt an excess of KCl is added, **B** rearranges presumably by a β-hydrogen elimination/reductive elimination sequence (equivalent to a 1,2-hydrogen shift) to the neutral η^2-butadiene complex **3**. The vacant coordination site of the resulting 16-electron intermediate is occupied by the incoming chloride.

The stereochemistry of **4** and **5**, difficult to determine by NMR methods, is established on the basis of the products formed from the reaction with CF_3COOH at room temperature included in Scheme 3. In this way the corresponding olefin complexes **3′** [(*Z*) and (*E*) isomers] with the vinyl side chain are formed. Under this experimental condition no isomerization takes place and the stereochemistry of the butadienyl fragment is readily apparent from the vicinal coupling constant $^3J_{HH}$ of the vinyl moiety (about 11 and 16 Hz in case of a *cis* and *trans* arrangement, respectively). From this it is concluded that the enynyl carbon atom of η^3-butadienyl complexes is nucleophilic, which offers the possibility of further kinds of functionalization by treating them with electrophiles. In fact, **4a** reacts with I_2 to yield complex **6** in essentially quantitative yield (Scheme 4). The NMR spectra of **6** are similar to those of **3** and are not discussed here. The solid-state structure of **6** is depicted in Figure 3 with selected bond lengths and angles given in the caption. The overall structures of **6** and **3** are very similar. The three Ru−N(Tp) bond lengths show only minor variations [on average the Ru−N(tp) distance is 2.141(1) Å] and are within the range of other ruthenium(tp) complexes. The Ru−I(1) and C(9)−I(2) distances are 2.780(1) and 2.126(2) Å, respectively. Additionally, a weak intermolecular interaction between the two I(2) atoms of pairs of neighboring molecules is observed, where the I(2)···I(2) distance is found to be 3.67 Å. Despite this interaction molecular packing is not very efficient in crystalline **6** and the structure contains voids of about 40 $Å^3$ per unit cell. If an excess of I_2 is present during crystallization of **6**, a new kind of crystal, **6**·0.5 I_2, is readily formed which will be reported elsewhere.

It may be mentioned that the above reactions are not restricted to COD complexes. In similar fashion to **1**, [Ru(tp){η^3-(*P*,*C*,*C*)-$Ph_2PCH{=}CHC(Ph){=}CH_2$}Cl] (**2**) was found to react with HC≡CR (R = Ph, C_6H_9) to give the η^3-butadienyl complexes **7a**,**b** (Scheme 5). In addition to full spectroscopic and analytical characterizations of the products, the solid-state structure of **7b** was determined by X-ray crystallography. As shown in Figure 4 the coordination geometry around the ruthenium center is a distorted octahedron in which three coordination positions are occupied by the tp ligand, and the remaining three are taken by the phosphorus atom and the butadienyl fragment of the $Ph_2PCH{=}CHC(Ph)CHCCHC_6H_9$ ligand. The Ru−C(24), Ru−C(25), and Ru−C(26) bond lengths are 2.255(3), 2.110(3), and 2.077(3) Å, respectively. Similar to the other η^3-butadienyl complexes,[5] the two allyl carbon atoms, C(24), C(25), are significantly further from the Ru center than is the enynyl carbon atom C(26). The bond lengths between the two allyl and the enynyl carbon atoms are 1.419(4) and 1.445(4) Å. The C(26)−C(27) bond length is 1.341(4) Å. The Ru−N(tp) and Ru−P bond lengths are within the usual ranges.[10][12] The cyclohexene ring consisting of C(34) through C(39) has an envelope conformation with an up/down disorder of C(37a)/C(37b) and C(38a)/C(38b). Only the b-orientation [C(37b/(C(38b)] is shown in Figure 4.

Conclusion

It is shown that selective coupling of olefins and terminal acetylenes is feasible in the coordination sphere of Ru^{II}. Although in the present case there is particular assistance by

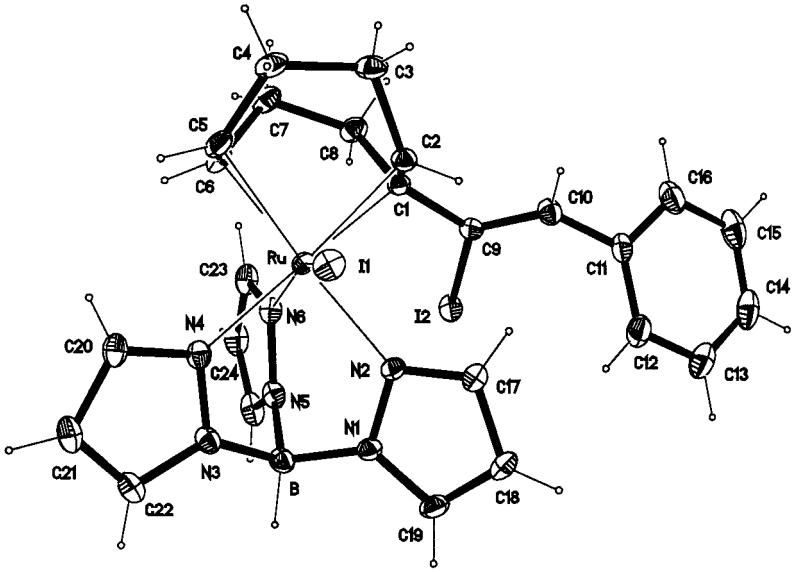


Figure 3. Structural view of **6**; selected bond lengths [Å]: Ru−N(2) 2.114(2), Ru−N(4) 2.133(2), Ru−N(6) 2.177(2), Ru−C(2) 2.206(2), Ru−C(6) 2.227(2), Ru−C(5) 2.249(2), Ru−C(1) 2.267(2), Ru−I(1) 2.780(1), I(2)−C(9) 2.126(2), C(1)−C(9) 1.498(3), C(9)−C(10) 1.329(3)

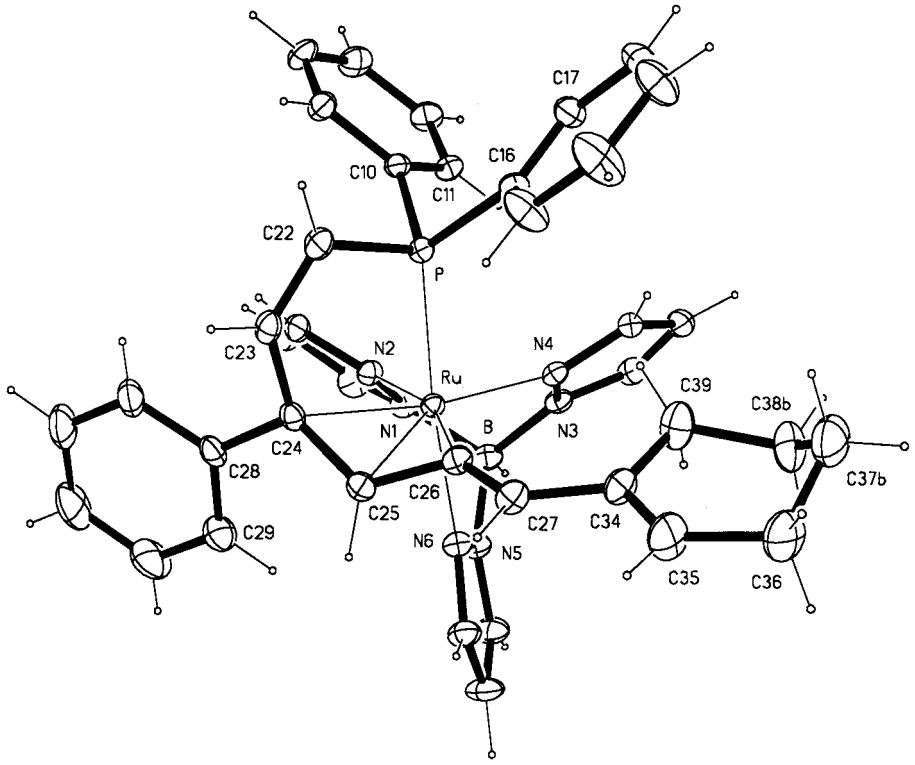
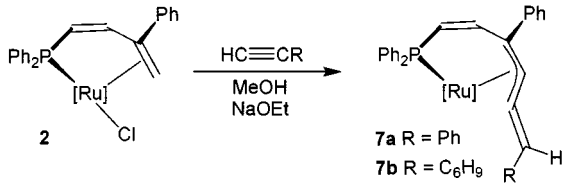


Figure 4. Structural view of **7b**; selected bond lengths [Å] and angles [°]: Ru−C(24) 2.255(3), Ru−C(25) 2.110(3), Ru−C(26) 2.077(3), Ru−N(2) 2.164(2), Ru−N(4) 2.151(2), Ru−N(6) 2.183(2), Ru−P 2.280(1), C(22)−C(23) 1.312(4), C(23)−C(24) 1.490(4), C(24)−C(25) 1.419(4), C(24)−C(28) 1.501(4), C(25)−C(26) 1.445(4), C(26)−C(27) 1.341(4), C(27)−C(34) 1.468(4), C(34)−C(35) 1.344(4); N(4)−Ru−N(2) 84.6(1), N(4)−Ru−C(24) 171.5(1), C(24)−Ru−P 80.5(1)



Scheme 5. Reaction of **2** with HC≡CR (R = Ph, C_6H_9)

the intramolecular mode with favorable stereochemical conditions imposed by an anchoring group, an extension to the intermolecular mode should be conceivable. The deprotonation pathway for the onward reaction of the metallacyclobutane complex has not yet been considered. The butadienyl fragment is nucleophilic at the enynyl carbon atom and is capable of reacting with electrophiles such as H^+ and I_2 to give the 1,3-diene unit. We believe this work may initiate a systematic search of coupling olefins with acetylenes into functionalized 1,3-dienes in a synthetically useful fashion

Experimental Section

General Techniques: All compounds were manipulated with standard Schlenk techniques and/or a glove box under purified argon. All chemicals were of standard reagent grade and used without further purification. The solvents were purified according to standard procedures.[15] The deuterated solvents were purchased from Aldrich and dried with 4-Å molecular sieves. For column chromatography silica gel purchased from Merck, grade 60, 70−230 mesh, 60 Å, or neutral MN aluminum oxide, purchased from Macherey−Nagel, was used. [Ru(tp)(COD)Cl] (**1**) and [Ru(tp){η^3-(*P*,*C*,*C*)-$Ph_2PCH{=}CH(Ph){=}CH_2$}Cl] (**2**) were prepared according to the literature.[7][10] − ^{1}H-, ^{13}C{^{1}H}-, and ^{31}P{^{1}H}-NMR spectra were recorded with a Bruker AC-250 spectrometer operating at 250.13, 62.86, and 101.26 MHz, respectively, and were referenced to $SiMe_4$ and to H_3PO_4 (85%). − Microanalysis were done by Microanalytical Laboratories, University of Vienna.

Synthetic Studies

Ru(tp)(η^4-1,5-cyclooctadiene)H: A suspension of **1** (100 mg, 0.22 mmol) and NaOEt (14.9 mg, 0.22 mmol) in MeOH (5 mL) was heated under reflux for 2.5 h. The reaction mixture was cooled to room temperature and the resulting yellow precipitate was collected on a glass frit, washed with MeOH (5 × 1.5 mL) and Et_2O (2 × 1 mL), and dried under vacuum. Yield: 65 mg (70%). In the absence of base the conversion is completed after about 20 h with 64% yield of isolated [Ru(tp)(η^4-1,5-cyclooctadiene)H]. The NMR spectra are in agreement with the published values.[11]

Ru(tp){(1,2-η;5,6-η)-1-[(*Z*)-2-phenylethenyl]cyclooctadiene}Cl (3): To a suspension of **1** (200 mg, 0.44 mmol) in MeOH (4 mL), KCl (200 mg, 2.68 mmol) and HC≡CPh (144 μL, 1.32 mmol) were added and heated at reflux for 20 h. The reaction mixture was then cooled to 0 °C and the resulting orange precipitate was collected on a glass frit and washed twice with methanol (1.5 mL). The crude product was redissolved in CH_2Cl_2 and insoluble materials were removed by filtration. After removal of the solvent, analytically pure product was obtained. Yield 180 mg (74%). − $C_{25}H_{28}BClN_6Ru$ (559.86): calcd. C 53.63, H 5.04, N 15.01; found C 53.64, H 5.12, N 14.88. − ^{1}H NMR ($CDCl_3$, 20 °C): δ = 8.24

(d, J = 2.2 Hz, 1 H, tp), 7.88 (d, J = 2.2 Hz, 1 H, tp), 7.80 (d, J = 2.2 Hz, 1 H, tp), 7.67 (d, J = 2.2 Hz, 1 H, tp), 7.59 (d, J = 2.2 Hz, 2 H, tp), 7.29−7.18 (m, 5 H, Ph), 6.82 (d, $^3J_{HHcis}$ = 11.7 Hz, CH=CH), 6.58 (d, $^3J_{HHcis}$ = 11.7 Hz, CH=CH), 6.25 (t, J = 2.2 Hz, 2 H, tp), 6.19 (t, J = 2.2 Hz, 1 H, tp), 4.91 (m, 1 H, olefinic H of COD), 3.90 (m, 2 H, olefinic H of COD), 3.31 (m, 1 H, aliphatic H), 2.74−1.91 (m, 7 H, aliphatic H). − $^{13}C\{^1H\}$NMR ($CDCl_3$, 20°C): δ = 145.8 (tp), 143.2 (tp), 142.2 tp), 138.8 (tp), 138.4 (C_{COD}-CH=CHPh), 138.2 (Ph^1), 136.0 tp), 135.2 (tp), 130.0 (C_{COD}-CH=CHPh), 129.1 (2 C, $Ph^{3,5}$), 128.6 (2 C, $Ph^{2,6}$), 127.3 (Ph^4), 107.4 (C_{COD}-CH=CHPh), 106.9 (tp), 106.8 (tp), 105.8 (tp), 91.5 (olefinic C of COD), 88.5 (olefinic C of COD), 85.8 (olefinic C of COD), 38.4 (aliphatic C of COD), 32.5 (aliphatic C of COD), 30.1 (aliphatic C of COD), 27.8 (aliphatic C of COD).

Ru(tp){(5,6-η;η^3)-1-[(*Z*)-2-phenylethenylidene]-5-cyclooctenyl} (4a): To a suspension of **1** (370 mg, 0.81 mmol) in MeOH (5 mL), NaOEt (55 mg, 0.81 mmol) and HC≡CPh (266 μL, 2.42 mmol) were added and heated under reflux for 20 h. The reaction mixture was cooled to 0 °C and the resulting yellow precipitate was collected on a glass frit, washed twice with 1.5 mL of MeOH, and dried under vacuum. Yield: 340 mg (80%). − $C_{25}H_{27}BN_6Ru$ (523.41): calcd. C 57.37, H 5.20, N 16.06; found C 57.40, H 5.21, N 15.97. − ^1H NMR ($CDCl_3$, 20°C): δ = 8.33 (d, J = 1.9 Hz, 1 H, tp), 8.08 (d, 1 H, J = 1.9 Hz, tp), 7.78 (d, J = 2.3 Hz, 1 H, tp), 7.76 (d, J = 2.3 Hz, 1 H, tp), 7.48 (d, J = 2.6 Hz, 1 H, tp), 7.34−7.27 (m, 4 H, Ph), 7.09 (m, 1 H, Ph), 6.47 (d, 1 H, J = 2.3 Hz, tp), 6.40 (vt, J = 2.3 Hz, 1 H, tp), 6.36 (dd, J = 2.3 Hz, J = 1.9 Hz, 1 H, tp), 5.90 (s, 1 H, C=C*H*Ph), 5.86 (dd, J = 2.3 Hz, J = 1.9 Hz, 1 H, tp), 3.81 (m, 1 H, olefinic H of COD), 3.45 (m, 1 H, olefinic H of COD), 3.03 (d, J = 5.0 Hz, 1 H, olefinic H of COD), 2.91−2.11 (m, 7 H), 1.70 (m, 1 H). − $^{13}C\{^1H\}$ NMR ($CDCl_3$, 20°C): δ = 181.2 (C_{COD}=*C*=CHPh), 143.9 (tp), 143.0 (tp), 141.3 tp), 137.6 (Ph^1), 135.8 (tp), 135.4 (tp), 134.1 (tp), 129.0 (2 C, $Ph^{3,5}$), 126.3 (2 C, $Ph^{2,6}$), 124.9 (Ph^4), 114.4 (C_{COD}=C=*C*HPh), 106.3 (tp), 106.2 (tp), 104.8 (tp), 90.8 (C_{COD}=C=CHPh), 82.8 (olefinic C of COD), 80.7 (olefinic C of COD), 63.2 (olefinic C of COD), 33.3 (aliphatic C of COD), 33.0 (aliphatic C of COD), 30.4 (aliphatic C of COD), 26.8 (aliphatic C of COD).

Ru(tp){(5,6-η;η^3)-2-[(*Z*)-2-deuterio-2-phenylethenylidene]-5-cyclooctenyl} ([D_1]4a): This complex was prepared analogously to **4a** (77 mg, 0.168 mmol) in [D_4]MeOH (1 mL) as the solvent, with **1**, NaOEt (11.4 mg, 0.168 mmol), and DC≡CPh (55 μL, 0.504 mmol) as the starting materials. Yield: 61 mg (69%). − $C_{25}H_{26}BDN_6Ru$ (524.42): calcd. C 57.37, H 5.20, N 16.06; found C 57.43, H 5.26, N 15.92. − ^1H NMR ($CDCl_3$, 20°C): δ = 8.35 (d, J = 1.9 Hz, 1 H, tp), 8.11 (d, 1 H, J = 1.9 Hz, tp), 7.78 (d, J = 2.3 Hz, 1 H, tp), 7.76 (d, J = 2.3 Hz, 1 H, tp), 7.51 (d, J = 2.6 Hz, 1 H, tp), 7.34−7.27 (m, 4 H, Ph), 7.09 (m, 1 H, Ph), 6.47 (d, 1 H, J = 2.3 Hz, tp), 6.40 (vt, J = 2.3 Hz, 1 H, tp), 6.36 (dd, J = 2.3 Hz, J = 1.9 Hz, 1 H, tp), 5.86 (dd, J = 2.3 Hz, J = 1.9 Hz, 1 H, tp), 3.81 (m, 1 H, olefinic H of COD), 3.45 (m, 1 H, olefinic H of COD), 3.03 (d, J = 5.0 Hz, 1 H, olefinic H of COD), 2.91−2.11 (m, 7 H), 1.70 (m, 1 H). − $^{13}C\{^1H\}$ NMR ($CDCl_3$, 20°C): δ = 181.1 (C_{COD}=*C*=CDPh), 144.0 (tp), 143.0 (tp), 141.3 (tp), 137.6 (Ph^1), 135.8 (tp), 135.4 (tp), 134.1 (tp), 129.0 (2 C, $Ph^{3,5}$), 126.3 (2 C, $Ph^{2,6}$), 124.9 (Ph^4), 114.1 (t, $^1J_{DC}$ = 22.7 Hz, C_{COD}=C=*C*DPh), 106.3 (tp), 106.2 (tp), 104.8 (tp), 90.1 (C_{COD}=C=CDPh), 82.9 (olefinic C of COD), 80.8 (olefinic C of COD), 63.2 (olefinic C of COD), 33.3 (aliphatic C of COD), 33.1 (aliphatic C of COD), 30.5 (aliphatic C of COD), 26.8 (aliphatic C of COD).

Ru(tp){(5,6-η;η^3)-1-[(*E*)-2-phenylethenylidene]-5-cyclooctenyl} (5a): To a suspension of Ru(tp)(η^4-1,5-cyclooctadiene)H (62 mg, 0.146 mg) in methanol (4 mL), NaOEt (9.5 mg, 0.146 mmol) and HC≡CPh (48 μL, 0.439 mmol) were added and heated at reflux for 20 h. The solvent was evaporated and the crude reaction mixture was purified by column chromatography (neutral Al_2O_3). The first yellow band was eluted with CH_2Cl_2. Yield: 27 mg (35%). − $C_{25}H_{27}BN_6Ru$ (523.41): calcd. C 57.37, H 5.20, N 16.06; found C 57.48, H 5.29, N 16.22. − ^1H NMR ($CDCl_3$, 20°C): δ = 8.29 (d, J = 1.9 Hz, 1 H, tp), 7.89 (d, 1 H, J = 1.9 Hz, tp), 7.84 (d, J = 2.8 Hz, 1 H, tp), 7.56 (d, J = 2.4 Hz, 1 H, tp), 7.48 (d, J = 2.3 Hz, 1 H, tp), 6.91 (s, 1 H, C=C*H*Ph), 6.86 (d, 1 H, J = 2.4 Hz, tp), 6.87−6.71 (m, 3 H, $Ph^{3,4,5}$), 6.55 (d, 2 H, $Ph^{2,6}$), 6.39 (dd, J = 2.4 Hz, J = 1.9 Hz, 1 H, tp), 6.22 (dd, J = 2.4 Hz, J = 1.9 Hz, 1 H, tp), 5.86 (vt, J = 2.4 Hz, 1 H, tp), 3.73 (m, 1 H, olefinic H of COD), 3.48 (m, 1 H, olefinic H of COD), 3.01−2.02 (m, 7 H), 1.20 (m, 2 H), 0.94 (m, 1 H). − $^{13}C\{^1H\}$ NMR ($CDCl_3$, 20°C): δ = 176.8 (C_{COD}=*C*=CHPh), 145.4 (tp), 142.6 (tp), 141.5 (tp), 139.7 (Ph^1), 135.78 (tp), 135.5 (tp), 134.5 (tp), 128.0 (2 C, $Ph^{3,5}$), 126.7 (2 C, $Ph^{2,6}$), 125.0 (Ph^4), 117.3 (C_{COD}=C=*C*HPh), 106.3 (tp), 106.2 (tp), 105.5 (tp), 91.1 (C_{COD}=C=CHPh), 83.3 (olefinic C of COD), 82.8 (olefinic C of COD), 63.2 (olefinic C of COD), 33.5 (aliphatic C of COD), 32.4 (aliphatic C of COD), 31.5 (aliphatic C of COD), 30.1 (aliphatic C of COD).

Ru(tp){(5,6-η;η^3)-1-[(*Z*)-2-(1-cyclohexenyl)ethenylidene]-5-cyclooctenyl} (4b): The (*Z*) isomer **4b** was obtained by adding *n*-hexane to the methanolic filtrate of **5b**. The resulting solid was collected on a glass frit, and dried under vacuum. Yield: 32 mg (14%). − $C_{25}H_{31}BN_6Ru$ (527.44): calcd. C 56.93, H 5.92, N 15.93; found C 57.12, H 6.12, N 15.73. − ^1H NMR ($CDCl_3$, 20°C): δ = 8.30 (d, J = 2.0 Hz, 1 H, tp), 8.02 (d, 1 H, J = 2.0 Hz, tp), 7.74 (d, J = 2.0 Hz, 1 H, tp), 7.70 (d, J = 2.3 Hz, 1 H, tp), 7.47 (d, J = 2.0 Hz, 1 H, tp), 6.42 (d, 1 H, J = 2.0 Hz, tp), 6.36 (dd, J = 2.3 Hz, J = 2.0 Hz, 1 H, tp), 6.31 (vt, J = 2.0 Hz, 1 H, tp), 5.94 (dd, J = 2.3 Hz, J = 2.0 Hz, 1 H, tp), 5.48 (s, 1 H, C=C*H*C_6H_9), 5.26 (m, 1 H, olefinic H of C_6H_9), 3.79−3.56 (m, 2 H, olefinic H of COD), 2.81−0.84 (m, 17 H). − $^{13}C\{^1H\}$ NMR ($CDCl_3$, 20°C): δ = 176. (C_{COD}=*C*=CHC_6H_9), 143.8 (tp), 143.0 (tp), 141.8 (tp), 135.8 (C_6H_9), 135.6 (tp), 135.1 (tp), 134.0 (tp), 121.9 (C_6H_9), 118.2 (C_{COD}=C=*C*HC_6H_9), 106.2 (tp), 106.1 (tp), 104.6 (tp), 90.4 7 (C_{COD}=C=CHC_6H_9), 82.0 (olefinic C of COD), 80.3 (olefinic C of COD), 62.1 (olefinic C of COD), 33.3 (aliphatic C of COD), 33.1 (aliphatic C of COD), 30.5, 29.4 (aliphatic C of COD and aliphatic C of C_6H_9), 27.0, 26.2, 23.7, 23.5 (aliphatic C of COD and aliphatic C of C_6H_9).

Ru(tp){(5,6-η;η^3)-1-[(*E*)-2-(1-cyclohexenyl)ethenylidene]-5-cyclooctenyl} (5b): This compound was prepared analogously to **4a** with **1** (203 mg, 0.443 mmol), NaOEt (30.2 mg, 0.443 mmol), and HC≡CC_6H_9 (156 μL, 1.33 mmol) as the starting materials. Yield: 145 mg (62%). − $C_{25}H_{31}BN_6Ru$ (527.44): calcd. C 56.93, H 5.92, N 15.93. found: C 56.99, H 6.05, N 15.88. − ^1H NMR ($CDCl_3$, 20°C): δ = 8.26 (d, J = 2.0 Hz, 1 H, tp), 7.97 (d, 1 H, J = 2.0 Hz, (tp), 7.73 (d, J = 2.0 Hz, 1 H, (tp), 7.70 (d, J = 2.3 Hz, 1 H, tp), 7.55 (d, J = 2.0 Hz, 1 H, tp), 6.80 (d, 1 H, J = 2.0 Hz, (tp), 6.47 (s, 1 H, C=C*H*C_6H_9), 6.35 (dd, J = 2.3 Hz, J = 2.0 Hz, 1 H, (tp), 6.25 (vt, J = 2.0 Hz, 1 H, (tp), 5.99 (dd, J = 2.3 Hz, J = 2.0 Hz, 1 H, (tp), 5.27 (m, 1 H, olefinic H of C_6H_9), 3.78−3.58 (m, 2 H, olefinic H of COD), 2.83−0.86 (m, 16 H), 0.53−0.41 (m, 1 H). − $^{13}C\{^1H\}$ NMR ($CDCl_3$, 20°C): δ = 172.0 (C_{COD}=*C*=CHC_6H_9), 144.8 (tp), 142.6 (tp), 142.3 (tp), 138.4 (C_6H_9), 135.6 (tp), 135.3 (tp), 134.4 (tp), 123.7 (C_6H_9), 120.6 (C_{COD}=C=*C*HC_6H_9), 106.2 (tp), 105.7 (tp), 104.9 (tp), 91.7 (C_{COD}=C=CHC_6H_9), 82.6 (olefinic C of COD), 81.9 (olefinic C of COD), 63.0 (olefinic C of COD), 33.7 (aliphatic C of COD), 32.3 (aliphatic C of COD), 31.4, 30.2

(aliphatic C of COD and aliphatic C of C_6H_9), 26.4, 25.6, 23.5, 23.2 (aliphatic C of COD and aliphatic C of C_6H_9).

Ru(tp){(5,6-η;η^3)-1-[(*E*)-2-ferrocenylethenylidene]-5-cyclooctenyl} (5c): This compound was prepared analogously to **4a** with **1** (123 mg, 0.269 mmol), NaOEt (18.3 mg, 0.269 mmol) and ferrocenylacetylene (67.7 mg, 0.322 mmol) as the starting materials. Yield: 122 mg (72%). − $C_{29}H_{31}BFeN_6Ru$ (631.33): calcd. C 55.17, H 4.95, N 13.31; found C 55.06, H 5.04, N 13.19. − ^{1}H NMR ($CDCl_3$, 20°C): δ = 8.27 (d, *J* = 1.6 Hz, 1 H, tp), 7.78−7.70 (m, 4 H, tp), 6.91 (d, 1 H, *J* = 2.1 Hz, tp), 6.62 (s, 1 H, C=C*H*-Fc), 6.38 (vt, *J* = 2.1 Hz, 1 H, tp), 6.15−6.13 (m, 2 H, tp), 3.98−3.91 (m, 2 H, Fc), 3.90 (s, 5 H, Fc) 3.71 (m, 1 H, olefinic H of COD), 3.60−3.48 (m, 4 H, Fc, olefinic H of COD), 2.92 (m, 1 H, aliphatic H of COD), 2.80−2.62 (m, 2 H, aliphatic H of COD), 2.48−2.35 (m, 3 H, aliphatic H of COD), 2.19−2.11 (m, 1 H, aliphatic H of COD), 1.80−1.67 (m, 1 H, aliphatic H of COD). − ^{13}C{^{1}H} NMR ($CDCl_3$, 20°C): δ = 173.6 (C_{COD}=*C*=CHFc), 145.3 (tp), 142.6 (tp), 141.7 (tp), 135.5 (tp), 135.3 (tp), 134.5 (tp), 112.8 (C_{COD}=C=*C*HFc), 106.2 (tp), 106.1 (tp), 105.2 (tp), 90.1 (*C*$_{COD}$=C=CHFc), 87.1 (Fc^1), 82.2 (olefinic C of COD), 81.9 (olefinic C of COD), 69.1 (5 C, Fc), 67.9 (Fc), 67.7 (Fc), 67.1 (Fc), 66.7 (Fc), 64.1 (olefinic C of COD), 33.1, 32.6, 31.3, 30.3 (aliphatic C of COD).

Ru(tp){(5,6-η;η^3)-1-[(*Z*)-3-phenylpropenylidene]-5-cyclooctenyl} (4d): This compound was prepared analogously to **4a** with **1** (308 mg, 0.672 mmol), NaOEt (46 mg, 0.672 mmol), and HC≡CCH$_2$Ph (250 µL, 2.02 mmol) as the starting materials. Yield: 300 mg (83%). − $C_{26}H_{29}BN_6Ru$ (537.44): calcd. C 58.11, H 5.48, N 15.64; found C 58.22, H 5.58, N 15.61. − ^{1}H NMR ($CDCl_3$, 20°C): δ = 8.29 (d, *J* = 2.1 Hz, 1 H, tp), 8.04 (d, 1 H, *J* = 2.1 Hz, (tp), 7.76 (d, *J* = 2.5 Hz, 1 H, tp), 7.74 (d, *J* = 2.5 Hz, 1 H, tp), 7.55 (d, *J* = 2.5 Hz, 1 H, tp), 7.31−7.11 (m, 3 H, Ph), 6.98 (m, 2 H, Ph), 6.81 (d, 1 H, *J* = 2.1 Hz, tp), 6.37 (vt, *J* = 2.1 Hz, 1 H, tp), 6.21 (dd, *J* = 2.5 Hz, *J* = 2.1 Hz, 1 H, tp), 5.96 (t, *J* = 7.1 Hz, 1 H, C=C*H*-CH$_2$Ph), 5.96 (dd, *J* = 2.5 Hz, *J* = 2.1 Hz, 1 H, tp), 3.73 (m, 1 H, olefinic H of COD), 3.49 (m, 2 H, olefinic H of COD), 3.06−2.96 (m, 1 H, diastereotopic CH$_2$), 2.83−2.13 (m, 8 H), 1.71 (m, 1 H). − ^{13}C{^{1}H} NMR ($CDCl_3$, 20°C): δ = 175.2 (C_{COD}=*C*=CH-CH$_2$Ph), 144.8 (tp), 144.0 (Ph^1), 142.8 (tp), 141.6 (tp), 135.6 (tp), 135.8 (tp), 135.4 (tp), 134.2 (tp), 129.0 (2 C, Ph^{3,5}), 128.6 (2 C, Ph^{2,6}), 125.7 (Ph^4), 112.6 (C_{COD}=C=*C*H-CH$_2$Ph), 106.2 (tp), 105.6 (tp), 104.8 (tp), 89.2 (*C*$_{COD}$=C=CH-CH$_2$Ph), 81.4 (olefinic C of COD), 81.2 (olefinic C of COD), 63.0 (olefinic C of COD), 37.7 (*C*H$_2$-Ph), 33.7 (aliphatic C of COD), 32.8 (aliphatic C of COD), 30.7 (aliphatic C of COD), 30.4 (aliphatic C of COD).

Ru(tp){(5,6-η;η^3)-1-[(*E*)-3-phenylpropenylidene]-5-cyclooctenyl} (5d): This isomer could not be obtained in pure form. The ratio of (*Z*)/(*E*) diastereomers of 94:6 was determined by ^{1}H-NMR spectroscopy.

Ru(tp){(5,6-η;η^3)-1-[(*E*/*Z*)-1-hexenylidene]-5-cyclooctenyl} (4e, 5e): To a suspension of **1** (200 mg, 0.437 mmol) in MeOH (5 L), NaOEt (29.7 mg, 0.437 mmol) and HC≡C*n*Bu (150 µL, 1.311 mmol) were added and the solution was kept at reflux for 20 h. The reaction mixture was allowed to cool to room temperature and the solvent was removed under reduced pressure. The crude product (orange oil) was purified by column chromatography (neutral Al_2O_3). The first yellow band was eluted with CH_2Cl_2. Yield: 300 mg (83%) of a mixture of (*Z*) and (*E*) diastereomeres in a 2:1 ratio. The diastereomers could not be seperated. − $C_{23}H_{31}BN_6Ru$ (503.42): calcd. C 54.88, H 6.21, N 16.69; found C 54.62, H 6.28, N 16.61. − ^{1}H NMR for the (*Z*) diastereomer **4e** ($CDCl_3$, 20°C): δ = 8.32 (d, *J* = 1.7 Hz, 1 H, tp), 8.08 (d, 1 H, *J* = 2.1 Hz, tp), 7.77 (d, *J* = 2.5 Hz, 1 H, tp), 7.76 (d, *J* = 2.1 Hz, 1 H, tp), 7.56 (d, *J* = 2.1 Hz, 1 H, tp), 6.84 (d, 1 H, *J* = 2.5 Hz, tp), 6.39 (vt, *J* = 2.1 Hz, 1 H, tp), 6.29 (vt, *J* = 2.8 Hz, 1 H, tp), 5.99 (vt, *J* = 2.1 Hz, 1 H, tp), 5.96 (t, *J* = 7.2 Hz, 1 H, C=C*H*-*n*Bu), 3.73 (m, 1 H, olefinic H of COD), 3.49 (m, olefinic H of COD), 2.86−2.01 (m, 5 H), 1.75−0.99 (m, 10 H), 0.96 (t, *J* = 7.2 Hz, 3 H). − ^{13}C{^{1}H} NMR ($CDCl_3$, 20°C): δ = 174.0 (C_{COD}=*C*=CH-*n*Bu), 144.6 (tp), 142.7 (tp), 141.6 (tp), 135.5 (tp), 135.1 (tp), 134.0 (tp), 113.5 (C_{COD}=C=*C*H-*n*Bu), 106.1 (tp), 105.4 (tp), 104.4 (tp), 88.7 (*C*$_{COD}$=C=CH-*n*Bu), 80.9 (olefinic C of COD), 80.7 (olefinic C of COD), 62.7 (olefinic C of COD), 33.7, 33.5, 32.9, 31.0, 30.4, 28.8, 28.5, 23.2 (aliphatic C of COD and *n*Bu). − ^{1}H NMR for the (*E*) diastereomer **5e** ($CDCl_3$, 20°C): δ = 8.34 (d, *J* = 2.1 Hz, 1 H, tp), 8.06 (d, 1 H, *J* = 1.7 Hz, tp), 7.74 (d, *J* = 2.1 Hz, 1 H, tp), 7.61 (d, *J* = 2.5 Hz, 1 H, tp), 7.52 (d, *J* = 2.5 Hz, 1 H, tp), 6.67 (d, 1 H, *J* = 2.1 Hz, tp), 6.39 (vt, *J* = 2.1 Hz, 1 H, tp), 6.29 (dd, *J* = 2.5 Hz, *J* = 2.1 Hz, 1 H, tp), 6.22 (vt, *J* = 2.1 Hz, 1 H, tp), 4.79 (t, *J* = 6.8 Hz, 1 H, C=C*H*-*n*Bu), 3.73 (m, 1 H, olefinic H of COD), 3.46 (m, 1 H, olefinic H of COD), 2.86−2.01 (m, 5 H), 1.75−0.99 (m, 10 H), 0.78 (t, *J* = 7.2 Hz, 3 H). − ^{13}C{^{1}H} NMR ($CDCl_3$, 20°C): δ = 173.8 (C_{COD}=*C*=CH-*n*Bu), 143.8 (tp), 143.0 (tp), 141.2 (tp), 135.5 (tp), 135.1 (tp), 133.7 (tp), 113.4 (C_{COD}=C=*C*H-*n*Bu), 105.9 (tp), 105.6 (tp), 104.3 (tp), 87.9 (*C*$_{COD}$=C=CH-*n*Bu), 81.5 (olefinic C of COD), 79.5 (olefinic C of COD), 63.1 (olefinic C of COD), 33.8, 33.5, 33.0, 31.0, 30.4, 28.6, 28.5, 23.2 (aliphatic C of COD and *n*Bu).

Reaction of 4 and 5 with CF_3COOH. − Formation of Ru(tp){(1,2-η;5,6-η)-1-[(*E*/*Z*)-2-R-ethenyl]cyclooctadiene}(OCOCF$_3$) (R = Ph, C_6H_9, ferrocenyl, CH_2Ph, *n*Bu) (3′): Typically, a 5-mm NMR tube was charged with either **4** or **5** (30 mg) and was capped with a septum. A solution of CF_3COOH (ca. 2 equiv.) in $CDCl_3$ (0.5 mL) was added by syringe and the sample was transferred into a NMR probe. ^{1}H-NMR spectra were immediately recorded. The following coupling constants were observed for the reactions with **4a**: δ = 6.82 (d, $^3J_{HHcis}$ = 11.7 Hz, CH=CH), 6.58 (d, $^3J_{HHcis}$ = 11.7 Hz, CH=CH); with **5a**: δ = 6.92 (d, $^3J_{HHtrans}$ = 16.3 Hz, CH=CH), 5.95 (d, $^3J_{HHtrans}$ = 16.3 Hz, CH=CH); with **4b**: δ = 6.48 (d, $^3J_{HHcis}$ = 11.6 Hz, CH=CH), 6.01 (d, $^3J_{HHcis}$ = 11.6 Hz, CH=CH); with **5b**: δ = 6.51 (d, $^3J_{HHtrans}$ = 16.3 Hz, CH=CH), 5.45 (d, $^3J_{HHtrans}$ = 16.3 Hz, CH=CH); with **5c**: δ = 6.50 (d, $^3J_{HHtrans}$ = 15.9 Hz, CH=CH), 5.58 (d, $^3J_{HHtrans}$ = 15.9 Hz, CH=CH); with **4d**: δ = 6.18 (d, $^3J_{HHcis}$ = 11.1 Hz, CH=CH), 5.90 (ddd, $^3J_{HHcis}$ = 11.1 Hz, CH=CH); with **5d**: could not be observed; with **4e**: δ = 6.03 (d, $^3J_{HHcis}$ = 11.8 Hz, CH=CH), 5.68 (ddd, $^3J_{HHcis}$ = 11.7 Hz, CH=CH); with **5e**: δ = 6.80 (d, $^3J_{HHtrans}$ = 15.7 Hz, CH=CH), 5.40 (ddd, $^3J_{HHtrans}$ = 15.7 Hz, CH=CH).

Ru(tp){(1,2-η;5,6-η)-1-[(*Z*)-1-iodo-2-phenylethenyl]cyclooctadiene}I (6): To a solution of **4a** (70 mg, 0.134 mmol) in CH_2Cl_2 (2 mL), I_2 (37 mg, 0.150 mmol) was added and stirred for 2 h at room temperature. The volume of the solution was reduced to about 0.5 mL and the product was precipitated upon addition of Et_2O. The residue was collected on a glass frit, washed twice with 1.5 mL of Et_2O, and dried under vacuum. Yield: 85 mg (82%). − $C_{25}H_{27}BI_2N_6Ru$ (777.21): calcd. C 38.63, H 3.05, N 10.81; found C 38.55, H 3.02, N 10.62. − ^{1}H NMR ($CDCl_3$, 20°C): δ = 8.28 (d, *J* = 2.2 Hz, 1 H, tp), 7.87 (d, 1 H, *J* = 2.6 Hz, tp), 7.86 (d, *J* = 2.2 Hz, 1 H, tp), 7.75 (d, *J* = 2.2 Hz, 1 H, tp), 7.71 (d, *J* = 2.2 Hz, 1 H, tp), 7.67 (d, 1 H, *J* = 2.2 Hz, tp), 7.23−7.20 (m, 4 H, Ph), 6.96 (m, 1 H, Ph), 6.42 (dd, *J* = 2.2 Hz, *J* = 2.6 Hz, 1 H, tp), 6.26 (dd, *J* = 2.2 Hz, *J* = 1.8 Hz, 1 H, (tp), 6.20 (dd, *J* = 2.2 Hz, *J* = 1.8 Hz, 1 H, tp), 5.74−5.69 (m, 2 H, CI=C*H*-Ph and olefinic H of COD), 5.14 (m, 1 H, olefinic H of COD), 4.03 (m, 1 H, olefinic H of COD), 3.80−3.59 (m, 1 H, COD), 3.31−2.85 (m, 4 H), 2.78−2.46 (m, 1 H), 2.30−2.02 (m, 2 H). − ^{13}C{^{1}H} NMR ($CDCl_3$, 20°C):

Table 2. Crystallographic data for **3**, **4a**, **6**, and **7b**

	3	**4a**	**6**	**7b**
Empirical formula	$C_{25}H_{28}BClN_6Ru$	$C_{25}H_{27}BN_6Ru$	$C_{25}H_{27}BI_2N_6Ru$	$C_{39}H_{38}BN_6PRu$
Molecular mass	559.86	523.41	777.21	733.60
Crystal size [mm]	0.45 × 0.25 × 0.15	0 30 × 0.10 × 0.03	057 × 0.20 × 0.10	0.20 × 0.05 × 0.03
Space group	$P\bar{1}$ (No. 2)	$P2_1/n$ (No. 14)	$P\bar{1}$ (No. 2)	$P2_1/n$ (No. 14)
a [Å]	8.191(1)	8.180(2)	8.287(2)	9.647(2)
b [Å]	9.852(1)	11.252(3)	12.157(3)	15.155(3)
c [Å]	16.335(2)	25.335(6)	13.987(3)	24.373(6)
α [deg]	103.53(1)	90	76.350(1)	90
β [deg]	93.55(1)	98.85(1)	86.260(1)	95.19(1)
γ [deg]	109.04(1)	90	77.690(1)	90
V [Å^3]	1197.7(2)	2304(1)	1337.7(5)	3549(1)
Z	2	4	2	4
$\rho_{calcd.}$ [g cm^{-3}]	1.552	1.509	1.930	1.373
T [K]	295(2)	303(2)	299(2)	295(2)
μ [mm^{-1}] (Mo-K_α)	0.793	0.706	2.920	0.524
Absorption correction	multi scan	multi scan	multi scan	multi scan
F(000)	572	1072	748	1512
Transmission factor, min/max	0.86/0.73	0.93/0.74	0.69/0.45	0.96/0.84
θ_{max} [°]	30	27	30	25
Index ranges	$-11 \le h \le 11$ $-13 \le k \le 13$ $-23 \le l \le 22$	$-11 \le h \le 11$ $-15 \le k \le 15$ $-35 \le l \le 35$	$-11 \le h \le 11$ $-17 \le k \le 17$ $-19 \le l \le 19$	$-11 \le h \le 11$ $-18 \le k \le 18$ $-29 \le l \le 29$
Number of relections measured	13687	29227	21311	58041
Number of unique reflections	6815	5029	7765	6265
Number of reflections with $I > 2\sigma(I)$	6136	3760	6550	5112
Number of parameters	317	307	317	453
R_1 [$I > 2\sigma(I)$]	0.024	0.032	0.023	0.031
R_1 (all data)	0.029	0.057	0.031	0.046
wR_2 (all data)	0.056	0.066	0.056	0.070
Difference Fourier peaks, min/max. [eÅ^{-3}]	−0.46/0.36	−0.31/0.30	−1.01/1.17	−0.31/0.75

$R_1 = \Sigma||F_o| - |F_c||/\Sigma|F_o||$; $wR_2 = [\Sigma\{w(F_o^2 - F_c^2)^2\}/\Sigma\{w(F_o^2)^2\}]^{1/2}$.

δ = 147.9 (tp), 145.9 (tp), 145.4 (tp), 139.8 (C_{COD}-CI=*C*HPh), 138.7 (Ph[1]), 137.9 (tp), 136.5 (tp), 135.4 (tp), 129.1 (2 C, Ph[3,5]), 128.3 (2 C, Ph[2,6]), 128.0 (Ph[4]), 113.0 (C_{COD}=C=CHPh), 107.5 (tp), 106.8 (tp), 106.6 (tp), 97.1 (olefinic C of COD), 94.1 (olefinic C of COD), 87.2 (olefinic C of COD), 82.3 (C_{COD}-*C*I=CHPh), 37.9 (aliphatic C of COD), 37.3 (aliphatic C of COD), 32.8 (aliphatic C of COD), 27.6 (aliphatic C of COD).

Ru(tp){(κ^1(*P*);2,3,4-η)-1,4-diphenyl-6-diphenylphosphanyl-1,3,5-hexatrien-2-yl} (7a): A suspension of **2** (155 mg, 0.229 mmol) in MeOH (4 mL) was treated with HC≡CPh (75.6 μL, 0.688 mmol) and NaOEt (15.6 mg, 0.229 mmol) and heated at reflux for 20 h. The reaction mixture was then cooled to room temperature and the solvent was removed under reduced pressure. The crude product was purified by column chromatography (neutral Al_2O_3). The first yellow band was eluted with CH_2Cl_2. Yield: 98 mg (59%). − $C_{39}H_{34}BN_6PRu$ (729.59): calcd. C 64.20, H 4.70, N 11.52; found C 64.26, H 4.79, N 11.48. − ^{1}H NMR ($CDCl_3$, 20°C): δ = 8.14 (d, J = 1.9 Hz, 1 H, tp), 7.85 (m, 1 H, tp), 7.81 (m, 2 H, tp), 7.70 (d, J = 2.3 Hz, 1 H, tp), 7.65−7.00 (m, 19 H), 6.86−6.79 (m, 2 H), 6.77−6.66 (m, 1 H), 6.28 (d, J = 2.3 Hz, 1 H, tp), 6.24 (m, 1 H), 6.10 (vt, J = 2.3 Hz, 1 H, tp), 5.98 (d, J = 1.9 Hz, 1 H, tp), 5.38 (vt, J = 2.3 Hz, 1 H, tp), 4.64 (m, 1 H, tp). − ^{13}C{^{1}H} NMR ($CDCl_3$, 20°C): δ = 164.8 [d, $^2J_{PC}$ = 13.8 Hz, P-CH=CH-C(Ph)=CH=*C*=CH-Ph], 155.4 [d, $^2J_{PC}$ = 23.6 Hz, P-CH=*C*H-C(Ph)=CH=C=CH-Ph], 147.2 [d, $^3J_{PC}$ = 1.9 Hz, (tp), 146.4 (quaternary C of a Ph], 144.1 (tp), 142.4 (quaternary C of a Ph), 141.9 (tp), 140.0 (d, $^5J_{PC}$ = 2.4 Hz, tp), 136.7 (d, $^1J_{PC}$ = 48.1 Hz, PPh[1]), 136.2 (d, $^5J_{PC}$ = 2.4 Hz, tp), 135.6 (tp), 133.9, 133.8, 133.2 (quaternary C), 133.1 (quaternary C), 132.7, 132.1, 129.6−128.0 (m, 11C), 126.4 (d, J_{PC} = 1.4 Hz), 126.0, 125.6, 125.5, 125.2, 105.8 (d, $^4J_{PC}$ = 2.4 Hz, 1 C, tp), 104.7 (tp), 104.6 (tp), 86.0 [d, J_{PC} = 4.8 Hz, P-CH=CH-*C*(Ph)=CH=C=CH-Ph], 74.9 [P-CH=CH-C(Ph)=*C*H=C=CH-Ph]. − ^{31}P{^{1}H} NMR ($CDCl_3$, 20°C): δ = 70.1.

Ru(tp){(κ^1(*P*);2,3,4-η)-1-(1-cyclohexenyl)-4-phenyl-6-(diphenylphosphanyl)-1,3,5-hexatriene-2-yl} (7b): This compound was prepared analogously to **7a** with **2** (68 mg, 0.101 mmol), NaOEt (6.8 mg, 0.229 mmol) and HC≡CC_6H_9 (35.5 μL, 0.303 mmol) as the starting materials. Upon cooling the reaction mixture to room temperature a precipitate was formed, which was collected on a glass frit, washed with methanol and *n*-hexane, and dried under vacuum. Yield: 32 mg (43%). − $C_{39}H_{38}BN_6PRu$ (733.60): calcd. C 63.85, H 5.22, N 11.46; found C 63.99, H 5.35, N 11.32. − ^{1}H NMR ($CDCl_3$, 20°C): δ = 8.00 (d, J = 2.1 Hz, 1 H, tp), 7.67 (d, J = 2.1 Hz, 1 H, tp), 7.59 (d, J = 2.1 Hz, 1 H, tp), 7.52−6.61 (m, 19 H), 6.20 (m, 2 H), 6.02 (vt, J = 2.1 Hz, 1 H, tp), 5.87 (d, J = 2.1 Hz, 1 H, tp), 5.62 (m, 1 H), 5.29 (vt, J = 2.1 Hz, 1 H, tp), 4.39 (m, 1 H, tp), 2.01−1.85 (m, 4 H), 1.45−1.23 (m, 4 H). − ^{13}C{^{1}H} NMR ($CDCl_3$, 20°C): δ = 159.2 [d, $^2J_{PC}$ = 14.3 Hz, P-CH=CH-C(Ph)=CH=*C*=CHC_6H_9], 155.7 [d, $^2J_{PC}$ = 23.4 Hz, P-CH=*C*H-C(Ph)=CH=C=CHC_6H_9], 146.7 (d, $^3J_{PC}$ = 2.3 Hz, tp), 144.4 (1 C, quaternary C of Ph), 140.2 (tp), 139.2 (tp), 138.4 (d, $^1J_{PC}$ = 48.2 Hz, PPh[1]), 135.8 [d, $^1J_{PC}$ = 38.6 Hz, P-*C*H=CH-C(Ph)=CH=C=CHC_6H_9], 134.2 (tp), 134.1 (tp), 131.2 (d, $^1J_{PC}$ = 45.3 Hz, PPh[1′]), 131.6, 129.6−128.3 (m, 13 C), 126.3, 126.1, 125.6 (d, J = 3.8 Hz), 125.0, 123.0, 105.8 (d, $^4J_{PC}$ = 1.9 Hz, 1 C, tp), 104.7 (tp), 104.5 (tp), 85.0 [d, J_{PC} = 4.7 Hz, P-CH=CH-*C*(Ph)=CH=C=CHC_6H_9], 75.8 [P-CH=CH-C(Ph)=*C*H=C=CHC_6H_9], 28.5, 26.4, 23.34, 23.27. − ^{31}P{^{1}H} NMR ($CDCl_3$, 20°C): δ = 69.9.

Crystallographic Structure Determinations: Crystal, data collection, and refinement parameters for complexes **3**, **4a**, **6**, and **7b** are given

in Table 2. Crystals were obtained by diffusion of diethyl ether into CH_2Cl_2 solutions, except for **7b**, where crystals were grown by layering of *n*-hexane over a CH_2Cl_2 solution. All X-ray data were collected with a Siemens Smart CCD area detector diffractometer (graphite-monochromated Mo-K_α radiation, $\lambda = 0.71073$ Å, 0.3° ω-scan frames). Corrections for Lorentz and polarization effects, for crystal decay, and for absorption were applied. The structures were solved by direct or Patterson methods.[16] All non-hydrogen atoms were refined anisotropically. Hydrogen atoms were inserted in idealized positions and were refined riding with the atoms to which they were bonded. The structures were refined against F^2.[17] Crystallographic data (excluding structure factors) for the structures reported in this paper have been deposited with the Cambridge Crystallographic Data Centre as supplementary publication no. CCDC-105597/105598/105599/105600. Copies of data can be obtained free of charge on application to CCDC, 12 Union Road, Cambridge CB2 1EZ, UK [Fax: + 44-1223/336-033; E-mail: deposit@ccdc.cam.ac.uk].

Acknowledgments

Financial support by the Jubliäumsfond der Österreichischen Nationalbank is greatfully acknowledged (Project No. 6474).

[1] P. J. Stang, F. Diederich, *Modern Acetylene Chemistry*, VCH, Weinheim, FRG, **1995**.

[2] [2a] H. E. Selnau, J. S. Merola, *J. Am. Chem. Soc.* **1991**, *113*, 4008. – [2b] R. Wiedmann, P. Steinert, M. Schäfer, H. Werner, *J. Am. Chem. Soc.* **1993**, *115*, 9864. – [2c] H. Werner, R. Wiedmann, P. Steinert, J. Wolf, *Chem. Eur. J.* **1997**, *3*, 127. – [2d] P.-C. Ting, Y.-C. Lin, G.-H. Lee, M.-C. Cheng, Y. Wang, *J. Am. Chem. Soc.* **1996**, *118*, 6433. – [2e] C. Bianchini, P. Innocenti, M. Peruzzini, A. Romerosa, F. Zanobini, *Organometallics* **1996**, *15*, 272. – [2f] S.-M. Yang, M. C.-W. Chan, K.-K. Cheung, C.-M. Che, S.-M. Peng, *Organometallics* **1997**, *16*, 2819. – [2g] Y. Wang, M. G. Finn, *J. Am. Chem. Soc.* **1995**, *117*, 8045. – [2h] C. A. Merlic, M. E. Pauly, *J. Am. Chem. Soc.* **1996**, *118*, 11319. – [2i] H. M. Lee, J. Yao, G. Jia, *Organometallics* **1997**, *16*, 3927. – [2j] D. Huang, M. Olivan, J. C. Huffman, O. Eisenstein, K. J. Caulton, *Organometallics* **1998**, *17*, 4700. – [2k] M. A. Esteruelas, L. A. Oro, C. Valero, *Organometallics* **1995**, *14*, 3596.

[3] [3a] R. Beckhaus, *Angew. Chem.* **1997**, *109*, 695. – [3b] R. Beckhaus, J. Sang, T. Wagner, B. Ganter, *Organometallics* **1996**, *15*, 1176. – [3c] H. G. Alt, H. E. Engelhardt, M. D. Rausch, L. B. Kool, *J. Organomet. Chem.* **1987**, *329*, 61. – (Vinylidene)-ruthenium complexes in ROMP: [3d] H. Katayama, F. Ozawa, *Chem. Lett.* **1998**, 67. – (Allenylidene)ruthenium in RCM: [3e] A. Fürstner, M. Picquet, C. Bruneau, P. H. Dixneuf, *J. Chem. Soc., Chem. Commun.* **1998**, 1415.

[4] [4a] K. McNeill, R. A. Anderson, R. G. Bergman, *J. Am. Chem. Soc.* **1997**, *119*, 11244. – [4b] A. Kinoshita, N. Sakakibara, M. Mori, *J. Am. Chem. Soc.* **1997**, *119*, 12388. – [4c] J. M. O′Connor, K. Hiibner, R. Merwin, P. K. Gantzel, B. S. Fong, M. Adams, A. L. Rheingold, *J. Am. Chem. Soc.* **1997**, *119*, 3631.

[5] For related η^3-butadienyl complexes see: [5a] C. S. Yi, N. Liu, A. L. Rheingold, L. M. Liable-Sands, *Organometallics* **1997**, *16*, 3910. – [5b] M. I. Bruce, D. N. Duffy, M. J. Liddell, E. R. T. Tiekink, B. K. Nicholson, *Organometallics* **1992**, *11*, 1527. – [5c] M. I. Bruce, T. W. Hambly, M. J. Liddell, M. R. Snow, A. G. Swincer, E. R. T. Tiekink, *Organometallics* **1990**, *9*, 96. – [5d] M. I. Bruce, T. W. Hambly, M. R.; Snow, A. G. Swincer, *Organometallics* **1985**, *4*, 501. – [5e] M. I. Bruce, J. R. Rodgers, M.R. Snow, A. G. Swincer, *J. Chem. Soc., Chem. Commun.* **1981**, 271.

[6] C. Slugovc, K. Mereiter, R. Schmid, K. Kirchner, *J. Am. Chem. Soc.* **1998**, *120*, 6175.

[7] C. Slugovc, P. Wiede, K. Mereiter, R. Schmid, K. Kirchner, *Organometallics* **1997**, *16*, 2768.

[8] [8a] B. M. Trost, G. Dyker, R. Kulawiec, *J. Am. Chem. Soc.* **1990**, *112*, 7809. – [8b] M. I. Bruce, B. C. Hall, N. N. Zaitseva, B. W. Skelton, A. H. White, *J. Organomet. Chem.* **1996**, *522*, 307.

[9] C. Slugovc, D. Doberer, C. Gemel, R. Schmid, K. Kirchner, B. Winkler, F. Stelzer, *Monatsh. Chem.* **1998**, *129*, 221.

[10] C. Gemel, G. Trimmel, C. Slugovc, S. Kremel, K. Mereiter, R. Schmid, K. Kirchner, *Organometallics* **1996**, *15*, 3998.

[11] [11a] T. V. Ashworth, E. Singleton, J. J. Hough, *J. Chem. Soc., Dalton Trans.* **1977**, 1809. – [11b] B. Moreno, S. Sabo-Etienne, B. Chaudret, A. Rodriguez, F. Jalon, S. Trofimenko, *J. Am. Chem. Soc.* **1995**, *117*, 7441.

[12] [12a] N.-Y. Sun, S. J. Simpson, *J. Organomet. Chem.* **1992**, *434*, 341. – [12b] N. W. Alcock, I. D. Burns, K. S. Claire, A. F. Hill, *Inorg. Chem.* **1992**, *31*, 2906. – [12c] N. W. Alcock, A. F. Hill, R. B. Melling, *Organometallics* **1991**, *10*, 3898. – [12d] A. F. Hill, *J. Organomet. Chem.* **1990**, *395*, C35. – [12e] M. M. deV. Steyn, E. Singleton, S. Hietkamp, D. C. Liles, *J. Chem. Soc., Dalton Trans.* **1990**, 2991. – [12f] A. M. McNair, D. C. Boyd, K. R. Mann, *Organometallics* **1986**, *5*, 303. – [12g] G. Trimmel, C. Slugovc, P. Wiede, K. Mereiter, V. N. Sapunov, R. Schmid, K. Kirchner, *Inorg. Chem.* **1997**, *36*, 1076.

[13] [13a] M. I. Bruce, *Chem. Rev.* **1991**, *91*, 197. – [13b] C. Slugovc, V. N. Sapunov, P. Wiede, K. Mereiter, R. Schmid, K. Kirchner, *J. Chem. Soc., Dalton Trans.* **1997**, 4209. – [13c] I. de los Rios, M. J. Tenorio, M. C. Puerta, P. Valerga, *J. Am. Chem. Soc.* **1997**, *119*, 6529.

[14] Unpublished results.

[15] D. D. Perrin, W. L. F. Armarego, *Purification of Laboratory Chemicals*, 3rd ed., Pergamon, New York, **1988**.

[16] G. M. Sheldrick, *SHELXS97*, *Program for the Solution of Crystal Structures*, University of Göttingen, Germany, **1997**.

[17] G. M. Sheldrick, *SHELXL97*, *Program for Crystal Structure Refinement*, University of Göttingen, Germany, **1997**.

Received December 4, 1998
[I98417]

Applications of Photoelectron Spectroscopy to Molecular Properties, 52[+] Gas-Phase Characterization of an Unhindered Germaimine by UV-Photoelectron Spectroscopy

Séverine Foucat,[a] Thierry Pigot,[a] Geneviève Pfister-Guillouzo,*[a] Stéphane Mazières,[b] and Hélène Lavayssière[b]

Keywords: Germacyclopentene / Germaimine / Photoelectron spectroscopy / Ab initio calculations / Germanium

An unhindered germaimine has been generated and characterized by the coupling of flash vacuum pyrolysis of two different precursors with UV-photoelectron spectroscopy. The Ge=N unit exhibits two ionizations in the low-energy region, corresponding to the ejection of an electron from the nitrogen atom lone pair and from the $\pi_{Ge=N}$ orbital, respectively.

Introduction

The chemistry of low-coordinated group-14 and -15 elements of the third and fourth periods has undergone considerable development over the past 35 years. The first experimental characterizations of the C≡P triple bond[1] and of the Si=C double bond appeared in the 1960s.[2] Soon after, germanium compounds with multiple bonds were reported. These species showed greater overall kinetic instability when they were slightly sterically hindered.

The germaimines, compounds with a Ge=N double bond, were first characterized indirectly using various trapping reagents.[3] Only in the last ten years have sufficiently stable germaimines been synthesized to allow their analysis in the solid state (XR, IR) or in solution (IR, NMR).[4−7] However, there have been no reports of the characterization of germaimines in the gas phase, other than that by Lee[8] concerning $H_2Ge{=}NCF_3$. This latter exhibited a surprising stability and proved to be resistant to hydrolysis (!).

We present in this paper the first characterization of an unhindered germaimine by UV-photoelectron spectroscopy (UV-PES), specifically *N-tert*-butyl-3,4-dimethyl-1-germacyclopent-3-en-1-imine (**1**).

Results and Discussion

The aforementioned germaimine was generated by flash vacuum thermolysis (FVT) of the fluorogermacyclopentene **2** and the cyclodigermazane **3**, and was analyzed by photoelectron spectroscopy (UV-PES). The coupling of FVT with UV-PES has turned out to be particularly well suited for the detection of highly reactive species and has recently been used in studies of *N*-alkylated and *N*-silylated silaimines.[9][10]

The precursor **2** was synthesized by condensation of the corresponding lithiated amine with germacyclopentene difluoride. After several weeks at ambient temperature under inert atmosphere, **2** had undergone spontaneous conversion into a white crystalline solid corresponding to the cyclodigermazane **3**, which was fully characterized by MS and NMR analysis.

The photoelectron spectrum of the precursor **2** (Figure 1a) features a first well-resolved band at 8.4 eV, corresponding to the ejection of an electron from the nitrogen atom lone pair[11] and the $\pi_{C=C}$ orbital.[12] The broader signal seen at 10.3 eV is associated with ionization from the σ_{Si-C} orbitals. The latter signal shows an obvious shoulder at 9.7 eV, which corresponds to ionization from the σ_{Ge-C} orbitals. The following ionization, which is attributed to the ejection of an electron from the σ_{Ge-N} orbital, is poorly resolved (11.6 eV).

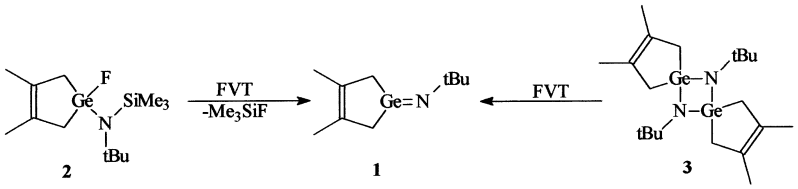
The PE spectrum of the cyclodigermazane **3** (Figure 1c) is characterized by two bands in the low-energy region, at 7.4 eV and 8.2 eV. We attribute the band at 7.4 eV to ionizations from the antibonding and bonding combinations of the nitrogen atom lone pairs. Ionizations of the antibonding and bonding $\pi_{C=C}$ orbital combinations are responsible for the broad signal at 8.2 eV. The bands above 9.0 eV correspond to the ejection of an electron from the σ_{Ge-C} and σ_{Ge-N} bonds.

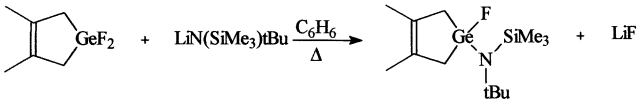
The short-path thermolysis spectrum of **2** at 673 K is displayed in Figure 1b. In the low-energy region, a broad signal at 7.0 eV, and an intense band at 8.7 eV with a marked shoulder at 8.1 eV can be seen. Beyond these signals, an ionization at 10.9 eV with a shoulder at 10.3 eV, and another signal at 11.4 eV can be noted. The ionization energy at 10.9 eV corresponds to Me_3SiF, formation of which was unambiguously proven when long-path thermolysis experiments were performed (520 K). An identical spectrum (lacking the band at 10.9 eV) was obtained upon

[+] For Part 51, see ref.[10]

[a] Laboratoire de Physico-Chimie Moléculaire, CNRS UMR 5624, Avenue de l'Université, F-64000 Pau, France
Fax: (internat.) + 33-5/59808344
E-mail: genevieve.pfister@univ-pau.fr
[b] Laboratoire d'Hétérochimie Fondamentale et Appliquée, 118, route de Narbonne, F-31062 Toulouse, France

 © WILEY-VCH Verlag GmbH, D-69451 Weinheim, 1999 1434−1948/99/0707−1151 $ 17.50+.50/0





heating the cyclic dimer **3** at the same temperature. Thus, it seems as though the same species was generated in each case, namely the germaimine **1**.

In order to verify the assigned natures of the ionizations, we have theoretically evaluated the energies of the first three ionic states of a structurally similar germaimine, **1′** (*N*-methyl rather than *N*-*tert*-butyl). These calculations were performed using the density functional method with the hybrid functional B3LYP[13] and the LANL2DZ(d) basis set.[14][15] The optimized structure of this molecule is shown in Figure 2. The calculated Ge=N bond length (1.696 Å) is in excellent agreement with both the experimental[7] and a previous theoretical value.[16]

The magnitudes and assignments of the first three vertical ionization energies are summarized in Table 1. We note that the ionization energies of the nitrogen atom lone pair and $\pi_{C=C}$ double-bond orbitals of *N*-alkylated germaimine are very close (7.78 eV and 7.71 eV). Moreover, the destabilizing effect of a *tert*-butyl group on the nitrogen atom compared to a methyl group has previously been observed for ionization from the n_N and $\pi_{Si=N}$ orbitals of dimethylsilaimines (0.5 eV and 0.9 eV, respectively).[9]

Table 1. Calculated [B3LYP/LANL2DZ(d), ΔSCF] and experimental first ionic states energies of **1** and **1′** [eV]

Ionic states	Calculated energies of **1′**	Experimental energies of **1**
$^2A'$ (n_N)	7.71	7.0
$^2A''$ ($\pi_{Ge=N}$)	7.78	7.0
$^2A''$ ($\pi_{C=C}$)	7.93	8.1

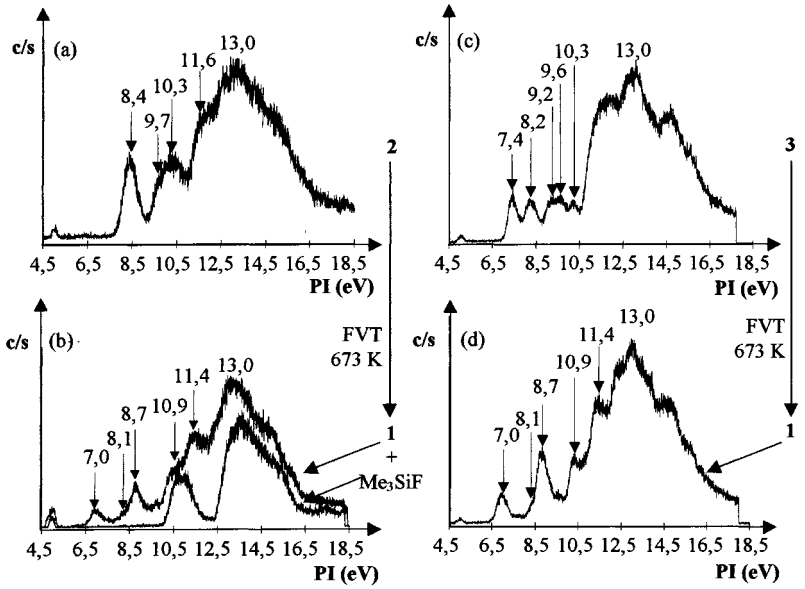


Figure 1. PE spectra of **2** at 300 K (a), at 673 K (b), of **3** at 300 K (c), and at 673 K (d)

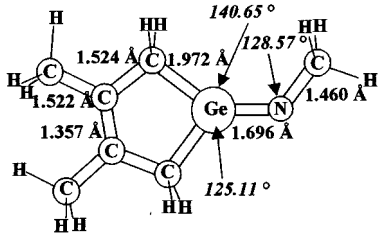


Figure 2. Geometrical parameters of the *N*-methylated germaimine **1′** [B3LYP/LANL2DZ(d)]

Thus, it seems reasonable to attribute the broad signal centered at 7.0 eV to ionizations from the nitrogen atom lone pair and $\pi_{Ge=N}$ bond, and the third ionization energy at 8.1 eV, the shoulder of the band at 8.7 eV in the PE spectrum, to the ejection of an electron from the $\pi_{C=C}$ cyclic bond (calculated at 7.93 eV). The ionizations of the antibonding and bonding combinations of the Ge−C bonds are observed at higher energies of 9.7 and 10.3 eV, respectively.[12] The intense signal at 8.7 eV is characteristic of the first ionization of 2,3-dimethylbuta-1,3-diene. Thus, at this temperature we observed the onset of the loss of 2,3-di-

methylbuta-1,3-diene, corresponding to a second decomposition process (confirmed when long-path thermolysis experiments were conducted at 673 K).

Conclusion

To the best of our knowledge, this work constitutes the first gas-phase characterization of a germaimine generated by flash vacuum thermolysis. This compound displays two characteristic ionizations in the low-energy region, corresponding to electron abstraction from the nitrogen atom lone pair and the Ge=N double bond. As in the case of silaimines, a $\pi_{Ge=N}$ orbital destabilization relative to the imines is in evidence. This stems from the kinetic instability and higher reactivity of the germaimines.

Experimental Section

Photoelectron Spectroscopy: Photoelectron spectra were recorded with a Helectros 0078 spectrometer, monitored by a microcomputer system supplemented by a digital analog converter (DAC). The spectra were built up from 2000 points and are accurate to within ±0.1 eV. They were recorded with 21.21 eV HeI radiation as the photon supply and were calibrated against the well-known helium ionization at 4.98 eV and nitrogen ionizations at 15.59 eV and 16.98 eV. Two types of pyrolysis experiments were performed, in combination with photoelectron spectroscopy. In short-path pyrolyses, the furnace was placed inside the ionization chamber of the UV spectrometer. The pressure in the ionization chamber was 10^{-5} mbar prior to introduction of the sample, and less than 10^{-4} mbar when the product was present. This first experimental procedure permitted analysis of species of short lifetime as well as their decomposition products. The second thermolysis system was external from the spectrometer. Thermolysis was performed in a vacuum device (oven pressure: 10^{-3} mbar without sample) connected to the spectrometer. In this case, only the stable species could be characterized after cryogenic distillation. Unstable compounds decompose and/or polymerize because of the considerable distance between the oven and the ionization head (around 1 m).

Synthesis of Precursors 2 and 3

1-[*tert*-Butyl(trimethylsilyl)amino]-1-fluoro-3,4-dimethyl-1-germacyclopent-3-ene (2): Germacyclopentene difluoride (6.65 g, 34.5 mmol) was added to a solution of LiN(*t*Bu)$SiMe_3$ (5.21 g, 34.5 mmol) in 20 mL of dry THF. The resulting yellow solution was stirred for 2 h at ambient temperature. Then, the THF was evaporated and pentane was added. LiF was eliminated by centrifugation and the organic layer was purified by vacuum distillation to yield 4.39 g (40%); b.p. 88°C/0.04 Torr. − MS (70 eV); *m/z*: 319 [M^+]. − ^{1}H NMR ($CDCl_3$): δ = 0.22 [s, 9 H, $Si(CH_3)_3$], 1.34 [s, 9 H, $C(CH_3)_3$], 1.74 (m, 6 H, cyclic CH_3), 1.84 (m, 2 H, cyclic CH_2), 1.92 (m, 2 H, cyclic CH_2). − ^{19}F NMR ($CDCl_3$): δ = −85.6 (m).

3: Compound **3** was obtained by spontaneous transformation of **2**. After one month under inert atmosphere, **2** was transformed into yellow crystals of **3** as Me_3SiF was given off; m.p. 174−176°C. − MS (70 eV); *m/z*: 452 [M^+]. − ^{1}H NMR ($CDCl_3$): δ = 1.15 [s, 18 H, $C(CH_3)_3$], 1.71−1.75 (m, 10 H, cyclic H).

Calculation Method: The theoretical evaluations were performed by means of an ab initio molecular orbital calculation method as implemented in the Gaussian 94 program package.[15] The geometrical parameters of neutral species were optimized by functional density theory using the B3LYP analytical function in conjunction with the LANL2DZ (D95 on H, C, N,[13] Los Alamos ECP plus DZ on Si, Ge[14]) basis set, extended with d orbitals (exponents: 0.8 for C and N; 0.202 for Ge). Ionization potentials (IPs) were evaluated at the ΔSCF level (IPs = $E_{neutral} - E_{ion}$).

Acknowledgments

Financial support of this work by the CNRS (France) is gratefully acknowledged. We also thank the Institut du Développement des Ressources Scientifiques (IDRIS, Orsay, France), under the administration of the CNRS, for use of the calculation facilities, and Dr. Gijs Schaftenaar for allowing us to use his graphics program Molden.

[1] T. E. Gier, *J. Am. Chem. Soc.* **1961**, *83*, 1769.
[2] L. E. Gusel′nikov, M. C. Flowers, *Chem. Commun.* **1967**, 864−865.
[3] J. Barrau, J. Escudié, J. Satgé, *Chem. Rev.* **1990**, *90*, 283−319.
[4] M. Rivière-Baudet, J. Satgé, F. El-Baz, *J. Chem. Soc., Chem. Commun.* **1995**, 1687−1688.
[5] T. Tsumuraya, W. Ando, *Chem. Lett.* **1989**, 1043−1046.
[6] C. Glidewell, D. Lloyd, K. W. Lumbard, J. S. McKechnie, *Tetrahedron. Lett.* **1987**, *28*, 343−344.
[7] A. Meller, G. Ossig, W. Maringgele, D. Stalke, R. Herbst-Irmer, S. Freitag, G. M. Sheldrick, *J. Chem. Soc., Chem. Commun.* **1991**, 1123−1124.
[8] H. G. Ang, F. K. Lee, *J. Chem. Soc., Chem. Commun.* **1989**, 310−311.
[9] V. Metail, S. Joanteguy, A. Chrostowska-Senio, G. Pfister-Guillouzo, A. Systermann, J. L. Ripoll, *Inorg. Chem.* **1997**, *36*, 1482−1487.
[10] V. Metail, S. Joanteguy, A. Chrostowska-Senio, G. Pfister-Guillouzo, A. Systermann, J. L. Ripoll, *Main Group Chem.* **1997**, *2*, 97−106.
[11] [11a] D. H. Harris, M. F. Lappert, J. B. Pedley, G. J. Sharp, *J. Chem. Soc., Dalton Trans.* **1976**, 945−950. − [11b] K. A. O. Starzewski, H. T. Dieck, H. Bock, *J. Organomet. Chem.* **1974**, *65*, 311−325.
[12] C. Guimon, G. Pfister-Guillouzo, G. Manuel, P. Mazerolles, *J. Organomet. Chem.* **1978**, *149*, 149−159.
[13] T. H. Dunning, Jr., P. J. Hay, *Modern Theoretical Chemistry* (Ed.: H. F. Schaefer III), Plenum, New York, **1976**, p. 1−28.
[14] P. J. Hay, W. R. Wadt, *J. Chem. Phys.* **1985**, *82*, 270−283; W. R. Wadt, P. J. Hay, *J. Chem. Phys.* **1985**, *82*, 284−298; P. J. Hay, W. R. Wadt, *J. Chem. Phys.* **1985**, *82*, 299−310.
[15] M. J. Frisch, G. W. Trucks, H. B. Schlegel, P. M. W. Gill, B. G. Johnson, M. A. Robb, J. R. Cheeseman, T. A. Keith, G. A. Petersson, J. A. Montgomery, K. Raghavachari, M. A. Al-Laham, V. G. Zakrzewski, J. V. Ortiz, J. B. Foresman, J. Cioslowski, B. B. Stefanov, A. Nanayakkara, M. Challacombe, C. Y. Peng, P. Y. Ayala, W. Chen, M. W. Wong, J. L. Andres, E. S. Replogle, R. Gomperts, R. L. Martin, D. J. Fox, J. S. Bingley, D. J. Defrees, J. Baker, J. P. Stewart, M. Head-Gordon, C. Gonzalez, J. A. Pople, *Gaussian 94* (Revision D.1), Gaussian, Inc., Pittsburgh PA, **1995**.
[16] G. Trinquier, J. C. Barthelat, J. Satgé, *J. Am. Chem. Soc*. **1982**, *104*, 5931−5936.

Received December 14, 1998
[I98421]

On the Bonding Properties of Diphosphanylmethanide Complexes with the Group-14 Elements Silicon, Germanium, Tin, and Lead in Their Divalent Oxidation States

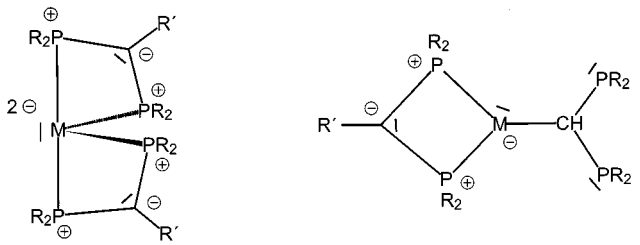
Wolfgang W. Schoeller,*[a] Andreas Sundermann,[a] Markus Reiher,[a] and Alexander Rozhenko[a]

Keywords: Ab initio calculations / Chelates / Donor–acceptor systems / P ligands

The mono- and bidentate chelation of the main-group elements silicon, germanium, tin, and lead through the phosphorus atoms of the diphosphanylmethanide ligand has been studied by means of quantum chemical methods. In accord with experimental investigations, the species are found to adopt a ψ-tbp conformation of high flexibility. The various distortional modes causing the axial and equatorial positions to become equivalent have also been investigated. In addition, the bonding situations in the electronically related bis(diamino)- and the higher element homologue bis(diarsanyl)methanide ligand systems have been studied. The bonding situation in the hitherto experimentally unknown bis(diamino)methanide ligands is predicted to be similar to that in bis(amidinate) complexes. An analysis of the electron distributions (natural bond orbital population analysis) in these compounds reveals that the central main-group element is positively charged and weakly chelated by the surrounding ligands.

Introduction

Divalent silicon compounds are currently of interest due to their high potential in new synthetic routes. Archetypal compounds in this field are $(C_5Me_5)Si$ with η^5-bonded ligands (silicocene)[1] and the intramolecular donor-stabilized diphosphanylmethanide complexes **1** (M = Si).[2] For the higher element homologues with M = Ge[3] and Sn,[4] corresponding compounds have also been characterized experimentally. Besides the connectivity seen in **1**, chelation of the main-group element can also occur in three-fold coordinated compounds such as **2** (Scheme 1).



M = Si, Ge, Sn
R = phenyl
R´= SiMe3

1 **2**

Scheme 1

Species of this kind are known for M = Ge, Sn, and Pb.[5] Recently, a diphosphanylmethanide complex was reported with phosphorus as the central main-group element.[6] For the Group-14 elements, chelation has been well documented in the amidinate chemistry of these species, which has been extensively investigated for tin and lead[7–10] as well as for germanium.[11] For silicon, bidentate amidinate chelation could be deduced on the basis of NMR investigations.[12] A first quantum chemical interpretation of the various structural alternatives in amidinate chemistry has recently been presented.[13]

The extremely rich chemistry in this field prompted us to investigate diphosphanylmethanide structures containing a Group-14 element (Si, Ge, Sn, Pb) as the central atom by quantum chemical methods. We report here the results of ab initio calculations on the chelated main-group elements in their divalent oxidation states, utilizing relativistic effective core potentials for the description of the higher main-group elements. In particular, we have analyzed the following aspects of the complexes: (a) bis(diphosphanyl)methanide chelation, and (b) the likelihoods of various geometrical arrangements at the central atom, i.e. trigonal-pyramidal (C_2) or planar (D_{2h}) environments. From experimental investigations it is known that these structures preferentially adopt pseudo-trigonal-bipyramidal (Ψ-tbp) geometries, which can easily be distorted. In solution, the structures undergo geometrical rearrangements that may be observed as dynamic processes by NMR spectroscopy.[4][5] All these aspects have been analyzed by means of quantum chemical calculations. Details of the quantum chemical methodology are given in the Appendix.

Results and Discussion

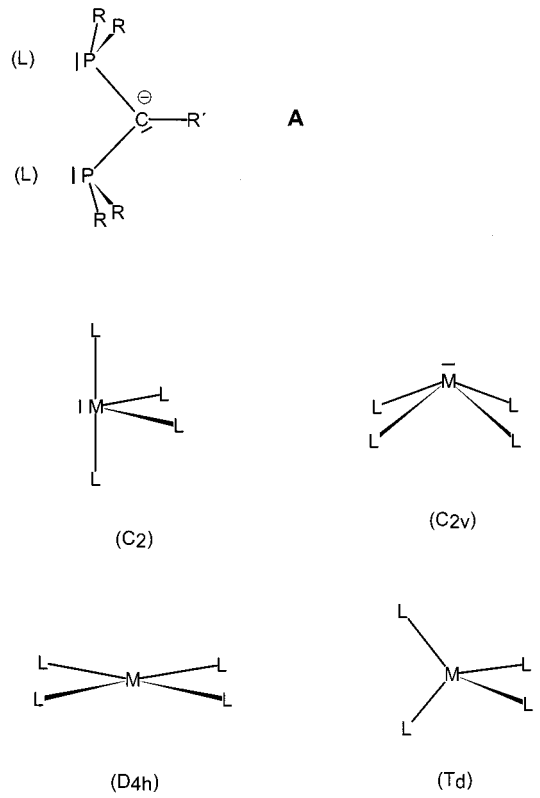
(a) The Ligand Field of the p-Block Elements

We begin our analysis with a discussion of some qualitative aspects. The formation of diphosphanylmethanide complexes can be considered in terms of the coordination of a

[a] Fakultät für Chemie, Universität Bielefeld,
Postfach 100131, D-33501 Bielefeld, Germany

 © WILEY-VCH Verlag GmbH, D-69451 Weinheim, 1999 1434–1948/99/0707–1155 $ 17.50+.50/0

central element M (Si, Ge, Sn, etc.) in a ligand field[14] that is spanned by the diphosphanylmethanide ligands **A** (Scheme 2).

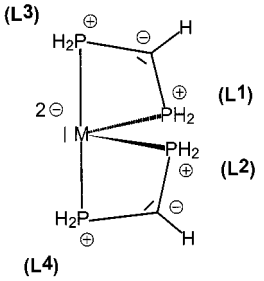


Scheme 2

The ligand **A** refers to two two-electron donors (denoted here as L). In other words, each two-electron donor is confined to a non-bonding lone pair at the (terminal) phosphorus atoms and each phosphorus atom of the diphosphanylmethanide ligand supplies two electrons to the central atom M. Various a priori possible conformations can be drawn. In each of them, the ligand exerts a ligand field[14] on the central atom. The orbital splitting for the different geometrical arrangements can be deduced from symmetry considerations, as has been shown previously for coordination of a central atom M with amidinato ligands.[13] In the C_2 and C_{2v} conformations, a non-bonding lone-pair orbital is operative at the central element M. The latter differs from the former geometry in that all M−L bonds are equivalent. It can be considered as the transition state geometry for interchange of the equatorial and axial bond positions in the dynamic rearrangement.[3] Possible planar (D_{4h}) or tetrahedral (T_d) conformations are not observed experimentally, and are thus not included in our considerations. For the corresponding amidinate complexes, the latter tetrahedral structure incorporates four strong bonds between the central atom M and the ligands, and can be assigned to a structure with a high degree of open-shell character.[13] For a more exhaustive discussion on the action of the ligand field on the orbitals of the central element M, the reader might like to refer to a recent report.[13]

(b) Bidentate Chelation

In this section, we report the numerical results obtained for the parent bis(diphosphanyl)methanide structures **B** (R = H). We first studied their equilibrium geometries with the main-group element M being varied by descending the group Si, Ge, Sn, and Pb. As ligands L^i (i = 1 to 4), the diamino- (L^i = N), diphosphanyl- (L^i = P), and diarsanylmethanide (L^i = As) components were chosen (Scheme 3). Experimentally, only the case of L^i = P is known, so our calculations make predictions for a variety of structures of experimentally unknown homologues. In all calculations we replaced the substituents at L^i and at the carbon atoms by hydrogen atoms. In the actual experimental situation the bis(diphosphanyl)methanide complexes are kinetically protected by bulky substituents (aryl, alkyl) at the chelating phosphorus atoms. Hence, our present calculations cannot account for these steric effects, but should accurately reflect the trends in bonding. The relevant equilibrium bonding parameters (bond lengths in Å, bond angles in degrees), obtained by energy optimizations of the equilibrium structures, are collected in Table 1.



Scheme 3

The most stable structure is found to be the ψ-tbp geometry, in accord with experiment. Two ligands L^1 and L^2 occupy equatorial while the other two L^3 and L^4 occupy axial positions. All of the equilibrium geometries could be ascertained by corresponding vibrational analyses. As expected, the equatorial bonds are invariably shorter than the axial ones. This is a common feature of the trigonal-bipyramid surrounding a central main-group element.[15] The actual equilibrium geometry of the ψ-tbp complex is determined by the electronegativity of the chelating axial and equatorial atoms (groups). We may discuss this for the case M = Si, L^i = N (diaminomethanide ligand), for which corresponding experimental structures are unknown. Here, the two axial bonds are equivalent in length, hence this molecule strictly adopts C_2 symmetry. On the other hand, replacement of N by P (diphosphanylmethanide ligand) makes the two axial bonds asymmetrical. The trend increases in the order (L^4/L^3, N = 1.0, P 1.35, As 1.41). However, with increasing atomic size of the central element M (Si < Ge < Sn < Pb), the asymmetry of the axial bonds becomes less marked. In fact, for M = Sn the two axial bonds in the ψ-tbp geometries are invariably symmetrical. The effects on the equatorial bonds are almost negligible so

Table 1. Equilibrium geometries of complexes **1** (bond lengths in Å; bond angles in degrees)

M	L^i	Symmetry	M−L^1	M−L^2	M−L^3	M−L^4	∠ L^1ML^2	∠ L^3ML^4
Si	N	C_2	1.956	1.956	2.165	2.165	96.0	142.0
	P	C_1	2.331	2.338	2.401	3.245	93.5	138.2
	As	C_1	2.435	2.459	2.502	3.514	90.6	135.2
Ge	N	C_2	2.079	2.079	2.284	2.284	94.8	137.8
	P	C_2	2.432	2.432	2.749	2.749	92.8	140.9
	As	C_1	2.525	2.548	2.664	3.200	89.6	139.3
Sn	N	C_2	2.301	2.301	2.417	2.417	89.9	130.4
	P	C_2	2.639	2.639	2.900	2.900	90.5	132.7
	As	C_2	2.731	2.731	3.008	3.008	87.8	133.8
Pb	N[a]	C_2	2.420	2.420	2.462	3.462	85.1	131.8
	P	C_2	2.691	2.691	2.929	2.929	90.6	131.6
	As	C_2	2.776	2.776	3.021	3.021	89.1	134.1

[a] Unstable (transition state) structure, rearranges to **d**.

that these have similar lengths in all cases. We note that for M = Pb and L^i = N the corresponding structure **B** is not stable on the electronic hypersurface, but further rearranges to its isomer **d** (vide infra) without having to surmount an energy barrier.

It is of interest to inspect the population analyses (NBO) of the resulting equilibrium geometries. These are presented in Table 2.

Table 2. Wiberg bond indices and NBO charges of complexes **1**

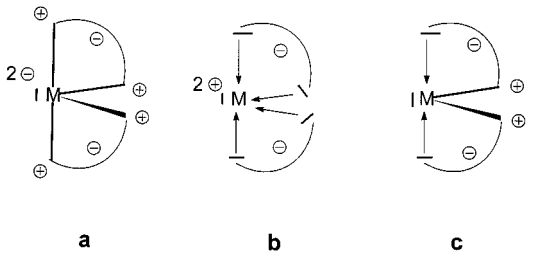
M	L^i	M−L^1	M−L^2	M−L^3	M−L^4	q(M)
Si	N	0.37	0.37	0.24	0.24	1.28
	P	0.84	0.80	0.72	0.10	0.24
	As	0.86	0.80	0.75	0.06	0.22
Ge	N	0.32	0.32	0.20	0.20	1.36
	P	0.77	0.77	0.40	0.40	0.39
	As	0.81	0.78	0.60	0.17	0.36
Sn	N	0.21	0.21	0.17	0.16	1.48
	P	0.66	0.66	0.37	0.37	0.64
	As	0.67	0.67	0.36	0.36	0.64
Pb	N	0.16	0.16	0.15	0.15	1.51
	P	0.63	0.63	0.34	0.34	0.73
	As	0.63	0.63	0.33	0.33	0.74

In general, the Wiberg bond indices for the axial bonds are smaller than those for the equatorial bonds. Nevertheless, for L^i = N, M = Si both the equatorial and the axial bonds are even weaker than a half bond. Replacing the ligands L^i by more electropositive elements (P, As) increases the strengths of the equatorial bonds, but makes the axial bonds more asymmetrical. As a further consequence, one axial bond becomes much stronger than the other (e.g. M = Si, L^i = P). As will be shown below by energetic considerations (vide infra), the overall energy differences resulting from the increased strength of one axial bond and the simultaneous weakening of the other are fairly small. With the higher element homologues as the central atom, M = Ge > Sn > Pb, the trend towards asymmetry of the two axial bonds is diminished.

It is notable that the axial bonds of the diphosphanylmethanide structures can easily become asymmetrical. Thus, one axial bond lengthens while the other shortens, and the energy difference between these forms and the highly symmetrical structure (C_2 symmetry) is fairly small. In order to further support this argument we have performed calculations at a higher level for the case M = Si, L^i = P. The two stationary points, with either C_2 symmetry (transition state structure) or C_1 symmetry (equilibrium structure) were taken into consideration. At the MP2 level, we obtained the following energy differences (in kJ/mol) as a function of the basis sets: (a) 6-31g** level 3.9, (b) 6-31+g** 5.1, (c) 6-311+g** 3.6. Thus, at higher computational levels our findings compare extremely well with the results obtained with the effective core potential basis sets. In other words, the more refined calculations are supportive of the present discussion. In the actual experiment, however, the structures are substituted by bulky substituents, which exert a steric hindrance. Hence, the subtle energy differences revealed by the quantum chemical theory for the unsubstituted cases can be neglected in comparison with the steric effects exerted by the substituents. The calculations also predict that the trend towards decreased symmetry should increase with decreasing positive charge at the central main-group element, e.g. for M = Si, in the order N < P < As.

We have also analyzed the extent of a bonding interaction between the negatively charged methanide carbon atoms and the central atom M. Overall, the Wiberg bond indices, i.e. the bond orders, are negligible (≤ 0.05) for the cases M = Si to Pb. Of interest is the charge at the central atom M. For L^i = N (diaminomethanide ligand) this amounts to ca. +1.3 to +1.5, while for the higher element homologues L^i = P, As it is much less (ca. +0.2 to +0.7). Such a description also holds true for the related amidinate complexes.[13] On the basis of the charge densities and the Wiberg bond indices, one can view the bonding situation in the complexes in terms of the three canonical structures **a** to **c** (Scheme 4).

In **a**, the central element M is tetravalent but additionally bears a lone pair orbital. Thus, this canonical structure formally refers to a 10-electron configuration at M. In comparison, in the canonical structure **b** the central atom M is chelated by four two-electron donating groups. In this structure, M is assigned a formal charge of +2. Finally, we may add a third canonical structure **c**. It is characterized by equatorial single bonds and two axial bonds fixed by a



Scheme 4

donor−acceptor interaction with the central atom. According to the population analyses, the various complexes can be divided into two categories: (a) In cases where the donating atoms are strongly electronegative (e.g. with the diaminomethanide ligand), the resulting compounds are best described by canonical structure **b**. In these cases, the Wiberg bond indices indicate a bond order of less than a half for the equatorial *and* axial bonds. However, the latter bonds are invariably stronger than the former ones. (b) On the other hand, in the case of L^i = P, As (diphosphanyl-, diarsanylmethanide ligands) the equatorial and, to a much lesser extent, the axial bonds become stronger. This supports the predominance of canonical structure **c** for the overall bonding description. Interestingly, for the structures with asymmetrical bonds, the shorter axial bond becomes much stronger, while the longer axial bond is weakened (e.g. M = Si, L^i = P).

Besides the ψ-tbp conformations with symmetrical (C_2 symmetry) or asymmetrical (C_1) axial bonds, we also explored structures in which the axial and equatorial bonds in the complexes were of equal length. This refers to the case of C_{2v} symmetry and represents the transition state for pseudorotation, i.e. the positional interchange of the equatorial and axial bonds. We will not present here the details of the equilibrium structures, but all geometries refer to transition states established from the corresponding vibrational analyses. They are in accordance with one imaginary vibration in these C_{2v} geometries. A summary of the energies of the ψ-tbp geometries and their corresponding C_{2v} geometries is also given in Table 3.

Table 3. Relative energies (in kJ/mol) for complexes **1**

M	L^i	$E(C_1)$	$E(C_2)$	$E(C_{2v})$
Si	N	0.0	0.0	21.9
	P	0.0	3.8	34.0
	As	0.0	6.1	41.7
Ge	N	−	0.0	15.0
	P	−	0.0	33.6
	As	0.0	0.6	38.1
Sn	N	−	0.0	6.2
	P	−	0.0	15.7
	As	−	0.0	20.0
Pb	N	−	0.0	9.6
	P	−	0.0	11.9
	As	−	0.0	15.0

The numerical data indicate that the energy differences between the two conformations are fairly small. The values decrease in the order M = Si > Ge > Sn > Pb and with increasing electronegativity of the chelating atoms, N < P < As. In the same order, canonical structure **b** comes to the fore.

These results allow a clear-cut assignment of the various mechanisms for the dynamic rearrangement of the bis(diphosphanyl)methanides. It has been noted that these species undergo exchange of the equatorial and axial phosphorus atoms and even more facile exchange of the axial and *exo*-phosphanyl groups.[3] The mechanism for the latter process is outlined in Scheme 5.

One axial bond is readily extended, while the other is strengthened. This is followed by a facile rotation about the P−C bond (I) and subsequent ring-closure (II). Along this reaction coordinate, the phosphanyl groups undergo positional interchange. Considering the presented results, such a process is easy to understand. While one axial bond is stretched, the other is shortened and the overall energy expense for such a process is fairly small.

There is another point that needs to be considered here. It has been reported that certain bis(diphosphanyl)methanide structures undergo irreversible reaction of the ψ-tbp geometry[4] to give a structure in which one diphosphanylmethanide ligand is linked through an M−C bond (structure **d**, Scheme 6).

In order to gain an insight into the stability of the latter geometry, we have calculated the energy balances for various cases (different M, L^i and R′, R = H) (Table 4).

In all cases, the structures **d** are found to be more stable than the ψ-tbp structures. Furthermore, the investigations indicate that with various substituents R the energy balances between the two structures are not significantly affected. This indicates that silyl or phosphanyl groups[16] at the carbon atom in structure **d** do not exert strongly stabilizing effects on the ψ-tbp geometries.

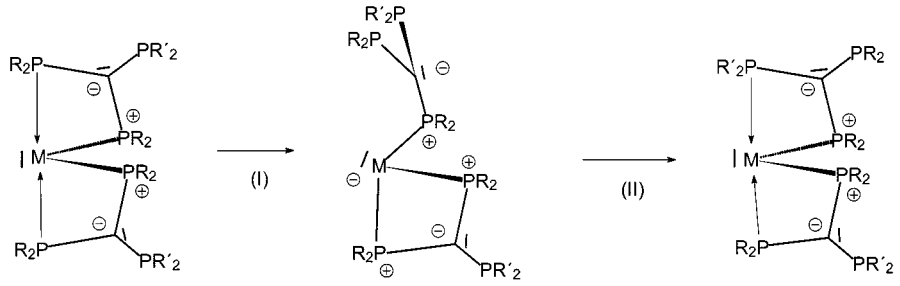
Conclusions

The results of our investigation can be summarized as follows:

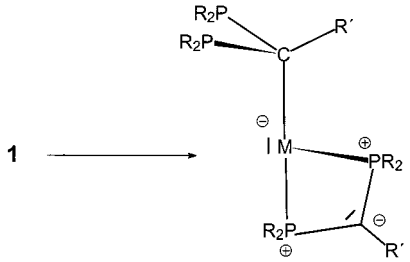
1. The bis(diphosphanyl)methanide complexes with Group-14 central elements have been studied by quantum chemical methods at an effective core potential level. They have been found to be capable of facile pseudorotation over a C_{2v} symmetrical structure. The energy barrier for the degenerate rearrangement decreases in the order Si > Ge > Sn > Pb. Rearrangement is also facilitated with increasing difference in electronegativity between the central and chelating atoms, As > P > N.

2. The structures with the diphosphanylmethanide and diarsanylmethanide ligands are best described as having equatorial single bonds and weak axial bonds, which can distort to form asymmetrical trigonal bipyramids. This explains the experimentally observed facile rearrangement of these species.

3. A "true" chelation, i.e. the formation of partial bonds between the central atom M and the ligands is observed only for the case L^i = N, i.e. the hitherto experimentally



Scheme 5



d

Scheme 6

Table 4. Energy differences (in kJ/mol) between ψ-tbp and geometries **d**

M	L^i	X = H	SiH_3	PH_2
Si	N	168.3	–	–
	P	131.5	109.7	107.1
Ge	N	157.5	–	–
	P	116.5	–	–
Sn	N	124.1	–	–
	P	97.5	–	–
Pb	N	76.4	–	–
	P	96.4	–	–

unknown diaminomethanide ligand. In this case, an extremely facile exchange of the equatorial and axial ligating atoms can be expected.

4. Structures in which one diphosphanylmethanide ligand is linked through an M−C bond are considerably lower in energy and the energy differences are found to be almost independent of the substituents R′ attached to the carbon atoms.

Experimental Section

All quantum chemical calculations were carried out at the MP2 level of theory using the Gamess set of programs.[17] The relativistically corrected effective core potential basis sets were taken from Stevens, Basch, and Krauss,[18] with a double-ζ basis set expansion for the valence space. All heavy atoms were augmented by a single set of polarization functions, as provided by Schmidt et al.[19] The energy optimizations of structures were performed at the MP2 level utilizing analytically determined nuclear coordinate gradients.[20] The force constants for the ECP(d) calculations were derived by the method of numerical differences. The population analyses at the given computational level were performed according to the Weinhold−Reed partitioning scheme.[21]

Acknowledgments

This work was supported by the Deutsche Forschungsmeinschaft and the Fonds der Chemischen Industrie.

[1] P. Jutzi, D. Kanne, C. Krüger, *Angew. Chem.* **1986**, *98*, 163−164; *Angew. Chem. Int. Ed. Engl.* **1986**, *25*, 164−165.
[2] H. H. Karsch, U. Keller, S. Gamper, G. Müller, *Angew. Chem.* **1990**, *102*, 297−298; *Angew. Chem. Int. Ed. Engl.* **1990**, *29*, 295−296.
[3] H. H. Karsch, B. Deubelly, G. Hanika, J. Riede, G. Müller, *J. Organomet. Chem.* **1988**, *344*, 153−161.
[4] [4a] H. H. Karsch, A. Appelt, G. Müller, *Angew. Chem.* **1985**, *97*, 404−406; *Angew. Chem. Int. Ed. Engl.* **1985**, *24*, 402−404. − [4b] H. H. Karsch, A. Appelt, G. Müller, *Organometallics* **1986**, *5*, 1664−1670.
[5] H. H. Karsch, A. Appelt, G. Hanika, *J. Organomet. Chem.* **1986**, *312*, C1−C5.
[6] H. H. Karsch, E. Witt, F. E. Hahn, *Angew. Chem.* **1996**, *108*, 2380−2382; *Angew. Chem. Int. Ed. Engl.* **1996**, *35*, 2242−2244.
[7] Y. Zhou, D. S. Richeson, *Inorg. Chem.* **1997**, *36*, 501−504.
[8] S. Appel, F. Weller, K. Dehnicke, *Z. Anorg. Allg. Chem.* **1990**, *583*, 7−16.
[9] U. Kilimann, M. Noltemeyer, F. T. Edelmann, *J. Organomet. Chem.* **1993**, *443*, 35−42.
[10] F. T. Edelmann, *Coord. Chem. Rev.* **1994**, *137*, 403−481.
[11] H. H. Karsch, P. A. Schlüter, M. Reisky, *Eur. J. Inorg. Chem.* **1998**, 433−436.
[12] H. W. Roesky, B. Meller, M. Noltemeyer, H.-G. Schmidt, U. Scholz, G. M. Sheldrick, *Chem. Ber.* **1988**, *121*, 1403−1406.
[13] W. W. Schoeller, A. Sundermann, M. Reiher, *Inorg. Chem.* **1999**, *38*, 29−37.
[14] R. McWeeny, *Coulson's Valence*, Oxford University Press, Oxford, **1979**.
[15] T. A. Albright, J. K. Burdett, M. H. Whangbo, *Orbital Interactions in Chemistry*, John Wiley & Sons, New York, **1985**.
[16] For the abilities of the phosphanyl group to stabilize a negative charge, see: W. W. Schoeller, U. Tubbesing, *J. Mol. Struct. (Theochem)* **1995**, *343*, 49−55.
[17] M. W. Schmidt, K. K. Baldridge, J. A. Boatz, S. T. Elbert, M. S. Gordon, J. H. Jensen, S. Koseki, N. Matsunaga, K. A. Nguyen, S. J. Su, T. L. Windus, M. Dupuis, J. A. Montgomery, *J. Comput. Chem.* **1993**, *14*, 1347−1363.
[18] W. J. Stevens, H. Basch, M. Krauss, *J. Chem. Phys.* **1984**, *81*, 6026. W. J. Stevens, H. Basch, M. Krauss, P. Jasien, *Can. J. Chem.* **1992**, *70*, 612−630. T. Cundari, W. J. Stevens, *J. Chem. Phys.* **1993**, *98*, 5555−5565.
[19] See reference manual in the GAMESS program.
[20] M. J. Frisch, M. Head-Gordon, J. A. Pople, *Chem. Phys. Lett.* **1990**, 166, 275−280. M. J. Frisch, M. Head-Gordon, J. A. Pople, *Chem. Phys. Lett.* **1990**, *166*, 281−289. C. Møller, M. S. Plesset, *Phys. Rev.* **1934**, *46*, 618−622.
[21] A. Reed, L. A. Curtiss, F. Weinhold, *Chem. Rev.* **1988**, *88*, 899−926.

Received December 15, 1998
[I98430]

Bonding Analysis in Inorganic Transition-Metal Cubic Clusters, 5[+] $M_8(\mu_8\text{-}E')(\mu_4\text{-}E)_6L_8$ Species Centered and Hexacapped by Main-Group Atoms

Régis Gautier,[a] François Ogliaro,[a] Jean-François Halet,*[a] Jean-Yves Saillard,*[a] and Evert Jan Baerends[b]

Keywords: Electron count / Electronic structure / Density functional calculations / Transition metals / Cluster compounds / Interstitial element / Main-group elements

The bonding in main-group atom-centered hexacapped transition-metal cubic clusters $M_8(\mu_8\text{-}E')(\mu_4\text{-}E)_6L_8$ has been analyzed by means of density functional theory (DFT) calculations. Although only one example of such compounds has been characterized so far, DFT results indicate that it should be possible for other members of this family to be synthesized. As for their metal-centered parents, there are several "magic" electron numbers that are able to satisfy the closed-shell requirement for such species, depending on the nature of the metal and the capping ligands. The most probable cluster valence electron counts that imply significant M–M bonding are 120 and 122. The former value is favored when E′ is an early main-group element while the latter value is favored when E′ is a late main-group element. Owing to the high connectivity between the atoms, such a regular cubic architecture may also be observed with open-shell electron configurations, as observed for the 119-cluster-valence-electron cluster $Ni_8(\mu_8\text{-}As)(\mu_4\text{-}As)_6(PPh_3)_8$.

Introduction

Among the simplest polyhedral architectures encountered in transition-metal clusters, the M_4 tetrahedral and M_6 octahedral arrangements are by far the most common.[1–4] However, an increasing number of compounds having an M_8 cubic or distorted-cubic cluster core have been characterized in recent years.[5–10] These cubic arrays may be empty[6][7] or centered by an interstitial atom.[8–10] In previous papers, we have analysed the electronic structure of cubic empty clusters of general formula $M_8(\mu_4\text{-}E)_6L_n$ (E = main-group atom or ligand),[11] as well as metal-centered $M_8(\mu_8\text{-}M)(\mu_4\text{-}E)_6L_8$ clusters[12] and other related compounds.[13] These geometries are characterized by a large range of allowed cluster valence electron (CVE) counts, most of which correspond to open-shell configurations or small HOMO–LUMO gaps. The high atom connectivity present in these clusters considerably reduces their Jahn–Teller instability. The largest allowed CVE count generally corresponds to a magic number satisfying the closed-shell requirement for stable diamagnetic molecules.

The possibility of the existence of hexacapped transition-metal cubic clusters centered by a main-group atom has been suggested by Wheeler[14] based on extended Hückel (EH) calculations on $Ni_8(\mu_8\text{-}Te)(\mu_4\text{-}Te)_6L_8$ models, for which he predicted two favored closed-shell CVE counts, namely 110 and 126. On the other hand, the application to these species of Mingos' inclusion principle,[15] which allows prediction of closed-shell electron counts for centered clusters, leads to the values of 114 CVEs and 120 CVEs. More recently, the 119-CVE cluster $Ni_8(\mu_8\text{-}As)(\mu_4\text{-}As)_6(PPh_3)_8$ (**1a**) was synthesized and characterized in the group of D. Fenske.[16] The X-ray molecular structure of this compound (see Figure 1) has exact C_i and approximate O_h symmetries, with the following average bond lengths [Å]: Ni–Ni = 2.89; Ni–(μ_8-As) = 2.50; Ni–(μ_4-As) = 2.32; Ni–P = 2.21; (μ_8-As)···(μ_4-As) = 2.54. This prompted us to undertake a density functional theory (DFT) analysis of the electronic structure of **1a** as well as that of various model clusters of the general type $M_8(\mu_8\text{-}E')(\mu_4\text{-}E)_6L_8$ (E′ = main-group atom; E = main-group atom or ligand) in order to rationalize the bonding, stability and properties of these centered clusters with respect to their possible CVE counts.

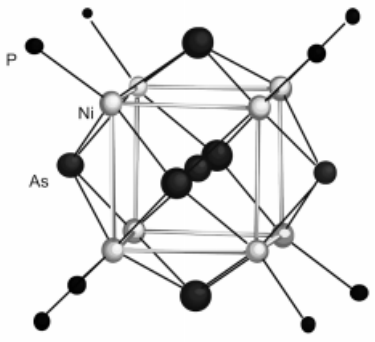


Figure 1. X-ray molecular structure of the 119-CVE cluster $Ni_8(\mu_8\text{-}As)(\mu_4\text{-}As)_6(PPh_3)_8$ (**1a**);[16] the phenyl groups are not shown for the sake of clarity

[+] Part 4: Ref.[13b]

[a] Laboratoire de Chimie du Solide et Inorganique Moléculaire, UMR CNRS 6511,
Université de Rennes 1, F-35042 Rennes Cedex, France
Fax: (internat.) + 33-2/99383487
E-mail: halet@univ-rennes1.fr
[b] Scheikundig Laboratorium der Vrije Universiteit,
De Boelelaan 1083, NL-1081 HV Amsterdam, The Netherlands

 © WILEY-VCH Verlag GmbH, D-69451 Weinheim, 1999 1434–1948/99/0707–1161 $ 17.50+.50/0

Qualitative Approach

The electronic structure of an $M_8(\mu_8\text{-}E')(\mu_4\text{-}E)_6L_8$ compound of approximate O_h symmetry can be qualitatively analysed in a similar way to that previously described by us for the metal-centered $M_8(\mu_8\text{-}M)(\mu_4\text{-}E)_6L_8$ species,[12] i.e. resulting from the interaction of the $M_8(\mu_4\text{-}E)_6L_8$ empty cage with the interstitial atom. We have shown that, as long as there is substantial M−M bonding, a noncentered $M_8(\mu_4\text{-}E)_6L_8$ cube should present a significant HOMO−LUMO gap for the ideal 120-CVE count, separating the more or less nonbonding d-type levels (the d-band) from the significantly antibonding levels.[11] This situation satisfying the closed-shell requirement is represented in the top-middle of Figure 2. The electron configuration corresponding to the 120-CVE magic electron count of the empty cage will be written as $[116](e_g)^4$ in the following discussion.

The interstitial E′ atom has four valence orbitals of a_{1g} (s) and t_{1u} (p) symmetry. They are expected to interact mainly with some metallic counterparts in the d-manifold, which are close in energy and available for bonding. If the four E′ orbitals interact strongly, the resulting antibonding

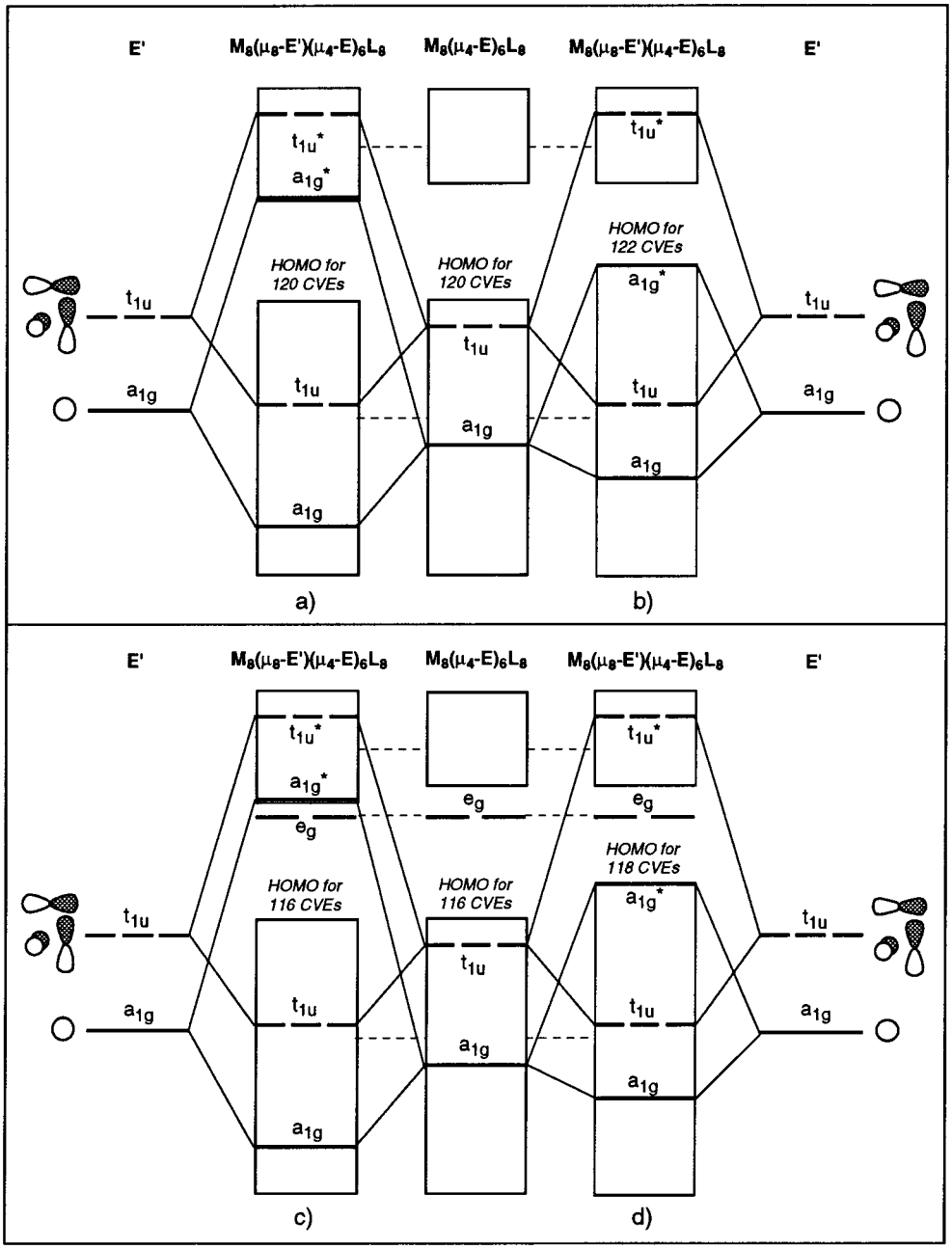


Figure 2. Qualitative MO interaction diagrams for four possible closed-shell configurations in the case of $M_8(\mu_8\text{-}E')(\mu_4\text{-}E)_6L_8$ species in which significant M−M bonding is present: (a) the four s (a_{1g}) and p (t_{1u}) E′ valence AOs interact strongly with the cubic host; (b) only the E′ valence p (t_{1u}) AOs interact significantly; (c) and (d) particular situation where the interactions are similar to those in (a) and (b), respectively, but the capping ligand E is a single main-group atom that tends to destabilize the highest e_g level of the d-band.

combinations will lie at high energy, leaving the same number of bonding and nonbonding levels as in the empty $M_8(\mu_4\text{-}E)_6L_8$, as shown in Figure 2a. In such a situation, the closed-shell requirement is expected to be satisfied for the same 120-CVE count as for the noncentered $M_8(\mu_4\text{-}E)_6L_8$ species, and with the same $[116](e_g)^4$ configuration.

Another closed-shell situation may occur if the E′ atom retains an s-type lone pair, as some heavy main-group atoms often do. This would correspond to a weak a_{1g} interaction, leaving at low energy the weakly antibonding a_{1g} combination. In such a case, a significant HOMO/LUMO gap is expected for the 122-CVE count, corresponding to the $[116](e_g)^4(a_{1g})^2$ configuration. This situation is shown in Figure 2b.

Finally, mention should be made of the special effect induced by the capping E ligands when they are single heavy main-group atoms. This *bare-atom-capping* effect tends to destabilize the highest e_g level of the metallic d-block, whether the cage is centered or not.[12] If this effect is moderate, open-shell configurations will be favored with partial occupation of the e_g level. On the other hand, if this effect is strong enough, the e_g orbitals will become unavailable, leading to the 116-CVE closed-shell count for the empty $M_8(\mu_4\text{-}E)_6L_8$ cluster, with the $[116](e_g)^0$ configuration, as shown in the bottom-middle of Figure 2. In the case of the centered $M_8(\mu_8\text{-}E')(\mu_4\text{-}E)_6L_8$ species, this would correspond to the 116- and 118-CVE possible magic numbers, depending on whether the a_{1g} interaction is strong or not, respectively. These two particular hypothetical closed-shell situations are represented in Figure 2c and d.

The 119-CVE Cluster $Ni_8(\mu_8\text{-}As)(\mu_4\text{-}As)_6(PH_3)_8$

In order to reduce computational effort, cluster **1a** was modeled by changing the PPh_3 ligands into PH_3 phosphanes. Single-point spin-polarized DFT calculations were first performed on $Ni_8(\mu_8\text{-}As)(\mu_4\text{-}As)_6(PH_3)_8$ (**1b**), with an idealized O_h geometry obtained by averaging the experimental structure of **1a** and assuming P−H distances of 1.42 Å. The ground state was found to be a doublet, with the configuration $[116](a_{1g})^2(e_g)^1$. Unfortunately, no experimental data about the magnetic properties have been reported so far for **1a** to confirm this doublet spin state. The level ordering corresponding to spin-restricted calculations is shown in Figure 3. The $5e_g$ and $6a_{1g}$ levels are close in energy and lie in the middle of a large gap separating the nonbonding levels from the antibonding ones. Clearly, the magnitude of the a_{1g} interaction as well as the magnitude of the e_g destabilizing effect due to the bare capping As atoms are both intermediate between strong and weak. The $5e_g$ and $6a_{1g}$ orbitals are plotted in Figure 4. Both are Ni−Ni bonding. The $6a_{1g}$ MO is Ni−(μ_4-As) bonding, whereas the $5e_g$ MO is antibonding along these contacts. As qualitatively predicted (Figure 2), $6a_{1g}$ is Ni−(μ_8-As) antibonding. This orbital is also (μ_8-As)···(μ_4-As) antibonding. The $6a_{1g}$ and $5e_g$ levels are situated in the middle of a large energy gap and so the closed-shell requirement for this kind of cluster should be satisfied for two different electron configurations (among the four predicted above): $[116](a_{1g})^2(e_g)^4$ (122 CVEs) and $[116](a_{1g})^0(e_g)^0$ (116 CVEs).

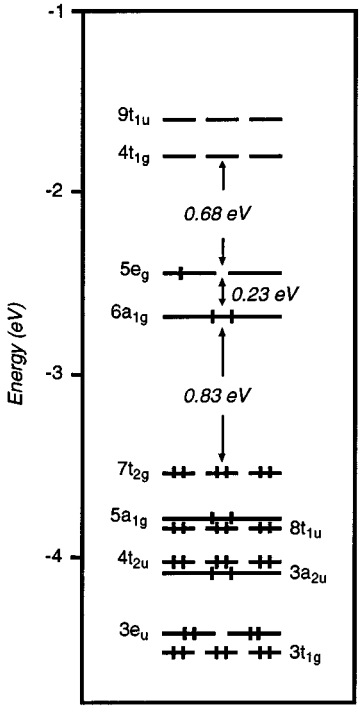


Figure 3. MO level ordering for model **1b** (spin-restricted calculations)

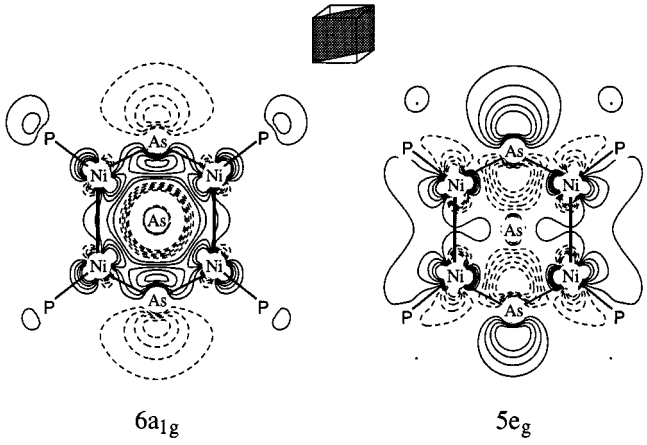


Figure 4. Contour plots of the $6a_{1g}$ and one of the $5e_g$ orbitals of **1b** in one diagonal plane (shaded) containing four Ni atoms and two capping As atoms; contour values are ±0.01, ±0.02, ±0.05, ±0.10, ±0.20, ±0.50 (e $bohr^{-3})^{1/2}$

In a further step, spin-polarized geometry optimizations of **1b** were performed for the three lowest spin states, corresponding to the $[116](a_{1g})^2(e_g)^1$, $[116](a_{1g})^1(e_g)^2$, and $[116](e_g)^3(a_{1g})^0$ configurations, still assuming O_h symmetry. The computed energies and metrical parameters are given in Table 1, together with the data corresponding to the single-point calculations on the averaged experimental structure. The three configurations lead to similar optimized P−H, Ni−(μ_4-As), and Ni−P bond lengths. The latter is in a reasonable agreement with the averaged Ni−PPh_3 exper-

imental value, while the optimized Ni−(μ_4-As) distance is somewhat longer than the averaged experimental one. The Ni−Ni and consequently the Ni−(μ_8-As) separations are found to be strongly dependent upon the electron configuration. Depopulating the $6a_{1g}$ orbital results in decreasing of the size of the cube. This can be attributed to the Ni−(μ_8-As) antibonding character of this orbital. The fact that the Ni−(μ_4-As) distance does not change with the orbital occupations is probably the result of compensating effects associated with the Ni−(μ_4-As) bonding and (μ_8-As)···(μ_4-As) antibonding characters of the a_{1g} orbital.

Other Electron Counts

Geometry optimizations were also performed on model **1b** with different electron counts: 118 CVEs (**1b**$^+$), 120 CVEs (**1b**$^-$), 116 CVEs (**1b**$^{3+}$), and 122 CVEs (**1b**$^{3-}$). The major results are given in Table 1. Again, one can see that the size of the cube strongly depends on the a_{1g} occupation. The other structural parameters primarily vary with the CVE count, almost independently from the electron configuration. It is noteworthy that an increase of the CVE count induces a shortening of the Ni−P distance and an increase of the pyramidalization of the PH_3 ligands. Adding electrons weakens the bonding within the cluster core and reinforces the Ni−PR_3 bonds through π back-bonding. As for **1b**, the three computed electron configurations of **1b**$^+$ and **1b**$^-$ are close in energy, with the lowest state corresponding to an empty $6a_{1g}$ orbital. In this situation, the bonding interaction between the interstitial As atom (considered as neutral) and its cage is maximum. Although significant, the HOMO/LUMO gaps associated with the closed-shell configurations of **1b**$^+$, **1b**$^-$, **1b**$^{3+}$, and **1b**$^{3-}$ are rather small. In order to find examples of clusters having favored CVE counts secured by larger HOMO/LUMO gaps, we have undertaken calculations on different model clusters.

Table 1. Optimized geometries, corresponding HOMO/LUMO gaps and selected bonding energies of cluster **1b** for different cluster valence electron (CVE) counts and electronic configurations

Compound	**1b**$^{3+}$	**1b**$^+$			**1b**			**1b**$^-$			**1b**$^{3-}$
CVE	116	118			119			120			122
Electronic configuration	$(6a_{1g})^0(5e_g)^0$	$(6a_{1g})^2(5e_g)^0$	$(6a_{1g})^1(5e_g)^1$	$(6a_{1g})^0(5e_g)^2$	$(6a_{1g})^2(5e_g)^1$	$(6a_{1g})^1(5e_g)^2$	$(6a_{1g})^0(5e_g)^3$	$(6a_{1g})^2(5e_g)^2$	$(6a_{1g})^1(5e_g)^3$	$(6a_{1g})^0(5e_g)^4$	$(6a_{1g})^2(5e_g)^4$
Ni−Ni [Å]	2.90	3.01	2.91	2.82	2.94	2.86	2.78	2.94	2.87	2.77	2.96
Ni−(μ_8-As) [Å]	2.51	2.61	2.52	2.44	2.55	2.48	2.41	2.55	2.48	2.40	2.56
Ni−(μ_4-As) [Å]	2.47	2.49	2.48	2.49	2.45	2.45	2.45	2.47	2.51	2.47	2.54
(μ_8-As)−(μ_4-As) [Å]	2.83	2.79	2.84	2.89	2.77	2.81	2.85	2.80	2.92	2.88	2.91
Ni−P [Å]	2.36	2.33	2.31	2.30	2.25	2.25	2.26	2.22	2.26	2.24	2.19
P−H [Å]	1.43	1.43	1.43	1.43	1.44	1.43	1.44	1.44	1.45	1.45	1.46
Ni−P−H [°]	119.1	120.9	120.9	120.9	121.8	121.7	121.6	122.7	122.5	122.5	124.1
HOMO/LUMO gap [eV]	0.46	0.44	[a]	[a]	[a]	[a]	[a]	[a]	[a]	0.38	0.63
BE[b] [eV]	−166.72	−185.37	−185.43	−185.61	−190.12	−190.30	−190.37	−192.24	−192.53	−192.77	−188.30
BE_f[c] [eV]	−3.27	−3.44	−3.07	−5.15	−2.23	−2.33	−4.90	−2.25	−4.06	−4.68	−3.53

[a] Open-shell configuration. − [b] Bonding energy with respect to fragmentation in individual neutral atoms. − [c] Bonding energy between the neutral interstitial As atom and its cubic host $Ni_8As_6(PH_3)_8$.

The ADF program allows the calculation of the bonding energy between two or several fragments of a molecule.[19] The bonding energy between the central As atom and its $Ni_8(\mu_4\text{-As})_6(PH_3)_8$ cage in **1b** is given in Table 1 for the three electron configurations considered. Consistent with the Ni−(μ_8-As) and (μ_4-As)−(μ_8-As) antibonding characters of the $6a_{1g}$ orbital, the bonding is stronger when this level is vacant. On the other hand, the depopulation of $6a_{1g}$ to the benefit of $5e_g$ weakens the Ni−Ni and Ni−(μ_4-As) bonding to a similar extent, since the three configurations are close in energy. They lie within a range of 0.25 eV, a value barely significant at the considered level of calculations for such a large cluster. In particular, one should note that the potential energy surface associated with the variation of the Ni−Ni and Ni−(μ_4-As) distances in the O_h symmetry was found to be rather flat. Moreover, **1b** is associated with an open-shell configuration, which may present some Jahn−Teller distortion away from the ideal O_h symmetry. As a matter of fact, the crystal structure of **1a** is of C_i symmetry in the solid state and exhibits some dispersion of the Ni−Ni and Ni−(μ_4-As) separations.[16] Geometry optimizations with lower symmetries, which could allow first-order Jahn−Teller distortion to occur, give results that are not significantly different from those of the $(a_{1g})^2(e_g)^1O_h$ configuration. We therefore conclude that the restriction to the O_h symmetry is a satisfying approximation for analysing the bonding in this type of cluster, owing to their soft flexibility with respect to Ni−Ni distance variation.

Changing the Nature of the Capping and Interstitial Ligands

The 120-CVE and 122-CVE Models $[Ni_8(\mu_8\text{-}E')(\mu_4\text{-}GeH)_6(CO)_8]^{q-}$ (E′ = Si, Ge, P, As, S, Se; $q = 0-4$)

The choice of these hypothetical models was driven by the fact that the diamagnetic 124-CVE metal-centered cluster $Ni_8(\mu_8\text{-Ni})(\mu_4\text{-GeEt})_6(CO)_8$ is known,[8a] and was calculated to present a large HOMO/LUMO gap.[12] Indeed, the presence of Ge−R groups as capping ligands allows to alleviate the destabilizing effect of the cluster e_g frontier level

caused by the μ_4-As bare atoms in **1b**$^{3+/+/-/3-}$. This is expected to particularly favor the 120-CVE and/or 122-CVE magic numbers (see Figure 2a and 2b). In the $[Ni_8(\mu_8\text{-}E')(\mu_4\text{-}GeH)_6(CO)_8]^{q-}$ models (denoted as **[2-E′]**$^{q-}$ in the following discussion), the interstitial main-group atom is varied in order to tune the magnitude of the a_{1g} interaction with respect to the electronegativity and size of E′. The reported calculations correspond to the CVE counts of 120 and 122 for E′ = Si, Ge, P, As, S, and Se. Geometry optimizations have been carried out assuming O_h symmetry. In any case, a single minimum was found on the potential energy hypersurface. The major results are given in Table 2. The computed one-electron level orderings are shown in Figure 5. As expected and in contrast to the case of **1b**, the $5e_g$ level for all the **[2-E′]**$^{q-}$ species lies deep in energy. They are not shown in Figure 5. The highest level of the band occupied for the 120-CVE count is now the $8t_{2g}$ level, which corresponds to the $7t_{2g}$ level in **1b**. In the following discussion the configuration designated above as $[116](e_g)^4$ will be alternatively written as $[110](e_g)^4(t_{2g})^6$. Most of the free anions which were calculated have occupied MOs associated with a positive energy, indicating instability with respect to electron loss. However, when a cationic environment is mimicked by positive point charges introduced in the calculations, these levels are in most of the cases significantly stabilized to negative energies. This is a quite common result for stable anionic clusters.[17] Moreover, it is clear that the hypothetical **[2-E′]**$^{q-}$ clusters should be considered as a series of models for more realistic compounds (see below).

As mentioned above for **1b**, the Ni−Ni separation is very sensitive to the a_{1g} occupation number. In the case of the 120-CVE $[110](e_g)^4(t_{2g})^6(a_{1g})^0$ configuration, this distance lies in the range 2.7−2.9 Å, whereas for the 122-CVE $[110](e_g)^4(t_{2g})^6(a_{1g})^2$ configuration it is longer by ca. 0.2 Å. This difference is smaller in the cases where E′ = S and Se because the a_{1g} level is still occupied in the corresponding 120-CVE configuration. Electron-electron repulsion is also responsible for the long Ni−Ni separations in the negatively charged **[2-E′]**$^{4-}$ (E′ = Si, Ge) and **[2-E′]**$^{3-}$ (E′ = P, As) models. Indeed, the replacement of the CO ligands by isoelectronic NO^+ units in **[2-Ge]**$^{4-}$ leads to shorter optimized Ni−Ni distances in the 122-CVE $[Ni_8(\mu_8\text{-}Ge)(\mu_4\text{-}GeH)_6(NO)_8]^{4+}$ cationic model.

The results on the **[2-E′]**$^{q-}$ series illustrate nicely the trend accompanying the variation of the nature of E′ across the periodic table. When E′ is an early main-group element, the a_{1g} interaction is strong, favoring the closed-shell 120-CVE count. Conversely, with late main-group encapsulated atoms the a_{1g} interaction is weak, favoring the closed-shell 122-CVE count. This is exemplified for the clusters **[2-Si]**$^{2-}$ and **[2-Ge]**$^{2-}$ (120 CVEs), and **[2-S]**$^{4-}$ and **[2-Se]**$^{4-}$ (122 CVEs) for which large HOMO/LUMO gaps are computed.

The 116-CVE and 118-CVE Models: $[Ni_8(\mu_8\text{-}Ge)(\mu_4\text{-}Ge)_6(CO)_8]^{4-}$ and $[Ni_8(\mu_8\text{-}Se)(\mu_4\text{-}Ge)_6(CO)_8]^{4-}$

Starting for example from **[2-Ge]**$^{2-}$ (120 CVEs) and **[2-Se]**$^{4-}$ (122 CVEs), the MO diagrams of which correspond to the general cases of Figure 2a and 2b, the formal removal of the H substituents on the Ge atoms is expected to induce a destabilization of a low-lying e_g level (see above) leading to the general cases of Figure 2c and 2d. In order to check this hypothesis, calculations were carried out on the "deprotonated" models $[Ni_8(\mu_8\text{-}Ge)(\mu_4\text{-}Ge)_6(CO)_8]^{4-}$ (116 CVEs) and $[Ni_8(\mu_8\text{-}Se)(\mu_4\text{-}Ge)_6(CO)_8]^{4-}$ (118 CVEs). They fully confirm the hypothesis illustrated in Figure 2c and 2d, with significant HOMO/LUMO gaps computed for the $[116](eg)^0$ (1.04 eV) and $[116](a_{1g})^2(eg)^0$ (0.88 eV), respectively. As for the **[2-E′]**$^{4-}$ models, the size of the cube is

Table 2. Optimized geometries, HOMO energies and bonding energies for 120-CVE and 122-CVE $[Ni_8(\mu_8\text{-}E')(\mu_4\text{-}GeH)_6(CO)_8]^{q-}$ (**[2-E′]**$^{q-}$) models

E′	Si		Ge		P		As		S		Se	
CVE	120	122	120	122	120	122	120	122	120	122	120	122
Charge ($q-$)	2−	4−	2−	4−	1−	3−	1−	3−	0	2−	0	2−
Ni−Ni [Å]	2.80	3.00	2.87	3.10	2.70	2.89	2.81	2.99	2.75	2.82	2.85	2.94
Ni−E′ [Å]	2.43	2.60	2.49	2.68	2.34	2.50	2.43	2.59	2.38	2.45	2.47	2.54
Ni−Ge [Å]	2.42	2.51	2.46	2.55	2.42	2.48	2.46	2.51	2.44	2.46	2.48	2.50
E′−Ge [Å]	2.80	2.83	2.83	2.84	2.83	2.84	2.85	2.85	2.84	2.84	2.87	2.85
Ge−H [Å]	1.59	1.66	1.59	1.66	1.57	1.62	1.57	1.62	1.56	1.60	1.56	1.60
Ni−C [Å]	1.82	1.80	1.82	1.80	1.83	1.83	1.82	1.80	1.81	1.82	1.81	1.82
C−O [Å]	1.17	1.19	1.17	1.19	1.16	1.18	1.16	1.18	1.16	1.17	1.16	1.17
HOMO energy [eV]	0.86	7.24	0.90	6.51	−1.96	4.21	−2.04	3.78	−5.20	0.87	−5.22	0.76
BE[a] [eV]	−212.37	−202.41	−209.73	−200.70	−211.09	−208.24	−208.74	−206.56	−204.53	−209.15	−202.93	−207.62

[a] Bonding energy with respect to fragmentation in individual neutral atoms.

Closed-shell ground-state configurations, namely $[116](e_g)^4(a_{1g})^0$ {or $[110](e_g)^4(t_{2g})^6(a_{1g})^0$} and $[116](e_g)^4(a_{1g})^2$ {or $[110](e_g)^4(t_{2g})^6(a_{1g})^2$}, were found for all the 120-CVE and 122-CVE models, respectively, except two of them. In the case of the 120-CVE species having E′ = S and Se, the $[110](e_g)^4(a_{1g})^2(t_{2g})^4$ open-shell ground-state configuration was found. This result suggests that with the more electronegative chalcogen elements as encapsulated atoms, the a_{1g} interaction is weak, requiring its occupation even for the 120-CVE count, for which a partially depopulated t_{2g} HOMO is preferred.

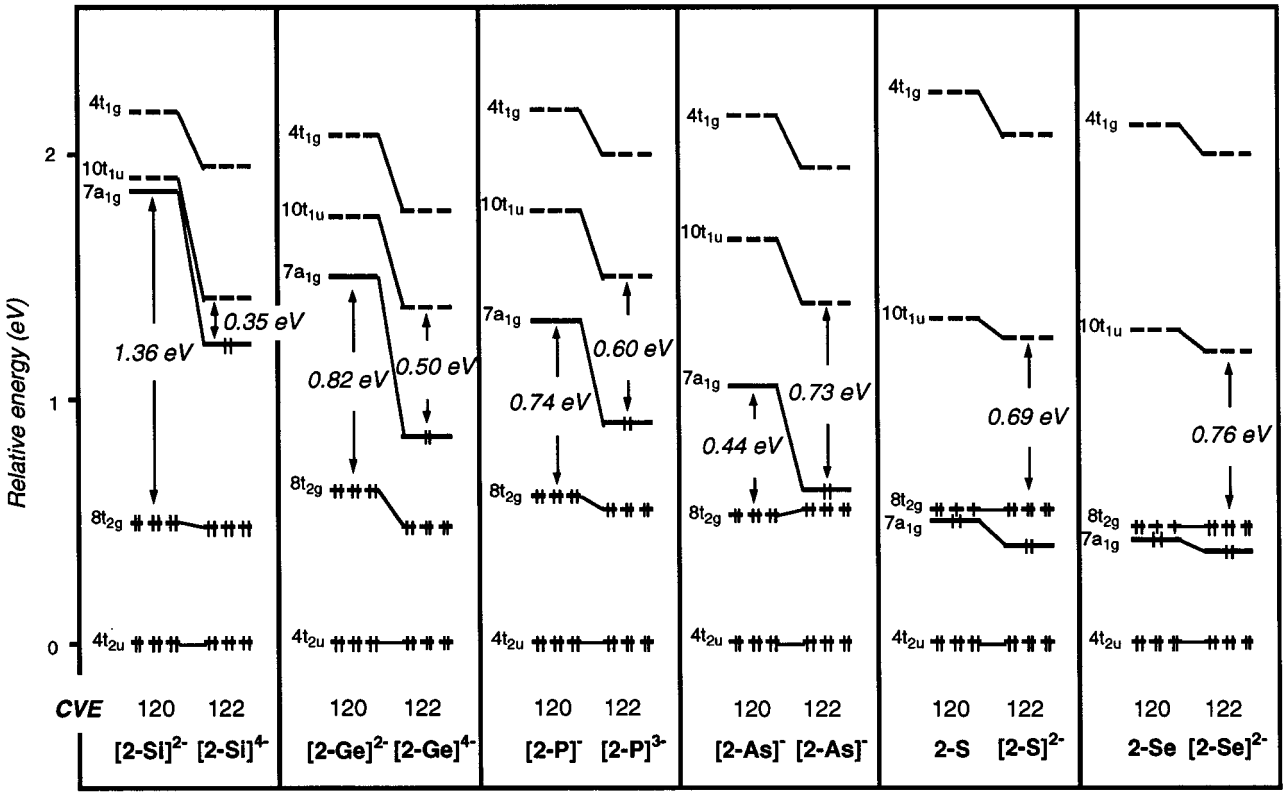


Figure 5. MO level orderings for the 120-CVE and 122-CVE cluster models **[2-E′]**$^{q-}$ (in all cases, the zero energy has been arbitrarily set to be the energy of the $4t_{2u}$ level)

rather large in these highly charged anions (Ni−Ni ca. 3.1 Å). Calculations on the isoelectronic cation $[Ni_8(\mu_8\text{-Ge})(\mu_4\text{-Ge})_6(NO)_8]^{4+}$ (116 CVEs) lead to a similar electronic configuration, with a HOMO/LUMO gap of 1.07 eV. In this latter model, the optimized Ni−Ni and Ni−(μ_4-Ge) distances are 2.79 Å and 2.42 Å, respectively.

Other Possible Electron Counts

The MO diagrams of **[2-E′]**$^{2-/4-}$ (E′ = Si, Ge) and of **[2-E′]**$^{-/3-}$ (E′ = P, As) exhibit a significant gap below the occupied $8t_{2g}$ level. This suggests that the count of 114 CVEs could be a possible closed-shell electron count for some members of the $M_8(\mu_8\text{-E}')(\mu_4\text{-E})_6L_8$ series. This is confirmed by calculations on the $[Co_8(\mu_8\text{-P})(PH)_6(CO)_8]^{3+}$ model (see Table 3), which show a significant HOMO/LUMO gap of 0.60 eV for the $[110](e_g)^4(t_{2g})^0$ ground-state configuration. The $8t_{2g}$ orbitals are mainly localized on the Co atoms (64%) with a very weak participation of the d-type polarization function of the encapsulated atom (its s and p valence orbitals do not have the proper t_{2g} symmetry). They exhibit some Co−Co and Co−(μ_4-P) antibonding character. The monoccupation of these MOs in $[Co_8(\mu_8\text{-P})(PH)_6(CO)_8]^{3+}$ tends to reinforce the corresponding bonds, as illustrated by comparing the corresponding bond lengths with their homologs in the 120-CVE **[2-P]**$^-$ cluster (see Table 2).

Table 3. Optimized geometries and corresponding bonding energies for the 114-CVE $[Co_8(\mu_8\text{-P})(\mu_4\text{-PH})_6(CO)_8]^{3+}$ and the 128-CVE $[Cu_8(\mu_8\text{-S})(\mu_4\text{-GeH})_6(CO)_8]$ species

Model compound	$[Co_8(\mu_8\text{-P})(\mu_4\text{-PH})_6(CO)_8]^{3+}$	$Cu_8(\mu_8\text{-S})(\mu_4\text{-GeH})_6(CO)_8$
CVE	114	128
M−M [Å]	2.68	2.88
M−(μ_8-E) [Å]	2.32	2.50
M−(μ_4-E′) [Å]	2.33	2.59
(μ_8-E)−(μ_4-E′) [Å]	2.69	3.04
P/Ge−H [Å]	1.44	1.60
M−C [Å]	1.87	1.91
C−O [Å]	1.15	1.15
BE_f[a] [eV]	−5.25	−3.80

[a] Bonding energy between the neutral interstitial E′ atom and its cubic host $M_8(\mu_4\text{-E})_6(CO)_8$.

On the other hand, the MO diagrams of **[2-E′]** and **[2-E′]**$^{2-}$ (E′ = S, Se) exhibit large $10t_{1u}/4t_{1g}$ separations, suggesting that the $[110](e_g)^4(a_{1g})^2(t_{2g})^6(t_{1u})^6$ configuration should satisfy the closed-shell requirement in the case of electron-rich metals. This is confirmed by calculations on the 128-CVE $Cu_8(\mu_8\text{-S})(GeH)_6(CO)_8$ model (see Table 3). The optimized Cu−Cu and Cu−Ge distances are long, indicating weak bonding. The $10t_{1u}$ orbitals are predominantly localized on the Cu (28%) and Ge (31%) atoms, with

a smaller S (18%) participation. Although it exhibits some Cu−S antibonding character, this level cannot be identified as being the t_{1u}* level shown in the diagrams of Figure 2. In fact, this $10t_{1u}$ level is better described as being associated with the Cu−Ge bonds.[11] Therefore, its occupation is expected to weaken these bonds (see above) or to induce a Jahn−Teller distortion of the octahedral architecture. Such a distortion is unlikely to occur, as shown by geometry optimizations carried out under the T_d and D_{4h} symmetry constraints, which provide results not significantly different from those obtained under the O_h symmetry.

One may be tempted to compare the 128-CVE face-capped $Cu_8(\mu_8\text{-}S)(GeH)_6(CO)_8$ model and a series of Cu_8 edge-capped cubic 128-CVE clusters synthesized by Fackler, Coucouvanis and co-workers[7] in which the Cu−Cu separations (2.8−2.9 Å) are similar to that optimized in $Cu_8(\mu_8\text{-}S)(GeH)_6(CO)_8$ (2.88 Å). The similarity is, in fact, fortuitous. In the edge-capped clusters the bonding can be simply described by a 2-electron/2-center bonding scheme in which the Cu atoms are 16-electron centers, with no formal Cu−Cu bonding.[5][7] Such a description does not apply at all for the highly delocalized $Cu_8(\mu_8\text{-}S)(GeH)_6(CO)_8$ system. There is also no simple relationship between this latter cluster and the recently characterized edge-capped Cu_8 clusters centered by other main-group atoms.[10]

The 122-CVE count is likely to be the upper limit of the allowed CVE range, since adding more electrons would result in the occupation of strongly antibonding levels. The lowest CVE limit is probably much lower, owing to the fact that the lowest predicted and observed (so far) values for the noncentered $M_8(\mu_4\text{-}E)_6L_8$ species are 76[11] and 99,[6] respectively.

Conclusion

Although only one example of main-group atom-centered hexacapped cubic clusters of the type $M_8(\mu_8\text{-}E')(\mu_4\text{-}E)_6L_8$ is known so far, namely **1a**,[16] DFT calculations that we carried out indicate that there is no reason for this kind of compound to be unstable. It is therefore very likely that other members of this family will be characterized in the future. The major challenge for their synthesis appears to be the accomplishment of the right combinations of the various M, E, E′, and L building blocks in such a way that they would fit with an allowed CVE count and a reasonable ionic charge (if any).[18]

As for their metal-centered parents,[12] there are several "magic" electron numbers susceptible to satisfy the closed-shell requirement for stable $M_8(\mu_8\text{-}E')(\mu_4\text{-}E)_6L_8$ molecules. The most probable electron counts are 120 and 122. The former is favored when E′ is an early main-group element while the latter is favored when E′ is a late main-group element. These two CVE counts are the corresponding values of the most commonly encountered 120-CVE number in noncentered $M_8(\mu_4\text{-}E)_6L_8$ clusters.[5][11] They imply substantial M−M bonding. In the particular case where the capping ligand E is a bare heavy main-group atom, these two closed-shell electron counts diminish to 116 and 118, respectively. In the case of stronger M−M overlap, the highest level of the d-manifold, of t_{2g} symmetry, can become unavailable, favoring the 114-CVE count. Conversely, weak M−M overlap allows the occupation of the lowest M−E antibonding level, of t_{1u} symmetry, leading to the closed-shell count of 128 CVEs. It is likely that this value constitutes the upper limit of the allowed CVE range, since adding more electrons would result in the occupation of strongly antibonding levels. As for their noncentered and metal-centered relatives, there must be a continuum within this allowed range of electron counts for $M_8(\mu_8\text{-}E')(\mu_4\text{-}E)_6L_8$ species.[6][8] Most of these electron counts should correspond to open-shell configurations or small HOMO/LUMO gaps associated with the absence of, or only weak, Jahn−Teller instability, as suggested by the calculations we performed on some of them. A similar stability with respect to the capped cubic architecture was found for the noncentered and metal-centered relatives.[5,11−13] The lowest limit of the allowed CVE range is probably much lower than the closed-shell 114 count, owing to the fact that the lowest predicted and (so far) observed values for the noncentered $M_8(\mu_4\text{-}E)_6L_8$ species are 76[11] and 99,[6] respectively. Assuming orbital interactions as depicted in Figure 1a, the lowest hypothetical limit is also 76 CVE. Such a value should be approached with M = Fe or earlier transition metals.

Regardless of the real limits of the allowed range of electron counts within the whole $M_8(\mu_8\text{-}E')(\mu_4\text{-}E)_6L_8$ series of compounds, its large width suggests that one particular member of this family should have by itself a significant range of allowed CVE counts, i.e. should behave as an electron reservoir and/or sink. For example, compound **1a** is a very good electron donor, owing to the ionization potential calculated for model **1b** (4.8 eV). This value is close to that of the famous 19-electron electron-reservoir $(\eta^5\text{-}C_5H_5)Fe(\eta^6\text{-}C_6Me_6)$ complex.[19] It is likely that, as for $(\eta^5\text{-}C_5H_5)Fe(\eta^6\text{-}C_6Me_6)$, the kinetic stability of **1a** is partly due to the protection of the reactive centers by bulky ligands.

Experimental Section

Density functional calculations were carried out on $Ni_8(\mu_8\text{-}As)(\mu_4\text{-}As)_6(PH_3)_8$ and related species using the Amsterdam Density Functional (ADF) program.[20] Becke exchange[21] and Perdew correlation[22] nonlocal gradient corrections were included in the local density approximation.[23][24] The geometry optimization was based on the method developed by Versluis and Ziegler.[25] The Slater-type basis was of triple-ζ quality. The Ni, Co, and Cu (1s−3p); C and O (1s); Si, P, and S (1s−2p); Ge, As, and Se (1s−3d) cores were kept frozen.[26] Single-ζ 4p polarization functions were included in the Ni, Co, and Cu valence sets, as well as a single-ζ 3d one in the C and O valence sets, a single-ζ 4d one in the Si, P, S, Ge, As, and Se valence sets and a single-ζ 2p one in the H basis set. Test calculations carried out with f polarization functions on Ni and As atoms give results similar to those carried out without f polarization functions.

Acknowledgments

Exchanges between the groups in Amsterdam and Rennes have been made possible through a European Human Capital and Mobility Network Grant (ERBCHRXCT-930156). J.-F. H. and J.-Y. S. thank the Centre de Ressources Informatiques (CRI) of Rennes and the Institut de Développement et de Ressources en Informatique Scientifique du Centre National de la Recherche Scientifique (IDRIS-CNRS) of Orsay for computing facilities. We are grateful to Prof. D. Fenske (Karlsruhe) for helpful discussions.

[1] D. M. P. Mingos, D. J. Wales, *Introduction to Cluster Chemistry*, Prentice-Hall, Englewood Cliffs, New Jersey, **1990**.
[2] *Clusters and Colloids, From Theory to Applications* (Ed.: G. Schmid), VCH, Weinheim, **1994**.
[3] C. Mealli, J. A. Lopez, Y. Sun, M. J. Calhorda, *Inorg. Chim. Acta* **1993**, *213*, 199.
[4] Z. Lin, M.-F. Fan, *Struct. Bonding* **1997**, *87*, 35.
[5] J.-F. Halet, J.-Y. Saillard, *Struct. Bonding* **1997**, *87*, 81.
[6] [6a] L. D. Lower, L. F. Dahl, *J. Am. Chem. Soc.* **1976**, *98*, 5046. – [6b] D. Fenske, R. Basoglu, J. Hachgenei, F. Rogel, *Angew. Chem. Int. Ed. Engl.* **1984**, *23*, 160. – [6c] D. Fenske, J. Magull, *Z. Naturforsch.* **1990**, *45b*, 121. – [6d] D. Fenske, H. Krautscheid, M. Müller, *Angew. Chem. Int. Ed. Engl.* **1992**, *31*, 321. – [6e] D. Fenske, J. Hachgenei, J. Ohmer, *Angew. Chem. Int. Ed. Engl.* **1985**, *24*, 706. – [6f] D. Fenske, J. Ohmer, J. Hachgenei, K. Merzweiler, *Angew. Chem. Int. Ed. Engl.* **1988**, *27*, 1277. – [6g] D. Fenske, J. Hachgenei, F. Rogel, *Angew. Chem. Int. Ed. Engl.* **1984**, *23*, 982. – [6h] G. Christou, K. S. Hagen, J. K. Bashkin, R. H. Holm, *Inorg. Chem.* **1985**, *24*, 1010. – [6i] S. Pohl, U. Opitz, *Angew. Chem. Int. Ed. Engl.* **1993**, *32*, 863. – [6j] S. Pohl, W. Barklage, W. Saak, U. Opitz, *J. Chem. Soc., Chem. Commun.* **1993**, 1251. – [6k] C. Junghans, W. Saak, S. Pohl, *J. Chem. Soc., Chem. Commun.* **1994**, 2327. – [6l] S. Pohl, W. Saak, *Angew. Chem. Int. Ed. Engl.* **1984**, *23*, 907. – [6m] A. M. Arif, R. A. Jones, D. E. Heaton, C. M. Nunn, S. T. Scwab, *Inorg. Chem.* **1988**, *27*, 254.
[7] [7a] L. E. McCandlish, E. C. Bissell, D. Coucouvanis, J. P. Fackler, K. Knox, *J. Am. Chem. Soc.* **1968**, *90*, 7357. – [7b] F. J. Hollander, D. Coucouvanis, *J. Am. Chem. Soc.* **1974**, *96*, 5646. – [7c] A. Avdeef, J. P. Fackler, *Inorg. Chem.* **1978**, *17*, 2182.
[8] [8a] J. G. Brennan, T. Siegrist, S. Stuczynski, M. L. Steigerwald, *J. Am. Chem. Soc.* **1989**, *111*, 9240. – [8b] D. Fenske, H. Fleischer, C. Persau, *Angew. Chem. Int. Ed. Engl.* **1989**, *28*, 1665. – [8c] D. Fenske, C. Persau, *Z. Anorg. Allg. Chem.* **1991**, *593*, 61. – [8d] J. P. Zebrowski, R. K. Hayashi, A. Bjarnason, L. F. Dahl, *J. Am. Chem. Soc.* **1992**, *114*, 3121. – [8e] D. Fenske, J. Ohmer, K. Merzweiler, *Angew. Chem. Int. Ed. Engl.* **1988**, *27*, 1512.
[9] K. H. Whitmire, J. R. Eveland, *J. Chem. Soc., Chem. Commun.* **1994**, 1335.
[10] [10a] D. Wu, J. Q. Huang, Y. Lin, J. L. Huang, *Sci. Sin. Ser. B (Engl. Ed.)* **1988**, *31*, 800. – [10b] Z. H. Huang, S. F. Lu, J. Q. Huang, D. M. Wu, J. L. Huang, *Jiegou Huaxue* **1991**, *10*, 213. – [10c] I. Haiduc, D. B. Sowerby, S. F. Lu, *Polyhedron* **1995**, *14*, 3389. – [10d] C. W. Liu, T. Stubbs, R. J. Staples, J. P. Fackler, *J. Am. Chem. Soc.* **1995**, *117*, 9778. – [10e] C. W. Liu, H.-S. Chen, J.-C. Wang, T.-C. Keng, *J. Chem. Soc., Chem. Commun.* **1998**, 1831.
[11] E. Furet, A. Le Beuze, J.-F. Halet, J.-Y. Saillard, *J. Am. Chem. Soc.* **1994**, *116*, 274. See also: N. Rösch, L. Ackermann, G. Pacchioni, *Inorg. Chem.* **1993**, *32*, 2963.
[12] E. Furet, A. Le Beuze, J.-F. Halet, J.-Y. Saillard, *J. Am. Chem. Soc.* **1995**, *117*, 4936.
[13] [13a] B. Zouchoune, F. Ogliaro, J.-F. Halet, J.-Y. Saillard, J. R. Eveland, K. H. Whitmire, *Inorg. Chem.* **1998**, *37*, 5, 865. – [13b] R. Gautier, J.-F. Halet, J.-Y. Saillard, *Eur. J. Inorg. Chem.* **1999**, 673.
[14] R. A. Wheeler, *J. Am. Chem. Soc.* **1990**, *112*, 8737; *J. Am. Chem. Soc.* **1991**, *113*, 4046.
[15] [15a] D. M. P. Mingos, *J. Chem. Soc., Chem. Commun.* **1985**, 1353. – [15b] D. M. P. Mingos, Z. Lin, *J. Chem. Soc., Dalton Trans.* **1998**, 1657.
[16] [16a] D. Fenske, K. Vogt, unpublished results. – [16b] K. Vogt, Ph.D. Dissertation, University of Karlsruhe, Germany, **1994**.
[17] F. Ogliaro, S. Cordier, J.-F. Halet, C. Perrin, J.-Y. Saillard, M. Sergent, *Inorg. Chem.* **1998**, *37*, 6199.
[18] Unlike for most of the empty and metal-centered capped cubic clusters,[11–13] we found that extended Hückel calculations lead to conclusions that, even at a qualitative level, strongly disagree with DFT calculations. In particular, the a_{1g} interaction (see Figure 1) is always found to be very strong at the extended Hückel level, whatever is the nature of E′. In addition, the e_g effect caused by E when it is a bare atom appears to be systematically overestimated when compared to the DFT results. As a result, most of the favored electron counts as predicted by extended Hückel theory are likely to be unrealistic.
[19] D. Astruc, *Electron Transfer and Radical Processes in Transition Metal Chemistry*, VCH Publishers, **1995**.
[20] [20a] E. J. Baerends, D. E. Ellis, P. Ros, *Chem. Phys.* **1973**, *2*, 41. – [20b] *Amsterdam Density Functional (ADF) program, version 2.0.1*, Vrije Universiteit, Amsterdam, Netherlands, **1996**.
[21] A. D. Becke, *Phys. Rev. A* **1988**, *38*, 3098.
[22] J. P. Perdew, *Phys. Rev. B* **1986**, *33*, 8822; J. P. Perdew, *Phys. Rev. B* **1986**, *34*, 7046.
[23] S. H. Vosko, L. Wilk. M. Nusair, *Can. J. Phys.* **1980**, *58*, 1200.
[24] H. Stoll, E. Golka, E. Preuss, *Theoret. Chim. Acta* **1980**, *29*, 55.
[25] L. Versluis, T. Ziegler, *J. Chem. Phys.* **1988**, *88*, 322.
[26] [26a] E. J. Baerends, P. Ros, *Chem. Phys.* **1975**, *8*, 41. – [26b] E. J. Baerends, P. Ros, *Int. J. Quantum. Chem.* **1978**, *S12*, 169, and references cited therein.

Received December 18,1998
[I98448]

Reduction of Bis(phosphonio)isophosphindolides to Phosphane-Functionalized Benzo[*c*]phospholides

Dietrich Gudat,*[a] Volker Bajorat,[a] Stefan Häp,[a] Martin Nieger,[a] and Gisela Schröder[a]

Dedicated to Professor Dr. Edgar Niecke on the occasion of his 60th birthday

Keywords: Phosphorus heterocycles / Phospholides / Nickel complexes / Reductions / NMR spectroscopy

Bis(phosphonio)benzo[*c*]phospholides (isophosphindolides) **1a**,**b** have been found to react with magnesium or alkali metal naphthalenides $MC_{10}H_8$ (M = Li, Na, K) with reduction of one or both of the phosphonio groups. The main products are the mono- or bis(phosphanyl)-substituted heterocycles **2**, **3**, **6**, **7**, which have been characterized by in situ NMR studies and in some cases isolated. Subsequent reaction of **2** with excess $[Ni(CO)_4]$ gave the complex **4**, which has been characterized by X-ray diffractometry. Reactions of **1a** with alkali metals followed a more complicated course and gave a mixture of **2**, **3**, and the substitution product **8**, which was further reduced to the phosphanido-substituted benzo[*c*]phospholide **9**. The latter could be formed selectively by first converting **1a** into **8** by treatment with PhNa and then treating this with lithium. NMR data of the phosphane-substituted benzo[*c*]phospholides and the structural features of **4** are discussed.

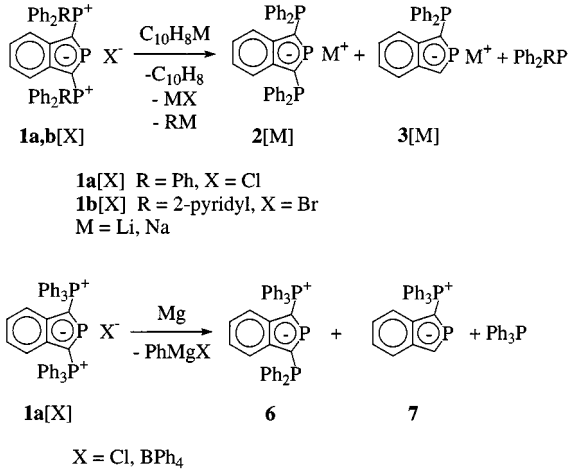
Introduction

Phospholides[1] are hetero analogues of cyclopentadienide anions and are distinguished by both high aromatic character[2] and versatile ligand properties. The phospholide moiety is not only capable of acting as a 6e π-donor ligand similar to an η^5-coordinated cyclopentadienide, but may also coordinate as a terminal 2e donor through the phosphorus lone pair, or, through a combination of σ and π coordination, as a bridging 4e or 8e ligand.[1] Whereas recent developments in the field of cyclopentadienides have been focused on derivatives bearing additional ligand groups attached either directly to the ring or on pendant side chains,[3] reports on analogous phospholide derivatives are scarce.[4][5] In view of the fact that a general route to tertiary phosphanes involves reductive cleavage of phosphonium salts,[6] we have examined the potential of reduction of bis(phosphonio)-substituted isophosphindolides incorporating a fused benzo[*c*]phospholide ring system.[7] We found that this reaction gives access to previously unknown[8] neutral and anionic benzo[*c*]phospholides bearing exocyclic phosphane functionalities.

Results

Reactions

Reactions of the bis(triphenylphosphonio)isophosphindolide salts **1a**[Cl][9] and **1b**[Br] (R = 2-pyridyl)[10] with four equivalents of lithium naphthalenide in THF were found to proceed with selective cleavage of one P−C bond in each exocyclic phosphonium moiety, thereby affording a mixture of the phosphane-substituted benzophospholide anions **2** and **3**. The by-products produced included the cleavage products C_6H_5Li or C_5H_4NLi along with triphenylphosphane or diphenylpyridylphosphane, respectively, as well as some $LiPPh_2$ arising from further reduction of the latter (Scheme 1).



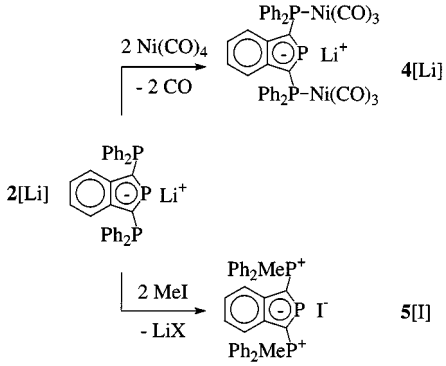
Scheme 1. X = Cl, Br, BPh_4; M = Li, Na; R = Ph (**1a**), 2-pyridyl (**1b**)

The anions **2**, **3** were generated in a ratio of approximately 3:1 almost irrespective of the reaction temperature. Mixtures of similar composition were also obtained in other solvents (DME, liq. NH_3) or when sodium naphthalenide was used as the reducing agent. No further intermediates could be detected; only mixtures of **2**, **3** and unreacted starting material were produced when the reactions were performed with less than four equivalents of the metal naphthalenide.

[a] Anorganisch Chemisches Institut der Universität Bonn, Gerhard-Domagk-Straße 1, D-53121 Bonn, Germany
Fax: (internat.) + 49(0)228/73-5327
E-mail: dgudat@uni-bonn.de

 © WILEY-VCH Verlag GmbH, D-69451 Weinheim, 1999 1434−1948/99/0707−1169 $ 17.50+.50/0

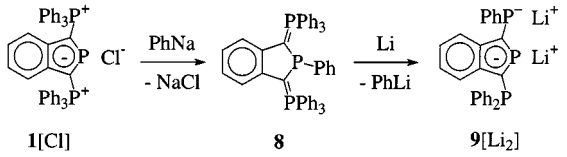
All reaction products were identified in situ by multinuclear 1D- and 2D-NMR studies (see Experimental Section). A salt **2**[Li(THF)$_x$] was isolated in crude form (approximately 95% pure on the basis of ^{31}P- and ^{1}H-NMR data) after quenching the remaining lithiated species with a stoichiometric amount of $FeCl_2$, filtering, and precipitation of the product with diethyl ether/hexane. Attempted purification of the product by recrystallization was unsuccessful, but a crystalline derivative could be obtained after reaction of either crude **2**[Li], or the reaction mixture containing both anions **2** and **3**, with excess $Ni(CO)_4$, followed by repeated recrystallization of the formed complex **4**[Li(THF)$_4$] from THF/diethyl ether. Likewise, reaction of crude **2**[Li] with excess MeI afforded the quaternization product **5**[I], which could be isolated in pure form after recrystallization from CH_2Cl_2/THF (Scheme 2).



Scheme 2

Only one phosphonium moiety was reduced in reactions of **1a**[X] (X = Cl, BPh_4) with magnesium. As in the case of the naphthalenide reduction, two main products were formed, which were identified by ^{31}P-NMR spectroscopy as the neutral species **6** and **7** (Scheme 1; the generation of **7** was accompanied by the formation of Ph_3P). The exact reaction conditions and the product ratio varied with the specific physical state of the employed metal: The use of magnesium turnings required activation by treatment with I_2 or CCl_4 and produced some 25−50% of the cleavage product **7**; in contrast, application of a suspension of magnesium powder, freshly prepared by thermal decomposition of magnesium−anthracene,[11] resulted in shorter overall reaction times and a higher selectivity, giving up to 80% of the phosphane-substituted heterocycle **6**. Isolation and further spectroscopic characterization of this product was feasible after solvent extraction of the reaction mixture and recrystallization from toluene. The by-product **7** decomposed during the workup procedure and could not be further characterized.

A different and more complicated reaction pathway was observed when alkali metals were used instead of their naphthalenides as reducing agents. NMR-spectroscopic monitoring of the early stages of the reactions of **1a**[Cl] with Li or Na revealed, besides the presence of the anions **2**, **3** [and concomitant formation of the cleavage products C_6H_5Li(Na) and Ph_3P], the formation of the substitution product **8** (Scheme 3). The concentration of the latter decreased during the course of the reaction as a new species appeared, which was later identified as the phosphanide-substituted benzophospholide **9**[M_2] (M = Li, Na). In total, **2**, **3**, and **9** constituted approximately 90% of all the phosphorus-containing species; a higher percentage was prevented by unspecified side reactions and slow cleavage to give $MPPh_2$. Prolonged reaction times or elevated temperatures led to the decomposition of all other species, leaving the phosphanides $MPPh_2$ as the only well-defined phosphorus-containing reaction products.



Scheme 3

The formation of **8** by substitution of the cation **1a** by C_6H_5M (which was generated in the initial reduction of **1a** to give **2** and **3**) was proven by its independent synthesis from **1a**[Cl] and one equivalent of C_6H_5Na. Since a control experiment revealed that lithium reduction of an isolated sample of **2** under similar conditions did not yield any detectable amount of **9**[M_2], formation of this product can be assumed to occur exclusively through the intermediate **8**. This was confirmed by an investigation of the reaction of pure **8** with lithium under ultrasound sonification, which gave **9**[M_2] together with a small amount (10−15%) of $LiPPh_2$ as the only reaction products detectable by ^{31}P-NMR spectroscopy. Even though all attempts to isolate **9**[M_2] from any of the reaction mixtures have hitherto been unsuccessful, it could be characterized in situ by multinuclear NMR spectroscopy (see below).

NMR-Spectroscopic Investigations

The identities of the neutral and anionic benzophospholides **2**−**4**, **6**, **7**, and **9**, the benzophosphole **8**, and the cation **5** were unequivocally established from their ^{1}H-, ^{13}C-, and ^{31}P-NMR data. Substitution patterns at the fused ring system were easily assigned from the habit of the ^{31}P{^{1}H}-NMR spectra, which featured characteristic A_2X (**2**, **4**, **5**), A_2B (**8**), AMX (**6**, **9**), or AX patterns (**3**, **7**). Consequently, the ^{1}H-NMR spectra displayed ABCD (**3**, **6**, **7**, **9**) or AA′BB′ patterns (**2**, **4**, **5**, **8**) for the four protons of the benzenoid fragment of the fused ring system. In addition, the spectra of **3** and **7** also featured a resonance for the 2-H proton, showing characteristic splitting due to coupling with the two phosphorus atoms. Discrimination between phosphonio (Ph_3P−), phosphane (Ph_2P−), and phosphanido [Ph(M)P−] substituents was feasible on the basis of characteristic ^{31}P chemical shift differences (Table 1). Signals for the first two types of substituents appear in common spectral regions, while the resonance of the phosphanide group in **9** appears at much higher field than in simple diarylphosphanides [δ^{31}P = −22.5, −36 for Ph_2P(Na, Li)[12]]. The resonances of the Ph(M)P and Ph_2P

Table 1. ^{31}P- and selected ^{13}C-NMR data of **2**–**9**

	$\delta^{31}P$	$J_{P,P}$ [Hz]	$\delta^{13}C$	$J_{P,C}$ [Hz]
2[Li]	−20.0 (P^APh_2) 216.4 (−P^X−)	130	124.4 (P^X−C−P^A)	51 ($J_{P(X),C}$), 13 ($J_{P(A),C}$), 10 ($J_{P(A'),C}$)
3[Li]	−21.9 (P^APh_2) 174.0 (−P^X−)	219	–[a]	–[a]
4[Li]	10.3 (P^APh_2) 237.3 (−P^X−)	164	–[a]	–[a]
5[I]	12.5 (P^APh_3) 229.0 (−P^X−)	92	109.4 (P^X−C−P^A)	54 ($J_{P(X),C}$), 96 ($J_{P(A),C}$), 14 ($J_{P(A'),C}$)
6	−21.4 (P^APh_2) 14.7 ($P^MPh_3^+$) 218.4 (−P^X−)	76 ($J_{P(A),P(X)}$) 82 ($J_{P(M),P(X)}$)	92.8 (P^X−C−P^M) 143.2 (P^X−C−P^A)	99 ($J_{P(M),C}$), 60 ($J_{P(X),C}$), 10 ($J_{P(A),C}$) 53 ($J_{P(M),C}$), 14 ($J_{P(A),C}$), 12 ($J_{P(X),C}$)
7	15.1 (P^APh_3) 190.2 (−P^X−)	88	–[a]	–[a]
8	8.0 ($P^APh_3^+$) 14.0 (P^BPh)	122	33.3 (P^A−C−P^B)	119.2 ($J_{P(A),C}$), 11.4 ($J_{P(B),C}$), −9.3 ($J_{P(A)',C}$)[b]
9[Li_2]	−87.1 (P^APhLi) −20.8 (P^MPh_2) 194.2 (−P^X−)	108 ($J_{P(A),P(X)}$) 61 ($J_{P(M),P(X)}$)	116.0 (P^X−C−P^A) 139.2 (P^X−C−P^M)	52 ($J_{P(X),C}$), 8 ($J_{P(A),C}$), 5 ($J_{P(M),C}$) 46 ($J_{P(X),C}$), 30 ($J_{P(M),C}$), 6 ($J_{P(A),C}$)
9[Na_2]	−86.2 (P^APhNa) −20.8 (P^MPh_2) 193.2 (−P^X−)	106 ($J_{P(A),P(X)}$) 66 ($J_{P(M),P(X)}$)	–[a]	–[a]

[a] Not determined. – [b] Spectral analysis as $[A]_2BX$ system gave $J_{P(B),C}/J_{P(B'),C} < 0$ and $^4J_{P(B),P(B')} = 5.5$ Hz.

fragments in **9** are further distinguished by different multiplicities in ^1H non-decoupled ^{31}P spectra, showing coupling to two or four *ortho* protons, respectively. The chemical shifts of the phospholide P atoms in **2**, **4**, **6**, and **9** are seen to be somewhat more shielded as in **1a** ($\delta^{31}P = 241.8$[9]), but significantly less shielded than in monocyclic phospholides ($\delta^{31}P = 55-142$[1b]). This trend could be confirmed by a comparison with calculated[13] $\delta^{31}P$ values of model compounds (Table 2). This revealed that the deshielding of the resonance of **1a** (as well as of **2** and **4**) compared to those of the monocyclic phospholides can be attributed to similar contributions from both the benzanellation and the influence of the phosphonio (phosphane) substituents. Inspection of the results of calculations suggests that the deshielding shows a correlation with both a continuously decreasing energy gap between the phosphorus lone pair and the lowest π* orbital, and an increasing shift of π electron density from the two-coordinate phosphorus atom to the adjacent carbon atoms, which tends to impose some "ylidic" character on the P−C bond.

Comparison of $\delta^{31}P$ values for the corresponding nuclei in the lithium and sodium salts of the anions **2**, **3**, and **9** indicates some influence of the counterion, which is less pronounced for the monoanions **2**, **3** than for **9** and suggests some degree of ionic association (contact ion pair formation) in solution. Of diagnostic relevance in the ^{13}C-NMR spectra are the signals of the ring carbon atoms adjacent to the two-coordinate phosphorus atoms: Carbon atoms bearing exocyclic phosphonio groups display similar chemical shifts and exocyclic $^1J(P,C)$ couplings as seen in **1a**, whereas those bearing phosphanyl groups exhibit lower $^1J(P,C)$ values and chemical shifts appear further downfield resembling those due to the α-carbon atoms in phospholides.[1]

Table 2. Calculated [GIAO-B3LYP/6−311+g(2d,d,p)//B3LYP/6−31+g(d,p)] ^{31}P chemical shifts of phospholides and of the parent and 1,3-disubstituted benzo[*c*]phospholides[12]

	$\delta^{31}P$
$[C_4H_4P]^-$	139.4
$[C_8H_6P]^-$ (benzo[*c*]phospholide)	200.5
$[1,3\text{-}(H_2P)_2\text{-}C_8H_4P]^-$	306.0
$[1,3\text{-}(H_3P)_2\text{-}C_8H_4P]^+$	311.5

Crystal Structure of Compound 4

The results of an X-ray crystal structure analysis of **4**[$Li(THF)_4$] revealed a salt-like composition with two independent, only slightly different pairs of $[Li(THF)_4]^+$ cations and benzophospholide anions per asymmetric unit (Figure 1). The bonding parameters in the fused ring systems of the anions do not differ significantly from those in the phosphonio-substituted cation **1a**.[14] On the other hand, the exocyclic P−C distances (1.774−1.789 Å) are longer than the corresponding bonds in **1a** (1.747−1.749 Å[14]) but shorter than the peripheral P−C(phenyl) distances (1.825−1.847 Å). The P−Ni distances in **4** are comparable with typical values in PPh_3−Ni complexes (2.225 ± 0.070 Å).[15] The remaining bond parameters display no peculiarities. On the whole, these findings suggest that electronic perturbation of the 10π system in **4** by hyperconjugation with the substituents[7] is lower than that in **1a**. In view of the rather low degree of electronic interaction between the five- and six-membered rings in a structurally characterized benzo[*b*]phospholide,[8] the anion **4** would seem to represent the first example of a benzophospholide with a unique 10π electron system having an electronic structure comparable to that found in heteronaphthalenic benzodithiaphospholium cations.[16]

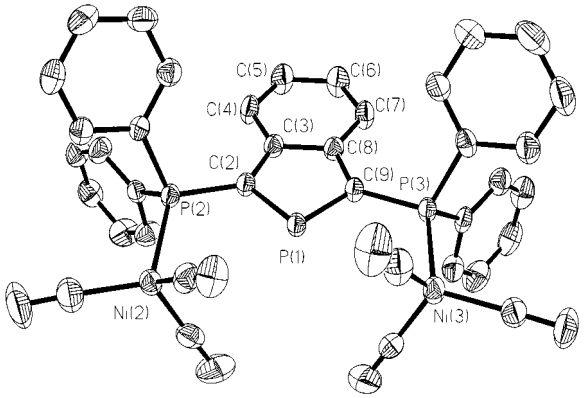


Figure 1. Representation of one of the two crystallographically independent anions in crystalline **4**[Li(THF)$_4$] (50% thermal ellipsoids); selected bond lengths [Å] and angles [°] (data of the second anion in brackets): P(1)−C(2) 1.732(4) [1.747(4)], P(1)−C(9) 1.736(4) [1.744(4)], C(2)−C(3) 1.441(5) [1.423(5)], C(2)−P(2) 1.789(4) [1.777(4)], C(3)−C(4) 1.416(5) [1.416(5)], C(3)−C(8) 1.432(5) [1.440(5)], C(4)−C(5) 1.367(5) [1.371(5)], C(5)−C(6) 1.399(6) [1.401(5)], C(6)−C(7) 1.372(5) [1.380(5)], C(7)−C(8) 1.413(5) [1.400(5)], C(8)−C(9) 1.440(5) [1.431(5)], C(9)−P(3) 1.780(4) [1.774(4)], P(2)−Ni(2) 2.241(1) [2.238(1)], P(3)−Ni(3) 2.241(1) [2.240(1)]; C(2)−P(1)−C(9) 93.0(2) [92.6(2)]

Discussion

The reported reactions of the bis(phosphonio)isophosphindolide cations **1a**, **b** conform to the general scheme of the reduction of phosphonium salts through cleavage of P−C bonds to give phosphanes and carbanions. The latter may be protonated to give the corresponding hydrocarbons during workup.[6] For the bis(phosphonium) cations studied here, the extent of the reduction appears to be controlled by the reductive power of the metal: The reaction with magnesium stops after reduction of the first phosphonium functionality, while the stronger reducing agent alkali metal/naphthalene attacks both substituents. The failure to observe the neutral species **6**, **7** as intermediates under these conditions, which would be expected if a stepwise reaction is assumed, may be attributed to kinetic factors: The second reaction step may be faster, presumably due to the low solubility of the starting material in the solvents employed.

The formation of product mixtures in the observed reactions reflects the presence of different types of P−C single bonds: Starting from the cation **1a**, cleavage of a peripheral phenyl group affords the phosphane-substituted phospholide **6** and the corresponding phenylmetal compound, both of which were observed in the reaction mixtures, while fission of a P−C(ring) bond should liberate Ph_3P and an α-deprotonated benzophospholide anion. The latter was not directly detected and is most likely quenched by abstraction of a proton (presumably from a solvent molecule) to afford the neutral compound **7**, which could be isolated in the course of the reaction with magnesium. Further reduction of **6** and **7** with alkali metals can be expected to afford a mixture of **2** and **3**, together with Ph_3P and the parent benzophospholide anion. The latter was not observed, suggesting that the second reduction step occurs either with selective P−C(phenyl) bond fission, or that this product decomposes under the reaction conditions. If one considers that the ease of reductive P−C cleavage in phosphonium salts generally parallels the ability of the leaving group to stabilize a negative charge,[6] the observed product ratio in the reduction of **1a** suggests a slightly higher charge-stabilizing capacity of a triphenylphosphoniobenzophospholide as compared to a phenyl moiety, whereas selective cleavage of pyridyl instead of phenyl groups in the reduction of **1b** suggests that the pyridyl group is superior to both.

The outcome of the reduction of **1a** with alkali metals in the absence of naphthalene is consistently explained in terms of two competing reaction channels, viz. reduction of the cation **1a** and its substitution by the formed metal phenyl to give **8**. The successful competition of the two different pathways under these conditions is again attributable to kinetic factors: the reduction proceeds at a much lower rate when solid metals are used rather than soluble metal naphthalenides, so that the slower substitution of the formed phenylmetal compound with still present starting material to give **8** may take place. Further conversion of **8** to the dimetallated species **9**[M_2] requires the reductive cleavage of phenyl groups from both the two exocyclic ylide moieties and the endocyclic phosphorus atom. Both types of reactions are known in principle. Reductive cleavage of triphenylphosphonium ylides has been reported, and even though this process is not fully understood, it is considered to follow a different mechanism than the reduction of phosphonium salts,[17] thus accounting for the different nature of the obtained product. Reductive cleavage of P−Ph bonds in phospholes has been extensively studied, in particular by Mathey and co-workers.[1] Since no further intermediates were identified, the exact mechanism of the reaction from **8** to **9** cannot be further elucidated. Nonetheless, it appears reasonable to assume reduction of one of the phosphonium moieties as the first step.

Conclusion

Our investigations have shown that bis(phosphonio)isophosphindolides can be reduced with preservation of the fused aromatic ring system to give phosphane-substituted benzo[*c*]phospholides. Despite the formation of mixtures of products, which arise from the presence of different P−C bonds in the starting materials that may possibly be cleaved, the novel phosphane-substituted benzophospholide **6** and the anionic nickel complex **4** could be isolated. Further investigations into the syntheses and reactivities of other phosphane-substituted (poly)phospholide derivatives, in particular with respect to a side-on π coordination to transition metal ions, are currently in progress.

Experimental Section

General Remarks: NMR spectra were recorded at 30°C with a Bruker AMX 300 spectrometer (300.13, 121.50, and 75.46 MHz for ^{1}H, ^{31}P, and ^{13}C). Chemical shifts are referenced to external TMS (^{1}H, ^{13}C) or 85% H_3PO_4. ^{13}C,^{31}P{^{1}H}INEPT spectra were recorded with a 5-mm triple-resonance probe head equipped with an inner

tunable coil adjusted to ^{13}C and a second coil double-tuned to ^{1}H and ^{31}P. The spectra of **3** and **6** were recorded directly from the reaction mixtures with suppression of the solvent signals by presaturation. Signal assignments were made with the aid of (semi)selective 1D $^{13}C,^{31}P\{^{1}H\}$-INEPT and 2D $^{1}H,^{1}H$-COSY/TOCSY, $^{1}H,^{13}C$-HMQC, and $^{1}H,^{31}P$-HMQC-TOCSY spectra. The atoms of the benzophospholide moiety are denoted by C-1 to C-7a and 1-H to 7-H, the carbon atoms of the phenyl groups by C_{para}, C_{meta} etc., and the designation of the phosphorus nuclei is as given in Table 1. Resonances in the ^{13}C spectra forming part of $[A]_2MY$ or $[A]_2Y$ spin systems (A, M = ^{31}P) were in some cases analyzed using the program WINDAISY; in the remaining cases the given values of ΣJ and J_M denote the sum of the couplings to the isochronous ^{31}P nuclei of the $[A]_2$ fragments and the coupling to the endocyclic phosphorus atom, respectively. − IR spectra: Nicolet Magna 550 FT-IR spectrometer.

Reduction of 1a[Cl] with Lithium Naphthalenide: A freshly prepared solution of lithium napththalenide [obtained from 180 mg (30 mmol) of Li and 3.84 g (30 mmol) of $C_{10}H_8$] in 150 mL of THF was slowly added to a stirred suspension of **1a**[Cl] (5.45 g, 7.5 mmol) in 50 mL of THF at 0 °C. Stirring was continued for 1 h. Anions **2**, **3**, Ph_3P, and PhLi were identified in situ in the dark-red mixture by multinuclear NMR analyses. A stoichiometric amount of $FeCl_2$ was then added to quench the PhLi, and the resulting mixture was stirred for a further 2 h. After addition of 10 mL of Et_2O, stirring was continued for another 30 min, then the mixture was filtered. The filtrate was concentrated in vacuo to a volume of 15 mL and 100 mL of a Et_2O/hexane (2:1) mixture was added. The resulting precipitate was collected by filtration, redissolved in a little THF, and reprecipitated with Et_2O/hexane. ^{31}P- and ^{1}H-NMR analysis revealed that the product consisted of approximately 95% **2**[Li(THF)$_x$]; yield 3.00 g (50%). The same protocol was used for the reduction of **1a**[Cl] with $C_{10}H_8Li$ and for that of **1a**,**b**[Cl] with $C_{10}H_8Na$. − **2**[Li]: ^{1}H NMR (THF): δ = 7.53 (m, 8 H, H_{ortho}), 7.45 (m, 2 H, 4-H/7-H), 7.08 (m, 8 H, H_{meta}), 7.04 (m, 4 H, H_{para}), 6.49 (m, 2 H, 5-H/6-H). − $^{13}C\{^{1}H\}$NMR (THF): δ = 145.2 (m, ΣJ = 18.2 Hz, J_M = 2.2 Hz, C_{ipso}), 144.1 (m, ΣJ = 15.1 Hz, J_M = 7.6 Hz, C-3a/C-7a), 132.9 (m, $^{3}J_{P(A),C}$ = 18.7 Hz, $^{5}J_{P(M),C}$ = 1 Hz, C_{meta}), 126.9 (m, spectral analysis gave $^{4}J_{P(A),P(A)'}$ = 1.8 Hz, $^{2}J_{P(A),C}$ = 5.5 Hz, C_{ortho}), 125.6 (s, C_{para}), 124.4 (ddd, $^{1}J_{P(M),C}$ = 51.0 Hz, $J_{P(A)/A',C}$ = 13, 10 Hz, C-1/C-3), 119.4 (m, ΣJ = 10 Hz, J_M = 6.8 Hz, C-4/C-7), 115.1 (s, C-5/C-6). − **3**[Li]: ^{1}H NMR (THF): δ = 7.58 (dd, $^{2}J_{H,P(X)}$ = 39.3 Hz, $^{4}J_{H,P(A)}$ = 2.9 Hz, 1 H, 3-H), 7.50 (m, 4 H, H_{meta}), 7.47 (m, 1 H, 4-H), 7.34 (m, 1 H, 7-H), 7.07 (m, 4 H, H_{ortho}), 7.02 (m, 2 H, H_{para}), 6.52 (m, 1 H, 6-H), 6.40 (m, 1 H, 5-H).

Reduction of 1b[Br] with Lithium Naphthalenide: The reduction of **1b**[Br] (1.94 g, 2.5 mmol) with lithium naphthalenide [obtained from 60 mg (10 mmol) of Li and 1.28 g (10 mmol) of $C_{10}H_8$] was carried out under analogous conditions as described above. Anions **2**, **3**, (2-py)Ph_2P, and (2-py)Li were identified in situ in the dark-red solution by ^{31}P- and ^{1}H-NMR analyses. No further workup of the reaction mixture was attempted.

Nickel Complex 4[Li(THF)$_4$]: A solution of 1.00 g (1.25 mmol) of crude **2**[Li(THF)$_x$] in 10 mL of THF was added dropwise with stirring to a freshly prepared solution of 1.2 mL of $Ni(CO)_4$ in 10 mL of THF. After stirring for a further 2 h, the mixture was concentrated to a volume of 5 mL, treated with 5 mL of Et_2O, and filtered. Storage of the filtrate at 2 °C for several weeks led to the deposition of a colorless precipitate, which was recrystallized once from THF to give 540 mg (40%) of complex **4**[Li(THF)$_4$], m.p. 150 °C (dec.), as colorless cubic crystals. − ^{1}H NMR ($CDCl_3$): δ = 7.56 [m, 8 H, $H_{meta}(PPh_2)$], 7.20−7.05 [m, 12 H, $H_{ortho/para}(PPh_2)$], 6.96 (m, 2 H, 4-H/7-H), 6.28 (m, 2 H, 5-H/6-H). − IR (THF): $\tilde{\nu}$ (CO) = 2056 (s), 1982 (vs), 1972 (vs) cm^{-1}.

Bis(methyldiphenylphosphonio)isophosphindolide Iodide (5[I]): A solution of 0.50 g (3.5 mmol) of methyl iodide in 5 mL of THF was added dropwise to a solution of 1.00 g (1.25 mmol) of crude **2**[Li(THF)$_x$] in 10 mL of THF. The mixture was refluxed for 10 min, allowed to cool to room temperature, and then concentrated to dryness. The residue was extracted with 10 mL of CH_2Cl_2, the extract was filtered, and the filtrate was concentrated to a volume of 5 mL. Addition of 15 mL of THF led to the deposition of 620 mg (63%) of an off-white precipitate of **5**[I], m.p. 185 °C, which was collected by filtration and dried in vacuo. − ^{1}H NMR ($CDCl_3$): δ = 7.75−7.53 (m, 20 H, C_6H_5), 7.08 (m, 2 H) and 6.93 (m, 2 H, C_6H_4), 2.77 (dd, 6 H, $^{2}J_{H,P}$ = 12.8 Hz, $^{4}J_{H,P}$ = 1.4 Hz, CH_3). − $^{13}C\{^{1}H\}$NMR (CH_2Cl_2): δ = 143.5 (m, ΣJ = 25.4 Hz, J_M = 2.2 Hz, C-3a/C-7a), 133.7 (s, C_{para}), 132.4 (m, ΣJ = 10.7 Hz, C_{ortho}), 129.4 (m, ΣJ = 13.1 Hz, C_{meta}), 122.8 (dd, $J_{P(A),C}$ = 89.0 Hz, $J_{P(X),C}$ = 2.9 Hz, C_{ipso}), 120.8 (s) and 119.8 (m) (C-4/C-7 and C-5/C-6), 109.4 (ddd, $J_{P,C}$ = 95.5, 54.3 and 14.3 Hz, C-1/C-3), 12.6 (dd, $J_{P(A),C}$ = 61.2 Hz, $J_{P(X),C}$ = 7.9 Hz, CH_3). − $C_{34}H_{30}I_2P_3$ (785.34): calcd. C 52.00, H 3.85; found C 51.5, H 3.8.

Reduction of 1a[Cl] with Magnesium: To a stirred suspension of 3.0 g (12.3 mmol) of Mg powder (freshly prepared by decomposition of $C_{14}H_{10}Mg$[11]) in 150 mL of THF was added 6.91 g (10 mmol) of **1a**[Cl]. Once the reaction had commenced, stirring was continued overnight. ^{31}P-NMR-spectroscopic assay of the dark-red mixture confirmed the formation of **6** (ca. 80%) and **7**/Ph_3P (ca. 20%). The mixture was subsequently treated with 40 mL of Et_2O, filtered, and the filtrate was concentrated in vacuo. The residue was suspended in 120 mL of DME/Et_2O (5:1), stirred for 1 h, and then filtered. The volume of the filtrate was reduced to 40 mL, and the product was precipitated by addition of 100 mL of MeOH. Recrystallization from toluene afforded 3.35 g (58%) of **6** as a yellow powder, m.p. 150 °C. − ^{1}H NMR ($CDCl_3$): δ = 7.67 (m, 1 H, 4-H), 7.60 [m, 6 H, $H_{ortho}(PPh_3)$], 7.48 [m, 4 H, $H_{ortho}(PPh_2)$], 7.35−7.45 [m, 9 H, $H_{meta/para}(PPh_3)$], 7.15−7.25 [m, 6 H, $H_{meta/para}(PPh_2)$], 6.91 (m, 1 H, 7-H), 6.85 (m, 1 H, 6-H), 6.74 (m, 1 H, 5-H). − $^{13}C\{^{1}H\}$NMR ($CDCl_3$): δ = 146.3 (ddd, $^{3}J_{P(A),C}$ = 17.2 Hz, $^{2}J_{P(M),C}$ = 15.3 Hz, $^{2}J_{P(X),C}$ = 6.5 Hz, C-7a), 144.3 (ddd, $^{2}J_{P(A),C}$ = 10.2 Hz, $^{2}J_{P(X),C}$ = 5.4 Hz, $^{3}J_{P(M),C}$ = 1.2 Hz, C-3a), 143.2 (ddd, $^{1}J_{P(X),C}$ = 53.4 Hz, $^{1}J_{P(A),C}$ = 14.1 Hz, $^{3}J_{P(M),C}$ = 11.9 Hz, C-3), 140.4 [dd, $^{1}J_{P(A),C}$ = 10.7 Hz, $^{3}J_{P(X),C}$ = 8.8 Hz, $C_{ipso}(PPh_2)$], 134.0 [dd, $^{2}J_{P(M),C}$ = 10.3 Hz, $^{4}J_{P(X),C}$ = 1.1 Hz, $C_{ortho}(PPh_3)$], 133.3 [dd, $^{3}J_{P(A),C}$ = 18.3 Hz, $^{5}J_{P(X),C}$ = 1.2 Hz, $C_{meta}(PPh_2)$], 132.9 [d, $^{4}J_{P(M),C}$ = 3.1 Hz, $C_{para}(PPh_3)$], 129.1 [d, $^{3}J_{P(M),C}$ = 12.8 Hz, $C_{meta}(PPh_3)$], 127.8 [d, $^{2}J_{P(A),C}$ = 6.9 Hz, $C_{ortho}(PPh_2)$], 127.4 [s, $C_{para}(PPh_2)$], 125.2 [dd, $^{1}J_{P(M),C}$ = 89.7 Hz, $^{3}J_{P(X),C}$ = 1.9 Hz, $C_{ipso}(PPh_3)$], 120.7 (dd, $^{3}J_{P(A),C}$ = 12.1 Hz, $^{3}J_{P(X),C}$ = 7.5 Hz, C-4), 120.0 (d, $J_{P,C}$ = 4.2 Hz, C-7), 119.4 (d, $J_{P,C}$ = 3.1 Hz, C-5), 118.3 (s, C-6), 92.8 (ddd, $^{1}J_{P(X),C}$ = 98.8 Hz, $^{1}J_{P(M),C}$ = 60.0 Hz, $^{3}J_{P(A),C}$ = 10.1 Hz, C-1). − $C_{38}H_{29}P_3$ (578.57): calcd. C 78.89, H 5.05; found C 78.0, H 4.9.

Reduction of 1a[Cl] with Lithium: To a stirred suspension of **1a**[Cl] (1.45 g, 2 mmol) in 15 mL of THF was added approximately 60 mg (10 mmol) of freshly cut lithium wire. After 30 min, ^{31}P-NMR-spectroscopic monitoring revealed, besides the presence of unreacted **1a**, the formation of **2**, **3**, Ph_3P, Ph_2PLi (from cleavage of Ph_3P), as well as of the substitution product **8**. Prolonged reaction times led to a decay of the signals due to **8**, while those due to a new product **9** intensified. Continuation of the reaction for several days, or heating, led to the disappearance of all resonances other

than that due to Ph_2PLi. Similar results were obtained when the reduction of **1a**[Cl] was performed with sodium.

Benzophosphole 8: A freshly prepared solution of phenyllithium (26.6 mmol) in 100 mL of THF was added dropwise to a suspension of **1a**[Cl] (15.7 g, 21.7 mmol) in 80 mL of THF at 0°C. The mixture was stirred for 5 h at 0°C, then treated with 20 mL of Et_2O, and filtered. The filtrate was concentrated to dryness, the residue was refluxed for 1 h with 250 mL of toluene, and the hot solution was filtered. Slow cooling of the filtrate resulted in the deposition of a crystalline precipitate, which was collected by filtration and dried in vacuo to give 14.3 g (90%) of **8** as black needles; m.p. 160°C. – ^{1}H NMR ($CDCl_3$): δ = 7.55 [m, 12 H, $H_{meta}(PPh_3)$], 7.38 [m, 6 H, $H_{para}(PPh_3)$], 7.27 [m, 12 H, $H_{ortho}(PPh_3)$], 7.21–7.15 [m, 3 H, $H_{ortho/para}(PPh)$], 6.91 [m, 2 H, $H_{meta}(PPh)$], 6.08 (m, 2 H, 5-H/6-H), 5.94 (m, 2 H, 4-H/7-H). – $^{13}C\{^1H\}$ NMR ($CDCl_3$):[18] δ = 154.6 [m, $^1J_{P(B),C}$ = 58.7 Hz, ΣJ = 2.6 Hz, $C_{ipso}(PPh)$], 148.3 (m, ΣJ = 29 Hz, $^2J_{P(B),C}$ = 0.5 Hz, C-3a/C-7a), 133.9 [m, $^2J_{P(A),C}$ = 9.6 Hz, $^4J_{P(B),C}$ = 2.0 Hz, $C_{ortho}(PPh_3)$], 130.8 [m, $^4J_{P(A),C}$ = 2.3 Hz, $C_{para}(PPh_3)$], 129.7 [m, $^1J_{P(A),C}$ = 86.7 Hz, $^3J_{P(B),C}$ = +3.1 Hz, $C_{ipso}(PPh_3)$], 128.2 [d, $^3J_{P(B),C}$ = 6.9 Hz, $C_{meta}(PPh)$], 127.8 [m, $^3J_{P(A),C}$ = 11.1 Hz, $C_{meta}(PPh_3)$], 126.4 [d, $^2J_{P(B),C}$ = 4.6 Hz, $C_{ortho}(PPh)$], 125.7 [s, $C_{para}(PPh)$], 116.6 (m, ΣJ = 1.9 Hz, C-4/C-7), 116.3 (s, C-5/C-6), 33.3 (m, $^1J_{P(A),C}$ = 119.2 Hz, $^3J_{P(A)',C}$ = −9.3 Hz, $^1J_{P(B),C}$ = 11.4 Hz, C-1/C-3). – $C_{50}H_{39}P_3$ (732.78): calcd. C 81.95, H 5.36; found C 81.0, H 5.1.

Reduction of Benzophosphole 8 with Lithium: To a solution of 1.00 g (1.37 mmol) of **8** in 25 mL of THF was added an excess of lithium powder, and the resulting mixture was allowed to react for 30 min under sonification with ultrasound. ^{1}H- and ^{31}P-NMR-spectroscopic assays confirmed the formation of **9**[Li_2] (accounting for ca. 85–90% of the phosphorus-containing material), some Ph_2PLi (ca. 10–15%), and phenyllithium. Characterization of the major product **9**[Li_2] was achieved in situ by multinuclear (^{1}H-, ^{13}C-, ^{31}P-)NMR analyses. All attempts to isolate and further purify the product were unsuccessful, invariably resulting in partial or complete decomposition. – **9**[Li_2]: ^{1}H NMR ($CDCl_3$): δ = 7.60 (m, 1 H, 6-H), 7.44 [m, 4 H, $H_{meta}(PPh_2)$], 7.38 (m, 1 H, 4-H/5-H), 7.22 (m, 1 H, 5-H/4-H), 7.13 [m, 2 H, $H_{meta}(PPh)$], 6.91 [m, 4 H, $H_{ortho}(PPh_2)$], 6.80 (m, 1 H, 7-H), 6.68 [m, 2 H, $H_{ortho}(PPh)$], 6.40 [m, 2 H, $H_{para}(PPh_2)$], 6.28 [m, 1 H, $H_{para}(PPh)$]. – $^{13}C\{^1H\}$NMR ($CDCl_3$): δ = 160.2 [dd, $^1J_{P(A),C}$ = 45.8 Hz, $^3J_{P(X),C}$ = 7.6 Hz, $C_{ipso}(PPh)$], 146.6 [dd, $^1J_{P(M),C}$ = 14.3 Hz, $^3J_{P(X),C}$ = 5.0 Hz, $C_{ipso}(PPh_2)$], 144.8 (dd, $^1J_{P(M)/A,C}$ = 15.0 Hz, $^3J_{P(X),C}$ = 7.2 Hz, C-3a/C-7a), 144.5 (dd, $^1J_{P(M)/A,C}$ = 7.5, 1 Hz, $^3J_{P(X),C}$ = 1 Hz, C-7a/C-3a), 139.2 (ddd, $^1J_{P(X),C}$ = 46.1 Hz, $^1J_{P(M),C}$ = 30.3, $^3J_{P(A),C}$ = 6.3 Hz, C-3), 133.6 [dd, $^3J_{P(M),C}$ = 18.7 Hz, $^5J_{P(X),C}$ = 1.5 Hz, $C_{meta}(PPh_2)$], 128.2 [dd, $^3J_{P(A),C}$ = 17.8 Hz, $^5J_{P(X),C}$ = 2.0 Hz, $C_{meta}(PPh)$], 126.9 [d, $^3J_{P(M),C}$ = 5.7 Hz, $C_{ortho}(PPh_2)$], 126.1 [d, $^3J_{P(M),C}$ = 5.7 Hz, $C_{ortho}(PPh)$], 120.6 (dd, $^3J_{P(A),C}$ = 7 Hz, $^3J_{P(X),C}$ = 6 Hz, C-7), 120.4 (dd, $^4J_{P(A)/M,C}$ = 4 Hz, $^4J_{P(X),C}$ = 6 Hz, C-4/C-5), 119.7 (ddd, $^4J_{P(A)/M,C}$ = 5.5, 1.7 Hz, $^4J_{P(X),C}$ = 12.0 Hz, C-5/C-4), 118.6 (dd, $^3J_{P(M),C}$ = 15.7 Hz, $^4J_{P(X),C}$ = 4.8 Hz, C-6), 116.5 [s, C_{para} (PPh_2)], 116.0 [s, $C_{para}(PPh)$], 116.0 (ddd, $^1J_{P(X),C}$ = 52 Hz, $^1J_{P(A),C}$ = 8 Hz, $^3J_{P(M),C}$ = 5 Hz).

X-ray Crystal Structure Determination of 4[Li(THF)$_4$]: $C_{38}H_{24}Ni_2O_6P_3 \cdot Li(THF)_4 \cdot Et_2O$, colorless, M_r = 1156.4; monoclinic, space group $P2_1/c$ (No. 14), a = 32.3511(7) Å, b = 13.8186(5) Å, c = 29.4593(8) Å, β = 116.262(2)°, V = 11810.3(6) Å^3, Z = 8, μ(Mo-K_α) = 0.78 mm^{-1}, T = 123(2) K, 68443 reflections measured ($2\theta_{max}$ = 50°), 19310 independent reflections used for structure solution (direct methods) and refinement (on F^2 anisotropic with SHELXL-93), 1348 parameters, 2915 restraints, H atoms as a riding model, $wR2(F^2)$ = 0.145, $R[F, I > 2\sigma(I)]$ = 0.049. Crystallographic data (excluding structure factors) for the structure reported in this paper have been deposited with the Cambridge Crystallographic Data Centre as supplementary publication no. CCDC-101915. Copies of the data can be obtained free of charge on application to CCDC, 12 Union Road, Cambridge CB2 1EZ, U.K. [Fax: (internat.) + 44-1223/336033; E-mail: deposit@ccdc.cam.ac.uk].

Acknowledgments

Financial support by the Deutsche Forschungsgemeinschaft and the Fonds der Chemischen Industrie is gratefully acknowledged.

[1] [1a] F. Mathey, *Coord. Chem. Rev.* **1994**, *137*, 1. – [1b] K. B. Dillon, F. Mathey, J. F. Nixon, *Phosphorus: The Carbon Copy*, J. Wiley & Sons, Chichester, **1998**, p. 227.
[2] [2a] E. J. Padma Malar, *J. Org. Chem.* **1992**, *57*, 3694. – [2b] D. B. Chesnut, L. D. Quin, *J. Am. Chem. Soc.* **1994**, *116*, 9638. – [2c] B. Goldfuss, P. v. R. Schleyer, F. Hampel, *Organometallics* **1996**, *15*, 1755.
[3] See, for example: P. Jutzi, T. Redeker, *Eur. J. Inorg. Chem.* **1998**, 663, and references cited therein
[4] [4a] A. Espinosa Ferao, B. Deschamps, F. Mathey, *Bull. Soc. Chim. Fr.* **1993**, *130*, 695. – [4b] S. Holand, M. Jeanjean, F. Mathey, *Angew. Chem.* **1997**, *109*, 117; *Angew. Chem. Int. Ed. Engl.* **1997**, *36*, 98.
[5] For the generation of side-chain-functionalized phospholides in metal coordination spheres, see: [5a] B. Deschamps, F. Mathey, *Organometallics* **1992**, *11*, 1411. – [5b] C. Ganter, L. Brassat, C. Glinsböckel, B. Ganter, *Organometallics* **1997**, *16*, 2862. – [5c] C. Ganter, L. Brassat, B. Ganter, *Chem. Ber.* **1997**, *130*, 1771.
[6] H. J Cristau, F. Plenat, in *The Chemistry of Organophosphorus Compounds*, vol. 3 (Ed.: F. R. Hartley), J. Wiley & Sons, Chichester, **1994**, p. 45.
[7] D. Gudat, V. Bajorat, M. Nieger, *Bull. Soc. Chim. Fr.* **1995**, *132,* 280.
[8] For the synthesis and characterization of a benzo[*b*]phospholide, see: E. Niecke, M. Nieger, P. Wenderoth, *Angew. Chem.* **1994**, *106*, 362; *Angew. Chem. Int. Ed. Engl.* **1994**, *33*, 353.
[9] A. Schmidpeter, M. Thiele, *Angew. Chem.* **1991**, *103*, 333; *Angew. Chem. Int. Ed. Engl.* **1991**, *30*, 308.
[10] D. Gudat, *Phosphorus Sulfur Silicon* **1993**, *77*, 238.
[11] W. A. Herrmann, C. Zybill, in *Synthetic Methods of Organometallic and Inorganic Chemistry*, vol. 1 (Ed.: W. A. Herrmann), Georg Thieme Verlag, Stuttgart, **1996**, p. 41.
[12] J. C. Tebby, in *Phosphorus-31 NMR Spectroscopy in Stereochemical Analysis* (Eds.: J. G. Verkade, L. D. Quin), VCH, Deerfield Beach, **1987**, p. 1.
[13] All calculations were performed with the Gaussian 94 package: M. J. Frisch, G. W. Trucks, H. B. Schlegel, P. M. W. Gill, B. G. Johnson, M. A. Robb, J. R. Cheeseman, T. Keith, G. A. Petersson, J. A. Montgomery, K. Raghavachari, M. A. Al-Laham, V. G. Zakrzewski, J. V. Ortiz, J. B. Foresman, C. Y. Peng, P. Y. Ayala, W. Chen, M. W. Wong, J. L. Andres, E. S. Replogle, R. Gomperts, R. L. Martin, D. J. Fox, J. S. Binkley, D. J. Defrees, J. Baker, J. P. Stewart, M. Head-Gordon, C. Gonzalez, J. A. Pople, *Gaussian 94, Rev. B.3*, Gaussian, Inc., Pittsburgh PA, **1995**.
[14] D. Gudat, M. Nieger, M. Schrott, *Chem. Ber.* **1995**, *128*, 259.
[15] *International Tables for Crystallography*, vol. C (Ed.: A. J. C. Wilson), Kluwer Academic Publishers, Dordrecht, **1992**, p. 680.
[16] [16a] N. Burford, B. W. Royan, A. Linden, T. S. Cameron, *Inorg. Chem.* **1989**, *28*, 144. – [16b] N. Burford, A. I. Dipchand, B. W. Royan, P. S. White, *Inorg. Chem.* **1990**, *29*, 4938. – [16c] N. Burford, A. I. Dipchand, B. W. Royan, P. S. White, *Acta Crystallogr.* **1989**, *C45*, 1485.
[17] A. W. Johnson, *Ylides and Imines of Phosphorus*, J. Wiley & Sons, New York, **1993**, p. 139.
[18] Couplings in higher order multiplets were determined by spectral analysis and by using $^4J_{P(B),P(B')}$ = 5.5 Hz.

Received December 28, 1998
[I98453]

X-ray Structures of a Phenanthroline-Strapped Porphyrin and Its Dihydrated Zinc(II) Complex: Convergent Distal Hydrogen Bonds and "CH···O" Interactions

Philippe Ochsenbein,[a] Michel Bonin,[b] Kurt Schenk,[b] Jérôme Froidevaux,[c] Jennifer Wytko,[c] Ernest Graf,[d] and Jean Weiss*[c]

Dedicated to the memory of Dr. Michael Momenteau

Keywords: Hydrogen bonds / Inclusion compounds / Solid-state structures / Porphyrinoids / Zinc

The X-ray structure of a phenanthroline-(phen-)strapped 1,10-diphenylporphyrin **1** has been resolved. From the structure obtained, it is apparent that in spite of the rigidity of the strap the porphyrin ring is only slightly distorted, and that the substituents on the phen moiety define what would seem to be a hydrophobic pocket. Metallation of the free base **1** with zinc(II) acetate yields a metallic complex (**1**)Zn with a free axial coordination site. Crystallization of the zinc complex in the presence of a hindered base (*N*-methylimidazole, denoted *N*-MeIm) in organic solvents affords single crystals of a porphyrinatozinc(II) species, in which two water molecules are surprisingly present in the encumbered (distal) pocket of the phen site. One water molecule is axially bound to the zinc(II) ion, while the other is doubly hydrogen-bonded, as an H-bond donor to the phenanthroline and as an H-bond acceptor to the axial water ligand.

Introduction

Metalloporphyrins capable of forming hydrogen bonds (H bonds) have been extensively studied due to their involvement in photosynthetic processes of higher plants, either as main pigments such as chlorophyll a, or as accessory pigments such as chlorophyll b. Zinc and magnesium porphyrins and chlorin derivatives constitute the majority of models studied to date. H-bond formation can occur either at the periphery of the tetraaza ligand or along the axis defined by the metal $4p_z$ and $4d_{z^2}$ orbitals, but in either case is associated with selective assembling processes. These assembling processes include substrate recognition[1] and axial ligand selection (e.g. CO/O_2),[2] dimer formation,[3] and anchoring to proteins and membranes.[4][5] Water molecules may play a crucial role in bridging H-bond donors and H-bond acceptors, leading to superstructures;[6] thus, H bonding may originate from a water molecule coordinated axially to a metalloporphyrin.

An example of a self-assembling process of a porphyrin derivative mediated by an axially bound water molecule, leading to a dimeric porphyrin−quinone assembly, has recently been described by Fajer.[7] This type of interaction has been envisaged for decades,[8] and analysis of several metalloporphyrin structures, including those of mono-[9] and dihydrated[10] chlorophyll, has suggested that hydrogen bonding plays an important role in the anchoring of pigments on proteins. A confirmation of the role of water in the three-dimensional structure of a peridin-chlorophyll light-harvesting complex was reported by Hofmann and Welte.[11] In this case, a histidine imidazole ring of the pigment, which is stacked with ring II of the chlorophyll, is H-bonded through a water molecule coordinated at the central Mg. Coordination of water to the central metal in pigments may also be involved in the modification and control of the redox properties of charged radical intermediate species.[12] Thus, H bonding contributes in various ways to a better control of electron transfer in natural systems,[13] and in this regard it is important that well-defined hydrated structures of metalloporphyrins are obtained. In this paper, we present the structure of a dihydrated zinc porphyrin complex, together with that of the corresponding free base.[14]

In a search for controlled architectures combining porphyrins and either metal- or H-binding sites, we have described the synthesis of a phenanthroline-(phen-)strapped porphyrin **1**.[14] The formation of copper and silver mixed-valence complexes with this heteroditopic ligand has illustrated its coordination capabilities.[15] In the course of the synthesis of a heterodinuclear zinc-copper complex of ligand **1**, we found that it was possible to crystallize the free base and the dihydrated zinc(II) complex. The X-ray structures[16] of both are described and compared herein. Moreover, the H-bond network of the two water molecules found

[a] Synthélabo Recherche,
10, rue des Carrières, F-92500 Rueil-Malmaison, France
[b] Département Sciences Physiques, Université de Lausanne,
CH-1015 Lausanne-Dorigny, Switzerland
[c] Laboratoire d'Electrochimie, UMR 7512 au CNRS, Université Louis Pasteur,
4, rue Blaise Pascal, F-67070 Strasbourg, France
Fax: (internat.) + 33-3/88611553
E-mail: jweiss@chimie.u-strasbg.fr
[d] Laboratoire de Chimie de Coordination Organique, UMR 7513 au CNRS, Université Louis Pasteur,
4, rue Blaise Pascal, F-67070 Strasbourg, France

 © WILEY-VCH Verlag GmbH, D-69451 Weinheim, 1999 1434−1948/99/0707−1175 $ 17.50+.50/0

in the hydrophobic environment of the phenanthroline pocket in the case of the Zn^{II} porphyrin is discussed.

Results and Discussion

Crystals of the free base **1** were obtained by slow diffusion of hexane and traces of methanol into a concentrated (10^{-2} M) solution of the porphyrin in dichloromethane. The structure depicted in Figure 1 clearly shows that the tetrapyrrolic macrocycle is only slightly distorted.

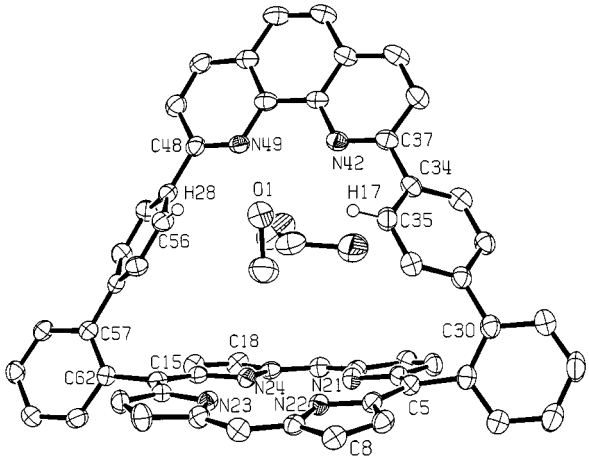


Figure 1. Crystallographic view of **1**; hydrogen atoms are omitted for the sake of clarity and only atoms discussed in the text are labelled; selected bond lengths and angles are discussed in the text

There had previously been some doubt as to the degree of planarity of the porphyrin ring, as the rate of metallation of **1** is three orders of magnitude faster than that of regular tetraphenylporphyrin (TPP).[15] The deviation from planarity shows that the conformation adopted by the (24-atom) core is saddled with respect to the orientation of the pyrrole rings and ruffled when considering the *meso* positions [maximum deviation from planarity of 0.24 Å for the *meso*-(C5) and β-carbon atoms (C8)]. The phenyl spacers between the porphyrin and phenanthroline units are tilted away from the phen plane (by 41° and 49°), which is in agreement with previously reported 2,9-diphenylphenanthroline structures.[17] The frozen orientation of the phenyl spacers is observed only in the solid state; ^{1}H-NMR data are consistent with their free rotation in solution. A tilt of the strap towards one side of the porphyrin is also seen in the crystal, while solution ^{1}H-NMR data are consistent with a mirror plane containing the phen subunit (apparent C_{2v} symmetry).[14] The cleft, or cavity, defined by the two phenyl spacers should be referred to as the distal pocket, in accordance with standard mono-*ansa*-porphyrin nomenclature. The width of this pocket is ca. 11.0 Å (C30−C57) above the porphyrin plane (between the two *meso*-phenyl groups), and ca. 6.7 Å (C37−C48) near the phenanthroline unit (between the two phenyl spacers in the 2- and 9-positions of the phen). A methanol guest molecule resides in the pocket, held in position by a set of four weak interactions. There are two hydrogen bonds to the phenanthroline nitrogen atoms, with distances of 3.19(2) Å between O1 (methanol) and N42 and 3.21(2) Å between O1 and N49. In addition, two strong "CH···O" interactions[23] are present between O1 and C35−H17 and C56−H28 with H···O distances (CHO angles) of 2.41(2) Å (147.7°) and 2.45(2) Å (139.4°), respectively. As depicted in the unit-cell view (Figure 2), intermolecular π interactions may be responsible for the bending of the phen strap. This distortion of the free base cannot be guest-induced, as might be the case for the corresponding zinc(II)-imidazole complex and for the dihydrated porphyrinatozinc(II) complex (vide infra).

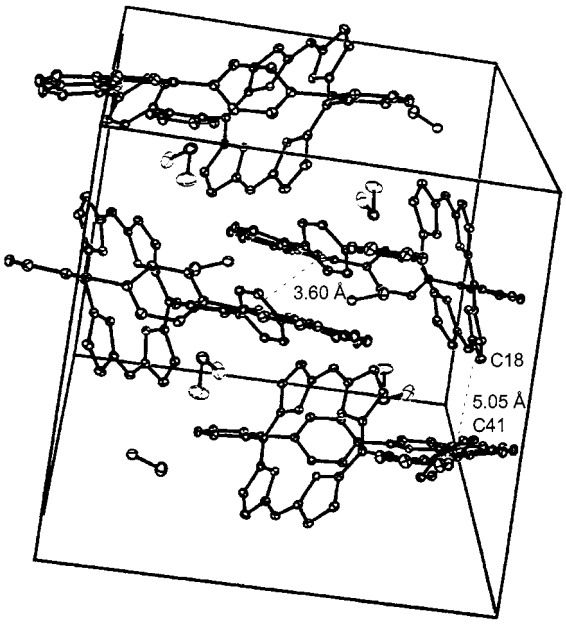


Figure 2. Packing of **1** in the unit cell; additional methanol molecules occupy free spaces defined by the head-to-tail arrangement of **1**

A π-stacking interaction at van der Waals distances is present between two phenyl spacers of neighboring molecules, with maximum and minimum interplanar distances of 3.611(4) and 3.590(4) Å for C34 and C35, respectively, from the mean plane of the neighboring phenyl spacer. As depicted in Figure 2, these two particular aromatic rings are parallel in the solid state, with a dihedral angle of 0.00(9)° and a centroid−centroid distance of 3.807(5) Å. Edge-on (or T-shaped) σ−π interactions[19] between the *meso* and β positions of one porphyrin unit and the phen nucleus of another are also observed with, for example, a minimum distance of 5.03(5) Å between C18 and C41 (see Figure 2). The structure of the free base would appear to be well-suited for the formation of mixed-valence homobinuclear complexes, as reported previously.[15] Moreover, due to the allowed bending of the phen strap, the inclusion of substrates within the cleft, already observed for monometallic species,[18] should also be possible in a bimetallic complex.

Metallation of the free base with zinc acetate in refluxing DMF afforded [(**1**)Zn(H_2O)$_2$] in 80% yield after purification by chromatography on alumina (CH_2Cl_2 + traces of pyridine).[19] Crystals of [(**1**)Zn(H_2O)$_2$] were obtained by diffusion of hexane into a dilute solution of (**1**)Zn in dichloromethane containing one equivalent of *N*-methylimidazole

(*N*-MeIm). Initially, *N*-MeIm was added to complete the coordination sphere of zinc(II) on the expected proximal side of the porphyrinatozinc(II) species, but subsequent binding studies revealed a low affinity of *N*-MeIm for the zinc complex.[18] Instead, the coordination sphere of the pentacoordinated zinc(II) cation is completed by an oxygen atom of a water molecule, as depicted in Figure 3.

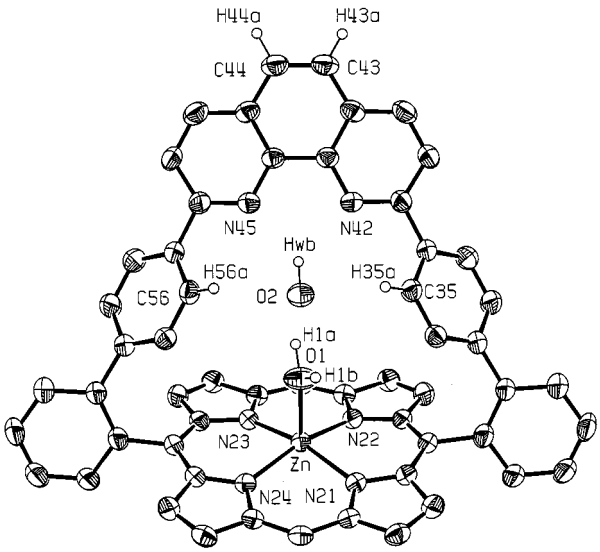


Figure 3. Front view and selected atom numbering for [(**1**)Zn(H_2O)$_2$]; only the hydrogen atoms involved in the H-bond network found by Fourier difference techniques are represented; selected bond lengths and angles are discussed in the text

The conformation of the porphyrin (24-atom) core is changed from ruffled in the solid state to domed, as would be expected for the coordination of large metal cations. This variation of conformation of the (24-atom) core does not affect the phenanthroline strap, the distance between the two *meso*-carbon atoms remaining unchanged. This confirms that no conformational restraints are imposed by the rigid phen strap. The unexpected presence of two water molecules within the distal pocket merits special comment.

The slightly domed porphyrin ring bears a resemblance to reported conformations of pentacoordinated zinc porphyrin complexes with oxygen donors occupying the fifth coordination site.[2,7,9a,9b,12,22] The coordination sphere around the zinc(II) atom is a slightly distorted tetragonal pyramid. The Zn−O1 bond [2.09(2) Å] is perpendicular to the (24-atom) core in that the N−Zn−O1 angles for N21 to N24 are 98.58(8), 98.52(8), 98.34(8), and 98.19(8)°, respectively. While the hydrogen atoms were added to the ligand using a routine treatment of the data, high resolution of the structure allowed us to establish the precise locations, by Fourier difference analysis (see Crystallographic Studies), of the two hydrogen atoms of the axially bound water molecule, as well as that remotely bound to the phenanthroline moiety. As depicted in Figure 3, the plane containing the axial water molecule is orthogonal to the phen plane and is oriented above the unsubstituted $C_{meso}-C_{meso}$ axis with an H1a−O1−H1b angle of 108(3)° and Zn−O1−H1a and Zn−O1−H1b angles of 126(2)° and 123(2)°, respectively. The O1−H1b bond length of 0.92(2) Å is slightly shorter than the O1−H1a distance [0.97(2) Å] due to the hydrogen bonding of H1a with O2. The detailed drawing of the H-bond network given in Figure 4 shows that the 1.69(2) Å distance between H1a and O2 corresponds to a strong H bond, with an oxygen−oxygen distance of 2.621(2) Å.

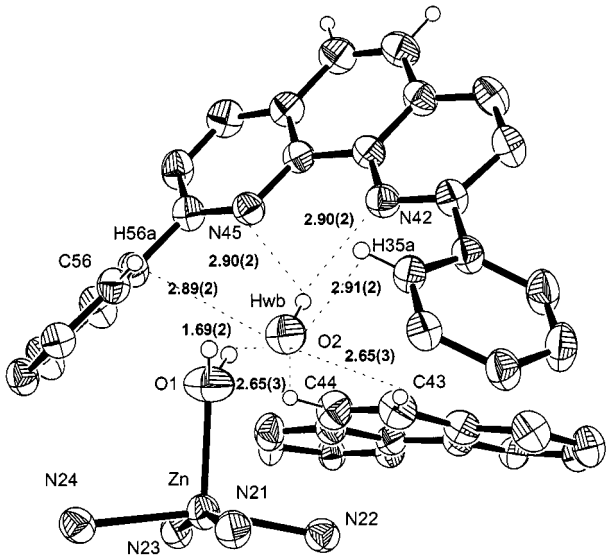


Figure 4. Crystallographic detail of the H-bond (3) and "CH···O" (4) interactions; the direct environment of the O2 water oxygen atom is represented; only the parts of the molecules involved in the binding are depicted; distances are given in Å; an additional van der Waals contact is observed between C44 and C43 and the porphyrin plane (C10) with equal distances of 3.40(2) Å

The angle of 114(2)° between H1a and the uncoordinated O2−Hwb bond, coupled with the precise location of Hwb at 2.27(3) and 2.21(3) Å from the phen nitrogen atoms N42 and N45, respectively, would seem to indicate that there is a direct interaction between H1a and the uncoordinated oxygen lone pairs, and that the second hydrogen atom of the uncoordinated water molecule is disordered in the crystal. This water molecule is fixed in the crystal by means of four "CH···O" interactions.[23] Two bonds of this type are found between the uncoordinated oxygen atom and the two top-central carbon atoms (C44 and C43) of the neighboring adjacent phenanthroline backbone, with identical H···O distances of 2.65(3) Å. The other two "CH···O" interactions are found between the aromatic *ortho* protons of the phenyl spacer and the uncoordinated oxygen atom, with shorter H···O distances of 2.89(2) and 2.91(2) Å. The three hydrogen bonds and four "CH···O" interactions are depicted in detail in Figure 4.

The packing of the metalloporphyrin in the crystal, as depicted in Figure 5, shows that additional π interactions are also present, mainly between the phenanthroline nuclei and open faces of the porphyrin rings. Each porphyrin unit resides on the phen strap of the molecule below, thereby forming Z-shaped stacks (a herringbone arrangement) of porphyrin units. The stacks are mutually interpenetrated by a partial overlap of the back of the phen moiety with the unsubstituted edge of the porphyrin ring in the next stack,

which allows the formation of the inter-stack "CH···O" interactions described above. As indicated in Figure 5, distances corresponding to strong aromatic-ring-stacking interactions, as well as edge-on interactions are observed within and between the zig-zag columns of the porphyrin units.

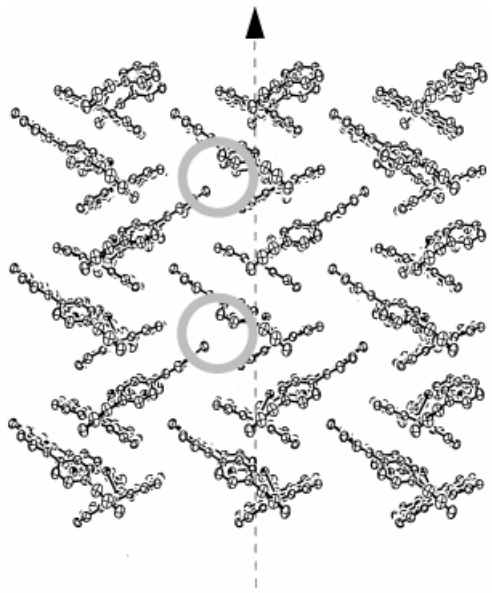


Figure 5. Packing of [(**1**)Zn(H_2O)$_2$]; the crystal consists of parallel arrangements of layers made up of zig-zag stacks (along the --- axis) of [(**1**)Zn(H_2O)$_2$] connected by "CH···O" interactions (identified by grey circles for the left stack); CH_2Cl_2 molecules are omitted for the sake of clarity

The presence of these additional intermolecular interactions certainly contributes in making the observed "CH···O" interactions quite strong (C···O distance: ca. 3.29 Å; CHO angle: ca. 124°) compared to the range of strengths previously reported in the literature.[24] Indeed, the particular nature of the C44−C43 bond in the phenanthroline defines the H44 and H43 atoms involved in the "CH···O" bond as vinylic protons rather than aromatic protons, which usually exhibit "C···O" distances in the range 3.55 to 3.65 Å,[25] with CHO angles commonly in the range 140−180°.[26]

A possible explanation for the high affinity for water shown by the hindered side of the porphyrin ligand is that the coordination of water does not induce any major conformational changes in the ligand. Indeed, the tilt of the *meso*-phenyl substituents on the porphyrin ring in the free base is very similar to that observed in the dihydrated zinc(II) complex. The measured dihedral angles between the *meso*-phenyl groups and the porphyrin plane are 67.86(6)° and 72.07(8)° in the zinc(II) complex and 66.83(10)° and 71.14(11)° in the free base. Furthermore, the dihedral angle between the phen subunit and the porphyrin core remains unchanged during the metallation/hydration process (ca. 61°). Thus, the energetic requirements for accommodating the two water molecules are minimized. Moreover, the lipophilic nature of the solvent (CH_2Cl_2) in which the crystals were grown might have been more conducive to *O* coordination of water at the zinc center than to *N* coordination of the imidazole.

Conclusion

The structure of a mono-*ansa*-porphyrin bearing a phenanthroline strap maintained at a fixed distance by means of two phenyl spacers has been resolved, as has that of the corresponding zinc(II) complex. The structure of the free base shows a relatively large cavity within the strap, with a distance of approximately 6 Å between the two coordination sites. The structure of the zinc complex obtained in the presence of *N*-MeIm does not show binding of an axial nitrogen ligand, but two water molecules are found to be present in the phenanthroline pocket. One water molecule is axially bound to the zinc atom, while the second completes the hydrogen-bond "network" to the phenanthroline nitrogen atoms. Experiments to determine the affinity of **1** for water in solution and the exchange rate of water are currently in progress, as are investigations in which the zinc ion is replaced by a magnesium ion to allow comparison of the photophysical properties of metalloporphyrin cores in the presence and absence of coordinated water.

Experimental Section

General: All solvents and reagents used were of commercial analytical grade. − Ligand **1** was prepared according to ref.[14] − ^{1}H-NMR spectra were recorded with a Bruker WP 300 MHz instrument; data were processed using WINNMR software available from Bruker, with residual non-deuteriated solvent as chemical-shift reference (CH_2Cl_2 at δ = 5.29). − UV/Vis spectra were recorded with a Hewlett-Packard HP8452A diode-array spectrophotometer (2 nm resolution).

[1(Zn)]: To a solution of the free base **1** (50 mg, $6.5\cdot10^{-5}$ mol) in 20 mL of DMF was added Zn(OAc)$_2$ (100 mg, $45.5\cdot10^{-5}$ mol) and the solution was refluxed under argon until the Soret band at 412 nm had disappeared from the UV/Vis spectra of withdrawn aliquots (ca. 4 h). The resulting mixture was then poured into water (200 mL). The pink-red precipitate was collected by filtration, washed with water, and dried by azeotropic distillation with toluene and ethanol, to afford the pure zinc(II) complex as a red solid (47 mg, $5.5\cdot10^{-5}$ mol, 85%); m.p. > 250°C. − ^{1}H NMR (300 MHz, CD_2Cl_2): δ = 10.15 (s, 2 H), 9.28 (d, *J* = 4.4 Hz, 4 H), 9.01 (d, *J* = 4.4 Hz, 2 H), 8.75 (d, *J* = 7.4 Hz, 2 H), 7.96 (d, *J* = 8.2 Hz, 2 H), 7.89 (m, 6 H), 7.49 (d, *J* = 8.2 Hz, 2 H), 7.48 (s, 2 H), 6.62 (d, *J* = 8.3 Hz, 4 H), 6.51 (d, *J* = 8.3 Hz, 4 H). − [**1**(Zn)] + CH_2Cl_2 + 3/2 H_2O: $C_{57}H_{37}Cl_2N_6O_{1.5}Zn$ (968.2): calcd. C 70.86, H 3.86, N 8.70; found C 71.06, H 4.02, N 8.72. − UV/Vis (CH_2Cl_2): λ_{max} [nm] (ε [$M^{-1}\cdot cm^{-1}$]): 284 (28000), 308 (29000), 418 (259000), 546 (11000), 578 (2000). − Positive-ion FAB MS; *m/z*: calcd. for $[M]^+ = [C_{56}H_{32}N_6Zn]^+$ 852; found 853.

X-ray Crystallographic Study:[16] Crystals of **1** were obtained by vapor diffusion of hexane into a CH_2Cl_2/MeOH (95:5) solution of the porphyrin. Crystal data for $C_{56}H_{34}N_6\cdot CH_2Cl_2\cdot CH_3OH$: M_r = 907.91, monoclinic, space group $P2_1/c$, *a* = 17.763(5), *b* = 16.800(4), *c* = 15.759(3) Å, β = 111.59(2)°, *V* = 4372(3) Å^3, *Z* = 4, $\rho_{calcd.}$ = 1.38 gcm^{-3}, μ(Cu-K_α) = 1.743 mm^{-1}. Data were collected with a Philips PW 1100/16 diffractometer using Cu-K_α

graphite-monochromated radiation (λ = 1.5418 Å) at −100°C. A dark-red crystal of dimensions 0.40 × 0.40 × 0.40 mm was used and a total of 5517 reflections were collected, $3° < \theta < 53°$ (max θ limited by cooling device). 4178 reflections with $I > 3\sigma(I)$ were used for the structure determination and refinement. The structure was solved using direct methods and refined against $|F|$. Hydrogen atoms were introduced as fixed contributors. Empirical absorption corrections, transmission factors: 0.64, 1.00. For all computations, the Nonius OpenMoleN package[20] was used. Final results: R_f = 0.052, wR (F) = 0.080, GooF on F: 1.537, maximum residual electronic density: 0.58 eÅ^{-3}. Crystals of [(**1**)Zn(H_2O)$_2$] were obtained by slow diffusion of hexane into a dichloromethane solution of (**1**)Zn containing one equivalent of *N*-methylimidazole. − Crystal structure of [(**1**)Zn(H_2O)$_2$]: $C_{57}H_{35}Cl_2N_6O_2Zn$, M_r = 972.18, red rectangular plates, monoclinic, space group *Ia*, a = 12.355(3), b = 12.658(3), c = 28.639(6) Å, β = 89.99(3)°, V = 4479(3) Å^3, Z = 4. Data were collected at room temperature with a STOE-IPDS diffractometer using Mo-K_α graphite-monochromated radiation (λ = 0.70910 Å). Structure solution and anisotropic refinement were performed with the SHELXTL package[21] using 6664 independent reflections of the 14456 reflections collected. Hydrogen atoms were geometrically positioned with all distances X−H being free to refine, except for those attached to oxygen atoms, which were located by Fourier difference techniques. Final results: R_1 = 0.0342 [$I > 2\sigma(I)$], wR_2 = 0.0865 (all data), GooF on F^2: 1.342, maximum residual density: 0.405 eÅ^{-3}.

Acknowledgments

The Centre National de la Recherche Scientifique (C.N.R.S.) is gratefully acknowledged for financial support.

[1] T. Mizutani, T. Kurahashi, T. Murakami, N. Matsumi, H. Ogoshi, *J. Am. Chem. Soc.* **1997**, *119*, 8991−9001.
[2] K. M. Barkigia, D. Melamed, R. M. Sweet, K. M. Smith, J. Fajer, *Spectrochim. Acta, Part A* **1997**, *53*, 463−469.
[3] [3a] M. F. Perutz, *Ann. Rev. Biochem.* **1979**, *48*, 327−386 and references cited therein. − [3b] M. Momenteau, C. A. Reed, *Chem. Rev.* **1994**, *94*, 659.
[4] O. El-Kabbani, C.-W. Chang, D. Tiede, J. Norris, M. Schiffer, *Biochemistry* **1991**, *30*, 5361−5369.
[5] [5a] E. J. Bylina, C. Kirmaier, L. McDowell, D. Holten, D. C. Youvan, *Nature* **1988**, *336*, 182−184 and references cited therein. − [5b] W. Kühlbrandt, D. N. Wang, *Nature* **1991**, *350*, 130−134.
[6] L. R. McGilliwray, J. L. Atwood, *Nature* **1997**, *389*, 469−472.
[7] J. Fajer, K. M. Barkigia, D. Melamed, R. M. Sweet, H. Kurrek, J. von Gersdorff, M. Plato, H.-C. Rohland, G. Elger, K. Möbius, *J. Phys. Chem.* **1996**, *100*, 14236−14239.
[8] M. S. Fischer, D. H. Templeton, A. Zalkin, M. Calvin, *J. Am. Chem. Soc.* **1972**, *94*, 3613−3619. Very valuable information on H bonding and magnesium(II) or zinc(II) in porphyrins has been compiled by: K. M. Barkigia, J. Fajer in *The Photosynthetic Reaction Center* (Eds.: J. Deisenhoffer, J. R. Norris), Academic Press, San Diego, CA, **1993**, vol. II, pp. 513−539.
[9] [9a] B. Cheng, R. Scheidt, *Inorg. Chim. Acta* **1995**, *237*, 5−11. − [9b] O. C. Choon, V. McKee, G. A. Rodley, *Inorg. Chim. Acta* **1986**, *123*, 11−14. − [9c] C. Kratky, H. P. Isenring, J. D. Dunitz, *Acta Crystallogr.* **1977**, *B33*, 547−549. − [9d] R. Timkovich, A. Tulinsky, *J. Am. Chem. Soc.* **1969**, *91*, 4430−4432. − [9e] M. D. Glick, G. H. Cohen, J. L. Hoard, *J. Am. Chem. Soc.* **1967**, *89*, 1996−1998.
[10] [10a] R. Serlin, H.-S. Chow, C. E. Strouse, *J. Am. Chem. Soc.* **1975**, *97*, 7237−7242. − [10b] H.-S. Chow, R. Serlin, C. E. Strouse, *J. Am. Chem. Soc.* **1975**, *97*, 7230−7237. − [10c] C. Kratky, J. D. Dunitz, *Acta Crystallogr.* **1975**, *B31*, 1586−1589.
[11] E. Hofmann, P. M. Wrench, F. P. Sharples, R. G. Hiller, W. Welte, K. Diederichs, *Science* **1996**, *272*, 1788−1791.
[12] For X-ray studies on charged radical species, see: H. Song, R. D. Orosz, C. A. Reed, W. R. Scheidt, *Inorg. Chem.* **1990**, *29*, 4274−4282; H. Song, N. P. Rath, C. A. Reed, W. R. Scheidt, *J. Am. Chem. Soc.* **1989**, *119*, 8991−9001. For ESR and ENDOR studies, see: A. Forman, M. S. Davis, E. Fujita, L. K. Hanson, K. M. Smith, J. Fajer, *Isr. J. Chem.* **1981**, *21*, 265−269. For redox structural analysis, see: K. M. Barkigia, L. Chantranupong, K. M. Smith, J. Fajer, *J. Am. Chem. Soc.* **1988**, *110*, 7566−7567. For a global analysis, see: M. W. Renner, R. J. Cheng, C. K. Chang, J. Fajer, *J. Phys. Chem.* **1990**, *94*, 8508−8511.
[13] A. Forman, M. W. Renner, E. Fujita, K. M. Barkigia, M. C. W. Evans, K. M. Smith, J. Fajer, *Isr. J. Chem.* **1989**, *29*, 57−64.
[14] For the synthesis of the ligand, see: J. A. Wytko, E. Graf, J. Weiss, *J. Org. Chem.* **1992**, *57*, 1015−1018.
[15] A. Giraudeau, J.-P. Gisselbrecht, M. Gross, J. Weiss, *J. Chem. Soc., Chem. Commun.* **1993**, 1103−1105.
[16] Crystallographic data (excluding structure factors) for the structures reported in this paper have been deposited with the Cambridge Crystallographic Data Centre as supplementary publication nos. CCDC-113533, -113534. Copies of the data can be obtained free of charge on application to CCDC, 12 Union Road, Cambridge CB2 1EZ, U.K. [Fax: (internat.) + 44-1223/336-033; E-mail: deposit@ccdc.cam.ac.uk].
[17] C. Pascard, J. Guilhem, S. Chardon-Noblat, J. P. Sauvage, *New J. Chem.* **1993**, *17*, 331−335.
[18] The presence of the phen strap allows the selective binding of imidazole and 2-methylimidazole within the phen pocket with respective log K_a values of 6.1 and 7.3, while *N*-methylimidazole is bound on the open side with a log K_a value of 4.7 under the same conditions (CH_2Cl_2, 25°C). For details, see: J. Froidevaux, P. Ochsenbein, M. Bonin, K. Schenk, P. Maltese, J.-P. Gisselbrecht, J. Weiss, *J. Am. Chem. Soc.* **1997**, *119*, 12362−12363.
[19] C. Hunter, J. K. M. Sanders, *J. Am. Chem. Soc.* **1990**, *112*, 5525−5534.
[20] C. K. Fair in *MoleN, An Interactive Intelligent System for Crystal Structure Analysis*, Nonius, Delft, The Netherlands, **1990**.
[21] G. M. Sheldrick, *SHELXTL-Plus*, Rel. 5.03, Siemens Analytical X-ray Instruments Inc., Madison, Wisconsin, **1995**.
[22] [22a] L. D. Spaulding, P. G. Eller, J. A. Bertrand, R. H. Felton, *J. Am. Chem. Soc.* **1974**, *96*, 982−987. − [22b] M. M. Williamson, C. M. Prosser-McCartha, S. Mukudan, Jr., C. L. Hill, *Inorg. Chem.* **1988**, *27*, 1061−1068. − [22c] C. Comte, C. P. Gros, S. Koeller, R. Guilard, D. J. Nurco, K. M. Smith, *New J. Chem.* **1998**, 621−626.
[23] For a recent paper representative of the growing importance of "CH···O" interactions in molecular recognition (and *not* in crystal engineering), see: R. A. Musah, G. M. Jensen, R. J. Rosenfeld, D. E. McRee, D. B. Goodin, *J. Am. Chem. Soc.* **1997**, *119*, 9083−9084.
[24] "CH···O" interactions in the coordination of water have been extensively analyzed: T. Steiner, W. Saenger, *J. Am. Chem. Soc.* **1993**, *115*, 4545−4547.
[25] G. R. Desiraju, *Acc. Chem. Res.* **1996**, *29*, 441−449.
[26] T. Steiner, G. R. Desiraju,*Chem. Commun.* **1998**, 891−892.

Received January 18, 1999
[I99014]

New Chelating Nitroxide Free Radical Ligands For Heterospin-Magnetic Engineering

Kira E. Vostrikova,[a] Elie Belorizky,[b] Jacques Pécaut,[a] and Paul Rey*[a]

Keywords: Nitronyl nitroxides / Coordination chemistry / Magnetic properties / Radicals / Chelates / Chelates

Polychelating nitroxide ligands derived from *N*-methylethylenediamine and piperazine have been prepared by reactions of 2-bromomethyl nitronyl nitroxide with the corresponding polyamines. Two of these ligands have been structurally and magnetically characterized, along with some of their transition metal complexes, the magnetic properties of which are compared to those of previously reported related species. In particular, the properties of a nickel(II) derivative of a pentadentate tris(nitroxide), the ground spin-state of which is a quadruplet, are discussed in detail.

The popularity of nitroxide free radicals stems from their high stability and the well-studied, sophisticated organic chemistry.[1−3] Thus, ease of chemical modification allows the synthesis of nitroxides specially designed for use in fields as different as spin labelling[4][5] and materials chemistry.[6−9] In recent years, there has been increasing interest in the incorporation of nitroxide spin carriers into large homo-[9−11] and heterospin assemblies[6−8,12−15] of exchange-coupled species.

Coordination compounds incorporating nitroxide ligands are especially attractive since ligation through the nitroxyl oxygen atom ensures significant magnetic interactions. Moreover, overlap of magnetic orbitals of different types, d and p, may result in special situations where these orbitals are orthogonal and the interaction is ferromagnetic.[6][7] Among the various types of nitroxides, nitronyl nitroxides[16][17] have attracted special interest because of their delocalized electronic structures and their bridging properties, which have been exploited in the construction of extended structures made up of interacting organic and metallic spin carriers. The coordination chemistry of nitroxide free radicals is, however, highly dependent on the weakly basic character of ligands of this type, which precludes coordination to metal ions other than those bearing electron-withdrawing groups.[18−21] Enhancement of the Lewis acid properties of the metal center may easily be achieved, but most of the coordination sites would then be occupied by ancillary ligands and structures of high dimensionality would not be accessible, other than for high-spin polyradicals.[8] Consequently, most of the extended species described to date are one-dimensional alternating arrays of metal ions and nitroxide ligands which are ordered at low temperature.[22−24] In an attempt to circumvent this difficulty, we have investigated the coordination properties of a few nitronyl nitroxides in which the substituent bears a donor such as a nitrogen atom, which enforces the coordination of the nitroxyl oxygen atom through the chelate effect.[12,14,25] The results of these preliminary investigations have prompted us to develop a more general method, which should allow the design of paramagnetic ligands suitable for developing the field of molecular nitroxide-based magnetic coordination compounds.

We report herein on the preparation of a reactive nitroxide synthon, **1** (Figure 1), which couples with *N*-methylethylenediamine to afford tri- (**2**) and tetranitroxide (**3**) ligands, and with piperazine to give a biradical (**4**). The magnetic properties of these polychelating ligands have been investigated and two of them (**3**, **4**) have been structurally characterized. In a preliminary step, and for comparison with previously reported species, complexes of metal hexafluoroacetylacetonates **6** {**4**[$Mn(hfac)_2]_2$}, **7** {**4**[$Co(hfac)_2]_2$}, and **8** {**4**[$Ni(hfac)_2]_2$} have been prepared and their structural and magnetic properties have been investigated. Finally, we report the synthesis and magnetic behavior of a pentacoordinate nickel(II) complex, **5** {**2**[$Ni(ClO_4)_2] \cdot H_2O$}, which illustrates the potential of ligands of this type in the design of new molecular magnetic materials.

Results and Discussion

Although the yield of **1** was rather low (ca. 30%), the one-pot synthesis from the readily available 2,3-dimethyl-2,3-dinitrobutane described here affords samples of the compound from which the amino derivatives can conveniently be prepared. Synthesis of a similar synthon, the chloro compound analogous to **1**, has been described previously.[26] This chloro compound was used in the preparation of 2-(phenyloxymethyl)imidazoline-*N,N′*-dioxyl derivatives, but it is unreactive toward amines.

The synthesis of metal complexes did not present any problems; the chelating nature of these ligands ensures coordination of the nitroxyl groups to the metal center, as

[a] Département de Recherche Fondamentale sur la Matière Condensée, Service de Chimie Inorganique et Biologique, Laboratoire de Chimie de Coordination (Unité de Recherche Associée au CNRS No. 1194),
CEA-Grenoble, F-38054 Grenoble Cedex 09, France
E-mail: rey@drfmc.ceng.cea.fr
[b] Laboratoire de Spectrométrie Physique (CNRS-UMR 5588), Université Joseph Fourier Grenoble 1,
B. P. 87, F-38402 Saint Martin d′Hères Cedex, France

 © WILEY-VCH Verlag GmbH, D-69451 Weinheim, 1999 1434−1948/99/0707−1181 $ 17.50+.50/0

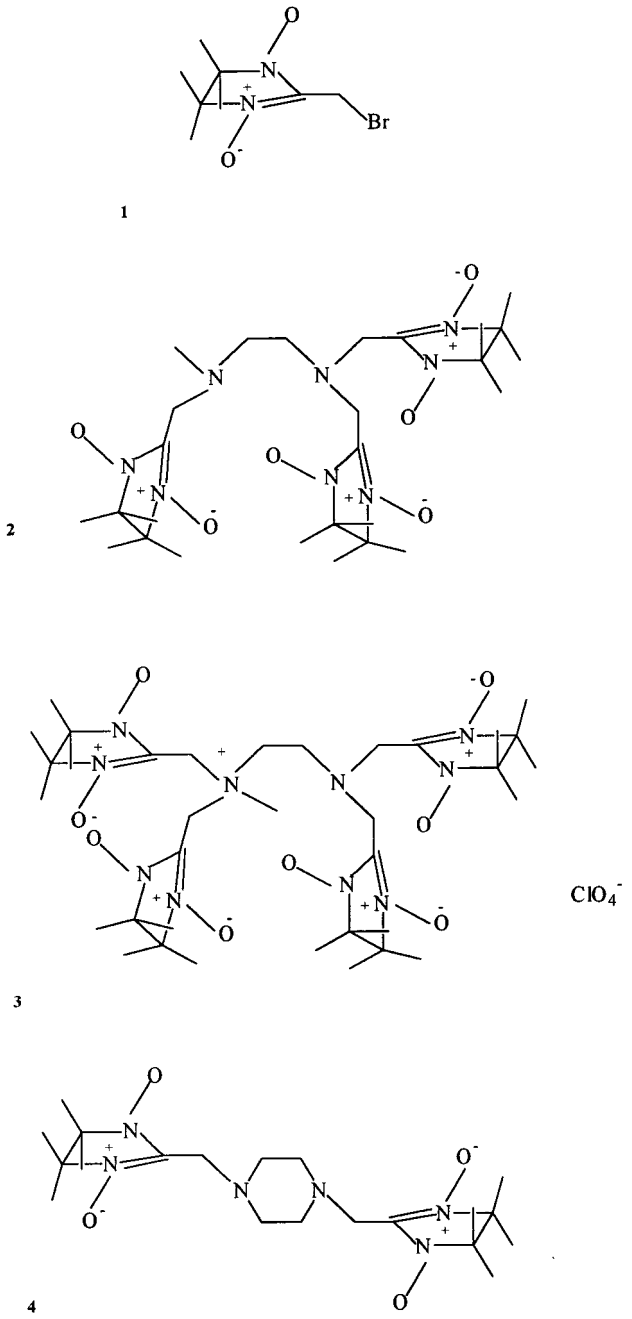


Figure 1. Chemical structure of the nitroxide synthon **1** and of the polychelating ligands **2**−**4**

observed for the Mn^{II} (**6**), Co^{II} (**7**), and Ni^{II} (**8**) derivatives of **4**, the X-ray structures of which have been determined.

Structural Studies

Since only one structure of a 2-aminomethyl derivative of a nitronyl nitroxide has been reported previously,[26] it seemed worthwhile to structurally characterize a few of these ligands.

Views of the molecular structures of $\mathbf{3}^+$ and **4** are depicted in Figures 2 and 3, respectively. In both compounds, the imidazoline *N*-oxide *N*′-oxyl fragments exhibit struc-

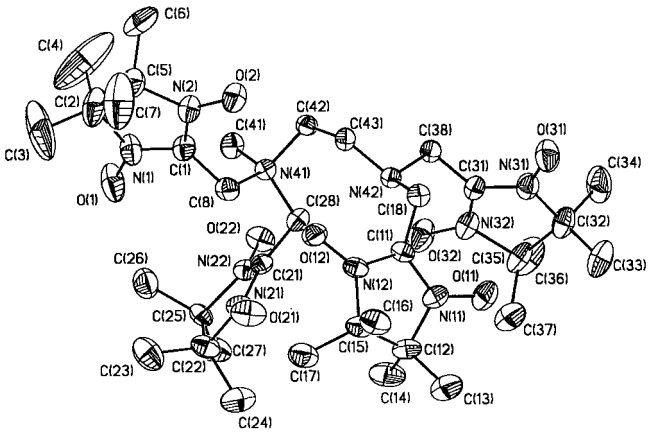


Figure 2. Molecular structure of ligand $\mathbf{3}^+$ showing the atom numbering scheme; thermal ellipsoids are drawn at a 30% probability level; selected bond lengths [Å] and angles [°]: Oi−Ni (av.) = 1.281(6), Ci1−Ci8 (av.) = 1.470(6), C8−N41 = 1.514(4), C28−N41 = 1.530(6), C18−N42 = 1.490(5), C38−N42 = 1.470(4); C1−C8−N41 = 114.3(4), C11−C18−N42 = 112.4(3), C21−C28−C41 = 112.9(3), C31−C38−N42 = 114.6(4)

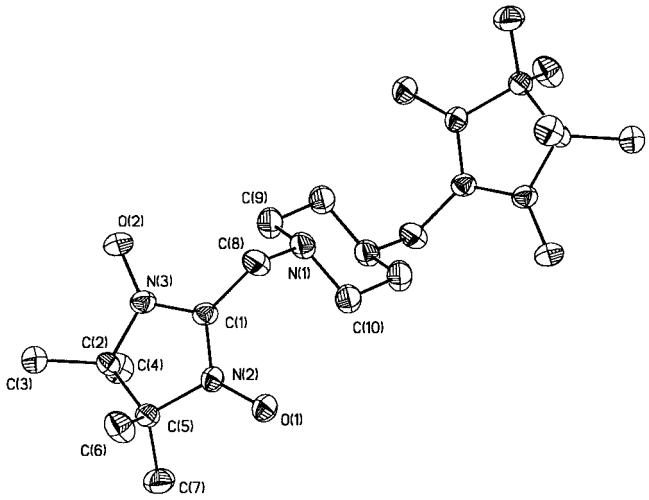


Figure 3. Molecular structure of ligand **4** showing the atom numbering scheme; thermal ellipsoids are drawn at a 30% probability level; selected bond lengths [Å] and angles [°]: N2−O1 = 1.272(4), N3−O2 = 1.285(4), C1−C8 = 1.489(5), C8−N1 = 1.461(5); C1−C8−N1 = 117.0(3)

tural features characteristic of nitronyl nitroxides,[6] such as NO bond lengths in the range 1.26−1.29 Å. Regarding the 2-aminomethyl moiety, one observes the following structural features: (i) In both ligands, the imidazoline ring is almost perpendicular to the plane defined by the sp^2-hybridized carbon atom (C1; Figure 2) and the aminomethyl group (84.6−93.5°). This can be rationalized by considering the steric requirements, since in this arrangement the oxyl groups are far removed from the organic fragment bearing the amino function. (ii) In **3**, the relative arrangement of the four imidazoline-*N*,*N*′-dioxyl groups is such that two of them are almost parallel [12.4(4)°] and each group within this pair is almost perpendicular (83−87°) to the other two. (iii) In **4**, the C1−C8−N1 plane is roughly orthogonal to

both the imidazole ring and the mean plane of the piperazine fragment. Finally, the ethylenediamino group in **3** is in a gauche conformation, while in the centrosymmetric compound **4** the six-membered piperazine ring adopts a chair form. Numerous weak intermolecular interactions involving the oxyl groups are observed, with distances larger than 5 Å.

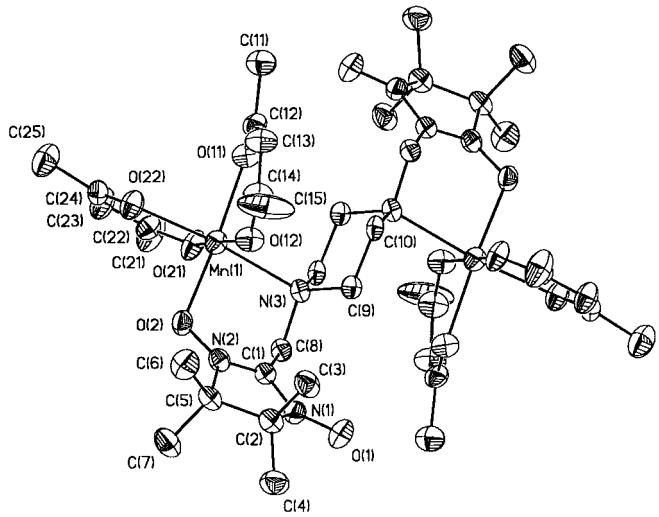


Figure 4. Molecular structure of complex **6** showing the atom numbering scheme; thermal ellipsoids are drawn at a 30% probability level; selected bond lengths [Å] and angles [°]: N1−O1 = 1.266(7), O2−N2 = 1.309(7), Mn−O2 = 2.158(5), Mn−N3 = 2.463(5); O2−Mn−N3 = 88.7(2), O2−Mn−O11 = 163.3(2), N3−Mn−O22 = 163.3(2), C1−C8−N3 = 112.0(5)

Although complex **6** {**4**[Mn(hfac)$_2$]$_2$} on the one hand, and the isostructural complexes **7** {**4**[Co(hfac)$_2$]$_2$} and **8** {**4**[Ni(hfac)$_2$]$_2$} on the other, do not crystallize in the same space group (*P*1 and *P*21/*n*, respectively), their molecular structures (Figure 4) are very similar. They are centrosymmetric species incorporating a piperazine ring in a chair conformation. The metal coordination spheres are octahedral, with that of the manganese ion being more distorted than those of the cobalt and nickel ions. It is worth noting that each metal center is chiral, but since the molecular structures are centrosymmetric the complexes exist in inactive forms. In both molecular structures, the chelate ring involving the nitroxide oxygen atom adopts a boat conformation, and the N−O distance in the coordinated nitroxyl group is larger than that in the uncoordinated one by as much as 0.03 Å. This latter feature is diagnostic of significant metal−nitroxide magnetic coupling. Furthermore, the chelate ring is distorted because, due to steric factors, the metal−nitrogen(piperazine) distance is much larger than usual [2.463(5) Å in **6** and 3.300(6) Å in **7**]. Finally, the smallest intermolecular distances are observed between symmetry-related uncoordinated oxyl groups, with distances as small as 3.41 Å in **6**. Therefore, the magnetic behavior of these metal complexes may depend not only on intramolecular metal−nitroxide couplings, but also on intermolecular nitroxide−nitroxide interactions.

Magnetic Studies

Ligands **2**−**4** exhibit similar magnetic behavior characterized by obeyance of the Curie law down to ca. 40 K, followed by a decrease of the product of the magnetic susceptibility and the temperature, indicative of antiferromagnetic interactions. In biradical **4**, the saturated piperazine moiety is not expected to mediate sizeable intramolecular interactions between the two nitroxide spin carriers. Indeed, the Bleaney−Bowers expression[27] was not able to reproduce the experimental data. However, fairly good results were obtained by considering independent spins interacting with neighboring molecules[28] [^{z}J = −2.4(3) cm^{-1}, R = 6.2·10^{-4}].[29] As mentioned above, in tetraradical **3** intra- and intermolecular contacts are of the same order of magnitude. Consequently, good agreements were obtained either by considering a four-spin system with identical intramolecular interactions being operative between the nitroxide fragments [J = −2.1(2) cm^{-1}, R = 2.4·10^{-4}] or an S = 1/2 spin interacting with an unknown number (z) of neighbors [^{z}J = −6.8(2) cm^{-1}, R = 1.7·10^{-4}]. This latter model could also be successfully applied to triradical **2** [^{z}J = −5.9(3) cm^{-1}, R = 3.5·10^{-4}], for which structural information is not available. Although the magnetic behavior of the ligands is somewhat unremarkable, the small magnitudes of the coupling constants suggest that analysis of the magnetic properties of the complexes could be performed neglecting inter-nitroxide coupling within the metal coordination sphere.

Curie behavior is observed for complex **6**. The almost constant value of χT from room temperature (6.06 cm^3·K·mol^{-1}) down to 5 K (5.97 cm^3·K·mol^{-1}) precludes any quantitative analysis of the coupling constant. This value of $\chi T \approx 6$ cm^3·K·mol^{-1} is consistent with the presence of two independent S = 2 spins, resulting from a large metal−nitroxide antiferromagnetic interaction at both complexing sites of the molecule. Indeed, the value at room temperature indicates that the magnitude of the coupling constant should be as large as −100 cm^{-1}, and that intermolecular interactions should be negligible. Such large Mn^{II}−nitroxide interactions have been reported previously, but it has been suggested that geometric constraints imposed by the chelation usually lessen the extent of magnetic interaction.[25] Indeed, if one considers that the interaction primarily originates from overlap of the π* orbital of the nitroxyl group with the metal orbital directed towards the oxyl oxygen atom, chelation would result in unfavorable local structural parameters for overlap and strong coupling. In **6**, these parameters (M−O−N angle 116.5°; angle between the M−O−N and N−C−N planes 51.4°) are similar to those observed in the related complex Mn(hfac)$_2$NIT · 2 Py (120° and 42°),[25] where the chelating donor atom is a pyridyl nitrogen atom and the Mn^{II}−nitroxide interaction has a magnitude of just −65 cm^{-1}.

Similarly, antiferromagnetic behavior is shown by the analogous nickel(II) complex **8**, for which the value of χT decreases from 2.04 to 0.91 cm^3·K·mol^{-1} over the 300−2 K temperature range and the ground spin-state is the sum of

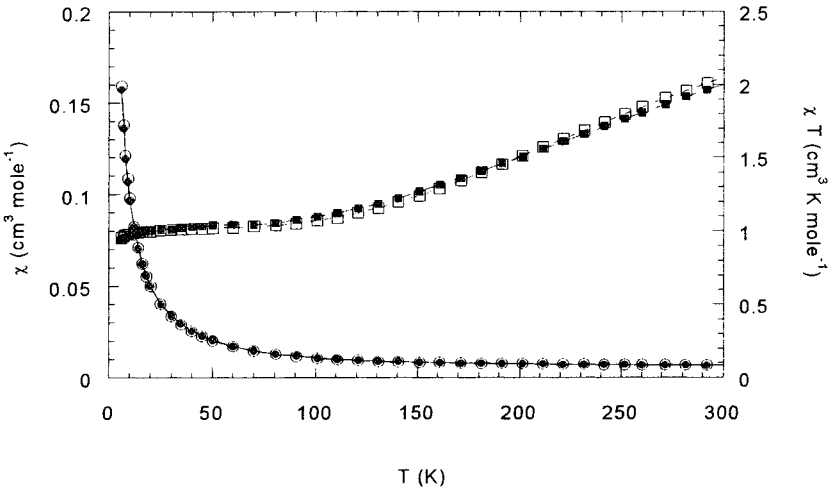


Figure 5. Magnetic behavior of complex **8** displayed as χ (full circle: experimental; open circle: calculated; see text) and χT (full square: experimental; open square: calculated)

two doublets. However, in this case the variation of χT is sufficiently large (Figure 5) to allow calculation of a reliable value of $J_{Ni-nitroxide} = -131(4)$ cm^{-1} [$g = 2.11(1)$, $R = 3.4 \cdot 10^{-4}$], which is smaller than that found for the Ni^{II} complex of the pyridyl-substituted radical (-161 cm^{-1}).[25] Structural parameters relating to magnetic orbital overlap in these two compounds are also similar. Therefore, these two examples illustrate how slight structural modifications within the metal coordination sphere can have a significant influence on the magnitude of the metal−radical magnetic interaction.

In the case of complex **7** {**4**[Co(hfac)$_2$]$_2$}, one observes a decrease in χT, which is probably the result of antiferromagnetic metal−nitroxide interactions. Owing to the significant orbital contribution to the magnetic behavior of octahedral Co^{II} species, no attempts have been made to determine a coupling constant.

The magnetic behavior of complex **5** is depicted in Figure 6. On decreasing the temperature, χT increases from 2.31 emu·K·mol^{-1} (independent spins) to 2.53 emu·K·mol^{-1} at 38 K, and then decreases to ca. 1.0 emu·K·mol^{-1} at 2 K. The presence of dominant ferromagnetic interactions is confirmed by a positive θ value of 8.6 K, as shown by the temperature dependence of $1/\chi$. Although Ni^{II}−nitroxide interactions are usually antiferromagnetic, recent reports have documented special situations where ferromagnetic couplings can be attributed to specific structural features of the coordination sphere.[30] In the present case, structural information is not available but, as shown in Figure 7, the complex may exist in two isomeric forms, namely OC-6-25 (*mer*) and OC-6-35 (*fac*). Of these, the *mer* configuration is probably more stable due to steric factors, as has been observed previously for related nickel(II) complexes of other chelating nitroxide ligands.[13]

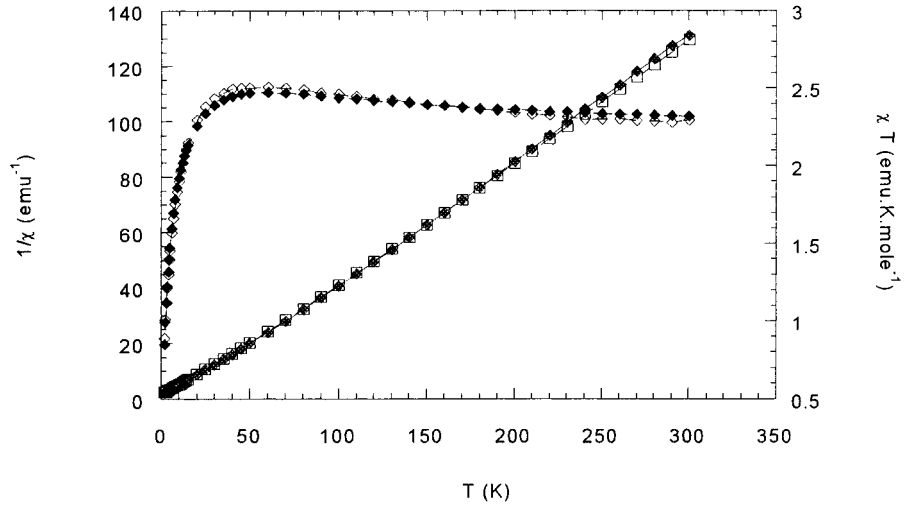


Figure 6. Temperature dependence of χT (full circle: experimental; open circle: calculated) and $1/T$ (full square: experimental; open square: calculated) for complex **5**

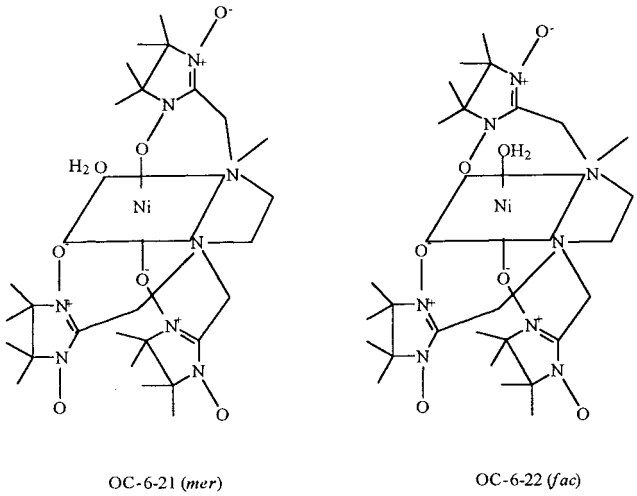


Figure 7. Sketch of the possible isomeric modifications of complex **5**; enantiomeric modifications are not represented

From a magnetic point of view, there are two different sets (axial and equatorial) of coordinated nitroxide ligands, irrespective of the configuration. Accordingly, a model including two different Ni−nitroxide coupling constants was considered, which led to the following parameters: $J_{Ni-C} = -5.3(6)$ cm^{-1}, $J_{Ni-A} = J_{Ni-B} = +12(3)$ cm^{-1}, $g = 2.13(2)$, and furthermore indicated a weak intermolecular interaction of 0.45(2) cm^{-1} ($R = 8.2 \cdot 10^{-4}$). This coupling scheme suggests that the ground spin-state of the "isolated" complex is a quadruplet. Figure 8 shows plots of the theoretical Brillouin function for $S = 3/2$ ($g = 2.13$) and the magnetization data of the complex collected at $T = 2$ K. These two curves have been extrapolated to high field using a sum of exponential functions for the experimental data. Although at low field the data deviate markedly from the calculations, one observes that at high field the experimental magnetization extrapolates to a value close to that of a quadruplet state. The discrepancy observed at low field is most likely attributable to zero-field effects, which split the ground state into two Kramer doublets.

Concluding Remarks

We have presented a general strategy for the incorporation of donor atoms in chelating positions to the oxyl group in nitronyl nitroxides. The method allows the preparation of metal−nitroxide exchange-coupled species with weakly acidic metal centers. The variety of amino-functionalized organic fragments that can be used as precursors for designing nitroxide ligands makes this strategy very attractive for magnetochemists. For example, complex **5**, which has a spin quadruplet ground state and a free coordinating position, can be used to build up high-spin clusters. Work along these lines using this $S = 3/2$ complex as a terminal building block for metal hexacyanates is currently in progress.

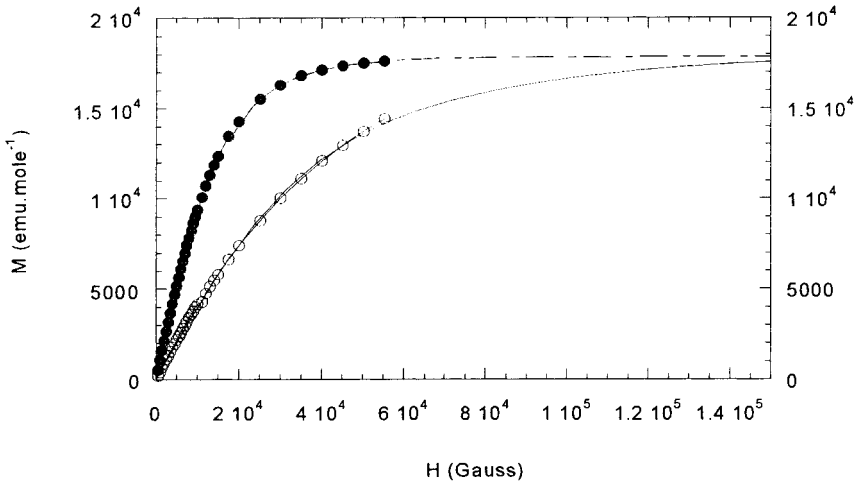


Figure 8. Field dependence of the magnetization for complex **5** (full circle: theoretical Brillouin curve for $S = 3/2$ and $g = 2.13$; open circle: experimental data)

Experimental Section

Synthesis of 2-Bromomethyl-4,5-dihydro-4,4,5,5-tetramethyl-1-oxy-1*H*-imidazolyl 3-Oxide (1): This compound was synthesized directly from 2,3-dimethyl-2,3-dinitrobutane.[31] The precursor (10 g, 57 mmol) and ammonium chloride (5 g) were dissolved in a mixture of water (20 mL) and THF (80 mL). Subsequent reduction to the bis(hydroxylamino) derivative was performed by adding zinc powder (13 g) over a period of 1 h at 10°C. The resulting slurry was stirred for 5 h at room temperature and then filtered. The filtrate was acidified to pH = 1 with HCl and the THF was evaporated in vacuo. The remaining aqueous solution was treated with 8 mL of 2-bromoacetaldehyde dimethylacetal and the resulting mixture was stirred at 10°C for 2 d. The solution was subsequently extracted with diethyl ether and the aqueous phase was neutralized to pH = 7 with $NaHCO_3$. Then, 200 mL of dichloromethane was added, the mixture was cooled to 5°C, and oxidation was carried out by adding 7 g of sodium periodate in 50 mL of water over a period of 1 h. The organic phase was subsequently dried and concentrated in vacuo and the crude deep-red compound was chromatographed (SiO_2; diethyl ether) to afford 2.6 g (18%); m.p. 126°C (dec.). The product was found to be stable for months at −28°C, but only for a few hours at room temperature. Thus, it had to be used promptly in the subsequent reactions.

Synthesis of *N*-Methylethylenediamine Derivatives: Celite (5 g) and *N*-methylethylenediamine (100 mg, 1.35 mmol) were mixed in 30 mL of acetonitrile. A solution of 1.0 g (4.0 mmol) of bromomethyl nitronyl nitroxide in 20 mL of MeCN was then added dropwise at room temperature and stirring was continued for a further 2 h. Filtration and evaporation of the solvent from the filtrate afforded a crude mixture, which was chromatographed on alumina (Woelm, activity grade V). Compounds **2** and **3** were successively eluted. − **2**: With dichloromethane/acetonitrile, 60:40; 423 mg (72%); m.p. 145°C (dec.); $C_{27}H_{52}N_8O_6$ (585): calcd. C 55.46, H 8.96, N 19.16; found C 55.58, H 8.72, N 18.97. − Bromide **3:** With acetonitrile. **3** was dissolved in a mixture of methanol/water (1:1) containing one equiv. of sodium perchlorate. After allowing the mixture to stand for 2 d, the crystals deposited were collected by filtration; yield 158 mg (17%); m.p. 189°C (dec.); $C_{35}H_{71}ClN_{10}O_{12} \cdot 4\,H_2O$: calcd. C 45.37, H 8.05, N 15.12, Cl 3.83; found C 45.18, H 8.12, N 15.26, Cl 4.08. Crystals of this compound proved suitable for an X-ray diffraction study.

Synthesis of a Piperazine Derivative: Using the same procedure as above, starting from 1.0 g (4.0 mmol) of **1** and 172 mg of piperazine (2.0 mmol), chromatography on alumina (Woelm activity grade V, CH_2Cl_2/CH_3CN, 70:30) afforded 428 mg (50%) of **4**; m.p. 156°C; $C_{20}H_{36}N_6O_4$ (424.5): calcd. C 56.58, H 8.55, N 19.80; found C 56.78, H 8.53, N 19.92. Crystals suitable for an X-ray diffraction study were obtained by slow evaporation of the solvents from acetone/hexane solutions. Other compounds were present in small quantities, which were not characterized.

Metal Complexes

Nickel(II) 5: Ligand **2** (100 mg, 0.17 mmol) was dissolved in 8 mL of methanol. To this solution, a solution of Ni(ClO4)2·6H2O (70 mg, 0.2 mmol) in 5 mL of MeOH was added portionwise. A red powder (128 mg, 95%) was immediately precipitated, which, after drying in vacuo, gave a satisfactory analysis for $C_{27}H_{51}Cl_2N_8NiO_{15}$ (786.4): calcd. C 37.83, H 6.00, N 13.07, Ni 6.85; found C 37.59, H 5.93, N 13.12, Ni 6.94. All attempts to grow single crystals from solutions in various solvents were unsuccessful.

Manganese(II) Complex 6: Manganese(II) hexafluoroacetylacetonate dihydrate (250 mg, 0.5 mmol) was dissolved in 30 mL of boiling heptane and reflux was continued in order to obtain an anhydrous solution of the metal salt. A solution of ligand **4** (100 mg, 0.23 mmol) in 5 mL of dichloromethane was added to the solution at ca. 50°C. Precipitation occurred on cooling and acetone was added until the solid redissolved. Subsequent slow evaporation of the solvent led to well-formed crystals of complex **6** (223 mg, 33%; m.p. 188°C); $C_{40}H_{40}F_{24}Mn_2N_6O_{12}$ (1362.6): calcd. C 35.26, H 2.96, Mn 8.06, N 6.17; found C 34.98, H 3.11, Mn 7.97, N 6.04.

Cobalt(II) Complex 7 and Nickel(II) Complex 8: Crystals suitable for X-ray diffraction experiments were obtained starting from the appropriate metal salt and following the same procedure as above.

Crystal Structure Determinations: All crystals (**3**, **4**, **6**, **7**) were analyzed using a Siemens SMART CCD area detector three-circle diffractometer (Mo-K_α radiation, graphite monochromator, λ = 0.71073 Å). The cell parameters were determined from intensities detected in three batches of 15 frames with a 10-s exposure time for each. For three settings of Φ and 2Θ, 1200 narrow data frames were collected for successive increments in ω of 0.3°. A full hemisphere of data was collected for each complex. At the end of collection, the first 50 data frames were re-examined in order to check for decay during the data collection. Unique intensities with $I > 10\sigma(I)$ selected from all the data frames using the SAINT program were used to refine the cell parameters. The substantial degree of redundancy in the data allowed empirical absorption corrections to be applied using multiple measurements of equivalent reflections with the SADABS program. Space groups were derived from systematic absences and were later confirmed by the successful solutions of the structures.[32] The structures were solved by direct methods as implemented in the SHELXTL 5.05 package and all atoms were located on difference Fourier maps. Non-hydrogen atoms were refined anisotropically on F^2, while hydrogen atoms, located by calculation, were refined isotropically. For compound **4**, use of the data collected at 20°C led to a structural scheme in which the perchlorate anion was highly disordered. Attempts to collect the data at low temperature were unsuccessful owing to disintegration of the crystals. Therefore, the anion was tentatively modelled on two different chlorine locations with equal occupancies and the oxygen atoms were distributed over a sphere. Although this disorder has a significant effect on the *R* factor values, it does not hamper the chemical interpretation of the cationic part of the molecule. The nickel(II) complex **8** was found to be isostructural with the cobalt(II) analogue **7**.

Magnetic Susceptibility Measurements: Magnetic susceptibility data were collected using a Quantum Design MPMSR2 magnetometer working at a 0.5-T field strength over the 2−300 K temperature range. Squid outputs were corrected for the contribution of the sample holder and susceptibility data were corrected for the diamagnetic contribution of the constituent atoms using Pascal constants.

Acknowledgments

Financial support from the Commissariat à l'Energie Atomique (CEA), C.N.R.S., and the TMR research network 3MD (ERBFMRXCT-980181) of the European Community is gratefully acknowledged.

[1] E. G. Rozantsev, *Free Nitroxyl Radicals* (Ed.: H. Ulrich), Plenum Press, New York, **1970**.
[2] A. R. Forrester, J. M. Hay, R. H. Thomson, *Organic Chemistry of Stable Free Radicals*, Academic Press, London, **1968**.
[3] J. F. W. Keana, *Chem. Rev.* **1978**, *78*, 37.

[4] S. H. W. Wu, H. M. McConnell, *Biochemistry* **1974**, *14*, 847.
[5] L. J. Berliner, *Spin Labeling − Theory and Applications*, Academic Press, New York, **1976**.
[6] A. Caneschi, D. Gatteschi, P. Rey, *Prog. Inorg. Chem*. **1991**, *39*, 331.
[7] A. Caneschi, D. Gatteschi, R. Sessoli, P. Rey, *Acc. Chem. Res.* **1989**, *22*, 392.
[8] K. Inoue, H. Iwamura, *J. Am. Chem. Soc.* **1994**, *118*, 1803.
[9] M. Kinoshita, Ph. Turek, M. Tamura, K. Nozawa, D. Shiomi, Y. Nakazawa, M. Ishikawa, M. Takahashi, K. Awaga, T. Inabe, Y. Maruyama, *Chem. Lett.* **1991**, 1225.
[10] E. Hernandez, M. Mas, E. Molins, C. Rovira, J. Veciana, *Angew. Chem. Int. Ed. Engl.* **1993**, *32*, 882.
[11] M. M. Matsushita, A. Izuoka, T. Sugawara, T. Kobayashi, N. Wada, N. Takeda, M. Ishikawa, *J. Am. Chem. Soc*. **1997**, *119*, 4369.
[12] K. Fegy, D. Luneau, T. Ohm, C. Paulsen, P. Rey, *Angew. Chem. Int. Ed. Engl.* **1998**, *37*, 1270.
[13] K. Fegy, N. Sanz, D. Luneau, E. Belorizky, P. Rey, *Inorg. Chem*. **1998**, *37*, 4518.
[14] K. Fegy, D. Luneau, E. Belorizky, M. Novac, J.-L. Tholence, P. Rey, *Inorg. Chem*. **1998**, *37*, 4523.
[15] L. B. Volodarsky, V. A. Reznikov, V. I. Ovcharenko, *Synthetic Chemistry of Stable Nitroxides*, CRC Press, London, **1994**.
[16] E. F. Ullman, L. Call, J. H. Osiecki, *J. Org. Chem*. **1970**, *35*, 3623.
[17] E. F. Ullman, J. H. Osiecki, D. G. B. Boocock, R. Darcy, *J. Am. Chem. Soc.* **1972**, *94*, 7049.
[18] Y. Y. Lim, R. S. Drago, *J. Am. Chem. Soc.* **1971**, *93*, 891.
[19] R. A. Zelonka, M. C. Baird, *J. Am. Chem. Soc.* **1971**, *93*, 6066.
[20] O. P. Anderson, T. C. Kuechler, *Inorg. Chem*. **1980**, *19*, 1417.
[21] M. H. Dickman, R. J. Doedens, *Inorg. Chem*. **1981**, *20*, 2677.
[22] A. Caneschi, D. Gatteschi, P. Rey, R. Sessoli, *Inorg. Chem*. **1988**, *27*, 1756.
[23] A. Caneschi, D. Gatteschi, J.-P. Renard, P. Rey, R. Sessoli, *Inorg. Chem*. **1989**, *28*, 1976.
[24] A. Caneschi, D. Gatteschi, J.-P. Renard, P. Rey, R. Sessoli, *Inorg. Chem*. **1989**, *28*, 2940.
[25] D. Luneau, G. Risoan, P. Rey, A. Grand, A. Caneschi, D. Gatteschi, J. Laugier, *Inorg. Chem.* **1993**, *32*, 5616.
[26] G. Ulrich, Ph. Turek, R. Ziessel, A. de Cian, J. Fisher, *J. Chem. Soc., Chem. Commun*. **1996**, 2461.
[27] B. Bleaney, K. D. Bowers, *Proc. Roy. Soc., Ser. A* **1952**, *214*, 451.
[28] R. L. Carlin, *Magnetochemistry*, Springer-Verlag, Berlin, **1986**.
[29] The magnetic properties were analysed using our own program, which diagonalizes numerically the appropriate hamiltonian ($H = -2J\ SiSj$). The agreement factor R is defined as $R = \Sigma(\chi_{calcd.} - \chi_{obsd.})^2/\Sigma(\chi_{obsd.})^2$.
[30] D. Luneau, F. Romero, R. Ziessel, *Inorg. Chem*. **1998**, *37*, 4524.
[31] L. W. Seigle, H. B. Hass, *J. Org. Chem*. **1940**, *5*, 100.
[32] Crystallographic data (excluding structure factors) for the reported structures have been deposited with the Cambridge Crystallographic Data Centre. Copies of the data (deposition numbers CCDC-113692−113695) may be obtained free of charge on application to CCDC, 12 Union Road, Cambridge CB2 1EZ, U.K. [Fax: (internat.) + 44-1223/336-033, E-mail: deposit@ccdc.cam.ac.uk].

Received January 21, 1999
[I99017]

Unsaturated Hetero Chains, VIII[+]

First Metal Complexes of Oligonitrile Ligands: Palladium(II) Complexes of *N*-Methoxycarbonyl- and *N*-Thiobenzoyl-1,3,5,7-tetraazaoctatetraenes

Nicola C. Aust,[a] Anke Beckmann,[a] Ria Deters,[a] Roland Krämer,*[a] Lothar Terfloth,[a] Sabine Warzeska,[b] and Ernst-Ulrich Würthwein*[a]

Dedicated to Professor Bernt Krebs at the occasion of his 60th birthday

Keywords: Palladium(II) complexes / Oligonitriles / N ligands / S ligands / *N*-Acylimine

Two mononuclear six-membered chelate $PdCl_2$ complexes **2a**, **b** of the two different types of tetrameric oligonitriles **1a**, **b** have been synthesized. Both contain square-planar palladium(II) with a *cis* arrangement of the chloride atoms. In complex **2a** of the ω-amino-substituted *N*-methoxycarbonyl oligonitrile **1a** the metal center is coordinated by the nitrogen atoms N1 and N3. Within the chelate ring alternating bond lengths for the C–N bonds are observed, whereas the non-complexed, more flattened part of the oligonitrile chain shows almost equal C–N bond lengths, indicating strong donor-acceptor interactions involving the terminal amino group and the N3–Pd moiety of the molecule. The complex **2b** is derived from the thiobenzoyl ligand **1b** bearing a terminal (*R*)-fenchylidene group. In **2b** the sulfur atom S1 and the nitrogen atom N2 are involved in complexation. In contrast to **2a**, strong bond-length alternation is observed in **2b** for the complexed and the non-complexed part of the ligand. From the NMR spectra of both complexes no indication for a migration of the $PdCl_2$ unit along the chain could be derived.

Introduction

Recently, variably substituted oligonitriles became available for the first time in monodisperse, well-defined form.[1−4] Although these substances are isoelectronic with polyacetylenes (polyenes), their structural and electronic properties are entirely different. For instance they adopt nonplanar three-dimensional structures (often helices in the crystalline state) without far-reaching conjugation. Of special interest is their behavior in complexation and redox reactions as well as their electrical conductivity[5] and the NLO properties.

In this paper we report on our investigations of the complexation ability of oligonitriles using palladium(II) as metal counterpart. Oligonitriles are expected to serve as potent polydentate ligands since each imine nitrogen atom is a potential σ donor. Furthermore, the numerous C=N bonds may give rise to π complexation. High molecular flexibility due to low barriers of rotation around the C−N single bonds is expected to facilitate complexation additionally.

Results and Discussion

Two different types of substituted oligonitrile molecules have been used, both carrying four adjacent imino bonds ("tetramers") and one additional terminal C=X functionality. Substance **1a** bears a methoxycarbonyl moiety at nitrogen atom N1 whereas **1b** is a thiobenzoyl derivative. For the formation of the complexes the ligands were dissolved in acetonitrile, and bis(benzonitrile)palladium dichloride was added. Crystallization was achieved by adding a surplus of diethyl ether, yielding metal complex **2a**, and **2b**.[6]

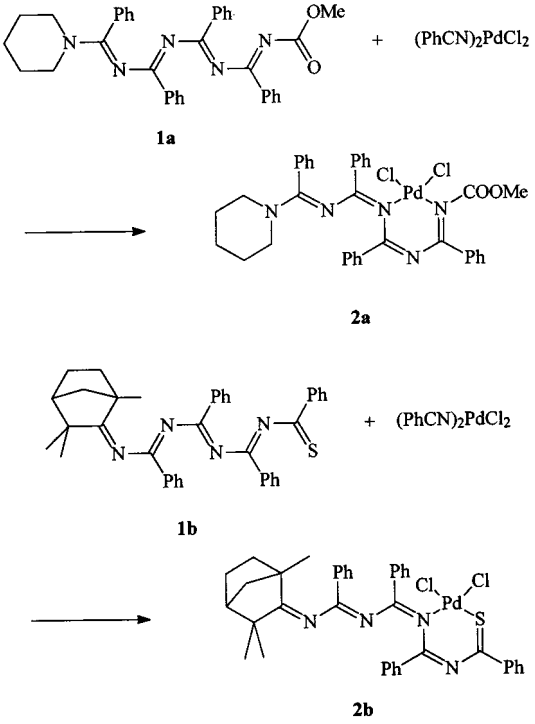
Both new compounds **2a** and **2b** were subjected to X-ray analysis. Both are mononuclear 1:1 complexes with a *cis*-$PdCl_2$ unit.

The methoxycarbonyl compound **1a** leads to metal complex **2a** by complexation of nitrogen atom N1 and N3 (crystallographic numbering) to Pd forming a six-membered chelate ring (Figure 1). The palladium center is tetracoordinate forming the expected square-planar geometry[7] as indicated by the sum of angles around palladium (359.88°). Coordinative bond lengths are in the typical range of $Pd^{II}-N(sp^2)$ and $Pd^{II}-Cl$ bonds. As expected for a palladium compound, coordination to nitrogen atoms is clearly preferred over complexation to oxygen atoms of the methoxycarbonyl group. The chelate ring deviates strongly from planarity leading to a twisted-boat-shaped structure. The two other nitrogen atoms N4 and N5 are not involved in complexation. This observation may be explained by

[+] Part VII: ref.[3]

[a] Institute of Organic Chemistry, Westfälische Wilhelms-Universität,
Corrensstraße 40, D-48149 Münster, Germany
Fax: (internat.) + 49(0)251/83-39772
[b] Institute of Inorganic Chemistry, Westfälische Wilhelms-Universität,
Wilhelm-Klemm-Straße 8, D-48149 Münster, Germany

 © WILEY-VCH Verlag GmbH, D-69451 Weinheim, 1999 1434−1948/99/0707−1189 $ 17.50+.50/0



Scheme 1

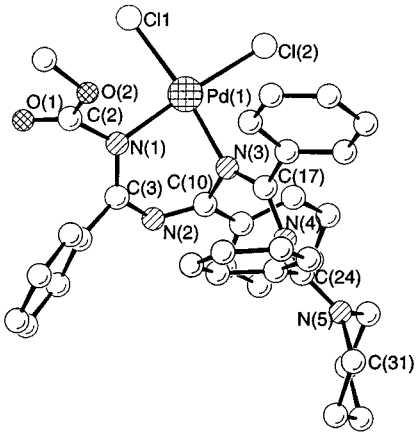


Figure 1. Molecular structure of **2a** (hydrogen atoms omitted for clarity); selected bond lengths [Å], bond angles [°], and torsional angles [°]: bond lengths [Å]: Pd−Cl(1) 2.282(1), Pd−Cl(2) 2.276(1), Pd−N(1) 2.041(2), Pd−N(3) 2.017(2), O(1)−C(2) 1.187(4), C(2)−N(1) 1.434(4), N(1)−C(3) 1.295(4), N(2)−C(3) 1.381(4), N(2)−C(10) 1.285(4), N(3)−C(10) 1.407(4), N(3)−C(17) 1.322(4), N(4)−C(17) 1.330(4), N(4)−C(24) 1.328(4), N(5)−C(24) 1.322(4); bond angles [°]: Cl(1)−Pd−Cl(2) 92.93(3), N(1)−Pd−N(3) 83.45(10), Cl(1)−Pd−N(1) 91.04(7), Cl(2)−Pd−N(3) 92.46(7), O(1)−C(2)−N(1) 123.4(3), C(2)−N(1)−C(3) 120.2(3), N(1)−C(3)−N(2) 120.7(3), C(3)−N(2)−C(10) 121.0(3), N(2)−C(10)−N(3) 120.6(3), C(10)−N(3)−C(17) 118.8(2), N(3)−C(17)−N(4) 118.3(3), C(17)−N(4)−C(24) 124.2(3), N(4)−C(24)−N(5) 118.1(3); torsional angles [°]: O(1)−C(2)−N(1)−C(3) −58.8, C(2)−N(1)−C(3)−N(2) 162.0, N(1)−C(3)−N(2)−C(10) 45.0, C(3)−N(2)−C(10)−N(3) 3.5, N(2)−C(10)−N(3)−C(17) 113.2, C(10)−N(3)−C(17)−N(4) 7.1, N(3)−C(17)−N(4)−C(24) −149.2, C(17)−N(4)−C(24)−N(5) −153.5, N(4)−C(24)−N(5)−C(31) −164.4

strong interactions of the two chlorine atoms to the palladium center which could not be replaced by the nitrogen functionalities.[7] In the six-membered chelate ring of **2a** alternating C=N double bonds (1.29−1.30 Å) and C−N single bonds (1.38−1.41 Å) are found. This structural feature is typical for the free oligonitriles which form nonplanar solid-state structures with alternating bond lengths.[1][2] Similarly, UV/Vis spectra of oligonitriles including **1a** do not indicate long-range conjugation in solution. Much in contrast to this, the exocyclic oligonitrile chain (N3 to N5) of **2a** bears C−N bonds with almost equal bond lengths (1.32−1.33Å). This (*Z*,*E*,*E*)-configured part of **2a** does not deviate much from planarity as the torsional angles indicate (see Figure 1). Both observations indicate a strong conjugative donor−acceptor interaction of N5 (lone pair) and Pd^{II} coordinated to N3, similar to 2-azavinamidinium-type structures.[8] Unfortunately, interpretation of the UV/Vis spectra of this chromophore is difficult due to strong UV absorptions of Pd^{II}. These favorable electronic interactions as well as steric factors based on the bulky substituents at N4 may lead to the unexpected regioselectivity of the complexation reaction which does not involve the nitrogen atoms N2, N4 or N5 which present better donor groups than the acceptor-substituted N1.

The thiobenzoyl-substituted oligonitrile **1b** also forms a six-membered chelate **2a** on reaction with $PdCl_2(PhCN)_2$, but now the sulfur atom is involved in coordination to the palladium center (Figure 2). This is not unexpected in view of the high affinity of the soft Pd^{II} ion for S ligands. Again a square planar coordination geometry of the palladium center (sum of angles 360.0°) is observed. Due to the chiral (*R*)-fenchyl group, which was introduced enantiomerically pure into the molecule, a chiral space group is required for the crystallization of the substance. However, good adaption was achieved by calculating for the monoclinic space group $P2_1/c$ whereas refinement assuming chiral space groups was unsuccessful. Large U_{iso} values of fenchyl C atoms, which were refined isotropically, and high residual electron density around the fenchyl group may in part be a consequence of the structure solution in the achiral space group. Attempts to apply a split-atom model to the fenchyl group were unsuccessful; however, it is quite likely that (*E*/*Z*) isomers with regard to the N5−C29 bond of **2b** give rise to these difficulties. The C−N bond lengths alternate strongly in the chelate ring and − in contrast to **2a** − also in the uncomplexed part of the chain. This observation supports the postulated donor−acceptor interaction in **2a**, since the imine nitrogen atom N4 and the fenchyl group in **2b** do not have the donor properties of N5 in **2a**. All C=N double bonds show (*Z*) configuration as it is often found in the structures of oligonitriles.[2]

NMR Spectra

The ^{1}H-NMR spectra of complexes **2a** and **2b** at 25 °C in $CDCl_3$ display broad and poorly resolved signals for the phenyl protons and the piperidyl and fenchyl protons,

respectively, due to dynamic properties of the complexes. However, the presence of a single, sharp CO_2CH_3 signal of **2a** at $\delta = 3.8$ (0.3 ppm downfield relative to **1a** in $CDCl_3$[2]) indicates that the N1−N3 coordination in the solid state is retained in solution since metal coordination at N1 reduces the electron density of the ester group. Alternatively, magnetic anisotropy caused by sterically hindered phenyl groups may be responsible for this chemical shift. At −50 °C the phenyl and the alkyl signals of **2a** are much sharper but the CO_2CH_3 signal is very broad. We interpret this effect by a sterically hindered, slow rotation of the ester group around the C2−N1 bond. The ^{13}C-NMR spectrum of **2a** at both 20 °C and −50 °C supports the presence of a single isomer in $CDCl_3$ solution. No indications for a migration of the $PdCl_2$ unit along the chain could be detected in the temperature range used.

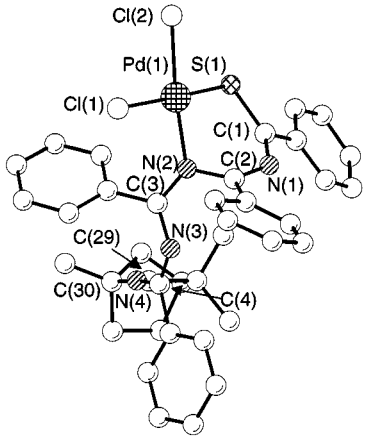


Figure 2. Molecular structure of **2b** (hydrogen atoms omitted for clarity); selected bond lengths [Å], bond angles [°], and torsional angles [°]: bond lengths [Å]: Pd−Cl(1) 2.341(1), Pd−Cl(2) 2.291(1), Pd−S 2.237(1), Pd−N(2) 2.039(4), S−C(1) 1.677(5), N(1)−C(1) 1.372(6), N(1)−C(2) 1.303(7), N(2)−C(2) 1.396(6), N(2)−C(3) 1.310(6), N(3)−C(3) 1.350(6), N(3)−C(4) 1.302(7), N(4)−C(4) 1.347(6), N(4)−C(29) 1.273(7); bond angles [°]: Cl(1)−Pd−Cl(2) 95.34(5), S−Pd−N(2) 89.57(12), S−Pd−Cl(2) 83.46(5), Cl(1)−Pd−N(2) 91.63(12), S−C(1)−N(1) 122.9(4), C(1)−N(1)−C(2) 125.2(4), N(1)−C(2)−N(2) 122.0(5), C(2)−N(2)−C(3) 120.1(4), N(2)−C(3)−N(3) 119.7(5), C(3)−N(3)−C(4) 125.2(4), N(3)−C(4)−N(4) 125.0(5), C(4)−N(4)−C(29) 136.2(5), N(4)−C(29)−C(39) 121.7(5); torsional angles [°]: S−(1)−N(1)−C(2) −38.6(7), C(1)−N(1)−C(2)−N(2) −11.8(8), N(1)−C(2)−N(2)−C(3) −113.8(6), C(2)−N(2)−C(3)−N(3) −10.6(7), N(2)−C(3)−N(3)−C(4) 142.6(5), C(3)−N(3)−C(4)−N(4) −5.9(9), N(3)−C(4)−N(4)−C(29) −100.5(8), C(4)−N(4)−C(29)−C(30) −172.4(6)

Experimental Section

Materials and Methods: Compounds **1a** and **1b** were prepared as previously described.[2][3] Commercially available solvents (p.a. quality) were used without further purification. − CHN analyses were performed with a DiaCHN 240 (Perkin−Elmer). − IR spectra were recorded with a Bruker FT-IR IFS 48 spectrophotometer as KBr pellets. − UV/Vis spectra were recorded using an HP 8453 diode array spectrophotometer (Hewlett-Packard). − ^{1}H- and ^{13}C-NMR spectra were obtained using a Bruker AC 200 and Varian Unity 600 spectrometer.

$PdCl_2$ Complex of *N*-Methoxycarbonyl-2,4,6,8-tetraphenyl-8-piperidino-1,3,5,7-tetraazaoctatetraene (2a): 27 mg (0.049 mmol) of **1a**[2] was treated at room temperature with 19 mg (0.049 mmol) of $(PhCN)_2PdCl_2$ in 1 mL of acetonitrile. After stirring for 10 min, a clear, orange solution was formed, which was treated with 1 mL of diethyl ether. Later, 10 mL of diethyl ether and 10 mL of pentane were added carefully in such a way that an upper layer was formed. After 5 d, red crystals of **2a** were collected [31 mg (0.042 mmol), 21% yield]. − UV/Vis($CDCl_3$): λ_{max} [nm] (ε) = 445 (100), 375 (shd), 300 (2900). − ^{1}H NMR(600 MHz, 298 K, $CDCl_3$): δ = 1.31 (br., 4 H, CH_2), 1.52 (br., 2 H, CH_2), 3.07 (br., 4 H, NCH_2), 3.80 (s, 3 H, OCH_3), 6.35, 6.85, 7.10, 7.35, 7.54 (br., phenyl-CH), 7.55, 7.63 (t, phenyl-CH), 7.80, 7.99 (s, br., phenyl-CH), 8.25 (br., phenyl-CH). − ^{13}C NMR(150.85 MHz, 298 K, $CDCl_3$): δ = 23.72, 24.78, 26.40 (CH_2), 49.76 (NCH_2), 54.71 (OCH_3), 128.19, 128.64, 128.89, 128.98, 130.42, 130.60 (CH), 131.69, 132.51 (C_i), 132.91, 133.24 (CH), 137.68 (C_i), 157.94, 162.54, 164.85, 166.76 (CN, CO). $-C_{35}H_{33}Cl_2N_5O_2Pd \cdot Et_2O$ (807.08): calcd. C 57.71 H 4.97 N 9.09; found C 57.26 H 5.13 N 9.02.

X-ray Diffraction Analysis of $2a \cdot Et_2O$ ($C_{35}H_{33}Cl_2N_5O_2Pd \cdot Et_2O$):[9] The red single crystals were analyzed with a Siemens P3 diffractometer using Mo-K_α radiation (λ = 0.71073 Å) and a graphite monochromator at 170(2) K. Crystal system: monoclinic, space group $P2_1/n$ with cell parameters a = 10.186(2), b = 22.633(5), c = 16.221(3) Å, β = 95.73(3)°, V = 3720.9(13) Å^3, $\rho_{calcd.}$ = 1.441 g cm^{-3}, Z = 4. Crystal size: 0.38 × 0.34 × 0.15 mm. 8573 reflections were collected leading to 8118 independent and 6422 observed [$I > 2\,\sigma(I)$] reflections. Absorption coefficient μ = 0.687 mm^{-1}, no absorption correction, 452 refined parameters. Non-hydrogen atoms were refined anisotropically. H atoms were geometrically positioned (riding model). $R(F)$ = 0.0417, $wR(F^2)$ = 0.0904; residual electron density: 0.551/−1.097 e Å^{-3}. The structure was solved and refined using SHELXS-86 and SHELXL-93.[10]

$PdCl_2$ Complex of 2,4,6,8-Tetraphenyl-8-(1,3,3-trimethylbicyclo-[2.2.1]hept-2-ylidene)amino-1-thia-1,3,5,7-octatetraene (2b): 24 mg (0.042 mmol) of **1b**[3] was suspended in 1 mL of acetonitrile and treated with a solution of 18.8 mg (0.049 mmol) of $(PhCN)_2PdCl_2$ in 2 mL of acetonitrile. After stirring for 5 min, a clear, deeply red solution has formed, from which after 30 min a red, powder-like solid precipitated. The solid was separated by filtration, washed with little acetonitrile and dried in vacuo. Yield: 17 mg (0.022 mmol; 53%). − IR (KBr): $\tilde{\nu}$ [cm^{-1}] = 3058 (w), 2962−2868 (w), 1734 (m), 1585 (m), 1560 (s), 1495 (s), 1478 (s), 1450 (s), 1345 (m), 1323 (m), 1309 (m), 1285 (m), 1267 (m), 1205 (m), 766 (m), 696 (m). − $C_{38}H_{36}Cl_2N_4PdS$(758.07): calcd. C 60.20 H 4.78 N 7.39; found C 59.04 H 5.06 N 7.68.

X-ray Diffraction Analysis of 2b ($C_{38}H_{36}Cl_2N_4PdS$):[9] The red single crystals were analyzed at 170(2) K with a Siemens P3 diffractometer using Mo-K_α radiation (λ = 0.71073 Å) and a graphite monochromator. Crystal system: monoclinic, space group $P2_1/c$ (see text) with cell parameters a = 11.244(2), b = 30.714(4), c = 11.562(2) Å, β = 118.42(3)°, V = 3511.7(10) Å^3, $\rho_{calcd.}$ = 1.434 g cm^{-3}, Z = 4; crystal size 0.12 × 0.20 × 0.38 mm). 8037 reflections were collected leading to 7657 independent and 5399 observed [$I > 2\,\sigma(I)$] reflections. Adsorption coefficient μ = 0.773 mm^{-1}, no absorption correction. 379 refined parameters. Non-hydrogen atoms were refined anisotropically with exception of the fenchyl C atoms which were refined isotropically. H atoms were geometrically positioned (riding model). $R(F)$ = 0.0594, $wR(F^2)$ = 0.1625; residual electron density: 2.072/−0.887 e Å^{-3}. The structure was solved and refined using SHELXS-97 and SHELXL-97.[10]

Acknowledgments

The authors thank Prof. Dr. B. Krebs for the use of a Siemens P3 diffractometer and Dr. R. Fröhlich for his valuable help with the X-ray diffraction analyses. We gratefully acknowledge financial support by the Deutsche Forschungsgemeinschaft (SFB 424) and by the Fonds der Chemischen Industrie. R. D. thanks the Fonds der Chemischen Industrie for a Ph. D. fellowship.

[1] M. Buhmann, M. H. Möller, U. Rodewald, E.-U. Würthwein, *Angew. Chem.* **1994, 106,** 2386; *Angew. Chem. Int. Ed. Engl.* **1994**, *33*, 2337.
[2] N. C. Aust, R. Fröhlich, J. Hecht, E.-U. Würthwein, *Liebigs Ann.* **1997**, 1593.
[3] A. Beckmann, R. Fröhlich, E.-U. Würthwein, *Tetrahedron Lett.* **1997**, *38*, 5481; see also: A. Beckmann, Ph.D. thesis, Univ. of Münster, **1996**.
[4] N. Schulte, R. Fröhlich, J. Hecht, E.-U. Würthwein, *Liebigs Ann.* **1996**, 371.
[5] D. Wöhrle, *Makromol. Chem.* **1974**, *175*, 1751−1760.
[6] From **1a** and $[Pd(MeCN)_4]^{2+}(BF_4^-)_2$ a yellow oil was obtained which could not be crystallized. Due to broad ^{1}H-NMR signals, a satisfying structural assignment was not possible.
[7] C. F. Barnard, M. J. H. Russel, in *Comprehensive Coordination Chemistry*, vol 5 (Eds.: G. Wilkinson, R. D. Gillard, J. A. McCleverty), Pergamon Press, Oxford, **1987**, p. 1115.
[8] H. Pritzkow, H. Hartl, *Acta Crystallogr.* **1973**, *B29*, 1777−1784.
[9] Crystallographic data (excluding structure factors) for the structures reported in this paper have been deposited with the Cambridge Crystallographic Data Centre as supplementary publication no. CCDC-112052 (**2a**) and -112053(**2b**). Copies of the data can be obtained free of charge on application to CCDC, 12 Union Road, Cambridge, CB2 1EZ, UK (Fax: + 44-1223/336-033; E-mail: deposit@ccdc.cam.ac.uk).
[10] G. M. Sheldrick, *SHELXS-86, Program for crystal structure solution*, Universität Göttingen, Germany, **1986**. G. M. Sheldrick, *SHELXL-93, Program for the refinement of crystal structures*, Universität Göttingen, Germany, **1993**; G. M. Sheldrick, *SHELX-97*, Universität Göttingen, **1997**.

Received January 21, 1998
[I99020]

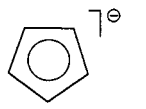
Synthesis, Structure and Reactivity of 3,4-Dihydro-2*H*-1,2,4,3-triazaboroles

Lothar Weber,*[a] Markus Schnieder,[a] Hans-Georg Stammler,[a] Beate Neumann,[a] and Wolfgang W. Schoeller[a]

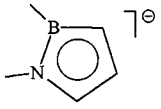
Keywords: Boron / Triazaboroles / Heterocycles / Halogens / Cyanides

3,4-Dihydro-2,4-diphenyl-2*H*-1,2,4,3-triazaboroles **3a**, **3b**, and **4** were synthesized by cyclocondensation of N^1,N^3-diphenylformamidrazone (**1**) with dibromophenylborane, dibromomethylborane, and boron trichloride. 3-Chloro-3,4-dihydro-2,4-diphenyl-2*H*-1,2,4,3-triazaborole (**4**) was converted into 3,4-dihydro-2,4-diphenyl-2*H*-1,2,4,3-triazaborole (**5**) by treatment with $LiAlH_4$. The corresponding 3-cyanato and 3-cyano derivatives **6** and **7** resulted from the reaction of **4** with AgOCN and AgCN, respectively. Compound **7** was transformed into the bis(1,2,4,3-triazaborolyl)oxane **8** by silver oxide. Compounds **1–8** were characterized by elemental analyses and spectroscopic methods (^{1}H, ^{11}B, and ^{13}C NMR; IR; MS). The molecular structure of **8** was established by single-crystal X-ray diffraction analysis.

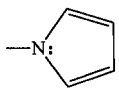
Replacing a pair of adjacent carbon atoms in the cyclopentadienide anion **I** by the isoelectronic B−N combination affords the dihydro-1,2-azaborolyl anion **II**. With pyrrol **III** and imidazole **V** the same formalism leads to 2,3-dihydro-1*H*-1,3,2-diazaboroles **IV** and 3,4-dihydro-2*H*-1,2,4,3-triazaboroles **VI**, respectively.



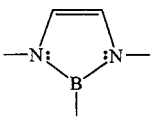
I



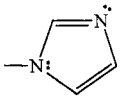
II



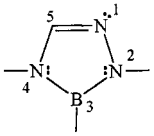
III



IV

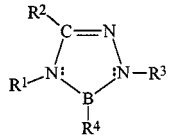


V

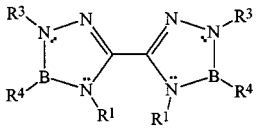


VI

Whereas the chemistry of 1,2-azaborolyl anions **II** has been thoroughly studied, especially with respect to its ligating properties,[1][2] and a series of papers has dealt with 1,3,2-diazaboroles **IV**,[3][4] information on 3,4-dihydro-2*H*-1,2,4,3-triazaboroles is scarce. 3,4-Dihydro-2,3,4,5-tetraphenyl-2*H*-1,2,4,3-triazaborole was formed in 5% yield during the cothermolysis of the pyridine adduct of diphenylboron azide and 2,5-diphenyltetrazole at 210°C.[5] In a brief communication the preparation of eight 1,2,4,3-triazaboroles **VI** by cyclocondensation of amidrazones $R^2C(NHR^1)=NNHR^3$ with boronic acid derivatives R^4BX_2 (X = Cl, OMe, OEt, OH, NMe_2) was reported.[6] Similarly, four bis(1,2,4,3-triazaborole)s **VII** were obtained from $PhB(OH)_2$ or $BuB(OH)_2$ and oxamidrazones.[7] No spectroscopic details were given for **VI** and **VII**.



VI a: $R^1 = R^3 = H$; $R^2 = Me$, $R^4 = Ph$
b: $R^1 = H$; $R^2 = R^3 = Me$; $R^4 = Ph$
c: $R^1 = R^4 = Ph$; $R^2 = R^3 = H$
d: $R^1 = R^3 = H$; $R^3 = 2$-py; $R^4 = Ph$
e: $R^1 = R^3 = R^4 = Ph$; $R^2 = H$
f: $R^1 = R^2 = R^4 = Ph$; $R^3 = H$
g: $R^1 = R^2 = R^3 = R^4 = Ph$
h: $R^1 = R^2 = Ph$; $R^3 = H$; $R^4 = n$-Bu



VII a: $R^1 = R^3 = H$; $R^4 = Ph$
b: $R^1 = R^3 = H$; $R^4 = n$-Bu
c: $R^1 = H$; $R^3 = R^4 = Ph$
d: $R^1 = R^4 = Ph$; $R^3 = H$

Bezuglaya et al. were concerned with IR,[8] mass[9], electronic absorption,[10] and X-ray photoelectron spectra,[11] as well as electrochemical studies,[12] acylation[13] and protonation reactions on 2,3,5-triaryl-1,2,4,3-triazaboroles[14] in which the aryl rings were *para*-substituted phenyl groups. Theoretical studies on the 2,3,5-triphenyl derivative as well as the UV spectra are not in accordance with heteroaromaticity.[10] Interestingly, in all the described 1,2,4,3-triazaboroles no other substitutents than phenyl (or *para*-substituted phenyl) rings and the *n*-butyl group are ligated to the boron atom.

We decided to investigate the chemistry of this ring system in more detail and from our experience with 2-halo-1,3,2-diazaboroles first envisaged the synthesis of 3-halo-1,2,4,3-triazaboroles. For synthetic and spectroscopic reasons the carbon atom of the ring should bear a hydrogen atom.

Results and Discussions

For the preparation of 3-halo-1,2,4,3-triazaboroles and derivatives thereof it was necessary to explore the experimental conditions in more detail and, moreover, provide

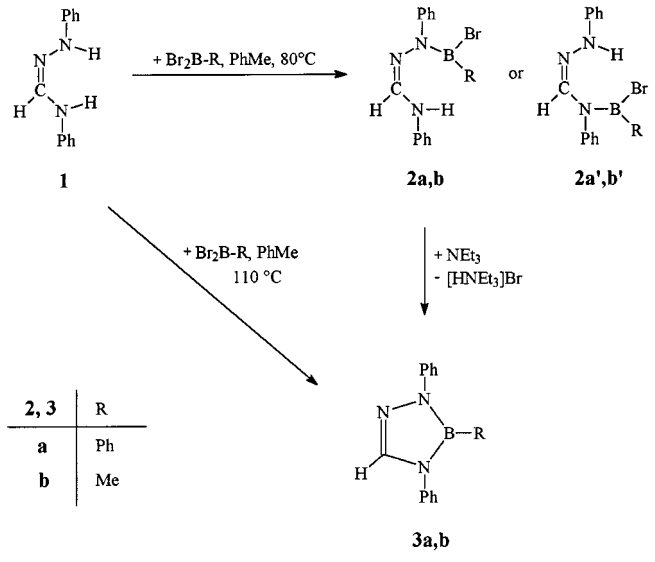
[a] Fakultät für Chemie der Universität Bielefeld,
Universitätsstraße 25, D-33615 Bielefeld, Germany
Fax: (internat.) + 49(0)5201/106-6146
E-mail: lothar.weber@uni-bielefeld.de

 © WILEY-VCH Verlag GmbH, D-69451 Weinheim, 1999 1434−1948/99/0707−1193 $ 17.50+.50/0

the NMR data that was lacking for some of the known species.

Combination of equimolar amounts of $PhBBr_2$ with formamidrazone **1** in toluene at 80°C for 1 h did not lead to the ring system **3a** as indicated in ref.[6] Instead the acyclic bromo(hydrazino)phenylborane derivative **2a/2a′** was obtained as a colorless crystalline solid (62% yield). Similarly, the bromo(hydrazino)methylborane derivative **2b/2b′** resulted from the reaction of **1** with $MeBBr_2$ in toluene at 80°C (52%). The air- and moisture-sensitive compounds display singlets at δ = 28.9 and 29.1 in the $^{11}B\{^1H\}$-NMR spectra. The amidine hydrogen atoms in the ^1H-NMR spectra of **2a/2a′** and **2b/2b′** give rise to singlets at δ = 8.93 and 9.03. In the $^{13}C\{^1H\}$-NMR spectrum the corresponding carbon atoms of **2a/2a′** and **2b/2b′** were observed as singlets at δ = 141.3 and 140.8. Basicly, the boryl group can be attached to the hydrazino group as indicated in **2a** and **2b** or alternatively to the anilino function as shown in **2a′** and **2b′**. No unambigious differentation between the two isomers was possible only by means of the spectroscopic data. Unfortunately, crystals of **2a/2a′** or **2b/2b′** suitable for an X-ray analysis were not available.

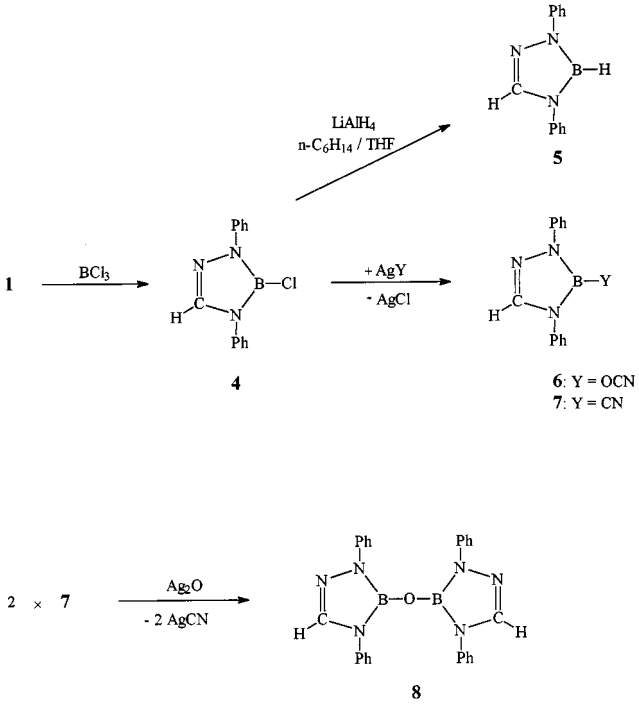
Cyclization of **2a/2a′** and **2b/2b′** to **3a** and **3b**, respectively, was effected by dehydrobromination with triethylamine. Alternatively the heterocycles were directly obtained by cyclocondensation of **1** with equimolar amounts of $PhBBr_2$ or $MeBBr_2$ in boiling toluene. By this method improved yields (74 and 69%) were achieved. In a control experiment the cyclization also occurred by heating a toluene solution of **2a/2a′** to 110°C.



Scheme 1

Heating a toluene solution of boron trichloride with a threefold excess of **1** at 90°C for 2.5 h led to the formation of the 3-chloro-1,2,4,3-triazaborole **4**, which was isolated as a colorless, extremely moisture-sensitive solid in 63% yield. This compound proved to be a valuable starting material for a series of other 1,2,4,3-triazaborole derivatives. Thus, formation of **3b** from **4** and an equimolar amount of methyllithium cleanly occurred in 83% yield.

Lithium aluminium hydride reduction of **4** in an *n*-hexane/THF mixture afforded the colorless crystalline 3-hydro-substituted 1,2,4,3-triazaborole **5** (84%). Treatment of **4** with equimolar amounts of silver cyanate or silver cyanide in acetonitrile in the absence of light smoothly generated the compounds **6** and **7** in 68% and 63% yield. Like **4** both products are extremely moisture-sensitive colorless solids. Their great propensity for hydrolysis is evident from impurities, revealed as bis(1,2,4,3-triazaborolyl)oxane (**8**) (δ ^{11}B = 20.5). A clean high-yield synthesis of **8** made use of the reaction of 3-cyano derivative **7** with silver oxide in acetonitrile (Scheme 2).



Scheme 2

The $^{11}B\{^1H\}$-NMR spectra of the triazaboroles described here display an increased shielding as follows: **3b** (δ = 27.8) > **3a** (26.4) > **4** (22.8) > **5** (21.5) > **8** (20.5) > **6** (17.1) > **7** (13.9). A comparable order was observed with the corresponding *N*-arylated 1,3-diazaboroles. Thus, in $PhN^a-C(Me)=C(Me)N^b(Ph)B-Me(N^a-B)$,[15] $XylN^aC(H)=C(H)-N^b(Xyl)BCl(N^a-B)$,[4a] $XylN^a-C(H)=C(H)-N^b(Xyl)BH(N^a-B)$, and $XylN^aC(H)=C(H)-N^b(Xyl)BCN(N^a-B)$ (Xyl = 2,6-$Me_2C_6H_3$) ^{11}B-NMR signals were recorded at δ = 28.0,[15] 21.1,[4a] 21.9,[4c] and 13.5[4a]. In the proton-coupled ^{11}B-NMR spectrum of **5** a doublet ($^1J_{B-H}$ = 162.5 Hz) was observed. The corresponding doublet in the diazaborole $tBuN^a-CH=CH-N^b(tBu)BH(N^a-B)$ at δ = 21.9 showed a coupling constant $^1J_{B-H}$ = 158 Hz.[4c] In the ^1H-NMR spectra of **3a,b–8** the CH protons of the heterocycle were observed as singlets at δ = 7.33–7.87. In the $^{13}C\{^1H\}$-NMR spectra the corresponding ^{13}C atoms gave rise to singlets at δ = 138.39–141.03. Interestingly, in the ^1H-NMR spectrum of **5** a broad 1:1:1:1 quadruplet at δ = 5.39 ($^1J_{B-H}$ = 158 Hz) appeared for the proton at the boron atom. In *t*BuN-

$^{a}C(H)=C(H)N^{b}(tBu)BH(N^{a}-B)$ a quadruplet at $\delta = 4.78$ ($^{1}J_{B-H} = 150$ Hz) was attributed to this proton.[4c]

The IR spectrum of **5** displayed a week, sharp band at $\tilde{\nu} = 2645$ cm^{-1} for the BH stretching vibration. A weak band at $\tilde{\nu} = 2224$ cm^{-1} in the IR spectrum of **7** was assigned to the stretching mode of the cyano group. The antisymmetric NCO vibration gave rise to a strong band at $\tilde{\nu} = 2309$ cm^{-1} in the IR spectrum of **6**. In isocyanato boranes of the type $(R_2N)_2BNCO$ intense bands for ν_{as}(NCO) were measured in the range $\tilde{\nu} = 2290 \pm 15$ cm^{-1}.[16]

X-ray Structural Analysis of 8

In the crystal, molecule **8** (Figure 1) has an overall similarity to the bent twisted structures of the bis(1,2,3-diazaborolyl)oxane **9**[4b] and tetramesityldiboroxane,[17] which display B−O−B angles of 157.1(3)° and 165.5(12)°, respectively. In **8**, however, the valence angle at the oxygen atom is more compressed [133.6(3)°]. Both BCN_3 rings in **8** are planar, enclosing an interplanar angle $\Psi = 66.0°$. Due to the bulky *tert*-butyl group in **9** the diazaborole rings in **9** are mutually orthogonal.

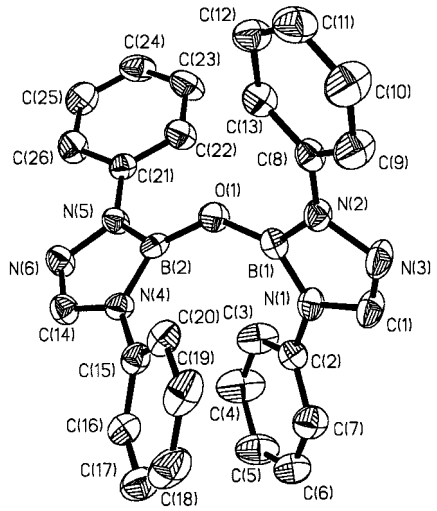
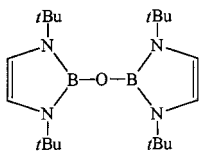
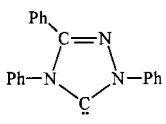


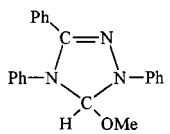
Figure 1. Crystal molecular structure of **8**; selected bond lengths [Å] and angles [°]: O(1)−B(1) 1.365(4), O(1)−B(2) 1.370(4), B(1)−N(1) 1.434(5), B(1)−N(2) 1.427(4), B(2)−N(4) 1.429(5), B(2)−N(5) 1.426(4), N(2)−N(3) 1.409(4), N(5)−N(6) 1.406(4), N(3)−C(1) 1.283(4), N(1)−C(1) 1.377(4), N(1)−C(2) 1.425(4), N(2)−C(8) 1.414(4), N(4)−C(14) 1.379(4), N(6)−C(14) 1.294(4), N(4)−C(15) 1.425(4), N(5)−C(21) 1.417(4); B(1)−O(1)−B(2) 133.6(3), O(1)−B(1)−N(2) 126.6(3), O(1)−B(1)−N(1) 129.3(3), O(1)−B(2)−N(4) 128.8(3), O(1)−B(2)−N(5) 127.0(3), N(1)−B(1)−N(2) 104.1(3), N(4)−B(2)−N(5) 104.2(3), B(1)−N(2)−N(3) 109.8(3), B(1)−N(1)−C(1) 105.1(3), N(2)−N(3)−C(1) 105.2(3), N(1)−C(1)−N(3) 115.8(3), B(2)−N(5)−N(6) 110.0(3), B(2)−N(4)−C(14) 105.3(3), N(4)−C(14)−N(6) 115.4(3), N(5)−N(6)−C(14) 105.1(3), B(1)−N(1)−C(2) 132.1(3), B(1)−N(2)−C(8) 134.1(3), C(1)−N(1)−C(2) 122.3(3), N(3)−N(2)−C(8) 115.8(3), B(2)−N(4)−C(15) 130.2(3), B(2)−N(5)−C(21) 132.5(3), C(14)−N(4)−C(15) 124.5(3), N(6)−N(5)−C(21) 117.4(3)



9



10



11

The respective bond lengths and bond angles within both 1,2,4,3-triazaborole units of **8** are identical within experimental error. The B−N distances [av. 1.429(5) Å] fall in the range of 1.407(3) to 1.450(7) Å measured for B−N bond lengths in a series of 1,3,2-diazaboroles and indicate multiple bond character. The endocyclic bond lengths N(1)−C(1) [1.377(4) Å] and N(4)−C(14) [1.379(4) Å] are significantly shorter than the exocyclic N−C (sp^2) bonds [av. 1.421(4) Å]. Within experimental error they are comparable to the N(Ph)−C(Ph) distances in 4,5-dihydro-1,3,4-triphenyl-1*H*-1,2,4-triazole-5-ylidene (**10**) [1.391(2) Å] and 4,5-dihydro-5-methoxy-1,3,4-triphenyl-1*H*-1,2,4-triazole (**11**) [1.391(6) Å].[18] The endocyclic bonds N(3)−C(1) [1.283(4) Å] and N(6)−C(14) [1.294(4) Å] are also close to those in **10** [1.304(3) Å] and **11** [1.296(6) Å], and are thus not significantly elongated relative to the calculated C=N bond length in formaldehyde imine [1.283 Å][18] or the experimentally determined C=N bond length in formaldehyde oxime [1.276 Å].[19] The interatomic distance N(2)−N(3) in **8** [1.409(4) C] is similar to the N−N bond length in **11** [1.394(6)] C,[18] and has to be regarded as a localized single bond.

The endocyclic angles B(1)−N(2)−N(3) [109.8(3)°] and B(2)−N(5)−N(6) [110.0(3)°] in **8** are more obtuse than the endocyclic angles B(1)−N(1)−C(1) [105.1(3)°] and B(2)−N(4)−C(14) [105.1(3)°]. The latter values compare well with the corresponding angles B−N−C in **9** [105.7(3)−106.5(2)°]. The angles at the endocyclic carbon atoms in **9** [110.3(3)−110.5(3)°] are markedly compressed relative to the endocyclic angles at C(1) [115.8(3)°] and C(14) [115.8(3)°] in **8**. The angles at the dicoordinate ring nitrogen atoms N(3) and N(6) are 105.2(3) and 105.1(3)°. In conclusion, the structural parameters of **8** provided by the X-ray analysis give no support for a 6π-electron delocalization within the 1,2,4,3-triazaborole ring as claimed in ref.[6]

In order to analyze this aspect in more detail we performed quantum-chemical ab initio calculations[20] at RHF/6-31g* and density functional level (B3LYP/6-31g*)[21] on **8** and its parent compound without the phenyl groups. Corresponding Molden plots[22] of the computed equilibrium geometries are given in Figure 2.

In the parent compound the two five-membered ring units are twisted (torsion angle N−B−O−B 23.2°). The RHF and density functional calculations yield almost similar bond lengths within the ring geometries. The structure of the diborolyloxane changes markedly on the introduction of the four phenyl substituents. It adopts an equilibrium structure which is in perfect agreement with the results of the X-ray investigations (torsion angle N−B−O−B 45.0°). Consequently, the actual structure of **8** is largely determined by the steric demand of the phenyl groups. Since from the computed structure it is not clear how the π bonds are delocalized in the heterocyclic units, we performed population analyses at the given equilibrium geometries, utilizing the natural bond orbital scheme.[23] The results of these investigations will not be recorded here in detail. However, an inspection of the corresponding Wiberg bond

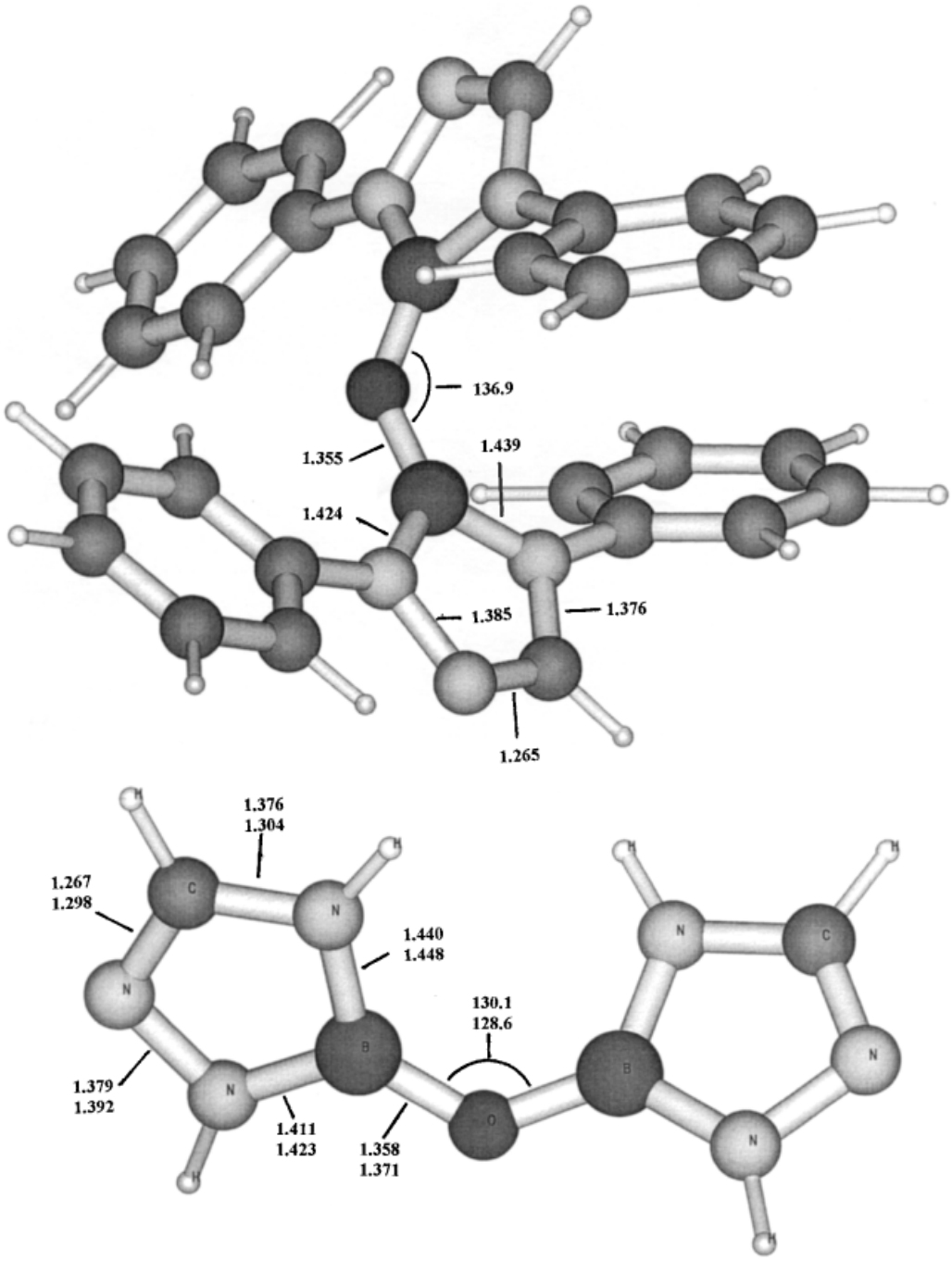


Figure 2. Computed equilibrium structures of 8 (A) and parent compound (B) (bond lengths in Å) at RHF/6-31g* (top) and B3LYP/6-31g* (bottom) level.

indices[23] indicates that the π bonds in the five-membered rings are essentially localized. In other words these results do not indicate significant π delocalization in **8**. These considerations are equally true for all computed structures and agree with the results reported in ref.[10]

Experimental Section

General: All manipulations were performed under dry argon. Solvents were rigorously dried with an appropriate drying agent and distilled before use. The following compounds were prepared as described in the literature: ethyl *N*-phenylformimidate,[24] dibromophenylborane,[25] dibromomethylborane.[25] Boron trichloride, boron tribromide, tetraphenylstannane, tetramethylstannane, lithium aluminium hydride, phenylhydrazine, silver cyanide, silver cyanate, and silver oxide were purchased commercially. − IR spectra: Bruker FT IR IFS66. − ^{1}H-, ^{11}B-, and ^{13}C-NMR spectra: Bruker AC 100 (^{1}H, 100.13 MHz) and Bruker Avance DRX 500 (^{1}H, 500.13 MHz; ^{11}B, 160.46 MHz; ^{13}C, 125.75 MHz); references: $SiMe_4$ (^{1}H, ^{13}C), $BF_3 \cdot OEt_2$ (^{11}B). − Mass spectra (EI): VG Autospec sector-field mass spectrometer (Micromass) 70 eV.

***N*^{1},*N*^{3}-Diphenylformamidrazone (1):** A mixture of ethyl *N*-phenylformimidate (10.0 g, 67.0 mmol) and phenylhydrazine (7.24 g,

67.0 mmol) in ethanol (20 mL) was stirred at 20°C for 16 h. The resulting viscous red solution was layered with *n*-pentane (50 mL) and stored overnight at −18°C. Orange crystals were collected by filtration and washed with *n*-pentane (2 × 50 mL) to afford 12.81 g (90%) of **1**. − ^{1}H NMR (CD_3OD): δ = 6.74 (t, J_{H-H} = 7.3 Hz, 1 H, C_6H_5), 6.96 (m, 3 H, C_6H_5), 7.05 (d, J_{H-H} = 8.0 Hz, 2 H, C_6H_5), 7.17 (t, J_{H-H} = 7.32 Hz, 2 H, C_6H_5), 7.28 (t, J_{H-H} = 7.6 Hz, 3 H, C_6H_5 and HC=N). − $^{13}C\{^1H\}$ NMR (CD_3OD): δ = 114.24, 116.42, 120.15, 122.95, 129.91, 130.60, 136.71, 142.17 (C-phenyl), 148.76 (HC=N). − MS/EI (70 eV); *m/z* (%): 212 (65) [M^+ + H], 119 (10) [M^+ − HNPh], 91 (100) [PhN]. − $C_{13}H_{13}N_3$ (211.24): calcd: C 73.98, H 6.18, N 19.83; found C 73.60, H 6.14, N 19.98.

PhN(H)C(H)=N−N(Ph)B(Br)Ph (2a) or PhN(BBrPh)C(H)=N−N-(H)Ph (2a′): A solution of dibromophenylborane (5.21 g, 21.0 mmol) in 30 mL of toluene was added dropwise to a chilled toluene solution (100 mL, 0°C) of **1** (4.44 g, 21.0 mmol). After warming to room temp., the mixture was heated at 80°C for 1 h. Cooling to 20°C led to the separation of an ocher precipitate. Volatile compounds were removed in vacuo, and the tan solid residue was dissolved in 200 mL of CH_2Cl_2. It was filtered and the filtrate was concentrated to 50 mL. Storing at 4°C for 16 h afforded 4.92 g (62%) of colorless crystalline **2a**. − ^{1}H NMR (CD_2Cl_2): δ = 7.26−7.51 (m, 15 H, Ph), 8.93 (s, 1 H, HC=N). − $^{13}C\{^1H\}$ NMR (CD_2Cl_2): δ = 124.87, 125.23, 128.56, 128.83, 129.13, 129.82, 130.16, 130.99, 134.44, 136.45, 136.61 (C-phenyl), 141.28 (HC=N). − $^{11}B\{^1H\}$ NMR (CD_2Cl_2): δ = 28.9.

PhN(H)C(H)=NN(Ph)B(Br)(Me) (2b) or PhN(BBrMe)C(H)=N−N-(H)Ph (2b′): Analogously, the combination of dibromomethylborane (3.34 g, 18.0 mmol) and 3.80 g (18.0 mmol) of **1** in 130 mL of toluene gave 4.32 g (52%) of colorless crystalline **2b**. − ^{1}H NMR (CD_2Cl_2): δ = 0.85 (s, 3 H, CH_3), 7.10−7.52 (m, 10 H, C_6H_5), 9.03 (s, 1 H, HC=N). − $^{13}C\{^1H\}$ NMR (CD_2Cl_2): δ = 123.28, 124.35, 127.91, 128.61, 129.67, 130.04, 136.42, 136.74 (C-phenyl), 140.77 (HC=N). − $^{11}B\{^1H\}$ NMR (CD_2Cl_2): δ = 29.1. − $C_{14}H_{15}BBrN_5$ (316.01): calcd: C 53.21, H 4.78, N 13.30; found C 53.14, H 4.89, N 13.38.

PhN^a−N=C(H)−N(Ph)BPh(*N*^{a}−*B*) (3a): A solution of 4.13 g (16.6 mmol) of dibromophenylborane in toluene (30 mL) was added dropwise at 0°C to a stirred solution of 3.52 g (16.6 mmol) of **1** in toluene (100 mL). After warming to room temp., the mixture was refluxed for 3 h. Cooling to ambient temp. was accompanied by the formation of an ocher precipitate. Solvent and all volatile components were removed at 10^{-2} Torr. The red-brown residue was dissolved in CH_2Cl_2 (100 mL) and filtered. The ocher filtrate was concentrated to 50 mL and stored for 16 h at −18°C to afford 3.65 g (74%) of colorless crystals. − ^{1}H NMR (CD_2Cl_2): δ = 7.13−7.40 (m, 15 H, C_6H_5), 7.74 (s, 1 H, HC=N). − $^{13}C\{^1H\}$ NMR (CD_2Cl_2): δ = 121.83, 124.63, 124.85, 126.56, 128.63, 129.01, 129.28, 129.58, 134.17, 139.69 (C-phenyl), 141.03 (HC=N), 143.76 (C-phenyl). − $^{11}B\{^1H\}$ NMR (CD_2Cl_2): δ = 26.4. − MS/EI; *m/z*: 297 (100) [M^+]. − $C_{19}H_{16}BN_3$(297.15): calcd. C 76.79, H 5.42, N 14.14; found C 74.83, H 5.35, N 12.40.

PhN^{a}N=C(H)−N(Ph)BMe(*N*^{a}−*B*) (3b). − Path 1: A solution of 2.49 g (13.4 mmol) of dibromomethylborane in 30 mL of toluene was added dropwise at 0°C to a solution of 2.83 g (13.4 mmol) of **1** in 50 mL of toluene and allowed to warm to 20°C with stirring. Then the mixture was heated at reflux for 2 h. Solvent and volatiles were removed in vacuo to yield a red-brown residue. The residue was dissolved in 20 mL of CH_2Cl_2 and filtered. The violet filtrate was stored overnight at −18°C to afford 2.16 g (69%) of colorless crystalline **3b**. − **Path 2:** A solution of triethylamine (0.55 g, 5.43 mmol) in 10 mL of toluene was added dropwise to the solution of **2b/2b′** (2.50 g, 5.43 mmol) in 30 mL of toluene at room temp. After 1 h of stirring, the mixture was concentrated to dryness and the light brown residue was extracted with 50 mL of *n*-pentane and filtered. The filtrate was concentrated to dryness to afford 0.83 g of **3b**. − **Path 3:** An *n*-hexane solution made of 0.75 mL of 1.6 M ethereal methyllithium solution (1.20 mmol) in 30 mL of *n*-hexane was added dropwise to a chilled solution (−20°C) of **4** (0.30 g, 1.17 mmol) in 150 mL of *n*-hexane. It was slowly warmed to room temp. Precipitated LiCl was removed by filtration. The filtrate was concentrated to 50 mL and stored overnight at −18°C to give 0.23 g (83%) of **3b**. − ^{1}H NMR (CD_2Cl_2): δ = 0.87 (s, 3 H, CH_3), 7.16 (t, J_{H-H} = 7.5 Hz, 1 H, *p*-C_6H_5), 7.29 (m, 2 H, C_6H_5), 7.31 (t, J_{H-H} = 7.6 Hz, 1 H, *p*-C_6H_5), 7.39 (t, J_{H-H} = 7.8 Hz, 2 H, C_6H_5), 7.46 (t, J_{H-H} = 7.8 Hz, 2 H, C_6H_5), 7.50 (d, J_{H-H} = 7.5 Hz, 2 H, C_6H_5), 7.63 (s, 1 H, CH=N). − $^{13}C\{^1H\}$ NMR (CD_2Cl_2): δ = 120.69, 123.95, 124.29, 126.33, 129.24, 129.81, 140.05 (C-phenyl), 140.46 (CH=N), 144.28 (C-phenyl). − $^{11}B\{^1H\}$ NMR (CD_2Cl_2): δ = 27.8. − MS/EI; *m/z* (%): 235 (100) [M^+]. − $C_{14}H_{14}BN_3$ (235.13): calcd. C 71.45, H 6.00, N 17.87; found C 71.11, H 6.01, N 17.55.

PhN^a−N=C(H)−N(Ph)BCl(*N*^{a}−*B*) (4): A chilled solution (−30°C) of boron trichloride (1.76 g, 15.0 mmol) in toluene (30 mL) was added dropwise within 2 h to a chilled suspension (−35°C) of **1** (5.44 g, 40 mL) in toluene (160 mL). The mixture was allowed to warm to room temp., and then was stirred for 2.5 h at 90°C. The resulting suspension was cooled to 20°C and filtered. The filtrate was concentrated to dryness. The residue was extracted with *n*-hexane (100 mL) during the course of 4 h. Removal of solvent from the extract yielded 2.15 g (63%) of **4** as a colorless solid. − ^{1}H NMR (CD_2Cl_2): δ = 7.22 (t, J_{H-H} = 7.5 Hz, 1 H, *p*-C_6H_5), 7.36−7.49 (m, 7 H, C_6H_5), 7.71 (d, J_{H-H} = 7.3 Hz, 2 H, *o*-C_6H_5), 7.72 (s, 1 H, HC=N). − $^{13}C\{^1H\}$ NMR (CD_2Cl_2): δ = 120.74, 123.89, 125.28, 127.15, 129.29, 129.89, 138.08 (C-phenyl), 140.53 (HC=N), 142.31 (C-phenyl). − $^{11}B\{^1H\}$ NMR (CD_2Cl_2): δ = 22.8. − MS/EI; *m/z* (%): 255 (100) [M^+]. − $C_{13}H_{11}BClN_3$ (255.07): calcd. C 61.16, H 4.35, N 16.47; found C 61.32, H 4.42, N 16.56.

PhN^a−N=C(H)N(Ph)BH(*N*^{a}−*B*) (5): A sample of solid $LiAlH_4$ (0.23 g, 6.0 mmol) was added to a solution of 1.53 g (6.0 mmol) of **4** in a mixture of *n*-hexane (80 mL) and THF (20 mL). The slurry was stirred for 30 min at room temp., then filtered and the filtrate was concentrated to dryness. The residue was dissolved in *n*-hexane (100 mL) and stored overnight at −18°C to yield 1.11 g (84%) of colorless crystalline **5**. − IR (KBr): $\tilde{\nu}$ [cm^{-1}] = 2645 w−m [ν(B−H)]. − ^{1}H NMR (CD_2Cl_2): δ = 5.39 (q, J_{B-H} = 158.3 Hz, 1 H, BH), 7.15 (t, J_{H-H} = 7.3 Hz, 1 H, *p*-C_6H_5), 7.28 (t, J_{H-H} = 7.2 Hz, 1 H, *p*-C_6H_5), 7.37−7.47(m, 6 H, C_6H_5), 7.66 (d, J_{H-H} = 7.1 Hz, 2 H, *o*-C_6H_5), 7.87 (s, 1 H, HC=N). − $^{13}C\{^1H\}$ NMR (CD_2Cl_2): δ = 118.10, 121.30, 124.45, 126.16, 129.47, 130.01 (C-phenyl), 139.54 (HC=N), 143.38 (C-phenyl). − ^{11}B NMR (CD_2Cl_2): δ = 21.5 (d, J_{B-H} = 162.5 Hz). − MS/EI; *m/z* (%): 221 (100) [M^+]. − $C_{13}H_{12}BN_3$ (221.11): calcd. C 70.55, H 5.47, N 19.00; found: C 70.58, H 5.59, N 18.65.

PhN^a−N=CHN(Ph)BNCO(*N*^{a}−*B*) (6): A mixture of **4** (2.10 g, 8.24 mmol) and silver cyanate (1.23 g, 8.24 mmol) in acetonitrile (50 mL) was stirred at room temp. in the dark for 3 h. The slurry was then concentrated to dryness, and the residue was extracted with *n*-hexane (3 × 50 mL). The combined filtered extracts were liberated from solvent to afford 1.68 g (68%) of **6** as a colorless solid. − IR (KBr): $\tilde{\nu}$ [cm^{-1}] = 2309 s [ν_{as}(NCO)]. − ^{1}H NMR (CD_2Cl_2): δ = 7.18 (m, 1 H, *p*-C_6H_5), 7.42−7.55 (m, 7 H, C_6H_5), 7.61 (d, J_{H-H} = 7.5 Hz, 2 H, *o*-C_6H_5), 7.65 (s, 1 H, HC=N). −

$^{13}C\{^1H\}$ NMR (CD_2Cl_2): δ = 119.45 (C-phenyl), 121.44 (NCO), 122.93, 124.87, 126.95, 129.51, 130.18, 138.16 (C-phenyl), 139.55 (HC=N), 142.46 (C-phenyl). − $^{11}B\{^1H\}$ NMR (CD_2Cl_2): δ = 17.1. − MS/EI; *m/z* (%): 262 (4) [M^+]. − $C_{14}H_{11}BN_4$ (262.10): calcd. C 64.10, H 4.23, N 21.37; found: C 64 17, H 4.46, N 20.65.

$PhN^a-N=CHN(Ph)BCN$*(N^a-B) **(7):** Analogously, **4** (3.06 g, 12.0 mmol) and 1.61 g (12.0 mmol) of silver cyanide were allowed to react in acetonitrile (50 mL). The mixture was filtered, and the filtrate was concentrated to 20 mL. Storage overnight at −18°C afforded 1.86 g (63%) of **7** as colorless needles. − IR (KBr): $\tilde{\nu}$ [cm^{-1}] = 2224 w [ν(CN)]. − ^1H NMR (CD_2Cl_2): δ = 7.42−7.55 (m, 8 H, C_6H_5), 7.75 (d, J_{H-H} = 7.5 Hz, 2 H, *o*-C_6H_5), 7.85 (s, 1 H, HC=N). − $^{13}C\{^1H\}$ NMR (CD_2Cl_2): δ = 120.17, 123.05, 126.50, 127.88, 129.69, 130.33, 137.55 (C-phenyl), 140.90 (HC=N), 141.73 (C-phenyl). − $^{11}B\{^1H\}$ NMR (CD_2Cl_2): δ = 13.9 . − MS/EI; *m/z* (%): 246 (4) [M^+]. − $C_{14}H_{11}BN_4$ (246.11): calcd. C 68.26, H 4.50, N 22.76; found: C 68.02, H 4.61, N 22.35.

$[PhN^a-CH=NN(Ph)B]_2O$*(N^a-B) **(8):** A sample of silver oxide (2.07 g, 9.00 mmol) was added to a solution of **7** (2.13 g, 8.66 mmol) in a mixture of acetonitrile (50 mL) and THF (10 mL), and stirred for 24 h at room temp. Solvent and volatile components were removed in vacuo. The residue was extracted with *n*-hexane (3 × 50 mL). After filtration, the combined extracts were freed from solvent to give 1.64 g (83%) of **8** as colorless solid. − ^1H NMR (CD_2Cl_2): δ = 6.87 (m, 2 H, *o*-C_6H_5), 7.09 (m, 1 H, *p*-C_6H_5), 7.18 (m, 1 H, *p*-C_6H_5), 7.24 (m, 2 H, *m*-C_6H_5), 7.33 (m, 3 H, *m*-C_6H_5 and HC=N). − $^{13}C\{^1H\}$ NMR (CD_2Cl_2): δ = 118.40, 122.34, 123.69, 126.15, 129.35, 129.67, 137.74 (C-phenyl), 138.39 (HC=N), 142.85 (C-phenyl). − $^{11}B\{^1H\}$ NMR (CD_2Cl_2): δ = 20.5. − MS/EI; *m/z* (%): 456 (100) [M^+], 211 (80) [1^+]. − $C_{26}H_{22}B_2N_6O$ (456.20): calcd. C 68.39, H 4.86, N 18.42; found C 68.04, H 4.97, N 18.36.

X ray Structural Analysis of 8:[26] Colorless single crystals from *n*-pentane. A crystal of appoximate dimensions 0.08 × 0.1 × 0.3 mm was examined with a Siemens SMART CCD area detector system with three-axis geometry using Mo-K_α radiation (λ = 0.71073 Å) at 173 K. Crystal data and refinement details: Crystal system triclinic, cell dimensions *a* = 10.6800(13), *b* = 10.8811(14), *c* = 12.0371(15) Å, α = 70.006(2), β = 68.868(2), γ = 66.777(2)°, *V* = 1166.0(3) $Å^3$ (refined from 1396 reflections) *Z* = 2, $d_{calcd.}$ = 1.299 g cm^{-3}, μ = 0.082 mm^{-1}, space group $P\bar{1}$, hemisphere data collections in ω at 0.3° scan width in three runs with 606, 435, and 230 frames (φ = 0.88 and 180°) at a detector distance of 5 cm (2 Θ_{max} = 54°), data reduction with the SAINT programm (V 4.028 Siemens) by which more than 95.3% of the data are converted, empirical absorption correction with redundant data (SADABS programm, Siemens) max/min transmission 1.000/0.768; 6811 intensities collected, 4870 unique (R_{int} = 0.0438); structure solution and refinement on F^2 with SHELX 97, 317 parameters, hydrogen atoms treated as riding groups with a 1.5-fold isotropic *U* value of the equivalent *U* value of the corresponding C atom. *R*1 = 0.0777; *wR*2 = 0.1761 for all data, $w^{-1} = \sigma(F_o^2) + (0.0580P)^2$ where $P = [\max(F_o^2,0) + 2F_c^2]/3$, maximum/minimum residual electron densities 0.271 and −0.250 $eÅ^{-3}$.

Acknowledgments

This work was financially supported by the Deutsche Forschungsgemeinschaft and the Fonds der Chemische Industrie.

[1] Review: G. Schmid, *Comm. Inorg. Chem.* **1985**, *4*, 17−32.
[2] G. Schmid, W. Meyer-Zaika, R. Boese, N. Augart, *Angew. Chem.* **1988**, *100*, 956−957; *Angew. Chem. Int. Ed. Engl.* **1988**, *27*, 952 and refs. cited therein.
[3] G. Schmid, M. Polk, R. Boese, *Inorg. Chem.* **1990**, *29*, 4421−4429 and ref. cited therein.
[4] [4a] L. Weber, E. Dobbert, R. Boese, M. T. Kirchner, D. Bläser, *Eur. J. Inorg. Chem.* **1998**, 1145−1152. − [4b] L. Weber, E. Dobbert, H.-G. Stammler, B. Neumann, R. Boese, D. Bläser, *Chem. Ber.* **1997**, *130*, 705−710. − [4c] L. Weber, E. Dobbert, H.-G. Stammler, B. Neumann, R. Boese, D. Bläser, *Eur. J. Inorg. Chem.* **1999**, 491−497.
[5] P. I. Paetzold, *Z. Anorg. Allg. Chem.* **1963**, *326*, 64−69.
[6] M. J. S. Dewar, R. Golden, P. A. Spanninger, *J. Am. Chem. Soc.* **1971**, *93*, 3298−3299.
[7] M. J. S. Dewar, P. A. Spanninger, *Tetrahedron* **1972**, *28*, 959−961.
[8] G. V. Avramenko, Z. V. Bezuglaya, B. I. Stepanov, V. S. Troitskaya, V. G. Vinokurov, *Zh. Prikl. Spectrosk.* **1988**, *48*, 952−957; *Chem. Abstr.* **1988**, *109*, 118491.
[9] Z. V. Bezuglaya, G. A. Avramenko, B. I. Stepanov, *Zh. Vses. Khim. O-va* **1988**, *33*, 355−357; *Chem. Abstr.* **1988**, *109*, 118491.
[10] Z. V. Bezuglaya, G. V. Avramenko, V. N. Listyutenko, B. E. Zaitsev, B. I. Stepanov, *Zh. Obsch. Khim.* **1988**, *58*, 2683−2694; *Chem. Abstr.* **1989**, *111*, 7459a
[11] B. E. Zaitsev, Z. V. Bezuglaya, G. V. Avramenko, T. M. Ivanova, V. N. Lisyutenko, B. I. Stepanov, *Zh. Obshch. Khim.* **1985**, *55*, 1398−1403; *Chem. Abstr.* **1986**, *104*, 168531.
[12] V. A. Shapovalov, Yu. M. Kargin, B. I. Stepanov, Z. V. Bezuglaya, V. D. Bezuglyi, G. V. Avramenko, *Zh. Obshch. Khim.* **1984**, *54*, 148−151, *Chem. Abstr.* **1984**, *100*, 156676.
[13] Z. V. Bezuglaya, G. V. Avramenko, B. I. Stepanov, *Zh. Obshch. Khim.* **1980**, *50*, 2811−2812; *Chem. Abstr.* **1981**, *94*, 139702.
[14] Z. V. Bezuglaya, S. M. Lukin, G. V. Avramenko, B. I. Stepanov, *Zh. Vses. Khim. O-va* **1981**, *26*, 348−350; *Chem. Abstr.* **1981**, *95*, 132074.
[15] L. Weber, G. Schmid, *Angew. Chem.* **1974**, *86*, 519−520.; *Angew. Chem. Int. Ed. Engl.* **1974**, *13*, 467.
[16] M. F. Lappert, H. Pyszora, *J. Chem. Soc. A* **1967**, 854−860.
[17] C. J. Cardin, H. E. Parge, J. W. Wilson, *J. Chem. Res. Synopsis* **1983**, *93*; *J. Chem. Res. Miniprint* **1983**, 0801.
[18] D. Enders, K. Breuer, G. Raabe J. Rusink, J. H. Teles, J.-P. Melder, K. Ebel, S. Brode, *Angew. Chem.* **1995**, *107*, 1119−1122; *Angew. Chem. Int. Ed. Engl.* **1995**, *34*, 1021−1023.
[19] I. N. Levine, *J. Chem. Phys.* **1963**, *28*, 2326.
[20] All calculations were performed with the Gaussian-94 set of programs: M. J. Frisch, G. W. Trucks, H. B. Schlegel, P. M. W. Gill, B. G. Johnson, M. A. Robb, J. R. Cheesman, T. A. Keith, G. A. Petersson, J. A. Montgomery, K. Raghavachari, M. A. Al-Laham, V. G. Zakrzewski, J. V. Ortiz, J. B. Foresman, J. Cioslowski, B. B. Stefanov, A. Nanayakkara, M. Challacombe, C. Y. Peng, P. Y. Ayala, W. Chen, M. W. Wong, J. L. Andres, E. S. Replogle, R. Gomperts, R. L. Martin, D. J. Fox, J. S. Binkley, D. J. Defrees, J. Baker, J. P. Stewart, M. Head-Gordon, C. Gonzalez, J. A. Pople *Gaussian 94, Revision D.4*, Gaussian, Inc., Pittsburgh, PA, **1995**.
[21] A. D. Becke, *J. Chem. Phys.* **1993**, *98*, 5648.
[22] Program Molden written by: G. Schaftonaar, www.caos.-kun.nl/˜schaft/molden/molden.html
[23] A. F. Reed, L. A. Curtiss, F. Weinhold, *Chem. Rev.* **1988**, *88*, 899.
[24] R. M. Roberts, P. J. Vogt, *Org. Synth. Coll. Vol.* **1963**, *IV*, 464.
[25] H. Nöth, H. Vahrenkamp, *J. Organomet. Chem.* **1968**, *11*, 399−405.
[26] Crystallographic data (excluding structure factors) for the structure reported in this paper have been deposited with the Cambridge Crystallographic Data Centre as supplementary publication no. CCDC-118940. Copies of the data can be obtained free of charge on application to CCDC, 12 Union Road, Cambridge CB2 1EZ, UK [Fax: int. code + 44-1223/336-033; E-mail: deposit@ccdc.cam.ac.uk).

Received November 20, 1998
[I98403]

Platination of the Exocyclic Amino Group of the Adenine Nucleobase by Pt^{II} Migration

Jorma Arpalahti*[a] and Karel D. Klika[a]

Keywords: Metal migration / NMR spectroscopy / Nucleobases / Platinum / Structure elucidation

Migration of coordinated Pt^{II} from the endocyclic N(1) site to the exocyclic nitrogen atom in 9-methyladenine occurs at high pH values. The resulting N(6)-platinated complex has been characterized by X-ray crystal structure analysis and by ^{1}H- and ^{195}Pt-NMR spectroscopy. The ^{1}H-NMR spectra show that the Pt^{II}(dien) unit at N(6) can adopt either a *syn* or an *anti* conformation with respect to the N(1) site, and that protonation of the ring nitrogen atoms N(1) and/or N(7) perturbs the *syn*/*anti* equilibrium.

The ability of Pt^{II} to form kinetically inert complexes with the base residues in DNA is crucial for the biological activity of various platinum anticancer drugs.[1][2] Although different Pt^{II} compounds show a clear preference for the guanine N(7) site followed by the adenine N(7) atom,[3] coordination to other sites cannot be excluded when assessing the active binding mode of Pt drugs. For example, the selectivity of the N(7) site most probably results from kinetic factors, since in 9-substituted purine nucleobases the Pt−N(1) bond seems to be thermodynamically more stable than the Pt−N(7) bond.[4] Because of the differing basicities of the purine nitrogen atoms, the distribution of Pt^{II} between the N(1) and N(7) sites can be affected by (de)protonation of the purine nucleobases.[3][5] When coordination to these sites is hindered, Pt^{II} binding to N(3) may be observed,[5][6] but only in very rare cases is platination of the exocyclic amino or oxo groups of 9-substituted purines observed.[5] For example, coordination of Pt^{II} to C(6)−NH_2 in adenosine and 2′-deoxyadenosine has been proposed with 4-picoline(2,2′:6,2′′-terpyridine)platinum(II), but only *after* the initial N(1) platination.[7] There are also a few reported cases of structurally characterized complexes exhibiting N(6) binding mode with other metal ions.[8] Hence, in the search for unusual Pt^{II} binding patterns we report here the preparation, X-ray crystal structure determination, and NMR-spectroscopic characterization of the model nucleobase 9-methyladenine (9-made) bearing a Pt^{II}(dien) unit (dien = diethylenetriamine) at N(6).

In general, metal-ion binding to the exocyclic amino group of the adenine moiety requires proton abstraction from the NH_2 group and it is the high pK_a value (ca. 17) of the NH_2 group which makes direct complexation at this site very difficult.[5][8] However, it is known that coordination of electrophilic Pt^{II} to the adenine N(1) and N(7) sites lowers the pK_a value of the exocyclic NH_2 group by ca. 4 log units.[5] In addition, the N(6) atom seems to be spatially quite close to Pt^{II} in N(1)-platinated adenine derivatives.[4b] These considerations prompted us to employ an indirect strategy to accomplish Pt^{II} binding to the N(6) site, i.e. via the N(1)-platinated species. Although the reaction of aquated Pt^{II}(dien) with an excess of 9-made initially gives the N(1)-bound complex as the minor species, a slow N(7) → N(1) isomerization takes place at elevated temperatures analogous to that found earlier with adenosine.[4b] The employment of [Pt(dien)(9-made-*N*1)]$(ClO_4)_2$ (**1**) as the starting material enables the facile preparation of the N(6)-platinated species, [Pt(dien)(9-made-*N*6)]$(ClO_4)_2$ (**2**), in strongly basic solution.

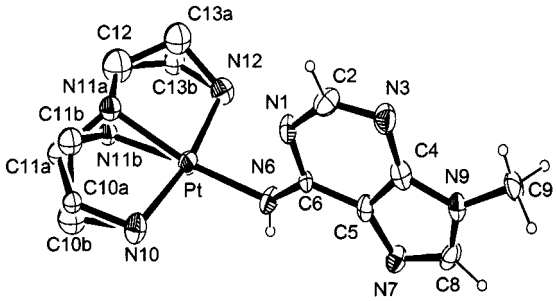


Figure 1. Structure of the cation of [Pt(dien)(9-made-*N*6)]$(ClO_4)_2$; selected interatomic distances [Å] and angles [°] with estimated deviations in parentheses: Pt−N(6) 2.010(18), Pt−N(10) 2.079(17), Pt−N(11a) 2.09(4), Pt−N(11b) 2.04(3), Pt−N(12) 2.081(18), N(6)−C(6) 1.30(3), N(6)−Pt−N(11a) 167.0(14), N(6)−Pt−N(11b) 171.5(12), N(6)−Pt−N(10) 98.8(8), N(6)−Pt−N(12) 92.8(8), N(10)−Pt−N(12) 168.3(6), C(6)−N(6)−Pt 128.9(13)

The X-ray crystal structure of **2** confirms Pt^{II} binding to the deprotonated amino group (Figure 1).[9] Comparison with **1** reveals that the N(1) → N(6) migration of Pt^{II} does not substantially change the nucleobase geometry. Since **2** was isolated at pH = 6, the nucleobase moiety of the dication is expected to bear a proton.[10] Unfortunately, unambiguous assignment of the protonation site was not forthcoming from the X-ray data. Although all the ring nitrogen atoms N(1), N(3), and N(7) display nonbonded contacts, only the N(1) site seems to act as a donor [N(1)···O(13a) 2.83(6) Å, N(1)···O(14b) 3.16(4) Å].[11] It is worth noting that the distance of 3.96 Å between N(1) and N(12) does not indicate an intramolecular H bond in *dicationic* **2**, even

[a] Department of Chemistry, University of Turku, FIN-20014, Turku, Finland
Fax: (internat.) + 358-2/333-6700
E-mail: jorma.arpalahti@utu.fi

 © WILEY-VCH Verlag GmbH, D-69451 Weinheim, 1999 1434−1948/99/0808−1199 $ 17.50+.50/0

though this interaction may be present in the *syn* conformer of deprotonated **2** (vide infra). These findings suggest that it is the N(1) site that bears the required proton, as was also observed in the N(6)-bound Hg^{II} complex.[8b] In fact, both dicationic **2** and the Hg^{II} complex[8b] represent a metalated form of the rare imino tautomer of the adenine nucleobase. However, the internal ring angle C(2)−N(1)−C(6) does not unambiguously verify N(1) as the protonation site[8b] since the value of 122.8(16)° found for **2** has only increased by 2.2σ[12] from that in free 9-made,[13] viz. 118.7(1)°. For comparison, in the N(6)-bound Hg^{II} complex the C(2)−N(1)−C(6) angle [126(1)°] increases by 7.3σ upon N(1) protonation.[8b]

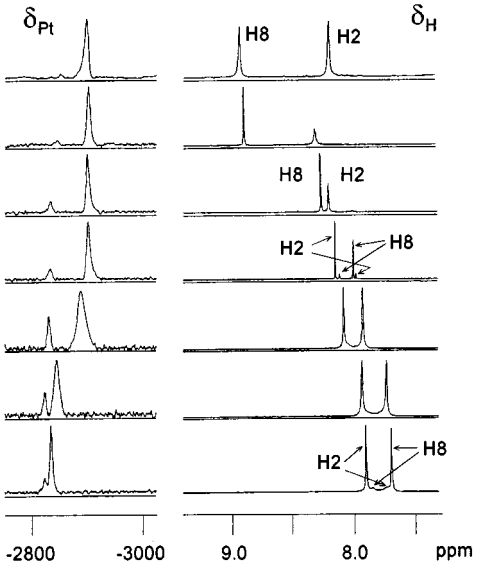


Figure 2. Sections of the ^{195}Pt- and ^{1}H-NMR spectra of **2** in D_2O/water solutions at different pH values (from bottom to top: 12.6, 8.5, 7.4, 6.0, 1.4, 0.6, ca. 0); the assignments of H(2) and H(8) are based on long-range C−H correlations (major conformer) and exchange correlations (minor conformer)

Both, ^{195}Pt- and ^{1}H-NMR spectra show pH-dependent dynamic processes for **2** (Figure 2),[14] which may be attributed predominantly to the restricted rotation about the C(6)−N(6) bond.[4b] Thus, the Pt^{II}(dien) unit may adopt either a *syn* or an *anti* orientation with respect to the N(1) site.[8b] In the deprotonated (monocationic) **2**, the major *syn* conformation is concomitant with an apparent H bond formed between dien−NH_2 and the N(1) site bearing a (partial) negative charge resulting in a stronger deshielding of H(2) relative to H(8). In the minor *anti* conformer, the reversal of the H(2) and H(8) chemical shifts may be attributed to H-bond formation between dien−NH_2 and the N(7) site. With decreasing pH value all of the ^{1}H signals shift downfield suggestive of an effect from both protonation and a shift in the conformational equilibrium. In the formation of dicationic **2**, N(1) protonation in the major species eliminates the H bonding from dien−NH_2 to N(1) and may cause a shift in the *syn* ⇌ *anti* equilibrium. As a consequence, both H(2) and H(8) are shifted downfield in the major species, the former due to protonation and the latter due to H bonding. Because two sets of aromatic protons are again detected for dicationic **2**, also with a reverse of the order of H(2) and H(8) chemical shifts in the minor conformer, there seems to be, in addition to the restricted rotation about the C(6)−N(6) bond, also a concomitant prototropic tautomeric equilibrium in effect between N(1) and N(7). The larger downfield shift of H(8) over H(2) in the minor species of the dicationic **2** suggests that in this case it is the N(7) site which is protonated with the Pt^{II}-(dien) unit in the *syn* conformation. This is implied by the comparable chemical shifts for H(2) in the monocationic, major species and in the dicationic, minor species, where in both cases H bonding can be in effect between dien−NH_2 and the N(1) site, and for H(8) in the monocationic, minor species and in the dicationic, major species where similarly in both cases H bonding can be in effect between dien−NH_2 and the N(7) site. Unfortunately, we were unable to independently confirm the proposed conformations. Further acidification down to pH < 0 results in a marked downfield shift only for H(8) suggesting that the second protonation occurs predominantly at N(7). Although the *syn* and *anti* conformers are no longer resolvable in the aromatic protons, the two species remain discernible in the ^{195}Pt-NMR spectra.

Two mechanistic explanations may be given for the adenine N(1) → N(6) isomerization, both of which require deprotonation of the C(6)−NH_2 group. First, the migration of Pt may be analogous to the Dimroth rearrangement, in which an alkyl group migrates from a heterocyclic nitrogen atom to an α-amino or α-imino group.[15] Alternatively, the imino group at C6 may directly attack Pt^{II} in the starting compound resulting in a 5-coordinate intermediate, where cleavage of the expectedly weaker Pt−N(1) bond gives the N(6)-bound species. It is worth noting that in **1** the distance between N(6) and Pt^{II} is 3.19(1) Å, very similar to that found in the corresponding adenosine complex, viz. 3.25 Å (unit A) and 3.16 Å (unit B).[4b] At this stage both explanations are feasible, although the proposed simultaneous binding of Pt to the endocyclic and exocyclic N atoms in pyrimidine complexes[16] lends support to the latter explanation. We note, however, that the bond rearrangement in the adenine moiety must still be mechanistically different from that in the pyrimidine complex, since the latter occurs in acidic solution via Pt^{IV}, while the adenine N(1) → N(6) migration proceeds in strongly basic solution without any detectable redox reaction

Experimental Section

[Pt(dien)(9-made-*N*1)](ClO$_4$)$_2$ (1): A mixture of aquated Pt^{II}(dien) {1.0 mmol, prepared by treating [PtI(dien)]I with 1.9 equiv. of $AgClO_4$[17]} and 9-made[18] (2.0 mmol) in 15 mL of water was stirred for 7 d at 75−85°C. According to HPLC analysis the initial N(1)/N(7) ratio of 2:3 increased to 2:1 during this treatment. After concentration to ca. 5 mL, the pH of the solution was adjusted to 1.5 using 1.0 M $HClO_4$. The addition of $NaClO_4$ (4 mmol) afforded 460 mg of crystalline product. Recrystallization from 0.1 M $HClO_4$ gave clear prisms of [Pt(dien)(9-made-*N*1)](ClO$_4$)$_2$ (**1**). Based on HPLC analysis, the product was analytically pure. The crystals were washed with cold water and air-dried; yield 220 mg (45% from

Pt). The N(1)-binding mode in **1** was confirmed by X-ray crystal structure analysis.[19][20]

[Pt(dien)(9-made-*N*6)](ClO$_4$)$_2$ (2): For the preparation of **2**, 71 mg (0.11 mmol) of **1** was dissolved in 5 mL of 0.1 M NaOH. The solution (pH = 12.8) was stirred for 3 h at 60−65°C after which the pH value was adjusted to 6.5 by using 1 M $HClO_4$. The solution was concentrated to ca. 0.5 mL, and left at 4°C to afford [Pt(dien)(9-made-*N*6)](ClO$_4$)$_2$ (**2**) as thick, clear plates or prisms; yield 55 mg (77%). Satisfactory elemental analysis (C, H, N) was obtained. − $C_{10}H_{20}Cl_2N_8O_8Pt$ (646.33): calcd. C 18.58, H 3.12, N 17.34; found C 18.65, H 3.18, N 17.21.

Acknowledgments

Support by COST Action D8/004/97 is kindly acknowledged.

[1] S. L. Bruhn, J. H. Toney, S. J. Lippard in *Progress in Inorganic Chemistry*, vol. 38 (Ed.: S. J. Lippard), Wiley, New York, **1990**, p. 477−516.
[2] J. Reedijk, *Chem Commun*. **1996**, 801−806.
[3] J. Arpalahti in *Metal Ions in Biological Systems*, vol. 32 (Eds.: A. Sigel, H. Sigel), Marcel Dekker, New York, **1996**, p. 379−395.
[4] [4a] R. B. Martin in *Platinum, Gold and Other Metal Chemotherapeutic Agents* (Ed.: S. J. Lippard), ACS Symposium Series 209, American Chemical Society, Washington DC, **1983**, p. 231−244. − [4b] J. Arpalahti, K. D. Klika, R. Sillanpää, R. Kivekäs, *J. Chem. Soc., Dalton Trans.* **1998**, 1397−1402.
[5] B. Lippert in *Progress in Inorganic Chemistry*, vol. 37 (Ed.: S. J. Lippard), Wiley, New York, **1989**, p. 1−97.
[6] C. Meiser, B. Song, E. Freisinger, M. Peilert, H. Sigel, B. Lippert, *Chem. Eur. J.* **1997**, *3*, 388−398.
[7] G. Lowe, T. Vilaivan, *J. Chem. Soc., Perkin Trans. 1* **1996**, 1499−1503.
[8] [8a] L. Y. Kuo, M. G. Kanatzidis, M. Sabat, A. L. Tipton, T. J. Marks, *J. Am. Chem. Soc*. **1991**, *113*, 9027−9045. − [8b] F. Zamora, M. Kunsman, M. Sabat, B. Lippert, *Inorg. Chem*. **1997**, *36*, 1583−1587. − [8c] See also: M. J. Clarke, *J. Am Chem. Soc*. **1978**, *100*, 5068−5075.
[9] Crystal structure analysis of **2**: $C_{10}H_{20}Cl_2N_8O_8Pt$ (M_r = 646.33), orthorhombic, space group *Pna*21 (no. 33), a = 18.652(2), b = 11.3199(12), c = 9.4299(7) Å, V = 1991.0(4) Å^3, Z = 4, $\rho_{calcd.}$ = 2.156 g cm^{-3}, F(000) = 1248; Rigaku AFC5S diffractometer, ambient temperature, Mo-K_α radiation (λ = 0.71069 Å), μ = 7.373 mm^{-1}, ω/2θ scan technique with 4.2° ≤ 2θ ≤ 50.04°, absorption correction: ψ scan (T_{min}/T_{max} = 0.51/1.00), 1874 measured reflections and 1873 observed reflections with $I > 2\sigma(I)$ (248 parameters) gave $R1$ = 0.0426 and $wR2$ = 0.0915, $R1$ = 0.0838 and $wR2$ = 0.1033 (all data), max/min residual electron density: 0.732/−1.185 eÅ^{-3}. The structure was solved by standard Patterson and difference Fourier methods and refined by full-matrix least-squares calculations on F^2 by employing SHELXL-97.[21] In the base moiety, the NH hydrogen atom was found from the electron density map and was refined, whilst the CH_3 and ring hydrogen atoms are at calculated positions. The dien hydrogen atoms were not included due to the disorder of the dien ligand. The perchlorate oxygen atoms also suffered disordering.[20]
[10] p$K_{\alpha1}$ = 1.2 ± 0.1, p$K_{\alpha2}$ = 7.65 ± 0.05 determined at 298.2 K in 0.1 M $NaClO_4$ using the potentiostatic technique described earlier, see: H. Lönnberg, J. Arpalahti, *Inorg. Chim. Acta* **1980**, *55*, 39−42.
[11] Shortest nonbonded contacts for N(3) and N(7) in **2**: N(10)···N(3^{i}) 3.31(3) Å, N(11a)···N(7^{ii}) 3.44(5) Å; symmetry operations: i) 0.5 − x, y − 0.5, z − 0.5, ii) 0.5 − x, 0.5 + y, z − 0.5.
[12] σ defined as $\sigma = (\sigma_1^2 + \sigma_2^2)^{1/2}$ with σ_1 and σ_2 being the errors in angles that are compared.[8b]
[13] T. J. Kistenmacher, M. Rossi, *Acta Crystallogr*. **1977**, *B33*, 253−257.
[14] The minor species is well resolved only at pD = 6 {broad signals at pD = 12: δ = 7.72 [H(2)], 7.88 [H(8)]; very broad, partially unresolved signals at pD = 8.5 and 7.4}. The NMR measurements were carried out as previously described.[4b]
[15] T. Fujii, T. Itaya, *Heterocycles* **1998**, *48*, 359−390.
[16] [16a] F. Pichierri, D. Holtenrich, E. Zangrando, B. Lippert, L. Randaccio, *J. Biol. Inorg. Chem*. **1996**, *1*, 439−445. − [16b] J. Müller, E. Zangrando, N. Pahlke, E. Freisinger, L. Randaccio, B. Lippert, *Chem. Eur. J.* **1998**, *4*, 397−405.
[17] J. Arpalahti, P. Lehikoinen, *Inorg. Chem*. **1990**, *29*, 2564−2567.
[18] H. Lönnberg, J. Ylikoski, J. Arpalahti, E. Ottoila, A. Vesala, *Acta Chem. Scand.* **1985**, *A39*, 171−180.
[19] F. Schwarz, B. Lippert, H. Schöllhorn, U. Thewalt, *Inorg. Chim. Acta* **1990**, *176*, 113−121.
[20] Crystallographic data (excluding structure factors) for the structures reported in this paper have been deposited with the Cambridge Crystallographic Data Centre as supplementary publication no. CCDC-113725 (**1**) and -113726 (**2**). Copies of the data can be obtained free of charge on application to CCDC, 12 Union Road Cambridge, CB2 1EZ, UK [Fax: + 44-1223/336-033; E-mail: deposit@ccdc.cam.ac.uk].
[21] G. M. Sheldrick, *SHELXL 97, Program for the Refinement of Crystal Structures*, University of Göttingen, **1997**.

Received March 25, 1999
[99106]

Combined Quantum Chemical and Mass Spectrometry Study of $[Ge,C,H]^+$ and Its Neutral Counterpart

Phillip Jackson,[a] Martin Diefenbach,[a] Detlef Schröder,[a] and Helmut Schwarz*[a]

Dedicated to Professor Hans Bock on the occasion of his 70th birthday

Keywords: Organogermanium ions / Mass spectrometry / *Ab initio* theory / NBO

The cation $[Ge,C,H]^+$ has been generated by the electron ionisation of trichloromethylgermane. Collisional activation experiments were used to establish a Ge–C–H connectivity in this species, for which a significant fraction of the ion population was found to survive neutralisation-reionisation mass spectrometry (NRMS) experiments. Thus, the neutral counterpart $[Ge,C,H]^0$ is stable on a microsecond timescale. Becke's 3 parameter hybrid density functional (B3LYP) was used to map the ion and neutral potential-energy surfaces, in conjunction with double-zeta and triple-zeta basis sets. The computational results obtained using the triple-zeta basis sets suggest that, for the cation, the global minimum is the high spin $^3\Sigma$ $GeCH^+$, with the first Ge–C–H excited state, $^1\Sigma$ $GeCH^+$, approximately 39 kcal mol^{-1} less stable. The lowest energy ion structure with H–Ge–C connectivity is bent ($^3A''HGeC^+$, $\angle$H–Ge–C = 126.3) and 69 kcal mol^{-1} less stable than the global minimum. For the neutral, a doublet ($^2\pi$) with Ge–C–H connectivity is predicted to be the global minimum. The classical barrier for the neutral 1,2-hydrogen shift reaction on the doublet surface is negligible (0.1 kcal mol^{-1}), while the smallest barrier for the cation is 13.0 kcal mol^{-1}, corresponding to ($^3A''$) $HGeC^+ \rightarrow$ ($^3\Sigma$) $GeCH^+$. Natural bond order analysis has been used to establish the order of the metal–carbon bond for selected states of both the neutral and the ion. Neutral and cationic isomers with Ge–C triple bonds were found to be high-energy excited states, with the metal–carbon bonds in the cation and neutral ground states of order 2.0 and 2.5, respectively. The instability of Ge–C triple bonded species is attributed to the energy required for electronic promotion in the metal in order to achieve a hybrid configuration suitable for the formation of such a bond.

Introduction

In 1991, neutral [Si,C,H] was detected by means of neutralisation-reionisation mass spectrometry (NRMS).[1] Collisional activation (CA) experiments established the connectivity in the cation precursor as Si−C−H, for which a subsequent NR recovery signal was detected. Thus, the CA and NRMS results together vindicated the predictions of ab initio calculations, which suggested that the radical $SiCH^\bullet$ was 2.6 eV more stable than the $CSiH^\bullet$ isomer, and that $SiCH^+$ is more stable than $HSiC^+$ by at least 3.0 eV.[2] In the years since 1991, a plethora of molecules whose existence has only been proposed by spectroscopists or theoreticians have been detected using this technique.[3]

Whereas the number of challenges remaining in the area of silicon chemistry are now few,[4] the chemistry of germanium is still largely unexplored. This is perhaps due to a low terrestrial abundance[5] and broad similarities in the chemistry of main-group elements as one progresses from the third to fifth rows, which enable predictions based on the behaviour of lighter or heavier congeners. It is interesting to note that there has been recent interest in the electronic structure and gas-phase chemistry of homonuclear germanium clusters.[6] Several small germanium-hydrocarbon molecules have been previously generated in the gas phase, but still very little is known of their structures. Operti et al. were able to generate $GeCH_n^+$ (n = 1−5) and some digermanium-organo cations from ion-molecule reactions between germane and methylgermane in a high pressure source,[7] although studies towards structural characterisation were not undertaken. Willett and coworkers[6c] were able to generate $GeC_2H_3^+$, $GeC_3H_5^+$, and $Ge_nCH_2^+$ (n = 1,2) via the reactions of laser ablated Ge^+, Ge_2^+ with cyclopropane. While $Ge_2CH_2^+$ was the only reaction product observed for Ge_2^+, branching for Ge^+ yielded $GeCH_2^+$ as the major product, followed by $GeC_2H_3^+$ and $GeC_3H_5^+$. Density functional theory (BLYP/6-31G*) investigations of $[Ge_2,C,H_2]^+$ suggests that the disubstituted methane isomer Ge−CH_2−Ge is more stable than the isomer with Ge−Ge−CH_2 connectivity by approximately 15 kcal mol^{-1}.[6c] Although it was established that both structures were minima on the PES, and the disubstituted methane structure is probably the ground state, it must be noted that no structures with Ge−H bonds were investigated.[8]

Concerning other small germanium molecules and ions, $[Ge,O,H]^{0/+}$ have been studied using double- and triple-zeta basis sets in conjunction with the coupled cluster theory.[9] The most stable isomer for the ion was linear and possessed Ge−O−H connectivity, whereas a bent structure, with analogous connectivity, was found to be the ground state of the neutral. Results from a kinetic study of the neutral-neutral reaction between germylene (GeH_2) and germane

[a] Institut für Organische Chemie, Technische Universität Berlin, Straße des 17. Juni 135, D-10623 Berlin
Fax: (internat.) + 49(0)30/314-21102
E-mail: schw0531@www.chem.tu-berlin.de

 © WILEY-VCH Verlag GmbH, D-69451 Weinheim, 1999 1434−1948/99/0808−1203 $ 17.50+.50/0

(GeH_4) have appeared recently,[10] and the experimental evidence suggests the rate of the association reaction leading to Ge_2H_6 depends on collisional cooling by a third body. The structures of the triatomic halogermylenes HGeX (X = Cl, Br) have been proposed on the basis of high level ab initio calculations[11] and rovibrational bands observed in laser-induced fluorescence experiments.[12] In the last year, this technique has been employed to characterise HGeI.[13]

This paper is divided into two sections: in the first, experimental results for $[Ge,C,H]^{0/+}$ are presented. In the second section, the results of density functional calculations are discussed in relation to the ground states of $GeCH^{0/+}$ and the possible existence of $HGeC^{0/+}$ isomers. The 1,2 hydrogen shift barrier, and results from Ge−C bond order analyses of selected ion and neutral isomers are then examined. The nature of multiple bonds involving heavier main-group elements are the focus of current interest and speculation.[3e,14] According to criteria proposed by Goubeau in 1957,[15] double bonds stable towards polymerisation are achievable if the sum of the electronegativities of the bonding partners exceeds the approximate value of 5. Using the literature values for the Mulliken electronegativities[16] of Ge ($4sp^3$), 2.50, and C (2sp), 3.29,[17] the sum obviously exceeds this value, suggesting there is a good chance of forming a Ge−CH bond of order 2 or greater.

Results and Discussion

Mass Spectrometry

The CA-mass spectrum of $GeCH^+$ is presented in Figure 1. Loss of $CH^\bullet$ is the major fragmentation observed under single collision conditions (66% fragment ion current), suggesting a Ge−C−H connectivity in the ion. It is interesting to note that there is also a minor signal corresponding to GeH^+ at *m/z* 71 (5% fragment ion current), indicating that there may be small amounts of an isomer with H−Ge−C connectivity, or that post-collisional isomerisation precedes fragmentation. If the barrier for the associated 1,2-shift lies above the GeC^+ + H and GeH^+ + C dissociation asymptotes, then the CA spectrum unequivocally confirms the existence of $HGeC^+$ (see below). In contrast, there was an additional source of uncertainty regarding the assignment of the fragment at *m/z* 29 in the CA spectrum of the silicon congener,[1] due to the small but non-negligible abundance of the ^{29}Si isotope.

The NR-mass spectrum of $[Ge,C,H]^+$ yields a distinct recovery signal for the parent ion (Figure 2), thus demonstrating that [Ge,C,H] is a stable molecule on the microsecond timescale. The most intense fragment ion that results from the reduction and subsequent oxidation of $[Ge,C,H]^+$ is Ge^+, which suggests that the Ge−C bond length in the neutral is displaced from the bond length in the ion, resulting in vertical transitions to high vibrational levels. Although it appears that there is a peak of low intensity at *m/z* 71 corresponding to loss of C, the uncertainty due to the higher signal to noise ratio suggests that only a tentative assignment can be made in this instance. In summary, the precursor structure as well as the CA and the NR spectra of $[Ge,C,H]^+$ are in accord with a Ge−C−H connectivity.

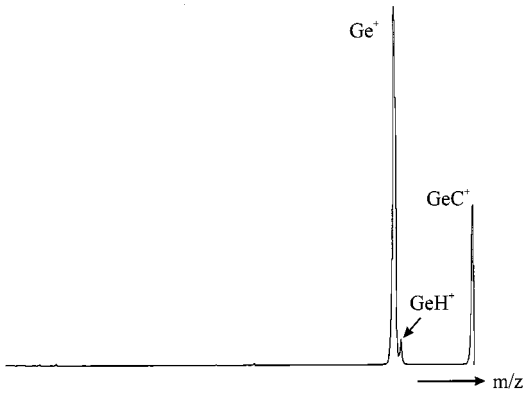


Figure 1. CA-mass spectrum of B(1)/E(1) mass-selected $^{70}GeCH^+$ generated by electron ionisation of methyltrichlorogermane

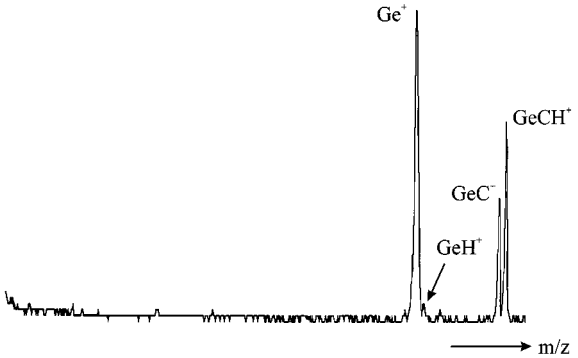


Figure 2. NR-mass spectrum of B(1)/E(1) mass-selected $^{70}GeCH^+$ generated by electron ionisation of methyltrichlorogermane

Theoretical Calculations

In order to map the potential-energy surfaces (PES) of neutral and cationic $[Ge,C,H]^{0/+}$, the relative energies were investigated for various spin isomers in linear and bent geometries for the connectivities Ge−C−H and H−Ge−C. Although the various cation and neutral minima were investigated using both BS-I and BS-II, only the results obtained using BS-II are presented here. The corresponding BS-I results can be provided on request.

(i) $[Ge,C,H]^+$ Potential Energy Surface: A schematic of the cation PES is presented in Figure 3. For the sake of clarity, we have omitted high-lying excited states. In Table 2, we present the bond energies of any associated diatomics and the zero-point corrected energies required to effect various ion dissociations. Only the lowest energy asymptotes corresponding to each particular dissociation are shown.

The global minimum on the $[Ge,C,H]^+$ PES corresponds to linear $^3\Sigma$ $GeCH^+$. This state lies approximately 110 kcal mol^{-1} below the lowest energy Ge^+ + CH dissociation asymptote, and almost 82 kcal mol^{-1} below the transition structure ^{3}TS for the associated 1,2 H-shift. The lowest energy cation isomer with H−Ge−C connectivity is $^3A''$

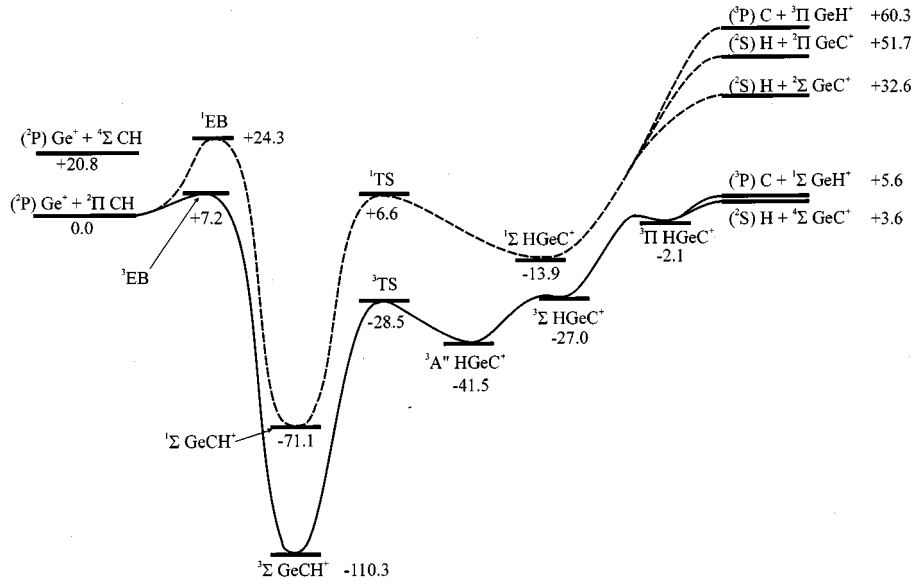


Figure 3. PES for $[Ge,C,H]^+$ from B3LYP/6-311++G(d,p) calculations; refer to Table 1 for details of particular structures, and Table 2 for details regarding asymptotes

Table 1. Total energies (E_{SCF}, Ha), bond lengths (r_e, in Å), bond angles (α, in degrees), and absolute relative energies (E_{rel}, in kcal mol^{-1}) of stationary points for electronic states of $[Ge,C,H]^+$ at B3LYP/6-311++G(d,p) level of theory

Structure	State	E_{SCF}	r_e(Ge−C)	r_e (C−H)	r_e (Ge−H)	α	E_{rel}
$GeCH^+$	$^3\Sigma$	−2115.2903912	1.894	1.090			0.0
	$^1\Sigma$	−2115.2284407	1.914	1.092			39.2
	$^3\Pi$	−2115.2042964	1.739	1.092			54.5
	$^3\Sigma$	−2115.1892111	1.725	1.091			64.0
	$^1\Sigma$	−2115.0613128	1.636	1.113			145.0
^{1}EB [a]	$^1\Sigma$	−2115.0777673	6.219	1.122			134.6
^{1}EB [a]	$^3\Sigma$	−2115.1048022	6.084	1.122			117.5
^{3}TS	$^3A''$	−2115.1611256	1.925		1.579	90.8	81.8
^{1}TS	$^1A'$	−2115.1058258	1.801		1.582	88.0	116.8
$HGeC^+$	$^3A''$	−2115.1631782	1.899		1.548	126.3	68.8
	$^3\Sigma$	−2115.1588284	1.906		1.549		83.3
	$^3\Pi$	−2115.1193585	1.714		1.510		108.2
	$^1\Sigma$	−2115.1380349	1.918		1.548		96.4
	$^1\Sigma$	−2115.0098613	1.629		1.511		177.5

$D^0(Ge^+-CH)$[b] = 107.7 kcal mol^{-1}
$D^0(GeC^+-H)$[c] = 104.9 kcal mol^{-1}

[a] These structures correspond to the entrance channel barriers depicted in Figure 3. − [b] Evaluated using zero point energies derived from BS-I vibrational frequencies for $^3\Sigma$ $GeCH^+$ and $^2\Pi$ CH, calculated at the BS-I optimised geometries: $^3\Sigma$ $GeCH^+$, r_e(Ge−C) = 1.919 Å; r_e(C−H) = 1.094 Å, ZPE = 9.9 kcal mol^{-1}. $^2\Pi$ CH, r_e(C−H) = 1.151 Å, ZPE = 3.9 kcal mol^{-1}. − [c] Evaluated using zero point energies derived from BS-I vibrational frequencies for $^3\Sigma$ $GeCH^+$ (see footnote 2) and $^4\Sigma$ GeC^+, calculated at the BS-I-optimised geometries: $^4\Sigma$ GeC^+, r_e(Ge−C) = 1.973 Å, ZPE = 0.9 kcal mol^{-1}.

$HGeC^+$. According to B3LYP/BS-II, the classical barrier for the 1,2 H-shift reaction on the triplet surface is 13.0 kcal mol^{-1}, which may suffice for the detection of $HGeC^+$ from suitable precursors.

Although several linear isomers of $HGeC^+$ were found as minima on the triplet surface at the B3LYP/BS-I level, all are less stable than the bent structure. Moreover, transition state searching failed to locate a barrier linking the linear and bent isomers, suggesting the linear species reside in shallow minima and should convert into bent structures with minimal activation.

From Figure 3, it is apparent that there is only one curve crossing between the singlet and triplet surfaces, and this is near the Ge^+ + CH dissociation limit. A distinctive feature of the singlet PES is the large energy required to couple the ground states of Ge^+ ($^2\Pi$) and CH ($^2\Pi$) to form $^1\Sigma$ $GeCH^+$. Although pure DFT methods are largely considered unsuitable for the calculation of van der Waals and charge-exchange complexes,[18] hybrid DFT often performs better in this regard, and because this barrier is much larger than typical rotational barriers (of the order of a few kcal mol^{-1}), it must be associated with an electron promotion

Table 2. States, total energies (E_{SCF}, Ha), bond lengths (r_e, in Å), calculated ionization energies (IE, in eV), and bond dissociation energies (D^0, in kcal mol^{-1}) of various atomic and diatomic fragments used in the calculations of bond energies and dissociation asymptotes at B3LYP/6-311++G(d,p) level of theory. Tabulated dissociation energies include zero point energy corrections calculated using the frequencies obtained with BS-I.[a]

	State	E_{SCF} (ha)	r_e	IE	D^0(X−Y)
H	^{2}S	− 0.50225698			
C	^{3}P	−37.85726708			
Ge	^{3}P	−2076.90984966		7.83	
Ge^+	^{2}P	−2076.62207107			
CH	$^2\Pi$	−38.49410314	1.126		81.3
CH	$^4\Sigma$	−38.46117836	1.096		59.9
GeH	$^2\Pi$	−2077.52295375	1.598	7.30	67.5
GeH	$^4\Sigma$	−2077.44569581	1.578		18.8
GeH^+	$^1\Sigma$	−2077.25460678	1.592		79.6
GeH^+	$^3\Pi$	−2077.16815521	1.695		25.9
GeC	$^1\Sigma$	−2114.86335882	1.715		59.7
GeC	$^3\Pi$	−2114.92334025	1.806	8.58	99.9[b]
GeC	$^3\Sigma$	−2114.89668382	1.900		82.7
GeC^+	$^2\Pi$	−2114.52648018	1.812		30.8
GeC^+	$^2\Sigma$	−2114.55672709	1.962		49.8
GeC^+	$^4\Sigma$	−2114.60816155	1.928		80.6

[a] Geometries and harmonic frequencies calculated using BS-I: $^2\Pi$ CH, r_e = 1.151 Å, ω_e = 2671 cm^{-1}. $^4\Sigma$ CH, r_e = 1.103 Å, ω_e = 3046 cm^{-1}. $^2\Pi$ GeH, r_e = 1.630 Å, ω_e = 1812 cm^{-1}. $^4\Sigma$ GeH, r_e = 1.588 Å, ω_e = 1709 cm^{-1}. $^1\Sigma$ GeH^+, r_e = 1.607 Å, ω_e = 1944 cm^{-1}. $^3\Pi$ GeH^+, r_e = 1.673 Å, ω_e = 1267 cm^{-1}. $^1\Sigma$ GeC, r_e = 1.744 Å, ω_e = 864 cm^{-1}. $^3\Pi$ GeC, r_e = 1.844 Å, ω_e = 742 cm^{-1}. $^3\Sigma$ GeC, r_e = 1.981 Å, ω_e = 479 cm^{-1}. $^2\Pi$ GeC^+, r_e = 1.856 Å, ω_e = 641 cm^{-1}. $^2\Sigma$ GeC^+, r_e = 1.992 Å, ω_e = 545 cm^{-1}. $^4\Sigma$ GeC^+, r_e = 1.973 Å, ω_e = 617 cm^{-1}. − [b] Experimental value: D^0(GeC) = 109.8 kcal mol^{-1}, from ref.[19].

Table 3. Total energies (E_{SCF}, Ha), bond lengths (r_e, in Å), bond angles (α, in degrees), and absolute relative energies (E_{rel}, in kcal mol^{-1}) of stationary points for electronic states of [Ge,C,H] at B3LYP/6−311++G(d,p) level of theory

Structure	State	E_{SCF}	r_e(Ge−C)	r_e(C−H)	r_e(Ge−H)	α	E_{rel}
GeCH	$^2\Pi$	−2115.5843426	1.774	1.082			0.0
	$^2\Sigma$	−2115.5286932	1.667	1.078			35.2[a]
	$^4\Sigma$	−2115.4093521	1.813	1.078			110.7
	$^2\Pi$	−2115.2723698	1.710	1.090			197.4
	^{4}A′′	−2115.5165009	2.001	1.099		131.2	42.9
^{4}TSa	$^4\Pi$	−2115.5101950	2.011	1.087			46.9
^{4}TSb	^{4}A′′	−2115.4414048	2.032		1.662	50.0	90.5
^{4}TSc	$^4\Pi$	−2115.4167485	2.055		1.548		106.0
HGeC	^{4}A′′	−2115.4770732	1.960		1.597	97.1	67.9
	^{4}A′	−2115.4207679	2.051		1.547	128.8	103.5
	^{2}A′[b]	−2115.5026479	1.789		1.554	117.2	51.7
^{2}TSa	^{2}A′	−2115.5025132	1.797		1.567	101.1	51.8
^{2}TSb	$^2\Pi$	−2115.4812352	1.791		1.539		65.2
	$^2\Sigma$	−2115.4488889	1.659		1.492		85.7
	$^4\Sigma$	−2115.3429078	1.801		1.492		152.8

D^0(Ge−CH) [c] = 110.8 kcal mol^{-1}
D^0(GeC−H) [c] = 94.3 kcal mol^{-1}
IE_{ad} (GeCH) = 8.00 eV

[a] A second $^2\Sigma$ GeCH minimum was located using Gaussian 94, lying 44.4 kcal mol^{-1} above the global minimum with a slightly shorter r_e(Ge−C) = 1.664 Å, than the lowest energy $^2\Sigma$ state. Analysis of the molecular orbitals and populations revealed this minimum to be an artefact (identical to the lowest $^2\Sigma$ GeCH). − [b] A second ^{2}A′ HGeC minimum was located using Gaussian 94, lying 61.1 kcal mol^{-1} above the global minimum with bond lengths r_e(Ge−C) = 1.780 Å, r_e(Ge−H) = 1.544 Å and ∠H−Ge−C = 121.3°. Analysis of the molecular orbitals and populations revealed this minimum to be an artefact (identical to the lowest ^{2}A′ HGeC). − [c] Evaluated using zero point energies derived from BS-I vibrational frequencies for $^2\Pi$ GeCH, $^2\Pi$ CH or $^3\Pi$ GeC, calculated at the BS-I-optimised geometries: $^2\Pi$ GeCH, r_e(Ge−C) = 1.798 Å; r_e(C−H) = 1.086 Å, ZPE = 7.3 kcal mol^{-1}. $^2\Pi$ CH, r_e(C−H) = 1.151 Å, ZPE = 3.9 kcal mol^{-1}. $^3\Pi$ GeC, r_e(Ge−C) = 1.844, ZPE = 1.1 kcal mol^{-1}.

in the diatomic fragment. Even though the coupling energy required is close to the calculated B3LYP first excitation energy of CH ($^4\Sigma \leftarrow {}^2\Pi$, 20.8 kcal mol^{-1}: B3LYP/BS-II), this state does not correlate with the singlet surface. Rather, it must correspond to either an $a^2\Pi$ or $^2\Sigma$ excitation.

The lowest energy minimum on the singlet surface is $^1\Sigma$ $GeCH^+$, which is ca. 71 kcal mol^{-1} below the ground state Ge^+ + CH dissociation asymptote, and almost 78 kcal mol^{-1} below ^{1}TS. No bent minima could be located, so ^{1}TS effectively connects two linear isomers. This was verified by following the reaction coordinate downhill from the saddle-point. The classical barrier to the 1,2 H-shift on the singlet surface is 20.5 kcal mol^{-1}, which is larger than the triplet barrier. In summary, we conclude that $^3\Sigma$ $GeCH^+$ is by far

the most stable $[Ge,C,H]^+$ species, whereas all other conceivable states and/or structures are much more energy demanding. These results support our assignment of a Ge−C−H ion structure derived from the fragmentation patterns in the CA and NR experiments (see above).

(ii) $[Ge,C,H]^0$ Potential Energy Surface: The neutral PES is presented in Figure 4. For further information regarding the various minima depicted or higher excited states not shown in this figure, consult Table 3. In contrast to the cation PES, the global minimum of the neutral corresponds to a *low* spin Ge−C−H isomer, $^2\Pi$ GeCH. This state lies more than 114 kcal mol^{-1} below the lowest energy $^3\Pi$ Ge + $^2\Pi$ CH dissociation asymptote, almost 43 kcal mol^{-1} below the most stable bent quadruplet state $^4A''$ GeCH, and more than 61 kcal mol^{-1} below the lowest energy structure with H−Ge−C connectivity, $^2A'$ HGeC. It is important to note that all linear structures having H−Ge−C connectivity were characterised as transition structures using BS-I. In order to unambiguously establish the instability of linear HGeC isomers towards rearrangement, vibrational analysis of $^2\Pi$ HGeC using BS-II was undertaken, which revealed this species is indeed a transition structure. It should also be noted that the PES in the vicinity of the $^2A'$ HGeC minimum is very flat, and ^{2}TSa, which links $^2\Pi$ GeCH and $^2A'$ HGeC (1,2 H-shift barrier), lies only 0.1 kcal mol^{-1} above the bent minimum. For the quadruplet PES, the classical barrier for the 1,2 H-shift reaction is 22.6 kcal mol^{-1}, and is of a similar magnitude to the singlet barrier on the cation PES. No barrier was encountered for the coupling of Ge and CH on the doublet PES.

(iii) Natural Bond Order (NBO) Analyses: A qualitative MO diagram for the linear Ge−C−H ground states of both $[Ge,C,H]^{0/+}$ is presented in Figure 5. For the $^3\Sigma$ ground state of the cation, the uncoupled electrons reside in π-bonding MOs with 18% Ge and 82% C character. Note that the next MO lower in energy than the π-bonding MOs is a σ-nonbonding MO, which is occupied by both 4s electrons of Ge. This implies that the CH unit, or more precisely C, is the source of the two π-electrons, as the remaining Ge electron is involved in formation of the Ge−C σ-bond. Thus, we deduce that the electronic configuration of Ge^+ in $^3\Sigma$ $GeCH^+$ is $4s^24p^1$, which also corresponds to the electron configuration of the $^2\Pi$ Ge^+ ground state. The NBO evaluation of the natural electron configuration of the constituent atoms yields $Ge(4s^{1.89}4p^{0.83})$ $C(2s^{1.54}2p^{2.90})$ $H(1s^{0.80})$, in agreement with empirical deductions. Moreover, the C atom is sp^3 hybridised, and the Ge^+−C σ-bond contribution from the metal is $4s^{0.08}4p^{0.92}$. The order of the Ge^+−C bond was evaluated by (i) summing the orbital populations of the σ- and π-*bonding* MOs, and subtracting from this, (ii) the sum of the populations of the Ge^+−C σ- and π-*antibonding* MOs. This result is then divided by two to yield a value of 1.99 for the Ge^+−C bond in $^3\Sigma$ $GeCH^+$. It should be noted that the derived bond order of 1.99, does

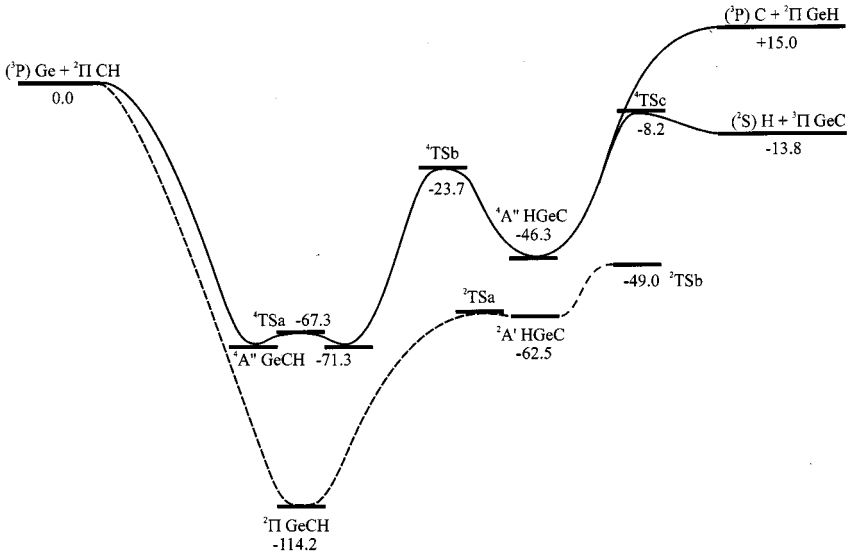


Figure 4. PES for $[Ge,C,H]^0$ from B3LYP/6-311++G(d,p) calculations; refer to Table 3 for details of particular structures, and Table 2 for details regarding asymptotes

The (quadruplet) 1,2 H-shift barrier height suggests that $HGeC^+$ isomers may be detectable in matrix isolation or other spectroscopic experiments. Unfortunately, the barrier for the bent to linear conversion of the neutral is negligible, and given the finite possibility for spin inversion, generation of long-lived HGeC appears unlikely.[3d] Finally, the isomerisation barriers on the singlet and triplet surfaces of the cation, are either lower than, or close in energy to, the lowest energy exit channels. Thus the CA results regarding the formation of H−Ge−C isomers are inconclusive, as the keV ion-neutral collisions excite the ions to dissociative vibrational levels well above the barriers associated with interconversion between GeCH and HGeC.

not imply the presence of formally paired π-electrons on both the germanium and carbon centres. The addition of an electron to one of the π-bonding MOs of $^3\Sigma$ $GeCH^+$ leads to some minor electronic and geometrical adjustments in the transition to the neutral ground state. The minor increase in Ge−C bond strength for the ground state neutral (Tables 1 and 3) is expected; however, the large decrease

in the C−H bond strength could be considered unusual. Comparison of the MO energies reveals the C−H σ-bonding MO in $^2\Pi$ GeCH is inverted with respect to the Ge−C σ-bonding MO in $^3\Sigma$ $GeCH^+$, and the population of the C−H σ-antibonding MO is much higher in $^2\Pi$ GeCH than $^3\Sigma$ $GeCH^+$. The second order energy of interaction between the σ-nonbonding MO, localised on the metal, and the C−H σ-antibonding MO in the neutral is 13.5 kcal mol^{-1} (alpha + beta sum), while the Ge 3s/C−H σ-antibonding MO interaction energy amounts to 7.7 kcal mol^{-1}. It is evident that core polarisation effects, in particular electron donation to the C−H σ-antibonding MO, has a pronounced effect on the C−H bond *strength* in the neutral, but the expected effect on the bond length is not dramatic. In fact, a slight bond contraction is observed, which is ascribed to enhanced Coulombic attraction between the C and H atoms of the neutral. The atomic charges in the neutral and cation ground states verify this point i.e. $C^{-0.85e}H^{+0.18e}$ for $^2\Pi$ GeCH, and $C^{-0.45e}H^{+0.20e}$ for $^3\Sigma$ $GeCH^+$.

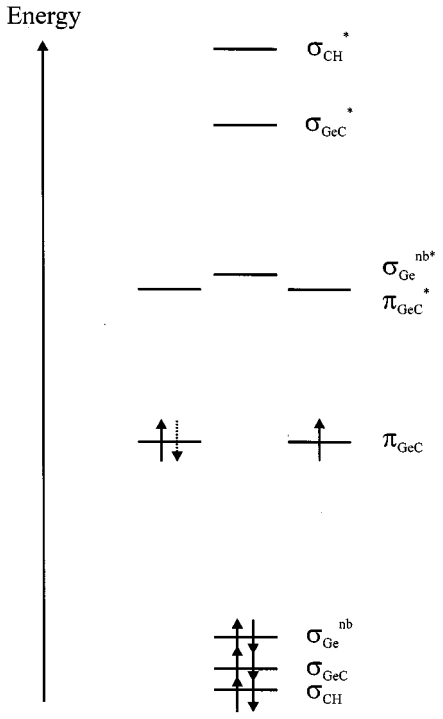


Figure 5. Qualitative MO diagram for the linear ground states of $[Ge,C,H]^{0/+}$; the dashed electron signifies the neutralisation of the cation to form the ground state configuration of the neutral

The Ge−C bond contraction upon formation of the ground state neutral (bond order 1.99) corresponds to 0.12 Å, which is significant considering the new Ge−C bond order is only 2.49, compared with 1.99 for the ground state cation. It is not surprising then that a significant signal for Ge^+ is detected in the NRMS spectrum of $GeCH^+$. For comparison, the typical bond length contraction for reduction of an alkane to an alkene is approximately 0.20 Å, and from an alkene to alkyne is 0.14 Å.[20]

The other noteworthy features of the NBO analysis of $^2\Pi$ GeCH are the extent to which the carbon atom is reduced, and the energy difference between the closed and half filled π-bonding MOs. To discuss the reduction of the carbon atom, first consider the natural electron configurations of the constituent atoms in $^2\Pi$ GeCH: $Ge(4s^{1.79}4p^{1.51})$ $C(2s^{1.44}2p^{3.41})$ $H(1s^{0.83})$. Comparison with the cation values presented above reveals the carbon atom to be sufficiently electronegative in the neutral to have gained $0.85e^-$, most of which comes from the metal. Even in the cation, the carbon atom has managed to extract 0.24 e^- from Ge. The origin of the energy splitting of the π MOs is more difficult to explain, but is probably due to closed-shell core-valence repulsions.

We have also performed NBO analyses for some of the neutral and cation excited states, and interesting aspects of the bonding and electronic features of these isomers is discussed in the following paragraphs. The first excited neutral state, $^2\Sigma$ GeCH, r_{GeC} = 1.667 Å, has a bond order of 2.99, and probably represents the best possibility of generating and observing a Lewis-type triple bond between Ge and C. Destabilisation of this isomer with respect to the ground state is due to excitation of a metal 4s electron from the σ-nonbonding orbital to the nearest π-bonding orbitals. This excitation costs 35.2 kcal mol^{-1}, ignoring additional molecular stabilisation gained by bond adjustments. The electronic configurations of the constituent atoms of this isomer are: $Ge(4s^{1.25}4p^{1.89})$ $C(2s^{1.30}2p^{3.77})$ $H(1s^{0.76})$. This suggests the electron promotion gives rise to a highly polar bonding arrangement in which a metal 4s electron is virtually transferred to the carbon atom, as confirmed by the calculated atomic charges: $Ge^{+0.85e}C^{-1.08e}H^{+0.24e}$. The first cation excited state is formed by the spin inversion of one of the two parallel-spin π-bonding electrons of the ground state isomer. Most of the inherent bonding features of this isomer are described in the NBO analysis of ground state $^3\Sigma$ $GeCH^+$, and no further discussion is warranted.

Before continuing with the relative structures of high energy excited states, it is acknowledged that at the full-CI level of theory, the particular cation configurations examined in the following paragraphs could correspond to transition structures on the potential energy hypersurface. For an understanding of the origins of Ge−C triple bond instability, a discussion of these structures cannot be overlooked.

The species with the shortest Ge−C bond lengths, and highest Ge−C bond orders, are the high energy excited states $^1\Sigma$ $GeCH^+$, r_{GeC} = 1.636 Å, and $^1\Sigma$ $HGeC^+$, r_{GeC} = 1.629 Å (see Table 2). The electronic configurations of the various constituent atoms in each isomer are: $Ge(4s^{0.94}4p^{1.50})$ $C(2s^{1.35}2p^{3.60})$ $H(1s^{0.61})$ and $H(1s^{0.83})$ $Ge(4s^{1.07}4p^{1.94})$ $C(2s^{1.30}2p^{2.87})$. It is immediately apparent that the electronic configuration of Ge in these high energy structures is approximately $4s^14p^2$, which corresponds to the excited cation state ^4P Ge^+. According to B3LYP/BS-II, the promotion energy required for hybridisation of Ge^+, in the absence of electric fields, is 6.5 eV ($^2\Pi$ $Ge^+ \rightarrow$ $^4\Pi$ Ge^+). The corresponding neutral value is 5.5 eV, whereas the promotion energy for CH (see Table 1), which for simplicity can be extracted from the $^2\Pi$ CH → $^4\Sigma$ CH excitation energy, amounts to 0.85 eV. It is clear that little, if

any, of this energy is recovered by GeC triple-bond stabilisation. Thus, it appears that the energy required to hybridise heavy group 14 congeners for triple-bond formation accounts for any relative destabilisation. The other characteristic feature of the excited states with short Ge−C bonds is the nature of the Ge−C σ bonding orbital. In the cation and neutral ground states, this orbital is a Ge($4p_z$) C($2sp_z$) hybrid, whereas the hybridisation for the excited cationic states is Ge(4s) C($2sp_z$). Moreover, this orbital has 47% Ge character in $^1\Sigma$ $GeCH^+$, 32% Ge character in $^1\Sigma$ $HGeC^+$ but only 18% Ge character in the cation ground state $^3\Sigma$ $GeCH^+$. This suggests the greater the carbon character of the Ge−C σ-bond, the greater the stability of the isomer.

Finally, it is interesting to compare the relative atomic charges of $^1\Sigma$ $GeCH^+$ and $^1\Sigma$ $HGeC^+$, which are: $Ge^{+1.58e}C^{-0.96e}H^{+0.38e}$ and $H^{+0.17e}Ge^{+1.01e}C^{-0.18e}$. On the basis of these values, it is expected that the $^1\Sigma$ $GeCH^+$ excited state would be more reactive than the $^1\Sigma$ $HGeC^+$ state, due to the much higher polarity of the Ge−C bond. Electronic reorganisation of $^1\Sigma$ $GeCH^+$ to a more stable open shell configuration would be favourable on the grounds of simple entropy arguments.

Experimental Section

For a detailed description of the experiment and the instrument used, the reader is advised to consult the recent review by Schalley et al.[21] In brief, the experiments were performed using a four-sector modified HF-ZAB AMD 604 mass spectrometer with BEBE configuration, where B and E represent magnetic and electric sectors respectively. $^{70}GeCH^+$ was generated by the 100 eV electron ionisation of trichloromethylgermane (Gelest Inc., PA, USA). The isotopomer $^{70}GeCH^+$ was selected for analysis as there are no isobaric interferences at *m*/*z* 83 due to other possibilities such as $GeCH_n$ (n = 0−3). Typical electron ionisation source conditions are as follows: source temperature 200°C; trap current 100 μA; repeller voltage 15 V; ion extraction voltage 8 kV; $m/\Delta m \geq 1500$. Collisional activation of B(1)/E(1)-mass selected $GeCH^+$ was effected in collision cells, positioned between E(1) and B(2), using He as a target gas. The collision cell pressure was maintained such that 80% of the parent ion beam was recovered after passing through this cell. This corresponds to an average of 1.1−1.2 collisions per ion.[22] CA products were recorded by scanning the second magnetic sector B(2).

NRMS experiments were performed for B(1)/E(1)-mass selected $GeCH^+$, utilising the dual collision cells between sectors E(1) and B(2). Cation neutralisation was achieved by collision with Xe at 80% transmittance, while reionisation was achieved by collision of the neutrals with O_2, again at 80% transmittance. Any ions remaining after the first collision event were deflected from the primary neutral beam using an electrode maintained at a high voltage (2 kV) positioned before the second collision cell. In order to detect a reionisation signal, the neutral species must be stable for approximately one microsecond. NRMS spectra were averaged over 100 acquisitions in order to obtain a sufficient S/N ratios, while CA spectra were averaged over 20−50 acquisitions.

The B3LYP calculations were performed using the Gaussian 94 software[23] on IBM RS/6000 computers running AIX 4.2.1. The structures of $[Ge,C,H]^+$ were investigated as follows: first, geometry optimisations were performed using the 3-parameter hybrid density functional method of Becke (B3LYP)[24] in conjunction with valence basis sets of double-zeta quality, and an effective core potential (ECP) replacing the $1s^2-3d^{10}$ electrons of Ge.[25] These basis sets are collectively referred to hereafter as BS-I. The nature of each stationary point located at this level of theory was then established via subsequent frequency analysis.

The optimised structures obtained using BS-I were then re-optimised using the all-electron 6-311G basis set of Krishnan and coworkers for C and H,[26] and the basis set of McGrath, Curtiss and coworkers for Ge.[27] The respective all-electron basis sets were supplemented with single p and d functions for Ge, one p and one d function for C, and one s and one p function for H. These basis sets are referred to as BS-II. The natural bond orbital analyses were performed at the re-optimised BS-II geometries using version 3.0 of the NBO code of Weinhold and coworkers.[28] In some instances, frequency analyses were repeated using BS-II at the optimised BS-II geometry to unambiguously establish the nature of low energy stationary points.

Acknowledgments

This research was supported by the Deutsche Forschungsgemeinschaft, the Volkswagen-Stiftung, and the Fonds der Chemischen Industrie. The Konrad-Zuse Zentrum, Berlin, is acknowledged for generous allocation of computer time. We would also like to thank Prof. Yitzhak Apeloig, for providing the inspiration to undertake this work during a recent visit to TU Berlin.

[1] R. Srinivas, D. Sülzle, H. Schwarz, *J. Am. Chem. Soc.* **1991**, *113*, 52.
[2] [2a] B. T. Luke, J. A. Pople, M. B. Krogh-Jesperson, Y. Apeloig, M. Karni, J. Chandrasekhar, P. von Rague-Schleyer, *J. Am. Chem. Soc.* **1986**, *108*, 270. – [2b] M. R. Hoffmann, Y. Yoshioka, H. F. Schaefer, *J. Am. Chem. Soc.* **1983**, *105*, 1084.
[3] Representative examples include: [3a] D. Schröder, C. A. Schalley, N. Goldberg, J. Hrušàk, H. Schwarz, *Chem. Eur. J.* **1996**, *2*, 1235. – [3b] C. A. Schalley, S. Blanksby, J. N. Harvey, D. Schröder, W. Zummack, J. H. Bowie, H. Schwarz, *Eur. J. Org. Chem.* **1998**, 987. – [3c] M. Brönstrup, D. Schröder, I. Kretzschmar, C. A. Schalley, H. Schwarz, *Eur. J. Inorg. Chem.* **1998**, 1529. – [3d] D. Schröder, C. Heinemann, H. Schwarz, J. N. Harvey, S. Dua, S. Blanksby, J. H. Bowie, *Chem. Eur. J.* **1998**, *4*, 2550. – [3e] M. Karni, Y. Apeloig, D. Schröder, W. Zummack, R. Rabezzana, H. Schwarz, *Angew. Chem.* **1999**, *111,* 206.
[4] To place silicon chemistry in perspective, even in the gas-phase the behaviour of this element is well-characterised. See the chapter by N. Goldberg, H. Schwarz, *Gas Phase Ion Chemistry of Silicon-containing Molecules*, and references therein. In: *The Chemistry of Organic Silicon Compounds, Vol II.* (Eds. Z. Rappoport, Y. Apeloig), J. Wiley & Sons, New York, **1998**, p 1105.
[5] N. N. Greenwood, A. Earnshaw, *The Chemistry of the Elements*, Pergamon Press, Oxford, **1984**.
[6] [6a] D. Dai, K. Balasubramanian, *J. Chem. Phys.* **1996**, *105*, 5901. – [6b] G. R. Burton, C. C. Arnold, C. Xu, D. M. Neumark, *J. Chem. Phys.* **1996**, *104*, 2757. – [6c] P. Jackson, K. J. Fisher, I. G. Dance, G. E. Gadd, G. D. Willett, *Int. J. Mass Spectrom. Ion Proc.* **1997**, *164*, 45. – [6d] Y. Negishi, H. Kawamata, T. Hayase, M. Gomei, R. Kishi, F. Hayakawa, A. Nakajima, K. Kaya, *Chem. Phys. Lett.* **1997**, *269*, 199. – [6e] P. W. Deutsch, L. A. Curtiss, J. P. Bladeau, *Chem. Phys. Lett.* **1997**, *270*, 413.
[7] [7a] L. Operti, M. Splendore, G. A. Vaglio, P. Volpe, M. Speranza, G. Occhiucci, *J. Organomet. Chem.* **1992**, *433*, 35. – [7b] P. Antoniotti, P. Benzi, F. Grandinetti, P. Volpe, *J. Phys. Chem.* **1993**, *97*, 4945. – [7c] M. Castiglioni, L. Operti, R. Rabezzana, G. A. Vaglio, P. Volpe, *Int. J. Mass Spectrom.* **1998**, *179/180*, 277.
[8] P. Jackson, Ph.D Thesis, University of New South Wales, **1998**.
[9] [9a] Y. Yamaguchi, C. A. Richards, H. F. Schaefer, *J. Chem.*

Phys. **1995**, *103*, 7975. – [9b] Y. Yamaguchi, H. F. Schaefer, *J. Chem. Phys.* **1996**, *104*, 9841.
[10] R. Becerra, S. E. Boganov, M. P. Egorov, V. I. Faustov, O. M. Nefedov, R. Walsh, *J. Am. Chem. Soc.* **1998**, *120*, 12657.
[11] M. Benavides-Garcia, K. Balasubramanian, *J. Chem. Phys.* **1992**, *97*, 7537.
[12] W. W. Harper, D. J. Clouthier, *J. Chem. Phys.* **1997**, *106*, 4367.
[13] W. W. Harper, C. M. Klusek, D. J. Clouthier, *J. Chem. Phys.* **1998**, *109*, 9300.
[14] See for instance: K. W. Klinkhammer, *Angew. Chem. Int. Ed. Engl.* **1997**, *36*, 2320.
[15] J. Goubeau, *Angew. Chem.* **1957**, *69*, 3.
[16] R. S. Mulliken, *J. Chem. Phys.* **1934**, *2*, 782.
[17] J. E. Huheey, *Inorganic Chemistry: Principles of Structure and Reactivity*, Third Edition, Harper Collins, New York, **1983**, pp 146–148.
[18] [18a] J. M. Pérez-Jordá, A. D. Becke, *Chem. Phys. Lett.* **1995**, *233*, 134. – [18b] E. Ruiz, D. R. Salahub, A. Vela, *J. Am. Chem. Soc.* **1995**, *117*, 1141.
[19] I. Shim, M. Sai Baba, K. A. Gingerich, *J. Phys. Chem. A* **1998**, *102*, 10763.
[20] J. March, *Advanced Organic Chemistry: Reactions, Mechanisms and Structure.* Fourth Edition, J. Wiley & Sons, New York, **1992**.
[21] C. A. Schalley, G. Hornung, D. Schröder, H. Schwarz, *Chem. Soc. Rev.* **1998**, *27*, 91.
[22] J. L. Holmes, *Org. Mass Spectrom.* **1985**, *20*, 169.
[23] M. J. Frisch, G. W. Trucks, H. B. Schlegel, P. M. W. Gill, B. G. Johnson, M. A. Robb, J. R. Cheeseman, T. A. Keith, G. A. Petersson, J. A. Montgomery, K. Raghavachari, M. A. Al-Laham, V. G. Zakrzewski, J. V. Ortiz, J. B. Foresman, J. Cioslowski, B. B. Stefanov, N. Nanayakkara, M. Challacombe, C. Y. Peng, P. Y. Ayala, W. Chen, M. W. Wong, J. L. Andres, E. S. Replogle, R. Gomperts, R. L. Martin, D. J. Fox, J. S. Binkley, D. J. DeFrees, J. Baker, J. P. Stewart, M. Head-Gordon, C. Gonzales, J. A. Pople, *Gaussian 94*, Gaussian Inc., Pittsburgh, Pennsylvania, **1995**.
[24] [24a] A. D. Becke, *Phys. Rev. A* **1988**, *38*, 3088. – [24b] A. D. Becke, *J. Chem. Phys.* **1993**, *98*, 5648. – [24c] C. Lee, W.Yang, R. G. Parr, *Phys. Rev. B.* **1988**, *37*, 785.
[25] [25a] P. J. Hay, W. R. Wadt, *J. Chem. Phys.* **1985**, *82*, 270. – [25b] W. R. Wadt, P. J. Hay, *J. Chem. Phys.* **1985**, *82*, 284. – [25c] P. J. Hay, W. R. Wadt, *J. Chem. Phys.* **1985**, *82*, 299.
[26] R. Krishnan, J. S. Binkley, R. Seeger, J. A. Pople, *J. Chem. Phys.* **1980**, *72*, 650.
[27] [27a] R. C. Binning, L. A. Curtiss, *J. Comp. Chem.* **1990**, *11*, 1206. – [27b] L. A. Curtiss, M. P. McGrath, J.-P. Blandeau, N. E. Davis, R. C. Binning, L. Radom, *J. Chem. Phys.* **1995**, *103*, 6104. – [27c] M. P. McGrath, L. Radom, *J. Chem. Phys.* **1991**, *94*, 511.
[28] [28a] J. P. Foster, F. Weinhold, *J. Am. Chem. Soc.* **1980**, *102*, 7211. – [28b] A. E. Reed, F. Weinhold, *J. Chem. Phys.* **1985**, *83*, 1736. – [28c] A. E. Reed, L. A. Curtiss, F. Weinhold, *Chem. Rev.* **1988**, *88*, 899.

Received March 4, 1999
[I99084]

Compounds of Silicon and Homologues, 127[1] Unsaturated Compounds of Silicon and Homologues, 54[2]

Tetrasupersilyl-tristannaallene and -tristannacyclopropene (tBu$_3$Si)$_4$Sn$_3$ – Isomers with the Shortest Sn=Sn Double Bonds to Date

Nils Wiberg,*[a] Hans-Wolfram Lerner,[a] Sham-Kumar Vasisht,[a] Susanne Wagner,[a] Konstantin Karaghiosoff,[a][+] Heinrich Nöth,[a][++] and Werner Ponikwar[a][++]

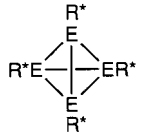
Dedicated to Professor Wolf-Peter Fehlhammer on the occasion of his 60th birthday

Keywords: Double Bonds / NMR Spectroscopy / Silicon / Tin / X-ray structure analyses

The dark blue, air- and moisture-sensitive, thermolabile tristannaallene R$^\star_2$Sn=Sn=SnR$^\star_2$ (**5**) (R* = SitBu$_3$) is prepared by reaction of Sn(OtBu)$_2$ or Sn[N(SiMe$_3$)$_2$]$_2$ with R*Na in pentane/benzene at –25°C. The dark red-brown, air-sensitive, moisture-insensitive, and thermostable cyclotristannene R$^\star_4$Sn$_3$ (**6**) with a –R*Sn=SnR*– moiety as part of a Sn$_3$ ring is obtained from the reaction of Sn(OtBu)$_2$ or Sn[N(SiMe$_3$)$_2$]$_2$ with R*Na in pentane at 25°C or from the isomerization of **5** at room temperature ($\tau_{1/2}$ = 9.8 h). According to the result of X-ray structural analyses the Sn$_3$ framework of chiral **5** is bent (156°) and the terminal Sn atoms have pyramidal surroundings. The SnSn double bonds in **5** (2.68 Å) are shorter than those found for the hitherto structurally investigated distannenes (2.77–2.91 Å). Even shorter is the double bond in **6** (2.59 Å). The unsaturated Sn atoms here have nearly planar surroundings in perfect analogy to the carbon atoms in CC double bonds. The SnSn double bond in **6** can therefore be considered as the first "true" Sn=Sn bond. The structures of **5** and **6** can be deduced also from ^{119}Sn- and ^{29}Si-NMR studies in solution.

The reaction of tin dichloride SnCl$_2$ with supersilyl sodium R*Na ("supersilyl" **R*** = tri-*tert*-butylsilyl SitBu$_3$) in tetrahydrofuran (THF) attracted our attention for two reasons:

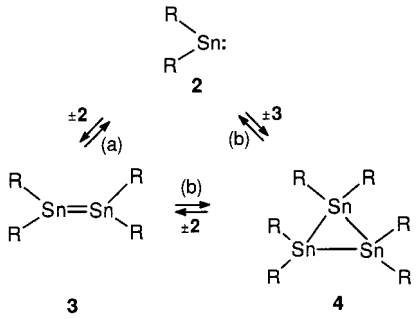
(i) By treating germanium dichloride (in form of its dioxane adduct) with an excess of supersilyl sodium in THF (molar ratio GeCl$_2$ to R*Na of 1:3) we synthesized in 1996 **1b**, the first molecular germanium compound with a Ge$_4$ tetrahedron[3]. Three years earlier we had already reported **1a**, the first molecular silicon compound with a Si$_4$ tetrahedron[4]. In continuation of our investigations we attempted the synthesis of **1c**, the first molecular tin compound bearing a Sn$_4$ tetrahedron by the analogous reaction of SnCl$_2$ with R*Na in THF.



R* = SitBu$_3$

1a : E = Si
1b : E = Ge
1c : E = Sn

(ii) The reaction of tin dichloride with the twofold molar amount of supersilyl sodium should yield in THF according to SnCl$_2$ + 2 R*Na → R*$_2$Sn + 2 NaCl the stannylene R*$_2$Sn as the first product. We hoped that it would be possible to isolate or detect the bis(supersilyl)stannylene as the monomer **2** or – less probable – as the dimer **3** or the trimer **4** at low enough temperatures [see Scheme 1, Equations (a) and (b), R = R*].



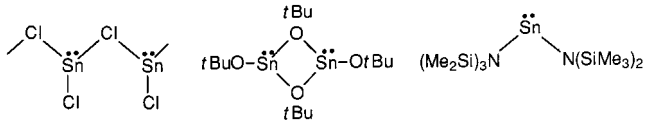
Scheme 1

In fact, a few distannenes of type **3** with organyl as well as silyl substituents R of *intermediate bulkiness* could be prepared and structurally characterized in the last years (see Table 1 and refs.[5–9]). NMR investigations reveal, however, that in solution these "bis(stannylenes)" **3** are in equilibrium with the corresponding "mono(stannylenes)" **2** and in one case[7] with the "tris(stannylene)" **4**. *Very bulky* organyl as well as silyl substituents (e.g. R = 2,4,6-tBu$_3$C$_6$H$_2$[9] and also R = R* [see below]) prevent the formation of distannenes **2** even in the solid state.

[a] Institut für Anorganische Chemie der Universität München, Butenandtstraße 5–13 (Haus D), D-81377 München, Germany
[+] NMR studies.
[++] X-ray structure analyses.

 © WILEY-VCH Verlag GmbH, D-69451 Weinheim, 1999 1434–1948/99/0808–1211 $ 17.50+.50/0

Electronegative substituents R can also stabilize the stannylenes **2**. In such cases with substituents of small, intermediate or large steric demand [e.g. R = Cl,[10] O*t*Bu,[11] or $N(SiMe_3)_2$[12]] they exist as oligomers, dimers, or monomers, respectively. In the oligomers and dimers R acts as a bridge between two tin atoms. As a consequence of the polymeric structure the dichloride **2a** is insoluble in hydrocarbons like pentane and soluble only in ethers like THF in which it forms adducts, whereas the dialkoxide **2b** and the diamide **2c** are soluble also in hydrocarbons.



2a: $(SnCl_2)_x$ **2b:** $[Sn(Ot\,Bu)_2]_2$ **2c:** $Sn[N(SiMe_3)_2]_2$

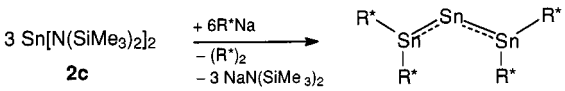
Here we first describe the reactions of the Sn^{II} compounds **2a**−**2c** with supersilyl sodium, which yield together with other products *tetrasupersilyl tristannaallene* **5** and *tetrasupersilyl tristannacyclopropene* **6** (referred to in the following as tristannaallene and cyclotristannene). The subsequent sections deal with the characterization as well as with multinuclear NMR and X-ray studies of the products **5** and **6**.

Preparation of the Tristannaallene 5 and Cyclotristannene 6

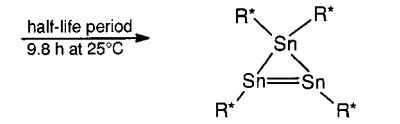
Some years ago[13] we observed that a solution of $SnCl_2$ (**2a**) in THF when added dropwise to a solution of the twofold molar amount of R*Na in THF at −78 °C followed by warming to ambient temperature gives a microcrystalline extremely air-sensitive blackish-brown *insoluble tin compound* (main product) and a dark brown solution. The latter contains a *soluble tin compound* as well as superdisilane $tBu_3Si{-}SitBu_3$.[14] We had obtained this soluble tin compound already as a product of the dehalogenation of disupersilyltin dichloride $R^*_2SnCl_2$ with sodium metal in benzene.[15] It is also formed from the reaction of $Sn(OtBu)_2$ (**2b**) or of $Sn[N(SiMe_3)_2]_2$ (**2c**) with supersilyl sodium in alkanes like pentane or heptane.

The chemical identity of the insoluble and the soluble tin compounds remained initially obscure. In a communication published recently[16] it is suggested that the insoluble tin compound probably has the tetrasupersilyl *tetrahedro* tetrastannane structure **1c**, whereas for the soluble tin compound a zwitterionic distannene structure $R^*_2Sn{\rightarrow}SnR^*_2$ was proposed. Both presumed structures are inconsistent with our results, however. According to our experience the tetrahedrane **1c** should be soluble in organic solvents and thus cannot account for the insoluble compound (cf. ref.[1]). Our analytical studies reveal that this compound must be a mixture of supersilyl, tin, and sodium containing products.[17] Chemical, NMR, and X-ray studies show the soluble tin compound to be the *cyclotristannene* **6** − a structure, which has been already reported by Sekiguchi et al. for the germanium homologue $R^*_4Ge_3$[18] and by Kira et al. for the silicon homologue $R_3R'Si_3$ ($R' = tBuMe_2Si$; $R = R'_3Si$).[19]

We could gain a deeper insight into the reaction pathway of Sn^{II} compounds with supersilyl sodium by studying the reaction of the diamide **2c** with donor free R*Na in pentane at low temperatures. It yields in the first stage according to Equation (1) together with superdisilane the *tristannaallene* **5** (at first we believed this product to be the expected tetrastannatetrahedrane **1c**[20]). The tristannaallene **5** rearranges at ambient temperature (25 °C), as shown by Equation (2) to the isomeric cyclotristannene **6**. This rearrangement implies the migration of one supersilyl substituent to the supersilyl free central tin atom with concomitant formation of a chemical bond between the outer tin atoms of the tristannaallene. An analogous reaction sequence is observed also for the reaction of **2b** with R*Na in pentane.

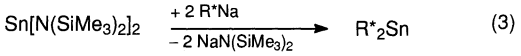


5 (1)

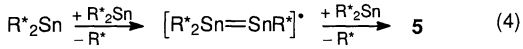


6 (2)

The formation of the tristannaallene **5** could proceed according to Equations (3) and (4) via the disupersilyl stannylene R^*_2Sn. The stannylene could subsequently add first one and than a second molecule R^*_2Sn with elimination of supersilyl radicals, which dimerize to give superdisilane. The intermediate formation of R^*_2Sn in pentane at −78 °C is supported by the fact that when the diamide **2c** is allowed to react with an equimolar amount of R*Na half of **2c** remains unchanged. Obviously due to steric reasons the stannylene R^*_2Sn cannot dimerize according to Equation (a) in Scheme 1, but loses, as shown by Equation (4), in the course of its "trimerization" two supersilyl groups. We have no proof for the existence of radicals $R^*_3Sn^{\bullet}_2$, which should form according to the mechanism suggested by Equation (4). We have noted, however, that in the course of the reaction of **2c** with R*Na in pentane at low temperatures the NMR signals of **2c** disappear, while a strong ESR signal appears. As the reaction proceeds further the ESR signal disappears and at the same time the NMR signals of **5** can be detected.



(3)

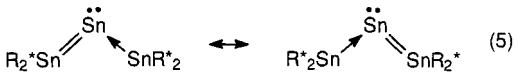


(4)

Characterization and Structure of the Tristannaallene 5

From a solution of **5** in 1.7 mL of pentane/0.1 mL of C_6D_6 at −25 °C, prepared from 0.7 mmol of $Sn[N(SiMe_3)_2]_2$ and 0.7 mmol of tBu_3SiNa in 0.7 mL of pentane/0.1 mL of C_6D_6 at −25 °C (cf. Experimental), dark blue crystals of **5** are formed within several days. These are sensitive to air as well as to moisture and slowly thermolyse at room temperature. Hereby, as shown in Equation (2) isomerization with formation of **6** takes place according to a first order reaction with half-life of 9.8 h at 25 °C.

The *structure* of the tristannaallene **5** results unambiguously from the $^{119}Sn\{^1H\}$- and $^{29}Si\{^1H\}$-NMR spectra, as well as from an X-ray structure analysis. In the *$^{119}Sn\{^1H\}$-NMR spectrum* (cf. Figure 1) two signals at low field (δ = 503, 2233, intensity ratio 2:1) are observed, which result from the isotopomers with ^{119}Sn in terminal and central position, respectively. The chemical shift of the terminal three-coordinate Sn atoms in **5** compares well with that of the distannene **3** with R = 2,4,6-iPr$_3$C$_6$H$_2$ (δ = 427.3[7]) − the only distannene known so far to be stable in solution at ambient temperature. In contrast, the NMR signal of the central two-coordinate Sn atom appears at much lower field in the same region where also the signals of the symmetrically and unsymmetrically substituted stannylenes **2** with $R_2 = (Me_3Si)_2C-CH_2-CH_2-C(SiMe_3)_2$ (δ = 2323[21]) as well as $[CH(SiMe_3)_2]_2$ (δ = 2328[22]) and R/R = 2,4,6-iPr$_3$C$_6$H$_2$/2,4,6-[(Me$_3$Si)$_2$CH]$_3$C$_6$H$_2$ (δ = 2208[23]) are found. This similarity suggests for the central tin atom in **5** a considerable stannylene character with a stereochemically active lone pair of electrons − a fact which is further supported by the bent Sn−Sn−Sn arrangement resulting from the X-ray structure analysis for the solid state (see below). Thus, the bonding situation in **5** is best described by the resonance formulae shown in Equation (5).



(5)

The ^{119}Sn-NMR signals of the central and terminal tin atoms are each accompanied by two pairs of satellites, which arise from the isotopomers having either one ^{119}Sn and one ^{117}Sn or two ^{119}Sn nuclei in one of the terminal positions and in the central position (Figure 1). The signal of the terminal tin atoms exhibits an additional pair of satellites, which results from the two-bond $^{119}Sn,^{117}Sn$ coupling of the isotopomer having one ^{119}Sn and one ^{117}Sn in the terminal positions. The observed value for the one-bond tin,tin coupling of 4302 Hz for $^1J(^{119}Sn,^{119}Sn)$ and 4117 Hz for $^1J(^{119}Sn,^{117}Sn)$ is considerably larger than $^1J(^{119}Sn,^{117}Sn)$ in the distannenes **3** with R = 2,4,6-iPr$_3$C$_6$H$_2$ (2930 Hz[24]) and R = CH(SiMe$_3$)$_2$ (1340 Hz, from the ^{119}Sn CPMAS spectrum[22]). This is in accord with the shorter Sn=Sn distance in **5** (2.68 Å) relative to the Sn=Sn distances reported so far for distannenes (2.76−2.94 Å; cf. Table 1). $^2J(^{119}Sn,^{117}Sn)$ is with 1679 Hz also remarkably large.[25]

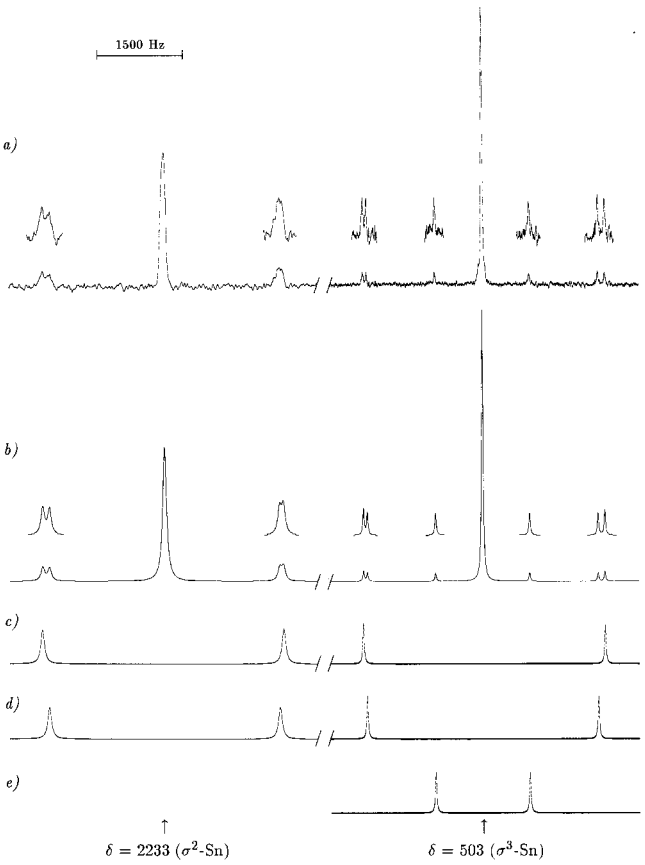


Figure 1. $^{119}Sn\{^1H\}$-NMR spectrum of the tristannaallene **5**: *a)* Observed spectrum at 100.7 MHz and −20 °C (ca. 0.1 M solution in [D$_8$]toluene, 10000 scans with 0.7 s repetition time). − *b)* Calculated total spectrum (Program DSYMPC, G. Hägele, R. Spiske, S. Goudetsidis, F. Mistry, University of Düsseldorf, **1994**), representing the sum of the spectra of all isotopomers with ^{119}Sn, and ^{119}Sn together with ^{117}Sn, weighted according to their natural abundances. The tin satellites of the low field signal originate from the superposition of the signals of the σ^2−Sn atom in the isotopomers with one additional ^{119}Sn (14.3% rel. intensity, $^1J(^{119}Sn,^{119}Sn)$ = 4302 Hz) and ^{117}Sn (12.7% rel. intensity, $^1J(^{119}Sn,^{117}Sn)$ = 4117 Hz) in the terminal positions. (cf. *c* and *d*) For the signal of the σ^3-Sn atoms the tin satellites result from the superposition of the signals of the isotopomers with one additional ^{119}Sn (7.2% rel. intensity) and ^{117}Sn (6.3% rel. intensity) in the central position, as well as ^{117}Sn (6.3% rel. int, $^2J(^{119}Sn,^{117}Sn)$ = 1679 Hz) in the other terminal position (cf. *c*, *d*, and *e*).

The *$^{29}Si\{^1H\}$-NMR spectrum* of **5** shows only one signal at δ = 77.3. It is accompanied by three pairs of satellites, arising from the isotopomers with one ^{119}Sn or ^{117}Sn nucleus in the three possible positions. From the satellites the values of 109 Hz for ^1J(Sn,Si), of 54 Hz for ^2J(Sn,Si), and of 12 Hz for ^3J(Sn,Si) can be estimated.

The dark-blue crystals of the tristannaallene, obtained from pentane/benzene at −25°C, contain according to the result of an *X-ray structure analysis* in the unit cell two independent molecules of **5**, which form an axially chiral pair of enantiomers. The structure of one of the molecules of **5**

in the unit cell is displayed in Figure 2 together with selected bond lengths and angles for both molecules **5**. Figure 3 shows Newman projections of both enantiomeric molecules **5** viewed in direction of the outer tin atoms of the Sn_3 chain together with selected fold and torsion angles.

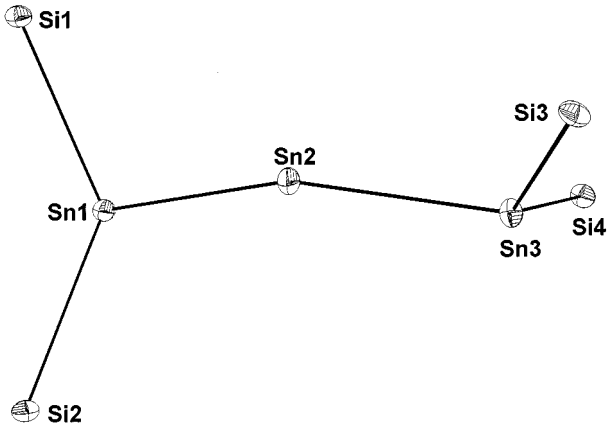


Figure 2. View of the crystal structure of one of the two enantiomers **5** in the unit cell (ORTEP, 25% thermal probability ellipsoide, tert-butyl groups omitted for clarity). Selected bond lengths [Å] and angles [°] (in brackets corresponding data of the other enantiomer **5** in the unit cell with Sn6/Sn5/Sn4/Si7/Si8/Si6/Si5 instead of Sn1/Sn2/Sn3/Si1/Si2/Si3/Si4; for folding and torsion angles see Figure 3): Sn1−Sn2 2.684 (1) [2.682(1)], Sn2−Sn3 2.675(1) [2.675(1)], Sn1−Si1 2.692(3) [2.694(3)], Sn1−Si2 2.689(3) [2.687(3)], Sn3−Si3 2.683(3) [2.701(3)], Sn3−Si4 2.696(3) [2.697(3)]. − Sn1−Sn2−Sn3 156.01(3) [155.81(3)], Si1−Sn1−Si2 134.29(9) [133.96(9)], Si1−Sn1−Sn2 100.58(7) [101.16(7)], Si2−Sn1−Sn2 109.39(7) [108.69(7)], Si3−Sn3−Si4 133.61(10) [134.38(10)], Si3−Sn3−Sn2 100.48(7) [99.94(6)], Si4−Sn3−Sn2 112.79(8) [113.01(8)].

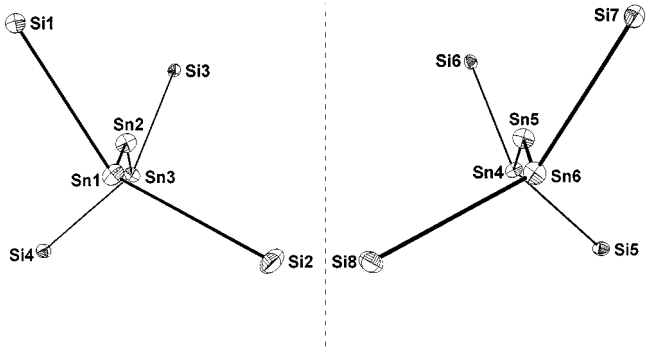
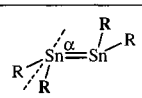


Figure 3. Newman projection of the two tristannaallene enantiomers **5** in the unit cell, viewed in direction Sn1−Sn3 and Sn6−Sn4. Folding angles [°] between the bisector b-Sn of the SiSnSi angles and the SnSn bonds as well as torsion angles [°] between the SiSn bonds of the two R^*_2Sn groups in **5** (for bond lengths and angles see Figure 2): b-Sn1/Sn1−Sn2 48.5, b-Sn3/Sn3-Sn2 43.4, b-Sn6/Sn6−Sn5 48.9, b-Sn4/Sn4−Sn5 43.3. − Si1−Sn1−Sn3−Si3 53.0, Si1−Sn1−Sn3−Si4 98.0, Si2−Sn1−Sn3−Si3 97.1, Si2−Sn1−Sn3−Si4 111.8, Si7−Sn6−Sn4−Si6 52.5, Si7−Sn6−Sn4−Si5 99.6, Si8−Sn6−Sn4−Si6 98.9, Si8−Sn6−Sn4−Si5 111.1.

The most striking feature of the structure of **5** are the short SnSn distances, for which an avarage value of 2.683 Å is found. The SnSn distances in **5** are thus shorter than all SnSn distances observed for distannenes so far

Table 1. Double bond lengths *d*(SnSn), fold angles α (cf. formula in the Table), and dihedral angles δ(**R**SnSn**R**) of distannenes **3** studied by X-ray structure analyses to date

R/R in 	*d* (SnSn)	α	δ(**R**SnSn**R**)	Ref.
$CH(SiMe_3)_2$ / $CH(SiMe_3)_2$	2.77 Å	41°	0°	[5]
R'_4C_6H / R'_4C_6H[a]	2.91 Å	21/64°	33/55°	[6]
Tip/Tip[b]	[b]			[7]
$Si(SiMe_3)_3$ / $Si(SiMe_3)_3$	2.83 Å	29°	63°	[8a]
$Si(SiMe_3)_3$ / 2,4,6-$(CF_3)_3C_6H_2$	2.83 Å	42°	0°	[8b]
Tristannaallene **5**[c]	2.68 Å	24/46°	—	present
Cyclotristannene **6**[c]	2.59 Å	< 5°		paper

[a] R'_4C_6H = 2-*t*Bu-4,5,6-Me_3C_6H. − [b] From solutions that contain 3 $(Tip_2Sn)_2$ ⇌ 2 $(Tip_2Sn)_3$ with Tip = 2,4,6-*i*$Pr_3C_6H_2$ only $(Tip_2Sn)_3$ crystallizes.[7] − [c] Mean values.

(2.77−2.91 Å; cf. Table 1), but longer than the one found for the Sn=Sn bond in **6** (2.59 Å, see below). This suggests, in accordance with the resonance formulae (5), a bond order between one and two for the SnSn bonds in **5**; in contrast, a bond order of nearly one for the "distannenes" is listed in Table 1 (cf. 2.85 Å for the Sn−Sn single bond length in **6**), as indicated by the resonance formulae

$$[R_2Sn{\rightarrow}SnR_2 \leftrightarrow R_2Sn{\leftarrow}SnR_2]. \quad (5)$$

Another interesting feature, which becomes evident from Figure 2, is − as already mentioned − the bent rather than linear Sn_3 chain in **5**. This is again in accordance with the resonance formulae (5), and consequently **5** does not represent a "real" homologue of an allene. Indeed, the observed SnSnSn bond angle of 155.9° is quite large (cf. NSnN angle in crystalline **2c**[12], 104.7°) − a consequence of the steric interactions of the supersilyl groups and perhaps also a consequence of a small participation of the lone pair of electrons at the central tin atom in the bond system of the Sn_3 fragment.

The two outer tin atoms of the Sn_3 chain in **5** have no planar surroundings, as is the case with the corresponding carbon atoms in allenes; they are located each at the top of a flat pyramid, the base of which is formed by two supersilyl groups and the inner Sn atom (sum of the angles at the outer Sn atoms on average 345.6°). The "folding angle" between the bisecting line of the SiSnSi angle and the bond axis between the outer and the central tin atoms falls with an average value of 46.0°, in the same range as the folding angles observed for distannenes (21−64°, cf. Table 1).

As a consequence of the steric pressure of the two Sn-bonded supersilyl groups the SiSnSi bond angle in the two R^*_2Sn groups of compound **5** is quite large and clearly exceeds 120° (on average 134.1°; cf. SiSnSi angle in $R^*_2SnCl_2$, 145.0°,[26] and in **6**, 131°, see below). The R^*_2Sn groups in **5** adopt − as the R_2C groups in allenes − a *gauche* configuration (cf. Figure 3). The four supersilyl groups in compound **5** occupy in close approximation the edges of a bis-

phenoid (cf. Figure 3). They cover the Sn_3 chain almost completely and prevent undesired reactions between the Sn_3 groups of different molecules. The SnSi distances (2.68−2.70 Å) are larger than the sum of the atomic radii $r_{Sn} + r_{Si}$ (1.40 + 1.17 = 2.57 Å[10]) − obviously a consequence of the mutual steric repulsion of the supersilyl groups.

Characterization and Structure of the Cyclotristannene 6

From a solution of **6** in 30 mL of *tert*-butyl methyl ether at −25 °C, prepared from 12 mmol of $Sn(OtBu)_2$ and 24 mmol of $tBu_3SiNa(THF)_2$ in 60 mL of pentane at −78 °C and 25 °C (cf. Experimental), dark red-brown crystals of **6** are formed within several days. These are sensitive to air, but stable to moisture at room temperature. As a solid, **6** decomposes at 166 °C; in benzene solution it slowly thermolyses at 100 °C with the formation of hexasupersilyl-*hexahedro*-octastannane $R^*_6Sn_8$.[17]

The *structure* of **6** − an isomere of tristannaallene **5** − with a distannene unit integrated in a Sn_3 ring is suggested by the $^{119}Sn\{^1H\}$- and the $^{29}Si\{^1H\}$-NMR spectra as well as by an X-ray structure analysis. The *$^{119}Sn\{^1H\}$-NMR spectrum* (cf. Figure 4) exhibits a signal at high field (δ = −694) together with a second signal at low field (δ = 412) with double intensity. The position of the low-field signal corresponds to that observed for the distannene **3** with R = 2,4,6-$iPr_3C_6H_2$ (δ = 427.3[7]) and for the terminal tin atoms in the tristannaallene **5** (s. above). Thus it can be unambiguously assigned to the three-coordinate tin atoms of the distannene unit in **6**. The high-field signal appears in the same region as the signals of the only cyclotristannanes **4** known so far with R = 2,6-$Et_2C_6H_3$ (δ = −416.5[6]) and with R = 2,4,6-$iPr_3C_6H_2$ (δ = −378.9[24]) and has to be assigned to the tetracoordinate tin atom in **6**.

The $^{119,117}Sn$ satellites originate from the isotopomer with two anisochronic ^{119}Sn nuclei and from the isotopomers with one ^{119}Sn and one ^{117}Sn nucleus and are clearly observable (Figure 4). The observed relative intensity of the tin satellites (22% for the low field signal and 28% for the high field signal) proves the presence of three tin atoms in the molecule and at the same time clearly excludes the zwitterionic distannene structure suggested in ref.[16]. The striking unsymmetrical arrangement of the satellites (Figure 4) is caused by the AX spectrum of the isotopomer with two anisochronous ^{119}Sn nuclei, which already slightly deviates from the first order. $^1J(^{119}Sn,^{117}Sn)$ between the two three-coordinate tin atoms of the distannene unit is 2110 Hz, almost half the coupling observed for **5** (see above), and roughly comparable to the Sn,Sn coupling constant in the distannene **3** with R = 2,4,6-$iPr_3C_6H_2$ (2930 Hz[7]). On the other hand the observed value is definitely larger than the one reported for the distannene **3** with R = $CH(SiMe_3)_2$ (1340 Hz[22]), for which an exceptionally weak Sn,Sn bond is discussed. The coupling constants $^1J(^{119}Sn,^{119}Sn)$ and $^1J(^{119}Sn,^{117}Sn)$ between the three- and the tetracoordinate

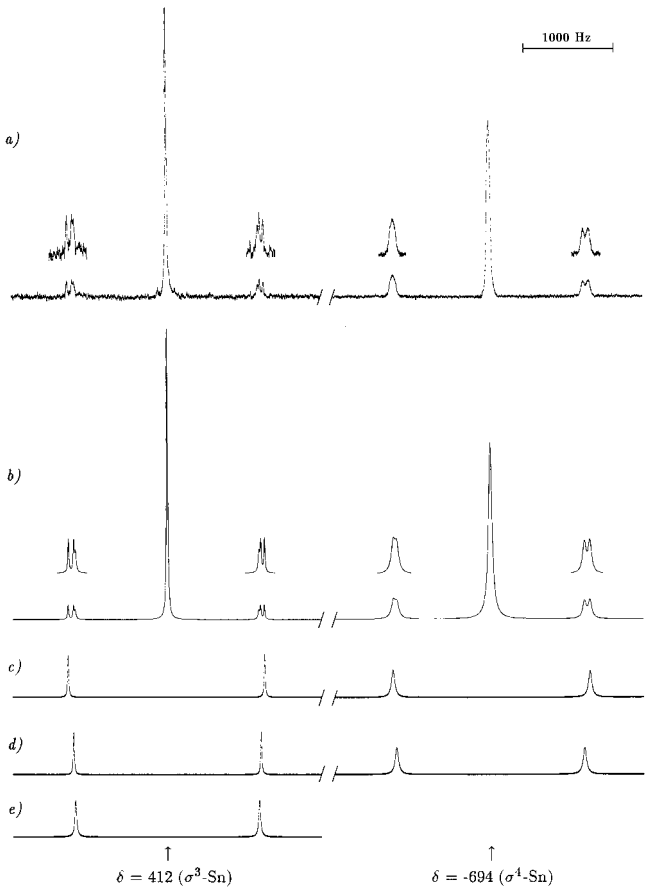


Figure 4. $^{119}Sn\{^1H\}$-NMR spectrum of the cyclotristannene **6**: *a)* Observed spectrum at 100.7 MHz (ca. 0.1 M solution in C_6D_6, 70000 scans with 0.7 s repetition time). − *b)* Calculated total spectrum (Program DSYMPC, G. Hägele, R. Spiske, S. Goudetsidis, F. Mistry, University of Düsseldorf, **1994**), resulting from the addition of the spectra of all isotopomers containing ^{119}Sn, and ^{119}Sn together with ^{117}Sn, weighted according to their natural abundances. The Sn satellites of the low-field signal originate from the superposition of signals of the σ^3-Sn atoms in the isotopomers with one additional ^{119}Sn in 3-position [7.2% rel. intensity, $^1J(^{119}Sn,^{115}Sn)$ = 2223 Hz], ^{117}Sn in 3-position (6.3% rel. intensity, $^1J(^{119}Sn,^{117}Sn)$ = 2123 Hz) and ^{117}Sn in 1(2)-position (6.3% rel. intensity, $^1J(^{119}Sn,^{117}Sn)$ = 2110 Hz) (cf. *c*, *d*, and *e*). For the high field signal the Sn satellites arise from the signals of the σ^4-Sn atom of the isotopomers with one additional ^{119}Sn (14.3% rel. intensity) and ^{117}Sn (12.7 rel. intensity) in 1(2)-position (cf. *c* and *d*).

Sn atoms in **6** of 2223 and 2123 Hz, respectively, are of the same order of magnitude as $^1J(^{119}Sn,^{117}Sn)$ in the cyclotristannanes **4** with R = 2,6-$Et_2C_6H_3$ (2285 Hz[6]) and with R = 2,4,6-$iPr_3C_6H_2$ (3017[24]).

The *$^{29}Si\{^1H\}$-NMR spectrum* of **6** shows, in accordance with the cyclotristannene structure, two signals of equal intensity at δ = 58.0 (for $Sn(SitBu_3)_2$) and at δ = 35.6 (for $SnSitBu_3$). Each of the two signals is accompanied by one pair of satellites, resulting from the isotopomers with one ^{119}Sn or ^{117}Sn directly bonded to the ^{29}Si nucleus. A $^1J(Sn,Si)$ of 81 Hz for the $SitBu_3$ groups at the distannene unit falls into the usual range. In contrast, an unusually small value[25] of $^1J(Sn,Si)$ = 12 Hz is observed for the $SitBu_3$ groups bonded to the tetracoordinate tin atom.

The dark red-brown crystals of the cyclotristannene, obtained from *tert*-butyl methyl ether at −25 °C, contain according to the result of an *X-ray structure analysis* two independent molecules **6** in the unit cell. Figure 5 shows the structure of one of the molecules **6**, as well as selected bond lengths and bond angles for both molecules. However, due to the poor quality of the crystals obtained from *t*BuOMe (no crystals could be obtained from heptane or benzene), only the positions of the Sn and Si atoms could be determined with sufficient accuracy.

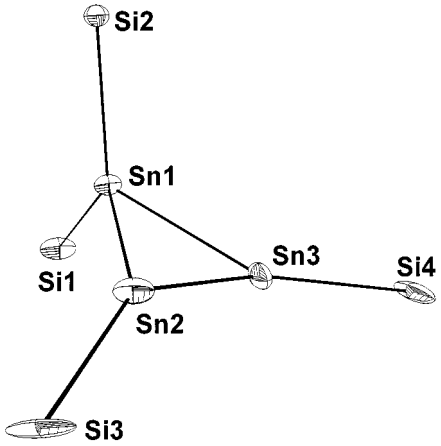


Figure 5. View of the molecular core of one of the two crystallographically independent cyclotristannene molecules **6** in the unit cell (ORTEP plot, 25% thermal probability ellipsoids, *tert*-butyl groups omitted for clarity). Selected bond lengths [A] and angles [°] (in brackets corresponding data of the second molecule **6** in the unit cell with Sn4/Sn5/Sn6 instead of Sn1/Sn2/Sn3): Sn1−Sn2 2.852(2) [2.841(3)], Sn1−Sn3 2.859(3) [2.846(2)], Sn2−Sn3 2.601(3) [2.582(4)]. − Sn2−Sn1−Sn3 54.19(7) [53.99(8)], Sn1−Sn2−Sn3 63.05(7) [63.07(8)], Sn2−Sn3−Sn1 62.76(6) [62.94(7)]. − Angle sum at Sn2/Sn3 350.8/355.8, at Sn5/Sn6 359.6/360.0.

The most striking feature in the structure of **6** is the SnSn double bond length in the Sn_3 rings, for which an average value of only 2.59 Å is found. The cyclotristannene **6** exhibits thus the shortest Sn=Sn bond of all structurally investigated distannenes so far (cf. Table 1). The Sn=Sn moiety has a nearly planar surrounding, formed by the directly attached Si atoms and by the tetracoordinate Sn atom. Thus the "distannene" **6** is the first compound with a Sn=Sn bond analogous to C=C bonds. As in the case of other analogous of the C=C bond, the length of a "true" Sn=Sn bond can be calculated as the sum of the atom radii, each reduced by 0.1 Å ($2 \times r_{Sn} - 0.2 = 2 \times 1.40 - 0.2 = 2.60$ Å[10]). The SnSn single bond lengths in the Sn_3 rings are with an average value of 2.85 Å somewhat longer than the sum of the Sn atom radii (2.80 Å).

The four supersilyl groups in compound **6** occupy roughly the edges of a tetrahedron, thus adopting a close packing. They cover the Sn_3 ring almost completely and prevent it from reacting with the Sn_3 ring of another molecule. The distances between the Si atoms and the attached unsaturated Sn atoms in **6** of 2.57−2.60 Å fall within the usual range ($r_{Sn} + r_{Si} = 1.40 + 1.17 = 2.57$ Å). On the other hand the distances of the Si atoms bonded to the saturated Sn atom in the cyclotristannene (2.72−2.76 Å) are clearly elongated as a consequence of the steric interactions between the two supersilyl groups.

Experimental Section

All experiments were carried out in flame-dried glass apparatus with the Schlenk technique under dry argon atmosphere. During all manipulations air and moisture were strictly excluded. *t*Bu_3SiNa (in pentane),[27] *t*Bu_3SiNa (in THF),[27] Sn(O*t*Bu)$_2$,[11] and Sn[N(SiMe$_3$)$_2$]$_2$[12] were prepared according to literature procedures. The solvents (pentane, benzene, tetrahydrofuran) were distilled from sodium/benzophenone immediately before use. − The NMR spectra were recorded with a JEOL GSX-270 (^{1}H/^{13}C/^{29}Si/^{119}Sn: 270.17/67.94/53.67/100.75 MHz) and a JEOL EX-400 (^{1}H/^{13}C/^{29}Si/^{119}Sn: 399.78/100.54/79.43/149.08 MHz) spectrometer. The ^{29}Si-NMR spectra were recorded with the INEPT pulse sequence using empirically optimized parameters for polarization transfer from the *t*Bu substituents. For the ^{119}Sn-NMR spectra an acquisition time of 0.3−0.4 s and a repetition rate of ca. 0.6 s were used; for 0.1 m solutions of the tin compounds typically 5000 scans were necessary to obtain spectra with satisfactory signal to noise ratio.

Formation of 5 from Sn[N(SiMe$_3$)$_2$]$_2$: A solution of 0.311 g (0.708 mmol) of Sn[N(SiMe$_3$)$_2$]$_2$ in 0.7 mL of pentane and 0.1 mL of C_6D_6 was added dropwise to 0.152 g (0.685 mmol) of solid *t*Bu_3SiNa at −196 °C. The resulting reaction mixture was warmed to −25 °C. At this temperature the reaction solution contains, according to the ^{119}Sn-NMR spectrum, **5** (see below), **6** (see below), Sn[N(SiMe$_3$)$_2$]$_2$,[12] and a still unidentified tin compound **7** bearing *t*Bu_3Si as well as Me_3Si groups and two equivalent tin atoms [integral ratio of the ^{119}Sn NMR signals of **5** (1 + 2 Sn atoms), **6** (1 + 2 Sn atoms), **7** (2 Sn atoms) = (7 + 14):(1/2 + 1):5].[28] In the ^{29}Si-NMR spectrum of the reaction solution at −25 °C in addition to **5**, **6**, Sn[N(SiMe$_3$)$_2$]$_2$, and **7**, as well as *t*Bu_3Si−Si*t*Bu_3 (δ = 35.2) and *t*Bu_3SiH (δ = 17.4) can be identified. The reaction solution was separated at −25 °C from the precipitate formed, which was then washed with pentane (1 mL). The combined pentane solutions are kept at −25 °C for several days during which time dark blue crystals of *tetrakis(tri-tert-butylsilyl)tristannaallene* (**5**) (0.040 g, 0.035 mmol, 20%) are formed. − ^{1}H NMR (C_6D_6, −25 °C, TMS internal reference (int.)): δ = 1.40 (s, 4 Si*t*Bu_3). − ^{29}Si NMR (C_6D_6, −25 °C, TMS external reference (ext.)) and ^{119}Sn NMR ($C_6D_5CD_3$, −20 °C, $SnMe_4$ ext.): Cf. general part and Figure 1. − X-ray structure analysis. Cf. Figure 2 and 3.

Formation of 5 from Sn(O*t*Bu)$_2$: In an NMR tube 0.055 g (0.207 mmol) of Sn(O*t*Bu)$_2$ and 0.046 g (0.207 mmol) of *t*Bu_3SiNa are dissolved in 0.6 mL of C_6D_6 and the solution was immediately cooled to −25 °C. The reaction mixture instantly adopts a black color. The ^{29}Si-NMR spectrum of the reaction solution shows after warming to ambient temperature the signals of *t*Bu_3Si−Si*t*Bu_3, *t*Bu_3SiH, and **5**.

Formation of 6 from Sn(O*t*Bu)$_2$: A solution of 3.179 g (12.00 mmol) of Sn(O*t*Bu)$_2$ in 20 mL of pentane was added dropwise at −78 °C to a solution of 8.799 g (24.00 mmol) of *t*Bu_3SiNa(THF)$_2$ in 60 mL of pentane. After stirring for 3 d at −78 °C and for further 2 d at ambient temperature the reaction solution contains, according to the ^{1}H-NMR spectrum, in addition to supersilane *t*Bu_3SiH (formed from the hydrolysis of *t*Bu_3SiNa) practically only *t*Bu_3Si−Si*t*Bu_3 and **6** in a molar ratio of 1.1 (in the case the formation of **6** would proceed exclusively via (1) and (2) the molar ratio should amount to 1.0). The solvent and all volatile components are removed in vacuo, the remaining brown residue was stirred with 50 mL of *n*-heptane, and the insoluble materials (mainly NaO*t*Bu and small

amounts of an insoluble tin compound) are separated by filtration. The solvent was removed from the filtrate in vacuo and the residue left dissolved in 20 mL of pentane. In the course of 2 weeks at −23 °C one part of the dissolved superdisilane crystallizes from the pentane solution and was separated by filtration. The pentane filtrate was subjected to flash chromatography on an Al_2O_3 column with *n*-heptane as mobile phase. The heptane was removed in vacuo and the residue dissolved in 30 mL of *t*BuOMe. After several days *1,2,3,3-tetrakis(tri-tert-butylsilyl)cyclotristannene* (**6**; 1.244 g, 1.080 mmol, 27%) crystallizes from this solution at −25 °C as dark red-brown rods. − ^{1}H NMR (C_6D_6, TMS int.): δ = 1.409 (s; 2 SnSi*t*Bu$_3$), 1.515 [s; Sn(Si*t*Bu$_3$)$_2$]. − ^{13}C{^{1}H} NMR ($C_6D_5CD_3$, TMS int.): δ = 29.05/34.66 (*C*Me$_3$/C*Me*$_3$ of 2 SnSi*t*Bu$_3$), 26.42/32.55 [*C*Me$_3$/C*Me*$_3$ of Sn(Si*t*Bu$_3$)$_2$]. − ^{29}Si (C_6D_6, TMS ext.) and ^{119}Sn NMR (C_6D_6, SnMe$_4$ ext.): Cf. General part and Figure 4. − X-ray structure analysis: Cf. Figure 5.

Thermolysis of 5: A solution of 0.152 g (0.306 mmol) of Sn[N(SiMe$_3$)$_2$]$_2$ in 0.6 mL of C_6D_6 was added to 0.059 g (0.265 mmol) of *t*Bu$_3$SiNa and the resulting blue reaction solution was investigated by ^{1}H and ^{29}Si NMR. Every 24 min a ^{1}H-NMR spectrum (16 scans, PD = 2.5 s) was recorded at 25 °C for a total of 27 ^{1}H-NMR spectra. Between every two ^{1}H experiments a ^{29}Si-NMR spectrum was recorded in order to control the course of the reaction. The first recorded ^{1}H-NMR spectrum showed the following signals: δ = 1.407 (**5**, rel. intensity 2.69), 1.476 and 1.378 (**6**, rel. intensity of both signals together 2.19), 1.365 (*t*Bu$_3$Si−Si*t*Bu$_3$, rel. intensity 1.67), 1.118 (*t*Bu$_3$SiH, rel. intensity 2.65), 1.343 and 0.456 (**7**, rel. intensity of both signals together 2.76), 0.274 {Sn[N(SiMe$_3$)$_2$]$_2$, rel. intensity 11.5}. The intensities of the ^{1}H-NMR signals as resulting from the evaluation of the integrals, are assumed to correspond to the relative concentrations of the single compounds in the reaction solution. To determine the reaction order ln(signal region **5** + signal region **6**/signal region **5**) was plotted against the time *t*, where signal regions **5** and **6** are the relative intensities of the ^{1}H-NMR signals of **5** and **6** (both signals of **5** as well as **6** together), respectively. The half-life of the first-order isomerization was determined to be 9.8 h at 25 °C.

X-ray Structure Determination of 5: Siemens P4 diffractometer, Mo-K_α radiation, graphite monochromator, CCD area detector, crystal dimensions 0.2 × 0.15 × 0.1 mm. The crystal was mounted in perfluoro ether oil, T = 183(2) K, $C_{48}H_{108}Si_4Sn_3$, M_r = 1153.77, deep purple prism, orthorhombic, a = 28.7513(6), b = 12.1963(2), c = 33.3574(2) Å, α = β = γ = 90°, V = 11697.1(4) Å^3, Z = 8; space group *Pca*2(1), ρ_{cacd} = 1.310 Mg m^{-3}, μ = 1.381 mm^{-1}, F(000) = 4816. *Data collection*: 2 θ from 2.44 to 58.38°, $-38 \le h \le 30$, $-15 \le k \le 15$, $-41 \le l \le 41$; of 64648 reflections 22638 were independent (R_{int} = 0.1221) and 14134 were observed [$F > 4\sigma(F)$], semiempirical absorption correction with SADABS (max./min. transmission 0.9765/0.8571), R_1 = 0.0708, wR_2 = 0.0801 [$F > 4\sigma(F)$], GOOF (F^2) = 0.989; maximum residual electron density 1.226 eÅ^{-3}. *Structure determination:* The structure was solved by direct methods (SHELXL-97). The absolute structure could not be determined. Three C atoms could only be refined with isotropic displacement parameters. The structure has not been completely refined until now.[29]

X-ray Structure Determination of 6: Siemens P4 diffractometer, Mo-K_α radiation, graphite monochromator, CCD area detector. It was extremely difficult to select a suitable crystal from the almost brown-black solution, and a large number of crystals were tested. The crystals were mounted in perfluoro ether oil, T = 183(2) K, $C_{48}H_{108}Si_4Sn_3$, M_r = 1153.77, deep red-brown plates. The best crystal 0.2 × 0.15 × 0.1 mm, gave the following monoclinic cell: a = 13.133(3), b = 29.956(6), c = 16.752(3) Å, β = 95.365(8)°, V = 6561.4 Å, Z = 4. In spite of absorption correction (SADABS), it was difficult to find an acceptable space group. For the best crystal it was space group *P*2(1). Structure solution by the heavy atom method revealed clearly the Sn_3Si_4 core of the molecule. The Sn−Si atom distances covered the range from 2.567(7) to 2.763(7) Å. Almost all *tert*-butyl groups showed rotational disorder. Therefore, the R_1 value of the "best" solution is only 17%. This is of course rather unsatisfactory; however, the data for the Sn−Sn distances are reliable if the esd′s are considered.

[1] Part 126: N. Wiberg, H.-W. Lerner, H. Nöth, W. Ponikwar, *Angew. Chem.* **1999**, *111*, 1176, *Angew. Chem. Int. Ed. Engl.* **1999**, *38*, 1103.

[2] Part 53: N. Wiberg, H. Auer, H. Nöth, J. Knizek, K. Polborn, *Angew. Chem.* **1998**, *110*, 3030; *Angew. Chem. Int. Ed. Engl.* **1998**, *37*, 2869.

[3] N. Wiberg, W. Hochmuth, H. Nöth, A. Appel, M. Schmidt-Amelunxen, *Angew. Chem*. **1996**, *108*, 1437; *Angew. Chem. Int. Ed. Engl.* **1996**, *35*, 1333.

[4] N. Wiberg, C. M. M. Finger, K. Polborn, *Angew. Chem.* **1993**, *105*, 1140; *Angew. Chem. Int. Ed. Engl.* **1993**, *32*, 1054.

[5] D. E. Goldberg, D. H. Harris, M. F. Lappert, K. M. Thomas, *J. Chem. Soc., Chem. Commun.* **1976**, 261; D. E. Goldberg, P. B. Hitchcock, M. F. Lappert, K. M. Thomas, T. Fjeldberg, A. Haarland, B. E. R. Schilling, *J. Chem. Soc., Dalton Trans.* **1986**, 2387 and refs. cited therein.

[6] G. Trinquier, J. P. Malrieu, *J. Am. Chem. Soc.* **1987**, *109*, 5303; M. A. D. Bona, M. C. Cassani, J. M. Keates, G. A. Lawlen, M. F. Lappert, M. Stürmann, M. Weidenbruch, *J. Chem. Soc., Dalton Trans.* **1998**, 1187 and refs. cited therein.

[7] S. Masamune, L. R. Sita, *J. Am. Chem. Soc.* **1985**, *107*, 6390.

[8] [8a] K. W. Klinkhammer, W. Schwarz, *Angew. Chem.* **1995**, *107*, 1448; *Angew. Chem. Int. Ed. Engl.* **1995**, *34*, 1334. − [8b] K. W. Klinkhammer, T. F. Fässler, H. Grützmacher, *Angew. Chem.* **1998**, *110*, 114; *Angew. Chem. Int. Ed. Engl.* **1998**, *27*, 124.

[9] M. Weidenbruch, J. Schlaefke, A. Schäfer, K. Peters, H.G.v. Schnering, H. Marsmann, *Angew. Chem.* **1994**, *106*, 1938; *Angew. Chem. Int. Ed. Engl*. **1994**, *33*, 1846.

[10] Holleman-Wiberg, *Lehrbuch der Anorganischen Chemie*, De-Gruyter, Berlin, **1995**.

[11] T. Fjeldberg, P. B. Hitchcock, M. F. Lappert, S. J. Smith, A. J. Thome, *J. Chem. Soc., Chem. Commun.* **1985**, 939.

[12] D. H. Harris, M. F. Lappert, *J. Chem. Soc., Chem. Commun.* **1974**, 895; T. Fjeldberg, H. Hope, M. F. Lappert, P. P. Power, A. J. Thorne, *J. Chem. Soc., Chem. Commun.* **1983**, 639.

[13] W. Hochmuth, Diploma Thesis, University of Munich, **1994**.

[14] N. Wiberg, H. Schuster, A. Simon, K. Peters, *Angew. Chem.* **1986**, *98*, 100; *Angew. Chem. Int. Ed. Engl.* **1986**, *25*, 79.

[15] T. Passler, PhD Thesis, University of Munich **1993**; N. Wiberg in *Progress in Organosilicon Chemistry* (Eds.: B. Marciniec, J. Chojnowski), Gordon and Breach Publishers, **1995**, 19−39.

[16] M. Weidenbruch, A. Stilter, H. Marsmann, K. Peters, H. G. von Schnering, *Eur. J. Inorg. Chem.* **1998**, 1333.

[17] [17a] Definite, poorly soluble products − namely R*$_6$Sn$_6$ with Sn_6 prismane framework (cf. ref.[1]) and R*$_6$Sn$_8$Na$_2$(THF)$_4$ with Sn_8 cubane framework (cf. ref.[17b]) − can be obtained when **2c** is added to R*Na in ethers (in alkanes the title compounds **5** and **6** are formed). − [17b] N. Wiberg, H.-W. Lerner, S. Wagner, H. Nöth, T. Seifert, *Z. Naturforsch., B*, in press.

[18] A. Sekiguchi, H. Yamazaki, C. Kabato, H. Sakurai, *J. Am. Chem. Soc.* **1995**, *117*, 8025; A. Sekiguchi, M. Tsukamoto, M. Ichinohe, *Science* **1997**, *275*, 60.

[19] T. Iwamoto, C. Kabuto, M. Kira, *J. Am. Chem. Soc.* **1999**, *121*, 886.

[20] N. Wiberg, *Coord. Chem. Rev.* **1997**, *163*, 217, cit. Refs.

[21] R. Kira, R. Yanchibara, R. Hirano, C. Kabato, H. Sakurai, *J. Am. Chem. Soc.* **1991**, *113*, 7785.

[22] W. Zilm, G. A. Lawless, R. M. Merill, J. M. Millar, G. G. Webb, *J. Am. Chem. Soc.* **1987**, *109*, 7236.

[23] N. Tokitoh, M. Saito, R. Okazaki, *J. Am. Chem. Soc.* **1993**, *115*, 2065.

[24] S. Masamune, L. R. Sita, D. J. Williams, *J. Am. Chem. Soc.* **1983**, *105*, 630.

[25] B. Wrackmeyer, *Ann. Rep. NMR Spectrosc.* **1985**, *16*, 73−186.

[26] N. Wiberg in *Progress in Organosilicon Chemistry* (Eds. B. Marciniec, J. Chojnowski), Gordon and Breach Publishers, Basel, **1995**, S. 31.
[27] N. Wiberg, K. Amelunxen, H.-W. Lerner, H. Schuster, H. Nöth, I. Krossing, M. Schmidt-Amelunxen, T. Seifert, *J. Organomet. Chem.* **1997**, *542*, 1.
[28] Compound **7** is formed in much better yield from the reaction of 0.381 g (1.713 mmol) of tBu$_3$SiNa with 0.369 g (0.840 mmol) of Sn[N(SiMe$_3$)$_2$]$_2$ in 15 mL of pentane at −78 °C, followed by complete evaporation of the pentane in vacuo, dissolution of the remaining residue in 10 mL of benzene and stirring of the benzene solution for several days.
[29] Crystallographic data (excluding structure factors) for compound **5** reported in this paper have been deposited with the Cambridge Crystallographic Data Centre as supplementary publication no. CCDC-117961. Copies of the data can be obtained free of charge on application to CCDC, 12 Union Road, Cambridge CB2 1EZ, UK [fax: (+44) 1223/ 336-033; E-mail: deposit@ccdc.cam.ac.uk].

Received April 9, 1999
[I99105]

Chiral Phosphoramidite Ligands Based on 8-Chloroquinoline and Their Rhodium(III), Palladium(II), and Platinum(II) Complexes

Giancarlo Franciò,[a] Carmela G. Arena,[a] Felice Faraone,*[a] Claudia Graiff,[b] Maurizio Lanfranchi,[b] and Antonio Tiripicchio[b]

Keywords: Phosphoramidite / Chiral ligands / Platinum / Rhodium

The new chiral ligands 2-butyl-8-chloro-1-(4,8-di-*tert*-butyl-2,10-dimethoxy-5,7-dioxa-6-phosphadibenzo[*a*,*c*]cyclohepten-6-yl)-1,2-dihydroquinoline (BIPHENPHOSHQUIN, **3**) and 2-butyl-8-chloro-1-(3,5-dioxa-4-phosphacyclohepta[2,1-*a*;3,4-*a*′]-dinaphthalen-4-yl)-1,2-dihydroquinoline (BINAPHOSHQUIN, **4**; **4a**: S_aR_C, **4b**: S_aS_C) have been synthesized starting from the rigid backbone of 8-chloroquinoline. The reactions of **3** and **4** with rhodium(I), palladium(II), and platinum(II) substrates are reported. The reaction of **3** with $[Rh(CO)_2Cl]_2$ in a 2:1 molar ratio in hexane afforded a binuclear chloro-bridged rhodium(III) species by intramolecular oxidative addition of the C–Cl bond of ligand **3** across the rhodium(I) centers. The rhodium(III) complex **5**, incorporating the enantiomers S_aR_C-**3** and R_aS_C-**3**, has been fully characterized by X-ray diffractometry. Reactions of $[Pd(PhCN)_2Cl_2]$ with the ligands **3** and **4a** in 1:2 molar ratio in toluene afforded the products *cis*-$[Pd(\mathbf{3})_2Cl_2]$ (**9**) and *cis*-$[Pd(\mathbf{4a})_2Cl_2]$ (**10**). Similarly, reaction of $[Pt(COD)I_2]$ with **4a** in a 1:2 molar ratio afforded the complex *cis*-$[Pt(\mathbf{4a})_2I_2]$ (**11**). An X-ray analysis has been carried out to obtain information on the effect of the ligand **4a** on the overall structure of **11**.

Introduction

Recently, much attention has been focused on the development of chiral ligand-modified catalysts for application in asymmetric synthesis.[1] Attempts have been made to correlate structural and electronic characteristics of the coordinated ligands with the catalytic activities of the resulting metal complexes. The structural features of the ligands, such as the "natural bite angle",[2] the rigidity, and the presence of bulky substituents, drastically influence the chemo- and regioselectivity of the catalytic process.[3] Recent contributions[4] have shown that diphosphites or a mixed phosphane/phosphite containing a chiral bridging moiety are efficient ligands in the rhodium-catalyzed asymmetric hydroformylation of olefinic substrates. Several mono- and bidentate phosphane ligands have been prepared starting from molecules with rigid polyaromatic backbones.[5] Their abilities in determining unusual geometries when coordinated to a metal center are of great interest.

The present work stems from our interest in developing large chiral mono- and bidentate ligands starting from the rigid backbone of quinolines, and to study the properties of their d^8-metal complexes, particularly in homogeneous catalysis. We report here the synthesis of large chiral monodentate phosphoramidites, and of their rhodium(III), palladium(II), and platinum(II) complexes, together with the X-ray structures of some representative compounds of this series. Recently,[6] phosphoramidite ligands have been used in homogeneous catalysis. Several metal complexes incorporating ligands based on quinolines, such as 8-(dimethylphosphanyl)quinoline, 8-(dimethylarsanyl)quinoline, 8-(diphenylphosphanyl)quinoline, 8-(diphenylarsanyl)quinoline, bis(6-methylquinolin-8-yl)phenylarsane, tris(6-methylquinolin-8-yl)phenylarsane, (*R*)- and (*S*)-methylphenyl(8-quinolyl)phosphane, and (*R*)- and (*S*)-methylphenyl(8-quinolyl)-arsane, have previously been reported.[7] Application of ligands **3** and **4** in copper-catalyzed enantioselective Michael addition will soon be reported.[8]

[a] Dipartimento di Chimica Inorganica, Chimica Analitica, Chimica Fisica, Università di Messina,
Salita Sperone, 31, Vill. S. Agata, I-98166 Messina, Italy
[b] Dipartimento di Chimica Generale ed Inorganica, Chimica Analitica, Chimica Fisica, Centro di Studio per la Strutturistica Diffrattometrica del C.N.R., Università di Parma,
Viale delle Scienze, 78, I-43110 Parma, Italy

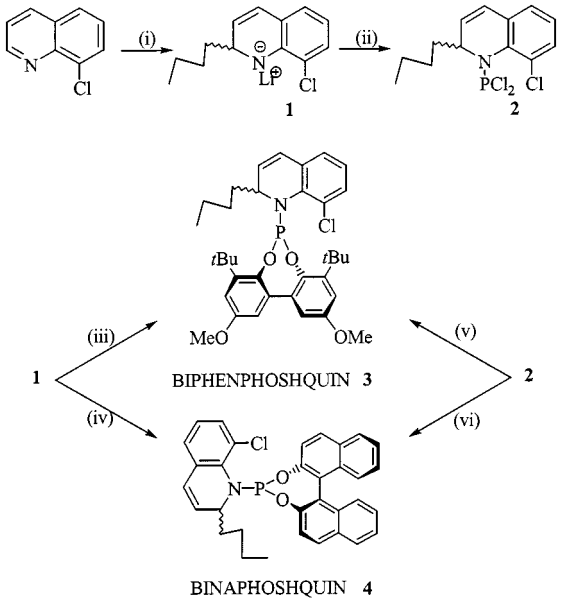
Results and Discussion

Synthesis of the Ligands

Reaction of 8-chloroquinoline with *n*BuLi[9] in a 1:1 molar ratio in tetrahydrofuran at −78 °C involves addition of the butyl group to the carbon atom in the 2-position and lithiation of the nitrogen atom. Consequently, the ring containing the nitrogen atom loses its aromaticity and the carbon atom in the 2-position becomes a stereogenic center. Addition of an excess of neat PCl_3 to the THF solution of anion **1** affords, after removal of the unreacted PCl_3 under reduced pressure, compound **2** (Scheme 1). Subsequent treatment of a solution of **2** in toluene at 0 °C with equimolar amounts of 3,3′-di-*tert*-butyl-2,2′-dihydroxy-5,5′-dimethoxybiphenyl and NEt_3 affords the ligand 2-butyl-8-chloro-1-(4,8-di-*tert*-butyl-2,10-dimethoxy-5,7-dioxa-6-phosphadibenzo[*a*,*c*]cyclohepten-6-yl)-1,2-dihydroquinoline (BIPHENPHOSHQUIN, **3**) (Scheme 1).

Compound **3** was also obtained by treating 4,8-di-*tert*-butyl-6-chloro-2,10-dimethoxy-5,7-dioxa-6-phosphadibenzo-

 © WILEY-VCH Verlag GmbH, D-69451 Weinheim, 1999 1434−1948/99/0808−1219 $ 17.50+.50/0



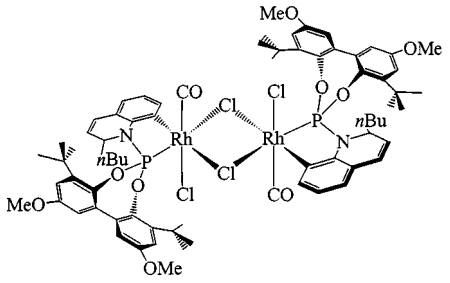
Scheme 1. (i) thf, −78°C, BuLi; (ii) thf, −78°C, PCl_3; (iii) thf, −78°C, 4,8-di-*tert*-butyl-6-chloro-2,10-dimethoxy-5,7-dioxa-6-phosphadibenzo[*a*,*c*]cycloheptene; (iv) thf, −78°C, (*S*)-4-chloro-3,5-dioxa-4-phosphacyclohepta[2,1-*a*;3,4-*a*′]dinaphthalene; (v) toluene, 0°C, Et_3N, 3,3′-di-*tert*-butyl-2,2′-dihydroxy-5,5′-dimethoxybiphenyl; (vi) toluene, 0°C, Et_3N, (*S*)-2,2′-dihydroxybinaphthyl

[*a*,*c*]cycloheptene with the anion **1** in THF solution. Because of the atropoisomerism of the biphenyl moiety and the presence of a stereogenic carbon atom, compound **3** may be obtained as a racemic mixture of two diastereoisomers [(S_aR_C), (R_aS_C), (S_aS_C), and (R_aR_C)]. The $^{31}P\{^1H\}$-NMR spectra in CD_2Cl_2 solution at 293 K and 193 K show a singlet at δ = 141.1 and are consistent with either the presence of only one of the two possible enantiomeric pairs, or with rapid atropoisomerization of the biphenyl moiety on the NMR time scale. In some cases, $^{31}P\{^1H\}$-NMR spectroscopy does not allow a distinction of species present in solution.[10] In the ^1H-NMR spectrum in $CDCl_3$, the *tert*-butyl groups display two different chemical shifts due to their diastereotopicity.

The ligand 2-butyl-8-chloro-1-(3,5-dioxa-4-phosphacyclohepta[2,1-*a*;3,4-*a*′]dinaphthalen-4-yl)-1,2-dihydroquinoline (BINAPHOSHQUIN, **4**) was similarly obtained either by addition of the enantiomer (S_a)-(−)-2,2′-dihydroxy-1,1′-binaphthyl in toluene to a solution of **2** in the same solvent, or by addition of (*S*)-4-chloro-3,5-dioxa-4-phosphacyclohepta[2,1-*a*;3,4-*a*′]dinaphthalene in THF to a solution of the anion **1** in the same solvent (Scheme 1). An improved procedure[4a] was utilized for the synthesis of (*S*)-4-chloro-3,5-dioxa-4-phosphacyclohepta[2,1-*a*;3,4-*a*′]dinaphthalene (see Experimental Section). Compound **4** was found to be moisture-sensitive and was obtained as a mixture of the two diastereoisomers [(S_aR_C)and (S_aS_C)]. Thus, the $^{31}P\{^1H\}$-NMR spectrum in $CDCl_3$ solution shows two peaks at δ = 137.6 and 145.1, while in the ^1H-NMR spectrum two sets of signals are seen. The synthesis method had an effect on the diastereoisomer ratio. Starting from **2**, the diastereoisomers were formed in a 50:50 ratio, whereas starting from the anion **1** an excess (70:30) of the (S_aS_C) diastereoisomer was obtained. The (S_aR_C) and (S_aS_C) diastereoisomers (**4a** and **4b**, respectively) could be separated as white solids by virtue of their different solubilities in hexane and were characterized by microanalysis and spectroscopic data. By comparison with the structure of *cis*-[Pt(**4a**)$_2$I$_2$] (**11**) (see below), it can be inferred that the diastereomer exhibiting a $^{31}P\{^1H\}$-NMR resonance at δ = 137.6 has the absolute configuration (S_aR_C).

Syntheses of the Complexes

We treated the ligands **3** and **4** with rhodium(I), palladium(II), and platinum(II) precursors. Addition of a hexane solution of ligand **3** to $[Rh(CO)_2Cl]_2$ in the same solvent in a 2:1 molar ratio afforded a yellow solid, which was recrystallized from CH_2Cl_2/hexane. The air-stable product **5** proved to be non-conducting in benzene solution and its structure was fully elucidated by an X-ray analysis of crystals of its hexane solvate (see below).



5

The IR spectrum (Nujol mull) of **5** shows a ν(CO) band at 2112 cm^{-1}, consistent with an oxidative process on the starting rhodium(I) center. It is noteworthy that the ^1H-NMR spectrum in $CDCl_3$ solution features two signals with very different shifts (δ = 1.75 and 1.08) due to the *tert*-butyl groups; a slight difference in the methoxy group resonances is also observed (δ = 3.86 and 3.87). The $^{31}P\{^1H\}$-NMR spectrum in $CDCl_3$ solution shows a single resonance at δ = 127.7 (J_{RhP} = 197 Hz).

In the crystals of **5** · 2 C_6H_{14}, dimeric rhodium(III) complexes, having an imposed C_i symmetry, are present, together with disordered molecules of hexane. A view of the dimer showing the atomic numbering system is presented in Figure 1. Selected bond lengths and angles are given in Table 1. Two Cl atoms bridge the two rhodium atoms in an asymmetric manner.

The metal has an octahedral coordination sphere, involving three Cl atoms (two bridging and one terminal), a carbonyl group, and the P1 and C3 atoms of the chelating ligand, derived from oxidative addition of **3**. The five-membered Rh−P1−N1−C2−C3 chelating ring is approximately planar. The Rh−Cl2 bond length, 2.328(4) Å, is much shorter than those involving the bridging Cl1 and Cl1′ atoms, which amount to 2.454(4) and 2.536(4) Å. In accordance with the *trans* influence, the Rh−Cl1 bond length (Cl1 *trans* to P1) is shorter than the Rh−Cl1′ bond length (Cl1′

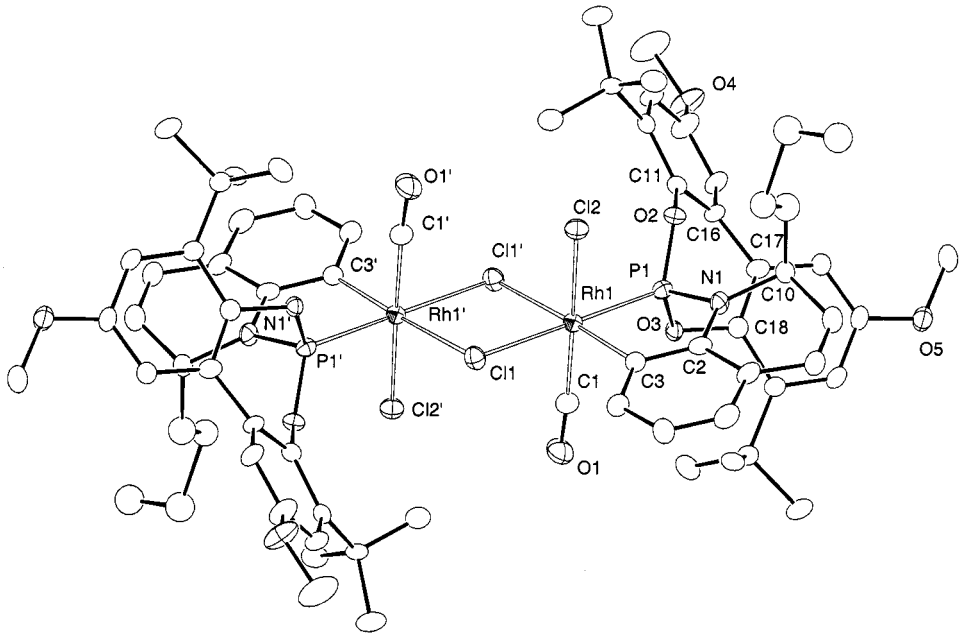


Figure 1. ORTEP view of the structure of complex **5** showing the atomic numbering scheme; thermal ellipsoids are drawn at a 30% probability level

Table 1. Selected bond lengths [Å] and angles [°] in $\mathbf{5} \cdot 2\,C_6H_{14}$; symmetry transformation used to generate equivalent atoms: $-x + 1, -y + 1, -z + 1$

Bond lengths			
Rh(1)−C(1)	1.89(2)	O(2)−C(11)	1.43(2)
Rh(1)−C(3)	2.02(2)	O(3)−C(18)	1.45(2)
Rh(1)−P(1)	2.206(4)	O(4)−C(14)	1.37(2)
Rh(1)−Cl(2)	2.328(4)	O(4)−C(31)	1.43(2)
Rh(1)−Cl(1)	2.454(4)	O(5)−C(21)	1.39(2)
Rh(1)−Cl(1′)	2.536(4)	O(5)−C(32)	1.45(2)
P(1)−O(2)	1.59(1)	N(1)−C(2)	1.45(2)
P(1)−O(3)	1.60(1)	N(1)−C(10)	1.50(2)
P(1)−N(1)	1.64(1)	C(9)−C(10)	1.52(2)
O(1)−C(1)	1.11(2)	C(16)−C(17)	1.47(2)
Bond angles			
C(1)−Rh(1)−C(3)	90.8(7)	N(1)−P(1)−Rh(1)	105.4(5)
C(1)−Rh(1)−P(1)	95.2(6)	C(11)−O(2)−P(1)	129.9(9)
C(3)−Rh(1)−P(1)	82.0(5)	C(18)−O(3)−P(1)	117.0(9)
C(1)−Rh(1)−Cl(2)	174.8(5)	C(14)−O(4)−C(31)	121(1)
C(3)−Rh(1)−Cl(2)	86.3(5)	C(21)−O(5)−C(32)	117(1)
P(1)−Rh(1)−Cl(2)	88.6(2)	C(2)−N(1)−C(10)	121(1)
C(1)−Rh(1)−Cl(1)	86.5(6)	C(2)−N(1)−P(1)	114(1)
C(3)−Rh(1)−Cl(1)	96.1(5)	C(10)−N(1)−P(1)	125(1)
P(1)−Rh(1)−Cl(1)	177.4(2)	Rh(1)−Cl(1)−Rh(1′)	96.4(1)
Cl(2)−Rh(1)−Cl(1)	89.5(2)	O(1)−C(1)−Rh(1)	175(2)
C(1)−Rh(1)−Cl(1′)	86.1(5)	C(8)−C(9)−C(10)	122(2)
C(3)−Rh(1)−Cl(1′)	176.9(5)	N(1)−C(10)−C(9)	108(1)
P(1)−Rh(1)−Cl(1′)	98.3(1)	N(1)−C(10)−C(1A)	111(1)
Cl(2)−Rh(1)−Cl(1′)	96.8(1)	C(9)−C(10)−C(1A)	111(1)
Cl(1)−Rh(1)−Cl(1′)	83.6(1)	C(15)−C(16)−C(11)	117(1)
O(2)−P(1)−O(3)	105.5(5)	C(15)−C(16)−C(17)	117(1)
O(2)−P(1)−N(1)	102.1(6)	C(11)−C(16)−C(17)	125(1)
O(3)−P(1)−N(1)	111.3(6)	C(18)−C(17)−C(22)	118(1)
O(2)−P(1)−Rh(1)	122.1(4)	C(18)−C(17)−C(16)	123(2)
O(3)−P(1)−Rh(1)	110.0(4)	C(22)−C(17)−C(16)	119(1)

trans to C3). As a result of the chelation, the mean plane of the fragment derived from the quinoline approximately bisects the O−P−O angle. The chiral C10 atom lies out of the plane formed by the other five atoms of the ring by 0.44(2) Å. The *n*-butyl groups are situated in axial positions so as to minimize steric repulsion with the biphenyl moiety and thus determine the configuration [(S_aR_C) and (R_aS_C)] of the atropoisomeric unit in complex **5**. The torsion angle, determining the axial chirality of the ligand [τ(C11−C16−C17−C18)], is 55(2)°. The nitrogen atom shows a remarkable degree of sp^2 character.

The packing of the complexes in the crystal leads to the formation of large channels that extend along the *b* axis, into which hexane molecules can insert in a disordered fashion (Figure 2).

It seems very likely that the formation of **5** occurs via an intermediate rhodium(I) species. In this way, an intramolecular redox process, due to the addition of the C−Cl bond of the coordinated ligand **3** across the rhodium(I) center, can account for the formation of the product **5**. The breaking of the C(aromatic)−Cl bond may be induced by the rigidity and steric requirements of **3**, which fix the chlorine atom in the proximity of the metal center in the rhodium(I) intermediate.

Nozaki et al.,[4a] using phosphane/phosphite ligands derived from reaction of optically active (*R*)-2-(diphenylphosphanyl)-1,1′-binaphthalen-2′-ol with the phosphorochloridite of biphenol in the rhodium(I)-catalyzed hydroformylation of olefins, found that a single species is present in solution and they proposed that the biphenyl is fixed in an (*S*) configuration. Analogously, the phosphane/phosphite ligand prepared starting from racemic 2-diphenylphosphanyl-2′-hydroxybiphenyl by reaction with the phosphorochloridite of (*R*)-binaphthol was obtained as a 55:45 equi-

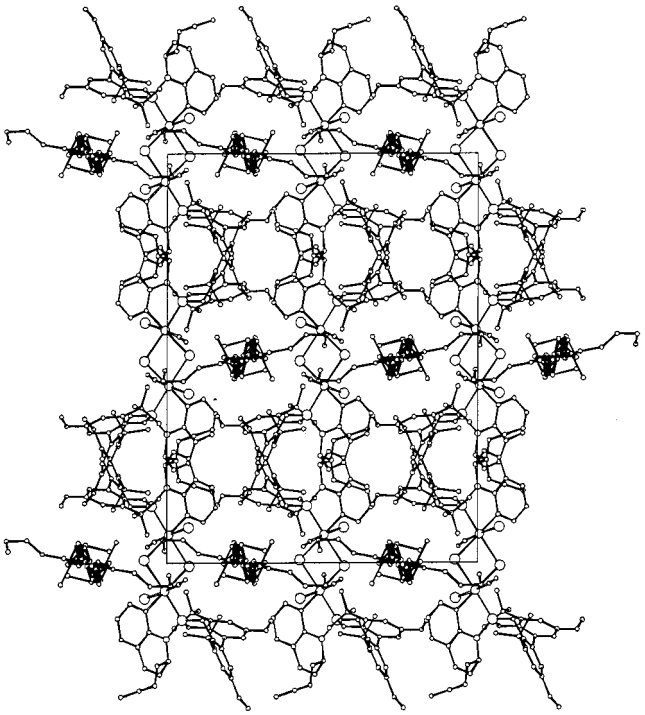
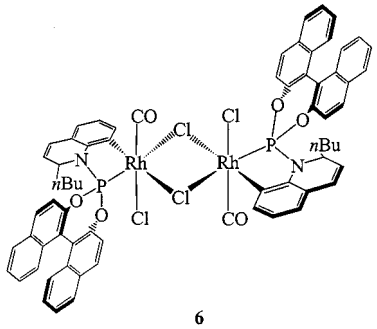


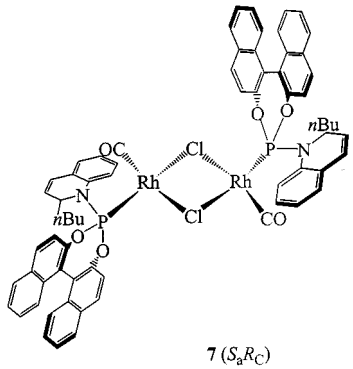
Figure 2. Projection of the structure of $\mathbf{5} \cdot 2\ C_6H_{14}$ along the *b* axis showing the channels into which the hexane molecules are inserted in a disordered manner

librium mixture of two diastereomers. Interconversion between the diastereomers seems to be inhibited by coordination to the rhodium(I) center and in the resulting compound the ligand adopts only one configuration.[4a] Other examples of the fixation of biphenyl rings following coordination to a metal center, using biphenol-derived bis(phosphites), have been reported in the literature.[11] Fixation of the biphenyl rings also occurs in compound **5** due to the presence of the substituents and the rigidity of the chelate quinoline ring.

The reaction of $[Rh(CO)_2Cl]_2$ with **4** proceeds differently to that with **3**. Addition of a twofold molar excess of diastereomer **4a** (S_aR_C) in hexane to a solution of $[Rh(CO)_2Cl]_2$ in the same solvent afforded a yellow solid. The IR spectrum shows ν(CO) bands at 2106 and 2012 cm^{-1}, indicating the presence of the rhodium(III) species **6** as the major product, together with the rhodium(I) species **7** (ratio 10:1.5). The $^{31}P\{^1H\}$-NMR spectrum of the mixture in $CDCl_3$ solution features a resonance at δ = 134.8 (J_{RPh} = 192 Hz) for the major product **6**, together with a resonance at δ = 135.0 (J_{RhP} = 191 Hz) of very low intensity. The similar values of the ^{31}P chemical shifts for **6** and **7** are consistent with structures in which the ligands *trans* to **4a** are the same. Assuming that **6** has a structure analogous to that of **5**, it is very likely that **7** has a binuclear structure with chloro bridges, i.e. $[Rh(CO)(\mathbf{4a})Cl]_2$. A similar intermediate, $[Rh(CO)(\mathbf{3})Cl]_2$, should be formed in the reaction of $[Rh(CO)_2Cl]_2$ with **3**. Compound **6** was obtained in an analytically pure state by several crystallizations from benzene/hexane. The ^1H-NMR spectrum of **6** in $CDCl_3$ solution shows a multiplet at δ = 5.15 and a doublet at δ = 6.28 (^3J = 10.2 Hz) due to the olefinic protons, while a multiplet at δ = 3.24 can be assigned to the proton on the stereogenic carbon atom.



6



7 (S_aR_C)

8 (S_aS_C)

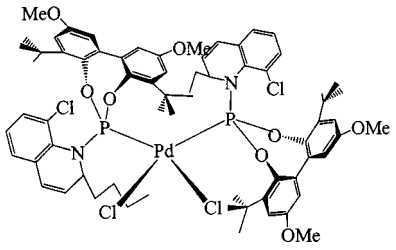
The reaction of $[Rh(CO)_2Cl]_2$ with **4b** in hexane gave only the rhodium(I) species, i.e. $[Rh(CO)(\mathbf{4b})Cl]_2$ (**8**) with the ν(CO) appearing at low wavenumbers. With this diastereoisomer, the intramolecular redox process of addition of the C−Cl bond across the rhodium(I) center seems to be hindered.

Binuclear chloro-bridged compounds, such as **7** and **8**, have been detected previously by NMR spectroscopy.[12] In the reactions with $[Rh(CO)_2Cl]_2$, the rigidity and steric requirements of the ligands **3**, **4a**, and **4b** might be a factor determining the nature of the reaction products. Thus, in reactions of $[Rh(CO)_2Cl]_2$ with sterically hindered ligand molecules, a CO substitution reaction might be preferred to cleavage of the chloro bridges. The C−Cl bond in haloarenes is rather inert. Unlike alkyl halides, haloarenes exhibit low reactivities toward nucleophiles.[13] The use of rhodium(I) complexes in catalytic transformations of chloroarenes is limited to a few examples of C−Cl bond hydrogenolysis.[13] Intramolecular activation of the C−Cl bonds in $[Rh(CO)(\mathbf{3})Cl]_2$, **7** and **8**, requires a proximity of the chlorine atom to the metal center. The diastereoisomers **4a** and **4b** behave differently in the intermediate, most probably because with the (S_aS_C) diastereomer **4b**, the C−Cl bond is positioned away from the rhodium(I) center.

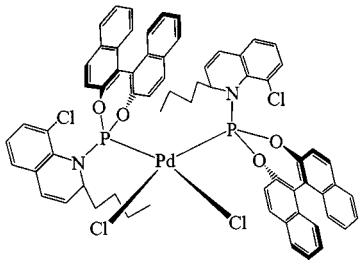
Overnight stirring of $[Pd(PhCN)_2Cl_2]$ and ligand **3** in a 1:2 molar ratio in toluene led to a bright-yellow solution. Workup of the reaction mixture furnished the product $[Pd(\mathbf{3})_2Cl_2]$ (**9**) as a yellow solid, which was found to be stable in air in the solid state and soluble in dichlorometh-

ane. In this case, in contrast to the situation in the rhodium(I) complex **5**, the ligand **3** acts as a monodentate ligand. Compound **9** was characterized by microanalysis and spectroscopic data. The $^{31}P\{^1H\}$-NMR spectrum in CD_2Cl_2 solution shows two partially overlapped singlets at $\delta = 134.1$ and $\delta = 134.2$, with an intensity ratio of ca. 1:0.7. This supports the presence of only two diastereomers, i.e. [Pd(R_C-**3**)(R_C-**3**)Cl_2] {[Pd(S_C-**3**)(S_C-**3**)Cl_2]} and [Pd(S_C-**3**)(R_C-**3**)Cl_2], assuming that the rapid atropoisomerism of the biphenyl moiety is still possible. In the ^1H-NMR spectrum in CD_2Cl_2 solution, at either 298 K or 193 K, only one set of signals is observed, hence there is no discrimination between the two diastereomers. The *tert*-butyl groups give rise to singlets with markedly different chemical shift values ($\delta = 0.95$ and 1.61), whereas only a slight difference is seen in the δ values of the methoxy groups ($\delta = 3.78$ and 3.84).

The reaction of [Pd$(PhCN)_2Cl_2$] with ligand **4a** in a 1:2 molar ratio proceeded similarly and the complex [Pd(**4a**)$_2Cl_2$] (**10**) was obtained in high yield as a yellow solid. The product was found to be stable in air in the solid state and soluble in benzene, acetone, and chlorinated solvents. Its $^{31}P\{^1H\}$-NMR spectrum in $CDCl_3$ shows a single peak at $\delta = 117.5$. In the ^1H-NMR spectrum in $CDCl_3$, the olefinic protons give rise to a double-doublet at $\delta = 4.50$ ($^3J = 5.4$ Hz, $^3J = 9.4$ Hz) and a doublet at $\delta = 6.40$ ($^3J =$ 9.4 Hz). The proton at the stereogenic center appears as a multiplet at $\delta = 3.95$. The appearance of two ν(PdCl) bands at about 335 and 300 cm^{-1} in the IR spectrum (Nujol mull) is indicative of a *cis* configuration for **9** and **10**.



9



10

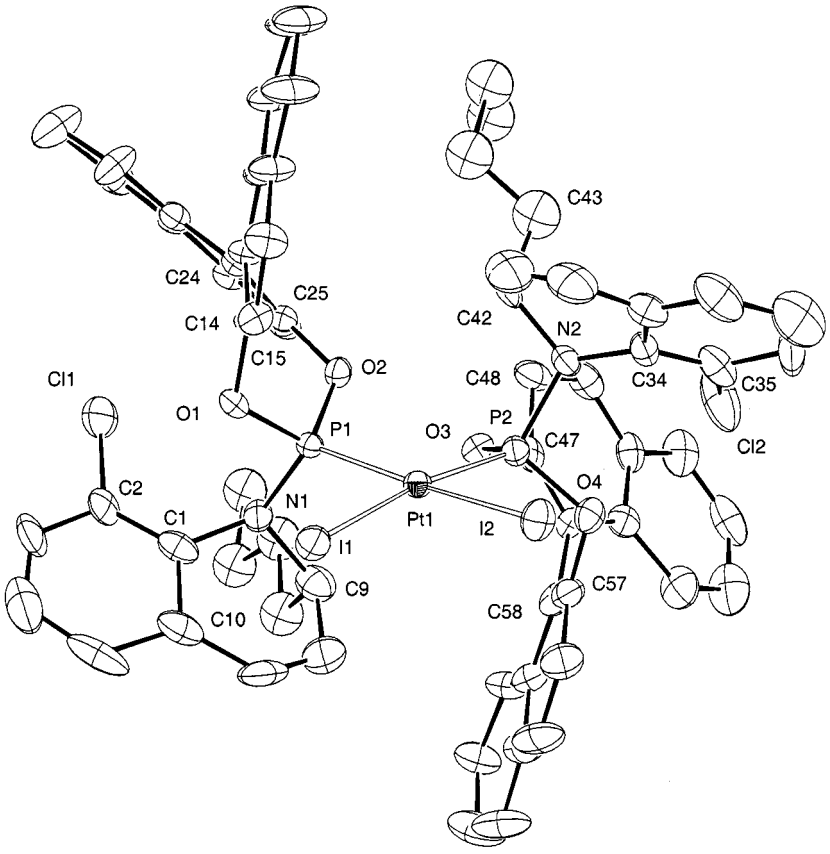
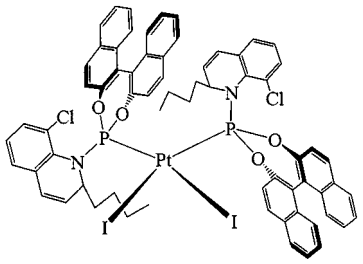


Figure 3. ORTEP view of the structure of complex **11** showing the atomic numbering scheme; thermal ellipsoids are drawn at a 30% probability level

Similarly, reaction of $[Pt(COD)I_2]$ with **4a** in a 1:2 molar ratio afforded *cis*-$[Pt(\mathbf{4a})_2Cl_2]$ (**11**) as a yellow crystalline solid. The compound was characterized by microanalysis and spectroscopic data. The effect of the coordinated ligand **4a** on the overall structure of **11** was assessed by X-ray analysis.



11

Table 2. Selected bond lengths [Å] and angles [°] in **11**

Bond lengths			
Pt(1)−P(2)	2.229(4)	O(2)−C(25)	1.42(2)
Pt(1)−P(1)	2.235(3)	O(3)−C(47)	1.43(1)
Pt(1)−I(1)	2.655(1)	O(4)−C(57)	1.44(2)
Pt(1)−I(2)	2.670(1)	N(1)−C(1)	1.47(2)
P(1)−O(1)	1.584(9)	N(1)−C(9)	1.55(2)
P(1)−O(2)	1.586(9)	N(2)−C(34)	1.42(2)
P(1)−N(1)	1.66(1)	N(2)−C(42)	1.51(2)
P(2)−O(4)	1.59(1)	Cl(1)−C(2)	1.70(2)
P(2)−O(3)	1.613(9)	Cl(2)−C(35)	1.77(2)
P(2)−N(2)	1.67(1)	C(23)−C(24)	1.49(2)
O(1)−C(14)	1.45(1)	C(56)−C(58)	1.49(2)
Bond angles			
P(2)−Pt(1)−P(1)	98.1(1)	C(10)−C(9)−C(8)	109(1)
P(2)−Pt(1)−I(1)	172.1(1)	C(10)−C(9)−N(1)	110(1)
P(1)−Pt(1)−I(1)	87.86(9)	C(23)−C(14)−C(15)	124.8(12)
P(2)−Pt(1)−I(2)	86.8(1)	C(23)−C(14)−O(1)	119.3(12)
P(1)−Pt(1)−I(2)	172.56(9)	C(15)−C(14)−O(1)	115.5(12)
I(1)−Pt(1)−I(2)	87.80(4)	C(14)−C(23)−C(22)	116.3(13)
O(1)−P(1)−O(2)	102.5(5)	C(14)−C(23)−C(24)	120.3(11)
O(1)−P(1)−N(1)	98.1(5)	C(22)−C(23)−C(24)	123.1(12)
O(2)−P(1)−N(1)	108.5(6)	C(25)−C(24)−C(33)	117.8(13)
O(1)−P(1)−Pt(1)	118.2(3)	C(25)−C(24)−C(23)	120.7(12)
O(2)−P(1)−Pt(1)	108.2(3)	C(33)−C(24)−C(23)	121.5(13)
N(1)−P(1)−Pt(1)	119.8(4)	C(24)−C(25)−O(2)	120.3(12)
O(4)−P(2)−O(3)	104.0(5)	C(24)−C(25)−C(26)	123.5(13)
O(4)−P(2)−N(2)	101.3(6)	O(2)−C(25)−C(26)	116.2(12)
O(3)−P(2)−N(2)	106.8(6)	C(35)−C(34)−N(2)	125.5(15)
O(4)−P(2)−Pt(1)	115.8(4)	C(35)−C(34)−C(39)	116.8(16)
O(3)−P(2)−Pt(1)	109.6(4)	N(2)−C(34)−C(39)	117.5(15)
N(2)−P(2)−Pt(1)	118.2(5)	C(41)−C(42)−N(2)	110.6(18)
C(14)−O(1)−P(1)	115.8(8)	C(41)−C(42)−C(43)	116.6(17)
C(25)−O(2)−P(1)	123.7(8)	N(2)−C(42)−C(43)	103.1(17)
C(47)−O(3)−P(2)	120.3(8)	C(56)−C(47)−O(3)	122.4(14)
C(57)−O(4)−P(2)	114.2(9)	C(56)−C(47)−C(48)	124.1(13)
C(1)−N(1)−C(9)	115(1)	O(3)−C(47)−C(48)	113.5(13)
C(1)−N(1)−P(1)	121.2(9)	C(47)−C(56)−C(55)	117.9(14)
C(9)−N(1)−P(1)	112(1)	C(47)−C(56)−C(58)	118.6(13)
C(34)−N(2)−C(42)	112(1)	C(55)−C(56)−C(58)	123.5(13)
C(34)−N(2)−P(2)	127(1)	C(58)−C(57)−C(66)	123.7(16)
C(42)−N(2)−P(2)	111.0(9)	C(58)−C(57)−O(4)	121.4(13)
C(2)−C(1)−C(6)	120(2)	C(66)−C(57)−O(4)	114.9(15)
C(2)−C(1)−N(1)	126(1)	C(57)−C(58)−C(59)	117.7(15)
C(6)−C(1)−N(1)	115(2)	C(57)−C(58)−C(56)	119.8(14)
C(8)−C(9)−N(1)	111(1)	C(59)−C(58)−C(56)	122.4(14)

A view of complex **11** showing the atomic numbering system is depicted in Figure 3. Selected bond lengths and angles are given in Table 2. The Pt atom has a distorted square-planar coordination sphere involving two iodine atoms and the P atoms of two **4a** ligands.

The *cis* arrangement of these very bulky ligands leads to a remarkable distortion of the coordination geometry. The two P atoms deviate above and below the mean square plane by about 0.20(1) Å. The absolute configuration of both ligands is (S_aR_C). The two binaphthyl fragments reside on opposite sides with respect to the coordination plane, and the torsion angles determining the axial chirality [τ(C14−C23−C24−C25) and τ(C47−C56−C58−C57)] are 48(2)° and −54(2)°, respectively. In contrast to the nitrogen atoms in ligand **3** in complex **5**, the nitrogen atoms of the coordinated ligand **4a** in complex **11** show a remarkable degree of sp^3 hybridization, such that these atoms can be considered as chiral centers. In both ligands, the nitrogen atoms are of (*S*) configuration. In accordance with the observed structure, the $^{31}P\{^1H\}$-NMR spectrum shows a single resonance at δ = 94.5 (J_{PtP} = 5296 Hz), while the ^1H-NMR spectrum in $CDCl_3$ solution features a double-doublet at δ = 4.36 and a doublet at δ = 6.20 due to the vinylic protons, and a multiplet at δ = 4.05 attributable to the proton at the stereogenic center.

Surprisingly the compound $[Pt(COD)I_2]$ does not react with **3** in solution, even if an excess of the ligand is used. Most probably, the presence of OMe and *t*Bu substituents on the biphenyl ring of the ligand **3** prevents the formation of a *cis* square-planar platinum(II) complex.

Experimental Section

The compounds 3,3′-di-*tert*-butyl-2,2′-dihydroxy-5,5′-dimethoxybiphenyl and 4,8-di-*tert*-butyl-6-chloro-2,10-dimethoxy-5,7-dioxa-6-phosphadibenzo[*a,c*]cycloheptene were prepared according to literature procedures.[5a,14] 8-Chloroquinoline was purchased from Tokyo Kasei Organic Chemicals, whereas all other reagents were purchased from Sigma/Aldrich and were used as supplied. Solvents were dried by standard procedures. All experiments were performed under purified nitrogen. − IR spectra were obtained from Nujol mulls on KBr plates using a Perkin−Elmer FT-IR 1720 spectrophotometer. − ^1H- and $^{31}P\{^1H\}$-NMR spectra were recorded with a Bruker AMX R300 instrument. ^1H-NMR spectra are referenced to internal tetramethylsilane and $^{31}P\{^1H\}$-NMR spectra to external 85% H_3PO_4; positive chemical shifts for all nuclei refer to higher frequencies. − Elemental analyses were performed by Redox s.n.c., Cologno Monzese, Milano.

2-Butyl-8-chloro-*N*-(dichlorophosphanyl)-1,2-dihydroquinoline (2): To a solution of 8-chloroquinoline (1.00 g, 6.1 mmol) in tetrahydrofuran (20 mL) at −78°C, 3.9 mL of a 1.6 M hexane solution of *n*-butyllithium was added dropwise. The reaction mixture was allowed to warm to −50°C, stirred for 1 h, then cooled to −78°C once more. Excess PCl_3 (8.37 g, 61.1 mmol) was then rapidly added to the lithium reagent. The reaction mixture was slowly allowed to warm to room temperature and then stirred for 2 h. After removal of the solvents and the excess PCl_3, the residue was extracted with toluene (40 mL). Evaporation of the solvent from the combined extracts afforded the product as a pale-yellow oil, which was used without further purification. Yield: 1.47 g (75%). − ^1H NMR

($CDCl_3$): δ = 6.94 (d, ^3J = 6.0 Hz, 1 H, Ar-H), 6.56 (m, 2 H, Ar-H), 6.05 (d, ^3J = 9.6 Hz, 1 H, CH=CH), 5.80 (dd, ^3J = 9.6 Hz, ^3J = 5.6 Hz, 1 H, CH=CH), 4.68 (m, 1 H, CH), 1.38−1.13 (m, 6 H, CH_2), 0.82 (t, ^3J = 7.2 Hz, CH_3). − $^{31}P\{^1H\}$ NMR ($CDCl_3$): δ = 160.7 (s).

(*S*)-4-Chloro-3,5-dioxa-4-phosphacyclohepta[2,1-*a*;3,4-*a*′]dinaphthalene: A suspension of (*S*)-2,2′-dihydroxybinaphthyl (1.00 g, 3.5 mmol) and 1-methyl-2-pyrrolidone (0.001 g, 0.01 mmol) in PCl_3 (7.21 g, 52.5 mmol) was warmed to 75°C and then stirred for 5 min. After this time, a clear solution was obtained. The bulk of the excess PCl_3 was removed under reduced pressure and then the final traces were removed by azeotropic distillation with toluene (10 mL) in vacuo. A white solid corresponding to the title compound was obtained.

2-Butyl-8-chloro-1-(4,8-di-*tert*-butyl-2,10-dimethoxy-5,7-dioxa-6-phosphadibenzo[*a*,*c*]cyclohepten-6-yl)-1,2-dihydroquinoline (3). − Method A: A solution of 3,3′-di-*tert*-butyl-2,2′-dihydroxy-5,5′-dimethoxybiphenyl (1.11 g, 3.1 mmol) and Et_3N (1.57 g, 15.5 mmol) in toluene (10 mL) was added dropwise over a period of 1 h to a solution of **2** (1.00 g, 3.1 mmol) in the same solvent (20 mL) at 0°C. The mixture was stirred at room temp. for 40 min and then the precipitate of $Et_3N \cdot HCl$ formed was removed by filtration. The toluene was evaporated from the filtrate and the residue was extracted with hexane (50 mL). Removal of the solvent from the combined extracts afforded **3** (1.69 g, 90%) as a white foam. − ^1H NMR ($CDCl_3$): δ = 7.34 (d, ^4J = 3.0 Hz, 1 H, Ar-H), 7.23 (d, ^4J = 3.0 Hz, 1 H, Ar-H), 6.89 (d, ^4J = 3.0 Hz, 1 H, Ar-H), 6.86 (d, ^4J = 3.0 Hz, 1 H, Ar-H), 6.75 (m, 3 H, Ar-H), 6.33 (d, ^3J = 9.5 Hz, 1 H, CH=CH), 5.83 (dd, ^3J = 9.5 Hz, ^3J = 5.7 Hz, 1 H, CH=CH), 4.48 (m, 1 H, CH), 3.49 (s, 3 H, OCH_3), 3.47 (s, 3 H, OCH_3), 1.83 [s, 9 H, $C(CH_3)_3$], 1.45 [s, 9 H, $C(CH_3)_3$], 1.56−1.53 (m, 2 H, CH_2), 1.24−1.12 (m, 4 H, CH_2), 0.84 (t, ^3J = 7.2 Hz, 3 H, CH_3). − $^{31}P\{^1H\}$ NMR ($CDCl_3$): δ = 141.1 (s). − $C_{35}H_{43}ClNO_4P$ (608.16): calcd. C 69.12, H 7.13, Cl 5.83, N 2.30; found C 68.85, H 7.01, Cl 5.59, N 2.15. − **Method B:** To a solution of 8-chloroquinoline (1.00 g, 6.1 mmol) in tetrahydrofuran (20 mL) cooled in an acetone/dry-ice bath, 3.9 mL of a 1.6 M hexane solution of *n*-butyllithium was added dropwise. The reaction mixture was allowed to warm to −50°C, stirred for 1 h, and cooled to −78°C once more. A precooled solution of 4,8-di-*tert*-butyl-6-chloro-2,10-dimethoxy-5,7-dioxa-6-phosphadibenzo[*a*,*c*]cycloheptene (2.58 g, 6.1 mmol) in THF (3 mL) was then rapidly added to the lithium reagent (anion). The reaction mixture was slowly allowed to warm to room temperature and then stirred for 2 h. After removal of the THF, the residue was extracted with hexane (50 mL). Removal of the solvent from the combined extracts afforded **3** as a white foam. Yield: 2.97 g, 80%.

2-Butyl-8-chloro-1-(3,5-dioxa-4-phosphacyclohepta[2,1-*a*;3,4-*a*′]-dinaphthalen-4-yl)-1,2-dihydroquinoline (4). Method A: In analogy to Method A for the preparation of compound **3**, compound **4** was synthesized from (*S*)-2,2′-dihydroxybinaphthyl (1.00 g, 3.5 mmol), Et_3N (1.76 g, 17.5 mmol), and **2** (1.13 g, 3.5 mmol). The ^1H- and $^{31}P\{^1H\}$-NMR spectra of the crude reaction mixture were consistent with the formation of an approximately 1:1 mixture of two diastereoisomers. Recrystallization from hexane allowed the components to be separated. The compound more soluble in hexane (0.56 g, 30%) proved to be the (S_aR_C) diastereoisomer **4a** (assignment based on X-ray studies of the corresponding diiodoplatinum complex). − ^1H NMR ($CDCl_3$): δ = 8.04−7.88 (m, 3 H, Ar-H), 7.64 (m, 1 H, Ar-H), 7.44−7.28 (m, 9 H, Ar-H), 7.23−7.03 (m, 2 H, Ar-H), 6.52 (d, ^3J = 9.5 Hz, 1 H, CH=CH), 5.74 (dd, ^3J = 9.5 Hz, ^3J = 5.6 Hz, 1 H, CH=CH), 4.35 (m, 1 H, CH), 1.48−1.20 (m, 6 H, CH_2), 0.61 (t, ^3J = 7.2 Hz, 3 H). − $^{31}P\{^1H\}$ NMR ($CDCl_3$): δ = 137.6 (s). − $C_{33}H_{27}ClNO_2P$ (536.01): calcd. C 73.95, H 5.08, N 2.61, Cl 6.61; found C 73.75, H 5.02, N 2.71, Cl 6.45. − The compound less soluble in hexane (0.75 g, 40%) proved to be the (S_aS_C) diastereomer **4b**. − ^1H NMR ($CDCl_3$): δ = 7.96−7.89 (m, 3 H, Ar-H), 7.65 (m, 1 H, Ar-H), 7.45−7.26 (m, 9 H, Ar-H), 7.28−7.26 (m, 2 H, Ar-H), 6.36 (d, ^3J = 9.3 Hz, 1 H, CH=CH), 5.92 (dd, ^3J = 9.3 Hz, ^3J = 5.6 Hz, 1 H, CH=CH), 3.72 (m, 1 H, CH), 1.52−1.22 (m, 6 H, CH_2), 0.72 (t, ^3J = 7.2 Hz, 3 H, CH_3). − $^{31}P\{^1H\}$ NMR ($CDCl_3$): δ = 145.1 (s). − $C_{33}H_{27}ClNO_2P$ (536.01): calcd. C 73.95, H 5.08, Cl 6.61, N 2.61; found C 73.78, H 5.07, Cl 6.55, N 2.63. − **Method B:** In analogy to Method B for the preparation of compound **3**, compound **4** was synthesized from 8-chloroquinoline (0.3 g, 0.18 mmol), *n*BuLi (1.6 M in hexane, 0.56 mL), and (*S*)-4-chloro-3,5-dioxa-4-phosphacyclohepta[2,1-*a*;3,4-*a*′]dinaphthalene (0.643 g, 0.18 mmol). In this case, the diastereomeric ratio was 70:30, with the (S_aS_C) diastereomer constituting the major product.

[Rh(CO)(P−C)Cl$_2$]$_2$ [P−C = 2-Butyl-1-(4,8-di-*tert*-butyl-2,10-dimethoxy-5,7-dioxa-6-phosphadibenzo[*a*,*c*]cyclohepten-6-yl)-1,2-dihydro-8-quinolyl] (5): A solution of **3** (0.317 g, 0.52 mmol) in hexane (15 mL) was added to a stirred solution of $[Rh(CO)_2Cl]_2$ (0.100 g, 0.26 mmol) in the same solvent (15 mL) at room temp. A yellow precipitate was deposited during the course of the addition. This solid was collected, washed with petroleum ether, and dried. Yield 0.382 g (95%). − IR (KBr, Nujol): ν(CO) = 2112 cm^{-1}. − ^1H NMR ($CDCl_3$): δ = 7.19 (d, ^4J = 2.9 Hz, 1 H, Ar-H), 6.97 (d, ^4J = 2.9 Hz, 1 H, Ar-H), 6.72 (m, 3 H, Ar-H), 6.68 (d, ^4J = 2.9 Hz, 1 H, Ar-H), 6.62 (d, ^4J = 2.9 Hz, 1 H, Ar-H), 6.19 (d, ^3J = 9.6 Hz, 1 H, CH=CH), 5.33 (br. dd, 1 H, CH=CH), 3.87 (s, 3 H, OCH_3), 3.86 (s, 3 H, OCH_3), 3.60 (br. m, 1 H, CH), 1.75 [s, 9 H, $C(CH_3)_3$], 1.08 [s, 9 H, $C(CH_3)_3$], 1.82−0.86 (m, 6 H, CH_2), 0.71 (t, ^3J = 7.3 Hz, 3 H, CH_3). − $^{31}P\{^1H\}$ NMR ($CDCl_3$): δ = 127.7 (d, J_{RhP} = 197 Hz). − $C_{36}H_{43}Cl_2NO_5PRh$ (774.53): calcd. C 55.83, H 5.60, Cl 9.15, N 1.81; found C 55.78, H 5.68, Cl 8.91, N 2.01.

[Rh(CO)(P′−C)Cl$_2$]$_2$ [P′−C = (S_aR_C)-2-Butyl-1-(3,5-dioxa-4-phosphacyclohepta[2,1-*a*;3,4-*a*′]dinaphthalen-4-yl)-1,2-dihydro-8-quinolyl] (6): A solution of **4a** (0.279 g, 0.52 mmol) in hexane was slowly added at room temp. to a stirred solution of $[Rh(CO)_2Cl]_2$ (0.100 g, 0.26 mmol) in the same solvent (15 mL) until the CO stretching bands of the reagent disappeared from the IR spectrum. A yellow precipitate was deposited during the course of the addition. This solid was collected and washed with petroleum ether. After repeated recrystallization from benzene/hexane, the pure title compound was obtained. Yield: 0.255 g (70%). − IR (KBr, Nujol): ν(CO) = 2106 cm^{-1}. − ^1H NMR ($CDCl_3$): δ = 8.08−7.36 (m, 12 H, Ar-H), 6.91−6.86 (m, 3 H, Ar-H), 6.28 (d, ^3J = 10.2 Hz, 1 H, CH=CH), 5.15 (m, 1 H, CH=CH), 3.24 (m, 1 H, CH), 1.24−0.76 (m, 6 H, CH_2), 0.54 (t, ^3J = 7.3 Hz, 3 H, CH_3). − $^{31}P\{^1H\}$ NMR ($CDCl_3$): δ = 134.8 (d, J_{RhP} = 192 Hz). − $C_{34}H_{27}Cl_2NO_3PRh$ (702.38): calcd. C 58.14, H 3.87, Cl 10.10, N 1.99; found C 58.35, H 3.93, Cl 9.89, N 2.03.

***cis*-[Pd(3)$_2$Cl$_2$] (9):** A solution of **3** (0.475 g, 0.78 mmol) in toluene (10 mL) was added to a solution of $[Pd(PhCN)_2Cl_2]$ (0.150 g, 0.39 mmol) in the same solvent (20 mL) cooled in an ice bath. The reaction mixture was then stirred overnight at room temperature. The yellow solution was subsequently concentrated to a volume of 5 mL and upon addition of 30 mL of diethyl ether a lemon-yellow solid was deposited. This solid was collected, washed with diethyl ether, and dried in vacuo. Yield: 0.489 g (90%). − IR (CsI, Nujol): ν(PdCl) = 335, 302 cm^{-1}. − ^1H NMR (CD_2Cl_2): δ = 7.62−7.54 (m, 3 H, Ar-H), 7.29 (d, ^3J = 7.4 Hz, 1 H), 7.13 (br., 1 H), 7.07

(d, ^4J = 3.0 Hz, 1 H, Ar-H), 6.86 (d, ^4J = 3.0 Hz, 1 H, Ar-H), 6.71 (d, ^4J = 3.0 Hz, 1 H, Ar-H), 6.65 (d, ^4J = 3.0 Hz, 1 H, Ar-H), 4.55 (m, 1 H, CH), 3.84 (s, 3 H, OCH_3), 3.78 (s, 3 H, OCH_3), 1.61 [s, 9 H, $C(CH_3)_3$], 1.48−1.22 (m, 6 H, CH_2), 0.95 [s, 9 H, $C(CH_3)_3$], 0.85 (t, ^3J = 7.1 Hz, 3 H, CH_3). − $^{31}P\{^1H\}$ NMR ($CDCl_3$): δ = 131.6 (s). − $C_{70}H_{86}Cl_4N_2O_8P_2Pd$ (1393.6): calcd. C 60.33, H 6.22, Cl 10.18, N 2.01; found C 60.45, H 6.28, Cl 9.96, N 2.03.

***cis*-[Pd(4a)$_2$Cl$_2$] (10):** A solution of **4a** (0.418 g, 0.78 mmol) in toluene (10 mL) was added to a stirred solution of $[Pd(PhCN)_2Cl_2]$ (0.150 g, 0.39 mmol) in the same solvent (20 mL) cooled in an ice bath. The reaction mixture was then stirred overnight at room temperature, resulting in the deposition of an orange precipitate. This was filtered off, washed with toluene (in which the product is slightly soluble), and dried. Yield: 0.195 g (40%). − IR (CsI, Nujol): ν(PdCl) = 335, 301 cm^{-1}. − ^1H NMR ($CDCl_3$): δ = 8.33 (d, ^3J = 9.2 Hz, 1 H, Ar-H), 8.08−7.98 (m, 3 H, Ar-H), 7.55−7.35 (m, 9 H, Ar-H), 6.87 (m, 1 H, Ar-H), 6.80−6.76 (m, 2 H, Ar-H), 6.40 (d, ^3J = 9.4 Hz, 1 H, CH=CH), 4.50 (dd, ^3J = 9.4 Hz, ^3J = 5.4 Hz, 1 H, CH=CH), 3.95 (m, 1 H, CH), 0.88−0.68 (m, 6 H, CH_2), 0.56 (t, ^3J = 7.2 Hz, 3 H, CH_3). − $^{31}P\{^1H\}$ NMR ($CDCl_3$): δ = 117.5 (s). − $C_{66}H_{54}Cl_4N_2O_4P_2Pd$ (1249.3): calcd. C 63.45, H 4.36, Cl 11.35, N 2.24; found C 63.35, H 4.28, Cl 11.12, N 2.15.

***cis*-[Pt(4a)I$_2$] (11):** At room temp. a solution of **4a** (0.097 g, 0.18 mmol) in toluene was added to a stirred solution of $[Pt(COD)I_2]$ (0.050 g, 0.09 mmol) in the same solvent (20 mL). After 4 h, the bright-yellow solution was concentrated to a volume of ca. 5 mL and upon addition of 30 mL of diethyl ether a light-yellow solid was deposited. This solid was collected, washed with diethyl ether, and dried in vacuo. Yield: 0.123 g (90%). Recrystallization from $CHCl_3$/hexane gave yellow single crystals suitable for X-ray diffraction analysis. − ^1H NMR ($CDCl_3$): δ = 8.49 (d, ^3J = 9.2 Hz, 1 H, Ar-H), 8.04−7.95 (m, 3 H, Ar-H), 7.51−7.31 (m, 8 H, Ar-H), 6.89 (m, 1 H, Ar-H), 6.80−6.75 (m, 2 H, Ar-H), 6.20 (d, ^3J = 9.6 Hz, 1 H, CH=CH), 4.36 (dd, ^3J = 9.6 Hz, ^3J = 5.4 Hz, 1 H, CH=CH), 4.05 (m, 1 H, CH), 0.95−0.74 (m, 6 H, CH_2), 0.51 (t, ^3J = 7.2 Hz, 3 H, CH_3). − $^{31}P\{^1H\}$ NMR ($CDCl_3$): δ = 94.5 (J_{PtP} = 5296 Hz). − $C_{66}H_{54}Cl_2I_2N_2O_4P_2Pt$ (1520.9): calcd. C 52.12, H 3.58,, Cl 4.66, I 16.69 N 1.84; found C 52.26, H 3.60, Cl 4.76, I 16.47, N 1.89.

Crystal Structure Determination of Complexes 5 · 2 C$_6$H$_{14}$ and 11: Intensity data for **5** · 2 C_6H_{14} were collected at room temperature (22°C) with an Enraf-Nonius CAD-4 single-crystal diffractometer using graphite-monochromated Cu-K_α radiation. Intensity data for **11** were collected at room temperature (22°C) with a Philips PW 1100 single-crystal diffractometer using graphite-monochromated Mo-K_α radiation. In both cases, the θ/2θ scan technique was employed. Final unit-cell parameters were obtained from least-squares refinements using 24 (**5** · 2 C_6H_{14}) and 30 (**11**) reflections. Crystallographic and experimental details pertaining to both structures are summarized in Table 3.

Data were corrected for Lorentz and polarization effects in the usual manner. A correction for absorption was made for both complexes [maximum and minimum values for the transmission coefficients 1.000 and 0.7101 (**5** · 2 C_6H_{14}) and 1.000 and 0.3741 (**11**)].[15] Both structures were solved by Patterson and Fourier methods and refined by full-matrix least-squares procedures (based on F_o^2) with anisotropic thermal parameters in the final cycles of the refinement for all non-hydrogen atoms other than the carbon atoms of the *n*-butyl moiety and of the solvent molecules in **5** · 2 C_6H_{14}. The *n*-butyl group was found to be disordered and distributed over two positions with the first carbon atom (C1A) in common, with occupancy factors of 0.62 and 0.38, respectively. The

Table 3. Crystal data and structure refinement for **5** · 2 C_6H_{14} and **11**; $R1 = \Sigma||F_o| - |F_c||/\Sigma|F_o|$; $wR2 = \{\Sigma[w(F_o^2 - F_c^2)^2]/\Sigma[w(F_o^2)^2]\}^{1/2}$

Formula	$C_{72}H_{86}Cl_4N_2O_{10}P_2Rh_2 \cdot 2\ C_6H_{14}$	$C_{66}H_{54}Cl_2I_2N_2O_4P_2Pt$
Formula weight	1721.34	1520.84
Temperature	293(2) K	293(2) K
Wavelength	1.54184 Å	0.71073 Å
Crystal system	orthorhombic	orthorhombic
Space group	*Pbca*	$P2_12_12_1$
Unit cell dimensions	a = 26.499(5) Å	a = 20.479(5) Å
	b = 17.869(3) Å	b = 20.546(5) Å
	c = 20.200(4) Å	c = 16.757(4) Å
Volume	9565(3) Å^3	7051(3) Å^3
Z	4	4
Density (calculated)	1.195 Mg/m^3	1.433 Mg/m^3
Absorption coefficient	45.30 cm^{-1}	30.29 cm^{-1}
F(000)	3600	2976
Crystal size [mm]	0.32 × 0.25 × 0.21	0.18 × 0.24 × 0.27
θ range (°)	3.34−60.02	3.06−28.00
Index ranges	$0 \le h \le 29$,	$0 \le h \le 27$,
	$0 \le k \le 20$,	$0 \le k \le 27$,
	$-22 \le l \le 0$	$0 \le l \le 22$
Reflections collected	6802	9215
Independent reflections	6802	9215
Obsd. reflns. [$I > 2\sigma(I)$]	2638	4729
Refinement method	Based on F^2	Based on F^2
Data/restr./param.	6798/27/486	9215/0/677
Flack index	−	−0.04(1)
Goodness-of-fit on F^2	0.818	0.928
Final R indices [$I > 2\sigma(I)$]	$R1$ = 0.0659,	$R1$ = 0.0450,
	$wR2$ = 0.1728	$wR2$ = 0.1162
R indices (all data)	$R1$ = 0.1841,	$R1$ = 0.1196,
	$wR2$ = 0.2520	$wR2$ = 0.1411
Largest diff. peak and hole	0.701 and −0.715 eÅ^{-3}	0.958 and −1.364 eÅ^{-3}

hexane molecules of solvation were found to be disordered over three different positions within the channels present in the crystal structure. The hydrogen atoms (other than those of the disordered *n*-butyl group and of the hexane molecules in **5** · 2 C_6H_{14}) were placed in geometrically calculated positions and were refined riding on the corresponding carbon atoms. In the final cycles of the refinement, weighting schemes $w = 1/[\sigma^2F_o^2 + (0.1275P)^2]$ (**5** · 2 C_6H_{14}) and $w = 1/[\sigma^2F_o^2 + (0.0668P)^2]$ (**11**), where $P = (F_o^2 + 2F_c^2)/3$, were used. All calculations were carried out with the CNRDIF computers of the Centro di Studio per la Strutturistica Diffrattometrica del CNR, Parma, using the SHELXS-86 and SHELXL-92 packages of crystallographic computer programs.[16,17] Supplementary material available for both structures includes lists of atomic coordinates for the non-H atoms, of calculated coordinates for the hydrogen atoms, and of anisotropic thermal parameters. Details of the crystal structure determinations have been deposited at the Cambridge Crystallographic Data Centre as supplementary publication nos. CCDC-110254 (**5** · 2 C_6H_{14}) and -110253 (**11**). Copies of the data can be obtained free of charge on application to the CCDC, 12 Union Road, Cambridge CB2 1EZ, U.K. [Fax: (internat.) + 44-1223/336-033; E-mail: deposit@ccdc.cam.ac.uk].

[1] [1a] G. W. Parshall, S. D. Ittel, *Homogeneous Catalysis*, Wiley-Interscience Publications, New York, **1992**. – [1b] *Catalytic Asymmetric Synthesis* (Ed.: I. Ojima), VCH, Weinheim, **1995**. – [1c] R. Noyori, *Asymmetric Catalysis in Organic Synthesis*, Wiley-Interscience Publications, New York, **1994**.

[2] [2a] C. P. Casey, G. T. Whiteker, M. G. Melville, L. M. Petrovich, J. A. Gavney, Jr., D. R. Powell, *J. Am. Chem. Soc.* **1992**, *114*, 5535. – [2b] C. P. Casey, G. T. Whiteker, *Isr. J. Chem.* **1990**, *30*, 299.

[3] [3a] A. Togni, C. Breutel, A. Schnyder, F. Spindler, H. Landert, A. Tijani, *J. Am. Chem. Soc.* **1994**, *116*, 4062. – [3b] S. Cserépi, J. Bakos, *J. Chem. Soc., Chem. Commun.* **1997**, *635*. – [3c] G. J. H. Buisman, L. A. van der Veen, P. C. J. Kamer, P. W. N. M. van Leeuwen, *Organometallics* **1997**, *16*, 5681 and references therein. – [3d] A. von Rooy, P. C. J. Kamer, P. W. N. M. van Leeuwen, K. Goubitz, J. Fraanje, N. Veldman, A. L. Spek, *Organometallics* **1996**, *15*, 835 and references therein.

[4] [4a] K. Nozaki, N. Sakai, T. Nanno, T. Higashijima, S. Mano, T. Horiuchi, H. Takaya, *J. Am. Chem. Soc*. **1997**, *119*, 4413. – [4b] K. Nozaki, T. Nanno, H. Takaya, *J. Organomet. Chem*. **1997**, *527*, 103. – [4c] T. Horiuchi, E. Shirakawa, K. Nozaki, H. Takaya, *Organometallics* **1997**, *16*, 2981.

[5] [5a] S. D. Pastor, S. P. Shum, R. K. Rodebaugh, A. D. Debellis, *Helv. Chim. Acta* **1993**, *76*, 900. – [5b] S. D. Pastor, J. L. Hyun, P. A. Odorisio, R. K. Rodebaugh, *J. Am. Chem. Soc*. **1988**, *110*, 6547. – [5c] M. W. Haenel, D. Jakubik, E. Rothenberger, G. Schroth, *Chem. Ber*. **1991**, *124*, 1705. – [5d] S. D. Pastor, J. D. Spivack, L. P. Steinhuebel, *J. Heterocycl. Chem*. **1984**, *21*, 1285. – [5e] S. D. Pastor, S. P. Shum, *Tetrahedron: Asymmetry* **1998**, *9*, 543. – [5f] N. J. De Stefano, D. K. Johnson, L. M. Venanzi, *Angew. Chem. Int. Ed. Engl.* **1974**, *86*, 133. – [5g] U. Baltensperger, J. R. Gunther, S. Kagi, G. Kahr, W. Marty, *Organometallics* **1983**, *2*, 571. – [5h] M. Kranenburg, Y. E. M. van der Burgt, P. C. J. Kamer, P. W. N. M. van Leeuwen, K. Goubitz, J. Fraanje, *Organometallics* **1995**, *14*, 3081. – [5i] M. Stolmàr, C. Floriani, G. Gervasio, D. Viterbo, *J. Chem. Soc., Dalton Trans.* **1997**, 1119. – [5j] J. Sakaki, W. B. Schweizer, D. Seebach, *Helv. Chim. Acta* **1993**, 76, 2654. – [5k] S. D. Pastor, A. Togni, *Inorg. Chim. Acta* **1989**, *159*, 3. – [5l] S. D. Pastor, R. K. Rodebaugh, P. A. Odorisio, *Helv. Chim. Acta* **1991**, *74*, 1175.

[6] [6a] A. H. M. de Vries, A. Meetsma, B. L. Feringa, *Angew. Chem. Int. Ed. Engl.* **1996**, *35*, 2374. – [6b] B. L. Feringa, M. Pineschi, L. A. Arnold, R. Imbos, A. H. M. de Vries, *Angew. Chem. Int. Ed. Engl.* **1997**, *36*, 2620. – [6c] A. K. H. Knobel, I. H. Escher, A. Pfaltz, *Synlett* **1997**, 1429. – [6d] N. Sewald, V. Wendisch, *Tetrahedron: Asymmetry* **1998**, *9*, 1341. – [6e] N. Krause, *Angew. Chem. Int. Ed. Engl*. **1998**, *37*, 283.

[7] [7a] D. G. Allen, G. M. McLaughlin, G. B. Robertson, W. L. Steffen, G. Salem, S. B. Wild, *Inorg. Chem*. **1982**, *21*, 1007. – [7b] R. D. Feltham, H. G. Metzger, *J. Organomet. Chem.* **1971**, *33*, 347. – [7c] G. L. Roberts, B. W. Skelton, A. H. White, S. B. Wild, *Aust. J. Chem*. **1982**, *35*, 2193. – [7d] H. A. Hudali, J. V. Kingston, H. A. Tayim, *Inorg. Chem*. **1979**, *18*, 1391. – [7e] G. A. Barclay, M. A. Collard, C. M. Harris, J. V. Kingston, *J. Chem. Soc. A* **1969**, 830. – [7f] G. Salem, S. B. Wild, *Inorg. Chem.* **1992**, *31*, 581. – [7g] T. Suzuki, K. Kashiwabara, J. Fujita, *Bull. Chem. Soc. Jpn.* **1995**, *68*, 1619.

[8] F. Faraone et al., work in progress.

[9] J. W. Suggs, G. D. N. Pearson, *J. Org. Chem*. **1980**, *45*, 1514.

[10] G. T. Whiteker, A. M. Harrison, A. G. Abatjoglou *J. Chem. Soc., Chem. Commun.* **1995**, 1805.

[11] M. J. Baker, K. N. Harrison, A. G. Orpen, P. G. Pringle, G. Shaw, *J. Chem. Soc., Chem. Commun.* **1991**, 803.

[12] E. Rotondo, G. Battaglia, G. Giordano, F. Priolo Cusmano, *J. Organomet. Chem.* **1993**, *450*, 245 and references therein.

[13] V. V. Grushin, H. Alper, *Chem. Rev.* **1994**, *94*, 1047.

[14] F. R. Hewgill, D. G. Hewitt, *J. Chem. Soc. C* **1967**, 726.

[15] N. Walker, D. Stuart, *Acta Crystallogr., Sect. A* **1983**, *39* 158; F. Ugozzoli, *Comput. Chem.* **1987**, *11*, 109.

[16] G. M. Sheldrick, *SHELXS-86, Program for the Solution of Crystal Structures*, University of Göttingen, Germany, **1986**.

[17] G. M. Sheldrick, *SHELXL-93, Program for the Refinement of Crystal Structures*, University of Göttingen, Germany, **1993**.

Received December 9, 1998
[I98420]

Synthesis and Structural Characterization of Monomeric Zinc(II), Cadmium(II), and Mercury(II) Arenethiolates with a Chelating Oxazoline Ligand

G. Mugesh,[a] Harkesh B. Singh,*[a] and Ray J. Butcher[b]

Keywords: Metal thiolates / Helical chirality / Spontaneous resolution / Disulfide / Intramolecular coordination

The synthesis and characterization of homoleptic zinc(II), cadmium(II), and mercury(II) thiolates derived from 4,4-dimethyl-2-phenyloxazoline (**1**) are described. The disulfide [Ox_2S_2 (**3**), Ox = 2-(4,4-dimethyl-2-oxazolinyl)phenyl] is prepared by the oxidation of lithium arenethiolate OxS^-Li^+ (**2**), and structurally characterized. The disulfide **3** is chiral and enantiomerically pure in the solid state. The thiolate derivatives, $M[S(Ox)]_2$ [M = Zn (**4**), or Cd (**5**)], are prepared in good yield by the metathesis reactions of MCl_2 with lithium arenethiolate **2**. The mercury complex **6** is synthesized by treating **3** with elemental mercury. The complexes are quite stable and highly soluble in common nonpolar organic solvents. X-ray diffraction results show that the zinc thiolate **4** and cadmium thiolate **5** are monomeric in the solid state. The geometry around the metal ion in these two complexes is found to be distorted tetrahedral. The zinc complex is chiral and has crystallized in two different crystalline modifications. The single crystal structures have been determined for both the crystalline modifications, a monoclinic modification (**4a**) and an orthorhombic one (**4b**). The crystal structure of **4a** shows that the complex is "helically" chiral and enantiomerically pure whereas the crystal structure of **4b** shows the modification to be racemic. The spontaneous splitting of the racemates, which is responsible for the isolation of optically active compound, indicates that there should be some solubility differences between the racemates and pure enantiomers. ^1H- and ^{13}C-NMR measurements indicate that the complex **4** retains its "helical" structure in solution.

Introduction

There is considerable general interest in the bonding and unusual structures adopted by chalcogenolate complexes of the Group 12 elements.[1] Besides their importance as single-source stoichiometric precursors to Group 12−16 semiconductors,[2] the metal-chalcogen chemistry of these elements has yielded many surprising results with respect to structural features, method of preparation, and degree of aggregation.[3]

As part of our work on intramolecularly coordinated organochalcogens,[4] we have recently isolated some stable monomeric mercury selenolates using *ortho*-chelating [(dimethylamino)benzyl]- and [(dimethylamino)ethyl]ferrocenyl ligands[5] and well-characterized examples of zinc, cadmium and mercury selenolato complexes by using a more rigid 4,4-dimethyl-2-phenyloxazoline substrate.[6] Interestingly, the zinc selenolato complex derived from 4,4-dimethyl-2-phenyloxazoline was found to be chiral at room temperature and the cadmium selenolate showed chirality at low temperatures. Although the corresponding tellurolate complexes of zinc and cadmium showed chirality at low temperatures, the complexes could not be crystallized due to their instability in solution.[7] In order to investigate the effect of the chalcogen atom on the chirality in Group 12 chalcogenolates, we extended our approach to the thiolate chemistry since the high affinity of zinc ions towards thiolates and the very marked preference for ZnN_2S_2 coordination may allow the isolation of "helically" chiral metal complexes.

In this paper, we describe the use of a phenyloxazoline-derived ligand to prepare monomeric Group 12 metal thiolates including a novel "helically" chiral zinc thiolate **4** and its spontaneous resolution. Structurally characterized "mono-helical" complexes of zinc are very rare[8] and this is the first example, to the best of our knowledge, where the two optically active forms have been spontaneously resolved in a four-coordinate zinc thiolate complex. We also describe the synthesis and structure of a novel chiral disulfide stabilized by intramolecular S···N interactions. In addition, the thermal behavior of the zinc, cadmium, and mercury thiolates provided some insight into their utility as CVD precursors.

Results and Discussion

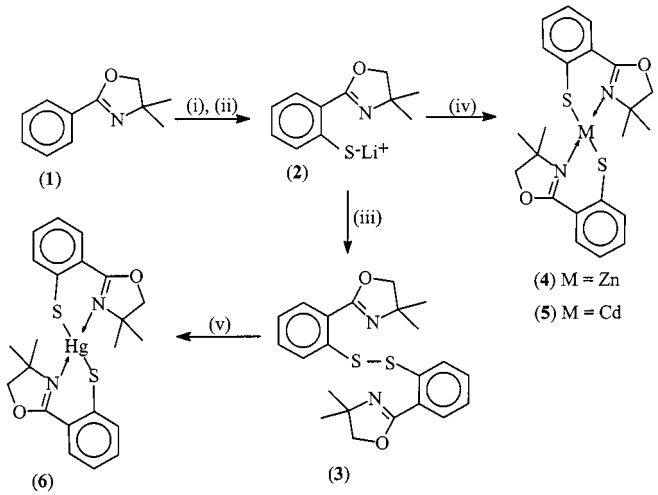
Monomeric Thiolates

Synthesis of the thiolate complexes was approached by the metathesis reaction of the lithium arenethiolate with the corresponding MCl_2 in ether according to our recently reported method for the synthesis of metal selenolates (Scheme 1).[6] The 2:1 molar reactions of **2** and anhydrous MCl_2 (M = Zn, Cd) in ether afforded the desired products in moderate yields. Attempts to synthesize the mercury thi-

[a] Department of Chemistry, Indian Institute of Technology, Powai, Bombay 400076, India
Fax: (internat.) + 91-22/578-3480,
E-mail: chhbsia@chem.iitb.ernet.in
[b] Department of Chemistry, Howard University, Washington, D.C. 20059, USA

 © WILEY-VCH Verlag GmbH, D-69451 Weinheim, 1999 1434−1948/99/0808−1229 $ 17.50+.50/0

olate by the reaction of **2** with $HgCl_2$ were unsuccessful. The 2:1 molar reactions of **2** and anhydrous $HgCl_2$ afforded the corresponding disulfide **3** resulting, presumably, due to the oxidation of **2** with $HgCl_2$. Recently, we have shown that pure monomeric mercury selenolate complexes could be obtained in two further steps, whereby the lithium areneselenolate was oxidized to the diselenide (which was air-stable and readily purified), followed by the oxidative addition of mercury.[5,6] Therefore, we have approached the synthesis of **6** by the reaction of **3** with elemental mercury. In contrast to the synthesis of corresponding diselenide[4f] and ditelluride,[7] the synthesis of disulfide by aerial oxidation of the lithium arenethiolate **2** was found to be difficult due to higher stability of the arenethiol produced by the addition of the lithium arenethiolate to water, and, therefore, vigorous oxidation was required to convert the thiol to disulfide. The reaction of **3** with elemental mercury then afforded, after several days of stirring at room temperature, **6** in 60% yield.



Scheme 1. Synthesis of M^{II} complexes; reagent and conditions: (i) *n*BuLi, hexane, room temp., 1 h; (ii) S powder, ether, 0°C, 2 h; (iii) O_2, H_2O; (iv) anhydrous MCl_2, 0°C, 1 h, and room temp., 18 h; (v) elemental mercury, methanol, room temp., 5 d

The significant feature of the chemistry of the entire class of complexes **4**–**6** is their excellent solubility in both nonpolar and slightly polar solvents at room temperature which is generally not a feature of metal chalcogenolate chemistry. They are, however, almost insoluble in highly polar solvents like DMSO and methanol.

Complex **4**, obtained as a yellow solid, shows some interesting features. The complex affords two types of crystals; yellow needle-shaped (**4a**, enantiomerically pure) and white plates (**4b**, racemic) crystals due to spontaneous crystallization of the enantiomers (vide infra). The complex **4** shows very good solubility in ether but the solubility is reduced for the enantiomers in the same solvent. The differences observed between **4a** and **4b** may also be ascribed to the different speed of crystallization. The crystals of **4a** were obtained from a mixture of chloroform/hexane within a day whereas the crystals of **4b** were separated from the solution after five days.

NMR-Spectroscopic Studies

In order to investigate the solution behavior of **3** and the complexes **4**–**6**, we have studied the ^{1}H- and ^{13}C-NMR spectra in $CDCl_3$. Although the crystal structure shows that **3** is chiral (vide infra), the room-temperature NMR (^{1}H, ^{13}C) spectra are not indicative of chirality. A sharp singlet for the methylene protons and another sharp singlet for the methyl protons observed in the ^{1}H-NMR spectrum of **3** at room temperature infer that the nonbonded S···N interactions are weak in the solution. The room-temperature ^{1}H-NMR spectrum of **4** contains a well-resolved AB doublet of doublets for the methylene protons and two sharp singlets for the methyl protons (Figure 1). The AB pattern for the methylene protons implies that the strong coordination of the "hard" imine nitrogen atom with the "hard" zinc(II) ion removes the erstwhile enantiotopic nature of these protons. The protons become diasteriotopic resulting in chirality of the complex. We[6] and others[8b,9] have noted a similar AB spin behavior of methylene protons in other complexes and have used it as a diagnostic probe of chirality. The inequivalence of the methylene group protons and two methyl group protons even at 55°C indicates a strong coordination of the nitrogen atom to the metal center and retention of the "helicity" even at higher temperatures. The spectra of both the crystalline modifications [yellow needles (**4a**) and white square plates (**4b**)] are identical.

The room-temperature ^{1}H-NMR spectrum of **5** consists of a sharp singlet for the methylene protons and another sharp singlet for the methyl protons. At −60°C, the methyl protons give rise to two singlets, however, the signal for the methylene protons is observed as a broad singlet (Figure 2). This is in contrast to the spectra of the corresponding cadmium selenolate[6] and cadmium tellurolate[7] where an AB doublet of doublets for the methylene protons was observed at −60°C. This indicates that the complex is probably not rigid even at −60°C. For complex **6**, the signals for the methylene and methyl protons are observed as sharp singlets. Since the exchange between "helical" and "nonhelical" arrangements is very fast, the splitting of the signals due to chirality could not be detected even at −60 °C. At this temperature only a slight broadening of the signals was observed.

From the current results and their comparison with those of corresponding selenolates[6] and tellurolates,[7] it is observed that the chemical shift values in all the complexes lie almost in the same region and there is no drastic change in the chemical shift values by changing the metal atom or changing the chalcogen atom. However, the signals due to the methyl and methylene protons are shifted upfield compared with the corresponding dichalcogenides probably due to the d^{10} configuration of the metal ions.

The ^{13}C-NMR spectra of the complexes are not very informative. The chemical shift values for the methyl and methylene carbon atoms are very close to the values observed for the disulfide. However, the ^{13}C-NMR spectrum of complex **4** gives some information about the chirality of the complex. Two signals at δ = 26.99 and 28.28 observed

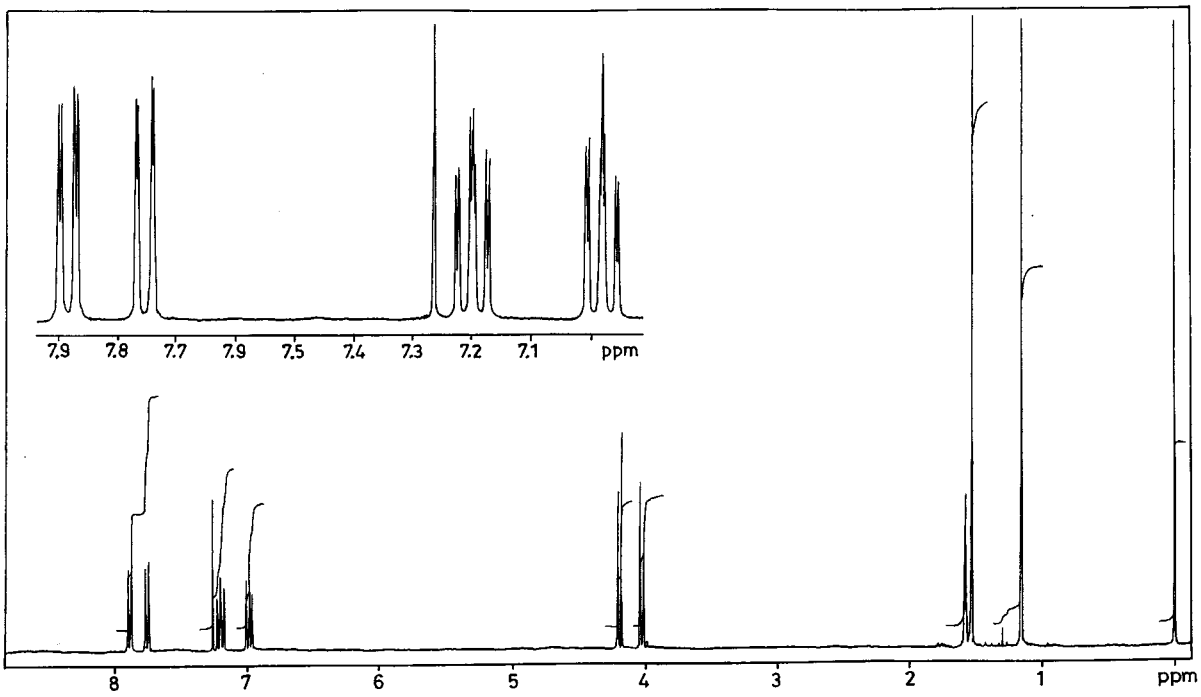


Figure 1. Room-temperature ^{1}H-NMR spectrum of **4a** ($CDCl_3$, 300 MHz)

for the methyl group carbon atoms clearly indicate that the two methyl groups present in the complex are nonequivalent.

Mass-Spectrometric Studies and Thermal Behavior

The mass spectra were recorded for complexes **4** and **5**. The mass spectra of complexes **4** and **5** are indicative of the presence of both monomeric and dimeric species in the gas phase {**4**; *m/z*: 477 [$Zn(SOx)_2^+$], 750 [$Zn_2(SOx)_3^+$]; **5**; *m/z*: 525 [$Cd(SOx)_2^+$], 844 [$Cd_2(SOx)_3^+$]}. The molecular ion peaks and the peaks due to other fragments containing S and M exhibit the expected isotope patterns.

The complexes have sharp melting points in the range 120−195°C giving clear liquids. To further know the volatility of the complexes and the decomposition pathway, TGA and DTA were recorded for all three complexes. The DTA curves of complexes **4**, **5** and **6** showed a phase transition (endothermic peak) in the range 130−200°C which corresponds to their melting. The TGA of complexes **4** and **5** showed the formation of expected metal sulfides (MS: M = Zn, Cd) at 530 and 390°C, respectively at ambient pressure. The mercury complex **6** showed complete weight loss in this temperature range probably due to the high volatility of this complex.

Molecular Structure of Compound 3

The crystal structure of **3** is shown in Figure 3 and the bond lengths and angles are given in Table 1. The interesting feature in this structure is that compound **3** crystallizes in the chiral space group $P2_12_12_1$ of the orthorhombic system. The structure is different from that of the corresponding diselenide[4f] and ditelluride[7] which are not chiral. Refinement of the Flack enantiopole parameter[10] shows that the compound has crystallized in enantiomerically pure form. Generally, the S···N interactions are expected to be weak compared with Se···N and Te···N interactions. However, in compound **3** the S···N interactions are found to be quite strong. The S(1)···N(1) and S(2)···N(2) bond lengths (2.815 and 2.787 Å) are considerably shorter than the sum of the van der Waals radii (3.35 Å) of these two atoms. In contrast to the selenium and tellurium analogues, the two S···N distances are almost equal. The S−S bond length of 2.053(1) Å is comparable to the single-bond covalent radii (2.08 Å).[11] The S(1)−C(11) and S(2)−C(21) bond lengths [1.798(3) Å and 1.790(3) Å] are also comparable to the corresponding single-bond covalent radii (1.81 Å). The angles N(1)···S(1)−S(2) and S(1)−S(2)···N(2) are 173.5° and 172.9°, respectively, indicating an almost linear arrangement of N···S−S···N atoms. The torsion angle C(11)−S(1)−S(2)−C(21) is −79.47°.

Molecular Structure of Compound 4

Complex **4** crystallizes in two different enantiomorphs (**4a** and **4b**). The structures of both crystalline modifications were determined.

Molecular Structure of Compound 4a

The structure of complex **4a** is consistent with the solution data. Interestingly, complex **4a** crystallizes in a chiral space group $P2_1$ with two molecules per unit cell. Crystals

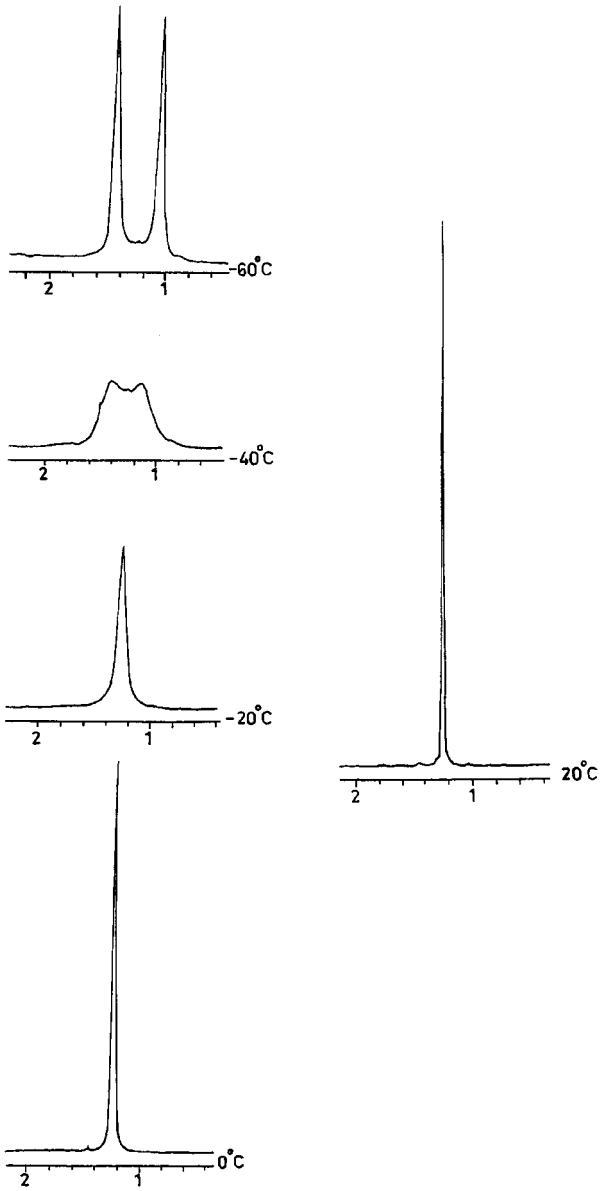


Figure 2. Variable-temperature ^{1}H-NMR ($CDCl_3$, 300 MHz) spectra (in part only) of **5**; at −60°C, the signals due to the CH_3 protons split into two singlets

of the complex **4a** belong to the monoclinic system. The ORTEP[12] view of the molecule is shown in Figure 4 and selected bond lengths and angles are given in Table 2. The structure is similar to that of the corresponding zinc selenolate complex,[6] which also crystallized in the same space group and almost with same cell parameters [the cell in **4** corresponds to $P2_1$ with a = 9.371(1), b = 11.397(1), c = 10.881(1) Å and β = 97.351(9)°; the cell in selenolate[6] corresponds to $P2_1$ with a = 9.390(1), b = 11.618(2), c = 10.882(1) Å and β = 98.245(8)°] and, therefore, the two compounds appear to be isostructural. Although, tetrahedral complexes with AB-type chelate ligands are expected to be chiral, to our knowledge, no optically pure chiral tetrahedral thiolatozinc complexes have been reported so far (generally they crystallize as racemates). Refinement of the Flack enantiopole parameter[10] led to a value of ca.

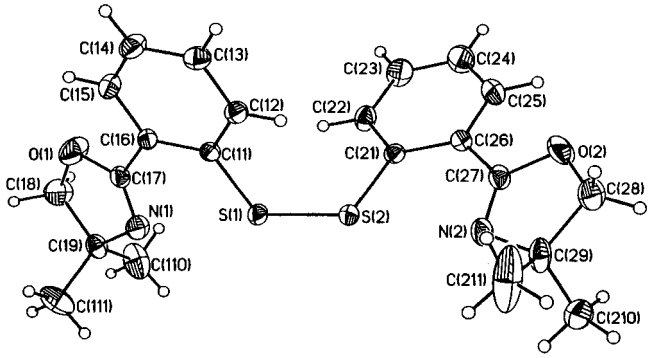


Figure 3. Crystal structure of disulfide **3**

Table 1. Selected bond lengths [Å] and angles [°] for **3**

S(1)−N(1)	2.815(3)	S(2)−N(2)	2.787(3)
S(1)−C(11)	1.798(3)	S(2)−C(21)	1.790(3)
O(1)−C(17)	1.357(4)	O(1)−C(18)	1.437(6)
O(2)−C(27)	1.352(4)	O(2)−C(28)	1.438(6)
N(1)−C(17)	1.244(4)	N(1)−C(19)	1.485(4)
N(2)−C(27)	1.254(4)	N(2)−C(29)	1.492(4)
S(1)−S(2)	2.053(1)		
C(26)−C(21)−S(2)	119.4(2)	C(12)−C(11)−S(1)	121.0(2)
C(11)−S(1)−S(2)	105.6(1)	C(16)−C(11)−S(1)	119.7(2)
C(21)−S(2)−S(1)	105.5(1)	C(22)−C(21)−S(2)	121.5(2)

zero for **4a** thus confirming the enantiomeric purity of the crystals.

The complex is monomeric with the zinc atom coordinated to two nitrogen and two sulfur atoms forming a distorted tetrahedron. As a consequence of the interaction of the two chelating ligands which causes the complex to distort in a helical way, chirality is induced at the metal center. The average Zn−S bond length 2.270(1) Å is close to the Zn−S length reported for an $(N_2S_2)Zn^{II}$ Schiff base complex incorporating pyrazole [Zn−S: 2.293(1) Å][13] but slightly shorter than that reported for a chiral five-coordinate Zn^{II} complex (2.34 Å)[8a] and for $Zn(SAr)_2(imid)_2$ (2.315 Å).[14] The Zn−N bond lengths [Zn−N(1): 2.043(3); Zn−N(2): 2.036(4) Å] are very close to the Zn−N length reported for the pyrazole Schiff base complex [2.039(3) Å][13] and for $Zn(SAr)_2(imid)_2$ (2.048Å)[14] and that reported for zinc and typical N-donor ligands which normally range from 2.04 Å to 2.14 Å. However, this bond is much stronger than the Zn−N bond reported for the chiral five-coordinate Zn^{II} complex (2.21 Å).[8a] The C−S bond lengths [S(1)−C(11): 1.758(4) Å; S(2)−C(21): 1.756(5) Å] are intermediate between that of a thione (C−C=S: 1.6 Å) and that of a thiol (C−C−SH 1.8 Å)[15] which is normal for N_2S_2 Schiff base complexes.[16] The chelate bite angles of S(1)−Zn−N(1) and S(2)−Zn−N(2) are 96.16(9) and 97.18(9)°, respectively. The larger bite angle leads to relatively smaller N−Zn−N and S−Zn−S angles of 106.45(14) and 116.47(9)°, respectively.

Interestingly, in the case of the selenium analogue[6] of **4**, the N−Zn−N and Se−Zn−Se bond angles [106.6(2)° and 113.49(4)°] are close to ideal tetrahedral angles and in this case we have isolated optically pure complex whereas in the oxygen analogue, the deviation from the ideal tetrahedral

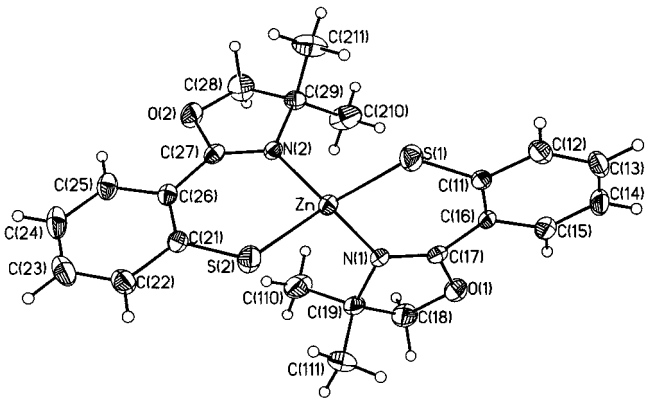


Figure 4. Crystal structure of monomeric Zn^{II} complex **4a**

Table 2. Selected bond lengths [Å] and angles [°] for **4a**

Zn−N(2)	2.036(4)	Zn−N(1)	2.043(3)
Zn−S(2)	2.268(1)	Zn−S(1)	2.273(1)
S(1)−C(11)	1.758(4)	S(2)−C(21)	1.756(5)
O(1)−C(17)	1.350(4)	O(1)−C(18)	1.442(5)
O(2)−C(27)	1.357(5)	O(2)−C(28)	1.456(6)
N(1)−C(17)	1.277(5)	N(1)−C(19)	1.493(5)
N(2)−C(27)	1.282(5)	N(2)−C(29)	1.501(5)
N(2)−Zn−N(1)	106.5(1)	N(2)−Zn−S(2)	97.18(9)
N(1)−Zn−S(2)	120.98(9)	N(2)−Zn−S(1)	120.9(1)
N(1)−Zn−S(1)	96.16(9)	S(2)−Zn−S(1)	116.47(7)

geometry is even higher [N−Zn−N: 121.13(9); O−Zn−O: 117.73(9)] and in this case no optically pure enantiomer could be isolated.[17]

Molecular Structure of Compound 4b

The colorless crystals of complex **4b** belong to the space group *Pbca* of the orthorhombic system with 8 molecules per unit cell. Surprisingly, although the crystals of **4b** exhibited optical rotation, the space group indicates the formation of racemic crystals. This indicates that **4b** is probably a mixture of optically pure and racemic forms. An ORTEP view of the structure is shown in Figure 5 and selected bond lengths and angles are given in Table 3. The geometry around the metal center is distorted tetrahedral. Although the bond lengths around the metal ion are found to be similar to that of **4a**, the bond angles show significant differences. The N(1)−Zn−N(2) [110.6(1)°] and S(1)−Zn−S(2) [118.34(6)°] angles are slightly larger than the corresponding angles observed in complex **4a**. The N(1)−Zn−S(2) [114.4(1)°] and N(2)−Zn−S(1) [117.0(1)°] bond angles are considerably smaller than the corresponding angles observed in **4a** [N(1)−Zn−S(2): 120.98(9)°; N(2)−Zn−S(1): 120.9(1)°]. The average chelate bite angle of 98.6° is larger than that of **4a** [96.67(9)°].

Molecular Structure of Compound 5

The colorless crystals of **5** belong to the space group *Pbca* of the orthorhombic system with 8 molecules per unit

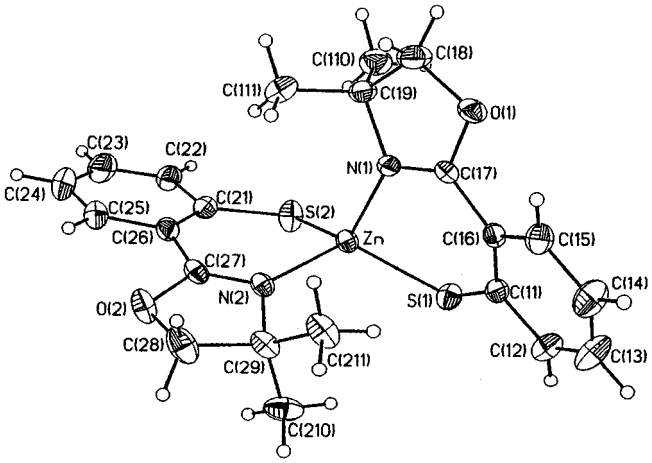


Figure 5. Crystal structure of monomeric Zn^{II} complex **4b**

Table 3. Selected bond lengths [Å] and angles [°] for **4b**

Zn−N(2)	2.021(3)	Zn−N(1)	2.027(3)
Zn−S(2)	2.271(1)	Zn−S(1)	2.264(1)
S(1)−C(11)	1.739(5)	S(2)−C(21)	1.745(5)
O(1)−C(17)	1.357(5)	O(1)−C(18)	1.436(6)
O(2)−C(27)	1.353(4)	O(2)−C(28)	1.441(6)
N(1)−C(17)	1.287(5)	N(1)−C(19)	1.497(5)
N(2)−C(27)	1.286(5)	N(2)−C(29)	1.498(5)
N(2)−Zn−N(1)	110.6(1)	N(2)−Zn−S(2)	98.6(1)
N(1)−Zn−S(2)	114.4(1)	N(2)−Zn−S(1)	117.0(1)
N(1)−Zn−S(1)	98.6(1)	S(2)−Zn−S(1)	118.34(6)

cell. From the space group and the cell parameters, complex **5** can be considered as isostructural with the corresponding selenolate.[6] An ORTEP diagram of the structure is shown in Figure 6. The bond lengths and angles are given in Table 4. The geometry around the metal center is distorted tetrahedral. In contrast to other cadmium thiolates, **5** is monomer without any close intermolecular contacts. The Cd−S bond lengths [Cd(1)−S(1): 2.453(3); Cd(1)−S(2): 2.459(3) Å] are much smaller than the corresponding lengths reported for $[Cd(C_5H_4NS)_2]_n$ (2.81 Å)[18] and $[Cd(C_7H_4N_2S)_2]_n$ (2.55 Å).[18] The Cd−N bond lenghts [Cd(1)−N(1): 2.286(8); Cd(1)−N(2): 2.261(8) Å] are, however, comparable to that reported for $[Cd(C_5H_4NS)_2]_n$ (2.34 Å) and $[Cd(C_7H_4N_2S)_2]_n$ (2.28 Å). The bond angle S(1)−Cd−S(2) [139.1(1)°] and the chelate ring bite angle S−Cd−N [88.2(2)°] are much larger than that of $[Cd(C_5H_4NS)_2]_n$ in which the S−Cd−S bond angle is 103.4(3)° and the chelate bite angle is 60.80°. In contrast to the zinc complex **4**, complex **5** is not chiral which indicates that the interactions between the nitrogen atom and the cadmium ion are not strong enough to create the required distortion around the metal center.

The bond lengths and angles for the oxazoline rings in all the cases reflect certain similarities with other five-membered heterocycles containing O and N atoms such as isoxazoline[19] and oxazolo[20] compounds. The O(1)−C(17) lengths [1.357(4) Å and 1.36(1) Å] in complexes **4a** and **4b**, respectively are significantly shorter than the O(1)−C(18) bond lengths [1.442(5) Å and 1.46(1) Å], while the same is

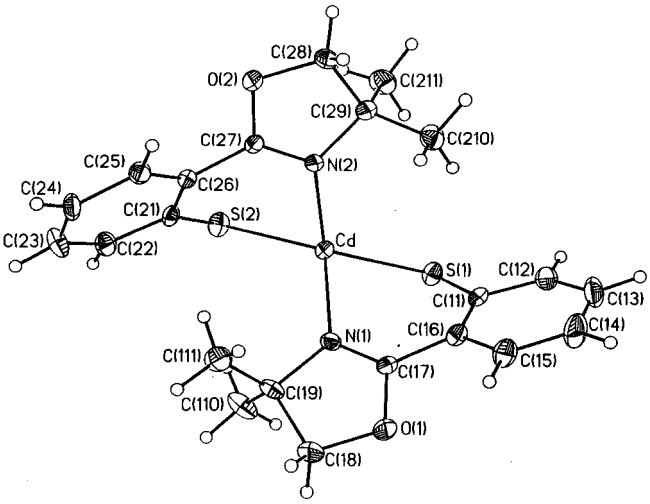


Figure 6. Crystal structure of monomeric Cd^{II} complex **5**

Table 4. Selected bond lengths [Å] and angles [°] for **5**

Cd(1)−N(1)	2.286(8)	Cd(1)−N(2)	2.261(8)
Cd(1)−S(1)	2.453(3)	Cd(1)−S(2)	2.459(3)
S(2)−C(21)	1.763(10)	S(1)−C(11)	1.766(10)
O(1)−C(17)	1.357(11)	O(1)−C(18)	1.464(14)
O(2)−C(27)	1.350(11)	O(2)−C(28)	1.440(12)
N(1)−C(17)	1.257(12)	N(1)−C(19)	1.508(12)
N(2)−C(27)	1.294(11)	N(2)−C(29)	1.49 (1)
N(2)−Cd−N(1)	107.0(3)	N(2)−Cd(1)−S(2)	88.1(2)
N(1)−Cd−S(1)	88.3(2)	N(2)−Cd(1)−S(1)	116.7(2)
N(1)−Cd(1)−S(2)	116.4(2)	S(1)−Cd(1)−S(2)	113.1(1)

true for the N(1)−C(17) lengths [1.244(4) Å and 1.26(1) Å] with respect to the N(1)−C(19) bond lengths [1.485(4) Å and 1.51(1) Å]. This indicates a similar double-bond character in both O(1)−C(17) and N(1)−C(17). The O(1)−C(17) bond lengths are slightly shorter than the corresponding length observed for the zinc selenolate [1.362(8) Å].[6] Complex **5** also shows similar double-bond character in both O(1)−C(17) and N(1)−C(17).

Conclusion

The intramolecularly coordinating 2-(4,4-dimethyloxazolino)benzenethiolate ligand can be successfully used for the isolation of a series of monomeric four-coordinate Group 12 metal thiolate complexes, including the rare example of a "helically" chiral zinc complex. The high affinity of zinc ions towards thiolates and the strong coordination of the imine nitrogen atom to the metal center facilitate the separation of two enantiomorphs by crystallization. The AB spin behavior of methylene protons present in the oxazoline ring can be used as a diagnostic probe of chirality in the complexes. The thiolate ligand shows chirality only with the zinc ion, whereas the selenolate and tellurolate ligands show chirality with the zinc and cadmium ions. The isolation of "helically" chiral zinc complex is much more facile in the case of thiolate compared with selenolate and tellurolate. However, the chirality observed in these complexes at either room temperature or low temperatures shows the general tendency of the oxazoline ligand to form "helical" metal complexes. As expected, the stability of the Group 12 metal complexes decreases in the order S > Se > Te. In addition, the low molecularity, excellent solubility in hydrocarbon solvents, low melting points and relatively high volatility of the complexes render them of interest as single-source precursors to Group 12−16 thin-film semiconductors.

Experimental Section

General Procedures: All reactions were carried out under nitrogen or argon using standard vacuum-line techniques. Solvents were purified by standard procedures[21] and were freshly distilled prior to use. Mercury and $ZnCl_2$ were purified prior to use.[21] Commercially available $CdCl_2$ and $HgCl_2$ were used as received. − Melting points were recorded in capillary tubes and are uncorrected. − ^{1}H- and ^{13}C-NMR spectra were obtained at 300 and 75.42 MHz, respectively, in $CDCl_3$ with a Varian VXR 300S spectrometer. Chemical shifts are cited with respect to $SiMe_4$ as internal standard. − Elemental analyses were performed with a Carlo-Erba model 1106 elemental analyzer. − Fast atom bombardment (FAB) mass spectra were recorded at room temperature with a JEOL SX 102 DA-6000 mass spectrometer/data system with xenon (6 kV, 10 mV) as the bombarding gas. The acceleration voltage was 10 kV and *m*-nitrobenzyl alcohol was used as the matrix with positive-ion detection. In case of isotopic patterns the value given is for the most intense peak. − Thermal analyses were performed at atmospheric presure with a Shimadzu D30 thermal analyser under nitrogen with the heating rate of 10°C/min. − Optical rotations were measured with a JASCO Model DIP 370 digital polarimeter.

Synthesis of Ox_2S_2 (3): To a suspension of 4,4-dimethyl-2-oxazolinylphenyl lithium[6] (1.82 g, 10 mmol) in dry ether (30 mL), elemental sulfur (0.32 g, 10 mmol) was added rapidly at 0°C. After 3 h, all sulfur was consumed to give a yellow solution of **2**. To this, distilled water (10 mL) was added and complete oxidation was affected by passing oxygen through the mixture for 2 h. The resulting organic layer and the ether extracts from the aqueous layer were combined, dried with anhydrous sodium sulfate, and concentrated in vacuo to give a yellow oil. Crystallization of this from chloroform/methanol (1:1) afforded **3** as white needles. Yield: 0.8 g, (40%); m.p. 142−144°C. − $C_{22}H_{24}N_2O_2S_2$ (412.6): calcd. C 63.98, H 5.82, N 6.79; found C 63.86, H 5.42, N 5.94. − ^{1}H NMR (300 MHz, $CDCl_3$): δ = 1.44 (s, 12 H, CH_3), 4.12(s, 4 H, CH_2), 7.17−7.22 (m, 2 H, Ar-H), 7.26−7.35 (m, 2 H, Ar-H), 7.71−7.74 (m, 2 H, Ar-H), 7.78−7.81 (m, 2 H, Ar-H). − ^{13}C NMR ($CDCl_3$): δ = 27.97, 68.68, 78.70, 124.66, 125.81, 126.69, 128.97, 131.64, 138.51, 160.57.

Synthesis of $Zn[S(Ox)]_2$ (4): To the lithium arenethiolate (2.14 g, 10 mmol), prepared as described above, was added anhydrous $ZnCl_2$ (0.68 g, 5 mmol) and stirring was continued for 1 h at 0 °C and 18 h at room temperature. The resulting solution was filtered through Celite and concentrated to give a yellow compound. The compound was recrystallized from a chloroform/hexane (1:1) mixture to give **4**. The spontaneous resolution of the racemate was observed during the crystallization process. The crude yellow compound (1.62 g) was dissolved in chloroform (20 mL) and hexane (20 mL) was added. Evaporation of the solvent at room temperature afforded the crystals of the two enantiomorphs. Fast crystallization (in 24 h) in an open vessel resulted in pale yellow crystals (**4a**) whereas slow evaporation of the remaining solvent (in 5 d) in

a flask covered with a rubber septum with a small hole resulted in white crystals (**4b**).

4a: Yellow crystals. Yield: 1.07 g (45%); m.p. 192−194°C. − $C_{22}H_{24}N_2O_2S_2Zn$ (477.9): calcd. C 55.30, H 5.03, N 5.87; found C 54.68, H 4.82, N 5.12. − ^{1}H NMR (300 MHz, $CDCl_3$): δ = 1.16 (s, 6 H, CH_3), 1.38 (s, 6 H, CH_3), 4.01−4.18 (dd, 4 H, CH_2), 6.95−6.98 (m, 2 H, Ar-H), 7.00−7.22 (m, 2 H, Ar-H), 7.73−7.77 (m, 2 H, Ar-H), 7.86−7.90 (m, 2 H, Ar-H). − ^{13}C NMR ($CDCl_3$): δ = 26.99, 28.28, 68.50, 78.15, 121.97, 122.78, 131.30, 131.62, 136.54, 150.45, 167.46. − MS; *m/z* (%): 652 [$C_{33}H_{36}N_3O_3S_3Zn_2^+$], 587 [$C_{33}H_{36}N_3O_3S_3Zn^+$], 477 [$M^+$, $C_{22}H_{24}N_2O_2S_2Zn^+$], 412 [$C_{22}H_{24}N_2O_2S_2^+$], 380 [$C_{22}H_{24}N_2O_2S^+$], 206 (100) [$C_{11}H_{12}NOS^+$]. − $[\alpha]_D^{25}$ = −6.158 (*c* = 1.0, $CHCl_3$).

4b: White crystals. Yield: 0.48 g (20%). m.p. 190−192°C. − $C_{22}H_{24}N_2O_2S_2Zn$ (477.9): calcd. C 55.30, H 5.03, N 5.87; found C 55.50, H 5.02, N 5.25. − $[\alpha]_D^{25}$ = +5.080 (*c* = 1.0, $CHCl_3$). − ^{1}H- and ^{13}C-NMR chemical shifts are in full accordance with the values reported for **4a**.

Synthesis of Cd[S(Ox)]$_2$ (5): Compound **5** was prepared according to the method described for **4** using 1.82 g (10 mmol) of 4,4-dimethyl-2-oxazolinylphenyllithium,[6] 0.32 g (10 mmol) of elemental sulfur and 0.917 g (5 mmol) of anhydrous $CdCl_2$. The crude product was recrystallized from a chloroform/hexane (1:1) mixture to give white crystals of **5**. Yield: 1.36 g (52%); m.p. 186−188°C. − $C_{22}H_{24}CdN_2O_2S_2$ (524.9): calcd. C 50.34, H 4.58, N 5.34; found C 50.49, H 4.45, N 5.28. − ^{1}H NMR(300 MHz, $CDCl_3$): δ = 1.25 (s, 12 H, CH_3), 4.09(s, 4 H, CH_2), 6.97−7.02 (m, 2 H, Ar-H), 7.15−7.20 (m, 2 H, Ar-H), 7.73−7.76 (m, 2 H, Ar-H), 7.75−7.81 (m, 2 H, Ar-H). − ^{13}C NMR ($CDCl_3$): δ = 27.91, 68.18, 77.82, 122.66, 124.99, 130.77, 131.30, 137.17, 147.66, 167.11. − MS; *m/z* (%): 746 [$C_{33}H_{36}Cd_2N_3O_3S_3^+$], 524 [$M^+$, $C_{22}H_{24}CdN_2O_2S_2^+$], 380 [$C_{22}H_{24}N_2O_2S^+$], 318 [$C_{11}H_{12}CdNOS^+$], 206 (100) [$C_{11}H_{12}NOS^+$].

Synthesis of Hg[S(Ox)]$_2$ (6). − Method A: Synthesis of compound **6** was approached by the method described for **4** from 10 mmol of 4,4-dimethyl-2-oxazolinylphenyllithium,[6] 0.32 g (10 mmol) of elemental sulfur and 1.358 g (5 mmol) of anhydrous $HgCl_2$. Elemental analysis and other analytical data for the white solid obtained from the reaction indicated the formation of the disulfide **3**. The crude product was recrystallized from a chloroform/hexane (1:1) mixture. Yield: 2.12 g (60%). All analytical data are in full accordance with the values reported for **3**.

Method B: To a stirred solution of **3** (0.413 g, 1 mmol) in methanol (20 mL) was added an excess of mercury (1 g, 5 mmol) at room temperature. The reaction mixture was stirred for 5 d to give an almost colorless solution. This was filtered through a Celite-padded filter frit to remove the unchanged mercury. The filtrate was concentrated to give a colorless crystalline product (0.5 g). This was recrystallized from a chloroform/methanol (1:1) mixture to give colorless crystals of **6**. Yield: 0.37 g (60%); m.p. 122−124°C. − $C_{22}H_{24}HgN_2O_2S_2$ (612.6): calcd. C 43.12, H 3.92, N 4.52; found C 42.95, H 3.86, N 4.10. − ^{1}H NMR (300 MHz, $CDCl_3$): δ = 1.17 (s, 12 H,CH_3), 3.99 (s, 4 H, CH_2), 7.06−7.11 (m, 2 H, Ar-H), 7.24−7.28 (m, 2 H, Ar-H), 7.67−7.71 (m, 2 H, Ar-H), 7.74−7.78 (m, 2 H, Ar-H). − ^{13}C NMR ($CDCl_3$): δ = 28.05, 68.53, 77.92, 124.76, 126.87, 132.67, 133.35, 139.32, 148.93, 165.23.

Caution: Cadmium and mercury complexes are expected to be toxic and must be handled with care.

X-ray Crystallographic Studies: The diffraction measurements for compounds **3**, **4a**, **4b**, and **5** were performed at room temperature (293 K) with a Siemens R3m/V diffractometer using graphite-monochromated Mo-K_α radiation (λ = 0.7170 Å). The unit cell was determined from 25 randomly selected reflections using the automatic search index and least-squares routine. For **3**, the θ range for data collection was from 2.61 to 30.00° whereas for **4a**, **4b**, and **5** it ranged from 2.60 to 27.50°, 2.52 to 27.50° and 2.53 to 27.50°, respectively. The index range for **3** was $0 \le h \le 11$, $0 \le k \le 21$, $0 \le l \le 23$ while for **4a**, **4b**, and **5** it was $0 \le h \le 12$, $-14 \le k \le 0$, $-14 \le l \le 14$; $0 \le h \le 11$, $-26 \le k \le 0$, $0 \le l \le 30$; and $-16 \le h \le 0$, $0 \le k \le 23$, $0 \le l \le 27$, respectively. The data for **4b** and **5** were corrected for Lorentz, polarization and absorption effects. The maximum/minimum transmission values of the correction factors for compounds **4b** and **5** were 0.9471/0.5626 and 0.8588/0.5163, respectively. The data were monitored by measuring two standard reflections every 60 min of X-ray exposure time. The structures were solved by routine heavy-atom (using SHELXS 86[22]) and Fourier methods and refined by full-matrix least squares

Table 5. Crystal data and structure refinement for **3**, **4a**, **4b**, and **5**

	3	**4a**	**4b**	**5**
empirical formula	$C_{22}H_{24}N_2O_2S_2$	$C_{22}H_{24}N_2O_2S_2Zn$	$C_{22}H_{24}N_2O_2S_2Zn$	$C_{22}H_{24}CdN_2O_2S_2$
mol. mass	412.55	477.92	477.92	524.95
crystal system	orthorhombic	monoclinic	orthorhombic	orthorhombic
space group	$P2_12_12_1$	$P2_1$	*Pbca*	*Pbca*
a [Å]	8.657(1)	9.371(1)	9.531(2)	12.504(2)
b [Å]	15.581(2)	11.397(1)	20.118(2)	17.773(2)
c [Å]	16.387(2)	10.881(1)	23.351(3)	21.019(3)
β [°]	90	97.35(1)	90	90
V [Å^3]	2210.3(5)	1152.6(2)	4477.5(11)	4671(10)
Z	4	2	8	8
D(calcd.) [Mg/m^3]	1.260	1.377	1.418	1.493
crystal size [mm]	0.36×0.99×0.50	0.24×0.52×0.30	0.23×0.82×0.40	0.27×0.82×0.72
abs. coeff. [mm^{-1}]	0.240	1.266	1.304	1.333
obsd. reflxns. [$I > 2\sigma$]	3486	2746	4944	4847
final $R(F)$ [$I > 2\sigma(I)$][a]	0.0454	0.0307	0.0500	0.0633
$wR(F^2)$ indices [$I > 2\sigma(I)$]	0.1161	0.0638	0.1002	0.1458
absolute structure parameter	0.11(11)	0.96(3)	−	−
data/restrains/parameters	3480/0/281	2745/1/291	4944/0/290	4783/0/290
goodness of fit on F^2	1.04	1.04	1.02	1.19

[a] Definitions: $R(F_o) = \Sigma||F_o| - |F_c||/\Sigma|F_o|$ and $wR(F_o^2) = \{\Sigma[w(F_o^2 - F_c^2)^2]/\Sigma[w(F_c^2)^2]\}^{1/2}$.

with the nonhydrogen atoms anisotropic and hydrogen atoms with fixed isotropic thermal parameters of 0.07 Å^2 using the SHELXL 93 program.[23] The hydrogen atoms were partially located from difference electron density maps and the rest were fixed at calculated positions. Scattering factors were from common sources.[24] Only the observed reflections were used in the final refinements. Some details of data collection and refinement are given in Table 5. Crystallographic data (excluding structure factors) for the structures reported in this paper have been deposited with the Cambridge Crystallographic Data Centre as supplementary publication no. CCDC-111948 (**3**), -111950 (**4a**), -111949 (**4b**), -111951 (**5**). Copies of the data can be obtained free of charge on application to CCDC, 12 Union Road, Cambridge CB2 1EZ, UK [Fax: + 44-1223/336-033; E-mail: deposit@ccdc.cam.ac.uk].

Acknowledgments

We are grateful to the Department of Science and Technology (DST), New Delhi and Board of Research in Nuclear Sciences (BRNS), Department of Atomic Energy, Bombay for funding this work. Additional help from the Regional Sophisticated Instrumentation Centre (RSIC), Indian Institute of Technology (IIT), Bombay for 300-MHz NMR spectroscopy, RSIC, Central Drug Research Institute (CDRI), Lucknow for Mass spectra and Tata Institute of Fundamental Research (TIFR), Bombay for 500-MHz NMR spectroscopy is gratefully acknowledged. R. J. B. wishes to acknowledge the DoD-ONR program for funds to upgrade the diffractometer.

[1] [1a] A. Müller, E. Diemann, in *Comprehensive Coordination Chemistry* (Ed.: G. Wilkinson), Pergamon, London, **1987**, vol. 2, p. 515. – [1b] I. G. Dance, *Polyhedron* **1986**, *5*, 1037. – [1c] P. G. Blower, J. R. Dilworth, *Coord. Chem. Rev.* **1987**, *76*, 121. – [1d] J. Arnold, "The Chemistry of Metal Complexes with Selenolate and Tellurolate Ligands" in *Progress in Inorganic Chemistry* (Ed.: K. D. Karlin), John Wiley & Sons, Inc.,**1995**, vol. 43, p. 353.

[2] [2a] J. G. Brennan, T. Siegrist, S. Stuczynski, C. Carroll, L. Brus, M. Steigerwald, *Chem. Mater.* **1990**, *2*, 403. – [2b] M. B. Hursthouse, M. A. Malik, M. Motevalli, P. O′Brien, *Organometallics* **1991**, *10*, 730. – [2c] M. A. Malik, M. Motevalli, J. R. Walsh, P. O′Brien, *Organometallics* **1992**, *11*, 3136. – [2d] M. A. Malik, M. Motevalli, T. Saeed, P. O′Brien, *Adv. Mater.* **1993**, *5*, 653. – [2e] M. Bochmann, *Chem. Vap. Deposition* **1996**, *2*, 85. – [2f] H. B. Singh, N. Sudha, *Polyhedron* **1996**, *15*, 745. – [2g] A. L. Seligson, J. Arnold, *J. Am. Chem. Soc.*, **1993**, *115*, 8214. – [2h] P. J. Bonasia, J. Arnold, *Inorg. Chem.* **1992**, *31*, 2508.

[3] [3a] I. G. Dance, R. G. Garbutt, D. C. Craig, M. L. Scudder, *J. Chem. Soc., Chem. Commun.* **1987**, 1164. – [3b] I. G. Dance, R. G. Garbutt, T. D. Bailey, *Inorg. Chem.* **1990**, *29*, 603. – [3c] I. G. Dance, R. G. Garbutt, M. L. Scudder, *Inorg. Chem.* **1990**, *29*, 1571. – [3d] T. Alsina, W. Clegg, K. A. Fraser, J. Sola, J. *J. Chem. Soc., Dalton Trans.* **1992**, 1393.

[4] [4a] H. B. Singh, N. Sudha, *Coord. Chem. Rev.* **1994**, *135–136*, 469. – [4b] R. Kaur, H. B. Singh, R. J. Butcher, *Organometallics* **1995**, *14*, 4755. – [4c] S. C. Menon, H. B. Singh, J. M. Jasinski, J. P. Jasinski, R. J. Butcher, *Organometallics* **1996**, *15*, 1707. – [4d] R. Kaur, S. C. Menon, H. B. Singh, *Proc. Indian Acad. Sci. (Chem. Sci.)* **1996**, *108*, 159. – [4e] S. C. Menon, H. B. Singh, R. P. Patel, K. Das, R. J. Butcher, *Organometallics* **1997**, *18*, 563. – [4f] G. Mugesh, A. Panda, H. B. Singh, N. S. Punekar, R. J. Butcher, *Chem. Commun.* **1998**, 2227. – [4g] G. Mugesh, H. B. Singh, R. J. Butcher, *Tetrahedron: Asymm.* **1999**, *10*, 237. – [4h] G. Mugesh, A. Panda, H. B. Singh, R. J. Butcher, *Chem. Eur. J.* **1999**, *5*, 1411.

[5] R. Kaur, H. B. Singh. R. P. Patel, S. K. Kulshreshtha, *J. Chem. Soc., Dalton Trans.* **1996**, 461.

[6] G. Mugesh, H. B. Singh, R. P. Patel, R. J. Butcher, *Inorg. Chem.* **1998**, *37*, 2663.

[7] G. Mugesh, H. B. Singh, R. J. Butcher, *J. Organomet. Chem.* **1999**, *577*, 243.

[8] [8a] L. F. Lindoy, D. H. Busch, V. Goedken, V. *J. Chem. Soc., Chem. Commun*. **1972**, 683. – [8b] T. Adatia, N. Beynek, B. P. Murphy, *Polyhedron* **1995**, *14*, 335. – [8c] R. Chotalia, E. C. Constable, M. Neuburger, D. R. Smith, M. Zehnder, *J. Chem. Soc., Dalton Trans.* **1996**, 4207.

[9] [9a] S. Ruttimann, C. Piguet, G. Bernardinelli, B. Bocquet, A. F. Williams, *J. Am. Chem. Soc.* **1992**, *114*, 4230. – [9b] A. Bilyk, M. M. Harding, *J. Chem. Soc., Dalton Trans.* **1994**, 77.

[10] H. Flack, *Acta Crystallogr., Sect. A* **1983**, *39*, 876.

[11] L. Pauling, in *The Nature of the Chemical Bond*, 3rd ed. Cornell University Press, Ithaca, New York, **1960**, p. 224.

[12] C. K. Johnson, *ORTEPII*; Report ORNL-5138, Oak Ridge National Laboratory, Oak Ridge, TN, **1976**.

[13] O. P. Anderson, A. la Cour, M. Findeisen, L. Hennig, O. Simonsen, L. F. Taylor, H. Toftlund, *J. Chem. Soc., Dalton Trans.* **1997**, 111.

[14] M. Bochmann, G. C. Bwembya, R. Grinter, A. K. Powell, K. J. Webb, M. B. Hursthouse, K. M. A. Malik, M. A. Mazid, *Inorg. Chem*. **1994**, *33*, 2290.

[15] F. H. Allen, O. Kennard, D. G. Watson, L. Bremmer, A. G. Orpen, R. Taylor, *J. Chem. Soc., Perkin Trans. 2* **1987**, S1.

[16] A. D. Garnowski, A. L. Nivorozhkin, V. I. Minkin, *Coord. Chem. Rev.* **1993**, *126*, 1.

[17] G. Mugesh, H. B. Singh, R. J. Butcher, *Inorg. Chem.*, under revision.

[18] M. B. Hursthouse, O. F. Z. Khan, M. Mazid, M. Motevalli, P. O′Brien, *Polyhedron* **1990**, *9*, 541.

[19] [19a] D. C. Rodiou, S. C. Kokkou, P. J. Rentzeperis, *Acta Crystallogr., Sect. B* **1978**, 13. – [19b] A. P. Bozopoulos, S. C. Kokkou, P. J. Rentzeperis, *Acta Crystallogr., Sect. B* **1980**, 1326.

[20] [20a] R. Jaunin, W. E. Oberhansli, J. Hellerbach, *Helv. Chim. Acta* **1972**, *55*, 2975. – [20b] K. Kamiya, Y. Wada, M. Nishikawa, *Chem. Pharm. Bull.* **1973**, *21*, 1520.

[21] D. D. Perrin, W. L. F. Armarego, D. R. Perrin, *Purification of Laboratory Chemicals*, 2nd ed., Pergamon, Oxford, **1980**.

[22] G. M. Sheldrick, *Crystallographic Computing 3*, Oxford University Press, Oxford, **1985**, p 175.

[23] G. M. Sheldrick, *SHELX 93*, Program for Crystal Structure Determination, University of Göttingen, **1993**.

[24] *International Tables for X-ray Crystallography*, Kynoch Press, Birmingham, **1974**, vol. 4, pp. 99, 149.

Received December 10, 1998
[I98424]

On the Influence of the Bite Angle of Bidentate Phosphane Ligands on the Regioselectivity in Allylic Alkylation

Richard J. van Haaren,[a] Henk Oevering,[b] Betty B. Coussens,[b] Gino P. F van Strijdonck,[a] Joost N. H. Reek,[a] Paul C. J. Kamer,[a] and Piet W. N. M. van Leeuwen*[a]

Keywords: Palladium / Phosphane ligands / Bite angle / Allylic alkylation / Molecular modelling

The natural bite angle of bidentate phosphane ligands influences the isomer distribution (*syn* and *anti*) in (1-methylallyl)(bisphosphane)Pd OTf complexes. It was found (^{31}P- and ^{1}H-NMR studies) that the *syn*/*anti* ratio changes from 12 (dppp) to 1.3 (sixantphos). Molecular orbital calculations [PM3(tm) level] indicate that for ligands inducing a large bite angle, the phenyl rings of the ligand embrace the allyl moiety, thus influencing the *syn*/*anti* ratio. This bite-angle effect on the *syn*/*anti* ratio is transferred to the regioselectivity in stoichiometric allylic alkylation. Ligands inducing large bite angles direct the regioselectivity towards the formation of the branched product **2**. Catalytic alkylation of (*E*)-2-butenyl acetate showed that for ligands with a small bite angle the regioselectivity of the catalytic and stoichiometric alkylation are in good agreement. This correspondence is worse for ligands with a larger bite angle, which is rationalised in terms of the relative rates of *syn*/*anti* isomerisation and alkylation. The ligand with the largest bite angle (sixantphos) gives the most active catalytic species.

The palladium-catalysed allylic alkylation reaction receives much interest.[1–7] Most of the research in this field focuses on asymmetric induction. Less effort is put into understanding the regioselectivity found in the alkylation of nonsymmetrically substituted allyl fragments.[5,13] Åkermark[5] has shown that the cone angle of substituted phenanthrolines has a large influence on both the isomer distribution of (1-methylallyl)Pd complexes and the regioselectivity of stoichiometric alkylation. The methyl substituents on the 2,9-dimethyl-1,10-phenanthroline ligand interfere with the methyl substituent on the allyl moiety. This causes the *anti* isomer of the complex to prevail over the otherwise more stable *syn* isomer. It was shown that stoichiometric alkylation of the *syn* complex resulted in almost exclusive formation of the linear (*E*) product (**1**). The *anti* complex reacted to the branched (**2**) and the linear *cis* product (**3**) in an approximately 1:1 ratio.

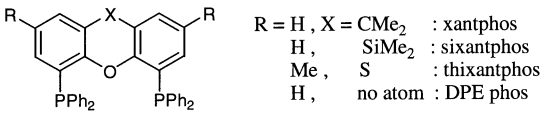


Figure 1. Generic xantphos structure

In our research group much research has been conducted concerning the effect of the natural bite angle[21] (β_n) of bidentate phosphane ligands on transition-metal-catalysed reactions.[15] This research led to the development of a new class of ligands that enforces (very) large bite angles up to 110° (the xantphos-type ligands: see Figure 1). Significant dependencies of the catalyst performance on the natural bite angle have been observed in reactions such as the rhodium-catalysed hydroformylation[8] and the nickel-catalysed hydrocyanation.[9] Recently, we communicated on the effect found in the alkylation of (*E*)-2-hexenyl acetate with sodium diethyl 2-methylmalonate.[11] Ligands with a large natural bite angle were found to direct the regioselectivity to the linear (*E*) product **1** resulting in smaller amounts of the branched product.

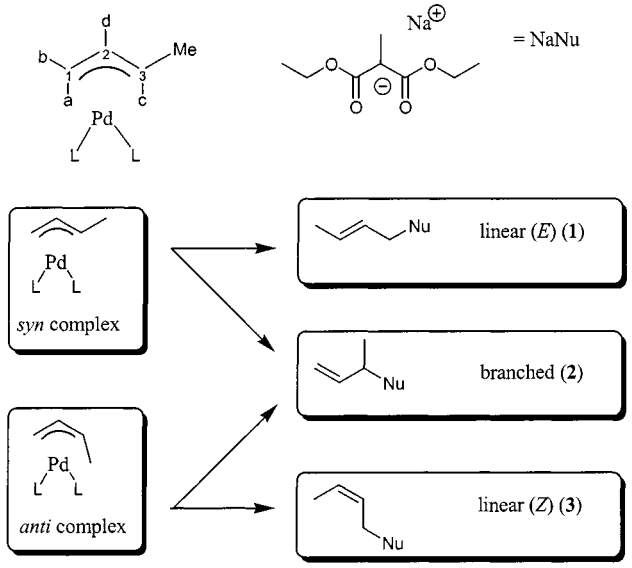


Figure 2. Numbering scheme and formation of regioisomers in the stoichiometric alkylation of (bisphosphane)(1-methylallyl)PdOTf complexes

In order to further investigate the nature of this bite angle effect, we have prepared and isolated (bisphosphane)(1-methylallyl)PdOTf complexes of several bisphosphane ligands. NMR studies (^{1}H and ^{31}P) of these compounds show that they exist as an equilibrium mixture of the *syn*

[a] Institute for Molecular Chemistry, University of Amsterdam, Nieuwe Achtergracht 166, NL-1018 WV, Amsterdam, The Netherlands
[b] D. S. M. Research N. V., P. O. Box 18, NL-6160 MD, Geleen, The Netherlands

 © WILEY-VCH Verlag GmbH, D-69451 Weinheim, 1999 1434–1948/99/0808–1237 $ 17.50+.50/0

and *anti* isomers. The *syn*/*anti* ratio is dependent on the bite angle of the ligand and is significantly lower in complexes of ligands inducing larger bite angles (Table 1).

To understand the effect of the P−Pd−P angle[20] (β) on the structure of the (allyl)Pd complex, molecular orbital calculations [semiempirical PM3(tm) level] were carried out on the cationic (1-methylallyl)(bisphosphane)Pd^+ complexes. The P−Pd−P angle (β), taken from the calculated structures, varies from 85° (dppe) to 110° (sixantphos). The allyl moiety is found to be embraced by the phenyl rings of the ligand. When the bite angle is larger, the embracing becomes more pronounced. This is visualised in Figure 3.

In all the complexes studied using molecular modelling, the *syn* isomer has a lower energy than the *anti* isomer. The energy *difference* between the *syn* and *anti* isomer, however, decreases with larger bite angle. This is in agreement with the experimental data: a lower *syn*/*anti* ratio is observed when ligands inducing larger bite angles are applied (Table 1). The embracing effect in complexes of ligands inducing a *small* bite angle, however, is of minor influence. The relatively high *syn*/*anti* ratio of (dppp)(1-methylallyl)PdOTf is therefore the result of electronic rather than steric effects. This special case will be discussed in more detail elsewhere.[16]

The percentage of **3** remains almost constant along the bite angle range studied.

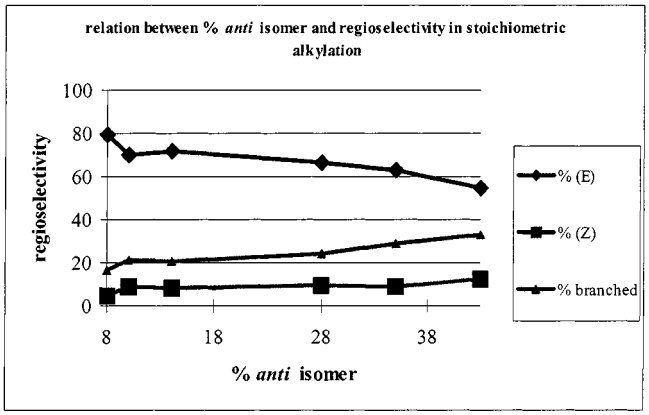


Figure 4. Relation between isomer distribution in cationic (bisphosphane)(1-methylallyl)PdOTf complexes and the regioselectivity of stoichiometric alkylation

It has been suggested[1] that in allylic alkylation reactions the structure of the allyl complex determines the (enantio)-selectivity in an early transition state. Recent developments,[4,6,12−15] however, indicate that in many cases a late transition state is more likely. In an early transition state the steric accessibility of the two carbon atoms of the allyl moiety will determine the selectivity. Due to steric hindrance between the substituent on the allyl moiety and the ligand, it will be bent out of the allyl plane, away from the palladium centre. Therefore the substituted allyl carbon atom C-3 will be less accessible for nucleophilic attack and consequently alkylation of the unsubstituted allyl carbon atom C-1 will prevail.

In a late transition state, nucleophilic attack of the malonate anion at the substituted allyl carbon atom C-3 will cause a change in the hybridisation on C-3 from sp^2 to sp^3. This causes the substituent to bend towards a phenyl ring of the ligand. A large bite angle results in an increase of the steric hindrance in this stage of the reaction (Figure 3), which hampers the formation of **2**.[11]

With a small group like a methyl substituent on the allyl moiety the steric hindrance during the nucleophilic attack is of less influence. Consequently, electronic factors may be-

Table 1. Relation between the bite angle and 1) Δ*E* (*syn*/*anti*) calculated by molecular modelling [PM3(tm) level] and obtained from experimental data (NMR), and 2) the regioselectivity in stoichiometric alkylation of the equilibrium mixtures of (bisphosphane)(1-methylallyl)PdOTf complexes

Complex (ligand)	β[a] [°]	% *syn*	% *anti*	Δ*E* (NMR) [kJ·mol^{-1}]	Δ*E*[b] [pm3(tm)] [kJ·mol^{-1}]	% **1**	% **3**	% **2**
I (dppe)	85	90	10	−5.4	−23.7	70.0	8.9	21.1
II (dppp)	95	92	8	−6.1	−21.9	79.2	4.6	16.2
III (dppb)	99	86	14	−4.5	−20.0	71.7	8.0	20.3
IV (dppf)	106	78	22	−3.1	−18.9	68.9	8.9	22.2
V (DPEphos)	108	72	28	−2.3	−15.4	66.4	9.6	24.0
VI (sixantphos)	110	57	43	−0.7	−12.5	54.5	12.4	33.1

[a] β Obtained from the calculated (bisphosphane)(1-methylallyl)Pd complexes. − [b] The relative large energy difference in the calculations is most likely the result of the absence of solvent and anion.

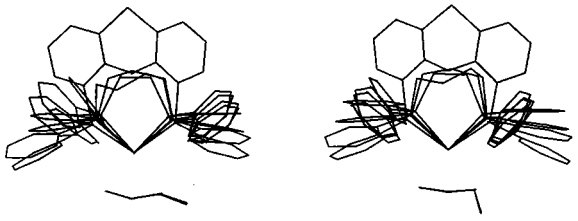


Figure 3. The embracing effect of the phenyl rings cause the substituent on the allyl moiety to bend out of the allyl plane; left = *syn*, right = *anti*

The *syn*/*anti* ratio governs the regioselectivity of the stoichiometric alkylation (Table 1, Figure 4). In (bisphosphane)(1-methylallyl)PdOTf complexes of ligands inducing a *small* bite angle the *syn* isomer largely prevails and the relative amount of the linear (*E*) product **1** is high. Going to a larger bite angle (from dppp to sixantphos), the percentage of *syn* isomer as well as the selectivity to **1** drops, whereas the selectivity to the branched product **2** increases.

come more important. This would explain the good correlation between the *syn*/*anti* ratio and the observed regioselectivity. Therefore it is concluded that in the alkylation of (bisphosphane)(1-methylallyl)PdOTf complexes the transition state of the reaction is not late. The relative importance of steric and electronic factors is dependent on the nature of the ligand and the (*syn* or *anti*) orientation of the substituents on the allyl moiety.

In addition to these stoichiometric experiments we have also carried out the *catalytic* alkylation of (*E*)-2-butenyl acetate. The catalytic experiments have been performed using the isolated (bisphosphane)(1-methylallyl)PdOTf complexes, instead of using a precursor, such as $Pd(dba)_2$, or $Pd(OAc)_2$, and the ligand. This procedure excludes an incubation step which is necessary for the formation of the catalytically active species, as well as the possibility of preequilibria by complexation of dba to Pd.[18] The retarding effect of dba is clear, if we compare the reaction rates presented in Table 2 with the reaction rates presented in a previous communication of the bite angle effect on allylic alkylation.[11] The difference in the rate of reaction is at least one order of magnitude.[16] Remarkably, the observed trend in reaction rate does not remain the same. Starting from the isolated (bisphosphane)(1-methylallyl)PdOTf complex, sixantphos is found to yield the most active catalytic species, whereas use of $Pd(dba)_2$ results in DPEphos or dppb to yield the most active catalyst.[11] Obviously, the catalytically active species is less easily formed from $Pd(dba)_2$ when a rigid ligand inducing a large bite angle is used.

In contrast to most literature procedures for allylic alkylation reactions only one equivalent of ligand per palladium atom is used. When a precursor, such as $Pd(OAc)_2$ is used, an additional equivalent of ligand might be required to reduce the Pd^{II} to the active Pd^0 species.[17] The presence of an excess of ligand will also reduce the rate of the reaction, by complexation to the Pd^0 species which is formed after alkylation. Before coordination of the substrate dissociation of the extra ligand is necessary. This can retard the overall reaction rate.

The bite-angle effect as observed in the *stoichiometric* alkylation of (bisphosphane)(1-methylallyl)PdOTf complexes is less obvious in the *catalytic* alkylation of (*E*)-2-butenyl acetate. The starting complex enters the catalytic cycle by alkylation of the starting (bisphosphane)(1-mehylallyl)-PdOTf complex. The next step involves oxidative addition of the substrate to the thus formed Pd^0 species. As the substrate configuration is mainly (*E*) (95%), initially the *syn*-(bisphosphane)(1-methylallyl)PdOAc complex is formed as the main product. This complex is cationic, so the acetate leaving group will remain as a counterion in the coordination sphere. Interaction of the counterion with the palladium centre is known to increase the rate of dynamic behaviour of the allyl moiety.[19] This results in an isomerisation of the *syn* complex to the *anti* complex and vice versa. The resulting regioselectivity of the catalytic reaction (Table 2) is dependent on the relative rates of *syn*/*anti* isomerisation and alkylation.

NMR experiments with the (bisphosphane)(1-methylallyl)PdOTf complexes used in the alkylation reactions, indicate that the *syn*/*anti* isomerisation in these complexes is slow relative to stoichiometric alkylation. The isomerisation, however, may play a significant role when acetate instead of the weakly co-ordinating triflate is the counterion, as is the case in the catalytic experiments.

The correlation between the regioselectivity in stoichiometric and catalytic alkylation is good for ligands inducing a small bite angle, such as dppe and dppp, but also for dppf (Table 1 and 2). Going to a larger bite angle, the selectivity follows a different trend as that in the stoichiometric reaction. The sixantphos ligand directs the regioselectivity towards 85% of the linear (*E*) product. This can be rationalised in terms of a fast alkylation rate, relative to isomerisation, of the complexes with ligands inducing a large bite angle.

In conclusion, we have shown that for (bisphosphane)(1-methylallyl)PdOTf complexes with ligands inducing a large bite angle the *syn*/*anti* ratio is much lower than in the corresponding complexes with ligands with a small bite angle. Molecular modelling studies indicate that this is caused by an increasing embracement of the allyl moiety by the phenyl rings of the ligand. This bite-angle effect on the *syn*/*anti* ratio can be transferred to the regioselectivity in stoichiometric allylic alkylation. Ligands inducing large bite angles direct the regioselectivity towards the formation of **2**. In the *catalytic* alkylation of (*E*)-2-butenyl acetate, however, the regioselectivity is also determined by the relative rates of *syn*/*anti* isomerisation and alkylation. The correlation between the regioselectivity found in the stoichiometric and

Table 2. Catalytic alkylation of (*E*)-2-butenyl acetate using the equilibrium mixtures of (bisphosphane)(1-methylallyl)PdOTf complexes

Complex (ligand)	β[a] [°]	t.o.f.[b] [$\times 10^3$ mol·h^{-1}]	Yield[c] (%)	% **1**	% **3**	% **2**
I (dppe)	85	2.0	37.3	68.8	11.1	20.0
I (dppp)	95	2.9	37.1	76.0	6.6	17.4
III (dppb)	99	8.9	90.3	79.0	3.1	17.9
IV (dppf)	106	8.0	81.5	74.1	2.5	23.4
V (DPEphos)	108	8.7	86.0	80.1	2.5	17.4
VI (sixantphos)	110	9.1	88.3	85.7	1.4	12.9

[a] β Obtained from the calculated (bisphosphane)(1-methylallyl)Pd complexes. – [b] t.o.f. is the initial turn over frequency, determined after 10 min of reaction time. – [c] Based on the formation of **1**, **2**, and **3**, as determined after 30 min by GC, using the internal standard method. The catalytic reactions were performed in THF (10 mL), using 0.05 mol-% of catalyst (0.00050 mmol), 1.0 mmol of substrate, and 2.0 mmol of sodium diethyl 2-methylmalonate. The reaction was monitored by GC using decane as the internal standard.

the catalytic alkylation is best for ligands inducing a small bite angle. The ligands with the largest bite angle (sixantphos) is found to result in the most active catalytic species.

Experimental Section

^{1}H- (300 MHz, TMS, $CDCl_3$) and ^{31}P-NMR spectra (121.5 MHz external 85% H_3PO_4, $CDCl_3$) were recorded with a Bruker AMX-300 spectrometer. − Elemental analyses were performed with an Elementar Vario EL (Foss Electric). − All calculations were carried out using the commercially available SPARTAN program (version 5.0.3). The geometry optimisation was performed on the semiempirical pm3(tm) level. − The product distribution was measured with an Interscience Mega2 apparatus, equipped with a DB1 column, length 30 m, inner diameter 0.32 mm, film thickness 3.0 μm, and an F.I.D detector. − All experiments were carried out using standard Schlenk techniques. All solvents were freshly distilled prior to use. − Sodium diethyl 2-methylmalonate (0.5 M in THF) was prepared from diethyl 2-methylmalonate and NaH in THF at 273 K. − The stoichiometric alkylation reactions were performed by adding an excess of sodium diethyl 2-methylmalonate (0.1 mL of a 0.5 M solution in THF) to a solution of 10 mg of the Pd complex in 1 mL of THF. Reaction was instantaneous and after 1 min, the mixture was worked up with water, filtered through silica gel, and analysed by GC. − The catalytic reactions were performed in THF (10 mL), using 0.05 mol-% of catalyst (0.00050 mmol), 1.0 mmol of substrate, and 2.0 mmol of sodium diethyl 2-methylmalonate. The reaction was monitored by taking samples from the reaction mixture which, after aqueous workup, were analysed by GC using decane as the internal standard. − The Pd complexes were prepared in CH_2Cl_2 from [(1-methylallyl)Pd(μ-Cl)]$_2$ by adding 2 equiv. of ligand and abstracting the Cl atom with AgOTf. The complexes were isolated in quantitative yield (white microcrystalline powder) as their analytically pure equilibrium mixtures and were used as such in the alkylation reaction. The syntheses of DPEphos and sixantphos have been published elsewhere.[6] Dppe, dppp, dppb, and dppf were obtained from Acros chemicals and used as received. − Analytical data of the (ligand)(1-methylallyl)-PdOTf complexes are given for their equilibrium mixtures. The NMR signals of the *syn* and *anti* isomers could easily be distinguished. The *syn*/*anti* ratio was determined by comparing the intensities of the signals of the methyl substituent on the allyl moiety. NMR data of the complexes were obtained in $CDCl_3$ (δ values).

(dppe)(1-methylallyl)PdOTf (Is+a): Obtained in a *syn*/*anti* ratio of 90:10. − $C_{32}H_{31}F_3O_3P_2PdS$ (721.005) (**Ia+s**): calcd. C 52.51, H 4.38; found C 52.08, H 4.30.

(dppe)(*syn*-1-methylallyl)PdOTf (Is): ^{1}H NMR: δ = 1.69 (ddd, J_1 = 6.3 Hz, J_2 = 8.4 Hz, J_3 = 8.4 Hz, 3 H, Me), 2.4−3.0 (m, 4 H, 2 × CH_2 bridge), 3.1 (dd, J_1 = 12.1 Hz, J_2 = 12.1 Hz, 1 H, H-a), 4.37 (m, 1 H, H-c), 4.6 (dd, J_1 = 7.2 Hz, J_2 = 7.2 Hz, 1 H, H-b), 5.7 (ddd, J_1 = 7.4 Hz, J_2 = 13.1 Hz, J_3 = 13.1 Hz, 1 H, H-d), 7.3−7.7 (m, 20 H, Ar). − ^{31}P{^{1}H} NMR: δ = 48.5 (d, J = 33 Hz), 49.6 (d, J = 33 Hz).

(dppe)(*anti*-1-methylallyl)PdOTf (Ia): ^{1}H NMR: δ = 0.9 (ddd, J_1 = 6.9 Hz, J_2 = Hz, J_3 = Hz, 3 H, Me), 2.4−3.0 (m, 4 H, 2 × CH_2 bridge), 3.5 (dd, 1 H, H-a), 4.15 (m, 1 H, H-c), 4.7 (dd, 1 H, H-b), 5.6 (m, 1 H, H-d), 7.3−7.7 (m, 20 H, Ar). − ^{31}P{^{1}H} NMR: δ = 49.9 (d, J = 35 Hz), 52.6 (d, J = 35 Hz).

(dppp)(1-methylallyl)PdOTf (IIs+a): Obtained in a *syn*/*anti* ratio of 92:8. − $C_{33}H_{33}F_3O_3P_2PdS$ (735.032) (**IIa+s**): calcd. C 53.16, H 4.60; found C 52.58, H 4.74.

(dppp)(*syn*-1-methylallyl)PdOTf (IIs): ^{1}H NMR: δ = 1.14 (ddd, J_1 = 6.7 Hz, J_2 = 8.9 Hz, J_3 = 8.9 Hz, 3 H, Me), 2.6−3.0 (m, 4 H, 2 × CH_2 bridge), 3.0 (dd, J_1,J_2 > 7 Hz, 1 H, H-a), 3.65 (dd, J_1,J_2 < 7 Hz, 1 H, H-b), 4.2 (m, 1 H, H-c), 5.5 (ddd, J_1 = 12.4 Hz, J_2 = 12.4 Hz, J_3 = 7.4 Hz, 1 H, H-d), 7.2−7.6 (m, 20 H, Ar). − ^{31}P{^{1}H} NMR: δ = 6.75 (d, J = 65.3 Hz), 8.01 (d, J = 65.3 Hz).

(dppp)(*anti*-1-methylallyl)PdOTf (IIa): ^{1}H NMR: δ = 0.88 (ddd, J_1 = 7.1 Hz; J_2 = 7.1 Hz, J_3 = 7.1 Hz, 3 H, Me), 2.6−3.0 (m, 4 H, 2 × CH_2 bridge), 3.2 (dd, J_1,J_2 > 7, 1 Hz, 1 H, H-a), 4.0 (dd, J_1 = 6.9 Hz, J_2 = 6.9 Hz 1 H, H-b), 4.0 (dd, J_1 = 6.9 Hz, J_2 = 6.9 Hz, 1 H, H-b), 4.7 (m, 1 H, H-c), 5.5 (m, 1 H, H-d), 7.2−7.6 (m, 20 H, Ar). − ^{31}P{^{1}H} NMR: δ = 7.1 (d), 7.9 (d).

(dppb)(1-methylallyl)PdOTf (IIIs+a): Obtained in a *syn*/*anti* ratio of 86:14. − $C_{34}H_{35}F_3O_3P_2PdS$ (749.059) (**IIIa+s**): calcd. C 53.78, H 4.79; found C 52.60, H 4.73.

(dppb)(*syn*-1-methylallyl)PdOTf (IIIs): ^{1}H NMR: δ = 1.15 (ddd, J_1 = 9.4 Hz, J_2 = 7.2 Hz, J_3 = 7.2 Hz, 3 H, Me), 1.7−2.0 (m, 4 H, 2 × CH_2 bridge), 2.5−2.8 (m, 4 H, 2 × CH_2 bridge), 2.95 (dd, J_1 = 11.3 Hz, J_2 = 11.3 Hz, 1 H, H-a), 3.7 (dd, J_1 = 6.5 Hz, J_2 = 6.5 Hz, 1 H, H-b), 4.85 (m, 1 H, H-c), 5.5 (ddd, J_1 = 7.4 Hz, J_2 = 13.0 Hz, J_3 = 13.0 Hz, 1 H, H-d), 7.4−7.7 (m, 20 H, Ar). − ^{31}P{^{1}H} NMR: δ = 20.4 (d, J = 20.8 Hz), 21.2 (d, J = 20.8 Hz).

(dppb)(*anti*-1-methylallyl)PdOTf (IIIa): ^{1}H NMR: δ = 0.64 (ddd, J_1 = 6.7 Hz, J_2 = 6.7 Hz, J_3 = 6.7 Hz, 3 H, Me), 1.7−2.0 (m, 4 H, 2 × CH_2 bridge), 2.5−2.8 (m, 4 H, 2 × CH_2 bridge), 3.05 (dd, 1 H, H-a), 4.0 (dd, 1 H, H-b), 5.7 (m, 1 H, H-d), 7.4−7.7 (m, 20 H, Ar). − ^{31}P{^{1}H} NMR: δ = 20.7 (d, overlap with signals of *syn* complex), 21.2 (d, overlap with signals of *syn* complex).

(dppf)(1-methylallyl)PdOTf (IVs+a): Obtained in a *syn*/*anti* ratio of 78:22. − $C_{40}H_{35}F_3FeO_3P_2PdS$ (876.973) (**IVa+s**): calcd. C 54.15, H 4.05; found 53.71, H 4.11.

(dppf)(*syn*-1-methylallyl)PdOTf (IVs): ^{1}H NMR: δ = 1.08 (ddd, J_1 = 6.7 Hz, J_2 = 6.7 Hz, J_3 = 10.3 Hz, 3 H, Me), 3.23 (dd, J_1 = 11.0 Hz, J_2 = 11.0 Hz, 1 H, H-a), 3.50 (dd, J_1 = 4.0 Hz, J_2 = 4.0 Hz, 1 H, H-b), 3.83 (s, 1 H, Cp-H), 3.94 (s, 1 H, Cp-H), 4.27 (s, 1 H, Cp-H), 4.32 (s, 1 H, Cp-H), 4.35−4.55 (m, contains Cp-H and H-c), 4.37 (s, 1 H, Cp-H), 4.46 (s, 1 H, Cp-H), 4.63 (s, 1 H, Cp-H), 4.83 (s, 1 H, Cp-H), 5.64 (ddd, J_1 = 12.9 Hz, J_2 = 12.9 Hz, J_3 = 7.4 Hz, 1 H, H-d), 7.3−7.8 (m, 20 H, Ar, *syn* and *anti*). − ^{31}P{^{1}H} NMR: δ = 24.9 (d, J = 47.5 Hz), 23.6 (d, J = 47.5 Hz).

(dppf)(*anti*-1-methylallyl)PdOTf (IVa): ^{1}H NMR; some signals appear as shoulders on signals of **IVs**, others appear as separate signals: δ = 0.90 [ddd, J_1 = J_2 = J_3 = 6.8 Hz, 3 H, Me], 3.2 [shoulder on signals of **IVs** (H-a), H-a], 3.93 (s, 1 H, Cp-H), 4.35−4.55 (m, contains Cp-H), 4.40 (s, 1 H, Cp-H), 4.43 (s, 1 H, Cp-H), 4.51 (s, 1 H, Cp-H), 4.56 (s, 1 H, Cp-H), 4.66 (s, 1 H, Cp-H), 4.74 (ddd, J_1 = J_2 = J_3 = 6.8 Hz, 1 H, H-c), 7.3−7.8 (m, 20 H, Ar, *syn* and *anti*). − ^{31}P{^{1}H} NMR: signals appear as shoulders on signals of **IVs**.

(DPEphos)(1-methylallyl)PdOTf (Vs+a): Obtained in a *syn*/*anti* ratio of 72:28. − $C_{42}H_{35}F_3O_4P_2PdS$ (861.148) (**Va+s**): calcd. C 57.99, H 4.15; found C 57.60, H 4.08.

(DPEphos)(*syn*-1-methylallyl)PdOTf (Vs): ^{1}H NMR: δ = 1.1 (ddd, J_1 = 10.7 Hz, J_2 = 6.6 Hz, J_3 = 6.6 Hz, 3 H, Me), 3.4 (m, 2 H, H-a and H-b), 4.4 (m, 1 H, H-c), 5.6 (ddd, J_1 = 7.4 Hz, J_2 = 12.7 Hz, J_3 = 12.7 Hz, 1 H, H-d), 6.4−7.6 (m, Ar). − ^{31}P{^{1}H} NMR: δ = 10.3 (d, J = 39.6 Hz), 17.1 (d, J = 39.6 Hz).

(DPEphos)(anti-1-methyl-allyl)PdOTf (Va): ^{1}H NMR: δ = 0.9 (ddd, J_1 = 6.6 Hz, J_2 = 6.6 Hz, J_3 = 6.6 Hz, 3 H, Me), 3.0 (dd, J_1 = 9.1 Hz, J_2 = 14.1 Hz, 1 H, H-a), 4.2 (dd, J_1 = 6.4 Hz, J_2 = 6.1 Hz, 1 H, H-b), 4.4 (m, 1 H, H-c), 5.8 (ddd, J_1 = 14.0 Hz, J_2 = 7.7 Hz, J_3 = 7.7 Hz, 1 H, H-d), 6.4−7.6 (m, Ar). − ^{31}P{^{1}H} NMR: δ = 10.6 (d, J = 40 Hz), 16.4 (d, J = 40 Hz).

(sixantphos)(1-methylallyl)PdOTf (VIs+a): Obtained in a *syn*/*anti* ratio of 57:43. − $C_{44}H_{39}F_3O_4P_2PdSSi$ (917.287) (**VIa+s**): calcd. C 55.88, H 4.46; found C 56.31, H 4.35.

(sixantphos)(*syn*-1-methylallyl)PdOTf (VIs): ^{1}H NMR: δ = 0.57 (s, 3 H, MeSi), 0.61 (s, 3 H, MeSi), 0.8 (ddd, J_1 = 11.3 Hz, J_2 = 6.3 Hz, J_3 = 6.3 Hz, 3 H, Me), 3.4 (dd, J_1 = 11.7 Hz, J_2 = 11.7 Hz, 1 H, H-a), 3.55 (dd, J_1 = 6.4 Hz, J_2 = 6.4 Hz, 1 H, H-b), 4.4 (m, 1 H, H-c), 5.4 (ddd, J_1 = 12.8 Hz, J_2 = 12.8 Hz, J_3 = 7.3 Hz, 1 H, H-d), 6.9−7.5 (m, Ar, *syn* and *anti*), 7.7 (q, Ar, *syn* and *anti*). − ^{31}P{^{1}H} NMR: δ = 9.8 (d, J = 39.3 Hz), 10.6 (d, J = 39.3 Hz).

(sixantphos)(*anti*-1-methylallyl)PdOTf (VIa): ^{1}H NMR: δ = 0.57 (s, 3 H, MeSi), 0.61 (s, 3 H, MeSi), 0.9 (ddd, J_1 = 6.2 Hz, J_2 = 6.2 Hz, J_3 = 6.2 Hz, 3 H, Me), 3.4 (dd, J_1 = 11.7 Hz, J_2 = 11.7 Hz, 1 H, H-a), 3.7 (dd, J_1 = 7.1 Hz, J_2 = 7.1 Hz, 1 H, H-b), 4.65 (m, 1 H, H-c), 5.9 (ddd, J_1 = 13.8 Hz, J_2 = 8.0 Hz, J_3 = 8.0 Hz, 1 H, H-d), 6.9−7.5 (m, Ar, *syn* and *anti*), 7.7 (q, Ar, *syn* and *anti*). − ^{31}P{^{1}H} NMR: δ = 5.8 (d, J = 35.2 Hz), 7.0 (d, J = 35.2 Hz).

Acknowledgments

D. S. M. Research N. V. is acknowledged gratefully for financial support.

[1] J. Tsuji, *Tetrahedron* **1986**, *42*, 4361−4401.
[2] B. M. Trost, D. L. Van Vranken, *Chem. Rev.* **1996**, *96*, 395−422, and references therein.
[3] P. S. Pregosin, R. Salzmann, *Coord. Chem. Rev.* **1996**, *155*, 35−68.
[4] P. Dierkes, S. Ramdeehul, L. Barloy, A. De Lian, J. Fischer, P. C. J. Kamer, P. W. N. M. van Leeuwen, J. A. Osborn, *Angew. Chem. Int. Ed. Engl.* **1998**, *37*, 3116.
[5] M. P. T. Sjögren, S. Hansson, B. Åkermark, A. Vitagliano, *Organometallics* **1994**, *13*, 1963−1971.
[6] P. E. Blöchl, A. Togni, *Organometallics* **1996**, *15*, 4125−4132, and references therein.
[7] B. M. Trost, R. C. Bunt, *J. Am. Chem. Soc*. **1998**, *120*, 70−79.
[8] M. Kranenburg, Y. E. M. van der Burgt, P. C. J. Kamer, P. W. N. M. van Leeuwen, *Organometallics* **1995**, *14*, 3081−3089.
[9] M. Kranenburg, P. C. J. Kamer, P. W. N. M. van Leeuwen, D. Vogt, W. Keim, *J. Chem. Soc., Chem. Commun*. **1995**, 2177−2178.
[10] M. Kranenburg, J. P. G. Delis, P. C. J. Kamer, P. W. N. M. van Leeuwen, N. Veldman, A. L. Spek, K. Goubitz, J. Fraanje, *J. Chem. Soc., Dalton Trans.* **1997**, 1839−1849.
[11] M. Kranenburg, P. C. J. Kamer, P. W. N. M. van Leeuwen, *Eur. J. Inorg. Chem*. **1998**, 25−27.
[12] [12a] M. Kawatsura, Y. Uozomi, T. Hayashi, *J. Chem. Soc., Chem. Commun*. **1998**, 217−218. − [12b] . Hayashi, M. Kowatsura, Y. Uozumi, *J. Am. Chem. Soc*. **1998**, *120*, 1681−1687.
[13] K. J. Szabó, *J. Am. Chem. Soc*. **1996**, *118*, 7818−7826.
[14] S. Ramdeehul, P. Dierkes, R. Aguado, P. C. J. Kamer, P. W. N. M. van Leeuwen, J. A. Osborn, *Angew. Chem. Int. Ed. Engl.* **1998**, *37*, 3118.
[15] P. Dierkes, P. W. N. M. van Leeuwen, *J. Chem. Soc., Dalton Trans.*, in press.
[16] R. J. van Haaren, Henk Oevering, Betty B. Coussens, Gino P. F. van Strijdonck, et al., to be published.
[17] [17a] C. Amatore, A. Jutand, M. A. M′Braki, *Organometallics* **1992**, *11*, 3009−3013. − [17b] C. Amatore, E. Carré, A. Jutand, M. A. M′Braki, *Organometallics* **1995**, *14*, 1818−1826.
[18] C. Amatore, A. Jutand, F. Khalil, M. A. M′Barki, L. Mottier, *Organometallics* **1993**, *12*, 3168−3178.
[19] K. Vrieze, P. W. N. M. van Leeuwen, *Dynamic Nuclear Magnetic Resonance Spectroscopy*, Academic Press, New York, **1975**.
[20] β obtained from the calculated (bisphosphane)(1-methylallyl)Pd complexes.
[21] C. P. Casey, G. T. Whiteker, *Isr. J. Chem.* **1990**, *30*, 299−304.

Received December 23, 1998
[I98455]

Linear Five-Centred Chromium Multiple Bonds Bridged by Four $tpda^{2-}$ Ligands [$tpda^{2-}$ = tripyridyldiamido dianion] – Synthesis and Structural Studies

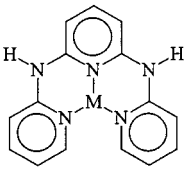
Hsiao-Chi Chang,[a] Jia-Tzung Li,[a] Chih-Chieh Wang,[a] Tzu-Wei Lin,[a] Hsiao-Ching Lee,[a] Gene-Hsiang Lee,[a] and Shie-Ming Peng*[a]

Keywords: Metal string complexes / Multicentered metal–metal multiple bond / Quadruple bonds / Metal-metal interactions / Chromium

The linear pentanuclear chromium complexes $[Cr^{II}_5(\mu_5\text{-tpda})_4Cl_2]$ (**1**), $[Cr^{II}_5(\mu_5\text{-tpda})_4(NCS)_2]$ (**2**), $[Cr^{III}Cr^{II}_4(\mu_5\text{-tpda})_4F_2](BF_4)$ (**3**), and $[Cr^{III}Cr^{II}_4(\mu_5\text{-tpda})_4F(OTf)](OTf)$ (**4**), with four all-*syn* tri(α-pyridyl)diamido dianion ($tpda^{2-}$) ligands, have been prepared and structurally characterized. Compounds **1** and **2** possess a delocalized $Cr^{(II)}$–$Cr^{(II)}$–$Cr^{(II)}$–$Cr^{(II)}$–$Cr^{(II)}$ five-centred metal–metal bond of order 1.5. In both **1** and **2** two values for Cr^{II}–Cr^{II} bond lengths are found both; the outer ones connected with axial ligands are 2.284(1) and 2.285(2) Å, and the inner ones are 2.2405(8) and 2.246(1) Å, for **1** and **2,** respectively. When compound **1** reacts with 2 equiv. of $AgBF_4$ or Ag(OTf), a oxidation reaction takes place and one of the terminal chromium(II) ions is oxidized to produce $[Cr^{III}Cr^{II}_4(\mu_5\text{-tpda})_4F_2]BF_4$ (**3**) or $[Cr^{III}Cr^{II}_4(\mu_5\text{-tpda})_4F(OTf)](OTf)$ (**4**). Two short Cr–Cr distances [1.969(2) and 2.138(2) Å for **3**, 1.846(1) and 1.922(1) Å for **4**] are found, with the presence of two quadruple bonds among four adjacent Cr^{II} ions. The fifth Cr^{III} ion, which is separated from the neighboring Cr^{II} ion by 2.487(2) Å for **3** and 2.610(1) Å for **4**, is simply a square pyramidal unit with no metal–metal bonding interaction.

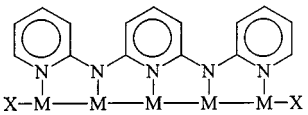
Introduction

The coordination chemistry of oligo-α-pyridylamino ligands[1] is an interesting topic, not only on the subject of the synthetic varieties of *all-anti* and *all-syn* complexes, but also as concerns the specific conformations and chemical properties of these complexes.[1–9]



All *anti*-form

M = Fe, Co, Ni, Cu, Zn



All *syn*-form

M = Co, Ni

Previous reports on the extension of di-nuclear metal complexes[10–12] to metal string complexes supported by oligo-α-pyridylamino ligands were focused on the tri-nuclear $[M_3(dpa)_4X_2]$ (M = Cr,[2] Co,[3,4] Ni,[5] Cu,[6] Rh,[7] Ru;[7] dpa^- = dipyridylamido anion), and pentanuclear $[M_5(tpda)_4X_2]$ (M = Co, Ni; $tpda^{2-}$ = tripyridyldiamido dianion) systems.[8,9] There is good correlation between the metal–metal distance obtained from structural analysis and the bond order predicted by qualitative M. O. calculations for the tri-nuclear metal string complexes $[M_3(dpa)_4X_2]$. The M–M distances are affected by the axial ligands, and the magnetic behavior of the M^{II}_5 unit in $[Ni_5(tpda)_4X_2]$ and $[Co_5(tpda)_4X_2]$ complexes has been studied in detail. In order to achieve a complete bonding scheme for five-centred metal–metal multiple bonds, the early transition metal string complexes $[Cr_5(tpda)_4Cl_2]$ (**1**), $[Cr_5(tpda)_4(NCS)_2]$ (**2**) have been synthesized. In addition, two oxidation products of $[Cr^{III}Cr^{II}_4(tpda)_4F_2](BF_4)$ (**3**) and $[Cr^{III}Cr^{II}_4(tpda)_4F(CF_3SO_3)](CF_3SO_3)$ (**4**) are reported. The structural analyses are described and discussed in detail (see Table 5).

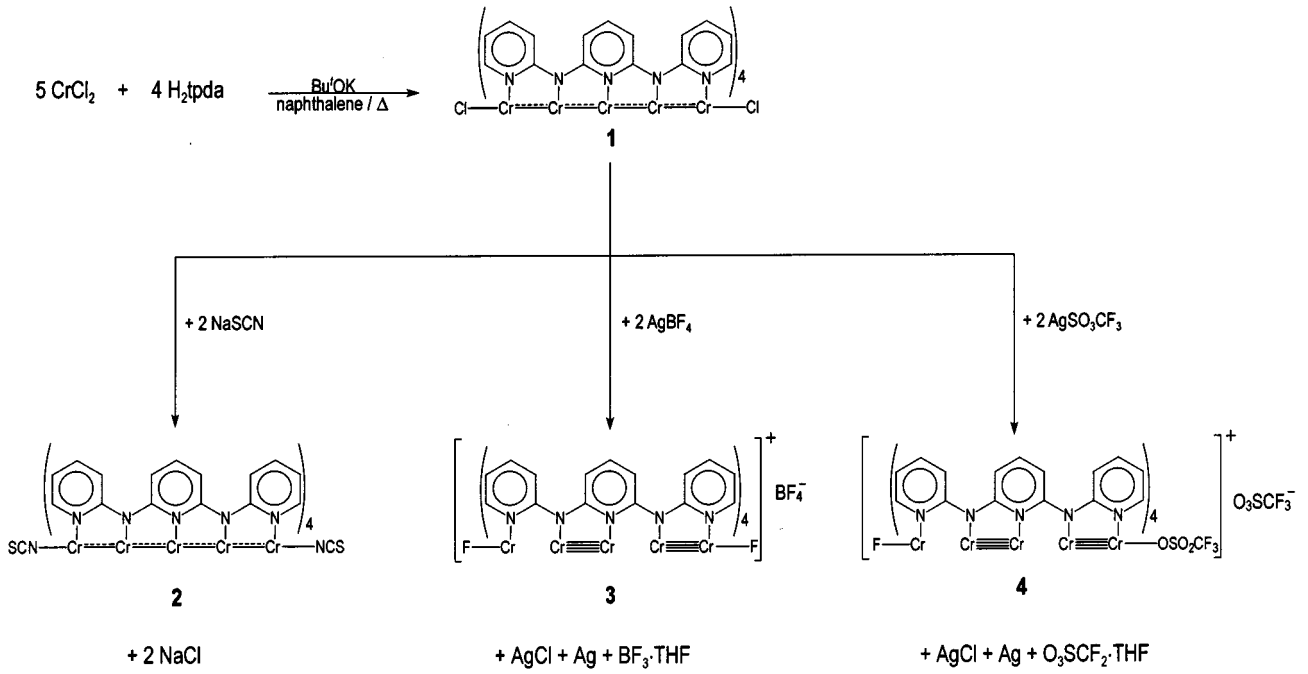
Results and Discussions

The synthetic procedures for compounds **1**, **2**, **3**, and **4** are summarized in Scheme 1. Compound **1** can be synthesized under nitrogen using anhydrous $CrCl_2$ and the H_2tpda ligand as the starting materials, and naphthalene as the solvent. *t*BuOK was used as a base to deprotonate the H atom on the amido group of the H_2tpda ligand. Compound **2** was synthesized via the axial ligand replacement method with the NCS^- ligand instead of the Cl^- ligand in **1**. Compounds **3** and **4** are the products of the oxidation reactions of compound **1** with **2** equiv. of $AgBF_4$ and AgOTf, respectively. The presence of the F^- ion in **3** and **4** can be explained by considering the dissociation in THF of the BF_4^- and $SO_3CF_3^-$ anion, respectively.[2a]

For compounds **1** and **2**, each structure basically consists of a linear chain of five chromium atoms bridged by four $tpda^{2-}$ ligands. The steric crowding of the β-carbon hydrogen atoms on the pyridyl rings forces the $tpda^{2-}$ ligand to

[a] Department of Chemistry, National Taiwan University, Taipei, Taiwan, ROC
Fax: (internat.) +886-2/ 2363 6359
E-mail: smpeng@chem35.ch.ntu.edu.tw

 © WILEY-VCH Verlag GmbH, D-69451 Weinheim, 1999 1434–1948/99/0808–1243 $ 17.50+.50/0



Scheme 1. Synthetic routes for compounds **1**, **2**, **3** and **4**

bind helically with the metal ion. Both are essentially isostructural with $[M_5(\mu_5\text{-tpda})_4X_2]$ (M^{II} = Co, X = Cl^-, NCS^-, N_3^-, CH_3CN and M^{II} = Ni, X = Cl^-, CN^-, NCS^-, N_3^-, CH_3CN).[8,9] Complex **1** crystallizes in the *C*2/*c* space group with the Cr(3) atom located at the crystallographic 2-fold axis. The molecular structure of **1** is shown in Figure 1. Complex **2** crystallizes in the *I*4/*m* space group with the Cr(3) atom located at the crystallographic 4/*m* symmetry, and the asymmetric unit contains only one eighth of the complex. The atomic positions of the complex **2** are averaged, because the right-turn and left-turn helical complexes are seriously disordered in the crystal. The eight nitrogen atoms from the amido group (occupancy 0.5) coordinated to chromium ions [Cr(2)], and the α-carbon atoms of the pyridyl groups have high anisotropic thermal parameters. One of the helical structures of **2** is shown in Figure 2. All of the Cr ions and two axial ligands for **1** and **2** are nearly co-linear. The five-centred Cr^{II} delocalized

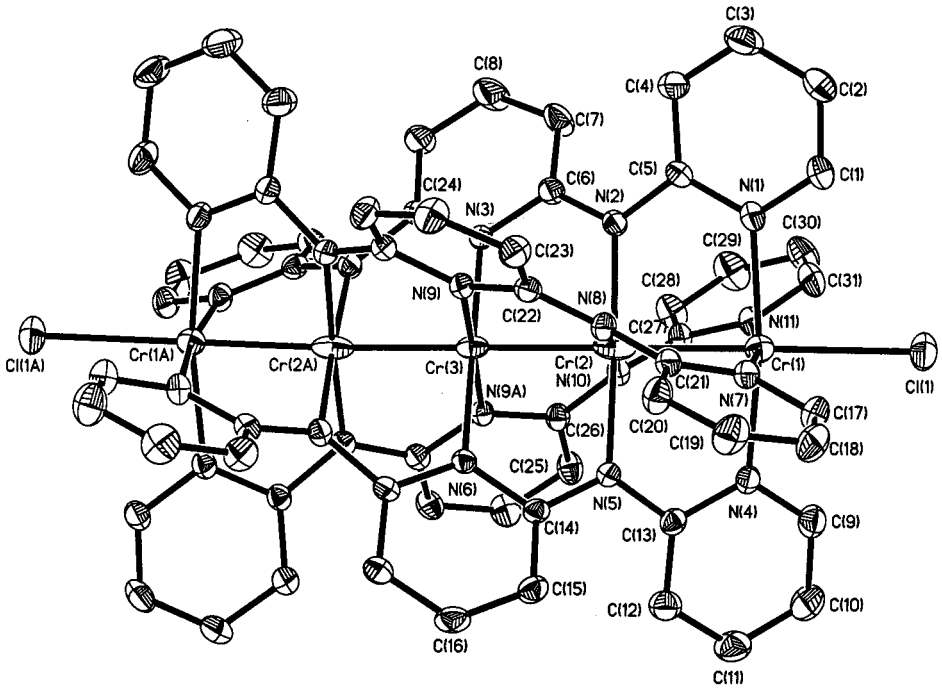


Figure 1. Crystal structure of $[Cr_5(\mu_5\text{-tpda})_4Cl_2]$ **1**. Atoms are shown as 20% vibrational thermal ellipsoids

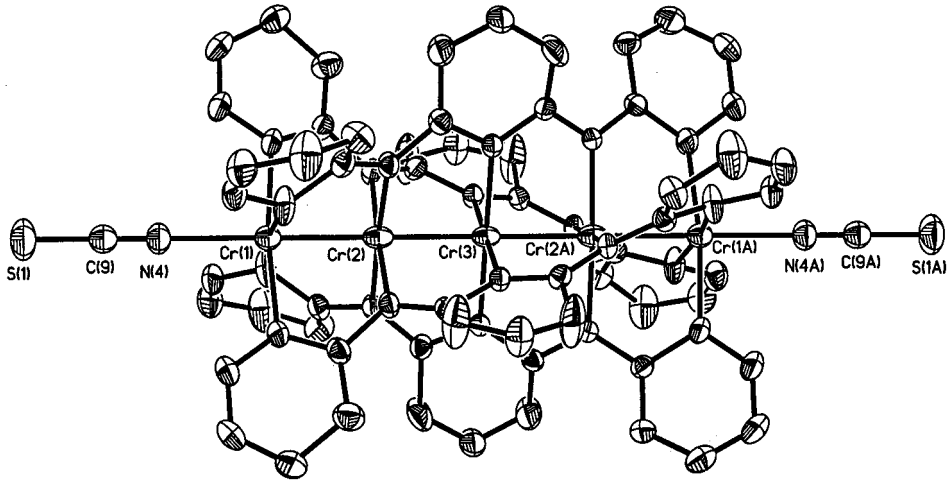


Figure 2. Crystal structure of $[Cr_5(\mu_5\text{-tpda})_4(NCS)_2]$ **2**. Atoms are shown as 20% vibrational thermal ellipsoids

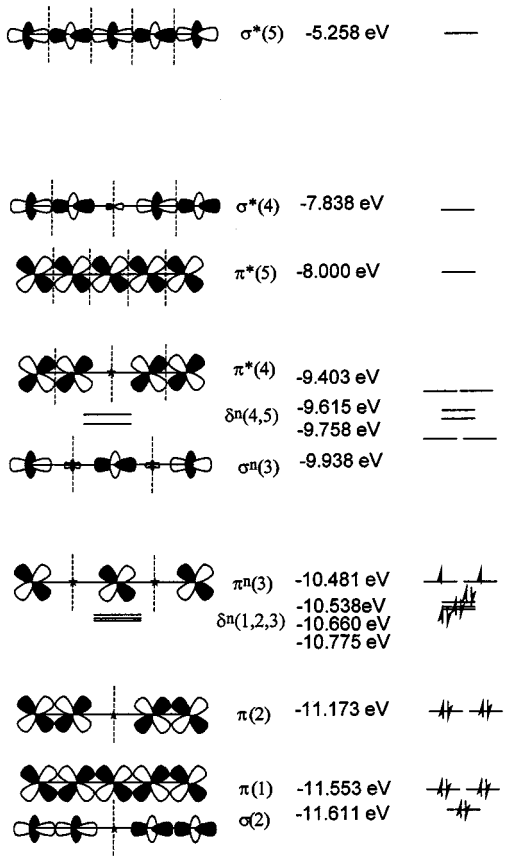


Figure 3. The qualitative molecular orbital diagram of linear five $Cr^{II}-Cr^{II}-Cr^{II}-Cr^{II}-Cr^{II}$ system for $[Cr_5(\mu_5\text{-tpda})_4Cl_2]$ **1**

multiple bond is the focus of this study. Two types of Cr−Cr bond lengths are found in **1** and **2**. The outer ones connected to the axial ligands are 2.284(1) and 2.285(2) Å, and the inner ones are 2.2405(8) and 2.246(1) Å, for **1** and **2** respectively. Both are shorter than those found in trinuclear complexes {2.365(1) Å in $[Cr_3(dpa)_4Cl_2]$[2]} and dichromium(II) tetracarboxylate complexes {2.29−2.53 Å in $[Cr_2(O_2CR)_4X_2]$[10]}, but much longer than those in super-short dichromium(II) complexes bridged by N,N-containing ligands {e.g. 1.843(2) Å in $[Cr_2(MeNC(Ph)NMe)_4]$,[19] 1.870(3) Å in $[Cr_2(Me\text{-pyridylamido})_4]$,[20] 1.858(1) Å in $[Cr_2(PhN_3Ph)_4]$[21]}. They are also comparable with the values of 2.28 Å and 2.23 Å found in the $[Co_5(\mu_5\text{-tpda})_4X_2]$ complex, which exhibits a double bond among the $Co^{II}{}_5$ unit.[8] The qualitative molecular orbital analysis of the Cr−Cr−Cr−Cr−Cr system, according to the atomic coordinates of **1** derived from the X-ray data, is shown in Figure 3. The bonding features among the five Cr atoms are similar to those of $[Co_5(tpda)_4(NCS)_2]$ and $[Ni_5(tpda)_4(NCS)_2]$, with a linear combination of the d_{z^2} orbitals of the five Cr atoms forming five σ orbitals, the (d_{xz}, d_{yz}) of the five Cr atoms forming ten π orbitals and the ($d_{x^2-y^2}$ or d_{xy}) orbitals of the five Cr atoms forming five nonbonding orbitals.[9] A total of twenty d electrons of Cr^{II} ions fill up to n_π degenerate orbitals leading to the configuration of $\sigma_1{}^2\sigma_2{}^2\pi_1{}^4\pi_2{}^4\delta_{n1}{}^2\delta_{n2}{}^2\ \delta_{n3}{}^2\pi_{n(dxz)}{}^1\pi_{n(dyz)}{}^1$. This configuration shows that two unpaired electrons are delocalized among the $Cr^{II}-Cr^{II}-Cr^{II}-Cr^{II}-Cr^{II}$ unit and that the bond order is 1.5 for each $Cr^{II}-Cr^{II}$ bond (the δ bonds are regarded as nonbonding orbitals for the helical conformation of the $tpda^{2-}$ ligand). The temperature independent magnetic susceptibility measurement of compound **1** is shown in Figure 4 with μ = 4.0 B.M, which is consistent with the M.O. prediction. This measured magnetic value is larger than the spin-only value (μ = 2.82 B.M), and this may be due to the orbital contribution of π-nonbonding orbitals. [The magnetic moment (μ_{eff}) is 3.6 B. M. for $[Cr_3(dpa)_4Cl_2]$ which is also larger than spin-only value (2.82).] If the M−M distances in the $[M_5(\mu_5\text{-tpda})_4X_2]$ system are compared with the distances for those systems having the axial ligands Cl^- and NCS^- for different metal centers (listed in Table 1) it can be seen that, i) in the Ni case, the outer M−M distance is obviously changed from 2.385(2) Å to 2.369(2) Å when the axial ligand is changed from Cl^- to NCS^- with the Ni−Ni bond order being zero,[8,9] ii) in compounds **1** and **2**, the outer Cr−Cr distance is nearly the same [2.284(1) and 2.285(2) Å] whether the axial ligand is Cl^- or NCS^-, with the Cr−Cr bond order being 1.5. These results indicate that, in the $[M_5(\mu_5$-

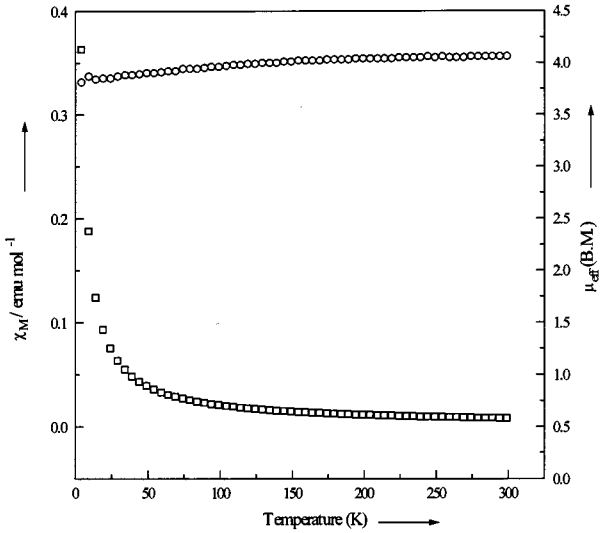
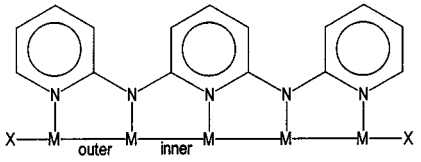


Figure 4. Magnetic measurement for compound **1**. □ indicates the observed magnetic susceptibility (χ_M) and ○ the observed effect magnetic moment (μ_{eff})

Table 1. Comparison of M−M bond length [Å] in $[M_5(tpda)_4X_2]$ complexes (M = Cr, Co, Ni; X = Cl, NCS)



Compound	Outer M−M distance	Inner M−M distance	Bond order
$[Cr_5(tpda)_4Cl_2]$ (**1**)	2.284(1)	2.2405(8)	1.5
$[Cr_5(tpda)_4(NCS)_2]$ (**2**)	2.285(2)	2.246(1)	1.5
$[Co_5(tpda)_4Cl_2]$[a]	2.281(4)	2.234(4)	0.5
$[Co_5(tpda)_4(NCS)_2]$[a]	2.277(2), 2.274(2)	2.232(2), 2.229(2)	0.5
$[Ni_5(tpda)_4Cl_2]$[a]	2.385(2)	2.305(1)	0.0
$[Ni_5(tpda)_4(NCS)_2]$[a]	2.367(2), 2.371(2)	2.289(2), 2.294(2)	0.0

[a] Ref.[8] and ref.[9]

tpda)$_4X_2$] system, the outer M−M distance could be affected or not affected by the axial ligands, and that the bonding strength of M−M bond is an important factor. When the M−M interaction is weak {in $[Ni_5(tpda)_4X_2]$ case}, the outer M−M distance is easily affected by the different axial ligands,[9] but the M−M distance is not influenced by the axial ligand when the metal−metal bond is strong {in the case of $[Cr_5(tpda)_4X_2]$}. However, such structural characterizations should be studied further by synthesizing more $[M_5(\mu_5\text{-tpda})_4X_2]$ complexes, with different metal center and axial ligands, and supporting the results by theoretical calculations.

Compounds **3** and **4** crystallize in $P2_1/n$ and $P2_1/c$ space groups, respectively, with both molecules residing in general positions. As for the compounds **1** and **2**, all of the Cr ions and two axial ligands are nearly co-linear and the five Cr centers are also helically wrapped by four $tpda^{2-}$ ligands. One of the terminal Cr^{II} atoms in these compounds is oxidized to Cr^{III}, connected with the axial ligand F^-, and the other terminal Cr^{II} ion is connected with the axial ligand F^- and $CF_3SO_3^-$ (**3** and **4**, respectively). The crystal structures of **3** and **4** are shown in Figures 5 and 6. Four unsym-

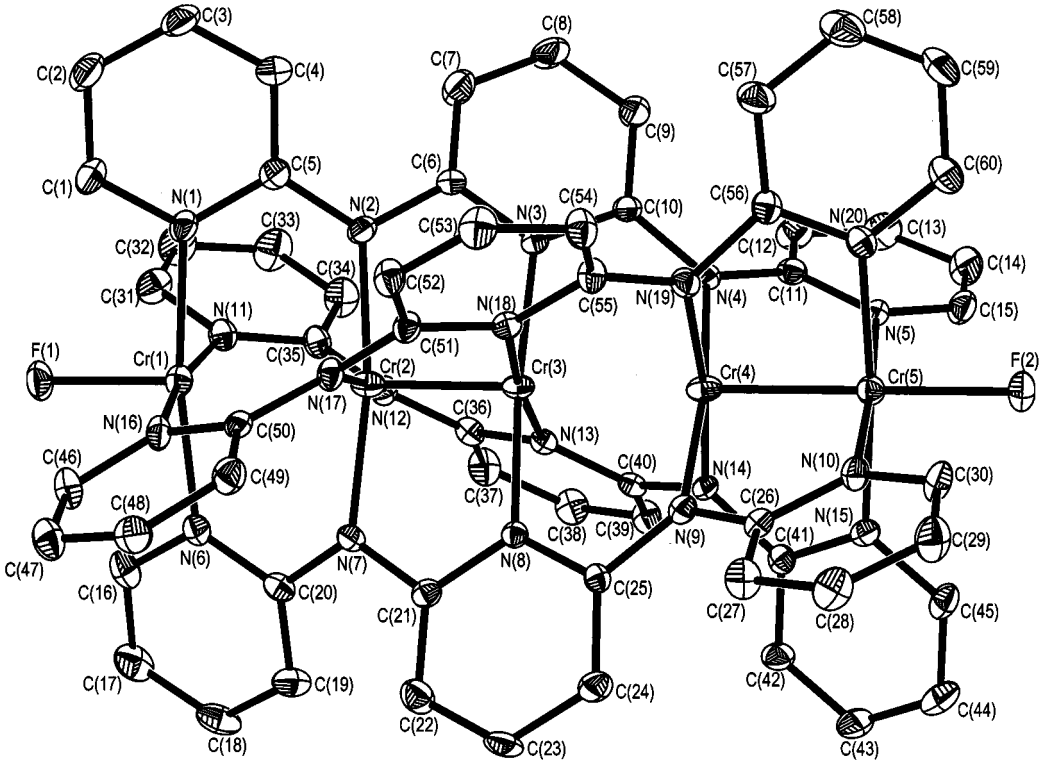


Figure 5. Crystal structure of $[Cr_5(\mu_5\text{-tpda})_4F_2]^+$ **3**. Atoms are shown as 20% vibrational thermal ellipsoids

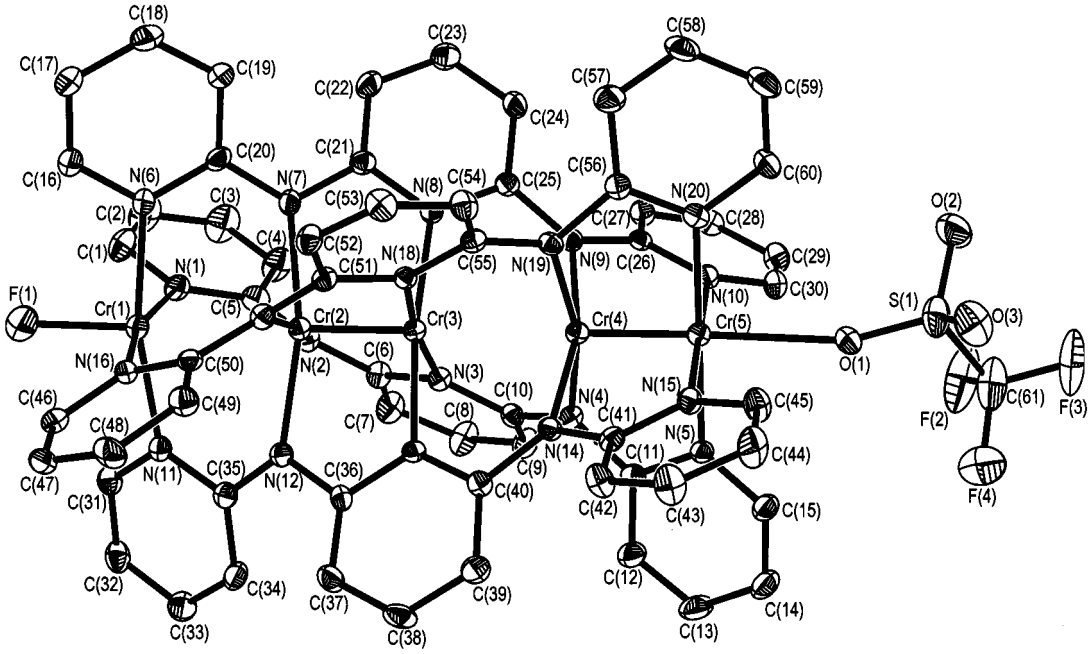
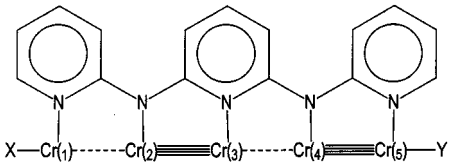


Figure 6. Crystal structure of $[Cr_5(\mu_5\text{-tpda})_4F(SO_3CF_3)]^+$ **4**. Atoms are shown as 20% vibrational thermal ellipsoids

metric Cr−Cr distances listed in Table 2 are observed in both compounds. Two short Cr−Cr distances [1.969(2) and 2.138(2) Å for **3**, 1.846(1) and 1.922(1) Å for **4**] are found along with the presence of two quadruple bonds among four adjacent Cr^{II} ions. The longer distances of 1.922(1), 1.969(2), and 2.138(2) Å are comparable with those found in the dichromium(II) complexes (1.937−2.354 Å) bridged by N,N- or N,O-containing ligands (e.g. formamidinate and 2-oxopyridinates),[10] and in the trichromium(II) complexes bridged by the dpa^- ligand {1.9952(8) Å in $[Cr_3(dpa)_4Cl(BF_4)]$}.[2] The shortest distance of 1.846(1) Å is comparable with those found in the super-short dichromium(II) complexes which are bridged by N,N-containing ligands {e.g. 1.843(2) Å in $[Cr_2(MeNC(Ph)NMe)_4]$,[19] 1.870(3) Å in $[Cr_2(Me\text{-}pyridylamido)_4]$,[20] 1.858(1) Å in $[Cr_2(PhN_3Ph)_4]$[21]}. Complexes **3** and **4** are so far the only cases found in the literature where two Cr−Cr quadruple bonds co-exist in a molecule. In the dichromium(II) complex an unusually wide range of Cr−Cr bond lengths (1.828−2.541 Å) are exhibited.[10] The presence or absence of axial ligand was found to be the determining factor over the Cr−Cr bond length when considering the same bridging ligands. In complexes **3** and **4**, the influence of the axial ligand on the Cr−Cr quadruple bond is also significant (Table 2). The intermediate Cr(2)−Cr(3) bond lengths [**3**, 1.969(2) Å; **4**, 1.846(1) Å] are obviously shorter than the terminal Cr(4)−Cr(5) bond lengths [**3**, 2.138(2) Å; **4**, 1.922(1) Å] with one axial ligand (**1**, F^-; **2**, $SO_3CF_3^-$) connected to Cr(5). Meanwhile, the terminal Cr(4)−Cr(5) distance is shortened from 2.138(2) Å to 1.922(1) Å when the axial ligand connected on Cr(5) is changed from a strong σ-donating F^- ligand to a weak $CF_3SO_3^-$ ligand. The distances [Cr(3)−Cr(4)] between the two quadruple bonds are long [2.419(2) and 2.596(1) Å for **3** and **4** respectively] which can be explained by the absence of a metal−metal bonding interaction. The fifth Cr^{III} [Cr(1)] ion connected with F^-, which is separated from the neighboring Cr^{II} ion by 2.487(2) and 2.610(1) Å (**3** and **4** respectively), is simply

Table 2. Selected bond lengths [Å] for $[Cr_5(tpda)_4F_2](BF_4)$ and $[Cr_5(tpda)_4F(OTf)](OTf)$



Compound	Cr(1)−X[a]	Cr(1)−Cr(2)	Cr(2)−Cr(3)	Cr(3)−Cr(4)	Cr(4)−Cr(5)	Cr(5)−Y[a]
$[Cr_5(tpda)_4F_2](BF_4)$	1.840(4)	2.487(2)	1.969(2)	2.419(2)	2.138(2)	1.931(4)
$[Cr_5(tpda)_4F(OTf)](OTf)$	1.863(5)	2.610(1)	1.846(1)	2.596(1)	1.922(1)	2.353(5)

[a] X = F^-, Y = F^- or $SO_3CF_3^-$.

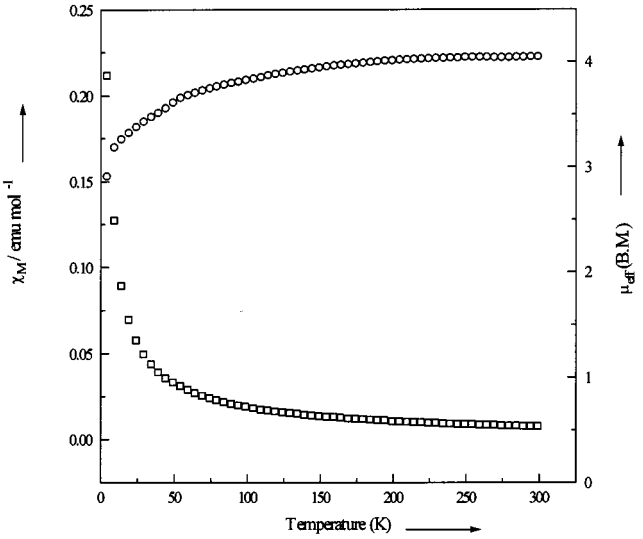
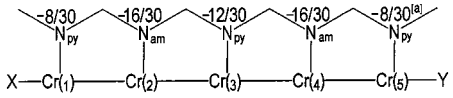


Figure 7. Magnetic measurement for compound **3**. □ indicates the observed magnetic susceptibility (χ_M) and ○ the observed effect magnetic moment (μ_{eff})

a square pyramidal $F-Cr^{III}-N_4$ unit without a metal−metal bonding interaction. The $Cr^{III}-F$ distances of 1.840(4) Å (**3**) and 1.863(5) Å (**4**) are comparable with those of 1.824(7) and 1.802(6) Å in the $[Cr_3(dpa)_4F(BF_4)](BF_4)$ complex.[2] The magnetic measurement of compound **3** is shown in Figure 7. The temperature independent magnetic moment of μ_B = 4.0 B.M. indicates that there are three unpaired electrons. These can be assigned to the $Cr^{3+}(d^3)$ species; the two quadruply bonded fragments would not be expected to contribute to the paramagnetism of the molecule.

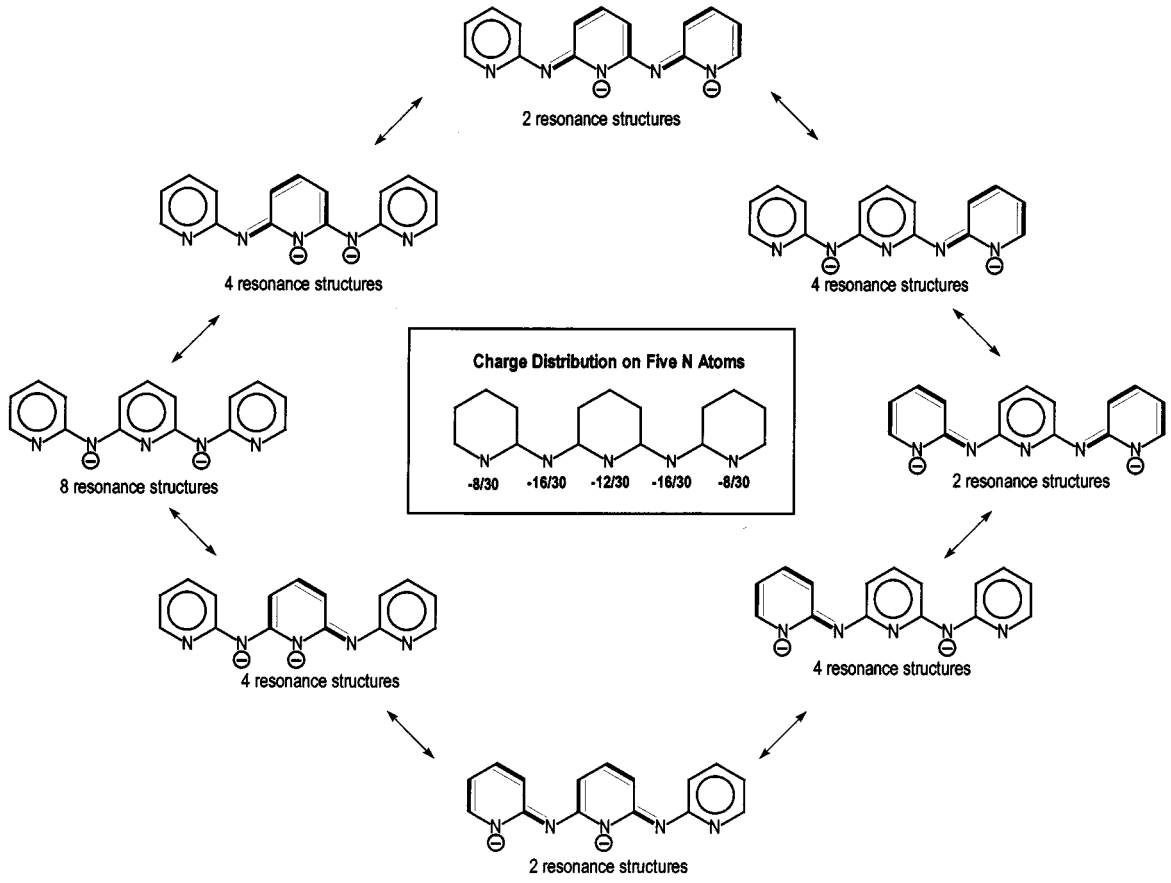
Table 3. The averaged Cr−N distances [Å] for compounds **1**, **2**, **3**, and **4**



Compound	Cr(1)−N	Cr(2)−N	Cr(3)−N	Cr(4)−N	Cr(5)−N
1	2.119(3)	2.021(3)	2.050(3)	2.021(3)	2.119(3)
2	2.086(3)	2.019(5)	2.055(3)	2.019(5)	2.086(3)
3	2.070(7)	2.004(6)	2.034(6)	1.992(6)	2.079(6)
4	2.081(6)	2.014(5)	2.053(5)	2.031(5)	2.095(5)

[a] Charges on the nitrogen atoms according to 30 resonance structures.

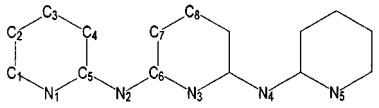
According to the structural analyses listed in Table 3, the Cr−N distances are in the order $Cr-N_{amido}$ [Cr(2)−N] < the central $Cr-N_{py}$ [Cr(3)−N] < the terminal $Cr-N_{py}$ [Cr(1)−N] for compounds **1**, **2**, **3**, and **4**. This result could be due to the charge distribution on the $tpda^{2-}$ ligand. The resonance structures of the $tpda^{2-}$ ligand is described in Scheme 2. The probability of two negative charges distri-



Scheme 2. Resonance structures of $tpda^{2-}$ ligand

buting on the terminal N_{py}, the N_{amido}, and the central N_{py} atoms are 8:30, 16:30, and 12:30, respectively. From this negative charge distribution, the bond interaction between Cr and N atoms should be in the sequence of the Cr−N_{amido} > the central Cr−N_{py} > the terminal Cr−N_{py} bond. Such a result will reflect directly on the Cr−N distance giving the order Cr−N_{amido} < the central Cr−N_{py} < the terminal Cr−N_{py}. The Cr−N distance predicted from the resonance structures of the $tpda^{2-}$ ligand is in a good agreement with those obtained from structural analyses. No matter what the oxidation state of terminal Cr ion is (2+ or 3+), or what the axial ligand is, the averaged terminal Cr−N_{py} distances are always the longest and the averaged Cr−N_{amido} bond lengths are the shortest. This result is also found in $[Ni_5(\mu_5\text{-tpda})_4X_2]$ and $[Co_5(\mu_5\text{-tpda})_4X_2]$ complexes.[8][9] Beside the Cr−N bond lengths, the π bond orders of C−N and C−C bonds obtained from the resonance structures shown in Scheme 2 are also consistent with those observed for the $tpda^{2-}$ ligands in compounds **1**, **3**, and **4** (Table 4).

Table 4. The averaged N−C and C−C distances [Å] for compounds **1**, **3**, and **4**



Bond type	π-Bond order[a]	1	3	4
N1−C1	11/30	1.356(5)	1.357(10)	1.359(9)
N1−C5	11/30	1.363(5)	1.357(10)	1.359(9)
N2−C5	8/30	1.373(4)	1.384(10)	1.373(8)
N2−C6	6/30	1.379(5)	1.387(10)	1.385(8)
N3−C6	9/30	1.366(4)	1.369(9)	1.361(8)
C1−C2	19/30	1.361(6)	1.370(13)	1.356(11)
C2−C3	11/30	1.385(7)	1.383(14)	1.378(12)
C3−C4	19/30	1.374(6)	1.372(13)	1.363(11)
C4−C5	11/30	1.404(5)	1.401(12)	1.406(10)
C6−C7	15/30	1.396(5)	1.386(11)	1.394(9)
C7−C8	15/30	1.379(6)	1.374(13)	1.373(10)

[a] π bond order was calculated according to 30 resonance structures.

Conclusions

In summary, a five-centred multiple bonding scheme has been successfully demonstrated for both late transition metal ions (M = Ni, Co)[8][9] and an early transition metal ion (M = Cr) (compounds **1** and **2**). According to the structural analyses two types of Cr−Cr−Cr−Cr−Cr unit are observed in the $[Cr_5(tpda)_4]$ fragments. One is a delocalized Cr^{II}_5 system (compounds **1** and **2**) with four nearly equal Cr−Cr distances, the other is a localized $[C^{III}\cdots C^{II}_4]$ system (compounds **3** and **4**) with four asymmetric Cr−Cr distances. Two short quadruple bonds are found. The magnetic behaviors of these two systems are in accordance with the structural analysis and qualitative theoretical predictions.

Experimental Section

Spectroscopic Measurements: IR: Nicolet Fourier-Transform IR, MAGNA-IR 500 spectrometer in the range of 500−4000 cm^{-1}, KBr discs. − UV/Vis: Hewlett Packard (HP) 8453 spectrophotometer. − Temperature dependent magnetic susceptibility: SQUID system with 10,000 Gauss external magnetic field. − Molar magnetic susceptibility: recorded every 5 K in the range of 5−300 K. The H_2tpda ligand was synthesized according to the literature.[1,8a]

Preparation and Characterization of $[Cr_5(\mu_5\text{-tpda})_4Cl_2]$ (1): Anhydrous $CrCl_2$ (0.369 g, 3 mmol), H_2tpda (0.526 g, 2 mmol) and potassium *tert*-butoxide (0.44 g, 4 mmol) were placed in an Erlenmeyer flask, and naphthalene (10 g) added under nitrogen in the glove box. The mixture was refluxed under nitrogen and heated to 180−200°C for 6 h. After the mixture had cooled, *n*-hexane was added to wash out the naphthalene. The remaining solid was extracted with CH_2Cl_2 and re-crystallized from a $CHCl_3$/ether solution. Deep brown crystals were obtained (yield: 30%). − IR (KBr): $\tilde{\nu}$ = 1602 cm^{-1}, 1578, 1547 (C=C). − MS (FAB); *m/z* (%): 1376 (7) $[M]^+$. − UV/Vis (CH_2Cl_2): λ_{max} (ε) = 283 nm ($7.56\cdot10^4$ M^{-1} cm^{-1}), 326 ($5.58\cdot10^4$ M^{-1} cm^{-1}), 390 ($4.20\cdot10^4$ M^{-1} cm^{-1}), 710 ($8.15\cdot10^3$ M^{-1} cm^{-1}). − $\mathbf{1}\cdot CHCl_3\cdot O(C_2H_5)_2$: calcd. C 49.74, H 3.53, N, 17.85; found C 49.66, H 3.66, N 17.84.

Preparation and Characterization of $[Cr_5(\mu_5\text{-tpda})_4(NCS)_2]$ (2): $[Cr_5(\mu_5\text{-tpda})_4(Cl)_2]$ (0.05 g, 0.036 mmol) was placed in an Erlenmeyer flask in THF (40 mL). The brown solution was stirred for 5 min and filtered off. NaSCN (0.06 g, 0.72 mmol) was added to the filtrate and stirring continued for 2 d. Then water (50 mL) was added to dissolve unchanged NaSCN. The solution was extracted with CH_2Cl_2 (3× 60 mL) and Na_2SO_4 added to remove water. The remaining solvent was removed by rotary evaporator and recrystallized from a CH_2Cl_2/ether solution. Deep brown crystals were obtained (yield: 30%). − IR (KBr): $\tilde{\nu}$ = 1604 cm^{-1}, 1577, 1546 (C=C), 2033 (C≡N). − MS (FAB); *m/z* (%): 1421 (1) $[M]^+$. − UV/Vis (CH_2Cl_2): λ_{max} (ε) = 288 nm ($1.19\cdot10^5$ M^{-1} cm^{-1}), 332 ($7.84\cdot10^4$ M^{-1} cm^{-1}), 392 ($7.52\cdot10^4$ M^{-1} cm^{-1}), 721 ($9.02\cdot10^3$ M^{-1} cm^{-1}). − $\mathbf{2}\cdot CH_2Cl_2\cdot 6\,H_2O$: calcd. C 46.86, H 3.62, N 19.08; found C 47.70, H 3.71, N 19.08.

Preparation and Characterization of $[Cr^{III}Cr^{II}_4(\mu_5\text{-tpda})_4F_2]BF_4$ (3): $[Cr_5(\mu_5\text{-tpda})_4(Cl)_2]$ (0.1 g, 0.072 mmol) and silver tetrafluoroborate ($AgBF_4$, 0.028 g, 0.14 mmol) were placed in a 50 mL flask containing THF (20 mL). After 1 h of stirring, the solution was filtered to remove AgCl and Ag solid, leaving a clear dark brown solution. The solution was concentrated and a brown powder obtained. The powder was recrystallized from CH_3CN/ether solution. Deep brown crystals were obtained (yield: 35%). − IR (KBr): $\tilde{\nu}$ = 1606 cm^{-1}, 1581, 1547 (C=C). − UV/Vis (CH_2Cl_2): λ_{max} (ε) = 290 nm ($9.03\cdot10^4$ M^{-1} cm^{-1}), 396 ($6.00\cdot10^4$ M^{-1} cm^{-1}), 716 ($5.38\cdot10^3$ M^{-1} cm^{-1}). − MS (FAB): *m/z* (%): 1343 (60) $[M]^+$. − $\mathbf{3}\cdot 2\,CH_2Cl_2\cdot 3\,H_2O$: calcd. C 43.07, H 3.32, N 15.95; found: C 43.27, H 3.23, N 15.95.

Preparation and Characterization of $[Cr^{III}Cr^{II}_4(\mu_5\text{-tpda})_4F(CF_3SO_3)](CF_3SO_3)$ (4): $[Cr_5(\mu_5\text{-tpda})_4(Cl)_2]$ (0.05 g, 0.036 mmol) and $AgCF_3SO_3$ (0.019 g, 0.072 mmol) were placed in 50 mL flask containing THF (20 mL). After 1 h of stirring, the solution was filtered to remove AgCl and Ag solid, leaving a clear dark brown solution. The solution was concentrated and a brown powder obtained. The powder was recrystallized from $CHCl_3$/ether solution. Deep brown crystals were obtained (yield: 30%). − IR (KBr): $\tilde{\nu}$ = 1604 cm^{-1}, 1581, 1547 (C=C). − MS (FAB); *m/z* (%): 1454 (21) $[M]^+$.

Crystal Structure Determinations: Data collection was carried out on a Siemens SMART diffractometer with a CCD detector with

Table 5. Crystal data for compounds **1**, **2**, **3**, and **4**

Compound	**1**·2 $O(C_2H_5)_2$·4 $CHCl_3$	**2**	**3**·1.5 CH_3CN·2 H_2O·THF	**4**·SO_3CF_3·2 $CHCl_3$
Formula	$C_{72}H_{68}Cl_{14}Cr_5N_{20}O_2$	$C_{62}H_{44}Cr_5N_{20}S_2$	$C_{67}H_{52.5}BCr_5N_{21.5}O_3$	$C_{64}H_{46}Cl_6Cr_5F_7N_{20}O_6S_2$
Molecular weight	2001.76	1417.28	1591.61	1861.03
Crystal system	Monoclinic	Tetragonal	Monoclinic	Monoclinic
Space group	*C*2/*c*	*I*4/*m*	$P2_1/n$	$P2_1/c$
Color of crystal	Brown	Brown	Brown	Brown
a [Å]	28.5053(3)	10.8142(2)	16.7514(1)	13.7588(1)
b [Å]	14.0725(2)		17.5659(2)	17.8995(1)
c [Å]	25.1033(1)	26.1892(7)	23.1206(3)	31.0298(2)
β [°]	122.87		100.882(1)	93.620(1)
V [Å^3]	8457.9(2)	3062.8(1)	6681.0(1)	7626.64(9)
Z	4	2	4	4
R_F, $R_w(F^2)$ (all data)	0.1004, 0.1669	0.0696, 0.1729	0.1448, 0.2462	0.1361, 0.2092
R_F, $R_w(F^2)$ [$I > 2\sigma(I)$]	0.0672, 0.1419	0.0543, 0.1575	0.0899, 0.2163	0.0758, 0.1750
GOF	1.114	1.067	1.078	1.033

[a] $R_F = \Sigma|F_o - F_c|/\Sigma|F_o|$; $R_w(F^2) = [\Sigma w|F_o^2 - F_c^2|^2/\Sigma w(F_o^4)]^{1/2}$.

Mo radiation (λ = 0.71073 Å) at room temp. A preliminary orientation matrix and unit cell parameters were determined from 3 runs of 15 frames each, each frame correspond to a 0.3° scan in 20 s, following by spot integration and least-squares refinement. For each structure, data were measured using ω scans of 0.3° per frame for 20 s until a complete hemisphere had been collected. Cell parameters were retrived using SMART[13] software and refined with SAINT on all observed reflections. Data reduction was performed with the SAINT[14] software and corrected for Lorentz and polarization effects. Absorption corrections were applied with the program SADABS.[15] The detail crystal data of compounds **1**, **2**, **3**, and **4** are listed in Table 5.

Crystal Data of 1·2 $O(C_2H_5)_2$·4 $CHCl_3$: A brown crystal of approximation dimensions 0.5 × 0.4 × 0.3 mm was mounted on a glass capillary. A total of 27034 reflections in 1650 frames were collected with a final resolution of 0.75 Å. Sadabs absorption correction (T_{min} 0.59 and T_{max} 0.72), 9601 unique reflections (2θ < 55°, R_{int} = 0.058) were used in the refinement. Full-matrix least-square refinement on F^2 converged to R_F = 0.1004 (all data), 0.0672 [$I > 2\sigma(I)$] and $R_w(F^2)$ = 0.1669 (all data), 0.1419 [$I > 2\sigma(I)$].

Crystal Data of 2: A brown crystal of approximation dimensions 0.4 × 0.2 × 0.2 mm was mounted on a glass capillary. A total of 10471 reflections in 1680 frames were collected with a final resolution of 0.75 Å. Sadabs absorption correction (T_{min} 0.58 and T_{max} 0.80), 1614 unique reflections (2θ < 52.7°, R_{int} = 0.040) were used in the refinement. Full-matrix least-square refinement on F^2 converged to R_F = 0.0696 (all data), 0.0543 [$I > 2\sigma(I)$] and $R_w(F^2)$ = 0.1729 (all data), 0.1575 [$I > 2\sigma(I)$].

Crystal Data of 3·1.5 CH_3CN·2 H_2O·THF: A brown crystal of approximation dimensions 0.4 × 0.2 × 0.1 mm was mounted on a glass capillary. A total of 42784 reflections in 1666 frames were collected with a final resolution of 0.75 Å. Sadabs absorption correction (T_{min} 0.51 and T_{max} 0.71), 11400 unique reflections (2θ < 50°, R_{int} = 0.106) were used in the refinement. Full-matrix least-square refinement on F^2 converged to R_F = 0.1448 (all data), 0.0899 [$I > 2\sigma(I)$] and $R_w(F^2)$ = 0.2462 (all data), 0.2163 [$I > 2\sigma(I)$].

Crystal Data of 4·2 $CHCl_3$: A brown crystal of approximation dimensions 0.4 × 0.1 × 0.04 mm was mounted on a glass capillary. A total of 41618 reflections in 1666 frames were collected with a final resolution of 0.75 Å. Sadabs absorption correction (T_{min} 0.65 and T_{max} 0.86), 13463 unique reflections (2θ < 50°, R_{int} = 0.089) were used in the refinement. Full-matrix least-square refinement on F^2 converged to R_F = 0.1361 (all data), 0.0758 [$I > 2\sigma(I)$] and $R_w(F^2)$ = 0.2090 (all data), 0.1750 [$I > 2\sigma(I)$].

The structures of **1**, **2**, **3**, and **4** are solved by direct methods with the SHELX-93[15] program and refined by full-matrix least-squares methods on F^2 with SHELXTL-PC V 5.03.[16] All nonhydrogen atomic positions were located in difference Fourier maps and refined anisotropically. Hydrogen atoms were placed in their geometrically generated positions.

Crystallographic data (excluding structure factors) for the structures reported in this paper have been deposited with the Cambridge Crystallographic Data Centre as supplementary publication no. CCDC-113116 {$[Cr_5(tpda)_4Cl_2]$}, -113117 {$[Cr_5(tpda)_4(NCS)_2]$}, -113118 {$[Cr_5(tpda)_4F_2](BF_4)$}, -113119 {$[Cr_5(tpda)_4(F)(OTf)](OTf)$}. Copies of the data can be obtained free of charge on application to CCDC, 12 Union Road, Cambridge CB2 1EZ, UK [Fax: int. code + 44-1223/336-033; E-mail: deposit@ccdc.cam.ac.uk].

Molecular Orbital Calculation: A simple molecular orbital calculation namely Extended Hückel Molecular Orbital method (EHMO) was chosen to apply on such a large system for the purpose of investigating the bonding features of five-centred Cr−Cr−Cr−Cr−Cr bond qualitatively. The EHMO is performed using the program ICON.[17] The atomic coordinates are derived directly from the X-ray diffraction data of $[Cr_5(tpda)_4Cl_2]$ (**1**). The basis functions of Cl, C, N, and H are taken from the default values of the program. The basis functions for Cr is as follows:[18] $H_{ii}(4s) = -8.66$ eV, $\zeta = 1.70$; $H_{ii}(4p) = -5.24$ eV, $\zeta = 1.70$; $H_{ii}(3d) = -11.22$ eV, $\zeta_1 = 4.95$, $C_1 = 0.488$, $\zeta_2 = 1.60$, $C_2 = 0.721$.

Acknowledgments

The authors thank the National Science Council of the Republic of China for financial support.

[1] M. H. Yang, T. W. Lin, C. C. Chou, H. C. Lee, H. C. Chang, G. H. Lee, M. K. Leung, S. M. Peng, *Chem. Commun.* **1997**, 2279.
[2] [2a] F. A. Cotton, L. M. Daniels, C. A. Murillo, I. Pascual, *J. Am. Chem. Soc.* **1997**, *119*, 10223. – [2b] F. A. Cotton, L. M. Daniels, C. A. Murillo, X. Wang, *Chem. Commun.* **1998**, 39.
[3] E. C. Yang, M. C. Cheng, M. S. Tsai, S. M. Peng, *J. Chem. Soc., Chem. Commun.* **1994**, 2377.
[4] [4a] F. A. Cotton, L. M. Daniels, G. T. Jordan IV, *Chem. Commun.* **1997**, 421. – [4b] F. A. Cotton, L. M. Daniels, G. T. Jordan IV, C. A. Murillo, *J. Am. Chem. Soc.* **1997**, *119*, 10377.
[5] [5a] L. P. Wu, P. Field, T. Morrisey, C. Murphy, P. Nagle, B. Hathaway, C. Simmons, P. Thornton, *J. Chem. Soc., Dalton Trans.* **1990**, 3835. – [5b] G. J. Pyrka, M. El-Mekki, A. A. Pinkerton, *J. Chem. Soc. Chem. Commun.* **1991**, 84.

[6] S. Aduldecha, Hathaway, B. *J. Chem. Soc., Dalton Trans.* **1991**, 993.
[7] J. T. Sheu, C. C. Liu, I. Chao, C. C. Wang, S. M. Peng, *Chem. Commun.* **1996**, 315.
[8] S. J. Shieh, C. C. Chou, G. H. Lee, C. C. Wang, S. M. Peng, *Angew. Chem. Int. Ed. Engl.,* **1997**, *36*, 56.
[9] [9a] C. C. Wang, W. C. Lo, C. C. Chou, G. H. Lee, J. M. Chen, S. M. Peng, *Inorg. Chem.* **1998**, *37*, 4059. – [9b] S. Y. Lai, T. Z. Lin, Y. H. Chen, C. C. Wang, G. H. Lee, M. H. Yang, M. K. Leung, S. M. Peng, *J. Am. Chem. Soc.* **1999**, *121*, 250.
[10] F. A. Cotton, R. A. Walton, *Multiple Bonds Between Metal Atoms*, 2nd edn.; Clarendon Press: Oxford, U.K., **1993**.
[11] F. A. Cotton, G. Wilkinson, *Advanced Inorganic Chemistry*, 5th edn.; Wiley: New York, **1988**, Chap. 23.
[12] *Metal–Metal Bonds Clusters in Chemistry and Catalysis*, Plenum, New York, **1989**.
[13] *SMART V 4.043 Software for the CCD Detector System*; Siemens Analytical Instruments Division: Madison, WI, **1995**.
[14] *SAINT V 4.035 Software for the CCD Detector System*; Siemens Analytical Instruments Division: Madison, WI, **1995**.
[15] G. M. Sheldrick, *SHELXL-93, Program for the Refinement of Crystal Structures*; University of Göttingen: Göttingen, Germany, **1993**.
[16] *SHELXTL 5.03 (PC-Version), Program Liberary for Structure Solution and Molecular Graphics*; Siemens Analytical Instruments Division: Madison, WI, **1995**.
[17] J. Howell, A. Rossl, D. Wallace, K. Haraki, R. Hoffmann, ICON Program for Extended Hückel molecular orbital calculation. Quantum chemistry program exchange, University of Indiana, Bloomington, IN, **1977**.
[18] T. A. Albright, R. Hoffmann, J. C. Thiberult, D. L. Thorn, *J. Am. Chem. Soc.* **1979**, *101*, 3801.
[19] A. Bino, F. A. Cotton, W. Kaim, *Inorg. Chem.* **1979**, *18*, 3566.
[20] F. A. Cotton, R. H. Niswander, J. C. Sekutowski, *Inorg. Chem.* **1978**, *17*, 3541.
[21] F. A. Cotton, G. W. Rice, J. C. Sekutowski, *Inorg. Chem.* **1978**, *18*, 1143.

Received January 12, 1999
[I99008]

Syntheses and Characterization of New Tertiary Phosphane Ligands Prepared from *p*-Anisyl- and *p*-Thioanisyldichlorophosphanes

Riitta H. Laitinen,*[a] Helena Riihimäki,[a] Matti Haukka,[b] Sirpa Jääskeläinen,[b] Tapani A. Pakkanen,[b] and Jouni Pursiainen[a]

Keywords: Phosphane ligands / ^{31}P-NMR spectrometry / Substituent increments / Electronic and steric properties

The syntheses and spectroscopic parameters of the new tertiary phosphane ligands (*p*-$MeOC_6H_4$)(*o*-$MeOC_6H_4$)$_2$P (**1**), (*p*-$MeOC_6H_4$)(*o*-$MeSC_6H_4$)$_2$P (**2**), (*p*-$MeSC_6H_4$)(*o*-$MeSC_6H_4$)$_2$P (**3**), (*p*-$MeSC_6H_4$)(*o*-$MeOC_6H_4$)$_2$P (**4**), (*p*-$MeOC_6H_4$)(*o*-NC_5H_4)$_2$P (**5**), and (*p*-$MeSC_6H_4$)(*o*-NC_5H_4)$_2$P (**6**) are reported. Single-crystal X-ray structures of all the compounds (**1–6**) have been determined. The dependence of the ^{31}P-NMR chemical shifts on the substituent groups of the phosphanes is discussed.

Introduction

Aromatic tertiary phosphanes, such as triphenylphosphane, are important ligands that find widespread use in homogeneous organometallic catalysts. They stabilize the low oxidation states of the metal centers and can be used to modify both the electronic and steric properties of the catalysts. The incorporation of substituents at the *ortho*-, *meta*-, or *para*-positions of the aromatic rings offers a means of tailoring the properties of the ligands. Such substituents affect both the metal−phosphorus bond lengths and the associated angles.[1]

Ways of quantifying the electronic and steric properties of phosphanes have been extensively studied since 1970. Tolman′s electronic and steric parameters (ν and θ, respectively) have formed the basis for these studies over the last 30 years.[1,2,3] The improvements in NMR techniques and molecular modelling have introduced new possibilities for delineating the properties of phosphanes.[4,5,6,7]

In the present study, we have prepared and characterized a series of new ligands derived from *p*-anisyl- and *p*-thioanisyldichlorophosphanes. The ligands have been designed with a view to modifying triphenylphosphane by introducing heteroatoms at various positions on the phenyl rings. This should allow different coordination modes in metal complexes. The electronic and steric properties of these ligands, assessed on the basis of their experimental ^{31}P-NMR shifts and crystal structures, are discussed.

Results and Discussion

Syntheses

The new mixed *ortho*/*para*-substituted tertiary phosphane ligands were prepared from *para*-substituted aryldichlorophosphanes. Friedel−Crafts reaction of phosphorus trichloride with anisole or thioanisole in the presence of aluminium chloride as catalyst furnished the desired aryldichlorophosphanes.[8] These were then allowed to react with *ortho*-substituted organolithium compounds, which were obtained by halogen−metal interchange reactions.[9] Organolithium compounds bearing anisyl-, thioanisyl-, and pyridyl groups were employed in order to modify the functionality of the new ligands. These groups induce both steric and electronic changes in the phosphane ligands. The ligands thus obtained, bearing *o*-anisyl and *o*-thioanisyl substituent groups, are potentially tridentate. However, experimental findings indicate that the *o*-thioanisyl ligands behave as bidentate ligands in metal complexes,[10] while the *o*-anisyl ligands behave mainly as monodentate ligands.[11][12] The *o*-pyridyl ligands are also potentially tridentate, but in fact form either monodentate complexes or behave as bridging ligands so as to form bimetallic coordination compounds.[13][14] The introduction of pyridyl groups can also have a modifying effect on the solubilities of phosphanes and their complexes.[15]

^{31}P-NMR Spectra

The behaviour of phosphanes as ligands is dependent on the electron-donating and -accepting properties of the phosphorus atom. The catalytic properties of phosphanes are, for example, regulated by the basicities of these ligands. ^{31}P-NMR spectrometry is an important tool for obtaining information concerning the chemical nature of the phosphorus atom. The ^{31}P-NMR chemical shifts have been shown to be dependent on the R groups of a phosphane PR_3.[16][17] Indeed, the chemical shifts of tertiary phosphane ligands can be estimated empirically (Equation 1):[16]

$$\delta = -62 + \sum_{n=1}^{3} \sigma_n^P$$

[a] Department of Chemistry, University of Oulu,
P. O. Box 3000, FIN-90401 Oulu, Finland
Fax: (internat.) + 358-8/552-1603
E-mail: Riitta.Laitinen@oulu.fi
[b] Department of Chemistry, University of Joensuu,
P. O. Box 111, FIN-80101 Joensuu, Finland

 © WILEY-VCH Verlag GmbH, D-69451 Weinheim, 1999 1434−1948/99/0808−1253 $ 17.50+.50/0

Here, σ^P values are increments that are characteristic for each substituent group. The reference value corresponds to PMe_3 ($\delta = -62$ vs. 85% H_3PO_4).

The increments (σ^P) for the various substituent groups incorporated in the new tertiary phosphane ligands reported herein can be calculated from the published ^{31}P-NMR chemical shifts (Table 1). In these ligands, all three substituent groups are similar. On using the aforementioned increments to calculate theoretical ^{31}P-NMR chemical shifts for the six new ligands prepared in this work, a relatively good agreement with the experimental values is observed (Table 2). This indicates that with information on the substituent increments at hand, the electronic properties of the phosphane can be predicted with reasonable accuracy. This helps in the targeted modification of the phosphanes towards known applications.

Table 1. Increments of substituted phenyl groups

Ligand	Empirical shift [ppm]	σ^P increment [ppm]
(o-$MeSC_6H_4$)$_3$P	−30.2[18]	10.60
(p-$MeSC_6H_4$)$_3$P	−8.3[19]	17.90
(o-$MeOC_6H_4$)$_3$P	−37.1[18], −38.5[19]	8.30, 7.83
(p-$MeOC_6H_4$)$_3$P	−10.2[19], −9.60[20]	17.27, 17.47
(o-NC_5H_4)$_3$P	−1.3[21]	20.23

Table 2. Comparison of empirical and theoretical ^{31}P-NMR shifts of the new ligands

Ligand	Empirical shift [ppm]	Theoretical shift [ppm]
1	−27.7	−28.13
2	−23.1	−23.53
3	−21.1	−22.90
4	−25.9	−27.50
5	−2.3	−4.27
6	−1.6	−3.64

Tolman[2] has estimated the electron-donating properties of tertiary phosphanes by measuring the IR frequencies of the carbonyl groups in $Ni(CO)_3(PR_3)$. The frequencies obtained with various ligands were compared to that with tri-*tert*-butylphosphane, which proved to be the most basic ligand in the series. Based on the experimental results, Tolman calculated the substituent contributions (χ_i) of various attached groups. The relationship can be expressed empirically by Equation 2:

$$\nu(CO) = 2056.1 + \sum_{i=1}^{3} \chi_i \, cm^{-1}$$

Here, the frequency 2056.1 cm^{-1} is that seen with tri-*tert*-butylphosphane attached to Ni. The larger the χ_i value, the less basic the ligand.

Tolman and Allman recognized that there is no general correlation between basicity and ^{31}P-NMR chemical shifts of phosphane ligands.[3][22] However, the basicities of the corresponding phosphane oxides have been shown to be directly related to the ^{31}P-NMR chemical shifts.[23] Phosphane oxides were chosen to minimize the effect of the lone pair on phosphorus on the chemical shift, which allows the electronic effects to dominate. However, it seems that within certain chemically related groups of phosphanes, a relationship between ^{31}P-NMR shifts and basicity can be found. For example, the values for trialkylphosphanes correlate quite well: P(tBu)$_3$: ν(CO) = 2056.1 cm^{-1} vs. δ = 63; P(iPr)$_3$: ν(CO) = 2059.2 cm^{-1} vs. δ = 19.4; PEt_3: ν(CO) = 2061.7 cm^{-1} vs. $\delta = -20.0$; PMe_3: ν(CO) = 2064.1 cm^{-1} vs. $\delta = -62$.[2][3]

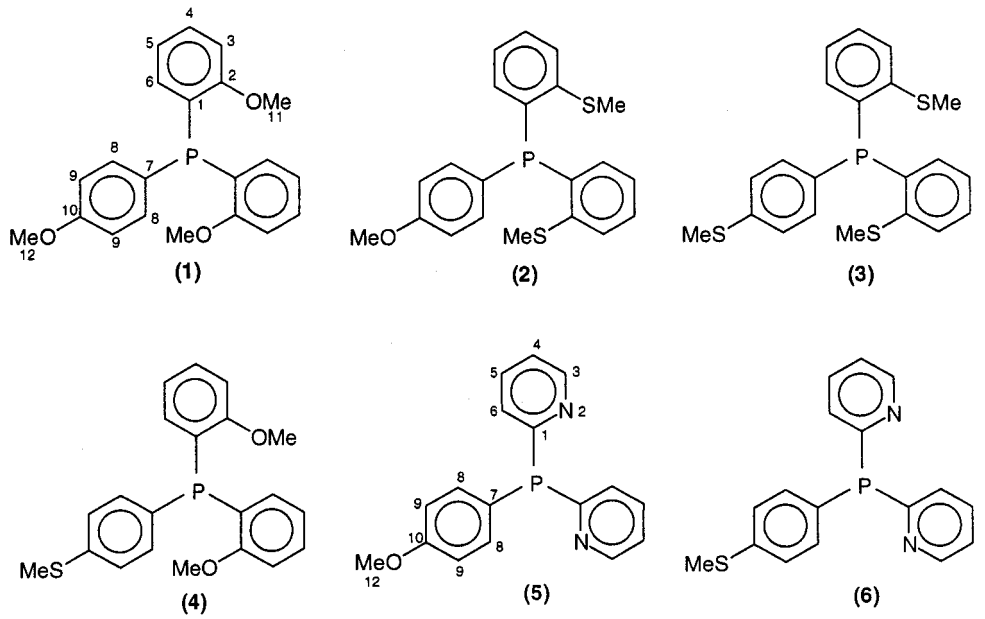
A similar kind of correlation, although of opposite direction, can be noted in the series of anisyl-substituted phosphane ligands. ν(CO) values of these ligands can be calculated by using the substituent contributions of o-$C_6H_4OCH_3$ (0.9 cm^{-1}) and p-$C_6H_4OCH_3$ (3.4 cm^{-1}) reported by Tolman.[2] When the experimental ^{31}P-NMR shifts are compared with these calculated ν(CO) values, a reasonably good agreement is seen: (o-$MeOC_6H_4$)$_3$P: ν(CO) = 2058.8 cm^{-1} vs. $\delta = -37.1$; (p-$MeOC_6H_4$)(o-$MeOC_6H_4$)$_2$P: ν(CO) = 2061.3 cm^{-1} vs. $\delta = -27.7$; (p-$MeOC_6H_4$)$_3$P: ν(CO) = 2066.3 cm^{-1} vs. $\delta = -10.2$.

The fairly good correlation of ν(CO) values and ^{31}P-NMR shifts in these examples suggests that ^{31}P-NMR chemical shifts give adequately reliable information concerning the basicities of closely related phosphane ligands. Therefore, the basicity order of the new ligands should be **6 > 5 > 3 > 2 > 4 > 1**. This order is also supported by the observation that electron-donating substituents increase while electron-withdrawing substituents decrease the basic strengths of the ligands.[2][24]

Molecular Structures

The X-ray crystal structures of all six ligands are essentially very similar. There are no significant differences in bond lengths or bond angles between the ligands. For example, the C−P bond lengths all fall within a range of just 0.025 Å. Similarly, the variations in the C_{arom}−O, C_{methyl}−O, C_{arom}−S, and C_{methyl}−S bond lengths are relatively small: 0.017, 0.021, 0.023, and 0.055 Å, respectively. Furthermore, the relative orientation of the MeO or MeS groups does not seem to have a systematic effect on the bond lengths. The small geometrical variations suggest that the structural impact of the *ortho* or *para* groups or the pyridyl ring on the overall form of the ligands is only minor. The X-ray crystal structures of the ligands **2** and **6** are presented in Figures 1 and 2.

The steric effects of phosphanes as ligands are often expressed in terms of the Tolman cone angles θ.[1][3] These are estimated by assuming an average M−P bond length of 2.28 Å. Substituent groups in the *para* positions of the aryl rings do not significantly influence the steric properties of the ligands. This is illustrated by the similar cone angles found for PPh_3 and (pTol)$_3$P, both $\theta = 145°$.[1] Of the ligands prepared in this work, (p-$MeOC_6H_4$)(o-NC_5H_4)$_2$P (**5**) and (p-$MeSC_6H_4$)(o-NC_5H_4)$_2$P (**6**) should therefore resemble PPh_3 from a steric point of view. The four other ligands (p-$MeOC_6H_4$)(o-$MeOC_6H_4$)$_2$P (**1**), (p-$MeOC_6H_4$)(o-



Scheme 1. Schematic structures of the reported ligands; numbering corresponds to the NMR data

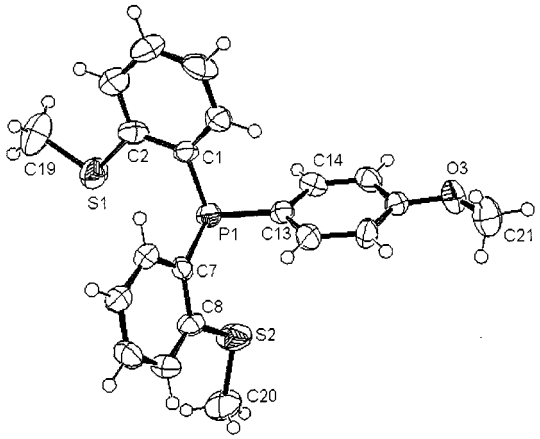


Figure 1. X-ray crystal structure of (p-$MeOC_6H_4$)(o-$MeSC_6H_4$)$_2$P (**2**)

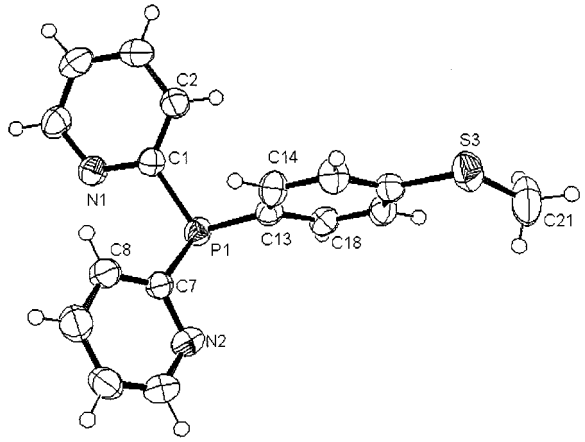


Figure 2. X-ray crystal structure of (p-$MeSC_6H_4$)(o-NC_5H_4)$_2$P (**6**)

$MeSC_6H_4$)$_2$P (**2**), (p-$MeSC_6H_4$)(o-$MeSC_6H_4$)$_2$P (**3**), and (p-$MeSC_6H_4$)(o-$MeOC_6H_4$)$_2$P (**4**) should be sterically analogous to (o-$MeOC_6H_4$)$_2$PPh and (o-$MeSC_6H_4$)$_2$PPh ligands. The steric requirements of these ligands are affected by the conformations of the o-anisyl and o-thioanisyl groups, and therefore the cone angles may not have strictly defined values. The cone angles of these ligands have not been determined

Experimental Section

The ligands were characterized mainly on the basis of ^{1}H-, ^{13}C-, and ^{31}P-NMR data. NMR spectra were recorded on Bruker AM200 and Bruker DPX400 spectrometers. ^{1}H- and ^{13}C-NMR spectra were referenced to TMS; ^{31}P-NMR spectra to 85% H_3PO_4. − Elemental analyses were carried out on a Perkin−Elmer 2400 Series II CHNS/O analyzer. − Exact mass peaks were measured on a Kratos MS-80 spectrometer. − X-ray crystal structures were determined with either an Enraf−Nonius Kappa-CCD or a Nicolet R3m diffractometer. − Commercial reagents were used without further purification. Diethyl ether was distilled from sodium/benzophenone ketyl under nitrogen prior to use. Standard Schlenk techniques were used for the syntheses.

Starting Materials: p-Anisyldichlorophosphane and p-thioanisyldichlorophosphane were prepared according to a published procedure for p-anisyldichlorophosphane.[25][26] The reaction time for the preparation of p-thioanisyldichlorophosphane was extended to 90 h. p-Anisyldichlorophosphane was collected at 98−100°C/0.3 Torr; p-thioanisyldichlorophosphane at 125−126°C/0.15 Torr.

(p-Methoxyphenyl)bis(o-methoxyphenyl)phosphane (1): o-Bromoanisole (1.0 g, 0.7 mL, 5.4 mmol) was lithiated with n-butyllithium (nBuLi) (2.2 mL, 2.5 M in hexane, 5.4 mmol) in sodium-dried diethyl ether (Et_2O) (20 mL) at 0°C. The mixture was stirred for 1 h at 0°C, and then a solution of p-anisyldichlorophosphane (0.6 g, 2.7 mmol) in Et_2O (15 mL) was added. The resulting mixture was stirred for a further 1 h at 0°C and the precipitate formed was filtered off and dried in vacuo. The product (0.5 g, 1.5 mmol, 55.1%) was recrystallized from ethanol. Single crystals suitable for X-ray crystallographic analysis were obtained by slow evaporation

of the solvents from a dichloromethane/hexane solution at −20°C. M.p. 146−149°C. − $C_{21}H_{21}O_3P$: calcd. C 71.6, H 6.0; found C 71.7, H 6.0. − ^{1}H NMR (400 MHz, $CDCl_3$): δ = 3.7 (s, 6 H, H^{11}), 3.8 (s, 3 H, H^{12}), 6.7 (dd, $^3J_{H-H}$ = 6.0 Hz, $^3J_{H-P}$ = 2.2 Hz, 2 H, H^6), 6.8 (m, 6 H, H^3, H^5, and H^9), 7.2 (t, $^3J_{H-H}$ = 7.6 Hz, 2 H, H^8), 7.3 (t, $^3J_{H-H}$ 7.7 Hz, 2 H, H^4). − $^{13}C\{^1H\}$ NMR (100 MHz, $CDCl_3$): δ = 55.1 (s, 1 C, C^{12}), 55.6 (s, 2 C, C^{11}), 110.1 (s, 2 C, C^3), 113.9 (d, $^2J_{C-P}$ = 7.9 Hz, 2 C, C^8), 120.8 (s, 2 C, C^5), 125.7 (d, $^1J_{C-P}$ = 12.3 Hz, 2 C, C^1), 126.8 (d, $^1J_{C-P}$ = 6.9 Hz, 1 C, C^7), 130.0 (s, 2 C, C^4), 133.5 (s, 2 C, C^6), 135.6 (d, $^3J_{C-P}$ = 22.5 Hz, 2 C, C^9), 160.1 (s, 1 C, C^{10}), 161.2 (d, $^2J_{C-P}$ = 15.9 Hz, 2 C, C^2). − $^{31}P\{^1H\}$ NMR (162 MHz, $CDCl_3$): δ = −27.7 (s).

(*p*-Methoxyphenyl)bis(*o*-thiomethylphenyl)phosphane (2): *o*-Bromothioanisole (2.0 g, 1.3 mL, 9.8 mmol) was lithiated with *n*BuLi (3.9 mL, 2.5 M in hexane, 9.8 mmol) in sodium-dried diethyl ether (20 mL) at 0°C. The mixture was stirred for 2 h at 0°C, and then a solution of *p*-anisyldichlorophosphane (1.0 g, 4.9 mmol) in Et_2O (20 mL) was added. The resulting mixture was stirred for a further 2 h at 0°C and the precipitate formed was filtered off and dried in vacuo. The product (1.1 g, 2.9 mmol, 59.2%) was recrystallized from ethanol/toluene. Single crystals suitable for X-ray crystallographic analysis were obtained by slow evaporation of the solvents from a dichloromethane/hexane solution. M.p. 155−157°C. − $C_{21}H_{21}OPS_2$: calcd. C 65.6, H 5.5, S 16.7; found C 65.5, H 5.5, S 16.3. − ^{1}H NMR (200 MHz, $CDCl_3$): δ = 2.4 (s, 6 H, H^{11}), 3.8 (s, 3 H, H^{12}), 6.7 (dd, $^3J_{H-H}$ = 7.5 Hz, $^3J_{H-P}$ = 3.8 Hz, 2 H, H^6), 6.9 (d, $^3J_{H-H}$ = 7.7 Hz, 2 H, H^9), 7.1 (m, 2 H, H^5), 7.2 (t, $^3J_{H-H}$ = 7.8 Hz, 2 H, H^8), 7.3 (m, 4 H, H^3 and H^4). − $^{13}C\{^1H\}$ NMR (50 MHz, $CDCl_3$): δ = 17.3 (d, $^4J_{C-P}$ = 8.7 Hz, 2 C, C^{11}), 55.1 (s, 1 C, C^{12}), 114.4 (d, $^2J_{C-P}$ = 8.7 Hz, 2 C, C^8), 125.3 (s, 2 C, C^5), 125.9 (d, $^1J_{C-P}$ = 7.3 Hz, 1 C, C^7), 126.8 (d, $^3J_{C-P}$ = 4.4 Hz, 2 C, C^3), 129.2 (s, 2 C, C^4), 133.1 (s, 2 C, C^6), 136.1 (d, $^3J_{C-P}$ = 23.2 Hz, 2 C, C^9), 136.8 (d, $^1J_{C-P}$ = 8.7 Hz, 2 C, C^1), 143.5 (d, $^2J_{C-P}$ = 27.6 Hz, 2 C, C^2), 160.5 (s, 1 C, C^{10}). − $^{31}P\{^1H\}$ NMR (162 MHz, $CDCl_3$): δ = −23.1 (s).

(*p*-Thiomethylphenyl)bis(*o*-thiomethylphenyl)phosphane (3): *o*-Bromothioanisole (2.0 g, 1.3 mL, 9.8 mmol) was lithiated with *n*BuLi (3.9 mL, 2.5 M in hexane, 9.8 mmol) in sodium-dried diethyl ether (30 mL) at 0°C. The mixture was stirred for 2 h at 0°C, and then a solution of *p*-thioanisyldichlorophosphane (1.1 g, 4.9 mmol) in Et_2O (20 mL) was added. The resulting mixture was stirred for a further 2 h at 0°C and the precipitate formed was filtered off and dried in vacuo. The product (0.9 g, 2.2 mmol, 45.0%) was twice recrystallized, first from ethanol/toluene and then from hexane/ethanol. Crystals were used for X-ray crystallographic analysis without further crystallization. M.p. 144°C. − $C_{21}H_{21}PS_3$: calcd. C 63.0, H 5.3, S 24.0; found C 62.9, H 5.4, S 24.0. − ^{1}H NMR (200 MHz, $CDCl_3$): δ = 2.4 (s, 6 H, H^{11}), 2.5 (s, 3 H, H^{12}), 6.7 (dd, $^3J_{H-H}$ = 7.3 Hz, 2 H, H^6), 7.1 (m, 2 H, H^5), 7.2 (m, 4 H, H^8 and H^9), 7.3 (m, 4 H, H^3 and H^4). − $^{13}C\{^1H\}$ NMR (50 MHz, $CDCl_3$): δ = 15.1 (s, 1 C, C^{12}), 17.3 (d, $^4J_{C-P}$ = 8.7 Hz, 2 C, C^{11}), 125.3 (s, 2 C, C^5), 126.1 (d, $^2J_{C-P}$ = 8.7 Hz, 2 C, C^8), 126.8 (d, $^3J_{C-P}$ = 4.4 Hz, 2 C, C^3), 129.3 (s, 2 C, C^4), 131.3 (d, $^1J_{C-P}$ = 10.2 Hz, 1 C, C^7), 133.3 (s, 2 C, C^6), 134.7 (d, $^3J_{C-P}$ = 20.3 Hz, 2 C, C^9), 136.2 (d, $^1J_{C-P}$ = 10.2, 2 C, C^1), 140.0 (s, 1 C, C^{10}), 143.7 (d, $^2J_{C-P}$ = 29.1 Hz, 2 C, C^2). − $^{31}P\{^1H\}$ NMR (162 MHz, $CDCl_3$): δ = −21.1 (s).

(*p*-Thiomethylphenyl)bis(*o*-methoxyphenyl)phosphane (4): *o*-Bromoanisole (1.9 g, 1.2 mL, 9.8 mmol) was lithiated with *n*BuLi (3.9 mL, 2.5 M in hexane, 9.8 mmol) in sodium-dried diethyl ether (30 mL) at 0°C. The mixture was stirred for 1 h at 0°C, and then a solution of *p*-thioanisyldichlorophosphane (1.1 g, 4.9 mmol) in Et_2O (20 mL) was added. The resulting mixture was stirred for a further 2

Table 3. Crystallographic data

Ligand	**1**	**2**	**3**	**4**	**5**	**6**
Chemical formula	$C_{21}H_{21}O_3P$	$C_{21}H_{21}OPS_2$	$C_{21}H_{21}PS_3$	$C_{21}H_{21}O_2PS$	$C_{17}H_{15}N_2OP$	$C_{17}H_{15}N_2PS$
Molecular weight [g mol^{-1}]	352.35	384.47	400.53	368.41	294.28	310.34
Crystal size [mm]	0.2 × 0.2 × 0.2	0.3 × 0.3 × 0.3	0.1 × 0.1 × 0.3	0.4 × 0.4 × 0.2	0.4 × 0.4 × 0.2	0.3 × 0.3 × 0.2
Color	Colorless	Colorless	Colorless	Colorless	Colorless	Colorless
Crystal system	Monoclinic	Monoclinic	Triclinic	Triclinic	Monoclinic	Monoclinic
Space group	$P2_1/c$	$P2_1/c$	P-1	P-1	$P2_1/n$	$P2_1/c$
Unit cell dimensions [°]						
a [nm]	7.678(2)	8.002(2)	8.083(2)	8.357(2)	8.300(2)	9.406(2)
b [nm]	30.928(6)	14.917(3)	10.110(2)	11.126(2)	10.944(2)	9.350(2)
c [nm]	7.780(2)	16.304(3)	13.454(3)	11.786(2)	16.967(3)	17.877(4)
α [°]	90	90	72.09(3)	103.57(3)	90	90
β [°]	102.45(3)	92.63(3)	74.97(3)	107.60(3)	100.84(3)	98.50(3)
γ [°]	90	90	82.52(3)	104.49(3)	90	90
Volume [nm^3]	1804.1(6)	1944.1(7)	1008.9(4)	952.5(3)	1513.7(5)	1554.9(6)
Z	4	4	2	2	4	4
Density$_{calcd.}$ [Mg m^{-3}]	1.297	1.314	1.319	1.285	1.291	1.326
Absorption coefficient μ [mm^{-1}]	0.169	0.362	0.448	0.265	0.181	0.305
F(000)	744	808	420	388	616	648
θ range [°]	2.72−24.99	2.50−25.00	3.03−25.00	2.01−28.22	3.07−26.00	2.46−26.00
h range	−8 → 9	0 → 9	−9 → 9	−11 → 11	−10 → 10	0 → 11
k range	−36 → 29	0 → 17	−12 → 12	−13 → 14	−13 → 13	0 → 11
l range	−9 → 8	−19 → 19	−15 → 15	−15 → 15	−20 → 20	−22 → 21
No. of collected reflns.	7645	3749	6761	12254	18305	3047
No. of unique reflns.	3068	3409	3488	4456	2952	3047
No. of obsd. reflns., $I > 2\sigma(I)$	2317	1404	2163	3894	2637	2705
No. of parameters	227	227	227	227	235	190
Final R indices $I > 2\sigma(I)$	0.0651	0.0730	0.0551	0.0523	0.0371	0.0333
w$R2$ $I > 2\sigma(I)$	0.1586	0.1076	0.1305	0.1448	0.0984	0.0821
Goodness-of-fit	1.094	1.006	1.045	1.055	1.037	1.048
T [K]	120(2)	293(2)	293(2)	293(2)	293(2)	293(2)

Table 4. Selected bond lengths [Å]

	(**1**)	(**2**)	(**3**)	(**4**)	(**5**)	(**6**)
P(1)−C(1)	1.842(4)	1.842(6)	1.843(3)	1.8332(16)	1.8395(16)	1.8373(16)
P(1)−C(7)	1.834(4)	1.833(6)	1.838(3)	1.8283(17)	1.8392(16)	1.8439(17)
P(1)−C(13)	1.836(4)	1.826(6)	1.829(4)	1.8352(17)	1.8194(16)	1.8288(16)
C(2)−S(1)		1.759(6)	1.759(4)			
C(8)−S(2)		1.768(6)	1.753(4)			
C(16)−S(3)			1.762(4)	1.7763(19)		1.7613(17)
C(16)−O(3)	1.377(5)	1.366(7)			1.360(2)	
S(1)−C(19)		1.783(6)	1.795(4)			
S(2)−C(20)		1.769(6)	1.756(5)			
S(3)−C(21)			1.740(5)	1.776(3)		1.780(2)
C(2)−O(1)	1.375(5)			1.365(2)		
C(8)−O(2)	1.369(5)			1.368(2)		
C(16)−S(3)				1.7763(19)		1.7613(17)
O(1)−C(19)	1.429(5)			1.423(2)		
O(2)−C(20)	1.435(5)			1.414(3)		
O(3)−C(21)	1.431(5)	1.426(7)			1.422(3)	
N(1)−C(1)					1.345(2)	1.351(2)
N(1)−C(5)					1.337(2)	1.333(2)
N(2)−C(7)					1.343(2)	1.347(2)
N(2)−C(11)					1.338(2)	1.341(3)

Table 5. Selected bond angles [°]

	(**1**)	(**2**)	(**3**)	(**4**)	(**5**)	(**6**)
C(1)−P(1)−C(7)	102.57(18)	101.8(3)	102.74(15)	102.04(8)	103.03(7)	102.52(7)
C(1)−P(1)−C(13)	100.94(18)	100.3(3)	100.74(15)	101.12(8)	103.02(7)	103.36(7)
C(7)−P(1)−C(13)	102.60(18)	103.4(3)	103.38(16)	103.81(8)	103.57(7)	100.63(7)
C(16)−O(3)−C(21)	116.4(3)	117.5(5)			118.98(16)	
C(16)−S(3)−C(21)			103.7(2)	103.30(12)		104.77(10)
C(2)−O(1)−C(19)	117.5(3)			118.54(17)		
C(8)−O(2)−C(20)	117.5(3)			118.51(19)		
C(2)−S(1)−C(19)		104.4(3)	103.44(19)			
C(8)−S(2)−C(20)		104.5(3)	105.6(2)			

h at 0°C and then the precipitate formed was filtered off and dried in vacuo. The product (1.1 g, 3.1 mmol, 62.0%) was recrystallized from ethanol. Single crystals suitable for X-ray crystallographic analysis were obtained by slow evaporation of the solvent from a dichloromethane solution. M.p. 151−152°C. − $C_{21}H_{21}O_2PS$: calcd. C 68.5, H 5.8, S 8.7; found C 68.0, H 5.5, S 9.1. − ^{1}H NMR (200 MHz, $CDCl_3$): δ = 2.5 (s, 3 H, H^{12}), 3.7 (s, 6 H, H^{11}), 6.7 (dd, $^3J_{H-H}$ = 7.3 Hz, $^3J_{H-P}$ = 1.7 Hz, 2 H, H^6), 6.8 (t, $^3J_{H-H}$ = 7.7 Hz, 2 H, H^5), 6.9 (t, $^3J_{H-H}$ = 5.1 Hz, 2 H, H^3), 7.2 (d, $^3J_{H-H}$ = 4.3 Hz, 4 H, H^8 and H^9), 7.3 (t, $^3J_{H-H}$ = 6.8 Hz, 2 H, H^4). − $^{13}C\{^1H\}$ NMR (100 MHz, $CDCl_3$): δ = 15.2 (s, 1 C, C^{12}), 55.7 (s, 2 C, C^{11}), 110.2 (s, 2 C, C^3), 120.9 (s, 2 C, C^5), 125.1 (d, $^1J_{C-P}$ = 12.2 Hz, 2 C, C^1), 125.8 (d, $^2J_{C-P}$ = 7.0 Hz, 2 C, C^8), 130.1 (s, 2 C, C^4), 132.4 (d, $^1J_{C-P}$ = 9.7 Hz, 1 C, C^7), 133.7 (s, 2 C, C^6), 134.4 (d, $^3J_{C-P}$ = 21.6 Hz, 2 C, C^9), 139.1 (s, 1 C, C^{10}), 161.3 (d, $^2J_{C-P}$ = 15.9 Hz, 2 C, C^2). − $^{31}P\{^1H\}$ NMR (162 MHz, $CDCl_3$): δ = −25.9 (s).

(*p*-Methoxyphenyl)bis(*o*-pyridyl)phosphane (5): A solution of *n*BuLi (10 mL, 2.5 M in hexane, 25 mmol) in sodium-dried diethyl ether (40 mL) was cooled to −100°C by means of an ethanol/liquid nitrogen bath. A solution of *o*-bromopyridine (2.5 mL, 25 mmol) in diethyl ether (30 mL) was then rapidly added and the mixture was stirred for 1.5 h at −100°C. A solution of *p*-anisyldichlorophosphane (2.61 g, 12.5 mmol) in diethyl ether (30 mL) was then added dropwise and stirring was continued at −100°C for 1 h. After slowly warming to room temperature, the light-brown mixture was extracted with H_2SO_4 (2 N, 30 mL) and the aqueous layer was separated and made alkaline with NaOH. The crude product was extracted from the aqueous phase with diethyl ether. The solvent was evaporated from the combined extracts and the oily crude product was washed with methanol. The product (3.06 g, 10.4 mmol, 83.2%) was dried in vacuo. Single crystals were grown by vapor diffusion of hexane into a methanol/dichloromethane solution of the pyridylphosphane. M.p. 100−101°C. − ^{1}H NMR (200 MHz, $CDCl_3$): δ = 3.8 (s, 3 H, H^{12}), 7.0 (d, $^3J_{H-H}$ = 8.5 Hz, 2 H, H^9), 7.3 (m, 4 H, H^6 and H^8), 7.5 (t, $^3J_{H-H}$ = 7.3 Hz, 2 H, H^4), 7.7 (t, $^3J_{H-H}$ = 7.7 Hz, $^4J_{H-P}$ = 1.7 Hz, 2 H, H^5), 8.6 (m, 2 H, H^3). − $^{13}C\{^1H\}$ NMR (50 MHz, $CDCl_3$): δ = 55.5 (s, 1 C, C^{12}), 115.2 (d, $^2J_{C-P}$ = 8.7 Hz, 2 C, C^8), 123.1 (s, 2 C, C^4), 127.0 (d, $^1J_{C-P}$ = 7.3 Hz, 1 C, C^7), 128.7 (d, $^2J_{C-P}$ = 18.9 Hz, 2 C, C^6), 136.4 (d, $^3J_{C-P}$ = 2.9 Hz, 2 C, C^5), 137.7 (d, $^3J_{C-P}$ = 23.2 Hz, 2 C, C^9), 150.8 (d, $^3J_{C-P}$ = 11.6 Hz, 2 C, C^3), 162.0 (s, 1 C, C^{10}), 164.8 (d, $^1J_{C-P}$ = 4.4 Hz, 2 C, C^1). − $^{31}P\{^1H\}$ NMR (162 MHz, $CDCl_3$): δ = −2.3 (s). − MS: Exact mass: 294.0886.

(*p*-Thiomethoxyphenyl)bis(*o*-pyridyl)phosphane (6): A solution of *n*BuLi (4 mL, 2.5 M in hexane, 10 mmol) in sodium-dried diethyl ether (20 mL) was cooled to −100°C by means of an ethanol/liquid nitrogen bath. A solution of *o*-bromopyridine (1.0 mL, 10 mmol) in diethyl ether (20 mL) was then rapidly added and the mixture was stirred for 75 min at −100°C. A solution of *p*-thioanisyldichlorophosphane (1.13 g, 5 mmol) in diethyl ether (20 mL) was then added dropwise and stirring was continued at −100°C for 1 h. After slowly warming to room temperature, the light-yellow mixture was extracted with H_2SO_4 (2 N, 30 mL) and the aqueous layer was separated and made alkaline with NaOH. The white solid

product was obtained by extraction of the aqueous phase with diethyl ether. The product (0.60 g, 1.93 mmol, 38.7%) was dried in vacuo. Single crystals were grown by vapor diffusion of hexane into a methanol/dichloromethane solution of the pyridylphosphane. M.p. 122−123°C. − ^{1}H NMR (200 MHz, $CDCl_3$): δ = 2.5 (s, 3 H, H^{12}), 7.2 (m, 6 H, H^6, H^8, and H^9), 7.4 (t, $^3J_{H-H}$ = 7.7 Hz, 2 H, H^4), 7.6 (t, $^3J_{H-H}$ = 7.7 Hz, $^4J_{H-P}$ = 1.9 Hz, 2 H, H^5), 8.7 (d, $^3J_{H-H}$ = 4.7 Hz, 2 H, H^3). − $^{13}C\{^1H\}$ NMR (50 MHz, $CDCl_3$): δ = 14.8 (s, 1 C, C^{12}), 123.3 (s, 2 C, C^4), 126.5 (d, $^2J_{C-P}$ = 8.7 Hz, 2 C, C^8), 128.9 (d, $^2J_{C-P}$ = 20.3 Hz, 2 C, C^6), 132.3 (d, $^1J_{C-P}$ = 10.2 Hz, 1 C, C^7), 136.2 (s, 2 C, C^5), 136.6 (d, $^3J_{C-P}$ = 2.9 Hz, 2 C, C^9), 142.0 (s, 1 C, C^{10}), 150.9 (d, $^3J_{C-P}$ = 11.6 Hz, 2 C, C^3), 164.1 (d, $^1J_{C-P}$ = 4.4 Hz, 2 C, C^1). − $^{31}P\{^1H\}$ NMR (162 MHz, $CDCl_3$): δ = −1.6 (s). − MS: Exact mass: 310.0727.

X-ray Crystallography: X-ray diffraction data were collected with an Enraf−Nonius Kappa-CCD (compounds **1** and **3−6**) or a Nicolet R3m (compound **2**) diffractometer using Mo-K_α radiation (λ = 0.71073 Å). For **2**, cell parameters were obtained from 25 automatically centered reflections. Data collection (ω scan mode), data reduction, and cell refinement were carried out with the P3/P4 diffractometer program V4.27.[27] For the other compounds, the data were collected using ϕ or combined ϕ−ω scans with the Collect[28] data collection program. Denzo and Scalepack[29] programs were used for cell refinements and data reduction. All structures were solved by direct methods using either SHELXS-97[30] or SIR-97[31] programs with the WinGX[32] graphical user interface, or by using the SHELXTL v5.1[33] program package. Structure refinements were carried out with SHELXL-97.[34] All non-hydrogen atoms were refined anisotropically. For compounds **1−5**, the hydrogens were constrained to ride on their parent atom [U_{iso} = 1.2(C_{eq}) for aromatic hydrogens and U_{iso} = 1.5(C_{eq}) for methyl H atoms]. For compound **6**, all hydrogens were located from the difference Fourier map and refined isotropically with constant U_{iso} = 0.05 for aromatic hydrogens and U_{iso} = 0.08 for methyl hydrogens. Crystallographic data are summarized in Table 3 and selected bond lengths and angles are given in Tables 4 and 5.

Crystallographic data (excluding structure factors) for the structures reported in this paper have been deposited with the Cambridge Crystallographic Data Centre as supplementary publication nos. CCDC-114003 to CCDC-114008. Copies of the data can be obtained free of charge on application to CCDC, 12 Union Road, Cambridge CB2 1EZ, U.K. [Fax: (internat.) +44 (0)1223/ 336033; E-mail: deposit@ccdc.cam.ac.uk].

[1] C. A. Tolman, *Chem. Rev.* **1977**, *77*, 313−348.
[2] C. A. Tolman, *J. Am. Chem. Soc.* **1970**, *92*, 2953−2956.
[3] C. A. Tolman, *J. Am. Chem. Soc.* **1970**, *92*, 2956−2965.
[4] C. J. Elsevier, B. Kowall, H. Kragten, *Inorg. Chem.* **1995**, *34*, 4836−4839.
[5] S. Song, E. C. Alyea, *Can. J. Chem.* **1996**, *74*, 2304−2320.
[6] T. L. Brown, K. J. Lee, *Coord. Chem. Rev.* **1993**, *128*, 89−116.
[7] J. M. Smith, B. C. Taverner, N. J. Coville, *J. Organomet. Chem.* **1997**, *530*, 131−140.
[8] J. A. Miles, M. T. Beeny, K. W. Ratts, *J. Org. Chem.* **1975**, *40*, 343−347.
[9] R. G. Jones, H. Gilman, *Org. React.* **1951**, *6*, 339−356.
[10] L. Hirsivaara, M. Haukka, S. Jääskeläinen, R. H. Laitinen, E. Niskanen, T. A. Pakkanen, J. Pursiainen, *J. Organomet. Chem.*, in press.
[11] L. Hirsivaara et al., to be published.
[12] K. R. Dunbar, J. S. Sun, S. C. Haefner, J. H. Matonic, *Organometallics* **1994**, *13*, 2713−2720.
[13] J. P. Farr, M. M. Olmstead, A. L. Balch, *J. Am. Chem. Soc.* **1980**, *102*, 6654−6656.
[14] A. Maisonnet, J. P. Farr, M. M. Olmstead, C. T. Hunt, A. L. Balch, *Inorg. Chem.* **1982**, *21*, 3961−3967.
[15] A. S. C. Chan, C. C. Chen, R. Cao, M. R. Lee, S. M. Peng, G. H. Lee, Organometallics **1997**, *16*, 3469−3473.
[16] J. G. Verkade, L. D. Quin (Eds.), *Phosphorus-31 NMR Spectroscopy in Stereochemical Analysis*, VCH Publishers, Inc., Deerfield Beach, FL, U.S.A., **1987**, p. 88−92.
[17] S. O. Grim, W. McFarlane, E. F. Davidoff, *J. Org. Chem* **1967**, *31*, 781−784.
[18] P. Suomalainen, R. H. Laitinen et al., to be published.
[19] S. O. Grim, A. W. Yankowsky, *Phosphorus and Sulfur* **1977**, *3*, 191−195.
[20] Y. Yamashoji, T. Matsushita, M. Tanaka, T. Shono, *Polyhedron* **1989**, *8*, 1053−1059.
[21] R. J. Bowen, A. C. Garner, S. J. Berners-Price, I. D. Jenkins, R. E. Sue, *J. Organomet. Chem.* **1998**, *554*, 181−184.
[22] T. Allman, R. G. Goel, *Can. J. Chem.* **1982**, *60*, 716−722.
[23] T. T. Derencsenyi, *Inorg. Chem.* **1981**, *20*, 665−670.
[24] C. A. Streuli, *Anal. Chem.* **1960**, *32*, 985−987.
[25] A. Michaelis, *Annalen* **1896**, *293*, 249−257.
[26] W. C. Davies, F. G. Mann, *J. Chem. Soc.* **1944**, 276−283.
[27] *P3/P4 Diffractometer Program* V4.27, Siemens Analytical X-ray Instruments, **1989−1991**.
[28] *Collect*, Data collection software, Enraf−Nonius, Delft, The Netherlands, **1998**.
[29] Z. Otwinowski, W. Minor, *Processing of X-ray Diffraction Data Collected in Oscillation Mode*, Methods in Enzymology, Vol. *276*, *Macromolecular Crystallography, Part A* (Eds.: C. W. Carter, Jr., R. M. Sweet), Academic Press, **1997**, p. 307−326.
[30] G. M. Sheldrick, *SHELXS-97, Program for Crystal Structure Determination*, University of Göttingen, Germany, **1997**.
[31] A. Altomare, C. Cascarano, C. Giacovazzo, A. Guagliardi, A. G. G. Moliterni, M. C. Burna, G. Polidori, M. Camalli, R. Spagna, *SIR-97*, *A Package for Crystal Structure Solution by Direct Methods and Refinement*, University of Bari, Italy, **1997**.
[32] L. J. Farrugia, *WinGX − A Windows Program for Crystal Structure Analysis*, University of Glasgow, Scotland, **1998**.
[33] G. M. Sheldrick, *SHELXTL* Version 5.1, Bruker Analytical X-ray Systems, Inc., Madison, Wisconsin, USA, **1998**.
[34] G. M. Sheldrick, *SHELXL-97*, *Program for Crystal Structure Refinement*, University of Göttingen, Germany, **1997**.

Received February 8, 1999
[I99042]

Charge-Transfer Complexes of Metal Dithiolenes XXVI[+] Azobipyridinium Dications and Radical Monocations as Acceptors

Carsten Handrosch,[a] Robert Dinnebier,[b] Gennadij Bondarenko,[c] Eberhard Bothe,[d] Frank Heinemann,[a] and Horst Kisch*[a]

Keywords: Metal dithiolenes / Charge-transfer complexes / Azo compounds / Electrical conductivity / High-resolution X-ray powder diffractometry

Combination of the planar redox-active ions $[ML_2]^{2-}$ (L = mnt^{2-} = maleonitrile-1,2- dithiolate; M = Ni (**1**), Pd (**2**), Pt (**3**); $dmit^{2-}$ = 2-thioxo-1,3-dithiol-4,5-dithiolate: M = Ni (**4**), Pd (**5**) and *trans*-4,4′-azobis(1-methyl-pyridinium), ($\mathbf{a}^{2+}$) affords 1:1 ion pairs exhibiting partial and complete electron transfer as evidenced by UV-Vis and EPR spectra. Replacement of planar $\mathbf{a}^{2+}$ by a non-planar dipyridinium ketone $\mathbf{b}^{2+}$ leads to the complexes **1b** and **4b**. **1a**, **2a**, and **3a** are predominantly composed of dications and dianions while **4a**, **5a**, and **4b** are rare examples of ion pairs consisting of two radical ions. Single crystal X-ray structural analyses was performed on **4a**, $\mathbf{a}(PF_6)_2$, and $\mathbf{a}(MeSO_4)_2$ while the structure of **1a** was resolved by powder X-ray diffractometry. The latter consists of mixed stacks of planar dianions and dications forming a slipped arrangement with the centers of the two ions displaced relative to each other by 250 pm. The short interplanar distances of 340 pm are in agreement with the presence of a weak charge-transfer interaction as indicated by the corresponding absorption band at about 1400 nm. A mean reorganization energy of 0.85 ±0.04 eV is calculated from the Hush equation for complexes **1a, 2a**, and **3a**. No ion pair charge-transfer band is observable for **4a**, **5a**, and **4b**. Surprisingly, in the solid state structure of **4a** the $[Ni(dmit)_2]^-$ monoanions do not form segregated columns as found in the many ion pairs with redox inert counterions, but prefer a mixed stack arrangement as observed also for **1a.** The specific electrical conductivity of pressed powder pellets of complexes exhibiting a charge-transfer band is in the range of 2×10^{-7} to 1×10^{-5} $\Omega^{-1}cm^{-1}$, increasing with increasing driving force of electron transfer in accordance with previous results. Different to that, the conductivity of the other complexes does not depend on driving force and is much higher (2×10^{-4} to 4×10^{-4} $\Omega^{-1}cm^{-1}$).

Introduction

The control of physical properties of a solid by variation of molecular parameters is a central topic in materials science.[2] In recent work we have found that ion-pair charge-transfer (IPCT) complexes consisting of redoxactive components provide ideal conditions to study the influence of weak supramolecular CT interactions on the electrical conductivity. It was found that for class I complexes of the type $\{A^{2+}[ML_2]^{2-}\}$ wherein the acceptor A^{2+} is a planar dicationic 4,4′- or 2,2′-bipyridinium derivative and the $[ML_2]^{2-}$ donor is a planar dithiolene metalate, L = 2-thioxo-1,3-dithiol-4,5-dithiolate ($dmit^{2-}$) and maleonitrile-1,2-dithiolate (mnt^{2-}), M = Ni, Pd, Pt, the electrical conductivity (σ) of pressed powder pellets increases linearly on a logarithmic scale from 10^{-11} to 10^{-3} $\Omega^{-1}cm^{-1}$ when the driving force of electron transfer from the donor to the acceptor (ΔG_{12}) is varied from 0.7 to −0.1 eV.[3][4] As ΔG_{12} is easily obtained from the solution redox potentials of the two components, the conductivity of the solid IPCT salts can be quantitatively predicted from these molecular parameters. Although the CT interaction is very weak as indicated by the small fraction of an electron transferred from the donor to the acceptor, which is 0.01 to 1%,[5] σ varies over eight orders of magnitude. No similar correlation existed when the d^8 central metal was replaced by a d^7 ion like Co(II).[6] In addition to this strong electronic influence on the electrical properties we have shown that steric alterations like *cis*-*trans* isomerization of the acceptor component may have also a significant effect. While in the case of $[Ni(mnt)_2]^{2-}$ the σ value does not change when the counterion *trans*-DPE-Me^{2+} (Figure 1) is replaced by the *cis*-isomer, it increases by one order of magnitude for the $[Ni(dmit)_2]^{2-}$ complex.[7] This finding suggested that a controlled change of conductivity through photoisomerization may become feasible. In order to investigate whether the observed effect is a unique property of DPE-Me^{2+} or of more general importance, in the present work the acceptor was modified by replacing the bridging ethene fragment by an azo group, well-known to undergo photoisomerization. In the following we report on the synthesis, solid state structure and electrical conductivity of ion pair complexes containing the *trans*-isomer of the new acceptor DPD-Me^{2+} (Figure 1).

[+] Part XXV: See ref.[1]

[a] Institut für Anorganische Chemie der Universität Erlangen-Nürnberg
Egerlandstraße 1, D-91058 Erlangen, Germany
[b] Lehrstuhl für Kristallographie der Universität Bayreuth, Universitätsstraße 30, D-95440 Bayreuth, Germany
[c] Department of Physical Chemistry, Rostov University Zorge St. 7, 344092 Rostov-on-Don, Russia
[d] Max-Planck-Institut für Strahlenchemie, Stiftstraße 34−36, D-45470 Mülheim / Ruhr, Germany

 © WILEY-VCH Verlag GmbH, D-69451 Weinheim, 1999 1434−1948/99/0808−1259 $ 17.50+.50/0

Out of the four structures investigated by X-ray analysis three of them were resolved by the conventional single crystal method and one by the more unconventional powder diffractometry.

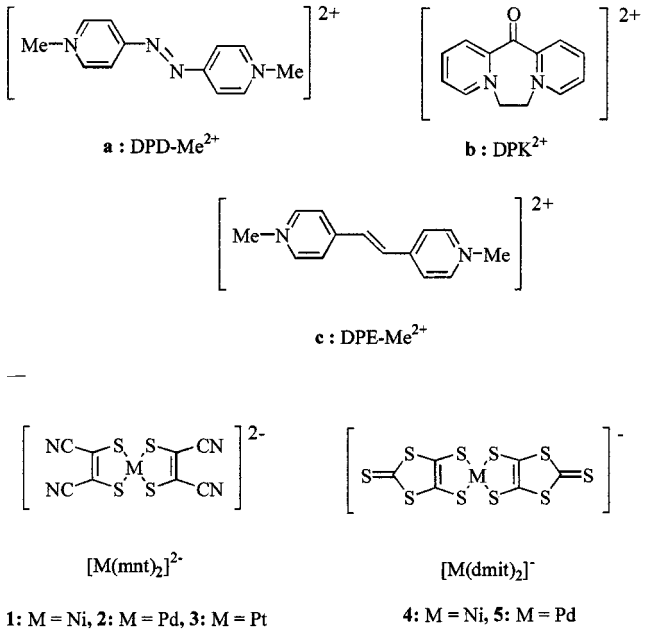


Figure 1. Isolated complexes

Results

DPD-Me(X)$_2$ [X = MeSO$_4$, PF$_6$]

The azoviologen salt **a**(MeSO$_4$)$_2$ was synthesized as described recently[8] and converted into **a**(PF$_6$)$_2$ by metathesis with NH_4PF_6. Single crystals of both salts were obtainable and their structures were solved by X-ray analysis. The observed bond lengths and angles for both compounds are equal within experimental error and therefore only the structure of **a**(PF$_6$)$_2$ × 2 (Me$_2$CO) is shortly discussed (Figure 2, Table 1) but the crystal data of **a**(MeSO$_4$)$_2$ are included in the Experimental Section. The N=N and C−N bond lengths of 123.6 and 143.5 pm agree well with the values of 123 and 141 pm reported for azobenzene[9] and with 127.3 and 143.3 pm calculated for a 4-[4-(dimethylamino)phenyl]azopyridinium salt.[10] Various attempts to isomerize $\mathbf{a}^{2+}$ failed. In all cases no change was observable in the UV-Vis spectrum upon irradiation at various wavelengths.

The cyclic voltammogram of **a**(PF$_6$)$_2$ in acetonitrile exhibits two reversible redox waves at −0.207 V and −0.536 V (vs. Ferrocene), which are assigned to the DPD-Me^{2+}/DPD-Me$^{\bullet+}$ and DPD-Me$^{\bullet+}$/DPD-Me^0 redox steps, respectively (Figure 3a). While the well-known radical cation of methylviologen [11a−d] is blue, DPD-Me$^{\bullet+}$ is deep red. It was generated in a spectroelectrochemical experiment by reduction of the dication at −0.3 V (vs. ref.). This electrolysis led to a constant absorbance at 452 nm ($\varepsilon_{452} = 4.4 \times 10^4$ M^{-1} cm^{-1}). In addition to this sharp band, a broad absorption developed in the range from 500 to 600 nm as depicted in Figure 3b.

Table 1. Selected bond lengths [pm] and angles [°] of **a**(PF$_6$)$_2$ × 2(Me$_2$CO) with estimated standard deviations in parentheses

N(1)−C(16)	147.7(4)
N(1)−C(11)	133.5(4)
N(2)−C(13)	143.5(4)
C(11)−C(12)	136.9(4)
C(12)−C(13)	138.7(4)
C(13)−C(14)	138.3(4)
C(14)−C(15)	137.0(4)
N(1)−C(15)	134.0(4)
N(2)−N(2′)	123.6(5)
C(12)−C(13)−N(2)	115.5(3)
C(14)−C(13)−N(2)	124.4(3)
N(2′)−N(2)−C(13)	113.2(3)

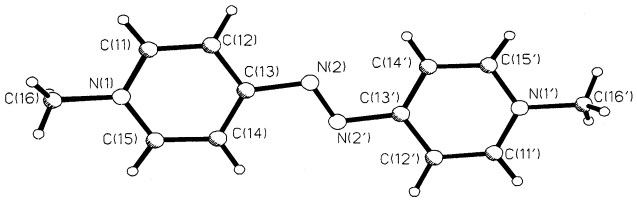


Figure 2. Molecular structure of **a**(PF$_6$)$_2$ × 2 (Me$_2$CO)

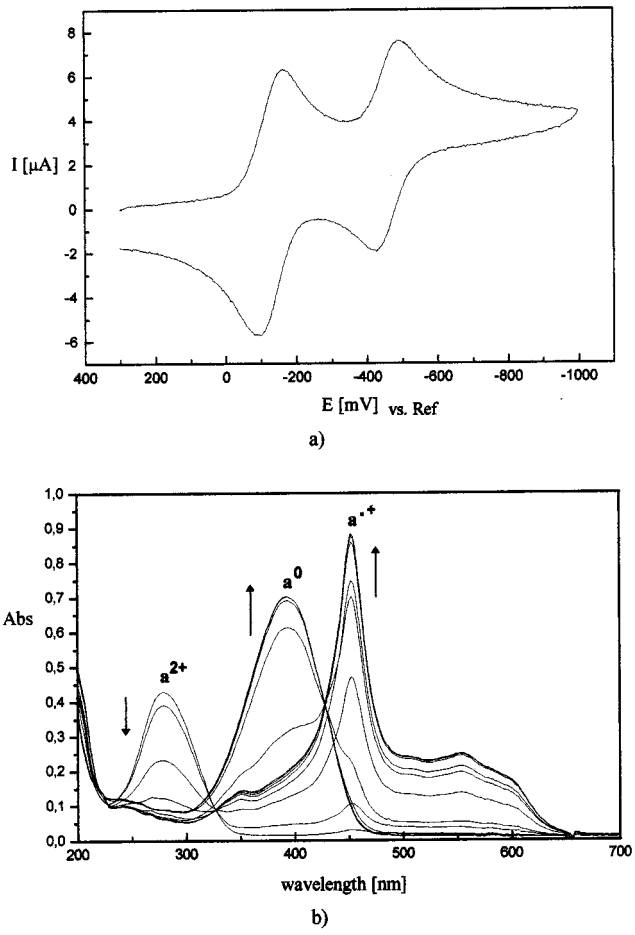


Figure 3. a) Cyclic voltammogram of **a**(PF$_6$)$_2$ in MeCN; v = 0.2 Vs^{-1}; MeCN; E vs. Ag/0.01 M $AgNO_3$; b) Spectroelectrochemistry of **a**(PF$_6$)2 in MeCN

These data agree very well with the one reported for the ethyl derivative DPD-Et$^{\bullet+}$ which was also generated electrochemically.[11c] But different to DPD-Me$^{\bullet+}$, no structural information is available for this ethyl or any other derivative. Further reduction at −0.7 V (vs. ref.) led to the yellow-colored neutral diimine with a single absorption band at 392 nm ($\varepsilon_{392} = 3.5 \times 10^4$ M^{-1} cm^{-1}). Isosbestic points are observed at 325 and 425 nm (Figure 3b).

Chemical reduction of DPD-Me^{2+} to the radical cation can be performed with $S_2O_3^{2-}$, NEt_3, Zn/HOAc, $[Zn(mnt)_2]^{2-}$, Na_2mnt or simply photochemically by dissolving **a**$(PF_6)_2$ in MeOH under diffuse daylight. The resulting red solutions were stable for several days when kept under dinitrogen at −25°C.

In agreement with the slightly twisted structure[12b] DPK^{2+} (Figure 1) is a slightly worse acceptor than DPD-Me^{2+} as indicated by the first reduction potential of −0.06 V (MeCN, vs. SCE)[3] (congruent with −0.45 V vs. ferrocene). Although the radical cation was generated electrochemically[12a] and characterized by resonance raman spectroscopy,[12b] no electronic absorption spectrum was reported. While DPK^{2+} starts absorbing only at about 400 nm, the deep red acetone solution of DPK$^{\bullet+}$, generated under dinitrogen through reduction with aqueous sodium thiosulfate, exhibits a broad maximum already at 507 nm ($\Delta\tilde{\nu}_{1/2} = 1435$ cm^{-1}).

Powder X-Ray Diffractometry of 1a

The complexes **1a** to **5a** were all precipitated by adding slowly a acetone solution of the dication to the dissolved dianion, as described recently.[3][6] All complexes gave satisfactory elemental analyses except **4a**, for which non-stoichiometric compositions of (DPD-Me)$_x$[Ni(dmit)$_2$], $x = 0.7$ to 0.9 were found (vide infra).

Since no single crystals of **1a** could be obtained, the structure was solved by powder X-ray structural analysis.[13] The resulting bond lengths suggest that the nickel component is present as dianion (Table 2). This is indicated by the observed mean Ni−S length of 219.1(4) pm, which is close to the Ni−S bond length of 217.4(2) pm in $\{MV^{2+}[Ni(mnt)_2]^{2-}\}$[14] and comparable $[Ni(mnt)_2]^{2-}$ complexes.[15] The corresponding value in $[Ni(mnt)_2]^-$ compounds is 214.3(2) pm.[16][17] Different to that, the observed N−N length of 131.2(2) pm strongly deviates both from the values of 123.6(5) and 135.5(8) pm observed for the dication (Table 1) and radical cation (Table 4), respectively, while the C−N bond length of 142.8(2) pm is not significantly different from 143.5(4) pm as found for the dication. On the other hand, the difference between the C−N and N=N length is 19.9 and 11.6 pm in DPD-Me^{2+} and **1a**, respectively, while it is negligible in DPD-Me$^{\bullet+}$. It is therefore proposed that the structure of **1a** consists of DPD-Me^{2+} and $[Ni(mnt)_2]^{2-}$ ions. These are arranged as mixed stacks (Figure 4), as also found in other class I IPCT complexes like $\{(MV)^{2+}[Ni(mnt)_2]^{2-}\}$,[14] $\{(DPE\text{-}R)^{2+}[Ni(mnt)_2]^{2-}\}$, [R = $(CH_2)_4CN$],[7] and $\{(MV)^{2+}[Pd(mnt)_2]^{2-}\}$.[18a] As observed in these structures, the two components of **1a** are slipped along the longest molecule axis by about 250 pm. Short interplanar distances are slightly below or above the corresponding sum of the van der Waals radii (Table 3).[18b,19] The average value of 340 pm is characteristic for dithiolene metalate IPCT complexes.[7][18][20]

Table 2. Selected bond lengths [pm] and angles [°] of **1a** with estimated standard deviations in parentheses

DPD-Me^{2+}		$[Ni(mnt)_2]^{2-}$	
N(3)−N(3a)	131.2(2)	Ni(1)−S(1)	219.9(4)
N(3)−C(5)	142.8(2)	Ni(1)−S(2)	218.3(4)
C(5)−C(9)	138.0(2)	S(1)−C(1)	167.8(2)
C(8)−C(9)	134.1(2)	S(2)−C(2)	174.9(2)
N(4)−C(8)	145.8(2)	C(1)−C(2)	136.0(2)
N(4)−C(7)	131.8(2)	C(1)−C(4)	153.5(2)
C(6)−C(7)	138.3(2)	C(4)−N(1)	119.4(2)
C(5)−C(6)	135.7(2)	C(2)−C(3)	147.5(2)
		C(3)−N(2)	105.6(2)
		S(1)−Ni(1)−S(2)	93.33(1)

Single Crystal X-Ray Analysis of 4a

Suitable, dark-green single crystals of **4a** × DMF were obtained by crystallization from DMF/acetone under nitrogen atmosphere. The Ni−S bond lengths of 215−216 pm indicate the presence of the monoanion $[Ni(dmit)_2]^-$[21] since a value of 221 pm is expected for the dianion (Figure 5a, Table 4).[22] This is corroborated by the characteristic electronic absorption spectra (vide infra). The structure of the cationic component in **4a** significantly differs from that of the DPD-Me^{2+} dication as indicated by the comparison of the central CNNC fragments. In the dication the C13−N2 and N2−N2′ bond lengths are 143.5(4) and 123.6(5) pm, respectively, while in **4a** the values of the corresponding C13−N2, C7−N1 and N1−N2 bonds are 134.7(8), 137.7(8) and 135.5(8) pm. Thus, while for DPD-Me^{2+} the C−N bond is about 20 pm longer than the N=N bond, no significant difference is observed for the cation present in **4a**. Accordingly, complex **4a** is composed of two radical ions, a combination hitherto unknown for dithiolene metalate−viologen ion pairs. Contrary to the structure of **1a**, the two components are slipped only marginally relative to each other. In the resulting structure one of the azo nitrogen atoms (N1) is located 362 pm perpendicular above the central nickel ion. Although the distance is much longer than 318 pm, the sum of the corresponding van der Waals radii,[18b,19] it may suggest a weak coordinative interaction and would rationalize the much smaller slipping as compared to **1a**.

Compared to the interplanar distances within **1a**, those in **4a** are remarkably longer (Table 5) and the mean value of 365 pm is in the range of interplanar anion distances as reported for $[Ni(dmit)_2]^-$ complexes with more simple countercations.[21] All values are about 20 pm longer than the sum of the corresponding van der Waals radii. If at all,

Table 3. Shortest interplanar distances in **1a**

	Ni(1a)···C(9a)	S(2a)···N(3a)	C(2a)···N(3)	C(3a)···C(5)	N(2a)···C(9)	S(1)···C(7a)
[pm]	344	337	345	334	333	344
[pm][a]	333	335	325	340	325	335

[a] sum of the corresponding van der Waals radii[19]

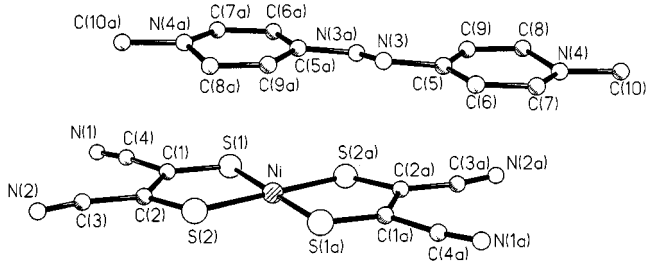
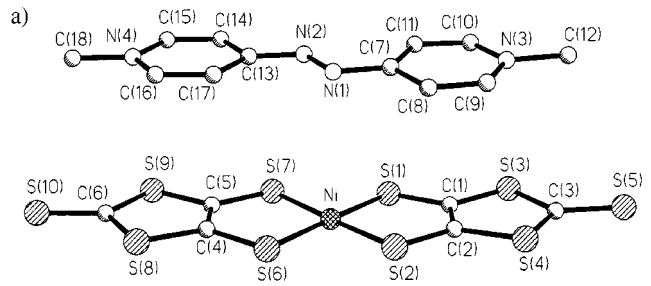


Figure 4. Molecular structure of **1a**



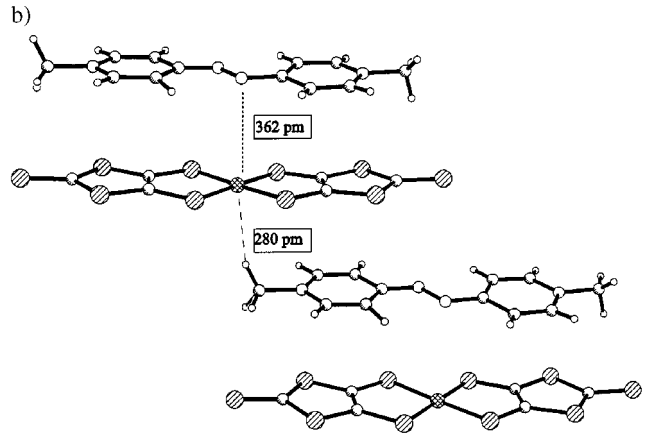


Figure 5. Molecular structure of **4a** × DMF; a) isolated ion pair, b) neighboring pairs

this points to only very weak π interactions between the two components. The presence of weak hydrogen bonding between the ion pairs is suggested by the distance of 280 pm between the methyl group hydrogen atom of DPD-Me$^{\bullet+}$ and the nickel ion; the corresponding sum of the van der Waals radii is 283 pm.

As already mentioned in the discussion of the interplanar distances, the packing structure of **4a** significantly differs from the one generally observed for $[Ni(dmit)_2]^-$ monoanions. In the latter the anions form isolated stacks

Table 4. Selected bond lengths [pm] and angles [°] of **4a** × DMF with estimated standard deviations in parentheses

DPD-Me$^{\bullet+}$	**$[Ni(dmit)_2]^-$**		
N(3)−C(10)	132.9(9)	Ni(1)−S(6)	215.5(2)
N(3)−C(9)	135.2(8)	Ni(1)−S(1)	215.6(2)
N(3)−C(12)	147.6(8)	Ni(1)−S(7)	216.3(2)
N(1)−N(2)	135.5(8)	Ni(1)−S(2)	216.7(2)
N(1)−C(7)	137.7(8)	S(1)−C(1)	172.6(6)
N(4)−C(15)	135.5(9)	S(2)−C(2)	171.8(6)
N(4)−C(16)	136.2(9)	S(3)−C(3)	171.7(7)
N(4)−C(18)	146.8(9)	S(3)−C(1)	174.2(6)
N(2)−C(13)	134.7(8)	S(4)−C(3)	173.7(6)
C(10)−C(11)	137.0(9)	S(4)−C(2)	174.3(6)
C(7)−C(11)	141.6(10)	S(5)−C(3)	165.5(6)
C(7)−C(8)	140.6(10)	S(6)−C(4)	173.2(6)
C(8)−C(9)	135.7(9)	S(7)−C(5)	172.9(6)
C(16)−C(17)	136.5(9)	S(8)−C(6)	172.7(7)
C(13)−C(17)	143.3(10)	S(8)−C(4)	173.9(5)
C(13)−C(14)	142.1(10)	S(9)−C(6)	172.0(6)
C(14)−C(15)	134.7(10)	S(9)−C(5)	175.4(5)
C(17)−C(13)−N(2)	129.3(7)	S(10)−C(6)	165.3(6)
C(13)−N(2)−N(1)	114.4(6)	C(1)−C(2)	133.9(8)
C(7)−N(1)−N(2)	114.6(6)	C(4)−C(5)	132.4(8)
N(1)−C(7)−C(11)	124.3(7)		

which are separated by the cations.[21] In contrast to that, the structure of **4a** consists of mixed anion-cation stacks as typically observed for class I IPCT complexes like MV[Ni(mnt)$_2$],[4][14] although these contain a dication and dianion. These mixed stacks are orientated along the [010] direction as depicted in Figure 6.

Within a stack each DPD-Me[Ni(dmit)$_2$] pair is slipped relative to the other by nearly half of the ion pair length resulting in a steplike arrangement (Figure 5b). Viewed perpendicular to the planar components, parallel stacks appear which are separated by the DMF molecules preventing short interstack contacts between the thioxo sulfur atoms of neighboring dithiolenes, a type of interaction which is generally observable in the many complexes where $[Ni(dmit)_2]^-$ possesses a non-redoxactive counterion.[21] On the other hand when viewed along the components planes there is no separation by solvent molecules and strong interstack interactions between the non-thioxo sulfur atoms become feasible. All corresponding distances of 331 to 362 pm are shorter than the sum of the van der Waals radii (370 pm[19]) and are characteristic for such type of S···S interactions.[21] Furthermore the distance of 331 pm is shorter than ever reported for a 3-dimensional network of $[Ni(dmit)_2]^-$ anions. The overall arrangement in the solid can be viewed as consisting of wavy sheets of distorted nickel dithiolene hexagons, hold together by strong interstack S···S interactions. The latter is typical for $[M(dmit)_2]^-$ (M = Ni, Pd, Pt) as reported for many complexes with more simple counter

Table 5. Shortest interplanar distances in **4a** × DMF

	S(2a)···C(14a)	C(2a)···C(14a)	C(2a)···C(15a)	S(4a)···C(15a)	(S3a)···N(11a)
[pm]	372	355	361	371	367
[pm][a]	350	340	340	350	335

[a] sum of the corresponding van der Waals radii[19]

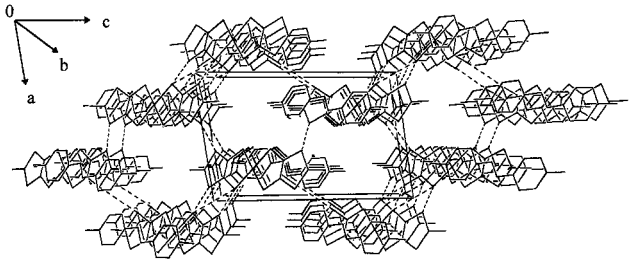


Figure 6. Crystal structure of **4a** × DMF viewed along the *b* axis [010]; dashed lines represent the interstack S···S interactions; DMF molecules are omitted

cations.[21] The ″holes″ in the $[Ni(dmit)_2]$ sheets are occupied by two DPD-$Me^{\bullet+}$ molecules. But in spite of the close packing of the radical cations, there is no evidence for a dimerization as known e.g. for $MV^{\bullet+}$ [11a,11b,23].

General Properties

Since the single-crystal structural analysis of **4a** × DMF revealed the presence of singly charged ions, electron transfer (ET) from $[Ni(dmit)_2]^{2-}$ to DPD-Me^{2+} must have occurred during the synthesis. This is thermodynamically feasible in all cases as indicated by the moderate to strong driving force of the reaction calculated from the redox potentials which were corrected for the actually involved concentrations (Table 6). Only the palladium complex **2a** and the DPK^{2+} ion pair **1b** have rather small ΔG_{12}(corr.) values of −0.08 eV and −0.07 eV, respectively. Accordingly, the UV-Vis-NIR solution absorption spectra of all DPD-Me^{2+} ion pairs except **2a** and **1b** indicate the presence of radical ions. For the mnt complexes **1a** and **3a** the diagnostic absorption of the $[Ni(mnt)_2]^-$ monoanion[24] appears at 862 nm and the DPD-$Me^{\bullet+}$ radical cation is observable at 452, 550(sh) and 600(sh) nm (Figure 7a). Based on a monoanion extinction coefficient of 8000 and 11700 M^{-1} cm^{-1} for M = Ni and Pt at 862 and 855 nm,[24] respectively, one calculates that the concentration of $[M(mnt)_2]^-$ is only 25 (**1a**) and 6% (**3a**), of the theoretical value. This suggests that the major species present is the dianion as also corroborated by the EPR spectra (vide infra). An almost complete ET can be deduced from the high absorbance of the $[Ni(dmit)_2]^-$ monoanion at 1145 nm (ε = 16250 M^{-1} cm^{-1})[25] and 1414 nm (ε = 18050 M^{-1} cm^{-1})[26] in the case of the dmit-complexes **4a**, **4b** and **5a,** respectively (Figure 7b). Small amounts of remaining dianion could form the ion pair $\{(DPD\text{-}Me^{\bullet+})_2[Ni(dmit)_2]^{2-}\}$ which would account for the non-stoichiometric composition of **4a** (vide supra). Absorptions of the radical cation are evident only in the spectrum of **5a** while they probably are superimposed by monoanion bands in the case of **4a** and **4b**.

The fact that no radical ion absorptions are observable in the spectra of **1b** and **2a** can be rationalized by the unfavorable driving force of ET (Table 6).

The diffuse reflectance spectra of **1a** and **3a** both exhibit very broad absorption bands reaching from around 700 nm to the NIR region at 2200 respectively 2400 nm (Figure 8a).

This is at much lower energy as compared to hitherto observed IPCT bands of mnt complexes which did not extend beyond λ_{max} = 1000 nm while the absorption maxima of **1a** and **3a** are around 1400 nm. As expected, the onset of this low-energy band correlates with the driving force of ET from the dianion to the dication and is therefore assigned to an IPCT transition. According to the Hush equation ($E_{IPCT} = \chi + \Delta G_{12}$) the reorganization energy χ is about the same for the DPD-Me^{2+} complexes **1a**, **2a**, and **3a** resulting in an average value of 0.85 ± 0.04 eV as calculated from the data summarized in Table 6 while 0.89 is obtained for the DPK compound **1b**. This indicates, that the different structure of the acceptor component in **1a** and **1b** does not lead to a significant change of the reorganisation energy.

The diffuse reflectance spectra of **4a**, **4b** and **5a** do not contain evidence for the presence of an IPCT band, in accordance with the absence of short interionic distances typical for π,π interactions (vide supra). The maxima at 1190 and 1490 nm can be assigned to the monoanions $[Ni(dmit)_2]^-$ and $[Pd(dmit)_2]^-$.[26] Although the low-energy tailing of **4a** and **5a** may suggest an IPCT character, its independence on the donor component excludes this possibility. More likely is the assignment to an interanion charge-transfer transition along the 3-D network of the dithiolene metalate as proposed for comparable systems.[27]

The presence of different amounts of radical ions in the mnt and dmit complexes, respectively, is suggested from the UV-Vis-NIR solution spectra. This is corroborated by ESR spectroscopy of the complexes **1a** and **4a**. The powder ESR spectra of **1a** at 77 K exhibits the three signals of the $[Ni(mnt)_2]^-$ monoanion (g_1 = 2.152, g_2 = 2.043, g_3 = 1.997) and an intense signal of the DPD-$Me^{\bullet+}$ radical cation (g = 2.006) (Figure 9a), which overlaps with the less intensive g_3 signal of the monoanion. The observed g values of the dithiolene metalate anion are in excellent agreement with the literature (g_1 = 2.160, g_2 = 2.042, g_3 = 1.998).[28] Due to the separated rhombic spectra of the monoanion and the signal of the DPD-$Me^{\bullet+}$ radical cation, it can be concluded that there are no magnetic interactions between them. For in that case only a single signal of the monoanion

Table 6. Redox potentials of the components; ΔG_{12} and E_{IPCT} of the complexes

	redox potential [V][a]			ΔG_{12} [eV]		E_{IPCT}[e] [eV]	ΔG_{12}* [eV]
	$A^{2+/+}$	$D^{-/2-}$	$D^{-/0}$	corr.[d]	uncorr.		corr.[d]
1a	+ 0.18	+ 0.23[b]	+ 1.03[b]	−0.31	+ 0.05	0.64	0.11
1b	−0.06[c]	+ 0.23[b]	+ 1.03[b]	−0.07	+ 0.29	0.82	0.19
2a	+ 0.18	+ 0.46[b]	n.d.[b]	−0.08	+ 0.28	0.79	0.18
3a	+ 0.18	+ 0.21[b]	n.d.[b]	−0.33	+ 0.03	0.60	0.10
4a	+ 0.18	−0.14[c]	+ 0.18[c]	−0.68	−0.32	–	–
4b	−0.06[c]	−0.14[c]	+ 0.18[c]	−0.43	−0.08	–	–
5a	+ 0.18	−0.02[c]	n.d.[c]	−0.56	−0.20	–	–

[a] from cyclic voltammetry in MeCN, V vs. SCE. – [b] See ref.[17] – [c] See ref.[3] – [d] calculated after correcting the redox potentials via Nernst's equation with $[D^{2-}]_0 = [A^{2+}]_0 = 10^{-3}$ M; $[D^{-}]_0 = [A^{\cdot+}]_0 = 10^{-6}$ M. – [e] onset energy as obtained from diffuse reflectance spectra (see Experimental Section)

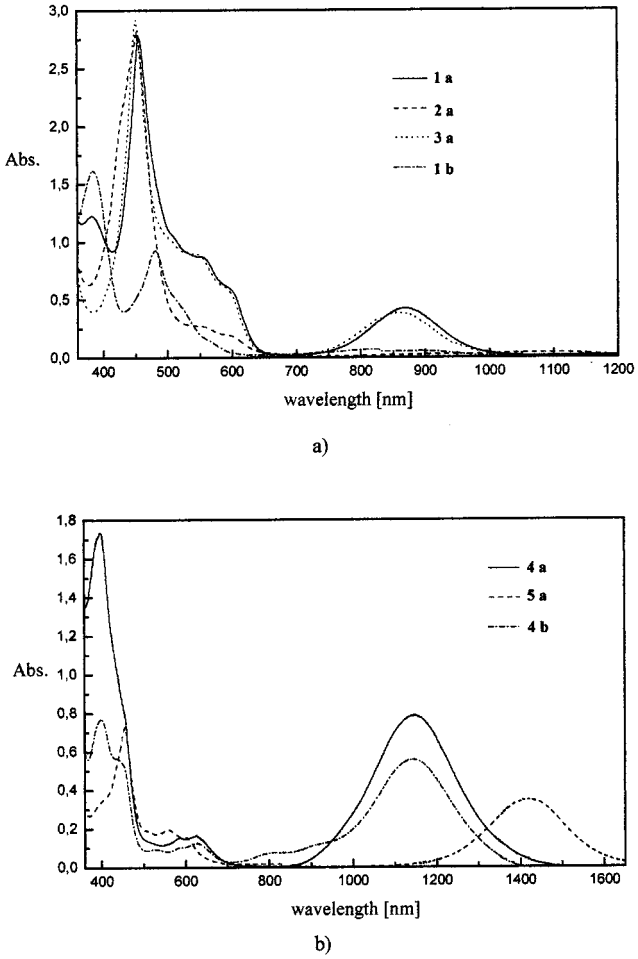


Figure 7. UV-Vis-NIR spectra in DMF; a) mnt complexes, b) dmit complexes, **5a** was measured in DMF/THF = 1 : 4 (*v*/*v*)

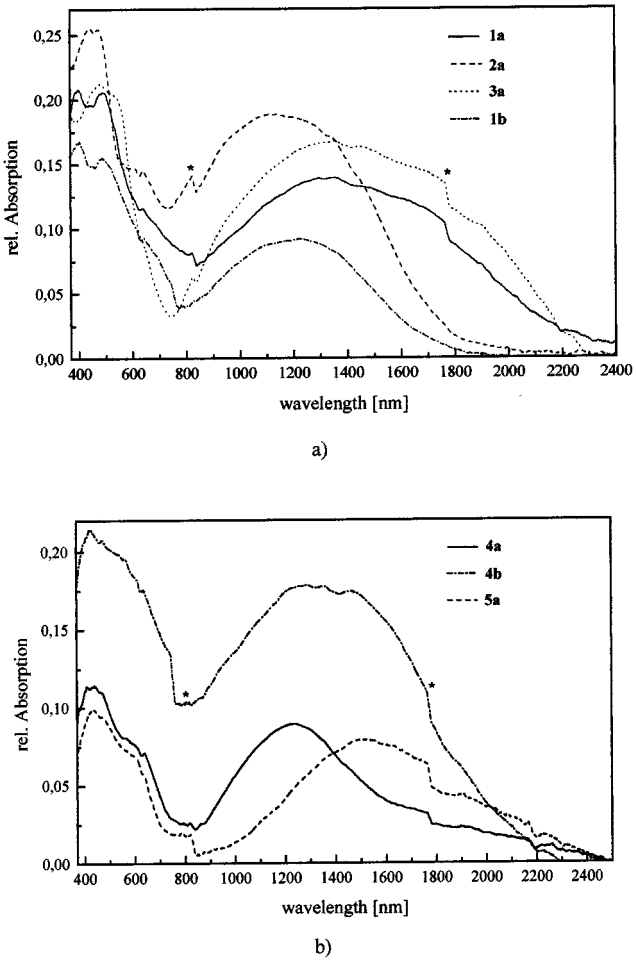


Figure 8. Diffuse reflectance spectra; a) mnt complexes, b) dmit complexes

would have been observed, as in $(NBu_4)[Ni(mnt)_2]$. This lack of interaction between the radicals is confirmed by the comparison of the spectra at room temp. and at 77 K. At both temperatures there are sharp signals of the two components, which are more intensive at the lower temperature (77 K). This is contrary to a mutual antiferromagnetic interaction between the components, in which case less intensive signals would be observed at 77 K than at room temp. From these results it is concluded that both components are magnetically diluted in the diamagnetic complex $\{DPD\text{-}Me^{2+}[Ni(mnt)_2]^{2-}\}$, which is in accordance with the electronic solution spectra showing only a small amount of the anion.

Contrary to that, the dmit complex **4a** exhibits an intensive broad signal at about $g = 2.046$ at room temperature (Figure 9b). At 77 K this apparently isotropic signal disappears, while peaks at $g_1 = 2.003$, $g_2 = 2.047$, $g_3 = 2.118$ emerge (Figure 9c). The small shoulder at the g_2 signal of the monoanion might be caused by the radical cation. These results suggest that the broad signal may be caused

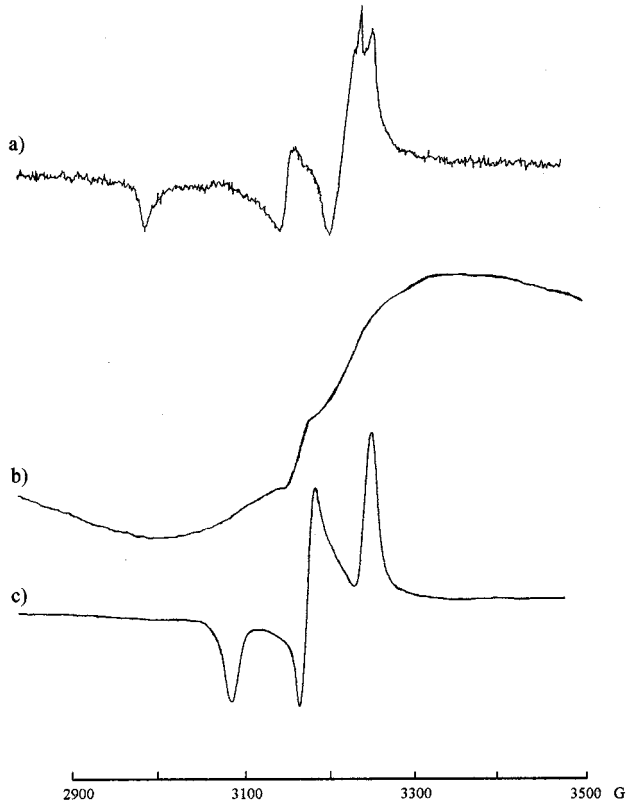


Figure 9. Powder ESR spectra; a) **1a** at 77 K, b) **4a** at room temp., c) **4a** at 77 K

by antiferromagnetic interactions between paramagnetic centers in partially oxidized (DPD-Me)[Ni(dmit)$_2$] containing also magnetically diluted monoanions. A similar broad signal was also reported for the partially oxidized (DEPZ)$_{0.35}$[Ni(dmit)$_2$], (DEPZ = diethylpyrazinium), but contrary to our results this broad signal persisted even at 77 K.[29] This antiferromagnetic interaction between the radicals in **4a** can be detected due to their much higher concentration than in **1a**. This is again in accordance with the high amounts of monoanions observed in the solution UV-spectra of the dmit complexes.

Electrical Conductivity

As expected from our previous findings that σ increases with a more negative driving force of ET when both components are planar and an IPCT band is present (class I complexes),[3] the conductivity increases from 2×10^{-7} over 4×10^{-6} to 1×10^{-5} Ω^{-1}cm^{-1} as ΔG_{12}(corr.) varies from −0.08 (**2a**) over −0.31 (**1a**) to −0.33 (**3a**) eV. The DPK^{2+} complex **1b** [ΔG_{12}(corr.) = −0.07 eV] does not follow this correlation which suggests that another factor must be responsible for this unexpected low conductivity of 1×10^{-9} Ω^{-1} cm^{-1}. Corresponding activation energies of 0.24 and 0.44 eV were measured for **1a** and **1b**, respectively, in the temperature range of 25 to 95°C. This remarkable difference is in sharp contrast to the only slightly different ΔG_{12}* (corr.) values of both complexes (**1a**: 0.11 eV; **1b**: 0.19 eV). It may be rationalized by recalling that the measured activation energy is composed of two components. The energy which is necessary for generation of conducting electrons and the energy barrier for electron transport through the crystal lattice. Since the former should be not too different as suggested by the solution ΔG_{12}*(corr.) values, it seems likely that the latter value is much higher for **1b**. The different acceptor geometries should lead to different crystal structures imposing unfavorable steric constraints for charge transport in the case of **1b**. A significant contribution of the radical species seems to be negligible since the conductivity of **3a** is about half an order of magnitude higher as compared to **1a** although the corresponding radical contents are 6 (**3a**) and 25% (**1a**, vide supra).

Contrary to the mnt complexes, the conductivity of the dmit compounds (4×10^{-4}, 3×10^{-4}, 2×10^{-4} Ω^{-1} cm^{-1} for **4a**, **4b** and **5a**, respectively) does not change significantly upon variation of the metal and acceptor. This suggests a different conduction mechanism which does not depend on electronic interaction between the two components but rather on the strong interstack S···S interactions between the monoanions (Figure 6), a well-known effect for [Ni(dmit)$_2$]$^-$ systems.[21]

Experimental Section

General Methods: Unless noted otherwise, all reactions and operations were carried out under nitrogen using standard Schlenk techniques. Solvents were dried and distilled before use. Spectra were recorded with the following instruments: NMR: Jeol FT-JNM-GX 270, EX 270 and Lambda LA 400. − ^{1}H NMR: The protio-solvent signal was used as an internal reference. Chemical shifts are quoted on the δ scale relative to tetramethylsilane. − ESR spectra were measured on a Radiopan 2543 spectrometer working in X band. − Elemental analyses: Carlo−Erba EA 1106 and 1108. − UV/Vis: Shimadzu UV-3101 PC. − Electrochemical investigations were performed with a three electrode cell with a Ag/0.01 M $AgNO_3$ reference, Pt counter and 2-mm diameter glassy carbon (CV) or Pt-gauze (spectroelectrochemistry) working electrode. Sample solutions were 4×10^{-4} M and TBA(PF$_6$) (10^{-1} M) was the supporting electrolyte. Potentials were referred to *Fc*/*Fc*$^+$ which was added to the solution as internal standard at the end of the measurement prior to the last scan. − For diffuse reflectance measurements the substances were spread on a corundum carrier (Ceram Tec) which also served as reflectance standard. The spectrometer was equipped with an intergrating shere unit. The onset of the absorption band of lowest energy was determined according to the method by Karvaly and Hevesi, originally developed for inorganic semiconductors,[30] which is independent on the sample concentration. Within the linear decrease of absorption on the low-energy side of the band, 5−6 points are selected and the term $[F(R_\infty)h\nu]^2$, with $F(R_\infty) = (1 - R_\infty)^2/2\ R_\infty$ (Kubelka−Munk function) is calculated for each of them. A plot of the first term vs. $h\nu$ affords a straight line which intersects the abscissa at the value E_{IPCT}. − Conductivity: Specific resistivities were measured for compacted pellets at ambient conditions by the conventional two-probe method as described previously.[3] Average values are given as obtained from 3−4 powder pellets; the mean deviation in these measurements was ± 18%. Activation energies E_a were measured in the range of 25−95°C at 5−6 temperatures in a thermostated oil

bath.[3] Arrhenius plots of log σ vs. $1/T$ exhibited excellent linearity with regression coefficients of 0.99 or better.

Powder X-ray Diffraction: For the powder X-ray diffraction experiments, several samples were sealed in glass capillaries (Hilgenberg glass no.50) of 0.5 mm diameter. High resolution powder diffraction data were collected at room temperature at the SUNY X3B1 beamline at the National Synchrotron Light Source, Brookhaven National Laboratory (Figure 10).

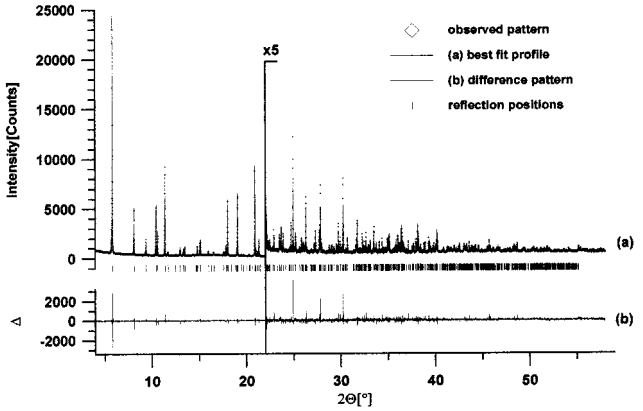


Figure 10. Rietveld plot of monoclinic **1a**. The asymmetric unit contains 23 atoms (17 non-hydrogen atoms). The spikes in the difference curve are the same as in the leBail type of fit and can be attributed to some anisotropical peak broadening which has not been refined.

X-rays of wavelength 1.14946(2) Å were selected by a double Si(111) monochromator. Wavelength and zero-point shift were determined from 8 well-defined reflections of the NIST1976 flat plate alumina standard. The diffracted beam was analyzed with a Ge(111) crystal and detected with a Na(Tl)I scintillation counter with a pulse-height discriminator in the counting chain. The incoming beam was monitored by an ion chamber for normalization for the decay of the primary beam. In this parallel beam configuration, the resolution is determined by the analyzer crystal instead of by slits. Data were taken for 3.3 s at each 2Θ from 2° to 56.805° 2Θ, for 4.3 s at each 2Θ from 40° to 48.3540° 2Θ and for 6.3 s at each 2Θ from 40° to 58.055° 2Θ in steps of 0.005° 2Θ during 2.5 GeV operation (max. 350 mA current). The three data sets were added up and normalized against 10^6 monitor counts.

Although Θ scans did not show serious crystallite size effects, the sample was spinned around the Θ axis during measurement for better statistics. Low angle diffraction peaks from (DPD-Me)[Ni(mnt)$_2$] showed strong asymmetry due to axial divergence and had a FWHM of 0.011° 2Θ, not significantly broader than the resolution of the spectrometer.

The diffraction pattern could be indexed based on a triclinic lattice using the program ITO.[31] The number of formula units per unit cell (Z) was found by geometrical considerations. Since Z was equal to 1 and the DPD-Me^{2+} cation as well as the [Ni(mnt)$_2$]$^{2-}$ ion contain a center of inversion, P-1 was chosen as the most likely space group, which was later confirmed by Rietveld refinement. A Le-Bail fit[32] using the program GSAS[33] worked well to extract 728 reflections up to 57.7° 2Θ. The peak profile function was modeled using a multiterm Simpson′s rule integration of the pseudo-Voigt function.[34] The strong asymmetry in the low-angle region was modeled by a lately implemented function[35] which accounts for the asymmetry due to axial divergence, leading to an strongly improved fit and therefore better profile R factors. Mainly because of the well-resolved peaks over the entire powder pattern, a minor non-constant shift of the peak positions was detected, which could be attributed to a small shift of wavelength. This effect could be satisfactory described by refining an additional sin Θ-depending term in addition to the zero point. A manual fit background using the program GUFI[36] was used in combination with a refinable 4-term cosine-series. The final profile agreement factors obtained were R-p = 5.35% and R-wp = 7.02%.

For the determination of the structure, two different procedures were used. In a direct method approach, the previously extracted intensities were used as input for the program SIRPOW92.[13c] It was possible to detect almost the entire [Ni(mnt)$_2$]$^{2-}$ anion and some fragment of the DPD-Me^{2+} cation. Alternatively, refinable starting parameters for the position and the orientation of the two independent molecules could also be derived from the single-crystal structure determination of the similar compound (MV)-[Ni(mnt)$_2$].[14] For the consecutive Rietveld refinements[37] in GSAS, all background, lattice and profile parameters obtained by the Lebail type of fit were fixed.

Since the shape of the two distinct molecules is known in very narrow limits, this additional information was used to stabilize the refinement by setting up rigid bodies derived from similar structures. Since both, the [Ni(mnt)$_2$]$^{2-}$ anion and DPD-Me^{2+} cation were located on a center of inversion, this reduced the number of refinable parameters for both molecules from 24 positional to 3 rotational parameters each. In order to allow the molecules to relax, the length, the width and in case of the [Ni(mnt)$_2$]$^{2-}$ anion also some out of plane bending of the outer atoms were refined as additional parameters. The refinement converged to a R-Bragg value around 15%.

Due to the high quality of the powder data, all (non-hydrogen) positional parameters remained very close to their rigid-body positions after turning them loose in a final cycle of refinement. Both molecules can be regarded as flat within the error limits. It was also possible to refine individual temperature factors. The final R values were R-p = 6.18%, R-wp = 8.47% and R-F = 7.53%, referring to the Rietveld criteria of fit for profile, weighted profile, and structure factor, respectively, defined in ref.[13a] Esd′s are a factor of six larger than Rietveld statistical estimates, as discussed in ref.[13a]

Single-Crystal X-ray Structure Analyses: Intensity data for the structural analyses of **a**(MeSO$_4$)$_2$, **a**(PF$_6$)2 × 2 (Me$_2$CO) and **4a** × DMF were collected on an automatic four-circle diffractometer (Siemens P4) at 200 K using Mo-K_α radiation (graphite monochromator). Data were corrected for Lorentz and polarization effects. In case of **4a** × DMF a semi-empirical absorption correction has been carried out. For **a**(MeSO$_4$)$_2$ and **a**(PF$_6$)2 × 2-(Me$_2$CO) absorption effects have been neglected. The structures were solved by direct methods and refined using full-matrix least-squares methods on F^2 (SHELXTL 5.03).[38] All non-hydrogen atoms with anisotropic displacement parameters. Hydrogen atom positions were taken from a difference fourier synthesis (exept for the H atoms of the DMF molecules in **4a** × DMF, which were geometrically positioned) and either refined isotropically [**a**(MeSO$_4$)$_2$, **a**(PF$_6$)2 × 2(Me$_2$CO)] or refined with a fixed isotropic displacement parameter (**4a** × DMF).

Orange platelets of **a**(MeSO$_4$)$_2$ were obtained when a saturated solution in methanol was layered with the same volume of acetone and allowed to cool from 20 to −20°C.

Long, orange-colored platelets of **a**(PF$_6$)2 × 2 (Me$_2$CO) were obtained when a saturated solution in acetone was layered with the same volume of 2-propanol and allowed to cool from 20 to −20°C.

Table 7. Selected crystallographic data of **a**$(MeSO_4)_2$, **a**$(PF_6)_2 \times 2\ (Me_2CO)$, **1a**, and **4a** × DMF

compound	**a**$(MeSO_4)_2$	**a**$(PF_6)_2 \cdot 2\ (Me_2CO)$	**1a**	**4a** · DMF
emp. formular	$C_{14}H_{20}N_4O_8S_2$	$C_{18}H_{26}F_{12}N_4O_2P_2$	$C_{20}H_{14}N_8NiS_4$	$C_{21}H_{21}N_5NiOS_{10}$
M_r [g/mol]	436.07	620.37	553.31	738.74
crystal size [mm]	0.40 × 0.30 × 0.30	0.60 × 0.42 × 0.16	–	0.42 × 0.35 × 0.15
F (000)	456	632	282	756
space group	$P2_1/n$	$P2_1/m$	P-1	P-1
cryst. syst.	monoclinic	monoclinic	triclinic	triclinic
a [pm]	621.60(12)	978.9(1)	818.816(3)	979.8(2)
b [pm]	1500.0(3)	1111.2(2)	1143.430(5)	1033.1(2)
c [pm]	1077.7(2)	1287.4(1)	635.682(3)	1535.0(3)
α [°]	90.0	90.0	96.64540(30)	78.19(1)
β [°]	106.41(3)	107.09(1)	93.00920(30)	80.29(1)
γ [°]	90.0	90.0	82.2175(4)	80.58(1)
V [nm^3]	0.9639(3)	1.3397(2)	5.85309(4)	1.4856(5)
Z	2	2	1	2
$D_{calcd.}$ [g/cm^3]	1.504	1.538	1.570	1.651
μ [mm^{-1}]	0.327	0.269	–	1.383
diffractometer	Siemens P4	Siemens P4	Huber 2-circle	Siemens P4
radiation [pm]	Mo-K_α (λ = 71.073)	Mo-K_α (λ = 71.073)	114.946(2)	Mo-K_α (λ = 71.073)
temperature [K]	200	200	295	200
scan technique	ω scan	ω scan	Θ/2Θ	ω scan
2Θ range [°]	4.7–54.2	4.0–54.0	2.0–58.06	4.0–54.0
scan speed [°/min]	3.00–30.00	6.00–40.00	11.00–21.00	8.00
meas. reflections	3580	3976	740	7612
indep. reflections	2110	3079	–	6458
$R_{int.}$ [%]	2.89	2.83	7.53	4.82
obsd. reflections	1336	2057	–	3283
σ criterion	$F \geq 4\ \sigma\ (F)$	$F \geq 4\ \sigma\ (F)$	–	$F \geq 4\ \sigma\ (F)$
R; R_w [%]	5.23; 13.60	6.03; 17.07	6.18; 8.47[a]	5.82; 16.07
refined parameters	168	284	66	387

[a] As defined in ref.[13a]

Dark-green platelets of **4a** × DMF were obtained when a saturated solution in $DMF_{abs}/MeOH_{abs}$ (v/v = 1:3) was allowed to cool slowly from 80 to −20°C.

Syntheses: 4,4′-Azopyridine,[39] DPD-Me$(MeSO_4)_2$ **a**$(MeSO_4)_2$,[8] DPK$(PF_6)_2$ **b**$(PF_6)_2$,[40] $(NBu_4)_2$[Ni$(mnt)_2$],[20] $(NBu_4)_2$[Pd$(mnt)_2$], $(NBu_4)_2$[Pt$(mnt)_2$],[25] $(NBu_4)_2$[Ni$(dmit)_2$] and $(NBu_4)_2$[Pd$(dmit)_2$][41] were prepared according to literature methods. – 4,4′-Azopyridine has been chromatographed prior to use on silica gel (eluent: acetone/petroleum ether/ethyl acetate, 1:3:1) under air. Until noted otherwise all syntheses were carried out under inert gas atmosphere in absolute solvents.

a$(PF_6)_2$: This synthesis was carried out under air. 1.5 g (8.16 × 10^{-3} mol) of 4,4′-azopyridine were dissolved in 36 mL of dimethylsulfate. An orange-colored precipitate was formed after 2 min and stirring at ambient temperature was continued for half an hour. The separated precipitate was dissolved in 500 mL of methanol/ethanol/acetone (v/v = 2 : 2 : 1) and 2.85 g (17.5 × 10^{-3} mol) of NH_4PF_6 in 30 mL of water/methanol (v/v = 1 : 1) were added to the dark-orange solution. After storing in the refrigerator for 2 h, the small orange-colored needles were filtered off through a filter funnel, washed twice with 10 mL of ethanol and dried in vacuo. Yield: 3.6 g (88%) of **a**(PF_6), orange-colored needles. – UV/Vis (acetone): λ_{max} = 280 nm, 450. – ^{1}H NMR (270 MHz, [D$_6$]acetone): δ = 4.80 [d, 6 H, NCH_3], 8.67 [d, 4 H, *3,3′*-, *5,5′*-aromatic H], 9.45 [d, 4 H, *2,2′*-, *4,4′*-aromatic H]. – $C_{12}H_{14}N_4P_2F_{12}$ (504.0): calcd. C 28.57, H 2.80, N 11.11; found C 28.61, H 2.77, N 11.01.

1a: A solution of 201.6 mg (0.40 × 10^{-3} mol) of **a**$(PF_6)_2$ in 40 mL of acetone was added dropwise to 330.0 mg (0.40 × 10^{-3} mol) of $(NBu_4)_2$[Ni$(mnt)_2$] in 50 mL of acetone. Rapidly a dark-brown precipitate was formed which was collected by filtration after standing in the refrigerator for 2 h. The microcrystalline solid was carefully washed both with 10 mL of methanol and acetone and dried in vacuo.Yield: 215 mg (97%) of **1a**, dark-brown microcrystalline powder. UV/Vis (solid): λ_{max} = 398 nm, 474, 1300. – UV/Vis (DMF): λ_{max} = 382 nm, 456, 550, 600, 872. – $C_{20}H_{14}N_8NiS_4$ (553.31): calcd. C 43.41, H 2.55, N 20.25, S 23.18; found C 43.27, H 2.46, N 20.16, S 23.00.

1b: To a solution of 741 mg (0.90 × 10^{-3} mol) of $(NBu_4)_2$[Ni$(mnt)_2$] in 30 mL of acetone, a solution of 453 mg (0.90 × 10^{-3} mol) of **b**$(PF_6)_2$ in 150 mL of acetone was added dropwise. Immediately a dark-brown solid started to precipitate and stirring was carried on for 45 min and the mixture was kept in the refrigerator for 3.5 h. The precipitate was filtered off through a filter funnel, washed three times with 5-mL portions of acetone and dried in vacuo. Yield: 450 mg (91%) of **1b**, dark-brown powder. UV/Vis (solid): λ_{max} = 410 nm, 489, 641(sh), 1224. – UV/Vis (DMF): λ_{max} = 385 nm, 481, 816. – $C_{21}H_{12}N_6NiOS_4$ (550.70): calcd. C 45.76, H 2.18, N 15.25, S 23.24; found C 45.84, H 1.99, N 15.24, S 23.83.

2a: A solution of 355 mg (0.70 × 10^{-3} mol) of **a**$(PF_6)_2$ in 50 mL of acetone was added dropwise within 30 min to 610 mg (0.70 × 10^{-3} mol) of $(NBu_4)_2$[Pd$(mnt)_2$] in 90 mL of acetone. Rapidly an olive-brown, microcrystalline precipitate was formed. Stirring was continued for half an hour, after which the precipitate was collected by filtration, washed twice with 10 mL of acetone and dried in vacuo. Yield: 410 mg (98%) of **2a**, olive-brown microcrystalline powder. UV/Vis (solid): λ_{max} = 350 nm, 449, 469, 639, 1124. – UV/Vis (DMF): λ_{max} = 452 nm, 550, 600, 1100. – $C_{20}H_{14}N_8PdS_4$ (600.04): calcd. C 39.97, H 2.33, N 18.65, S 21.32; found C 39.79, H 2.36, N 18.51, S 21.31.

3a: A solution of 86 mg (0.17 × 10^{-3} mol) of **a**$(PF_6)_2$ in 17 mL of acetone was added within 20 min dropwise to a solution of 166 mg (0.17 × 10^{-3} mol) of $(NBu_4)_2$[Pt$(mnt)_2$] in 26 mL of acetone. Rapidly an violet-brown, microcrystalline precipitate was formed. Stir-

ring was continued for 30 min, after which the precipitate was filtered off. After washing with 5 mL of acetone, the complex was recrystallized from 5 mL of DMF. After two weeks in the refrigerator the black, microcrystalline product was filtered off, washed twice with 2 mL of acetone and dried in vacuo. Yield: 85 mg (73%) of **3a**, dark-brown microcrystalline powder. UV/Vis (solid): λ_{max} = 486 nm, 1357. – UV/Vis (DMSO): λ_{max} = 460 nm, 550(sh), 600(sh), 870. – $C_{20}H_{14}N_8PtS_4$ (689.70): calcd. C 34.83, H 2.05, N 16.25, S 18.59; found C 34.71, H 1.85, N 16.10, S 18.50.

(DPD-Me)$_x$[Ni(dmit)$_2$]; x = 0.7–1.0 (4a): To a cooled (−35°C) solution of 280 mg (0.30×10^{-3} mol) of $(NBu_4)_2[Ni(dmit)_2]$ in 80 mL of acetone was added dropwise within 20 min a cooled (−30°C) solution of 150 mg (0.30×10^{-3} mol) of **a**$(PF_6)_2$ in 50 mL of acetone. During the addition the temperature of the mixture was kept between −35 and −30°C. The brown product started to precipitate immediately. The mixture was then cooled down to −40°C and the precipitate was filtered off as fast as possible (25 min). During the filtration the mixture was allowed to warm up to 0°C. After washing once with 5 mL of acetone and twice with 5 mL of methanol at room temp. the product was dried in vacuo.Yield: 185 mg (93%) of **4a**, dark-brown microcrystalline powder. UV/Vis (solid): λ_{max} = 440 nm, 1243. – UV/Vis (DMF): λ_{max} = 399 nm, 584, 626, 1145. – $C_{18}H_{14}N_4NiS_{10}$ (664.70): calcd.(x = 1.0) C 32.50, H 2.11, N 8.42, S 48.14; found C 32.56, H 2.29, N 8.30, S 47.56.; these values could not be reproduced, two new syntheses gave the following results: $C_{16.8}H_{12.6}N_{3.6}NiS_{10}$ (643.30): calcd.(x = 0.9) C 31.34, H 1.96, N 7.83; found C 31.10, H 1.43, N 8.03; and $C_{15.6}H_{11.2}N_{3.2}NiS_{10}$ (621.90): calcd.(x = 0.8) C 30.10, H 1.80, N 7.20; found C 29.92, H 1.72, N 6.92, respectively.

4b: To a solution of 720 mg (0.77×10^{-3} mol) of $(NBu_4)_2[Ni(dmit)_2]$ in 62 mL of acetone, a solution of 286 mg (0.77×10^{-3} mol) of **b**$(Br)_2$ in 11 mL of acetone/water (v/v = 2:1) was added dropwise. Immediately a grey solid started to precipitate and stirring was carried on for 30 min and the mixture was kept in the refrigerator overnight. The precipitate was filtered off through a filter funnel, washed three times with 5-mL portions of acetone and once with 5 mL of water and dried in vacuo. Yield: 485 mg (95%) **4b**, dark-grey powder. UV/Vis (solid): λ_{max} = 410 nm, 570 (sh), 600 (sh), 1300. – UV/Vis (DMF): λ_{max} = 400 nm, 450 (sh), 630 (sh), 800 (sh), 900 (sh), 1140. – $C_{19}H_{12}N_2NiOS_{10}$ (662.70): calcd. C 34.40, H 1.81, N 4.23, S 48.29; found C 34.77, H 1.86, N 4.25, S 47.54.

5a: A solution of 150 mg (0.30×10^{-3} mol) of **a**$(PF_6)_2$ in 20 mL of acetone was added dropwise within 20 min to a solution of 296 mg (0.30×10^{-3} mol) of $(NBu_4)_2[Pd(dmit)_2]$ in 63 mL of acetone/methanol (v/v = 20 : 1). Rapidly, brown microcrystals started to precipitate. Stirring was carried on for 30 min. After standing in the refrigerator overnight, the product was filtered off, washed twice with 5 mL of acetone and dried in vacuo. Yield: 65 mg (30%) of **5a**, dark-grey microcrystalline powder. UV/Vis (solid): λ_{max} = 434 nm, 1529. – UV/Vis (DMF/THF = 1:4): λ_{max} = 320 nm, 456, 559, 610, 1414. – $C_{18}H_{14}N_4PdS_{10}$ (712.40): calcd. C 30.32, H 1.97, N 7.86, S 44.92; found C 30.60, H 2.10, N 7.78, S 43.34.

Acknowledgments

This work was supported by Volkswagen-Stiftung (C. H., H. K.), Deutsche Forschungsgemeinschaft (R. D.), and Deutscher Akademischer Auslandsdienst (G. B.). Part of the work was carried out at the National Synchrotron Light Source at Brookhaven National Laboratory, which is supported by the U.S. Department of Energy, Division of Materials Sciences and Division of Chemical Sciences. The SUNY X3 beamline at NSLS is supported by the Division of Basic Energy Sciences of the U.S. Department of Energy under grant DE-FG02−86ER45231.

[1] U. Ammon, C. Chiorboli, W. Dümler, G. Grampp, F. Scandola, H. Kisch, *J. Phys. Chem. A* **1997**, *101*, 6876−6882.
[2] [2a] G. J. Ashwell (Ed.), *Molecular Electronics,* Research Studies Press Ltd., Taunton, Somerset, England, **1992**. – [2b] F. L. Carter (Ed.), *Molecular Electronic Devices*, Marcel Dekker Inc., New York, Basel, **1992**.
[3] I. Nunn, B. Eisen, R. Benedix, H. Kisch, *Inorg. Chem.* **1994**, *33*, 5079−5085.
[4] [4a] H. Kisch, *Coord. Chem. Rev.* **1993**, *125*, 155−172. – [4b] H. Kisch, *Coord. Chem. Rev.* **1997**, *159*, 385−396.
[5] As estimated from the parameter α^2 obtained from application of the Hush model (see ref.[3]).
[6] G. Schmauch, F. Knoch, H. Kisch, *Chem. Ber.* **1995**, *128*, 303.
[7] G. Schmauch, F. Knoch, H. Kisch, *Chem. Ber.* **1994**, *127*, 287−294.
[8] J. E. Rockley, L. A. Summers, *Aust. J. Chem.* **1981**, *34*, 2683−2686.
[9] H. Rau, *Angew. Chem*. **1973**, *85*, 248−258.
[10] C. H. Huang et al. *J. Phys.Chem.***1996**, *100*, 15525−15531.
[11] [11a] E. M. Kosower, J. L. Cotter, *J. Am. Chem. Soc.* **1964**, *86*, 5524−5527. – [11b] M. Wolszczak, Cz. Stradowski, *Radiat. Phys. Chem.* **1989**, *33*, 355−359. – [11c] S. Hünig, D. Scheutzow, P. Cársky, R. Zahradnik, *J. Phys. Chem.* **1971**, *75*, 335−339. – [11d] T. Watanabe, K. Honda, *J. Phys. Chem.***1982**, *86*, 2617−2619.
[12] [12a] A. L. Black, L. A. Summers, *J. Chem. Soc. (C)* **1970**, 2394−2395. – [12b] D. J. Barker, L. A. Summers, R. P. Cooney, G. R. Clark, C. E. F. Rickard, *J. Mol. Struct.* **1987**, *159*, 265−278.
[13] [13a] J. I. Langford, D. Louër, *Rep. Prog. Physics* **1996**, *59*, 131−234. – [13b] N. Masciocchi, A. J. Sironi, *J. Chem. Soc. Dalton Trans.* **1997**, 4643−4650. – [13c] C. Giacovazzo, *Acta Cryst.* **1996**, *A52*, 331−339. – [13d] K. D. M. Harris, M. Tremayne, *Chem. Mater.* **1996**, 2554−2570. – [13e] U. M. Schmidt, R. E. Dinnebier, *J. Appl. Cryst.* **1998**, in press.
[14] H. Kisch, A. Fernández, Y. Wakatsuki, H. Yamazaki, *Z. Naturforsch.* **1985**, *40b*, 292−297.
[15] B.-Z. Shan, X.- M. Zhang, X.- Z. You, H.- K. Fun, K. Sivakumar, *Acta Cryst*. **1996**, *C52*, 1148−1150.
[16] J. Morgado, I. C. Santos, L. F. Veiros, R. T. Henriques, M. T. Duarte, M. Almeida, L. Alcacer: *J. Mater. Chem.* **1997**, *7*, 2387−2392.
[17] J. A. McCleverty, *Prog. Inorg. Chem.* **1968**, *10*, 49−219.
[18] [18a] M. Lemke, F. Knoch, H. Kisch, *Acta Cryst.* **1993**, *C49*, 1630−1632. – [18b] To take distances lower than the sum of the van der Waals radii as criterion is not unambiguous since weak electrostatic forces reach much longer. e.g. T. Steiner, *J. Chem. Soc. Chem. Commun*. **1997**, 727.
[19] A. Bondi, *J. Phys. Chem.* **1964**, *68*, 441−451.
[20] E. Billig, R. Williams, I. Bernal, J. H. Waters, H. Gray, *Inorg. Chem.* **1964**, *3*, 663−666.
[21] [21a] O. Lindqvist, L. Andersen, J. Sieler, G. Steinmecke, E. Hoyer, *Acta Chem. Scand. A* **1982**, *36*, 855−856. – [21b] R. Kato, T. Mori, A. Kobayashi, Y. Sasaki, H. Kobayashi, *Chem. Lett.* **1984**, 1−4. – [21c] L. Valade, J.-P. Legros, M. Bousseau, P. Cassoux, *J. Chem. Soc. Dalton Trans.* **1985**, 783−794. – [21d] D. Mentzafos, A. Hountas, A. Terzis, *Acta Cryst.* **1988**, *C44*, 1550−1553. – [21e] P. Cassoux, L. Valade, *Coord. Chem. Rev.* **1991**, *110*, 115−160. – [21f] Kochurani, H. B. Singh, J. P. Jasinski, E. S. Paight, R. J. Butcher, *Polyhedron* **1997**, *16*, 3505−3510. –
pf1[g] Sh. Sun, P. Wu, D. Zhu, *Synth. Met.* **1997**, *88*, 243−247.
[22] O. Lindqvist, L. Sjölin, J. Sieler, G. Steinmecke, E. Hoyer, *Acta Chem.Scand. A* **1979**, *33*, 445−448.
[23] [23a] C. L. Bird, A. T. Kuhn, *J. Chem. Soc. Rev.* **1980**, *10*, 49−82. – [23b] H. Wolkers, R. Stegmann, G. Frenking, K. Dehnicke, D. Fenske, G. Baum, *Z. Naturforsch.* **1993**, *48 b*, 1341−1347.
[24] A. Davison, N. Edelstein, R. H. Holm, A. H. Maki, *Inorg.Chem*. **1963**, *6*, 1227−1232.
[25] A. Davison, R. H. Holm, *Inorg. Synth.* **1966**, 8−26.
[26] B. Eisen, *Doctoral Thesis*, University of Erlangen-Nürnberg, **1995**.
[27] A. E. Underhill et al., *J. Phys. Cond. Matter.* **1991**, *3*, 933−954.

[28] R. D. Schmitt, A. H. Maki, *J. Am. Chem. Soc.* **1968**, *90*, 2288−2292.
[29] Y. Sakamoto, G. E. Matsubayashi, T. Tanaka, *Inorg. Chim. Acta* **1986**, *113*, 137− 141.
[30] B. Karvaly, I. Hevesi, *Z. Naturforsch.* **1971**, *26a,* 245.
[31] J. W. Visser, *J. Appl. Cryst.* 1969, *2*, 89−95.
[32] A. leBail, H. Duroy, J. L. Fourquet, *Mat. Res. Bull.* **1988**, *23*, 447−452.
[33] A. C. Larson, R. B. Von Dreele, *Los Alamos National Laboratory Report* LAUR, **1990**, 86−748.
[34] P. Thompson, D. E. Cox, J. B. Hastings, *J. Appl. Cryst.* **1987**, *20*, 79.
[35] L. W. Finger, D. E. Cox, A. P. Jephcoat, *J. Appl. Cryst.* **1994**, *27*, 892.
[36] R. E. Dinnebier**,** Dinnebier, GUFI*, a program for measurement and evaluation of powder pattern*: Heidelberger Geowiss. Abh. 68, ISBN 3−89257−067−1, 1993.
[37] H. M. Rietveld, *J. Appl. Cryst.* **1969**, *2*, 65−71.
[38] SHELXTL 5.03 for Siemens Crystallographic Research Systems, Copyright **1995** by Siemens Analytical X-ray Instruments Inc., Madison, WI, USA.
[39] N. Campbell, A. W. Henderson, D. Taylor, *J. Chem. Soc.* **1953**, 1281−1285.
[40] [40a] A. L. Black, L. A. Summers, *J. Chem. Soc. (C)* **1970**, 2394 f. – [40b] R. F. Homer, T. E. Tomlinson, *J. Chem. Soc.* **1960**, 2498 ff.
[41] G. Steinmecke, H. J. Sieler, R. Krimse, E. Hoyer, *Phosphorus and Sulfur* **1979**, *7*, 49.

Received February 11, 1999
[I99049]

Predetermined Chirality in Mono- and Dinuclear Cyclometalated Rhodium(III) Complexes

Liana Ghizdavu,[a] Brunhilde Kolp,[a] Alex von Zelewsky,*[a] and Helen Stoeckli-Evans[b]

Keywords: Chirality / Dinuclear complexes / Rhodium

Dinuclear and polynuclear metal complexes with octahedral centers coordinated to di- or polydentate ligands are often obtained as complicated mixtures of various stereoisomers. Stereospecific synthesis of such species is therefore of high current interest. Chiral derivatives of pyridine can be used for this purpose. Dinuclear μ-chloro-bridged Rh^{III} complexes with two didentate, cyclometalated thienylpyridine-type ligands at each metal center are formed stereoselectively when pinene groups are fused to the pyridine rings. The two octahedral Rh^{III} centers have homochiral configurations, ΔΔ and ΛΛ. The heterochiral diastereomer ΔΛ is not observed. With (8*R*,10*R*)-2-(2′-thienyl)-4,5-pinenopyridine [Hth4,5-(*R*,*R*)ppy] the ΔΔ to ΛΛ ratio is 9:1 when the separation eluent contains NaCl. Modeling the ΛΛ and the ΔΔ isomers of the dinuclear species shows crowding of the pinene groups in both cases; however, the strain can be released by relatively small distortions only in the case of the ΛΛ isomer. NO_3^- cleaves the dichloro bridge, yielding the mononuclear species Δ[$Rh(L_2)_2(NO_3)$] (**2**) in a completely stereoselective manner when NaCl is replaced by KNO_3 in the eluent mixture. The molecular structure has been determined by X-ray structure analysis for both the ΔΔ and the mononuclear complex Δ[$Rh(L_2)_2(NO_3)$] (**2**) in order to confirm the configuration at the metal center. ^{1}H-NMR, ^{13}C-NMR and CD spectra were measured and the latter shows that the CD activity is solely due to the chirality at the metal center.

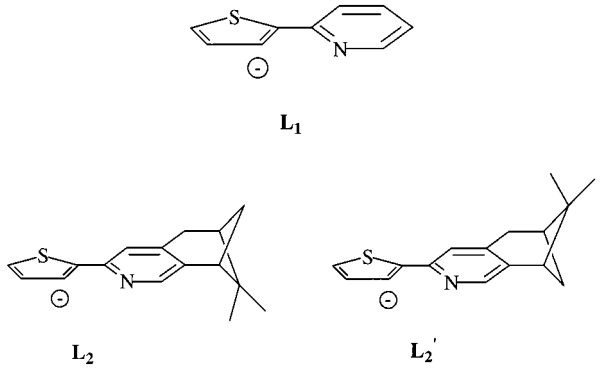
Introduction

The selective generation of chiral metal centers in a predetermined configuration has been reported already in 1920 by Smirnoff,[1] who worked with A. Werner. In contrast to organic chemistry, where *stereoselective synthesis* was developed to a high degree of sophistication, progress in this field was rather slow in coordination chemistry. A recent, fairly comprehensive review[2] on the subject reveals a strongly increased interest in metal-centred chirality in recent years.

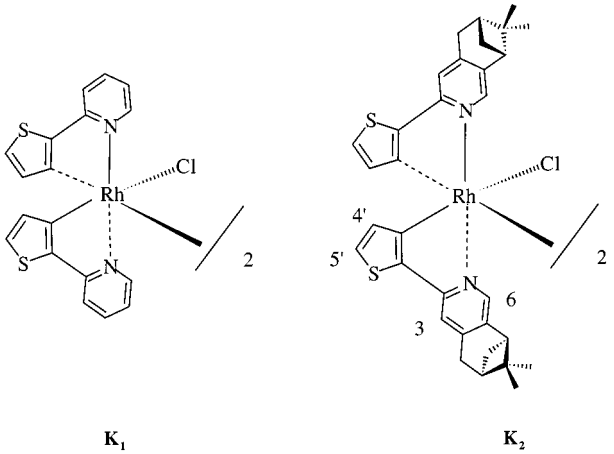
In earlier contributions, we reported the formation of dinuclear cyclometalated Rh^{III} complexes with thienylpyridine[3] or phenylpyridine.[4] 2-(2-Thienyl)pyridine (**L$_1$**, Scheme 1) gives, through a spontaneous cyclometalation, the dinuclear complex di-μ-chlorobis{bis[2-(thien-2′-yl)pyridinato-*N*,*C*$^{3'}$]rhodium} (**K$_1$**, Scheme 2).

It was shown that the formation of this complex is completely regioselective, i.e. only *C*,*C*-*cis*,*N*,*N*-*trans* isomers are obtained. The chirality at the metal centers follows an almost statistical distribution, yielding a ratio of ΔΔ/ΛΛ/ΔΛ of 1:1:2.[5][6] The two enantiomers ΔΔ and ΛΛ occur, of course, in an exact 1:1 ratio.

The introduction of a new family of chiral, enantiomerically pure pyridine-type ligands[7] prompted us to investigate the ability of these versatile molecules to form the dinuclear complexes in a stereoselective manner and to obtain derived mononuclear species with predetermined chirality at the metal center. For this purpose we used (8*R*,10*R*)-



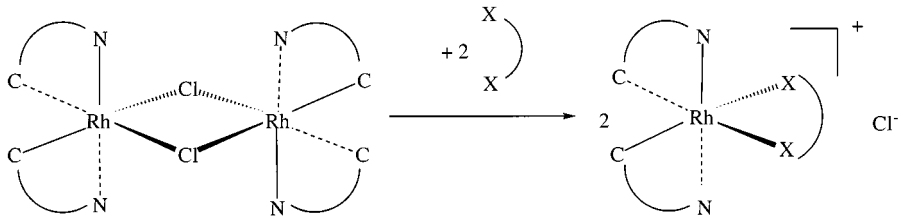
Scheme 1. 2-(2-Thienyl)pyridine [thpy] (**L$_1$**), (8*R*,10*R*)-2-(2′-thienyl)-4,5-pinenopyridine [th4,5(*R*,*R*)ppy] (**L$_2$**) and (8*S*,10*S*)-2-(2′-thienyl)-4,5-pinenopyridine [th4,5(*S*,*S*)ppy] (**L$_2$′**)



Scheme 2

[a] Contribution from the Institute of Inorganic Chemistry, University of Fribourg,
Pérolles, CH-1700 Fribourg, Switzerland
[b] Institute of Chemistry, University of Neuchâtel,
Avenue de Bellevaux 51, CH-2000 Neuchâtel, Switzerland

 © WILEY-VCH Verlag GmbH, D-69451 Weinheim, 1999 1434−1948/99/0808−1271 $ 17.50+.50/0



Scheme 3

2-(2′-thienyl)-4,5-pinenopyridine (**L_2**, in Scheme 1) for the preparation of dinuclear complexes. This ligand forms SP-4 Pt^{II} complexes, which significantly deviate from planarity.[8] The enantiomeric purity of **L_2** is due to its synthesis from a chiral-pool precursor, (−)-myrtenal, which is commercially available in high enantiomeric purity. A first question was the stereochemical outcome of the formation of **K_2** (Scheme 2). If we assume the same regioselectivity as in the case of **K_1** (this assumption is a posteriori justified by our investigations), the three isomers ΔΔ, ΛΛ, ΔΛ are now all diastereomers.

In order to obtain more information about the stereochemistry of such complexes, cleaving reactions (Scheme 3) can be carried out with chiral and nonchiral diimines, diamines and other chelating ligands.[3] Further investigations of such reactions and their products are in progress. Cleavage of the dinuclear species with NO_3^- occurred unintentionally upon separation on TLC plates, and also with acetonitrile in an attempt to obtain crystals of an artificial racemate (vide infra).

Results and Discussion

The replacement of the achiral 2-(2-thienyl)pyridine **L_1** by the enantiomerically pure (8*R*,10*R*)-2-(2′-thienyl)-4,5-pinenopyridine **L_2** renders the ΔΔ/ΛΛ isomers of the dinuclear species diastereomers. Separation with ordinary chromatographic methods becomes therefore possible. TLC (preparative thin layer chromatography, with a mixture of solvents and NaCl) gave the ΔΔ.ΛΛ isomers in a ratio of ca. 9:1, indicating that no cleavage occurred. When replacing NaCl with KNO_3, (see Experimental Section) three products in a mass ratio of 61:28:11 are obtained. The major product can clearly be identified as the ΔΔ isomer.

Single-crystal structure determination of this shows a D_2-symmetric species, where the sterical constraints of ligand/ligand interactions are relatively small. Figure 1 is a representation of the experimentally determined structure (see Table 1 for detailed structural information). The two minor products isolated (28% and 11%) were found to be the Δ[Rh(L$_2$)$_2$(NO$_3$)] (**2**) and the Λ[Rh(L$_2$)$_2$(NO$_3$)] (**3**) complexes, respectively. Both species were examined by X-ray diffraction, and the structures are shown in Figures 3 and 4. These two monomeric, isomerically pure compounds behave in some respects almost as enantiomers, in others, however, their diastereomeric nature is quite evident. Since the CD activity is mainly determined by the configuration around the metal center, the respective spectra are almost mirror images (Figure 7). The NMR spectra are also very similar, small differences in shift values are, however, noticeable. The two compounds behave quite differently with respect to crystallization, which shows the importance of intermolecular interactions in the crystal packing.

The isomer ΔΔ, where the structure could be determined experimentally, shows a relatively low crowding in the region where the pineno moieties of the ligands of the two Rh centers make their closest approach. The observed angle of 170° for N−Rh−N at one center is the same as in the mononuclear complex Δ[Rh(L$_2$)$_2$(NO$_3$)] (**2**), which will be discussed in more detail later. This indicates that the deviation of the N−Rh−N angle from 180° is a purely "local" phenomenon, due to the bite angle of ca. 81° of the cyclometalated ligand. Because of the relatively low quality of the structural analysis of the ΔΔ dimer (see Experimental Section) an attempt was made to prepare an artificial ΔΔ.ΛΛ racemate, using the enantiomeric ligands L_2 and L_2', respectively. The dimers ΔΔ[Rh(L$_2$)$_2$(μ-Cl)]$_2$ (**1**) and ΛΛ[Rh(L$_2'$)$_2$(μ-Cl)]$_2$ (**5**) behave as true enantiomers and are identical in every respect, except for their CD spectra, which are mirror images. Mixing the two enantiomers in order to form the artificial racemate, however, yielded a product that was no longer soluble in pure CH_2Cl_2. CH_3CN had to be added and crystallization was carried out in a CH_3CN/CH_2Cl_2 solvent mixture. The resulting crystalline material turned out to be {Δ[Rh(L$_2$)$_2$Cl(CH$_3$CN)] Λ[Rh(L$_2'$)$_2$Cl(CH$_3$CN)]} (**6**) (Figure 5), indeed a racemate, but of one of the cleaved dimers, containing the monomeric enantiomers. Thus, the dimers are obviously not sufficiently inert towards the solvent (CH_3CN).

In order to gain more insight into the effects that influence the formation or (non-)formation of the three dinuclear diastereomers, the non-existing configurations were graphically constructed on computer (with the MSI Cerius[2] program) by "manual" manipulation of the X-ray structure of the ΔΔ isomer (Figure 2a). The "models" of the ΔΛ and the ΛΛ diasteromers were obtained using the same coordinates as for the ΔΔ isomer except for the μ-dicloro bridge (vide infra), but changing the absolute configuration at the metal centers to ΔΛ and ΛΛ, respectively. This was done by simply breaking the Rh−C bonds and inverting the ligand′s orientation on both sides of the ΛΛ diasteromer and only for one metal center for ΔΛ diasteromer.

In the ΔΛ and the ΛΛ "models" severe crowding of the pineno groups occurs. Figure 2b represents a structure in which the twist angle of the two N−Rh−N directions,

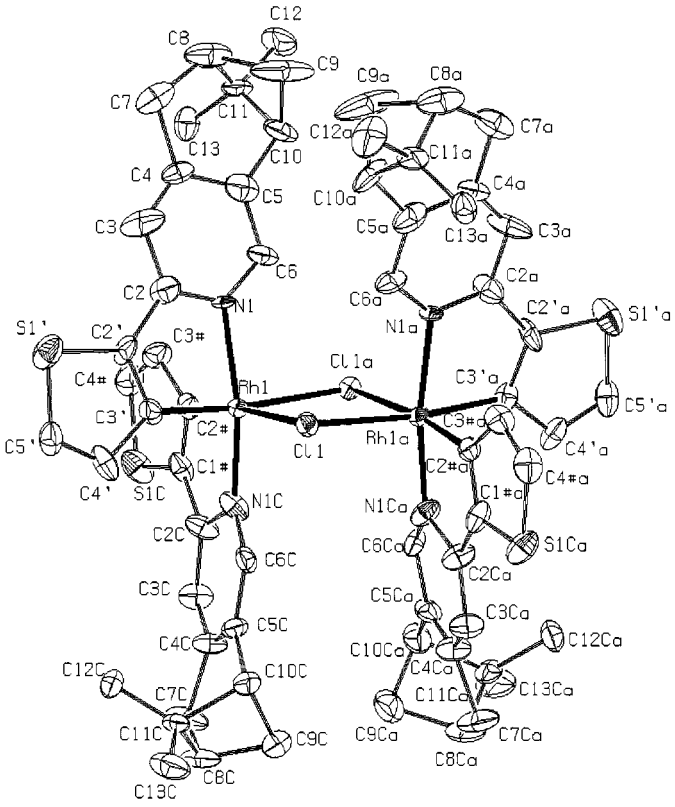


Figure 1a. Numbered ORTEP[18] plot with thermal ellipsoids drawn at 30% probability level of **1**

bution of ΔΔ/Δ/Λ of 61:28:11, mirrors the relative reactivities of the possible diastereomers of the dinuclear species. Only the ΔΔ isomer could be isolated, demonstrating the much higher reactivities towards the cleavage reaction of the ΛΛ and of the ΔΛ isomers that are most probably formed as intermediates.

A model of the "*meso*" isomer ΔΛ, which is still chiral due to the pineno groups, is shown in Figure 2c. Here the internal coordinates were taken from the ΔΔ isomer and the configuration at one Rh center was inverted. This reduces the symmetry of the dinuclear complex from D_2 to C_2. Figure 2c shows that the aromatic groups of the ligands on the two different Rh centers are now nearly perpendicular. The concomitant steric strain cannot be avoided through "distortions" of the complex. Experimentally no evidence indicated that the ΔΛ isomer is formed in this synthesis. From these observations it is concluded that only the ΔΔ isomer of the dimer shows a sufficiently low reactivity to be isolable. Another dimer must be formed as intermediate, which, however, reacts rapidly under the experimental conditions to yield the monomeric species Λ[Rh(L$_2$)$_2$(NO$_3$)] (**3**). Most probably this intermediate is the ΛΛ dimer, already observed in small proportions after separation of the raw product.

The third product obtained after separation on the TLC plates (61:*28*:11) was identified by X-ray diffraction methods as a mononuclear species Δ[Rh(L$_2$)$_2$(NO$_3$)] (**2**) (Figures 3a and 3b). Evidently, the enantiomerically pure mononuclear complex is obtained through cleavage of the dichloro

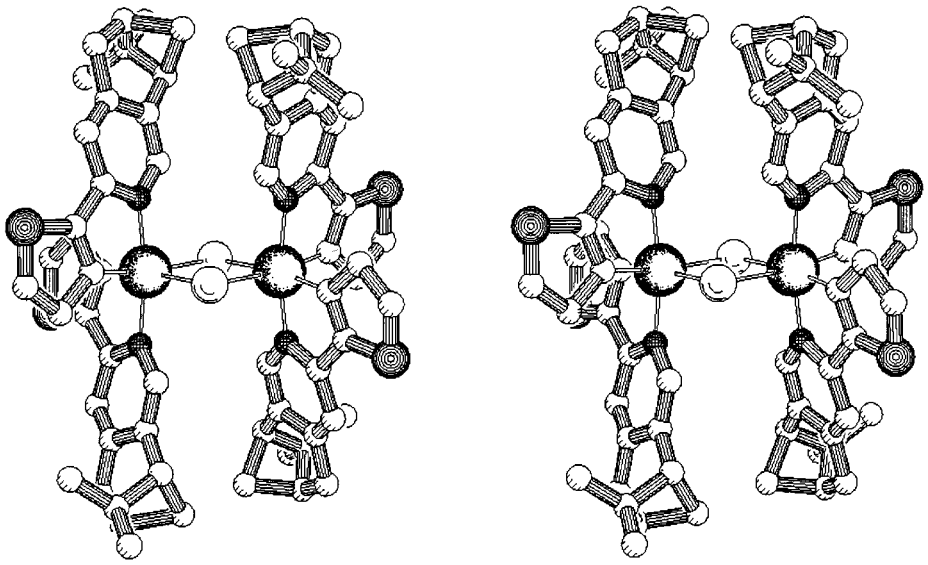


Figure 1b. Stereoview of the molecular structure of ΔΔ[Rh(L$_2$)$_2$(μ-Cl)]$_2$ (**1**); the hydrogen atoms have been omitted for clarity

which is 0° in the ΔΔ isomer, has been changed to 15° in the ΛΛ isomer. This distortion along one of the C_2 axes of the dinuclear species relieves the steric strains due to interligand repulsion considerably. It is therefore predicted that the ΛΛ isomer shows a "distortion" of this type, where the D_2 symmetry is conserved and the parallel orientation of the aromatic parts is maintained, but where the pineno groups are in less crowded positions. The product distribridge by NO_3^- used in the eluent during chromatography. As we will show in a forthcoming publication about a number of mononuclear complexes obtained through cleavage of the dinuclear species, it is a general phenomenon that the former can be obtained in enantiomerically pure form with predetermined chirality. Thus, the complex Δ[Rh(L$_2$)$_2$(NO$_3$)] (**2**) is the first example of a mononuclear species obtained from a diastereoselectively prepared dinuclear

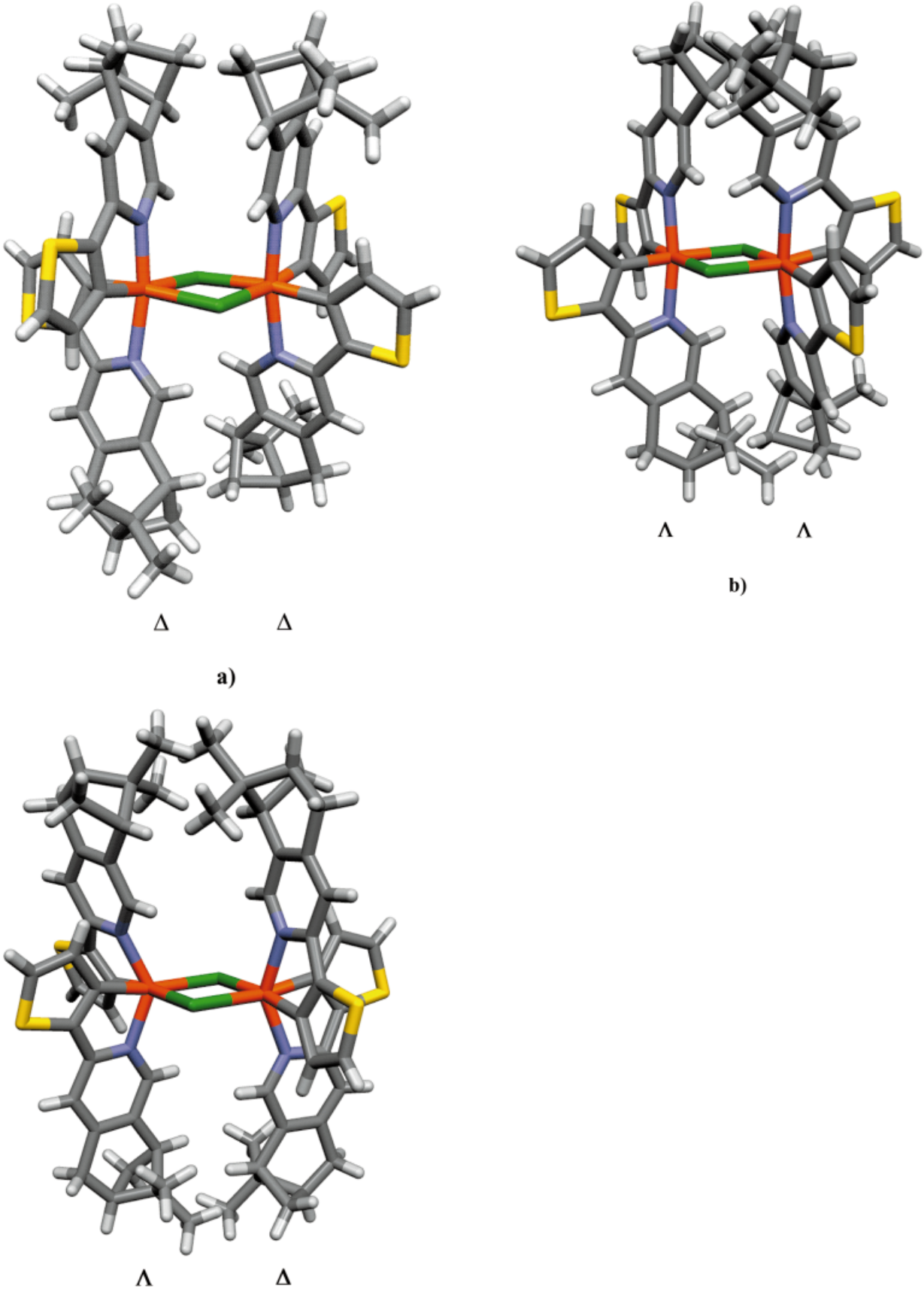


Figure 2. Cylinder plot of the molecular structure of ΔΔ[Rh(L_2)$_2$(μ-Cl)]$_2$ (**1**) (a), models of the ΛΛ structures (b) and ΔΛ (c) using the same internal coordinates as those measured in the ΔΔ isomer

compound that shows a *completely* predetermined chirality at the metal center.

NMR Spectroscopy

Figure 6 illustrates the aromatic region of the ^{1}H-NMR spectra for the $\Delta\Delta[Rh(L_2)_2(\mu\text{-}Cl)]_2$ (**1**), $\Delta[Rh(L_2)_2(NO_3)]$

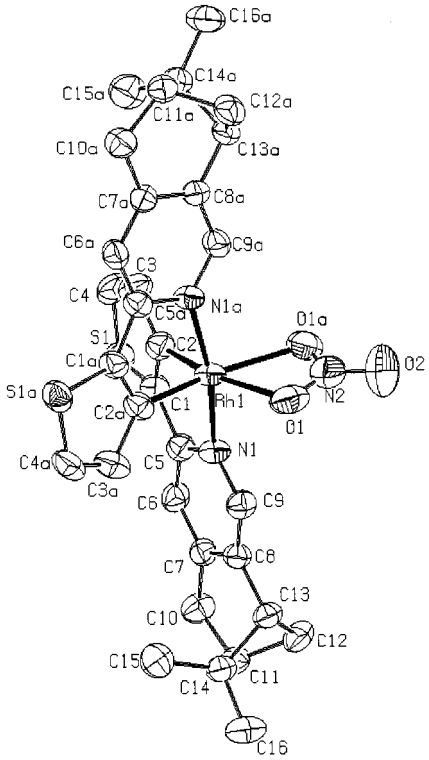


Figure 3a. Numbered ORTEP[18] plot with thermal ellipsoids represented at 50% probability level of **2**

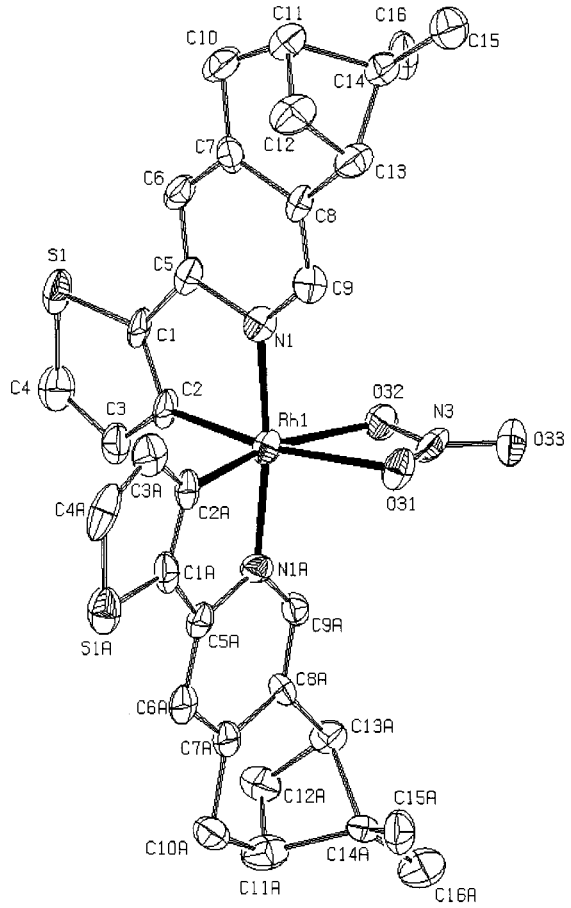


Figure 4. Numbered ORTEP[18] plot with thermal ellipsoids represented at 30% probability level of the molecular structure of $\Lambda[Rh(L_2)_2(NO_3)]$ (**3**); the hydrogen atoms have been omitted for clarity

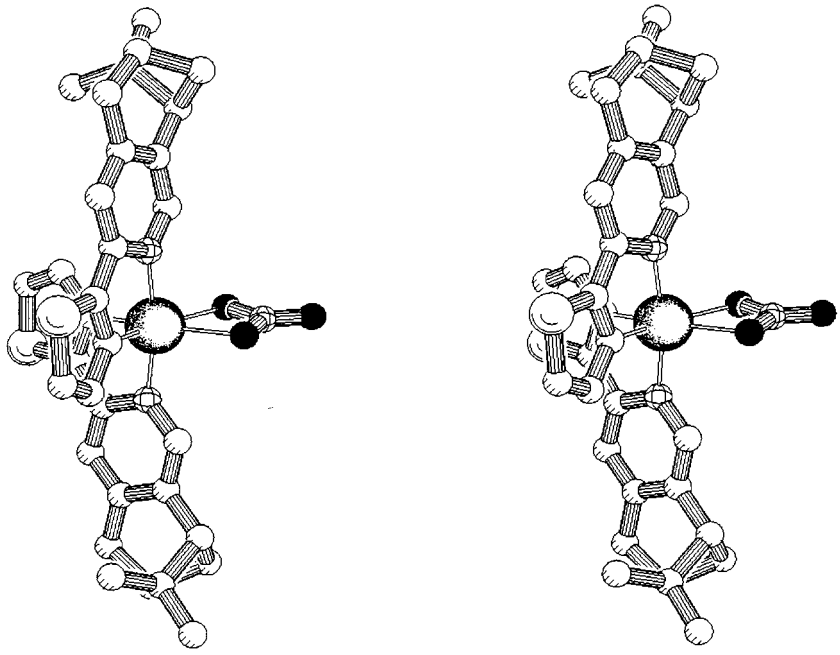


Figure 3b. Stereoview of the molecular structure of $\Delta[Rh(L_2)_2(NO_3)]$ (**2**); the hydrogen atoms have been omitted for clarity

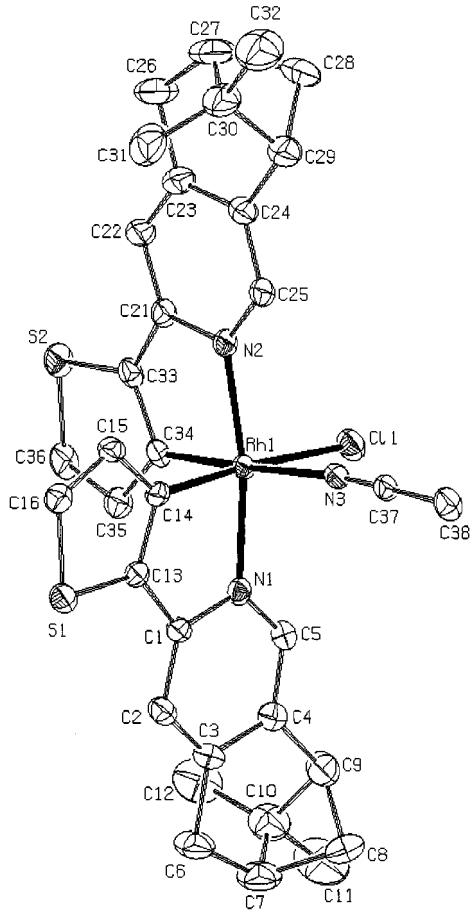


Figure 5. Numbered ORTEP[18] plot with thermal ellipsoids represented at 30% probability level of the molecular structure of $\Lambda[Rh(L_2')_2Cl(CH_3CN)]$ (**6**); the hydrogen atoms have been omitted for clarity

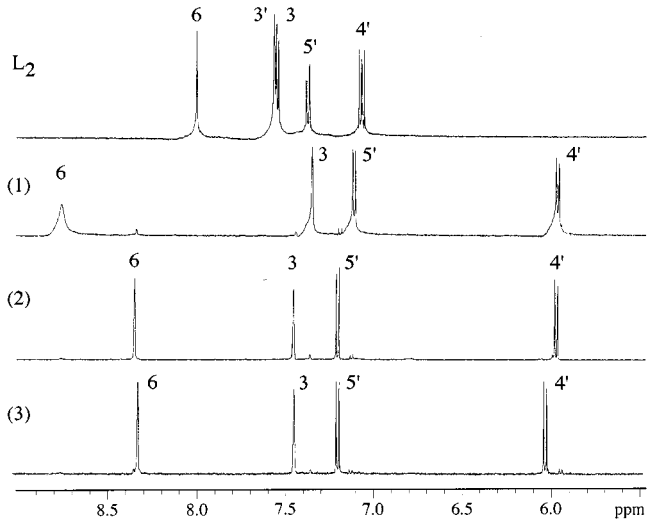


Figure 6. ^{1}H-NMR aromatic region spectra of $\Delta\Delta[Rh(L_2)_2(\mu\text{-}Cl)]_2$ (**1**), $\Delta[Rh(L_2)_2(NO_3)]$ (**2**), $\Lambda[Rh(L_2)_2(NO_3)]$ (**3**), (8*R*,10*R*)-2-(2′-thienyl)-4,5-pinenopyridine ($\mathbf{L_2}$)

(**2**), $\Lambda[Rh(L_2)_2(NO_3)]$ (**3**) complexes and the free ligand $\mathbf{L_2}$: (8*R*,10*R*)-2-(2′-thienyl)-4,5-pinenopyridine. Upon complexation with Rh^{III}, the signal corresponding to the proton 3′-H in the free (8*R*,10*R*)-2-(2′-thienyl)-4,5-pinenopyridine disappears. In agreement with the data from X-ray structure determination, the ^{1}H- and ^{13}C-NMR spectra indicate that the dinuclear complex $\Delta\Delta[Rh(L_2)_2(\mu\text{-}Cl)]_2$ (**1**) has D_2 symmetry and therefore all four ligands are equivalent. The ^{13}C-NMR spectrum of the $\Delta\Delta$ isomer shows 16 resonances; the signal at lowest field attributed to C-3′ is split due to the ^{13}C-^{103}Rh coupling (J_{Rh-C} = 36 Hz). The aromatic region of the ^{1}H-NMR spectra of the complexes is simple: Only four signals are observed due to the high symmetry. Relative to the free-ligand spectrum (see Figure 6) the proton chemical shifts of 4′-H, 5′-H and 3-H in all complexes appear upfield due to the positive ring current of the neighboring ligand coordinated at the same metal center. While the 5′-H and 3-H signals are only slightly shifted upfield, an important shift of ca. 1 ppm occurs for the signal of the 4′-H proton, which is pointing inside the pyridine ring of the neighboring ligand. There are three possible effects on the shift of the proton 6-H: (i) a deshielding by coordination to rhodium, (ii) a close proximity to the bridging Cl ligand, (iii) a negative ring current of the ligand situated at the other metal center. The corresponding signals of the two mononuclear complexes show a small downfield shift, and those of the $\Delta\Delta$ complex a much larger one. It seems therefore that in the mononuclear complexes Δ and Λ the shift of 6-H is mainly determined by the coordination to the rhodium center, whereas in the $\Delta\Delta$ isomer an additional influence in the same direction is observed, which is due to (iii). The limited solubility of the $\Delta[Rh(L_2)_2(NO_3)]$ (**2**) and $\Lambda[Rh(L_2)_2(NO_3)]$ (**3**) complexes in CD_3CN renders ^{13}C-NMR measurements impossible.

Electronic Spectra

The UV/Vis spectra of the dinuclear and mononuclear complexes show essentially two absorption bands at 282 and at 375 nm. These bands are likely to be due to charge transfer transitions.[5,9,10] Figure 7 shows the CD spectra of the Δ and Λ diastereomers of the mononuclear species. The near mirror symmetry of these spectra shows that the whole CD activity in this spectral range is mainly determined by the chiral configuration of the metal center.

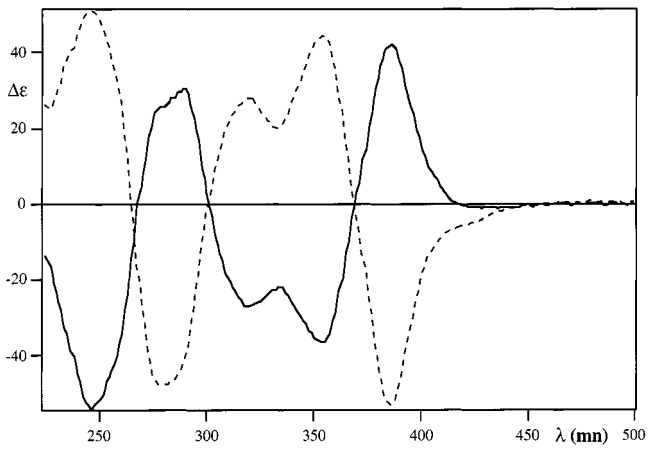


Figure 7. CD spectra of −−− $\Delta[Rh(L_2)_2(NO_3)]$ (**2**) and ---- $\Lambda[Rh(L_2)_2(NO_3)]$ (**3**) (c = 1.45 10^{-5} M in CH_3CN)

Conclusions and Outlook

The synthesis of the rhodium complexes with chiral thienylpyridine ligands yields two homochiral dimers (ΔΔ and ΛΛ), which are diastereomers, in a ratio of 9:1. The heterochiral dinuclear complex (ΔΛ) does not occur in measurable amounts. Through interactions between chiral ligands located at two adjacent metal centers, the absolute configurations of the latter are determined with a high selectivity. Cleavage of the dichloro bridge with NO_3^- or CH_3CN yields mononuclear species with predetermined chirality, since the configuration is retained during the cleavage reaction. As preliminary results indicate, stereochemically especially interesting reactions of this type occur with chiral diimines and diamines. The use of easily accessible chiral ligands thus gives the possibility of preparing stereoselectively Rh^{III} chelate complexes of various compositions. Such complexes may have interesting applications in the fields of bioinorganics[11] and photochemistry,[12][13] as well as in catalysis.

Experimental Section

General: All chemicals and reagent-grade products were obtained from Fluka, Aldrich or Merck and used, unless noted, without further purification. (+)-α-Pinene (> 97%; $[\alpha]_D^{20} = +45$), and (1*R*)-(−)-myrtenal (> 97%, $[\alpha]_D^{20} = -14.6$) were obtained from Fluka. The ligand $\mathbf{L_2}$ [(8*R*,10*R*)-2-(2′-thienyl)-4,5-pinenopyridine] and (2-thienylacetyl)pyridinium bromide were prepared according to literature procedures.[8] The enantiomer of $\mathbf{L_2}$ [(8*S*,10*S*)-2-(2′-thienyl)-4,5-pinenopyridine (abbreviated $\mathbf{L_2}'$)] was obtained analogously, starting from (+)-α-pinene, which was transformed into (+)-(*S*)-myrtenal by known procedures.[14] The product of crystallization of the artificial racemate {ΔΔ[Rh(L_2)$_2$Cl]$_2$ **(1)** ΛΛ[Rh(L_2')$_2$Cl]$_2$ **(5)**} was, in fact, {Δ[Rh(L_2)$_2$Cl(CH_3CN)] Λ[Rh(L_2')$_2$Cl(CH_3CN)]} (**6**) (see Results and Discussion), and was only characterized by X-ray structure analysis (see Figure 5).

Measurements: UV/Vis spectra were recorded with a Perkin-Elmer Lambda 5 and Perkin-Elmer Lambda 40 spectrometers; λ_{max} in nm, ε in <emphasis type="scaps">m^{-1} cm^{-1}. − NMR spectra were measured with a Varian Gemini-300 spectrometer operating at 300 MHz (for ^{1}H) and 75.46 MHz (for ^{13}C); δ in ppm with solvent as internal standard relative to $SiMe_4$, *J* in Hz. CD spectra: Jobin-Yvon and JASCO J-715 specropolarimeters; λ_{max} (Δε) in nm. − IR-spectral data were obtained with Perkin−Elmer 683 and Perkin−Elmer 16 PC FT-IR spectrometers; samples (1%) were compressed KBr pellets. − MS: VG-Instruments 7070E mass spectrometer equipped with an FAB inlet system. The elemental analyses were performed by CIBA Specialty Chemicals, Marly, Switzerland.

X-ray Structure Determination of ΔΔ[Rh(L_2)$_2$(μ-Cl)]$_2$ (1), Δ[Rh(L_2)$_2$(NO_3)] (2), Λ[Rh(L_2)$_2$(NO_3)] (3) and {Δ[Rh(L_2)$_2$Cl(CH_3CN)] Λ[Rh(L_2')$_2$Cl(CH_3 CN)]} (6). − Data Collection: Suitable orange block-like crystals of compounds **1** and **2**, and red block-like crystals of compound **3** were grown by slow diffusion of diethyl ether into CH_2Cl_2 solutions of the respective compounds. Suitable crystals of **6** were grown from a solution of CH_2Cl_2/CH_3CN as yellow plates. − Intensity data for compounds **1**, **2** and **6** were collected at 223 K with a Stoe Image Plate Diffraction System using graphite-monochromated Mo-K_α radiation (λ = 0.71073 Å) and equipped with a φ circle. The image plate distance was 70 mm, φ scans of 0−200°, step Δφ = 1°, 2θ range 3.27−52.1°, resolution limits $d_{min} - d_{max}$ = 12.45−0.81 Å. − Intensity data for compound **3** was collected at room temperature with a Stoe AED2 4-circle diffractometer using graphite-monochromated Mo-K_α radiation (λ = 0.71073 Å) with ω.2θ scans in the 2θ range 5−51°. Further crystallographic data are summarized in Tables 1 and 2.

Structure Solution and Refinement: The structure of compounds **1**, **2**, **3** and **6** were solved by direct methods with the program SHELXS-97.[15] The refinements and all further calculations were carried out with the program SHELXL-97.[16] For all four compounds the H atoms were included in calculated positions and treated as riding atoms with SHELXL-97[16] default parameters. The non-H atoms in all four compounds were refined anisotropically, using weighted full-matrix least squares on F^2. No corrections for extinction or absorption were applied. For all four compounds the coordinates correspond to the absolute structure of the molecules in the crystals. This is confirmed by reference to the absolute structure of the ligand used and the absolute structure factor parameters,[17] 0.13(9) for **1**, −0.16(7) for **2** and 0.03(5) for **3**. Compound **1** possesses crystallographic twofold symmetry and is associated with one whole molecule of diethyl ether, which is disordered over two sites related by a 2-fold axis (occupancy 0.5). Atoms C(9) and C(10) of one of the pinene ligands undergo considerable thermal motion. An attempt to split these atoms was unsuccessful leading to poor bond lengths and bond angles. Complex **2** crystallized with one molecule of dichloromethane per molecule of **2**. For compound **6** there are two independent molecules and two complete molecules of CH_3CN, one of which is disordered over two sites with occupancies of 0.5 each. The molecular structures and crystallographic numbering schemes are illustrated in the PLATON[18] drawings, Figures 1a, 3a, 4 and 5. − The CIF files, including complete tables of bond lengths, bond angles and torsion angles, have been deposited with the Cambridge Crystallographic Data Centre, 12 Union Road, Cambridge CB2 1EZ (UK). Deposition numbers are CCDC-114591 (**1**), -114592 (**2**), -114593 (**3**), -114594 (**6**).

Synthesis and Characterization

[Rh(L_2)$_2$(μ-Cl)]$_2$: With a modified literature procedure,[3] a mixture of $RhCl_3 \cdot 3H_2O$ (264 mg, 1 mmol) and th4,5ppy (766 mg, 3 mmol) was suspended in 20 mL of 2-methoxyethanol and dispersed during 10 min in an ultrasonic bath. The resulting solution, refluxed for 4 h, was concentrated and after addition of Et_2O, the brownish-orange precipitate was filtered off. Because the reaction was not complete, the unchanged ligand was recovered. The purification and separation of different diastereoisomers was done by preparative thin layer plate silica gel chromatography with CH_3CN/BuOH/H_2O/KNO_3 (4:1:1:0.1) as eluent. ΔΔ[Rh(L_2)$_2$(μ-Cl)]$_2$/Δ[Rh(L_2)$_2$(NO_3)]/Λ[Rh(L_2)$_2$(NO_3)] = 61.27:28.17:10.56. If KNO_3 is replaced by NaCl, a ratio ΔΔ[Rh(L_2)$_2$(μ-Cl)]$_2$/ΛΛ[Rh(L_2)$_2$(μ-Cl)]$_2$ of 9:1 is observed.

ΔΔ[Rh(L_2)$_2$(μ-Cl)]$_2$ (1): Yield (separation): 87 mg (27%). − ^{1}H NMR (CD_3CN, 300 MHz): δ = 8.76 (s, 4 H, 6-H), 7.37 (s, 4 H, 3-H), 7.13 (d, 4 H, ^3J = 4.8 Hz, 5′-H), 5.98 (d, 4 H, ^3J = 4.73 Hz, 4′-H), 3.14 (d, 8 H, ^3J = 2.48 Hz, 7-H), 2.97 (d×d, 4 H, ^4J = 5.5 Hz, ^3J = 5.5 Hz, 10-H), 2.78 (d×d×d, 4 H, ^2J = 9.7 Hz, ^3J = 5.8 Hz, ^3J = 5.9 Hz, 9-H^{exo}), 2.35 (t×d×d, 4 H, ^4J = 5.6 Hz, ^3J = 5.7 Hz, ^3J = 2.8 Hz, 8-H), 1.44 (s, 12 H, 13-H), 1.31 (d, 4 H, ^2J = 9.7 Hz, 9-H^{endo}), 0.78 (s, 12 H, 12-H). − ^{13}C NMR (CD_3CN, 75 MHz): δ = 165.59, 165.12 (quat), 160.3 (quat), 148.7 (tert), 147.4 (tert), 140.4 (quat), 135.5 (quat), 131.4 (tert), 127 (quat), 126.7 (tert), 45.4 (tert), 40.9 (tert), 40.1 (quat), 33.6 (sec), 32.3 (sec),

Table 1. Experimental crystallographic data for ΔΔ[Rh(L$_2$)$_2$(μ-Cl)]$_2$ (**1**), Δ[Rh(L$_2$)$_2$(NO$_3$)] (**2**) and Λ[Rh(L$_2$)$_2$(NO$_3$)] (**3**)

	1	**2**	**3**
Empirical formula	$C_{64}H_{64}Cl_2N_4Rh_2S_4\cdot(CH_3CH_2OCH_2CH_3)$	$C_{32}H_{32}N_3O_3RhS_2$	$C_{32}H_{32}N_3O_3RhS_2\cdot(CH_2Cl_2)$
Molecular mass	1368.27	673.64	758.56
Temperature [K]	223(2)	293(2)	223(2)
Crystal system	monoclinic	tetragonal	orthorhombic
Space group	*I*2 (no. 5)	$P4_32_12$ (no. 96)	$P2_12_12_1$ (no. 19)
Crystal color	orange	red	orange
Unit cell dimensions: *a* [Å]	14.2978(13)	10.4991(10)	10.6163(7)
b [Å]	16.3132(12)	10.4991(10)	14.9196(12)
c [Å]	14.3462(13)	27.740(3)	20.932(2)
β [°]	95.025(11)°	90°	90°
α°= γ [°]	90°	90°	90°
V [Å^3]	3333.3(5)	3057.8(5)	3315.4(5)
Z	2	4	4
Calculated density [g/cm^{-3}]	1.363	1.463	1.520
Absorption coeff. [mm^{-1}]	0.744	0.732	0.841
F [000]	1412	1384	1552
Crystal size [mm]	0.50 × 0.40 × 0.30	0.49 × 0.42 × 0.38	0.50 × 0.10 × 0.10
Independent reflns.	5172	2848	5173
Observed refls. [$I < 2\sigma(I)$]	4357	2350	2627
Final *R* indices [$I > 2\sigma(I)$]	*R*1 = 0.0838 *wR*2 = 0.2189	*R*1 = 0.0346 *wR*2 = 0.0720	*R*1 = 0.0567 *wR*2 = 0.1218
R indices (all data)	*R*1 = 0.0942 *wR*2 = 0.2260	*R1* = 0.0484 *wR*2 = 0.0898	*R*1 = 0.1132 *wR*2 = 0.1372
Goodness-of-fit (obsd. data)	1.045	1.091	0.801
Residual density [e/Å^3]	1.126/−0.794	0.362/−0.312	0.355/−0.576

[a] $R1 = \Sigma(F_o - F_c)/\Sigma(F_o)$; $wR2 = [\Sigma(w(F_o^2 - F_c^2)^2\}/\Sigma\{w(F_o^4)\}]^{1/2}$.

Table 2. Experimental crystallographic data for the artificial racemate {Δ[Rh(L$_2$)$_2$Cl(CH$_3$CN)] Λ[Rh(L$_2$′)$_2$Cl(CH$_3$CN)]} (**6**)

Empirical formula	**6** $C_{36}H_{38}ClN_4RhS_2\cdot C_{36}H_{35}ClN_3RhS_2CH_3CN$
Molecular mass	729.18
Temperature [K]	223(2)
Crystal system	triclinic
Space group	*P*1bar (no. 2)
Crystal color	yellow
Unit cell dimensions: *a* [Å]	15.4610(13)
b [Å]	15.6988(13)
c [Å]	16.2503(15)
α [°]	99.914(10)
β [°]	106.810(10)
γ [°]	92.586(10)
V [Å^3]	3700.4(6)
Z	4
Calculated density [g/cm^{-3}]	1.306
Absorption coeff. [mm^{-1}]	0.675
F(000)	1500
Crystal size [mm]	0.3 × 0.18 × 0.05
Independent reflns.	13296
Observed refls. [$I < 2\sigma(I)$]	7482
Final *R* indices [$I > 2\sigma(I)$]	*R*1 = 0.0432, *wR*2 = 0.0991
R indices (all data)	*R*1 = 0.0890, *wR*2 = 0.1089
Goodness-of-fit (obsd. data)	0.833
Residual density [e/Å^3]	0.920/−0.600

[a] $R1 = \Sigma(F_o - F_c)/\Sigma(F_o)$; $wR2 = [\Sigma(w(F_o^2 - F_c^2)^2\}/\Sigma\{w(F_o^4)\}]^{1/2}$.

26.1 (prim), 21.68 (prim). − MS (FAB); *m*/*z* (%): 1259 (13) [M$^+$ − Cl$^-$], 646 (100) [Rh(th4,5ppy)$_2$Cl − H$^+$], 612 (100) [Rh(th4,5ppy)$_2$], 356 (50) [Rh(th4,5ppy) − H$^+$], 256 (32) [Hth4,5ppy]. − UV/Vis (CH$_3$CN): λ (ε) = 376 (18582), 282 (56137). − IR (KBr): ṽ = 3423 (w), 2926 (m), 2362 (w), 2342 (w), 1619 (m), 1490 (s), 1428 (m), 1384 (w), 1260 (w),1239 (w), 1134 (w), 874 (m), 757 (w), 703 (m) cm^{-1}. − CD (CH$_3$CN): λ (Δε) = 389 (49.9), 355 (−43.5), 323 (−40.8), 290 (44.5), 247 (−59.8). − $C_{64}H_{64}Cl_2N_4Rh_2S_4$ (1294.39): calcd. C 59.38, H 4.98, N 4.33; found C 59.08, H 5.34, N 4.16.

Δ[Rh(L$_2$)$_2$(NO$_3$)] (2): Yield (separation): 40 mg (12%). − ^{1}H NMR (CD$_3$CN, 300 MHz): δ = 8.35 (s, 2 H, 6-H), 7.46 (s, 2 H, 3-H), 7.2 (d, 2 H, ^3J = 4.9 Hz, 5′-H), 5.97 (d, 2H, ^3J = 4. 9 Hz, 4′-H), 3.17 (d, 4 H, ^3J = 2.75 Hz, 7-H), 3.02 (d×d, 2 H, ^4J = 5.5 Hz, ^3J = 5.5 Hz, 10-H), 2.8 (d×d×d, 2 H, ^2J = 9.8 Hz, ^3J = 5.74 Hz, ^3J = 5.9 Hz, 9-H^{exo}), 2.37 (txdxd, 2H, ^4J = 5.65 Hz, ^3J = 5.8 Hz, ^3J = 2.9 Hz, 8-H); 1.46 (s, 6H, 13-H); 1.29 (d, 2H, ^2J = 9.8 Hz, H−C(9 endo)); 0.78 (s, 6 H, 12-H). − MS (FAB); *m*/*z* (%): 612 (100) [Rh(th4,5ppy)$_2$], 356 (43) [Rh(th4,5ppy)-H$^+$], 256 (25) [Hth4,5ppy]. − UV/Vis (CH$_3$CN): λ (ε) = 375 (7457), 282 (21842). − IR (KBr): ṽ = 3424 (m), 2933 (m), 2362 (m), 2342 (m), 1619 (m), 1491 (s), 1433 (w), 1384 (m), 1249 (w), 1131 (w), 873 (w), 729 (w) cm^{-1}. − CD (CH$_3$CN): λ (Δε) = 386 (42.4), 353 (−36.5), 320 (−26.9), 289 (30.9), 246 (−54). − $C_{32}H_{32}N_3O_3RhS_2\cdot Et_2O\cdot CH_2Cl_2$ (832.80): calcd. C 53.36, H 5.33, N 5.04; found C 53.38, H 4.62, N 5.40.

Λ[Rh(L$_2$)$_2$(NO$_3$)] (3): Yield (separation): 15 mg (4.58%). − ^{1}H NMR (CD$_3$CN, 300 MHz): δ = 8.33 (s, 2 H, 6-H), 7.46 (s, 2 H, 3-H), 7.2 (d, 2 H, ^3J = 4.9 Hz, 5′-H), 6.06 (d, 2 H, ^3J = 4.9 Hz, 4′-H), 3.16 (d, 4 H, ^3J = 2.75 Hz, 7-H), 3.02 (d×d, 2 H, ^4J = 5.5 Hz, ^3J = 5.8 Hz, 10-H), 2.8 (d×d×d, 2 H, ^2J = 9.9 Hz, ^3J = 5.9 Hz, ^3J = 5.7 Hz, 9-H^{exo}), 2.37 (t×d×d, 2 H, ^4J = 5.7 Hz, ^3J = 5.9 Hz, ^3J = 3.0 Hz, 8-H), 1.46 (s, 6 H, 13-H), 1.29 (d, 2 H, ^2J = 9.8 Hz,

9-H^{endo}), 0.74 (s, 6 H, 12-H). − MS (FAB); *m/z* (%): 612 (100) [Rh(th4,5ppy)$_2$], 356 (45) [Rh(th4,5ppy) − H$^+$], 256 (25) [Hth4,5ppy]. − UV/Vis (CH_3CN): λ (ε) = 375 (8853), 281 (26307). − IR (KBr): $\tilde{\nu}$ = 3440 (m), 2924 (w), 1619 (m), 1490 (m), 1431 (w), 1384 (s), 1243 (w), 1099 (m), 874 (w), 709 (w) cm^{-1}. − CD (CH_3CN): λ (Δε) = 386 (−55), 355 (45), 319 (28.5), 281 (−48.6), 246 (51.4). − $C_{32}H_{32}ClN_3O_3RhS_2$ (709.20): calcd. C 54.19, H 4.55, N 5.92; found: C 53.65, H 4.61, N 5.75.

(8*S*,10*S*)-2-(2′-Thienyl)-4,5-pinenopyridine (L_2') (4): A method analogous to that already described for $\mathbf{L}_2$[8] was applied. A mixture of (2-thienylacetyl)pyridinium bromide (1.65 g, 6 mmol) in 10 mL of formamide, ammonium acetate (0.897 g, 11.6 mmol) (added under vigorous stirring) and (0.87 g, 6 mmol) of (+)-myrtenal was refluxed at 60°C for 16 h. The reaction was quenched by addition of water (10 mL) and the brownish solution was extracted with hexane (8 × 50 mL). After the mixture was dried with $MgSO_4$, the solvent was removed and an orange oil that solidified at 4°C was obtained. Yield: 75% (1.11 g). − ^{1}H NMR ($CDCl_3$, 300 MHz): δ = 8.07 (s, 1 H, 6-H), 7.50 (d×d, 1 H, ^3J = 3.7 Hz, ^4J = 1.2 Hz, 3′-H), 7.44 (s, 1 H, 3-H), 7.31 (d×d, 1 H, ^3J = 5.0 Hz, ^4J = 1.2 Hz, 5′-H), 7.07 (d×d, 1 H, ^3J = 5.0 Hz, ^3J = 3.7 Hz, 4′-H), 2.97 (d, 2 H, ^3J = 2.7 Hz, 7-H), 2.80 (d×d, 1 H, ^4J = 5.6 Hz, ^3J = 5.6 Hz, 10-H), 2.68 (d×d×d, 1 H, ^2J = 9.6 Hz, ^3J = 5.6 Hz, ^3J = 5.6 Hz, 9-H^{exo}), 2.28 (t×d×d, 1 H, ^4J = 5.6 Hz, ^3J = 5.6 Hz, ^3J = 2.7 Hz, 8-H), 1.38 (s, 3 H, 13-H), 1.20 (d, 2 H, ^2J = 9.6 Hz, 9-H^{endo}), 0.63 (s, 3 H, 12-H). − ^{13}C NMR ($CDCl_3$, 75 MHz): δ = 150.8 (quat), 145.7 (quat), 145.5 (quat), 145.2 (tert), 141.2 (quat), 127.8 (tert), 126.6 (tert), 123.5 (tert), 118.3 (tert), 44.4 (tert), 40.0 (tert), 39.3 (quat), 32.8 (sec), 31.9 (sec), 26.0 (prim), 21.4 (prim). − MS (EI); *m/z* (%): 255 (20) [M$^+$], 240 (10) [M$^+$ − CH_3], 212 (100) [M$^+$ − C_3H_7]. − UV/Vis (CH_2Cl_2): λ (ε) = 307 (15545), 292 (sh), 229 (6281). − IR (KBr): $\tilde{\nu}$ = 2920 (s), 1596 (w), 1536 (w), 1474 (m), 1384 (m), 1262 (w), 1220 (w), 1128 (w), 1054 (w), 942 (w), 828 (w), 692 (s) cm^{-1}. − $C_{16}H_{17}NS$ (255.38): calcd. C 75.25, H 6.71, N 5.48, S 12.55; found C 74.98, H 6.72, N 5.63, S 12.63.

ΛΛ[Rh(L_2')$_2$(μ-Cl)]$_2$ (5): This compound was synthesized as described for [Rh(L_2)$_2$m-Cl)]$_2$. Preparative thin layer plate silica gel chromatography with CH_3CN/BuOH/H_2O/KCl/NaCl (4:1:1:0.05:0.05) as eluent was used for the purification and separation of the different diastereoisomers. A ratio of ΛΛ[Rh(L_2')$_2$(μ-Cl)]$_2$/ΔΔ[Rh(L_2')$_2$(μ-Cl)]$_2$ = 9:1 was obtained. All data are identical with those of ΔΔ[Rh(L_2)$_2$(μ-Cl)]$_2$ except for the mirror-image CD spectra.

{Δ[Rh(L_2)$_2$Cl(CH_3CN)] Λ[Rh(L_2')$_2$Cl(CH_3CN)]} (6): This compound was obtained by "crystallization" of ΔΔ[Rh(L_2)$_2$(μ-Cl)]$_2$ and ΛΛ[Rh(L_2')$_2$(μ-Cl)]$_2$ from a CH_2Cl_2/CH_3CN mixture.

Acknowledgments

The authors wish to thank Raf Bruyndonckx for graphical representation of the ΛΛ and ΔΔ diastereomers and the Swiss National Science Foundation for financial support.

[1] A. P. Smirnoff, *Helv. Chim. Acta* **1920**, *3*, 177−195.
[2] U. Knof, A. von Zelewsky, *Angew. Chem. Int. Ed.* **1999**, *38*, 302−322.
[3] U. Maeder, A. von Zelewsky, H. Stoeckli-Evans, *Helv. Chim. Acta* **1992**, *75*, 1320−1332.
[4] U. Maeder, T. Jenny, A. von Zelewsky, *Helv. Chim. Acta* **1986**, *69*, 1085−1087.
[5] S. Sprouse, K. A. King, P. J. Spellane, R. J. Watts, *J. Am. Chem. Soc.* **1984**, *106*, 6647−6653.
[6] P. J. Steel, *J. Organomet. Chem.* **1991**, *408*, 395−402.
[7] P. Hayoz, A. von Zelewsky, *Tetrahedron Lett.* **1992**, *33*, 5165−5168.
[8] M. Gianini, A. Forster, P. Haag, A. von Zelewsky, H. Stoeckli-Evans, *Inorg. Chem.* **1996**, *35*, 4889−4895.
[9] D. Sandrini, M. Maestri, V. Balzani, U. Maeder, A. von Zelewsky, *Inorg. Chem.* **1988**, *27*, 2640−2643.
[10] M. Maestri, D. Sandrini, V. Balzani, U. Maeder, A. von Zelewsky, *Inorg. Chem.* **1987**, *26*, 1323−1327.
[11] N. Y. Sardesai, K. Zimmermann, J. K. Barton, *J. Am. Chem. Soc.* **1994**, *116*, 7502−7508.
[12] M. R. Arkin, E. D. A. Stemp, C. Turro, N. J. Turro, J. K. Barton, *J. Am. Chem. Soc.* **1996**, *118*, 2267−2274.
[13] M. R. Arkin, E. D. A. Stemp, R. E. Holmlin, J. K. Barton, A. Hoerman, E. J. C. Olson, P. F. Barbara, *Science* **1996**, *273*, 475−480.
[14] R. K. de Richter, M. Bonato, M. Follet, J-M. Kamenka, *J. Org. Chem.* **1990**, *55*, 2855−2860
[15] G. M. Sheldrick, "SHELXS-97, Program for Crystal Structure Determination", *Acta Crystallogr.* **1990**, *A46*, 467.
[16] G. M. Sheldrick, *SHELXL-97, Program for Crystal Structure Refinement*, Universität Göttingen, Göttingen, Germany, **1997**.
[17] H. D. Flack, *Acta Crystallogr.* **1983**, *A39*, 876.
[18] A. L. Spek, "PLATON/PLUTON", *Acta Crystallogr.* **1990**, *A46*, C34.

Received February 18, 1999
[I99055]

A Density Functional Study of the Dimerization of Phosphaalkynes in the Presence of Transition Metal Fragments

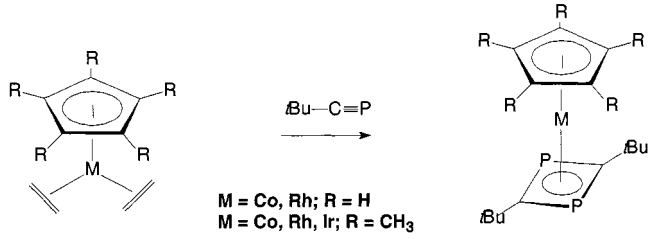
Steven Creve,[a] Minh Tho Nguyen,*[a] and Luc G. Vanquickenborne[a]

Keywords: Phosphaalkynes / Dimerization mechanism / Diphosphacyclobutenes / Density functional theory / Ab initio calculations

The dimerization of phosphaalkynes (R–C≡P, R = H, Me, *t*Bu) without and with the presence of transition metal fragments, including CpCo (Cp = cyclopentadienyl) and COT–Ti (COT = cyclooctatetraene), has been probed using density functional theory calculations (B3LYP with different basis sets). MP2 and CCSD(T) calculations were also performed for the $[H_2C_2P_2]$ systems. In an attempt to address the exciting controversy and uncertainty about phosphaalkyne dimerization, a number of dimer formation mechanisms proposed in the literature have been examined. Some new and plausible intermediates have also been identified.

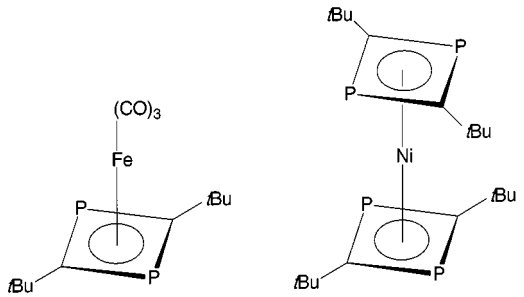
1. Introduction

In 1986, two independent groups[1][2] first reported the cyclodimerization of a phosphaalkyne (R−C≡P) in the coordination sphere of cobalt, rhodium, and iridium centers, yielding a 1,3-diphosphacyclobutadiene ring (referred to hereafter as 1,3-DPCB), as shown in Scheme 1.



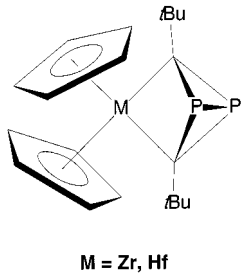
Scheme 1. Formation of 1,3-DPCB in metal complexes

Soon afterwards, other similar complexes containing iron were discovered,[3][4] as well as a sandwich complex of nickel containing two 1,3-DPCB rings[5] (Scheme 2).



Scheme 2. Observation of 1,3-DPCB in Fe and Ni complexes

With Zr or Hf as metallic center, however, a 1,3-diphosphabicyclo[1.1.0]butanediyl ligand was shown to be formed[6][7] (Scheme 3).



Scheme 3. Observation of bicyclic dimers in Zr, Hf complexes

Interestingly, it has been proven extremely difficult, if not impossible, to displace the η^4-ligated $P_2C_2tBu_2$ rings from any of these cornplexes, which is in clear contrast to the behavior of analogous cyclobutadiene rings.

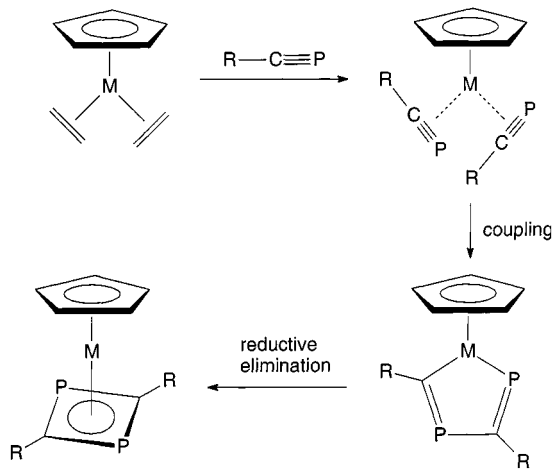
As far as the formation of the 1,3-DPCB complexes is concerned (Scheme 4), it has been assumed that first a bis(π-phosphaalkyne) complex is formed, followed by a coupling process to give a 1-metalla-2,4-diphosphacyclopentadienyl complex. The latter can than undergo a reductive elimination yielding the product 1,3-DPCB complex. This mechanism was postulated by analogy to the reaction sequence taking place when cyclobutadiene complexes are formed out of alkynes.[8][9]

Further evidence for this reaction mechanism was provided by Binger et al. who found the existence of a 1,4-diphospha-2-rhodacyclopentadiene species as intermediate in the formation of the 1,3-DPCB complex[10] (Scheme 5). These authors were able to characterize the 1,4-diphospha-2-rhodacyclopentadiene species by X-ray diffraction studies.

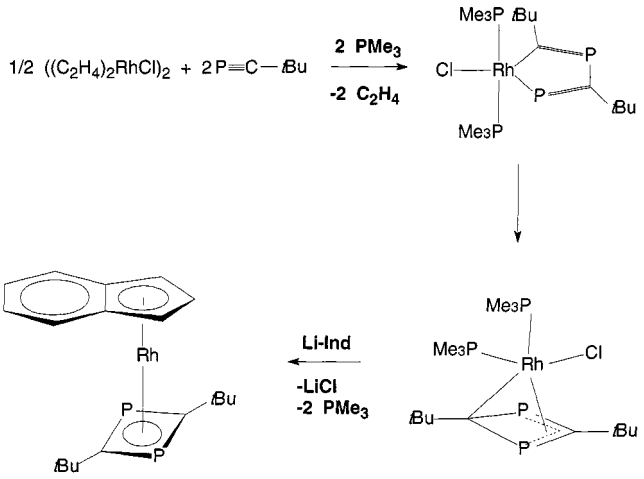
However, no clear-cut evidence has been found yet proving or disproving that the mechanisms of formation of other complexes (such as shown in Schemes 1 and 2) also proceed via 1-metalla-2,4-diphosphacyclopentadienyl inter-

[a] Department of Chemistry, University of Leuven, Celestijnenlaan 200F, B-3001 Leuven, Belgium

 © WILEY-VCH Verlag GmbH, D-69451 Weinheim, 1999 1434−1948/99/0808−1281 $ 17.50+.50/0



Scheme 4. Proposed formation mechanism of 1,3-DPCB involving metallacyclobutadiene intermediate

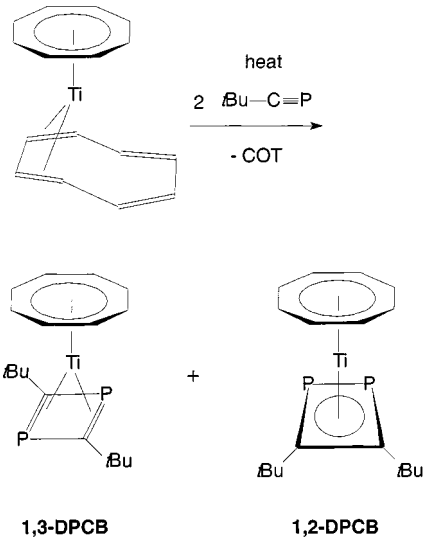


Scheme 5. Proposed formation mechanism of 1,3-DPCB in Rh complexes

mediates. Another interesting point is that, when using Co or Rh as metallic center, a 1,2-diphosphacyclobutadiene complex has never been detected (referred to hereafter as 1,2-DPCB). In fact, the first example of a 1,2-DPCB complex has only recently been characterized by making use of titanium[11][12] (Scheme 6).

In the case of Ti, both the 1,3-DPCB and 1,2-DPCB complexes have been found. While the latter has a large delocalization of electrons within the ring, the former shows two short and two long P−C bonds. Again, this is in contrast to the 1,3-DPCB complexes of Co and Rh, where the carbon-phosphorus ring is also largely delocalized. Without the presence of metal compounds, a cyclotetramerization of phosphaalkynes has been found upon heating, which leads to a tetraphosphacubane.[13] Formation of the latter has been postulated to involve a 1,3-DPCB intermediate.

In our previous work,[14] different equilibrium and transition structures on the $[C_2H_2P_2]$ potential energy surface have been calculated. It turned out that 1,2-DPCB tends to be more stable than the 1,3-DPCB by about 30−40 kJ/mol.



Scheme 6. Formation of both 1,3- and 1,2-DPCB when Ti complexes were used

Moreover, the activation energy for 1,2-DPCB formation in a head-to-head approach is also smaller.

All facts considered, a number of intriguing questions remain unanswered:

- Why is, in the case of Co and Rh, only the 1,3-DPCB complex found, and not the 1,2-DPCB, although the latter is more stable in free form, as found in previous work?[14]
- Concerning the free DPCB species, what is the influence of bulkier substituents on the carbon atoms, i.e. how large are steric effects in these systems? As a matter of fact, the available experiments have usually been carried out with phosphaalkynes R−C≡P where R = *t*Bu or other sterically hindered substituents.
- With Ti as metallic center, both 1,2-DPCB and 1,3-DPCB complexes are found. Remarkably, however, the 1,3-DPCB complex shows two different P−C bond lengths, in contrast to the Co and Rh cases, where a more delocalized DPCB ring is obtained.
- Finally, is the mechanism via metallacyclobutadiene intermediates indeed a valid reaction scheme?

In an attempt to obtain more insight into this interesting area of low-coordinated phosphorus chemistry, a computational study has been carried out on free DPCB species on the one hand ($R_2C_2P_2$, with R = H, CH_3, and *t*Bu), and some representative metal complexes on the other hand [Cp−Co−($R_2C_2P_2$), with R = H, CH_3, and Cp = cyclopentadienyl; COT−Ti-($H_2C_2P_2$) with COT = cyclooctatetraene].

2. Computational Details

The species considered include the important $[R_2C_2P_2]$ isomers with R = H, CH_3, and *t*Bu, [Cp−Co−($R_2C_2P_2$)] isomers (R = H, CH_3; Cp = cyclopentadienyl), and a number of COT−Ti-$[H_2C_2P_2]$ isomers (COT = eyclooctatetra-

ene). For the sake of comparison, we also calculated some isomers of Cp−Co−[H_4C_4].

All geometries have been optimized using the B3LYP density functional[15][16] with the 6−31G(d,p) basis set. For the metal elements, a (14s,9p,5d)/[8s,5p,3d] basis set was used,[17] augmented by two p functions,[18] one d function,[19] and one f function. For the free species ($R_2C_2P_2$) with R = H and CH_3, harmonic vibrational analyses have been performed as well at the B3LYP/6−31G(d,p) level. MP2 geometry optimizations using the 6−31G(d,p) basis set have been performed for the [$H_2C_2P_2$] compounds, including vibrational analysis. To obtain improved relative energies, coupled cluster CCSD(T)/6−311+G (2df,p) single-point calculations using the MP2-optimized geometries as well as B3LYP/6−311+G(2df,p) single-point calculations have also been carried out for the [$H_2C_2P_2$] isomers.

While the Gaussian 98 electronic structure program[20] was used for calculating the uncomplexed species, the Mulliken software[21] was used for calculations on complexed species. Both the geometry optimizations in Gaussian 98 and in the Mulliken software were performed with a convergence criterion of $4.5 \cdot 10^{-4}$ Hartree/Bohr for the gradients.

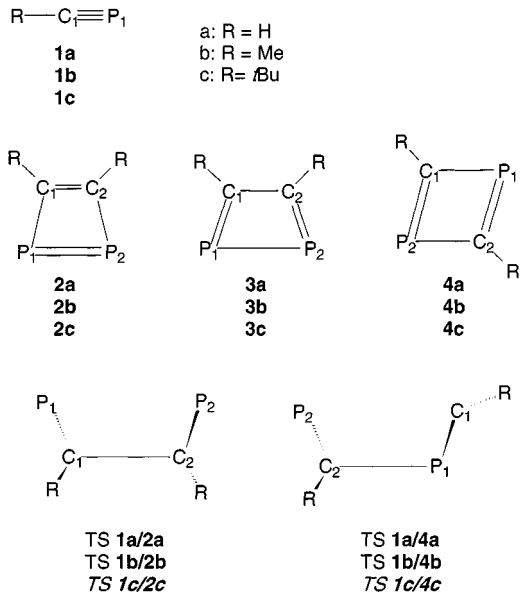


Figure 1. Schematic representations of noncomplexed species considered, along with the labeling conventions; labels in *italics* refer to species mentioned in the text, but not actually computed in this work

3. Results and Discussion

3.1 Uncomplexed Dimerization Products

Figure 1 shows schematic representations of the uncomplexed species considered in this work, along with the labeling conventions used throughout. Tables 1 and 2 contain the optimized geometrical parameters and relative energies, respectively. The minima considered include the free phosphaalkynes **1a−c**, the two valence isomers of 1,2-DPCB **2a−c** and **3a−c**, and 1,3-DPCB **4a−c**. While **1a/2a** and **1b/2b** are transition states for the so-called "head-to-head" cycloaddition of two RCP molecules leading to 1,2-DPCB, **1a/4a** and **1b/4b** describe the "head-to-tail" reaction yielding 1,3-DPCB. In the following paragraphs, mentioned geometrical parameters refer to the B3LYP-optimized values, unless otherwise noted.

Table 1. B3LYP/6−31G(d,p)-optimized bond lengths [Å] and angles [°] for the differently substituted uncomplexed diphosphacyclobutadienes under consideration; values in parentheses refer to MP2/6−31G(d,p)-optimized parameters (see Figure 1 for definition of structures and atom labels)

	C_1P_1		RC_1			
1a	1.543	(1.561)	1.074	(1.070)		
1b	1.550		1.460			
1c	1.552		1.473			
	C_1P_1	C_1C_2	P_1P_2	$C_1C_2P_2$	$P_1P_2C_2$	RC_1C_2
2a	1.924	1.330	2.071	101.1	78.9	129.7
	(1.900)	(1.339)	(2.081)	(101.3)	(78.7)	(129.5)
2b	1.926	1.339	2.067	100.9	79.1	132.3
2c	1.942	1.351	2.053	100.4	79.5	137.3
3a	1.698	1.463	2.488	107.6	72.4	125.0
	(1.702)	(1.460)	(2.455)	(107.0)	(73.0)	(125.7)
3b	1.703	1.488	2.447	106.4	73.6	124.5
3c	1.708	1.533	2.371	104.1	75.8	133.0
	C_1P_1	C_1P_2	RC_1	$C_1P_1C_2$	$P_1C_2P_2$	
4a	1.925	1.679	1.086	81.1	98.9	
	(1.897)	(1.682)	(1.080)	(81.4)	(98.6)	
4b	1.931	1.692	1.482	80.6	99.4	
4c	1.934	1.694	1.499	80.7	99.3	
	C_1C_2	P_1P_2	C_1P_1	$P_1C_1C_2$	P_1C_1R	$P_1C_1C_2P_2$
1a/2a	1.908	4.068	1.593	117.3	143.5	107.2
	(1.868)	(4.200)	(1.608)	(120.2)	(140.6)	(114.9)
1b/2b	1.885	4.000	1.608	112.1	141.6	116.6
	C_1P_2	C_2P_1	C_1P_1	C_2P_2	$C_1P_1C_2$	$C_1P_1C_2P_2$
1a/4a	3.051	1.960	1.720	1.607	102.2	74.3
	(3.015)	(2.045)	(1.674)	(1.596)	(99.8)	(75.4)
1b/4b	3.234	1.996	1.713	1.613	99.2	91.2

3.1.1 Dimerization of the Parent H−C≡P

Concerning the dimerization products of HCP, it is seen from Table 2 that these products are all bound with respect to the free phosphaalkynes. This fact is reproduced at all levels of theory, including B3LYP, MP2, and CCSD(T), with one exception, being **4a** at the MP2 level.

Both valence isomers **2a** and **3a** of the head-to-head dimers exist. While **2a** clearly shows a C=C bond (1.330 Å) and a P=P bond (2.071 Å), the reverse is seen for **3a**, having single C−C and P−P bonds (1.463 and 2.488 Å, respectively) and double C=P bonds (1.698 Å). Both **2a** and **3a** possess a trapezoid structure. Of the two valence isomers, **2a** with C=C and P=P π bonds is the most stable, lying 11 kJ/mol below **3a** at the B3LYP level and 12 kJ/mol at the C0SD(T) level.

The head-to-tail dimer **4a** has a parallelogram structure, with clearly distinguishable alternating single C−P and double C=P bonds (1.925 and 1.679 Å, respectively). The C−P−C angles turn out to be somewhat smaller than 90° (81.10); consequently, the P−C−P angles are larger than 90° (98.9°). **4a** turns out to be the least stable of the isomers considered here. Although it is bound by more than 20 kJ/mol with respect to the free phosphaalkyne at the B3LYP

Table 2. Relative energies [kJ/mol] of uncomplexed species considered

	B3LYP[a]	MP2[b]	B3LYP[a]	CCSD(T)[b]
	6-31G(d,p)		6-311+G(2df,p)	
1a	0.0	0.0	0.0	0.0
2a	-74.4	-21.4	-69.3	-66.3
3a	-68.1	-14.3	-58.8	-54.3
4a	-21.1	15.3	-21.2	-23.8
TS 1a/2a	107.5	105.8	98.2	100.2
TS 1a/4a	177.0	258.1	164.9	185.0

	B3LYP[a]		B3LYP[c]
	6-31G(d,p)		6-31G(d,p)
1b	0.0	**1c**	0.0
2b	-46.3	**2c**	-5.7
3b	-36.7	**3c**	9.8
4b	2.0	**4c**	-3.1
TS 1b/2b	129.5		
TS 1b/4b	203.5		

[a] Based on B3LYP geometries and including ZPE(B3LYP). – [b] Based on MP2 geometries and including ZPE(MP2). – [c] Based on B3LYP geometries and without ZPE.

and CCSD(T) levels, MP2 predicts it to be less stable than the separated monomers.

For the dimerization reaction, two transition states have been located. While TS **1a/2a** connects the free HCP molecules to the 1,2-DPCB having C=C and P=P π bonds, TS **1a/4a** represents the transition structure for head-to-tail dimerization. At the B3LYP level, the head-to-head process has an energy barrier of 98 kJ/mol, and the head-to-tail reaction passes over a 165 kJ/mol energy barrier. While MP2 is in good agreement with B3LYP and CCSD(T) concerning the former process, the MP2 head-to-tail energy barrier is considerably overestimated with respect to the B3LYP or CCSD(T) values. Most likely, this is due to the fact that MP2 is not able to treat nondynamical correlation energy, whereas the DFT and CCSD(T) can do so to some extent (vide infra). Qualitatively, however, all levels of theory confirm that the head-to-head product **2a** is both kinetically and thermodynamically favored over its head-to-tail counterpart.

In agreement with results of previous work,[14] the two HCP monomers approach each other in nearly perpendicular planes to form the 1,2- and 1,3-DPCB (TS **1a/2a** and **1a/4a**). In TS **1a/2a**, formation of the CP bond has clearly progressed further than the PP bond (C_1C_2 = 1.908 Å, in contrast to P_1P_2 = 4.068 Å). The same behavior is seen in TS **1a/4a**, where one forming CP bond is markedly shorther than the other (C_2P_1 = 1.960 Å versus C_1P_2 = 3.051 Å). Both transition structures thus imply a highly asynchronous formation of the two new chemical bonds. This suggests a radical mechanism for this symmetry-forbidden [2+2] cycloaddition.

In general, no severe geometrical differences between the MP2- and B3LYP-optimized structures are found. Concerning relative energies, however, a close examination of Table 2 shows that, while B3LYP yields results in excellent agreement with the CCSD(T) values, MP2 is often in considerable error with the CCSD(T) level.

It has to be noted, finally, that a proper description of the dimerization process of R−C≡P species requires a treatment using a multi-configurational wavefunction (MCSCF).

However, such a treatment is beyond the scope of the present work. Note also that density functional methods are generally believed to incorporate at least some part of the nondynamical correlation. Therefore, in view of the good agreement between our B3LYP and CCSD(T) calculations, we think that the present calculations provide a sufficiently accurate basis for drawing the conclusions described above.

3.1.2 Dimerization of Me−C≡P and *t*Bu−C≡P

In an attempt to tackle the question posed in the introduction concerning the influence of bulkier substituents on C, B3LYP calculations have been carried out for the heavier phosphaalkynes MeCP and *t*BuCP. Due to limitations in computational resources, harmonic frequency calculations have not been carried out for the latter, and TS **1c/2c** and **1c/4c** have not been calculated.

Substitution of H in the parent phosphaalkyne by CH_3 yields the following relative energy ordering for the dimers: **2b** < **3b** <**4b**, in analogy with the parent species. However, the stability with respect to the free phosphaalkynes is considerably changed upon Me substitution. The 1,3-DPCB **4b** lies now even higher in energy than the monomers. The reason for this alteration of relative stabilities has probably to be found in the stabilization of the monomers by larger alkyl substituents. The energy difference between **2b** and **4b** amounts to 48 kJ/mol, and has thus been decreased with respect to the unsubstituted case (53 kJ/mol). This fact possibly points to a slight destabilization of the 1,2-DPCB **2b** due to steric interactions between the two methyl groups. Another indication for steric repulsion between the methyl groups is found in the RC_1C_2 angle of **2b** which is 2.6° larger than the corresponding value for **2a**. The transition structures for head-to-head and head-to-tail cycloaddition reactions are found at 130 kJ/mol and 204 kJ/mol, respectively, relative to the monomers. As a consequence, the energy barriers have been increased with respect to the HCP case (due to stabilization of the MeCP monomers), whereas the relative ordering of the two TSs has remained nearly constant. Proceeding in the opposite direction, both DPCBs become less stable with regard to cycloreversion.

Replacing the hydrogen atom by the sterically demanding *t*Bu groups has considerable consequences on the relative stabilities. Only the 1,2-DPCB **2c** and 1,3-DPCB **4c** are stabilized with respect to the free monomers. The corresponding stabilization energies, however, amount to only 6 and 3 kJ/mol, respectively. It thus seems that replacing Me by *t*Bu further stabilizes the monomers. The energy gap between the two valence isomers **2c** and **3c** has further increased to 16 kJ/mol, whereas it was 6 kJ/mol for **2a-3a** and 10 kJ/mol for **2b-3b**. Most remarkable is the fact that the energy difference between the head-to-head adduct **2c** and

the head-to-tail dimer **4c** has decreased to only 3 kJ/mol, in favor of the former. This points to a considerable destabilization of **2c** by steric hindrance of the *t*Bu groups. Again, this observation is in agreement with an RC_1C_2 angle of 137.3° in **2c**, as compared with that of 129.7° for **2a**.

3.2 Metal Complexes of the R−C≡P Dimers

Overviewing the results gathered from calculations on the free R−C≡P dimers, it turns out that in all cases considered, the 1,2-DPCB dimer is the more stable. Therefore, it is most intriguing why, in the presence of transition metal fragments of Co, Rh, Ir, Fe, and Ni (see Schemes 1 and 2), only the 1,3-DPCB complexes are found. Interestingly, when Ti is used, both dimers are found (see Scheme 6). We have therefore carried out calculations on the model compounds shown in Figure 2. Two transition metal fragments have been considered: the 14e⁻ CpCo fragment (Cp cyclopentadiene) and the 12e⁻ COT−Ti fragment (COT = cyclooctatetraene). The calculations include full B3LYP geometry optimizations and energy calculations. The basis sets used are specified in a previous section. Optimized geometrical parameters and relative energies of the complexes considered are shown in Tables 3 and 4, respectively.

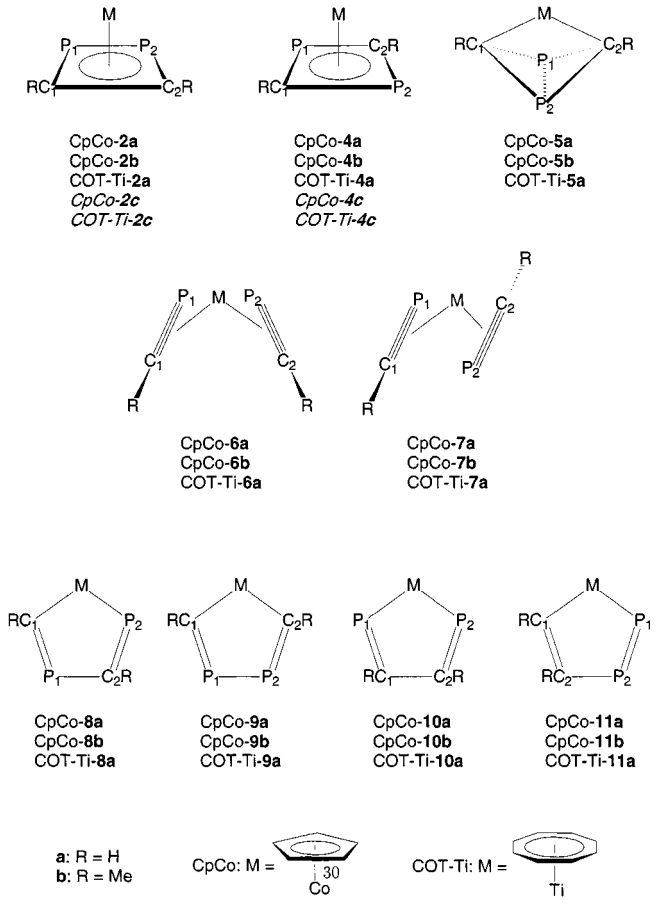


Figure 2. Schematic representations of the complexes considered, along with the labeling conventions; labels in *italics* refer to species mentioned in the text, but not actually computed in this work

Table 3. B3LYP/6−31G(d,p)-optimized bond lengths [Å] and angles [°] for the various complexed species under consideration (see Figure 2 for definition of structures and atom labels)

	MP_1	MC_1	C_1P_1	C_1C_2	P_1P_2	$C_1P_1P_2$	$C_1C_2P_2$
CpCo-**2a**	2.293	2.037	1.812	1.416	2.238	76.9	103.1
CpCo-**2b**	2.286	2.052	1.820	1.423	2.230	77.2	102.8
COT-Ti-**2a**	2.523	2.313	1.811	1.404	2.232	76.8	103.2
exp.[a]	2.491	2.387	1.811	-	2.175	78.1	101.9
	MP_1	MC_1	C_1P_1	C_1P_2	$C_1P_1C_2$	$P_1C_1P_2$	$C_1P_1P_2C_2$
CpCo-**4a**	2.267	2.050	1.801	1.801	79.6	100.0	169.3
CpCo-**4b**	2.267	2.048	1.808	1.809	80.3	99.2	168.7
exp.[b]	2.243	2.058	1.797	1.797	80.9	98.9	172.0
COT-Ti-**4a**	2.530	2.302	1.795	1.795	80.1	99.3	167.6
exp.[c]	2.5180	2.333	1.747	1.836	81.8	97.8	-
	MP_1	MC_1	C_1P_1	P_1P_2			$C_1P_1P_2C_2$
CpCo-**5a**	2.822	1.897	1.904	2.126			92.1
CpCo-**5b**	2.807	1.900	1.911	2.133			93.4
exp.[d]	-	-	1.900	2.147			70
COT-Ti-**5a**	2.985	2.087	1.895	2.146			95.6
	MC_1	MP_2	C_1P_1	P_1C_2	C_2P_2		
CpCo-**8a**	1.778	2.267	1.717	1.808	1.684		
CpCo-**8b**	1.776	2.276	1.736	1.818	1.685		
COT-Ti-**8a**	2.096	2.593	1.682	1.841	1.687		
	MC_1	C_1P_1	P_1P_2				
CpCo-**9a**	1.844	1.671	2.309				
CpCo-**9b**	1.876	1.682	2.271				
COT-Ti-**9a**	2.122	1.680	2.299				
	MP_1	P_1C_1	C_1C_2				
CpCo-**10a**	2.230	1.707	1.435				
CpCo-**10b**	2.221	1.718	1.453				
COT-Ti-**10a**	2.560	1.703	1.452				
	MC_1	MP_1	C_1C_2	C_2P_2	P_1P_2		
CpCo-**11a**	1.857	2.182	1.341	1.828	2.067		
CpCo-**11b**	1.882	2.186	1.351	1.828	2.055		

[a] Experimental parameters for the *t*Bu analog COT−Ti-**2c**, ref.[11] — [b] Experimental parameters for the *t*Bu analog CpCo-**4c**, ref.[22] — [c] Experimental parameters for the *t*Bu analog COT−Ti-**4c**, ref.[11] — [d] Experimental parameters for the Cp_2Zr complex of the 2,4-di-*tert*-butyl-1,3-diphosphabicyclo[1.1.0]butanediyl ligand, ref.[6]

Table 4. Relative energies [kJ/mol] of the complexes considered

	B3LYP		B3LYP		B3LYP
CpCo-**2a**	0.0	CpCo-**2b**	0.0	COT-Ti-**2a**	0.0
CpCo-**4a**	45.9	CpCo-**4b**	52.3	COT-Ti-**4a**	53.8
CpCo-**5a**	256.2	CpCo-**5b**	269.4	COT-Ti-**5a**	173.9
CpCo-**6a**	247.2	CpCo-**6b**	227.5	COT-Ti-**6a**	272.5
CpCo-**7a**	245.3	CpCo-**7b**	220.4	COT-Ti-**7a**	277.2
CpCo-**8a**	347.9	CpCo-**8b**	359.0	COT-Ti-**8a**	229.6
CpCo-**9a**	349.0	CpCo-**9b**	372.0	COT-Ti-**9a**	248.5
CpCo-**10a**	326.1	CpCo-**10b**	349.3	COT-Ti-**10a**	183.7
CpCo-**11a**	308.3	CpCo-**11b**	319.9	COT-Ti-**11a**	-
CpCo-**12a**	181.4	CpCo-**12b**	190.4	COT-Ti-**12a**	162.7

	B3LYP
A	0.0
B	236.5
C	173.3
D	354.3

3.2.1 Cobalt Complexes of H−C≡P Dimers

While the uncomplexed 1,2-DPCB and 1,3-DPCB clearly show alternating single and double bonds, their complexed counterparts CpCo-**2a** and CpCo-**4a** have bond lengths between single and double [r(CC) ≈ 1.41 Å, r(CP) ≈ 1.81 Å, and r(PP) ≈ 2.23 Å). Complexation of the dimers thus yields a shortening of the single bonds and a lengthening of the double bonds. This is a geometrical indication that the DPCB rings become less antiaromatic if complexed to

a CpCo fragment. Another indication of this behavior is the fact that complexation of **4a**, which has a parallelogram structure, leads to CpCo-**4a** where the diphosphacyclobutadiene unit exhibits a rhombic structure with four equal CP bond lengths.

Concerning the relative stabilities of both CpCo-**2a** and CpCo-**4a**, it seems that complexation has not much altered the situation with respect to the free dimers. While in free form, 1,2-DPCB lies 53 kJ/mol below 1,3-DPCB (B3LYP), in complexed form this energy gap is slightly decreased to 46 kJ/mol. Experimentally observed complexes of CpCo, however, are formed of *t*BuCP instead of HCP. In the previous seetion, it was calculated that the **2a − 4a** energy gap decreases from 53 kJ/mol to 3 kJ/mol for **2c − 4c**. By transferring this energy effect to the CpCo-**2a** − CpCo-**4a** energy difference, one can estimate the energy gap between CpCo-**2c** and CpCo-**4c** to be −5 kJ/mol, in favor of the latter. Even if such a crude approximation would be correct, the energy difference is too small and as such it could not explain why exclusively CpCo-**4a** complexes are found experimentally, and not the CpCo-**2a** complexes. Therefore, it seems necessary to take a closer look at the way the DPCB complexes are formed.

It has been proposed in the literature,[6][22] that the formation of diphosphacyclobutadiene complexes proceeds by the reaction sequence shown in Scheme 4, in analogy with that of cyclobutadiene complexes resulting from bis(π-acetylene) complexes.[8][9] Therefore, a number of additional structures have also been calculated. These include the bis(π-phosphaalkyne) complexes CpCo-**6a** and CpCo-**7a**, and four possible cobalt species CpCo-**8a**−CpCo-**11a**. For the sake of comparison, the all-carbon analogues, shown in Figure 3, have been computed as well. For the latter molecules, Table 4 shows that the bis(π-acetylene) complex **B** lies higher in energy than the CpCoCb complex **A** by 237 kJ/mol. The cobalt complex **C** is found at an intermediate position of 173 kJ/mol. Hence, the **B** → **C** → **A** reaction seems possible for these species, and it has indeed been found experimentally.[8][9] A different situation appears when the acetylene molecules are replaced by H−C≡P species. Two bis(π-phosphaacetylene) complexes are possible, CpCo-**6a** and CpCo-**7a**. While in the former complex, the two HCP molecules are side-on coordinated in a head-to-head fashion, the latter complex has them oriented in a head-to-tail manner. The complexes are found at 247 and 245 kJ/mol above CpCo-**2a**, respectively, which is very similar to the situation of **A** and **B**. However, the cobalt complexes CpCo-**8a**, CpCo-**9a**, CpCo-**10a**, and CpCo-**11a** are found at a much higher relative energy than the bis(π-phosphaacetylene) complexes. Note that CpCo-**11a** has been calculated only for the sake of completeness, since it seems not possible that CpCo-**11a** can be formed starting from CpCo-**6a** or CpCo-**7a**. The relative energies of these cobalt complexes range from 308 to 349 kJ/mol, with respect to CpCo-**2a**. Hence, it is unlikely that these species intervene as intermediates, such as shown in Scheme 4. In this respect, it is noteworthy that direct fragmentation of a complexed cyclobutadiene ligand into two acetylene ligands, without prior formation of a cobaltacyclopentadiene intermediate, has been observed.[23] This result suggests that the reverse − direct formation of cyclobutadiene out of two acetylene ligands − is also possible. Since the cobalt intermediates appear to be too high in relative energy in the case of diphosphacyclobutadiene complexes, it is tempting to say that a direct reaction of CpCo-**6a** or CpCo-**7a** to CpCo-**2a** or CpCo-**4a** might be possible.

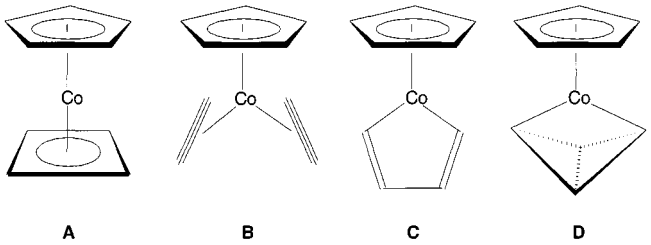


Figure 3. Schematic representations of the all-carbon complexes considered, along with the labeling conventions

Since Zr and Hf complexes containing a 1,3-diphosphabicyclo[1.1.0]butanediyl ligand have been found experimentally[6][7] (Scheme 3), the cobalt analog CpCo-**5a** has also been calculated. It is found at 256 kJ/mol relative to CpCo-**2a**. Note that CpCo-**5a** was optimized within C_s symmetry (MC_1C_2 mirror plane). Releasing all symmetry constraints yielded CpCo-**12a**, shown in Figure 4, which still possesses C_s symmetry, but now with an MP_1P_2 mirror plane. This structure, which has so far not been reported in the literature, possesses a tilted 1,3-diphosphabicyclo[1.1.0]-butanediyl ligand, so that a bond between Co and P_1 is formed. Selected geometrical parameters of this molecule are given in Table 5. While the C_1P_1 bond length amounts to 1.951 Å, indicating a single bond, the C_1P_2 distance of 1.811 Å suggests a partial double bond character between the C_1 and P_2 atoms. The folding angle $C_1P_1P_2C_2$ of 100.4° shows that the 1,3-diphosphabicyclo[1.1.0]butanediyl unit has opened up by about 8° with respect to CpCo-**5a**. The most striking feature of this molecule, however, is its energy. CpCo-**12a** is found at 181 kJ/mol relative to CpCo-**2a** and thus well below the bis(π-phosphaalkyne) complexes CpCo-**6a** and CpCo-**7a** (Table 4). Most likely, flattening of the 1,3-diphosphabicyclo[1.1.0]butanediyl unit in CpCo-**12a** *uniquely* leads to the 1,3-DPCB complex CpCo-**4a**. Therefore, CpCo-**12a** should be regarded as an important candidate for an intermediate in the formation of CpCo-**4a**.

3.2.2 Cobalt Complexes of CH_3−C≡P Dimers

In order to check the influence of larger R substituents on phosphaalkynes, the methyl analogues CpCo-**2b**−CpCo-**11b** have also been calculated (see Figure 2). It is seen from Table 4 that substituting H by CH_3 has a rather moderate effect on the relative energies. The energy gap between the 1,2-DPCB complex CpCo-**2b** and the 1,3-DPCB complex CpCo-**4b** has slightly increased with respect to the hydrogen analogues. The cobalt complexes CpCo-**8b**−CpCo-**11b** are now found at an even higher relative energy than was the

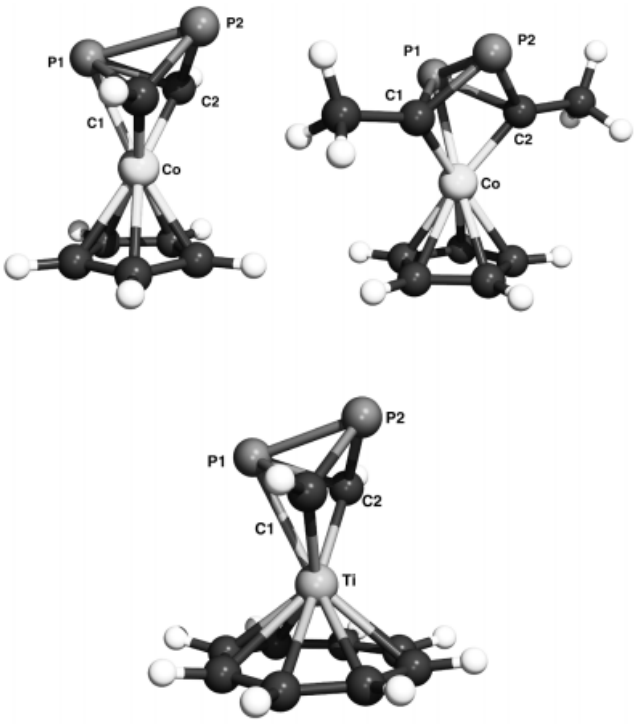


Figure 4. B3LYP-optimized structures of CpCo-**12a**, CpCo-**12b** and COT−Ti-**12a**

Table 5. B3LYP/6-31G(d,p)-optimized bond lengths [Å] and angles [°] of the CpCo-**12a**, CpCo-**12b** and COT−Ti-**12a** structures

	CpCo-**12a**	CpCo-**12b**	COT-Ti-**12a**
MP_1	2.299	2.299	2.625
MP_2	2.891	2.877	3.123
MC_1	1.907	1.908	2.104
C_1P_1	1.951	1.964	1.953
C_1P_2	1.811	1.818	1.831
C_1C_2	2.306	2.335	2.330
P_1P_2	2.262	2.262	2.187
$C_1P_1C_2$	72.4	72.9	73.2
C_1CoC_2	74.4	75.5	67.3
$C_1P_1P_2C_2$	100.4	101.1	98.2

case for their hydrogen analogues. Hence, in the case of methyl substitution, it is also likely that the proposed reaction mechanism of Scheme 4 is not valid. The complex containing a tilted 1,3-diphosphabicyclo[1.1.0]butanediyl ligand CpCo-**12b** has also been located and is found at a relative energy of 190 kJ/mol. Hence, similar to the case for R = H, it possibly represents an important intermediate in the formation of DPCB complexes. As CpCo-**4b** represents the best approximation to the structure of the experimentally known CpCo-**4c**, some geometrical parameters of the latter have also been included in Table 3. While the calculated metal−phosphorus distances are somewhat longer than the experimental value (by about 0.02 Å), the metal−carbon bond is slightly underestimated by 0.01 Å. The other parameters are in good agreement with experimental values, and the geometry obtained using B3LYP optimization thus seems very reliable.

Since the Cp_2Zr complex of the 2,4-di-*tert*-butyl-1,3-diphosphabicyclo[1.1.0]butanediyl ligand is known[6] (see Scheme 3), it is also worth comparing the experimental geometry with calculated values for CpCo-**5b**. Table 3 shows that B3LYP yields good values for the C_1P_1 and P_1P_2 distances. The folding angle $C_1P_1P_2C_2$, however, is considerably overestimated with respect to the experimental one (93.4° versus 70°). Note, though, that the latter effect could be due to steric interactions of the two Cp ligands with the *t*Bu groups.

3.2.3 Titanium Complexes of H−C≡P Dimers

The situation changes quite drastically when COT−Ti is used as the complexing metal fragment (COT = cyclooctatetraene). Only complexes of the HCP molecule have been investigated in conjunction with this metal fragment, since our available computational resources did not allow larger systems to be calculated.

The energy difference between the 1,2-DPCB complex COT−Ti-**2a** and the 1,3-DPCB complex COT−Ti-**4a** amounts to 54 kJ/mol, in favor of the former. Both bis(π-phosphaalkyne) complexes COT−Ti-**6a** and COT−Ti-**7a** are found at about 270 kJ/mol above COT−Ti-**2a**.

So far, the situation is quite analogous to the case of cobalt complexes. However, more serious differences appear when turning our attention to the metalla complexes. The complexes COT−Ti-**8a** and COT−Ti-**10a** are now lying well below the bis(π-phosphaalkyne) complexes in relative energy. As such, for COT−Ti complexes, these findings support the reaction mechanism shown in Scheme 4. Another important difference − as compared with the cobalt complexes − concerns the COT−Ti-**5a** species, which contains a 1,3-diphosphabicyclo[1.1.0]butanediyl ligand. While in the case of Co, it was found at relative energies of 250−270 kJ/mol, it is now located at 174 kJ/mol. Hence, COT−Ti-**5a** is likely to be accessible from the bis(π-phosphaalkyne) complexes, and thus it possibly represents an important intermediate. In analogy to the CpCo-**12a** complex, containing a tilted 1,3-diphosphabicyclo[1.1.0]butanediyl ligand, COT−Ti-**12a** has also been located. While its geometry is shown in Figure 4, the corresponding optimized parameters are given in Table 5. Apart, of course, from the MC and MP distances, all values are very similar to the ones derived for CpCo-**12a** and CpCo-**12b**. The relative energy of the species COT−Ti-**12a** is calculated to be 163 kJ/mol with respect to COT−Ti-**2a**. Hence it is only 11 kJ/mol more stable than its analog containing a nontilted 1,3-diphosphabicyclo[1.1.0]butanediyl ligand. The species COT−Ti-**5a** and -**12a** as well as the metalla complexes COT−Ti-**8a**−COT−Ti-**10a** should be considered accessible from the bis(π-phosphaalkyne) complexes. This implies that all of them possibly represent important intermediates in the formation of DPCB complexes. Note that, in the case of Ti complexes, the complex COT−Ti-**11a** could not be located, in contrast to CpCo-**11a** and CpCo-**11b**.

As far as geometry is concerned, both COT−Ti-**2c** and COT−Ti-**4c** have been characterized experimentally by X-

ray diffraction.[11] Their geometrical parameters are also shown in Table 3. For these species, B3LYP seems to overestimate slightly the metal−phosphorus bond lengths by about 0.02 Å, while the reverse trend is noted for the metal −carbon distances (an underestimation of about 0.05 Å). The most striking discrepancy between experimental and optimized geometries is the fact that, for the 1,3-DPCB complex, B3LYP yields a rhombic C_2P_2 ligand, having four equal C−P distances, while the experimentally resolved structure shows alternating single and double C−P bonds. At this point, however, it is not elear whether such an inconsistency originates from either a shortcoming of the B3LYP method or an effect of crystal packing or even an electronic effect of the *t*Bu groups.

4. Conclusions

In an attempt to tackle some points of controversy and uncertainty concerning the formation and relative stabilities of DPCB complexes, calculations have been carried out on a number of important isomers of $[R_2C_2P_2]$ with R = H, CH_3, and *t*Bu, [Cp−Co−$(R_2C_2P_2)$] isomers (R = H, CH_3; Cp = cyclopentadienyl), and isomers of COT−Ti-$[H_2C_2P_2]$. Several of these points have been addressed, which lead to new insights into the chemistry of DPCB complexes.

• Concerning the uncomplexed species, the calculations confirm the previous results that the valence isomer of 1,2-DPCB having π bonds between the two C atoms and between the two P atoms tends to be the most stable diphosphacyclobutadiene. The other isomer is found 6 kJ/mol higher in energy for R = H, 10 kJ/mol for R = Me and 16 kJ/mol for R = *t*Bu. The 1,3-DPCB is considerably less stable than 1,2-DPCB for both R = H and Me (53 and 48 kJ/mol, respectively). Only for R = *t*Bu, the 1,2 and 1,3 dimers are found rather close in energy. The fact that the head-to-head dimer turns out to be the most stable, even when large substituents are used, emphasizes its intrinsic stability.

Calculation of the energy barriers for the cycloaddition of two R−C≡P molecules, confirms that the head-to-head reaction is not only thermodynamically favored, but also kinetically.

For the parent species (R = H), MP2, and CCSD(T) calculations show that B3LYP yields good results as compared to CCSD(T), whereas the MP2 method is often in considerable deviation with the CCSD(T) level.

• Calculations on the diphosphacyclobutadiene complexes of CpCo show that the relative stability of the head-to-head product versus the head-to-tail product remains almost unchanged as compared to the uncomplexed dimers. In order to check the reaction mechanism proposed in the literature, a number of additional complexes have been calculated, including cobalta species. Due to their high energy content, it is suggested that the 1-cobaltadiphosphacyclopentadiene complexes are unlikely to act as intermediates in the formation of diphosphacyclobutadiene ligands out of bis(π-phosphaalkyne) complexes. This observation is in sharp contrast to the available experimental observations for the all-carbon CpCoCb complexes. However, a rather remarkable and so far unknown species has been located theoretically, containing a tilted 1,3-diphosphabicyclo-[1.1.0]butanediyl ligand. In view of its relative energy, the latter complex is more likely to be an intermediate in the formation of diphosphacyclobutadiene complexes than the cobalta species.

An extension has also been made from R = H to R = Me. Theoretical findings show, however, that substituting H by Me does not affect the conclusions drawn above.

• While the COT−Ti complexes behave rather analogously to the CpCo complexes, one major difference is detected. The metalla ring intermediates, that turn out to be too high in relative energy in the case of CpCo complexes, seem now to be valuable candidates to intervene in the formation of COT−Ti DPCB complexes. As such, in the case of Ti complexes, several routes leading from the bis(π-phosphaalkyne) to the diphosphacyclobutadiene complexes seem to be possible. This fact may explain the experimental detection of complexes of both the 1,2- and 1,3-dimers.

A characterization of the complexes considered in this work by harmonic frequency analysis, as well as the location of transition structures connecting the various complexed species, seem thus necessary for a full understanding of the formation of diphosphacyclobutadiene complexes. At this very moment, these calculations are unfortunately quite beyond our computational limits. Nevertheless, we believe that the presented results add several new insights into this interesting problem in low-coordinated phosphorus chemistry.

Acknowledgments

The authors are indebted to the FWO-Vlaanderen and the GOA program for continuing support.

[1] P. B. Hitchcock, M. J. Maah, J. F. Nixon, *J. Chem. Soc., Chem. Commun.* **1986**, 737.
[2] P. Binger, R. Milczarek, R. Mynott, M. Regitz, W. Rösch, *Angew. Chem. Int. Ed. Engl.* **1986**, *25*, 644.
[3] M. Driess, D. Hu, H. Pritzkow, H. Schäufele, U. Zenneck, M. Regitz, W. Rösch, *J. Organomet. Chem.* **1987**, *334*, C35.
[4] P. Binger, B. Biedenbach, R. Schneider, M Regitz, *Synthesis* **1989**, 960.
[5] T. Wettling, G. Wolmershäuser, P. Binger, M. Regitz, *J. Chem. Soc., Chem. Commun.* **1990**, 1541.
[6] P. Binger, B. Biedenbach, C. Krüger, M. Regitz, *Angew. Chem.* **1987**, *99*, 798.
[7] T. Wettling, B. Geissler, R. Schneider, S. Barth, P. Binger, M. Regitz, *Angew. Chem.* **1992**, *104*, 761.
[8] K. Jonas, *Angew. Chem.* **1985**, *97*, 292.
[9] K. P. C. Vollhardt, *Angew. Chem.* **1984**, *96*, 525.
[10] P. Binger, B. Biedenbach, R. Mynott, C. Krüger, P. Betz, M. Regitz, *Angew. Chem.* **1988**, *100*, 1219.
[11] P. Binger, G. Glaser, S. Albus, C. Krüger, *Chem. Ber.* **1995**, *128*, 1261.
[12] P. Binger, G. Glaser, J. Stannek, *Phosphorus Sulfur Silicon* **1996**, *109−110*, 149.
[13] T. Wettling, J. Schneider, O. Wagner, C. Kreiter, M. Regitz, *Angew. Chem. Int. Ed. Engl.* **1989**, *28*, 1013.
[14] M. T. Nguyen, L. Landuyt, L. G. Vanquickenborne, *J. Org. Chem.* **1993**, *58*, 2817.

[15] A. D. Becke, *J. Chem. Phys.* **1993**, *98*, 5648.
[16] C. Lee, W. Yang, R. G. Parr, *Phys. Rev. B* **1988**, *37*, 785.
[17] A. Schäfer, H. Horn, R. Ahlrichs, *J. Chem. Phys.* **1992**, *97*, 2571.
[18] A. J. H. Wachters, *J. Chem. Phys.* **1970**, *52*, 1033.
[19] P. J. Hay, *J. Chem. Phys.* **1977**, *66*, 4377.
[20] M. J. Frisch, G. W. Trucks, H. B. Schlegel, G. E. Scuseria, M. A. Robb, J. R. Cheeseman, V. G. Zakrzewski, J. A. Montgomery, Jr.; R. E. Stratmann, J. C. Burant, S. Dapprich, J. M. Millam, A. D. Daniels, K. N. Kudin, M. C. Strain, O. Farkas, J. Tomasi, V. Barone, M. Cossi, R. Cammi, B. Mennucci, Pomelli, 0.; C. Adamo, S. Clifford, J. Ochterski, G. A. Petersson, P. Y. Ayala, Q. Cui, K. Morokuma, D. K. Malick, A. D. Rabuck, K. Raghavachari, J. B. Foresman, J. Cioslowski, J. V. Ortiz, B. B. Stefanov, G. Liu, A. Liashenko, P. Piskorz, I. Komaromi, R. Gomperts, R. L. Martin, D. J. Fox, T. Keith, M. A. Al-Laham, C. Y. Peng, A. Nanayakkara, C. Gonzalez, M. Challacombe, P. M. W. Gill, B. Johnson, W. Chen, M. W. Wong, J. L. Andres, C. Gonzalez, Head-M. Gordon, E. S. Replogle, J. A. Pople, *GAUSSL4N 98, Rev. A.5*, Gaussian Inc., Pittsburgh PA, **1998**.
[21] IBM Research Division, Chemical Services and Applications, Almaden Research Center, 650 Harry Road San Jose, CA 95120−6099, USA, *Mulliken, version 1.1.0*, **1994**.
[22] P. Binger, R. Milczarek, R. Mynott, C. Krüger, Y.-H. Tsay, E. Raabe, M. Regitz, *Chem. Ber.* **1987**, *121*, 637.
[23] G. A. Ville, K. P. C. Vollhardt, M. J. Winter, *Organometallics* **1984**, *3*, 1177.

Received October 20, 1998
[I98361]

Synthesis and Characterization of the Heterometallic Aggregate $Pb_2Al_5(\mu_3\text{-}O)(\mu_4\text{-}O)(\mu\text{-}O\textit{i}Pr)_9(O\textit{i}Pr)_3(\mu\text{-}OAc)_3$

Ashutosh Pandey,[a] Vishnu D. Gupta,*[a] and Heinrich Nöth[b]

Keywords: Aluminum / Lead / O ligands / Alkoxy carboxylates / Structure elucidation

A novel heterometallic aggregate $Pb_2Al_5(\mu_3\text{-}O)(\mu_4\text{-}O)(\mu\text{-}O\textit{i}Pr)_9(O\textit{i}Pr)_3(\mu\text{-}OAc)_3$ obtained from the interaction of $Pb(OAc)_2$ and $Al(O\text{–}\textit{i}Pr)_3$ is the first structurally characterized example based on lead and aluminum. This compound has been isolated in high yield and examined by ^{1}H-, ^{13}C-, and ^{27}Al NMR, and in the solid state by X-ray crystallography.

Introduction

The use of heterometallic alkoxides[1–3] as precursors for mixed metal oxides has increased significantly in recent times, with efforts directed towards understanding the relationship, with regard to both structure and properties, between the precursor and the final material.[4] Structural data, even for heterobimetallic alkoxides,[1] is still scarce. Lead and aluminum are important components of many such materials.[5]

The difficulty in preparing lead(II) alkoxides[6] has been overcome by using commonly accessible salts such as nitrate,[7] acetate,[8] halides, hydroxides, or β-diketonates.[9][10] In general metal acetates are the most common precursors associated with metal alkoxides. Structural features of the products[11] obtained by treating metal acetates with metal alkoxides show that the acetate ligand is bridging, or bridge-chelating, indicating the role of the carboxylate group in maintaining the stoichiometry during the various stages of the transformation that leads to mixed metal oxides.

This work reports on the synthesis and characterization of a heterobimetallic aggregate, $Pb_2Al_5(\mu_3\text{-}O)(\mu_4\text{-}O)(\mu\text{-}O\textit{i}Pr)_9(O\textit{i}Pr)_3(\mu\text{-}OAc)_3$, based on lead and aluminum. This compound represents a unique example in which aluminum is present in three different coordination environments. The pentacoordination around the lead center observed in this system is rare in molecular compounds, and has been reported to be found in high-T_c superconductors.[12]

Results and Discussion

Reactions between metal alkoxides and metal acetates have generally been reported to give oxo products by the elimination of an ester.[11] Simple addition products[8] have also been reported in room-temperature reactions. However, under refluxing conditions the formation of oxo species is spontaneous. The product $Pb_2Al_5(O)_2(O\textit{i}Pr)_{12}(OAc)_3$ was obtained in a high and reproducible yield, which excludes formation by accidental hydrolysis.

In the IR spectrum of the compound the difference of 150 cm^{-1} in the $\nu(CO_2)$ absorption frequency of the asymmetric (1610 cm^{-1}) and symmetric (1460 cm^{-1}) bands is indicative of the acetate group acting as bidentate ligand. The absorptions observed at 1090 cm^{-1} and 1020 cm^{-1} account for the presence of terminal and bridging isopropoxy groups, respectively.

At ambient temperature ^{1}H- and ^{13}C-NMR spectra of the compound are not structurally informative. However, the ^{27}Al-NMR spectrum shows a broad peak (δ = 32–58) centered at δ = 42.24, which is at a position characterisitic of both octahedral and tetrahedral symmetries around the aluminum centers.[13]

The X-ray crystallography and molecular structure of the compound is given in Figure 1 and the core is shown in Figure 2.

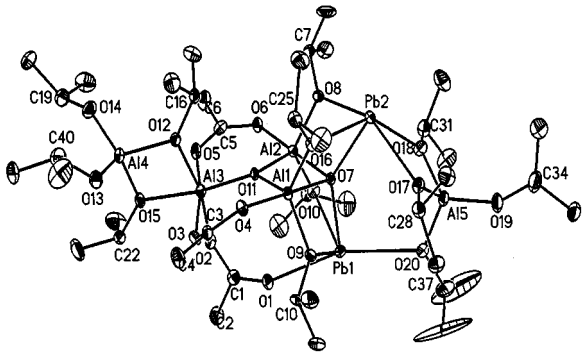


Figure 1. Molecular structure of $Pb_2Al_5(\mu_3\text{-}O)(\mu_4\text{-}O)(\mu\text{-}O\textit{i}Pr)_9(O\textit{i}Pr)_3(\mu\text{-}OAc)_3$; thermal ellipsoids are represented with 25% probability; hydrogen atoms have been omitted for clarity

Selected bond dimensions are summarized in Table 1. The compound has a Pb_2Al_5 unit linked by acetato, isopropoxo, and oxo groups, making a complex and interesting structure. There are two tetrahedral aluminum atoms [Al(5), Al(4)] which differ environmentally, two trigonal bipyramidal aluminum centers [Al(2) and Al(1)], and one which is octrahedrally surrounded [Al(3)]. This constitutes the first example of a system containing the same metal atom in three different coordination environments. Both the lead atoms are pentacoordinate, having different geometries

[a] Department of Chemistry, Faculty of Science, Banaras Hindu University,
Varanasi 221005, India
[b] Institute of Inorganic Chemistry, University of Munich,
Meiserstraße 1, D-80333 Munich, Germany

 © WILEY-VCH Verlag GmbH, D-69451 Weinheim, 1999 1434–1948/99/0808–1291 $ 17.50+.50/0

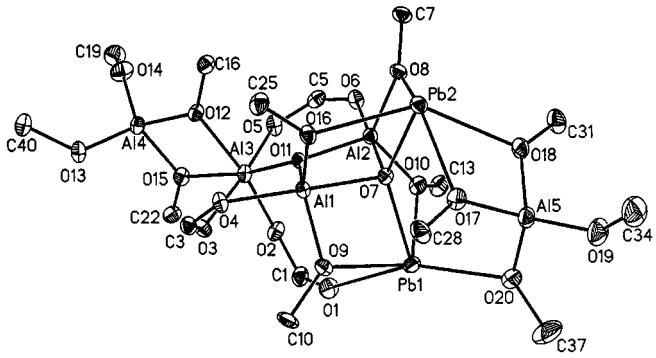


Figure 2. Plot of the core of $Pb_2Al_5(\mu_3\text{-}O)(\mu_4\text{-}O)(\mu\text{-}OiPr)_9(OiPr)_3(\mu\text{-}OAc)_3$

but each essentially that of a distorted teragonal pyramid with a lone pair.

Table 1. Selected bond dimensions for compound $Pb_2Al_5(O)_2(OiPr)_{12}(OAc)_3$

Bond lengths[Å]			
Pb(1)−O(7)	2.250(4)	Pb(1)−O(9)	2.440(4)
Pb(1)−O(10)	2.454(5)	Pb(1)−O(1)	2.535(5)
Pb(1)−O(20)	2.686(5)	Pb(2)−O(7)	2.234(4)
Pb(2)−O(17)	2.485(5)	Pb(2)−O(18)	2.476(5)
Pb(2)−O(8)	2.487(5)	Pb(2)−O(16)	2.491(4)
Al(1)−O(16)	1.790(5)	Al(1)−O(9)	1.808(5)
Al(1)−O(11)	1.822(5)	Al(1)−O(4)	1.878(5)
Al(1)−O(7)	1.920(5)	Al(2)−O(8)	1.788(5)
Al(2)−O(10)	1.797(5)	Al(2)−O(11)	1.806(4)
Al(2)−O(6)	1.869(5)	Al(2)−O(7)	1.909(5)
Al(3)−O(11)	1.825(5)	Al(3)−O(2)	1.857(5)
Al(3)−O(5)	1.920(5)	Al(3)−O(3)	1.926(5)
Al(3)−O(12)	1.942(5)	Al(3)−O(15)	1.960(5)
Al(4)−O(14)	1.694(6)	Al(4)−O(13)	1.717(5)
Al(4)−O(15)	1.784(5)	Al(4)−O(12)	1.787(5)
Al(5)−O(19)	1.694(6)	Al(5)−O(20)	1.747(6)
Al(5)−O(18)	1.757(5)	Al(5)−O(17)	1.763(5)
O(1)−C (1)	1.228(9)	O(2)−C(1)	1.295(9)
Bond angles [°]			
O(7)−Pb(1)−O(9)	65.1(2)	O(7)−Pb(1)−O(10)	65.2(2)
O(9)−Pb(1)−O(10)	116.5(2)	O(7)−Pb(1)−O(1)	102.6(2)
O(9)−Pb(1)−O(1)	73.2(2)	O(10)−Pb(1)−O(1)	81.7(2)
O(7)−Pb(1)−O(20)	95.3(2)	O(9)−Pb(1)−O(20)	108.0(2)
O(10)−Pb(1)−O(20)	113.5(2)	O(1)−Pb(1)−O(20)	160.4(2)
O(7)−Pb(2)−O(17)	82.75(2)	O(7)−Pb(2)−O(18)	83.4(2)
O(17)−Pb(2)−O(18)	61.9(15)	O(7)−Pb(2)−O(8)	64.82(2)
O(17)−Pb(2)−O(8)	142.2(2)	O(18)−Pb(2)−O(8)	94.2(2)
O(7)−Pb(2)−O(16)	65.73(2)	O(17)−Pb(2)−O(16)	92.12(2)
O(18)−Pb(2)−O(16)	142.4(2)	O(8)−Pb(2)−O(16)	91.6(2)
O(16)−Al(1)−O(4)	93.3(2)	O(9)−Al(1)−O(4)	95.1(2)
O(11)−Al(1)−O(4)	97.1(2)	O(16)−Al(1)−O(7)	87.8(2)
O(9)−Al(1)−O(7)	85.3(2)	O(11)−Al(1)−O(7)	81.44(2)
O(4)−Al(1)−O(7)	178.5(2)	O(8)−Al(2)−O(6)	92.6(2)
O(10)−Al(2)−O(6)	94.6(2)	O(11)−Al(2)−O(6)	97.5(2)
O(8)−Al(2)−O(7)	86.7(2)	O(10)−Al(2)−O(7)	86.5(2)
O(11)−Al(2)−O(7)	82.1(2)	O(6)−Al(2)−O(7)	178.9(2)
O(11)−Al(3)−O(2)	100.1(2)	O(11)−Al(3)−O(5)	96.0(2)
O(11)−Al(3)−O(3)	94.6(2)	O(5)−Al(3)−O(3)	169.3(2)
O(11)−Al(3)−O(15)	168.7(2)	O(5)−Al(3)−O(15)	85.7(2)
O(3)−Al(3)−O(15)	84.0(2)	O(12)−Al(3)−O(15)	74.9(2)
O((14)−Al(4)−O(15)	119.1(3)	O(14)−Al(4)−O(12)	112.9(3)
O(15)−Al(4)−O(12)	83.2(2)	O(19)−Al(5)−O(18)	118.1(3)
O(19)−Al(5)−O(17)	117.6(3)	O(18)−Al(5)−O(17)	92.1(2)

The coordination around Al(5) is completed by one terminal and three doubly bridging O*i*Pr groups. The angles subtended by O(20) are normal tetrahedral angles, while the acute angle [O(18)−Al(5)−O(17), 92.1°] due to the four-membered ring [−Pb(2)−O(17)−Al(5)−O(18)−] leads to a widening of the other two angles (average 117.8°). The second tetrahedral aluminum atom, Al(4), has two terminal and two μ-O*i*Pr groups. Four of the tetrahedral angles are almost normal. The larger deviations in case of the angles O(15)−Al(4)−O(12) [83.2(2)°] and O(14)−Al(4)−O(15) [119.1(3)°] are caused by two isopropoxy groups bridging to the octahedral Al(3). The former is quite comparable to the corresponding angle (83.1°) in $[Al(OiPr)_3]_4$.[14]

Al(2) and Al(1) are pentacoordinate with similar environments. The coordination around Al(1) is completed by two μ-O*i*Pr groups bridging with Pb(1) and Pb(2), and two oxo groups μ_3-O(11) and μ_4-O(7) and one bidentate acetate group bridging to Al(3). Al(1) and Al(2) almost lie in the plane constituted by O(11), O(10), O(8) and O(9), O(11), O(16), respectively. Bond angles at the pentacoordinated Al atoms to the axial oxygen atoms are close to linear, e.g. O(6)−Al(2)−O(7) = 178.9°. Octahedral Al(3), along with the coordination by oxo functionality O(1), is linked by three bridging OAc groups, two aluminum atoms [Al(1) and Al(2)] and one lead atom [Pb(1)], and two μ-O*i*Pr groups with Al(4), allowing the metal center to reach its most common coordination number six. Due to the complexity of the structure the angles for the octahedron range from 74.9(2)−100.1(2)°.

Among the Al−O*i*Pr bond lengths the terminal Al−O distances (average 1.701 Å) of the tetrahedral Al(4) and Al(5) are the shortest. In the bridging distances the pattern is Al−O (tetrahedral) (average 1.767 Å) < Al−O (trigonal-bipyramidal (average 1.797 Å) < Al−O (octahedral) (average. 1.951 Å). These are well within the range already reported in the literature.[14−16] The aluminum−oxygen bond lengths due to the bridging acetate groups are almost equal, whereas that of the bridging Pb(1) is somewhat shorter (see Table 1) The coordination around Pb(1) is completed by three μ-O*i*Pr groups bridging Al(1), Al(2), and Al(5), and a bidentate acetate group bridging Al(3) and μ_4-O(7). Pb(2) is surrounded by four bridging oxygen atoms of isopropoxy groups, two with Al(5) and one each with Al(1) and Al(2) and μ_4-O(7). Thus Pb_2O_9 essentially constitutes a bitetragonal-pyramidal geometry. The tetragonal angles for Pb(1) range from 73.2(2)° [O(9)−Pb(1)−O(1)] to 113.5(2)° [O(10)−Pb(1)−O(20)], while for Pb(2) the range is 61.9(2)° [O(17)−Pb(2)−O(18)] to 94.2(2)° [O(18)−Pb(2)−O(8)]. This difference is obviously a consequence of the different degree of constraint imposed by the coordinating groups. For Pb(1) the lead−oxygen distances cover the unusually wide range from 2.250(4) to 2.686(5) Å. However, for Pb(2) the range [2.234(4)−2. 491(4) Å] is comparable to reported[8] values.

The coordination geometry of the μ_3-O(11) group is almost planar (Σangles = 357.6°) while that around μ_4-O(7) is distorted tetrahedrally with angles ranging from 94.0(2)−138.6(2)°. This distortion is not as severe as ob-

served in the case of $Pb_2Ti_2(\mu_4\text{-}O)(\mu_3\text{-}OiPr)_2(\mu\text{-}OiPr)_4(OiPr)_4$[17] where the angles around μ_4-O range from 95.0(5) to 163.0(7)°.

For the two acetato moieties, bridging aluminum atoms, the C−O distances (average 1.259 Å) are almost similar. However, some asymmetry [C(1)−O(1) 1.228(9) Å, C(1)−O(2) 1.295(9) Å] is introduced for the third one attached to lead and aluminum atoms.

Conclusions

The first structurally characterized heterometallic aggregate based on lead and aluminum is found to have a high degree of asymmetry. It is the first reported occurence of the presence of the three identical metal centers (aluminum) in three different coordination environments. The asymmetry is also reflected by the fact that the pair of tetrahedral aluminum atoms and the tetragonal-pyramidal lead centers also differ in their coordinating groups.

Experimental Section

General: The reaction was performed under dry argon using standard Schlenck and glove-box techniques. Toluene and $CDCl_3$ were dried by standard procedures and stored over molecular sieves. Aluminum isopropoxide (Aldrich) was distilled prior to use. Anhydrous lead acetate was obtained by refluxing $Pb(OAc)_2 \cdot 3\,H_2O$ (BDH) with acetic anhydride (Qualigens). − IR: JASCO FT IR-5300; Nujol mulls between NaCl plates. − ^1H,^{13}C, and ^{27}Al NMR: JEOL-FX 90Q spectrometer ($CDCl_3$); $SiMe_4$ internal reference for ^1H- and ^{13}C-NMR spectra, $[Al(H_2O)_6]^{3+}$ external reference for ^{27}Al spectrum. Lead was estimated as lead chromate and aluminum as aluminum oxinate. O*i*Pr analysis was done by the method described by Bradley et al.[18]

Crystallography: The structure determination was performed by using a Siemens P4 diffractometer equipped with a CCD area detector and low-temperature device LTL. Mo-K_α radiation with λ = 0.71013 Å was used and the sample cooled to 193 K. Data reduction was performed with the program SAINT and absorption by SADABS. Computer calculations were carried out by using the SHELXS-97 (Sheldrick, **1990**) program package and the structure was solved by the heavy-atom method. The refinement was performed by SHELXL-97 (Sheldrick, **1997**) program with anisotropic thermal parameters for the non-hydrogen atoms. Hydrogen atoms were placed in calculated positions and refined as a riding model. The carbon atoms of one isopropyl group shows large anisotropic motion.

Crystallographic Data: $C_{42}H_{92}Al_5O_{20}Pb_2$; molecular mass 1466.44; a = 13.1182(3), b = 23.6499(4), c = 20.16104(3) Å; β = 96.885(1)°, V = 6348.1(2) Å^3, monoclinic system, space group $P2_1/n$, Z = 4, d = 1.534·10^{-9} g/cm^{-3}, μ = 5.427 mm^{-1}, 2θ = 2−49.42°, index range $-15 < h < 15$, $-22 < k < 27$, $-24 < l < 24$, max./min. transmission: 0.483/0.283, measured/unique/observed reflections: 29924/9671/7677 (R_{int} = 4.46%), no. of variables: 622, $R1$ = 0.0411, $wR2$ (all data) = 0.0970, weight (x/y) = 0.0442/12.2106, Goodness-of-fit = 1.090, $\Delta\rho$ = 1.411e/Å. The weighting scheme is $w^{-1} = \sigma^2F_o^2 + (xP)^2 + yP$ with $P = (F_o^2 + 2F_o^2)/3$. It should be noted that atoms C(38) and C(39) have large thermal parameters indicating rotational disorder. Calculations with split positions did not improve the result significantly. Additional data (except structure factor tables) have been deposited with the Cambridge Crystallographic Data Centre as supplementary publication no. CCDC-104505. Copies may be obtained free of charge on application to CCDC, 12 Union Road, Cambridge CB2 1EZ, UK [Fax: (internat.) + 44-1223/336-033; E-mail: deposit@cam.ac.uk].

$Pb_2Al_5(O)_2(OiPr)_{12}(OAc)_3$: A suspension of lead acetate (2.41 g, 7.41 mmol) in toluene (ca. 25 mL) was added dropwise to a solution of aluminum isopropoxide (3.02 g, 14.8 mmol) in toluene (ca. 30 mL) with stirring at room temp. (25°C). The reaction mixture was heated slowly by raising the bath temperature to 100°C. At this stage all the acetate had dissolved and the stirring was continued for 1 h while maintaining the bath temp. A very small quantity of solid suspension was filtered off and the solution concentrated to 20 mL and kept at −15°C to afford a white crystalline product (4.51 g, yield 83%). − $C_{42}H_{93}Al_5O_{20}Pb_2$ (1467.49): calcd. Pb 28.25, Al 9.19, O*i*Pr 48.29; found Pb 28.50, Al 8.91, O*i*Pr 48.19. − ^1H NMR (25°C): δ = 1.24, [d, CH_3 (O*i*Pr)], 4.42 (sept., CH), 2.00 [s, CH_3 (OAc)]. − ^{13}C NMR: δ = 174.72, 177.37, 179.50 [CO (OAc)], 64.11, 64.31 (CH), 27.31 and 27.69 [CH_3 (O*i*Pr and OAc)]. − Single crystals were grown from toluene at −15°C.

Acknowledgments

A. P. is grateful to U. G. C., New Delhi for financial support.

[1] R. C. Mehrotra, A. Singh, S. Sogani, *Chem. Rev.* **1994**, *94*, 1643−1660.
[2] K. G. Caulton, L. G. Hubert-Pfalzgraf, *Chem. Rev.* **1990**, *90*, 969−995
[3] M. Vieth, *Chem. Rev.* **1990**, *90*, 3−15.
[4] Y. W. Chen, W. B. Klemperer, C. W. Park, Mat. Res. Soc. *Symp.Proc*. **1992**, *271*, 57−63.
[5] L. G. Hubert-Pfalzgraf, *Chemical Processing of Ceramics* (Eds.: B. I. Pope, E. J. A. Pope), **1994**, p. 24−57.
pf1[6] R. Papiernik, L. G. Hubert-Pfalzgraf, M. C. Massiani, *Polyhedron* **1991**, *10*, 1657−1662.
[7] L. R. Pederson, G. D. Mupin, W. J. Weber, D. J. McReady, R. W. Stephens, *Mater. Lett*. **1991**, *10*, 437−439.
[8] L.G. Hubert-Pfalzgraf, *Mater. Res. Soc. Symp. Proc*. **1992**, *271*, 15−25.
[9] C. Sirio, O. Poncelet, L. G. Hubert-Pfalzgraf, J. C. Daran, J. Vaissermann, *Polyhedron* **1992**, *11*, 177−184.
[10] M. Veith, S. Mathur, V. Huch, *Inorg. Chem*. **1997**, *36*, 2391−2399.
[11] L. G. Hubert-Pfalzgraf, *Polyhedron* **1994**, *13*, 1181−1195.
[12] R. J. Cava, B. Batlogg, J. J. Krajewski, L. W. Rupp, L. F Schneemeyer, T. Siegrist, R. B. Vandover, P. Marsh, W. F. Peck Jr., P. K. Gallagher, S. H. Glarum, J. H. Marshall, R. C. Farrow, J. V. Waszczak, R. Hull, P. Trever, *Nature* **1988**, *33*, 211−216.
[13] S. J. Karlik, E. Tarien, G. A. Elgavish, G. L.Eichhorn, *Inorg.Chem*. **1983**, *22*, 525−529.
[14] N. Ya. Turova, Y. A. Kozunov, A. I. Yanovskii, N. G. Bokii, Yu. T. Struchkov, B. L. Tarnopolskii, *J. Inorg. Nucl. Chem*. **1979**, *41*, 5−11.
[15] A. Juliane, M. Marktscheffel, R. Fukuchi, M. Kido, G. Tachibana, C. M. Jenson, J. W. Gilji, *Chem. Mater*. 1**993, 5**, 755−757.
[16] S. A. Sangokoya, W. T. Pennington, J. B. Hill, G. H. Robinson, R. D. Rogers, *Organometallics* **1993**, *2*, 2429−2431.
[17] S. Daniele, R. Papiernik, L. G. Hubert-Pfalzgraf, S. Jagner, M. Hakansson, *Inorg. Chem*. **1995**, *34*, 628−632.
[18] D. C. Bradley, F. M. A. Halim, W. Wardlaw, *J. Chem. Soc*. **1950**, 3450−3454.

Received October 21, 1998
[I98362]

Directed Syntheses of New Quaternary Niobium Oxysulfides: Crystal Structures and Properties of $K_4Nb_2S_{10}O$ and $Rb_4Nb_2S_{10}O$ Compared to $K_4Nb_2S_{11}$

Oliver Krause,[a] Peter Dürichen,[a] Christian Näther,[a] and Wolfgang Bensch*[a]

Keywords: Solid-state chemistry / Structure elucidation / Reactive flux syntheses / Oxysulfides / Niobium chalcogenides

The new compounds $K_4Nb_2S_{10}O$ and $Rb_4Nb_2S_{10}O$ have been synthesized by the reaction of potassium or rubidium alkaline polychalcogenides with NbO_2, Nb_2O_5, or mixtures of Nb and NbO. Their structures consist of discrete $[Nb_2Q_{11}]^{4-}$ anions (Q = O, S) built up of two face-sharing pentagonal bipyramids, which are connected via the alkali metal cations.

Introduction

Difficulties are encountered in syntheses of oxysulfides and oxyselenides of the Group 5 transition metals owing to the high oxophilicity of these metals. If there is a competition between the hard O^{2-} anion and the more polarizable chalcogenide anions Q^{2-} (Q = S, Se, Te), Group 5 metals (M = V, Nb, Ta) prefer to bond to oxygen. Previously reported compounds containing both oxygen and another chalcogen bound to the metal atom were obtained serendipitously because oxygen-contaminated starting materials were used in the attempted synthesis of other compounds. Traces of such oxygen-containing compounds are sufficient to partially substitute heavier chalcogenide anions, hence oxysulfides or oxometallates are obtained as side products. However, such compounds are of special interest because they combine the physical properties of pure transition metal chalcogenides with those of the pure oxides. Therefore, the directed synthesis of oxysulfides and oxyselenides is a challenge for the preparative solid-state chemist.

In the field of classical solvent-based chemistry, several compounds containing thiooxometallate units have been synthesized. It is assumed that an important step in the addition of oxygen is the hydrolysis of sulfidic species. Examples of such compounds reported previously are $R_2[Nb(O)(S_2)_2SH]$ and $R_4\{[Nb(S)_3]_2O\}$ (with R = Ph_4P^+, Et_4N^+),[1a] $R_2\{[(S_2)_2MoO]_2S\}$ and $R_2\{[(S_2)_2MoO]_2S]S\}_2$ (with R = Et_4N^+).[1b] The vanadium compound $(NH_4)_6(V_4S_{20}O_4) \cdot 5\ bpy \cdot 7\ H_2O$[2] is also known. It must also be noted that numerous ternary alkali oxysulfides of the composition $[MO_{4-x}S_x]^{2-}$ (M = Mo, W, Re) have been precipitated from aqueous solutions.[3a–3f]

In contrast to the numerous solvent-mediated reactions, examples of alkali or alkaline earth transition metal oxysulfides and -selenides prepared by solid-state reactions are rare. Examples are $Ba_6(NbS_4)(NbS_3O)_3$,[4] $Na_{1.9}Cu_2Se_2 \cdot Cu_2O$,[5] $Ba_6Ti_5S_{15}O$,[6] $Na_{1.9}Cu_2Se_2 \cdot Cu_2O$,[5] $A_4(UO_2)(S_2)$ (A = Na, Cs),[7] and $Na_4(UO_2)Cu_2S_4$.[8] $Ba_6(NbS_4)(NbS_3O)_3$ was obtained as a by-product during a classical high-temperature synthesis at 1273 K, the oxygen source being identified as $BaSO_4$.[4] The other compounds were prepared using the reactive flux method.

In the course of our investigations of A–M(V)–Q systems (A = alkali metal; M = V, Nb, Ta; Q = S, Se, Te), we have prepared several new compounds containing M_2Q_{11} units as basic building blocks.[9,10a] In this unit, the Nb atoms are sevenfold coordinated by chalcogen atoms and the polyhedron may be described as a distorted pentagonal bipyramid.

This unit can be connected in many different modes. In $K_4Nb_2S_{11}$[9,10a] and $Rb_4Ta_2S_{11}$,[9,10b] isolated monomeric species are found, whereas in $K_4Nb_2S_{14}$[10c] this unit is expanded by an additional polychalcogenide ligand. In $A_6Nb_4S_{22}$ (A = Rb, Cs),[10d] two of these units are directly connected, while in $K_6Nb_4S_{25}$ they are joined via one additional S_3 fragment.[10e] For the selenides, predominantly polymeric structures are found. $K_{12}Nb_6Se_{35}$ and $Rb_{12}Nb_6Se_{35}$[10f] are built up from infinite $_\infty{}^1[Nb_6Se_{35}]^{12-}$ anionic chains, in which the Nb_2Q_{11} units are linked either directly or through one Se atom. It must be pointed out that all geometrical changes on going from monomeric to dimeric or polymeric species can be rationalized on the basis of a simple topological description.[9] In the course of our efforts to synthesize further polymeric compounds, we have obtained two new compounds, which surprisingly contain oxygen in one of the terminal positions of the bipyramid. In $K_4Nb_2Se_{11}O$,[10g] infinite anionic chains are found, in which the M_2Q_{11} units are connected through one Se atom. In contrast, crystals of $Cs_4Nb_2Se_{11}O$[10g] contain both discrete monomeric anions and polymeric anions, where the latter are built up of Nb_2Q_{11} units connected either directly or through one additional Se_2 unit.

A careful analysis of the experimental conditions showed that the source of oxygen was a contamination of the niobium metal with niobium oxides. However, the accidental synthesis of the new niobium oxyselenides prompted us to

[a] Institut für Anorganische Chemie, Universität Kiel, Olshausenstraße 40, D-24098 Kiel, Germany
Fax: (internat.) + 49(0)431/880-1520
E-mail: wbensch@ac.uni-kiel.de

 © WILEY-VCH Verlag GmbH, D-69451 Weinheim, 1999 1434–1948/99/0808–1295 $ 17.50+.50/0

try to prepare oxysulfides and -selenides in a directed way. For the first investigations we selected the simplest compounds containing discrete monomeric Nb_2Q_{11} units. Here, we report on the directed syntheses of the two new oxysulfides $K_4Nb_2S_{10}O$ and $Rb_4Nb_2S_{10}O$. The structural and optical properties of these two new compounds are compared with those of the previously reported oxygen-free potassium compound.[10a]

Results and Discussion

Crystal Structures

$K_4Nb_2S_{10}O$ and $Rb_4Nb_2S_{10}O$ are isotypic with the potassium polysulfide $K_4Nb_2S_{11}$[10a] and crystallize in the noncentrosymmetric space group $Pca2_1$. Their structures consist of well-separated $[Nb_2S_{10}O]^{4-}$ anions connected through the alkali metal ions. In the complex anion $[Nb_2S_{10}O]^{4-}$, one of the two Nb atoms is bound to a terminal monosulfide S^{2-}, while the other is coordinated by the terminal O^{2-} ligand (Figure 1, A and B). The environment about the Nb atoms is completed by one η^2-S_2^{2-} unit, one μ^2-S^{2-} unit that bridges the two Nb atoms, and one additional S_2^{2-} anion, which is bound in an η^2 fashion to one Nb while one S atom of this unit serves as a second bridging atom to the opposite Nb. Hence, the coordination mode of the anion may be described as $[Nb_2(\mu\text{-}S)(\mu\text{-}\eta^2,\eta^1\text{-}S_2)_2(\eta^2S_2)_2(S)(O)]^{4-}$ (Figure 1, A and B). The resulting coordination polyhedron can be described as being composed of two distorted pentagonal bipyramids sharing common faces. The Nb−Nb bond length of 3.538 Å in the rubidium compound and 3.522 Å in the potassium compound are significantly longer than that in metallic Nb (2.858 Å), too long for an Nb−Nb bond (Table 1). Hence, the formal oxidation state of Nb can be assigned as +5.

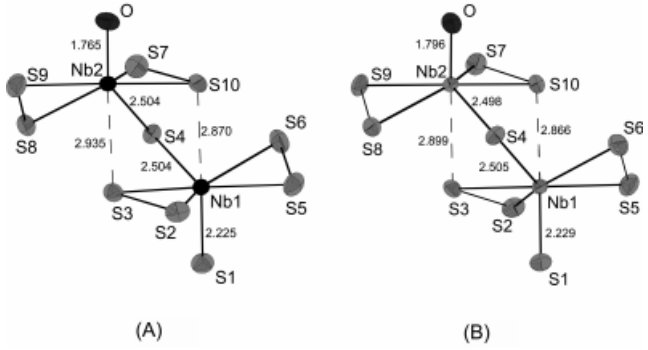


Figure 1. Structure of the $[Nb_2S_{10}O]^{4-}$ anion in (A) $Rb_4Nb_2S_{10}O$ and (B) $K_4Nb_2S_{10}O$ showing atom labelling (bond lengths are given in Å; displacement ellipsoids are drawn at a 50% probability level)

All interatomic distances in the anions of the two compounds are comparable (Table 1). The interatomic Nb−S distances may be divided into three groups. One short [Rb compound: Nb(1)−S(1): 2.225(3) Å; K compound: 2.229(3) Å], five more typical distances [Rb: Nb(1): 2.440(2) to 2.504(2) Å, Nb(2): 2.484(2) to 2.504(2) Å; K: Nb(1): 2.435(3) to 2.505(3) Å, Nb(2): 2.463(3) to 2.498(3) Å], and one longer separation [Rb: Nb(1)−S(10): 2.870(2), Nb(2)−S(3): 2.935(2) Å; K: 2.866(3), 2.899(3) Å] (Table 1). As was demonstrated in a previous communication, the long Nb−S separation must be treated as a weak interaction, while the short Nb−S bond lengths are close to an Nb−S double-bond length.[9] The S−S distances in the S_2^{2-} units range from 2.071(4) to 2.077(4) Å and are thus typical for S−S single bonds (Table 1). The Nb atoms are shifted from the plane of the pentagonal bipyramid towards the terminal chalcogen atoms by about 0.474 Å [Nb(1)] and 0.470 Å [Nb(2)] in the rubidium compound, and by 0.475 Å [Nb(1)] and 0.473 Å [Nb(2)] in the potassium compound (Table 1).

Table 1. Selected bond lengths [Å], deviation of the Nb atoms from the pentagonal plane [Å], and angles between the pentagonal planes [°] for $Rb_4Nb_2S_{10}O$, $K_4Nb_2S_{10}O$, and $K_4Nb_2S_{11}$

Bond lengths	$Rb_4Nb_2S_{10}O$	$K_4Nb_2S_{10}O$	$K_4Nb_2S_{11}$[10a]
Nb(1)−S(1)	2.225(3)	2.229(3)	2.221(3)
Nb(1)−S(2)	2.440(2)	2.435(3)	2.457(3)
Nb(1)−S(3)	2.500(3)	2.503(3)	2.497(3)
Nb(1)−S(4)	2.504(2)	2.505(3)	2.502(2)
Nb(1)−S(5)	2.496(3)	2.487(3)	2.512(3)
Nb(1)−S(6)	2.456(3)	2.452(3)	2.436(3)
Nb(1)−S(10)	2.870(2)	2.866(3)	2.856(3)
Nb(2)−O	1.765(7)	1.796(7)	−
Nb(2)−S(11)	−	−	2.182(3)
Nb(2)−S(3)	2.935(2)	2.899(3)	2.859(3)
Nb(2)−S(4)	2.504(2)	2.498(3)	2.504(2)
Nb(2)−S(7)	2.460(3)	2.463(3)	2.464(2)
Nb(2)−S(8)	2.494(3)	2.488(3)	2.463(3)
Nb(2)−S(9)	2.484(3)	2.493(3)	2.491(3)
Nb(2)−S(10)	2.494(2)	2.481(3)	2.486(3)
S(2)−S(3)	2.071(4)	2.071(4)	2.061(3)
S(5)−S(6)	2.077(4)	2.071(5)	2.060(4)
S(7)−S(10)	2.074(4)	2.073(4)	2.070(3)
S(8)−S(9)	2.076(4)	2.073(4)	2.078(4)
Deviation of Nb from the pentagonal plane	Nb(1) 0.474 Nb(2) 0.470	Nb(1) 0.475 Nb(2) 0.473	Nb(1) 0.479 Nb(2) 0.474
Angle between pentagonal planes	128.4°	128.3°	129.4°

The Nb−O bond length of 1.765(7) Å [1.796(7) Å in $K_4Nb_2S_{10}O$] can be regarded as corresponding to an Nb=O double bond, and is comparable to those reported for $R_4\{[Nb(O)(Se_2)_2]_2Se_4\}$ (Nb−O: 1.671 Å) and $R_4\{[Nb(Se)_3]_2O\}$ ($R = Ph_4P^+$, Et_4N^+)[1a] (Nb−O: 1.682 Å), where Nb is sevenfold coordinated. In the binary oxides NbO and NbO_2, with Nb in a quadratic-planar environment, the Nb−O bond lengths are about 2.105 Å and 2.046 Å, respectively. The average Nb−O distance in a tetrahedral environment, as found in Nb_2O_5, is 1.725 Å.[11a] We note that Nb−O distances are scattered over a wide range, even those in NbO_6 octahedra (e.g. 1.751 to 2.554 Å in $Nb_{12}O_{29}$;[11b] 1.635 to 2.331 Å in $NaNbO_3$;[11c] 1.867 to 2.107 Å in $Rb_4Nb_{11}O_{30}$[11d]) and an NbO_7 pentagonal bipyramid (1.896 to 2.435 Å and 1.761 to 2.161 Å in $LaNb_5O_{14}$[11e]).

The packing of anions and cations in the rubidium compound is depicted in Figure 2, A and B. A projection onto the $a-b$ plane reveals an almost hexagonal arrangement of

the anions, with channels running parallel to the *c* axis, whereas a view parallel to [0 1 0] shows the separation of the anions by the alkali metal cations. The shortest intermolecular nonbonding S−S distances are 3.239 Å in $Rb_4Nb_2S_{10}O$ and 3.252 Å in $K_4Nb_2S_{10}O$, both of which are significantly shorter than the sum of the van der Waals radii of sulfur. The alkali metal cations are coordinated by S and O atoms in irregular polyhedra and have coordination numbers between 8 and 10. The A···S and A···O distances lie in the expected ranges for K^+ and Rb^+ cations and S^{2-} and O^{2-} anions[10d,12a,12b] (Table 2).

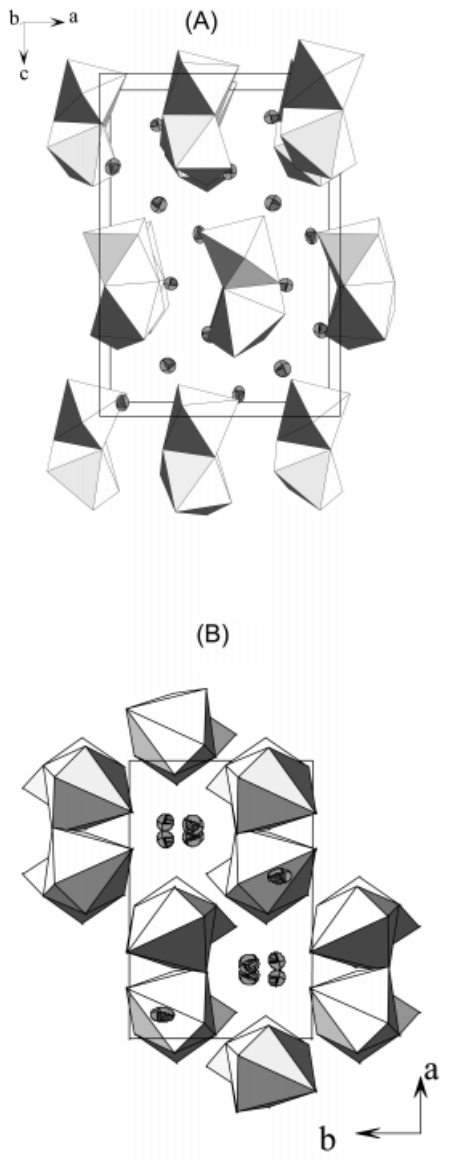


Figure 2. Crystal structure of $A_4Nb_2S_{10}O$ (A = K, Rb) showing (A) a view parallel to [0 1 0], and (B) a view parallel to [0 0 1]

Comparison of the interatomic distances in the $[Nb_2S_{10}O]^{4-}$ anion of $K_4Nb_2S_{10}O$ with those in the $[Nb_2S_{11}]^{4-}$ anion of $K_4Nb_2S_{11}$ shows that the introduction of the oxygen atom only slightly influences the distinct Nb−S distances (Table 1) The most marked deviation is observed for the Nb(2)−S(3) distance, positioned *trans* to Nb(2)−O, which is 0.040 Å longer than in $K_4Nb_2S_{11}$. The angle between the two pentagonal planes amounts to 128.3° in $K_4Nb_2S_{10}O$ and 129.4° in $K_4Nb_2S_{11}$ (Table 1).

Table 2. Coordination numbers (CN), shortest (min.), longest (max.), and average (< >) A···S distances, as well as A···O distances [Å] for the alkali metal cations (A) in $K_4Nb_2S_{10}O$, $Rb_4Nb_2S_{10}O$, and $K_4Nb_2S_{11}$ (cut-off$_K$ = 3.81 Å; cut-off$_{Rb}$ = 4.01 Å)

$Rb_4Nb_2S_{10}O$	Rb(1)	Rb(2)	Rb(3)	Rb(4)
CN	10	9	9	8
Rb···S min.	3.330(3)	3.333(3)	3.208(3)	3.347(3)
Rb···S max.	3.658(3)	3.704(3)	3.751(3)	3.804(3)
< Rb···S >	3.517(3)	3.466(3)	3.478(3)	3.532(3)
Rb···O	3.321(8)	2.993(6)	–	2.793(7)
$K_4Nb_2S_{10}O$	K(1)	K(2)	K(3)	K(4)
CN	10	9	9	8
K···S min.	3.210(4)	3.228(4)	3.103(4)	3.239(4)
K···S max.	3.614(4)	3.591(4)	3.753(4)	3.807(4)
< K···S >	3.427(4)	3.382(4)	3.387(4)	3.422(4)
K···O	3.258(8)	2.913(7)	–	2.605(8

Synthetic Aspects

As pointed out in the Experimental Section, direct syntheses of the title compounds can be carried out using several Nb oxides such as NbO, NbO_2, or Nb_2O_5, as well as mixtures of elemental Nb with these oxides. However, if only small amounts of niobium oxides are present, e.g. only slightly contaminated Nb metal is used for the syntheses, mixtures of oxysulfides and the pure sulfides are obtained. This is exemplified by the synthesis of the two new compounds, $K_4Nb_2S_{10.7}O_{0.3}$ and $Rb_4Nb_2S_{10.7}O_{0.3}$, which were isolated in the course of our investigations. Because these compounds are isotypic with the title compounds, having only very small differences in their cell parameters, their identification by means of X-ray powder diffraction is not possible. Significant differences are only observed upon refinement of single-crystal data, and only with an oxygen content of several%. For an effective control of the syntheses of pure chalcogenides, oxysulfides, or oxyselenides, this is not an adequate method. Therefore, a much more sensitive method is needed for the fast and non-destructive characterization of these compounds. For this purpose, extremely sensitive spectroscopic methods are ideal. If small amounts of oxysulfides or oxyselenides are present, this can clearly be detected by the appearance of Nb−O absorption peaks in the IR spectra. The vibration of the Nb−O bond in $Rb_4Nb_2S_{10}O$ gives rise to a strong absorption near 850 cm^{-1} (see Figure 3, B and C), whereas for the pure sulfide this band is absent (Figure 3, A). Therefore, IR spectroscopy is a suitable tool for monitoring the synthesis of compounds of this class.

It should be noted that in the title compounds only one of the two terminal positions is occupied by oxygen. Therefore, several attempts were made to substitute both axial S atoms by O atoms. A large number of experiments were carried out using different combinations of Nb with Nb oxides (NbO, NbO_2, and Nb_2O_5) as well as only Nb oxides

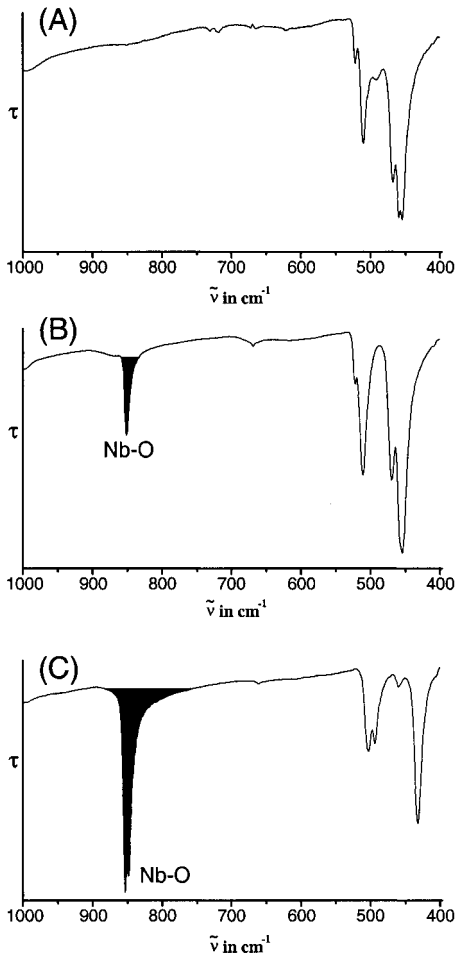


Figure 3. MIR spectra of (A) $K_4Nb_2S_{11}$, (B) $K_4Nb_2S_{10.7}O_{0.3}$, and (C) $K_4Nb_2S_{10}O$ (τ in arbitrary units)

as starting materials. However, the products of all these reactions consisted only of $Rb_4Nb_2S_{10}O$ or $K_4Nb_2S_{10}O$, alkali metal oxoniobates, and A_3NbS_4[13] (A = K, Rb) as the minor phases. In the case of the pure oxides, this is an interesting reaction from several points of view. First of all, most of the oxygen atoms of the niobium oxide must be replaced by sulfur atoms, which would be expected to be difficult considering the highly oxophilic character of Nb. Secondly, it is not obvious why only one oxygen remains unchanged, while in the products of the solution-mediated reactions both terminal positions are invariably occupied by oxygen. Concerning the reaction mechanism in the case of pure Nb_2O_5, a redox reaction between low-valent Nb and the S_x^{2-} polyanions in the melt can be excluded. Instead, it involves replacement of most of the oxygen by sulfur, where the large excess of sulfur does not allow the retention of oxygen at both the axial positions. However, even at lower concentrations, only one of the two possible positions is occupied by O. A further decrease of the sulfur content is not possible because no flux is generated. The reasons for this surprising reaction remain unclear, hence further investigations are needed.

UV/Vis Measurements

For a comparison of the optical properties, UV/Vis reflectance spectra of $K_4Nb_2S_{10}O$ and the pure sulfide were measured (Figure 4). Both compounds show a sharp absorption, from which an optical-band gap of 1.99 eV can be estimated for $K_4Nb_2S_{10}O$, while in the case of $K_4Nb_2S_{11}$ this band gap is shifted to higher energy by about 0.1 eV. The colour of the new material, as well as the value for the band gap, are consistent with its semiconducting nature.

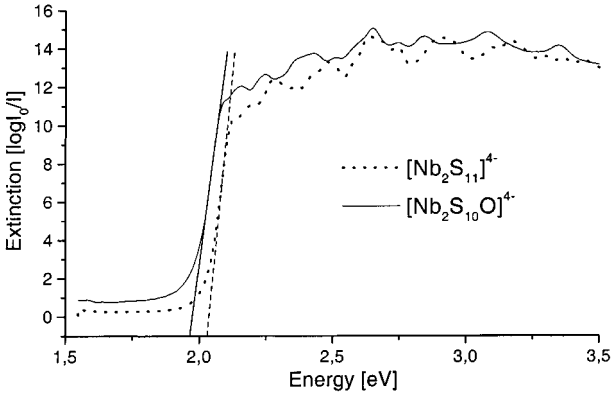


Figure 4. UV/Vis spectra of $K_4Nb_2S_{10}O$ and $K_4Nb_2S_{11}$

Conclusion

In the present paper we have shown that oxysulfides of niobium can be synthesized in a directed way by employing niobium oxides as starting materials. This synthetic approach can also be applied to selenide chemistry and we have shown that the polymeric oxyselenides first obtained accidentally can also be prepared using NbO, NbO_2, or Nb_2O_5. It can be assumed that the directed introduction of oxygen is generally applicable. However, in contrast to what is known from solution chemistry, in the reaction in the alkali metal polychalcogenide melts only one of the two terminal positions is selectively occupied by oxygen. Such reactions are not only of considerable interest from a synthetic point of view, but also to dramatically increase the number of new compounds in several ternary and multinary transition metal polychalcogenide systems. Moreover, the directed introduction offers the possibility of influencing or even modelling the physical properties of the compounds at a molecular level.

Experimental Section

Syntheses: The requisite alkali metal sulfides were first prepared by reactions of stoichiometric amounts of the elements in liquid ammonia. $K_4Nb_2S_{10}O$ and $Rb_4Nb_2S_{10}O$ were then synthesized by reactions of K_2S_3 and Rb_2S_3 with S and NbO in molar ratios of 2:4:1. As mentioned above, the preparation could also be carried out using several mixtures of Nb/NbO and NbO_2 or Nb_2O_5. The starting reagents were thoroughly mixed in a nitrogen-filled glovebox and then transferred to a Pyrex ampoule. The ampoule was evacuated to $6 \cdot 10^{-5}$ mbar and flame-sealed. The sample was heated

to 623 K and maintained at this temperature for 5 d. It was then cooled to 473 K at a rate of 3 K/h and to room temperature at a rate of 30 K/h. The excess polysulfide flux was removed by washing with dry DMF and diethyl ether and the residue was dried in vacuo. After optimization of the reaction parameters, yields of 50% based on niobium were achieved. The homogeneity of the product was checked by means of X-ray powder diffraction and MIR spectroscopy.

General Remarks: Single-crystal X-ray investigations were performed with a STOE AED II diffractometer (Mo-K_α radiation, graphite monochromator). The intensities were reduced to F_o. Lorentz, polarization, and empirical absorption corrections using ψ-scan data were applied. Both structures were solved by direct methods using SHELXS-86. Full-matrix least-squares refinements were performed against F^2 using SHELXL-93. All atoms were refined using anisotropic displacement parameters. Additional material relating to the structure determination can be ordered from the Fachinformationszentrum Karlsruhe, Gesellschaft für wissenschaftlich-technische Information mbH, D-76344 Eggenstein-Leopoldshafen, Germany, on quoting the numbers. CSD-410820 and -410821, the names of the authors, and the full journal citation. − MIR spectra were recorded with a Genesis FT-IR spectrometer (ATI Mattson) in the range 400−4000 cm^{-1} with a resolution of 2 cm^{-1}. Samples of the compounds were prepared as KBr pellets. − UV/Vis diffuse-reflectance measurements were made with a Leica Orthoplan microscope equipped with a Leica MPV-SP, an ICS quartz UV optic, and a xenon lamp as light source. The resolution was 1 nm and $BaSO_4$ was used as a standard for 100% reflectance. Absorption data were calculated from the reflectance data using the Kubelka−Munk function. The approximate band gap was determined from the intersection point on the energy axis of the line extrapolated from the linear part of the absorption edge in an $[F(R)]^2$ plot. − Powder diffraction measurements were made using a STADI P transmission powder diffractometer from STOE & CIE.

X-ray Crystallographic Study. − $K_4Nb_2S_{10}O$: Mol. mass 678.82, red crystal, size: 0.3 × 0.2 × 0.2 mm, a = 12.714(3) Å, b = 7.532(2) Å, c = 17.828(3) Å, V = 1707.2(7) $Å^3$ (room temp.), $\rho_{calc.}$ = 2.641 g cm^{-3}, orthorhombic, $Pca2_1$ (No. 29), Z = 4, μ = 3.517 mm^{-1}, 2824 reflections measured in the range 3° < 2θ < 53°, 2307 independent reflections used for refinement, R_{int} = 0.0466, 154 parameters, $w = 1/[\sigma^2(F_o^2) + (0.0417 \times P)^2 + (1.06 \times P)]$, R for 1765 $F_o > 4\sigma(F_o)$ = 0.0350, $wR2$ for all 2307 data = 0.0829, GooF = 1.028, residual electron density 1.23/−0.80 $eÅ^{-3}$. The absolute structure was determined and is in agreement with the selected setting: Flack x parameter = 0.03(12). − **$Rb_4Nb_2S_{10}O$:** Mol. mass 864.3, red crystal, size: 0.3 × 0.2 × 0.2 mm, a = 12.967(1) Å, b = 7.790(1) Å, c = 18.085(2) Å, V = 1826.7 $Å^3$ (room temp.), $\rho_{calc.}$ = 3.143 g cm^{-3}, orthorhombic, $Pca2_1$ (No. 29), Z = 4, μ = 12.97 mm^{-1}, 3843 reflections measured in the range 3° < 2θ < 54°, 3040 independent reflections used for refinement, R_{int} = 0.0320, 155 parameters, $w = 1/[\sigma^2(F_o^2) + (0.0361 \times P)^2 + (0.0 \times P)]$, R for 2439 $F_o > 4\sigma(F_o)$ = 0.0316, $wR2$ for all 3040 data = 0.0714, GooF = 1.013, residual electron density 0.90/−0.79 $eÅ^{-3}$. The absolute structure was determined and is in agreement with the selected setting: Flack x parameter = 0.018(9).

Acknowledgments

Financial support by the State of Schleswig-Holstein and the Deutsche Forschungsgemeinschaft (DFG) is gratefully acknowledged.

[1] [1b] B. S. Mandimutsira, S.-J. Chen, K. D. Demadis, D. Coucouvanis, *Inorg. Chem.* **1995**, *34*, 2267−2268. − [1b] D. Coucouvanis, A. Hadjikyriacou, *Inorg. Chem.* **1987**, *26*, 1−2.
[2] C. Simonnet-Jégat, S. Delalande, S. Halut, B. Marg, F. Sécheresse, *J. Chem. Soc., Chem. Commun.* **1996**, 423−424.
[3] [3a] A. Müller, B. Krebs, W. Rittner, M. Stockburger, *Ber. Bunsenges.* **1967**, 182−189. − [3b] A. C. Ranade, A. Müller, E. Diemann, *Z. Anorg. Allg. Chem.* **1970**, *373*, 258−264. − [3c] A. Müller, W. Rittner, A. Neumann, R. C. Sharma, *Z. Anorg. Allg. Chem.* **1981**, *472*, 69−74. − [3d] M. Herbold, G. X. Jin, A. Müller, M. Penk, *Z. Naturforsch.* **1991**, *46b*, 25−34. − [3e] A. Müller, W. Jaegermann, W. Hellmann, *J. Mol. Struct.* **1983**, *100*, 559−570. − [3f] A. Müller, O. Glemser, E. Diemann, H. Hofmeister, *Z. Anorg. Allg. Chem.* **1969**, *371*, 74−80.
[4] L. E. Rendon-Diazmiron, C. F. Campana, H. Steinfink, *J. Solid State Chem.* **1983**, *47*, 322−327.
[5] Y. P. Park, D.C. DeGroot, J. Schindler, C. R. Kannewurf, M. G. Kanatzidis, *Chem. Mater.* **1993**, *5*, 8−10.
[6] A. C. Sutorik, M. G. Kanatzidis, *Chem. Mater.* **1994**, *6*, 1700−1704.
[7] A. C. Sutorik, M. G. Kanatzidis, *Polyhedron* **1997**, *16*, 3921−3927.
[8] A. C. Sutorik, M. G. Kanatzidis, *J. Am. Chem. Soc.* **1997**, *119*, 7901−7902.
[9] W. Bensch, P. Dürichen, C. Näther, *Eur. J. Solid State Inorg. Chem.*, in press.
[10] [10a] W. Bensch, P. Dürichen, *Eur. J. Solid State Inorg. Chem.* **1996**, *33*, 527−536. − [10b] P. Dürichen, W. Bensch, *Acta Crystallogr.* **1998**, *C54*, 706. − [10c] W. Bensch, P. Dürichen, *Inorg. Chim. Acta* **1997**, *261*, 103. − [10d] W. Bensch, P. Dürichen, *Z. Anorg. Allg. Chem.* **1996**, *622*, 1963−1967. − [10e] W. Bensch, P. Dürichen, *Eur. J. Solid State Inorg. Chem.* **1996**, *33*, 1233. − [10f] P. Dürichen, M. Bolte, W. Bensch, *J. Solid State Chem.* **1998**, *140*, 97−102. − [10g] P. Dürichen, O. Krause, W. Bensch, *Chem. Mater.* **1998**, *10*, 2127−2134.
[11] [11a] B. M. Gatehouse, A. D. Wadsley, *Acta Crystallogr.* **1964**, *17*, 1545. − [11b] R. Norin, *Acta Chem. Scand.* **1966**, *20*, 871−880. − [11c] R. von der Muehl, A. Sadel, P. Hagenmüller, *J. Solid State Chem.* **1984**, *51*, 176−182. − [11d] J. C. Dewan, A. J. Edwards, G. R. Jones, *J. Chem. Soc., Dalton Trans.* **1978**, 968−972. − [11e] R. Hofmann, R. Gruehn, *Z. Anorg. Allg. Chem.* **1990**, *590*, 81−92.
[12] [12a] P. Boettcher, *Z. Kristallogr.* **1979**, *150*, 65−73. − [12b] M. Serafin, R. Hoppe, *J. Less-Common Met.* **1980**, *76*, 299−316.
[13] O. Krause, C. Näther, I. Jeß, W. Bensch, *Acta Crystallogr.* **1998**, *C54*, 902−904.

Received December 23, 1998
[I98454]

Pyrazolato Metal Complexes – Synthesis, Characterization, and X-ray Crystal Structures of Heterotrimetallic Re–M_2 Derivatives (M = Cu, Ag, Au)

G.Attilio Ardizzoia,*[a][+] Girolamo La Monica,[a][+] Angelo Maspero,[a] Norberto Masciocchi,[b][+] and Massimo Moret*[b]

Keywords: Pyrazolato ligands / Rhenium / Group-11 metals / Heterometallic complexes

By treating $[(CO)_3Re(Hpz)_2(pz)]$ (Hpz = pyrazole) with $[Cu(CH_3CN)_4]BF_4$, $AgNO_3$, or [Au(tht)Cl] (tht = tetrahydrothiophene) in acetonitrile in the presence of Et_3N, the corresponding trinuclear complexes $\{(CO)_3Re(pz)_3[M(CH_3CN)]_2\}$ (**1a–c**) have been obtained. Treatment of complexes **1a–c** with cyclohexyl isocyanide (*c*-$C_6H_{11}NC$) afforded the derivatives $\{(CO)_3Re(pz)_3[M(c\text{-}C_6H_{11}NC)]_2\}$ (**2a–c**). Complexes **2a–c** have been characterized in solution by ^{1}H-NMR spectroscopy and in the solid state by single-crystal X-ray diffraction analysis.

Introduction

The synthesis of di- and polynuclear complexes bearing ligands that hold the metal centers in close proximity is an important objective in metal coordination chemistry. Interest in such systems arises mainly because of their potential role in multi-metal-centered catalysis, both in biological and industrial reactions.[1] The major effort in this field is to find convenient binucleating ligands capable of producing the desired activities. Deprotonated pyrazoles (pyrazolate anions) represent a significant class of binucleating ligands because of their ability to coordinate in an *exo*-bidentate fashion.[2][3]

We have recently described the synthesis and structural properties of the mononuclear bis(pyrazole)pyrazolate complex of rhenium(I), $[(CO)_3Re(Hpz)_2(pz)]$ (Hpz = pyrazole).[4] This species belongs to a limited class of complexes that, from a coordination point of view, are comparable to protonated tris(pyrazolyl)borate molecules.[5] The other reported members of this class, $[(\eta^5\text{-}C_5Me_5)Ir(Hpz)(pz)_2]$,[6] $[(\eta^6\text{-}p\text{-cymene})Ru(Hpz)(pz)_2]$,[7] and $[(\eta^6\text{-mesitylene})Ru(Hpz)(pz)_2]$,[8] when deprotonated to give the anionic species $[(\eta^5\text{-}C_5Me_5)Ir(pz)_3]^-$, $[(\eta^6\text{-}p\text{-cymene})Ru(pz)_3]^-$, and $[(\eta^6\text{-mesitylene})Ru(pz)_3]^-$, have been shown to behave, in some respects, akin to the tris(pyrazolyl)borate anion, acting as organometallic ligands toward a variety of metal ions.[8][9]

We report herein on the reactivity of $[(CO)_3Re(Hpz)_2(pz)]$ towards Group-11 metal ions and show that, in the presence of an appropriate deprotonating agent, this complex gives rise to the formally dianionic species $[(CO)_3Re(pz)_3]^{2-}$, which is capable of coordinating two different metal centers through the lone pairs of its three monodentate pyrazolate groups. This leads to trimetallic species of general formula $[(CO)_3Re(pz)_3(ML)_2]$ [M = Cu^I, Ag^I, Au^I; L = CH_3CN, *c*-$C_6H_{11}NC$].

Results and Discussion

Reactions of $[(CO)_3Re(Hpz)_2(pz)]$ with $[Cu(CH_3CN)_4]BF_4$, $AgNO_3$, and [Au(tht)Cl] (tht = tetrahydrothiophene) in acetonitrile in the presence of Et_3N led to the formation of trimetallic species formulated as $\{(CO)_3Re(pz)_3[M(CH_3CN)]_2\}$ [M = Cu (**1a**), Ag (**1b**), Au (**1c**)] (Equation 1).

$$[(CO)_3Re(Hpz)_2(pz)] + 2\ ML_nX \xrightarrow[-Et_3NHX,\ -\ n\ L]{Et_3N\ /\ CH_3CN} [(CO)_3Re(pz)_3\{M(CH_3CN)\}_2] \qquad [1]$$

*(ML_nX = [Cu(CH$_3$CN)$_4$]BF$_4$, AgNO$_3$ or [Au(tht)Cl], for **1a-c**, respectively)*

The very low thermal stability of complexes **1a–c**, leading to loss of coordinated CH_3CN ligands and the formation of decomposition by-products, hampered any further characterization of these species. However, when reaction according to Equation 1 was carried out in the presence of stoichiometric amounts of *c*-$C_6H_{11}NC$, the readily characterizable species $\{(CO)_3Re(pz)_3[M(c\text{-}C_6H_{11}NC)]_2\}$ [M = Cu (**2a**), Ag (**2b**), Au (**2c**)] were obtained.

The IR spectra of all three species feature three strong ν(CO) bands in the 2000–1800 cm^{-1} region, typical for a *fac* stereochemistry at the rhenium center[10] and reminiscent of the spectrum of the starting rhenium complex $[Re(CO)_3(Hpz)_2(pz)]$. The positions of these absorptions are only marginally affected by the nature of the Group-11 metal (see Table 1). Moreover, no absorption attributable to the N–H stretching was detected, confirming the presence, in species **2**, of the $[(CO)_3Re(pz)_3]^{2-}$ core.

The pattern of the IR bands in the ν(NC) region merits further comment. While the copper (**2a**) and the silver (**2b**) derivatives show two absorptions (2210, 2164 and 2225, 2192 cm^{-1}, respectively), suggesting similar structures for

[a] Dipartimento di Chimica Inorganica, Metallorganica e Analitica, Università di Milano e Centro CNR,
Via Venezian, 21, I-20133 Milano, Italy
E-mail: attilio@csmtbo.mi.cnr.it
[b] Dipartimento di Chimica Strutturale e Stereochimica Inorganica, Università di Milano e Centro CNR,
Via Venezian, 21, I-20133 Milano, Italy
[+] On leave from: Dipartimento di Scienze Chimiche, Fisiche e Matematiche, Università dell'Insubria, Via Lucini, 3, I-22100 Como, Italy

 © WILEY-VCH Verlag GmbH, D-69451 Weinheim, 1999 1434–1948/99/0808–1301 $ 17.50+.50/0

Table 1. Characteristic IR frequencies [cm^{-1}] for complexes **2a**−**c** (Nujol mulls)

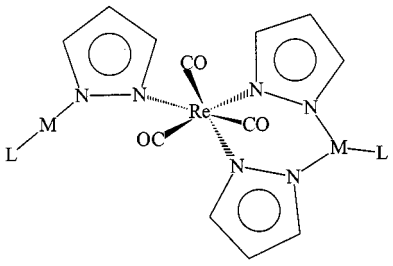
Complex	ν(CO)	ν(NC)
2a	2002, 1885, 1868	2210, 2164
2b	1999, 1882, 1860	2225, 2192
2c	2002, 1884, 1860	2253

both complexes, marked differences are observed for the gold derivative **2c**. Indeed, this species shows only one ν(NC) stretching at 2253 cm^{-1}, suggesting a structure distinct from that of the copper and silver derivatives.

As far as complexes **2a** and **2b** are concerned, taking into account that three pyrazolato groups (elemental analyses) and three CO molecules (IR) complete the coordination sphere about the rhenium center, the presence of two cyclohexyl isocyanide ligands bound to two copper (or silver) centers in different coordinative environments can be inferred. Given the ability of silver and copper to sustain digonal and trigonal geometries, it can be presumed that both such stereochemistries are present in the heterometallic species **2a** and **2b**. Under this assumption, the ν(NC) absorption at lower energy (2164 cm^{-1} for **2a**; 2192 cm^{-1} for **2b**) can be attributed to the cyclohexyl isocyanide group coordinated to the (more electron-rich) trigonal Cu^{I} and Ag^{I} centers.

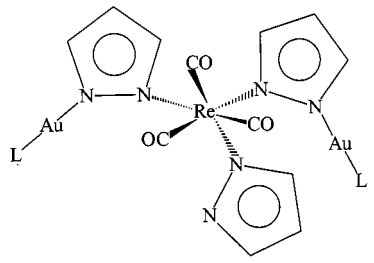
The different situation found in complex **2c** can be rationalized by taking into account the strong tendency of gold(I) to maintain a linear digonal coordination geometry; indeed, the presence in **2c** of two Au^{I} centers bonded to one pyrazolate nitrogen atom and one cyclohexyl isocyanide ligand each is consistent with the observation of a single ν(NC) absorption.

The proposed stuctures of **2a**−**c** (Scheme 1) have been unequivocally confirmed by single-crystal X-ray diffraction studies.



M = Ag, Cu L = c-$C_6H_{11}NC$

(A)



L = c-$C_6H_{11}NC$

(B)

Scheme 1. Schematic drawing of the connectivity patterns for complexes **2a**−**2b** (a) and **2c** (b)

Crystal Structures of 2a, 2b, and 2c

Crystals of compounds **2a**−**2c** are built up from neutral heterotrimetallic molecules held together by van der Waals interactions (see below for a more detailed description of the intermolecular interactions in **2c**). Figures 1−3 show ORTEP views of the molecular conformations of each compound, as observed in the solid state. Salient geometrical parameters are summarized in Table 2.

All three complexes contain an octahedral Re^{I} center bearing three carbonyl groups in a *fac* arrangement and three pyrazolato ligands able to connect to a second metal ion in an *exo*-bidentate mode. In **2a** and **2b**, two pyrazolate ligands are linked to the same Group-11 metal center M(1) [Cu(1) and Ag(1) for **2a** and **2b**, respectively] resulting in an Re−[N−N]$_2$−M(I) six-membered ring in the typical boat conformation. The difference in the ionic radii of the Cu^{I} and Ag^{I} species is mainly reflected in the M−N(2) and M−N(4) distances, which are about 0.25 Å longer in the Ag derivative. This leads to a remarkable narrowing of the

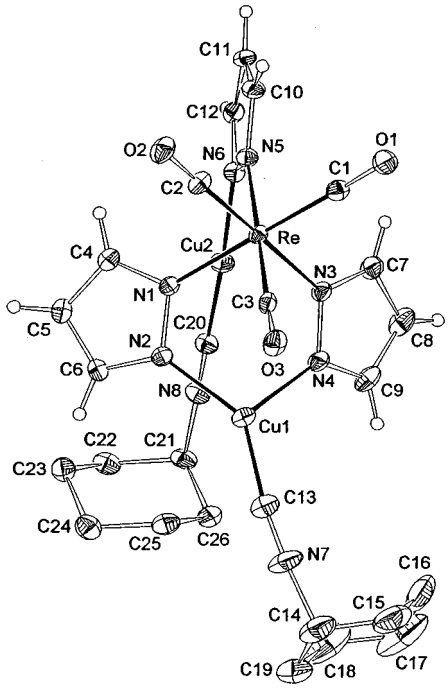


Figure 1. ORTEP drawing of complex **2a**, with partial labelling scheme; thermal ellipsoids are drawn at a 30% probability level; hydrogen atoms were given arbitrary radii

N(2)−M−N(4) angle in **2b** (see Table 2). The Cu^{I} [or Ag^{I}] center is further coordinated by a cyclohexyl isocyanide ligand, and therefore attains a planar-trigonal coordination environment [deviations from the coordination plane

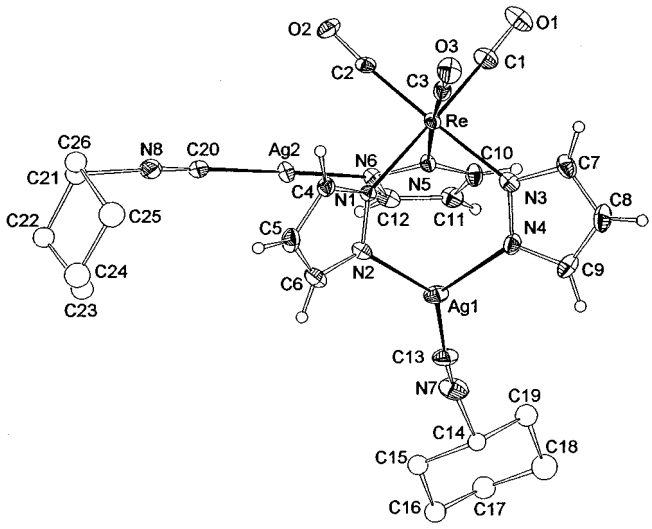


Figure 2. ORTEP drawing of complex **2b**, with partial labelling scheme; thermal ellipsoids are drawn at a 30% probability level; only the major component of the disordered cyclohexyl rings is drawn; hydrogen atoms were given arbitrary radii

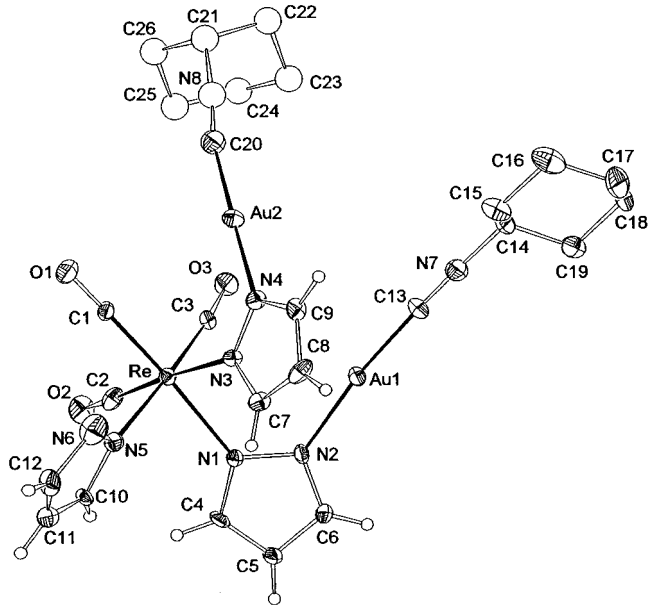


Figure 3. ORTEP drawing of complex **2c**, with partial labelling scheme; thermal ellipsoids are drawn at a 30% probability level; only the major component of the disordered cyclohexyl rings is drawn; hydrogen atoms were given arbitrary radii

amount to 0.084(4) and 0.016(4) Å for Cu(1) and Ag(1), respectively].

The remaining pyrazolate ligand is connected to the second Cu (**2a**) [or Ag (**2b**)] atom, the digonal coordination sphere of which is completed by another cyclohexyl isocyanide ligand. In this way, both molecules **2a** and **2b** contain one linearly coordinated and one trigonal-planar Group-11 metal ion, as was presumed on the basis of spectroscopic data. Nevertheless, the conformations of the Cu and Ag derivatives differ markedly in the solid state. Indeed, in **2a**, the Cu(1)−Re−N(5)−N(6) torsion angle is −0.2(5)° and

Table 2. Selected bond lengths [Å] and angles [°] for **2a−c** with e.s.d.′s in parentheses

Compound M	**2a** Cu	**2b** Ag	**2c** Au
Re−C(1)	1.902(8)	1.884(8)	1.891(11)
Re−C(2)	1.898(7)	1.919(8)	1.920(12)
Re−C(3)	1.903(8)	1.892(7)	1.886(11)
Re−N(1)	2.173(5)	2.199(5)	2.205(8)
Re−N(3)	2.181(5)	2.147(6)	2.189(8)
Re−N(5)	2.178(5)	2.170(5)	2.168(8)
M(1)−C(13)	1.828(8)	2.035(8)	1.920(11)
M(1)−N(2)	1.960(5)	2.218(5)	1.992(8)
M(1)−N(4)	1.986(6)	2.269(6)	
M(2)−N(4)			2.010(9)
M(2)−C(20)	1.834(7)	2.025(8)	1.946(14)
M(2)−N(6)	1.881(5)	2.096(5)	
O(1)−C(1)	1.151(8)	1.182(8)	1.161(11)
O(2)−C(2)	1.160(8)	1.138(7)	1.136(12)
O(3)−C(3)	1.162(8)	1.160(7)	1.163(11)
C(13)−M(1)−N(2)	139.7(3)	139.7(3)	173.4(5)
C(13)−M(1)−N(4)	117.7(3)	128.4(3)	
N(2)−M(1)−N(4)	102.0(2)	91.9(2)	
C(20)−M(2)−N(4)			176.9(4)
C(20)−M(2)−N(6)	169.3(3)	175.8(3)	
O(1)−C(1)−Re	178.3(7)	179.1(7)	178.4(10)
O(2)−C(2)−Re	177.8(6)	175.7(6)	176.7(11)
O(3)−C(3)−Re	177.0(6)	178.3(7)	173.3(10)

thus Cu(2) is nearly symmetrically buried within the pz(1−2) and pz(3−4) ligands, with an idealized mirror plane passing through Cu(1), Cu(2), Re, N(5), and N(6). On the contrary, the Ag(2)−CNC_6H_{11} moiety in **2b** is almost orthogonal to the Re−Ag(1) hinge [Ag(1)−Re−N(5)−N(6) 94.3(5)°]. Moreover, in terms of their "apparent" ionic radii, the Cu and Ag centers are about 0.1 Å larger in the trigonal than in the digonal environment.

In spite of the fact that all three complexes have the same general formula, the gold derivative **2c** has a completely different arrangement of the pyrazolate ligands. Owing to the lower tendency of gold for tricoordination, we observe a solid-state conformation with two digonally coordinated gold atoms, each bearing an isocyanide ligand and one nitrogen atom of a pyrazolato ligand. Thus, the third pyrazolato ligand is terminally bonded only to the rhenium atom in a monodentate fashion, leaving the second nitrogen lone pair unused.

While molecules **2a** and **2b** do not show significantly short intermolecular contacts in the crystals (which we have frequently observed for a number of Cu and Ag diazolato systems[11]), the packing of molecules **2c** reveals some additional features that merit further comment. Indeed, the crystal structure of **2c** reveals intermolecular interactions involving the gold atoms: Au(2)···Au(2)′ interactions of ca. 3.27 Å [relating molecules (x, y, z) and ($1-x$, $-y$, $-z$)] generate "dimeric" supramolecular entities; if the much looser Au(1)···Au(1)″ interactions [ca. 3.60 Å, relating (x, y, z) and ($-x$, $-y$, $-z$) molecules] are taken into account, an infinite 1-D concatenation of dimers can be envisaged, with pseudo-hexagonally packed chains of molecules running parallel to the a axis.

Solution Behaviour of 2a, 2b, and 2c

The structural analogies between complexes **2a** and **2b** found in the solid state were also seen in solution. The ^{1}H-NMR spectrum of **2b** recorded in CD_2Cl_2 at 303 K shows, beside the signals attributable to the cyclohexyl rings of the *c*-$C_6H_{11}NC$ ligands, a triplet centered at $\delta = 6.22$ ($J = 1.83$ Hz) attributable to C(4)−H of the pyrazolato rings, and two doublets ($\delta = 7.51$ and $\delta = 7.43$) attributable to C(3)−H and C(5)−H (Figure 4a). The observation of only one set of signals for each pyrazolato proton indicates that dynamic processes are operative that render all the pyrazolato groups present in the heterometallic species indistinguishable.

On lowering the temperature to 173 K, the ^{1}H-NMR spectrum of **2b** exhibits six signals at $\delta = 6.14$, 6.22, 7.07, 7.28, 7.45, and 8.03 in a 2:1:2:1:2:1 ratio, clearly attributable to C(4)−H (the two upfield signals) and C(3,5)−H of distinct pyrazolato groups (in a 2:1 ratio) (Figure 4c). Thus, although a partial broadening of the signals is still evident at this temperature, the observed pattern is consistent with the solid-state structure, indicating the almost complete freezing of the aforementioned dynamic process. At intermediate temperatures, the situation is less clear: The signals attributable to the protons in the 3- and 5-positions of the pyrazolate ligands collapse into a single resonance centered at $\delta = 7.41$ (Figure 4b). These features are seen over the 203−243 K range (with an increasing broadening of the signals); above 243 K, splitting into the two resonances observed at room temperature occurs.

An interpretation of the fluxional behaviour based on a concerted mutual exchange between the trigonal and digonal silver centers (as depicted in Scheme 2) can explain the limiting spectra at low and high exchange rates,[12] but is not able to account for the equivalence of the six protons in the 3- and 5-positions of the pyrazolate rings detected at intermediate exchange rates.

The spectroscopic observations may be rationalized by assuming that the exchange between the trigonal and digonal silver centers shown in Scheme 2 passes through transient intermediate species (species B_i in Scheme 3, $i = 1-3$) containing two singly bridged and one monodentate pyrazolato, as found in the solid state for the gold(I) derivative **2c**.

In fact, two exchange processes may be operative: one relating to the equilibrium between the doubly bridged and singly bridged species, $A_i - B_i$ (Scheme 3), and the second, responsible for rendering the 3- and 5-positions of the pyrazolate rings indistinguishable, involving N(1)/N(2) scrambling ($B_i - B'_i$), which is frequently found in complexes containing anionic monodentate pyrazolate ligands.[13] Hence, the ^{1}H-NMR pattern can be attributed to the relative rates of these two processes. Schematically, we can write the equilibrium as shown in Equation 2.

In the intermediate temperature range, the lifetime of the species B_i is sufficiently long to permit "hopping" of the metal atom between the two nitrogen atoms of the monodentate pyrazolate ring, making the 3- and 5-protons indis-

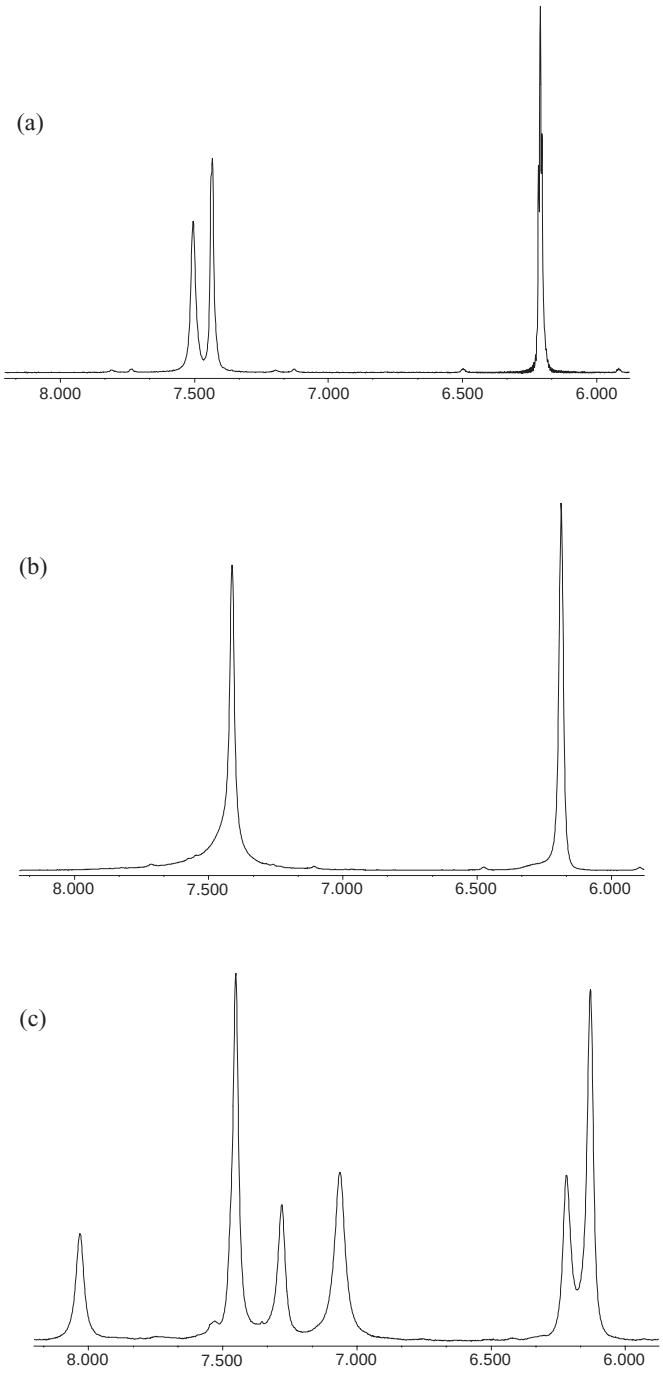
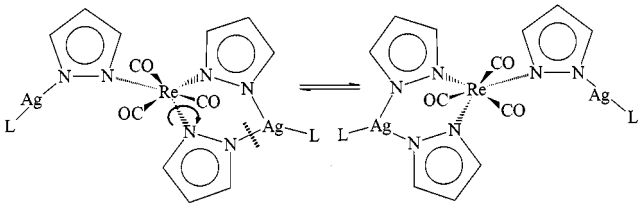
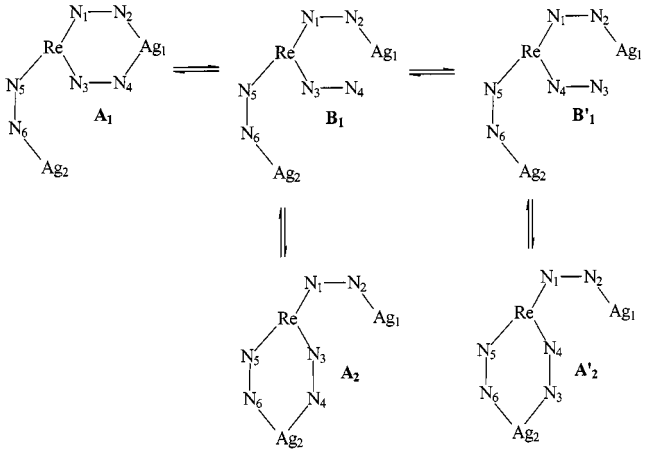


Figure 4. ^{1}H-NMR spectra (CD_2Cl_2 solution) in the pyrazolate-H region for compound **2b**: (a) at room temp., (b) at 213 K, and (c) at 173 K



Scheme 2. Concerted mutual exchange between the trigonal and digonal silver centers in complex **2b**



Scheme 3. Proposed mechanism for the dynamic process involving complex **2b**; similar equilibria are seen for all A_j species (see text)

$$A_i \rightleftharpoons \{B_i, B'_i\} \rightleftharpoons A_j \qquad [2]$$

tinguishable. At higher temperatures, the rapid opening/closure of the Ag−[N−N]$_2$−Ag metallocycle hampers this scrambling and hence the equilibration of the 3- and 5-positions. In terms of kinetic parameters (Arrhenius law), this corresponds qualitatively to rather different temperature dependences for the two processes, i.e. $\Delta E^{\neq}_{\text{open-close}} > \Delta E^{\neq}_{\text{scramble}}$ and $\ln A_{\text{open-close}} > \ln A_{\text{scramble}}$.

The room-temperature ^{1}H-NMR spectrum of the copper derivative **2a** closely matches that of species **2b** [two doublets centered at δ = 7.50 and 7.45, respectively; J = 1.92 Hz; a pseudo triplet at δ = 6.23]. On lowering the temperature to 173 K, all signals are broadened, but the overall spectral features do not change significantly. Indeed, the ^{1}H-NMR spectra of complex **2a** over the entire 303−173 K range are similar to those of **2b** in the "high" temperature range (above 243 K). This fact, assuming that the same fluxional processes active in **2b** also occur in **2a**, seems to indicate lower rigidity of the copper derivative compared to its silver counterpart.

As far as complex **2c** is concerned, the room-temperature ^{1}H-NMR spectrum shows, in the region of the pyrazole sig-

Table 3. Summary of single-crystal X-ray data and structure refinement parameters

Compound	**2a**	**2b**	**2c**
Empirical formula	$C_{26}H_{31}Cu_2N_8O_3Re$	$C_{26}H_{31}Ag_2N_8O_3Re$	$C_{26}H_{31}Au_2N_8O_3Re$
Molecular mass	816.87	905.53	1083.72
Crystal system	monoclinic	triclinic	monoclinic
Space group	$P2_1/c$	$P-1$	$P2_1/c$
a [Å]	18.631(6)	9.686(1)	13.521(1)
b [Å]	10.124(3)	13.344(1)	11.215(1)
c [Å]	16.660(7)	13.527(4)	21.016(1)
α [°]		109.43(1)	
β [°]	102.59(3)	100.70(1)	104.67(1)
γ [°]		102.24(1)	
V [Å^3]	3066.9(19)	1547.9(5)	3083.1(3)
Z	4	2	4
F(000)	1600	872	2000
D(calcd.) [g cm^{-3}]	1.769	1.943	2.335
Temperature [K]	293(2)	293(2)	293(2)
Diffractometer	CAD4	SMART	SMART
Radiation [Å]	0.71073	0.71073	0.71073
Absorption coefficient [mm^{-1}]	5.352	5.193	13.451
Crystal size [mm]	0.05 × 0.25 × 0.25	0.12 × 0.12 × 0.20	0.03 × 0.03 × 0.10
Scan method	ω	ω	ω
Scan interval [°]	1.5 + 0.35tanθ	0.3[a]	0.3[a]
Max time per refln. [s]	75	30[a]	60[a]
θ range [°]	3.0−25.0	2.2−28.5	2.0−28.0
Index ranges	$-22 \le h \le 21$	$-8 \le h \le 12$	$-13 \le h \le 16$
	$0 \le k \le 12$	$-17 \le k \le 17$	$-14 \le k \le 14$
	$0 \le l \le 19$	$-17 \le l \le 11$	$-25 \le l \le 26$
Reflections collected	5349	9774	16706
Independent reflections	5349 (R_{int} = 0.00)	7141 (R_{int} = 0.030)	6451 (R_{int} = 0.056)
Crystal decay	7%	none	none
Absorption correction	Ψ-scan	Sadabs	Sadabs
Min. transmission factor	0.44	0.695	0.742
Observed reflection criterion		all reflections	
Refinement method		full-matrix least squares on F_o^2	
Data/restraints/parameters	5349/0/361	7141/48/351	6451/15/326
Goodness-of-fit[b] on F_o^2	1.006	0.778	0.957
$R1$, $wR2$ indices[c] [$F_o > 4\sigma(F_o)$]	0.0305, 0.0691	0.0383, 0.0738	0.0492, 0.0724
$R1$, $wR2$ indices (all data)	0.0864, 0.0823	0.0772, 0.0817	0.1090, 0.0850
Largest diff. peak and hole [eÅ^{-3}]	1.214, −0.987	1.248, −1.386	1.023, −1.036
Weighting scheme:[d] a, b	0.0418, 2.5380	0.0333, 0	0.0306, 0

[a] Frame width and exposure time per frame. − [b] GoF = $[\Sigma w(F_o^2 - F_c^2)^2/(n-p)]^{1/2}$ where n is the number of reflections and p is the number of refined parameters. − [c] $R1 = \Sigma||F_o| - |F_c||/\Sigma|F_o|$, $wR2 = [\Sigma w(F_o^2 - F_c^2)/\Sigma wF_o^4]^{1/2}$. − [d] $w = 1/[\sigma(F_o^2) + (aP)^2 + bP]$ where $P = (F_o^2 + 2F_c^2)/3$.

nals, three doublets (6 H, in a 1:1:1 ratio) centered at δ = 7.77 (J = 1.92 Hz), δ = 7.53 (J = 1.75 Hz), and δ = 7.43 (J = 1.75 Hz), respectively, along with two triplets (3 H, in a 1:2 ratio) centered at δ = 6.25 and δ = 6.21, respectively. On lowering the temperature, the second doublet and the downfield triplet broaden and disappear, and finally, at −40°C, only three signals remain. Further lowering of the temperature leads to a drastic change in the spectrum with the appearance of new, partially overlapped signals. Presently, we are unable to give a complete explanation of this behaviour. This effect might be a manifestation of exchange processes similar to those observed for **2b**, but the non-equivalence of the Re−[N−N]$_2$−Au fragments further increases the complexity of the spectrum.

Conclusions

We have demonstrated herein that the organometallic complex [(CO)$_3$Re(Hpz)$_2$(pz)], once deprotonated, can act as a multidentate ligand towards a variety of metal atoms. The analogy with the tris(pyrazolyl)borate anion is, however, partially obscured by the fact that "tripod-like" coordination of Group-11 metal atoms was not observed, probably because of the specific electronic/steric requirements of the present systems, which favour low coordination numbers. Preliminary studies of Re−Mn derivatives have revealed that triply bridged [(CO)$_3$Re(μ-pz)$_3$MnL$_n$] systems can indeed be prepared, but these will be reported in a forthcoming paper.

Additionally, variable-temperature NMR analyses have clearly revealed the nonrigidity of the isolated species and have indicated that fluxionality can be attributed to simultaneous scrambling of monodentate pyrazolato ligands and ring-opening/closure equilibria, leading to a rather complex "argentotropic" behaviour.[12]

Experimental Section

General: Solvents were dried and purified by standard methods. Pyrazole (Aldrich Chemical Co.) was used as supplied. − Infrared spectra were recorded with a Bio Rad FT-IR 7 instrument. − ^{1}H-NMR spectra were acquired with a Bruker AC-300 FT spectrometer operating at 300.13 MHz. − Elemental analyses were performed at the Microanalytical Laboratory of this university (C, H, N). − All reactions were carried out under dry nitrogen using standard Schlenk techniques.

{(CO)$_3$Re(μ-pz)$_3$[Cu(CyNC)]$_2$} (2a): [(CO)$_3$Re(Hpz)$_2$(pz)][4] (150 mg, 0.317 mmol) was dissolved in acetonitrile (10 mL) and solid [Cu(CH$_3$CN)$_4$](BF$_4$)[14] (210 mg, 0.668 mmol) was added under stirring. Triethylamine (0.5 mL) was then added and the yellow solution was stirred for a further 15 min. A solution of cyclohexyl isocyanide (90 μL) in degassed CH_2Cl_2 (ca. 2 mL) was then added, leading to a colorless solution. After stirring for 30 min, the solvent was completely evaporated, the residue was treated with ethanol, and the white solid was collected by filtration, washed with ethanol, and dried in vacuo (155 mg, 60% yield). − $C_{26}H_{31}Cu_2N_8O_3Re$ (816.87): calcd. C 38.23, H 3.83, N 13.73; found C 38.06, H 3.78, N 13.38. − Crystals suitable for X-ray structure analysis were obtained by slow diffusion of *n*-hexane into dichloromethane solutions of the complex.

{(CO)$_3$Re(μ-pz)$_3$[Ag(CyNC)]$_2$} (2b): To a solution of [(CO)$_3$Re(Hpz)$_2$(pz)] (100 mg, 0.21 mmol) in acetonitrile (4 mL), was added a solution of $AgNO_3$ (94 mg, 0.55 mmol) in water (ca. 2 mL). Triethylamine (0.5 mL) was then added dropwise to the colorless solution, resulting in the sudden deposition of a white solid. The suspension was stirred for a further 15 min, and then the solid was collected by filtration, washed with water, and dried in vacuo (compound **1b**). **1b** was suspended in CH_2Cl_2 (ca. 2 mL) and cyclohexyl isocyanide (60 μL) was added to the white suspension, giving a colorless solution. The solvent was then evaporated in vacuo and the residue was treated with Et_2O, filtered, and dried in vacuo (108 mg, 57% yield). − $C_{26}H_{31}Ag_2N_8O_3Re$ (905.53): calcd. C 34.51, H 3.46, N 12.39; found C 34.83, H 3.54, N 12.35. − Crystals suitable for X-ray structure analysis were obtained by slow diffusion of *n*-hexane into dichloromethane solutions of the complex.

{(CO)$_3$Re(μ-pz)$_3$[Au(CyNC)]$_2$} (2c): To a stirred solution of [(CO)$_3$Re(Hpz)$_2$(pz)] (200 mg, 0.422 mmol) in acetonitrile (ca. 6 mL) at 0°C under nitrogen, was added [Au(tht)Cl][15] (tht: tetrahydrothiophene) (269 mg, 0.883 mmol). Tributylamine (0.5 mL) was then added dropwise. After a few minutes, a white solid separated from the colorless solution. The suspension was kept at 0°C and stirred for a further 3 h. The white solid was then collected by filtration and dried in vacuo (compound **1c**). Cyclohexyl isocyanide (60 μL) was added to a suspension of **1c** in CH_2Cl_2 (ca. 3 mL), giving a colorless solution. This solution was then concentrated to dryness and the residue was treated with ethanol. The white solid obtained was filtered off, washed with ethanol, and dried in vacuo (261 mg, 57% yield). − $C_{26}H_{31}Au_2N_8O_3Re$ (1083.72): calcd. C 28.78, H 2.88, N 10.33; found C 28.81, H 2.80, N 10.26. − Crystals suitable for X-ray structure analysis were obtained by slow diffusion of *n*-hexane into dichloromethane solutions of the complex, with protection from light.

Crystallography:[16] Crystals of **2a−c** were studied by conventional single-crystal X-ray methods; an overview of the methodology used can be found in ref.[11b] Owing to disorder involving the cyclohexyl moieties in **2b** and **2c**, special procedures were adopted during the structure refinement. For **2b**, the cyclohexyl rings were each described by two models having 62/38% and 52/48% occupancy factors, respectively. In **2c**, only one cyclohexyl ring was found to be disordered (with a 54/46% ratio) but required, in order to achieve least-squares stability, a common (isotropic) atomic displacement parameter. Hydrogen atoms of the disordered groups were omitted from the structure factor calculations. A list of crystal data, refinement parameters, and final agreement factors is presented in Table 3.

Acknowledgments

This work was supported by the Ministero dell'Università e della Ricerca Scientifica e Tecnologica (MURST) and by the Italian Consiglio Nazionale delle Ricerche (CNR). The technical support of Mr. Gianni Mezza is also acknowledged.

[1] [1a] R. Poilblanc, *Inorg. Chim. Acta* **1982**, *62*, 75−89. − [1b] C. Tejel, J. M. Villoro, M. A. Ciriano, J. A. López, E. Eguizábal, F. J. Lahoz, V. I. Bakhmutov, L. A. Oro, *Organometallics* **1996**, *15*, 2967−2978.

[2] [2a] S. Trofimenko, *Chem. Rev.* **1972**, *72*, 497−509. − [2b] S. Trofimenko, *Prog. Inorg. Chem.* **1986**, *34*, 115−210. − [2c] G. La Monica, G. A. Ardizzoia, *Prog. Inorg. Chem.* **1997**, *46*, 151−238.

[3] A few *endo*-bidentate pyrazolate complexes have been structurally characterized: [3a] C. W. Eigenbrot, Jr., K. N. Raymond, *Inorg. Chem.* **1981**, *20,* 1553−1556. − [3b] C. W. Eigenbrot, Jr., K. N. Raymond, *Inorg. Chem.* **1982**, *21,* 2653−2660. − [3c] D. Röttger, G. Erker, M. Grehl, R. Frölich, *Organometallics* **1994**, *13*, 3897−3902. − [3d] I. A. Guzei, G. A. Baboul, G. P. A. Yap, A. L. Rheingold, H. B. Schegel, C. H. Winter, *J. Am. Chem. Soc.* **1997**, *119*, 3387−3388. − [3e] J. E. Cosgriff, G. B. Deacon, *Angew. Chem.* **1998**, *110*, 298−299; *Angew. Chem. Int. Ed. Engl.* **1998**, *37*, 286−287 and references therein. − [3f] D. Pfeiffer, M. J. Heeg, C. H. Winter, *Angew. Chem.* **1998**, *110*, 2674−2676; *Angew. Chem. Int. Ed. Engl.* **1998**, *37,* 2517−2519.

[4] G. A. Ardizzoia, G. La Monica, A. Maspero, M. Moret, N. Masciocchi, *Eur. J. Inorg. Chem.* **1998**, 1503−1511

[5] S. Trofimenko, *Chem. Rev.* **1993**, *93*, 943−980.

[6] D. Carmona, L. A. Oro, M. P. Lamata, J. Elguero, M. C. Apreda, C. Foces-Foces, F. H. Cano, *Angew. Chem. Int. Ed. Engl.* **1986**, *25*, 1114−1115.

[7] D. Carmona, J. Ferrer, L. A. Oro, M. C. Apreda, C. Foces-Foces, F. H. Cano, J. Elguero, M. L. Jimeno, *J. Chem. Soc., Dalton Trans.* **1990**, 1463−1476.

[8] D. Carmona, F. J. Lahoz, R. Atencio, A. J. Edwards, L. A. Oro, M. P. Lamata, M. Esteban, S. Trofimenko, *Inorg. Chem.* **1996**, *35*, 2549−2557.

[9] [9a] D. Carmona, F. J. Lahoz, L. A. Oro, M. P. Lamata, S. Buzarra, *Organometallics* **1991**, *10*, 3123−3131. − [9b] D. Carmona, L. A. Oro, M. P. Lamata, M. L. Jimeno, J. Elguero, A. Belguise, P. Lux, *Inorg. Chem.* **1994**, *33*, 2196−2203. − [9c] D. Carmona, J. Ferrer, R. Atencio, F. Lahoz, L. A. Oro, M. P. Lamata, *Organometallics* **1995**, *14*, 2057−2065.

[10] R. J. Angelici, F. Basolo, A. J. Poe, *J. Am. Chem. Soc.* **1963**, *85*, 2215−2219.

[11] [11a] G. A. Ardizzoia, S. Cenini, G. La Monica, N. Masciocchi, A. Maspero, M. Moret, *Inorg. Chem.* **1998**, *37*, 4284−4292. − [11b] G. A. Ardizzoia, G. La Monica, A. Maspero, M. Moret, N. Masciocchi, *Inorg. Chem.* **1997**, *36*, 2321−2328. − [11c] N. Masciocchi, M. Moret, P. Cairati, A. Sironi, G. A. Ardizzoia, G. La Monica, *J. Chem. Soc., Dalton Trans.* **1995**, 1671−1675. − [11d] N. Masciocchi, M. Moret, P. Cairati, A. Sironi, G. A. Ardizzoia, G. La Monica, *J. Am. Chem. Soc.* **1994**, *116*, 7668−7676.

[12] This *argentotropism* has previously been reported for related species such as $\{(Cp^*)Ir(pz)_3[Ag(PPh_3)]_2\}^+$ and {(*p*-cymene)$Ru(pz)_3[Ag(PPh_3)]$}; see refs.[7,9b]

[13] [13a] A. L. Bandini, G. Banditelli, F. Bonati, G. Minghetti, F. Demartin, M. Manassero, *J. Organomet. Chem.* **1984**, *269*, 91−105. − [13b] D. Röttger, G. Erker, M. Grehl, R. Fröhlich, *Organometallics* **1994**, *13*, 3897−3902.

[14] G. J. Kubas, *Inorg. Synth.* **1979**, *19*, 90−91

[15] R. Uson, A. Laguna, M. Laguna, *Inorg. Synth.* **1989**, *26*, 85−86

[16] Crystallographic data for the structures reported in this paper have been deposited with the Cambridge Crystallographic Data Centre as supplementary publications nos. CCDC-112751 (**2a**), -112752 (**2b**), and -112753 (**2c**). Copies of the data can be obtained free of charge on application to CCDC, 12 Union Road, Cambridge CB2 1EZ, U.K. [Fax: (internat.) + 44-1223/336-033; E-mail: deposit@ccdc.cam.ac.uk].

Received December 30, 1998
[I98457]

Synthesis and Investigations on Nitrido(phthalocyaninato)rhenium Complexes

Karsten Frick,[a] Ulrich Ziener,[a] and Michael Hanack*[a]

Keywords: Phthalocyanines / Rhenium / Nitrido(octa-*n*-alkylphthalocyaninato)rhenium compounds / Nucleophilic additions

The reactions of nitrido(tetra-*tert*-butylphthalocyaninato)-rhenium (**1**) with boron tribromide leading to (tBu$_4$Pc)-ReNBBr$_3$ (**4**) and with acetone to give the imido complex (tBu$_4$Pc)Re[NC(CH$_3$)$_2$CH$_2$C(O)CH$_3$]OH (**2b**) and its μ-oxo dimer **3** are reported. Starting from the corresponding 4,5-di-*n*-alkylphthalonitriles and ammonium perrhenate four soluble nitrido(octa-*n*-alkylphthalocyaninato)rhenium complexes **5**–**8** were synthesized. Nitrido(octa-*n*-pentylphthalocyaninato)rhenium (**6**) was treated with boron tribromide to afford [(C$_5$H$_{11}$)$_8$Pc]ReNBBr$_3$ (**9**).

To investigate the chemical and optoelectronic properties of hitherto unknown nitrido-bridged phthalocyaninato transition-metal/main-group complexes (PcMNPcM′: M = Re, Mo, W; M′ = Si, Ge, Sn) a suitable synthetic procedure was needed. The heavier transition-metal ions in high oxidation states, which are suitable to form the M−N triple bond, are used to prepare the nitrido complexes. N^{3-} (nitride) containing a triple bond is known as one of the strongest π-donor ligands.[1] Some (nitrido)metal complexes of porphyrins, e.g. (TPP)MnN,[2] (OEP)ReN[3] and others[4] have been prepared, some nitrido complexes with phthalocyanines are also known, namely PcMnN,[5] PcTcN,[6] PcReN[7] and the dinuclear complexes (PcFe)$_2$N[8] and (PcRu)$_2$N.[9] These nitrido(phthalocyaninato) complexes are practically all insoluble in organic solvents. Recently, we published the first soluble (phthalocyaninato)rhenium compound, (tBu$_4$Pc)ReN (**1**),[10] which exists in four structural isomers.

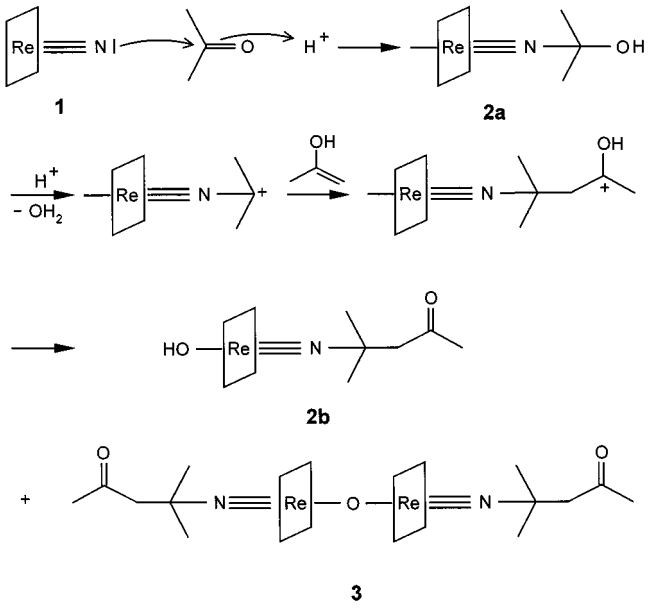
Here we report on the reaction of (tBu$_4$Pc)ReN (**1**) with boron tribromide leading to (tBu$_4$Pc)ReNBBr$_3$ (**4**) and the reaction of **1** with acetone to afford (tBu$_4$Pc)Re-[NC(CH$_3$)$_2$CH$_2$C(O)CH$_3$]OH (**2b**) and {(tBu$_4$Pc)Re-[NC(CH$_3$)$_2$CH$_2$C(O)CH$_3$]}$_2$O (**3**), which are the first μ-nitrido(phthalocyaninato) complexes between rhenium and boron or carbon, respectively. In addition we describe the synthesis of the octasubstituted (phthalocyaninato)rhenium complexes [(C$_4$H$_9$)$_8$Pc]ReN (**5**), [(C$_5$H$_{11}$)$_8$Pc]ReN (**6**), [(C$_6$H$_{13}$)$_8$Pc]ReN (**7**) and [(C$_7$H$_{15}$)$_8$Pc]ReN (**8**) and the reaction of **6** with BBr$_3$.

The reaction of a mixed-ligand nitridorhenium(V) complex, [ReN(Cl)(Me$_2$PhP)$_2$R$_2$tcb] [R$_2$tcb = *N*-(*N*,*N*-dialkylthiocarbamoyl)benzamidinate] with HCl and HBr in acetone to form a nitrene-like compound, Re[NC(CH$_3$)$_2$-CH$_2$C(O)CH$_3$]X$_3$(Me$_2$PhP)$_2$ (X = Cl, Br) was recently described.[11] On addition of few drops of concentrated HCl to a suspension of tBu$_4$PcReN (**1**) in acetone a colour change from blue to blue-green occurs with dissolution of the solid. A UV/Vis spectrum of this solution exhibits broader bands with a red shift of the Q band of 30 nm relative to that of the starting material. The change in colour may be due to protonation of either the isoindoline nitrogen atoms of **1**[12] or the nitrido N atom. In the mechanism given in ref.[11], firstly the formation of diacetone alcohol due to the addition of HCl and secondly the attack of the nitrido nitrogen atom at the C−OH group are described. A direct way seemed more appropriate to us, namely a nucleophilic attack of the nitrido N atom to the carbonyl C atom of acetone to form **2a**, which reacts with a second molecule of acetone to form **2b** as shown in Scheme 1. This suggestion avoids the formation of diacetone alcohol in the first step which is very much dependent upon the acid concentration and temperature. After a reaction time of several days, the condensation product **2b** of diacetone alcohol and **1** was isolated (Scheme 1). For charge compensation, the *trans* position at the rhenium atom is occupied by OH^-. While purifying the crude product by column chromatography on aluminium oxide a small amount of the μ-oxo dimer {(tBu$_4$Pc)Re[NC-(CH$_3$)$_2$CH$_2$C(O)CH$_3$]}$_2$O (**3**) is eluted (see below).

A comparison of the IR spectra of (tBu$_4$Pc)Re-[NC(CH$_3$)$_2$CH$_2$C(O)CH$_3$]OH (**2b**) with that of (tBu$_4$Pc)ReN (**1**) reveals the disappearance of $\tilde{\nu}_{Re\equiv N}$ = 978 cm^{-1} in **2b**, while additional bands at $\tilde{\nu}$ = 1123, 1148 and 3651 cm^{-1} appear. One of the two bands at $\tilde{\nu}$ = 1123 cm^{-1} and $\tilde{\nu}$ = 1148 cm^{-1} is assigned to the stretching vibration $\tilde{\nu}_{Re\equiv N}$.[1] There is no possible assignment for the origin of the other band. The C=O vibration of **2b** can be attributed to the band at $\tilde{\nu}_{C=O}$ = 1718 cm^{-1}. **A** weak but sharp band at $\tilde{\nu}$ = 3651 cm^{-1} is caused by the OH group. The ^{1}H-NMR spectrum of **2b** shows, besides the expected signals for the *tert*-butyl protons (δ = 1.74−1.95) and the protons in the aromatic region (δ = 8.13 and 9.35), three groups of signals at δ = 0.14, −0.80 and −2.08 in the ratio 3:2:6. They are assigned to CH$_3$ in the neighbourhood of the carbonyl group, the CH$_2$ group and the equivalent CH$_3$ groups, respectively. The splitting of these groups is either caused by aggregation effects or is due to the four isomers

[a] Institut für Organische Chemie, Lehrstuhl II,
Universität Tübingen
Auf der Morgenstelle 18, D-72076 Tübingen, Germany
Fax: (internat.) + 49(0)7071/295244
E-mail: hanack@uni-tuebingen.de

 © WILEY-VCH Verlag GmbH, D-69451 Weinheim, 1999 1434−1948/99/0808−1309 $ 17.50+.50/0



Scheme 1. Possible mechanism leading to **2b** and **3**

present in tetrasubstituted phthalocyanines.[13] The structure of **2b** is also proved by its ^{13}C-NMR spectrum. In addition to the signals already observed for **1**,[10] five signals for **2b** at δ = 202.07, 65.51, 47.40, 29.17 and 21.65 corresponding to the six C atoms of the axial ligand are observed.

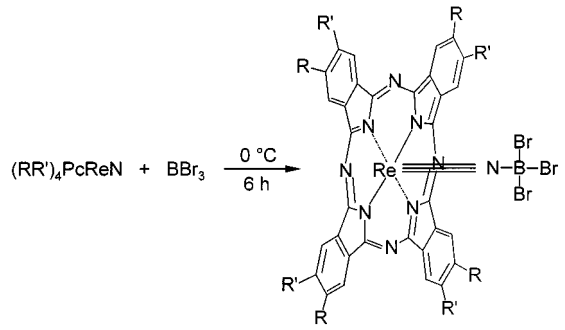
Besides some changes in intensity, the IR spectrum of **3** shows two new bands at $\tilde{\nu}$ = 727 and 802 cm^{-1}, which cannot be assigned and consequently no O−H vibration $\tilde{\nu}$ = 3651 cm^{-1} was observed. Dimeric phthalocyanines with a coplanar arrangement of the macrocycles and an ideal D_{4h} symmetry show a blue shift of the Q band,[14] which is also observed in **3** by 37 nm relative to **1**. From this shift the exciton coupling can be estimated to be about 1600 cm^{-1}, which is in accordance with the value for dimeric phthalocyanines.[14]

The ^{1}H-NMR spectrum of **3** exhibits in all regions sharp signals in the expected ratio of intensity. In the aromatic region several signals between δ = 9.46 and 8.20 are found besides signals due to the *tert*-butyl protons between δ = 2.63 and 2.05, which are attributed to the higher number of isomers. The low-field shift of the *tert*-butyl protons by about 0.5 ppm and the high-field shift of the protons of the axial imido ligand at δ = −0.63, −1.68 and −3.01 of about 0.7 to 1.0 in **3** are caused by the additional ring current of the second macrocycle.

The unsubstituted PcReN does not react with acetone/HCl even after several days. This is due to the poor solubility of PcReN.

(Nitrido)metal complexes are suitable precursors to complexes with nitrogen bridges between the transition-metal rhenium (M) and main-group elements such as, for example, boron (M′) (M≡N−M′). We investigated the possibility of a reaction of **1** and $(C_5H_{11})_8$PcReN (**6**) with BBr_3. Nitrogen-bridged rhenium−boron complexes like $Br_4ReNBBr_3$,[15a] $Re(NBCl_3)Cl_2[P(CH_3)_2C_6H_5]_3$[15b] and $(PEt_2C_6H_5)_3X_2ReNBY_3$ (X = Cl, Br; Y = F, Cl, Br)[15c] are known.

The reaction of (tBu$_4$Pc)ReN (**1**) with the Lewis acid BBr_3 in dichloromethane at 0°C for 6 h leads to a bonding of the boron atom to the axial nitrogen atom of **1** (Scheme 2). After removing the solvent and the excess of BBr_3 under vacuum, (tBu$_4$Pc)ReNBBr$_3$ (**4**) was obtained, which is sensitive to moisture.



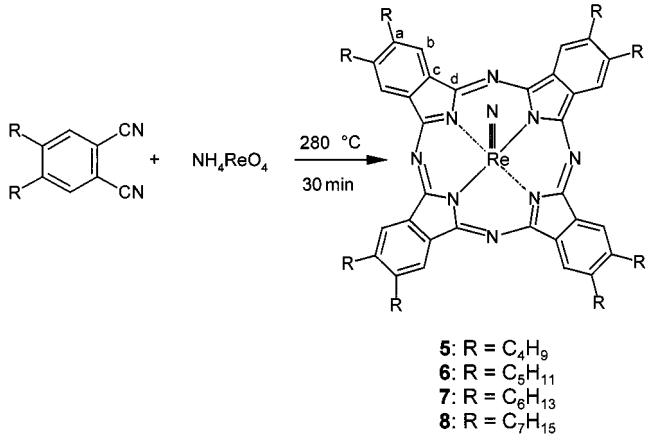
1: R = H, R' = *t*Bu
6: R = R' = C_5H_{11}
4: R = H, R' = *t*Bu (D_{4h}-isomer)
9: R = R' = C_5H_{11}

Scheme 2. Synthesis and Structure of (tBu$_4$Pc)ReNBBr$_3$ (**4**) and [$(C_5H_{11})_8$Pc]ReNBBr$_3$ (**9**)

In the FD MS and ionspray MS the M$^+$ peak of **4** was absent. However, (tBu$_4$Pc)ReNBBr$_2$, (tBu$_4$Pc)ReNBBr and BBr_3 were detected at m/z = 1107.5, 1029.6 and 250.8, respectively. The peak for **1** is also found in these spectra due to adventitious moisture present, which decomposes **4** to HBr, $B(OH)_3$ and **1**. The IR spectrum of **4** shows new vibrations compared to **1**. The Re−N triple bond vibration at $\tilde{\nu}_{Re\equiv N}$ = 978 cm^{-1} is shifted to 1196 cm^{-1}. This band matches with the vibrations reported for a nitrido bridge between the rhenium and the boron atom, which is assigned at $\tilde{\nu}$ = 1170 and 1180 cm^{-1}.[15b] This absorption at lower wavelength of $\tilde{\nu}_{Re\equiv N}$ is caused by the coupling with the B−N vibration of the presumably linear axis Re≡N−B.[15b] The extent of this coupling is lower than in complexes like Re≡N−C ($\tilde{\nu}_{Re\equiv N}$ = 1123 or 1148 cm^{-1} for **2b**) due to the higher frequency of $\tilde{\nu}_{N-C}$ relative to $\tilde{\nu}_{N-B}$. The latter appears at $\tilde{\nu}_{N-B}$ = 645 cm^{-1} and the BBr_3 stretching vibration at $\tilde{\nu}_{B-Br}$ = 671 cm^{-1}. In general, the N−B vibrations are located between 650 and 780 cm^{-1}.[16] The absorption at longer wavelength is due to the coupling with $\tilde{\nu}_{Re\equiv N}$. In the UV/Vis spectrum of **4** the Q band is red-shifted from λ = 697 to 725 nm due to the electron-withdrawing effect of the BBr_3 group. The band is broadened and shows a shoulder at λ = 755 nm. Furthermore, the ^{11}B-NMR spectrum of **4** gave unambiguous evidence for a boron−nitrogen bond. Relative to that of BBr_3 (δ = 38.15), the ^{11}B signal of (tBu$_4$Pc)ReNBBr$_3$ (**4**) is shifted to δ = −12.90 showing the influence of the aromatic Pc ring.

To improve the stability of nitrido-bridged (phthalocyaninato)rhenium complexes and keep the good solubility we replaced the large *tert*-butyl groups by alkyl chains. Therefore the (octaalkylphthalocyaninato)rhenium complexes, [$(C_4H_9)_8$Pc]ReN (**5**), [$(C_5H_{11})_8$Pc]ReN (**6**), [$(C_6H_{13})_8$Pc]ReN

(**7**) and [$(C_7H_{15})_8$Pc]ReN (**8**) were synthesized by treating the respective 4,5-di-*n*-alkylphthalodinitriles with ammonium perrhenate.[10] The phthalocyanines were purified by Soxhlet extraction with methanol followed by column chromatography with dichloromethane. The yields are lower than that of unsubstituted PcReN[17] but similar to the yield of (tBu$_4$Pc)ReN (**1**)[10] (Scheme 3).



Scheme 3. Synthesis and Structure of **5**−**8**

The IR spectra of **5**−**8** resemble other octa-*n*-alkyl-substituted (phthalocyanine)metal complexes[18] except in the region between 950 and 1000 cm^{-1}. A band of low intensity is observed in all IR spectra of **5**−**8**, which is assigned to the Re−N triple-bond stretching vibration.[1] These bands are in agreement with those found for PcReN[6] and (tBu$_4$Pc)ReN (**1**).[10] The UV/Vis spectra of the **5**−**8** show the Q band at λ = 705 nm (π-π* transition) for **5** and vibronic transitions at λ = 673 and 633 nm (in toluene) [**6** (CH_2Cl_2): λ = 708, 676, 638; **7** (toluene): λ = 704, 671, 634; **8** (CH_2Cl_2): λ = 708, 676, 638]. The slight blue shift of the Q band in **5**,**7** relative to **6**,**8** is caused by the change of solvent. Compounds **5**−**8** show a red shift of the Q band of about 30 nm relative to that of other octasubstituted phthalocyanines.[18] This difference may be caused by the high oxidation state of rhenium (+V). Similarly for (tBu$_4$Pc)ReN (**1**), the Q band is red-shifted by about 25 nm to λ = 697 nm.[10][20] We have no indication for exciton interaction of dimers or even larger aggregates,[21] so monomeric units of **5**−**8** were assumed in solution. The B band of **5**−**8** shows two maxima for **5** at λ = 369 and 351 nm [**6** (CH_2Cl_2): 361, 347 nm; **7** (toluene): 369, 350 nm; **8** (CH_2Cl_2): 361, 347 nm]. The FD MS spectra of **5**−**8** exhibit the expected peaks at 1161.5 (**5**; M^+), 1274.0 (**6**; M^+), 1385.7 (**7**; M^+) and 1498.3 (**8**; M^+) showing all the calculated isotope distribution. A singlet at low field in the ^{1}H-NMR spectrum of **5**−**8** is due to their high symmetry: For **5** this signal appears at δ = 9.21, at δ = 8.75 for **6**, at δ = 8.81 for **7** and at δ = 9.13 for **8** and is assigned to the eight aromatic protons. For **1**[10] three multiplets are found in the aromatic region due to the four isomers of tetrasubstituted phthalocyanines (C_{4h}, C_{2v}, D_{2h}, C_s) at δ = 8.39, 9.46, and 9.56 in the ratio of 1:1:1. The alkyl chains in **5**−**8** show the usual and expected signals at higher field. The methyl groups appear as triplets with coupling constants J = 7.04 Hz for **5**, 7.08 Hz for **6**, 6.88 Hz for **7** and 6.71 Hz for **8** (Figure 1). In the ^{13}C-NMR spectra of **5**−**8** four signals in the aromatic region for the carbon atoms C-a [144.28 (**8**)−144.08 (**6**)], C-b [122.84 (**5**)−122.66 (**6**)], C-c [135.12 (**8**)−134.98 (**6**)] and C-d [148.30 (**8**)−148.04 (**6**)] are observed. This pattern matches well with other octasubstituted phthalocyanines.[18] However, (tBu$_4$Pc)ReN (**1**) shows ten signals at lower field, which are all split or show at least a shoulder due to its structural isomers.[10] In the higher field between δ = 34.13 and 14.19 the expected number of signals for alkyl carbon atoms for compounds **5**−**8** are found (Figure 1).

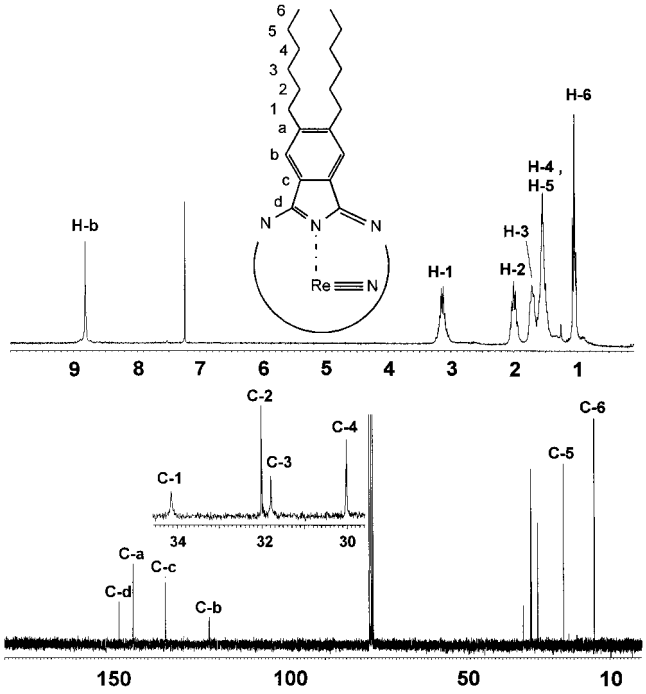


Figure 1. ^{1}H-and ^{13}C-NMR of ($C_6H_{13})_8$PcReN (**7**)

The solubility of **5**−**8** is good in common organic solvents (e.g. $CHCl_3$, toluene, THF, pyridine), but less than that of (tBu$_4$Pc)ReN (**1**). The solubility increases from [$(C_4H_9)_8$Pc]ReN (**5**) to [$(C_7H_{15})_8$Pc]ReN (**8**). However, they are quite insoluble in hexane, methanol and diethyl ether.

[$(C_5H_{11})_8$Pc]ReN (**6**) was treated with BBr_3 under the same conditions as for **4** to investigate the stability of the formed complex [$(C_5H_{11})_8$Pc]ReNBBr$_3$ (**9**) (Scheme 2). Compound **9** is less sensitive to moisture than **4** and hence it was possible to obtain the M^+ peak in the FAB MS at 1531.5 (M^+ + matrix) proving the higher stability of **9**. Peaks at 1450.4, 1372.4, 1286.5 and 1273.6 for [$(C_5H_{11})_8$Pc]ReNBBr$_2$, [$(C_5H_{11})_8$Pc]ReNBBr, [$(C_5H_{11})_8$Pc]-ReNB and [$(C_5H_{11})_8$Pc]ReN (**6**) have been also observed. The Re−N triple-bond stretching vibration in the IR spectrum of **9** is found in the expected region similar to that of **4** at $\tilde{\nu}_{Re\equiv N}$ = 1194 cm^{-1}. Furthermore, the vibrations of $\tilde{\nu}_{B-Br}$ = 677 cm^{-1}, $\tilde{\nu}_{N-B}$ = 650 cm^{-1} and the usual vibrations for octasubstituted phthalocyanines give definite evidence for the suggested structure of **9**. The Q band in

the UV/Vis spectrum of **9** is broadened and red-shifted to $\lambda = 738$ nm. The extent of this shift (30 nm) is the same as for (tBu$_4$Pc)ReNBBr$_3$ (**4**). The vibronic transitions at $\lambda = 676$ and 638 nm in **6** are also red-shifted to $\lambda = 701.5$ and 667.5 nm, respectively, due to the electron-withdrawing effect of the BBr_3 group, which is in accordance with **4**. In the same way the B band exhibits its maximum at $\lambda = 380$ nm. The ^{11}B-NMR spectrum of **9** shows a signal at $\delta = -12.75$, similar to the one observed for **4** ($\delta = -12.90$).

Experimental Section

4,5-Di-*n*-alkylphthalodinitriles were synthesized according to ref.[18] NH_4ReO_4 was prepared from Re metal,[21] which was a gift from Degussa AG. The solvents were purified by known procedures. − FT IR: Bruker IFS 48. − UV/Vis: Shimadzu UV−365. − MS: Varian Mat 711 (EI, FD). − ^{1}H, ^{13}C, ^{11}B NMR: Bruker AC 250 (^{1}H: 250.133 MHz; ^{13}C: 62.902; ^{11}B: 80.251). − Elemental analyses: Carlo Erba Elemental Analyser 1104, 1106.

(tBu$_4$Pc)Re[NC(CH$_3$)$_2$CH$_2$C(O)CH$_3$]OH (2b) and {tBu$_4$PcRe-[NC(CH$_3$)$_2$CH$_2$C(O)CH$_3$]}$_2$O (3): (tBu$_4$Pc)ReN (**1**)[10] (97 mg, 0.1 mmol) was suspended in 10 mL of acetone and treated with 5 drops of conc. HCl leading to dissolution and change of colour from blue to blue-green. After stirring at room temperature for 4 d in the dark, the solvent was removed and the residue chromatographed on Al_2O_3 with toluene as eluent to eliminate unchanged **1**. Two blue-green compounds were eluted with CH_2Cl_2 the first being the dimer **3** and the second the monomer **2b**. 59 mg (54%) of **2b** and 5 mg (2%) of **3**, both blue-green microcrystalline solids, were obtained.

2b: IR (KBr): $\tilde{\nu} = 3651$ cm^{-1}, 3076, 2959, 2903, 2866, 1718, 1614, 1485, 1337, 1281, 1258, 1155, 1148, 1123, 1113, 1090, 1049, 935, 833, 768, 756. − UV/Vis (CH_2Cl_2): λ (lg ε) = 246 nm (4.70), 270 (4.54), 286 (4.47), 356 (4.79), 557 (3.06), 579 (3.58), 601 (3.83), 626 (4.40), 695 (5.08). − MS (FD); *m/z* (%): 1053.4 (100) [M$^+$]. − ^{1}H NMR ($CDCl_3$): $\delta = -2.13$ to -2.08 [m, 6 H, C(CH_3)$_2$], 0.80 (m, 2 H, CH_2), 0.11−0.14 [m, 3 H, C(O)CH_3], 1.74−1.94 (m, 36 H, *t*Bu), 8.13−9.31 (m, 8 H, aromatic H). − ^{13}C NMR ($CDCl_3$): $\delta = 21.65$ [m, C(*C*H$_3$)$_2$], 29.17 [m, C(O)*C*H$_3$], 31.90−32.18 [m, C(*C*H$_3$)], 36.04−36.14 [m, *C*(CH$_3$)$_3$], 47.70 (m, *C*H$_2$), 65.51 [m, *C*(CH$_3$)$_2$], 119.30−119.40 (m, *C*H$_2$), 122.90 (m, C-b), 127.95 (m, C-a), 135.14−135.30 (m, C-c,), 137.78−138.00 (s, C-c′), 147.05−147.75 (m, C-d, C-d′), 153.61−153.78 (m, C-a′), 202.07 (C-O). − $C_{54}H_{60}N_9O_2Re$ (1053.3): calcd. C 61.58, H 5.74, N 11.97; found C 61.43, H 5.54, N 11.65.

3: IR (KBr): $\tilde{\nu} = 3071$ cm^{-1}, 2961, 2924, 2866, 1709, 1616, 1485, 1259, 1144, 1122, 1090, 802, 727. − UV/Vis (CH_2Cl_2): λ (lg ε) = 257 nm (4.65), 289 (4.48), 340 (4.48), 353 (4.52), 554 (3.50), 575 (3.57), 603 (3.91), 634 (4.14), 659 (4.85). − MS (FD); *m/z* (%): 2088.6 (100) [M$^+$]. − ^{1}H NMR ($CDCl_3$): $\delta = -3.03$ to -2.95 [m, 12 H, 2 × C(CH_3)$_2$], −1.73 to −1.64 (m, 4 H, 2 × CH_2), −0.66−0.63 [m, 6 H, 2 × C(O)CH_3], 1.99−2.21 (m, 72 H, *t*Bu), 8.20−9.37 (m, 24 H, aromatic H). − ^{13}C NMR (H/C COSY; $CDCl_3$): $\delta = 22.26$ [m, C(*C*H$_3$)$_2$], 29.65 [m, C(O)*C*H$_3$], 33.65 [m, C(*C*H$_3$)], 49.39 (m, *C*H$_2$), 119.89 (m, C-b′), 124.36 (m, C-b), 128.23. − $C_{108}H_{118}N_{18}O_3Re_2$ (2088.7): calcd. C 62.11, H 5.69, N 12.07; found C 64.86, H 6.88, N 9.17.

(tBu$_4$Pc)ReNBBr$_3$ (4) and [(C$_5$H$_{11}$)$_8$Pc]ReNBBr$_3$ (9): 0.053 mmol of the nitrido(phthalocyaninato)rhenium complexes (**1**,**6**)[10] was dissolved in 10 mL of CH_2Cl_2. Then 0.1 mL (1 mmol) BBr_3 was added dropwise at 0°C showing a change of colour from blue to green. The temperature was maintained for 6 h. Removal of the solvent and excess BBr_3 under vacuum gave 62.9 mg (100%) **4**, and 80.7 mg (100%) **9**, dark-green microcrystalline solids.

4: IR (KBr): $\tilde{\nu} = 3221$ cm^{-1}, 2961, 2905, 1612, 1481, 1408, 1366, 1331, 1283, 1257, 1196, 1155, 1092, 1051, 935, 833, 810, 766, 754, 671, 645. − UV/Vis (CH_2Cl_2): $\lambda = 382$ nm, 725, 775. − MS (FD); *m/z* (%): 1107.5 (5) [M$^+$ − Br], 937.7 (100) [M$^+$ − BBr_3], 921.8 (35) [M$^+$ − $NBBr_3$]. − MS (ionspray); *m/z* (%): 1029.6 (100) [M$^+$ − 2 × Br], 938.4 (80) [M$^+$ − BBr_3], 378.2 (10) [$ReNBBr_2$], 294.6 (57) [$ReNBBr_3$], 250.8 (69) [BBr_3] − ^{11}B NMR ($CDCl_3$/BF3·Et2O): $\delta = -12.90$ (s, 1B).

9: IR (KBr): $\tilde{\nu} = 3215$ cm^{-1}, 2955, 1616, 1456, 1337, 1259, 1194, 1109, 1036, 883, 804, 754, 735, 677, 650. − UV/Vis (CH_2Cl_2): $\lambda = 380$ nm, 668, 702, 738. − MS (FAB); *m/z* (%): 1531.5 (3) [M$^+$ + matrix], 1450.4 (4) [M$^+$ − Br + matrix], 1372.4 (7) [M$^+$ − 2 × Br + matrix], 1286.5 (18) [M$^+$ − 3 × Br + matrix], 1273.6 (100) [M$^+$ − BBr_3]. − ^{11}B NMR ($CDCl_3$/BF3·Et2O): $\delta = -12.75$ (s, 1 B).

Nitrido(octa-*n*-alkylphthalocyaninato)rhenium(V) [(R$_8$Pc)ReN] 5−8: 0.21 mmol of the appropriate 4,5-di-*n*-alkylphthalodinitriles was heated with 0.048 mmol NH_4ReO_4 to 280°C for 30 min. After cooling, the dark green reaction mixture was first chromatographed on Al_2O_3 (neutral, 10% H_2O) with dichloromethane as eluent (2 ×) to remove most of the impurities. Then the excess of dinitrile was extracted with methanol for 12 h by using a Soxhlet apparatus. 55 mg (5%) of **5,** 65 mg (5%) of **6**, 55 mg (4%) of **7** and 60 mg (4%) of **8** were obtained as dark green powders.

5: IR (KBr): $\tilde{\nu} = 2957$ cm^{-1}, 2930, 1620, 1497, 1456, 1403, 1335, 1113, 1082, 1030, 964, 905, 754, 733. − UV/Vis (toluene): $\lambda = 351$ nm, 369, 633, 673, 705. − MS (FD); *m/z* (%): 1161.5 (100) [M$^+$]. − ^{1}H NMR ($CDCl_3$): $\delta = 1.18$ (t, $J = 7.04$ Hz, 24 H, CH_3), 1.63−1.81 (m, 16 H, CH$_3$CH_2), 1.87−2.09 (m, 16 H, CH$_3$CH$_2$CH_2), 3.04−3.27 (m, 16 H, ArCH_2), 8.91 (s, 8 H, aromatic H). − ^{13}C NMR ($CDCl_3$): $\delta = 14.25$ (s, *C*H$_3$), 23.35 (s, CH$_3$*C*H$_2$), 33.81 (s, CH$_3$CH$_2$*C*H$_2$), 33.91 (s, Ar*C*H$_2$), 122.84 (s, C-b), 135.11 (s, C-c), 144.22 (s, C-a), 148.27 (s, C-d). − $C_{64}H_{72}N_9Re$ (1161.6): calcd. C 66.18, H 6.94, N 10.85; found C 66.39, H 6.53, N 10.45.

6: IR (KBr): $\tilde{\nu} = 2954$ cm^{-1}, 2927, 2868, 1618, 1498, 1456, 1406, 1337, 1110, 1079, 1018, 965, 891, 754, 732. − UV/Vis (CH_2Cl_2): $\lambda = 347$ nm, 361, 638, 676, 708. − MS (FD); *m/z* (%): 1274.0 (100) [M$^+$]. − ^{1}H NMR ($CDCl_3$): $\delta = 1.11$ (t, $J = 7.08$ Hz, 24 H, CH_3), 1.51−1.78 (m, 32 H, CH$_3$CH_2CH_2), 1.90−2.10 (m, 16 H, ArCH$_2$CH_2), 2.98−3.22 (m, 16 H, ArCH_2), 8.75 (s, 8 H, aromatic H). − ^{13}C NMR ($CDCl_3$): $\delta = 14.29$ (s, *C*H$_3$), 22.83 (s, CH$_3$*C*H$_2$), 31.46 (s, CH$_3$CH$_2$*C*H$_2$), 32.52 (s, ArCH$_2$*C*H$_2$), 34.07 (s, Ar*C*H$_2$), 122.66 (s, C-b), 134.98 (s, C-c), 144.08 (s, C-a), 148.04 (s, C-d). − $C_{72}H_{96}N_9Re$ (1273.8): calcd. C 67.89, H 7.60, N 9.90; found C 66.66, H 7.87, N 8.65.

7: IR (KBr): $\tilde{\nu} = 2955$ cm^{-1}, 2926, 1618, 1496, 1456, 1406, 1337, 1109, 1080, 1024, 964, 900, 802, 754, 731. − UV/Vis (toluene): $\lambda = 350$ nm, 369, 634, 671, 704. − MS (FD); *m/z* (%): 1385.7 (100) [M$^+$]. − ^{1}H NMR ($CDCl_3$): $\delta = 1.04$ (t, $J = 6.88$ Hz, 24 H, CH_3), 1.45−1.61 (m, 32 H, CH$_3$CH_2CH_2), 1.65−1.75 (m, 16 H, ArCH$_2$CH$_2$CH_2), 1.91−2.07 (m, 16 H, ArCH$_2$CH_2), 3.02−3.24 (m, 16 H, ArCH_2), 8.81 (s, 8 H, aromatic H). − ^{13}C NMR ($CDCl_3$): $\delta = 14.25$ (s, *C*H$_3$), 22.88 (s, CH$_3$*C*H$_2$), 30.01 (s, CH$_3$CH$_2$*C*H$_2$), 31.79 (s, ArCH$_2$CH$_2$*C*H$_2$), 32.01 (s, ArCH$_2$*C*H$_2$), 34.13 (s, Ar*C*H$_2$), 122.75 (s, C-b), 135.04 (s, C-c), 144.14 (s, C-a), 148.10 (s, C-d). − $C_{80}H_{112}N_9Re$ (1386.0): calcd. C 69.33, H 8.14, N 9.10; found C 70.27, H 8.17, N 8.91.

8: IR (KBr): $\tilde{\nu} = 2956$ cm^{-1}, 2925, 1619, 1497, 1456, 1405, 1387, 1112, 1080, 1027, 977, 887, 752, 730. − UV/Vis (CH_2Cl_2): $\lambda =$

347 nm, 361, 638, 676, 708. – MS (FD); *m/z* (%): 1498.3 (100) [M^+]. – ^{1}H NMR ($CDCl_3$): δ = 0.98 (t, *J* = 6.71 Hz, 24 H, CH_3), 1.38–1.77 (m, 60 H, $CH_3CH_2CH_2CH_2CH_2$), 1.89–2.12 (m, 16 H, $ArCH_2CH_2$), 3.01–3.27 (m, 16 H, $ArCH_2$), 8.92 (s, 8 H, aromatic H). – ^{13}C NMR ($CDCl_3$): δ = 14.19 (s, CH_3), 22.81 (s, CH_3CH_2), 29.44 (s, $CH_3CH_2CH_2$), 30.26 (s, $CH_3CH_2CH_2CH_2CH_2$), 31.84 (s, $ArCH_2CH_2CH_2$), 32.05 (s, $ArCH_2CH_2$), 34.12 (s, $ArCH_2$), 122.80 (s, C-b), 135.12 (s, C-c), 144.28 (s, C-a), 148.30 (s, C-d). – $C_{88}H_{128}N_9Re$ (1498.3): calcd. C 70.49, H 8.61, N 8.41; found C 69.35, H 8.10, N 9.05.

Acknowledgments

We wish to thank the Deutsche Forschungsgemeinschaft (Schwerpunktprogramm "Nitridobrücken", II C10–3221008) for financial support of this work and Mr. R. Süßmuth for the MS (ionspray) measurements.

[1] [1a] K. Dehnicke, J. Strähle, *Angew. Chem.* **1981**, *93*, 451; *Angew. Chem. Int. Ed. Engl.* **1981**, *20*, 413. – [1b] K. Dehnicke, J. Strähle, *Angew. Chem.* **1992**, *104*, 978; *Angew. Chem. Int. Ed. Engl.* **1992**, *31*, 955.
[2] J. W. Buchler, C. Dreher, K. L. Lay, *Z. Naturforsch., B: Anorg. Chem. Org. Chem.* **1982**, *37*, 1155.
[3] J. W. Buchler, A. De Cian, J. Fischer, S. B. Kruppa, R. Weiss, *Chem. Ber.* **1990**, *123*, 2247.
[4] C. Tong, L. Bottomley, *Inorg. Chem.* **1996**, *35*, 5108.
[5] H. Grunewald, H. Homborg, *Z. Naturforsch., B: Chem. Sci.* **1990**, *45*, 483.
[6] S. Rummel, M. Hermann, K. Schmidt, *Z. Chem.* **1985**, *25*, 152.
[7] [7a] A. Mrwa, S. Rummel, M. Starke, *Z. Chem.* **1985**, *5*, 186.
[7b] A. Mrwa, H. Giegenhack, M. Starke, *Cryst. Res. Technol.* **1988**, *23*, 773.
[8] [8a] V. L. Goedken, C. Ercolani, *J. Chem. Soc., Chem. Commun.* **1984**, 378. – [8b] L. A. Bottomley, J.-N.Gorce, V. L. Goedken, C. Ercolani, *Inorg. Chem.* **1985**, *24*, 3733. – [8c] B. J. Kennedy, K. S. Murray, H. Homborg, W. Kalz, *Inorg. Chim. Acta* **1987**, *134*, 19.
[9] G. Rossi, M. Gardini, G. Pennesi, C. Ercolani, V. L. Goedken, *J. Chem. Soc., Dalton Trans.* **1989**, 193.
[10] [10a] U. Ziener, M. Hanack, *Chem. Ber.* **1994**, *127*, 1681. – [10b] U. Ziener, K. Dürr, M. Hanack, *Synth. Met.* **1995**, 2285.
[11] S. Ritter, U. Abram, *Z. Anorg. Allg. Chem.* **1994**, *620*, 1786.
[12] B. D. Berezin, *J. Gen. Chem. USSR (Engl. Transl.)* **1974**, *43*, 2714.
[13] G. Schmid, M. Sommerauer, M. Geyer, M. Hanack in *Phthalocyanines, Properties and Applications*, vol. 4 (Eds. C. C. Leznoff, A. B. P. Lever), VCH Publishers, New York, **1996**, p. 1.
[14] M. J. Stillman, T. Nyokong in *Phthalocyanines, Properties and Applications*, vol. 1 (Eds. C. C. Leznoff, A. B. P. Lever), VCH Publishers, New York, **1989**, p. 133.
[15] [15a] W, Kaffitz, F. Weller, K. Dehnicke, *Z. Anorg. Allg. Chem.* **1982**, *490*, 175. – [15b] R. Dantona, E. Schweda, J. Strähle, *Z. Naturforsch.* **1984**, *39b,* 733. – [15c] J. Chatt, B. T. Heaton, *J. Chem. Soc. A* **1971**, 705.
[16] J. Weidlein, U. Müller a. K. Dehnicke, *Schwingungsfrequenzen I*, G. Thieme Verlag, Stuttgart, **1981**.
[17] [17a] E. Merz, *Nukleonik* **1966**, *8*, 248. – [17b] K. Yoshihara, G. K. Wolf and F. Baumgärtner, *Radiochim. Acta* **1974**, *21*, 96. – [17c] H. Przywarska-Boniecka, *Roczniki Chemii* **1966**, *40*, 1627; *Chem. Abstr.* **1967**, *66*, 72008. – [17d] H. Przywarska-Boniecka, *Roczniki Chemii* **1967**, *41*, 1703; *Chem. Abstr.* **1968**, *69*, 32582. – [17e] H. Przywarska-Boniecka, *Roczniki Chemii* **1968**, *42*, 211; *Chem. Abstr.* **1968**, *69*, 14810. – [17f] G. Pfrepper, *Z. Chem.* **1970**, *10*, 76.
[18] M. Hanack, M. Lang, *Adv. Mater.* **1994**, *6*, 487.
[19] S. A. Mikhalenko, S. V. Barkanova, O. L. Lebedev, E. A. Luk′yanets, *Zh. Obshch. Khim.* **1971**, *41*, 2735; *J. Gen. Chem. USSR* **1971**, *41*, 2770.
[20] E. A. Lucia, F. D. Verderame, *J. Chem. Phys.* **1970**, *52*, 2307.
[21] L. S. Crocker, G. L. Gould, D. M. Heinekey, *J. Organomet. Chem.* **1988**, *342*, 243.

Received January 20, 1999
[I99016]

Roles of π-Alkyne, Hydride–Alkynyl, and Vinylidene Metal Species in the Conversion of Alkynes into Vinylidene: New Theoretical Insights

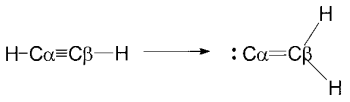
Enrique Peréz-Carreño,[a][+] Paola Paoli,[b] Andrea Ienco,[a] and Carlo Mealli*[a]

Keywords: Ab initio calculations / EHMO / Vinylidene complexes / Cobalt / Rhodium

The transformation of acetylene into vinylidene, as promoted by the metal fragment $[(pp_3)Co]^+$ [$pp_3 = P(CH_2CH_2PPh_2)_3$], is unimolecular and features the hydride–acetylide species as an intermediate. The paper describes a detailed ab initio study of the reaction, in particular with regard to the step involving 1,3-H shift. The best computational results are obtained by mimicking the pp_3 ligand with actual ethylenic chains rather than with single PH_3 molecules. The keypoints along the two-step reaction path (π-acetylene, hydride–acetylide, and vinylidene complexes, as well as intermediate transition states) have been optimized for Co^I and Rh^I derivatives at the MP2 level. For the fragment $[(pp_3)Co]^+$, the barrier associated with transformation of the hydride–acetylide intermediate to vinylidene (20.6 kcal/mol) is easier to surmount compared to that for reversion to the reactants (28.6 kcal/mol). The situation is reversed for the analogous Rh^I system, with the initial π-acetylene adduct being slightly more stable. Although higher in energy, the hydride–acetylide species is the experimentally detected product of the reaction of acetylene with the fragment $[(pp_3)Rh]^+$. The salient chemical aspects of the 1,3-H shift are discussed in terms of perturbation theory arguments. Parallel EHMO calculations, which have provided a relatively good consistency with the ab initio results, allow the proposal of an orbital rationale for the mode of migration of the hydride ligand along the substantially linear $Co–C_\alpha–C_\beta$ grouping.

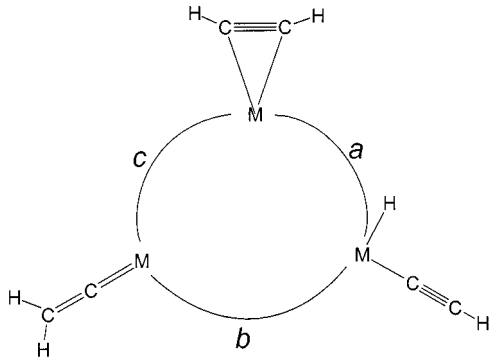
Introduction

The conversion of unsubstituted or monosubstituted acetylene into vinylidene has been widely investigated both experimentally[1] and theoretically.[2] The strongly endothermic reaction $HC{\equiv}CH \rightarrow :C{=}CH_2$ (ca. 45 kcal/mol) becomes more feasible in the presence of numerous ancillary metal fragments. Following the first EHMO studies,[3] the problem of the metal-promoted interconversion has also been tackled by several groups using higher-level ab initio theory.[4] Briefly, we wish to summarize what is known about the reaction **I**, which may follow alternative pathways.



I

The least-motion 1,2-shift seems to be best promoted by d^6 metal fragments, which initially form π-adducts with the alkyne. For example, the early EHMO analysis was consistent with the latter mechanism in the case of $[CpMn(CO)_2]$.[3] More recent ab initio calculations were supportive of the same pathway for the fragment $Cl_2(PH_3)_2Ru$.[4a] There are cases, however, for which the formation of a metal hydride−acetylide species has been documented[5−7] and the question remains open as to whether the latter is the actual intermediate en route to the vinylidene complex (steps *a* and *b* in **II**, correspond to C−H oxidative addition followed by 1,3-H shift) or is merely formed as a side-product. If the latter were to be the case, the formation of vinylidene would also imply the reverse of step *a* (reductive elimination) followed by the 1,2-H shift itself (step *c*).



II

This point is still the subject of a passionate debate involving both experimentalists and theoreticians. The situation may vary considerably depending on the nature of the metal fragment. For example, in a recent theoretical study[4c] the possibility that 1−2 tautomerization or hydride−

[a] Istituto per lo Studio della Stereochimica ed Energetica dei Composti di Coordinazione, CNR,
Via J. Nardi 39, I-50132 Firenze, Italy
Fax: (internat.) +39 55 2478366
E-mail: mealli@fi.cnr.it
[b] Dipartimento di Energetica, Università di Firenze,
Via Santa Marta, I-50100 Firenze, Italy
[+] On leave from the Departamento de Química Física y Analítica, Universidad de Oviedo, Spain.

 © WILEY-VCH Verlag GmbH, D-69451 Weinheim, 1999 1434−1948/99/0808−1315 $ 17.50+.50/0

acetylide formation might be involved in acetylene polymerization promoted by electron-deficient metal fragments [e.g. X_4W (X = F, Cl)] was ruled out. On the other hand, Werner et al.[5] reported that the hydride−acetylide is formed in the presence of the d^8 planar fragment $[Cl(PR_3)_2Rh]^+$. However, an ad hoc theoretical study[4b] showed that the straightforward 1,3-H shift cannot be pursued. More probably, the vinylidene species forms through a bimolecular mechanism where the hydrogen atom coordinated to one metal is transferred to the C_β acetylide atom of a second, properly oriented, complex molecule. The coordinated hydrogen atom in the latter follows the parallel path in the opposite direction. Although novel and interesting, the bimolecular mechanism cannot be invoked in all cases involving the hydride−acetylide species. We refer in particular to the chemistry supported by the ancillary d^8 metal fragment $[(pp_3)Co]^+$ [pp_3 = $P(CH_2CH_2PPh_2)_3$][6] or by the d^6 metal fragment $[Cp^*(dippe)_2Ru]^+$ dippe = $iPr_2PCH_2CH_2PiPr_2$].[7] Kinetic and spectroscopic studies of these species provide evidence that the reaction leading to vinylidene is first-order unimolecular. Most probably, the bulkiness of the phenyl substituents in pp_3 makes docking of two molecules difficult. Finally, the hydride−acetylide complexes $[(pp_3)CoH(C{\equiv}CR)]^+$ (the derivative with R = $SiMe_3$ could be structurally characterized since it is inert to further transformation[6]) generally undergo transformation into the most stable vinylidene complex, even in the solid state, i.e. simply upon warming the crystals. Mainly because of spatial constraints within the lattice, the unimolecular reaction implies minimal geometrical rearrangement. Thus, especially in the presence of a bulky acetylene substituent such as phenyl, it is unthinkable that the hydride−acetylide can undergo reversion to the π-adduct, and hence that the reaction proceeds through a 1,2-H shift. In any event, by disregarding the spatial constraints of the solid state, it is interesting to evaluate the barrier for the reverse C−H reductive elimination of the hydride−acetylide and, where possible, that for the conversion of the π-adduct into the final vinylidene complex.

In order to focus more intently on this point, and since the system reported by Bianchini et al.[6] {that involving the d^8 metal fragment $[(pp_3)Co]^+$} has never been theoretically investigated in detail, we have performed specific ab initio calculations (the MP2 level was selected to be consistent with the approach adopted in ref.[4b]). The same set of calculations has been carried out for the isoelectronic fragment $[(pp_3)Rh]^+$, which is reported to yield only the hydride−acetylide species.[8] The sufficiently satisfactory numerical results are reported herein. We also outline some important chemical implications using the qualitative language of Perturbation Theory. In fact, a pictorial MO analysis (EHMO method using the CACAO package[9]) allows the evolution of the MOs between structural key-points on the reaction coordinate, already indicated by the ab initio results, to be monitored. The two approaches are not inconsistent, so that ultimately the quantitative and qualitative theoretical inferences allow a good understanding of the system based on common chemical intuition.

Computational Details

EHMO Calculations

In MO calculations of the extended Hückel type,[10] a weighted-modified Wolfsberg−Helmholz formula[11] was used. Literature STO parameters were used for Co,[12] while standard values were used for the main group elements. The 3D drawings, correlation and interaction diagrams were generated using the program CACAO.[9]

Ab Initio Calculations

The ab initio calculations were performed with the Gaussian-94[13] program at the MP2 level (electron correlation by second-order Møller−Plesset perturbation) using the ECP (effective core potential) approximation for some atoms. Specifically, the 17-electron ECP of Hay and Wadt[14] was adopted by using the [3s3p2d]/(5s5p5d) and [3s3p2d]/(5s5p4d) basis functions for cobalt and rhodium, respectively. Moreover, in order to further reduce the computational burden, 10- and 2-electron ECPs were adopted for phosphorus and carbon atoms, respectively, by using the [2s2p]/(4s4p) basis set.[15] For the H atoms, the D95 set was adopted.[16] Single-point energy calculations on the optimized structures were carried out using the same effective core potential for the metal and the 6-31G* basis set[17] for the other atoms. Unless otherwise specified, we discuss energies at these highest basis sets. Finally, to test the reliability of the ECP approximation, the computations were repeated using the ECP only for the transition metal, while a 6−31G basis set was used for the remaining atoms. The differences are not substantial, as can be seen on inspection of the data in Table 1.

In all cases, the geometries of the stationary points were fully optimized at the MP2 level using the analytical gradient under the C_s symmetry constraint. The transition state structures were relaxed after introducing small perturbations to ensure that they were indeed associated with the corresponding reactants and products. In the complexes with independent PH_3 ligands, the true minima or the transition state points on the potential energy surface were detected by calculating the second energy derivative matrix. Only for one of the optimized structures containing the actual model of the ligand pp_3 (refer later to **3a** in Figure 1) were the frequencies calculated. Although one imaginary frequency was found (not unexpectedly in view of the imposed C_s symmetry, see the later discussion), the optimized structures were still considered acceptable from a chemical viewpoint.

Results and Discussion

Ab Initio Calculations: Modelling Strategies and Energetic Trends

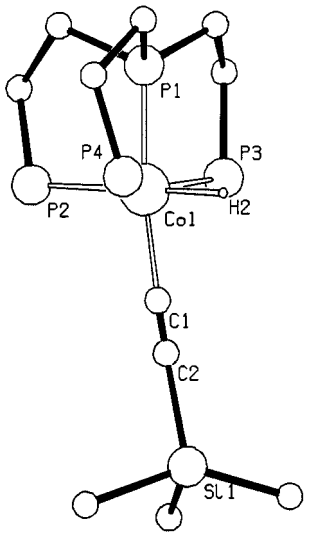
The tripodal ligand pp_3 was first mimicked with four independent PH_3 molecules, as is a common practise in MO calculations. As a result, various isomers of the general for-

Table 1. Experimental and calculated distances and angles for Co^{I}-vinylidene cationic complexes

	Ligand pp_3				Four (PH_3) ligands		
	Expt. Struct.[a]	ECP-31G[b]	ECP-31G[b]	6-31G[b]	Expt. Struct.[c]	ECP-31G[b]	6-31G[b]
Symmetry	C_1	Cs	C_1	Cs	C_1	C_{2v}	C_{2v}
$Co-P_1$	2.185	2.16	2.16	2.14	2.252	2.30	2.33
$Co-P_2$	2.21	2.23	2.24	2.24	2.246	2.30	2.33
$Co-P_3$	2.20	2.11	2.11	2.11	2.214	2.14	2.15
$Co-P_4$	2.205	2.11	2.11	2.11	2.219	2.14	2.15
$Co-C_1$	1.71	1.67	1.67	1.67	1.728	1.68	1.68
$C1-C_2$	1.34	1.38	1.38	1.34		1.38	1.34
P_1-Co-P_2	87.0	90.41	90.43	90.06	109.58	99.64	97.78
P_1-Co-P_3	85.0	89.36	89.24	89.44	92.02	95.83	96.43
$P1-Co-P_4$	84.3	89.36	89.49	89.44	95.87	95.83	96.43
P_2-Co-P_3	108.8	102.35	103.18	102.44	95.58	95.83	96.42
P_2-Co-P_4	109.1	102.35	101.34	102.44	95.27	95.83	96.42
P_3-Co-P_4	140.0	155.28	155.45	155.10	163.60	161.88	160.40
P_1-Co-C_1	164.5	154.83	154.36	155.56	133.51	130.20	131.09
P_2-Co-C_1	107.5	114.76	115.20	114.38	116.37	130.17	131.13
P_3-Co-C_1	91.5	85.37	85.45	85.46	81.61	80.94	80.19
P_4-Co-C_1	89.0	85.37	85.17	85.46	82.58	80.94	80.19
$Co-C_1-C_2$	168.5	177.16	177.26	177.20		180.00	180.00

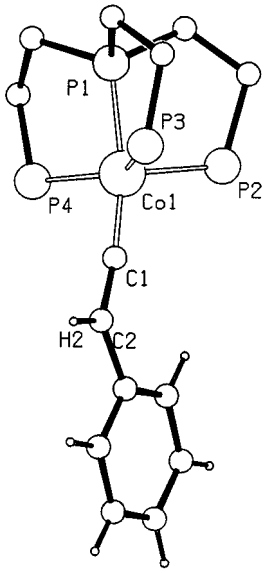
[a] Average values of the two complex cations $[(pp_3)Co-C{=}CHPh]^+$ reported in ref.[6] – [b] For metal atoms, the effective core potential (ECP) of Hay and Wadt was chosen. – [c] Values for the complex $[(PH_3)_4Co-CO]^+$ reported in ref.[18]

mula $[(PH_3)_4Co(C_2H_2)]^+$ could be optimized, although the geometries were not fully consistent with the structural data available for $[(pp_3)Co(C_2HR)]^+$.[6] Data are available for the hydride–acetylide species with R = $SiMe_3$ (**III**), which is sufficiently stable for X-ray analysis. Conversely, the vinylidene isomer is most easily obtained for R = phenyl (**IV**). In this case, the transformation starting from the corresponding hydride–acetylide complex proceeds even in the solid state, simply upon warming the crystals.



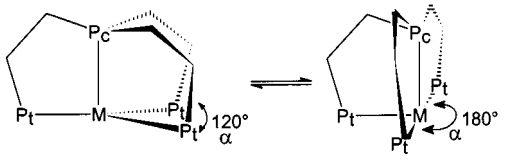
III

The most obvious difference between **III** and **IV** is the shape of the L_4M ancillary fragment. While the skeleton of $(pp_3)Co$ is approximately trigonal-pyramidal in **III**, a butterfly shape (*pseudo*-C_{2v} symmetry) is observed in the hydride–acetylide complex **IV**. Because of the constraints due to the ethylenic chains, the interconversion can only occur through the pathway **V**. Thus, all of the P_c-M-P_t angles remain close to 90°, while one of the P_t-M-P_t angles



IV

opens out towards 180°. The latter angle, α, can be considered as a governing parameter in this type of reactivity as promoted by $(pp_3)M$ fragments (vide infra).



V

As mentioned above, the inadequacy of $(PH_3)_4Co$ as an ancillary fragment is evident as some parameters diverge significantly from the experimental values. In particular, one of the angles P_c-Co-P_t, which are all close to 90° in the actual fragment $(pp_3)Co$, is found to be as large as

145.5° at the transition state along the pathway **a** (see **II**). Another aspect is that the free PH_3 ligands are clearly subject to steric hindrance. Thus, in the optimized pseudo-octahedral hydride−acetylide complex, the two *trans*-axial phosphane ligands are not perfectly linear but are bent away from the equatorial ligands in order to avoid short contacts (angle of 157.7°). The same feature has been observed in the structure of $[(PH_3)_4CoCO]$[18] (the structural parameters of the latter are reported in Table 1), which would, however, be unattainable with the ligand pp_3. In fact, no vinylidene complex with four independent phosphane ligands has ever been reported. Indirectly, this may suggest that the variations of the stereochemistry about the metal atom impose a subtle orbital control on the acetylene−vinylidene transformation. Thus, we then focused on the results of MP2 calculations where the ligand pp_3 was mimicked with the model $P(CH_2CH_2PH_2)_3$ (terminal hydrogen atoms in place of the phenyl substituents). The need for the actual tripodal ligands in ab initio calculations has recently been stressed by other authors.[19]

To reduce the computational burden and to exploit at least one symmetry element, the skeletal atoms of one $P_cCH_2CH_2P_t$ arm as well as the cobalt atom were forced to be planar, thus ignoring the propensity of the aliphatic chains to be chiral. Indeed, use of this C_s approximation for the models **1a**, **2a**, and **3a** (see Figure 1) did not dramatically affect the results.[20] Moreover, comparison with the experimental cobalt structures **III** and **IV** was sufficiently satisfactory (see Table 1).

In the vinylidene model **3a**, the $C{=}CH_2$ group is not perfectly *trans* to the central P_1 atom (the calculated $C_\alpha{-}Co{-}P_1$ angle is 154.8° cf. the value of 164.5° found in the experimental structure). The P_4Co unit in the hydride−acetylide model **2a** even diverges significantly from the pseudo-C_{2v} symmetry found for the $(PH_3)_4Co$ model. In particular, the angle α defined in **V** is rather small (158.8°), in spite of the presence of the H ligand in its bisector. The corresponding angle in **3a**, $P_3{-}Co{-}P_4$, does not vary significantly (155.3°), although the experimental value is smaller (140.0°).

The transition states **4a** and **5a** were determined using the appropriate Gaussian-94 algorithm (STQN[21]), which exploits structural knowledge of both the reactant and the product, namely the pairs **1a**−**2a** and **2a**−**3a**, respectively. Furthermore, since our present computational capabilities are limited, no attempt was made to confirm that the detected transition states (**4a** and **5a**) were indeed the correct ones through calculation of the frequencies. Nevertheless, the latter species do not only exhibit a satisfactorily correct geometry for the P_4Co chromophore, but also appear chemically realistic. In particular, **4a** corresponds to the expected *agostic*-type adduct, which precedes the oxidative addition, while **5a** sheds new light on the mechanism leading to the formation of the vinylidene product. In fact, this structure differs somewhat from that calculated by Morokuma′s group[4a] for the process supported by the fragment $[Cl_2(PH_3)_2Ru]$, for which the formation of a hydride−acetylide species was ruled out. In the latter, the transferring

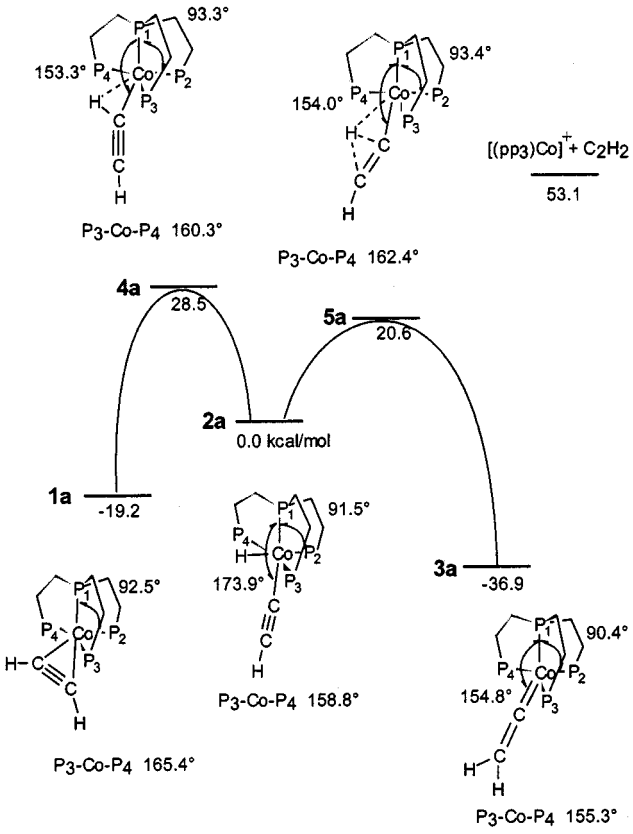


Figure 1. Optimized structures and relative energetics (MP2 level) along the pathway of interconversion between acetylene and vinylidene as promoted by the fragment $[P(CH_2CH_2PH_2)_3Co]^+$

hydrogen is strongly linked to the C_α atom (1.13 Å) and is far removed from C_β. Conversely, in **5a** a quasi-symmetrical bridging mode of hydrogen over the C−C linkage is observed. This is similar to the transition state detected[4b] for the unimolecular conversion of $[Cl(PH_3)_2RhH(C{\equiv}CH)]$ into $[Cl(PH_3)_2Rh(C{=}CH_2)]$, a process which is, however, disfavored with respect to the bimolecular one.

Before commenting on the energetics involved and on their evaluation in relation to the mechanism of the cobalt-induced reactions, we also present the parallel results (Figure 2) calculated using the fragment $[(pp_3)Rh]^+$. The latter is experimentally known to prevent the ultimate formation of the vinylidene complex[8b] starting from the hydride−acetylide isomer. Indeed, this species is the only stable product of the reaction of acetylene at the metal.

The structural keypoints are essentially similar to those in Figure 1. Perhaps the most obvious difference concerns the vinylidene structure **3b**, where the angle $P_1{-}Rh{-}C$ is smaller than that in **3a** (143.7° vs. 154.8°). This would seem to reveal a tendency of the $C{=}CH_2$ group to become better aligned with the bisector of the angle $P_1{-}M{-}P_2$, thus approaching more closely the behavior of the free phosphane model. In the latter C_{2v} structure, the $P_1{-}Co{-}C$ angle is as small as 130.2°.

Comparison of the data in Figures 1−2 and Table 1 reveals that the vinylidene species is most stabilized in the cobalt complex ($\Delta E = -36.9$ kcal/mol for **3a**) and that the

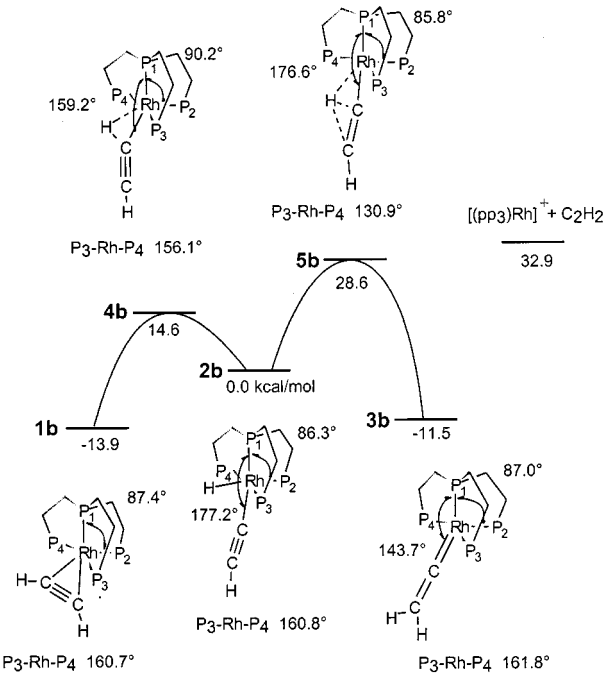


Figure 2. Optimized structures and relative energetics (MP2 level) along the pathway of interconversion between acetylene and vinylidene as promoted by the fragment $[P(CH_2CH_2PH_2)_3Rh]^+$

barrier associated with its formation is not large (20.6 kcal/mol for **5a**). In comparison, the rhodium vinylidene **3b** is much less stabilized (only −11.5 kcal/mol) and its associated barrier is larger (28.6 kcal/mol for **5b**). Furthermore, it is remarkable for rhodium that the barrier to reversion to the starting π-adduct is only 14.6 kcal/mol, practically half the magnitude of that calculated for cobalt. Concerning the transition states **4** in the direction of formation of the hydride−acetylide, the C−H oxidative addition of acetylene has a critically large value for cobalt (over 40 kcal/mol). Nevertheless, this does not seem unreasonable considering that the experimental reaction requires heating.[6] It must also be mentioned that, while the transition states of type **5**, i.e. between hydride−acetylide and vinylidene complexes (path *b* in **II**) have easily been detected, location of the transition states of type **4**, i.e. those involving an *agostic* interaction (path *a* in **II**), has proved much more time-consuming. The latter could only be determined through a trial and error approach based on small geometric modifications of the π-acetylene complexes **1**. Finally, like other authors before us,[4] we have not been able to detect a transition state between π-acetylene **1** and vinylidene **3** (path *c* in **II**). Only the most recent calculations[4c] on the system based on the fragment F_4W have led to the location of the corresponding transition state, following a systematic search after removing any possible symmetry.

In summary, the C−H oxidative addition process yielding complex **2** from **1** has been shown to be much more facilitated by rhodium than by cobalt, as is also the case for the reverse reductive elimination process. Moreover, the calculations have confirmed what was experimentally known, i.e. that the transformation **2** → **3** is quite straightforward with cobalt (it occurs in the solid state), but is impossible with rhodium. Besides having a larger associated barrier, the rhodium vinylidene complex does not seem to possess the necessary stability to be a terminal product. Another interesting numerical result, which confirms the better propensity of the cobalt fragment to function as an activator of acetylene, is contained in Figures 1 and 2. The energy of the separated fragments is distinctly higher for cobalt than for rhodium (53.1 vs. 32.9 kcal/mol), thus confirming the greater propensity of cobalt to promote this chemistry.

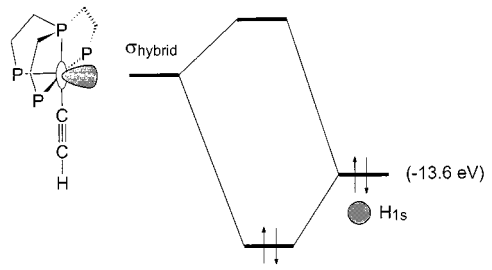
Considerations from the Viewpoint of Qualitative MO Theory

In this section, we mainly try to develop interpretational arguments concerning the second part of the pathway, leading from hydride−acetylide to vinylidene. The Hoffmann group, besides addressing the overall process of alkyne activation,[3] has also dedicated much attention to step of the C−H activation relative to the parallel dichotomy between η^2-ethylene and vinyl−hydride complexes.[22]

An intriguing aspect of the H migration ensuing from the hydride−acetylene adduct is the nature of the migrating hydrogen itself, i.e. whether it has proton or hydride character. Bianchini et al.[6] have reported that the vinylidene complex $[(pp_3)Co(C{=}CRH)]^+$ may be obtained not only through tautomerization of the alkyne HC≡CR by the 16-electron fragment $[(pp_3)Co]^+$, but also through straightforward protonation of the 18-electron acetylide complex $[(pp_3)Co(C{\equiv}CR)]$. More recently, de los Ríos et al.[7] reported that the isomerization of the hydride−acetylide species $[Cp^*RuH(C{\equiv}CR)(dippe)]^+$ to vinylidene is inhibited by strong acids such as HBF_4. While these facts are indicative of the strongly nucleophilic character of the acetylide C_β atom in the 18-electron complexes, it is difficult to envisage a proton migrating all the way from the metal atom.

In pseudo-octahedral Co^{III} complexes of type **III**, the orbital of the H ligand is energetically well below the σ hybrid of the fragment ML_5, **VI**. The latter, mainly z^2 in character, is destabilized by an antibonding interaction with the *trans*-axial phosphane, which promotes hybridization with the higher *s* and *pz* orbitals. In agreement with chemical intuition, the hydride is a donor.

In principle, a cooperating base could extract the H ligand as a proton and transfer it elsewhere. This is also the essence of the bimolecular mechanism proposed by Morokuma et al.,[4a] where the metal of the second molecule itself acts as the extracting base. In the present case, however, the process, which also occurs in the solid state, is not assisted by any external agent, nor is it feasible for two highly hindered complex molecules to get sufficiently close to one another. In the crystal, it is also hard to imagine a structural rearrangement that could bring the nucleophilic C_β atom sufficiently near the metal to extract the proton. Moreover,



VI

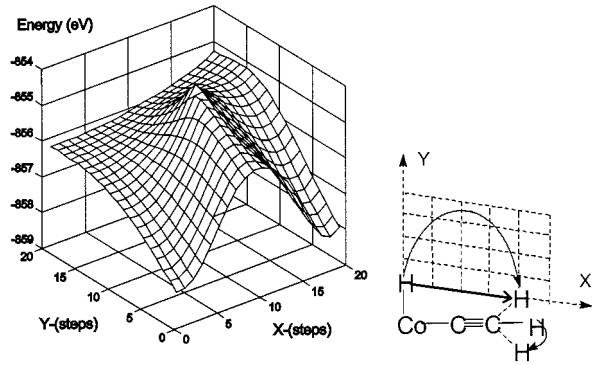


Figure 3. Potential energy surface (PES) calculated (EHMO method) on the small two-dimensional grid; the origin of the latter corresponds to the complex $[(PH_3)_4CoH(C{\equiv}CH)]^+$, with the *y* coordinate corresponding to the progressive separation of the H atom from the linear grouping $Co-C_\alpha-C_\beta$; the non-orthogonal *x* axis, which accounts for the non-equivalence of the $Co-H$ and $C_\beta-H$ bond lengths, describes the H shifting along the same grouping; irrespective of the *y* value, the $C_\alpha-C_\beta-H$ angle begins to bend as soon as the vectors $Co-C_\alpha-C_\beta$ and $C_\beta-H$ become orthogonal

if H^+ could separate from M^-, there would remain a hole in the overall MO picture (i.e. the empty H_{1s} orbital would lie below the occupied metal d block, including the high-lying metal σ lone pair). Thus, at least in the early stages of $M-H$ dissociation, the bonding electron pair is more reasonably assigned to the H atom. In any event, even though a net separation of charges may not be realistic, the extreme viewpoints of migration of a proton or a hydride are helpful in delineating the actual situation.

Although the ab initio calculations indicate that at the transition state the migrating H atom is close-bridging between the C_α and C_β atoms, a migration out of the domains of the latter atoms cannot, in principle, be excluded. However, since this would correspond to the heterolysis of two charged species, unassisted by any solvent, no satisfactory response can be expected based on ab initio theory. Indeed, as the calculations are based on a gaseous system, the attractive electrostatic interactions would overwhelm any opposing repulsive effect. An indirect confirmation of the possible coexistence of hydride and the species $[(pp_3)Co(C{\equiv}CR)]^{2+}$ might perhaps be provided by a straightforward optimization of the latter. Experimentally, the stability of the 16-electron pentacoordinated complex is confirmed by several crystal structures involving d^6 metals, mainly of the second and third transition rows,[23] and further support is provided by theoretical studies, including ab initio calculations with a proper orbital rationale.[24] In contrast, we are not aware of any stable Co^{III} species having a 16-electron count. Moreover, all our attempts to reach convergence for the model $[(pp_3)Co(C{\equiv}CR)]^{2+}$ (at the MP2 level) were unsuccessful because of large oscillations about the energy minimum. Thus, not even an indirect proof of the M^+-H^- heterolysis could be obtained.

While the existence of the *ion pair* cannot readily be demonstrated at the ab initio level, the extended Hückel method neglects the electrostatic term. Thus, in order to compare the MO behavior at any limiting geometrical situation, Figure 3 shows the EHMO 3D potential energy surface (PES). The latter is constructed on the two-dimensional grid appearing at the lower right-hand side of the figure, where the axes correspond to the increasing $M-H$ separation (positive *y*) and to the shifting of the H atom along the $M-C_\alpha-C_\beta-R$ direction (positive *x*). The origin corresponds to the hydride−acetylide Co^{III} complex itself.

In the early stages, the $[(pp_3)Co(C{\equiv}CR)]^{2+}$ fragment is kept in a fixed geometry and, in particular, the critical angle α, P_3-Co-P_4 (see **V**), is fixed at 150°. On approaching the final vinylidene product, narrowing of the terminal $C_\alpha-C_\beta-R$ angle is allowed. Interestingly, on the side of the surface facing the observer, there is a barrier which reproduces, at least geometrically, the transition state **5a** obtained by MP2 calculations (at EHMO level the barrier is large, ca. 50 kcal/mol). On the other hand, on descending the *y* axis (on the left side), the energetic cost of the $Co-H$ cleavage remains comparable so that, in principle, the hydride could migrate isolated behind the highest peak of the PES until it falls towards the C_β atom.

Some sound chemical inferences may be gained from the Walsh diagrams shown in Figure 4, which refer to alternative pathways indicated by the arrows in the small grid of Figure 3.

In the diagram on the far left, complete $M-H$ *heterolysis* is followed by coupling of the hydride with the C_β atom. The HOMO−LUMO gap, fairly large and constant over the central region, becomes small (ca. 0.5 eV) at some later point, so that even a change of the ground state can be hypothesized (singlet → triplet). Conversely, for the *close-contact* H migration, the gap is never smaller than 2 eV and none of the latter complications can be expected.

As the H atom moves parallel to the $Co-C_\alpha-C_\beta$ direction, the effects on some important MOs may be generalized, even if their extent depends on the initial $M-H$ separation. Figure 5 focuses on the behavior of only four levels. Starting from the left, these are the pair of occupied/empty σ and σ^*_{M-H} MOs of the hydride−acetylide species (see **VI**), and the pair of occupied/empty MOs corresponding to the in-plane π and π* levels of the acetylide.

As the H_{1s} orbital moves away from the direction of the metal σ hybrid, their overlap diminishes so that the σ^*_{M-H} level (LUMO) is stabilized. For an already long $M-H$ distance, this effect cannot be large as the LUMO energy would quickly reach the constant minimum, essentially the energy of the metal σ hybrid itself. In the left-hand diagram

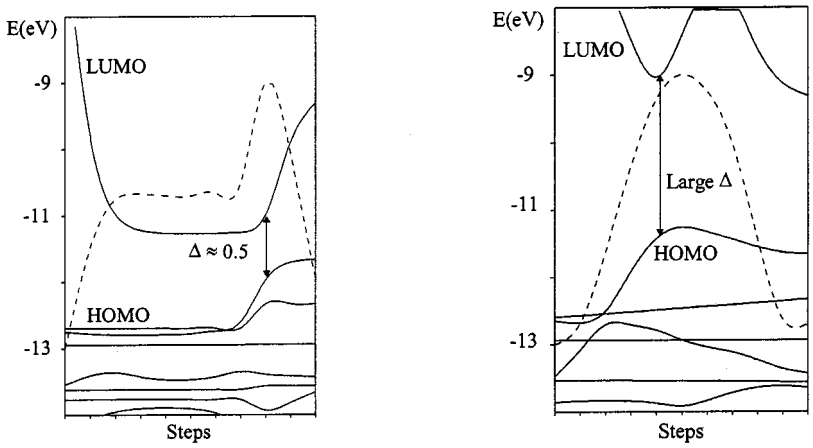


Figure 4. Walsh diagrams (EHMO calculations) relating to the two pathways indicated by the curved and straight arrows in the small grid of Figure 3, respectively; the far left-hand diagram corresponds to a H atom that migrates while physically separated from the rest of the molecule; the far right-hand diagram goes through the bridging H mode, corresponding to the ab initio transition state **5a** as depicted in Figure 1; the dashed lines refer to the total energy, for which each increment on the *y* axis corresponds to 0.6 eV

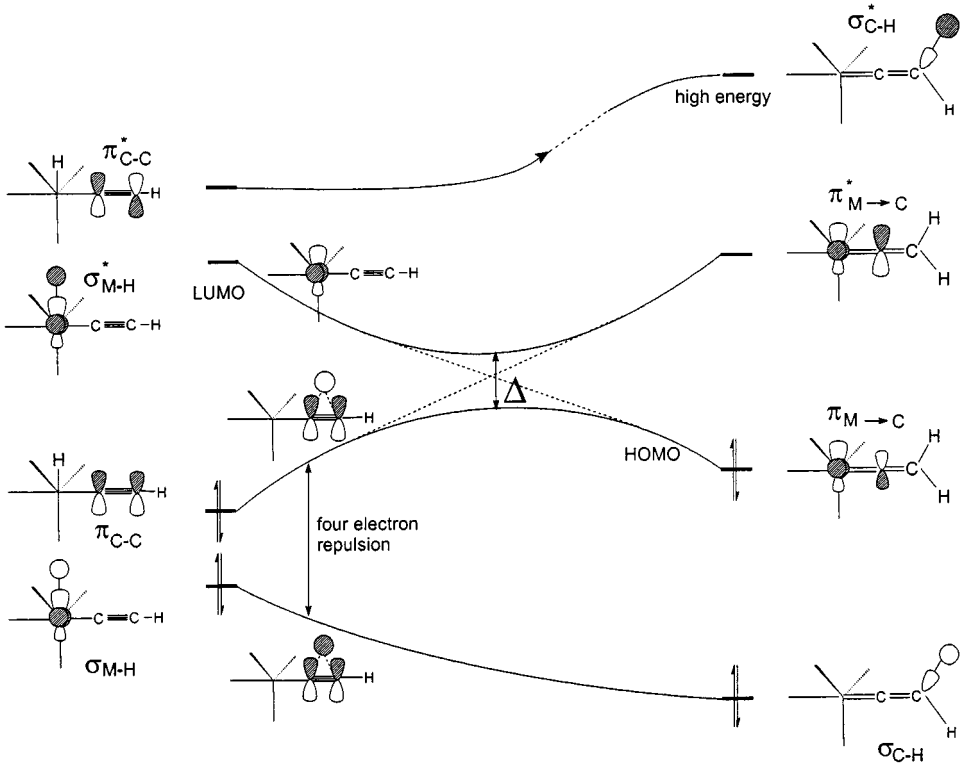


Figure 5. Schematic evolution of selected *in-plane* frontier MOs upon shifting of the H atom (initially the hydride ligand bound to the metal) along the linear grouping $Co-C_\alpha-C_\beta$; a four-electron repulsion between the hydride and one π-acetylene electron pair causes the destabilization of the HOMO, and hence is the origin of the barrier; the effect is subsequently counterbalanced by an interplay of orbital mixings, which brings metal character to the HOMO x^2-y^2 and involvement in some sort of back-donation

of Figure 4, the LUMO takes on C−H σ* character in the final steps and rises again until all of the character is transferred into high-lying MOs. Conversely, when the hydrogen atom is closer to the C−C linkage (right-hand diagram in Figure 4), the LUMO destabilizes soon after the initial stabilization. At the same time, a low-lying occupied level increases in energy and becomes the new HOMO.

Essentially, the origin of the *avoided* HOMO−LUMO crossing, highlighted in Figure 5, can be described as follows. On moving away from the metal, H_{1s} begins to interact with the π_{C-C} bonding MO, giving rise to diverging *in-phase* and *out-of-phase* combinations (the latter being the HOMO, as shown in Figure 5). At least initially, due to the shortness of the C≡C triple bond, π^*_{C-C} is too high to mix into the HOMO so as to alter the depicted repulsion between H_{1s} and π_{C-C}-based orbitals. Subsequently, the intermixing between all of the levels of Figure 5 (isosymmetric) becomes more significant. Thus, the descending LUMO (σ^*_{M-H}) and the rising HOMO evidently undergo an *avoided crossing*, which involves π^*_{C-C} as well. By virtue of

the latter, the pπ contribution from C_β disappears from both levels, which acquire a sort of π and π* character relative to $M-C_\alpha$ (see below). As mentioned above, the $C_\beta-H$ σ* character is only temporarily observed in the LUMO and is quickly transferred to higher levels.

Ultimately, the HOMO is largely centered on the metal and it can be assumed that its formal reduction has occurred, involving the electrons formerly on the hydride ligand. More precisely, the x^2-y^2 component, although not strictly a dπ orbital, can make some back-donation into the $C_\alpha p_\pi$ orbital through its most hybridized lobe, so that the M=C=C bonding formulation is reasonable. Moreover, it can be shown that the nature and extent of the back-donation are subtly governed by the geometrical flexibility of the pp_3 ligand (vide infra).

Recall that the vinylidene complex containing four independent PH_3 ligands was optimized with C_{2v} symmetry, as was the fragment $[(PH_3)_4Co]^+$. The latter of the type d^8-L_4M and with butterfly shape is characterized by an equatorial, occupied d_ϕ hybrid,[25] which is most suitable for back-donation. Significantly, in this complex, the grouping $C=CH_2$ is perfectly aligned with the bisector of the two angles P_1-Co-P_2 and P_3-Co-P_4. The same picture does not quite apply to the fragment $[(pp_3)Co]^+$, which is at most C_s and is somewhat reminiscent of threefold symmetry (Figure 1). Under these circumstances, the coordinated $C=CH_2$ grouping remains close to one apical position of the trigonal bipyramid (*trans* to P_1), with the angle P_1-Co-C_α deviating from linearity by only 15° (experiment[6]) or 25.2° (MP2 structure **3a** in Figure 1). As already discussed, the angle P_1-Co-P_2 is almost fixed at 90°, while the angle P_3-Co-P_4 (α in **V**) is free to open from 120° (up to 140° in the experimental structure and even more so in the optimized structure **3a**, i.e. 155.3°).

The angle P_3-Co-P_4 plays a major role in governing the dπ back-donation capabilities of d^8-L_4M fragments. Figure 6 shows the evolution of the frontier MOs of the trigonal-pyramidal fragment $[(PH_3)_4Co]^+$ (left side) on widening one equatorial P−Co−P angle over the range 120−180°. At the right-hand side, the fragment has a butterfly shape with the typical FMOs ($t_{2g} + d_\phi + \sigma_{hybrid}$).[25]

At the trigonal-pyramidal stage, the metal orbitals consist of two *e* sets (*xz*/*yz* orbitals, unperturbed, and *xy*/x^2-y^2 orbitals partially destabilized by the equatorial ligands) and of a higher a_1 level (σ_{hybrid}, largely z^2 in character and destabilized by the axial ligand). On widening of the angle, 1*e* and a_1 remain unaffected, but the 2*e* components diverge. In fact, the two equatorial ligands slip off two consecutive lobes of *xy* and progressively point more towards the nodes of the orbital, while an opposite trend is seen for x^2-y^2. Ultimately, *xy* becomes equivalent to *xz* and *yz* ("octahedral" t_{2g} set), while x^2-y^2 is so destabilized that its crossing with the higher z^2 (a_1) is attempted but *avoided* because of the equal symmetry (*a′* in C_s). The resultants of a z^2/x^2-y^2 mixing, usually difficult to visualize, are well illustrated by the CACAO pictures[9] in Figure 6. Thus, the former a_1 level reorientates the main σ lobe up to 45° in the plane *xz* and maintains the original σ character, albeit with

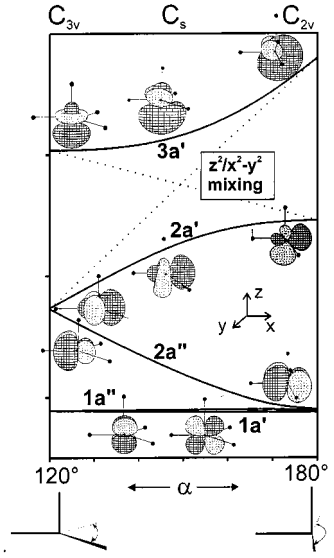


Figure 6. Evolution of the metal d orbitals during the interconversion of an L_4M metal fragment from trigonal-pyramidal to butterfly geometry, the unique governing factor being the opening of one equatorial L−M−L angle; avoided crossing between x^2-y^2 and z^2 slowly develops d_ϕ character at the former orbital, which is occupied in the d^8 configuration

reduced d orbital contribution. At the same time, the mixing transforms the most extended lobes of the somewhat hybridized z^2 and x^2-y^2 orbitals into a new orbital with progressively greater dπ character. At α = 180°, the well known d_ϕ hybrid typical of the L_4M fragments with butterfly shape is observed.[25] The ethylenic chains in the fragment $[(pp_3)Co]^+$ are resistant to full P−Co−P opening, so that an intermediate geometry can be stabilized as soon as the d_ϕ character is sufficient to allow back-donation into the vinylidene unit. This is most likely the key factor in interpreting the influence of the geometry of the ancillary ligand on the stability of the vinylidene complex.

Concluding Remarks

The experimental data and the present ab initio results indicate that, at least for the system $(pp_3)Co^I$, the hydride−acetylide species is the key basic intermediate en route to vinylidene. The essential qualitative arguments are shown schematically in Figure 7. The acetylene molecule adds to the d^8 metal through donation of its π bonding electron pairs into the acceptor σ hybrid orbital typical of the trigonal-pyramidal fragments. The metal bears a lone pair based on the occupied x^2-y^2 orbital, which is relatively high in energy. On opening of one P−M−P angle (α, see **V**), the metal develops the necessary d_ϕ character to trigger C−H oxidative addition (see Figure 6) and the pseudo-octahedral hydride−acetylide complex is formed.

Formally, the hydrogen ligand abstracts the lone pair from the metal so that a total of 12 valence electrons is consistently assigned to the whole grouping $H^- + CCH^-$. As soon as the hydride falls away from the position of maximum overlap with the σ metal hybrid, its electrons are re-

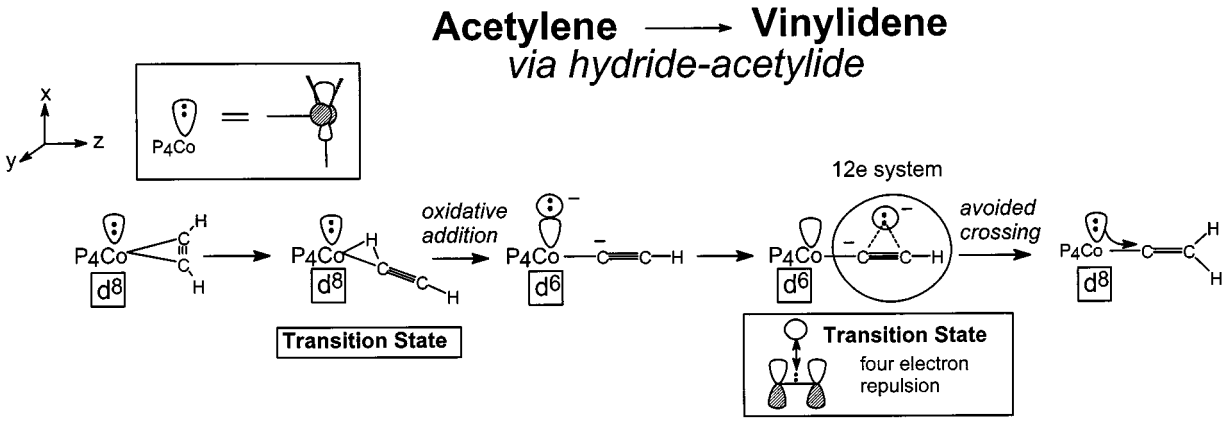


Figure 7. Structural highlights for the 1,3-shifts promoted by d^8 metal fragments; along this pathway, oxidative addition and reductive elimination of the metal involve a suitably modified orbital (originally x^2-y^2)

pelled by the electron cloud of the coplanar C−C π bond, as indicated in Figure 5. The four-electron repulsion is maximized at some point where the hydrogen bonds the two carbon atoms (transition state). The barrier is directly related to the destabilization of the HOMO, and the trend is inverted by an *avoided crossing mechanism.* By virtue of the latter, the hydride electron pair is returned to a metal orbital. This is essentially x^2-y^2, which characterizes the descending LUMO and ultimately concentrates into the HOMO. The final step on the pathway corresponds to the simple protonation of the C_β atom of the 18-electron acetylide complex, which occurs easily.[6]

At the transition state, the C_α−H and C_β−H distances are critically long, and are likely to limit the effects of the aforementioned four-electron repulsion. The calculated MP2 values are 1.32 and 1.48 Å, respectively. At longer C−H bridging distances, the energetics of the system would go steeply uphill toward the highest peak of the EHMO PES shown in Figure 3. Alternatively, the system might go around the peak by first elongating the M−H distance. In this case, the barrier would be essentially the energy of the M−H bond, which is too high. In fact, this is estimated to be no lower than 50 kcal/mol and significantly larger for second- and third-row transition metals.[26] Most probably because of the latter reason, the rhodium system stabilizes the hydrido−acetylide species and the barrier to vinylidene formation is distinctly higher than in the case of cobalt.

Even though the EHMO method neglects the important electrostatic component when charges are separated, it reveals an orbital drawback to the heterolysis. Namely, a small HOMO−LUMO gap along the pathway (left-hand diagram of Figure 4) would imply a necessity for a change in the ground state. If complete M−H heterolysis appears improbable, the hydrogen must start its migration as a hydride. When the C_β atom bears too great a negative charge, as is the case when it is bound to an electropositive silyl substituent, the migration may be inhibited and the hydride−acetylide species is stabilized.[6]

The general reactivity studied here has already received much theoretical attention. Despite this, no generalization of the results can yet be made. In the present study, we have not only performed ab initio calculations on a system which follows possibly unique pathways, but we have also offered some interpretations by exploiting the concepts of perturbation theory as well as by applying chemical intuition. From a quantitative point of view, it has become apparent that sufficiently good results are only obtainable with the most realistic model (use of the pp_3 ligand). At the same time, monitoring of the MO behavior along the reaction pathways has helped to resolve some major chemical ambiguities.

Acknowledgments

E. P.-C. is grateful to the Spanish Ministerio de Educacion y Cultura for a Postdoctoral grant. Financial support from EC contract ERBIC15CT-960746 is gratefully acknowledged. We thank the "Area della Ricerca CNR di Firenze" (in particular, Dr. Alberto Tronconi and Mr. Stefano Cerreti) for the providing computing time and facilities.

[1] K. M. Ervin, J. Ho, W. C. Lineberger, *J. Chem. Phys.* **1989**, *91*, 5974−5992.
[2] W.-C. Chen, C.-H. Yu, *Chem. Phys. Lett.* **1997**, *277*, 245−251 and references therein.
[3] J. Silvestre, R. Hoffmann, *Helv. Chim. Acta* **1985**, *68*, 1461−1506.
[4] [4a] Y. Wakatsuki, N. Koga, H. Yamazaki, K. Morokuma, *J. Am. Chem. Soc.* **1994**, *116*, 8105−8111. − [4b] Y. Wakatsuki, N. Koga, H. Werner, K. Morokuma, *J. Am. Chem. Soc.* **1997**, *119*, 360−366. − [4c] R. Stegmann, G. Frenking, *Organometallics* **1998**, *17*, 2089−2095.
[5] [5a] H. Werner, U. Brekau, *Z. Naturforsch.* **1989**, *44b*, 1438−1448. − [5b] T. Rappert, O. Nürnberg, N. Mahr, J. Wolf, H. Werner, *Organometallics* **1992**, *11*, 4156−4164. − [5c] H. Werner, M. Baum, D. Schneider, B. Windmüller, *Organometallics* **1994**, *13*, 1089−1089. − [5d] M. Oliván, E. Clot, O. Eisenstain, K. G. Caulton, *Organometallics* **1998**, *17*, 897−901.
[6] C. Bianchini, M. Peruzzini, A. Vacca, F. Zanobini, *Organometallics* **1991**, *10*, 3697−3707.
[7] I. de los Ríos, M. J. Tenorio, M. C. Puerta, P. Valerga, *J. Am. Chem. Soc.* **1997**, *119*, 6529−6538.
[8] [8a] C. Bianchini, A. Meli, M. Peruzzini, F. Zanobini, P. Zanello, *Organometallics* **1990**, *9*, 241−250. − [8b] C. Bianchini, D. Masi, A. Meli, M. Peruzzini, J. A. Ramirez, A. Vacca, F. Zanobini, P. Zanello, *Organometallics* **1989**, *8*, 2179−2189.
[9] C. Mealli, D. M. Proserpio, *J. Chem. Educ.* **1990**, *67*, 399−402.
[10] [10a] R. Hoffmann, W. N. Lipscomb, *J. Chem. Phys.* **1962**, *36*,

2872−2883. − [10b] R. Hoffmann, W. N. Lipscomb, *J. Chem. Phys.* **1962**, *37*, 3489−3493.
[11] J. H. Ammeter, H.-B. Bürgi, J. C. Thibeault, R. Hoffmann, *J. Am. Chem. Soc.* **1978**, *100*, 3686−3692.
[12] R. H. Summerville, R. Hoffmann, *J. Am. Chem. Soc.* **1976**, *98*, 7240−7254.
[13] M. J. Frisch, G. W. Trucks, H. B. Schlegel, P. M. W. Gill, B. G. Johnson, M. A. Robb, J. R. Cheeseman, T. A. Keith, G. A. Petersson, J. A. Montgomery, K. Raghavachari, M. A. Al-Laham, V. G. Zakrzewski, J. V. Ortiz, J. B. Foresman, J. Cioslowski, B. B. Stefanov, A. Nanayakkara, M. Challacombe, C. Y. Peng, P. Y. Ayala, W. Chen, M. W. Wong, J. L. Andres, E. S. Replogle, R. Gomperts, R. L. Martin, D. J. Fox, J. S. Binkley, D. J. Defrees, J. Baker, J. P. Stewart, M. Head-Gordon, C. Gonzalez, J. A. Pople, *Gaussian-94*, Gaussian Inc., Pittsburgh, PA, **1995**.
[14] P. J. Hay, W. R. Wadt, *J. Chem. Phys.* **1985**, *82*, 299−310.
[15] W. J. Stevens, H. Basch, M. Krauss, *J. Chem. Phys.* **1984**, *81*, 6026−6033.
[16] T. H. Dunning, P. J. Hay, *Modern Theoretical Chemistry* (Ed.: H. F. Schaefer III), Plenum, New York, **1976**, 1−28.
[17] [17a] P. C. Hariharan, J. A. Pople, *Theor. Chim. Acta* **1973**, *28*, 213−222. − [17b] M. M. Francl, W. J. Petro, W. J. Hehre, J. S. Binkley, M. S. Gordon, D. J. DeFree, J. A. Pople, *J. Chem. Phys.* **1982**, *77*, 3654.
[18] Y. Pérès, M. Dartiguenave, Y. Dartiguenave, *Organometallics* **1990**, *9*, 1041−1047.
[19] [19a] H. Jacobsen, H. Berke, *Chem. Eur. J.* **1997**, *3*, 881−886. − [19b] C. Bianchini, D. Masi, M. Peruzzini, M. Casarin, C. Maccato, G. A. Rizzi, *Inorg. Chem.* **1997**, *36*, 1061−1069.
[20] Frequencies were calculated for the most stable isomer **3b**. The only imaginary value has the largest components, indicating that the two C atoms in the mirror plane vibrate out of it, in opposite directions. In order to get an idea of the error introduced, complex **3b** was also optimized in C_1 symmetry. Since structural (Table 1) and energetic differences are small (< 2 kcal/mol), the C_s symmetry was retained for all of the key structures, including the transition states, **4a** and **5a**.
[21] C. Peng, H. B. Schlegel, *Isr. J. Chem.* **1993**, *33*, 449−454.
[22] J. Silvestre, M. J. Calhorda, R. Hoffmann, P. O. Stoutland, R. G. Bergaman, *Organometallics* **1986**, *5*, 1841−1851.
[23] [23a] C. R. S. M. Hampton, I. R. Butler, W. R. Cullen, B. R. Jones, J.-P. Charland, J. Simpson, *Inorg. Chem.* **1992**, *31*, 5509−5520. − [23b] R. L. Harlow, D. L. Thorn, R. T. Baker, N. L. Jones, *Inorg. Chem.* **1992**, *31*, 993−997. − [23c] M. D. Fryzuk, P. A. MacNeil, R. L. Massey, R. G. Ball, *J. Organomet. Chem.* **1989**, *368*, 231−247. − [23d] M. D. Fryzuk, P. A. MacNeil, R. G. Ball, *J. Am. Chem. Soc.* **1986**, *108*, 6414−6416. − [23e] H. Werner, A. Höhn, M. Dziallas, *Angew. Chem. Int. Ed. Engl.* **1986**, *12*, 1090−1092.
[24] [24a] M. Ogasawara, S. A. Macgregor, W. E. Streib, K. Folting, O. Eisenstein, K. G. Caulton, *J. Am. Chem. Soc.* **1995**, *117*, 8869−8870. − [24b] J. T. Poulton, M. P. Sigalas, K. Folting, W. E. Streib, O. Eisenstein, K. G. Coulton, *Inorg. Chem.* **1994**, *33*, 1476−1485.
[25] A. Albright, J. K. Burdett, M. H. Whangbo, *Orbital Interactions in Chemistry*, Wiley, New York, **1985**.
[26] F. Calderazzo. *Insertion Reactions: Principles and Applications*, Wiley, in preparation.

Received February 9, 1999
[I99032]

Di- and Tripalladium(II) and -platinum(II) Complexes Containing 7-Amino-1,8-naphthyridin-2-one as a Bridging Ligand − Oxidation of a $[Pt_3]^{6+}$ Core to $[Pt_3]^{8+}$

Bernhard Oskui[a] and William S. Sheldrick*[a]

Keywords: Platinum / Palladium / Platinum blues / Naphthyridine complexes / Trinuclear complexes

All three dinuclear complexes $[Pd_2(donp)_2(bpy)_2]$ (**1**) (H_2donp = 1,8-naphthyridin-2,7-dione), $[Pd_2(H_2nonp)_2(bpy)_2](ClO_4)_2$ (**2**), and $[Pt_2(H_2nonp)_2(bpy)_2](PF_6)_2$ (**3**) (H_3nonp = 7-amino-1,8-naphthyridin-2-one) exhibit the μ-1κN^1:2κN^8 bridging mode for their *head/tail* orientated naphthyridine ligands. Whereas **1** and **3** may be prepared by direct reaction of the dinucleating ligand with $[MCl_2(bpy)]$, formation of competing tripalladium(II) complexes must be avoided for **2** by employment of the precursor $H_2acnonp$ (7-acetamido-1,8-naphthyridin-2-one), which affords $[H_2nonp]^-$ on cleavage of its original acetyl group. A mixture of the *head/tail* (**4a**) and *head/head* (**4b**) isomers of $[Pd_3(Hnonp)_2(bpy)_3](ClO_4)_2$ is obtained when H_3nonp is treated with $[PdCl_2(bpy)]$ and LiOH at room temperature for 2 d, followed by precipitation with $LiClO_4$. Contrastingly exclusive formation of **4a** is observed upon refluxing this reaction mixture for 3 d in aqueous solution. The $[Hnonp]^{2-}$ ligands exhibit a μ$_3$-1κN^1:2κN^8:3κN^7 bridging mode that leads to short Pd···Pd interactions of 2.781(2) and 2.775(2) Å. Similar metal–metal distances of 2.771(3) and 2.816(3) Å are observed in *head/head*-$[Pt_3(acnonp)(Hnonp)(bpy)_3]Cl_2$ (**5**). An in situ 2e$^-$-oxidation (Ag^+/Ag) of the $[Pt_3]^{6+}$ core in triplatinum(II) species such as **5** formed by the reaction of $[PtCl_2(bpy)]$ with $H_2acnonp$ allows the isolation of diamagnetic dark-brown *head/head*-$[Pt_3(Hnonp)_2(NO_3)(bpy)_3](ClO_4)_2(NO_3)$ (**6**) with an average oxidation state of Pt (2.67+). The Pt–Pt distances of 2.723(2) and 2.670(2) Å are markedly shorter than in **5**.

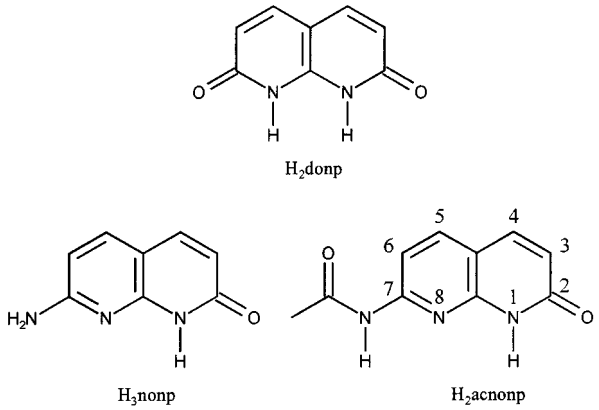
Although the oligomeric class of molecules known as the platinum blues all formally contain Pt^{III}, the average oxidation state of their Group 10 metal atoms is usually much lower than +3.0.[1] Following the first report of the prototype platinum-acetamide blues in 1908,[2] some 70 years were to pass before Lippard et al.[3] were finally successful in structurally characterising *cis*-$[\{Pt_2(\mu\text{-}C_5H_4NO)_2(NH_3)_4\}_2](NO_3)_5$ (C_5H_4NO = α-pyridonate) as an adequate model analog. This paramagnetic tetranuclear complex (S = 1/2), with its average oxidation state of +2.25, exhibits a Pt−Pt distance of 2.775(1) Å in its outer α-pyridonate bridged dimeric sub-units, that are linked through an inner Pt−Pt interaction of length 2.877(1) Å. Similar alternating short supported [2.880(2), 2.778(1) Å] and longer unsupported [2.900(1), 2.934(1) Å] Pt−Pt bonds were subsequently established for the diamagnetic centrosymmetric octanuclear platinum−acetamide complex $[\{Pt_2(NHCOCH_3)_2(NH_3)_4\}_4](NO_3)_{10} \cdot 4\,H_2O$, in which the average oxidation state is once again +2.25.[4] Significantly shorter metal-metal distances of 2.702(6), 2.710(5), and 2.706(6) Å in the linear Pt_4 chain of $[\{Pt_2(C_4H_3NO)_2(NH_3)_4\}_2](NO_3)_6 \cdot 2\,H_2O$[5] ($C_4H_3NO$ = α-pyrrolidonate) are consistent with this so-called "α-pyrrolidone tan" being in the higher average oxidation state of Pt (2.5+). The spectroscopic, redox, and chemical properties of μ-*N,O*-pyrimidinate bridged (1-MeU = 1-methyluracilate, 1-MeT = 1-methylthyminate) blue and green oligomeric platinum complexes closely mirror those of the α-pyridone blues and an average oxidation state of Pt (2.75+) has been established for $[\{Pt_2Cl_2(1\text{-}MeT)_2(NH_3)_2\}_2Cl]PtCl_6 \cdot 6\,H_2O$.[6] However, this complex contains two individual diplatinum units [Pt−Pt distance, 2.699(1) Å], that are connected by a single chloride bridge, and is not, therefore, strictly comparable with the typical Pt_4 linear clusters discussed above.

Mixed intensely golden-tan trinuclear Pt_2Pd complexes of the type *cis*-$[L_2'Pt(\mu\text{-}L)_2Pd(\mu\text{-}L)_2PtL_2']X_2$ (L′ = en/2, NH_3; L = 1-MeU, 1-MeT; X = NO_3^-, ClO_4^-) have been characterised by Lippert and co-workers[7][8] and can be oxidised by conc. HNO_3 to deep purple-blue trications with an average oxidation state M (2.33+) and Pt−Pd distances in the range 2.634(1)−2.646(1) Å. This posed the question as to whether similar linear homonuclear Pt_3 complexes can also be prepared in the presence of suitable di- or trinucleating ligands and led to our recent characterisation[9] of the 1,8-naphthyridin-2,7-dionato (H_2donp, Scheme 1) compounds *cis*-$[M_3(donp)_2(bpy)_3]^{2+}$ (M = Pd, Pt), which exhibit relatively short supported $M^{II}\cdots M^{II}$ distances in the range 2.801−2.807 Å. The blue-green triplatinum(II) complex displays one-electron transfer waves at $E_{1/2}$ = 0.65 V to blue-violet *cis*-$[Pt_3(donp)_2(bpy)_3]^{3+}$ and $E_{1/2}$ = 1.30 V (in CH_3CN, vs. Ag/AgCl) to violet *cis*-$[Pt_3(donp)_2(bpy)_3]^{4+}$. As we were unsuccessful in isolating either the Pt (2.33+) or the Pt (2.67+) complex, we have now extended our studies to 7-amino-1,8-naphthyridin-2-one (H_3nonp) and 7-acetamido-1,8-naphthyridin-2-one ($H_2acnonp$, Scheme 1), in the expectation that the change in the sites of protonation from

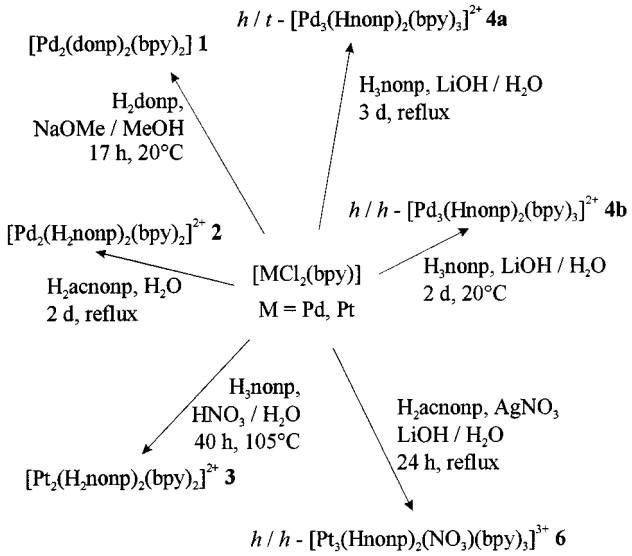
[a] Lehrstuhl für Analytische Chemie, Ruhr-Universität Bochum
D-44780 Bochum, Germany
Fax: (internat.) + 49(0)234/7094-420
E-mail: shel@anachem.ruhr-uni-bochum.de

 © WILEY-VCH Verlag GmbH, D-69451 Weinheim, 1999 1434−1948/99/0808−1325 $ 17.50+.50/0

N^1/N^8 in H_2donp to N^1/N^7 in these ligands might help to stabilise a triplatinum(III, II, III) species.



Scheme 1. The ligands H_2donp, H_3nonp and H_2acnonp with the numbering scheme



Scheme 2. Synthesis of complexes **1**–**6**

Results

The reaction of H_2donp with [MCl_2(bpy)] (M = Pd, Pt) and LiOH at 1:1:2 molar ratio in refluxing aqueous solution generates the trinuclear complexes *cis*-[M_3(donp)$_2$(bpy)$_3$]$^{2+}$ rather than the stoichiometrically expected μ-N^1,N^8-bridged dimers *cis*-[M_2(donp)$_2$(bpy)$_2$].[9] Lowering the reaction temperature to 20 °C does, indeed, lead to precipitation of a sparingly soluble dinuclear Pd neutral complex, albeit in low yield. We could now show that *cis*-[Pd_2(donp)$_2$(bpy)$_2$] (**1**) can, in fact, be isolated as an orange precipitate in satisfactory yield (63%) by changing the solvent/base combination to CH_3OH/CH_3ONa and performing the reaction at room temperature. The formation of tripalladium(II) complexes of the type [Pd_3(Hnonp)$_2$(bpy)$_3$]$^{2+}$ (**4a**, **4b**) can likewise be avoided by treating [$PdCl_2$(bpy)] with H_2acnonp at an equimolar ratio in refluxing water in the absence of base. Addition of $LiClO_4$ leads to precipitation of *cis*-[Pd_2(H_2nonp)$_2$(bpy)$_2$](ClO_4)$_2$ (**2**), in which the naphthyridine monoanions H_2nonp$^-$, formed by cleavage of the acetyl group in the original ligand, adopt the bridging μ-N^1,N^8 coordination mode. The analogous diplatinum(II) complex *cis*-[Pt_2(H_2nonp)$_2$(bpy)$_2$](PF_6)$_2$ (**3**) can be isolated by adding an excess of NH_4PF_6 to an aqueous reaction solution of [$PtCl_2$(bpy)] and H_3nonp kept at pH 2 to suppress the metalation of the 7-amino function, which leads to formation of the preferred trinuclear dications.

Figures 1 and 2 depict the structures of the neutral dipalladium(II) complex **1** and the dication of the $Pt^{(II,II)}$ complex **3**. All three dinuclear species **1**–**3** display the μ-1κN^1:2κN^8 coordination mode with *head/tail* positioning of their bridging naphthyridine ligands. This binding pattern was also established for [Ru_2(monp)$_4$][10] (Hmonp = 7-methyl-1,8-naphthyridin-2-one) and [Ru_2(mphonp)$_4$(H_2O)][11] (Hmphonp = 5-methyl-7-phenyl-1,8-naphthyridin-2-one) and should be electronically favourable for [M_2]$^{4+}$ cores with occupied antibonding orbitals (e.g. [Ru_2]$^{4+}$, [Rh_2]$^{4+}$, [Pd_2]$^{4+}$), as it will enhance the interaction between the δ* orbitals of the dimetal unit and the π* molecular orbitals of the bridging aromatic anions[11]. In contrast, the dinucleating monp$^-$ ligands in [Mo_2(monp)$_4$] exhibit the alternative μ$_2$-1κN^1:2κO^2 coordination mode[10].

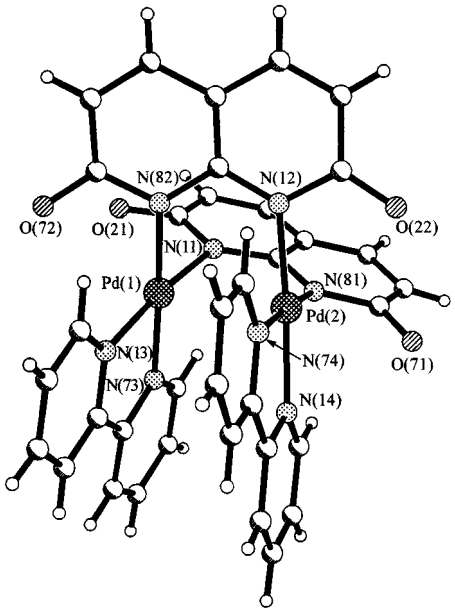


Figure 1. Molecular structure of [Pd_2(donp)$_2$(bpy)$_2$] (**1**)

The M···M distances of respectively 2.779(1) (M = Pd) and 2.789(1) Å (M = Pt) in the H_2nonp$^-$ complexes **2** and **3** are marginally shorter than that of 2.797(1) Å in the $Pd^{(II,II)}$ compound **1** (Table 1). This latter value lies in the range 2.794–2.804 Å established[9] for the analogous dinuclear complexes [M_2(onp)$_2$(bpy)$_2$]$^{2+}$ (Honp = 1,8-naphthyridin-2-one) and [M_2(monp)$_2$(bpy)$_2$]$^{2+}$ (M = Pd, Pt), which themselves are markedly shorter than the metal–metal distances of 2.841–2.974 Å previously reported for similar 1-methylthyminato- and 1-methyluracilato-bridged complexes.[12–17] The Pt···Pt separation of 2.899(2) Å in the di-

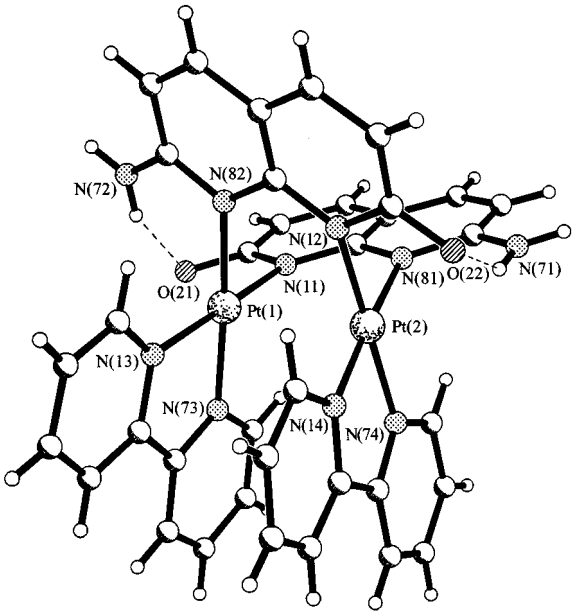


Figure 2. Structure of dication $[Pt_2(H_2nonp)_2(bpy)_2]^{2+}$ of **3**

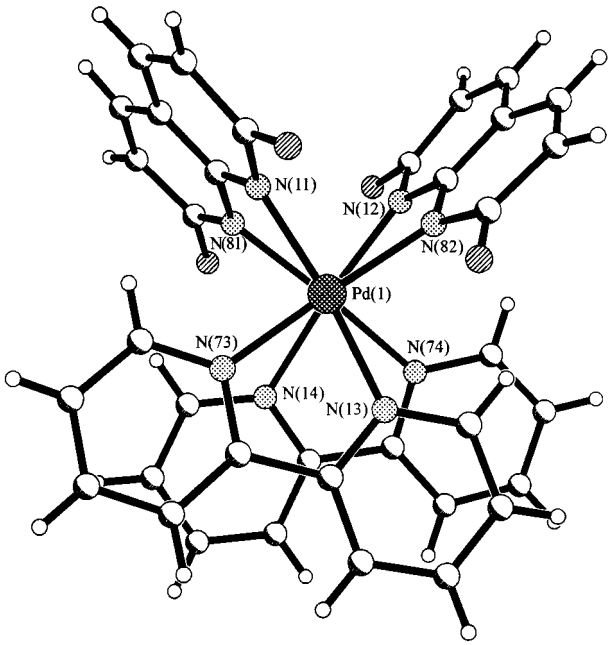


Figure 3. Projection of the structure of (**1**) along the Pd(1)···Pd(2) axis to demonstrate the pronounced relative twisting of the $donp^{2-}$ and bpy ligands

nuclear (bpy)Pt^{II} cation of $[Pt_2(C_4H_6NO)_2(bpy)_2](ClO_4)_2$ (C_4H_6NO = α-pyrrolidonate) also lies within this typical longer range.[18] μ-1κN^1:2κN^8 metal coordination in **1**−**3** leads to a significant widening of the $N^1\cdots N^8$ bite distance (respectively 2.34, 2.35, 2.40 Å) in comparison to the separation of these donor atoms in free naphthyridine ligands [e.g. 2.293(6) Å in Hmonp[19]]. Interestingly, the $N^1-M^1\cdots M^2$ angles in the H_2nonp^- complexes **2** [81.6(2)°] and **3** [81.5(4), 82.3(4)°] are considerably narrower than those observed for $N^8-M^2\cdots M^1$ [85.8(2)° in **2**, 85.8(4) and 86.3(5)° in **3**]. The analogous angles for the symmetrically 2,7-disubstituted $donp^{2-}$ ligands of **1** all lie within the range 81.3(2)−83.0(2) and are, therefore, similar to those for $N^1-M^1\cdots M^2$ in **2** and **3**. As the Pd^{II} and Pt^{II} atoms in **1**−**3** are not significantly displaced from the least-squares planes of their respective coordination spheres, the narrow $N^1\cdots N^8$ separations of the bridging naphthyridine ligands cause the square-planar MN_4 units to tilt away from one another at dihedral angles of 19.4(3) (**1**), 17.9(2) (**2**), and 18.0(4)° (**3**). Close intramolecular contacts between adjacent O^2 and O^7 atoms of the *cis*-positioned $donp^{2-}$ ligands in **1** lead to pronounced rotation of the naphthyridine (npy) and 2,2′-bipyridyl moieties relative to one another about the Pd(1)···Pd(2) axis. This state of affairs is illustrated in Figure 3 and manifests itself in the large average N(npy)−Pd(1)−Pd(2)−N(npy)′ and N(bpy)−Pd(1)−Pd(2)−N(bpy)′ torsion angles of 19.4(3) and 22.6(3)° in this compound. In contrast to **1**, the *head*/*tail* arrangement of the bridging H_2nonp^- ligands in **2** and **3** is stabilised by the formation of intramolecular O2···H−N^7 hydrogen bonds (Figure 2), with the consequence that the degree of twisting for the naphthyridine and 2,2′-bipyridyl ligands is significantly less pronounced in these complexes (Table 1).

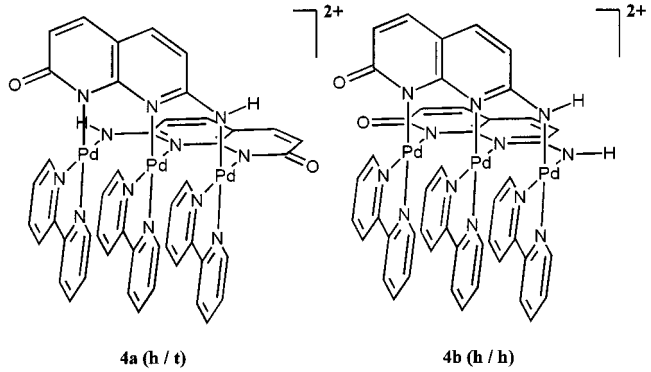
Trinuclear Pd^{II} and Pt^{II} Complexes

Treatment of H_2donp[9] and H_3nonp with $[MCl_2(bpy)]$ (M = Pd, Pt) in aqueous solution in the presence of base leads to preferred formation of trinuclear complexes even at an equimolar ratio of the starting materials. A *head*/*head* positioning of the μ_3-1κN^1:2κN^8:3κO^7 coordinated $donp^{2-}$ ligands in $[M_3(donp)_2(bpy)_3]^{2+}$ (M = Pd, Pt) would afford the less favourable polar complexes, with formal charge balance at M^1 and M^2. Such isomers would also exhibit unfavourable short intramolecular contacts between adjacent O^2 atoms. As a result of these electronic and steric factors, favoured formation of the charge balanced *head*/*tail* isomers is observed upon refluxing aqueous solutions of this naphthyridine derivative with $[MCl_2(bpy)]$ and LiOH for 1−3 d at a 2:3:4 molar ratio.[9] In contrast to H_2donp with its protonated aromatic nitrogen atoms N^1 and N^8, the likewise dibasic H_3nonp is protonated at N^1 and the endocyclic amino nitrogen N^7, with the consequence that for a μ_3-1κN^1:2κN^8:3κN^7 bridging mode both the *head*/*head* and *head*/*tail* isomers of $[M_3(Hnonp)_2(bpy)_3]^{2+}$ will exhibit formal charge balance at M^1 and M^3 of a linear $[M_3]^{6+}$ core. Inspection of the structures of these isomers (Scheme 3) indicates, however, that, whereas the *head*/*tail* isomers could be stabilised by intramolecular $N^7-H\cdots O^2$ bonding between adjacent substituents, close contacts between neighbouring O^2 atoms of the *cis* sited $Hnonp^{2-}$ ligands in the *head*/*head* isomer would lead to pronounced relative twisting of the naphthyridine and 2,2′-bipyridyl ligands about the M···M axes, as in $[Pd_2(donp)_2(bpy)_2]$ **1**.

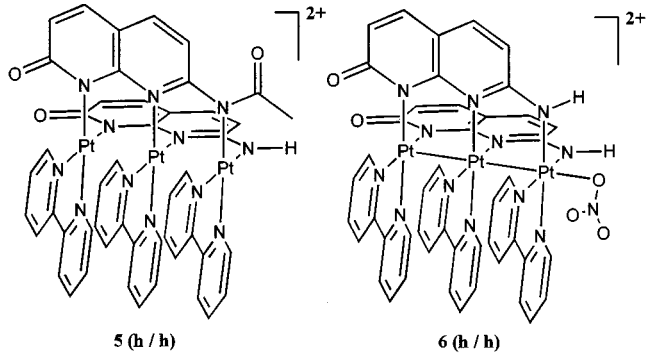
The reaction of H_3nonp with $[PdCl_2(bpy)]$ and LiOH in refluxing water does, indeed, lead to exclusive formation of the preferred isomers, *head*/*tail* $[Pd_3(Hnonp)_2(bpy)_3]^{2+}$ after 3 d. This dication, whose X-ray structure is depicted in Fig-

Table 1. M−M distances [Å] and average N−M−M′−N′ torsion angles in di- and trinuclear naphthyridine-bridged complexes

Complex	Coordination mode	d(M−M′)	N(npy)−M−M′−N(npy)′	N(bpy)−M−M′−N(bpy)′
1, *cis*-$[Pd_2(donp)_2(bpy)_2]$	μ-1κN^1:2κN^8	2.797(1)	19.4(3)	22.6(3)
2, *cis*-$[Pd_2(H_2nonp)_2(bpy)_2]^{2+}$	μ-1κN^1:2κN^8	2.779(1)	9.9(2)	13.7(2)
3, *cis*-$[Pt_2(H_2nonp)_2(bpy)_2]^{2+}$	μ-1κN^1:2κN^8	2.789(1)	12.2(1)	14.2(5)
4a, *h*/*t*-$[Pd_3(Hnonp)_2(bpy)_3]^{2+}$	μ_3-1κN^1:2κN^8:3κN^7	2.781(1), 2.775(2)	14(1), 19.3(5)	17(1)
5, *h*/*h*-$[Pt_3(acnonp)(Hnonp)(bpy)_3]^{2+}$	μ_3-1κN^1:2κN^8:3κN^7	2.771(3), 2.816(3)	20(2), 21(1)	23(3)
6, *h*/*h*-$[Pt_3(Hnonp)_2(NO_3)(bpy)_3]^{3+}$	μ_3-1κN^1:2κN^8:3κN^7	2.723(2), 2.670(2)	2(1), 3(1)	2(1)



Scheme 3. *head*/*tail* and *head*/*head* isomers (**4a**, **4b**) of $[Pd_3(Hnonp\text{-}\mu_3\text{-}1\kappa N^1{:}2\kappa N^8{:}3\kappa N^7)_2(bpy)_3](ClO_4)_2$



Scheme 4. *head*/*head*-$[Pt_3(acnonp)(Hnonp)(bpy)_3]^{2+}$ (**5**) and *head*/*head*-$[Pt_3(Hnonp\text{-}\mu_3\text{-}1\kappa N^1{:}2\kappa N^8{:}3\kappa N^7)_2(NO_3)(bpy)_3](ClO_4)_2(NO_3)$ (**6**)

ure 4, can be precipitated as its dark-orange perchlorate (**4a**) by addition of $LiClO_4$ to the reaction solution. The closely similar Pd(1)···Pd(2) and Pd(2)···Pd(3) distances of 2.781(2) and 2.775(2) Å in **4a**, which are associated with a Pd(1)···Pd(2)···Pd(3) angle of 170.9(1)° are significantly shorter than those in the analogous $donp^{2-}$ complex $[Pd_3(donp)_2(bpy)_3](PF_6)_2$ (2.801(1), 2.804(1) Å). As observed in the dinuclear complexes **1**−**3**, tilting of the metal coordination planes dihedral angles $Pd(1)N_4$−$Pd(2)N_4$ 19.2(5)°, $Pd(2)N_4$−$Pd(3)N_4$ 19.6(4)°] is accompanied by marked twisting of the $Hnonp^{2-}$ and bpy ligand positions relative to the Pd(1)···Pd(2) and Pd(2)···Pd(3) vectors in **4a** (Table 1). Due to the fact that the Pd···Pd separations are markedly longer than the bridging N1···N8 and N8···N7 bite distances, wide C^9−N^1−Pd [128.0(7), 128.3(7)°) and C^7−N^7−Pd (129.3(8), 128.9(8)°] angles are required in this trinuclear complex.

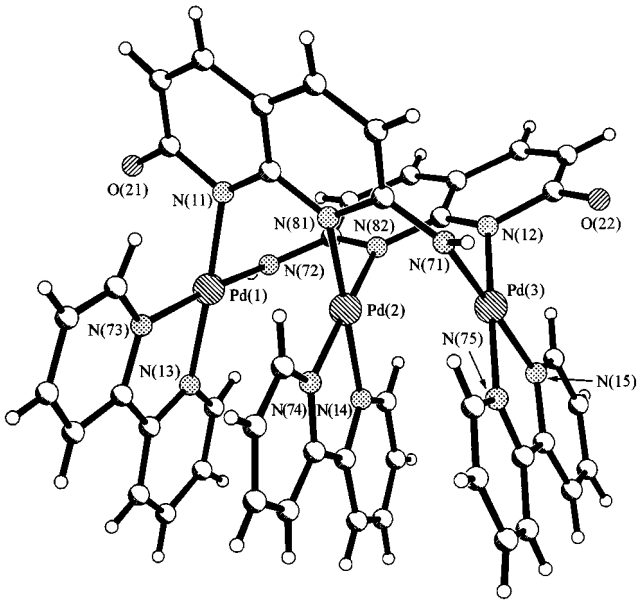


Figure 4. X-ray structure of the dication of *head*/*tail*-$[Pd_3(Hnonp)_2(bpy)_3](ClO_4)_2$ (**4a**)

A mixture of the *head*/*head* and *head*/*tail* isomers of $[Pd_3(Hnonp)_2(bpy)_3]^{2+}$ is obtained when H_3nonp is treated with $[PdCl_2(bpy)]$ and LiOH at room temperature for 2 d. The major product of this reaction **4b** (*head*/*head*) can be isolated in 32% yield by extracting the more soluble *head*/*tail* isomer **4a** with pyridine. **4b** was characterised by elemental analysis, mass spectrometry, and ^{1}H NMR spectroscopy. As both the C_2 symmetric *head*/*tail* and C_s symmetric *head*/*head* isomers exhibit 5 naphthyridine and 12 2,2′-bipyridyl magnetically inequivalent protons, it is not possible to distinguish **4a** and **4b** on the basis of their ^{1}H-NMR patterns. However, characteristic differences are apparent in Figure 5 for the bpy chemical shifts and the $Hnonp^{2-}$ amino H^7 resonance, which moves upfield from δ = 6.49 in **4a** to 6.28 in **4b**.

In contrast to the tripalladium(II) complex, an aqueous reaction solution of $Hnonp^{2-}$ and $[PtCl_2(bpy)]$ still contains a mixture of the *head*/*head* and *head*/*tail* isomers of $[Pt_3(Hnonp)_2(bpy)_3]^{2+}$, even after refluxing for periods longer than 3 d. It proved impossible to separate these products by solvent extraction or liquid chromatography, even though ^{1}H-NMR spectra indicated a predominance

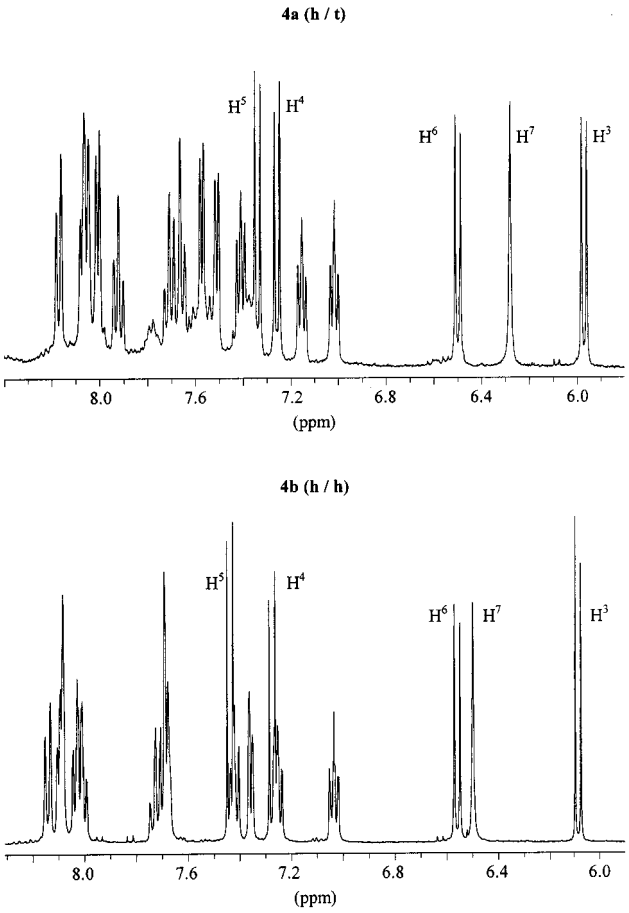


Figure 5. Proton NMR spectra ([D_6]DMSO) of the *head/tail* and *head/head* isomers (**4a**, **4b**) of $[Pd_3(Hnonp)_2(bpy)_3](ClO_4)_2$

(ca. 4:1) of the energetically more favourable *head/tail* isomer. The formation of trimers was confirmed by the presence of molecular ions $[M - PF_6]^+$ (*m/z* 1517) and $[M - 2\,PF_6]^+$ (*m/z* 1371) in the FAB mass spectrum of the product mixture. This lack of success in separating the isomers of $[Pt_3(Hnonp)_2(bpy)_3]^{2+}$ prompted us to study the reaction of H_2acnonp with $[PtCl_2(bpy)]$ in alkaline solution. As discussed previously, the facile cleavage of the 7-acetyl function of this naphthyridine derivative (presumably after initial coordination) enables the preparation of $[Pd_2(H_2nonp)_2(bpy)_2](ClO_4)_2$ **2**. After refluxing an aqueous 2:3:4 molar mixture of H_2acnonp, $[PtCl_2(bpy)]$ and LiOH for 1 d, addition of excess NH_4PF_6 leads to precipition of a dark-green solid, whose FAB mass spectrum contains (among others) the following molecular ions (*m/z*, %): 1559 (23) $[Pt_3(acnonp)(Hnonp)(bpy)_3(PF_6)]^+$, 1518 (4) $[Pt_3(Hnonp)_2(bpy)_3(PF_6)]^+$, 1414 (14) $[Pt_3(acnonp)(Hnonp)(bpy)_3]^+$, 1375 (5) $[Pt_3(Hnonp)_2(bpy)_3]^+$. Although satisfactory separation of the products contained in this mixture could not be achieved, a few green-blue crystals of *head/head*-$[Pt_3(Hacnonp)(Hnonp)(bpy)_3]Cl_2 \cdot x\,H_2O$ (**5**) could, on one occasion, be isolated by slow evaporation of a reaction solution. The X-ray structure of this triplatinum(II) complex, which exhibits Pt(1)···Pt(2) and Pt(2)···Pt(3) separations of 2.771(3) and 2.816(3) Å, is depicted in Figure 6. Tilt angles of 19.3(8) and 22.0(9)° are observed for the terminal PtN_4 coordination planes relative to the central PtN_4 unit and are associated with a Pt(1)···Pt(2)···Pt(3) angle of 168.0(1)°.

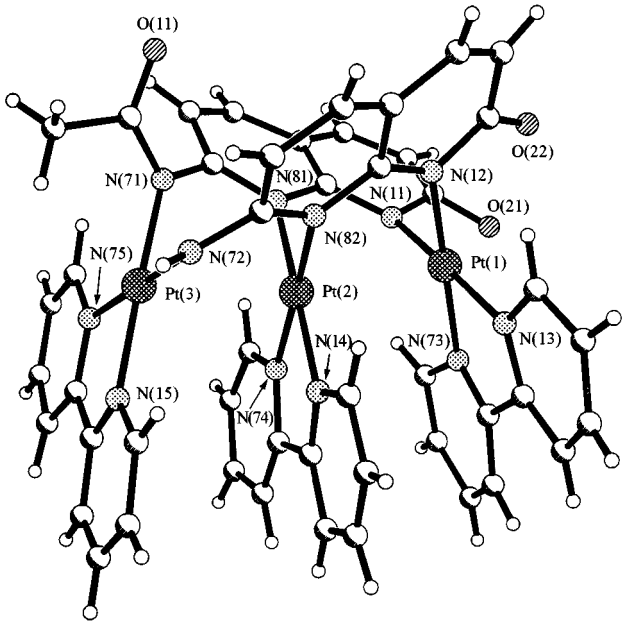


Figure 6. X-ray structure of the dication of *head/head*-$[Pt_3(acnonp)(Hnonp)(bpy)_3]Cl_2 \cdot x\,H_2O$ (**5**)

A Linear $[Pt_3]^{8+}$ Core

We have previously reported the CV characterisation of reversible one-electron oxidation steps for the $[Pt_3]^{6+}$ core in $[Pt_3(donp)_2(bpy)_3]^{2+}$ to $[Pt_3]^{7+}$ and $[Pt_3]^{8+}$, at respectively $E_{1/2}$ 0.65 and 1.30 V (vs. Ag/AgCl). Oxidation is accompanied by a shift in the main absorption maximum in the visible range to lower wavelengths and the appearance of a second maximum for the tri- and tetracations: $[Pt_3]^{6+}$ blue-green, λ_{max} = 710 nm, 555 nm, $[Pt_3]^{8+}$ violet, λ_{max} = 695 nm, 540 nm. Attempts to prepare $[Pt_3]^{7+}$ or $[Pt_3]^{8+}$ species were carried out with oxidants such as HNO_3 (conc.), $Na_2S_2O_8$, and $NOBF_4$. The first member of this list, HNO_3, was, for instance, used by Matsumoto to prepare violet $[\{Pt_2(GI)_2(bpy)_2\}_2](NO_3)_5 \cdot 2\,H_2O$ (GI = glutarimidate)[20]. However, only the addition of $NOBF_4$ to an acetonitrile solution of $[Pt_3(donp)_2(bpy)_3]^{2+}$ did, in fact, lead to a characteristic colour change from blue-green to violet, but did not allow the isolation of a solid oxidation product. As we had previously been unsuccessful in separating the *head/head* and *head/tail* isomers of $[Pt_3(Hnonp)_2(bpy)_3]^{2+}$, oxidation experiments were carried out directly on the aqueous reaction solutions obtained by treatment of $Hnonp^{2-}$ or $acnonp^{2-}$ with $[PtCl_2(bpy)]$. $[Pt_3]^{7+}$, or $[Pt_3]^{8+}$ species could, once again, not be isolated with the above oxidants.

The Ag^+/Ag couple has also occasionally been employed for the oxidation of platinum(II) complexes. For instance, both Kuyper[21] and Cotton[22] have demonstrated that Ag^I

can extract two electrons from dinuclear Pt^{II} complexes to afford $Pt(^{III, III})$ species with a Pt−Pt single bond. Although the mechanism of this redox process has not been fully elucidated, Lippert et al.[23][24] have isolated heteronuclear Pt_4Ag and Pt_2Ag complexes, which can be regarded as precursors. This approach finally led to the isolation of dark-brown *head/head*-$[Pt_3(Hnonp)_2(NO_3)(bpy)_3](ClO_4)_2(NO_3)$ (**6**) in low (23%) but reproducible yields by refluxing 2:3:4 aqueous solutions of H_2acnonp, $[PtCl_2(bpy)]$, and LiOH for 24 h in the presence of an excess of $AgNO_3$. After filtration of a black precipitate and addition of $LiClO_4$, crystals of **6** · 2 H_2O can be grown by gas diffusion of acetone into a nitromethane solution of the resulting dark-brown solid. The δ values of the aromatic protons of **6** (Figure 7) are shifted on average by 0.3 ppm to lower field (^{1}H NMR spectrum, [D_6]DMSO) in comparision to those recorded for the mixture of *head/head* and *head/tail* isomers of the triplatinum(II) complex $[Pt_3(Hnonp)_2(bpy)_3]^{2+}$. Cleavage of the original acetyl functions of the bridging naphthyridine ligands is confirmed by the absence of CH_3C(O) methyl resonances in this spectrum and by the X-ray structure presented in Figure 8, which also establishes the presence of the novel $[Pt_3]^{8+}$ core with its average oxidation state of Pt (2.67+). The diamagnetic trinuclear cation exhibits Pt(1)−Pt(2) and Pt(2)−Pt(3) distances of 2.723(2) and 2.670(2) Å, that are similar to those of 2.702(6)−2.710(5) in the respectively tetranuclear Pt (2.5+) and Pt (2.75+) complexes $[\{Pt_2(C_4H_3NO)_2(NH_3)_4\}_2](NO_3)_6 \cdot 3\,H_2O$ and $[\{Pt_2Cl_2(1\text{-MeT})_2(NH_3)_2\}_2Cl]PtCl_6 \cdot 6\,H_2O$.[6] One of the nitrate counterions in **6** is axially coordinated to Pt(3) at a distance of 2.42(3) Å, that is longer than that of the analogous interaction in the dinuclear complex $[Pt_2(\mu\text{-}C_5H_4NO)_2(NO_3)(H_2O)(NH_3)_4](NO_3)_3$ [2.193(7) Å].[25] This axial ligand is disordered in **6** at two different sites with site occupation factors of 0.52 and 0.48. In contrast to **4a** and **5**, the terminal metal atoms in **6**, Pt(1) and Pt(3), are displaced by respectively 0.064(8) and 0.071(8) Å towards the central atom Pt(2) and the chelating 2,2′-bipyridyl ligands adopt an effectively eclipsed orientation (Figure 9). The metrical data for **6** and the fact that the trinuclear cation is diamagnetic are in accordance with the presence of a $[Pt_3]^{8+}$ core, for which the Pt(1) and Pt(3) atoms can be assigned a formal oxidation state of 3+, with the central metal atom Pt(2) remaining at 2+. Interestingly the trimetal core retains the 48E electron count of tripalladium(II) or triplatinum(II) complexes such as **4a** or **5**, by means of its additional axial coordination of an NO_3^- anion.

6 represents, to our knowledge, the first example of a homonuclear triplatinum complex with an average oxidation state above 2+. Its isolation confirms the suitability of 2(7)-substituted naphthyridines as trinucleating ligands capable of supporting two metal−metal bonds. Previous examples are limited to the 46E $[Ru_3]^{2+}$ complex $[Ru_3(\mu\text{-mponp})_2(CO)_6]$ (hpmonp = 5-methyl-7-phenyl-1,8-naphthyridin-2-one)[26] with its Ru−Ru distances of 2.701(2) and 2.702(3) Å and the paramagnetic 47E complexes $[Rh_xIr_y(\mu\text{-dmonp})_2(CO)_2(cod)_2]^{2+}$ ($x = 0, 2$; $y = 3 - x$; Hdmonp = 5,7-dimethyl-1,8-naphthyridin-2-one), for which the Rh_2Ir cluster could be characterised by X-ray anaysis (Rh−Ir bond lengths, 2.768(2), 2.773(2) Å].[27]

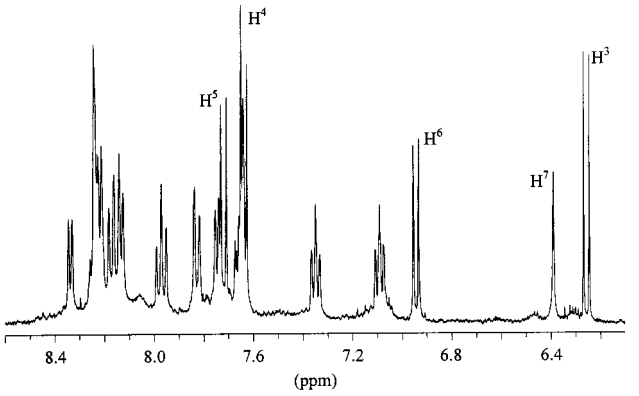


Figure 7. ^{1}H NMR spectrum of *head/head*-$[Pt_3(Hnonp)_2(NO_3)(bpy)_3]^{3+}$ (**6**) in [D_6]DMSO solution

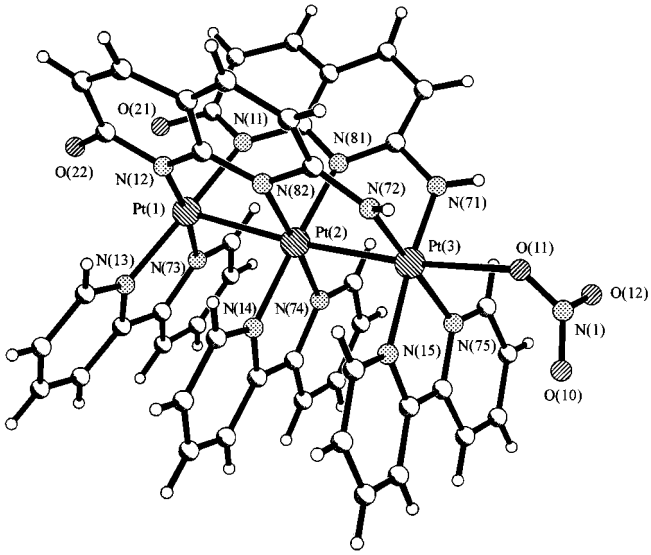


Figure 8. X-ray structure of the trication of *head/head*-$[Pt_3(Hnonp)_2(NO_3)(bpy)_3](ClO_4)_2(NO_3)$ (**6**)

Experimental Section

FAB MS: Fisons VG Autospec with 3-nitrobenzyl alcohol as matrix. − ^{1}H NMR: Bruker DRX 400; chemical shifts are reported as δ values relative to the signal of the deuterated solvent. − ^{195}Pt NMR: Bruker DRX 400, using a saturated K_2PtCl_4 solution as external standard with δ = −1628. − UV/Vis: Perkin−Elmer Lambda 15, λ_{max} is in nm, ε $dm^3 \cdot mol^{-1} \cdot cm^{-1}$. − Elementary analyses: Beller, Mikroanalytisches Labor, Göttingen. The naphthyridine derivatives H_3nonp[28] and H_2acnonp[29] were synthesized according to literature procedures; the starting compounds $[MCl_2(bpy)]$ (M = Pd, Pt) were prepared[30] from K_2MCl_4.

$[Pd_2(donp)_2(bpy)_2]$ (1): H_2donp (16.2 mg, 0.1 mmol) were stirred with 0.2 mL of 1 M NaOMe in 15 mL of MeOH for 30 min. $[PdCl_2(bpy)]$ (33.2 mg, 0.1 mmol) was added to the yellow solution and the suspension stirred for 17 h at room temperature. The resulting light orange precipitate was filtered off, washed with MeOH, and dried in vacuo to afford **1**. Yield 28.9 mg (63%). − $C_{36}H_{24}N_8O_4Pd_2 \cdot 4\,H_2O$ (917.5): calcd. C 47.1, H 3.5, N 12.2;

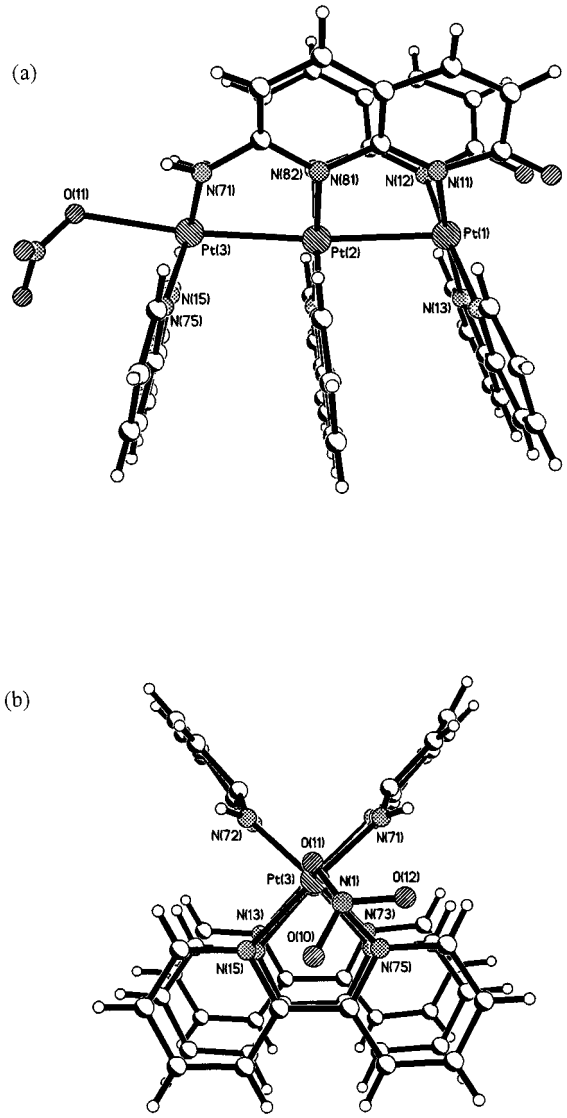


Figure 9. Projections of the trication of *head/head*-$[Pt_3(Hnonp)_2(NO_3)(bpy)_3](ClO_4)_2(NO_3)$ **6**: (a) parallel to the plane of the central 2,2′-bipyridyl plane and (b) along the Pt_3 axis

found C 47.7, H 3.7, N 12.2. − FAB MS; *m/z* (%): 845 (36) $[M]^+$, 685 (12) $[M - donp]^+$, 534 (29) $[M - 2\,bpy]^+$, 422 (100) $[M - donp - bpy - Pd]^+$. − UV/Vis (DMSO): λ_{max} (ε): 258 (2642), 308 (2637), 330 (2567), 344 (2561), 360 sh (1480), 440 sh (133). Crystals of **1** · 3.5 $C_7H_7NO_3$ for X-ray analysis were obtained by gas diffusion of acetone into a 3-nitrobenzyl alcohol solution of **1**.

$[Pd_2(H_2nonp)_2(bpy)_2](ClO_4)_2$ (2): $[PdCl_2(bpy)]$ (33.2 mg, 0.1 mmol) and H_2acnonp (20.3 mg, 0.1 mmol) were stirred in 20 mL of refluxing water for 2 d. After cooling, an excess of $LiClO_4$ was added to the solution and following centrifugation the resulting yellow precipitate dried in vacuo to afford **2**. Yield 45.4 mg (87%). − $C_{36}H_{28}Cl_2N_{10}O_{10}Pd_2 \cdot 2\,H_2O$ (1080.5): calcd. C 40.0, H 3.0, N 13.0; found C 40.0, H 3.0, N 13.1. − FAB MS; *m/z* (%): 945(31) $[M - ClO_4]^+$, 846 (27) $[M - 2\,ClO_4]^+$, 688 (19) $[M - 2\,ClO_4 - bpy]^+$, 534 (38) $[M - 2\,ClO_4 - 2\,bpy]^+$, 422 (100) $[M - 2\,ClO_4]^{2+}$, 260 (52) $[Pd(bpy)]^+$. − ^{1}H NMR ([D$_6$]DMSO): δ = 6.50 (d, 2 H, 3-H), 6.62 (d, 2 H, 6-H), 7.08 (m, 4 H, bpy), 7.53 (dd, 2 H, bpy), 7.61 (d, 2 H, bpy), 7.81 (d, 2 H, 4-H), 7.93 (d, 2 H, 5-H), 8.07 (dd, 2 H, bpy), 8.16 (dd, 2 H, bpy), 8.21 (d, 2 H, bpy), 8.26 (d, 2 H, bpy), 8.94 (s, 4 H, NH_2). − UV/Vis (DMSO): λ_{max} (ε): 262 (3501), 308 (5006), 325 sh (5000), 343 (7156), 368 sh (3012), 420 sh (216).

$[Pt_2(H_2nonp)_2(bpy)_2](PF_6)_2$ (3): $[PtCl_2(bpy)]$ (42.2 mg, 0.1 mmol) and H_3nonp (16.2 mg, 0.1 mmol) were mixed in 15 mL of water, whose pH was subsequently adjusted to 2 by addition of 0.1 M HNO_3. After heating for 40 h at 105 °C the deep-red solution was filtered and an excess of NH_4PF_6 added to the filtrate. The resulting violet precipitate was filtered off and dried in vacuo to afford **3**. Yield 45.9 mg (70%). − $C_{36}H_{28}F_{12}N_{10}O_2P_2Pt_2$ (1312.8): calcd. C 32.9, H 2.1, N 10.7; found C 32.3, H 1.9, N 10.8. − FAB MS; *m/z* (%): 1167 (30) $[M - PF_6]^+$, 1022 (60) $[M - 2\,PF_6]^+$, 861 (6) $[M - 2\,PF_6 - H_2nonp]^+$, 704 (11) $[M - 2\,PF_6 - H_2nonp - bpy]^+$, 511 (100) $[M - 2\,PF_6 - H_2nonp - bpy - Pt]^+$. − ^{1}H NMR ([D$_6$]DMSO): δ = 6.49 (d, 2 H, 3-H), 6.60 (d, 2 H, 6-H), 7.14 (dd, 2 H, bpy), 7.49 (d, 2 H, bpy), 7.53 (dd, 2 H, bpy), 7.79 (d, 2 H, 4-H), 7.91 (d, 2 H, 5-H), 8.01 (d, 2 H, bpy), 8.12 (dd, 2 H, bpy), 8.22 (d, 4 H, bpy), 8.27 (d, 2 H, bpy), 8.76 (s, 4 H, NH_2). − ^{195}Pt NMR ([D$_6$]DMSO): δ = −2285. − UV/Vis (DMSO): λ_{max} (ε): 259 (3442), 311 (3258), 349 (3960), 370 sh (2262), 460 sh (155), 550 (166). Crystals of **3** · 3 C_3H_7NO for X-ray analysis were grown by gas diffusion of *tert*-butyl methyl ether into a dimethylformamide (dmf) solution.

***headltail*-$[Pd_3(Hnonp)_2(bpy)_3](ClO_4)_2$ (4a):** A mixture of H_3nonp (32.2 mg, 0.2 mmol), $[PdCl_2(bpy)]$ (100.1 mg, 0.3 mmol) and $LiOH \cdot H_2O$ (16.8 mg, 0.4 mmol) was stirred at reflux in 40 mL of H_2O for 3 d. Following cooling, addition of an excess of $LiClO_4$ led to precipitation of dark-orange **4a**, which was dried in vacuo after centrifugation. Yield 79.6 mg (61%). − $C_{46}H_{34}Cl_2N_{12}O_{10}Pd_3 \cdot 4\,H_2O$ (1377.1): calcd. C 40.1, H 3.1, N 12.2; found C 40.3, H 3.7, N 12.3. − FAB MS; *m/z* (%): 1205 (43) $[M - ClO_4]^+$, 1106 (49) $[M - 2\,ClO_4]^+$, 951 (17) $[M - 2\,ClO_4 - bpy]^+$, 792 (31) $[M - 2\,ClO_4 - 2bpy]^+$, 638 (74) $[M - 2\,ClO_4 - 3\,bpy]^+$, 552 (100) $[M - 2\,ClO_4]^{2+}$. − ^{1}H NMR ([D$_6$]DMSO): δ = 6.08 (d, 2 H, 3-H), 6.49 (s, 2 H, NH), 6.55 (d, 2 H, 6-H), 7.03 (dd, 2 H, bpy), 7.25 (dd, 2 H, bpy), 7.27 (d, 2 H, 4-H), 7.35 (d, 2 H, bpy), 7.41 (dd, 2 H, bpy), 7.43 (d, 2 H, 5-H), 7.72 (m, 6 H, bpy), 8.00 (dd, 2 H, bpy), 8.02 (dd, 2 H, bpy), 8.09 (m, 4 H, bpy), 8.13 (d, 2 H, bpy). − UV/Vis (DMSO): λ_{max} (ε): 263 (7242), 307 (9065), 325 sh (7102), 352 (6250), 440 sh (1208), 530 sh (277). Crystals of **4a** · 7 H_2O for X-ray diffraction were obtained by slowly evaporating an acetone/water solution of the product.

***head/head*-$[Pd_3(Hnonp)_2(bpy)_3](ClO_4)_2$ (4b):** $[PdCl_2(bpy)]$ (100.1 mg, 0.3 mmol) was added to a suspension of H_3nonp (32.2 mg, 0.2 mmol) and $LiOH \cdot H_2O$ (16.8 mg, 0.4 mmol) in 40 mL of H_2O and the reaction mixture then stirred for 2 d at room temperature. After addition of an excess of $LiClO_4$, the resulting orange precipitate was washed with acetone and **4a** extracted with pyridine to leave **4b**, which was dried in vacuo. Yield 41.8 mg (32%). − $C_{46}H_{34}Cl_2N_{12}O_{10}Pd_3$ (1305.0): calcd. C 42.3, H 2.6, N 12.9; found C 42.5, H 2.7, N 12.8. − FAB MS; *m/z* (%): 1205 (51) $[M - ClO_4]^+$, 1106 (35) $[M - 2\,ClO_4]^+$, 951 (21) $[M - 2\,ClO_4 - bpy]^+$, 792 (36) $[M - 2\,ClO_4 - 2\,bpy]^+$, 638 (70) $[M - 2\,ClO_4 - 3\,bpy]^+$, 552 (100) $[M - 2\,ClO_4]^{2+}$. − ^{1}H NMR ([D$_6$]DMSO): δ = 5.97 (d, 2 H, 3-H), 6.28 (s, 2 H, NH), 6.50 (d, 2 H, 6-H), 7.03 (dd, 2 H, bpy), 7.16 (dd, 2 H, bpy), 7.26 (d, 2 H, 4-H), 7.34 (d, 2 H, 5-H), 7.41 (dd, 4 H, bpy), 7.52 (d, 2 H, bpy), 7.57 (d, 2 H, bpy), 7.68 (m, 2 H, bpy), 7.93 (dd, 2 H, bpy), 8.01 (d, 2 H, bpy), 8.07 (m, 4 H, bpy), 8.17 (d, 2 H, bpy). − UV/Vis (DMSO): 263 (5888), 306 (7221), 325 (5211), 353 (5549), 440 sh (1201), 530 sh (331).

***head/head*-$[Pt_3(Hnonp)_2(NO_3)(bpy)_3](ClO_4)_2(NO_3)$ (6):** H_2acnonp (20.3 mg, 0.1 mmol), $LiOH \cdot H_2O$ (8.4 mg, 0.2 mmol) and $[PtCl_2(bpy)]$ (63.4 mg, 0.15 mmol) were stirred at reflux in 30 mL

of H_2O for 24 h in the presence of $AgNO_3$ (203.8 mg, 1.2 mmol). After filtration of the black precipitate and addition of an excess of $LiClO_4$ to the filtrate, the resulting dark-brown solid was dried in vacuo. Crystals of **5** · 2 H_2O were obtained from a nitromethane solution of the product mixture by gas diffusion of acetone. Yield 19.9 mg (23%). − $C_{46}H_{34}Cl_2N_{14}O_{16}Pt_3 \cdot 2\,H_2O$ (1731.0): calcd. C 31.9, H 2.2, N 11.3; found C 31.6, H 2.3, N 11.1. − ^1H NMR ([D_6]DMSO): δ = 6.26 (d, 2 H, 3-H), 6.39 (s, 2 H, NH), 6.94 (d, 2 H, 6-H), 7.09 (dd, 2 H, bpy), 7.35 (dd, 2 H, bpy), 7.63 (d, 2 H, 4-H), 7.64 (m, 2 H, bpy), 7.72 (d, 2 H, 5-H), 7.74 (d, 2 H, bpy), 7.83 (d, 2 H, bpy), 7.97 (dd, 2 H, bpy), 8.13 (d, 2 H, bpy), 8.16 (dd, 2 H, bpy), 8.23 (m, 6 H, bpy), 8.34 (d, 2 H, bpy). − UV/Vis (DMSO): 259 (8418), 309 (7288), 327 sh (6242), 388 sh (4749), 437 sh (1734), 478 sh (1274), 539 sh (678), 773 (364).

X-ray Structural Analyses: Siemens P4 diffractometer graphite-monochromated Mo-K_α radiation (λ = 0.71073 Å), T = 295 K. Semi-empirical absorption corrections were applied to the intensity data for **1**, **3**, **4a**, and **5** on the basis of ψ scans; DIFABS[31] was employed for the data set of **3**. The structures were solved by Patterson syntheses or direct methods and refined by full-matrix least squares against F^2 using SHELXL-93.[32] Where appropriate, hydrogen atoms were included at calculated positions with isotropic temperature factors.[33]

$[Pd_2(donp)_2(bpy)_2]\cdot 3.5C_7H_7NO_3$ (1): $C_{36}H_{24}N_8O_4Pd_2 \cdot 3.5\,C_7H_7NO_3$ $_M$ = 1381.4, monoclinic space group $P2_1/c$ (no. 14), a = 17.193(3), b = 23.616(4), c = 15.747(2) Å, β = 96.60(1)°, V = 6352(2) Å^3, Z = 4, D_{calcd} = 1.445 g·cm^{-3}, μ = 0.64 mm^{-1}. Crystal size: 0.65 × 0.45 × 0.22 mm; ω-scan; scan range 4° ≤ 2θ ≤ 50° (−20 ≤ h ≤ 20, 0 ≤ k ≤ 28, 0 ≤ l ≤ 18), 11169 symmetry independent reflections; max./min. transmission 0.93/0.86; 704 parameters refined; R = 0.082 [$I > 2\sigma(I)$], wR_2 = 0.271 (all data), Δρ max./min 1.39/−0.78 eÅ^{-3}. With one exception, all of the solvent 3-nitrobenzyl alcohol molecules are disordered.

$[Pd_2(H_2nonp)_2(bpy)_2](ClO_4)_2 \cdot 2\,H_2O$ (2): $C_{36}H_{32}Cl_2N_{10}O_{12}Pd_2$ $_M$ = 1080.4, orthorhombic space group *Pbcm* (no. 57), a = 12.708(2), b = 14.639(3), c = 23.702(3) Å, V = 4409.1(13) Å^3, Z = 4, D_{calcd} = 1.628 g·cm^{-3}, μ = 1.01 mm^{-1}. Crystal size: 0.68 × 0.22 × 0.20 mm; ω scan; scan range 4° ≤ 2θ ≤ 50° (0 ≤ h ≤ 15, 0 ≤ k ≤ 17, 0 ≤ l ≤ 28), 3978 symmetry-independent reflections; max./min. transmission 0.33/0.31; 305 parameters refined; R = 0.048 [$I > 2\sigma(I)$], wR_2 = 0.198 (all data), Δρ max./min. 0.83/−0.76 eÅ^{-3}. The water oxygens exhibit multiple disorder.

$[Pt_2(H_2nonp)_2(bpy)_2](PF_6)_2 \cdot 3\,C_3H_7NO$ (3): $C_{45}H_{49}F_{12}N_{13}O_5P_2Pt_2$, M = 1532.1, triclinic space group $P\bar{1}$ (no. 2), a = 14.436(2), b = 15.684(2), c = 16.036(3) Å, α = 62.01(1), β = 70.36(1), γ = 68.47(1)°, V = 2922.4(7) Å^3, Z = 2, D_{calcd} = 1.741 g·cm^{-3}, μ = 4.93 mm^{-1}. Crystal size: 0.42 × 0.33 × 0.09 mm; ω scan; scan range 4° ≤ 2θ ≤ 45° (−14 ≤ h ≤ 15, 0 ≤ k ≤ 16, −15 ≤ l ≤ 17), 7553 symmetry-independent reflections; max./min. transmission 0.70/0.26; 707 parameters refined; R = 0.070 [$I \le 2\sigma(I)$], wR_2 = 0.198 (all data), Δρ max./min. 0.91/−0.99 eÅ^{-3}. The F atoms of the counterions are disordered, as is one of the solvent dmf molecules.

***headltail*-$[Pd_3(Hnonp)_2(bpy)_3](ClO_4)_2 \cdot 7\,H_2O$ (4a):** $C_{46}H_{48}Cl_2N_{12}O_{17}Pd_3$, M = 1431.1, triclinic space group $P\bar{1}$ (no. 2), a = 12.651(3), b = 14.248(3), c = 18.427(3) Å, α = 81.87(2), β = 70.34(1), γ = 79.75(2)°, V = 3066(1) Å^3, Z = 2, D_{calcd} = 1.550 g·cm^{-3}, μ = 1.03 mm^{-1}. Crystal size: 0.72 × 0.30 × 0.12 mm; ω scan; scan range 4° ≤ 2θ ≤ 45° (−14 ≤ h ≤ 15, 0 ≤ k ≤ 16, −21 ≤ l ≤ 21), 10758 symmetry-independent reflections, max./min. transmission 0.88/0.83; 674 parameters refined; R = 0.082 [$I \le 2\sigma(I)$], wR_2 = 0.294 (all data), Δρ max./min. 0.91/−0.82 eÅ^{-3}. Whereas the first of the ClO_4^- counterions is disordered with s. o. f. s of 0.8 and 0.2, the second perchlorate could not be satisfactorily located in difference syntheses.

***headhead*-$[Pt_3(acnonp)(Hnonp)(bpy)_3]Cl_2 \cdot x\,H_2O$ (5):** $C_{48}H_{58}Cl_2N_{12}O_{14}Pt_3$ (x = 11), M = 1683.2, monoclinic space group $P2_1/c$ (no. 14), a = 12.045(2), b = 22.696(5), c = 22.236(4) Å, β = 92.96(3)°, V = 6071(2) Å^3, Z = 4, $D_{calcd.}$ = 1.842 g·cm^{-3}, μ = 7.05 mm^{-1}. Crystal size: 0.22 × 0.15 × 0.13 mm; ω scan; scan range 4° ≤ 2θ ≤ 47.5° (0 ≤ h ≤12, 0 ≤ k ≤24, −23 ≤ l ≤ 23), 6951 symmetry-independent reflections, max. /min. transmission 0.94/0.45; 415 parameters refined; R = 0.083 [$I \le 2\sigma(I)$], wR_2 = 0.196 (all data), Δρ max./min. 0.89/−0.70 eÅ^{-3}. The disordered water oxygens were assigned appropriate s. o. f. s for x = 11. One of the chloride counterions is disordered with s. o. f. s 0.4, 0.3 and 0.3.

***headhead*-$[Pt_3(Hnonp)_2(NO_3)(bpy)_3](ClO_4)_2(NO_3) \cdot 2\,H_2O$ (6):** $C_{46}H_{38}Cl_2N_{14}O_{18}Pt_3$, M = 1731.1, monoclinic space group $P2_1/n$ (no. 14), a = 12.233(2), b = 18.126(4), c = 27.234(5) Å, β = 90.01(3)°, V = 6039(2) Å^3, Z = 4, $D_{calcd.}$ = 1.904 g·cm^{-3}, μ = 7.10 mm^{-1}. Crystal size: 0.24 × 0.22 × 0.18 mm; ω scan; scan range 4° ≤ 2θ ≤ 45° (−1 ≤ h ≤ 13, −1 ≤ k ≤ 19, −29 ≤ l ≤ 29), 7723 symmetry-indepent reflections, max./min. transmission 0.045/0.028; 323 parameters refined; R = 0.070 [$I \le 2\sigma(I)$], wR_2 = 0.182 (all data), Δρ max./min. 0.71/−0.75 eÅ^{-3}. Both NO_3^- counterions are disordered, with that coordinated directly to Pt(3) displaying s. o. f. s of 0.52 and 0.42 and the other s. o. f. s of 0.57, 0.25 and 0.18.

[1] L. S. Hollis, S. J. Lippard, *J. Am. Chem. Soc.* **1981**, *103*, 1230−1232.
[2] K. A. Hofmann, G. Bugge, *Ber. Dtsch. Chem. Ges.* **1908**, *41*, 312−314.
[3] J. K. Barton, H. N. Rabinowitz, D. J. Szalda, S. J. Lippard, *J. Am. Chem. Soc.* **1977**, *99*, 2827−2829; J. K. Barton, D. J. Szalda, H. N. Rabinowitz, J. V. Waszczak, S. J. Lippard, *J. Am. Chem. Soc.* **1979**, *101*, 1434−1441.
[4] K. Sakai, K. Matsumoto, *J. Am. Chem. Soc.* **1989**, *111*, 3074−3075.
[5] K. Matsumoto, K. Fuwa, *J. Am. Chem. Soc.* **1982**, *104*, 897−898; K. Matsumoto, H. Takahashi, K. Fuwa, *Inorg. Chem.* **1983**, *22*, 4086−4090.
[6] O. Renn, A. Albinati, B. Lippert, *Angew. Chem. Int. Ed. Engl.* **1990**, *29*, 84−86.
[7] W. Micklitz, G. Müller, J. Riede, B. Lippert, *J. Chem. Soc., Chem. Commun.* **1987**, 76−78.
[8] W. Micklitz, G. Müller, B. Huber, J. Riede, F. Rashwan, J. Heinze, B. Lippert, *J. Am. Chem. Soc.* **1988**, *110*, 7084−7092.
[9] B. Oskui, M. Mintert, W. S. Sheldrick, *Inorg. Chim. Acta* **1999**, *287*, 72−81.
[10] W. S. Sheldrick, M. Mintert, *Inorg. Chim. Acta* **1994**, *219*, 23−29.
[11] M. Mintert, W. S. Sheldrick, *Inorg. Chim. Acta* **1995**, *236*, 13−20.
[12] R. Fraggiani, C. J. L. Lock, R. J. Pollock, B. Rosenberg, G. Turner, *Inorg. Chem.* **1981**, *20*, 804−807.
[13] C. J. L. Lock, H. J. Peresie, B. Rosenberg, G. Turner, *J. Am. Chem. Soc.* **1978**, *100*, 3371−3374.
[14] D. Neugebauer, B. Lippert, *Inorg. Chim. Acta* **1982**, *67*, 151−158.
[15] H. Engelking, B. Krebs, *J. Chem. Soc., Dalton Trans.* **1996**, 2409−2416.
[16] M. Grehl, B. Krebs, *Inorg. Chem.* **1994**, *33*, 3877−3885.
[17] H. Schöllhorn, U. Thewalt, B. Lippert, *Inorg. Chim. Acta* **1984**, *93*, 19−26.
[18] K. Matsumoto, K. Harashima, H. Moriyama, T. Sato, *Inorg. Chim. Acta* **1992**, *197*, 217−226.
[19] M. Mintert, Dissertation, Ruhr-Universität Bochum, **1995**.
[20] K. Matsumoto, H. Urata, *Chemistry Letts.* **1994**, 307−310.
[21] J. Kuyper, K. Vrieze, *Transition Met. Chem.* **1976**, *1*, 208−211.
[22] D. P. Bancroft, F. A. Cotton, L. R. Falvello, W. Schwotzer, *Inorg. Chem.* **1986**, *25*, 766−770.
[23] B. Lippert, D. Neugebauer, *Inorg. Chem.* **1982**, *21*, 451−452.

[24] B. Lippert, H. Schöllhorn, U. Thewalt, *Inorg. Chem.* **1987**, *26*, 1736−1741.
[25] D. P. Bancroft, F. A. Cotton, L. R. Falvello, W. Schwotzer, *Inorg. Chem.* **1986**, *25*, 763.
[26] M. Mintert, W. S. Sheldrick, *J. Chem. Soc., Dalton. Trans.* **1995**, 2663−2669.
[27] B. E. Villarroya, L. A. Oro, F. J. Lahoz, A. J. Edwards, M. A. Ciriano, P. J. Alonso, A. Tiripicchio, M. Tiripicchio Camellini, *Inorg. Chim. Acta* **1996**, *250*, 241−264.
[28] G. H. Newcome, S. J. Garbis, V. K. Majestic, F. R. Fronczek, G. Chiari, *J. Org. Chem*. **1981**, *46*, 833−839.
[29] E. V. Brown, *J. Org. Chem.* **1965**, *30*, 1607−1619.
[30] J. McCormik, E. N. Janges, R. I. Kaplan, *Inorg. Synth.* **1972**, *13*, 216−218.
[31] N. Walker, D. Stuart, *Acta Crystallogr., Sect. A* **1983**, *39*, 158−166.
[32] G. M. Sheldrick, *SHELXL-93*, *A Program, for Structure Refinement*, Göttingen, **1993**.
[33] Crystallographic data (excluding structure factors) for the structures reported in this paper have been deposited with the Cambridge Crystallographic Data Centre. Copies of the data (deposit numbers (CCDC-113920−113925) may be obtained free of charge on application to CCDC, 12 Union Road, Cambridge CB2 1EZ, UK (Fax: +44−1223/ 336-033, E-mail: deposit@ccdc. cam. ac. uk).

Received February 3, 1999
[I99033]

Oxygen Transfer from Chromyl Chloride to Alkynes and Allene − IR-Spectroscopic Identification of η^1-Ketene and Cyclopropanone Complexes of $O{=}CrCl_2$

Tobias Wistuba,[a] and Christian Limberg*[a]

Keywords: Photolysis / Alkynes / Matrix isolation / DFT / Oxygenations

Photolytically-induced reactions of chromyl chloride with acetylene and but-2-yne (dimethylacetylene) in low-temperature argon matrices yield *end-on* ketene and dimethylketene complexes of $O{=}CrCl_2$, respectively. The product formation probably results from an electrophilic attack of a Cr=O linkage on the C≡C triple bonds, leading to radical-like transition states or intermediates, which subsequently rearrange through 1,2-H or 1,2-methyl shifts. Consequently, allene is attacked at its central carbon and the allyl radical thus generated undergoes subsequent ring-closure to give a cyclopropanone complex of $O{=}CrCl_2$.

Introduction

The oxidation of olefins by chromyl chloride, which was established in the 19th century,[1] is still employed for the functionalization of C=C double bonds yielding epoxides, chlorohydrins, and dichlorides.[2] Although the associated mechanism has been the subject of extensive studies,[3] until recently the detailed course of these reactions remained speculative, and there was no evidence to support the intermediacy of the species that had been proposed to account for the experimental findings. Cook and Mayer wrote: "The nature and the chemistry of such intermediate chromium species is perhaps the most difficult aspect of these reactions to unravel",[4a] and indeed, this matter has received significant attention in the past.[2a,5] Substantial progress has, however, been made, especially within the last two years: Ziegler et al. have postulated, on the basis of exemplary DFT calculations in the case of ethylene,[6] that interactions with the $Cr(=O)_2$, Cr(=O)Cl, or $CrCl_2$ moieties represent the initial steps responsible for the formation of the three observed products (vide supra) when this olefin is oxidized. At the same time, we have been able to show that it is possible to photolytically induce olefin oxidations by chromyl chloride at 10 K in argon matrices. In this way, it has been possible to matrix-isolate complexes of ketones, aldehydes, and epoxides with the hitherto unknown oxo-metal halide $O{=}CrCl_2$, which represent the primary products of oxo-transfer reactions combined, in some cases, with 1,2-H migrations (cf. Scheme 1).[7] In fact $O{=}CrCl_2{\cdots}$epoxide complexes have been proposed as intermediates accounting for epoxide formation by others,[2a,6b] but the mechanism of the reactions occurring under photolytic matrix conditions is probably different from that which is operative under thermal conditions. The former most likely involves photoexcited chromyl chloride in its triplet state,[7b] which is not accessible under thermal conditions. Once in the excited state, chromyl chloride is capable of oxygenating olefins either via an epoxide-like or a radical-like transition state. The latter rearranges through a 1,2-H shift to generate a carbonyl complex, while the former yields epoxide complexes that have been postulated as being formed after a spin-crossover via glycolates in the thermal process (Scheme 1).[6b] Consequently, in spite of different initial transition states and intermediate geometries, the minima corresponding to the matrix-isolated species are common to the potential energy surfaces of both processes, making their identification, characterization, and investigation an important issue.

[a] Universität Heidelberg, Anorganisch-Chemisches Institut, Im Neuenheimer Feld 270, D-69120 Heidelberg, Germany
Fax: (internat.) + 49-6221/545707
E-mail: Limberg@sun0.urz.uni-heidelberg.de

Results and Discussion

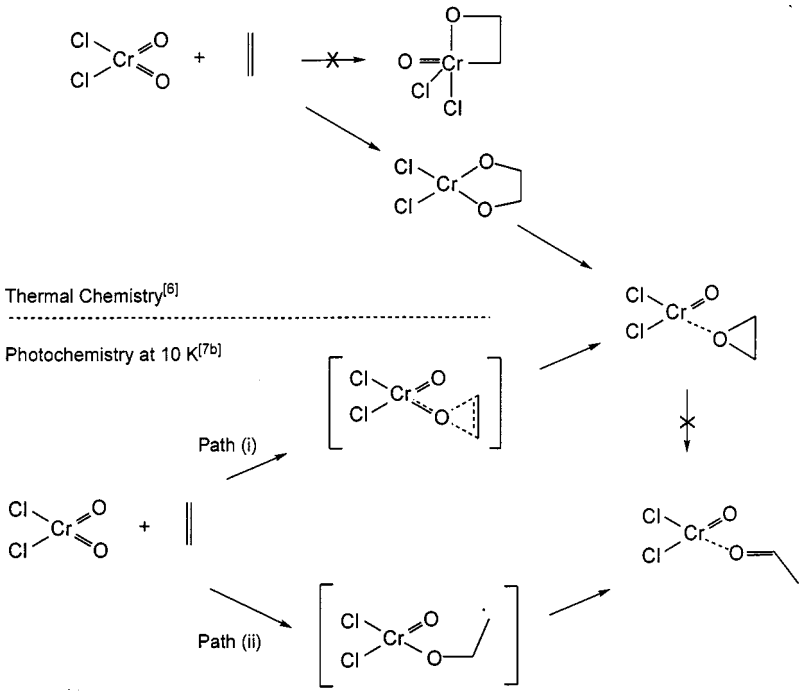
We have expanded our investigations concerning the photoreactions of chromyl chloride with unsaturated systems under matrix conditions from alkenes to alkynes and allene.

(a) CrO_2Cl_2/HCCH

Literature concerning the products of alkynes in oxidations with chromyl chloride under preparative conditions is scarce, but where reported diketones or α-C oxidation products have been obtained.[8] If the principles found for the matrix oxidations of olefins by chromyl chloride[7] also hold for alkynes, interesting products may be expected: an analogous route to path (i) in Scheme 1 would lead to an oxirene complex, while that corresponding to path (ii) would generate a η^1-ketene complex, as shown in Scheme 2 in the case of acetylene. Both are attractive targets:

(i) There have been many attempts to synthesize and characterize oxirenes. Such species have frequently been proposed as intermediates during the Wolff rearrangement or during oxidation reactions involving alkynes, and have

 © WILEY-VCH Verlag GmbH, D-69451 Weinheim, 1999 1434−1948/99/0808−1335 $ 17.50+.50/0



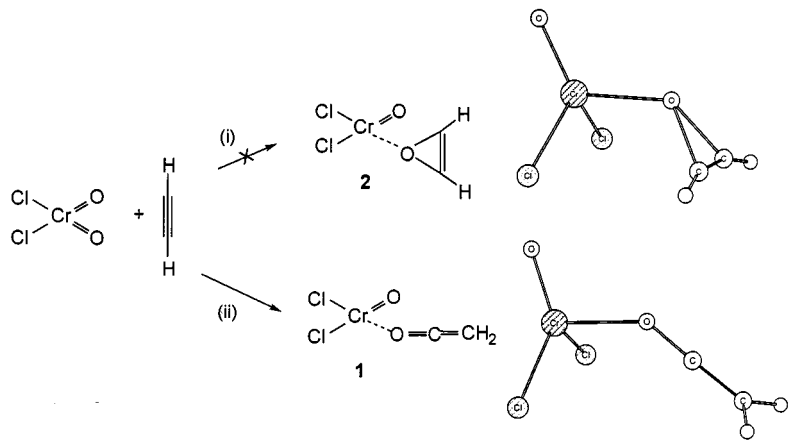
Scheme 1. Mechanistic possibilities for the photolytic olefin oxidation with CrO_2Cl_2 under matrix conditions[7b] vs. calculated intermediates[6]

been the subject of numerous theoretical investigations.[9] To date, only one successful oxirene synthesis (photodecomposition of α-diazo ketones in Ar matrices[10]) has been reported, but as a stabilization can be expected from its coordination to a transition metal (cf. the case of cyclobutadiene[11]), the complex **2** shown in Scheme 2 seemed to be a reasonable product.

(ii) Although various complexes of ketenes have been analysed structurally,[12–15] none of these shows an *end-on* coordination mode.

DFT calculations (B3LYP/LANL2DZ) proved that for both complexes of the type $O{=}CrCl_2{\cdots}O{=}C{=}CH_2$, **1**, and $O{=}CrCl_2{\cdots}O(CH)_2$, **2**, minima can be found on the potential energy surface (triplet state structures of C_1 symmetry were optimized as shown in Scheme 2) but that, not surprisingly, **1** is more stable than **2** by 258.6 kJ/mol.

Our investigation of the reaction of chromyl chloride with alkynes in low-temperature matrices started with the simplest alkyne, i.e. acetylene, under conditions[7] that had already enabled the characterization of intermediates such as those depicted in Scheme 1. Since molecules do not undergo diffusion in the solid low-temperature matrices, the reservoir of collisional reactant pairs formed upon deposition is depleted as the photolytically-induced chemical reaction proceeds. The line-widths of the new bands observed were found to be independent of the chromyl chloride concentration and the relatively broad appearance of some of them is probably due to conformational isomers.



Scheme 2. Possible routes for a photolytically-induced reaction of chromyl chloride with acetylene at 7 K; optimized structures of **1** and **2** (B3LYP/LANL2DZ)

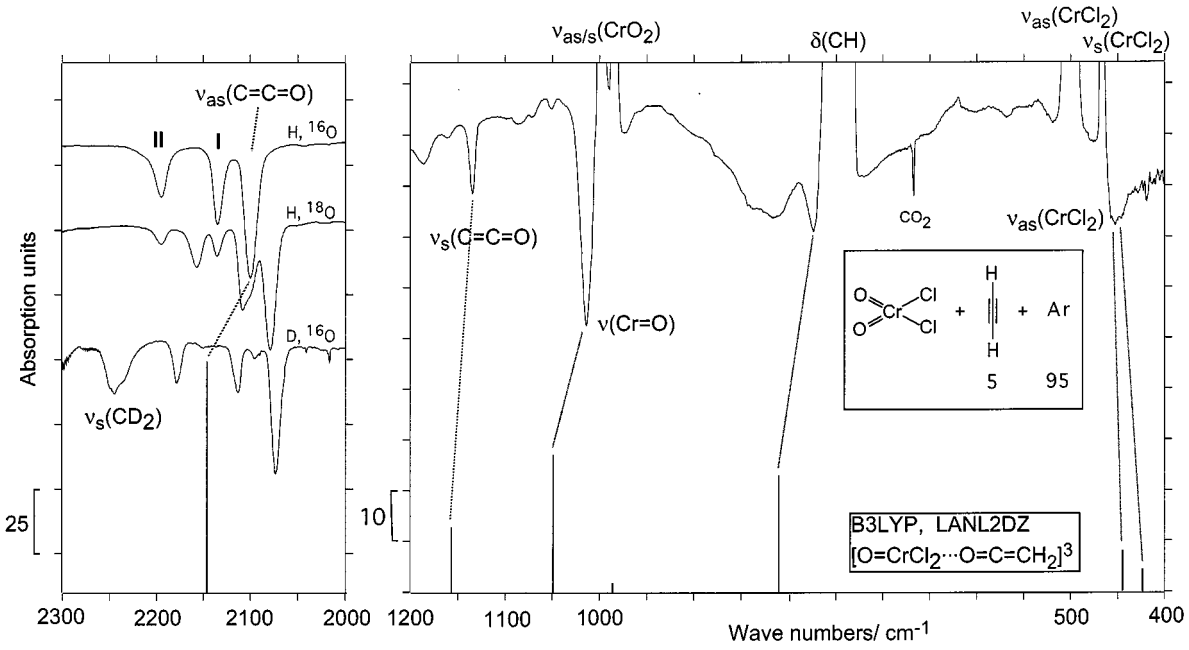


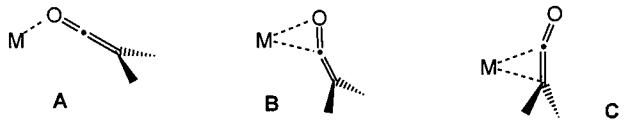
Figure 1. Upper trace: Difference between the IR spectrum (1800−350 cm^{-1}) of CrO_2Cl_2 isolated in an argon matrix doped with 5 mol-% acetylene at 7 K and the spectrum recorded of the same matrix after photolysis at 411 nm for 20 min. Lower trace: Line diagrams for the IR spectrum calculated for **1**; the upper trace of the offset shows the 2000−2200 cm^{-1} region of the spectrum, the middle trace the effects of the ^{18}O enrichment on this region, and the lower trace the effects of complete deuteriation

Identification of 1: Co-condensation of a mixture of acetylene in argon (5%) with chromyl chloride at 7 K yielded an IR spectrum of the unperturbed starting materials, which was subtracted from a spectrum recorded after subsequent photolysis (15 min at 411 nm). The result is shown in Figure 1 (the negative bands are attributable to consumed starting material). The band at 1014 cm^{-1} can be assigned to $\nu(Cr{=}O)$ of an $O{=}CrCl_2$ fragment, by analogy with the CrO_2Cl_2/ethylene case (1009 cm^{-1}).[7a] The band due to $\nu_{as}(CrCl_2)$, which had previously been observed at 452 cm^{-1}, can be discerned as a broad feature at 424 cm^{-1}, while the corresponding $\nu_s(CrCl_2)$ band, expected to appear around 380 cm^{-1}, is probably broadened into the base line (not shown in Figure 1).

In addition, a new intense band can be seen at 2095 cm^{-1}, which is accompanied by two less intense bands at 2132 and 2195 cm^{-1}. These are discussed separately below. The findings point to ketene as the oxidation product, since free ketene shows a $\nu_{as}(C{=}C{=}O)$ band at 2142 cm^{-1},[16] which can be expected to be red-shifted upon coordination to $O{=}CrCl_2$. The observed shift of 47 cm^{-1} is of the same order as that found for acetaldehyde[7a] (60 cm^{-1}). Since the absorption cross-section of $\nu_{as}(CCO)$ found for free ketene exceeds that of any other IR absorption by at least one order of magnitude (and can even be expected to be enhanced on complexation), all other IR absorptions due to the ketene ligand should have very low intensities in Figure 1. Indeed, apart from the absorptions mentioned so far, only two other definite bands − namely a weak but sharp band at 1135 cm^{-1} and a broad, low-intensity band at 773 cm^{-1} − can be detected. These show the same growth behaviour as the 2095 cm^{-1} band. All these observations thus provide further support for the formation of an $O{=}CrCl_2{\cdots}O{=}C{=}CH_2$ complex.

In principle, there are three possible coordination modes for ketene at a metal centre, which are depicted in Scheme 3: *end-on* **A**, *side-on* (O=C) **B**, and *side-on* (C=C) **C**. A few compounds are known where type **B** or **C** structures have been established by X-ray crystal structure analysis. Not surprisingly, ketene complexes of early, very oxophilic transition metals all display mode **B**,[12][13] while type **C** has mainly been observed by X-ray diffraction analysis of some structurally closely related complexes of Mn.[14] However, only recently, the first bond isomerism of a ketene metal complex has been demonstrated.[15] In order to permit assignment of the coordination mode of the ketene ligand in $O{=}CrCl_2{\cdots}O{=}C{=}CH_2$ as **A**, **B**, or **C**, DFT calculations (B3LYP, LANL2DZ), which have previously been shown to provide reliable information concerning the IR spectra and the corresponding isotopic shifts of such species,[7] were performed for individual complexes. Bearing in mind the results presented in Scheme 1, the theoretical investigation was started with a frequency calculation for complex **1** based on the structure shown in Scheme 2, which is, of course, only one of several possible conformations for type **A** coordination. The result has been included in Figure 1 in the form of a line diagram. As can be seen, the band pattern and the intensity ratios of the experimental spectrum are nicely reproduced. Additional support for the assignment of the experimental spectrum to **1** with an *end-on*-coordinated ketene ligand was provided by experiments employing ^{18}O-enriched CrO_2Cl_2: apart from $\nu(Cr{=}O)$, which is shifted by 43 cm^{-1} as $\nu(Cr{=}O)$ of $O{=}CrCl_2{\cdots}O{=}CHCH_3$,[7a] and $\nu_{as}(CCO)$ (21 cm^{-1}), the band at 1135 cm^{-1} also shows a

significant shift (22 cm^{-1}) and hence it can confidently be assigned to ν_s(CCO). Moreover, the ^{18}O shifts observed are in excellent agreement with those predicted by the calculation (cf. Table 1). Additional experiments employing C_2D_2 were performed, and the resulting shifts are also compared with the calculated values in Table 1. Naturally, these shifts are larger than those obtained upon ^{18}O enrichment, and hence the deviations between the experimental and calculated values are correspondingly higher. However, such deviations can arise from very small differences between the theoretical and actual structures.[17] Deuteriation additionally allows the observation of $\nu_{as}(CD_2)$ at 2260 cm^{-1}, which was the only other observable band besides ν_{as}(CCO) when free deuteriated ketene was generated by NO_2 oxidation of [D_2]acetylene in an Ar matrix.[18] Further calculations ruled out the two possible η^2-coordination modes **B** and **C** (vide infra). Taken together, the aforementioned results strongly support the assignment of all new bands below 2100 cm^{-1} to compound **1**, a metal complex with a ketene ligand in the *end-on* coordination mode **A**. The underlying reasons for the preference of $O{=}CrCl_2{\cdots}O{=}C{=}CH_2$ to adopt coordination mode **A** can be traced to the oxophilic nature of the *hard* d^2 Cr centre, which is electron-



Scheme 3. Possible coordination modes for ketenes at metal centres

poor and therefore not suitable for efficient back-bonding.

The Additional Bands: The above assignments leave only the two bands at 2132 cm^{-1} (**I**) and 2194 cm^{-1} (**II**) unaccounted for. The left-hand part of Figure 1 shows their positions and intensities, as well as their behaviour on isotopic enrichment in comparison to ν_{as}(CCO) of **1**. While the upper trace corresponds to the right-hand part of Figure 1, the middle trace is the result of an $^{18}O_2CrCl_2$ reaction (note that the satellites beside the shifted bands are due to the ^{16}O isotopomers, which formed simultaneously due to incomplete ^{18}O enrichment). D_2C_2 gave rise to the lower trace. The wavenumbers of **I** and **II** are rather high, and their ^{18}O shifts indicate that the corresponding vibrations should involve a significant motion of the oxygen. On the other hand, there must also be a contribution from the C−H vibrations, as indicated by the D shifts observed for these bands, although these are smaller than the shift found for ν_{as}(CCO) of **1**. The fact that the bands still appear in the same region after isotopic enrichment proves that they are *not* the result of a Fermi resonance or an overtone. Their characteristics are therefore also indicative of ν_{as}(CCO) vibrations, but as they show markedly different isotopic shifts and positions in comparison to ν_{as}(CCO) of **1**, they have to be assigned to ν_{as}(CCO) vibrations of two independent species that are related to, but are nevertheless significantly different from **1**. Interestingly, it proved possible to decrease the intensity of the ν_{as}(CCO) band of **1** in favour of the bands **I** and **II** by irradiation with light of the wavelengths 313 and 545 nm.

By optimizing the structures of over a dozen different complexes and calculating their IR spectra (plus isotopic shifts), the following facts could be established:

(i) Neither different matrix sites nor different conformations are responsible for these bands, as these could not explain the significantly different positions and isotopic shifts of **I** and **II**.

(ii) The change of spin state from triplet to singlet has a large effect on the IR properties of the $O{=}CrCl_2$ fragment, but the effects on the $O{=}C{=}CH_2$ unit are negligible.

(iii) A coordination mode of type **B** would not be expected to cause a shift of $\nu_{as}(C{=}C{=}O)$ to higher wavenumbers compared to that in **1**. Moreover, a structure with a corresponding starting geometry changed its mode to **A** during the optimization.

(iv) A mode of type **C** would, in fact, cause a shift of $\nu_{as}(C{=}C{=}O)$ to higher wavenumbers, but a corresponding complex would additionally show a band half as intense as $\nu_{as}(C{=}C{=}O)$ at ca. 890 cm^{-1}. No band can be seen in this region of the experimental spectrum (Figure 1).

(v) Oxirene or formyl carbene complexes do not show bands of significant intensity in the region 2000−2200 cm^{-1}, nor does oxiranylidene, which has recently been identified in low-temperature matrices.[19]

Consequently, a reaction of **1** with an excess of acetylene was then considered as a possible explanation for bands **I**

Table 1. Frequencies obtained experimentally on photolysis of $Cr^{16}O_2Cl_2$ and $Cr^{18}O_2Cl_2$ isolated in HCCH (or DCCD)/Ar matrices (5%), as well as calculated frequencies for **1** (B3LYP/LANL2DZ) in cm^{-1} (intensities given in parentheses); the assignments are based on the spectrum of free ketene,[16] as well as on the results of the calculation

Bands [cm^{-1}]	calculated [cm^{-1}]	$\Delta^{18}O$ found [cm^{-1}]	$\Delta^{18}O$ calcd. [cm^{-1}]	ΔD found [cm^{-1}]	ΔD calcd. [cm^{-1}]	Assignment
2195 (0.47)		37		17		**II**
2132 (0.55)		27		19		**I**
2095 (1.00)	2146 (1.00)	21	20	22	35	$\nu_{as}(C{=}C{=}O)$
	1405 (0.02)	−	0	−	186	$\delta(CH_2)$
1135 (0.25)	1157 (0.14)	22	27	242	216	$\nu_s(C{=}C{=}O)$
1014 (0.85)	1049 (0.30)	43	45	0	0	$\nu(Cr{=}O)$
	986 (0.02)	−	1	−	154	$\delta_s(CH_2)$
773 (0.19)	818 (0.25)	0	2	216	172	$\delta_s(CH_2)$
450 (0.31)	445 (0.09)	3	2	5	7	$\nu_{as}(CrCl_2)$
	424 (0.05)		3		61	$\nu(CrO)$/ $\delta(CH_2)$

and **II**, even though the concentrations and conditions chosen do not usually permit reactions with significantly more than one equivalent of a substrate. However, acetylene is a very special case in that it forms aggregates even at very low pressures in the gas phase.[20a] A real matrix *isolation* of acetylene can therefore only be achieved by diluting it with argon to such a low concentration that would preclude study of its reaction with chromyl chloride as the number of collisional pairs formed upon co-condensation would become too low. The concentration amounted to 5% in the experiment described above, and consequently oligomers of acetylene were also isolated in the matrices, as indicated by their characteristic bands.[20] As a result, the structures of the matrices could not, of course, be treated statistically: the ratio of chromyl chloride molecules with just *one* acetylene molecule as a nearest neighbour to those with more than one such neighbour was significantly decreased compared to the situation under standard conditions. Thus, the bands **I** and **II** may well result from species incorporating more than one equivalent of acetylene, and indeed, a decrease of the acetylene concentration down to the lowest possible level of 2% (where the signal-to-noise ratio is still acceptable in the difference spectrum following irradiation) led to a significant decrease in the intensities of these bands in relation to the intensity of ν_{as}(CCO) attributable to **1**. Bearing in mind the effects observed upon photolysis at 313 and 545 nm, respectively, the corresponding species must be accessible by direct reaction of **1** with acetylene. A reaction of the ketene moiety can be excluded as no product can be envisaged that would still exhibit a band at a higher wavenumber than 2100 cm^{-1} (with a significant ^{18}O shift). The most likely reaction at the metal centre is a complex formation (i.e. a weak or even strong binding of acetylene). Unfortunately, DFT calculations are not adequate for describing the simultaneous complexation of acetylene and ketene at an $O{=}CrCl_2$ fragment (at least not with the B3LYP functional),[21] hence it was not possible to unequivocally assign the bands **I** and **II** to alkyne complexes of **1**.

(b) CrO_2Cl_2/CH_3CCCH_3

Next, but-2-yne was employed as a reactant in order to find out whether the corresponding dimethylketene derivative $O{=}CrCl_2{\cdots}O{=}C{=}C(CH_3)_2$, **3**, is formed, or whether the methyl groups prevent rearrangement by 1,2-migration (no methyl shift has ever been observed for any analogous olefin reactions[7b]). Provided that the above arguments in the case of acetylene are correct, formation of **3** should also be accompanied by the generation of two additional species. The concentrations of the latter, however, should be much lower: in contrast to acetylene, but-2-yne does not show a pronounced tendency to aggregate, so that a reaction of chromyl chloride molecules with *two* equivalents of alkyne should, on statistical grounds, only be possible for the small fraction of molecules that have two alkyne neighbours in the solid matrix (ca. 10% for a 5:95 ratio of butyne/Ar vs. 34% with just *one* neighbour[22]).

Following the reaction of but-2-yne with chromyl chloride, the bands for the $O{=}CrCl_2$ fragment could be found as before. In addition, a band at 2072 cm^{-1} was observed, suggesting that a dimethylketene complex **3** had indeed been formed. This was further corroborated by repeating the experiment with $^{18}O_2CrCl_2$ (leading to shifts comparable to those found previously for **1**), as well as by calculations (B3LYP/LANL2DZ) concerning the structure and frequencies of such a complex, the latter being in good agreement with the experimental frequencies (cf. Table 2). As anticipated (vide supra), two additional bands could be observed at higher wavenumbers beside the ν_{as}(C=C=O) band of **3**, albeit with only minor intensities.

The fact that **3** was formed by a 1,2-methyl migration suggests that such a shift should, in principle, also be possible in the case of olefins. However, in the latter case, a low degree of methylation leaves open too many alternative 1,2-H migration routes, while permethylation makes path (i) in Scheme 1 more favourable. The transition state associated with the analogous path (i) in Scheme 2 is of course very high in energy (**2** itself was calculated to form in an *endothermic* reaction, while formation of **1** is exothermic by −246 kJ/mol). The transition state energy will be lowered only slightly if H is substituted by Me. Consequently, there is only one low-energy path open for alkynes, which probably involves attack of a Cr=O bond at the triple bond in a fashion analogous to path (ii) in Scheme 1. After passing through the corresponding radical-like transition state, a methyl shift yields **3**. The postulation of such a transition state prompted a further experiment that might support its existence: thus, allene was employed as the unsaturated component.

(c) $CrO_2Cl_2/CH_2{=}C{=}CH_2$

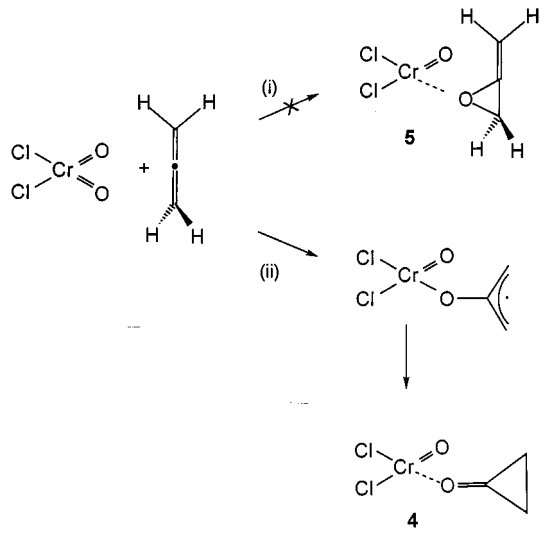
If radical-like transition states, produced by attack of the Cr=O function at the unsaturated bonds, do indeed govern product formation in the reactions of alkenes and alkynes, allene can be expected to be attacked at the central carbon, as this would lead to a resonance stabilized allyl radical as shown in Scheme 4. A downhill route involving a 1,2-H or 1,2-Me shift would then not be accessible, but the reaction could proceed through a subsequent ring-closure to yield a cyclopropanone complex (NO_2 oxidation of allene in low-temperature matrices leads to cyclopropanone).[24]

A terminal attack at the allene followed by a 1,2-H shift would yield acrolein, or, alternatively, an epoxidation of one olefinic bond may be envisaged [compare path (i) in Scheme 4].

Following co-condensation of a 5% allene/argon mixture with chromyl chloride, the usual photolysis at 411 nm led to the bands of $O{=}CrCl_2$, which were seen at 1012 and 447 cm^{-1}. Additionally, an intense matrix-split band was observed at 1800 cm^{-1}, which must be attributable to a ν(C=O) vibration in view of the marked ^{18}O-shift and the negligible D-shift observed when experiments were performed with $^{18}O_2CrCl_2$ and $D_2C{=}C{=}CD_2$, respectively. All

Table 2. Frequencies obtained experimentally on photolysis of $Cr^{16}O_2Cl_2$ and $Cr^{18}O_2Cl_2$ isolated in CH_3CCCH_3/Ar matrices (5%), as well as calculated frequencies for **3** (B3LYP/LANL2DZ) in cm^{-1} (intensities given in parentheses); the assignments are based on the spectrum of free dimethylketene,[23] as well as on the results of the calculation

Bands [cm^{-1}]	calculated [cm^{-1}]	$\Delta^{18}O$ found [cm^{-1}]	$\Delta^{18}O$ calcd. [cm^{-1}]	Assignment
2126 (0.08)				
2089 (0.14)				
2072 (0.47)	2114 (1)	18	16	ν_{as}(C=C=O)
1453 (0.33)	1513 (0.07)	0	0	CH_3 bend
1436 (0.43)	1505 (0.04)	0	0	CH_3 bend
1369 (0.20)	1450 (0.03)	0	0	CH_3 bend
1360 (0.18)	1436 (0.02)	0	0	CH_3 bend
1339 (0.15)		0		CH_3 bend
1254 (0.52)	1361 (0.21)	11	16	$\delta(CH_2)$, wag
1157 (0.13)	1196 (0.01)	0	0	$\rho(CH_3)/\delta(CCC)$
1145 (0.13)		5		
1082 (0.14)		–		$\rho(CH_3)/\delta(CCC)$
1061 (0.15)	1107 (0.01)	0	1	$\rho(CH_3)/\delta(CCC)$
1009 (1)	1045/1050 (0.44)	41	41	ν(Cr=O)
451 (0.50)	431 (0.16)	3	0	$\nu_{as}(CrCl_2)$



Scheme 4. Proposed mechanism of the photolytically-induced reaction of chromyl chloride with allene at 7 K

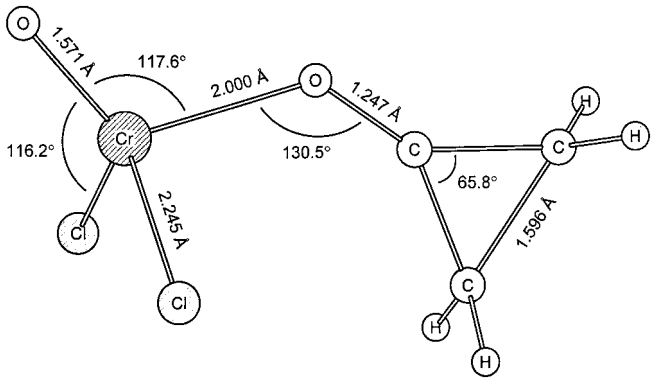


Figure 2. The optimized structure calculated for $OCrCl_2$···cyclopropanone, **4**, by means of DFT using LANL2DZ basis sets (B3LYP); selected bond lengths and angles are given in Å and°

bands and their isotopic shifts are shown in Table 3, along with the theoretical frequencies and the calculated isotopic shifts for an optimized structure of the cyclopropanone···$Cr(O)Cl_2$ complex **4** (Figure 2). As can be seen, the agreement is very good, hence it can safely be concluded that **4** was indeed formed. This supports the hypothesis of a radical-like transition state in carbonylations with chromyl chloride under matrix conditions. The simultaneous formation of the allene oxide complex **5** in Scheme 4 can be ruled out on the basis of further calculations concerning its frequencies.[26] This finding is not surprising as the barrier leading to **5** is probably much higher than that associated with the conversion of the allyl radical to **4**. Moreover, **5** itself is less stable than **4** by 59 kJ/mol.

Conclusions

We have shown herein that the reactions of chromyl chloride with acetylene and but-2-yne (dimethylacetylene) under matrix conditions yield η^1-ketene and -dimethylketene complexes of $O{=}CrCl_2$, respectively. The oxidation of allene leads exclusively to a cyclopropanone complex, probably through an initial radical-like attack of a Cr=O functionality at the central carbon, with subsequent ring-closure. The formation of all products is consistent with the general reactivity pattern observed previously for chromyl chloride in reactions with olefins,[7] and supports the idea that radical-like transition states are involved in the corresponding carbonylation reactions.

In the past, H-atom transfers by metal-oxo species have been rationalized in terms of intuitions based on analogy with organic radical chemistry, i.e. unpaired electron density was thought to be transferred to the oxygen of the metal compounds, which then determined its propensity to take part in radical reactions. In the meantime, it has been established that chromyl chloride – a d^0 system having no unpaired spin density – can in fact abstract hydrogen atoms from saturated organic systems. This has led to progress in current thinking, from considerations of radicals and spin density to a new approach based on the thermochemistry of the H-atom transfer step and, therefore, on the bond strengths.[27]

Table 3. Frequencies obtained experimentally on photolysis of $Cr^{16}O_2Cl_2$ and $Cr^{18}O_2Cl_2$ isolated in $H_2C{=}C{=}CH_2$ (or $D_2C{=}C{=}CD_2$)/Ar matrices (5%), as well as calculated frequencies for **4** (B3LYP/LANL2DZ) in cm^{-1} (intensities given in parentheses); the assignments are based on the spectrum of free cyclopropanone,[25] as well as on the results of the calculation

Bands [cm^{-1}]	calculated [cm^{-1}]	$\Delta^{18}O$ found [cm^{-1}]	$\Delta^{18}O$ calcd. [cm^{-1}]	ΔD found [cm^{-1}]	ΔD calcd. [cm^{-1}]	Assignment
1807/1800 (0.81)	1830 (1)	20	24	3	7	$\nu_{as}(C{=}O)$
1392 (0.05)	1434 (0.07)	0	0	222	292	$\delta(CH_2)$
1107 (0.07)	1080 (0.27)	2	1	10	23	$\nu(CC)$
1107 (0.07)	1075 (0.11)	2	1	60	47	ring wag
1012 (1)	1053 (0.52)	47	46	1	0	$\nu(Cr{=}O)$
703 (0.13)	705 (0.09)	8	11	–	148	ring
447 (0.44)	428 (0.24)	1	0	0	0	$\nu_{as}(CrCl_2)$

These fundamental discoveries made for the *C–H activation* by chromyl chloride naturally raise questions concerning the initial steps of its reactions with *unsaturated systems*. It could be envisaged that in these oxidations chromyl chloride might also follow one reaction route (among others) where it behaves akin to a fleeting main group oxygen radical, giving rise to a radical intermediate or transition state, which finally undergoes rearrangement to produce the isolated carbonyl products. This is exactly what we seem to have found for the matrix reactions of chromyl chloride under photolytic conditions as outlined in the above. However, under thermal conditions (−80°C), an analogous reactivity can only be postulated provided that a necessary condition holds, i.e. that the thermochemistry is favourable or at least only slightly unfavourable,[27] in other words that the CrO–C bond formed in the course of the Cr=O attack at the carbon of an unsaturated bond must be sufficiently strong to drive the reaction in the direction of carbonylation. Addition of an organic radical to a Cr=O function is indeed likely to be very exothermic,[4b] and the CrO–C bond energy released can therefore easily overcompensate the loss of π-bonding energy if a similar addition is considered for an unsaturated bond. This has certainly been the case in our experiments, which have, however, started from chromyl chloride in an excited state.[7b] Therefore, it is not yet certain as to whether CrO–C bond formation is sufficiently exothermic to make a corresponding attack energetically favourable under thermal conditions as well. This subtle problem will only be resolved following an experimental determination of the Cr(V)O–C bond energy

Experimental Section

Computational Methods: Density functional calculations were carried out using the Gaussian-94/DFT[28] series of programs. The structures of **1–3** were optimized with the LANL2DZ basis set using in each case the B3LYP formulation of density functional theory, i.e. Becke's three-parameter exchange functional and the Lee–Yang–Parr correlation functional. Harmonic vibrational frequencies and infrared intensities were predicted at these levels by numerical second derivatives using analytically calculated first derivatives. No scaling was applied and no negative frequencies were obtained.

Experimental: Liquid helium cooling gave temperatures of ca. 7 K inside a shroud maintained at a pressure below 10^{-7} Torr. Mixtures were prepared in a vacuum line using standard manometric techniques and were then deposited on the cold support. A CsI window was used for all the IR experiments; the slow spray-on deposition was favoured for CrO_2Cl_2 with the sample maintained at −65°C.

The photolysis source was a 200 W medium-pressure arc. The radiation was filtered with a Balzers interference filter (band-pass ca. 15 nm). IR spectra were recorded in transmission mode over the ranges 4000–300 and 1000–200 cm^{-1}, with a resolution of 1 cm^{-1}, on a Bruker IFS 88 spectrophotometer.

CrO_2Cl_2 (99.99% pure), but-2-yne, and acetylene (99% pure) were supplied by Aldrich and further purified by fractional condensation in high vacuum prior to use. Argon (99.999% pure, Messer Grieshheim), [D_2]acetylene (99% pure, Campro Scientific), and [D_4]allene (98% pure, Campro Scientific) were used as received.

^{18}O-enrichment of CrO_2Cl_2 can be achieved according to a published procedure. Allene was synthesized according to ref.[7b]

Acknowledgments

Financial support by the Deutsche Forschungsgemeinschaft (scholarship for C. L. and SFB 247) and the Fonds der Chemischen Industrie is gratefully acknowledged. Further, we would like to thank Prof. M. Driess and Prof. emer. W. Sundermeyer for the provision of equipment, as well as Prof. G. Huttner for his generous support. We are also grateful to Prof. T. Ziegler for providing us with a preprint.[6b]

[1] M. A. Etard, H. M. Moissan, *C. R. Hebd. Seances Acad. Sci.* **1893**, *116*, 434–437.
[2] [2a] K. B. Sharpless, A. Y. Teranishi, J.-E. Bäckvall, *J. Am. Chem. Soc*. **1977**, *99*, 3120–3128. – [2b] F. Freeman in *Organic Syntheses by Oxidation with Metal Compounds* (Eds.: W. J. Mijs, C. R. H. I. de Jonge), Plenum, New York, **1986**, chapter 2, pp. 41–118.
[3] S. J. Cristol, K. R. Eilar, *J. Am. Chem. Soc.* **1950**, *72*, 4353–4356; R. A. Stairs, D. G. M. Diaper, A. L. Gatzke, *Can. J. Chem.* **1963**, *41*, 1059–1064; F. Freeman, P. J. Cameran, R. H. Dubois, *J. Org. Chem*. **1968**, *33*, 3970–3972; N. Miyaura, J. K. Kochi, *J. Am. Chem. Soc*. **1983**, *105*, 2368–2378; F. Freeman, R. H. Dubois, N. J. Yamachika, *Tetrahedron* **1969**, *25*, 3441–3446; F. Freeman, P. D. McCart, N. J. Yamachika, *J. Am. Chem. Soc.* **1970**, *92*, 4621–4626; F. Freeman, K. W. Arledge, *J. Org. Chem.* **1972**, *37*, 2656–2662; K. B. Sharpless, A. Y. Teranishi, *J. Org. Chem.* **1973**, *38*, 185–186.
[4] [4a] G. K. Cook, J. M. Mayer, *J. Am. Chem. Soc.* **1994**, *116*, 1866. – [4b] G. K. Cook, J. M. Mayer, *J. Am. Chem. Soc.* **1995**, *117*, 7152.
[5] F. Freeman, N. J. Yamachika, *J. Am. Chem. Soc.* **1970**, *92*, 3730–3733; F. Freeman, N. J. Yamachika, *J. Am. Chem. Soc.* **1972**, *92*, 1214–1219; F. Freeman, N. J. Yamachika, *Tetra-*

hedron Lett. **1969**, *41*, 9615−9618; A. K. Rappé, W. A. Goddard III, *J. Am. Chem. Soc.* **1982**, *104*, 3287−3294; A. Fiedler, I. Kretzschmar, D. Schröder, H. Schwarz, *J. Am. Chem. Soc.* **1996**, *118*, 9941−9952.

[6] [6a] M. Torrent, L. Deng, T. Ziegler, *Inorg. Chem.* **1998**, *37*, 1307−1314. − [6b] M. Torrent, L. Deng, M. Duran, M. Solá, T. Ziegler, *Can. J. Chem.* **1999**, submitted.

[7] [7a] C. Limberg, R. Köppe, H. Schnöckel, *Angew. Chem.* **1998**, *110*, 512−515; *Angew. Chem. Int. Ed. Engl.* **1998**, *37*, 496−499. − [7b] C. Limberg, R. Köppe, *Inorg. Chem.* **1999**, *38*, 2106−2116.

[8] W. B. Sheats, L. K. Olli, R. Stout, J. T. Lundeen, R. Justus, W. G. Nigh, *J. Org. Chem.* **1979**, *44*, 4075−4078 and references therein.

[9] G. Maier, H. P. Reisenauer, T. Sayrac, *Chem. Ber.* **1982**, *115*, 2192−2201; E. R. Lovjoy, C. B. Moore, *J. Chem. Phys.* **1993**, *98*, 7846−7854; G. Vacek, J. M. Galbraith, Y. Yamaguchi, H. F. Schaefer III, A. P. Scott, L. Radom, *J. Phys. Chem.* **1994**, *98*, 8660−8665; J. D. Gezelter, W. H. Miller, *J. Chem. Phys.* **1995**, *103*, 7868−7875.

[10] C. Bachmann, T. Y. N′Guessan, F. Debu, M. Monnier, J. Pourcin, J.-P. Aycard, H. Bodot, *J. Am. Chem. Soc.* **1990**, *112*, 7488; evidence has also been presented for the observation of a substituted oxirene by laser flash photolysis during a Wolff rearrangement: K. Tanigaki, T. W. Ebbesen, *J. Am. Chem. Soc.* **1987**, *109*, 5883.

[11] P. M. Maitlis, *Adv. Organomet. Chem*. **1966**, *4*, 95.

[12] For a literature collection, see: P. Hofmann, L. A. Perez-Moya, O. Steigelmann, J. Riede *Organometallics* **1992**, *11*, 1167−1176.

[13] G. S. Bristow, P. B. Hitchcock, M. F. Lappert, *J. Chem. Soc., Chem. Commun.* **1982**, 462−463; J. D. Meinhart, B. D. Santarsiero, R. H. Grubbs, *J. Am. Chem. Soc.* **1986**, *108*, 3318; R. Birk, H. Berke, H.-U. Hund, G. Huttner, L. Zsolnai, L. Dahlenburg, U. Behrens, T. Sielisch, *J. Organomet. Chem.* **1989**, *372*, 397; A. Antinolo, A. Otero, M. Fajardo, C. Lopez-Mardomingo, D. Lucas, Y. Mugnier, M. Lanfranchi, M. A. Pellinghelli, *J. Organomet. Chem.* **1992**, *435*, 55; D. B. Grotjahn, H. C. Lo, *Organometallics* **1995**, *14*, 5463; S. Gambarotta, M. Pasquali, C. Floriani, A. Chiesi-Villa, C. Guastini, *Inorg. Chem.* **1981**, *20*, 1173−1178; R. Flügel, O. Gevert, H. Werner, *Chem. Ber.* **1996**, *129*, 405−410.

[14] A. D. Redhouse, W. A. Herrmann, *Angew. Chem.* **1976**, *88*, 652; *Angew. Chem. Int. Ed. Engl.* **1976**, *15*, 615; W. A. Herrmann, J. Plank, M. Ziegler, K. Weidenhammer, *J. Am. Chem. Soc.* **1979**, *101*, 3133; W. A. Herrmann, J. Plank, G. W. Kriechbaum, J. L. Ziegler, H. Pfisterer, J. L. Atwood, R. D. Rogers, *J. Organomet. Chem.* **1984**, *264*, 2327.

[15] E. Bleuel, M. Laubender, B. Weberndörfer, H. Werner, *Angew. Chem.* **1999**, *111*, 222−225; *Angew. Chem. Int. Ed. Engl.* **1999**, *38*, 156−159.

[16] R. Hochstrasser, J. Wirz, *Angew. Chem.* **1990**, *102*, 454−455; *Angew. Chem. Int. Ed. Engl.* **1990**, *29*, 411−412.

[17] A. Bérces, T. Ziegler, *J. Phys. Chem.* **1995**, *99*, 11417; A. Bérces, *J. Phys. Chem*. **1996**, *100*, 16538.

[18] J. A. Harrison, H. Frei, *J. Phys. Chem.* **1994**, *98*, 12142−12151.

[19] G. Maier, H. P. Reisenauer, M. Cibulka, *Angew. Chem.* **1999**, *111*, 110−113; *Angew. Chem. Int. Ed. Engl.* **1999**, *38*, 105−108.

[20] [20a] R. D. Pendley, G. E. Ewing, *J. Chem. Phys.* **1983**, *78*, 3530−3540. − [20b] E. S. Kline, Z. H. Kafafi, R. H. Hauge, J. L. Margrave, *J. Am. Chem. Soc.* **1985**, *107*, 7559; N. I. Bagdanskis, M. O. Bulanin, *Opt. Spektrosk*. **1972**, *32*, 525; T. Szymanska-Buzar, A. J. Downs, T. M. Greene, A. S. Marshall, *J. Organomet. Chem.* **1995**, *495*, 149−161; G. Maier, C. Lantz, *Eur. J. Org. Chem.* **1998**, 769.

[21] The structures of five different complexes were optimized but none of the results could be accepted as reasonable.

[22] H. Bandow, H. Akimoto, *J. Phys. Chem.* **1985**, *89*, 845−849.

[23] W. H. Fletcher, W. B. Barish, *Spectrochim. Acta* **1965**, *21*, 1647−1661.

[24] M. Nakata, H. Frei, *J. Am. Chem. Soc.* **1992**, *114*, 1363−1372.

[25] K. A. Singmaster, G. C. Pimentel, *J. Mol. Struct.* **1989**, *194*, 215−238.

[26] **5** should show an intense ν_s(COC) band at around 850 cm^{-1}, which corresponds to a region heavily masked by $\omega(CH_2)$ of the starting material (842 cm^{-1}). However, according to the calculation, the ν(C=C) mode of free allene oxide[25] at 1824 cm^{-1} **5** should shift by 15 cm^{-1} to higher wavenumbers on complexation with $OCrCl_2$ and there is no detectable band in the region between 1880 and 1820 cm^{-1}.

[27] Review: J. M. Mayer, *Acc. Chem. Res.* **1998**, *31*, 441−450.

[28] M. J. Frisch, G. W. Trucks, H. B. Schlegel, P. M. W. Gill, B. G. Johnson, M. A. Robb, J. R. Cheeseman, T. Keith, G. A. Petersson, J. A. Montgomery, K. Raghavachari, M. A. Al-Laham, V. G. Zakrzewski, J. V. Ortiz, J. B. Foresman, C. Y. Peng, P. Y. Ayala, W. Chen, M. W. Wong, J. L. Andres, E. S. Replogle, R. Gomperts, R. L. Martin, D. J. Fox, J. S. Binkley, D. J. Defrees, J. Baker, J. P. Stewart, M. Head-Gordon, C. Gonzalez, J. A. Pople, *Gaussian 94*, revision E.2, Gaussian Inc., Pittsburgh PA, **1995**.

Received February 3, 1999
[I99036]

Synthesis and Single-Crystal X-ray Diffraction Studies on New Methylindium(III) Alkoxides

Michael Veith,*[a] Sven Hill,[a] and Volker Huch[a]

Keywords: Indium / O ligands / N ligands / C ligands

New heteroleptic indium compounds have been synthesized starting from indium(III) halides and hexamethyldisilazyllithium to form $MeXInN(SiMe_3)_2$ [X = Cl (**1**), Br (**2**)], and then subsequent alcoholysis to afford the molecules $[ClMeIn(OtBu)]_2$ (**3**), $[BrMeIn(OtBu)]_2$ (**4**), $\{ClMeIn[O(C_6H_4)OMe]\}_2$ (**5**), $\{[(SiMe_3)_2N]MeIn(OtBu)\}_2$ (**6**) and $[MeIn(OtBu)_2]_2$ (**7**). The molecular structures of molecules **3**–**7** have been obtained by single crystal X-ray diffraction studies. The structures of the compounds **3**–**7** are almost identical: **3**–**5** crystallize in the monoclinic crystal system with two dimeric molecules per unit cell in the space group $P2_1/c$, **6** crystallizes in the monoclinic space group $C2/c$ with four molecules per unit cell, and compound **7** crystallizes in the triclinic crystal system with one dimeric molecule per unit cell in the space group $P\bar{1}$. The central centrosymmetric In_2O_2 ring, common to all the compounds, is achieved by two bridging oxygen atoms. Due to the additional coordination by an oxygen atom of the methoxy group, the coordination number of the metal center rises from 4 to "4+1" if the O*t*Bu ligand (compounds **3**, **4**, **6**, and **7**) is exchanged for a methoxyphenol ligand (compound **5**). In addition to the In_2O_2 ring the compound **5** possesses two annealed five-membered InO_2C_2 rings. The common indium methyl group of all compounds, which is transfered by an original route from the silicon to the indium atom, is used to compare structural and spectroscopic properties of the molecules, as there is a correlation between the In–C bond length and the chemical shift of the methyl group which depends on the ligand system used.

Introduction

The interest in organometallic precursors for use in the area of surface coating has been growing over the last few years. In particular the use of metal alkoxides in metal-organic chemical vapor deposition (MOCVD) or in the sol-gel process has become increasingly popular. In the field of indium alkoxides, however, few studies have been made when contrasted with the lower homologous aluminum and gallium. Indium compounds and ceramics possess a wide variety of interesting properties, which are important in modern technologies. Pure indium oxides, for example, are used as heat insulators,[1] and mixed indium-tin oxides for transparent and conductive ceramics.[2][3] Furthermore, indium compounds find applications in the solar[4–6] and the semiconductor industries.[7] Only a few indium compounds, however, are known to be used in CVD. Indium alkoxides used as an In/O source might be interesting precursors for MOCVD.[8] Apart from some indium compounds of the type $R_2In(OR)$,[9–11] some indium aryloxides,[12–14] some $In(OR)_3$[15] compounds and some heterometallic alkoxides of the type $In[M(OiPr)_4]_3$ with M = Al, Ga,[16] only two dialkylindium alkoxides $[(tBu_2InOEt)_2$[17] and $(tBu_2InOMe)_2$[18]] have been fully characterized by single-crystal X-ray analysis to date.

The authors report here on the synthesis and X-ray crystal-structure analysis (see Table 2) of some new (alkoxo)indium compounds as well as the first monoalkylindium dialkoxide. The principle idea of the reactions described was to introduce selected ligands into indium-centered molecules, and to analyze the structural changes brought about by these ligands. These changes should be monitored in the solid state by X-ray diffraction techniques.

Syntheses of the Indium-Centered Molecules 1–7

Tris(hexamethyldisilazyl)indium, $In[N(SiMe_3)_2]_3$, has been described previously together with $Ga[N(SiMe_3)_2]_3$ and $Al[N(SiMe_3)_2]_3$.[19][20] It is easily obtained by the reaction of $InCl_3$ with three equivalents of $LiN(SiMe_3)_2$.[19] This silylamide was synthesized by Bürger et al. in 1971 and structurally characterized by Power et al. in 1993.[19][20] In the present work the interest is in the reactions of $InCl_3$ with $LiN(SiMe_3)_2$ in molar ratios which differ from 1:3. A molar ratio of 1:2 was first tried. The nonpolar solvent toluene was used to exclude the donation of a basic solvent to the metal center (Equation 1). The reaction solution of $LiN(SiMe_3)_2$ and $InCl_3$ was refluxed for 24 h as the reaction rate was too slow at room temp. The surprising result of this synthesis was a monochloro substitution and migration of a methyl group from an $[N(SiMe_3)_2]$ group to the metal atom to form compound **1**. The first evidence of the methyl group transfer was given by the spectroscopic analysis of the product; the ^{1}H-NMR spectrum of the resulting product $ClMeIn[N(SiMe_3)_2]$ (**1**) shows two signals with an integration ratio of 1:6, in contrast to the singlet expected for the disubstituted product $ClIn[N(SiMe_3)_2]_2$. The ^{13}C-NMR spectrum also shows two NMR signals, indicating the migration of a methyl group. Similar methyl-group transfers are known for gallium compounds.[21][22] The C/H/N, In,

[a] Institute of Inorganic Chemistry, University of Saarland, D-66041 Saarbrücken, Germany
Fax: (internat.) + 49(0)681/302-3995
E-mail: veith@rz.uni-sb.de

 © WILEY-VCH Verlag GmbH, D-69451 Weinheim, 1999 1434–1948/99/0808–1343 $ 17.50+.50/0

and Cl analyses performed also give values which correspond exactly with those calculated for **1**. So far, it has not been possible to select a suitable crystal for single-crystal X-ray analysis.

$$2\ LiN(SiMe_3)_2 + InCl_3 \rightarrow \underset{\mathbf{1}}{MeClIn[N(SiMe_3)_2]} + LiCl\ \downarrow\ + \text{side products} \quad (1)$$

If the reaction is carried out in an equimolar ratio the result is similar except that the yield of **1** is less. The change to a polar solvent, such as diethyl ether or THF, also leads to the same results.

In order to insert the first alkoxo ligand into the molecule, **1** was subjected to an alcoholysis reaction (Equation 2). The reaction solution was again refluxed for 24 h to speed up the reaction rate. The alcohol was added in excess to secure a complete reaction.

$$MeClIn[N(SiMe_3)_2] + 2\ HO\mathit{t}Bu \rightarrow \underset{\mathbf{3}}{ClMeIn(O\mathit{t}Bu)} + HN(SiMe_3)_2 + HO\mathit{t}Bu \quad (2)$$

After removing the volatiles under reduced pressure and dissolving the residue in hexane, **3** was crystallized from hexane at low temperatures (−30°C) and purified by sublimation (10^{-2} Torr/120°C; yield: 64%). The ^{1}H-NMR spectrum of **3** shows two signals in an integration ratio of 3:1, corresponding to the ratio of the methyl protons of the *tert*-butyl group and the methyl group. The ^{13}C-NMR spectrum shows three signals as expected, corresponding to the metal-bonded methyl group and two signals for the *tert*-butyl group. In the hope of increasing the yield, the more reactive $InBr_3$ was used as a starting compound instead of $InCl_3$. Compound **2** BrMeIn[N(SiMe$_3$)$_2$] was synthesized according to the same procedure reported for compound **1** (Equation 3).

$$2\ LiN(SiMe_3)_2 + InBr_3 \rightarrow \underset{\mathbf{2}}{MeBrIn[N(SiMe_3)_2]} + LiBr\ \downarrow\ + \text{side products} \quad (3)$$

The ^{1}H- and ^{13}C-NMR spectra of **2** are similar to that of **1**. The following alcoholysis of **2** was carried out under the same conditions as described for **3** (Equation 4). The yield of the reaction (70%) was not much higher than for the reaction with $InCl_3$, for which reason $InCl_3$ was used again in subsequent syntheses. The ^{1}H- and ^{13}C-NMR spectra of **4** are very similar to that of **3**.

$$MeBrIn[N(SiMe_3)_2] + 2\ HO\mathit{t}Bu \rightarrow \underset{\mathbf{4}}{BrMeIn(O\mathit{t}Bu)} + HN(SiMe_3)_2 + HO\mathit{t}Bu \quad (4)$$

With the introduction of the MeO(C$_6$H$_4$)O ligand to the indium atom instead of the O*t*Bu ligand, a further possibility of coordination was offered to the metal center. In this way attempts were made to prevent the molecule from dimerising. The synthesis of **5** is almost analogous to the synthesis of **3** and **4** (Equation 5), with the exception that crystallization of **5** did not occur from hexane at low temperatures, but directly from the mother liquor (yield: 60%). The ^{1}H-NMR spectrum of **5** shows a signal for the metal-bonded methyl group and one signal for the methoxy group. In the ^{13}C-NMR spectrum only two signals are found, corresponding to the metal-bonded methyl group and the OMe group.

$$MeClIn[N(SiMe_3)_2] + 2\ HO(C_6H_4)OMe \rightarrow \underset{\mathbf{5}}{ClMeIn[O(C_6H_4)OMe]} + HN(SiMe_3)_2 + HO(C_6H_4)OMe \quad (5)$$

For the synthesis of MeIn(O*t*Bu)[N(SiMe$_3$)$_2$] (**6**) an analogous procedure to that for **3**, **4**, and **5** was chosen to introduce the [N(SiMe$_3$)$_2$] ligand into the system. The reaction of **3** with Li[N(SiMe$_3$)$_2$] in a molar ratio of 1:1 was performed under refluxing toluene. During this reaction no methyl-group transfer of trimethylsilyl to indium was observed and **6** was formed together with lithium chloride (Equation 6).

$$ClMeIn(O\mathit{t}Bu) + LiN(SiMe_3)_2 \rightarrow \underset{\mathbf{6}}{[(SiMe_3)_2N]MeIn(O\mathit{t}Bu)} + LiCl \quad (6)$$

Compound **6** could be isolated by crystallization from hexane at low temperatures (yield: 60%). The ^{1}H-NMR spectrum of **6** shows three signals in a ratio of 1:3:6 corresponding to the signals of the metal-bonded methyl group, the *tert*-butyl group and the [N(SiMe$_3$)$_2$] group. Within the ^{13}C-NMR spectrum, four signals are visible in accordance with the singlets of the methyl group, the [N(SiMe$_3$)$_2$] group and the two signals of the *tert*-butyl group.

In order to replace the amino function by an alcohol group, **6** was subject of an alcoholysis. The synthesis was carried out in refluxing toluene with a double equivalent of *tert*-butyl alcohol (Equation 7). After removing the volatiles in vacuo and dissolving the residue in hexane, MeIn(O*t*Bu)$_2$ (**7**) was separated from the solvent by crystallization at low temperatures (−30°C).

$$[(SiMe_3)_2N]MeIn(O\mathit{t}Bu) + 2\ HO\mathit{t}Bu \rightarrow \underset{\mathbf{7}}{MeIn(O\mathit{t}Bu)_2} + HN[SiMe_3]_2 + HO\mathit{t}Bu \quad (7)$$

An adequate yield of **7** (60%) was only possible if the reaction took place in a very dilute solution. In a concentrated solution, a mixture of **3**, **6**, and **7** was obtained. After purification of **7** by sublimation (10^{-2} Torr/120°C), the ^{1}H-NMR spectrum shows two signals (ratio 1:6) corresponding to the metal-bonded methyl group and the two *tert*-butyl groups. As expected in the ^{13}C-NMR spectra three signals are visible.

Metal alkoxides are often synthesized by the reaction of alkylmetal compounds with alcohol.[23] Therefore, **7** was treated with *tert*-butyl alcohol in toluene and refluxed for several hours to replace the methyl group by the *tert*-butyl group. Surprisingly, even after refluxing the solvent for

24 h, no reaction took place (Equation 8). In conclusion, the metal−carbon bond in **7** seems to be remarkably stable.

$$MeIn(OtBu)_2 + 2\ HOtBu \not\rightarrow In(OtBu)_3 + CH_4 \uparrow + HOtBu \quad (8)$$

Crystal Structures of Compounds 3, 4, 5, 6, and 7

The molecular structures of the compounds **3**, **4**, **5**, **6**, and **7** have been determined by single-crystal X-ray analysis. The crystal structures of the molecules are shown in Figures 1−5. Selected bond lengths and angles are given in Table 1.

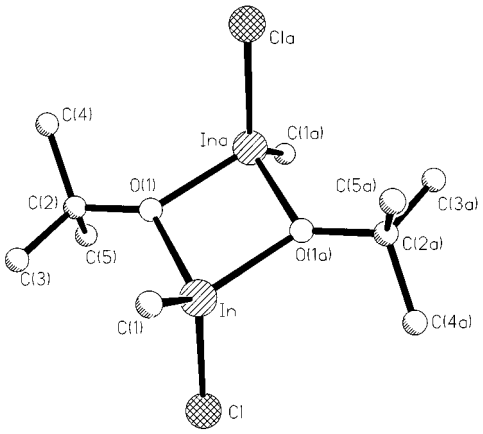


Figure 1. Molecular structure of $[ClMeIn(OtBu)]_2$ (**3**); hydrogen atoms are omitted for clarity

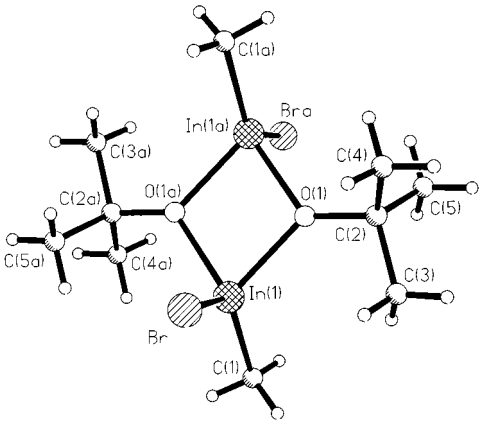


Figure 2. Molecular structure of $[BrMeIn(OtBu)]_2$ (**4**)

Crystal Structures of 3 and 4

The compounds $[ClMeIn(OtBu)]_2$ (**3**) and $[BrMeIn(OtBu)]_2$ (**4**) are similar, except for the different halogen atoms. Both compounds crystallize in a monoclinic crystal system with two molecules per unit cell, in the space group $P2_1/c$, and are isostructural. The compounds form centrosymmetric dimers (crystal symmetry: C_i). The dimerisation is achieved by two bridging oxygen atoms. The In_2O_2 ring is planar by symmetry requirements. The indium atoms in both compounds are present in a strongly distorted tetrahedral environment. The oxygen atoms in both the structures possess an almost trigonal planar coordination sphere (358.3° for **3**; 358.7° for **4**) and thus are sp^2-hybridized. The bond lengths within the In_2O_2 ring of both the molecules are rather similar [211.5(7) pm in **3** and 212.1(7) pm in **4**]. The In−C lengths in both compounds are also within the same range [211.8(6) pm for **3** and 210(1) pm for **4**], but

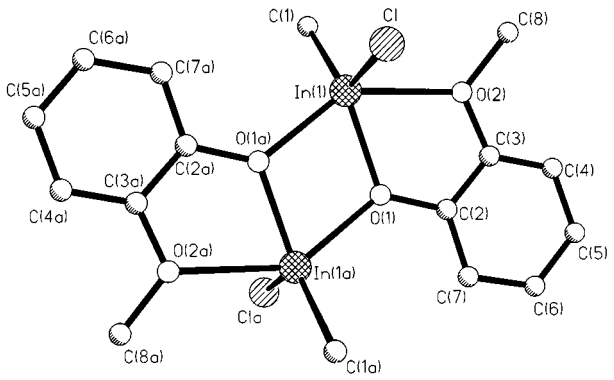


Figure 3. Molecular structure of $[ClMeIn(OC_6H_4OMe)]_2$ (**5**); hydrogen atoms are omitted for clarity

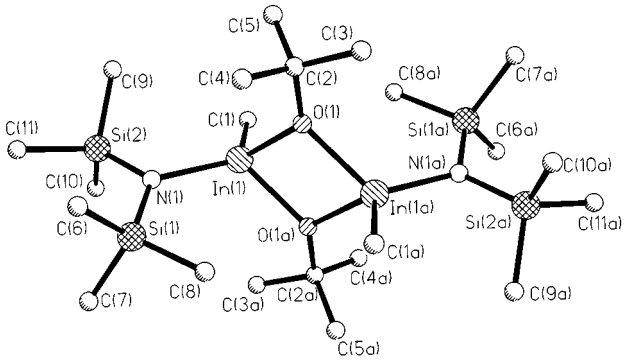


Figure 4. Molecular structure of $\{[N(SiMe_3)_2]MeInOtBu\}_2$ (**6**); hydrogen atoms are omitted for clarity

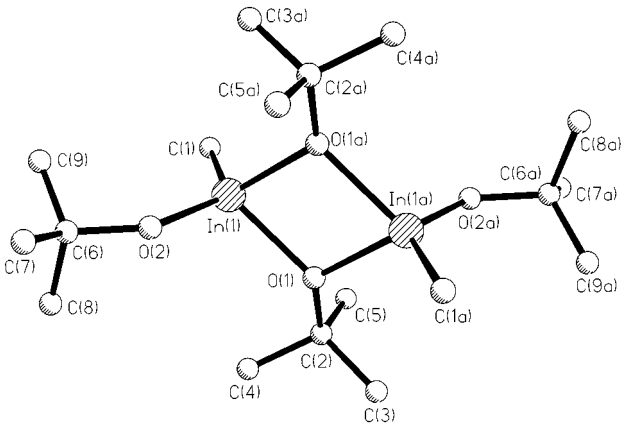


Figure 5. Molecular structure of $[MeIn(OtBu)_2]_2$ (**7**)

Table 1. Selected bond lengths [pm] and angles [°] of **3**–**7**

$C_{10}H_{24}Cl_2In_2O_2$ (**3**)							
In–O(1a)	210.9(3)	In–Cl	237.2(2)	O(1)–In(a)	210.9(3)	C(2)–C(5)	152.6(8)
In–C(1)	211.8(6)	In–In(a)	331.2(9)	C(2)–C(3)	151.7(7)		
In–O(1)	212.2(4)	O(1)–C(2)	144.0(6)	C(2)–C(4)	152.1(8)		
O(1a)–In–C(1)	122.9(2)	O(1a)–In–Cl	103.8(1)	O(1a)–In–In(a)	38.6(9)	Cl–In–In(a)	107.6(5)
O(1a)–In–O(1)	77.0(2)	C(1)–In–Cl	122.4(2)	C(1)–In–In(a)	129.8(2)	In(a)–O(1)–In	103.0(1)
C(1)–In–O(1)	117.3(2)	O(1)–In–Cl	103.6(1)	O(1)–In–In(a)	38.3(8)		
$C_{10}H_{24}Br_2In_2O_2$ (**4**)							
In(1)–C(1)	210(1)	In(1)–Br	251.0(2)	O(1)–In(1a)	211.3(7)	C(2)–C(5)	154(2)
In(1)–O(1a)	211.4(7)	In(1)–In(1a)	332.0(2)	C(2)–C(4)	148(2)		
In(1)–O(1)	212.9(8)	O(1)–C(2)	145.6(1)	C(2)–C(3)	153(2)		
C(1)–In(1)–O(1a)	121.8(5)	C(1)–In(1)–Br	124.5(4)	C(1)–In(1)–In(1a)	127.6(4)	Br–In(1)–In(1a)	107.6(5)
C(1)–In(1)–O(1)	115.4(4)	O(1A)–In(1)–Br	103.8(2)	O(1A)–I-n(1)–In(1a)	38.7(2)	In(1a)–O(1)–In(1)	103.0(3)
O(1A)–In(1)–O(1)	77.0(3)	O(1)–In(1)–Br	103.6(2)	O(1)–In(1)–In(1a)	38.3(2)		
$C_{16}H_{20}Cl_2In_2O_4$ (**5**)							
In(1)–C(1)	212.9(7)	In(1)–O(2)	240.6(5)	O(2)–C(3)	139.3(8)	C(3)–C(4)	135(1)
In(1)–O(1)	213.6(4)	In(1)–In(1a)	350.1(1)	O(2)–C(8)	143.7(9)	C(7)–C(6)	138(1)
In(1)–O(1a)	220.4(4)	O(1)–C(2)	136.4(8)	C(2)–C(7)	138(1)	C(4)–C(5)	137(1)
In(1)–Cl	236.7(2)	O(1)–In(1a)	220.4(4)	C(2)–C(3)	139(1)	C(5)–C(6)	138(1)
C(1)–In(1)–O(1)	129.2(3)	C(1)–In(1)–Cl	121.7(2)	C(1)–In(1)–O(2)	95.7(3)	Cl–In(1)–O(2)	91.3(1)
C(1)–In(1)–O(1a)	110.2(3)	O(1)–In(1)–Cl	107.6(2)	O(1)–In(1)–O(2)	70.3(2)	C(1)–In(1)–In(1a)	127.1(2)
O(1)–In(1)–O(1a)	72.4(2)	O(1a)–In(1)–Cl	97.1(2)	O(1a)–In(1)–O(2)	142.6(2)	Cl–In(1)–In(1a)	105.2(7)
O(2)–In(1)–In(1a)	107.1(1)	C(2)–O(1)–In(1)	122.5(4)	C(2)–O(1)–In(1a)	129.3(4)	In(1)–O(1)–In(1a)	107.5(2)
$C_{22}H_{60}In_2N_2O_2Si_4$ (**6**)							
In(1)–N(1)	209.3(4)	In(1)–In(1a)	340.5(9)	Si(1)–C(7)	186.8(6)	Si(2)–C(10)	187.6(7)
In(1)–O(1)	213.8(3)	Si(1)–N(1)	172.3(4)	Si(2)–N(1)	173.8(4)	O(1)–C(2)	145.9(5)
In(1)–O(1a)	215.3(3)	Si(1)–C(8)	184.9(6)	Si(2)–C(9)	185.8(6)	O(1)–In(1a)	215.3(3)
In(1)–C(1)	216.0(5)	Si(1)–C(6)	186.3(6)	Si(2)–C(11)	187.5(6)		
N(1)–In(1)–O(1)	113.2(1)	O(1A)–In(1)–C(1)	109.3(2)	C(8)–Si(1)–C(6)	105.0(3)	Si(1)–N(1)–Si(2)	120.5(2)
N(1)–In(1)–O(1a)	117.7(1)	N(1)–In(1)–In(1a)	122.8(1)	N(1)–Si(1)–C(7)	111.3(3)	Si(1)–N(1)–In(1)	125.1(2)
O(1)–In(1)–O(1a)	75.0(1)	C(1)–In(1)–In(1a)	117(1)	C(8)–Si(1)–C(7)	107.8(3)	Si(2)–N(1)–In(1)	113.0(2)
N(1)–In(1)–C(1)	119.5(2)	N(1)–Si(1)–C(8)	111.5(2)	C(6)–Si(1)–C(7)	107.9(3)		
O(1)–In(1)–C(1)	114.1(2)	N(1)–Si(1)–C(6)	113.0(3)	In(1)–O(1)–In(1a)	105.0(1)		
$C_{18}H_{42}In_2O_4$ (**7**)							
In(1)–O(2)	200.6(4)	In(1)–In(1a)	334.6(1)	C(2)–C(3)	151.7(9)	C(6)–C(7)	152(1)
In(1)–O(1)	212.6(4)	O(1)–C(2)	145.1(6)	C(2)–C(4)	151.8(9)	C(6)–C(8)	153(1)
In(1)–O(1a)	213.1(4)	O(1)–In(1a)	213.1(4)	C(2)–C(5)	152.6(9)		
In(1)–C(1)	213.6(7)	O(2)–C(6)	143.1(7)	C(6)–C(9)	150(1)		
O(2)–In(1)–O(1)	104(2)	O(2)–In(1)–C(1)	129.0(3)	O(2)–In(1)–In(1a)	105.6(1)	C(2)–O(1)–In(1a)	126.2(3)
O(2)–In(1)–O(1a)	99(2)	O(1)–In(1)–C(1)	116.8(3)	C(1)–In(1)–In(1a)	125.3(2)	In(1)–O(1)–In(1a)	103.6(2)
O(1)–In(1)–O(1a)	76.4(2)	O(1a)–In(1)–C(1)	117.3(3)	C(2)–O(1)–In(1)	126.8(3)	C(6)–O(2)–In(1)	127.6(4)

about 10 pm shorter than in other comparable compounds.[17] The In–X bond lengths (X = halogen atom) are normal by comparison with standard compounds.[24] As a consequence of the short In–C length, compared to the In–X length, the carbon atoms experience a stronger repulsion to the bridging oxygen atoms. This leads to different C–In–In and X–In–In angles. The C–In–In angle in compound **3**, for example, is found to be 129.8(2)°; 22.2° larger than the X–In–In angle [107.6(5)°]. In compound **4** the effect is similar: The C–In–In angle [127.6(4)°] is 20.4° larger than the X–In–In angle [107.2(5)°]. The difference in the C–In–In angles of compounds **3** and **4** can be explained by the different halogen atoms; thus, the X–In–C angle in **4** [124.5(4)°] is larger than the corresponding angle in **3** [122.4(2)°] because of the larger bromine atom. The bonding angles within the In_2O_2 rings of the two compounds are almost identical (see Table 1). The larger In–O–In angles are due to the hard-shell oxygen atoms, whereas the soft-shell indium atoms allow more acute angles.

Table 2. Crystal data and data-collection parameters of the compounds **3**–**7**

	3	**4**	**5**	**6**	**7**
Empirical formula	$C_{10}H_{24}Cl_2In_2O_2$	$C_{10}H_{24}Br_2In_2O_2$	$C_{16}H_{20}Cl_2In_2O_4$	$C_{22}H_{60}In_2N_2O_2Si_4$	$C_{18}H_{42}In_2O_4$
Formula weight	476.83	565.75	576.86	726.72	552.16
Space group	$P2_1/c$	$P2_1/c$	$P2_1/n$	$C2/c$	$P-1$
Crystal system	monoclinic	monoclinic	monoclinic	monoclinic	triclinic
a [pm]	796.6(2)	809.2(2)	1043.9(2)	1022.9(2)	876.1(2)
b [pm]	1307.3(3)	1342.0(3)	875.6(2)	1532.0(4)	929.2(2)
c [pm]	892.1(2)	909.0(2)	1125.7(2)	2338.0(5)	967.4(2)
α [°]	90	90	90	90	117.07(3)
β [°]	103.7(3)	104.01(3)	97.75(3)	97.53(3)	95.99(3)
γ [°]	90	90	90	90	109.95(3)
V [Å^3]	905.0(4)	944.9(4)	1019.5(4)	3632.2(13)	626.7(2)
Z	2	2	2	4	1
$d_{calcd.}$ [g/cm^3]	1.750	1.988	1.879	1.329	1.463
Absorpt. coeff.[mm^{-1}]	2.83	6.66	2.54	1.42	1.86
F(000)	464	536	560	1504	280
Crystal size [mm]	0.5 × 0.5 × 0.7	0.8 × 0.6 × 0.5	0.5 × 0.5 × 0.6	0.7 × 0.2 × 0.5	0.7 × 0.5 × 0.3
Crystal color	colorless	colorless	colorless	colorless	colorless
Data collection					
Diffractometer used	Siemens/Stoe AED 2	Siemens/Stoe AED 2	Siemens/Stoe AED 2	Siemens/Stoe AED 2	Siemens/Stoe AED 2
Monochromator	graphite	graphite	graphite	graphite	graphite
Radiation	Mo-K_α	Mo-K_α	Mo-K_α	Mo-K_α	Mo-K_α
Wavelength (Mo-K_α) [Å]	0.71073	0.71073	0.71073	0.71073	0.71073
Temperature [K]	293(2)	293(2)	293(2)	293(2)	293(2)
2θ range [°]	2.62–22.48	2.59–22.50	2.50–22.51	1.76–22.50	2.49–24.99
Scan type	ϖ-θ	ϖ-θ	ϖ-θ	ϖ-θ	ϖ-θ
Observed reflections [$I > 2F(I)$]	1110	1113	1261	2079	2115
Independent reflections	1174	1230	1331	2368	2205
Refinement					
No. of refined parameters	73	73	109	145	109
Goodness-of-fit on F^2	1.277	1.563	1.013	1.153	1.112
Final R indices	$R_1 = 0.0290$	$R_1 = 0.0618$	$R_1 = 0.0443$	$R_1 = 0.0338$	$R_1 = 0.0244$
[$I > 2\sigma(I)$]	$wR_{1=0}$.0778	$wR_1 = 0.1685$	$wR_1 = 0.1393$	$wR_1 = 0.1026$	$wR_1 = 0.0673$
Final R indices (all data)	$R_2 = 0.0306$,	$R_2 = 0.0691$	$R_2 = 0.0460$	$R_2 = 0.0398$	$R_2 = 0.0256$
	$wR_2 = 0.0793$	$wR_2 = 0.1847$	$wR_2 = 0.1426$	$wR_2 = 0.1095$	$wR_2 = 0.0702$
Min./max. residual density [eÅ^{-3}]	0.357/−0.933	0.950/−1.799	0.765/−1.139	0.343/−0.960	0.749/−0.64

Crystal Structure of 5

The compound $\{ClMeIn[O(C_6H_4)OMe]\}_2$ (**5**) crystallizes in the monoclinic crystal system with two molecules per unit cell in the space group $P2_1/c$. The dimerisation of "monomers" to form the centrosymmetric dimer **5** can be understood in terms of the tendency of indium(III) to achieve higher coordination numbers, while a polycycle is formed due to the presence of further basic ligands (methoxy group) (see Figure 3). Besides an In_2O_2 ring, the dimeric molecule contains two five-membered InO_2C_2 rings and two six-membered phenyl rings, all fused together. The central In_2O_2 ring with respect to the bridging oxygen atoms is the same as that described for **3** and **4**. The In_2O_2 ring is planar because of centrosymmetry, whereas the phenyl ring is planar due to electronic considerations. On the other hand the atoms within the InO_2C_2 ring are not equiplanar and have a dihedral angle which differs by about 5° from planarity. In contrast to the compounds described above, the indium atoms in **5** possess a "4+1" coordination sphere with a strongly distorted tetrahedral environment: $In(ClCO_2)$ plus additional coordination by an oxygen atom of the $O(C_6H_4)OMe$ group. The O–In–O angles within the In_2O_2 ring are more acute, and the In–O–In angles even larger, when compared to **3** and **4**. The In–O bond lengths are also longer compared to **3** and **4**; the mean value of the bonds [220.4(4) pm] being 9 pm longer when compared to those of **3** and **4**. The bond between In(1) and O(2) within the InO_2C_2 ring [240.6(5) pm] may be classified as coordinative due to its length. From a general point of view, the In–O lengths are comparable to values of the oxopentaindium alkoxide cluster reported by Bradley et al.[25] Alcock et al. described an indium compound, $[Me_2In(OC_6H_4CHO)]_2$, which is similar to **5**.[14] The dimeric molecule consists of a central In_2O_2 ring, two six-membered InO_2C_3 rings, and two phenyl rings all fused together. The O–In–O angles inside the In_2O_2 ring are larger [74.8(1)°] and the In–O–In angles more acute [105.2(1)°] compared to those of **5**. The mean value of the In–O bond lengths in $[Me_2In(OC_6H_4CHO)]_2$ [228.6(3) pm] is about 8 pm longer compared to

that of **5**. The In−C bond lengths hardly differ between $[Me_2In(OC_6H_4CHO)]_2$ [212.1(2) pm] and **5**. The bond lengths between In−C and In−Cl hardly differ between compounds **5** and **3**. This is very surprising, because the coordination numbers of the indium atoms are not equal in the two compounds. All oxygen atoms in **5** possess a more or less distorted trigonal environment and are sp^2-hybridized. The distortion of O(2) (356.4°) is higher as compared to that of O(1) (359.35°).

Crystal Structure of 6

As with **3**, **4**, and **5** compound $\{MeIn(OtBu)[N(SiMe_3)_2]\}_2$ (**6**) crystallizes in the monoclinic crystal system with four molecules per unit cell in the space group *C*2/*c*. The crystal-structure analysis shows again a centrosymmetric dimer (crystal symmetry: C_i) with a planar In_2O_2 ring, which originates by a base attack of the more electronegative oxygen atoms (as compared to the nitrogen atoms) on the indium atom. In contrast to **3**, **4**, and **5**, no halogen atom is bonded to the metal atom but a nitrogen atom, belonging to a $[N(SiMe_3)_2]$ ligand, is present. The In−O−In angle [105.40(1)°] within the In_2O_2 ring is slightly smaller than in **5**, but larger than in **3** or **4**. The In−O lengths within the In_2O_2 ring [214.50 (7) pm] are longer than for **3** and **4**, which could be explained by the less electronegative $N(SiMe_3)_2$ ligand when compared to the halogen atom. The indium atoms possess a highly distorted tetrahedral coordination sphere. The oxygen atoms are almost trigonal planar coordinated (359.04°) and thus are sp^2-hybridized. The In−C and In−N bond lengths are within the range of values described in the literature.[26] The C−In−In and N−In−In angle in compound **6** are almost the same as the corresponding angles in **3** and **4**, due to the almost equal bond lengths between In−C and In−N.

Crystal Structure of 7

Compound $[MeIn(OtBu)_2]_2$ (**7**) crystallizes in a triclinic crystal system with one dimeric molecule per unit cell in the space group *P*−1. As for the compounds **3**−**6**, **7** also exists as a centrosymmetric dimer (crystal symmetry: C_i). At the metal atom, three alkoxo ligands are present besides the methyl group (Figure 5). The bond angles within the In_2O_2 ring [In−O−In 103.6(2)°, O−In−O 76.4(2)°] are comparable with both the corresponding angles in **3** and **4** and those of the ethoxy compound, $[tBu_2In(OEt)]_2$, described by Hursthouse et al.[17] The indium atoms have a distorted tetrahedral coordination sphere. The oxygen atoms O(1) and O(1a) possess a slightly distorted trigonal-planar environment, whereas O(2) and O(2a) are in the apices of an angle. The In−O bond lengths within the In_2O_2 ring [212.8(8) pm] are comparable to the bond lengths in compounds **3**−**6** and $[tBu_2In(OEt)]_2$. The In−O bond lengths to the terminal oxygen atoms are 12 pm shorter than the bond lengths within the In_2O_2 ring, due to the different coordination numbers of the oxygen atoms.

Conclusion

All compounds reported here have a metal-bound methyl group in common. This group can be used as a sensor to compare the different compounds with different ligand spheres. One way to use this sensor is to compare the dependence on the ligands of the In−C bond length in the molecules. It was expected that there would be a correlation between the electronegativity of the ligands and the In−C bond length. Generally speaking, the more electronegative chlorine atom in compound **3** should cause an electron withdrawal from the indium atom and therefore lead to a smaller In−C bond length than in the case of compound **4** where there is a less electronegative bromine atom. Inspection of the In−C bond lengths confirms this assumption, except for compounds **3** and **4** (Table 1). The In−C bond in **3** [211.8(6) pm] is surprisingly slightly longer than in **4** [210(12) pm], but if the halogen atom is substituted by a nitrogen atom, as in **6**, which is less electronegative, the In−C bond [216(5) pm] is elongated. In compound **7**, where the halogen atom is substituted by a more electronegative oxygen atom, the bond length [213.6 (7) pm] is reduced compared to **6** and is in the region of that found for **3** and **4**. In compound **5**, the situation is more complicated; because of the change of the coordination number from 4 to "4+1", the In−C bond should be quite long but with 212.9(7) pm the bond length has a mean value which seems to be the result of the three electronegative oxygen ligands. In any case the electronegativity is not the only parameter which has to be considered in the change of the In−C bond length; the size and the steric requirement of the ligand must also be taken into account. On this theme, the most sterically demanding ligand, the $[N(SiMe_3)_2]$ group in **6**, gives the longest In−C bond length. The O*t*Bu group in **7**, which is sterically less demanding than the $[N(SiMe_3)_2]$ group, leads to a slightly shorter In−C bond length. The $MeO(C_6H_4)O$ group in **5** is sterically not as demanding as the $[N(SiMe_3)_2]$ and the O*t*Bu group, but the ligand does offer an additional intramolecular coordination site such that the coordination number of the metal atom and the

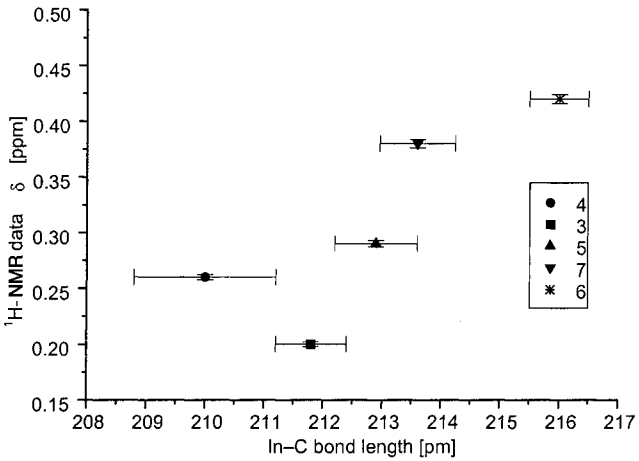


Figure 6. Chemical shift of the molecules **3**−**7** vs. In−C bond lengths

In−C bond lengths are increased, however not as much as expected because of the electronegativity of the ligands. In our experiment, we find a correlation between the ^{1}H-NMR data and the In−C bond lengths. The compound with the longest In−C bond, compound **6**, has the highest chemical shift (δ = 0.42) followed by compound **7** and compound **5**. The ^{1}H-NMR shifts for **3** and **4**, however, are reversed (Figure 6).

Experimental Section

General: All manipulations were performed under purified and dried nitrogen using a modified Stock apparatus. Solvents were distilled from Na/K alloy prior to use. $InCl_3$ and $InBr_3$ were prepared according to known procedures.[27] *tert*-Butyl alcohol was dried by distillation from sodium. − ^{1}H and ^{13}C NMR: Bruker AC 200 spectrometer, quoted to [D$_6$]benzene by using the solvent signal as internal reference. − Elemental analyses: LECO CHN 900 analyser. − Metal and halogen analyses: Standard methods. − The crystal structures of compounds **3**−**7** were obtained from X-ray diffraction of single crystals. The most important parameters for the crystals and the structure determination have been summarized in Table 2. Diffraction data were collected with a Stoe AED 2 diffractometer. The structures were solved by direct methods (SHELXS-86)[28] and refined by full-matrix least-squares procedures on all F^2 values (SHELXS-97).[29] All nonhydrogen atoms were refined anisotropically. Crystallographic data for the structures reported in this paper have been deposited with the Cambridge Crystallographic Data Centre as supplementary publication CCDC-121777−121781 (**3**−**7**). Copies of the data can be obtained free of charge on application to CCDC, 12 Union Road, Cambridge CB2 IEZ, UK [Fax: (internat.) + 44-1223/336-033; E-mail: deposit@ccdc.cam.ac.uk].

Synthesis of {ClMeIn[N(SiMe$_3$)$_2$]}$_2$ (1): A solution of $LiN(SiMe_3)_2$ (3.0 g,17.92 mmol) in toluene (40 mL) was added dropwise to a stirred suspension of $InCl_3$ (1.98 g, 8.96 mmol) in toluene (30 mL). A weak exothermic reaction took place. The reaction solution was refluxed for 24 h, and after removing the volatiles under reduced pressure, the product purified by sublimation (10^{-2} Torr/100°C). Yield: 1.89 g, 65.0% (based on $InCl_3$). − ^{1}H NMR: δ = 0.30 (s, 3 H, $InCH_3$), 0.28 {s, 18 H, N[Si(CH_3)$_3$]}. − ^{13}C NMR: δ = 5.03 {s, 6 C, N[Si(CH_3)$_3$]$_2$}, 6.60 (s, 1 C, In*C*H$_3$). − $C_7H_{21}ClInNSi$ (325.67): calcd. C 30.57, H 7.64, Cl 7.52, In 24.37, N 5.94; found C 30.28, H 7.47, Cl 7.26, In 23.96, N 5.65.

Synthesis of {BrMeIn[N(SiMe$_3$)$_2$]}$_2$ (2): Compound **2** was synthesized in an analogous manner to **1**. Yield: 1.47 g, 70.0% (based on $InBr_3$). − ^{1}H NMR: δ = 0.30 (s, 3 H, $InCH_3$), 0.28 {s, 18 H, N[Si(CH_3)$_3$]}. − ^{13}C NMR: δ = 5.03 {s, 6 C, N[Si(CH_3)$_3$]$_2$}, 6.60 (s, 1 C, $InCH_3$).

Synthesis of [ClMeIn(O*t*Bu)]$_2$ (3): An excess of *tert*-butyl alcohol (0.88 mL, 9.2 mmol) was added to a stirred solution of ClMeIn[N(SiMe$_3$)]$_2$ (**1**) (1.50 g, 4.6 mmol) in toluene (25 mL). The reaction solution was refluxed for 24 h, and, after removing the volatiles under reduced pressure, the residue dissolved in a small amount of hexane. The product crystallized at low temperatures (−30°C) within 12 h and was further purified by sublimation (10^{-2} Torr/120°C). Yield 0.7 g, 64% (based on $InCl_3$). − ^{1}H NMR: δ = 0.20 (s, 3 H, $InCH_3$), 1.13 [s, 9 H, C(CH_3)$_3$]. − ^{13}C NMR: δ = 6.8 (s, $InCH_3$), 33.45 [s, C(*C*H$_3$)$_3$], 75.00 [s, *C*(CH$_3$)$_3$]. − $C_5H_{12}ClInO$ (238.41): calcd. C 25.16, H 5.03, Cl 14.87, In 48.16; found C 24.39, H 5.02, Cl 14.75, In 48.96.

Synthesis of [BrMeIn(O*t*Bu)]$_2$ (4): Compound **4** was synthesized in an analogous manner to **3**. Yield: 1.02 g, 70% (based on $InBr_3$). − ^{1}H NMR: δ = 0.26 (s, 3 H, $InCH_3$), 1.13 [s, 9 H, C(CH_3)$_3$]. − ^{13}C NMR: δ = 6.93 (s, $InCH_3$), 33.55 [s, C(*C*H$_3$)$_3$], 75.42 [s, *C*(CH$_3$)$_3$]. − $C_5H_{12}BrInO$ (282.87): calcd. C 21.22, H 4.24, Br 28.26, In 40.60; found C 20.88, H 4.23, Br 29.87, In 41.50.

Synthesis of {ClMeIn[O(C$_6$H$_4$)OMe]}$_2$ (5): An excess of 2-methoxyphenol (3.0 mL, 27.0 mmol) was added to a stirred solution of ClMeIn[N(SiMe$_3$)$_2$] (**1**) (4.40 g, 13.5 mmol) in toluene (80 mL). The reaction solution was refluxed for 24 h and the product crystallized from the mother liquor while cooling. Yield 2.30 g, 60% (based on $InCl_3$). − ^{1}H NMR: δ = 0.29 (s, 3 H, $InCH_3$), 3.13 (s,3 H, OCH_3). − ^{13}C NMR: δ = 6.8 (s, $InCH_3$), 55.88 (s, OCH_3). − $C_8H_{10}ClInO_2$ (288.43): calcd. C 33.30, H 3.46, Cl 12.30, In 39.80; found C 33.20, H 3.87, Cl 12.40, In 39.70.

Synthesis of {Me[N(SiMe$_3$)$_2$]In(O*t*Bu)}$_2$ (6): A solution of LiN(SiMe$_3$)$_2$ (2.53 g, 15.2 mmol) in toluene (50 mL)was added dropwise to a stirred solution of ClMeIn(O*t*Bu) (**3**) (3.3 g, 15.2 mmol) in toluene (150 mL). The reaction solution was refluxed for 24 h and, after removing the volatiles under reduced pressure, the residue dissolved in a small amount of hexane. The product crystallized at low temperatures (−30°C) within 12 h and was further purified by sublimation (10^{-2} Torr/115°C). Yield 3.30 g, 60% (based on $InCl_3$). − ^{1}H NMR: δ = 0.34 [s, 18 H, Si(CH_3)$_3$], 0.42 (s, 3 H, $InCH_3$), 1.27 [s, 9 H, C(CH_3)$_3$]. − ^{13}C NMR: δ = 5.78 (s, $SiMe_3$), 6.8 (s, $InCH_3$), 33.95 [s, C(*C*H$_3$)$_3$], 73.93 [s, *C*(CH$_3$)$_3$]. − $C_{11}H_{60}InNOSi_2$ (363.36): calcd. C 36.34, H 8.25, In 31.61, N 3.85; found C 36.29, H 8.66, In 32.00, N 3.67.

Synthesis of [MeIn(O*t*Bu)$_2$]$_2$ (7): An excess of *tert*-butyl alcohol (1.74 mL, 18.2 mmol) was added to a stirred solution of Me[N(SiMe$_3$)$_2$]In(O*t*Bu) (**6**) (3.3 g, 9.10 mmol) in toluene (150 mL). The reaction solution was refluxed for 24 h, and, after removing the volatiles under reduced pressure, the residue dissolved in a small amount of hexane. The product crystallized at low temperatures (−30°C) within 2 d and was purified by sublimation (10^{-2} Torr/120°C). Yield 1.50 g, 60% (based on $InCl_3$). − ^{1}H NMR: δ = 0.38 (s, 3 H, $InCH_3$), 1.39 [s, 18 H, C(CH_3)$_3$]. − ^{13}C NMR: δ = 6.92 (s, $InCH_3$), 34.71 [s, C(*C*H$_3$)$_3$], 69.91 [s, *C*(CH$_3$)$_3$]. − $C_9H_{21}InO_2$ (276.08): calcd. C 39.15, H 7.6, In 41.61; found C 39.30, H 7.82, In 41.3.

Acknowledgments

The authors thank Dr. Charu Mathur for reading the manuscript.

[1] Römpp, *Chemie Lexikon*, 9th ed., Thieme-Verlag, Stuttgart − New York, **1995**.
[2] Y. Shigesato, I. Yasui, *Ceram. Jpn*. **1996**, *31*, No. 10,842.
[3] T.-S. Kim, C.-H. Kim, M.-H. Oh, *J. Appl. Phys.* **1994**, *76*, 4316.
[4] T. Ishida, H. Kouno, H. Kobayashi, *J. Electrochem. Soc*. **1994**, *141*, 1357.
[5] H. Kobayashi, Y. Kogetsu, T. Ishida, Y. Nakato, *J. Appl. Phys.* **1993**, *74*, 4756.
[6] S. Noguchi, M. Mizuhashi, H. Sakata, *Glastech. Ber.* **1992**, *65*, 9.
[7] H. Shiomi, M. Nakamura, K. Satou, T. Kobayashi, *J. Ceram. Soc. Jpn., Int. Ed.* **1993**, *101*, 528.
[8] A. Melas, CVD, Inc., USA, Patent number US 5147688, **1992**; *Chem. Abstr.* **1993**, *118*, 30657s.
[9] *Gmelin Handbook of Inorganic and Organometallic Chemistry*, "Organoindium Compounds", Part 1, 8th ed., Springer-Verlag, Berlin, **1991**.
[10] H. Schmidbaur, *Angew. Chem*. **1965**, *77*, 169; *Angew. Chem. Int. Ed. Engl.* **1965**, *4*, 152.

[11] H. C. Clark, A. L. Pickard, *J. Organomet. Chem*. **1968**, *13*, 61.
[12] D. A. Atwood, A. H. Cowley, R. D. Schluter, M. R. Bond, C. J. Carrano, *Inorg. Chem.* **1995**, *34*, 2186.
[13] T. Kräuter, B. Neumüller, *Chem. Eur. J.* **1997**, *3*, 568.
[14] N. W. Alcock, I. A. Degnan, S. M. Roe, M. G. H. Wallbridge, *J. Organomet. Chem.* **1991**, *414*, 285.
[15] S. Chatterjee, S. R. Bindal, R. C. Mehrotra, *J. Ind. Chem. Soc.* **1976**, *53*, 867.
[16] A. Mehrotra, R. C. Mehrotra, *Inorg. Chem*. **1972**, *11*, 2170.
[17] D. C. Bradley, D. M. Frigo, M. B. Hursthouse, B. Hussain, *Organometallics* **1988**, *7*, 1112.
[18] A. J. Canti, L. A. Titcombe, B. W. Skelton, A. H. White, *Inorg. Chim. Acta* **1986**, *117*, L 35.
[19] H. Bürger, J. Cichon, U. Goetze, U. Wannagat, H. J. Wismar, *J. Organomet. Chem*. **1971**, *33*, 1.
[20] M. A. Petrie, K. Ruhlandt-Senge, H. Hope, P. P. Power, *Bull. Soc. Chim. Fr*. **1993**, *130*, 851−855.
[21] M. Veith, *Nova Acta Leopold.* **1985**, *59* (264), 321.
[22] M. Veith, F. Goffing, V. Huch, *Z. Naturforsch.* **1988**, *43b*, 846.
[23] D. C. Bradley, R. C. Mehrotra, D. P. Gaur, *Metal Alkoxides*, Academic Press, London, **1978**.
[24] M. Veith, O. Recktenwald, *J. Organomet. Chem*. **1984**, *264*, 19.
[25] D. C. Bradley, H. Chudzynska, D. M. Frigo, M. B. Hursthouse, M. A. Mazid, *J. Chem. Soc., Chem. Commun.* **1988**, 1258.
[26] J. Kim, S. G. Bott, D. M. Hoffman, *Inorg. Chem*. **1998**, *37*, 3835.
[27] G. Brauer, *Handbuch der Präparativen Anorganischen Chemie*, vol. II, F. Enke, Verlag, Stuttgart, **1978**.
[28] G. M. Sheldrick, *SHELXS-86, Program for Crysta Structure Determination*, University of Göttingen, **1986**.
[29] G. M. Sheldrick, *SHELXS-97, Program for Crysta Structure Refinement*, University of Göttingen, **1997**.

Received February 4, 1999
[I99037]

Halogenation of Alkenes in Five-Coordinate Platinum(II) Complexes – A Route to Stable (β-Haloalkyl)platinum(IV) Species

Francesco Paolo Fanizzi,*[a] Luciana Maresca,[a] Concetta Pacifico,[a] Giovanni Natile,*[a] Maurizio Lanfranchi,[b] and Antonio Tiripicchio[b]

Keywords: Haloalkyl complexes / Five-coordinate platinum complexes / Alkene complexes / Olefin halogenation / Oxidative addition / Platinum

Five-coordinate complexes $[PtX_2(olefin)(2,9\text{-}Me_2\text{-}phen)]$ (**1**; 2,9-Me_2-phen = 2,9-dimethyl-1,10-phenanthroline; olefin = ethene denoted by **a**, propene by **b**, 1-butene by **c**; X = Cl denoted by **x**, Br by **y**) undergo photoactivated reactions with Cl_2 and Br_2 to give the (β-haloalkyl)platinum(IV) complexes $[Pt(CH_2CHRX)(2,9\text{-}Me_2\text{-}phen)X_3]$ (**2**). Bromination of the chloro species **1ax** leads to the formation of the Pt^{IV} species **2axy** containing the bromide, the bromoalkyl, and the phenanthroline ligands in the equatorial plane and two chloride ions in axial positions. The iodo complexes **1**(**a**–**c**)**z** are not oxidized by iodine even under UV irradiation but react readily with Cl_2 or Br_2 to give **2**(**a**–**c**)**x** and **2**(**a**–**c**)**y**. The structure of **2ay**, the first structurally characterized (β-haloalkyl)platinum complex, has been determined by X-ray diffraction methods. The stereochemistry of the (β-haloalkyl)platinum(IV) complexes is in accord with a simultaneous addition of two halogen atoms to the coordinated olefin and to the metal center.

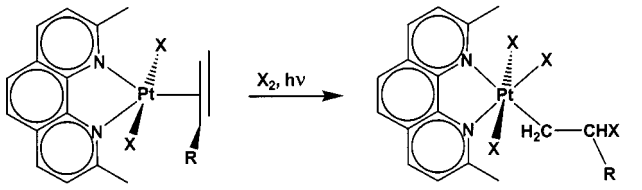
Introduction

Although free olefins are very easily halogenated, only few reports have dealt with the halogenation of olefins coordinated to a metal center.[1] In the particular case of (olefin)platinum(II) complexes, reaction with X_2 generally leads to oxidation of the metal center and release of the π-olefin ligand to form Pt^{IV} species. In some cases the reaction also involves the π-coordinated olefin, giving rise to the formation of an organic fragment which is retained by the metal center.[2] For instance the chelate *o*-styryldimethylarsane complex $\{PtBr_2[o\text{-}(AsMe_2)C_6H_4CH{=}CH_2]\}$ reacts with bromine to give a Pt^{IV} product containing a metal−carbon σ bond, $\{PtBr_3[o\text{-}(AsMe_2)C_6H_4CHBrCH_2]\}_2$.[3] Similarly, the Zeise salt $K[PtCl_3(C_2H_4)]$ reacts with chlorine gas in water to give $[Pt(CH_2CH_2Cl)Cl_5]^{2-}$ together with some $[Pt(CH_2CH_2OH)Cl_5]^{2-}$.[4] The latter products have been extensively investigated as model compounds for the functionalization of alkanes mediated by platinum salts.[5] To the best of the authors knowledge $[Pt(CH_2CH_2Cl)Cl_5]^{2-}$ is the only example of a (β-haloalkyl)platinum complex so far reported.

The reason for which β-haloalkyl complexes are extremely rare in transition metal chemistry is to be found in the propensity of these species to undergo β-elimination reactions.[6] An alternative route to the synthesis of haloalkyl compounds is the oxidative addition of terminal dihaloalkanes $[X(CH_2)_nX]$ to transition metal complexes to yield $\{ML_m[(CH_2)_nX]\}$ compounds, which can be used as building blocks for the synthesis of homo- and heterometallic polymethylene-bridged dendritic macromolecules.[7] Again the isolation of the ω-haloalkyl complexes $\{ML_m[(CH_2)_nX]\}$ is easily accomplished when $n = 1$ or $n > 2$, whereas for $n = 2$ the β-haloalkyl species is much more difficult to prepare. As an example the oxidative addition of 1,2-diiodoethane to the $[PtMe_2(phen)]$ complex results in the formation of $[PtMe_2(phen)X_2]$ and the evolution of ethylene gas together with dimethylene-bridged dimeric or polymeric species.[8] Having investigated the reactivity of olefins in 4-coordinate platinum(II) complexes[9] attention was directed to the reactivity of olefins in five-coordinate substrates and, in particular, their reaction with halogens. These species were considered to be appealing substrates[10] because of: i) their thermodynamic stability, ii) their coordination geometry (the saturated coordination sphere should prevent direct attack of the halide on the metal center), and iii) the increased electronic charge on the olefinic carbon atoms (due to the efficient π-back donation from filled platinum d orbitals) which could render the alkene prone to the attack by electrophiles. Here the halogenation of the five-coordinate trigonal bipyramidal Pt compounds $[PtX_2(olefin)(2,9\text{-}Me_2phen)]$ (**1**) (2,9-Me_2-phen = 2,9-dimethyl-1,10-phenanthroline; olefin = ethene denoted by **a**, propene by **b**, 1-butene by **c**; X = Cl denoted by **x**, Br by **y**) to give the (β-haloalkyl)platinum(IV) complexes $[Pt(CH_2CHRX)(2,9\text{-}Me_2\text{-}phen)X_3]$ (**2**) (Scheme 1) is reported, together with the X-ray structure of **2ay** [the first for a (β-haloalkyl)platinum complex].

[a] Dipartimento Farmaco-Chimico, Università di Bari,
via E. Orabona 4, I-70125, Bari, Italy
Fax: (internat.) + 39-080/544-2724
E-mail: fanizzi@farmchim.uniba.it
natile@farmchim.uniba.it
[b] Dipartimento di Chimica Generale ed Inorganica, Chimica Analitica, Chimica Fisica, Università di Parma, Centro di Studio per la Strutturistica Diffrattometrica del C.N.R.,
Viale delle Scienze, I-43100 Parma, Italy

 © WILEY-VCH Verlag GmbH, D-69451 Weinheim, 1999 1434−1948/99/0808−1351 $ 17.50+.50/0



X = Cl, R = H, 1ax; Me, 1bx; Et, 1cx
X = Br, R = H, 1ay; Me, 1by; Et, 1cy

X = Cl, R = H, 2ax; Me, 2bx; Et, 2cx
X = Br, R = H, 2ay; Me, 2by; Et, 2cy

Scheme 1

Results and Discussion

The Five-Coordinate Precursor

Five-coordinate trigonal bipiramydal Pt^{II} complexes [Pt(N−N)(olefin)XY] (X=halide, Y= halide or hydrocarbyl group; N−N = bidentate nitrogen ligand) represent a well-characterized class of platinum compounds.[10] The presence on the trigonal plane of a π-acceptor olefin ligand which draws electron charge from the metal center, so favouring the coordination of both ends of the bidentate nitrogen donor, plays a crucial role in stabilizing the five-coordinate geometry in these species.[11][12]

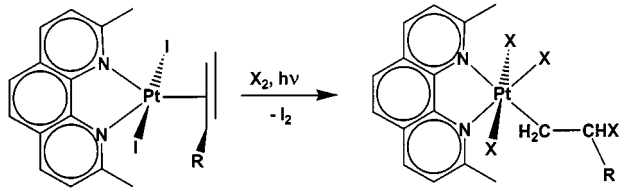
When N−N = 2,9-Me_2-1,10-phenanthroline the five-coordinate complexes are particularly stable if compared to analogous species with other bidentate nitrogen ligands.[10] Such a stabilization stems from the release, in the five-coordinate species, of the steric interaction between the *ortho*-methyl substituents of the phenanthroline and the *cis*-halogen ligands built up in square planar [$Pt^{II}X_2$(2,9-Me_2-phen)][13] and octahedral [$Pt^{IV}X_4$(2,9-Me_2-phen)][14] complexes.

Due to the steric strain the [PtX_2(2,9-Me_2-phen)] complexes easily dissociate one end of the phenanthroline chelate to form a T-shaped, coordinatively unsaturated, platinum species which is highly susceptible to addition reactions.[13][15] The addition product, [$Pt^{II}X_2$(2,9-Me_2-phen)(L)], can be either a square-planar species [L = CO, PPh_3, Me_2SO, Me_2S, PhNO, Py, $NH_2(CH_2)_2CH_3$], with the phenanthroline ligand monocoordinate to the platinum center (and exchanging in solution the donor nitrogen atoms at the coordination site) or, in the case of L = alkene[11] and alkyne,[16] a five-coordinate trigonal-bipyramidal (tbp) species with the halogen ions in the axial positions and the phenanthroline ligand acting as chelate and lying, together with the L ligand, in the trigonal plane.

Octahedral [PtX_4(2,9-Me_2-phen)] complexes also react with excess C_2H_4 to give reductive elimination of halogen (which, in turn, reacts with excess C_2H_4 to give 1,2-dihaloethane) and formation of the five-coordinate Pt^{II} species [$PtX_2(C_2H_4)$(2,9-Me_2-phen)].[14]

The Halogenation Reaction

In $CHCl_3$ solution and in the presence of light the five-coordinate complexes [PtX_2(olefin)(2,9-Me_2-phen)] (**1**) (olefin = ethene denoted by **a**, propene by **b**; 1-butene by **c**; X = Cl denoted by **x**, Br by **y**) react with Cl_2 and Br_2 to give the β-haloalkyl complexes [$Pt^{IV}(CH_2CHRX)$(2,9-Me_2-phen)X_3] (**2**) (see Scheme 1). The reaction requires photoactivation which is not required in the case of oxidative addition of X_2 to either the square-planar species [Pt(2,9-Me_2-phen)X_2][14] or to the free olefins. The iodo complexes **1(a−c)z** are not oxidized by iodine even under UV irradiation, while they react readily with Cl_2 or Br_2 to give **2(a−c)x** and **2(a−c)y**, respectively (see Scheme 2).

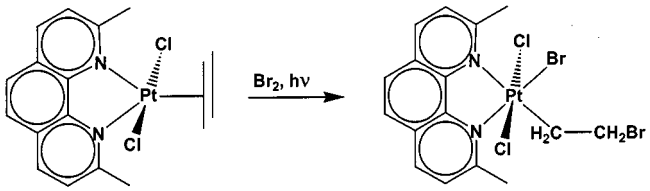


R = H, 1az; Me, 1bz; Et, 1cz

X = Cl, R = H, 2ax; Me, 2bx; Et, 2cx
X = Br, R = H, 2ay; Me, 2by; Et, 2cy

Scheme 2

The bromination of the chloro species **1ax** leads to the formation of a Pt^{IV} species **2axy** containing, besides the phenanthroline and the two chloride ligands, one bromide and a bromoalkyl ligand (see Scheme 3). Comparison of the ^{1}H-NMR spectra of the mixed halide complex with those of the chloro and bromo complexes **2ax** and **2ay** (Figure 1) led to the conclusion that the bromide, the bromoalkyl, and the phenanthroline ligands occupy equatorial positions while the two chloride ions occupy axial sites. The presence of a single sharp IR absorption (330 cm^{-1}) typical of two chloride ions mutually *trans* in an octahedral environment is in accord with this conclusion.[17]



1ax 2axy

Scheme 3

The use of $PhICl_2$, instead of chlorine gas, in the halogenation of **1ax**, did not eliminate the need for photoactivation, indicating that the reactive species is the Cl_2 released from the iodobenzene complex. Moreover, as observed for other photochlorination reactions,[18] the rate of halogenation of **1ax** by Cl_2 or $PhICl_2$ is strongly reduced if the reaction is carried out in benzene instead of chloroform. On the other hand the reaction of **1ax** with *N*-chlorosuccinimide (as substituted for the halogen) in the absence or presence of a radical initiator (benzoyl peroxide) did not give a significant amount of **2ax**.

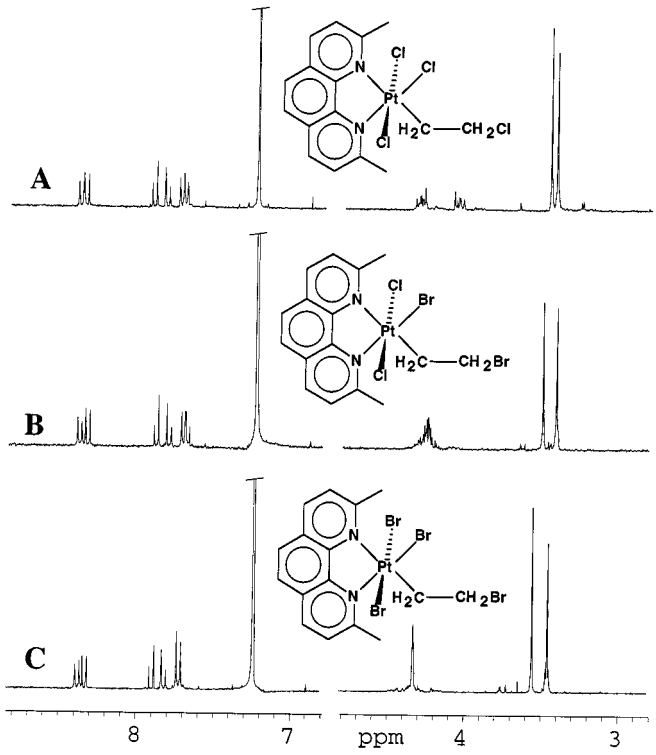
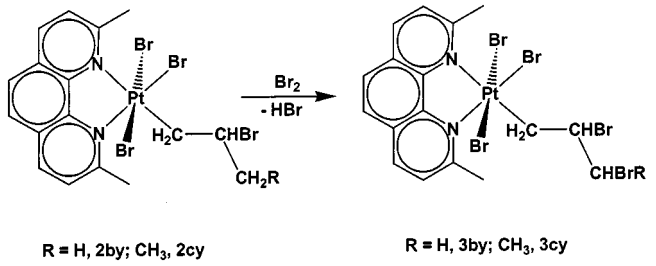


Figure 1. Comparison of the ^{1}H-NMR spectra for **2ax** (**A**), **2axy** (**B**), and **2ay** (**C**) complexes

The haloethyl complexes **2a**(**x**, **y**) are stable for days in chloroform solution and, if kept in the dark, can also withstand an excess of halogen. For prolonged reaction time with excess bromine the complexes **2**(**b**, **c**)**y** undergo substitution at the γ-carbon atom with formation of the β,γ-dihaloalkyl species [Pt($CH_2CHBrCH_2Br$)(2,9-Me_2-phen)Br_3] (**3by**) and [Pt($CH_2CHBrCHBrMe$)(2,9-Me_2-phen)Br_3] (**3cy**), respectively (see Scheme 4). This γ-halogenation reaction is much faster for **2cy** than for **2by** and does not take place, under similar conditions, for the chloro species **2**(**b**, **c**)**x**. Analogous effects of substituents (activation by alkyl radicals and deactivation by halogens, with Cl stronger deactivator than Br) are observed in the halogenation of alkanes.[19] It should be noted that in the case of **3cy** the presence of two chiral centres at the β- and γ-carbon atoms leads to the formation of two diastereoisomers. Interestingly ^{1}H-NMR experiments show a kinetic preference for one of the two diastereoisomers (ratio of major, **M** to minor, **m**, isomer of 80:20) (Figure 2).



Scheme 4

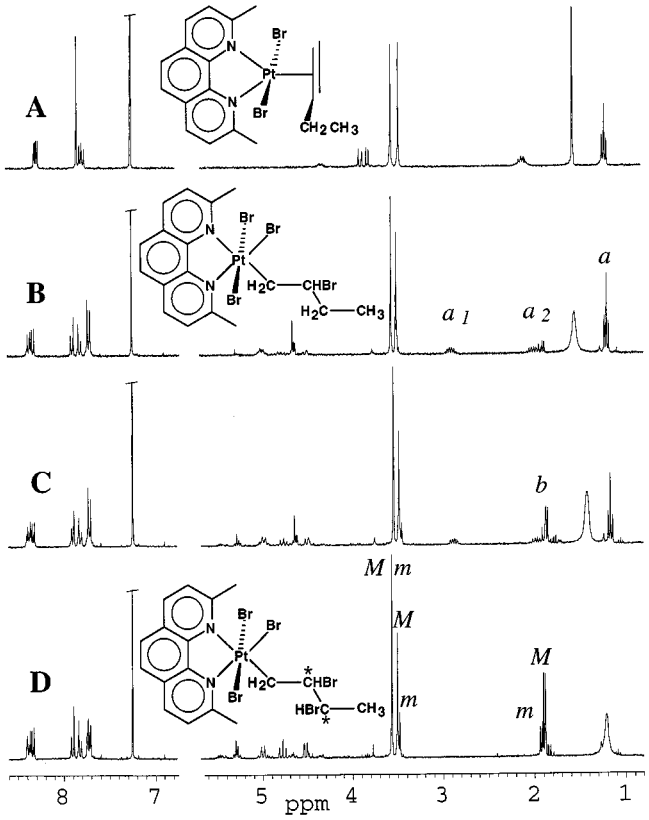


Figure 2. ^{1}H-NMR spectra recorded during the reaction of **1cy** (**A**) with Br_2; the initially formed **2cy** species (**B**), characterized by the terminal CH_3 (a) and the two diastereotopic CH_2 protons (a1 and a2) reacts further (spectra **C** and **D**) to give two new species in which the terminal CH_3 is a doublet (only one proton in γ position) and correspond to different isomers (major and minor) of **3cy**; spectra were taken: (**B**) 8 min after Br_2 addition under neon light irradiation, (**C**) and (**D**) after 20 and 60 min incubation in the dark, respectively

Stereochemistry of the β-Haloalkyl Complexes

^{1}H-NMR spectra of the new Pt^{IV} complexes are reported in Table 1. The protons of one half of the coordinated phenanthroline ligand do not show measurable coupling with ^{195}Pt as a consequence of the weakening of the Pt−N bond *trans* to the haloalkyl ligand.

In the case of the ethene (**a**) precursor the α- and β-CH_2 protons give rise to an AA′XX′ spin system of various complexity. Both the $C_α$-H_2 and $C_β$-H_2 protons show ^{195}Pt coupling, however only in the case of **2ax** could both α-H_2 and β-H_2 values be given, in all other cases only the values for $C_α$-H_2 were measured.

In the case of 1-propene and 1-butene complexes halogenation occurs specifically at the alkyl-substituted carbon atom in accord with the preference expected for an electrophilic attack. In the β-halopropyl complexes **2bx** and **2by** the $C_α$-H_2 protons exhibit two different ^3J(H−H) couplings (ca. 10 and 2 Hz, respectively) indicating that one is *anti* and the other *gauche* to $C_β$-H. (Figure 3). A connectivity (^{1}H NOESY experiments) between the β-Me group and only one of the $C_α$-H protons suggests that the Me group is *gauche* and the halide ion *anti* to the platinum center. The

Table 1. ^{1}H-NMR data (δ, downfield from $SiMe_4$; $CDCl_3$ solvent) for (β-haloalkyl)- and (β,γ-dihaloalkyl)(phenanthroline)platinum(IV) complexes

Compound	Phen[a] Me(2,9)	H(3,8)	H(4,7)	H(5,6)
2ax	3.42[6]	7.71d(8)[12]	8.36d(8)	7.83d(8)
	3.46	7.74d(8)	8.39d(8)[6]	7.92d(8)
2axy	3.43[6]	7.70d(8)[12]	8.35d(8)	7.82d(8)
	3.52	7.72d(8)	8.40d(8)[6]	7.90d(8)
2ay	3.44[6]	7.72d(8)[12]	8.33d(8)	7.82d(8)
	3.54	7.72d(8)	8.38d(8)[6]	7.90d(8)
2bx	3.44[6]	7.70d(8)[12]	8.35d(8)	7.82d(8)
	3.46	7.73d(8)	8.38d(8)[6]	7.91d(8)
2by	3.48[6]	7.71d(8)[12]	8.32d(8)	7.81d(8)
	3.54	7.71d(8)	8.37d(8)[6]	7.89d(8)
3by	3.45[6]	7.72d(8)[12]	8.35d(8)	7.83d(8)
	3.55	7.73d(8)	8.40d(8)[6]	7.91d(8)
2cx	3.45[6]	7.70d(8)[12]	8.35d(8)	7.82d(8)
	3.46	7.73d(8)	8.38d(8)[6]	7.90d(8)
2cy	3.48[6]	7.71d(8)[12]	8.32d(8)	7.81d(8)
	3.54	7.71d(8)	8.37d(8)[6]	7.90d(8)
3cyM	3.48[6]	7.72d(8)[12]	8.34d(8)	7.82d(8)
	3.54	7.73d(8)	8.39d(8)[6]	7.91d(8)
3cym	3.46[6]	7.74d(8)[12]	8.35d(8)	7.83d(8)
	3.54	7.74d(8)	8.40d(8)[6]	7.92d(8)

Compound	Haloalkyl[a] α-CH_2-	β-CH(R)X	R
2ax	4.06 m[79]{2}	4.30 m[18]{2}	–
2axy	4.25 m[79]{2}	4.28m{2}	
2ay	4.31 m[84]{2}	4.33m{2}	
2bx	4.10dd(10,10)[72]{1}	4.92dqd(10,7,2)[18]{1}	1.95d(7){3}
	4.35dd(10,2)[93]{1}	–	–
2by	4.56dd(11,10)[72]{1}	5.19dqd(11,7,2)[18]{1}	2.22d(7){3}
	4.64dd(10,2)[102]{1}	–	–
3by	4.55dd(11,11)[54]{1}	5.12dddd(11,8,3,2)[18]{1}	3.84dd(11,8){1}
	4.62dd(11,3)[105]{1}	–	4.91dd(11,2){1}
2cx	4.18dd(10,10)[69]{1}	4.69dddd(10,9,3,2)[18]{1}	1.13t(7){3}
	4.32dd(10,2)[96]{1}	–	1.88ddq(15,9,7){1}
	–	–	2.70ddq(15,3,7){1}
2cy	4.63 m[88]{2}	4.99m{1}	1.15t(7){3}
	–	–	1.95ddq(15,9,7){1}
	–	–	2.88ddq(15,3,7){1}
3cyM	4.50dd(11,2)[104]{1}	4.46ddd(11,2,1)[18]{1}	1.86d(6){3}
	4.76dd(11,11)[70]{1}	–	5.27qd(6,1){1}
3cym	4.43dd(11,11)[70]{1}	5.42ddd(11,2,2)[18]{1}	1.90d(6){3}
	4.51dd(11,2)[105]{1}	–	5.44qd(6,2){1}

[a] Values of J_{H-H} (in parentheses) and J_{Pt-H} [in brackets] are given when assignable. Integral values are given in braces.

Me substituent of the phenanthroline ligand *cis* to the β-haloalkyl group (easily distinguishable from that *trans* to the β-haloalkyl group because of its coupling with ^{195}Pt) has a cross peak [NOESY spectrum of **2b**(**x**, **y**)] with the C_α-H weakly coupled with the C_β-H (2 Hz) indicating that this C_α-H is *anti* to the β-Me group. The resulting preferred conformation of the β-haloalkyl group is that shown in the formula of Figure 3. The different couplings of the two C_α-H protons with the platinum center [$^2J(Pt-H) \approx 100$ and 70 Hz, respectively], and the relatively small value of the $^3J(Pt-C_\beta-H)$ coupling (18 Hz), are also in accord with this conformation of the β-haloalkyl group.

In the β-halo-*n*-buthyl complexes **2c**(**x**, **y**) the α-CH_2 signals are quite similar to those found for **2b**(**x**, **y**). Moreover two multiplets (ca. 0.9 ppm apart from each other) are observed for the diastereotopic γ-CH_2 protons, and a triplet for the terminal CH_3.

X-ray Structure of 2ay

The X-ray structure of [Pt(CH_2CH_2Br)(2,9-Me_2-phen)Br_3] (**2ay**) is shown in Figure 4 together with the atomic labeling scheme; relevant bond lengths and angles are reported in Table 2. The octahedral complex adopts a *mer* configuration with the two N(1) and N(2) atoms from the 2,9-Me_2-phen chelating ligand and the σ-bonded C(15) atom of the β-bromoethyl group lying in the same plane.

The three Pt−Br bonds have nearly equal length, whereas the Pt−N(2) bond [2.217(10) Å] is much longer than the Pt−N(1) bond [2.110(10) Å] reflecting the much greater *trans* influence of the haloalkyl group with respect to the bromide ion. The Pt and Br(4) atoms are, as expected, in *anti* positions [Pt−C(15)−C(16)−Br(4) torsion angle of −170.8(6)°]. Due to the lengthening of the Pt−N(2) bond the clash between the methyl substituent C(14) of the phen

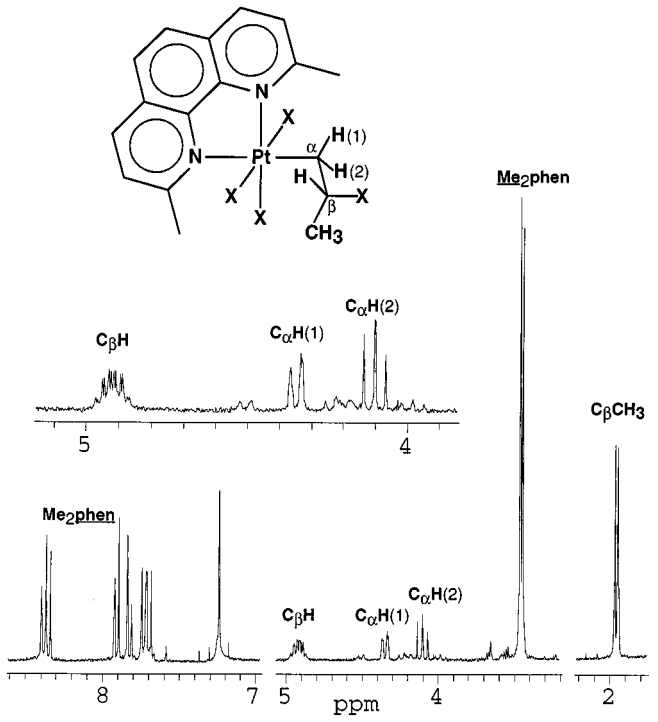


Figure 3. ^{1}H-NMR spectrum of **2bx** showing that J_{HH} and J_{PtH} for the α and β protons of the haloalkyl group are in accord with a preferred conformer having the Me and halide substituents on the β-carbon atom, respectively, *gauche* and *anti* to the Pt atom

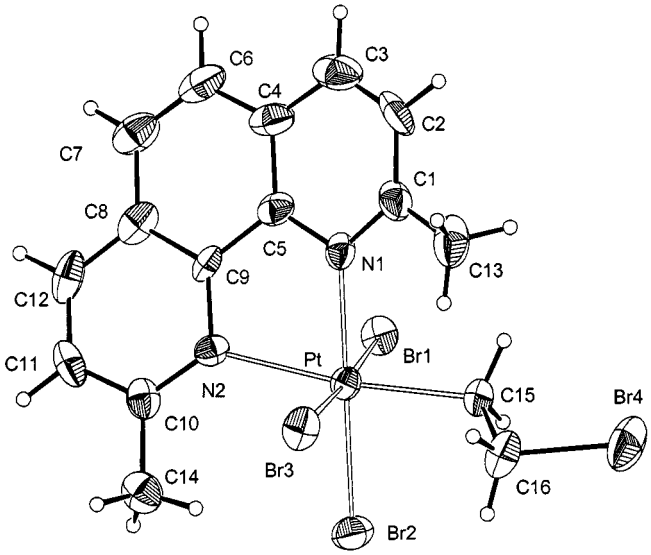


Figure 4. View of the complex molecule [Pt(CH_2CH_2Br)(2,9-Me_2-phen)Br_3] (**2ay**) with the atomic numbering scheme (30% probability ellipsoids)

ligand and the Br(2) atom is smaller than that between the second methyl group of phen C(13) and the α-carbon atom C(15) of the bromoethyl group [the Pt−N(2)−C(10)−C(14) and Pt−N(1)−C(1)−C(13) torsion angles are 18(2)° and −27(2)° respectively].

The steric interaction between the 2,9-methyl substituents of phen and other ligands in the coordination sphere causes

Table 2. Selected bond lengths [Å] and angles [°] for **2ay**

Pt−Br(1)	2.469(2)	C(1)−C(13)	1.49(2)
Pt−Br(2)	2.446(2)	C(4)−C(5)	1.39(2)
Pt−Br(3)	2.460(2)	C(4)−C(6)	1.41(2)
Pt−N(1)	2.110(10)	C(5)−C(9)	1.45(2)
Pt−N(2)	2.217(10)	C(6)−C(7)	1.38(3)
Pt−C(15)	2.121(12)	C(7)−C(8)	1.40(2)
N(1)−C(1)	1.36(2)	C(8)−C(9)	1.40(2)
N(1)−C(5)	1.40(2)	C(8)−C(12)	1.40(2)
N(2)−C(10)	1.34(2)	C(10)−C(11)	1.41(2)
N(2)−C(9)	1.36(1)	C(10)−C(14)	1.48(2)
C(1)−C(2)	1.35(2)	C(11)−C(12)	1.37(2)
C(2)−C(3)	1.35(3)	C(15)−C(16)	1.50(2)
C(3)−C(4)	1.42(3)	Br(4)−C(16)	1.96(2)
N(1)−Pt−C(15)	96.6(5)	N(2)−Pt−Br(1)	87.3(2)
N(1)−Pt−N(2)	77.6(4)	Br(2)−Pt−Br(1)	88.3(1)
C(15)−Pt−N(2)	171.7(4)	Br(3)−Pt−Br(1)	175.9(1)
N(1)−Pt−Br(2)	175.9(3)	C(1)−N(1)−C(5)	117.2(12)
C(15)−Pt−Br(2)	83.8(4)	C(1)−N(1)−Pt	131.2(9)
N(2)−Pt−Br(2)	101.6(2)	C(5)−N(1)−Pt	110.7(8)
N(1)−Pt−Br(3)	91.7(3)	C(10)−N(2)−C(9)	118.1(11)
C(15)−Pt−Br(3)	97.6(4)	C(10)−N(2)−Pt	132.7(9)
N(2)−Pt−Br(3)	88.6(2)	C(9)−N(2)−Pt	108.2(8)
Br(2)−Pt−Br(3)	92.3(1)	C(16)−C(15)−Pt	114.4(9)
N(1)−Pt−Br(1)	87.6(3)	C(15)−C(16)−Br(4)	107.7(10)
C(15)−Pt−Br(1)	86.5(4)		

the same type of distortion already observed for (2,9-dimethylphenanthroline)platinum(II)[13] and -platinum(IV)[14] complexes: a) tilting of the plane of the chelating moiety (N−C−C−N) with respect to the equatorial coordination plane [dihedral angle between N(1)−C(5)−C(9)−N(2) and Br(2)−Pt−C(15) planes of 32.9(5)°]; b) narrowing of the angle between the *cis* ligands coplanar with Me_2-phen [Br(2)−Pt−C(15) = 83.8(4)°]; c) bowlike distortion of the phen ligand [dihedral angle between the outer rings of the phen ligand of 15.0(5)°]. It is to be noted that the presence of the two axial ligands reduces the tilting of the phen ligand with respect to the equatorial coordination plane which is smaller than that found in [$PtBr_2$(2,9-Me_2-phen)][13] [angles between the N−C−C−N and Br−Pt−Br planes of 41.9(4)°]. A decrease in the tilting angle of the phenanthroline on going from square planar Pt^{II} to octahedral Pt^{IV} species has already been observed in the case of [PtI_2(2,9-Me_2-4,7-Ph_2phen)] and [PtI_4(2,9-Me_2-4,7-Ph_2-phen)] complexes.[14]

Insight Into the Halogenation Mechanism

The experimental results of the present investigation strongly suggest that the radical species $X^\bullet$ is responsible for the attack on the coordinated olefin. In accord with this hypothesis are: i) The scarce reactivity of our substrates with iodine (halogenation of olefins by a radical mechanism requires a much higher activation energy in the case of iodine with respect to chlorine and bromine).[20] ii) The use of $PhICl_2$ (instead of Cl_2) which could act as an ion source (Cl^+) does not eliminate the need for photoactivation. iii)

The reduced reactivity of chlorine in benzene due to the formation of chlorine atom−benzene π complexes.[18]

It is noteworthy that the bromination of **1ax** leads to the formation of the mixed-halide Pt^{IV} species **2axy**, which contains the phenanthroline, the bromide, and the bromoalkyl ligand in equatorial positions and the two chloride ions in axial positions. This stereochemistry gives an indication of a nearly simultaneous addition of the halogen atoms to the olefin and to the metal center, preventing a possible scrambling of ligands in the five-coordinate intermediate formed after the addition of one halogen atom to the π-olefin. Also the observation that *N*-chlorosuccinimide (as substitute of the halogen) under radical conditions (presence of benzoyl peroxide) does not react with the five-coordinate olefin complexes to yield the β-haloalkyl species, can be taken as evidence that the photoactivation of the halogen must take place while the halogen molecule is already close to the platinum center and to the olefin ligand.

In spite of the several investigations concerned with the oxidative addition of halogens to square-planar platinum complexes,[21] only in a few cases were (olefin)platinum complexes involved, and the reaction very rarely gave products which retained the organic fragment bound to the platinum center. Oxidative addition of halogen or alkyl halide to three-coordinate Pt^0 species [Pt(2,9-Me_2-phen)(olefin)] results in an electrophilic attack to the metal center and formation of the five-coordinate trigonal-bipyramidal Pt^{II} complexes [Pt(olefin)(2,9-Me_2-phen)XY] (X = halide Y = hydrocarbyl or halide).[22] Only in one case was evidence found of a further oxidation reaction involving the five-coordinate species, but no attempt was made to characterize the products.[22] Successful halogenation of the coordinate olefin has been reported, so far, for the bromination of [$PtBr_2${*o*-(Me_2As)C_6H_4CH=CH_2}][3] and the chlorination of Zeise′s salt in water.[4] In the former case the reaction with bromine led to a Pt^{IV} dimer, {$PtBr_3$[*o*-(Me_2As)C_6H_4CHBrCH_2]}$_2$, in which the olefin of the chelate dimethyl(*o*-styryl)arsane ligand was converted into a β-haloalkyl group σ-bonded to the metal center. A synchronous *cis* addition of a polarized bromine molecule with the negative end attacking the platinum center and the positive end attacking the double bond was suggested.

In the reaction of Zeise′s salt with chlorine, $[Pt(CH_2CH_2Cl)Cl_5]^{2+}$, together with some $[[Pt(CH_2CH_2OH)Cl_5]^{2+}$, was formed and the reaction mechanism was assumed to imply external attack of halogen to ethene subsequent to oxidation of platinum(II) to platinum(IV) as observed for olefin complexes of palladium.[23] The oxidation of Zeise′s salt in water with $[PtCl_6]^{2-}$ produces only $[Pt(CH_2CH_2OH)Cl_5]^{2+}$, and in the latter case the reverse sequence of reactions, that is nucleophilic attack of the solvent on the coordinated ethylene ligand followed by oxidation of the (β-hydroxyalkyl)platinum(II) species just formed was suggested.[24] A cross oxidation involving simultaneously the metal center and the olefin ligand can be envisaged in this case, where the coordinatively saturated trigonal-bipyramidal platinum(II) species does not allow an attack on the metal center as first step.

Conclusions

The five-coordinate complexes [PtX_2(olefin)(2,9-Me_2-phen)] react in the presence of light with Cl_2 and Br_2 to give the β-haloalkyl complexes [Pt^{IV}(CH_2CHRX)(2,9-Me_2-phen)X_3]. The reaction requires photoactivation which is not required in the oxidative addition of X_2 to either the square-planar species [Pt(2,9-Me_2-phen)X_2] or to the free olefins. Experimental data suggest that the radical species $X^{\cdot}$ is responsible for attack on the coordinated olefin ligand in the five-coordinate platinum(II) species, by a cross oxidation which involves also the metal center. Such a reaction is completely different from other reported halogenation reactions of square-planar Pt^{II} complexes for which the oxidation to Pt^{IV} precedes the attack on the coordinated olefin ligand. Further work is in progress to elucidate the mechanism of the halogenation reaction in coordinatively saturated five-coordinate (olefin)platinum(II) complexes.

Experimental Section

General: Commercial reagent-grade chemicals, ethylene, propene, 1-butene, chlorine (Matheson); bromine, iodine, *N*-chlorosuccinimide (NCS), and benzoyl peroxide (Aldrich) were used without further purification. $PhICl_2$ was prepared according to a literature method.[25] Starting complexes [PtX_2(2,9-Me_2-phen)] (**1**) (2,9-Me_2-phen = 2,9-dimethyl-1,10-phenanthroline; X = Cl, **x**; Br, **y**; I, **z**) were prepared as already described.[11] − ^{1}H NMR: Bruker AM 300 instrument. COSY and NOESY spectra were recorded by using the automated Bruker microprograms, a mixing time of 1 s was used in the NOESY experiments. − IR: KBr pellets with Perkin−Elmer 283 and FT 1600 spectrophotometers. − Microanalyses: Dipartimento Farmaco-chimico Microanalytical Service (Bari University) with a Carlo Erba 1106 Elemental Analyzer.

Synthesis of the Five-Coordinate Complexes: [PtX_2(olefin)(2,9-Me_2-phen)] (olefin = ethylene, **a**; propene, **b**; 1-butene, **c**; X = Cl, **x**; Br, **y**; I, **z**) were prepared from the corresponding square-planar species **1**(**x**−**z**) by direct uptake of the olefin.[11]

Synthesis of the (β-Haloalkyl)platinum(IV) Complexes: [Pt(CH_2CHRX)(2,9-Me_2-phen)X_3] (**2**); X= Cl (**x**) or Br (**y**); R= H (**a**), Me (**b**) or Et (**c**). The five-coordinate olefin complex [PtX_2(olefin)(2,9-Me_2-phen)] (0.2 mmol) was dissolved in chloroform (10 mL) and treated with excess halide (chlorine gas was bubbled for 5 min through the solution while bromine was added as pure liquid (0.4 mL). The solution was left under neon light (two OSRAM L36 W/10 Daylight tubes) for 5 min (**1cy**) or 10 min (all other complexes), then the (β-chloroalkyl)- (yellow) or (β-bromoalkyl)platinum(IV) complexes (orange) were precipitated by addition of *n*-pentane to the filtered solution. The solid was collected, washed with *n*-pentane and dried in air. The oxidation of the chloro complex **1ax** with bromine gave the mixed Pt^{IV} halide complex [Pt(CH_2CH_2Br)(2,9-Me_2-phen)Cl_2Br] (**2axy**). Yields of the isolated products were always above 80%. − $C_{16}H_{16}Cl_4N_2Pt$ (**2ax**; 573.2): calcd. C 33.5, H 2.8, N 4.9; found C 33.3, H 2.7, N 4.7. − $C_{16}H_{16}Br_2Cl_2N_2Pt$ (**2axy**; 662.1): calcd. C 29.0, H 2.4, N 4.2; found C 28.9, H 2.5, N 4.1. − $C_{16}H_{16}Br_4N_2Pt$ (**2ay**; 751.0): calcd. C 25.6, H 2.1, N 3.7; found C 25.7, H 2.0, N 3.5. − $C_{17}H_{18}Cl_4N_2Pt$ (**2bx**; 587.2): calcd. C 34.8, H 3.1, N 4.8; found C 34.6, H 3.2, N 4.7. − $C_{17}H_{18}Br_4N_2Pt$ (**2by**; 765.0): calcd. C 26.7, H 2.4, N 3.7; found C 26.6, H 2.3, N 3.5. − $C_{18}H_{20}Cl_4N_2Pt$ (**2cx**; 601.3): calcd. C 36.0, H 3.4, N 4.7; found C 35.8, H 3.2, N 4.5. − $C_{18}H_{20}Br_4N_2Pt$ (**2cy**; 779.1): calcd. C 27.8,

H 2.6, N 3.6; found C 27.6, H 2.5, N 3.4. − The reaction of the iodo complexes **1az** with excess I_2 (1:10 molar ratio) was performed in an NMR tube (ca. $5\cdot10^{-3}$ M in $CDCl_3$) and monitored by ^1H NMR. No oxidation of the starting complex was detected after several h even after prolonged UV irradiation. The analogous reactions of **1az** with excess Cl_2 (bubbled for 5 min trough the solution) or Br_2, monitored by ^1H NMR, showed, after exposure to a neon light for 10 min, the formation of **2ax** or **2ay,** respectively. − The oxidation of **1ax** with excess $PhICl_2$ was also performed in an NMR tube exposed to neon light (ca. $2\cdot10^{-3}$ M in $CDCl_3$; 1:5 complex/oxidant molar ratio) and monitored by ^1H NMR. When the solvent was $CDCl_3$, complete conversion of **1ax** into **2ax** was observed within 2 h of light exposure. In contrast, when the solvent was C_6D_6 only 5% conversion was observed after 2 h of light exposure. − Reactions of **1ax** with *N*-chlorosuccinimide (1:10, complex/oxidant molar ratio), in the absence and presence of a radical promoter (1:1, oxidant/benzoyl peroxide molar ratio) were also performed (complex concentration ca. $5\cdot10^{-3}$ M in $CDCl_3$) in an NMR tube exposed to neon light. In both cases no conversion of **1ax** into **2ax** was observed after 24 h (^1H NMR).

Synthesis of the (β,γ-Dibromoalkyl)platinum(IV) Complexes [Pt($CH_2CHBrCH_2Br$)(2,9-Me_2-phen)Br_3] (3by) and [Pt($CH_2CHBrCHBrMe$)(2,9-Me_2-phen)Br_3] (3cy): Besides the β-haloalkyl complexes described above the reaction of the five-coordinate complexes **1by** and **1cy** with excess Br_2 can also afford products of further halogenation. The reactants were placed in an NMR tube (complex concentration ca. $5\cdot10^{-3}$ M, Br_2 concentration ca. 10^{-1} M, in $CDCl_3$), exposed for 10 min to neon light irradiation, and than post-incubated in the dark (1 h in the case of **1by**; 12 h in the case of **1cy**). Quantitative formation of new species was detected by ^1H NMR. The new species could be isolated as orange solids by addition of pentane to the filtered solution and were identified, on the basis of their ^1H-NMR spectra and microanalytical data, as the β,γ-dihaloalkyl complexes [Pt($CH_2CHBrCH_2Br$)(2,9-Me_2-phen)Br_3] (**3by**) and [Pt($CH_2CHBrCHMeBr$)(2,9-Me_2-phen)Br_3] (**3cy**), respectively. The latter compound is found in two diastereoisomeric forms (major and minor, 80:20 molar ratio), due to the presence of two chiral centers. Yields of the isolated products **3by** and **3cy** were above 70%. − $C_{17}H_{17}Br_5N_2Pt$ (**3by**; 843.9): calcd. C 24.2, H 2.0, N 3.3; found C 24.0, H 1.9, N 3.1. − $C_{18}H_{19}Br_5N_2Pt$ (**3cy**; 858.0): calcd. C 25.2, H 2.2, N 3.3; found C 25.1, H 2.2, N 3.2.

X-ray Data Collection, Structure Determination, and Refinement of Complex 2ay: Crystals of **2ay** were obtained from CH_2Cl_2/Et_2O solution. The crystallographic data are summarized in Table 3. Accurate unit-cell parameters were determined by least-squares refinement of the setting angles of 30 randomly distributed and carefully centered reflections with θ in the range 24−44°. The data collection was performed at 293 K with a Siemens AED diffractometer by using the θ/2θ scan mode. One standard reflection was monitored every 100 measurements, no significant decay was noticed over the time of data collection. The structure was solved by direct methods (SIR92[26]) and refined by full-matrix least squares based on F_o^2 using the SHELXL-97 program,[27] first with isotropic then with anisotropic thermal parameters for all the non-hydrogen atoms. All the hydrogen atoms were placed at their geometrically calculated positions and refined "riding" on their parent carbon atoms. The weighting scheme used was $w = 1/[\sigma^2(F_o^2) + (0.1028P)^2 + 11.5518P]$ where $P = (F_o^2 + 2F_c^2)/3$. All calculations were carried out with the ENCORE 91 of the "Centro di Studio per la Strutturistica Diffrattometrica" del CNR, Parma. Crystallographic data (excluding structure factors) for the structure reported in this paper have been deposited with the Cambridge Crystallographic data Centre, registration number CCDC-111824. Copies of the data may be obtained free of charge on application to CCDC, 12 Union Road, Cambridge CB2 1EZ, UK [Fax: (internat.) + 44-1223/336-033; E-mail: deposit@ccdc.cam.ac.uk].

Table 3. Crystal data and structure refinement for **2ay**

Formula	$C_{16}H_{16}Br_4N_2Pt$
Molecular weight	751.04
Temperature [K]	273(2)
Wavelength	1.54184 Å
Crystal system, space group	monoclinic, $P2_1/n$
Cell constants	
a [Å]	11.084(5)
b [Å]	14.729(6)
c [Å]	12.236(5)
β [°]	109.23(2)
V [Å^3]	1886.1(14)
Z, calculated density	4, 2.645 Mg/m^3
Absorption coefficient	23.836 mm^{-1}
F(000)	1376
Crystal size	0.28 × 0.18 × 0.12 mm
θ range [°]	4.86−69.93
Index ranges	$-13 \le h \le 12$, $-17 \le k \le 7$, $-13 \le l \le 14$
Reflections collected/unique	3735/3574 [R(int) = 0.0672]
Completeness to 2Θ = 69.93°	95.6%
Max. and min. transmission	1.000 and 0.450
Refinement method	Full-matrix least squares on F^2
Data/restraints/parameters	3574:0:211
Goodness-of-fit on F^2	1.124
Final R indices [$I > 2\sigma(I)$]	$R1$ = 0.0630, $wR2$ = 0.1643
R indices (all data)	$R1$ = 0.0748, $wR2$ = 0.1807
Largest diff. peak and hole	2.073 and −1.771 e·Å^{-3}

Acknowledgments

This work was financially supported by the Ministero della Università e della Ricerca Scientifica e Tecnologica (Cofinanziamento MURST), the University of Bari and the University of Parma (contribution 60%).

[1] *Comprehensive Organometallic Chemistry I* (Eds.: E. W. Abel; F. G. A. Stone, G. Wilkinson), Academic Press, London, and New York, **1974**, vol 6, p. 708 and refs. therein.
[2] U. Belluco, *Organometallic and Coordination Chemistry of Platinum* (Eds.: P. M. Maitlis; F. G. A. Stone, R. West), Academic Press, London, and New York, **1974**, p. 443.
[3] M. A. Bennet, G. J. Erskine, R. S. Nyholm, *J. Chem Soc. A* **1967**, 1260.
[4] J. Halpern, R. A. Jewsbury, *J. Organomet. Chem.* **1979**, *181*, 223.
[5] A. Gerrit, J. A. Luinstra, J. E. Bercaw, *J. Am. Chem. Soc.* **1993**, *115*, 3004.
[6] H. B. Friedrich, J. R. Moss, *Adv. Organomet. Chem.* **1991**, *33*, 235.
[7] E. J. Starr, M. Naidoo, A. T. Hutton, J. R. Moss, *J. Organomet. Chem.* **1966**, *526*, 321 and refs. therein.
[8] P. K. Monaghan, R. J. Puddephatt, *J. Chem Soc., Dalton Trans.* **1988**, 595. P. K. Monaghan, R. J. Puddephatt, *Organometallics* **1986**, *5*, 218.
[9] F. P. Fanizzi, L. Maresca, G. Natile, C. Pacifico, *Gazz. Chim. Ital.* **1994**, *124*, 137. F. P. Fanizzi, L. Maresca, G. Natile, C. Pacifico, *J. Chem Soc., Dalton Trans.* **1994**, 949. L. Maresca, G. Natile, *Comments Inorg. Chem.* **1994**, *16*, 95. F. P. Fanizzi, F. P. Intini, L. Maresca, G. Natile, F. Gasparrini, *J. Chem Soc., Dalton Trans.* **1990**, 1019.
[10] V. G. Albano, G. Natile, A. Panunzi, *Coord. Chem. Rev.* **1994**, *133*, 67.
[11] F. P. Fanizzi, F. P. Intini, L. Maresca, G. Natile, M. Lanfranchi, A. Tiripicchio, *J. Chem Soc., Dalton Trans.* **1991**, 1007.

[12] F. P. Fanizzi, L. Maresca, G. Natile, M. Lanfranchi, A. Tiripicchio, G. Pacchioni, *J. Chem. Soc., Chem. Commun.* **1992**, 333.
[13] R. J. H. Clark, F. P. Fanizzi, G. Natile, C. Pacifico, G. C. van Rooyen, D. A. Tocher, *Inorg. Chim. Acta* **1995**, *235*, 205.
[14] F. P. Fanizzi, G. Natile, M. Lanfranchi, A. Tiripicchio, F. Laschi, P. Zanello, *Inorg. Chem.* **1996**, *35,* 3173.
[15] F. P. Fanizzi, M. Lanfranchi, G. Natile, A. Tiripicchio, *Inorg. Chem.* **1994**, *33*, 3331.
[16] F. P. Fanizzi, G. Natile, M. Lanfranchi, A. Tiripicchio, G. Pacchioni, *Inorg. Chim. Acta* **1998**, *275–276*, 500.
[17] K. Nakamoto, *Infrared and Raman Spectra of Inorganic and Coordination Compounds*, 4th ed., Wiley and Sons, New York, **1986**, p.147 and refs. therein.
[18] N. J. Bunce, K. U. Ingold, J. P. Landers, J. Lusztyk, J. C. Scaiano, *J. Am. Chem. Soc.* **1985**, *107*, 5464.
[19] J. March, *Advanced Organic Chemistry*, 4th ed., John Wiley & Sons, New York, **1992**, p. 689 and refs. therein.
[20] J. March, *Advanced Organic Chemistry*, 4th ed., John Wiley & Sons, New York, **1992**, p.812. and refs. therein.
[21] L. M. Rendina, R. J. Puddephatt, *Chem. Rev.* **1997**, *97*, 1735.
[22] V. De Felice, M. Funicello, A. Panunzi, F. Ruffo, *J. Organomet. Chem.* **1991**, *403*, 243.
[23] J. K. Stille, D. E. James, *J. Am. Chem. Soc.* **1975**, *97*, 674. J. K. Stille, R. J. Divakaruni, *J. Organomet. Chem. Soc.* **1979**, *169*, 239. P. M. Henry, *Adv. Organomet. Chem.* **1975**, *13*, 363.
[24] G. A. Luinstra, L. Wang, S. S. Stahl, J. A. Labinger, J. E. Bercaw, *J. Organomet. Chem.* **1995**, *504,* 75.
[25] H. J. Lucas, E. R. Kennedy, *Organic Synthesis Collection*, John Wiley & Sons, New York, **1988**, vol. 3, p. 482.
[26] A. Altomare, G. Cascarano, C. Giacovazzo, A. Guagliardi, M. C. Burla, G. Polidori, M. Camalli, *J. Appl. Crystallogr.* **1994**, *27*, 435.
[27] G. M. Sheldrick, *SHELXL-97 – Program for Crystal Structure Determination*, University of Göttingen, Göttingen, Germany, **1997**.

Received February 12, 1999
[I99048]

Synthesis, Chemistry, and Characterization of Perfluoroaromatic Selenium Derivatives

Thomas M. Klapötke,*[a] Burkhard Krumm,[a] and Kurt Polborn[a][+]

Dedicated to Professor W.-P. Fehlhammer on the occasion of his 60th birthday

Keywords: Selenium / Fluorine / Multinuclear NMR / Raman spectroscopy / X-ray crystallography

The reaction of perfluoroaryllithium RC_6F_4Li, where R = F or 4-$CF_3C_6F_4O$, respectively, with selenium gives the known diselanes $(RC_6F_4Se)_2$ (**1a**, **1b)**. Redox reactions of **1** with hydrogen peroxide result in the formation of the seleninic acids RC_6F_4SeOOH which crystallize as hydrates (**2a**, **2b**); with mercury give the bis(arylseleno)mercuries $(RC_6F_4Se)_2Hg$ (**3a**, **3b**); with sulfuryl chloride or bromine give the selenenyl chlorides (**4a**, **4b**) or selenenyl bromides (**5a**, **5b**). Selenenyl chlorides (**4a**, **4b**) react with a variety of trimethylsilyl reagents Me_3SiX (X = Br, CN, NMe_2, NEt_2) to form **5a**, **5b**; selenocyanates RC_6F_4SeCN (**6a**, **6b**); selenenyl amides $RC_6F_4SeNMe_2$ (**7a**, **7b**) and $RC_6F_4SeNEt_2$ (**8a**, **8b**). A new synthetic route to diorgano selanes is developed by reaction of **4a**, **4b** with perfluoroaryllithium to give the symmetric $(RC_6F_4)_2Se$ (**9a**, **9b**). All derivatives are thoroughly characterized and in addition the molecular structures of **2a**, **6a**, and **9a** are established by X-ray crystallography.

Introduction

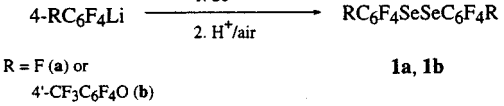
Selenium compounds with perfluorinated substituents have been known for three decades.[1][2] A considerable part consists of selenium species bound to perfluoroalkyl groups, which is reviewed by Haas.[3] However, the chemistry of perfluoroaromatic selenium species is rather limited to a few compounds. The diselanes $C_6F_5SeSeC_6F_5$ and (4-$CF_3C_6F_4)_2Se_2$, as well as the selane $C_6F_5SeC_6F_5$, have been reported to be synthesized by either rather low yield methods and/or requiring high temperatures,[4] or by reaction of the appropriate Grignard R_FMgBr (R_F = C_6F_5 or 4-$CF_3C_6F_4$) where in addition considerable amounts of the unwanted selane $(R_F)_2Se$ are formed.[5] Very recently, a high-yield synthesis of a new diselane [4-(4′-$CF_3C_6F_4O)C_6F_4]_2Se_2$ was reported by reaction of in situ generated 4-(4′-$CF_3C_6F_4O)C_6F_4Li$ with selenium.[6] This method is extended in this report to the synthesis of the known $C_6F_5SeSeC_6F_5$. Our findings show, that in the reaction of C_6F_5MgBr, which is easily formed by reacting C_6F_5Br and magnesium, with selenium no formation of the diselane is observed. This fact is likely to be attributed to the significantly increased reactivity of C_6F_5Li than C_6F_5MgBr towards selenium.

Pentafluorobenzeneselenenyl chloride, C_6F_5SeCl, is reported to be synthesized by chlorination of C_6F_5SeH as well as pentafluorobenzeneseleninic acid, C_6F_5SeOOH, by hydrolysis of $C_6F_5SeCl_3$.[5] The preparation of the bis(arylseleno)mercury $(C_6F_5Se)_2Hg$ is reported to proceed at elevated temperatures.[2] For those materials simplified routes were found and employed.

For some of the mentioned derivatives NMR data have been published.[7–10] The to date only crystal structure of a pentafluorophenylselenium derivative is established for the diselane $C_6F_5SeSeC_6F_5$.[11]

Results and Discussion

Suitable stable starting materials for the chemistry done in this work are the diselanes $C_6F_5SeSeC_6F_5$ (**1a**) and [4-(4′-$CF_3C_6F_4O)C_6F_4]_2Se_2$ (**1b**). As already indicated, they are accessible via the respective aryllithium reagents, generated in situ by lithiation of C_6F_5H, respectively 4-(4′-$CF_3C_6F_4O)C_6F_4H$,[12] with *n*-butyllithium (Scheme 1).



Scheme 1

The diselanes **1a**, **1b** undergo oxidation reactions with hydrogen peroxide, sulfuryl chloride, and bromine to give the seleninic acids **2a**, **2b**, the selenenyl chlorides **4a**, **4b**, and bromides **5a**, **5b**. Reduction with elemental mercury results in the formation of the bis(arylseleno)mercuries **3a**, **3b**. All reactions occur readily at ambient temperature. Sulfuryl chloride and bromine have to be employed in large excess, otherwise the back reaction occurs (Scheme 2).

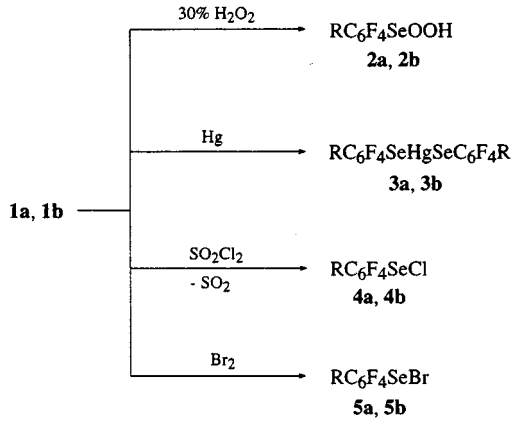
The selenenyl chlorides **4a**, **4b** are useful precursors for further chemistry at the selenium center.

The trimethylsilyl nucleophiles Me_3SiX (X = Br, CN, NMe_2, NEt_2) react readily at 25°C under loss of trimethyl-

[+] X-ray structure analysis.

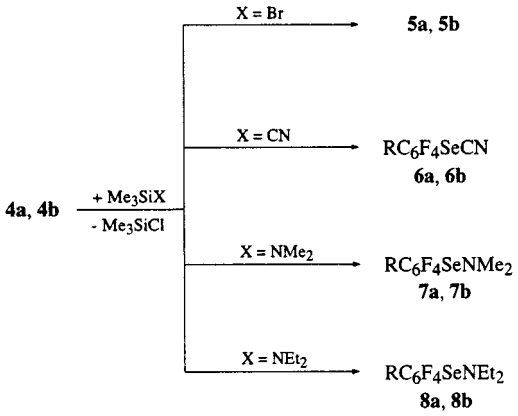
[a] Institut für Anorganische Chemie der Universität München
Meiserstr. 1, D-80333 München, Germany
Fax: (internat.) +49 (0)89/ 5902382
E-mail: tmk@anorg.chemie.uni-muenchen.de

 © WILEY-VCH Verlag GmbH, D-69451 Weinheim, 1999 1434–1948/99/0808–1359 $ 17.50+.50/0



Scheme 2

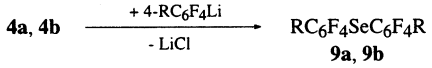
silylchloride to give **5a**, **5b**, the selenocyanates **6a**, **6b**, and the selenenylamides **7a**, **7b** and **8a**, **8b** (Scheme 3).



Scheme 3

Compounds **5**, **7**, and **8** are extremely moisture and light sensitive materials and tend to decompose at 25°C under re-formation of **1**, which can be suppressed by storage in the dark at 0°C. The reaction of **4** with Me_3SiBr displays an alternative route to synthesize **5**.

The reaction of **4a**, **4b** with 4-RC_6F_4Li is a new straightforward synthesis of diorganoselanes, here shown for the symmetric $(C_6F_5)_2Se$ (**9a**) and the new [4-(4′-$CF_3C_6F_4O)C_6F_4]_2Se$ (**9b**) (Scheme 4).



Scheme 4

Spectra

Table 1 illustrates the influence of the substituent attached to selenium for RC_6F_4Se derivatives on the ^{77}Se- and ^{19}F-NMR shift. For ^{19}F NMR are listed the resonances of the *ortho*-fluorine atoms (in 2- and 5-position to Se). In general, the resonances of the aromatic fluorine atoms appear in the ^{19}F-NMR spectrum as parts of AA′BB′, respectively AA′BB′X for C_6F_5Se, patterns. While the *ortho*- and *meta*-fluorine resonances were referred to multiplets, the resonances of the *para*-fluorine atoms in C_6F_5Se derivatives **1a**−**9a** can be solved first order (triplets of triplets, see Experimental Section). Changing from R = F to 4-$CF_3C_6F_4O$ results in a small but significant low field shift of 0.1−0.5 ppm for the *ortho*-fluorine resonances in the ^{19}F-NMR spectrum. This effect is much more pronounced for the ^{77}Se resonances (0−11 ppm). The ^{77}Se resonances are split into triplets due to coupling to the *ortho*-fluorine atoms (pentets for **9a/b**); the value for the $^3J_{SeF}$ coupling constant is in the range 13−28 Hz. A high field shift of the ^{77}Se resonance occurs for the here investigated derivatives in the following order: −SeCl (**4a/b**), $-SeNMe_2$ (**7a/b**), $-SeNEt_2$ (**8a/b**), −SeBr (**5a/b**), −SeSe− (**1a/b**), −SeCN (**6a/b**), −Se− (**9a/b**). A similar tendency is observed and discussed in detail for CF_3Se derivatives.[13] The derivatives −SeOOH (**2a/b**) and −SeHgSe− (**3a/b**) represent the most extreme ^{77}Se-NMR shifts in this work, but are measured in different solvents than the above.

Table 1. ^{77}Se and *ortho*-F ^{19}F-NMR data [ppm] of RC_6F_4Se derivatives, $^3J_{SeF}$ in parentheses [Hz][a]

R	$\delta^{77}Se$ F	$\delta^{77}Se$ 4-$CF_3C_6F_4O$	$\delta^{19}F$ F	$\delta^{19}F$ 4-$CF_3C_6F_4O$
$(RC_6F_4Se)_2$ (**1**)	373 (20.8)	377 (19.7)	−125.6	−125.4
RC_6F_4SeCl (**4**)	801 (20.5)	801 (20.8)	−122.5	−122.3
RC_6F_4SeBr (**5**)	619 (21.6)	617 (21.6)	−122.3	−122.1
RC_6F_4SeCN (**6**)	184 (14.9)	189 (14.6)	−124.4	−124.2
$RC_6F_4SeNMe_2$ (**7**)	768 (26.3)	774 (27.6)	−122.9	−122.8
$RC_6F_4SeNEt_2$ (**8**)	633 (br)	640 (br)	−123.1	−123.0
$(RC_6F_4)_2Se$ (**9**)	122 (14.0)	133 (13.4)	−126.6	−126.4
RC_6F_4SeOOH[b] (**2**)	1215 (br)	1220 (br)	−142.4	−142.1
$(RC_6F_4Se)_2Hg$[c] (**3**)	55 (22.7)	64 (br)	−126.2	−125.7

[a] $CDCl_3$. − [b] CD_3CN. − [c] C_6D_6.

Table 2 summarizes the ^{13}C-NMR data of C_6F_5Se derivatives **1a-9a** (from recording of ^{13}C-NMR data of the $CF_3C_6F_4OC_6F_4Se$ derivatives **1b**−**9b** was refrained due to the increased complexity of the resonances, requiring significantly higher number of accumulations). All resonances are split into multiplets due to couplings to the entire fluorine atoms present in the ring. Remarkable are the shift differences of the resonances of the C-1 carbon atoms, depending on the nature of the substituent bonded to selenium (range of δ = 95−123). The resonances of C-2/3/4 appear mainly at the same position (C-2 δ = ca. 137, C-3 δ = ca. 147 and C-4 δ = ca. 143). The values of the $^nJ_{CF}$ coupling constants are in the range of ca. 2−260 Hz (n = 1−4) (omitted in the Experimental Section). Further NMR characterization include $^{14}N/^{15}N$ NMR data of **6a**, **7a** and **8a**, as well as ^{199}Hg-NMR shifts for **3a/3b** (see Experimental Section).

Additionally to IR spectra the Raman spectra were recorded. In the Raman spectra are some important selenium containing vibrations visible which are difficult to observe in IR. Figure 1 depicts the Raman spectrum of the selenocyanate **6a** as a representative example. The CN stretching frequency is very intense at 2167 cm^{-1} (of medium to weak

Table 2. ^{13}C NMR data [ppm] of C_6F_5Se derivatives[a]

	C-1	C-2	C-3	C-4
$(C_6F_5Se)_2$ (**1a**)	102.9	137.3	147.3	143.1
C_6F_5SeCl (**4a**)	104.3	137.5	147.0	144.6
C_6F_5SeBr (**5a**)	101.8	137.4	147.5	144.3
C_6F_5SeCN[d] (**6a**)	94.9	137.9	146.8	143.9
$C_6F_5SeNMe_2$[e] (**7a**)	99.6	137.2	147.1	142.8
$C_6F_5SeNEt_2$[f] (**8a**)	101.1	137.1	147.4	142.5
$(C_6F_5)_2Se$ (**9a**)	100.5	137.6	147.0	142.7
C_6F_5SeOOH[b] (**2a**)	122.6	138.6	146.5	144.7
$(C_6F_5Se)_2Hg$[c] (**3a**)	100.1	137.8	146.6	140.1

[a] $CDCl_3$. – [b] CD_3CN. – [c] C_6D_6. – [d] $\delta = 97.2$ (SeCN, s, $^1J_{C-Se} = 241.3$ Hz). – [e] $\delta = 52.2$ (SeNC, s, $^2J_{C-Se} = 9.3$ Hz). – [f] $\delta = 54.7$ (SeNC, s, $^2J_{C-Se} = 8.5$ Hz), 14.9 (CH_3, s).

intensity in IR). The frequencies of νSeSe 282 (**1a**)/284 (**1b**) cm^{-1}, νSeCl 398 (**4a**)/375 (**4b**) cm^{-1}, νSeBr 289 (**5a**)/292 (**5b**) cm^{-1}, and νSeN 552 (**7a**) are assigned and appear as the strongest absorptions in Raman and very weak or not observable in IR. The SeN vibration for **8a** is tentatively assigned at 515 cm^{-1}. Definite assignment of the νSeC vibration is not possible.

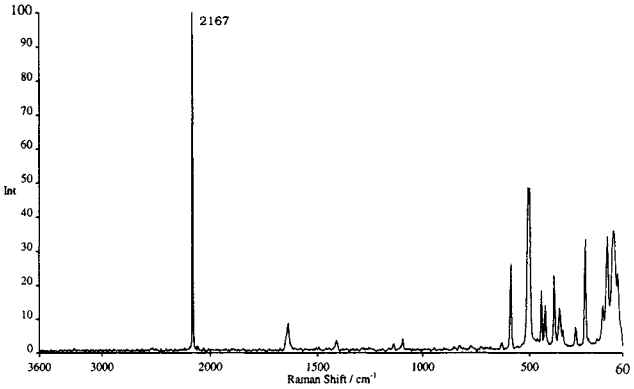


Figure 1. Raman spectrum of **6a**

Crystal Structures

As already indicated, the only crystal structure available of a selenium species having attached a C_6F_5 group, is established for the diselane $C_6F_5SeSeC_6F_5$.[11] The seleninic acid **2a** is recrystallized from water and forms crystals of a monohydrate. A view of the unit cell is shown in Figure 2. Strong hydrogen bonding is present on H(1)···O(3) = 1.76 Å and weak on O(2)···H(3Z) = 2.09 Å. The SeC distance Se(1)−C(1) = 1.962 Å is slightly lengthened compared to regular SeC bonds (see below), probably due to the strong electron-withdrawing effect of the SeOOH moiety. Interestingly, the molecular structure of the nonfluorinated analogue, C_6H_5SeOOH, is anhydrous, though crystallized from water.[14] Here, as well as in *p*-ClC_6H_4SeOOH,[15] strong intermolecular hydrogen bonds between two discrete SeOOH moieties are present.

The structure of the selenocyanate **6a**, shown in Figure 3, consists of two independent molecules. The phenyl rings

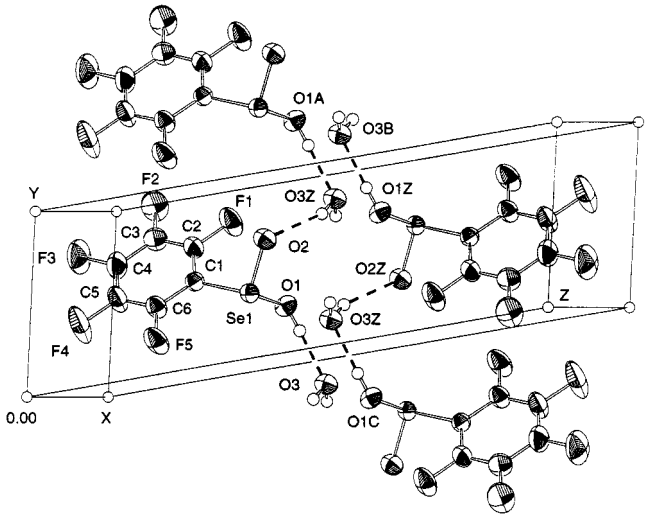


Figure 2. ORTEP plot of **2a** (unit cell); selected bond lengths [Å], angles [°]: Se(1)−O(1) 1.741(3), Se(1)−O(2) 1.638(3), Se(1)−C(1) 1.962(4), O(1)−H(1) 0.82, H(1)···O(3) 1.76, O(2)···H(3Z) 2.09; O(2)−Se(1)−O(1) 102.0(2), O(1)−Se(1)−C(1) 94.2(2), C(6)−C(1)−Se(1) 119.5(3), C(2)−C(1)−Se(1) 122.8(3), C(6)−C(1)−C(2) 117.6(4), F(1)−C(2)−C(1) 120.5(4), F(5)−C(6)−C(1) 119.7(4)

of both molecules are tilt by 35.0° to each other. The out of plane angle between the SeCN moiety and the phenyl ring is 71.5°, respectively 69.9°. There are two short intermolecular contacts involving the Se and N atom in each chain of identical molecules of N(1)···Se(1B) = 2.964 Å and N(1A)···Se(1C′) = 2.957 Å. Between the two independent molecules exist no direct Se···N contacts. The Se(1)−C(7) distance of 1.850 Å, respectively Se(1A)−C(7A) of 1.850 Å, is significantly shorter than a regular SeC bond, than expected, due to the greater contribution of *s* character by the cyano C atom, creating partial double-bond character. The Se(1)−C(1) bond length of 1.920 Å, respectively, Se(1A)−C(1A) of 1.906 Å, represents a typical SeC single bond. The CN bond length for N(1)−C(7) = 1.120 Å, respectively N(1A)−C(7A) = 1.111 Å, is consistent with cyano triple bonds. The only other existing crystal structures of aromatic selenocyanates are of 1,4-diselenocyanatobenzene, *p*-$C_6H_4(SeCN)_2$,[16] and of 3-selenocyanatopyridine, *m*-$C_5H_4N(SeCN)$.[17] Both structures show similar features and intermolecular SeN contacts of 3.06/3.32 Å[16] and 2.84/3.39 Å.[17]

The crystal structure of the selane **9a** is shown in Figure 4. Compound **9a** crystallizes in the noncentrosymmetric space group $P2_1$, allowing the determination of the absolute configuration of the structure. Flack′s parameter refined to −0.006(9) which suggests the correctness of the absolute configuration. The SeC distances Se(1)−C(1) = 1.920 Å, Se(1)−C(7) = 1.903 Å are similar to those found for $C_6F_5SeSeC_6F_5$ 1.899/1.921 Å.[11] The dihedral angle C(2)−C(1)−Se(1)−C(7) is 60.9°; the angle between the planes of both rings is 82.8°. The CSeC angle of 96.61(14)°, is as expected smaller than found for $(C_6F_5)_2S$ [CSC 100.6(5)°][18] and 4-$CF_3C_6F_4OC_6F_5$ [COC 116.2(2)°][12] but larger than found for $(C_6F_5)_2Te$ [CTeC 93.3(5)°].[19]

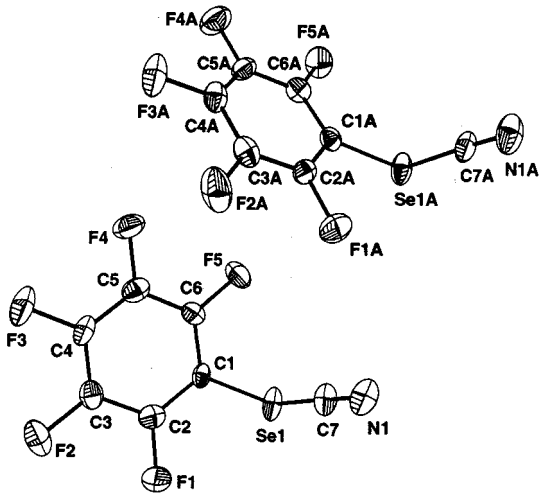


Figure 3. ORTEP plot of **6a**; selected bond lengths [Å], angles [°]: Se(1)−C(7) 1.850(10), Se(1)−C(1) 1.920(7), N(1)−C(7) 1.120(11), Se(1A)−C(7A) 1.856(11), Se(1A)−C(1A) 1.906(8), N(1A)−C(7A) 1.111(12); C(7)−Se(1)−C(1) 95.3(4), N(1)−C(7)−Se(1) 177.4(9), C(7A)−Se(1A)−C(1A) 94.7(4), N(1A)−C(7A)−Se(1A) 175.4(9)

Conclusion

Perfluoroaromatic diselanes, obtained in high yields from perfluoroaromatic lithium reagents, were used to prepare selenenyl chlorides and related derivatives. Further exploration of their synthetic potential is underway.

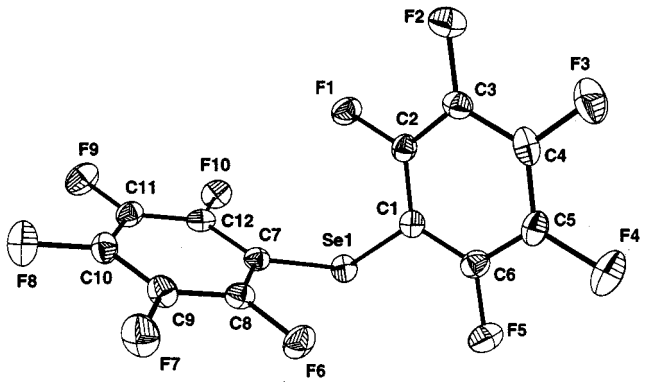


Figure 4. ORTEP plot of **9a**; selected bond lengths [Å], angles [°]: Se(1)−C(1) 1.920(4), Se(1)−C(7) 1.903(4); C(7)−Se(1)−C(1) 96.61(14), C(6)−C(1)−C(2) 117.4(4), C(6)−C(1)−Se(1) 121.0(3), C(2)−C(1)−Se(1) 121.6(3), C(2)−C(1)−Se(1)−C(7) 60.91

Experimental Section

General: The solvents were dried with common methods. Commercially available chemicals were used as received. − NMR: JEOL GSX270 and EX400; chemical shifts are reported with respect to $(CH_3)_4Si$ (^1H, ^{13}C), CH_3NO_2 (^{14}N, ^{15}N), $CFCl_3$ (^{19}F), $(CH_3)_2Se$ (^{77}Se) and $(CH_3)_2Hg$ (^{199}Hg). − IR: Nicolet 520 FT-IR (as KBr pellets or neat liquids). − Raman: Perkin−Elmer Spectrum 2000R NIR FT (Nd: YAG laser, 1064 nm). − MS: Finnigan MAT 90. Multi-isotope containing fragments refer to the isotope with the highest abundance (for example ^{80}Se). − Elemental analyses: C,H,N: in-house; F: Mikroanalytisches Labor Beller, Göttingen. − All reactions are carried out under dry nitrogen atmosphere.

Table 3. Crystal data and structure refinements for **2a**, **6a**, and **9a**

Compound	**2a**	**6a**	**9a**
Empirical Formula	$C_6H_3F_5O_3Se$	C_7F_5NSe	$C_{12}F_{10}Se$
Formula mass	297.04	272.04	413.08
Temperature [K]	293(2)	293(2)	293(2)
Crystal size [mm]	0.40 × 0.30 × 0.27	0.43 × 0.33 × 0.07	0.53 × 0.27 × 0.13
Crystal system	triclinic	monoclinic	monoclinic
Space group	$P\bar{1}$	$P2_1/c$	$P2_1$
a [Å]	4.6849(6)	9.946(3)	9.2495(9)
b [Å]	5.3270(8)	5.9196(12)	7.4686(8)
c [Å]	17.427(4)	29.154(9)	9.3933(9)
a [°]	81.42(2)		
β [°]	88.49(2)	98.87(3)	106.508(8)
γ [°]	84.608(12)		
Volume [Å^3]	428.10(13)	1696.0(8)	622.15(11)
Z	2	8	2
ρ (calcd.) [mg/m^3]	2.304	2.131	2.205
μ_{Mo} [mm^{-1}]	4.455	4.466	3.138
F(000)	284	1024	392
θ range [°]	3.55−23.97	2.68−23.97	2.73−23.97
Index ranges	$-5 \le h \le 5$	$0 \le h \le 11$	$-10 \le h \le 10$
	$-6 \le k \le 0$	$0 \le k \le 6$	$-8 \le k \le 8$
	$-19 \le l \le 19$	$-33 \le l \le 32$	$0 \le l \le 10$
Reflections collected	1509	2827	2082
Independent reflections	1343 (R_{int} = 0.0107)	2656 (R_{int} = 0.0374)	1953 (R_{int} = 0.0114)
Observed reflections	1228	1720	1758
Max. and min. transmission	0.9994 and 0.8719	0.9985 and 0.3956	0.9990 and 0.7133
Data/restraints/parameters	1343/0/137	2656/0/253	1953/1/208
Goodness-of-fit on F^2	1.187	1.166	1.039
$R1$, $wR2$ [$I>2\sigma(I)$]	0.0302, 0.0753	0.0582, 0.1106	0.0235, 0.0534
$R1$, $wR2$ (all data)	0.0352, 0.0789	0.0927, 0.1239	0.0300, 0.0577
Larg. Diff. peak/hole [e/Å^3]	0.557/−0.483	0.550/−0.408	0.209/−0.301
Flack parameter			−0.006(9)

X-ray Crystallography: An Enraf Nonius CAD 4 diffractometer was employed for data collection using Mo-K_α radiation. The structures were solved by direct methods (SHELXS86) and were refined by means of the full-matrix least squares procedures using SHELXL93 (Table 3). All nonhydrogen atoms were refined anisotropically. For the hydrogen atoms in **2a** a riding model was employed. Further details of the crystal-structure investigations may be obtained from the Fachinformationszentrum Karlsruhe, D-76344 Eggenstein-Leopoldshafen, Germany, on quoting the depository numbers CSD-410719, -410718 and -410720 for **2a**, **6a**, and **9a**, respectively.

CAUTION! *Experiments involving perfluoroaromatic lithium reagents should be handled with care, conducted at low temperatures and under strict exclusion of moisture!*

Bis(pentafluorophenyl)diselane (1a): Into a solution of 30 mmol of pentafluorobenzene in 150 mL of anhydrous ether, 30 mmol of *n*BuLi (2.5 M in hexane) is added dropwise at −70°C during a period of 30 min. After 1 h stirring at −70°C, 35.5 mmol of selenium is added in one portion. The resulting mixture is allowed to warm up to ambient temperature within 4 h. 20 mL of 10% HCl and 20 mL of H_2O are added for hydrolysis. After filtration from excess selenium and several extractions with ether/water the combined etheral extracts are dried with anhydrous $MgSO_4$. The etheral solution is stirred for 24 h in the presence of air. After removal of the solvent the residue is sublimed at 40°C/0.01 Torr and yielded orange needles of **1** (81%), m.p. 52−54°C (ref.[5] 49−50°C). − ^{19}F NMR ($CDCl_3$): δ = −125.6 (2-F, m, 2 F), −149.0 (4-F, tt, 1 F, $^3J_{F-F}$ = 20.8 Hz, $^4J_{F-F}$ = 3.5 Hz), −159.7 (3-F, m, 2 F). − IR (KBr): $\tilde{\nu}$ = 1641 m, 1633 m, 1587 w, 1513 s, 1489 s, 1393 m, 1376 m, 1349 w, 1282 m, 1249 w, 1146 m, 1105 m, 1086 s, 1081 s, 1029 w, 1014 m, 974 s, 819 s, 722 w, 626 w, 379 w, 310 w cm^{-1}. − Raman (100 mW): $\tilde{\nu}$ = 1634 (34), 1494 (8), 1395 (32), 1284 (10), 821 (30), 626 (9), 588 (43), 498 (54), 444 (31), 390 (34), 362 (18), 282 (100) [νSeSe], 242 (30), 225 (21), 164 (35), 100 (18) cm^{-1}. − EI MS (70 eV): *m/z* (%) = 494 (28) [M$^+$], 414 (1) [M$^+$ − Se], 334 (13) [M$^+$ − 2 Se], 327 (2) [$C_6F_5Se_2^+$], 247 (100) [$C_6F_5Se^+$], 197 (24) [$C_5F_3Se^+$], 167 (79) [$C_6F_5^+$], 155 (24) [$C_5F_5^+$], 117 (21) [$C_5F_3^+$], 93 (9) [$C_3F_3^+$]. − ^{19}F NMR data in CCl_4 given in ref.[2]; elemental analysis given in ref.[4]

Bis(4-(4′-trifluoromethyl-tetrafluorophenoxy)tetrafluorophenyl)-diselane (1b): 1b is prepared analogously and fully characterized according to ref.[6] − Raman (100 mW): $\tilde{\nu}$ = 1661 (47), 1632 (61), 1489 (6), 1432 (7), 1394 (64), 1344 (6), 1279 (7), 1226 (5), 1142 (5), 878 (5), 825 (22), 801 (9), 719 (18), 656 (6), 642 (8), 539 (16), 498 (82), 443 (30), 389 (42), 361 (13), 284 (100) [νSeSe], 246 (27), 162 (22), 151 (24), 116 (14) cm^{-1}.

Pentafluorobenzeneseleninic Acid Monohydrate (2a), 4-(4′-Trifluoromethyltetrafluorophenoxy)tetrafluorobenzeneseleninic Acid Monohydrate (2b): Into a solution of 1.0 mmol **1a** in 5 mL of CH_2Cl_2 is added 3 mL of H_2O_2 (30% in water). Immediate decolorization occurred and the mixture is stirred for 1 h. After removal of all volatiles in vacuum, the residue is recrystallized from water.

2a is obtained as colorless crystals (80%), m.p. 132−133°C (ref.[5] 123−123.5°C). − ^{1}H NMR (CD_3CN): δ = 3.65 (s). − ^{19}F NMR (CD_3CN): δ = −142.4 (2-F, m, 2 F), −150.6 (4-F, tt, 1 F, $^3J_{F-F}$ = 19.9 Hz, $^4J_{F-F}$ = 5.2 Hz), −161.9 (3-F, m, 2 F). − IR (KBr): $\tilde{\nu}$ = 3480/3258/2900/2408 vbr [νOH], 1672 m, 1640 m, 1588 w, 1521 s, 1486 s, 1470 m, 1385 m, 1379 m, 1349 w, 1294 m, 1276 w, 1110 m, 1099 s, 1040 w, 1016 m, 974 s, 931 m, 862 s, 841 m, 804 w, 756 w, 722 w, 684 m, 622 m, 586 w, 550 w, 495 w, 391 m, 353 m, 318 m, 300 m cm^{-1}. − Raman (100 mW): $\tilde{\nu}$ = 3250 (6), 1640 (22), 1140 (9), 1102 (14), 859 (99), 807 (17), 685 (62), 586 (69), 497 (83), 443 (46), 392 (100), 357 (39), 301 (22), 279 (21), 242 (30), 202 (71), 185 (48), 166 (27), 118 (32) cm^{-1}. − EI MS (70 eV): *m/z* (%) = 264 (19) [$C_6F_5SeOH^+$], 247 (44) [$C_6F_5Se^+$], 197 (9) [$C_5F_3Se^+$], 184 (36) [$C_6F_5OH^+$], 168 (100) [$C_6F_5H^+$], 155 (15) [$C_5F_5^+$], 117 (13) [$C_5F_3^+$], 93 (7) [$C_3F_3^+$]. Elemental analysis given in ref.[5]

2b (colorless powder, 72%, m.p. 152−155°C (dec.) is prepared from **1b** in a similar fashion and recrystallized from acetonitrile/water. − ^{1}H NMR (CD_3CN): δ = 3.52 (s). − ^{19}F NMR (CD_3CN): δ = −57.4 (4′-CF_3, t, 3 F, $^4J_{F-F}$ = 21.7 Hz), −142.1 (2-F, m, 2 F), −142.5 (3′-F, m, 2 F), −155.7 (2′-F, m, 2F), −156.6 (3-F, m, 2 F). − IR (KBr): $\tilde{\nu}$ = 3480 / 2870 / 2413 vbr [νOH], 1661 m, 1635 m, 1512 s, 1489 s, 1430 m, 1390 m, 1350 s, 1278 w, 1234 s, 1192 m, 1153 s, 1125 m, 1029 m, 1003 s, 979 s, 921 w, 878 m, 857 m, 837 m, 795 w, 718 m, 695 m, 643 w, 496 w, 420 w, 373 m, 320 m, 297 w cm^{-1}. − Raman (100 mW): $\tilde{\nu}$ = 1663 (20), 1637 (17), 1490 (7), 1429 (7), 1392 (9), 1352 (8), 1134 (7), 916 (7), 861 (9), 816 (27), 789 (12), 721 (20), 705 (18), 540 (17), 496 (62), 443 (28), 413 (20), 388 (37), 308 (14), 286 (17), 215 (16), 145 (26), 85 (100) cm^{-1}. − EI MS (70 eV): *m/z* (%) = 478 (2) [$CF_3C_6F_4OC_6F_4SeOH^+$], 461 (23) [$CF_3C_6F_4OC_6F_4Se^+$], 382 (100) [$CF_3C_6F_4OC_6F_4H^+$], 363 (39) [382 − F$^+$], 313 (19) [382 − CF_3^+], 244 (6) [$OC_6F_4Se^+$], 217 (7) [$CF_3C_6F_4^+$], 149 (16) [$C_6F_4H^+$], 117 (5) [$C_5F_3^+$]. − $C_{13}H_3F_{11}O_4Se$ (511.12): calcd. C 30.55, H 0.59, F 40.89; found C 30.49, H 0.38, F 40.6.

Bis(pentafluorophenylseleno)- and Bis[4-(4′-trifluoromethyltetrafluorophenoxy)tetrafluorophenylseleno]mercury (3a) and (3b): Into a solution of 1.0 mmol of **1a** in 10 mL of benzene is added 2.2 mmol of mercury. After stirring for 24 h the mixture is filtered from excess mercury. After removal of the solvent, the residue is recrystallized from chloroform to give pale yellow-green crystals **3a**, m.p. 173−175°C (ref.[2] 171−173°C) (86%). − ^{19}F NMR (C_6D_6): δ = −126.2 (2-F, m, 2 F), −156.1 (4-F, t, 1 F, $^3J_{F-F}$ = 21.7 Hz), −161.4 (3-F, m, 2 F). ^{19}F-NMR data in ether given in ref.[2] − ^{199}Hg NMR (C_6D_6): δ = −1562 (s). − IR (KBr): $\tilde{\nu}$ = 1638 m, 1633 m, 1586 w, 1518 s, 1483 s, 1394 m, 1369 m, 1343 w, 1293 w, 1141 m, 1101 m, 1094 m, 1086 m, 1014 m, 972 s, 821 s, 722 w, 622 w, 370 w, 312 w cm^{-1}. − Raman (100 mW): $\tilde{\nu}$ = 1636 (25), 1395 (31), 1289 (10), 824 (42), 625 (11), 588 (45), 499 (47), 445 (27), 396 (33), 373 (16), 364 (19), 284 (8), 243 (42), 228 (19), 202 (100), 177 (47), 151 (31), 100 (24) cm^{-1}. − EI MS (70 eV): *m/z* (%) = 696 (15) [M$^+$], 616 (1) [M$^+$ − Se], 494 (30) [M$^+$ − Hg], 414 (1) [M$^+$ − HgSe], 334 (2) [M$^+$ − Hg − 2 Se], 327 (2) [$C_6F_5Se_2^+$], 247 (100) [$C_6F_5Se^+$], 202 (12) [Hg$^+$], 197 (14) [$C_5F_3Se^+$], 167 (37) [$C_6F_5^+$], 155 (15) [$C_5F_5^+$], 117 (9) [$C_5F_3^+$], 93 (4) [$C_3F_3^+$]. − $C_{12}F_{10}HgSe_2$ (692.63): calcd. C 20.81, F 27.43; found C 20.92, F 27.6.

3b (pale yellow powder, m.p. 175−177 °C (dec.) (71%) is prepared from **1b** in a similar fashion and recrystallized from dichloromethane. − ^{19}F NMR (C_6D_6): δ = −56.4 (4′-CF_3, t, 3 F, $^4J_{F-F}$ = 21.7 Hz), −125.7 (2-F, m, 2 F), −140.8 (3′-F, m, 2 F), −155.9 (2′-F/3-F, m, 4 F). − ^{199}Hg NMR (C_6D_6): δ = −1573 (s). − IR (KBr): $\tilde{\nu}$ = 1658 m, 1630 w, 1513 s, 1483 s, 1430 m, 1394 w, 1352 s, 1273 w, 1232 s, 1193 m, 1160 m, 1127 m, 1026 m, 997 s, 972 m, 879 m, 824 w, 797 w, 719 m, 641 w, 378 w cm^{-1}. − Raman (100 mW): $\tilde{\nu}$ = 1660 (4), 1630 (5), 1394 (5), 826 (4), 725 (3), 540 (4), 503 (15), 440 (6), 394 (15), 280 (6), 245 (13), 226 (9), 198 (47), 148 (24), 83 (100) cm^{-1}. − EI MS (70 eV): *m/z* (%) = 1124 (6) [M$^+$], 1105 (1) [M$^+$ − F], 1044 (2) [M$^+$ − Se], 964 (4) [M$^+$ − 2 Se], 922 (24) [M$^+$ − Hg], 903 (2) [M$^+$ − Hg − F], 842 (4) [M$^+$ − HgSe], 762 (18) [M$^+$ − Hg − 2 Se], 461 (100) [$CF_3C_6F_4OC_6F_4Se^+$], 442 (5) [461 − F$^+$], 381 (74) [$CF_3C_6F_4OC_6F_4H^+$], 362 (29) [381 − F$^+$], 312 (17) [381 − CF_3^+], 244 (14) [$OC_6F_4Se^+$], 228 (6) [$C_6F_4Se^+$], 217 (11) [$CF_3C_6F_4^+$], 202 (42) [Hg$^+$], 148 (13) [$C_6F_4^+$], 117 (11) [$C_5F_3^+$], 69

(7) [CF_3^+]. − $C_{26}F_{22}HgO_2Se_2$ (1120.77): calcd. C 27.86, F 37.30; found C 27.75, F 37.3.

Pentafluorobenzeneselenenyl Chloride (4a), 4-(4′-Trifluoromethyltetrafluorophenoxy)tetrafluorobenzeneselenenyl Chloride (4b): Into a solution of 8.5 mmol of **1a** in 50 mL of CH_2Cl_2 is added 35 mL of sulfuryl chloride and heated 1 h to reflux. Then the solvent and excess sulfuryl chloride is slowly distilled off (under SO_2 evolution and darkening of the solution). The liquid residue is distilled in vacuum, the receiving flask is cooled with ice. Dark red **4a** is obtained in 70% yield, b.p. 25−26°C/0.01 Torr (ref.[5] 80°C/10 Torr). − ^{19}F NMR ($CDCl_3$): δ = −122.5 (2-F, m, 2 F), −145.5 (4-F, tt, 1 F, $^3J_{F-F}$ = 20.8 Hz, $^4J_{F-F}$ = 5.2 Hz), −159.1 (3-F, m, 2 F). − IR (liquid film/KBr): $\tilde{\nu}$ = 1633 m, 1514 s, 1492 s, 1396 m, 1377 w, 1350 w, 1288 m, 1259 w, 1152 w, 1108 m, 1091 s, 1013 w, 980 s, 824 m, 724 w, 627 w, 393 w cm^{-1}. − Raman (100 mW): $\tilde{\nu}$ = 1635 (31), 1494 (4), 1398 (26), 1290 (7), 1152 (4), 826 (20), 588 (37), 499 (51), 444 (22), 398 (100) [νSeCl], 381 (65), 283 (9), 245 (17), 225 (12), 156 (14), 133 (19) cm^{-1}. − EI MS (70 eV): *m/z* (%) = 282 (1) [M^+], 263 (1) [M^+ − F], 247 (100) [$C_6F_5Se^+$], 197 (11) [$C_5F_3Se^+$], 167 (18) [$C_6F_5^+$], 155 (6) [$C_5F_5^+$], 117 (5) [$C_5F_3^+$], 93 (3) [$C_3F_3^+$]. Elemental analysis given in ref.[5]

4b: (red-brown crystals, m.p. 50−52°C) is prepared from **1b** in a similar fashion and purified by sublimation at 40−50°C/0.01 Torr (91%). − ^{19}F NMR ($CDCl_3$): δ = −56.4 (4′-CF_3, t, 3 F, $^4J_{F-F}$ = 21.7 Hz), −122.3 (2-F, m, 2 F), −139.6 (3′-F, m, 2 F), −154.0 (2′-F, m, 2 F), −154.6 (3-F, m, 2 F). − IR (KBr): $\tilde{\nu}$ = 1659 m, 1630 m, 1605 w, 1513 s, 1490 s, 1431 m, 1394 m, 1344 s, 1262 w, 1229 s, 1193 m, 1156 m, 1122 m, 1029 m, 1002 s, 980 s, 877 m, 822 w, 798 w, 717 m, 643 w, 498 w cm^{-1}. − Raman (100 mW): $\tilde{\nu}$ = 1662 (8), 1630 (14), 1483 (2), 1429 (3), 1395 (17), 1348 (3), 1268 (2), 1232 (2), 1145 (3), 1117 (2), 827 (8), 719 (8), 658 (2), 647 (2), 633 (2), 568 (5), 538 (12), 500 (27), 452 (9), 441 (15), 412 (6), 390 (46), 375 (100) [νSeCl], 305 (5), 281 (8), 246 (10), 232 (5), 169 (12), 144 (14), 128 (19) cm^{-1}. − EI MS (70 eV): *m/z* (%) = 496 (9) [M^+], 477 (1) [M^+ − F], 461 (31) [M^+ − Cl], 381 (100) [M^+ − SeCl], 362 (41) [381 − F^+], 312 (23) [381 − CF_3^+], 244 (5) [$OC_6F_4Se^+$], 228 (2) [$C_6F_4Se^+$], 217 (6) [$CF_3C_6F_4^+$], 148 (16) [$C_6F_4^+$], 117 (7) [$C_5F_3^+$], 69 (13) [CF_3^+]. − $C_{13}ClF_{11}OSe$ (495.54): calcd. C 31.51, F 42.18; found C 31.39, F 41.9.

Pentafluorobenzeneselenenyl Bromide (5a), 4-(4′-Trifluoromethyltetrafluorophenoxy)tetrafluorobenzeneselenenyl Bromide (5b): A solution of 25 mmol of bromine in 3 mL of CH_2Cl_2 is added to a solution of 3 mmol of **1a** in 10 mL of CH_2Cl_2 at 25°C. The mixture is stirred for 2 h (^{19}F NMR shows reaction completed after 1 h) and all volatile materials are removed in vacuum at 25°C. The remaining residue is distilled under light exclusion (nevertheless under decomposition) to give **5a** as a black-red liquid, b.p. ca. 38°C/0.01 Torr (59%). The solid yellow residue consisted of the diselane **1a**, which can be recovered and rebrominated to form **5a**.

Alternative procedure: Into a solution of 1.0 mmol of **4a** in 10 mL of CH_2Cl_2 is added 2.0 mmol of Me_3SiBr at 25°C. The mixture is stirred for 10 h and after removal of all volatile materials in vacuum, the residue is distilled under light exclusion to give **5a** (60%). The yellow residue consisted of the diselane **1a**, which can be recovered and recycled to form **4a**.

5a: ^{19}F NMR ($CDCl_3$): δ = −122.3 (2-F, m, 2 F), −146.2 (4-F, tt, 1 F, $^3J_{F-F}$ = 19.9 Hz, $^4J_{F-F}$ = 5.2 Hz), −159.3 (3-F, m, 2 F). − IR (liquid film/KBr): $\tilde{\nu}$ = 1633 m, 1513 s, 1491 s, 1395 m, 1377 w, 1349 w, 1287 m, 1255 w, 1150 w, 1107 m, 1090 s, 1033 w, 1012 m, 980 s, 823 m, 723 w, 626 w cm^{-1}. − Raman (100 mW): $\tilde{\nu}$ = 1633 (25), 1397 (25), 1289 (13), 825 (19), 588 (26), 498 (32), 444 (17), 383 (16), 289 (100) [νSeBr], 243 (17), 223 (15), 153 (14), 119 (14) cm^{-1}. − EI MS (70 eV): *m/z* (%) = 326 (7) [M^+], 247 (100) [$C_6F_5Se^+$], 197 (15) [$C_5F_3Se^+$], 167 (8) [$C_6F_5^+$], 155 (18) [$C_5F_5^+$], 117 (11) [$C_5F_3^+$], 93 (5) [$C_3F_3^+$]. − C_6BrF_5Se (325.92): calcd. C 22.11, F 29.15; found C 22.03, F 29.1.

5b: (chocolate-brown solid, m.p. 64−66°C) is prepared from **1b** (and alternatively **4b**) in a similar fashion and purified by vacuum sublimation (51%). Compound **5b** as well partly decomposes under bromine evolution and formation of **1b** (residue). − ^{19}F NMR ($CDCl_3$): δ = −56.4 (4′-CF_3, t, 3 F, $^4J_{F-F}$ = 21.7 Hz), −122.1 (2-F, m, 2 F), −139.6 (3′-F, m, 2 F), −154.1 (2′-F, m, 2 F), −154.6 (3-F, m, 2 F). − IR (KBr): $\tilde{\nu}$ = 1659 m, 1629 m, 1608 w, 1513 s, 1490 s, 1431 m, 1394 m, 1344 s, 1278 w, 1263 w, 1229 s, 1193 m, 1156 m, 1122 m, 1029 m, 1001 s, 979 s, 877 m, 824 w, 797 w, 717 m, 644 w, 498 w cm^{-1}. − Raman (100 mW): $\tilde{\nu}$ = 1660 (16), 1630 (20), 1429 (5), 1393 (22), 1344 (6), 828 (11), 724 (11), 539 (9), 501 (39), 440 (12), 392 (31), 358 (6), 292 (100) [νSeBr], 279 (17), 245 (15), 160 (12), 141 (16), 127 (12) cm^{-1}. − EI MS (70 eV): *m/z* (%) = 540 (3) [M^+], 461 (14) [M^+ − Br], 381 (100) [M^+ − SeBr], 362 (44) [381 − F^+], 313 (21) [381 − CF_3^+], 217 (4) [$CF_3C_6F_4^+$], 148 (17) [$C_6F_4^+$], 117 (5) [$C_5F_3^+$]. − $C_{13}BrF_{11}OSe$ (539.99): calcd. C 28.91, F 38.70; found C 29.16, F 38.8.

Pentafluorophenylselenocyanate (6a), 4-(4′-Trifluoromethyltetrafluorophenoxy)tetrafluorophenylselenocyanate (6b): Into a solution of 1.5 mmol of **4a** in 5 mL of CH_2Cl_2 is added 2.0 mmol of Me_3SiCN at 25°C. Immediate decolorization occurred and the mixture is stirred for 30 min. After removal of all volatiles in vacuum, the residue is sublimed at 35°C/0.01 Torr. **6a** is obtained as colorless crystals, m.p. 41−42°C (83%). − ^{19}F NMR ($CDCl_3$): δ = −124.4 (2-F, m, 2 F), −146.2 (4-F, tt, 1 F, $^3J_{F-F}$ = 20.8 Hz, $^4J_{F-F}$ = 5.2 Hz), −157.8 (3-F, m, 2 F). − ^{14}N NMR ($CDCl_3$): δ = −91 (br, $\Delta\nu_{1/2}$ = 800 Hz). − ^{15}N NMR ($CDCl_3$): δ = −91.1 (s). − IR (KBr): $\tilde{\nu}$ = 2167 m [νCN], 1646 m, 1638 m, 1589 w, 1519 s, 1493 s, 1409 m, 1379 m, 1352 w, 1293 w, 1255 w, 1147 w, 1108 m, 1096 s, 1083 m, 1015 m, 1006 w, 975 s, 825 s, 722 m, 628 m, 507 m, 426 w, 353 w, 344 w, 312 w cm^{-1}. − Raman (100 mW): $\tilde{\nu}$ = 2167 (100) [νCN], 1639 (9), 1412 (4), 1099 (4), 629 (3), 588 (26), 507 (48), 500 (48), 445 (18), 428 (14), 386 (23), 362 (13), 346 (4), 285 (8), 241 (33), 157 (14), 136 (34), 107 (36) cm^{-1}. − EI MS (70 eV): *m/z* (%) = 273 (100) [M^+], 254 (1) [M^+ − F], 247 (53) [$C_6F_5Se^+$], 197 (26) [$C_5F_3Se^+$], 193 (73) [M^+ − Se], 167 (21) [$C_6F_5^+$], 155 (24) [$C_5F_5^+$], 117 (56) [$C_5F_3^+$], 93 (18) [$C_3F_3^+$], 80 (38) [Se^+]. − C_7F_5NSe (272.04): calcd. C 30.90, F 34.92, N 5.15; found C 30.70, F 35.0, N 5.14.

6b is prepared from **4b** in a similar fashion and obtained as colorless crystals, purified by vacuum sublimation at 70°C/0.01 Torr, m.p. 85−87°C (85%). − ^{19}F NMR ($CDCl_3$): δ = −56.4 (4′-CF_3, t, 3 F, $^4J_{F-F}$ = 21.7 Hz), −124.2 (2-F, m, 2 F), −139.4 (3′-F, m, 2 F), −152.7 (2′-F, m, 2 F), −154.5 (3-F, m, 2 F). − IR (KBr): $\tilde{\nu}$ = 2164 w [νCN], 1660 m, 1632 m, 1519 s, 1497 s, 1431 m, 1406 w, 1343 s, 1280 w, 1228 s, 1197 m, 1158 m, 1126 m, 1029 m, 1005 s, 981 s, 877 m, 828 w, 797 w, 716 m, 644 w, 509 w cm^{-1}. − Raman (100 mW): $\tilde{\nu}$ = 2165 (100) [νCN], 1662 (21), 1633 (16), 1491 (4), 1433 (7), 1406 (12), 1346 (7), 1274 (4), 1228 (4), 1149 (4), 720 (16), 570 (9), 542 (17), 501 (78), 441 (26), 390 (40), 281 (14), 243 (14), 160 (22), 125 (40) cm^{-1}. − EI MS (70 eV): *m/z* (%) = 487 (100) [M^+], 468 (13) [M^+ − F], 461 (89) [M^+ − CN], 407 (69) [M^+ − Se], 381 (20) [M^+ − SeCN], 362 (6) [381 − F^+], 338 (11) [M^+ − Se − CF_3], 254 (34) [$C_6F_4SeCN^+$], 244 (20) [$OC_6F_4Se^+$], 217 (21) [$CF_3C_6F_4^+$], 148 (17) [$C_6F_4^+$], 117 (14) [$C_5F_3^+$]. − $C_{14}F_{11}NOSe$ (486.11): calcd. C 34.59, F 42.99, N 2.88; found C 34.35, F 42.4, N 2.69.

***N,N*-Dimethyl(pentafluorobenzene)selenenylamide (7a), *N,N*-Dimethyl-4-(4′-trifluoromethyltetrafluorophenoxy)tetrafluorobenzene-**

selenenylamide (7b): Into a solution of 2.0 mmol of **4a** in 5 mL of CH_2Cl_2 is added 3.0 mmol of Me_3SiNMe_2 at 25°C. Immediate decolorization occurred and the mixture is stirred for 30 min. After removal of all volatiles in vacuum, the residue is distilled in vacuum. **7a** is obtained as a colorless liquid, b.p. 30−31°C/0.01 Torr (94%). − ^{1}H NMR ($CDCl_3$): δ = 2.79 (CH_3, t, $^6J_{H-F}$ = 1.3 Hz, $^3J_{H-Se}$ = 14.5 Hz). − ^{19}F NMR ($CDCl_3$): δ = −122.9 (2-F, m, 2 F), −149.0 (4-F, t, 1 F, $^3J_{F-F}$ = 20.8 Hz), −160.0 (3-F, m, 2 F). − ^{14}N NMR ($CDCl_3$): δ = −350 (vbr, $\Delta\nu_{1/2}$ = 1300 Hz). − ^{15}N NMR ($CDCl_3$): δ = −352.9 (s). − IR (liquid film/CsBr): $\tilde{\nu}$ = 2989/2936/2860/2824/2784 m [νCH], 1633 m, 1584 w, 1512 s, 1482 s, 1469 m, 1449 m, 1426 w, 1403 w, 1382 m, 1349 w, 1280 m, 1261 w, 1224 w, 1181 m, 1140 m, 1083 s, 1029 m, 1015 m, 975 s, 940 m, 806 m, 723 w, 626 m, 552 m, 493 w, 407 m, 348 w, 332 w, 312 w, 285 w cm^{-1}. − Raman (100 mW): $\tilde{\nu}$ = 2994 (15)/2937 (46)/2881 (13)/2859 (12)/2826 (19)/2783 (25) [νCH], 1634 (28), 1510 (3), 1466 (10), 1447 (11), 1403 (7), 1385 (6), 1272 (4), 1224 (12), 1180 (3), 1140 (6), 1088 (3), 1030 (3), 941 (11), 808 (6), 626 (8), 585 (48), 552 (100) [νSeN], 493 (68), 443 (30), 389 (28), 357 (35), 347 (51), 220 (21), 178 (8), 152 (18), 130 (17) cm^{-1}. − EI MS (70 eV): *m/z* (%) = 291 (3) [M^+], 262 (1) [$C_6F_5SeNH^+$], 247 (10) [$C_6F_5Se^+$], 197 (2) [$C_5F_3Se^+$], 167 (100) [$C_6F_5^+$], 155 (4) [$C_5F_5^+$], 117 (10) [$C_5F_3^+$], 93 (6) [$C_3F_3^+$], 45 (4) [$HN(CH_3)_2^+$]. − $C_8H_6F_5NSe$ (290.11): calcd. C 33.12, H 2.09, N 4.83; found C 32.94, H 2.12, N 4.83.

7b: (colorless solid, m.p. 66−68°C) is prepared from **4b** in a similar fashion and purified by vacuum sublimation at 60°C/0.01 Torr (74%). − ^{1}H NMR ($CDCl_3$): δ = 2.81 (CH_3, t, $^6J_{H-F}$ = 1.2 Hz, $^3J_{H-Se}$ = 14.5 Hz). − ^{19}F NMR ($CDCl_3$): δ = −56.4 (4′-CF_3, t, 3 F, $^4J_{F-F}$ = 21.7 Hz), −122.8 (2-F, m, 2 F), −139.9 (3′-F, m, 2 F), −154.6 (2′-F, m, 2 F), −154.9 (3-F, m, 2 F). − ^{13}C NMR ($CDCl_3$): δ = 52.3 (SeNC, s, $^2J_{C-Se}$ = 9.8 Hz). − IR (KBr): $\tilde{\nu}$ = 3003/2938/2865/2828/2784 w−m [νCH], 1659 m, 1629 m, 1510 s, 1488 s, 1450 w, 1431 m, 1404 w, 1385 w, 1346 s, 1266 w, 1228 s, 1193 m, 1162 s, 1116 m, 1083 s, 1027 m, 1000 s, 977 s, 943 m, 878 m, 812 w, 792 w, 718 m, 698 w, 640 w, 630 w, 553 w, 499 w, 419 m, 350 w cm^{-1}. − Raman (100 mW): $\tilde{\nu}$ = 3001 (27)/2954 (35)/2863 (12)/2831 (21)/2788 (26) [νCH], 1658 (38), 1628 (39), 1465 (12), 1422 (17), 1407 (11), 1382 (15), 1339 (11), 1266 (6), 1222 (19), 1161 (6), 1139 (8), 1029 (6), 940 (23), 879 (5), 810 (13), 789 (6), 761 (7), 719 (26), 699 (14), 645 (20), 629 (11), 558 (88), 538 (33) [νSeN], 496 (100), 451 (28), 439 (47), 420 (19), 393 (44), 384 (54), 349 (78), 322 (21), 270 (22), 199 (12), 158 (23), 140 (31), 117 (35) cm^{-1}. − EI MS (70 eV): *m/z* (%) = 505 (77) [M^+], 486 (6) [M^+ − F], 461 (61) [M^+ − $N(CH_3)_2$], 425 (26) [M^+ − Se], 381 (100) [M^+ − $SeN(CH_3)_2$], 362 (34) [381 − F^+], 312 (12) [381 − CF_3^+], 244 (12) [$OC_6F_4Se^+$], 218 (31) [$CF_3C_6F_4H^+$], 199 (31) [$CF_2C_6F_4H^+$], 149 (21) [$C_6F_4H^+$], 117 (18) [$C_5F_3^+$], 69 (9) [CF_3^+], 45 (17) [$HN(CH_3)_2^+$]. − $C_{15}H_6F_{11}NOSe$ (504.18): calcd. C 35.73, H 1.20, N 2.78; found C 35.60, H 1.29, N 2.82.

***N,N*-Diethyl(pentafluorobenzene)selenenylamide (8a), *N,N*-Diethyl-4-(4′-Trifluoromethyltetrafluorophenoxy)tetrafluorobenzeneselenenylamide (8b):** Compounds **8a** and **8b** are prepared analogously to **7a** and **7b** except using Me_3SiNEt_2. **8a** is obtained as a colorless liquid, b.p. 39−40°C/0.01 Torr (84%). − ^{1}H NMR ($CDCl_3$): δ = 2.78 (CH_2, q, 2 H, $^3J_{H-H}$ = 7.0 Hz), 1.19 (CH_3, t, 3 H). − ^{19}F NMR ($CDCl_3$): δ = −123.1 (2-F, m, 2 F), −149.8 (4-F, tt, 1 F, $^3J_{F-F}$ = 20.8 Hz, $^4J_{F-F}$ = 3.5 Hz), −160.2 (3-F, m, 2 F). − ^{14}N NMR ($CDCl_3$): δ = −310 (vbr, $\Delta\nu_{1/2}$ = 3000 Hz). − ^{15}N NMR ($CDCl_3$): δ = −316.8 (s). − IR (liquid film/CsBr): $\tilde{\nu}$ = 2975/2935/2873/2837 m [νCH], 1634 m, 1582 w, 1511 s, 1482 s, 1447 m, 1378 m, 1359 w, 1337 w, 1279 m, 1264 w, 1174 m, 1154 m, 1140 m, 1130 w, 1087 s, 1028 w, 1014 m, 975 s, 877 w, 817 m, 802 m, 743 m, 722 w, 625 m, 580 w, 513 w, 492 w, 453 w, 429 w, 410 w, 395 w, 314 w, 283 w cm^{-1}. − Raman (100 mW): $\tilde{\nu}$ = 2978 (41)/2938 (88)/2875 (42)/2852 (23) [νCH], 1635 (39), 1449 (31), 1386 (12), 1273 (10), 1056 (16), 1030 (13), 879 (16), 803 (13), 627 (19), 585 (93), 515 (54) [νSeN], 494 (90), 445 (41), 390 (39), 358 (41), 332 (20), 217 (25), 119 (28), 84 (100) cm^{-1}. − EI MS (70 eV): *m/z* (%) = 319 (53) [M^+], 304 (100) [M^+ − CH_3], 247 (49) [$C_6F_5Se^+$], 197 (8) [$C_5F_3Se^+$], 167 (22) [$C_6F_5^+$], 155 (10) [$C_5F_5^+$], 117 (6) [$C_5F_3^+$], 93 (3) [$C_3F_3^+$]. − $C_{10}H_{10}F_5NSe$ (318.17): calcd. C 37.75, H 3.17, N 4.40; found C 37.22, H 3.31, N 4.41.

8b is obtained as a colorless solid, m.p. 47−48°C, purified by vacuum sublimation at 40°C/0.01 Torr (90%). − ^{1}H NMR ($CDCl_3$): δ = 2.80 (CH_2, q, 2 H, $^3J_{H-H}$ = 6.9 Hz), 1.18 (CH_3, t, 3 H). − ^{19}F NMR ($CDCl_3$): δ = −56.4 (4′-CF_3, t, 3 F, $^4J_{F-F}$ = 21.7 Hz), −123.0 (2-F, m, 2 F), −140.0 (3′-F, m, 2 F), −154.8 (2′-F, m, 2 F), −155.0 (3-F, m, 2 F). − ^{13}C NMR ($CDCl_3$): δ = 54.8 (SeNC, s, $^2J_{C-Se}$ = 7.6 Hz), 14.9 (CH_3, s). − IR (KBr): $\tilde{\nu}$ = 2983 / 2937 / 2872 / 2849 w-m [νCH], 1660 m, 1629 m, 1512 s, 1486 s, 1446 w, 1425 m, 1400 w, 1382 m, 1348 s, 1262 w, 1229 s, 1191 m, 1155 m, 1117 m, 1080 w, 1061 w, 1025 m, 999 s, 978 s, 879 m, 810 m, 793 m, 718 m, 689 w, 647 w, 631 w, 513 w, 495 w, 447 w, 429 m, 374 w cm^{-1}. − EI MS (70 eV): *m/z* (%) = 533 (50) [M^+], 518 (100) [M^+ − CH_3], 461 (76) [M^+ − $N(CH_2CH_3)_2$], 381 (55) [M^+ − $SeN(CH_2CH_3)_2$], 362 (21) [381 − F^+], 312 (11) [381 − CF_3^+], 244 (10) [$OC_6F_4Se^+$], 217 (7) [$CF_3C_6F_4^+$], 198 (8) [$CF_2C_6F_4^+$], 148 (9) [$C_6F_4^+$], 117 (6) [$C_5F_3^+$], 73 (31) [$HN(CH_2CH_3)_2^+$]. − $C_{17}H_{10}F_{11}NOSe$ (532.24): calcd. C 38.36, H 1.90, N 2.63; found C 37.66, H 1.83, N 2.45.

Bis(pentafluorophenyl)selane (9a), Bis[4-(4′-trifluoromethyltetrafluorophenoxy)tetrafluorophenyl]selane (9b): Into a stirred solution of 2.0 mmol of C_6F_5Li in ether (see prep. of **1a**), 2.0 mmol of **4a** is added at −70°C. Immediate decolorization of the deep red **4a** occurs and resulted in an almost colorless solution. The mixture is stirred for 1 h and then slowly warmed to ambient temperature; then the lithium chloride precipitated. After evacuation of all volatile material the residue is sublimed at 40−50°C/0.01 Torr. Colorless crystals in X-ray diffraction quality are obtained in 61% yield, m.p. 76−77°C (ref.[4] 71−72°C). − ^{19}F NMR ($CDCl_3$): δ = −126.6 (2-F, m, 2 F), −150.0 (4-F, tt, 1 F, $^3J_{F-F}$ = 20.8 Hz, $^4J_{F-F}$ = 3.5 Hz), −159.7 (3-F, m, 2 F). − IR (KBr): $\tilde{\nu}$ = 1640 m, 1588 w, 1519 s, 1511 s, 1490 s, 1398 m, 1378 m, 1353 w, 1341 w, 1288 m, 1153 m, 1113 m, 1092 s, 1047 w, 1016 m, 1003 m, 972 s, 827 m, 817 s, 722 w, 631 m, 619 w, 394 m, 363 w, 313 m cm^{-1}. − Raman (100 mW): $\tilde{\nu}$ = 1639 (42), 1516 (5), 1445 (5), 1404 (19), 1305 (5), 1275 (11), 1255 (7), 1142 (8), 1090 (6), 975 (4), 827 (18), 770 (6), 721 (6), 632 (10), 586 (79), 498 (100), 445 (62), 386 (61), 362 (39), 284 (16), 252 (22), 225 (22), 184 (10), 161 (21), 137 (21), 120 (13), 100 (19) cm^{-1}. ^{19}F-NMR data in CCl_4 and mass spectrum given in ref.[2]; elemental analysis given in ref.[4]

9b: (colorless solid, m.p. 122−124°C) is prepared in a similar fashion by reaction of **4b** with $CF_3C_6F_4OC_6F_4Li$ and purified by vacuum sublimation at 100°C/0.01 Torr (47%). − ^{19}F NMR ($CDCl_3$): δ = −56.4 (4′-CF_3, t, 3 F, $^4J_{F-F}$ = 21.7 Hz), −126.4 (2-F, m, 2 F), −139.7 (3′-F, m, 2 F), −154.2 (2′-F, m, 2 F), −154.7 (3-F, m, 2 F). − IR (KBr): $\tilde{\nu}$ = 1659 m, 1630 m, 1508 s, 1495 s, 1485 s, 1431 m, 1397 w, 1350 s, 1342 s, 1278 w, 1227 s, 1189 m, 1154 m, 1111 m, 1028 m, 1001 m, 994 s, 973 s, 878 m, 822 w, 795 w, 718 m, 701 w, 640 w, 499 w, 420 w, 376 w cm^{-1}. − Raman (100 mW): $\tilde{\nu}$ = 1660 (43), 1631 (42), 1431 (22), 1404 (32), 1350 (19), 1226 (17), 1028 (15), 828 (18), 771 (16), 737 (16), 719 (36), 703 (16), 651 (16), 571 (22), 538 (38), 499 (100), 452 (34), 438 (51), 392 (75), 357 (22), 306 (24), 251 (26), 224 (17), 200 (17), 143 (34), 129 (24) cm^{-1}. − EI MS (70 eV): *m/z* (%) = 842 (100) [M^+], 823

(10) [$M^+ - F$], 762 (12) [$M^+ - Se$], 545 (7) [762 − $CF_3C_6F_4^+$], 461 (12) [$CF_3C_6F_4OC_6F_4Se^+$], 362 (3) [$CF_2C_6F_4OC_6F_4^+$], 244 (6) [$OC_6F_4Se^+$], 217 (4) [$CF_3C_6F_4^+$], 148 (3) [$C_6F_4^+$], 117 (2) [$C_5F_3^+$]. − $C_{26}F_{22}O_2Se$ (841.22): calcd. C 37.12, F 49.69; found C 37.56, F 49.7.

Acknowledgments

Financial support of this research by the University of Munich and the Fonds der Chemischen Industrie is gratefully acknowledged.

[1] *Gmelin Handbook of Inorganic and Organometallic Chemistry*, Perfluorohaloorgano Compounds of Main Group Elements, 2nd Supplement, 8th Edn.; Springer Verlag Berlin, **1995**, Vol. 2.
[2] S. C. Cohen, A. G. Massey, *Advances in Fluorine Chemistry* (Eds.: J. C. Tatlow, R. D. Peacock, H. H. Hyman); Butterworths & Co., London, **1970**, Vol. 6.
[3] A. Haas, *J. Fluorine Chem.* **1986**, *32*, 415−439.
[4] S. C. Cohen, M. L. N. Reddy, A. G. Massey, *J. Organomet. Chem.* **1968**, *11*, 563−566.
[5] G. G. Furin, T. V. Terent′eva, G. G. Yakobson, *Izv. Sib. Otd. Akad. Nauk SSSR* **1972**, *6*, 78−88.
[6] B. Krumm, R. L. Kirchmeier, J. M. Shreeve, *Inorg. Chem.* **1997**, *36*, 5222−5230.
[7] G. G. Furin, A. I. Rezvukhin, M. A. Fedotov, G. G. Yakobson, *J. Fluorine Chem.* **1983**, *22*, 231−252.
[8] A. I. Rezvukhin, G. G. Furin, G. A. Kalabin, S. A. Krupoder, V. G. Storozhenko, V. M. Polonov, D. F. Kushnarev, G. G. Yakobson, *Izv. Sib. Otd. Akad. Nauk SSSR* **1982**, *5*, 94−102.
[9] A. Haas, K. Schinkel, *Chem. Ber.* **1990**, *123*, 685−689.
[10] T. M. Klapötke, M. Broschag, *Compilation of Reported ^{77}Se NMR Chemical Shifts*, John Wiley & Sons, Chichester, **1996**.
[11] C. M. Woodard, D. S. Brown, J. D. Lee, A. G. Massey, *J. Organomet. Chem.* **1976**, *121*, 333−344.
[12] B. Krumm, A. Vij, R. L. Kirchmeier, J. M. Shreeve, *Inorg. Chem.* **1997**, *36*, 366−381.
[13] W. Gombler, *Z. Naturforsch.* **1981**, *36b*, 535−543.
[14] J. H. Bryden, J. D. McCullough, *Acta Cryst.* **1954**, *7*, 833−838.
[15] J. H. Bryden, J. D. McCullough, *Acta Cryst.* **1956**, *9*, 528−533.
[16] W. S. McDonald, L. D. Pettit, *J. Chem. Soc. (A)* **1970**, 2044−2046.
[17] S. J. Dunne, L. A. Summers, E. I. Von Nagy-Felsobuki, *Acta Cryst.* **1994**, *C50*, 971−974.
[18] R. Minkwitz, H. Preut, J. Sawatzki, *Z. Anorg. Allg. Chem.* **1989**, *569*, 158−168.
[19] K. Polborn, private communication.

Received February 26, 1999
[I99069]

Synthesis, Mesomorphism, and Spectroscopic Characterization of Bis[4-(*n*-alkoxy)-5-(*p*-*n*-tetradecylphenylazo)]-Substituted (*N*,*N*′-Salicylidenediaminato)nickel(II) Complexes

Iolinda Aiello,[a] Mauro Ghedini,*[b] Massimo La Deda,[a] Daniela Pucci,[a] and Oriano Francescangeli[c]

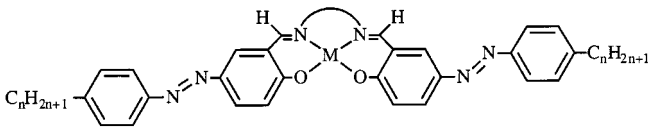
Keywords: Metallomesogens / Nickel / Salicylidenediamines / Azo compounds / (*E*)/(*Z*) photoisomerization / Isomerizations

The bis[4-(*n*-$C_mH_{2m+1}O$)-5-(*p*-$C_{14}H_{29}C_6H_4N{=}N$)]-substituted *N*,*N*′-salicylidenediamines $H_2[L_N(m,14)]$ (*N* = 1: 1,2-diaminoethane; *N* = 2: 1,3-diaminopropane; *N* = 3: 1,3-diamino-2,2-dimethylpropane; *m* = 6 or 18) have been synthesized. Both the *N* = 2 and 3 series of compounds display a smectic C (SmC) mesophase, with clearing points well below 100 °C. By treating the $H_2[L_N(m,14)]$ ligands with an Ni^{II} salt, liquid crystalline mononuclear complexes with "unconventional" (lateral-tailed) molecular shape form. These $Ni[L_N(m,14)]$ complexes, showing nematic and smectic disordered phases, are stable over a quite large temperature range and have been characterized by different spectroscopic techniques. The newly synthesized mesogens exhibit lower transition temperatures and higher thermal stability than homologous complexes $Ni[L_N(14)]$ with a "conventional" rod-like molecular geometry.

Introduction

The photoisomerization of liquid crystals containing an azobenzene core has been envisaged as useful tool in designing optical switching materials based on light-induced isothermal phase transitions.[1,4] In an endeavour to improve or explore possible new applications of mesomorphic species, metal atoms have been incorporated into mesogenic molecular structures and a further class of materials (*metallomesogens*), for which some physical properties (e.g. optical, electrical, or magnetic) depend on the nature of the metal centre, is now available.[5] In principle, new materials can be obtained from compounds whose molecular structures combine different features; thus, in particular, photoisomerizable metal-based liquid crystals could be relevant for applications in electrooptic devices.

We are currently concerned with the design and synthesis of metallomesogens[6,7] and with reference to the abovementioned uses have recently reported[8] rod-like thermotropic complexes of Ni^{II}, Cu^{II}, or VO^{2+} with a series of bis[5-(*p*-*n*-alkylphenylazo)]-substituted *N*,*N*′-salicylidenediamines (see Scheme 1). The results of such a comparative investigation indicate that: i) the mesomorphism appears for N⌒N = 1,2-diaminoethane or 1,3-diaminopropane only; ii) the lowest clearing temperatures are shown by the Ni^{II} species and iii) the better mesomorphic properties (namely larger mesomorphic range) are obtained for the ligands bearing the *n*-$C_{14}H_{29}$ alkyl chains. However, all these mesogens display poor thermal stability, and strong decomposition is observed when, at about 300 °C, the mesophase to isotropic liquid transition occurs. This drawback severely limits any practical applications; therefore, in order to preserve chemical stability, the melting transition temperatures of these materials must decrease − i.e. a different molecular structure has to be considered.



M[L_N(n)]

M = Cu, Ni, VO ; n = 6,14

⌒ = CH_2-CH_2 ; CH_2-CH_2-CH_2 ; CH_2-$C(CH_3)_2$-CH_2

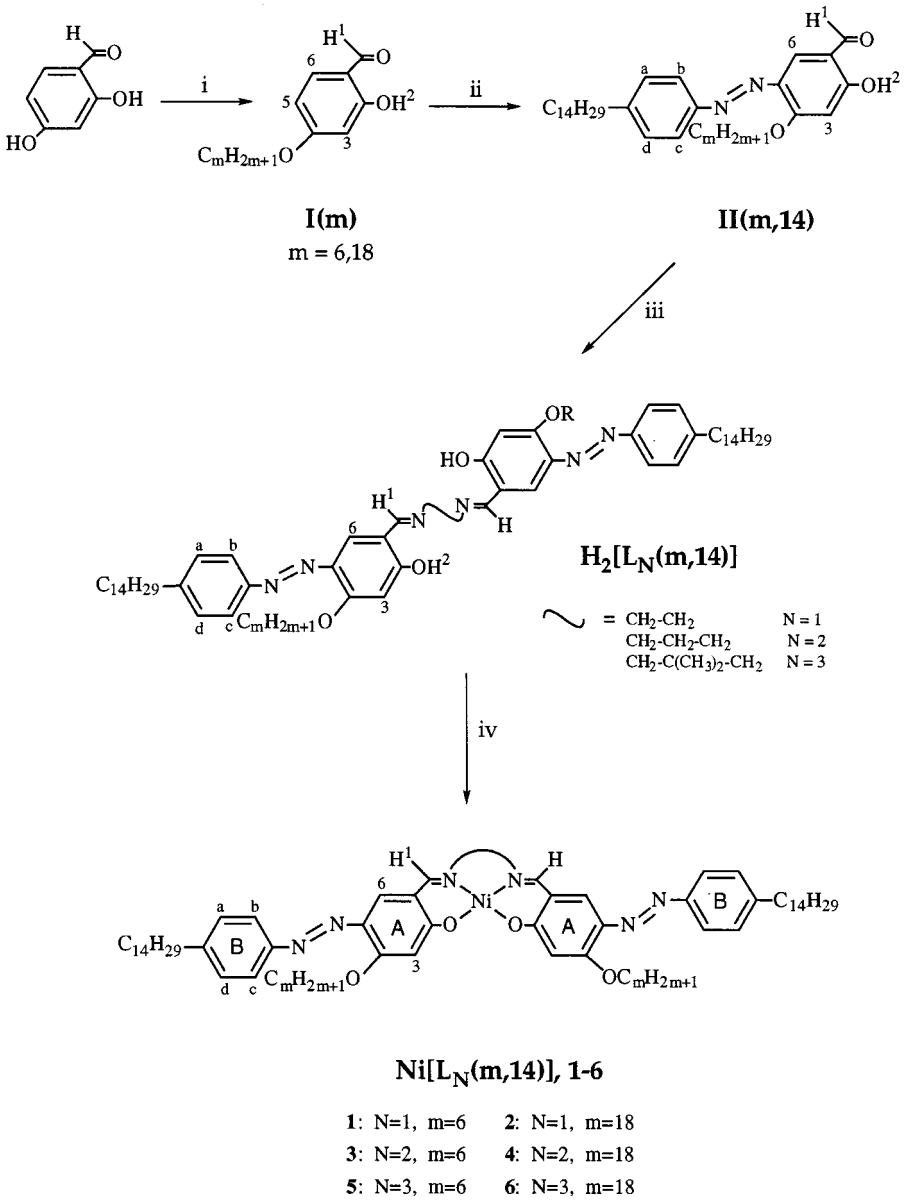
Scheme 1. General formula of the $M[L_N(n)]$ complexes (ref.[8])

The relationship between chemical structure and mesogenic properties is an extensively investigated area in the field of liquid crystal chemistry and, although the greater part of the available data concerns organic species,[9] some rules could also be of use for the metallomesogens. In particular, it has been proven that lateral addition of long alkyl chains to a rod-like molecular structure gives rise to a class of "nonconventional" liquid crystals, whose mesophase-isotropic transition temperatures are significantly lower than those of the corresponding rod-like compounds.[10] Thus, speculating on this trend, low-temperature phase transitions could be predicted for metallomesogens with similar structural features.

The target of the research work we are presently involved in is to obtain thermally stable photoactive metal-contain-

[a] Dipartimento di Chimica, Università della Calabria, I-87030 Arcavacata (CS), Italy
[b] Dipartimento di Chimica, Università della Calabria, I-87030 Arcavacata (CS), Italy
Fax: (internat.) + 39-0984/492062
E-mail: m.ghedini@unical.it
[c] Dipartimento di Scienze dei Materiali e della Terra and Istituto Nazionale per la Fisica della Materia, Università di Ancona, Via Brecce Bianche, I-60131 Ancona, Italy

 © WILEY-VCH Verlag GmbH, D-69451 Weinheim, 1999 1434−1948/99/0808−1367 $ 17.50+.50/0



Scheme 2. Synthetic route to Ni[L_N(*m*,14)] complexes **1**–**6**; reagents and conditions: i) KOH, *n*-$C_mH_{2m+1}Br$, ethanol; ii) 4-(*n*-tetradecyl)-aniline, HCl, $NaNO_2$, NaOH, water; iii) *N* = 1,2-diaminoethane or 1,3-diaminopropane or 1,3-diamino-2,2-dimethylpropane, ethanol; iv) $Ni(CH_3COO)_2 \cdot 4\,H_2O$, ethanol

ing liquid crystals. As an extension of the previous study,[8] this paper reports on the synthesis, mesomorphic behaviour, and spectroscopic properties of the complexes that the Ni^{II} ion forms with a series of salicylidenediamino ligands obtained by the symmetric addition of two aliphatic tails to the bis[5-(*p*-*n*-tetradecylphenylazo)]-substituted *N*,*N*′-salicylidenediamine skeleton (see Scheme 2).

Results and Discussion

Synthesis

The H_2[L_N(*m*,14)] ligands were synthesized in satisfactory yields as outlined in Scheme 2. The starting material, 2,4-dihydroxybenzaldehyde, was treated first with the appropriate alkyl bromide *n*-$C_mH_{2m+1}Br$ [intermediates **I(6)** for *m* = 6 and **I(18)** for *m* = 18], and then coupled with the diazonium chloride obtained from the 4-*n*-tetradecylaniline. Finally, the new formed intermediates **II(6,14)** and **II(18,14)** were condensed with the selected diamines (namely 1,2-diaminoethane, *N* = 1; 1,3-diaminopropane, *N* = 2; and 1,3-diamino-2,2-dimethylpropane, *N* = 3). The H_2[L_N(*m*,14)] compounds are orange solids which, by treatment with nickel(II) acetate tetrahydrate, give the corresponding Ni[L_N(*m*,14)] complexes **1**–**6** (Scheme 2) as brown to red solids.

The ligands and complexes were characterized by IR and ^{1}H-NMR spectroscopies and their purity confirmed by elemental analysis (see Experimental Section). These data as a whole account for the general formula shown in

Scheme 2. Moreover, both the IR and ^{1}H-NMR spectra, except for the signal attributable to the *n*-$C_mH_{2m+1}O$ chain, compare well with those of the previously described $H_2[L_N(n)]$ and $Ni[L_N(n)]$ compounds (see Scheme 1).[8] Thus, for complexes **1**–**6**, an $[L_N(m,14)]$ bonding mode, like that which the $[L_N(n)]$ groups exhibit in $Ni[L_N(n)]$ and expected for ligands containing the salicylidenediaminato core, is proposed (see Scheme 2).

Mesomorphism

The thermal behaviour of all the newly synthesized compounds belonging to the three homologous series $N = 1-3$, was investigated by combining polarized optical microscopy (POM), miscibility tests with reference compounds, differential scanning calorimetry (DSC) and variable-temperature low-angle X-ray diffraction (XRD) measurements.

The transition temperatures and associated enthalpies for both the ligands $H_2[L_N(m,14)]$ and their related Ni^{II} complexes are reported in Tables 1 and 2, respectively.

Table 1. Transition temperatures, phase assignments[a] and enthalpy changes for the $H_2[L_N(m,14)]$ ligands

Ligand	Transition	T [°C]	ΔH [kJmol^{-1}]
$H_2[L_1(6,14)]$	Cr−I	94.5	69.1
$H_2[L_1(18,14)]$	Cr−Cr′	85.6	28.4
	Cr′−I	106.4	72.7
$H_2[L_2(6,14)]$	Cr−SmC	61.8	83.3
	SmC−I	83.4	39.5
$H_2[L_2(18,14)]$	Cr−Cr′	52.5	47.9
	Cr′−I	65.9	2.7
	I−SmC[b]	61.7	2.5
	SmC−Cr	42.5	44.6
$H_2[L_3(6,14)]$	Cr−SmC	49.7	27.5
	SmC−I	62.9	18.0
$H_2[L_3(18,14)]$	Cr−SmC	48.1	4.1
	SmC−I	51.9	24.1

[a] Cr: crystal; Sm: smectic; I: isotropic liquid. – [b] Monotropic transition.

Table 2. Transition temperatures, phase assignments[a] and enthalpy changes for the $Ni[L_N(m,14)]$ complexes **1**–**6**

Compound	Transition	T [°C]	ΔH [kJmol^{-1}]
1 $\{Ni[L_1(6,14)]\}$	Cr−I	213.7	46.7
2 $\{Ni[L_1(18,14)]\}$	Cr−SmC	65.5	46.0
	SmC−I	101.2	2.5
3 $\{Ni[L_2(6,14)]\}$	Cr−N	127.3	49.6
	N−I	226.0[b]	
4 $\{Ni[L_2(18,14)]\}$	Cr−SmC	89.5	29.9
	SmC−SmA	102.2	1.0
	SmA−I	180.0[b]	
5 $\{Ni[L_3(6,14)]\}$	Cr−SmA	128.1	61.8
	SmA−I	293.0[b]	
6 $\{Ni[L_3(18,14)]\}$	Cr−SmA	117.8	31.1
	SmA−I	190.1	5.0

[a] Cr: crystal; Sm: smectic; N: nematic; I: isotropic liquid. – [b] From optical microscopy.

Ligands

None of the $H_2[L_1(m,14)]$ ligands displays mesomorphic behaviour, melting directly to an isotropic liquid at about 100°C; a crystal-to-crystal transition at 86°C (DSC, XRD) appears only for the $m = 18$ homologues.

Increasing the bridge size promotes liquid crystalline behaviour ($N = 2$ and 3 series). The smectic C (SmC) mesophase is the only one observed in these compounds, irrespective of the bridging diamine or the length of the lateral *n*-$C_mH_{2m+1}O-$ group. In particular, an enantiotropic ($m = 6$) or monotropic ($m = 18$) SmC phase, featuring the typical schlieren texture, is exhibited by the $H_2[L_2(m,14)]$ couple, showing clearing temperatures ranging from 66°C ($m = 18$) to 83°C ($m = 6$). Worthy of note is an exothermic peak detected at 65°C (DSC) for the $H_2[L_2(6,14)]$ sample just after the formation of the SmC phase, indicating a transition to a thermodynamically more stable form before reaching the isotropic liquid. In contrast, in the $H_2[L_2(18,14)]$ compound, a crystal-to-crystal transition is observed at 52°C (DSC, XRD). For both the $H_2[L_2(m,14)]$ species, an SmC mesophase first appears on cooling from the isotropic liquid but, on further cooling, crystallization does not occur and the samples solidify into a glassy state retaining the structure of the SmC phase.

Finally, both the $N = 3$ compounds give an SmC phase showing a sanded texture. On cooling down from the isotropic liquid, the SmC phase is not restored for $H_2[L_3(6,14)]$ and the sample becomes an amorphous solid (POM, DSC, XRD).

At room temperature, the compound with the longest lateral chain, $H_2[L_3(18,14)]$, is a viscous material, slightly birefringent when sheared, whose XRD patterns reveals a semicrystalline structure with a hexagonal smectic-like structure. As the temperature is increased, the material becomes more fluid and an SmC phase is observed at 48°C, before reaching the clearing point at 52°C. Upon cooling, the SmC phase reappears at 41°C and the SmC texture remains until solidification (without crystallization) occurs.

As expected, the results obtained for the $N = 2$ and 3 series demonstrate that longer lateral tails or bulkier bridges gradually decrease the transition temperatures, whereas the thermal stability of the mesophase progressively reduces. Moreover, since liquid crystalline properties were not observed for any of the $[L_N(14)]$ series,[8] the $H_2[L_N(m,14)]$ thermal behaviour is a further example of the role the lateral *n*-$C_mH_{2m+1}O-$ chains could play in mesomorphism.[9]

Complexes

All the $Ni[L_N(m,14)]$ complexes (except for **1**) are liquid crystals which exhibit higher clearing points and larger mesomorphic ranges than those of the corresponding ligands.

Of the $N = 1$ species, **1** ($m = 6$) melts directly to the isotropic liquid at 214°C but the lengthening of the lateral aliphatic chain to $m = 18$ (complex **2**), induces mesomorphism. Indeed **2** shows an enantiotropic SmC phase, stable in

the range 65−101°C. Upon cooling, this mesophase reappears at 88°C and is supercooled to room temperature.

The mesomorphic behaviour of the Ni[L_2(*m*,14)] series proves to be quite sensitive to changes in the lateral alkoxy tail length and confirms the general trend that longer chains promote more ordered phases. Thus, compound **3** (*m* = 6) displays a nematic (N) phase showing a homeotropic texture over its entire temperature range, whereas the upper homologues **4** (*m* = 18) exhibits an SmC (blurred "schlieren" texture) followed by an SmA phase. This latter mesophase becomes more and more fluid and displays homeotropic zones as the temperature is increased. However, both complexes exhibit mesogenic behaviour over a temperature range of about 100°C; the corresponding clearing peaks, only detected by POM observations, were not observed in the DSC scans. When cooled from the isotropic liquid to room temperature, both compounds **3** and **4** transformed into an amorphous solid (XRD).

Finally, of the *N* = 3 derivatives, the Ni[L_3(*m*,14)] complexes **5** and **6** exhibit an SmA phase, identified from the appearance, via batônnetes, of the focal conic fan texture at 128°C (**5**) and 118°C (**6**). On cooling from the isotropic liquid, in compound **5** the SmA phase develops at 280°C and remains stable until, at 103°C, crystallization takes place (POM, XRD). In contrast, for compound **6** no crystallization or glass transition was observed until −20°C.

However, for these three series of Ni[L_N(*m*,14)] complexes it is possible to conclude that the clearing points decrease by about 50°C (for *N* = 2) or 100°C (for *N* = 1,3) as the lateral chain changes from $C_6H_{13}O$ to $C_{18}H_{37}O$, while they rise only slightly as the number of the carbon atoms of the bridging diamine increases (from 2, *N* = 1, to 3, *N* = 2, 3). A similar trend is not observed for the melting transitions and, consequently, for the stability range of the different mesophases.

Azobenzene (*E*)/(Z) Photoisomerization Measurements

Experiments concerning the (*E*)/(*Z*) photoisomerization were performed at room temperature in dichloromethane solutions on Ni[L_2(18,14)] and, for the sake of comparison, on its rod-like homologues Ni[L_2(14)] and on both of the uncomplexed ligands H_2[L_2(18,14)] and H_2[L_2(14)].

The absorption spectra of azobenzenes in their thermally stable (*E*) configuration exhibit absorption maxima at about 350 and 450 nm, and it was observed that irradiation at about 360 nm induces (*E*)/(*Z*)-N=N isomerization.[11] Absorptions at similar wavelengths were also recognized in the spectra of the azo compounds considered; nevertheless under the experimental conditions used, no spectral changes attributable to (*Z*) isomers were detected after irradiation.

Based on the spectral features, Rau[11] classified the substituted azobenzenes into three different classes depending on the electronic effects the different substituents exert: namely, the azobenzene type, the aminobenzene type, and the pseudo stilbenes, the latter class containing the azobenzenes substituted with electron-donating and -accepting groups. Each of these classes behave differently as far as the (*Z*)/(*E*) isomerization is concerned and, in particular, the donor-acceptor azobenzenes isomerize on a millisecond time scale at room temperature.[11] The lack of spectral evidence for the (*E*)/(*Z*) isomerization of Ni[L_2(18,14)], Ni[L_2(14)], H_2[L_2(18,14)], or H_2[L_2(14)] could therefore be ascribed to a very fast (*Z*)/(*E*) thermal isomerization process which takes place in the time required to move the sample from the irradiating lamp to the spectrometer (see Experimental Section). These results suggest that in the compounds examined each molecular half (see Scheme 2) behaves as a pseudo stilbene. Moreover, since the *n*-$C_{14}H_{19}$ chain is a common feature of these species, an investigation comparing the ligands with the corresponding Ni^{II} complexes and the rod-like molecules with the lateral alkoxy-substituted ones indicates that neither complexation to an Ni^{II} ion nor the addition of a lateral alkoxy chain to the aromatic ring A (Scheme 2) changes the photophysical properties of these N=N-containing molecules significantly.

Conclusions

The present investigation was planned in order to explore a convenient synthetic route to prepare thermally stable photoisomerizable metallomesogens. All the members of the Ni[L_N(*m*,14)] series display thermotropic mesomorphism except for the complex Ni[L_1(6,14)]. In no case was decomposition observed, the mesophases are stable over a rather large temperature range, and the clearing temperatures decrease as the lateral chains increase in length.

These results prove that the addition of two lateral *n*-alkoxy tails to bis[5-(*p*-*n*-alkylphenylazo)]-substituted *N*,*N*′-salicylidenediaminato species produces the correct molecular geometry for nematic and smectic metal-containing liquid crystalline compounds with good thermal stability. Indeed, a comparison of the newly synthesized mesogens with the corresponding rod-like complexes[8] (Scheme 1) shows that the lateral chains i) lower both the melting and clearing temperatures by some 100°C (*N* = 2) or 200°C (*N* = 1), ii) promote mesomorphism in the *N* = 3 derivatives, and iii) cause more disordered mesophases (N and S_A) to appear in the *N* = 1 and 2 series. Thus, as far as the thermal behaviour is concerned, the addition of lateral groups to metallomesogens with a rod-like structure induces effects similar to those observed for organic liquid crystals.[10]

Practical applications which require metal-based mesogenic optical switching materials can now be considered. Moreover, it has been recently reported that some complexes containing the (salicylidenediaminato)nickel(II) core display second-order nonlinear optical properties,[12] and this makes coordination compounds such as those reported herein even more attractive materials.

Experimental Section

General: IR: Perkin−Elmer F.T.2000; as KBr pellets. − ^{1}H NMR: Bruker WH-300 spectrometer; in $CDCl_3$ solutions, with TMS as internal standard. − Elemental analyses: Perkin−Elmer 2400 analyzer. − Phase transitions and optical textures: Zeiss Axioscope polarizing microscope equipped with a Linkam C0 600 heating stage. − Transition temperatures and enthalpies: Perkin−Elmer DSC-7 differential scanning calorimeter (DSC) operating at a scanning rate of 10.0 °C/min; the apparatus was calibrated with indium (156.6 °C, 3.3 kJ mol). − X-ray diffraction: INEL CPS-120 powder diffractometer using a monochromatized Cu-K_α radiation (λ = 1.54 Å). − Room-temperature absorption spectra of aerated dichloromethane solutions: Perkin−Elmer Lambda 5 spectrometer. − Irradiation experiments: At selected wavelengths by using the 150-W xenon lamp of a Spex Fluorolog II Spectrofluorimeter. − All the commercially available chemicals were used without further purification. The reference compounds $H_2[L_2(14)]$ and $Ni[L_2(14)]$ were prepared as previously reported.[8]

4-(*n*-Hexyloxy)-2-hydroxybenzaldehyde [I(6)]: KOH (0.81 g, 14.5 mmol) and subsequently an ethanolic solution (10 mL) of 1-bromohexane (3.5 mL, 21.7 mmol) was added to a solution of 2,4-dihydroxybenzaldehyde (2.0 g, 14.5 mmol) in ethanol (30 mL). The resulting mixture was heated at reflux for 24 h, allowed to cool to room temp. and 15 mL of H_2O was added. The brownish solid formed was filtered and washed with diethyl ether. The organic layer was dried with Na_2SO_4 and the solvent removed under reduced pressure to afford a yellow oil, which was purified by column chromatography on silica gel (diethyl ether/petroleum ether, 1:1 v:v). Yield 1.82 g (55%). − IR (KBr): $\tilde{\nu}$ = 1677 cm^{-1} (CHO). − ^{1}H NMR ($CDCl_3$): δ = 11.49 (s, 1 H, H^2), 9.70 (s, 1 H, H^1), 7.42 (d, 1 H, H^6), 6.53 (dd, 1 H, H^5), 6.41 (d, 1 H, H^3), 4.03 (t, 2 H, OCH_2).

2-Hydroxy-4-(*n*-octadecyloxy)benzaldehyde [I(18)]: Compound **I(18)** was prepared according to the procedure decribed for **I(6)**. The white solid afforded was purified by recrystallization from ethanol. Yield 2.86 g (50)%. M.p. 60 °C. − IR (KBr): $\tilde{\nu}$ = 1676 cm^{-1} (CHO). − ^{1}H NMR ($CDCl_3$): δ = 11.50 (s, 1 H, H^2), 9.70 (s, 1 H, H^1), 7.41 (d, 1 H, H^6), 6.52 (dd, 1 H, H^5), 6.41 (d, 1 H, H^3), 4.00 (t, 2 H, OCH_2). − $C_{25}H_{42}O_3$ (390.6): calcd. C 76.87, H 10.84; found C 76.67, H 10.84.

4-(*n*-Hexyloxy)-2-hydroxy-5-{[*p*-(*n*-tetradecyl)phenyl]azo}benzaldehyde [II(6,14)]: 4-(*n*-Tetradecylyl)aniline (1.3 g, 45.0 mmol) was dissolved in water (15 mL) and HCl (1.12 mL, 13.49 mmol). The solution was cooled to 0 °C and an aqueous solution (8 mL) of $NaNO_2$ (0.3 g, 48.6 mmol) was added dropwise. **I(6)** (1 g, 45.0 mmol), dissolved in NaOH (5.17 mL, 2 N) and ethanol (3 mL), was added to the solution of the diazonium salt. The reaction mixture was stirred for 1 h at 0 °C and then allowed to warm slowly to room temp. The brown solid formed was filtered, washed several times with H_2O and dissolved in dichloromethane. The organic layer was dried with anhydrous Na_2SO_4, the solvent removed and the crude product purified by column chromatography on silica gel (diethyl ether/petroleum ether, 1:4 v:v). Further purification by recrystallization from methanol afforded the pure product as a yellow solid. Yield 0.70 g (30%). M.p. 81 °C. − IR (KBr): $\tilde{\nu}$ = 1653 cm^{-1} (CHO). − ^{1}H NMR ($CDCl_3$): δ = 14.62 (s, 1 H, H^2), 9.81 (s, 1 H, H^1), 7.93 (s, 1 H, H^6), 7.81 (d, 2 H, $H^{b,c}$), 7.30 (d, 2 H, $H^{a,d}$), 6.58 (s, 1 H, H^3), 4.21 (t, 2 H, OCH_2), 2.67 (t, 2 H, CH_2). − $C_{33}H_{50}N_2O_3$ (522.77): calcd. C 75.82, H 9.64, N 5.36; found C 75.78, H 9.60, N 5.15.

2-Hydroxy-4-(*n*-octadecyloxy)-5-{[4-(*n*-tetradecyl)phenyl]azo}benzaldehyde [II(18,14)]: Compound **II(18,14)** was prepared according to the procedure decribed for **II(6,14)**. Yellow. Yield 0.70 g (40%). M.p. 79 °C. − IR (KBr): $\tilde{\nu}$ = 1653 cm^{-1} (CHO). − ^{1}H NMR ($CDCl_3$): δ = 11.63 (s, 1 H, H^2), 9.82 (s, 1 H, H^1), 7.95 (s, 1 H, H^6), 7.82 (d, 2 H, $H^{b,c}$), 7.31 (d, 2 H, $H^{a,d}$), 6.59 (s, 1 H, H^3), 4.22 (t, 2 H, OCH_2), 2.68 (t, 2 H, CH_2). − $C_{45}H_{74}N_2O_3$ (691.09): calcd. C 78.21, H 10.19, N 4.05; found C 78.31, H 10.15, N 4.34.

***N,N'*-Bis[4-(*n*-hexyloxy)-2-hydroxy-5-{[*p*-(*n*-tetradecyl)phenyl]azo}-benzylidene]ethylenediamine {$H_2[L_1(6,14)]$}:** A mixture of **II(6,14)** (0.25 g, 0.47 mmol) and 1,2-diaminoethane (0.016 mL, 0.23 mmol) in ethanol (15 mL) was refluxed for 4 h. The precipitate was then filtered off and purified by recrystallization from chloroform/ethanol to yield 0.21 g (82%) of a red solid. − ^{1}H NMR ($CDCl_3$): δ = 14.07 (br. s, 2 H, H^2), 8.31 (s, 2 H, H^1), 7.78 (d, 4 H, $H^{b,c}$), 7.69 (s, 2 H, H^6), 7.28 (d, 4 H, $H^{a,d}$), 6.54 (s, 2 H, H^3), 4.16 (t, 4 H, OCH_2), 3.90 (s, 4 H, NCH_2), 2.67 (t, 4 H, CH_2). − $C_{68}H_{102}N_6O_4$ (1069.61): calcd. C 76.36, H 9.80, N 7.86; found C 76.39, H 9.83, N, 7.24.

$H_2[L_1(18,14)]$: Prepared according to the procedure described for $H_2[L_1(6,14)]$ with the appropriate diamine. Yellow orange. Yield 0.230 g (75%). − ^{1}H NMR ($CDCl_3$): δ = 14.10 (br. s, 2 H, H^2), 8.31 (s, 2 H, H^1), 7.77 (d, 4 H, $H^{b,c}$), 7.68 (s, 2 H, H^6), 7.27 (d, 4 H, $H^{a,d}$), 6.53 (s, 2 H, H^3), 4.17 (t, 4 H, OCH_2), 3.69 (s, 4 H, NCH_2), 2.66 (t, 4 H, CH_2). − $C_{92}H_{152}N_6O_4$ (1404.26): calcd. C 78.58, H 10.89, N 5.98; found C 78.88, H 11.24, N 5.80.

$H_2[L_2(6,14)]$: Prepared as described for $H_2[L_1(6,14)]$ with the appropriate diamine. Orange, yield 0.21 g (81%). − ^{1}H NMR ($CDCl_3$): δ = 14.30 (br. s, 2 H, H^2), 8.28 (s, 2 H, H^1), 7.77 (d, 4 H, $H^{b,c}$), 7.68 (s, 2 H, H^6), 7.27 (d, 4 H, $H^{a,d}$), 6.52 (s, 2 H, H^3), 4.17 (t, 4 H, OCH_2), 3.69 (t, 4 H, NCH_2), 2.66 (t, 4 H, CH_2), 2.12 (m, 2 H, NCH_2CH_2). − $C_{69}H_{104}N_6O_4$ (1081.62): calcd. C 76.62, H 9.69, N 7.77; found C 76.70, H 9.70, N 7.75.

$H_2[L_2(18,14)]$: Prepared according to the procedure decribed for $H_2[L_1(6,14)]$ with the appropriate diamine. Yellow orange, yield 0.28 g (90%). − ^{1}H NMR ($CDCl_3$): δ = 14.26 (br. s, 2 H, H^2), 8.29 (s, 2 H, H^1), 7.78 (d, 4 H, $H^{b,c}$), 7.69 (s, 2 H, H^6), 7.27 (d, 4 H, $H^{a,d}$), 6.53 (s, 2 H, H^3), 4.17 (t, 4 H, OCH_2), 3.69 (t, 4 H, NCH_2), 2.66 (t, 4 H, CH_2), 2.13 (m, 2 H, NCH_2CH_2). − $C_{93}H_{154}N_6O_4$ (1420.28): calcd. C 78.65, H 10.93, N 5.92; found C 78.60, H 10.70, N 5.99.

$H_2[L_3(6,14)]$: Prepared according to the procedure decribed for $H_2[L_1(6,14)]$ with the appropriate diamine. Dark red, yield 0.21 g (70%). − ^{1}H NMR ($CDCl_3$): δ = 14.48 (br. s, 2 H, H^2), 8.25 (s, 2 H, H^1), 7.78 (d, 4 H, $H^{b,c}$), 7.70 (s, 2 H, H^6), 7.27 (d, 4 H, $H^{a,d}$), 6.53 (s, 2 H, H^3), 4.18 (t, 4 H, CH_2), 3.46 (s, 4 H, NCH_2), 2.66 (t, 4 H, OCH_2), 1.32 [s, 6 H, $C(CH_3)_2$]. − $C_{71}H_{108}N_6O_4$ (1109.68): calcd. C 76.85, H 9.81, N 7.50; found C 76.81, H 9.79, N 7.55.

$H_2[L_3(18,14)]$: Prepared according to the procedure decribed for $H_2[L_1(6,14)]$ with the appropriate diamine. Dark orange, yield 0.23 g (73%). − ^{1}H NMR ($CDCl_3$): δ = 14.51 (br. s, 2 H, H^2), 8.25 (s, 2 H, H^1), 7.77 (d, 4 H, $H^{b,c}$), 7.70 (s, 2 H, H^6), 7.27 (d, 4 H, $H^{a,d}$), 6.53 (s, 2 H, H^3), 4.17 (t, 4 H, OCH_2), 3.46 (s, 4 H, NCH_2), 2.66 (t, 4 H, CH_2), 1.25 [s, 6 H, $C(CH_3)_2$]. − $C_{95}H_{158}N_6O_4$ (1448.34): calcd. C 78.78, H 5.80, N 11.00; found C 78.72, H 5.90, N 11.50.

$Ni[L_1(6,14)]$ (1): A mixture of nickel(II) acetate tetrahydrate (0.02 g, 0.09 mmol) and an equimolar amount of $H_2[L_1(6,14)]$ (0.1 g) in ethanol (15 mL) was refluxed for 4 h. The dark red solid formed was filtered off and the pure product was obtained by recrystallization from chloroform/ethanol. Yield 0.09 g (86%). − ^{1}H NMR ($CDCl_3$): δ = 7.70 (d, 4 H, $H^{b,c}$), 7.55 (s, 2 H, H^6), 7.32 (br. s, 2 H, H^1), 7.19 (d, 4 H, $H^{a,d}$), 6.60 (s, 2 H, H^3), 4.09 (t, 4 H, OCH_2), 3.33 (s, 4 H, NCH_2), 2.61 (t, 4 H, CH_2). − $C_{68}H_{102}N_6NiO_4$

(1126.29): calcd. C 72.52, H 9.13, N 7.46; found C 72.62, H 9.12, N 7.46.

Ni[L_1(18,14)] (2): Prepared according to the procedure decribed for Ni[L_1(6,14)] with the appropriate ligand. Brick red, yield 0.073 g (70%). − ^{1}H NMR ($CDCl_3$): δ = 7.72 (d, 4 H, $H^{b,c}$), 7.57 (s, 2 H, H^6), 7.39 (d, 2 H, H^1), 7.22 (d, 4 H, $H^{a,d}$), 6.62 (s, 2 H, H^3), 4.09 (t, 4 H, OCH_2), 3.37 (s, 4 H, NCH_2), 2.63 (t, 4 H, CH_2). − $C_{92}H_{150}N_6NiO_4$ (1462.93): calcd. C 75.53, H 10.33, N 5.74; found C 75.60, H 10.59, N 5.88.

Ni[L_2(6,14)] (3): Prepared according to the procedure decribed for Ni[L_1(6,14)] with the appropriate ligand. Brown, yield 0.057 g (53%). − ^{1}H NMR ($CDCl_3$): δ = 7.73 (d, 4 H, $H^{b,c}$), 7.57 (s, 2 H, H^6), 7.25 (d, 6 H, $H^{a,d}$ and H^1), 6.60 (s, 2 H, H^3), 4.10 (t, 4 H, OCH_2), 3.50 (t, 4 H, NCH_2), 2.64 (t, 4 H, CH_2), 1.89 (m, 2 H, NCH_2CH_2). − $C_{69}H_{102}N_6NiO_4$ (1138.30): calcd. C 72.81, H 9.03, N 7.38; found C 72.80, H 9.10, N 7.40.

Ni[L_2(18,14)] (4): Prepared according to the procedure decribed for Ni[L_1(6,14)] with the appropriate ligand. Ochre yellow, yield 0.095 g (92%). − ^{1}H NMR ($CDCl_3$): δ = 7.73 (d, 4 H, $H^{b,c}$), 7.57 (s, 2 H, H^6), 7.25 (d, 6 H, $H^{a,d}$ and H^1), 6.60 (s, 2 H, H^3), 4.10 (t, 4 H, OCH_2), 3.50 (t, 4 H, NCH_2), 2.64 (t, 4 H, CH_2), 1.89 (m, 2 H, NCH_2CH_2). − $C_{93}H_{152}N_6NiO_4$ (1476.96): calcd. C 75.63, H 10.37, N 5.69; found C 75.73, H 10.46, N 5.70.

Ni[L_3(6,14)] (5): Prepared according to the procedure decribed for Ni[L_1(6,14)] with the appropriate ligand. Brown, yield 0.060 g (57%). − ^{1}H NMR ($CDCl_3$): δ = 7.74 (d, 4 H, $H^{b,c}$), 7.59 (s, 2 H, H^6), 7.26 (d, 4 H, $H^{a,d}$), 7.13 (s, 2 H, H^1), 6.62 (s, 2 H, H^3), 4.11 (t, 4 H, CH_2), 3.26 (s, 4 H, NCH_2), 2.65 (t, 4 H, OCH_2), 1.48 (s, 6 H, $C(CH_3)_2$). − $C_{71}H_{106}N_6NiO_4$ (1166.37): calcd. C 73.11, H 9.16, N 7.21; found C 73.40, H 9.25, N 7.32.

Ni[L_3(18,14)] (6): Prepared according to the procedure decribed for Ni[L_1(6,14)] with the appropriate ligand. Red, yield 0.097 g (94%). − ^{1}H NMR ($CDCl_3$): δ = 7.74 (d, 4 H, $H^{b,c}$), 7.59 (s, 2 H, H^6), 7.26 (d, 4 H, $H^{a,d}$), 7.12 (s, 2 H, H^1), 6.62 (s, 2 H, H^3), 4.10 (t, 4 H, CH_2), 3.25 (s, 4 H, NCH_2), 2.65 (t, 4 H, OCH_2), 1.26 [s, 6 H, $C(CH_3)_2$). − $C_{95}H_{156}N_6NiO_4$ (1505.01): calcd. C 75.82, H 10.45, N 5.58; found C 75.73, H 10.75, N 5.83.

Acknowledgments

This work was partially supported by the Italian Ministero dell′Università e della Ricerca Scientifica e Tecnologica (MURST), Consiglio Nazionale delle Ricerche (CNR) and Regione Calabria (POP 94/99). We thank Dr. Francesco Barigelletti (Istituto FRAE-CNR, Bologna) for his help during the (*E*)/(*Z*) photoisomerization experiments.

[1] S. Xie, A. Natansohn, P. Rochon, *Chem. Mater.* **1993**, *5*, 403−411.
[2] J. Newton, H. Walton, H. Coles, P. Hodge, *Mol. Cryst. Liq. Cryst.* **1995**, *260*, 107−113.
[3] O. Tsutsumi, T. Shiono, T. Ikeda, G. Galli, *J. Phys. Chem. B* **1997**, *101*, 1332−1337 and references therein.
[4] S. Furumi, H. Akiyama, S. Morino, K. Ichimura, *J. Mater. Chem.* **1998**, *8*, 65−70.
[5] [5a] D. W. Bruce in: *Inorganic Materials* (Eds.: D.W. Bruce, D. O′Hare), Wiley, Chichester, **1992**. − [5b] J. L. Serrano, *Metallomesogens*, VCH, Weinheim, **1996**. − [5c] A. M. Giroud-Godquin in *Handbook of Liquid Crystals*, vol. 2B (Eds.: D. Demus, J. Goodby, G. W. Gray, H. W. Spiess, V. Vill), Wiley-WCH, Weinheim, **1998**.
[6] F. Neve, M. Ghedini, O. Francescangeli, S. Campagna, *Liq. Cryst.* **1998**, *24*, 673−680.
[7] M. Ghedini, F. Neve, D. Pucci, *Eur. J. Inorg. Chem.* **1998**, 501−504.
[8] I. Aiello, M. Ghedini, F. Neve, D. Pucci, *Chem. Mater.* **1997**, *9*, 2107−2112.
[9] D. Demus in *Handbook of Liquid Crystals*, vol. 1 (Eds.: D. Demus, J. Goodby, G. W. Gray, H. W. Spiess, V. Vill), Wiley-WCH, Weinheim, **1998**.
[10] W. Weissflog in *Handbook of Liquid Crystals*, vol. 2B (Eds.: D. Demus, J. Goodby, G. W. Gray, H. W. Spiess, V. Vill), Wiley-WCH, Weinheim, **1998**.
[11] H. Rau in *Photochromism* (Eds.: H. Durr, H. Bouas-Laurent), Elsevier, Amsterdam, **1990**, chapter 4.
[12] S. Di Bella, I. Fragalà, I. Ledoux, M. A. Diaz-Garcia, T. J. Marks, *J. Am. Chem. Soc.* **1997**, *119*, 9550−9957.

Received December 21, 1998
[I98445]

Metal Tetrahydridoborates and Tetrahydroborato Metallates, 24[+] Solvates of Sodium Bis(borane)dimethylamide

Heinrich Nöth*[a] and Steffen Thomas[a]

Keywords: Sodium bis(borane)dimethylamide solvates / X-ray structure / Reduction

The reaction of sodium metal with dimethylamine–borane in THF yields $Na[(H_3B)_2NMe_2]$ (**1**) which can be isolated as $\{Na[(H_3B)_2NMe_2]\}_5$·THF or as $Na[(H_3B)_2NMe_2]$·15-crown-5 (**2**) and $Na[(H_3B)_2NMe_2]$·benzo-15-crown-5 (**3**) after addition of the appropriate crown ether to the THF solution of **1**. Reaction of **1** with $ZrCl_4$ yields $Me_2HN–BH_2–NMe_2–BH_3$ (**4**), the structure of which has been determined. In THF solution, **1** reduces aldehydes, ketones, acyl chlorides, and esters to the corresponding alcohols. It also reacts slowly with nitriles and allylbenzene. Compound $(\mathbf{1})_5$·THF crystallizes in an extended three-dimensional lattice, in which the Na atoms are coordinated by 6–9 hydridic H atoms, while **3** is a molecular compound in the solid state. Only one hydrogen atom of each BH_3 group coordinates to the sodium center. On the other hand, **4** forms dimeric associates in the solid state through N–H···H–B interactions.

Introduction

As reducing agents, lithium dialkylamidotrihydridoborates, $Li(H_3BNR_2)$, have many advantages over MBH_4 compounds (M = Li, Na) and, in some respects, over $LiAlH_4$ as well.[2] The structures of the solvates of these amidotrihydridoborates $M(R_2NBH_3)$·*n*L depend on the type and number of ligands L;[3] all of them are characterized by metal−nitrogen bonds as well as M···H−B interactions. A metal−nitrogen interaction is not possible in alkali metal salts of the anion $H_3B-NMe_2-BH_3^-$ because the nitrogen atom is tetracoordinated. However, the hydridic atoms of this anion with an alkali metal cation is of interest, particularly in comparison to solvates of alkali metal tetrahydridoborates.[1]

Synthesis

Compound $Na[H_3B-NMe_2-BH_3]$ (**1**) was first obtained by addition of NaH to $Me_2NB_2H_5$[4] according to Equation 1. It was isolated as a hemidioxanate. **1** is also formed when $NaBH_4$ is allowed to react with $Me_2NB_2H_5$ in diglyme, as described by Equation 2.[5] A possible synthesis from $NaNMe_2$ and BH_3·THF is difficult to perform because pure $NaNMe_2$ is not readily accessible. We now report an efficient synthesis starting from the readily available $Me_2NH·BH_3$ and elemental sodium in the presence of THF. This process is described by Equation 3.

$$\mu\text{-}Me_2NB_2H_5 + NaH \rightarrow Na[H_3B-NMe_2-BH_3]\ (\mathbf{1}) \quad (1)$$

$$\mu\text{-}Me_2NB_2H_5 + 2\ NaBH_4 \rightarrow Na[H_3B-NMe_2-BH_3] + NaB_2H_7 \quad (2)$$

$$4\ Me_2NH·BH_3 + 2\ Na \rightarrow 2\ Na[H_3B-NMe_2-BH_3] + H_2 + 2\ Me_2NH \quad (3)$$

Compound **1** slowly decomposes in THF solution with formation of $NaBH_4$ and dimeric dimethylaminoborane (Equation 4). In addition, small amounts of $(Me_2N)_2BH$ [$\delta^{11}B = 29.7$, $^1J(^{11}BH) = 132$ Hz][6] can be detected in the ^{11}B-NMR spectrum of the solution. Experimental evidence has shown that the faster the rate of formation of **1**, the lower the amount of by-products. A higher reaction rate can be achieved by providing an excess of sodium metal, if possible in a highly dispersed form. The shortest reaction times were achieved by using sodium metal dispersed on an Al_2O_3 support, which allowed the conversion of 0.1 mol of $Me_2NH·BH_3$ into **1** within 30 min.

$$2\ \mathbf{1} \rightarrow 2\ NaBH_4 + [Me_2NBH_2]_2 \quad (4)$$

Following the dissolution of solid **1**·*n*THF in toluene, single crystals were obtained, which were shown to be $\{Na[H_3B-NMe_2-BH_3]\}_5$·THF by X-ray structure analysis. Addition of 15-crown-5 or benzo-15-crown-5 to the THF solution of **1** yielded the 1:1 solvates of the crown ethers $[Na(15\text{-crown-5})][H_3B-NMe_2-BH_3]$ (**2**) and $[Na(\text{benzo-15-crown})][H_3B-NMe_2-BH_3]$ (**3**). Single crystals could only be obtained in the case of **3**.[7]

IR and NMR Spectra

While the IR spectra of covalently bonded BH_4 groups, particularly of mononuclear tetrahydroborates, usually provide conclusive evidence with regard to the bonding mode of the BH_4 ligand,[8] this is not the case if highly polar tetrahydridoborates are present, as would be expected for **1**.[9] Nevertheless, the IR spectra of 3 different compounds derived from **1**, depicted in Figure 1, show quite drastic differences in the B−H stretching region. Consequently, the

[+] Part 23: Ref.[1]

[a] Institute of Inorganic Chemistry, University of Munich, Butenandtstr. 5−13, Haus D, D-81377 München, Germany

 © WILEY-VCH Verlag GmbH, D-69451 Weinheim, 1999 1434−1948/99/0808−1373 $ 17.50+.50/0

structures of **1** in THF solution, in solid $(\mathbf{1})_5$·THF, and in **3** must be significantly different. We attribute the strong band of **1** seen at 2291 cm^{-1} to $\nu_{as}BH_3$, and the band of medium intensity at 2251 cm^{-1} to ν_sBH_3.

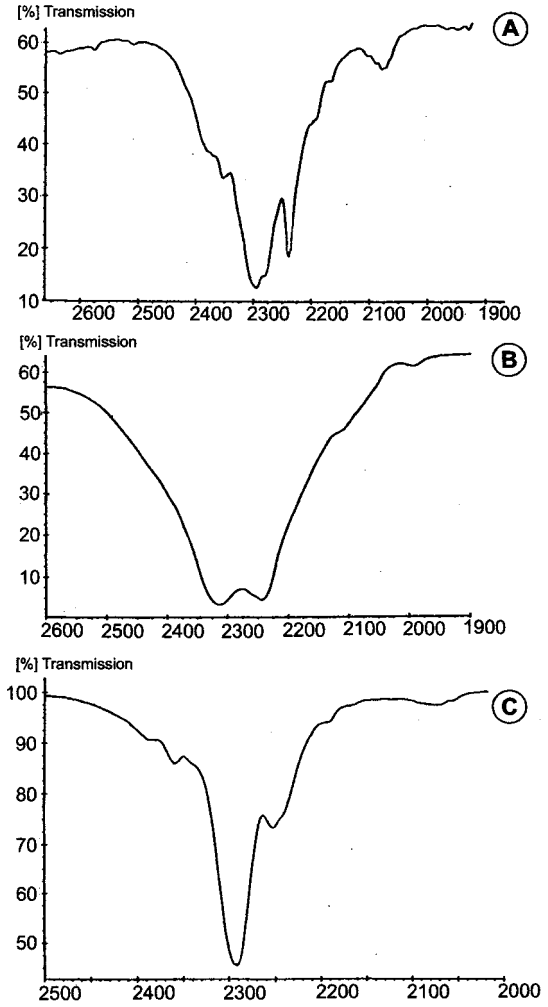


Figure 1. IR spectra in the B−H stretching band region of (A) solid $(\mathbf{1})_5$·THF, (B) **1** in THF solution, and (C) **3** in nujol

On the other hand, the IR spectrum of $(\mathbf{1})_5$·THF in nujol shows two strong bands at 2312 and 2244 cm^{-1}, along with shoulders, which cannot be unequivocally assigned. These observations suggest that the anion in **1** must have a different structure to that seen in THF solution. Compound **3** gives a better resolved IR spectrum. The three intense bands at 2294, 2281 and 2239 cm^{-1}, correspond to BH_3 groups in which a single hydrogen bond is present (ν_{MHB} = 2239 cm^{-1}), with the strongest bands being attributable to $\nu_{as}BH_3$. The presence of BH_3 groups in **1**−**3** is clearly demonstrated by 1:3:3:1 quadruplets in the ^{11}B-NMR spectrum with $^1J(^{11}B^1H)$ values ranging from 90 to 92 Hz, typical for tetracoordinated B atoms.

Reactions

Compound **1** may be a useful reducing agent having properties akin to those of $NaBH_4$. Some "standard" reductions were therefore tested, employing an acyl chloride, an aldehyde, two ketones, an ester and amide, as well as a nitrile, a carboxylic acid, and allylbenzene. Alcohols were obtained as reduction products of benzoyl chloride, benzaldehyde, acetophenone, and cyclohexanone. All other functional groups were reduced only slowly. Moreover, not all of the available hydride was utilized in the reactions (Table 1). The reaction of $ZrCl_4$ with **1** in a 1:4 molar reaction yielded small quantities of $Me_2NH{-}BH_2{-}NMe_2{-}BH_3$ (**4**). This compound is well known.[10] Its crystal structure has now been determined (vide infra).

X-ray Structures

The crown ether complex **3** was shown to be a molecular compound (or contact ion pair) in the solid state by X-ray crystallography. The compound crystallizes from THF solution in the monoclinic system, space group *Cc*, $Z = 8$.

Figure 2 shows that the anion $H_3B{-}NMe_2{-}BH_3^-$ coordinates to the sodium center through one hydridic H atom per BH_3 group. Thus, the coordination number at the sodium center is seven, resulting from two hydrogen and five oxygen atoms. The latter are arranged almost in a plane, and the Na atom resides above this plane with Na−O lengths ranging from 2.426(3) to 2.513(3) Å. Two different Na−B lengths [2.944(5) and 3.110(6) Å] indicate that the anion is not symmetrically coordinated to the metal center. On the other hand, the B−N−B bond angle is close to the ideal tetrahedral angle.

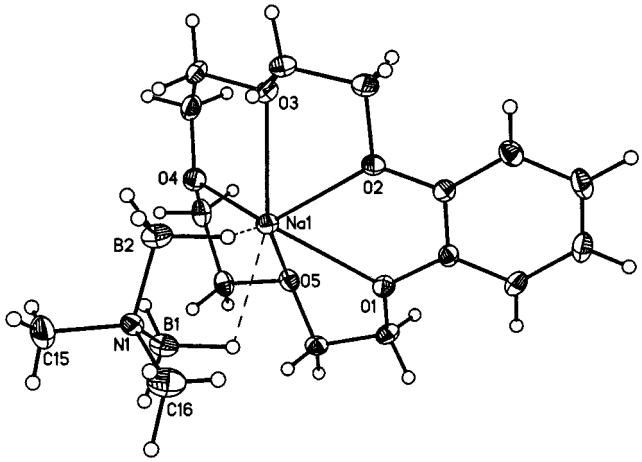


Figure 2. Molecular structure of **3** in the crystal; thermal ellipsoids represent a 25% probability; estimated standard deviations are shown in parentheses; selected atom distances [Å] and bond angles [°]: Na1−O1 2.469(3), Na1−O2 2.465(3), Na1−O3 2.449(3), Na1−O4 2.426(3), Na1−O5 2.513(3), Na1···B1 2.944(5), Na1···B2 3.110(6), N1−B1 1.580(6), N1−B2 1.580(6); O2−Na1−O1 63.9(1), O3−Na1−O2 65.9(1), O4−Na1−O3 68.0(1), O4−Na1−O5 67.64(9), O1−Na1−O5 65.29(1), B1−Na1−B2 51(1), C15−N1−C16 108.3(3), B1−N1−B2 110.9(3), B1−N1−C15 109.9(3), B2−N1−C15 109.2(3)

In contrast to **3**, the structure of compound $(\mathbf{1})_5$·THF is much more complex in the solid state. There are five different "molecules" of **1** in the asymmetric unit. This is rep-

resented in Figure 3, while Figure 4 shows a plot of the three-dimensional array.

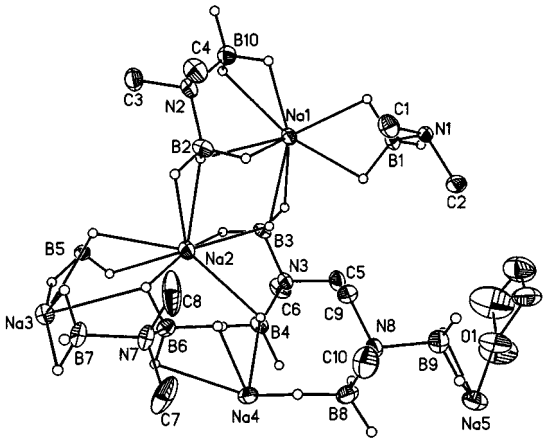


Figure 3. Atoms in the asymmetric unit of $(\mathbf{1})_5$·THF in an ORTEP representation with thermal ellipsoids at a 25% probability level; selected atom distances [Å] and bond angles [°]: Na1···B1 2.828(4), Na1···B2 2.899(3), Na1···B3 2.850(5), Na1···B10 2.888(5), Na2···B6 2.943(5), Na4···B6 2.970(5), Na5···B9 2.795(6), Na5−O1 2.310(4), N1−B1 1.588(5), N2−B2 1.581(6), N2−B10 1.588(5); B1−Na1−B3 107.6(2), B1−Na1−B2 124.5(2), B1−Na1−B10 118.5(2), B2−Na1−B10 53.4(2), B3−Na2−B2 88.7(2), B3−Na2−B6 135.9(1), B3−Na2−B5 119.5(2), B3−Na2−B4 51.4(1), B7−Na3−B7′ 86.9(1), B7−Na3−B5 135.6(1), B7−Na3−B4′ 120.2(1), B7−Na3−B6 51.7(1), B1′−Na4−B4 86.9(1), B1′−Na4−B6 122.5(1), Ba′−Na4−B8 86.2(1), B1′−Na4−B5′ 53.2, O1−Na5−B9 109.0(2), O1−Na5−B10′ 109.0(2), O1−Na5−B5′ 103.4(2), B9−Na5−B10′ 129.4(2), B3−N3−B4 110.7(3), B2−N2−B10 110.2(3), C3−N2−C4 108.9(3)

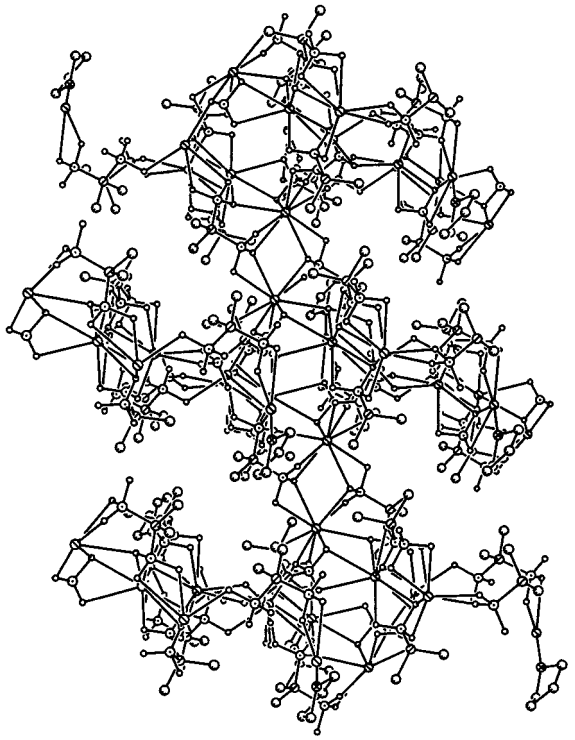


Figure 4. Plot of the three-dimensional array of the unit $(\mathbf{1})_5$·THF; view down the *b* axis

All hydrogen atoms of the BH_3 groups are involved in Na···H−B interactions; one shows contacts with two different Na atoms (as a $\mu^2{}_1$ bridge), while the other two H atoms coordinate either through a $\mu^1{}_1$ interaction to two different Na atoms or through a $\mu^1{}_2$ interaction to one Na center (see the "coordination polyhedra" in Figure 5). If we consider only the corresponding boron atoms ($NaOB_3$ polyhedron), then a slightly distorted tetrahedral array is observed with O−Na5−B bond angles ranging from 103.4(2)° to 109.0(2)°. Atom Na1 is surrounded by five boron atoms at distances of 2.828(4) to 2.899(5) Å, as well as by nine H atoms. Nine H atoms are associated with atom Na3, while Na4, like Na2, is coordinated by eight hydridic hydrogen atoms. In contrast, but in line with expectation, the B−N−B bond angles of all five different $H_3B{-}NMe_2{-}BH_3^-$ anions are close to the ideal tetrahedral bond angle, varying only from 108.9(3) to 110.2(3)°. Moreover, the B−N bond lengths are equal within the standard deviation, the average value being 1.58 Å, which is typical for a B−N single bond involving sp^3-type atoms (in cubic BN 1.56 Å[11]). Figure 4 depicts the three-dimensional array of atoms in the solid state of compound (**1**)5·THF. One must assume that this lattice is broken up into smaller units upon dissolution in solvents such as THF.

Figure 6 shows the molecular structure of two molecules of the amine−borane **4**. This species represents the BN analogue of 2,2,4,4-tetramethylbutane. The two terminal B−N bonds [1.600(2), 1.599(2) Å] have equal lengths, while the central B−N bond is slightly but significantly shorter [1.583(2) Å]. Interestingly, the B−N−B and the N−B−N bond angles are slightly wider than might be expected for tetracoordinated N and B atoms [113.4(1), 113.9(1)°].

N−C bond lengths in **4** lie in the expected range (1.477−1.487 Å) for single bonds.[12] The most interesting aspect of the structure of **4** in the solid state is its association. Crystallographically, there is a center of inversion between each pair of molecules, resulting in close contacts between the NH proton with two hydridic hydrogen atoms of the BH_3 group (H1−H3c 2.27 Å, H1a−H3b 2.38 Å; angle N1a−H1a−H3c 151°, N1a−H1a−H3b 135°) . This implies that the observed packing is a result of a dipolar interaction between hydrogen atoms of opposite polarization. Such interactions have previously been observed in the case of $H_3N{-}BH_3$,[13] and other amine−boranes[14] and have also been invoked as being responsible for determining the conformations of BH_3 adducts of triazacyclohexanes and heteroatom-azacyclohexanes $[S_{2-n}(NMe)_{n+1}(CH_2)_3]$.[15]

Discussion

Sodium bis(borane)dimethylamide is readily obtained in excellent yield by allowing elemental sodium to react with dimethylamine−borane in the presence of THF. Under similar conditions, elemental Li reacts with $Me_2NH{\cdot}BH_3$ with formation of $Li(Me_2NBH_3)$ but not of $Li(H_3B{-}NMe_2{-}BH_3)$.[16] It seems likely that $Na(Me_2NBH_3)$, which should be formed initially, is a very

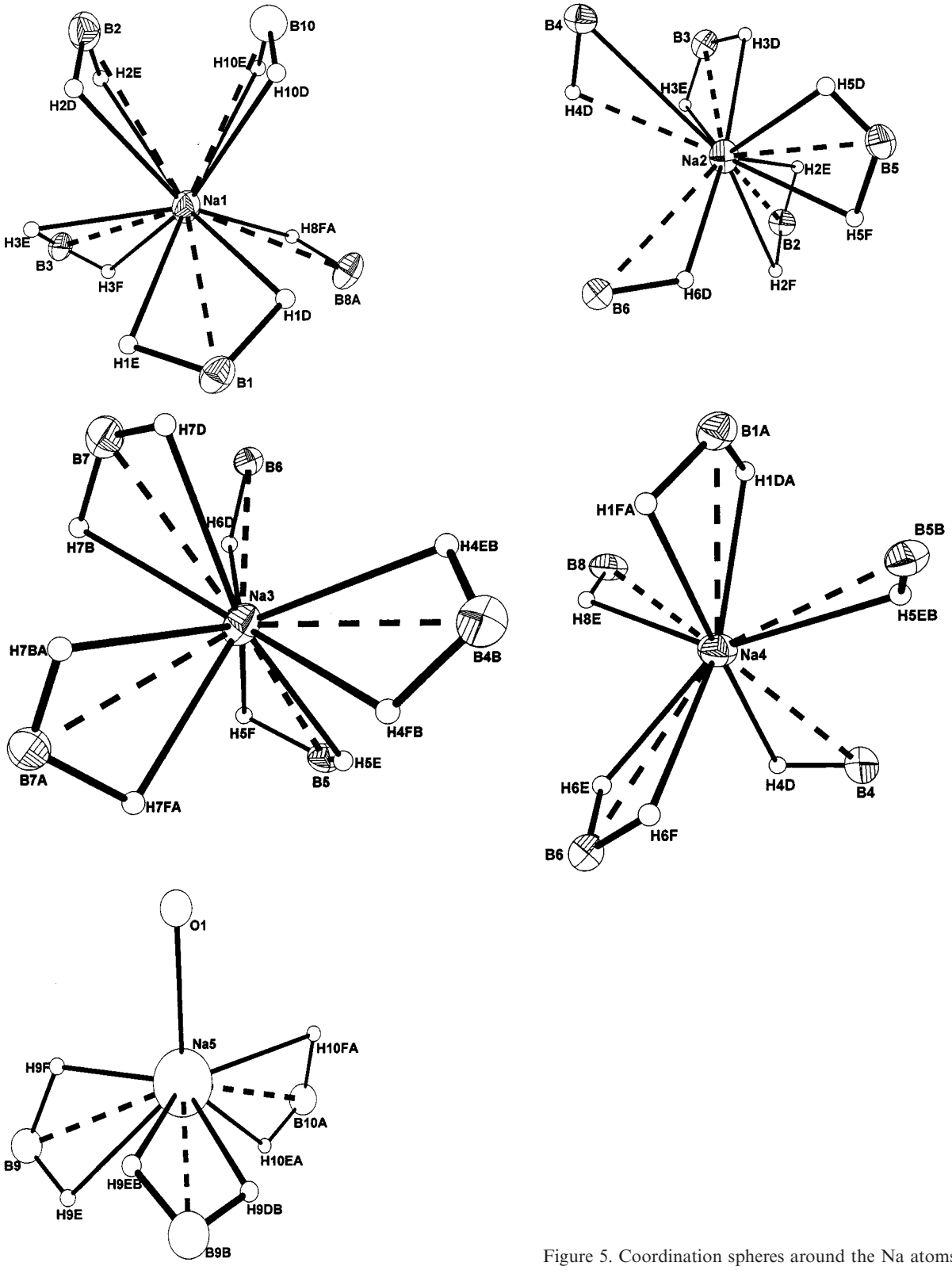


Figure 5. Coordination spheres around the Na atoms in $(\mathbf{1})_5$·THF

strong base and thus displaces Me_2NH from the amine–borane according to Equation 5.

$$Na(Me_2NBH_3) + Me_2NH{\cdot}BH_3 \rightarrow Na(H_3B{-}NMe_2{\cdots}BH_3) + Me_2NH \quad (5)$$

Compound **1** is soluble in THF (up to 1.57 M at 25°C) and may be present in solution as an ion pair $(THF)_nNa(H_3B{-}NMe_2{-}BH_3)$, possibly with a structure similar to that adopted by the crown-ether solvate **3**. On the other hand, differences are seen in the IR spectra of a

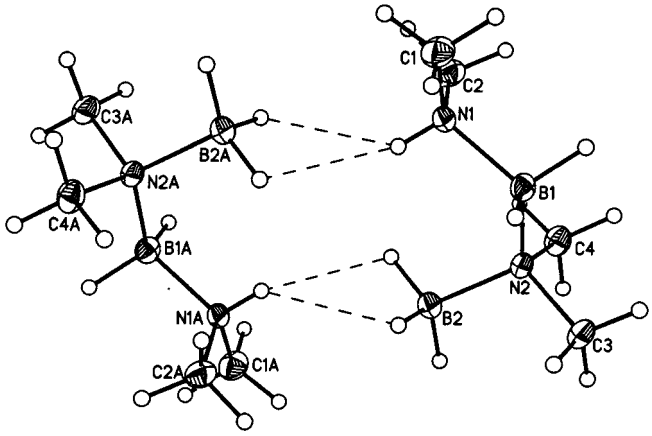


Figure 6. ORTEP plot of two molecules of **4**; thermal ellipsoids are depicted at a 25% probability level; selected bond lengths [Å] and bond angles [°]: B1−N1 1.599(2), B1−N2 1.589(2), B2−N2 1.600(2), N2−C3 1.488(2), N2−C4 1.481(2), N1−C2 1.477(2), N1−C1 1.483(2); N1−B1−N2 113.9(1), B2−N2−B1 113.4(1), C3−N2−B1 105.0(1), C3−N2−B2 108.3(1), C2−N1−B1 116.5(1)

THF solution of **1** and of the well-defined compound **3**. Nevertheless, these spectra are not too dissimilar when compared to that of $(\mathbf{1})_5$·THF.

The good solubility of **1** in THF is in remarkable contrast to the limited solubility of $NaBH_4$ in this solvent. Therefore, **1** in THF solution may represent a promising reducing agent, as has been shown for typical organic functional groups. Compared to $NaBH_4$, compound **1** is a stronger reducing agent in that it also reduces benzoic acid, benzamide, ethyl benzoate, and benzonitrile. It also acts as a mild hydroboration agent, for example attacking styrene. The structures of (**1**)5·THF and **3** have no precedent in the field of alkali metal hydridoborates. Thus, **3** is the first example where "single" M···H−B bridges are present, while (**1**)5·THF forms a three-dimensional array comprising 7−9 coordinated sodium atoms (taking into account only O and H atoms), involving all hydridic hydrogen atoms of the anion $H_3B-NMe_2-BH_3$. The bridging mode of the BH_3 units resembles that of BH_4 groups in dimeric $LiBH_4$·TMEDA[17] and in dimeric $NaBH_4$·PMDETA,[1] e.g. two hydrogen atoms bridge to two different Na centers, while one hydrogen atom connects to two metal centers.

Conclusion

Compound **1** is a nice example where changes in the coordination mode of the $H_3B-NMe_2-BH_3^-$ anion, as brought about by different ligands, can be studied. It is evident from the examples presented here that an expected three-dimensional structure of **1** (which is not yet known) breaks up into smaller units upon solvation. $(\mathbf{1})_5$·THF still retains the three-dimensional association, which most likely breaks down into ion pairs in THF solution or upon addition of a crown ether. This is in agreement with previous structural studies on $Li(R_2NBH_3)$ ether solvates[3] and on $LiBH_4$ ether solvates.[9][18] Although $NaBH_4$ has been known for more than 40 years, its structural chemistry remains largely unexplored. Compound **1** would seem to represent another reducing agent that may compete with lithium amidohydridoborates as a convenient and easy to handle reagent.

Experimental Section

General: All experiments were performed under anhydrous conditions in flame-dried glassware using Schlenk techniques and N_2 as a protecting gas. − NMR spectra were recorded with a Bruker AC 200 or a JEOL GSX 270 instrument (^1H, ^{13}C: reference C_6D_6 or $SiMe_4$; ^{11}B: ext. BF3·OEt2; ^7Li ext. aq. LiCl). − IR: Nicolet 520 FT-IR spectrometer.

Preparation of a Solution of Sodium Bis(borane)dimethylamide (1) in THF: Sodium pieces (2.00 g, 87 mmol) were suspended in stirred THF (150 mL). Then, a concentrated solution of $Me_2NH{\cdot}BH_3$ (5.1 g, 87 mmol) in THF was added and the mixture was refluxed for 6 d. A turbid solution was formed and a gas was evolved, leaving sodium pellets. The solution showed the following ^{11}B-NMR signals: δ = −42.4 (very weak, $NaBH_4$), −12.5 [q, $^1J(^{11}B^1H)$ = 91 Hz, **1**], 6.3 [very weak t, $(Me_2NBH_2)_2$], 29.7 [d, $^1J(^{11}B^1H)$ = 128 Hz, $(Me_2N)_2BH$]. 1.0 g (43 mmol) of Na was recovered. All volatile materials were then removed from the solution in vacuo (down to 10^{-3} Torr). Yield: 3.8 g of **1** (ca. 92%) as a fine white powder. − Solubility: 1.57 M in THF at 25°C. − IR (cm^{-1}, BH region): $\tilde{\nu}$ = 2384 w, 2359 w, 2291 vs, 2251 m. − $C_2H_{12}B_2NNa$ (94.73): calcd. B 22.82, N 14.79, Na 22.99; found B 22.1, N 13.9, Na 20.5.

Pentakis[sodium bis(borane)dimethylamide]·Tetrahydrofuran [$(\mathbf{1})_5$·THF]: Prepared as described for **1**. All volatiles were removed at 10 Torr. The solid residue was then suspended in toluene (20 mL) and the suspension was heated to reflux. Insoluble material was then removed from the hot solution by filtration through a G3 glass frit. Pentane (10 mL) was added to the filtrate, which subsequently became turbid. After cooling to −20°C, crystals of m.p. 7°C were deposited. The supernatant solution was separated by means of a syringe. Further crystals separated from this solution. Although these were largely intergrown, single crystals could easily be separated. − ^{11}B NMR (THF): δ = −10.1 [q, $^1J(^{11}B^1H)$ = 91 Hz]. − ^1H NMR (C_6D_6): δ = 2.33 (s, 30 H), 3.56 (m, 8 H, THF). − IR (cm^{-1}, Nujol): $\tilde{\nu}$ = 2312 vs, 2244 vs, 1627 w, 1579 w, 1469 vs, 1445 m, 1427 w, 1398 w, 1384 w, 1370 w, 1214 vs, 1177 vs, 1159 vs, 1032 s, 1031 vs, 935 m, 914 m, 819 m. − $C_{14}H_{68}B_{10}N_5Na_5O$ (545.77): calcd. C 30.81, H 12.56, N 12.83; found C 30.62, H 12.52, N 12.65.

Sodium Bis(borane)dimethylamide·15-Crown-5 (2): (**1**)5·THF (1.1 g, 2.02 mmol) was dissolved in THF (10 mL) and 15-crown-5 (2 mL, 10 mmol) was added to the stirred solution by means of a syringe. The solution showed ^{11}B-NMR signals at δ = −9.4 [q, $^1J(^{11}B^1H)$ = 91 Hz, **1**] and −12.4 (s) in a 21:1 ratio. Crystals separated from the solution within 2 d at −14°C. They were extensively intergrown and no single crystal could be separated. Yield: 2.3 g of **2** (73%); m.p. 175°C. − ^{11}B NMR: δ = −7.6 [q, $^1J(^{11}B^1H)$ = 92 Hz] in DMF; δ = −9.2 [q, $^1J(^{11}B^1H)$ = 91 Hz] in glyme, besides very weak signals at δ = 21.0 and 11.9; δ = −9.3 [q, $^1J(^{11}B^1H)$ = 91 Hz] in toluene, δ = −9.4 [q, $^1J(^{11}B^1H)$ = 93 Hz] in diethyl ether; δ = −9.3 [q, $^1J(^{11}B^1H)$ = 90 Hz] in benzene. − IR (cm^{-1}, BH region): $\tilde{\nu}$ = 2340 s, 2293 vs, 2237 s, 2163 m. − $C_{12}H_{32}B_2NNaO_5$ (315.00): calcd. C 45.76, H 10.24, B 6.86, N 4.45; found C 47.30, H 10.45, B 6.50, N 3.93.

Sodium Bis(borane)dimethylamide·Benzo-15-crown-5 (3): The crown ether (1.34 g, 5 mmol) was dissolved in THF (20 mL) with stirring.

To this solution was added a solution of **1** in THF (3.36 mL, 1.49 M). After concentrating the solution in vacuo to a volume of ca. 10 mL, crystals separated within 2 months at −14°C, which were eventually isolated. Yield: 1.49 g of **2** (82%); m.p. 129°C (dec.). − ^{11}B NMR (DMSO): δ = −7.9 [q, $^{1}J(^{11}B^{1}H)$ = 90 Hz]. − IR (cm^{-1}, BH region): $\tilde{\nu}$ = 2295 vs, 2281 vs, 2239 vs, 2168 sh, 2194 sh. − $C_{18}H_{32}B_2NNaO_5$ (363.04): calcd. C 52.93, H 8.88, B 5.96, N 3.86; found C 53.12, H 8.91, B 5.74, N 3.44.

Reductions: To a 1.57 M solution of **1** in THF (32 mL, 50 mmol) was added the appropriate organic compound (usually 50 mmol). The mixture was refluxed for 2 h (5 min in the case of benzoyl chloride). After cooling to ambient temperature, 15 mL of a 6 M HCl solution was added, followed by NaOH until the solution was basic. The mixture was extracted with diethyl ether (3 × 15 mL), the combined extracts were dried with $MgSO_4$, and the reaction product was finally isolated by distillation. All compounds were characterized by their ^{1}H- and ^{13}C-NMR spectra.

Benzyl Alcohol from Benzoyl Chloride: From C_6H_5COCl (7.05 g, 50 mmol) was obtained $C_6H_5CH_2OH$. Yield: 4.49 g (83%); b.p. 93°C/10 Torr.

Table 1. Hydrogen consumptions for some reductions using **1** in THF solution

Substrate	Hydride equiv.	H_2 evolved	Hydride consumed
Ethyl benzoate	42	345 cm^3, 15.6 mmol	26.5 mmol
Benzamide	42	525 cm^3, 23.7 mmol	18.3 mmol
Benzonitrile	42	550 cm^3, 24.8 mmol	17.2 mmol
Benzoic acid	63	790 cm^3, 35.7 mmol	27.3 mmol
Allylbenzene	21	345 cm^3, 15.6 mmol	5.4 mmol

[a] $w^{-1} = \sigma^2F_o^2 + (xP)^2 + yP$; $P = (F_o^2 + 2F_c^2)/3$.

Benzyl Alcohol from Benzaldehyde: From C_6H_5CHO (5.30 g, 50 mmol) was obtained $C_6H_5CH_2OH$. Yield: 4.32 g (80%); b.p. 90−93°C/10 Torr.

1-Phenylethanol from Acetophenone: From $C_6H_5COCH_3$ (6.00 g, 50 mmol) was obtained $C_6H_5CH_2CH_2OH$. Yield: 4.58 g (75%); b.p. 95−97°C/10 Torr.

Cyclohexanol from Cyclohexanone: From $C_6H_{10}O$ (4.90 g, 50 mmol) was obtained $C_6H_{11}OH$. Yield: 3.81 g (76%); b.p. 58−62°C/10 Torr.

Hydride Consumption by Various Organic Compounds: A solution of **1** in THF (4.5 mL, 1.57 M) was placed in a two-necked flask. Then, the organic compound (20 mmol) was slowly added and the mixture was refluxed for 3 d. The hydrogen gas released after addition of 15 mL of a 6 M HCl solution was collected, the volume of which allowed the hydride consumption to be determined. The results of these experiments are collected in Table 1.

Dimethylamine−Dimethylaminoborane−Borane (4): $ZrCl_4$ (1.16 g, 5.00 mmol) was suspended in THF (80 mL). To the stirred brownish suspension was added a solution of **1** in THF (13.6 mL, 1.47 M, 20 mmol). A clear solution resulted, which was stored at −78°C. Crystals of **4** separated over a period of 2 weeks. The yield of **4** was not determined, but was rather low. − ^{11}B NMR (THF): δ = −13.2 [q, $^{1}J(^{11}B^{1}H)$ = 198 Hz], 2.0 [t, $^{1}J(^{11}B^{1}H)$ = 96 Hz]. − ^{1}H NMR (C_6D_6): δ = 5.0 (br., NH, 1 H) 2.3 (NMe, 6 H), 1.8 (Me_2NH, 6 H), 2.0 (q, ^{1}J = 108 Hz), 1.95 (q, ^{1}J = 96 Hz). − ^{13}C NMR (C_6D_6): δ = 52.4 (NMe_2), 42.7 ($HNMe_2$). − IR (cm^{-1}, νBH region): $\tilde{\nu}$ = 2447 s, 2390 vs, 2353 vs, 2345 vs, 2315 vs, 2293 vs, 2283 s, 2253 s, 2165 m, 2109 m, 2084 m, 2061 m. − $C_4H_{18}B_2N_2$ (115.82): calcd. C 52.93, H 8.88, B 5.96, N 3.82; found C 53.12, H 8.91, B 5.74, N 3.44.

X-ray Structure Determinations: Crystals were transferred into cooled perfluoroether oil, a single crystal was selected and placed

Table 2. Summary of crystallographic data and information relating to data collection and refinement

Compound	**3**	(**1**)$_5$·THF	**4**
Empirical formula	$C_{16}H_{32}B_2NNaO_5$	$C_{14}H_{68}B_{10}N_5Na_5O$	$C_4H_{18}B_2N_2$
Formula mass	363.04	672.25	115.82
Crystal size	0.2×0.45×0.45	0.3×0.45×0.56	0.25×0.32×0.5
Crystal system	monoclinic	monoclinic	monoclinic
Space group	*Cc*	*P*2(1)/*c*	*P*2(1)/*n*
a [Å]	8.5440(10)	10.529(2)	6.2774(3)
b [Å]	29.262(5)	19.439(5)	10.0411(5)
c [Å]	9.1030(10)	20.101(4)	13.8360(6)
α [°]	90	90	90
β [°]	114.65(1)	100.24(1)	102.519(1)
γ [°]	90	90	90
V [Å^3]	2068.5(5)	4048.6(15)	851.38(7)
Z	4	4	4
ρ(calcd.) [Mg/m^3]	1.166	0.895	0.904
μ [mm^{-1}]	0.100	0.097	0.052
F(000)	784	1200	264
Index range	$-9 \le h \le 9$	$0 \le h \le 12$	$-8 \le h \le 6$
	$0 \le k \le 34$	$-22 \le k \le 22$	$-12 \le k \le 12$
	$-10 \le l \le 10$	$-23 \le l \le 22$	$-17 \le l \le 16$
2θ [°]	48.98	48.00	57.70
Temperature [K]	196	213	233
Refl. collected	3605	7066	4320
Refl. unique	3350	6209	1721
Refl. observed (4σ)	2835	3145	1342
R (int.)	0.0344	0.0569	0.0595
No. of variables	242	347	146
Weighting scheme[a] *x*/*y*	0.0753/3.1604	0.0607/1.7723	0.0813/0.1664
GOOF	1.033	1.033	1.125
Final *R* (4σ)	0.0504	0.0645	0.0462
Final *wR*2	0.1338	0.1332	0.1386
Largest res. peak [e/Å^3]	0.163	0.201	0.221

on top of a glass fibre, which was mounted on the goniometer head of the diffractometer. Most measurements were performed with a Siemens P4 diffractometer equipped with a graphite monochromator, an Mo-K_α tube, an LT2 low-temperature device, and an area detector. For one compound, a Siemens P3m diffractometer was employed. − Reflection data sets were collected either in the hemisphere mode (SMART program) with $\Delta\varphi = 0.3°$ per frame, or in the $\omega/2\Theta$ mode. Lorentz and polarization corrections were applied in the data reduction, but not an absorption correction. The structures were solved by direct methods (SHELXT programs). Non-hydrogen atoms were refined anisotropically, while all H atoms bound to boron atoms were refined isotropically in their found positions. Hydrogen atoms attached to carbon atoms were placed in calculated positions and included in the refinement as a riding model. The THF molecule in compound $(\mathbf{1})_5$·THF was found to be disordered; atoms were placed in split positions and SOFs were refined for two different sites. A summary of the relevant crystallographic data and information relating to the data collection, structure solution, and refinement is given in Table 2. − Additional data (except F_o/F_c tables) have been deposited with the Cambridge Crystallographic Data Centre as supplementary publication no. CCDC-125203−125205 Copies of the data can be obtained free of charge on application to CCDC, 12 Union Road, Cambridge CB2 1EZ, U.K. [Fax: (internat.) + 44-1223/336-033; E-mail: deposit@ccdc.cam.ac.uk].

Acknowledgments

We thank the Fonds der Chemischen Industrie and particularly Chemetall GmbH for support of our research.

[1] H. H. Giese, H. Nöth, W. Ponikwar, St. Thomas, M. Warchhold, *Inorg. Chem*., submitted.
[2] G. B. Fisher, J. C. Fuller, J. Harrison, S. G. Alvares. E. R. Burkhart, C. T. Goralski, B. Singaram, *J. Org. Chem*. **1994**, *59*, 6378−6385; J. Harrison, J. C. Fuller, C. T. Goralski, B. Singaram, *Tetrahedron Lett*. **1994**, *29*, 5201−5204.
[3] H. Nöth, St. Thomas, M. Schmidt, *Chem. Ber*. **1996**, *129*, 451−458.
[4] A. B. Burg, J. Sandhu, *Inorg. Chem*. **1965**, *4*, 1467−1473.
[5] C. Keller, *Inorg. Chem*. **1971**, *10*, 2256−2259.
[6] H. Nöth, H. Vahrenkamp, *Chem. Ber*. **1966**, *99*, 1049−1067.
[7] Although crystals of **2** were isolated, they proved to be twins or were strongly intergrown. Consequently, the structure could not be determined.
[8] T. J. Marks, J. R. Kolb, *Chem. Rev*. **1977**, *77*, 263−293.
[9] H. H. Giese, H. Nöth, H. Schwenk, St. Thomas, *Eur. J. Inorg. Chem*. **1998**, 941−949.
[10] G. A. Hahn, R. Schaefer, *J. Am. Chem. Soc*. **1964**, *86*, 1503−1504.
[11] Gmelin, *Handbuch der Anorganischen Chemie*, 8th ed., Ergänzungswerk, vol. 13, pp. 28 ff.
[12] *Interatomic Distances*, Special Publ., Supplement, Chem. Soc., London, **1965**.
[13] E. W. Hughes, *J. Am. Chem. Soc*. **1956**, *78*, 502−504; E. L. Lippert, W. N. Lipscomb, *J. Am. Chem. Soc*. **1958**, *80*, 503; M. Bühl, T. Steinke, P. von R. Schleyer, R. Boese, *Angew. Chem*. **1991**, *103*, 1179−1181; *Angew. Chem. Int. Ed. Engl*. **1991**, *30*, 1160.
[14] R. H. Crabtree, *Science* **1998**, *282*, 2000−2001.
[15] A. Flores-Para, S. S. Sanchez-Ruiz, C. Gundanama, H. Nöth, R. Contreras, *Eur. J. Inorg. Chem*., submitted.
[16] H. Nöth, St. Thomas, P. Rittmayer, U. Wietelmann, German Patent 4441064.6−09 of November 18, **1994**; *Chem. Abstr*. **1996**, *125*, 114842f.
[17] D. R. Armstrong, W. Clegg, H. M. Colquhuon, J. A. Daniels, R. E. Mulvey, I. R. Stephenson, K. Wade, *J. Chem. Soc., Chem. Commun*. **1987**, 630−632.
[18] A. Heine, D. Stalke, *J. Organomet. Chem*. **1997**, *542*, 25−28.

Received January 7, 1999
[I99006]

Intermediates and Products of the Hexachlorodisilane Cleavage of Group 14 Element Phosphanes and Amines − Molecular Structure of Di-*tert*-butyl(trichlorosilyl)phosphane in the Gas Phase Determined by Electron Diffraction and *ab Initio* Calculations

Wolf-W. du Mont,*[a] Lars Müller,[a] Reiner Martens,[a] Paul M. Papathomas,[b] Bruce A. Smart,[b] Heather E. Robertson,[b] and David W. H. Rankin*[b]

Keywords: Phosphanes / Disilanes / Disilanylamines / Germanes / Stannanes / Stannanes

Reactions of dialkyl(trimethylsilyl)phosphanes RR′PSiMe$_3$ (**1**: R, R′ = *t*Bu; **3**: R, R′ = *i*Pr; **5**: R = *i*Pr, R′ = *t*Bu) with Si_2Cl_6 provide stable trichlorosilylphosphanes RR′PSiCl$_3$ (**2**, **4**, **6**); the reactions of silyl- and stannylamines of *i*Pr$_2$NMMe$_3$ (M = Si: **11**; M = Sn: **12**) with Si_2Cl_6, however, provide the stable pentachlorodisilanylamine *i*Pr$_2$NSi$_2$Cl$_5$ (**13**). Heating of **1** with the technical mixture Me$_2$(Cl)SiSiCl$_2$Me/(MeCl$_2$Si)$_2$ yields the stable silylphosphane *t*Bu$_2$PSiMe$_2$Cl (**8**) and the disilanylphosphane *t*Bu$_2$PSi(Me)(Cl)Si(Me)Cl$_2$ (**9**). Methylation of **9** with MeLi gave *t*Bu$_2$PSi$_2$Me$_5$ **10**, which was isolated in a pure state. Reactions of *t*Bu(*i*Pr)PSiMe$_3$ (**5**) and of organometal phosphanes *t*Bu(*i*Pr)PMR$_3$ (**14**: M = Ge, R = Me; **17a–c**: M = Sn; R = Me, Et, *n*Bu) with Si_2Cl_6 were monitored by ^{31}P, ^{29}Si, and ^{119}Sn NMR. – In the first step of these reactions, new *t*Bu(*i*Pr)PSi$_2$Cl$_5$ (**7**) is formed. **7** is accompanied by increasing amounts of *t*Bu(*i*Pr)PSiCl$_3$ (**6**) and Me$_3$GeSiCl$_3$ (**15**)/(Me$_3$Ge)$_2$Si(SiCl$_3$)$_2$ (**16**) or traces of compounds R$_3$SnSiCl$_3$ (**19a–c**) that decompose providing (R$_3$Sn)$_2$Si(SiCl$_3$)$_2$ (**18a–c**) and *n*Bu$_3$SnSi(SiCl$_3$)$_3$ (**20c**). Subsequently, compounds **19a–c** decompose providing increasing amounts of **18a–c**. Stannylphosphane **17b** is also cleaved by SiCl$_4$ leading to **6** with liberation of Et$_3$SnCl, whereas **17b** *is formed* from the reaction of **5** with Et$_3$SnCl under liberation of Me$_3$SiCl. The suggestion of an extra stabilisation of P–Si bonds of trichlorosilylphosphanes was subjected to direct evidence through the structure determination of the trichlorosilylphosphane *t*Bu$_2$PSiCl$_3$ (**2**) in the gas phase by electron diffraction. This crowded molecule has a "normal" P–Si bond length of 225.0(12) pm; its C_1 symmetric conformation with both *t*Bu groups and the SiCl$_3$ group twisted about 17° from the perfectly staggered positions, and with each of the three groups tilted about 6° away from each other, allows to reduce steric strain.

Introduction

Trihalosilyl compounds are of importance as trifunctional precursors for the synthesis of highly functionalised silicon compounds. The cleavage of trimethylgermyl and -stannyl phosphanes with hexachlorodisilane was reported to furnish trichlorosilylphosphanes as well as trichlorosilyltrimethylgermane and trichlorosilyltrimethylstannane.[1] This novel reductive trichlorosilylation of Me$_3$Ge and Me$_3$Sn groups attached to phosphorus was thought to be due to nucleophilic attack of Me$_3$Ge and Me$_3$Sn groups by latent trichlorosilyl anions. Such anions are generated from one SiCl$_3$ group of Si_2Cl_6 when the other silicon atom is attacked by a phosphorus nucleophile leading to an adduct.[2] Because in situ-generated trichlorosilyl anions are also the key precursors in reactions of trichlorosilane/triethylamine mixtures with various organic halides leading to products of reductive *C*-trichlorosilylations,[3,4] we recently used the "Benkeser" type of reaction of chlorotrimethylstannane with the trichlorosilane/triethylamine reagent as an alternative route to trichlorosilyltrimethylstannane.[5] In the course of the extension of this type of reductive trichlorosilylation for the preparation of trihalosilyl derivatives of main group elements, we were surprised by the nature of the products from the trichlorosilane/triethylamine reagent with chlorotrimethylgermane[6] and dichlorodimethylgermane.[6,7] Contradictory data concerning liquid Me$_3$Ge−SiCl$_3$ and solid (Me$_3$Ge)$_2$Si(SiCl$_3$)$_2$[1,6] led us to study the "Benkeser" type of reaction of organotin and organogermanium halides with the trichlorosilane/triethylamine reagent in detail by heteronuclear NMR.[6,7]

$$Me_3GeCl + HSiCl_3 + NEt_3 \longrightarrow Me_3GeSiCl_3 + (Me_3Ge)_2Si(SiCl_3)_2 + HNEt_3Cl + SiCl_4\ (ref.^{[7]}) \quad (1)$$

$$4\ Me_3GeSiCl_3 \longrightarrow (Me_3Ge)_2Si(SiCl_3)_2 + SiCl_4 + 2\ Me_3GeCl \quad (2)$$

The observation of unexpected products of the constitution (Me$_3$M)$_2$Si(SiCl$_3$)$_2$ (M = Ge, Sn) from these reactions led us to reinvestigate also, by heteronuclear NMR-spectroscopy, the course of the hexachlorodisilane cleavage of P−Ge and P−Sn bonds which yields trichlorosilylphos-

[a] Institut für Anorganische und Analytische Chemie der Technischen Universität Braunschweig,
Hagenring 30, D−38106 Braunschweig, Germany
Fax: (internat.) +49 (0)531/ 391 5387
E mail: w.du-mont@tu-bs.de
[b] Department of Chemistry, The University of Edinburgh,
West Mains Road, Edinburgh, EH9 3JJ, U. K.
Fax: (internat.) +44 (0)131/ 650 6452
E mail: d.w.h.rankin@ed.ac.uk

 © WILEY-VCH Verlag GmbH, D-69451 Weinheim, 1999 1434−1948/99/0808−1381 $ 17.50+.50/0

phanes accompanied by new trichlorosilyl compounds containing Si−Ge and Si−Sn bonds.[1] These reactions are expected to be related to the known cleavage of trimethylsilylphosphanes tBu$_2$PSiMe$_3$ (**1**) and tBuP(SiMe$_3$)$_2$ with hexachlorodisilane, which allowed the isolation of the related trichlorosilylphosphanes tBu$_2$PSiCl$_3$ (**2**) and tBuP(SiMe$_3$)(SiCl$_3$) in high yields.[8] As "model" phosphanes we chose silyl-, germyl-, and stannylphosphane derivatives containing the tBu(iPr)P group, which are moderately bulky and fairly accessible from the corresponding chlorophosphane on the HSiCl$_3$/NEt$_3$ pathway[5] followed by methylation and transmetalation reactions.[9]

Reactions of Hexachlorodisilane with Silyl-, Germyl-, and Stannylphosphanes Followed by NMR Spectroscopy

1. Reactions of Chlorodisilanes with Silylphosphanes

The reaction of Si$_2$Cl$_6$ with tBu$_2$PSiMe$_3$ (**1**) was reported to provide trichlorosilylphosphane tBu$_2$PSiCl$_3$ (**2**) in high yield under mild conditions.[8] Similarly, iPr$_2$PSiMe$_3$ (**3**) was easily cleaved to give iPr$_2$PSiCl$_3$ (**4**) in fair yield. After distillation of **2** and **4**, the residues contained orange oils that are expected to contain yet undefined polysilanes, possibly with a certain degree of SiPR$_2$ functions. Addition of Si$_2$Cl$_6$ to tBu(iPr)PSiMe$_3$ (**5**) at 0°C provided a red-brown solution, which turned brown on warming to room temperature. ^{31}P-NMR spectra showed that 5 min after mixing the compounds about 75% **5** was accompanied by about 8% of tBu(iPr)PSiCl$_3$ (**6**), 8% of tBu(iPr)PSi$_2$Cl$_5$ (**7**), and about 3−4% each of two other new phosphorus compounds. After 80 min compound **7** appeared as the main product. After 13 h, **5** was completely consumed and **6** became the main product (about 55%), accompanied by **7** (about 40%) and two other phosphanes. After 10 d at room temp. more than 90% of **6** and less than 10% of other phosphanes were present in solution.

$$\underset{\mathbf{1,3}}{R_2PSiMe_3} + Si_2Cl_6 \longrightarrow \underset{\mathbf{2,4}}{R_2PSiCl_3} + Me_3SiCl + \textit{other products} \quad (3)$$

1, 2: R = tBu[1]
3, 4: R = iPr

$$\underset{\mathbf{5}}{(t\text{Bu})(i\text{Pr})PSiMe_3} + Si_2Cl_6 \longrightarrow \underset{\mathbf{6}}{(t\text{Bu})(i\text{Pr})PSiCl_3} + \underset{\mathbf{7}}{(t\text{Bu})(i\text{Pr})PSi_2Cl_5} + SiCl_4 + Me_3SiCl + \textit{other products} \quad (4)$$

$$\mathbf{1} + Me_2(Cl)SiSiCl_2Me + (MeCl_2Si)_2 \longrightarrow \underset{\mathbf{8}}{t\text{Bu}_2PSiMe_2Cl} + \underset{\mathbf{9}}{t\text{Bu}_2PSi(Me)(Cl)Si(Me)Cl_2} \quad (5)$$

The reaction of tBu$_2$PSiMe$_3$ (**1**) with an excess of the industrial disilane fraction Me$_2$(Cl)SiSiCl$_2$Me/(MeCl$_2$Si)$_2$ required heating for several hours. Distillation provided satisfactory yields of the silylphosphane tBu$_2$PSiMe$_2$Cl (**8**)[10] as first fraction and the new disilanylphosphane tBu$_2$PSi(Me)(Cl)Si(Me)Cl$_2$ **9** as second fraction. Both compounds are thermally stable at room temperature, but very sensitive to oxygen and moisture. The constitution of **9** was confirmed by ^{1}H-, ^{13}C-, ^{29}Si-, and ^{31}P-NMR spectra. Disilanylphosphane **9** (about 50% yield) is obviously the product of a transsilylation of **1** with (MeCl$_2$Si)$_2$. The formation of **8** from **1** (24%) with Me$_2$(Cl)SiSiCl$_2$Me is more surprising. The formation of **8** by transsilylation of **1** with Me$_2$SiCl$_2$ is known to proceed significantly more slowly than the reaction of **1** with MeSiCl$_3$.[10] Adding **9** to an excess of methyllithium led to permethylation giving tBu$_2$PSi$_2$Me$_5$ (**10**), which was then isolated in a pure state.

2. Reactions of Si$_2$Cl$_6$ with iPr$_2$NMMe$_3$ (11: M = Si; 12: M = Sn)

Heating the mixture of Si$_2$Cl$_6$ and iPr$_2$NSiMe$_3$ (**11**) for 6 h at 60°C led to complete consumption of **11**. Distillation provided iPr$_2$NSi$_2$Cl$_5$ (**13**) in fair yield. The stannylamine **12** is more reactive: after mixing **12** and Si$_2$Cl$_6$ at 0°C and warming to room temperature, the formation of crude **13** and Me$_3$SnCl was quantitative.

$$\underset{\mathbf{11}: M = Si;\ \mathbf{12}: M = Sn}{i\text{Pr}_2NMMe_3} + Si_2Cl_6 \longrightarrow \underset{\mathbf{13}}{i\text{Pr}_2NSi_2Cl_5} + Me_3MCl \quad (6)$$

$$\underset{\mathbf{14}}{(t\text{Bu})(i\text{Pr})PGeMe_3} + Si_2Cl_6 \longrightarrow \mathbf{6} + \underset{\mathbf{15}}{\mathbf{7}} + Me_3GeSiCl_3 + \underset{\mathbf{16}}{(Me_3Ge)_2Si(SiCl_3)_2} + SiCl_4 + Me_3GeCl \quad (7)$$

3. Reaction of Si$_2$Cl$_6$ with tBu(iPr)PGeMe$_3$ (14)

Five minutes after mixing the starting materials, about 30% of **14** was consumed in favour of five new phosphorus compounds, among them **6** and **7**. After 3 h, 50% of **14** had been consumed, **6** was the main product and small amounts of **7** (among other P-containing compounds) were also present. A ^{29}Si-NMR spectrum confirmed the presence of Me$_3$GeSiCl$_3$ (**15**) (a rather broad signal, ^{29}Si = +17.7)[7] and (Me$_3$Ge)$_2$Si(SiCl$_3$)$_2$ (**16**) (two signals, at δ ^{29}Si = +16.8 and −84.9, the upfield one being less intense)[7] as well as SiCl$_4$. One peak of the ^{29}Si doublet, doublet pattern of **6** (from Si,P and Si,H couplings) shows "enhanced intensity", possibly due to accidental overlap with the singlet signal of another new germylsilane [δ ^{29}Si = +10.1; probably Me$_3$GeSi(SiCl$_3$)$_3$[9]]. This signal is quite intense in the earliest stage of the reaction. After several days, when **14** had been completely consumed and the crude yield of **6** was close to 90%, the ^{29}Si-NMR pattern of **6** exhibited the expected four lines of equal intensity. Evidence for the formation of Me$_3$GeCl was provided by ^{13}C-NMR spectra of the reaction mixture.

4. Reaction of Si$_2$Cl$_6$ with Stannylphosphanes tBu(iPr)PSnR$_3$ (17a−c: R = Me, Et, nBu)

***t*Bu(*i*Pr)PSnMe$_3$ (17a):** Twenty minutes after mixing the starting materials **17a** had been completely consumed. Silylphosphane **6** and the branched bis(stannyl)silane **18a** were the main products; small amounts of disilanylphosphane **7** (less than 10% of **6**, by ^{31}P-NMR), stannylsilane **19a** (about 25% of **18a**), and a further stannylsilane [δ ^{29}Si = +11.3

and −88; probably $Me_3SnSi(SiCl_3)_3$[9]] were also present. After 15 h, the crude yields (by NMR) of **6** and of **18a** were both more than 90%.

***t*Bu(*i*Pr)PSnEt$_3$ (17b):** After 5 min, **17b** had been consumed and large amounts of the disilanylphosphane **7** were present. Tin-NMR spectra showed the presence of large amounts of $Et_3SnSiCl_3$ (**19b**) accompanied by **18b**[7] and Et_3SnCl. From such a sample, mass spectrometric evidence for **19b** ($M^+ - Et$) was provided. Within one hour, however, trichlorosilylphosphane **6** and the branched bis(stannyl)silane **18b** became the main products at the expense of **7** and **19b**. Besides **18b**, the presence of a further branched silylstannane was indicated by ^{29}Si-NMR ($\delta\ ^{29}Si = +11.7$ and −88).

In an additional experiment, **17b** was mixed with $SiCl_4$ at room temperature. NMR spectra revealed that **17b** was consumed and that trichlorosilylphosphane **6** and Et_3SnCl were formed, accompanied by some *t*Bu(*i*Pr)PH.

$$\underset{\textbf{17a–c}}{(t\text{Bu})(i\text{Pr})\text{PSnR}_3} + \text{Si}_2\text{Cl}_6 \longrightarrow \textbf{6} + \textbf{7} + \underset{\textbf{19a–c}}{\text{R}_3\text{SnSiCl}_3} + \underset{\textbf{18a–c}}{(\text{R}_3\text{Sn})_2\text{Si}(\text{SiCl}_3)_2} \quad (8)$$

a: R = Me
b: R = Et
c: R = *n*Bu

$$+ \underset{\textbf{20a–c}}{\text{R}_3\text{SnSi}(\text{SiCl}_3)_3} + \text{SiCl}_4 + \text{R}_3\text{SnCl}$$

$$\underset{\textbf{17b}}{(t\text{Bu})(i\text{Pr})\text{PSnEt}_3} + \text{SiCl}_4 \longrightarrow \underset{\textbf{6}}{(t\text{Bu})(i\text{Pr})\text{PSiCl}_3} + \text{Et}_3\text{SnCl} \quad (9)$$

***t*Bu(*i*Pr)PSn(*n*Bu)$_3$ (17c):** as in the cases described above, consumption of the stannylphosphane **17c** was very fast. After 2 h, **7** and **19c**[7] were the main products and after 12 d, **6** and $n\text{Bu}_3\text{SnSi}(\text{SiCl}_3)_3$ (**20c**) were the predominant species. After an even longer reaction time (2 months), stannylsilane **19c** was completely decomposed and in addition to **20c**, the branched bis(stannyl)silane **18c** could also be detected by ^{29}Si- and ^{119}Sn-NMR.[7]

Discussion of the Reactions

1. Cleavage of Sn−N and Sn−P Bonds with Si_2Cl_6

Si_2Cl_6 cleaves stannylamines and stannylphosphanes quantitatively within a few minutes under mild conditions by transmetalation-like SnR_3/Si_2Cl_5 exchange reactions providing large amounts of the corresponding pentachlorodisilanylamines and -phosphanes and the trialkylchlorostannanes (Equation 6, Equation 10a). From such reactions, diisopropyl(pentachlorodisilanyl)amine **13** can be isolated in pure state; pentachlorodisilanylphosphane **7**, however, serves as a source of $SiCl_2$ or $SiCl_3^-$ moieties towards the trialkylchlorostannanes, leading by $Cl^-/SiCl_3^-$ exchange to trichlorosilylstannanes $R_3SnSiCl_3$ **19** (Equation 10b).

$$\textbf{17} + \text{Si}_2\text{Cl}_6 \xrightarrow{(10a)} \textbf{7} + \text{R}_3\text{SnCl} \xrightarrow{(10b)} \textbf{6} + \textbf{19} \quad (10)$$

$$4\ \textbf{19} \longrightarrow \textbf{18} + 2\ \text{R}_3\text{SnCl} + \text{SiCl}_4 \quad (11)$$

$$4\ \textbf{19} \longrightarrow \textbf{20} + 3\ \text{R}_3\text{SnCl} \quad (12)$$

$$\textbf{19} + 3\ \textbf{7} \longrightarrow \textbf{20} + 3\ \textbf{6} \quad (13)$$

These compounds can be detected by NMR in solution, but they are not persistent under the reaction conditions (presence of phosphorus nucleophiles). Their decomposition furnishes new branched stannylsilanes $(R_3Sn)_2Si(SiCl_3)_2$ **18** and $R_3SnSi(SiCl_3)_3$ **20** (Equations 11, 12). The previous assignments of NMR data of compounds **15** and **19a** made in ref.[1] have to be withdrawn (see the following section, Table 1). The isolated solids were not **15** and **19a**,[1] but **16** and **18a**.[7] The formation of compounds **20** from **19** (which is favoured by bulkier alkyl groups at tin) can be explained as being reaction steps analogous to those that occur in the course of the base-catalysed disproportionation of Si_2Cl_6, i.e. $Cl^-/SiCl_3^-$ exchange or $SiCl_2$ insertion at the most branched Si atom of an oligochlorosilane.[11–13] Disilanylphosphane **7** can also be a source of $SiCl_3^-$ or $SiCl_2$ (Equation 13). The predominant formation of bis(stannyl)silanes **18a**, **b** and the related germanium compound **16**[7] deserves further investigation; the formation of a second Si−Sn or Si−Ge bond leading from **15/19** to intermediates $(R_3M)_2SiCl_2$ (M = Ge, Sn) as precursors for **16/18** is apparently affected by bulkier alkyl groups at Ge or Sn.

2. Cleavage of Trimethylgermylphosphane 14 by Si_2Cl_6

This reaction proceeds much more slowly than the reaction of stannylphosphanes **17**. Disilanylphosphane **7** is already being consumed by its reaction with Me_3GeCl before its formation by the cleavage of **14** can be quantitative. Formation of trichlorosilylphosphane **6** is slower than in the stannylphosphane reactions, but finally it is also close to quantitative. Contribution of a *direct* $GeMe_3/SiCl_3$ exchange (that was previously proposed[1]) to the formation of $Me_3GeSiCl_3$ (**15**) and **6** cannot be ruled out. Even at an early phase of the reaction, approximately equal amounts of **15** and the branched bis(germyl)silane **16** are present in solution. Experiments with pure **15** show that the presence of Me_3GeCl (its decomposition product !) inhibits the base-catalysed decomposition.[7] The formation of deeply coloured precipitates on addition of Si_2Cl_6 to the phosphanes at 0°C deserves further attention. Phosphanes are known to catalyse the disproportionation,[14] they can coordinate with Si_2Cl_6,[2] and they can activate disilanes for radical reactions with $n\text{Bu}_3\text{SnH}$.[15]

3. Cleavage of Trimethylsilylphosphanes by Si_2Cl_6 and by the Disilane Fraction

Silylphosphane **5** reacts more slowly than the stannylphosphanes but faster than the germylphosphane **14** with Si_2Cl_6 (silylphosphane **5** requires more than 2 h, germylphosphane **14** about a day, and stannylphosphanes **17a-c** less than 20 min to be consumed completely). In the course of the decomposition of disilanylphosphane **7** in the presence of Me_3SiCl, the compound $Me_3SiSiCl_3$ was not detected by ^{29}Si NMR. This compound is known to disproportionate in the presence of N- or P-nucleophiles.[16] Silylphosphane **1** reacts with $(MeCl_2Si)_2$ by transsilylation yielding $t\text{Bu}_2\text{PSi(Me)(Cl)Si(Me)Cl}_2$ (**9**), a stable disilanylphosphane. $Me_2(Cl)SiSiCl_2Me$, however, suffered from Si−Si bond cleavage by **1** by attaching the chlorodimethylsilyl group to phosphorus, i.e. "the more electrophilic sily-

lene" MeSiCl (that allows better base-stabilisation) was lost when tBu$_2$PSiMe$_2$Cl (**8**) was formed. Whether **8** is in fact the *kinetic* product, i.e. whether the higher chlorinated silylphosphanes (like R$_2$PSiCl$_2$Me, R$_2$PSiCl$_3$) profit from extra stabilisation of their P−Si bonds compared with di- and trialkylsilylphosphanes, deserves further investigation.

Characterisation of New Germyl- and Stannylsilanes by NMR Spectroscopy

Assignments were supported by measurements on pure samples of **15** and **18a** from independent syntheses using the trichlorosilane/triethylamine route.[7]

In the series of compounds Me$_3$E−SiCl$_3$ (E = C, Si, Ge) the ^{29}Si resonances of the trichlorosilyl groups appear in the range 18 ± 1 ppm (Table 1). The ^{29}Si nuclei of the SiCl$_3$ groups of the branched compounds (Me$_3$E)$_2$Si(SiCl$_3$)$_2$ exhibit rather similar resonances. Our previous assignments of **15** and **19a**, however, were wrong[1]. Contributions from the electric field gradient (from the p-electron imbalance at Si) to σ_{para} will overcome inductive effects on δ^{29}Si (electronegativity range C >> Ge > Si, Sn). In the case of compounds Me$_3$ESiCl$_3$, however, the ^{13}C resonances of the methyl groups adjacent to C (δ = +24.4), Ge (δ = −2.8), and Sn (δ = −8.1) follow the inductive trend. Again, the related resonances of the branched compounds **16** and **18a** appear not far from those of **15** and **19a**.

The central silicon atoms of the branched bis(germyl)- and bis(stannyl)silanes (R$_3$E)$_2$Si(SiCl$_3$)$_2$ appear at rather low frequency, the tin compounds **18a−c** even lower frequency than the germanium derivative **16**. The ^{29}Si shift of the central atom of stannylsilane **20c** appears at significantly higher frequqency than that of the bis(stannyl)silane **18a**. The ^{119}Sn resonances of compounds **18a-c**, **19a-c**, and **20c** appear in a narrow range from δ = −45 to −70.[7]

Table 1. ^{13}C-, ^{29}Si-, and ^{119}Sn NMR shifts of trichlorosilyl derivatives of C, Si, Ge, and Sn and reference compounds

	δ^{13}C	δ^{29}Si	δ^{119}Sn
Me$_3$CSiCl$_3$	+24.37 [*C*H$_3$], +26.14 [*C*C$_3$]	+17.3	
Me$_3$SiSiCl$_3$[12]	*	+17.5 [*Si*Cl$_3$], −7.2 [*Si*Me$_3$]	
Me$_3$GeSiCl$_3$ **15**	−2.8	+17.8	
Me$_3$SnSiCl$_3$ **19a**	−8.6	*	−70[7]
Et$_3$SnSiCl$_3$ **19b**	*	*	−59
nBu$_3$SnSiCl$_3$ **19c**	*	*	−72
Si(SiCl$_3$)$_4$[17]		+3.5 [*Si*Cl$_3$], −80.0 [*Si*Si$_4$]	
(Me$_3$Ge)$_2$Si(SiCl$_3$)$_2$ **16**	+0.8	+17.2 [*Si*Cl$_3$], −84.2 [Ge$_2$*Si*Si$_2$]	
(Me$_3$Sn)$_2$Si(SiCl$_3$)$_2$ **18a**	−8.0	+19.6 [*Si*Cl$_3$], −106.4 [Sn$_2$*Si*Si$_2$]	−55.2
(Et$_3$Sn)$_2$Si(SiCl$_3$)$_2$ **18b**	+3.8 [Sn*C*] +12.1 [SnC*C*]	+21.0 [*Si*Cl$_3$], −108.2 [Sn$_2$*Si*Si$_2$]	−45.0
(nBu$_3$Sn)$_2$Si(SiCl$_3$)$_2$ **18c**	+12.2 [Sn*C*], +14.0 [SnC$_3$*C*], +27.8 [SnC$_2$*C*], +30.3 [SnC*C*]	+21.3 [*Si*Cl$_3$], −107.4 [Sn$_2$*Si*Si$_2$]	−52.7
nBu$_3$SnSi(SiCl$_3$)$_3$ **20c**		+12.0 [*Si*Cl$_3$,] −88.3 [Sn*Si*Si$_3$	−46.8

* Not available.

Table 2. ^{29}Si- and ^{31}P-NMR data of disilanylphosphanes and hexachlorodisilane adducts (δ in ppm, magitudes of J in Hz)

	δ ^{31}P	δ ^{29}*Si*(−P) |(^{1}J ^{29}Si, ^{31}P)|	δ ^{29}*Si*(−Si−P) |(^{2}J ^{29}Si, ^{31}P)|
tBu(iPr)PSiCl$_2$SiCl$_3$ **7**	8.3	13.2 (*125.5*)	−0.4 (*24.0*)
tBu$_2$PSiMeClSiMeCl$_2$ **9**	8.6	12.1 (*100.2*)	26.8 (*21.9*)
tBu$_2$PSiMe$_2$SiMe$_3$ **10**	5.6	−25.2 (*63.4*)	−14.9 (*12.1*)
iPr(iPr$_2$N)PSiCl$_2$SiCl$_3$[2]	42.7	8.9 (*132.0*)	1.1 (*16.6*)
iPr(iPr$_2$N)(Cl)PSiCl$_3$SiCl$_3$[2]	57.1	−69.6 (*160.7*)	9.8 (*24.8*)
tBu(Et$_2$N)PSiCl$_2$SiCl$_3$[2]	77.4	* (*134.2*)	* (*not resolved*)
tBu(Et$_2$N)(Cl)PSiCl$_3$SiCl$_3$[2]	98.0	* (*166.2*)	* (*24.3*)

Characterisation of New Disilanylphosphanes by NMR

Characteristic coupling patterns allowed safe assignments of the ^{31}P-NMR and ^{29}Si-NMR spectra of transient and persistent disilanylphosphanes (Table 2). Compared with organic subsituents or hydrogen, chlorine atoms at silicon lead to increased couplings ^1J and ^2J (^{31}P, ^{29}Si).[10,18] ^{29}Si-NMR shifts allow distinction between disilanylphosphanes (CN 4 at both Si) and phosphane-hexachlorodisilane adducts (one Si with CN 5 [low frequency], one Si with CN 4).[2]

Experimental and Calculated Structure of 2

Ab initio Calculations

Preliminary calculations on tBu$_2$PSiCl$_3$ were carried out at the 3-21G*/SCF level, assuming C_s symmetry. Vibrational-frequency calculations revealed the presence of a single imaginary frequency (74i cm^{-1}), indicating that the C_s structure represents a transition state connecting two equivalent C_1 minima. This structure can be regarded as

Table 3. Selected theoretical bond lengths, bond angles, and dihedral angles[a]

Parameter	3-21G*/ SCF	6-31G*/ SCF	6-31G*/ MP2
P−Si	225.0	227.0	224.9
Si−Cl(mean)	204.8	206.1	205.8
P(1)−C(6)	189.6	191.8	190.7
P(1)−C(19)	189.8	192.0	191.0
C−C(mean)	155.0	154.0	153.4
C−H(mean)	108.3	108.4	109.4
P(1)−Si(2)−Cl(3)	118.2	118.2	118.4
P(1)−Si(2)−Cl(4)	108.8	109.0	108.5
P(1)−Si(2)−Cl(5)	111.9	112.0	111.5
Si(2)−P(1)−C(6)	105.5	106.3	104.9
Si(2)−P(1)−C(19)	104.6	105.4	103.9
C(6)−P(1)−C(19)	111.4	111.8	111.0
P(1)−C(6)−C(7)	106.4	106.2	105.7
P(1)−C(19)−C(20)	108.5	108.2	107.6
C−C−H(mean)	110.7	111.2	110.8
Cl(5)−Si(2)−P(1)−C(19)	−164.7	−166.1	−164.8
C(20)−C(19)−P(1)−C(6)	−161.3	−162.4	−160.8
C(8)−C(6)−P(1)−Si(2)	−163.4	−164.0	−162.6

[a] All distances (r_a) in pm, all angles in°. See Figure 1 for atom numbering.

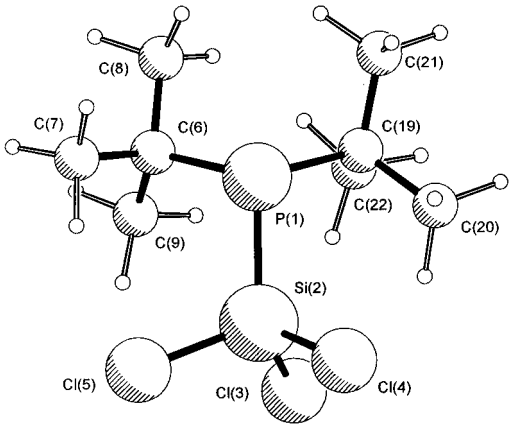


Figure 1. The molecular structure of tBu$_2$PSiCl$_3$ as determined by gas-phase electron diffraction

being derived from a fully staggered structure with *tert*-butyl and $SiCl_3$ groups twisted in the same sense by around 15−20°, increasing the minimum distance between H atoms on neighbouring *tert*-butyl groups from 195.4 pm (C_s) to 211.1 pm (C_1) and reducing the molecular energy by 16.8 kJ mol^{-1} at the 3-21G*/SCF level of theory. All subsequent calculations were carried out in C_1 symmetry. Selected geometric parameters are shown in Table 3 and the atom numbering is shown in Figure 1.

The computational facilities available to us restricted geometry optimisations to the 3-21G*/SCF, 6-31G*/SCF, and 6-31G*/MP2 levels, which should give an acceptably accurate geometry, since tBu$_2$PSiCl$_3$ is not expected to contain any significant multiple-bond character and there are few electronegative atoms.

With the 6-31G* basis set, raising the level of theory from SCF to MP2 produced little change (Table 3). Bond lengths were generally within ca. 1 pm; for example, the Si(2)−Cl(3) bond length is predicted to be 206.6 and 206.5 pm at the SCF and MP2 levels, respectively, and similarly the P(1)−C(19) bond length to be 192.0 and 191.0 pm at the same levels. Only the P−Si bond length changed appreciably, shortening from 227.0 pm to 224.9 pm. Bond angles generally varied by little more then 1°, although angles around the central phosphorus atom differed by up to 2°. At the SCF level the Si−P−C(6), Si−P−C(19), and C(6)−P−C(19) bond angles were predicted to be 106.3°, 105.4°, and 111.8° and to 104.9°, 103.9°, and 111.0° at the higher level.

Although the overall symmetry of tBu$_2$PSiCl$_3$ is predicted to be C_1, the $SiCl_3$ and two *tert*-butyl groups were all found to exhibit approximate local C_3 symmetry. At the 6-31G*/MP2 level, the calculated Si−Cl bond lengths lie in the range 205.4 to 206.5 pm, with internal Cl−Si−Cl angles ranging from 105.3° to 106.5°. Similarly, for the *tert*-butyl groups the C−C bond lengths are calculated to range from 153.0 to 153.7 pm, with internal P−C−C angles from 106.9° to 109.9°.

Molecular Model

The large number of geometric parameters needed to define the structure of tBu$_2$PSiCl$_3$ in C_1 symmetry made it necessary to introduce a number of assumptions into the GED refinement. At first the tBu and $SiCl_3$ groups had no symmetry and 9 parameters were used to define the C-(methyl) and Cl positions in each groups. The number of parameters was reduced only when (a) they were shown to be defined effectively entirely by restraints and (b) they were uncorrelated with the refining parameters. This procedure allows deviations from local symmetry to be fully explored rather than applying local symmetry without testing the validity of the assumptions. In this case the refined structures of *tert*-butyl and $SiCl_3$ groups showed insignificant variation from C_3 local symmetry. Therefore all further refinements were carried out assuming this symmetry. Moreover, within the levels of experimental uncertainty all six C−C bond lengths were also found to be indistinguishable and therefore were constrained to be equal. Since hydrogen

Table 4. Refined and calculated geometric parameters (distances in pm, angles in°) from the GED study[a]

No.	Parameter	GED(r_a)	6−31G*/MP2 (r_e)
a) independent parameters			
p_1	C−H	113.6(4)	109.4[b]
p_2	C−C	153.6(2)	153.4[b]
p_3	P−C (mean)	192.5(10)	190.9
p_4	P−C (diff)	−0.1(5)	−0.3
p_5	Si−Cl	204.7(3)	205.8[b]
p_6	P−Si	225.0(12)	224.9
p_7	C−C−H	109.2(9)	110.0[b]
p_8	P−C−C (mean)	109.2(4)	110.6
p_9	P−C−C (diff)	0.05(51)	−0.07
p_{10}	P−Si−Cl (mean)	112.9(2)	113.1
p_{11}	$SiCl_3$ torsion	194.1(15)	
p_{12}	$SiCl_3$ axial tilt	6.0(6)	
p_{13}	$SiCl_3$ equat. tilt	−0.5(19)	
p_{14}	Methyl twist	6.2(19)	
p_{15}	Methyl tilt	0.0(fixed)	
p_{16}	Butyl torsion (mean)	18.1(21)	
p_{17}	Butyl torsion (diff)	288.3(10)	
p_{18}	Butyl axial tilt (mean)	5.9(6)	
p_{19}	Butyl axial tilt (diff)	−1.2(14)	
p_{20}	Butyl equat. tilt (mean)	−0.7(4)	
p_{21}	Butyl equat. tilt (diff)	−4.0(7)	
p_{22}	Butyl dip (mean)	−31.5(8)	
p_{23}	Butyl dip (diff)	4.4(27)	
p_{24}	Butyl dihedral	105.4(7)	
b) dependent parameters			
p_{25}	C(6)−P−C(19)	110.6(13)	111.0
p_{26}	Si−P−C(6)	103.4(8)	104.9
p_{27}	Si−P−C(19)	102.8(6)	103.9
p_{28}	P−Si−Cl(3)	118.8(7)	118.4
p_{29}	P−Si−Cl(4)	108.9(16)	108.5
p_{30}	P−Si−Cl(5)	110.6(16)	111.5
p_{31}	P−C(6)−C(7)	104.9(10)	105.7
p_{32}	P−C(6)−C(8)	107.6(10)	108.5
p_{33}	P−C(6)−C(9)	114.9(10)	116.2
p_{34}	P−C(19)−C(20)	106.3(8)	107.6
p_{35}	P−C(19)−C(21)	105.3(8)	106.4
p_{36}	P−C(19)−C(22)	115.7(9)	116.8
p_{37}	Cl(5)−Si−P−C(19)	−163.4(16)	−164.8
p_{38}	C(20)−C(19)−P−C(6)	−156.5(23)	−160.8
p_{39}	C(8)−C(6)−P−Si	−161.8(21)	−162.6

[a] See text for atom numbering and parameter definitions. − [b] *ab initio* values quoted are mean values.

atom positions are poorly defined by the experimental data, all CH_3 groups were assumed to be identical and to have local C_{3v} symmetry.

In total 24 independent geometrical parameters were used to describe the structure of tBu$_2$PSiCl$_3$ in C_1 symmetry (Table 4). The bond length parameters are C−H, p_1, C−C, p_2, the mean and difference of P(1)−C(6) and P(1)−C(19), p_3 and p_4, Si−Cl, p_5, and P−Si, p_6. The bond angles are C−C−H, p_7, the average of the P−C−C bond angles, p_8, the difference between the averages of the P−C−C bond angles found in each of the *tert*-butyl groups, p_9, and the average P−Si−Cl angle, p_{10}.

The remaining parameters are best described with a coordinate system in which the P−Si bond defines the z axis, with P(1) at the origin and Si(2) in the positive z direction. The Cl atoms are arranged initially so that the z axis is an axis of local 3-fold symmetry, with Cl(3) lying in the xz plane in the positive x direction. By assuming a right-handed set of coordinate axes the y axis is also defined.

The $SiCl_3$ torsion angle is a rotation about the z axis, p_{11}, anticlockwise when viewed down the axis from Si to P. The $SiCl_3$ axial and equatorial tilts are anticlockwise rotations at Si(2) about the y axis, p_{12}, and the x axis, p_{13}, respectively. All subsequent torsion and tilt angle directions are anticlockwise when viewed down the rotation axis.

The *tert*-butyl groups were generated by initially placing a methyl group carbon at the origin [i.e. same position as P(1)] so that its three H atoms were arranged with local C_{3v} symmetry about the z axis and one H in the xz plane in the positive x direction. The methyl torsion, p_{14}, and tilt, p_{15}, are rotations about the z axis and x axis, respectively. The methyl group is then translated along the positive z axis by the average C−C bond length and the central carbon of the *tert*-butyl group is placed at the origin. The correct P−C−C bond angle is generated by rotating the methyl group about the y axis. The two remaining methyl groups are defined by replicating the first methyl group and then rotating about the z axis by 120° and −120°, respectively. The *tert*-butyl torsion angle is a rotation of the group about the z axis, while the axial and equatorial tilts are rotations about the y axis and x axis, respectively. Positive axial tilts move *tert*-butyl or $SiCl_3$ groups towards the phosphorus lone pair and equatorial tilts move these groups around the 3-fold belt. Parameters introduced here are the mean and difference of the butyl torsion angles, p_{16} and p_{17}, mean and difference of the butyl axial tilts, p_{18} and p_{19}, and the mean and difference of the butyl equatorial tilts, p_{20} and p_{21}. The *tert*-butyl groups are then translated along the positive z axis by their respective P−C bond lengths.

The three groups that were initially placed along the z axis are moved into their final positions by rotating both *tert*-butyl groups about the y axis by their respective "dip" angles to allow a nonplanar PC_2Si fragment, and then about the x axis by an equal amount in opposite directions to give the correct angles about phosphorus. This introduces three final parameters: the mean and difference of the butyl dip angles, p_{22} and p_{23}, and the *tert*-butyl rotation angle, p_{24}.

Electron Diffraction Refinement

The radial distribution curve for tBu$_2$PSiCl$_3$ (Figure 2) consists of five distinct peaks at distances of ca. 110, 155, 205, 280, and 340 pm together with shoulders and weaker peaks above 400 pm. The peaks at 110 and 155 pm correspond to C−H and C−C scattering, respectively, and the intense peak at 205 pm to scattering from Si−Cl bonds, broadened by contributions associated with the P−Si and P−C bonds. The peak at 280 pm consists mainly of scattering from P···C non-bonded pairs, while the intense broad peak at 340 pm is attributed to scattering from a number of nonbonded atom pairs, with major contributions from Cl···Cl and P···Cl pairs.

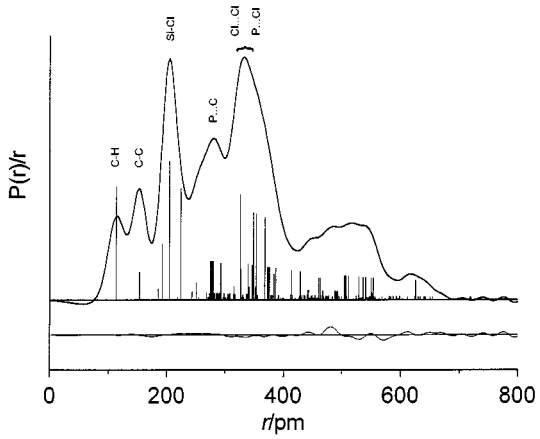


Figure 2. Experimental and difference (experimental − theoretical) radial distribution curves, $P(r)/r$, for tBu$_2$PSiCl$_3$. Before Fourier inversion the data were multiplied by $s\cdot\exp(-0.00002s^2)/(Z_{Si} - f_{Si})(Z_{Cl} - f_{Cl})$.

The starting parameters for the r_a structure refinement were taken from the theoretical geometry optimised at the 6-31G*/MP2 level. The program ASYM40[19] was used to convert the theoretical (6-31G*/SCF) Cartesian force field to one described by symmetry coordinates and this was scaled to obtain root-mean-square amplitudes of vibration (u). Scaling factors were chosen to be 0.90, 0.85, and 0.80 for bond stretches, angle bends and torsions, respectively. The presence of a large number of low-frequency vibrational modes led to overestimated predictions of the perpendicular amplitudes of vibration (k). Since these values were considered to be unreliable, corrections for shrinkage effects were not included.

Since the molecular structure contained a large number of similar interatomic distances, the SARACEN method[20] was employed in the GED refinements. Twelve geometrical and twelve vibrational amplitude restraints were used (Table 5). Values for geometrical restraints were taken to be those predicted at the 6-31G*/MP2 level, while amplitude restraints were based upon the force-field calculations at the 6-31G*/SCF level. Uncertainties were 0.5 pm for bond length differences, 1° for bond angles and 0.5° for bond angle differences. Torsion angles were assigned uncertainties of 2°, and 1° for differences. Uncertainties of 10% were assigned to vibrational amplitude restraints. The methyl tilt

Table 5. Flexible restraints

Number	Description	Parameter definition	Calculated value (Uncertainty)	Refined value
Geometrical restraints:				
1	P−C bond length difference	p_4	−0.2(5)	−0.14
2	Mean C−C−H angle	p_7	109.5(10)	109.2
3	P−C−C angle difference	p_9	−0.07(50)	0.05
4	Methyl torsion angle	p_{11}	4.0(20)	6.2
5	$SiCl_3$ torsion angle	p_{13}	194.0(20)	194.1
6	Butyl torsion angle difference	p_{17}	288.0(10)	288.3
7	C(6)−P−C(19) angle	p_{25}	111.0(10)	110.6
8	[Si−P−C(6)] − [Si−P−C(19)]	$p_{26} - p_{27}$	1.03(50)	0.6
9	P−C(6)−C(7) angle	p_{31}	105.7(10)	104.9
10	[P−C(6)−C(8)] − [P−C(6)−C(9)]	$p_{32} - p_{33}$	−7.7(10)	−7.3
11	[P−C(19)−C(20)] − [P−C(19)−C(21)]	$p_{34} - p_{35}$	1.1(5)	1.0
12	P−C(19)−C(22) angle	p_{36}	116.9(10)	115.7
Vibrational Restraints:				
13	P(1)−Si(2)	u_1	5.9(6)	5.5
14	P(1)···C(6)	u_2	5.8(6)	5.6
15	P(1)···Cl(3)	u_7	10.1(10)	8.9
16	Si(2)···C(6)	u_{16}	9.2(10)	9.3
17	Si(2)···C(7)	u_{18}	12.5(10)	12.4
18	Si(2)···C(8)	u_{19}	9.5(10)	10.7
19	Si(2)···C(9)	u_{20}	15.3(10)	15.4
20	Cl(3)···C(6)	u_{25}	18.9(20)	19.8
21	Cl(3)···C(7)	u_{27}	20.5(20)	22.7
22	Cl(3)···C(8)	u_{28}	20.0(20)	21.5
23	Cl(3)···C(9)	u_{29}	27.8(30)	24.8
24	Cl(4)···C(8)	u_{36}	12.3(10)	12.6

parameter, p_{12}, which helped define the position of the hydrogen atoms, was fixed, since little information is contained in the experimental data because of the poor scattering ability of hydrogen.

The use of flexible restraints allowed the refinement of 41 independent parameters, comprising 23 geometrical parameters and 18 amplitudes of vibration.

In the final refinement the R factors R_G and R_D were 0.091 and 0.077 respectively. Experimental and calculated radial distribution curves are shown in Figure 2, while Figure 3 displays the experimental and calculated molecular scattering intensity curves. Final refined parameters are listed in Table 4, selected interatomic distances and the corresponding amplitudes of vibration in Table 6 and the least-squares correlation matrix in Table 7.

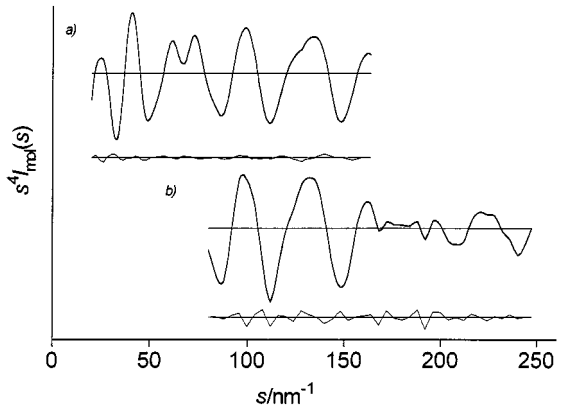


Figure 3. Experimental and final weighted difference (experimental − theoretical) molecular scattering intensities for tBu$_2$PSiCl$_3$. Camera distances were *(a)* 259 mm and *(b)* 95 mm

Discussion

The SARACEN method[20] has allowed the refinement of all significant structural parameters for tBu$_2$PSiCl$_3$. The highest possible molecular symmetry is C_s, but the perfectly staggered arrangement of all *tert*-butyl and $SiCl_3$ groups leads to parallel 1:3 interactions between two methyl groups or between a methyl group and a chlorine atom. The steric interactions of Y(MX$_3$)$_3$ groups are typically minimised by twisting the three groups by 15−20°, and this is what happens in this case, reducing the symmetry to C_1.

Overall, good agreement between theory and experiment was found; theoretical bond-length, bond-angle, and dihedral-angle predictions were in general found to be within one or two standard deviations of the experimental value. The introduction of electron correlation at the MP2 level is seen to be important in obtaining an accurate prediction of the P−Si distance; the 6-31G*/MP2 value at 224.9 pm is essentially identical to the experimental value of 225.0(12) pm, whilst the 6-31G*/SCF uncorrelated computation overestimates the distance at 227.0 pm. The P−Si bond length is also effectively identical to those found by GED in other compounds such as silylphosphane[21] [224.9(3) pm], silylmethylphosphane[21] [224.8(3) pm] and silyldimethylphosphane[21] [224.5(3) pm]. In H_2P-SiF_3, P−Si has been found[22] to be 220.7(3) pm, consistent with the fact that fluorine substituents at silicon result in a significant shortening of the P−Si bond length relative to that of H-substituted compounds. Substitution of the less electronegative chlorine for the silyl hydrogens does not seem to have a significant effect.[2]

Table 6. Selected interatomic distances (r_a) and root-mean-square amplitudes of vibration for tBu$_2$PSiCl$_3$ from the GED study[a]

Number	Atom pair	r_a/pm	u/pm
1	P−Si	225.0(12)	6.9(5)
2	P−C(6)	192.4(10)	5.6(1)
3	P−C(19)	192.5(10)	5.6(tied to u_2)
4	Si−Cl	204.7(3)	4.2(5)
5	C−C	153.6(2)	4.2(6)
6	C−H	113.6(2)	6.9(5)
7	P···Cl(3)	370.1(20)	8.9(9)
8	P···Cl(4)	350.0(40)	9.8(tied to u_7)
9	P···Cl(5)	353.5(33)	9.8(tied to u_7)
10	P···C(7)	275.4(18)	9.8(10)
11	P···C(8)	280.1(16)	10.1(tied to u_{10})
12	P···C(9)	292.4(16)	9.3(tied to u_{10})
13	P···C(20)	277.9(13)	10.0(tied to u_{10})
14	P···C(21)	276.1(13)	9.7(tied to u_{10})
15	P···C(22)	293.8(18)	9.4(tied to u_{10})
16	Si···C(6)	328.2(40)	9.2(10)
17	Si···C(19)	329.9(38)	9.0(tied to u_{16})
18	Si···C(7)	375.4(62)	12.4(10)
19	Si···C(8)	463.6(29)	10.7(9)
20	Si···C(9)	340.2(53)	15.4(10)
21	Si···C(20)	327.1(72)	13.4(tied to u_{20})
22	Si···C(21)	460.8(34)	10.9(tied to u_{19})
23	Si···C(22)	384.0(36)	13.5(tied to u_{18})
24	Cl(3)···Cl(4)	326.7(6)	10.1(6)
25	Cl(3)···C(6)	429.9(68)	19.8(19)
26	Cl(3)···C(19)	388.0(70)	15.5(tied to u_{28})
27	Cl(3)···C(7)	511.9(88)	22.7(19)
28	Cl(3)···C(8)	551.2(62)	21.5(13)
29	Cl(3)···C(9)	369.0(106)	24.8(27)
30	Cl(3)···C(20)	375.1(124)	23.8(tied to u_{28})
31	Cl(3)···C(21)	541.2(66)	18.5(tied to u_{27})
32	Cl(3)···C(6)	369.1(68)	19.3(tied to u_{28})
33	Cl(4)···C(6)	505.2(42)	12.4(tied to u_{26})
34	Cl(4)···C(19)	415.3(64)	15.3(tied to u_{24})
35	Cl(4)···C(7)	536.4(61)	19.4(tied to u_{27})
36	Cl(4)···C(8)	625.7(38)	12.6(9)
37	Cl(4)···C(9)	541.6(50)	15.8(tied to u_{27})
38	Cl(4)···C(20)	340.0(93)	16.5(tied to u_{28})
39	Cl(4)···C(21)	529.7(80)	18.9(tied to u_{27})
40	Cl(4)···C(22)	507.0(59)	20.9(tied to u_{26})
41	Cl(5)···C(6)	375.2(50)	13.3(tied to u_{28})
42	Cl(5)···C(19)	506.3(25)	11.5(tied to u_{26})
43	Cl(5)···C(7)	345.1(90)	15.0(tied to u_{28})
44	Cl(5)···C(8)	528.1(50)	15.9(tied to u_{27})
45	Cl(5)···C(9)	372.3(66)	21.6(tied to u_{28})
46	Cl(5)···C(20)	528.1(62)	14.1(tied to u_{27})
47	Cl(5)···C(21)	625.0(29)	12.2(tied to u_{35})
48	Cl(5)···C(22)	553.3(29)	17.4(tied to u_{27})
49	C(7)···C(8)	251.3(7)	4.5(9)

[a] See Figure 1 for atom numbering; all other distances were included in the refinement, but are not listed here.

All P−Si−Cl angle predictions were within one standard deviation of the experimentally determined values, and angles about the central phosphorus within two standard deviations. The angles about the central phosphorus [C−P−C 110.6(3)° and Si−P−C 103.6(3)°] are considerably larger than for the corresponding angles in silyldimethylphosphane[20] [C−P−C 100.8(12)° and Si−P−C 99.0(5)°], but can be attributed to the strong electron withdrawing character of the $SiCl_3$ group and to steric interactions between the *tert*-butyl groups. Axial tilts are all close to 6°, implying that $SiCl_3$ and *tert*-butyl groups are all tilted away from each other and towards the phosphorus lone pair. The equatorial tilts of the *tert*-butyl groups are smaller (ca. 2°) and towards one another. This implies that the residual steric interactions between two *tert*-butyl groups (after widening of the angle) are less than those between *tert*-butyl and $SiCl_3$ groups

Table 7. Least-squares correlation matrix (×100) for tBu$_2$PSiCl$_3$[a]

	p_3	p_5	p_6	p_{11}	p_{16}	p_{18}	u_1	u_5	u_6	u_{24}	k_1
p_6		74									
p_8	−64						−53				
p_{12}				−58							
p_{13}					−50						
p_{20}					−53						
p_{24}		−54	−62								
u_2		−53									
u_4							60				
u_{10}						68					
u_{49}			−50								
k_1	−50		50					73	52	57	
k_2			59					64	51	58	83

[a] Only elements with absolute values ≥ 50% are shown; k_1 and k_2 are scale factors.

Experimental Section

General: ^{1}H-, ^{13}C-, ^{29}Si-, and ^{31}P-NMR spectra: Bruker AC-200 spectrometer (200 MHz for ^{1}H, 50.3 MHz for ^{13}C, 81 MHz for ^{31}P, 39.8 MHz for ^{29}Si); solvent [D$_6$]benzene; shifts are given relative to TMS (^{1}H, ^{13}C, ^{29}Si) and 85% H_3PO_4 (^{31}P). − MS: Finnigan Mat 8430. − Elemental analyses: Carlo Erba analytical gas chromatograph. − All experiments were carried out under deoxygenated dry nitrogen as inert gas; solvents were dried according to standard procedures.

Ab initio Calculations: All calculations were performed on Dec Alpha 1000 4/200 and 8400 3/500 computers using the GAUSSIAN94 program.[23] Geometry optimisations were performed using the standard 3-21G*[24−26] and 6-31G*[27−29] basis sets at the SCF level and at the correlated MP2 level with the 6-31G* basis. Vibrational frequencies were calculated from analytic second derivatives at the 3-21G*/SCF and 6-31G*/SCF levels to determine the nature of stationary points and to provide estimates of amplitudes of vibration (u) for use in the GED refinements.

Electron Diffraction Measurements: Electron scattering intensities were recorded on Kodak Electron Image plates with the Edinburgh gas-diffraction apparatus operating at ca. 44.5 kV (electron wavelength ca. 5.7 pm).[30] Nozzle-to-plate distances for the metal inlet nozzle were 94.7 and 259.2 mm yielding data in the range s 20−360 nm^{-1}; four and three plates were exposed at the short and long distances, respectively. The sample and nozzle temperatures were maintained at ca. 423 and 448 K respectively during the exposure periods.

The scattering pattern of benzene was also recorded for the purpose of calibration; this was analysed in exactly the same way as for tBu$_2$PSiCl$_3$ so as to minimise systematic errors in the wavelengths and camera distances. Nozzle-to-plate distances, weighting functions used to set up the off diagonal weight matrix, correlation parameters, final scale factors and electron wavelengths for the measurements are collected in Table 8.

The electron scattering patterns were converted into digital form with a computer-controlled Joyce Loebl MDM6 microdensitometer and a scanning program described elsewhere.[31] The programs used for data reduction[31] and least squares refinement[32] have been

Table 8. Nozzle-to-plate distances [mm], weighting functions [nm^{-1}], correlation parameters and electron wavelengths [pm] used in the electron diffraction study

Nozzle-to-plate distance[a]	Δs	s_{min}	sw_1	sw_2	s_{max}	Correlation Parameter	Scale Factor[b]	Electron Wavelength
94.67	4	80	100	210	248	0.391	0.432(19)	5.653
259.17	2	20	40	140	164	0.411	0.638(24)	5.708

[a] Determined by reference to the scattering pattern of benzene. – [b] Values in parentheses are estimated standard deviations.

Table 9. ^{31}P-NMR data of *t*Bu(*i*Pr)PSiMe$_3$ (**5**), *t*Bu(*i*Pr)PSi$_2$Cl$_5$ (**7**), and *t*Bu(*i*Pr)PSiCl$_3$ (**6**)

time	**5**		**7**		**6**		other signals	
	[ppm]	relative intensity	[ppm]	relative intensity	[ppm]	relative intensity	[ppm]	relative intensity
5 min	−17.4	100	7.9	9	6.4	10	9.6	4
							10.8	5
30 min	−17.4	100	8.0	78	6.5	64	9.7	6
							10.1	5
							10.9	12
80 min	−17.5	51	8.1	100	6.5	82	1.8	14
							10.9	5
13 h			8.3	73	6.6	100	2.2	11
							9.9	3
43 h			8.3	46	6.7	100	2.3	1
							10.0	3
61 h			8.3	27	6.7	100	10.0	3
85 h			8.3	20	6.7	100	10.0	4
10 d			8.4	7	6.7	100	10.0	3

described previously; the complex scattering factors were those listed by Ross et al.[33]

Reaction of Diisopropyl(trimethylsilyl)phosphane 3 with Si_2Cl_6: Hexachlorodisilane (3.15 g, 11.7 mmol) was added dropwise to ice-cooled **1** (2.2 g, 11.6 mmol). A strongly exothermic reaction occurred. After 2 h stirring at room temperature, trimethylchlorosilane was distilled off from the red liquid; subsequent distillation at 2.5 mbar provided 2.3 g (78%) **4** as a colourless liquid, b.p. 65 °C.[34]

Reaction of *tert*-Butyl(isopropyl)(trimethylsilyl)phosphane 5[9] with Si_2Cl_6 Followed by Heteronuclear NMR: Hexachlorodisilane (0.43 g, 1.6 mmol) is added dropwise to ice-cooled **5** (0.33 g, 1.6 mmol). After warming up to room temperature, the brown liquid was transferred into an NMR tube. For results see Table 9.

NMR data of disilanylphosphane **7**: δ^{31}P 8.3 [s, $^1J(^{31}P, ^{29}Si) \pm 126.0$ Hz; $^2J(^{31}P, ^{29}Si) \pm 22.2$ Hz]; δ^{29}Si 13.2 [d, d, $^1J(^{31}P, ^{29}Si) \pm 125.5$ Hz; $^3J(^{29}Si, ^1H) \pm 8.7$ Hz], −0.4 [d, $^2J(^{31}P, ^{29}Si) \pm 24.0$ Hz].

Reaction of Di-*tert*-butyl(trimethylsilyl)phosphane (1) with the Disilane Fraction: A mixture of 6.21 g (28.43 mmol) of silylphosphane **1** and 12.52 g of a freshly distilled *WACKER AG.* technical disilane fraction sample [$Me_2(Cl)SiSiCl_2Me/(MeCl_2Si)_2$ ratio about 1:1; corresponding to about 28 mmol of each of the two disilanes] was heated to 100 °C. After 16 h, a ^{31}P-NMR spectrum confirms complete consumption of silylphosphane **1**. Distillation at 1 mbar allowed separation of two fractions: b.p. 55−60 °C, 1.6 g (24%) *t*Bu$_2$PSiMe$_2$Cl (**8**),[10] and b.p. 110−114 °C, 4.4 g (48%) *t*Bu$_2$PSi(Me(Cl)Si(Me)Cl$_2$ (**9**).

8: ^{1}H NMR: $\delta = 1.28$ (d, $J = \pm 11.4$ Hz, 18 H), 0.6 (d, $J = \pm 3.5$ Hz); ^{31}P NMR: $\delta = 0.8$ (s, ^1J (^{31}P, ^{29}Si = ± 67.5 Hz).[10]

NMR data of **9**: ^{1}H NMR: $\delta = 1.26$ [d, $^3J(^{31}P, ^1H) \pm 12$ Hz, PCCH_3, 18 H], 0.87 [d, $^3J(^{31}P, ^1H) \pm 3.7$ H, PSiCH_3,, 3 H], 0.78 (s, SiSiCH_3, 3 H). – ^{13}C NMR: $\delta = 34.2$ [d, $^1J(^{31}P, ^{13}C) \pm 26.5$ Hz, P*C*], 33.1 [d, $^2J(^{31}P, ^{13}C) \pm 12.4$ Hz, C-*C*H$_3$], 7.1 (s, SiSi-*C*), 4.9 [d, $^2J(^{31}P, ^{13}C) \pm 8.3$ Hz, PSi-*C*]. – ^{29}Si NMR: $\delta = 12.1$ [d, $^1J(^{31}P, ^{29}Si) \pm 100.2$ Hz, P-*Si*], 26.8 [d, $^2J(^{31}P, ^{29}Si) \pm 21.9$ Hz, PSi-*Si*]. – ^{31}P NMR: $\delta = 8.6$ [s, ^1J (^{31}P, ^{29}Si) ± 100.8 Hz, ^2J (^{31}P, ^{29}Si) ± 22.0 Hz].

Synthesis of Di-*tert*-butyl(pentamethyldisilanyl)phosphane (10): Methyllithium dissolved in ether (28.5 mL of a 1.6 M solution, 45.6 mmol) was added slowly to a solution of 4.52 g (13.8 mmol) **19** in ether at −20 °C. Stirring was continued for 2 h at room tempature, and subsequently the mixture was heated under reflux for 30 min. After separation of the solution from lithium chloride, dis-

Table 10. ^{31}P-NMR data of *t*Bu(*i*Pr)PGeMe$_3$ (**14**) and *t*Bu(*i*Pr)PSiCl$_3$ (**6**)

time	**14** [ppm]	relative intensity	**6** [ppm]	relative intensity	other signals [ppm]	relative intensity
5 min	−1.5	100	6.0	10	1.4	7
					3.0	7
					7.5 (*)	12
					11.8	4
3 h	−1.6	100	6.1	53	1.4	13
					3.1	14
					7.5 (*)	9
					11.7	4
15 h	−1.6	23	6.2	100	1.4	12
					3.5	22
					11.4	3
					11.9	3
6 d			6.5	100	1.5	8
					3.9	6

(*) Probably *t*Bu(*i*Pr)PSiCl$_2$SiCl$_3$ (**7**).

Table 11. ^{29}Si-NMR: of $Me_3GeSiCl_3$ **15**, $(Me_3Ge)_2Si(SiCl_3)_2$ **16**, $SiCl_4$

time	**15** [ppm]	relative intensity	**16** [ppm]	relative intensity	$SiCl_4$ [ppm]	relative intensity	other signals [ppm]	relative intensity
3 h	17.5	11	16.9	11	−19.0	100	10.1	43 (*)
15 h	17.7	19	16.8−84.9	307	−19.0	100	**3** (d,d): 10.1 (+), 10.4, 13.1, 13.3	38 (+), 27, 23, 25
7 d	17.9 (broad)	89	16.9	76	−19.0	89	**3**: 11.8 (d,d) **3**: 11.8	100 (++)
26 d	17.8 (broad)	71	16.9	74	−19.0	64	(d,d)	100 (++)

(*) Reasonable assignment: $Me_3GeSi(SiCl_3)_3$; (+) intensity of this peak of the d,d pattern enhanced due to overlap with the singlet at δ = 10.1 of (*); (++) normal intensity d,d pattern.

Table 12. ^{31}P-NMR data of *t*Bu(*i*Pr)$PSiCl_3$ (**6**), and *t*Bu(*i*Pr)PSi_2Cl_5 (**7**)

time	**7** [ppm]	relative intensity	**6** [ppm]	relative intensity	other signals [ppm]	relative intensity
20 min	8.1	6	6.3	100	1.2[a] 4.1	35
15 h			6.2	100	1.1[a]	2

[a] *t*Bu(*i*Pr)PH.

Table 13. ^{29}Si-NMR data of $(Me_3Sn)_2Si(SiCl_3)_2$ (**19a**), and *t*Bu(*i*Pr)$PSiCl_3$ (**3**)

time	**19a** [ppm]	relative intensity	$SiCl_4$ [ppm]	relative intensity	other signals [ppm]	relative intensity
60 min	19.4	58	−19.2	100	11.2 (*) **3:** 11.8 (d,d)	36 38, 38, 36, 25
15 h	19.4 −106.6	64 11	−19.2	100	**3**: 11.8 (d,d) 11.3 (*), −88 (*)	35, 35, 33, 33 21, 3

(*) $Me_3SnSi(SiCl_3)_3$ (**20a**).

tillation yielded 2.5 g (66%) of disilanylphosphane **10** as a colourless liquid. − ^{1}H NMR: δ = 1.29 [d, ^3J (^{31}P, ^{1}H) ± 11.1 Hz, PCC*H*$_3$, 18 H], 0.38 [d, ^3J(^{31}P, ^{1}H) ± 4.1 Hz, PSiC*H*$_3$, 6 H], 0.18 [s, SiSiC*H*$_3$), 9H]. ^{13}C NMR: δ = 33.5 [d, ^2J(^{31}P, ^{13}C) ± 12.1 Hz, C*C*H$_3$], 32.8 [d, ^1J(^{31}P, ^{13}C) ± 24.9 Hz, P*C*], 4.9 [d, ^2J(^{31}P, ^{13}C) ± 11 Hz, PSi-*C*]. −0.6 [d, ^3J(^{31}P, ^{13}C) ± 1.2 Hz, SiSi-*C*]. − ^{29}Si NMR: δ = −25.2 [d, ^1J(^{31}P, ^{29}Si) ± 63.4 Hz, P-*Si*], −14.9 [d, ^2J(^{31}P, ^{29}Si) ± 12.1 Hz, PSi-*Si*]. − ^{31}P NMR: δ = 5.6 [s, ^1J (^{31}P, ^{29}Si) ± 63.6 Hz, ^2J (^{31}P, ^{29}Si) ± 12.5 Hz]. − MS (EI, 70 eV) *m*/*z*(%): 276 (3, M^+), 131 (22, $Me_5Si_2^+$), 73 (60, Me_3Si^+), 58 (100, $C_4H_{10}^+$). − IR (liquid between KBr) [cm^{-1}] 2970 (s), 2950 (vs), 2900 (s), 2870 (s) 1475 (m), 1395 (m), 1370 (m), 1250 (s), 1200 (w), 1165 (m), 1045 (m), 1005 (m), 945 (m), 920 (m), 895 (w), 835 (s), 810 (s), 780 (m), 740 (vw), 690 (vw), 675 (w), 620 (w), 540 (vw), 495 (w), 440 (vw). − $C_{13}H_{33}PSi_2$ (276.55), found (calc.) C 56.19 (56.46), H 11.83 (12.02), P 11.13 (11.20).

Reaction of Diisopropyl(trimethylsilyl)amine (11) with Si_2Cl_6: Hexachlorodisilane (7.35 g, 27.3 mmol) was added to 4.5 g (26 mmol) diisopropyl(trimethylsilyl)amine. After heating the mixture for 6 h at 60°C complete consumption of the silylamine was indicated by NMR. Distillation at 0.5 mbar gave 6.24 g (72%) diisopropyl(pentachlorodisilanyl)amine as a moisture-sensitive colourless liquid, b.p. 61°C.[35] − ^{1}H NMR: δ = 1.02 [d, ^3J($^{1\,H,\,1}$H) ± 6.7 Hz, C*H*$_3$,, 12 H], 3.26 [sept, ^3J($^{1\,H,\,1}$H) ± 6.7 Hz, C*H*, 2 H]. − ^{13}C NMR: δ = 23.55 (s, *C*H$_3$), 47.25 (s, *C*H). ^{29}Si NMR: δ = −1.8 (s), −26 (s). − MS (EI, 70 eV): *m*/*z* (%) 318 (14) [M^+ − CH_3]; 276 (14) [M^+ − CH_3, − C_3H_6]; 176 (12) [M^+ − CH_3, − C_3H_6, − $SiCl_2$]; 133 (18) [$SiCl_3^+$]; 98 (4) [$SiCl_2^+$], 44 (100) [$C_3H_8^+$]. − IR $\tilde{\nu}$ (liquid between KBr) [cm^{-1}]: 2970 (s), 2939 (s), 2880 (s), 2850 (m) 1460 (m), 1385 (m), 1370 (s), 1305 (w), 1205 (w), 1175 (m), 1155 (w), 1000 (w), 885 (m), 840 (m), 815 (w), 800 (w), 645 (m), 570 (vs, broad), 510 (s), 485 (m), 445 (s), 375 (m). − $C_6H_{14}Cl_5NSi_2$ (336.62) found (calcd.) C 21.56 (21.41), H 4.14 (4.19), Cl 53.03 (52.66).

Reaction of Diisopropyl(trimethylstannyl)amine 12 with Si_2Cl_6: Hexachlorodisilane (2.7 g, 10 mmol) was added slowly at 0°C to 2.45 g (9.3 mmol) diisopropyl(trimethylstannyl)amine. After warming up to room temperature, complete consumption of the stannylamine was indicated by NMR. After removal of Me_3SnCl by crystallisation from pentane, distillation at 0.8 mbar gave 1.3 g (40%) diisopropyl(pentachlorodisilanyl)amine (**13**) as a moisture-sensitive colourless liquid,[35] b.p. 65°C (see above).

Table 14. ^{119}Sn-NMR data of $Me_3SnSiCl_3$ (**18a**) and $(Me_3Sn)_2Si(SiCl_3)_2$ (**19a**)

time	**18a** [ppm]	relative intensity	**19a** [ppm]	relative intensity
15 min	−66.3	26	−53.5	100
15 h	−66.5	4	−53.5	100

Table 15. ^{31}P-NMR data of *t*Bu(*i*Pr)$PSiCl_3$ (**6**), and *t*Bu(*i*Pr)PSi_2Cl_5 (**7**)

time	**7**		**6**		other signals	
	[ppm]	relative intensity	[ppm]	relative intensity	[ppm]	relative intensity
5 min	8.5	100	6.7	19	1.1	27
					4.3	2
30 min	8.4	63	6.6	100	1.2	26
					4.3	2
70 min	8.4	16	6.6	100	1.2	8
					4.2	1
5 h			6.5	100	1.1	6
3 d			6.6	100	1.2	1

Table 16. ^{119}Sn-NMR data of $Et_3SnSiCl_3$ (**18b**), $(Et_3Sn)_2Si(SiCl_3)_2$ (**19b**), and Et_3SnCl

time	**18b** [ppm]	relative intensity	**19b** [ppm]	relative intensity	Et_3SnCl [ppm]	relative intensity
25 min	−58.4	100	−44.6	17	150 (*)	6
60 min	−58.5	87	−44.7	100	145 (*)	7
330 min	−58.7	12	−44.8	100	136 (*)	7
24 h	−58.6	9	−44.8	100	135 (*)	7
3 d	−58.6	7	−44.8	100	135 (*)	8
9 d	−58.5	8	−44.8	100	135 (*)	8

(*) Broad.

Reaction of *tert*-Butyl(isopropyl)(trimethylgermyl)phosphane 14 with Si_2Cl_6 Followed by Heteronuclear NMR: Hexachlorodisilane (0.35 g, 1.3 mmol) was added dropwise to ice-cooled **14** (0.33 g, 1.3 mmol). A violet precipitate could be observed. After warming up to room temperature, the brown liquid was transferred into an NMR tube. For NMR results see Tables 10 and 11.

Reaction of *tert*-butyl(isopropyl)(trimethylstannyl)phosphane 17a with Si_2Cl_6 followed by heteronuclear NMR: Hexachlorodisilane (0.4 g, 1.5 mmol) was added dropwise to ice-cooled **17a** (0.41 g, 1.4 mmol). A red precipitate could be observed. After warming up to room temperature, the yellow liquid was transferred into an NMR tube. For NMR results see Tables 12, 13, and 14.

Reaction of *tert*-Butyl(isopropyl)(triethylstannyl)phosphane (17b) with Si_2Cl_6 Followed by Heteronuclear NMR: Hexachlorodisilane (0.24 g, 0.89 mmol) was added dropwise to ice-cooled **17b** (0.29 g, 0.86 mmol). The liquid turned red, then yellow and, at room temperature, green. The green liquid was transferred into an NMR tube. For NMR results see Table 15.

^{29}Si-NMR after 5 h: [$SiCl_4$: relative intensity = 100%] δ^{29}Si = 21.0/−108.1 (50%/9%) [$(Et_3Sn)_2Si(SiCl_3)_2$ (**19b**)], 11.8 (d,d) (4 lines, 20% each) [*t*Bu(*i*Pr)$PSiCl_3$ (**6**)], 12.1 (35%)[20b]; in a separate experiment, a spectrum with about 12 h acquisition time allowed the resolution of two signals for **20b**: δ^{29}Si = 11.7 ($SiCl_3$), −88.0 [$Si(SiCl_3)_3$]. For NMR results see Table 16.

Reaction of *tert*-Butyl(isopropyl)(tri-*n*-butylstannyl)phosphane (17c) with Si_2Cl_6 Followed by Heteronuclear NMR: Hexachlorodisilane (0.27 g, 1.0 mmol) was added dropwise to ice-cooled **17c** (0.4 g, 0.95 mmol). After warming up to room temperature, the greenish-yellow solution was transferred into an NMR tube (see the following tables).

Adding excess of the disilane (0.4 g, 1.5 mmol) at −20 °C to **17c** (0.27 g, 1.0 mmol) led qualitatively to the same products, but in a quite different distribution (faster consumption of **7** and of **18c**;

Table 17. ^{31}P-NMR data of *t*Bu(*i*Pr)$PSiCl_3$ (**6**) and *t*Bu(*i*Pr)$PSiCl_2SiCl_3$ (**7**)

time	**7**		**6**		other signals	
	[ppm]	relative intensity	[ppm]	relative intensity	[ppm]	relative intensity
2 h	7.3	100	5.9	9	1.4	3
					10.3	3
2.5 h	7.3	100	5.9	21	1.4	3
					10.3	.
12 d	7.0	3	5.9	100		

Table 18. ^{119}Sn-NMR data of *n*$Bu_3SnSiCl_3$ (**18c**), $(nBu_3Sn)_2Si(SiCl_3)_2$ (**19c**) and *n*$Bu_3SnSi(SiCl_3)_3$ (**20c**)

time	**18c** [ppm]	relative intensity	**20c** [ppm]	relative intensity	other signals [ppm]	relative intensity
2.5 h	−72.3	100			45.5	57
12 d	−72.7	21	−48.1	100		
75 d			−47.8	100	−53.8 (*)	64
					142.0 (**)	59

(*) **19c**; (**) *n*Bu_3SnCl.

about 5:4 intensity ratio of the ^{119}Sn-NMR signals of **19c** and **20c** after 30 days). For NMR results see Tables 17 and 18.

Acknowledgments

We thank the Deutsche Forschungsgemeinschaft, Bonn-Bad Godesberg, and the Fonds der Chemischen Industrie, Frankfurt, for financial support, the WACKER AG, Burghausen, for a sample of the disilane fraction, and Professor Uwe Klingebiel (Universität Göttingen) for a ^{29}Si-NMR measurement. We thank the U. K. Engineering and Physical Sciences Research Council for a research studentship (P. M. P.), for support of the Edinburgh gas electron diffraction Service (grant GR/K 44411) and *ab initio* calculations (grant GR/K 04194) and for provision of microdensitometer facilities at the Daresbury Laboratory.

[1] R. Martens, W.-W. du Mont, *Chem. Ber.* **1993**, *126*, 1115−1117.
[2] L.-P. Müller, W.-W. du Mont, J. Jeske, P. G. Jones, *Chem. Ber.* **1995**, *128*, 615; L.-P. Müller, A. Zanin, W.-W. du Mont, J. Jeske, P. G. Jones, *Chem. Ber.* **1997**, *130*, 377.
[3] R. A. Benkeser, *Acc. Chem. Res.* **1971**, *4*, 94.
[4] R. A. Benkeser, K. M. Foley, J. B. Grutzner, W. E. Smith, *J. Am. Chem. Soc.* **1970**, *92*, 697.
[5] W.-W. du Mont, L.-P. Müller, L. Müller, S. Vollbrecht, A. Zanin, *J. Organomet. Chem.* **1996**, *521*, 417.
[6] W.-W. du Mont, L.-P. Müller, L. Müller, S. Vollbrecht, A. Zanin, XI. Int. Symp. on Organosilicon Chemistry, Montpellier **1996**, Abstract.
[7] L. Müller, W.-W. du Mont, F. Ruthe, P. G. Jones, H. C. Marsmann, *J. Organomet. Chem.*, in print
[8] R. Martens, W.-W. du Mont, *Chem. Ber.* **1992**, *125*, 657.
[9] L. Müller, W.-W. du Mont, F. Ruthe, P. G. Jones, to be published; L. Müller, Ph.D. thesis, TU Braunschweig, **1998**.
[10] H. Schumann, W.-W. du Mont, *Z. Anorg. Allg. Chem*. **1975**, *418*, 259.
[11] G. D. Cooper, A. R. Gilbert, *J. Am. Chem. Soc.* **1960**, *82*, 5042.
[12] G. Urry, *Acc. Chem. Res.* **1970**, *3*, 306.
[13] U. Herzog, R. Richter, E. Brendler, G. Roewer, *J. Organomet. Chem.* **1996**, *507*, 221.
[14] H. J. Emeleus, M. Tufail, *J. Inorg. Nucl. Chem.* **1967**, *29*, 2081.
[15] U. Herzog, G. Roewer, U. Pätzold, *J. Organomet. Chem.* **1996**, *494*, 143.
[16] U. Herzog, G. Roewer, *J. Organomet. Chem.* **1997**, *544*, 217.
[17] K. G. Sharp, P. A. Sutor, E. A. Williams, J. D. Cargioli, T. C. Farrar, K. Ishibitsu, *J. Amer. Chem. Soc.* **1976**, *98*, 1977.
[18] G. Fritz, H. Schäfer, *Z. Anorg. Allg. Chem.* **1974**, *407*, 295.
[19] ASYM 40, version 3.0, update to program ASYM 20: L. Hedberg, I. M. Mills, *J. Mol. Spectrosc.* **1993**, *160*, 117.
[20] A. J. Blake, P. T. Brain, H. McNab, J. Miller, C. A. Morrison, S. Parsons, D. W. H. Rankin, H. E. Robertson, B. A. Smart, *J. Phys. Chem.*, **1996**, *100*, 12280; P. T. Brain, C. A. Morrison, S. Parsons, D. W. H. Rankin, *J. Chem. Soc.*, *Dalton Trans.*, **1996**, 4589.
[21] C. Glidewell, P.M. Pinder, A.G. Robiette, G.M. Sheldrick, *J. Chem. Soc.*, *Dalton Trans.*, **1972**, 1402.
[22] R. Demuth, H. Oberhammer, *Z. Naturforsch. A*, **1973**, *28*, 1862.
[23] *Gaussian 94* (Revision C.2), M. J. Frisch, G. W. Trucks, H. B. Schlegel, P. M. W. Gill, B. G. Johnson, M. A. Robb, J. R. Cheesman, T. A. Keith, G. A. Petersson, J. A. Montgomery, K. Raghavachari, M. A. Al-Laham, V. G. Zakrzewski, J. V. Ortiz, J. B. Foresman, J. Cioslowski, B. B. Stefanov, A. Nanayakkara, M. Challacombe, C. Y. Peng, P. Y. Ayala, W. Chen, M. W. Wong, J. L. Andres, E. S. Replogle, R. Gomperts, R. L. Martin, D. J. Fox, J. S. Binkley, D. J. Defrees, J. Baker, J. P. Stewart, M. Head-Gordon, C. Gonzalez, J. A. Pople, Gaussian Inc., Pittsburgh, PA, **1995**.
[24] J. S. Binkley, J. A. Pople, W. J. Hehre, *J. Am. Chem Soc.*, **1980**, *102*, 939.
[25] M. S. Gordon, J. S. Binkley, J. A. Pople, W. J. Pietro, W. J. Hehre, *J. Am. Chem. Soc*., **1982**, *104*, 2797.
[26] W. J. Pietro, M. M. Francl, W. J. Hehre, D. J. Defrees, J. A. Pople, J. S. Binkley, *J. Am. Chem. Soc.*, **1982, 104**, 5039.
[27] W. J. Hehre, R. Ditchfield, J. A. Pople, *J. Chem. Phys.*, **1972, 56**, 2257.
[28] P. C. Hariharan, J. A. Pople, *Theor. Chim. Acta*, **1973**, *28*, 213.
[29] M. S. Gordon, *Chem. Phys. Lett*. **1980**, *76*, 163.
[30] C. M. Huntley, G. S. Laurenson, D. W. H. Rankin, *J. Chem. Soc.*, *Dalton Trans.* **1980,** 954.
[31] S. Cradock, J. Koprowski, D. W. H. Rankin, *J. Mol. Struct.* **1981**, *77*, 113.
[32] A. S. F. Boyd, G. S. Laurenson, D. W. H. Rankin, *J. Mol. Struct.* **1981**, *71*, 217.
[33] A. W. Ross, M. Fink, R. Hildebrandt, in: *International Tables for Crystallography*, Vol. C, (Ed.: A. J. C. Wilson), Kluwer Academic Publishers, Dordrecht, **1992**, p. 245.
[34] R. Martens, W.-W. du Mont, L. Lange, *Z. Naturforsch. B* **1991**, *46*, 1609.
[35] H. Schuh, T. Schlosser, P. Bissinger, H. Schmidbaur, *Z. Anorg. Allg. Chem.* **1993**, *619,* 1347.

Received December 28, 1998
[I98451]

Synthesis, Crystal Structure, Spectroscopy, and Theoretical Investigations of Tetrahedrally Distorted Copper(II) Chelates with $[CuN_2S_2]$ Coordination Sphere

Stephan Knoblauch,[a] Roland Benedix,[b] Martin Ecke,[a] Thomas Gelbrich,[c] Joachim Sieler,[a] Fernando Somoza,[a] and Horst Hennig*[a]

Keywords: Copper chelates / EPR spectroscopy / Electronic structure / Schiff base ligands / Structure elucidation

A series of tetrahedrally distorted copper(II) complexes with thiolate and imine coordination were synthesized. Schiff bases derived from 4-benzoyl-3-methyl-1-phenyl-2-pyrazoline-5-thione and various diamines were used as tetradentate ligands to obtain tetrahedrally distorted metal chelates with $[CuN_2S_2]$ complex units. Crystal structures of the complexes **1**, **2**, **5** and **6** and of ligand H_2**5** have been determined by means of single-crystal X-ray structure analysis. The structure data show a strong influence of the diamine building blocks on the tetrahedral distortion of the copper(II) complexes. Results of Extended Hückel LCAO calculations correlate strongly with structural, electrochemical, UV/Vis- and EPR-spectroscopic features obtained experimentally. The calculations confirm for the whole complex series a strong delocalization of the frontier orbitals. The highest fully occupied molecular orbital shows a weak contribution, resulting from thiolate donor atoms, whereas the antibonding singly occupied molecular orbitals (SOMOs) are distributed between the copper(II) centre (ca. 35–40%) and the N_2S_2 donor set. The SOMO energy significantly lowers with increasing tetrahedral distortion of the coordination sphere. The influence of the tetrahedral distortion of copper(II) complexes on redox potentials, UV/Vis and EPR spectra is discussed.

Introduction

Numerous examples of copper coordination in the active sites of proteins are known.[1][2] These highly specialized molecules fulfil special requirements to manage electron and dioxygen transfer.[3][4] Particularly the Cu^I/Cu^{II} redox couple is a matter of importance.[5] Since the elucidation of crystal structures of plastocyanin (e.g. *Populus nigra*[6]) and azurin (e.g. *Pseudomonas aeruginosa*[7]), much attention is focused on modelling these *Type I* copper active sites,[8][9] also with respect to their unusual spectroscopic and electronic properties.[10][11] Moreover, the Cu_A electron transfer site in *cytochrome c oxidase* contains copper thiolate bonds.[12] With respect to the biomimetic modelling of these active sites, the chemistry of copper complexes with simultaneous imine and thiolate coordination has expanded during the last two decades.

The uncommon electron transfer properties of copper(II) ions in a low-symmetry environment of imino and thiolato donor sets led us to photochemical studies of various copper(II) chelates of $[CuN_2S_2]$ constitution.[13] It could be shown, that $[CuN_2S_2]$ chelates with Schiff base ligands derived from appropriate pyrazoline-5-thiones lead to unusual photo-induced electron transfer reactions, when irradiated in the presence of (porphyrin)metal(III) compounds and cycloolefins like α-pinene.[14–16] However, the role of the $[CuN_2S_2]$ complexes in these coupled electron transfer processes could not be sufficiently explained.

The $[CuN_2S_2]$ complexes **1**–**4**, **7**, and **9** and the corresponding ligands (H_2**1**–H_2**4**, H_2**7**, and H_2**9**) were synthesized for the first time whereas **5**, **6**, and **8** are already known from the literature.[17][18] The complex series **1**–**9** belong to the relatively few examples of stable copper(II) complexes with thiolate coordination[19] and are characterized by UV/Vis-spectroscopic similarity to Blue copper proteins.[20–23] The Schiff base ligands (see Figure 1) were obtained by condensation of 4-benzoyl-3-methyl-1-phenyl-2-pyrazoline-5-thione with selected diamines as proposed by Toftlund.[17] The choice of the bridging diamines was planned with the aim to control the geometry around the copper centre. Parallel with the structural changes of the Schiff base ligands a change in the spectral features of the corresponding Cu^{II} complexes occurs.[24][25] However, the UV/Vis spectra of that kind of copper(II) Schiff base complexes featuring large π-systems are not very well understood. EHT-LCAO calculations were carried out, therefore, as an approach to better understand the spectroscopic as well as electronic properties of these compounds. The calculations are based on crystal-structure data obtained for complexes **1**, **2**, **5**, and **6**. Crystal-structure data of the 2,2′-biphenylene-bridged compound **8** were taken from the literature.[17]

The goal of this study is to find the geometrical parameters introduced by the different ligand backbones which govern the deformations of the usually preferred planar coordination sphere for copper(II) ions in $[CuN_2S_2]$ chelates. An attempt is made to correlate EHMO data with UV/Vis-

[a] Institut für Anorganische Chemie der Universität Leipzig, Talstraße 35, D-04103 Leipzig, Germany
Fax: (internat.) +49(0)341/9604600
E-mail: hennigho@sonne.tachemie.uni-leipzig.de
[b] Bereich Naturwissenschaften der HWTK Leipzig, Postfach 66, D-04251 Leipzig, Germany
[c] University of Southampton, Department of Chemistry, Highfield, Southampton SO17 1BJ, United Kingdom

 © WILEY-VCH Verlag GmbH, D-69451 Weinheim, 1999 1434–1948/99/0808–1393 $ 17.50+.50/0

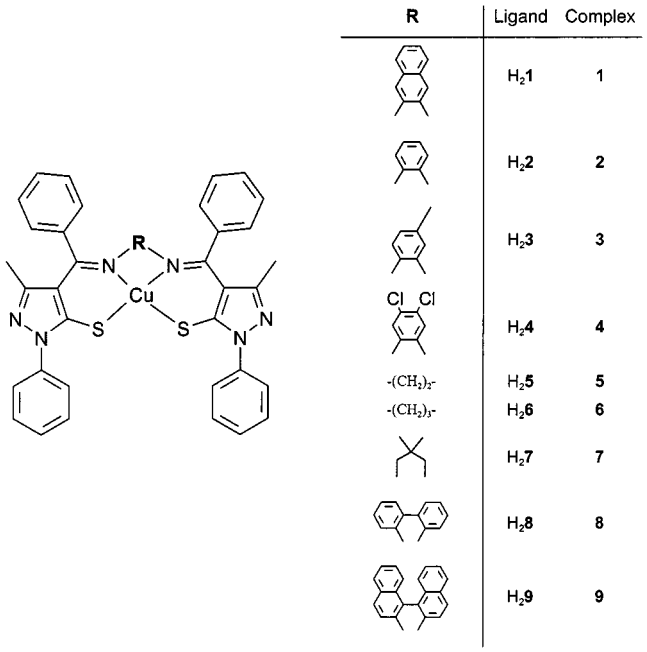


Figure 1. Formula scheme of copper(II) complexes **1**−**9**

and EPR-spectroscopic results as well as previously reported electrochemical parameters.[13]

Results and Discussion

Structures of the Schiff Base Ligand H_2**5** and of the Copper(II) Complexes 1, 2, 5, and 6

The crystal structure of the ligand H_2**5** has been determined to estimate the influence of the metal ion on the structural changes which occur upon deprotonation and coordination (see Figure 2 and Table 1).

Because no viable solution resulted perceiving $Z = 8$ and *C*2/*c*, space group *Cc* was applied yielding two independent molecules in the asymmetric unit. Figure 3 displays these molecules superimposed along the ethylenediamine fragments N(1)−C(35)−C(36)−N(2) and N(7)−C(71)−C(72)−N(8), respectively. This proves that the two molecules within the asymmetric unit are conformationally independent. Both molecules crystallize in the thioketone tautomeric form and show no symmetry. Considering the C(35)−C(36) [or C(71)−C(72)] axis, H_2**5** shows an antiperiplanar conformation which is changed to a gauche arrangement upon deprotonation and coordination of copper(II) ions. In addition, the ligand H_2**5** is characterized by two weak hydrogen bonds between the pyrazolinethione S atoms and the N atoms of the bridging ethylenediamine unit (Figure 2 and Table 2).

In agreement with available crystal-structure data of **8**,[17] none of the investigated complexes show two-fold symmetry. In general, neither **1**, **2**, **5**, nor **6** can be ordered to any symmetry element (C_1). The intermolecular distances between single molecules of **1**, **2**, **5**, and **6** in the corresponding crystal lattices refer to discrete monomeric species without any interactions. Crystal data of **1**, **2**, **5**, and **6** are listed in Table 1. Selected bond lengths and angles are given in Table 3 and perspective views are displayed in Figures 4, 5, and 6.

The copper(II) centre in all considered complexes is surrounded by a more or less flattened tetrahedron of two imine nitrogen atoms and two thiolate sulfur atoms. Figure 7 visualizes the most important geometrical parameters of the coordination spheres in **1**, **2**, **5**, **6**, and **8**. The deviation from the planar arrangement can be assessed in a first approach by means of the interplanar angles between the two planes defined by the atoms N(1)−Cu−S(1) and N(2)−Cu−S(2)

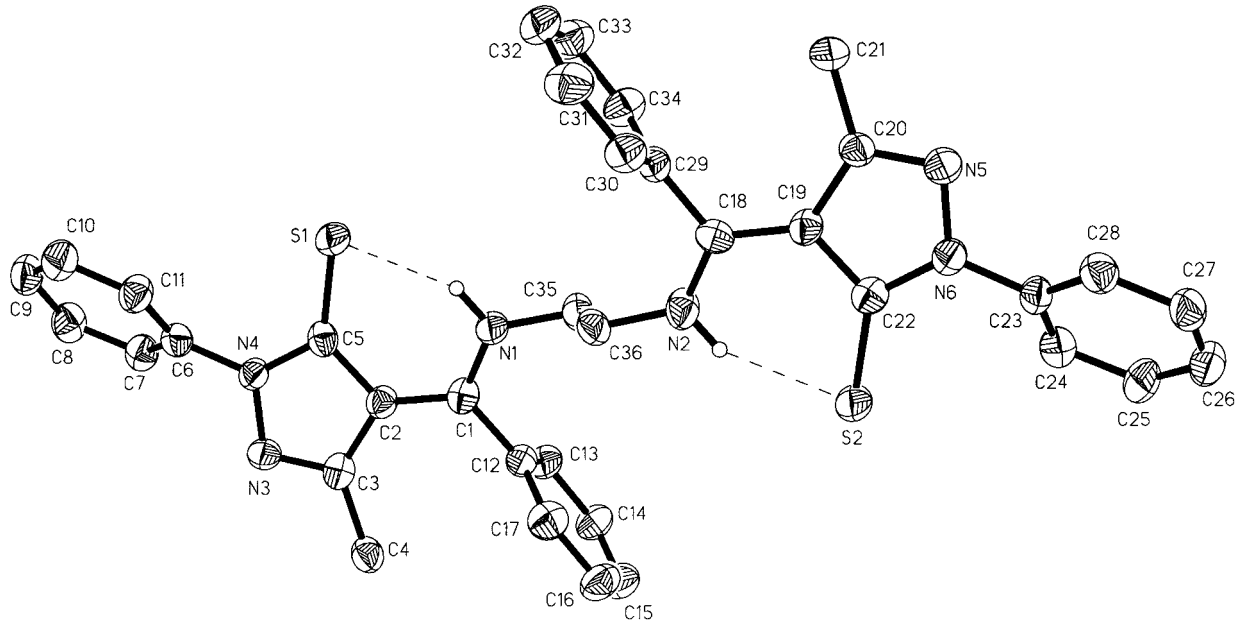


Figure 2. Molecular structure and numbering scheme of ligand H_2**5**; with exception of N(1)H and N(2)H hydrogen atoms are omitted for clarity (ORTEP drawing with 50% probability ellipsoids)

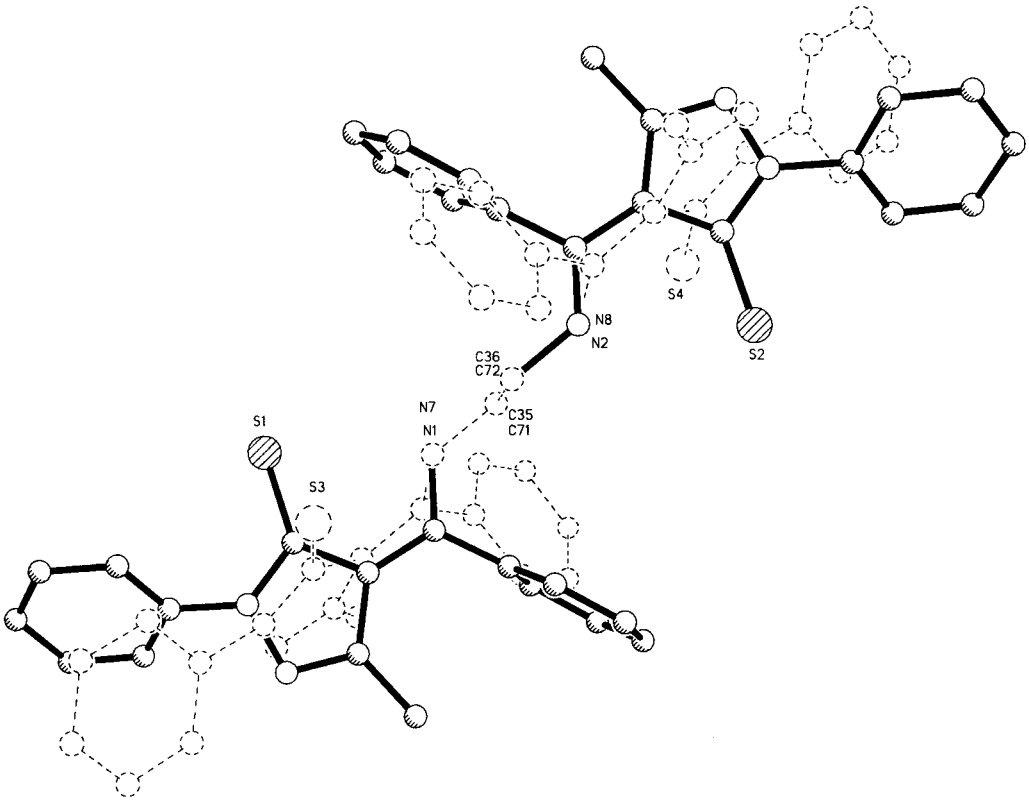


Figure 3. View of the two molecules of H_2**5** (solid lines and dashed lines, respectively) as present in the crystal; hydrogen atoms are omitted for clarity (ORTEP drawing with 50% probability ellipsoids)

Table 1. Crystallographic data and data related to data acquisition and refinement for compounds H_2**5**, **1**, **2**, **5,** and **6**

	H_2**5**	**1**	**2**	**5**	**6**
Empirical formula	$C_{36}H_{32}N_6S_2$	$C_{44}H_{32}CuN_6S_2$	$C_{40}H_{30}CuN_6S_2{\cdot}CHCl_3$	$C_{36}H_{30}CuN_6S_2{\cdot}H_2O$	$C_{37}H_{32}CuN_6S_2$
Molecular mass	612.81	772.42	841.72	692.32	687.35
Crystal size [mm]	0.25 × 0.12 × 0.10	0.40 × 0.20 × 0.20	0.26 × 0.20 × 0.20	0.50 × 0.20 × 0.20	0.30 × 0.24 × 0.24
Crystal system	monoclinic	monoclinic	monoclinic	orthorhombic	hexagonal
Space group	*Cc*	$P2_1/n$	$P2_1/n$	$Pna2_1$	$P6_1$
Unit cell dimensions					
a [Å]	12.143(1)	10.0339(7)	10.569(1)	13.050(3)	14.2559(6)
b [Å]	19.172(1)	26.005(2)	34.605(5)	10.550(2)	14.2559(6)
c [Å]	26.638(1)	16.054(1)	10.696(2)	23.990(5)	28.510(2)
α [°]	90	90	90	90	90
β [°]	94.10(1)	94.1520(10)	95.24(2)	90	90
γ [°]	90	90	90	90	120
V [Å^3]	6176.9(3)	4178.0(5)	3896(1)	3303(1)	5017.9(4)
Z	8	4	4	4	6
ρ(calcd.) [g/cm^3]	1.305	1.228	1.435	1.388	1.367
μ [mm^{-1}]	0.286	0.659	0.912	0.827	0.814
Absorption correction		SADABS	ψ scans	SADABS	SADABS
θ range for data collection	1.53° < θ < 26.00°	1.49° < θ < 26.14°	2.00° < θ < 25.98°	1.70° < θ < 26.28°	1.65° < θ < 26.23°
Reflections collected	44478	18221	7302	15133	22883
Independent reflections	12045	7272	5719	4789	6150
Final *R* indices [$I > 2\sigma(I)$]	$R = 0.0566$	$R = 0.0566$	$R = 0.0525$	$R = 0.0344$	$R = 0.0528$
	$wR_2 = 0.1330$	$wR_2 = 0.1427$	$wR_2 = 0.1051$	$wR_2 = 0.0685$	$wR_2 = 0.1329$
R indices (all data)	$R = 0.0830$	$R = 0.1181$	$R = 0.2285$	$R = 0.0464$	$R = 0.0718$
	$wR_2 = 0.1440$	$wR_2 = 0.1746$	$wR_2 = 0.1570$	$wR_2 = 0.0733$	$wR_2 = 0.1526$
Absolute structure parameter	0.07(6)	–	–	0.01(1)	0.02(2)

(θ), or by the sum (Σ) of each of the four angles N(1)−Cu−S(1), S(1)−Cu−S(2), S(2)−Cu−N(2), and N(2)−Cu−N(1) (Σ = 360° for an ideal planar arrangement and Σ = 437.6° for an ideal tetrahedral arrangement of all donor atoms in CuN_2S_2 units).

In complex **1**, the copper(II) ion is bound to the imine and thiolate donors in an essentially planar arrangement (see Figure 4). The copper ion in the crystal lattice of **1** deviates by 0.0413 Å from the calculated least-squares plane of the four donor atoms $N_{(1)}-N_{(2)}-S_{(1)}-S_{(2)}$. As expected,

Table 2. Bond lengths [Å] and bond angles [°] for hydrogen bonds in H_2**5**

D−H···A	*d*(D−H)	*d*(H···A)	*d*(D···A)	<(DHA)
N(1)−H(1)···S(1)	0.88	2.25	3.018(3)	145.3
N(2)−H(2)···S(2)	0.88	2.26	3.022(4)	145.3
N(7)−H(7A)···S(3)	0.88	2.32	3.039(4)	138.8
N(8)−H(8A)···S(4)	0.88	2.30	3.025(4)	140.2

θ increases in the order **1**, **2**, **5**, **6**, and **8** due to increasing steric demands of the different diamine backbones (Table 3). Depending on the amine bridge used, five- [**1**−**5**, Cu−N(1)−C(35)−C(36)−N(2)], six- [**6**−**7**, Cu−N(1)−C(35)−C(36)−C(37)−N(2)], or seven-membered chelate rings (**8**−**9**) form.

Even though complexes **1** and **5** both feature five-membered chelate rings, complex **1** with a bridging naphthyl unit shows distinct differences in θ values from the dihedral angle determined for complex **5**. This can be attributed to the different ligand flexibilities resulting from hindered rotation around the bond C(35)−C(36) in **1** or to larger conjugative effects of the aromatic bridging units forcing the system **1** into a planar donor arrangement to attain a more efficient π overlap.

In agreement with complexes containing comparably combined *N*,*S*-coordinating ligands,[26] a larger bite angle for the two N donors (N_1−Cu−N_2 in Figure 7) increases the tendency to form a pseudotetrahedral coordination sphere. This angle is influenced by both the steric demands of the corresponding backbone **R** connecting the N donors and the conformational flexibility of **R**. Consequently, a stronger distortion was observed for **6** [N(1)−Cu−N(2): 91.6°, θ = 42.5°] and **8** than for **1**, **2** and **5** due to the larger N(1)−Cu−N(2) bite angle.

A comparable Schiff base Cu^{II} complex synthesized by Gullotti consisting of 3-formyl-1-phenyl-2(1*H*)-pyridinethione and a propylene bridge shows a weaker effect on the coordination geometry (N−Cu−N′: 89.2°; N−Cu−N′/S−Cu-S′: 19.6°).[27] On the other hand, Bereman observed a particularly strong tetrahedral distortion of 53° for [*N*,*N*′-trimethylenebis(methyl 2-amino-1-cyclopentenedithiocarboxylato)]copper(II) (N−Cu−N′: 93.1°; N−Cu−N′/S−Cu−S′: 53°).[28] Steric influence of the different ligand frameworks and bonding behaviour of the coordinating sulfur donors may be responsible for the observed differences.

The geometry of the pyrazole units of the chelates **1**, **2**, **5**, and **6** shows no significant changes due to the influence of different backbones **R** (see Table 3). The pyrazole rings including the sulfur donors are almost planar in all cases and none of the atoms in the units S(1)−N(3)−N(4)−C(2)−C(3)−C(5) and S(2)−N(5)−N(6)−C(19)−C(20)−C(22), deviate more than 0.0618 Å [S(1) in **1**] from the least-squares planes defined by these atoms.

The sulfur−sulfur distances (3.13, 3.17, 3.08 Å) and S(1)−Cu−S(2) angles (88.3, 90.2, 87.3°) for **1**, **5**, **6**, respectively are also nearly uneffected by the different diamine bridges. This finding shows that, if in a first approximation the S_2Cu fragment remains almost unchanged, the geometrical changes forcing the system from planar to pseudotetrahedral donor arrangements are mainly a result of the different positions of the imine donors relative to the copper ion, and the different modes of coordination are obtained through simultaneous torsions along the bisector of the S_1−Cu−S_2 angle (Figure 7).

EHMO Calculations Related with UV/Vis, EPR, and Electrochemical Data

The UV/Vis spectra of H_2**1**−H_2**9** were used to estimate the spectral changes occurring upon deprotonation and coordination of the copper(II) ion. All ligands feature three intense bands in the region between 270 and 450 nm (Table 4). The two bands in the ultraviolet part of the spectrum are, in accordance to their intensities, attributable to π-π* transitions within the aromatic system and the azomethine or the thiolate chromophore, respectively. These absorptions appear at lower energies for the Schiff bases with aromatic coupling between the two imine groups via phenyl or biphenyl units (H_2**1**−H_2**4**, H_2**8**−H_2**9**), since the larger system of conjugated double bonds gives rise to a smaller energy gap between the highest occupied (HOMO) and the lowest unoccupied molecular orbitals (LUMO). The third absorption peaks in the visible region are less intense for H_2**1**−H_2**9**, but they can also be attributed to π-π* transitions since their intensities are too high for forbidden n-π* transitions. These bands disappear upon coordination of the metal ion.

To elucidate the electronic structure of copper complexes **1**−**9** in relation to their spectroscopic features, Extended Hückel MO calculations were performed. According to L. Hennig,[17] the UV/Vis spectra of the analogous complexes with hydrogen atoms instead of phenyl groups bound to the imine functions are nearly identically with those of **1**−**9**. This shows that electronic transitions are not significantly influenced by the phenyl groups on C(1) and C(18). In order to simplify molecules **1**−**9**, the smaller hydrogen-substituted systems were used as model fragments for the EHMO calculations, and the two hydrogen atoms were calculated in ideal positions.

Figure 8 displays the frontier orbital region of the fragment derived from the ethylene-bridged [CuN_2S_2] complex **5** belonging to the point group C_1. In agreement with previous MO calculations on copper dithiolates,[29][30] the highest singly occupied MO (SOMO) correlates with an antibonding orbital. It is formed by σ-type lone-pair orbitals of the ligand and a copper d orbital described as an admixture of d_{xy}, d_{xz}, and $d_{x^2-y^2}$ functions. The orbital mixing correlates with the absence of any symmetry element. The intricate stereochemistry of **1**−**9** prevents σ/π separation of the interacting orbitals.

As expected, the orbital structure of the lower lying MOs differs remarkably when compared with copper complexes of the [CuN_2S_2] type with saturated ligands (aliphatic thiol-

Table 3. Selected bond lengths [Å], angles, torsion angles [°], and dihedral angles [°] of **1**, **2**, **5**, **6**, **8** (e.s.d.s in parentheses)

Bond lengths [Å]	**1**	**2**	**5**	**6**	**8**[17]
Cu−N(1)	2.001(3)	2.014(6)	1.984(3)	1.994(4)	
Cu−N(2)	2.005(3)	1.986(6)	1.990(3)	2.011(4)	
Cu−S(1)	2.231(1)	2.253(2)	2.217(1)	2.247(2)	
Cu−S(2)	2.262(1)	2.221(2)	2.263(1)	2.219(2)	
N(1)−C(1)	1.319(5)	1.318(8)	1.296(4)	1.295(6)	
C(1)−C(2)	1.429(6)	1.431(9)	1.450(5)	1.454(7)	
C(2)−C(5)	1.402(6)	1.415(9)	1.401(5)	1.398(7)	
C(5)−S(1)	1.716(5)	1.711(7)	1.717(4)	1.718(5)	
C(2)−C(3)	1.438(6)	1.436(9)	1.432(5)	1.417(7)	
C(3)−C(4)	1.512(7)	1.518(9)	1.490(6)	1.500(7)	
C(3)−N(3)	1.311(6)	1.307(9)	1.322(5)	1.322(7)	
N(3)−N(4)	1.383(5)	1.397(7)	1.369(4)	1.373(5)	
N(4)−C(5)	1.425(6)	1.360(8)	1.355(4)	1.354(6)	
N(2)−C(18)	1.312(5)	1.314(9)	1.287(5)	1.303(6)	
C(18)−C(19)	1.425(6)	1.407(9)	1.439(5)	1.445(7)	
C(19)−C(22)	1.418(6)	1.415(9)	1.416(5)	1.405(7)	
C(22)−S(2)	1.721(5)	1.731(8)	1.725(4)	1.718(5)	
C(19)−C(20)	1.429(7)	1.451(9)	1.416(5)	1.444(7)	
C(20)−C(21)	1.497(8)	1.504(9)	1.508(5)	1.512(7)	
C(20)−N(5)	1.317(6)	1.312(9)	1.321(5)	1.302(6)	
N(5)−N(6)	1.381(5)	1.408(8)	1.385(4)	1.372(6)	
N(6)−C(22)	1.346(6)	1.333(9)	1.360(4)	1.358(6)	
N(1)−C(35)	1.425(5)	1.421(9)	1.477(5)	1.469(6)	
N(2)−C(36)	1.418(5)	1.418(9)	1.462(5)	–	
N(2)−C(37)	–	–	–	1.473(6)	
C(35)−C(36)	1.446(6)	1.403(9)	1.506(7)	1.523(8)	
C(36)−C(37)	1.364(6)	1.369(9)	–	1.522(8)	
Angles [°]					
S(1)−Cu(1)−S(2)	88.3(1)	91.5(1)	90.2(1)	87.3(1)	88.1
S(1)−Cu(1)−N(1)	96.2(1)	92.6(2)	98.8 (1)	96.7(1)	99.6
N(1)−Cu(1)−N (2)	81.7(1)	80.7(3)	86.0(1)	91.6(2)	98.1
N(2)−Cu(1)−S(2)	93.7(1)	95.5(2)	96.5(1)	98.5(1)	100.2
S(1)−Cu(1)−N(2)	177.2(1)	168.8(2)	153.8(1)	154.5(1)	
S(2)−Cu(1)−N(1)	174.9(1)	175.6(2)	154.0(1)	147.5(1)	
Cu(1)−S(1)−C(5)	103.2(2)	97.2(2)	104.7(1)	104.1(2)	
Cu(1)−S(2)−C(22)	99.7(2)	102.0(3)	103.4(1)	106.7(2)	
Cu(1)−N(1)−C(1)	128.8(3)	127.7(5)	133.4(2)	131.7(3)	
Cu(1)−N(2)−C(18)	128.6(3)	129.4(6)	130.2(3)	131.8(3)	
Cu(1)−N(1)−C(35)	108.1(1)	124.6(7)	106.3(2)	108.1(3)	
Cu(1)−N(2)−C(36)	107.8(3)	106.5(5)	109.8(2)	–	
N(1)−C(35)−C(36)	114.3(4)	113.0(8)	108.9(3)	110.1(4)	
N(2)−C(36)−C(35)	114.6(3)	116.5(8)	109.0(4)	–	
N(1)−C(1)−C(2)	121.5(4)	119.3(7)	122.1(3)	122.3(4)	
N(2)−C(18)−C(19)	121.8(4)	120.9(7)	124.1(3)	123.6(4)	
C(1)−C(2)−C(5)	127.4(4)	125.9(6)	126.6(3)	126.8(4)	
C(18)−C(19)−C(22)	126.9(4)	127.9(8)	126.5(3)	128.0(4)	
C(2)−C(5)−S(1)	131.5(3)	131.5(6)	133.4(3)	131.3(4)	
C(19)−C(22)−S(2)	129.7(4)	130.6(7)	130.6(3)	131.4(4)	
Cu(1)−N(2)−C(37)	–		–	109.0(3)	
C(35)−C(36)−C(37)	–		–	112.5(5)	
N(2)−C(37)−C(36)	–	–	–	110.1(4)	
Torsion angles [°]					
N(1)−C(35)−C(36)−N(2)	1.6	−1.3	48.5	–	
N(1)−C(35)−C(36)−C(37)	–	–	–	−33.5	
N(2)−C(37)−C(36)−C(35)	–	–	–	−48.8	
Cu(1)−N(1)−C(1)−C(2)	18.3	−15.3	−8.0	1.9	
Cu(1)−N(2)−C(18)−C(19)	−12.7	19.6	7.6	1.5	
N(1)−C(1)−C(2)−C(5)	13.4	−20.1	7.5	18.4	
N(2)−C(18)−C(19)−C(22)	−15.1	11.5	15.6	0.7	
C(1)−C(2)−C(5)−S(1)	−13.6	3.0	2.2	−7.4	
C(18)−C(19)−C(22)−S(2)	−3.0	−7.0	−6.4	−2.6	
C(2)−C(5)−S(1)−Cu(1)	−12.1	34.9	−8.4	−16.0	
C(19)−C(22)−S(2)−Cu(1)	34.4	−19.8	−17.3	1.8	
C(5)−S(1)−Cu(1)−N(1)	27.0	−44.5	5.8	23.1	
C(22)−S(2)−Cu(1)−N(2)	−40.2	31.6	25.8	0.0	
S(1)−Cu(1)−N(1)−C(1)	−36.4	47.1	0.8	−21.7	
S(2)−Cu(1)−N(2)−C(18)	39.8	−39.8	−27.1	−1.6	
Dihedral angles [°]					
θ	3.3	9.0	34.7	42.5	52.1

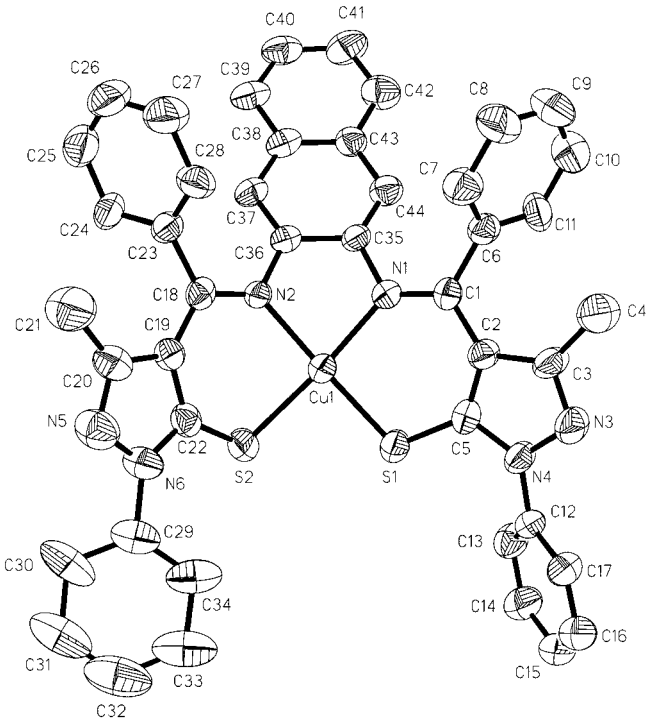


Figure 4. Molecular structure of complex **1** ($\theta = 3.3°$); hydrogen atoms and solvent molecules are omitted for clarity (ORTEP drawing with 50% probability ellipsoids)

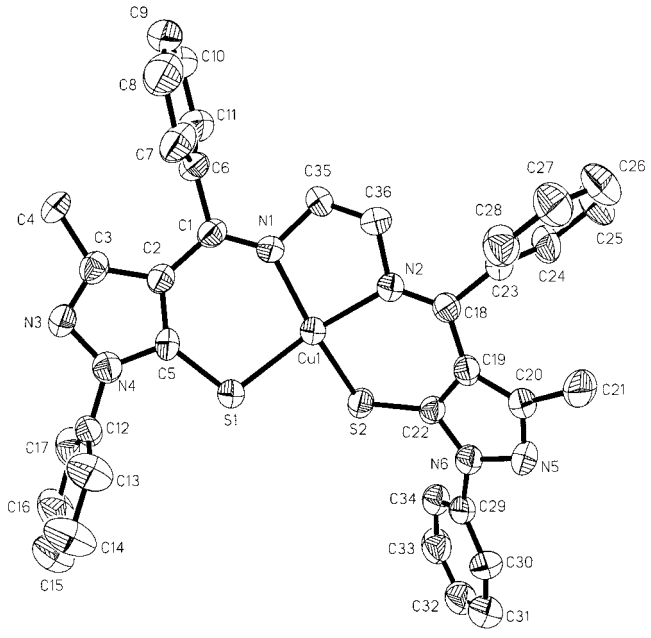


Figure 5. Molecular structure of complex **5** ($\theta = 34.7°$); hydrogen atoms and solvent molecules are omitted for clarity (ORTEP drawing with 50% probability ellipsoids)

ates).[31] In this case, the MOs arranged below the SOMO are typical sulfur lone-pair orbitals, whereas **1**−**9** are distinguished by largely delocalized MOs. The doubly occupied orbitals 6*a* and 5*a* are delocalized over the phenylpyrazole building block of the ligand with a ca. 20% contribution of the sulfur donor atoms. The following four orbitals at lower energies are mainly delocalized within the imine and pyrazole fragment with a more (4*a*, 1*a*) or less (3*a*, 2*a*) strong contribution of the thiolate sulfur. The three lowest unoccupied MOs calculated are mainly localized at the imine and pyrazole fragment.

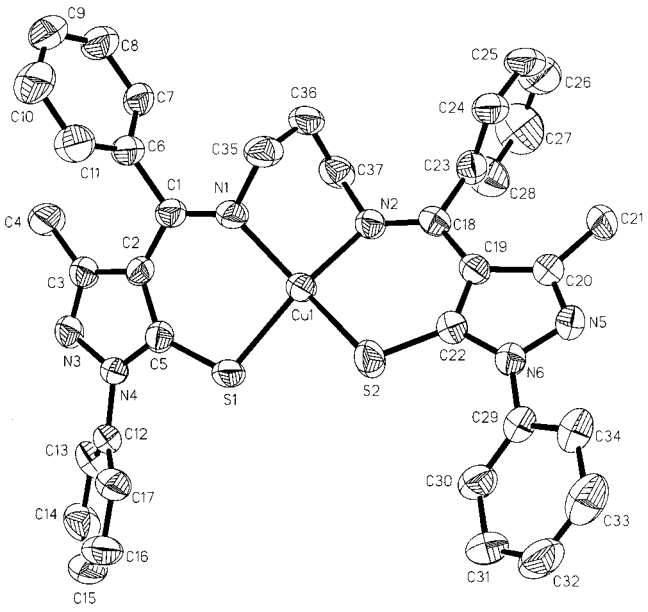


Figure 6. Molecular structure of complex **6** ($\theta = 42.5°$); hydrogen atoms and solvent molecules are omitted for clarity (ORTEP drawing with 50% probability ellipsoids)

The orbital characteristics obtained for the ethylene-bridged ligand system **5** agree with those of **1**, **6** and **8** distinguished by different *N*,*N*′-diamine backbones. Interestingly, the nearly planar complex **1** shows primarily an MO-localized at the imine functions arranged between the S-containing orbitals.

Single vacancy on the copper-containing SOMO and the existence of lower lying sulfur lone-pair orbitals should lead to the appearance of LMCT absorption in the low-energy region of the electronic spectra of the $[CuN_2S_2]$ complexes **1**−**9** (Table 5). Usually, the UV/Vis spectra of these complexes are dominated by three LMCT bands of σ and π symmetry in the range 350−500 nm.[25] In the electronic spectra of the complexes with the pyrazole-based thiolate ligands **1**−**9** two absorption bands in the regions 484−660 nm and 410−530 nm were assigned to transitions from sulfur-containing MOs to the SOMO.[19] A third absorption at shorter wavelength should be superimposed by the long-wavelength side of the intraligand (IL) π-π* absorption bands. Due to the strong delocalization calculated for the S-containing donor orbitals of the electronic transitions, the lowest energy absorption of the complexes **1**−**9** should possess π-π* character.

Increasing tetrahedral distortion of $[CuN_2S_2]$ complexes leads to red-shifted absorption in the UV/Vis spectra.[10][32] EHMO calculations confirm these experimental findings. With an increasing dihedral angle θ between the planes N_1CuS_1 and N_2CuS_2, the energy of the SOMO (its antibonding nature is the largest in the planar arrangement) is

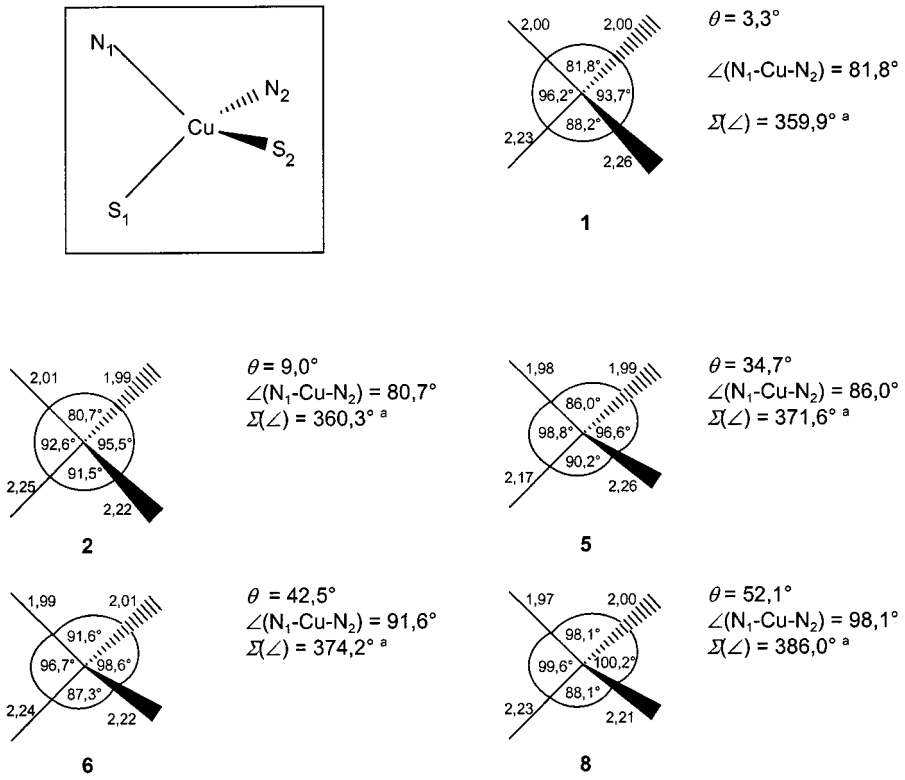


Figure 7. Comparison of the geometrical changes in the coordination polyhedra **1**, **2**, **5**, **6**, and **8** and enlargement of the N_1-Cu-N_2 bite angle dependent on the bridging diamine unit **R** [$\Sigma(\angle) = 360°$ ideal planar arrangement, $\Sigma(\angle) = 437.6°$ ideal tetrahedral arrangement of all donor atoms around the central ion Cu^{2+}]

Table 4. UV/Vis-spectroscopic data of the ligands H_2**1**$-H_2$**9**

Ligand	Backbone **R**	λ_{max} (ε) [nm (in L mol^{-1} cm^{-1})] {293 K; $CHCl_3$}
H_2**1**	2,3-naphthyl	271 (37300), 321 (34000), 419 (11700)
H_2**2**	1,2-phenyl	276 (35500), 318 (35800), 421 (11900)
H_2**3**	4-methylphenyl	275 (34800), 317 (35100), 419 (12300)
H_2**4**	3,4-dichlorophenyl	271 (36000), 321 (36000), 426 (10900)
H_2**5**	$-CH_2-CH_2-$	277 (26100), 314 (31200), 399 (11700)
H_2**6**	$-CH_2-CH_2-CH_2-$	281 (24500), 310 (29900), 394 (11100)
H_2**7**	$-CH_2-C(CH_3)_2-CH_2-$	282 (25600), 311 (31200), 394 (11400)
H_2**8**	2,2′-biphenyl	271 (32800), 321 (26300), 419 (10600)
H_2**9**	2,2′-binaphthyl	284 (37900), 344 (28300), 446 (12100)

successively decreased with increasing θ, whereas the energies of the doubly occupied S-containing MOs and the lowest unoccupied MOs remain nearly constant. In order to make the energetical changes in the frontier orbital region more obvious and to simplify the MO analysis by excluding the backbones between the two imine nitrogen atoms a purposely idealized C_{2v} model system **A** with planar NC_3S groups has been considered (Figure 9). Fixed averaged bond lengths and angles obtained from the structural data of complexes **1**, **5**, and **6** have been used as idealized geometrical parameters of the NS ligands. The hydrogen atoms were calculated in ideal positions.

The results of EHT calculations clearly show the overlap between d functions and ligand orbitals of appropriate symmetry to be most effective for $\theta = 0$. One ligand of the model fragment was fixed and the other ligand was stepwise rotated around the bisector of the N_1-Cu-S_1 angle simulating an increasing θ. This method has limitations in fitting to the actual structures that are in contrast to the actual molecules, the S_1-Cu-S_2 bite angles are successively increased in the model fragment with increasing θ. Regardless of this limitation, the more the ligand field is distorted (pointgroup changes from C_{2v} for $\theta = 0$ to C_2 for $\theta > 0$), the more the SOMO is stabilized (Figure 10). The SOMO ($2b_2$ for $\theta = 0$ or $3b$ for $\theta > 0$) is an antibonding orbital constructed with σ-type lone-pair orbitals from the four donor atoms and the copper d_{xy} AO. A considerable admixture of Cu p functions to $3b$ is observed for the nonplanar C_2 systems.

The highest fully occupied MO ($1a_2$ for $\theta = 0$, $2a$ for $\theta > 0$) is vice versa destabilized with increasing θ, but no orbital crossing occurs between SOMO $3b$ and the fully occupied orbital $2a$ for $0 \leq \theta \leq 90°$. The unoccupied π* MOs $3a$ and $4b$ and the π MO $2b$ are nearly unaffected by the

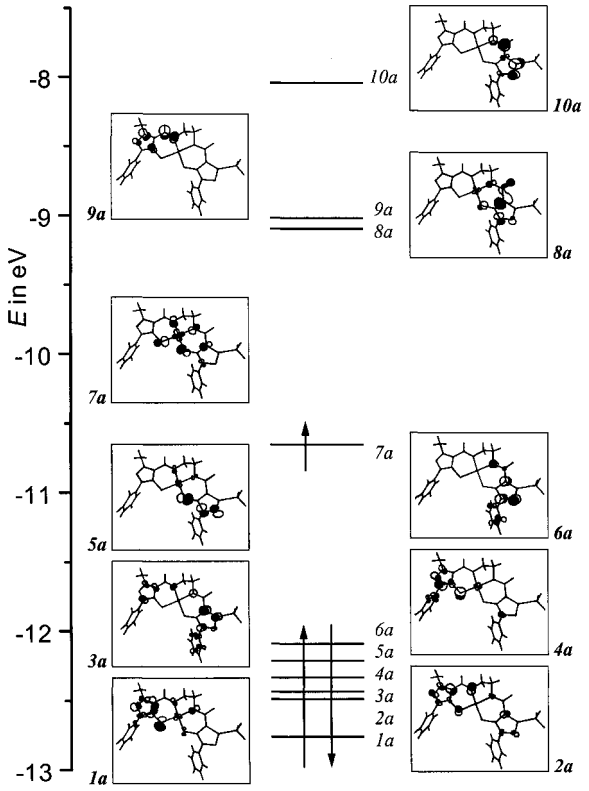


Figure 8. MO diagram of the model complex derived from **5**

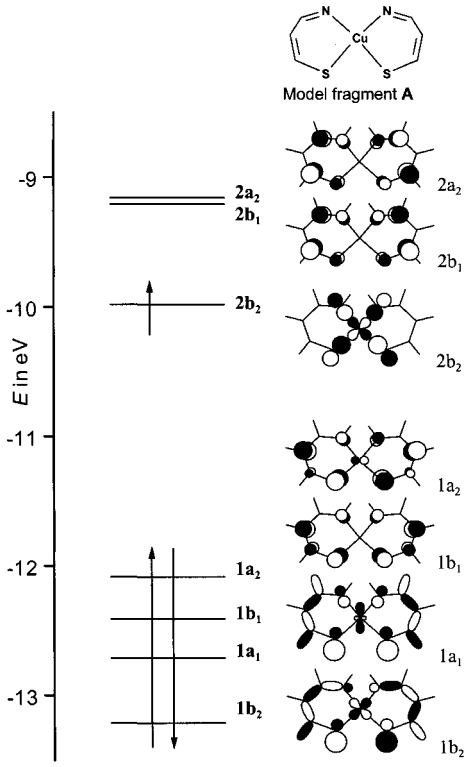


Figure 9. MO diagram of the C_{2v} model fragment **A**

Table 5. UV/Vis-spectroscopic data of the complexes **1**−**9**

Complex	Backbone **R**	λ_{max} (ε) [L mol^{-1} cm^{-1}] {293 K; $CHCl_3$}
1	2,3-naphthyl	484 (sh) (4300), 410 (sh) (16200), 336 (41600), 275 (41400)
2	1,2-phenyl	500 (sh) (2500), 405 (sh) (11900), 344 (32900), 275 (37500)
3	(4-methyl)phenyl	500 (sh) (2500), 410 (sh) (12200), 345 (33600), 277 (39400)
4	(3,4-dichloro)phenyl	505 (sh) (2500), 410 (sh) (14100), 350 (33700), 317 (28400), 279 (34000)
5	$-CH_2-CH_2-$	520 (sh) (1600), 438 (3500), 346 (sh) (10800), 275 (35600)
6	$-CH_2-CH_2-CH_2-$	610 (sh) (1900), 476 (3900), 339 (12100), 274 (36700)
7	$-CH_2-C(CH_3)_2-CH_2-$	599 (1900), 473 (3700), 341 (11500), 272 (35500)
8	2,2′-biphenyl	630 (sh) (1400), 522 (2100), 350 (sh) (10800), 279 (35500)
9	2,2′-binaphthyl	659 (1600), 530 (1800), 355 (sh) (17000), 290 (51800)

geometrical changes, and the levels 1*b* and 1*a* display only minor shifts. Generally it is hard to detect any further trends for these levels and for the interpretation of the electronic spectra of complexes **1**−**9**, because of the orbital mixing of all close-lying orbitals of the same symmetry type (*a* or *b*).

The results of the EHMO calculations are also in good agreement with the EPR data for complexes **1**−**9**. All complexes considered display typical Cu^{II} EPR signals with the four copper lines showing additional hyperfine splitting due to the coordination of two nitrogen donors (Table 6). The a_0^{Cu} values for **1**−**4** are as expected for planar Cu^{II} chromophores ($79-80\times10^{-4}$ cm^{-1}), while **5** shows a decreased a_0^{Cu} value due to a noticeable tetrahedral distortion. With a stronger deviation from the planar donor arrangement, the a_0^{Cu} values decline considerably, with the lowest value being obtained for **9**.

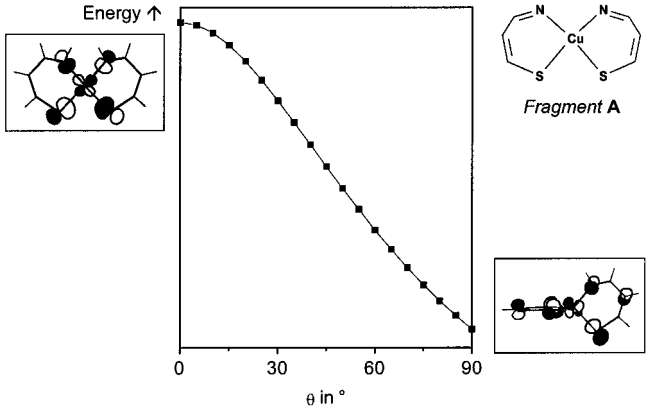


Figure 10. SOMO energy of the model fragment **A** in correlation to the dihedral angle θ

Table 6. EPR[a] (g_0, a_0^{Cu} at 293 K; $g_\parallel$, $g_\perp$, $A_\parallel^{Cu}$, $A_\perp^{Cu}$ at 130 K) and electrochemical data[b] of the complexes **1**−**9**

Complex	293 K g_0	a_0^{Cu} [10^{-4} cm^{-1}]	$g_\parallel$	$g_\perp$	130 K $A_\parallel^{Cu}$ [10^{-4} cm^{-1}]	$A_\perp^{Cu}$ [10^{-4} cm^{-1}]	Redox potentials[13] vs. Fc/Fc$^+$ $E_{p,c}$(red) [V]	$E_{p,a}$(ox) [V]
1	2.069	80.20	2.173	2.038	160	26	−1.03[d]	0.31[d]
2	2.070	80.32	2.135	2.037	173	36	−1.04[d]	0.34[d]
3	2.069	80.20	2.175	2.039	162	30	−1.06[d]	0.32[d]
4	2.069	79.45	2.152	2.027	194	25	−0.94[d]	0.42[d]
5	2.066	77.66	2.128	2.035	169	34	−1.23[c]	0.27[c]
6	2.070	69.32	2.137	2.034	161	26	−1.04[c]	0.23[d]
7	2.070	67.04	2.137	2.033	150	25	−1.02[c]	0.24[d]
8	2.072	68.19	2.147	2.035	148	28	−0.89[c]	0.25[d]
9	2.065	66.60	2.132	2.031	141	29	−0.84[c]	0.29[d]

[a] In $CHCl_3$. − [b] In butyronitrile at 293 K. − [c] Electrochemically reversible. − [d] Electrochemically irreversible

Because of the relatively low g values, the copper d orbital contribution to the SOMO of **1**−**9** was estimated from the EPR data.[33] The results obtained are comparable with data from MO calculations yielding a copper contribution to the SOMO of approximately 30−40%. The overall copper contribution on this orbital splits between the p and d functions and remains unaffected by the tetrahedral twist, but the more distorted systems show weaker contributions of the d functions to the SOMO. This finding points to an increased covalency in the tetrahedrally more distorted complexes.

The stepwise decrease of the energy of the SOMO with an increasing dihedral angle θ also influences the redox potentials of compounds **1**−**9**. A detailed description of this electrochemical behaviour of **1**−**9** is given elsewhere,[13] but the trend is that the higher the degree of distortion, the easier the compound can be reduced (Table 6). However, the positive shift of the reduction potentials with increasing tetrahedral distortion within the complex series can only be found after separating the aromatic bridged complexes **1**−**4**, **8**, and **9** from the aliphatic bridged compounds **5**−**7**. This result shows the limits of EHMO calculations in predicting the electrochemical behavior of the considered complexes. The oxidation potentials of **1**−**9** seem to be independent of the coordination geometry. In correlation to the calculated orbitals, the nature of the orbital where the electron is removed from is obviously similar for all considered complexes.

Conclusions

The tetrahedral distortion of the donor sphere in the considered complexes can be influenced by the choice of diamines used for the preparation of the Schiff base ligands. The stereochemistry observed for the different complexes is mainly a result of the interaction between the steric requirements introduced by the ligands and the increasing stabilizing bonding interactions (SOMO) which occur when the ligand field is distorted from planarity. The MO studies of these complexes are complicated by the orbital mixing correlating with the absence of any symmetry elements. The presented results confirm that the unpaired electron is localized in an antibonding orbital formed by σ-type lone pairs of the ligand and a mixed copper p and d contribution. The energy of the SOMO drops and the Cu p contribution increases with larger tetrahedral distortion of the [CuN_2S_2] group. These effects are reflected in bathochromically shifted CT absorptions in the UV/Vis spectra and positively shifted reduction potentials. The increased covalence nature in the tetrahedrally distorted complexes is manifested in declining coupling constants a_0^{Cu} in the EPR spectra of the studied complexes.

Experimental Section

General: Analytical-grade chemicals were used as received from Fluka (several diamines), Laborchemie Apolda [$Cu(CH_3COO)_2$-H_2O] and Merck (solvents for spectroscopy). Elemental analysis were carried out with a Heraeus CHN-O-RAPID analysator. NMR spectra were recorded with a 400-MHz spectrometer (Unity 400, Varian) at room temperature in $CDCl_3$. Electronic spectra were measured with a CARY 3 UV/Vis spectrometer (Varian). An ESP 300E (Bruker) spectrometer (X-band 9.8 GHz) was used to record the ESR spectra at 293 K and at 130 K. − The Schiff base ligands H_2**5**, H_2**6**, and H_2**8** were synthesized according to a literature procedure.[18] This method was extended to prepare the new ligands H_2**1**−H_2**4**, H_2**7**, and H_2**9**.

Schiff Base $H_2$1: M.p. 267°C. − ^{1}H NMR ($CDCl_3$): δ = 7.21−7.83 (m, aromatic H), 1.58 (s, −CH_3), 16.10 (s, >N−H···). − ^{13}C NMR ($CDCl_3$): δ = 15.62 (s, −CH_3), 151.65 (s, >C=N−N), 113.46 (s, >C=), 168.95 (s, >C=S), 166.29 (s, >C=N), 125.50−139.25 (m, aromatic C). − $C_{44}H_{34}N_6S_2$ (710.9): calcd. C 74.34, H 4.82, N 11.82, S 9.02; found C 73.4, H 4.9, N 11.3, S 9.1.

Schiff Base $H_2$2: M.p. 259−261°C. − ^{1}H NMR ($CDCl_3$): δ = 6.75−7.85 (m, aromatic H), 1.56 (s, −CH_3), 15.98 (s, >N−H···). − ^{13}C NMR ($CDCl_3$): δ = 16.06 (s, −CH_3), 152.05 (s, >C=N−N), 113.71 (s, >C=), 169.53 (s, >C=S), 166.64 (s, >C=N), 125.96−139.66 (m, aromatic C). − $C_{40}H_{32}N_6S_2$ (660.9): calcd. C 72.70, H 4.88, N 12.72, S 9.70; found C 73.0, H 4.9, N 12.6, S 9.34.

Schiff Base $H_2$3: M.p. 248−249°C. − ^{1}H NMR ($CDCl_3$): δ = 6.55−7.85 (m, aromatic H), 1.54 (s, −CH_3), 1.56 (s, −CH_3), 15.88 (s, >N−H···), 2.01 (s, −CH_3). − ^{13}C NMR ($CDCl_3$): δ = 16.05 (s, −CH_3), 16.01 (s, −CH_3), 152.09 (s, >C=N−N), 112.80 (s, >C=), 113.63 (s, >C=), 169.12 (s, >C=S), 166.79 (s, >C=N); 166.73 (s, >C=N), 125.96−139.18 (m, aromatic C), 21.27 (s, −CH_3). −

$C_{41}H_{34}N_6S_2$ (674.9): calcd. C 72.97, H 5.08, N 12.45, S 9.50; found C 72.7, H 5.0, N 12.4, S 9.4.

Schiff Base $H_2$4: M.p. 271−273°C. − ^{1}H NMR ($CDCl_3$): δ = 6.76−7.83 (m, aromatic H), 1.56 (s, $-CH_3$), 15.68 (s, >N−H···). − ^{13}C NMR ($CDCl_3$): δ = 16.10 (s, $-CH_3$), 152.10 (s, >C=N−N), 114.06 (s, >C=), 170.01 (s, >C=S), 165.78 (s, >C=N), 125.83−139.30 (m, aromatic C). − $C_{40}H_{30}Cl_2N_6S_2$ (729.8): calcd. C 65.83, H 4.14, Cl 9.72, N 11.52, S 8.79; found C 65.6, H 4.5, Cl 10.2, N 11.5, S 8.9.

Schiff Base $H_2$5: M.p. 284−286°C. − ^{1}H NMR ($CDCl_3$): δ = 7.16−7.76 (m, aromatic H), 1.37 (s, $-CH_3$), 14.54 (s, >N−H···), 3.50 (m, $-CH_2-$). − ^{13}C NMR ($CDCl_3$): δ = 15.28 (s, $-CH_3$), 151.49 (s, >C=N−N), 112.29 (s, >C=), 169.03 (s, >C=S), 167.79 (s, >C=N), 125.39−139.55 (m, aromatic C), 44.80 (s, $-CH_2-$). − $C_{36}H_{32}N_6S_2$ (612.8): calcd. C 70.56, H 5.26, N 13.71, S 10.46; found C 70.0, H 5.4, N 13.5, S 10.8.

Schiff Base $H_2$6: M.p. 212−214°C. − ^{1}H NMR ($CDCl_3$): δ = 7.30−7.80 (m, aromatic H), 1.35 (s, $-CH_3$), 14.37 (s, >N−H···), 3.39 (m, $-CH_2-$N), 1.92 (m, C$-CH_2-$C). − ^{13}C NMR ($CDCl_3$): δ = 15.30 (s, $-CH_3$), 151.74 (s, >C=N−N), 112.19 (s, >C=), 169.66 (s, >C=S), 167.78 (s, >C=N), 126.24−140.85 (m, aromatic C), 43.36 (s, $-CH_2-$N=), 30.05 ($-CH_2-$). − $C_{37}H_{34}N_6S_2$ (626.9): calcd. C 70.89, H 5.47, N 13.41, S 10.23; found C 71.0, H 5.4, N 13.4, S 10.8.

Schiff Base $H_2$7: M.p. 206−208°C. − ^{1}H NMR ($CDCl_3$): δ = 7.22−7.84 (m, aromatic H), 1.41 (s, $-CH_3$), 14.41 (s, >N−H···), 3.30 (m, $-CH_2-$), 1.18(s, $-CH_3$). − ^{13}C NMR ($CDCl_3$): δ = 15.25 (s, $-CH_3$), 151.40 (s, >C=N−N), 112.32 (s, >C=), 168.89 (s, >C=S), 167.05 (s, >C=N), 125.87−139.35 (s, arom. C), 36.08 (s, >C<), 54.13 (s, $-CH_2$), 24.54 (s, $-CH_3-$). − $C_{39}H_{38}N_6S_2$ (654.9): calcd. C 71.53, H 5.85, N 12.83, S 9.79; found C 71.4, H 5.5, N 11.7, S 9.9.

Schiff Base $H_2$8: M.p. 214−217°C. − ^{1}H NMR ($CDCl_3$): δ = 6.75−7.85 (m, aromatic H), 1.45 (s, $-CH_3$), 15.53 (s, >NH···). − ^{13}C NMR ($CDCl_3$): δ = 16.01 (s, $-CH_3$), 151.62 (s, >C=N−N), 114.05 (s, >C=), 170.03 (s, >C=S), 166.87 (s, >C=N), 125.86...139.48 (m, arom. C). − $C_{46}H_{36}N_6S_2$ (737.0): calcd. C 74.98, H 4.92, N 11.40, S 8.70; found C 74.2, H 5.4, N 11.8, S 8.3.

Schiff Base $H_2$9: M.p. 310−315°C. − ^{1}H NMR ($CDCl_3$): δ = 6.70−7.79 (m, aromatic H), 1.44 (s, $-CH_3$), 15.65 (s, >N−H···). − ^{13}C NMR ($CDCl_3$): δ = 16.38 (s, $-CH_3$), 151.32 (s, >C=N−N), 133.49 (s, >C=), 169.08 (s, >C=S), 163.90 (s, >C=N), 125.25−139.62 (m, aromatic C). − $C_{54}H_{40}N_6S_2$ (837.1): calcd. C 77.48, H 4.82, N 10.04, S 7.66; found C 76.1, H 5.2, N 9.3, S 7.8.

Complexes **1−9** were synthesized with the appropriate ligands and $Cu(CH_3COO)_2{\cdot}H_2O$ in ethanol according to a literature procedure.[17]

Cu Complex 1: M.p. 338°C. − $C_{44}H_{32}CuN_6S_2$ (772.5): calcd. C 68.41, H 4.18, Cu 8.23, N 10.88, S 8.30; found C 67.8, H 4.0, Cu 8.8, N 10.5, S 7.9.

Cu Complex 2: M.p. 329−331°C. − $C_{40}H_{30}CuN_6S_2$ (722.4): calcd. C 66.51, H 4.19, Cu 8.80, N 11.62, S 8.88; found C 66.7, H 4.3, Cu 8.7, N 11.8, S 8.6.

Cu Complex 3: M.p. 302°C. − $C_{41}H_{32}CuN_6S_2{\cdot}CHCl_3$(855.8): calcd. C 58.95, H 3.88, Cl 12.43, Cu 7.42, N 9.83, S 7.49; found C 58.7, H 3.7, Cl 12.6, Cu 6.9, N 9.7, S 8.2.

Cu Complex 4: M.p. 333−336°C. − $C_{40}H_{28}Cl_2CuN_6S_2$ (791.3): calcd. C 60.71, H 3.57, Cl 8.96, Cu 8.04, N 10.62, S 8.10; found C 60.7, H 3.8, Cl 8.7, Cu 9.5, N 10.8, S 8.1.

Cu Complex 5: M.p. 324−326°C. − $C_{36}H_{30}CuN_6S_2$ (674.3): calcd. C 64.12, H 4.48, Cu 9.42, N 12.46, S 9.52; found C 63.9, H 4.8, Cu 9.1, N 12.5, S 10.0.

Cu Complex 6: M.p. 282−285°C. − $C_{37}H_{32}CuN_6S_2$ (688.4): calcd. C 64.56, H 4.69, Cu 9.23, N 12.21, S 9.31; found C 64.2, H 5.1, Cu 9.6, N 12.1, S 8.2.

Cu Complex 7: M.p. 262°C. − $C_{39}H_{36}CuN_6S_2$ (716.4): calcd. C 65.39, H 5.06, Cu 8.87, N 11.73, S 8.95; found C 64.2, H 5.1, Cu 9.6, N 12.1, S 8.2.

Cu Complex 8: M.p. > 306°C (decomp.). − $C_{46}H_{34}CuN_6S_2$ (798.5): calcd. C 69.19, H 4.29, Cu 7.97, N 10.52, S 8.03; found C 68.7, H 4.4, Cu 7.7, N 10.4, S 7.7.

Cu Complex 9: M.p. 346°C (decomp.). − $C_{54}H_{38}CuN_6S_2$ (898.6): calcd. C 72.18, H 4.26, Cu 7.07, N 9.35, S 7.14; found C 71.6, H 4.3, Cu 8.0, N 9.3, S 7.9.

X-ray Crystal-Structure Determination: Detailed structure data for H_2**5**, **1**, **2**, **5**, and **6** can be obtained from the Cambridge Crystallographic Data Centre. The deposition numbers are CCDC-101708 (H_2**5**), -101711 (**1**), -101712 (**2**), -101710 (**5**), and -101713 (**6**). Suitable crystals were obtained by diffusion of *n*-decane or *n*-hexane into saturated solutions of **1**, **2** and **6** in $CHCl_3$. Crystals of **5** precipitated during slow concentration of a saturated ethanolic solution at −20°C, single crystals of H_2**5** precipitated from an EtOH/$CHCl_3$ mixture. Crystallographic data for H_2**5**, **1**, **2**, **5**, and **6** are listed in Table 1. Selected bond lengths and angles are given in Tables 2 and 3. Figures 2−6 display thermal-ellipsoid drawings of 50% probability. Crystals were mounted on a glass pin. Data were collected at room temperature with a Siemens CCD diffractometer (SMART) operating in the ω-scan mode (**1**, **5**, **6**) or a Stoe four-circle diffractometer (STADI 4) operating in the ω/2θ-scan mode (**2**). Data for H_2**5** were collected with a Nonius CCD diffractometer. All diffractometers were equipped with a monochromator utilizing Mo-K_α radiation (λ = 0.7107 Å). Empirical absorption correction (SADABS[34]) was applied for **1**, **5**, and **6.** A ψ-scan correction was used for **2.** All observed reflections of H_2**5**, **1**, **5**, and **6** were used for refinement of unit-cell parameters. 80 reflections with 20° < Θ < 25° were selected for complex **2**. All structures were solved using direct methods (SHELXS[35]). Parameters were refined by full-matrix least-squares techniques (SHELXL[36]). Partly, the hydrogen atoms were calculated in ideal positions and their isotropic thermal parameters were fixed. For **5**, the water hydrogen atoms could not be localized in the structure.

Calculational Methods: The Extended Hückel LCAO Calculations[37] were carried out using methods as proposed by Mealli.[38] Considering the calculation of transition metal complexes, the weighted H_{ij} formula (modified Wolfberg-Helmholtz relation) for the off-diagonal elements (H_{ij}) was used, to take into consideration the counterintuitive orbital mixing.[39] Single Slater-type orbitals were used for the main-group elements as well as for the s and p functions of the metal ion, whereas d wave functions were taken as contracted linear combinations of two Slater-type functions as proposed by Richardson.[40] The crystallographic data (atomic coordinates) of the complexes **1**, **2**, **5**, **6**, and **8** (Cambridge Crystallographic Data Centre) were taken for the calculations to fit the molecular geometry. In all cases the phenyl rings on C(1) and C(18) were replaced by hydrogen atoms calculated in ideal positions. Atomic coordinates for dimethyl *N*,*N*′-ethylenebis(L-cysteinato)-*S*,*S*′]copper(II) were included for comparison (Cambridge Crystallographic Data Centre).

Acknowledgments

This work was supported by the Deutsche Forschungsgemeinschaft and the Fonds der Chemischen Industrie. We thank Prof. R. Kirmse and A. Voigt (University of Leipzig) for the EPR investigations.

[1] S. Otsuka, T. Yamanaka, *Metalloproteins − Chemical and Biological Effects*, *Bioactive Molecules*, Elsevier Science Publ., Amsterdam, **1988**, vol. 8.
[2] T. G. Spiro (Ed.), *Copper Proteins*, Wiley & Sons, New York, **1981**.
[3] K. D. Karlin, Y. Gultneh, *Prog. Inorg. Chem.*, **1987**, *35*, 219.
[4] A. Messerschmidt, *Adv. Inorg. Chem*. **1993**, *40*, 121.
[5] W. Kaim, J. Rall, *Angew. Chem.* **1996**, *108,* 47.
[6] P. M. Colman, H. C. Freeman, J. M. Guss, M. Murata, V. A. Norris, J. A. M. Ramshaw, M. P. Venkatappa, *Nature*, **1978**, *160*, 309.
[7] E. T. Adman, R. E. Stenkamp, L. C. Sieker, L. H. Jensen, *J. Mol. Biol.* **1978**, *123*, 35.
[8] A. G. Sykes, *Adv. Inorg. Chem.* **1991**, *36*, 377.
[9] B. P. Murphy, *Coord. Chem. Rev.* **1990**, *124*, 63.
[10] E. I. Solomon, M. J. Baldwin, M. D. Lowery, *Chem. Rev.* **1992**, *92*, 521.
[11] N. Kitajima, Adv. *Inorg. Chem.* **1993**, *39*, 1.
[12] T. Tsukihara, H. Aoyama, E. Yamashita, T. Tomizaki, H. Yamaguchi, K. Shinzawa-Itoh, R. Nakashima, R. Yaono, S. Yoshikawa, *Science* **1995**, *269*, 1069.
[13] S. Knoblauch, F. Hartl, D. J. Stufkens, H. Hennig, *Eur. J. Inorg. Chem.* **1999**, 303.
[14] H. Hennig, S. Knoblauch, D. Scholz, *New J. Chem.* **1997**, *21*, 701.
[15] M. Grosche, Dissertation, Universität Leipzig, **1993**.
[16] J. Behling, Dissertation, Universität Leipzig, **1994**.
[17] L. Hennig, R. Kirmse, O. Hammerich, S. Larsen, H. Frydendahl, H. Toftlund, J. Becher, *Inorg. Chim. Acta* **1995**, *234*, 67.
[18] L. Hennig, G. Mann, *Z. Chem.* **1988**, *28*, 364.
[19] S. Mandal, G. Das, R. Singh, R. Shukla, P. K. Bharadwaj, *Coord. Chem. Rev.* **1997**, *160,* 191.
[20] E. I. Solomon, K. W. Penfield, D. E. Wilcox, *Struct. Bonding* **1983**, *53*, 1.
[21] A. G. Sykes, *Struct. Bonding* **1990**, *75*, 175.
[22] H. B. Gray, E. I. Solomon, in *Copper proteins* (Ed.: T.G. Spiro), Wiley & Sons, New York, **1981**.
[23] A. Messerschmidt, *Struct. Bonding* **1998**, *90*, 37.
[24] H. Toftlund, J. Becher, P. H. Olesen, J. Z. Pedersen, *Israel J. Chem.* **1985**, *25*, 56.
[25] H. J. Schugar, *Copper Coordination Chemistry*, Adenine Press, New York, **1984**, p. 43.
[26] S. Mandal, R. Shukla, P. K. Bharadwaj, *Polyhedron* **1995**, *14*, 2063.
[27] M. Gullotti, L. Casella, A. Pintar, E. Suardi, P. Zanello, S. Mangani, *J. Chem. Soc., Dalton Trans.* **1989**, 1979.
[28] R. D. Bereman, M. R. Churchill, G. Shields, *Inorg. Chem.* **1979**, *18*, 3117.
[29] T. Yamabe, K. Hori, T. Minato, K. Fukui, Y. Sugiura, *Inorg. Chem.* **1982**, *21*, 2040.
[30] R. Cini, A. Cinquantini, P. L. Orioli, C. Mealli, M. Sabat, *Can. J. Chem.* **1984**, *62*, 2908−2913.
[31] P. K. Bharadwaj, J. A. Potenza, H. J. Schugar, *J. Am.Chem. Soc.* **1986**, *108*, 1351.
[32] R. L. Harlow, W. J. Wells, G. W. Watt, S. H. Simonsen, *Inorg. Chem.* **1975**, *14*, 1768.
[33] J. R. Morton, K. F. Preston, *J. Magn. Reson.* **1978**, *30*, 577.
[34] R. H. Blessing, *Acta Crystallogr.* **1995**, *51A*, 33.
[35] G. M. Sheldrick, *SHELXS-86*, Universität Göttingen, **1986**.
[36] G. M. Sheldrick, *SHELXL-97*, Universität Göttingen, **1997**.
[37] R. Hoffmann, *Chem. Phys.* **1963**, *39*, 1397.
[38] C. Mealli, D. M. Prosperio, *J. Chem. Educ.* **1990**, *76*, 399.
[39] J. H. Ammeter, H. B. Bürgi, J. C. Thibeault, R. Hoffmann, *J. Am. Chem. Soc.* **1978**, *100*, 3686.
[40] J. W. Richardson, W. C. Nieuwpoort, R. Powell, W. F. Edgel, *J. Chem. Phys.* **1962**, *36*, 1057.

Received August 12, 1998
[I98274]

The First Oligomeric Samarium(II) Silylamide: Coordinative Saturation through Agostic Sm···SiH Interactions

Iris Nagl,[a] Wolfgang Scherer,[a] Maxim Tafipolsky,[a] and Reiner Anwander*[a]

Keywords: Agostic interactions / Samarium / Silylamide / Transsilylamination / Trinuclear complex

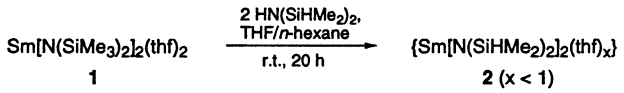
$Sm[N(SiMe_3)_2]_2(thf)_2$ reacts with 1,1,3,3-tetramethyldisilazane by a transsilylamination reaction to form the hexane-soluble $Sm[N(SiHMe_2)_2]_2(thf)_x$ in high yield. An X-ray diffraction study reveals a novel trinuclear complex of composition $Sm\{[\mu\text{-}N(SiHMe_2)_2]_2Sm[N(SiHMe_2)_2](thf)\}_2$ featuring a bent array of metal centers. Multiple metal···SiH β-agostic interactions sterically and electronically saturate the samarium(II) centers implying a new coordination mode of the bridging amide ligands.

Introduction

Sterically encumbered amide ligands are known to stabilize the lower oxidation states of transition metals efficiently.[1][2] However, complexes of strong reductants such as $Sm^{(II)}$ ($E_0 = -1.55$ V) display an intrinsic instability in the presence of β-H atoms and functional groups.[3] Donor ligand coordination and ate complex formation usually add to complex stability by counteracting oligonuclear aggregation and subsequent disproportionation reactions.[2][4] Recently, we introduced the bis(dimethylsilyl)amide ligand, $N(SiHMe_2)_2$, into organolanthanide chemistry which imparts (i) increased complex stability relative to the similarly sized $NiPr_2$ ligand, and (ii) enhanced steric flexibility relative to the commonly employed $N(SiMe_3)_2$ ligand.[5] In addition, the Si−H moiety proved to be an excellent spectroscopic probe prone to unique agostic, "Ln···SiH", interactions.[6] This paper describes how the Si−H functionality can also provide a stabilizing environment in samarium(II) chemistry.

Results and Discussion

When $SmI_2(thf)_2$[7] was allowed to react with 1.95 equivalents of $Li[N(SiHMe_2)_2]$, in THF at ambient temperature, the color of the suspension turned from dark green to black. Evaporation of the solvent gave a residue whose IR spectrum showed the presence of samarium-bonded $N(SiHMe_2)_2$ ligands. However, tractable $Sm^{(II)}$ species soluble in *n*-hexane or toluene could not be isolated.



Scheme 1. Synthesis of complex **2**

In order to exclude any ate complex formation or alkali metal salt contamination, we performed a transsilylamination reaction, using $Sm[N(SiMe_3)_2]_2(thf)_2$[4a] (**1**) and $HN(SiHMe_2)_2$ as reagents (Scheme 1). A similar transsilylamination reaction was recently used to form $Na[N(SiHMe_2)_2]$ by exploiting the difference in the pK_a values of the parent silylamines [pK_a(THF): 25.8 $HN(SiMe_3)_2$), 22.6 $HN(SiHMe_2)_2$].[8] Following this procedure, the compound $Sm[N(SiHMe_2)_2]_2(thf)_x$ (**2**) was obtained in almost quantitative yield. IR spectroscopy confirmed the coordination of the bis(dimethylsilyl)amide ligand by the appearance of a very strong SiH stretching vibration at 2040 cm^{-1} (free silylamine: 2118 cm^{-1}). Additionally, a broad lower energy shoulder at approximately 1936 cm^{-1}, indicative of agostic interactions, was observed. The ^1H NMR spectrum of **2**, measured in [D_8]tetrahydrofuran, showed two resonances at $\delta = -2.47$ and -12.18 in a ratio of 6:1, respectively, as would be expected for an intact $N(SiHMe_2)_2$ ligand. Recrystallization of compound **2** from *n*-hexane/THF (4:1) solutions at −35°C yielded black, rhombic single crystals (**2a**). Both the crude reaction product **2** and the crystals **2a** gave similar ^1H NMR spectra in [D_6]benzene displaying at least five resonances. Although a variable-temperature ^1H NMR spectroscopic study showed the coalescence of some signals at −60°C, which is in agreement with the presence of differently coordinated amide ligands, the resonances ranging from $\delta = 14$ to -40 proved of little diagnostic value.

An X-ray crystallographic study of **2a** revealed an unprecedented, trinuclear molecular structure of composition $Sm\{[\mu\text{-}N(SiHMe_2)_2]_2Sm[N(SiHMe_2)_2](thf)\}_2$. As shown in Figure 1, three samarium(II) atoms are arranged in a bent fashion ("Sm···Sm···Sm" 130°). In contrast, the structurally related heteroleptic complexes $Yb\{[\mu\text{-}DAC]Yb[N(SiMe_3)_2]\}_2$ (DAC = deprotonated 4,13-diaza-18-crown-6)[3c] and $Mn\{[\mu\text{-}NHC_6H_3iPr_2\text{-}2,6]_2Mn[N(SiMe_3)_2]\}_2$[9] show almost linear arrays of metal centers ["M···M···M" 176.9(1)° and 170.3(1)°, respectively]. The central Sm(1) is formally four-coordinate − the nitrogen atoms of the bridging amide ligands producing a distorted tetrahedral SmN_4 core coordination ["N−Sm(1)−N"

[a] Anorganisch-chemisches Institut, Technische Universität München
Lichtenbergstraße 4, D-85747 Garching, Germany
Fax: (internat.) + 49-89/289-13473
E-mail: reiner.anwander@ch.tum.de

 © WILEY-VCH Verlag GmbH, D-69451 Weinheim, 1999 1434−1948/99/0909−1405 $ 17.50+.50/0

84.00(7)−143.83(7)°]. The formal four-coordination of the terminal samarium atoms, which are approximately related by a C_2 axis through Sm(1), is completed by terminal amide and THF donor ligands.

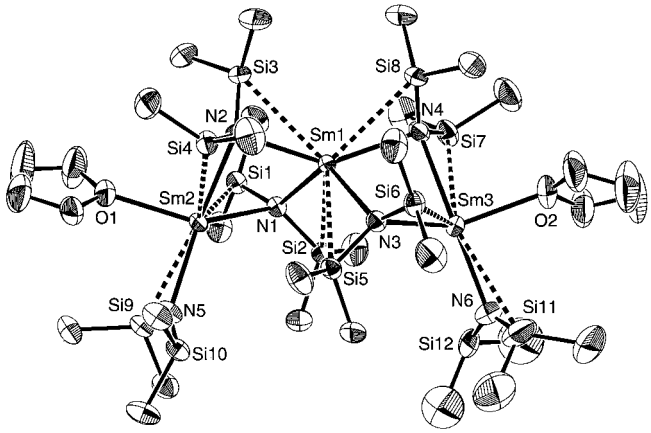


Figure 1. Molecular structure of **2a** (PLATON, 50% probability level). Hydrogen atoms and one part of the disordered Si(12)Me_2 group are omitted for clarity. Selected interatomic distances (Å) and angles (°): Sm(1)−Sm(2) 3.6920(2), Sm(1)−Sm(3) 3.6999(3), Sm···Si 3.2317(9)-3.342(1); N−Sm(2)−N 81.09(7)-146.27(7), N−Sm(2)−O(1) 88.35(8)-136.76(7), N−Sm(3)−N 82.48(7)−152.8(1), N−Sm(3)−O(2) 89.5(1)-134.61(9), Sm(1)−N(1)−Si(1) 132.7(1), Sm(1)−N(1)−Si(2) 96.04(9), Sm(1)−N(2)−Si(3) 94.7(1), Sm(1)−N(2)−Si(4) 128.0(1), Sm(1)−N(3)−Si(5) 96.10(9), Sm(1)−N(3)−Si(6) 130.5(1), Sm(1)−N(4)−Si(7) 127.7(1), Sm(1)−N(4)−Si(8) 95.0(1), Sm(2)−N(1)−Si(1) 92.1(1), Sm(2)−N(1)−Si(2) 122.4(1), Sm(2)−N(2)−Si(3) 127.9(1), Sm(2)−N(2)−Si(4) 93.7(1), Sm(2)−N(5)−Si(9) 100.5(1), Sm(2)−N(5)−Si(10) 130.8(1), Sm(3)−N(3)−Si(5) 122.3(1), Sm(3)−N(3)−Si(6) 92.9(1), Sm(3)−N(4)−Si(7) 94.5(1), Sm(3)−N(4)−Si(8) 127.6(1), Sm(3)−N(6)−Si(11) 106.8(2).

The coordination mode of the bridging amide ligands is asymmetric since the N atoms are located closer to the central Sm(1) atom [av. Sm(1)−N 2.633 Å]. The remaining Sm−N bond lengths associated with the bridging amide ligands range from 2.664(2) to 2.723(2) Å and are the longest Sm−N σ-bonds observed so far. In comparison, the bridging Sm−N bond lengths in $MSm[N(SiMe_3)_2]_3$ average 2.560(6) Å (M = Na) and 2.529(3) Å (M = K), respectively,[2] while the Sm−N bond lengths in $Sm[HB(3,5\text{-}Me_2pz)_3]_2$ (pz = pyrazolyl) are 2.617(4) Å.[10] The two terminal amide ligands are *cis*-orientated and have Sm−N lengths [av. 2.470 Å] comparable with those of the formally four-coordinate complex **1** [av. 2.433 Å]. The Sm−O distances average 2.552 Å and are in the expected range {**1**, av. 2.596 Å; $Sm[N(SiMe_3)(C_6H_3iPr_2\text{-}2,6)]_2(thf)_2$, av. 2.550 Å}.[4]

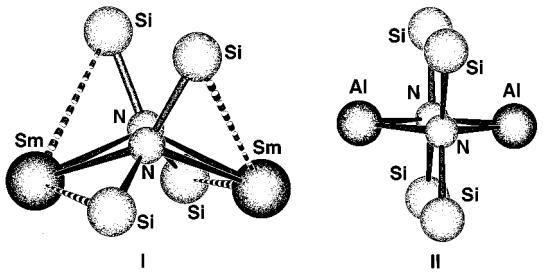


Figure 2. Bridging modes of the $N(SiHMe_2)_2$ ligand

A closer examination of the bridging silylamide ligands reveals a novel coordination mode featuring "SiNSi moieties" tilted towards the metal centers (**I** in Figure 2). This asymmetric ligand coordination is confirmed by the Sm−N−Si angles, which vary between 92.1(1) and 132.7(1)°. Apparently, coordinatively unsaturated and electron-deficient Sm^{II} centers favor the formation of close Sm···SiH β-agostic interactions involving all of the $SiHMe_2$ groups. The resulting Sm−Si (av. 3.273 Å) and Sm−H contacts (av. 2.75 Å) are remarkably short. In contrast, the shortest Sm−Si distance in **1** showing Sm···$SiCH_3$ contacts is 3.467 Å.[4a] The two terminal amide ligands in complex **2a** also show close Sm···SiH contacts. Taking the Sm···SiH β-agostic interactions into account a coordination number of 8 and 7 can be assigned to the central and terminal Sm atoms, respectively. The complex $\{Me_2Al[(\mu\text{-}N(SiHMe_2)_2]\}_2$ displays an unperturbated geometry (**II** in Figure 2) due to minimum attractive Al···SiH interactions [Al−N−Si 111.5(1)°].[11]

Conclusions

We have reported the first homotrinuclear samarium(II) amide featuring an unusual oligomeric structure. Considering the solid-state structures of mononuclear, solvated $Sm[N(SiMe_3)_2]_2(thf)_2$ (**1**) and dinuclear, unsolvated $\{Yb[N(SiMe_3)_2]_2\}_2$,[12] on one hand this novel structural motif might be attributable to the decreased steric bulk of $N(SiHMe_2)_2$,[5] which favors aggregation. On the other hand β-agostic Sm···SiH interactions seem to be markedly stronger than Sm(Yb)···$SiCH_3$ γ-agostic interactions as evidenced by the displacement of donor (THF) molecules. The toleration of SiH functionalities might have implications for the use of $Sm^{(II)}$ reagents in organic synthesis. We are currently investigating the feasibility of ligand exchange reactions of $Sm[N(SiHMe_2)_2]_2(thf)_x$ (**2**) with bulky protic subtrates.

Experimental Section

General: All manipulations were performed in a argon-filled glovebox (MBraun MB150B-G-II). Solvent pretreatment and physical characterizations were conducted as described previously.[5] $SmI_2(thf)_2$,[7] $Li[N(SiHMe_2)_2]$[8] and **1**[4a] were synthesized according to known procedures.

Sm^{II} Silylamide 2 (2a): A solution of 1,1,3,3-tetramethyldisilazane (0.587 g, 4.40 mmol) in THF (5 mL) was added to a solution of **1** (1.231 g, 2.00 mmol) in THF (15 mL) and stirred at ambient temperature for 20 h, whereupon the color of the solution turned from purple to black. Evaporation of the THF afforded a black powder **2** (yield > 95%) which completely dissolved in *n*-hexane and gave crystals of **2a** after recrystallization from *n*-hexane/THF. − IR (Nujol): $\tilde{\nu}$ = 2040 s, 1936 m sh, 1243 vs, 1039 vs, 954 vs, 893 vs, 836 vs, 785 s, 762 s, 680 m, 626 m, 599 w cm^{-1}. − ^1H NMR (270.16 MHz, $[D_8]$THF): δ = −2.47 (s, 6 H), −12.18 (s, 1 H). − ^{13}C (67.93 MHz, $[D_8]$THF): δ = 14.7. − MS (CI); *m/z* (%): 547 {2, $Sm[N(SiHMe_2)_2]$}, 532 [3, $\{Sm[N(SiHMe_2)_2]_3 - Me\}^+$], 415 {21, $Sm[N(SiHMe_2)_2]_2$}. − $C_{32}H_{100}N_6O_2Si_{12}Sm_3{\cdot}C_6H_{14}$ (1475.47): calcd. C 30.93, H 7.79, N 5.70; found (**2**) C 29.5, H 7.4, N 5.6; found (**2a**) C 29.7, H 7.6, N 5.6.

X-ray Crystal Structure Analysis of 2a: $C_{32}H_{100}N_6O_2Si_{12}Sm_3$, M = 1389.35; monoclinic, space group $P2_1/c$, a = 11.4620(7), b = 28.873(2), c = 22.064(1) Å, β = 96.605(6), V = 7253.4(8) Å^3, T = 173(1) K, Z = 4, $F(000)$ = 2816, D_c = 1.272 g cm^{-3}, μ = 2.62 mm^{-1}. 122106 (17029 unique) Bragg reflections with $\sin\Theta/\lambda_{max}$ = 0.66 Å^{-1} were collected on an image plate system from STOE IPDS[13] with a rotating anode generator (Nonius FR591; Mo-K_α, λ = 0.71073 Å). 12806 independent reflections. Full-matrix least-squares refinement of 537 parameters against 11255 observed reflections reflections ($\sin\Theta/\lambda_{max}$ = 0.6 Å^{-1}) converged to $R1$ = 0.023, $wR2$ = 0.061, residual electron density: +0.95/-0.46 eÅ^{-3}.[14] The terminal Si(12)Me_2 moiety was described by a disordering model with two split Si positions. One of the resulting $SiMe_2$ groups (occupation factor 0.43) displays an additional Sm···SiH β-agostic interaction. The positions of the agostic hydrogen atoms in the nondisordered $SiHMe_2$ groups were refined. Furthermore, disordered *n*-hexane molecules were located in a potential solvent accessible area of 243 Å^3. However, the BYPASS method[15] was applied to account for the disordered solvent contribution to the structure factor in the final refinements. Structure graphics were performed with the programs PLATON[16] and SCHAKAL.[17] Crystallographic data (excluding structure factors) for the structure reported in this paper have been deposited with the Cambridge Crystallographic Data Centre as supplementary publication no. CCDC-118713. Copies of the data can be obtained free of charge on application to CCDC, 12 Union Road, Cambridge CB2 1EZ, UK [Fax: (internat.) + 44-1223/336-033; E-mail: deposit@ccdc.cam.ac.uk].

Acknowledgments

We thank the Deutsche Forschungsgemeinschaft and Degussa-Hüls AG for generous support of this work. Additionally, support from Professor W. A. Herrmann is gratefully acknowledged.

[1] M. F. Lappert, P. P. Power, A. R. Sanger, R. C. Srivastava, *Metal And Metalloid Amides*, Ellis Horwood, Chichester, 1980.
[2] R. Anwander, *Top. Curr. Chem.* **1996**, *179*, 33−112.
[3] [3a] A. Recknagel, A. Steiner, S. Brooker, D. Stalke, F. T. Edelmann, *J. Organomet. Chem.* **1991**, *415*, 315−326. − [3b] D. Drees, J. Magull, *Z. Anorg. Allg. Chem.* **1994**, *620*, 814−818. − [3c] L. Lee, D. J. Berg, G. W. Bushnell, *Inorg. Chem.* **1994**, *33*, 5302−5308. − [3d] R. K. Minhas, Y. Ma, J.-I. Song, S. Gambarotta, *Inorg. Chem.* **1996**, *35*, 1866−1873.
[4] [4a] W. J. Evans, D. K. Drummond, H. Zhang, J. L. Atwood, *Inorg. Chem.* **1988**, *27*, 575−579. − [4b] W. J. Evans, G. W. Rabe, J. W. Ziller, *Organometallics* **1994**, *13*, 1641−1645. − [4c] G. B. Deacon, G. D. Fallon, C. M. Forsyth, H. Schumann, R. Weimann, *Chem. Ber.* **1997**, *130*, 409−415.
[5] R. Anwander, O. Runte, J. Eppinger, G. Gerstberger, E. Herdtweck, M. Spiegler, *J. Chem. Soc., Dalton Trans.* **1998**, 847−858 and references therein.
[6] W. A. Herrmann, J. Eppinger, O. Runte, M. Spiegler, R. Anwander, *Organometallics* **1997**, *16*, 1813−1815.
[7] J. L. Namy, P. Girard, H. B. Kagan, *Nouv. J. Chim.* **1977**, *1*, 5−7.
[8] J. Eppinger, E. Herdtweck, R. Anwander, *Polyhedron* **1998**, *17*, 1195−1201.
[9] D. K. Kennepohl, S. Brooker, G. M. Sheldrick, H. W. Roesky, *Z. Naturforsch.* **1992**, *47b*, 9−16.
[10] J. Takats, X. W. Zhang, V. W. Day, T. A. Eberspacher, *Organometallics* **1993**, *12*, 4286−4288.
[11] J. J. Byers, W. T. Pennington, G. H. Robinson, D. C. Hrncir, *Polyhedron* **1990**, *9*, 2205−2210.
[12] T. D. Tilley, R. A. Andersen, A. Zalkin, *Inorg. Chem.* **1984**, *23*, 2271−2276.
[13] STOE & CIE. GMBH, *IPDS Operating System Version 2.6.* **1995**, Darmstadt, Germany.
[14] G. M. Sheldrick, *SHELXL 93*, Universität Göttingen, Germany, **1993**.
[15] P. Van der Sluis, A. L. Spek, *Acta Crystallogr.* **1990**, *A46*, 194−201.
[16] A. L. Spek, *Acta Crystallogr.* **1990**, *A46*, C34.
[17] E. Keller, *SCHAKAL*, Universität Freiburg, Germany, **1988**.

Received April 13, 1999
[I99129]

Absorption and Emission Properties of Di- and Trinuclear Ruthenium(II) Rack-Type Complexes

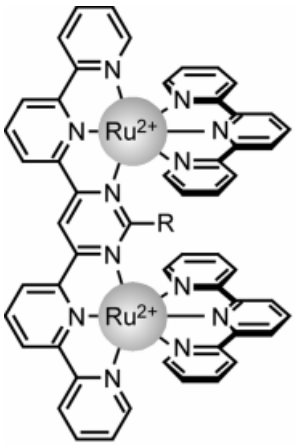
Paola Ceroni,[a] Alberto Credi,[a] Vincenzo Balzani,*[a] Sebastiano Campagna,*[b] Garry S. Hanan,[c] Claudia R. Arana,[c] and Jean-Marie Lehn*[c]

Keywords: Ruthenium complexes / Luminescence / Bridging ligands / Terpyridine ligands / Polynuclear metal complexes

The absorption spectra and the luminescence properties of three dinuclear Ru^{II} complexes and one trinuclear Ru^{II} complex have been investigated. All the complexes have rack-type structures. The dinuclear complexes **1**, **2**, and **3** incorporate a bis-tridentate bridging ligand made up of a pyrimidine and four pyridine moieties, as well as two 2,2′:6′,2"-terpyridyl (tpy) ligands. The trinuclear complex **4** incorporates a tris-tridentate bridging ligand made up of two pyrimidine and five pyridine moieties, as well as three tpy ligands. The absorption spectra of the complexes show a large number of ligand-centered (LC) and metal-to-ligand charge-transfer (MLCT) bands. All the complexes exhibit emission from a triplet MLCT state, with maxima in the spectral range 840–950 nm (lifetimes between 40 and 80 ns) at 298 K in fluid solution, and in the spectral range 760–810 nm (lifetimes between 2 and 3 μs) at 77 K in rigid matrices. A fine tuning of the absorption and luminescence properties of complexes **1**–**3** can be achieved by changing the substituents on the pyrimidine ring of the bridging ligand. Efficient energy transfer within the rack structure **4** occurs from the (upper-lying) central metal-based chromophore to the (lower-lying) peripheral ones.

Introduction

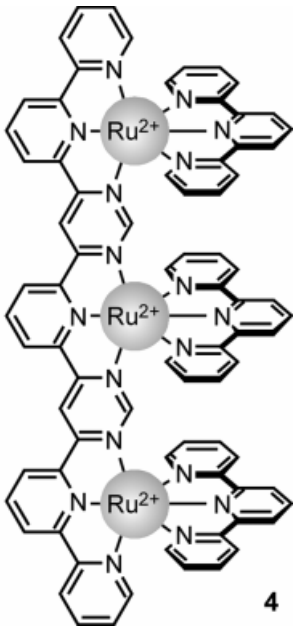
The assembly of molecular components into large, well-defined, and functional arrays (supramolecular species) is currently a major research theme.[1][2] Ruthenium(II) and osmium(II) complexes with polypyridine-type and related ligands are particularly useful units in the design of photo- and redox-active multi-component systems.[3] Some of us have recently reported the synthesis of rack-type polynuclear Ru^{II} complexes based on bis-tridentate and tris-tridentate bridging ligands made up of pyrimidine and pyridine coordinating moieties, as well as 2,2′:6′,2″-terpyridyl (tpy) ligands.[4][5] Such systems, as well as the related ladder-[6a] and grid-type[6b−6d] multi-metallic assemblies, exhibit structures of potentially great interest for the development of photonic and electronic devices.[1−3,7] We report herein the results of an investigation on the absorption spectra and luminescence properties of three dinuclear Ru^{II} complexes **1**−**3** and a trinuclear Ru^{II} complex **4** with rack-type structures. The synthesis and NMR characterization of the trinuclear complex are also described.



1 : R = H

2 : R = methyl

3 : R = phenyl



4

Results and Discussion

The dinucleating bis-tridentate ligands of complexes **1**−**3** differ only in the nature of the substituents attached at the pyrimidine unit. X-ray crystal structure analyses[4] of **1**−**3** have shown that the metal-to-metal distance and the center-to-center distance of the central pyridine units of the tpy ligands increase with increasing size of the substituent. Non-negligible differences have also been found in the pinching angle of the bis-tridentate ligand and in the convergence angle of the two ancillary tpy ligands. The sub-

[a] Dipartimento di Chimica "G. Ciamician", Università di Bologna, via Selmi 2, I-40126 Bologna, Italy
Fax: (internat.) +39-051/2099456
[b] Dipartimento di Chimica Inorganica, Chimica Analitica e Chimica Fisica, Università di Messina, Villaggio S. Agata, I-96166 Messina, Italy
Fax: (internat.) +39-090/393756
[c] Laboratoire de Chimie Supramoléculaire, Institut Le Bel, Université Louis Pasteur, 4 rue Blaise Pascal, F-67000 Strasbourg, France

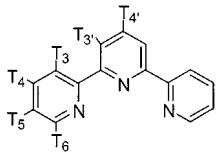
 © WILEY-VCH Verlag GmbH, D-69451 Weinheim, 1999 1434−1948/99/0909−1409 $ 17.50+.50/0

stituents can, of course, also be expected to influence the electronic properties of the ligands.

NMR Characterization of Complex 4

The proton chemical shifts measured for the three terpyridine (tpy) ligands and the tris-tridentate ligand present in **4** are collected in Tables 1 and 2, respectively. Also included in Table 1 are the chemical shift differences (in ppm) between the tpy units of complex **4** and $[Ru(tpy)_2]^{2+}$ **5** ($\Delta\delta$ **5**),[8] and in Table 2, the chemical shift differences (in ppm) between **4** and **1** ($\Delta\delta$ **1**). The importance of comparing the ^1H chemical shifts to those of a related complex rather than to those of the free ligand should be clear. Shielding effects exist between the terminal pyridines in the free ligand because of nitrogen lone pair induced helication.[9] On forming the trimetallic complex, these shielding effects are no longer present, making most of the protons in the free ligand strongly deshielded in the metal complex. The assignments were made by the following methods: comparing proton coupling constants, decoupling experiments, comparing spectra, and verifying heterocycle connectivity using NOE.[10]

Table 1. Proton chemical shifts (in ppm) of terpyridine ligands in **4** and chemical shift differences between **4** and $[Ru(tpy)_2]^{2+}$ **5**[a] in CD_3CN; T denotes peripheral tpy hydrogens and T* denotes central tpy hydrogens



	T6	T5	T4	T3	T3′	T4′
4 (H_T)	7.01	6.94	7.80	8.34	8.65 [b]	8.51 [b]
$\Delta\delta$ **5**	−0.32	−0.21	−0.11	−0.14	−0.09	+0.11
4 (H_{T*})	6.80 [b]	6.80 [b]	7.74	8.29	8.65 [b]	8.64 [b]
$\Delta\delta$ **5**	−0.53	−0.50	−0.17	−0.19	−0.09	+0.24

[a] Data for **5** taken from ref.[8] – [b] Central position of multiplet.

In the trimetallic complex **4**, the tpy protons are in a peripheral-to-central ratio of 2:1. The central tpy protons (H_{T*}) are more shielded than the peripheral tpy protons (H_T), as would be expected as the central tpy site is flanked by two peripheral tpy′s, whereas the peripheral tpy′s have only the central one in their vicinity.

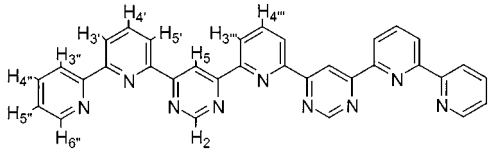
Comparison of the chemical shifts of central pyridine in the ligand with those of the central pyridines in $[Ru(tpy)_2]^{2+}$ (**5**) allows determination of the $\Delta\delta$ **5** values for $H_{3'''}$ and $H_{4'''}$. The values are indicative of greater deshielding for $H_{3'''}$ than for $H_{4'''}$. This may be due to the preferred orientation of the terminal pyridine on the central terpyridine towards one side of the central pyridine of **L**, resulting in greater deshielding at $H_{3'''}$ and H_5 (Figure 1). The large deshielding value for H_5 in **4** as compared to **1** ($\Delta\delta$ **1**) may be explained in terms of the distorted positioning of the terminal pyridine of the central and peripheral terpyridines in **4** (Figure 1). The individual terpyridines sites in **1** are disymmetric in the solid state, as shown by the X-ray structure.[4] The terpyridines in **4** may behave similarly. This is also supported by NOE interactions, which are found between H_{T5} and H_{T5*} as well as H_{T6} and H_{T5*}. The motion represented in Figure 1, which is expected to be fast on the NMR timescale, leads to an averaged symmetry.

Absorption Spectra

The absorption spectra of compounds **1**, **2**, and **4** (acetonitrile solution, 298 K) are shown in Figures 2 and 3. The wavelengths of the absorption maxima and the values of the molar absorption coefficients for complexes **1**−**4** and the model compound $[Ru(tpy)_2]^{2+}$ (**5**) in the visible region are listed in Table 3.

The UV region of the absorption spectrum of each of the complexes is dominated by a variety of intense bands that can be assigned to ligand-centered (LC) transitions of the tpy ligands and of the multi-tridentate bridging ligands. In the visible region, several weaker bands are present, attributable to metal−to−ligand charge-transfer (MLCT) transitions.[3] At first glance, one could distinguish three types

Table 2. Proton chemical shifts and chemical shift differences in the free tris-tridentate ligand **L** and **4**; for the assignments, see the sketch below



	6′′	5′′	4′′	3′′	5′	4′	3′	5	2	3′′′	4′′′
L [a]	8.31	6.85	6.72	8.31	8.62	8.02	8.38	9.99	9.44	8.70	8.14
4 [b]	7.27	7.14	7.92	8.46	9.12	8.51	8.82	9.92	6.15	9.20	8.64
$\Delta\delta$ **1** [c]	0	0	−0.01	+0.01	+0.01	+0.01	0	+0.66	−0.09	+0.46	+0.24
$\Delta\delta$ **5** [d]											

[a] In $CDCl_3$; data from G. S. Hanan, U. S. Schubert, D. Volkmer, E. Rivière, J.-M. Lehn, N. Kyritsakas, J. Fischer, *Can. J. Chem.* **1997**, *75*, 169. – [b] In CD_3CN. – [c] Data for **1** taken from ref.[4] – [d] Data for **5** taken from ref.[8]

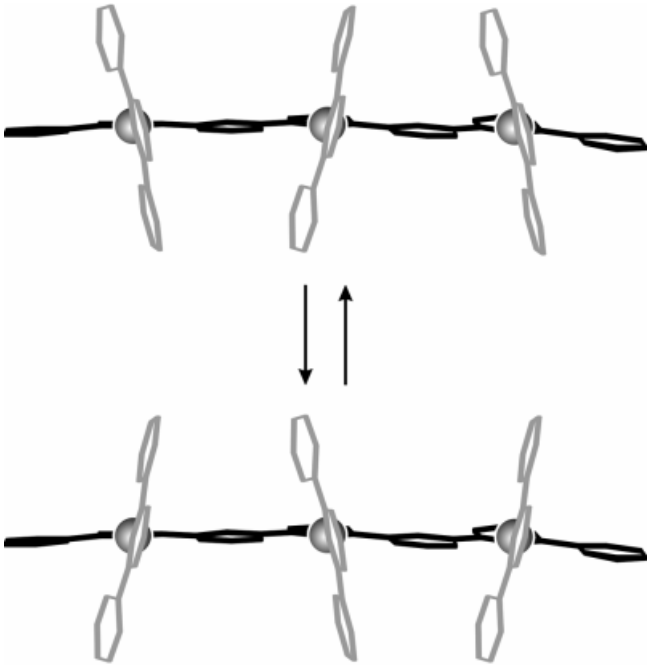


Figure 1. Proposed averaging motion of terpyridines in **4**

of ligand units (tpy, bpy, and pyrimidine) in the metal coordination spheres, but it should be noted that the latter two units are conjugated so that it is probably more correct to treat the multi-tridentate bridging ligands as single large molecules.[2]

Complexes 1−3: Electrochemical measurements[4] show that these complexes undergo two (metal-centered) oxidation processes at about +1.4 and +1.5 V vs. SCE, and several (ligand-centered) reduction processes. The separation between the two oxidation waves of the formally equivalent Ru^{II} ions shows that the metal−metal interaction through the bis-tridentate ligands is not negligible, as is typical for this kind of bridging ligand.[3d] The first two reduction processes, which occur around −0.5 and −1.1 V, can be assigned to successive reductions of the bridging ligand. As expected,[3a] reduction of the tpy ligands occurs at more negative potentials (around −1.5 V).

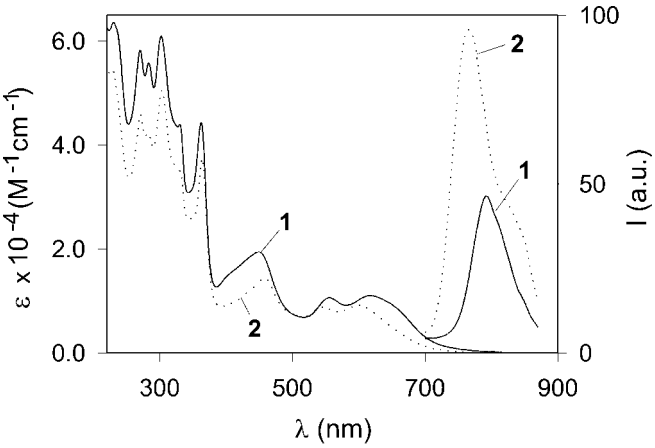


Figure 2. Absorption spectra in acetonitrile solution at 298 K (left scale) and emission spectra in a rigid butyronitrile matrix at 77 K (λ_{ex} = 480 nm; right scale) of compounds **1** and **2**

The three MLCT absorption bands observed for compounds **1**−**3** in the visible region (Figure 2 and Table 3) can be straightforwardly assigned in the light of the electrochemical results. The two low energy bands, with maxima around 600 and 550 nm, are due to CT transitions to the first and second LUMO′s of the bridging ligand, respectively, while the higher energy band, with a maximum at around 450 nm, is due to a transition to the first LUMO of the tpy ligands. The difference between the potentials of the first and second reduction waves is much larger than the energy separation between the two lowest energy absorption bands because the second wave is associated with reduction of an already reduced ligand. This interpretation is consistent with the results obtained for a closely related dinuclear Ru^{II} rack containing an anthryl subunit.[11]

As can be seen from Figure 2, the presence of the methyl substituent on the pyrimidine ring in **2** displaces the

Table 3. Absorption and luminescence data for complexes **1**−**4** and for the model compound $[Ru(tpy)_2]^{2+}$ **5**

Compound	Absorption 298 K[a,b]		Luminescence 298 K[a]		77 K[c]	
	λ_{max}, nm	ε_{max}, M^{-1} cm^{-1}	λ_{max},[d] nm	τ, ns	λ_{max},[d] nm	τ, μs
1	448	19400	845	77	792	2.4
	555	10600				
	615	11000				
2	458	14700	845	51	767	3.3
	544	9900				
	597	9300				
3	457	11700	845	37	786	2.5
	555	7700				
	606	7900				
4	405[e]	25500	920	40	810[f]	2.8
	450[e]	25000				
	543	14500				
	624	19000				
$[Ru(tpy)_2]^{2+}$ **5**[g]	474	10400	629	< 1	598	10.6

[a] Air-equilibrated acetonitrile solution. − [b] Only the absorption bands in the visible region are indicated. − [c] Butyronitrile rigid matrix. − [d] Corrected values. − [e] Overlapping bands, see Figure 3. − [f] λ_{max} and highest energy feature of a structured band, see Figure 3. − [g] Data taken from ref.[8]

Ru→bridging ligand bands to higher energy and the Ru→tpy band to lower energy compared to the situation in **1**. This is due to the electron-donating nature of the methyl group, which has two effects: (i) it increases the electron density on the bridging ligand and therefore raises the energy of its LUMO′s; (ii) by increasing the σ-donor power of the pyrimidine nitrogens, it increases the electron density on the metal and therefore decreases the energy of the MLCT band involving the tpy ligands, which are unaffected by the pyrimidine substituent. The phenyl substituent present in **3** has a similar, albeit smaller, effect.

Complex 4: In the trinuclear compound **4**, the two lateral subunits are equivalent, but different from the central one. As expected, because of the larger number of subunits, the molar absorbance is enhanced compared to that of the dinuclear compounds over the entire UV/vis domain (Figures 2 and 3, Table 3). The lowest-lying MLCT band is displaced to lower energy compared to that of the dinuclear species, due to the more extended electronic delocalization on the bridging ligand (BL), which leads to a stabilization of its LUMO. Such a low-lying MLCT band (as well as the MLCT band involving the second LUMO of the bridging ligand) should receive contributions from two different Ru→BL transitions because, as mentioned above, the peripheral Ru^{II} metal ions are different from an electronic viewpoint compared to the central Ru^{II} metal ion, since the latter is coordinated by two pyrimidine rings. The central metal ion should be more difficult to oxidize than the peripheral ones, because pyrimidines are better electron acceptors than pyridines.[12] Indeed, this was confirmed by electrochemical studies. In fact, **4** exhibits a two-electron oxidation at +1.47 V vs. SCE in acetonitrile solution, associated with the peripheral non-interacting metal centers, followed by a one-electron oxidation process at +1.88 V, attributable to oxidation of the central metal subunit.[5] Although the lowest-lying MLCT band for **4** is large and exhibits a pronounced shoulder in its red tail, the expected two bands are not resolved, probably owing to their broadness and slight energy difference (Figure 3). Interestingly, two bands are evident in the absorption spectrum of the complex in the region corresponding to the Ru→tpy CT transitions (compare the 400−500 nm region in the absorption spectra shown in Figures 2 and 3). On the basis of the above considerations and the redox properties of **4**, these absorption bands can be assigned, in order of increasing energy, to Ru(peripheral)→tpy CT transition(s) and Ru(central)→tpy CT transition(s), respectively.

Luminescence Properties

The emission spectra of compounds **1**, **2**, and **4** (rigid butyronitrile matrix at 77 K) are shown in Figures 2 and 3. The wavelengths of the emission maxima and the excited-state lifetimes of all the complexes are collected in Table 3.

On the basis of the emission energies, spectra, and lifetimes,[3] the relatively weak emission exhibited by all the complexes can be assigned to the lowest ^{3}MLCT level,

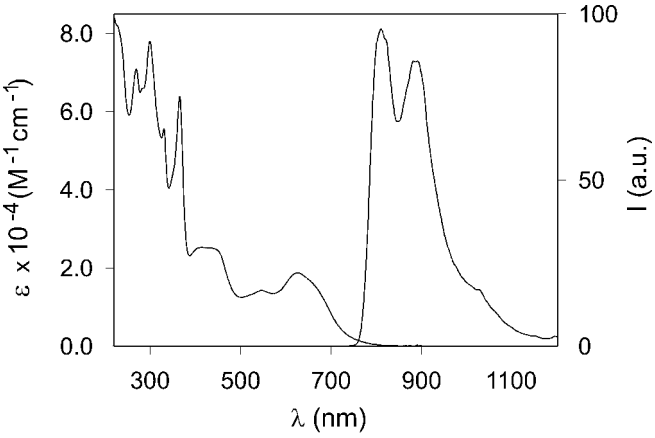


Figure 3. Absorption spectrum in acetonitrile solution at 298 K (left scale) and emission spectrum in a rigid butyronitrile matrix at 77 K (λ_{ex} = 488 nm; right scale) of compound **4**

which is associated with the bridging ligand. As already discussed for the absorption spectra, the nature of the substituent on the pyrimidine ring of the bridging ligand is responsible for fine-tuning the emission energy in **1**−**3**, with **2** exhibiting the highest energy emission (Table 3). The emission energy of **4** is lower than those of **1**−**3**, as expected considering the electronic and redox properties of the bridging ligand in **4**,[5] and according to the interpretation of the absorption data.

Compared with $[Ru(tpy)_2]^{2+}$,[3] the luminescence lifetimes of compounds **1**−**3** are longer at room temperature and shorter at 77 K (Table 3). This can be explained by recalling that the radiationless decay of the luminescent excited state in Ru^{II} polypyridine compounds occurs via an upper-lying metal-centered triplet (^{3}MC) level at high temperature and by vibronic coupling directly to the ground state at low temperature.[3] Since in compounds **1**−**3** the luminescent level is lower in energy than in $[Ru(tpy)_2]^{2+}$,[3] the activation energy for radiationless decay via the upper-lying MC level should be larger (with the reasonable assumption that in these complexes the ^{3}MC excited state has approximately the same energy), and the coupling with the ground state should be stronger. The shorter lifetime at room temperature and the longer lifetime at 77 K for **2** compared with **1** (Table 3) is in line with such an interpretation.

As mentioned above, the two metal-based chromophores of **1**−**3** are identical, whereas in **4** the central metal-based chromophore is different from the peripheral ones. Considering the different acceptor abilities of pyridine and pyrimidine rings and the oxidation behaviour of the complex (see above), the lowest ^{3}MLCT state of each peripheral subunit should be lower in energy than the corresponding level involving the central subunit. Because **4** contains two *different* metal-based chromophores, potentially luminescent from their respective lowest-lying ^{3}MLCT level,[3] two emissions could in principle occur. The insensitivity of the emission spectrum of **4** to the excitation wavelength (both at 77 K and at room temperature), the matching between the absorption and excitation spectra, and the pres-

ence of a single exponential luminescence decay with the same lifetime under all the experimental conditions, indicate that only the lowest-lying MLCT level of the assembly, associated with the peripheral chromophores, undergoes deactivation through radiative decay, whereas the upper-lying MLCT level, associated with the central subunit, transfers its electronic energy to the nearby chromophore. Thus, efficient energy transfer from the central chromophore to the peripheral ones occurs within the trinuclear rack.

Finally, the luminescence lifetimes of **1**−**3** at 77 K roughly obey the energy gap law,[13] but **4** exhibits a longer lifetime than expected in comparison with the dinuclear systems (**1**−**3**). This is probably due to the greater delocalization of the acceptor ligand of the MLCT luminescent level in **4**, which decreases the vibronic coupling between excited and ground states, thereby reducing the Franck−Condon factors for non-radiative decay.[14]

Conclusion

The absorption spectra and the luminescence properties of one trinuclear and three dinuclear ruthenium(II) rack-type complexes have been studied. The absorption spectra of the complexes show a multitude of LC and MLCT bands. All the complexes exhibit luminescence from the lowest-lying ^{3}MLCT level, both at 298 K in fluid solution and at 77 K in rigid matrices. The absorption and emission properties of the dinuclear compounds **1**−**3** are fine-tuned by the substituents on the pyrimidine ring incorporated in the bridging ligand framework. Excited-state decays are governed by direct vibronic coupling with the ground state at 77 K and by thermally-activated population of a close-lying ^{3}MC level at room temperature. In **4**, efficient electronic energy transfer occurs from the upper-lying central chromophore to the lower-lying peripheral ones. This result is of interest with regard to the possible development of larger (disymmetric) racks exhibiting vectorial energy and/or electron transfer within their structures

Experimental Section

The syntheses, characterization, and structures of compounds **1**−**3** have been described in detail elsewhere;[4] synthetic procedures for the preparation of **4** have also been outlined previously.[5] NMR instrumentation and methods used were as reported previously.[4]

Absorption and Luminescence Measurements: Absorption spectra were recorded with a Perkin−Elmer λ6 spectrophotometer in acetonitrile solution at room temperature. Luminescence experiments were performed in dilute (ca. 10^{-5} M) acetonitrile solution at room temperature and in rigid butyronitrile matrices at 77 K. Corrected luminescence spectra in the 700−850 nm range were obtained with a Perkin−Elmer LS-50 spectrofluorimeter. Corrected luminescence spectra in the 800−1200 nm range were obtained with an in-house constructed near-infrared spectrofluorimeter consisting of an Ar ion laser as excitation source (λ_{ex} = 488 nm), a monochromator (Edinburgh) with a grating of 1200 L/mm, and a liquid nitrogen cooled germanium detector and preamplifier (Northcoast, model EO-817 L). The sample (air-equilibrated CH_3CN solution) was placed in a 10 mm × 10 mm cuvette, and a beam chopper (Stanford Research, model SR540) was placed between the excitation source and the sample; luminescence was monitored at right angles to the excitation. A muon filter (Northcoast, model 829B) was used as an electronic signal filter, after the signal had been sent to a lock−in amplifier (Stanford Research, model SR510). Luminescence lifetimes were measured with an Edinburgh single-photon counting apparatus (D_2 lamp, λ_{ex} = 310 nm). Estimated errors are as follows: molar absorption coefficients, 10%; absorption maxima, ±2 nm; emission maxima in the visible range, ±2 nm; emission maxima in the near-infrared range, ±4 nm; emission quantum yields, 20%; excited-state lifetimes, 10%.

Preparation of Complex 4: To $Ru(tpy)Cl_3$ (0.0324 g, 0.0735 mmol) and free tris-tridentate ligand (0.0102 g, 0.0188 mmol) was added propan-2-ol/water (20 mL, 1:1) and *N*-ethylmorpholine (0.5 mL). The mixture was heated under reflux for 40 h, then cooled to room temperature and filtered. Excess aqueous NH_4PF_6 was added to the solution and the precipitate was collected. The solid was purified by successive recrystallizations from acetonitrile/toluene to afford **4** (0.0264 g, 58%) as a green solid. − M.p. > 300°C. − ^{1}H NMR (CD_3CN, 400 MHz); the subscript T indicates protons of the peripheral terpyridine ligands and T* indicates protons of the central terpyridine ligand: δ = 9.29 (s, 1 H, H_5), 9.20 (d, *J* = 8.4 Hz, 2 H, $H_{3''''}$), 9.12 (d, *J* = 8.4 Hz, 2 H, $H_{5'}$), 8.82 (d, *J* = 8.2 Hz, 2 H, $H_{3'}$), 8.65 (d, *J* = 8.4 Hz, 6 H, $H_{T3',\ T3'*}$), 8.64 (m, 2 H, $H_{4'''',T4'*}$), 8.51 (m, 4 H, $H_{4',T4'}$), 8.46 (d, *J* = 7.2 Hz, 2 H, $H_{3''}$), 8.34 (d, *J* = 8.2 Hz, 4 H, H_{T3}), 8.29 (d, *J* = 8.0 Hz, 2 H, H_{T3*}), 7.92 (td, *J* = 7.8, 1.5 Hz, 2 H, $H_{4''}$), 7.80 (td, *J* = 8.0, 1.5 Hz, 4 H, H_{T4}), 7.74 (td, *J* = 8.2, 1.9 Hz, 2 H, H_{T4*}), 7.27 (d, *J* = 5.0 Hz, 2 H, $H_{6''}$), 7.14 (ddd, *J* = 7.5, 5.7, 1.2 Hz, 2 H, $H_{5''}$), 7.01 (d, *J* = 5.5 Hz, 4 H, H_{T6}), 6.94 (ddd, *J* = 7.4, 5.7, 1.5 Hz, 4 H, H_{T5}), 6.80 (m, 4 H, $H_{T6*,T5*}$), 6.15 (d, *J* = 0.8 Hz, 1 H, H_2). − ^{13}C{^{1}H} NMR (CD_3COCD_3, 100 MHz): δ = 166.89, 165.32, 161.39, 158.43, 157.96, 157.07, 156.89, 155.57, 155.07, 154.67, 154.51, 153.92, 153.81, 153.16, 140.31, 140.16, 139.68, 139.65, 138.64, 137.13, 136.97, 129.59, 128.95, 128.86, 128.67, 127.93, 126.83, 125.67, 125.19, 124.98, 124.50, 118.50 (one overlapped resonance). − FAB: *m*/*z* (%): 2272 (40) $[M - PF_6]^+$, 2126 (100) $[M - 2\ PF_6]^+$, 1981 (62) $[M - 3\ PF_6]^+$, 1063 (36) $[M - 2\ PF_6]^{2+}$, 991 (78) $[M - 3\ PF_6]^{2+}$, 918 (33) $[M - 4\ PF_6]^{2+}$. − $C_{78}H_{54}F_{36}N_{18}P_6Ru_3{\cdot}4CH_3CN$: calcd. C 40.02, H 2.58, N 11.94; found C 40.33, H 2.81, N 11.40.

Acknowledgments

We thank MURST (Progetto Dispositivi Supramolecolari), the University of Bologna (Funds for Selected Research Topics), and the EU (contract FMRX−CT96−0031) for financial support. G. S. H. thanks the NSERC of Canada for a graduate fellowship. We also acknowledge Patrick Maltese for performing the NOE experiments.

[1] J.-M. Lehn, *Supramolecular Chemistry: Concepts and Perspectives*, VCH, Weinheim, **1995**.
[2] V. Balzani, F. Scandola, *Supramolecular Photochemistry*, Ellis Horwood, Chichester, **1991**.
[3] [3a] A. Juris, V. Balzani, F. Barigelletti, S. Campagna, P. Belser, A. Von Zelewsky, *Coord. Chem. Rev.* **1988**, *84*, 85. − [3b] T. J. Meyer, *Acc. Chem. Res.* **1989**, *22*, 163. − [3c] J.-P. Sauvage, J.-P. Collin, J.-C. Chambron, S. Guillerez, C. Coudret, V. Balzani, F. Barigelletti, L. De Cola, L. Flamigni, *Chem. Rev.* **1994**, *94*, 993. − [3d] V. Balzani, A. Juris, M. Venturi, S. Campagna, S. Serroni, *Chem. Rev.* **1996**, *96*, 759.
[4] G. S. Hanan, C. R. Arana, J.-M. Lehn, G. Baum, D. Fenske, *Chem. Eur. J.* **1996**, *2*, 2019.

[5] G. S. Hanan, C. R. Arana, J.-M. Lehn, D. Fenske, *Angew. Chem. Int. Ed. Engl.* **1995**, *34*, 1122.
[6] [6a] P. N. W. Baxter, G. S. Hanan, J.-M. Lehn, *J. Chem. Soc., Chem. Commun.* **1996**, 2019. – [6b] P. N. W. Baxter, J.-M. Lehn, J. Fischer, M.-T. Youinou, *Angew. Chem. Int. Ed. Engl.* **1994**, *33*, 2284. – [6c] G. S. Hanan, D. Volkmer, U. S. Schubert, J.-M. Lehn, G. Baum, D. Fenske, *Angew. Chem. Int. Ed. Engl.* **1997**, *36*, 1842. – [6d] A. Garcia, F. Romero-Salguero, D. M. Bassani, J.-M. Lehn, G. Baum, D. Fenske, *Chem. Eur. J.* **1999**, *5*, 1803.
[7] See also, for example: [7a] O. Waldmann, J. Hassmann, P. Müller, G. S. Hanan, D. Volkmer, U. S. Schubert, J.-M. Lehn, *Phys. Rev. Lett.* **1997**, *78*, 3390. – [7b] D. Astruc, *Acc. Chem. Res.* **1997**, *30*, 383.
[8] M. Maestri, N. Armaroli, V. Balzani, E. C. Constable, A. M. W. Cargill Thompson, *Inorg. Chem.* **1995**, *34*, 2759.
[9] G. S. Hanan, J.-M. Lehn, N. Kyritsakas, J. Fischer, *J. Chem. Soc., Chem. Commun.* **1995**, 765.
[10] Trimetallic complex **4** exhibits all of the expected interannular NOE interactions.
[11] A. Credi, V. Balzani, S. Campagna, G. S. Hanan, C. R. Arana, J.-M. Lehn, *Chem. Phys. Lett.* **1995**, *243*, 105.
[12] P. Ford, D. F. D. Rudd, R. Gaunder, H. Taube, *J. Am. Chem. Soc.* **1968**, *90*, 1187.
[13] [13a] W. Siebrand, *J. Chem. Phys.* **1967**, *46*, 440. – [13b] J. V. Caspar, E. M. Kober, B. P. Sullivan, T. J. Meyer, *J. Am. Chem. Soc.* **1982**, *104,* 630. – [13c] J. V. Caspar, T. J. Meyer, *J. Phys. Chem.* **1983**, *87*, 952. – [13d] T. J. Meyer, *Pure Appl. Chem.* **1986**, *58*, 1193.
[14] [14a] G. F. Strouse, J. R. Schoonover, R. Duesing, S. Boyde, W. E. Jones Jr., T. J. Meyer, *Inorg. Chem.* **1995**, *34*, 473. – [14b] A. C. Benniston, V. Grosshenny, A. Harriman, R. Ziessel, *Angew. Chem. Int. Ed. Engl.* **1994**, *33*, 1884.

Received February 25, 1999
[I99065]

Dynamic Combinatorial Chemistry: Substrate H-Bonding Directed Assembly of Receptors Based on Bipyridine-Metal Complexes

Ivan Huc,[a] Michael J. Krische,[a] Daniel P. Funeriu,[a] and Jean-Marie Lehn*[a]

Keywords: Combinatorial chemistry / Molecular recognition / Functionalized bipyridine metal complexes / Janus molecules / Hydrogen bonding

The functionalized ligands **1** and **2** bearing hydrogen-bonding recognition groups have been synthesized. Their assembly by metal ions such as Cu^{I} and Pd^{II} having different coordination geometries generates different receptor architectures for the binding of suitable substrates. Addition of the complementary bis(imide) Janus molecules (**4**–**7**) to [**1a**, **2a**, CuTf] or to [**1b**, **2b**, $Pd(BF_4)_2$] mixtures leads to a moderate selective increase of the fraction of the $[(\mathbf{1a})_2Cu]^+$ or $[(\mathbf{1b})_2Pd]^{2+}$ complex depending on the Janus substrate used. Largest enhancements are observed for those Janus substrates that may be expected to display highest geometrical complementarity with the two complexes. These results represent a process directed by target binding based on dynamic combinatorial chemistry.

Introduction

The reversible connection of molecular building blocks generates potentially a set of molecular or supramolecular entities containing in principle all possible combinations of the constituents whose proportions are controlled by thermodynamic equilibria. This process may be considered as defining a dynamic combinatorial chemistry (DCC) that gives access to virtual combinatorial libraries (VCLs). In the presence of a species that binds one of the (real or virtual) members of such a library, a selective increase of the amount of this specific constituent may be expected, amounting to a target-directed enhancement of a member of the library. This is the case in the selective self-assembly of a pentameric circular helicate induced by the strong binding of a chloride ion, which led us to the DCC/VCL concept.[1] The latter was formulated in detail and extended to the recognition-induced assembly of an enzyme inhibitor.[2a] A major aspect of DCC is the search for suitable reversible processes.

Dynamic combinations of building blocks have made use of covalent linkages, such as the reversible formation of imines,[2] esters,[3] disulfides,[4] or the photoisomerization of alkenes[5] for the generation of equilibrating combinatorial libraries of receptor or substrate molecules. They may also be based on non-covalent linkages such as metal coordination,[1][6] hydrophobic effects,[7] or hydrogen bonding.[8] In the present work, we have taken advantage of the reversible assembly of ligands bearing recognition groups on a transition metal center for generating dynamic mixtures of artificial receptors.

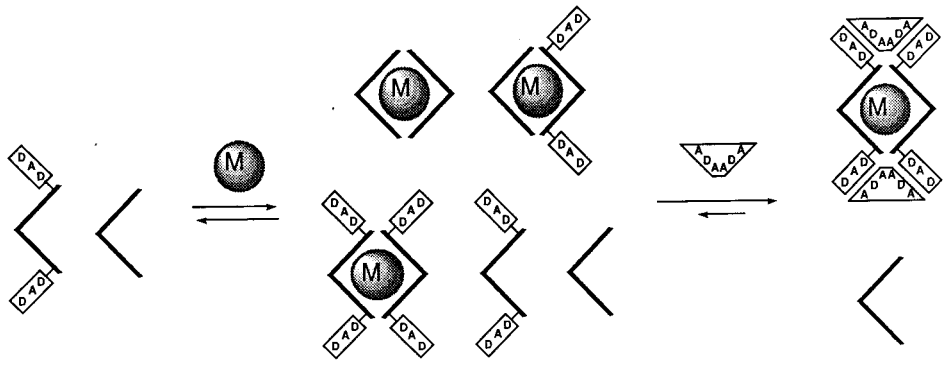
The coordination of organic ligands to metal ions has proved an efficient approach to create cavities of defined shape and size and to preorganize recognition groups in space to generate binding cavities.[9] The combination of different ligands or the formation of coordination isomers has led to the construction of libraries of self-assembled receptors, in systems where each receptor was studied as a separate entity.[10] The use of *reversible* coordination to metal centers for assembling receptors has also been reported. It was shown that an appropriate guest can act as a template for the preferential formation of the receptor.[11]

In the present study, we take advantage of this phenomenon to identify, in a dynamic mixture of coordination receptors bearing hydrogen-bonding units, those presenting best complementarity to a particular substrate molecule of Janus type,[12] i.e. a molecule having two recognition faces. As depicted in Scheme 1, the mixture is based on the *reversible* coordination of pairs of ligands to a transition metal ion. Using two different ligands, a mixture of three different complexes can be generated. Each complex is defined by a recognition capability, which results from the combination of the recognition elements of its ligands. Thus, a complex made of two ligands possessing hydrogen-bonding functions with a Donor-Acceptor-Donor (DAD) pattern, potentially has an enhanced affinity for Janus molecules having twice the complementary ADA hydrogen-bonding pattern. Indeed, this complex may form six hydrogen bonds with the two faces of a Janus molecule, whilst the free ligand or a complex bearing only one such ligand can only form three hydrogen bonds with one face. Thus, a better recognition may be achieved by a combination of the recognition elements of two ligands than from one ligand only.

The main consequence of the involvment of two ligands from the same complex in the recognition event is the selective stabilization of the complex since the Janus molecule bridges the ligands through noncovalent interactions. The equilibria should thus be shifted towards the formation of the complex displaying the best complementarity to the Janus molecule. The free energy associated with this equilibrium shift corresponds to the differential binding energy of

[a] Laboratoire de Chimie Supramoléculaire, ISIS − ULP − CNRS ESA-7006
4 rue Blaise Pascal, F-67000 Strasbourg, France
Fax: (internat.) + 33-3/88411020
E-mail: lehn@chimie.u-strasbg.fr

 © WILEY-VCH Verlag GmbH, D-69451 Weinheim, 1999 1434−1948/99/0909−1415 $ 17.50+.50/0



Scheme 1. Dynamic mixture of ligands and complexes formed upon coordination of two different ligands to a transition metal; stabilization of a receptor complex (molding) with a complementary Janus substrate molecule; one ligand bears two recognition groups with DAD hydrogen-bonding pattern; the Janus-type substrate presents two complementary ADA patterns

the Janus molecule to one complex with respect to the other components of the mixture.

Another consequence of the equilibrium shift is the release of the other ligand from the complexes. Using an appropriate stoichiometry of ligands, metal ion, and Janus substrate molecule, this may ultimately lead to a situation where only one ligand participates to the coordination, the other remaining free in solution (Scheme 1). A good receptor is thus identified simply from the fact that it becomes more abundant in the presence of its complementary substrate.

Ligand Components

As metal coordination components, 2,2′-bipyridine units bearing diacylaminopyridine DAD hydrogen-bonding motifs in position 4 and 4′ were used (Figure 1). Molecules such as **1** possess one bidendate metal-binding center and can hydrogen-bond to two imide functions via a complementary DAD/ADA array of three hydrogen bonds.[13] Ligands **2** also have 4,4′-carboxamide groups, but lack the diacylaminopyridine moiety. This should confer on them electronic properties and affinities for transition metals

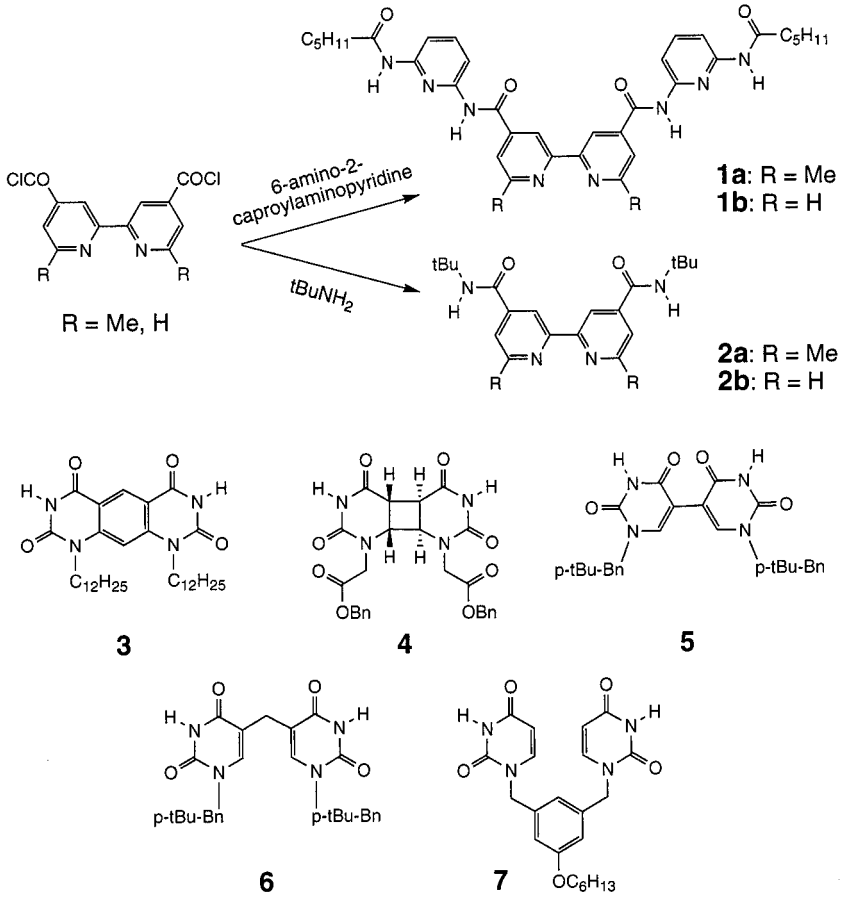


Figure 1. Functionalized ligands and substrate Janus molecules

similar to that of **1**, while keeping low hydrogen-bonding capacity to imide functions. Ligands **1** and **2** were prepared from the coupling of a 2,2′-bipyridine-4,4′-dicarbonyl chloride and either tBuNH$_2$ or 6-amino-2-caproylaminopyridine.

Janus molecules **3**−**7** all possess two hydrogen-bonding ADA imide functions as prime recognition elements. They thus all belong to the same interactional space and only differ by their geometrical properties. In **3** and **4**, the imide groups are rigidly held in parallel planes. In **5**, **6**, and **7** the imides are separated by an increasing number of single bonds, a feature that goes along with reduced preorganization and larger conformational freedom.

Copper(I) Complexes

Formation

Cu^I ions coordinate two bipyridine ligands in a distorted tetrahedral geometry, thus holding them in an approximately perpendicular arrangement ($\Phi \approx 90°$ in Figure 2). The 2,2′-bipyridine ligands **1a** and **2a** having methyl groups in the 6,6′ positions were preferred to **1b** and **2b** because their complexes with Cu^I are less labile, and less sensitive to oxidation by air. In pure chloroform at room temperature, the ligands exchange slowly on the NMR time scale. The signals observed in the ^{1}H-NMR spectrum of a solution of **1a**, **2a** (1 mM each) and CuTf (0.5 mM) can be assigned to a mixture of the five possible species by comparison with the individual spectra of **1a**, **2a**, (**1a**)$_2$CuTf, and (**2a**)$_2$CuTf. A series of six singlets is seen at $\delta = 2-2.8$, that correspond to the signals of the methyl substituents *ortho* to the bipyridine nitrogen atom (Figure 3A): one singlet for each free ligand, one singlet for each homocomplex, and two singlets of equal intensity for the mixed complex (**1a**)(**2a**)CuTf. Integration of these signals allows to measure the proportion of each species in the mixture. Due to a slightly higher intrinsic affinity of **2a** for Cu^I, (**2a**)$_2$CuTf is more abundant than (**1a**)$_2$CuTf, and **2a** and **1a**, respectively, represent 27% and 73% of the free ligands.

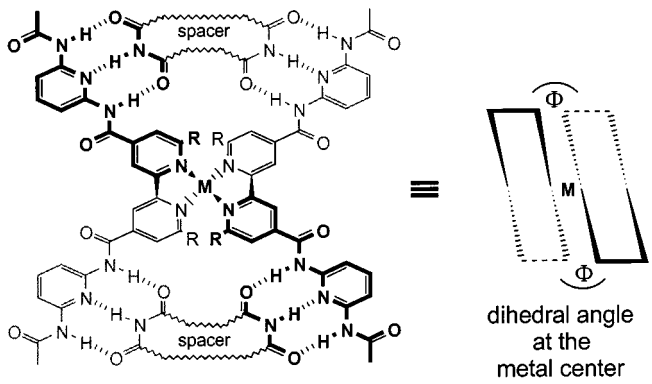


Figure 2. Schematic representation of the bridging of two ligands of a transition metal complex through hydrogen bonding to Janus molecules; the coordination sphere of the metal center determines the relative orientation of the aminopyridine moieties (Φ); the degree of complementarity of the Janus molecules is set by their spacer

Binding of Substrate Molecules

When a substrate **3**, **4**, **5**, or **7** (1 mM) is added to the mixture of complexes and ligands, the ratios [**1a**]/[**2a**] and [(**1a**)$_2$CuTf]/[(**2a**)$_2$CuTf] remained unchanged (Figure 3B). The signals assigned to **1a**, (**1a**)$_2$CuTf, and (**1a**)(**2a**)CuTf shifted upon the formation of hydrogen-bonded complexes, while those corresponding to **2a** and (**2a**)$_2$CuTf did not shift. This indicates that hydrogen bonding occurs between the imide and the diacylaminopyridine groups without specificity. None of these Janus molecules is capable of bridging two ligands on a same complex. On the other hand, hydrogen bonding of the Janus molecules to **2a** and (**2a**)$_2$CuTf is negligible. These results also indicate that hydrogen bonding to **1a** does not enhance its affinity for copper through any electronic effect.

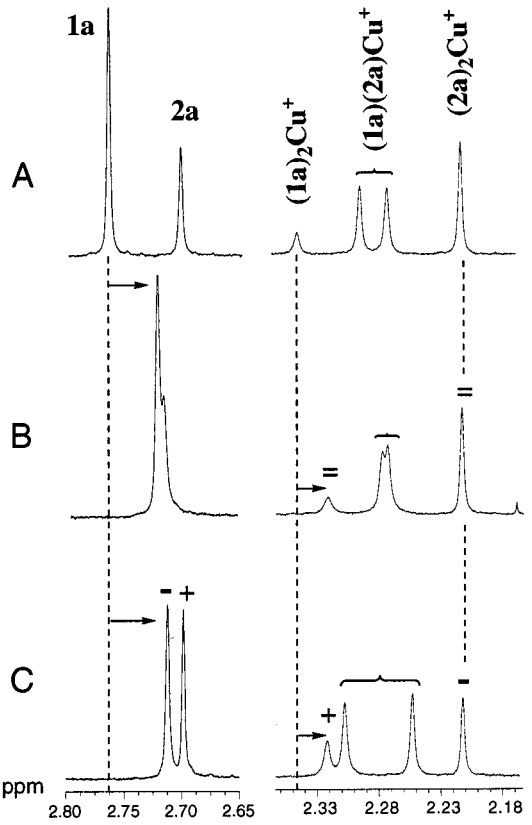


Figure 3. Part of the 500-MHz ^{1}H-NMR spectrum of a $CDCl_3$ solution of **1a**, **2a** (1 mM each) and CuTf (0.5 mM) at 298 K; the region at $\delta = 2.36-2.65$ is omitted for clarity; arrows indicate some of the shifts observed upon the addition of bis(imide) Janus substrate; A: no substrate added; B: **5** added (1 mM); C: **6** added (1 mM)

When the bis(imide) **6** (1 mM) was added to the mixture, similar shifts were observed, but the proportions between the different species were also modified (Figure 3C). The amount of (**1a**)$_2$CuTf was multiplied by a factor 2.3, and the proportions of **1a** in the free ligand decreased from 73 to 52%. Concomitantly the amount of (**2a**)$_2$CuTf decreased whilst the proportion of **2a** in the free ligands increased from 27 to 48%. The free energy difference between the two entities formed may be estimated to be about 4 kJ/mol.

The diacylaminopyridine groups of two different ligands in a Cu^{I} complex are more or less perpendicular. The capability of a Janus molecule to stabilize $(\mathbf{1a})_2$CuTf upon forming simultaneously hydrogen bonds with both ligands of the complex is thus linked to its ability of positioning its imide groups perpendicularly to each other. The results indicate that only **6** is able to do so at sufficiently low entropic and enthalpic costs. Thus, these experiments allowed to identify one Janus molecule to which $(\mathbf{1a})_2$CuTf binds selectively. However, the affinity for **6** remained small, and we searched for larger effects by changing the geometry of the complex. This was achieved by using Pd^{II} instead of Cu^{I}.

Palladium(II) Complexes

Formation

Pd^{II} can coordinate two 2,2′-bipyridines such as **1b** and **2b** which have no substituents in the 6 and 6′ positions in a square-planar arrangement ($\Phi \approx 0°$ in Figure 2). As a consequence, within a complex with **1b**, the aminopyridine moieties are held in the same plane. To form hydrogen bonds to both ligands of this complex, a Janus molecule should thus have coplanar imides diverging at an angle of ca. 120°, such as in **3** and **4**.

The bis(bipyridine)$-Pd(BF_4)_2$ complexes are not readily soluble in pure chloroform. In the following experiments this was circumvented by adding small amounts of DMSO (5%) to the mixtures, resulting in a satisfactory solubility whilst keeping competing hydrogen-bonding to the solvent low. In this solvent however, the ligand exchange is fast on the NMR time scale. For a mixture of **1b**, **2b**, and $Pd(BF_4)_2$, each ligand appears as one set of signals in the ^{1}H-NMR spectrum. The chemical shift of each signal is an average of its value for the free ligand and for the ligand complexed to Pd^{II}. From the chemical shift, one can access the proportion of free and complexed ligand, as illustrated by the titration experiment shown in Figure 4.

Increasing amounts of $Pd(BF_4)_2$ were added to a solution of **1b** and **2b** (1 mM each). Coordination to Pd^{II} causes a downfield shift of the bipyridines 3-H/3′-H, and amide NH signals. It is interesting to note that the 3-H/3′-H signal of **2b** shifts more at the beginning of the titration before reaching its limit value, whilst the 3-H/3′-H signal of **1b** follows a sigmoidal curve. As with Cu^{I}, this arises from a slightly larger affinity of ligand **2b** for Pd^{II}. During the titration, **1b** is involved in the complexes only in a second step, when the amount of free **2b** becomes smaller. When $[Pd(BF_4)_2]$ = 0.5 mM, 65% of **2b** and 35% of **1b** are coordinated to Pd^{II}.

Substrate Binding

The effect of the presence of the Janus molecules on the ^{1}H-NMR signals was first evaluated on **1b**, $(\mathbf{1b})_2Pd(BF_4)_2$, **2b**, $(\mathbf{2b})_2Pd(BF_4)_2$ individually. For **1b** and $(\mathbf{1b})_2Pd(BF_4)_2$ the introduction of imide units resulted in shifts similar to those observed for **1a** and $(\mathbf{1a})_2$CuTf: downfield shift of the amide NH signals, and upfield shift of the bipyridine 3-H/3′-H signals. Since shifts occur both upon hydrogen bonding of **1b** to imides and upon its coordination to metal centers, these signals cannot be used as reliable probes for either phenomenon. However, the presence of the Janus molecules had no effect on the spectra of **2b** and $(\mathbf{2b})_2Pd(BF_4)_2$, as was also the case for **2a** and $(\mathbf{2a})_2$CuTf. Thus, a shift of the signals of **2b**, and in particular of the signals of 3-H/3′-H, can be assigned directly to its coordination to Pd^{II}.

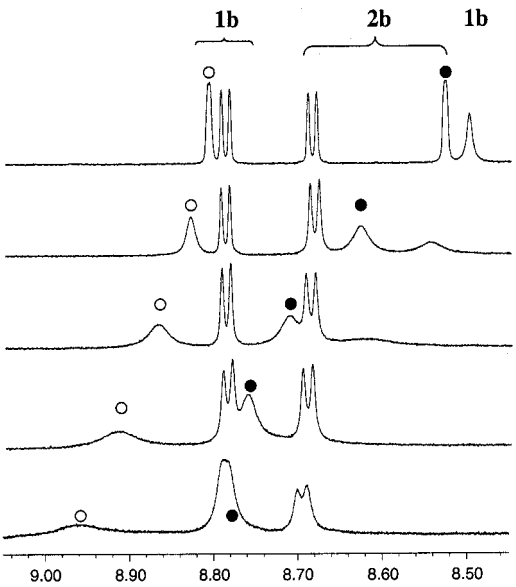


Figure 4. Part of the 500-MHz ^{1}H-NMR spectrum of a 95:5 $CDCl_3$/[D_6]DMSO solution of **1b**, **2b** (1 mM each) and $Pd(BF_4)_2$ (0, 0.25, 0.5, 0.75 and 1 mM from top to bottom) at 298 K; the circles mark the signals assigned to the bipyridine 3-H and 3′-H of **1b** (o) and **2b** (•); these signals shift upon the formation of bipyridine−palladium complexes; the doublets at δ = 8.79 and 8.69 were assigned to **1b** and **2b**, respectively (bipyridine 5-H and 5′-H); the singlet at δ = 8.50 (top spectrum) was assigned to **1b** (pentyl−CON*H*−)

In a last series of experiments, we measured the effect of the addition of Janus molecules (1 mM) on a dynamic mixture of **1b**, **2b** (1 mM each) and $Pd(BF_4)_2$ (0.5 mM). The results are summarized in the Table 1. They show that Janus molecules cause a release of **2b** from the Pd^{II} complexes, and therefore an increase of the coordination of **1b** to Pd^{II}. This is best explained by a selective stabilization of $(\mathbf{1b})_2Pd(BF_4)_2$ upon formation of hydrogen-bonded bridges between these Janus molecules and the ligands. This occurs despite the presence of DMSO in the solvent. The effect can be enhanced upon cooling the mixture down to 273 K (Figure 5): association becomes stronger, and the proportion of **2b** involved in coordination to Pd^{II} drops below 5% in the case of **3**.

Nevertheless, the selectivity for **3** remains low, and despite their structural differences, all the Janus molecules have some effectiveness to shift the equilibrium towards a better coordination of **1b** to Pd^{II}. One possible explanation is a flexibility in the positioning of the ligands about the metal center. The angle Φ (Figure 2) may deviate substan-

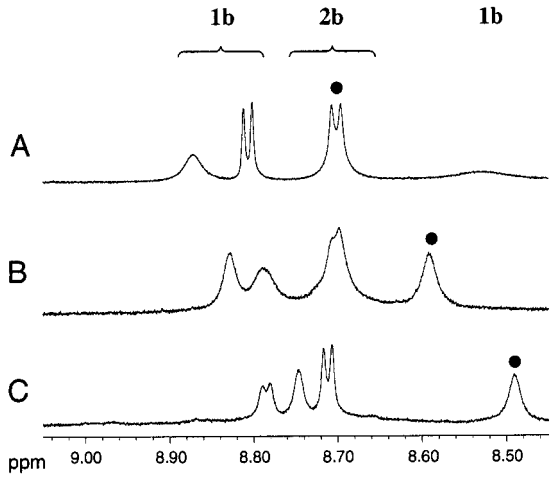


Figure 5. Part of the 500-MHz ^{1}H-NMR spectrum of a 95:5 $CDCl_3$/[D_6]DMSO solution of **1b**, **2b** (1 mM each), and $Pd(BF_4)_2$ (0.5 mM) at 298 K; A: no wedge added; B: **3** added (1 mM); C: same as B at 213 K; the circle marks the bipyridine 3-H and 3′-H of **2b**; in A, this signal overlaps with the bipyridine 5-H and 5′-H of **2b**

tially from zero, thus allowing $(\mathbf{1b})_2Pd(BF_4)_2$ to accommodate imides at various distances and orientations.

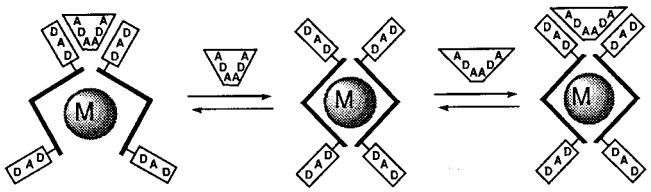
Table 1. Proportions (± 5%) of **1b** and **2b** involved in the coordination with Pd^{II} in a mixture of **1b**, **2b** (1 mM each), $Pd(BF_4)_2$ (0.5 mM), and various Janus molecules (1 mM)[a]

	Janus molecule						
	none	**3**	**3**[b]	**4**	**5**	**6**	**7**
Proportion (%) of **1b** coordinated to Pd^{II}	35	70	95	65	55	60	65
Proportion (%) of **2b** coordinated to Pd^{II}	65	30	5	35	45	40	35

[a] At 298 K. The proportion of the different complexes was calculated from the chemical shift of the bipyridine 3-H/3′-H signal in **2b**. – [b] At 273 K.

Cooperativity

The metal complexes involving two ligands **1** have two binding sites for Janus molecules (Scheme 2). The experiments above were performed using two equivalents of Janus molecule (1 mM) with respect to the metal. We looked for the conceivable presence of some degree of cooperativity between these two binding sites by examining the effect of *a single equivalent* (0.5 mM) of Janus molecule on the same dynamic mixtures as above ([**1**] = [**2**] = 1 mM, [metal] = 0.5 mM). In the case of a strong negative cooperativity between the binding sites, one equivalent of Janus molecule should be as effective as two for the stabilization of complexes $(\mathbf{1})_2$(metal) (Scheme 2). In the case of a strong positive cooperativity, one equivalent of Janus molecule should have a stabilizing effect of exactly half the effect of two equivalents. In none of our systems, however, we observed a clear cooperativity, and the results were always between these ideal cases.



Scheme 2. Negative (left) and positive (right) cooperativity; the binding of a Janus molecule to the complex may favor or disfavor the binding of a second Janus molecule

Conclusion

The present results demonstrate a selective enhancement of a constituent of a dynamic combinatorial set of metal complexes acting as receptors for the binding of a complementary substrate species. They are based on the simultaneous operation of reversible metal ion coordination for the exploration of the combinatorial space and of substrate binding through hydrogen bonding, for the amplification of a given constituent of the dynamic library.

A variety of other reversible molecular or supramolecular processes may be envisaged for gaining access to dynamic combinatorial libraries, real or virtual, adapted to the molecular recognition of specific partners.

Experimental Section

General: ^{1}H- and ^{13}C-NMR spectra were recorded with a Bruker WM-200 (200 MHz) or a Bruker 500 (500 MHz) spectrometer at 298 K. Chemical shifts are reported as δ values relative to the residual solvent peak. – Yields are calculated on isolated compounds and are unoptimized. The following compounds were prepared according to literature procedures: 2,2′-bipyridine-4,4′-dicarbonyl chloride,[14] 6,6′-dimethyl-2,2′-bipyridine-4,4′-dicarbonyl chloride,[15] 2-amino-6-caproylaminopyridine,[16] Janus molecule **3**,[12] uracil photodimer **4**,[17] 5,5′-diuracil and methylene 5,5′-diuracil.[18]

General Procedure for the Preparation of Ligands 1 and 2: 2,2′-Bipyridine-4,4′-dicarbonyl chloride (0.5 mmol) was dissolved in anhydrous toluene (5 mL), and either freshly distilled tBuNH$_2$ (5 equiv.) or 2-amino-6-caproylaminopyridine (2.1 equiv.) was added. The suspension was stirred at room temperature for 24 h under an anhydrous atmosphere. The solvent was then evaporated and the solid residue triturated in saturated aqueous $NaHCO_3$. The suspension was filtered and the solid was washed thoroughly with saturated aqueous $NaHCO_3$ and water, and finally dried under vacuum. Recrystallization from EtOAc/EtOH afforded analytically pure **1a**, **1b**, **2a**, and **2b**.

4,4′-Bis[(6-caproylamino-2-pyridyl)carboxamido]-2,2′-bipyridine (1b): White solid m.p. 260°C. – ^{1}H NMR ($CDCl_3$, 10% [D_6]DMSO, 200 MHz): δ = 10.87 (br, s, 2 H, NH), 10.21 (br, s, 2 H, NH), 8.94 (d, 2 H, J = 5 Hz, 6-H, 6′-H bipy), 8.88 (d, 2 H, J = 1.5 Hz, 3-H, 3′-H bipy), 7.97 (dd, 2 H, J = 5 Hz, J = 1.5 Hz, 5-H, 5′-H bipy), 7.90–7.76 (m, 6 H, H py), 2.41 (t, 4 H, J = 7.2 Hz, CH_2–NH), 1.59 (q, 4 H, J = 7.2 Hz, CH_2–CH_2–NH), 1.29 (m, 8 H, CH_3–CH_2–CH_2-), 0.87 (t, 6 H, J = 7.2 Hz, CH_3). – ^{13}C NMR ([D_6]DMSO, 50 MHz): d = 172.2, 164.4, 155.2, 150.6, 150.0, 149.6, 142.7, 139.9, 122.3, 118.7, 110.6, 110.0, 35.9, 30.7, 24.6, 21.8, 13.7. – $C_{34}H_{38}N_8O_4$ (622.73): calcd. C 65.57, H 6.15, N 17.99; found C 65.14, H 6.16, N 17.86.

4,4′-Bis[(6-caproylamino-2-pyridyl)carboxamido]-6,6′-dimetyl-2,2′-bipyridine (1a): White solid m.p. 225°C. − ^{1}H NMR ([D$_6$]DMSO, 200 MHz): δ = 10.80 (br, s, 2 H, NH), 10.20 (br, s, 2 H, NH), 8.64 (s, 2 H, 3-H, 3′-H bipy), 7.87−7.78 (m, 8 H, H py and 5-H, 5′-H bipy), 2.69 (s, 6 H, CH_3), 2.44 (t, 4 H, J = 7.2 Hz, CH_2−NH), 1.57 (q, 4 H, J = 7.2 Hz, CH_2−CH_2−NH), 1.29 (m, 8 H, CH_3−CH_2−CH_2−), 0.87 (t, 6 H, J = 7.2 Hz, CH_3). − ^{13}C NMR ([D$_6$]DMSO, 50 MHz): δ = 172.2, 158.7, 154.8, 150.6, 149.7, 143.0, 139.9, 121.5, 115.9, 110.5, 110.0, 35.9, 30.7, 24.5, 24.1, 21.7, 13.7. − High Resolution MS; $C_{36}H_{43}N_8O_4^+$: calcd. 651.3407; found 651.3414.

4,4′-Bis(*tert*-butylcarboxamido)-6,6′-dimethyl-2,2′-bipyridine (2a): White solid m.p. 287.2°C. − ^{1}H NMR ($CDCl_3$, 200 MHz): δ = 8.35 (d, 2 H, J = 0.8 Hz, 3-H, 3′-H), 7.54 (dd, 2 H, J = 4.4 Hz, J = 0.8 Hz, 5-H, 5′-H), 6.18 (br, s, 2 H, NH), 2.67 (s, 6 H, CH_3 bipy), 1.48 (s, 18 H, CH_3). − ^{13}C NMR ([D$_6$]DMSO, 50 MHz): δ = 165.1, 158.0, 154.7, 144.5, 121.1, 115.6, 51.0, 28.3, 24.1. − High Resolution MS; $C_{22}H_{31}N_4O_2^+$: calcd. 383.2447; found 383.2436. − The crystal structure of this compound was determined and will be reported elsewhere.

4,4′-Bis(*tert*-butylcarboxamido)-2,2′-bipyridine (2b): White solid, m.p. 272°C. − ^{1}H NMR ($CDCl_3$, 200 MHz): δ = 8.80 (d, 2 H, J = 4.4 Hz, 6-H, 6′-H), 8.58 (d, 2 H, J = 0.8 Hz, 3-H, 3′-H), 7.76 (dd, 2 H, J = 4.4 Hz, J = 0.8 Hz, 5-H, 5′-H), 6.18 (br, s, 2 H, NH), 1.51 (s, 18 H, CH_3). − ^{13}C NMR ([D$_6$]DMSO, 50 MHz): δ = 164.7, 155.2, 149.6, 144.2, 122.0, 118.3, 51.1, 28.3. − High Resolution MS; $C_{20}H_{27}N_4O_2^+$: calcd. 355.2134; found 383.2135.

Cu(2a)$_2$Tf: Red crystals. − ^{1}H NMR ($CDCl_3$, 200 MHz): δ = 8.60 (s, 2 H, 3-H, 3′-H), 7.76 (s, 2 H, 5-H, 5′-H), 7.09 (br, s, 2 H, NH), 2.21 (s, 6 H, CH_3 bipy), 1.54 (s, 18 H, CH_3 $_{tert}$-butyl). − ^{13}C NMR ([D$_3$]MeCN, 50 MHz): δ = 165.0, 159.1, 152.9, 146.2, 125.0, 118.7, 53.0, 28.8, 25.3. − The crystal structure of this compound was determined and will be reported elsewhere.

Pd(2b)$_2$[BF$_4$]$_2$: Yellow crystals. − ^{1}H NMR ($CDCl_3$, 200 MHz, 10% [D$_6$]DMSO, 200 MHz): δ = 8.81 (s, 2 H, 3-H, 3′-H), 8.70 (d, 2 H, J = 5.5 Hz, 6-H, 6′-H), 8.18 (d, 2 H, J = 5.5 Hz, 5-H, 5′-H), 7.69 (br, 2 H, NH), 1.43 (s, 18 H, CH_3 $_{tert}$-butyl). − ^{13}C NMR ([D$_3$]MeCN, 50 MHz): δ = 163.6, 158.2, 153.3, 149.9, 127.7, 124.1, 53.9, 29.1.

Acknowledgments

We thank R. Graff for NMR measurements and Dr. T. Carell for providing us with a sample of compound **4**.

[1] B. Hasenknopf, J.-M. Lehn, B. O. Kneisel, G. Baum, D. Fenske, *Angew. Chem.* **1996**, *108*, 1987−1990; *Angew. Chem. Int. Ed. Engl.* **1996**, *35*, 1838−1840; B. Hasenknopf, J.-M. Lehn, N. Boumediene, A. Dupont-Gervais, A. Van Dorsselaer, B. Kneisel, D. Fenske, *J. Am. Chem. Soc.* **1997**, *119*, 10956−10962.

[2] [2a] I. Huc, J.-M. Lehn, *Proc. Natl. Acad. Sci. USA* **1997**, *94*, 2106−2110. − [2b] For a related template directed imine formation see: J. T. Goodwin, D. G. Lynn, *J. Am. Chem. Soc.* **1992**, *114*, 9197−9198.

[3] P. A. Brady, R. P. Bonar-Law, S. J. Rowan, C. J. Suckling, J. K. M. Sanders, *Chem. Commun.* **1996**, 319−320; S. J. Rowan, J. K. M. Sanders, *Chem. Commun*. **1997**, 1407−1408; P. A. Brady, J. K. M. Sanders, *J. Chem. Soc., Perkin Trans. 1* **1997**, 3237−3253.

[4] H. Hioki, W. C. Still, *J. Org. Chem.* **1998**, *63*, 904−905.

[5] A. V. Eliseev, M. I. Nelen, *Chem. Eur. J.* **1998**, *4*, 825−834.

[6] B. Klekota, M. H. Hammond, B. L. Miller *Tetrahedron Lett.* **1997**, *38*, 8639−8642.

[7] X. Cha, K. Ariga, M. Onda, T. Kunitake, *J. Am. Chem. Soc.* **1995**, 11833−11838.

[8] M. Crego Calama, R. Hulst, R. Fokkens, N. M. M. Nibbering, P. Timmerman, D. N. Reinhoudt, *Chem. Commun.* **1998**, 1021−1022.

[9] [9a] For exoreceptor complexes bearing nucleoside residues, e.g. metallonucleates, see: U. Koert, M. Harding, J.-M. Lehn, *Nature* **1990**, *346*, 339; M. Harding, J.-M. Lehn, unpublished work cited in J.-M. Lehn, *Angew. Chem.* **1988**, *100*, 91−116; *Angew. Chem. Int. Ed. Engl.* **1988**, *27*, 89−112, structures **41**, **42**. − [9b] For peptide-bearing complexes see for instance: M. Lieberman, T. Sasaki, *J. Am. Chem. Soc.* **1991**, *113*, 1470−71; M. R. Ghadiri, C. Soares, C. Choi, *J. Am. Chem. Soc.* **1992**, *114*, 4000−4002. − [9c] M. S. Goodman, A. D. Hamilton, J. Weiss, *J. Am. Chem. Soc.* **1995**, *117*, 8447−8455. − [9d] J. L. Lee, A. W. Schwabacher, *J. Am. Chem. Soc.* **1994**, *116*, 8382−8383; I. Prévot-Halter, T. J. Smith, J. Weiss *Tetrahedron Lett.* **1996**, *37*, 1201−1204. − [9e] For the generation of cage complexes see: P. N. W. Baxter in *Comprehensive Supramolecular Chemistry* (Eds.: J. L. Atwood, J. E. D. Davies, D. D. MacNicol, F. Vögtle, J.-M. Lehn), Pergamon, Oxford, **1996**, *9*, 165; M. Fujita, *Comprehensive Supramolecular Chemistry* **1996**, *9*, 253.

[10] S. Sakai, T. Sasaki, *J. Am. Chem. Soc.* **1994**, *116*, 1587−1588; M. S. Goodman, V. Jubian, B. Linton, A. D. Hamilton *J. Am. Chem. Soc.* **1995**, *117*, 11610−11611.

[11] M. Yamamoto, M. Takeuchi, S. Shinkai, *Tetrahedron Lett.* **1998**, *39*, 1189−1192; A. Bilyk, M. M. Harding *J. Chem. Soc. Chem. Commun.* **1995**, 1697−1698; M. Fujita, J. Yazaki, K. Ogura, *J. Am. Chem. Soc.* **1990**, *112*, 5645−5647; S. Sakai, Y. Shigemasa, T. Sasaki, *Tetrahedron Lett.* **1997**, *38*, 8145−8148.

[12] A. Marsh, E. G. Nolen, K. M. Gardinier, J.-M. Lehn, *Tetrahedron Lett.* **1994**, *35*, 397−400; N. Kimizuka, S. Fujikawa, H. Kuwahara, T. Kunitake, A. Marsh, J.-M. Lehn, *J. Chem. Soc. Chem. Commun.* **1995**, 2103−2104.

[13] J. Rebek, Jr., B. Askew, P. Ballester, C. Buhr, S. Jones, D. Nemeth, K. Williams, *J. Am. Chem. Soc.* **1987**, *109*, 5033−5035; A. D. Hamilton, D. Van Engen, *J. Am. Chem. Soc.* **1987**, *109*, 5035−5036.

[14] G. Sprintschnik, H. W. Sprintschnik, P. P. Kirsh, D. G. Whitten, *J. Am. Chem. Soc.* **1977**, *99*, 4947−4954.

[15] M. H. Harding, J.-M. Lehn, *Aust. J. Chem.* **1996**, *49*, 1023−1027.

[16] T. Paolo, V. Jubian, A. D. Hamilton, *Tetrahedron* **1995**, 435−448.

[17] T. Carell, R. Epple, V. Gramlich, *Angew. Chem.* **1996**, *108*, 676−679; *Angew. Chem. Int. Ed. Engl.* **1996**, *35*, 620−623.

[18] F. Perin, A. Cier, C. Nofre, *Bull. Soc. Chim. Fr.* **1964**, 1877−1880.

Received March 4, 1999
[I99082]

Self-Assembly, Structure, and Physical Properties of Tetranuclear Zn_{II} and Co_{II} Complexes of [2 × 2] Grid-Type

Javier Rojo,[a] Francisco J. Romero-Salguero,[a] Jean-Marie Lehn,*[a] Gerhard Baum,[b] and Dieter Fenske[b]

Keywords: Grid complexes / Self-assembly / Co / Zn / Coordination chemistry / Bis(tridentate) ligands

The tretrametallic [2 × 2] grid-type complexes **1–4** are formed by self-assembly of the bis(tridentate) ligands **5** and **6** with Zn^{II} and Co^{II} cations. They have been characterized by spectroscopic studies in solution as well as by crystal structure determination. The substituents in the central pyrimidine ring play an important role in terms of geometry and physical properties of the complexes. They induce an orthogonal orientation of the ligand in the complexes which is critical for the formation of ordered monolayers and extended self-organized arrays of grids. The physical properties of the complexes such as metal–metal interaction and π-π* stacking between the ligands may be modulated by changing these substituents.

Introduction

The self-assembly of suitable polydentate ligands with metal ions allows the preparation of well-defined inorganic supramolecular architectures in solution. In recent years, much effort has focused on the generation of inorganic arrays of various types in view of their promising physicochemical properties and their potential application in nanotechnology.[1−10]

The design of the ligand is the crucial for controlling the structure and properties of the final assemblies. Recently, our laboratory has reported the synthesis of bidentate ligands based on terpyridine subunits[11] and their self-assembly with metal ions of octahedral coordination to generate complexes of grid-type geometry.[12] The physicochemical properties of the [2 × 2] cobalt(II) grids formed indicate an electronic communication between the metallic centers suggesting that these inorganic assemblies could have applications in molecular information storage.[13] Moreover, the self-organization of such building blocks could lead to highly ordered monolayers[14] (e.g. "grids of grids") presenting magnetic domains or into which it might be possible to write information in the form of different metal redox states using for instance scanning probe microscopy techniques.

For generating such extended arrays, it is necessary that the basic grid components present regular, undistorted structures where the ligands are arranged in orthogonal fashion. Based on previous results, this arrangement depends in particular on the substituent present at the C^2 position of the pyrimidine ring.[15]

[a] Laboratoire de Chimie Supramoléculaire, ISIS − ULP − CNRS ESA-7006
4 rue Blaise Pascal, F-67000 Strasbourg, France
Fax: (internat.) + 33-3/88411020
E-mail: lehn@chimie.u-strasbg.fr
[b] Institut fur Anorganische Chemie, Universität Karlsruhe, D-76128 Karlsruhe, Germany

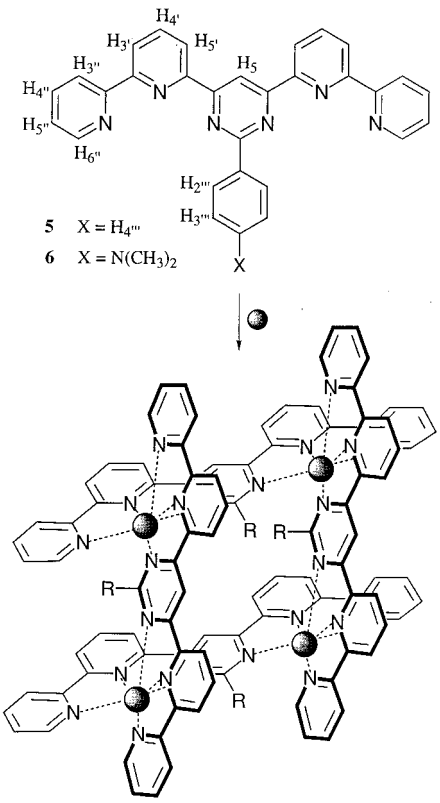
In the present work, we describe the formation as well as the structural and physico-chemical properties of the [2 × 2] grid-type complexes **1−4** obtained by the self-assembly of zinc(II) and cobalt(II) ions with the ligands **5** and **6** bearing a phenyl and a *p*-(dimethylamino)phenyl substituent, respectively, on the central pyrimidine (Scheme 1). The interaction between the phenyl ring and the pyridine units of the perpendicular ligands in the complexes induces an orthogonal arrangement suitable for applications in self-organizing systems.

Results and Discussion

Synthesis of Ligands 5 and 6 and of the Corresponding Grid Complexes 1−4

The synthesis of the bis(tridentate) ligand **5** has been reported previously.[11] Ligand **6** was obtained as described in Scheme 2. The reaction of equivalent amounts of ligands **5** or **6** and of the metal salts $Co(BF_4)_2$, $Co(DMSO)_4Tf_2$, or $ZnTf_2$ in acetonitrile leads to clear solutions from which the metal complexes **1−4** were isolated by precipitation with ethyl ether and centrifugation (**1** and **2**) or by simply removing the solvent under reduced pressure (**3** and **4**) (Scheme 1). These compounds were purified by recrystallization from acetonitrile/ethyl ether and characterized by physical and spectroscopic techniques as described below. The assembly rates of ligands **5** and **6** with Co^{II} and Zn^{II} ions to give complexes **1** and **2**, are appreciably slower than when the ligand does not present a phenyl substituent in the 2-position of the pyrimidine ring.[12] In the latter case, the self-assembly takes a few hours in contrast to the one night to two days for ligands **5** and **6**. This may be attributed to the steric hindrance introduced by the central phenyl substituent which must insert between two other ligands in the final grid complex (see below). All new compounds had spectral and analytical properties in agreement with their structure.

 © WILEY-VCH Verlag GmbH, D-69451 Weinheim, 1999 1434−1948/99/0909−1421 $ 17.50+.50/0

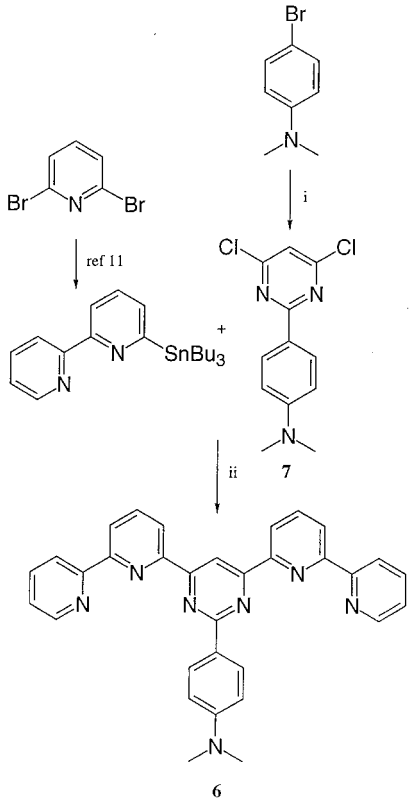


Scheme 1. Self-assembly of the [2 × 2] grid complexes **1**−**4** from the ligands **5**, **6**, and metal salts

^{1}H-NMR Spectra

The metal complexation leads to remarkable changes in the proton-NMR spectra with large modifications in the chemical shifts of the protons of the ligand. The metal binding induces a conformational change in the ligand. The most stable conformation of the ligand is that which adopts a *transoid* conformation around all C−C bonds linking the heterocyclic units;[11,16,17] in this form the nitrogen lone pairs of the heterocycle deshield the ligand protons adjacent to the interannular bonds (5-H, 5′-H, 3′-H, and 3′′-H). In the metal complex, the ligand presents a *cisoid* conformation to allow the formation of chelating coordination bonds with the metal centers and this deshielding effect disappears. The formation of the coordinative nitrogen−metal bonds as well as the positioning of the ligands in the complex also contribute to the chemical shift changes.

The proton-NMR spectra of ligand **5** and its Zn complex **1** as well as of ligand **6** and its Zn complex **3** are represented in Figures 1 and 2, respectively. The corresponding chemical shifts are listed in Table 1. The spectra of the cobalt(II) complexes **2** and **4** present special features due to the magnetic anisotropy effects of the ions; they will be described elsewhere.[18]



Scheme 2. Synthesis of the ligand **6**, i) *n*BuLi, THF, 4,6-dichloropyrimidine; ii) $Pd(Ph_3P)_4$, toluene

The major changes observed in the NMR spectra on complexation reside in the shielding of the phenyl protons. In the free ligand, these protons appear as a multiplet at low field corresponding to the *ortho* protons centered at δ = 8.78 and another multiplet centered at δ = 7.59 for the *meta* and *para* protons in the case of ligand **5** and an AA′BB′ system at δ = 8.79 and 6.87 for ligand **6**. The *ortho* protons are deshielded due to the presence of the two nitrogen lone pairs of the pyrimidine ring. When the zinc complexes **1** and **3** are formed, the multiplets are split into five and three well defined signals, respectively. The *ortho*, *ortho′* and *meta*, *meta′* protons of the phenyl ring, which are equivalent in ligands **5** and **6**, become nonequivalent in the complexes **1** and **3**. Moreover, all the aromatic protons are markedly shielded giving signals between δ = 7.0 and 4.96. These two observations suggest that in solution the complexes **1** and **3** adopt a very compact structure where the phenyl rings of the two ligands on one face of the grid structure insert between the two ligands on the other face. As a result, the phenyl protons are subject to strong shielding effects due to the heteocyclic units, thus inducing large shifts; furthermore, rotation around the phenyl−pyrimidine C−C bond is blocked, leading to nonequivalence of the *o*, *o′* and *m*, *m′* protons. This has been confirmed by a ROESY NMR experiment where a NOE interaction between 3′′′-H and 3′-H and 4′-H as well as between 3′′′-H^i and 5-H and 5′-H is observed for complex **1**.

In the Zn complex **3**, the signal of the methyl substituents on the amino group appears as a broad resonance centered

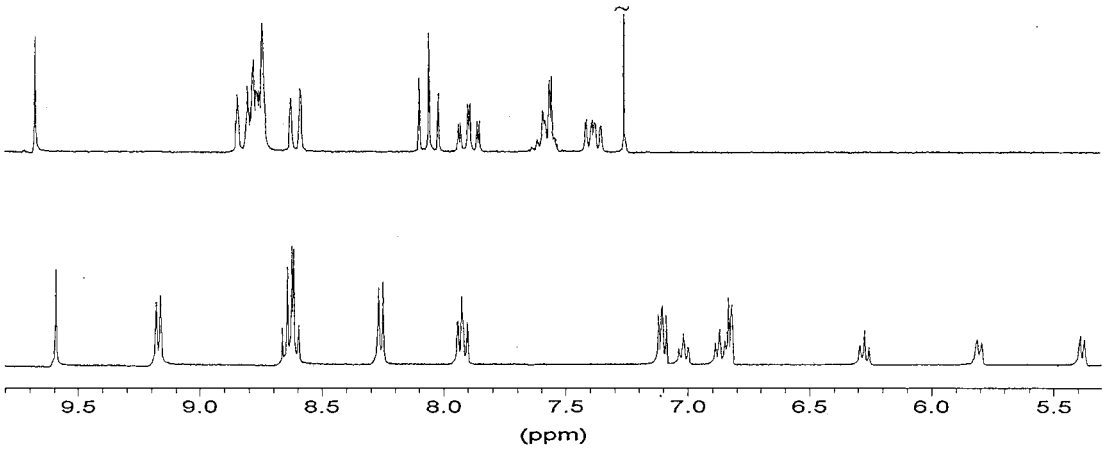


Figure 1. Proton-NMR spectra of ligand **5** at 200 MHz in $CDCl_3$ (top) and the Zn_4 complex **1** at 400 MHz in CD_3CN (bottom); for signal assignments, see Experimental Section

Table 1. Chemical shifts and chemical shift differences for proton-NMR signals of cornplexes **1** and **3** (in CD_3CN) and ligands **5** and **6** (in $CDCl_3$)[a]

Compound	5-H	5′-H	4′-H	3′-H	3′′-H	4′′-H	5′′-H	6′′-H	2′′′-H^o	2′′′-H^i	3′′′-H^o	3′′′-H^i	4′′′-H
5	9.69		8.08		8.84	7.91	7.40	8.76	8.78	8.78	7.59	7.59	7.59
1	9.57	9.17	8.63	8.63	8.25	7.92	7.10	6.82	5.80	5.38	7.00	6.27	6.87
Δδ	−0.12		+0.55		−0.59	+0.01	−0.30	−1.94	−2.98	−3.40	−0.59	−1.32	−0.72
6	9.54		8.07			7.91	7.38	8.79	8.79	8.79	6.87	6.87	
3	9.67	9.29	8.54	8.61		7.90	7.09	6.86	5.34	5.49	4.96	5.49	
Δδ	+0.13		+0.47			−0.01	−0.29	−1.93	−3.45	−3.30	−1.91	−1.38	

[a] *i* and *o* designate the inner and outer *ortho* and *meta* protons, respectively, on the phenyl substituent.

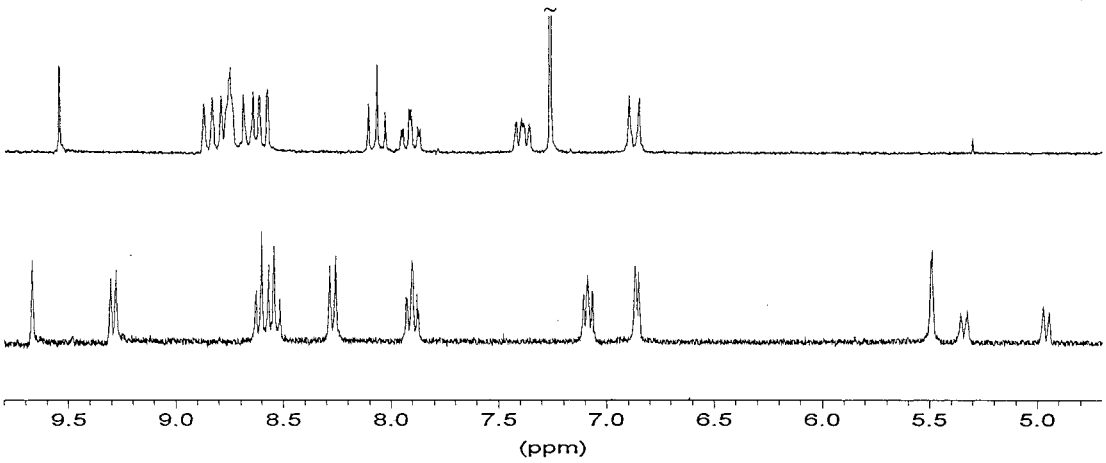


Figure 2. Proton-NMR spectra of ligand **6** at 200 MHz in $CDCl_3$ (top) and the Zn_4 complex **3** at 300 MHz in CD_3CN (bottom); for signal assignments, see Experimental Section

at δ = 3.07 in the proton-NMR spectrum. Due to the complex structure the rotation around the N−C bond is hindered. A variable-temperature experiment was performed (Figure 3). When the sample was heated to 333 K the broad band sharpened to a fine singlet for the two chemically equivalent methyl groups. When the temperature was lowered to 243 K, the signal at δ = 3.07 split into two singlets at δ = 3.25 and 2.88. A NOESY experiment allowed the assignment of the low-field peak as the signal of internal methyl group and the other one of the external methyl group. With a coalescence temperature T_c of 290 K a free energy of activation $\Delta G_c^{\geq}$ for the rotation around the N−C bond may be calculated as $\Delta G_c^{\geq} = 4.57T_c\cdot(9.97 + \log T_c/\delta\nu)$ where δν is the chemical shift difference between the two signals,[19] giving a value of 13.6 kcal/mol.

In this variable-temperature experiment the other signals in the spectrum did not change except those corresponding to the phenyl ring which may be affected by small changes in the complex structure with temperature. The data also show that at the highest temperature reached, rotation of

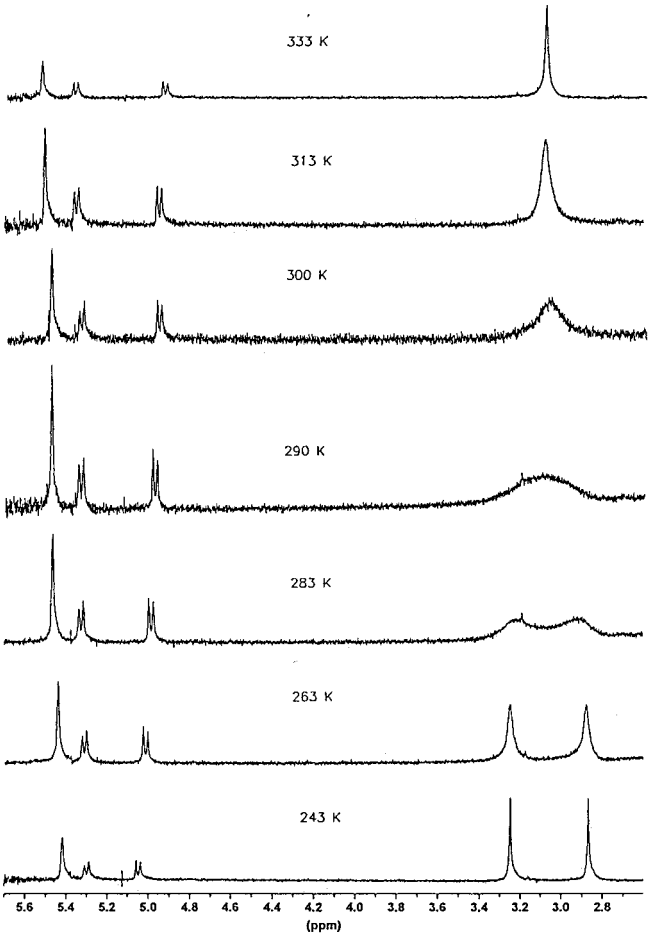


Figure 3. Proton-NMR spectra at different temperatures for the Zn_4 complex **3** at 300 MHz in CD_3CN (heteroaromatic protons not shown)

the phenyl group with respect to the pyrimidine ring is still slow on the NMR time scale, indicating that no significant dissociation of the complex is taking place. One may note that the phenyl ring rotation is thus a probe for investigating the kinetics of ligand exchange in such grid complexes.[18]

Crystal Structures of the Complexes 1, 2, and 4

The structures of the Zn^{II} and Co^{II} complexes **1**, **2**, and **4** of ligands **5** and **6** were investigated by X-ray crystallography. Those of **1** and **2** are represented in Figures 4 and 5. In all three structures the complexes present a [2 × 2] grid-type architecture in which the four metal ions form a square and lie close to an average common plane.

In the complex $\{[\mathbf{5}_4Zn_4](CF_3SO_3)_8\}$ (**1**) the Zn^{II} ions display a distorted octahedral coordination (Figure 4). The Zn−Zn distances lie in the range of 6.584−6.767 Å. The Zn−N bond lengths are between 2.053 and 2.184 Å for the pyridine nitrogen atoms and between 2.231 and 2.373 Å for the pyrimidine nitrogen atoms. The distances between the heteroaromatic rings of one ligand and the phenyl ring of the orthogonal one (3.25−3.50 Å) indicate van der Waals contact and π−π stacking interaction.

The complex $\{[\mathbf{5}_4Co_4](BF_4)_8\}$ (**2**) crystallizes with two molecules per unit cell. The metal ions also display a distorted octahedral coordination with Co,Co distances between 6.453−6.570 Å (Figure 5). The Co−N bond lengths lie between 2.041−2.175 Å for pyridine nitrogens and are slighly longer (2.213−2.309 Å) for the pyrimidine nitrogens. Again the short distances between phenyl and pyridine rings indicate π, π stacking.

In the case of $\{[\mathbf{6}_4Co_4](CF_3SO_3)_8\}$ (**4**), the overall quality of the crystal structure data is at this stage too low for a detailed description. However, the analysis indicates without doubt the [2 × 2] grid-type arrangement. Crystals of better quality are required for improving the structural data.

The central substituent in position 2 of the pyrimidine ring plays an important role in the geometrical features of the final complexes. It has been shown that in the case of rack-type metal ion coordination arrays, a methyl substituent was the best suited for the formation of complexes presenting the least distorted ligand geometry.[15] In the case of a cobalt(II) [2 × 2] grid complex of the type studied here, the presence of a methyl substituent on the central pyrimidine ring was found to cause a divergent, outward bending of the planes of the ligands, a CH_3 group being apparently somewhat too large.[12] On the contrary, when there is no substituent in that position, the situation is opposite and an inward, convergent bending is observed in the corresponding $(Zn^{II})_4$ complex.[20] An intermediate situation is found in the present case of a phenyl substituent which has a thickness intermediate between the steric requirements of CH_3 and H. Insertion of the phenyl group between two ligands in complexes **1** and **2** induces an almost parallel arrangement of the average planes of the ligands, thus leading to an overall geometry of the [2 × 2] grid complexes close to a regular square (Figures 4 and 5).

UV/Vis Absorption and Emission Spectra

The absorption maxima (λ_{max}) and extinction coefficients (ε) for ligands **5** and **6** in chloroform and for complexes **1**, **2**, **3**, and **4** in acetonitrile are listed in Table 2. The UV region of the absorption spectra shows strong absorption bands at 280−290 and 350−375 which correspond to ligand-centered (LC) π-π* transition bands. In the ligands, these bands appear at higher energies.

In the case of complexes **2**, **3**, and **4**, absorption bands are observed in the visible region. The zinc complex **3** presents a remarkable deep red color, corresponding to an intense absorption band at 516 nm which could be due to a donor-acceptor charge transfer transition between the electron-rich (dimethylamino)phenyl group and the pyridine rings held in stacking position by the structure of the complex. The broad bands centered between 400−475 and 532 nm in the Co complexes **2** and **4**, respectively, could correspond to Co^{II}−bipyridine MLCT and the very broad

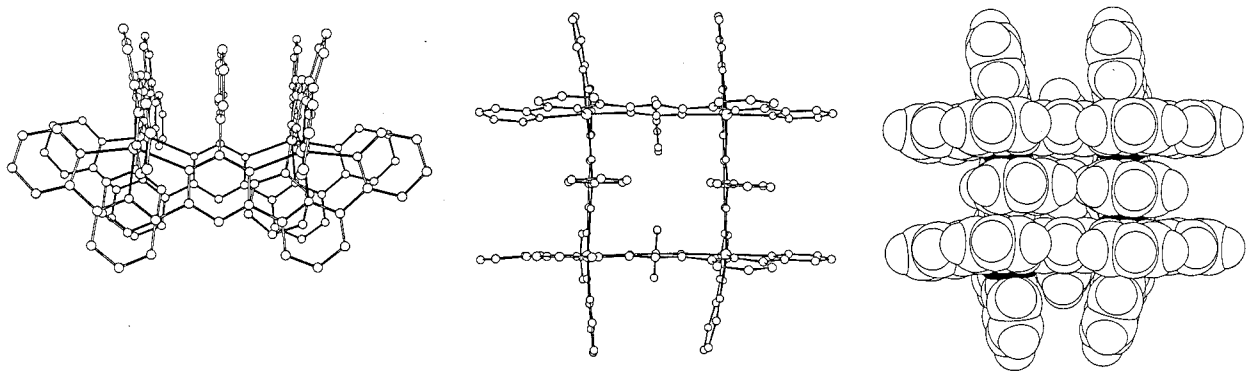


Figure 4. X-ray structure of the [2 × 2] Zn_4 grid complex **1**: side view (left); top view (center); top view, space-filling representation (right)

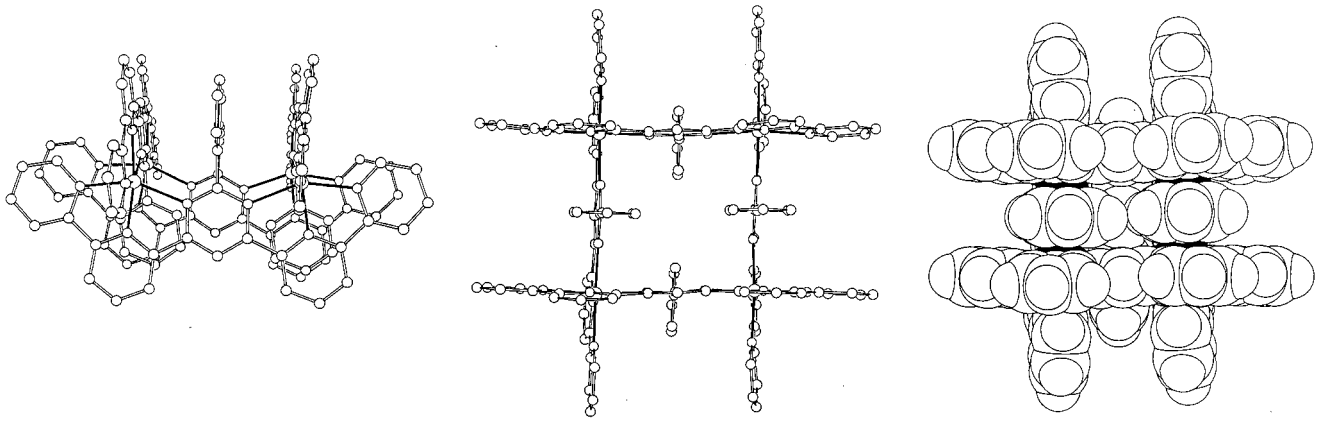


Figure 5. X-ray structure of the [2 × 2] Co_4 grid complex **2**: side view (left); top view (center); top view, space-filling representation (right); this is one of the two grid complexes present in the unit cell

Table 2. Electronic absorption spectral data for the complexes **1**–**4** and the ligands **5** and **6** in acetonitrile, λ in nm (ε in 10^4 $M^{-1}cm^{-1}$)

Compound		π-π* (LC)
5		333 (1.0), 332 (1.4), 284 (3.5), 274 (3.8), 256 (3.2), 236 (4.8)
1		375 (6.5), 358 (7.2), 294 (4.2), 282 (4.9)
2	430 (0.1)[a]	371 (0.8), 361 (0.9), 291 (0.7), 279 (18)
6	402 (0.7)[b]	348 (8.4), 312 (7.9), 284 (10.0)
3	516 (5.5)[b]	371 (1.3), 357 (1.3), 295 (0.8), 282 (0.9), 261 (1.3)
4	532 (1.1)[a]	365 (18.5), 292 (13.2), 267 (19.8)

[a] Metal-to-ligand charge-transfer transitions. – [b] Ligand-centered transitions, probably of donor-acceptor type for **3**.

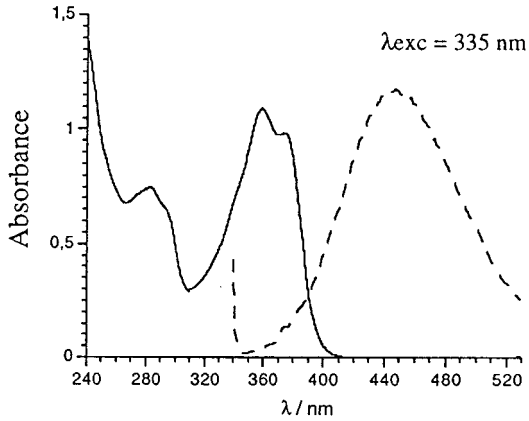


Figure 6. Electronic absorption and emission (broken line) spectra of the Zn_4 grid complex **1** in acetonitrile

shoulder at lower energy to Co^{II}–pyrimidine MLCT transitions.

The strong fluorescence of the zinc complex **1** is noteworthy. Whereas ligand **5** in chloroform exhibits only a weak emission at about 410 nm when irradiated at 272 nm, complex **1** in acetonitrile presents an intense emission at 450 nm under excitation at 335 nm at room temperature (Figure 6).[21] Since the Zn^{II} ions are of d^{10} electronic configuration and possess no low-lying metal-centered excited states, the fluorescence of **1** may be ascribed to emission from the lowest ligand-centered excited singlet level, its high intensity being due to the rigidity of the complex, which decreases the radiationless decay relative to that for the free ligand **5**. The absence of emission for the cobalt complex **2** is due to the presence of the low-lying nonemissive Co^{II}-centered MLCT excited state which inhibits luminescence,

as has been previously observed for other cobalt complexes.[22] Ligand **6** and its metal complexes **3** and **4** show no emission. Radiationless decay of the ligand-centered levels may take place in **3** and **4** through the low-energy charge transfer and MLCT excited states.

Electrochemical Properties

Preliminary studies indicated that the present grid-type species, in particular the Co^{II} complexes **2** and **4** present remarkable electrochemical properties, in line with those reported earlier for the related $(Co^{II})_4$ grid bearing no phenyl group on the pyrimidine rings.[12] Thus, for instance, eight successive reductions are observed for **2** at about −0.10, −0.24, −0.45, −0.77, −1.00, −1.22, −1.38, and −1.54 V (in DMF). Similar values are also found for **4**. Detailed investigations are in progress and will be reported together with data on related complexes.

Conclusion

The formation of the four tetrametallic complexes **1**−**4** from the ligands **5** and **6** and Co^{II} and Zn^{II} metal ions with octahedral coordination confirms the generality of the self-assembly of such grid-type architectures. The stacking interactions introduced by the phenyl ring provide high stability to the complexes as well as structural features suitable for their use as components in extended self-organized arrays. The introduction of an electron-donating group on the phenyl ring provides means for modulating the electronic properties of the ligand and therefore the properties of the final complexes. The control which may thus be progressively achieved over both the structural and electronic features of these tetrametallic grid complexes makes them particularly attractive as components in the construction of inorganic architectures for multicellular ion-dot supramolecular devices.

Experimental Section

Materials: Precipitates were isolated by high-speed spinning in a Hettich Universal centrifuge (ca. 3000 rpm, 5 min). − Unless otherwise noted, ^{1}H-NMR spectra were measured in CD_3CN calibrated to the residual solvent peak at 200 MHz with a Bruker AC 200 spectrometer. − Melting points were obtained with a digital Thomas Hoover (Electrotherma) apparatus. − Infrared absorption spectra were recorded on a Perkin−Elmer 1600 series FTIR spectrometer in KBr, an electronic absortion espectra on a Cary 219 spectrometer in CH_3CN with λ_{max} in nm and ε ($\times 10^4$) in M^{-1} cm^{-1}. − Fast atom bombardment (FAB) mass spectrometry was performed on a ZAB-HF VG spectrometer with *m*-nitrobenzyl alcohol as the matrix and electrospray (ES) mass spectra were obtained with a triple quadrupole mass spectrometer Quattro II (Micromass) mass spectrometry. Spectroscopic studies were performed in spectroscopic-grade solvents. − All solvents were reagent-grade and used without further purification.

Complex $(5_4Zn_4)(CF_3SO_3)_8$ (1): To a suspension of 4,6-bis(2′′,2′-bipyrid-6′-yl)-2-phenylpyrimidine[11] (20 mg, 0.043 mmol) in acetonitrile (6 mL) was added zinc triflate (16 mg, 0.043 mmol) and the mixture was stirred at room temperature for 18 h. Diethyl ether was added to the reaction and the precipitate was isolated by centrifugation and purified by recrystallization from acetonitrile/diethyl ether to afford **1** as a white solid (22 mg, 63%). − M.p. > 300 °C. − ^{1}H NMR (400 MHz): δ = 9.57 (s, 1 H, 5-H), 9.17 (d, 2 H, *J* = 6.3 Hz, 5′-H), 8.63 (m, 4 H, 4′-H, 3′-H), 8.25 (d, 2 H, *J* = 8.2 Hz, 3′′-H), 7.92 (t, 2 H, *J* = 7.7 Hz, 4′′-H), 7.10 (dd, 2 H, *J* = 6.5, 5.2 Hz, 5′′-H), 7.00 (t, 1 H, *J* = 7.4 Hz, 3′′′-H^i), 6.87 (t, 1 H, *J* = 7.6 Hz, 4′′′-H), 6.82 (d, 2 H, *J* = 5.2 Hz, 6′′-H), 6.27 (t, 1 H, *J* = 7.6 Hz, 3′′′-H), 5.80 (d, 1 H, *J* = 7.2 Hz, 2′′′-H^i), 7.38 (d, 1 H, *J* = 7.6 Hz, 2′′′-H). − FAB MS; *m*/*z* (%): 3123 (2) [*M* − 149 (− Tf)], 3014 (7) [*M* − 298 (− 2 Tf)], 2863 (8) [*M* − 447 (− 3 Tf)], 2714 (5) [*M* − 596 (−4 Tf)], 2566 (3) [*M* − 745 (−5 Tf)]. − $C_{128}H_{80}F_{24}N_{24}O_{24}S_8Zn_4$ (3312.17): calcd. C 46.42, H 2.43, N 10.15; found C 46.46, H 2.15, N 10.04. − IR (KBr): $\tilde{\nu}$ = 3089, 1600, 1465, 1256, 1162, 1029, 776, 637. − UV/Vis: λ (ε_{max}) = 282 (4.9), 294 (4.2), 358 (7.2), 375 (6.5).

Complex $(5_4Co_4)(BF_4)_8$ (2): To a suspension of 4,6-bis(2′′,2′-bipyrid-6′-yl)-2-phenylpyrimidine[11] (20 mg, 0.043 mmol) in acetonitrile (6 mL) was added cobalt tetrafluoroborate (15 mg, 0.043 mmol) and the mixture was stirred at reflux for 2 d. Diethyl ether was added to the reaction and the precipitate was isolated by centrifugation and purified by recrystallization from acetonitrile/diethyl ether to afford **2** as a slightly brown solid (23 mg, 77%). − M.p. > 300 °C. − FAB MS; *m*/*z* (%): 2701 (20) [*M* − 87 (− BF_4)], 2614 (81) [*M* − 174 (− 2 BF_4)], 2528 (95) [*M* − 261 (− 3 BF_4)], 2441 (48) [*M* − 348 (− 4 BF_4)], 2354 (16) [*M* − 435 (− 5 BF_4)], 1307 (37) [{*M* − 174 (− 2 BF_4)}/2], 1264 (100) [{*M* − 261 (− BF_4)}/2], 1220 (83) [{*M* − 348 (− 4 BF_4)}/2]. − $C_{120}H_{80}B_8Co_4F_{32}N_{24}$ (2788.31): calcd. C 51.69, H 2.89, N 12.06; found C 51.47, H 2.90, N 11.87. − IR (KBr): $\tilde{\nu}$ = 3072, 1600, 1463, 1228, 773, 656. − UV/Vis: λ (ε_{max}) = 279 (1.8), 291 (0.7), 361 (0.9), 371 (0.8), 430 (0.1).

4,6-Dichloro-2-[4′-(dimethylamino)phenyl]pyrimidine (7): To *p*-bromo(dimethylamino)benzene (5 g, 24.988 mmol) in ethyl ether (80 mL) at room temperature under argon was added one equiv. of 1.6 M *n*BuLi in hexane (15.6 mL, 24.988 mmol). The mixture was stirred for 5 min and then cooled at −70 °C. Then, one equiv. of 4,6-dichloropyrimidine (3.7 g, 24.988 mmol) was added. After 1 h 15 min, the temperature of the mixture was allowed to rise to 0 °C, a solution of acetic acid, water, and THF (1.6:0.25:5 mL) was added dropwise, and the mixture was immediately treated with a solution of DDQ (5.9 g, 26 mmol) in THF (25 mL). The solution was stirred at room temperature for 15 min, cooled to 0 °C and a cold 3 M aqueous solution of NaOH (10 mL, 30 mmol) was added followed by water (10 mL) 15 min later. The organic phase was removed and the aqueous layer was extracted with chloroform (5 × 100 mL). The combined organic layers were dried (Na_2SO_4) and the solvent was removed under low pressure. The residue was purified by chromatography on silica gel using hexane/ethyl acetate (6:1) as eluent giving 1.33 g (20% yield) of **7** as yellow needles. − M.p. 174−175 °C. − ^{1}H NMR: δ = 8.29 (d, 2 H, *J* = 8.9 Hz, Ar), 7.06 (s, 1 H, 4-H), 6.71 (d, 2 H, *J* = 8.9 Hz, Ar), 3.07 [s, 6 H, $(CH_3)_2N$]. − ^{13}C NMR: δ = 166.1, 161.5, 153.1, 130.5, 122.2, 116.2, 111.3, 40.1. − EI MS; *m*/*z* (%): 269 (64) [M^+ + 1], 268 (14) [M^+], 267 (100) [M^+ − 1]. − $C_{12}H_{11}Cl_2N_3$ (268.14): calcd. C 53.93, H 4.15, N 15.73; found C 53.65, H 4.05, N 15.71. − IR (KBr): $\tilde{\nu}$ = 3109, 2899, 1609, 1536, 1385, 1190, 1093, 819, 778.

4,6-Bis(2′′,2′-bipyrid-6′-yl)-2-[4′′-(dimethylamino)phenyl]pyrimidine (6): To 4,6-dichloro-2-[4′-(dimethylamino)phenyl]pyrimidine (**7**) (250 mg, 0.9323 mmol), 1.5 equiv. of 6-tributylstannyl-2,2′-

bipyridine[11] (622 mg, 1.3984 mmol) and 10% of tetrakis(triphenylphosphane)palladium (0) (108 mg, 0.0932 mmol) was added toluene (15 mL) and the mixture was refluxed overnight under argon. Then, the solvent was removed under low pressure and the residue was washed with MeOH (10 mL). Without further purification, again 1.5 equiv. of 6-tributylstannyl-2,2′-bipyridine (622 mg, 1.3984 mmol), 10% of tetrakis(triphenylphosphane)palladium(0) (108 mg, 0.0932 mmol), and toluene (15 mL) were added to the solid. The mixture was heated at reflux for 24 h under argon. The solvent was removed and the slurry residue was treated with MeOH (10 mL). The solid was filtered and washed with more MeOH (10 mL) to give 230 mg (53%) of **6** as a yellow solid. − M.p. 302−304 °C (calcination). − ^{1}H NMR: δ = 9.54 (s, 1 H, 5-H), 8.85 (d, 2 H, *J* = 7.9 Hz, 3′′-H), 8.79 (m, 4 H, 6′′-H, Ar), 8.66 (d, 2 H, *J* = 8.9 Hz, 3′-H or 5′-H), 8.59 (d, 2 H, *J* = 7.8 Hz, 3′-H or 5′-H), 8.07 (t, 2 H, *J* = 7.8 Hz, 4′-H), 7.91 (dt, 2 H, *J* = 7.8, 1.8 Hz, 4′′-H), 7.38 (dd, 2 H, *J* = 6.7, 4.9 Hz, 5′′-H) 6.87 (d, 2 H, *J* = 9 Hz, Ar), 3.11 (s, 6 H, 2× CH_3). − ^{13}C NMR: δ = 172.7, 163.9, 158.1, 155.5, 149.2, 137.9, 136.7, 129.7, 129.5, 123.9, 122.7, 122.2, 121.7, 121.3, 121.0, 111.7, 110.1, 40.3. − MS (FAB); *m*/*z*: 508 [M^+ + 1]. − HRMS: $C_{32}H_{26}N_7$: calcd. 508.2250, found: 508.2235. − UV/Vis: λ(ε_{max}) = 284 (10.0), 312 (7.9), 348 (8.4); 402 (0.7). − The reaction was tried in a single step using double amount of reagents but only poor yields were obtained.

Complex $(6_4Zn_4)(CF_3SO_3)_8$ (3): To a suspension of 4,6-bis(2′′,2′-bipyrid-6′-yl)-2-[4′′-(dimethylamino)phenyl]pyrimidine (**6**) (20 mg, 0.039 mmol) in acetonitrile (8 mL) was added zinc triflate (14 mg, 0.039 mmol) and the mixture was refluxed for 48 h under argon. The solvent was removed under low pressure and the solid recrystallized from acetonitrile/diethyl ether to afford **3** as a deep red solid (27 mg, 79%). − M.p. > 300 °C. − ^{1}H NMR (300 MHz): δ = 9.67 (s, 1 H, 5-H), 9.29 (d, 2 H, *J* = 7.4 Hz, 5′-H), 8.61 (d, 2 H, *J* = 7.5 Hz, 3′-H), 8.54 (t, 2 H, *J* = 8.1 Hz, 4′-H), 8.27 (d, 2 H, *J* = 8.2 Hz, 3′′-H), 7.90 (dt, 2 H, *J* = 7.8, 1.6 Hz, 4′′-H), 7.09 (dd, 2 H, *J* = 7.6, 6.1, 5′′-H), 6.86 (d, 2 H, *J* = 5.2 Hz, 6′′-H), 5.49 (S_b, 2 H, 2′′-H^i, 3′′′-H^i), 5.34 (d, 1 H, *J* = 9.0 Hz, 2′′′-H), 4.96 (d, 1 H, *J* = 8.0 Hz, 3′′′-H), 3.07 (S_b, 6 H, 2 × CH_3). − ES MS; *m*/*z*: 1593.7 [M − 298 (− 2 Tf)], 1012.6 [M − 447 (− 3 Tf)], 720 [M − 596 (− 4 Tf)]. − $C_{136}H_{100}F_{24}N_{28}0_{24}S_8Zn_4$ (3484.45): calcd. C 46.88, H 2.89, N 11.26; found C 47.12, H 3.06, N 11.00. − UV/Vis: λ(ε_{max}) = 261 (1.3), 282 (0.9), 295 (0.8), 357 (1.3), 371 (1.3), 516 (5.5).

Complex $(6_4Co_4)(CF_3SO_3)_8$ (4): To a suspension of 4,6-bis(2′′,2′-bipyrid-6′-yl)-2-[4′′-(dimethylamino)phenyl]pyrimidine (**6**) (10 mg, 0.0197 mmol) in acetonitrile (5 mL) was added cobalt triflate tetrakis(DMSO) (16 mg, 0.0197 mmol) and the mixture was refluxed for 48 h under argon. The solvent was removed under low pressure and the solid recrystallized from acetonitrile/diethyl ether to afford **4** as a dark solid (10 mg, 60%). − M.p. > 300 °C. − FAB MS; *m*/*z* (%): 3309.7 (4) [M − 149 (− Tf)], 3159.4 (9) [M − 298 (− 2 Tf)], 3010.5 (7) [M − 447 (− 3 Tf)], 2861.6 (3) [M − 596 (− 4 Tf)], 2713.5 (1) [M − 745(− 5 Tf)]. − $C_{136}H_{100}Co_4F_{24}N_{28}O_{24}S_8$ (3458.66): calcd. C 47.23, H 2.91, N 11.34; found C 47.49, H 2.62, N 11.31. − UV/Vis: λ(ε_{max}) = 267 (19.8), 292 (13.2), 365 (18.5), 532 (1.1).

Crystal Structure Determinations: The measurements were carried out with a STOE-IPDS diffractometer with graphit-monochromatized Mo-K_α radiation. Table 3 summarizes the crystal data, data collection, and refinement parameters. All calculations were performed with the SHELX-97 package.[24] All structures were solved by direct methods and were refined by full-matrix least squares based on F^2. All hydrogen atoms, disordered anions and solvent molecules with an occupation factor less than 1.0 were refined isotropically. All of the C−H hydrogen atoms in all structures were placed in calculated positions with U(H) = 1.5U_{eq}(C) for methyl groups and U(H) = 1.2U_{eq}(C) for all other. Molecular graphics performed with SCHAKAL96.[25] Single crystals of the complexes were obtained by slow vapor diffusion of diethyl ether into aceto-

Table 3. Crystal data and structure refinement for complexes **1** and **2**

	Complex **1**	Complex **2**
Empirical formula	$C_{120}H_{80}N_{24}Zn_4{\cdot}(SO_3CF_3)_8{\cdot}(MeCN)_{4.5}$	$C_{120}H_{80}N_{24}Co_4{\cdot}8BF_4{\cdot}13.5MeCN{\cdot}0.75Et_2O{\cdot}0.5H_2O$
M_r [g mol^{-1}]	3496.86	3407.10
T [K]	198(1)	200(1)
Wavelength [Å]	0.71073	0.71073
Crystal system	monoclinic	triclinic
Space group	*C*2/*c*	*P*1bar
a [Å]	53.751(11)	18.118(4)
b [Å]	20.281(4)	27.476(6)
c [Å]	30.748(6)	32.602(7)
α [°]	90	97.54(3)
β [°]	120.02(3)	100.33(3)
γ [°]	90	98.03(3)
Volume [Å]	29023(10)	15605(5)
Z	8	4
$\rho_{calcd.}$ [g cm^{-3}]	1.601	1.45
μ(Mo-K_α [mm^{-1}]	0.879	0.521
F(000)	14168	6950
Crystal size [mm]	0.20 × 0.15 × 0.10	0.30 × 0.20 × 0.20
Θ [°]	2.05 − 25.05	1.87−25.07
Index ranges	$-63 \le h \le 54$, $-24 \le k \le 24$, $-29 \le l \le 36$	$-21 \le h \le 21$, $-31 \le k \le 32$, $-38 \le l \le 33$
Reflections collected	58633	76177
R(int)	0.0430	0.0581
Independent reflections	24149	49669
Data/restraints/parameters	24149/885/2140	49669/2350/4262
GoF *S*	1.382	1.023
Final *R* indices [$I > 2\sigma(I)$]	R_1 = 0.0678, wR_2 = 0.1845	R_1 = 0.0761, wR_2 = 0.2159
R indices (all data)	R_1 = 0.0884, wR_2 = 0.1955	R_1 = 0.0945, wR_2 = 0.2346
Largest diff. peak/hole [eÅ^{-3}]	1.637/−1.208	1.745/−0.807

nitrile solutions. The Zn^{II} complex **1** crystallized with several acetonitrile molecules. The dark brown crystals of the Co^{II} complex **2** contained several solvent molecules (CH_3CN, Et_2O, and H_2O). Crystallographic data (excluding structure factors) for the structures of complexes **1** and **2** have been deposited with the Cambridge Crystallographic Data Centre as supplementary publication no. CCDC-120674 for **1** and -120673 for **2**. Copies of the data can be obtained free of charge on application to CCDC, 12 Union Road, Cambridge CB2 1EZ, UK [Fax: + 44-1223/336-033; E-mail: deposit@ccdc.cam.ac.uk].

Acknowledgments

We thank the French Goverment (J. R.) and the Ministerio de Educación y Ciencia (Spain) (F. J. R. S.) for postdoctoral fellowships. We also thank Hélène Nierengarten and Emmanuelle Leize for the ESMS determinations, Patrick Maltèse for the NOESY NMR experiments, and Mario Ruben for some spectroscopic measurements.

[1] *Comprehensive Supramolecular Chemistry* (Eds.: J. L. Atwood, J. E. D. Davies, D. D. MacNicol, F. Vögtle, J.-M. Lehn), Pergamon, Oxford, **1996**; P. N. W. Baxter, vol. 9, pp. 166−211; E. C. Constable, vol. 9, pp. 213−252; M. Fujita, vol. 9 pp. 254−282.
[2] E. C. Constable, *Progress in Inorganic Chemistry* (Ed.: K. D. Karlin), John Wiley and Sons, New York, **1994**, vol. 42, pp. 67−138.
[3] J.-M. Lehn, *Supramolecular Chemistry: Concepts and Perspectives*, VCH, Weinheim, **1995**, chapter 9.
[4] P. N. W. Baxter, J.-M. Lehn, J. Fischer, M.-T. Youinou, *Angew. Chem.* **1994**, *106*, 2432; *Angew. Chem. Int. Ed. Engl.* **1994**, *33*, 2284.
[5] B. Hasenknopf, J.-M. Lehn, B. O. Kneisel, G. Baum, D. Fenske, *Angew. Chem.* **1996**, *108*, 1987; *Angew. Chem. Int. Ed. Engl.* **1996**, *36*, 1838.
[6] P. N. W. Baxter, G. S. Hanan, J.-M. Lehn, *J. Chem. Soc., Chem. Commun.* **1996**, 2019.
[7] B. Hasenknopf, J.-M. Lehn, G. Baum, D. Fenske, *Proc. Natl. Acad. Sci. USA* **1996**, *93*, 1397
[8] B. Hasenknopf, J.-M. Lehn, N. Boumediene, A. Dupont-Gervais, A. Van Dorsselaer, B. Kneisel, D. Fenske, *J. Am. Chem. Soc.* **1997**, *119*, 10956.
[9] D. P. Funeriu, J.-M. Lehn, G. Baum, D. Fenske, *Chem. Eur. J.* **1997**, *3*, 99.
[10] E. C. Constable, A. M. W. Cargill-Thompson, P. Harveson, L. Macko, M. Zehnder, *Chem. Eur. J.* **1995**, *1*, 360.
[11] G. S. Hanan, U. S. Schubert, D. Volkmer, E. Rivière, J.-M. Lehn, N. Kyritsakas, J. Fischer, *Can. J. Chem.* **1997**, *75*, 169.
[12] G. S. Hanan, D. Volkmer, U. S. Schubert, J.-M. Lehn, G. Baum, D. Fenske, *Angew. Chem.* **1997**, *109*, 1929; *Angew. Chem. Int. Ed. Engl.* **1997**, *36*, 1842.
[13] O. Waldmann, J. Hassmann, P. Müller, G. S. Hanan, D. Volkmer, U. S. Schubert, J.-M. Lehn, *Phys. Rev. Lett.* **1997**, *78*, 3390.
[14] I. Weissbuch, P. N. W. Baxter, S. Cohen, K. Kjaer, P. B. Howes, J. Als-Nielsen, G. S. Hanan, U. S. Schubert, J.-M. Lehn, L. Leiserowitz, M. Lahav, *J. Am. Chem. Soc.* **1998**, *120*, 4850.
[15] G. S. Hanan, C. R. Arana, J.-M. Lehn, G. Baum, D. Fenske, *Chem. Eur. J.* **1996**, *2*, 1292.
[16] G. S. Hanan, J.-M. Lehn, N. Kyritsakas, J. Fischer, *J. Chem. Soc., Chem. Commun.* **1995**, 765.
[17] D. M. Bassani, J.-M. Lehn, G. Baum, D. Fenske, *Angew. Chem.* **1997**, *109*, 1931; *Angew. Chem. Int. Ed. Engl.* **1997**, *36*, 1845; D. M. Bassani, J.-M. Lehn, *Bull. Soc. Chim. Fr.* **1997**, *134*, 897.
[18] J.-P. Kintzinger, P. Maltèse, J. Rojo, F. J. Romero-Salguero, J.-M. Lehn, to be published.
[19] H. Günther, *NMR-Spektroskopie*, Georg Thieme Verlag, Stuttgart, **1973**.
[20] J. Rojo, F. J. Romero-Salguero, J.-L. Lehn, unpublished results.
[21] Related species gave emission quantum yields of $< 1.10^{-3}$ and 0.11 for the ligand and the Zn^{II}_4 grid complex, respectively: I. Manet, V. Balzani, D. Volkmer, J.-M. Lehn, unpublished results.
[22] See for example: N. Armoroli, L. De Cola, V. Balzani, J.-P. Sauvage, C. O. Dietrich-Buchecker, J.-M. Kern, A. Bailal *J. Chem. Soc., Dalton Trans.* **1993**, 3241.
[23] Quantum-dot cells, each with four dots of [2 × 2] grid-type, have been used in the realization of multicellular automata: A. O Orlov, I. Ambani, G. H. Bernstein, C. S. Lent, G. L. Snider, *Science* **1997**, *277*, 928; J. Glanz, *Science* **1997**, *277*, 898.
[24] G.M. Sheldrick, *SHELX-97*, University of Göttingen, Germany, **1997**.
[25] E. Keller, *SCHAKAL97*, University of Freiburg, Germany, **1997**.

Received March 8, 1999
[I99090]

A Tetranuclear Platinum Compound Designed to Overcome Cisplatin Resistance

Bart A. J. Jansen,[a] Judith van der Zwan,[a] Jan Reedijk,*[a] Hans den Dulk,[b] and Jaap Brouwer[b]

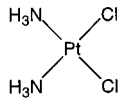
Keywords: Antitumor drugs / Platinum / DNA / Dendrimers / L1210 Mouse leukemia

The synthesis and characterisation of the first generation of a poly(propyleneimine) dendrimer DAB(PA)$_4$, substituted with four *trans*-diamminechloroplatinum moieties is reported. The compound DAB(PA-tPt-Cl)$_4$ was designed to overcome two problems often associated with cisplatin resistance in cancer cells: (i) deactivation of the platinum species by intracellular thiolates and (ii) improved repair of crosslinks with DNA. The four-armed molecule can be expected to form crosslinks with DNA that are very different from the adducts formed by cisplatin. Also, the tetranuclear compound has four leaving groups, while cisplatin has only two. Therefore, DAB(PA-tPt-Cl)$_4$ would be less susceptible towards inactivation by reaction with intracellular thiolates. A reaction with an excess of the model nucleobase guanosine 5′-monophosphate (GMP) confirmed that the tetranuclear compound is capable of binding a maximum of four nucleobases. Therefore, the inactivation of one or two arms would still leave the molecule with enough reactivity to form crosslinks with DNA. Cytotoxicity tests were performed on two mouse leukemia L1210 cell lines, both sensitive and resistant towards cisplatin, and in seven human tumor cell lines. In all cell lines, the tetranuclear compound showed a low cytotoxicity. It is suggested that the low activity is related to the structure of the compound. Probably the high charge (+6) at physiological pH and its branched structure hamper the molecule in crossing the cell membranes.

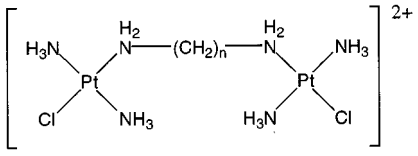
Introduction

Since the discovery of cisplatin as antitumor drug, much effort has been undertaken to find new platinum compounds applicable as a drug against cancer.[1−3] One of the main objectives in platinum antitumor chemistry is to find compounds with activity against cancer cells having intrinsic or acquired resistance against cisplatin.[3] It is now generally accepted that the antitumor activity of cisplatin stems from the complex events that occur after its binding to DNA.[1−3] Known mechanisms for cisplatin resistance include improved recognition of DNA adducts by DNA repair mechanisms, decreased drug accumulation in the cell (due to decreased influx) and increased intracellular levels of the heavy-metal scavengers glutathione (GSH) and metallothionein (MT).[4−6]

Many derivatives with structures similar to cisplatin were found to be cross resistant with cisplatin. One approach to overcome cisplatin resistance is the preparation of drugs that bind to DNA in a structurally different way compared to cisplatin.[1] In this respect, the dinuclear 1,1/t,t platinum complexes,[7][8] with the general formula [{*trans*-PtCl(NH$_3$)$_2$}μ-{NH$_2$(CH$_2$)$_n$NH$_2$}](NO$_3$)$_2$ (n = 4, 6), are very interesting (Scheme 1). These compounds consist of two monofunctional [PtCl(NH$_3$)$_2$] moieties connected by a flexible diamine linker. This type of compounds was found to be active against cisplatin resistant cancers in vivo.[8] The striking difference in DNA binding behavior of such compounds is illustrated by the hairpin structure of an interstrand adduct of 1,1/t,t (n = 4) with a dsDNA octamer.[9] Binding of cisplatin to DNA is mainly restricted to intrastrand crosslinks between adjacent purine bases, with only 5−10% interstrand crosslinks.[10][11] In contrast, the number of interstrand crosslinks is reported to be much larger (50%) for dinuclear platinum compounds.[12]



Cisplatin



1,1/t,t (n=4, 6)

Scheme 1. Cisplatin and a dinuclear compound of the 1,1/t,t type

Recently, the diaminoalkyl linker was replaced by the naturally occurring polyamines spermine and spermidine.[13] The protonated, noncoordinating secondary amines in these molecules may have an additional interaction with

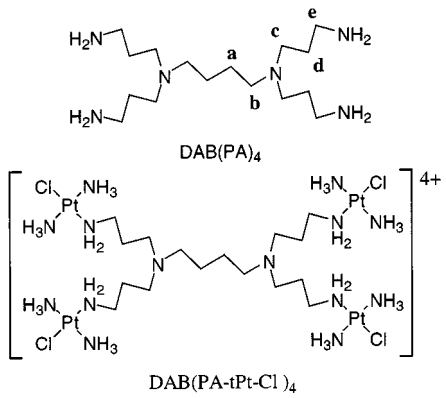
[a] Leiden Institute of Chemistry, Gorlaeus Laboratories, Leiden University,
P. O. Box 9502, NL-2300 RA Leiden, Netherlands
Fax: (internat.) +31 715274451
E-mail: reedijk@chem.leidenuniv.nl
[b] Molecular Genetics, Leiden Institute of Chemistry, Gorlaeus Laboratories, Leiden University,
P. O. Box 9502, NL-2300 RA Leiden, Netherlands

 © WILEY-VCH Verlag GmbH, D-69451 Weinheim, 1999 1434−1948/99/0909−1429 $ 17.50+.50/0

DNA by hydrogen bonding and electrostatic interaction. At the moment, the most promising variation appears to be the bifunctional trinuclear compound BBR 3464 [μ-*trans*-$Pt(NH_3)_2\{transPtCl(NH_3)_2[NH_2(CH_2)_6NH_2]\}_2](NO_3)_4$.[14][15] This cationic compound can be seen as a linear molecule with two ends capable of DNA binding, and a central platinum moiety that is restricted to noncovalent interactions. BBR 3464, with a total charge of +4, has now entered clinical trials.[14]

It has been suggested that the increased number of interstrand crosslinks is the reason for the high activity of dinuclear compounds against cisplatin-resistant cell lines.[12] From this point of view, it is interesting to investigate variatons on the dinuclear 1,1/t,t compounds with a number of DNA-binding moieties higher than two. One way to obtain more DNA-binding moieties is to increase the number of platinated "arms". A dinuclear molecule may be considered as having two arms. Statistically, additional arms should increase the number of interstrand adducts formed compared to dinuclear compounds. An additional advantage of this type of compound could be that after deactivation of one, or even two, of its arms by GSH or MT, the molecule still retains enough active arms left to form a bifunctional adduct with DNA.

In this paper, the synthesis and characterisation is reported of a novel tetranuclear platinum compound $DAB(PA\text{-}tPt\text{-}Cl)_4$ based on the first generation of the commercially available butanediamine poly(propyleneimine) dendrimer $DAB(PA)_4$ (Scheme 2). This first generation dendrimer provides four amine end-groups that can be functionalized by platinum. The structure was characterized by ^{195}Pt NMR, elemental analysis, and a pH titration followed by ^1H NMR spectroscopy. The reactivity of the platinated arms towards DNA was checked by a test reaction with guanosine monophosphate (GMP), monitored by ^1H NMR. The in vitro cytotoxicity was tested on L1210 mouse leukemia cell lines, including cell lines resistant towards cisplatin. As a reference, cisplatin was tested as well.



Scheme 2. The first generation poly(propyleneimine) dendrimer $DAB(PA)_4$, and the tetranuclear platinum complex $DAB(PA\text{-}tPt\text{-}Cl)_4$

Results and Discussion

Synthesis and Characterisation

For the preparation of the dendritic platinum complex $DAB(PA\text{-}tPt\text{-}Cl)_4$, a variation on the common synthesis of dinuclear compounds was applied.[16] The polyamine was reacted with an excess of the monoactivated solvent species *trans*-$[PtCl(NH_3)_2(dmf)]NO_3$. The chloride salt of the tetranuclear complex was obtained by quenching the reaction with an excess of LiCl. The excess of LiCl is later removed by extraction with ethanol or methanol. *trans*-$[PtCl_2(NH_3)_2]$ is easily separated from the product, while it has a low solubility in water, in contrast to $(PA\text{-}tPt\text{-}Cl)_4$.

^{195}Pt shows a single signal at $\delta = -2425$, which is identical to that of the $[PtClN_3]$ coordination sphere found for the dinuclear 1,1/t,t compounds.[17] The two tertiary amine atoms present in $DAB(PA)_4$ are potential coordination sites for platinum, although they are poorer donors than the four primary amines. In order to confirm the coordination site, pH titrations of the complex and the free ligand were followed by ^1H NMR spectroscopy (Figure 1). The spectrum shows shifted peaks and a different pH dependence compared to the free ligand.

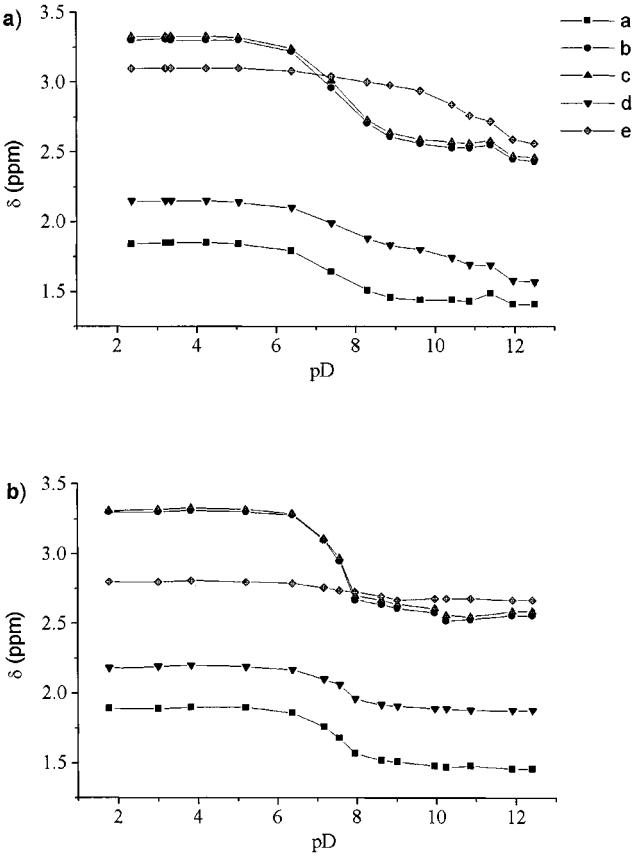


Figure 1. Titration curves of the proton signals of a) the ligand $DAB(PA)_4$ and b) the platinum complex $DAB(PA\text{-}tPt\text{-}Cl)_4$

The titration curve of $DAB(PA)_4$ is in general agreement with the data recently determined for this compound using natural abundant ^{15}N spectroscopy.[18] Upon lowering the

pH, first the primary and then the tertiary nitrogens are protonated. The protons shifted most upfield show only small pH dependence and are identified as protons **a** and **d** (Scheme 2). Protons **b** and **c** show overlapping signals at all pH values, and are identified by their total integral value of 12 protons. The remaining peak is assigned to **e**. The assignment was confirmed by a [^{1}H,^{1}H] COSY NMR experiment. Metalation should protect the amines from protonation. In the titration of the complex, pH dependence of the shift of proton **e** is only marginal compared to its behavior in the free ligand. In contrast protons **b** and **c** show a strong pH dependence in both titrations. This allows the conclusion that platinum is coordinated at the primary amines. At physiological pH, the tertiary amines are hydronated, thus giving the molecule a total charge of +6. This high positive charge is likely to give strong coulomb interactions with a polyanion like DNA.

Reaction with GMP, a Model Nucleobase

The coordination of DAB(PA-tPt-Cl)$_4$ with the model nucleobase guanine-5′-monophosphate (GMP) was studied by ^{1}H NMR spectroscopy. The reaction was performed in D_2O at 313 K, with a molar ratio of 5:1 ([GMP]:[DAB(PA-tPt-Cl)$_4$]). Results are summarized in Table 1. Signals of a platinated product appeared immediately after mixing the two compounds. After four days the reaction was judged to be complete. The single signal in ^{195}Pt NMR at $\delta = -2560$ proves that all platinum has reacted. Also, the ratios of platinated and free GMP were found constant. This ratio was determined from the integral values of the GMP H8 signals at $\delta = 8.05$ (H8, free) and $\delta = 8.72$ (H8*, platinated). The ratio of the integral values of H1′ at $\delta = 5.87$ and of H1′* at $\delta = 5.96$ was constant as well.

Table 1. NMR Data for the complexation of DAB(PA-tPt-Cl)$_4$ with GMP

	δH8	δH1′	$J_{1'-2'}$ (Hz)	δ^{195}Pt
GMP	8.05	5.87	5.7 (d)	–
DAB(PA-tPt-GMP)$_4$	8.72	5.96	3.6 (d)	−2560
DAB(PA-tPt-Cl)$_4$	–	–	–	−2425

The values of H8* and H1′* are indicative of platination at N7. Also, the decrease in the coupling constant $J_{1'-2'}$ agrees with that observed before in the reaction of dinuclear 1,1/t,t compounds with GMP.[17] The ^{195}Pt value of the GMP adduct lies near the values for dinuclear compounds as well. Apparently all four arms of the tetranuclear compound are available for binding to DNA. The binding of each separate arm is comparable to that of the ends of dinuclear 1,1/t,t compounds. However, the actual number of "arms" binding to DNA may be smaller in cells due to partial inactivation by binding to other cellular targets like GSH. This illustrates a feature of tetrafunctional compounds that might be advantageous compared to bifunctional compounds like cisplatin or the 1,1/t,t compounds. The tetrafunctional compound is still able to form crosslinks with DNA even after two of its functional groups are deactivated.

Biological Activity

Cisplatin and the tetranuclear compound DAB(PA-tPt-Cl)$_4$ were tested on L1210/0 mouse leukemia cells, and on the cisplatin resistant L1210/2 cell line. These cell lines are described in literature.[19][20] The drug concentrations at 50% growth inhibition (IC_{50}) are presented in Table 2. As expected, cisplatin was found to be cytotoxic against the L1210/0 cells, and less cytotoxic in the resistant lines. The found IC_{50} values are comparable to literature.[19][20] The resistance factor (rf, IC_{50} for the resistant cell line divided by the IC_{50} for the sensitive cells) was found to be 3.1. In contrast, the tetranuclear compound appeared to be equally toxic in L1210/0 and L1210/2 (rf = 0.8). However, the cytotoxicity of DAB(PA-tPt-Cl)$_4$ was low compared to cisplatin in both cell lines.

Table 2. IC_{50} values obtained in cisplatin-sensitive L1010/0 mouse leukemia cells (A) and the resistant L1210/2 cell line (B). Resistance factors (*rf*) for cisplatin and DAB(PA)$_4$ were calculated (*rf* = B/A)

	IC_{50} (μM) L1210/0 (A)	Resistance factor L1210/2 (B)	*rf* = B/A
DAB(PA-tPt-Cl)$_4$	12.4	9.3	0.8
cisplatin	1.5	4.6	3.1

DAB(PA-tPt-Cl)$_4$ was also tested in 7 human tumor cell lines. IC_{50} values are shown in Table 3. The tetranuclear compound showed a low cytotoxicity in all cell lines, which is in accordance with the results in L1210 mouse leukemia. In some cell lines, the IC_{50} value could not be determined because it was out of the used concentration range. In the other cases, the IC_{50} value of DAB(PA-tPt-Cl)$_4$ was found 13−20 times higher than that of cisplatin.

Conclusion

The results in this paper show that it is possible to functionalize the four amino endgroups of the first generation of a poly(propyleneimine) dendrimer DAB(PA)$_4$ selectively with *trans*-diamminechloroplatinum moieties in high yield. The tetranuclear platinum compound DAB(PA-tPt-Cl)$_4$ is able to bind four molecules of GMP at their N7 positions. The arms of the tetranuclear compound are capable of binding GMP in a way similar to the ends of dinuclear 1,1/t,t compounds. The compound shows low cytotoxicity towards L1210/0 and L1210/2 mouse leukemia cell lines and seven human tumor cell lines. The low cytotoxicity may as well be caused by transport problems across the cell membranes the compound has to pass to reach DNA. The high charge (+6 at neutral or acidic pH) in combination with the branched structure may cause these problems. The high charge makes diffusion through the apolar membrane un-

Table 3. IC_{50} values determined in seven human tumor cell lines using the microculture sulforhodamine B (SRB) test

	IC_{50} (μM) MCF7	EVSA-T	WIDR	IGROV	M19	A498	H226
DAB(PA-tPt-Cl)$_4$	30.9	26.7	> 40	8.9	26.2	> 40	> 40
cisplatin	2.3	1.4	3.2	0.6	1.9	7.5	10.9

likely. However, the efficient uptake of the trinuclear compound BBR 3464 (with a charge of +4) in L1210 cells[15] shows that a high charge does not necessarily hamper the influx of a compound. In literature it has been suggested that charged linear dinuclear compounds may enter the cell through the same gates and channels as the structurally related polyamines spermine and spermidine.[1] Such gates may be unable to accommodate transport of a compound with a branched structure such as DAB(PA-tPt-Cl)$_4$.

In order to establish a structure-activity relationship, we are currently preparing a family of di- and polynuclear platinum compounds. It would be interesting to study their cellular uptake and cytotoxicity, related to their charge and structure. This should improve our insight into the mechanism of action of this new class of platinum compounds.

The authors are indebted to the EU for a grant as Host Institute in the EU programme Human Capital and Mobility. Also support and sponsorship by COST Action D8/00097/97 (biocoordination chemistry) is kindly acknowledged. The authors wish to thank Johnson & Matthey (Reading, UK) for their generous loan of K_2PtCl_4. This work has been performed under auspices of the joint BIOMAC Research Graduate School of Leiden University and Delft University of Technology.

Experimental Section

General Remarks: The complex *trans*-[$PtCl_2(NH_3)_2$] was prepared according to literature procedures[20] from K_2PtCl_4. K_2PtCl_4 was obtained from Johnson & Matthey (Reading, UK). Other chemicals were obtained from Aldrich and were used without further purification.

Titrations were carried out in D_2O. The pH was adjusted by adding trace amounts of 1 M DCl and NaOD to the NMR solutions. pH Measurements were carried out with a Radiometer PHM 80 pH meter, using a Hamilton combination glass electrode. The pH was corrected for the deuterium isotope effect by adding 0.4 units to the display readout. − NMR spectra were taken on a Bruker DPX 300 spectrometer with a 5-mm multi-nucleus probe. Temperature was kept constant by a variable temperature unit. ^{1}H NMR spectra were determined with respect to external TMS. ^{195}Pt spectra were calibrated by using K_2PtCl_4 as an external reference at δ = −1614.

Syntheses

[DAB(PA-*trans*-Pt(NH_3)$_2$Cl]Cl_4 (DAB(PA-tPt-Cl)$_4$): This synthesis was based on literature procedures for the preparation of dinuclear 1,1/t,t compounds.[16] *trans*-$PtCl_2(NH_3)_2$ (0.70 g, 2.3 mmol) was activated by treatment with $AgNO_3$ (0.30 g, 2.3 mmol) in 13 mL of DMF. After stirring overnight in the dark, AgCl was removed by filtration. A solution of the ligand DAB(PA)$_4$ (0.16 g, 0.5 mmol) in 1 mL of DMF was added dropwise and the reaction mixture was stirred at 40°C in the dark. After 16 hours the reaction was quenched with a tenfold excess of LiCl. DMF was removed in vacuo, and the remaining yellow gel was treated with small portions of warm EtOH to remove LiCl. Unreacted *trans*-$PtCl_2(NH_3)_2$ was removed by adding a minimum amount of cold water, after which the remaining yellow solid was filtered off. Lyophilization of the solution yields an off-white solid (564 mg, 0.37 mmol, yield 90%). In some batches, small amounts of a brown sticky material developed after standing at room temperature for several weeks. This problem could be circumvented by storage at −20°C. More pure product has been obtained by repeated washing of the crude material with MeOH and warm EtOH. Mixing of the remaining solid with water, followed by filtration of the solution and lyophilization results in a white powder (0.13 g, 0.09 mmol, yield 17%). Analysis: ^{1}H NMR (D_2O, pD = 12) δ (ppm) = 2.67 (t (J = 7.2 Hz), 8 H, e), 2.60−2.45 (m, 12 H, b+c), 1.88 (m, 8 H, d), 1.46 (s, 4 H, a); ^{195}Pt NMR (D_2O): δ (ppm) = −2425; calculated for $C_{16}H_{64}N_{14}Cl_8Pt_4$ (1516.72): C 12.67, H 4.25, N 12.93; found C 12.92, H 4.29, N 12.04. Although the nitrogen analysis is slightly lower (7%) than calculated, only one signal was observed in ^{195}Pt NMR. Therefore it is concluded that the impurity is unlikely to be a platinum compound interfering in the cytotoxicity tests.

Cytotoxic Studies

Cytoxicity assays in L1210 cell lines were based on literature procedures.[19][20] The cell lines L1210/0 and L1210/2 were cultured in McCoy's 5a medium supplemented with 10% fetal calf serum(Gibco, Paisley, Scotland), penicillin (100 units/ml: Duchefa, Netherlands) and streptomycin (100μg/ml: Duchefa, Netherlands). During growth, the cells grew partly in suspension and partly weakly adherent to the flasks. The cytotoxicity of cisplatin and DAB(PA-tPt-Cl)$_4$ were determined by measuring the inhibition of cell growth (cell growth assay, CGA). For the CGA, cells (5×10^4/mL) were pre-cultured in 24 multi-well plates for 24 h at 37°C in an incubator with 5% CO_2 and subsequently treated with at least three different concentrations of cisplatin (0−16 μM) or DAB(PA-tPt-Cl)$_4$ (0−66 μM) for 3 days. Cell numbers were determined with a counting chamber. Each platinum concentration was tested in at least two independent experiments.

In vitro cytotoxicity assays in human tumor cell lines were performed at the Dr. Daniel den Hoed Kliniek (Rotterdam Cancer Institute), Department of Medical Oncology (Rotterdam, the Netherlands). The seven well-characterized cell lines used were MCF7 and EVSA-T (breast cancer), WIDR (colon cancer), IGROV (ovarian cancer), M19 (melanoma), A498 (renal cancer) and H226 (nonsmall cell lung cancer). ID_{50} values were determined using the microculture sulforhodamine B test (SRB).[22]

[1] T. W. Hambley, *Coord. Chem. Rev.* **1997**, *166*, 181−223.
[2] M. J. Bloemink, J. Reedijk, *Metal Ions Biol. Syst.* **1996**, *32*, 641−685.
[3] J. Reedijk, *Chem. Commun.* **1996**, 801−806.
[4] S. G. Chaney, A. Sancar, *J. Nat. Cancer Inst.* **1996**, *88(19)*, 1346−1360.
[5] G. Chu, *J. Biol. Chem.* **1994**, *269(2)*, 787−790.
[6] D. P. Gately, S. B. Howell, *Br. J. Cancer* **1993**, *67*, 1171.
[7] N. Farrell, Y. Qu, L. Feng, B. Van Houten, *Biochemistry* **1990**, *29*, 9522.
[8] N. Farrell, *Cancer Invest.* **1993**, *11(5)*, 578−589.
[9] D. Yang, S. S. G. E. van Boom, J. Reedijk, J. H. van Boom, N. Farrell, A. H.-J. Wang, *Nature Struct. Biol.* **1995**, *2(7)*, 577−585.
[10] A. M. Fichtinger-Schepman, J. L. van der Veer, J. H. den Hartog, P. H. Lohman, J. Reedijk, *Biochemistry* **1985**, *24*, 707−713.
[11] A. Eastman, *Biochemistry* **1986**, *25*, 3912−3915.
[12] Y. Qu, N. Farrell, *J. Inorg. Biochem.* **1990**, *40*, 255.
[13] H. Rauter, R. Di Domenico, E. Menta, A. Oliva, Y. Qu, N. Farrell, *Inorg. Chem.* **1997**, *36*, 3919−3927.
[14] N. Farrell, E. Menta, M. Valsecchi, R. Di Domenico, G. Da Re, C. Manzotti, G. Pezzoni, F. C. Giuliani, S. Spinelli, *J. Inorg. Biochem.* **1997**, *67*, 173 (abstract).
[15] P. Di Blasi, A. Bernareggi, G. Beggiolin, L. Piazzoni, E. Menta, A. L. Formento, *Anticancer Res.* **1998**, *18*, 3113−3118.
[16] Y. Qu, N. Farrell, *Inorg. Chem.* **1992**, *31*, 930−932.
[17] Y. Qu, N. Farrell, *J. Am. Chem. Soc.* **1991**, *113*, 4851−4857.
[18] G. J. M. Koper, M. H. P. van Genderen, C. Elissen-Román, M. W. P. L. Baars, E. W. Meijer, M. Borkovec, *J. Am. Chem. Soc.* **1997**, *119*, 6512−6521.
[19] F. A. Blommaert, B. G. J. Floot, H. C. M. van Dijk-Knijnenburg, F. Berends, R. A. Baan, J. H. Schornagel, L. den Engelse, A. M. J. Fichtinger-Schepman, *Chemico-Biol. Interactions* **1998**, *108*, 209−225.
[20] A. Eastman, N. Schulte, *Biochemistry* **1988**, *27*, 275−280.
[21] G. B. Kaufman, D. O. Cowan, *Inorg. Synth.* **1963**, *7*, 239.
[22] Y. P. Kepers, G. J. Peters, J. Van Ark-Otte, B. Winograd, H. M. Pinedo, *Eur. J. Cancer* **1991**, *27*, 897−900.

Received March 4, 1999
[I99083]

Enantioselective Organic Syntheses Using Chiral Transition Metal Complexes, 8[+] Chiral Rhenium Complexes of Functionalized Thioaldehydes

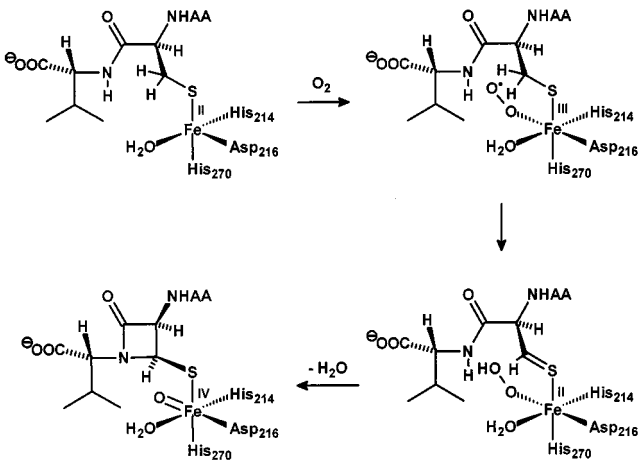
Nicolai Burzlaff[a] and Wolfdieter A. Schenk*[a]

Dedicated to Professor Helmut Werner on the occasion of his 65th birthday

Keywords: Captopril / Cysteine / Rhenium / S ligands / Thioaldehydes

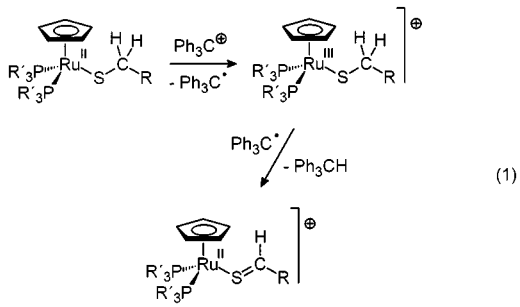
Chiral racemic rhenium thioaldehyde complexes [CpRe(NO)(PPh$_3$)(η^2-S=CHR)]PF$_6$ (**2a–g**) bearing functionalized aliphatic groups R [R = CH$_2$Ph (**a**), COOEt (**b**), CH$_2$COOMe (**c**), CH$_2$C(O)NHCH$_2$Ph (**d**), (*R*)-CH(NC$_8$H$_4$O$_2$)COOMe (**e**), (*S*,*S*)-CH(Me)C(O)NC$_4$H$_7$COOMe (**f**), C$_4$H$_3$O (**g**)] have been obtained by hydride abstraction from the corresponding thiolate complexes [CpRe(NO)(PPh$_3$)(SCH$_2$R)] (**1a–g**). With the exception of **2b**, only single stereoisomers with *like* configurations at rhenium and the thioaldehyde carbon atom were obtained. In some cases, the corresponding sulfinate complexes [CpRe(NO)(PPh$_3$)(SO$_2$CH$_2$R)] (**3d–f**) were formed as by-products. The analogous toluenesulfinate complex [CpRe(NO)(PPh$_3$){SO$_2$(4-C$_6$H$_4$CH$_3$)}] (**3a**) has been prepared from [CpRe(NO)(PPh$_3$)(THF)]BF$_4$ (**8**), and the structure of **3e** has been determined by X-ray crystallography. The use of phosphorus ligands other than PPh$_3$ was briefly explored with the synthesis of [CpRe(NO)(PR′$_3$)(η^2-S=CHR)]PF$_6$ (**5a–d**) [R′ = OPh, R = Ph (**a**), 4-C$_6$H$_4$Cl (**b**), R′ = *i*Pr, R = Ph (**c**), H (**d**)]. Nucleophilic addition of NaSMe to [CpRe(NO)(PPh$_3$){η^2-S=CH(4-C$_6$H$_4$OMe)}]PF$_6$ (**5e**) gave the dithioacetal complex [CpRe(NO)(PPh$_3$){SCH(SMe)(4-C$_6$H$_4$OMe)}] (**9**) in high yield and with low diastereoselectivity. Diels–Alder additions of **5a**, **e** with 2,3-dimethylbutadiene and 2,3-dimethoxybutadiene gave complexes of cyclic thioethers (**10a–c**). From the relative rates of reaction (**5a** >> **5e**) and the low diastereoselectivity, it was concluded that the cycloadditions as well as the nucleophilic addition proceed via the linkage isomers [CpRe(NO)(PR′$_3$)(η^1-S=CHR)]PF$_6$.

The central step of penicillin biosynthesis leading to the formation of the β-lactam ring is initiated by a hydrogen atom abstraction from the α position of an iron(III)-coordinated cysteine moiety. The thioaldehyde intermediate thus formed undergoes nucleophilic attack by the deprotonated amide group of the cysteine[2] (Scheme 1).



Scheme 1. Hydride abstraction and ring closure steps of penicillin biosynthesis[2]

We have in the past reported a similar and very efficient synthesis of ruthenium thioaldehyde complexes from the corresponding thiolates and triphenylcarbenium salts.[3] Mechanistically, this reaction proceeds through a one-electron oxidation of Ru^{II} to Ru^{III}, followed by hydrogen atom abstraction (Equation 1).[4]



For ruthenium, this synthesis appears to be limited to complexes of aromatic thioaldehydes. However, the same reaction carried out on rhenium thiolates of the type [CpRe(NO)(PPh$_3$)(SCH$_2$R)] also gave the corresponding thioaldehyde complexes with R = H, CH$_3$.[5] We report herein on an extension of this methodology to complexes of aliphatic thioaldehydes, particularly those bearing functional groups on the side chain.

Complexes of aliphatic thioaldehydes have hitherto attracted only limited attention. Cobalt and rhodium thioacetaldehyde complexes have been synthesized either by nucleophilic substitution of α-(bromoethyl) complexes or by

[+] Part 7: Ref.[1]

[a] Institut für Anorganische Chemie der Universität, Am Hubland, D-97074 Würzburg, Germany
Fax: (internat.) + 49(0)931/888-4605
E-mail: wolfdieter.schenk@mail.uni-wuerzburg.de

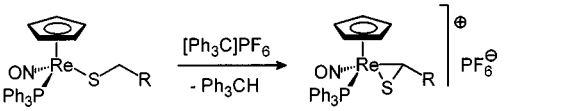
 © WILEY-VCH Verlag GmbH, D-69451 Weinheim, 1999 1434–1948/99/0909–1435 $ 17.50+.50/0

hydrogenation of a thioketene complex.[6][7] A phenylthioacetaldehyde complex of ruthenium has been obtained by H_2S addition to the corresponding vinylidene complex.[8] Thioaldehyde complexes of titanium and zirconium are generally accessible by intramolecular methane elimination from $[L_nM(CH_3)(SCH_2R)]$ complexes[9][10] or simply by α-deprotonation of thiolate ligands.[11] Complexes of η^4-coordinated unsaturated thioaldehydes have been obtained by metal-induced ring-opening of thietes.[12] However, in none of these cases have any substrates bearing functional groups on the side chain been involved.

Results

Synthesis of Thioaldehyde Complexes

Treatment of the thiolate complexes **1a**−**c**[1] with triphenylcarbenium hexafluorophosphate at −70°C as described previously[5] gave the expected thioaldehyde complexes **2a**−**c** in fair to good yields (Equation 2).



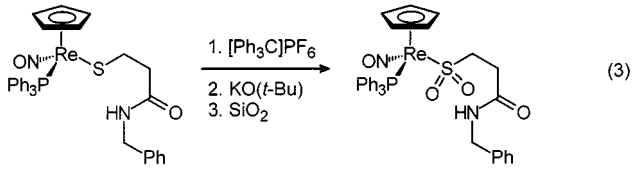
(2)

1a - c

R: CH_2Ph (**a**), C(O)OEt (**b**), $CH_2C(O)OMe$ (**c**)

2a (81%)
2b (76%)
2c (58%)

The method has its limitations, however. Similar reactions with R = $CH{=}CH_2$, CH_2NHAc, or $CH_2C(O)NHCH_2Ph$ gave inseparable mixtures of products, among which the expected thioaldehyde complexes could only be identified spectroscopically. In one such case, base hydrolysis of the reaction mixture led to the formation of the corresponding sulfinate complex **3d** along with some starting material **1d** (Equation 3).

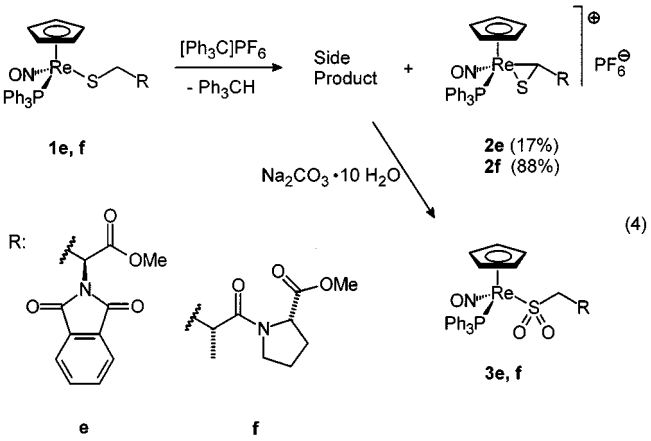


(3)

1d **3d** (25%)

Similarly, the thiolate complexes derived from the methyl esters of (*R*)-*N*-phthaloylcysteine (**1e**) and *N*-[(*S*)-3-mercapto-2-methylpropionyl]-(*S*)-proline (Captopril) (**1f**) gave the corresponding thioaldehyde complexes in poor (**2e**) and good yields (**2f**). The formation of side products became more pronounced at low temperature; their hydrolysis again gave the sulfinate complexes **3e**, **f** (Equation 4), which could be isolated by chromatography.

The new thioaldehyde complexes were obtained as brownish-yellow microcrystalline materials, which were found to be soluble only in polar organic solvents such as dichloromethane or acetone. A dominant feature of their



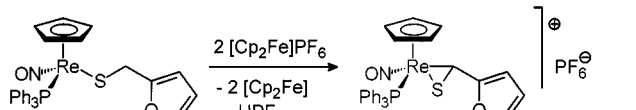
(4)

1e, f **2e** (17%) **2f** (88%) **3e, f**

e **f**

infrared spectra, besides the absorptions of the ester and amide groups, is an intense NO stretching absorption around 1750 cm^{-1}. In the ^1H- and ^{13}C-NMR spectra, the thioformyl group gives resonances near $\delta(^1H) = 6$ and $\delta(^{13}C) = 45$, which confirms the $\eta^2(C,S)$-coordination of the thioaldehyde ligand.[5] For this coordination mode, the existence of diastereoisomers with *syn* and *anti* arrangements of the Cp ligand and the substituent at the thioformyl group can be expected. For **2b**, two isomers in an 80:20 ratio were indeed found, whereas **2a** and **2c** were obtained as single diastereoisomers. Low-temperature NMR spectra did not reveal any dynamic phenomena down to −60°C. The complexes **1e**, **f**, which contain enantiomerically pure thiolate ligands, were employed in this synthesis as diastereomeric mixtures with opposing configurations at rhenium. As a consequence, **2e**, **f** were obtained as 1:1 mixtures of diastereoisomers. The same reaction carried out on diastereomerically pure (R_{Re},R_C)-**1e**[1] gave **2e** as a single isomer, indicating that the hydride abstraction proceeds with retention of configuration at rhenium.

Treatment of the (2-furyl)methylthiolate complex **1g** with triphenylcarbenium hexafluorophosphate gave only an intractable, dark-purple mixture. As noted previously, the dehydrogenation of thiolate complexes may in some cases be brought about using ferrocenium hexafluorophosphate as a one-electron oxidant.[4] Using this method we obtained the expected (2-furyl)methanethial complex **2g** in acceptable yield as a single diastereoisomer (Equation 5).



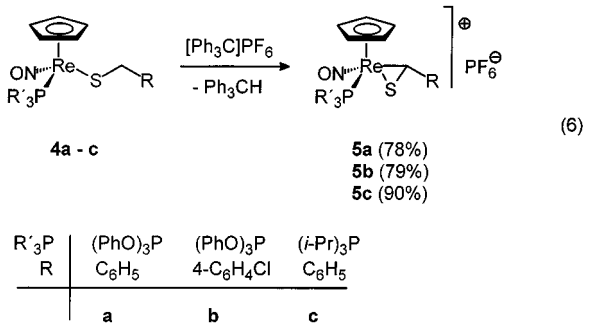
(5)

1g **2g** (41%)

Again, **2g** was obtained as a yellow crystalline compound and its spectroscopic properties were very similar to those of the analogous thiobenzaldehyde complex.[5]

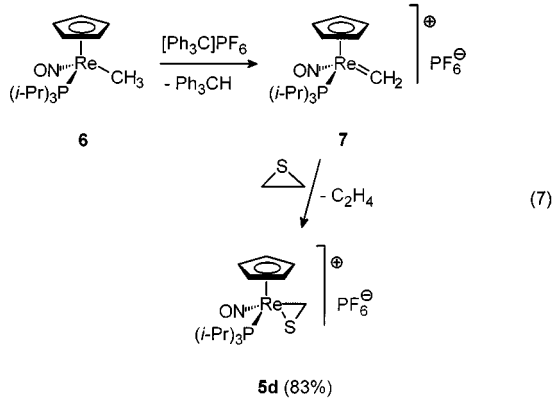
The use of other rhenium complexes with different steric and electronic properties was investigated briefly. The triphenylphosphite complexes **4a**, **b** and the triisopropylphosphane complex **4c**[13] reacted cleanly with triphenylcarbenium hexafluorophosphate, giving good yields of the corre-

sponding thiobenzaldehyde complexes **5a**−**c**, again as single diastereoisomers (Equation 6).



(6)

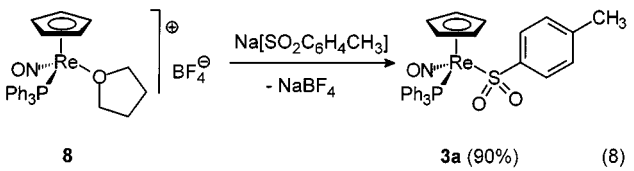
Finally, the thioformaldehyde complex **5d** was obtained from the methyl complex **6** by a reaction sequence closely analogous to the synthesis of $[CpRe(NO)(PPh_3)(S{=}CH_2)]PF_6$ originally reported by Gladysz[14] (Equation 7).



(7)

The thioaldehyde complexes **5a**−**d** are spectroscopically very similar to their triphenylphosphane analogues. The variation of the electron density at rhenium is apparent from the shift of ν(NO) to higher frequencies for L = $P(OPh)_3$ and, for L = $P(iPr)_3$ in particular, from the 5 ppm upfield shift of the ^{13}C resonance of the thiocarbonyl carbon atom.

Since rhenium sulfinate complexes $[CpRe(NO)(PPh_3)(SO_2R)]$ have not been described previously, we decided to prepare an authentic example by a ligand substitution reaction (Equation 8).



(8)

Complexes **3a**, **d**−**f** were obtained as light-yellow materials and were found to be readily soluble in dichloromethane and chloroform. Their infrared spectra show an intense ν(NO) absorption around 1700 cm^{-1} and two medium-intensity bands at 1150−1180 and 1038−1055 cm^{-1} due to $\nu_{asym}(SO_2)$ and $\nu_{sym}(SO_2)$. A further characteristic feature of sulfinate complexes is a low field ^{13}C-NMR signal[15] due to the α-carbon atom, which is found at δ = 157 for **3a** and at δ = 70 for **3d**.

Crystal and Molecular Structure of 3e

The identity of the sulfinate complexes was finally confirmed by an X-ray structure determination of the cysteine derivative **3e**. The compound crystallized as an acetone solvate in the centrosymmetric space group $P\bar{1}$, which indicates that racemization of the cysteine-derived ligand must have occurred en route to **3e**. Indeed, the sample of **1e** used in this reaction had been obtained under sufficiently alkaline conditions (NaOEt/HOEt) to effect racemization at the α carbon atom.[1] Figure 1 shows a view of the molecule in its (*S*,*S*) configuration.

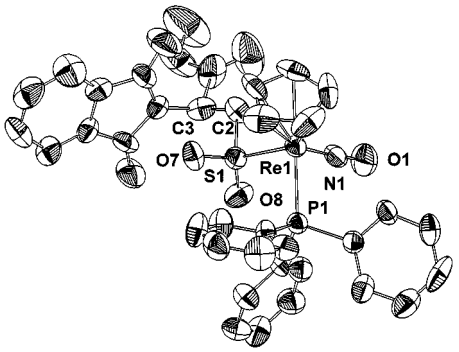


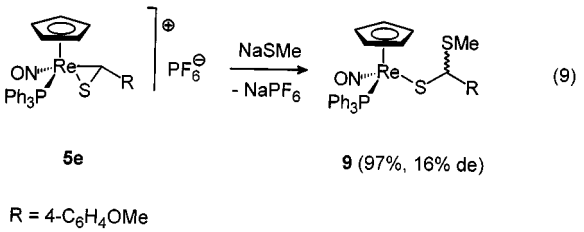
Figure 1. Molecular structure $[CpRe(NO)(PPh_3)\{SO_2CH_2CH(NC_8H_4O_2)COOMe\}]$ (**3e**). Selected distances [pm] and angles [°] (standard deviations in parentheses): Re(1)−S(1) 235.8(4), Re(1)−P(1) 236.8(4), Re(1)−N(1) 174(2), N(1)−O(1) 121(2), S(1)−C(2) 178(2), S(1)−O(7) 146.3(11), S(1)−O(8) 145.3(11),; S(1)−Re(1)−P(1) 92.82(14), S(1)−Re(1)−N(1) 94.2(4), P(1)−Re(1)−N(1) 90.9(4), Re(1)−S(1)−C(2) 103.4(5), Re(1)−S(1)−O(7) 111.2(4), Re(1)−S(1)−O(8) 117.8(5), O(7)−S(1)−O(8) 114.4(7); P(1)−Re(1)−S(1)−C(2) 161.5(12).

It is interesting to compare the molecular dimensions of **3e** with those of the starting thiolate complex **1e**.[1] All relevant bond lengths except those involving the sulfur atom are the same within one standard deviation. The S−Re and S−C bonds in **3e** are 4 pm shorter due to the contraction of the valence orbitals at the sulfur atom resulting from the increase of the formal oxidation state and the attachment of two highly electronegative oxygen atoms, respectively. The most conspicuous difference between the structures of **1e** and **3e** concerns the bond angles at rhenium. In **1e**, the angle S−Re−N is widened to 102.35(11)°.[1] A similar distortion has been found in other thiolate complexes, e.g. $[CpRe(NO)(PPh_3)\{SCH(Ph)(2\text{-}C_6H_4Me)\}]$ [101.3(2)°][16] and $[CpRe(NO)\{P(iPr)_3\}(SCH_3)]$ [102.2(4)°].[13] In **3e**, however, the N−Re−S angle [94.2(4)°] is close to the value of a regular octahedron, despite the fact that a sulfinate ligand is sterically more demanding than a thiolate group.

Reactions of Thioaldehyde Complexes

Typical reactions of transition metal thioaldehyde complexes include nucleophilic additions and [2+4]-cycload-

ditions.[17–19] We have found previously that thiolates add rapidly to cationic η^1-thioaldehyde complexes of ruthenium.[4] In a similar experiment, **5e**[5] was treated with sodium methylthiolate in acetone. An almost quantitative yield of the dithioacetal complex **9** was isolated as a mixture of two diastereoisomers (Equation 9).



(9)

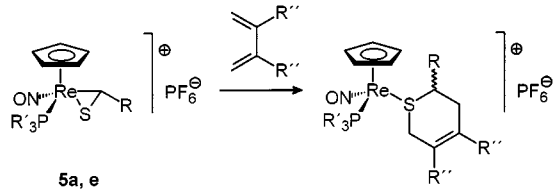
5e

9 (97%, 16% de)

R = 4-C_6H_4OMe

Complex **9** was obtained as a yellow oil and was found to be soluble in most common organic solvents. The spectroscopic properties of **9** are very similar to those of other thiolate complexes of the type [CpRe(NO)(PPh_3)(SR)].[1] Particularly characteristic is an intense ν(NO) absorption at ca. 1650 cm^{-1} and, in the ^{13}C-NMR spectrum, two low field signals due to the α carbon at sulfur in the two diastereoisomers, 1 ppm apart and split into doublets through coupling with phosphorus.

The complexes were next subjected to Diels–Alder-type additions with 2,3-dimethylbutadiene and 2,3-dimethoxybutadiene (Equation 10).



5a, e

10a (63%, 46% de)
10b (78%, 24% de)
10c (12%, 55% de)

R′$_3$P	(PhO)$_3$P	(PhO)$_3$P	Ph$_3$P
R	C_6H_5	C_6H_5	4-C_6H_4OMe
R′′	CH_3	OCH_3	CH_3
	5a	**5a**	**5e**
	10a	**10b**	**10c**

(10)

The triphenylphosphane complex **5e** reacted sluggishly; even after 5 d at room temperature the isolated yield of the adduct **10c** was only 12%. In contrast, the triphenylphosphite complex **5a** gave good yields of the cycloaddition products **10a**, **b** in less than 1 h. Again, the diastereoselectivity was disappointingly low. **10a–c** were obtained as yellow crystalline solids. In the ^{1}H-NMR spectra, some of the signals of the minor diastereoisomers of **10a**, **b** are broadened due to slightly hindered inversion at sulfur.[20][21] In this regard, **10a**, **b** are quite similar to the analogous cycloadducts of the ruthenium thioaldehyde complexes reported previously.[4]

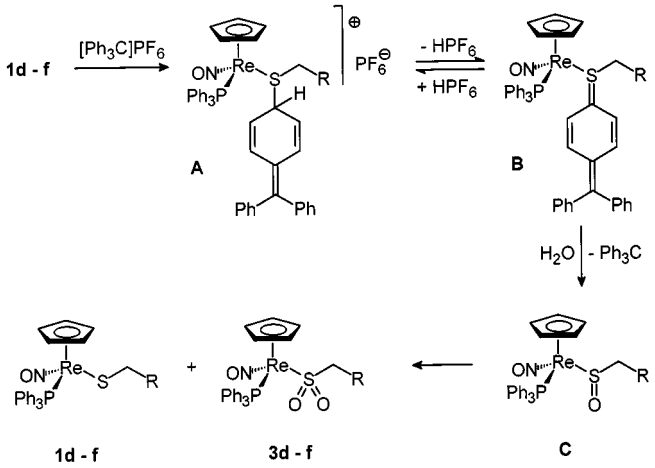
Discussion

There is a striking similarity between the synthesis of thioaldehyde complexes through β-hydride abstraction discovered in this laboratory (Equation 1)[3][4] and the formation of the thioaldehyde intermediate in penicillin biosynthesis (Scheme 1).[2] Both involve the coordination of a thiolate group to a d^6 transition metal complex followed by a one-electron oxidation to give the corresponding d^5 system, and H atom abstraction from the carbon atom in the position β to the metal. In view of this, it seemed a worthwhile undertaking to extend our investigations to thioaldehyde complexes derived from cysteine and other functionalized thiolates. Reactivity studies would then perhaps provide a deeper insight into the inner workings of isopenicillin N synthase (IPNS).

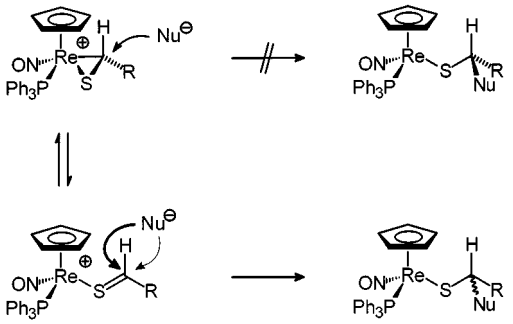
The coordination of prochiral alkenes and heteroalkenes to the chiral Lewis acid $[CpRe(NO)(PPh_3)]^+$ is, in general, accompanied by a high degree of diastereoselectivity.[22] For purely steric reasons, an *anti* arrangement of the Cp ring at rhenium and the substituent R is preferred. This is apparently also true for thiobenzaldehydes[5] and the aliphatic thioaldehydes forming the basis of this study. In the case of the thioacetaldehyde complex [CpRe(NO)(PPh_3)(S=$CHCH_3$)]PF_6, we have been able to detect the minor (*RS*,*SR*)-diastereoisomer by low-temperature NMR.[5] The equilibration of the diastereoisomers proceeds via the corresponding η^1-(*S*) isomers, which can often be observed separately,[23][24] e.g. in the case of the similar ruthenium complexes [CpRu(PMe_3)$_2$(S=CHR)]PF_6.[4] This is in contrast to the thioformaldehyde complexes [CpRe(NO)(PPh_3)(S=CH_2)]PF_6[14] and **5d**, as well as the ester derivative **2b**, which are static at room temperature. The energy of the π* level of the C=S double bond, which is raised by +I substituents and lowered by −M substituents, obviously determines the activation energy for the $\eta^2 \rightarrow \eta^1 \rightarrow \eta^2$ rearrangement.

Although in general the hydride abstraction with triphenylcarbenium salts gave good results, it was not always devoid of side reactions. Thus, starting from the thiolate complexes **1d–f**, the ^{31}P-NMR spectra of the crude reaction mixtures invariably featured a prominent signal at δ = 11, which is typical of thioether complexes [CpRe(NO)(PPh_3)(SRR′)]PF_6.[5] Attempted isolation of these byproducts led to further decomposition, which, after workup under basic conditions, ultimately resulted in the formation of the sulfinate complexes **3d–f** (Equation 3, 4). A likely explanation for this course of events is summarized in Scheme 2.

Electrophilic attack by the trityl cation gives an unstable thioether complex **A**. Under basic conditions, provided for example by chromatography on silica, **A** is deprotonated to give a resonance-stabilized metallated sulfur ylide **B**, which, in turn, is hydrolyzed to a sulfenate complex **C**. Transition metal sulfenate complexes remain a rare and little-understood class of compounds.[25] While there are some examples of quite stable complexes,[25–27] others seem to have a pronounced tendency to undergo a redistribution of their oxygen atoms.[28] Such a disproportionation would ulti-



Scheme 2. Formation of sulfinate side products **3d**−**f**



Scheme 3. Stereochemical course of nucleophilic attack at the carbon atom

mately produce the observed sulfinate complexes **3d**−**f** along with the starting compounds **1d**−**f**.

A comparison of spectroscopic and structural data of the sulfinate complex **3e** and the corresponding thiolate **1e**[1] reveals further insights into the bonding in low-valent transition metal thiolate complexes. The importance of antibonding interactions between the p-type lone pairs at sulfur and the occupied d orbitals at the metal has been stressed repeatedly.[29][30] In sulfinate complexes such as **3e** the sulfur electrons are no longer available for such π interactions. As a consequence, the electron density at rhenium is lowered compared to that in **1e**, which is most obvious from a 50 cm^{-1} hypsochromic shift of ν(NO). Furthermore, the N−Re−S angle, which in **1e** is widened to more than 102° to minimize antibonding,[13] is now lowered again to 94°. Thus, in hindsight the structure of **3e** offers additional proof of our contention that bond angles in low-valent transition metal thiolate complexes are influenced by π-antibonding interactions to a similar extent as bond lengths and dihedral angles.[29]

The disappointingly low diastereoselectivity of the nucleophilic addition (Equation 9) deserves some comment. If this reaction were analogous to the addition of nucleophiles to coordinated alkenes,[31][32] i.e. backside attack by Nu^- accompanied by cleavage of the metal−carbon bond, then the diastereoselectivity should somehow reflect the high diastereoisomer ratio of the starting thioaldehyde complexes. If, on the other hand, the η^2-thioaldehyde complexes described here are in rapid equilibrium with their η^1-isomers − such equilibria have been observed in many other cases, including the closely related ruthenium complexes $[CpRu(PR'_3)_2(S{=}CHR)]$[4] − then a much lower asymmetric induction would be expected (Scheme 3).

In the Diels−Alder addition (Equation 10), the less stable but more reactive η^1-isomers also play a decisive role. We have seen previously that with decreasing electron donation from the supporting phosphane ligands, the isomer ratio shifts in favor of the η^1 form.[4] As a consequence, the triphenylphosphite complex **5a** reacts with dienes much more rapidly than the triphenylphosphane complex **5e** does. The diastereoselectivity, on the other hand, is again too low to be synthetically useful.

Conclusions

We have demonstrated herein that the synthesis of thioaldehyde complexes through β-hydride abstraction can be extended to aliphatic thioaldehydes, and that it tolerates ester and amide functionalities. In particular, the successful synthesis of the cysteine-derived thioaldehyde complex **2e** offers additional proof of the mechanism of penicillin biosynthesis proposed by Baldwin.[2] Nucleophilic additions and cycloadditions at the C=S function proceed via the more reactive η^1 linkage isomers. In order to achieve high diastereoselectivities in these reactions, it will be necessary to employ less electron-donating and sterically more demanding phosphorus ligands.

Experimental Section

All experiments were carried out in Schlenk tubes under an atmosphere of nitrogen using suitably purified solvents. − IR: Perkin−Elmer 283, Bruker IFS 25. − ^{1}H NMR: Bruker AMX 400, δ values relative to TMS. − ^{13}C NMR: Bruker AMX 400, δ values relative to TMS; assignments were routinely checked by DEPT; in some cases the ^{13}C-NMR signals of quaternary carbon atoms were too weak to be detected. − ^{31}P NMR: Bruker AMX 400, δ values relative to 85% H_3PO_4. The ^{1}H- and ^{13}C-NMR signals of phenyl groups are unremarkable and have therefore been omitted from the lists of spectral data. − Elemental analyses: Analytical Laboratory of the Institut für Anorganische Chemie. The following starting materials were obtained as described in the literature: [CpRe(NO)(PPh$_3$)(SR)] (**1a**−**g**),[1] [CpRe(NO)(PR′$_3$)(SR)] (**4a**−**c**),[13] [CpRe(NO)(PPh$_3$){η^2-S=CH(4-C_6H_4OMe)}]PF_6 (**5e**),[5] [CpRe(NO){P(*i*Pr)$_3$}(CH_3)] (**6**),[13] [CpRe(NO)(PPh$_3$)(OC_4H_8)]BF_4 (**8**),[33] sodium methylthiolate.[34] All other reagents were used as purchased.

[CpRe(NO)(PPh$_3$)(η^2-S=CHCH$_2$Ph)]PF_6 (2a): At −70°C, a solution of $[Ph_3C]PF_6$ (66 mg, 0.17 mmol) in dichloromethane (5 mL) was added to a solution of **1a** (102 mg, 0.15 mmol) in the same solvent (10 mL). The mixture was allowed to warm to 20°C and then concentrated in vacuo to a volume of 2 mL. Addition of diethyl ether led to precipitation of the product, which was filtered off, washed with diethyl ether, and dried in vacuo. Yield 100 mg (81%); m.p. 108°C. − ^{1}H NMR (400 MHz, [D$_6$]acetone, 20°C):

δ = 3.03 [dd, ^2J(H,H) = 13.8 Hz, ^3J(H,H) = 9.6 Hz, 1 H, CH_2], 3.93 [dd, ^2J(H,H) = 13.8 Hz, ^3J(H,H) = 3.0 Hz, 1 H, CH_2], 6.00 [ddd, ^3J(H,H) = 9.6 Hz, ^3J(H,H) = 3.6 Hz, ^3J(P,H) = 2.0 Hz, 1 H, SCH], 6.33 (s, 5 H, C_5H_5). − ^{13}C NMR (100 MHz, [D$_6$]acetone, 20°C): δ = 48.5 (s, SCH_2), 54.0 (s, SCH), 101.4 (s, C_5H_5). − ^{31}P NMR (162 MHz, [D$_6$]acetone, 20°C): δ = 6.9 (s). − IR (CH_2Cl_2): $\tilde{\nu}$ = 1744 cm^{-1} (NO). − $C_{31}H_{28}F_6NOP_2ReS$ (824.8): calcd. C 45.14, H 3.42, N 1.70, S 3.89; found C 44.97, H 3.63, N 1.71, S 3.84.

[CpRe(NO)(PPh$_3$)(η^2-S=CHCOOEt)]PF$_6$ (2b): This compound was prepared analogously from **1b**. Yield 92 mg (76%), m.p. 212°C (dec.). − Major diastereoisomer: ^{1}H NMR (400 MHz, [D$_6$]acetone, 20°C): δ = 1.27 [t, ^3J(H,H) = 7.2 Hz, 3 H, CH_3], 4.21, 4.26 [q of AB systems, ^2J(H,H) = 10.9 Hz, ^3J(H,H) = 7.1 Hz, 2 H, OCH_2], 5.87 [d, ^3J(P,H) = 1.2 Hz, 1 H, SCH], 6.51 [d, ^3J(P,H) = 0.9 Hz, 5 H, C_5H_5]. − ^{13}C NMR (100 MHz, [D$_6$]acetone, 20°C): δ = 14.8 (s, CH_3), 39.9 (s, SCH), 62.2 (s, OCH_2), 102.3 (s, C_5H_5), 171.8 (s, C=O). − ^{31}P NMR (162 MHz, [D$_6$]acetone, 20°C): δ = 8.0 (s). − Minor diastereoisomer: ^{1}H NMR (400 MHz, [D$_6$]acetone, 20°C): δ = 1.36 [t, ^3J(H,H) = 7.2 Hz, 3 H, CH_3], 4.37, 4.39 [q of AB systems, ^2J(H,H) = 4.1 Hz, ^3J(H,H) = 7.1 Hz, 2 H, OCH_2], 5.08 [d, ^3J(P,H) = 1.7 Hz, 1 H, SCH], 6.23 [d, ^3J(P,H) = 0.8 Hz, 5 H, C_5H_5]. − ^{13}C NMR (100 MHz, [D$_6$]acetone, 20°C): δ = 14.6 (s, CH_3), 43.7 (s, SCH), 62.9 (s, OCH_2), 103.4 (s, C_5H_5), 174.9 (s, C=O). − ^{31}P NMR (162 MHz, [D$_6$]acetone, 20°C): δ = 6.2 (s). − IR (CH_2Cl_2): $\tilde{\nu}$ = 1764 (NO), 1719 cm^{-1} (COOR). − $C_{27}H_{26}F_6NO_3P_2ReS$ (806.7): calcd. C 40.20, H 3.25, N 1.74, S 3.97; found C 40.52, H 3.46, N 1.69, S 4.02.

[CpRe(NO)(PPh$_3$)(η^2-S=CHCH$_2$COOMe)]PF$_6$ (2c): This compound was prepared analogously from **1c**. The purple-black crude product was suspended in acetone and stirred for 24 h. **2c** was precipitated from the filtered solution by adding diethyl ether. Yield 70 mg (58%), m.p. 100°C. − ^{1}H NMR (400 MHz, [D$_6$]acetone, 20°C): δ = 3.19, 3.56 [d of AB systems, ^2J(H,H) = 17.0 Hz, ^3J(H,H) = 6.4 Hz, ^3J(H,H) = 5.6 Hz, 2 H, CH_2], 3.70 (s, 3 H, OCH_3), 5.88 (br. t, 1 H, SCH), 6.34 (s, 5 H, C_5H_5). − ^{13}C NMR (100 MHz, [D$_6$]acetone, 20°C): δ = 45.5 (s, SCH), 52.3 (s, OCH_3), 69.3 (s, CH_2), 101.7 (s, C_5H_5), 172.8 (s, C=O). − ^{31}P NMR (162 MHz, [D$_6$]acetone, 20°C): δ = 6.8 (s). − IR (CH_2Cl_2): $\tilde{\nu}$ = 1744 cm^{-1} (NO). − $C_{27}H_{26}F_6NO_3P_2ReS$ (806.7): calcd. C 40.20, H 3.25, N 1.74, S 3.97; found C 40.46, H 3.45, N 1.81, S 4.07.

[CpRe(NO)(PPh$_3$){η^2-S=CHCH(NC$_8$H$_4$O$_2$)COOMe}]PF$_6$ (2e): This compound was prepared from a 1:1 diastereomeric mixture of (R_{Re},R_C/S_{Re},R_C)-**1e**.[1] The dark-brown crude product was suspended in acetone and stirred for 24 h. After evaporation of the solvent to dryness, the residue was washed with benzene and treated again with acetone as above. Crystallization from dichloromethane/diethyl ether/pentane finally gave pure **2e**. Yield 24 mg (17%), m.p. 117°C. − (R_{Re},R_C,R_C)-Diastereoisomer: ^{1}H NMR (400 MHz, [D$_6$]acetone, 20°C): δ = 3.83 (s, 3 H, OCH_3), 4.81 [d, ^3J(H,H) = 9.6 Hz, 1 H, CH], 6.30 [dd, ^3J(H,H) = 9.2 Hz, ^3J(P,H) = 1.8 Hz, 1 H, SCH], 6.52 (s, 5 H, C_5H_5). − ^{13}C NMR (100 MHz, [D$_6$]acetone, 20°C): δ = 46.3 (s, SCH), 53.9 (s, OCH_3), 68.3 (s, CH), 102.7 (s, C_5H_5), 167.3 (s, C=O), 168.0 (s, C=O). − ^{31}P NMR (162 MHz, [D$_6$]acetone, 20°C): δ = 7.3 (s). − (S_{Re},S_C,R_C)-Diastereoisomer: ^{1}H NMR (400 MHz, [D$_6$]acetone, 20°C): δ = 3.79 (s, 3 H, OCH_3), 4.62 [d, ^3J(H,H) = 10.0 Hz, 1 H, CH], 6.45 [dd, ^3J(H,H) = 9.6 Hz, ^3J(P,H) = 2.0 Hz, 1 H, SCH], 6.34 (s, 5 H, C_5H_5). − ^{13}C NMR (100 MHz, [D$_6$]acetone, 20°C): δ = 45.7 (s, SCH), 53.8 (s, OCH_3), 69.2 (s, CH), 102.3 (s, C_5H_5), 167.9 (s, C=O), 168.7 (s, C=O). − ^{31}P NMR (162 MHz, [D$_6$]acetone, 20°C): δ = 7.0 (s). − IR (CH_2Cl_2): $\tilde{\nu}$ = 1778 (CO), 1748 (NO), 1722 cm^{-1} (CO). − $C_{35}H_{29}F_6N_2O_5P_2ReS$ (951.8): calcd. C 44.17, H 3.07, N 2.94, S 3.37; found C 43.67, H 3.43, N 2.91, S 3.43.

Using the same procedure, diastereomerically pure (R_{Re},R_C,R_C)-**2e** was obtained from pure (R_{Re},R_C)-**1e**.

[CpRe(NO)(PPh$_3$){SO$_2$CH$_2$CH(NC$_8$H$_4$O$_2$)COOMe}] (3e): This compound was isolated as a 1:1 mixture of diastereoisomers from the combined benzene extracts by partial evaporation and precipitation with pentane. A complete separation from **2e** and traces of unidentified decomposition products could not be achieved. However, the compound was fully characterized by X-ray crystallography. − Both diastereoisomers: ^{1}H NMR (400 MHz, [D$_6$]acetone, 20°C): δ = 3.70 (s, 3 H, OCH_3), 3.71 (s, 3 H, OCH_3), 3.68−3.80 (m, 1 H, CH_2), 3.88−4.01 (m, 2 H, CH_2), 4.16−4.24 (m, 1 H, CH_2), 5.34 (s, 5 H, C_5H_5), 5.38 (s, 5 H, C_5H_5), 5.53−5.57 (m, 2 H, CH). − ^{13}C NMR (100 MHz, [D$_6$]acetone, 20°C): δ = 47.2 (s, CH), 47.6 (s, CH), 53.1 (s, OCH_3), 53.1 (s, OCH_3), 66.3 (s, CH_2), 68.0 (s, CH_2), 93.9 (s, C_5H_5), 93.9 (s, C_5H_5), 167.3 (s, C=O), 167.4 (s, C=O), 169.0 (s, C=O), 169.2 (s, C=O). − ^{31}P NMR (162 MHz, [D$_6$]acetone, 20°C): δ = 13.3 (s), 13.8 (s). − IR (CH_2Cl_2): $\tilde{\nu}$ = 1778 (CO), 1748 (COOR), 1722 (CO), 1700 cm^{-1} (NO).

[CpRe(NO)(PPh$_3$){η^2-S=CHCH(Me)C(O)NC$_4$H$_7$COOMe}]PF$_6$ (2f): This compound was prepared as a 1:1 mixture of diastereoisomers from (R_{Re},S_C,S_C/S_{Re},S_C,S_C)-**1f**[1] and [Ph$_3$C]PF$_6$ at 20°C. Yield 121 mg (88%), m.p. 72°C (dec.). − Both diastereoisomers: ^{1}H NMR (400 MHz, [D$_6$]acetone, 20°C): δ = 1.43 [d, ^3J(H,H) = 6.8 Hz, 3 H, CH_3], 1.57 [d, ^3J(H,H) = 6.8 Hz, 3 H, CH_3], 1.90−2.20 (m, 2 × 2 H, CH_2), 2.72 [dq, ^3J(H,H) = 9.6 Hz, ^3J(H,H) = 6.8 Hz, 1 H, CH], 2.77 [dq, ^3J(H,H) = 9.6 Hz, ^3J(H,H) = 6.8 Hz, 1 H, CH], 3.65 (s, 3 H, OCH_3), 3.69 (s, 3 H, OCH_3), 4.20−4.46 (m, 2 × 2 H, CH_2), 5.61 (m, 1 H, CH), 5.83 (m, 1 H, CH), 5.82 [dd, ^3J(H,H) = 9.4 Hz, ^3J(P,H) = 2.0 Hz, 1 H, SCH], 5.90 [dd, ^3J(H,H) = 9.6 Hz, ^3J(P,H) = 2.2 Hz, 1 H, SCH], 6.31 [d, ^3J(P,H) = 0.4 Hz, 5 H, C_5H_5], 6.47 [d, ^3J(P,H) = 0.8 Hz, 5 H, C_5H_5]. − ^{13}C NMR (100 MHz, [D$_6$]acetone, 20°C): δ = 18.2 (s, CH_3), 25.3 (s, CH_2), 25.4 (s, CH_2), 25.9 (s, CH_3), 29.2 (s, CH_2), 29.3 (s, CH_2), 47.8 (s, CH_2), 47.8 (s, CH_2), 50.0 (s, SCH), 52.1 (s, OCH_3), 52.2 (s, OCH_3), 52.7 (s, SCH), 55.9 (s, CH), 56.5 (s, CH), 59.4 (s, CH), 59.6 (s, CH), 101.6 (s, C_5H_5), 101.9 (s, C_5H_5), 173.0 (s, C=O), 173.1 (s, C=O), 173.4 (s, C=O), 175.4 (s, C=O). − ^{31}P NMR (162 MHz, [D$_6$]acetone, 20°C): δ = 6.8 (s), 7.2 (s). − IR (CH_2Cl_2): $\tilde{\nu}$ = 1747 (NO), 1641 cm^{-1} (CO). − $C_{33}H_{35}F_6N_2O_4P_2ReS$ (917.9): calcd. C 43.18, H 3.84, N 3.05, S 3.49; found C 42.89, H 4.09, N 2.90, S 3.40.

[CpRe(NO)(PPh$_3$){SO$_2$CH$_2$CH(Me)C(O)NC$_4$H$_7$COOMe}] (3f): Treatment of **1f** with [Ph$_3$C]PF$_6$ at −70°C gave a mixture of compounds, which was hydrolyzed with an excess of $Na_2CO_3 \cdot 10\,H_2O$ in THF. After concentration to dryness, the residue was dissolved in dichloromethane and chromatographed by passage through a short (20 cm) silica column with dichloromethane/acetone, 2:1, as eluent. The yellow band containing **3f** was concentrated to dryness and the residue was recrystallized from dichloromethane/pentane. Yield 41 mg (34%), m.p. 190°C (dec.). − Both diastereoisomers: ^{1}H NMR (400 MHz, $CDCl_3$, 20°C): δ = 1.09 [d, ^3J(H,H) = 7.2 Hz, 3 H, CH_3], 1.25 [d, ^3J(H,H) = 7.2 Hz, 3 H, CH_3], 1.80−2.20 (m, 2 × 4 H, CH_2), 2.95 [dd, ^2J(H,H) = 13.2 Hz, ^3J(H,H) = 2.8 Hz, 1 H, SO_2CH_2], 3.06 [dd, ^2J(H,H) = 13.4 Hz, ^3J(H,H) = 4.2 Hz, 1 H, SO_2CH_2], 3.14 (m, 1 H, CH), 3.29 (m, 1 H, CH), 3.50−3.60 (m, 2 H, CH_2), 3.65 (s, 3 H, OCH_3), 3.67 (s, 3 H, OCH_3), 3.78 (m, 2 H, CH_2), 3.81 [dd, ^2J(H,H) = 13.2 Hz, ^3J(H,H) = 6.8 Hz, 1 H, SO_2CH_2], 3.89 [dd, ^2J(H,H) = 12.8 Hz, ^3J(H,H) = 8.8 Hz, 1 H, SO_2CH_2], 4.43 [dd, ^3J(H,H) = 8.8 Hz, ^3J(H,H) = 4.4 Hz, 1 H, CH], 4.51 [dd, ^3J(H,H) = 8.8 Hz, ^3J(H,H) = 4.4 Hz, 1 H, CH],

5.33 (s, 5 H, C_5H_5), 5.34 (s, 5 H, C_5H_5). − ^{13}C NMR (100 MHz, $CDCl_3$, 20°C): δ = 17.8 (s, CH_3), 18.2 (s, CH_3), 24.7 (s, CH_2), 24.8 (s, CH_2), 29.0 (s, CH_2), 29.0 (s, CH_2), 31.8 (s, CH), 33.8 (s, CH), 46.8 (s, CH_2), 46.8 (s, CH_2), 51.9 (s, OCH_3), 52.0 (s, OCH_3), 58.6 (s, CH), 58.9 (s, CH), 73.9 (s, SO_2CH_2), 75.3 (s, SO_2CH_2), 93.8 (s, C_5H_5), 94.0 (s, C_5H_5), 173.0 (s, C=O), 173.1 (s, C=O), 174.0 (s, C=O), 174.6 (s, C=O). − ^{31}P NMR (162 MHz, $CDCl_3$, 20°C): δ = 14.0 (s). − IR (CH_2Cl_2): $\tilde{\nu}$ = 1747 (COOR), 1699 (NO), 1645 ($CONR_2$), 1177 (SO), 1045 cm^{-1} (SO). − $C_{33}H_{36}N_2O_6PReS$ (805.9): calcd. C 49.18, H 4.50, N 3.48, S 3.98; found C 48.85, H 4.59, N 3.20, S 3.74.

[CpRe(NO)(PPh$_3$){SO$_2$CH$_2$CH$_2$C(O)NHCH$_2$Ph}] (3d): Treatment of **1d** (111 mg, 0.15 mmol) with $[Ph_3C]PF_6$ (66 mg, 0.17 mmol) at −70°C as described above for **2a** gave a mixture of compounds, which was solvolyzed with an excess of KO(*t*Bu) in THF. After concentration to dryness, the residue was dissolved in dichloromethane and chromatographed by passage through a short (20 cm) silica column with dichloromethane/acetone, 4:1, as eluent. A first eluted yellow band was found to contain **1d** and some unidentified material. A second, light-yellow band containing **3d** was concentrated to dryness and the residue was recrystallized from dichloromethane/pentane. Yield 29 mg (25%), m.p. 55°C. − ^{1}H NMR (400 MHz, $CDCl_3$, 20°C): δ = 2.67 [t, ^3J(H,H) = 6.0 Hz, 2 H, CH_2], 3.44 [t, ^3J(H,H) = 6.4 Hz, 2 H, CH_2], 4.20 [t, ^3J(H,H) = 5.6 Hz, 1 H, NH], 4.37 [d, ^3J(H,H) = 5.2 Hz, 2 H, NCH_2], 5.33 (s, 5 H, C_5H_5). − ^{13}C NMR (100 MHz, $CDCl_3$, 20°C): δ = 30.0 (s, CH_2), 43.4 (s, CH_2), 67.6 (s, SCH_2), 93.7 (s, C_5H_5), 171.8 (s, CO). − ^{31}P NMR (162 MHz, $CDCl_3$, 20°C): δ = 13.6 (s). − IR (CH_2Cl_2): $\tilde{\nu}$ = 1693 (NO), 1152 (SO), 1038 cm^{-1} (SO). − $C_{33}H_{32}N_2O_4PReS$ (769.9): calcd. C 51.48, H 4.19, N 3.64, S 4.16; found C 50.77, H 4.61, N 3.54, S 4.27.

[CpRe(NO)(PPh$_3$)(η^2-S=CHC$_4$H$_3$O)]PF$_6$ (2g): A solution of **1g** (111 mg, 0.17 mmol) and $[Cp_2Fe]PF_6$ (0.52 g, 1.57 mmol) in acetone (20 mL) was stirred for 2 d at 20°C. The mixture was then concentrated to dryness and the residue was dissolved in dichloromethane and chromatographed on a short (20 cm) silica column with dichloromethane/acetone, 10:1, as eluent. The first eluted bright-yellow band was found to contain ferrocene. A second, brownish-yellow band containing **2g** was concentrated to dryness and the residue was recrystallized from dichloromethane/diethyl ether. Yield 56 mg (41%), m.p. 88°C (dec.). − ^{1}H NMR (400 MHz, CD_3CN, 20°C): δ = 6.41 (s, 5 H, C_5H_5), 6.51 [dd, ^3J(H,H) = 3.2 Hz, ^3J(H,H) = 1.6 Hz, 1 H, CH], 6.56 [d, ^3J(H,H) = 3.2 Hz, 1 H, CH], 6.80 (s, 1 H, SCH), 7.41 [d, ^3J(H,H) = 1.2 Hz, 1 H, CH]. − ^{13}C NMR (100 MHz, [D$_6$]acetone, 20°C): δ = 42.0 (s, SCH), 101.8 (s, C_5H_5), 110.2 (s, CH), 111.7 (s, CH), 144.0 (s, OCH), 157.7 (s, OC). − ^{31}P NMR (162 MHz, [D$_6$]acetone, 20°C): δ = 7.9 (s). − IR (CH_2Cl_2): $\tilde{\nu}$ = 1751 cm^{-1} (NO). − $C_{28}H_{24}F_6NO_2P_2ReS$ (800.7): calcd. C 42.00, H 3.02, N 1.75, S 4.00; found C 41.76, H 3.23, N 1.74, S 4.01.

[CpRe(NO){P(OPh)$_3$}(η^2-S=CHPh)]PF$_6$ (5a): This compound was prepared as described above for **2a**. Yield 100 mg (78%), m.p. 228°C (dec.). − ^{1}H NMR (400 MHz, [D$_6$]acetone, 20°C): δ = 6.59 (s, 5 H, C_5H_5), 6.99 (s, 1 H, SCH). − ^{13}C NMR (100 MHz, CD_3NO_2, 20°C): δ = 53.5 (s, SCH), 100.8 (s, C_5H_5). − ^{31}P NMR (162 MHz, [D$_6$]acetone, 20°C): δ = 77.0 (s). − IR (CH_2Cl_2): $\tilde{\nu}$ = 1767 cm^{-1} (NO). − $C_{30}H_{26}F_6NO_4P_2ReS$ (858.7): calcd. C 41.96, H 3.05, N 1.63, S 3.73; found C 41.76, H 2.83, N 1.65, S 3.85.

[CpRe(NO){P(OPh)$_3$}{η^2-S=CH(4-C$_6$H$_4$Cl)}]PF$_6$ (5b): This compound was prepared analogously to **2a**. Yield 106 mg (79%), m.p. 110°C (dec.). − ^{1}H NMR (400 MHz, [D$_6$]acetone, 20°C): δ = 6.58 (s, 5 H, C_5H_5), 6.92 (s, 1 H, SCH). − ^{13}C NMR (100 MHz, CD_3NO_2, 20°C): δ = 51.7 (s, SCH), 100.9 (s, C_5H_5). − ^{31}P NMR (162 MHz, [D$_6$]acetone, 20°C): δ = 76.7 (s). − IR (CH_2Cl_2): $\tilde{\nu}$ = 1767 cm^{-1} (NO). − $C_{30}H_{25}ClF_6NO_4P_2ReS$ (893.2): calcd. C 40.34, H 2.82, N 1.57, S 3.59; found C 40.33, H 2.94, N 1.59, S 3.79.

[CpRe(NO){P(*i*Pr)$_3$}(η^2-S=CHPh)]PF$_6$ (5c): This compound was prepared analogously to **2a**. Yield 96 mg (90%), m.p. 150°C (dec.). − ^{1}H NMR (400 MHz, [D$_6$]acetone, 20°C): δ = 1.44 [dd, ^3J(P,H) = 15.6 Hz, ^3J(H,H) = 7.2 Hz, 9 H, CH_3], 1.48 [dd, ^3J(P,H) = 16.4 Hz, ^3J(H,H) = 7.2 Hz, 9 H, CH_3], 3.25 [dsept, ^2J(P,H) = 9.6 Hz, ^3J(H,H) = 7.2 Hz, 3 H, CH], 6.72 (s, 5 H, C_5H_5), 6.89 (s, 1 H, SCH). − ^{13}C NMR (100 MHz, [D$_6$]acetone, 20°C): δ = 20.1 [d, ^2J(P,C) = 2 Hz, CH_3], 20.3 [d, ^2J(P,C) = 2 Hz, CH_3], 31.4 [d, ^1J(P,C) = 28 Hz, CH], 45.9 (s, SCH), 100.3 (s, C_5H_5). − ^{31}P NMR (162 MHz, [D$_6$]acetone, 20°C): δ = 22.2 (s). − IR (CH_2Cl_2): $\tilde{\nu}$ = 1740 cm^{-1} (NO). − $C_{21}H_{32}F_6NOP_2ReS$ (708.7): calcd. C 35.59, H 4.55, N 1.98, S 4.52; found C 35.51, H 4.58, N 1.94, S 4.58.

[CpRe(NO){P(*i*Pr)$_3$}(η^2-S=CH$_2$)]PF$_6$ (5d): To a solution of **6** (105 mg, 0.23 mmol) in dichloromethane (5 mL) at −70°C was added $[Ph_3C]PF_6$ (90 mg, 0.23 mmol). The mixture was stirred at this temperature for 30 min. Thiirane (20 μL, 0.33 mmol) was then added and the mixture was allowed to warm to 20°C. It was then concentrated in vacuo to a volume of 1 mL. Addition of diethyl ether led to precipitation of the product, which was filtered off and dried in vacuo. Yield 121 mg (83%), m.p. 188°C (dec.). − ^{1}H NMR (400 MHz, [D$_6$]acetone, 20°C): δ = 1.35 [dd, ^3J(P,H) = 15.6 Hz, ^3J(H,H) = 7.2 Hz, 9 H, CH_3], 1.45 [dd, ^3J(P,H) = 14.8 Hz, ^3J(H,H) = 7.2 Hz, 9 H, CH_3], 3.13 [dsept, ^2J(P,H) = 9.6 Hz, ^3J(H,H) = 7.2 Hz, 3 H, CH], 3.30 [dd, ^3J(P,H) = 1.2 Hz, ^2J(H,H) = 1.2 Hz, 1 H, SCH], 4.84 [dd, ^3J(P,H) = 1.2 Hz, ^2J(H,H) = 1.2 Hz, 1 H, SCH], 6.61 (s, 5 H, C_5H_5). − ^{13}C NMR (100 MHz, [D$_6$]acetone, 20°C): δ = 20.0 [d, ^2J(P,C) = 3 Hz, CH_3], 20.3 [d, ^2J(P,C) = 2 Hz, CH_3], 25.2 (s, SCH), 30.7 [d, ^1J(P,C) = 28 Hz, CH], 99.5 (s, C_5H_5). − ^{31}P NMR (162 MHz, [D$_6$]acetone, 20°C): δ = 22.7 (s). − IR (CH_2Cl_2): $\tilde{\nu}$ = 1744 cm^{-1} (NO). − $C_{15}H_{28}F_6NOP_2ReS$ (632.6): calcd. C 28.48, H 4.46, N 2.21, S 5.07; found C 28.77, H 4.45, N 2.14, S 5.31.

[CpRe(NO)(PPh$_3$){SO$_2$(4-C$_6$H$_4$Me)}] (3a): A solution of **8** (281 mg, 0.40 mmol) and $NaSO_2(4\text{-}C_6H_4Me) \cdot H_2O$ (157 mg, 0.80 mmol) in THF (20 mL) and ethanol (20 mL) was stirred for 1 h at 20°C. The mixture was then concentrated to dryness and the residue was extracted with benzene. After filtration through Celite, the benzene was partially evaporated and the product was precipitated by adding pentane. Yield 252 mg (90%), m.p. 214°C (dec). − ^{1}H NMR (400 MHz, $CDCl_3$, 20°C): δ = 2.28 (s, 3 H, CH_3), 5.04 (s, 5 H, C_5H_5). − ^{13}C NMR (100 MHz, $CDCl_3$, 20°C): δ = 21.1 (s, CH_3), 94.0 (s, C_5H_5). − ^{31}P NMR (162 MHz, $CDCl_3$, 20°C): δ = 13.8 (s). − IR (CH_2Cl_2): $\tilde{\nu}$ = 1695 (NO), 1182 (SO), 1054 cm^{-1} (SO). − $C_{30}H_{27}NO_3PReS$ (698.8): calcd. C 51.56, H 3.89, N 2.00, S 4.59; found C 51.33, H 3.98, N 1.99, S 4.47.

[CpRe(NO)(PPh$_3$){SCH(SMe)(4-C$_6$H$_4$OMe)}] (9): To a solution of **5e** (69 mg, 0.08 mmol) in acetone (6 mL) at −50°C was added NaSMe (20 mg, 0.29 mmol). The mixture was allowed to warm to 20°C and then concentrated to dryness. The yellow residue was redissolved in THF and chromatographed by passage through a short (20 cm) silica column with THF/diethyl ether, 2:1, as eluent. A first yellow band was collected, the solvents were evaporated, and the residue was recrystallized at low temperature from dichloromethane/pentane. Owing to its semi-solid nature, the product could not be rigorously freed of solvent. Yield 57 mg (97%). − Major diastereoisomer: ^{1}H NMR (400 MHz, $CDCl_3$, 20°C): δ = 2.12 (s, 3 H, SCH_3), 3.77 (s, 3 H, OCH_3), 4.73 (s, 1 H, CH), 4.93

(s, 5 H, C_5H_5). − ^{13}C NMR (100 MHz, $CDCl_3$, 20°C): δ = 17.0 (s, SCH_3), 55.3 (s, OCH_3), 65.1 [d, ^3J(P,C) = 8 Hz, CH], 90.9 (s, C_5H_5). − ^{31}P NMR (162 MHz, $CDCl_3$, 20°C): δ = 19.3 (s). − Minor diastereoisomer: ^{1}H NMR (400 MHz, $CDCl_3$, 20°C): δ = 2.00 (s, 3 H, SCH_3), 3.78 (s, 3 H, OCH_3), 4.71 (s, 1 H, CH), 5.10 (s, 5 H, C_5H_5). − ^{13}C NMR (100 MHz, $CDCl_3$, 20°C): δ = 16.7 (s, SCH_3), 55.3 (s, OCH_3), 64.2 [d, ^3J(P,C) = 8 Hz, CH], 91.3 (s, C_5H_5). − ^{31}P NMR (162 MHz, $CDCl_3$, 20°C): δ = 19.0 (s). − IR (CH_2Cl_2): $\tilde{\nu}$ = 1653 cm^{-1} (NO).

[CpRe(NO){P(OPh)$_3$}(SC$_5$H$_5$PhMe$_2$)]PF$_6$ (10a): A solution of **5a** (117 mg, 0.14 mmol) and 2,3-dimethylbutadiene (275 μL, 2.34 mmol) in dichloromethane (15 mL) was kept at 20°C. The orange colour of the starting material faded gradually. After 4 h, the mixture was concentrated to dryness. ^{1}H-NMR analysis of the crude residue indicated complete conversion with 46% *de*. Recrystallization from dichloromethane/pentane gave analytically pure **10a**. Yield 80 mg (63%), m.p. 226°C (dec.). − Major diastereoisomer: ^{1}H NMR (400 MHz, [D$_6$]acetone, 20°C): δ = 1.81 (s, 3 H, CH_3), 1.85 (s, 3 H, CH_3), 2.85, 2.92 [d of AB systems, ^2J(H,H) = 18.6 Hz, ^3J(H,H) = 7.6 Hz, ^3J(H,H) = 2.8 Hz, 2 H, CH_2], 3.81, 4.27 [AB system, ^2J(H,H) = 16.4 Hz, 2 H, SCH_2], 4.40 [dd, ^3J(H,H) = 7.6 Hz, ^3J(H,H) = 5.2 Hz, 1 H, CH], 5.08 (s, 5 H, C_5H_5). − ^{13}C NMR (100 MHz, [D$_6$]acetone, 20°C): δ = 19.6 (s, CH_3), 19.8 (s, CH_3), 38.1 (s, CH_2), 44.2 (s, CH_2), 58.0 (s, CH), 92.6 (s, C_5H_5), 123.3 (s, C=C), 128.8 (s, C=C). − ^{31}P NMR (162 MHz, [D$_6$]acetone, 20°C): δ = 105.5 (s). − Minor diastereoisomer: ^{1}H NMR (400 MHz, [D$_6$]acetone, 20°C): δ = 1.75 (s, 3 H, CH_3), 1.79 (s, 3 H, CH_3), 2.69 (m, 2 H, CH_2), 3.54, 3.92 [AB system, ^2J(H,H) = 17.4 Hz, 2 H, SCH_2], 4.40 (m, 1 H, CH), 5.52 (s, 5 H, C_5H_5). − ^{13}C NMR (100 MHz, [D$_6$]acetone, 20°C): δ = 19.3 (s, CH_3), 20.0 (s, CH_3), 40.1 (s, CH_2), 46.9 (s, CH_2), 56.9 (s, CH), 93.2 (s, C_5H_5), 123.3 (s, C=C), 129.2 (s, C=C). − ^{31}P NMR (162 MHz, [D$_6$]acetone, 20°C): δ = 104.3 (s). − IR (CH_2Cl_2): $\tilde{\nu}$ = 1733 cm^{-1} (NO). − $C_{36}H_{36}F_6NO_4P_2ReS$ (940.9): calcd. C 45.96, H 3.86, N 1.49, S 3.41; found C 46.16, H 3.67, N 1.48, S 3.32.

[CpRe(NO){P(OPh)$_3$}{SC$_5$H$_5$Ph(OMe)$_2$}]PF$_6$ (10b): This compound was prepared analogously from **5a** (143 mg, 0.17 mmol) and 2,3-dimethoxybutadiene (210 μL, 1.75 mmol). The orange colour of the starting material faded within 15 min. ^{1}H-NMR analysis of the crude product indicated complete conversion with 24% *de*. Yield 127 mg (78%), m.p. 83°C (dec.). − Major diastereoisomer: ^{1}H NMR (400 MHz, [D$_6$]acetone, 20°C): δ = 3.09, 3.17 [d of AB systems, ^2J(H,H) = 17.9 Hz, ^3J(H,H) = 8.5 Hz, ^3J(H,H) = 4.9 Hz, 2 H, CH_2], 3.68 (s, 3 H, OCH_3), 3.74 (s, 3 H, OCH_3), 3.90, 4.54 [AB system, ^2J(H,H) = 15.0 Hz, 2 H, SCH_2], 4.57 [dd, ^3J(H,H) = 8.6 Hz, ^3J(H,H) = 4.9 Hz, 1 H, CH], 5.08 (s, 5 H, C_5H_5). − ^{13}C NMR (100 MHz, [D$_6$]acetone, 20°C): δ = 34.0 (s, CH_2), 40.7 (s, CH_2), 58.1 (s, OCH_3), 58.8 (s, CH), 59.3 (s, OCH_3), 92.7 (s, C_5H_5), 135.7 (s, C=C), 138.5 (s, C=C). − ^{31}P NMR (162 MHz, [D$_6$]acetone, 20°C): δ = 104.5 (s). − Minor diastereoisomer: ^{1}H NMR (400 MHz, [D$_6$]acetone, 20°C): δ = 2.88 (m, 2 H, CH_2), 3.65 (s, 3 H, OCH_3), 3.68 (s, 3 H, OCH_3), 3.95−4.10 (m, 2 H, SCH_2), 4.54 (m, 1 H, CH), 5.57 (s, 5 H, C_5H_5). − ^{13}C NMR (100 MHz, [D$_6$]acetone, 20°C): δ = 35.6 (s, CH_2), 42.0 (s, CH_2), 57.1 (s, CH), 58.1 (s, OCH_3), 59.3 (s, OCH_3), 93.3 (s, C_5H_5), 136.4 (s, C=C), 138.4 (s, C=C). − ^{31}P NMR (162 MHz, [D$_6$]acetone, 20°C): δ = 103.7 (s). − IR (CH_2Cl_2): $\tilde{\nu}$ = 1735 cm^{-1} (NO). − $C_{36}H_{36}F_6NO_6P_2ReS$ (972.9): calcd. C 44.44, H 3.73, N 1.44, S 3.30; found C 44.45, H 3.68, N 1.29, S 3.00.

[CpRe(NO)(PPh$_3$){SC$_5$H$_5$Me$_2$(4-C$_6$H$_4$OMe)}]PF$_6$ (10c): A solution of **5e** (146 mg, 0.17 mmol) and 2,3-dimethylbutadiene (0.60 mL, 5.30 mmol) in acetone (4 mL) was kept for 5 d at 20°C. The mixture was then concentrated to dryness and the crude product was chromatographed by passage through a short (20 cm) silica column using dichloromethane/acetone, 20:1, as eluent. A first yellow band was found to contain the product, while the second consisted of unchanged **5e**. Both were collected and worked-up by evaporation of the solvents and recrystallization of the residues from dichloromethane/diethyl ether. Yield 20 mg (12%), m.p. 125°C (dec.). − Major diastereoisomer: ^{1}H NMR (400 MHz, $CDCl_3$, 20°C): δ = 1.33 (s, 3 H, CH_3), 1.64 (s, 3 H, CH_3), 2.47 [d, ^2J(H,H) = 15.6 Hz, 1 H, SCH_2], 2.60 [d, ^2J(H,H) = 18.2 Hz, 1 H, CH_2], 2.82 (m, 1 H, CH_2), 2.89 [d, ^2J(H,H) = 16.9 Hz, 1 H, SCH_2], 3.85 (s, 3 H, OCH_3), 4.00 [dd, ^3J(H,H) = 9.8 Hz, ^3J(H,H) = 4.3 Hz, 1 H, CH], 4.96 (s, 5 H, C_5H_5). − ^{13}C NMR (100 MHz, $CDCl_3$, 20°C): δ = 19.2 (s, CH_3), 19.7 (s, CH_3), 39.6 (s, CH_2), 44.2 (s, CH_2), 55.6 (s, OCH_3), 57.4 (s, CH), 92.8 (s, C_5H_5), 122.0 (s, C=C), 128.3 (s, C=C). − ^{31}P NMR (162 MHz, $CDCl_3$, 20°C): δ = 12.1 (s). − Minor diastereoisomer: ^{1}H NMR (400 MHz, $CDCl_3$, 20°C): δ = 1.39 (s, 3 H, CH_3), 1.60 (s, 3 H, CH_3), 2.06 [d, ^2J(H,H) = 14.7 Hz, 1 H, SCH_2], 2.60 (m, 1 H, CH_2), 3.53 [d, ^2J(H,H) = 15.7 Hz, 1 H, CH_2], 3.81 (s, 3 H, OCH_3), 4.04 (m, 1 H, CH), 5.23 (s, 5 H, C_5H_5). − ^{13}C NMR (100 MHz, $CDCl_3$, 20°C): δ = 19.0 (s, CH_3), 19.7 (s, CH_3), 55.4 (s, OCH_3), 57.7 (s, CH), 92.5 (s, C_5H_5), 123.1 (s, C=C), 127.8 (s, C=C). − ^{31}P NMR (162 MHz, $CDCl_3$, 20°C): δ = 11.4 (s). − IR (CH_2Cl_2): $\tilde{\nu}$ = 1712 cm^{-1} (NO). − $C_{37}H_{38}F_6NO_2P_2ReS$ (922.9): calcd. C 48.15, H 4.15, N 1.52; found C 47.82, H 3.82, N 1.84.

X-ray Structure Determination of [CpRe(NO)(PPh$_3$){SO$_2$CH$_2$CH(NC$_8$H$_4$O$_2$)COOMe}] · [D$_6$]acetone (3e · [D$_6$]acetone): $C_{35}H_{30}N_2O_7PReS \cdot C_3D_6O$: molecular mass 904.0, crystal size 0.3 × 0.15 × 0.05 mm, obtained from a saturated [D$_6$]acetone solution; triclinic crystal system, space group $P\bar{1}$ (No. 2), a = 8.4564(4), b = 13.229(2), c = 18.647(3) Å, α = 102.036(14)°, β = 93.63(2)°, γ = 102.69(2)°; V = 1977.1(10) Å^3, Z = 2, d_{calcd} = 1.519 g cm^{-3}; μ(Mo-K_α) = 1.82 cm^{-1}. Data were collected at 293 K in the range 2° < θ < 23° from one-half of the reflection sphere (Enraf−Nonius CAD4 diffractometer, graphite monochromator, Mo-K_α radiation, λ = 0.70930 Å). Of the 5926 measured reflections, 5485 were symmetry-independent and 3044 were classified as observed [$I_O > 2\sigma(I_O)$]. An empirical absorption correction based on the counts of 4 reflections was applied. The structure was solved by the Patterson method by using the program package SHELXS-86[35] with hydrogen atoms included in their calculated positions. Refinement using the program package SHELXL-93[36] gave R_1 = 0.066, wR_2 = 0.121. The 5 highest maxima of a final difference Fourier map were below 0.895 e·Å^{-3}. Further details of the structure determination may be obtained from the Fachinformationszentrum Karlsruhe, D-76344 Eggenstein-Leopoldshafen, on quoting the depository number CSD-408460.

Acknowledgments

This work was supported by the Deutsche Forschungsgemeinschaft (SFB 347 "Selektive Reaktionen Metall-aktivierter Moleküle").

[1] N. Burzlaff, W. A. Schenk, *Eur. J. Inorg. Chem.* **1998**, 2055−2061.
[2] P. L. Roach, I. J. Clifton, C. M. H. Hensgens, N. Shibata, C. J. Schofield, J. Hajdu, J. E. Baldwin, *Nature* **1997**, *387*, 827−830.
[3] W. A. Schenk, T. Stur, E. Dombrowski, *Inorg. Chem.* **1992**, *31*, 723−724.
[4] W. A. Schenk, T. Stur, E. Dombrowski, *J. Organomet. Chem.* **1994**, *472*, 257−273.
[5] W. A. Schenk, N. Burzlaff, H. Burzlaff, *Z. Naturforsch.*, *B* **1994**, *49*, 1633−1639.

[6] H. Werner, L. Hofmann, J. Wolf, G. Müller, *J. Organomet. Chem.* **1985**, *280*, C55−C59.
[7] H. Werner, W. Paul, W. Knaup, J. Wolf, G. Müller, J. Riede, *J. Organomet. Chem.* **1988**, *358*, 95−121.
[8] C. Bianchini, L. Glendenning, M. Peruzzini, A. Romerosa, F. Zanobini, *J. Chem. Soc., Chem. Commun.* **1994**, 2219−2220.
[9] S. L. Buchwald, R. B. Nielsen, J. C. Dewan, *J. Am. Chem. Soc.* **1987**, *109*, 1590−1591.
[10] A. V. Firth, D. W. Stephan, *Organometallics* **1997**, *16*, 2183−2188.
[11] Y. Huang, M. Etkin, R. R. Heyn, T. T. Nadasdi, D. W. Stephan, *Organometallics* **1996**, *15*, 2320−2330.
[12] E. J. Parker, J. R. Bodwell, T. C. Sedergran, D. C. Dittmer, *Organometallics* **1982**, *1*, 517−522, and references cited therein.
[13] N. Burzlaff, M. Hagel, W. A. Schenk, *Z. Naturforsch.*, *B* **1998**, *53*, 893−899.
[14] W. E. Buhro, M. C. Etter, S. Georgiou, J. A. Gladysz, F. B. McCormick, *Organometallics* **1987**, *6*, 1150−1156.
[15] W. A. Schenk, P. Urban, T. Stährfeldt, E. Dombrowski, *Z. Naturforsch.*, *B* **1992**, *47*, 1493−1500.
[16] P. C. Cagle, O. Meyer, D. Vichard, K. Weickhardt, A. M. Arif, J. A. Gladysz, *Organometallics* **1996**, *15*, 194−204.
[17] H. Fischer, U. Gerbing, J. Riede, *J. Organomet. Chem.* **1989**, *364*, 155−167.
[18] H. Fischer, U. Gerbing, K. Treier, J. Hofmann, *Chem. Ber.* **1990**, *123*, 725−732.
[19] H. Fischer, K. H. Fluck, C. Troll, *Chem. Ber.* **1992**, *125*, 2675−2680.
[20] E. W. Abel, S. K. Bhargava, K. G. Orrell, *Prog. Inorg. Chem.* **1984**, *32*, 1−118.
[21] N. Q. Mendez, A. M. Arif, J. A. Gladysz, *Organometallics* **1991**, *10*, 2199−2209.
[22] J. A. Gladysz, B. J. Boone, *Angew. Chem.* **1997**, *109*, 566−602; *Angew. Chem. Int. Ed. Engl.* **1997**, *36*, 550−583.
[23] H. Fischer, S. Zeuner, *Z. Naturforsch.*, *B* **1985**, *40*, 954−960.
[24] H. Fischer, S. Zeuner, U. Gerbing, J. Riede, C. G. Kreiter, *J. Organomet. Chem.* **1989**, *377*, 105−122.
[25] W. Weigand, R. Wünsch, *Chem. Ber.* **1996**, *129*, 1409−1419.
[26] T. A. George, D. D. Watkins, *Inorg. Chem.* **1973**, *12*, 398−402.
[27] W. G. Jackson, A. M. Sargeson, *Inorg. Chem.* **1988**, *27*, 1068−1073, and references cited therein.
[28] C. A. Grapperhaus, M. Y. Darensbourg, *Acc. Chem. Res.* **1998**, *31*, 451−459.
[29] M. T. Ashby, J. H. Enemark, D. L. Lichtenberger, *Inorg. Chem.* **1988**, *27*, 191−197.
[30] M. T. Ashby, *Comments Inorg. Chem.* **1990**, *10*, 297−313.
[31] S. G. Davies, M. L. H. Green, D. M. P. Mingos, *Tetrahedron* **1978**, *34*, 3047−3077.
[32] L. S. Hegedus in: *The Chemistry of the Metal−Carbon Bond*, Vol. 2 (Eds.: F. R. Hartley, S. Patai), Wiley, New York **1985**, chapter 6.
[33] S. K. Agbossou, J. M. Fernandez, J. A. Gladysz, *Inorg. Chem.* **1990**, *29*, 476−480.
[34] A. Schöberl, A. Wagner in: *Methoden der Organischen Chemie (Houben-Weyl)*, 4th Edition, Vol. 9, Thieme, Stuttgart, **1955**, pp. 43−45.
[35] G. M. Sheldrick, *SHELXS-86, Program for Crystal Structure Solution*, Universität Göttingen, Germany, **1986**.
[36] G. M. Sheldrick, *SHELXL-93, Program for Crystal Structure Refinement*, Universität Göttingen, Germany, **1993**.

Received March 5, 1999
[I99088]

New Inorganic Metallacycles and the First Six-Membered Covalent "True" Heterocycle − Oxidation of $RC(E)NHPPh_2$ (E = O or S; R = H_2N, Ph, or Py) with O, S, or Se to Give $RC(E)NHP(E')Ph_2$ (E′ = O, S, Se) and Their Coordination Chemistry

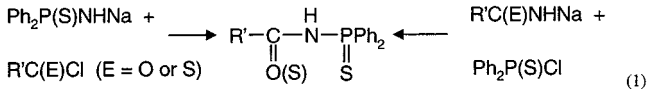
David J. Birdsall,[a] Jason Green,[a] Tuan Q. Ly,[a] Josef Novosad,[b] Marek Necas,[b] Alexandra M. Z. Slawin,[a] J. Derek Woollins,*[a] and Zdirak Zak[b]

Keywords: Metallacycles / Solid-state structures / Heterocycles / Oxidations

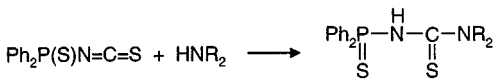
Direct oxidation of $PhC(O)NHPPh_2$, $H_2NC(S)NHPPh_2$, $(C_5H_4N)C(S)NHPPh_2$ with O_2, S_8, or Se gives $[PhC(O)NHP(O)Ph_2]$ (**1**), $[H_2NC(S)NHP(S)Ph_2]$ (**2**), $[H_2NC(O)NHP(S)Ph_2]$ (**3**), $[PhC(O)NHP(S)Ph_2]$ (**4**), $[(C_5H_4N)C(S)NHP(S)Ph_2]$ (**5**), and $[H_2NC(S)NHP(Se)Ph_2]$ (**6**). Deprotonation of **1**, **2**, **4**–**6** with potassium *tert*-butoxide gives $K[PhC(O)NP(O)Ph_2]$ (**7**), $K[H_2NC(S)NP(S)Ph_2]$ (**8**), $K[PhC(O)NP(S)Ph_2]$ (**9**), $K[(C_5H_4N)C(S)NP(S)Ph_2]$ (**10**), and $K[H_2NC(S)NP(Se)Ph_2]$ (**11**). Reaction of **4** with KOBu and $[Cu(Ph_3P)_2][NO_3]$ gives $[Cu(Ph_3P)(PhC(O)NP(S)Ph_2)]$ (**12**) which is the first crystallographically characterised example of a non-ionic six-membered "true" heterocycle (i.e. a ring in which every heterocatom is different). **9** and **10** were treated with $[PdCl_2(COD)]$ to give $[Pd\{PhC(O)NP(S)Ph_2\}_2]$ (**13**) and $[Pd\{(C_5H_4N)C(O)NP(S)Ph_2\}_2]$ (**14**), respectively The anion of **8** coordinates to zinc forming $[Zn\{H_2NC(S)NP(S)Ph_2\}_2]$ (**15**). Treatment of **2** or **8** with $[PtCl_2(COD)]$ gives $[Pt\{H_2NC(S)NP(S)Ph_2\}\{H_2NC(S)NHP(S)Ph_2\}]^+Cl^-$ (**16**) and $[Pt\{H_2NC(S)NP(S)Ph_2\}_2]$ (**17**), respectively. The X-ray structures of **12**, **15–17** are reported.

Introduction

We have reported extensively[1] on the coordination chemistry of imidophosphinates in part as a consequence of their relationship to *acac*. Furthermore, monochalcogenides and molecules of the type $[Ph_2PNHP(E)Ph_2]$ (E = O, S, or Se)[2−11] have been developed and shown to chelate to range of late transition metals through both phosphorus and chalcogen donor atoms. The chemistry of phosphane derivatives of urea and thiourea were first studied during the 1960s. Three known methods of preparing such derivatives are shown below (Equation 1 and 2).[12−20]



(1)



(2)

Schmutzler et al. reported that the reaction of thiourea and chlorodiphenylphosphane at −20 °C did not give the expected *N*,*N*′-bis(diphenylphosphanyl)thiourea, $Ph_2PHNC(S)NHPPh_2$, but only gave $Ph_2P-P(S)Ph_2$.[21] Later, Bhattacharyya et al. carried out the reaction at room temperature and obtained *N*,*N*′-bis(diphenylphosphanyl)-thiourea in up to 46 % yield.[22] We have recently described[23] the formation of some phosphanylurea and related systems Here, we report on the oxidation of the phosphanylurea and phosphanyl-thiourea derivatives. Demonstrative examples of coordination complexes are also described, including the first example of a non-ionic six-membered "true" heterocycle.

Results and Discussion

The ligands were synthesised by direct oxidation of the phosphanylureas or phosphanylthioureas with the appropriate oxidising reagents generalised in Equation 1. $PhC(O)NHPPh_2$ oxidises readily with oxygen by dissolving it in tetrahydrofuran and stirring overnight exposed to air. However, $H_2NC(S)NHPPh_2$ is more stable and does not oxidise in air, when treated with aqueous hydrogen peroxide as well as the oxidation of P^{III} to P=O, most of the C=S is converted into C=O in the course of the reaction, the by-product, $H_2NC(O)NHP(O)Ph_2$,was identified by ^{31}P-NMR, infrared, and mass spectroscopy.

Oxidation of the phosphanylurea/thiourea derivatives by elemental sulfur is readily achieved in tetrahydrofuran at room temperature. $H_2NC(O/S)NHPPh_2$ react with S_8 to form (Equation 3) $[H_2NC(S)NHP(S)Ph_2]$ (**2**) and $[H_2NC(O)NHP(S)Ph_2]$ (**3**), respectively. Treatment of $RC(O)NHPPh_2$ (R = Ph and Py, 3-C_5H_4N, Py = pyridyl) with S_8 gave $[PhC(O)NHP(S)Ph_2]$ (**4**) and $[PyC(O)NHP(S)Ph_2]$ (**5**), respectively.

$[H_2NC(S)NHP(Se)Ph_2]$ (**6**) was prepared by allowing $H_2NC(S)NHPPh_2$ to react with grey selenium in tetrahydrofuran with warming for one hour. The solution was then filtered and its solvent removed to give a white powder.

[a] Department of Chemistry, University of St Andrews, St Andrews, Scotland KY16
E-mail: J.D.Woollins@st-and.ac.uk
[b] Department of Chemistry, Masaryk University, Czech Republic

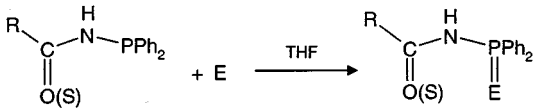
 © WILEY-VCH Verlag GmbH, D-69451 Weinheim, 1999 1434−1948/99/0909−1445 $ 17.50+.50/0

Table 1. ^{31}P-{^{1}H} NMR [ppm, relative to 85% H_3PO_4] for compounds **1**−**11**

	δ =		δ =
1 [PhC(O)NHP(O)Ph_2]	24	**7** K[PhC(O)NP(O)Ph_2]	17
2 [H_2NC(S)NHP(S)Ph_2]	52	**8** K[H_2NC(S)NP(S)Ph_2]	37
3 [H_2NC(O)NHP(S)Ph_2]	53		
4 [PhC(O)NHP(S)Ph_2]	56	**9** K[PhC(O)NP(S)Ph_2]	44
5 [PyC(O)NHP(S)Ph_2]	56	**10** K[PyC(O)NP(S)Ph_2]	41
6 [H_2NC(S)NHP(Se)Ph_2]	45	**11** K[H_2NC(S)NP(Se)Ph_2]	29
Note: Py = 3-C_5H_4N	[^{1}J(PSe) 783]		[^{1}J(PSe) 530]

Table 2. Selected infrared data [cm^{-1}] in compounds **1**−**11**

	ν(NH)	ν(CO, S)	ν(CN)	ν(PN)	ν(PO, S, Se)
1 [PhC(O)NHP(O)Ph_2]	3107m-sh, 3066 s	1669 vs	1456 vs	838 s, 807 w	1199 vs
2 [H_2NC(S)NHP(S)Ph_2]	3381 w, 3294 s, 3074 s	1054 s	1484 vs	835 s, 810 s	642 s, 632 s
3 [H_2NC(O)NHP(S)Ph_2]	3492m, 3333m, 3187m	1704 vs, 1682 vs, 1650 vs	1477 vs	912m, 872 w	636m
4 [PhC(O)NHP(S)Ph_2]	3159m, 3070m	1651 vs	1454 vs	880 w, 832m	636 vs
5 [PyC(O)NHP(S)Ph_2]	3368 vw, 3182 s	1656 vs	1482m	842m, 815m	639 vs
6 [H_2NC(S)NHP(Se)Ph_2]	3364 w, 3284m, 3072m	1052m	1482 vs	832 s, 807 s	555 vs
7 K[PhC(O)NP(O)Ph_2]		1523 vs	1591 s	896 s, 842 s	1141 s
8 K[H_2NC(S)NP(S)Ph_2]	3364m, 3280m, 3164 w			856 vw, 836 vw	624m, 607 s
9 K[PhC(O)NP(S)Ph_2]		1519 vs	1588m	895 w, 838 s	627 s, 612 s
10 K[PyC(O)NP(S)Ph_2]	3322 vw, 3237 vw	1526 vs	1590 vs	906 s, 830 vs	626 vs, 613 vs
11 K[H_2NC(S)NP(Se)Ph_2]	3353m, 3162m			885 w, 851 w	544 vs



(3)

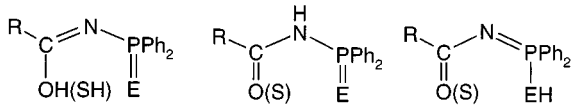


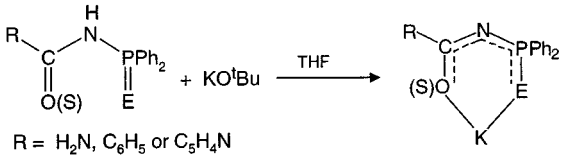
Figure 1. Tautomeric forms of RC(E)NHP(E′)Ph_2 (E = O or S; E′ = O, S, or Se)

After trituration with diethyl ether the product was obtained in 67 % yield.

All of the compounds are air stable colourless solids except **6** which turns red when exposed to air over a week; it can be stored under nitrogen almost indefinitely. The ^{31}P-NMR showed the shifts of P^{III} to P^{V} shown in Table 1. All the P=O, S, and Se derivatives display singlets in their phosphorus NMR spectra.

Compounds **1**−**6** can exist in three tautomeric forms (**A** − **C**, Figure 1). Their infrared spectra (Table 2) suggest form (**B**) is predominant in the solid state. The spectra of the compounds show peaks at around 3200 cm^{-1} indicating ν(NH) character. The vibrations at around 1665 cm^{-1} and 1100 cm^{-1} are indicative of ν(C=O) and ν(C=S) double bonds. The bands at around 1470 cm^{-1} are characteristic of ν(C−N) single bond [lower than ca. 1650 cm^{-1} for ν(C=N)]. All these compounds also have bands around 850 cm^{-1} reflecting the single bond character of ν(PN) compared to the double bond vibration at higher frequency around 1300 cm^{-1}. Furthermore vibrations at around 630 cm^{-1} and 1180 cm^{-1} for ν(P=S) and ν(P=O) support structure (**B**) in solid state.

Compounds **1**, **2**, **4**−**6** were easily deprotonated upon treatment with KO*t*Bu in THF at room temperature to give K[PhC(O)NP(O)Ph_2] (**7**), K[H_2NC(S)NP(S)Ph_2] (**8**), K[PhC(O)NP(S)Ph_2] (**9**), K[PyC(O)NP(S)Ph_2] (**10**), and K[H_2NC(S)NP(Se)Ph_2] (**11**) (Equation 4). The solutions were filtered through celite and the solvent removed to give the products analytically pure. All the compounds are colourless in appearance.



(4)

It can be seen by ^{31}P NMR that the displacement of an amino proton by an electropositive element (potassium) in general shields the nucleus under scrutiny and it is observed at lower frequency (Table 1). Upon deprotonation the ν(C=O) vibration shifts around 130 cm^{-1} to lower frequency, whilst the ν(C=S) cannot be easily identified. Concurrently the bond order of the P−N bond has increased and the & uψ;(CN) is observed at higher frequency in the deprotonated compounds.

The X-ray structure of **4** shows[24] the compound is in the keto form with the proton bonded to the nitrogen and not to the terminal chalcogen atoms. The geometry of this compound can be compared with [*i*Pr_2P(S)NHP(S)*i*Pr_2]

which also exists in a *syn* conformation.[27] The molecular structure of K[PhC(O)NP(S)Ph_2] **9** shows the ligand is coordinated to potassium via oxygen and sulfur donor atoms in a six-membered chelate ring arrangement in which the ring can be viewed as a true heterocycle containing six different atoms from Groups 1, 14, 15, and 16 of the periodic table. There are few previous crystallographic determinations to make comparisons. The most appropriate is K[N{P(S)Ph_2}$_2$].[28]

Reaction of K[PhC(O)NP(S)Ph_2] **9** with Cu(PPh_3)$_2$(NO_3) gives Cu(PhC(O)NP(S)Ph_2)(PPh_3) **12** which is the first example of a non-ionic six-membered true heterocycle. In **12** the X-ray structure (Table 3, Figure 2) reveals that copper is trigonal [Cu lies 0.03 Å out of the Cu−O−S−P(2) mean plane) and that the Cu−S−P−N−C−O ring is non-planar in what can best be described as a pseudo boat conformation. The P(1)−S−Cu−O mean plane [max. deviation 0.16 Å for Cu] is inclined by 142° to the O−C(37)−N−P(1) mean plane [max. deviation 0.01 Å for C(37)].

Table 3. Selected bond lengths [Å] and angles [°] in [Cu(PPh_3)-(PhC(O)NP(S)Ph_2)] **12**

Cu−O 2.013(2)	P(1)−N 1.621(3)
Cu−P(2) 2.1897(10)	N−C(37) 1.326(4)
Cu−S 2.223(1)	C(37)−O 1.270(3)
S−P(1) 2.011(1)	
O−Cu−P(2) 112.4(1)	N−P(1)−S 119.0(1)
O−Cu−S 106.2(1)	C(37)−N−P(1) 121.1(2)
P(2)−Cu−S 141.3(4)	O−C(37)−N 126.4(3)
P(1)−S−Cu 92.3(1)	C(37)−O−Cu 125.7(2)

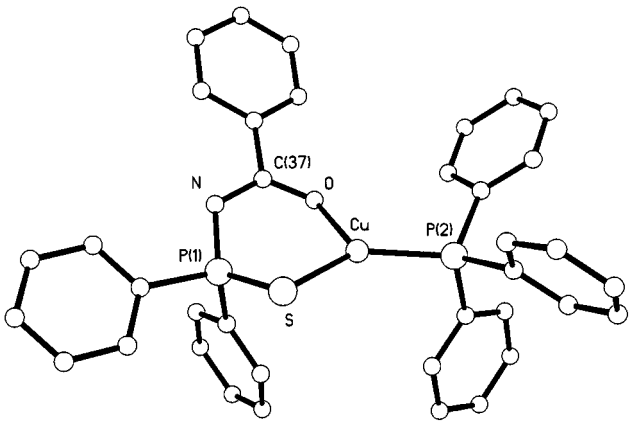


Figure 2. Molecular structure of [Cu(PPh_3)(PhC(O)NP(S)Ph_2)] **12** in the crystal

Two equivalents of the ligand salt K[PhC(O)NP(S)Ph_2] (**9**) was treated with [$PdCl_2$(COD)] in dichloromethane to give an orange solution immediately (Equation 5). The product [Pd{PhC(O)NP(S)Ph_2}$_2$] (**13**) was triturated with petroleum ether and a yield of 57 % was collected. [Pd{PyC(O)NP(S)Ph_2}$_2$] (**14**) was prepared in the same way with K[PyC(O)NP(S)Ph_2] (**10**) and [$PdCl_2$(COD)] and was isolated as red powder (93 %). The compounds **13** and **14** show the correct parent ion mass numbers [779 and 780 *m/z*] and isotope distributions in their FAB mass spectra and have satisfactory elemental analysis. The $^{31}P\{^1H\}$ NMR spectra display a singlet for both compounds at δ = 30 for **13** and 31 for **14** whilst their infrared spectra show similar features with the vibrational patterns simplified compared to the ligand salts and free ligands. The P=S vibrational frequencies have shifted around 50 cm^{-1} lower compared to the free ligands. In compound **13** the ν(CO) band is reduced significantly by 166 cm^{-1} which is in the range of a C−O single bond. The ν(CO) band for **14** appears to be a lot more complicated and are assigned at 1609, 1585, 1551, and 1508 cm^{-1}. The ν(PN) band in the palladium complexes have shifted [926 and 804 cm^{-1} for **13**; 920 and 818 cm^{-1} for **14**] to a higher frequency indicating an increase in the P−N bond order. The ligands seem to have coordinated to a palladium atom through their PS and CO donor groups to form metal complexes as six-membered chelate compounds. There are two possible isomers, *cis* or *trans*, that these compounds can form.

$$[PdCl_2(COD)] + 2K[RC(O)NP(S)Ph_2] \longrightarrow$$

R = C_6H_5 or C_5H_4N

$$[Pd\{RC(O)NP(S)Ph_2\}_2] + 2KCl \quad (5)$$

Ojima et al.[14][15] proposed that some diphenylphosphanylthioylthioureato metal(II) complexes have a chelate structure consisting of five different atoms − C, N, P, 2 S, and M^{II}. One of those complexes, where M = Ni, was later confirmed by Iwamoto et al.[29] with a molecular structure from X-ray crystallography studies however there has been little further work done in this area.

The zinc complex [Zn{H_2NC(S)NP(S)Ph_2}$_2$] (**15**) was obtained by the addition of $ZnCl_2$ to a tetrahydrofuran solution of K[H_2NC(S)NP(S)Ph_2] (Equation 6) in 75 % yield.

$$ZnCl_2 + 2K[H_2NC(S)NP(S)Ph_2] \longrightarrow$$

$$[Zn\{H_2NC(S)NP(S)Ph_2\}_2] + 2KCl \quad (6)$$

The X-ray structure of **15** (Table 4, Figure 3) reveals the expected tetrahedral coordination at zinc with the ZnS_2PCN ring adopting an approximately boat conformation Zn(1)−S(1)−S(2)−C(1) [max. deviation 0.08 Å for S(2)] is inclined by 137° to P(1)−N(1)−C(1)−S(1) [max. deviation 0.29 Å for N(1)].

Table 4. Selected bond lengths [Å] and angles [°] in [Zn{H_2NC-(S)NP(S)Ph_2}$_2$] **15**

Zn(1)−S(1) 2.351(2)	Zn(1)−S(2) 2.338(2)
P(1)−S(1) 2.014(2)	P(1)−N(1) 1.637(5)
N(1)−C(1) 1.334(8)	N(2)−C(1) 1.343(8)
C(1)−S(2) 1.748(6)	
S(1)−Zn(1)−S(2) 107.1(1)	Zn(1)−S(1)−P(1) 95.5(1)
S(1)−Zn(1)−S(1A) 116.1(1)	S(1)−Zn(1)−S(2A) 106.5(1)
S(1)−P(1)−N(1) 116.9(2)	P(1)−N(1)−C(1) 125.3(9)
N(1)−C(1)−N(2) 116.2(5)	N(2)−C(1)−S(2) 114.7(5)
N(1)−C(1)−S(2) 129.0(5)	C(1)−S(2)−Zn(1) 109.3(2)

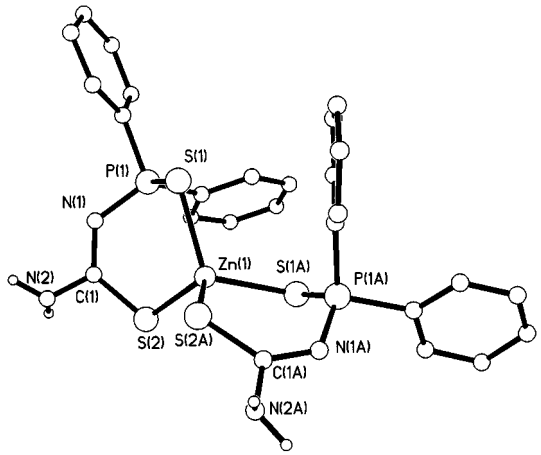


Figure 3. Molecular structure of $[Zn\{H_2NC(S)NP(S)Ph_2\}_2]$ **15** in the crystal

Reaction of equimolar amounts of $[H_2NC(S)NHP(S)Ph_2]$ (**2**) and $[PtCl_2(COD)]$ in dichloromethane was expected to give a six-membered chelate complex $PtCl_2\{H_2NC(S)NHP(S)Ph_2\}$. However, two singlets with unresolved ^2J platinum satellites were observed in the ^{31}P-NMR spectrum. Mass spectrometry reveals that two ligands have coordinated to the metal centre. The two NMR signals may be assigned to a neutral and a deprotonated ligand in $Pt\{H_2NC(S)NHP(S)Ph_2\}\{H_2NC(S)NP(S)Ph_2\}]Cl$ (**16**) (vide infra). The reaction was repeated using 2 molar equivalents of $K[H_2NC(S)NP(S)Ph_2]$, in dichloromethane to give the yellow crystalline $[Pt\{H_2NC(S)NP(S)Ph_2\}_2]$ (**17**) (Equation. 7).

$$[PtCl_2(COD)] + 2K[H_2NC(S)NP(S)Ph_2] \longrightarrow [Pt\{H_2NC(S)NP(S)Ph_2\}_2] + 2KCl \quad (7)$$

Compound **17** displays a singlet [δ = 33] with characteristic ^2J platinum coupling [^2J(P−Pt) = 114 Hz]. Compound **16** and **17** both displayed the correct mass values with the appropriate isotope distributions for $[Pt\{H_2NC(S)NP(S)Ph_2\}_2]$ obtained from FAB mass spectroscopy. Confirmation of the stoichiometry in the complexes was obtained from satisfactory elemental analysis data.

The infrared spectrum of compound **16** shows a close similarity to[23] $[Pt\{H_2NC(S)NHPPh_2\}_2]^{2+} \cdot 2\,Cl^-$ but with additional peaks at 598 and 576 cm^{-1} due to the two different phosphorus-sulfur vibrations Two broad ν(PN) vibrations are observed at 922 and 883 cm^{-1}. Close inspection of the peaks due to the NH_2 groups reveals two overlapping peaks resulting in very broad bands. Compound **17** displays an infrared spectrum which is very similar to that of **15**; with the ν(PS) vibration in **17** seen at 577 cm^{-1} and the ν(PN) vibration as a broad band at 883 cm^{-1}.

The X-ray structure of **16** (Table 5, Figure 4) shows that the two chelates are bound to a platinum atom by four sulfur donor atoms forming two six-membered rings in the *trans* configuration. Interestingly only one ligand is deprotonated which is supported by the notable differences in the P−N bond lengths for the two rings [P(1)−N(1) 1.56(3) P(21)−N(21) 1.65(2) Å] with deprotonation giving the shorter P−N length which is comparable to those in **15**. Furthermore the presence of the N−H proton in chelate **A** is supported by the close proximity of the chloride counter ion which H-bonds to the NH and NH_2 groups [N(22)···Cl(1) 3.38 Å, N−H···Cl 154°; N(21)···Cl(1) 3.10 Å, N−H···Cl 125°] to give a six-membered H−N−C−N−H−Cl ring. The chloride ion also H-bonds to the adjacent cation [N(2′)···Cl(1) 3.40 Å, N−H···Cl 160°] thus linking the cations and anions into chains. The square planar complex contains two six-membered rings though there are significant differences in ring conformation which may be due to one chelate ring being deprotonated. In chelate **A** (neutral ligand) the two Pt−S bond lengths are 2.317(7) and 2.322(8) Å with no significant differences between the sulfur donors bound by carbon and phosphorus atoms; the P=S bond length [1.97(1) Å] is similar to those in $[PhC(O)NHP(S)Ph_2]$ [1.94(6) Å] and $[\{(PhO)_2P(S)NC(S)N(nPr)_2\}_2Ni]$[30] which haa a P−S bond with substantial delocalisation and a bond length of 1.978(1) Å. The P−N and N−C bonds distances are appropriate for a limited degree of delocalisation and compare well with those in $[Pt\{H_2NC(S)NHPPh_2\}_2]^{2+} \cdot 2\,Cl^-$ [1.676(1) and 1.38(2) Å]. The most dramatic change observed is the lengthening of the C=S bond by about 0.1 Å compared to that in $[Pt\{H_2NC(S)NHPPh_2\}_2]^{2+} \cdot 2\,Cl^-$ to an observed single bond value [1.75(3) Å] similar to that in $[\{Ph_2(S)PNC(S)NH(CH_3)\}_2Ni]$ [1.760(9) Å].[29] There are significant differences in bond lengths in chelate **B** (deprotonated anionic ligand). The two Pt−S and P=S bond lengths are similar to those in chelate **A**. The P−N appears to be partially double [1.56(3) Å] and the C−N and C=S are similar to those in the neutral ligand The ring conformations are different; **A** is a "twist chair" conformation whilst **B** contains a relatively planar fragment −S(2)−P(1)−N(1)−C(1)−S(1) [max deviation 0.25 Å for N(1)] which is inclined by 63° to the Pt(1)−S(1)−S(2) plane.

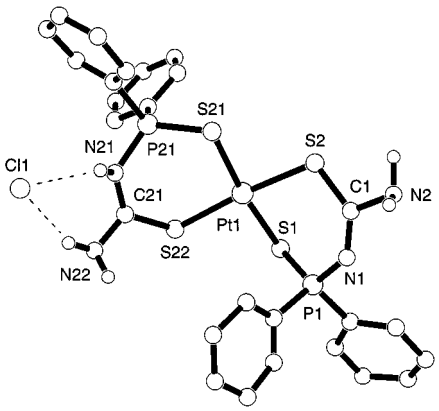


Figure 4. Molecular structure of *trans*-$[Pt\{H_2NC(S)NP(S)Ph_2\}\{H_2NC(S)NHP(S)Ph_2\}]^+Cl^-$ **16** in the crystal

Table 5. Selected bond lengths [Å] and angles [°] in *trans*-[Pt{$H_2NC(S)NP(S)Ph_2$}{$H_2NC(S)NHP(S)Ph_2$}]$^+Cl^-$ **16**

Chelate **A**		Chelate **B** (deprotonated)	
Pt−S(21)	2.316(7)	Pt−S(1)	2.324(7)
Pt−S(22)	2.322(8))	Pt−S(2)	2.313(8)
S(21)−P(21)	1.97(1)	S(1)−P(1)	1.98(1)
P(21)−N(21)	1.65(2)	P(1)−N(1)	1.56(3)
N(21)−C(21)	1.30(3)	N(1)−C(1)	1.30(3)
C(21)−S(22)	1.75(3)	C(1)−S(2)	1.73(3)
C(21)−N(22)	1.34(3)	C(1)−N(2)	1.40(3)
S(21)−Pt−S(22)	101.9(3)	S(1)−Pt−S(2)	90.6(3)
S(2)−Pt−S(21)	83.7(3)	S(1)−Pt−S(22)	83.9(3)
Pt−S(22)−C(21)	112(1)	Pt−S(2)−C(1)	108(1)
Pt−S(21)−P(21)	102.0(4)	Pt−S(1)−P(1)	97.4(4)
S(22)−C(21)−N(21)	127(2)	S(2)−C(1)−N(1)	134(2)
C(21)−N(21)−P(21)	125(2)	C(1)−N(1)−P(1)	126(2)
N(1)−C(1)−N(2)	115(3)	N(21)−C(21)−N(22)	121(2)
N(21)−P(21)−S(21)	113.4(9)	N(1)−P(1)−S(1)	118(1)
S(22)−C(21)−N(22)	112(2)	S(2)−C(1)−N(2)	110(2)

The X-ray structure of **17** (Table 6, Figure 5) reveals that the two deprotonated ligands are bound to the square planar platinum atom in a *cis* configuration. The PtS_4 coordination sphere resembles that in bis(dithiobiureto)palladium(II)[31] and imidodiphosphinatoplatinum(II).[32] The bond lengths within the rings of **17** are similar to those of ring **B** in **16** and the ring conformations mostly closely resembles that of the deprotonated ring **B** in **16**. In **17** both rings consist of fairly planar S−P−N−C−S backbones [max. deviations for the two rings being 0.25 Å for C(1) and 0.31 Å for C(21)] which are inclined to the coordination plane by 60° in each case.

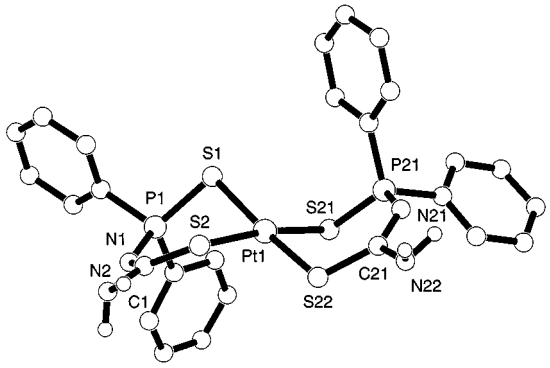


Figure 5. Molecular structure of *cis*-[Pt{$H_2NC(S)NP(S)Ph_2$}$_2$]·(Et_2O) **17** in the crystal

When we attempted to react [$H_2NC(S)NHP(Se)Ph_2$] **6** with [$PtCl_2$(COD)], red selenium deposited out of solution. The reaction was monitored by ^{31}P NMR which revealed a signal at 70 ppm with platinum-satellites which identified the product as [Pt{$H_2NC(S)NHPPh_2$}$_2$]$^{2+}$ · 2 Cl^-.

This work has demonstrated the ease of formation of hybrid organic/inorganic ligands which have elements of *acac* and imidophosphinate ligand systems. The usefulness of these ligands in metal specific coordination and catalysis awaits investigation.

Table 6. Selected bond lengths [Å] and angles [°] in *cis*-[Pt{$H_2NC(S)NP(S)Ph_2$}$_2$] · (Et_2O) **17**

Pt−S(1)	2.322(4)	Pt−S(21)	2.330(4)
Pt−S(2)	2.312(4)	Pt−S(22)	2.307(4)
S(1)−P(1)	1.987(7)	S(21)−P(21)	2.004(7)
P(1)−N(1)	1.62(1)	P(21)−N(21)	1.61(1)
N(1)−C(1)	1.34(2)	N(21)−C(21)	1.32(2)
C(1)−S(2)	1.70(2)	C(21)−S(22)	1.72(2)
C(1)−N(2)	1.37(2)	C(21)−N(22)	1.37(2)
S(1)−Pt−S(2)	93.0(1)	S(21)−Pt−S(22)	93.0(1)
S(1)−Pt−S(21)	90.6(2)	S(2)−Pt−S(22)	84.2(1)
Pt−S(2)−C(1)	108.6(6)	Pt−S(22)−C(21)	109.7(6)
Pt−S(1)−P(1)	99.0(2)	Pt−S(21)−P(21)	98.2(2)
S(1)−P(1)−N(1)	120.5(5)	S(21)−P(21)−N(21)	119.8(6)
P(1)−N(1)−C(1)	127(1)	P(21)−N(21)−C(21)	129(1)
N(1)−C(1)−N(2)	112(2)	N(21)−C(21)−N(22)	116(1)
N(1)−C(1)−S(2)	133(1)	N(21)−C(21)−S(22)	132(1)
S(2)−C(1)−N(2)	114(1)	S(22)−C(21)−N(22)	112(1)

Experimental Section

General: Diethyl ether, petroleum ether (60−80 °C) and tetrahydrofuran were purified by reflux over sodium and distillation under nitrogen. Dichloromethane was heated to reflux over powdered calcium hydride and distilled under nitrogen. − Infrared spectra were recorded from KBr discs on a Perkin−Elmer system spectrometer. − ^{31}P NMR spectra on a Jeol FX90Q operating at 36.21MHz; ^1H-, ^{13}C-, and ^{31}P-NMR spectra on a Bruker AC250 operating at 250, 62.9, and 101.3MHz respectively. − Fast atom bombardment mass spectra were measured by the Swansea mass spectrometry service.

[PhC(O)NHP(O)Ph_2] (1): A solution of $PhC(O)NHPPh_2$ (760 mg, 2.49 mmol) in THF (50 mL) was stirred overnight in air. The solution was filtered and the filtrate was reduced to dryness to give a white powder. It was recrystallised from CH_2Cl_2/Et_2O to give a yield of 795 mg (99 %). M.p. 197−199 °C. − ^{31}P NMR ($CDCl_3$): δ = 24. − IR (KBr disc, cm^{-1}): 3159 m, 3066 s, 2842 mw, 1669 vs, 1591 m, 1500 s, 1456 vs, 1439 vs, 1267 s, 1199 vs, 1128 vs, 1108 s, 1072 m, 1027 m, 998 w, 875 m, 838 s, 807 w, 754 s, 728 vs, 711 vs, 692 vs, 525 vs, 476 w, 296 w. − FAB (*m/z*): 344 $[M + Na]^+$ and 322 $[M + H]^+$. − $C_{19}H_{16}NO_2P$ (321.32): found C 70.66, H 4.72, N 3.87; (calcd. C 71.02, H 5.02, N 4.36 %).

[$H_2NC(S)NHP(S)Ph_2$] (2): To a suspension of $H_2NC(S)NH_2$ (8.5 g, 112 mmol) in THF (300 mL) was added Et_3N (15.5 mL, 111 mmol) and DMAP (100 mg, 10 mmol). A THF (200 mL) solution of Ph_2PCl (15 mL, 83 mmol) was then added dropwise over 3 h. The solution was filtered into another flask containing S (2.7 g, 83 mmol) and the residue washed with THF (100 mL). After 30 min of stirring the solution was evaporated to dryness and extracted with CH_2Cl_2 (200 mL). The extract was concentrated and triturated with Et_2O to give a microcrystalline product 9.4 g (39 %). Mp: 144−145 °C. − ^{31}P NMR ($CDCl_3$): δ = 52. − IR (KBr disc, cm^{-1}): 3381 w, 3294 s, 3141 m−sh, 3074 s, 2943 w, 2877 w, 1619 vs, 1586 w, 1484 vs, 1425 vs, 1309 w, 1278 m, 1111 s, 1102 s, 1054 s, 1029 m, 997 m, 835 s, 810 s, 749 s, 719 vs, 690 s, 642 s, 632 s, 614 m, 572 m, 521 vs, 495 s, 482 s, 464 m, 418 w, 404 m, 347 w, 301 m. − FAB (*m/z*): 315 $[M + Na]^+$ and 293 $[M]^+$. − $C_{13}H_{13}N_2PS_2$ (292.35): found C 53.18, H 4.46, N 9.91; (calcd. C 53.41, H 4.48, N 9.58 %).

[$H_2NC(O)NHP(S)Ph_2$] 3: To a solution of $H_2NC(O)NHPPh_2$ (3.5 g, 14.3 mmol) in THF (100 mL) was added S (451 mg, 14.1 mmol). The reaction was stirred for 4 h. The solution was filtered and the solvent removed to give a yield of 2.5 g (62 %). Mp: 162−166 °C. − ^{31}P NMR ($CDCl_3$): δ = 53. − IR

(KBr disc, cm^{-1}): 3492 m, 3333 m, 3187 m, 3056 w, 2956 vw, 1704 vs, 1682 vs, 1650 vs, 1615 vs, 1461 vs, 1436 vs, 1343 m, 1246 w, 1178 w, 1106 vs, 998 w, 912 m, 872 w, 747 s, 716 vs, 692 vs, 656 m, 634 m, 613 m, 590 m, 513 m, 496 s, 460 w. − FAB (*m*/*z*): 299 $[M + Na]^+$ and 277 $[M]^+$. $C_{13}H_{13}N_2OPS$ (276.29): found C 55.88, H 4.74, N 10.14; (calcd. C 56.51, H 4.74, N 10.64 %)

[PhC(O)NHP(S)Ph$_2$] 4: To a solution of $PhC(O)NH_2$ (3.2 g, 7.7 mmol) in THF (150 mL) was added Et_3N (3.9 mL, 30 mmol), DMAP (200 mg, 20 mmol) and neat Ph_2PCl (5 mL, 27.9 mmol) − the solution was heated at reflux overnight. S (1.78 g, 55.7 mmol) was added and stirred overnight at room temperature. The solution was filtered and the filtrate was reduced to dryness to a white powder. It was then triturated with Et_2O (200 mL) to give a yield of 6.43 g (34 %). Mp: 186−190 °C. − ^{31}P NMR ($CDCl_3$): δ = 56. − IR (KBr disc, cm^{-1}): 3159 m, 3060 w, 2857 vw, 1651 vs, 1600 m, 1581 w, 1496 m, 1480 w, 1454 vs, 1436 vs, 1266 s, 1180 vw, 1102 s, 1071 w, 1024 w, 999 w, 952 vw, 880 w, 832 m, 796 w, 745 s, 726 vs, 715 vs, 690 vs, 669 m, 636 vs, 615 m, 516 s, 497 s, 398 w. FAB (*m*/*z*): 361 $[MH + Na]^+$ and 337 $[MH + H]^+$. − $C_{19}H_{16}NOPS$ (337.38): found C 67.25, H 4.54, N 4.02; (calcd. C 67.64, H 4.78, N 4.15 %).

[PyC(O)NHP(S)Ph$_2$] 5: To a solution of $PyC(O)NH_2$ (3.4 g, 27.8 mmol) in THF (150 mL) was added Et_3N (3.9 mL, 30 mmol), DMAP (200 mg, 20 mmol) and neat Ph_2PCl (5 mL, 27.9 mmol) − the solution was heated at reflux overnight. S (890 mg, 27.8 mmol) was added and the raction was stirred for 1 h. at room temperature. The solution was filtered and the filtrate reduced to dryness to a white powder. The product was recrystallised from CH_2Cl_2/Et_2O to give 4.4 g (47 %). Mp: 195−198 °C. − ^{31}P NMR ($CDCl_3$): δ = 56. − IR (KBr disc, cm^{-1}): 3368 vw, 3182 s, 3077 w, 1656 vs, 1588 s, 1573 m, 1482 m, 1457 vs, 1437 s, 1413 s, 1269 s, 1104 s, 1020 m, 998 w, 878 m, 842 m, 815 m, 742 vs, 724 s, 715 vs, 7703 s, 691 vs, 662 m, 639 vs, 615 m, 516 m, 499 s, 477 w, 457 w, 412 w, 402 w, 297 w. − FAB (*m*/*z*): 361 $[M + Na]^+$ and 339 $[M + H]^+$. − $C_{18}H_{15}N_2OPS$ (338.36): found C 64.15, H 4.41, N 8.19; (calcd. C 63.89, H 4.47, N 8.28 %).

[H$_2$NC(S)NHP(Se)Ph$_2$] 6: To a solution of $H_2NC(S)NHPPh_2$ (2.20 g, 8.45 mmol) in THF (50 mL) was added Se (0.67 g, 8.45 mmol) and the mixture stirred for 1 h. The solution was filtered through celite and reduced to dryness to give 1.63 g (67 %) of white powder. Mp: 141−144 °C. − ^{31}P NMR (THF/C_6D_6): δ = 45 [^1J(PSe) 783 Hz]. − IR (KBr disc, cm^{-1}): 3364 w, 3284 m, 3072 m, 2940 w, 2875 w, 1619 vs, 1482 vs, 1424 vs, 1308 w, 1278 m, 1107 m, 1052 m, 996 w, 832 s, 807 s, 748 vs, 715 s, 701 vs, 688 vs, 640 m, 555 vs, 515 vs, 490 s, 473 m, 409 m, 396 m, 304 w m 284 m. − FAB (*m*/*z*): 339 $[M]^+$. − $C_{13}H_{13}N_2PSSe$ (339.25): found C 45.98, H 3.76, N 8.30; (calcd. C 46.02, H 3.86, N 8.26 %).

K[PhC(O)NP(O)Ph$_2$] 7: To a solution of $[PhC(O)NHP(O)Ph_2]$ (500 mg, 1.56 mmol) in THF (50 mL) was added KO*t*Bu (0.57 g, 5.12 mmol). After stirring overnight the solution was filtered through celite, and then reduced to dryness to give 557 mg (100 %) of white powder. Mp: 286−290 °C. − ^{31}P NMR (THF/C_6D_6): δ = 17. − IR (KBr disc, cm^{-1}): 3397 w, 3056 m, 2974 w, 2866 w, 1649 m, 1624 m, 1591 s, 1523 vs, 1481 m, 1436 s, 1376 vs, 1298 m, 1171 s, 1153 s, 1141 s, 1120 s, 1101 s, 1066 s, 1026 s, 896 vs, 842 vs, 755 s, 719 vs, 701 vs, 547 vs, 527 vs, 459 m, 435 m, 324 m, 303 m. − FAB (*m*/*z*): 360 $[M + H]^+$. − $C_{19}H_{15}KNO_2P$ (338.38): found C 63.23, H 4.35, N 3.74; (calcd. C 63.50, H 4.21, N 3.90 %).

K[H$_2$NC(S)NP(S)Ph$_2$] 8: Was prepared in a similar fashion to **7**, yield 1.3 g 79 %. Mp: 155−157 °C. − ^{1}H NMR ([D$_6$]DMSO): 7.85 (aromatic), 7.34 (aromatic) and 3.30 (2 H, s, NH). − ^{13}C NMR: 189 (CS), 142 (C_6H_5) 141 (C_6H_5), 131 (C_6H_5), 130 (C_6H_5) and 128 (C_6H_5). − ^{31}P NMR: 37 ppm. − IR (KBr disc, cm^{-1}): 3364 s, 3280 m, 3164 w, 3054 w, 1604 s, 1479 s, 1431 vs, 1402 s, 1307 s, 1291 s, 1104 s, 1055 vw, 1026 vw, 999 vw, 884 vw, 856 vw, 836 vw, 809 vw, 746 s, 712 vs, 693 s, 624 m, 607 s, 521 s, 416 vw. − FAB (*m*/*z*): 331 M + H]$^+$. − $C_{13}H_{12}KN_2PS_2$ (330.44): found C 47.18, H 3.75, N 7.99; (calcd. C 47.25, H 3.66, N 8.48 %).

K[PhC(O)NP(S)Ph$_2$] 9: Was prepared in a similar fashion to **7**, yield 1.1 g, 100 %. Mp: 286−290 °C. − ^{31}P NMR ([D$_6$]DMSO): δ = 44. − IR (KBr disc, cm^{-1}): 3434 w, 3053 w, 2968 w, 2852 w, 1588 m, 1519 vs, 1479 w, 1436 m, 1360 vs, 1297 w, 1102 m, 1068 m, 1024 m, 895 m, 884 w, 838 s, 816 w, 748 w, 723 vs, 710 s, 695 s, 672 w, 627 s, 612 s, 516 m, 503 s, 306 w. − FAB (*m*/*z*): 399 $[MH + Na]^+$, 377 $[MH + H]^+$. − $C_{19}H_{15}KNOPS$ (375.4): found C 60.34, H 4.12, N 3.45; (calcd. C 60.78, H 4.03, N 3.73 %).

K[PyC(O)NP(S)Ph$_2$] 10: Was prepared in a similar fashion to **7**, yield 2.30 g, 94 %. Mp: 308−312 °C. − ^{31}P NMR (THF/C_6D_6): δ = 41. − IR (KBr disc; cm^{-1}): 3322 vw, 3237 vw, 3072 w, 3053 w, 1676 w, 1590 vs, 1526 vs, 1476 m, 1436 s, 1417 m, 1371 vs, 1314 m, 1305 m, 1193 m, 1164 s, 1102 s, 1028 s, 906 s, 893 m, 830 vs, 748 vs, 717 s, 707 vs, 694 vs, 626 vs, 613 vs, 503 vs, 413 w, 305 m. − FAB (*m*/*z*): 377 $[M + H]^+$. − $C_{18}H_{14}KN_2OPS$ (376.45): found C 57.25, H 3.37, N 7.01**;** (calcd. C 57.43, H 3.75, N 7.44 %).

K[H$_2$NC(S)NP(Se)Ph$_2$] 11: Was prepared in a similar fashion to **7**, yield 317 mg, 59 %. Mp: 120−125 °C. − ^{31}P NMR (THF/C_6D_6): δ = 29 [^1J(PSe) 530 Hz]. − IR (KBr disc, cm^{-1}): 3353 m, 3162 w, 3051 w, 1605 vs, 1476 s, 1431 vs, 1306 vs, 1103 vs, 1025 m, 999 m, 885 w, 851 w, 743 vs, 712 s, 699 vs, 544 vs, 516 vs, 408 m. − FAB (*m*/*z*): 346 $[M - S]^+$. − ($C_{13}H_{12}KN_2PSSe$ (377.34): found C 41.29, H 3.43, N 6.97; calcd. C 41.38, H 3.21, N 7.42 %).

[Cu(PPh$_3$)(PhC(O)NP(S)Ph$_2$)] 12: To a suspension of $PhC(O)NP(S)Ph_2$ (0.21 g, 0.62 mmol) in methanol (20 mL) was added KO*t*Bu (0.07 g, 0.62 mmol), after stirring for 10 minutes a solution of $Cu(PPh_3)_2(NO_3)$ (0.40 g, 0.62 mmol) in $CHCl_3$ (25 mL) was added dropwise. The mixture was refuxed for two hours, cooled and the white precipitate was filtered off, washed with diethyl ether and dried in vacuo. Yield 0.24 g, 59%, M.p. 246 °C. ^{31}P δ = 28.4. − $C_{37}H_{30}CuNOP_2S$ (662.20): Found C 67.10, H 4.65, N 2.02, S 4.80 (calcd. C 67.11, H4.57, N 2.12, S 4.84%). − IR (KBr disc, cm^{-1}): 3058 w, 1500 m, 1435 m, 1376 vs, 1304 w, 1180 w, 1111 m, 1109 w, 822 m, 718 s, 695 s, 593 s, 528 m 508 m. − Mass Spec. Parent ion not observed.

[Pd{PhC(O)NP(S)Ph$_2$}$_2$] 13: To a solution of $[PdCl_2(COD)]$ (30 mg, 105 μmol) in CH_2Cl_2 (10 mL) was added $K[PhC(O)NP(S)Ph_2]$ (80 mg, 213 μmol). After 1 h of stirring the solution was filtered through celite and reduced to dryness. After trituration with petroleum ether, 47 mg (57 %) of product was collected. Mp: 136−139 °C. − ^{31}P NMR (DCM/C_6D_6): δ = 30. − IR (KBr disc, cm^{-1}): 3052 w, 3055 m, 1588 m, 1485 vs, 1436 vs, 1372 vs, 1304 m, 1181 m, 1113 s, 1103 s, 1068 w, 1026 m, 998 w, 926 m, 795 m, 804 m, 745 m, 720 s, 701 vs, 689 vs, 618 w, 590 vs, 552 m 511 vs, 489 m, 418 w, 337 w. − FAB (*m*/*z*): 802 $[M + Na]^+$ and 779 $[M]^+$. − $C_{38}H_{30}N_2O_2P_2PdS_2$ (779.16): found C 58.66, H 3.88, N 3.24; (calcd. C 58.58, H 3.88, N 3.60 %).

[Pd{PyC(O)NP(S)Ph$_2$}$_2$] 14: To a solution of $[PdCl_2(COD)]$ (38 mg, 133 μmol) in CH_2Cl_2 (10 mL) was added K[PyC(O)NP(S)Ph$_2$] (100 mg, 266 μmol), which gave a red solution immediately. After overnight stirring the solution was filtered through celite and reduced to dryness. The compound was then triturated with petroleum ether (60−80 °C) gave a yield of 97 mg (93 %). Mp: 155−158 °C. − ^{31}P NMR (CH_2Cl_2/C_6D_6): δ = 31. − IR (KBr disc, cm^{-1}): 3053 w, 2923 w, 1609 s, 1585 s, 1551 s, 1508 s, 1479 w, 1436 s,

Table 7. Details of the crystal data and refinements

Compound	**12**	**15**	**16**	**17**
Empirical formula	$C_{37}H_{30}CuNP_2S$	$C_{28}H_{27.5}Cl_5N_4P_2S_4Zn$	$C_{26}H_{26}N_4P_2S_4PtClO_{0.5}$	$C_{30}H_{34}N_4P_2S_4PtO$
Formula weight	662.2	852.8	823.2	851.9
Colour	Colourless	Colourless	Yellow	Yellow
Size [mm]	0.25 × 0.25 × 0.15	0.25 × 0.15 × 0.1	0.1 × 0.1 × 0.1	0.1 × 0.03 × 0.1
Crystal system	Triclinic	Monoclinic	Monoclinic	Triclinic
Space Group	*P*-1	*C*2/*c*	*C*2/*c*	*P*-1
a	10.828(2)	19.074(1)	23.176(5)	12.645(5)
b	12.704(3)	12.801(1)	14.04(1)	13.988(3)
c	13.161(3)	19.411(1)	26.237(5)	10.838(2)
α	100.50(3)	90	90	99.25(2)
β	105.86(3)	114.53(1)	122.92(1)	100.98(2)
γ	106.95(3)	90	90	65.49(2)
Volume [Å^3]	1597	4311	7166	1705
Z	2	4	8	2
Density (calc.) [g/cm^3]	1.38	1.31	1.53	1.66
μ [mm^{-1}]	0.88	1.17	10.9	10.8
F(000)	684	1730	3224	844
Ind.Refl./Observed Refl	4617/4219	3073/3019	5743/1864	5077/3659
Final*R*1/*wR*2	0.030/0.080	0.076/0.207	0.059/0.067	0.080/0.083
Largest Difference Peak/Hole [eÅ^{-3}]	0.25, −0.265	1.00, −0.551	1.03, −0.63	1.44, −2.05

1375 s, 1341 vs, 1307 s, 1174 m, 1103 s, 1058 w, 1026 w, 998 w, 920 w, 818 m, 746 s, 720 m, 690 vs, 619 w, 572 vs, 505 s, 415 w. − FAB (*m*/*z*): 780 [M]$^+$. − $C_{36}H_{28}N_4O_2P_2PdS_2$ (781.13): found C 55.33, H 3.91, N 6.79; (calcd. C 55.35, H 3.61, N 7.17 %).

[Zn{$H_2NC(S)NP(S)Ph_2$}$_2$] 15: To a solution of K[$H_2NC(S)NP(S)Ph_2$] (61 mg, 184 μmol) in THF (20 mL) was added $ZnCl_2$ (50 mg, 367 μmol). After stirring overnight, the solution was filtered through celite, and the filtrate reduced to dryness to give a white powder (178 mg, 75 %). Mp: 132−136 °C. − ^{31}P NMR (THF/C_6D_6 insert): δ = 41. − IR (KBr disc, cm^{-1}): 3464 w, 3306 m, 3160 w, 3053 w, 2970 vw, 1588 vs, 1478 vs, 1436 vs, 1311 s, 1161 m, 1104 s, 1027 w, 998 w, 873 s, 748 m, 719 s, 707 vs, 691 s, 638 m, 577 vs, 556 s, 499 m. − FAB (*m*/*z*): 671 [MH_2 + Na]$^+$ and 649 [MH_2 + H]$^+$. − $C_{26}H_{24}N_4P_2S_4Zn$ (648.07): found C 48.04, H 3.76, N 8.32; (calcd. C 48.18, H 3.73, N 8.64 %).

[Pt{$H_2NC(S)NHP(S)Ph_2$}{$H_2NC(S)NP(S)Ph_2$}]$^+$Cl$^-$ 16: To a solution of [$H_2NC(S)NHP(S)Ph_2$] (78 mg, 267 μmol) in CH_2Cl_2 (20 mL) was added [$PtCl_2$(COD)] (100 mg, 267 μmol) giving yellow precipitates immediately. After overnight stirring the residue was filtered to give a yield of 96 mg (85 %). Decomp. temp: >160 °C. − ^{31}P NMR (CH_3OH/C_6D_6 insert): δ = 29.25, 29.54 [^2J(P−Pt) broad unresolved]. − IR (KBr disc, cm^{-1}): 3261 m, 3055 m, 2697 vw, 1603 s, 1500 s, 1437 vs, 1390 m, 1312 s, 1184 w, 1163 vw, 1106 vs, 998 w, 922 vw, 883 w, 748 m, 708 s, 688 s, 618 w, 598 m, 576 s, 551 m, 495 m, 365 vw. − FAB (*m*/*z*): 777 [M − H]$^+$. − $C_{26}H_{26}ClN_4P_2PtS_4$ (815.24): found C 38.66, H 3.10, N 7.05; (calcd. C 38.41, H 2.97, N 6.88 %).

[Pt{$H_2NC(S)NP(S)Ph_2$}$_2$] 17: To a suspension of K[$H_2NC(S)NP(S)Ph_2$] (61 mg, 184 μmol) in CH_2Cl_2 (10 mL) was added [$PtCl_2$(COD)] (32 mg, 85 μmol) gave a yellow solution. After 1 h stirring the solution was filtered through celite and the filtrate kept in a refrigerator overnight; a yellow crystalline product was collected (35 mg, 53 %). Mp: 144−148 °C. − ^{31}P NMR (CH_2Cl_2/C_6D_6 insert): δ = 33 [^2J(P−Pt) 114 Hz]. − IR (KBr disc, cm^{-1}): 3460 w, 3328 w, 3157 vw, 3053 vw, 1588 vs, 1484 vs, 1436 vs, 1308 s, 1161 m, 1112 s, 1105 s, 1027 vw, 999 w, 883 s, 748 m, 720 s, 707 vs, 691 s, 577 vs, 558 s, 502 m, 356 vw. − FAB (*m*/*z*): 778 [M + H]$^+$ and 777 [M]$^+$. − $C_{26}H_{24}N_4P_2PtS_4$ (777.77): found C 39.75, H 2.81, N 6.81; (calcd. C 40.15, H 3.11, N 7.20 %).

Crystallography: Details of the data collections and refinements are summarised in Table 7 Experimental details for **1** and **9** have been previously reported.[24] Data were collected at room temperature using a KUMA KM-4 and Mo radiation for **12** or with a SMART system for **15** and using Cu radiation with ω scans with a Rigaku AFC7S diffractometer for **16** and **17**. Intensities were corrected for Lorentz-polarisation and for absorption. The structures were solved by the heavy atom method or by direct methods. The positions of the hydrogen atoms were idealised. Refinements were by full-matrix least squares based on *F* using teXsan[25] (**16**, **17**) or using F^2 and SHELXTL[26] (**12**, **15**). Crystallographic Data for the structural analyses has been deposited with the Cambridge Crystallographic data centre, CCDC Nos: 115899, 115900, 115901, and 115902 Copies of this information may be obtained free of charge from The Director CCDC, 12 Union Road, Cambridge, CB2 1EZ UK. (Fax +44 1223/ 336-033 or Email deposit@ccdc.cam.ac.uk or www: http://www.ccdc.cam.ac.uk).

Acknowledgments

We are grateful to the JREI for an equipment grant. JN is grateful to the Royal Society of Chemistry for a journal grant for international authors. JN, MN and ZZ wish to express their gratitude to the Grant Agency of the Czech Republic for Grant Nos. 203/97/0955, 203/98/0676 abd 203/99/0067.

[1] J. D.Woollins, *J. Chem. Soc., Dalton Trans.* **1996**, 2893.
[2] R. Rossi, L. Marvelli, A. Marchi, L. Magon, V. Bertolasi, V. Ferretti, *J. Chem. Soc*., *Dalton Trans.* **1994**, 339.
[3] D. Pohl, E. Ellermann, F. A. Knoch, M. J. Moll, *J. Organomet. Chem.* **1995**, *495*, C6.
[4] A. M. Z. Slawin, M. B. Smith, J. D. Woollins, *J. C.hem. Soc*., *Dalton Trans.* **1996**, 1283.
[5] P. Bhattacharyya, A. M. Z. Slawin, M. B. Smith, J. D. Woollins, *Inorg. Chem.* **1996**, *35*, 3675.
[6] A. M. Z. Slawin, M. B. Smith, J. D. Woollins, *Polyhedron* **1996**, *15*, 1579.

[7] M. S. Balakrishna, R. Klein, S. Uhlenbrock, A. A. Pinkerton, R. G. Cavell, *Inorg. Chem.* **1993**, *32*, 5676.
[8] P. Bhattacharyya, A. M. Z. Slawin, D. J. Williams, J. D. Woollins, *J. Chem. Soc*., *Dalton Trans.* **1995**, 3189
[9] A. M. Z. Slawin, M. B. Smith, J. D.Woollins, *J. Chem. Soc., Dalton Trans.* **1996**, 4575.
[10] A. M. Z. Slawin, M. B. Smith, J. D.Woollins, *J. Chem. Soc., Dalton Trans.* **1996**, 1283.
[11] T. Q. Ly, F. E. Mabbs, A. M. Z. Slawin, J. D. Woollins. *Inorganic Chemistry Communications*, **1998**, *1*, 143
[12] D. T. Elmore, J. R. Ogle, *J. Chem. Soc*. **1959**, 2286.
[13] A. Schmidpeter, H. Groeger, *Chem. Ber*. **1967**, *100*, 3052; H. Groeger, A. Schmidpeter, *Chem. Ber*. **1967**, *100*, 3216.
[14] I. Ojima, T. Iwamoto, T. Onishi, N. Inamoto, K. Tamaru, *Chem*. *Commun*. **1969**, 1501.
[15] I. Ojima, T. Iwamoto, T. Onishi, N. Inamoto, K. Tamaru, *Bull*. *Chem. Soc. Japan* **1971**, *44*, 2150.
[16] I. Ojima, K.-Y. Akiba, N. Inamoto, *Bull*. *Chem. Soc. Japan* **1973**, *46*, 2559.
[17] A. Spencer, J. M. Swan, H. B. Wright, *Aust. J. Chem*. **1969**, *22*, 2359.
[18] A. Ziegler, V . P. Botha, I. Haiduc, *Inorg. Chim. Acta* **1975**, *15*, 123.
[19] J. Bödeker, H. Zärtner, *J. Prakt. Chem.* **1976**, *318*, 149.
[20] N. G. Zabirov, V. N. Solov′ev, F. M. Shamsevaleev, R. A. Cherkasov, A. N. Chekhlov, A. G. Tsifarkin, I. V. Martynov, *J. Gen. Chem. USSR* **1991**, *61*, 597.
[21] M. Gruber, P. G. Jones, R. Schmutzler, *Chem. Ber*. **1990**, *123*, 1313.
[22] P. Bhattacharyya, A. M. Z. Slawin, M. B. Smith, D. J. Williams, J. D. Woollins, *J. Chem. Soc*., *Dalton Trans.* **1996**, 3647.
[23] T. Q.Ly, A. M. Z.Slawin, J. D.Woollins, *Polyhedron*, in press.
[24] T. Q.Ly, A. M. Z.Slawin, J. D.Woollins, *Angew.Chem.Int.Ed.-Engl.* **1998**, *37*, 2501.
[25] *TeXsan*, Molecular Structure Corporation, The Woodlands, Texas (**1992**, **1996**)
[26] *SHELXTL*. Siemens X-Ray Madison (**1998**).
[27] D. Cupertino, R. Keyte, A. M. Z. Slawin, D. J. Williams, J. D. Woollins, *Inorg. Chem*. **1996**, *35*, 2695.
[28] A. M. Z. Slawin, J. Ward, D. J. Williams, J. D. Woollins, *J. Chem. Soc*., *Chem. Commun*. **1994**, 421.
[29] T. Iwamoto, F. Ebina, H. Nakazawa, C. Nakatsuka, *Bull*. *Chem. Soc. Japan*. **1979**, *52*, 1857.
[30] Z. Zák, T. Glowiak, N. T. T. Chau, E. Herrmann, *Z. Anorg. Allg. Chem*. **1990**, *586*, 136.
[31] R. L. Girling, E. L. Amma, *Chem. Commun*. **1968**, 1487.
[32] J. Phillips, A. M. Z. Slawin, A. J. P. White, D. J. Williams, J. D. Woollins, *J. Chem. Soc*., *Dalton Trans.* **1995**, 2467.

Received March 12, 1999
[I99097]

Formation of the [(*s-trans*-η⁴-Butadiene)TaCp*Cp]⁺ Cation and Its Reaction with Organic Carbonyl Derivatives

Hans Christian Strauch,[a] Gerhard Erker,*[a] Roland Fröhlich,[a][+] and Maija Nissinen[a][+]

Keywords: Group-5 bent metallocene cation complexes / (Butadiene)tantalocene cation / (*s-trans*-η⁴-Butadiene)metal complex / Ethene polymerization / Metallocenes / Homogeneous catalysis

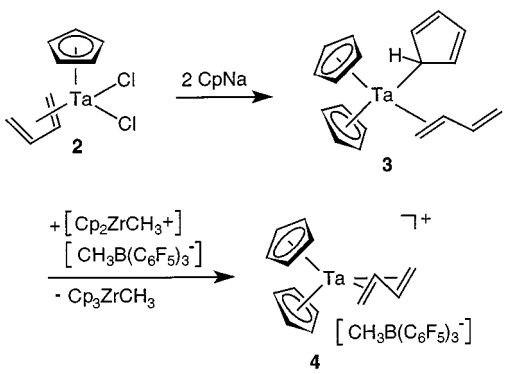
(Butadiene)TaCp*Cl_2 (**6**) was treated with CpNa to yield (η²-butadiene)TaCp*CpCl (**7**). Subsequent reaction with $[Cp_2ZrCH_3^+][CH_3B(C_6F_5)_3^-]$ resulted in transfer of the chloride ligand from tantalum to zirconium with formation of the [(*s-trans*-η⁴-butadiene)TaCp*Cp]⁺ cation [**8**, with $CH_3B(C_6F_5)_3^-$ anion]. Complex **8** was characterized spectroscopically and by an X-ray crystal structure analysis. The group-5 [(*s-trans*-η⁴-C_4H_6)TaCp*Cp]⁺ bent metallocene cation complex **8** reacts with ketones (acetone, adamantanone) to yield the corresponding seven-membered 2-tantalatetrahydrooxepine cation complexes (**9**, **10**). 1-Cyanoadamantane reacts with **8** to yield the 2-tantala-3,6-dihydro-2*H*-azepine cation system **11**. Activation of **8** with methylalumoxane gives an active ethene polymerization catalyst.

Introduction

(Butadiene)zirconocene (**1**) was the first organometallic example exhibiting a stable *s-trans*-η⁴-conjugated diene coordination to a single transition metal center.[1] Since then a variety of additional examples have been found and described,[2] but mononuclear (*s-trans*-η⁴-butadiene)metal complexes are still not too frequently encountered. The (butadiene)zirconocene system has turned out to be a very useful reagent in organic and organometallic synthesis, serving as a mildly nucleophilic C_4-building block,[3] and it has successfully been applied as a suitable catalyst precursor in homogeneous metallocene Ziegler catalysis.[4] Therefore, we considered it desirable to expand the scope of such (butadiene) bent metallocene chemistry and search for additional examples of (η⁴-butadiene)metallocenes that are structurally and chemically related to the parent system **1** and its congeners.

We have recently synthesized the group-5 metal analogue of (butadiene)hafnocene. Our synthesis started from the readily available complex (η-cyclopentadienyl)(*s-cis*-η⁴-butadiene)$TaCl_2$ (**2**)[5] that was treated with two molar equivalents of CpNa to yield $(\eta^5\text{-Cp})_2(\eta^1\text{-Cp})(\eta^2\text{-butadiene})$tantalum (**3**). Subsequent treatment with $[Cp_2ZrCH_3^+][CH_3B(C_6F_5)_3^-]$[6] led to a clean transfer of a Cp-anion ligand to give the neutral Cp_3ZrCH_3[7] and the [(*s-trans*-η⁴-butadiene)$TaCp_2$]⁺ cation complex **4** (isolated with $CH_3B(C_6F_5)_3^-$ anion).[8] Spectroscopically and structurally complex **4** behaves as an isoelectronic analogue of the neutral (*s-trans*-η⁴-butadiene)hafnocene. The system **4** appears to be the first simple cationic group-5 equivalent of the well-established group-4 (η⁴-conjugated diene)metallocene complexes.[9] First scouting experiments have revealed that **4** also adds a variety of unsaturated reagents, similarly as **1**, to yield heterometallacyclic ring systems,[10] although the reactivity of the cationic group-5 metal complex system **4** seemed to be lower than that of the group-4 analogue **1**.

We have now developed a synthetic pathway to a second example of a group-5 (*s-trans*-η⁴-butadiene)metallocene cation system. The system contains a pentamethylcyclopentadienyl ligand that allows for a different synthetic entry and results in increased activities of the group-5 bent metallocene systems. Moreover, the presence of two differently substituted cyclopentadienide moieties at tantalum introduces an additional stereochemical marker into the system that has been useful in controlling the dynamic features of a variety of derived organometallic ring systems. The preparation of [(*s-trans*-η⁴-butadiene)TaCp*Cp]⁺ (**8**), its structural and spectroscopic characterization and the preliminary results of a few representative addition reactions are described in this article.



Scheme 1

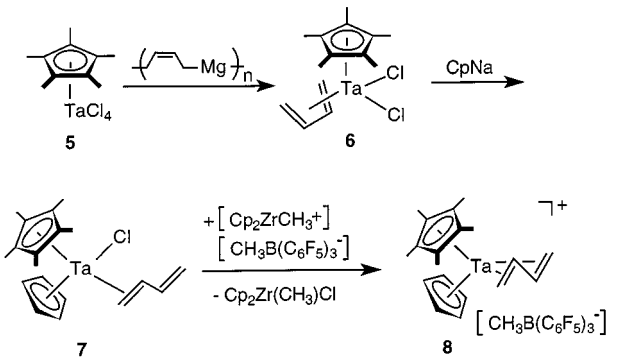
[a] Organisch-Chemisches Institut der Universität Münster, Corrensstraße 40, D-48149 Münster, Germany
Fax: (internat.) + 49(0)251/8336503
E-mail: erker@uni-muenster.de
[+] X-ray crystal structure analysis.

 © WILEY-VCH Verlag GmbH, D-69451 Weinheim, 1999 1434–1948/99/0909–1453 $ 17.50+.50/0

Results and Discussion

Our synthesis of the new group-5 (butadiene) bent metallocene cation system **8** starts from Cp^*TaCl_4 (**5**) which is readily available by treatment of $TaCl_5$ with (trimethylsilyl)-pentamethylcyclopentadiene, as described by W. A. Herrmann et al.[11] This was then treated with ca. one molar equivalent of the oligomeric (butadiene)magnesium reagent,[12] according to the procedure developed by H. Yasuda et al.,[13] to yield (*s-cis*-η^4-butadiene)$TaCp^*Cl_2$ (**6**). We have then treated **6** with ca. one molar equivalent of sodium cyclopentadienide in tetrahydrofuran at 0 °C. This resulted in the formation of the (η^2-butadiene)TaCp*CpCl complex **7**, isolated in 45% yield as a pale brown solid.

The η^2-coordination of the butadiene ligand to the tantalum center in **7** was deduced from its NMR spectra.[14] The ^{13}C-NMR spectrum shows two pairs of butadiene resonances at δ = 111.2 and 157.4 (noncoordinated $H_2C^4{=}C^3H$ moiety) and δ = 42.4 and 60.4 (η^2-coordinated $H_2C^1{=}C^2H$ unit). The η^2-butadiene ligand features ^{1}H-NMR resonances at δ = 0.88, 1.37 (1-H, 1-H′), 0.71 (2-H) of the coordinated vinyl group and δ = 6.33 (3-H), 4.27, and 4.00 (4-H,H′) of the free butadiene vinyl moiety.



Scheme 2

Complex **7** was then treated with $[Cp_2ZrCH_3^+]$-$[CH_3B(C_6F_5)_3^-]$[6] at room temperature in toluene solution. The tantalum-containing product precipitated as an oil, and it was shown by NMR spectroscopy that the supernatant toluene phase contained the neutral zirconium product $Cp_2Zr(CH_3)Cl$.[15] The oil was recovered and solidified by treatment with pentane and shown to consist of [CpCp* Ta(butadiene)$^+$][$CH_3B(C_6F_5)_3^-$] (**8**, isolated in > 80% yield). Thus, treatment of Cp*Cp(η^2-butadiene)TaCl (**7**) with the $Cp_2ZrCH_3^+$ cation has selectively resulted in transfer of the chloride ligand from tantalum to zirconium. The resulting tantalum complex contains an *s-trans*-η^4-butadiene ligand. This is evident from the NMR spectra which are to be compared with the characteristic NMR features of the *s-trans*-η^4-C_4H_6 ligand system in (*s-trans*-η^4-butadiene)zirconocene[1][9] [^{1}H NMR: δ = 1.2 (1-,4-H_{anti}), 3.2 (1-,4-H_{syn}), 2.9 (2-,3-H)] or in [(*s-trans*-η^4-C_4H_6)$TaCp_2$]$^+$ cation (**4**)[8] [^{1}H NMR: δ = 1.45 (1-,4-H_{anti}), 3.15 (1-,4-H_{syn}), 2.95 (2-,3-H) in [D_5]bromobenzene; ^{13}C NMR: δ = 57.8 (C-1, -4), 90.1 (C-2, -3) in [D_2]dichloromethane]. Due to the lower symmetry (**4**: C_2; **8**: C_1) the [(*s-trans*-η^4-butadiene)TaCp*Cp]$^+$ cation exhibits four ^{13}C-NMR signals of the η^4-coordinated *s-trans*-C_4H_6 ligand at δ = 59.8 (C-1), 64.3 (C-4), 91.2 (C-2), and 93.6 (C-3). As expected, all six butadiene hydrogen atoms are different due to the unsymmetric structure of **8** in solution. The corresponding ^{1}H-NMR signals appear in the very characteristical range as expected for the (*s-trans*-η^4-butadiene)Ta$^+$ moiety at δ = 0.88 (1-H_{anti}), 2.91 (1-H_{syn}), 1.61 (4-H_{anti}), 2.53 (4-H_{syn}), 3.04 (2-H), 1.61 (3-H).

Pentane vapor was allowed to diffuse into a solution containing 30 mg of **8** in 2 mL of dichloromethane to give single crystals suited for the X-ray crystal structure analysis (see Figure 1). This analysis confirmed the formation of the [(*s-trans*-η^4-butadiene)TaCp*Cp]$^+$ cation complex. The Ta−C(butadiene) distances are between 2.35 and 2.28 Å. Unfortunately, the structure suffers from considerable disorder problems (for details see the Experimental Section) so that structural details will not be discussed (Cp-ring and the butadiene ligand were refined with restraints).

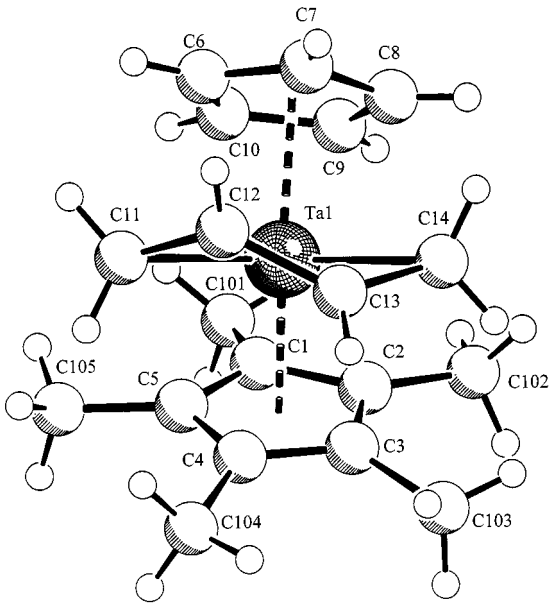


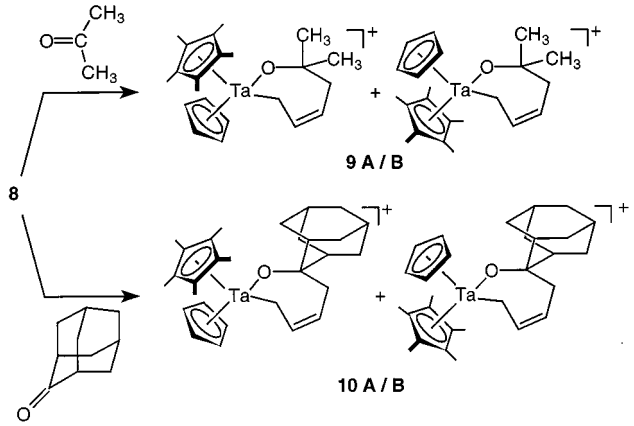
Figure 1. Molecular geometry of **8** in the crystal (cation only)

Both (butadiene)zirconocene and (butadiene)tantalocene cation react with a variety of organic carbonyl compounds and derivatives to yield the corresponding seven-membered 2-metalla-tetrahydrooxepine systems.[8−10] In order to characterize the chemical behavior of **8** we have consequently treated the [(*s-trans*-η^4-butadiene)TaCp*Cp]$^+$ cation complex with a few selected ketones and with a nitrile.

Complex **8** reacts with excess acetone at 50 °C (3 h) resulting in the incorporation of one equivalent of the carbonyl compound. The tantalatetrahydrooxepine cation **9** was isolated in ca. 70% yield. The NMR spectra show that two isomers were formed in a 1:1 ratio. These exhibit the same atom connectivity. They constitute two conformational isomers (isotopomers).[16] It is well-known that such metallatetrahydrooxepines contain nonplanar seven-

membered ring frameworks.[10] To a first approximation these contain two nearly planar subunits (in **9** the planes are defined by the atoms C3,Ta,O,C7,C6 and C3−C6) with an angle between these two planes of ca. 40−50°. Thus, in the case of **9** the two diastereoisomers are characterized by having the $C^4{=}C^5$ double bond oriented *syn* or *anti* to the Cp* ligand. Often such isotopomers rapidly equilibrate on the NMR time scale,[8][10] but in the case of **9** the thermally induced ring-inversion process seems to be kinetically hindered, potentially by an unfavorable transannular Cp*/CH_3 1,3-interaction in the transition state, so that the isomers **9A** and **9B** are distinguished by their separate NMR signals at 150/600 MHz at ambient temperature.

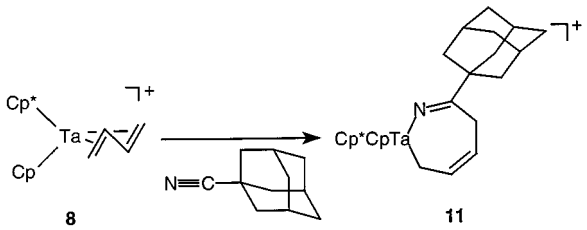
We observe a ^{1}H NMR Cp singlet for **9A** at δ = 5.78, for **9B** at δ = 6.04. Complex **9A** exhibits two methyl singlets at δ = 1.40 and 1.22; the corresponding 7-CH_3 signals of **9B** are at δ = 1.49 and 1.09, and each of the complexes exhibits distinctly different AB-type multiplets of their C^6H_2 and C^3H_2 groups (for details see the Experimental Section).



Scheme 3

Even the bulky ketone 2-adamantanone reacts analogously with the [(*s-trans*-η⁴-butadiene)TaCp*Cp]⁺ cation (**8**). The seven-membered metallacyclic cation complex **10** [with $CH_3B(C_6F_5)_3^-$ anion] was isolated from the reaction mixture in close to 60% yield. Again, a mixture of two isotopomers was observed by NMR spectroscopy at ambient temperature in a 70:30 ratio. The major isomer **10A** exhibits a ^{1}H-NMR Cp singlet at δ = 5.77, whereas the minor **10B** shows the corresponding Cp signal at δ = 6.01 (for additional spectroscopic data see the Experimental Section).

1-Cyanoadamantane reacts cleanly with **8** to yield the 3,6-dihydro-2-tantala-2*H*-azepine cation **11** (> 70% isolated). In this case only a single set of NMR resonances was observed (^{1}H-NMR Cp signal at δ = 5.67, 6-H/H′ multiplet at δ = 3.32 and 1.77, 3-H/H′ multiplet at δ = 1.55 and 0.85). From these data it is not clear whether only a single isotopomer of **11** is present or if the two possible diastereomers **11A/B** are rapidly interconverting by thermally induced ring inversion which is rapid on the NMR time scale under the conditions of the measurement.[8]



Scheme 4

Both the complexes [(*s-trans*-η⁴-butadiene)TaCp$_2$]⁺ cation (**4**) and [(*s-trans*-η⁴-butadiene)TaCp*Cp]⁺ (**8**) may serve as organometallic precursors for the generation of active homogeneous metallocene Ziegler catalyst systems. In a few scouting experiments we have treated **4** or **8** with a large excess of methylalumoxane in toluene. Subsequent introduction of ethene led to the formation of polyethylene (for details see Table 1 and the Experimental Section).

Table 1. Ethene polymerization with the homogeneous **4**/MAO and **8**/MAO Ziegler catalysts[a]

Precursor	μmol of cat.	Al/Ta	*T* [°C]	g of PE	m.p.	act[b]
4	22.4	1470	40	2.4	127	107
4	22.4	1470	50	2.8	128	125
4	22.4	1470	70	4.4	129	196
8	20.8	1580	40	4.1	127	198
8	20.8	1580	50	4.8	128	231
8	20.8	1580	70	7.3	129	351

[a] Reactions in 220 mL of toluene, Büchi glass autoclave at 2 bar ethene pressure. − [b] kg [PE]/mol(cat)·bar·h.

Our study has shown that [Cp*CpTa(*s-trans*-η⁴-butadiene)]⁺ cation as a second example of a stable (*s-trans*-η⁴-conjugated diene)tantalocene cation complex is readily available. The *s-trans*-η⁴-diene coordination mode appears to be even more favored at the group-5 than at the group-4 bent metallocene − the corresponding isoelectronic hafnocene complexes feature a thermodynamically favored *s-cis*-η⁴-diene coordination[17] [the (*s-trans*-η⁴-diene)HfCp$_2$ isomers can be generated photochemically at low temperature].[9] The (butadiene)tantalocene cation examples known so far seem to react cleanly with a variety of unsaturated organic substrates by selective carbon−carbon coupling. These new readily available reagents are potentially useful as stoichiometric C_4-delivering building blocks in organic synthesis and as catalyst precursors.

Experimental Section

Reactions were carried out under argon using Schlenk-type glassware or in a glovebox. Solvents (including deuterated solvents used for the spectroscopic characterization) were dried and distilled under argon prior to use {dichloromethane, bromobenzene: P_4O_{10} (Sicapent); ether, pentane: $LiAlH_4$; THF: potassium/benzophenone; toluene: sodium/benzophenone; CD_2Cl_2, $CDCl_3$: P_4O_{10}

(Sicapent); [D_6]benzene, [D_8]THF: sodium/potassium alloy; [D_5]bromobenzene: CaH_2; [D_8]toluene: potassium}. For more general information including a list of spectrometers and instrumentation used for physical characterization see ref.[8] The complexes Cp^*TaCl_4 (**5**),[11] (butadiene)$TaCp^*Cl_2$ (**6**),[13] and the reagents "butadiene-magnesium"[12] and $[Cp_2ZrCH_3^+][CH_3B(C_6F_5)_3^-]$[6] were prepared according to literature procedures. For a compilation of 1D- and 2D-NMR experiments used for spectroscopic characterization see ref.[18]

Preparation of (η^2-Butadiene)(η^5-cyclopentadienyl)(η^5-pentamethylcyclopentadienyl)tantalum Chloride (7): A solution of sodium cyclopentadienide (479 mg, 5.44 mmol) in 10 mL of tetrahydrofuran was added at 0 °C to a solution of 2.00 g (4.53 mmol) of (butadiene)$TaCp^*Cl_2$ (**6**) in 50 mL of THF. The reaction mixture was stirred for 15 h at room temperature. The solvent was removed in vacuo. The residue was taken up in 30 mL of toluene and filtered. The filtrate was concentrated to dryness in vacuo and the remaining solid stirred with 30 mL of pentane. The product was collected by filtration, washed twice with pentane (2 × 20 mL), and dried to yield 962 mg (45%) of **7** as a pale brownish solid, m.p. 150 °C (decomp.). − ^{1}H NMR ([D_8]THF, 599.8 MHz, 298 K): δ = 6.33 (ddd, $^3J_{HH}$ = 16.9 Hz, $^3J_{HH}$ = 10.1 Hz, $^3J_{HH}$ = 5.7 Hz, 1 H, 3-H), 5.08 (s, 5 H, Cp-H), 4.27 (ptd, $^3J_{HH}$ = 16.9 Hz, $^2J_{HH}$ = 1.2 Hz, 1 H, 4-H′), 4.00 (ddd, $^3J_{HH}$ = 10.1 Hz, $^2J_{HH}$ = 1.2 Hz, $^4J_{HH}$ = 1.5 Hz, 1 H, 4-H), 1.74 [s, 15 H, $C_5(CH_3)_5$], 1.37 (dd, $^3J_{HH}$ = 12.6 Hz, $^2J_{HH}$ = 6.7 Hz, 1 H, 1-H′), 0.88 (dd, $^3J_{HH}$ = 9.7 Hz, $^2J_{HH}$ = 6.7 Hz, 1 H, 1-H), 0.71 (m, 1 H, 2-H). − 1D-TOCSY NMR ([D_8]THF, 599.8 MHz, 298 K): Isomer **A**: irradiation at δ = 1.37 (1-H′), response at δ = 6.33 (3-H), 4.27 (4-H′), 4.00 (4-H), 0.88 (1-H), 0.70 (2-H). − GCOSY NMR ([D_8]THF, 599.8 MHz, 298 K): δ = 6.33/4.27, 4.00, 0.73 (3-H/4-H′, 4-H, 2-H), 4.27/6.33, 4.00 (4-H′/3-H, 4-H), 4.00/6.33, 4.27 (4-H/3-H, 4-H′),1.37/0.88, 0.73 (1-H′/1-H, 2-H), 0.88/1.37, 0.73 (1-H/1-H′, 2-H), 0.73/6.33, 1.37, 0.88 (2-H/3-H, 1-H′). − ^{13}C NMR ([D_8]THF, 150.8 MHz, 298 K): δ = 157.4 (C-3), 119.6 [$C_5(CH_3)_5$], 114.9 (C-Cp), 111.2 (C-4), 60.4 (C-2), 42.4 (C-1), 20.6 [$C_5(CH_3)_5$]. − GHSQC ([D_8]THF, 150.8 MHz/599.8 MHz, 298 K): δ = 157.4/6.33 (C-3/3-H), 114.9/5.08 (C-Cp/Cp-H), 111.2/4.27 (C-4/4-H′), 111.2/4.00 (C-4/4-H), 60.4/0.70 (C-2/2-H), 42.4/1.37 (C-1/1-H′), 42.4/0.88 (C-1/1-H), 20.6/1.74 [$C_5(CH_3)_5$]. − IR (KBr): $\tilde{\nu}$ = 3108 (vw), 3085 (vw), 2906 (m), 2857 (m), 1593 (w), 1485 (vw), 1434 (m), 1377 (s), 1260 (w), 1100 (s), 1081 (s), 1028 (s), 1011 (s), 831 (vs), 808 (s), 715 (vs), 663 (w) cm^{-1}. − $C_{19}H_{26}ClTa$ (470.8): calcd. C 48.47, H 5.57; found C 48.44, H 5.65.

Preparation of (*s-trans*-η^4-Butadiene)(η^5-cyclopentadienyl)(η^5-pentamethylcyclopentadienyl)tantalum Methyltris(pentafluorophenyl)-borate (8): The reagent $[Cp_2ZrCH_3^+][CH_3B(C_6F_5)_3^-]$ was generated in situ by treatment of 1.50 g (2.93 mmol) of $B(C_6F_5)_3$ with 753 mg (3.00 mmol) of $Cp_2Zr(CH_3)_2$ in 20 mL of toluene. The resulting orange-colored solution was added with stirring at ambient temperature to a solution of 1.55 g (3.30 mmol) of **7** in 20 mL of toluene. The reaction mixture was stirred for 10 min. Then the oily product was allowed to separate from the solution. The supernatant liquid was removed. The remaining oil was washed with toluene (3 × 15 mL) and dried in vacuo. The dark grey solid was suspended in 20 mL of pentane and then collected by filtration, washed with pentane (2 × 20 mL) and then dried in vacuo to yield 2.29 g (81%) of **8**, m.p. 191 °C (decomp.). − ^{1}H NMR ([D_2]dichloromethane, 599.8 MHz, 298 K): δ = 5.13 (s, 5 H, Cp-H), 3.75−3.68 (m, 1 H, 2-H), 3.46 (dd, $^2J_{HH}$ = 5.4 Hz, $^3J_{HH}$ = 7.7 Hz, 1 H, 1-H′), 3.09−3.07 (m, 1 H, 4-H′), 2.20−2.17 (m, 2 H, 3-H, 4-H), 1.88 [s, 15 H, $C_5(CH_3)_5$], 1.42 (ddd, $^2J_{HH}$ = 5.4 Hz, $^3J_{HH}$ = 16.2 Hz, $^4J_{HH}$ = 1.2 Hz, 1 H, 1-H), 0.48 [br. s, 3 H, *Me*-$B(C_6F_5)_3$]. − ^{1}H NMR ([D_5]bromobenzene, 599.8 MHz, 298 K): δ = 4.44 (s, 5 H, Cp-H), 3.07−3.01 (m, 1 H, 2-H), 2.91 (m, 1 H, 1-H′), 2.53 (m, 1 H, 4-H′), 1.61 (m, 2 H, 3-H, 4-H), 1.32 [s, 15 H, $C_5(CH_3)_5$], 0.88 (dd, $^2J_{HH}$ = 4.0 Hz, $^3J_{HH}$ = 16.0 Hz, 1 H, 1-H), 1.12 [br. s, 3 H, *Me*-$B(C_6F_5)_3$]. − 1D-TOCSY NMR ([D_2]dichloromethane, 599.8 MHz, 298 K): irradiation at δ = 3.71 (2-H): response at δ = 3.46 (1-H′), 3.08 (4-H′), 2.18 (3-H, 4-H), 1.42 (1-H). − GCOSY NMR ([D_2]dichloromethane, 599.8 MHz, 298 K): δ = 3.71/3.46, 2.18, 1.42 (2-H/1-H′, 3-H, 1-H), 3.46/3.71, 1.42 (1-H′/2-H, 1-H), 3.08/2.18 (4-H′/3-H, 4-H), 2.18/3.71, 3.08 (3-H, 4-H/2-H, 4-H′), 1.42/3.71, 3.46 (1-H/2-H, 1-H′). − ^{13}C NMR ([D_2]dichloromethane, 150.8 MHz, 298 K): δ = 148.7 [d, $^1J_{CF}$ = 232 Hz, *o*-$B(C_6F_5)_3$], 137.8 [d, $^1J_{CF}$ = 234 Hz, *p*-$B(C_6F_5)_3$], 136.8 [d, $^1J_{CF}$ = 235 Hz, *m*-$B(C_6F_5)_3$], 129.1 [br. m, *ipso*-$B(C_6F_5)_3$], 109.5 [$C_5(CH_3)_5$], 98.6 (C-Cp), 93.6 (C-3), 91.2 (C-2), 64.3 (C-4), 59.8 (C-1), 12.2 [$C_5(CH_3)_5$], 10.4 [br. s, *Me*-$B(C_6F_5)_3$]. − ^{13}C NMR ([D_5]bromobenzene, 150.8 MHz, 298 K): δ = 148.7 [d, $^1J_{CF}$ = 230 Hz, *o*-$B(C_6F_5)_3$], 137.6 [d, $^1J_{CF}$ = 232 Hz, *p*-$B(C_6F_5)_3$], 136.5 [d, $^1J_{CF}$ = 234 Hz, *m*-$B(C_6F_5)_3$], 108.3 [$C_5(CH_3)_5$], 97.4 (C-Cp), 92.9 (C-3), 90.6 (C-2), 63.8 (C-4), 59.2 (C-1), 11.2 [$C_5(CH_3)_5$], 11.0 [br. s, *Me*-$B(C_6F_5)_3$] (*ipso*-C of C_6F_5 not found). − GHSQC ([D_2]dichloromethane, 150.8/599.8 MHz, 298 K): δ = 98.6/5.13 (C-Cp/Cp-H), 93.6/2.18 (C-3/3-H), 91.2/3.71 (C-2/2-H), 64.3/3.08 (C-4/4-H′), 64.3/2.18 (C-4/4-H), 59.2/3.46 (C-1/1-H′), 59.2/1.42 (C-1/1-H), 12.2/1.88 ($C_5(CH_3)_5$/$C_5(CH_3)_5$), 11.0/0.48 (*Me*-$B(C_6F_5)_3$). − ^{11}B NMR ([D_2]dichloromethane, 64.2 MHz): δ = 15.0. − ^{19}F NMR ([D_2]dichloromethane, 282.4 MHz, 298 K): δ = −130 [m, 6 F, *o*-$CH_3B(C_6F_5)_3$], −163 [m, 3 F, *p*-$CH_3B(C_6F_5)_3$], −166 [m, 6 F, *m*-$CH_3B(C_6F_5)_3$]. − IR (KBr): $\tilde{\nu}$ = 3132 (vw), 2963 (w), 2921 (w), 1642 (m), 1512 (vs), 1456 (vs), 1383 (w), 1265 (m), 1087 (vs), 979−934 (br. m), 842 (m), 804 (w) cm^{-1}. − $C_{38}H_{29}BF_{15}Ta$ (962.4): calcd. C 47.43, H 3.04; found C 46.87, H 3.62.

X-ray Crystal Structure Analysis of 8: Formula $C_{19}H_{26}Ta \cdot B(C_6F_5)_3CH_3 \cdot CH_2Cl_2$, M = 1047.30, red crystal, 0.40 × 0.30 × 0.15 mm, a = 9.369(1), b = 12.479(1), c = 17.647(1) Å, α = 102.13(1), β = 102.11(1), γ = 102.59(1)°, V = 1896.7(3) Å^3, $\rho_{calcd.}$ = 1.834 g cm^{-3}, F(000) = 1024 e, μ = 31.43 cm^{-1}, absorption correction by SORTAV (0.366 ≤ T ≤ 0.650), Z = 2, triclinic, space group $P\bar{1}$ (No. 2), λ = 0.71073 Å, T = 198 K, φ and ω scans, 16502 reflections collected (±h, ±k, ±l), [(sinθ)/λ] = 0.67 Å^{-1}, 9284 independent and 8161 observed reflections [$I \geq 2\,\sigma(I)$], 470 refined parameters, R = 0.056, wR^2 = 0.145, max. residual electron density 2.07 (−1.75) e Å^{-3}, hydrogen atoms calculated and refined as riding atoms. The butadiene unit is severely disordered, carbon atoms C11−C14 are refined isotropically and with restraints [DFIX 1.38(1) for C11−C12 and C13−C14, DFIX 1.47(1) for C12−C13, SADI (0.1) for C11−C13 and C12−C14]. This disorder affects also the neighboring Cp ring, especially the closest carbon atoms C6, C7, and C8 show large displacement parameters. Therefore the Cp ring is refined isotropically as rigid group. All other non-hydrogen atoms including the solvent molecule CH_2Cl_2 are refined anisotropically. The data set was collected with a Nonius Kappa CCD diffractometer, equipped with a rotating anode generator FR591. Programs used: data collection COLLECT, data reduction DENZO-SMN, absorption correction SORTAV, structure solution SHELXS-97, structure refinement SHELXL-97, graphics SCHAKAL-92. Crystallographic data (excluding structure factors) for the structures reported in this paper have been deposited with the Cambridge Crystallographic Data Centre as supplementary publication no. CCDC-115170. Copies of the data can be obtained free of charge on application to CCDC, 12 Union

Road, Cambridge CB2 1EZ, UK [Fax: int. code + 44-1223/336-033; E-mail: deposit@ccdc.cam.ac.uk.].

Preparation of 2-(η⁵-Cyclopentadienyl)-7,7-dimethyl-2-(η⁵-pentamethylcyclopentadienyl)-2,3,6,7-tetrahydro-2-tantalaoxepine Methyltris(pentafluorophenyl)borate (9): Acetone (36.2 mg, 620 μmol) was added to a solution of 300 mg (310 μmol) of **8** in 5 mL of bromobenzene at ambient temperature. The mixture was stirred for 3 h at 50 °C. The product was then precipitated at room temperature by the addition of 10 mL of pentane. The solvent was decanted off. The residue was dissolved in 5 mL of dichloromethane and the product again precipitated by adding 10 mL of pentane. The solvents were removed and the product dried in vacuo, then suspended in 10 mL of pentane and collected by filtration. Yield of **9**: 230 mg (72%), m.p. 74°C (decomp.). − ^{1}H NMR ([D$_2$]dichloromethane, 599.8 MHz, 298 K): The ^{1}H-NMR spectrum shows the presence of two isomers, **9A** and **9B** in a 50:50 ratio. Isomer **A**: δ = 6.43 (m, 1 H, 4-H), 5.78 (s, 5 H, Cp-H), 4.48 (m, 1 H, 5-H), 1.99 [s, 15 H, C$_5$(CH$_3$)$_5$], 1.57 (pt, J_{HH} = 6.6 Hz, 1 H, 6-H), 1.40 (s, 3 H, 7-CH$_3$), 1.38 (pt, J_{HH} = 11.2 Hz, 1 H, 3-H), 1.22 (s, 3 H, 7-CH$_3$′); 6-H′ and 3-H′ resonances under C$_5$(C*H*$_3$)$_5$ signal. Isomer **B**: δ = 6.48 (m, 1 H, 4-H), 6.04 (s, 5 H, Cp-H), 5.35 (m, 1 H, 5-H), 2.13 [s, 15 H, C$_5$(CH$_3$)$_5$], 1.96 (dd, $^2J_{HH}$ = 8.9 Hz, $^3J_{HH}$ = 13.5 Hz, 6-H′), 1.91 (m, 1 H, 3-H′), 1.82 (m, 1 H, 3-H), 1.65 (dd, $^2J_{HH}$ = 8.9 Hz, $^3J_{HH}$ = 14.7 Hz, 1 H, 6-H), 1.49 (s, 3 H, 7-CH$_3$), 1.09 (s, 3 H, 7-CH$_3$′); the C*H*$_3$[B] resonance is at δ = 0.49. − 1D TOCSY NMR ([D$_2$]dichloromethane, 599.8 MHz, 298 K): Isomer **A**: 1. irradiation at δ = 4.48 (5-H): response at δ = 6.43 (4-H), 2.18 (6-H′), 2.12 (3-H′), 1.57 (6-H), 1.38 (3-H); 2. irradiation at δ = 1.40 (8-H): response at δ = 6.43 (4 H), 4.48 (5-H), 2.12 (3-H′), 1.38 (3-H). Isomer **B**: 1. irradiation at δ = 5.35 (5-H): response at δ = 6.48 (4-H), 1.96 (6-H′), 1.91 (3-H′), 1.83 (3-H), 1.65 (6-H); 2. irradiation at δ = 1.09 (9-H): response at δ = 6.48 (4-H), 5.35 (5-H), 1.96 (6-H′), 1.65 (6-H), 1.49 (8-H). − GCOSY NMR ([D$_2$]dichloromethane, 599.8 MHz, 298 K): Isomer **A**: δ = 6.43/4.48, 2.12, 1.38 (4-H/5-H, 3-H′, 3-H), 4.48/6.43, 2.18, 1.57 (5-H/4-H, 6-H′, 6-H), 2.18/4.48, 1.57 (6-H′/5-H, 6-H), 1.57/4.48, 2.18 (6-H/5-H, 6-H′), 2.12/6.43, 1.38 (3-H′/6-H, 3-H), 1.38/6.43, 2.12 (3-H/6-H, 3-H′). Isomer **B**: δ = 6.48/5.35, 1.91, 1.83 (4-H/5-H, 3-H′, 3-H), 5.35/6.48, 1.96, 1.65 (5-H/4-H, 6-H′, 6-H), 1.96/5.35, 1.65 (6-H′/5-H, 6-H), 1.91/6.48, 1.83 (3-H′/4-H, 3-H), 1.83/6.48, 1.91 (3-H/4-H, 3-H′), 1.65/5.35, 1.96 (6-H/5-H, 6-H′). − ^{13}C NMR ([D$_2$]dichloromethane, 150.8 MHz, 298 K): Isomer **A**: δ = 146.6 (C-4), 119.2 [*C*(CH$_3$)$_5$], 110.3 (C-5), 107.2 (C-Cp), 99.1 (C-7), 48.8 (C-3), 42.6 (C-6), 37.1 (C-8), 30.1 (C-9), 11.9 (C(CH$_3$)$_5$). Isomer **B**: δ = 137.6 (C-4), 124.0 (C-5), 123.0 [C(CH$_3$)$_5$], 115.4 (C-7), 110.4 (C-Cp), 44.8 (C-3), 37.3 (C-6), 33.4 (C-8), 25.7 (C-9), 12.3 [C(CH$_3$)$_5$]. CH$_3$B(C$_6$F$_5$)$_3$$^-$: δ = 148.5 [d, $^1J_{CF}$ = 235 Hz, *o*-B(C$_6$F$_5$)$_3$], 137.8 [d, $^1J_{CF}$ = 236 Hz, *p*-B(C$_6$F$_5$)$_3$], 136.7 [d, $^1J_{CF}$ = 238 Hz, *m*-B(C$_6$F$_5$)$_3$], 129.3 [br. m, *ipso*-B(C$_6$F$_5$)$_3$], 10.5 [br. s, *Me*-B(C$_6$F$_5$)$_3$]. − GHSQC NMR ([D$_2$]dichloromethane, 150.8/599.8 MHz): Isomer **A**: δ = 146.6/6.43 (C-4/4-H), 110.3/4.48 (C-5/5-H), 107.2/5.78 (C-Cp/Cp-H), 48.8/2.12 (C-3/3-H′), 48.8/1.38 (C-3/3-H), 42.6/2.18 (C-6/6-H′), 42.6/1.57 (C-6/6-H), 37.1/1.40 (C-8/8-H), 30.1/1.22 (C-9/9-H), 11.9/1.99 (C(*C*H$_3$)$_5$/C(C*H*$_3$)$_5$). Isomer **B**: δ = 137.6/6.48 (C-4/4-H), 124.0/5.35 (C-5/5-H), 110.4/6.04 (C-Cp/Cp-H), 44.8/1.91 (C-3/3-H′), 37.3/1.96 (C-6/6-H′), 37.3/1.65 (C-6/6-H), 33.4/1.49 (C-8/8-H), 25.7/1.09 (C-9/9-H), 12.3/2.13 [C(*C*H$_3$)$_5$/C(C*H*$_3$)$_5$]. [*Me*-B(C$_6$F$_5$)$_3$]: δ = 10.5/0.49. − ^{11}B NMR ([D$_2$]dichloromethane, 64.2 MHz): δ = −15.0. − ^{19}F NMR ([D$_2$]dichloromethane, 282.4 MHz, 298 K): δ = −130 [m, 6 F, *o*-CH$_3$B(C$_6$F$_5$)$_3$], −163 [m, 3 F, *p*-CH$_3$B(C$_6$F$_5$)$_3$], −166 [m, 6 F, *m*-CH$_3$B(C$_6$F$_5$)$_3$]. − IR (KBr): $\tilde{\nu}$ = 3124 (w), 2925 (m), 1641 (w), 1511 (vs), 1458 (vs), 1378 (vw), 1362 (vw), 1265 (m), 1084 (vs), 993−953 (br. s), 847 (s), 803 (w) cm^{-1}. − C$_{41}$H$_{35}$BF$_{15}$OTa (1020.5): calcd. C 48.26, H 3.46; found C 48.03, H 3.28.

Reaction of 8 with Adamantanone, Preparation of 10: Adamantanone (51.5 mg, 340 μmol) was added to a solution of 300 mg (310 μmol) of **8** in 5 mL of bromobenzene. The mixture was stirred for 3 h at 50 °C. The product was precipitated by adding 10 mL of pentane. The supernatant liquid was decanted from the oil. The oily product was dissolved in 5 mL of dichloromethane and again precipitated with 10 mL of pentane. The solvent was decanted and the product dried in vacuo. Yield of **10**: 199 mg (57%), m.p. 176 °C (decomp.). − ^{1}H NMR ([D$_2$]dichloromethane, 599.8 MHz, 298 K): The ^{1}H-NMR spectrum shows the presence of two isomers, **10A** and **10B**, in a 70:30 ratio. Isomer **A**: δ = 6.43 (m, 1 H, 4-H), 5.77 (s, 5 H, Cp-H), 4.64 (m, 1 H, 5-H), 3.01 (dd, $^3J_{HH}$ = 5.0 Hz, $^2J_{HH}$ = 11.8 Hz, 1 H, 3-H′), 2.11 [s, 16 H, 6-H′, C$_5$(C*H*$_3$)$_5$], 1.55 (pt, J_{HH} = 6.5 Hz, 1 H, 6-H), 1.08 (pt, J_{HH} = 11.8 Hz, 1 H, 3-H). Isomer **B**: δ = 6.53 (m, 1 H, 4-H), 6.01 (s, 5 H, Cp-H), 5.31 (m, 1 H, 5-H), 2.85 (br. m, 1 H, 6-H′), 2.01 [s, 15 H, C$_5$(C*H*$_3$)$_5$], 1.11 (br. m, 1 H, 6-H), 3-H/H′ signals under adamantyl signals at δ = 2.10−1.58 (br. m, 30 H, both isomers), C*H*$_3$[B] signal at δ = 0.47. − 1D-TOCSY NMR ([D$_2$]dichloromethane, 599.8 MHz, 298 K): Isomer **A**: irradiation at δ = 4.64 (5-H): response at δ = 6.42 (4-H), 3.01 (3-H′), 2.11 (6-H′), 1.55 (6-H), 1.08 (3-H). Isomer **B**: irradiation at δ = 5.32 (5-H): response at δ = 6.52 (4-H), 2.80 (6-H′),1.90 (3-H′), 1.83 (3-H), 1.10 (6-H). − GCOSY NMR ([D$_2$]dichloromethane, 599.8 MHz, 298 K): Isomer **A**: 6.42/4.64, 3.01, 1.08 (4-H/5-H, 3-H′, 3-H), 4.64/6.42, 2.11, 1.55 (5-H/4-H, 6-H′, 6-H), 3.01/6.42, 1.08 (3-H′/4-H, 3-H), 2.11/4.64, 1.55 (6-H′/5-H, 6-H), 1.55/4.64, 2.11 (6-H/5-H, 6-H′), 1.08/6.42, 3.01 (3-H/4-H, 3-H′). Isomer **B**: 6.52/5.32, 1.90, 1.83 (4-H/5-H, 3-H′, 3-H), 5.32/6.52, 2.80, 1.10 (5-H/4-H, 6-H′, 6-H), 2.80/5.32, 1.10 (6-H′/5-H, 6-H), 1.90/6.52, 1.83 (3-H′/4-H, 3-H), 1.83/6.52, 1.90 (3-H/4-H, 3-H′), 1.10/5.32, 2.80 (6-H/5-H, 6-H′). − ^{13}C NMR ([D$_2$]dichloromethane, 150.8 MHz, 298 K): Isomer **A**: δ = 140.9 (C-4), 118.8 [*C*(CH$_3$)$_5$], 115.6 (C-7), 111.4 (C-5), 110.4 (C-Cp), 43.2 (C-3), 42.3 (C-6), 47.4, 37.5, 36.4, 36.3, 35.7, 34.8, 33.7, 27.5, 26.8 (C-adamantyl fragment), 11.8 [C(C*H*$_3$)$_5$]. Isomer **B**: δ = 137.2 (C-4), 123.8 [*C*(CH$_3$)$_5$], 122.3 (C-5), 110.4 (C-Cp), 109.3 (C-7), 45.2 (C-3), 45.0 (C-6), 46.4, 39.2, 38.9, 38.3, 36.1, 36.0, 33.2, 27.0, 26.6, 11.8 [C$_5$(C*H*$_3$)$_5$]. CH$_3$B(C$_6$F$_5$)$_3$$^-$: δ = 148.6 (d, $^1J_{CF}$ = 233 Hz, *o*-B(C$_6$F$_5$)$_3$], 137.9 [d, $^1J_{CF}$ = 235 Hz, *p*-B(C$_6$F$_5$)$_3$], 136.5 [d, $^1J_{CF}$ = 237 Hz, *m*-B(C$_6$F$_5$)$_3$], 129.1 [br. m, *ipso*-B(C$_6$F$_5$)$_3$], 10.5 [br. s, *Me*-B(C$_6$F$_5$)$_3$]. − GHSQC NMR ([D$_2$]dichloromethane, 150.8/599.8 MHz, 298 K): Isomer **A**: δ = 140.9/6.42 (C-4/4-H), 111.4/4.64 (C-5/5-H), 110.4/5.77 (C-Cp/Cp-H), 43.2/3.01 (C-3/3-H′), 43.2/1.08 (C-3/3-H), 42.3/2.11 (C-6/6-H′), 42.3/1.55 (C-6/6-H), 11.8/2.11 [C(*C*H$_3$)$_5$/C(C*H*$_3$)$_5$]. Isomer **B**: δ = 137.2/6.52 (C-4/4-H), 122.3/5.32 (C-5/5-H), 110.4/6.01 (C-Cp/Cp-H), 45.2/1.90 (C-3/3-H′), 45.2/1.83 (C-3/3-H), 42.3/2.80 (C-6/6-H), 42.3/1.10 (C-6/6-H′), 11.8/2.01 [C$_5$(*C*H$_3$)$_5$/C$_5$(C*H*$_3$)$_5$]; δ = 10.5/0.47 [*Me*-B(C$_6$F$_5$)$_3$]. − IR (KBr): $\tilde{\nu}$ = 3120 (vw), 2915 (w), 2858 (w), 1640 (w), 1510 (s), 1457 (vs), 1381 (w), 1266 (w), 1085 (s), 995−933 (br. m), 842 (w), 804 (w) cm^{-1}. − C$_{48}$H$_{43}$BF$_{15}$OTa (1112.6): calcd. C 51.82, H 3.89; found C 52.12, H 4.26.

Preparation of 7-(1-Adamantyl)-2-(η⁵-cyclopentadienyl)-3,6-dihydro-2-(η⁵-pentamethylcyclopentadienyl)-2-tantala-2*H*-azepine Methyltris(pentafluorophenyl)borate (11): 1-Cyanoadamantane (55.3 mg, 340 μmol) was added to a solution of 300 mg (310 μmol) of **8** in 10 mL of bromobenzene. The mixture was kept for 2 h at 50 °C. Pentane (15 mL) was added to precipitate the product. The supernatant liquid was decanted. The residue was dissolved in 5 mL of

dichloromethane and the product again precipitated by adding 10 mL of pentane. The solvent was decanted off and the product dried in vacuo, suspended in 10 mL of pentane and then collected by filtration to yield 252 mg (72%) of **11**, m.p. 205 °C (decomp.). – ^{1}H NMR ([D$_2$]dichloromethane, 599.8 MHz, 298 K): δ = 6.34 (m, 1 H, 4-H), 5.67 (s, 5 H, Cp-H), 4.82 (m, 1 H, 5-H), 3.32 (dd, $^2J_{HH}$ = 12.7 Hz, $^3J_{HH}$ = 8.4 Hz, 1 H, 6-H′), 2.01 [s, 15 H, C$_5$(CH_3)$_5$], 2.10–2.07, 1.86–1.79, 1.75–1.65 (m, 15 H, adamantyl), 1.77 (ddd, $^2J_{HH}$ = 12.7 Hz, $^3J_{HH}$ = 7.1 Hz, $^4J_{HH}$ = 2.0 Hz, 1 H, 6-H), 1.55 (dd, $^2J_{HH}$ = 10.4 Hz, $^3J_{HH}$ = 7.9 Hz, 1 H, 3-H′), 0.85 (ddd, $^2J_{HH}$ = 10.4 Hz, $^3J_{HH}$ = 7.8 Hz, $^4J_{HH}$ = 1.8 Hz, 1 H, 3-H), 0.47 [br. s, 3 H, *Me*-B(C$_6$F$_5$)$_3$]. – 1D-TOCSY NMR ([D$_2$]dichloromethane, 599.8 MHz, 298 K): irradiation at δ = 4.82 (5-H): response at δ = 6.35 (4-H), 3.32 (6-H′), 1.77 (6-H), 1.55 (3-H′), 0.85 (3-H). – GCOSY NMR ([D$_2$]dichloromethane, 599.8 MHz, 298 K): δ = 6.35/4.82, 1.55, 0.85 (4-H/5-H, 3-H′, 3-H), 4.82/6.35, 3.32, 1.77 (5-H/4-H, 6-H′, 6-H), 3.32/4.82, 1.77 (6-H′/5-H, 6-H), 1.77/4.82, 3.32 (6-H/5-H, 6-H′), 1.55/6.35, 0.85 (3-H′/4-H, 3-H), 0.85/6.35, 1.55 (3-H/4-H, 3-H′). – ^{13}C NMR ([D$_2$]dichloromethane, 150.8 MHz, 298 K): δ = 190.1 (C-7), 148.6 [d, $^1J_{CF}$ = 231 Hz, *p*-B(C$_6$F$_5$)$_3$], 139.6 (C-4), 137.8 [d, $^1J_{CF}$ = 233 Hz, *p*-B(C$_6$F$_5$)$_3$], 136.4 [d, $^1J_{CF}$ = 232 Hz, *m*-B(C$_6$F$_5$)$_3$], 118.1 [C_5(CH$_3$)$_5$], 112.5 (C-5), 107.5 (C-Cp), 35.2 (C-3), 27.6 (C-6), 43.3, 38.7, 36.5, 28.2 (C-adamantyl), 11.9 [C$_5$(*C*H$_3$)$_5$], 10.4 [br. s, *Me*-B(C$_6$F$_5$)$_3$]. – GHSQC ([D$_2$]dichloromethane, 150.8/599.8 MHz, 298 K): δ = 139.6/6.35 (C-4/4-H), 112.5/4.82 (C-5/5-H), 107.5/5.67 (C-Cp/Cp-H), 35.2/1.55 (C-3/3-H′), 35.2/0.85 (C-3/3-H), 27.6/3.32 (C-6/6-H′), 27.6/1.77 (C-6/6-H), 11.9/2.01 [C$_5$(*C*H$_3$)$_5$/C$_5$(CH_3)$_5$], 10.4/0.48 [*Me*-B(C$_6$F$_5$)$_3$]. – ^{11}B NMR ([D$_2$]dichloromethane, 64.2 MHz): δ = –15.0. – ^{19}F NMR ([D$_2$]dichloromethane, 282.4 MHz): δ = -130 [m, 6 F, *o*-CH$_3$B(C$_6$F$_5$)$_3$], –163 [m, 3 F, *p*-CH$_3$B(C$_6$F$_5$)$_3$], –166 [m, 6 F, *m*-CH$_3$B(C$_6$F$_5$)$_3$]. – IR (KBr): $\tilde{\nu}$ = 3120 (vw), 2959 (w), 2915 (m), 2852 (w), 1665 (w), 1640 (w), 1510 (s), 1457 (vs), 1381 (w), 1264 (m), 1085 (vs), 1016–951 (br. m), 838 (m), 803 (m) cm^{-1}. – C$_{49}$H$_{44}$BNF$_{15}$Ta (1123.6): calcd. C 52.38, H 3.95, N 1.25; found C 52.79, H 4.24, N 1.14.

Ethene Polymerization Reactions: The ethene polymerization reactions were carried out in a Büchi glass autoclave. The reaction vessel was charged with 200 mL of toluene and 20 mL (0.033 mol) of a 10.5% solution of methylalumoxane in toluene. The mixture was brought to the preset reaction temperature and saturated with ethene at 2 bar for 1 h with stirring (700 min^{-1}). Then the polymerization reaction was started by the injection of 2 mL of a toluene solution of the catalyst precursors **4** or **8** (see Table 1). The polymerization was stopped after 30 min by quenching with CH$_3$OH/2 N aqueous HCl (1:1) and the polyethylene isolated (m.p. by DSC). For further details see Table 1.

Acknowledgments

Financial support from the Fonds der Chemischen Industrie, the Bundesministerium für Bildung, Wissenschaft, Forschung und Technologie (stipend to H.C.S.), the Deutsche Forschungsgemeinschaft, and the Academy of Finland (M. N.) is gratefully acknowledged.

[1] [1a] G. Erker, J. Wicher, K. Engel, F. Rosenfeldt, W. Dietrich, C. Krüger, *J. Am. Chem. Soc*. **1980**, *102*, 6344; G. Erker, J. Wicher, K. Engel, C. Krüger, *Chem. Ber*. **1982**, *115*, 3300; G. Erker, K. Engel, C. Krüger, A.-P. Chiang, *Chem. Ber*. **1982**, *115*, 3311. – [1b] H. Yasuda, Y. Kajihara, K. Mashima, K. Nagasuna, K. Lee, A. Nakamura, *Organometallics* **1982**, *1*, 388; Y. Kai, N. Kanehisa, K. Miki, N. Kasai, K. Mashima, K. Nagasuna, H. Yasuda, A. Nakamura, *J. Chem. Soc., Chem. Commun*. **1982**, 191.

[2] For recent examples see e.g.: S. A. Benyunes, J. P. Day, M. Green, A. W. Al-Saadoon, T. L. Waring, *Angew. Chem.* **1990**, *102*, 1505; *Angew. Chem. Int. Ed. Engl*. **1990**, *29*, 1416; G. Herberich, U. Englert, K. Linn, P. Roos, J. Runsink, *Chem. Ber*. **1991**, *124*, 975; R. D. Ernst, E. Melendez, L. Stahl, M. L. Ziegler, *Organometallics* **1991**, *10*, 3635; J. D. Debad, P. Legzdins, M. A. Young, R. J. Batchelor, F. W. B. Einstein, *J. Am. Chem. Soc.* **1993**, *115*, 2051; U. Böhme, K.-H. Thiele, A. Rufinska, *Z. Anorg. Allg. Chem*. **1994**, *620*, 1455; C. Gemel, K. Mereiter, R. Schmid, K. Kirchner, *Organometallics* **1997**, *16*, 2623; L.-S. Wang, J. C. Fettinger, R. Poli, *J. Am. Chem. Soc.* **1997**, *119*, 4453; K. Mashima, H. Fukumoto, K. Tani, M. Haga, A. Nakamura, *Organometallics* **1998**, *17*, 410, and references cited therein.

[3] For selected examples see: H. Yasuda, T. Okamoto, Y. Matsuoka, A. Nakamura, Y. Kai, N. Kanehisa, N. Kasai, *Organometallics* **1989**, *8*, 1139; G. Erker, F. Sosna, P. Betz, S. Werner, C. Krüger, *J. Am. Chem. Soc.* **1991**, *113*, 564; G. Erker, R. Pfaff, D. Kowalski, E.-U. Würthwein, C. Krüger, R. Goddard, *J. Org. Chem.* **1993**, *58*, 6771; M. Berlekamp, G. Erker, B. Schönecker, R. Krieg, A. L. Rheingold, *Chem. Ber*. **1993**, *126*, 2119; L. López, M. Berlekamp, D. Kowalski, G. Erker, *Angew. Chem*. **1994**, *106*, 1168; *Angew. Chem. Int. Ed. Engl.* **1994**, *33*, 1114; G. Erker, M. Berlekamp, L. López, M. Grehl, B. Schönecker, R. Krieg, *Synthesis* **1994**, 212. Review: G. Erker, *Angew. Chem*. **1989**, *101*, 411; *Angew. Chem. Int. Ed. Engl*. **1989**, *28*, 397.

[4] K. Mashima, S. Fujikawa, A. Nakamura, *J. Am. Chem. Soc.* **1993**, *115*, 10990; B. Temme, G. Erker, J. Karl, H. Luftmann, R. Fröhlich, S. Kotila, *Angew. Chem*. **1995**, *107*, 1867; *Angew. Chem. Int. Ed. Engl*. **1995**, *34*, 1755; D. D. Devore, F. J. Timmers, D. L. Hasha, R. K. Rosen, T. J. Marks, P. A. Deck, C. L. Stern, C. L. *Organometallics* **1995**, *14*, 3132; K. Mashima, S. Fujikawa, Y. Tanaka, H. Urata, T. Oshiki, E. Tanaka, A. Nakamura, *Organometallics* **1995**, *14*, 2633; B. Temme, J. Karl, G Erker, *Chem. Eur. J.* **1996**, *2*, 919; J. Karl, G. Erker, R. Fröhlich, *J. Am. Chem. Soc*. **1997**, *119*, 11165; G. J. Pindado, M. Thornton-Pett, M. Bowkamp, A. Meetsma, B. Hessen, M. Bochmann, *Angew. Chem.* **1997**, *109*, 2457; *Angew. Chem. Int. Ed. Engl*. **1997**, *36*, 2358; J. Karl, M. Dahlmann, G. Erker, K. Bergander, *J. Am. Chem. Soc.* **1998**, *120*, 5643.

[5] H. Yasuda, K. Tatsumi, T. Okamoto, K. Mashima, K. Lee, A. Nakamura, Y. Kai, N. Kanehisa, N. Kasai, *J. Am. Chem. Soc.* **1985**, *107*, 2410.

[6] X. Yang, C. L. Stern, T. J. Marks, *J. Am. Chem. Soc.* **1994**, *116*, 10015.

[7] T. Brackemeyer, G. Erker, R. Fröhlich, *Organometallics* **1997**, *16*, 531.

[8] H. C. Strauch, G. Erker, R. Fröhlich, *Organometallics* **1998**, *17*, 5746.

[9] [9a] Reviews: H. Yasuda, K. Tatsumi, A. Nakamura, *Acc. Chem. Res.* **1985**, *18*, 120; G. Erker, C. Krüger, G. Müller, *Adv. Organomet. Chem.* **1985**, *24*, 1. – [9b] For a description of the special bonding features of (*s-trans*-η^4-conjugated diene) bent metallocene complex see: K. Tatsumi, H. Yasuda, A. Nakamura, A. *Isr. J. Chem*. **1983**, *23*, 145; G. Erker, K. Engel, U. Korek, P. Czisch, H. Berke, P. Caubère, P. Vanderesse, *Organometallics* **1985**, *4*, 1531.

[10] H. Yasuda, Y. Kajihara, K. Mashima, K. Nagasuna, A Nakamura, *Chem. Lett*. **1981**, 671; Y. Kai, N. Kanehisa, K. Miki, N. Nasai, M. Akita, H. Yasuda, A. Nakamura, *Bull. Chem. Soc. Jpn*. **1983**, *56*, 3735; G. Erker, K. Engel, J. L. Atwood, W. E. Hunter, *Angew. Chem*. **1983**, *95*, 506; *Angew. Chem. Int. Ed. Engl*. **1983**, *22*, 494, *Angew. Chem. Suppl.* **1983**, 675; H. Yasuda, A. Nakamura, *Angew. Chem.* **1987**, *99*, 745; *Angew. Chem. Int. Ed. Engl*. **1987**, *26*, 723; T. Okamoto, H. Yasuda, A. Nakamura, Y. Kai, N. Kanehisa, N. Kasai, *Organometallics* **1988**, *7*, 2266; H. Yasuda, T. Okamoto, K. Mashima, A. Nakamura, *J. Organomet. Chem*. **1989**, *363*, 61.

[11] W. A. Herrmann, W. W. Kalcher, H. Biersack, I. Bernal, *Chem. Ber*. **1981**, *114*, 3558.

[12] Y. Nakano, K. Natsukawa, H. Yasuda, H. Tani, *Tetrahedron Lett*. **1972**, 2833; K. Fujita, Y. Ohuma, H. Yasuda, H. Tani, *J. Organomet. Chem.* **1976**, *113*, 201; H. Yasuda, Y. Nakano, K. Natsukawa, H. Tani, *Macromolecules* **1978**, *11*, 586; Y. Kai, N. Kanehisa, K. Miki, N. Kasai, K. Mashima, H. Yasuda, A. Nakamura, *Chem. Lett*. **1982**, 1277.

[13] H. Yasuda, T. Okamoto, A. Nakamura, *Organometallic Syn-*

thesis (Ed.: R. B. King, J. J. Eisch), **1988**, vol. 4; see also ref.[5]
[14] See for a comparison: J. L. Thomas, *Inorg. Chem*. **1978**, *17*, 1507; A. Sen, J. Halpern, *Inorg. Chem*. **1980**, *19*, 1073; W. Beck, K. Raab, U. Nagel, W. Sacher, *Angew. Chem.* **1985**, *97*, 498; *Angew. Chem. Int. Ed. Engl*. **1985**, *24*, 505.
[15] J. R. Surtees, *J. Chem. Soc., Chem. Commun*. **1965**, 567.
[16] G. Binsch, E. L. Eliel, H. Kessler, *Angew. Chem.* **1971**, *83*, 618; *Angew. Chem. Int. Ed. Engl*. **1971**, *10*, 570.
[17] C. Krüger, G. Müller, G. Erker, U. Dorf, K. Engel, *Organometallics* **1985**, *4*, 215, and references cited therein.
[18] S. Braun, H. Kalinowski, S. Berger, *100 and More Basic NMR Experiments*, VCH, Weinheim **1996**, and references cited therein.

Received March 3, 1999
[I99080]

Group 5 Metal Complexes with Cyclooctatetraene: Formation and Characterization of (Butadiene)(cyclooctatetraene)(cyclopentadienyl)tantalum Systems

Hans Christian Strauch,[a] Klaus Bergander,[a][+] Gerald Kehr,[a][+] Roland Fröhlich,[a][++] and Gerhard Erker*[a]

Keywords: Diene complexes / η^3-Cyclooctatetraene metal complex / $B(C_6F_5)_3$ addition / Tantalum / Bicyclo[5.1.0]octadienyl metal complex

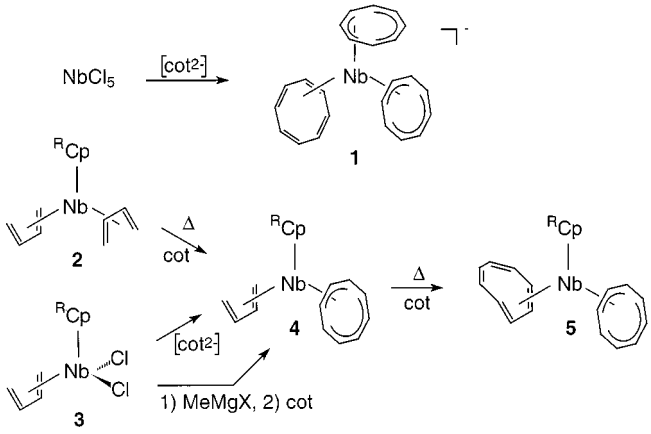
The [(η^4-diene)(η^5-^{R}Cp)$TaCl_2$] complexes **6a-e** (diene = butadiene, isoprene or 2,3-dimethylbutadiene; ^{R}Cp = pentamethylcyclopentadienyl, methylcyclopentadienyl or cyclopentadienyl) react with cyclooctatetraene dianion (employed as [(cot)Li_2]) to yield the (η^4-diene)(η^3-cyclooctatetraene)(η^5-^{R}Cp)tantalum complexes **7**. The η^3-cot coordination was confirmed by an X-ray crystal structure analysis of the compound [(*supine*-*s*-*cis*-η^4-C_4H_6)(η^3-cot)(η^5-Cp*)Ta] **7a**. In solution, the cot ligand of all the complexes **7** is fluxional. Two isomers [*supine* and *prone* orientation of the (diene)CpTa subunit] were found for the (η^4-butadiene)(η^3-cot)CpTa system (**7e**/**7e**′ = 95:5). Complex **7e** cleanly adds the organometallic Lewis acid $B(C_6F_5)_3$ to yield the betaine system [(η^4-C_4H_6){$C_8H_8B(C_6F_5)_3$}Cp*Ta] **8**, which contains a substituted bicyclo[5.1.0]octadienyl ligand.

Introduction

Cyclooctatetraene binds to the electropositive d-block metals of the left side of the periodic table (and to the f-elements) in a variety of coordination modes.[1] η^8-Coordination, η^4-conjugated diene-like and also η^2-bonding of the cot ligand can be found[2−4] and, most interestingly, η^3-coordination is not uncommon.[5] In these cases a π^5-section of the C_8H_8 ligand remains uncoordinated, which formally leads to an unsymmetrical, potentially dipolar electronic distribution at the M(η^3-C_8H_8) subunit. Such complexes were first reported by Schrock et al. The [(η^4-cot)(η^3-cot)$_2$Nb]$^-$ anion (**1**) is a typical example.[5] Recent examples include the [(*supine*-η^4-*s*-*cis*-butadiene)CpNb(η^3-cot)] system (**4**)[6] and its Cp*Nb analogue.[7] We have now prepared a series of related tantalum complexes. This work supplements the Nb-series, reported recently, but also has revealed a variety of subtle, but important, differences and variations.

Results and Discussion

Most examples of Cp- and Cp*Nb(η^4-butadiene)(η^3-cyclooctatetraene) complexes known so far have been prepared either by butadiene ligand displacement starting from [Cp(η^4-butadiene)$_2$Nb] **2** or by trapping of the bent metallocene analogue Cp*(η^4-butadiene)Nb, generated in situ, with cyclooctatetraene.[5−7] For this study we have exclusively used the [^{R}Cp(η^4-diene)$TaCl_2$] complexes **6** as precursors[8] and treated them with the cyclooctatetraene dianion[9] to form the corresponding [^{R}Cp(η^4-diene)(η^3-cyclooctatetraene)Ta] complexes **7** [^{R}Cp = η^5-C_5H_5, η^5-$C_5H_4(CH_3)$ or η^5-$C_5(CH_3)_5$; diene = butadiene, isoprene or 2,3-dimethylbutadiene].



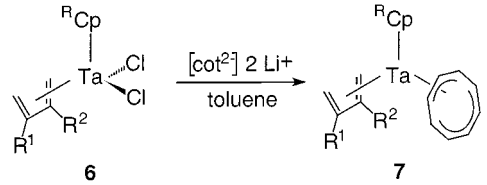
Scheme 1. Previous syntheses of (cot)Nb complexes

A typical example is the reaction of [(η^4-butadiene)(η^5-pentamethylcyclopentadienyl)$TaCl_2$] **(6a)** with the cyclooctatetraene dianion (employed as the corresponding dilithium salt). The reaction is carried out in toluene solution and takes about 15 h at 50°C to go to completion. Workup gives the product **7a** as a very dark-colored solid in approximately 50% yield. Dark red single crystals suitable for an X-ray crystal structure analysis were obtained from a toluene/pentane solution.

Complex **7a** has a central tantalum atom that is surrounded by a trigonal array of three π ligands. The pentamethylcyclopentadienyl ligand is η^5-coordinated [average Ta−C(Cp*) distance = 2.439(6) Å]. The η^4-*s*-*cis*-butadiene

[a] Organisch-Chemisches Institut der Universität Münster, Corrensstr. 40, D-48149 Münster, Germany
Fax: (internat.) + 49-(0)251/8336503
E-mail: erker@uni-muenster.de
[+] NMR spectroscopy.
[++] X-ray crystal structure analysis.

 © WILEY-VCH Verlag GmbH, D-69451 Weinheim, 1999 1434−1948/99/0909−1461 $ 17.50+.50/0



6 7

	RCp	R1	R2
a	η^5-$C_5(CH_3)_5$	H	H
b	η^5-$C_5(CH_3)_5$	CH_3	H
c	η^5-$C_5(CH_3)_5$	CH_3	CH_3
d	η^5-$C_5H_4(CH_3)$	H	H
e	η^5-C_5H_5	H	H

Scheme 2. Preparation of the (η^4-diene)(η^3-cot)^{R}CpTa complexes **7**

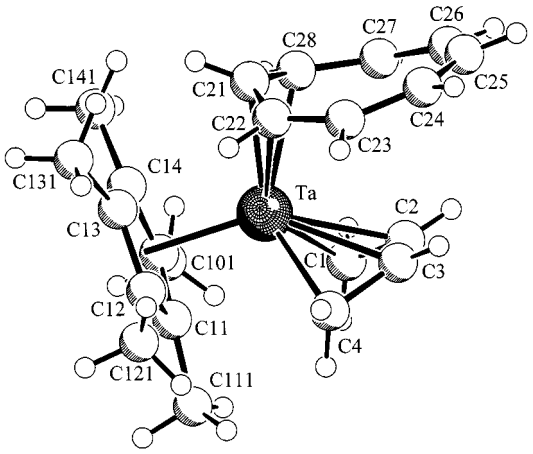


Figure 1. Molecular structure of **7a** with unsystematical atom numbering scheme

ligand opens toward the Cp* ligand (i.e. *supine*[8] oriented) and the Ta−C_4H_6 subunit exhibits some metallacyclopentene structural properties. It can probably best be described as approaching a metallacyclic σ^2,π-type structure as is often observed for early transition metal conjugated diene complexes.[10−12] This description is supported by the observed long-short-long bond alternation of the carbon framework of the butadiene ligand in complex **7a** (see Table 1). Also, the bonds between tantalum and the terminal diene ligand carbon atoms are markedly shorter [Ta−C1 = 2.252(6), Ta−C4 = 2.240(6) Å] than the bonds to the internal butadiene carbon centers [Ta−C2 = 2.433(5), Ta−C3 = 2.424(5) Å]. Similar conjugated diene C−C lengths were observed for both the [Cp*(η^4-butadiene)(η^3-cot)Nb] complex **4a**[7] and the related [(MeCp)(η^4-cot)(η^3-cot)Nb] complex **5a**.[6] These three systems, however, differ markedly in their relative M−C(diene) lengths (see Table 1). From these data a trend becomes apparent and it is possible to assign to the new tantalum complex **7a** the most pronounced σ-complex character of the M(diene) subunit in this series of compounds.

The cot ligand in **7a** is only η^3-coordinated. The central Ta−C21 bond length is 2.239(5) Å. It is the shortest metal to carbon bond of this group. The adjacent (η^3-cot)Ta linkages are slightly longer at 2.426(5) Å (Ta−C28) and 2.455(5) Å (Ta−C22). The next pair of distances (Ta···C27: 3.228(5) Å and Ta···C23: 3.333(5) Å) lie outside the range of a significant bonding interaction. The η^3-cot ligand in **7a** is coordinated in a *prone* orientation[8] and the ligand is slightly folded away from tantalum (see Table 1). There is no significant bond alternation visible in the η^3-C_8H_8 framework, so it appears that the cot ligand in **7a** has substantially retained its aromatic character with regard to its structural properties. It is structurally apart from the examples of "semiaromatic" cot character, that have recently been reported in the literature.[8b,13]

Table 1. A comparison of selected structural parameters of the complexes **7a, 4a** and **5a**[a]

	7a (Ta)	**4a** (Nb)	**5a** (Nb)
M−C1	2.252(6)	2.307(4)	2.453(5)
M−C2	2.433(5)	2.424(4)	2.363(4)
M−C3	2.424(5)	2.393(4)	2.375(3)
M−C4	2.240(6)	2.270(4)	2.456(3)
C1−C2	1.414(8)	1.415(6)	1.418(6)
C2−C3	1.392(8)	1.382(6)	1.394(8)
C3−C4	1.448(9)	1.423(6)	1.401(7)
α (C1, C4)[b]	104.5	101.9	[c]
M−C21	2.239(5)	2.255(4)	2.259(4)
M−C22	2.455(5)	2.452(4)	2.421(3)
M−C28	2.426(5)	2.424(4)	2.463(4)
M···C23	3.333(5)	[c]	3.192(4)
M···C27	3.228(5)	[c]	3.287(4)
α (C22, C28)[b]	25.3	[c]	23.6
α (C23, C27)[b]	12.7	[c]	11.8
α (C24, C26)[b]	4.9	[c]	4.2
C21−C28	1.423(7)	1.415(6)	1.408(6)
C21−C22	1.438(7)	1.415(6)	1.423(5)
C22−C23	1.411(7)	1.411(6)	1.401(5)
C23−C24	1.387(8)	1.411(6)	1.365(5)
C24−C25	1.412(9)	1.385(7)	1.384(7)
C25−C26	1.382(9)	1.384(7)	1.375(6)
C26−C27	1.396(8)	1.376(7)	1.382(6)
C27−C28	1.394(8)	1.392(6)	1.413(6)

[a] **7a**: [Cp*(*supine-s-cis*-η^4-C_4H_6)(*prone*-η^3-cot)Ta], this work; **4a**: [Cp*(*supine-s-cis*-η^4-C_4H_6)(*prone*-η^3-cot)Nb], from ref.[7]; **5a**: [(MeCp)(*supine*-η^4-cot)(*prone*-η^3-cot)Nb], from ref.[6] bond lengths in Å, angles in deg. − [b] Angles of fold along the indicated vectors. − [c] Values not given.

In solution, complex **7a** shows a singlet for the methyl groups of the Cp* ligand in the ^{1}H NMR spectrum at δ = 1.46 ([D_8]toluene, ^{13}C NMR: δ = 109.7 and 10.6). There is only a single resonance for the cot ligand in the ^{1}H NMR spectrum which remains sharp even down to 143 K (δ = 5.18 in $CDCl_2F/CDClF_2$).[14] The resonance in the ^{13}C NMR spectrum for the cot ligand of **7a** is observed at δ = 102.5 ([D_8]toluene), which is between the corresponding resonances of free cyclooctatetraene (δ = 131) and Li_2(cot) (δ = 90). We assume that a rapid interchange is responsible for this symmetrized appearance of the cot ligand in the ^{1}H/^{13}C NMR spectra.[15] We regard it unlikely that **7a** exhibits a fundamentally different structure in solution and in the solid state. An η^8-cot bonding situation would mean that **7a** would have more than 18 valence electrons as the other ligands have retained their coordination character as η^5-Cp* and (σ^2,π)η^4-C_4H_6 (see below). We therefore regard it very likely that a rapid equilibration on the NMR times-

Table 2. A comparison of selected ^{1}H NMR and ^{13}C NMR spectroscopic data of the complexes **7**[a] and **4a**[b]

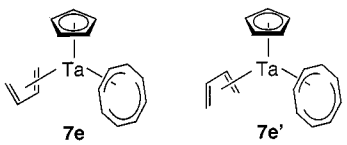
^{1}H NMR	Compd. 1-/4-H$_{anti}$	1-/4-H$_{syn}$	2-/3-H	cot-H	^{13}C NMR C-1/-4	C-2/-3	C-cot
7a	−0.92	3.05	4.45	5.08	47.4	127.5	102.5
7b	−0.97	2.82	−	5.10	49.8	135.8	102.4
	−0.93	2.57	3.50		46.1	114.6	
7c	−0.83	2.70	−	5.02	51.8	120.2	102.2
7d	−0.98	3.48	4.25	5.20	46.6	126.0	101.0
7e	−1.05	3.56	4.20	5.22	45.3	125.4	100.7
7e′	1.50	2.45	4.79	5.22	45.4	122.8	100.4
4a	−0.36	3.05	4.51	5.16	53.6	126.4	103.6

[a] Complexes **7** in [D$_8$]toluene at 298 K, this work. − [b] **4a** in [D$_6$]benzene at 303 K, from ref.[7]

cale of the (η^3-cot)Ta subunit causes the simple spectroscopic features that were observed.

In solution a single set of signals in the NMR spectrum is observed, i.e. only a single stereoisomer is present in solution. This is likely to contain the η^4-butadiene ligand in the *supine* orientation, with its "open" side pointing toward the Cp* ligand as was observed in the X-ray crystal structure of **7a**. The complex shows the typical signals in the ^{1}H NMR spectrum of a σ^2,π-structured η^4-butadiene ligand at the metal center[10−12] [δ = −0.92 (1-/4-H$_{anti}$), 3.05 (1-/4-H$_{syn}$), 4.45 (2-/3-H)]. The corresponding signals in the ^{13}C NMR spectrum of the butadiene ligand of **7a** are observed at δ = 47.4 (C1/4) and δ = 127.5 (C2/3).

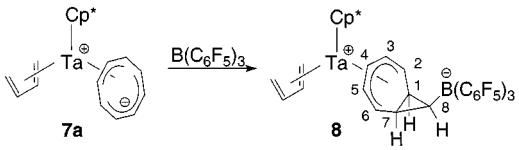
The complexes **7b** and **7c** show very similar NMR spectra (see Table 2). In each case a single isomer of the [Cp*(η^4-diene)(cot)Ta] system is observed. This is also the case for the [(MeCp)(butadiene)(cot)Ta] complex **7d**, but a different situation is encountered with the [Cp(η^4-butadiene)(cot)Ta] system. In this case, a mixture of two stereoisomers **7e** and **7e′** in a ratio of 95:5 is observed in solution by NMR spectroscopy. Each shows the typical single resonance for the cot ligand in the ^{1}H and ^{13}C NMR spectra (δ = 100.7, major isomer **7e**; δ = 100.4, minor isomer **7e′**). Both complexes also exhibit sets of resonances in their ^{1}H- and ^{13}C NMR spectra which are typical for σ^2,π-type *s-cis*-η^4-butadiene ligands at the group 5 metal center,[8][12] but the two are quite different from each other. We therefore assume that this is the first case in this series of complexes where we observe both a *supine* and a *prone* [Cp(butadiene)(cot)Ta] isomer. In view of the spectroscopic similarity with the other members of the series of complexes **7** (and **4a**, see Table 2) we assign to the major isomer (**7e**) the "conventional" *supine*-type structure, and to the minor isomer (**7e′**) the *prone* orientation of the C_4H_6 and Cp ligands at the tantalum center.



Scheme 3. The (*supine* and *prone*-η^4-diene)(η^3-cot)CpTa isomers **76e** and **7e′**

We have recently shown that (butadiene)zirconocene and related group 4 metal complexes add the organometallic Lewis acid B(C$_6$F$_5$)$_3$[16] to a terminal carbon atom of the butadiene ligand to form a (π-allyl)metalloceneborate betaine complex that is of interest as an active, single-component Ziegler-type catalyst.[17] Complex **7a** was, therefore, also treated with B(C$_6$F$_5$)$_3$ but reacted differently. A single compound (**8**) that still contained the intact η^4-butadiene ligand was formed. This is evident from the typical features of the ^{1}H and ^{13}C NMR spectra of the C_4H_6 moiety [δ = 0.18, 2.86 (1-/4-H), 5.48 (2-H); δ = 54.2 (C1) and 118.6 (C2)]. The B(C$_6$F$_5$)$_3$ reagent was found to add to the cot ligand. In contrast to compounds **7**, complex **8** exhibits signals in the ^{1}H and ^{13}C NMR spectra of a static cot-derived subunit. By a combination of pertinent 1D and 2D NMR experiments the structure of the $C_8H_8B(C_6F_5)_3$ ligand was established as being of the bicyclo[5.1.0]octadienyl type. The ^{1}H/^{13}C NMR spectroscopic assignments (including their very characteristic $^1J_{CH}$ coupling constants) are as follows (see Scheme 4 for the atom numbering scheme): δ = 1.23/39.4 ($^1J_{CH}$ = 165 Hz, C1/7−H), 6.66/158.7 (157 Hz, C2/6−H), 3.30/91.8 (155 Hz, C3/5−H), 3.86/71.4 (167 Hz, C4−H), 3.33/(^{13}C signal not observed, C8−H). The newly formed ligand is probably η^5-coordinated to tantalum. Addition of the B(C$_6$F$_5$)$_3$ Lewis acid has apparently occurred at the central carbon atom of the open, noncoordinated π^5-pentadienyl anion section of the cot ligand in **7a**, which resulted in a rapid subsequent disrotatory ring closure to give the bicyclic cot-B(C$_6$F$_5$)$_3$-derived ligand in **8**. In principle four different diastereoisomers of **8** could have been formed in this reaction, depending on whether B(C$_6$F$_5$)$_3$ had attacked from "inside" or from "outside" the complex framework of **7a**, each attack being followed by two possible modes of disrotatorial ring closure. Apparently, one of these electrophilic addition/ring closure combinations has prevailed here, leading to a single observed diastereoisomer **8** of the [Cp*(η^4-C$_4$H$_6$){8-B(C$_6$F$_5$)$_3$-η^5-bicyclo[5.1.0]-octadienyl}Ta] system. We assume that the structure depicted in Scheme 4 is favored, with the B(C$_6$F$_5$)$_3$ substituent *endo* to the bicyclic framework (the observed ^3J(1-H/8-H) coupling constant of ca. 8 Hz would be in accord with the *cis* substitution pattern at the three-membered ring), and the Cp*(η^4-C$_4$H$_6$)Ta "metallocene" η^5-coordinated from the *exo*-face, as was observed for a remotely related example

in the early (cot)Nb chemistry described by Schrock et al.[5b]



Scheme 4. Reaction of **7a** with $B(C_6F_5)_3$ and atom numbering scheme for **8**

Conclusion

Our study has shown that [^{R}Cp(η^4-butadiene)$TaCl_2$] complexes react cleanly with the cot dianion to yield the [^{R}Cp(η^4-butadiene)(η^3-cot)Ta] complexes **7**. These complexes exhibit a slightly greater σ^2,π-character of the (η^4-butadiene) ligand than their niobium analogues. Most of the complexes **7** exhibit a *supine*-oriented butadiene ligand, but for the [Cp(η^4-butadiene)(η^3-cot)Ta] system we have for the first time observed the *prone* isomer as a minor equilibrium component in solution. This probably indicates that steric factors dominate this equilibrium situation. In the complexes **7** the ^{R}Cp(η^4-diene)Ta subunit seems to function structurally and chemically in a similar manner to the Cp_2M bent metallocene unit in group 4 metal chemistry:[19] treatment of **7a** with $B(C_6F_5)_3$ leaves the bent metallocene surrogate intact; the attack occurs exclusively at the adjacent cot ligand. This ligand system seems to be chemically active in these complexes. It serves as a carbon nucleophile at the center of its uncomplexed pentadienyl moiety to yield the addition product **8**. Further chemical reactions and the catalytic potential of the complexes **7** will be investigated in our laboratory

Experimental Section

All reactions were carried out under argon using Schlenk-type glassware or in a glovebox. Solvents were dried and distilled under argon prior to use. For additional general information including a list of instruments used for the spectroscopic and physical characterization of the compounds see ref.[20] The [^{R}Cp(η^4-diene)$TaCl_2$] complexes **6** were prepared analogously as described by Yasuda et al.[8][21] The [(cot)Li_2] reagent was prepared according to a literature procedure.[9]

Synthesis of (η^4-Butadiene)(η^3-cyclooctatetraene)(η^5-pentamethylcyclopentadienyl)tantalum (7a): A solution of **6a** (1.00 g, 2.70 mmol) in toluene (20 mL) was added to a suspension of [(cot)Li_2] (330 mg, 2.80 mmol) in 20 mL of toluene. The mixture was stirred for 15 h at 50°C, then filtered and the solvent removed from the filtrate in vacuo. The crude reaction product was stirred for 10 h in 10 mL of pentane, then the product was collected by filtration to give 653 mg (54%) of **7a** as a black solid. Single crystals of **7a** suitable for an X-ray crystal structure analysis were obtained from a solution containing 100 mg of **7a** in 3 mL of toluene and 8 mL of pentane. − M.p. 185°C (decomp.). − IR (KBr): $\tilde{\nu}$ = 3050, 2984, 2904, 1547, 1496, 1422, 1375, 1229, 1159, 1147, 1054, 1041, 1023, 902, 840, 805, 797, 686, 614 cm^{-1}. − ^{1}H NMR ([D$_8$]toluene, 599.8 MHz, 298 K): δ = 5.16 (s, 8 H, cot-H), 4.40 (m, 2 H, 2-H), 3.04 (m, 2 H, 1-H′), 1.46 [s, 15 H, $C_5(CH_3)_5$], −0.93 (m, 2 H, 1-H). − ^{1}H NMR [$CDClF_2$/$CDCl_2F$ (2:1), 599.8 MHz, 143 K]: δ = 5.18 (s, 8 H, cot-H), 3.97 (m, 2 H, 2-H), 3.08 (m, 2 H, 1-H′), 1.86 [s, 15 H, $C_5(CH_3)_5$], −0.97 (m, 2 H, 1-H). − 1D TOCSY ([D$_8$]toluene, 599.8 MHz, 298 K): irradiation at δ = 4.45 (2-H): response at 3.05 (1-H′) and −0.92 (1-H). − GCOSY ([D$_8$]toluene, 599.8 MHz, 298 K): δ = 4.45/3.05, −0.92 (2-H/1-H′, 1-H), −0.92/4.45, 3.05 (1-H/2-H, 1-H′). − ^{13}C NMR ([D$_8$]toluene, 599.8 MHz, 298 K): δ = 127.0 (C2), 109.7 [$C_5(CH_3)_5$], 102.5 (C-cot), 46.9 (C1), 10.6 [$C_5(CH_3)_5$]. − GHSQC ([D$_8$]toluene, 150.8/599.8 MHz, 298 K): δ = 127.0/4.45 (C2, 2-H), 102.5/5.16 (C-cot/cot-H), 46.9/3.05 (C1/1-H′), 46.9/−0.92 (C1/1-H), 10.6/1.93 $C_5(CH_3)_5$/$C_5(CH_3)_5$. − $C_{22}H_{29}Ta$ (474.4): calcd. C 55.70, H 6.16; found C 56.06, H 6.60.

X-ray Crystal Structure Analysis of 7a: Formula $C_{22}H_{29}Ta$, M = 474.40, dark red crystal, 0.45 × 0.35 × 0.15 mm, a = 12.134(1), b = 11.086(1), c = 14.376(1) Å, β = 112.31(1)°, V = 1789.1(3) Å^3, ρ_{calc} = 1.761 g cm^{-3}, F(000) = 936 e, μ = 61.42 cm^{-1}, absorption correction by SORTAV (0.169 ≤ T ≤ 0.459), Z = 4, monoclinic, space group $P2_1/c$ (No. 14), λ = 0.71073 Å, T = 198 K, ω and φ scans, 8258 reflections collected (±h, ±k, ±l), [(sinθ)/λ] = 0.67 Å^{-1}, 4056 independent and 3555 observed reflections [$I \geq 2\,\sigma(I)$], 213 refined parameters, R = 0.054, wR^2 = 0.141, max. residual electron density 5.893 (−4.069) eÅ^{-3} less than 1 Å from Ta, hydrogen atoms calculated and refined as riding atoms. The data set was collected with a Nonius Kappa CCD diffractometer, placed on a rotating anode generator FR591. Programs used: data collection COLLECT, data reduction DENZO-SMN, absorption correction SORTAV, structure solution SHELXS-86, structure refinement SHELXL-97, graphics SCHAKAL-92. Crystallographic data (excluding structure factors) for the structure reported in this paper have been deposited with the Cambridge Crystallographic Data Centre as supplementary publication no. CCDC-118700. Copies of the data can be obtained free of charge on application to: CCDC, 12 Union Road, Cambridge CB2 1EZ, UK [Fax: internat. + 44-1223/336-033, E-mail: deposit@ccdc.cam.ac.uk].

Preparation of (η^3-Cyclooctatetraene)(η^4-isoprene)(η^5-pentamethylcyclopentadienyl)tantalum (7b): The reaction between **6b** (1.00 g, 2.20 mmol) and [(cot)Li_2] (285 mg, 2.41 mmol) in 50 mL of toluene was performed as described above. The product (**7b**) was suspended in pentane for purification, collected by filtration, washed with pentane (2 × 5 mL) and dried in vacuo to yield 666 mg (62%) of **7b** as a black solid. − m.p. 178°C (decomp.). − IR (KBr): $\tilde{\nu}$ = 3049, 2981, 2953, 2856, 1556, 1519, 1488, 1446, 1433, 1376, 1367, 1260, 1091, 1026, 868, 807, 800, 686, 615, 584 cm^{-1}. − ^{1}H NMR ([D$_8$]toluene, 599.8 MHz, 298 K): δ = 5.10 (s, 8 H, cot-H), 3.50 (m, 1 H, 2-H), 2.82 (pt, J_{HH} = 8.9 Hz, 1 H, 1-H′), 2.57 (dd, $^2J_{HH}$ = 10.0 Hz, $^4J_{HH}$ = 2.0 Hz, 1 H, 4-H′), 2.31 (s, 3 H, 2-CH_3), 1.47 [s, 15 H, $C_5(CH_3)_5$], −0.93 (dd, $^2J_{HH}$ = 10.0 Hz, $^4J_{HH}$ = 2.1 Hz, 1 H, 4-H), −0.97 (m, 1 H, 1-H). − GCOSY ([D$_8$]toluene, 599.8 MHz, 298 K): δ = 3.49/2.82, −0.97 (2-H/1-H′, 1-H), 2.82/3.49, −0.97 (1-H′/2-H, 1-H), 2.57/3.49, −0.93 (4-H′/2-H, 4-H), −0.93/3.49, 2.57 (4-H/2-H, 4-H′), −0.97/3.49, 2.82 (1-H/2-H, 1-H′). − ^{13}C NMR ([D$_8$]toluene, 150.8 MHz, 298 K): δ = 135.8 (C3), 114.6 (C2), 109.9 [$C_5(CH_3)_5$], 102.4 (C-cot), 49.8 (C4), 46.1 (C1), 30.2 (2-CH_3), 10.6 [$C_5(CH_3)_5$]. − GHSQC ([D$_8$]toluene, 150.8/599.8 MHz, 298 K): δ = 114.6/3.49 (C2, 2-H), 102.4/5.10 (C-cot/cot-H), 49.8/2.57 (C4/4-H′), 49.8/−0.93 (C4/4-H), 46.1/2.82 (C1/1-H′), 46.1/−0.97 (C1/1-H), 30.2/2.31 (2-CH_3/2-CH_3), 10.6/1.47 $C_5(CH_3)_5$/$C_5(CH_3)_5$. − $C_{23}H_{31}Ta$ (488.44): calcd. C 56.55, H 6.40; found C 56.47, H 6.80.

Preparation of (η^3-Cyclooctatetraene)(η^4-2,3-dimethylbutadiene)(η^5-pentamethylcyclopentadienyl)tantalum (7c): The reaction between

6c (1.00 g, 2.13 mmol) and [(cot)Li_2] (277 mg, 2.34 mmol) was performed as described above to yield 482 mg (45%) of **7c**. − m.p. 155°C (decomp.). − IR (KBr): $\tilde{\nu}$ = 3104, 3093, 3074, 2993, 2953, 2920, 2866, 1546, 1494, 1438, 1306, 1235, 1078, 1054, 1029, 856, 826, 688, 611 cm^{-1}. − ^1H NMR ([D_8]toluene, 599.8 MHz, 298 K): δ = 5.02 (s, 8 H, cot-H), 2.70 (d, $^2J_{HH}$ = 10.1 Hz, 2 H, 1-H′), 1.79 (pd, $^4J_{HH}$ = 1.0 Hz, 6 H, 2-CH_3), 1.46 [s, 15 H, $C_5(CH_3)_5$], −0.83 (dd, J_{HH} = 10.5 Hz, 2 H, 1-H). − GCOSY ([D_8]toluene, 599.8 MHz, 298 K): δ = 2.70/−0.83 (1-H′/1-H), 1.79/−0.83 (2-CH_3, 1-H), −0.83/2.70, 1.79 (1-H/1-H′, 2-CH_3). − ^{13}C NMR ([D_8]toluene, 150.8 MHz, 298 K): δ = 120.0 (C2), 110.0 [$C_5(CH_3)_5$], 102.2 (C-cot), 51.8 (C1), 25.5 (2-CH_3), 10.4 [$C_5(CH_3)_5$]. − GHSQC ([D_8]toluene, 150.8/599.8 MHz, 298 K): δ = 102.2/5.02 (C-cot/cot-H), 51.8/2.70 (C1/1-H′), 51.8/−0.83 (C1/1-H), 25.5/1.79 (2-CH_3/2-CH_3), 10.4/1.46 $C_5(CH_3)_5$/$C_5(CH_3)_5$. − $C_{24}H_{33}Ta$ (502.47): calcd. C 57.37, H 6.62; found C 57.13, H 6.83.

Preparation of (η⁴-Butadiene)(η³-cyclooctatetraene)(η⁵-methylcyclopentadienyl)tantalum (7d): The reaction between **6d** (1.00 g, 2.60 mmol) and [(cot)Li_2] (337 mg, 2.85 mmol) was performed as described above to yield 720 mg (66%) of **7d** as a dark-brown solid. − m.p. 148°C (decomp.). − IR (KBr): $\tilde{\nu}$ = 3097, 3074, 2990, 2956, 2942, 1547, 1493, 1456, 1438, 1429, 1305, 1230, 1054, 1029, 857, 825, 807, 689, 613 cm^{-1}. − ^1H NMR ([D_8]toluene, 599.8 MHz, 298 K): δ = 5.24 (s, 8 H, cot-H), 4.83 (d, J_{HH} = 2.5 Hz, 2 H), 4.35 (pt, J_{HH} = 2.5 Hz, 6 H, C_5H_4), 4.24 (m, 2 H, 2-H), 3.48 (m, 2 H, 1-H′), 1.74 (s, 3 H, CH_3), −0.98 (m, 2 H, 1-H). − ^{13}C NMR ([D_8]toluene, 150.8 MHz, 298 K): δ = 126.0 (C2), 113.4, 103.0, 99.7 (C_5H_4), 101.0 (C-cot), 46.6 (C1), 14.3 (CH_3). − GHSQC ([D_8]toluene, 150.8/599.8 MHz, 298 K): δ = 126.0/4.24 (C2/2-H), 113.5/4.83 (C_5H_4/C_5H_4), 101.0/5.24 (C-cot/cot-H), 99.7/4.35 (C_5H_4/C_5H_4), 46.6/3.48 (C1/1-H′), 46.6/−0.98 (C1/1-H). − $C_{18}H_{21}Ta$ (418.31): calcd. C 51.68, H 5.06; found C 52.16, H 5.32.

Preparation of the (η⁴-Butadiene)(η³-cyclooctatetraene)(η⁵-cyclopentadienyl)tantalum Isomers 7e and 7e′: The reaction between **6e** (1.50 g, 4.04 mmol) and [(cot)Li_2] (525 mg, 4.45 mmol) was performed as described above to yield 902 mg (55%) of a 95:5 mixture of **7e** and **7e′**. − m.p. 147°C (decomp.). − IR (KBr): $\tilde{\nu}$ = 3098, 3085, 2998, 2947, 1437, 1429, 1367, 1236, 1070, 1020, 1011, 817, 844, 822, 690, 612, 430 cm^{-1}. − ^1H NMR ([D_8]toluene, 599.8 MHz, 298 K): **7e** (major isomer): δ = 5.22 (s, 8 H, cot-H), 4.79 (d, 5 H, Cp-H), 4.20 (m, 2 H, 2-H), 3.56 (m, 2 H, 1-H′), −1.04 (m, 2 H, 1 H). **7e′** (minor isomer): δ = 5.22 (s, 8 H, cot-H, under signal of the major isomer), 4.81 (d, 5 H, Cp-H), 4.78 (m, 2 H, 2-H, under **7e** resonance), 2.45 (m, 2 H, 1-H′), 1.50 (m, 2 H, 1-H). − 1D TOCSY ([D_8]toluene, 599.8 MHz, 298 K): **7e**: irradiation at δ = 3.56 (1-H′): response at δ = 4.20 (2-H) and −1.05 (1-H). **7e′**: irradiation at δ = 1.50 (1-H): response at δ = 4.79 (2 H) and 2.45 (1-H′). − GCOSY ([D_8]toluene, 599.8 MHz, 298 K): **7e**: δ = 4.20/3.56, −1.05 (2-H/1-H′, 1-H), 3.56/4.20, −1.05 (1-H′/2-H, 1-H), −1.05/4.20, 3.56 (1-H/2-H, 1-H′). **7e′**: δ = 4.79/2.45, 1.50 (2-H/1-H′, 1-H), 2.45/4.79, 1.50 (1-H′/2-H, 1-H), 1.50/4.79, 2.45 (1-H/2-H,1-H′). − ^{13}C NMR ([D_8]toluene, 150.8 MHz, 298 K): **7e**: δ = 125.4 (C2), 100.7 (C-cot), 100.6 (C−Cp), 45.3 (C1). **7e′**: δ = 122.8 (C2), 100.4 (C-cot), 99.6 (C−Cp), 45.4 (C1). − GHSQC ([D_8]toluene, 150.8/599.8 MHz, 298 K): **7e**: δ = 125.4/4.20 (C2/2-H), 100.5/5.22 (C-cot/cot-H), 100.6/4.74 (C−Cp/Cp-H). 45.3/3.56 (C1/1-H′), 45.3/−1.05 (C1/1-H). **7e′**: δ = 122.8/4.79 (C2/2-H), 100.4/5.22 (C-cot/cot-H), 99.6/4.81 (C-Cp/Cp-H), 45.4/2.45 (C1/1-H′), 45.4/−1.50 (C1/1-H). − $C_{17}H_{19}Ta$ (404.29): calcd. C 50.51, H 4.74; found C 50.12, H 4.73.

Reaction of Complex 7a with $B(C_6F_5)_3$. − Generation of 8: (The reaction was carried out in deuterated solvent and the product was not isolated. At room temperature complex **8** starts to decompose after about 2 h; therefore some NMR experiments had to be carried out at low temperature.) An NMR tube was charged with a sample of **7a** (50 mg, 54.1 μmol) and a solution of $B(C_6F_5)_3$ (81.0 mg, 158 μmol) in 0.8 mL of [D_2]dichloromethane was added at −78°C. The sample was warmed to +10°C inside the NMR spectrometer. After ca. 1 h, the addition reaction to give **8** was complete and the sample was cooled to −30°C to collect the NMR spectroscopic data. − ^1H NMR ([D_2]dichloromethane, 599.8 MHz, 223 K, bco = bicyclo[5.1.0]octadienyl): δ = 6.66 (m, 2 H, bco-2/6-H), 5.42 (m, 2 H, butadiene-2-H), 3.86 (m, 1 H, bco-4-H), 3.33 (m, 1 H, bco-8-H), 3.30 (m, 2 H, bco-3/5-H), 2.86 (m, 2 H, butadiene-1-H′), 1.94 [s, 15 H, $C_5(CH_3)_5$], 1.23 (m, 2 H, bco-1/7-H), 0.17 (m, 2 H, butadiene-1-H). − 1D TOCSY ([D_2]dichloromethane, 599.8 MHz, 223 K): (i) irradiation at δ = 5.42 (butadiene-2-H): response at δ = 2.86 (1-H′), 0.17 (1-H). (ii) irradiation at δ = 6.66 (bco-2/6-H): response at δ = 3.86 (4-H), 3.33 (8-H), 3.30 (3/5-H), 1.23 (1/7-H). − GCOSY ([D_2]dichloromethane, 599.8 MHz, 223 K): δ = 6.66/3.30, 1.23 (bco-2/6-H//3/5-H, 1/7-H), 5.42/2.86, 0.17 (butadiene-2-H/1-H, 1-H′), 3.86/3.30 (bco-4-H//3/5-H), 3.33/1.23 (bco-8-H//1/7-H), 3.30/3.86, 6.66 (bco-3/5-H//4-H, 2/6-H), 2.86/5.42, 0.17 (butadiene-1-H′//2-H, 1-H), 1.23/3.33 (bco-1/7-H//8-H), 0.17/5.42, 2.86 (butadiene-1-H//2-H, 1−1H′). − ^{13}C NMR ([D_2]dichloromethane, 150.8 MHz, 223 K): δ = 158.7 ($^1J_{CH}$ = 157 Hz, bco-C2/6), 148.2 [$^1J_{CF}$ = 249 Hz, *o*-$B(C_6F_5)_3$], 144.7 [$^1J_{CF}$ = 260 Hz, *p*-$B(C_6F_5)_3$], 137.1 [$^1J_{CF}$ = 251 Hz, *m*-$B(C_6F_5)_3$], 113.2 (butadiene-C2), 110.1 [$C_5(CH_3)_5$], 91.8 ($^1J_{CH}$ = 155 Hz, bco-C3/5), 71.4 ($^1J_{CH}$ = 167 Hz, bco-C4), 39.4 ($^1J_{CH}$ = 165 Hz, bco-C1/7), 10.6 [$C_5(CH_3)_5$], *ipso*-C of $B(C_6F_5)_3$ and bco-C8 not observed, butadiene-C1 hidden by solvent. − GHSQC ([D_2]dichloromethane, 150.8 MHz, 223 K): δ = 158.7/6.66 (bco-C2/6//2/6-H), 113.3/5.42 (butadiene-C2/2-H), 91.8/3.30 (bco-C3/5//3/5-H), 71.4/3.86 (bco-C4//4-H), 65.1/3.33 (bco-C8//8-H), 54.1/2.86, 0.17 (butadiene-C1//1-H/H′), 39.4/1.23 (bco-C1/7//1/7-H), 10.6/1.94 (Cp*). − ^{11}B NMR ([D_2]dichloromethane, 64.2 MHz, 243 K): δ = −14.0. − ^{19}F NMR ([D_2]dichloromethane, 564.3 MHz, 243 K): δ = −130.4 [m, 6 F, *o*-$B(C_6F_5)_3$], −161.7 [m, 3 F, *p*-$B(C_6F_5)_3$], −165.6 [m, 6 F, *m*-$B(C_6F_5)_3$].

Acknowledgments

Financial support from the Fonds der Chemischen Industrie, the Deutsche Forschungsgemeinschaft, and the Ministerium für Schule und Weiterbildung, Wissenschaft und Forschung des Landes Nordrhein-Westfalen is gratefully acknowledged.

[1] General review: M. A. Bennett, *Adv. Organomet. Chem.* **1996**, *4*, 353.
[2] K. O. Hodgson, F. Mares, D. F. Starks, A. Streitwieser, *J. Am. Chem. Soc.* **1973**, *95*, 8650; A. Streitwieser, U. Müller-Westerhoff, G. Sonnichsen, F. Mares, D. Morrell, K. O. Hodgson, *J. Am. Chem. Soc.* **1973**, *95*, 8644; A. Streitwieser, *Organometallics of the f-Elements* (Eds.: T. J. Marks, R. D. Fischer), Reidel, Dordrecht, **1979**, chapter 5; D. G. Karraker, J. A. Stone, E. R. Jones, N. Edelstein, *J. Am. Chem. Soc.* **1970**, *92*, 4841. C. J. Burns, B. E. Bursten, *Comments Inorg. Chem.* **1989**, *9*, 61.
[3] H. Dietrich, M. Soltwisch, *Angew. Chem.* **1969**, *81*, 785; *Angew. Chem. Int. Ed. Engl.* **1969**, *8*, 765; D. J. Brauer, C. Krüger, *J. Organomet. Chem.* **1972**, *42*, 129; J. Schwartz, J. E. Sadler, *J. Chem. Soc., Chem. Commun.* **1973**, 172; H. Lehmkuhl, S. Kintopf, K. Mehler, *J. Organomet. Chem.* **1972**, *46*, C1; H.-J. Kablitz, R. Kallweit, G. Wilke, *J. Organomet. Chem.* **1972**, *44*, C49; H.-J. Kablitz, G. Wilke, *J. Organomet. Chem.* **1972**, *51*, 241; B. B. King, C. D. Hoff, *J. Organomet. Chem.* **1982**, *225*, 69; D. M. Rogers, S. R. Wilson, G. S. Girolami, *Organometallics* **1991**, *10*, 2419.
[4] [4a] N. I. Pyshograeva, V. N. Setkina, V. G. Andrianov, Yu. T.

Struchkov, D. N. Kursanov, *J. Organomet. Chem*. **1981**, *206*, 169; N. C. Baenziger, G. F. Richards, J. R. Doyle, *Inorg. Chem*. **1964**, *3*, 1529. – [4b] I. Bach, K.-R. Pörschke, B. Proft, R. Goddard, C. Kopinske, C. Krüger, A. Rufinska, K. Seevogel, *J. Am. Chem. Soc.* **1997**, *119*, 3773.

[5] [5a] L. J. Guggenberger, R. R. Schrock, *J. Am. Chem. Soc.* **1975**, *97*, 6693. – [5b] R. R. Schrock, L. J. Guggenberger, A. D. English, *J. Am. Chem. Soc.* **1976**, *98*, 903.

[6] G. E. Herberich, U. Englert, P. Roos, *Chem. Ber.* **1991**, *124*, 2663.

[7] K. Mashima, Y. Nakayama, M. Kaidzu, N. Ikushia, A. Nakamura, *J. Organomet. Chem*. **1998**, *557*, 3.

[8] H. Yasuda, K. Tatsumi, T. Okamoto, K. Mashima, K. Lee, A. Nakamura, Y. Kai, N. Kanehisa, N. Kasai, *J. Am. Chem. Soc.* **1985**, *107*, 2410.

[9] W. Reppe, O. Schlichting, K. Klager, T. Töpel, *Liebigs Ann. Chem*. **1948**, *1*, 560; J. M. Bellama, J. B. Davison, *J. Organomet. Chem*. **1975**, *86*, 69; N. Hu, L. Gong, Z. Jin, W. Chen, *J. Organomet. Chem*. **1988**, *352*, 61; D. M. Rogers, S. R. Wilson, G. S. Girolami, *Organometallics* **1991**, *10*, 2419.

[10] [10a] Zr: H. Yasuda, K. Tatsumi, A. Nakamura, *Acc. Chem. Res.* **1985**, *18*, 120; H. Yasuda, Y. Kajihara, K. Mashima, K. Nagasuna, K. Lee, A. Nakamura, *Organometallics* **1981**, *1*, 388; Y. Kai, N. Kanehisa, K. Miki, N. Kasai, K. Mashima, K. Nagasuna, H. Yasuda, A. Nakamura, *J. Chem. Soc., Chem. Commun*. **1982**, 191. – [10b] G. Erker, K. Engel, C. Krüger, A. P. Chiang, *Chem. Ber*. **1982**, *115*, 3311; G. Erker, C. Krüger, G. Müller, *Adv. Organomet. Chem.* **1985**, *24*, 1.

[11] Hf: H. Yasuda, Y. Kajihara, K. Mashima, K. Lee, A. Nakamura, *Chem. Lett*. **1981**, 519; C. Krüger, G. Müller, G. Erker, U. Dorf, K. Engel, *Organometallics* **1985**, *4*, 215; B. Hessen, J. H. Teuben, *J. Organomet. Chem*. **1988**, *358*, 135.

[12] Nb: H. Yasuda, A. Nakamura, *Angew. Chem.* **1987**, *99*, 745; *Angew. Chem. Int. Ed. Engl*. **1987**, *26*, 723; T. Okamoto, H. Yasuda, A. Nakamura, Y. Kai, N. Kanehisa, N. Kasai, *J. Am. Chem. Soc.* **1988**, *110*, 5008; G. E. Herberich, U. Englert, K. Linn, P. Roos, J. Runsink, *Chem. Ber*. **1991**, *124*, 975.

[13] K. Verkade, A. Westerhof, H. J. Liefde Meijer, *J. Organomet. Chem*. **1978**, *154*, 371.

[14] . S. Siegel, F. A. L. Anet, *J. Org. Chem*. **1988**, *53*, 2629.

[15] F. A. Cotton, *Acc. Chem. Res.* **1968**, *1*, 257.

[16] A. G. Massey, A. J. Park, F. G. A. Stone, *Proceedings Chem. Soc*. **1963**, 212; A. G. Massey, A. J. Park, *J. Organomet. Chem*. **1964**, *2*, 245; A. G. Massey, A. J. Park, *Organometallic Synthesis* (Eds.: R. B. King, J. J. Eisch), Elsevier, New York, **1986**, vol. 3, p. 461.

[17] B. Temme, J. Karl, G. Erker, H. Luftmann, R. Fröhlich, S. Kotila, *Angew. Chem.* **1995**, *107*, 1867; *Angew. Chem. Int. Ed. Engl*. **1995**, *34*, 1755. B. Temme, J. Karl, G. Erker, *Chem. Eur. J.* **1996**, *2*, 919; J. Karl, M. Dahlmann, G. Erker, K. Bergander, *J. Am. Chem. Soc.* **1998**, *120*, 5643; M. Dahlmann, G. Erker, M. Nissinen, R. Fröhlich, *J. Am. Chem. Soc.* **1999**, *121*, 2820.

[18] For related H^+ addition reactions to cot ligands see e.g. J. Evans, B. F. G. Johnson, J. Lewis, D. J. Yarrow, *J. Chem. Soc., Dalton Trans.* **1974**, 2375; M. Brookhart, E. R. Davis, *Tetrahedron Letters* **1971**, 4349; M. Brookhart, E. R. Davis, D. L. Harris, *J. Am. Chem. Soc.* **1972**, *94*, 7853.

[19] J. W. Lauher, R. Hoffmann, *J. Am. Chem. Soc.* **1976**, *98*, 1729.

[20] For related $Cp_2Ta(butadiene)^+$ cation chemistry see: H. C. Strauch, G. Erker, R. Fröhlich, *Organometallics* **1998**, *17*, 5746; H. Strauch, G. Erker, R. Fröhlich, M. Nissinen, *Eur. J. Inorg. Chem.*, in press.

[21] Y. Yasuda, T. Okamoto, A. Nakamura, *Organometallic Syntheses* (Eds.: R. B. King, J. J. Eisch), vol. 4, Elsevier, Amsterdam, **1988**.

Received April 20, 1999
[I99139]

Mechanism of the Catalytic Oxidation of Tertiary Alcohols by the Water-Soluble Mn-TMPyP/$KHSO_5$ System: β-Fragmentation versus *O*-Neophyl Rearrangement

Karine Wietzerbin,[a] Jean Bernadou,*[a] and Bernard Meunier*[a]

Keywords: Oxidations / Tertiary alcohol / Porphyrins / Neophyl rearrangement / Cleavage reactions / β-Scission

Oxidation of 4-(1-hydroxy-1-phenylethyl)benzoic acid HPEBA with a water-soluble metalloporphyrin as catalyst and $KHSO_5$ as oxygen atom donor gives the major products, acetophenone AC and acetylbenzoic acid ABA, by a C_{aliph}–C_{Ar} bond cleavage, but a minor product, benzoyloxybenzoic acid BOBA, requires the insertion of an oxygen atom to form the ester. This compound becomes the main oxidation product on increasing the amount of acetonitrile in the reaction medium, and its formation is oxygen-dependent. The conversion is drastically lowered by using D_2O instead of H_2O, suggesting that an alkoxyl radical is formed in the rate-determining step. Labeling experiments using $^{18}O_2$ or $H_2{}^{18}O$ under different reaction conditions show that the carbonyl oxygen atoms of AC and ABA originate either from substrate, water or dioxygen. However, the carbonyl oxygen atom in the ester group of BOBA originates from dioxygen while the other oxygen atom of the ester remains unlabeled. These results can be explained by an *O*-neophyl rearrangement of the initial alkoxyl radical to afford a carbon-based radical which then reacts with dioxygen or Mn^{IV}-OH/water. In a competitive reaction pathway, direct β-scission of the alkoxyl radical leads to unlabeled products. The oxidation of other tertiary diaryl alcohols is also discussed.

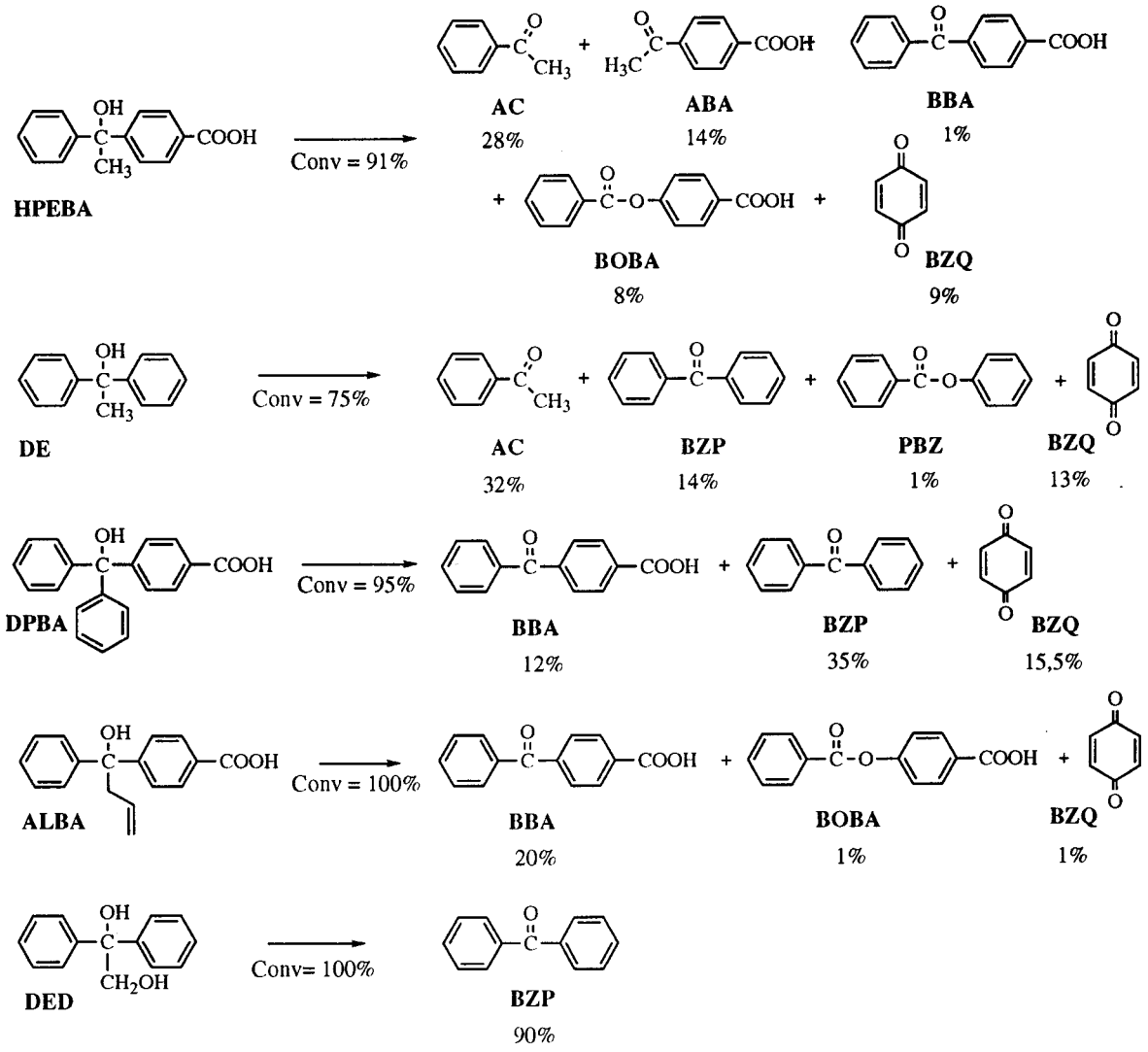
Introduction

Little is known about the oxidative C–C bond cleavage by biomimetic catalysts, although it is a key step in several reactions catalyzed by cytochrome P-450 in steroidal hormone biosynthesis such as estrogen biosynthesis or the side chain cleavage of cholesterol.[1] In the latter case, the cleavage is achieved by three successive oxidations; two hydroxylation steps at C-20 and C-22 produce a vicinal diol which is then oxidatively cleaved in the third step into two carbonyl compounds. With the aim of simulating this last scission step, the oxidation of aryl-substituted ethane-1,2-diols by chromium(III) tetraphenylporphyrin/4-cyano-*N,N*-dimethylaniline *N*-oxide without[2] and under photocatalysis,[3] or by iron(III) tetraphenylporphyrin/O_2/dihydropyridine[4][5] was shown to induce C–C bond cleavage selectively to give aldehydes and ketones. The photochemical cleavage of 1,2-diphenylethane-1,2-diols has also been observed with water-soluble iron porphyrin complexes to produce benzaldehyde and small amounts of benzoic acid, in which experimental yields and bleaching of the catalyst depend on the presence of O_2.[6][7] Aromatization of a synthetic androgen analogue by a peroxo iron(III) porphyrin complex results in C–C bond cleavage and allows the authors to mimic the third step of aromatase, the enzyme responsible for the conversion of androgens to estrogens in humans, which involves loss of the C-19 aldehyde and aromatization of the A ring of the steroid.[8]

As part of our mechanistic studies on the biomimetic Mn-TMPyP/$KHSO_5$ system – a water-soluble manganese porphyrin complex as catalyst with potassium monopersulfate as oxygen atom donor – we show here how some intermediate tertiary alcohol models can give ketones through cleavage of a C–C bond. As opposed to primary and secondary alcohols, tertiary alcohols are usually resistant to oxidation, and examples of such oxidative conversions are rather unusual and generally related to some structural peculiarity. Chromium(VI) can oxidize allylic- or α-cyclopropyl tertiary alcohols to give rearrangements,[9–11] δ- or γ- unsaturated tertiary alcohols to afford cyclization products,[12][13] and tertiary cycloalkanols to produce fragmentations.[14] Cerium(IV) salts and cobalt(III) complexes can also induce C–C bond cleavage by oxidation of tertiary alcohols, leading mainly to fragmentation reactions.[15][16] Synthetic metalloporphyrins, used as models for cytochrome P-450, are highly efficient catalysts for the oxidation of various substrates but only some rare examples of oxidation of tertiary alcohols are described in the literature. Recently, we have shown that the biomimetic water-soluble Mn-TMPyP/$KHSO_5$ system gives mainly C_{aliph}–C_{aliph} and C_{aliph}–C_{Ar} bond cleavage through a β-fragmentation mechanism in the course of the oxidation of aryl and diaryl tertiary alcohol derivatives.[17][18] We now report a mechanistic study based on a careful examination of the oxidation products of tertiary alcohols, and labeling experiments, which emphasizes, besides the initial observation of β-fragmentation as a possible mechanism to explain the observed product distribution, the role of *O*-neophyl rearrangement. This latter mechanism allows us to understand not only the partial incorporation of oxygen from water and dioxygen in oxidation products but also the formation of an unexpected

[a] Laboratoire de Chimie de Coordination du CNRS,
205 route de Narbonne, F-31077 Toulouse cedex 4, France
E-Mail: bernadou@lcc-toulouse.fr
bmeunier@lcc-toulouse.fr

 © WILEY-VCH Verlag GmbH, D-69451 Weinheim, 1999 1434–1948/99/0909–1467 $ 17.50+.50/0



Scheme 1. Identified products and yields from oxidation of HPEBA, DE, DPBA, ALBA and DED with the Mn-TMPyP/$KHSO_5$ system

ester derivative which is characteristic of such a reaction pathway.

Results

Oxidation of HPEBA With Mn-TMPyP/$KHSO_5$

The metalloporphyrin-catalyzed oxidation of 4-(1-hydroxy-1-phenylethyl)benzoic acid HPEBA was performed in air at pH 5 in aqueous phosphate buffer containing 10% acetonitrile, with the manganese(III) *meso*-tetrakis(1-methylpyridinium-4-yl)porphyrin (Mn-TMPyP) as catalyst and $KHSO_5$ as oxidant. Final concentrations of substrate, catalyst and oxidant were 500 μM, 10 μM and 10 mM, respectively. The reaction was monitored by HPLC. After 10 min, the substrate conversion was 90%. Products (Scheme 1) were identified by HPLC co-injection of authentic samples (benzoyloxybenzoic acid, BOBA, which is not commercially available, was synthesized) and by GC-MS analysis of a reaction sample after esterification of the carboxylic groups with diazomethane.

In the case of benzoquinone BZQ, which is not easily detectable by GC-MS, it should be noted that its HPLC peak disappeared after addition of a small amount of sodium dithionite ($Na_2S_2O_4$), which is a specific reductant of benzoquinones. Product yields and selectivities are given in Table 2. The major products, acetophenone AC and *p*-acetylbenzoic acid ABA, are derived from a $C_{aliph}-C_{ar}$ bond cleavage, while a very small amount of *p*-benzoylbenzoic acid BBA resulting from a $C_{aliph}-C_{aliph}$ bond cleavage was obtained. The formation of the unexpected ester BOBA requires the loss of a methyl group and the insertion of an oxygen atom. Surprisingly, the isomeric ester monophenylterephthalate MPTP, corresponding to insertion of the oxygen atom on the phenyl side of the carbonyl ester function, was not detected. This fact was confirmed by preparing an authentic sample of this compound, which proved to have almost the same HPLC elution time as BOBA, but different GC behavior and different NMR and EI-MS spectra. MPTP was not observed, either by GC-MS analysis of the reaction mixture or by NMR spectroscopic analysis of the

collected HPLC peak (the NMR spectrum corresponded to that of BOBA only). When replacing $KHSO_5$ by the same molar amount of H_2O_2, no conversion was observed, and the use of methanol instead of acetonitrile inhibited the oxidation, probably through trapping of the high valent metal-oxo species.[19] We also checked that no reaction occurred in the absence of catalyst and that ABA, BBA, AC and BZQ were stable under the catalytic oxidation conditions. However, in the case of BOBA, 70% conversion was obtained after 10 min, the only identified product being a small amount of benzoquinone. The same behavior was observed with MPTP but, in this case, conversion was 90%. We then decided to study the competitive oxidation of a mixture of substrate and one of the two esters. For a mixture of HPEBA and BOBA, the conversion of HPEBA was almost 100%, while only 10−15% of BOBA was converted. Therefore, the yield of BOBA resulting from the catalytic oxidation is barely affected by further oxidation. The same experiment with MPTP revealed an 85% conversion of the ester. These observations led us to conclude that MPTP was not detected among the reaction products because either: (i) it was further oxidized under the reaction conditions, or (ii) it was not formed during the catalytic reaction. These two possibilities will be discussed later.

Influence of the Acetonitrile/Buffer Ratio

Increasing the acetonitrile content from 10% to 45% in the buffered medium resulted in a decrease in the conversion, from 90% to 35%, and also in a significant change in the product distribution. Figure 1 shows that, with more than 40% acetonitrile, BOBA becomes the main product, while the selectivity in the other four products is slightly lowered. In fact, acetonitrile seems to favor the formation of BOBA. These results highlight the peculiar behaviour of BOBA over that of the other products, and suggest that there are several reaction pathways operating at the same time (at least two), one of them leading only to BOBA.

Influence of Dioxygen

In order to assess the influence of the reaction atmosphere, we carried out the oxidation under different pressures of dioxygen (to avoid leaks, we always added nitrogen to maintain a pressure of 1 atm). For these experiments we used 10% catalyst so that, in each case, the conversion was close to 100%. Figure 2 indicates the evolution of product selectivities as the amount of dioxygen is raised. Once again, the yield of BOBA increases while the yield of the other products is lowered indicating that formation of BOBA is oxygen-dependent. Furthermore, Figure 2 also shows that the yields of BOBA and AC are inversely correlated. In other words, as the yield of BOBA increases, the yield of AC decreases by the same amount, so that the value ([BOBA] + [AC]) remains constant (see also Table 1). This suggests that AC and BOBA have a common intermediate in their formation pathway. This intermediate is able to react with molecular oxygen to give BOBA, or to follow an alternative route leading to AC.

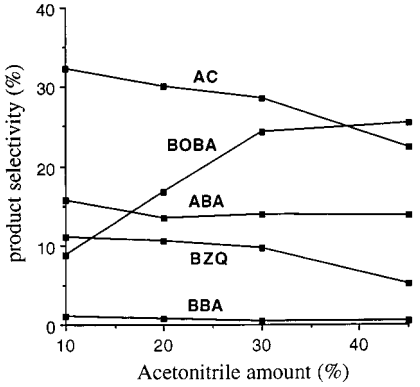


Figure 1. Influence of acetonitrile on selectivity

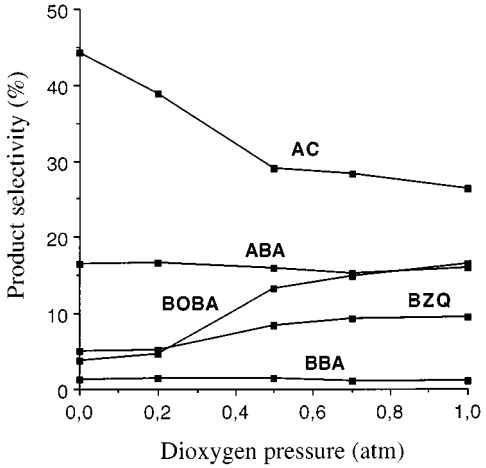


Fig. 2. Influence of dioxygen on selectivity

Table 1. Yields of AC, ABA and BOBA obtained from oxidation of HPEBA under dioxygen or nitrogen atmosphere

Products	Yield (%)	
	under O_2	under N_2
AC	26	44
ABA	16	16
BOBA	16	4

Labeling Experiments

In order to obtain more information about the reaction mechanism, we performed labeling experiments. To this end, we prepared the trideuteriated substrate CD_3-HPEBA, where the CH_3 has been replaced by a CD_3, and subjected it to the Mn-TMPyP/$KHSO_5$ system. Substrate conversion, product yields and selectivities are shown in Table 2. First of all, we observed that the conversion rate is almost the same as the oxidation rate of HPEBA. The absence of an isotope effect allows us to conclude that the rate-determining step of the oxidation does not involve an H-abstraction

Table 2. Yields and selectivities of products obtained from Mn-TMPyP/$KHSO_5$ oxidation of HPEBA in H_2O or D_2O and CD_3-HPEBA in H_2O[a]

Substrate Products	HPEBA in H_2O Yield (%)[b]	Selectivity (%)[b,c]	CD3-HPEBA in H_2O Yield (%)[b]	Selectivity (%)[b,c]	HPEBA in D_2O Yield (%)	Selectivity (%)[c]
AC	28 ± 1	31 ± 1	28 ± 1	34 ± 1	6	19
ABA	14 ± 0.5	15.3 ± 0.4	15.2 ± 0.3	19 ± 0.5	9	21
BBA	0.8 ± 0.1	0.9 ± 0.1	2.6 ± 0.3	3.2 ± 0.4	0.5	1
BOBA	7.7 ± 0.3	8.7 ± 0.3	6.8 ± 0.2	8.0 ± 0.1	2	6
BZQ	9.2 ± 0.4	10.6 ± 0.2	8.0 ± 0.4	9.8 ± 0.3	2	6
Conversion (%)	*91 ± 4*		*83 ± 3*		*37*	

[a] Experiments were performed under the same conditions, with 10% acetonitrile (substrate, $KHSO_5$ and Mn-TMpyP concentrations were respectively 500 μM, 10 mM and 10 μM). – [b] Experimental errors were obtained from three independent experiments. – [c] Selectivity is defined as the ratio of product yield divided by substrate conversion.

from the methyl group. No major changes in product selectivity were observed, except for BBA, whose selectivity, although it remained very low, increased significantly by a factor of 3.5. Thus replacing CH_3 by CD_3 in HPEBA influences only the formation of BBA. The reaction mixture resulting from the oxidation of CD_3-HPEBA was also analyzed by GC-MS. The mass spectra of AC and derivatized ABA showed a unique molecular peak at M + 3 (*m*/*z* 123 and *m*/*z* 181, respectively). These data clearly demonstrate that during the formation of ABA and AC, the methyl group remains unchanged since the three deuterium atoms are still present in the oxidation products.

Another experiment was performed in D_2O instead of H_2O, using HPEBA. An important isotopic effect was detected: the product distribution was not really affected, but the conversion decreased to 37% instead of the 91% observed in H_2O over the same reaction time (Table 2). When the substrate was placed in D_2O, its alcoholic hydrogen was exchanged for a deuterium. The decreased conversion indicates the major role played by the alcoholic hydrogen in the reaction mechanism. Additionally, we checked that with a substrate without exchangeable hydrogen, no such isotopic effect was observed. For example, the epoxidation of carbamazepine with Mn-TMPyP/$KHSO_5$, performed in D_2O, gave 97% conversion, the value obtained in H_2O being 95% in the same reaction conditions.[20] We can therefore conclude that the isotope effect observed with HPEBA is not a solvent isotope effect, but must be related to an isotope effect of the substrate itself.

In order to investigate the origin of the oxygen incorporated in the oxidation products, we performed experiments in the presence of ^{18}O-labeled water or dioxygen. The reactions were carried out with 10% catalyst and 20% acetonitrile for 10 min, so that the conversion was almost complete, and the yield of BOBA was optimized to provide suitable conditions for GC-MS analyses. In control experiments, we checked that HPEBA, AC, BBA and BOBA did not exchange their oxygen with water under these reaction conditions. A small exchange (7%) was found in the case of ABA. Also, $KHSO_5$ itself does not exchange its oxygen with water.[21] The labeling of BZQ was not studied since it was not detected by GC-MS under our conditions. Experiments were performed under air or under 1 atm of nitrogen or dioxygen either labeled or not. The dependence of the amount of labeled oxygen incorporated into each product on the reaction conditions is indicated in Table 3. The percentages were determined by calculating the relative abundances of molecular ions at M, M + 2 and M + 4, corresponding to the incorporation of none, one or two heavy oxygen atoms (the latter case concerns only BOBA). For BOBA, the relative abundances of the peaks at *m*/*z* 105 and 107 ($[Ph-C=O]^+$) provided the separate labeling of the carbonyl oxygen.

These results give us several key data. First, the oxygen incorporated in BOBA comes only from dioxygen, and is selectively introduced at the carbonyl position (no M + 4 peak was detected, and M + 2/M and 107/105 relative abundances were both close to 100% when the reaction was performed under $^{18}O_2$). In other words, 100% of the carbonyl oxygen atom of BOBA originates from dioxygen, while the oxygen atom of the ester remains unlabeled. This is consistent with the fact that BOBA formation is oxygen-dependent (see Figure 2). In contrast, the other three products incorporate labeled-oxygen atoms either from water or dioxygen. With AC and ABA, the labeling depends on the reaction conditions: as the quantity of dioxygen decreases, the amount of oxygen atoms from water increases (runs 2–4, Table 3). Interestingly, when the reaction was performed under 1 atm of dioxygen, AC was found to contain 24% of water-derived oxygen atoms and 65% of dioxygen-derived oxygen atoms. The total contribution of both water and dioxygen is thus 89%, which nearly corresponds to the amount of oxygen atoms incorporated from water when the reaction is performed under nitrogen (*i.e.* 85%). The same observation can be made with ABA. This suggests that there are two competitive pathways leading to AC and ABA, one involving a reaction with water, and the other involving a reaction with dioxygen. As the amount of dioxygen decreases, the preferred pathway become the water-dependent one. In the case of BBA, the labeling does not depend on the reaction conditions, since the amount of oxygen atoms from water remains unchanged whether the reaction is performed under nitrogen or under dioxygen (runs 2 and 4, Table 3).

Oxidation of Other Tertiary Alcohols

For a better understanding of the reactivity of HPEBA we decided to study the catalytic oxidation of some other tertiary alcohols. 1,1-Diphenylethan-1-ol DE (Scheme 1) was chosen to study the influence of the carboxylic group. Under the same experimental conditions as with HPEBA, the conversion was 75% and the oxidation products were the same as those resulting from oxidation of HPEBA, but without the carboxylic group, *i.e.* AC, BZQ, benzophenone BZP and the phenylbenzoate ester PBZ. The small amount of PBZ detected (Scheme 1) may be due to its poor stability in the reaction medium, since a control experiment showed that PBZ is completely oxidized by Mn-TMPyP/$KHSO_5$ in 10 min. The more striking fact is the large amount of BZP formed relative to the very low quantity of BBA obtained from HPEBA. This suggests that removal of the carboxylic group influences the rate of the $C_{aliph}-C_{aliph}$ bond cleavage pathway.

4-(Diphenylhydroxymethyl)benzoic acid DPBA and 4-(1-hydroxy-1-phenylbut-3-en-1-yl)benzoic acid ALBA (Scheme 1), analogous to HPEBA but with a phenyl or an allyl group instead of the methyl susbstituent, were also prepared and oxidized by Mn-TMPyP/$KHSO_5$ under the same conditions as HPEBA. The reactions were followed by HPLC and GC-MS. In both cases, the conversion was almost complete. The identified products and yields are indicated in Scheme 1. In the case of DPBA, the products are formed from the three possible $C_{aliph}-C_{ar}$ bond cleavages. Despite the fact that the loss of the phenyl group is statistically favored, the major product is BZP, resulting from the loss of the *p*-carboxyphenyl group. This is consistent with the selectivity observed for oxidation of HPEBA, where AC, deriving from the loss of the *p*-carboxyphenyl, is formed preferentially over ABA, resulting from the loss of the phenyl group. In contrast, no product deriving from the loss of one of the aromatic rings was detected by GC-MS analysis of the reaction mixture obtained from catalytic oxidation of ALBA. Instead, the major product is formed by loss of the allyl substituent, and we found a small amount of BZQ and BOBA. These observations suggest that the nature of the substituents of the carbinol plays a crucial role in the cleavage selectivity.

The last compound studied was 1,1-diphenylethane-1,2-diol DED (Scheme 1). In the presence of Mn-TMPyP/$KHSO_5$, substrate conversion was complete, and the only identified product was BZP, which was obtained in 90% yield. We also performed the oxidation with labeled water or dioxygen. In both cases, no labeled oxygen was found in the BZP, indicating that the carbonyl oxygen atom of BZP comes from the oxygen of the tertiary alcohol.

Discussion

Formation of Unlabeled Products

In a previous communication,[17] we suggested, based on product distribution from catalytic oxidation of HPEBA, that ABA, BBA, and AC are formed from the β-scission of the alkoxyl radical intermediate **1** by abstraction from the substrate of either H·, or an electron followed by H^+ loss (Scheme 2). Either type of abstraction may be performed by the high-valent $Mn^V=O$ species, generated by $KHSO_5$ with Mn-TMPyP, which is the active species operating in this catalytic system.[20][22] Taking into consideration the present labeling results, we now know that the pathway leading to these products must involve, at least in part, molecular oxygen and water. Since some products remain unlabeled, a β-scission must occur, but it is not the only reaction pathway operating. The experiments performed with CD_3-HPEBA demonstrate that, during the formation of AC and ABA, the methyl group is not modified, allowing us to discard any mechanism involving an oxidative attack on this group. On the other hand, the important role of the alcoholic hydrogen atom is shown by the experiment in D_2O where the conversion is significantly lowered. All these data are consistent with the formation of an alkoxy radical in a rate-determining step, as initially proposed. This radical can undergo β-fragmentation in competition with alternative pathways involving water and/or dioxygen. Thus, we can attribute the formation of the unlabeled fraction of AC, ABA and BBA to the β-scission of the alkoxy radical intermediate **1** (Scheme 2): the three products originate from the three possible cleavages, producing phenyl, *p*-carboxyphenyl and methyl radicals but the loss of the aryl groups is highly preferred, since very small amounts of BBA are formed. Previous studies on the decomposition of the cumyloxyl radical[23][24] and its derivative bearing a *p*-COOH substituent on the phenyl ring[18] revealed a predominent elimination of the methyl group, leading to acetophenone derivatives. Actually, β-scission is a process involving a late tran-

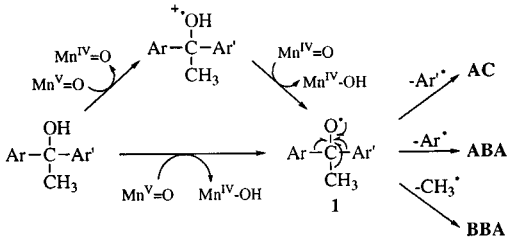
Table 3. ^{18}O-incorporation in AC, ABA, BBA and BOBA during the oxidation of HPEBA by Mn-TMPyP/$KHSO_5$ with $H_2{}^{18}O$ or $^{18}O_2$ (● = ^{18}O-labeled oxygen atom)

Run	Conditions	AC C=●	ABA C=●	BBA C=●	BOBA −C=●	−●−
1	$H_2O/●_2$	65%	23%	15%	95%	0
2	$H_2●/O_2$	24%	14%	22%	0	0
3	$H_2●$/Air	46%	19%	13%[a]	0	0
4	$H_2●/N_2$	85%	38%	22%	0	0

[a] The GC peak corresponding to BBA was too small in this experiment (yield of BBA from oxidation of HPEBA was 1%) to afford an accurate value.

sition state.[25] Consequently, the reaction rate depends on the stability of the generated radical and also of the carbonyl product formed. In our case, and in the case of cumyloxyl radicals, very unstable radicals are released (methyl or aryl radicals), so the orientation of the C−C bond cleavage should be controlled by the stability of the carbonyl products. Thus, the cleavage orientation can be rationalized by the enhanced stability of acetophenone derivatives over benzophenone derivatives (or acetone in the case of loss of a phenyl group from cumyloxyl radicals).[24] Furthermore, other factors such as diminution of the steric strain by expulsion of bulky groups can also influence a β-scission reaction.[24]

In contrast with HPEBA, none of the aryl groups were cleaved during the oxidation of ALBA (see Scheme 1). Instead, the only product detected results from cleavage of the allyl group. Assuming that the β-scission is the only pathway, we propose that, in this case, the much higher stability of the allyl radical[26] over the phenyl and *p*-carboxyphenyl radicals is the driving force for the reaction. Thus, the release of the allyl radical is highly favored, and there is only a minor influence of the stability of the carbonyl products formed concomitantly, or of any other factor.



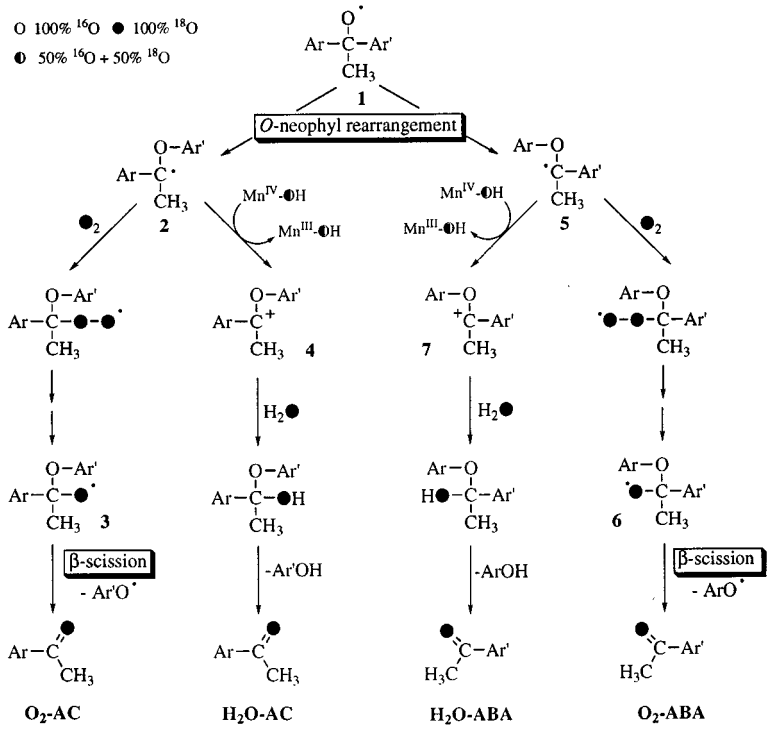
Scheme 2. Formation of unlabeled AC, ABA and BBA through β−scission of the alkoxyl radical **1**; Ar = phenyl and Ar′ = *p*-carboxyphenyl.

Formation of Labeled AC, ABA and BOBA

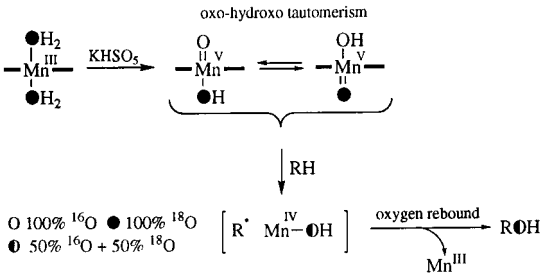
Following the idea that the alkoxy radical is the key intermediate in the oxidation reaction, we decided to investigate how this alkoxy radical can lead to AC, ABA, and BOBA with incorporation of oxygen atoms from water and dioxygen in the carbonyl function (in the case of AC and ABA) or from dioxygen only (in the case of BOBA). Obviously, the observed ^{18}O-incorporation and, more importantly, the formation of the ester BOBA require the involvement of a rearrangement. Aryl-substituted alkoxyl radicals are known to undergo an *O*-neophyl rearrangement, consisting of a 1,2 migration of an aryl group from the carbon to the oxygen, which gives rise to a new, more stable, carbon-centred radical (see for example Scheme 3).[27][28]

Usually, this rearrangement occurs on alkoxy radicals substituted by three α-aryl groups, generating an efficiently stabilized carbon radical, although the 1,1-diphenylethoxyl radical is also known to rearrange in such a way.[29−32] Considering that: (i) the structure of the 1-*p*-carboxyphenyl-1-phenylethoxyl radical **1** is very close to that of 1,1-diphenylethoxyl radical, and (ii) that 1,1-diphenylethanol exhibits a similar reactivity to HPEBA under the present oxidative conditions (see above), we can reasonably suppose that the alkoxyl radical **1** may also undergo an *O*-neophyl rearrangement (Scheme 3). Thus, if either phenyl (Ar) or *p*-carboxyphenyl (Ar′) migrates, two new carbon-centred radicals **2** and **5** are formed, which may escape from the solvent cage and react with dioxygen or Mn^{IV}-OH/water to provide AC and ABA, with a carbonyl oxygen atom from either dioxygen or water. Clearly, if the *p*-carboxyphenyl group migrates to the oxygen, the carbon-centred radical **2** is formed. This radical can react with dioxygen to produce a peroxy radical which can dimerize and provide a new alkoxy radical **3** after a Russell fragmentation. The β-scission of **3** releases a *p*-carboxyphenoxy radical and acetophenone, with a dioxygen-derived carbonyl oxygen atom (O_2-AC). Such a process was shown to occur with the 1,1-diphenylethoxy radical by Ingold *et al.*[29] Alternatively, the *O*-neophyl-rearranged radical can suffer electron abstraction by Mn^{IV}-OH. Reaction of the resulting cation **4** with water produces a hemiacetal, which can subsequently be hydrolysed to form acetophenone containing a water-derived carbonyl oxygen atom (H_2O-AC). Another possible pathway leading to H_2O-AC could be that the radical **2** gives the hemiacetal by a classical oxygen rebound route with Mn^{IV}-OH. However, it has been established that, in water, the active species Mn^{V}=O undergoes an oxo-hydroxo tautomerism,[20][22] leading to a 50% labeled active species Mn^{V}=O if ^{18}O-labeled water is used (Scheme 4).

Thus, after H-abstraction, a 50% labeled Mn^{IV}-OH species is generated. Therefore an oxygen rebound mechanism should lead to a 50% incorporation of labeled oxygen from water in the resulting product. In our case, since there are other pathways operating, there should be less than 50% incorporation of water-derived oxygen atoms in AC, and we should obtain at least the same amount of nonlabeled AC. However, the incorporation of labeled oxygen from water was found to be 85% under a nitrogen atmosphere (run 4, Table 3), and 24% under a dioxygen atmosphere (run 2) but with only 11% of nonlabeled H_2O-AC (runs 1 and 2: 11% = 100% − 65% − 24%). Thus, an oxygen rebound mechanism to explain the incorporation of water-derived oxygen atoms can be ruled out, at least as a main mechanism. A similar pathway, involving an initial migration of the phenyl group instead of the *p*-carboxyphenyl of the alkoxyl radical **1**, leads to O_2-ABA and H_2O-ABA. This mechanism explains why the incorporation of oxygen from water increases as the amount of dioxygen in the reaction atmosphere decreases. Indeed, the carbon-centred radicals **2** and **5** can follow two competitive routes, one involving water and the other involving dioxygen. The importance of each route depends on the amount of dioxygen (or water) available and, when the reaction is performed under nitrogen, the only pathway operating must be the water-dependent one. This is in agreement with the fact that, when the reaction is performed under nitrogen, the number of oxygen atoms from water is equal to the total number of oxygen atoms coming from water + dioxygen when the reaction is performed under dioxygen (run 4 and runs 1, 2, respectively, Table 3).



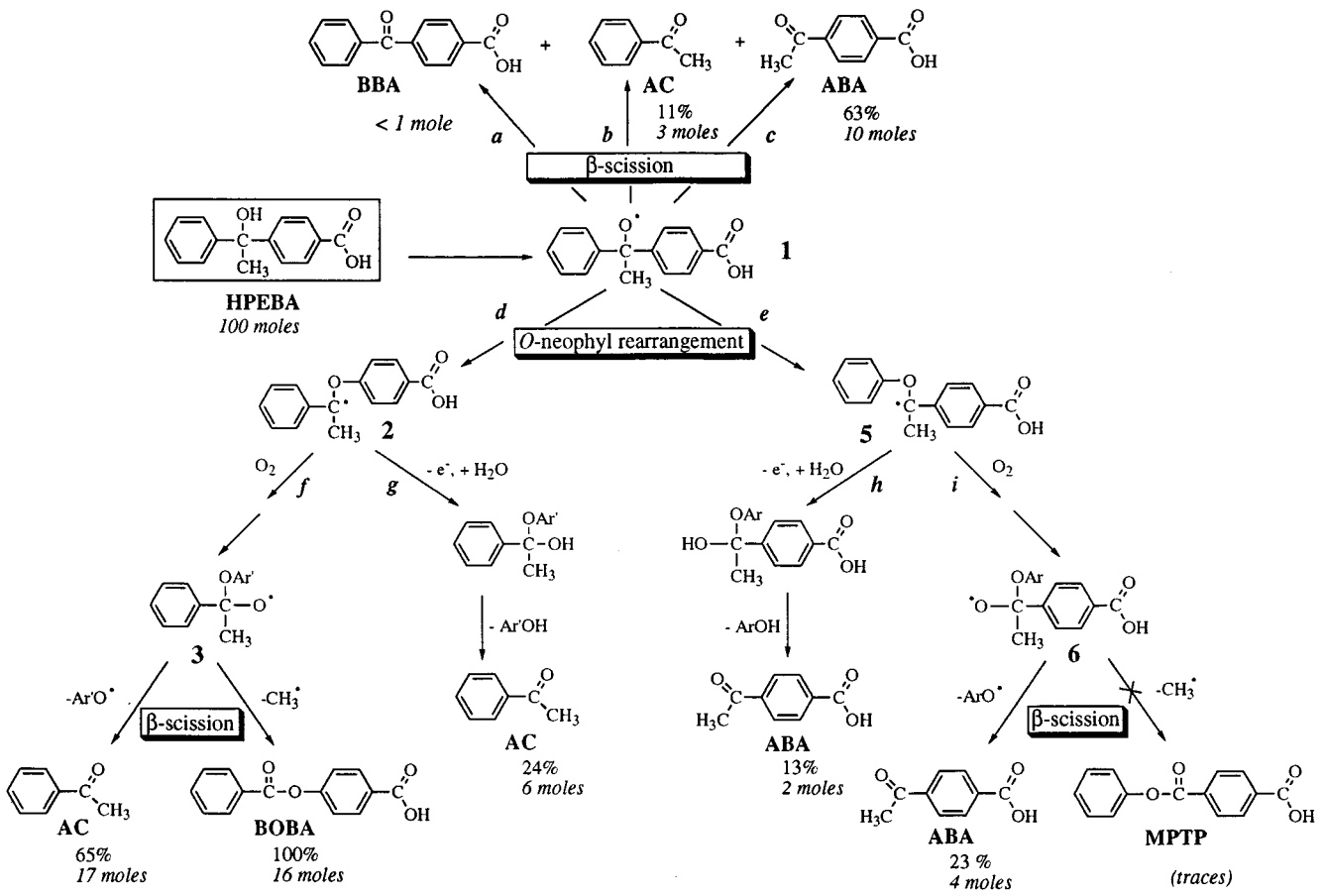
Scheme 3. Formation of ^{18}O-labeled AC and ABA after an *O*-neophyl rearrangement of intermediate **1**, using $H_2{}^{18}O$ or $^{18}O_2$ (direct β-scission from radical **1** generates unlabeled products); Ar = phenyl, Ar′ = *p*-carboxyphenyl



Scheme 4. Oxo-hydroxo tautomerism and oxygen rebound in $KHSO_5$ hydroxylation reaction catalyzed by Mn-TMPyP and performed in $H_2{}^{18}O$

A study of the influence of dioxygen showed that AC and BOBA probably have a common intermediate since, when the amount of dioxygen increases, the quantity of BOBA produced increases as well, but at the expense of AC formation. In addition, BOBA does not derive from a Baeyer-Villiger reaction on BBA because we checked that BBA is stable under the catalytic oxidation conditions. Furthermore, BOBA must incorporate a dioxygen-derived oxygen atom exclusively on the carbonyl position, the other ester oxygen atom being substrate-derived. According to these data, we propose that BOBA is formed through the β-scission of the alkoxy radical **3** (Scheme 5) with loss of a methyl radical. This C-β-scission pathway is in competition with the O-β-scission leading to acetophenone with loss of *p*-carboxyphenoxyl radical. It should be noted that, as far as we are aware, such an alternative between O- and C-β-scission has not previously been reported. A small difference between the bond dissociation energy of a C−C bond or a C−O bond in radical **3** would explain the formation of BOBA and AC from the same radical intermediate. The O_2-dependent pathway to BOBA formed at the expense of AC can now be explained as follows: under anaerobic conditions, the carbon-centred radical **2** (Scheme 3 and 5) follows a water-dependent route leading to AC containing a water-derived carbonyl oxygen atom, but under aerobic conditions, an oxygen-dependent pathway competes with this, leading to AC and BOBA both containing dioxygen-derived carbonyl oxygen atoms.

In a similar manner, the loss of a methyl radical from the oxygen-centred radical **6** (Scheme 5) could lead to MPTP with the same labeling as BOBA. However, MPTP was not detected among the reactions products, but careful analysis of the GC-MS spectra obtained from the labeling experiments showed traces of MPTP with a dioxygen-derived carbonyl oxygen atom. Since it is not stable under the reaction conditions, we wonder whether MPTP is formed and further oxidized, or whether only traces are formed. Our view is that if MPTP is formed, like BOBA, in significant amounts, then the production of ABA should be influenced in the same way as AC by the increase in acetonitrile or dioxygen concentrations. Since ABA proved to be indifferent to these changes of reaction conditions (see Figure 1 and 2), this fact precludes a competitive route leading to MPTP at the expense of ABA formation. Thus, we propose that MPTP is not formed in significant amounts during the reaction. However, we have presently no explanation to rationalize this particular difference in selectivity between C- and O-β-scissions of radicals **3** and **6**.



Scheme 5. Formation pathway of AC, ABA, BOBA and unlabeled BBA; the percentages indicate the part of the product formed through the considered route under a dioxygen atmosphere; the number of mols is the amount of each product formed if the initial amount of HPEBA is 100 mols

Formation of Labeled BBA

The reaction pathways presented in Scheme 5 do not explain the production of partially labeled BBA in the experiments performed in $H_2{}^{18}O$ or under $^{18}O_2$ (Table 3). Although BBA represents only 1% of the products, some additional experimental data were collected to try to understand the role of dioxygen and water in its formation, besides the direct β-fragmentation process. A conceivable pathway which could lead to BBA, after an initial hydroxylation of the methyl group and further oxidation of the resulting 1,1-diarylethane-1,2-diol, can be discarded since: (i) the catalytic oxidation of the related compound 1,1-diphenylethane-1,2-diol DED by Mn-TMPyP/$KHSO_5$ only produces unlabeled products in experiments performed in $H_2{}^{18}O$ or under $^{18}O_2$, and (ii) BBA is more efficiently produced when the methyl group of the substrate is trideuterated (see Table 2), this inverse deuterium isotope effect allows us to eliminate the possibility of an initial hydroxylation of the methyl group. In addition, this isotope effect is different from that observed for the loss of $CD_3^\bullet$ or $CH_3^\bullet$ from $C_6H_6C(CH_3)(CD_3)O^\bullet$ by β-scission (k_H/k_D = 1.15).[25] A carbon-centred radical such as Ar−C·(OH)-Ar′ is a possible intermediate since analogous radicals have been proposed in oxidations catalyzed by cytochrome P-450 or chemical models.[33][34] At present, these results do not allow us to propose a convincing mechanism to explain the available data on this minor reaction product.

Overall Mechanism for HPEBA Oxidation

An overall mechanism, presented in Scheme 5, can now be established with the involvement of two possible evolution pathways for the alkoxy radical **1**: direct β-scission or *O*-neophyl rearrangement. Both AC and ABA can form from **1** through either a direct β-scission (top of Scheme 5) or an *O*-neophyl rearrangement followed (bottom, on the left and on the right) or not (bottom, in the middle) by a β-scission in the ultimate step. BOBA is only produced from **1** through a *O*-neophyl rearrangement followed, after dioxygen addition, by a β-scission in the last step of the reaction (bottom, on the left). BBA is partially produced by direct β-scission of **1** (top) but other pathway(s) remain unidentified at the moment. In Scheme 5, the percentages under the products indicate the part of each product formed through the considered route under 1 atm of dioxygen. Assuming a starting quantity of 100 mols of HPEBA, we obtained for each product the quantities indicated below the percentages. These calculations afford an additional demonstration that

the proposed mechanism is coherent. Indeed, according to this scheme, if the reaction is performed under nitrogen instead of O_2 (according to Table 1, 4 mols of BOBA were still produced under N_2, probably due to the presence of traces of residual dioxygen), routes d + g should lead to 35 mols of AC (17 + 16 + 6 − 4 mols of residual BOBA) containing a water-derived oxygen atom. Adding the 3 mols of AC generated by β-scission gives a total number of 38 mols of AC produced. This quantity is consistent with the 44% yield experimentally observed under nitrogen (see Table 1). In addition, the fact that formation of BOBA was favored by increase in acetonitrile concentration (see Figure 1) can be explained by the decreasing polarity of the medium, which disfavors the β-scission pathway.[35]

Formation of Benzoquinone

Benzoquinone probably derives from the further oxidation of the aryl radicals (phenyl, *p*-carboxyphenyl, phenoxy and *p*-carboxyphenoxy radicals) released in the different β-scission processes. We have checked that phenol, benzoic acid and *p*-hydroxybenzoic acid, three putative evolution products of the aryl radicals (phenol and *p*-hydroxybenzoic acid are also formed through the water-dependent route, see Scheme 5), are quickly oxidized to BZQ by the catalytic system. An additional argument is that the oxidation of ALBA and DED, where almost no aryl radicals are released, gives only 1% of benzoquinone (Scheme 1). In contrast, a significant amount of BZQ is obtained from oxidation of HPEBA, DE and DPBA, for which the oxidation products are derived mainly from a $C_{aliph}-C_{ar}$ bond cleavage with release of aryl radicals (Scheme 1). Consequently, the formation of BZQ can be considered as proof of formation of aryl radicals during the oxidation process.

Conclusions

The catalytic oxidation of several tertiary diaryl alcohols has been achieved with $KHSO_5$ in the presence of Mn-TMPyP. The use of this biomimetic catalytic system represents an alternative and efficient process for oxidative conversion of tertiary alcohols, which are resistant to conventional oxidants. Interestingly, the reaction led to acetophenone and benzophenone derivatives, and also to an unexpected ester. This product distribution, and additional labeling experiments, provide useful insights into the mechanism of the C−C bond cleavage by this cytochrome P-450 model system. The key intermediate in this catalytic oxidation is an alkoxy radical which follows a β-scission route or, alternatively, undergoes an *O*-neophyl rearrangement. This latter route explains the formation of products containing dioxygen- or water-derived oxygen atoms. In addition the unprecedented formation of an ester derivative during the catalytic oxidation of tertiary diaryl alcohols can be considered as a proof of the involvement of an *O*-neophyl rearrangement in the reaction mechanism

Experimental Section

Materials: Potassium monopersulfate (the triple salt $[KHSO_5]_2[KHSO_4][K_2SO_4]$, Curox®) was kindly donated by Peroxid Chemie GmbH. Mn-TMPyP (pentaacetate form) was prepared according to ref.[36] AC, ABA, BBA, BZQ, BZP, PBZ and DE were purchased from Aldrich. $H_2{}^{18}O$ (96.5 atom%) was supplied by Eurisotop (Gif sur Yvette, France) and $^{18}O_2$ (96.8 atom%) was supplied by Leman (Saint Quentin en Yvelines, France).

Instrumentation: HPLC analyses were performed on a Waters Millipore chromatograph equipped with a U6 K injector, a diode array detector (Kontron Instrument) and a 10 μm Nucleosil C18 column (Interchrom). The eluent was a mixture of acetonitrile/triethylammonium acetate buffer 0.1M (pH = 6.5) in proportions 35:65 or 25:75 (v/v) for oxidation of HPEBA, DPBA and ALBA and 45:55 (v/v) for oxidation of DE and DED. The flow rate was 1 mL/min Detection was performed at 240 nm. GC-MS analyses were performed on a Hewlett Packard HP 6890 instrument coupled with a MSD 5973 mass spectrometer, using electron impact ionization at 70 eV. The GC column used was a non polar capillary column [25 m × 0.2 mm HP-5MS, cross-linked diphenyl (5%) and dimethylpolysiloxane (95%)] and the carrier gas was helium. The injector temperature was 250°C, and analyses were performed at 80°C for 2 min, then up to 200°C (10°C/min) where the temperature was maintained for 15 min. MS spectra were obtained on a Nermag R10/10H instrument. ^{1}H NMR spectra were recorded with a Bruker WM 250 spectrometer.

Preparation of HPEBA: The three-step procedure was adapted from ref.[37] and improved in terms of solvent used, purification and yields. *p*-Benzoylbenzoic acid (1 g, 4.4 mmol), (−)-menthol (2.8 g, 18 mmol) and *p*-toluenesulfonic acid (42 mg, 0.2 mmol) were heated for 8 h at 180°C. The crude product was dissolved in 50 mL ether/toluene 1/1 (v/v) and washed three times with a saturated solution of sodium carbonate. After addition of water, the organic layer was steam distilled up to 140°C in order to remove the excess menthol. The aqueous residue was then extracted with toluene, and the extracts were dried with sodium sulfate. After removal of solvent under vacuum, menthyl *p*-benzoylbenzoate was obtained as a brown oil (1.52 g, yield = 94%). − ^{1}H NMR ([D$_6$]DMSO): δ = 0.88 [d, ^3J(H,H) = 6.9 Hz, 3 H, CH_3], 1.02 (m, 7 H, $2CH_3$ + CH), 1.25 (m, 2 H, CH_2), 1.56−1.88 (m, 4 H, 2 CH_2), 2.00 (m, 1 H, CH), 2.13 (m, 1 H, CH), 5.01 (m, 1 H, CH), 7.70 [t, ^3J(H,H) = 7.3 Hz, 2 H, 2 aromatic CH], 7.79−7.92 (m, 3 H, 3 aromatic CH), 7.97 [d, ^3J(H,H) = 8.5 Hz, 2 H, 2 aromatic CH], 8.23 [d, ^3J(H,H) = 8.5 Hz, 2 H, 2 aromatic CH].

Methylmagnesium iodide (3.7 mmol) was added dropwise to a stirred solution of menthyl *p*-benzoylbenzoate (674 mg, 1.8 mmol) in 9 mL anhydrous toluene under nitrogen at room temperature. After hydrolysis with 2 M aqueous hydrochloric acid, the organic layer was washed with water, dried over sodium sulfate and concentrated under vacuum. A brown solid was obtained and identified as menthyl *p*-(1-hydroxy-1-phenylethyl)benzoate (562 mg, yield = 82%). − ^{1}H NMR ([D$_6$]DMSO): δ = 0.84 [d, ^3J(H,H) = 6.9 Hz, 3 H, CH_3], 0.99 (m, 7 H, $2CH_3$ + CH), 1.21 (m, 2 H, CH_2), 1.64 (m, 2 H, CH_2), 1.79 (m, 2 H, CH_2), 1.97 (m, 4 H, CH+CH_3), 2.08 (m, 1 H, CH), 4.93 (m, 1 H, CH), 6.01 (s, 1 H, OH), 7.33−7.48 (m, 3 H, 3 aromatic CH), 7.54 [d, 2 H, ^3J(H,H) = 7.2 Hz, 2 aromatic CH], 7.68 [d, ^3J(H,H) = 8.4 Hz, 2 H, 2 aromatic CH], 7.98 [d, ^3J(H,H) = 8.5 Hz, 2 H, 2 aromatic CH].

Menthyl-*p*-(1-hydroxy-1-phenylethyl)benzoate (474 mg, 1.3 mmol) was dissolved in 30 mL aqueous ethanol containing 2.5 M KOH. The solution was refluxed for 4 hours. After removal of ethanol

under vacuum, menthol was extracted with ether. The aqueous layer was then acidified with hydrochloric acid until a brown oil precipitated, which was extracted with dichloromethane. The organic phase was washed with water saturated in sodium chloride until neutral pH and dried over sodium sulfate. Solvent was removed under vacuum. The resulting product was recrystallized from a dichloromethane/hexane mixture to yield pure HPEBA as a white powder (177 mg, yield = 58%). − ^{1}H NMR ([D$_6$]DMSO): δ = 1.96 (s, 3 H, CH$_3$), 5.97 (s, 1 H, OH), 7.29 [t, ^3J(H,H) = 7.3 Hz, 1 H, aromatic CH], 7.40 [t, ^3J(H,H) = 7.3 Hz, 2 H, 2 aromatic CH], 7.54 [d, ^3J(H,H) = 7.0 Hz, 2 H, 2 aromatic CH], 7.64 [d, ^3J(H,H) = 8.4 Hz, 2 H, 2 aromatic CH], 7.96 [d, ^3J(H,H) = 8.4 Hz, 2 H, 2 aromatic CH], 12.97 (br s, 1 H, COOH). − $C_{15}H_{14}O_3$(242.28): calcd. C 74.36, H 5.82; found C 74.12, H 5.74. − MS (DCI/NH$_3$): *m/z*: 260 [$M^+ + NH_4^+$], 242 [M^+], 225 [$(M - OH)^+$].

Preparation of CD$_3$-HPEBA: The procedure was the same as for HPEBA except that in the second step, methylmagnesium iodide was replaced by trideuterated methylmagnesium iodide (3 mmol). Reaction with menthyl *p*-benzoylbenzoate (727 mg, 2 mmol) followed by saponification gave CD$_3$-HPEBA as a white powder (277 mg, yield = 56% for the two steps). − ^{1}H NMR ([D$_6$]DMSO): δ = 5.97 (s, 1 H, OH), 7.29 [t, ^3J(H,H) = 7.3 Hz, 1 H, aromatic CH], 7.40 [t, ^3J(H,H) = 7.3 Hz, 2 H, aromatic CH], 7.54 [d, ^3J(H,H) = 7.0 Hz, 2 H, 2 aromatic CH], 7.64 [d, ^3J(H,H) = 8.4 Hz, 2 H, 2 aromatic CH], 7.96 [d, ^3J(H,H) = 8.4 Hz, 2 H, 2 aromatic CH], 12.97 (br s, 1 H, COOH); − $C_{15}D_3H_{11}O_3$(245.29): calc. C 73.47, H 5.71; found C 73.24, H 5.55. − MS (DCI/NH$_3$): *m/z*: 263 [$M^+ + NH_4^+$], 245 [M^+], 228 [$(M - OH)^+$].

Preparation of DPBA: The procedure was the same as for HPEBA except that in the second step, methylmagnesium iodide was replaced by phenylmagnesium iodide (3.2 mmol) and hydrolysis was performed with 2M aqueous NH_4Cl instead of 2N HCl. Reaction with menthyl *p*-benzoylbenzoate (787 mg, 2.2 mmol) followed by saponification gave DPBA as a cream-colored solid (330 mg, yield = 48% for the two steps). ^{1}H NMR ([D$_6$]DMSO): δ = 6.74 (s, 1 H, OH), 7.29−7.50 (m, 12 H, aromatic H), 8.00 [d, ^3J(H,H) = 8.4 Hz, 2 H, 2 aromatic CH], 12.96 (br s, 1 H, COOH) − $C_{20}H_{16}O_3 \cdot 0.2\ H_2O$ (307.95): calcd. C 78.00, H 5.37; found C 77.94, H 5.13.

Preparation of ALBA: The procedure was the same as for HPEBA except that in the second step, methylmagnesium iodide was replaced by allylmagnesium bromide (7 mmol) and hydrolysis was performed with 2M aqueous NH_4Cl instead of 2M HCl. Reaction with menthyl *p*-benzoylbenzoate (768 mg, 2.1 mmol) followed by saponification and purification by chromatography on silica gel (eluent used was CH_2Cl_2/MeOH 96/4, v/v) gave ALBA as a yellow oil which solidified under vacuum (79 mg, yield = 14% for the two steps). ^{1}H NMR ([D$_6$]DMSO): δ = 3.19 [d, ^3J(H,H) = 6.7 Hz, 2 H, CH$_2$], 4.95−5.20 (m, 2 H, CH$_2$), 5.78 (m, 1 H, CH), 5.93 (s, 1 H, OH), 7.28 [t, ^3J(H,H) = 7.4 Hz, 1 H, aromatic CH], 7.40 [t, ^3J(H,H) = 7.4 Hz, 2 H, 2 aromatic CH], 7.57 [d, ^3J(H,H) = 8.0 Hz, 2 H, 2 aromatic CH], 7.67 [d, ^3J(H,H) = 8.3 Hz, 2 H, 2 aromatic CH], 7.95 [d, ^3J(H,H) = 8.2 Hz, 2 H, 2 aromatic CH], 12.95 (br s, 1 H, COOH). − MS (DCI/NH$_3$): *m/z*: 303 [$(M^+ + N_2H_7^+$], 286 [$(M^+ + NH_4^+$], 268 [$(M - OH + NH_3)^+$], 251 [$(M - OH)^+$].

Preparation of DED: Phenylmagnesium bromide (3.6 mmol) was added dropwise to a stirred solution of ethyl glycolate (110 mg, 1.06 mmol) in anhydrous toluene (10 mL) under nitrogen at room temperature. After hydrolysis with 2M aqueous NH_4Cl, the organic layer was washed with water, dried over sodium sulfate and concentrated under vacuum. The resulting product was recrystallized from a dichloromethane/hexane mixture to yield pure DED as a white solid (141 mg, yield = 62%). − ^{1}H NMR ($CDCl_3$): δ = 1.8 (br s, 1 H, OH), 3.15 (br s, 1 H, OH), 4.17 (s, 2 H, CH$_2$), 7.25−7.45 (m, 10 H, aromatic H). − $C_{14}H_{14}O_2$ 0.2 H_2O (214.26): calc. C 78.48, H 6.59; found C 78.25, H 6.26.

Preparation of BOBA: Benzoyl chloride (1.3 mL, 10.8 mmol) was added dropwise to a stirred solution of *p*-hydroxybenzoic acid (1 g, 7.2 mmol) and triethylamine (2.6 mL, 18 mmol) in 45 mL of acetonitrile under nitrogen at room temperature. After stirring for 3 h, the mixture was poured into 35 mL diethyl ether and washed with water. The aqueous layer was acidified with hydrochloric acid to precipitate the product, which was extracted with diethyl ether. The organic layer was dried over sodium sulfate and the solvent removed under vacuum. The resulting solid was recrystallized from hot ethanol to give a white powder identified as BOBA (262 mg, yield = 15%). − ^{1}H NMR ([D$_6$]DMSO): δ = 7.55 [d, ^3J(H,H) = 8.6 Hz, 2 H, 2 aromatic CH], 7.74 [t, ^3J(H,H) = 7.7 Hz, 2 H, 2 aromatic CH], 7.89 [t, ^3J(H,H) = 7.4 Hz, 1 H, aromatic CH], 8.16 [d, ^3J(H,H) = 8.5 Hz, 2 H, 2 aromatic CH], 8.27 [d, ^3J(H,H) = 7.2 Hz, 2 H, 2 aromatic CH], 13.1 (br s, 1 H, COOH). − $C_{14}H_{10}O_4 \cdot 0.2H_2O$ (242.23): calc. C 69.42, H 4.16; found C 69.25, H 3.97. − MS (DCI/NH$_3$): *m/z:* 277 [$M^+ + N_2H_7^+$], 260 [$M^+ + NH_4^+$].

Preparation of MPTP: A solution of phenol (100 mg, 1.06 mmol) in 5 mL acetonitrile was added dropwise to a stirred solution of terephthaloyl chloride (1.08 g, 5.3 mmol) and triethylamine (500 μL, 3.6 mmol) in 25 mL of acetonitrile under nitrogen at room temperature. After stirring for 1 h, the mixture was poured into water and extracted with dichloromethane. The organic layer was dried over sodium sulfate and solvent was removed under vacuum. The product was purified by chromatography on silica gel (the eluent was dichloromethane/ethanol 95:5, v/v) as it was found to contain terephthalic acid as a by-product of the reaction. **MPTP** (62 mg, yield = 24%) was obtained as a white powder. ^{1}H NMR ([D$_6$]DMSO): δ = 7.40−7.49 (m, 3 H, 3 aromatic CH), 7.61 [t, ^3J(H,H) = 7.5 Hz, 2 H, 2 aromatic CH], 8.25 [d, ^3J(H,H) = 8.4 Hz, 2 H, 2 aromatic CH], 8.36 [d, ^3J(H,H) = 8.5 Hz, 2 H, 2 aromatic CH], 13.6 (br s, 1 H, COOH).

General Catalytic Oxidation Conditions: Unless otherwise stated, the reaction medium (1 mL of water/acetonitrile 9:1, v/v) contained 66 mM phosphate buffer pH 5, 500 μM substrate (introduced as a 25 mM solution in CH_3CN), 10 mM $KHSO_5$ (introduced as a 250 mM solution in water) and 200 μM *p*-diacetylbenzene (used as internal standard). Mn-TMPyP (10 μM) was introduced as a 1 mM solution in water in five consecutive 2 nmol additions, every two min. The first addition initiated the reaction. Reactions were performed at room temperature and monitored by HPLC. Yields were calculated after 10 min from the initial amount of substrate by comparison with calibration curves. For the oxidation of carbamazepine, a previously reported procedure was used.[19]

Competitive Oxidation of HPEBA with BOBA or MPTP: The reaction was carried out as described above, but with addition of 150 μM of BOBA or MPTP. After 10 min, the products were analyzed by HPLC. The amount of ester coming from the catalytic oxidation was estimated from the substrate conversion, so that the conversion of BOBA or MPTP initially introduced could be calculated.

Experiments Under Different Pressures of Dioxygen: In this case, the mixture contained 20% acetonitrile instead of 10%, and the Mn-TMPyP concentration was 50 μM. The reaction medium was placed in a Schlenk tube connected to a pressure captor and degassed by three consecutive freeze-thaw cycles under vacuum. It was then repressurized with the desired pressure of dioxygen, and nitrogen was added to maintain a final pressure of 1 atm. Mn-

TMPyP (previously degassed) was added in five consecutive additions by gas-tight syringe. HPLC analysis was performed after 10 min.

Experiments with D_2O: Solutions of the required concentrations and volume of buffer plus $KHSO_5$ on the one side, and Mn-TMPyP on the other side, were prepared and lyophilized using a Speed-Vac. Substrate and internal standard in CH_3CN and appropriate volumes of D_2O were added (in this case the total volume was 500 μL). The reaction was then carried out as described above.

Experiments with $H_2{}^{18}O$: In this case, the mixture contained 20% acetonitrile instead of 10%, and the Mn-TMPyP concentration was 50 μM. Solutions of the required concentration and volume of buffer plus $KHSO_5$ on the one side, and Mn-TMPyP on the other side, were prepared and lyophilized using a Speed-Vac. Substrate in CH_3CN and appropriate volumes of $H_2{}^{18}O$ were added (in this case the total volume was 500 μL). In the case of the reaction under dioxygen or nitrogen, the reaction medium was placed in a Schlenk tube connected to a pressure captor and degassed by three consecutive freeze-thaw cycles under vacuum. It was then repressurized with 1 atm of dioxygen or nitrogen. Mn-TMPyP (previously degassed) was added in five consecutive additions by gastight syringe. After 10 min, the mixture was saturated with NaCl and extracted with three 1 mL portions of dichloromethane. The organic phase was concentrated, and a solution of diazomethane in dichloromethane (prepared with an Aldrich MNNG diazomethane generation apparatus) was added to convert the carboxylic functions into methyl esters. After concentration, the sample was analysed by GC-MS (to analyze AC, which does not require prior derivatization, a 30 μL sample was taken after the first extraction and analyzed by GC-MS without further treatment). The percentage of ^{18}O incorporated in each product was determined by the relative abundances of the peaks at: *m/z* 120 and 122 [M^+], and *m/z* 105 and 107 [$(M - CH_3)^+$] for **AC**, *m/z* 178 and 180 [M^+], and *m/z* 163 and 165 [$(M - CH_3)^+$] for ABA methyl ester, *m/z* 240 and 242 [M^+], and *m/z* 209 and 211 [$(M - OCH_3)^+$] for BBA methyl ester, *m/z* 256, 258 and 260 [M^+], and *m/z* 105 and 107 [$(M - OC_6H_4COOCH_3)^+$] for BOBA methyl ester. The values obtained were corrected considering the ^{18}O content of the labeled water. Since BOBA and HPEBA methyl esters had the same mass and almost the same elution time, it was necessary to add 10% catalyst instead of 2% to ensure a complete conversion. In addition, a peak at *m/z* 241 [$(M - CH_3)^+$] corresponding only to HPEBA methyl ester allowed us to check the possible presence of small amounts of nonconverted substrate and to calculate its contribution to the molecular peak. Control experiments to check if the products exchanged their oxygen with $H_2{}^{18}O$ were performed under the same conditions using 200 μM AC, ABA, BBA or BOBA instead of HPEBA.

Experiments with $^{18}O_2$: The reaction conditions were the same as for experiments under different pressures of dioxygen, but in this case the Schlenk tube was repressurized with 1 atm of $^{18}O_2$ and the total volume was 500 μL. After 10 min, the sample was treated and analyzed as described for the $H_2{}^{18}O$ experiments. The values obtained from ^{18}O incorporations were corrected considering the ^{18}O content of the labeled dioxygen.

Acknowledgments

We thank Dr. Massimo Bietti (University of Rome) for fruitful discussions on the neophyl rearrangement.

[1] P. R. O. d. Montellano, *Cytochrome P-450: Structure, Mechanism and Biochemistry*, Plenum Press, New York, **1995**.
[2] T. S. Calderwood, W. A. Lee, T. C. Bruice, *J. Am. Chem. Soc.* **1985**, *107*, 8272−8273.
[3] R. I. Murray, S. G. Sligar, *J. Am. Chem. Soc.* **1985**, *107*, 2186−2187.
[4] T. Okamoto, K. Sasaki, M. Shimada, S. Oka, *J. Chem. Soc., Chem. Commun.* **1985**, 381−383.
[5] T. Okamoto, K. Sasaki, S. Oka, *J. Am. Chem. Soc.* **1988**, *110*, 1187−1196.
[6] Y. Ito, K. Kunimoto, S. Miyachi, T. Kako, *Tetrahedron Lett.* **1991**, *32*, 4007−4010.
[7] Y. Ito, *J. Chem. Soc., Chem. Commun.* **1991**, 622−624.
[8] D. L. Wertz, M. F. Sisemore, M. Selke, J. Driscoll, J. S. Valentine, *J. Am. Chem. Soc.* **1998**, *120*, 5331−5332.
[9] J. H. Babler, M. J. Coghlan, *Synth. Commun.* **1976**, *6*, 469−474.
[10] W. G. Dauben, D. M. Michno, *J. Org. Chem.* **1977**, *42*, 682−685.
[11] E. Wada, M. Okawara, *J. Org. Chem.* **1979**, *44*, 2952−2954.
[12] T. G. Waddell, A. D. Carter, T. J. Miller, *J. Org. Chem.* **1992**, *57*, 381−383.
[13] M. F. Schlecht, H. J. Kim, *J. Org. Chem.* **1989**, *54*, 583−587.
[14] J. Rocek, A. M. Martinez, G. E. Cushmac, *J. Am. Chem. Soc.* **1973**, *95*, 5425−5426.
[15] W. S. Trahanovsky, D. B. Macaulay, *J. Org. Chem.* **1973**, *38*, 1497−1499.
[16] D. G. Hoare, A. W. William, *J. Chem. Soc.* **1964**, 2552−2560.
[17] K. Wietzerbin, B. Meunier, J. Bernadou, *Chem. Commun.* **1997**, 2321−2322.
[18] R. J. Balahura, A. Sorokin, J. Bernadou, B. Meunier, *Inorg. Chem.* **1997**, *36*, 3488−3492.
[19] J. T. Groves, R. Quinn, T. J. McMurry, G. Lang, B. Boso, *J. Chem. Soc., Chem. Commun.* **1984**, 1455−1456.
[20] J. Bernadou, A.-S. Fabiano, A. Robert, B. Meunier, *J. Am. Chem. Soc.* **1994**, *116*, 9375−9376.
[21] R. Song, A. Sorokin, J. Bernadou, B. Meunier, *J. Org. Chem.* **1997**, *62*, 673−678.
[22] J. Bernadou, B. Meunier, *Chem. Commun.* **1998**, 2167−2173.
[23] E. Baciocchi, F. d′Acunzo, C. Galli, M. Ioele, *J. Chem. Soc., Chem. Commun.* **1995**, 429−430.
[24] C. Walling, A. Padwa, *J. Am. Chem. Soc.* **1962**, *85*, 1593−1596.
[25] A. A. Zavitsas, S. Seltzer, *J. Am. Chem. Soc.* **1964**, *86*, 3836−3840.
[26] D. F. McMillen, D. M. Golden, *Ann. Rev. Phys. Chem.* **1982**, *33*, 493−532.
[27] M. S. Kharasch, A. C. Poshkus, A. Fono, W. Nudenberg, *J. Org. Chem.* **1951**, 1458−1470.
[28] W. H. Urry, M. S. Kharasch, *J. Am. Chem. Soc.* **1944**, *66*, 1438−1440.
[29] J. A. Howard, K. U. Ingold, *Can. J. Chem.* **1969**, *47*, 3797−3801.
[30] J. A. Howard, K. Academic, K. U. Ingold, *Can. J. Chem.* **1969**, *47*, 3793−3795.
[31] J. T. Banks, J. C. Scaiano, *J. Phys. Chem.* **1995**, *99*, 3527−3531.
[32] D. E. Falvey, B. S. Khambatta, G. B. Schuster, *J. Phys. Chem.* **1990**, *94*, 1056−1059.
[33] E. Baciocchi, S. Belvedere, M. Bietti, O. Lanzalunga, *Eur. J. Org. Chem.* **1998**, 299−302.
[34] A. D. N. Vaz, M. J. Coon, *Biochemistry* **1994**, *33*, 6442−6449.
[35] D. V. Avila, C. E. Brown, K. U. Ingold, J. Lusztyk, *J. Am. Chem. Soc.* **1993**, *115*, 466−470.
[36] J. Bernadou, G. Pratviel, F. Bennis, M. Girardet, B. Meunier, *Biochemistry* **1989**, *28*, 7268−7275.
[37] M. M. J. Kubitscheck, W. A. Bonner, *J. Org. Chem.* **1961**, *26*, 2194−2197.

Received April 24, 1999
[I99158]

Tungsten Carbonyl Complexes of 1*H*-Diphosphirenes and Diphosphirenylium Salts

Didier Bourissou,[a] Yves Canac,[a] Heinz Gornitzka,[a] Colin J. Marsden,[b] Antoine Baceiredo,[a] and Guy Bertrand*[a]

Keywords: Phosphorus heterocycles / Cations / Tungsten complexes / Coordination modes / Phosphaalkenes

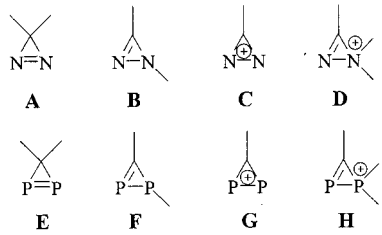
The 1,1,3-tris(diisopropylamino)diphosphirenium salt **1** reacts with lithium aluminium hydride leading to the *P*-hydrogeno-*C*-phosphinophosphaalkenes **2**, which on treatment with a catalytic amount of $BF_3{\cdot}OEt_2$ afford the 1,3-bis(diisopropylamino)-1*H*-diphosphirene **3**. The corresponding η^1-coordinated 1*H*-diphosphirene **6** can be prepared by treatment of **2** or **3** with one equivalent of $[W(CO)_5(thf)]$. Alternatively, the diphosphirenium salt **1** reacts with an excess of $[W(CO)_5(thf)]$, affording the corresponding η^1-coordinated diphosphirenium salt complex **4**, which is converted into the *P*-hydrogenophosphaalkene complex **5** with lithium aluminium hydride. The dinuclear tungsten complexes **7** and **8** are obtained by treatment of the free 1*H*-diphosphirene **3** with two equivalents of $[W(CO)_5(thf)]$ or one equivalent of $[W(CO)_4(thf)_2]$, respectively. Compound **6** reacts with two equivalents of hydrogen chloride, giving the 1-chloro-3-diisopropylamino-1*H*-diphosphirene **9**, which can be subsequently converted into the 1-diisopropylamino-, 1-azido, or 1-phenyl-3-diisopropylamino-1*H*-diphosphirenes **6**, **10** and **11** by nucleophilic substitution with diisopropylamine, azidotrimethylsilane or sodium tetraphenylborate, respectively. The [η^2-(3-diisopropylaminodiphosphirenylium salt)·$W(CO)_5$] complexes **12a-c** can be prepared by reaction of **9** with silver trifluoromethanesulfonate, aluminium or gallium trichloride or, alternatively, by treatment of **6** with two equivalents of trifluoromethanesulfonic acid. Reaction of **12a** with diisopropylamine, water, bis(triphenylphosphoranylidene)-ammonium chloride or tetrabutylammonium fluoride gives the corresponding 1*H*-diphosphirene complexes **6**, **13**, **9**, or **14**, respectively. Compound **12a** also reacts with one or two equivalents of $[W(CO)_5(thf)]$, leading to the di- and trinuclear complexes **15** and **16**, respectively.

Introduction

Three-membered rings, in particular the dinitrogen- and diphosphorus-containing unsaturated heterocycles **A**−**H** (Scheme 1), are not only fascinating species for scientists because of their inherent ring strain, but also valuable starting materials. The chemistry of the 3*H*-diazirines **A**, which are good precursors for transient carbenes, has been extensively explored,[1] whereas only one anti-aromatic 1*H*-diazirine **B** has been spectroscopically characterized.[2] In contrast, for the analogous phosphorus-containing series, one 1*H*-diphosphirene, **F**, has been isolated,[3] while no 3*H*-diphosphirenes **E**, which feature a weak P=P bond,[4] have been characterized.[5] As far as cationic derivatives are concerned,[6] none of the nitrogen-containing systems **C** or **D** has been observed and even the postulated involvement[7] of diazirinium salts, **C**, in the exchange reaction of nucleophiles with halodiazirines has been refuted.[8] The replacement of nitrogen atoms by phosphorus centres decreases the ring strain, and a diphosphirenium salt **H**[9] has been isolated.[10]

Although no complexes featuring 1*H*-diazirines **B** or diazirinium salts **C** and **D** as ligands are known, the coordination chemistry of 3*H*-diazirines **A** constitutes a well-established field in organometallic chemistry.[1c] It is important to note that the cyclic diazirine moiety is retained when bound to group VI metal carbonyls; the diazirine adopts an end-on coordination mode and both mono- and dimetallic complexes have been obtained.

For the diphosphorus-containing series, only two complexes of 1*H*-diphosphirenes **F** have been reported.[11] Here we report experimental and theoretical results concerning the coordination chemistry of heterocycles **F**−**H**. We have evidence for various coordination modes of the 1*H*-diphosphirenes **F** and diphosphirenylium salt **G** to the $W(CO)_5$ fragment.



Scheme 1. Structure of dinitrogen- and diphosphorus-containing heterocycles **A**−**H**

[a] Laboratoire d'Hétérochimie Fondamentale et Appliquée, Université Paul Sabatier,
118, route de Narbonne, F-31062 Toulouse Cédex 04, France
Fax: (internat.) + 33-5/61558204
E-mail: gbertran@ramses.ups-tlse.fr
[b] Laboratoire de Physique Quantique, IRSAMC, UMR 5626-CNRS, Université Paul Sabatier,
118, route de Narbonne, F-31062 Toulouse Cédex, France

 © WILEY-VCH Verlag GmbH, D-69451 Weinheim, 1999 1434−1948/99/0909−1479 $ 17.50+.50/0

Results and Discussion

Synthesis of Free and Coordinated 1*H*-diphosphirenes

We have already[12] shown that the 1*H*-diphosphirene **3** is readily available (52% yield) from the diphosphirenium salt **1**[9] via the *P*-hydrogeno phosphaalkenes **2** (Scheme 2). Single crystals of **2**, suitable for an X-ray diffraction study, were obtained from a pentane solution at −20°C (Figure 1, Table 1). The asymmetric unit contains two independent molecules of **2**. Although Fourier synthesis reveals a disorder for the phosphorus-bonded hydrogen atom positions, it is quite clear that both *cis* and *trans* isomers are present in the solid state. The P1−C1−N3−P2−H fragment is nearly planar (average torsion angle: 10°). The planar geometry around N3 (sum of the angles 359.7°), along with the shortness of the C1−N3 bond [1.368(2) Å], suggests an interaction between the nitrogen lone pair and the π system of the P−C bond. This is corroborated by the value of the central C1−P2 bond length [1.713(2) Å], which is at the upper limit for localized C=P double bonds (1.71 Å)[13] although significantly shorter than in HP=C(NMe$_2$)$_2$ [1.740(1) Å].[14] Finally, probably due to severe steric constraints around C1, the C1−P1 bond is elongated [1.899(2) Å] relative to the expected value for a P−C single bond (1.83−1.84 Å).[15]

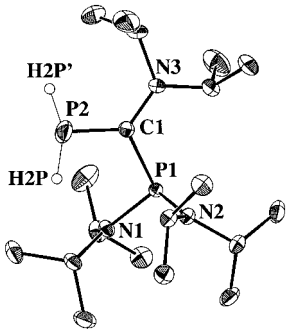


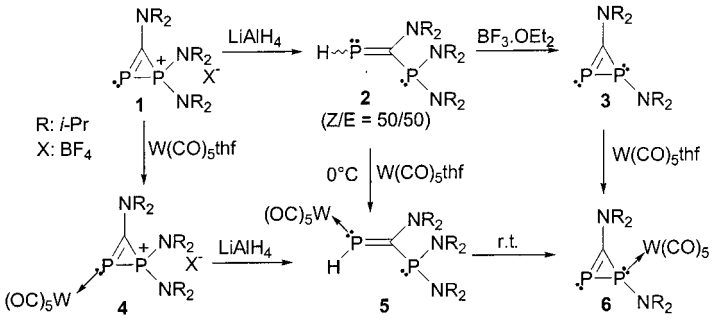
Figure 1. Thermal ellipsoid diagram (30% probability) of **2** showing the atom numbering scheme. Both positions for the disordered hydrogen atom are represented. Selected bond lengths (A) and bond angles (°): P1−C1 1.899(2), P1−N1 1.685(2), P1−N2 1.687(2), C1−N3 1.368(2), C1−P2 1.713(2), P2−H2P 1.226, P2−H2P′ 1.206; P1−C1−N3 114.5(1), P1−C1−P2 118.7(1), N3−C1−P2 126.5(1), C1−P2−H2P 103.2, C1−P2−H2P′ 110.0.

The coordinated 1*H*-diphosphirene **6** can be easily obtained in 65% yield by treatment of **3** with [W(CO)$_5$(thf)]. The end-on coordination of the σ^3-phosphorus centre to the pentacarbonyltungsten fragment was clearly established from the characteristic[16] ^1J(P,W) coupling constant of 295 Hz. Interestingly, **6** can also be prepared directly from phosphaalkenes **2** in 80% yield (Scheme 2). In this case, evidence for the transient formation of the phosphaalkene complex **5** (*E* isomer) has been provided by ^{31}P NMR spectroscopy at 0°C.[12] The metal fragment can even be introduced at the σ^2-phosphorus atom of the diphosphirenium salt **1**. Indeed, treatment of **1** with an excess of [W(CO)$_5$(thf)] in THF at room temperature quantitatively leads to complex **4**. Due to the lability of the P-W bond, this compound was only characterized by ^{31}P NMR spectroscopy [δ = −33.9 (d, *J*(P,P) = 130 Hz, P$^+$), +39.9 (d, *J*(P,P) = 130 Hz, ^1J(P,W) = 249 Hz, σ^{2}P)]. It is noteworthy that the reduction of the coordinated diphosphirenium salt **4** with lithium aluminium hydride affords the coordinated *P*-hydrogeno phosphaalkene **5** (Scheme 2).

Table 1. Crystallographic data for compounds **2** and **8**.

	2	**8**
Chem. formula	$C_{19}H_{43}N_3P_2$	$C_{17}H_{28}ClN_2O_4P_2W$
fw	375.50	611.66
Cryst. syst.	monoclinic	orthorhombic
Space group	$P2_1/c$	$P2_12_12$
a, Å	14.641(1)	13.480(3)
b, Å	21.573(2)	18.390(4)
c, Å	16.302(1)	10.303(2)
β, deg	114.51(1)	90
V, Å^3	4685.0(6)	2554.1(9)
F(000)	1664	1200
Z	8	4
D_{calc}, g cm^{-3}	1.065	1.591
T [K]	198	193
μ (Mo-K_α), mm^{-1}	0.192	4.774
2θ range, deg	5−46	5.4−45.4
no. of data collected	27536	10010
no. of unique data	6502	3296
R(int)	0.0663	0.0704
no. of parameters varied	473	261
Goodness-of-fit	1.034	0.971
*R*1	0.0364	0.0471
*wR*2	0.0969	0.1114
$(\Delta/\rho)_{max}$,	0.191	0.976
$(\Delta/\rho)_{min}$, eÅ^{-3}	−0.360	−1.169

Clearly, the reduction/cyclisation sequence can be achieved with free compounds or in the coordination sphere of the tungsten, and the diphosphirenium salt **1** can thereby be converted into the corresponding 1*H*-diphosphirene complex **6**. Moreover, these new synthetic routes can be used on multi-gram scales allowing for the development of the chemistry of 1*H*-diphosphirenes.

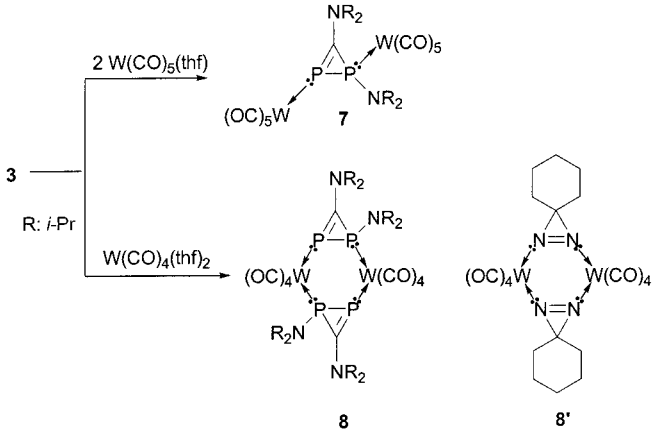


Scheme 2. Synthesis of the mononuclear diphosphirene complex **6**

In **6**, the tungsten is coordinated to the σ^3-phosphorus atom.[17] However, the σ^2-phosphorus atom can also be implicated in the coordination of a transition metal. Indeed, the dinuclear complex **7** is obtained in near quantitative yield when a two-fold excess of [W(CO)$_5$(thf)] is used (Scheme 3). Derivative **7** has been isolated as yellow crystals (mp. 128−129°C) and fully characterized. The coordination of both phosphorus centres is clearly established by ^{31}P NMR spectroscopy {δ = −86.9 [d, *J*(P,P) = 111 Hz, ^1J(P,W) = 296 Hz, P−NR$_2$], −6.3 [d, *J*(P,P) = 111 Hz,

^1J(P,W) = 209 Hz, P=C]}. The IR spectrum features characteristic $\tilde{\nu}_{CO}$ absorption bands at 1934, 1972, 2067 and 2079 cm^{-1}. Among them, the band at 2067 cm^{-1} can be assigned to the $(R_2N)P-W(CO)_5$ fragment by comparison with that observed for the mononuclear complex **6** (2069 cm^{-1}). The absorption at 2079 cm^{-1} can similarly be assigned to the $W(CO)_5$ moiety bonded to the σ^2-phosphorus atom, which suggests a stronger π back donation.[18]

In the nitrogen-containing series, the related 3*H*-diazirines have been used as "structurating" 1,2-bidentate ligands to prepare an original dinuclear double-bridged complex **8′**.[19] This derivative, in which two 3*H*-diazirines coordinate two $W(CO)_4$ fragments, is organised around a *planar* six-membered dimetallacycle. The free 1*H*-diphosphirene **3** was analogously treated with one equivalent of $[W(CO)_4(thf)_2]$.[20] After displacement of the two labile ligands, the dinuclear double-bridged complex **8** was isolated as yellow crystals (M.p. 166−167°C) in 60% yield (Scheme 3). The dimeric structure of **8** was indicated by an A_2B_2 spin system present in the ^{31}P NMR spectrum [δ = −129.4 (P−NR_2), −28.6 (P=C)]. Single crystals of **8**, suitable for an X-ray diffraction study, were grown from a dichloromethane/pentane solution at −20°C. In the solid state (Figure 2), complex **8** is organised around a twofold axis, the six-membered ring adopts an unusual slightly distorted *boat conformation*, and the two three-membered rings occupy equatorial positions. The geometry of the 1*H*-diphosphirene fragment is very similar to that previously observed for the only known free derivative.[3] Interestingly, the boat conformation induces an unusual twist (ca. 42.5°) of the P=C double bond. In most η^1-coordinated complexes the phosphaalkene moiety is nearly planar,[21] whereas twisted P=C bonds have only been reported in sterically congested systems.[22]



Scheme 3. Synthesis of the dinuclear diphosphirene complexes **7** and **8**

Synthesis and Reactivity of Coordinated Diphosphirenylium Salts

Halogenophosphane complexes are very good precursors for coordinated functionalised phosphanes and coordinated

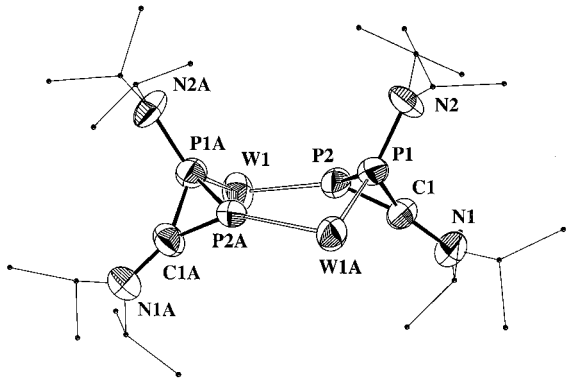
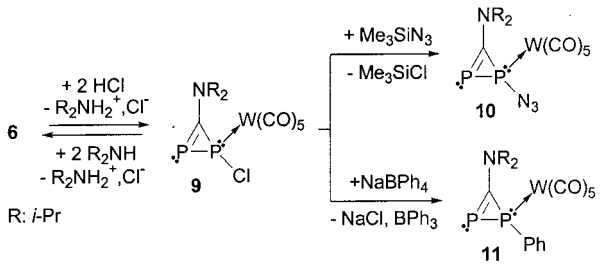


Figure 2. Thermal ellipsoid diagram (30% probability) of **8** showing the atom numbering scheme. All the carbonyl groups have been omitted, and the isopropyl groups have been simplified. Selected bond lengths (Å) and bond angles (°): P1−C1 1.798(15), P1−N2 1.680(11), C1−N1 1.327(18), C1−P2 1.686(15), P1−P2 2.130(5), P2−W1 2.508(3), P1−W1A 2.529(4); P1−C1−N1 138.1(12), P2−C1−N1 146.6(13), P1−C1−P2 75.3(6), C1−P1−P2 49.9(5), C1−P1−N2 113.7(7), P2−P1−N2 113.0(4), C1−P1−W1A 117.4(5), N2−P1−W1A 122.0(5), P2−P1−W1A 120.17(18), C1−P2−P1 54.7(5), C1−P2−W1 150.3(5), P1−P2−W1 143.5(2), P2−W1−P1A 82.6(12).

phosphenium salts, by nucleophilic exchange of the halogen atom and heterolytic cleavage of the P−X bond,[23] respectively. Therefore, *P*-halo-1*H*-diphosphirene complexes seemed to be ideal precursors for coordinated *P*-functionalised-1*H*-diphosphirenes as well as coordinated diphosphirenylium salts. Reaction of **6** with two equivalents of hydrogen chloride[24] in pentane gives the *P*-chloro-1*H*-diphosphirene **9** as a yellow oil in 69% yield (Scheme 4). Although the solubility of **9** in pentane leaves no doubt about the covalent nature of the P−Cl bond, it is interesting to note that the mass spectrum features fragment peaks corresponding to both complexed and uncomplexed diphosphirenylium salts {CI, CH_4, *m/z* = 534 MH^+, 498 $(M - Cl)^+$ and 174 $[M - Cl - W(CO)_5]^+$}.

The chlorine atom of derivative **9** can easily be substituted for an amino substituent, an azido or a phenyl group. Indeed, complex **6** was isolated (85% yield) after treatment of **9** with two equivalents of diisopropylamine in pentane. On addition of a THF solution of azidotrimethylsilane at 45°C, **9** afforded the *P*-azido-1*H*-diphosphirene complex **10** in 40% yield.[25] The replacement of the chlorine atom by an azido group at the λ^3-phosphorus centre was apparent from the mass (CI, $CH_{4,\ m/z}$ = 540), the IR ($\tilde{\nu}_{N3}$ 2130 cm^{-1}) and the ^{31}P NMR spectra [δ = −96.6 (d, J(P,P) = 210 Hz, ^1J(P,W) = 310 Hz, P−N_3), −5.0 (d, J(P,P) = 210 Hz, P=C)]. Finally, treatment of **9** with sodium tetraphenylborate in dichloromethane at room temperature afforded the *P*-phenyl-1*H*-diphosphirene **11** (60% yield) (Scheme 4, Table 2). The formation of **11** probably results from the ionization of the P−Cl bond of **9** leading to a transient diphosphirenylium salt, which abstracts a phenyl group from the tetraphenylborate counterion.[26]

In order to prevent nucleophile transfer, ionization of **9** was carried out in dichloromethane solution at −78°C with either silver trifluoromethanesulfonate,[27] or aluminium or gallium trichloride. The corresponding coordinated diphos-



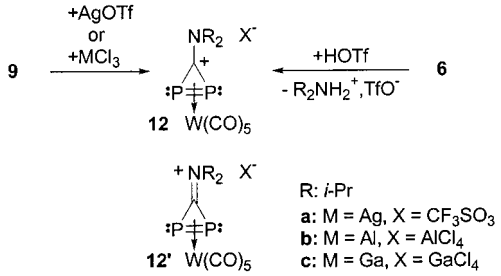
Scheme 4. Synthesis of the *P*-functionalised 1*H*-diphosphirene complexes **9**−**11**

Table 2. Selected spectroscopic data (δ in ppm, *J* in Hz) for the 1*H*-diphosphirene complexes **6**, **9**, **10**, **11**, **13** and **14**.

	6	**9**	**10**	**11**	**13**	**14**
δ(P=C)	+15.0	+34.6	−5.0	−60.0	+33.7	+43.2[a]
δ(σ^4-P)	−123.0	−75.5	−96.6	−177.5	−67.4	−12.1[b]
J(P,P)	164	218	210	148	199	238
^1J(P,W)	295	308	310	257	305	323

[a] *J*(P,F) = 121 Hz. − [b] *J*(P,F) = 1116 Hz.

phirenylium salts **12a**−**c** were isolated as highly air- and moisture-sensitive brown oils in high yields (90−95%). Note that the heterolytic cleavage of the P−N bond of complex **6** with 2 equivalents of trifluoromethanesulfonic acid directly afforded the diphosphirenylium cation **12a** in near quantitative yield (Scheme 5). The structure of derivatives **12a**−**c** and, in particular, the η^2-coordination of the heterocycle (through the P=P bond), has been clearly established by multinuclear NMR and IR spectroscopy, and mass spectrometry.[12] The stability of **12a**−**c** (stable for weeks in solution at room temperature) is almost certainly due to the presence of the metal fragment, but also to the effective π-donation of the nitrogen: **12′** is likely to be the major contributing resonance structure.



Scheme 5. Synthesis of the mononuclear diphosphirenylium salt complexes **12**

Computational Studies

In order to gain more of an insight into the role of the amino substituent and to rationalize the η^2-coordination mode, theoretical calculations were performed on model derivatives **G1**,**2** and **12d**−**g** at the SCF/DZP and B3LYP/DZP levels. The optimized geometric data and atomic charges of derivatives **G1** and **G2** (R = H and NH_2, respectively) are listed in Table 3. Both cations adopt perfectly planar geometries with C_{2v} symmetry. Amino-substitution induces a significant shortening of the P−P bond while the P−C bonds are slightly elongated. The C−N bond length in **G2** is typical for C=N double bonds and comparable with the value found in the tris(dimethylamino)cyclopropenium salt.[28] These data, along with the values of Mulliken and π-charges calculated for **G2**, strongly suggest that the positive charge is shifted outside the ring toward the nitrogen atom. Therefore, the well-established[29] effect of amino substituents on the stability of cyclopropenium salts is also effective for the related diphosphorus-containing species **G**.

It is of further interest to analyse the frontier orbital systems in **G1**,**2**. A detailed listing of the orbitals HOMO-2, HOMO-1, and HOMO is presented in Table 4. It must be noted that as all orbital energies are taken from the results of the energy-optimized RHF calculation of the geometries, orbital energies are meaningful only for the occupied orbitals. In the parent system **G1**, the HOMO and HOMO-1 refer to symmetric and antisymmetric combinations of the two phosphorus lone pairs (a_1 and b_2 orbitals, respectively) while the HOMO-2 corresponds to a π_{PP}-orbital (b_1) which is perpendicular to the ring. The situation is totally different for the amino-substituted cation **G2**. Indeed, the HOMO now refers to the π_{PP}-orbital (b_1) whereas the HOMO-1 and HOMO-2 are almost degenerate and correspond to the a_1 and b_2 orbitals (Figure 3). Thus, the frontier orbital system of **G2** is in agreement with the observed η^2-coordination mode and, in order to complete the theoretical study, the geometry of the isomeric η^1- and η^2-complexes **12d** and **12e** (R = NH_2) were optimized at the B3LYP/DZ(P) level (Figure 4). It is interesting to note that the geometries of the three-membered rings are very similar to those calculated for the free derivative **G2**. The only noticeable difference is the entirely understandable elongation of the P−P bond for the η^1-complex **12d** (**G2** 2.11 Å; **12d** 2.23 Å) and to an even greater extent for the η^2-complex **12e** (2.31 Å). As expected, the η^2-complex **12e** is the more stable isomer, but it is interesting to note that it lies only 16 kJ mol^{-1} below the corresponding η^1-complex **12d**. The influence of the amino group on the coordination mode is shown by the calculations performed for the related complexes **12f,g** featuring the parent cation **G1** as ligand. Indeed, geometry optimization of an η^2-complex of type **12e** results in the η^3-complex **14g**. The tungsten interacts with all the atoms of the three-membered ring of **14g**, as shown by the deviation of the C−H bond from the ring plane (21°) and by the W−P and W−C bond lengths (2.72 and 2.39 Å, respectively, relative to 2.73 and 3.06 Å for **12e**). This η^3-coordination mode results in a reinforced diphosphirenylium salt-metal binding energy (240 kJ mol^{-1} compared to 166 kJ mol^{-1} for **12e**), and thus, the corresponding η^1-complex **12f** is substantially higher in energy (57 kJ mol^{-1}). As far as we are aware, there are no previous examples in which the $W(CO)_5$ fragment is η^3-coordinated.

In the hope of preparing hitherto unknown 3*H*-diphosphirenes **E**, the diphosphirenylium salt complex **12a** was

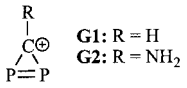


Table 3. Optimized geometry (bond lengths in Å and bond angles in degrees) and atomic charges for derivatives **G1** and **G2**.

	G1 SCF/DZP	**G1** B3LYP/DZP	**G2** SCF/DZP	**G2** B3LYP/DZP
P−P	2.108	2.159	2.059	2.110
P−C	1.706	1.729	1.7051	1.773
C−R	1.075	1.088	1.298	1.312
PCP	76.4	77.3	72.0	73.0
PCR	141.8	141.4	144.0	143.5
q(P)[a]	0.5	0.5	0.38	0.37
q(C)[a]	0	0	0.03	−0.08
q(R)[a]	−	−	0.21	0.34
q(P)[b]	0.38	0.38	0.20	0.2
q(C)[b]	0.24	0.24	0.24	0.15
q(R)[b]	−	−	0.36	0.45

[a] Mulliken charge. − [b] π-charge.

Table 4. Frontier orbital energies (in eV) of cations **G1** and **G2**.

	HOMO-2	HOMO-1	HOMO
G1	−18.4 (b_1)	−17.8 (b_2)	−17.0 (a_1)
G2	−16.7 (b_2)	−16.6 (a_1)	−15.7 (b_1)

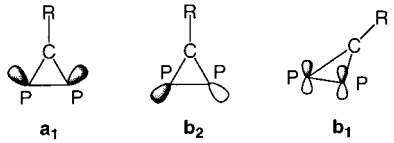


Figure 3. Schematic representation of the molecular orbitals calculated for the model diphosphirenylium salts **G1** and **G2**.

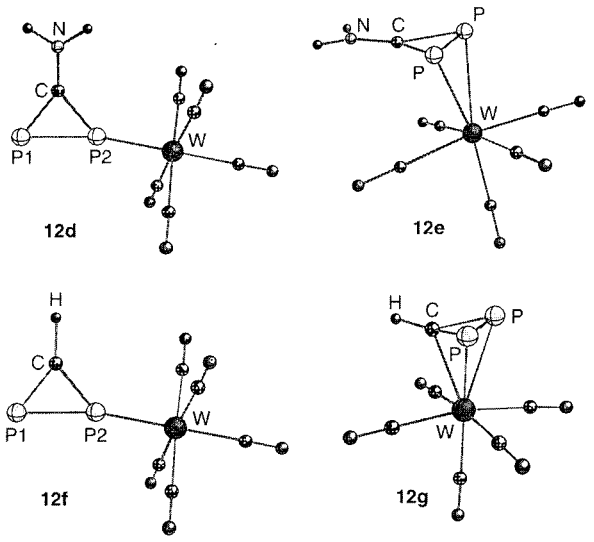
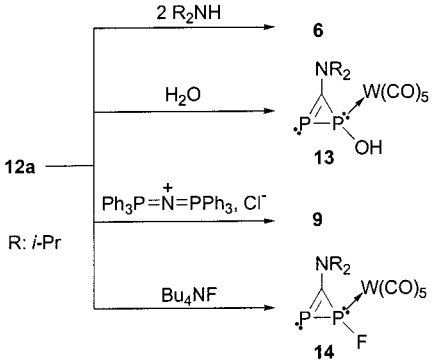


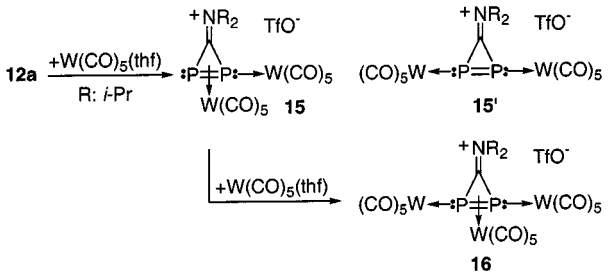
Figure 4. Ball-and-stick views of the calculated structures (at the B3LYP/DZP level) of the η^1-, η^2- and η^3-diphosphirenylium salt complexes **12d−g**. Selected bond lengths (Å): **12d**: N−C 1.33, C−P1 1.78, C−P2 1.77, P2−W 2.40; **12e**: N−C 1.32, C−P1 1.80, P1−P2 2.20, P1−W 2.73; **12f**: H−C 1.09, C−P1 1.73, C−P2 1.75, P2−W 2.37; **12g**: H−C 1.32, C−P 1.79, P−P 2.20, P−W 2.72, C−W 2.39.

then treated with various nucleophiles. However, using diisopropylamine (two equivalents), water, bis(triphenylphosphoranylidene)ammonium chloride (PPNCl) or tetrabutylammonium fluoride, the corresponding 1*H*-diphosphirene complexes **6**, **13**,[30] **9** and **14** were, according to ^{31}P-NMR spectroscopy, formed quantitatively (Scheme 6). In all cases, the presence of the 1*H*-diphosphirene moiety was evidenced by the typical AX spin system observed in the ^{31}P-NMR spectra (Table 2). The presence of the hydroxy or fluoro functionality was deduced from the mass spectrum of **13** (CI, CH_4, m/z = 544), and the ^{31}P and ^{19}F NMR spectra of **14** {^{31}P: δ = −12.1 [dd, J(P,P) = 238 Hz, ^1J(P,W) 323 Hz, J(P,F) = 1116 Hz, P−F], 43.2 [dd, J(P,P) = 238 Hz, J(P,H) = 121 Hz, P=C]; ^{19}F: δ = −14.1 [dd, J(P,F) = 1116 and 121 Hz]}.



Scheme 6. Reaction of the diphosphirenylium salt complex **12a** with various nucleophiles

We then studied the coordination chemistry of the diphosphirenylium salt **12a**, since it can potentially act as a 2-, 4- or 6-electron ligand. The reaction of **12a** with [W(CO)$_5$(thf)] in dichloromethane solution was monitored by ^{31}P NMR spectroscopy. On addition of one equivalent of [W(CO)$_5$(thf)], the sharp singlet corresponding to **12a** (δ = −157.4) disappears to give a broad signal centred at δ = −130. Addition of an excess of [W(CO)$_5$(thf)] subsequently converts the broad signal into a sharp singlet at δ = −74.1.



Scheme 7. Synthesis of the di- and trinuclear diphosphirenylium salt complexes **15** and **16**

This chemical shift, in the range expected for a three-membered phosphorus heterocycle,[32] and the presence of three different *J*(P,W) coupling constants (176, 61 and 45 Hz)[33] strongly support the trinuclear structure **16** (Scheme 7). In addition, the ^{13}C NMR spectrum of **16** reveals the presence of two types of $W(CO)_5$ fragment {δ = 193.6 [t, *J*(P,C) < 1 Hz, ^1J(C,W) = 127 Hz, CO_e], 194.5 (s, CO_a) and 213.6 (s, CO_e), 214.7 (s, CO_a)}. By comparison with those observed for **12a** {δ = 189.3 [t, *J*(P,C) = 4 Hz, ^1J(C,W) = 122 Hz, CO_e], 194.4 [t, *J*(P,C) < 1 Hz, CO_a]}, the signals at δ = 193.6 and 194.5 can be assigned to the η^2-$PW(CO)_5$ moiety while the deshielding of the other two signals (Δδ ≈ 20 ppm) can be classically[34] attributed to the η^1-coordination mode of the corresponding $W(CO)_5$ fragments. Taking into account the trinuclear structure of **16**, the intermediate broad signal detected by ^{31}P NMR spectroscopy is probably due to the dinuclear tungsten complex, for which an equilibrium between the structures **15** and **15′** is likely to occur. Indeed, calculations have clearly shown a small energy difference between η^1- and η^2-coordination modes for the model compounds **12d** and **12e** (see above). The formation of the mono-, di- and trinuclear diphosphirenylium complexes **12**, **15** and **16**, respectively, shows that the coordination chemistry of diphosphirenylium salts **G** shows some resemblance to that of diphosphenes RP=PR.[35]

Conclusion

We have shown that the 1*H*-diphosphirene **3**, which is easily available from the corresponding diphosphirenium salt **1**, can act as a 2- or 4-electron ligand to afford mono- and dinuclear tungsten complexes. Furthermore, not only can this ligand be modified in the coordination sphere of tungsten, but several coordinated diphosphirenylium salts have been prepared and isolated.[36]

These results as a whole clearly demonstrate that diphosphirenylium salts **G** merit further study, and that the synthesis of a noncomplexed derivative remains an exciting challenge. Moreover, the reactivity of these cations has up to now been governed by the electrophilicity of the phosphorus centres, and it would be particularly interesting to attempt to force the system to react at the carbon atom, which should lead to the hitherto unknown 3*H*-diphosphirenes **E**.

Experimental Section

All manipulations were performed under argon with standard Schlenk techniques. Dry, oxygen-free solvents were employed. ^1H, ^{13}C, and ^{31}P NMR spectra were recorded on Bruker AC80, AC200, WM250 or AMX400 spectrometers. Chemical shifts are reported in ppm relative to Me_4Si as external standard (^1H and ^{13}C) or with a positive sign, in ppm, relative to external 85% H_3PO_4 (^{31}P). Infrared spectra were recorded on a Perkin−Elmer FT-IR Spectrometer 1725 X. Mass spectra were obtained on a Ribermag R10 10E instrument.

***C*-Diisopropylamino-*C*-[bis(diisopropylamino)phosphino]phosphaalkenes (2)**: To a THF solution (5 mL) of the diphosphirenium salt **1** (0.46 g, 1 mmol) was added, at −78°C, 1 equiv. of $LiAlH_4$ (38 mg, 1 mmol). The solution was warmed to room temp., the solvent removed in vacuo, and the residue extracted with pentane (15 mL). After filtration and evaporation of pentane, compound **2** (as a 50:50 mixture of *Z* and *E* isomers) was obtained as a yellow powder (0.30 g, 80%). − M.p. 25−30°C. − ^1H NMR (C_6D_6): δ = 1.20−1.35 (m, 72 H, CH_3), 3.7−4.0 (m, 12 H, CHN), 4.66 (dd, ^1J(P,H) = 174 Hz, ^3J(P,H) = 1.0 Hz, 1 H, P−H, isomer 1), 4.96 (dd, ^1J(P,H) = 138 Hz, ^3J(P,H) = 7.4 Hz, 1 H, P−H, isomer 2). − $^{13}C\{^1H\}$ NMR (C_6D_6): δ = 205.1 (dd, ^1J(P,C) = 97.6 and 40.1 Hz, PCP), 212.3 (dd, ^1J(P,C) = 65.4 and 58.8 Hz, PCP). − ^{31}P NMR (C_6D_6): δ = 23.8 (dd, ^2J(P,P) = 40 Hz, ^1J(P,H) = 138 Hz, P−H, isomer 1), 34.3 (d, ^1J(P,H) = 174 Hz, P−H, isomer 2), 53.7 (d, ^2J(P,P) = 40 Hz, P−N*i*Pr_2, isomer 1), 55.9 (s, P−N*i*Pr_2, isomer 2). − $C_{19}H_{43}N_3P_2$ (375.3): calcd. C 60.77, H 11.54, N 11.19; found C 60.52, H 11.38, N 11.00.

1,3-Bis(diisopropylamino)-1*H*-diphosphirene (3): To a THF solution (5 mL) of phosphinophosphaalkenes **2** (0.37 g, 1 mmol) was added, at −78°C, a catalytic amount of $BF_3{\cdot}Et_2O$ (14 mg, 0.1 mmol). The solution was warmed to room temp., and stirred for 1 h (the reaction being monitored by ^{31}P NMR spectroscopy). The solvent was then removed in vacuo and the residue extracted with pentane (15 mL). After filtration and evaporation of pentane, compound **3** was obtained as a yellow oil (0.17 g; 62%). − ^1H NMR (C_6D_6): δ 0.95 (d, ^3J(H,H) = 6.6 Hz, 6 H, CH_3), 1.13 (d, ^3J(H,H) = 6.7 Hz, 6 H, CH_3), 1.15 (d, ^3J(H,H) = 6.6 Hz, 6 H, CH_3), 1.32 (d, ^3J(H,H) = 6.7 Hz, 6 H, CH_3), 3.60 (sept, ^3J(H,H) = 6.7 Hz, 2 H, CHN), 4.19 (sept d, ^3J(H,H) = 6.6 Hz, ^3J(P,H) = 1.8 Hz, 2 H, CHN). − $^{13}C\{^1H\}$ NMR (C_6D_6): δ = 19.1 (d, *J*(P,C) = 4.9 Hz, CH_3), 20.1 (d, *J*(P,C) = 2.7 Hz, CH_3), 21.6 (d, *J*(P,C) = 2.1 Hz, CH_3), 21.8 (s, CH_3), 24.2 (d, *J*(P,C) = 12.2 Hz, CH_3), 24.5 (d, *J*(P,C) = 5.2 Hz, CH_3), 43.4 (d, *J*(P,C) = 5.6 Hz, CHN), 51.3 (s, CHN), 58.4 (t_{like}, *J*(P,C) = 4.2 Hz, CHN), 191.2 (dd, *J*(P,C) = 82.2 and 77.9 Hz, PCP). − $^{31}P\{^1H\}$ NMR (C_6D_6): δ = −121.7 (d, *J*(P,P) = 121 Hz, P−N*i*Pr_2), −23.7 (*J*(P,P) = 121 Hz, σ^2-P). − MS (NH_3, CI); *m*/*z*: 275 (MH^+). − $C_{13}H_{28}N_2P_2$ (274.2): calcd C 56.92, H 10.29, N 10.21; found C 57.04, H 10.43, N 9.87.

[1,1,3-Tris(diisopropylamino)diphosphirenium Salt][$W(CO)_5$] (4): To a THF solution (30 mL) of the diphosphirenium salt **1** (0.46 g, 1 mmol) was added, at −78°C, an excess of [$W(CO)_5$(thf)] (10 mL, 0.3 M solution in THF, 3 mmol). The solution was warmed to room temp. and stirred for 1 h at room temp. Complex **4** was characterized in solution without further purification. − ^{31}P NMR (THF): δ = −33.9 (d quint, *J*(P,P) = 130 Hz, ^3J(P,H) = 20 Hz, P−N*i*Pr_2), 39.9 (d, *J*(P,P) = 130 Hz, ^1J(P,W) = 249 Hz, P=C).

{*C*-Diisopropylamino-*C*-[bis(diisopropylamino)phosphino]phosphaalkene}[$W(CO)_5$] (5): To a THF solution (5 mL) of phosphinophosphaalkenes **2** (0.37 g, 1 mmol) was added, at −78°C, 1 equiv. of [$W(CO)_5$(thf)] (5 mL, 0.2 M solution in THF, 1 mmol). The solu-

tion was warmed to 0°C, the solvent removed in vacuo, the residue redissolved in deuterated toluene and complex **5** characterized in solution at 0°C. – ^{1}H NMR (C_7D_8): δ = 1.10–1.60 (m, 36 H, CH_3), 3.30–4.20 (m, 6 H, CHN), 4.95 (d, 1 H, ^1J(P,H) = 267 Hz, P–H); ^{13}C{^{1}H} NMR (C_7D_8): δ = 20.0–25.0 (m, CH_3), 50.2 (s, CHN), 55.7 (d, J(P,C) = 45.9 Hz, CHN), 58.7 (d, J(P,C) = 29.7 Hz, CHN), 199.9 (s, ^1J(C,W) = 126.1 Hz, CO_e), 203.3 (d, ^2J(P,C) = 7.7 Hz, CO_a), 233.3 (dd, ^1J(P,C) = 72.3 and 50.3 Hz, PCP). – ^{31}P NMR (C_7D_8): δ = –71.0 (d, ^1J(P,H) = 267 Hz, ^1J(P,W) = 129 Hz, P–H), 66.5 (s, P–N*i*Pr$_2$). – Complex **5** was also obtained by adding an excess of lithium aluminium hydride to a THF solution of the diphosphirenium salt complex **4** at –78°C.

[1,3-Bis(diisopropylamino)-1*H*-diphosphirene][W(CO)$_5$] (6): To a THF solution (5 mL) of 1*H*-diphosphirene **3** (0.27 g, 1 mmol) was added, at –78°C, 1 equiv. of [W(CO)$_5$(thf)] (5 mL, 0.2 M solution in THF, 1 mmol). The solution was warmed to room temp., the solvent removed in vacuo and the residue extracted with pentane (15 mL). After filtration and evaporation of pentane, complex **6** was obtained as a yellow oil (0.39 g; 65%). – ^{1}H NMR (C_6D_6): δ = 1.18 (d, ^3J(H,H) = 6.9 Hz, 6 H, CH_3), 1.25 (d, ^3J(H,H) = 6.9 Hz, 6 H, CH_3), 1.29 (d, ^3J(H,H) = 6.7 Hz, 3 H, CH_3), 1.37 (d, ^3J(H,H) = 6.6 Hz, 3 H, CH_3), 1.39 (d, ^3J(H,H) = 6.6 Hz, 3 H, CH_3), 1.51 (d, ^3J(H,H) = 6.7 Hz, 3 H, CH_3), 3.63 (sept d, ^3J(H,H) = 6.9 Hz, ^3J(P,H) = 13.8 Hz, 2 H, CHNP), 3.97 (sept, ^3J(H,H) = 6.6 Hz, 1 H, CHN), 4.51 (sept, ^3J(H,H) = 6.7 Hz, 1 H, CHN). – ^{13}C{^{1}H} NMR (C_6D_6): δ = 18.3 (d, J(P,C) = 5.6 Hz, CH_3), 19.0 (d, J(P,C) = 3.5 Hz, CH_3), 20.7 (s, CH_3), 23.8 (s, CH_3), 48.8 (s, CHN), 49.2 (d, J(P,C) = 7.7 Hz, CHNP), 62.4 (dd, J(P,C) = 5.8 and 3.8 Hz, CHN), 195.9 (dd, J(P,C) = 80.6 and 48.4 Hz, PCP), 197.6 (d, ^2J(P,C) = 8.7 Hz, ^1J(C,W) = 126.9 Hz, CO_e), 200.2 (d, ^2J(P,C) = 33.1 Hz, ^1J(C,W) = 149.9 Hz, CO_a). – ^{31}P{^{1}H} NMR (C_6D_6): δ = –123.0 (d, J(P,P) = 164 Hz, ^1J(P,W) = 295 Hz, P–N*i*Pr$_2$), 15.0 (J(P,P) = 164 Hz, σ^2-P). – IR (THF): $\tilde{\nu}$ = 1930 (vs), 1938 (vs) and 2069 (s) cm^{-1} (CO). – $C_{18}H_{28}N_2O_5P_2W$ (598.1): calcd C 36.14, H 4.72, N 4.68; found C 36.35, H 4.53, N 4.62.

[1,3-Bis(diisopropylamino)-1*H*-diphosphirene][W(CO)$_5$]$_2$ (7): To a THF solution (5 mL) of 1*H*-diphosphirene **3** (0.27 g, 1 mmol) was added, at –78°C, 2 equiv. of [W(CO)$_5$(thf)] (5 mL, 0.4 M solution in THF, 2 mmol). The solution was warmed to room temp., the solvent removed in vacuo and the residue extracted with pentane (15 mL). After filtration, complex **7** crystallized from the pentane solution as a yellow, microcrystalline powder (0.85 g; 92%). – M.p. 128–129°C (dec). – ^{1}H NMR (C_6D_6): δ = 0.86 (d, ^3J(H,H) = 6.7 Hz, 3 H, CH_3), 1.08 (d, ^3J(H,H) = 6.7 Hz, 3 H, CH_3), 1.10 (d, ^3J(H,H) = 6.9 Hz, 6 H, CH_3), 1.19 (d, ^3J(H,H) = 6.9 Hz, 6 H, CH_3), 1.21 (d, ^3J(H,H) = 6.8 Hz, 3 H, CH_3), 1.32 (d, ^3J(H,H) = 6.8 Hz, 3 H, CH_3), 3.39 (sept, ^3J(H,H) = 6.8 Hz, 1 H, CHN), 3.66 (sept d, ^3J(H,H) = 6.9 Hz, ^3J(P,H) = 15.5 Hz, 2 H, CHNP), 4.27 (sept, ^3J(H,H) = 6.7 Hz, 1 H, CHN). – ^{13}C{^{1}H} NMR (C_6D_6): δ 20.0 (d, J(P,C) = 3.2 Hz, CH_3), 20.3 (d, J(P,C) = 2.1 Hz, CH_3), 20.4 (d, J(P,C) = 2.5 Hz, CH_3), 20.9 (d, J(P,C) = 2.1 Hz, CH_3), 24.4 (s, CH_3), 24.6 (d, J(P,C) = 3.1 Hz, CH_3), 49.7 (d, J(P,C) = 1.7 Hz, CHN), 50.4 (d, J(P,C) = 9.0 Hz, CHN), 61.5 (d, J(P,C) = 8.0 Hz, CHN), 188.3 (dd, J(P,C) = 46.4 and 37.5 Hz, PCP), 195.7 (d, ^2J(P,C) = 6.2 Hz, ^1J(C,W) = 126.4 Hz, CO_e), 197.6 (dd, J(P,C) = 7.8 and 1.7 Hz, ^1J(C,W) = 127.0 Hz, CO_e), 199.4 (d, ^2J(P,C) = 34.9 Hz, CO_a), 199.7 (d, ^2J(P,C) = 35.2 Hz, CO_a). – ^{31}P{^{1}H} NMR (C_6D_6): δ = –86.9 (d, J(P,P) = 111 Hz, ^1J(P,W) = 296 Hz, P–N*i*Pr$_2$), –6.3 (J(P,P) = 111 Hz, ^1J(P,W) = 209 Hz, P=C). – IR (THF): $\tilde{\nu}$ = 1934 (vs), 1972 (vs), 2067 (s) and 2079 (s) cm^{-1} (CO). – $C_{23}H_{28}N_2O_{10}P_2W_2$ (922.0): calcd C 29.96, H 3.06, N 3.04; found C 30.12, H 2.88, N 2.92.

{[1,3-Bis(diisopropylamino)-1*H*-diphosphirene][W(CO)$_4$]}$_2$ (8): To a THF solution (5 mL) of 1*H*-diphosphirene **3** (0.27 g, 1 mmol) was added, at –78°C, 1 equiv. of [W(CO)$_4$(thf)$_2$] (2.5 mL, 0.4 M solution in THF, 1 mmol). The solution was warmed to room temp., the solvent removed in vacuo and the residue extracted with pentane (15 mL). After filtration, complex **8** crystallized from a pentane/dichloromethane solution at –20°C as yellow crystals (0.26 g; 60%). – M.p. 166–167°C (dec). – ^{1}H NMR (C_6D_6): δ = 1.24 (d, ^3J(H,H) = 6.7 Hz, 6 H, CH_3), 1.33 (d, ^3J(H,H) = 6.7 Hz, 6 H, CH_3), 1.35 (d, ^3J(H,H) = 6.7 Hz, 12 H, CH_3), 1.37 (d, ^3J(H,H) = 6.7 Hz, 12 H, CH_3), 1.39 (d, ^3J(H,H) = 6.7 Hz, 6 H, CH_3), 1.45 (d, ^3J(H,H) = 6.7 Hz, 6 H, CH_3), 3.40 (m, 2 H, CHN), 3.86 (m, 2 H, CHN), 4.04 (sept, ^3J(H,H) = 6.7 Hz, 2 H, CHN), 4.42 (sept, ^3J(H,H) = 6.7 Hz, 2 H, CHN). – ^{13}C{^{1}H} NMR (C_6D_6): δ = 19.3 (s, CH_3), 19.7 (s, CH_3), 20.6 (s, CH_3), 20.8 (s, CH_3), 23.8 (s, CH_3), 24.4 (s, CH_3), 47.8 (s, CHN), 50.1 (s, CHN), 61.7 (d, J(P,C) = 5.7 Hz, CHN), 194.3 (dd, J(P,C) = 52.6 and 37.7 Hz, PCP), 198.2 (s, ^1J(C,W) 129.3 Hz, CO_a), 201.0 (d, ^2J(P,C) = 6.7 Hz, ^1J(C,W) = 130.6 Hz, CO_a), 204.2 (d, ^2J(P,C) = 35.6 Hz, ^1J(C,W) = 158.2 Hz, CO_e), 207.3 (dd, J(P,C) = 37.3 and 6.5 Hz, CO_e). – ^{31}P{^{1}H} NMR (C_6D_6): A_2B_2 system δ –129.4 (P–N*i*Pr$_2$), –28.6 (P=C). – $C_{34}H_{56}N_4O_8P_4W_2$ (1140.2): calcd C 35.81, H 4.95, N 4.91; found C 36.05, H 4.80, N 4.82.

[1-Chloro-3-diisopropylamino-1*H*-diphosphirene][W(CO)$_5$] (9): To an ether solution (6 mL) of complex **6** (0.12 g, 0.2 mmol) was added, at –78°C, 400 μL of a 1 M Et_2O solution of HCl (2 equiv). The solution was warmed to room temp., the solvent removed in vacuo and the residue extracted with pentane (20 mL). After filtration and evaporation of pentane, complex **9** was obtained as a yellow oil (0.07 g; 69%). – ^{1}H NMR (C_6D_6): δ 0.86 (d, ^3J(H,H) = 6.7 Hz, 3 H, CH_3), 1.03 (d, ^3J(H,H) = 6.7 Hz, 3 H, CH_3), 1.04 (d, ^3J(H,H) = 6.7 Hz, 3 H, CH_3), 1.12 (d, ^3J(H,H) = 6.7 Hz, 3 H, CH_3), 3.27 (sept, ^3J(H,H) = 6.7 Hz, 1 H, CHN), 4.71 (sept, ^3J(H,H) = 6.7 Hz, 1 H, CHN). – ^{13}C{^{1}H} NMR (C_6D_6): δ = 19.3 (d, J(P,C) = 4.2 Hz, CH_3), 19.5 (d, J(P,C) = 4.6 Hz, CH_3), 20.4 (s, CH_3), 20.5 (s, CH_3), 50.2 (d, J(P,C) = 3.3 Hz, CHN), 63.4 (dd, J(P,C) = 7.3 and 4.8 Hz, CHN), 189.0 (dd, J(P,C) = 88.6 and 34.7 Hz, PCP), 196.7 (d, ^2J(P,C) = 8.6 Hz, ^1J(C,W) = 127.1 Hz, CO_e), 199.5 (d, ^2J(P,C) = 46.8 Hz, CO_a). – ^{31}P{^{1}H} NMR (C_6D_6): δ = –78.5 (d, J(P,P) = 218 Hz, ^1J(P,W) = 308 Hz, P–Cl), 34.6 (d, J(P,P) = 218 Hz, σ^2-P). – IR (pentane): $\tilde{\nu}$ = 1949 (vs), 1959 (vs) and 2079 (s) cm^{-1} (CO). – MS (CH_4, CI); *m*/*z*: 534 (MH^+), 498 [(M–Cl)$^+$], 442 [(M–Cl-*i*Pr)$^+$], 174 {[M–Cl-W(CO)$_5$]$^+$}. – $C_{12}H_{14}ClNO_5P_2W$ (532.9): calcd C 27.02, H 2.65, N 2.63; found C 26.75, H 2.50, N 2.42.

Reaction of complex 9 with *i*Pr$_2$NH: To a THF solution (5 mL) of complex **9** (0.36 g, 0.7 mmol) was added, at room temp., 2 equiv. of diisopropylamine (0.14 g, 1.4 mmol). The solution was warmed to room temp., the solvent removed in vacuo and the residue extracted with pentane (15 mL). After filtration and evaporation of pentane, complex **6** was obtained as a yellow oil (0.40 g; 95%).

[1-Azido-3-diisopropylamino-1*H*-diphosphirene][W(CO)$_5$] (10): To a THF solution (5 mL) of complex **9** (0.36 g, 0.7 mmol) was added, at room temp., 1 equiv. of Me_3SiN_3 (0.08 g, 0.7 mmol). The solution was warmed to 45°C and stirred for 1 h (the reaction was monitored by ^{31}P NMR spectroscopy). The solvent was then removed in vacuo and the residue extracted with pentane (20 mL). After filtration and evaporation of pentane, complex **10** was obtained as a brown oil (0.15 g; 40%). – ^{1}H NMR (C_6D_6): δ = 0.86 (d, ^3J(H,H) = 6.8 Hz, 3 H, CH_3), 1.02 (d, ^3J(H,H) = 6.8 Hz, 3 H, CH_3), 1.06 (d, ^3J(H,H) = 6.8 Hz, 3 H, CH_3), 1.12 (d, ^3J(H,H) = 6.8 Hz, 3 H, CH_3), 3.30 (sept, ^3J(H,H) = 6.8 Hz, 1 H, CHN), 4.71

(sept, ^3J(H,H) = 6.8 Hz, 1 H, CHN). − $^{13}C\{^1H\}$ NMR (C_6D_6): δ = 19.1 (d, J(P,C) = 4.5 Hz, CH_3), 19.5 (d, J(P,C) = 4.2 Hz, CH_3), 20.4 (s, CH_3), 20.7 (s, CH_3), 51.3 (d, J(P,C) = 3.3 Hz, CHN), 62.5 (dd, J(P,C) = 36.4 and 4.3 Hz, CHN), 196.4 (d, ^2J(P,C) = 8.8 Hz, ^1J(C,W) = 109.3 Hz, CO_e), 199.0 (d, ^2J(P,C) = 41.9 Hz, CO_a), PCP was not observed. − $^{31}P\{^1H\}$ NMR (C_6D_6): δ = −96.6 (d, J(P,P) = 210 Hz, ^1J(P,W) = 310 Hz, P−N_3), −5.0 (d, J(P,P) = 210 Hz, σ²-P). − IR (THF): $\tilde{\nu}$ = 2130 (vs) cm^{-1} (NN). − MS (CH_4, CI) *m/z*; 540 (MH^+), 498 [(M-N_3)$^+$]. − $C_{12}H_{14}N_4O_5P_2W$ (540.0): calcd C 26.69, H 2.61, N 10.37; found C 26.83, H 2.74, N 10.23.

[1-Phenyl-3-diisopropylamino-1*H*-diphosphirene][W(CO)$_5$] (11): To a CH_2Cl_2 solution (2 mL) of complex **9** (0.07 g, 0.14 mmol) was added, at −78°C, a CH_2Cl_2 solution (2 mL) of 1 equiv. of $NaBPh_4$ (0.05 g, 0.14 mmol). The solution was warmed to room temp., the solvent removed in vacuo and the residue extracted with pentane (15 mL). After filtration and evaporation of pentane, complex **11** was obtained as a yellow oil (0.05 g; 60%). − ^1H NMR (C_6D_6): δ 0.82 (d, ^3J(H,H) = 6.7 Hz, 3 H, CH_3), 1.30 (d, ^3J(H,H) = 6.7 Hz, 3 H, CH_3), 1.38 (d, ^3J(H,H) = 6.7 Hz, 3 H, CH_3), 1.47 (d, ^3J(H,H) = 6.7 Hz, 3 H, CH_3), 3.88 (sept d, ^3J(H,H) = 6.7 Hz, J(P,H) = 2.1 Hz, 1 H, CHN), 4.28 (sept, ^3J(H,H) = 6.7 Hz, 1 H, CHN), 6.9−7.1 (m, 3 H, $H_{m,p}$), 7.65 (ddd, ^3J(H,H) = 8.0 Hz, ^4J(H,H) = 1.5 Hz, J(P,H) = 13.2 Hz, 2 H, H_o). − $^{13}C\{^1H\}$ NMR (C_6D_6): δ = 19.0 (d, J(P,C) = 3.2 Hz, CH_3), 19.2 (d, J(P,C) = 4.0 Hz, CH_3), 20.2 (s, CH_3), 20.3 (s, CH_3), 49.4 (d, J(P,C) = 3.2 Hz, CHN), 63.2 (dd, J(P,C) = 7.3 and 4.3 Hz, CHN), 129.0 (d, J(P,C) = 10.2 Hz, C_{arom}), 130.5 (d, J(P,C) = 2.0 Hz, C_{arom}), 132.5 (d, J(P,C) = 15.8 Hz, C_{arom}), 197.7 (d, ^2J(P,C) = 8.0 Hz, ^1J(C,W) = 126.3 Hz, CO_e), 199.1 (d, ^2J(P,C) = 30.4 Hz, CO_a), C_i and PCP were not observed. − $^{31}P\{^1H\}$ NMR (C_6D_6): δ = −177.5 (d, J(P,P) = 148 Hz, ^1J(P,W) = 257 Hz, P−Ph), −60.0 (d, J(P,P) = 148 Hz, σ²-P). − IR (THF): $\tilde{\nu}$ = 1935 (vs), 1943 (vs) et 2071 (s) cm^{-1} (CO). − MS (NH_3, CI) *m/z*; 576 (MH^+), 498 [(M−Ph)$^+$].

[η^2-(3-Diisopropylaminodiphosphirenylium Salt)][W(CO)$_5$] (12): To a CH_2Cl_2 solution (3 mL) of complex **9** (0.15 g, 0.28 mmol) was added, at −78°C, 1 equiv. of $AgCF_3SO_3$ (0.07 g, 0.28 mmol). The solution was warmed to room temp., and silver salts were removed by filtration. Evaporation of CH_2Cl_2 gave the complex **12a** as a yellow oil (0.16 g; 90%). − ^1H NMR ($CDCl_3$): δ = 1.39 (d, ^3J(H,H) = 6.7 Hz, 6 H, CH_3), 1.44 (d, ^3J(H,H) = 6.7 Hz, 6 H, CH_3), 4.34 (sept, ^3J(H,H) = 6.7 Hz, 2 H, CHN). − $^{13}C\{^1H\}$ NMR ($CDCl_3$): δ 20.2 (s, CH_3), 20.9 (s, CH_3), 63.2 (s, CHN), 119.7 (q, ^1J(C,F) = 319 Hz, CF_3), 189.3 (t, ^2J(P,C) = 4.3 Hz, ^1J(C,W) = 121.5 Hz, CO_e), 194.4 (t, ^2J(P,C) < 1 Hz, CO_a), 205.1 (t, ^1J(P,C) = 90.9 Hz, PCP). − $^{31}P\{^1H\}$ NMR ($CDCl_3$): δ = −157.4. − IR (CH_2Cl_2): $\tilde{\nu}$ = 1950 (vs) and 2055 (s) cm^{-1} (CO). − MS (CH_4, CI) *m/z*; 498 (M^+), 470 [(M−CO)$^+$], 442 {[M-2(CO)]$^+$}. − The same salt **12a** was obtained in near quantitative yield (95%) by adding, at −78°C, 2 equivalents of CF_3SO_3H to a CH_2Cl_2 solution of complex **6**. Starting from complex **9** and using $AlCl_3$ or $GaCl_3$ as Lewis acids, complexes **12b** and **12c** could also be obtained in 90% yield. − $C_{12}H_{14}Cl_4GaNO_5P_2W$ (707.6): calcd C 20.31, H 1.99, N 1.97; found C 19.60, H 2.39, N 2.10.

Reactivity of Complex 12a:

− *i*Pr_2NH: To a CH_2Cl_2 solution (4 mL) of complex **14a** (0.14 g, 0.22 mmol) was added, at −78°C, 2 equiv. of *i*Pr_2NH (0.04 g, 0.44 mmol). The solution was warmed to room temp., the solvent removed in vacuo and the residue extracted with pentane (15 mL). After filtration and evaporation of pentane, complex **6** was obtained as a yellow oil (0.12 g; 95%).

− H_2O: A CH_2Cl_2 solution (4 mL) of complex **12a** (0.08 g, 0.13 mmol) was stirred in contact with air for 1 h. Compound **13** (obtained in quantitative yield according to ^{31}P NMR spectroscopy) was analyzed without further purification. − $^{31}P\{^1H\}$ NMR (C_6D_6): δ = −67.4 (d, J(P,P) = 199 Hz, ^1J(P,W) = 305 Hz, P−OH), 33.7 (d, J(P,P) = 199 Hz, σ²-P). − MS (CH_4, CI); *m/z*: 544 (M+29), 516 (M+1), 498 [(M−OH)$^+$].

− $Ph_3P{=}N{=}PPh_3^+,Cl^-$: To a CH_2Cl_2 solution (4 mL) of complex **12a** (0.14 g, 0.22 mmol) was added, at −78°C, 1 equiv. of $Ph_3P{=}N{=}PPh_3^+.Cl^-$ (0.13 g, 0.22 mmol). The solution was warmed to room temp., the solvent removed in vacuo and the residue extracted with pentane (15 mL). After filtration and evaporation of pentane, complex **9** was obtained as a yellow oil (0.11 g; 94%).

− Bu_4NF: To a CH_2Cl_2 solution (4 mL) of complex **12a** (0.14 g, 0.22 mmol) was added, at −78°C, 1 equiv. of Bu_4NF (0.06 g, 0.22 mmol). The solution was warmed to room temp. and compound **14** (obtained in quantitative yield according to ^{31}P NMR spectroscopy) was analyzed without further purification. − ^{19}F NMR (C_6D_6): δ = −14.1 (dd, ^1J(P,F) = 1116 Hz, ^2J(P,F) = 121 Hz) − $^{31}P\{^1H\}$ NMR (CH_2Cl_2): δ = −12.1 (dd, J(P,P) = 238 Hz, ^1J(P,F) = 1116 Hz, ^1J(P,W) = 323 Hz, P−F), 43.2 (dd, J(P,P) = 238 Hz, ^2J(P,F) = 121 Hz, σ²-P).

[η^2-(3-Diisopropylaminodiphosphirenylium Salt)][W(CO)$_5$]$_2$ (15): To a $C_2H_4Cl_2$ solution (4 mL) of complex **12a** (0.19 g, 0.3 mmol) was added, at −78°C, 1 equiv. of [W(CO)$_5$(thf)] (3 mL, 0.1 M solution in THF, 0.3 mmol). The solution was warmed to room temp., stirred for 1 h, and compound **15** was analyzed without further purification. − $^{31}P\{^1H\}$ NMR ($C_2H_4Cl_2$): δ = −130 (broad).

[η^2-(3-Diisopropylaminodiphosphirenylium Salt)][W(CO)$_5$]$_3$ (16): To a CD_2Cl_2 solution (4 mL) of complex **12a** (0.19 g, 0.3 mmol) was added, at −78°C, 2 equiv. of [W(CO)$_5$(thf)] (6 mL, 0.1 M solution in THF, 0.6 mmol). The solution was warmed to room temp., stirred for 1 h, the solvent removed in vacuo, and the compound **16** (obtained in quantitative yield according to ^{31}P NMR spectroscopy) was analyzed without any further purification. − ^1H NMR (CD_2Cl_2): δ = 1.60 (d, ^3J(H,H) = 6.8 Hz, 6 H, CH_3), 1.63 (d, ^3J(H,H) = 6.8 Hz, 6 H, CH_3), 4.48 (sept, ^3J(H,H) = 6.8 Hz, 2 H, CHN). − $^{13}C\{^1H\}$ NMR (CD_2Cl_2): δ = 20.1 (s, CH_3), 21.3 (s, CH_3), 59.3 (s, CHN), 118.5 (q, ^1J(C,F) = 318 Hz, CF_3), 193.6 (t, J(P,C) < 1 Hz, ^1J(C,W) = 127.1 Hz, CO_e), 194.5 (s, CO_a), 213.6 (s, CO_a), 214.7 (s, CO_e), PCP was not observed. − $^{31}P\{^1H\}$ NMR (CD_2Cl_2): δ = −74.1 (J(P,W) = 176, 61 and 45 Hz).

X-Ray Crystal Structure Determination of 2 and 8: Crystal data for all structures are presented in Table 1. Data for **2** and **8** were collected at low temperatures using an oil-coated, shock-cooled crystal[37] on a Stoe-IPDS with Mo-*Kα* (λ = 0.71073 Å) radiation. The structures were solved by direct methods using SHELXS-97[38] and refined with all data on F^2 using SHELXL-97.[39] All non-hydrogen atoms were refined anisotropically. The hydrogen atoms of the molecules were geometrically idealized and refined using a riding model. A numerical absorption correction was employed for structure **8**,[40] the min./max. transmissions are 0.4325/0.568. Refinement of an inversion twin parameter[41] [x = 0.49(2), where × = 0 for the correct absolute structure and +1 for the inverted structure] confirmed a racemic twinning of **8**. The two positions for the disordered hydrogen atoms in **2** were localized by Fourier synthesis and refined by using distance restraints. In **8** two half molecules of CH_2Cl_2 located on the twofold axis are refined anisotropically. 80 ADP and distance restraints were used for the refinement of **8**.

Crystallographic data (excluding structure factors) for the structures reported in this paper have been deposited with the Cam-

bridge Crystallographic Data Centre as supplementary publications nos. CCDC-121633 (2) and −121634 (8). Copies of the data can be obtained free of charge on application to CCDC, 12 Union Road, Cambridge CB2 1EZ, UK [Fax: (internat.) + 44(1223)336−033; E-mail: deposit@ccdc.cam.ac.uk].

Computational details. We have used standard, well-calibrated computational methods incorporated into the Gaussian 92 program.[42] In view of the size of the molecules concerned, typical approximations were made so that the computations were actually performed on model compounds, in which the diisopropylamino substituent was replaced by an hydrogen atom, or an amino group. Geometries were optimized with the complete DZP basis set[43] at both SCF and B3LYP[44] levels. For the free species, vibrational frequencies were calculated for the various stationary points located, to check that these are true minima. Pseudo-potentials were adopted for W[45] and P[46] atoms in calculations on complexes **12d−g**; the use of these pseudopotentials was shown to lead to trivial differences relative to all-electron results for the ligands G1,2. Geometries for **12d−g** were fully optimized under C_s symmetry at the B3LYP level, employing a basis with polarisation functions on P atoms only. Final binding energies (B3LYP) were obtained with a basis containing polarisation functions on all atoms (f-type exponent 0.5 for W).

Acknowledgments

Thanks are due to the CNRS for financial support of this work.

[1] [1a] M. T. H. Liu, *Chem. Soc. Rev.* **1982**, *11*, 127. − [1b] H. W. Heine, *Small Ring Heterocycles, Part 2* (Ed.: A. Hassner), The Chemistry of Heterocyclic Compounds, vol. 42, Wiley, New York, **1983**, p 588. − [1c] *Chemistry of Diazirines* (Ed. M. T. H. Liu), CRC Press, Inc., Boca Raton, FL, **1987**, vols. I and II.

[2] N. Dubau-Assibat, A. Baceiredo, G. Bertrand, *J. Am. Chem. Soc.* **1996**, *118*, 5216.

[3] E. Niecke, R. Streubel, M. Nieger, D. Stalke, *Angew. Chem. Int. Ed. Engl.* **1989**, *28*, 1673.

[4] According to calculations, 1*H*-diphosphirenes are more stable than the corresponding 3*H*-diphosphirenes: N. J. Fitzpatrick, D. F. Brougham, P. J. Groarke, M. T. Nguyen, *Chem. Ber.* **1994**, *127*, 969.

[5] The transient formation of a 3*H*-diphosphirene has been postulated: E. Niecke, R. Streubel, M. Nieger, *Angew. Chem. Int. Ed. Engl.* **1991**, *30*, 90.

[6] For a review on diheteroatom-containing cyclopropenylium salt analogues, see: D. Bourissou, G. Bertrand, *Acc. Chem. Res.* in press.

[7] [7a] W. H. Graham, *J. Am. Chem. Soc.* **1965**, *87*, 4396. − [7b] K. Krogh-Jespersen, C. M. Young, R. A. Moss, M. Wostowski, *Tetrahedron Lett.* **1982**, *23*, 2339. − [7c] R. A. Moss, J. Terpinski, D. P. Cox, D. Z. Denney, K. Krogh-Jespersen, *J. Am. Chem. Soc.* **1985**, *107*, 2743. − [7d] M. T. H. Liu, N. Paike, *Tetrahedron Lett.* **1987**, *28*, 3763. − [7e] M. T. H. Liu, M. P. Doyle, K.-L. Loh, S. M. Anand, *J. Org. Chem.* **1987**, *52*, 323. − [7f] R. A. Moss, *Acc. Chem. Res.* **1989**, *22*, 15.

[8] [8a] W. P. Dailey, *Tetrahedron Lett.*, **1987**, *28*, 5801. − [8b] K. E. Bainbridge, W. P. Dailey, *Tetrahedron Lett.* **1989**, *30*, 4901. − [8c] X. Creary, A. F. Sky, *J. Am. Chem. Soc.* **1990**, *112*, 368. − [8d] X. Creary, *Acc. Chem. Res.* **1992**, *25*, 31.

[9] [9a] F. Castan, A. Baceiredo, J. Fischer, A. De Cian, G. Commenges, G. Bertrand, *J. Am. Chem. Soc.* **1991**, *113*, 8160. − [9b] M. Soleilhavoup, Y. Canac, A. M. Polozov, A. Baceiredo, G. Bertrand, *J. Am. Chem. Soc.* **1994**, *116*, 6149. − [9c] M. Soleilhavoup, A. Baceiredo, F. Dahan, G. Bertrand, *J. Chem. Soc., Chem. Commun.* **1994**, 337. − [9d] Y. Canac, M. Soleilhavoup, L. Ricard, A. Baceiredo, G. Bertrand, *Organometallics* **1995**, *14,* 3614. − [9e] Y. Canac, A. Baceiredo, H. Gornitzka, D. Stalke, G. Bertrand, *Angew. Chem. Int. Ed. Engl.* **1995**, *34,* 2677. − [9f] Y. Canac, A. Baceiredo, W. W. Schoeller, D. Gigmes, G. Bertrand, *J. Am. Chem. Soc.* **1997**, *119*, 7579.

[10] Note that a diazirinyl radical has been characterized by ESR at −75°C (Y. Maeda, K. U. Ingold, *J. Am. Chem. Soc.* **1979**, *101*, 837), and that diphosphirenyl radicals dimerize through π*-π* interaction affording a tetraphosphabenzene valence isomer with one-electron phosphorus-phosphorus bonds (Y. Canac, D. Bourissou, A. Baceiredo, H. Gornitzka, W. W. Schoeller, G. Bertrand, *Science* **1998**, *279*, 2080).

[11] [11a] F. Mercier, L. Ricard, F. Mathey, M. Regitz, *J. Chem. Soc., Chem. Commun.* **1991**, 1305. − [11b] R. Streubel, L. Ernst, J. Jeske, P. G. Jones, *J. Chem. Soc., Chem. Commun.* **1995**, 2113.

[12] For preliminary results, see: [12a] D. Bourissou, Y. Canac, M. I. Collado, A. Baceiredo, G. Bertrand, *J. Am. Chem. Soc.* **1997**, *119*, 9923. − [12b] D. Bourissou, Y. Canac, M. I. Collado, A. Baceiredo, G. Bertrand, *J. Chem. Soc., Chem. Commun.* **1997**, 2399.

[13] R. Appel, *Multiple Bonds and Low Coordination in Phosphorus Chemistry* (Eds.: M. Regitz, O. J. Scherer), Georg Thieme Verlag, Stuttgart, **1990**, p. 160.

[14] A. N. Chernega, M. Yu. Antipin, Yu. T. Struchkov, T. V. Sarina, V. D. Romanenko, *Zh. Strukt. Khim.* **1986**, *27*, 78.

[15] [15a] H. Schmidbaur, R. Herr, J. Riede, *Chem. Ber.* **1984**, *117*, 2322. − [15b] J. Bruckmann, C. Kruger, F. Lutz, *Z. Naturforsch* **1995**, *50b*, 351.

[16] See for example: F. Mercier, F Mathey, C. Afiong-Akpan, J. F. Nixon, *J. Organomet. Chem.* **1988**, *348*, 361 and references therein.

[17] Calculations predict that complexation of the σ^3-phosphorus atom strongly stabilizes 1*H*-phosphirenes: D. Gonbeau, G. Pfister-Guillouzo, A. Marinetti, F. Mathey, *Inorg. Chem.* **1985**, *24*, 4133.

[18] A similar effect has been observed going from diazetidine to 3*H*-diazirine complexes.[1c]

[19] W. Beck, W. Danzer, *Z. Naturforsch* **1975**, *30b*, 716.

[20] The *cis*-$[W(CO)_4(thf)_2]$ precursor was prepared by photolysis of $[W(CO)_6]$ in THF solution under a stream of N_2: [20a] L. W. Arndt, M. Y. Darensbourg, T. Delord, B. T. Bancroft, *J. Am. Chem. Soc.* **1986**, *108*, 2617. − [20b] D. J. Darensbourg, C. J. Bischoff, J. H. Reibenspies, *Inorg. Chem.* **1991**, *30*, 1144.

[21] [21a] T. C. Klebach, R. Lourens, F. Bickelhaupt, C. H. Stam, A. Van Herk, *J. Organomet. Chem.* **1981**, *210*, 211. − [21b] J. F. Nixon, *Chem. Rev.* **1988**, *88*, 1327.

[22] R. H. Neilson, R. J. Thoma, I. Vickovic, W. H. Watson, *Organometallics* **1984**, *3*, 1132.

[23] [23a] R. G. Montemayor, D. T. Sauer, S. Fleming, D. W. Bennett, M. G. Thomas, R. W. Parry, *J. Am. Chem. Soc.* **1978**, *100*, 2231. − [23b] A. H. Cowley, R. A. Kemp, J. C. Wilburn, *Inorg. Chem.* **1981**, *20*, 4289.

[24] Examples of conversion of aminophosphane complexes into the corresponding chlorophosphane complexes have already been described: [24a] R. B. King, F.-J. Wu, E. M. Holt, *J. Am. Chem. Soc.* **1988**, *110*, 2775. − [24b] R. B. King, F.-J. Wu, E. M. Holt, *Inorg. Chem.* **1988**, *27*, 1241. − [24c] F. Mercier, B. Deschamps, F. Mathey, *J. Am. Chem Soc.* **1989**, *111*, 9098.

[25] O. Wagner, M. Ehle, M. Regitz, *Angew. Chem. Int. Ed. Engl.* **1989**, *28*, 225.

[26] A similar process has been suggested for 1*H*-phosphirenes: K. K. Laali, B. Geissler, O. Wagner, J. Hoffmann, R. Armbrust, W. Eisfeld, M. Regitz, *J. Am. Chem. Soc.* **1994**, *116*, 9407.

[27] A covalent *P*-trifluoromethanesulfoxy-1*H*-phosphirene was obtained by treating a *P*-chloro-1*H*-phosphirene with silver trifluoromethanesulfonate.[26]

[28] A. T. Ku, M. Sundaralingam, *J. Am. Chem. Soc.* **1972**, *94*, 1688.

[29] Z. Yoshida, *Top. Curr. Chem.* **1973**, *40*, 47.

[30] The *P*-hydroxy-1*H*-diphosphirene complex 13 has only been characterized in solution due to its intrinsic[31] instability.

[31] Isolated group VI carbonyl complexes of phosphinous acids generally benefit from supplementary inter- or intra-molecular stabilising interactions: [31a] C. S. Kraihanzel, C. M. Bartish, *J. Am. Chem. Soc.* **1972**, *94*, 3572. − [31b] G. M. Gray, C. S. Kraihanzel, *J. Organomet. Chem.* **1978**, *146*, 23. − [31c] S. Al-Jibori, M. Hall, A. T. Hutton, B. L. Shaw, *J. Chem. Soc., Chem. Commun.* **1982**, 1069. − [31d] S. Al-Jibori, M. Hall, A. T. Hutton, B. L. Shaw, *J. Chem. Soc., Dalton Trans.* **1984**, 863. − [31e] F. A. Cotton, L. R. Falvello, M. Tomas, G. M. Gray, C. S. Kraihanzel, *Inorg. Chim. Acta* **1984**, *82*, 129.

[32] F. Mathey, *Chem. Rev.* **1990**, *90*, 997.

[33] Three *J*(P,W) coupling constants with similar values (138, 103 and 30 Hz) have been observed for the trinuclear diphosphene

complex (PhP=PPh)·[W(CO)$_5$]$_3$: F. Mathey, private communication.
[34] Such a phenomenon has already been observed for iron phosphaalkene complexes: R. Appel, C. Casser, F. Knoch, *J. Organomet. Chem.* **1985**, *293*, 213.
[35] L. Weber, *Chem. Rev.* **1992**, *92*, 1839.
[36] For comparison, the two phosphirenylium complexes reported so far feature the cationic 2-π-electron three-membered ring η^3- or η^1-ligated: [36a] A. G. Avent, F. Geoffrey, N. Cloke, K. R. Flower, P. B. Hitchcock, J. F. Nixon, D. M. Vickers, *Angew. Chem. Int. Ed. Engl.* **1994**, *33*, 2330. – [36b] J. Simon, U. Bergsträsser, M Regitz, K. K. Laali, *Organometallics* **1999**, *18*, 817.
[37] D. Stalke, *Chem. Soc. Rev.* **1998**, *27*, 171.
[38] G. M. Sheldrick, *Acta Crystallogr. Sect. A.* **1990**, *46*, 467.
[39] G. M. Sheldrick, Program for Crystal Structure Refinement, Universität Göttingen, **1997**.
[40] H. D. Flack, *Acta Crystallogr. Sect. A.* **1983**, *39*, 876.
[41] X-SHAPE A Crystal Optimisation For Numerical Absorption Correction STOE and Cie (X-SHAPE is based on the program "HABITUS" by Dr. W. Herrendorf, Institut für Anorganische Chemie, Universität Giessen).
[42] Gaussian 92, M. J. Frisch, G. W. Trucks, M. Head-Gordon, P. M. W. Gill, M. W. Wong, J. B. Foresman, B. G. Johnson, H. B. Schlegel, M. A. Robb, E. S. Replogle, R. Gomperts, J. L. Andres, K. Raghavachari, J. S. Binkley, C. Gonzalez, R. L. Martin, D. J. Fox, D. J. Defrees, J. Baker, J. J. P. Stewart, S. Topiol, J. A. Pople, Gaussian Inc.: Pittsburgh, PA **1992**.
[43] T. H. Dunning, P. J. Hay, *Modern Quantum Chemistry* (Ed.: H. F. Schaefer), Plenum, New York, **1976**, Vol. 3, Chap.1.
[44] [44a] A. D. Becke, *J. Chem. Phys.*, **1993**, *98*, 1372 and 5648. – [44b] C. Lee, W. Yang, R. G. Parr, *Phys. Rev. B*, **1988**, *37*, 785.
[45] D. Andrae, U. Häussermann, M. Dolg, H. Stoll, H. Preuss, *Theor. Chim. Acta* **1990**, *77*, 123.
[46] Y. Bouteiller, C. Mijoule, M. Nizam, J.-C. Barthelat, J.-P. Daudey, M. Pelissier, B. Silvi, *Mol. Phys.* **1988**, *65*, 295.

Received May 17, 1999
(I99181]

Histidine-Containing Bisperoxovanadium(V) Compounds: Insight Into the Solution Structure by an ESI-MS and ^{51}V-NMR Comparative Study

Olga Bortolini,*[c] Mauro Carraro,[a] Valeria Conte,*[a,b] and Stefano Moro[d]

Keywords: Peroxo complexes / Vanadium / Mass spectrometry / ^{51}V-NMR spectroscopy / Vanadium dependent bromoperoxidases

ESI mass spectrometry and ^{51}V-NMR spectroscopy have been used to study the reactions occurring between bisperoxo vanadates and a number of histidine and histidine-like ligands, in aqueous alcoholic solutions. Coordination of one and two molecules of ligand is observed with all the compounds investigated affording $[VO_5L]^-$ and $[VO_52L]^-$, respectively. Characterization of these species has been achieved by MS^n experiments, which have allowed specific fragmentations of the peroxidic moiety to be distinguished. In particular, with $[VO_52L]^-$, two distinct modes of decomposition were observed, depending on the presence in the ligand of a free carboxylic function. – Possible biochemical implications related to vanadium haloperoxidase enzymes are discussed.

Introduction

Haloperoxidase enzymes catalyze the oxidation of halides by hydrogen peroxide.[1][2] The presence of vanadium in the oxidation state 5+ in vanadium-dependent chloro- and bromoperoxidases has been firmly established by using a variety of techniques. The binding of hydrogen peroxide to the metal, to yield a peroxo species as active intermediate, has been established as the initial step in the catalytic cycle. The oxidized halide is likely formed upon nucleophilic attack of X^- on the protonated peroxide group. In the absence of an organic halogen acceptor, the halogenating intermediate reacts with a second molecule of hydrogen peroxide thus producing halide, water and dioxygen, in its singlet state.

On the basis of several mechanistic studies, the catalytic cycle of the haloperoxidase enzymes can be outlined as it follows in Figure 1.[1][2]

Recently the X-ray structures of the native and peroxide form of V^V containing chloroperoxidase (V-ClPO) from the fungus *Curvularia inaequalis*[3] have been solved and possible implications for the catalytic mechanism have also been offered.[4][5] These recent crystallographic studies confirmed that the apical nitrogen donor bound to the metal center in the active site of the enzyme is an histidine imidazole. The other interactions of the prosthetic group with the proteic residues are hydrogen bonds to surrounding, positively charged or hydrophilic protein functions. A second molecule of histidine (His 404) is close to the active site. A very similar environment around the vanadium atom has been detected in the peroxide form of the enzyme.[4][5]

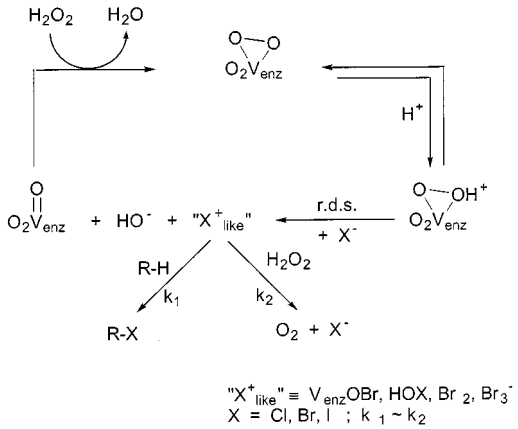


Figure 1. Mechanism for halides oxidation with hydrogen peroxide catalyzed by V-HalPO enzymes

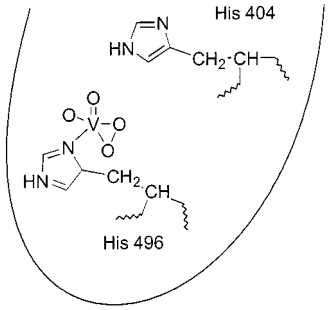


Figure 2. Schematic representation of the vanadium containing active site in the peroxide form of V-ClPO from *Curvularia inaequalis* taken from ref.[5]; hydrogen bonds network with water molecules has been removed for clarity

The occurrence of a protonation step in the catalytic cycle, see Figure 1, is strongly supported from mechanistic

[a] Centro Studi Meccanismi Reazioni Organiche del CNR, Dipartimento di Chimica Organica, Università di Padova, via Marzolo 1, I-35131 Padova, Italy,
Fax: (internat.) + 39-(0)49/ 8275239
E-mail: CONTE@CHOR.UNIPD.IT
[b] Facoltà di Agraria II, Foggia, Università di Bari Via Napoli 25, I-71100 Foggia, Italy
[c] Dipartimento di Chimica, Università di Ferrara, via Borsari 46, I-44100 Ferrara, Italy,
Fax: (internat.) + 39-(0)532/ 240709
E-mail: BRL@DNS.UNIFE.IT
[d] Dipartimento di Scienze Farmaceutiche, Università di Padova via Marzolo 5, I-35131 Padova, Italy

 © WILEY-VCH Verlag GmbH, D-69451 Weinheim, 1999 1434–1948/99/0909–1489 $ 17.50+.50/0

studies both on the enzyme and on model systems.[2][6] In the enzyme such a role appears to be played by protonated histidine 404, which is in the appropriate position to activate, by protonation, the peroxidic complex through hydrogen bonding interactions.

Several functional models for vanadium dependents HalPO have been reported,[2] the simplest one being *cis*-dioxovanadium(V), VO_2^+, in acidic conditions in the presence of hydrogen peroxide.[7] It is well-known that depending on the acidity of the medium and on the concentration of precursors both mono- and bisperoxovanadium species can be formed.[8][9] We have recently proposed as functional models for V-BrPO a two-phase procedure, the oxidation of bromide is carried out, in the aqueous acidic phase, by either monoperoxo- or bisperoxovanadium derivatives which are formed from NH_4VO_3 and H_2O_2.[10–12] Subsequently, the reactive intermediate can brominate the substrate in the organic phase. The vanadium bisperoxo complex appears to be reactive toward bromide ions only when it is protonated.[6][13]

In almost neutral conditions, bisperoxovanadium complexes are quite stable species,[14] therefore we envisaged the possibility of using such complexes, in the presence of histidine-like ligands,[15] as simple models for the analysis of structural features in solution of peroxovanadium complexes in order to collect information related the behavior of the enzyme. The idea of studying a bisperoxovanadate species as a model of the enzyme is based on the knowledge of the crystal structure of V-ClPO,[5] see Figure 2. In fact, the prosthetic group of the enzyme is a monoperoxo-metavanadate moiety[5] bound to the protein only through histidine 496. Therefore, there is significant correspondence between the structure of a bisperoxovanadate[15] eventually containing an imidazole ring and the prosthetic group of V-ClPO from *C. inaequalis*.

We report here a study on the chemistry in solution of histidine-containing bisperoxovanadium compounds, by using ^{51}V-NMR and ESI-MS analyses. The latter technique has been already successfully used for the analysis of cationic mono-peroxovanadium compounds in acid conditions.[16]

Results and Discussion

Speciation of Bisperoxovanadates

Ammonium vanadate ($4\cdot10^{-3}$ mol L^{-1}), dissolved in water at pH ca. 6.8 shows in ^{51}V-NMR the known distribution pattern of mono- and oligomeric vanadate species.[17] In particular the prevailing species are monomeric, dimeric and tetrameric metavandates, respectively, indicated by the resonances at $\delta = -559$, -572, and -577, in agreement with literature data. When the same solution is diluted with ethanol, signals appear at $\delta = -552$, -556, -561, and -571, thus showing the possible formation also of the pentameric derivative. The addition of alcohol results in downfield shifts of the resonances and a broadening of the signals. This latter behavior can be assigned to fast exchange between water and alcohol molecules in the coordination sphere of the metal.[18]

The analysis of the same solutions by ESI-MS, in negative ion mode, shows the occurrence of the following species: $[VO_3]^-$ (*m*/*z* 99, relative abundance 3%), $[VO_3(H_2O)]^-$ (*m*/*z* 117, 14%), $[VO_3(EtOH)]^-$ (*m*/*z* 145, 44%), $[OV(O)(OEt)_2]^-$ (*m*/*z* 173, 100%), the dimeric $[\{OV(O)\}_2O(OH)]^-$ (*m*/*z* 199, 2%) and $[\{OV(O)\}_2O(OEt)]^-$ (*m*/*z* 227, 28%), as well as the less intense trimeric and tetrameric ions $[\{OV(O)\}_3O(OEt)(OH)]^-$ (*m*/*z* 327, 3%), $[\{OV(O)\}_3O(OEt)_2]^-$ (*m*/*z* 355, 8%), $[\{OV(O)\}_4O(OH)_3]^-$ (*m*/*z* 399, 2%).

When hydrogen peroxide is added to vanadate solutions in water/ethanol, a number of peroxovanadates are formed.[8,9,19] The relative abundance of the different species depends on the ratio H_2O_2/vanadate, pH, and on vanadium concentration. Under acidic conditions, in the presence of equimolar amounts of H_2O_2 with respect to vanadium, the predominant species are cationic monoperoxo complexes with different coordination sphere, whose ESI-MS behavior has been already reported.[16]

Aqueous solutions of peroxovanadium species were initially analyzed by employing mixtures of water and methanol. However, the presence in the coordination sphere of the metal of both the peroxo O_2^{2-} moiety and the methanol molecule having the same molecular weight (32 Da) caused difficulties in assigning some of the fragmentation patterns. Therefore, water and water/ethanol mixtures have been used as solvent. See Experimental Section for details regarding the preparation of the solutions. The preferential formation of bisperoxovanadium monoanion complexes was monitored by increasing the amount of hydrogen peroxide up to a 2.4:1 ratio with respect to vanadium, for pH values of 1.3, 6.9, 8.2. ^{51}V-NMR spectra at pH 1.3 revealed the presence of similar concentration of mono- and bisperoxo complexes, as indicated by signals at $\delta = -521$ ($W_{1/2}$ 501 Hz) and -681 ($W_{1/2}$ 468 Hz), respectively. On the other hand, in ESI-MS experiments, carried out both in positive and negative ion mode, the absence of any detectable species suggests that in these conditions, mono- and protonated bisperoxo compounds do not survive to the electrospray ionization conditions. In agreement with this observation, we have found that the decomposition reaction of bisperoxovanadium solutions at various pHs is faster as the concentration of $HClO_4$ increases, see Figure 3.

^{51}V-NMR experiments at almost neutral pH indicate the presence of a single species at $\delta = -689$ ($W_{1/2}$ 270 Hz) identified as the bisperoxovanadium compound. When the same solution is analyzed by ESI-MS, most of the observed peaks can be attributed to bisperoxo species containing different solvent molecules in the coordination sphere: $[VO_5]^-$ (*m*/*z* 131, 100%), the solvent bound species $[VO_5(EtOH)]^-$ (*m*/*z* 177, 55%) and $[VO_5(EtOH,H_2O)]^-$ (*m*/*z* 195, 5%), see Figure 4.

Other peroxidic compounds are observed at higher *m*/*z* values such as the dimeric species $[\{VO(OO)_2\}_2(H)]^-$ (*m*/*z* 263, 5%) and the water containing $[\{VO(OO)_2\}_2(H,H_2O)]^-$

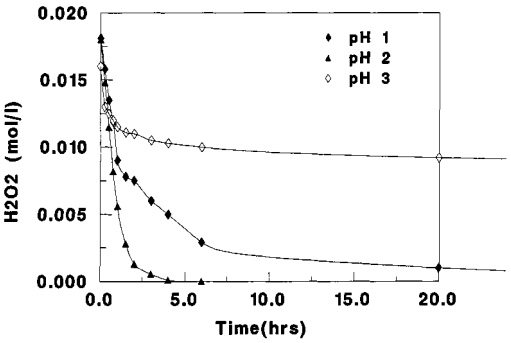


Figure 3. Disappearance of H_2O_2 (0.0.2 mol L^{-1})as a function of the time in the presence of NH_4VO_3 (0.01 mol L^{-1}) in water at 25 °C, at various pH ($HClO_4$); ▲ = pH 1.1 ($[VO(O_2)]^+ \sim [VO(O_2)_2]^-$ as measured by ^{51}V-NMR), ◆ = pH 2.0; (only $[VO(O_2)_2]^-$), ◇ = pH 3.0 (only $[VO(O_2)_2]^-$)

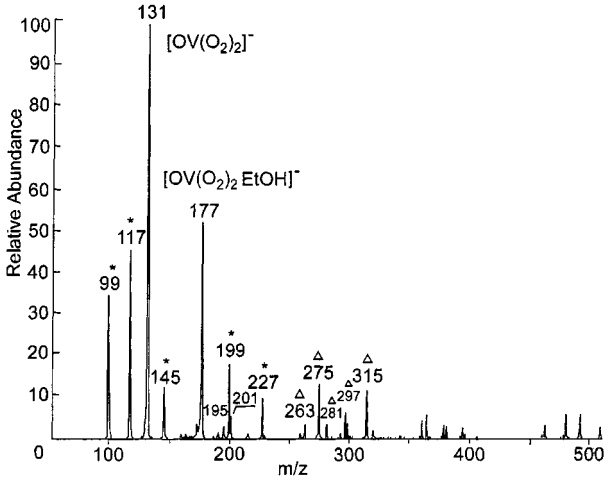


Figure 4. ESI mass spectrum of VO_3^- ($2\cdot10^{-3}$ mol L^{-1}) in the presence of 2.4 equivalents of H_2O_2 in ethanol/water 1:1, pH 6.9; (*) non-peroxidic species, (Δ) peroxospecies with a ratio $O_2^{2-}/V \geq 2$

ion (*m/z* 281, 5%). It is worth of noting that very recently the crystal structure of this latter dimeric compound has been solved.[20] Furthermore, species having a peroxo-to-vanadium ratio higher than two have been detected at *m/z* 315 and 361. As far as the possibility of observing the formation of the previously reported[19] triperoxo compound is concerned, under such experimental conditions even though a small peak is detected at the correct *m/z* value corresponding to $[OV(O_2)_3(H_2O)_2(H)_2]^-$ (*m/z* 201, < 5%), we could not confirm its nature with collision induced-decomposition experiments (MS^n) because of the low intensity of the signal.

MS^n mass spectra were used to identify some of the above-mentioned species. The "naked" bisperoxovanadium compound, at *m/z* 131, fragments to the non-peroxidic species $[VO_3]^-$ (*m/z* 99). This decomposition is followed by the coordination of water or ethanol to $[VO_3]^-$ affording ions at *m/z* 117 and 145, respectively, Figure 5a. Support for this behavior was obtained by independent experiments on the isolated $[VO_3]^-$ which showed addition of water or ethanol, see Figure 5b. $[VO_5]^-$ with an ethanol molecule in the coordination sphere, is more prone to add neutrals, as found in the MS/MS mass spectrum of $[VO_5(EtOH)]^-$ (*m/z* 177) where coordination of water and ethanol is observed, affording the ions $[VO_5(EtOH,H_2O)]^-$ *m/z* 195 and $[VO_5(EtOH)_2]^-$ *m/z* 223, the latter in much lower relative intensity. An increase of the pH of the medium promotes the formation of oligomeric vanadium peroxo compounds in most cases having a peroxo-to-vanadium ratio higher than two.[19] As expected, also the increase of the concentration of vanadium favors the oligomerization process.

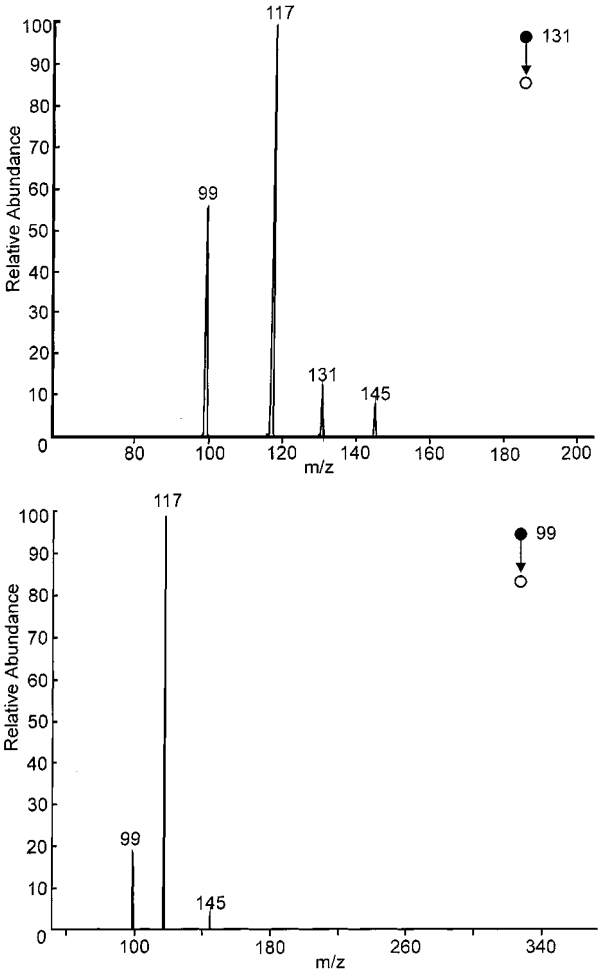
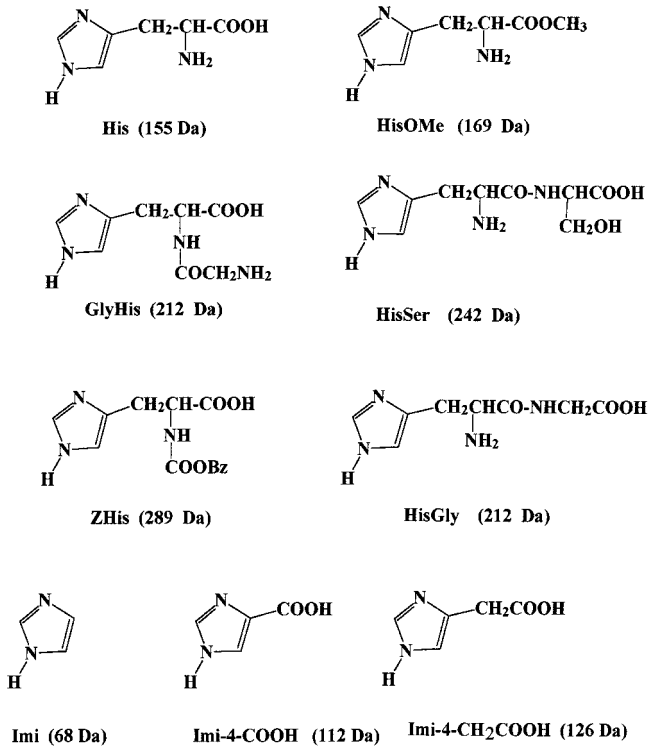


Figure 5. MS/MS mass spectrum of (a) the bisperoxovanadium $[VO_5]^-$ and of (b) the non-peroxidic species $[VO_3]^-$, in ethanol/water, 1:1, pH 6.9

We recently reported[16] that the tandem use of ^{51}V-NMR and ESI-MS analyses allows a better characterization of rapidly exchanging monoperoxovanadium species with different coordination sphere composition. Analogously, in the present study, the evidence that the line width of the NMR signals related to bisperoxocompounds significantly increases in passing from water to water/alcohol mixtures suggests the occurrence of new equilibria, regardless, a detailed snapshot of the equilibrating species, not feasible on NMR time scale, is accessible with the ESI-MS technique.

Histidine-Like Ligands for Bisperoxovanadates

Vanadium imidazole complexes have recently received significant attention in connection with the evidence that haloperoxidases contain histidine residues coordinated to vanadium.[3−5] Taking advantage of the results reported above we analyzed bisperoxo vanadium compounds at neutral pH in the presence of histidine and histidine-like ligands, i.e. methyl histidine (HisOMe), carbobenzoxy histidine (ZHis); dipeptides: GlyHis, HisSer, HisGly; imidazole (Imi), and carboxyimidazole derivatives (Imi−4-COOH) and (Imi−4-CH_2COOH), see Scheme 1. For example, upon addition of 2 to 6 equivalents of histidine to the bisperoxovanadium solution, at pH 6.9, together with the ^{51}V-NMR signal located at ca. $\delta = -690$, two new peaks are observed at $\delta = -729$ ($W_{1/2}$ not measured due to low intensity) and $\delta = -742$ ($W_{1/2} = 291$ Hz). This latter value is very close to the chemical shift ($\delta = -744$) reported by Crans et al.[15] for the bisperoxovanadium imidazole monoanion thus confirming that the coordination of histidine to $[VO_5]^-$ occurs via the imidazole moiety. The former signal has been assigned by Tracey et al.[21], even though with no firm evidence, to a species containing histidine bound to vanadium through the second imidazole nitrogen.



Scheme 1

The coordination properties of all the ligands used, see Scheme 1, were tested via ^{51}V-NMR technique in aqueous solution (pH ca. 6.9) and in water-ethanol mixture, by changing the [ligand]/$[VO_5]^-$ ratio from 1 to 6. In all cases the main peak observed is located between $\delta = -738$ and -750, depending from the ligand and from the solvent, thus indicating that the binding to the bisperoxovanadium complex always occurs through the imidazole sp^2 nitrogen. In agreement with previous data, ^{51}V-NMR analysis of solutions containing Imi and Imi−4-CH_2COOH as ligands shows the occurrence of bisperoxovanadates (at δ ca. -700) and $[VO_5L]^-$ (at δ ca. -740) species. On the other hand, by using Imi−4-COOH, three signals were detected pertaining to bisperoxovanadate ($\delta = -690$), $[VO_5$Imi−4-COOH$]^-$ ($\delta = -740$) and to a new species, located at $\delta = -770$. As far as its nature is concerned, we suggest the formation a dimeric bisperoxovanadate, possibly containing one or two molecules of Imi−4-COOH. Characterization of such species is currently in progress. Solutions of bisperoxovanadates in the presence of two equivalents of histidine were analyzed by ESI-MS, and additional signals are observed at *m/z* 286 and 441, corresponding to $[VO_5$His$]^-$ and $[VO_5$2His$]^-$, respectively, see Figure 6.

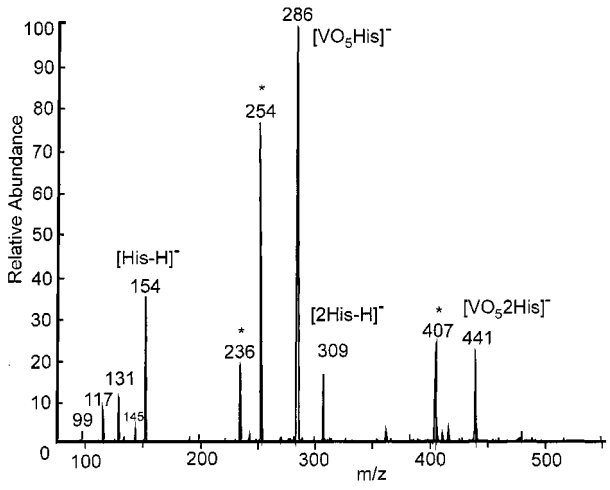


Figure 6. ESI mass spectrum of VO_3^- ($2\cdot10^{-3}$ mol L^{-1})/H_2O_2 (2.4 equivalents) in ethanol/water, 1:1, pH 6.9. in the presence of histidine (2 equivalents); (*) signals due to fragmentation of $[VO_5$His$]^-$ and $[VO_5$2His$]^-$, respectively, see text

It is important to emphasize that both *m/z* values correspond to the insertion of intact histidine molecule(s), although at this point we shall not specifically address where the protons are located. As will be discussed later on in the paper, this is a crucial point in the reactivity of the species. MS^n mass spectra of $[VO_5$His$]^-$ and $[VO_5$2His$]^-$ were also collected and the relevant data are inserted in Table 1. In particular, the different behavior of $[VO_5$His$]^-$ with respect to $[VO_5$2His$]^-$ deserves comments. The collision-induced decomposition (MS^2) of the $[VO_5$His$]^-$ complex shows a new peak at *m/z* 254 corresponding to the loss of 32 Da. On the other hand, $[VO_5$2His$]^-$ under the same CID conditions, shows formation of peaks at *m/z* 407 and 286 related to the loss of 34 and 155 Da. The $[VO_5$2His -155 Da$]^-$ ion is easily attributed to the release of a neutral histidine molecule. In order to better understand the nature of the 32 and 34 Da fragments observed in the decomposition of $[VO_5$His$]^-$ and $[VO_5$2His$]^-$ respectively, we have extended the analysis to the other ligands listed in Scheme 1, see Table 1.

Table 1. Relative abundances of $[VO_5L]^-$ and $[VO_52L]^-$ ionic species in ESI mass spectra of bisperoxovanadium compounds in the presence of histidine and histidine-like ligands and related MS/MS fragmentations[a]

Species	*m/z*	rel. abund.%	MS/MS[a]
[M]$^-$ ≡ $[VO_5His]^-$	286	100	**[M - 32]$^-$**
[M′]$^-$ ≡ $[VO_5(His)_2]^-$	441	25	**[M′ - 34]$^-$** **[M′ -His]$^-$**
[M]$^-$ ≡ $[VO_5ZHis]^-$	420	60	**[M - 32]$^-$**
[M′]$^-$ ≡ $[VO_5(ZHis)_2]^-$	709	55	**[M′ - 34]$^-$** **[M′ − ZHis]$^-$**
[M]$^-$ ≡ $[VO_5GlyHis]^-$	343	100	**[M - 32]$^-$**
[M′]$^-$ ≡ $[VO_5(GlyHis)_2]^-$	555	30	**[M′ - 34]$^-$** **[M′ − GlyHis]$^-$**
[M]$^-$ ≡ $[VO_5HisOMe]^-$	300	35	**[M - 32]$^-$**
[M′]$^-$ ≡ $[VO_5(HisOMe)_2]^-$	469	15	**[M′ − HisOMe]$^-$**
[M]$^-$ ≡ $[VO_5HisOMe(HCl)]^-$ [b]	336	45	**[M - 32]$^-$**
[M′]$^-$ ≡ $[VO_5(HisOMe)_2(HCl)]^-$ [b]	505	16	**[M′ − HisOMe]$^-$**
[M]$^-$ ≡ $[VO_5HisSer]^-$	373	100	**[M - 32]$^-$**
[M′]$^-$ ≡ $[VO_5(HisSer)_2]^-$	614	15	**[M′ - 34]$^-$** **[M′ − HisSer]$^-$**
[M]$^-$ ≡ $[VO_5HisGly]^-$	343	100	**[M - 32]$^-$**
[M′]$^-$ ≡ $[VO_5(HisGly)_2]^-$	555	40	**[M′ - 34]$^-$** **[M′ − HisGly]$^-$**
[M]$^-$ ≡ $[VO_5Imi]^-$	199	80	**[M - 32]$^-$**
[M′]$^-$ ≡ $[VO_5(Imi)_2]^-$	267	< 1	signal too low
[M]$^-$ ≡ $[VO_5Imi\text{-}4\text{-}COOH]^-$	243	80	**[M - 32]$^-$**
[M′]$^-$ ≡ $[VO_5(Imi\text{-}4\text{-}COOH)_2]^-$	355	4	**[M′ - 34]$^-$** **[M′ − Imi-4-COOH]$^-$**
[M]$^-$ ≡ $[VO_5Imi\text{-}4\text{-}CH_2COOH]^-$	257	80	**[M - 32]$^-$**
[M′]$^-$ ≡ $[VO_5(Imi\text{-}4\text{-}CH_2COOH)_2]^-$	383	2	Signal too low

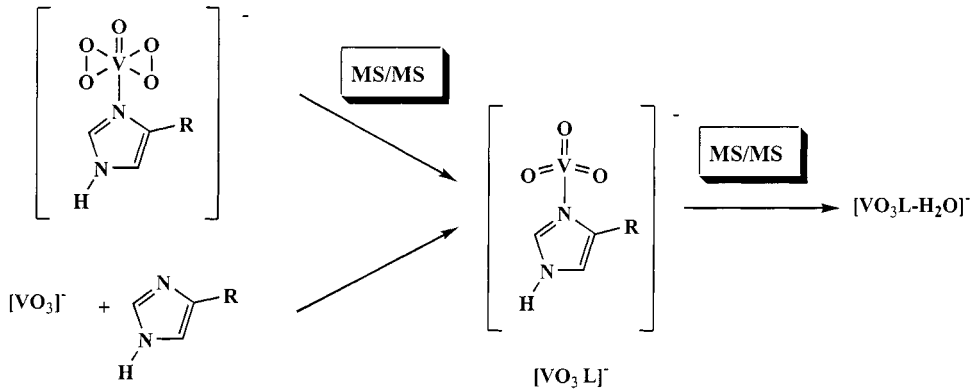
[a] MS/MS fragmentations of the selected $[M]^-$ and $[M']^-$ ions, respectively. − [b] These signals are due to the use as ligand of the commercially available HisOMe(HCl).

The overall picture obtained with these ligands by ESI-MS is very close to that observed for histidine. The data reported in the Table show that all the vanadium bisperoxo species containing one heteroligand in the coordination sphere are prone to release the 32 Da fragment, whereas the presence of two heteroligands on $[VO_5]^-$ appears to favor the expulsion of 34 Da only when a carboxy group is present in the framework of the ligand. The loss of 32 Da fragment from $[VO_5L]^- \equiv [M]^-$ has been attributed to the decomposition of both peroxidic moieties, which gives rise to the formation of the non-peroxidic species $[VO_3L]^-$ on the basis of the identical decomposition pattern of $[M - 32\ Da]^-$ ions and the isobaric ions obtained from ligands containing vanadates solutions, see Scheme 2. On the other hand, the loss of 34 Da fragment from $[VO_52L]^- \equiv [M']^-$, observed when L has a free carboxylic function, has been attributed to the release of H_2O_2. In fact upon isolation of the $[M' - 34]^-$ ion, loss of an intact L molecule is observed, thus proving that fragmentation of the ligands is not taking place, Scheme 3. Furthermore, the $[M' - 34]^-$ ions have to have an intact "side on" peroxidic group otherwise they would not be monoanions and therefore observed at a different *m/z* value.

A plausible explanation for the above-reported data takes into account the protonation a peroxidic oxygen by the carboxylic function of the ligands. When two ligands are involved in the coordination, the loss of hydrogen peroxide is made possible. Protonation of a peroxidic moiety likely results in an opening of the three-membered ring.[14] Such a process may allow a direct coordination to the metal of a second molecule of ligand. The resulting species has the peculiar ESI-MS fragmentation pattern discussed above, i.e. 34 Da loss. In the absence of a free carboxy group, as it is the case of HisOMe, HisOMe(HCl), and IMI, the second molecule of ligand in $[VO_5L_2]^-$, can be seen as external to the first coordination sphere of the metal, as it is in the crystal structure of $[VO_5Imi]^-(ImiH)^+$, where the imidazolium cation acts as counterion. Ab initio calculations are currently in progress in order to obtain further support to this hypothesis.

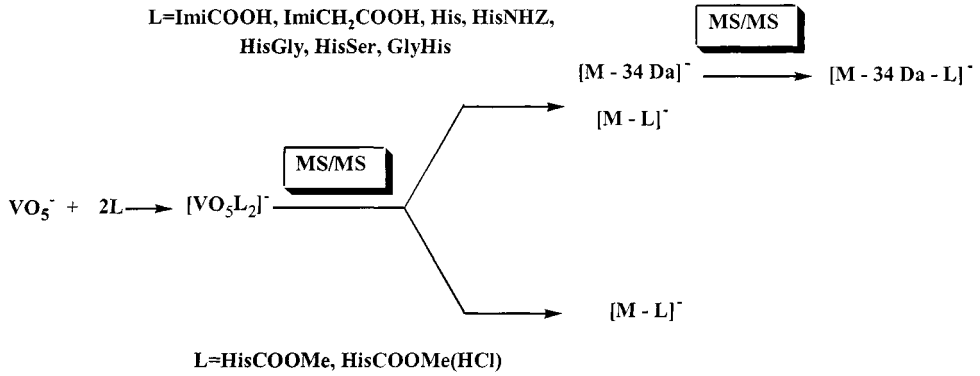
Conclusion

In summary, this study shows that the correct choice of the model for V-HalPO enzymes and its analysis with appropriate techniques allows the collection of significant structural and mechanistic data. In this respect, we have obtained direct[6] and independent evidence that the protonation of the peroxidic moiety is a crucial step in the activation of vanadium peroxocompounds. Such a mechanism of activation is also involved in the reactivity of V-HalPO enzymes.[5] The role of two different molecules of histidine and histidine-like ligands as proton donors has been also directly observed.



R = CO_2H, CH_2CO_2H, $CH_2CH(NH_2)CO_2H$, $CH_2CH(NH_2)CO_2CH_3$, $CH_2CH(NHCOOBz)CO_2H$, $CH_2CH(NH_2)CONHCH_2CO_2H$, $CH_2CH(NH_2)CONHCH(CH_2OH)CO_2H$, $CH_2CH(NHCOCH_2NH_2)CO_2H$

Scheme 2. Decomposition pattern of $[VO_3L]^-$ ions obtained from $[VO_5L]^-$ (MS^3 experiment) or of ligand containing vanadate solutions (MS^2 experiment), respectively



Scheme 3. Decomposition patterns of $[VO_5L_2]^-$ ions (MS^2 and MS^3 experiments) as a function of the ligand L

Experimental Section

General Remarks: The ESI-MS measurements were obtained using a Finnigan MAT LCQ instrument (San Jose, CA) by using the following parameters: solution flow rate 8 μL min^{-1}, capillary temperature 120−140 °C, spray voltage 3.4 kV, capillary voltage comprised between −5 and −20 V, nebulizing gas N_2 (40 units flow rate). Parameters related to octapoles and detector were those achieved by the automatic set-up procedure. Collision induced decompositions of selected ions (MS^n, n = 2, 3) were obtained by applying a supplementary r.f. voltage (tickle voltage) to the end cap electrodes of the ion trap (resonance activation). Typical tickle voltage values for fragmentation were 3−5 V. The vanadate and peroxovanadate solutions were introduced into the instrument by direct injection. The vanadate solutions at pH 6.9 are prepared by dissolving NH_4VO_3 ($2\cdot10^{-3}$ mol L^{-1}), in CH_3CH_2OH/H_2O, 1:1. The peroxovanadium solutions are prepared by dissolving NH_4VO_3 ($4\cdot10^{-3}$ mol L^{-1}) in water. 2.4 equivalents of H_2O_2 are subsequently added and pH is finally adjusted to the desired value [1.3 ($HClO_4$), 6.9 (natural value), and 8.2 (NH_3)]. The solutions are then diluted 1:1 with ethanol. Ligands are added in due time (1−8 equivalents with respect to V^V) to the aqueous solution of peroxovanadates before pH adjustment.

No significant variation on the qualitative distribution of the species was observed by repeating the measurements. However, the intrinsic nature of the ESI-MS technique does not allow to estimate the relative concentration of the ions detected. This event, nevertheless, does not interfere with the conclusion drawn in the present work.

Decomposition Reactions: The appropriate amount (2 equivalents) of H_2O_2, in water, is added to a aqueous solution of NH_4VO_3 ($1\cdot10^{-3}$ mol L^{-1}), at pH = 1 and 25 °C. When needed, pH adjustment (at values of 2 and 3) is settled with NH_3. Consumption of peroxide content is analyzed at chosen time interval with standard iodometric titration. Reproducibility of the kinetic behavior was checked for each pH with triplicate runs.

NMR experiments were carried out as already described.[9][12]

Acknowledgments

We acknowledge the Italian Ministry of the University and of the Scientific Research (MURST) for financial support to the research project: "Efficient processes for the Controlled Oxidations of Organic Compounds". O. B. thanks the University of Ferrara for financial support.

[1] [1a] A. Butler, J. V. Walker, *Chem. Rev.* **1993**, *105*, 1937. – [1b] A. Butler, A. H. Baldwin in: *Metal Sites in Protein and Models, Structure and Bonding* vol. 89, Springer Verlag Berlin-Heidelberg; Dordrecht, **1997**, pp. 108–132.
[2] C. Slebodnick, B. J. Hamstra, V. L. Pecoraro in: *Metal Sites in Protein and Models, Structure and Bonding* vol. 89, Springer Verlag Berlin-Heidelberg; Dordrecht, **1997**, pp. 51–108.
[3] J. W. P. M. van Schijndel, E. G. M. Vollenbroek, R. Wever, *Biochim. Biophys. Acta* **1993**, *1161*, 249.
[4] A. Messerschmidt, R. Wever, *Proc. Natl. Acad. Sc.* **1996**, *93*, 392.
[5] A. Messerschmidt, L. Prade, R. Wever, *Biol. Chem.* **1997**, *378*, 309.
[6] B. J.Hamstra, G. J.Colpas, V. L. Pecoraro, *Inorg. Chem*. **1998**, *37*, 949.
[7] [7a] F. Secco *Inorg. Chem*. **1980**, *19*, 2722. – [7b] R. I. de la Rosa, M. J. Claugue, A. Butler, *J. Am. Chem. Soc.* **1995**, *117*, 3475.
[8] A. Butler, M. J. Claugue, G. E. Meister, *Chem. Rev.* **1994**, *94*, 625.
[9] V. Conte, F. Di Furia, S. Moro, *J. Mol. Catal.* **1994**, *94*, 323.
[10] V. Conte, F. Di Furia, S. Moro, *Tetrahedron Lett*. **1994**, *35*, 7429.
[11] M. Andersson, V. Conte, F. Di Furia, S. Moro, *Tetrahedron Lett*. **1995**, *36*, 2675.
[12] V. Conte, F. Di Furia, S. Moro, S. Rabbolini, *J. Mol. Catal.* **1996**, *113*, 175.
[13] V. Conte, M. Carraro, S. Moro, manuscript in preparation.
[14] V. Conte, F. Di Furia, S. Moro, *J. Mol. Catal.* **1997**, *120*, 93.
[15] D. C. Crans, A. D. Keramidas, H. Hoover-Litty, O. P. Anderson, M. M. Miller, L. M. Lemoine, S. Pleastic-Williams, M. Vandenberg, A. J. Rossomando, L. J. Sweet, *J. Am. Chem. Soc* **1997**, *119*, 5447.
[16] O. Bortolini, V. Conte, F. Di Furia, S. Moro, *Eur. J. Inorg. Chem.* **1998**, 1193.
[17] [17a] N. D. Chasteen, *Vanadium in Biological Systems*; Kluwer Academic Publishers; Dordrecht, **1990**. – [17b] *Metal Ions in Biological Systems. Vol.31. Vanadium and its Role in Life* (Eds.: H. Sigel, A. Sigel, Marcel Dekker inc.: New York NY, **1995**.
[18] V. Conte, F. Di Furia, S. Moro, *Inorg. Chim. Acta*, **1998**, *272*, 62.
[19] [19a] O. W. Howarth, J. R. Hunt, *J. Chem. Soc. Dalton Trans.* **1979**, 1388. – [19b] O. W. Howarth, A. T. Harrison, *J. Chem. Soc. Dalton Trans.***1985**, 1173. – [19c] J. S. Jaswal, A. S. Tracey, *Inorg. Chem.* **1991**, *30*, 3718.
[20] V. Suchá, M. Sivák, J. Tyršelová, J. Marek, *Polyhedron* **1997**, *16*, 2837.
[21] J. S. Jaswal, A. S. Tracey, *J. Am. Chem. Soc.* **1993**, *115*, 5600.

Received February 10, 1999
[I99045]

Optically Active Transition-Metal Complexes, 8[+]

Transition-Metal Complexes of the Optically Active Cyclopentadienyl Ligand PinCp*: Crystal Structure of (S_{Re})-(η^5-PinCp*)Re(NO)(PPh_3)[$CONHCH(CH_3)C_{10}H_7$]

Albrecht Salzer,*[a] Annegret Hosang,[a] Jutta Knuppertz,[a] and Ulli Englert[a]

Dedicated to Professor Helmut Werner on the occasion of his 65th birthday

Keywords: Half-sandwich complexes / Molybdenum / Optically active complexes / Rhenium / Tungsten

The synthesis of (η^5-PinCp*)Re($CO)_3$ [PinCp* = tetramethyl(pinanyl)cyclopentadienyl] is described. Successive substitution of two CO ligands by NO^+ and PPh_3 generates a 1:1 diastereomeric mixture of chiral-at-metal [(S_{Re})/(R_{Re})-(PinCp*)Re(CO)(NO)(PPh_3)]BF_4. The diastereomers are converted with sodium methoxide into the derivative "esters" (S_{Re})/(R_{Re})-(PinCp*)Re($COOCH_3$)(NO)(PPh_3), and then with (+)-(*R*)-(1-naphthylethyl)amine to the "amides" (S_{Re})/(R_{Re})-(PinCp*)Re(NO)(PPh_3)[$CONHCH(CH_3)C_{10}H_7$] [(S_{Re})/(R_{Re}) = 1:1]. Fractional crystallisation separates the (S_{Re}) isomer with an optical purity of > 98%. The latter compound has been characterized by X-ray structure analysis. By treating the (S_{Re})-amide with CF_3CO_2H and $NaBF_4$, (S_{Re})-(PinCp*)Re(CH_3)(NO)(PPh_3) can be generated. Protolysis of this compound with HBF_4/Et_2O in CD_2Cl_2 at –78 °C leads to the solvent-stabilized complex (S_{Re})-[(PinCp*)Re(NO)(PPh_3)($ClCD_2Cl$)]$^+BF_4^-$. The thermal and configurational stability of this chiral Lewis acid is investigated at various temperatures. The syntheses of [PinCp*$RhCl_2]_2$, PinCp*$TiCl_3$ and PinCp*$M(CO)_2$(NO) (M = Mo, W) are also described. Starting with PinCp*$M(CO)_2$(NO), the relatively stable 16-VE complexes PinCp*MCl_2(NO) and PinCp*$W(CH_2SiMe_3)_2$(NO) are synthesized.

Introduction

Chiral Lewis acids, derived from transition-metal complexes, play an increasingly important role in enantioselective organic synthesis.[1–4] Both their thermal as well as their configurational stability are essential for their application as catalysts in asymmetric synthesis. While Gladysz et al.[4] have investigated the stability of the chiral-at-metal Lewis acid (S_{Re})-[(η^5-C_5H_5)Re(NO)(PPh_3)($ClCD_2Cl$)]$^+$ BF_4^-, our group has studied the behaviour of a chiral Lewis acid incorporating an optically active cyclopentadienyl ligand, namely (S_{Re})-[(η^5-PCp)Re(NO)(PPh_3)-($ClCD_2Cl$)]$^+$-BF_4^- (PCp = "pinene-fused cyclopentadienyl").[5][6] Gladysz determined the configurational stability of (S_{Re})-[(η^5-C_5H_5)Re(NO)(PPh_3)($ClCD_2Cl$)]$^+BF_4^-$ by either investigating the optical purity of the decomposition products formed after warming above −20°C, or by analysing the products generated when nucleophiles are added at low temperatures. The configurational stability of (S_{Re})-[(η^5-PCp)Re(NO)(PPh_3)($ClCD_2Cl$)]$^+BF_4^-$, on the other hand, was determined by low-temperature ^{31}P-NMR spectrocopy, where the optically active cyclopentadienyl ligand served as an internal spectroscopic probe of diastereomeric purity. Both systems show no inversion of configuration at the stereogenic metal centre up to their decomposition points at −20°C.

Recently, Gladysz et al.[7] have extended their studies to the peralkylated derivative (S_{Re})-[(η^5-C_5Me_5)Re(NO)-(PPh_3)($ClCD_2Cl$)]$^+BF_4^-$, under the assumption that peralkylated ligands should enhance the thermal and configurational stability of the chiral Lewis acid by either shielding the central metal atom through the bulk of the ligand, or by stabilizing the cationic centre through the electron-donating effect of the five alkyl groups. Surprisingly, they found that decomposition of (S_{Re})-(η^5-C_5Me_5)Re(NO)(PPh_3)-($ClCD_2Cl$)]$^+BF_4^-$ seems to occur even below −35°C. They also noticed that products formed by addition of nucleophiles at lower temperatures were only recovered with a maximum enantiomeric purity of 90%. Because spectroscopic methods for directly determining the conformational stability of enantiomers are limited, Gladysz et al. were not able to fully rationalize their observations.

As our previous work[6] had shown that the fate of a stereogenic metal centre could be easily monitored by low-temperature NMR spectroscopy when an optically active cyclopentadienyl ligand is present, we also investigated the synthesis and stability of a chiral Lewis acid derived from a peralkylated, optically active ligand such as PinCp* [PinCp* = tetramethyl(pinenyl)cyclopentadienyl], a ligand that has been first introduced by Lai et al.[8] This ligand, like PCp used by us before, should serve as an internal chiral probe to directly determine the stability of peralkylated derivatives of Gladysz' chiral Lewis acids. We also wanted

[+] Part 7: Ref.[27]

[a] Institut für Anorganische Chemie, RWTH Aachen, D-52056 Aachen, Germany
Fax: (internat.) + 49-(0)241/888-8288
E-mail: albrecht.salzer@ac.rwth-aachen.de

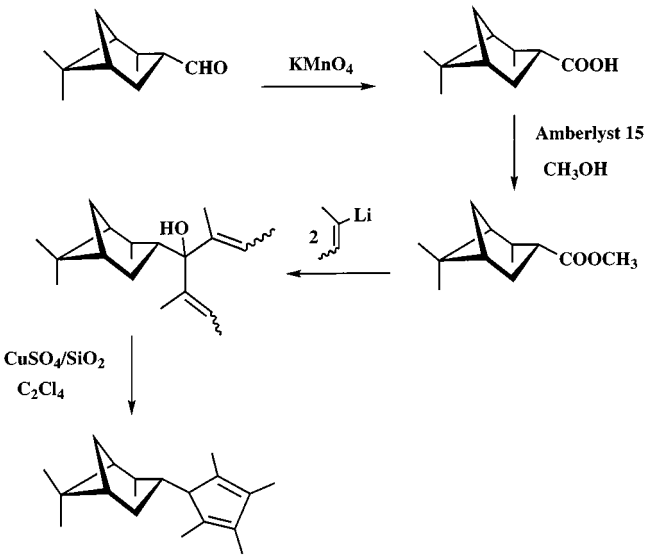
 © WILEY-VCH Verlag GmbH, D-69451 Weinheim, 1999 1434–1948/99/0909–1497 $ 17.50+.50/0

to show that this ligand could be universally used as a chiral replacement for Cp* by incorporating it into a series of other organometallic compounds.

Results and Discussion

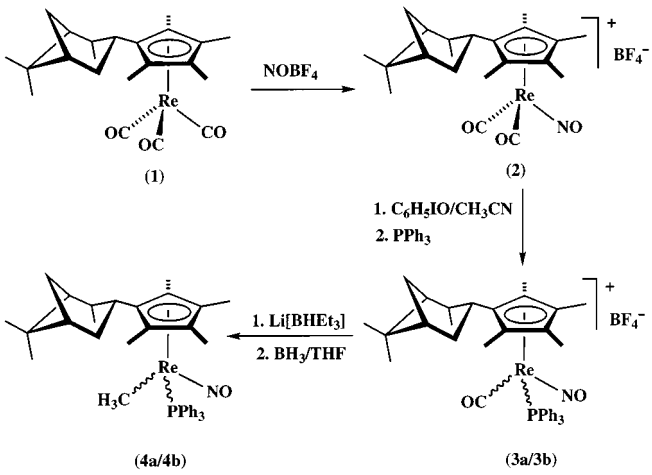
1. Synthesis of a Diastereomeric Mixture of (S_{Re})/(R_{Re})-(η^5-PinCp*)Re(CH_3)(NO)(PPh_3)

The ligand PinCp* was prepared from optically active (+)-pinanaldehyde,[9] which was oxidized to the (+)-carboxylic acid and then converted in several steps into a peralkylated cyclopentadiene ligand, as described by Lai for the other enantiomer[8] (Scheme 1).



Scheme 1

Following the same method as before,[6] (η^5-PinCp*)-Re($CO)_3$ (**1**) was synthesized in good yield by reaction of [Re($CO)_3$($THF)_2$]Cl with PinCp*Li in THF (Scheme 2). Because the peralkylated ligand has homotopic faces, only one product is generated and no separation step is required. In line with the work of Gladysz et al.,[10] the tricarbonyl complex was treated with freshly prepared $NOBF_4$ in CH_2Cl_2 at 0°C to form [(η^5-PinCp*)Re($CO)_2$(NO)]$^+$ (**2**) as yellow crystals after workup. The two diastereotopic CO groups could now be distinguished in the ^{13}C-NMR spectrum as two singlets. Because PPh_3 is less π-accepting than CO, the second CO ligand could not be substituted directly. In a first step, one of the CO groups had to be oxidized with iodosobenzene in acetonitrile. The intermediate acetonitrile complex was then treated with an excess of PPh_3 to give a diastereomeric mixture of (S_{Re})/(R_{Re})-[(η^5-PinCp*)-Re(CO)(NO)(PPh_3)]$^+BF_4^-$ (**3a/3b**), which was obtained in excellent yield and purity. The IR spectrum contains two bands for the CO and NO ligands. The ^{1}H- and ^{13}C-NMR spectra each have two sets of signals due to the two diastereomers. The signals of the diastereomeric CO ligands are quite interesting, because they appear as two doublets at δ = 202, each with a coupling constant of 8.3 Hz. There was, unexpectedly, only one signal for both diastereomers in the ^{31}P-NMR spectrum, both in [D_6]acetone and in [D_3]nitromethane.



Scheme 2

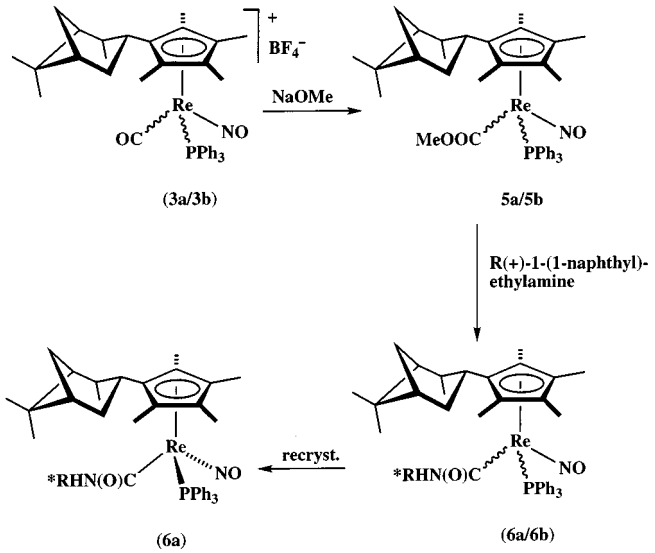
The reduction of the CO ligand to a methyl group was achieved in a two-step reaction with Li(C_2H_5)BH_3 and BH_3·THF.[11] After workup, (S_{Re})/(R_{Re})-(η^5-PinCp*)-Re(CH_3)(NO)(PPh_3) (**4a/4b**) was obtained as a red powder. The IR spectrum had one characteristic band for the NO ligand, while the ^{1}H- and ^{13}C-NMR spectra again contained two sets of signals for the two diastereomers. In the ^{1}H-NMR spectrum, the four methyl groups of the five-membered ring and the three methyl groups of the pinanyl part of each diastereomer overlapped. These signals therefore cannot be assigned unambiguously. Two signals, one at δ = 25.7 and one at δ = 23.4, appeared in the ^{31}P-NMR spectrum of the diastereomeric complexes. Because one of these signals is sharp and the other one is broad, it appears as if one of the two diastereomers is undergoing hindered ligand rotation. Measurements at low temperature confirmed that the broadened signal disappears below 0°C; two new signals, at a 3.5:1 ratio, appeared below −25°C. The sharp signal for the other diastereomer is retained throughout this experiment. That the original spectrum was observed again after the NMR sample was warmed up, confirms that hindered ligand rotation is a likely explanation for this phenomenon. It is interesting, but not yet explained why the two diastereomers should show such disparate behaviour and which type of rotation is involved.

The two signals of **4a/4b** appeared in a ratio of 1:1 in the ^{31}P-NMR spectrum, at room temp. The optically active PinCp* ligand therefore caused no asymmetric induction at the rhenium stereogenic centre. A reason for this may be the high temperature required for the substitution of the second CO group.

2. Resolution of Optically Active (S_{Re})-(PinCp*)Re(CH_3)(NO)(PPh_3) (4a)

Usually, mixtures of diastereomers can be separated by fractional crystallization or by chromatography. In our case, fractional crystallization was not possible because of the poor crystallinity of the mixture of (S_{Re})/(R_{Re})-(η^5-PinCp*)-Re(CH_3)(NO)(PPh_3). Also, no solvent mixture could be found to separate the diastereomers by preparative MPLC. We therefore followed the route of Gladysz et al. for the separation of (S_{Re})/(R_{Re})-(η^5-C_5Me_5)Re(CH_3)(NO)(PPh_3)[7] by using a suitable derivative.

The starting material for the separation was the complex (S_{Re})/(R_{Re})-[(η^5-PinCp*)Re(CO)(NO)(PPh_3)]$^+BF_4^-$ (**3a/3b**), which was treated with sodium methoxide in methanol to give the methyl ester (S_{Re})/(R_{Re})-[(η^5-PinCp*)Re(COOMe)(NO)(PPh_3) (**5a/5b**) in excellent yield (Scheme 3). The ^{31}P-NMR spectrum contained two sharp singlets in a ratio of 1:1. We could determine the ratio of the two diastereomers by using the two singlets of the methoxy groups at $\delta = 3$ in the ^{1}H-NMR spectrum. The CO groups appear in the ^{13}C-NMR spectrum as two doublets at $\delta = 203$ and 202, with $J_{C-P} = 13.8$ Hz.



Scheme 3

The methyl ester complexes were then treated with commercially available (+)-(*R*)-(1-naphthyl)ethylamine in CH_2Cl_2 to obtain the amide complexes **6a/6b**. The solvent was evaporated and the residual orange oil was stirred in *n*-hexane. An orange solid separated, which was collected by filtration, and recrystallized from benzene/*n*-hexane as crystals of one single diastereomer in an optical purity of > 98%, as determined by ^{1}H- and ^{31}P-NMR spectra (Scheme 3).

This less soluble diastereomer was identified by a crystal-structure determination to be (S_{Re})-(η^5-PinCp*)Re(NO)(PPh_3)[CONHCH(CH_3)$C_{10}H_7$] (**6a**) (Figure 1). These observations agree with Gladysz′ findings for (η^5-C_5Me_5)Re(NO)(PPh_3)[CONHCH(CH_3)$C_{10}H_7$], where the symmetrical products (S_{Re},S_{amid}) and (R_{Re},R_{amid}) were also more soluble than the mixed products (S_{Re},R_{amid}) and (R_{Re},S_{amid}).[7] The pinanyl substituent in **6a** adopts a conformation in which the methyl group points away from the metal centre and the dimethylmethylene bridge lies parallel to the plane of the cyclopentadienyl ring. This is very similar to the stereochemistry found in Lai′s molybdenum compound.[8]

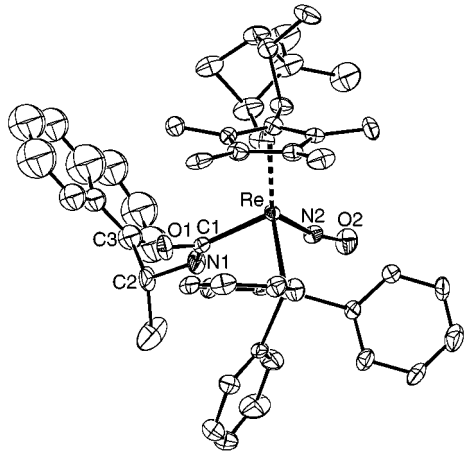


Figure 1. Crystal structure of (S_{Re})-(η^5-PinCp*)Re(NO)(PPh_3)-[CONHCH(CH_3)$C_{10}H_7$] (**6a**)

The enantiomerically pure amide was treated with trifluoroacetic acid at 0°C, which recovered the cationic, optically pure carbonyl complex, which was then isolated as the tetrafluoroborate salt (S_{Re})-[(η^5-PinCp*)Re(CO)-NO(PPh_3)]$^+BF_4^-$ (**3a**). By following this procedure with the other diastereomer, recovered by concentration of the mother liquor of the resolution step, the (R_{Re})-carbonyl complex could also be obtained in 80% optical purity. The reduction of pure **3a** to the methyl complex **4a** was carried out as described above for the diastereomeric mixture. The ^{31}P-NMR spectrum of (S_{Re})-(η^5-PinCp*)Re(CH_3)(NO)-(PPh_3) (**4a**) shows the broadened signal of the diastereomer undergoing hindered rotation. This signal, upon cooling, underwent the same changes as described before.

3. Formation and Stability of the Diastereomeric Mixture of (S_{Re})/(R_{Re})-[(η^5-PinCp*)-Re(NO)(PPh_3)($ClCD_2Cl$)]$^+BF_4^-$ (7a/7b) and Its Optically Pure (S_{Re}) Isomer

The chiral Lewis acid (S_{Re})/(R_{Re})-[(η^5-PinCp*)-Re(NO)(PPh_3)($ClCD_2Cl$)]$^+BF_4^-$ (**7a/7b**) was generated as described before.[5][12] The diastereomers were dissolved in CD_2Cl_2 in an NMR tube and treated with HBF_4 at −78°C. The ^{31}P-NMR spectrum, measured directly after shaking the reaction mixture, had three sharp signals of different intensity at $\delta = 14$, assignable to the two diastereomeric cations where one cation is a mixture of two rotamers. Additional signals appeared at $\delta = 15$ and 11 and seem to be decomposition products. When the solution was warmed, one of the three signals of the chiral Lewis acid remained unchanged, while the two others became broad. This behav-

iour is similar to that of the diastereomeric mixture of the complex (S_{Re})/(R_{Re})-[(η^5-PinCp*)Re(CH_3)(NO)(PPh_3) described above. Warming to −20°C resulted in a rapid decrease in the intensity of the three signals and a concomitant growth of the signals at δ = 11 and 15. The signal at δ = 11 appeared as two singlets in a ratio of 1:1, one of them sharp, the other one broadened.

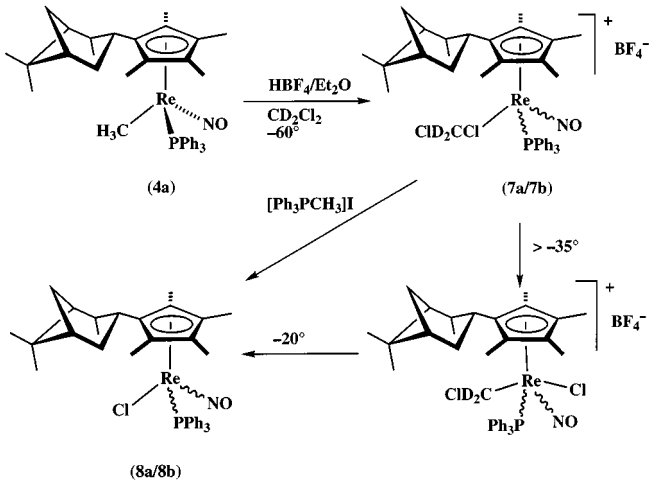
We then repeated the same experiment with optically pure (S_{Re})-[(η^5-PinCp*)Re(CH_3)(NO)(PPh_3). We expected to see only the two signals of the (S_{Re}) isomer, but surprisingly we also immediately observed the third signal due to the second diastereomer. This indicates that inversion at the metal centre starts taking place directly after mixing the compounds at −80°C. A noticeable amount of decomposition products was also observed at this temperature. At −60°C, the two diastereomers approached a ratio of 1:1, which was reached at −40°C. At −20°C, the cation had completely disappeared and the two signals at δ = 11 were again apparent as one sharp and one broadened signal. The IR spectrum of the reaction mixture, measured at room temperature, contained two NO signals, one at 1746 cm^{-1}, and one at 1641 cm^{-1}; they are assigned to the main decomposition products at δ = 11 and 15.

These results clearly show that the chiral Lewis acid (S_{Re})-[(η^5-PinCp*)Re(NO)(PPh_3)($ClCD_2Cl$)]$^+BF_4^-$ has an extremely low configurational stability. Even at −80°C, a small amount of the inversion product can be detected and at −40°C complete inversion has occurred. These conclusions could be drawn solely on the basis of low-temperature ^{31}P-NMR spectroscopy and they confirm the results obtained by Gladysz et al. for the Cp* complex. Gladysz′ observations, that the optically purity of the Lewis acid diminishes on reaction with another nucleophile can now be explained: Inversion at the metal centre already starts occurring shortly before the CD_2Cl_2 ligand is exchanged for a new nucleophile.

To find an explanation for the thermal and configurational instability of the complex [(η^5-Cp*)-Re(NO)(PPh_3)($ClCD_2Cl$)]$^+BF_4^-$, Gladysz et al. examined the products formed on warming the solution. They found that oxidative addition of the dichloromethane fragment takes place to give the cationic complex [(η^5-PinCp*)-Re(NO)(PPh_3)(CD_2Cl)Cl]$^+BF_4^-$. This Re^{III} species gives rise to a singlet at δ = 11 in its ^{31}P-NMR spectrum and an NO band at 1739 cm^{-1} in its IR spectrum. It was rationalized that the electron-rich permethylated complex confers stability to this unexpected Re^{III} species; this favours the formation of a higher oxidation species, which, contrary to expectations, lowers the stability of the chiral Lewis acid.

As we also saw two signals at δ = 11 in the ^{31}P-NMR spectra and a signal at 1746 cm^{-1} in the IR spectra, we tried to isolate [(η^5-PinCp*)Re(NO)(PPh_3)(CD_2Cl)Cl]$^+$-BF_4^- by dissolving the dried residue of the NMR sample in a small amount of THF and precipitating it with ether. A solid appeared, which dissolved again after being stirred for a short time. If this precipitate was in fact the Re^{III} species, of which we are sure, it must be quite unstable in the case of the PinCp* complex.

The chiral Lewis acid decomposition products whose signals were observed at δ = 15 appeared to be more stable. By comparing[12][13] the ^{31}P-NMR and IR data of the analogous PCp and Cp* complexes, we deduced this species to be a diastereomeric mixture of (S_{Re})/(R_{Re})-(η^5-PinCp*)-ReCl(NO)(PPh_3) (**8a/8b**). This could have formed directly by nucleophilic substitution of the stabilizing solvent molecule by a chloride anion, available from a small amount of DCl in the solvent. On the other hand, it could have formed by loss of CD_2Cl^+ from the Re^{III} species. We favour the second pathway because the signal at 1746 cm^{-1} disappears in favour of the signal at 1641 cm^{-1} (Scheme 4).



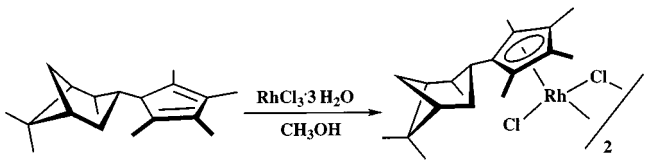
Scheme 4

To confirm this, we synthesized the chloride complex independently, following the route that Gladysz used for the Cp* complex.[13] After formation of the chiral Lewis acid, methyltriphenylphosphonium iodide was added. The solution turned red and the product could be identified by IR, ^{1}H-, ^{13}C-, ^{31}P-NMR, and MS data to be the expected chloride species (**8a/8b**). The IR and ^{31}P-NMR signals were identical to those of the previous NMR experiments. The ^{31}P-NMR spectrum of **8a/8b** contained a sharp and a broad signal. The broadened signal disappeared upon cooling below 0°C and two new signals appeared upon further cooling. The sharp signal does not change during this time. The same behaviour was previously observed for (S_{Re})/(R_{Re})-[(η^5-PinCp*)Re(CH_3)(NO)(PPh_3). Again, a hindered ligand rotation associated most likely with the bulky PinCp* ligand occurs within the (S_{Re}) isomer, but not in the case of the (R_{Re}) isomer. It remains unclear why this phenomenon should so persistently be restricted to only one of the two diastereomers.

4. Synthesis of Other Metal Complexes of the Chiral Cyclopentadienyl Ligand PinCp*

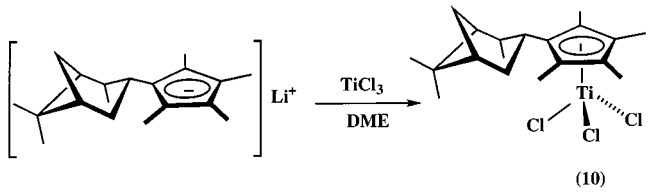
As rhodium complexes with a chiral cyclopentadienyl ligand are known to be useful in asymmetric hydrogenations,[14] we also synthesized a corresponding PinCp* complex. We prepared [PinCp*$RhCl_2$]$_2$ (**9**) by heating

$RhCl_3 \cdot 3H_2O$ and PinCp*H in methanol under reflux for a few days (Scheme 5). After the solvent was evaporated, a red solid was collected in reasonable yields, which was characterized by ^1H- and ^{13}C-NMR spectroscopy and elemental analysis. We are currently trying to perform these experiments in the presence of zeolites to prepare a corresponding "ship-in-the-bottle" complex and to test **9** as a catalyst precursor in enantioselective hydrogenation.



Scheme 5

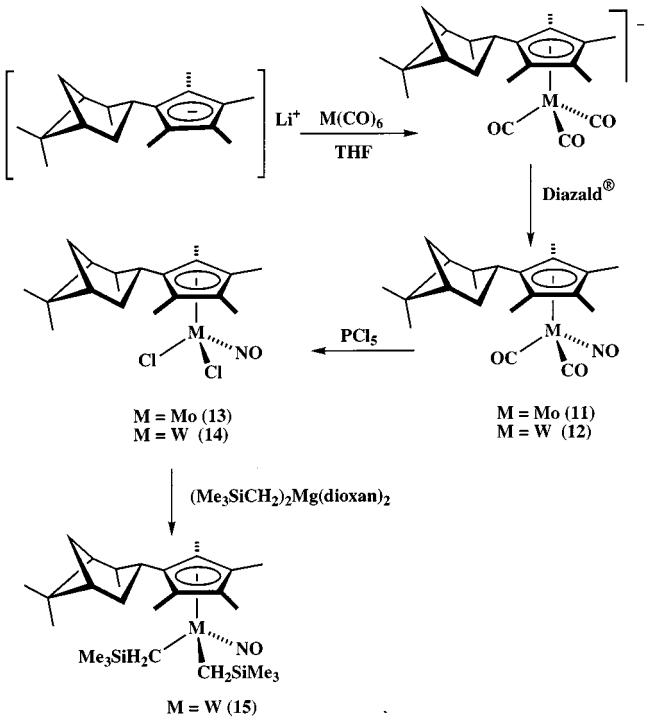
Chiral cyclopentadienyl ligands are also often attached to early transition metals like Ti, Zr, and Hf.[15] Such complexes may be efficient Ziegler-Natta polymerization catalysts, or catalyse enantioselective synthesis. We prepared the complex (PinCp*)$TiCl_3$ (**10**) by treating $TiCl_3 \cdot 3THF$ with PinCp*Li in DME under reflux.[16] After workup, a red solid was isolated and characterized by ^1H- and ^{13}C-NMR and MS data to be PinCp*$TiCl_3$. Extraction of the remaining solid with CCl_4 did not lead to the isolation of the expected doubly substituted product (PinCp*)$_2TiCl_2$. The reaction with PinCp* therefore takes a different route from that with Cp*, where Cp*$_2TiCl_2$ is the major product under the same reaction conditions (Scheme 6).



Scheme 6

Legdzins et al. have prepared many complexes with the 14-VE backbone Cp′M(NO) [M = Mo, W; Cp′ = C_5H_5 or C_5Me_5].[17] Their aim was to synthesize stable 16-VE complexes of the type Cp′M(NO)(R)(R′), where the alkyl or aryl substituents could be equivalent or different from each other. To synthesize such a complex with the chiral ligand PinCp* we followed the procedure published for Cp*.[18] [(η^5-PinCp*)M$(CO)_3$]$^-$ was synthesized by treating $M(CO)_6$ with PinCp*Li in THF. The anion was then directly converted into the neutral, coordinatively saturated complexes (η^5-PinCp*)M$(CO)_2$(NO) (**11**,**12**) without further purification by treating the tricarbonyl complex with Diazald. The product was purified by sublimation and excess Diazald was separated by column chromatography (hexane/ether, 4:1). The reaction of the nitrosyl complexes with PCl_5 in ether yielded the 16-VE complexes (PinCp*)MCl_2(NO) (**13**,**14**) as poorly soluble, green solids (Scheme 7).

The nitrosyl dichloride complex was alkylated with $(Me_3SiCH_2)_2Mg \cdot (dioxane)_2$ at very low temperatures.[19] As the Cp* tungsten complex was more stable than the corresponding molybdenum compounds,[20] we restricted our investigations to the former. The NO group of the dialkylated product (PinCp*)W(NO)$(CH_2SiMe_3)_2$ (**15**) has an IR absorption at 1582 cm^{-1} which agrees with a weakening of the N−O bond as found by Legdzins et al. in crystal structures. The ^1H- and ^{13}C-NMR spectra contain two signals for the diastereotopic $SiMe_3$ groups. The compound does not appear to be as stable in solution as the corresponding Cp* complex, but it can be stored at room temperature as a solid. We could also obtain a monoalkylated product as a red oil by using only half an equivalent of the magnesium reagent and strict temperature control, but this product was too unstable to be isolated and fully characterized in analytically pure form.



Scheme 7

We also tried to generate a new stereogenic centre at the metal atom by a thermal or photochemical substitution of one of the CO groups in (PinCp*)W$(CO)_2$(NO). Brunner[21] had reported an efficient substitution of PPh_3 for CO to generate the complex CpMo(CO)(NO)(PPh_3) in refluxing toluene. He obtained quantitative yields, while another group[22] claimed that this substitution does not take place even at very high temperatures. We treated (PinCp*)Mo$(CO)_2$(NO) with PPh_3 in refluxing toluene over several hours. No substitution could be observed, which may be either because the PinCp* ligand is more electron-donating or because of steric hindrance. A photochemical ligand exchange also did not occur by irradiation in toluene, where after one hour the starting material had completely decomposed.

PinCpH* also reacts with carbonyliron and -ruthenium complexes to form dimeric carbonyl complexes. These will be described elsewhere.

Conclusion

The optically active peralkylated ligand PinCp*H can be introduced into a series of metal complexes of titanium, molybdenum, tungsten, rhenium and rhodium. In most cases, these new complexes have properties similar to those of the corresponding Cp* complexes. The PinCp* ligand can serve as an internal spectroscopic probe for the configurational stability of the chiral-at-metal Lewis acid [PinCp*ReNO(PPh_3)($ClCD_2Cl$)]$^+$.

Experimental Section

General Remarks: All experiments were performed under purified nitrogen using standard vacuum-line and Schlenk-tube techniques. Diethyl ether and THF were distilled from sodium benzophenone ketyl. Acetonitrile and dichloromethane were distilled from calcium hydride. Dimethoxyethane (DME) and *n*-hexane were dried with molecular sieves. [$Re(CO)_3(THF)_2$]Cl,[23] $NOBF_4$,[24] iodosobenzene,[25] [$(Me_3Si)CH_2Mg$]·(dioxane)$_2$[26] and PinCp*[8] were prepared as described in the literature. (+)-3-Formylpinane was a gift from BASF. − Infrared spectra were recorded with a Perkin−Elmer 1750 FT spectrophotometer as solutions in *n*-hexane, CH_2Cl_2, or DME in NaCl cells. − NMR spectra were recorded with either a Varian VXR 300 or a Varian Unity 500 spectrometer in $CDCl_3$ or C_6D_6 unless otherwise stated. ^{1}H- and ^{13}C-NMR spectra were referenced to tetramethylsilane (TMS) or from internal solvent peaks; ^{31}P-NMR spectra were referenced to H_3PO_4 (external). All ^{13}C- and ^{31}P-NMR data are of proton-decoupled (broadband) spectra.

(+)-(1*S*,2*S*,3*S*,5*R*)-Pinane-3-carboxylic Acid: (+)-3-Formylpinane (49.8 g, 0.30 mol) was dissolved in acetone and treated slowly with a cold saturated aqueous solution of $KMnO_4$ (31.6 g, 0.2 mol). The solution was stirred for 2 h at room temperature and the precipitate of MnO_2 was filtered off with a Buchner funnel, and through Celite/cotton wool. The solution was treated with solid KOH to an approximate pH value of 12 and extracted 3 times with ether. After acidification with concd. HCl, the aqueous solution was again extracted 3 times with ether. The organic phases were combined and dried with $MgSO_4$. The solvent was evaporated under reduced pressure in a rotary evaporator, leaving a pale-yellow oil, yield 52.8 g (0.29 mol, 98%). This product was used for the further synthesis of PinCp*.[8]

[(η^5-PinCp*)Re(CO)$_3$ (1): PinCp*H (5.16 g, 20.0 mmol) was dissolved in 80 mL of THF and cooled to −78°C. *n*BuLi (1.6 M in hexane, 20 mmol, 12.5 mL) was added by syringe while the solution was stirred. The mixture was allowed to warm to room temperature and was then refluxed for 14 h. PinCp*Li precipitated as a white solid. The solvent was removed by vacuum distillation and the product was washed twice with 100 mL of *n*-hexane. The white solid was dissolved in 50 mL of THF, cooled to 0°C, and a solution of 20.0 mmol of [$Re(CO)_3(THF)_2$]Cl in THF was added dropwise. The solution was then refluxed for 12 h and, after cooling to room temperature, the solvent was removed by vacuum distillation. The residue was extracted with hot *n*-hexane and filtered hot through Celite. After concentrating the solution, the product precipitated at −30°C as an off-white solid; yield: 10.00 g (19.0 mmol, 95%). − IR (*n*-hexane): $\tilde{\nu}_{(CO)}$ = 2014 (s), 1923 (s) cm^{-1}. − ^{1}H NMR ($CDCl_3$): δ = 2.94 (q, J_{H-H} = 9.5 Hz, 1 H, H-4), 2.38 (m, 1 H), 2.27 (s, 3 H, C_5Me_4), 2.21 (s, 3 H, C_5Me_4), 2.17 (d, J_{H-H} = 7.3 Hz, 6 H, C_5Me_4), 2.08 (m, 3 H, H-9), 1.90 (t, J_{H-H} = 5.5 Hz, 2 H), 1.26 (s, 3 H, H-9), 1.19 (s, 1 H), 1.16 (s, 3 H, H-8), 1.02 (d, J_{H-H} = 7.0 Hz, 2 H). − ^{13}C NMR ($CDCl_3$): δ = 198.1 (CO), 105.5, 100.9, 98.4, 96.9 (C_5Me_4), 49.2 (C-5), 43.2 (C-1), 39.42, 34.4 (C-2/6/10), 39.1 (br., C-3), 33.9 (C-4), 28.7, 23.5 (C-8/9), 21.2 (C-7), 12.0, 10.9, 10.8 (C_5Me_4). − $C_{22}H_{29}O_3Re$ (527.66): calcd. C 50.08, H 5.54; found C 50.08, H 5.52.

[(η^5-PinCp*)Re(CO)$_2$(NO)]$^+$BF$_4^-$ (2): Compound **1** (2.30 g, 4.36 mmol) was dissolved in 100 mL of CH_2Cl_2 and cooled to 0°C. Freshly prepared $NOBF_4$ (0.79 g, 6.77 mmol) was added in small portions and CO started to evolve immediately. After 3 h of stirring, the solution was poured into 300 mL of diethyl ether and a light yellow precipitate formed. The solid was collected by filtration and washed with diethyl ether. Recrystallisation from CH_2Cl_2/*n*-hexane gave a yellow compound **2**; yield: 2.63 g (4.27 mmol, 98%). − IR (hexane): $\tilde{\nu}_{(CO)}$ = 2093 (s), 2040 (s); $\tilde{\nu}_{(NO)}$ = 1799 (m) cm^{-1}. − ^{1}H NMR ([D$_6$]acetone): δ = 3.37 (q, *J* = 9.5 Hz, 1 H, H-4), 2.64 (s, 3 H, C_5Me_4), 2.57 (s, 3 H, C_5Me_4), 2.50 (d, J_{H-H} = 2.8 Hz, 6 H, 2∞ C_5Me_4), 2.47 (m, 1 H), 2.35 (m, 2 H), 2.12 (m, 1 H), 1.99 (m, 2 H), 1.30 (s, 3 H, H-9), 1.28 (s, 1 H), 1.22 (s, 3 H, H-8), 1.12 (d, J_{H-H} = 7.0 Hz, 3 H, H-7). − ^{13}C NMR ([D$_6$]acetone): δ = 187.0, 186.9 (CO), 112.1, 109.2 (C_5Me_4), 49.9 (C-5), 43.8 (C-1/3), 40.1, 38.3, 34.9 (C-2/6/10), 35.2 (C-4), 29.0, 23.7 (C-8/9), 21.4 (C-7), 11.9, 11.7, 10.5, 10.3 (C_5Me_4). − $C_{21}H_{29}BF_4NO_3Re$ (616.47): calcd. C 40.91, H 4.74, N 2.27; found C 40.56, H 2.25, N 2.25.

(*S*$_{Re}$)/(*R*$_{Re}$)-[(η^5-PinCp*)Re(CO)(NO)(PPh_3)]$^+$BF$_4^-$ (3a/3b): The nitrosyl complex **2** (2.56 g, 4.16 mmol) was dissolved in 50 mL of acetonitrile and freshly prepared iodosobenzene (1.05 g, 4.78 mmol) was added at 0°C. CO_2 evolution started immediately and the solution was stirred until the solid had dissolved (about 1.5 h). The solution was filtered through 2 cm of silica gel and after evaporation of the solvent (*S*$_{Re}$)/(*R*$_{Re}$)-[(η^5-PinCp*)Re(CH_3CN)(NO)(PPh_3)]$^+$BF$_4^-$ was obtained as a brown oil. − IR (CH_3CN): $\tilde{\nu}_{(CO)}$ = 2010 (s), $\tilde{\nu}_{(NO)}$ = 1743 cm^{-1}. − The oil was dissolved in 2-butanone and PPh_3 (1.33 g, 5.09 mmol) was added in small portions while stirring. The dark-brown mixture was refluxed for 12 h and the solvent was removed afterwards by vacuum distillation. The residue was recrystallized from acetone/Et_2O; yield of yellow **3a/3b**: 3.18 g (3.74 mol, 90%). − IR (CH_2Cl_2): $\tilde{\nu}_{(CO)}$ = 2005 (s), $\tilde{\nu}_{(NO)}$ = 1747 (s) cm^{-1}. − ^{1}H NMR ([D$_6$]acetone): δ = 7.70−7.50 (m, 30 H, PPh_3), 3.45 (q, J_{H-H} = 9.46 Hz, 1 H, H-4), 3.40 (q, J_{H-H} = 7.02, 1 H, H-4′), 2.85 (s, 3 H), 2.50 (s, 3 H), 2.46 (m, 1 H), 2.38 (m, 3 H), 2.31 (s, 3 H), 2.27 (s, 3 H), 2.16 (m, 3 H), 2.00 (m, 2 H), 1.86 (s, 3 H), 1.71 (s, 3 H), 1.51 (s, 3 H), 1.33(s, 1 H), 1.30 (m, 6 H), 1.27 (s, 3 H), 1.24 (s, 3 H), 1.12 (m, 6 H). − ^{13}C NMR ([D$_6$]acetone): δ = 201.8 (d, J_{C-P} = 12.6 Hz, CO), 201.4 (d, J_{C-P} = 12.6 Hz, CO′), 134.3 (d, J_{C-P} = 11.4 Hz, C-b), 134.1 (d, J_{C-P} = 11.4 Hz, C-b′), 133.3 (dd, J_{C-P} = 6.6 Hz, C-d/d′), 131.2 (d, J_{C-P} = 12.6 Hz, C-a/a′), 130.7 (d, J_{C-P} = 11.4 Hz, C-c), 130.6 (d, J_{C-P} = 11.4 Hz, C-c′), 115.5, 114.7, 109.7, 107.5, 106.0 (C_5Me_4), 50.2 (C-5/5′), 44.4 (br. s, C-3/3′), 43.9, 43.7 (C-1/1′), 40.2, 40.1 (C-10/10′), 37.8, 36.3 (C-4/4′), 35.9, 35.6, 34.9 (C-2/2′/6/6′), 29.4, 29.0, 23.9, 23.7 (C-8/8′/9/9′), 21.8, 21.7 (C-7/7′), 15.1, 11.8, 11.6, 10.2, 10.0, 9.8, 9.4 (C_5Me_4). − ^{31}P NMR ([D$_6$]acetone): δ = 12.9. − $C_{38}H_{44}BF_4NOPRe$ (834.71): calcd. C 53.65, H 5.21, N 1.65; found C 52.98, H 5.22, N 1.64.

(*S*$_{Re}$)/(*R*$_{Re}$)-(η^5-PinCp*)Re(CH_3)(NO)(PPh_3) (4a/4b): The diastereomeric mixture of **3** (1.56 g, 1.83 mmol) was suspended in 50 mL of THF and 3.7 mL of Li(C_2H_5)$_3$BH in THF (1 M in THF, 3.7 mmol) was injected. The precipitate dissolved slowly, while the colour of the solution became honey-brown. Then 9.2 mL of 0.776 M BH_3·THF in THF (7 mmol) was added. H_2 evolution occurred immediately and the solution was stirred for 30 min. The

solvent was then removed and the residue extracted with toluene and passed through a short silica gel column. The solvent was evaporated to give complex **4a/4b** as a red powder; yield 1.31 g (1.74 mmol, 95%). − IR (hexane): $\nu_{(NO)}$ = 1634 (s) cm^{-1}. − ^1H NMR ($CDCl_3$): δ = 7.50−7.32 (m, 30 H, PPh_3), 3.22 (q, J_{H-H} = 9.46 Hz, 1 H, H-4), 3.13 (q, J_{H-H} = 9.46 Hz, 1 H, H-4′), 2.38 (m, 2 H), 2.28 (m, 2 H), 2.21 (m, 2 H), 2.06 (s, 3 H), 2.00(m, 1 H), 1.90 (m, 4 H), 1.82 (s, 3 H), 1.80 (s, 3 H), 1.53(s, 3 H), 1.50 (s, 3 H), 1.29−1.23 (6 s, 18 H), 1.11 (d, J_{H-H} = 7.02 Hz, 3 H), 1.06 (d, J_{H-H} = 7.02 Hz, 3 H), 0.84 (d, J_{H-P} = 7.02, 3 H, Re−Me), 0.79 (d, J_{H-P} = 7.02 Hz, 3 H, Re−Me′), 0.68 (s, 3 H), 0.5 (s, 3 H). − ^{13}C NMR ($CDCl_3$): δ = 136.4, 136.0 (d, J_{C-P} = 47.7 Hz, C-a), 136.0, 135.6 (d, 47.7 Hz, C-a′), 134.08, 134.01 (d, J_{C-P} = 9.8 Hz, C-b), 134.04, 133.96 (d, 10.4 Hz, C-b′), 129.5 (C-d/d′), 128.1, 128.0 (C-c/c′), 107.5, 105.9, 103.7, 103.6, 100.4, 96.6, 95.6, 94.7 (C_5Me_4), 49.6, 49.5 (C-5/5′), 43.8 (br., C-3/3′), 43.2, 43.1 (C-1/1′), 39.6, 39.5 (C-10/10′), 35.7, 35.4, 34.8, 34.6,34.4 (C-4/4′/2/2′/6/6′), 28.9, 23.6, 23.5 (C-8/8′/9/9′), 21.6, 21.5 (C-7/7′), 11.9,11.8, 10.8, 10.7, 10.6, 7.6, 7.3 (C_5Me_4), −22.7 (d, J_{C-P} 7.0 Hz, Re−Me), −24.7 (d, J_{C-P} = 7.2 Hz, Re−Me). − ^{31}P NMR (C_6D_6): δ = 25.7 (br.), 23.4. − $C_{38}H_{47}NOPRe$ (750.92): calcd. C 60.78, H 6.31, N 1.87; found C 59.96, H 6.33, N 1.87

(S_{Re})/(R_{Re})-(η⁵-PinCp*)Re(COOCH₃)(NO)(PPh₃) (5a/5b): The diastereomeric mixture of **3a/3b** (1.04 g, 1.23 mmol) was dissolved in 30 mL of dichloromethane and 2.7 mL of 4.37 M sodium methoxide in MeOH (10.68 mmol) was added while stirring. The progress of the reaction was monitored by IR spectroscopy. After the disappearance of the starting material, the solvent was removed. The residue was extracted with hot *n*-hexane, filtered and concentrated. Slow cooling gave a yellow precipitate which was purified by washing with a small amount of *n*-hexane. Yield of **5a/5b**: 1.15 g (1.14 mmol, 93%). − IR (CH_2Cl_2): $\tilde{\nu}_{(NO)}$ = 1646 (s), $\tilde{\nu}_{(COOMe)}$ = 1576 (m) cm^{-1}. − IR (MeOH): $\tilde{\nu}_{(NO)}$ = 1663 (s), $\tilde{\nu}_{(COOMe)}$ = 1550 (m) cm^{-1}. − ^1H NMR ($CDCl_3$): δ = 7.47 (m, 12 H, PPh_3), 7.36(m, 18 H, PPh_3), 3.27 (q, J_{H-H} = 9.46 Hz, 1 H, H-4), 3.17 (q, J_{H-H} = 9.46 Hz, 1 H, H-4′), 3.03 (s, 3 H, OCH_3), 2.98 (s, 3 H, OCH_3), 2.36 (m, 3 H), 2.25 (s, 4 H), 2.16 (s, 2 H), 2.07 (m, 3 H), 1.97 (s, 1 H), 1.91 (m, 2 H), 1.87 (s, 6 H), 1.72 (s, 3 H), 1.47 (s, 2 H), 1.31 (s, 2 H), 1.29 (s, 1 H), 1.28 (s, 3 H), 1.24 (s, 6 H), 1.21 (m, 1 H), 1.16 (s, 9 H), 1.08 (d, J_{H-H} = 7.02 Hz, 3 H), 1.02 (d, J_{H-H} = 7.02 Hz, 3 H), 0.95 (d, 3 H). − ^{13}C NMR ($CDCl_3$): δ = 203.2 (d, J_{C-P} = 13.7 Hz, CO), 202.6 (d, J_{C-P} = 13.7 Hz, CO), 135.0 (d, J_{C-P} = 25 Hz, C-a), 134.6 (d, J_{C-P} = 25 Hz, C-a′), 134.2, 134.1 (d, J_{C-P} = 3.8 Hz, C-b), 134.1, 134.0 (d, J_{C-P} = 3.8 Hz, C-b′), 130.0, 129.9 (C-d/d′), 128.1, 128.0 (C-c/c′), 111.2, 110.6, 104.5, 104.1, 100.1, 100.0 (C_5Me_4), 49.7, 49.5, 49.4, 49.1 (C-5/5′/OCH_3/OCH_3′), 44.5, 44.1 (br., C-3/3′), 43.3, 43.2 (C-1/1′), 39.6, 39.5 (C-10/10′), 36.5, 35.4 (C-4/4′), 34.8, 34.7, 34.4, 34.3 (C-2/2′/6/6′), 28.8, 28.7, 23.6, 23.4 (C-8/8′/9/9′), 21.7, 21.6 (C-7/7′), 11.9, 11.8, 11.6, 11.1, 10.9, 9.9, 8.9, 8.7 (C_5Me_4/C_5Me_4′). − ^{31}P NMR ($CDCl_3$): δ = 18.7, 18.1. − $C_{39}H_{47}NO_3PRe$ (794.97): calcd. C 58.92, H 5.96, N 1.76; found C 58.88, H 5.89, N 1.74.

(S_{Re})/(R_{Re})-(η⁵-PinCp*)Re(NO)(PPh₃)[CONHCH(CH₃)C₁₀H₇] (6a/6b): Compound **5a/5b** (1.02 g, 1.28 mmol) was dissolved in 30 mL of CH_2Cl_2 and (+)-(*R*)-1-(1-naphthyl)ethylamine (0.42 mL, 2.56 mmol) was added dropwise via a syringe. The solution was stirred at room temperature until the reaction was completed (reaction monitoring by IR spectroscopy). The solvent was then removed and the oily residue was stirred in *n*-hexane until a yellow precipitate formed. The solid was collected by filtration and recrystallized from CH_2Cl_2/*n*-hexane. After a few days, orange crystals of (S_{Re})-(η⁵-PinCp*)Re(NO)(PPh_3)[CONHCH(CH_3)$C_{10}H_7$] (**6a**) had formed. Yield: 0.35 g (0.38 mmol, 60%) of optical purity: > 98% *de*. − IR (CH_2Cl_2): $\tilde{\nu}_{(NO)}$ = 1624 (s), $\tilde{\nu}_{(CO)}$ = 1533 (m) cm^{-1}. − ^1H NMR ($CDCl_3$): δ = 8.16 (d, J_{H-H} = 7.32 Hz, 1 H), 7.78 (d, J_{H-H} = 7.94 Hz, 1 H), 7.67 (dd, J_{H-H} = 1.83 Hz, J<inf'H−H</INF' = 6.91 Hz, 1 H), 7.55 (t, J_{H-H} = 8.55 Hz, 6 H, H-b), 7.39 (m, 13 H, H-c/d/naphthyl), 5.76 (quint, J_{H-H} = 6.87 Hz, 1 H, NCH), 5.26 (s, 1 H, NH), 3.08 (q, J<inf'H&NDASH;H</INF' = 9.36 Hz, 1 H, H-4), 2.17 (t, J_{H-H} = 7.48 Hz, 2 H), 2.10 (s, 3 H, CH_3), 2.03 (s, 3 H, CH_3), 1.89 (m, 1 H), 1.78 (t, J_{H-H} = 5.56 Hz, 1 H), 1.52 (s, 3 H, CH_3), 1.43 (s, 1 H), 1.26 (s, 1 H), 1.18 (s, 3 H, CH_3), 1.10 (s, 3 H, CH_3), 1.05 (s, 3 H, CH_3), 0.95 (s, 3 H, CH_3), 0.84 (d, J_{H-H} = 6.41, 1 H), 0.78 (d, J_{H-H} = 6.71 Hz, 3 H, $NCCH_3$). − ^{13}C NMR ($CDCl_3$): δ = 199.5 (d, J_{H-H} = 11.6 Hz, CO), 141.4 (C-Naph1), 134.2 (C-NCH), 133.9 (C-a PPh_3), 131.3 (C-Naph8/9), 139.8, 128.3, 128.2, 128.1 (d, J_{H-H} = 9.8 Hz), 127.1, 125.7, 125.3, 125.2, 124.5, 122.2 (CH-Naph, PPh_3), 111.7, 101.1, 98.6 (C_5Me_4), 49.3 (C-5), 43.9, 42.9 (C-3/NaphCH_3), 43.5 (C-1), 39.3, 34.8, 34.4 (C-2/6/10), 35.0 (C-4), 28.8, 23.4 (C-8/9), 20.3 (C-7), 12.0, 11.5, 10.2, 8.1 (C_5Me_4). − ^{31}P NMR ($CDCl_3$): δ = 19.5. − $C_{50}H_{46}O_2N_2PRe$ (924.10): calcd. C 64.29, H 6.04, N 3.00; found C 64.19, H 6.11, N 3.04.

(S_{Re})-(η⁵-PinCp*)Re(NO)(PPh_3)(CH_3) (4a): The optically pure amide **6a** (0.34 g, 0.36 mmol) was dissolved in 5 mL of dichloromethane and CF_3COOH (68.0 mL, 0.90 mmol) was added dropwise at 0 °C. The solution was stirred at this temperature for 10 min; the orange colour changed to yellow. The solvent was removed and the residue was dissolved in 5 mL of MeOH. Then $NaBF_4$ (0.075 g, 0.72 mmol), dissolved in 2 mL of water, was added dropwise. An additional 6 mL of water was then added and a yellow precipitate formed. Stirring was continued for 15 min, the solid was collected by filtation and dried in vacuo. Yield of **3a** (S_{Re})-[(η⁵-PinCp*)-Re(CO)(NO)(PPh_3)]$^+BF_4^-$: 0.30 g (0.36 mmol, 99%). − ^{13}C NMR ([D_6]acetone): δ = 206.0 (CO), 134.3, 134.1 (d, J_{C-P} = 11.5 Hz, C-b), 133.3 (C-d), 131.5 (C-a), 130.7, 130.5 (d, J_{C-P} = 11.4 Hz, C-c), 116.9, 116.1, 110.2, 107.6, 106.3 (C_5Me_4), 50.4 (C-5), 44.3 (br., C-3), 43.9 (C-1), 40.2 (C-10), 36.5 (C-4), 36.0, 35.0 (C-2/6), 38.9, 23.9 (C-8/9), 21.8 (C-7), 12.3, 11.7, 10.1, 9.6 (C_5Me_4). − The yellow precipitate of **3a** was dissolved in 20 mL of THF and 0.71 mL of Li[(C_3H_5)$_3$BH] in THF (1 M in THF, 0.71 mmol) was added. After 20 min of stirring, 1.25 mL of BH3·THF (0.94 M in THF, 1.34 mmol) was added dropwise. While the solution was stirred for 30 min, it turned red. The solvent was removed in vacuo, the residue taken up in toluene and passed through 3 cm of silica gel. After evaporating the solvent in vacuo, the red solid was recrystallized from *n*-hexane. Yield of **4a**: 0.26 g (0.34 mmol, 95%). − IR (*n*-hexane): nu tilde$_{(NO)}$ = 1634 (s) cm^{-1}. − ^1H NMR ($CDCl_3$): δ = 7.50−7.32 (m, 15 H, PPh_3), 3.22 (q, J_{H-H} = 9.46 Hz, 1 H, H-4), 2.38 (m, 1 H), 2.28 (m, 1 H), 2.21 (m, 1 H), 2.06 (s, 1 H), 2.00 (m, 1 H), 1.90 (m, 1 H), 1.82 (s, 3 H), 1.50 (s, 3 H), 1.29 (s, 3 H), 1.23 (s, 3 H), 1.06 (d, J_{H-H} = 7.02 Hz, 3 H), 0.84 (d, J_{H-P} = 7.02, 3 H, ReMe), 0.5 (s, 3 H). − ^{13}C NMR ($CDCl_3$): δ = 136.4, 136.1 (d, J_{C-P} = 47.6 Hz, C-a), 134.1, 134.0 (d, J_{C-P} = 10.4 Hz, C-b), 129.6 (C-d), 128.1, 128.0 (d, J_{C-P} = 9.8 Hz, C-c), 96.6, 94.7 (C_5Me_4), 49.6 (C-5), 43.6 (br., C3), 43.1 (C-1), 39.6 (C-10), 35.4 (C-4), 34.9, 34.4 (C-2/6), 28.0, 23.6 (C-8/9), 21.6 (C-7), 11.8, 10.8, 10.6, 7.3 (C_5Me_4), 22.7, −22.8 (d, J_{C-P} = 6.5 Hz, ReCH_3). − ^{31}P NMR ($CDCl_3$): δ = 24.8 (br.) (25 °C); 25.4 (br.), 23.1 (br.) (−20 °C); 25.5, 23.1 (−50 °C). − $C_{38}H_{47}NOPRe$ (750.92): calcd. C 60.78, H 6.31, N 1.87; found C 60.82, 6.38, N 1.85.

(S_{Re})/(R_{Re})-[(η⁵-PinCp*)Re(NO)(PPh_3)($ClCD_2Cl$)]$^+BF_4^-$ (7a/7b) (NMR Experiment): A 5-mm NMR tube was filled with a solution of **4a/4b** (60.0 mg, 0.08 mmol) in 0.7 mL of CD_2Cl_2. The NMR tube was cooled to −78 °C and 11 μL of HBF_4·Et_2O (54% in Et_2O, 0.081 mmol) was added by syringe. The tube was sealed, shaken

quickly and a ^{31}P-NMR spectrum was measured at −80°C immediately. − ^{31}P NMR (CD_2Cl_2): δ = 14.7, 14.3, 14.2 (−80°C); 14.6, 14.1, 14.0 (−60°C); 14.5 (v br.), 14.0, (br.), 13.9 (−40°C); 13.9 (v br.), 13.8 (−20°C).

(S_{Re})-[(η^5-PinCp*)Re(NO)(PPh_3)($ClCD_2Cl$)]$^+BF_4^-$ (7a) (NMR Experiment): Optically pure **4a** was treated the same way as the diastereomeric mixture. − ^{31}P NMR (CD_2Cl_2): δ = 14.7, 14.3 (−80°C); 14.6, 14.1 (−60°C); 14.5 (v br.), 14.0, (br.) (−40°C); 13.9 (v br.) (−20°C).

(S_{Re})/(R_{Re})-(η^5-PinCp*)ReCl(NO)(PPh_3) (8a/8b): Complexes **4a/4b** (60 mg, 0.08 mmol) were dissolved in 10 mL of CH_2Cl_2 and cooled to −78°C. 11.8 µL HBF_4·Et_2O (54% in Et_2O, 0.087 mmol) was added by syringe and the mixture was stirred at this temperature for 10 min. Then $[Ph_3PCH_3]^+I^-$ (39.5 mg, 0.098 mmol) was added and the cooling bath was removed. The solution was warmed to room temperature, passed through 3 cm of silica gel and dried. Yield of a red solid **8a/8b**: 49.3 mg (0.06 mmol, 80%). − IR (CH_2Cl_2) $\tilde{\nu}_{(NO)}$ = 1641 cm^{-1}. − ^{1}H NMR ($CDCl_3$): δ = 7.60−7.52 (m, 6 H, H-b), 7.37 (m, 9 H, H-c/d), 3.14 (q, J_{H-H} = 9.46 Hz, 1 H, H-4), 3.06 (q, J_{H-H} = 9.46 Hz, 1 H, H-4′), 2.49 (m, 1 H), 2.34 (m, 2 H), 2.29 (m, 1 H), 2.20 (m, 2 H), 2.05 (m, 4 H), 1.96 (s, 1 H), 1.92 (m, 1 H), 1.89 (m, 2 H), 1.75 (s, 3 H), 1.73 (s, 3 H), 1.65 (s, 3 H), 1.3 (s, 3 H), 1.28−1.16 (6s, 18 H), 1.14 (d, J_{H-H} = 6.7 Hz, 3 H), 1.11 (d, 7.0 Hz, 3 H), 0.85 (m, 3 H), 0.78 (s, 3 H). − ^{13}C NMR ($CDCl_3$): δ = 134.32, 134.24 (d, J_{C-P} = 10.4 Hz, C-b), 134.29, 134.21 (d, J_{C-P} = 9.9 Hz, C-b′), 130.0 (C-d/d′), 128.3, 128.2 (C-c/c′), 115.9, 115.5, 107.9, 105.3, 103.8, 97.3, 95.7, 93.2, 90.7 (C_5Me_4), 49.5, 49.3 (C-5/5′), 43.3 (br., C-3/3′), 43.0, 42.9 (C-1/1′), 39.5 (C-10/10′), 36.4, 34.7, 34.5, 34.3 (C-2/2′/6/6′), 34.9 (C-4/4′), 28.8, 28.7, 23.5, 23.4 (C-8/8′/9/9′), 21.6, 21.4 (C-7/7′), 12.1, 11.6, 11.4, 10.9, 10.7, 10.6, 8.4, 7.0 (C_5Me_4/C_5Me_4′). − ^{31}P NMR ($CDCl_3$): δ = 17.0 (br.), 15.2 (25°C); 17.5 (v br.), 15.4 (0°C); 18.1 (br.), 16.3 (v. br.), 15.5 (−25°C); 18.4, 16.6, 15.6 (−50°C). − MS (EI); *m*/*z* (%): 771 (10) [M$^+$].

[(η^5-PinCp*)$_2$$RhCl_2$]$_2$ (9): PinCp*H (2.00 g, 7.70 mmol) was dissolved in 50 mL of methanol and Rh_3·$3H_2O$ (0.96 g, 37.4% Rh, 3.50 mmol) was added. The light red solution was refluxed for 5 d and the solvent was concentrated to 10 mL afterwards. Storage at 5°C for several hours gave a red solid, which was filtered, washed with diethyl ether and dried. Compound **9** can be recrystallized from CH_2Cl_2/Et_2O. Yield of the red solid **9**: 1.52 g (1.76 mmol, 50%). − ^{1}H NMR ($CDCl_3$): δ = 2.82 (q, J_{H-H} = 9.46 Hz, 1 H, H-4), 2.49 (m, 1 H), 2.35 (m, 1 H), 2.06 (m, 2 H), 1.90 (m, 2 H), 1.83 (s, 3 H), 1.80 (s, 3 H), 1.65 (s, 3 H), 1.61 (s, 3 H), 1.24 (s, 3 H), 1.14 (s, 3 H), 0.95 (d, J_{H-H} = 10.1 Hz), 0.98 (d, J_{H-H} = 6.7 Hz). − ^{13}C NMR ($CDCl_3$): δ = 100.1, 98.2, 96.3, 93.1, 90.8 (C_5Me_4), 48.8 (C-5), 42.2 (C-1), 41.3 (br., C-3), 39.6, 34.3 (C-2/6), 32.7 (C-4), 32.5 (C-10), 28.8, 23.5 (C-8/9), 21.6 (C-7), 11.6, 11.1, 10.0, 9.2 (C_5Me_4). − $C_{38}H_{58}Cl_4Rh_2$ (862.5): calcd.: C 52.92, H 6.78; found C 53.41, H 6.75.

(η^5-PinCp*)$TiCl_3$ (10): PinCp*Li (0.86 g, 3.46 mmol) was dissolved in DME and $TiCl_3$·3THF (0.43 g, 1.15 mmol) was added at −78°C. The solution was warmed to room temp. and refluxed for 2 d. Concd. HCl (2.7 mL) was added carefully at −30°C, followed by 10 mL of chloroform. The layers were separated and the organic layer was dried with $NaSO_4$. The solvent was removed and the nearly dry residue was transferred to a Soxhlet extractor. The extraction was performed with pentane saturated with HCl gas. The red solution, obtained after 30 min, was dried and a red solid was obtained. Yield of the red solid **10**: 0.13 g (0.32 mmol, 28%). − ^{1}H NMR ($CDCl_3$): δ = 3.63 (q, J_{H-H} = 9.46 Hz, 1 H, H-4), 2.67 (s, 3 H), 2.47 (s, 3 H), 2.46 (s, 3 H), 2.43−2.34 (m, 1 H), 2.27 (s, 3 H), 2.22−2.17 (m, 1 H), 2.13 (m, 1 H), 1.90 (m, 1 H), 1.80 (m, 1 H), 1.28 (s, 3 H), 1.26 (m, 2 H), 1.23 (s, 3 H), 0.95 (d, J_{H-H} = 7.02 Hz, 3 H). − ^{13}C NMR ($CDCl_3$): δ = 148.8, 141.2, 137.9, 137.1, 134.3 (C_5Me_4), 49.4 (C-5), 43.8 (br., C-3), 42.6 (C-1), 39.6 (C-10), 37.6 (C-4), 34.4, 33.5 (C-2/6), 28.8, 23.5 (C-8/9), 21.7 (C-7), 16.6, 15.6, 15.2, 14.0 C_5Me_4). − MS (EI): *m*/*z* (%): 375 (7) [M$^+$ − Cl], 256 (80) [PinCp*$^+$]. − $C_{19}H_{29}Cl_2Ti$ (411.7): calcd.: C 55.43, H 7.10; found C 56.18, H 7.21.

(η^5-PinCp*)$Mo(CO)_2(NO)$ (11): PinCp*Li (3.54 g, 13.41 mmol) was dissolved in THF and, after addition of $Mo(CO)_6$ (3.33 g; 13.41 mmol), the reaction mixture was heated under reflux for 12 h. After cooling the solution, Diazald (2.7 g, 12.60 mmol), dissolved in 10 mL of THF, was added dropwise, so that the temperature did not exceed room temp. Stirring was continued for 3 h, with a continuous slight flow of nitrogen over the solution. The solvent was distilled off and the residue was sublimed at 140°C and 10^{-3} bar. The sublimed product was then purified by chromatography (Al_2O_3; hexane/ether, 4:1) to give red crystals after evaporation of the solvent. Yield: 3.60 g (8.19 mmol, 65%). − IR (hexane): $\tilde{\nu}_{(CO)}$ = 2004 (s), 1930 (s), $\tilde{\nu}_{(NO)}$ = 1667 cm^{-1}. − ^{1}H NMR ($CDCl_3$): δ = 3.03 (q, J_{H-H} = 9.77 Hz, 1 H, H-4), 2.37 (m, 1 H) 2.17 (s,3 h), 2.12 (m, 3 H), 2.07 (s, 3 H), 2.03 (s, 3 H), 2.03 (s, 3 H), 1.85 (m, 2 H), 1.26 (s, 3 H), 1.21 (m, 1 H), 1.17 (s, 3 H) 1.02 (d, J_{H-H} = 7.02 Hz, 3 H). − ^{13}C NMR ($CDCl_3$): δ = 230.7, 230.6 (CO), 114.8, 108.2, 106.0, 105.1 (C_5Me_4), 49.2 (C-5), (43.5 (br., C-3) 43.1 (C-1) 39.5 (C-2/6), 38.0 (C-10), 34.5 (C-4), 28.8, 23.5 (C-8,9), 21.5 (C-7), 12.1, 12.0, 10.9, 10.8 (C_5Me_4). − $C_{21}H_{29}NO_3Mo$ (439.4): calcd.: C 57.40, H 6.65, N 3.19; found: C 57.62, H 6.72, N 3.15.

(η^5-PinCp*)$W(CO)_2NO$ (12): (η^5-PinCp*)$W(CO)_2NO$ (**12**) was prepared in a similar way to **11** from PinCp*Li (3.00 g 11.40 mmol) and $W(CO)_6$ (4.05 g, 11.50 mmol) after 5 d of reflux. Diazald (2.44 g, 11.4 mmol) was added as before. Yield: 3.61 g (6.84 mmol, 60%), red crystals. − IR (hexane): $\tilde{\nu}_{(CO)}$ = 1995 (s), 1918 (s), $\tilde{\nu}_{(NO)}$ = 1661 cm^{-1}. − ^{1}H NMR ($CDCl_3$): δ = 3.03 (q, J_{H-H} = 9.2 Hz, 1 H, H-4), 2.35 (m, 1 H) 2.27 (s, 3 H), 2.18 (s, 3 H), 2.14 (s, 3 H), 2.10 (s, 3 H), 1.89 (m, 2 H), 1.25 (s, 3 H), 1.19 (m, 1 H), 1.16 (s, 3 H) 0.99 (d, J_{H-H} = 7.0 Hz, 3 H). − ^{13}C NMR ($CDCl_3$): δ = 222.4 (2CO), 113.4, 106.4, 104.6, 104.0 (C_5Me_4), 49.4 (C-5), (43.4 (C-3) 43.2 (C-1) 39.4 (C-10))34.8 (C-2/6), 34.5 (C-4), 28.8, 23.4 (C-8,9), 21.1 (C-7), 11.8, 10.7, 10.6 (C_5Me_4). − $C_{21}H_{29}NO_3W$ (527.31): calcd.: C 47.83, H 5.54, N 2.66; found C 48.51, H 5.61, N 2.70.

(η^5-PinCp*)$MoCl_2(NO)$ (13): Compound **11** (0.85 g, 1.94 mmol) was dissolved in ether and treated slowly at 0°C with solid PCl_5 (0.40 g, 1.94 mmol). Stirring was continued for 12 h at room temp.; the solution turned a vivid green with a green solid precipitate. After addition of 30 mL of hexane, the volume was reduced to 10 mL under vacuum. The green solid was filtered, washed with a small amount of cold ether and dried. Yield 0.75 g (1.65 mmol, 85%). − IR (THF): $\tilde{\nu}_{(CO)}$ = 1660 cm^{-1}. − ^{1}H NMR ($CDCl_3$): δ = 3.13 (q, J_{H-H} = 9.46 Hz, 1 H, H-4), 2.38 (m, 1 H), 2.23 (s, 3 H), 2.19 (m, 3 H), 2.10 (s, 3 H), 2.06 (m, 3 H) 1.95 (s, 3 H) 1.86 (m, 2 H), 1.26 (s, 3 H), 1.18 (m, 1 H) 1.14 (s, 3 H) 1.00 (d, J_{H-H} = 7.02 Hz), 3 H). − ^{13}C NMR ($CDCl_3$): δ = 127.0, 125.8, 124.6, 119.1 (C_5Me_4), 49.2 (C-5), 43.1 (br., C-3) 42.4 (C-1), 39.5, 34.5 (C-2/6), 34.9 (C-4). 33.2 (C-10) 28.8, 23.4 (C-8/9), 21.8 (C-7), 12.9, 12.6, 10.7, 10.3 (C_5Me_4). − MS: *m*/*z* (%): 455 (20) [M$^+$], 425 (95) [M$^+$ − NO], 385 (25) [M$^+$ − 2 Cl]. − $C_{19}H_{29}Cl_2NOMo$ (454.27): calcd.: C 48.88, H 6.60; found C 48.63, H 6.49.

(η^5-PinCp*)$WCl_2(NO)$ (14): Compound **12** (1.07 g, 2.03 mmol) was dissolved in ether and was treated slowly at 0°C with solid PCl_5 (0.42 g, 2.03 mmol). Reaction and workup as above. Yield

0.95 g(1.75 mmol, 86%). − IR (THF): $\tilde{\nu}_{(CO)}$ = 1632 cm^{-1}. − ^1H NMR ($CDCl_3$): δ = 3.15 (q, J_{H-H} = 9.53 Hz, 1 H, H-4), 2.42 (s, 3 H), 2.25 (s, 3 H), 2.21 (s, 3 H), 2.15 (m, 2 H), 2.04 (m, 3 H) 2.02−1.78 (m, 4 H) 1.86 (m, 2 H), 1.26 (s, 3 H), 1.21 (m, 1 H) 1.16 (s, 3 H) 1.00 (d, J_{H-H} = 7.02 Hz, 3 H). − ^{13}C NMR ($CDCl_3$): δ = 124.2, 123.2, 119.3, 117.3 (C_5Me_4), 49.9 (C-5), 43.4 (br., C-3) 43.1 (C-1), 39.9, 35.5 (C-2/6), 34.4 (C-4). 33.2 (C-10) 29.0, 23.6 (C-8/9), 21.8 (C-7), 12.5, 12.3, 10.8, 10.3 (C_5Me_4). − MS: *m*/*z* (%): 543 (40) [M^+], 490 (70) [M^+ − Cl, − NO], 385 (30) [M^+ − 2 Cl, − NO]. − $C_{19}H_{29}Cl_2NOW$ (542.18): calcd.: C 40.78, H 5.51; found C 40.52, H 5.39.

(η⁵-PinCp*)W(CH_2SiMe_3)$_2$NO (15): Compound **14** (346.9 mg, 0.64 mmol) and [$(CH_3)_3Si(CH_2)_2Mg$]·(dioxan)$_2$ (246.1 mg, 0.64 mmol) were mixed as solids in a Schlenk tube. After cooling to −196°C, 20 mL of THF was slowly condensed into the tube under vacuum. After waiting for 10 min, the Schlenk tube was transferred into a Dewar cooled to −78°C. The temperature was allowed to rise to −50°C and kept at this temperature for 12 h. The solution assumed a deep purple colour. The solvent was evaporated at 0°C, the residue taken up in cold ether and filtered at −20°C through Celite. A purple residue was obtained after evaporating the solvent at 0°C, yield 315.9 mg (0.51 mmol, 80%). − IR (hexane): $\tilde{\nu}_{(CO)}$ = 1582 (s) cm^{-1}. − ^1H NMR (C_6D_6): δ = 3.03 (q, J_{H-H} = 9.15 Hz, 1 H, H-4), 2.28 (m, 2 H), 2.13 (m, 1 H), 1.90 (s, 3 H), 1.82 (s, 3 H), 1.78 (m, 1 H), 1.71 (d, J_{H-H} = 11.58, 1 H, H-a1), 1.68 (S, 3 H), 1.66 (d, J_{H-H} = 11.29 Hz, 1 H, H-b1), 1.49 (s, 3 H), 1.33−1.22 (m, 2 H), 1.17 (s, 3 H), 1.10 (m, 1 H), 1.08 (s, 3 H), 0.93 (d, J_{H-H} = 7.01 Hz, 3 H), 0.38 (2 s, 18 H, $SiMe_3$), −1.21 (d, J_{H-H} = 11.29 Hz, 1 H, H-b2), −1.29 (d, J_{H-H} = 11.58 Hz, 1 H, H-a2). − ^{13}C NMR (C_6H_6): δ = 119.2, 117.2, 113.6, 112.2 (C_5Me_4), 65.2, 63.4, (2 × C-11), 49.6 (C-5), 43.0 (br., C-3), 42.8 (C-1), 39.5, 35.0 (C-2/6), 34.9 (C-4), 30.1 (C-10), 28.9, 23.5 (C-8/9) 21.8 (C-7), 14.3, 12.0, 9.7, 9.5 (C_5Me_4), 1.41, 1.37 ($SiMe_3$). − $C_{27}H_{51}NOSi_2W$ (645.72): calcd. C 49.28, H 8.11; found C 49.64, H 8.23.

X-ray Crystallographic Study: (S_{Re})-[(η⁵-PinCp*)Re(COOMe)NO-(PPh_3) (**5a**) crystallizes in the orthorhombic space group $P2_12_12_1$ (no. 19). Crystal data: $C_{50}H_{56}N_2O_2PRe$, formula mass 934.19 g mol^{-1}, *a* = 11.522(5), *b* = 18.789(2), *c* = 20.116(6) Å, *V* = 4355(2) $Å^3$, *Z* = 4, $d_{calcd.}$ = 1.425 g cm^{-3}, μ(Mo-K_α) = 29.02 cm^{-1}, *F*(000) = 1904. Intensity data were collected at 203 K on an orange rod of approximate dimensions 0.47 × 0.18 × 0.15 mm with an ENRAF-Nonius CAD4 diffractometer in the ω mode up to θ_{max} = 26°. A total of 11726 reflections were corrected for Lorentz and polarization effects and for absorption (numerical by Gaussian integration;[28] min. transmission 0.5339, max. transmission 0.6826). After averaging symmetry-equivalent data, the structure was solved[29] by Patterson and subsequent Fourier difference synthesis. Full-matrix least-squares refinement on *F*[29] of 428 variables for 7010 independent observations with $I > 1.0\ \sigma(I)$ converged at *R* = 0.057, R_w = 0.058 [$w^{-1} = \sigma^2(F_o)$], *GOF* = 1.338. During refinement the naphtyl moiety was treated as a rigid group, all other non-hydrogen atoms were assigned anisotropic displacement parameters, and hydrogen atoms were included as riding in calculated positions [C−H = 0.98 Å, U_{iso}(H) = 1.3 U_{eq}(C)]. A final Fourier difference synthesis showed a residual electron density of ca. 3 $eÅ^{-3}$ in the region of the disordered naphtyl moiety. Crystallographic data (excluding structure factors) for the structure reported in this paper have been deposited with the Cambridge Crystallographic Data centre as supplementary publication no. CCDC-114499. Copies of the data can be obtained free of charge on application to CCDC, 12 Union Road, Cambridge CB2 1EZ, UK [Fax: (internat.) + 44-1223/336-033; E-mail: deposit@ccdc.cam.ac.uk].

Acknowledgments

The authors gratefully acknowledge financial support by the *Deutsche Forschungsgemeinschaft* (DFG) within the Collaborative Research Centre (SFB) 380: "Asymmetric Syntheses with Chemical and Biological Means", and by the Fonds der Chemischen Industrie.

[1] T. Mukaiyama, H. Uchiro, S. Kobayashi, *Chem. Lett.* **1989**, 1001−1005.
[2] K. Futura, S. Shimizu, Y. Miwa, H. Yamamoto, *J. Org. Chem.* **1989**, *54*, 1483−1486.
[3] K. Mikami, M. Terada, T. Nakai, *J. Am. Chem. Soc.* **1990**, *112*, 3949−3952.
[4] J. A. Gladysz, J. M. Fernandez, *Organometallics,* **1989**, *8*, 207−219.
[5] A. Salzer, U. Englert, B. Pfister, *Organometallics* **1995**, *14*, 5561−5565.
[6] A. Salzer, W. H. Bosch, U. Englert, B. Pfister, R. Stauber, *J. Organomet. Chem.* **1996**, *506*, 273−285.
[7] J. A. Gladysz, Y.-H. Huang, F. Niedercorn, A. M. Arif, *J. Organomet. Chem.* **1990**, *383*, 213−225.
[8] R. Lai, L. Bousquet, A. Heumann, *J. Organomet. Chem.* **1993**, *444*, 115−119.
[9] W. Himmele, H. Siegel, *Tetrahedron Lett.* **1976**, 907−914.
[10] J. A. Gladysz, A. T. Patton, C. E. Strouse, C. B. Knobler, *J. Am. Chem. Soc.* **1983**, *105*, 5804−5811.
[11] H. C. Brown, E. F. Knights, C. G. Scouten, *J. Am. Chem. Soc.* **1974**, *96*, 7765−7767.
[12] T. S. Peng, C. H. Winter, J. A. Gladysz, *Inorg. Chem.* **1994**, *33*, 2534−2542.
[13] J. A. Gladysz, J. H. Merrifield, C. E. Strouse, *Organometallics* **1982**, *1*, 1204−1211.
[14] P. A. Schofield, H. Adams, N. A. Bailey, E. Cesarotti, C. White, *J. Organomet. Chem.* **1991**, *412*, 273−289.
[15] R. L. Halterman, *Chem. Rev.* **1992**, *92*, 965−994.
[16] H. H. Brintzinger, J. A. Smith, *J. Organomet. Chem.* **1981**, *218*, 159−165.
[17] P. Legzdins, J. E. Veltheer, *Acc. Chem. Res.* **1993**, *26*, 41−48.
[18] P. Legzdins, J. E. Veltheer, "Synthetic Methods of Organometallic and Inorganic Chemistry" in *Transition Metals*, vol. 8, part 2 (Ed.: W. A. Herrmann), Georg Thieme, Stuttgart, **1997**, p. 79−83.
[19] P. Legzdins, J. D. Debad, S. Rettig, J. E. Veltheer, *J Organomet. Chem.* **1993**, *12*, 2714−2725.
[20] N. H. Dryden, P. Legzdins, S. J. Rettig, J. E. Veltheer, *Organometallics* **1992**, *11*, 2583−2590.
[21] H. Brunner, *J. Organomet. Chem.* **1968**, *16*, 119−124.
[22] H. Behrens, H. Schindler, *Z. Naturforsch.* **1968**, *23b*, 1110−1112
[23] B. N. Stornhoff, H. C. Lewis, *Synth. React. Inorg. Metal-Org. Chem.* **1974**, *4*, 467−475.
[24] N. G. Connelly, P. T. Draggett, M. Green, T. A. Kuc, *J. Chem. Soc., Dalton Trans.* **1977**, 70−75.
[25] H. Saltzman, J. G. Sharefkin, in *Organic Syntheses* (Ed.: H. E. Baumgarten), Wiley, New York, **1973**, p. 658−660.
[26] N. H. Dryden, P. Legzdins, J. Trotter, V.C. Yee, *Organometallics* **1991**, *10*, 2857−2862.
[27] B. Pfister, R. Stauber, A. Salzer, *J. Organomet. Chem.* **1997**, *533*, 131−141.
[28] P. Coppens, L. Leiserowitz, D. Rabinovich, *Acta Crystallogr.* **1965**, *18*, 1035−1038.
[29] ENRAF-Nonius, *SDP Version 5.0*, Delft, The Netherlands, **1989**.

Received February 22, 1999
[I99061]

Modified Bipyridines: 5,5′-Diamino-2,2′-bipyridine Metal Complexes Assembled into Multidimensional Networks via Hydrogen Bonding and π–π Stacking Interactions

Christoph Janiak,*[a] Stephan Deblon,[a] He-Ping Wu,[a] Mario J. Kolm,[a] Peter Klüfers,*[b] Holger Piotrowski,[b] and Peter Mayer[b]

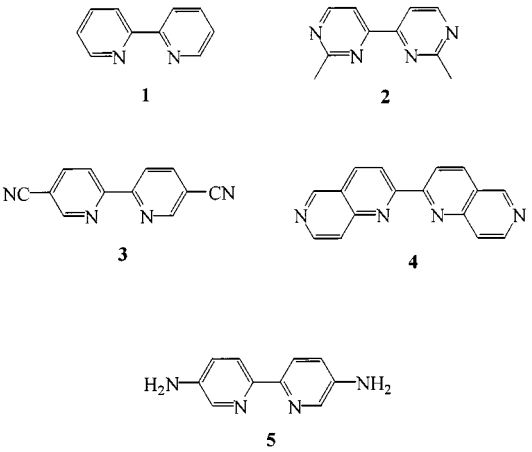
Keywords: 2,2′-Bipyridines / Chelate complexes / Hydrogen bonding / π–π stacking / Crystal structure

A new synthetic route for the synthesis of 5,5′-diamino-2,2-bipyridine (**5**) based on the coupling of 2-chloro-5-aminopyridine in the presence of $NiCl_2 \times 6\ H_2O/PPh_3/Zn$ in dimethylformamide is described. The reactions of the potentially ambidentate ligand **5** with salts of the transition metals Mn, Fe, Ni, Cu, Zn, Ag, and Cd gave a variety of 13 metal–ligand complexes depending on the anion, the crystallization conditions and the metal-to-ligand ratio. The complexes obtained were characterized by thermal analyses, NMR including ^{113}Cd-NMR, IR, and for the iron complex ^{57}Fe-Mößbauer spectroscopy. The structure of eight of the compounds was elucidated by X-ray crystallography. All of these metal complexes show a bipyridine–metal coordination. The amino functionality was never involved in metal coordination. The intermolecular arrangement is dictated by hydrogen bonding from the amino functionality and by π–π stacking of the bipyridine rings.

Introduction

Metal complexes of chelating 2,2′-bipyridine (bipy, **1**) and secondary terminal or chelating amines are of constant and general interest in metal-coordination chemistry.[1] We have recently engaged into a program to study the coordination behavior of modified 2,2′-bipyridine ligands such as 2,2′-dimethyl-4,4′-bipyrimidine (**2**),[2] 5,5′-dicyano-2,2′-bipyridine (**3**),[3] 2,2′-bi-1,6-naphthyridine (**4**),[4] and modified tris(pyrazolyl)borate ligands.[5] As part of this program we report here the coordinating properties of ambidentate 5,5′-diamino-2,2′-bipyridine (**5**). The idea behind the use of such ambidentate ligands is to have tetrahedral (**6**) or octahedral building blocks (**7**) for supramolecular assemblies based on the chelation of two or three ligands, respectively with an appropriate metal center. The intermolecular connectivity should then be controlled through an NH_2→metal coordination or through hydrogen bonding.[6][7] The amino group on the aromatic ring is a good candidate for hydrogen bonding as has been exploited in the self-assembly of supramolecular entities with 2,4,6-triaminopyrimidine units, for example.[8] The related ligand 2,2′-bipyridine-5,5′-dicarboxylate forms tris(chelate) complexes which are then connected by hydrogen bonding.[9]

Rigid bridging ligands have recently gained considerable interest in the synthesis of (rectangular) two-dimensional network structures.[10] The generation of such frameworks is a promising path in the search for stable microporous metal-organic networks that exhibit reversible guest exchange and possibly selective catalytic activity.[11]



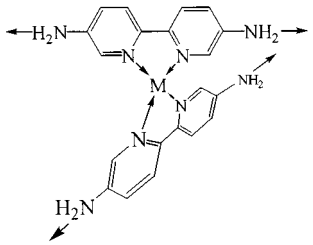
Results and Discussion

Ligand Synthesis

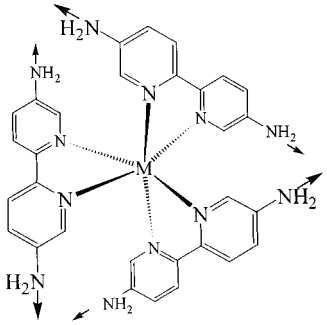
The synthesis of **5** has been achieved according to a route suggested by Whittle (Scheme 1):[12] 5,5′-Dimethyl-2,2′-bipyridine (**9**) is obtained in medium yield by a Raney nickel catalyzed coupling reaction from β-picoline (**8**).[13][14] Oxidation with $KMnO_4$ and esterification of the acid then yields the 5,5′-diester **10**.[15] Hydrazinolysis of the ester group and hydrazine-azide transformation gives the acyl azide **11**. In a Curtius rearrangement this acyl azide is converted by pyrolysis to the isocyanate (R−N=C=O) from which in the presence of ethanol the dicarbamate **12** is derived. Alkaline hydrolysis and sublimation leads to the final

[a] Institut für Anorganische und Analytische Chemie, Universität Freiburg,
Albertstraße 21, D-79104 Freiburg, Germany
E-mail: janiak@uni-freiburg.de
[b] Institut für Anorganische Chemie, Universität Karlsruhe,
Kaiserstraße 12, D-76131 Karlsruhe, Germany
Supporting Information for this article is available on the WWW under http://www.wiley-vch.de/home/eurjic or from the author.

 © WILEY-VCH Verlag GmbH, D-69451 Weinheim, 1999 1434−1948/99/0909−1507 $ 17.50+.50/0

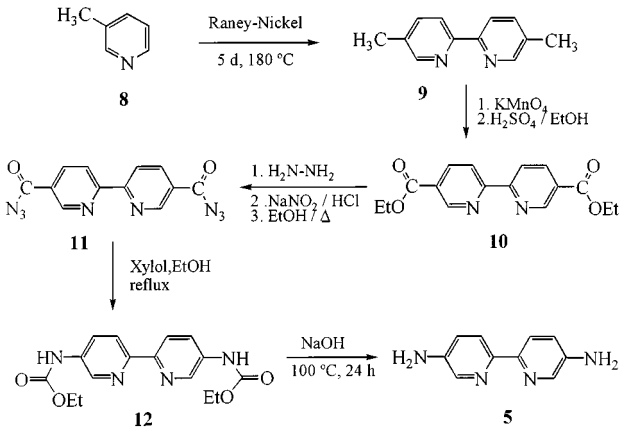


6



7

product **5** in an overall yield of 38% based on 5,5′-dimethyl-2,2′-bipyridine.



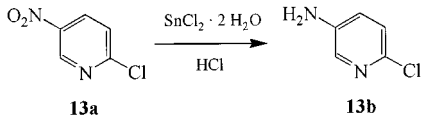
8 9 10 11 12 5

Scheme 1. Synthesis of **5** starting from 3-aminopyridine (**8**)

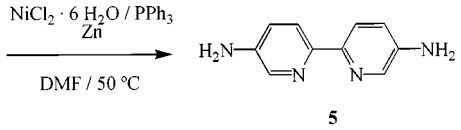
In order to shorten the synthesis of **5** and to improve the yield, we also tried a new method, namely the coupling of 5-amino-2-chloropyridine (**13**). It was reported in the literature that the coupling of haloaryl or halopyridine compounds in the presence of a catalytic system consisting of $NiCl_2 \times 6\ H_2O$/L/reducing agent could lead to the formation of bipyridine and biaryl derivatives. Such *ni*ckel-containing *c*omplex-*r*educing *a*gents are generally abbreviated as NiCRALs, L representing PPh_3 or 2,2′-bipyridine. Reducing agents can be zinc[16] or a mixture of sodium hydride and sodium *tert*-butoxide.[17][18] Zerovalent nickel complexes for the coupling of aryl halides were initially introduced by Semmelhack and co-workers.[19]

For the coupling of 5-amino-2-chloropyridine the use of sodium hydride as a reducing agent for the nickel complex to give the NiCRAL was unsuccesful. The necessary excess of NaH apparently deprotonates the amino function of the pyridine, which then coordinates to the nickel center so that the reaction is slowed down considerably. After 5 d under reaction conditions, the starting compound was still present and only traces of **5** were found. This is remarkable, since under the same conditions 2-amino-3-chloropyridine is coupled to the 2,2′-diamino-3,3′-bipyridine in 44% yield in 17 h.[17]

The use of zinc powder as a reducing agent for the NiCRAL was eventually successful: A solution of nickel(II) chloride hexahydrate and triphenylphosphane in DMF was reduced with zinc and was subsequently treated with a stoichiometric amount of 5-amino-2-halopyridine. No pyridine compound could be detected anymore after 2−2.5 h and workup yielded the coupling product **5** in over 60% yield (Scheme 2). The starting compound for the coupling reaction, the amino-substituted 2-halopyridine **13b** was obtained from the commercially available 2-chloro-5-nitropyridine (**13a**).[20]



13a 13b



5

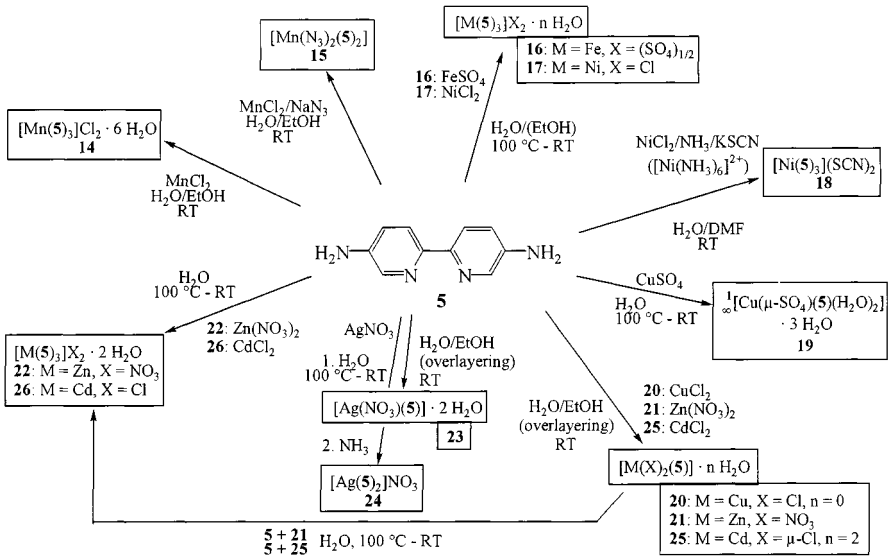
Scheme 2. Synthesis of **5** based on an NiCRAL−catalyzed coupling of 5-amino-2-chloropyridine (**13b**)

Syntheses of Metal Complexes of 5

Different methods were used for the syntheses of metal complexes of **5**. An overview of the prepared metal compounds is provided in Scheme 3.

In the case of the manganese complexes $[Mn(\mathbf{5})_3]Cl_2$ (**14**) and $[Mn(N_3)_2(\mathbf{5})_2]$ (**15**) it was sufficient to combine the reactands in solution and let them stand for some time. For the d^5-high-spin Mn^{2+} ion ligand substitution results only in a small gain of energy because of the theoretically zero ligand field stabilization energy (LFSE). Hence, the thermodynamic driving force for the formation of the manganese chelate complexes from the hexaaquametal ions is small and the reaction proceeds much slower than for iron, nickel and copper which have larger LFSE contributions.[21]

Heating an aqueous suspension or an ethanolic solution of **5** with a solution of the metal salt in water gave upon cooling the tris(5,5′-diamino-2,2′-bipyridine)metal complexes $[M(\mathbf{5})_3]^{2+}$ of iron as the sulfate (**16**), nickel as the chloride (**17**), zinc as the nitrate (**22**), and cadmium as the chloride (**26**). Furthermore, the mono(5,5′-diamino-2,2′-bipyridine)diaqua(μ-sulfato)copper compound **19** and a



Scheme 3. The metal complexes of 5,5′-diamino-2,2′-bipyridine (**5**)

mono(5,5′-diamino-2,2′-bipyridine)silver derivative (see **23**) was obtained by such a hydrothermal reaction. Also $[Zn(NO_3)_2(\mathbf{5})]$ (**21**) and $[Cd(\mu\text{-}Cl)_2(\mathbf{5})]$ (**25**) react with two equivalents of **5** under reflux to form the homoleptic tris(chelate) complexes $[Zn(\mathbf{5})_3](NO_3)_2$ (**22**) and $[Cd(\mathbf{5})_3]Cl_2$ (**26**), respectively. This observation agrees with the complexation behavior found for 2,2′-bipyridine.[22]

A different synthetic route was chosen for complexes where the coordination sphere was not completely constructed by the diaminobipyridine chelate ligand **5**. Such was the case for the compounds $[CuCl_2(\mathbf{5})]$ (**20**), $[Cd(\mu\text{-}Cl)_2(\mathbf{5})]$ (**24**), and the presumable silver complex $[Ag(NO_3)(\mathbf{5})]$ (**23**). Here the synthesis was carried out at room temperature mostly by overlayering the aqueous metal salt solution with an ethanolic solution of **5**. To slow down the diffusion of both solvents a layer of ethyl acetate was brought in between the water and the ethanol phase. In three cases it could be shown that the above heteroleptic complexes may be viewed as thermodynamically unstable intermediates along the reaction coordinate to the homoleptic compounds. The 1:1 ligand/metal complexes **21** and **25** react with two equivalents of **5** under reflux to the thermodynamically apparently more stable tris(chelate) complexes $[Zn(\mathbf{5})_3](NO_3)_2$ (**22**) and $[Cd(\mathbf{5})_3]Cl_2$ (**26**), respectively. A 1:1 ligand/silver complex (as **23**) is initially obtained from the reaction of two equivalents of **5** with one equivalent of Ag^+. This complex dissolves in concentrated aqueous ammonia and upon slow evaporation produces the 2:1 ligand/metal complex $[Ag(\mathbf{5})_2]NO_3$. Such a recrystallization involves formation of the intermediate $[Ag(NH_3)_2]^+$ complex and slow ligand exchange of the stronger, yet more volatile ammine ligand with **5**.[23] A similar ligand exchange was used in the synthesis of the complex $[Ni(\mathbf{5})_3](SCN)_2$ (**18**) which was obtained from mixing the reactands $NiCl_2$, **5**, and KSCN and adding concentrated ammonia, so that the rather stable amminenickel complex $[Ni(NH_3)_6]^{2+}$ is formed. In addition to the synthetic procedures described in the Experimental Section, the reactions were carried out with different concentrations and different ratios of ligand to metal salt (varied in a wide range between 1:1 and 5:1). In all cases the 3:1 ligand/metal complexes were obtained, though. The deep-red iron complex **16** was formed even in the case of a hundred-fold metal excess. The special stability of iron(II) complexes with 2,2′-bipyridine is well known[24] so that the unsubstituted bipyridine is applied as a test reagent for iron(II).

All of the above metal complexes are insoluble in aliphatic and aromatic solvents and in acetonitrile. The heteroleptic silver and cadmium complexes **23** and **25** are little water- but easily DMSO-soluble. The heteroleptic Cu^{2+} complexes **19** and **20** show a good solubility in water, but they do not dissolve in alcohol or THF. The homoleptic compounds **14** (Mn), **22** (Zn), and **26** (Cd) dissolve well in hot water and DMSO, the tris(chelate)iron and -nickel complexes **16** and **17** are well water-soluble but little in DMSO. Many of the crystalline metal complexes with **5** incorporate water of crystallization which is easily lost upon drying in air, so that the crystals have to be stored in water. The silver complexes **23** and **24** are light-sensitive and have to be stored in the dark.

An attempt was made to use the homoleptic tris(chelate) complexes as building blocks in the reaction with silver nitrate and to achieve the coordination through the amino function (to the silver atom) to give a heterobimetallic coordination polymer. However, a simple ligand exchange was observed when the zinc complex **22** was used (Equation 1) and a redox reaction occurred when the iron complex **16** was employed (Equation 2).

$$[Zn(\mathbf{5})_3]^{2+} + 2\,Ag^+ \xrightarrow{H_2O/EtOH\ (1:1)} [Zn(\mathbf{5})]^{2+} + 2\,[Ag(\mathbf{5})]^+ \quad (1)$$
22 **21**

$$[Fe(\mathbf{5})_3]^{2+} + Ag^+ \xrightarrow{H_2O/EtOH\ (1:1)} [Fe(\mathbf{5})_3]^{3+} + Ag\downarrow \quad (2)$$
16

Thermal Analyses

Some complexes were studied by thermogravimetry (TG) and differential scanning calorimetry (DSC) to gain information on the amount of the incorporated crystal water, the temperature of water loss and other phase transitions. The TG data on the water loss show good agreement with values from NMR experiments (see Table 1) and fit the elemental analyses data. For **16** and **17** the water content from the X-ray structural analyses is different. This may indicate a varying water content for each single crystal.

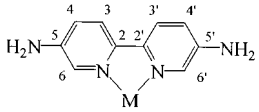
After the loss of solvent water, the manganese complex **14** looses a ligand molecule at 290°C and possibly forms a neutral complex of composition $[MnCl_2(\mathbf{5})_2]$, which in turn shows another phase transition at 361°C. Investigations on solvated tris(2,2′-bipyridine)iron complexes have shown that upon heating the loss of water of crystallization is followed by sequential loss of ligands.[25]

NMR Spectroscopy

Nuclear magnetic resonance spectroscopy is a valuable tool to judge the electronic effects in ligands, including bipyridinemetal chelate complexes.[26] Usually, the d^{10} ions Ag^+ and Cd^{2+} only cause a small down-field shift of the proton signals with respect to those of the free ligand ($\Delta\delta \approx 0.0-0.2$ ppm). A comparison of the chemical shift data for **5** and **22**–**26** in Table 2 confirms this statement. The small shift is due to the weak Lewis acidity and the small diamagnetic interaction of the ring current with the relatively large cations.[27] This is different for zinc and iron complexes. Since the iron compound **16** was not soluble enough in DMSO, it had to be measured in D_2O and the zinc complex **22** was investigated in both solvents to allow comparison between iron and silver complexes, and the free ligand.

A comparison between the two different solvents for **22** shows the effect of hydrogen bonding from water to the amino functions. This decreases the electron-donating (positive) inductive effect of the amino function to the heterocycle so that especially the signals of the protons in the 4- and 6-position experience a low-field shift compared to signals in DMSO. The significant high-field shift of 0.8−1 ppm of the signal of the proton in 6-position or α to the metal center in **22**/DMSO and **16**/D_2O versus the silver and cadmium complexes is due to the smaller ionic radii of the zinc and iron metal centers. This improves the diamagnetic interaction of the metal center with the ring current.[22][27]

Table 2. ^{1}H-NMR data of diamagnetic metal complexes of **5**



Compound	Solvent	H3, H3′	H4, H4′	H6, H6′
Free ligand **5**	$[D_6]$DMSO	7.92	6.95	7.84
$[Ag(NO_3)(\mathbf{5})]$ (**23**)	$[D_6]$DMSO	7.92	7.15	7.91
$[Ag(\mathbf{5})_2]NO_3$ (**24**)	$[D_6]$DMSO	7.91	7.12	7.90
$[CdCl_2(\mathbf{5})]$ (**25**)	$[D_6]$DMSO	7.92	7.14	7.98
$[Cd(\mathbf{5})_3]Cl_2$ (**26**)	$[D_6]$DMSO	7.90	7.09	7.88
$[Zn(\mathbf{5})_3](NO_3)_2$ (**22**)	$[D_6]$DMSO	8.08	7.19	7.08
	D_2O	8.43	7.84	7.79
$[Fe(\mathbf{5})_3]SO_4$ (**16**)	D_2O	7.99	7.28	6.85

The trends in the shifts in carbon-13 spectroscopy are less straightforward. The signals of the carbon atoms 2, 3, and 6 show only little chemical-shift difference to those of the free ligand (−0.5 to +0.8 ppm), the C4 signal experiences a slight down-field shift (1 to 7 ppm) and the C5 signal an up-field shift (2.8 to 4.2 ppm). These trends stem from two superimposing effects: The negative inductive effect of the coordinated metal ion leads in 2- and 6- (*ortho*) position to the nitrogen atom to a down-field shift and to a lesser extent also in the 4- (*para*) position. The interaction of the paired metal d electrons with the diamagnetic ring current, on the other hand, enhances the shielding and consequently induces an upfield shift, which weakens with increasing distance from the metal center.[27][28]

The ligand effect on a metal center was studied with the help of ^{113}Cd-NMR-spectroscopy. The Cd^{II} ion has a rather high relaxation time of 0.1−50 s. Labile complexes which experience rapid ligand exchange, including aqua ligands, then give a broad time-averaged signal. In the building block $[Cd(\mu\text{-}Cl)_2(\mathbf{5})]$ of the heteroleptic complex **25**, the coordination sphere can be concluded by aqua ligands so that the species $[CdCl_2(\mathbf{5})(H_2O)]$ and $[CdCl_2(\mathbf{5})(H_2O)_2]$ also exist in solution with a rapid interchange among them.[29][30]

Table 1. Thermogravimetic data on the crystal water content in **14**, **16**, and **17**

Compound	Temperature for H_2O loss [°C]	Mass loss [mass%]	ΔH [kJ/g]	Water content [1/formula unit] from TG	from NMR	from X-ray
$[Mn(\mathbf{5})_3]Cl_2 \times 6\ H_2O$ (**14**)	101−150	14.3	34.6	6.3	6.5	–
$[Fe(\mathbf{5})_3]SO_4 \times 6\ H_2O$ (**16**)	162−166	14.1	59.9	6.5	–[a]	9.0
$[Ni(\mathbf{5})_3]Cl_2 \times 6\ H_2O$ (**17**)	145−168	12.3	51.6	5.6	6.0	2.5

[a] Due to the low solubility in $[D_6]$DMSO the water content could not be verified by NMR.

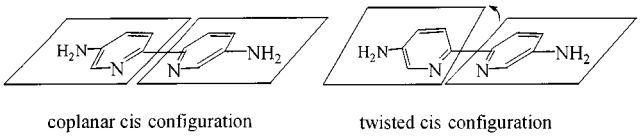
Hence, the signal for **25** was very broad and could not be clearly assigned. Whereas the tris(chelate) complex **26** gave a rather narrow singlet, which is indicative of the stable nature of $[Cd(\mathbf{5})_3]^{2+}$ in solution. The chemical shift of $\delta = 253$ for **26** [versus 2 M $Cd(ClO_4)_2$ as a standard] falls right in the range observed for other tris(bipyridine) and tris(phenanthroline) complexes: $[Cd(bipy)_3](ClO_4)_2$ ($\delta = 243$), $[Cd(4,4'\text{-}Me_2bipy)_3](ClO_4)_2$ ($\delta = 254$), and $[Cd(phen)_3](ClO_4)_2$ ($\delta = 254$ ppm) [all against 0.1 M $Cd(ClO_4)_2$ solution].[29]

Mößbauer Spectroscopy

The iron complex **16** is an exception with respect to its thermodynamic stability in the series of the analogous $[M(\mathbf{5})_3]^{2+}$ derivatives. It forms directly even at high metal excess. A possible explanation is the $3d^6$ low-spin configuration of the Fe^{II} ion which possesses a maximal ligand field stabilization energy.[31] Some bipyridineiron(II) complexes are known, e.g. $[Fe(bipy)_3](BF_4)_2 \times 2\ H_2O$[32][33] or $[Fe(3,3'\text{-}Me_2\text{-}bipy)_3](ClO_4)_2$[34] which exhibit a thermally induced low-spin to high-spin crossover. Such a spin crossover changes the spin state from singlet-$^1A_{1g}$ to quintuplet-$^5T_{2g}$ and as a consequence leads to an increase in ligand−metal bond length.[35] Mößbauer spectroscopy allows to discern the spin state of the iron complex. For $[Fe(\mathbf{5})_3]SO_4$ (**16**) in the solid state a pronounced doublet with an isomer shift $\delta(\alpha\text{-Fe}) = 0.30$ mm/s (at 293 K) and a half-width Γ of 0.25 mm/s was found. The quadrupole splitting ΔE_Q was 0.27 mm/s. These values are typical for tris(2,2′-bipyridine) complexes of iron in the low-spin state. The isomer shifts measured, for example, for $[Fe(bipy)_3](ClO_4)_2$, $[Fe(bipy)_3]Cl_2$, and $[Fe(bipy)_3]SO_4$ are 0.30, 0.33, and 0.24 mm/s, respectively.[25,33,36] The small quadrupole splitting in **16** indicates at the most a weak distortion from the octahedral $Fe-N_6$ coordination geometry. The DSC data for **16** exclude the existence of a thermally induced spin transition up to the decomposition temperature of 350 °C, because no reversible phase transition could be observed.[5][37] Another indication along the same lines is the deep-red color of **16** which stems from the $^1A_{1g} \rightarrow {}^1T_{1g}$ d-d transition. Upon heating, this color does not fade as would be expected from a spin crossover, because the smaller d-d splitting in the high-spin state shifts the absorption from the visible into the infrared regime.[5][38] Both negative indicators for a spin crossover behavior precluded a temperature-variable Mößbauer study.

Infrared Spectroscopy

Metal complexes with 2,2′-bipyridine ligands were the subject of intense IR-spectroscopical investigations.[39−41] All bands are now clearly assigned. Some of the many ring vibrations are sensitive to metal coordination and experience an hypsochromic shift (to higher wavenumbers or energy) of 10 to 20 wavenumbers.[40] The influence of the metal coordination on the vibrations of the amino function has been elucidated with the 2- and 3-aminopyridine ligand.[42][43] The in-plane ring-stretch vibrations of **5** are found at 1568, 1478 and 656 cm^{-1}.[44] The first two show in all metal complexes the aforementioned hypsochromic shift to 1579−1590 cm^{-1} and 1486−1497 cm^{-1}, respectively. The band at 656 cm^{-1} either remains almost unshifted (in **15**, **16**, **17**, **18**, **22**, **24**, and **25**) or is split into two bands (as in **14**, **19**, **23**, and **26**). Similarly, the corresponding band in $[Mn(bipy)_3](ClO_4)_2$ is split.[40][41] The explanation is sought in a substantial twist (over 10°) of the pyridine ring planes around the connecting C2−C2′ bond away from the almost coplanar to a twisted *cis* configuration (**27**).



coplanar cis configuration twisted cis configuration

27

To the extent of a few degrees the ring planes in a bipyridine pair are always twisted (see below).[45] An X-ray structure analysis of $[Mn(bipy)_3](ClO_4)_2$ confirmed the substantial twist, the dihedral angles between each pair of pyridine rings in all three bipyridine ligands lay between 13 and 25°.[46]

The structures collected here do not reveal a substantial twist in any case. The dihydral angles between the pyridine ring planes were 9.7° in **15**, 5.3, 5.7, and 11.3° in **18**, 3.3° in **19**, 2.3° in **20**, 5.2, 8.9, and 9.1° in **22**, and 0.1° in **25**. This finding coincides with the non-splitting of the band at around 656 cm^{-1} but does not agree with the splitting found for **19**. Hence, the IR analysis with respect to a twisted configuration should be applied with caution.

From aqueous solutions the ligand **5** crystallizes as the monohydrate. The IR spectrum of $\mathbf{5} \times H_2O$ then shows two sharp bands at 3425 and 3340 cm^{-1}, which are assigned to the symmetric and asymmetric NH stretch. Three additional and broader bands at 3376, 3315, and 3205 cm^{-1} are due to the formation of amino hydrogen bonds to the water oxygen atom. The NH deformation is found at 1632 cm^{-1}. In all metal complexes the position of this bending vibration remains rather unchanged, different to what would be expected in case of amino−metal complexation.[42]

X-ray Structural Studies

Generally, all of the metal complexes of **5** which are structurally elucidated here show a bipyridine−metal coordination of the potentially ambidentate diaminobipyridine ligand. The amino functionality was never involved in metal coordination, yet, could play a substantial role in hydrogen bonding (see below). Specific distances and angles and some figures for the hydrogen bonding networks which are not given here, can be found in the supporting information. The specific structures are described in some more detail in the following.

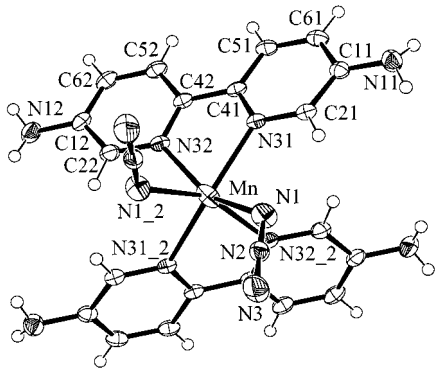


Figure 1. Molecular structure of $[Mn(N_3)_2(\mathbf{5})_2]$ (**15**); selected distances [Å] and angles [°]: Mn−N1 2.211(1), Mn−N31 2.265(1), Mn−N32 2.286(1), N1−N2 1.171(2), N2−N3 1.168(2); N1−Mn−N1#2 86.58(8), N1−Mn−N31#2 113.66(4), N1−Mn−N31 89.19(4), N31−Mn−N31#2 149.14(5), N1−Mn−N32 154.51(5), N1−Mn−N32#2 86.07(5), N31#2−Mn−N32#2 71.61(4), N31−Mn−N32#2 90.61(4), N32−Mn−N32#2 110.09(6), N1−N2−N3 178.1(1) (symmetry equivalent position #2 = 0.5 − *x*, *y*, −*z*)

$[Mn(N_3)_2(\mathbf{5})_2]$ (15)

Figure 1 illustrates the structure of this molecular complex. The two azide ligands are *cis*-coordinated, terminally bound and do not bridge between metal centers. The bonding mode is not unusual for coordinated azides.[47] The pseudooctahedral structure of **15** is similar to *cis*-$[Mn(NCS)_2(bipy)_2]$.[48] The M−N(bipy) bond lengths *trans* to the azide (or NCS) ligand show some lengthening. The crystal structure is stabilized by stacking interactions involving bipyridine ligands of adjacent molecules (π−π contacts down to 3.2 Å). Intermolecular hydrogen bonding from the amino functions to the N3 atom of the azide ligand is observed.

$[Fe(\mathbf{5})_3]SO_4 \times 9\ H_2O$ (16)

The tris(chelate) structure (cf. Figure 3) of the $[Fe(\mathbf{5})_3]^{2+}$ moiety is unremarkable (Table 3). Recent examples of $[Fe(bipy)_3]^{2+}$ complexes include the counterions $[Fe(NO)_2Cl_2]^-$,[49] $[Fe_2OCl_6]^{2-}$,[50] $[Fe_2(ox)_3]^{2-}$,[51] and

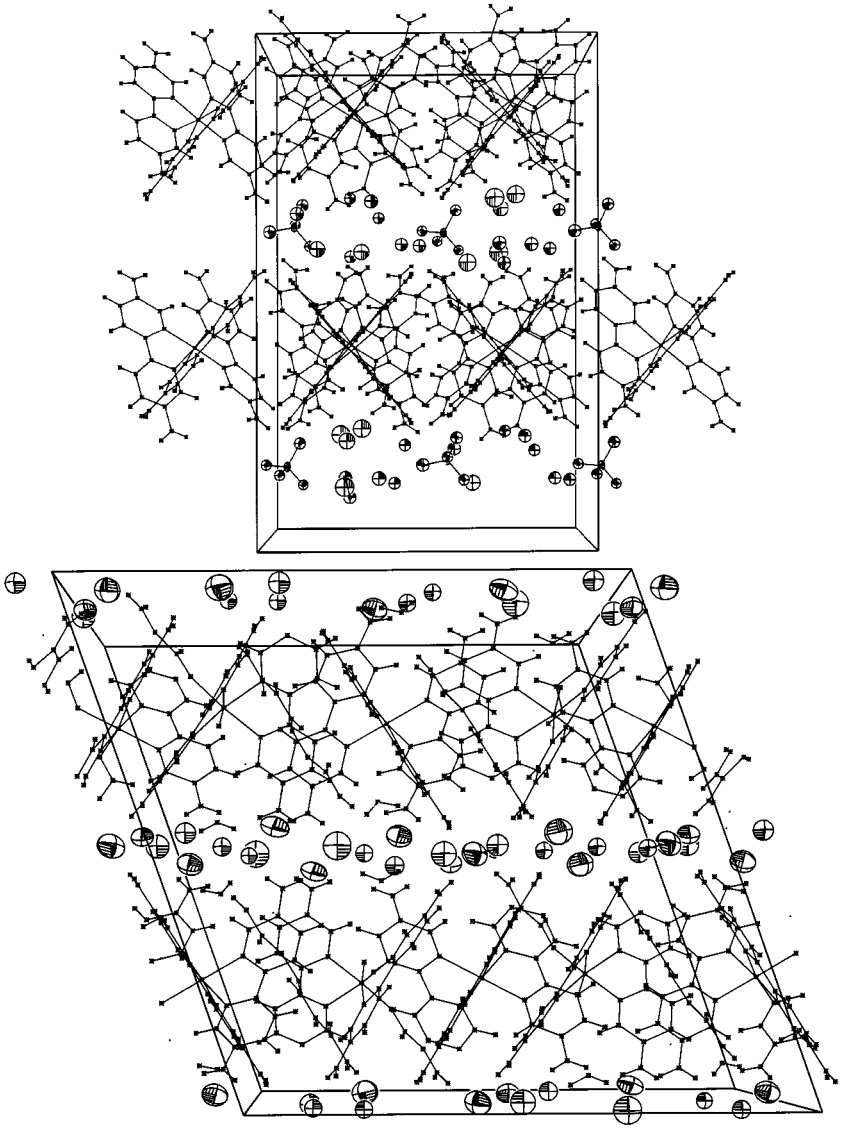


Figure 2. Layer arrangement of the $[M(\mathbf{5})_3]^{2+}$ cations and the anions (SO_4^{2-} or Cl^-) together with the water of crystallization in the structures of (a, top) $[Fe(\mathbf{5})_3]SO_4 \times 9\ H_2O$ (**16**) and (b, bottom) $[Ni(\mathbf{5})_3]Cl_2 \times 2.5\ H_2O$ (**17**); view along *a* (a) and *b* (b)

$[MC(ox)_3]^{2-}$,[52][53] (ox = oxalate, M = Ag, Na, Li). We just note that **16** is constructed from alternating layers of the tris(chelate) cations and layers of the sulfate anions together with the water of crystallization (Figure 2a). The interaction between the layers occurs through hydrogen bonding from the amino group to the oxygen centers.

$[Ni(5)_3]Cl_2 \times 2.5\ H_2O$ (17) and $[Ni(5)_3](SCN)_2$ (18)

The tris(chelate) structure around the nickel centers (Figure 3, Table 3) is common in a sizable number of tris(bipyridine)metal complexes which are described in the literature. Recent examples are $[Ni(bipy)_3][Mn_2(ox)_3]$,[53] $[Ni(bipy)_3]$-$NaAl(ox)_3]$,[54] $[Ni(bipy)_3][Ni(CN)_4] \times bipy \times 6\ H_2O$,[55] and $[Ni(bipy)_3]_2[Ag(CN)_2]_3Cl \times 9\ H_2O$.[56] The structure of **17** contains an analogous layer arrangement as seen before in **16** (Figure 2b). Noteworthy in **18** is the hydrogen bonding from the amino groups to both the sulfur and the nitrogen end of the SCN anions.

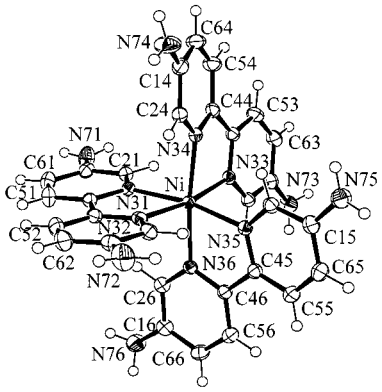


Figure 3. Exemplified view of the molecular structure of the tris-chelate)metal cations in $[Fe(5)_3]SO_4 \times 9\ H_2O$ (**16**), $[Ni(5)_3]Cl_2 \times 2.5\ H_2O$ (**17**), $[Ni(5)_3](SCN)_2$ (**18**, shown here), and in $[Zn(5)_3](NO_3)_2$ (**22**); selected distances and angles are given in Table 3

$^1{}_\infty[Cu(\mu\text{-}SO_4)(5)(H_2O)_2] \times 3\ H_2O$ (19)

Figure 4a shows a section of the 1-dimensional coordination polymer and Figure 4b displays the stabilizing π−π interaction (about 3.4 Å)[57] of adjacent strands. The chains

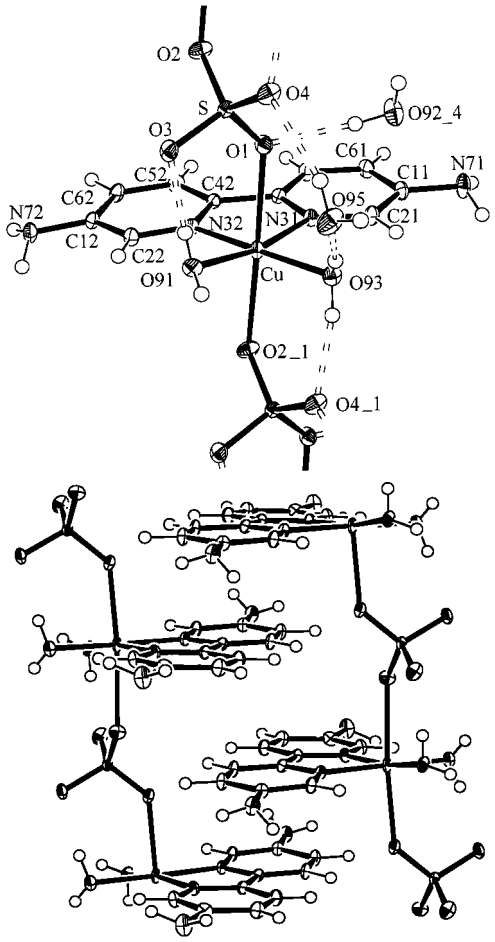


Figure 4. (a, top) Section of the one-dimensional coordination polymer $^1{}_\infty[Cu(\mu\text{-}SO_4)(5)(H_2O)_2] \times 3\ H_2O$ (**19**) indicating also part of the hydrogen bonding network with two water molecules of crystallization; selected distances [Å] and angles [°]: Cu−N31 2.010(2), Cu−N32 1.992(2), Cu−O91 2.006(2), Cu−O93 1.993(2), Cu−O1 2.468(2), Cu−O2#1 2.311(2); N32−Cu−O93 175.08(6), O91−Cu−N31 168.89(6), O1−Cu−O2#1 173.73(6), O93−Cu−O91 92.61(6), N32−Cu−N31 82.10(6), O1−Cu−N31 86.54(6), O1−Cu−O91 84.38(6), O91−Cu−O2#1 90.03(6), N31−Cu−O2 99.33(5), other angles between *cis*-positioned atoms range from 88.3 and 93.6° (symmetry equivalent position #1 = $x - 1, y, z$; #4 = $x - 0.5, -y + 0.5, z - 0.5$); (b, bottom) π-π stacking of neighboring strands, running along *a*

Table 3. Selected bond lengths and angles in the tris(chelate)metal complexes $[M(5)_3]^{2+}$

	$[Fe(5)_3]^{2+}$ (in **16**)[a]	$[Ni(5)_3]^{2+}$ (in **17**)[a]	$[Ni(5)_3]^{2+}$ (in **18**)	$[Zn(5)_3]^{2+}$ (in **22**)
M−N range [Å]	1.941(9)−1.995(9)	2.075(4)−2.095(3)	2.0742(15)−2.1152(16)	2.145(3)−2.212(3)
M−N average [Å]	1.968	2.084	2.094	2.167
N−M−N chelate bite angles [°]	81.9(4) (3 ×), 82.0(4), 82.2(3), 82.3(4)	78.9(2), 79.0(2), 79.1(2) (2 ×), 79.3(2), 79.4(2)	78.83(6), 79.04(6), 79.07(6)	76.4(1), 77.6(1), 77.9(1)
N−M−N *cis*, except chelate, range [°]	88.7(4)−96.9(4)	90.4(1)−96.8(1)	91.32(6)−97.26(6)	92.6(1)−97.1(1)
average N−M−N *cis*, except chelate [°]	92.7	93.8	93.89	94.6
N−M−N *trans* [°]	172.7(4), 173.2(4), 173.9(4), 175.1(4), 175.2(4), 175.6(4)	168.1(2), 169.4(1), 170.1(1), 170.5(2), 173.7 (2), 173.8(1)	169.05(6), 170.36(5), 173.13(6)	166.6(1), 167.3(1), 169.6(1)

[a] Two symmetically independent molecules in the unit cell.

are formed through the bridging action of the sulfato ligand, two of which are arranged *trans* around the copper center with Jahn−Teller-elongated Cu−O contacts. The aqua and sulfato ligands on the metal center and the water molecules of crystallization form a three-dimensional hydrogen-bonding network surrounding the π-interacting double strands from Figure 4.

[$CuCl_2$(5)] (20)

The structure of this molecular complex is displayed in Figure 5. The copper atom is four-coordinate with a coordination polyhedron between square-planar and tetrahedral. The dihedral angle between the plane of the five-membered chelate ring and the Cl−Cu−Cl plane is 41.1°. In the complex (3-amino-6,6′-dimethyl-2,2′-bipyridine)dichlorocopper(II) a (Jahn−Teller-)compressed tetrahedral structure is found since the methyl groups *ortho* to the coordinating nitrogen atom apparently prevent a more planar ligand arrangement.[58] An approximately square-planar coordination around Cu is observed in (2,2′-bipyridine-3,3′-dicarboxylic acid)dichlorocopper(II) monohydrate.[59] However, weak intermolecular interactions with a Cl atom (3.117 Å) and an O atom (2.678 Å away) on adjacent molecules complete an octahedral donor arrangement around the metal center. In **20** no such intermolecular interactions can be found; the next chlorine contact to a neighboring molecule is 5.28 Å. The absence of bridging chlorine atoms in **20** is unusual as in the related compounds dichloro(4,4′-dimethyl-2,2′-bipyridine)copper(II) hemihydrate[60] and in dichloro(2,2′-bipyridine)copper(II)[61] such intermolecular interactions are present leading to five- and six-coordinate copper centers in dimeric and polymeric structures, respectively. The chlorine atoms in **20** are involved in hydrogen bonding to the amino group (H···Cl 2.799 and 2.858 Å, see Figure 8a), yet, it is unclear if this is sufficient to prevent coordination to the copper atom (see below). That such intermolecular interaction are feasable is demonstrated with the structure of $^1{}_\infty$[Cd(μ-Cl)$_2$(**5**)] × 2 H_2O (**25**). The packing of the molecules of **20** (π−π distances around 3.4 Å) is discussed in combination with the related structure of **25** below.

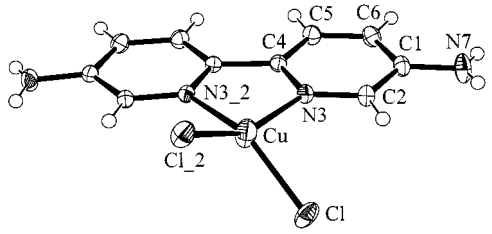


Figure 5. Molecular structure of [$CuCl_2$(**5**)] (**20**); selected distances [Å] and angles [°]: Cu−N3 1.981(1), Cu−Cl 2.2346(4); N3−Cu−N3#2 82.28(8), N3−Cu−Cl 97.41(4), N3−Cu−Cl#2 150.80(4), Cl−Cu−Cl#2 96.61(2) (symmetry equivalent position #2 = $-x + 1$, y, $-z + 0.5$)

[$Zn(5)_3$]$(NO_3)_2$ × 2 H_2O (22)

The unspectacular tris(chelate) structure is again found in **22** (cf. Figure 3, Table 3). We refer to [$Zn(bipy)_3$]$(SCN)_2$ × 7 H_2O[62] and to the various structures of [$Zn(bipy)_3$]-$ClO_4)_2$[63] as recent examples. Of more interest is an extended, two-dimensional hydrogen-bonded network formed by the nitrate anions, the water molecules of crystallization and the amino functions of the bipyridine ligands (Figure 6). These hydrogen-bonded grids separate and sandwich the layers build from the tris(chelate) complex molecules (and vice versa). Within such a network the amino groups hydrogen-bond either to one (N56) or two nitrate ions (N53, N54, N55) or bridge with their hydrogen atoms between a nitrate anion and a water molecule (N52) or between two water molecules (N51). One of the hydrogen atoms from N54 thereby forms a 3-center or bifurcated bridge to two oxygen atoms (O1 and O2) of a nitrate ion. One of the water molecules (O92) bridges between two nitrate anions and accepts a hydrogen bond from the other solvent water (O91). The latter forms hydrogen bonds between a nitrate ion and a water molecule and the oxygen atom accepts three hydrogen bonds from amino groups to become five-coordinate. Each of the nitrate ions is anchored by five or six hydrogen bonds, four of which are derived from the amino groups and the remaining one or two from water molecules. Figure 6 illustrates the hydrogen-bonded network and Table 4 provides further details.

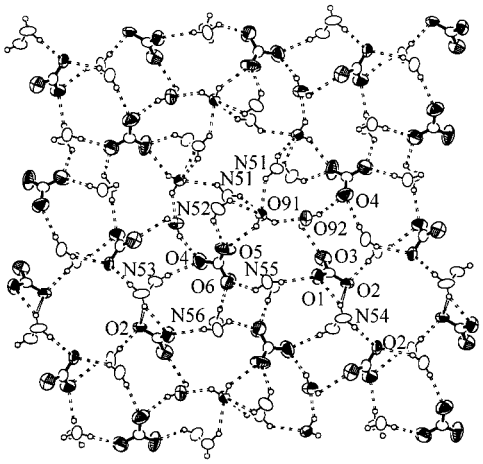


Figure 6. Two-dimensional hydrogen bonding network in [$Zn(5)_3$]$(NO_3)_2$ (**22**) in the *ab* plane; the nitrogen atoms of the amino groups are drawn as empty ellipsoids only; due to space requirements only part of the atom positions are labelled and symmetry operations are not shown

$^1{}_\infty$[Cd(μ-Cl)$_2$(5)] × 2 H_2O (25)

The building block for this one-dimensional coordination polymer is drawn in Figure 7a. At first sight, the structure is similar to the copper complex **20**. The dihedral angle between the plane of the five-membered chelate ring and the Cl−Cd−Cl plane is 17.8°. However, unlike **20** the cadmium compound forms 1D strands (Figure 7b). Polymer formation is based on the bridging action of the chloro ligands as is evident from Figure 7b. The distorted octahedral coordination sphere of cadmium thus consists of the two bipyridine nitrogen atoms and four bridging chlorine atoms. The cadmium−chlorine (2.561, 2.781 Å) and cadmium−cad-

Table 4. Hydrogen bonding interactions in $[Zn(\mathbf{5})_3](NO_3)_2 \times 2\ H_2O$ (**22**); symmetry equivalent positions: #4 = $-y - 0.25, -x + 0.75, z - 0.25$; #6 = $-x + 1, -y + 0.5, z$; #7 = $x - 0.25, -y + 0.25, z - 0.25$; #9 = $-x + 1, -y + 1, -z$; #12 = $-y + 1.25, x + 0.25, -z + 0.25$; #14 = $x, y + 0.5, -z$; #15 = $y - 0.25, -x + 1.25, -z + 0.25$

D−H···A	D−H [Å]	H···A [Å]	D···A [Å]	D−H···A [°]
N51−H51B···O91	0.880(4)	2.258(4)	3.048(6)	149.3(3)
N51−H51A···O91#15	0.879(4)	2.326(4)	3.051(5)	139.8(3)
N52−H52A···O91#4	0.880(5)	2.445(4)	3.038(6)	125.1(3)
N52−H52B···O5#4	0.881(5)	2.302(5)	3.061(7)	144.4(4)
N53−H53A···O2#6	0.882(4)	2.128(4)	2.923(5)	149.7(3)
N53−H53B···O4	0.879(5)	2.069(5)	2.889(7)	154.9(3)
N54−H54A···O1#7	0.881(4)	2.326(4)	3.148(6)	155.3(4)
N54−H54A···O2#7	0.881(4)	2.456(5)	3.217(6)	144.9(3)
N54−H54B···O2#9	0.879(5)	2.177(4)	3.029(6)	163.2(3)
N55−H55A···O6#15	0.880(4)	2.457(6)	3.114(7)	131.9(3)
N55−H55B···O1#15	0.878(4)	2.146(4)	3.004(5)	165.5(3)
N56−H56A···O6#14	0.880(4)	2.137(6)	3.010(7)	171.5(4)
O91−H911···O92	0.908(19)	1.881(19)	2.657(7)	142.1(19)
O91−H912···O5	0.89(2)	2.34(2)	2.901(6)	120.9(19)
O92−H921···O3	0.83(4)	2.31(5)	2.742(8)	113(3)
O92−H922···O4#12	0.82(3)	2.36(4)	2.892(8)	123(4)

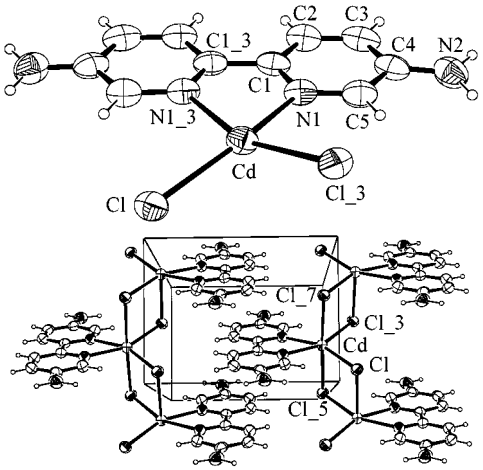


Figure 7. (a, top) Building block for the one-dimensional coordination polymer $^1{}_\infty[Cd(\mu\text{-}Cl)_2(\mathbf{5})] \times 2\ H_2O$ (**25**) and (b, bottom) partial packing diagram which shows the formation of one-dimensional strands; the water molecules of crystallization have been omitted for clarity; selected distances [Å] and angles [°]: Cd−N1 2.332(8), Cd−Cl,Cl#3 2.561(8), Cd−Cl#5,7 2.78(1); N1−Cd−N1#3 70.2(4), N1−Cd−Cl 159.6(11), N1−Cd−Cl#7 96.5(2), Cl−Cd−Cl#3 103.2(3), N1#3−Cd−Cl 94.5(3), N1#3−Cd−Cl#7 85.8(2), Cl−Cd−Cl#7 95.7(3), Cl#3−Cd−Cl#7 82.5(3) Cl#7−Cd−Cl#5 177.17(4) (symmetry transformations: #3 = $-x, y, -z + 0.5$; #5 = $-x, -y, -z$; #7 = $x, -y, z + 0.5$)

mium (4.04 Å) distances found here are typical for chloro-bridged cadmium compounds.[64] The amino groups are not involved in metal coordination but take part in the hydrogen bonding network build up by the water of crystallization.

The packing and strand formation in **25** by chlorine bridging can be compared to the packing of the molecular complexes of **20**. Figure 8 contrasts similar views of the unit cells of both compounds. It can be seen that the bipyridine π−π stacking (both from 3.4 Å on in **20** and in **25**)[57] is an important motif to control the intermolecular arrangement, as was also pointed out in Figure 4 for the copper complex **19**; π strands are formed with the MCl_2 moieties alternatingly facing to the left and right of these stacks. These π interactions may be more important in **20** than in **25**, since the ring overlap is larger in the copper than in the cadmium compound. On the basis of the molecular copper complex in Figure 8a, the metal−chlorine bridging in **25** (Figure 8b) can be developed by stretching the *a* axis and shortening the *b* axis. Cadmium−chlorine bridging can then occur along *b* between the $CdCl_2$ moieties which face each other. Starting from the complete ring overlap in **20** the bridging in **25** is enhanced at the cost of the bipyridine π overlap by moving the (bipy)$CdCl_2$ moieties to the left and right in the *b* direction, so that the ring overlap is greatly diminished.

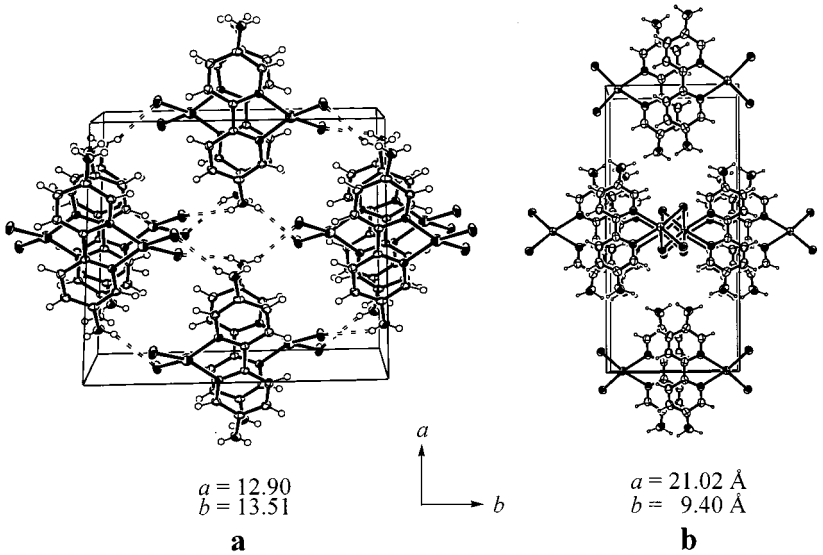


Figure 8. (a, left) unit cell of $[CuCl_2(\mathbf{5})]$ (**20**) and (b, right) unit cell of $^1{}_\infty[Cd(\mu\text{-}Cl)_2(\mathbf{5})] \times 2\ H_2O$ (**25**), both viewed approximately along *c*, to compare the relationship between the unbridged and chlorine-bridged packing; hydrogen−chlorine bonding is indicated in **20**; the water molecules of crystallization in **25** have been omitted for clarity

Conclusions

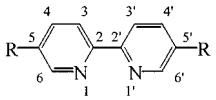
The expectation that the potentially ambidentate group 5,5′-diamino-2,2′-bipyridine (**5**) could function as a bridging and/or chelating bi- to tetradentate ligand in the coordination of transition metals has not been fulfilled. This may be traced to the delocalization of the amine lone-pair into the electron-deficient pyridine ring. The structural studies showed a well-developed coplanarity of the amino group with the aromatic ring. However, the amino function takes part in hydrogen bonding to the anions and to incorporated water molecules of crystallization. From this a two- to three-dimensional hydrogen-bonding network was created which was one of the factors in the packing of the molecular or extended ligand−metal complexes. The other key factor responsible for the supramolecular arrangement of the 5,5′-diamino-2,2′-bipyridine−metal entities is a face-to-face π−π stacking interaction between bipyridine ligands of neighboring ligand−metal fragments. The importance of such a π−π stabilization[57] for the ligand−metal packing has also been elucidated in the structures of the metal complexes with 2,2′-dimethyl-4,4′-bipyrimidine (**2**),[2] 5,5′-dicyano-2,2′-bipyridine (**3**),[3] and 2,2′-bi-1,6-naphthyridine (**4**).[4] These last three ligands also exhibit the sought for bridging and/or chelating bi- to tetradentate metal coordination.

Experimental Section

General: NMR: Bruker ARX 200 (200.1 MHz for ^{1}H, 50.3 MHz for ^{13}C) or Varian O-300 (300.0 MHz for ^{1}H, 75.4 MHz for ^{13}C); calibrated against the solvent signal ([D$_6$]DMSO: ^{1}H NMR: δ = 2.53; ^{13}C NMR: δ = 39.5; $CDCl_3$: ^{1}H NMR: δ = 7.26; ^{13}C NMR: δ = 77.0; C_6D_6: ^{1}H NMR: δ = 7.19; ^{13}C NMR: δ = 128.0). − Thermogravimetric analyses: simultaneous thermoanalysis apparatus STA 429 from Netsch. − IR spectra: Perkin−Elmer 783 infrared spectrophotometer as KBr disks or as Nujol mulls. − Mass spectra: GC/MS Finnigan MAT in solid-probe EI mode at an ionization energy of 70 eV. − Elemental analyses: Perkin−Elmer elemental analyzer E 240 C. − Commercial triphenylphosphane was dried for 24 h in vacuo at 50°C. Distilled water was carefully degassed prior to use. Dimethyl formamide (DMF) was of technical grade and was fractionally distilled with 10 vol-% of toluene and 2 vol-% of water. This prepurified DMF was stirred for 2 h over CaH_2 under argon and then distilled under vacuum. 5-Amino-2-chloropyridine (**13b**) was prepared as described in ref.[20] from 2-chloro-5-nitropyridine (**13a**) in 92% yield.

Synthesis of 5 from 3-Methylpyridine (8) (Scheme 1)

5,5′-Dimethyl-2,2′-bipyridine (9): ***CAUTION:*** Dry Raney nickel is highly pyrophoric! In a 250-mL three-necked flask 20 g of nickel/aluminum alloy were added under inert gas and ice-cooling in portions within 30 min to a solution of 25.6 g (0.64 mol) of NaOH in 100 mL of water. The temperature increased quickly to 80°C. After complete addition, stirring was continued at 80°C for 1 h. Then 100 mL of water was added and the solution was decanted from the Raney nickel. The latter was washed 20 times with 100 mL of H_2O each, which was decanted each time after 2 min of stirring. Afterwards the three-necked flask was fitted with a reflux condenser and a dropping funnel. The remaining water was first removed with a water aspirator at 60°C, eventually the Raney nickel was dried at 0.05 mbar at 80°C for 3 h. Then, 30 mL (0.29 mol) of 3-methylpyridine (**8**) was slowly added dropwise under ice-cooling and the reaction mixture was kept for 5 d at an oil-bath temperature of 180°C. The product was filtered hot through a D3 frit and the Raney nickel residue washed twice with hot toluene. (The Raney nickel was slowly dissolved with water, medium concentrated HCl and conc. HNO_3.) The filtrate was freed from the starting compound and toluene by vacuum distillation. The product was sublimed twice and obtained in colorless needle-shaped crystals (yield 9.5 g, 36%; ref.[13][14] 17%). − The procedure could easily scaled up six-fold: From 125 g of nickel/aluminum alloy, 160 g of NaOH, two times 600 mL of degassed water and 188 mL of 3-methyl-pyridine was obtained 55 g of **9** (31%). A 2-l flask was used as the reaction vessel and the reaction mixture was kept for 4 d at 180°C. The Raney nickel residue was washed three times with 80 mL of hot toluene, each. − M.p. 114°C (ref.[13] 114.5−115°C. − ^{1}H NMR ($CDCl_3$): δ = 8.41 (d, 2 H, J = 1.5 H, H6, H6′), 8.17 (d, 2 H, J = 9.0 Hz, H4, H4′), 7.52 (dd, 2 H, J_1 = 8.0 Hz, J_2 = 2.0 Hz, H3, H3′), 2.29 (s, 6 H, CH_3). − ^{13}C NMR ($CDCl_3$): δ = 153.7 (C2, C2′), 149.5 (C6, C6′), 137.3 (C4, C′), 132.9 (C5, C5′), 120.2 (C3, C3′), 18.2 (methyl-C). − The numbering for the NMR notation for **5**, **9−12** is as in Scheme 4.



Scheme 4. Numbering scheme for bipyridines

Diethyl 2,2′-Bipyridine-5,5′-dicarboxylate (10): 9.45 g (51 mmol) of **9** were added to a solution of 50.0 g (317 mmol) of $KMnO_4$ in 600 mL of water. The mixture was refluxed until decolorization had occurred. The solution was filtered from precipitated MnO_2 and the filtrate acidified with half-concentrated HCl. A fine colorless powder of 2,2′-bipyridine-5,5′-dicarboxylic acid precipitated. This intermediate (M.p. > 280°C) was separated by filtration, dried in vacuo and suspended in 200 mL of dried ethanol. After careful addition of 50 mL of conc. H_2SO_4, the reaction mixture was refluxed for 16 h to give a clear solution. The warm solution was poured onto ice. The hitherto obtained precipitate was filtered, washed several times with water, dried and recrystallized from ethanol to give **10** as colorless needles (yield 9.8 g, 64%). − M.p. 145°C (ref.[12]: 147°C) − ^{1}H NMR ([D$_6$]DMSO): δ = 9.18 (d, 2 H, J = 2.5 Hz, H6, H6′), 8.54 (dd, 2 H, J_1 = 8.6 Hz, J_2 = 2.5 Hz, H4, H4′), 8.44 (d, 2 H, J = 8.6 Hz, H3, H3′), 4.38 (q, 4 H, J = 7.1 Hz, OCH_2), 1.36 (t, 6 H, J = 7.1 Hz, CH_3). − ^{13}C NMR ($CDCl_3$): δ = 164.2 (*C*OOEt), 157.3 (C2, C2′), 149.8 (C6, C6′), 137.9 (C4, C4′), 126.2 (C5, C5′), 121.0 (C3, C3′), 61.0 (OCH_2), 13.8 (CH_3).

2,2′-Bipyridine-5,5′-dicarboxylic Diazide (11): 50 mL of an 80% hydrazine hydrate solution was added to a slurry of 8.20 g (27.3 mmol) of **10** in 50 mL of ethanol. The mixture was heated for 3 h at an oil-bath temperature of 120°C to give a viscous mass which was filtered, washed with hot ethanol and dried in vacuo. The intermediate dihydrazide (6.5 g) thus obtained was suspended at 0°C in 150 mL of conc. HCl. A solution of 3.88 g (56 mmol) of $NaNO_2$ in 30 mL of water was added dropwise to this slurry with the temperature kept always below 10°C. After a few hours, a clear yellow solution was obtained. Upon dilution with 750 mL of water a colorless precipitate was produced which was filtered, washed several times with water, twice with 30 mL of hot ethanol and dried in vacuo to yield 6.72 g (84%) of a white powder. − M.p. > 300°C. − IR (Nujol): $\tilde{\nu}$ = 3076 cm^{-1} w, 2730 w, 2182 w, 2143 w, 1728 w,

1696 s, 1595 m, 1556 w, 1560 w, 1467 s, 1380 m, 1290 m, 1282, 1238 m, 1182 m, 1238 w, 1182 w, 1160 w, 1130 w, 1120 w, 1058 w, 1034 w, 1000 w, 895 w, 870 w, 860 w, 751 w, 722 w.

5,5′-Bis(ethoxycarbonylamino)-2,2′-bipyridine (12): 6.00 g (20.4 mmol) of the diazide **11** was suspended in a mixture of 150 mL of *p*-xylene and 150 mL of dried ethanol and refluxed for 18 h to give a clear yellow solution. Upon cooling yellowish crystals were obtained which after filtration were recrystallized from ethanol. The yield of the now colorless product was 6.5 g (97%). − M.p. > 300°C. − ^{1}H NMR ([D$_6$]DMSO): δ = 9.92 (s, 2 H, NH), 8.67 (d, 2 H, *J* = 2.2 Hz, H6, H6′), 8.20 (d, 2 H, *J* = 8.8 Hz, H3, H3′), 7.97 (dd, 2 H, J_1 = 8.8 Hz, J_2 = 2.4 Hz, H4, H4′), 4.14 (q, 4 H, *J* = 7.1 Hz, OC*H*$_2$CH$_3$), 1.24 (t, 6 H, *J* = 7.1 Hz, CH$_2$C*H*$_3$). − ^{13}C NMR ([D$_6$]DMSO): δ = 159.3 (EtO*C*ONH), 155.0 (C2, C2′), 144.9 (C6, C6′), 141.5 (C4, C4′), 131.5 (C3, C3′), 125.6 (C5, C5′), 66.4 (OCH$_2$), 20.2 (CH$_3$).

5,5′-Diamino-2,2′-bipyridine (5): 5.00 g (15.2 mmol) of the diurethane **12** was refluxed for 24 h in a mixture of 200 mL of ethanol and 200 mL of 2 N NaOH. After cooling to room temperature, the solution was carefully neutralized and the alcohol distilled of at normal pressure. Upon cooling the hydrate of the diamine **5** crystallized as long needles which may be weakly pink colored due to traces of iron. Further purification was achieved by sublimation at 0.2 mbar and an oil-bath temperature of 190°C. Yield 1.97 g (70%). Analytical data are given after the following procedure.

Synthesis of 5 by Coupling of 5-Amino-2-chloropyridine (Scheme 2): In a 250-mL three-necked flask was placed 2.37 g (10 mmol) of nickel dichloride hexahydrate and 10.5 g (40 mmol) of triphenylphosphane. The flask was evacuated and refilled with argon for three times. 100 mL of dried dimethyl formamide was added under inert gas and the solution rapidly turned blue. After PPh_3 and $NiCl_2 \times 6\ H_2O$ had completely dissolved in DMF, 0.7 g (11 mmol) of zinc powder was added to the solution under inert gas at 50°C and the solution slowly turned brown-red. After stirring this mixture for 1 h, 10 mL of a DMF solution with 1.28 g (10 mmol) of 5-amino-2-chloropyridine was added dropwise to the mixture. Stirring was continued for 4 h at 50°C at which time the starting material could not be detected anymore by thin-layer chromatography (eluent ethyl acetate). The reaction mixture was then concentrated in vacuo to half of its volume. After adding 250 mL of water, the mixture was carefully poured into 150 mL of conc. ammonia and stirred for 18 h. The solution turned blue because of the formation of hexaamminenickel(II) complexes. The PPh_3 precipate was removed by filtration and the filtrate was extracted three times with 50 mL of dichloromethane each. The combined organic phases were treated with 50 mL of half-concentrated HCl for three times each to separate the diaminobipyridine from PPh_3. During this procedure strongly colored aminohydrochlorides of **5** were formed. The combined acidic aqueous phases were carefully neutralized with a 10% Na_2CO_3 solution. The product **5** separated as a yellowish solid and was sublimed as described above to give a colorless powder (yield 1.11 g, 60%). − M.p. 205°C (ref.[12] 205−206°C). − ^{1}H NMR ([D$_6$]DMSO): δ = 7.92 (d, 2 H, *J* = 2.8 Hz, H6, H6′), 7.84 (d, 2 H, *J* = 8.6 Hz, H3, H3′), 6.95 (dd, 2 H, J_1 = 8.6 Hz, J_2 = 2.5 Hz, H4, H4′), 5.30 [s (br.), 4 H, NH_2]. − ^{13}C NMR ($CDCl_3$): δ = 144.7 (C2, C2′),143.6 (C5, C5′), 134.9 (C6, C6′), 120.5 (C3, C3′), 119.0 (C4, C4′); ([D$_6$]DMSO): δ = 147.1, 145.5, 136.6, 123.5, 122.2. − IR (KBr): $\tilde{\nu}$ = 3424 cm^{-1} w, 3338 m, 3310 m, 3207 m, 3062 w, 3057 w, 3005 w, 1632 w, 1600 m, 1568 m, 1478 s, 1412 m, 1289 m, 1248 w, 1137 w, 1108 w, 1088 w, 1060 w, 1024 w, 920 w, 897 w, 846 m, 832 m, 737 w, 656 m, 552 m, 517 m, 509 w, 418 w.

Syntheses of Transition Metal Complexes

[Tris(5,5′-diamino-2,2′-bipyridine)manganese(II)] Chloride Hydrate (14): To a solution of 76.2 mg (0.38 mmol) of $MnCl_2 \times 4\ H_2O$ in 20 mL of distilled water was given a solution of 192.5 mg (1.03 mmol) of **5** in 25 mL of ethanol. The pale red solution was allowed to stand several days at room temperature. The bright red cubic crystals were separated by filtration. Upon standing in air the crystals slowly lose water of crystallization and turn opaque (yield 222 mg, 82%). − A thermogravimetric analysis shows the complete loss of crystal water at 101−145°C. At 290°C the loss of one diaminobipyridine ligand takes place with possible formation of [$MnCl_2$(**5**)$_2$]. Above 360°C decomposition is observed. − IR (Nujol): $\tilde{\nu}$ = 3420 cm^{-1} w (br.), 3305 m (br.), 3200 w (br.), 1632 m, 1598 s, 1585 m, 1487 m, 1430 m, 1325 w (br.), 1319 m, 1300 m, 1272 w (br.), 1262 w (br.), 1162 w, 1055 w, 1030 m, 1019 w, 965 w (br.), 890 w, 862 w, 852 w, 827 m, 758 w, 740 w, 728 m, 656 w, 650 w. − Tetrahydrate $C_{30}H_{38}Cl_2MnN_{12}O_4$ (756.56): calcd. C 47.62, H 5.06, N 22.21; found C 47.56, H 4.05, N 22.31.

[Diazidobis(5,5′-diamino-2,2′-bipyridine)manganese(II)] (15): 15 mL of an ethanolic solution of **5** (100 mg, 0.54 mmol) was added to 15 mL of an aqueous solution of $MnCl_2 \times 4\ H_2O$ (110 mg, 0.54 mmol) and stirred for 15 min. To this solution was added 5 mL of an aqueous solution of NaN_3 (88 mg, 1.35 mmol). The resulting yellow solution was left standing for 36 h at room temperature. Then some undissolved solid was filtered and the filtrate was then placed at ambient temperature. One month later, a yellow precipate had formed on the bottom of the flask. Two months later, the yellow precipate had transformed into well-formed red-orange crystals which were collected by filtration and washed with water and ethanol to give 123 mg of product (69%, based on **5**). − IR (KBr): $\tilde{\nu}$ = 3430 cm^{-1} w, 3372 s, 3304 s, 3207 s, 2078 s ν(N_3), 2020 s ν(N_3), 1620 s, 1604 s, 1588 s, 1485 s, 1438 s, 1350 w, 1328 m, 1311 s, 1295 m, 1275 s, 1165 m, 1125 w, 1060 w, 1030 m, 1025 m, 960 w, 934 m, 892 m, 865 w, 849 m, 838 s, 728 m, 698 w, 653 m, 630 m, 620 w, 592 w, 545 s, 520 m. − $C_{20}H_{20}N_{14}Mn$ (511.40): calcd. C 46.96, H 3.91, N 38.36; found C 46.76, H 3.92, N 38.33.

[Tris(5,5′-diamino-2,2′-bipyridine)iron(II)] Sulfate Hydrate (16): To a hot solution (90°C) of 532 mg (2.86 mmol) of **5** in 30 mL of distilled water was added dropwise a solution of 280 mg (1.01 mmol) of $FeSO_4 \times 7\ H_2O$ in 10 mL of distilled water. A red color immediately developed. After complete addition, the solution was allowed to cool and the precipitated crystals were washed with a few mL of ice-cooled water, then with dried ethanol and finally with diethyl ether. The crystals were briefly dried in air. Single crystals could best be obtained by cooling a saturated solution from room temperature to 0°C (yield 720 mg, 92%). − A thermogravimetric analysis shows the complete loss of water of crystallization at 166°C and decomposition above 350°C. − ^{1}H NMR (D_2O): δ = 7.99 (d, *J* = 8.8, H3, H3′), 7.29 (dd, J_1 = 8.8 Hz, J_2 = 2.4 Hz, H4, H4′), 6.85 (d, *J* = 2.4 Hz, H6, H6′). − ^{13}C NMR (D_2O): δ = 149.6 (C2, C2′), 144.7 (C5, C5′), 139.3 (C6, C6′), 123.1 (C4, C4′), 121.4 (C3, C3′). − IR (Nujol): $\tilde{\nu}$ = 3420 cm^{-1} w, 3340 w, 3205 w, 1632 s, 1602 s, 1580 m, 1575 w, 1488 s, 1429 m, 1368 s, 1352 m, 1328 m, 1310 s, 1292 m, 1268 m, 1206 m, 1165 m, 1028 w, 1019 w, 904 w, 860 w, 838 w, 832 w, 728 w, 655 w. − Hexahydrate $C_{30}H_{42}FeN_{12}O_{10}S$ (818.65): calcd. C 44.01, H 5.17, N 20.53; found C 44.16, H 4.20, N 20.50.

[Tris(5,5′-diamino-2,2′-bipyridine)nickel(II)] Chloride Hydrate (17): A solution of 158 mg (0.66 mmol) $NiCl_2 \times 6\ H_2O$ in 30 mL of distilled water was combined with a solution of 383 mg (2.05 mmol) of **5** in 25 mL of ethanol. The mixture was heated to reflux and a pale red solution formed. After cooling to room

temperature, the precipitate was filtered, washed with little cold water, ethanol, and diethyl ether and air-dried (yield 150 mg, 85%). Single crystals could be obtained by slow cooling of a saturated solution from room temperature to 0°C. The product crystallizes in bright red cubes, which slowly loose water of crystallization in air. − A thermogravimetric analysis shows the complete loss of water of crystallization at 168°C and decomposition above 280°C. − IR (Nujol): $\tilde{\nu}$ = 3420 cm^{-1} w (br.), 3320 w (br.), 3200 m (br.), 1630 m, 1602 s, 1579 m, 1486 s, 1432 m, 1321 m, 1300 m, 1272 m, 1260 w, 1161 w, 1060 w, 1054 w, 1031 w, 1019 w, 960 w (br.), 888 w, 868 w, 852 w, 828 m, 722 w, 654 m, 596 w, 532 w, 428 w. − Hexahydrate $C_{30}H_{42}Cl_2N_{12}NiO_6$ (796.34): calcd. C 45.25, H 5.31, N 21.11; tetrahydrate $C_{30}H_{38}Cl_2N_{12}NiO_4$ (760.31): calcd. C 47.39, H 4.99, N 22.10; 2.5-hydrate $C_{30}H_{35}Cl_2N_{12}NiO_{2.5}$ (733.28): calcd. C 49.13, H 4.81, N 22.92; found C 47.64, H 4.08, N 22.39.

[Tris(5,5′-diamino-2,2′-bipyridine)nickel(II)] Thiocyanate (18): To an aqueous solution (100 mL) of $NiCl_2 \times 6\ H_2O$ (0.64 g, 2.69 mmol or 0.32 g, 1.35 mmol) was added a DMF solution (10 mL) of **5** (0.50 g, 2.69 mmol). After stirring for 2 h, 50 mL of conc. ammonia was added and stirring was continued for 20 h. During this time the solution changed color from yellow to brown. 20 mL of the aforementioned solution (containing 80 mg/0.34 mmol or 40 mg/0.17 mmol of nickel and 62 mg/0.34 mmol of **5**) was used to overlayer 5 mL of an aqueous solution of 33 mg (0.34 mmol) of KSCN in a test tube. The solution was allowed to stand for 15 d at ambient temperature. The resulting orange-brown crystals were collected by filtration, washed with water and ethanol and dried under vacuum (yield 66−76 mg, 54−66% based on **5**). − $C_{32}H_{30}N_{14}NiS_2$ (733.50): calcd. C 52.41, H 4.09, N 26.75; found C 51.45, H 4.11, N 26.41. − IR (KBr): $\tilde{\nu}$ = 3438 cm^{-1} m, 3300 m, 3190 m, 2076 s ν(SCN), 2048 s ν(SCN), 1630 s, 1602 s, 1580 s, 1460 s, 1443 s, 1318 m, 1310 m, 1300 m, 1275 m, 1170 m, 1163 m, 1148 w, 1060 w, 1035 m, 1021 w, 858 w, 840 m, 825 m, 744 w, 725 m, 700 w, 660 s, 550 m. − $C_{32}H_{30}N_{14}NiS_2$ (733.50): calcd. C 52.41, H 4.09, N 26.75; found C 51.56, H 4.19, N 26.57.

$^1{}_\infty$[Diaqua(5,5′-diamino-2,2′-bipyridine)(μ-sulfato)copper(II)] Hydrate (19): A 25-ml flask was charged with mixture of $CuSO_4 \times 5\ H_2O$ (135 mg, 0.54 mmol), **5** (100 mg, 0.54 mmol) and 10 mL of water, sealed and heated in an oil bath to 120°C for 48 h. After cooling, the dark-green crystals formed were collected by filtration and washed with water and ethanol. Concentration of the filtrate by slow evaporation of the solvent at room temperature for 8 d gave another crop of well-formed dark-green crystals. A total yield of 183 mg (89%) was obtained. − IR (KBr): $\tilde{\nu}$ = 3420 cm^{-1} m, 3340 m, 3220 m, 1650 m, 1606 m, 1590 m, 1495 s, 1446 w, 1332 w to m, 1324 w, 1280 w, 1210 w, 1140 m, 1115 m, 1040 w, 955 w, 925 w, 850 w, 839 w, 718 w, 660 w, 550 w. − $C_{10}H_{14}CuN_4O_6S$ (381.86): calcd. C 31.45, H 3.67, N 14.68; found C 31.32, H 3.84, N 14.70.

[Dichloro(5,5′-diamino-2,2′-bipyridine)copper(II)] (20): 10 mL of an aqueous solution of $CuCl_2 \times 2\ H_2O$ (92 mg, 0.54 mmol) was carefully overlayered in a test tube with 10 mL of an ethanolic solution of **5** (100 mg, 0.54 mmol). The solution was allowed to stand for 7 d at room temperature. After this time, the well-formed rod-shaped dark-green crystals were collected by filtration and washed with cold water and ethanol to give 14 mg of product (82%). − IR (KBr):$\tilde{\nu}$ = 3448 cm^{-1} s, 3346 s, 3210 w, 1615 s, 1603 s, 1580 m, 1510 w, 1492 s, 1435 m, 1350 w to m, 1332 m, 1310 w, 1278 m, 1220 m, 1161 w, 1156 w, 1064 w, 1038 m, 1022 w, 968 w, 885 w, 836 s, 715 m, 665 w, 660 w, 550 m, 530 w. − $C_{10}H_{10}Cl_2CuN_4$ (322.66): calcd. C 37.44, H 3.12, N 17.47; found C 36.45, H 3.12, N 17.15. − The reaction of **5** in ethanol (or THF) with $CuCl_2 \times 2\ H_2O$ in water in the molar ratio of 1:2 also gave **20**.

[(5,5′-Diamino-2,2′-bipyridine)dinitratozinc(II)] (21): A solution of 64 mg (0.22 mmol) of $Zn(NO_3)_2 \times H_2O$ in 5 mL of distilled water was overlayered in a test tube first with 2 mL of ethyl acetate and then with a solution of 35 mg (0.19 mmol) of **5** in 4 mL of ethanol. After standing for several days, colorless rhombohedra had formed at the boundary layer, which were carefully separated, washed with little THF and air-dried (yield 55 mg, 77%). − When **21** was heated with two equivalents of **5** in water crystals formed upon cooling which were shown by analysis to have a 3:1 ligand/metal ratio as in **22**.

[Tris(5,5′-diamino-2,2′-bipyridine)zinc(II)] Nitrate Hydrate (22): To a solution of 167.5 mg (0.56 mmol) $Zn(NO_3)_2 \times 6\ H_2O$ in 20 mL of distilled water was added 332.8 mg (1.79 mmol) of **5** and the mixture heated to reflux for 30 min which led to a clear solution. After cooling to room temperature, the crystals formed were separated by filtration, washed with little ice-cooled water, ethanol and diethyl ether. After drying in air, the complex was obtained as a light yellow fine crystalline powder. Single crystals were obtained by slow cooling of a saturated solution from room temperature to 0°C (yield 320 mg, 69%). − A thermogravimetric analysis shows complete loss of the water of crystallization at 179°C and decomposition above 335°C. − ^{1}H NMR (D_2O):δ = 8.43 (d, J = 8.6, H3, H3′), 7.84 (dd, J_1 = 8.6 Hz, J_2 = 2.6 Hz, H4, H4′), 7.79 (d, J = 2.6 Hz, H6, H6′); ([D_6]DMSO): δ = 8.08 (d, J = 8.7, H3, H3′), 7.19 (dd, J_1 = 8.7 Hz, J_2 = 2.5 Hz, H4, H4′), 7.08 (d, J = 2.5 Hz, H6, H6′). − ^{13}C NMR (D_2O):δ = 145.5 (C2, C2′), 140.8 (C5, C5′), 134.4 (C6, C6′), 126.1 (C4, C4′), 122.2 (C3, C3′). − IR (Nujol): $\tilde{\nu}$ = 3430 cm^{-1} w (br.), 3325 w (br.), 3210 w (br.), 1630 m, 1602 s, 1582 m, 1488 m, 1378 m, 1342 m, 1320 m, 1316 m, 1272 m, 1160 w, 1152 w, 1142 w, 1080 w, 1060 w, 1031 w, 1019 w, 898 w, 892 w, 867 w, 850 w, 838 w, 828 m, 722 m, 658 w. − Dihydrate $C_{30}H_{34}N_{14}O_8Zn$ (784.07): calcd. C 45.94, H 4.37, N 25.00; found C 45.61, H 3.32, N 25.05.

[(5,5′-Diamino-2,2′-bipyridine)nitratosilver(I)] Hydrate (23): A solution of 122 mg (0.72 mmol) of $AgNO_3$ in 10 mL of distilled water was overlayered in a test tube first with 3 mL of dried ethyl acetate and then with a solution of 104 mg (0.56 mmol) of **5** in 15 mL of dried ethanol. After standing for several weeks at room temperature in the dark, yellowish fiber clusters had formed at the layer boundary. They were separated by filtration, washed with some cold water, ethanol and finally diethyl ether. Drying in air gave light yellow fibers (yield 1.66 mg, 76%). − M.p. > 195°C (dec.). − ^{1}H NMR ([D_6]DMSO): δ = 7.92 (d, J = 2.6 Hz, H6, H6′), 7.91 (d, J = 8.8 Hz, H3, H3′), 7.15 (dd, J_1 = 8.6 Hz, J_2 = 2.6 Hz, H4, H4′). − ^{13}C NMR ([D_6]DMSO): δ = 145.2 (C2, C2′), 140.4 (C5, C5′), 136.2 (C6, C6′), 121.9 (C4, C4′), 121.2 (C3, C3′). − IR (Nujol): $\tilde{\nu}$ = 3450 cm^{-1} w (br.), 3325 m (br.), 3210 w (br.), 1628 s, 1604 s, 1574 m, 1488 s, 1422 m, 1350 s, 1326 s, 1296 m, 1271 m, 1252 w, 1153 w, 1062 w, 1043 w, 1022 w, 1018 w, 879 w, 862 w, 843 w, 819 w, 722 m, 652 m, 646 m. − $C_{10}H_{14}AgN_5O_5$ (392.12): calcd. C 30.63, H 3.60, N 17.86; found C 30.22, H 3.18, N 17.63.

[Bis(5,5′-diamino-2,2′-bipyridine)silver(I)] Nitrate (24): A slurry of 225 mg (1.21 mmol) of **5** in 20 mL of distilled water was heated until complete dissolution. Then a hot solution of 110 mg (0.65 mmol) of $AgNO_3$ in 10 mL of water was added which immediately gave a colorless precipitate. This was shown by elemental analysis to have a 1:1 ligand/metal composition. Conc. aqueous ammonia was added dropwise until the precipitate had completely dissolved. The solution was kept at room temperature open to the air and after a few days thin platelets with a mother-of-pearl shine had formed. The crystals were collected by filtration, washed with diethyl ether and dried in vacuo (yield 171 mg, 52%). − M.p. >

230°C. – ^{1}H NMR ([D$_6$]DMSO): δ = 7.91 (d, J = 8.6 Hz, H3, H3′), 7.90 (d, J = 2.3 Hz, H6, H6′), 7.12 (dd, J_1 = 8.6 Hz, J_2 = 2.6 Hz, H4, H4′), 5.68 [s (br.), NH$_2$]. – ^{13}C NMR ([D$_6$]DMSO): δ = 145.1 (C2, C2′), 140.7 (C5, C5′), 136.0 (C6, C6′), 121.8 (C4, C4′), 121.0 (C3, C3′). – IR (Nujol): $\tilde{\nu}$ = 3420 cm^{-1} w, 3340 w, 3205 w, 1632 s, 1602 s, 1582 m, 1575 w, 1488 s, 1429 m, 1368 s, 1352 m, 1328 m, 1310 s, 1292 m, 1268 m, 1206 m, 1165 m, 1028 w, 1019 w, 904 w, 860 w, 838 w, 832 w, 728 w, 655 w. – $C_{20}H_{20}AgN_9O_3$ (542.31): calcd. C 44.30, H 3.70, N 23.25; found C 44.73, H 3.95, N 23.46.

$^1_\infty$[Di(μ-chloro)(5,5′-diamino-2,2′-bipyridine)cadmium(II)] Hydrate (25): A solution of 175 mg (0.87 mmol) $CdCl_2 \times H_2O$ in 10 mL of distilled water was overlayered in a test tube first with 3 mL of ethyl acetate and then with a solution of 130 mg (0.70 mmol) of **5** in 15 mL of ethanol. After standing for several days, colorless rhombohedra had formed at the boundary layer, which were carefully separated, washed with little THF and air-dried (yield 160 mg, 56%). – M.p. > 225°C. – ^{1}H NMR ([D$_6$]DMSO): δ = 7.98 [s (br.), H6, H6′], 7.92 (d, J = 8.7, H3, H3′), 7.14 (dd, J_1 = 8.7 Hz, J_2 = 2.7 Hz, H4, H4′), 5.85 [s (br.), NH$_2$]. – ^{13}C NMR ([D$_6$]DMSO): δ = 145.5 (C2, C2′), 138.0 (C5, C5′), 134.7 (C6, C6′), 122.8 (C4, C4′), 120.8 (C3, C3′). – IR (Nujol): $\tilde{\nu}$ = 3510 cm^{-1} w, 3338 m (br.), 3204 m (br.), 1638 m (br.), 1602 s, 1590 s, 1487 s, 1435 m, 1326 w, 1315 w, 1300 m, 1272 m, 1266 m, 1160 m, 1130 w (br.), 1064 w (br.), 1030 m, 918 m, 862 msh, 845 s, 827 m (br.), 727 m, 700 w, 655 w. – $C_{10}H_{14}CdCl_2N_4O_2$ (405.56): calcd. C 29.59, H 3.48, N 13.80; found C 30.55, H 3.22, N 13.23. – When **25** was heated with two equivalents of **5** in water crystals formed upon cooling which were shown by analysis to have a 3:1 ligand/metal ratio as in **26**.

[Tris(5,5′-diamino-2,2′-bipyridine)cadmium(II)] Chloride Hydrate (26): In 20 mL of an aqueous solution of 117.5 mg (0.58 mmol) of $CdCl_2 \times H_2O$ was suspended 336.0 mg (1.80 mmol) of **5** and heated under reflux for 30 min. From the bright yellow solution fine crystals formed upon cooling, which were filtered, washed with little ethanol and diethyl ether and air-dried. Upon storage in air the crystals slowly lost incorporated solvent water (yield 350 mg, 76%). – M.p. > 225°C. – ^{1}H NMR ([D$_6$]DMSO): δ = 7.90 (d, J = 8.6, H3, H3′), 7.88 (d, J = 2.6 Hz, H6, H6′), 7.09 (dd, J_1 = 8.6 Hz, J_2 = 2.6 Hz, H4, H4′). – ^{13}C NMR ([D$_6$]DMSO): δ = 144.9 (C2, C2′), 139.4 (C5, C5′), 134.6 (C6, C6′), 122.2 (C4, C4′), 120.4 (C3, C3′). – ^{113}Cd NMR (66.0 MHz, ([D$_6$]DMSO), standard is a 2.0 M cadmium perchlorate solution in D$_2$O): δ = 254 (s), half width 30 ppm. – IR (Nujol): $\tilde{\nu}$ = 3425 cm^{-1} w, 3310 w, 3205 w, 1628 s, 1604 m, 1586 w, 1495 s, 1440 s, 1330 m, 1322 w, 1280 w, 1269 w, 1172 w, 1168 w, 1130 w (br.), 1036 w, 1028 w, 970 w, 905 w, 888 w, 870 w, 833 m, 728 w, 668 w, 660 w. – Dihydrate $C_{30}H_{34}CdCl_2N_{12}O_2$ (778.00): calcd. C 46.29, H 4.40, N 21.59; found: C 45.59, H 3.85, N 21.48.

X-ray Structure Determinations: Data were collected with Mo-K_α radiation (λ = 0.71073 Å) and the use of a graphite monochromator. Structure solution was performed by direct methods using SHELXS-97.[65] Refinement: Full-matrix least-squares on F^2 [SHELXL-97 (version 97–2)];[65] all non-hydrogen positions found and refined with anisotropic temperature factors. Crystal data are

Table 5. Crystal data for compounds **15**–**20**, **22** and **25**

Compound	**15**	**16**	**17**	**18**	**19**	**20**	**22**	**25**
Empirical formula	$C_{20}H_{20}N_{14}Mn$	$C_{60}H_{96}Fe_2N_{24}O_{26}S_2$[f]	$C_{60}H_{70}Cl_4N_{24}Ni_2O_5$[f]	$C_{32}H_{30}N_{14}NiS_2$	$C_{10}H_{20}CuN_4O_9S$	$C_{10}H_{10}Cl_2CuN_4$	$C_{30}H_{34}N_{14}O_8Zn$	$C_{10}H_{14}CdCl_2N_4O_2$
M [g mol^{-1}]	511.405	2x872.68 [f]	2x733.28 [f]	733.500	435.899	322.665	784.07	405.56
Crystal size [mm]	0.45×0.35×0.25	0.50×0.30×0.05	0.80×0.50×0.40	0.25×0.15×0.09	1.08×0.15×0.09	0.46×0.08×0.08	0.76×0.39×0.25	0.30×0.20×0.20
Crystal description	prismatic	platelet	prismatic	prismatic	needle	needle	irregular	prismatic
Crystal color	red-brown	red	red	red	green	blue	yellow-brown	colorless
T [K]	200(3)	200(3)	200(3)	200(3)	200(3)	200(3)	200(3)	293(2)
Diffractometer	STOE-IPDS	STOE-IPDS	STOE-IPDS	STOE-IPDS	STOE-IPDS	STOE-IPDS	STOE-IPDS	Syntex P21
Scan type, 2 Θ range [°]	ω, 4.6–55.8	ω, 2.8–44.2	ω, 3.7–51.6	ω, 4.2–56.1	ω, 6.1–55.8	ω, 6.2–55.5	ω, 3.5–47.7°	ω, 8–40°
h; k; l range	–17, 17; –13, 14; –21, 20	–18, 18; –18, 18 –27, 27	–29, 29; –30, 24 –29, 27	–13, 13; –14, 14; –18, 18	–8, 9; –25, 25 –16, 16	–16, 16; –17, 17; –9, 9	–19, 12; –19, 19; –51, 48	0, 20; 0, 9; 0, 7
Crystal system	monoclinic	orthorhombic	monoclinic	triclinic	monoclinic	monoclinic	tetragonal	orthorhombic
Space group	*I*2/*a*	*Pna*2$_1$	*C*2/*c*	*P*$\bar{1}$	*P*2$_1$/*n*	*C*2/*c*	*I*4$_1$/*a*	*Pbcn*
a [Å]	13.6751(13)	17.4099(11)	24.5144(18)	10.4923(11)	6.8693(6)	12.9032(11)	17.5457(12)	21.02(12)
b [Å]	10.8010(6)	17.2792(16)	24.8858(15)	11.2927(12)	19.4875(13)	13.5149(10)	17.5457(12)	9.40(4)
c [Å]	16.0833(14)	26.3756(18)	24.3872(19)	14.3883(14)	12.7217(10)	7.3981(6)	46.380(4)	7.32(4)
α [°]	90	90	90	79.264(12)	90	90	90	90
β [°]	114.136(10)	90	109.325(9)	74.867(12)	105.212(9)	112.987(9)	90	90
γ [°]	90	90	90	89.259(12)	90	90	90	90
V [Å^3]	2165.7(14)	7934(1)	14039(2)	1615.7(12)	1643.3(14)	1187.74(15)	14278.2(19)	1446(13)
Z	4	4	8	2	4	4	16	8
$D_{calcd.}$ [g cm^{-3}]	1.568(1)	1.4681(2)	1.3877(2)	1.508(1)	1.7619(15)	1.7933(2)	1.4590(2)	1.862
F(000) [electrons]	1052	3664	6096	760	900	644	6496	800
μ [$^{-1}$]	6.53	5.09	7.53	7.79	15.1	22.7	7.58	18.82
Absorption correction	numerical	numerical	numerical	numerical	numerical	numerical	numerical	empirical
Max/min transmission		0.830/0.980	0.687/0.786	0.874/0.935	0.390/0.861	0.739/0.863	0.619/0.753	0.759/0.643
Measured reflections	9648	39521	26958	15188	15509	3746	20364	666
Unique reflect. for refinemt. (R_{int})	2511 (0.0254)	9855(0.12)	12059(0.0485)	7146 (0.0258)	3890 (0.0831)	1045 (0.0275)	5421 (0.0568)	666 (0.0830)
Observed reflection [I > 2 σ(I)]	2234	7381	7354	5406	3431	939	4364	545
Parameters refined	199	482	897	562	306	98	492	88
Max/min Δρ[a] [e Å^{-3}]	0.386/–0.212	0.780/–0.489	1.225/–0.580	0.345/–0.316	1.037/–0.732	0.304/–0.219	0.496/–0.302	0.742/–0.576
$R1$/$wR2$[b] [I > 2 σ(I)]	0.0271/0.0701	0.087/0.226[g]	0.061/0.169	0.0304/0.0688	0.0311/0.0829	0.0205/0.0520	0.0386/0.0855	0.0489/0.1233
$R1$/$wR2$[b] (all reflections)	0.0313/0.0718	0.108/0.235	0.098/0.188	0.0467/0.0731	0.0355/0.0846	0.0235/0.0528	0.0516/0.0889	0.0528/0.1330
GOF on F^2[c]	1.046	1.090	0.931	0.918	1.006	1.058	0.945	0.972
Weighting scheme w: a/b[d]	0.0481/0.4789	0.109/26.376	0.1262/0.0000	0.0436/0.0000	0.0555/0.0000	0.0381/0.0000	0.0547/0.0000	0.1098/0.0000

[a] Largest difference peak and hole. – [b] Largest difference peak and hole. – [c] $R1 = (\Sigma\ F_o - F_c)/\Sigma\ F_o$; $wR2 = \{\Sigma[w(F_o^2 - F_c^2)^2] / \Sigma[w(F_o^2)^2]\}^{1/2}$. – [d] Goodness-of-fit, Gof = $\{\Sigma\ [w(F_o^2 - F_c^2)^2]/(n - p)\}^{1/2}$. – [e] $w = 1/[\sigma^2(F_o^2) + (a{\cdot}P)^2 + b{\cdot}P]$ where $P = [\max(F_o^2 \text{ or } 0) + 2{\cdot}F_c^2]/3$. – [f] Two independent molecules in the unit cell. – [g] Structure refinement was hampered by the disorder in the anion-water layer.

listed in Table 5. The structure of compound **22** was refined as an axis twin (twin axis [010]). The volume fraction of the twin component from refinement was 0.5118(10), i.e. there is almost 1:1 twinning. Graphics were computed with ORTEP3 for Windows.[66] Crystallographic data (excluding structure factors) for the structures reported in this paper have been deposited with the Cambridge Crystallographic Data Center as supplementary publication no. CCDC-119339 (**15**), -119340 (**16**), -119341 (**17**), -119342 (**18**), 119343 (**19**), -119344 (**20**), -119345 (**22**), and -119346 (**25**). Copies of the data can be obtained free of charge on application to CCDC, 12 Union Road, Cambridge CB2 1EZ, UK [Fax: int. code + 44-1223/336-033; E-mail: deposit@ccdc.cam.ac.uk]. − Additional information (distances and angles) on hydrogen bonding which is not described in detail here can be found in the Supporting Information.

Acknowledgments

This work was supported by the Alexander von Humboldt Foundation (fellowship for H.-P. W.), the Fonds der Chemischen Industrie, the Deutsche Forschungsgemeinschaft (grant Ja 466/10-1), and the Graduate College "Unpaired Electrons" at the University of Freiburg.

[1] A. E. Martell, R. D. Hancock, *Metal Complexes in Aqueous Solutions*, Plenum Press, New York, **1996**; A. v. Zelewsky, *Stereochemistry of Coordination Compounds*, Wiley, Chichester, **1996**; J. M. Lehn, *Supramolecular Chemistry*, VCH, Weinheim, **1995**.
[2] C. Janiak, L. Uehlin, H.-P. Wu, P. Klüfers, H. Piotrowski, T. G. Scharmann, unpublished work.
[3] H.-P. Wu, C. Janiak, G. Rheinwald, H. Lang, *J. Chem. Soc., Dalton Trans.* **1999**, 183−190.
[4] H.-P. Wu, C. Janiak, L. Uehlin, P. Klüfers, P. Mayer, *Chem. Commun.* **1998**, 2637−2638.
[5] For our recent work with the ambidente hydrotris(triazolyl)boate ligand see for example: C. Janiak, T. G. Scharmann, J. C. Green, R. P. G. Parkin, M. J. Kolm, E. Riedel, W. Mickler, J. Elguero, R. M. Claramunt, D. Sanz, *Chem. Eur. J.* **1996**, *2*, 992−1000. C. Janiak, T. G. Scharmann, H. Hemling, D. Lentz, J. Pickardt, *Chem. Ber.* **1995**, *128*, 235−244.
[6] C. B. Aakeröy, A. M. Beatty, *Chem. Commun.* **1998**, 1067−1068. C. B. Aakeröy, A. M. Beatty, D. S. Leinen, *J. Am. Chem. Soc.* **1998**, *120*, 7383−7384. C. B. Aakeröy, K. R. Sneddon, *Chem. Soc. Rev.* **1993**, *22*, 397−407.
[7] B.-H. Ye, X.-M. Chen, G.-Q. Xue, *J. Chem. Soc. Dalton Trans.* **1998**, 2827−2831.
[8] J. M. Lehn, M. Mascal, A. DeCian, J. Fischer, *Chem. Commun.* **1990**, 479. J. M. Lehn, M. Mascal, A. DeCian, J. Fischer, *J. Chem. Soc. Perkin Trans. 2* **1992**, 461−467. C. M. Drain, R. Fischer, E. G. Nolen, J. M. Lehn, *J. Chem. Soc., Chem. Commun.* **1993**, 243.
[9] P. G. Desmartin, A. F. Williams, G. Bernardinelli, *New. J. Chem.* **1995**, *19*, 1109−1112.
[10] B. Olenyuk, A. Fechtenkötter, P. J. Stang, *J. Chem. Soc., Dalton Trans.* **1998**, 1707−1728. L. R. MacGillivray, R. H. Groeneman, J. L. Atwood, *J. Am. Chem. Soc.* **1998**, *120*, 2676−2677. A. J. Blake, S. J. Hill, P. Hubberstey, W.-S. Li, *J. Chem. Soc., Dalton Trans.* **1998**, 909−915. M.-L. Tong, X.-M. Chen, X.-L. Yu, T. C. W. Mak, *J. Chem. Soc., Dalton Trans.* **1998**, 5−6. P. Stang, B. Olenyuk, *Acc. Chem. Res.* **1997**, *30*, 502−518. O. M. Yaghi, H. Li, T. L. Groy, *Inorg. Chem.* **1997**, *36*, 4292−4293. P. Lossier, M. J. Zaworotko, *Angew. Chem. Int. Ed.* **1996**, *35*, 2779−2782. O. M. Yaghi, H. Li, *J. Am. Chem. Soc.* **1996**, *118*, 295−296. C. A. Hunter, *Angew. Chem. Int. Ed. Engl.* **1995**, *34*, 1079−1081.
[11] C. Janiak, *Angew. Chem. Int. Ed. Engl.* **1997**, *36*, 1431−1434. O. M. Yaghi, H. Li, C. Davies, D. Richardson, T. L. Groy, *Acc. Chem. Res.* **1998**, *31*, 474−484.
[12] C. Whittle, *J. Heterocycl. Chem.* **1977**, *14*, 191−194.
[13] F. Ebmeyer, F. Vögtle, *Chem. Ber.* **1989**, *122*, 1725−1727. W. H. F. Sasse, C. P. Whittle, *J. Chem. Soc.* **1961**, 1347−1350.
[14] M. Badger, F. Sasse, *J. Chem. Soc.* **1956**, 616−620.
[15] F. Case, *J. Am. Chem. Soc.* **1946**, *68*, 2574−2576.
[16] M. Tiecco, L. Testaferri, M. Tingoli, D. Chianelli, M. Montaucci, *Synthesis* **1984**, 736−738. K. S. Chan, A. K.-S. Tse, *Synth. Commun.* **1993**, *23*, 1929−1934.
[17] Y. Fort, S. Becker, P. Caubère, *Tetrahedron* **1994**, *50*, 11893−11902.
[18] M. Lourak, R. Vanderesse, Y. Fort, P. Caubère, *J. Org. Chem.* **1989**, *54*, 4840−4844. M. Lourak, R. Vanderesse, Y. Fort, P. Caubère, *J. Org. Chem.* **1989**, *54*, 4844−4848.
[19] M. F. Semmelhack, P. Helquist, L. D. Jones, L. Keller, L. Menelson, R. Speltz-Ryono, J. Gorszynski-Smith, R. D. Staufer, *J. Am. Chem. Soc.* **1981**, *103*, 6460.
[20] C. O. Okafer, *J. Org. Chem.* **1973**, *38*, 4383−4386.
[21] C. Janiak, T. G. Scharmann, W. Günther, F. Girgsdies, H. Hemling, W. Hinrichs, D. Lentz, *Chem. Eur. J.* **1995**, *1*, 637−644.
[22] B. Jezowska-Trzebiatowska, H. Kozlowski, L. Latos-Grazynski, T. Kowalik, *Chem. Phys. Lett*. **1975**, *30*, 355−357.
[23] For a similar recrystallization reaction from aqueous ammonia, see C. Janiak, T. G. Scharmann, W. Günther, W. Hinrichs, D. Lentz, *Chem. Ber.* **1996**, *129*, 991−995. C. Janiak, T. G. Scharmann, P. Albrecht, F. Marlow, R. Macdonald, *J. Am. Chem. Soc.* **1996**, *118*, 6307−6308.
[24] A. Vertes, I. Deszi, M. Suba, *Acta Chim*. **1970**, *64*, 347−350.
[25] H. Sato, T. Tominaga, *Bull. Chem. Soc. Jpn.* **1976**, *49*, 697−700.
[26] C. Tänzer, R. Price, E. Breitmaier, G. Jung, W. Voelter, *Angew. Chem.* **1970**, *82*, 957−958.
[27] B. Jezowska-Trzebiatowska, G. Formicka-Kozlowska, H. Kozlowski, L. Latos-Grazynski, T. Kowalik, *Chem. Phys. Lett*. **1975**, *30*, 358−362.
[28] C. J. Jameson, J. Mason, in *Multinuclear NMR* (J. Mason, Ed.), Plenum Press, New York, **1989**, ch. 3, p. 72−74.
[29] M. Munakata, S. Kitagawa, F. Yagi, *Inorg. Chem.* **1986**, *25*, 964−970.
[30] P. F. Rodesiler, R. W. Turner, N. G. Charles, E. A. H. Griffith, A. L. Amma, *Inorg. Chem.* **1984**, *23*, 999−1004.
[31] C. Janiak in *Moderne Anorganische Chemie* (E. Riedel, Ed.), de Gruyter, Berlin, **1998**, ch. 2, p. 206.
[32] S. Vadera, N. Kumar, *J. Radioanal. Nucl. Chem.* **1990**, *146*, 29−35.
[33] L. Y. Johansson, R. Larsson, *Chem. Phys. Lett*. **1974**, *24*, 508−513.
[34] D. C. Craig, H. A. Goodwin, D. Onggo, *Aust. J. Chem.* **1988**, *41*, 1157−1169.
[35] Reviews: P. Gütlich, A. Hauser, H. Spiering, *Angew. Chem. Int. Ed. Engl.* **1994**, *33*, 2024−2054. O. Kahn, *Molecular Magnetism*, VCH, Weinheim, **1993**, ch. 4, p. 53ff. J. Zarembowitch, *New. J. Chem.* **1992**, *16*, 255−267. P. Gütlich, A. Hauser, *Coord. Chem. Rev.* **1990**, *97*, 1−22. H. Toftlund, *Coord. Chem. Rev.* **1989**, *94*, 67−108. E. König, *Progr. Inorg. Chem.* **1987**, *35*, 527−622. P. Gütlich, *Struct. Bonding (Berlin)* **1981**, *44*, 83−195. H. A. Goodwin, *Coord. Chem. Rev.* **1976**, *18*, 293−325.
[36] L. M. Eppstein, *J. Chem. Phys.* **1964**, *40*, 435−439.
[37] C. Janiak, T. G. Scharmann, T. Bräuniger, J. Holubova, M. Nadvornik, *Z. Anorg. Allg. Chem.* **1998**, *624*, 769−774.
[38] C. Janiak, *Chem. Ber.* **1994**, *127*, 1379−1385.
[39] S. Ahuja, R. Singh, C. Rai, *J. Molec. Struct*. **1978**, *49*, 201−205. G. C. Percy, D. Thornton, *J. Molec. Struct*. **1972**, *14*, 313. C. Postmus, J. Ferraro, W. Wozniak, *Inorg. Chem*. **1967**, *6*, 2030−2032. A. Schilt, R. Taylor, *J. Inorg. Nucl. Chem*. **1959**, *9*, 211−221.
[40] D. Thornton, G. Watkins, *J. Coord. Chem*. **1992**, *24*, 299−315.
[41] R. Inskeep, *J. Inorg. Nucl. Chem*. **1962**, *24*, 763−776.
[42] Gmelin, *Handbook of Inorganic Chemistry, Silver*, part B6, Springer Verlag, Berlin, **1975**, p. 91−95 and literature cited therein.
[43] E. Uhlig, M. Mädler, *Z. Anorg. Allg. Chem.* **1965**, *338*, 199−208.
[44] M. Muniz-Miranda, L. Angeloni, E. Castelluci, *Spectrochim. Acta* **1983**, *39A*, 97−106. M. Muniz-Miranda, E. Castelluci, *Spectrochim. Acta* **1983**, *39A*, 107−113.
[45] A. Wada, N. Sakabe, J. Tanaka, *Acta Crystallogr.* **1976**, *B32*, 1121−1127.
[46] X.-M. Chen, R.-Q. Wang, Z.-T. Xu, *Acta Crystallogr.* **1995**, *C51*, 820−822.
[47] U. Müller, *Struct. Bonding* **1973**, *14*, 141−172. Z. Dori, R. F. Ziolo, *Chem. Rev.* **1973**, *73*, 247−254. W. Beck, W. P.

Fehlhammer, P. Pöllmann, E. Schuierer, K. Feldl, *Chem. Ber.* **1967**, *100*, 2335−2361.
[48] M. V. Veidis, B. Dockum, F. F. Charron, Jr., W. M. Reiff, T. F. Brennan, *Inorg. Chim. Acta* **1981**, *53*, L197−L199.
[49] H. L. K. Wah, M. Postel, F. Tomi, L. Mordenti, D. Ballivet-Tkatchenko, F. Dahan, F. Urso, *New J. Chem.* **1991**, *15*, 629−633.
[50] S. Bernès, F. Sécheresse, Y. Jeannin, *Inorg. Chim. Acta* **1992**, *194*, 105−112.
[51] S. Decurtins, H. W. Schmalle, P. Schneuwly, H. R. Oswald, *Inorg. Chem.* **1993**, *32*, 1888−1892.
[52] H. W. Schmalle, R. Pellaux, S. Decurtins, *Z. Kristallogr.* **1996**, *211*, 533−538.
[53] S. Decurtins, H. W. Schmalle, P. Schneuwly, J. Ensling, P. Gütlich, *J. Am. Chem. Soc.* **1994**, *116*, 9521−9528.
[54] P. Román, C. Guzmán-Miralles, A. Luque, *J. Chem. Soc., Dalton Trans.* **1996**, 3985−3989.
[55] J. Cernak, E. Lenyelova, K. Ahmadi, A.-M. Hardy, *J. Coord. Chem.* **1996**, *37*, 55−58.
[56] J. Cernak, M. Kanuchova, J. Chomic, I. Potocnak, J. Kameicek, Z. Zak, *Acta Crystallogr.* **1994**, *C50*, 1563−1566.
[57] Recent examples of π-π interaction: N. Yoshida, H. Oshio, T. Ito, *Chem. Commun.* **1998**, 63−64. M. Lämsä, J. Huuskonen, K. Rissanen, J. Pursiainen, *Chem. Eur. J.* **1998**, *4*, 84−92; E. Ishow, A. Gourdon, J.-P. Launay, *Chem. Commun.* **1998**, 1909−1910. D. Ranganathan, V. Haridas, R. Gilardi, I. L. Karle, *J. Am. Chem. Soc.* **1998**, *120*, 10793−10800; cf. also refs.[3][4]
[58] G. V. Long, M. M. Harding, P. Turner, T. W. Hambley, *J. Chem. Soc., Dalton Trans.* **1995**, 3905−3910.
[59] R. Goddard, B. Hemalatha, M. V. Rajasekharan, *Acta Crystallogr. C* **1990**, *46*, 33−35.
[60] O. Gonzalez, A. M. Atria, E. Spodine, J. Manzur, M. T. Garland, *Acta Crystallogr. C* **1993**, *49*, 1589−1591.
[61] M. T. Garland, D. Grandjean, E. Spodine, A. M. Atria, J. Manzur, *Acta Crystallogr. C* **1988**, *44*, 1209−1212.
[62] S. Baggio, M. I. Pardo, R. Baggio, M. T. Garland, *Acta Crystallogr. C* **1997**, *53*, 1570−1572.
[63] U. Klement, D. Trumbach, H. Yersin, *Z. Kristallogr.* **1995**, *210*, 228. X.-M. Chen, R.-Q. Wang, X.-L. Yu, *Acta Crystallogr. C* **1995**, *51*, 1545−1547. E. Krausz, H. Riesen, A. D. Rae, *Aust. J. Chem.* **1995**, *48*, 929−932.
[64] G. V. Long, S. E. Boyd, M. M. Harding, I. E. Buys, T. W. Hambley, *J. Chem. Soc., Dalton Trans.* **1993**, 3195−3180.
[65] G. M. Sheldrick, *SHELXL-97, Program for Crystal Structure Refinement*, Göttingen **1997**; *SHELXS-97, Program for Crystal Structure Solution*, Göttingen, **1997**.
[66] M. N. Burnett, C. K. Johnson, *ORTEP-III, Oak Ridge Thermal Ellipsoid Plot Program for Crystal Structure Illustrations*, Oak Ridge National Laboratory Report ORNL-6895, **1996**. L. J. Farrugia, *ORTEP3 for Windows*, version 1.0.1β, University of Glasgow, Scotland, **1997**.

Received March 2, 1999
[I99078]

Boryl and Bridged Borylene Complexes of Iron and Ruthenium

Holger Braunschweig,*[a] Carsten Kollann,*[a] and Karl W. Klinkhammer[b]

Keywords: Boron / Iron / Ruthenium / Boryl Complexes / Borylene Complexes

The reactivity of aminodihaloboranes R_2NBX_2 (R = Me, $SiMe_3$; X = Cl, Br) towards transition metal complexes of the type $Na[(\eta^5\text{-}C_5R'_5)M(CO)_2]$ (M = Fe, Ru; R′ = H, Me) was investigated. In the case of Me_2NBBr_2 and M = Fe the borylcomplexes $[(\eta^5\text{-}C_5R'_5)(CO)_2Fe\{BBr(NMe_2)\}]$ ($C_5R'_5$ = C_5H_5 **9a**; $C_5R'_5$ = C_5H_4Me **9b**; $C_5R'_5$ = C_5Me_5 **10**) were obtained. The compounds **9a** and **9b** were formed together with the corresponding bridged borylene complexes $[\mu\text{-}BNMe_2(\mu\text{-}CO)\{(\eta^5\text{-}C_5R'_5)Fe(CO)\}_2]$ ($C_5R'_5$ = C_5H_5 **11a**; $C_5R'_5$ = C_5H_4Me **11b**) in a 1:1 ratio, the latter, however, could be isolated from these mixtures as pure materials. In addition the novel boryl and borylene ruthenium complexes $[(\eta^5\text{-}C_5H_5)(CO)_2Ru\{BX(NMe_2)\}]$ (X = Cl **12a**; X = Br **12b**), $[(\eta^5\text{-}C_5H_5)(CO)_2Ru\{BCl\{NSiMe_3\{BClN(SiMe_3)_2\}\}\}]$ (**13**) and $[\mu\text{-}BN(SiMe_3)_2(\mu\text{-}CO)\{(\eta^5\text{-}C_5H_5)Ru(CO)\}_2]$ (**14**) were obtained by similar methods. All compounds were characterized by multinuclear NMR and IR spectroscopy. The structure of **13** in the solid state was determined by a single-crystal X-ray diffraction study.

Introduction

Transition metal complexes of boron, especially boryl and borylene complexes, have attracted considerable interest over the last decade.[1][2] The synthesis of boryl complexes, which are known to be versatile compounds for the functionalization of hydrocarbons,[3a−3c,4] is achieved mainly by the use of 1,2-dioxobenzo- or catecholborane and its derivatives.[5a−5j] More recently, however, nitrogen-substituted boranes have also proved to be well suited for the synthesis of such compounds. Examples include aminoboryl complexes,[6a,6b] diborane(4)yl complexes[7a,7b] and η^1-borazine complexes.[8]

In contrast to numerous reports on boryl complexes, only very few bridged[9−11] and terminal[12][13] borylene complexes are known. The first compounds of this class, bridged borylene complexes of the type $[\mu\text{-}BR\{(\eta^5\text{-}C_5H_5)Mn(CO)_2\}_2]$ (R = NMe_2 **1a**; R = *t*Bu **1b**), were obtained by an unprecedented reaction of diboranes(4) with cleavage of the boron boron bond[9a,9b] and, recently, the corresponding dinuclear cobalt complex $[\mu\text{-}BH(PMe_3)(\mu\text{-}CO)\{Co(CO)_3\}_2]$ (**2**) was obtained by a similar cleavage reaction of 1,2-bis(trimethylphosphane)diborane(4) (Scheme 1).[10] In the case of compounds **1** the range of bridged borylene complexes was broadened by utilizing substitution reactions at the metal-coordinated boron with preservation of the central Mn_2B core.[11] Both synthetic methods, however, are very specific and are restricted to the examples mentioned above. In order to open a more general access to bridged borylene complexes we investigated the reactions of aminodihaloboranes with anionic transition metal complexes. The compounds $[\mu\text{-}BN(SiMe_3)_2(\mu\text{-}CO)\{(\eta^5\text{-}C_5R'_5)Fe(CO)\}_2]$ ($C_5R'_5$ = C_5H_5 **3a**; $C_5R'_5$ = C_5H_4Me **3b**) represent the first borylene complexes obtained by this method (Scheme 1).[6b]

In the first part of the present paper we describe the synthesis of boryl and bridged borylene complexes from the reaction of Me_2NBBr_2 with $Na[(\eta^5\text{-}C_5R_5)Fe(CO)_2]$ (R = H, Me) and point out some differences with respect to the corresponding reactions of Me_2NBCl_2.[6b]

The second part of the paper reports on novel ruthenium complexes of boron, including the synthesis and spectroscopic characterization of the first bridged borylene complex of this transition metal.

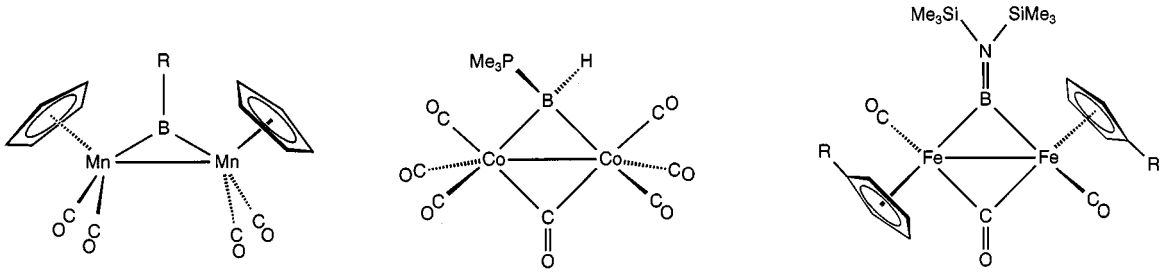
Results and Discussion

Iron Complexes

A number of iron complexes of boron were obtained by salt elimination reactions employing the strongly nucleophilic compound $Na[(\eta^5\text{-}C_5R_5)Fe(CO)_2]$ (R = H, Me) and suitable haloboranes. Examples include boryl complexes such as $[(\eta^5\text{-}C_5H_5)Fe(CO)_2)BCat]$ (Cat = 1,2-$O_2C_6H_4$) (**4**) and $[(\eta^5\text{-}C_5H_5)Fe(CO)_2)BPh_2]$ (**5**)[5a], the diborane(4)yl complex $[(\eta^5\text{-}C_5H_5)Fe(CO)_2\{B(NMe_2)BCl(NMe_2)\}]$ (**6**)[7a] and the η^1-borazine complexes $[\{(C_5R_5)(CO)_2Fe\}_n\text{-}Cl_{3-n}B_3N_3H_3]$ (*n* = 1, C_5R_5 = C_5Me_5 **7a**; *n* = 2, C_5R_5 = C_5H_4Me **7b**; *n* = 3, C_5R_5 = C_5H_5 **7c**).[8] In the case of aminodichloroboranes, corresponding reactions with the sterically less demanding Me_2NBCl_2 always resulted in the formation of monosubstituted boryl complexes $[(\eta^5\text{-}C_5R_5)(CO)_2Fe\{BCl(NMe_2)\}]$ (C_5R_5 = C_5Me_5 **8a**; C_5R_5 = C_5H_4Me **8b**; C_5R_5 = C_5H_5 **8c**) regardless of the iron to boron ratio.[6b] The more bulky, albeit more electrophilic $(Me_3Si)_2NBCl_2$, however, reacts with substitution of both the chloride ligands yielding the bridged borylene complexes $[\mu\text{-}BN(SiMe_3)_2(\mu\text{-}CO)\{(\eta^5\text{-}C_5R'_5)Fe(CO)\}_2]$ ($C_5R'_5$ = C_5H_5 **3a**; $C_5R'_5$ = C_5H_4Me **3b**).[6b]

[a] Institut für Anorganische Chemie der Technischen Hochschule, Templergraben 55, D-52056 Aachen
E-mail: holger.braunschweig@ac.rwth-aachen.de
[b] Institut für Anorganische Chemie der Universität Stuttgart, Pfaffenwaldring 55, D-70569 Stuttgart

 © WILEY-VCH Verlag GmbH, D-69451 Weinheim, 1999 1434−1948/99/0909−1523 $ 17.50+.50/0



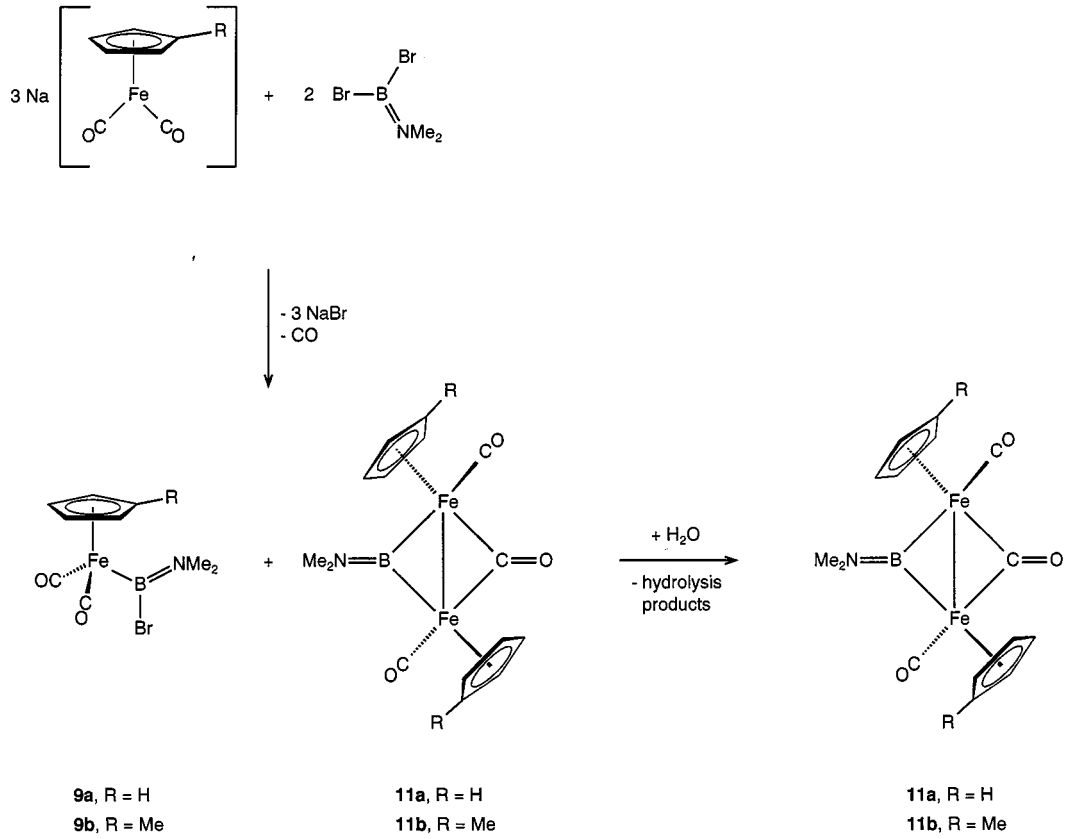
1a, R = NMe_2
1b, R = *t*Bu

2

3a, R = H
3b, R = Me

Scheme 1. Examples for bridged borylene complexes

Due to the weaker boron halide bonds,[14a,14b] Me_2NBBr_2 proves to be more reactive than the corresponding aminodichloroborane and reacts with $Na[(\eta^5\text{-}C_5R_5)Fe(CO)_2)]$ in benzene at ambient temperature to form a 1:1 mixture of the boryl complexes $[(\eta^5\text{-}C_5R'_5)(CO)_2Fe\{BBr(NMe_2)\}]$ ($C_5R'_5$ = C_5H_5 **9a**; $C_5R'_5$ = C_5H_4Me **9b**) and the corresponding bridged borylene complexes $[\mu\text{-}BNMe_2(\mu\text{-}CO)\{(\eta^5\text{-}C_5R'_5)Fe(CO)\}_2]$ ($C_5R'_5$ = C_5H_5 **11a**; $C_5R'_5$ = C_5H_4Me **11b**) according to Scheme 2. These mixtures were obtained as dark red solids from hexane at −30°C and attempts to seperate the boryl and borylene complexes by crystallisation or sublimation failed. The multinuclear NMR spectra of these mixtures, however, show no significant impurities and it was possible to assign all signals by comparison with the related compounds **8b**, **c** and **3a**, **b**, respectively. The boryl complexes **9a**, **b** are characterized by low-field-shifted signals in the ^{11}B-NMR spectra at δ = 54.5 (**9a**) and 55.0 (**9b**), and show the expected double sets of signals for the Me_2N groups in both ^{1}H- and ^{13}C-NMR spectra, indicating a hindered rotation of this group with respect to the boron nitrogen double bond. Interestingly, treatment of the obtained mixtures with water in diethyl ether under air (Scheme 2) resulted in a selective hydrolysis of the boryl complexes and the borylene complexes **11a**, **b** could subsequently be isolated as dark red crystals. The stability of **11a**, **b** towards air and water is in sharp contrast

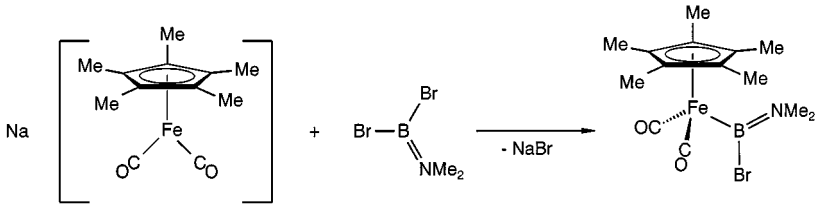


9a, R = H
9b, R = Me

11a, R = H
11b, R = Me

11a, R = H
11b, R = Me

Scheme 2. Syntheses of the bridged borylene complexes **11a**, **b**



10

to the known reactivity of $[\mu\text{-}BN(SiMe_3)_2(\mu\text{-}CO)\{(\eta^5\text{-}C_5R'_5)Fe(CO)\}_2]$ ($C_5R'_5 = C_5H_5$ **3a**; $C_5R'_5 = C_5H_4Me$ **3b**),[6b] which decompose under these conditions, whereas the related dimethylaminoborylene complex $[\mu\text{-}BNMe_2\{(\eta^5\text{-}C_5H_5)Mn(CO)_2\}_2]$ (**1a**)[9a,9b] exhibits a very similar stability. One might expect the electron-withdrawing effect of the nitrogen bound $SiMe_3$ groups and, hence, the enhanced electrophilicity of the boron atom in **3a**, **b** to be responsible for this different reactivity. The molecular structure of **11a**, **b** in solution can be deduced from the NMR and IR spectra. Due to the formation of two iron boron bonds these borylene complexes show highly deshielded signals in their ^{11}B-NMR spectra at $\delta = 103.5$ (**11a**) and 104.5 (**11b**). The presence of a bridging carbonyl group, which has already been found for **3a**, **b** is established by ^{13}C-NMR and IR spectroscopic data (**11a,** $\delta = 275.8$, $\tilde{\nu} = 1942$ cm^{-1}, 1776 cm^{-1}; **11b,** $\delta = 277.0$, $\tilde{\nu} = 1946$ cm^{-1}, 1778 cm^{-1}).

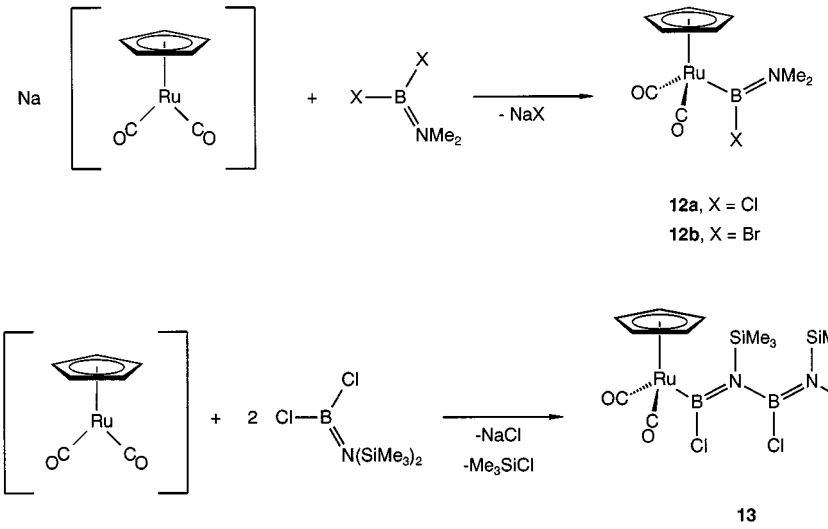
Similar reactions of Me_2NBBr_2 with the sterically demanding $Na[(\eta^5\text{-}C_5Me_5)Fe(CO)_2]$ result in the selective substitution of only one bromide and formation of the boryl complex $[(\eta^5\text{-}C_5Me_5)(CO)_2Fe\{BBr(NMe_2)\}]$ (**10**), which is isolated as a brown crystalline solid in 34% yield after recrystallization from hexane (Equation 1). The structure of **10** in solution is derived from the NMR and IR spectra, which resemble those of the related compounds **8a**−**c** and **9a**, **b**, e.g. the signal in the ^{11}B-NMR spectrum at $\delta = 57.2$ and the characteristic double sets of signals for the Me_2N group in both ^{1}H- and ^{13}C-NMR spectra. The CO stretching frequencies in the IR spectrum at 1991 cm^{-1} and 1933 cm^{-1} give no evidence for any iron-boron π-backbonding in solution, which corresponds to the findings for other nitrogen-substituted boryl complexes of iron.[6b,7a,8]

Ruthenium Complexes

Ruthenium complexes of boron, which are characterized by two-centre, two-electron bonds between ruthenium and boron are extremely rare. The few examples known, include the boryl complexes $[(\eta^5\text{-}C_5Me_5)Ru(CO)_2\{B(1,2\text{-}O_2\text{-}3,5\text{-}Me_2C_6H_2)\}]$[4] and $[Ru(BR_2)Cl(CO)(PPh)_3]$ (R = various ligands),[15] as well as the diborane(4)yl complex $[(\eta^5\text{-}C_5H_5)Ru(CO)_2\{B(NMe_2)BCl(NMe_2)\}]$.[7b] The latter represents the only structurally characterized compound of this type.

The anionic ruthenium moiety $[(\eta^5\text{-}C_5H_5)Ru(CO)_2]^-$ was reported to be less nucleophilic than the corresponding iron anion $[(\eta^5\text{-}C_5H_5)Fe(CO)_2]^-$ and hence one might expect a reduced, and probably more selective, reactivity with respect to salt eliminations.[16] Indeed, the reaction of $Na[(\eta^5\text{-}C_5H_5)Ru(CO)_2]$ with Me_2NBX_2 (X = Cl, Br) results in the selective formation of the borylcomplexes $[(\eta^5\text{-}C_5H_5)(CO)_2Ru\{BX(NMe_2)\}]$ (X = Cl **12a**; X = Br **12b**) with substitution of only one halide according to Equation 2. Both compounds can be isolated as dark yellow crystalline materials from hexane in yields of 77% (**12a**) and 41% (**12b**), respectively. These boryl complexes are stable at ambient temperature in hydrocarbon solution under nitrogen but decompose rapidly on contact with air or water. The structure of **12a, b** in solution is derived from multinuclear-NMR and IR spectroscopy. The signals in the ^{11}B-NMR spectra at $\delta = 50.3$ (**12a**) and 48.1 (**12b**) are considerably shifted to lower field with respect to the signals of the starting aminoboranes ($\delta \approx 30$),[17] thus appearing in the expected region for aminoboryl complexes. The double sets of signals for the Me_2N groups in the NMR spectra are again consistent with a hindered rotation of this group with respect to the boron nitrogen double bond. A variable temperature ^{1}H-NMR spectroscopic study of **12a** shows a coalescence of the two resonances at 98 °C from which a value of $\Delta G^{\neq} = 75.4$ kJ/mol for the rotation barrier can be calculated. This figure is in agreement with a value of $\Delta G^{\neq} = 72.3$ kJ/mol for the related iron complex $[(\eta^5\text{-}C_5R_5)(CO)_2Fe\{BCl(NMe_2)\}]$ ($C_5R_5 = C_5H_4Me$ **8b**).[6b] The IR spectra of both compounds show no evidence for a metal boron π-interaction, since the CO stretching frequencies (**12a**, 2019 cm^{-1}, 1956 cm^{-1}; **12b**, 2022 cm^{-1}, 1960 cm^{-1}) closely resemble those of the corresponding methyl ruthenium complex (2028 cm^{-1}, 1960 cm^{-1}).[18]

The compound $Na[(\eta^5\text{-}C_5H_5)Ru(CO)_2]$ exhibits a markedly different reactivity towards $(Me_3Si)_2NBCl_2$ and the nature of the reaction products depends on the reaction conditions and stoichiometry employed. According to Equation 3, $Na[(\eta^5\text{-}C_5H_5)Ru(CO)_2]$ reacts with two equivalents of $(Me_3Si)_2NBCl_2$ to form the boryl complex **13**, which can be isolated in 30% yield as a yellow crystalline material. This compound contains the unusual boryl ligand $-BCl(NSiMe_3)-BCl[N(SiMe_3)_2]$, which was formed by an intramolecular elimination of $ClSiMe_3$. The solution spectroscopic data indicate a structure for compound **13** similar to the ruthenium boryl complexes **12a**, **b**. This is indicated by a lowfield-shifted signal in the ^{11}B-NMR spectrum at $\delta = 60.3$ for the metal-coordinated boron atom ($\delta = 35.0$ for NBN) and the CO stretching frequencies at 2018 cm^{-1} and 1955 cm^{-1} in the IR spectrum. Crystals of **13** suitable



for an X-ray structure analysis were obtained after several days from hexane solutions at −30°C (Scheme 1). The complex crystallizes in the spacegroup $P\bar{1}$ and the molecule adopts C_1 symmetry in the crystal. The ruthenium-boron distance of 211.5(2) pm is 6 pm shorter than in the compound $[(\eta^5\text{-}C_5H_5)Ru(CO)_2\{B(NMe_2)BCl(NMe_2)\}]$,[7b] but still exceeds the sum of the covalent radii of both elements, thus giving no evidence for a ruthenium-boron π-interaction in the solid state. In the BNBN chain, two short boron-nitrogen distances of 141.5(2) pm (B1−N4) and 140.5(3) pm (B2−N5) are found, together with a significantly longer distance of 147.0(2) pm (B2−N4). These values, together with the dihedral angles between the bonding planes of B1/N4 (17.5°), B2/N4 (96.2°) and B2/N5 (17.7°), indicate boron nitrogen double bonds between B1 and N4, and between B2 and N5, and a single bond between B2 and N4.

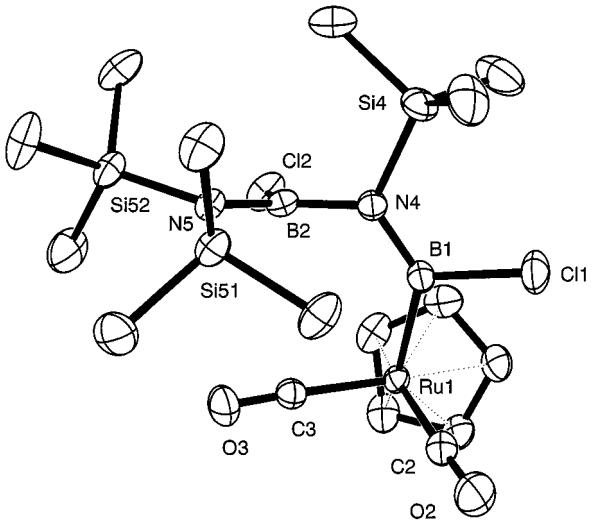


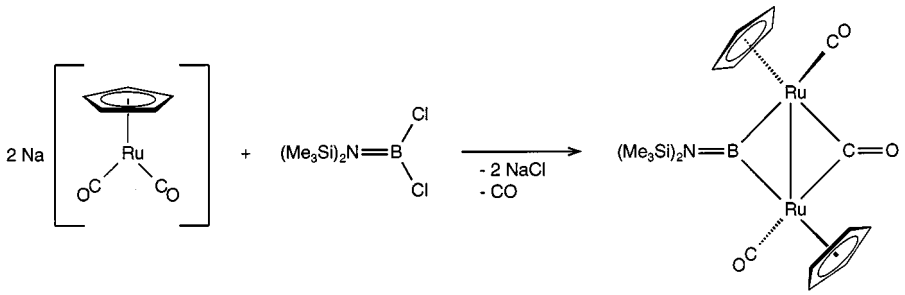
Figure 1. X-ray crystal structure of **13**. Selected bond lengths (pm) and angles (deg): Ru1−B1 211.5(2); B1−N4 141.5(2); B1−Cl1 185.4(2); N4−B2 147.0(2); B2−Cl2 182.2(2); B2−N5 140.5(2); Ru1−B1−Cl1 112.54(9); Ru1−B1−N4 133.29(12); Cl1−B1−N4 114.01(12); B1−N4−B2 120.90(14); N4−B2−Cl2 114.18(12); Cl2−B2−N5 118.76(13); N4−B2−N5 126.97(15).

The bridged borylene ruthenium complex $[\mu\text{-}BN(SiMe_3)_2(\mu\text{-}CO)\{(\eta^5\text{-}C_5H_5)Ru(CO)\}_2]$ (**14**) can be obtained from the reaction of $(Me_3Si)_2NBCl_2$ with two equivalents of $Na[(\eta^5\text{-}C_5H_5)Ru(CO)_2)]$, according to Equation 4, with elimination of one CO group. In order to prevent the formation of **13** as a by-product, the aminodichloroborane has to be added very slowly to a suspension of an excess of the anionic ruthenium complex. The borylene complex **14** can be isolated as a moderately air- and water-sensitive yellow amorphous solid from hexane at −30°C in 20% yield. The molecular structure of **14** in solution can be deduced from NMR and IR spectroscopic data and resembles that for the analogous iron compounds. The strongly deshielded signal at δ = 105.9 in the ^{11}B-NMR spectrum is in the expected region for aminobridged borylene complexes and the presence of a bridging CO group is established by the characteristic signal at δ = 250.2 in the ^{13}C-NMR spectrum and by a CO stretching frequency of 1776 cm^{-1} in the IR spectrum.

Conclusion

This study provides some insight into the reactivity of transition metal complexes of the type $Na[(\eta^5\text{-}C_5R_5)M(CO)_2)]$ (M = Fe, Ru) towards aminodihaloboranes. In the case of the strong nucleophiles $[(\eta^5\text{-}C_5R_5)Fe(CO)_2)]^-$ (C_5R_5 = C_5H_5, C_5H_4Me) the formation of bridged borylene complexes may be achieved not only by the use of electrophilic aminoboranes, such as $(Me_3Si)_2NBCl_2$, but also by employing dibromoboranes, which contain a more reactive boron halide bond. This is illustrated by the formation of $[\mu\text{-}BNMe_2(\mu\text{-}CO)\{(\eta^5\text{-}C_5R_5)Fe(CO)\}_2]$ (C_5R_5 = C_5H_5 **11a**; C_5R_5 = C_5H_4Me **11b**) from Me_2NBr_2. The reaction of Me_2NBr_2 with the very bulky $Na[(\eta^5\text{-}C_5Me_5)Fe(CO)_2)]$, however, results in the substitution of only one bromide and formation of the boryl complex $[(\eta^5\text{-}C_5Me_5)(CO)_2Fe\{Br(NMe_2)\}]$ (**10**).

The less nucleophilic ruthenium analogue $[(\eta^5\text{-}C_5H_5)Ru(CO)_2)]^-$ reacts with both Me_2NBCl_2 and Me_2NBBr_2 with selective substitution of only one halide



14

and formation of the boryl complexes $[(\eta^5\text{-}C_5H_5)(CO)_2Ru\{BX(NMe_2)\}]$ (X = Cl **12a**; X = Br **12b**). The first bridged borylene complex of ruthenium $[\mu\text{-}BN(SiMe_3)_2(\mu\text{-}CO)\{(\eta^5\text{-}C_5H_5)Ru(CO)\}_2]$ (**14**) was obtained from the reaction of $(Me_3Si)_2NBCl_2$ with two equivalents of $Na[(\eta^5\text{-}C_5H_5)Ru(CO)_2]$.

The reactivity of aminobridged borylene complexes of the type $[\mu\text{-}BNR_2\{ML_x\}_2]$ with respect to hydrolysis and oxidation depends on the electronic nature of the amino-group NR_2 and, to a lesser extent, on steric factors or on the transition metal. In the case where $NR_2 = N(SiMe_3)_2$, the electron-withdrawing effect of the silyl groups enhances the reactivity of the borylene complexes. The sterically less demanding, albeit stronger electron donating, Me_2N group, however, makes the corresponding borylene complexes rather unreactive towards air and/or water.

Experimental Section

All manipulations were carried out under dry nitrogen using standard Schlenk techniques, unless otherwise stated. Solvents and reagents were dried by standard procedures, distilled and stored under nitrogen over molecular sieves. Me_2NBCl_2,[19] Me_2NBBr_2,[19] $(Me_3Si)_2NBCl_2$,[20] $Na[(\eta^5\text{-}C_5R_5)Fe(CO)_2]$[21] and $Na[(\eta^5\text{-}C_5H_5)Ru(CO)_2]$[22] were synthesized according to literature procedures. − NMR: Varian Unity 500 at 499.843 MHz (^1H, standard TMS internal), 150.364 MHz (^{11}B, standard $BF_3{\cdot}OEt_2$ in C_6D_6 external), 125.639 MHz ($^{13}C\{^1H\}$, APT, standard TMS internal); all NMR spectra were recorded in C_6D_6 as solvent. − Mass spectra were recorded on a Finnigan MAT 95 (70 eV) and elemental analyses (C, H, N) were obtained from a Carlo−Erba elemental analyzer, model 1106. − IR: Perkin−Elmer FT-IR 1720x.

Reaction of $Na[(\eta^5\text{-}C_5H_5)Fe(CO)_2]$ with Me_2NBBr_2: $Na[(\eta^5\text{-}C_5H_5)Fe(CO)_2]$ (0.80 g, 4.00 mmol) was suspended in 25 mL of benzene and Me_2NBBr_2 (0.43 g, 2.00 mmol) was added dropwise at ambient temperature. After stirring for 15 min, all volatiles were removed in vacuo and the residue was treated with 20 mL of hexane, filtered and the remaining solid rinsed with 5 mL of hexane. The dark red filtrate was concentrated in vacuo to 15 mL and stored at −30°C for a period of 7 d. The dark red precipitate thus formed was found to be a 1:1 mixture of the boryl complex **9a** and the bridged borylene complex **11a**. − ^1H NMR: δ = 2.72 (s, 3 H, NMe, **9a**), 2.87 (s, 3 H, NMe, **9a**), 2.98 (s, 6 H, NMe_2, **11a**), 4.10 (s, 5 H, C_5H_5, **9a**), 4.39 (s, 10 H, C_5H_5, **11a**). − ^{11}B NMR: δ = 54.5 (s, 1 B, Fe−B−Br, **9a**), 103.5 (s, 1 B, Fe−B−Fe, **11a**). − ^{13}C NMR: δ = 35.3 (NMe, **9a**), 37.9 (NMe, **9a**), 43.1 (NMe_2, **11a**), 83.1 (C_5H_5, **9a**), 87.0 (C_5H_5, **11a**), 213.6 (CO, **11a**), 216.9 (CO, **9a**), 275.8 (μ-CO, **11a**).

Isolation of μ-Carbonyl-[μ-(dimethylamino)boranediyl]bis[carbonyl-(η^5-cyclopentadienyl)iron](*Fe−Fe*) (11a): The mixture of **9a/11a** was dissolved in 15 mL of raw diethyl ether and 10 mL of water were added without employing an inert gas atmosphere. After vigorously shaking the mixture for 3 min, the red organic layer was separated from the turbid, brownish aqueous phase and evaporated to dryness. The remaining red solid was recrystallized from 10 mL of hexane, yielding pure **11a** (0.08 g, 10.5%) as a dark red, crystalline solid. − ^1H NMR: δ = 2.98 (s, 6 H, NMe_2), 4.39 (s, 10 H, C_5H_5). − ^{11}B NMR: δ = 103.5 (s). − ^{13}C NMR: δ = 43.1 (NMe_2), 87.0 (C_5H_5), 213.6 (CO), 275.8 (μ-CO). − IR (toluene): $\tilde{\nu}$ = 1942 cm^{-1}, 1776 (CO). − $C_{15}H_{16}BFe_2NO_3$ (380.79): calcd. C 47.31, H 4.24; N 3.68; found C 46.85; H 4.39; N 3.80.

Reaction of $Na[(\eta^5\text{-}C_5H_4Me)Fe(CO)_2]$ with Me_2NBBr_2: This compound was prepared as described above, using $Na[(\eta^5\text{-}C_5H_4Me)Fe(CO)_2]$ (2.42 g, 11.31 mmol) and Me_2NBBr_2 (0.97 g, 4.53 mmol). The dark red solid obtained is a 1: 1 mixture of the boryl complex **9b** and the bridged borylene complex **11b**. − ^1H NMR: δ = 1.79 (s, 3 H, C_5H_4Me, **9b**), 1.86 (s, 6 H, C_5H_4Me, **11b**), 2.68 (s, 3 H, NMe, **9b**), 2.76 (s, 3 H, NMe, **9b**), 3.06 (s, 6 H, NMe_2, **11b**), 3.95−4.03 (m, 4 H, C_5H_4Me, **9b**), 4.08−4.48 (m, 8 H, C_5H_4Me, **11b**). − ^{11}B NMR: δ = 55.0 (s, 1 B, Fe−B−Br, **9b**), 104.5 (s, 1 B, Fe−B−Fe, **11b**). − ^{13}C NMR. δ = 12.9 (C_5H_4Me, **11b**), 13.1 (C_5H_4Me, **9b**), 34.7 (NMe, **9b**), 37.5 (NMe, **9b**), 43.2 (NMe_2, **11b**), 83.1, 85.2 (C_5H_4Me, **9b**), 83.7, 84.7, 86.2, 90.2 (C_5H_4Me, **11b**), 102.4 (*ipso*-C, C_5H_4Me, **9b**), 103.8 (*ipso*-C, C_5H_4Me, **11b**), 214.0 (CO, **11b**), 218.5 (CO, **9b**), 277.0 (μ-CO, **11b**).

Isolation of μ-Carbonyl-[μ-(dimethylamino)boranediyl]bis[carbonyl-(η^5-methylcyclopentadienyl)iron](*Fe−Fe*) (11b): The mixture of **9b/11b** was treated in the same way as described above. After recrystallisation from hexane, pure **11b** (0.19 g, 12.0%) was recovered at −30°C as a red, crystalline solid. − ^1H NMR: δ = 1.86 (s, 6 H, C_5H_4Me), 3.06 (s, 6 H, NMe_2), 4.08−4.48 (m, 8 H, C_5H_4Me). − ^{11}B NMR: δ = 104.5 (s). − ^{13}C NMR: δ = 12.9 (C_5H_4Me), 43.2 (NMe_2), 83.7, 84.7, 86.2, 90.2 (C_5H_4Me), 103.8 (*ipso*-C, C_5H_4Me), 214.0 (CO, **11b**), 277.0 (μ-CO). − IR (toluene): $\tilde{\nu}$ = 1946 cm^{-1}, 1778 (CO). − $C_{17}H_{20}BFe_2NO_3$ (408.84): calcd. C 49.94, H 4.93; N 3.43; found C 49.79; H 4.99; N 3.51.

[Bromo(dimethylamino)boryl]dicarbonyl(η^5-pentamethylcyclopentadienyl)iron (10): $Na[(\eta^5\text{-}C_5Me_5)Fe(CO)_2]$ (1.64 g, 6.07 mmol) was suspended in 30 mL of benzene and Me_2NBBr_2 (1.29 g,5.92 mmol) was added dropwise from a syringe at ambient temperature. After stirring for 15 min, all volatiles were removed in vacuo and the dark brown, solid residue was treated with 20 mL of hexane, filtered and the remaining solid rinsed with 10 mL of

hexane. The dark red filtrate was concentrated in vacuo to 15 mL and stored at −30°C overnight. Compound **10** (0.77 g, 33.7%) was obtained as red-brown needles. − ^{1}H NMR: δ = 1.52 (s, 15 H, C_5Me_5), 2.87 (s, 3 H, NMe), 3.06 (s, 3 H, NMe). − ^{11}B NMR: δ = 57.2. − ^{13}C NMR δ = 9.8 (C_5Me_5), 44.4 (NMe), 44.8 (NMe), 95.5 (C_5Me_5), 217.4 (CO). − IR (toluene): $\tilde{\nu}$ = 1991 cm^{-1}, 1933 (CO). − $C_{14}H_{21}BBrFeNO_2$ (381.89): calcd. C 44.03, H 5.54, N 3.67; found C 43.97, H 5.82, N 3.60.

[Chloro(dimethylamino)boryl]dicarbonyl(η^5-cyclopentadienyl)-ruthenium (12a): As described for **10**, Na[(η^5-C_5H_5)Ru(CO)$_2$] (0.65 g, 2.65 mmol) was treated with Me_2NBCl_2 (0.33 g, 2.65 mmol). Compound **12a** (0.64 g, 77.4%) was obtained as a brown-yellow, crystalline solid. − ^{1}H NMR: δ = 2.70 (s, 3 H, NMe), 2.91 (s, 3 H, NMe), 4.61 (s, 5 H, C_5H_5). − ^{11}B NMR: δ = 50.3. − ^{13}C NMR: δ = 40.7 (NMe), 44.4 (NMe), 87.4 (C_5H_5), 201.9 (CO). − IR (toluene): $\tilde{\nu}$ = 2019 cm^{-1}, 1956 (CO). − $C_9H_{11}BClNO_2Ru$ (312.51): calcd. C 34.59; H 3.55, N 4.48; found C 34.03, H 3.59, N 4.30.

[Bromo(dimethylamino)boryl]dicarbonyl(η^5-cyclopentadienyl)-ruthenium (12b): As described for **10**, 1.86 g (7.65 mmol) of Na[(η^5-C_5H_5)Ru(CO)$_2$] was treated with 1.64 g (7.65 mmol) Me_2NBBr_2. Compound **12b** (1.12 g, 40.1%) was obtained as brown-yellow crystals. − ^{1}H NMR: δ = 2.72 (s, 3 H, NMe), 2.99 (s, 3 H, NMe), 4.59 (s, 5 H, C_5H_5). − ^{11}B NMR: δ = 48.1. − ^{13}C NMR: δ = 43.5 (NMe), 45.0 (NMe), 87.8 (C_5H_5), 201.9 (CO). − IR (toluene): $\tilde{\nu}$ = 2022 cm^{-1}, 1960 (CO). − $C_9H_{11}BBrNO_2Ru$ (356.96): calcd. C 30.28; H 3.11, N 3.92; found C 30.19, H 3.34, N 4.08.

Dicarbonyl(chloro{chlorobis(trimethylsilylamino)boryl](trimethylsilyl)amino}boryl)(η^5-cyclopentadienyl)ruthenium (13): Na[(η^5-C_5H_5)Ru(CO)$_2$] (0.87 g, 3.55 mmol) was suspended in 25 mL of benzene and $(Me_3Si)_2NBCl_2$ (1.72 g, 7.10 mmol) was added all at once at ambient temperature. After stirring for 20 min, all volatiles were removed in vacuo and the brown, solid residue was treated with 25 mL of hexane, filtered and the remaining solid was rinsed with hexane (2 × 5 mL). The brown filtrate was concentrated in vacuo to 15 mL and stored at −30°C. After 72 h, **13** (0.60 g, 30.1%) was obtained as dark yellow crystals. − ^{1}H NMR: δ = 0.44 [s, 18 H, N(SiMe$_3$)$_2$], 0.49 (s, 9 H, NSiMe$_3$), 4.80 (s, 5 H, C_5H_5). − ^{11}B NMR: δ = 35.0 (s, 1 B, NBN), 60.3 (s, 1 B, NBRu). − ^{13}C NMR: δ = 3.8 [N(SiMe$_3$)$_2$], 5.3 (NSiMe$_3$), 89.3 (C_5H_5), 202.3 (CO). − IR (toluene): $\tilde{\nu}$ = 2018 cm^{-1}, 1955 (CO). − MS; *m/z* (%): 547 (5) [M$^+$ − Me], 534 (4) [M$^+$ − CO], 439 (6) [M$^+$ − Me − ClSiMe$_3$], 339 (40) [M$^+$ − (C_5H_5)Ru(CO)$_2$], 231 (100) [M$^+$ − ClSiMe$_3$ − (C_5H_5)Ru(CO)$_2$], 98 (75) [BNSiMe$_3^+$], 73 (90) [SiMe$_3^+$]. − $C_{16}H_{32}B_2Cl_2N_2O_2RuSi_3$ (562.29): calcd. C 34.17; H 5.74; N 4.98; found C 34.26; H 5.89; N 4.93.

{μ-[Bis(trimethylsilyl)amino]boranediyl}-μ-carbonylbis[carbonyl-(η^5-cyclopentadienyl)ruthenium](*Ru−Ru*) (14): A solution of $(Me_3Si)_2NBCl_2$ (0.38 g, 1.58 mmol) in 5 mL of benzene was added dropwise over a period of 10 min to a suspension of Na[(η^5-C_5H_5)Ru(CO)$_2$] (1.55 g, 6.32 mmol) in 20 mL of benzene at ambient temperature. The colour of the reaction mixture turned from dark yellow to brown during the addition. After stirring the mixture for another 10 min, all volatiles were removed in vacuo. The light brown residue was suspended in 20 mL of hexane and filtered. Compound **14** (0.18 g, 19.6%) was recovered from the filtrate at −30°C as an orange, amorphous solid. − ^{1}H NMR: δ = 0.29 (s, 18 H, SiMe$_3$), 4.90 (s, 10 H, C_5H_5). − ^{11}B NMR: δ = 105.9. − ^{13}C NMR: δ = 5.0 (SiMe$_3$), 90.2 (C_5H_5), 203.6 (CO), 250.2 (μ-CO). − IR (toluene): $\tilde{\nu}$ = 1932 cm^{-1}, 1776 (CO). − $C_{19}H_{28}BNO_3Ru_2Si_2$ (587.55): calcd. C 38.84, H 4.80; N 2.38; found C 38.26, H 4.58, N 2.08.

Crystal Structure Data Determination of 13: X-ray-quality crystals were removed from a Schlenk tube and immediately covered with a layer of viscous hydrocarbon oil (Paratone N, Exxon). A suitable crystal was selected, attached to a glass fiber and instantly placed in a low-temperature N_2 stream of a $P2_1$ four-circle diffractometer (Siemens). M_r = 562.30, triclinic, space group $P\bar{1}$, a = 911.6(2), b = 1133.7(2), c = 1465.4(3), α = 103.09(2), β = 102.72(2), γ = 111.000(15)°, V = 1.2994(5) mm^3, Z = 2, $\rho_{calc.}$ = 1.437 M gm^{-3}, $F(000)$ = 576, λ = 71.073 pm, T = 173 K, μ(MoK_α) = 0.962 mm^{-1}, crystal size: 0.4 × 0.4 × 0.3 mm, 3.02° < 2θ < 60°; of the 8516 reflections collected 7562 were unique and 7561 were used for refinement of 263 parameters; max./min. difference electron density: −866/744 e nm^{-3}. $R1$ = 0.027 [$F > 4\sigma(F)$] and wR_2 = 0.075 (all data) with $R1 = \Sigma||F_o| - |F_c||/\Sigma|F_o|$ and $wR2 = \{\Sigma w(F_o^2 - F_c^2)^2/\Sigma w(F_o^2)^2\}^{0.5}$. Calculations were carried out with the SHELXTL PC 5.03[23] and SHELXL-97[24] program system installed on a local PC. The phase problem was solved by direct methods and the structures were refined on F_o^2 by full-matrix least-squares refinement. An extinction correction was applied, extinction coefficient: 0.0115(7). Anisotropic thermal parameters were included for all non-hydrogen atoms. H atoms were placed geometrically and refined using a riding model, including free rotation of methyl groups. Their isotropic thermal parameters were constrained to 1.2 (cyclopentadienyl H) or 1.5 (methyl groups) times U_{eq} of the bonded carbon. Crystallographic data (excluding structure factors) have been deposited with the Cambridge Crystallographic Data Centre as supplementary publication no. CCDC-116235. Copies of the data can be obtained free of charge on application to CCDC, 12 Union Road, Cambridge CB2 1EZ, UK [Fax: + 44-1223/336−033; E-mail: deposit@ccdc.cam.ac.uk].

Acknowledgments

This work was supported by the Deutsche Forschungsgemeinschaft and the Fonds der Chemischen Industrie.

[1] H. Braunschweig, *Angew. Chem.* **1998**, *110*, 1882−1898, *Angew. Chem. Int. Ed. Engl.* **1998**, *37*, 1786−1801.
[2] G. I. Irvine, M. J. G. Lesley, T. B. Marder, N. C. Norman, C. R. Rice, E. G. Robins, W. R. Roper, G. R. Whittell, L. J. Wright, *Chem. Rev.* **1998**, *98*, 2685−2722.
[3] [3a] K. Burgess, M. J. Ohlmeyer, *Chem. Rev.* **1991**, *91*, 1179−1191. − [3b] I. Beletskaya, A. Pelter, *Tetrahedron*, **1997**, *53*, 4957−5026. − [3c] H. Wadepohl, *Angew. Chem.* **1997**, *109*, 2547−2550, *Angew. Chem. Int. Ed. Engl.* **1997**, *36*, 1787−1790. − [3d] T. B. Marder, N. C. Norman, "Transition Metal Catalysed Diboration", Topics in Catalysis **1998**, *5*, 63−73.
[4] K. M. Waltz, J. F. Hartwig, *Science*, **1997**, *277*, 211−213.
[5] [5a] J. F. Hartwig, S. Huber, *J. Am. Chem. Soc.* **1993**, *115*, 4908−4909. − [5b] J. F. Hartwig, S. R. de Gala, *J. Am. Chem. Soc.* **1994**, *116*, 3661−3662. − [5c] D. R. Lantero, D. H. Motry, D. L. Ward, M. R. Smith, *J. Am. Chem. Soc.* **1994**, *116*, 10811−10812. − [5d] K. M. Waltz, X. He, C. Muhoro, J. F. Hartwig, *J. Am. Chem. Soc.* **1995**, *117*, 11357−11358. − [5e] J. R. Knorr, J. S. Merola, *Organometallics* **1990**, *9*, 3008−3010. − [5f] S. A. Westcott, N. J. Taylor, T. B. Marder, R. T. Baker, N. J. Jones, J. C. Calabrese, *J. Chem. Soc. Chem. Commun.* **1991**, 304−305. − [5g] K. Burgess, W. A. van der Donk, S. A. Westcott, T. B. Marder, R. T. Baker, J. C. Calabrese, *J. Am. Chem. Soc.* **1992**, *114*, 9350−9359. − [5h] C. N. Iverson, M. R. Smith, *J. Am. Chem. Soc.* **1995**, *117*, 4403−4404. − [5i] J. F. Hartwig, Xiaoming He, *Angew. Chem.* **1996**, *108*, 352−354, *Angew. Chem. Int. Ed. Engl.* **1996**, *35,* 315−317. − [5j] C. Dai, G. Stringer, F. F. Corrigan, N. J. Taylor, T. B. Marder, N. C. Norman, *J. Organomet. Chem.* **1996**, *513*, 273−275.
[6] [6a] S. Onozawa, Y. Hatanaka, T. Sakakura, S. Shimada, M. Tanaka, *Organometallics,* **1996**, *15*, 5450−5452. − [6b] H. Braunschweig, C. Kollann, U. Englert, *Eur. J. Inorg. Chem.* **1998**, 465−468.

[7] [7a] H. Braunschweig, B. Ganter, M. Koster, T. Wagner, *Chem. Ber.* **1996**, *129*, 1099−1101. − [7b] H. Braunschweig, M. Koster, R. Wang, *Inorg. Chem.* **1999**, *38*, 415−416.
[8] H. Braunschweig, C. Kollann, M. Müller, *Eur. J. Inorg. Chem.* **1998**, 291−293.
[9] [9a] H. Braunschweig, T. Wagner, *Angew. Chem.* **1995**, *107*, 904−905; *Angew. Chem. Int. Ed. Engl.* **1995**, *34*, 825−826. − [9b] H. Braunschweig, B. Ganter, *J. Organomet. Chem.* **1997**, *545*, 163−167.
[10] M. Shimoi, S. Ikubo, Y. Kawano, *J. Am. Chem. Soc.* **1998**, *120*, 4222−4223.
[11] H. Braunschweig, M. Müller, *Chem. Ber.* **1997**, *130*, 1295−1298.
[12] H. Braunschweig, C. Kollann, U. Englert, *Angew. Chem.* **1998**, *110*, 3355−3357; *Angew. Chem. Int. Ed. Engl.* **1998**, *37*, 3179−3180.
[13] A. H. Cowley, V. Lomelí, A. Voigt, *J. Am. Chem. Soc.* **1998**, *120*, 6401−6402.
[14] [14a] E. Wiberg, W. Sütterlin, *Z. Anorg. Allg. Chem.* **1931**, *202*, 22−36. − [14b] F. L. Benton, T. E. Dillon, *J. Am. Chem. Soc.* **1942**, *64*, 1128−1129.
[15] G. J. Irvine, W. R. Roper, L. J. Wright, *Organometallics*, **1997**, *16*, 2291−2296.
[16] R. E. Dessy, R. L. Pohl, R. B. King, *J. Am. Chem. Soc.* **1966**, *88*, 5121−5124.
[17] H. Nöth, H. Vahrenkamp, *Chem. Ber.* **1967**, *100*, 3353−3356.
[18] A. Davison, J. A. McCloverty, G. Wilkinson, *J. Chem. Soc.* **1963**, 1133−1138.
[19] A. J. Banister, N. N. Greenwood, B. P. Straughan, J. Walker, *J. Chem. Soc.* **1964**, 995−1000.
[20] P. Geymeyer, E. G. Rochow, *Angew. Chem.* **1964**, *76*, 499−500.
[21] D. L. Reger, V. Fauth, M. D. Dukes, *Syn. React. Inorg. Metal-Org. Chem.* **1977**, *7*, 151−154.
[22] T. Blackmore, M. I. Bruce, F. G. A. Stone, *J. Chem. Soc. (A)* **1968**, 2158−2162.
[23] *SHELXTL PC 5.03*, Siemens Analytical X-Ray Instruments Inc., Madison, WI, **1994**.
[24] G. M. Sheldrick, *SHELXL-97*, Program for Crystal Structure Solution and Refinement, University of Göttingen, Germany, **1997**.

Received March 12, 1999
[I99098]

The Detection of $O{=}SiCl_2$ as an Intermediate During the Combustion Process of $SiCl_4$ with O_2

Markus Junker,[a] Andreas Wilkening,[b] Michael Binnewies,[b] and Hansgeorg Schnöckel*[a]

Dedicated to Professor G. Fritz on the occasion of his 80th birthday

Keywords: $SiCl_4$ Combustion / $OSiCl_2$ / Matrix isolation / Thermodynamic data / DFT calculations

During the technical important combustion of $SiCl_4$ with oxygen [$SiCl_4(g) + O_2(g) = SiO_2(s) + 2{\cdot}Cl_2(g)$] many intermediates have been detected in the past. However, the presence of the primary species $O{=}SiCl_2$ has been discussed controversially until today. With the help of matrix isolation technique we have now been successful to monitor $O{=}SiCl_2$ via its IR spectrum. With the help of quantum chemical calculations the thermodynamic data have been calculated first. On this basis it was possible to find the optimal conditions to trap $OSiCl_2$ from the high-temperature equilibrium. Furthermore it could be shown via IR spectroscopy and quantum chemical calculations, that the radical OSiCl does not play a significant role within this combustion process.

Introduction

The reaction of silicontetrachloride with oxygen at temperatures far above 1000 °C ends up with solid SiO_2, which can be obtained as an industrial produced fine grained aerosil, if special reaction conditions are applied. At temperatures of about 1000 °C a great variety of chlorosiloxanes have been isolated, which can be regarded as metastable intermediates of this reaction.[1] The large number of products − the reaction yields hundreds of different molecules − allows the conclusion, that there must be an high reactive species involved in a primary step of the reaction.

Some time ago we did the presumption that this reactive intermediate is $OSiCl_2$.[2] Assuming its existence, most resultant products can easily be elucidated, for example Si_2OCl_6 can be regarded as a reaction product between $OSiCl_2$ and $SiCl_4$. A reaction of $OSiCl_2$ with a catenasiloxan $Si_nO_{n-1}Cl_{2n+2}$ yields chain prolongation, an oligomerisation leads to cyclosiloxanes $Si_nO_nCl_{2n}$. The formation of higher condensed siloxanes [$n(O) > n(Si)$] can be explained via elimination of $SiCl_4$ from siloxanes containing a smaller amount of oxygen.

In order to prevent consecutive reactions yielding higher condensed siloxanes and to detect $OSiCl_2$, the reaction of $SiCl_4$ and O_2 was performed at very low pressure. Performing the reaction first in the inlet system of a mass spectrometer, only a significant increase of the signal at m/z = 44 (SiO) and no signal, that could be assigned to $OSiCl_2$, was found. Therefore we tried to detect this molecule via matrix IR-spectroscopy. These investigations are mainly reported in the following paper.

However, first of all we want to discuss the results of DFT calculations on OSiCl and $OSiCl_2$ and their thermodynamic data, which are the basis for the high-temperature gas-phase equilibrium calculations, which will presented further on.

[a] Institut für Anorganische Chemie der Universität Karlsruhe (TH),
Engesserstraße, Geb. 30.45, D-76128 Karlsruhe, Germany
Fax: (internat.) + 49(0)721/608-4854
E-mail: hg@achpc9.chemie.uni-karlsruhe.de
[b] Institut für Anorganische Chemie der Universität Hannover,
Callinstraße 9, D-30167 Hannover, Germany
Fax: (internat.) + 49(0)511/762-3006
E-mail: binn@mbox.aca.uni-hannover.de

Results and Discussion

Quantum Chemical Calculations

Though we have described matrix isolated $OSiCl_2$, generated via a photoinduced reaction between Cl_2 and SiO in solid argon, some years ago,[3] literature provides no direct information about the thermodynamic stability of this species. Though we have published some quantum chemical SCF calculations on the structure and energetic relation of this molecule, the results have not been analysed with respect to a possible gas-phase stability.[4] In order to test the reliability of our DFT-calculations presented here,[5] we first applied the similar method to get the well-known values of $\Delta H_f^0(298)$ and $S^0(298)$ of Cl_2CO. Due to the excellent agreement between both couples of values [$\Delta H_f^0(298)$: (exp.) −220.078 kJ/mol[17]/(theor.) −227.2 kJ/mol and $S^0(298)$: (exp.) 283.852 J/(mol·K)[17]/(theor.) 283.84 J/(mol·K)], we assessed the calculated data for $OSiCl_2$ as reliable too. First we determined the enthalpy and entropy of the following reaction (1) to be $\Delta H_R^0(298) = -336$ kJ/mol and $\Delta S_R^0(298) = -137$ J/(mol·K).

$$Cl_2(g) + SiO(g) = OSiCl_2(g) \quad (1)$$

On the basis of the experimental data of $Cl_2(g)$ and SiO(g),[17] the $\Delta H_f^0(298)$ and $S^0(298)$ values for $OSiCl_2$ can be calculated to be:

 © WILEY-VCH Verlag GmbH, D-69451 Weinheim, 1999 1434−1948/99/0909−1529 $ 17.50+.50/0

$$\Delta H_f^0(298) = -440.0\ \text{kJ·mol}^{-1}$$
$$S^0(298) = 302.4\ \text{J·(mol·K)}^{-1}$$

The geometry of $OSiCl_2$, which is a further result of these calculations, shows the expected differences to the former SCF calculation, e.g. the bond lengths are shortened [Si−O: 148.4 pm (SCF)/152.5 pm (DFT) and Si−Cl: 200.8 pm (SCF)/203.4 pm (DFT)], while the bond angles obtained by both methods are nearly identical: 109.1° (SCF)/ 108.9°(DFT). In order to calculate the thermodynamic data and to check the assignment of the matrix spectra, the following vibration frequencies (IR intensities [km/mol] in brackets) for $OSiCl_2$ have been determined.

Table 1. Calculated vibrational frequencies for $OSiCl_2$ (IR intensities [km/mol] in brackets)

Character	Frequencies in cm^{-1} (IR intensities in km/mol)		
A_1	1257.7 (99.4)	485.7 (24.1)	200.7 (2.8)
B_1	625.8 (249.2)	271.4 (25.3)	
B_2	274.7 (38.6)		

The excellent agreement between these calculated frequencies and the experimental values of the argon matrix isolated $OSiCl_2$ we published some years ago.[3]

[A_1: 1239.9/501.1 (200 estimated); B_1: 637.5/269.0; B_2: 279.9] confirms the reliability of the calculations about the high-temperature equilibrium presented further on.

During the combustion of $SiCl_4$ in principle one must also expect the radical species OSiCl, which recently has been characterised by our group.[6] The following thermodynamic values for OSiCl which are also the basis for the equilibrium calculations presented in the next chapter have been determined: $\Delta H_f^0(298) = -167.2\ \text{kJ·mol}^{-1}$; $S^0(298) = 279.1\ \text{J·(mol·K)}^{-1}$ [6]

Equilibrium State Considerations

To answer the question what should happen in the first steps of the considered reaction between $SiCl_4$ and O_2 we have carried out thermodynamic calculations of an equilibrium between the atoms and molecules given in Table 2. The computation was performed under the restriction, that no solid SiO_2 and higher molecular chlorosiloxanes are formed, that means only a homogeneous gas phase reaction is assumed.

The total pressure in the reaction tube cannot be measured exactly, therefore it is fixed to be 10^{-7} bar, which seems to be a realistic value, according to our experiments.

These data together with the presumed molar ratios 7:3, 5:5, and 3:7 of the species $SiCl_4$ and O_2 are the basis of our calculation. The results are shown in the diagrams Figure 1 to Figure 3, in which the partial pressures versus temperature are plotted.

Table 2. Thermodynamic data of those molecules which are involved in the equilibrium state calculations

Compound	$\Delta H°_{298}$/kJ/mol	$S°_{298}$/J/(K·mol)	Ref.
$SiCl_4$	−662.8	330.9	[17]
$SiCl_3$	−390.4	318.2	[17]
$SiCl_2$	−168.6	281.3	[17]
SiCl	198.3	237.8	[17]
Cl_2	0	223.1	[17]
Cl	121.3	165.2	[17]
O_2	0	205.1	[17]
O	249.2	161.1	[17]
SiO	−100.4	211.6	[17]
$OSiCl_2$	−440.0	302.4	cf. text
OSiCl	−167.2	279.1	cf. text

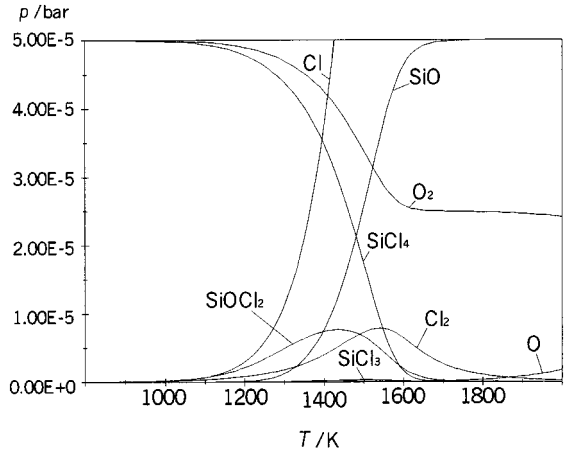


Figure 1. Equilibrium state partial pressures of the gaseous species in the system O/Si/Cl at a total pressure of 10^{-4} mbar; $SiCl_4$/ O_2 = 1:1

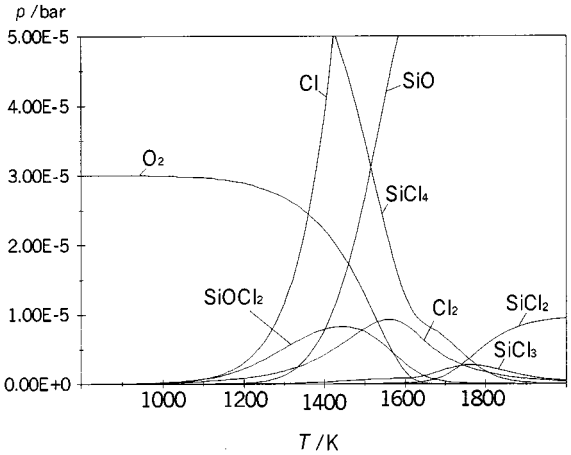


Figure 2. Equilibrium state partial pressures of the gaseous species in the system O/Si/Cl at a total pressure of 10^{-4} mbar; $SiCl_4$/ O_2 = 7:3

Although we cannot be sure that the system has been equilibrated all results of the computations are in good

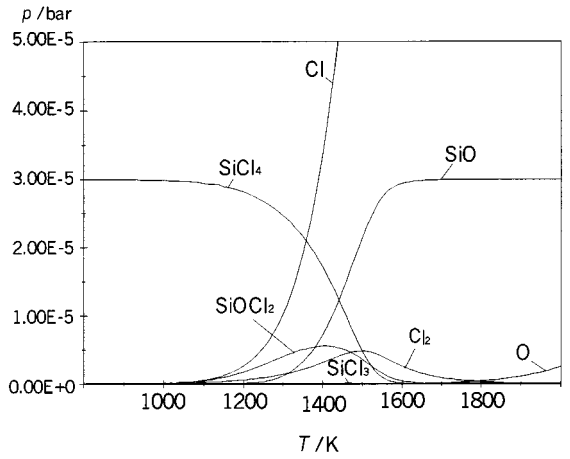


Figure 3. Equilibrium state partial pressures of the gaseous species in the system O/Si/Cl at a total pressure of 10^{-4} mbar; $SiCl_4$/O_2 = 3:7

agreement with experimental observations. It is evident that the reaction should start at a temperature of about 1000 K since the partial pressures of the starting materials $SiCl_4$ and O_2 begin to decrease there. Preparative and spectroscopic observations confirm this prediction. The formation of the oxygen containing species (e.g. $OSiCl_2$) is nearly completed at a temperature of 1400 K. Above this temperature mainly the dissociation of $SiCl_4$ and O_2 occurs. From all three diagrams it can be concluded that only two molecules containing Si and O appear at temperatures above 1000 K: SiO and $OSiCl_2$.[7]

The highest partial pressure of SiO is about one order of magnitude above that of $OSiCl_2$. The existence of the latter one is coupled to a rather narrow temperature range ΔT of about 300 to 400 K with a maximum of the partial pressure at about 1400 K. Based on these equilibrium state calculations the detection of $OSiCl_2$ via matrix IR spectroscopy should be possible without problems, because at a temperature of 1200 °C only SiO and $SiCl_4$ should be present in addition to $OSiCl_2$ and the IR-absorptions of the former ones are well-known and separated from those of $OSiCl_2$.

IR-Spectroscopic Investigations on Matrix-Isolated $OSiCl_2$

Matrix IR spectroscopy seemed to be the proper technique in order to investigate the combustion of $SiCl_4$ with O_2, since the starting materials as well as the products have already been studied by this method: $SiCl_4$,[8] SiO,[9] OSiCl,[6] and $OSiCl_2$.[3] Some time ago the $OSiCl_2$ molecule has been produced in the following way:[3] The high-temperature species SiO was cocondensed together with chlorine and a hundredfold excess of argon. The IR spectrum after cocondensation exhibited only the bands of SiO and its oligomers. Subsequently $OSiCl_2$ was generated from of SiO and Cl_2 in the matrix after irradiation with UV light of 254 nm. The IR spectrum of $OSiCl_2$ was analysed with the help of its isotopic shifts (^{16}O – ^{18}O/^{35}Cl – ^{37}Cl) and by means of a normal coordinate analysis.

In order to perform matrix investigations of the combustion process of $SiCl_4$ the gaseous components $SiCl_4$ and O_2 were first mixed in a ratio of 1:1. This gaseous mixture was passed under high-vacuum conditions through a high-temperature reactor at 1240 °C with a molar flow rate of 10^{-3} mmol/h. The mixture of gases leaving the high-temperature furnace was diluted with a hundredfold amount of gaseous argon and then was condensed onto a copper block of 15 K. The IR spectrum of a matrix after 30 minutes of condensation time of this gaseous mixture is shown in Figure 4.

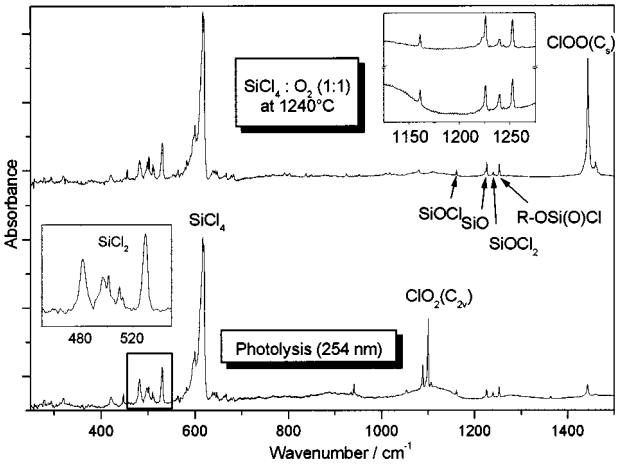


Figure 4. Top: argon matrix IR spectrum of the reaction products of the 1:1 $SiCl_4$/O_2-mixture at 1240 °C; below: following photolysis of the matrix with 254 nm for 10 min

The absorption bands of $OSiCl_2$ (1240 cm^{-1}, 637.5 cm^{-1}, 501.1 cm^{-1}), $SiCl_4$ (616.1 cm^{-1}), OSiCl (1161 cm^{-1}, 509.4 cm^{-1}), SiO (1226 cm^{-1}), $SiCl_2$ (512.0 cm^{-1}, 510.1 cm^{-1}, 501.4 cm^{-1}, 498.0 cm^{-1}), and ClO_2 (1100 cm^{-1}) can be observed. The molecule ClOO is formed spontaneously in the matrix by a reaction of chlorine atoms from the high-temperature equilibrium and O_2 molecules. The band at 1442 cm^{-1} can be assigned to the ClOO isomer (C_s symmetry).[10] After irradiation (254 nm) of the matrix the ClOO-molecule rearranges to the more stable C_{2v} isomer ClO_2 (1100 cm^{-1}). A spectrum over the whole range after photolysis is shown in Figure 4.

Starting with a molar ratio between $SiCl_4$ and O_2 of 5:1 a much smaller amount of ClO_2 is formed. This observation is plausible since no free O_2 molecules are present in the matrix due to the fact, that they have already reacted with the Si species which are present in large excess.

The most unexpected observation in Figure 4 is the larger intensity of the bands belonging to OSiCl, compared to those of $OSiCl_2$. Based on theoretical investigated integral extinction coefficients[14] of the "SiO absorption bands" (in [km/mol] SiO: 52.1; OSiCl: 56.8; $OSiCl_2$: 114) an OSiCl/$OSiCl_2$ ratio of about ten, averaged over eight experiments

is observed, whereas SiO and $OSiCl_2$ are produced in nearly equimolar amounts (with an light weight excess of SiO). While the molar ratio of SiO/$OSiCl_2$ roughly corresponds to our expectations of a high-temperature equilibrium at 1500 K, there is by far too much OSiCl in the matrix compared to the amount of $OSiCl_2$. This discrepancy can only be understood if OSiCl is not formed in the gas phase but in the matrix from SiO molecules and Cl atoms. To confirm this hypothesis some experiments have been performed, in which exclusively SiO and Cl atoms from two separate high-temperature reactors were cocondensed with an excess of argon.[6] The resulting spectra exhibited unchanged SiO and only OSiCl as a Si-containing species. No $OSiCl_2$ was formed. Even after a subsequent photolysis (254 nm) no $OSiCl_2$ is observed, i.e. in the high-temperature equilibrium nearly no Cl_2 was present, because, if it would be present, $OSiCl_2$ should be obtained after irradiation.[3]

The conclusion of all these experiments is, that the observed $OSiCl_2$ species during the matrix experiments are unambiguously formed in the high-temperature equilibrium. The observation of the first matrix experiments showing an OSiCl amount to be one or two orders of magnitude too high do not correspond to the equilibrium conditions at 1240 °C, for OSiCl is nearly exclusively produced by the spontaneous reaction of chlorine atoms and SiO in the matrix. However the higher concentrations of $OSiCl_2$ and SiO, concluded from the analysis of these matrix spectra after correction for spontaneously formed OSiCl, are in good agreement with the presented equilibrium calculations.

In the spectrum presented in Figure 4 a SiO valence band appears at 1250 cm^{-1}. It is only observed in those experiments starting with a molar ratio of $SiCl_4$ and O_2 of 1:1. With respect to the intensity of this band in several experiments it must be assigned to a different species than these discussed so far. Due to the high frequency range a −O(Cl)Si=O group can be expected, since ν(Si−O) in $OSiF_2$ is observed at 1309.4 cm^{-1}.[11] This estimation is confirmed by DFT calculations[12] from which the following SiO frequencies of the molecules under discussion result: SiO (1245 cm^{-1}), OSiCl (1149 cm^{-1}), $OSiCl_2$ (1258 cm^{-1}), and $Cl_3SiOSi(O)Cl$ (1299 cm^{-1},[13]). This variation in the frequency range reflects to a certain degree the variation in the SiO bond strength. However, for entropy reasons the species $Cl_3SiOSi(O)Cl$ should not exist in the high-temperature equilibrium, that means it should be formed in the matrix. However it is astonishing, that $Cl_3SiOSi(O)Cl$ and not the molecule $Cl_2SiO_2SiCl_2$ (with an central SiO_2Si four-membered ring) is formed, though according to analogous DFT calculations[12] the latter one is expected to be more stable by about 162 kJ/mol.

After the combustion of $SiCl_4$ we have also pyrolysed hexachlorodisiloxan (Figure 5) and octachlorotrisiloxan (Figure 6) at temperatures of 1240 °C.

These experiments clearly show the formation of the molecules SiO and $SiCl_4$. The species OSiCl and especially $OSiCl_2$ are only produced in small portions, that means the observed band intensities are below the limit of detection of this spectroscopic method.

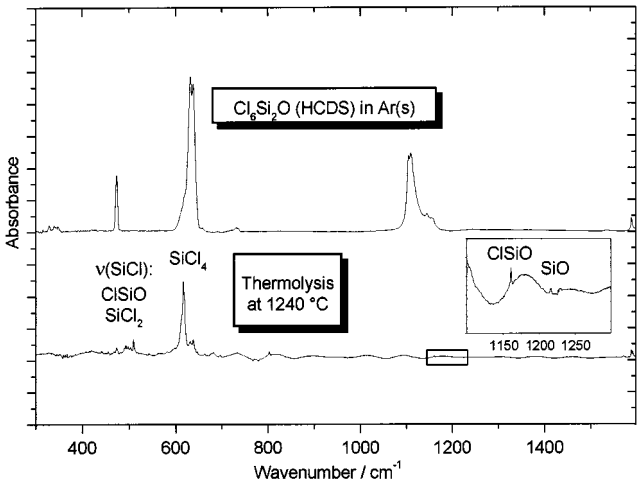


Figure 5. Top: argon matrix IR spectrum of hexachlordisiloxane, below: matrix IR spectrum of the thermolysis products (1240 °C)

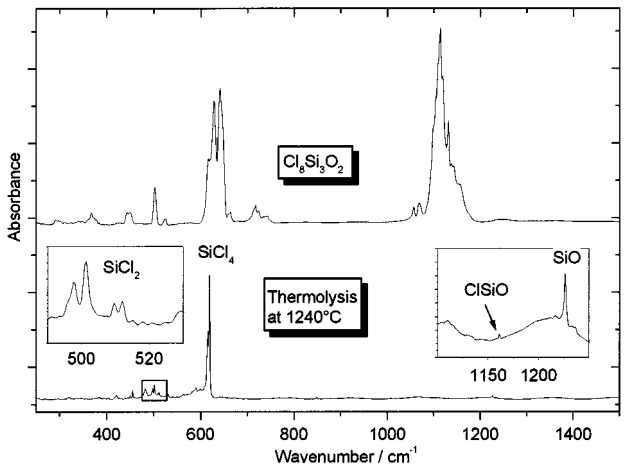


Figure 6. Top: matrix IR spectrum of octachlortrisiloxane in solid argon, below: matrix IR spectrum of the thermolysis products (1240 °C)

Conclusion

The quantumchemical calculations about the thermodynamic stability of OSiCl and $OSiCl_2$ and the equilibrium calculations based on these data are in good agreement with the experimental results of the matrix IR spectra. That means theory as well as experiments show that $OSiCl_2$ is an essential reactive intermediate in the combustion process of $SiCl_4$ with O_2. Therefore the presented results may be important as well for further synthetic investigations as for every kind of high-temperature processes, in which chlorine containing species are in a thermodynamic equilibrium with SiO containing species (e.g. chemical processes in quartz vessels). Since similar relations are expected for the reaction

between $SiBr_4$/SiI_4 and O_2, the analogous species $OSiBr_2$/$OSiI_2$ may also be important for the understanding of the gas phase reactions in halogen lamps.

Experimental Section

$SiCl_4$ (> 99 %, MERCK GaA, Darmstadt) and O_2 (4.8, MESSER-GRIESHEIM, Krefeld) were mixed in a glass vessel and the pressure was measured by means of a capacity instrument (MKS Instruments Deutschland GmbH). The same instrument was used in order to monitor the flow rate (10^{-5} mol/h) passing the reaction vessel (quartz) of the high-temperature furnace (alumina).

The relative amount of argon (4.8, MESSER-GRIESHEIM, Krefeld) mixed with the gaseous species after passing the high-temperature area to the Si/O/Cl species was estimated to be about 200:1. After a condensing period of 30 min, IR absorptions were recorded. The IR absorptions were recorded by means of a reflection unit, in which the copper plate for deposition of the matrix gases was cooled by a closed-cycle refrigerator (RGD 510, LEYBOLD Köln).

All spectra were recorded with a BRUKER IFS 113v FT-IR Spectrometer (BRUKER GmbH, Karlsruhe). A MCT detector and a Ge/KBr beamsplitter have been applied in order to obtain the spectra presented.

The DFT calculations were carried out on IBM RS 6000/390 workstations using the B3-LYP functional and a TZVPP basis. The program packages GAUSSIAN 94[14] and TURBOMOLE[15] have been used. Contour line diagrams have been realised using the program MOLDEN[16].

Photochemical activation has been performed with the help of a low-pressure Hg lamp (Gräntzel, Karlsruhe, Germany).

Atom	Basis	Contraction pattern	Exponent of the polarisation function
H	TZVPP	(5s2p1d) / [3s2p1d] {311/11/1}	η_p = 1.407; 0.388 η_d = 1.057
C	TZVPP	(11s6p2d1f) / [5s3p2d1f] {62111/411/11/1}	η_d = 1.097; 0.318 η_f = 0.761
O	TZVPP	(11s6p2d1f) / [5s3p2d1f] {62111/411/11/1}	η_d = 2.314; 0.645 η_f = 1.428
Si	TZVPP	(14s9p2d1f) / [5s5p2d1f] {73211/51111/11/1}	η_d = 0.481; 0.159 η_f = 1.428
Cl	TZVPP	(14s9p2d1f) / [5s5p2d1f] {73211/51111/11/1}	η_d = 1.046; 0.344 η_f = 0.706

[1] A. Kornick, M. Binnewies, *Z. Anorg. Allg. Chem.* **1990**, *587*, 157.
[2] M. Binnewies, M. Jerzembeck, A. Kornick, *Angew. Chem.* **1991**, *103*, 762.
[3] H. Schnöckel, *Z. Anorg. Allg. Chem.* **1980**, *460*, 37.
[4] H. Schnöckel, H. J. Göcke, R. Köppe, *Z. Anorg. Allg. Chem.* **1989**, *578*, 159.
[5] The DFT calculations have been performed using the B3-LYP functional (see for example: A. D. Becke, "Density-functional thermochemistry. III. The role of exact exchange", *J. Chem. Phys.* **1993**, *98*, 5648) and the following TURBOMOLE TZVPP basis sets:
[6] M. Junker, H. Schnöckel, *J. Chem. Phys.* **1999**, *110*, 3769
[7] Furthermore the radical OSiCl has also been involved in the equilibrium state calculations[6] which are presented in the diagrams 1−3. However, the resulting partial pressure of OSiCl is too small to be seen in these figures, it vanishes in the base line.
[8] F. Königer, A. Müller, W. J. Orville-Thomas, *J. Mol. Struct.* **1977**, *37*, 199; S. T. King, *J. Chem. Phys.* **1968**, *49*, 1321.
[9] H. Schnöckel, T. Mehner, H. S. Plitt, S. Schunk, *J. Am. Chem. Soc.* **1989**, *111,* 4578.
[10] M. M. Rochkind, G. C. Pimentel, *J. Chem. Phys.* **1967**, *46*, 4481; A. Arkell, J. Schwager, *J. Am. Chem. Soc.*, **1967**, *89,* 5999; J. L. Gole, *J. Phys. Chem.* **1980**, *84*, 1333.
[11] H. Schnöckel, *J. Mol. Struct.* **1980**, *65,* 115.
[12] B3-LYP functional, 6-31G** basis.
[13] Si1−O_t: 152 pm, Si1−Cl: 203 pm, Si−O−Si: 180°, Si2−Cl: 204 pm, $\angle_{Cl-Si2-Cl}$: 110°, $\angle_{O-Si-O}$: 127° .
[14] *GAUSSIAN 94*, Revision B.3, M. J. Frisch, G. W. Trucks, H. B. Schlegel, P. M. W. Gill, B. G. Johnson, M. A. Robb, J. R. Cheeseman, T. Keith, G. A. Petersson, J. A. Montgomery, K. Raghavachari, M. A. Al-Laham, V. G. Zakrzewski, J.V. Ortiz, J. B. Foresman, C.Y. Peng, P.Y. Ayala, W. Chen, M.W. Wong, J. L. Andres, E. S. Replogle, R. Gomperts, R. L. Martin, D. J. Fox, J. S. Binkley, D. J. Defrees, J. Baker, J. P. Stewart, M. Head-Gordon, C. Gonzalez, and J. A. Pople, Gaussian, Inc., Pittsburgh PA, **1995**.
[15] R. Ahlrichs, M. Bär, M. Häser, H. Horn, C. Kölmel, *Chem. Phys. Lett*. **1989**, *162*, 165
[16] MOLDEN a pre- and post processing program of molecular and electronic structure, G. Schaftenaar, CAOS/CAMM Center, the Netherlands, homepage: http://www.caos.kun.nl/schaft/molden/molden.html
[17] Ishan Barin, *Thermochemical Data of Pure Substances, Part I & II*, Verlag Chemie, Weinheim, **1989**.

Received April 23, 1999
[99145]

Structural and Functional Investigations on Diiron Complexes: Catalase-Like Activity and Mechanistic Studies on the Formation of (μ-Peroxo)diiron(III) Adducts

Roberto Than,[a] Antje Schrodt,[b] Lars Westerheide,[a] Rudi van Eldik,*[b] and Bernt Krebs*[a]

Dedicated to Professor Dirk Walther on the occasion of his 60th birthday

Keywords: Iron(III) / Peroxo Complexes / Kinetics / Hydrogen Peroxide / Catalase

The new diiron complex $[Fe_2(tbpo)\{O_2As(CH_3)_2\}(CH_3O)(CH_3OH)](ClO_4)_3 \cdot 5\ CH_3OH \cdot 2\ H_2O$ (**1**) containing a (μ-alkoxo)(μ-dimethylarsinato)diiron(III) core was synthesized using the heptadentate ligand *N*,*N*,*N*′,*N*′-Tetrakis(2-benzimidazolylmethyl)-1,3-diamino-2-propanol (Htbpo). The complex was characterized structurally by X-ray crystallography. **1** reproduces the coordination mode and the stoichiometry of the proposed purple acid phosphatase-arsenate inhibitor complex. More importantly, **1** is a good functional model for the activation of small molecules, since the solvent molecule in the coordination sphere of each iron ion can be substituted very easily by a small substrate molecule. This is confirmed by the comparatively high pH-dependent catalase-like activity of **1**. In order to study the influence of the cacodylate bridge on the formation of the metastable adduct with hydrogen peroxide, the analogous hydroxo-bridged complex $[Fe_2(tbpo)(OH)(NO_3)_2](NO_3)_2 \cdot CH_3OH \cdot 2\ H_2O$ (**2**) was employed. The reactions of **1** and **2** with H_2O_2 were studied as a function of $[H_2O_2]$, pH, temperature, and pressure, and the kinetic results including the activation parameters are reported. In the case of compound **2** the reaction proceeds in one step, and the observed first order rate constant, k_{obs}, shows a linear dependence on the hydrogen peroxide concentration with a zero intercept. For complex **1** the kinetic traces could be fitted to two exponential functions. One of the observed pseudo-first-order rate constants, k_{obs1}, exhibits a linear dependence on the hydrogen peroxide concentration with a zero intercept, whereas the other rate constant, k_{obs2}, was independent of the hydrogen peroxide concentration. A mechanistic interpretation is presented.

Introduction

Bridged diiron complexes can be regarded as structural and functional models for non-heme iron proteins.[1−5] Proteins belonging to this class include hemerythrin (Hr), ribonucleotide reductase (RR), methane monooxygenase (MMO), and purple acid phosphatase (PAP), whose X-ray structures are all available.[6−9] The spectroscopic and structural properties of the diiron centres of the metalloproteins have been modelled successfully by using various ligand systems.[10−16] There has been a particular interest in the oxygen activation at these diiron active sites in the last few years.[17−20] Therefore, the reaction of diiron complexes with either dioxygen or hydrogen peroxide has been studied very intensively.[21−24]

Recently, the structures of three dinuclear peroxo bridged iron complexes have been published, which were all generated by the reaction of dioxygen and the diferrous precursor compounds: $[Fe_2(O_2)(C_6H_5CH_2COO)_2\{(HB(pz')_3\}_2]$, $[Fe_2(N\text{-Et-tbpo})(O_2)(Ph_3PO)_2]^{3+}$, and $[Fe_2(Ph\text{-bimp})(C_6H_5COO)(O_2)]^{2+}$.[25−27] These peroxo complexes all show a μ-1,2-binding mode of the introduced peroxo ligand. The (1:1) peroxo adduct of $[Fe_2(tbpo)(OH)(NO_3)_2](NO_3)_2$ was described earlier in the literature,[28] but no X-ray structure was determined. The spectroscopic, magnetic and electrochemical investigations revealed a similar μ-1,2 coordination of the peroxide.

In this work we report the X-ray structure and catalase-like activity of the new μ-arsinato bridged diiron(III) complex $[Fe_2(tbpo)\{O_2As(CH_3)_2\}(CH_3O)(CH_3OH)](ClO_4)_3 \cdot 5\ CH_3OH \cdot 2\ H_2O$ (**1**) containing the heptadentate ligand *N*,*N*,*N*′,*N*′-Tetrakis(2-benzimidazolylmethyl)-1,3-diamino-2-propanol (Htbpo). In order to understand the rapid formation of the μ-peroxo complexes we carried out detailed kinetic studies on the reaction of species **1** and the related, well characterized species $[Fe_2(tbpo)(OH)(NO_3)_2](NO_3)_2 \cdot CH_3OH \cdot 2\ H_2O$ (**2**) with hydrogen peroxide in aqueous solution. The activation parameters for this reaction were determined and plausible mechanisms are postulated.

[a] Anorganisch-Chemisches Institut, Universität Münster
Wilhelm Klemm-Strasse 8, 48149 Münster, Germany
Fax: (internat.) + 49-(0)251/8338366
E-mail: krebs@uni-muenster.de
[b] Institut für Anorganische Chemie,
Universität Erlangen-Nürnberg
Egerlandstr. 1, 91058 Erlangen, Germany
Fax: (internat.) + 49-(0)9131/8527387
E-mail: vaneldik@anorganik.chemie.uni-erlangen.de

Supporting information for this article is available on the WWW under http://www.wiley-vch.de/home/eurjic or from the author.

 © WILEY-VCH Verlag GmbH, D-69451 Weinheim, 1999 1434−1948/99/0909−1537 $ 17.50+.50/0

Results and Discussion

Structural Studies on 1

The structure of **1** confirms a (μ-alkoxo)(μ-dimethylarsinato)diiron(III) core. **1** reproduces the coordination mode and the stoichiometry of the proposed purple acid phosphatase-oxoanion interaction.[31] Therefore **1** can be regarded as a model complex for the proposed structure of the oxidized arsenate complex of uteroferrin.

The cation of **1** is shown in Figure 1, while relevant bond lengths are collected in Table 1. Each iron ion is four-coordinated by the heptadentate ligand $tbpo^-$.

The metal ions are bound by two benzimidazole moieties, one tertiary non-aromatic nitrogen atom and the bridging oxygen atom. The metal centre in **1** exhibits a μ-alkoxo bridged diiron(III) unit with an additional dimethylarsinato bridge. The environments of the ions are completed by the coordination of one methanol and one methanolate ligand. The distance between the methanolic oxygens O4 and O5 (2.452 Å) indicates a strong "hydrogen bridge bond". The proton is assumed to be positioned between O4 and O5 at the same distance to each oxygen atom, so that it can be considered to be delocalized.

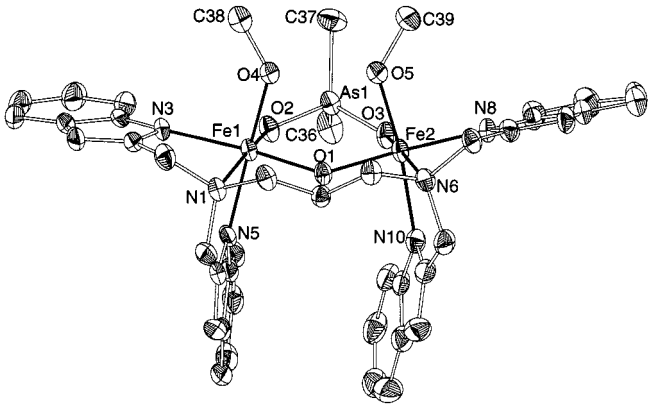


Figure 1. Structure of the cation in **1** showing 50% probability ellipsoids; hydrogen atoms have been omitted for clarity

Table 1. Selected bond lengths [Å] in **1**

Fe(1)···Fe(2)	3.445(1)	O(4)···O(5)	2.452(4)
Fe(1)···As	3.290(1)	Fe(2)···As	3.209(1)
Fe(1)−O(1)	1.941(3)	Fe(2)−O(1)	1.985(3)
Fe(1)−O(2)	1.894(3)	Fe(2)−O(3)	1.874(3)
Fe(1)−O(4)	1.993(3)	Fe(2)−O(5)	1.997(3)
Fe(1)−N(1)	2.293(4)	Fe(2)−N(6)	2.235(4)
Fe(1)−N(3)	2.032(3)	Fe(2)−N(8)	2.033(3)
Fe(1)−N(5)	2.091(4)	Fe(2)−N(10)	2.118(4)
As−O(2)	1.678(3)	As−O(3)	1.652(3)
As−C(36)	1.887(5)	As−C(37)	1.901(5)

Only two complexes containing a (μ-alkoxo)(μ-dimethylarsinato)diiron(III) core are known.[23] The Fe···Fe distance in **1** of 3.445 Å is shorter than the metal-metal separation in $[Fe_2(tbpo)\{O_2As(CH_3)_2\}(Cl)(H_2O)]^{3+}$ (3.58 Å)[23b] and $[Fe_2(mtbpo)\{O_2As(CH_3)_2\}(Cl)_2\ (CH_3OH)]^{2+}$ (3.54 Å)[23a]. The average Fe···As separation in **1** (3.25 Å) is in accordance with the Fe···As distances in $[Fe_2(tbpo)\{O_2As(CH_3)_2\}(Cl)(H_2O)]^{3+}$ and $[Fe_2(mtbpo)\{O_2As(CH_3)_2\}(Cl)_2(CH_3OH)]^{2+}$ with 3.31 Å and 3.28 Å, respectively.

Functional Studies on 1 and 2

The evolution of dioxygen was measured to investigate the hydrogen peroxide decomposition by complexes **1** and **2**. Figure 2 shows the initial decomposition rate after addition of the complexes **1**, **2**, or iron(III) salts (blind) to buffered aqueous hydrogen peroxide solutions. Both complexes exhibit only very little activity at pH 5 to 7 and no activity at pH 3 to 4, which is consistent with a completely protonated form of the substrate under these conditions. A little increase is observed at pH 8. The initial rate for the peroxide decomposition (0.90% O_2 per second) of complex **1** at pH 9 shows a significant increase in catalase-like activity at this pH. **2** has also a comparably high activity at pH 9 (0.48% O_2 per second). A solution containing iron(III) perchlorate instead of a complex shows no or very little activity at pH 3 to 9, which is also consistent with low solubility. Logarithm plots of the initial rates versus complex and peroxide concentrations, respectively, indicate that the reaction of **1** and **2** at pH 9 is first order in complex and peroxide concentration.

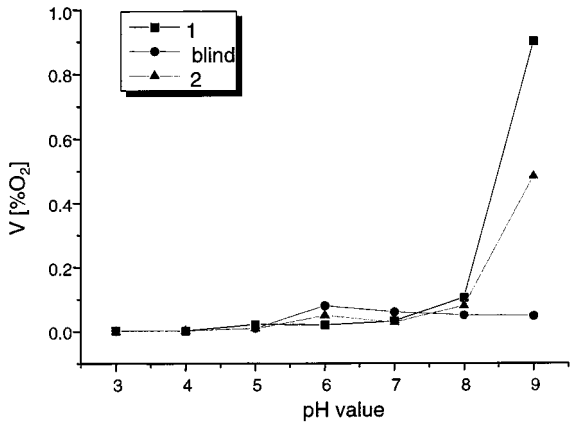


Figure 2. pH-dependence of the catalase-like activity of **1** and **2**

These experiments show that the decomposition of hydrogen peroxide is strongly pH dependent. **1** has approximately twice the activity than **2** to decompose hydrogen peroxide. Both complexes have a significantly higher catalase-like activity than iron(III) at pH 8 and 9. Activity at higher pH values could not be investigated due to solubility problems. **1** and **2** form metastable peroxide adducts at lower pH values. This adduct formation was investigated using kinetic methods.

Kinetic Measurements on the $[Fe_2(tbpo)(OH)(NO_3)_2](NO_3)_2$ Complex 2

A typical series of time resolved spectra observed during the reaction of the $[Fe_2(tbpo)(OH)(NO_3)_2](NO_3)_2$ complex **2** with an excess of hydrogen peroxide is shown in Figure 3.

The formation of the intensively blue coloured and metastabile peroxo species is accompanied by the formation of a new broad absorbance band at 550 nm, which strongly depends on the selected solvent[28] and is assigned to the iron–peroxo charge transfer. All subsequent kinetic measurements were performed at this wavelength.

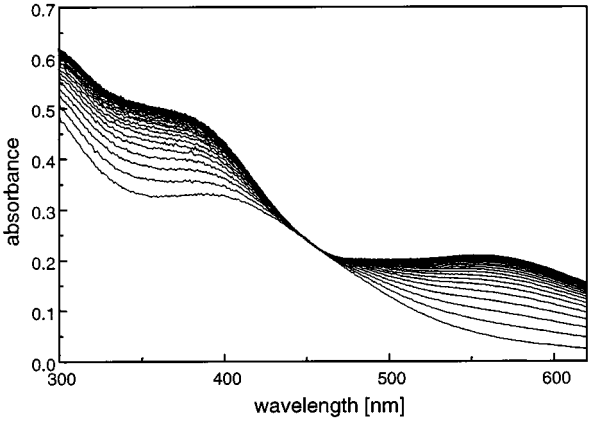


Figure 3. Typical time resolved spectra (10 ms) for the reaction of the hydroxo-bridged complex with a ten fold excess of H_2O_2. Experimental conditions: $[Fe_2(tbpo)(OH)] = 9.45 \cdot 10^{-5}$ M, ionic strength = 0.1 M, pH = 4.0, $T = 25.0$°C.

The reactions were followed for at least 5 half-lives and the kinetic traces, recorded in the presence of an excess of hydrogen peroxide, could all be fitted to a single exponential function under all experimental conditions. The observed pseudo-first-order rate constant, k_{obs}, exhibits a linear dependence on the hydrogen peroxide concentration with a zero intercept (Figure 4). An Eyring analysis of the kinetic data collected over the temperature range 5 to 35°C (Figure 5) allowed the estimation of the activation parameters listed in Table 2.

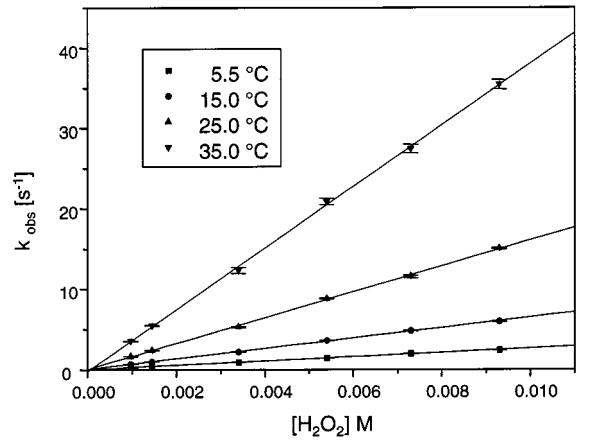


Figure 4. k_{obs} as a function of $[H_2O_2]$ and temperature. Experimental conditions: $[Fe_2(tbpo)(OH)] = 9.45 \cdot 10^{-5}$ M, ionic strength = 0.1 M, pH = 3.0, $T = 5.5–35.0$°C, $\lambda = 550$ nm

Stopped-flow measurements under high pressure showed that the reaction was practically independent of pressure, and the plot of ln k_{obs} vs. pressure gave a zero volume of activation. A preliminary pH dependence study of the reaction was performed in the range 2.0 to 4.0, since the complex showed its lowest catalase-like activity in this pH range. The pH range was limited by the decomposition of the complex occurring at lower pH and the formation of a precipitate at higher pH under the conditions selected for the kinetic measurements. The data showed an increase in the rate constant with increasing pH.

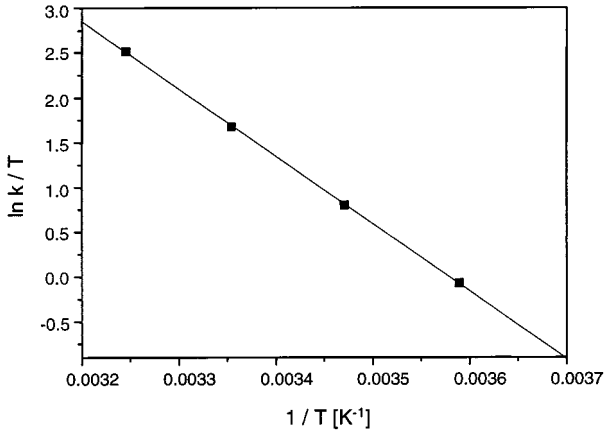


Figure 5. Eyring plot for the reaction of $[Fe_2(tbpo)(OH)]$ ($9.45 \cdot 10^{-5}$ M) with H_2O_2 based on the second-order rate constant determined from the kinetic measurements in the temperature range 5.5–35.0°C

Kinetic Measurements on the $[Fe_2(tbpo)\{O_2As(CH_3)_2\}(OCH_3)(HOCH_3)](ClO_4)_3$ Complex 1

Figure 6 shows a typical series of time resolved spectra observed during the reaction of the $[Fe_2(tbpo)\{O_2As(CH_3)_2\}(OCH_3)(HOCH_3)](ClO_4)_3$ complex with an excess of hydrogen peroxide.

The formation of the intensively blue coloured and metastable peroxo species is accompanied by the formation of a typical broad band at 550 nm, again assigned to the iron–peroxo charge transfer. This wavelength was selected for the kinetic investigations. The reactions were followed for at least 5 half-lives, but in contrast to complex **2** the kinetic traces recorded in the presence of an excess of hydrogen peroxide could not be fitted to a single, but rather to the sum of two exponential functions under all experimental conditions. One of the observed pseudo-first-order rate constants, k_{obs1}, exhibits a linear dependence on the hydrogen peroxide concentration with a zero intercept (Figure 7a), whereas the other rate constant, k_{obs2}, remains independent of the hydrogen peroxide concentration (Figure 7b). An Eyring analysis of the kinetic data collected over the temperature range 5 to 35°C (Figure 8a, b) afforded the activation parameters for k_1 and k_2 listed in Table 2.

The activation volume determined from the pressure dependence studied in the range 5 to 125 MPa is zero within the experimental error limits. The pH dependence was also studied in a preliminary way in the limited range 2.5 to 4.0, for the same reasons as outlined for complex **2**. Both k_{obs1} and k_{obs2} increased with increasing pH.

Table 2. Summary of rate and activation parameters for the reaction of **1** and **2** with H_2O_2 at pH 3.0.

complex	k_2 (s^{-1}) T = 25.0°C	k_1 (M^{-1} s^{-1}) T = 25.0°C	$\Delta H^{\#}$ (kJ mol^{-1})	$\Delta S^{\#}$ (J $mol^{-1}K^{-1}$)	$\Delta V^{\#}$ (cm^3 mol^{-1})
2		1600 ± 40	62.5 ± 0.5	26 ± 17	0 ± 2
1		1820 ± 40	57 ± 2	2 ± 9	0.2 ± 3
1	0.190 ± 0.010		79 ± 4	8 ± 13	−0.3 ± 0.9

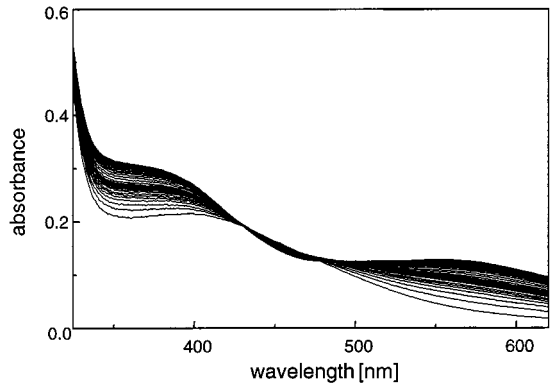


Figure 6. Typical time resolved spectra (10 ms) observed during the reaction of the $[Fe_2(tbpo)\{O_2As(CH_3)_2\}(OCH_3)(HOCH_3)](ClO_4)_3$ **1** complex with a ten fold excess of H_2O_2. Experimental conditions: $[Fe_2(tbpo)(OH)] = 9.45\cdot10^{-5}$ M, ionic strength = 0.1 M, pH = 3.0, T = 25.0°C.

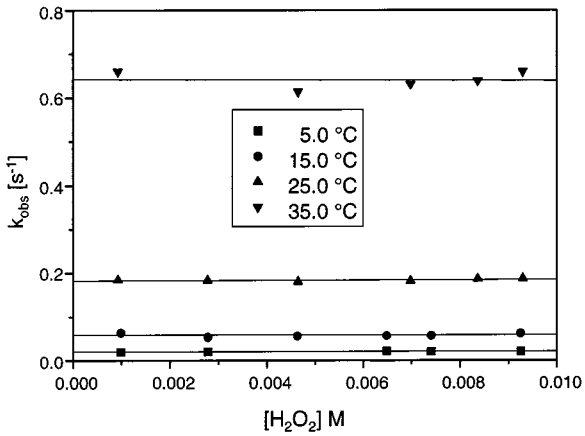


Figure 7b. k_{obs2} as a function of $[H_2O_2]$ and temperature. Experimental conditions: $[Fe_2(tbpo)\{O_2As(CH_3)_2\}] = 9.45\cdot10^{-5}$ M, ionic strength = 0.1 M, pH = 3.0, T = 5.0−35.0°C, λ = 550 nm

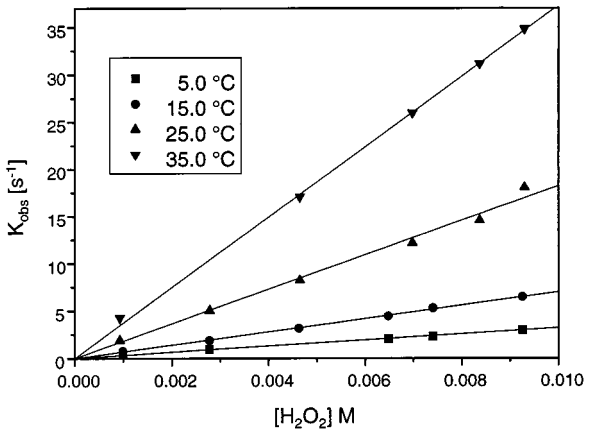


Figure 7a. k_{obs1} as a function of $[H_2O_2]$ and temperature. Experimental conditions: $[Fe_2(tbpo)\{O_2As(CH_3)_2\}] = 9.45\cdot10^{-5}$ M, ionic strength = 0.1 M, pH = 3.0, T = 5.0−35.0°C, λ = 550 nm

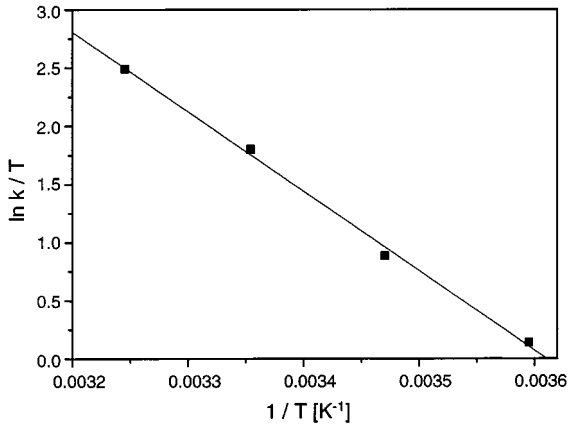


Figure 8a. Eyring plot for the reaction of $[Fe_2(tbpo)\{O_2As(CH_3)_2\}]$ ($9.45\cdot10^{-5}$ M) with H_2O_2 based on the second-order rate constant determined from the kinetic measurements in the temperature range 5.0−35.0°C at pH 3.0

Conclusion

At present no structural information is available on the peroxo products of both complexes **1** and **2.** From the literature[21][28] and our own spectroscopic investigations[32] we know that both complexes form a 1:1 adduct with H_2O_2. For the hydroxo-bridged complex the displacement of the hydroxo bridge during the formation of the peroxo complex is suggested in the literature,[28] whereas for the related benzoate-bridged complex $\{[Fe_2(tbpo)(OBz)](BF_4)_2\}$ no displacement of the benzoate bridge seems to occur.[21] In the X-ray structure of $[Fe_2(tbpo)(OH)(NO_3)_2](NO_3)_2$[33] two nitrates are coordinated to the iron centres, but in aqueous solution it is reasonable to expect that these will be displaced by water molecules. Similarly, in the cacodylate-bridged complex, two water molecules are coordinated to the iron centres, thereby replacing the methanol molecules. pH measurements after addition of two stoichiometrical amounts of acid to the complex solution showed that no protonation of the bridge occurs under these conditions. Spectrophotometric titrations could not be resolved in detail due to the complexity of the system.

The suggested reaction mechanisms for both complexes are shown in Schemes 1 and 2. For both complexes the first step is suggested to be the addition of H_2O_2 to one of the iron centres, which involves substitution of a more labile bond (e.g. coordinated water). In the case of the hydroxo-

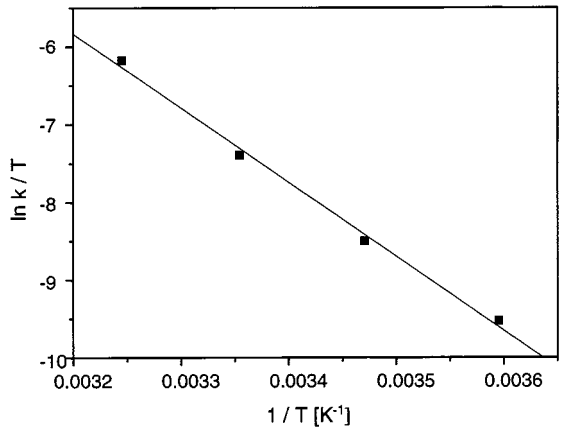
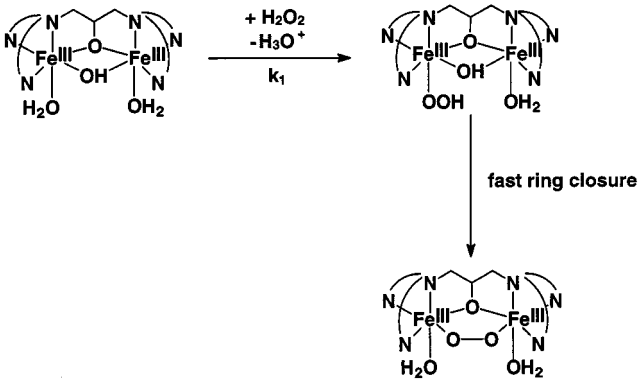


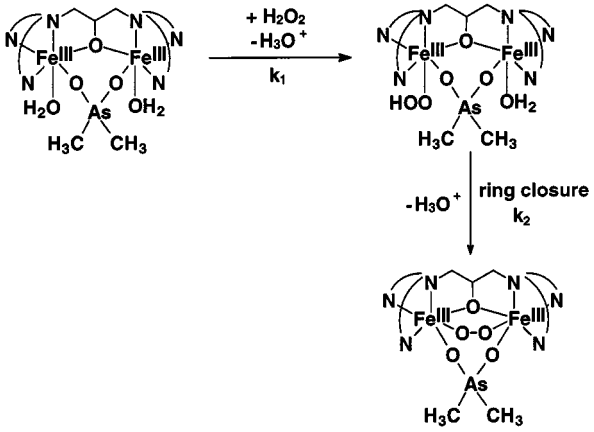
Figure 8b. Eyring plot for the reaction of $[Fe_2(tbpo)\{O_2As(CH_3)_2\}]$ ($9.45 \cdot 10^{-5}$ M) with H_2O_2 based on the first-order rate constant determined from the measurements in the temperature range 5.0−35.0°C at pH 3.0

bridged complex, a very fast ring closure follows which most probably involves the release of the hydroxo-bridge, which can be observed by magnetic and conductivity measurements.[28] In the other case the first reaction is the same, but the subsequent ring-closure reaction is much slower, and so it can be observed in the kinetics as k_2, a $[H_2O_2]$ independent rate constant. Due to the more stable binding of the cacodylate bridge it is not released during the formation of the peroxo adduct. This bulky bridge causes a steric hindrance during the ring-closure reaction, such that this reaction becomes much slower. The rate constant for the first step is similar to the rate constant for the hydroxo-bridged complex (see Table 2).



Scheme 1. Suggested mechanism for the reaction of the hydroxo-bridged complex with H_2O_2

The difference between the two complexes concerns the second step of the reaction, i.e. the bridge formation by the hydroperoxo ligand. In the case of the hydroxo-bridged complex the distance between the Fe^{III} centres (3.177 Å) is significantly shorter than in the case of the cacodylate-bridged complex.[33] This is consistent with the rapid bridge-formation step in the former complex and the much slower step in the latter complex.



Scheme 2. Suggested mechanism for the reaction of the cacodylate-bridged complex with H_2O_2

For both systems studied, preliminary data showed that the rate constants exhibit an increase with increasing pH over the limited pH range accessible. This can be related to the partial deprotonation of H_2O_2 (pK_a = 11.6), since HO_2^- will be orders of magnitude more nucleophilic than the fully protonated form. In a recent study[34] of the oxidation of hydrogen peroxide by different Ni^{III}, Fe^{III}, and Ru^{III} complexes, the authors also found an increase in the observed rate constants with increasing pH over a similar limited pH range. The data could be fitted to a model in which HO_2^- is up to 7 orders of magnitude more reactive than the fully protonated H_2O_2. A similar explanation can account for our observations, even in the case of the second reaction step observed for the cacodylate complex, since coordinated HO_2^- is expected to have a significantly lower pK_a value than the free ion. Alternatively, it is also possible that another ligand in the coordination sphere undergoes deprotonation at higher pH and results in an increase in reactivity.

The reactions are all characterised by almost zero entropies and volumes of activation. This is typical for a pure interchange substitution mechanism, where coordinated water is displaced during the first step, or by HO_2^- during the second bridge formation step. The similarity in the nature of the donor group and the associated partial molar volumes, can account for the zero volume change observed during the interchange of these ligands in the transition state. Thus the formation of the bridged peroxo complex is controlled by the displacement of the coordinated water molecules in both systems. The similarity in rate constants for the first reaction step indicates that the lability of the coordinated water molecules must be very similar in both complexes. This result also clearly supports the suggested displacement of the nitrate and the methanol/methanolate ligands, respectively, in aqueous solution.

Experimental Section

General Remarks: The heptadentate ligand Htbpo was synthesized as published previously,[23b] while all other chemicals were

Table 3. Crystal structure parameters of **1**

empirical formula	$C_{44}H_{70}N_{10}O_{24}Fe_2AsCl_3$
formula weight [g/mol]	1376.60
crystal system	triclinic
space group	$P\bar{1}$
lattice parameters [(Å) and (deg.)]	a = 12.441(2) α = 70.61(3) b = 13.746(3) β = 74.78(3) c = 19.098(4) γ = 81.16(3)
cell volume [Å^3]	2964.8
Z	2
density [g/cm^3] (calc.)	1.370
radiation	Mo-K_α (λ = 0.71073 Å)
temperature [K]	170
number of collected reflections	13937
number of independent reflections	13312 [R(int = 0.0267)]
number of observed reflections I > 2σ(I)	7445
number of parameters	807
R [$I > 2\sigma(I)$]	$R1$ = 0.0531, $wR2$ = 0.1402
weight	ω = 1/[σ^2(F_o^2) + (0.00731 P)^2+0 P]; P = (F_o+2F_c^2)/3

purchased commercially and used as received. Chemicals of analytical reagent grade and ultrapure water were used throughout this study. **Caution!** The perchlorate salts in this study are potentially explosive and should be handled with care.

Compound **1:** The reaction of equimolar amounts of Htbpo (100 mg) and the sodium salt of cacodylic acid with two equivalents of $Fe(ClO_4)_3 \cdot 9\,H_2O$ in 10 mL of a methanol/ethanol (5:2) solution leads to the formation of red crystals of $[Fe_2(tbpo)\{O_2As(CH_3)_2\}(CH_3O)(CH_3OH)](ClO_4)_3 \cdot 5\,CH_3OH \cdot 2\,H_2O$ (**1**).

Compound **2:** The complex $[Fe_2(tbpo)(OH)(NO_3)_2](NO_3)_2 \cdot CH_3OH \cdot 2\,H_2O$ **2** was synthesized according to literature procedures.[28] The complexes were checked by elemental analysis (CHN-O Rapid, Heraeus). − **1** ($C_{44}H_{70}AsCl_3Fe_2N_{10}O_{24}$): calcd. C 38.39, H 5.31, N 10.17; found C 38.18, H 5.10, N 10.31. − **2** ($C_{36}H_{43}Fe_2N_{14}O_{17}$): calcd. C 41.04, H 3.92, N 18.61; found: C 41.01, H 3.86, N 18.38.

For the kinetic studies both complexes **1** and **2** were dissolved in water and the ionic strength was adjusted with $NaClO_4$ or with $NaNO_3$. The pH of the solution was adjusted with NaOH, $HClO_4$, or HNO_3 and HEPES(I) was used as non-coordinating buffer. Hydrogen peroxide solutions were prepared from 30% hydrogen peroxide and standardized by titration with $KMnO_4$.

Crystallographic Studies:[35] The crystallographic data were collected on a Siemens P3/V diffractometer using monochromated Mo-K_α (λ = 0.71073 Å) radiation by the ω-scan method at 170 K. The crystal of **1** had approximate dimensions of 0.20 × 0.18 × 0.15 mm. Two standard reflections were measured every 99 reflections and remained constant throughout the data collection. The structure was solved using Patterson methods without absorption correction. All non-hydrogen atoms of the cation were refined anisotropically with the SHELX program suite.[36] Refinement was carried out on F^2 using full-matrix least-squares procedures. Hydrogen atoms were included with fixed distances and isotropic temperature factors 1.2 times those of their attached atoms. The R values are defined as $R_1 = \Sigma|F_o - F_c|/\Sigma F_o$ and $wR_2 = [\Sigma[w(F_o^2 - F_c^2)^2/\Sigma[w(F_o^2)^2]]^{1/2}$. Pertinent crystallographic details for **1** are collected in Table 3, and selected bond lenghts are tabulated in Table 1.

Functional Studies: The catalase-like activity measurements were done using a fiberoptical sensor (MOPS, microprocessor-controlled, optical, and portable oxygen sensor), which is based on fluorescence quenching of tris(4,7-diphenyl-1,10-phenanthroline)ruthenium(II) chloride by oxygen. The MOPS indicates dioxygen evolution as percent dioxygen in solution based on calibrations with saturated and unsaturated solutions. 5 mL of aqueous buffer solutions were saturated with nitrogen and different hydrogen peroxide solutions with concentrations between 0.16 and 0.28 mmol·dm^{-3} were added. The decomposition of hydrogen peroxide starts after the addition of a dioxygen-free methanolic complex solution (between 0.003 and 0.01 mmol·dm^{-3}). All reactions were carried out under nitrogen at room temperature in a 10 cm^3 reactor containing a stirring bar at pH values between 3 and 9 and observed over a 5 minute time periode.

Kinetic Studies: The kinetic experiments were performed on Biologic SFM-3 and Applied Photophysics SX.18MV (Leatherhead, UK) stopped-flow instruments, to which an online data acquisition system was connected. Time resolved spectra were recorded on an Applied Photophysics SX.18MV stopped flow (Leatherhead, UK) equipped with a J&M TIDAS 16−500 diode array spectrophotometer (Aalen, Germany). The kinetic measurements at pressures up to 150 MPa were carried out on a homemade high-pressure stopped-flow unit.[29][30] Data fitting was carried out using OLIS KINFIT (OLIS, Bogart, Georgia, USA) and Applied Photophysics (Leatherhead, UK) software. Complete tables of all rate constants (2 pages) are provided in the Supporting Information.

Acknowledgments

The authors gratefully acknowledge financial support from the Volkswagen Foundation, the Deutsche Forschungsgemeinschaft and the Fonds der Chemischen Industrie.

[1] S. J. Lippard, *Angew. Chem., Int. Ed. Engl*. **1988**, *27*, 344−361.
[2] J. Sanders-Loehr, W. D. Wheeler, A. K. Schiemke, B. A. Averill, T. M. Loehr, *J. Am. Chem. Soc.* **1989**, *111*, 8084−8093.
[3] D. M. Kurtz, Jr., *Chem. Rev.* **1990**, *90*, 585−606.
[4] J. B. Vincent, G. C. Lilley, B. A. Averill, *Chem. Rev.* **1990**, *90*, 1447−1467.
[5] L. Que, Jr., A. E. True, *Prog. Inorg. Chem.* **1990**, *38*, 97−200.
[6] M. A. Holmes, J. Le Trong, S. Turley, L. C. Sieker, R. E. Steinkamp, *J. Mol. Biol.* **1991**, *218*, 583−593.
[7] P. Nordlund, B.-M. Sjöberg, H. Eklund, *Nature* **1990**, *345*, 593−598.
[8] A. C. Rosenzweig, C. A. Frederick, S. J. Lippard, *J. Am. Chem. Soc.* **1993**, *366*, 357−543.
[9] [9a] N. Sträter, T. Klabunde, P. Tucker, H. Witzel, B. Krebs, *Science* **1995**, *268*, 1489−1492. − [9b] N. Sträter, W. N. Lipscomb, T. Klabunde, B. Krebs, *Angew. Chem., Int. Ed. Engl.* **1996**, *35*, 2024−2057.
[10] W. H. Armstrong, A. Spool, G. C. Papaefthymiou, R. B. Frankel, S. J. Lippard, *J. Am. Chem. Soc.* **1984**, *106*, 3653−3667.
[11] K. Wieghardt, K. Pohl, K. Gebert, *Angew. Chem., Int. Ed. Engl.* **1983**, *22*, 727−728.
[12] [12a] H. Toftlund, K. S. Murray, P. R. Zwack, L. F. Taylor, O. P. Anderson, *J. Chem. Soc., Chem. Commun.* **1986**, 191−192. − [12b] P. Gomez-Romero, N. Cassan-Pastor, A. Ben-Hussein, G. B. Jameson, *J. Am. Chem. Soc.* **1988**, *110*, 1988−1990.
[13] [13a] M. Kodera, H. Shimakoshi, M. Nishimura, H. Okawa, S. Iijima, K. Kano, *Inorg. Chem.* **1996**, *35*, 4967−4973. − [13b] H. Nie, S. M. J. Aubin, M. S. Mashuta, C.-C. Wu, J. F. Richardson, D. N. Hendrickson, R. M. Buchanan, *Inorg. Chem.* **1995**, *34*, 2382−2388. − [13c] C. Belle, I. Gautier-Luneau, J.-L. Pierre, C. Scheer, *Inorg. Chem.* **1996**, *35*, 3706−3708. − [13d] E. Lambert, B. Chabut, S. Chardon-Noblat, A. Deronzier, G. Chottard, A. Bousseksou, J.-P. Tuchagues, J. Laugier, M. Bardet, J.-M. Latour, *J. Am. Chem. Soc.* **1997**, *119*, 9424−9437.
[14] R. E. Norman, S. Ya, L. Que, Jr., G. Backes, J. Ling, J. Sanders-Loehr, J. H. Zhang, C. J. O′Connor, *J. Am. Chem. Soc.* **1990**, *112*, 1554−1562.

[15] [15a] R.E. Stenkamp, L. C. Sieker, L. H. Jensen, *J. Am. Chem. Soc.* **1984**, *106*, 618−622. − [15b] E. C. Niederhoffer, J. H. Timmons, A. E. Martell, *Chem. Rev.* **1984**, *84*, 137−203.
[16] [16a] B. Bremer, K. Schepers, P. Fleischhauer, W. Haase, G. Henkel, B. Krebs, *J. Chem. Soc., Chem. Commun.* **1991**, 510−512. − [16b] B. Krebs, K. Schepers, B. Bremer, G. Henkel, E. Althaus, W. Müller-Warmuth, K. Griesar, W. Haase, *Inorg. Chem.* **1994**, *33*, 1907−1914. − [16c] K. Schepers, B. Bremer, B. Krebs, G. Henkel, E. Althaus, B. Mosel, W. Müller-Warmuth, *Angew. Chem., Int. Ed. Engl.* **1990**, *29*, 532−534.
[17] J. M. Bollinger, Jr., D. E. Edmondson, B. H. Huynh, J. Filley, J. R. Norton, J. Stubbe, *Science* **1991**, *253*, 292−298.
[18] K. E. Liu, C. C. Johnson, M. Newcomb, S. J. Lippard, *J. Am. Chem. Soc.* **1993**, *115*, 939−947.
[19] [19a] S. K. Lee, B. G. Fox, W. A. Froland, J. D. Lipscomb, E. Münck, *J. Am. Chem. Soc.* **1993**, *115*, 6450−6451. − [19b] S. K. Lee, J. C. Nesheim, J. D. Lipscomb, *J. Biol. Chem.* **1993**, *268*, 21569−21577. − [19c] K. E. Liu, D. Wang, B. H. Huynh, D. E. Edmondson, A. Salifoglou, S. J. Lippard, *J. Am. Chem. Soc.* **1994**, *116*, 7465−7466. − [19d] K. E. Liu, A. M. Valentine, D. Wang, B. H. Huynh, D. E. Edmondson, A. Salifoglou, S. J. Lippard, *J. Am. Chem. Soc.* **1995**, *117*, 10174−10185.
[20] D. E. Edmonson, B. H. Huynh, *Inorg. Chim. Acta* **1996**, *252*, 399−404.
[21] L. Que, Jr., *J. Chem. Soc., Dalton Trans.* **1997**, 3933−3940.
[22] A. L. Feig, M. Becker, S. Schindler, R. van Eldik, S. J. Lippard, *Inorg. Chem.* **1996**, *35*, 2590−2601.
[23] [23a] B. Eulering, M. Schmidt, U. Pinkernell, U. Karst, B. Krebs, *Angew. Chem., Int. Ed. Engl.* **1996**, *35*, 618−619. − [23b] B. Eulering, F. Ahlers, F. Zippel, M. Schmidt, H.-F. Nolting, B Krebs, *J. Chem. Soc., Chem. Commun.* **1995**, 1305−1307.
[24] [24a] Y. Nishida, M. Takeuchi, H. Shimo, S. Kida, *Inorg. Chim. Acta* **1984**, *96*, 115−119. − [24b] Y. Hayashi, T. Kayatani, H. Sugimoto, M. Suzuki, K. Inomata, A. Uehara, Y. Mizutani, T. Kitagawa, Y. Maeda, *J. Am. Chem. Soc.* **1995**, *117*, 11220−11229. − [24c] R. H. Fish, M. S. Konings, K. J. Oberhausen, R. H. Fong, W. M. Yu, G. Christou, J. B. Vincent, D. K. Coggin, R. M. Buchanan, *Inorg. Chem.* **1991**, *30*, 3002−3006.
[25] K. Kim, S. J. Lippard, *J. Am. Chem. Soc.* **1996**, *118*, 4914−4915.
[26] T. Ookubo, H. Sugimoto, T. Nagayama, H. Masuda, T. Sato, K. Tanaka, Y. Maeda, H. Okawa, Y. Hayashi, A. Uehara, M. Suzuki, *J. Am. Chem. Soc.* **1996**, *118*, 701−702.
[27] Y. Dong, S. Yan, V. G. Young, Jr., L. Que, Jr., *Angew. Chem., Int. Ed. Engl.* **1996**, *35*, 618−620.
[28] B. A. Brennan, Q. Chen, C. Juarez-Garcia, A. E. True, C. J. O′Connor, L. Que, Jr., *Inorg. Chem.* **1991**, *30*, 1937−1943.
[29] R. van Eldik, D. A. Palmer, R. Schmidt, H. Kelm, *Inorg. Chim. Acta* **1981**, *50*, 131.
[30] R. van Eldik, W. Gaede, S. Wieland, J. Kraft, M. Spitzer, D. A. Palmer, *Rev. Sci. Instrum.* **1993**, *64*, 1355.
[31] [31a] A. E. True, R. C. Scarrow, C. R. Randall, R. C. Holz, L. Que, Jr., *J. Am. Chem. Soc.* **1993**, *115*, 4246−4251. − [31b] T. Klabunde, N. Sträter, R. Fröhlich, H. Witzel, B. Krebs, *J. Mol. Biol.* **1996**, *259*, 737−748.
[32] R. Than, L. Westerheide, B. Krebs, unpublished results
[33] J.-R Tzou, S. C. Chang, R. E. Norman, *J. Inorg. Biochem.* **1993**, *51*, 480.
[34] N. Koshino, S. Funahashi, H. D. Takagi, *J. Chem. Soc., Dalton Trans.* **1997**, 4175.
[35] The crystallographic data of the structure reported in this paper were deposited with the Cambridge Crystallographic Data Centre as CCDC-121762. Copies of the data can be obtained free of charge on application to CCDC, 12 Union Road, Cambridge CB2 1EZ, UK (Telefax: Int. +44-1223/336-033 E-mail: deposit@chemcrys.cam.ac.uk).
[36] G. M. Sheldrick, *SHELXS-97* and *SHELXL-97*, Programs for Crystal Structure Determination, Universität Göttingen, **1990** and **1997**.

Received February 26, 1999
[I99068]

Crystal Structure, Infrared, and Polarized Raman Spectra of $K_3Sm(PO_4)_2$

Mohamed Toumi,[a] Leila Smiri-Dogguy,[a] and Alain Bulou*[b]

Keywords: Phosphates / Structure / IR spectroscopy / Raman spectroscopy

The low-temperature form of $K_3Sm(PO_4)_2$ crystallizes in the monoclinic system [a = 7.4347(5) Å, b = 5.6270(5) Å, c = 9.4919(5) Å, β = 90.870(6)°, Z = 2, space group $P2_1/m$]. The structure has been determined using 1263 independent reflections (R = 0.045, R_w = 0.11) and is found to be of the glaserite type. The Raman and infrared spectra have been investigated: they are consistent with the proposed space group and an assignment of the observed frequencies is given.

Introduction

Compounds of the type $A_3M(TO_4)_2$ (M = Sc, Fe, Cr, rare earth; A = Na, K; T = P, V, As, S)[1−11] have structures built-up of isolated tetrahedra linked only by cations and exhibit pseudohexagonal symmetries. Their structures can be related to that of glaserite, $K_3Na(SO_4)_2$, which exhibits an ideal highly symmetrical arrangement (trigonal, $P\bar{3}\,m1$ space group, Z = 1, with a_0 = 5.547 Å c_0 = 7.070 Å in a hexagonal cell).[12] The latter consists of tetrahedral units separated by cavities, which are occupied by two kinds of atomic sequences (denoted E1 and E2) extending parallel to the c_0 axis. The E1 sequence involves potassium and sodium ions with coordination numbers of 12 and 6, respectively, while the E2 sequence involves ten-coordinated potassium ions.

In this work, we describe a new compound belonging to this structural family, namely $K_3Sm(PO_4)_2$. Such systems offer the possibility of doping by various rare earth ions, the luminescent properties of which can be useful in the field of lasers. The experimental conditions of preparation are given, along with details of the X-ray diffraction structure determination and the results of infrared and Raman investigations.

Results and Discussion

Structural Description and Discussion

Figure 1 shows a projection of the crystal structure in the [100] plane.[13] This arrangement is characterized by the presence of isolated $P(1)O_4$ and $P(2)O_4$ tetrahedra linked only by cations. All PO_4 tetrahedra have a mirror plane (a,c) and present a face almost parallel to the (b,c) plane.

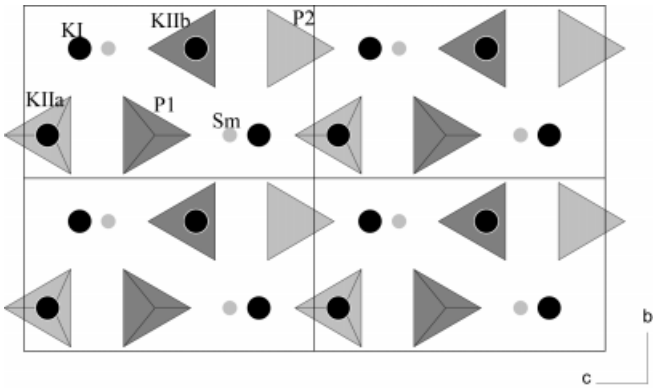


Figure 1. Projection of the $K_3Sm(PO_4)_2$ structure in the [001] plane

$P(1)O_4$ Tetrahedra: The average P(1)−O distance in the tetrahedra (1.542 Å; values range from 1.532 to 1.548 Å) is in good agreement with the value of 1.539 Å calculated by Baur and Khan.[14] The variance in the O−P−O bond angles, σ_1^2 = 2.37, is, however, larger than the value of 0.109 observed in $K_3Na(SO_4)_2$ [the variance σ^2 is defined as $\sigma^2 = 1/6\ \Sigma(\theta_i - 109.47)^2$, where θ_i represents the O−P−O bond angle and 109.47° is the ideal O−P−O bond angle in the PO_4 tetrahedron].

$P(2)O_4$ Tetrahedra: Again, the average P(2)−O distance (1.539 Å; range from 1.513 to 1.552 Å) is in good agreement with the calculated value. The variance σ_2^2 = 1.07 is much smaller than σ_1^2. The short P(2)−O(5) distance (1.513 Å) relates to the oxygen only bonded to potassium ions.

This structure can be described as comprising two types of sequences of atoms extending parallel to the a axis. The first sequence (E1) is formed by a regular succession of isolated PO_4 tetrahedra and potassium ions K(IIa) and K(IIb). The coordination numbers of K(IIa) and K(IIb) are 10 and 11, respectively. The second sequence (E2) consists of a regular succession of samarium and potassium ions. The coordination numbers are seven for samarium ions and nine for the potassium ions [K(I)].

The relationship between the $K_3Na(SO_4)_2$, β-K_2SO_4,[15] and $K_3Sm(PO_4)_2$ structures can easily be established by

[a] Laboratoire de Chimie Inorganique et Structurale, Faculté des Sciences de Bizerte,
7021 Zarzouna, Tunisia
[b] Laboratoire de Physique de l'Etat Condensé, UPRES-A CNRS no. 6087, Faculté des Sciences, Université du Maine,
F-72085 Le Mans Cedex 09, France

 © WILEY-VCH Verlag GmbH, D-69451 Weinheim, 1999 1434−1948/99/0909−1545 $ 17.50+.50/0

considering the coordination numbers (given in square parentheses) and the cell parameters:

$K_3Na(SO_4)_2$	$[K^{[12]}Na^{[6]}][K^{[10]}(SO)_4]_2$	(a_0, c_0, $P\bar{3}$ $m1$)
β-K_2SO_4	$[K^{[9]}K^{[9]}][K^{[10]}(SO_4)]_2$	($a = c_0$; $b = a_0\sqrt{3}$; $c = a_0$; *Pnma*
$K_3Sm(PO_4)_2$	$[K^{[9]}Sm^{[7]}][K^{[10]}(PO)_4]$-$[K^{[11]}(PO_4)]$	($a = c_0$; $b = a_0$; c = $a_0\sqrt{3}$; β = 90.870°; $P2_1/m$)

The structure of β-K_2SO_4 is derived from the glaserite type through a reorientation of the tetrahedra as well as a disordering of the K^+ ions of the E2 sequence. The structure of $K_3Sm(PO_4)_2$ is similar to this β-K_2SO_4 arrangement, with only a slight distortion. The variation in the coordination numbers of the cations can be attributed to a slight rotation and distortion of PO_4 tetrahedra.

The greater distortion of $P(1)O_4$ compared to that of $P(2)O_4$ may be explained by considering the nearest neighbors: in the former case, only three samarium and four potassium ions are found at distances less than 3.6 Å, while seven potassium ions are present in the latter case.

Spectroscopic Analysis

Group Theory Analysis

In accordance with the space group $P2_1/m$, the normal modes of vibration can be classified in the following irreducible representations of C_{2h} as:

$\Gamma_{optic} = 26A_g + 16B_g + 15A_u + 24B_u$

$\Gamma_{acoustic} = 1A_u + 2B_u$.

The A_g and B_g modes are Raman-active, while the A_u and B_u modes are infrared (IR)-active.

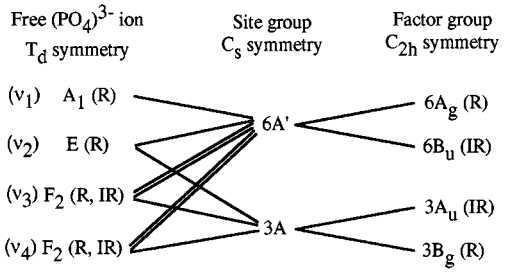
Vibrations of the PO_4 Groups

The free PO_4^{3-} tetrahedron exhibits T_d symmetry and so possesses four normal modes of vibration having A_1 (ν_1 mode), E (ν_2) and F_2 (ν_3 and ν_4) symmetries with average wave numbers of 938, 420, 1017, and 567 cm^{-1}, respectively.[16] All of these modes are Raman active, whereas only the triply-degenerate ν_3 and ν_4 modes are IR-active. The ν_1 and ν_2 modes represent the symmetric stretching and deformation vibrations, while ν_3 and ν_4 represent the corresponding asymmetric stretching and deformation vibrations. Since the other PO_4^{3-} ions occupy sites of lower symmetry than that of the free ion, anisotropic crystal fields may remove degeneracies in the normal modes and allow inactive modes to become active.

In the crystal cell, the two PO_4^{3-} ions occupy C_s-symmetric sites. The site method[17] can be applied in the analysis of the internal modes of the PO_4 groups. Table 1 shows the correlation diagram between the free PO_4^{3-} group vibrations in T_d symmetry and the lattice PO_4^{3-} internal vibrations in C_{2h} symmetry through the C_s symmetry of one PO_4 in the crystal. The correlation shows that 18 Raman and 18 IR lines are predicted:

Raman:
8 stretching modes: 2 ν_1 ($2A_g$); 6 ν_3 ($4A_g$, $2B_g$)
10 deformation modes: 4 ν_2 ($2A_g$, $2B_g$); 6 ν_4 ($4A_g$, $2B_g$)
IR:
8 stretching modes: 2 ν_1 ($2B_u$); 6 ν_3 ($4B_u$, $2A_u$)
10 deformation modes: 4 ν_2 ($2A_u$, $2B_u$); 6 ν_4 ($4B_u$, $2A_u$)

Table 1. Correlation scheme for the internal vibrations of the PO_4 group



Analysis of IR Spectra

In view of the paucity of infrared data in the frequency range below 300 cm^{-1}, only assignment of the internal modes of the PO_4 will be discussed.

In the IR spectrum (Figure 2) the bands in the 970−1100 cm^{-1} region can be assigned to the asymmetric stretching (ν_3) mode.

The two nondegenerate symmetric stretching (ν_1) modes, observed at 936 and 964 cm^{-1}, confirm the presence of two crystallographically distinct PO_4 groups. The IR bands are strongly influenced by the cation environments.

Only three bands are observed (410, 414, and 466 cm^{-1}) for the doubly-degenerate symmetric bending (ν_2).

The triply-degenerate asymmetric bending mode (ν_4) gives four bands at 545, 574, 585, and 601 cm^{-1}.

Analysis of Raman Spectra:

According to group theory analysis, of the 81 optical modes, 42 are Raman-active. With reference to the Raman tensors (Table 2), they can be distinguished by polarization investigations.

Polarized Raman spectra were recorded for different orientations of the crystal. The A_g modes were obtained in the $z(xx)\bar{z}$, $z(yy)\bar{z}$, $y(zz)\bar{y}$, and $y(zx)\bar{y}$ geometries, the B_g modes in the $x(zy)\bar{x}$ and $z(xy)\bar{z}$ geometries. The spectra are shown in Figure 3.

PO_4 Vibrations

A_g Modes

The two high-intensity bands at 938 and 970 cm^{-1} can be assigned to A_g components of the nondegenerate ν_1 mode corresponding to phosphates in sites 1 and 2.

Group theory analysis predicts four bands for the asymmetric bending mode ν_3 (A_g). Four bands at 989, 1026, 1050, and 1100 cm^{-1} are indeed observed for this mode in the $z(xx)\bar{z}$, $z(yy)\bar{z}$, and $y(zx)\bar{y}$ orientations of the Raman

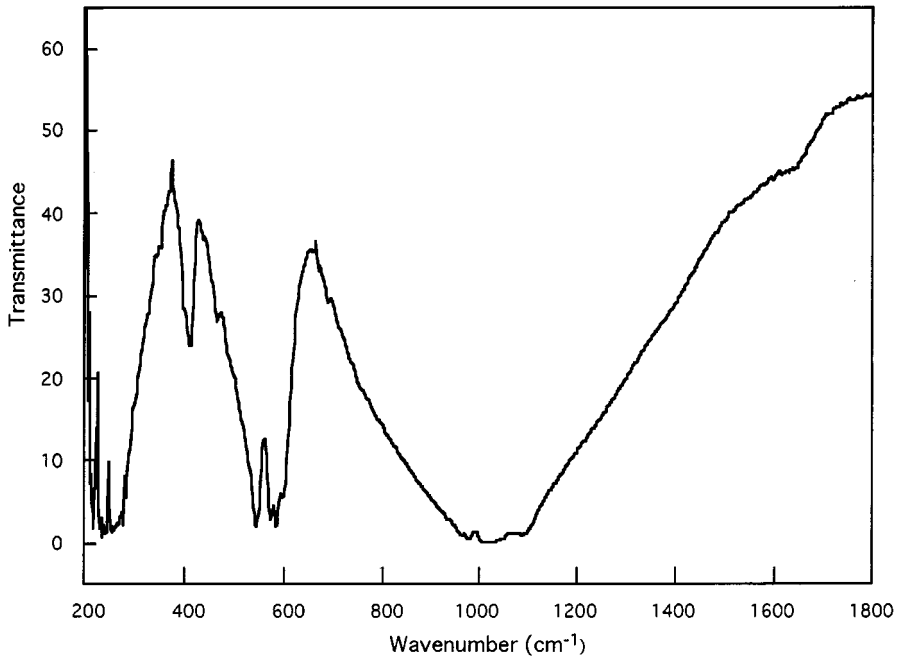


Figure 2. Infrared spectra of $K_3Sm(PO_4)_2$

Table 2. Raman tensors for the C_{2h} point group

	xx	0	*zx*		0	*yx*	0
A_g	0 xz	yy 0	0 zz	B_g	xy 0	0 yz	zy 0

spectra. In the $y(zz)\bar{y}$ orientation, only three bands at 989, 1050, and 1101 cm^{-1} are visible.

The polarized Raman bands observed at 561, 572, 589, and 609 cm^{-1} in the $z(xx)\bar{z}$, $z(yy)\bar{z}$, and $y(zz)\bar{y}$ spectra correspond to the asymmetric bending ν_4 (A_g) vibrations of the PO_4 group.

Factor group analysis predicts two bands for the symmetric bending ν_2 (A_g). Two bands at 415 and 450 cm^{-1} are indeed observed for this mode in the $z(yy)\bar{z}$ and $y(zx)\bar{y}$ orientations. In the $z(xx)\bar{z}$ and $y(zz)\bar{y}$ orientations, only one band at 450 cm^{-1} is seen.

B_g Modes

In the $x(zy)\bar{x}$ and $z(xy)\bar{z}$ geometries, 9 and 11 bands are observed, respectively.

$x(zy)\bar{x}$ 425, (450), 562, (572), (589), (938), (973), (988), 1009.

$z(xy)\bar{z}$ (416), 425, 447, 563, (573), 578, (589), (938), (972), (989), 1007.

According to group theory, only six lines are to be expected. In fact, detailed analysis shows that several lines correspond to A_g lines (frequencies in parentheses) and can be attributed to a contaminant that is difficult to completely eliminate for measurements under a microscope.

The bands at 425 and 447 cm^{-1} can be assigned to the $\nu_2(B_g)$ symmetric bending mode, those at 563 and 578 cm^{-1} to the $\nu_4(B_g)$ asymmetric bending mode, and those at 1007 and 1009 cm^{-1} to $\nu_3(B_g)$, the asymmetric bending mode.

In conclusion, the number of internal modes of the PO_4^{3-} anion observed in the Raman and IR spectra is consistent with predictions based on the proposed space group. The loss of symmetry compared to $K_3Na(SO_4)_2$[18] is clearly evident since the D_{3d} space group would lead to a much smaller number of Raman lines (Table 3).

External Modes

14 A_g and 10 B_g lines can be expected in the Raman low-frequency range, corresponding to external modes. In the absence of coupling, they would result from:

12 modes ($6A_g$ and $6B_g$) associated with the vibrations and translations of the PO_4 tetrahedra;

6 translational modes ($4A_g$ and $2B_g$) due to K^+ in K(IIa) and K(IIb) sites;

3 translational modes ($2A_g$ and $1B_g$) due to K^+ in a K(I) site;

3 translational modes ($2A_g$ and $1B_g$) due to Sm^{3+}.

Experimentally, 14 A_g modes and 10 B_g modes are indeed observed at the following wave numbers (cm^{-1}):

A_g mode: 73, 111, 121, 137, 151, 153, 161, 164, 179, 194, 209, 210, 228, 231,

B_g mode: 74, 82, 98, 126, 150, 165, 177, 188, 211, 234.

These modes are, as expected, well out of the frequency range of the internal modes of PO_4. However, it is very difficult to make assignments since the frequencies are al-

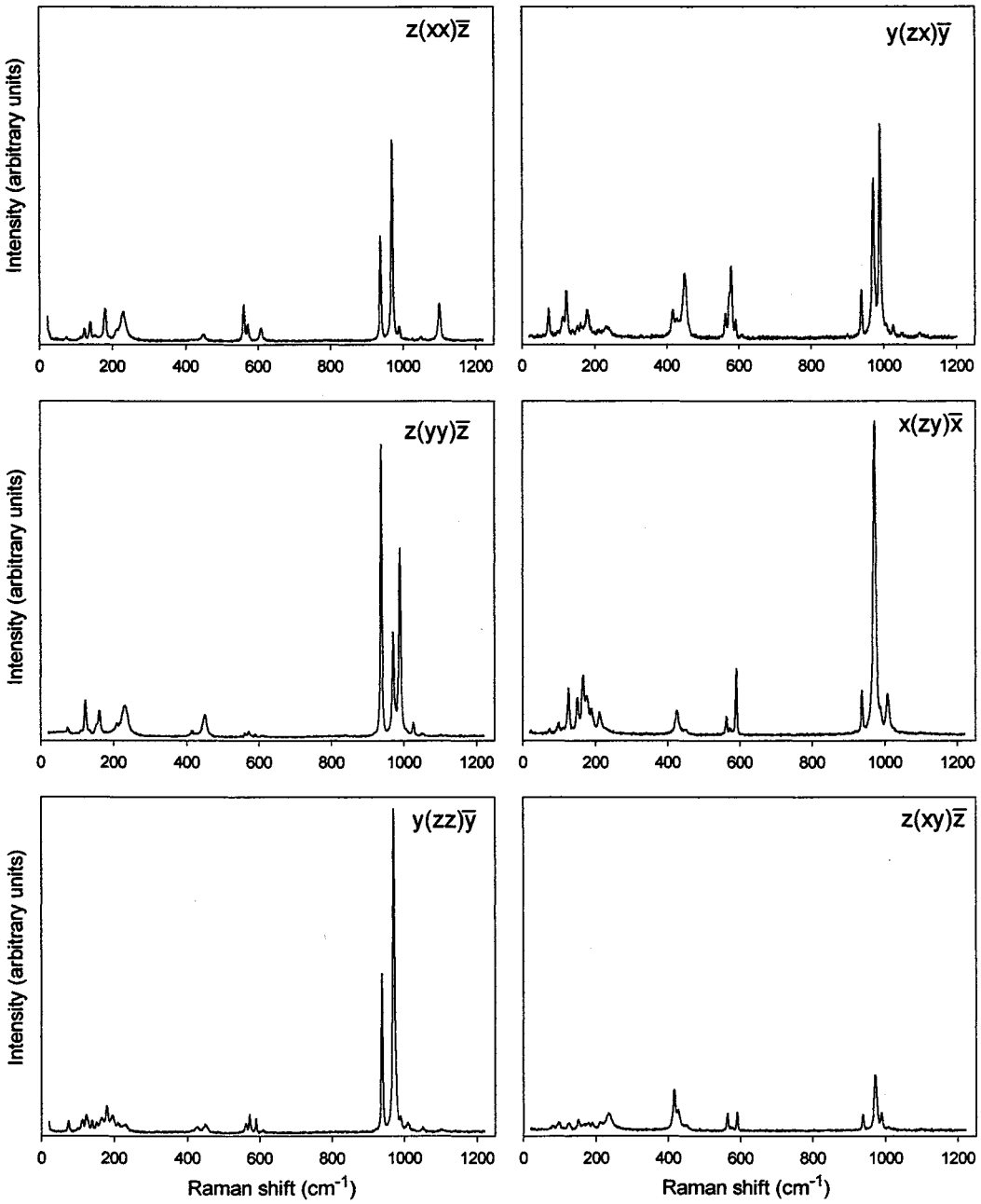


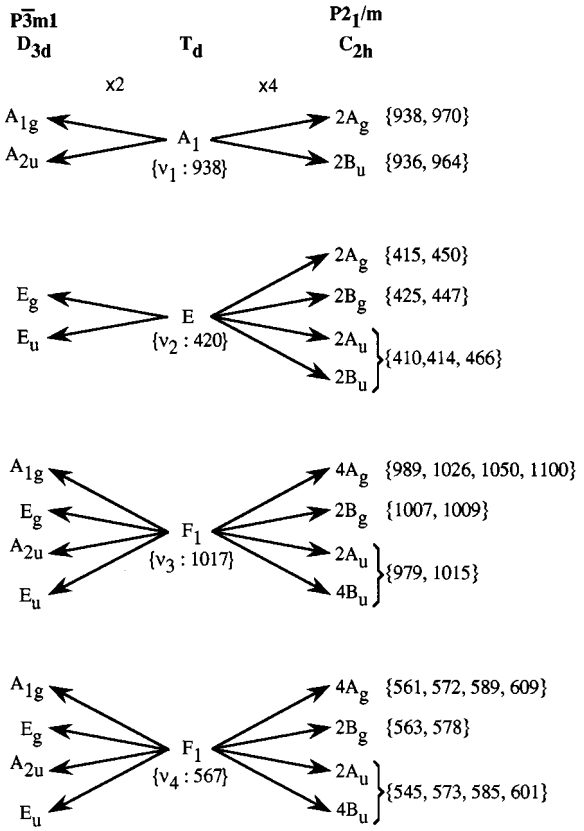
Figure 3. Raman spectra of $K_3Sm(PO_4)_2$ recorded in the various geometries indicated at the top right of each plot (the spectra recorded in cross-polarization mode are plotted with double scale)

most regularly spread and the various ionic displacements are presumably strongly coupled. Moreover, the compounds derived from glaserite[19] (space group $P\bar{3}\,m1$, $Z = 1$) that have so far been subjected to vibrational investigations,[20] such as $M^IM^{III}(XO_4)_2$ (M^I = K, Rb, Cs; M^{III} = In, Sc; X = Mo, W), do not possess the same ionic charges as in the present compound, neither for the cations nor for the molecular ions. Thus, it is not possible to extrapolate the frequencies merely from mass effects. A similar problem arises in the case of the Nasicon-type compounds Na_2-$M^{IV}(PO_4)_2$ (M^{IV} = Ti, Zr, Hf), also derived from glaserite, since the charge on samarium is just 3. However, with regard to the investigations of Barj et al.,[21] who assigned the translational modes of Ti, Zr, and Hf [setting on the K(I) site] at 195, 150, and 105 cm^{-1}, the modes involving samarium, with a lower charge, can be expected to appear at a lower frequency than 115 cm^{-1}. Indeed, several modes appear in this frequency range.

Conclusion

The crystal structure of $K_3Sm(PO_4)_2$ has been determined from single-crystal X-ray diffraction data. This structure is a derivative of the glaserite type.

Table 3. Relationship between the normal modes of vibration of the free PO_4 ions (center), those of $K_3Sm(PO_4)_2$ in the real $P2_1/m$ space (right), and those in the case of the ideal highly symmetrical glaserite (left)



The infrared and Raman spectra of single crystals of $K_3Sm(PO_4)_2$ have been measured and studied in detail on the basis of group theory analysis and by reference to other compounds derived from glaserite. The internal vibrations of the PO_4^{3-} anion could all be identified. The Raman and infrared spectra confirm the structural distortions deduced from the X-ray diffraction study.

Table 4. Crystallographic characteristics, measurement and refinement conditions for $K_3Sm(PO_4)_2$

Crystal data	
Chemical formula	$K_3Sm(PO_4)_2$
Crystal system	Monoclinic
Space group	$P2_1/m$
Lattice constants	a = 7.4347(5) Å; b = 5.6270(5) Å, c = 9.4919(5) Å and β = 90.870(6)°
Data collection	
Diffractometer	Enraf−Nonius CAD4
Radiation	λ(Mo-K_α) = 0.7107 Å
Scan mode	ω-2θ
(*hkl*) min., (*hkl*) max.	(−10,−7,−13), (10,1,0)
θ range	2−30°
Independent reflections	1263
Observed reflections	1191 [$F_O > 4\ \sigma(F_O)$]
Refinement	
Parameters	80
$R = \Sigma\|\|F_O\| - \|F_C\|\|/\Sigma\|F_O\|$	0.0455 [0.044 for $F_O > 4\ \sigma(F_O)$]
$Rw = [\Sigma\|\|F_O\| - \|F_C\|\|^2/\Sigma w\|F_O\|^2]^{1/2}$	0.1136

Table 5. Ionic coordinates and equivalent isotropic displacement factors for $K_3Sm(PO_4)_2$

Atoms	x	y	z	U_{eq}
P(1)	−0.1930(2)	1/4	0.5737(1)	0.0079(3)
P(2)	−0.2325(2)	3/4	0.0875(1)	0.0076(3)
O(1)	−0.2833(6)	1/4	0.4263(5)	0.0117(8)
O(2)	0.0102(7)	1/4	0.5994(5)	0.0242(13)
O(3)	0.2484(4)	−0.0262(6)	0.3426(3)	0.0139(6)
O(4)	−0.1755(6)	3/4	−0.0677(5)	0.0120(9)
O(5)	0.4349(6)	1/4	−0.1010(5)	0.0181(10)
O(6)	−0.1536(4)	−0.0260(6)	0.1612(3)	0.0137(6)
K(I)	−0.4940(1)	1/4	0.1923(1)	0.0148(3)
Sm	0.00705(3)	1/4	0.29098(3)	0.0077(2)
K(IIa)	−0.2035(2)	1/4	−0.0821(1)	0.0122(3)
K(IIb)	0.3627(2)	1/4	0.5920(1)	0.0155(3)

Experimental Section

Preparation: Single crystals of $K_3Sm(PO_4)_2$ were obtained by solid-state reaction of K_2CO_3, $(NH_4)_2HPO_4$, Sm_2O_3, and KF in a 3:4:1:10 molar ratio. After grinding, the mixture was heated at 400°C for 4 h, then at 900°C for 6 h, and was finally allowed to

Table 6. Bond lengths (Å) and selected angles (°) in $K_3Sm(PO_4)_2$

P(1)−O(2)	1.532(5)	O(2)−P(1)−O(2)	106.2(2)	P(2)−O(5)	1.513(5)
P(1)−O(1)	1.542(5)	O(2)−P(1)−O(3)	110.3(1) × 2	P(2)−O(4)	1.539(5)
P(1)−O(3)	1.548(4) × 2	O(1)−P(1)−O(3)	110.5(2) × 2	P(2)−O(6)	1.552(4) × 2
		O(3)−P(1)−O(3)	108.8(2)		
O(4)−P(2)−O(5)	111.7(2)			K(I)−O(1)	2.699(5)
O(5)−P(2)−O(6)	109.3(1) × 2	Sm−O(6)	2.305(3) × 2	K(I)−O(4)	2.710(5)
O(4)−P(2)−O(6)	110.9(1) × 2	Sm−O(3)	2.419(3) × 2	K(I)−O(5)	2.827(5)
O(6)−P(2)−O(6)	108.5(2)	Sm−O(2)	2.453(5)	K(I)−O(2)	2.863(4) × 2
		Sm−O(4)	2.478(5)	K(I)−O(5)	2.979(2) × 2
K(IIa)−O(5)	2.691(5)	Sm−O(1)	2.529(5)	K(I)−O(6)	2.988(4) × 2
K(IIa)−O(3)	2.790(4) × 2				
K(IIa)−O(6)	2.803(4)	K(IIb)−O(2)	2.646(5)	K(I)−O(1)	2.880(1)
K(IIa)−O(4)	2.824(1) × 2	K(IIb)−O(1)	2.880(1) × 2	K(I)−O(3)	2.946(4) × 2
K(IIa)−O(6)	3.043(4)	K(IIb)−O(5)	2.954(5)	K(I)−O(6)	3.099(4) × 2
K(IIa)−O(4)	3.138(5)	K(IIb)−O(1)	3.086(5)	K(I)−O(3)	3.205(4) × 2

cool to room temperature at a rate of 10°C/h. Small needles were separated from the flux by repeated washing in hot water.

X-ray Data Collection: The X-ray diffraction intensities from a single crystal ($0.05 \times 0.1 \times 0.12$ mm^3) were collected using a Nonius CAD4 four-circle diffractometer with graphite-monochromated Mo-K_α radiation ($\lambda = 0.7107$ Å). The unit cell parameters were determined by a least-squares fit of 25 randomly located reflections between 22° and 32° in 2 θ. The total sphere of reflection with index ranges $-10 \leq h \leq 10$, $-7 \leq k \leq 1$, $-3 \leq l \leq 0$ was measured and one standard reflection (−4 1 1) was monitored hourly. No absorption correction was applied ($R_\mu = 0.65$).

The experimental details are given in Table 4. The structure calculations were performed with the SHELXS-86[22] and SHELXL-93[23] programs. The atomic positions, selected bond lengths and angles are reported in Tables 5 and 6, respectively.

Raman Spectroscopy: The Raman spectra were recorded with a DILOR Z24 spectrometer. An argon laser (Coherent Innova 90.3) was used for the excitation: radiation of the wavelength 514.5 nm was chosen since the possible luminescence lines from samarium are weak and appear outside of the spectral range where the Raman signals appear. The spectral width (full-width at half-maximum) was less than 6 cm^{-1} and the error in the line positions was less than 1 cm^{-1}. The measurements were made at room temperature under a microscope (in the back-scattering geometry) with a × 50 objective with a long working distance. This was performed on micrometric samples (typically less than 0.1 mm in length) fixed on a goniometer head and suitably orientated for polarization analysis. The orientations were deduced from the growth faces of the crystals, which were needle-shaped with diamond-shaped bases. For the structure deriving from trigonal glaserite, the needle axis corresponds to the *c* direction and so to [100] of the monoclinic cell of $K_3Sm(PO_4)_2$.

Infrared Spectroscopy: The infrared absorption spectra in KBr pellets were obtained on a Perkin−Elmer FT-IR 1000 PC spectrophotometer in the range 4000−200 cm^{-1} with 4 cm^{-1} spectral resolution.

[1] R. Salmon, C. Parent, A. Berrara, R. Brochu, A. Daoudi, M. Vlasse, G. Le Flem, *C. R. Acad. Sci. Paris* **1975**, *280*, 805.
[2] R. Salmon, C. Parent, A. Daoudi, G. Le Flem, *Rev. Chim. Minér.* **1975**, *12*, 448.
[3] M. Vlasse, R. Salmon, C. Parent, *Inorg. Chem.* **1976**, *15*, 1440.
[4] R. Salmon, C. Parent, G. Le Flem, M. Vlasse, *Acta Cryst.* **1976**, *B32*, 2799.
[5] R. Salmon, C. Parent, G. Le Flem, M. Vlasse, *Mater. Res. Bull.* **1978**, *13*, 439.
[6] R. Salmon, C. Parent, G. Le Flem, *C. R. Acad. Sci. Paris* **1978**, *286*, 365.
[7] R. Salmon, C. Parent, G. Le Flem, M. Vlasse, *Mater. Res. Bull.* **1979**, *14*, 85.
[8] V. Aefremov, P. P. Melnikov, L. N. Komissarova, *Rev. Chim. Minér.* **1985**, *22*, 666.
[9] C. Parent, R. Salmon, G. Demazeau, G. Le Flem, *J. Solid State Chem.* **1980**, *35*, 83.
[10] J. Zah Letho, P. Houenou, R. Eholie, *C. R. Acad. Sci. Paris* **1988**, *307*, 1177.
[11] H. Y. P. Hong, S. R. Chinn, *Mat. Res. Bull.* **1976**, *11*, 421.
[12] K. Okada, J. Ossaka, *Acta Cryst.* **1980**, *B36*, 919.
[13] *International Tables for Crystallography*, vol. 1, Kynoch Press, Birmingham, **1974**.
[14] W. H. Baur, A. A. Khan, *Acta Cryst.* **1972**, *17*, 1195.
[15] J. A. McGinnety, *Acta Cryst.* **1972**, *B28*, 2845.
[16] K. Nakamoto, *Infrared Spectra of Inorganic and Coordination Compounds*, Wiley Interscience, New York, **1986**.
[17] H. Poulet, J. P. Mathieu, *Spectres de Vibration et Symétrie des Cristaux*, Gordon and Breach, Paris, **1970**; G. Turrel, *Infrared and Raman Spectra of Crystals*, Academic Press, London and New York, **1972**; B. Schrader (Ed.), *General Survey of Vibrational Spectroscopy in Infrared and Raman Spectroscopy*, VCH Verlagsgesellschaft mbH, Weinheim, **1995**, and references therein.
[18] M. Barj, G. Lucazeau, P. Colomban, Proceedings of the 8th International Conference on Raman Spectroscopy (6−11 Sept. **1982**, Bordeaux, France, Eds.: J. Lascombes, P. V. Huong), John Wiley & New York, **1982**, p. 461.
[19] M. Maczka, *Eur. J. Solid State Inorg. Chem.* **1996**, *T.33*, 783.
[20] R. F. Klevtsova, P. V. Klevtsov, *Kristallografiya* **1970**, *15*, 953.
[21] M. Barj, H. Pertuis, P. Colomban, *Solid State Ionics* **1983**, *11*, 157.
[22] *SHELXS-86*, in Crystallographic Computing 3 (Eds.: G. M. Sheldrick, C. Kruger, R. Goddard), Oxford University Press, **1985**.
[23] G. M. Sheldrick, *SHELXL-93: Program for the Refinement of Crystal Structures*, University of Göttingen, Germany, **1993**.

Received February 15, 1999

Received February 15, 1999
[99046]

Synthesis of Tumor-Inhibiting Complex Salts Containing the Anion *trans*-Tetrachlorobis(indazole)ruthenate(III) and Crystal Structure of the Tetraphenylphosphonium Salt

Wolfgang Peti,[a] Thomas Pieper,[a] Martina Sommer,[a] Bernhard K. Keppler,*[a] and Gerald Giester[b]

Dedicated to Prof. Dirk Walther on the occasion of his 60th birthday

Keywords: Ruthenium / Coordination chemistry / Paramagnetic complexes / Magnetic properties / Ion exchange / Antitumor agents / Colon tumors

Indazolium *trans*-tetrachlorobis(indazole)ruthenate(III) exhibits excellent results against different tumor models in vitro and in vivo. To improve the water solubility necessary for the introduction of this tumor-inhibiting compound into clinical trials, we synthesized the corresponding sodium salt in a two-step ion exchange via the tetramethylammonium salt. The sodium salt shows a 35-fold higher solubility in water relative to the indazolium salt. We also synthesized the *n*-butylammonium, *n*-octylammonium, and tetraphenylphosphonium salts, all of which showed improved solubility in organic solvents. The X-ray crystal structure of the latter could be solved, proving the *trans* configuration of the complex anion. In spite of the paramagnetic Ru^{III} center an assignement of the coordinated indazole protons could be made with the help of a COSY experiment.

Introduction

The development of ruthenium complexes as an alternative to platinum-based tumor inhibitors is of special interest. Antitumor and antimetastatic activity was found for different Ru^{II} and Ru^{III} complexes.[1–7] Ruthenium(III) complexes of the general formula $HL[RuCl_4L_2]$, where L is a heterocyclic ligand bound to ruthenium through nitrogen and HL the protonated ligand, show remarkable activity against different tumor models in vitro and in vivo. They exhibit excellent activity especially against autochthonous colorectal tumors in rats, with a tumor reduction of 70% to 90%.[8][9] This autochthonous tumor induced by intrarectal application of acetoxymethylnitrosamine (AMMN) is comparable to human colon tumors in its histological appearance and behavior toward chemotherapeutics. The metal-based antitumor drug *cisplatin* is completely inactive in this model. Furthermore, the Ru^{III} complexes show antiproliferative activity in two human colon cancer cell lines (SW707 and SW948).[10] The most promising complex contains two *trans*-standing indazole (L = ind) ligands. It exhibits antineoplastic effects on proliferation of clonogenic cells from freshly explanted human tumors in a capillary soft agar cloning system.[11] The problem with compound **1**, $HInd[RuCl_4ind_2]$ (see Figure 1),[12] is its poor water solubility, making a formulation for clinical trials difficult. To solve this problem, we synthesized new complex salts by ion exchange of the indazolium cation against a variety of cations. The complex anion, responsible for antitumor activity, remains unchanged. Especially the sodium salt **2** shows a much better water solubility, while the corresponding tetraphenylphosphonium salt, of which the crystal structure could be resolved, and the tetraalkylammonium salts are much more soluble in organic solvents, which might be of interest for further reactions with these complex salts.

Results and Discussion

Exchange of the indazole cation in the complex salt **1**, $HInd[RuCl_4ind_2]$, against a tetraalkylammonium or tetraphenylphosphonium cation can be achieved by adding the corresponding chloride salt to a nearly saturated solution of **1** in water (see Figure 1). Immediate precipitation of the complex salts **4**, **5**, or **6**, even less soluble in water than **1**, occurs. In the case of the tetramethylamonium salt **3** methanol is used as solvent instead of water because **3** is more soluble in water than **1**.

The more hydrophobic the substituents of the cation, the more soluble in organic solvents are the corresponding Ru-complex salts. Not surprisingly the tetraoctylammonium salt **5** exhibits the best solubility in less polar solvents like chloroform.

These solubility characteristics can be used in synthesizing the sodium salt **2**, $Na[RuCl_4ind_2]$, that cannot be obtained directly from **1**. Addition of sodium tetraphenylbo-

[a] University of Vienna, Institute of General and Inorganic Chemistry
Waehringerstraße 42, A-1090 Vienna, Austria
Fax: (internat.) +43-1/ 31367-2040
E-mail: keppler@merlin.ap.univie.ac.at
[b] University of Vienna, Institute of Mineralogy and Crystallography
University of Vienna, A-1090 Vienna, Austria

 © WILEY-VCH Verlag GmbH, D-69451 Weinheim, 1999 1434–1948/99/0909–1551 $ 17.50+.50/0

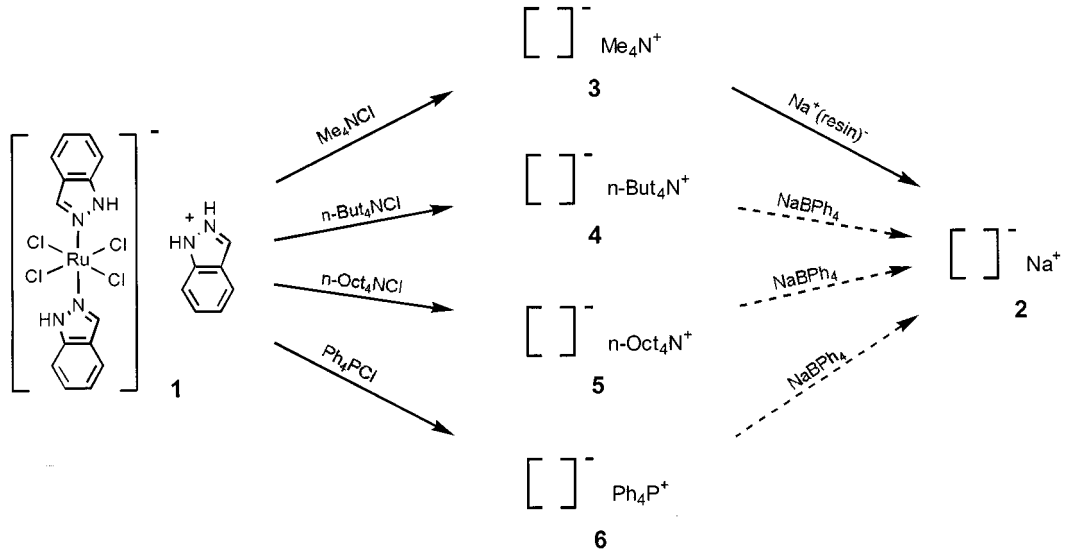


Figure 1. Synthesis of the complex salts **3**, **4**, **5**, and **6** ([ ]$^-$ represents the complex [$RuCl_4ind_2$]$^-$) and synthesis pathways from **1**, HInd[$RuCl_4ind_2$], to **2**, Na[$RuCl_4ind_2$]

rate to a solution of the complex salts **3**, **4**, **5**, or **6** in solvents like methanol, acetone or acetonitrile leads to precipitation of the corresponding tetraphenylborate salts, for example tetraphenylphosphonium tetraphenylborate in the case of **6**. The sodium salt **2** stays in solution and can be precipitated by addition of diethyl ether. Unfortunately, pure products cannot be obtained reproducibly. The best results were obtained with the tetraphenylphosphonium salt **6** in acetonitrile.

A more advantageous method of synthesizing the sodium salt **1** makes use of cation exchange resins. This method was only successful when the tetramethylammonium salt **3**, already more soluble in water than the indazolium salt **1**, was used. The sodium salt could not be prepared directly from the indazolium salt. Thus, a solution of **3** in water was mixed with a Dowex cation exchange resin preloaded with sodium. To avoid hydrolysis of the complex, the solution was frozen immediately after ion exchange, and water was removed under vacuum. After this lyophilization process the product **2**, sodium *trans*-tetrachlorobis(indazole)ruthenate(III), is obtained as a trihydrate. Its solubility in water (0.018 mol/l) is about 35 times higher than that of **1**.

The ^{1}H-NMR spectra of the complex salts show high-field shifts and peak broadening for the protons of the coordinated indazole ligands, because of the paramagnetic Ru^{III} center. In a [D_3]acetonitrile solution of the sodium salt **2** the signals for the protons at position 1 and 3 of the heterocycle, nearest to the Ru^{III} center, can be detected at a chemical shift of about $\delta = -7$ and -12, respectively. The signal at $\delta = -7$ can be assigned to the protons at N1 of the indazole rings, because it disappears due to rapid exchange upon addition of water. The other signals at $\delta = 2.45$ (2 H, at C4 or C7), 2.63 (2 H, at C7 or C4), 3.18 (2 H, at C5 or C6), and 4.32 (2 H, at C6 or C5), represent the protons at a greater distance from the paramagnetic Ru^{III} center. They were assigned in pairs with the help of a COSY experiment (see Figure 2).

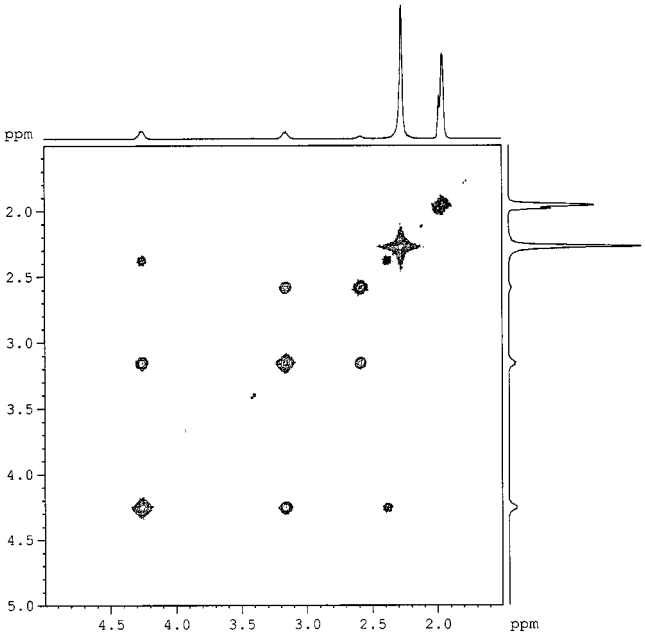


Figure 2. Detail of the COSY spectrum of **2**, Na[$RuCl_4ind_2$], in [D_3]acetonitrile, showing the signals at $\delta = 2.45$, 2.63, 3.18, and 4.32 that represent the indazole protons further from the paramagnetic Ru^{III} center (the signal at $\delta = 2.45$ in the projections is overlapped by the water signal of the solvent) than the two nearest protons, which cannot be detected in the COSY experiment.

In ^{13}C-NMR measurements the signals of the two quaternary carbons and the carbon beneath the coordinated nitrogen of each indazole ligand could not be detected. The detectable carbons at $\delta = 118.07$ (C5 or C6), 114.72 (C6 or C5), 98.29 (C4 or C7), and 97.77 (C7 or C4) could also be assigned in pairs because of the corresponding cross peaks in a H,C-correlated spectrum (HMQC, spectrum not shown).

The X-ray crystal structure of the tetraphenylphosphonium salt was solved, proving the *trans* configuration of

the complex anion $[RuCl_4ind_2]^-$ (see Figure 3, crystallographic data are collected in Table 1). The Ru atom is in the center of an octahedron. The two planes of the *trans* indazole ligands, bound through the N2 nitrogen, are twisted. The longest Ru−Cl bond is formed between Cl(2) and the Ru center [2.3723(8) Å], whereas the Ru−Cl(1) [2.3627(7) Å], Ru−Cl(3) [2.3618(7) Å] and especially the Ru−Cl(4) [2.3586(8) Å] bonds are slightly, but significantly shorter. The longer Ru−Cl(2) bond is due to hydrogen bonding between the Cl(2) and the N(4) of one indazole ligand. The N(4)−Cl(2) distance is 3.105 Å. The distance between Cl(2) and the hydrogen at the N(4) of the indazole ring, H(2), is 2.441 Å [N(4)−H(2): 1.094 Å]. Cl(2), Ru, N(3), N(4), and H(2) are nearly in a plane.

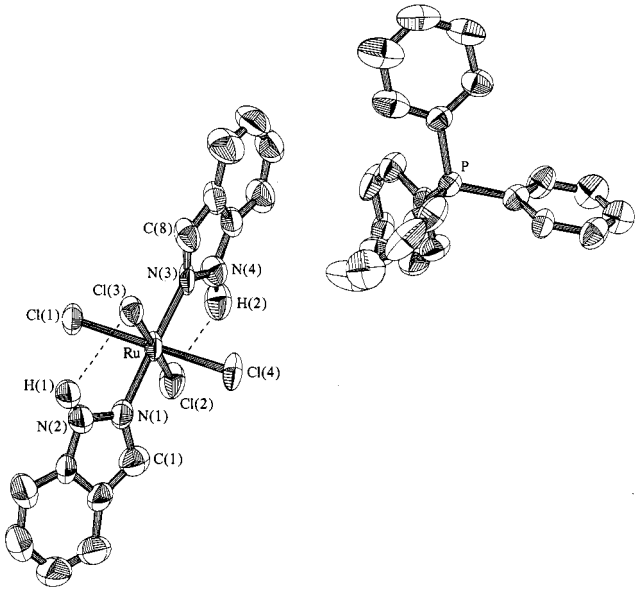


Figure 3. Perspective view of the crystal structure of **6**, $Ph_4P[RuCl_4ind_2]$. Selected bond lengths [Å] and angles [deg]: Ru−Cl(1) 2.3627(7), Ru−Cl(2) 2.3723(8), Ru−Cl(3) 2.3618(7), Ru−Cl(4) 2.3586(8), Ru−N(1) 2.0517(21), Ru−N(3) 2.0711(22), N(1)−N(2) 1.3498(31), N(3)−N(4) 1.3466(29), N(1)−C(1) 1.3338(36), N(3)−C(8) 1.3065(39), N(1)−Ru−N(3) 178.33(8), N(1)−Ru−Cl(1) 90.33(6), N(1)−Ru−Cl(2) 89.81(6), N(1)−Ru−Cl(3) 89.80(6), N(1)−Ru−Cl(4) 89.63(6), N(3)−Ru−Cl(1) 90.89(6), N(3)−Ru−Cl(2) 89.07(7), N(3)−Ru−Cl(3) 91.37(6), N(3)−Ru−Cl(4) 89.20(6), Cl(1)−Ru−Cl(2) 89.85(3), Cl(1)−Ru−Cl(3) 87.96(3), Cl(1)−Ru−Cl(4) 177.44(2), Cl(2)−Ru−Cl(3) 177.78(2), Cl(2)−Ru−Cl(4) 92.71(3), Cl(3)−Ru−Cl(4) 89.48(3)

In contrast, N(2) of the other indazole ligand exhibits only weak interactions with the chlorine Cl(3) through its H(1) atom [N(2)−Cl(3): 3.212 Å, Cl(3)−H(1): 2.750 Å, N(2)−H(1): 0.853 Å]. The N(2)−Cl(1) distance is 3.426 Å. Cl(4) is not involved in any hydrogen bonding and therefore exhibits the shortest Ru−Cl bond length.

In general, the Ru−Cl and Ru−N [Ru−N(1): 2.0517(21) Å, Ru−N(3): 2.0711(22) Å] bond lengths, as well as the bond lengths of the indazole rings, lie in the same range as those of the corresponding 1-methylindazole complex, the crystal structure of which has already been published[12]. The phosphorus of the tetraphenylphosphonium counterion is tetrahedrally coordinated by the phenyl rings, as could be expected

Experimental Section

Materials: All solvents and reagents were used as received and were of analytical grade. Indazolium *trans*-tetrachlorobis(indazole)ruthenate(III), $HInd[RuCl_4ind_2]$, was prepared as described previously[12].

Infrared Spectra: Infrared spectra were recorded on a Perkin−Elmer FTIR 2000 IR spectrophotometer.

NMR Spectra: The ^1H-, ^{13}C-, and 2D NMR experiments were performed at 400.13 MHz (^1H) and 100.61 MHz (^{13}C) on a Bruker DPX 400 spectrometer at 24 °C.

The gradient selected COSY and the HMQC (inverse H,C-correlation with BIRD selection and GARP decoupling in phase-sensitive mode using TPPI) experiments were performed with standard Bruker pulse programs.

X-ray Structure Determination: A single crystal of the tetraphenylphosphonium salt with the approximate dimensions of 0.30 × 0.25 × 0.15 mm was used for X-ray measurement on a Nonius KappaCCD diffractometer (Mo-*Kα* radiation) at room temperature. Denzo-SMN software was utilized for the data evaluation. The structure was solved by direct methods (SHELXS-97)[13] and refined (SHELXL-97)[14] including the positions of all hydrogen atoms. A summary of the crystal data and of the refinement procedures is given in Table 1. Atomic coordinates and displacement parameters are deposited in the Cambridge Crystallographic Data Centre as supplementary publication no. CCDC-112417.

Elemental Analyses: C,H,N analysis were carried out on a Perkin−Elmer 2400 CHN Elemental Analyzer. Cl was analyzed by argentometry.

Preparation of Compounds. Sodium *trans*-Tetrachlorobis(indazole)ruthenate(III) Trihydrate, $Na[RuCl_4ind_2] \cdot 3\ H_2O$ (2): A solution of $Me_4N[RuCl_4ind_2]$ (**3**; 100 mg, 0.18 mmol) in water (200 mL) was mixed with a Dowex 50WX2 acidic cation-exchange resin preloaded with sodium for 20 minutes. After filtration, the solution was immediately frozen with liquid nitrogen and lyophilized. The sodium salt was obtained as a voluminous, brown powder. Yield: 80 mg (89%). − $C_{14}H_{12}Cl_4N_4NaRu \cdot 3\ H_2O$ (556.19): calcd. C 30.23, H 3.26, Cl 25.50, N 10.07; found: C 30.20, H 2.62, Cl 25.47, N 9.80. − ^1H NMR (400 MHz, [D$_3$]acetonitrile): δ = 4.32 (2 H), 3.18 (2 H), 2.63 (2 H), 2.45 (2 H), −7.1 (2 H), −12.9 (2 H). − ^{13}C NMR (100 MHz, [D$_3$]acetonitrile): δ = 118.07, 114.72, 98.29, 97.77. IR (CsI): $\tilde{\nu}$ = 3459 s, 3316 s, 2925 w, 1627 vs, 1511 m, 1439 w, 1382 m, 1356 vs, 1280 w, 1241 s, 1154 m, 1124 m, 1085 s, 1004 m, 967 m, 900 w, 868 w, 838 m, 782 w, 750 vs, 667 s, 616 w, 435 m, 321 s, 291 m, 215 m cm^{-1}. − Thermogravimetric analysis (Mettler-Toledo TGA 850): The loss of one mol equivalent of water was achieved by heating up to 130 °C (nitrogen atmosphere). Further weight loss is observed at temperatures above 200 °C, resulting in decomposition of the complex.

Sodium *trans*-Tetrachlorobis(indazole)ruthenate(III), $Na[RuCl_4ind_2]$: $NaB[C_6H_5]_4$ (600 mg, 1.75 mmol) was added to a solution of **6** ($Ph_4P[RuCl_4ind_2]$, 500 mg, 0.61 mmol) in acetonitrile (25 mL). The precipitated $Ph_4PB[C_6H_5]_4$ was filtered off after stirring for five minutes. The sodium salt was precipitated by addition of diethyl ether to the filtrate. After standing at 4 °C for 30 minutes, $Na[RuCl_4ind_2]$ was filtered and dried in vacuum over P_2O_5. Yield: 266 mg (87%). − $C_{14}H_{12}Cl_4N_4NaRu$ (502.15): calcd. C, 33.49, H 2.41, N 11.16, Cl 28.24; found: C 33.09, H 2.67, N 11.04, Cl 26.79. − ^1H NMR (400 MHz, [D$_3$]acetonitrile): δ(cation) = 7.94 (4 H), 7.71 (m, 16 H); δ(anion) = 4.55 (2 H), 3.27 (2 H), 2.84 (2 H), 2.59 (2 H), −7.0 (2 H), −12.5 (2 H).

Table 1. Crystallographic data for $Ph_4P[RuCl_4ind_2]$ (**6**)

Empirical formula	$C_{38}H_{32}Cl_4N_4PRu$	$2\theta_{max}$[°]	53
space group	*P*1bar	measured reflections	13471
a [Å]	11.000(2)	unique data set	6802
b [Å]	13.503(2)	$R_{int.}$	0.017
c [Å]	14.471(2)	data with $F_o>4\sigma(F_o)$	5573
α [°]	65.42(1)	variables	562
β [°]	82.80(1)	*R*1 [for $F_o>4\sigma(F_o)$]	0.033
γ [°]	67.93(1)	*wR*2 [for all F_o^2]	0.088
V [Å^3]	1810.2	$R1 = \Sigma\|\|F_o\| - \|F_c\|\|/ \Sigma\|F_o\|$	
Z	2	$wR2 = [\Sigma w(F_o^2 - F_c^2)^2/\Sigma wF_o^4]^{1/2}$	
ρ_{calc} [gcm^{-3}]	1.50	$w = 1/[\sigma^2(F_o^2) + (0.045\times P)^2 + 0.3\times P]$	
μ(Mo-*Kα*) [$^{-1}$]	8.1	$P = \{[\max \text{ of } (0 \text{ or } F_o^2)] + 2F_c^2\}/3$	

Crystal−detector distance: 28 mm, 180 frames with 2° φ scan range and 2 × 150 s exposure time per frame.

Tetramethylammonium *trans*-Tetrachlorobis(indazole)ruthenate(III), $Me_4N[RuCl_4ind_2]$ (3): Tetramethylammonium chloride (368 mg, 3.36 mmol) was added to $HInd[RuCl_4ind_2]$ (500 mg, 0.84 mmol) in methanol (150 mL). After stirring for 30 min, the formed precipitate was filtered, washed with water and dried under vacuum over phosphorus pentaoxide. Yield: 326 mg (70%). − $C_{18}H_{24}Cl_4N_5Ru$ (553.1): calcd. C 39.07, H 4.37, Cl 25.63, N 12.66; found: C 38.90, H 4.29, Cl 25.52, N 12.36. − ^{1}H NMR (400 MHz, [D$_3$]acetonitrile): δ(cation) = 3.16 (s, 12 H); δ(anion) = 4.54 (2 H), 3.27 (2 H), 2.83 (2 H), 2.58 (2 H), −5.81 (2 H), −10.89 (2 H). − ^{13}C NMR (100 MHz, [D$_3$]acetonitrile): δ(cation) = 59.24; δ(anion) = 118.12, 113.91, 98.12, 97.81. − IR (CsI): $\tilde{\nu}$ = 3460 m, 3293 s, 3013 m, 1627 s, 1560 w, 1509 m, 1483 s, 1438 w, 1380 w, 1356 vs, 1276 w, 1239 s, 1149 w, 1119 w, 1082 m, 1002 m, 945 vs, 866 w, 836 w, 750 vs, 669 s, 522 m, 455 w, 435 m, 336 m, 321 s, 291 m, 266 w, 218 m cm^{-1}.

Tetra(*n*-butyl)ammonium *trans*-Tetrachlorobis(indazole)ruthenate(III), $(n\text{But})_4N[RuCl_4ind_2]$ (4): $HInd[RuCl_4ind_2]$ (200 mg, 0.34 mmol) was suspended in water (100 mL) and acetonitrile (5 mL) by ultrasonic treatment and then dissolved in water (400 mL). Tetra(*n*-butyl)ammonium chloride (186 mg, 0.69 mmol) was added to this solution and precipitation occurred immediately. To complete the reaction, the mixture was stirred overnight. The precipitate was filtered, washed with water, and dried under vacuum over phosphorus pentaoxide. Yield: 216 mg (89%). − $C_{30}H_{48}Cl_4N_5Ru$ (721.63): calcd. C 49.93, H 6.70, Cl 19.65, N 9.71; found: C 49.57, H 6.46, Cl 19.67, N 9.53. − ^{1}H NMR (400 MHz, [D$_3$]acetonitrile): δ(cation) = 3.20 (8 H), 1.76 (8 H), 1.40 (8 H), 1.01 (12 H); δ(anion) = 4.55 (2 H), 3.26 (2 H), 2.83 (2 H), 2.57 (2 H), −7.0 (2 H), −12.3 (2 H). − ^{13}C NMR (100 MHz, [D$_6$]DMSO): δ(cation) = 59.36, 24.39, 20.26, 14.53; δ(anion) = 118.39, 114.69, 99.79, 96.28. − IR (CsI): $\tilde{\nu}$ = 3307 s, 2960 s, 2874 m, 2360 m, 1626 s, 1506 w, 1478 vs, 1442 m, 1381 m, 1354 vs, 1275 w, 1243 s, 1152 s, 1089 m, 1002 m, 963 m, 838 m, 749 vs, 670 s, 628 s, 556 s, 434 m, 333 m, 320 s, 289 m, 217 m cm^{-1}.

Tetra(*n*-octyl)ammonium *trans*-Tetrachlorobis(indazole)ruthenate(III), $(n\text{Oct})_4N[RuCl_4ind_2]$ (5): To a solution of $HInd[RuCl_4ind_2]$ (250 mg, 0.42 mmol) in water (800 mL), prepared analogously to the above-mentioned procedure, were added tetra(*n*-octyl)ammonium chloride (420 mg, 0.84 mmol) in water (30 mL) and ethyl acetate (1 mL) to aid solution. After stirring for three days a green agglutinated precipitate formed and was filtered, washed with methanol, and dried under vacuum over phosphorus pentaoxide. Yield: 234 mg (59%). − $C_{46}H_{80}Cl_4N_5Ru$ (946.06): calcd. C 58.39, H 8.52, Cl 14.99, N 7.40; found: C 57.85, H 8.11, Cl 14.42, N 7.69. − ^{1}H NMR (400 MHz, $CDCl_3$): δ(cation) = 2.91 (8 H), 1.47 (16 H), 1.19 (32 H), 0.83 (12 H); δ(anion) = 4.11 (2 H), 3.11 (2 H), 2.40 (2 H), 2.27 (2 H), −7.7 (2 H), −14.3 (2 H). − ^{13}C NMR (100 MHz, $CDCl_3$): δ(cation) = 32.13, 30.19, 29.56, 29.02, 28.38, 23.04, 21.81, 14.55; δ(anion) = 116.88, 116.22, 99.40, 95.33. − IR (CsI): $\tilde{\nu}$ = 3296 s, 3096 w, 2955 s, 2926 vs, 2856 s, 1626 m, 1504 w, 1466 s, 1375 m, 1353 s, 1269 w, 1242 m, 1149 w, 1114 w, 1083 m, 998 w, 954 w, 830 w, 746 s, 671 m, 547 w, 442 w, 433 w, 328 s, 283 m, 218 m cm^{-1}.

Tetraphenylphosphonium *trans*-Tetrachlorobis(indazole)ruthenate(III), $Ph_4P[RuCl_4ind_2]$ (6): Tetraphenylphosphonium chloride (190 mg, 0.5 mmol) was added to a solution of $HInd[RuCl_4ind_2]$ (150 mg, 0.25 mmol) in water (500 mL), prepared analogously to the above-mentioned procedure, which resulted in immediate precipitation. After stirring overnight the precipitate was filtered and washed with water. Afterwards the crude product was dissolved in acetone and reprecipitated by addition of diethyl ether. The ocher-yellow precipitate was washed with diethyl ether/acetone (1:1) and dried under vacuum over phosphorus pentaoxide. Yield: 82 mg (40%). − $C_{38}H_{32}Cl_4N_4PRu$ (818.56): calcd. C 55.76, H 3.94, Cl 17.32, N 6.84; found: C 55.55, H 3.77, Cl 17.19, N 6.65. − ^{1}H NMR (400 MHz, [D$_3$]acetonitrile): δ(cation) = 7.94 (4 H), 7.71 (m, 16 H); δ(anion) = 4.54 (2 H), 3.26 (2 H), 2.82 (2 H), 2.58 (2 H), −7.1 (2 H), −12.5 (2 H). − ^{13}C NMR (100 MHz, [D$_6$]DMSO): δ(cation) = 136.88, 135.60 (d), 131.86 (d), 118.88 (d); δ(anion) = 118.42, 114.71, 99.82, 96.26. − IR (CsI): $\tilde{\nu}$ = 3475 s, 3351 s, 3057 m, 1626 s, 1584 m, 1508 m, 1482 m, 1437 vs, 1380 m, 1358 s, 1277 m, 1164 m, 1108 vs, 1087 w, 996 s, 962 m, 837 m, 764 vs, 723 vs, 690 vs, 666 s, 528 vs, 440 w, 435 w, 336 m, 321 s, 282 m, 216 m cm^{-1}. − Crystals for X-ray diffraction were obtained by slowly evaporating an acetonitrile solution.

Acknowledgments

The assistance of Mrs. Rosa Strobl in preparing the manuscript is gratefully acknowledged.

[1] M. J. Clarke, *Metal Complexes in Cancer Chemotherapy* (Ed.: B. K. Keppler), VCH Weinheim, **1993**, 129.
[2] E. Alessio, A. Balducci, A. Lutman, G. Mestroni, M. Calligaris, W. M. Attia, *Inorg. Chim. Acta* **1993**, *203*, 205.
[3] R. Vilaplana, M. A. Romero, M. Quiros, J. M. Salas, F. Gonzalez-Vilchez, *Metal Based Drugs* **1995**, *2*, 211.
[4] P. M. van Vliet, S. M. S. Toekimin, J. G. Haasnoot, J. Reedijk, O. Novakova, O. Vrana, V. Brabec, *Inorg. Chim. Acta* **1995**, *231*, 57.
[5] G. Mestroni, E. Alessio, S. Sava, S. Pacor, M. Coluccia, A. Boccarelli, *Metal Based Drugs* **1993**, *1*, 41.
[6] E. Alessio, G. Mestroni, G. Sava, A. Bergamo, M. Coluccia, L. Messori, *Cytotoxic, Mutagenic and Carcinogenic Potential of Heavy Metals Related to Human Environment* (Ed.: N. D. Had-

jiliadis), Kluwer Academic Publishers, Netherlands, **1997**, 457.
[7] S. Sava, I. Capozzi, K. Clerici, G. Gagliardi, E. Alessio, G. Mestroni, *Clin. Exp. Metastasis* **1998**, *16*, 371.
[8] B. K. Keppler, K. G. Lipponer, B. Stenzel, F. Kratz, *Metal Complexes in Cancer Chemotherapy* (Ed.: B. K. Keppler), VCH Weinheim, **1993**, 187.
[9] M. Seelig, M. R. Berger, B. K. Keppler, D. Schmähl, *Metal Ions in Biology and Medicine* (Eds.: Ph. Collery, L. A. Poirier, M. Manfait, J.C. Etienne), John Libbey Eurotext: Paris, **1990**, 476.
[10] A. Galeano, M. R. Berger, B. K. Keppler, *Arzneimittelforschung/Drug Research* **1992**, 42(I), *6*, 821.
[11] H. Depenbrock, S. Schmelcher, R. Peter, B. K. Keppler, G. Weirich, T. Block, J. Rastetter, A. R. Hanauske, *Europ. J. Cancer* **1997**, *33*, 2404.
[12] K. G. Lipponer, E. Vogel, B. K. Keppler, *Metal-Based Drugs* **1996**, *3*, 243.
[13] G. M. Sheldrick, *SHELXS-97, A Program for the Solution of Crystal Structures*, University of Göttingen, Germany, **1997**.
[14] G. M. Sheldrick, *SHELXL-97*, *A Program for Crystal Structure Refinement*, University of Göttingen, Germany, **1997**.

Received March 2, 1999
[I99077]

Synthesis and Metal-Ion Extraction Properties of *para-tert*-Butylcalixareneglycine Ester Acetamides

Burkhard König,*[a] Tom Fricke,[a] Karsten Gloe,*[b] and Christine Chartroux[b]

Dedicated to Professor Dirk Walther (Jena) on the occasion of his 60th birthday

Keywords: Calixarenes / Macrocycles / Silver / Radiotracer technique / Metal-ion extraction / Radiochemistry

Calixareneglycine ester acetamides **4a–c** have been synthesized from calixareneacetyl chlorides **5a–c** and glycine ethyl ester (**6**). Their ion-binding properties have been investigated by liquid-liquid extraction with radiotracer techniques. The experiments reveal a moderate affinity towards silver(I) ions, which increases with calixarene ring size.

Introduction

Calixarenes are most suitable precursors for the synthesis of selective ionophores.[1] As illustrated by many examples their unique molecular structure allows the arrangement of functional groups in space for the coordination of metal cations.[2] Receptor molecules with remarkable selectivities in cation binding have been developed, e.g. from calix[4]arene, which was anchored in a particular conformation of the macrocycle by suitable derivatization[1] and functionalized with crown ethers.[3] But even the introduction of much simpler functional groups, such as ethers, esters, amides or ketones has a profound effect on the binding ability of calixarenes. It has been well established that the phenolic functions of calixarenes can be alkylated with alkyl bromoacetates to form alkyl calixarene acetates **1** with significant ion-binding potential for mainly alkali metal cations.[4] The series has been extended to calixarene ketones **2**,[5] amides **3**,[6] thioamides and carboxylic acids,[7] and their alkali and alkaline earth cation binding properties have been determined. The principal findings of these studies were that calix[4]arene esters **1a**, ketones **2a** and *tert*-amides **3a**[8] show a clear preference for Na^+ ions, the pentamer series (**1d**, **2d**, **3d**), reflecting the larger receptor volume than the tetramers, favors the larger cations K^+, Rb^+ and Cs^+ over Na^+, and calix[6]arene (**1b**, **2b**, **3b**) and calix[8]arene derivatives (**1c**, **2c**, **3c**) are characterized by lower extraction ability and low levels of discrimination among the alkali cations. The *tert*-amides **3a** and **3b** also bind the alkaline earth metal ions Ca^{2+}, Sr^{2+} and Ba^{2+} with high efficiency, but without clear size preference. This was confirmed by stability-constant measurements and solvent-extraction studies.[2a] In contrast to the behavior of tertiary amides (R = R′ = alkyl) the related secondary amides **3a**, **3b**, **3c** (R = H; R′ = *n*Bu) extract alkali metal ions only very weakly.[9] With the alkaline earth metals the same compounds give size-dependent extractabilities, which are furthermore graduated in the order **3b > 3c > 3a**. Less data have been reported on the complexation of transition-metal cations in solution, with the exception of Ag^+, for which a broad range of stability constants in methanol is available.[2a,2b] With *para-tert*-butylcalixarene tetra- (**1a**), penta- (**1d**) and hexaesters (**1b**) log β values range between 3.1 and 4.3, and no size selectivity is observed. The stability of complexes is slightly higher for the tetraketone **2a** and much higher for the tetraamide **3a**. In the amide series there is a size effect: Compound **3d** shows a higher log β value than **3a** or **3b**.[2a,8] The calix[4]arene-*tert*-amide **3a** is a useful extractant for Ag^I from strongly acidic medium.[10]

In order to investigate the effect of functional groups simultaneously present in each arene moiety,[11] we have synthesized a series of new calixareneglycine ester acetamides **4**, which represent examples of simple calixarenes that bear both secondary amide *and* ester groups as potential coordination sites for metal ion binding. Their binding properties have been investigated by liquid-liquid extraction of aqueous solutions of metal picrates. A first example of this type, calix[4]areneglycine tetra-*tert*-butyl ester acetamide, was recently reported by Reinhoudt et al.[12]

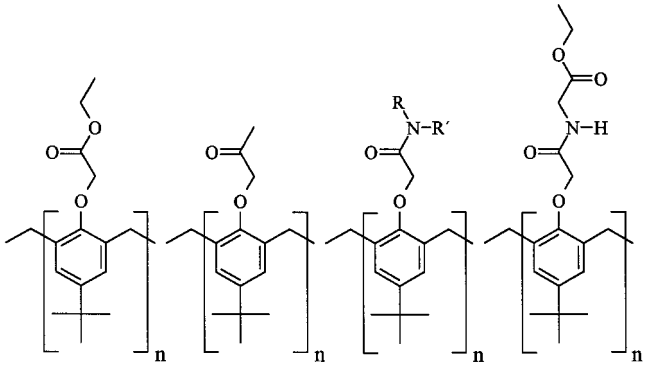
Results and Discussion

Synthesis

The synthesis of the *para-tert*-butylcalixareneglycine ester acetamides **4a–c** was achieved analogously to previously reported procedures for the synthesis of calixarene acetamides. The reaction of the *para-tert*-butylcalixareneacetyl chlorides **5a–c**[13] with glycine ethyl ester (**6**)[14] under standard conditions enabled the isolation of the glycine es-

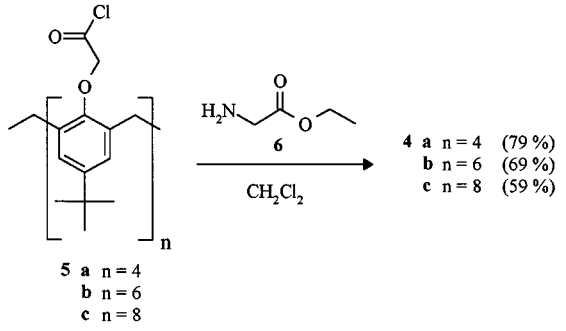
[a] Institut für Organische Chemie der Technischen Universität Braunschweig,
Hagenring 30, D-38106 Braunschweig, Germany
Fax: (internat.) + 49-(0)531/391-5388
E-mail: B.Koenig@tu-bs.de
[b] Institut für Anorganische Chemie der Technischen Universität Dresden,
Mommsenstraße 13, D-01062 Dresden, Germany
Fax: (internat.) + 49-(0)351/463-7287
E-mail: Karsten.Gloe@chemie.tu-dresden.de

 © WILEY-VCH Verlag GmbH, D-69451 Weinheim, 1999 1434–1948/99/0909–1557 $ 17.50+.50/0



Scheme 1. Calixarene ionophores

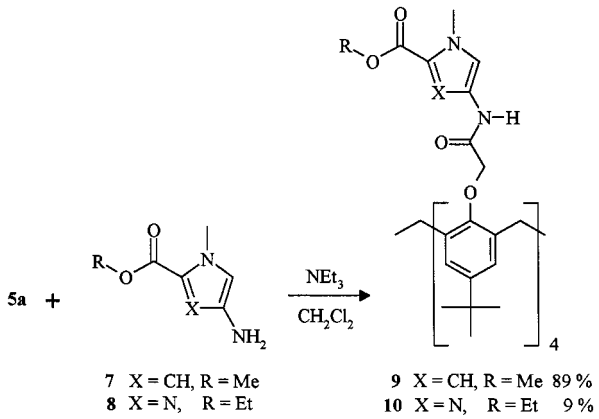
ter acetamides **4a–c** in 59–79% yields. As indicated by the broad resonance signals in the NMR spectra of **4b**, the compound has a restricted conformational mobility on the NMR time scale. Obviously, compound **4a** is, like **5a**, fixed in the cone conformation, whereas the macrocyclic ring of **4c** is large enough to allow rotation of the substituted arene units. The reaction of **5a** with heterocyclic amino acid esters, such as **7** and **8**, proceeds analogously, but is much less efficient for **8**.[15] Surprisingly, amides **9** and **10** show significant decomposition in chloroform solution at room temperature, which renders them unsuitable for extraction studies. *N*-Benzylamide **11** and compound **14** were synthesized from **5a** and benzylamine, and alkylation of **12** with **13**,[16] respectively, for comparison of their extraction properties with compound **4a**.



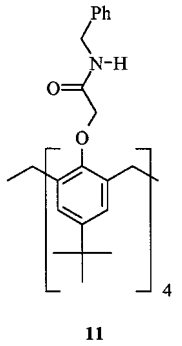
Scheme 2. Synthesis of *para-tert*-butylcalixareneglycine ester acetamides

Metal-Ion Extraction Properties

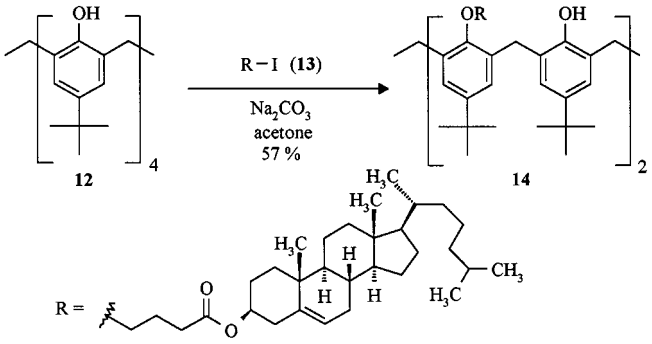
The binding properties of the new compounds were investigated by liquid-liquid extraction experiments. Aqueous solutions of the metal salts ($c = 1 \cdot 10^{-4}$ mol/l) and picric acid ($5 \cdot 10^{-3}$ mol/l), buffered to pH = 5.2 by NaOAc/HCl,[17] were extracted with chloroform solutions of the calixarene derivatives ($c = 1 \cdot 10^{-3}$ mol/l). The determination of the metal concentrations in both phases was carried out by measurement of the radiation of the corresponding



Scheme 3. Reaction of **5a** with heterocyclic amino acid esters



Scheme 4. *para-tert*-Butylcalix[4]arene *N*-benzylacetamide (**11**)



Scheme 5. Twofold alkylation of *para-tert*-butylcalix[4]arene

radionuclides.[18] As metal ions Na^+, Ba^{2+}, Tl^+, Pd^{2+}, Cu^{2+}, Zn^{2+}, Hg^{2+}, Eu^{3+} and Ag^+ were employed to obtain information about extraction properties towards alkali, alkaline earth and transition metal ions. Figure 1 summarizes the results. All glycine ester acetamides extract Ag^+, and the efficiency increases drastically from **4a** (1.8%) to **4b** (15%) and **4c** (57%).[19] For the large glycine ester acetamide **4c** some extraction of Cu^{2+} (7.1%), Hg^{2+} (5.5%), Eu^{3+} (3%) and Ba^{2+} (1.8%) was noted. Compound **4b** shows, besides Ag^+ binding, some uptake of Tl^+ (3.5%) but very low Hg^{2+}, Cu^{2+}, Eu^{3+} and Ba^{2+} extraction (< 2%). Extraction of Na^+ or Zn^{2+} was not observed in any case. The importance of the ester groups for extraction is illustrated by comparison with the *N*-benzylamide-substituted calix[4]arene **11**: None of the tested metal salts were ex-

tracted under the selected experimental conditions and only a small affinity towards Pd^{2+} could be detected.[20] Compound **14**, lacking ester and amide groups, did not show any extraction of metal salts within the error of the experiment.

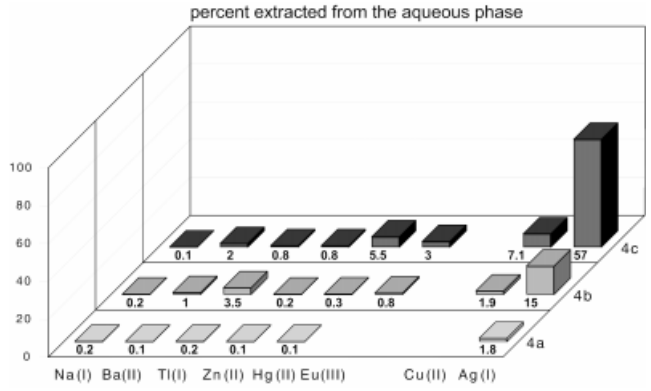


Figure 1. Extraction of metal picrates with compounds **4a**, **4b** and **4c**; $c_M = 1 \cdot 10^{-4}$ M; $c_{HPic} = 5 \cdot 10^{-3}$ M; pH = 5.2; $c_L = 1 \cdot 10^{-3}$ M/$CHCl_3$ a stoichometry of 1:1 for Hg^{2+}, Tl^+, Eu^+ complexes, and 1:1, 1:2 stoichometries for Ag^+ and Ba^{2+} complexes

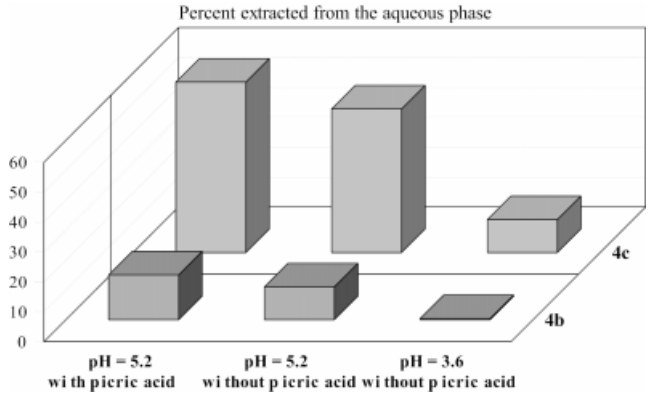


Figure 2. Influence of the pH value on the extraction of Ag^+ with **4b** and **4c**; $c_{Ag} = 1 \cdot 10^{-4}$ M; $c_L = 1 \cdot 10^{-3}$ M/$CHCl_3$

The extractability of Ag^+ with **4b** and **4c** strongly depends on the pH value of the aqueous phase. As it is shown in Figure 2 a decreasing pH value (from 5.2 to 3.6) led to a significant lower extraction (from 57% to 11% for **4c**; from 15% to 0.4% for **4b**). In contrast to this, amazingly, the influence of the picrate anion on the Ag^+ extraction is weak (see Figure 2). The extractability for **4c** in the absence of picrate is only 9%, and for **4b** 4% lower than with picrate present.

Some additional information about the stoichiometry of the calixarene metal complexes in the organic phase was derived from double log plots of distribution ratios of the metals versus ligand concentrations (Figure 3). The analysis suggests that **4b** and **4c** form 1:1 complexes with Hg^{2+}. The same composition is also obtained from **4b** with Tl^+ and Eu^{3+}; 1:1 and 1:2 complexes (M/L) are identified for Ag^+[21] with the calixarenes **4a** and **4b** and for Ba^{2+} with **4b**. The calculated extraction constants are summarized in Table 1. Preliminary molecular modeling studies give some evidence for the binding of the metal ion by ether and carbonyl oxygen donor atoms inside the cavity, similar to the known structures with tertiary amides.[2e] The limited extraction power of the novel compounds in comparison with *tert*-amides might be rationalized by a specific hydrogen-bonding pattern between the secondary amide and carbonyl oxygen functions in the molecule, as it is observed for compounds with related structure.[22] The interaction of the secondary amide with the solvent chloroform might also be taken into account.

Conclusion

In summary, calixarene derivatives that bear a secondary amide moiety and an ester group on each arene unit were obtained by reaction of calixareneacetyl chlorides **5** with glycine ethyl ester (**6**). The investigation of the binding

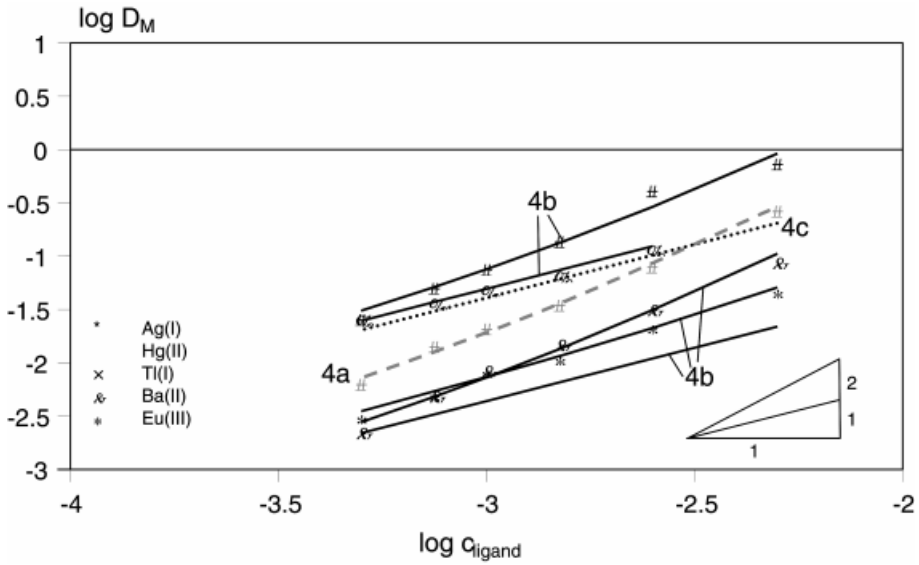


Figure 3. The double logarithmic plot suggests a stoichiometry of 1:1 for Hg^{2+} complexes in the organic phase, and 1:1, 1:2 or higher stoichiometries for Ag^+ complexes; $c_M = 1 \cdot 10^{-4}$ M; $c_{HPic} = 5 \cdot 10^{-3}$ M; pH = 5.2; $c_L = 5 \cdot 10^{-4} - 5 \cdot 10^{-3}$ M/$CHCl_3$

Table 1. Selected extraction constants for the calixarenes **4a−c**

Compound	**4a**	**4b**	**4c**
Ag^+	$\log K_{ex1} = 3.31$ $\log K_{ex2} = 6.29$	$\log K_{ex1} = 3.98$ $\log K_{ex2} = 6.76$	/
Hg^{2+}	/	$\log K_{ex1} = 2.94$	$\log K_{ex1} = 3.95$
Ba^{2+}	/	$\log K_{ex1} = 2.88$ $\log K_{ex2} = 5.84$	/
Tl^+	/	$\log K_{ex1} = 3.99$	/
Eu^{3+}	/	$\log K_{ex1} = 3.13$ $\log K_{ex2} = 5.15$	

properties of the new potential ionophores by liquid-liquid extraction of picrate salts revealed poor to moderate extraction of mainly silver(I) salts, in which the calix[8]arene derivative **4c** shows the largest extraction ability. For calixarenes bearing secondary amides on the lower rim efficient extraction of alkaline earth cations has been reported, and a little of this characteristic remains in compounds **4b** and **4c**. However, the affinity of calixareneacetates towards alkali cations[2a,8] is completely lost in **4**, where the ester is placed further away from the calixarene core and separated from it by an amide group. The ability of *para-tert*-butylcalixareneglycine ester acetamides **4** to bind Ag^+ ions is clearly surpassed by calixarene-*tert*-amides,[8] and in particular, -*tert*-thioamides.[23] In conclusion, calix[6]- and calix[8]areneglycine acetamides **4b** and **4c** show some affinity in metal ion extraction, but their efficiency and selectivity is inferior to other known calixarene ionophores.

Experimental Section

General Remarks: Melting points were taken with a hot-plate microscope apparatus and are not corrected. − NMR spectra were recorded at 400 MHz (^{1}H) and 100 MHz (^{13}C) in [D]chloroform solutions unless otherwise stated. The multiplicity of the ^{13}C signals was determined with the DEPT technique and quoted as: (+) for CH_3 or CH, (−) for CH_2 and (C_{quat}) for quaternary carbon atoms. CC means column chromatography on silica gel unless otherwise stated. PE means petroleum ether with a boiling range of 60−70°C, EA means ethyl acetate.

Determination of Metal-Ion Binding Properties by Liquid-Liquid Extraction: All extractions were performed at 25°C in agitated microreactors (2 cm^3). To reach the equilibrium of distribution the organic and aqueous phase of equal volumes were shaken for 30 min for all investigated metal ions. Only in the case of palladium was 2 h of shaking necessary to reach the equilibrium. The phases were separated, centrifuged and the concentration of metal ions in both phases was determined by the emission of the radionuclides which were used. The γ-radiation (^{203}Hg, ^{133}Ba, ^{110m}Ag, ^{109}Pd, ^{65}Zn, ^{64}Cu, ^{22}Na) was measured with an NaI(Tl) scintillation counter (Cobra II, Canberra Packard) and β-emission (^{204}Tl) was determined with a liquid scintillation counter (Tricarb 2500, Canberra Packard).

Calix[4]arene 4a: To a solution of the acyl chloride **5a** (0.24 g, 0.25 mmol) in 10 mL of CH_2Cl_2 was added glycine ethyl ester (**6**; 0.31 g, 3.0 mmol) in 10 mL of CH_2Cl_2 at 0°C, the reaction mixture was stirred at room temp. for 16 h, washed with saturated aqueous NH_4Cl solution, dried with $MgSO_4$ and the solvent was removed in vacuo. CC (Et_2O/EA, 5:1; R_f = 0.49) of the crude product gave 0.24 g (79%) of **4a** as a white solid, m.p. 230°C. − IR (KBr): $\tilde{\nu}$ = 3380 cm^{-1}, 1750, 1680, 1190. − UV/Vis (CH_3CN): λ_{max} (lg ε) = 194 nm (5.046), 216 (4.796). − ^{1}H NMR: δ = 7.92 (t, ^3J = 5.7 Hz, 4 H), 6.83 (s, 8 H), 4.58 (s, 8 H), 4.56 (d, ^2J = 13.9 Hz, 4 H), 4.19 (q, ^3J = 7.1 Hz, 8 H), 4.12 (s, 8 H), 3.31 (d, ^2J = 13.0 Hz, 4 H), 1.28 (t, ^3J = 7.1 Hz, 12 H), 1.09 (s, 36 H). − ^{13}C NMR: δ = 170.3 (C_{quat}), 170.1 (C_{quat}), 152.5 (C_{quat}), 146.1 (C_{quat}), 132.6 (C_{quat}), 125.9 (+), 74.1 (−), 61.2 (−), 41.0 (−), 33.9 (C_{quat}), 31.3 (+), 31.1 (−), 14.1 (+). − MS (MALDI-TOF); *m/z* (%): 1244.4 (100) [M + Na]$^+$. − C68H92N4O16·H2O (1239.5): calcd. C 65.89, H 7.64, N 4.52; found C 66.25, H 7.78, N 4.20.

Calix[6]arene 4b: To a solution of the acyl chloride **5b** (1.4 g, 1.0 mmol) in 30 mL of CH_2Cl_2 was added at 0°C glycine ethyl ester (**6**; 1.9 g, 18 mmol) in 30 mL of CH_2Cl_2; the mixture was stirred for 16 h at room temp. and was worked up as described for compound **4a**. The crude product was recrystallized from ethyl acetate (5 mL) and petroleum ether (30 mL) at −20°C overnight to yield 1.26 g (69%) of **4b** (R_f = 0.38 in Et_2O/EA, 5:1) as a white solid, m.p. 116−118°C. − IR (KBr): $\tilde{\nu}$ = 3410 cm^{-1}, 1750, 1680, 1190. − UV/Vis (CH_3CN): λ_{max} (lg ε) = 196 nm (5.264), 218 (4.995). − MS (MALDI-TOF); *m/z* (%): 1854.0 (100) [M + Na]$^+$. − $C_{102}H_{138}N_6O_{24}$ (1832.2): calcd. C 66.85, H 7.60, N 4.59; found C 66.53, H 7.66, N 4.29.

Calix[8]arene 4c: To a solution of the acyl chloride **5c** (1.4 g, 0.73 mmol) in 30 mL of CH_2Cl_2 was added at 0°C glycine ethyl ester (**6**; 1.9 g, 18 mmol), dissolved in 30 mL of CH_2Cl_2; the reaction mixture was stirred for 16 h at room temp. and worked up as described for **4c**. The crude product was recrystallized from CH_2Cl_2 (5 mL) and *n*-heptane (30 mL) at −20°C overnight to give 1.06 g (59%) of **4c** (R_f = 0.27 in Et_2O/EA, 5:1) as a white solid, m.p. 224−226°C. − IR (KBr): $\tilde{\nu}$ = 3430 cm^{-1}, 1750, 1690, 1200. − UV/Vis (CH_3CN): λ_{max} (lg ε) = 196 nm (5.366), 222 (5.075). − ^{1}H NMR: δ = 7.92 (t, ^3J = 5.7 Hz, 4 H), 6.83 (s, 8 H), 4.58 (s, 8 H), 4.56 (d, ^2J = 13.9 Hz, 4 H), 4.19 (q, ^3J = 7.1 Hz, 8 H), 4.12 (s, 8 H), 3.31 (d, ^2J = 13.0 Hz, 4 H), 1.28 (t, ^3J = 7.1 Hz, 12 H), 1.09 (s, 36 H). − ^{13}C NMR: δ = 169.9 (C_{quat}), 169.0 (C_{quat}), 151.9 (C_{quat}), 147.0 (C_{quat}), 132.0 (C_{quat}), 125.9 (+), 71.4 (−), 61.2 (−), 40.7 (−), 34.2 (C_{quat}), 31.3 (+), 31.2 (−), 14.0 (+). − MS (MALDI-TOF); *m/z* (%): 2466.1 (100) [M + Na]$^+$. − $C_{136}H_{184}N_8O_{32}$·H_2O (2461.0): calcd. C 66.38, H 7.62, N 4.55; found C 66.19, H 7.73, N 4.35.

Calix[4]arene 9: A mixture of methyl 1-methyl-4-nitropyrrole-2-carboxylate (0.5 g, 2.7 mmol) and Pd/C (0.15 g) in 200 mL of ethyl acetate and 100 mL of methanol was hydrogenated at an H_2 pressure of 4 bar for 16 h at room temp., the catalyst was removed by filtration and the solvent was removed in vacuo. The resulting amino acid **7** was dissolved in 30 mL of CH_2Cl_2, triethyl amine (2 mL, 14 mmol) and the acyl chloride **5a** (0.5 g, 0.52 mmol) were added at 0°C, the reaction mixture was stirred for 16 h at room temp., washed with saturated aqueous NH_4Cl solution, dried with Na_2SO_4 and the solvent was removed in vacuo. CC (CH_2Cl_2/MeOH, 97:3, R_f = 0.33) of the crude product gave 0.66 g (89%) of **9** as a white solid. − IR (KBr): $\tilde{\nu}$ = 3310 cm^{-1}, 1710, 1690, 1450, 1200. − UV/Vis (CH_3CN): λ_{max} (lg ε) = 204 nm (5.016), 228 (4.978), 284 (4.525). − ^{1}H NMR: δ = 9.56 (s, 4 H), 7.32 (d, ^4J = 1.9 Hz, 4 H), 6.85 (d, ^4J = 1.9 Hz, 4 H), 6.79 (s, 8 H), 4.57 (s, 8 H), 4.52 (d, ^2J = 12.9 Hz, 4 H), 3.75 (s, 12 H), 3.71 (s, 12 H), 3.23 (d, ^2J = 13.1 Hz, 4 H), 1.07 (s, 36 H). − ^{13}C NMR: δ = 167.4 (C_{quat}), 161.4 (C_{quat}), 153.4 (C_{quat}), 145.7 (C_{quat}), 132.8 (C_{quat}), 125.8 (+), 121.7 (+), 121.1 (C_{quat}), 119.8 (C_{quat}), 109.0 (+), 74.8 (−), 50.9 (+), 36.5 (+), 33.8 (C_{quart}), 31.4 (−), 31.3 (+). − MS (ESI); *m/z* (%): 1448.4 (90) [M + Na]$^+$, 732.4 (100) [M + K]$^{2+}$.

Calix[4]arene 10: A solution of ethyl 1-methyl-4-nitroimidazol-2-carboxylate (0.5 g, 2.5 mmol) in 200 mL of ethyl acetate and 100 mL of methanol was hydrogenated for 16 h at room temp. on Pd/C (0.15 g) at an H_2 pressure of 4 bar. The catalyst was removed by filtration, the solvent was distilled off in vacuo, CH_2Cl_2 (30 mL) and triethylamine (2 mL, 14 mmol) were added. The acyl chloride **5a** (0.5 g, 0.52 mmol) was added at 0°C, the reaction mixture was stirred for 16 h at room temp. and worked up as described for **9**. CC (CH_2Cl_2/MeOH, 97:3, R_f = 0.26) gave 70 mg (9%) of **10** as a solid. – ^{1}H NMR: δ = 9.91 (s, 4 H), 7.43 (s, 4 H), 6.75 (s, 8 H), 4.80 (s, 8 H), 4.58 (d, ^2J = 13.1 Hz, 4 H), 4.22 (q, ^3J = 7.1 Hz, 8 H), 3.85 (s, 12 H), 3.23 (d, ^2J = 13.3 Hz, 4 H), 1.22 (t, ^3J = 7.1 Hz, 12 H), 1.01 (s, 36 H). – ^{13}C NMR (100 MHz, $CDCl_3$): δ = 167.4 (C_{quat}), 158.8 (C_{quat}), 153.0 (C_{quat}), 145.6 (C_{quat}), 136.8 (C_{quat}), 132.7 (C_{quat}), 131.4 (C_{quat}), 129.3 (+), 125.7 (+), 74.7 (–), 61.1 (–), 35.8 (+), 33.8 (C_{quat}), 31.4 (–), 31.3 (+), 14.1 (+). – MS (ESI); *m/z* (%): 1507.6 (100) $[M + Na]^+$.

Calix[4]arene 11: To a solution of the acyl chloride **5a** (0.4 g, 0.42 mmol) and triethylamine (1.2 mL, 8.4 mmol) in 30 mL of CH_2Cl_2 was added benzylamine (0.2 mL, 1.8 mmol) at 0°C; the reaction mixture was stirred for 16 h at room temp. and worked up as described for **4a**. CC (CH_2Cl_2/MeOH, 49:1, R_f = 0.30) yielded 50 mg (10%) of **11** as a white solid, m.p. 277–278°C. – IR (KBr): $\tilde{\nu}$ = 3280 cm^{-1}, 1660, 1480, 1200. – UV/Vis (CH_3CN): λ_{max} (lg ε) = 194 nm (5.306), 202 (5.166), 276 (3.546). – ^{1}H NMR: δ = 7.81 (t, ^3J = 5.9 Hz, 4 H), 7.23 (m, 20 H), 6.75 (s, 8 H), 4.40 (m, 20 H), 3.14 (d, ^2J = 13.1 Hz, 4 H), 1.07 (s, 36 H). – ^{13}C NMR: δ = 169.5 (C_{quat}), 152.8 (C_{quat}), 145.8 (C_{quat}), 138.3 (C_{quat}), 132.6 (C_{quat}), 128.5 (+), 127.6 (+), 127.2 (+), 125.8 (+), 74.4 (–), 42.9 (–), 33.8 (C_{quat}), 31.4 (–), 31.3 (+). – MS (ESI); *m/z* (%): 1259.8 (100) $[M + Na]^+$, 1237.6 (40) $[M + H]^+$. – $C_{80}H_{92}N_4O_8$ (1236.7): calcd. C 77.64, H 7.49, N 4.53; found C 77.34, H 7.78, N 4.43.

Calix[4]arene 14: To a suspension of *para-tert*-butylcalix[4]arene (**12**; 0.5 g, 0.77 mmol) and Na_2CO_3 (0.5 g, 4.7 mmol) in 70 mL of acetone was added 2.7 g (4.6 mmol) of **13** and the reaction mixture was refluxed for 10 d. The solvent was removed, the solid residue was extracted with 20 mL of CH_2Cl_2 and the resulting suspension was filtered. The organic phase was washed with sat. aqueous NH_4Cl solution, dried with Na_2SO_4, and the solvent was removed in vacuo. CC (PE/EA, 20:1; R_f = 0.37) of the crude product yielded 0.68 g (57%) of **14**, as a white solid, m.p. 210°C. – IR (KBr): $\tilde{\nu}$ = 3430 cm^{-1}, 1730, 1470, 1170. – UV/Vis (CH_3CN): λ_{max} (lg ε) = 192 nm (5.553), 230 (4.006), 286 (3.618). – ^{1}H NMR: δ = 7.65 (s, 2 H), 7.03 (s, 4 H), 6.83 (s, 4 H), 5.34 (d, ^3J = 3.8 Hz, 2 H), 4.62 (m, 2 H), 4.24 (d, ^2J = 12.9 Hz, 4 H), 4.03 (t, ^3J = 5.9 Hz, 4 H), 3.31 (d, ^2J = 12.9 Hz, 4 H), 2.83 (t, ^3J = 7.2 Hz, 4 H), 1.67 (m, 60 H), 1.27 (s, 18 H), 1.00 (s, 6 H), 0.99 (s, 18 H), 0.92 (d, ^3J = 6.5 Hz, 6 H), 0.87 (d, ^3J = 6.6 Hz, 6 H), 0.86 (d, ^3J = 6.6 Hz, 6 H), 0.68 (s, 6 H). – ^{13}C NMR: δ = 172.7 (C_{quat}), 150.7 (C_{quat}), 149.5 (C_{quat}), 146.9 (C_{quat}), 141.3 (C_{quat}), 139.7 (C_{quat}), 132.7 (C_{quat}), 127.6 (C_{quat}), 125.5 (+), 125.1 (+), 122.5 (+), 75.1 (–), 74.0 (+), 56.7 (+), 56.1 (+), 50.0 (+), 42.3 (C_{quat}), 39.7 (–), 39.5 (–), 38.1 (–), 37.0 (–), 36.6 (C_{quat}), 36.2 (–), 35.8 (+), 33.9 (C_{quat}), 33.8 (C_{quat}), 31.9 (–), 31.8 (+), 31.7 (+), 31.0 (+), 28.2 (–), 28.0 (+), 27.7 (–), 25.5 (–), 24.3 (–), 23.8 (–), 22.8 (+), 22.5 (+), 21.0 (–), 19.3 (+), 18.7 (+), 11.8 (+). – MS (ESI); *m/z* (%): 1580.9 (55) $[M + Na]^+$, 524.2 (100). – $C_{106}H_{156}O_8$ (1558.4): calcd. C 81.70, H 10.09; found C 81.44, H 10.21.

Acknowledgments

This work was supported by the Deutsche Bundesstiftung Umwelt and the Fonds der Chemischen Industrie. T. F. thanks the ministry of education of Luxembourg, C. C. the DFG for a graduate scholarship.

[1] [1a] C. D. Gutsche, *Calixarenes*, Monographs in Supramolecular Chemistry (Ed.: J. F. Stoddart), The Royal Society of Chemistry, Cambridge, **1989**. – [1b] V. Böhmer, *Angew. Chem.* **1995**, *107*, 785–818; *Angew. Chem., Int. Ed. Engl.* **1995**, *34*, 713–746. – [1c] For recent examples, see: S. E. Bell, J. K. Browne, V. McKee, M. A. McKervey, J. F. Malone, M. O'Leary, A. Walker, *J. Org. Chem.* **1998**, *63*, 489–501. – [1d] A. F. D. De Namor, R. G. Hutcherson, F. J. S. Valarde, M. L. Zapata-Ormachea, L. E. P. Salazar, I. A. Jammaz, N. A. Rawi, *Pure Appl. Chem.* **1998**, *70*, 769–778 – [1e] A. F. Danil de Namor, R. M. Cleverley, M. L. Zapata-Ormachea, *Chem. Rev.* **1998**, *98*, 2495–2525.

[2] [2a] M. A. McKervey, M.-J. Schwing-Weill, F. Arnaud-Neu, in *Comprehensive Supramolecular Chemistry* (Eds.: J. L. Atwood, J. E. D. Davies, D. D. Macnicol, F. Vögtle, J.-M. Lehn, G. W. Gokel), Pergamon, Oxford, UK, **1996**, vol. 1, p. 537–603. – [2b] D. M. Roundhill, in *Progress in Organic Chemistry* (Ed.: K. D. Karlin), Wiley, New York, **1995**, vol. 43, p. 533–592. – [2c] C. Wieser, C. B. Dieleman, D. Matt, *Coord. Chem. Rev.* **1997**, *165*, 93–161. – [2d] A. Ikeda, S. Shinkai, *Chem. Rev.* **1997**, *97*, 1713–1734. – [2e] P. D. Beer, M. G. B. Drew, P. B. Leeson, M. I. Ogden, *J. Chem. Soc., Dalton Trans.* **1995**, 1273–1283.

[3] [3a] D. N. Reinhoudt, P. J. Dijkstra, P. J. A. in't Velt, K. E. Bugge, S. Harkema, R. Ungaro, E. Ghidini, *J. Am. Chem. Soc.* **1987**, *109*, 4761–4762. – [3b] P. J. Dijkstra, J. A. J. Brunink, K. E. Bugge, D. N. Reinhoudt, S. Harkema, R. Ungaro, F. Ugozzoli, E. Ghidini, *J. Am. Chem. Soc.* **1989**, *111*, 7567–7575. – [3c] E. Ghidini, F. Ugozzoli, R. Ungaro, S. Harkema, A. Abu El-Fade, D. N. Reinhoudt, *J. Am. Chem. Soc.* **1990**, *112*, 6979–6985.

[4] [4a] J. L. Atwood, S. G. Bott, in *Calixarenes, a Versatile Class of Macrocyclic Compounds* (Eds.: J. Vicens, V. Böhmer), Kluwer, Dordrecht, **1991**, p. 199–210. – [4b] R. Ungaro, A. Pochini, in *Calixarenes, a Versatile Class of Macrocyclic Compounds* (Eds.: J. Vicens, V. Böhmer), Kluwer, Dordrecht, **1991**, p. 127–147.

[5] [5a] F. Arnaud-Neu, E. M. Collins, M. Deasy, G. Ferguson, S. J. Harris, B. Kaitner, A. J. Lough, M. A. McKervey, E. Marques, B. L. Ruhl, M.-J. Schwing-Weill, E. M. Seward, *J. Am. Chem. Soc.* **1989**, *111*, 8681–8691. – [5b] G. Ferguson, B. Kaitner, M. A. McKervey, E. M. Seward, *J. Chem. Soc., Chem. Commun.* **1987**, 584–585.

[6] A. Arduini, E. Ghidini, A. Pochini, R. Ungaro, G. D. Andreetti, F. Ugozzoli, *J. Inclusion Phenom.* **1988**, *6*, 119.

[7] [7a] A. Arduini, A. Pochini, S. Reverberi, R. Ungaro, *J. Chem. Soc., Chem. Commun.* **1984**, 981–982. – [7b] F. Arnaud-Neu, G. Barrett, S. J. Harris, M. Owens, M. A. McKervey, P. Schwinté, *Inorg. Chem.* **1993**, 32–39.

[8] F. Arnaud-Neu, M.-J. Schwing-Weill, K. Ziat, S. Cremin, S. J. Harris, M. A. McKervey, *New J. Chem.* **1991**, *15*, 33–37.

[9] S. K. Chang, S. K. Kwon, I. Cho, *Chem. Lett.* **1987**, 947–948.

[10] K. Ohto, H. Yamaga, E. Murakami, K. Inoue, *Talanta* **1997**, *44*, 1123–1130.

[11] For a review of calixarenes with mixed ligating functional groups at different arene moieties, see: M.-J. Schwing-Weill, M. A. McKervey, in *Calixarenes, a Versatile Class of Macrocyclic Compounds* (Eds.: J. Vicens, V. Böhmer), Kluwer, Dordrecht, **1991**, p. 149–172.

[12] Tetra-*tert*-butyl ester: M. B. H. Grofe Gansey, W. Verboom, F. C. J. M. van Veggel, V. Vetrogon, F. Arnaud-Neu, M.-J. Schwing-Weill, D. N. Reinhoudt, *J. Chem. Soc., Perkin Trans. 2* **1998**, 2351–2360.

[13] F. Arnaud-Neu, G. Barrett, S. Cremin, M. Deasy, G. Ferguson, S. J. Harris, A. J. Lough, L. Guerra, M. A. McKervey, M.-J. Schwing-Weill, P. Schwinté *J. Chem. Soc., Perkin Trans. 2* **1992**, 1119–1125.

[14] D. Sahal, P. Balaram, *Biochemistry* **1986**, *25*, 6004–6013.

[15] E. E. Baird, P. B. Dervan *J. Am. Chem. Soc.* **1996**, *118*, 6141–6146.

[16] [16a] A. V. Bogatskii, A. I. Galatina, N. S. Novikova *J. Org. Chem. USSR (Engl. Transl.)* **1979**, *15*, 2333–2337. – [16b] N. Nakamura, T. Hanasaki, H. Onoi *Mol. Cryst. Liq. Cryst. Sci. Technol., Sect. A* **1993**, *225*, 269–278. – [16c] A. Arduini, A. Casnati in *Macrocycle Synthesis* (Ed.: D. Parker), Oxford University Press, Oxford **1996**, p. 156–158.

[17] In the case of $AgNO_3$ and $Cu(NO_3)_2$ a zwitterionic MES

(morpholine-4-ethanesulfonic acid)/NaOH buffer is used.
[18] [18a] K. Gloe; P. Mühl, *Isotopenpraxis* **1979**, *15*, 236−239. – [18b] K. Gloe; P. Mühl *Isotopenpraxis*, **1983**, *19*, 257−260. – [18c] M. Petrich, L. Beyer, K. Gloe, P. Mühl, *Anal. Chim. Acta* **1990**, *228*, 229−234. – [18d] F. Vögtle, S. Ibach, M. Nieger, C. Chartroux, T. Krüger, H. Stephan, K. Gloe, *Chem. Commun*. **1997**, 1809−1810. – [18e] J. Groß, G. Harder, F. Vögtle, H. Stephan, K. Gloe, *Angew. Chem*. **1995**, *107*, 523−526; *Angew. Chem. Int. Ed. Engl*. **1995**, *34*, 481−484. – [18f] H. Stephan, T. Krüger, K. Gloe, W. Hasse, B. Ahlers, K. Cammann, K. Rissanen, G. Brodesser, F. Vögtle, *Chem. Eur. J.* **1998**, *4*, 430−439.
[19] For a recent example of silver(I)-selective calixarenes, see: K. Kimura, K. Tatsumi, S. Yajima, S. Miyake, H. Sakamoto, M. Yokoyama, *Chem. Lett*. **1998**, 833−834.
[20]] A chiral derivative of **11** was previously reported by: N. Iki, F. Narumi, T. Suzuki, A. Sugawara, S. Miyano, *Chem. Lett.* **1998**, 1065−1066.
[21] An attempt to determine the location of Ag^+ binding to **4b** or **4c** by NMR spectrsocopy was not successful. Samples of both compounds in $CDCl_3$ or $[D_6]DMSO/CDCl_3$, 1:1, did not show any significant shifts in either proton or carbon resonances if treated with silver trifluoroacetate.
[22] H. Murakami, S. Shinkai, *J. Chem. Soc., Chem. Commun*. **1993**, 1533−1535.
[23] M.-J. Schwing-Weill, F. Arnaud-Neu, M. A. McKervey, *J. Phys. Org. Chem*. **1992**, *5*, 496−502.

Received March 2, 1999
[I99079]

Stanna-*closo*-dodecaborate: A Nucleophile in Transition Metal Chemistry

Lars Wesemann,*[a] Thiemo Marx,[a] Ulli Englert,[a] and Michael Ruck[b]

Keywords: Stannaborate cluster / Transition metal complexes / Tin / Coordination modes / Clusters / Boron

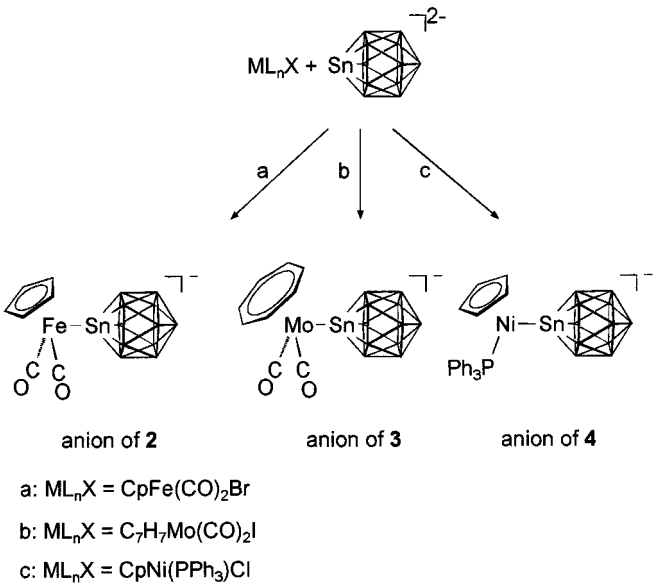
Reactions of the stannaborate salt $[NBu_4]_2[SnB_{11}H_{11}]$ (**1**) with the organometallic electrophiles $[CpFe(CO)_2Br]$, $[(C_7H_7)Mo(CO)_2I]$, and $[CpNi(PPh_3)Cl]$ resulted in substitution of the halide to give the stannaborate coordination products $[NBu_4][CpFe(CO)_2(SnB_{11}H_{11})]$ (**2**), $[NBu_4][(C_7H_7)Mo(CO)_2(SnB_{11}H_{11})]$ (**3**), and $[NBu_4][CpNi(PPh_3)(SnB_{11}H_{11})]$ (**4**) in high yields. Single crystals of the air- and moisture-stable products have been characterized by X-ray crystal structure analyses.

The incorporation of transition metals into the skeletons of boranes and heteroboranes has been extensively studied.[1] However, the direct coordination of a *closo* cluster at a transition metal centre has been realized in only a few cases.[2]

Recently, as part of a study on the chemistry of weakly coordinating anions, Strauss reported on the first structurally characterized example of a *closo*-monocarborane with an *exo* carbon−transition metal bond $\{[NBu_4]_2[CuCl(CB_{11}F_{11})]\}$.[3] The dianion $[CB_{11}F_{11}]^{2-}$ can be regarded as a new ligand in transition metal chemistry, offering the possibility of synthesizing complexes with zwitterionic structures incorporating weakly coordinating anions.

In our approach to this field, we set out to explore the synthetic potential of the *closo*-stannaborate dianion $[NBu_4]_2[SnB_{11}H_{11}]$ (**1**). This stannaborate was first synthesized by Todd starting from the readily accessible undecaborate cluster $[Me_3NH][B_{11}H_{14}]$.[4] Deprotonation with *n*-butyllithium and treatment with tin dichloride resulted in the formation of the *closo* cluster dianion **1**.

Although Todd has shown previously that the stannaborate reacts as a nucleophile with methyl iodide, the nucleophilic power of the dianion towards transition metal electrophiles has remained unexplored. In order to investigate the nucleophilicity of the cluster $[SnB_{11}H_{11}]^{2-}$, we studied its reaction with several transition metal halides. The stannaborate salt **1** was treated with $[CpFe(CO)_2Br]$, $[(C_7H_7)Mo(CO)_2I]$, and $[CpNi(PPh_3)Cl]$ in CH_2Cl_2. In all three cases the substitution product was straightforwardly obtained, in almost quantitative yield on the basis of ^{11}B-NMR spectroscopy. Besides the cluster coordination product, one equivalent of $[NBu_4]$[halide] was formed, which could be separated by extraction with water. The air- and moisture-stable transition metal complexes were crystallized by slow diffusion of hexane into a dichloromethane solution of the respective salt. Each transition metal complex was characterized by elemental analysis, NMR spectroscopy, and X-ray diffraction analysis of single crystals. In the ^{11}B-NMR spectrum of the cluster dianion **1** in solution, three signals in an intensity ratio of 1:5:5 for the eleven boron atoms indicate C_{5v} symmetry. The ^{11}B-NMR signals of the substitution products **2**, **3**, and **4** appear at higher field and the signals for the two B_5 groups are isochronic (Scheme 1). Thus, ^{11}B-NMR spectroscopy is an appropriate tool for monitoring the progress of the reactions. ^{119}Sn-NMR spectra were recorded in all three cases, although for the nickel derivative no resonance was observed. The ^{119}Sn-NMR spectra of **2** and **3** feature a single resonance at $\delta = -208$ ($W_{1/2} = 112$ Hz) and $\delta = -257$ ($W_{1/2} = 124$ Hz), respectively. The ^{119}Sn chemical shift depends on the oxidation state, the coordination number, and the solvent.[5] For the two oxidation states, the chemical shift ranges overlap markedly, thereby making impossible any assessment of the oxidation state on the basis of the observed chemical shifts. The measured chemical shifts can be compared with that of the methyl-substituted derivative $[MeSnB_{11}H_{11}]^-$ ($\delta = -196.5$).[4]



a: $ML_nX = CpFe(CO)_2Br$

b: $ML_nX = C_7H_7Mo(CO)_2I$

c: $ML_nX = CpNi(PPh_3)Cl$

Scheme 1. Syntheses of the organometallic stannaborate complexes

[a] Institut für Anorganische Chemie der Technischen Hochschule Aachen,
Prof.-Pirlet-Straße 1, D-52056 Aachen, Germany
E-mail: lars.wesemann@ac.rwth-aachen.de
[b] Institut für Anorganische Chemie, Universität Karlsruhe,
Engesserstraße, Geb. 30.45, D-76128 Karlsruhe, Germany

 © WILEY-VCH Verlag GmbH, D-69451 Weinheim, 1999 1434−1948/99/0909−1563 $ 17.50+.50/0

In each case, crystals suitable for X-ray diffraction analysis were obtained by slow diffusion of hexane into a dichloromethane solution of the respective salt. Views of the cluster anions of **2**, **3**, and **4** are depicted in Figures 1, 2, and 3, respectively. Selected interatomic lengths are listed in Table 1. In all three cases, the interatomic lengths between the cluster atoms indicate a close resemblance to the structure of $[MePPh_3][MeSnB_{11}H_{11}]$. The observed bond lengths between the tin atoms and the transition metal atoms [Fe−Sn 2.479(1) Å, Mo−Sn 2.711(1) Å, Ni−Sn 2.412(1) Å] fall within the ranges of known M−Sn lengths in related organometallic compounds [$CpFe(CO)_2SnBr_3$: Fe−Sn 2.462(2) Å, $CpFe(CO)_2SnCl_3$: Fe−Sn 2.467(2) Å, $CpFe(CO)_2SnPh_3$: Fe−Sn 2.536(2) Å],[6] [$(C_7H_7)Mo(CO)_2SnCl_3$: Mo−Sn 2.720(1) Å, $Cp_2Mo(Br)(SnBr_3)$: Mo−Sn 2.691(4) Å],[7] [$(CpNiPEt_3)_2SnCl_2$: Ni−Sn 2.468(1) Å, $(CpNiPEt_3)_3SnCl$: Ni−Sn 2.531(1) Å].[8]

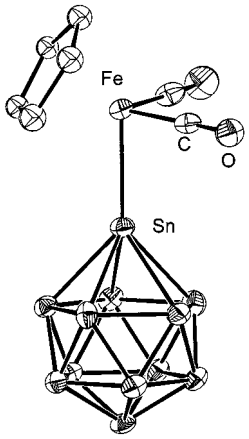


Figure 1. Molecular structure of the anion of **2**

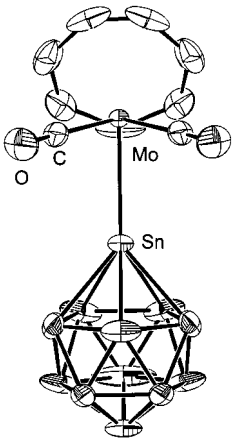


Figure 2. Molecular structure of the anion of **3**

The salts **2** and **4** crystallize in lattices built up of $[NBu_4]^+$ cations and $[L_nM(SnB_{11}H_{11})]^-$ anions. In the anion lattice, the charge-bearing stannaborates are directed towards the cation lattice.

In summary, the stannaborate cluster reacts as a nucleophile towards organometallic electrophiles and installs a negative charge in the complex, which is localized on the cluster atoms. The substitution products show remarkable stability towards air and moisture.

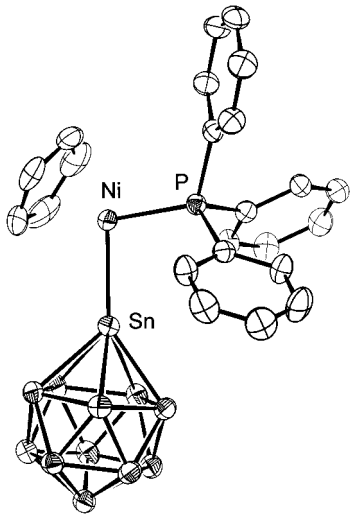


Figure 3. Molecular structure of the anion of **4** (the ellipsoids represent 50% probability)

Table 1. Selected interatomic distances [Å] in **2**, **3**, and **4**

	Fe	Mo	Ni
M−Sn	2.479(1)	2.711(1)	2.412(1)
Sn−B2	2.311(7)	2.266(9)	2.301(3)
Sn−B3	2.342(7)	2.266(9)	2.295(3)
Sn−B4	2.308(7)	2.30(1)	2.305(3)
Sn−B5	2.289(7)	2.30(1)	2.318(3)
Sn−B6	2.298(7)	2.32(1)	2.309(3)

Experimental Section

General: All manipulations were carried out under dry N_2 in Schlenk glassware. Solvents were dried and purified by standard methods and were stored under N_2. − NMR: Varian Unity 500 (^{1}H: 500 MHz, int. TMS; ^{13}C{^{1}H}: 126 MHz, int. TMS; ^{31}P: 202 MHz, ext. H_3PO_4; ^{11}B: 160 MHz, ext. $BF_3{\cdot}OEt_2$; ^{119}Sn: 186 MHz, ext. Me_4Sn). − MS: Finnigan MAT 95. − Elemental analysis: Institut für Anorganische Chemie RWTH Aachen, Carlo−Erba model 1106 elemental analyser.

$[NBu_4][CpFe(CO)_2SnB_{11}H_{11}]$ (2): A solution of 230 mg (257.1 g/mol, 0.89 mmol) of $CpFe(CO)_2Br$ in 10 mL CH_2Cl_2 was added at room temperature to a solution of 600 mg (733.8 g/mol, 0.82 mmol) of $[NBu_4]_2[SnB_{11}H_{11}]$ in 20 mL CH_2Cl_2. After stirring for 30 min, the solvent was evaporated in vacuo and the resulting brown waxy residue was stirred in 80 mL H_2O for 4 h. The remaining solid was filtered off, dried in vacuo, and crystallized from 20 mL CH_2Cl_2 by slow diffusion of hexane at +8°C to give 370 mg (67% yield) of **2** as orange-brown crystals. − ^{1}H{^{11}B} NMR (CD_2Cl_2): δ = 1.02 (t, 12 H, ^3J = 7.3 Hz, CH_2CH_3), 1.44 (m, 8 H, ^3J = 7.3 Hz, $CH_2CH_2CH_3$), 1.63 (m, 8 H, $CH_2CH_2CH_2$), 3.14 (m, 8 H, NCH_2CH_2), 5.32 (m, 5 H, C_5H_5). − ^{11}B{^{1}H} NMR (CD_2Cl_2): δ = −10.8 (s, B12), −15.1 (s, B2−6 and B7−11). − ^{13}C{^{1}H} NMR (CD_2Cl_2): δ = 12.7 (CH_2CH_3), 19.0 ($CH_2CH_2CH_3$), 23.2 ($CH_2CH_2CH_2$), 58.2 (NCH_2CH_2), 82.3 (C_5H_5), 210.4 (M−CO). − ^{119}Sn NMR (CD_2Cl_2): δ = −208.4. − MS (70 eV) SIMS; *m/z* (%):

248.0 (100) [M^- − $CpFe(CO)_2$]. − $C_{23}H_{52}B_{11}FeNO_2Sn$ (668.1): calcd. C 41.35, H 7.84, N 2.10; found C 41.11, H 7.93, N 1.93.

X-ray Crystallographic Study of 2: $C_{23}H_{52}B_{11}NO_2FeSn$; formula mass 668.13 g/mol; triclinic, space group $P\bar{1}$ (no. 2); a = 11.493(4), b = 11.852(6), c = 14.39(1) Å, α = 95.62(6), β = 90.55(6), γ = 120.44(3)°, V = 1678(2) Å^3, Z = 2, $d_{calcd.}$ = 1.322 g cm^{-3}, $\mu_{lin.}$ = 1.20 mm^{-1}. Enraf−Nonius CAD4 diffractometer; Mo-K_α radiation (λ = 0.71073 Å); graphite monochromator. Data collection at 203 K on a crystal of dimensions ca. 0.35 × 0.35 × 0.2 mm using ω scans in the range 2° ≤ θ ≤ 27° yielded 7197 reflections. The data were corrected for Lorentz and polarization effects, and an empirical absorption correction based on azimuthal scans[9] was applied. After merging symmetry equivalent data, 4856 unique observations with $I > 1.0\ \sigma(I)$ remained for structure solution[10] by Patterson and subsequent Fourier difference syntheses. Orientational disorder of the Cp ring was encountered. Least-squares refinement on structure factors[10] was performed with isotropic displacement parameters for the Cp carbon atoms, anisotropic displacement parameters for all other nonhydrogen atoms, and hydrogen atoms placed in calculated positions (C−H = 0.98 Å, B−H = 1.1 Å). Convergence was obtained for 349 variables, 4856 data, and R = 0.078, R_w = 0.068, GoF = 1.523. A final difference Fourier map showed fluctuations of less than 1.5 eÅ^{-3} close to the Sn atom.[11]

$[NBu_4][(C_7H_7)Mo(CO)_2SnB_{11}H_{11}]$ (3): A solution of 352 mg (371.0 g/mol, 0.95 mmol) of $(C_7H_7)Mo(CO)_2I$ in 10 mL CH_2Cl_2 was added to a solution of 696 mg (733.8 g/mol, 0.95 mmol) of $[NBu_4]_2[SnB_{11}H_{11}]$ in 20 mL CH_2Cl_2 at room temperature. After stirring for 30 min, the solvent was removed in vacuo and then the red waxy residue was treated with 80 mL H_2O for 4 h. The remaining dark-red solid was separated by filtration, dried in vacuo, and recrystallized from 20 mL CH_2Cl_2 by slow diffusion of hexane at +8°C to give 455 mg (65% yield) of **3** as dark-red needles. − $^1H\{^{11}B\}$ NMR (CD_2Cl_2): δ = 1.00 (t, 12 H, ^3J = 7.3 Hz, CH_2CH_3), 1.45 (m, 8 H, ^3J = 7.3 Hz, $CH_2CH_2CH_3$), 1.61 (m, 8 H, $CH_2CH_2CH_2$), 3.15 (m, 8 H, NCH_2CH_2), 5.73 (m, 7 H, C_7H_7). − $^{11}B\{^1H\}$ NMR (CD_2Cl_2): δ = −9.2 (s, B12), −14.4 (s, B2−6 and B7−11). − $^{13}C\{^1H\}$ NMR (CD_2Cl_2): δ = 13.8 (CH_2CH_3), 20.1 ($CH_2CH_2CH_3$), 24.3 ($CH_2CH_2CH_2$), 59.3 (NCH_2CH_2), 93.4 (C_7H_7), 215.1 (M−CO). − ^{119}Sn NMR (CD_2Cl_2): δ = −257.2. − $C_{25}H_{54}B_{11}MoNO_2Sn$ (735.3): calcd. C 40.89, H 7.41, N 1.91; found C 39.58, H 7.45, N 1.78.

X-ray Crystallographic Study of 3: $C_{25}H_{54}B_{11}MoNO_2Sn$; formula mass 734.27 g/mol; orthorhombic, space group *Pnma* (no. 62); a = 28.941(3), b = 10.684(4), c = 11.703(3) Å, V = 3619(2) Å^3, Z = 4, $d_{calcd.}$ = 1.348 g cm^{-3}, $\mu_{lin.}$ = 1.05 mm^{-1}. Enraf−Nonius CAD4 diffractometer; Mo-K_α radiation (λ = 0.71073 Å); graphite monochromator. Data collection at 293 K on a crystal of dimensions ca. 0.3 × 0.3 × 0.2 mm using ω-2θ scans in the diffraction range 3° < θ < 25° resulted in 13384 reflections. The data were corrected for Lorentz and polarization effects, and an empirical absorption correction based on azimuthal scans[9] was applied. After merging symmetry equivalent data, 3133 unique reflections remained for structure solution by direct methods.[12] The structure model was completed by Fourier difference synthesis: the cation was found to be disordered with respect to the crystallographic mirror plane. Tentative refinements in the noncentrosymmetric subgroup did not give satisfactory results and no Bijvoet differences could be detected, even though this subgroup should exhibit polarity. Least-squares refinement on structure factors[10] was performed with anisotropic displacement parameters for all nonhydrogen atoms except for the nitrogen atom in the cation close to the symmetry element. Hydrogen atoms were placed in calculated positions (C−H = 0.98 Å; B−H = 1.05 Å). Convergence was obtained for 266 variables, 2513 observed data with $I > 1.0\ \sigma(I)$ and R = 0.055, R_w = 0.055, GoF = 1.225. A final difference Fourier map showed fluctuations of less than 0.9 eÅ^{-3} close (0.8 Å) to B9.[11]

$[NBu_4][CpNi(PPh_3)SnB_{11}H_{11}]$ (4): A solution of 383 mg (421.6 g/mol, 0.91 mmol) of $CpNi(PPh_3)Cl$ in 10 mL CH_2Cl_2 was added at room temperature to a solution of 666 mg (733.8 g/mol, 0.91 mmol) of $[NBu_4]_2[SnB_{11}H_{11}]$ in 20 mL CH_2Cl_2. The reaction mixture was stirred for 30 min and then the solvent was evaporated in vacuo. The brown waxy residue was stirred in 80 mL H_2O. After filtration, the collected solid was dried and then recrystallized from 20 mL CH_2Cl_2 by slow diffusion of hexane at +8°C to give 574 mg (72% yield) of **4** as small golden-brown crystals. − $^1H\{^{11}B\}$ NMR (CD_2Cl_2): δ = 0.98 (t, 12 H, ^3J = 7.3 Hz, CH_2CH_3), 1.41 (m, 8 H, ^3J = 7.3 Hz, $CH_2CH_2CH_3$), 1.62 (m, 8 H, $CH_2CH_2CH_2$), 3.22 (m, 8 H, NCH_2CH_2), 5.32 (m, 5 H, C_5H_5), 7.50 (m, 5 H, C_6H_5). − $^{11}B\{^1H\}$ NMR (CD_2Cl_2): δ = −10.7 (s, B12), −15.2 (s, B2−6 and B7−11). − $^{13}C\{^1H\}$ NMR (CD_2Cl_2): δ = 14.0 (CH_2CH_3), 20.1 ($CH_2CH_2CH_3$), 24.3 ($CH_2CH_2CH_2$), 59.3 (NCH_2CH_2), 92.3 (C_5H_5), 128.7 (C_{meta}, C_{para}), 130.8 (C_{ortho}), δ = 134.2 (P−C). − ^{31}P NMR (CD_2Cl_2): δ = 42.3 (s, PPh_3). − $C_{40}H_{69}B_{11}Cl_2NNiPSn$ (877.3 + CH_2Cl_2): calcd. C 49.93, H 7.23, N 1.46, found C 48.55, H 7.26, N 1.35.

X-ray Crystallographic Study of 4: $C_{40}H_{69}B_{11}Cl_2NNiPSn$; formula mass 877.3 g/mol + CH_2Cl_2; monoclinic space group $P2_1/c$ (no. 14); a = 16.192(6), b = 15.000(8), c = 19.689(9) Å, α = 96.21(3)°, V = 4754(4) Å^3, Z = 4, $d_{calcd.}$ = 1.344 g cm^{-3}, $\mu_{lin.}$ = 1.10 mm^{-1}. Siemens/Stoe AED2 diffractometer; Mo-K_α radiation (λ = 0.71073 Å); graphite monochromator; data collection at 200(2) K on a single crystal of dimensions 0.2 × 0.3 × 0.6 mm, 1.5° ≤ θ ≤ 25°; 8106 independent reflections measured, 6634 "observed" [$I > 2\ \sigma(I)$]; Lorentz and polarization factors; structure solution by direct methods and difference Fourier synthesis,[13] F^2 refinement; anisotropic parameters for nonhydrogen atoms, CH_2Cl_2 disordered, hydrogen atoms placed in calculated positions (C−H = 0.98 Å; B−H = 1.12 Å). Convergence was obtained for 516 variables with wR_2 = 0.057, R_1 = 0.028, GoF = 1.031. Max./min residual density +1.12/−0.52 eÅ^{-3}.[14]

Acknowledgments

We wish to acknowledge the Deutsche Forschungsgemeinschaft and the Institut für Anorganische Chemie der TH Aachen for financial support.

[1] W. Siebert (Ed.), *Advances in Boron Chemistry*, Royal Society of Chemistry, Cambridge, **1997**.
[2] V. I. Bregadze, *Chem. Rev.* **1992**, *92*, 209−223; D. E. Hartwell, J. McMillan, C. B. Knobler, M. F. Hawthorne, *Inorg. Chem.* **1997**, *36*, 5951−5955.
[3] S. V. Ivanov, J. J. Rockwell, O. G. Polyakov, C. M. Gaudinski, O. P. Anderson, K. A. Solntsev, S. H. Strauss, *J. Am. Chem. Soc.* **1998**, *120*, 4224−4225.
[4] R. W. Chapman, J. G. Kester, K. Folting, W. E. Streib, L. J. Todd, *Inorg. Chem.* **1992**, *31*, 979−983.
[5] B. Wrackmeyer, *Ann. Rep. NMR Spectrosc.* **1985**, *16*, 73−186.
[6] P. T. Greene, R. F. Bryan, *J. Chem. Soc. A* **1970**, 1696−1702; G. A. Melson, P. F. Stokely, R. F. Bryan, *J. Chem. Soc. A* **1970**, 2247−2251.
[7] M. L. Ziegler, H.-E. Sasse, B. Nuber, *Z. Naturforsch., Teil B* **1975**, *30*, 22−25; T. S. Cameron, C. K. Prout, *J. Chem. Soc., Dalton Trans.* **1972**, 1447−1449.
[8] U. Denninger, J. J. Schneider, G. Wilke, R. Goddard, C. Krüger, *Inorg. Chim. Acta* **1993**, *213*, 129−140.

[9] A. C. T. North, D. C. Phillips, F. S. Mathews, *Acta Crystallogr.* **1968**, *A24*, 351−359.
[10] Enraf−Nonius SDP Version 5.0, Delft, The Netherlands, **1989**.
[11] Crystallographic data (excluding structure factors) for the structures of **2** and **3** reported in this paper have been deposited with the Cambridge Crystallographic Data Centre as supplementary publication nos. CCDC-116068 (**2**) and -116069 (**3**). Copies of the data can be obtained free of charge on application to CCDC, 12 Union Road, Cambridge CB2 1EZ, U.K. [Fax: (internat.) + 44-1223/336033; E-mail: deposit@ccdc.cam.ac.uk].
[12] G. M. Sheldrick, *SHELXS-86, Program for Structure Solution*, University of Göttingen, Göttingen, Germany, **1986**.
[13] G. M. Sheldrick, *SHELX-97, Program for Crystal Structure Determination*, University of Göttingen, Göttingen, Germany, **1997**.
[14] Crystallographic data (excluding structure factors) for the structure **4** reported in this paper have been deposited with the Cambridge Crystallographic Data Centre as supplementary publication no. CCDC-115869. Copies of the data can be obtained free of charge from the address given in ref.[11]

Received March 18, 1999
[I99089]

Chemistry of 2*H*-Azaphosphirene Complexes, 16[+]

Syntheses, Structures, and Reactions of *C*-Methoxycarbonyl-Functionalized Small- and Medium-Sized P-Heterocycle Complexes

Rainer Streubel,*[a] Hendrik Wilkens,[a] Udo Rohde,[a] Annette Ostrowski,[a] Jörg Jeske,[a] Frank Ruthe,[a] and Peter G. Jones[a]

Dedicated to Professor Reinhard Schmutzler on the occasion of his 65th birthday

Keywords: Phosphorus heterocycles / 2*H*-Azaphosphirene complexes / Water-soluble P ligands / Tungsten / Cyclizations

Thermal ring-opening of [{2-bis(trimethylsilyl)methyl-3-phenyl-2*H*-azaphosphirene-κ*P*}pentacarbonyltungsten(0)] (**8a**) in the presence of dimethyl acetylenedicarboxylate (DMAD) led to the 2,3-bifunctionalized 1*H*-phosphirene complex **9a** and the 4-phenyl-substituted 2*H*-1,2-azaphosphole complex **10a**, the latter as a by-product. If a small amount of benzonitrile was added, complex **10a** was obtained as the main product, along with a small amount of the decomplexed 2*H*-1,2-azaphosphole **11**, which could not be isolated. Reaction of complex **10a** with elemental sulfur furnished the corresponding P^V sulfide **13**. When the ring-opening of complex **8a** was performed in the presence of two equivalents of DMAD and two equivalents of dimethyl cyanamide, we obtained the 4-dimethylamino-substituted 2*H*-1,2-azaphosphole complex **10b**, together with the diastereomeric Δ^3-1,3,2-oxazaphospholene complexes **14a**,**b**. On reaction of [{2-pentamethylcyclopentadienyl-3-phenyl-2*H*-azaphosphirene-κ*P*}pentacarbonyltungsten(0)] (**8b**) and DMAD in toluene, the corresponding 1*H*-phosphirene complex **9b** was only formed as a transient species and the *P*-coordinated P,C-cage compound **15** was the final product. Using benzonitrile as solvent, the 4-phenyl-substituted 2*H*-1,2-azaphosphole complex **10c** was obtained, together with the 7-aza-1-phosphanorbornadiene complex **16**, the latter through partial decomposition of **10c** coupled with rearrangement and a Diels–Alder reaction; the ratio **10c/16** was found to depend strongly on the molar ratio of complex **8b** to DMAD. A cycloaddition reaction of the 2,3-bifunctionalized 1*H*-phosphirene complex **9a** with 2,3-dimethylbutadiene furnished the bicyclic phosphirane complex **19**, along with a small amount of the noncoordinated bicyclic phosphirane **20**. Reaction of complex **9a** with diethylamine yielded the phosphirane complex **21** as a 1,2-addition product, the diorganophosphane complex **22** through ring-opening of **9a**, and the 3,4-functionalized 1,2-dihydro-1-phosphet-2-one complex **23** through an unprecedented ring-expansion reaction; the products **21**, **22**, **23** were formed in a ratio of ca. 1:1:1. The structures of the 1*H*-phosphirene complex **9a**, the 4-dimethylamino-substituted 2*H*-1,2-azaphosphole complex **10b**, the bicyclic phosphirane complex **19**, the phosphirane complex **21**, and the 1,2-dihydro-1-phosphet-2-one complex **23** have been determined by single-crystal X-ray diffraction analysis.

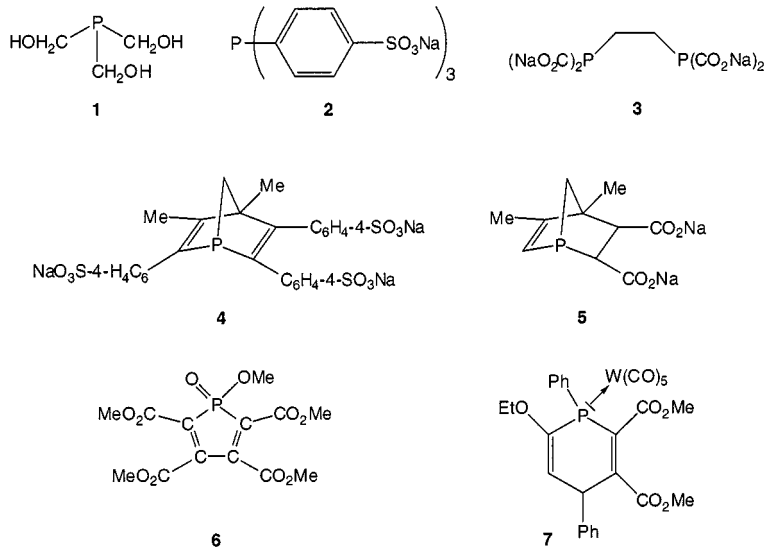
Introduction

The success of biphasic homogeneous catalytic reactions currently being achieved[2] using transition metals with triorganophosphane ligands has led to a great demand for ligands with enhanced water solubility.[3] Various concepts have been developed to satisfy this prerequisite, e.g. phosphanes bearing hydroxy-functionalized organic substituents such as the well-known tris(hydroxymethyl)phosphane **1**,[4] phosphanes bearing sodium *p*-phenylsulfonate groups as in triphenylphosphane trisodium sulfonate (TPPTS) **2**,[5] or sodium carboxylate groups as in **3**.[6] Moreover, water-soluble derivatives of P-heterocycles such as the 1-phosphanorbornadiene NORBOS **4**[7] have been successfully employed in catalytic processes, while others, such as the 1-phosphanorbornene **5**, seem likely to follow suit.[8] Apart from a very recent report on the catalytic use of complexes with polycyclic phosphane ligands having a phosphirane subunit,[9] knowledge of applications of small- and medium-sized P-heterocycle complexes as catalysts is still very limited. Equally apparent is the fact that unsaturated P^{III} heterocycles of different ring size with one or more *C*-methoxycarbonyl groups attached to the ring system are accessible only with difficulty,[10] although such systems are promising precursors for the respective carboxylic acid derivatives. This is in contrast to the situation for P^V phospholes such as **6**, which is accessible by reaction of trimethyl phosphite with dimethyl acetylenedicarboxylate (DMAD).[11] Unfortunately, the corresponding P^{III} derivative is still unknown. Apart from reactions of triorgano-

[+] Part 15: Ref.[1]

[a] Institut für Anorganische und Analytische Chemie der Technischen Universität Braunschweig,
Postfach 3329, D-38023 Braunschweig, Germany
Fax: (internat.) + 49-(0)531/391-5387
E-mail: r.streubel@tu-bs.de

 © WILEY-VCH Verlag GmbH, D-69451 Weinheim, 1999 1434–1948/99/0909–1567 $ 17.50+.50/0



Scheme 1. Water-soluble phosphanes (**1**−**5**) and phosphorus heterocycles bearing methoxycarbonyl groups (**6**,**7**)

phosphanes with DMAD, which are often unselective,[12] some more useful reactions exist, relying on DMAD as trapping reagent and leading, e.g., to complexes such as **7** with six-membered P^{III} heterocyclic ring systems.[13]

In view of the aforementioned factors, and bearing in mind that ring size variations could be a valuable additional instrument for tuning the attributes of the ligands, we decided to seek new routes to small- and medium-sized P-heterocycle complexes having *C*-methoxycarbonyl groups attached to the ring system. These, in turn, could give rise to the uncoordinated P-heterocycles by applying standard decomplexing methodologies.

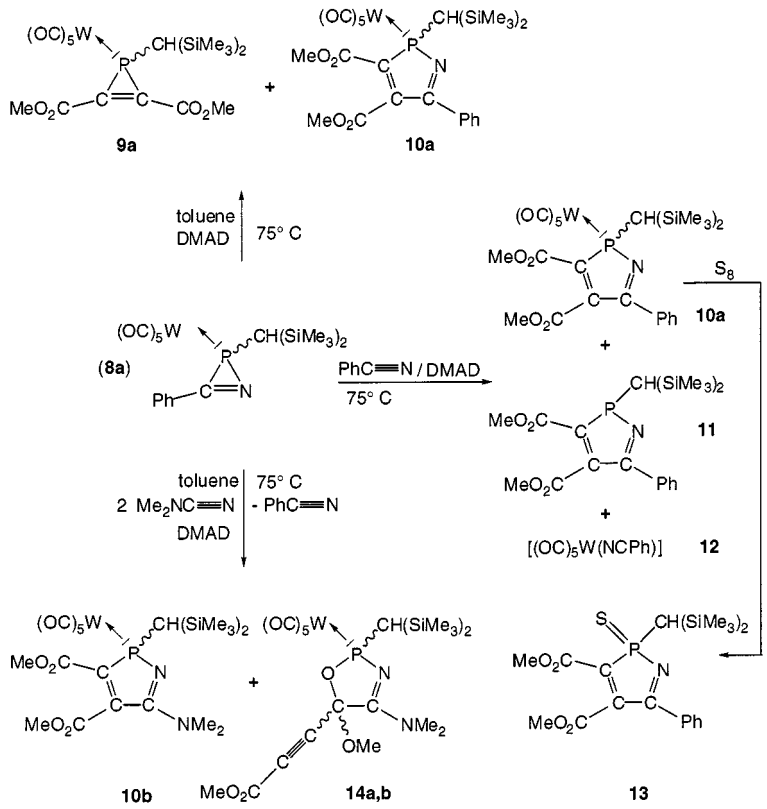
Recently, we demonstrated that ring-opening reactions of 2*H*-azaphosphirene complexes offer access to a wide variety of small- and medium-sized P-heterocycle complexes.[14−16] We also briefly reported on the syntheses of mono-,[17][18] bi-, and polycyclic P-heterocycles[1] with *C*-methoxycarbonyl-functionalized ring systems, using this methodology with dimethyl acetylenedicarboxylate (DMAD) as the trapping reagent.

In this paper, we show that the general reaction course to such *C*-methoxycarbonyl-functionalized heterocycle complexes depends largely on the solvent employed, and that the formation of the final products depends on the phosphorus substituent. Additionally, preliminary investigations of the reactivity of a 2,3-bifunctionalized 1*H*-phosphirene complex towards 2,3-dimethylbutadiene and diethylamine are presented. The latter reaction demonstrates how initial nucleophilic attack on the 1*H*-phosphirene ring system can give rise to three different reaction pathways, namely 1,2-addition to the C,C-double bond, ring-opening, and ring-expansion. The latter represents the first access to a ring-functionalized 1,2-dihydro-1-phosphet-2-one complex.

Results

A. Syntheses of *C*-Methoxycarbonyl-Functionalized Mono-, Bi-, and Polycyclic P-Heterocycles by Ring Opening of 2*H*-Azaphosphirene Complexes and Subsequent Trapping Reactions with DMAD

Apart from P^{V} phosphole derivatives such as **6**[11] and related compounds,[12] little is known about five-membered unsaturated P-heterocycles with one or more carboxylate groups bonded to the ring system.[13] Therefore, we became interested in developing a new synthetic methodology leading to such heterocycles. As we have already described in brief, thermally induced ring-opening of the 2*H*-azaphosphirene complex **8a**[19] in toluene and in the presence of DMAD leads to the 1*H*-phosphirene complex **9a** along with minor amounts of the 2*H*-1,2-azaphosphole complex **10a**.[17,18a] The yield of complex **10a** is significantly increased if the reaction is carried out in a mixture of toluene and benzonitrile. Under these reaction conditions, complex **10a** undergoes partial decomplexation leading to the benzonitrile−tungsten complex **12** and two other uncharacterized products exhibiting ^{31}P-NMR resonances at $\delta = 85.5$ and $\delta = 42.1$. Because of the $\Delta\delta$ value of the order of 25,[20] the former resonance would seem to be indicative of the 2*H*-1,2-azaphosphole **11**. Upon heating in benzonitrile with elemental sulfur, complex **10a** reacted selectively to give the 2*H*-1,2-azaphosphole *P*-sulfide **13**. When **8a** was heated in toluene in the presence of DMAD and two equivalents of dimethyl cyanamide, the reaction course was significantly altered; under these conditions the 2*H*-1,2-azaphosphole complex **10b**, along with the two diastereomeric Δ^3-1,3,2-oxazaphospholene complexes **14a**, **b** were formed.[18b] In this case, the transient formation of the nitrilium betaine-type complex



Scheme 2. Thermal ring-opening of 2*H*-azaphosphirene tungsten complex **8a** under various conditions in the presence of DMAD

$\{Me_2NCNP[CH(SiMe_3)_2]W(CO)_5\}$ via transylidation of **17a** seems to be operative (cf. Scheme 4).

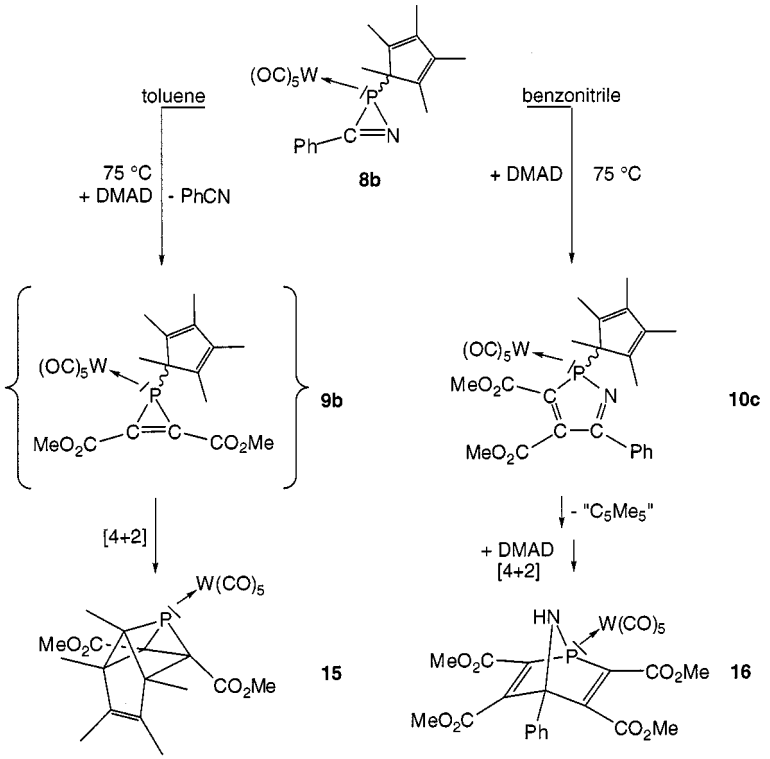
That the reaction course depends not only on the solvent, but also on the phosphorus substituent, was impressively demonstrated by investigations of the ring-opening of the 2*H*-azaphosphirene complex **8b**[20] in toluene and benzonitrile, both with DMAD as the trapping reagent (Scheme 3). In the first case, complex **15** was obtained as final product, whereas in the second case, the 7-aza-1-phosphanorbornadiene complex **16** was obtained.[1] The thermal instabilities of the transiently formed 1*H*-phosphirene complex **9b** and the 2*H*-1,2-azaphosphole complex **10c** were quite unexpected. Whereas the existence of the former is merely a plausible assumption, complex **10c** could be obtained using a different stoichiometry.

An explanation of these reaction pathways should take into account the roles of $[PhCNP(C_5Me_5)W(CO)_5]$ (**17c**) and the terminal phosphanediyl complex $[(OC)_5WPC_5Me_5]$ (**18b**) as intermediates (cf. Scheme 4). The fate of such intermediates seems to depend mainly on the solvent used for the reactions. The 1*H*-phosphirene complex **9b**, formed by [2+1] cycloaddition of **18b** to DMAD, undergoes rapid intramolecular [4+2] cycloaddition leading to the tungsten-coordinated P,C-cage compound **15**. In benzonitrile, complex **17b** reacts with the C,C π-system of DMAD to form the 2*H*-1,2-azaphosphole complex **10c** through a [3+2] cycloaddition. The next step could be an exocyclic P−C bond cleavage in complex **10c** with subsequent proton addition (the origin of which is still under investigation), to give a short-lived 1*H*-1,2-azaphosphole complex. This could then undergo rapid [4+2] cycloaddition with a second equivalent of DMAD, thereby yielding the 7-aza-1-phosphanorbornadiene complex **16**. Such a hypothesis of the intermediacy of a short-lived 1*H*-1,2-azaphosphole complex is further supported by an earlier observation by Mathey and co-workers that transiently formed 2*H*-phospholes undergo rapid [4+2] cycloaddition reactions leading to 1-phosphanorbornadienes[22] or 1-phosphanorbornenes[23] depending on the trapping reagent used.

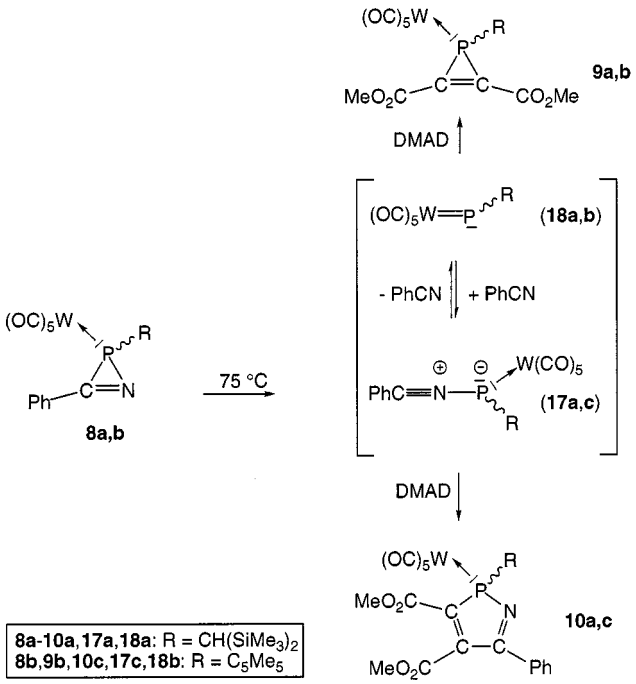
The main aspects of the aforementioned ring-opening reactions can be summarized as shown in Scheme 4. In all cases, the first step seems to be the transient formation of nitrilium phosphane−ylide complexes **17a**, **c**, which can decompose to give benzonitrile and the terminal phosphanediyl complexes **18a**, **b**. In toluene, complexes **18a**, **b** undergo subsequent [2+1] cycloaddition reactions to give complexes **9a**,**b**. In benzonitrile, however, reversion to the nitrilium phosphane−ylide complexes **17a**, **c** occurs preferentially, which show a tendency to undergo [3+2] cycloaddition reactions leading to the formation of 2*H*-1,2-azaphosphole complexes **10a**, **c**.

B. Cycloaddition, 1,2-Addition, Ring-Opening, and Ring-Expansion Reactions of *C*,*C*′-Methylcarboxylate-Functionalized 1*H*-Phosphirene Complex 9a

It has been demonstrated by Mathey and co-workers that a monofunctionalized *C*-carboxylate 1*H*-phosphirene com-



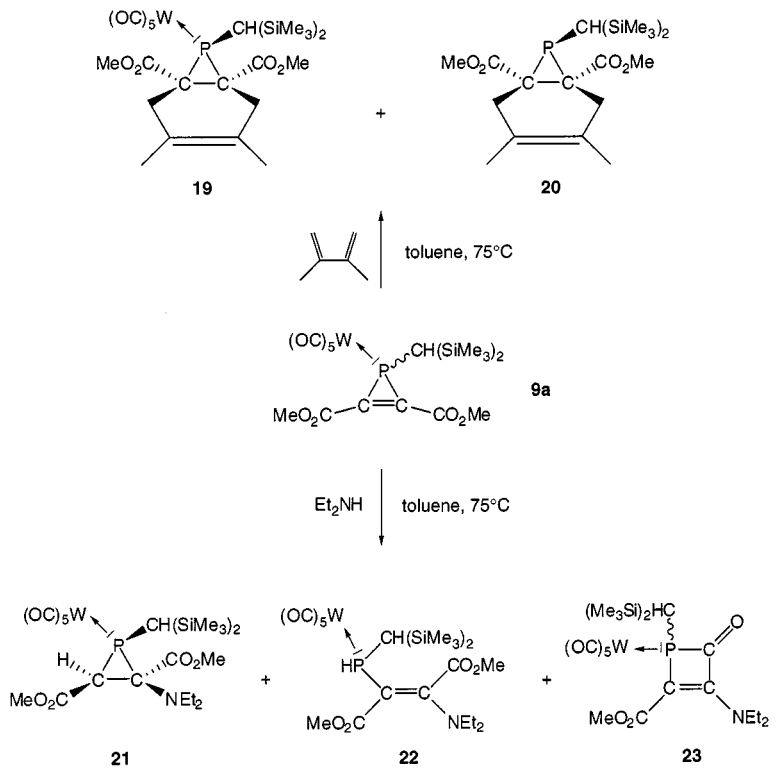
Scheme 3. Thermal ring-opening of 2*H*-azaphosphirene tungsten complex **8b** in various solvents in the presence of DMAD



Scheme 4. Proposed explanation for the generation and reactions of transiently formed nitrilium phosphane−ylide complexes

plex may react either with 1,3-dimethylbutadiene to give a bicyclic phosphirane complex through [4+2] cycloaddition, or with a secondary amine such as morpholine to yield a secondary vinylphosphane complex through ring-opening of the phosphirane ring.[24] These observations prompted us to investigate the reactivity of the bifunctionalized 1*H*-phosphirene complex **9a** towards 1,3-dimethylbutadiene and diethylamine. At 75°C, complex **9a** underwent a diastereoselective reaction with 1,3-dimethylbutadiene to give the [4+2] cycloadduct **19** together with a small amount of the bicyclic phosphirane **20**, the latter probably arising from partial decomplexation of complex **19** (Scheme 5). In both compounds, the six-membered ring moiety and the bis(trimethylsilyl)methyl substituent reside on the same side of the phosphirane ring plane, implying that the cycloaddition reaction is sterically controlled. In contrast to this relatively unsurprising reaction, the outcome of the reaction of complex **9a** with diethylamine at ambient temperature was unexpected: three phosphorus-containing products in a ratio of ca. 1:1:1 were formed, namely the 1,2-addition product **21**, the secondary vinylphosphane complex **22**, and the 1,2-dihydro-1-phosphet-2-one complex **23** (Scheme 5). In comparison to the other example mentioned above (PR = PPh),[24] the greater steric demand of the substituent at phosphorus in this case seems to increase the lifetime of the various intermediates, thus making possible three competing reaction pathways. Although the first 1,2-dihydro-1-phosphet-2-one complex[25] was also obtained by means of an insertion reaction (of carbon monoxide), the present example represents an unprecedented ring-expansion reaction in 1*H*-phosphirene chemistry.[26] A related ring-expansion has been reported for the reaction of a cyclopropene carboxylic acid derivative with $SOCl_2$.[27]

This reaction of complex **9a** can be rationalized by assuming the initial step to be a nucleophilic attack of the diethylamine nitrogen lone-pair on one carbon atom of the 1*H*-phosphirene ring, leading to the zwitterionic phosphir-



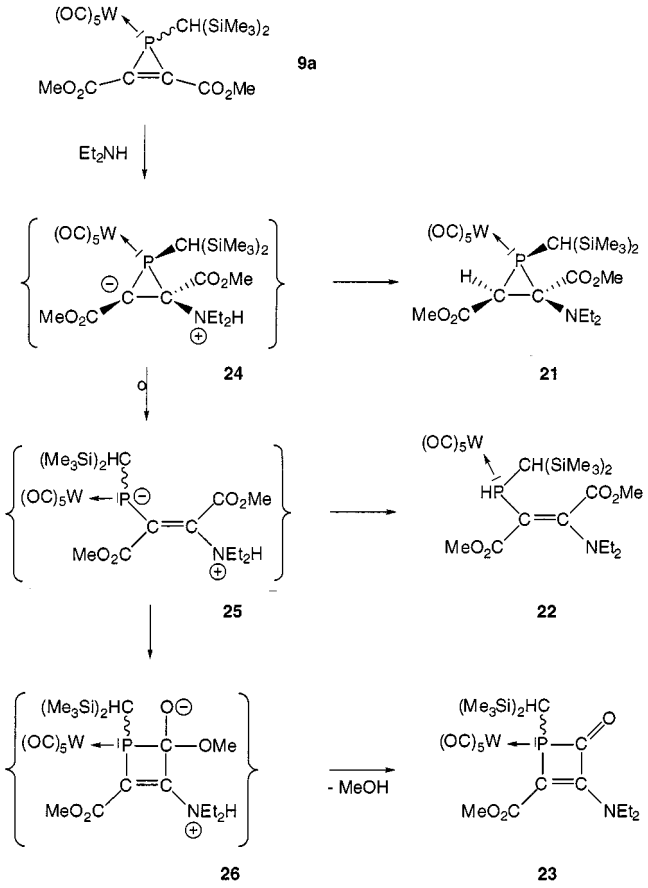
Scheme 5. Reactions of 1*H*-phosphirene tungsten complex **9a** with dimethylbutadiene and with diethylamine

ane complex **24**, which can either give rise to the 1,2-addition product **21** or undergo ring-opening to give **25** (Scheme 6). The latter can add a proton to furnish **22** or undergo ring-closure to yield **26** through an intramolecular attack of the phosphorus anion on the methoxycarbonyl carbon atom; the transient complex **26** subsequently eliminates methanol to give the 1,2-dihydro-1-phosphet-2-one complex **23**. The first step of this reaction cascade, i.e. the nucleophilic attack, also proceeds under steric control, leading exclusively to the phosphirane complex **21** with the pentacarbonyltungsten and diethylamino groups in a *trans* arrangement. The stereochemistry of the C−C double bond in **22** has not been determined but is expected to be *trans* (cf. ref.[25]). It should also be noted that no transformation of complex **21** into **22** (and vice versa) via prototropic rearrangement was observed.

C. Discussion of Selected NMR-Spectroscopic Data

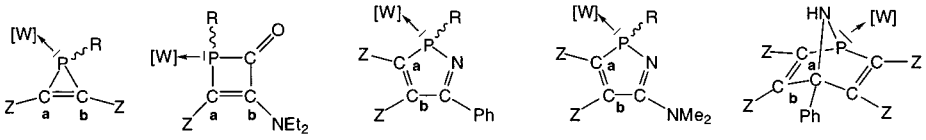
All of the reported complexes have been characterized by heteronuclear NMR experiments, IR spectroscopy, and mass spectrometry (see Experimental Section). Selected NMR data of the complexes are collected in Tables 1 and 2 and are discussed here; for X-ray data see Section D, Tables 1−3, and the Experimental Section.

A comparison of selected NMR data of the variously sized heterocycles of complexes **9a**, **10a**, **b**, **16**, and **23** (Table 1) shows, in all cases, significant resonances of the carbon nuclei of the C−C double bond units. Thus, the resonances of the carbons directly bonded to phosphorus appear at



Scheme 6. Proposed reaction course for the formation of complexes **21**−**23**

Table 1. Selected NMR [only absolute values of J(P,C) are given] and X-ray data of complexes **9a**, **23**, **10a**, **b**, and **16** (in order of ring-size); [W] = $W(CO)_5$, R = $CH(SiMe_3)_2$ and Z = CO_2Me; the X_3 plane in PR_3 units is defined by the three X atoms directly bonded to phosphorus

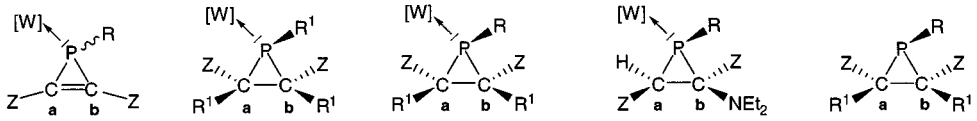


	9a	**23**	**10a**	**10b**	**16**
δ^{13}C-NMR [ppm]	C_a/C_b:	C_a/C_b:	C_a: 142.7 (25.9)	C_a: 139.2 (21.2)	C_a: 148.5 (13.3)
(J(P,C) [Hz])	143.2 (17.0)	119.4 (41.6)	C_b: 162.0 (1.4)	C_b: 161.8 (7.3)	C_b: 162.3 (16.3)
δ^{13}C-NMR [ppm]	C_a-CO_2Me:	C_a-CO_2Me:	C_a-CO_2Me:	C_a-CO_2Me:	C_a-CO_2Me:
(J(P,C) [Hz])	160.6 (8.5)	165.0 (14.5)	167.2 (11.5)	163.3 (7.3)	166.7 (2.1)
δ^{13}C-NMR [ppm]	C_b-CO_2Me:	C_b-CO_2Me:	C_b-CO_2Me:	C_b-CO_2Me:	C_b-CO_2Me:
(J(P,C) [Hz])	-	-	165.1 (14.2)	166.1 (14.6)	164.4 (9.7)
δ^{31}P-NMR [ppm]	-74.7	71.7	102.8	85.6	63.0
(^1J(W,P) [Hz])	(281.1)	(241.2)	(237.9)	(249.7)	(294.8)
P-atom/X_3-plane distance (Å)	0.9562	0.8737	0.785	0.7438	1.034
$\Sigma\,°(P_{PR3})(\pm2)$	265	293	306	310	272
d P-W (Å)	2.4749 (11)	2.5351 (13)	2.5045 (12)	2.5237 (11)	2.4525 (13)

higher field, while for the vicinal carbon atoms the opposite is true. All of the C_a carbons of **9a**, **10a**, **b**, **16**, and **23** exhibit absolute values of the carbon−phosphorus coupling constants in excess of 17 Hz, which depend specifically on the different scalar couplings (**9a** and **23**: $|^1J + {}^2J|$; **10a**, **b** and **16**: $|^1J + {}^4J|$). According to the ring size, the situation concerning the C_b carbons of **10a**, **b** and **16** is quite different from that in **23**; the former have absolute coupling constant values between 1.1 and 5.3 Hz ($|^2J + {}^3J|$), whereas for the latter the value is 56.2 Hz ($|^2J + {}^2J|$). Because of the approximately constant substitution pattern at phosphorus [with the exception of complex **16**, which has no $CH(SiMe_3)_2$ group] and the only slight variations at the other neighbouring atoms, the influence of the ring size on the phosphorus resonance can be delineated. The fact that the phosphorus nucleus becomes deshielded with increasing ring size has been widely documented for other P-heterocycles with different substitution patterns.[28] The magnitudes of the phosphorus−tungsten coupling constants show a marked dependence on the electronegativities of the phosphorus substituents[29] and, more surprisingly, on the ring size as well.

The 7-aza-1-phosphanorbornadiene complex **16** exhibits a phosphorus resonance δ = 63.0 with a large phosphorus−tungsten coupling constant of 294.8 Hz, indicating that the nitrogen fragment is directly bonded to the phosphorus. Compared to [pentacarbonyl(1,3,4-triphenyl-1,2-dihydro-1-phosphet-2-one)tungsten(0)][25a] [**27**; δ(^{31}P) = 86.9, ^1J(P,W) = 231.9 Hz], complex **23** shows similar ^{31}P-NMR data [δ = 71.7, ^1J(P,W) = 241.2 Hz]. Nevertheless, the π-donation of the diethylamino group is quite apparent throughout the ^{13}C-NMR resonances of the four-membered ring {δ = 119.4, [$^{(1+3)}J$(P,C) = 41.6 Hz, P*C*CO_2Me], 152.9 [$^{(2+2)}J$(P,C) = 56.2 Hz; PC*C*NEt_2]}, although the P*C*O carbon resonance seems to be largely unaffected {δ = 198.7, [$^{(1+3)}J$(P,C) = 35.7 Hz]; cf. **27:** δ = 190.72, [$^{(1+3)}J$(P,C) = 34.2 Hz]}. A comparison of the NMR data of the five-membered heterocycles **10a**, **b** and **13** reveals some noteworthy details. The phosphorus nuclei of **10a**, **b** and **13** exhibit resonances in the range δ = 85.6 to 103, whereas that in **10c** is significantly more deshielded (δ = 119.6). In these 2*H*-1,2-azaphosphole derivatives, the magnitudes of the phosphorus−tungsten coupling constants show a marked dependence on the nature of the substituents at phosphorus and the C^5-carbon; those in **10b** (J = 249.7 Hz) and **10c** (J = 248.1 Hz) are thus considerably greater than that in **10a** (237.9 Hz). Considering further the phosphorus−tungsten coupling constants, the effect of the oxygen atom directly bonded to phosphorus in the diastereoisomeric Δ^3-1,3,2-oxazaphospholene complexes **14a**, **b** is dominant (J = 303.1 and 305.9 Hz). Astonishingly, the imino carbon resonances of **10a**−**c**, **13**, and **14a**, **b** are hardly affected by variations in the bonding situation at the phosphorus atom. A comparison of selected NMR data of the three-membered heterocycle complexes having a mono- or polycyclic ring system (Table 2) shows that the phosphirane complexes **15**, **19**, and **21** exhibit phosphorus resonances in the same region as the 1*H*-phosphirene complex **9a**, which is not unexpected.[30] Complexes **9a**, **19**, and **21** show only slightly different phosphorus−tungsten coupling constants, whereas that of complex **15** is markedly smaller. Moreover, the nuclei of the three-membered ring of **15** are more deshielded. Taken together, the above results point to the dominating effect of the electronegativity of the phos-

Table 2. Selected NMR [only absolute values of *J*(P,C) are given] and X-ray data of complexes **9a, 15**, **19** and **21**; [W] = $W(CO)_5$, R = $CH(SiMe_3)_2$, R^1 = organic fragment and Z = CO_2Me; #: not determined; the X_3 plane in PR_3 units is defined by the three X atoms directly bonded to phosphorus



	9a	**15**	**19**	**21**	**20**
δ^{13}C-NMR [ppm]	C_a/C_b:	C_a/C_b:	C_a/C_b:	C_a: 41.4 (14.2)	C_a/C_b:
(J(P,C) [Hz])	143.2 (17.0)	70.4 (5.2)	40.2 (18.1)	C_b: 66.6 (16.0)	41.5 (47.7)
δ^{13}C-NMR [ppm]	C_a/C_b-CO_2Me:	C_a/C_b-CO_2Me:	C_a/C_b-CO_2Me:	C_a-CO_2Me: 167.1 (s)	C_a/C_b-CO_2Me:
(J(P,C) [Hz])	160.6 (8.5)	168.7 (s)	171.2 (3.7)	C_b-CO_2Me: 172.2 (s)	173.3 (14.2)
δ^{31}P-NMR [ppm]	-74.7	-67.2	-87.1	-81.1	-105.8
(^{1}J(W,P) [Hz])	(281.1)	(242.0)	(269.9)	(274.7)	(s)
P-atom/X_3-plane distance (Å)	0.9562	1.448	1.0131	1.0225	#
Σ °(P_{PR3}))(±2)	265	195	264	263	#
d P-W (Å)	2.4749 (11)	2.4569 (8)	2.5539 (7)	2.5351 (11)	#

phorus substituents (especially with regard to the hybridization of the carbon atoms) on the phosphorus−tungsten coupling constants. In this context, the very small bond angle sums of these complexes are of particular interest (see Section D).

D. Discussion of Selected X-ray Structural Data

The molecular structures of the complexes **9a**, **10b**, **19**, **21**, and **23** were confirmed in the solid state by X-ray crystallography (Figures 1−5); further details of the crystal data and structure refinement are given in Table 3.[31] Comparison of the structure of complex **9a** (Figure 1) with that of other 1*H*-phosphirene complexes[17b] having the same phosphorus fragment, [{$(Me_3Si)_2HCP$}$W(CO)_5$], reveals slightly shortened endo- and exocyclic carbon−carbon and phosphorus−carbon distances and a significantly shortened tungsten−phosphorus distance of 2.4749(11) Å (vs. ca. 2.50 Å)[17b] as the most interesting features. The latter is combined with a widened W−P−C(12) angle of 121.27(24)° (vs. ca. 118−119.5°)[17b] and an increased W−C(5) distance [2.001(5) Å] of the *trans* CO ligand, thus indicating weaker W−C and stronger W−P π-back bonding. The fact that there are no extended P−C distances (bonds) within the *P*-ligand is quite remarkable and is inconsistent with the current π-acceptor orbital bonding model, for which a substantial participation of σ*-orbitals has been proposed.[32][33]

For complex **10b**, the asymmetric unit contains two independent molecules, which are not significantly different from one another. The structure consists of discrete molecules with no unusual intermolecular distances. The heterocyclic ring of complex **10b** (Figure 2) is approximately planar, with the dimethylamino group subtending an interplanar angle to the five-membered ring of 11.4°. Apart

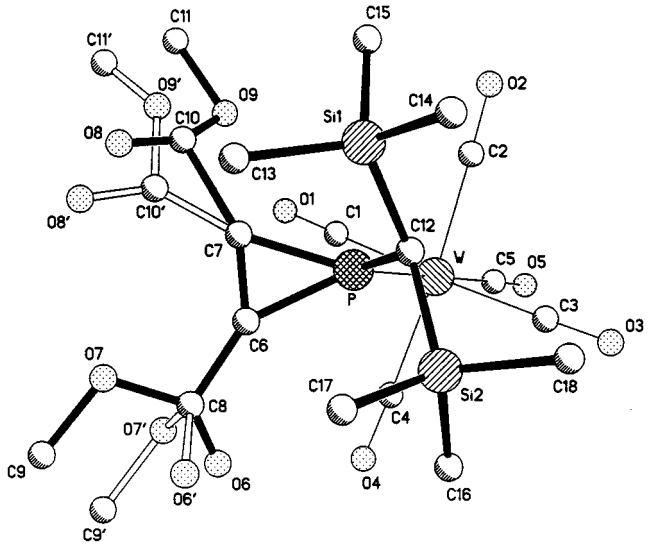


Figure 1. Molecular structure of **9a** in the crystal (both positions of the two disordered methoxycarbonyl groups are shown; hydrogen atoms are omitted for clarity); selected bond lengths [Å] and angles [°]: W−C(5) 2.001(5), W−C(4) 2.054(6), W−P 2.4749(11), P−C(12) 1.808(4), P−C(6) 1.791(5), P−C(7) 1.795(5), C(6)−C(7) 1.294(7); W−P−C(12) 121.27(14), C(6)−P−C(7) 42.3(2), C(6)−C(7)−P 68.7(3), C(7)−C(6)−P 69.0(3)

from localized endocyclic nitrogen−carbon and carbon−carbon double-bond lengths of 1.312(5) and 1.338(6) Å, respectively, the ring also has a substantially shortened exocyclic nitrogen−carbon bond length of 1.346(5) Å (cf. ref.[34]). Together with the angle sum of 360° at the N(2) nitrogen atom, this provides evidence for a $p_\pi-p_\pi$ electron interaction of the nitrogen lone-pair and the C−N π-bond. It is also noteworthy that this also affects the W−P distance, which amounts to 2.5237(11) Å in **10b** and 2.505(12) Å in **10a**.[18a]

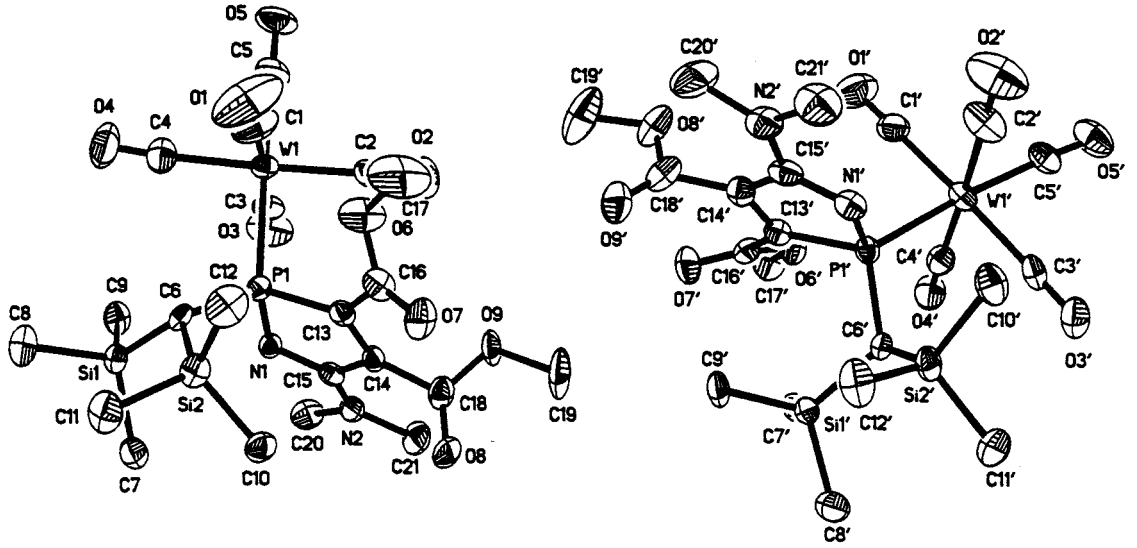


Figure 2. Two independent molecules of **10b** in the crystal (only one data set is given; ellipsoids represent 30% probability levels, hydrogen atoms are omitted for clarity); selected bond lengths [Å] and angles [°]: W(1)−C(5) 1.999(5), W(1)−C(1) 2.019(6), W(1)−C(2) 2.053(5), W(1)−P(1) 2.5237(11), P(1)−C(6) 1.836(4), P(1)−N(1) 1.674(4), N(1)−C(15) 1.312(5), N(2)−C(15) 1.346(5), C(15)−C(14) 1.492(6), C(14)−C(18) 1.338(6), C(13)−P(1) 1.839(4); W(1)−P−C(6) 119.26(14), C(13)−P(1)−N(1) 92.51(19), P(1)−N(1)−C(15) 112.1(3), N(1)−C(15)−C(14) 114.9(4), C(15)−C(14)−C(13) 111.6(4), C(14)−C(13)−P(1) 108.0(3)

Comparison of the structures of complexes **19** and **21** (Figures 3 and 4) with that of **9a** shows that the former have both significantly lengthened endocyclic bond lengths and slightly widened W−P−C(6) angles of 122.62(9) and 124.10(10)°, respectively. Detailed comparison between **19** and **21** cannot be made as the $CH(SiMe_3)_2$ groups adopt opposite orientations with respect to the $W(CO)_5$ fragment, which is very unusual in such P-heterocycle complexes. All three complexes have comparable angle sums [$\Sigma°(P_{PR3})$ values, Table 2] of ca. 264°, but distinctly different W−P distances. This finding most probably stems from different cone angles[35] of these P-ligands; unfortunately, much less data is currently available for such P-heterocycle ligands than for acyclic triorganophosphane ligands.[32][33] Comparing these findings to those for complex **15**,[1] for which a smaller bond angle sum [$\Sigma°(P_{PR3})$ value] and W−P distance were observed [ca. 195° and 2.4569(8) Å], this situation seemingly results from a reduction in the steric strain and an increase in the pyramidalization of the PR_3 ligand, as shown by the increasing distance of the phosphorus atom from the plane defined by the α-atoms of the three substituents (cf. Tables 2 and 3).[32][33] The latter aspect in particular merits further study. Although complexes **15**, **19**, **21** (and even **9a**) are quite similar, it is noteworthy that there is no simple correlation between X-ray structural parameters such as the $\Sigma°(P_{PR3})$ value and the W−P distance on one hand, and an NMR parameter such as the magnitude of the phosphorus−tungsten coupling constant on the other (cf. Table 2).

The molecular structure of the 1,2-dihydro-1-phosphet-2-one complex **23** (Figure 5) is characterized by an unsymmetrical, planar, four-membered ring system. Compared to the structure of complex **27**,[25a] the carbon−carbon bond length of the double bond unit is longer in **23** [1.399(5) vs. 1.36(1) Å (**27**)]. Moreover, it forms part of a

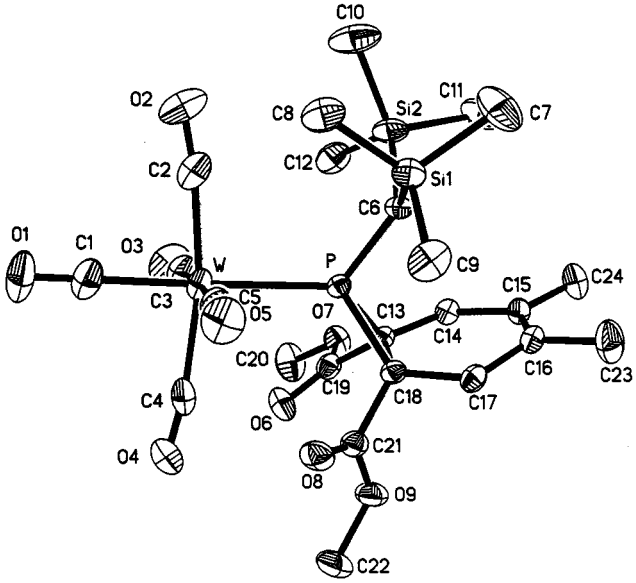


Figure 3. Molecular structure of **19** in the crystal (ellipsoids represent 50% probability levels, hydrogen atoms are omitted for clarity); selected bond lengths [Å] and angles [°]: W−C(1) 1.982(3), W−C(4) 2.063(3), W−C(5) 2.035(3), W−P 2.5539(7), P−C(6) 1.822(3), P−C(13) 1.908(3), P−C(18) 1.846(3), C(13)−C(18) 1.533(3), C(13)−C(19) 1.491(4), C(18)−C(21) 1.514(3); C(5)−W−P 87.95(8), C(4)−W−P 96.47(8), W−P−C(6) 122.62(9), C(13)−P−C(18) 48.18(10), P−C(13)−C(18) 63.78(13), C(13)−C(18)−P 68.03(13)

delocalized π-system consisting of the planar N−C(16)−C(13)−C(14) subunit [$\Sigma°(N_{NR3})$ value: 360; interplanar angle between the plane C(17)−N−C(19) and that of the four-membered ring 3.8°] and the planar N−C(16)−C(21)−O(8) subunit, which has significantly shortened exocyclic single bond lengths (cf. ref.[34]), [N−C(16) 1.328(5) Å and C(13)−C(14) 1.458(5) Å] for the

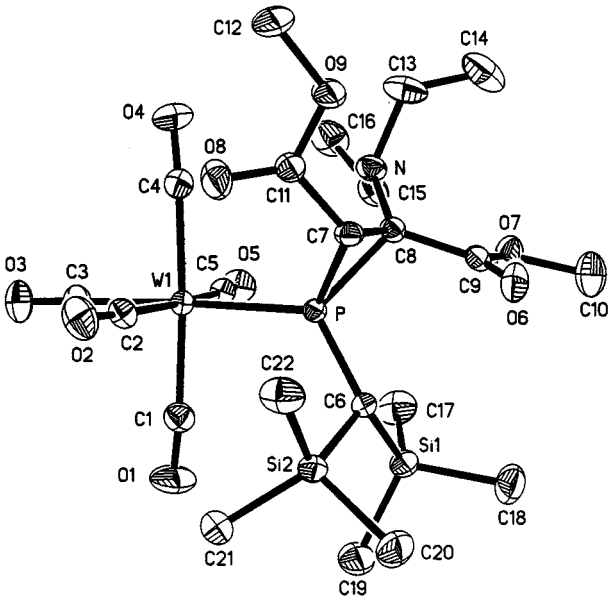


Figure 4. Molecular structure of **21** in the crystal (ellipsoids represent 50% probability levels, hydrogen atoms are omitted for clarity); selected bond lengths [Å] and angles [°]: W(1)−C(3) 1.987(3), W(1)−C(4) 2.057(3), W(1)−P 2.5351(11), P−C(6) 1.819(3), P−C(7) 1.816(3), P−C(8) 1.903(3), C(7)−C(8) 1.542(4), C(7)−C(11) 1.505(4), C(8)−C(9) 1.511(4), C(8)−N 143.1(4); C(2)−W(1)−P 88.43(9), C(5)−W(1)−P 98.29(9), W(1)−P−C(6) 124.10(10), C(7)−P−C(8) 48.91(12), P−C(7)−C(8) 68.5(2), C(7)−C(8)−P 62.60(14)

former and an increased carbon−oxygen distance for the latter [C(21)−O(8) 1.197(5) Å; **27**: 1.16(1) Å].

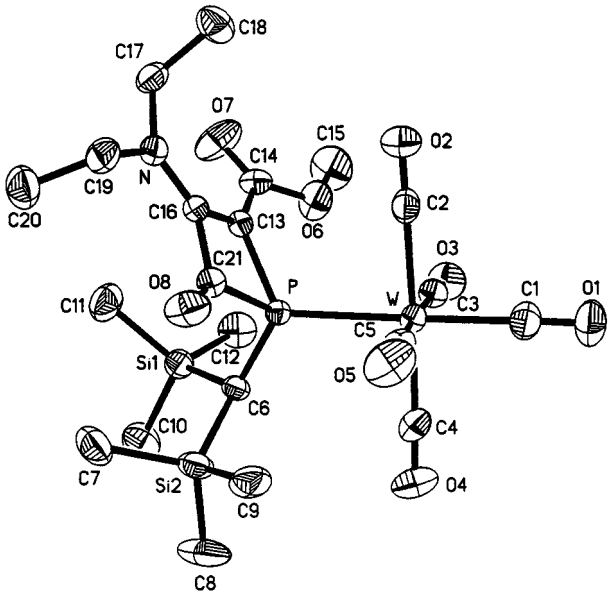


Figure 5. Molecular structure of **23** in the crystal (ellipsoids represent 50% probability levels, hydrogen atoms are omitted for clarity); selected bond lengths [Å] and angles [°]: W−C(1) 2.012(4), W−C(2) 2.044(4), W−P 2.4995(1), P−C(6) 1.836(4), P−C(13) 1.834(4), C(13)−C(16) 1.399(5), C(16)−C(21) 1.511(5), P−C(21) 1.880(4), C(13)−C(14) 1.458(5), N−C(16) 1.328(5), C(21)−O(8) 1.197(5); C(2)−W−P 85.91(11), C(3)−W(1)−P 92.57(11), W−P−C(6) 119.34(12), C(13)−P−C(21) 72.0(2), P−C(21)−C(16) 92.5(2), C(21)−C(16)−C(13) 97.2(3), C(16)−C(13)−P 98.3(2)

Experimental Section

General Procedures: All reactions and manipulations were carried out under an atmosphere of deoxygenated dry nitrogen, using standard Schlenk techniques with conventional glassware. Solvents were dried according to standard procedures. − NMR spectra were recorded on a Bruker AC-200 spectrometer (200 MHz for ^{1}H; 50.3 MHz for ^{13}C; 81.0 MHz for ^{31}P) with [D]chloroform and [D_6]benzene as solvents and internal standards; shifts are given relative to ext. tetramethylsilane (^{1}H, ^{13}C) and 85% H_3PO_4 (^{31}P). − Mass spectra were recorded on a Finnigan MAT 8430 (70 eV); apart from the *m*/*z* values of the molecular ions, only those peaks having intensities > 20% of the base-peak are listed. − Infrared spectra were recorded on a Biorad FT-IR 165 spectrometer (selected data given). − Melting points were measured on a Büchi 535 capillary apparatus. − Elemental analyses were performed using a Carlo Erba analytical gas chromatograph. − The κ*P* notation in the nomenclature is intended to differentiate between *P*- and *N*-coordination of the relevant heterocycle to the metal.

Pentacarbonyl[2-bis(trimethylsilyl)methyl-3,4-bis(methoxycarbonyl)-5-phenyl-2*H*-1,2-azaphosphole-κ*P*]tungsten(0) (10a): To a solution of the 2*H*-azaphosphirene tungsten complex **8a** (1.5 g, 2.4 mmol) in toluene (7.5 mL) and benzonitrile (2 mL) was added dimethyl acetylenedicarboxylate (0.6 mL, 5 mmol) and the mixture was heated at 75°C for 1.5 h under slow stirring. The solvent was then removed in vacuo and the product was separated by low-temperature column chromatography (SiO_2, −20°C, 10 × 4 cm, hexane/diethyl ether, 90:10). Evaporation of the solvent from the second fraction yielded **10a** as dark-red crystals. Yield: 680 mg (43%). − M.p. 121°C (dec.). − ^{1}H NMR ($CDCl_3$): δ = 0.15 (s, 9 H, $SiMe_3$), 0.39 (s, 9 H, $SiMe_3$), 1.35 [d, ^{2}J(P,H) = 2.4 Hz, 1 H, C*H*($SiMe_3$)$_2$], 3.87 (s, 3 H, OCH_3), 3.92 (s, 3 H, OCH_3), 7.50 (m_c, 3 H, C$H_{arom.}$), 7.79 (m_c, 2 H, C$H_{arom.}$). − $^{13}C\{^{1}H\}$ NMR ($CDCl_3$): δ = 2.6 [d, ^{3}J(P,C) = 1.9 Hz, $SiMe_3$], 3.2 [d, ^{3}J(P,C) = 2.4 Hz, $SiMe_3$], 18.9 [s, *C*H($SiMe_3$)$_2$], 53.0 (s, O*C*H$_3$), 53.2 (s, O*C*H$_3$), 128.4 (s, Ph), 128.8 (s, Ph), 131.7 (s, Ph), 134.4 [d, ^{3}J(P,C) = 16.6 Hz, Ph], 142.7 [d, ^{1}J(P,C) = 25.9 Hz, P*C*C], 162.0 [d, $^{(2+3)}J$(P,C) = 1.4 Hz, PC*C*], 162.7 [d, ^{3}J(P,C) = 13.1 Hz, *C*O$_2$Me], 165.1 [d, ^{3}J(P,C) = 14.2 Hz, *C*O$_2$Me], 167.7 [d, $^{(2+3)}J$(P,C) = 11.5 Hz, PN*C*], 196.7 [d, ^{2}J(P,C) = 6.5 Hz, *cis*-*C*O], 198.0 [d, ^{2}J(P,C) = 23.1 Hz, *trans*-*C*O]. − $^{31}P\{^{1}H\}$ NMR ($CDCl_3$): δ = 102.8 [s, ^{1}J(P,W) = 237.9 Hz]. − IR (KBr): $\tilde{\nu}$ = 2073 (s), 1992 (s), 1953 (vs), 1926 (vs), 1913 (vs) cm^{-1} (CO); 1745 (s), 1719 (s) cm^{-1} (CO_2); 1596 (m, sh), 1546 (m) cm^{-1} (C=N). − MS (70 eV, EI), (^{184}W); *m*/*z* (%): 759 (4) [M^+], 647 (50) [(M − 4 CO)$^+$·], 631 (100) [(M − 3 CO)$^+$·], 603 (40) [(M − 4 CO)$^+$·], 575 (35) [(M − 5 CO)$^+$·], 73 (100) [$SiMe_3^+$·]. − $C_{25}H_{30}NO_9PSi_2W$ (759.5): calcd. C 39.54, H 3.98, N 1.84; found C 39.73, H 3.85, N 1.76.

[2-Bis(trimethylsilyl)methyl-3,4-bis(methoxycarbonyl)-5-phenyl-2*H*-1,2-azaphosphole] *P*-Sulfide (13): A mixture of the 2*H*-1,2-azaphosphole tungsten complex **10a** (0.2 g, 0.25 mmol) and sulfur (0.08 g, 0.25 mmol) in benzonitrile (3 mL) was heated for 1.5 h at 75°C under slow stirring. The solvent was then removed in vacuo and the product was separated by low-temperature column chromatography of the residue (SiO_2, −20°C, 4 × 4 cm, dichloromethane). Crystallization from a small amount of pentane at −20°C afforded **13** as red crystals. Yield: 80 mg (65%). − M.p. 79°C (dec.). − ^{1}H NMR ($CDCl_3$): δ = 0.09 (s, 9 H, $SiMe_3$), 0.43 (s, 9 H, $SiMe_3$), 1.33 [d, ^{2}J(P,H) = 21.2 Hz, 1 H, C*H*($SiMe_3$)$_2$], 3.85 [d, ^{6}J(P,H) = 0.5 Hz, 3 H, OCH_3], 3.89 [d, ^{5}J(P,H) = 0.6 Hz, 3 H, OCH_3], 7.46 (m_c, 3 H, C$H_{arom.}$), 7.79 (m_c, 2 H, C$H_{arom.}$). − $^{13}C\{^{1}H\}$ NMR ($CDCl_3$): δ = 2.2 [d, ^{3}J(P,C) = 3.2 Hz, $SiMe_3$], 3.3 [d, ^{3}J(P,C) = 2.9 Hz, $SiMe_3$], 19.9 [d, ^{1}J(P,C) = 32.9 Hz, *C*H($SiMe_3$)$_2$], 53.0 (s, O*C*H$_3$),

53.1 (s, OCH_3), 128.6 (s, Ph), 128.8 (s, Ph), 133.2 (s, Ph), 134.0 [d, ^3J(P,C) = 23.7 Hz, Ph], 151.0 [d, ^1J(P,C) = 53.1 Hz, P*C*C], 161.3 [d, $^{(2+3)}J$(P,C) = 13.8 Hz, PN*C*], 164.8 [d, ^2J(P,C) = 22.4 Hz, PC*C*], 167.7 (s, *C*O_2Me), 170.7 [d, ^3J(P,C) = 7.5 Hz, *C*O_2Me]. − $^{31}P\{^1H\}$ NMR ($CDCl_3$): δ = 101.0 (s). − IR (KBr): ṽ = 1737 (vs), 1718 (vs) cm^{-1} (CO_2); 1610 (m), 1528 (m) cm^{-1} (C=N). − MS (70 eV, EI); *m/z* (%): 467 (25) [M^+·], 452 (50) [(M − CH_3)$^+$·], 408 (100) [(M − $C_2H_3O_2$)$^+$·]. − $C_{20}H_{30}NO_4PSi_2$ (467.7): calcd. C 51.37, H 6.47, N 3.00, S 6.86; found C 51.35, H 6.60, N 2.90, S 6.60.

Procedure for the Synthesis of 2*H*-1,2-Azaphosphole Tungsten Complex 10b and Δ^3-1,3,2-Oxazaphospholene Tungsten Complexes 14a, b: To a solution of 2*H*-azaphosphirene tungsten complex **8a** (1.5 g, 2.4 mmol) in toluene (3 mL), dimethylcyanamide (0.2 mL, 0.2 mmol), and dimethyl acetylenedicarboxylate (0.4 mL, 3 mmol) were added and the mixture was heated at 75°C for 1.5 h under slow stirring. After concentration to dryness, the products were separated by low-temperature column chromatography of the residue (SiO_2, −20°C, 10 × 2 cm, hexane/diethyl ether, 90:10) and subsequently crystallized from pentane at −20°C.

Pentacarbonyl[2-{bis(trimethylsilyl)methyl}-5-dimethylamino-3,4-bis(methoxycarbonyl)-2*H*-1,2-azaphosphole-κ*P*]tungsten(0) (10b): Yield: 130 mg (14%). − M.p. 123°C (dec.). − ^1H NMR ($CDCl_3$): δ = 0.05 (s, 9 H, $SiMe_3$), 0.35 (s, 9 H, $SiMe_3$), 1.13 [d, ^2J(P,H) = 5.6 Hz, 1 H, C*H*($SiMe_3$)$_2$], 3.13 [s, 6 H, N(CH_3)$_2$], 4.55 (s, 3 H, OCH_3), 4.76 (s, 3 H, OCH_3). − $^{13}C\{^1H\}$ NMR ($CDCl_3$): δ = 2.7 [d, ^3J(P,C) = 2.0 Hz, $SiMe_3$], 3.4 [d, ^3J(P,C) = 2.6 Hz, $SiMe_3$], 22.6 [s, *C*H($SiMe_3$)$_2$], 39.7 [s, N(*C*H_3)$_2$], 52.6 (s, O*C*H_3), 53.3 (s, O*C*H_3), 139.2 [d, ^1J(P,C) = 21.2 Hz, P*C*C], 158.4 [d, $^{(2+3)}J$(P,C) = 5.3 Hz, PN*C*], 161.8 [d, $^{(2+3)}J$(P,C) = 7.3 Hz, PC*C*], 163.2 [d, ^3J(P,C) = 7.3 Hz, *C*O_2Me], 166.1 [d, ^2J(P,C) = 14.6 Hz, *C*O_2Me], 197.7 [d, ^2J(P,C) = 7.2 Hz, *cis*-*C*O], 199.7 [d, ^2J(P,C) = 22.6 Hz, *trans*-*C*O]. − $^{31}P\{^1H\}$ NMR ($CDCl_3$): δ = 85.6 [s, ^1J(P,W) = 249.7 Hz]. − IR (KBr): ṽ = 2069 (s), 1983 (s), 1929 (vs sh) cm^{-1} (CO); 1742 (m), 1735 (m), 1720 (s) cm^{-1} (CO_2); 1596 (m), 1546 (m) cm^{-1} (C=N). − MS (70 eV, EI), (^{184}W); *m/z* (%): 726 (20) [M^+·], 698 (50) [(M − 1 CO)$^+$·], 614 (60) [(M − 4 CO)$^+$·], 586 (50) [(M − 5 CO)$^+$·], 558 (100) [M − 6 (CO)$^+$], 73 (80) [$SiMe_3^+$]. − $C_{21}H_{31}N_2O_9PSi_2W$ (726.5): calcd. C 34.72, H 4.30, N 3.86; found C 34.61, H 4.32, N 3.55.

Pentacarbonyl[2-{bis(trimethylsilyl)methyl}-5-dimethylamino-4-methoxy-4-(2-methoxycarbonylacetylenyl)-Δ^3-1,3,2-oxazaphospholene-κ*P*]tungsten(0) (14a,b): Compound **14a**: Yield: 125 mg (13%). − M.p. 164°C (dec.). − ^1H NMR ($CDCl_3$): δ = 0.17 (s, 9 H, $SiMe_3$), 0.29 (s, 9 H, $SiMe_3$), 1.49 [s, 1 H, C*H*($SiMe_3$)$_2$], 3.16 [s, 6 H, N(CH_3)$_2$], 3.63 (s, 3 H, OCH_3), 3.80 (s, 3 H, OCH_3). − $^{13}C\{^1H\}$ NMR ($CDCl_3$): δ = 2.5 (s, $SiMe_3$), 2.6 (s, $SiMe_3$), 37.8 [d, ^1J(P,C) = 5.9 Hz, *C*H($SiMe_3$)$_2$], 38.1 [s, N(*C*H_3)$_2$], 40.0 [s, N(*C*H_3)$_2$], 53.2 (s, O*C*H_3), 53.8 (s, O*C*H_3), 77.8 (s, C*C*CO_2Me), 79.9 (s, *C*CCO_2Me), 99.2 [d, $^{(2+3)}J$(P,C) = 4.0 Hz, PO*C*], 152.7 (s, *C*O_2Me), 158.0 [d, $^{(2+3)}J$(P,C) = 1.3 Hz, PN*C*], 197.1 [d, ^2J(P,C) = 8.8 Hz, ^1J(C,W) = 117.8 Hz, *cis*-*C*O], 201.1 [d, ^2J(P,C) = 29.1 Hz, *trans*-*C*O]. − $^{31}P\{^1H\}$ NMR ($CDCl_3$): δ = 191.6 [s, ^1J(P,W) = 305.9 Hz]. − IR (KBr): ṽ = 2073 (s), 1986 (s), 1952 (vs), 1930 (vs), 1919 (vs) cm^{-1} (CO); 1629 (s) cm^{-1} (CO_2). − MS (70 eV, EI), (^{184}W); *m/z* (%): 726 (50) [M^+·], 642 (30) [(M − 3 CO)$^+$·], 586 (40) [(M − 5 CO)$^+$·], 571 (50) [(M − 5 CO − CH_3)$^+$·], 558 (100) [(M − 6 CO)$^+$], 543 (60) [(M − 6 CO − CH_3)$^+$·], 73 (60) [$SiMe_3^+$].

Compound **14b**: Yield: 70 mg (8%). − M.p. 164°C (dec.). − ^1H NMR ($CDCl_3$): δ = 0.17 (s, 9 H, $SiMe_3$), 0.32 (s, 9 H, $SiMe_3$), 1.46 [s, 1 H, C*H*($SiMe_3$)$_2$], 3.16 [s, 3 H, N(CH_3)$_2$], 3.19 [s, 3 H, N(CH_3)$_2$], 3.61 (s, 3 H, OCH_3), 3.81 (s, 3 H, OCH_3). − $^{13}C\{^1H\}$ NMR ($CDCl_3$): δ = 2.1 [d, ^3J(P,C) = 2.9 Hz, $SiMe_3$], 2.3 [d, ^3J(P,C) = 1.3 Hz, $SiMe_3$], 36.8 [m_c, *C*H($SiMe_3$)$_2$], 38.5 [s, N(*C*H_3)$_2$], 39.9 [s, N(*C*H_3)$_2$], 52.9 (s, O*C*H_3), 53.2 (s, O*C*H_3), 74.6 (s, C*C*CO_2Me), 79.8 (s, *C*CCO_2Me), 99.1 [d, $^{(2+3)}J$(P,C) = 6.9 Hz, PO*C*], 152.7 (s, *C*O_2Me), 158.1 [d, $^{(2+3)}J$(P,C) = 1.1 Hz, PN*C*], 197.2 [d, ^2J(P,C) = 8.7 Hz, ^1J(C,W) = 126.1 Hz, *cis*-*C*O], 200.1 [d, ^2J(P,C) = 29.4 Hz, *trans*-*C*O]. − $^{31}P\{^1H\}$ NMR ($CDCl_3$): δ = 198.6 [s, ^1J(P,W) = 303.1 Hz]. − IR (KBr): ṽ = 2071 (s), 1983 (s), 1940 (vs), 1918 (vs) cm^{-1} (CO); 1726 (s) cm^{-1} (CO_2); 1618 (s) cm^{-1} (C=N). − MS (70 eV, EI), (^{184}W); *m/z* (%): 726 (40) [M^+·], 614 (30) [(M − 4 CO)$^+$·], 586 (100) [(M − 5 CO)$^+$·], 571 (80) [(M − 5 CO − CH_3)$^+$·], 543 (60) [(M − 6 CO − CH_3)$^+$·], 73 (35) [$SiMe_3^+$]. − $C_{21}H_{31}N_2O_9PSi_2W$ (726.5): calcd. C 34.72, H 4.30, N 3.86; found C 34.98, H 4.20, N 3.57.

Pentacarbonyl[3,4-bis(methoxycarbonyl)-2-pentamethylcyclopentadienyl-5-phenyl-2*H*-1,2-azaphosphole-κ*P*]tungsten(0) (10c): To a solution of 0.3 g (0.5 mmol) of the 2*H*-azaphosphirene tungsten complex **8b** in 3 mL of benzonitrile was added 0.5 mL (0.6 mmol) of dimethyl acetylenedicarboxylate and the mixture was stirred for 95 min at 62°C. The solution was then concentrated to dryness in vacuo (ca. 0.01 mbar) and the residue was subjected to low-temperature column chromatography on silica (−35°C, hexane/diethyl ether, 99:1). A red fraction was concentrated to dryness in vacuo and the product was crystallized from pentane. Yield: 118 mg (32%). − M.p. 132°C (dec.). − ^1H NMR: δ = 1.10 [d, ^2J(P,H) = 16.0 Hz, 3 H, Cp*-C1-CH_3], 1.82 [pseudo t, ^3J(P,H) = 6.0 Hz, 6 H, Cp*-C3/6-CH_3], 2.21 (s, 6 H, Cp*-C4/5-CH_3), 3.84 (s, 6 H, CO_2CH_3), 7.51 (m_c, 2 H, C$H_{arom.}$), 7.90 (m_c, 2 H, C$H_{arom.}$). − $^{13}C\{^1H\}$ NMR: δ = 11.3 [d, ^3J(P,C) = 1.6 Hz, Cp*-*C*H_3], 11.9 (s, Cp*-*C*H_3), 12.6 (s, Cp*-*C*H_3), 14.1 [d, ^4J(P,C) = 2.6 Hz, Cp*-C1-*C*H_3], 52.1 (s, O*C*H_3), 56.5 [d, ^4J(P,C) = 9.2 Hz, O*C*H_3], 62.9 [d, *J*(P,C) = 7.4 Hz, Cp*-C1], 128.5 (s, *i*-Ph), 128.7 (s, *p*-Ph), 131.7 (s, *o*-Ph), 134.1 (s, *m*-Ph), 136.2 (s, Cp*), 136.7 [d, *J*(P,C) = 2.0 Hz, Cp*], 141.6 [d, *J*(P,C) = 3.1 Hz, Cp*], 141.8 [d, *J*(P,C) = 2.4 Hz, Cp*], 144.8 [d, $^{(1+4)}J$(P,C) = 21.8 Hz, *C*3], 159.6 [d, $^{(2+3)}J$(P,C) = 4.2 Hz, *C*5], 162.8 [d, $^{(2+3)}J$(P,C) = 12.3 Hz, *C*4], 164.9 [d, ^2J(P,C) = 13.3 Hz, C3-*C*O_2CH_3], 168.3 [d, ^3J(P,C) = 13.2, Hz, C4-*C*O_2CH_3], 195.3 [d, ^2J(P,C) = 6.6 Hz, *cis*-*C*O], 197.4 [d, ^2J(P,C) = 26.3 Hz, *trans*-*C*O]. − $^{31}P\{^1H\}$ NMR ($CDCl_3$): δ = 119.6 [s, ^1J(P,W) = 248.1 Hz]. − IR (KBr): ṽ = 2075 (s), 1939 (vs, br), (CO); 1734 (s), 1719 (s) cm^{-1} (CO_2). − MS (positive CI, NH_3), (^{184}W) (%): 736 (12) [(M + H)$^+$], 602 (10) [(M + H − $C_{10}H_{14}$)$^+$], 135 (100) [$C_{10}H_{15}^+$]. − $C_{28}H_{26}NO_9PW$ (735.3): calcd. C 45.74, H 3.56, N 1.90; found C 45.91, H 4.09, N 1.81.

Procedure for the Preparation of Complexes 15 and 16: A mixture of 0.3 g (0.5 mmol) of the 2*H*-azaphosphirene tungsten complex **8b** and 0.5 mL (0.6 mmol) of dimethyl acetylenedicarboxylate was stirred for 25 min in 3 mL of toluene (**15**) or 3 mL of benzonitrile (**16**) at 75°C. The solution was then concentrated to dryness in vacuo (ca. 0.01 mbar), and the residue was subjected to low-temperature column chromatography on silica (−20°C, hexane/diethyl ether, 99:1). The eluents were concentrated to dryness in vacuo and the products were crystallized from pentane at −20°C (pale-yellow crystals in both cases).

Pentacarbonyl[3,4,5,6,8-pentamethyl-1-phosphatetracyclo-[4.1.1.1^{3,6}0^{2,7}]-2,7-bis(methoxycarbonyl)hept-4-ene-κ*P*]tungsten(0) (15): Yield: 0.25 g (81%). − M.p. 98°C (dec.). − ^1H NMR: δ = 0.58 [d, ^3J(P,H) = 19.0 Hz, 3 H, C8-CH_3], 1.52 (s, 6 H, C3/6-CH_3), 1.71 (s, 6 H, C4/5-CH_3), 3.62 (s, 6 H, CO_2CH_3). − $^{13}C\{^1H\}$ NMR: δ = 5.9 [d, ^3J(P,C) = 5.8 Hz, C8-*C*H_3], 14.0 (s, C3/6-*C*H_3), 14.1 [d, ^4J(P,C) = 2.6 Hz, C4/5-*C*H_3], 52.1 (s, O*C*H_3), 56.5 [d, ^4J(P,C) = 9.2 Hz, *C*3/6], 66.5 [d, *J*(P,C) = 32.2 Hz, *C*8], 70.4 [d, *J*(P,C) = 5.2 Hz, *C*2/7], 141.7 [d, *J*(P,C) = 10.4 Hz, *C*4/5], 168.7 (s, *C*O_2CH_3),

193.6 [d, ^2J(P,C) = 8.1 Hz, *cis*-*C*O], 197.4 [d, ^2J(P,C) = 35.5 Hz, *trans*-*C*O]. − ^{31}P{^{1}H} NMR ($CDCl_3$): δ = −74.6 [s, ^1J(P,W) = 281.1 Hz]. − IR (KBr): $\tilde{\nu}$ = 2079 (s), 1996 (s), 1946 (vs), 1922 (vs) cm^{-1} (CO); 1725 (s) cm^{-1}, 1718 (s) cm^{-1} (CO_2). − MS (negative CI, NH_3), (^{184}W); *m*/*z* (%): 631 (42) [M − H], 324 (100) [(C_5O_5W)], 308 (16) [M − (C_5O_5W)]. − $C_{21}H_{21}O_9PW$ (632.2): calcd. C 39.92, H 3.35; found C 39.92, H 3.46.

Pentacarbonyl[2,3,5,6-tetrakis(methoxycarbonyl)-4-phenyl-7-aza-1-phosphanorbornadiene-κ*P*]tungsten(0) (16): The assignments for C_a and C_b given in ref.[1] were erroneous!

Yield: 0.21 g (58%). − M.p. 152°C (dec.). − ^{1}H NMR: δ = 3.72 (s, 6 H, OCH_3), 3.76 [d, ^2J(P,H) = 5.1 Hz, 1 H, N*H*], 3.85 (s, 6 H, OCH_3), 7.45 (m_c, 3 H, $H_{arom.}$), 7.62 (m_c, 2 H, $H_{arom.}$). − ^{13}C{^{1}H} NMR: δ = 52.8 (s, O*C*H$_3$), 53.0 (s, O*C*H$_3$), 88.6 [d, J(P,C) = 5.4 Hz, *C*4], 126.1 (s, Ph), 129.0 (s, Ph), 129.6 (s, Ph), 132.5 [d, J(P,C) = 5.3 Hz, *i*-Ph], 148.5 [d, ^1J(P,C) = 13.3 Hz, *C*2/6], 162.3 [d, ^2J(P,C) = 16.3 Hz, *C*3/5], 164.4 [d, ^3J(P,C) = 9.7 Hz, *C*3/5-*C*O$_2$Me], 166.7 [d, ^2J(P,C) = 2.1 Hz, C2/6-*C*O$_2$Me], 194.2 [d, ^2J(P,C) = 8.2 Hz, *cis*-*C*O], 196.6 [d, ^2J(P,C) = 32.9 Hz, *trans*-*C*O]. − ^{31}P{^{1}H} NMR ($CDCl_3$): δ = 63.0 [s, ^1J(P,W) = 294.8 Hz]. − IR (KBr): $\tilde{\nu}$ = 3432 (s, br) (NH), 2082 (s), 1942 (vs, br), (CO); 1735 (s), 1724 (s) cm^{-1} (CO_2). − MS (positive CI, NH_3), (^{184}W); *m*/*z* (%): 761 (1) [(M + NH_4)$^+$], 602 (3) [(M + H − $C_6H_6O_4$)$^+$], 278 (100) [$C_{13}H_{13}NO_4P^+$]. − $C_{24}H_{18}NO_{13}PW$ (743.2): calcd. C 38.79, H 2.44, N 1.88; found C 38.92, H 2.52, N 1.94.

Procedure for the Diels−Alder Reaction of 1*H*-Phosphirene Tungsten Complex 9a with 2,3-Dimethylbutadiene: To a solution of the 1*H*-phosphirene tungsten complex **8a** (3.6 g, 0.55 mmol) in toluene (1.8 mL) was added 2,3-dimethylbutadiene (0.27 g, 3.3 mmol) and the mixture was heated at 75°C for 90 h under slow stirring. After concentration to dryness, the products were separated by low-temperature column chromatography of the residue (SiO_2, −20°C, 12 × 2 cm, hexane/diethyl ether, 98:2) and subsequently crystallized from pentane at −20°C.

Pentacarbonyl[1-{bis(trimethylsilyl)methyl}-2,7-bis(methoxycarbonyl)-4,5-dimethyl-1-phosphabicyclo[4.1.0^{2,7}]hept-4-ene-κ*P*]tungsten(0) (19): Yield: 100 mg (25%). − M.p. 117°C (dec.). − ^{1}H NMR (C_6D_6): δ = 0.27 (s, 18 H, $SiMe_3$), 0.94 [d, ^2J(P,H) = 14.4 Hz, 1 H, C*H*(SiMe$_3$)$_2$], 1.37 (s, 6 H, C*H*$_3$), 2.37 [dd, ^2J(H,H) = 17.1 Hz, ^3J(P,H) = 13.1 Hz, 2 H, C*H*$_2$], 2.87 [dd, ^2J(H,H) = 17.3 Hz, ^3J(P,H) = 10.6 Hz, 2 H, C*H*$_2$], 3.47 (s, 6 H, OCH_3). − ^{13}C{^{1}H} NMR (C_6D_6): δ = 2.6 (s, $SiMe_3$), 2.7 (s, $SiMe_3$), 12.7 [d, ^1J(P,C) = 34.2 Hz, *C*H(SiMe$_3$)$_2$], 18.4 (s, CH_3), 33.1 [d, ^2J(P,C) = 3.7 Hz, *C*H$_2$], 40.2 [d, ^1J(P,C) = 18.1 Hz, P*C*], 52.5 (s, O*C*H$_3$), 124.4 (s, *C*CH$_3$), 171.2 [d, ^3J(P,C) = 3.7 Hz, *C*O$_2$Me], 197.3 [d, ^2J(P,C) = 33.9 Hz, *trans*-*C*O], 197.4 [d, ^2J(P,C) = 7.4 Hz, *cis*-*C*O]. − ^{31}P{^{1}H} NMR ($CDCl_3$): δ = −87.1 [s, ^1J(P,W) = 269.9 Hz]. − IR (KBr): $\tilde{\nu}$ = 2075 (s), 2001 (s), 1932 (vs), 1910 (vs) cm^{-1} (CO); 1742 (vs) cm^{-1} (CO_2). − MS (70 eV, EI), (^{184}W); *m*/*z* (%): 710 (5) [(M − CO)$^+$·], 682 (25) [(M − 2 CO)$^+$·], 73 (100) [$SiMe_3^+$]. − $C_{24}H_{35}O_9PSi_2W$ (738.5): calcd. C 39.03, H 4.88; found C 40.12, H 5.13.

1-[Bis(trimethylsilyl)methyl]-2,7-bis(methoxycarbonyl)-4,5-dimethyl-1-phosphabicyclo[4.1.0^{2,7}]hept-4-ene (20): Yield: 50 mg (22%). − ^{1}H NMR (C_6D_6): δ = 0.16 [d, ^4J(P,H) = 0.8 Hz, 18 H, $SiMe_3$], 1.33 [d, ^2J(P,H) = 10.0 Hz, 1 H, C*H*(SiMe$_3$)$_2$], 1.57 (s, 6 H, C*H*$_3$), 2.25 [d, ^2J(H,H) = 19.2 Hz, 2 H, C*H*$_2$], 3.05 [dd, ^2J(H,H) = 17.6 Hz, 2 H, C*H*$_2$], 3.37 (s, 6 H, OCH_3). − ^{13}C{^{1}H} NMR (C_6D_6): δ = 1.6 (s, $SiMe_3$), 1.8 (s, $SiMe_3$), 6.8 [d, ^1J(P,C) = 81.5 Hz, *C*H(SiMe$_3$)$_2$], 18.6 (s, CH_3), 33.5 [d, ^2J(P,C) = 2.3 Hz, *C*H$_2$], 41.5 [d, ^1J(P,C) = 47.7 Hz, P*C*], 51.9 (s, O*C*H$_3$), 125.5 (s, *C*CH$_3$), 173.3 [d, ^3J(P,C) = 14.2 Hz, *C*O$_2$Me]. − ^{31}P{^{1}H} NMR ($CDCl_3$): δ = −105.8 (s). − MS (70 eV, EI), (^{184}W); *m*/*z* (%): 414 (15) [M$^+$·], 193 (100) [(Me$_3$Si)$_2$HCPH_2^+·], 73 (50) [$SiMe_3^+$].

Procedure for the Reaction of 1*H*-Phosphirene Tungsten Complex 9a with Diethylamine: To a solution of the 1*H*-phosphirene tungsten complex **9a** (0.25 g, 0.4 mmol) in toluene (5 mL) was added diethylamine (1 mL, 9.6 mmol) and the mixture was slowly stirred for 18 h at room temp. ^{31}P-NMR spectroscopic control showed that **21**, **22**, and **23** were formed in a ratio of 1:1:1. After concentration to dryness, the products were separated by low-temperature column chromatography of the residue (SiO_2, −20°C, 10 × 2 cm, hexane/diethyl ether, 98:2) and subsequently crystallized from pentane at −20°C. The crystals of **21**, **22**, and **23** were resolved manually using the Pasteur selection method.

Pentacarbonyl[1-{bis(trimethylsilyl)methyl}-2-(diethylamino)-2,3-bis(methoxycarbonyl)phosphirane-κ*P*]tungsten(0) (21): Yield: 55 mg (20%). − M.p. 114°C (dec.). − ^{1}H NMR (C_6D_6): δ = 0.20 (s, 9 H, $SiMe_3$), 0.29 (s, 9 H, $SiMe_3$), 0.93 [t, ^3J(H,H) = 6.7 Hz, 3 H, CH_2CH_3], 1.19 (m_c, 3 H, CH_2CH_3), 1.19 [d, ^2J(P,H) = 14.9 Hz, 1 H, C*H*(SiMe$_3$)$_2$], 2.70 (m_c, 2 H, CH_2CH_3), 3.18 (m_c, 1 H, CH_2CH_3), 3.35 [d, $^{(2+2)}J$(P,H) = 7.9 Hz, 1 H, PC*H*], 3.47 (m_c, 1 H, CH_2CH_3), 3.73 (s, 3 H, OCH_3), 3.80 (s, 3 H, OCH_3). − ^{13}C{^{1}H} NMR (C_6D_6): δ = 1.8 (s, $SiMe_3$), 2.0 (s, $SiMe_3$), 13.5 (s, CH_2CH_3), 14.0 (s, CH_2CH_3), 15.9 [d, ^1J(P,C) = 32.2 Hz, *C*H(SiMe$_3$)$_2$], 41.4 [d, $^{(1+2)}J$(P,C) = 14.2 Hz, P*C*HC], 46.6 [d, ^3J(P,C) = 5.4 Hz, *C*H$_2$CH$_3$], 49.5 (s, *C*H$_2$CH$_3$), 51.9 (s, O*C*H$_3$), 52.3 (s, O*C*H$_3$), 66.6 [d, $^{(1+2)}J$(P,C) = 16.0 Hz, P*C*N], 167.1 (s, *C*O$_2$Me), 172.2 (s, *C*O$_2$Me), 196.4 [d, ^2J(P,C) = 35.1 Hz, *trans*-*C*O], 197.1 [d, ^2J(P,C) = 7.0 Hz, *cis*-*C*O]. − ^{31}P{^{1}H} NMR ($CDCl_3$): δ = −81.1 [s, ^1J(P,W) = 274.7 Hz]. − IR (KBr): $\tilde{\nu}$ = 2038 (s), 1996 (s), 1935 (vs), 1911 (vs) cm^{-1} (CO); 1735 (s), 1700 (s) cm^{-1} (CO_2). − MS (70 eV, EI), (^{184}W); *m*/*z* (%): 729 (20) [M$^+$·], 486 (70) [(OC)$_4$WPCH(SiMe$_3$)$_2^+$·], 184 (100) [MeO$_2$C(H)CC(NEt$_2$)CO$^+$·]. − $C_{22}H_{36}NO_9PSi_2W$ (729.5): calcd. C 36.22, H 4.97, N 1.92; found C 36.36, H 5.08, N 1.98.

Pentacarbonyl{[bis(trimethylsilyl)methyl]-1-[2-(diethylamino)-1,2-bis(methoxycarbonyl)ethenyl]phosphane-κ*P*}tungsten(0) (22): Yield: 110 mg (40%). − M.p. 86°C (dec.). − ^{1}H NMR (C_6D_6): δ = 0.26 (s, 9 H, $SiMe_3$), 0.28 [d, ^4J(P,H) = 3.3 Hz, 9 H, $SiMe_3$], 0.77 [t, ^3J(H,H) = 7.0 Hz, 3 H, CH_2CH_3], 0.85 (m_c, 3 H, CH_2CH_3), 1.03 [dd, ^2J(P,H) = 11.1 Hz, ^3J(H,H) = 5.6 Hz, 1 H, C*H*(SiMe$_3$)$_2$], 2.80 [q, ^3J(H,H) = 7.3 Hz, 2 H, CH_2CH_3], 2.95 (m_c, 2 H, CH_2CH_3), 3.42 (s, 3 H, OCH_3), 3.55 (s, 3 H, OCH_3), 5.82 [dd, ^1J(P,H) = 330.1 Hz, ^3J(H,H) = 5.6 Hz, 1 H, C*H*]. − ^{13}C{^{1}H} NMR (C_6D_6): δ = 1.9 [d, ^3J(P,C) = 3.5 Hz, $SiMe_3$], 2.5 [d, ^3J(P,C) = 2.8 Hz, $SiMe_3$], 13.3 (s, CH_2CH_3), 17.3 [d, ^1J(P,C) = 5.5 Hz, *C*H(SiMe$_3$)$_2$], 46.1 (s, *C*H$_2$CH$_3$), 47.4 (s, *C*H$_2$CH$_3$), 51.3 (s, O*C*H$_3$), 52.3 (s, O*C*H$_3$), 95.7 [d, ^1J(P,C) = 39.9 Hz, P*C*C], 155.6 [d, ^3J(P,C) = 2.4 Hz, *C*O$_2$Me], 166.4 [d, ^2J(P,C) = 2.8 Hz, *C*O$_2$Me], 166.8 [d, ^2J(P,C) = 16.1 Hz, PC*C*], 198.5 [d, ^2J(P,C) = 6.8 Hz, *cis*-*C*O], 201.0 (m_c, *trans*-*C*O). − ^{31}P{^{1}H} NMR ($CDCl_3$): δ = −48.7 [s, ^1J(P,W) = 235.2 Hz]. − IR (KBr): $\tilde{\nu}$ = 2067 (s), 1975 (s), 1915 (vs) cm^{-1} (CO); 1730 (s), 1693 (s) cm^{-1} (CO_2). − MS (70 eV, EI), (^{184}W); *m*/*z* (%): 729 (2) [M$^+$·], 674 (50) [(M − 2 CO)$^+$·], 362 (100) [$C_{16}H_{31}NO_3Si_2P^+$·], 73 (80) [$SiMe_3^+$]. − $C_{22}H_{36}NO_9PSi_2W$ (729.5): calcd. C 36.22, H 4.97, N 1.92; found C 36.41, H 5.03, N 1.88.

Pentacarbonyl[1-{bis(trimethylsilyl)methyl}-3-dimethylamino-4-methoxycarbonyl-1,2-dihydro-1-phosphet-2-one-κ*P*]tungsten(0) (23): Yield: 55 mg (20%). − M.p. 100°C (dec.). − ^{1}H NMR (C_6D_6): δ = 0.11 (s, 9 H, $SiMe_3$), 0.33 [d, ^4J(P,H) = 0.3 Hz, 9 H, $SiMe_3$], 0.78 [t, ^3J(H,H) = 7.1 Hz, 6 H, CH_2CH_3], 1.24 [d, ^2J(P,H) = 8.7 Hz, 1 H, C*H*(SiMe$_3$)$_2$], 2.78 [q, ^3J(H,H) = 7.1 Hz, 2 H, CH_2CH_3], 2.56 (m_c, 2 H, CH_2CH_3), 3.55 (s, 3 H, OCH_3), 3.56 (s, 3 H, OCH_3). −

Table 3. Crystal data and structure refinement of complexes **9a**, **10b**, **19**, **21**, and **23**

Complex	**9a**	**10b**	**19**	**21**	**23**
Empirical formula	$C_{18}H_{25}O_9PSi_2W$	$C_{21}H_{31}N_2O_9PSi_2W$	$C_{24}H_{35}O_9PSi_2W$	$C_{22}H_{36}NO_9PSi_2W$	$C_{21}H_{32}NO_8P_2Si_2W$
Formula weight M_r [g mol^{-1}]	656.38	726.48	728.52	729.52	697.48
Crystal size [mm]	0.50 × 0.35 × 0.20	0.40 × 0.24 × 0.14	0.70 × 0.50 × 0.40	0.50 × 0.35 × 0.20	0.60 × 0.50 × 0.25
Crystal system	monoclinic	triclinic	triclinic	triclinic	triclinic
Space group	*C*2/*c*	*P*−1	*P*−1	*P*−1	*P*−1
a [Å]	33.558(3)	10.3286(14)	9.4580(10)	10.940(4)	10.050(4)
b [Å]	9.4981(10)	12.5475(16)	10.9450(10)	11.333(4)	10.239(4)
c [Å]	18.972(2)	23.393(2)	15.785(2)	13.579(5)	14.453(4)
α [°]	90	92.177(8)	75.416(10)	81.56(2)	100.64(4)
β [°]	120.544(5)	95.816(10)	88.493(10)	80.61(3)	94.53(4)
γ [°]	90	100.268(12)	73.844(10)	63.60(2)	98.98(4)
Volume [Å^3]	5207.9(9)	2962.9(6)	1517.3(3)	1482.6(9)	1434.8(9)
Z	8	4	2	2	2
Density D_X [Mg m^{-3}]	1.674	1.629	1.617	1.634	1.614
Absorption coefficient μ [mm^{-1}]	4.631	4.080	3.984	4.076	4.205
F(000)	2576	1440	736	728	692
Temperature *T* [°C]	−100	−100	−100	−130	−130
Data collection $2\theta_{max}$	50	50	50	50	50
Limiting indices (*h*, *k*, *l*)	−37/43, −12/9, −24/0	−12/12, −14/12, −27/27	−10/11, −12/12, −18/7	−13/12, −13/15, −15/16	−11/2, −12/12, −17/17
Reflections collected	11324	13786	8089	5518	6127
Independent reflections	5985	10415	5296	5219	5057
R_{int}	0.0312	0.0279	0.0135	0.0157	0.0271
Parameters	279	669	344	372	316
Restraints	103	36	169	150	123
Final $wR2(F^2)$ [all data]	0.071	0.053	0.044	0.046	0.064
Final $R1(F)$ [$I > 2\sigma(I)$]	0.032	0.028	0.019	0.019	0.025
Max. and min. Δρ [eÅ^{-3}]	1.143/−1.656	0.873/−0.714	0.658/−0.473	0.741/−0.364	1.110/−1.124

$^{13}C\{^1H\}$ NMR (C_6D_6): δ = 2.4 [d, ^3J(P,C) = 2.9 Hz, $SiMe_3$], 2.5 [d, ^3J(P,C) = 2.2 Hz, $SiMe_3$], 14.0 (m_c, CH_2CH_3), 27.8 [d, ^1J(P,C) = 21.0 Hz, $CH(SiMe_3)_2$], 45.5 (s, CH_2CH_3), 51.3 (s, OCH_3), 119.4 [d, $^{(1+3)}J$(P,C) = 41.6 Hz, $PCCO_2Me$], 152.9 [d, $^{(2+2)}J$(P,C) = 56.2 Hz, PC*C*], 165.0 [d, ^2J(P,C) = 14.5 Hz, CO_2Me], 197.7 [d, ^2J(P,C) = 6.9 Hz, *cis*-*C*O], 198.7 [d, $^{(1+3)}J$(P,C) = 35.7 Hz, P*C*O], 200.1 [d, ^2J(P,C) = 24.7 Hz, *trans*-*C*O]. − $^{31}P\{^1H\}$ NMR ($CDCl_3$): δ = 71.7 [s, ^1J(P,W) = 241.2 Hz]. − IR (KBr): $\tilde{\nu}$ = 2069 (s), 1942 (vs, br) cm^{-1} (CO); 1742 (s), 1693 (s) cm^{-1} (CO_2). − MS (70 eV, EI), (^{184}W); *m*/*z* (%): 698 (30) [M$^+$·], 557 (100) [(M − 4 CO − C_2H_5)$^+$·], 362 (100) [$C_{16}H_{31}NO_3Si_2P^+$], 73 (80) [$SiMe_3^+$]. − $C_{22}H_{36}NO_9PSi_2W$ (697.5): calcd. C 36.16, H 4.62, N 2.01; found C 36.35, H 4.79, N 1.91.

Data Collection, Structure Solution, and Refinement of 9a, 10b, 19, 21, and 23: Crystal data for all the structures are presented in Table 3. Structure determination of **9a**, **10b**, and **19**: A yellow prism (**9a**), a yellow tablet (**10b**), or a pale-yellow block (**19**) was mounted in inert oil and measured by ω-scans using Mo-K_α radiation (graphite monochromator) on a Siemens P4 diffractometer. After an absorption correction (ψ-scans), all unique data were used for the calculations (**9a**, **19**: program SHELXL-93;[37] **10b**: program SHELXL-97[38]). The structures were solved by direct methods (**9a**, **10b**) or the heavy-atom method (**19**) and refined anisotropically by full-matrix least-squares on F^2. All hydrogen atoms (except rigid methyl groups) were refined as a riding model. Structure determination of **21** and **23**: A colourless tablet (**21**) or an orange tablet (**23**) was mounted in inert oil and measured by ω/θ-scans using Mo-K_α radiation (graphite monochromator) on a Stoe STADI-4 diffractometer. Structure solution: heavy-atom method. Other details were as for **10b** above.

Acknowledgments

Support by the Deutsche Forschungsgemeinschaft and the Fonds der Chemischen Industrie, and MS measurements by Dr. Hans-Martin Schiebel (Technische Universität Braunschweig) are gratefully acknowledged.

[1] U. Rohde, J. Jeske, F. Ruthe, P. G. Jones, R. Streubel, *Angew. Chem.* **1999**, *111*, 158−160; *Angew. Chem. Int. Ed. Engl.* **1999**, *37*, 215−217.
[2] [2a] J. Manassen, in *Catalysis: Progress in Research* (Eds.: F. Basolo, R. L. Burwell), Plenum Press, London, **1973**, pp.177, 183. − [2b] E. G. Kuntz, *Chem. Tech.* **1987**, *17*, 570−575.
[3] Reviews: [3a] D. Sinou, *Bull. Soc. Chim. Fr.* **1987**, *3*, 480−486. − [3b] T. G. Southern, *Polyhedron* **1989**, *8*, 407−413. − [3c] P. Kalck, F. Monteil, *Adv. Organomet. Chem.* **1992**, *34*, 219−284. − [3d] W. A. Herrmann, C. W. Kohlpainter, *Angew. Chem.* **1993**, 105, 1588−1609; *Angew. Chem. Int. Ed. Engl.* **1993**, *32*, 1524−1544, and refs. cited therein.
[4] [4a] M. Reuter, L. Orthner, G. P. 1,035,135 (*Chem. Abstr.* **1960**, *54*, 14125a). − [4b] J. Chatt, G. J. Leigh, R. M. Slade, *J. Chem. Soc., Dalton Trans.* **1973**, 2021−2028.
[5] Rhône-Poulenc Recherche (E. Kuntz), FR 2.314.910, **1975**.
[6] J. Podlahová, J. Podlaha, *Collect. Czech. Chem. Commun.* **1980**, *45*, 2049−2053.
[7] W. A. Herrmann, C. W. Kohlpainter, R. B. Manatsberger, H. Bahrmann, H. Kottmann, *J. Mol. Catal. A* **1995**, *97*, 65.
[8] F. Mercier, F. Mathey, *J. Organomet. Chem.* **1993**, *462*, 103−106.
[9] C. Meyer, S. Boulmaaz, J. Liedtke, S. Loss, H. Schönberg, M. Wörle, H.-J. Grützmacher, *XIV International Conference on Phosphorus Chemistry*, Cincinnati, Ohio, **1998**, Lecture LW6-4.
[10] [10a] A. Marinetti, F. Mathey, *Tetrahedron Lett.* **1987**, *28*, 5021−5024. − [10b] A. Espinosa Ferao, B. Deschamps, F. Mathey, *Bull. Soc. Chim. Fr.* **1993**, *130*, 695−699. − [10c] S. Holand,

M. Jeanjean, F. Mathey, *Angew. Chem*. **1997**, *107*, 117−119; *Angew. Chem. Int. Ed. Engl.* **1997**, *36*, 98−100.
[11] J. C. Tebby, S. E. Willetts, D. V. Griffiths, *J. Chem. Soc., Chem. Commun.* **1981**, 420−421.
[12] [12a] N. E. Waite, J. C. Tebby, R. S. Ward, D. H. Williams, *J. Chem. Soc. C* **1969**, 1100−1104. − [12b] N. E. Waite, J. C. Tebby, *J. Chem. Soc. C* **1970**, 386−392. − [12c] D. G. Holah, A. N. Hughes, D. Kleemola, *J. Heterocycl. Chem.* **1978**, *15*, 1319−1330. − [12d] E. M. Hanawalth, K. M. Doxsee, G. S. Shen, T. J. R. Weakley, C. B. Knobler, H. Hope, *Heteroatom Chem.* **1998**, *9*, 9−19. − [12e] E. M. Hanawalth, K. M. Doxsee, G. S. Shen, T. J. R. Weakley, H. Hope, *Heteroatom Chem.* **1998**, *9*, 21−28. − [12f] J. Barluenga, M. Tomás, K. Bieger, S. García-Granda, R. Santiago-García, *Eur. J. Org. Chem.* **1998**, 1425−1429.
[13] [13a] N. H. Tran Huy, F. Mathey, *Tetrahedron Lett.* **1988**, *29*, 3077−3078. − [13b] H. Trauner, E. de la Cuesta, A. Marinetti, F. Mathey, *Bull. Soc. Chim. Fr.* **1995**, *132*, 384−393.
[14] [14a] R. Streubel, A. Kusenberg, J. Jeske, P. G. Jones, *Angew. Chem.* **1994**, *106*, 2564−2566; *Angew. Chem. Int. Ed. Engl.* **1994**, *33*, 2427−2428. − [14b] R. Streubel, A. Ostrowski, H. Wilkens, F. Ruthe, J. Jeske, P. G. Jones, *Angew. Chem.* **1997**, *109*, 409−413; *Angew. Chem. Int. Ed. Engl.* **1997**, *36*, 378−381.
[15] [15a] R. Streubel, L. Ernst, J. Jeske, P. G. Jones, *J. Chem. Soc., Chem. Commun.* **1995**, 2113−2114. − [15b] R. Streubel, U. Rohde, H. Wilkens, *Phosphorus Sulfur Relat. Elem.* **1998**, *124*/*125*, 545−548.
[16] [16a] H. Wilkens, J. Jeske, P. G. Jones, R. Streubel, *J. Chem. Soc., Chem. Commun.* **1997**, 2317−2318. − [16b] H. Wilkens, F. Ruthe, P. G. Jones, R. Streubel, *Chem. Eur. J.* **1998**, *4*, 1542−1553.
[17] [17a] A. Ostrowski, J. Jeske, P. G. Jones, *J. Chem. Soc., Chem. Commun.* **1995**, 2113−2114. − [17b] A. Ostrowski, J. Jeske, F. Ruthe, P. G. Jones, R. Streubel, *Z. Anorg. Allg. Chem.* **1997**, *623*, 1897−1902.
[18] [18a] R. Streubel, H. Wilkens, A. Ostrowski, C. Neumann, F. Ruthe, P. G. Jones, *Angew. Chem. Int. Ed. Engl.* **1997**, *109*, 1549−1550; *Angew. Chem. Int. Ed. Engl.* **1997**, *36*, 1492−1493. − [18b] H. Wilkens, F. Ruthe, P. G. Jones, R. Streubel, *J. Chem. Soc., Chem. Commun.* **1998**, 1529−1530.
[19] R. Streubel, S. Priemer, U. Rohde, F. Ruthe, P. G. Jones, *Eur. J. Inorg. Chem.* **1998**, 257−261.
[20] R. Streubel, U. Rohde, J. Jeske, F. Ruthe, P. G. Jones, *Eur. J. Inorg. Chem.* **1998**, 2005−2012.
[21] S. Berger, S. Braun, H. O. Kalinowski, in *NMR-Spektroskopie von Nichtmetallen*, vol. 3, Georg Thieme Verlag, Stuttgart, **1993**, p. 107.
[22] [22a] F. Mathey, F. Mercier, C. Charrier, *J. Am. Chem. Soc.* **1981**, *103*, 4595−4597. − [22b] P. Le Goff, F. Mathey, L. Ricard, *J. Org. Chem.* **1989**, *54*, 4754−4758. − [22c] S. Lelièvre, F. Mercier, F. Mathey, *J. Org. Chem.* **1996**, *61*, 3531−3533.
[23] [23a] F. Laporte, F. Mercier, L. Ricard, F. Mathey, *Bull. Soc. Chim. Fr.* **1993**, *130*, 843−850. − [23b] K. Maitra, J. H. Nelson, *Bull. Soc. Chim. Fr.* **1997**, *134*, 859−867.
[24] A. Marinetti, F. Mathey, *J. Am. Chem. Soc.* **1985**, *107*, 4700−4706.
[25] [25a] A. Marinetti, J. Fischer, F. Mathey, *J. Am. Chem. Soc.* **1985**, *107*, 5001−5002. − [25b] A. Marinetti, F. Mathey, *Organometallics* **1988**, *7*, 633−637.
[26] F. Mathey, M. Regitz, in: *Comprehensive Heterocyclic Chemistry II* (Eds.: A. R. Katritzky, C. W. Rees, E. F. V. Scriven), Pergamon, New York, **1997**, vol. 1A, p. 277−304.
[27] E. Schmitz, H. Sonnenschein, R. J. Kuban, *Tetrahedron Lett.* **1985**, *26*, 4911−4914.
[28] M. Baudler, *Angew. Chem.* **1982**, *94*, 520−539; *Angew. Chem. Int. Ed. Engl.* **1982**, *21*, 492−511.
[29] J. Mason, *Multinuclear NMR*, Plenum Press, New York, **1987**.
[30] F. Mathey, *Chem. Rev.* **1990**, *90*, 997−1025.
[31] Crystallographic data (excluding structure factors) for the structures reported in this paper have been deposited with the Cambridge Crystallographic Data Centre as supplementary publication nos. CCDC-114310, -114311, -114312, -114313, and -114314. Copies of the data can be obtained free of charge on application to CCDC, 12 Union Road, Cambridge CB2 1EZ, U.K. [Fax: (internat.) + 44-1223/336-033; E-mail: deposit@ccdc.cam.ac.uk].
[32] A. G. Orpen, N. G. Connelly, *Organometallics* **1990**, *9*, 1206−1210, and refs. cited therein.
[33] B. J. Dunne, R. B. Morris, A. G. Orpen, *J. Chem. Soc., Dalton Trans.* **1991**, 653−661, and refs. cited therein.
[35] F. H. Allen, O. Kennard, D. G. Watson, L. Brammer, A. G. Orpen, R. Taylor, *J. Chem. Soc., Perkin Trans. 2* **1987**, S1−S19.
[36] C. A. Tolman, *Chem. Rev.* **1977**, *77*, 313−348.
[37] G. M. Sheldrick, *SHELXL-93, Program for Crystal Structure Refinement*, University of Göttingen, **1993**.
[38] G. M. Sheldrick, *SHELXL-97, Program for Crystal Structure Refinement*, University of Göttingen, **1997**.

Received March 12, 1999
[I99093]

Diversity in Complexation of $[Rh^I(cod)]^+$ and $[Ir^I(cod)]^+$ by Pyridine-Amine-Pyrrole Ligands

Bas de Bruin,[a] Reinout J. N. A. M. Kicken,[a] Nicolaas F. A. Suos,[a] Maurice P. J. Donners,[a] Carolien J. den Reijer,[a] Albertus J. Sandee,[a] René de Gelder,[a] Jan M. M. Smits,[a] Anton W. Gal,*[a] and Anton L. Spek[b]

Keywords: Rhodium / Iridium / N ligands / Coordination modes / Polymerizations

Complexation of $[Rh^I(cod)]^+$ and $[Ir^I(cod)]^+$ by the new pyridine-amine-pyrrole ligands Py–CH_2–N(R)–CH_2–Pyr–H (HL_R; R = H, Bzl, Bu) and the corresponding pyridine-amine-pyrrolate ligands $[Py–CH_2–N(R)–CH_2–Pyr]^-$ (L_R^-; R = H, Bzl, Bu, CH_2Py) has been investigated. The neutral ligands HL_R (R = H, Bu, Bzl) give $[(HL_R)M^I(cod)]^+$ (M = Rh, Ir) in which HL_R acts as a didentate ligand via the pyridine nitrogen (N_{Py}) and the amine nitrogen (N^R_{amine}). The crystal structures of $[(HL_H)M^I(cod)]PF_6$ (M = Rh: **[1]**PF_6 and M = Ir: **[2]**PF_6) have been determined. Deprotonation of $[(HL_R)M^I(cod)]^+$ (M = Rh, Ir; R = H, Bzl, Bu) results in the neutral complexes $[(L_R)M^I(cod)]$ (M = Rh, Ir) of the mono-anionic ligands L_R^- (R = H, Bzl, Bu). In square-planar $[(L_H)M^I(cod)]$ (M = Rh: **3**, M = Ir: **4**), L_H^- is didentate via N^H_{amine} and the pyrrolate nitrogen (N_{Pyr}). The X-ray structures of **3** and **4** reveal that in both cases the uncoordinated N_{Py} accepts a hydrogen bond from N^H_{amine}. The X-ray structures of $[(L_{Bzl})M^I(cod)]$ (M = Rh: **5**, M = Ir: **6**), show that L_{Bzl}^- is didentate via N_{amine} and N_{Pyr} for M = Rh and tridentate for M = Ir. In solution L_{Bzl}^- is tridentate for both M = Rh and M = Ir. The neutral complexes $[\{Py–CH_2–N(R)–CH_2–Pyr\}M^I(cod)]$ (M = Rh, Ir) cannot be oxidised selectively with H_2O_2. This is in marked contrast to the previously observed selective oxidation of the corresponding cationic complexes $[\{Py–CH_2–N(R)–CH_2–Py\}Rh^I(cod)]^+$. Rhodium complex **5** is an active catalyst for the stereoregular polymerisation of phenylacetylene, whereas iridium complex **6** is inactive.

Introduction

Multidentate N-donor ligands ("N_x" ligands) have thusfar found limited application in the organometallic chemistry of rhodium(I) and iridium(I). Interesting reactivity has, however, been reported for triazacyclononane,[1][2] trispyrazolylborate,[2] and pyridine-2,6-diimine[3] complexes. We recently described the fast and selective mono-oxygenation of $[Rh^I(cod)]^+$ to $[Rh^{III}(oxabicyclononadiyl)]^+$ with aqueous hydrogen peroxide.[4] In this reaction $[Rh^I(cod)]^+$ is stabilised by the neutral tridentate pyridine-amine-pyridine ligands Py−CH_2−N(R)−CH_2−Py (R = H, Bu, Bzl). As part of our investigation into the tolerance of the observed oxygenation to changes in the nitrogen donor ligands, we have prepared and characterised a series of neutral complexes $[\{Py−CH_2−N(R)−CH_2−Pyr\}M^I(cod)]$ (M = Rh, Ir). In these, $[M^I(cod)]^+$ is stabilised by the potentially tridentate pyridine-amine-pyrrolate ligands $[Py−CH_2−N(R)−CH_2−Pyr]^-$ ($[L_R]^-$; R = H, Bzl, Bu). The complexes were obtained by deprotonation of the cationic complexes $[\{Py−CH_2−N(R)−CH_2−Pyr−H\}M^I(cod)]^+$ which result from reaction of $[\{(cod)M^I(\mu\text{-}Cl)\}_2]$ (M = Rh, Ir) with the neutral didentate ligands Py−CH_2−N(R)−CH_2−Pyr−H (HL_R;R = H, Bu, Bzl).

[a] Department of Inorganic Chemistry, University of Nijmegen, Toernooiveld 1, NL-6525 ED Nijmegen, The Netherlands
Fax: (internat.) +31-24/ 355-3450
E-mail: gal@sci.kun.nl
[b] Department of Crystal and Structural Chemistry, Bijvoet Centre for Biomolecular Research, University of Utrecht

Results and Discussion

Synthesis of the Ligands HL_R

The neutral ligands HL_R (R = H, Bzl, Bu; see Figure 1) were prepared via the synthesis routes shown in Scheme 1.

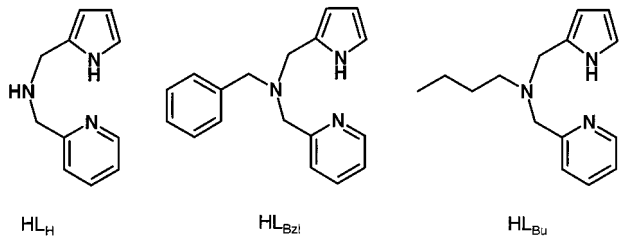
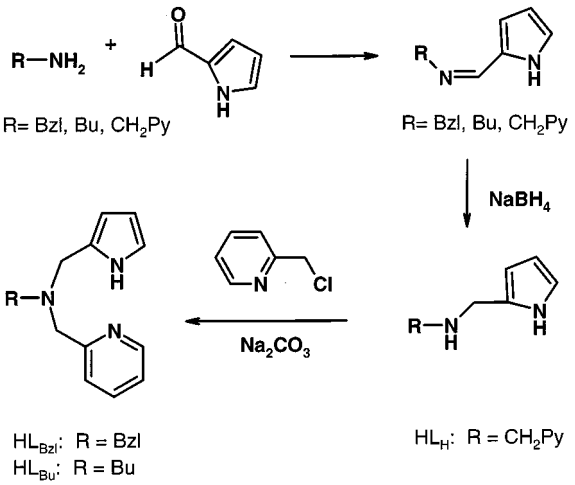


Figure 1. Pyridine-amine-pyrrole ligands HL_H, HL_{Bzl}, and HL_{Bu}

N-(2-pyridylmethyl)-*N*-(1*H*-2-pyrrolylmethyl)amine (HL_H) was prepared in two steps: condensation of 2-pyridylmethylamine and pyrrole-2-carboxaldehyde to the corresponding imine and subsequent reduction of the imine with $NaBH_4$. *N*-benzyl-*N*-(2-pyridylmethyl)-*N*-(1*H*-2-pyrrolylmethyl)-amine (HL_{Bzl}) and *N*-butyl-*N*-(2-pyridylmethyl)-*N*-(1*H*-2-pyrrolylmethyl)amine (HL_{Bu}) were prepared in three steps: *N*-benzyl-*N*-(1*H*-2-pyrrolylmethylidene)amine and *N*-butyl-*N*-(2-pyrrolylmethylidene)amine were obtained by condensation of pyrrole-2-carboxaldehyde with benzylamine and *n*-butylamine, respectively. The imines were reduced to the corresponding amines with $NaBH_4$. Alkylation of the amines with 2-picolyl chloride in a suspension of Na_2CO_3 in CH_3CN gave HL_{Bzl} and HL_{Bu}, respectively.

 © WILEY-VCH Verlag GmbH, D-69451 Weinheim, 1999 1434−1948/99/0909−1581 $ 17.50+.50/0



Scheme 1. Synthesis of the ligands HL_H, HL_{Bzl}, and HL_{Bu}

Structure of HL_H

Colourless crystals of compound HL_H were obtained by crystallisation from a hot saturated toluene solution. The structure of HL_H was determined by single-crystal X-ray diffraction (Figure 2).

In the crystal, the enantiomers (*R*) and (*S*) of HL_H occur as hydrogen-bridged dimers (*R*,*R*) and (*S*,*S*) in which the pyrrole N−H (N_{Pyr}−H) acts as a hydrogen bond donor, and the amine nitrogen (N_{amine}) as a hydrogen bond acceptor [N_{Pyr}−N_{amine} distance: 3.02(1) Å, H−N_{amine} distance: 2.09(6) Å, N_{Pyr}−H−N_{amine} angle: 169(4)°]. Selected bond lengths and angles are given in Tables 1 and 2. Crystallographic data are given in Table 4.

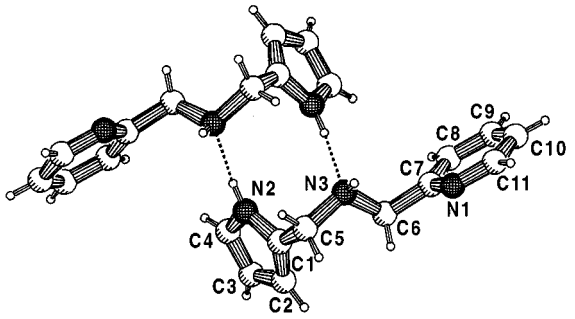


Figure 2. X-ray structure of ligand HL_H [the crystal contains the dimers (*R*,*R*) and (*S*,*S*) of the enantiomers (*R*) and (*S*); only (*R*,*R*) is shown]

Complexation of $[Rh^I(cod)]^+$ and $[Ir^I(cod)]^+$ by HL_H

Reaction of HL_H with $[\{(cod)Rh(\mu\text{-}Cl)\}_2]$ in methanol, followed by addition of an excess of NH_4PF_6, resulted in precipitation of $[(HL_H)Rh^I(cod)]PF_6$, [**1**]PF_6. Crystals of [**1**]PF_6 were obtained by cooling of a hot saturated solution of [**1**]PF_6 in methanol. The analogous reaction of HL_H with $[\{(cod)Ir(\mu\text{-}Cl)\}_2]$ in $MeOH/CH_2Cl_2$, followed by addition of excess KPF_6, led to precipitation of [**2**]PF_6. Crystals of [**2**]PF_6, were obtained by cooling of a saturated solution of [**2**]PF_6 in $MeOH/H_2O$ to 5 °C. The structures of [**1**]PF_6 and [**2**]PF_6 were determined by X-ray diffraction. The X-ray structure of $\mathbf{1}^+$ is shown in Figure 3. $\mathbf{2}^+$ was found to be isostructural. Selected bond lengths and angles for $\mathbf{1}^+$ and $\mathbf{2}^+$ are given in Tables 1 and 2.

Complexes $\mathbf{1}^+$ and $\mathbf{2}^+$ have the expected square-planar geometry. The ligand HL_H is didentate via the pyridine (N_{Py}) and amine (N_{amine}) nitrogens. No interaction is observed between the metal centre and the pyrrole N−H bond (N_{Pyr}−H). In both structures, the N_{Pyr}−H and N^H_{amine} protons are hydrogen bonded to two different PF_6^- counterions ($\mathbf{1}^+$: N_{amine}−F6 distance: 3.165(6) Å, H30−F6 distance: 2.33(7) Å, N_{amine}−H30−F6 angle: 173(6)°, N_{Pyr}−F3 distance: 3.118(6) Å, H20−F3 distance: 2.57(6) Å, N_{Pyr}−H20−F3 angle: 141(6)°; $\mathbf{2}^+$: N_{amine}−F6 distance: 3.098(7) Å, H30−F6 distance: 2.33(7) Å, N_{amine}−H30−F6 angle: 159(6)°, N_{Pyr}−F3 distance: 3.133(7) Å, H20−F3 distance: 2.54(7) Å, N_{Pyr}−H20−F3 angle: 152(8)°). In $[\mathbf{1}]^+$ the Rh−N_{Py} distance [Rh1−N1: 2.101(4) Å] and the Rh−N_{amine} distance [Rh1−N3: 2.144(4) Å] fall within the ranges of Rh−N_{sp2} (2.007−2.140 Å)[5] and Rh−N_{sp3} (2.111−2.178 Å)[5f,6] distances observed for other square planar "N_2"Rh^I(cod) complexes. The observed Rh−C and cod double bond lengths are also normal for "N_2"Rh^I(cod) complexes (Table 1).

The NMR data for [**1**]PF_6 and [**2**]PF_6 in [D_6]acetone are very similar, and are in accordance with their X-ray structure. The largest shift difference between $\mathbf{1}^+$ and $\mathbf{2}^+$ is observed for the *olefinic* cod fragment $(-CH=CH-)_{cod}$ (see Table 3). In the ^{1}H-NMR spectrum of [**1**]PF_6 the pyrrole signals appear at almost the same position as for the free HL_H, whereas the N^H_{amine} proton has shifted 2.75 ppm downfield (HL_H: δ = 2.24, [**1**]PF_6: δ = 4.99). The pyridine-H^6 signal has shifted 0.53 ppm upfield (HL_H: δ = 8.49, [**1**]PF_6: δ = 7.96) as a result of anisotropic shielding by η^4-cod. The N−CH_2−Pyr− and N−CH_2−Py signals appear as singlets at room temp. due to rapid dissociation, pyramidal inversion, and recoordination of N^H_{amine}. Combination of this inversion with rapid rotation of the η^4-cod fragment results in only one signal each for the vinylic, the allylic *exo* and the allyllic *endo* protons of cod. At −80 °C the pyramidal inversion at N_{amine} and rotation of cod are both frozen out. This results in two AB-type doublets for both N−CH_2−Pyr and N−CH_2−Py, each with an additional coupling to the N^H_{amine} proton. At this temperature each cod proton appears as a separate signal, with the exception of two overlapping allylic *exo* protons and two sets of two overlapping allylic *endo* protons.

Complexation of $[Rh^I(cod)]^+$ and $[Ir^I(cod)]^+$ by L_H^-

Reaction of HL_H with $[\{(cod)M^I(\mu\text{-}Cl)\}_2]$ (M = Rh, Ir) in methanol resulted in a solution of $[(HL_H)M^I(cod)]Cl$ M = Rh, Ir). The neutral complexes $[(L_H)M(cod)]$ (M = Rh: **3**; M = Ir: **4**) precipitated upon deprotonation of the uncoordinated pyrrole nitrogen (N_{Pyr}−H) by excess aqueous Na_2CO_3. Cooling of a saturated solution of rhodium

Table 1. Selected bond lengths [Å] for HL_H, **[1]**PF_6, **[2]**PF_6, **3**, $\mathbf{4^A}/\mathbf{4^B}$, **5**, and **6**[a]

	HLH	**[1]**PF_6 (M1 = Rh1)	**[2]**PF_6 (M1 = Ir1)	**3** (M1 = Rh1)	$\mathbf{4^A}$ (M1 = Ir1)	$\mathbf{4^B}$ (M1 = Ir1)	**5** (M1 = Rh)	**6** (M1 = Ir)
N1−M1		2.101(4)	2.083(4)	n. b.	n. b.	n. b	n. b.	2.235(7)
N2−M1		n. b.	n. b.	2.034(3)	2.020(5)	2.023(5)	2.039(3)	2.066(7)
N3−M1		2.144(4)	2.130(4)	2.164(3)	2.147(5)	2.150(5)	2.231(2)	2.397(7)
C12−M1		2.133(4)	2.117(5)	2.117(3)	2.120(6)	2.113(7)	2.106(3)	2.068(8)
C13−M1		2.143(4)	2.127(5)	2.126(3)	2.115(6)	2.098(6)	2.119(3)	2.055(8)
C16−M1		2.154(4)	2.136(5)	2.121(3)	2.125(6)	2.113(7)	2.156(3)	2.136(11)
C17−M1		2.146(4)	2.138(5)	2.145(8)	2.123(6)	2.132(6)	2.146(3)	2.129(10)
C12−C13		1.398(7)	1.403(8)	1.398(5)	1.406(10)	1.429(11)	1.393(5)	1.476(14)
C16−C17		1.392(7)	1.403(8)	1.398(5)	1.411(10)	1.417(10)	1.395(5)	1.414(16)
C6−C7	1.505(7)	1.506(6)	1.492(7)	1.521(5)	1.512(8)	1.519(9)	1.498(4)	1.488(11)
N3−C6	1.454(7)	1.494(6)	1.486(6)	1.458(5)	1.475(8)	1.476(8)	1.507(4)	1.499(11)
C1−C5	1.485(7)	1.479(7)	1.480(8)	1.484(5)	1.484(9)	1.487(9)	1.490(5)	1.493(13)
N3−C5	1.478(7)	1.498(6)	1.520(7)	1.498(4)	1.505(8)	1.506(8)	1.506(5)	1.477(11)
N3−C20	–	–	–	–	–	–	1.497(4)	1.474(12)
Pyridine								
N1−C7	1.331(6)	1.342(6)	1.366(7)	1.334(5)	1.352(9)	1.332(9)	1.356(5)	1.342(11)
C7−C8	1.384(7)	1.386(7)	1.387(7)	1.389(5)	1.377(10)	1.398(10)	1.389(5)	1.407(13)
C8−C9	1.372(8)	1.387(8)	1.386(9)	1.377(5)	1.384(11)	1.361(12)	1.390(7)	1.383(14)
C9−C10	1.369(8)	1.385(8)	1.381(9)	1.361(6)	1.370(12)	1.398(13)	1.373(9)	1.400(15)
C10−C11	1.365(8)	1.375(7)	1.392(8)	1.377(6)	1.385(11)	1.375(12)	1.361(7)	1.366(14)
C11−N1	1.330(7)	1.352(6)	1.336(7)	1.332(5)	1.343(9)	1.346(9)	1.354(5)	1.357(12)
Pyrrole								
N2−C1	1.371(7)	1.361(5)	1.350(8)	1.377(4)	1.384(8)	1.358(8)	1.364(4)	1.354(12)
C1−C2	1.362(7)	1.371(7)	1.371(8)	1.375(5)	1.380(9)	1.387(9)	1.379(4)	1.368(14)
C2−C3	1.408(7)	1.411(8)	1.399(10)	1.419(5)	1.411(10)	1.394(11)	1.403(6)	1.419(16)
C3−C4	1.354(9)	1.350(9)	1.344(11)	1.372(5)	1.382(10)	1.364(10)	1.371(5)	1.361(16)
C4−N2	1.375(6)	1.362(5)	1.360(8)	1.370(4)	1.379(8)	1.380(8)	1.368(4)	1.390(12)

[a] For atom labelling see Figure 2−6. Superscripts A and B refer to crystallographically independent molecules.

complex **3** in toluene resulted in crystals suitable for single-crystal X-ray diffraction. The analogous procedure for iridium complex **4** gave micro-crystalline material with a PXRD-pattern different from that of crystalline **3**. Single crystals of **4**, suitable for X-ray diffraction, could not be obtained from toluene. However X-ray quality crystals of $\mathbf{4} \cdot 1/2\ CH_2Cl_2$ were obtained by cooling a saturated solution in CH_2Cl_2. In the crystal of $\mathbf{4} \cdot 1/2\ CH_2Cl_2$, two independent iridium complexes $\mathbf{4^A}$ and $\mathbf{4^B}$, with geometries slightly different from rhodium complex **3** and from each other, are found in the asymmetric unit. The X-ray structure of **3** is given in Figure 4. Selected bond lengths and angles of **3** and **4** are given in Tables 1 and 2.

Both **3** and **4** have a square planar coordination geometry in which $[L_H]^-$ is didentate via N_{amine} and N_{Pyr}. Thus, deprotonation of $N_{Pyr}-H$ in $[\mathbf{1}]^+$ and $[\mathbf{2}]^+$ to a pyrrolate nitrogen (N_{Pyr}) results in a shift of $[M(cod)]^+$ (M = Rh, Ir) from the $N_{amine}-N_{Py}$ compartment to the $N_{amine}-N_{Pyr}$ compartment (Scheme 2).

In both **3** and $\mathbf{4} \cdot 1/2\ CH_2Cl_2$, N_{Py} accepts an intramolecular hydrogen bond from $N_{amine}-H$ (**3**: $N_{amine}-N_{Py}$ distance: 2.833(4) Å, $H-N_{Py}$ distance: 2.48(4) Å $N_{amine}-H-B_{Py}$ angle 105(3)°; $\mathbf{4^A}$: $N_{amine}-N_{Py}$ distance: 2.815(7) Å, $H-N_{Py}$ distance: 2.43 Å, $N_{amine}-H-N_{Py}$ angle: 104°, $\mathbf{4^B}$: $N_{amine}-N_{Py}$ distance: 2.824(8) Å, $H-N_{Py}$ distance: 2.46 Å, $N_{amine}-H-N_{Py}$ angle: 104°). Whereas in **3** the (*R*) and (*S*) enantiomers occur as monomers, in **4** they dimerise to (*R*,*R*) and (*S*,*S*) via additional intermolecular hydrogen-bonding interactions between $N_{amine}-H$ and N_{Py} (see $\mathbf{4^A}$ and $\mathbf{4^B}$ in Figure 5). [Intermolecular $N_{amine}-N_{Py}$ distances: 3.269(8) Å, 3.216(7) Å; intermolecular $H-N_{Py}$ distances: 2.47 Å, 2.41 Å intermolecular $N_{amine}-H-N_{Py}$ angles: 145°, 145°].

The additional intermolecular hydrogen bonding on going from **3** to **4**, could well reflect that the N^H_{amine} proton of iridium compound **4** is slightly more acidic than the N^H_{amine} proton of rhodium compound **3**, in accordance with its down-field ^{1}H-NMR shift on going from **3** (δ = 4.5) to **4** (δ = 5.3). This might also explain the difference in PXRD-pattern of crystalline **3** and **4** from toluene.

The $M-N_{Pyr}$ distances in **3** and **4** are approx. 0.06 Å shorter than the corresponding $M-N_{Py}$ distances in **[1]**PF_6 and **[2]**PF_6, respectively. This demonstrates the stronger interaction of the anionic pyrrolate nitrogen (N_{Pyr}) with the M^I center. The observed $M-N_{amine}$, $M-C_{olefin}$ and olefinic C−C distances in **3** and **4** are not significantly different from those in **[1]**PF_6 and **[2]**PF_6, respectively. As for $[\mathbf{1}]^+$, the Rh−N, Rh−C and olefinic C−C distances in **3** fall within the normal range for square planar "N_2"Rh^I(cod) complexes.[5][6]

The NMR spectra of **3** and **4** are very similar and correspond well with their solid state structure. As for $[\mathbf{1}]^+$and $[\mathbf{2}]^+$, the largest shift differences between **3** and **4** are observed for $(-CH=CH-)_{cod}$ signals (Table 3). In the ^{1}H-NMR spectrum of rhodium complex **3** at room temp. the pyramidal inversion at N_{amine} is frozen out (AB type signals with additional coupling to the N^H_{amine} proton for $N-CH_2-Py$ and $N-CH_2-Pyr$). Rapid rotation of the η^4-cod fragment results in one signal for the vinylic, two for the allylic *exo* and two for the allylic *endo* protons. The pyridine signals appear at almost the same position as in free HL_H. The N^H_{amine} proton (δ_{NH} = 4.50) has shifted

Table 2. Selected bond angles [°] for HL_H, [**1**]PF_6, [**2**]PF_6, **3**, $\mathbf{4^A/4^B}$, **5**, and **6**[a]

	HLH	[**1**]PF_6 (M1 = Rh1)	[**2**]PF_6 (M1 = Ir1)	**3** (M1 = Rh1)	$\mathbf{4^A}$ (M1 = Ir1)	$\mathbf{4^B}$ (M1 = Ir1)	**5** (M1 = Rh1)	**6** (M1 = Ir1)
N1−M1−N3	−	78.56(15)	78.62(17)	−	−	−	−	69.5(2)
N1−M1−N2	−	−	−	−	−	−	−	94.3(3)
N2−M1−N3	−	−	−	79.89(11)	79.36(19)	79.3(2)	78.15(10)	76.5(3)
N1−M1−C12	−	93.05(17)	92.98(19)	−	−	−	−	168.1(3)
N1−M1−C13	−	99.52(16)	99.62(19)	−	−	−	−	126.3(3)
N1−M1−C16	−	164.81(18)	163.9(2)	−	−	−	−	83.3(4)
N1−M1−C17	−	156.40(18)	156.9(2)	−	−	−	−	99.8(4)
N2−M1−C12	−	−	−	92.68(12)	97.8(2)	93.8(3)	89.89(12)	88.4(4)
N2−M1−C13	−	−	−	97.32(12)	92.6(2)	98.1(2)	96.47(12)	90.9(4)
N2−M1−C16	−	−	−	160.84(13)	159.5(3)	160.4(3)	165.17(13)	165.8(4)
N2−M1−C17	−	−	−	160.73(12)	161.2(2)	159.9(3)	156.92(13)	154.7(4)
N3−M1−C12	−	158.58(18)	157.7(2)	159.44(13)	158.0(2)	160.8(3)	155.54(12)	122.4(3)
N3−M1−C13	−	162.23(18)	162.8(2)	160.95(13)	161.8(2)	158.5(2)	162.83(13)	161.1(3)
N3−M1−C16	−	95.66(17)	95.62(18)	94.72(12)	100.2(2)	94.3(2)	99.33(11)	115.3(3)
N3−M1−C17	−	98.37(17)	98.27(19)	98.88(12)	93.9(2)	98.9(2)	101.11(11)	88.8(3)
C12−M1−C13	−	38.15(19)	38.6(2)	38.49(13)	38.8(3)	39.7(3)	38.50(14)	41.9(4)
C16−M1−C17	−	37.78(19)	38.3(2)	38.00(14)	38.8(3)	39.0(3)	37.82(14)	38.7(4)
M1−N2−C1	−	−	−	115.6(2)	117.0(4)	117.1(4)	114.1(2)	119.1(6)
N2−C1−C5	120.7(4)	−	−	117.3(3)	116.6(5)	116.8(5)	117.4(3)	116.5(8)
C1−C5−N3	111.9(4)	−	−	109.5(3)	108.6(5)	108.6(5)	109.2(3)	111.2(7)
C5−N3−M1	−	−	−	108.0(2)	109.8(4)	108.8(4)	101.81(17)	104.1(5)
M1−N1−C7	−	113.7(3)	113.8(3)	−	−	−	−	119.6(6)
N1−C7−C6	116.1(5)	115.7(4)	115.2(4)	117.6(3)	116.8(6)	117.2(6)	118.2(3)	117.1(8)
C7−C6−N3	112.7(5)	108.8(4)	109.1(4)	114.5(3)	114.7(5)	113.5(5)	114.3(2)	108.1(7)
C6−N3−M1	−	104.1(3)	105.1(3)	−	−	−	−	107.8(5)
Pyrrole								
N2−C4−C3	107.8(5)	107.9(5)	107.8(6)	110.4(3)	109.2(6)	108.9(6)	109.4(3)	110.0(9)
C4−C3−C2	107.8(5)	107.6(5)	107.8(6)	106.9(3)	107.7(6)	108.5(6)	107.4(3)	107.4(10)
C3−C2−C1	107.8(5)	107.5(5)	107.3(6)	105.9(3)	106.2(6)	105.5(6)	106.1(3)	105.0(9)
C2−C1−N2	107.5(5)	107.0(5)	107.1(5)	110.7(3)	110.1(6)	110.4(6)	109.9(3)	112.3(9)
C1−N2−C4	109.1(4)	110.1(5)	109.9(6)	106.0(3)	106.7(5)	106.7(5)	107.1(3)	105.2(8)
Pyridine								
N1−C11−C10	123.7(5)	121.9(5)	122.5(5)	124.5(4)	123.2(7)	123.2(8)	122.9(4)	123.6(9)
C11−C10−C9	118.3(5)	119.8(5)	118.9(5)	118.2(4)	118.3(7)	118.3(8)	119.1(4)	118.9(9)
C10−C9−C8	119.3(5)	118.2(5)	119.1(5)	118.8(4)	119.8(7)	119.1(8)	119.7(5)	118.4(9)
C9−C8−C7	118.7(5)	119.4(5)	119.6(5)	119.2(4)	118.6(7)	118.9(7)	118.7(5)	119.4(7)
C8−C7−N1	122.2(4)	121.9(4)	121.2(5)	122.4(3)	122.7(6)	122.8(6)	121.3(3)	121.8(8)
C7−N1−C11	117.7(4)	118.8(4)	118.8(4)	116.7(3)	117.4(6)	117.6(6)	118.5(4)	117.9(8)

[a] For atom labelling see Figure 2−6. Superscripts A and B refer to crystallographically independent molecules.

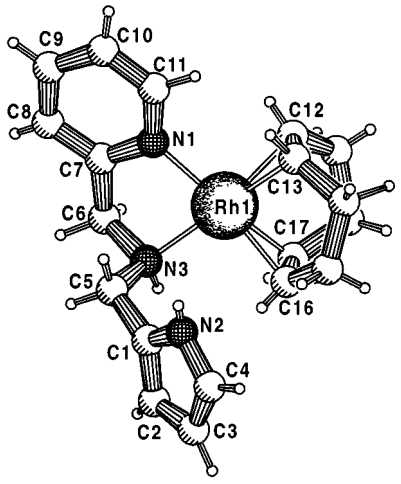


Figure 3. X-ray structure of $[\mathbf{1}]^+$ [only the (*S*) enantiomer is shown]

2.09 ppm downfield from that in the free ligand (δ_{NH} = 2.41). The pyrrole signals have all shifted up-field relative to HL_H. The chemical shift difference is most pronounced for Pyr−H^5 (Pyr−H^5: 0.42 ppm, Pyr−H^4: 0.13 ppm and Pyr−H^3: 0.26 ppm), probably due to anisotropic shielding by the η^4-cod fragment.

Complexation of $[Rh^I(cod)]^+$ and $[Ir^I(cod)]^+$ by $[L_{Bzl}]^-$ and $[L_{Bu}]^-$

Reaction of HL_{Bzl} with $[\{(cod)M^I(\mu\text{-}Cl)\}_2]$ (M = Rh, Ir) in methanol results in a solution of $[(HL_{Bzl})M^I(cod)]Cl$ (M = Rh, Ir). Subsequent addition of an excess of aqueous Na_2CO_3 results in deprotonation of N_{Pyr}−H and precipitation of the neutral complexes $[(L_{Bzl})M^I(cod)]$ (M = Rh: **5**, M = Ir: **6**). $[(L_{Bu})Rh^I(cod)]$, **7**, was obtained analogously. Crystals of **5** and **6** were obtained by cooling of a saturated solution in toluene. Their structures were determined by single-crystal X-ray diffraction (Figure 6). Selected bond lengths and angles are given in Tables 1 and 2.

In the crystal, complex **5** has a square planar geometry with didentate L_{Bzl}^- via N^{Bzl}_{amine} and N_{Pyr}, analogous to L_H^- in **3**. N_{Py} in **5** is not involved in any bonding interaction, whereas N_{Py} in **3** accepts a hydrogen bond from N^H_{amine}. The Rh−N_{Pyr} distances (N2−Rh1) in **5** and **3** are equal within experimental error, but the Rh−N^{Bzl}_{amine} dis-

Table 3. ^1H- and ^{13}C-NMR shifts of $(-HC{=}CH-)_{cod}$

	[1]PF_6[a] (M = Rh)	[2]PF_6[b] (M = Ir)	[3][b] (M = Rh)	[4][b] (M = Ir)	[5][b] (M = Rh)	[6][b] (M = Ir)	[7][c] (M = Rh)
^1H NMR	4.46	4.3 3.38	4.12	3.87 3.73	3.91 3.37	3.47 2.84	3.8 3.40
^{13}C NMR	82.2	68.0 (br)	79.3 78.8	62.3 61.5	77−74 (br)	57−54 (br)	– –

[a] Acetone[D_6]. – [b] CD_2Cl_2. – [c] $CDCl_3$.

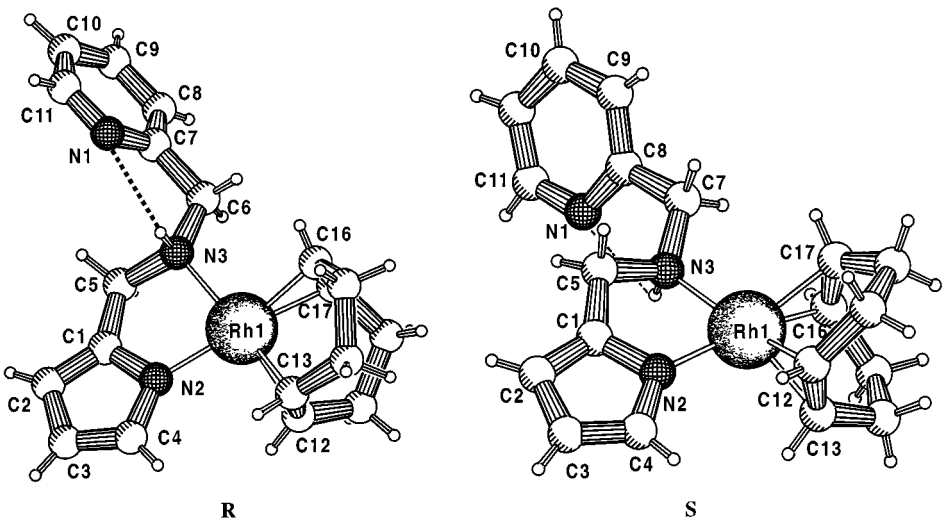
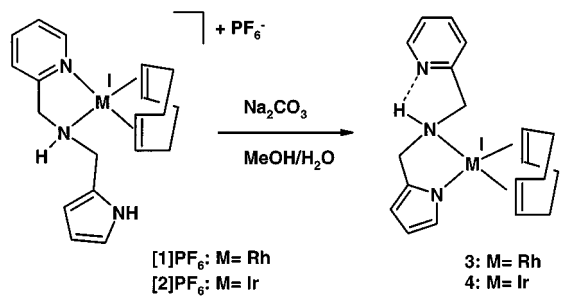


Figure 4. X-ray structure of **3** [the (*R*) and (*S*) enantiomers are shown]



Scheme 2. Dicompartimental ligand HL_H: Shift of $[M^I(cod)]^+$ from $N_{amine}-N_{Py}$ to $N_{amine}-N_{Pyr}$ compartment upon deprotonation of HL_H

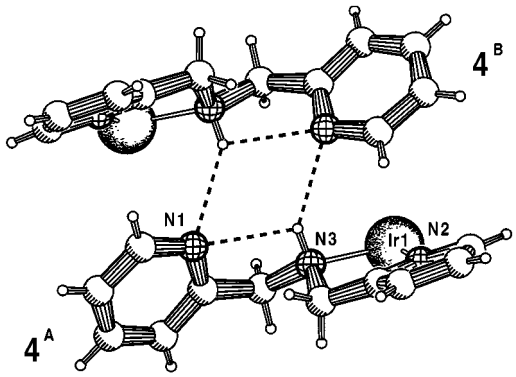


Figure 5. Hydrogen-bonding pattern in the X-ray structure of **4** · 1/2 CH_2Cl_2 [the crystal contains the dimers (*R,R*) and (*S,S*) of the enantiomers (*R*) and (*S*); only *R,R*) is shown]

tance in **5** [N3−Rh1 = 2.231(2) Å] is 0.07 Å longer than the Rh−N^H_{amine} distance in **3** [N3−Rh1 = 2.164(3) Å] and longer than Rh−N_{sp3} distances for square-planar "N_2"-ligand Rh^I complexes (2.111−2.178 Å) known so-far.[5][6] In accordance with this, the Rh−C distances *trans* to N^{Bzl}_{amine} in **5** are approx. 0.04 Å shorter than those trans to N_{Pyr}, whereas the corresponding distances in **3** are not significantly different. These effects all seem to indicate a substantial weakening of the Rh−N^R_{amine} interaction upon substitution of H by Bzl.

In contrast to the four-coordinate rhodium complex **5**, iridium complex **6** is five-coordinate. Complex **6** has a pseudo trigonal-pyramidal geometry with tridentate $[L_{Bzl}]^-$ (Figure 6). N_{Pyr} and one double bond of cod occupy the axial positions, whereas N_{Py} and N_{amine} together with the other double bond of cod occupy the equatorial positions.

Complex **6** contains two chiral centres; N^{Bzl}_{amine} and Ir. Nevertheless only the enantiomeric pairs *S,C* and *R,A*, and not their diastereomers *S,A* and *R,C* are observed. Because of the short "arms" of the ligand, the chiral centre on the amine nitrogen dictates the chirality at the iridium centre during complexation. The *S,A* and *R,C* forms are not accessible due to the geometrical constraints in the ligand.

For d^8-metals in a trigonal-bipyramidal geometry, theoretical and experimental results by Rossi and Hoffmann indicate that the strongest σ-donor prefers the axial position and that olefins are more strongly bound in the equatorial plane.[7] The axial position of the strongest σ-donor,

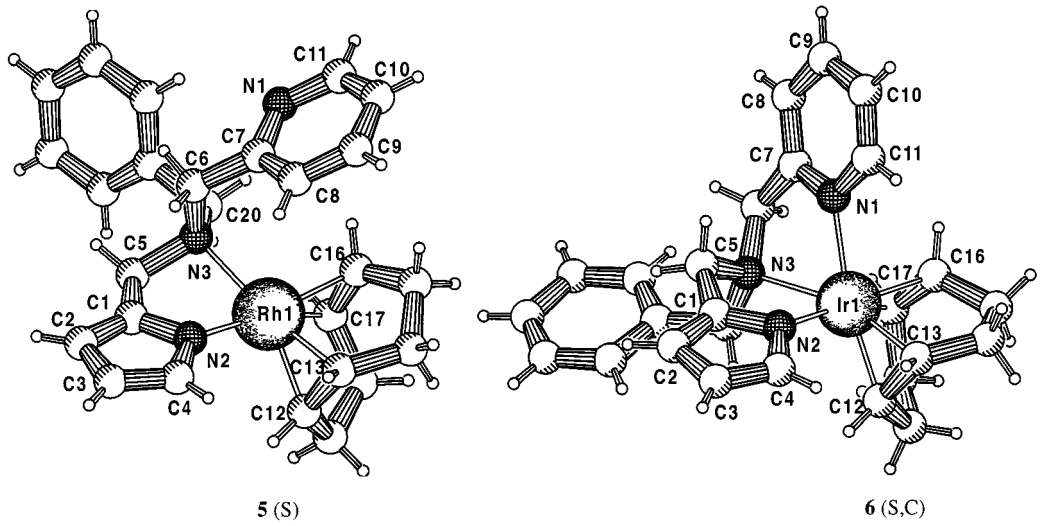
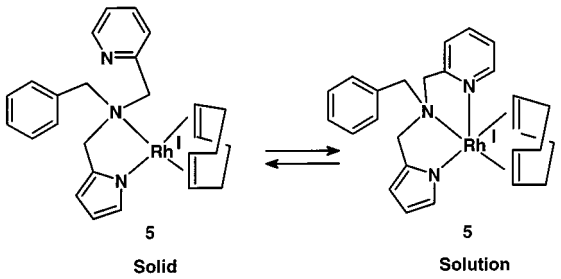


Figure 6. X-ray structures of **5** (*S* enantiomer) and **6** (*S,C* enantiomer), corresponding with enantiomer (*S*) of **3** in Figure 4

N_{Pyr}, at the shortest Ir−N distance (Ir−N2: 2.066 Å) and the shorter Ir−C distances for the equatorial double bond [Ir1−C12: 2.068(8) Å, Ir1−C13: 2.055(8) Å] relative to the axial double bond [Ir1−C16: 2.136(11) Å, Ir1−C17: 2.129(10) Å] are in accordance with theoretical and experimental results by Rossi and Hoffmann. In accordance with its "unfavourable" equatorial position, the $M-N^{Bzl}_{amine}$ distance (M1−N3) in the five-coordinate iridium complex **6** exceeds the $M-N^{Bzl}_{amine}$ distance in four-coordinate rhodium complex **5** by 0.17 Å, whereas the $M-N_{Pyr}$ distance (M−N2) in the "favourable" axial position is not significantly longer than in **5** (Table 1). Interestingly, **5** undergoes $\kappa^2-\kappa^3$ isomerisation on going from the solid state to solution (Scheme 3).



Scheme 3. $\kappa^2-\kappa^3$ isomerism for L_{Bzl}^- in **5**

In the ^{1}H-NMR solution spectrum of **5**, Py-H^6 of L_{Bzl}^- has shifted 0.69 ppm downfield relative to Py-H^6 of free HL_{Bzl} (HL_{Bzl}: δ = 8.56, HL_{Bzl}^- in **5**: δ = 9.25). This is in marked contrast with the situation for **3**, where we observed no significant shifts for Py-H^6 of the uncoordinated pyridine group of L_H^- compared to free HL_H (HL_H: δ = 8.48, L_H^- in **3**: δ = 8.55). Also, the Py-H^6 signal in **5** shows clear NOE contacts (counter phase to diagonal) with Pyr-H^5, and the two vinylic and the two allylic *exo* signals of cod. This shows that the structure of **5** in solution is predominantly five-coordinate. As was the case for $[\mathbf{1}]^+$ and **3**, the ^{1}H-NMR spectrum of **5** shows rapid rotation of the η^4-cod fragment. Two signals are observed for the vinylic protons, one for the allylic *exo* protons, and one for the allylic *endo* protons. At room temperature pyramidal inversion at N^{Bzl}_{amine} is slow on the ^{1}H-NMR time-scale (two AB-type doublets for each, $N-CH_2-Py$, $N-CH_2-Pyr$, and $N-CH_2-Ph$), but fast on the NOESY/EXSY time scale (exchange correlation peaks were observed for the two vinylic proton signals and for H_a and H_b of the three AB-patterns). On the basis of its ^{1}H-NMR spectrum, the solution structure of butylamine derivative **7** is similar to that of benzylamine derivative **5** (Table 3). As for **5**, the significant downfield shift of Py-H^6 (Δδ = 0.58 ppm) indicates that L_{Bu}^- is tridentate in solution.

Complex **6**, the iridium analogue of **5**, is also five-coordinate in solution. However **6** does not show N^{Bzl}_{amine} inversion on the ^{1}H-NOESY/EXSY time-scale. This seems to indicate the stronger preference of iridium for five-coordination.[8] Apart from the chemical shift differences for $(-HC=CH-)_{cod}$ (Table 3), the NMR spectra of **5** and **6** are very similar.

Thus, substitution of the N^H_{amine} proton in **3/4** by benzyl in **5/6** or butyl in **7** induces N_{Py} coordination in solution. This appears to be triggered by a weaker $N_{amine}-Rh$ interaction resulting from steric repulsions, and by the loss of stabilisation of the uncoordinated N_{Py} through hydrogen bonding with $N_{amine}-H$.

The ^{13}C-NMR signals for $(-CH=CH-)_{cod}$ of the iridium complexes appear at significant lower values than their corresponding rhodium analogues (Table 3), indicating stronger π-back donation for iridium.[8] Both for rhodium and for iridium, significant upfield shifts are observed for the $(-CH=CH-)_{cod}$ NMR signals on going from four-coordination to five-coordination (Table 3). The average NMR signals of $(-CH=CH-)_{cod}$ of four-coordinate **3** and **4** in CD_2Cl_2 [**3**: δ(^{1}H) = 4.1 and δ(^{13}C) = 79; **4**: δ(^{1}H) = 3.8 and δ(^{13}C) = 62] appear at significantly higher values than those of five-coordinate **5** and **6** [**5**: δ(^{1}H) = 3.6 and δ(^{13}C) = 77−74 (br); **6**: δ(^{1}H) = 3.2 and δ(^{13}C) = 57−54(br)]. For **7**, δ(^{1}H) = 3.7, which is close to the value

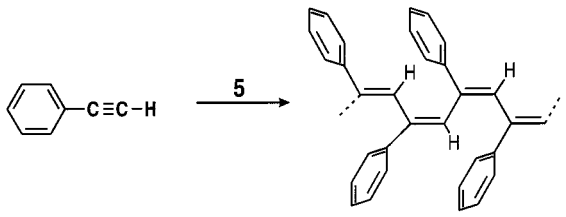
of **5**. This situation parallels that for 3,5-disubstituted tris(pyrazolyl)borate (Tp^{R2}) rhodium(I) cod complexes, where in $CDCl_3$ $\delta(^1H) = 4.1$ and $\delta(^{13}C) = 80$ for four-coordinate $[(\kappa^2\text{-}Tp^{R2})Rh^I(cod)]$ and $\delta(^1H) = 4.0$ and $\delta(^{13}C) = 73$ for five-coordinate $[(\kappa^3\text{-}Tp^{H2})Rh^I(cod)]$.[12e]

Reactivity towards H_2O, O_2, and H_2O_2

Solutions of the pyridine-amine-pyrrolate complexes **3**, **4**, **5**, **6**, and **7** show no reactivity towards water, but are oxidised in a nonselective way by air and aqueous H_2O_2. Sparingly soluble precipitates result, which have complex ^1H-NMR spectra with very broad lines.

Catalytic Polymerisation of Phenylacetylene

Complexes **5** and **7** are neutral "N_3"$Rh^I(cod)$ complexes that show $\kappa^2-\kappa^3$ isomerism, similar to tris(pyrazolyl)borate rhodium(I) cod complexes. Isomerisation of $[(\kappa^3\text{-}Tp^{R2})Rh^I(cod)]$ to $[(\kappa^2\text{-}Tp^{R2})Rh^I(cod)]$ has been suggested to be essential for its catalytic activity in the polymerisation of phenylacetylene.[9] In accordance with this we observed that rhodium complex **5**, but not iridium complex **6,** is an active catalyst for the polymerisation of phenylacetylene (Scheme 4).



Scheme 4. Polymerisation of phenylacetylene by **5**

Reaction of phenylacetylene in MeOH in the presence of 0.1 mol-percent of **5** resulted in precipitation of yellow poly(phenylacetylene) in 24% yield within 20 min. The molecular mass (M_n) and the high stereoregularity (head-to-tail cis-transoidal structure) of the obtained poly(phenylacetylene) are similar to those of poly(phenylacetylene) prepared with $(Tp^{R2})Rh^I(cod)$[9] and other rhodium catalysts.[10] The broad molecular weight distribution ($M_w/M_n = 4.7$) could be the result of partial precipitation during polymerisation.

Discussion

The pyridine-amine-pyrrolate complexes **3**−**7** are not oxidised selectively by H_2O_2 or O_2. Oxidation of the negatively charged pyrrolate group is probably responsible for these aselective oxidations. The new pyridine-amine-pyrrole and pyridine-amine-pyrrolate ligands display a diverse coordination chemistry towards $[Rh^I(cod)]^+$ and $[Ir^I(cod)]^+$.

The neutral pyridine-amine-pyrrole ligand HL_H in $[\mathbf{1}]^+$ and $[\mathbf{2}]^+$ is didentate via N^H_{amine} and N_{Py}. Deprotonation of the pyrrole group results in the potentially tridentate pyridine-amine-pyrrolate ligands L_H^-, L_{Bzl}^- and L_{Bu}^-. In both **3** (M = Rh) and **4** (M = Ir), L_H^- is didentate via N^H_{amine} and N_{Pyr} in the solid state *and* in solution. The observed difference between **3** and **4** in the solid state could well reflect that the N^H_{amine} proton of iridium compound **4** is slightly more acidic than the N^H_{amine} proton of rhodium compound **3**, in accordance with the down-field shift of the N^H_{amine} proton in the ^1H-NMR spectrum on going from **3** to **4**. The higher acidity is probably the result of stronger metal−ligand interaction for iridium(I) than for rhodium(I). In accordance with this, the ^{13}C-NMR olefinic cod signals of the iridium complexes are observed at higher field than those of their rhodium analogues (see Table 3).

L_{Bzl}^- in **5** (M = Rh) is predominantly tridentate via N_{Pyr}, N_{amine}, and N_{Py} in solution, but didentate via N_{Pyr} and N_{amine} in the solid state. Apparently, the free energy increase on going from κ^3-L_{Bzl} to κ^2-L_{Bzl} can easily be overcome by packing forces. The ^1H-NMR spectrum of **5** shows the occurrence of another mode of $\kappa^2-\kappa^3$ isomerism in solution, involving dissociation, pyramidal inversion and recoordination of N^{Bzl}_{amine}. The activity of **5** in polymerisation of phenylacetylene also reflects the occurrence of $\kappa^2-\kappa^3$ isomerism. L_{Bzl}^- in **6**, the Ir-analogue of **5**, shows no sign of pyramidal inversion of N^{Bzl}_{amine} via $\kappa^2-\kappa^3$ isomerism in solution, and is tridentate in the solid state. The observed differences between **5** and **6** in solution and in the solid state both appear to reflect the higher tendency of iridium for five coordination.[8]

Previously, $\kappa^2-\kappa^3$-isomerism has been observed for 3,5-disubstituted tris(pyrazolyl)borate[11] (Tp^{R2}) complexes $[(Tp^{R2})Rh^I(L_2)]$ (L_2 = diolefin or $(olefin)_2$).[12][13] Whereas a bulky R at the pyrazolyl-3-position in $[(Tp^{R2})Rh^I(cod)]$ favours four-coordination over five-coordination ($\kappa^2 > \kappa^3$), a bulky R at N^R_{amine} in $[(L_R^-)Rh^I(cod)]$ favours five-coordination over four-coordination ($\kappa^3 > \kappa^2$). Increased steric repulsion at N^R_{amine} in $[(L_R^-)Rh^I(cod)]$ induces a weaker $Rh-N^R_{amine}$ interaction. This is compensated by additional coordination of N_{Py}, and thus results in five coordination.

Experimental Section

General Methods: All reactions were performed under a nitrogen atmosphere using standard schlenk techniques, unless mentioned otherwise. Solvents (p. a.) were deoxygenated by bubbling through a stream of N_2 or by the freeze-pump-thaw method. The temperature indication room temp. corresponds to ca. 20 °C. $[\{(cod)Rh(\mu\text{-}Cl)\}_2]$[14] and $[\{(cod)Ir(\mu\text{-}Cl)\}_2]$[15] were prepared according to a literature procedure. All other chemicals are commercially available and were used without further purification. − IR spectra were measured on a Perkin−Elmer 1720X. − NMR experiments were carried out on a Bruker DPX200 (200 MHz and 50 MHz for ^1H and ^{13}C respectively), a Bruker AC300 (300 MHz and 75 MHz for ^1H and ^{13}C respectively) and a Bruker AM500 (500 MHz and 125 MHz for ^1H and ^{13}C respectively). Solvent shift reference for ^1H NMR: $[D_6]$acetone $\delta_H = 2.05$, THF-$[D_8]$ $\delta_H = 1.72$, CD_2Cl_2 $\delta_H = 5.31$, $CDCl_3$ $\delta_H = 7.28$. For ^{13}C NMR: $[D_6]$acetone $\delta_C = 29.50$, CD_2Cl_2 $\delta_C = 54.20$. Abbreviations used are s = singlet, d = doublet, dd = doublet of doublets, ddd = doublet of doublets of

doublets, t = triplet, m = multiplet and br = broad. − Elemental analysis (C,H,N) were carried out on a Carlo Erba NCSO-analyser. − Mass Spectra were recorded on a VG 7070 Mass spectrometer (FAB/EI) or on a JEOL JMS SX/SX102A four sector mass spectrometer (FD).

X-ray Diffraction: Crystals of [**1**]PF_6 and [**2**]PF_6 suitable for X-ray diffraction studies were obtained by cooling a saturated solution of the corresponding compound in MeOH to −20 °C. Crystals of HL_H, **3**, **5**, and **6** suitable for X-ray diffraction studies were obtained from hot saturated toluene solutions. Crystals of **4** suitable for X-ray diffraction studies were obtained by slow crystallisation from a saturated CH_2Cl_2 solution at −20°C. Single crystals were mounted in air on glass fibres. For [**1**]PF_6, [**2**]PF_6, **4**, **5**, and **6** an Enraf−Nonius CAD4 single-crystal diffractometer was used, graphite monochromatised Cu-*Kα* radiation, θ-2θ scan mode. The X-ray diffraction data for **3** were collected on a Enraf−Nonius CAD4T rotating anode diffractometer, graphite monochromatised Mo-*Kα* radiation, ω-scan mode. Semi-empirical absorption correction (*ψ*-scan) was applied.[16]

For HL_H an Enraf−Nonius CAD4 single-crystal diffractometer was used, graphite monochromatised Mo-*Kα* radiation, θ-2θ scan mode. No absorption correction was applied. Structures [**1**]PF_6, [**2**]PF_6, **3**, **4**, **5**, and **6** were solved by the program system DIRDIF[17] using the program PATTY[18] to locate the heavy atoms. The structure of HL_H was solved using the program CRUNCH.[19] All structures were refined with standard methods (refinement against F^2 of all reflections with SHELXL97[20]) with anisotropic parameters for the nonhydrogen atoms. Intensity data were corrected for Lorentz and polarisation effects. All hydrogen atoms were placed at calculated positions and were subsequently freely refined, however, for **4** and **6**, the hydrogen atoms were placed at calculated positions and were refined riding on the parent atoms. Details of the crystal parameters, data collections and structure refinements are given in Table 4. Crystallographic data (tables of structure determinations summaries, lists of anisotropic displacement parameters, lists of atom coordinates and full lists of bond lengths and angles, excluding structure factors) have been deposited with the Cambridge Crystallographic Data Centre as supplementary publication no. CCDC-115640 ([**1**]PF_6), 115641 (**3**), 115642 (**5**), 115643 (HL_H), 115644 ([**2**]PF_6), 115645 (**6**), and 115646 (**4**). Copies of the data can be obtained free of charge on application to The Director, CCDC, 12 Union Road, Cambridge CB2 1EZ, UK (fax: Int. Code +44 (1223) 336-033; E-mail: deposit@chemcrys.cam.ac.uk)

Syntheses

***N*-(2-Pyridylmethyl)-*N*-(1*H*-2-pyrrolylmethyl)amine (HL_H):** 6.8 g (0.064 mol) of 1*H*-pyrrole-2-carboxaldehyde was dissolved in 60 mL of EtOH and 6.0 g (0.063 mol) of picolylamine was added dropwise. The solution was heated to reflux for 10 min. Evaporation of the solvent under vacuum results in a yellow powder, from which *N*-(2-pyridylmethyl-*N*-(1*H*-pyrrolylmethylidene)amine was obtained as a white solid by recrystallisation from a hot saturated Et_2O solution. Yield 11.5 g (0.062 mol, 98%). − 11.3 g (0.061 mol) of *N*-(2-pyridylmethyl-*N*-(1*H*-pyrrolylmethylidene)amine was then dissolved in 200 mL of deoxygenated methanol. The solution was cooled to −10°C, and 2.9 g (0.076 mol) of $NaBH_4$ was added and some gas evolved from the solution. The solution was heated to 50°C for 3 h after which the solvent was partially evaporated. To this solution 50 mL water was added to destroy the excess $NaBH_4$. The water layer was extracted three times with 30 mL of Et_2O, and the combined Et_2O-fractions were dried with 10 g of $MgSO_4$. Filtration and evaporation of the solvent results in *N*-(2-pyridylmethyl)−*N*-(1*H*-2-pyrrolylmethyl)amine (HL_H) as a yellow powder, and was recrystallised from a hot saturated Et_2O solution. Yield 10.3 g (0.055 mol, 90%). Colourless crystals suitable for X-ray diffraction were obtained by crystallisation from toluene. − Mp: 59.0°C. − ^{1}H NMR (200 MHz, CD_2Cl_2, 298 K): δ = 9.40 (s, b, 1 H, Pyr−H1), 8.54 [d,1 H, ^3J(H,H) = 4.1 Hz, Py−H6], 7.65 [t, 1 H, ^3J(H,H) = 7.6 Hz, Py−H4], 7.26 [d, 1 H, ^3J(H,H) = 7.6 Hz, Py−H3], 7.16 [dd, 1 H, ^3J(H,H) = 7.6 Hz, ^3J(H,H) = 4.1 Hz, Py−H5], 6.67 (m, Pyr−H5), 6.05 (m, 1 H, Pyr−H4), 5.98 (m, 1 H, Pyr−H3), 3.86 (s, 2 H, N−CH_2−Py), 3.78 (s, 2 H, N−CH_2−Pyr), 2.41 (s, br, 1 H, NH). − ^{13}C {^{1}H} (75 MHz, [D$_6$]acetone, 298 K): δ = 161.4 (Py−C2), 149.9 (Py−C6), 137.2 (Py−C4), 131.6 (Pyr−C2), 122.9 (Pyr−C5), 122.2 (Py−C5), 117.8 (Py−C3), 108.7 (Pyr−C4), 106.9 (Pyr−C3), 54.9 (N−CH_2−Pyr), 46.8 (N−CH_2−Py). − EI-MS (*m*/*z*): 185 $[M]^+$, 118 $[M - Pyr + H]^+$, 107 $[M - CH_2Py]^+$, 93 $[CH_2Py + H]^+$. − $C_{11}H_{13}N_3$ (187.24): calcd. C 70.56, H 7.00, N 22.44; found C 70.55, H 7.03, N 21.95.

***N*-Benzyl-*N*-(2-pyridylmethyl)-*N*-(1*H*-2-pyrrolylmethyl)amine (HL_{Bzl}):** 9.5 g (0.09 mol) of 1*H*-pyrrole-2-carboxaldehyde was dissolved in 50 mL of freshly distilled THF and cooled to 0°C. 10.7 g (0.10 mol) of benzylamine was added drop wise. After 15 min the solution was allowed to warm up to room temp. and was stirred for 10 h. Evaporation of the solvent under vacuum results in a yellow powder, from which *N*-benzyl-*N*-(1*H*-pyrrolylmethylidene)-amine was obtained as a white solid by recrystallisation from a hot saturated Et_2O solution. Yield 17.7 g (0.085 mol, 96%). 9.2 g (0.049 mol) of *N*-benzyl-*N*-(1*H*-pyrrolylmethylidene)amine was then dissolved in 60 mL of deoxygenated methanol. The solution was cooled to 0°C, and 2.0 g (0.053 mol) of $NaBH_4$ was added and some gas evolved from the solution. The solution was heated to 50°C for 10 h after which the solvent was partially evaporated. To this solution 50 mL of water was added to destroy the excess $NaBH_4$. The water layer was extracted three times with 30 mL of Et_2O, and the combined Et_2O fractions were dried with 10 g of $MgSO_4$. Filtration and evaporation of the solvent results in 1*H*-pyrrol-2-ylmethylbenzylamine as a yellow oil, sufficiently pure for further reaction. Yield 7.87 g (0.061 mol, 71.3%). 100 mL of methanol was cooled to 0°C and 12 g of Na_2CO_3, dissolved in 20 mL of water, was added. To the resulting suspension 6.89 g (0.042 mol) of picolyl chloride hydrochloride and 7.9 g (0.042 mol) of (1*H*-pyrrol-2-ylmethyl)benzylamine were added. The pink solution was stirred for 10 h and gradually changed its colour to orange. The mixture was filtered and the filtrate was evaporated yielding a crude red solid. *N*-benzyl-*N*-(2-pyridylmethyl)-*N*-(1*H*-2-pyrrolylmethyl)amine (HL_{Bzl}) was obtained as a white solid by recrystallisation from a saturated Et_2O solution at −20°C. Yield 4.46 g (0.016 mol, 38%). − Mp: 86.0°C. − ^{1}H NMR (200 MHz, CD_2Cl_2, 298 K): δ = 9.84 (s, br, 1 H, Pyr−H1), 8.56 (m,1 H, Py−H6), 7.70 (m, 1 H, Py−H4, Py−H3), 7.8−7.2 (m, 6 H, Ph−H, Py−H4, Py−H5), 6.79 (m, Pyr−H5), 6.08 (m, 1 H, Pyr−H4), 5.99 (m, 1 H, Pyr−H3), 3.65 (s, 2 H, N−CH_2−Py), 3.62 (s, 2 H, N−CH_2−Pyr), 3.52 (s, 2 H, N−CH_2−Ph). − ^{13}C {^{1}H} (75 MHz, [D$_6$]acetone, 298 K): δ = 161.1 (Py−C2), 149.9 (Py−C6), 141.0 (Pyr−C2), 137.6 (Py−C4), 130.0 (Ph−C2, Ph−C3), 129.4 (Ph−C4), 128.1 (Ph−C1), 124.3 (Pyr−C5), 123.2 (Py−C5), 118.5 (Py−C3), 108.8 (Pyr−C4), 108.6 (Pyr−C3), 59.9 (N−CH_2−Ph), 58.9 (N−CH_2−Pyr), 51.1 (N−CH_2−Py). − EI-MS [*m*/*z* (%)]: 277 $[M]^+$ (0.13), 211 $[M - Pyr]^+$ (0.10), 197 $[M - CH_2Pyr]^+$ (37.10), 185 $[M - CH_2Py]^+$ (75.34), 93 $[CH_2Py + H]^+$ (100). − $C_{18}H_{19}N_3$ (277.37): calcd. C 77.95, H 6.90, N 15.15; found C 77.81, H 6.90, N 14.75.

***N*-Butyl-*N*-(2-pyridylmethyl)-*N*-(1*H*-2-pyrrolylmethyl)amine (HL_{Bu}):** *N*-Butyl-*N*-(2-pyridylmethyl)-*N*-(1*H*-2-pyrrolylmethyl)am-

Table 4. Crystallographic data for HL_H, [**1**]PF_6, [**2**]PF_6, **3**, **4** · 1/2 CH_2Cl_2, **5**, and **6**

	HL_H	[**1**]PF_6	[**2**]PF_6	**3**	**4** · 1/2 CH_2Cl_2	**5**	**6**
Emperical formula	$C_{11}H_{13}N_3$	$C_{19}H_{25}F_6N_3PRh$	$C_{19}H_{25}F_6IrN_3P$	$C_{19}H_{24}N_3Rh$	$C_{19.5}H_{25}ClIrN_3$	$C_{26}H_{30}N_3Rh$	$C_{26}H_{30}IrN_3$
Crystal size [mm]	0.37×0.33×0.29	0.37×0.33×0.17	0.25×0.22×0.12	0.22×0.22×0.12	0.48×0.16×0.06	0.46×0.29×0.20	0.17×0.13×0.12
Formula mass	187.24	543.30	632.59	397.32	529.08	487.44	576.73
T [K]	293(2)	208(2)	208(2)	173(2)	208(2)	293(2)	208(2)
Crystal system	Monoclinic	Triclinic	Triclinic	Monoclinic	Triclinic	Triclinic	Monoclinic
Space group	$C2/c$	$P-1$	$P-1$	$P2_1/c$	$P-1$	$P-1$	$P\,2_1/n$
a [Å]	15.85(4)	9.63157(17)	9.6377(3)	11.2479(5)	10.3279(3)	10.2385(3)	9.2972(6)
b [Å]	10.8942(15)	9.7229(3)	9.7205(3)	14.8328(8)	13.0692(3)	10.2554(2)	16.1521(8)
c [Å]	12.22(3)	13.8150(3)	13.7985(9)	10.3258(6)	15.1735(3)	11.2513(4)	14.8152(9)
α [°]	90	75.425(3)	75.408(6)	90	96.837(3)	79.957(3)	90
β [°]	106.5(3)	69.0584(17)	68.963(3)	111.157(4)	103.634(3)	72.835(3)	102.105(5)
γ [°]	90	60.680(3)	60.599(5)	90	105.233(2)	77.666(2)	90
V [Å^3]	2025(6)	1048.82(4)	1046.57(8)	1606.62(15)	1884.32(8)	1094.83(6)	2175.3(2)
$\rho_{calcd.}$ [gcm^{-3}]	1.229	1.720	2.007	1.643	1.865	1.479	1.761
Z	8	2	2	4	4	2	4
Diffractometer (scan)	Enraf−Nonius CAD4 (θ−2θ)	Enraf−Nonius CAD4 (θ−2θ)	Enraf−Nonius CAD4 (θ−2θ)	Nonius CAD4T rotating anode (ω−scan)	Enraf−Nonius CAD4 (θ−2θ)	Enraf−Nonius CAD4 (θ−2θ)	Enraf−Nonius CAD4 (θ−2θ)
Radiation	Mo-K_α	Cu-K_α	Cu-K_α	Mo-K_α	Cu-K_α	Cu-K_α	Cu-K_α
Wavelength [Å]	0.71073	1.54184	1.54184	0.71073	1.54184	1.54184	1.54184
F(000)	800	548	612	816	1028	504	1136
θ range [°]	2.64 to 26.26	3.44 to 69.97	3.44 to 69.97	1.94 to 27.46	3.05 to 69.90	4.14 to 69.95	4.10 to 70.02
Index ranges	$0 \le h \le 19$	$-11 \le h \le 10$	$-11 \le h \le 10$	$-14 \le h \le 14$	$-12 \le h \le 12$	$-12 \le h \le 12$	$-11 \le h \le 11$
	$0 \le k \le 13$	$-11 \le k \le 0$	$-11 \le k \le 11$	$-7 \le k \le 19$	$0 \le k \le 15$	$0 \le k \le 12$	$-19 \le k \le 19$
	$-15 \le l \le 14$	$-16 \le l \le 16$	$-16 \le l \le 0$	$-13 \le l \le 13$	$-18 \le l \le 18$	$-13 \le l \le 13$	$-18 \le l \le 0$
Range of rel. transm. fac.	−	0.784/1.655	0.827/1.515	0.964/1.049	0.724/2.183	0.790/1.373	0.816/1.227
Measured reflections	2095	4231	4145	7391	7465	4410	8395
Unique reflections	2022	3977	3970	3674	7130	4159	4120
Observed refl. [$Io > 2\sigma(Io)$]	1252	3936	3964	2799	6975	4145	3476
Refined parameters	180	372	372	304	443	392	271
Goodness-of-fit on F^2	1.166	1.135	1.144	1.023	1.117	1.123	1.051
R [$Io > 2\sigma(Io)$]	0.0915	0.0403	0.0309	0.0358	0.0427	0.0335	0.0674
$wR2$[all data]	0.3156	0.1331	0.0847	0.0732	0.1255	0.0934	0.1920
ρ_{fin} (max/min) [eÅ^{-3}]	0.352/−0.314	1.764/−1.463	2.103/−2.243	0.797/−0.395	3.732/−2.130	1.627/−1.125	6.529/−5.715

ine (HL_{Bu}) was obtained as a red oil by a procedure similar to that of *N*-benzyl-*N*-(2-pyridylmethyl)-*N*-(1*H*-2-pyrrolylmethyl)amine (HL_{Bzl}), starting from *n*-butylamine instead of benzylamine. The compound was purified by column chromatography over silica-60H with 10% MeOH/$CHCl_3$. Yield 0.64 g (2.63 mmol, 15.5%). − ^{1}H NMR (200 MHz, $CDCl_3$, 298 K): δ = 9.83 (s, br, 1 H, Pyr−H1), 8.52 [d, 1 H, ^3J(H,H) = 3.2 Hz, Py−H6], 7.61 (m, 1 H, Py−H4), 7.45 (m, 1 H, Py−H3), 7.15 (m, 1 H, Py−H5), 6.78 (m, 1 H, Pyr−H5), 6.11 (m, 1 H, Pyr−H4), 6.01 (m, 1 H, Pyr−H3), 3.69 (s, 2 H, N−CH_2−), 3.59 (s, 2 H, N−CH_2−), 2.48 [t, 2 H, ^3J(H,H) = 7.4 Hz, N−CH_2−C_3H_7], 1.51 (m, 2 H, N−CH_2−CH_2−C_2H_5), 1.31 (m, 2 H, N−C_2H_4−CH_2−CH_3), 0.85 [t, 3 H, ^3J(H,H) = 7.1 Hz, N−C_3H_6−CH_3]. − EI-MS [*m*/*z* (%)]: 244 $[M]^+$ (3), 186 $[M - Bu]^+$ (4), 163 $[M - Py]^+$ (39), 151 $[M - Bu - Pyr]^+$ (84), 107 $[M - Bu - Py]^+$, 93 $[CH_2Py + H]^+$ (100).

(η^4-Cycloocta-1,5-diene)[*N*-(2-pyridylmethyl)-*N*-(1*H*-2-pyrrolylmethyl)amine]rhodium(I) Hexafluorophosphate ([1]PF_6): 30.0 mg (0.16 mmol) of *N*-(2-pyridylmethyl)-*N*-(1*H*-2-pyrrolylmethyl)amine (HL_H) was dissolved in 5 mL of MeOH and 39.5 mg (0.08 mmol) of $[\{(cod)Rh(\mu\text{-}Cl)\}_2]$ was added, and stirred at room temp. for 1 h. Addition of 32.6 mg of NH_4PF_6 resulted in the precipitation of $[(HL_H)Rh^{I}(cod)]PF_6$ ([**1**]PF_6) as a yellow solid, which was collected by filtration, washed with small portions of water and MeOH and was vacuum-dried. Crystals suitable for X-ray diffraction were obtained by slow crystallisation from a saturated MeOH solution at −20°C. Yield 54 mg (62%). − ^{1}H NMR (500 MHz, [D$_6$]acetone, 298 K): 10.22 (s, br, 1 H, Pyr−H1), 8.10 [ddd, 1 H, ^3J(H,H) = 7.83 Hz, ^3J(H,H) = 7.10 Hz, ^4J(H,H) = 1.46 Hz, Py−H4], 7.96 [d, 1 H, ^3J(H,H) = 5.88 Hz, Py−H6], 7.76 [d, 1 H, ^3J(H,H) = 7.83 Hz, Py−H3], 7.54 [dd, 1 H, ^3J(H,H) = 7.10 Hz, ^3J(H,H) = 5.88 Hz, Py−H5], 6.80 (m, 1 H, Pyr−H5), 6.29 (m, 1 H, Pyr−H3), 6.06 (m, 1 H, Pyr−H4), 4.99 (s, br, 1 H, NH), 4.46 (m, br, 4 H, −HC=CH−), 3.98 (s, 2 H, N−CH_2−), 3.95 (s, 2 H, N−CH_2−), 2.47 (m, br, 4 H, −C=C−$CH_{2\ exo}$), 1.98 (m, br, 4 H, −C=C−$CH_{2\ endo}$). − ^{1}H NMR (500 MHz, [D$_6$]acetone, 193 K): δ = 10.65 (s, br, 1 H, Pyr−H1), 8.12 [ddd, ^3J(H,H) = 7.4 Hz, ^3J(H,H) = 7.4 Hz, ^4J(H,H) = 1.5 Hz, Py−H4], 7.98 [d, 1 H, ^3J(H,H) = 5.5 Hz, Py−H6], 7.79 [d, 1 H, ^3J(H,H) = 7.4 Hz, Py−H3], 7.56 [dd, 1 H, ^3J(H,H) = 7.4 Hz, ^3J(H,H) = 5.5 Hz, Py−H5], 6.87 [d, 1 H, ^3J(H,H) = 1.5 Hz, Pyr−H5], 6.25 (m, 1 H, Pyr−H3), 6.06 (m, 1 H, Pyr−H4), 5.16 (s, br, 1 H, NH), 4.74 (s, br, 1 H, −*HC*=*CH*−), 4.57 {dd[AB], 1 H, ^2J(H,H) = 16.0 Hz, ^3J(H,H) = 4.8 Hz, N−CH_2−}, 4.51 (s, br, 1 H, −*HC*=*CH*−), 4.30 {dd[AB], 1 H, ^2J(H,H) = 16.0 Hz, ^3J(H,H) = 2.9 Hz, N−CH_2−}, 3.95 {dd[AB], 1 H, ^2J(H,H) = 14.0 Hz, ^3J(H,NH) = 6.6 Hz, N−CH_2−}, 3.86 {dd[AB], 1 H, ^2J(H,H) = 14.0 Hz, ^3J(H,NH) = 6.6 Hz, N−CH_2−}, 3.64 (s, br, 1 H, −*HC*=*CH*−), 2.58 (m, br, 1 H, −C=C−$CH_{2\ exo}$), 2.46 (m, br, 1 H, −C=C−$CH_{2\ exo}$), 2.30 (m, br, 2 H, −C=C−$CH_{2\ exo}$), 2.02 (m, br, 2 H, −C=C−$CH_{2\ endo}$), 1.85 (m, br, 2 H, −C=C−$CH_{2\ endo}$). − ^{13}C NMR (50 MHz, [D$_6$]-acetone, 298 K): δ = 161.5 (Py−C2), 147.8 (Py−C6), 139. 8 (Py−C4), 124.8 (Pyr−C2), 124.0 (Py−C3), 122.9 (Py−C5), 118.6 (Pyr−C5), 109.6 (Pyr−C4), 108.2 (Pyr−C2), 82.2 (br., *C*=*C*), 56.5 (d, ^2J(C,Rh) = 4.6 Hz, N−CH_2−), 47.7 (N−CH_2), 29.8 (C=C−CH_2−). − FT-IR (KBr): $\tilde{\nu}$ = 3297 (NH), 1655 (C=C), 840 $[(PF_6)^-]$, 558 $[(PF_6)^-]$. − FAB-MS (*m*/*z*): 941 $[2\ M - PF_6]^+$, 398 $[M - PF_6]^+$. − $C_{19}H_{25}F_6N_3PRh$ (543.30): calcd. C 42.00, H 4.64, N 7.73; found C 41.87, H 4.46, N 7.61.

(η^4-Cycloocta-1,5-diene)-[*N*-(2-pyridylmethyl)-*N*-(1*H*-2-pyrrolylmethyl)amine]iridium(I) Hexafluorophosphate ([2]PF_6): 77 mg (0.41 mmol) of *N*-(2-pyridylmethyl)-*N*-(1*H*-2-pyrrolylmethyl)amine (HL_H) was added to a solution of 136 mg (0.20 mmol) of

[{(cod)Ir^{I}(μ-Cl)}$_2$] in 15 mL of MeOH/CH_2Cl_2 (2:1), and stirred at room temp. for 5 min. The dichloromethane was subsequently removed from the reaction mixture under reduced pressure. After addition of 500 mg (2.7 mmol) of KPF_6 and vigorous stirring for a further 5 min, 2 mL of water was added and the reaction mixture was stored at 5°C. Yellow, X-ray quality crystals of [(HL_H)Ir^{I}-(cod)]PF_6 ([**2**]PF_6) were formed overnight. The crystals were washed with water, ethanol, and ether in order to remove the excess KPF_6. The mother liquor was treated with water to cause further precipitation of [**2**]PF_6. – ^{1}H NMR (300 MHz, CD_2Cl_2, 298 K): 9.03 (s, br., 1 H, Pyr−H1), 8.01 (m., 2 H, Py−H4 and Py−H6), 7.61 [d, 1 H, ^3J(H,H) = 7.5 Hz, Py−H3], 7.43 [dd, 1 H, ^3J(H,H) = 6.3 Hz, Py−H5], 6.77 (m., 1 H, Pyr−H5), 6.17 (m., 1 H, Pyr−H3), 6.06 (m., 1 H, Pyr−H4), 4.91 (s., br., 1 H, NH), 4.45−4.10 (m., br., 2 H, −HC=CH− and 2 H, N−CH_2−Py), 3.99 (s.,1 H, N−CH_2−Pyr), 3.97 (s., 1 H, N−CH_2−Pyr), 3.83 (br., s., 2 H, −HC=CH−) 2.28 (m., br., 4 H, −C=C−CH_2− *exo*), 1.79 (s., br., 4 H, −C=C−CH_2− *endo*). – ^{13}C{^{1}H} NMR (75 MHz, CD_2Cl_2, 298 K): δ = 163.6 (Py−C2), 148.4 (Py−C6), 141.4 (Py−C4), 125.6 (Pyr−C2), 123.8 (Py−C3), 123.7 (Py−C5), 121.0 (Pyr−C5), 112.2 (Pyr−C4), 109.3 (Pyr−C2), 68.0 (s., br., C=C), 58.5 (N−CH_2−), 50.1 (N−CH_2), 31.7 (s., br., C=C−CH_2−). – FAB-MS (*m*/*z*): 488 and 486 [M − PF_6]$^+$, 408 [M − PF_6 − CH_2 − Pyr]$^+$, 376 [M − PF_6 − (cod)]$^+$. – $C_{19}H_{25}F_6IrN_3P$ (632.59): calcd. C 36.07, H 3.98, N 6.64; found C 35.96, H 4.31, N 6.50.

(η^4-Cycloocta-1,5-diene)[(*N*-(2-pyridylmethyl)-*N*-(2-pyrrolatomethyl)amine]rhodium(I) (3): 77.6 mg (0.41 mmol) of *N*-(2-pyridylmethyl)-*N*-(1*H*-2-pyrrolylmethyl)amine (HL_H) was dissolved in 10 mL of MeOH and 100.0 mg (0.20 mmol) of [{(cod)Rh(μ-Cl)}$_2$] was added, and stirred at room temp. for 1 h. Addition of a solution of 200 mg (1.89 mmol) of Na_2CO_3 in 5 mL of water resulted in the precipitation of [(L_H^-)Rh^{I}(cod)] (**3**) as a yellow solid, which was collected by filtration, washed three times with water, once with MeOH, and vacuum dried. Crystals suitable for X-ray diffraction were obtained by slow crystallisation from a saturated toluene solution at −20°C. Yield 90 mg (56%). – ^{1}H-NMR: (200 MHz, CD_2Cl_2, 298 K): δ = 8.55 [d, 1 H, ^3J(H,H) = 4.1 Hz, Py−H6], 7.67 (m, 1 H, Py−H4), 7.21 (m, 2 H, Py−H3, Py−H5), 6.23 (s, 1 H, Pyr−H5), 5.92 [dd, 1 H, ^3J(H,H) = 2.4 Hz, ^3J(H,H) = 2.9 Hz, Pyr−H4], 5.72 [d, 1 H, ^3J(H,H) = 2.4 Hz, Pyr−H3], 4.50 (s, br, 1 H, N*H*), 4.12 (m, br, 4H −CH=CH−), 3.94 {dd[AB], 1 H, ^2J(H,H) = 14.9 Hz, ^3J(H,NH) = 3.09 Hz, N−CH_2−}, 3.81 {dd[AB], 1 H, ^2J(H,H) = 13.3 Hz, ^3J(H,NH) = 5.1 Hz, N−CH_2−}, 3.73 {dd[AB], 1 H, ^2J(H,H) = 14.9 Hz, ^3J(H,NH) = 9.9 Hz, N−CH_2−}, 3.50 {dd[AB], 1 H, ^2J(H,H) = 13.3 Hz, ^3J(H,NH) = 7.6 Hz, N−CH_2−}, 2.55 (m, 2 H, −C=C−$CH_{2\ exo}$), 2.35 (m, 2 H, −C=C−$CH_{2\ exo}$), 2.05 (m, 2 H, −C=C−$CH_{2\ endo}$), 1.85 (m, 2 H, −C=C−$CH_{2\ endo}$). – After saturation of the N−H two AB-patterns are observed for the N−CH_2− groups of the ligand: 3.93 {d[AB], 1 H, ^2J(H,H) = 14.8 Hz, N−CH}, 3.72 {d[AB], 1 H, ^2J(H,H) = 14.8 Hz, N−CH}, 3.79 {d[AB], 1 H, ^2J(H,H) = 13.1 Hz, N−CH}, 3.49 {d[AB], 1 H, ^2J(H,H) = 13.1 Hz, N−CH}. – ^{13}C NMR (50 MHz, CD_2Cl_2, 298 K): δ = 156.5 (Py−C2). 150.5 (Py−C6), 139.6 (Pyr−C2), 137.6 (Py−C4), 123.7 (Py−C3), 123.6 (Py−C5), 123.3 [d, ^2J(C,Rh) = 2.6 Hz, Pyr−C5], 108.4 (Pyr−C4), 101.7 (Pyr−C3), 79.3 [d, ^1J(C,Rh) = 12.3 Hz, C=C], 78.8 [d, ^1J(C,Rh) = 12.6 Hz, C=C], 54.0 (N−*C*H_2−Pyr), 56.1 (N−*C*H_2−Py), 32.1 (C=C−*C*H_2), 30.6 (C=C−*C*H_2). – FT-IR (KBr, cm^{-1}): $\tilde{\nu}$ = 3236 (N−H), 1654 (C=C). – FAB-MS (*m*/*z*): 398 [M + H]$^+$, 319 [M − CH_2Pyr + H]$^+$, 288 [M − cod − H]$^+$, 209 [M − cod − CH_2Pyr]$^+$. – FD$^+$-MS: 397 [M] $^+$. – $C_{19}H_{24}N_3Rh$ (397.32): calcd. C 57.44, H 6.09, N 10.58; found C 57.02, H 6.05, N 10.35.

(η^4-Cycloocta-1,5-diene)[(*N*-(2-pyridylmethyl)-*N*-(2-pyrrolatomethyl)amine]iridium(I) (4): 125 mg (0.67 mmol) of *N*-(2-pyridylmethyl)-*N*-(1*H*-2-pyrrolylmethyl)amine (HL_H) (slight xs.) was added to a suspension of 210 mg (0.31 mmol) of [{(cod)Ir^{I}(μ-Cl)}$_2$] in 15 mL of MeOH, and stirred at room temp. for 10 min. Addition of a solution of 200 mg (0.70 mmol) of $Na_2CO_3 \cdot 10\ H_2O$ in 2 mL of water resulted in the precipitation of [(L_H^-)Ir^{I}(cod)] (**4**) as a yellow solid, which was collected by filtration. Crystals suitable for X-ray diffraction were obtained by slow crystallisation from a saturated CH_2Cl_2 solution at −20°C. – ^{1}H NMR: (300 MHz, CD_2Cl_2, 298 K): δ = 8.61 [d, 1 H, ^3J(H,H) = 4.8 Hz, Py−H6], 7.70 [dd, 1 H, average ^3J(H,H) = 7.5 Hz Py−H4], 7.26 [dd, 1 H, average ^3J(H,H) = 6 Hz, Py-H5], 7.19 [d, 1 H, ^3J(H,H) = 7.5 Hz, Py−H3], 6.47 [d, 1 H, ^3J(H,H) = 2.4 Hz, Pyr−H5], 6.02 [dd, 1 H, ^3J(H,H) = 2.4 Hz], 5.86 [d, 1 H, ^3J(H,H) = 2.4 Hz, Pyr−H3], 5.25 (s., br., 1 H, N−H), 4.18 {dd[AB], 1 H, ^2J(H,H) = 15.2 Hz, ^3J(H,NH) = 2.4 Hz, N−CH}, 3.95 {dd[AB], 1 H, ^2J(H,H) = 13.4 Hz, ^3J(H,NH) = 5.3 Hz, N−CH}, 3.87 (m., 2 H −CH=CH−), 3.86 {dd[AB], 1 H, ^2J(H,H) = 15 Hz, ^3J(H,NH) = 10.2 Hz, N−CH}, 3.73 (m., 2 H, −CH=CH−), 3.58 {dd[AB], 1 H, ^2J(H,H) = 13.4 Hz, ^3J(H,NH) = 7.0 Hz, N−CH}, 2.29 (m., 2 H, −C=C−$CH_{2\ exo}$), 2.14 (m., 2 H, −C=C−$CH_{2\ exo}$), 1.82 (m., 2 H, −C=C−$CH_{2\ endo}$), 1.48 (m., 2 H, −C=C−$CH_{2\ endo}$). – ^{13}C{^{1}H} NMR (75 MHz, CD_2Cl_2, 298 K): δ = 156.2 (Py−C2). 150.6 (Py−C6), 142.0 (Pyr−C2), 137.8 (Py−C4), 123.8 (Py−C3), 123.5 (Py−C5 and Pyr−C5), 109.8 (Pyr−C4), 101.7 (Pyr−C3), 62.3 (C=C), 61.5 (C=C), 55.3 (N−*C*H_2−Pyr), 57.0 (N−*C*H_2−Py), 33.1 (C=C−*C*H_2), 31.1 (C=C−*C*H_2). – FAB-MS (*m*/*z*): 488 and 486 [M + H]$^+$, 407 [M − Py]$^+$, 376 [M − cod − H]$^+$. – $C_{19}H_{24}N_3Ir$ (486.64): calcd. C 46.90, H 4.97, N 8.63; found C 47.17, H 4.72, N 8.31.

(η^4-Cycloocta-1,5-diene)[*N*-benzyl-*N*-(2-pyridylmethyl)-*N*-(2-pyrrolatomethyl)amine]-rhodium(I) (5): To 50 mL of methanol 200 mg Na_2CO_3 (18 mmol) in 2 mL of water and 400 mg (1.449 mmol) of *N*-benzyl-*N*-(2-pyridylmethyl)-*N*-(1*H*-2-pyrrolylmethyl)amine (HL_{Bzl}) was added. The suspension was stirred for 15 min and subsequently 350 mg (0.71 mmol) of [{(cod)Rh(μ-Cl)}$_2$] was added. The mixture was stirred for 2 h at room temp. and placed at −20°C for 10 h. The resulting precipitate was collected by filtration and the yellow residue was washed three times with 5 mL of a mixture of water and MeOH (1:1), subsequently dissolved in 10 mL of CH_2Cl_2 and filtered. The yellow filtrate was evaporated under vacuum to yield [(L_{Bzl}^-)Rh^{I}(cod)] (**5**) as a yellow powder. Crystals suitable for X-ray diffraction were obtained by crystallisation from a hot saturated solution of **5** in toluene. Yield 388 mg (55%). – ^{1}H NMR (200 MHz, CD_2Cl_2, 298 K): δ = 9.25 [d, 1 H, Py−H6, ^3J(H,H) = 4.7 Hz], 7.72−7.35 (m, 6 H, Ph−H, Py−H4), 7.25 (m, 1 H, Py−H5), 7.13 [d, 1 H, ^3J(H,H) = 7.6 Hz, Py−H3], 6.34 (s, br, 1 H, Pyr−H5), 5.76 [t, 1 H, ^3J(H,H) = 2.49 Hz, Pyr−H4], 5.64 (s, br, 1 H, Pyr−H3), 4.84 {d[AB], 1 H, ^2J(H,H) = 13.7 Hz, N−CH_2−Ph}, 4.66 {d[AB], 1 H, ^2J(H,H) = 13.7 Hz, N−CH_2−Ph}, 4.01 {d[AB], 1 H, ^2J(H,H) = 14.1 Hz, N−CH_2−Py}, 4.00 {d[AB], 1 H, ^2J(H,H) = 15.0 Hz, N−CH_2−Pyr}, 3.91 (m, 2 H, −CH=CH−), 3.54 {d[AB], 1 H, ^2J(H,H) = 14.1 Hz, N−CH_2−Py}, 3.37 (m, 2 H, −CH=CH−), 3.16 {d[AB], 1 H, ^2J(H,H) = 15.0 Hz, N−CH_2−Pyr}, 2.42 (m, 4 H, C=C−$CH_{2\ exo}$), 1.73 (m, 4 H, C=C−$CH_{2\ endo}$). – ^{13}C{^{1}H} NMR (75 MHz, CD_2Cl_2, 298 K): δ = 159.0 (Py−C2), 151.7 (Py−C6), 138.3 (Pyr−C2), 137.4 (Py−C4), 135.0 (Ph−C1), 132.21 (Ph−C2), 129.1 (Ph−C3), 128.7 (Ph−C4), 125.3 (Pyr−C5), 124.1 (Py−C5), 123.8 (Py−C3), 107.3 (Pyr−C4), 103.3 (Pyr−C3), 76.0 (br., C=C), 62.5 (N−*C*H_2−Ph), 60.25 (N−*C*H_2−Pyr), 56.90 (N−*C*H_2−Py), 31.9 (C=C−*C*H_2−), 31.7 (C=C−*C*H_2−). – FAB-MS (*m*/*z*): 488 [M + H]$^+$, 409 [M − Py]$^+$, 396 [M − CH_2Py +

H]$^+$, 211 $[Rh(cod)]^+$. − $C_{26}H_{30}N_3Rh$ (487.44): calcd. C 64.07, H 6.20, N 8.62; found C 64.49, H 6.29, N 8.33.

(η⁴-Cycloocta-1,5-diene)[*N*-benzyl-*N*-(2-pyridylmethyl)-*N*-(2-pyrrolatomethyl)amine]iridium(I) (6): To a suspension of 250 mg (0.37 mmol) of $[\{(cod)Ir(\mu\text{-}Cl)\}_2]$ in 10 mL of MeOH 210 mg (0.76 mmol) of *N*-benzyl-*N*-(2-pyridylmethyl)-*N*-(1*H*-2-pyrrolylmethyl)-amine (HL_{Bzl}) was added. The reaction mixture was stirred for 15 min and subsequently 500 mg (1.75 mmol) of $Na_2CO_3 \cdot 10\,H_2O$ in 3 mL of water was added. The resulting precipitate was collected by filtration and the yellow residue was dried in vacuo to yield $[(L_{Bzl}^-)Ir^I(cod)]$ (**6**) as a yellow powder. Crystals suitable for X-ray diffraction were obtained by crystallisation from a hot saturated solution of **6** in toluene. − ^{1}H NMR (300 MHz, CD_2Cl_2, 298 K): δ = 9.24 [d, 1 H, Py−H6, ^3J(H,H) = 4.4 Hz], 7.58 [dt, 1 H, ^3J(H,H) = 7.68 Hz, J(H,H) = 1.74 Hz, Py−H4], 7.45 (m., 5 H, Ph), 7.19 [t, 1 H, average ^3J(H,H) = 6.4 Hz, Py−H5], 7.05 [d, 1 H, ^3J(H,H) = 7.8 Hz], 6.51 (m., br., 1 H, Pyr−H5), 5.78 [t, 1 H, ^3J(H,H) = 2.6 Hz, Pyr−H4], 5.73 (s., br., 1 H, Pyr−H3), 4.93 {d[AB], 1 H, ^2J(H,H) = 14.0 Hz, N−CH_2−Ph}, 4.85 {d[AB], 1 H, ^2J(H,H) = 14.0 Hz, N−CH_2−Ph}, 4.17 {d[AB], 1 H, ^2J(H,H) = 15.1 Hz, N−CH_2−Pyr}, 3.95 {d[AB], 1 H, ^2J(H,H) = 14.5 Hz, N−CH_2−Py}, 3.73 {d[AB], 1 H, ^2J(H,H) = 15.3 Hz, N−CH_2−Pyr}, 3.47 (m., 2 H, −CH=CH−), 3.03 {d[AB], 1 H, ^2J(H,H) = 14.3 Hz, N−CH_2−Py}, 2.84 (m., 2 H, −CH=CH−), 2.23 (m., 4 H, C=C−$CH_{2\,exo}$), 1.49 (m., 4 H, C=C−$CH_{2\,endo}$). − ^{13}C{^{1}H} NMR (75 MHz, CD_2Cl_2, 298 K): δ = 160.5 (Py−C2), 152.8 (Py−C6), 140.3 (Pyr−C2), 137.4 (Py−C4), 134.8 (Ph−C1), 132.1 (Ph−C2), 129.2 (Ph−C3), 129.0 (Ph−C4), 124.6 (Pyr−C5 and Py−C5), 123.3 (Py−C3), 107.6 (Pyr−C4), 102.8 (Pyr−C3), 64.0 and 62.0 (N−CH_2−Ph and N−CH_2−Pyr), 56.20 (N−CH_2−Py), 55.7 (br., C=C) 33.3 (C=C−CH_2−), 33.0 (C=C−CH_2−). − FAB-MS (*m*/*z*): 576 and 574 $[M - H]^+$, 499 $[M - Ph]^+$. $C_{26}H_{30}IrN_3$ (576.73): calcd. C 54.14, H 5.24, N 7.29; found C 54.11, H 5.08, N 7.12.

(η⁴-Cycloocta-1,5-diene)[*N*-butyl-*N*-(2-pyridylmethyl)-*N*-(2-pyrrolatomethyl)amine]rhodium(I) (7): [(*N*-Butyl-*N*-(2-pyridylmethyl)-*N*-(2-pyrrolatomethyl)amine)Rh^I(cod)] (**7**) was prepared by a method similar to the preparation of $[(L_{Bzl}^-)Rh^I(cod)]$ (**5**), starting from *N*-butyl-*N*-(2-pyridylmethyl)-*N*-(1*H*-2-pyrrolylmethyl)amine (HL_{Bu}). − ^{1}H NMR (200 MHz, $CDCl_3$, 298 K): δ = 9.10 [d, 1 H, Py−H6, ^3J(H,H) = 5.0 Hz], 7.60 (m, 1 H, Py−H4), 7.17−7.32 (m, 2 H, Py−H3, Py−H5), 6.34 (s, br, 1 H, Pyr−H5), 5.99 (m, 1 H, Pyr−H4), 5.73 (s, br, 1 H, Pyr−H3), 3.95−3.80 (m, 4 H, N−CH_2−Py, −*HC*=*CH*−), 3.75 {d[AB], 1 H, ^2J(H,H) = 13.8 Hz, N−CH_2−Pyr}, 3.51 {d[AB], 1 H, ^2J(H,H) = 14.1 Hz, N−CH_2−Pyr}, 3.40 (m, 2 H, −CH=CH−), 3.37 (m, 2 H, −CH=CH−), 3.23 [dt, 1 H, ^2J(H,H) = 12.0 Hz, ^3J(H,H) = 4.2 Hz, N−CH_2−C_3H_7], 3.04 [dt, 1 H, ^2J(H,H) = 12.0 Hz, ^3J(H,H) = 4.2 Hz, N−CH_2−C_3H_7], 2.31 (m, 4 H, C=C−$CH_{2\,exo}$), 1.88 (m, 2 H, N−CH_2−*CH_2*−C_2H_5), 1.71 (m, 4 H, C=C−$CH_{2\,endo}$), 1.40 (m, 2 H, N−C_2H_4−*CH_2*−CH_3), 0.99 [t, ^3J(H,H) = 7.2 Hz, 3 H, N−C_3H_6−*CH_3*]. − FAB-MS (*m*/*z*): 454 $[M + H]^+$, 409 $[M-Py]^+$, 375 $[M - Py]^+$, 211 $[Rh(cod)]^+$. − $C_{23}H_{32}N_3Rh$ (453.43): calcd. C 60. 79, H 7.32, N 9.25; found C 60.88, H 7.04, N 9.39.

Polymerisation of Phenylacetylene: 0.82 g of Phenylacetylene was dissolved in 20 mL of MeOH. 5 mg of catalyst $[(L_{Bzl}^-)Rh^I(cod)]$ (**5**) was added to this solution. Almost immediate formation of poly(phenylacetylene) as a yellow/orange precipitate can be observed, and a gradual colour change of the solution from pale yellow to deep red. After 20 min the poly(phenylacetylene) precipitate was collected by filtration, washed with MeOH and dried under vacuum. Yield 0.20 g (24%). − IR (KBr): ṽ = 3053, 1596, 1488, 1444, 1073, 1028, 884, 756, 737, 696 cm^{-1}. − ^{1}H NMR (200 MHz, $CDCl_3$, 298 K): δ = 6.98 (s, br. Ph), 6.67 (m, br., Ph), 5.86 (s, br., vinyl). − GPC analysis (polystyrene standard): M_n = 14000, M_w = 65000, M_z = 137000, M_w/M_n = 4.7, M_z/M_w = 2.1, $[\eta]_{dv}$ = 0.292.

Acknowledgments

We thank Roel Fokkens of the University of Amsterdam for performing high resolution MS- measurements. We thank Johnson Matthey Ltd. for a generous loan of $RhCl_3 \cdot 3\,H_2O$ and $IrCl_3 \cdot 3\,H_2O$.

[1] $[(Cn^*)Rh^{III}(Me)]^+$ is active in polymerisation of ethene: [1a] L. Wang, T. C. Flood, *J. Am. Chem. Soc*. **1992**, *114*, 3169. − [1b] L. Wang, R. S. Lu, R. Bau, T. C. Flood, *J. Am. Chem. Soc*. **1993**, *115*, 6999.

[2] $[(Cn^*)Rh^I(PMe_3)]^+$ and $[(Tp^{Me2})Rh^I(CO)]$ oxidatively add C−H bonds: [2a] C. Wang, J. W. Ziller, T. C. Flood, *J. Am. Chem. Soc*. **1995**, *117*, 1647. − [2b] C. K. Ghosh, W. A. G. Graham, *J. Am. Chem. Soc*. **1987**, *109*, 4726. − [2c] C. K. Ghosh, W. A. G. Graham, *J. Am. Chem. Soc*. **1989**, *111*, 375. − [2d] P. E. Bloyce, J. Mascetti, A. J. Rest, *J. Organomet. Chem.* **1993**, *444*, 223. − [2e] A. A. Purwoko, A. J. Lees, *Inorg. Chem.* **1996**, *35*, 675.

[3] The α-chlorotolyl complex $[(2,6\text{-}(C(Me)=N-i\text{Pr})_2C_5H_3N)Rh^{II}Cl_2(CHClPh)]$ reacts with H_2O and O_2 to give benzaldehyde and H_2O_2: H. F. Haarman, F. R. Bregman, P. W. N. M. van Leeuwen, K. Vrieze, *Organometallics* **1997**, *16*, 979.

[4] B. de Bruin, M. J. Boerakker, J. J. J. M. Donners, B. E. C. Christiaans, P. P. J. Schlebos, R. de Gelder, J. M. M. Smits, A. L. Spek, A. W. Gal, *Angew. Chem*. **1997**, *109*, 2153; *Angew. Chem. Int. Ed. Eng*. **1997**, *36*, 2064.

[5] [5a] M. A. Esteruelas, F. J. Lahoz, A. M. Lopez, E. Onate, L. A. Oro, N. Ruiz, E. Sola, J. I. Tolosa, *Inorg. Chem.* **1996**, *35*, 7811. − [5b] P. G. Rasmussen, O. H. Bailey, J. C. Bayon, *Inorg. Chem*. **1984**, *23*, 343. − [5c] S. W. Kaiser, R. B. Saillant, W.M. Butler, P.G. Butler, P.G. Rasmussen, *Inorg. Chem*. **1976**, *15*, 2681. − [5d] M. Akita, K. Ohta, Y. Takahashi, S. Hikichi, Y. Moro-oka, *Organometallics* **1997**, *16*, 4121. − [5e] M. Bortolin, U. E. Bucher, H. Rüegger, L. M. Venanzi, A. Albinati, F. Lianza, S. Trofimenko, *Organometallics* **1992**, *11*, 2514. − [5f] H. Brunner, P. Beier, G. Riepl, I. Bernal, G. M. Reisner, R. Benn, A. Rufinska, *Organometallics* **1985**, *4*, 1732. − [5g] K. A. Beveridge, G. W. Bushnell, S. R. Stobart, J. L. Atwood, M. J. Zaworotko, *Organometallics* **1983**, *2*, 1447. − [5h] M. Cocivera, G. Ferguson, B. Kaitner, F. J. Lalor, D. J. O′Sullivan, M. Pavez, B. Ruhl, *Organometallics* **1982**, *1*, 1132. − [5i] M. A. Garalda, R. Hernandez, L. Ibarlucea, M. I. Arriotua, M. K. Urtiaga, *Inorg. Chim. Acta* **1995**, *232*, 9. − [5j] H. Brunner, G. Riepl, I. Bernal, W. H. Ries, *Inorg. Chim. Acta* **1986**, *112*, 65. − [5k] M. P. Garcia, A. M. Lopez, M. A. Esteruelas, F. J. Lahoz, L. A. Oro, *J. Chem. Soc., Chem. Comm.* **1988**, 793. − [5l] K. Yamamoto, H. Tateishi, W. Watanabe, T. Adachi, H. Matsubara, T. Ueda, T. Yoshida, *J. Chem. Soc., Chem. Comm* **1995**, 1637. − [5m] F. J. Lahoz, A. Tiripicchio, M. Tiripicchio Camellini, L. A. Oro, M. T. Pinillos, *J. Chem. Soc., Dalton Trans.* **1985**, 1487. − [5n] D. Sanz, M. D. Santa Maria, R. M. Claramunt, M. Cano, J. V. Heras, J. A. Campo, F. A. Ruiz, E. Pinilla, A. Monge, *J. Organomet. Chem*. **1996**, *523*, 179. − [5o] H. Brunner, B. Nubber, M. Prommesberger, *J. Organomet. Chem.* **1996**, *526*, 341. − [5p] W. S. Sheldrick, B. Gunther, *J. Organomet. Chem.* **1991**, *402*, 256. − [5q] W. S. Sheldrick, B. Gunther, *J. Organomet. Chem.* **1989**, *375*, 233. − [5r] A. Albinati, C. Arz, P. S. Preggosin, *J. Organomet. Chem*. **1988**, *356*, 367. − [5s] M. A. Esteruelas, L. A. Oro, M. C. Apreda, C. Foces-Foces, F. H. Cano, R. M. Claramunt, C. Lopez, J. Elguero, M. Begtrup, *J. Organomet. Chem*. **1988**, *344*, 93. − [5t] L. A. Oro, M Esteban, R. M. Claramunt, J. Elguero, C. Foces-Foces, F. H. Cano, *J. Organomet. Chem*. **1984**, 276, 79. − [5u] B.M Louie, S. J. Rettig, A. Storr, J. Trotter, *Can. J. Chem*. **1984**, *62*, 1057. − [5v] W. H. Watson, A. Nagl, A. P. Marchand, P. Annapurna, *Acta Crystallogr., Sect. C (Cr. Str. Comm.)* **1989**, *45*, 856.

[6] [6a] H. M. Colquhoun, S. M. Doughty, J. F. Stoddart, D. J. Williams, *J. Chem. Soc., Dalton Trans.* **1986**, 1639. − [6b] A. A. H.

van der Zeijden, G. Van Koten, R. A. Nordemann, B. Kojic-Prodic, A. L. Spek, *Organometallics* **1988**, *7*, 1957.
[7] A. R. Rossi, R. Hoffmann, *Inorg. Chem.* **1975**, *14* (2), 365.
[8] [8a] G. Winkhaus, H. Singer, *Chem. Ber.* **1966**, *99*, 3610. – [8b] G. Mestroni, A. Camus, G. Zassinovich, *J. Organomet. Chem.* **1974**, *73*, 119. – [8c] M. A. Esteruelas, L. A. Oro, M. C. Apreda, C. Foces-Foces, F. H. Cano, R. M. Claramunt, C. Lopex, J. Elguero, M. Bergtrup, *J. Organomet. Chem.* **1988**, *344*, 93.
[9] H Katayama, K. Yamamura, Y. Miyaki, F. Ozawa, *Organometallics* **1997**, *16*, 4497.
[10] [10a] Y. Kishimoto, P. Eckerle, T. Miyatake, T. Ikariya, R Noyori, *J. Am. Chem. Soc.* **1994**, *116*, 12131. – [10b] A. Escudero, R. Vilar, R. Salcedo, T. Ogawa, *Eur. Polym. J.* **1995**, *11*, 1135 and references quoted therein.
[11] [11a] S. Trofimenko, *Chem. Rev.* **1993**, *93*, 943. – [11b] N. Kitajima, W. B. Tolman, *Prog. Inorg. Chem.* **1995**, *43*, 419.
[12] Diene complexes: [12a] M. Akita, K. Ohta, Y. Takahashi, S. Hikichi, Y. Moro-oka, *Organometallics* **1997**, *16*, 4121. – [12b] M. Cocivera, T. J. Desmond, G. Ferguson, B. Kaitner, F. J. Lalor, D. J. O′Sullivan, *Organometallics* **1982**, *1*, 1125. – [12c] M. Cocivera, G. Ferguson, B. Kaitner, F. J. Lalor, D. J. O′Sullivan, M. Pavez, B. Ruhl, *Organometallics* **1982**, *1*, 1132. – [12d] M. Cocivera, G. Ferguson, F. J. Lalor, P. Szczecinski, *Organometallics* **1982**, *1*, 1139. – [12e] U. E. Bucher, A. Currao, R. Nesper, H. Rüegger, L. M. Venanzi, E. Younger, *Inorg. Chem.* **1995**, *34*, 66. – [12f] U. E. Bucher, T. F. Fässler, M. Hunziker, R. Nesper, H. Rüegger, L. M. Venanzi, *Gazz. Chim. Ital.* **1995**, *125*, 181. – [12g] D. Sanz, M. D. Santa Maria, R. M. Claramunt, M. Cano, J. V. Heras, J. A. Campo, F. A. Ruiz, E. Pinilla, A. Monge, *J. Organomet. Chem.* **1996**, *523*, 179.
[13] Olefin complexes: [13a] S. Trofimenko, *J. Am. Chem. Soc.* **1969**, *91*, 588. – [13b] W. J. Oldham, D. M. Heinekey, *Organometallics* **1997**, *16*, 467. – [13c] P. J. Pérez, M. L. Poveda, E. Carmona, *Angew. Chem. Int. Ed Engl.* **1995**, *34*, 66.
[14] G. Giordano, R. H. Crabtree, *Inorg. Synth.* **1990**, *28*, 88.
[15] J. L. Herde, J. C. Lambert, C. V. Senov, *Inorg. Synth.* **1974**, XV, 18.
[16] A. C. T. North, D. C. Phillips, F. C. Mathews, *Acta Cryst.* **1968**, *A24*, 351.
[17] P. T. Beurskens, G. Beurskens, W. P. Bosman, R. de Gelder, S. Garcia-Granda, R. O. Gould, R. Israel, J. M. M. Smits. *DIRDIF-96*. A computer program system for crystal structure determination by Patterson methods and direct methods applied to difference structure factors; Laboratory of Crystallography, Department of Inorganic Chemistry, University of Nijmegen: The Netherlands, **1996**.
[18] P. T. Beurskens, G. Beurskens, M. Strumpel, C. E. Nordman. In: *Patterson and Pattersons* (Eds.: J. P. Glusker, B. K. Patterson, M. Rossi); Clarendon Press: Oxford, **1987**; p. 356.
[19] R. de Gelder, R. A. G. de Graaff, H. Schenk, *Acta Cryst.* **1993**, A49, 297.
[20] G. M. Sheldrick, *SHELXL-97*. Program for the refinement of crystal structures; University of Göttingen: Germany, **1997**.

Received March 8, 1999
[I99095]

Main Group Metal Directed Self-Assembly in a Tetrameric Trimethyltin(IV) *N*-nitroso-*N*-phenylhydroxylaminato Complex Containing an Unprecedented 20-Membered Inorganic (Carbon-Free) Metallamacrocycle

Andrea Deák,[a,b] Ionel Haiduc,*[b] László Párkányi,[a] Monica Venter,[b] and Alajos Kálmán*[a]

Keywords: Metallamacrocycles / Structure elucidation / Supramolecular chemistry / Tin(IV) compounds / Vibrational spectroscopy

Tetrakis[trimethyl(*N*-nitroso-*N*-phenylhydroxylaminato)tin(IV)] was synthesized by reaction of cupferron ([PhN(O)NO]NH_4) with trimethyltin(IV) chloride. The complex was characterized by X-ray diffraction analysis, FT-IR and FT-Raman spectroscopy. An X-ray structural analysis of the title complex $[Me_3Sn(O_2N_2Ph)]_4$ reveals the first example of a bridging coordinated cupferronato ligand. This coordination pattern leads to an unprecedented inorganic 20-membered (carbon-free) metallamacrocycle $Sn_4O_8N_8$ in which four Me_3Sn and four PhN_2O_2 subunits are self-assembled.

Introduction

The rational design and construction of inorganic and organometallic metallamacrocycles by transition metal directed multicomponent self-assembly has had a major impact on supramolecular chemistry.[1−3] The incorporation of metal centres into supramolecular systems gives rise to novel electronic and/or magnetic properties[1] as well as fascinating structural features. Metallamacrocycles have been widely used in host-guest chemistry to understand self-assembly phenomena in natural systems.[3][4] Transition metal centres present a large variety of preferred coordination geometries (square-planar, tetrahedral or octahedral) which have been systematically used in the construction of supramolecular assemblies such as molecular racks,[5] ladders,[5] grids,[6] cylinders,[7] metallamacrocycles,[4][8] metallacyclic polygons[9] and helicates.[10] In contrast, the use of main group metals in supramolecular chemistry has been less well explored. Tin(IV) complexes are also known to display a wide range of coordination geometries around the metal centre, the most common being the penta- and hexacoordinate environments.[11] In the case of pentacoordination, the trigonal-bipyramidal (TBP) configuration is more common than square-pyramidal (SP). For example, the axial connections of nearly planar Me_3Sn(IV) units, with suitable bridging ligands, offer ready access to the preferred TBP coordination and may generate metallamacrocycles. This can be seen in the tetranuclear complexes $[Me_3Sn(O_2PPh_2)]_4$[12] and $\{Me_3Sn[C_5Me_5W(O)(\mu\text{-}O)_2]\}_4$[13] which contain 16-membered inorganic metallamacrocycles $Sn_4O_8E_4$ (E = P and/or W). In addition, the ligand subunits must have two binding sites in a correct arrangement and must be as rigid as possible in order to predispose the coordinating groups to the desired geometry.

The aim of this work is to design new metallamacrocycles exploring the structural features of the cupferronato ligand as well as the ability of the Me_3Sn(IV) unit to exhibit TBP geometry in inorganic ring systems.[12][13] We report an unprecedented 20-membered inorganic (carbon-free)[14][15] metallamacrocycle in the trimethyltin(IV) cupferronato complex $[Me_3Sn(O_2N_2Ph)]_4$. The compound was characterized by analytical and spectroscopic (FT-IR, FT-Raman) methods.[16] To elucidate the three dimensional structure of the macrocycle, X-ray diffraction analysis was performed.[16] The ammonium salt of *N*-nitroso-*N*-phenylhydroxylamine, [PhN(O)NO]NH_4 (cupferron) is a well-known analytical reagent for the quantitative determination of several metal ions.[17] The *N*-nitroso-*N*-phenylhydroxylaminato (cupferronato) anion, [PhN(O)NO^-] has been extensively used as a ligand in transitional metal chemistry behaving as a μ^3-bridging or, in most cases, as a bidentate chelating ligand.[18] In all cases, the X-ray diffraction analysis of the investigated cupferronato metal complexes has revealed a rigid and planar structure of the N(O)NO unit.[18] To the best of our knowledge, however, no bidentate bridging coordination pattern of the cupferronato ligand has been described.

Results and Discussion

Reaction of the cupferron with Me_3SnCl (1:1 ratio) in water yields the new tetranuclear trimethyltin(IV) cupferronato complex, $[Me_3Sn(O_2N_2Ph)]_4$ as a colourless crystalline solid. Single crystals suitable for an X-ray diffraction analysis were obtained by slow concentration of an *n*-heptane solution at ambient temperature.

[a] Institute of Chemistry, Chemical Research Center, Hungarian Academy of Sciences,
P. O. Box 17, H-1525 Budapest, Hungary
Fax: (internat.) + 36-1/325-7554
E-mail: akalman@cric.chemres.hu
[b] Chemistry Department, Babes-Bolyai University,
RO-3400 Cluj-Napoca, Romania
Fax: (internat.) + 40-64/190-818
E-mail: ihaiduc@chem.ubbcluj.ro

 © WILEY-VCH Verlag GmbH, D-69451 Weinheim, 1999 1434−1948/99/0909−1593 $ 17.50+.50/0

The molecular structure with atom-labeling scheme of $[Me_3Sn(O_2N_2Ph)]_4$ is shown in Figure 1 and relevant geometrical parameters are summarized in Table 1.

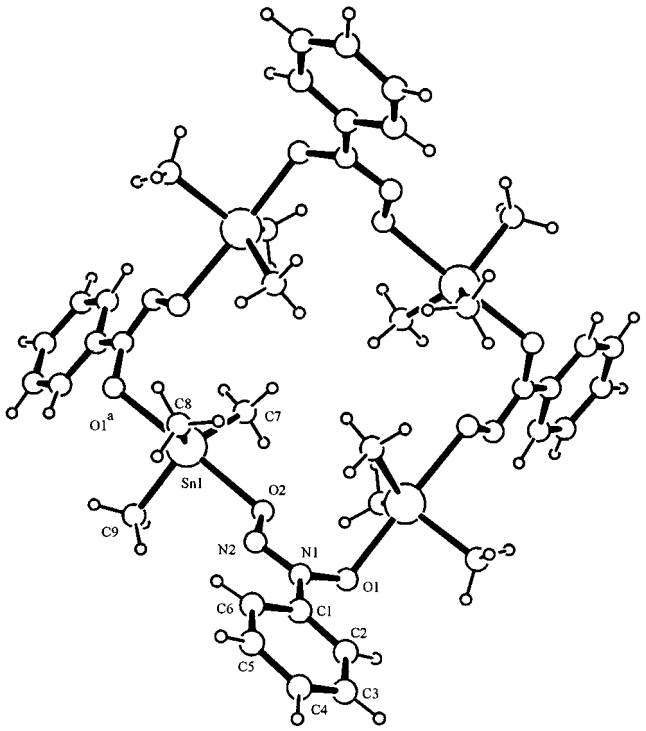


Figure 1. Molecular diagram of $[Me_3Sn(O_2N_2Ph)]_4$ with atom labeling for the asymmetric unit.

Table 1. Selected bond lengths (Å) and bond angles (°) for $[Me_3Sn(O_2N_2Ph)]_4$

Sn(1)−O(2)	2.3321(16)	O(1)[a]−Sn(1)−O(2)	175.79(6)
Sn(1)−O(1)[a]	2.2433(15)	O(1)−N(1)−N(2)	124.38(18)
O(1)−N(1)	1.321(2)	N(1)−N(2)−O(2)	112.63(18)
N(1)−N(2)	1.285(2)	C(7)−Sn(1)−C(8)	127.48(12)
N(2)−O(2)	1.293(2)	C(7)−Sn(1)−C(9)	116.83(13)
N(1)−C(1)	1.436(3)	C(8)−Sn(1)−C(9)	115.43(13)

[a] Equivalent atom generated by $1 - x, -1 + y, 2 - z$.

The molecular structure of $[Me_3Sn(O_2N_2Ph)]_4$ consists of a novel 20-membered macrocyclic inorganic ring system $Sn_4O_8N_8$, self-assembled from four Me_3Sn units, connected by four bridging *N*-nitroso-*N*-phenylhydroxylaminato anions. It provides the first example of the bridging coordination pattern of the cupferronato ligand. Each metal centre occupies an almost perfect TBP coordination site defined by the oxygen atoms of two cupferronato ligands in a *trans* axial array [O(1a)−Sn(1)−O(2) = 175.75(7)°] and three methyl groups in the equatorial plane [average C−Sn−C = 119.91(12)°]. The distortion from the idealized TBP geometry can be quantified by the τ factor, where the limits of τ = 0 or 1 are indicative[19] of perfect SP or TBP geometries, respectively. The calculated value of τ = 0.81 reveals a strong TBP character of the Sn(IV) coordination environment. The Sn(1)−O(1) bond length is shorter by 0.089 Å than that of Sn(1)−O(2), but both are significantly longer than the normal Sn−O covalent bond.[11] The intramolecular nonbonded Sn(1)···O(2a) distance of 3.273(2) Å suggests a weak secondary interaction.

In each cupferronato anion the N(O)NO moieties are essentially planar [r.m.s. deviation from the best plane is 0.0127 Å; torsion angle: O(1)−N(1)−N(2)−O(2) = 4.0(3)°] and nearly coplanar with that of the phenyl ring [O(1)−N(1)−C(1)−C(2) = 5.6(3)°]. These structural features reveal a rigid arrangement of all the atoms in the cupferronato moieties. A significant electron delocalisation along the N(O)NO group can be predicted, all N−N and N−O bond lengths being intermediate between that of the corresponding single and double bond lengths.[16]

The title complex with $P\bar{4}2_1$ symmetry consists of a 20-membered cup-shaped metallamacrocycle $Sn_4O_8N_8$ (see Figure 2) in which the four Sn(1)−O(2) bonds lie in the best plane of the symmetry related Sn(1) and O(2) atoms [r.m.s. deviation from the best plane is 0.212 Å; torsion angles: Sn(1)−O(2)−Sn(1a)−O(2a) = 1.12(7)°, O(2)−Sn(1)−O(2b)−Sn(1b) = 20.68(9)°, Sn(1a)−O(2a)−Sn(1b)−O(2b) = 1.12(7)°, O(2c)−Sn(1c)−O(2a)−Sn(1a) = 20.68(9)°]. The bridging ligands are placed alternatively above and below this plane. In the same manner, two of the three methyl groups on each tin atom protrude alternately above and below the $\{\cdots Sn(1)-O(2)\cdots\}_4$ plane. This arrangement leads to two narrow rings defined by the C(7), C(7a), C(7b), C(7c) and C(8,) C(8a), C(8b), C(8c) atoms, which are concentric with the 20-membered metallamacrocycle. There are weak intramolecular hydrogen bonds such as C−H···O [C(8)···O(2), O(2)···H(8A) distances, 3.368(3), 2.899(12) Å, C(8)−H(8A)···O(2) angle 115.04°] and C−H···N [C(7)···N(1), N(1)···H(7A) distances 3.282(3), 2.732(10) Å, C(7)−H(7A)···N(1) angle 122.60°; C(7)···N(2), N(2)···H(7A) distances 3.412(3), 2.874(14) Å, C(7)−H(7A)···N(2) angle 121.88°] between the methyl hydrogen atoms and an adjacent cupferronato group and weak Me···Ph [C(8)···π, H(8A)···π distances 3.793, 3.054 Å, C(8)−H(8A)···π angle 142.63°] interactions between neighbouring groups.

The molecules self-organise in the solid state leading to a column arrangement along the shortest unit cell edge of 7.383(1) Å, analogous to the β-type packing observed in crystalline aromatic hydrocarbons (see Figure 3). If we rescale the short axis ranges given by Desiraju and Gavezotti for crystalline aromatic hydrocarbons[20] by the ratio of the covalent radii of Sn/C (1.82), the short axis for a β-packing must be less than 7.6 Å.[21] Indeed, the shortest axis of the title compound falls in this range in agreement with the β-packing assumed by the cup-shaped metallamacrocycles. These symmetry-related columns then interact with each other through weak C−H···π contacts [C(4)···π, H(4)···π distances 3.854, 3.150 Å, C(4)−H(4)···π angle 133.36°].

The spectral data are consistent with the determined structure of the title compound. The FT-IR and Raman spectra were recorded for the $[Me_3Sn(O_2N_2Ph)]_4$ complex and its corresponding neutral ligand $[PhN(O)NO]NH_4$ (cupferron) in the 3500−100 cm^{-1} range. Selected bands and assignments are listed in Table 2.

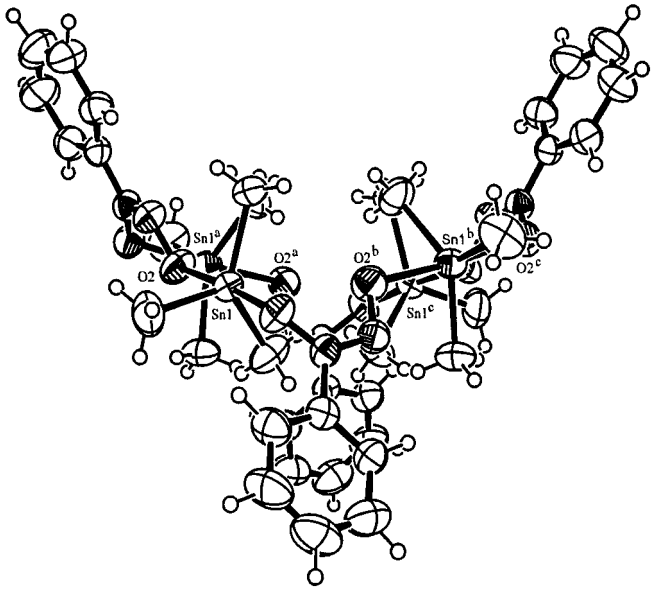


Figure 2. The side view of the molecular structure in $[Me_3Sn(O_2N_2Ph)]_4$; equivalent atoms are generated by: [a]: $1-x, -1+y, 2-z$; [b]: $-x, 2-y, z$; [c]: $1+x, 1-y, 2-z$

Table 2. Selected FT-IR/Raman data and vibrational assignments for cupferron and $[Me_3Sn(O_2N_2Ph)]_4$[a]

$[PhN(O)NO]NH_4$		$[Me_3Sn(O_2N_2Ph)]_4$		Assignment
IR	Raman	IR	Raman	
1335 s	1332 w	1344 s	1346 mw	ν(N−N)
1270 vs	1270 s	1224 vs	1221 vw	ν(N=O)
1220 vs	1226 m	1186 m	1187 w	
910 vs	910 mw	919 s	918 m	δ(ONNO)
		779 s		ρ(Me)
		555 m		$\nu_{as}(SnC_3)$
		542 m	546 mw	ν(Sn−C)
		520 w	516 s	$\nu_s(SnC_3)$
		387 vs		ν(Sn−O)
		142 s	141 m	$\delta(SnC_3$

[a] vw: very weak, w: weak, m: medium, mw: medium weak, s: strong, vs: very strong.

The assignments of the N−N and N=O stretching as well as ONNO bending modes − specific for the neutral ligand − in the 1500−800 cm^{-1} range of the IR and Raman spectra of the cupferron are in good agreement with similar IR data already published.[22][23] A comparison of IR and Raman spectra of the title complex with that of cupferron reveals significant changes in the position of the mentioned bands due to electron delocalisation over the coordinated ONNO unit. Thus, the ν(N−N) and δ(ONNO) modes are shifted to higher frequencies by 9 (IR)/14 (Raman) and 9 (IR)/8 (Raman) cm^{-1}, respectively, while the ν(N=O) mode is shifted to lower frequencies by 46/34 (IR) and 49/39 (Raman) cm^{-1}.

The vibrational modes specific to the coordination environment of tin may be assigned in the 800−100 cm^{-1} spectral range. The Me rocking vibration (779 cm^{-1} in the IR)[24] and the Sn−C stretching mode (542 in IR and 546 cm^{-1} in Raman)[24] are characteristic. Furthermore, the assignment of the three vibrational modes of the SnC_3 group (ν_{as}, ν_s and δ) in the IR spectrum of the complex are in good agreement with the vibrational behaviour proposed for a trigonal-plane arrangement of the Me groups about the tin(IV) centre.[24] The presence of the $\nu_s(SnC_3)$ − as a strong band − and $\delta(SnC_3)$ modes in the Raman spectrum support this structural feature.

Taking into account the coordination of the anionic cupferronato ligand to the metal centres through the oxygen atoms, the Sn−O stretching vibration, tentatively assigned at 565−560 cm^{-1},[22] was not found in the IR spectrum of the title complex. It is probably found at 387 cm^{-1}, as a very strong band.[23]

Experimental Section

General Remarks: All reagents and solvents were purchased from commercial suppliers and used without further purification. Elemental analyses were carried out in the laboratory of the University of Santiago de Compostela (Spain). FT-IR spectra were recorded on a Perkin−Elmer 2000 spectrometer. FT-Raman spectra

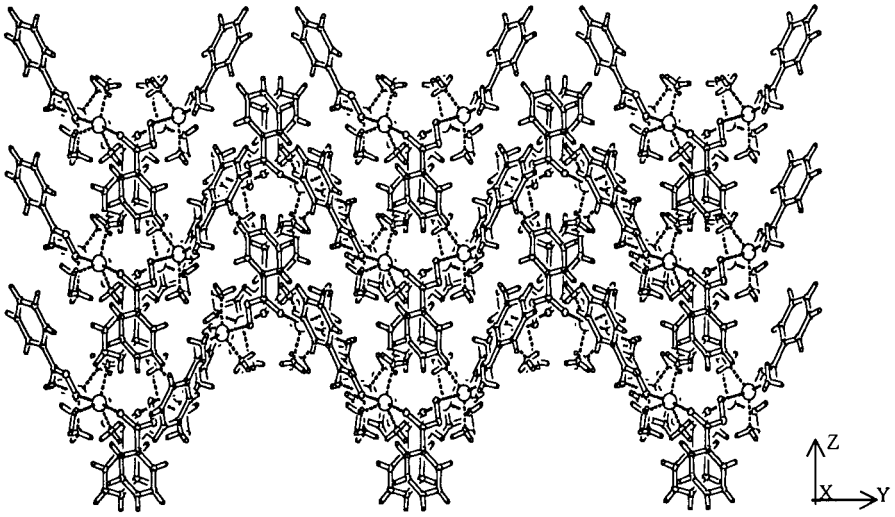


Figure 3. Crystal packing in $[Me_3Sn(O_2N_2Ph)]_4$; the molecules are stacked along the *c* axis

were recorded on a Bruker FT Raman spectrometer (IFS model 66).

Tetrakis[trimethyl(*N*-nitroso-*N*-phenylhydroxylaminato)tin(IV)]: NH_4[PhN(O)NO] (0.20 g, 1.29 mmol) was dissolved in 10 mL water and this solution was added to a solution of Me_3SnCl (0.26 g, 1.30 mmol) in 10 mL water. The product was formed immediately as a pale yellow precipitate. After stirring for 20 minutes at room temperature, the mother liquor was removed and the product was dried. Recrystallisation from n-heptane gave the title compound as colourless crystals. Yield: 0.24 g (62%); m.p. 81−85°C. − FT-IR (KBr): $\tilde{\nu}$ = 1594 cm^{-1} (C−H), 1487 (C−H), 1463 (C−H), 1344 (N−N), 1299 (C−H), 1224 (N=O), 1186 (N=O), 919 (ONNO), 779 (C−H), 755 (C−H), 689 (C−H), 555 (SnC_3), 542 (Sn−C), 520 (SnC_3), 387 (Sn−O), 280 (C−H), 230 (C−H), 142 (SnC_3). − FT-Raman: $\tilde{\nu}$ = 1594 cm^{-1} (C−H), 1491 (C−H), 1346 (N−N), 1288, 1221 (N=O), 1187 (N=O), 1003 (C−H), 918 (ONNO), 546 (Sn−C), 516 (SnC_3), 141 (SnC_3). − $C_{36}H_{56}N_8O_8Sn_4$ (1203.73): calcd. C 35.9, H 4.7, N 9.3; found C 36.0, H 4.4, N 9.4.

X-ray Crystallographic Study: Crystal data for $[Me_3Sn(O_2N_2Ph)]_4$: $C_{36}H_{56}N_8O_8Sn_4$, M = 1203.73, tetragonal, space group $P\bar{4}2_1c$ (No. 114), with $a = b$ = 18.084(3), c = 7.383(1) Å, $\alpha = \beta = \gamma$ = 90°, V = 2414.5(7) $Å^3$, Z = 8, ρ_{calcd} = 1.656 Mg/m^3, $F(000)$ = 1184, λ = 0.71073 Å, T = 293(2) K, μ(Mo-K_α) = 2.096 mm^{-1}, crystal size 0.45 × 0.25 × 0.24 mm. Intensity data of 11745 reflections were measured (2.25 ≤ 2Θ ≤ 34.98°) on an Enraf−Nonius CAD-4 diffractometer (ω-2Θ scans) of which 5245 were independent (R_{int} = 0.0197). The intensities of the standard reflections indicated a crystal decay of 28% which was corrected. A semi-empirical (ψ-scan) absorption correction was also applied (min/max transmission: 0.933/0.974). The structure was solved by direct methods (SHELXS-97)[25a] and refined by full-matrix least squares (SHELXL-97).[25b] 5245 reflections were employed in the structure refinement (138 parameters, 0 restraints). The final R values were $R1$ = 0.0238 [$I \geq 2\sigma(I)$] and $wR2$ = 0.0486 (all data); min/max residual electron density −0.467/0.262 $eÅ^{-3}$. All non-hydrogen atoms were refined anisotropically. Hydrogen atomic positions were generated from assumed geometries. A riding model refinement was applied for the hydrogen atoms. Crystallographic data (excluding structure factors) for the structure reported in this paper have been deposited with the Cambridge Crystallographic Data Centre as supplementary publication no. CCDC-114414. Copies of the data can be obtained free of charge on application to CCDC, 12 Union Road, Cambridge CB2 1EZ, UK [Fax: int. code +44−1223/336−033; E-mail: deposit@ccdc.cam.ac.uk].

[1] C. J. Jones, *Chem. Soc. Rev.* **1998**, *27*, 289−299.
[2] D. B. Amabilino, J. F. Stoddart, *Chem. Rev.***1995**, *95*, 2725−2828.
[3] D. Philp, J. F. Stoddart, *Angew. Chem.* **1996**, *108*, 1242−1286; *Angew. Chem. Int. Ed. Engl.* **1996**, *35*, 1154−1196.
[4] [4a] C. A. Hunter, *Angew. Chem.* **1995**, *107*, 1181; *Angew. Chem. Int. Ed. Engl.* **1995**, *34*, 1079−1081. − [4b] A. W. Maverick, M. L. Ivie, J. H. Waggenspack, F. R. Fronczek, *Inorg. Chem.* **1990**, *29*, 2403−2409.
[5] [5a] G. S. Hanan, C. R. Arana, J.-M. Lehn, D. Fenske, *Angew. Chem.* **1995**, *107*, 1191; *Angew. Chem. Int. Ed. Engl.* **1995**, *34*, 1122−1124. − [5b] H. Sleiman, P. Baxter, J.-M. Lehn, K. Rissanen, *J. Chem. Soc., Chem. Commun.* **1995**, 715−716.
[6] P. N. Baxter, J.-M. Lehn, J. Fischer, M.-T. Youinou, *Angew. Chem.* **1994**, *106*, 2432; *Angew. Chem. Int. Ed. Engl.* **1994**, *33*, 2284−2287.
[7] P. Baxter, J.-M. Lehn, A. DeCian, J. Fischer, *Angew. Chem.* **1993**, *105*, 92; *Angew. Chem. Int. Ed. Engl.* **1993**, *32*, 69−72.
[8] [8a] J. Manna, J. A. Whiteford, P. J. Stang, *J. Am. Chem. Soc.* **1996**, *118*, 8731−8732. − [8b] P. I. Jones, K. J. Byrom, J. C. Jeffery, J. A. McCleverty, M. D. Ward, *Chem. Commun.* **1997**, 1361−1362. − [8c] J. R. Farrell, C. A. Mirkin, I. A. Guzei, L. M. Liable-Sands, A. L. Rheingold, *Angew. Chem*. 1998, 110, 484−487; *Angew. Chem. Int. Ed. Engl*. 1998, 37, 465−467.
[9] P. J. Stang, *Chem. Eur. J.* **1998**, *4*, 19−27.
[10] [10a] M. Albrecht, *Chem. Soc. Rev.* **1998**, *27*, 281−287. − [10b] O. Mamula, A. von Zelewsky, G. Bernardinelli, *Angew. Chem.* **1998**, *110*, 301−305; *Angew. Chem. Int. Ed.* **1998**, *37*, 290−293.
[11] B. Y. K. Ho, J. J. Zuckerman, *J. Organomet. Chem.* **1973**, *49*, 1−84.
[12] M.G. Newton, I. Haiduc, R. B. King, C. Silvestru, *J. Chem. Soc., Chem. Commun.* **1993**, 1229−1230.
[13] M.S. Rau, C. M. Kretz, G. L. Geoffroy, *Organometallics* **1994**, *13*, 1624−1634.
[14] For a comprehensive review of inorganic ring systems, see:
[14a] I. Haiduc, *The Chemistry of Inorganic Ring Systems*, Wiley-Interscience, London, **1970**. − [14b] I. Haiduc, D.B. Sowerby, *The Chemistry of Inorganic Homo- and Heterocycles*, Academic Press, London, **1987**.
[15] A search of over 190307 entries in the Cambridge Crystal Structure Database (CSD) revealed only three 20-membered metallamacrocycles: − [15a] R. V. Slone, J. T. Hupp, C. L. Stern, T. E. Albrecht-Schmitt, *Inorg. Chem.* **1996**, *35*, 4096−4097, − [15b] W. S. Sheldrick, B. Günther, *J. Organomet. Chemistry* **1991**, *402*, 265−280, − [15c] J. Powell, M. J. Horvath, A. Lough, *J. Chem. Soc., Dalton Trans.* **1996**, 1669−1677. Each contains, however, four X−C−C−X spacers (X = N or I), the carbon atoms of which are part of an aromatic system.
[16] L. Párkányi, A. Kálmán, A. Deák, M. Venter, I. Haiduc, *Inorg. Chem. Commun.* **1999**, *2*, 265−268. Only a partial list of data is given here.
[17] F. Feigl, *Chemistry of Specific, Selective and Sensitive Reagents*, Academic Press, New York, **1949**, p. 262.
[18] [18a] G. B. Yi, M. A. Khan, G. B. Richter-Addo, *Inorg. Chem.* **1995**, *34*, 5703−5704. − [18b] S. S. Basson, J. G. Leipoldt, A. Roodt, J. A. Venter, *Inorg. Chim. Acta* **1987**, *128*, 31−37. − [18c] S. S. Basson, J. G. Leipoldt, J. A. Venter, *Acta Crystallogr.* **1990**, *C46*, 1324−1326. − [18d] S. S. Basson, J. G. Leipoldt, W. Purcell, J. A. Venter, *Acta Crystallogr.* **1992**, *C48*, 171−173. − [18e] Y. Ellerman, O. Atakol, I. Svoboda, M. Gesselle, *Acta Crystallogr.* **1995**, *C51*, 1520−1522. − [18f] N. Okabe, K. Tamaki, *Acta Crystallogr.* **1995**, *C51*, 2004−2005.
[19] A.W. Addison, T. N. Rao, J. Reedijk, J. van Rijn, G. C. Verschoor, *J. Chem. Soc. Dalton Trans.* **1984**, 1349−1356.
[20] G. R. Desiraju, A. Gavezotti, *J. Chem. Soc., Chem. Commun.* **1989**, 621−623.
[21] In principle *mutatis mutandis* the tin macrocycles may adopt one of the four packing types characterized by the rescaled ranges β [$sa \leq$ 7.6 Å], γ [8.4 ≤ sa ≤ 9.8 Å], herringbone [9.8 ≤ sa ≤ 14.5 Å] and sandwich herringbone [$sa \leq$; 14.5 Å] (sa: the shortest crystal axis). The applicability of the empirical rescaling was tested on a 16-membered inorganic tin macrocycles. The $[Me_3Sn(O_2PPh_2)]_4$[12] complex crystallizes in an orthorhombic system (space group *Pnma*) with a short crystal axis of 14.501 Å which suggests a herringbone or sandwich-herringbone packing. Indeed, in this complex a sandwich-herringbone packing can be recognized. In contrast, in the oblique unit cell (space group $P\bar{1}$) of $[Me_3Sn(C_5Me_5W(O)(\mu\text{-}O)_2)]_4$[13] complex no such packing rules can be realised.
[22] S. T. Srivastava, *J. Inorg. Nucl. Chem*. **1975**, *37*, 1546−1547.
[23] R. Kellner, P. Prokopowski, *Anal. Chim. Acta* **1976**, *86*, 175−184.
[24] D. Cunningham, L. A. Kelly, K. C. Molloy, J. J. Zuckerman, *Inorg. Chem*. **1982**, *21*, 1416−1421.
[25] [25a] G. M. Sheldrick, SHELXS97-Program for Crystal Structure Determination. − [25b] SHELXL97-Program for the Refinement of Crystal Structures, Universität Göttingen (Germany), **1997**.

Received April 28, 1999
[I99159]

Synthesis and Reactivity of Silicon Transition Metal Complexes, 43[+]

Iron and Ruthenium Fragment Substituted Disilanes $C_5R_5(OC)_2M–Si_2X_5$ (R = H, Me; M = Fe, Ru; X = Cl, H): Synthesis, Structural and Raman Spectroscopic Characterisation, DFT Calculation

Wolfgang Malisch,*[a] Heinrich Jehle,[a] Stephan Möller,[a] Gerhard Thum,[a] Joachim Reising,[a] Axel Gbureck,[b] Volker Nagel,[b] Claudia Fickert,[b] Wolfgang Kiefer,*[b] and Martin Nieger[c]

Dedicated to Professor Helmut Werner on occasion of his 65th birthday

Keywords: Metallo-disilanes / Ligand exchange at silicon / Transition metal effect / Raman spectroscopy / Density functional theory

Reaction of the sodium metalates $Na[M(CO)_2C_5R_5]$ [M = Fe, R = H (**1a**), Me (**1b**); M = Ru, R = H (**1c**), Me (**1d**)] with an equimolar amount of hexachlorodisilane yields the metallo-pentachlorodisilanes $C_5R_5(OC)_2M–SiCl_2–SiCl_3$ (**2a–d**), which can be converted into the pentahydrido analogues $C_5R_5(OC)_2M–SiH_2–SiH_3$ (**3a–c**) via Cl/H exchange with $LiAlH_4$. Due to the activating effect of the transition metal fragment chlorination of **3a–c** with CCl_4 or $HCCl_3$ occurs at the α-silicon to give $C_5R_5(OC)_2M–SiCl_2–SiH_3$ (**4a–c**). The metallo-disilanes were characterised by ^1H-, ^{13}C-, ^{29}Si-NMR, IR and especially Raman spectroscopy. The structures of $C_5H_5(OC)_2Fe–Si_2Cl_5$ (**2a**) and $C_5Me_5(OC)_2Fe–Si_2H_5$ (**3b**) have been determined by X-ray analysis; **2a,b**, **3a,b** were theoretically described by DFT calculations.

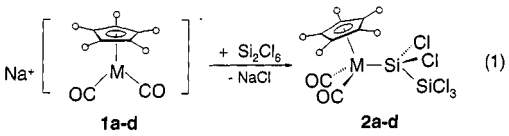
Introduction

Iron-substituted disilanes $Cp(OC)_2Fe–SiR_2–SiR_3$[1][2] have preferentially been the subject of studies concerning the photoinduced rearrangement to silyl(silylene) complexes $Cp(OC)Fe(=SiR_2)SiR_3$.[3] If organic substituents are attached to the silicon atoms this species represent a short-lived intermediate which is confirmed only by IR matrix studies[4] or by the isolated photolysis product $Cp(OC)_2Fe–SiR_3$.[3a–d] However, introduction of alkoxy groups at the β-silicon leads to oxygen stabilised cyclic (bis)silylene complexes $R_2Si^a–Cp(OC)Fe–SiR_2\cdots O^aR'(Si^a–O^a)$.[3e,f]

A limited number of investigations have been reported concerning complexes containing "inorganic" substituents at the silicon atoms, for instance hydrogen or halogen.[5][6] Therefore, we have undertaken efforts to establish efficient routes for the synthesis of metallo-pentachloro- and -pentahydridodisilanes.[6] These ligands offer the possibility to study the influence of the transition metal fragment on the exchange reactivities of the silicon atoms in α- or β-position as well as on the stability of the M–Si–Si bonding arrangement with respect to fragmentation. Support for the interpretation of the findings is expected from a detailed vibrational analysis using especially Raman spectroscopy combined with DFT calculations.

I. Preparative Results

In accordance with former experiments[6] a suspension of the sodium metalates **1a–d** in cyclohexane is combined with hexachlorodisilane in a molar ratio of 1:1 and the reaction mixture stirred at room temperature under exclusion of light for 3 to 48 hours to give the metallo-pentachlorodisilanes **2a–d** (Equation 1).



1a-d **2a-d** (1)

	a	b	c	d
M	Fe	Fe	Ru	Ru
—○	H	Me	H	Me

2a–d are isolated as pale yellow microcrystalline solids in good yields, which show considerable solubility in *n*-pentane and aromatic solvents. **2a–d** can be stored as solids under an atmosphere of nitrogen for months without decomposition.

Heterogeneous "salt elimination" according to Equation (1) is the only way to guarantee controlled mono-metallation of Si_2Cl_6 as analogous experiments with

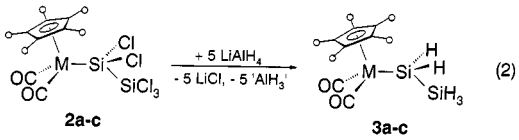
[+] Part 42: S. Möller, H. Jehle, W. Malisch, W. Seelbach in *Organosilicon Chemistry: From Molecules to Materials, Vol. 3,* (Eds.: N. Auner, J. Weis) VCH, Weinheim **1998**, 267–270.

[a] Institut für Anorganische Chemie der Universität Würzburg, Am Hubland, D-97074 Würzburg, Germany
Fax (internat.): +49 (0)931/888 4618
E-mail: Wolfgang.Malisch@mail.uni-wuerzburg.de
[b] Institut für Physikalische Chemie der Universität Würzburg, Am Hubland, D-97074 Würzburg, Germany
[c] Institut für Anorganische Chemie der Universität Bonn, Gerhard-Domagk-Straße 1, D-53121 Bonn, Germany

 © WILEY-VCH Verlag GmbH, D-69451 Weinheim, 1999 1434–1948/99/0909–1597 $ 17.50+.50/0

$Na[Fe(CO)_2Cp]$ (**1a**) performed by Hengge et al. proved using THF as a solvent.[5] In this case homogeneous reaction yields a mixture of **2a** and the bis(iron)disilane $[Cp(OC)_2Fe-SiCl_2]_2$ which makes separation necessary giving rise to a reduced yield of **2a** (41%).

The stability of the iron−silicon or ruthenium−silicon bonds of **2a−c** allows exchange reactions at the silicon atoms without Fe−Si bond cleavage. An attractive example in this context is the Cl/H exchange of the silicon bound chlorine atoms which is achieved by treatment of a solution of **2a−c** at −78°C in diethyl ether with $LiAlH_4$. For a molar ratio of 1:5 after 2 h of stirring at room temperature both silicons were fully hydrogen substituted (Equation 2).



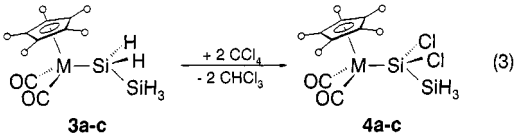
(2)

	a	b	c
M	Fe	Fe	Ru
R	H	Me	H

The metallo-disilanes **3a−c** are obtained after crystallisation from pentane at −78°C (**3b**) or sublimation in high vacuum (**3a,c**), respectively, as light yellow (**3a,b**) to colorless (**3c**) waxy solids, which show a good solubility in *n*-pentane and benzene.[7]

The pronounced electron releasing capacity of the transition metal fragment induces a highly hydridic character of the hydrogens at the α-silicon compared with that at the β-position, a fact that is clearly deduced from IR- and ^{29}Si-NMR data (see below).

As a consequence, the hydrogens of the metallo-pentahydridodisilanes **3a−c** next to the metal are selectively substituted by chlorine at room temperature after 3 hours using CCl_4 to give exclusively the metallo-dichlorodisilanes **4a−c** (Equation 3).



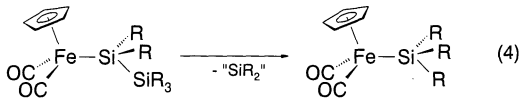
(3)

	a	b	c
M	Fe	Fe	Ru
—○	H	Me	H

The same procedure can be realised with $HCCl_3$, but more severe reaction conditions are necessary (40°C, 12 h). **4a−c**, which represent the first complexes bearing a dichloro-disilanyl ligand, are obtained as yellow solids in good yields, which are purified by crystallisation from pentane at −78°C. Solubility is comparable to that of **3a−c**.

A characteristic of ferrio-disilanes $Cp(OC)_2Fe-SiR_2-SiR_3$ (R = alykl) is the photoinduced rearrangement with elimination of the SiR_2 group to give the monosilyl complex $Cp(OC)_2Fe-SiR_3$ via oxidative addition of the Si−Si bond to the metal atom.[3] A comparable reaction, at least concerning the final product, is observed for the pentachloro- and pentahydridodisilanyl complexes **2a**,**c** and **3**.

In accordance with these results photolysis of **2a**/**3a** in benzene/cyclohexane at room temperature leads to the silyl iron complexes **5**[8] or **6**,[9] respectively, after 120 h. **2a** additionally shows this behaviour in the solid state (Equation 4).



(4)

The thermal stability of the metallo-disilanes **2, 3** decreases on going from the pentachloro- to the pentahydrido derivatives. Heating **2a** in cyclohexane to 65°C for 32 h does not result in any decomposition, while in the case of **3a** under these conditions $Cp(OC)_2Fe-SiH_3$ (**6**) is isolated quantitatively. A detailed examination of the silylene elimination involved in the photodegradation as well as trapping experiments concerning the silylenes SiH_2[10] and $SiCl_2$[11] are currently under way.

II. Spectroscopic Data

NMR Spectroscopy

Substantial information concerning the electronic character of the silicon atoms of **3a−c** is given by the ^1J(SiH) coupling. It is generally accepted that this parameter can be correlated with the s-electron density in the Si−H bond.[12] The SiH_2 units next to the transition metal give rise to a low value of the ^1J(SiH) coupling constants [179.5 Hz (**3a**), 172.4 Hz (**3b**), 181.0 Hz (**3c**)] compared to Si_2H_6[13] characterising the transition metal ligand as an efficient electron releasing group. The ^1J(SiH) value of the SiH_3 moiety is higher (184−186 Hz), but still below that of Si_2H_6 indicating a reduced "transition metal effect" on the β-silicon.

The difficulties of correlating the ^{29}Si-NMR shifts of organosilicon compounds on the basis of purely inductive effects have been pointed out in the literature.[14] Due to this fact only some empirical regularities of the ^{29}Si-NMR data will be discussed.

1.) The signals for **2** at low field (δ = −2 to +76) and **3** at high field (δ = −45 to −95) appear in the range characteristic of the corresponding disilanes Si_2R_6 [R = Cl (δ = −6.14);[15a] H (δ = −104.1)[15b]]. The metallo-dichlorodisilane **4a** with differing substituents at the silicon atoms follows these trends (**4a**: δ = +93 and −83). In each case the resonance of the metal-substituted silicon is characterised by an enormous low-field shift with the maximum for **4a** compared to the silicon in the β-position.

2.) The δ-value of the SiX_3 moiety is approximately identical for all species [δ = +1 to −2 (**2,** X = Cl), δ = −93 to −95 (**3,** X = H)]. In comparison to Si_2R_6 (R = Cl, H) the small low-field shift of this resonance of ca. 5−10 ppm indicates a minor influence of the transition metal fragment on the β-silicon of **2** and **3**. The largest difference (21 ppm)

is obtained for the SiH_3 resonance of the ferrio-dichlorodisilane **4a** ($\delta = -83$).

3.) Exchange of the iron against the ruthenium group causes a high-field shift of approximately 20 ppm for the α-silicon resonance. The chemical shift of the SiX_3 moieties remains unaffected.

Vibrational Spectroscopy and Density Functional Theory Calculations

Among the methods that can be used for the simulation of vibrational spectra, density functional methods are known to give very good results for vibrational wavenumbers compared to *ab initio* methods.[16]

a) Comparison of measured and calculated Raman bands of **2a**, **3a,b**:

The former assignments of the complex **3a** were based on normal coordinate analysis (NCA).[17] They agree with the results of DFT calculations. The simulation of vibrational spectra with NCA is based on a purely mechanical model, where an initial force constant matrix is chosen with a limited number of force constants [$(3N - 6)(3N - 5)/2$ in non-redundant internal coordinates for a nonlinear molecule], and then a force constant refinement is carried out.

Table 1. Comparison of measured (Raman spectra) and calculated wavenumbers of **3a** and **3b**

3a Measured [cm^{-1}]	**3a** Calculated [cm^{-1}]	**3b** Measured [cm^{-1}]	**3b** Calculated [cm^{-1}]	Mode description
2141	2177	/	2174	$\nu_{asym}(SiH_3)$
2132	2163	2135	2161	$\nu_{asym}(SiH_3)$
	2141		2141	$\nu_{sym}(SiH_3)$
2098	2126	2063	2108	$\nu_{asym}(SiH_2)$
2087	2098	2076	2082	$\nu_{sym}(SiH_2)$
2008	1906	2008	1887	$\nu_{sym}(CO)$
1959	1865	1959	1846	$\nu_{asym}(CO)$
1114	1102	594	575	Cp-ring breathing
606	611	606	617	$\nu_{asym}(FeC)$
441	425	449	425	ν(SiSi)
373	359	412	401	ν_{sym}(Fe-Cp)[a]

[a] Also partly a $C-CH_3$ out-of-plane bending vibration in Cp* compound.

Quantum mechanical calculations like DFT use another approach to obtain a force field: here, all necessary force constants are calculated by the second derivative of the energy with respect to the coordinates ($\partial^2 E/\partial q_i \partial q_j$). This method is more satisfying because of the avoidance of the empirical force constant refinement. Compared to conventional *ab initio*-methods, DFT has the advantage that an empirical scaling of force constants giving a *Scaled Quantum Mechanical* (SQM) force field of Pulay *et al.*[18] is not necessary to account for the lack of correlation energy. However, a scaling is often introduced to account for the anharmonicity. But we favoured to compare measured anharmonic wavenumbers with calculated *un*scaled harmonic wavenumbers rather than to introduce an empirical scaling procedure, because scaling does not change the fact we can get from the second derivatives only harmonic wavenumbers.

In comparison to NCA, the wavenumbers for the CH stretching vibrations obtained from DFT calculation and partly the SiH stretching vibrations were calculated to be too high.

Significant is the lowering of the ring breathing vibration to 575 cm^{-1}, according to the higher mass of the ring substituents.

Difficulties in the assignment of the pentamethylcyclopentadienyl complex **3b** arise from the great number of additional bands especially in the ν(C−C) and δ(CH) region due to the five methyl groups. Most of these vibrations are not summarized in Table 1.

Further complications originate from coupling of different internal coordinates: some formerly ″pure″ vibrations are coupled with vibrations of the substituent, e.g. the ν_{sym}-(Fe−Cp) is in the case of the pentamethylcyclopentadienyl complex also partly a $C-CH_3$ out-of-plane bending vibration. This gives the explanation for the unexpected shift in the calculations and in the spectra (because of the higher mass of the Cp*) towards higher wavenumbers [from 359 to 401 cm^{-1} (calc.), from 373 to 412 cm^{-1} (exp.)]. Consequently, the wavenumber shift in this case *cannot* be taken as a direct measure of bond strength. However, for the ν(CO) value, such an interpretation is possible, because this vibration is only coupled with the other CO stretching vibration. Both vibrations ν_{sym}(CO) and ν_{asym}(CO) are shifted by 35 cm^{-1} to lower wavenumbers switching from a cyclopentadienyl (Cp) to a pentamethylcyclopentadienyl (Cp*) ligand in the iron compounds **2a,b** and **3a,b**, respectively, which is in accordance with the higher electronic density in the case of **3b** causing a stronger back bonding from the metal to the carbonyl carbon and, consequently, a weaker CO bond. This shift is confirmed by the DF calculation, although the absolute value of ν_s(CO) and ν_{as}(CO) differ by nearly 100 cm^{-1} from the experimental data. In addition, the change of substituents at the silicon from H (**3a,b**) to Cl (**2a**) causes a shift of the ν(CO) band to higher wavenumbers. The identical spectral position of the carbonyl modes in **2b** and **3a** shows, that the difference in the −I-effect between the Cl atoms of **2b** and the H atoms of **3a** is compensated by the different electronic donor capacities of the Cp* and Cp ligands. Characterisation of the SiH stretching modes is an effective way to get information about the electronic structure of the Si atom and how it is influenced by the metal fragment. The IR spectra of **3a** show two weak bands at 2071 and 2133 cm^{-1}, which are assigned to the SiH stretching modes of the silylene and the silyl fragment.[19] In this case the signal at 2133 cm^{-1} can be assigned to an overlap of the symmetric and antisymmetric stretching modes of the silyl group.[20] Compound **3b**, with the better electron donating ligand C_5Me_5, shows the stretching modes of the silylene group at 2063 cm^{-1} [ν_{as}-(SiH_2)] and at 2076 cm^{-1} [ν_s(SiH_2)]. The symmetric and the antisymmetric stretching modes of the silyl group overlap in their spectral position and appear at 2135 cm^{-1}.

The SiSi stretching mode is found in a narrow spectral range around 445 cm^{-1} and its position is primarily independent from all the other ligands. The DFT calculations show that this vibration is indeed a pure SiSi stretching, and no other internal coordinates are involved. So, we can conclude that changes in the electronic density of the metal atom have no influence on this bond.

Table 2. Comparison of measured (FT Raman spectrum) and calculated wavenumbers of **2a**

Measured [cm^{-1}]	Calculated [cm^{-1}]	Mode description
2022	1937	ν_{sym}(CO)
1991	1901	ν_{asym}(CO)
1120	1102	Cp ring breathing
607	600	ν_{asym}(FeC)
528	523	ν(SiSi) + ν(SiCl)
493	496	ν(SiCl) + ν(SiSi) +
386	345	ν_{asym}(Fe-Cp)
290	321	ν_{asym}(Fe-Cp)
233	249	ν(FeSi) + δ(SiCl)
213	200	($SiCl_3$) in phase def. + ($SiCl_2$) bending
202	182	($SiCl_3$) in phase def.

The measured spectrum in Table 2 is a Fourier transform Raman spectrum with excitation in the NIR (1064 nm), because in the visible region decomposition in the laser focus occurred. The CO stretching vibrations appear at 2022 and 1991 cm^{-1}, indicating a higher CO stretching force constant than in the case of $Cp(OC)_2Fe-SiH_2SiH_3$ (2008 and 1959 cm^{-1}) which is in accordance with the higher electronegativity of the chlorine atom. The CC stretching vibrations of the coordinated cyclopentadienyl anion as well as the significant Cp ring breathing vibration do not change compared to $Cp(OC)_2Fe-SiH_2SiH_3$. For many other vibrations, the internal coordinates are more coupled than in $Cp(OC)_2Fe-SiH_2SiH_3$. This is an effect of the higher mass of chlorine, which is much closer to the mass of the other atoms compared to hydrogen. In contrast, for **3a,b** no band exists that can be assigned to be a pure Si−Si stretching vibration.

III. X-ray Analysis of $C_5H_5(OC)_2Fe-SiCl_2SiCl_3$ (2a), $C_5Me_5(OC)_2Fe-SiH_2SiH_3$ (3b) and Comparison to DFT Calculations

Final verification of the structures of **2a** and **3b** came from X-ray crystallographic studies (Figures 1−3). **3b** is to our knowledge the first structurally characterized metalloderivative of Si_2H_6.

The octahedral coordination sphere at the iron centre is in both cases indicated by the ligand-metal-ligand angles close to 90°. Larger angles are found between the carbonyl carbon atoms [94.2(11)° (**2a**); 96.0 (11)° (**3b**)] while the angles between the silicon atom and the CO ligands [88.4(8)°/88.3(8)° (**2a**); 85.5(8)°/88.5(8)° (**3b**)] are smaller. The Fe−Si bond length with a value of 2.224(7) Å (**2a**), 2.298(9) Å (**3b**) lies within the range of known iron silicon compounds[21a−h] with the usual trend of a bond shortage due to electronegative substituents like chlorine.[21c] The Si1−Si2 distance of 2.333(9) Å (**2a**), 2.335(11) Å (**3b**) is close to that of known disilanes (e. g. Me_6Si_2: 2.340 Å[22])

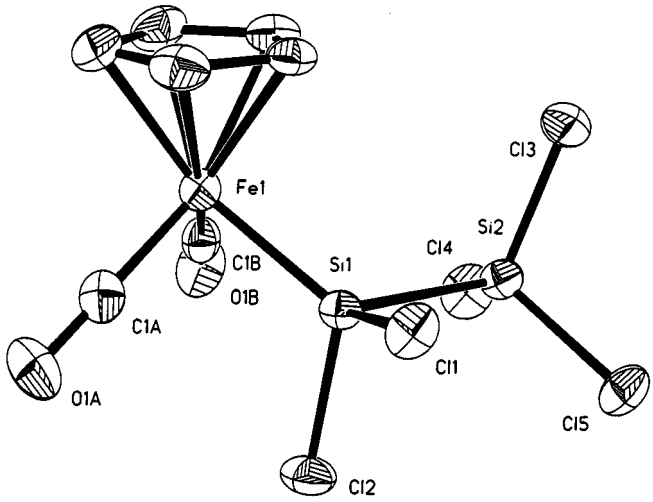


Figure 1. ORTEP view of $C_5H_5(OC)_2Fe-SiCl_2-SiCl_3$ (**2a**). Selected bond lenghts [Å], angles [°] and torsion angles [°]: Fe−Si1 2.2239(7), Si1−Si2 2.3333(9), Si1−Cl1 2.0859(8), Si1−Cl2 2.0811(9), Si2−Cl3 2.0410(9), Si2−Cl4 2.0421(9), Si2−Cl5 2.0358(9), Fe−C1a−O1a 178.9(3), Fe−C1b−O1b 178.8(9), Cl1−Si1−Si2 99.53(3), Cl3−Si2−Si1 111.60(4), Fe−Si1−Si2 119.20(3), C1a−Fe1−Si1 88.27(8), Fe1−Si1−Si2−Cl5 175.05(3), Fe1−Si1−Si2−Cl4 −63.76(5), Fe1−Si1−Si2−Cl3 55.53(4), Cl1−Si1−Si2−Cl5 46.59(5), C1a−Fe1−Si1−Cl1 −80.11(8), C1b−Fe1−Si1−Cl1 −174.37(8), Cp(Z)−Fe1−Si1−Si2 68.2, Cp(Z)−Fe1−Si1−Cl1 51.7, Cp(Z)−Fe1−Si1−Cl2 6.2.

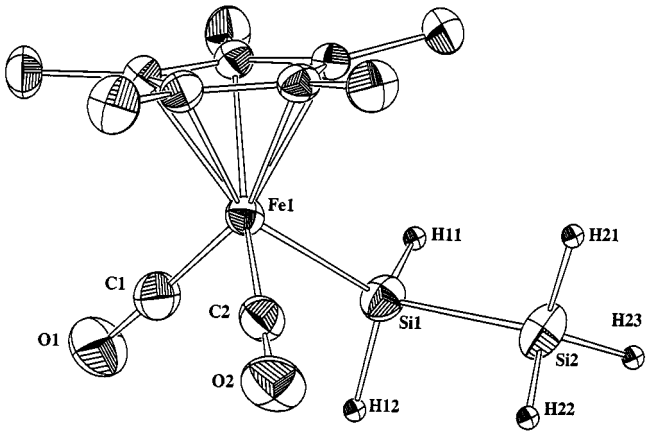


Figure 2. ORTEP view of $C_5Me_5(OC)_2Fe-SiH_2-SiH_3$ (**3b**). Selected bond lenghts [Å], angles [°] and torsion angles [°]: Fe−Si1 2.2980(9), Si1−Si2 2.3355(11), Si1−H11 1.43(2), Si1−H12 1.47(2), Si2−H21 1.41(3), Si2−H22 1.37(3), Si2−H23 1.42(3); C1−Fe1−Si1 85.46(8), C2−Fe1−Si1 88.52(8), H11−Si1−H12 102.7(12),H11−Si1−Fe 114.7(9), H12−Si1−Fe 113.4(9), H11−Si1−Si2 106.6(9), Si2−Si1−Fe 115.15(5), H21−Si2−H22 106.0(16), H21−Si2−Si1 111.4(12), H23−Si2−Si1 113.2(12), C1−Fe−C2 95.96(11), Fe−C1−O1 178.6(2), Fe−C2−O2 177.9(2); C2−Fe−Si1−Si2 −50.50(8), C1−Fe−Si1−Si2 −146.60(8), H11−Si1−Si2−H21 83.0(16), H11−Si1−Si2−H22 −159.3(14), H11−Si1−Si2−H23 −38.3(15), H12−Si1−Si2−H21 −169.3(16), H12−Si1−Si2−H22 −51.6(15), H12−Si1−Si2−H23 69.4(16), Fe−Si1−Si2−H21 −45.4(13), Fe−Si1−Si2−H22 −72.3(11), Fe−Si1−Si2−H23 −166.7(13), Cp(Z)−Fe1−Si1−Si2 82.56, Cp(Z)−Fe1−Si1−H11 41.72, Cp(Z)−Fe1−Si1−H12 159.25.

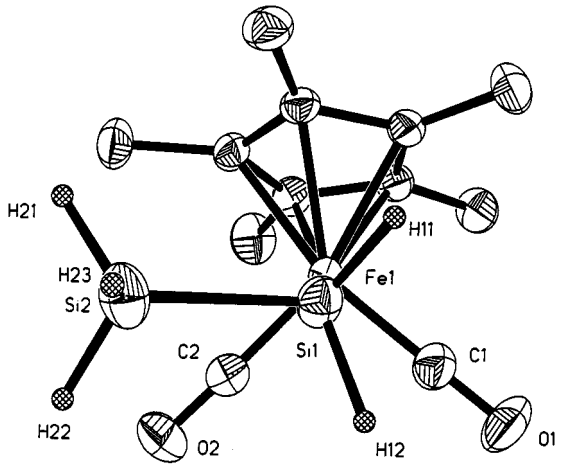


Figure 3. Newman like projection along the Fe−Si bond of **3b**

as well as to other disilanyl-metal-complexes[21f] including the tungsten derivative $C_5Me_5(OC)_2(Me_3P)W-SiCl_2-SiCl_3$ (Si1−Si2: 2.350 Å).[6] While Si−Cl distances of **2a** at Si2 (Si2−Cl3 2.0410(9), Si2−Cl4 2.0421(9), Si2−Cl5 2.0358(9) Å) are in the range of chlorosilanes,[21i] the analogous distances at the metal bound silicon exhibit a significant elongation (Si1−Cl1 [2.086(8) Å], Si1−Cl2 [2.081(9) Å]) due to the electron releasing capacity of the transition metal fragment. The Newman projection along the Fe−Si bond (Figure 3) reveals a staggered pseudo-ethane conformation with the following pairs of *"trans"*-arranged substituents: Cp*/X, CO/X, CO/SiX_3 (X = Cl, H).The gauche position of the SiX_3 group (X = H, Cl) with respect to the cyclopentadienyl unit found for **2a**, **3b** is typical for pseudo-tetrahedral halfsandwich iron complexes of the type $C_5R_5(OC)_2Fe-Si_2X_5$ (X = H, Cl, alkyl);[21h] at the metal centre more crowded complexes like the pseudo tetragonal monopyramidal tungsten compound$C_5Me_5(OC)_2(Me_3P)W-SiCl_2-SiCl_3$ prefer the trans arrangement.[6] Distorsion with respect to the ideal conformation of about 20° (**3b**)/ 8° (**2a**) for all the substituents at Si1 deduced from the dehedral angles Cp(Z)−Fe1−Si1−Si2 (82.6°)/(68.2°), Cp(Z)−Fe1−Si1−H11 (41.7°)/ Cp(Z)−Fe1−Si1−Cl1 (51.7°) and Cp(Z)−Fe1−Si1−H12 (159.3°)/ Cp(Z)−Fe1−Si1−Cl2 (6.2°) indicates the higher sterical demand of the SiX_3 group compared to the hydrogen or chlorine atoms.

The octahedral coordination sphere is also found in the calculation, and the corresponding bond angles show a very good agreement between the measured and calculated structures. In our calculations, the Si−Cl bond lengths of **2a** are somewhat overestimated, but they show the same behaviour concerning the effect of the iron fragment close to Si1, where the Si−Cl bonds are longer than those at Si2. Comparison of X-ray data of **3b** and the calculated structural data obtained by DFT method reveals a slightly different conformation, which is deduced from bond and torsion angles. The Si_2H_5 moiety is turned clockwise about 10° around the Fe−Si bond. However, the structural parameters reproduce reasonably the experimental values. An interesting aspect of the calculation are the Si−H bond lengths, which cannot be determined by X-ray structure analysis with satisfying accuracy. In the DFT calculation, the bond lengths at Si1 (next to the iron fragment) are elongated compared to the SiH_3-group, a result that parallels

Table 3. Comparison of selected structural parameters from X-ray data and DFT calculations for $C_5H_5(OC)_2FeSiCl_2-SiCl_3$ (**2a**), $C_5Me_5(OC)_2Fe-SiH_2-SiH_3$ (**3b**)

	X-ray data **2a**	calculated		X−ray data **3b**	calculated
Fe1−Si1	2.224	2.275	Fe1−Si1	2.298	2.362
Si1−Si2	2.333	2.397	Si1−Si2	2.336	2.364
Si1−Cl1	2.086	2.220	Si1−H11	1.43	1.507
Si1−Cl2	2.081	2.210	Si1−H12	1.47	1.512
Si2−Cl3	2.041	2.198	Si2−H21	1.41	1.501
Si2−Cl4	2.042	2.189	Si2−H22	1.37	1.497
Si2−Cl5	2.036	2.169	Si2−H23	1.42	1.501
Fe1−C1a	1.770	1.752	Fe1−C1		1.736
Fe1C1b	1.765	1.754	Fe1−C2		1.737
C1a−O1a	1.137	1.189	C1−O1		1.199
C1b−O1b	1.143	1.189	C1−O2		1.120
C1a−Fe1−Si1	88.3	88.9	C1−Fe1−Si1	85.5	84.7
C1b−Fe1−Si1	88.4	91.4	C2−Fe1−Si1	88.5	87.1
Cl1−Si1−Cl2	103.6	104.9	H11−Si1−H12	102.7	104.4
Cl1−Si1−Fe1	115.2	113.3	H11−Si1−Fe1	114.7	111.2
Cl2−Si1−Fe1	117.0	114.4	H12−Si1−Fe1	113.4	112.6
Cl1−Si1−Si2	99.5	102.4	H11−Si1−Si2	106.6	106.4
Cl3−Si2−Cl4	111.6	105.8	H21−Si2−H22	106.0	107.1
C1−Fe1−C2	94.2	94.1	C1−Fe1−C2	96.0	94.6
Fe1−C1a−O1a	178.9	177.0	Fe1−C1−O1	178.6	177.8
Fe1−C1b−O1b	178.8	176.5	Fe1−C2−O2	177.9	178.1
C1a−Fe1−Si1−Si2	160.0	169.0	C2−Fe1−Si1−Si2	−50.5	−59.0
C1b−Fe1−Si1−Si2	65.7	75.0	C1−Fe1−Si1−Si2	−146.6	−153.9
Cl1−Si1−Si2−Cl4	−178.4	−173.8	H11−Si1−Si2−H22	−159.3	−172.0
Fe1−Si1−Si2−Cl3	55.5	67.8	Fe1−Si1−Si2−H21	−45.4	−57.9
Cl1−Si1−Fe1−C1a	−80.1	−71.0	H11−Si1−Fe1−C1		82.9
Cl1−Si1−Fe1−C1b	−174.4	−165.0	H11−Si1−Fe1−C2		177.8

the finding for the Si_2Cl_5 derivative (*vide supra*) and offers a reasonable explanation for the higher reactivity of the SiH_2-group compared to the SiH_3 moiety. This difference is in addition established in the measured as well as in the calculated vibrational spectrum of **3b**.

Experimental Section

NMR: Bruker AMX 400 (400.1 MHz, 100.6 MHz and 79.5 MHz for ^1H, ^{13}C and ^{29}Si, respectively). [D_6]benzene as a solvent (used unless otherwise stated) $\delta_H = 7.15$, $\delta_C = 128.0$; for ^{29}Si ^2H-Lock internal, rel. TMS external. − IR: Perkin−Elmer 283. − MS: Varian MAT 112 S (70 eV). All reactions were performed under an atmosphere of purified nitrogen. Solvents were dried according to conventional procedures, distilled and saturated with N_2 prior to use. − DTA: Du Pont 9000. − Starting Materials: Na[Fe(CO)$_2$C$_5$R$_5$] (R = H,[23a] Me[23b]), Na[Ru(CO)$_2$C$_5$R$_5$] (R = H,[24a] Me[24]).

1. 1-[Dicarbonyl(η^5-cyclopentadienyl)ferrio]-1,1,2,2,2-pentachlorodisilane (2a): A suspension of 2150 mg (10.8 mmol) of Na[Fe(CO)$_2$Cp] (**1a**) in 50 mL of cyclohexane is treated with 3190 mg (12.0 mmol) of hexachlorodisilane and the mixture is stirred for 3 d at room temperature in the absence of light. After filtration of insoluble material (unreacted **1a** and formed NaCl), removal of the solvent and excess of hexachlorodisilane in vacuo the dark red residue is treated 6 times with 30 mL of pentane. The combined extracts are evaporated in vacuo to 15 mL and cooled to −78°C. Crystallised **2a** is filtered off, washed with 10 mL of cold pentane and dried in vacuo. − Yield 3800 mg (86%). − Pale yellow microcrystalline powder. − M.p. 63−64°C. − ^1H NMR: δ = 4.16 (s, H_5C_5). − ^{29}Si NMR ($CDCl_3$): δ = 76.81 (s, α-Si), −2.37 (s, β-Si). − IR (pentane): $\tilde{\nu}$ = 2035 cm^{-1} (vs), 1998 (vs) [ν(CO)]. − MS (rel. to ^{28}Si, ^{35}Cl and ^{56}Fe, 70 eV, 30°C): *m/z* (%) = 408 (3, $[M]^+$), 380 (8, $[M - CO]^+$), 352 (30, $[M - 2CO]^+$), 275 (55, $[M - SiCl_3]^+$), 254 (77, $[M - 2CO, - SiCl_2]^+$), 247 (11, $[M - CO, - SiCl_3]^+$), 156 (87, $[CpFeCl]^+$), 121 (44, $[CpFe]^+$), 93 (100, $[CpSi]^+$), 91 (22, $[FeCl]^+$). − $C_7H_5Cl_5FeO_2Si_2$ (410.40): calcd. C 20.48, H 1.23, Cl 43.19; found C 20.10, H 1.51, Cl 43.50.

2. 1-[Dicarbonyl(η^5-pentamethylcyclopentadienyl)ferrio]-1,1,2,2,2-pentachlorodisilane (2b): According to **1.** from 1880 mg (6.96 mmol) of Na[Fe(CO)$_2$C$_5$Me$_5$] (**1b**) and 2058 mg (7.65 mmol) of hexachlorodisilane in 60 mL of cyclohexane after 18 h. The obtained residue is stirred for 1 h with 35 mL of benzene, insoluble material filtered off and the clear filtrate evaporated in vacuo to 10 mL. After addition of 40 mL of *n*-pentane **2b** precipitates, is filtered off, washed with 20 mL of cold pentane and dried in vacuo. − Yield 2100 mg (63%). − Pale yellow microcrystalline powder. − M.p. 165°C. − ^1H NMR: δ = 1.50 [s, $(H_3C)_5C_5$]. − ^{13}C NMR: δ = 212.7 (s, CO), 97.76 [s, $C_5(CH_3)_5$], 9.16 [s, $(CH_3)_5C_5$]. − ^{29}Si NMR: δ = 75.65 (s, α-Si), −0.20 (s, β-Si). − IR (pentane): $\tilde{\nu}$ = 2013 cm^{-1} (s), 1981 (sh), 1975 (vs) [ν(CO)]. − MS (rel. to ^{28}Si, ^{35}Cl and ^{56}Fe, 70 eV, 80°C): *m/z* (%) = 478 (2, $[M]^+$), 450 (3, $[M - CO]^+$), 422 (15, $[M - 2CO]^+$), 345 (58, $[M - SiCl_3]^+$), 324 (12, $[M - 2CO, - SiCl_2]^+$), 289 (26, $[M - 2CO, - SiCl_3]^+$), 226 (100, $[C_5Me_5FeCl]^+$), 191 (83, $[C_5Me_5 - Fe]^+$), 163 (80, $[C_5Me_5Si]^+$). − $C_{12}H_{15}Cl_5FeO_2Si_2$ (480.55): calcd. C 29.99, H 3.15, Cl 36.89; found C 30.46, H 3.20, Cl 37.10.

3. 1-[Dicarbonyl(η^5-cyclopentadienyl)ruthenio]-1,1,2,2,2-pentachlorodisilane (2c): According to **1.** from 520 mg (2.12 mmol) of Na[Ru(CO)$_2$Cp] (**1c**) and 720 mg (2.90 mmol) of hexachlordisilane in 20 mL of cyclohexane after 14 h. − Yield 561 mg (58%). − Yellow microcrystalline powder. − M.p. 72°C (DTA). − ^1H NMR: δ = 4.44 (s, H_5C_5). − ^{13}C NMR: δ = 196.8 (s, CO), 87.84 (s, C_5H_5). − ^{29}Si NMR: δ = 58.31 (s, α-Si), −1.19 (s, β-Si). − IR (pentane): $\tilde{\nu}$ = 2043 cm^{-1} (vs), 1997 (vs) [ν(CO)]. − $C_7H_5Cl_5O_2RuSi_2$ (455.62): calcd. C 18.45, H 1.11, Cl 38.91; found C 19.14, H 1.23, Cl 38.46.

4. 1-[Dicarbonyl(η^5-pentamethylcyclopentadienyl)ruthenio]-1,1,2,2,2-pentachlorodisilane (2d): According to **1.** from 780 mg (2.35 mmol) of K[Ru(CO)$_2$C$_5$Me$_5$] (**1d**) and 760 mg (2.82 mmol) of hexachlorodisilane in 60 mL of cyclohexane after 18 h. − Yield 1005 mg (85%). − Yellow microcrystalline powder. − M.p. 62°C (decomp., DTA). − ^1H NMR: δ = 1.45 [s, $(H_3C)_5C_5$]. − ^{13}C NMR: δ = 199.5 (s, CO), 101.4 [s, $C_5(CH_3)_5$], 9.5 [s, $(CH_3)_5C_5$]. − ^{29}Si NMR: δ = 56.69 (s, α-Si), 1.29 (s, β-Si). − IR (pentane): $\tilde{\nu}$ = 2024 cm^{-1} (vs), 1980 (vs) [ν(CO)]. − $C_{12}H_{15}Cl_5RuO_2Si_2$ (525.76): calcd. C 27.41, H 2.88; found C 28.46, H 3.20.

5. 1-[Dicarbonyl(η^5-cyclopentadienyl)ferrio]disilane (3a): A suspension of 347 mg (9.14 mmol) $LiAlH_4$ in 40 mL of diethyl ether is cooled to −78°C and 750 mg (1.83 mmol) of Cp(OC)$_2$Fe−$SiCl_2$−$SiCl_3$ (**2a**), dissolved in 30 mL of diethyl ether, are added within 15 min. After 30 min of stirring the reaction mixture is warmed up to room temperature and stirred for another 2 h. Insoluble materials are filtered off, the solvent removed in vacuo and the oily residue extracted with 35 mL of petroleum ether (boiling range 50−70°C). After reducing the volume of the extract in vacuo to 6 mL and cooling to −78°C **3a** precipitates, is separated, washed with 5 mL of cold pentane and dried in vacuo. Further purification is achieved by sublimation at 80−85°C/10^{-2} Torr. − Yield 310 mg (71%). − Yellow, microcrystalline powder. − M.p. 16−17°C. − ^1H NMR: δ = 4.10 (s, 5 H, H_5C_5), 3.95 [q, ^1J(HSi) = 179.5 Hz, ^2J(HSiSi) = 4.6 Hz, ^3J(HSiSiH) = 3.2 Hz, 2 H, H_2Si], 3.66/3.30 [t, ^1J(HSi) = 186.1 Hz, ^{2}J(HSiSi) = 7.7 Hz, ^3J(HSiSiH) = 3.2 Hz, 3 H, H_3Si]. − ^{29}Si NMR: δ = −53.92 (SiH_2), −93.81 [^1J(SiSi) = 67.3 Hz, SiH_3]. − IR (pentane): $\tilde{\nu}$ = 2133 cm^{-1} (w, SiH_3), 2087 (w, SiH_2) [ν(SiH)]; 2007 (s), 1968 (vs) [ν(CO)]. − MS (rel. to ^{28}Si and ^{56}Fe, 70 eV, 35°C): *m/z* (%) = 238 (22, $[M]^+$), 210 (11, $[M - CO]^+$), 182 (19, $[M - 2CO]^+$), 179 (39, $[M - CO, - SiH_3]^+$), 151 (31, $[M - 2CO, - SiH_3]^+$), 149 (68, $[CpFe-Si]^+$), 121 (100, $[CpFe]^+$), 93 (71, $[CpSi]^+$). − $C_7H_{10}FeO_2Si_2$ (238.20): calcd. C 35.29, H 4.24; found C 35.84, H 4.51.

6. 1-[Dicarbonyl(η^5-pentamethylcyclopentadienyl)ferrio]disilane (3b): According to **5.** from 1010 mg (2.10 mmol) of $C_5Me_5(OC)_2Fe-SiCl_2-SiCl_3$ (**2b**) and 395 mg (10.5 mmol) of $LiAlH_4$ in 80 mL of diethyl ether after stirring for 4 h. **3b** is purified by recrystallisation from 15 mL of *n*-pentane. − Yield 630 mg (97%). − Deep yellow crystals. − M. p. 64°C. − ^1H NMR: δ = 3.75 [m, 5 H, ^1J(HSi) = 172.4 Hz (SiH_2), ^1J(HSi) = 184.4 Hz (SiH_3), H_5Si_2], 1.40 [s, 15 H, $(H_3C)_5C_5$]. − ^{13}C NMR: δ = 215.68 (s, CO), 95.12 [s, $C_5(CH_3)_5$], 9.42 [s, $(CH_3)_5C_5$]. − ^{29}Si NMR: δ = −45.19 (SiH_2), −95.61 (SiH_3). − IR (petroleum ether): $\tilde{\nu}$ = 2127 cm^{-1} (w, SiH_3), 2071 (w, SiH_2) [ν(SiH)]; 1994 (vs), 1947 (vs) [ν(CO)]. − MS (rel. to ^{28}Si and ^{56}Fe, 70 eV, 35°C): *m/z* (%) = 308 (15, $[M]^+$), 280 (60, $[M - CO]^+$), 252 (7, $[M - 2CO]^+$), 250 (55, $[M - CO, - SiH_2]^+$), 249 (23, $[M - CO, - SiH_3]^+$), 248 (100, $[M - Si_2H_5]^+$), 247 (24, $[M - Si_2H_6]^+$), 219 (87, $[C_5Me_5FeSi]^+$), 191 (48, $[C_5Me_5Fe]^+$), 163 (83, $[C_5Me_5Si]^+$). − $C_{12}H_{20}FeO_2Si_2$ (308.35): calcd. C 46.74, H 6.55; found C 47.05, H 6.68.

7. 1-[Dicarbonyl(η^5-cyclopentadienyl)ruthenio]disilane (3c): According to **5.** from 91 mg (2.39 mmol) of $LiAlH_4$ and 210 mg (0.47 mmol) of Cp(OC)$_2$Ru−$SiCl_2$−$SiCl_3$ (**2c**) in 30 mL of diethyl ether after stirring for 2 h at room temperature, extraction of the residue with 10 mL of petroleum ether (40−60) and sublimation at 40°C/10^{-5} Torr. − Yield 112 mg (82%). − Colorless waxy solid. −

M.p. −12 to −14)°C. − ^{1}H NMR: δ = 4.41 (s, 5 H, H_5C_5), 3.73 [q, ^3J(HSiSiH) = 3.36 Hz, 2 H, H_2Si], 3.66 [t, ^3J(HSiSiH) = 3.36 Hz, 3 H, H_3Si]. − ^{29}Si NMR: δ = −76.6 [dq, ^1J(SiH) = 181.0 Hz, ^2J(SiSiH) = 5.0 Hz, SiH_2], −94.0 [dt, ^1J(SiH) = 186.1 Hz, ^2J(SiSiH) = 6.6 Hz, SiH_3]. − IR (pentane): $\tilde{\nu}$ = 2129 cm^{-1} (w, SiH_3), 2084 (w, SiH_2) [ν(SiH)]; 2022 (vs), 1978 (vs) [ν(CO)]. − $C_7H_{10}O_2RuSi_2$ (283.39): calcd. C 29.67, H 3.56; found C 29.54, H 3.51.

8. 1-[Dicarbonyl(η^5-cyclopentadienyl)ferrio]-1,1-dichlorodisilane (4a): A solution of 175 mg (0.73 mmol) of $Cp(OC)_2Fe-SiH_2-SiH_3$ (**3a**) in 5 mL of cyclohexane is combined with 566 mg (3.68 mmol) of CCl_4 and the reaction mixture stirred for 3 h at room temperature and monitored by ^{1}H NMR. After removing volatile components (solvent, formed chloroform and excess of CCl_4) in vacuo the orange residue is extracted twice with 7 mL each of petroleum ether (50−70) and the volume of the extract is reduced in vacuo to 5 mL. **4a** crystallises after cooling for 3 h to −78°C, is filtered off and dried in vacuo at 10°C. − Yield 205 mg (91%). − Yellow microcrystalline powder. − M.p. 23−24°C. − ^{1}H NMR: δ = 4.07 (s, 5 H, H_5C_5), 3.83 (s, 3 H, HSi). − ^{13}C NMR: δ = 211.5 (s, CO), 85.07 (s, C_5H_5). − ^{29}Si NMR: δ = 93.6 (s, α-Si), −83.23 (s, β-Si). − IR (pentane): $\tilde{\nu}$ = 2150 cm^{-1} [w, ν(SiH)]; 2028 (s), 2021 (m), 1989 (vs), 1981 (s) [ν(CO)]. − MS (rel. to ^{28}Si, ^{35}Cl and ^{56}Fe, 70 eV, 35°C): *m/z* (%) = 306 (8, $[M]^+$), 278 (41, $[M - CO]^+$), 250 (7, $[M - 2CO]^+$), 247 (49, $[M - CO, - SiH_3]^+$), 219 (86, $[M - 2CO, - SiH_3]^+$), 149 (18, $[CpFeSi]^+$), 121 (37, $[CpFe]^+$), 93 (100, $[CpSi]^+$). − $C_7H_8Cl_2FeO_2Si_2$ (307.08): calcd. C 27.32, H 2.49, Cl 22.81; found C 27.38, H 2.63, Cl 23.00.

9. 1-[Dicarbonyl(η^5-pentamethylcyclopentadienyl)ferrio]-1,1-dichlorodisilane (4b): According to **8.** from 210 mg (0.68 mmol)/90 mg (0.29 mmol) of $C_5Me_5(OC)_2Fe-SiH_2-SiH_3$ (**3b**) and 7 mL of CCl_4/ 2 mL of $CHCl_3$ after 80 min at room temperature/12 h at 40°C. The brown residue obtained is extracted with 10 mL of a 1:1 mixture of petroleum ether (50−70)/methylcyclohexane, the extract evaporated in vacuo to dryness and the residue dissolved in 4 mL of pentane. **4b** crystallises on cooling to −78°C. − Yield 200 mg (77%)/ 98 mg (89%). − Yellow microcrystalline powder. − M.p. 119−120°C. − ^{1}H NMR: δ = 3.97 (s, 3 H, H_3Si), 1.49 [s, 15 H, $(H_3C)_5C_5$]. − ^{13}C NMR: δ = 215.6 (s, CO), 94.9 [s, $C_5(CH_3)_5$], 9.41 [s, $(CH_3)_5C_5$]. − IR (pentane): $\tilde{\nu}$ = 2141 cm^{-1} [w, ν(SiH)]; 2008 (s), 2001 (m), 1970 (vs), 1961 (s) [ν(CO)]. − MS (rel. to ^{28}Si, ^{35}Cl and ^{56}Fe, 70 eV, 60°C): *m/z* (%) = 376 (4, $[M]^+$), 348 (14, $[M - CO]^+$), 320 (8, $[M - 2CO]^+$), 289 (8, $[M - 2CO, - SiH_3]^+$), 226 (4, $[C_5Me_5FeCl]^+$), 191 (13, $[C_5Me_5Fe]^+$), 163 (100, $[C_5Me_5Si]^+$), 135 (19, $[C_5Me_5]^+$). − $C_{12}H_{18}Cl_2FeO_2Si_2$ (377.23): calcd. C 38.21, H 4.82, Cl 18.80; found C 38.33, H 4.92, Cl 18.55.

10. 1-[Dicarbonyl(η^5-cyclopentadienyl)ruthenio]-1,1-dichlorodisilane (4c): According to **8.** from 105 mg (0.37 mmol) of $Cp(OC)_2Ru-SiH_2-SiH_3$ (**3c**) in 15 mL of benzene and 550 mg (3.60 mmol) of CCl_4 after 15 h. After dissolving the beige residue in 1 mL of benzene and addition of 10 mL of pentane **4c** precipitates, is filtered off and dried in vacuo. − Yield 85 mg (65%). − Light beige powder. − M.p. 68°C (decomp.). − ^{1}H NMR: δ = 4.48 (s, 5 H, H_5C_5), 3.71 (s, 3 H, H_3Si). − IR (benzene): $\tilde{\nu}$ = 2151 cm^{-1} [w, ν(SiH)]; 2025 (s), 2017 (m), 1979 (vs), 1970 (s) [ν(CO)]. − $C_7H_8Cl_2O_2RuSi_2$ (352.29): calcd. C 23.87, H 2.29, Cl 20.13; found C 24.79, H 1.49, Cl 19.87.

11. Photolysis of $Cp(OC)_2Fe-SiCl_2-SiCl_3$ (2a): A solution of 100 mg (0.24 mmol) of $Cp(OC)_2Fe-SiCl_2-SiCl_3$ (**2a**) in 5 mL of benzene is irradiated for 120 h with UV-light (quartz lamp TQ 718, 700 W, Hanau). Insoluble materials are filtered off and the yellow filtrate is evaporated in vacuo to dryness. The residue is extracted with 10 mL of pentane, and the volume of the extract is reduced to 3 mL. After cooling to −78°C $Cp(OC)_2Fe-SiCl_3$ (**5**)[9a] precipitates. − Yield 43 mg (59%). − Light beige, microcrystalline powder.

12. Photolysis of $Cp(OC)_2Fe-SiH_2-SiH_3$ (3a): A solution of 93 mg (0.39 mmol) of $Cp(OC)_2Fe-SiH_2-SiH_3$ (**3a**) in 5 mL of cyclohexane is irridiated for 120 h with UV light (quartz lamp TQ 718, 700 W, Hanau). A white unidentified precipitate is separated and the filtrate evaporated in vacuo to dryness, yielding $Cp(OC)_2Fe-SiH_3$ (**6**).[8][21] − Yield 43 mg (53%).

13. Thermolysis of $Cp(OC)_2Fe-SiH_2-SiH_3$ (3a): A solution of 146 mg (0.61 mmol) of $Cp(OC)_2Fe-SiH_2-SiH_3$ (**3a**) in 8 mL of cyclohexane is heated to 65°C for 32 h. Workup according to **12.** yields $Cp(OC)_2Fe-SiH_3$ (**6**).[8][21] − Yield 93 mg (73%).

14. X-ray Crystal Structure Determination of 2a: Suitable single crystals of $Cp(OC)_2FeSi_2Cl_5$ were obtained from a saturated *n*-pentane solution at −20°C. Crystal data for $Cp(OC)_2FeSi_2Cl_5$**:** $C_7H_5Cl_5FeO_2Si_2$, M = 410.39, triclinic, space group P-1 (No. 2), yellow crystals, dimensions 0.20 × 0.20 × 0.30 mm^3, a = 12.1711(4), b = 8.7557(4), c = 13.9851(6) Å, α = 90°, β = 100.589(2)°, γ = 90°, V = 1465.0(2) Å^3, D_c = 1.861 Mg m^{-3}, Z = 4, μ (Mo-$K\alpha$) = 2.088 mm^{-1}, T = 123(2) K, F(000) = 808; 17118 reflections were collected on a Nonius Kappa CCD diffractometer ($2\theta_{max.}$ = 56.6°, $-16 \le h \le 16$, $-11 \le k \le 11$, $-17 \le l \le 16$), 3292 symmetry independent reflections (R_{int} = 0.1011) were used for the structure solution (Patterson methods)[1] and refinement (full-matrix least-squares on F^2,[2] 155 parameters, 0 restraints), non-hydrogen atoms were refined anisotropically, $wR2$ = 0.0572 [R_1 = 0.037 for 3292 $I > 2\ \sigma(I)$].Crystallographic data (excluding structure factors) for the structure reported in this paper have been deposited with the Cambridge Crystallographic Data Centre as supplementary publication no. CCDC-114922. Copies of the data can be obtained free of charge on application to The Director, CCDC, 12 Union Road, Cambrigde CB2 1EZ, UK (Fax: int. code +(1223)336−033; E-mail: teched@ccdc.cam.ac.uk).

15. X-ray Crystal Structure Determination of 3b: Yellow crystals of **3b**, suitable for X-ray diffraction were grown by slow diffusion of pentane into a saturated toluene solution of **3b** at −30°C. Crystal data: $C_{12}H_{20}FeO_2Si_2$, M = 308.31, triclinic, space group: P-1 (No. 2), a = 7.739(3) Å, b = 8.233(5) Å, c = 13.875(6) Å, α = 77.795(8)°, β = 84.945(8)°, γ = 63.262(9)°, V = 771.7(6) Å^3, Z = 2, $d_{calcd.}$: 1.327 gcm^{-3}, CAD4-diffractometer (Enraf−Nonius), radiation type: Mo-K_α, wavelength: λ = 0.71073 Å, graphite monochromator, crystal size: 0.55 × 0.50 × 0.50 mm, temperature: 173(2) K, ω/Θ-scan, scale range: 1.50° < Θ < 24.92°, F(000): 324, total reflections: 5300, independant reflections: 2691, observed reflections: 2310 with $I > 2\sigma(I)$, absorption coefficient: μ = 1.121 mm^{-1}, semi-empirical absorption correction (T_{min}/T_{max}: 0.9716/0.9983), structure solution: SHELXS-96[25a] with patterson methods, structure refinement: SHELXL-96[25b] (234 parameters), R_1 = 0.0249, wR_2 = 0.0614. The absorption correction was conducted semi-empirically with the help of of the SDP-program.[26] All atoms were determined by Fourier-transformation, the non-hydrogens refined anisotropically by the method of the smallest mean-square-errors (full-matrix least-squares) while the hydrogen atoms were refined isotropically.

Crystallographic data (excluding structure factors) for the structure reported in this paper have been deposited with the Cambridge Crystallographic Data Centre as supplementary publication no. CCDC-101420. Copies of the data can be obtained free of charge on application to CCDC, 12 Union Road, Cambridge CB2 1EZ, UK [Fax: int. Code + 44(1223)336−033; E-mail: deposit@ccdc.cam.ac.uk].

16. Matrix Isolation Raman Spectra of $Cp(OC)_2Fe-SiH_2-SiH_3$ (3a): For the Raman spectroscopic investigations of **3a** the sample was isolated in a krypton matrix at 20 K by using the ″slow-spray-on″ technique.[27] The matrix isolation apparatus consisted of a cryocooler (CTI Cryogenics, model 22C) and a turbo-pumping unit (Pfeiffer/Balzers, TPH 170).[28] The sample material was sublimated in a Knudsen cell at 308 K and a pressure of $10^{-7} - 10^{-8}$ mbar. Afterwards the gas was directly mixed with the matrix gas (krypton) in a heated nozzle, from where it was deposited on a highly polished gold plated copper cold head at 20 K. For excitation of the Raman spectra we used the 647 nm line of a krypton ion laser (Spectra Physics, model 2025). The laser beam was focussed on the matrix layer in a 30° angle to the target. The scattered light was dispersed by means of a double monochromator (Spex, model 1404) and the signal was detected by a CCD camera system (Photometrics, Spectra 9000). For the spectrum a resolution of 3 cm^{-1} was chosen. Data acquisition and spectra analyses were performed by a commercial software package (MAPS, Photometrics).

17. Density Functional Calculations of 2a, 3a: The quantum mechanical calculations were performed using Gaussian94.[29] For the best combination of exchange and correlation functionals concerning vibrational frequencies[30] we used Becke′s 1988 exchange functional[31] in combination with the Perdew-Wang 91 gradient-corrected correlation functional[32] (BPW91). As basis sets we tested the Los Alamos effective core potential (ECP) plus double zeta[33] on iron, silicon and chlorine, whereas for the rest of the atoms (all first-row elements) the Dunning/Huzinaga full double zeta basis set[34] was applied. All calculations were performed on DEC alphastations 500 [400 MHz]). Wavenumber calculations are only valid at a stationary point,so in every calculation a full geometry optimization had to be done first.

Acknowledgments

We gratefully acknowledge financial support from the Deutsche Forschungsgemeinschaft (Schwerpunktprogramm ″Spezifische Phänomene in der Siliciumchemie″; SFB 347 ″Selektive Reaktionen Metal-aktivierter Moleküle″) as well as from the Fonds der Chemischen Industrie.

[1] [1a] W. Malisch, *J. Organomet. Chem*. **1972**, *39*, C28−C30. − [1b] W. Malisch, *ibid.* **1974**, *82*, 185−199.
[2] [2a] R. B. King, K. H. Pannell, *Z. Naturforsch* **1969**, *24b*, 262. − [2b] B. K. Nicholson, J. Simpson, *J. Organomet. Chem.* **1974**, *72*, 211−220. − [2c] L. Parkanyi, K. H. Pannell, C. Hernandez, *J. Organomet. Chem*. **1983**, *252*, 127−132.
[3] [3a] K. H. Pannell, J. Cervantes, C. Hernandez, J. Cassias, S. Vincenti, *Organometallics* **1986**, *5*, 1056−1057. − [3b] K. H. Pannell, J. M. Rodzell Jr., C. Hernandez, *J. Am. Chem. Soc.* **1989**, *111*, 4482−4485. − [3c] H. Tobita, K. Ueno, H. Ogino, *Chem. Lett.* **1986**, 1777−1780. − [3d] K. H. Pannell, S.-H. Lin, R. N. Kapoor, F. Cervantes-Lee, M. Pinon, L. Parkanyi, *Organometallics* **1990**, *9*, 2454−2462. − [3e] H. Tobita, K. Ueno, M. Shimoi, H. Ogino, *J. Am. Chem. Soc.* **1990**, *112*, 3415−3420. − [3f] T. Takeuchi, H. Tobita, H. Ogino, *Organometallics* **1991**, *10*, 835−836.
[4] A. Haynes, M. W. George, M. T. Haward, M. Poliakoff, J. J. Turner, N. M. Boag, M. Green, *J. Am. Chem. Soc.* **1991**, *113*, 2011−2020.
[5] [5a] B. Stadelmann, P. Lassacher, H. Stüger, E. Hengge, *J. Organomet. Chem.* **1994**, *482*, 201−206. − [5b] M. J. Michalczyk, C. A. Recatto, J. C. Calabrese, M. J. Fink, *J. Am. Chem. Soc.* **1992**, *114*, 7955−7957.
[6] W. Malisch, R. Lankat, W. Seelbach, J. Reising, M. Noltemeyer, R. Pikl, U. Posset, W. Kiefer, *Chem. Ber.* **1995**, *128*, 1109−1115.
[7] **3a** has already been mentioned in ref.[5] but yields are considerable lower (41%) in those experiments.
[8] H.-U. Wekel, W. Malisch, *J. Organomet. Chem.* **1984**, *264*, C10−C13.
[9] [9a] W. Jetz, W. A. G. Graham, *J. Am. Chem. Soc.* **1967**, *89*, 2773−2775. − [9b] U. Schubert, G. Kraft, E. Walther, *Z. Anorg. Allg. Chem.* **1984**, *519*, 96−106.
[10] [10a] M. Schmeisser, P. Voss, *Z. Anorg. Allg. Chem.* **1964**, *334*, 50−56. − [10b] P. W. Schenk, H. Bloching, *ibid.* **1964**, *334*, 57−65. − [10c] K. Hassler, E. Hengge, W. Raml, *Monatshefte Chem.* **1980**, *111*, 581−590. − [10d] H. E. O′Neal, M. A. Ring, W. H. Richardson, G. F. Licciardi, *Organometallics* **1989**, *8*, 1968−1973. − [10e] R. Becerra, H. M. Frey, B. P. Mason, R. Walsh, M. S. Gordon, *J. Am. Chem. Soc.* **1992**, *114*, 2751−2752. − [10f] R. Becerra, H. M. Frey, B. P. Mason, R. Walsh, *J. Organomet. Chem.* **1996**, *521*, 343−349.
[11] [11a] A. Y. Vanderwielen, M. A. Ring, H. E. O′Neal, *J. Am. Chem. Soc.* **1975**, *97*, 993−998. − [11b] H. Bock, B. Solouki, G. Maier, *Angew. Chem.* **1985**, *97*, 205−206; *Angew. Chem. Int. Ed. Engl.* **1985**, *24*, 205−206. − [11c] J. M. Coffin, T. P. Hamilton, P. Pulay, I. Hargittai, *Inorg. Chem.* **1989**, *28*, 4092−4094. − [11d] M. S. Gordon, W. Nelson, *Organometallics* **1995**, *14*, 1067−1069.
[12] H. Marsmann, *29*Si-NMR-Spectroscopic Results in *NMR-Basic Principles and Progress*, Springer, Berlin-Heidelberg-New York, **1981**, Bd. 7, S. 65.
[13] R. L. Scholl, G. E. Maciel, W. K. Musker, *J. Am. Chem. Soc.* **1972**, *94*, 6376−6385.
[14] R. Loewer, M. Vongehr, H. C. Marsmann, *Chem.-Ztg.* **1975**, *99*, 33.
[15] H. C. Marsmann, H. G. Horn, *Z. Naturforsch.* **1972**, *27b*, 1448−1451.
[16] [16a] X. Zhou, C .J. M. Wheeless, R. Liu, *Vibrational Spectroscopy* **1996**, *12*, 53−63. − [16b] X. Zhou, R. Liu, *Vibrational Spectroscopy* **1996**, *12*, 65−71. − [16c] X. Zhou, S. J. Mole, R. Liu, *Vibrational Spectroscopy* **1996**, *12*, 73−79.
[17] C. Fickert, PhD thesis, Würzburg, **1998**.
[18] P. Pulay, G. Fogarasi, G. Pongor, J. E. Boggs, A. Vargha, *J. Am. Chem. Soc.* **1983**, *105*, 7037−7047.
[19] The infrared data concerning the ν(Si−H) values of **3a** differ considerably from those given by Hengge et al.[5]. These authors report only one band at 2030 cm^{-1} which is in accordance to that of $Cp(OC)_2Fe-SiH_3$, the decomposition product of **3a**.
[20] S. Schmitzer, U. Weis, H. Käb, W. Buchner, W. Malisch, T. Polzer, U. Posset, W. Kiefer, *Inorg. Chem*. **1993**, *32*, 303−306.
[21] [21a] W. Malisch, S. Möller, O. Fey, H.-U. Wekel, R. Pikl, U. Posset, W. Kiefer, *J. Organomet. Chem.* **1996**, *507*, 117−124. − [21b] W. Palitzsch, U. Bohme, G. Roewer, *J. Organomet. Chem.* **1997**, *540*, 83−88. − [21c] U. Schubert, G. Kraft, E. Walther, *Z. Anorg. Allg. Chem.* **1984**, *519*, 86. − [21d] R. West, E. K. Pham, *J. Organomet. Chem.* **1991**, *402*, 215. − [21e] L. Parkanyi, K. H. Pannell, C. Hernandez, *J. Organomet. Chem.* **1983**, *252*, 127. − [21f] T. J. Drahnak, R. West, J. C. Calabrese, *J. Organomet. Chem.* **1980**, *198*, 55. − [21g] W. Höhnle, H. G. von Schnering, *Z. Anorg. Allg. Chem.* **1980**, *464*, 139. − [21h] K. H. Pannell, S.-H. Lin, R. N. Kapoor, F. Cervantes-Lee, M. Pinon, L. Parkanyi, *Organometallics* **1990**, *9*, 2454−2462. − [21i] W. S. Sheldrick, in *The Chemistry of Organic Silicon Compounds* (Eds.: S. Patai, Z. Rappoport), John Wiley & Sons Ltd, New York, **1989,** 227.
[22] B. Beagly, J. J. Monaghan, *J. Molec. Struct.* **1971**, *8*, 401. − W. S. Sheldrick, in *The Chemistry of Organic Silicon Compounds* (Eds.: S. Patai, Z. Rappoport), John Wiley & Sons Ltd, New York, **1989**.
[23] [23a] T. S. Piper, G. Wilkinson, *J. Inorg. Nucl. Chem.* **1956**, *3*, 104−124. − [23b] T. Blackmore, M. I. Bruce, F. G. A. Stone, *J. Chem. Soc. (A)* **1968**, 2158−2162.
[24] [24a] D. H. Gibson, W.-L. Hsu, F. U. Ahmed, *J. Organomet. Chem.* **1981**, *215*, 379−401. − [24b] A. Stasunik, D. Wilson, W. Malisch, *J. Organomet. Chem.* **1984**, *270*, C18−C22.
[25] [25a] G. M. Sheldrick, SHELXS-96, *Program for Structure Solution*, Göttingen **1996**. − [25b] G. M. Sheldrick, SHELXL-96, *Program for Structure Determination*, Göttingen **1996**.
[26] Enraf.Nonius, *Structure-Determination-Package*, Enraf−Nonius, Delft, The Netherlands **1984**.
[27] M. J. Almond, A. J. Downs, in *Spectroscopy of Matrix Isolated Species, Advances in Spectroscopy*, (Eds.: R. J. H. Clark, R. E. Hester), Vol. 17, Wiley, Chichester, UK, **1989**, p.15.
[28] D. Gernet, W. Kiefer, *Fresenius J. Anal. Chem.* **1998**, *362*, in press.
[29] Gaussian94, Revision D.5, M. J. Frisch, G. W. Trucks, H. B. Schlegel, P. M. W. Gill, B. G. Johnson, M. A. Robb, J. R. Chee-

seman, T. Keith, G. A. Petersson, J. A. Montgomery, K. Raghavachari, M. A. Al-Laham, V. G. Zakrzewski, J. V. Ortiz, J. B. Foresman, J. Cioslowski, B. B. Stefanov, A. Nanayakkara, M. Challacombe, C. Y. Peng, P. Y. Ayala, W. Chen, M. W. Wong, J. L. Andres, E. S. Replogle, R. Gomberts, R. L. Martin, D. J. Fox, J. S.Binkley, D. J. Defrees, J. Baker, J. P. Stewart, M. Heat-Gordon, C. Gonzalez, J. A. Pople, Gaussian, Inc., Pittsburgh PA, **1995**.

[30] A. Gbureck, R. Pikl, W. Kiefer, *Asian J. Phys.*, submitted.

[31] A. D. Becke, *Phys. Rev. A* **1988**, *38*, 3098.

[32] J. P. Perdew, Y. Wang, *Phys. Rev. B* **1992**, *45*, 13244.

[33] [33a] P. J. Hay, W. R. Wadt, *J. Chem. Phys.* **1985**, *82*, 270−283. – [33b] W. R. Wadt, P. J. Hay, *J. Chem. Phys.* **1985**, *82*, 284−298. – [33c] P. J. Hay, W. R. Wadt, *J. Chem. Phys.* **1985**, *82*, 299−310.

[34] T. H. Dunning, Jr., P. J. Hay, in *Modern Theoretical Chemistry*, (Ed.: H. F. Schaefer), III, Plenum: New York, **1976**, 1−28.

Received April 22, 1998
[I98123]

Transition Metal Substituted Phosphaalkenes, 40[+] Transition Metal Substituted Arsaalkenes, 6[+]

Reactivity of Ferriophosphaalkene $[(\eta^5\text{-}C_5Me_5)(CO)_2Fe\text{–}P{=}C(NMe_2)_2]$ and Ferrioarsaalkene $[(\eta^5\text{-}C_5Me_5)(CO)_2Fe\text{–}As{=}C(NMe_2)_2]$ Towards Trimethylaluminium, -gallium and -indium

Lothar Weber,*[a] Matthias H. Scheffer,[a] Hans-Georg Stammler,[a] and Anja Stammler[a]

Dedicated to Professor Reinhard Schmutzler on the occasion of his 65th birthday

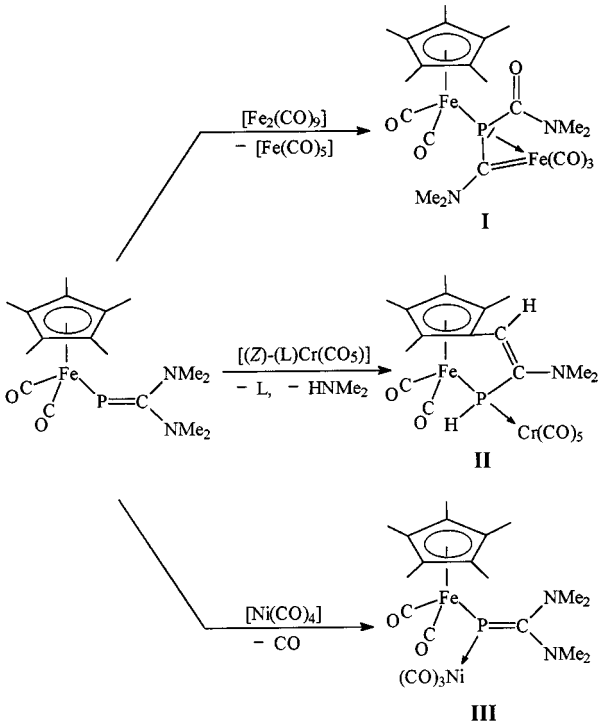
Keywords: Arsaalkenes / Phosphaalkenes / Aluminium / Gallium / Indium

Reaction of equimolar amounts of the ferriophosphaalkene $[(\eta^5\text{-}C_5Me_5)(CO)_2FeP{=}C(NMe_2)_2]$ (**1a**) or the ferrioarsaalkene $[(\eta^5\text{-}C_5Me_5)(CO)_2FeAs{=}C(NMe_2)_2]$ (**1b**) with trimethylaluminium, trimethylgallium and trimethylindium afforded the adducts $[(\eta^5\text{-}C_5Me_5)(CO)_2FeE\{MMe_3\}C(NMe_2)_2]$ with E = P; M = Al (**2a**), Ga (**3a**), In (**4a**) and E = As; M = Al (**2b**), Ga (**3b**), and In (**4b**). These compounds feature η^1-coordination of the phosphaalkene or the arsaalkene ligand towards the Lewis acid via the pnictogen atom. The molecular structures of **2a** and **3a** were elucidated by X-ray diffraction analyses.

Introduction

During the course of our investigations on the chemical properties of metallophospha- and metalloarsaalkenes $[(\eta^5\text{-}C_5Me_5)(CO)_2FeE{=}C(NMe_2)_2]$ (E = P, As)[1][2] we have studied their reactivity towards transition metal carbonyls. Whereas the treatment of the arsalkene with $[Ni(CO)_4]$, $[Fe_2(CO)_9]$ or [(*Z*)-cyclooctene$Cr(CO)_5$] afforded adducts of the type $[(\eta^5\text{-}C_5Me_5)(CO)_2FeAs\{M(CO)_n\}C(NMe_2)_2]$ ($[M(CO)_n$ = $[Ni(CO)_3]$, $[Fe(CO)_4]$, $[Cr(CO)_5]$)[3] the corresponding phosphaalkene and $[Fe_2(CO)_9]$ or [(*Z*)-cyclooctene$Cr(CO)_5$] gave rise to the formation of complexes **I** and **II**.[4]

With nickel carbonyl adduct **III** was obtained.[4] Moreover, the metallophosphaalkene was converted by $[(\eta^5\text{-}C_5H_5)(CO)_2Rh]$ into a complex analogous to **II** ($[(\eta^5\text{-}C_5H_5)(CO)Rh]$ instead of $[Cr(CO)_5]$) the arsaalkene was disintegrated to the η^2-diarsene complex $[\{(\eta^5\text{-}C_5Me_5)(CO)_2Fe\text{-}As\}_2Rh(CO)(\eta^5\text{-}C_5H_5)]$.[5] In view of these results it was obvious to extent our studies on the reactivity of the title compounds to electrophiles derived from main group metals.



Scheme 1

Results and Discussion

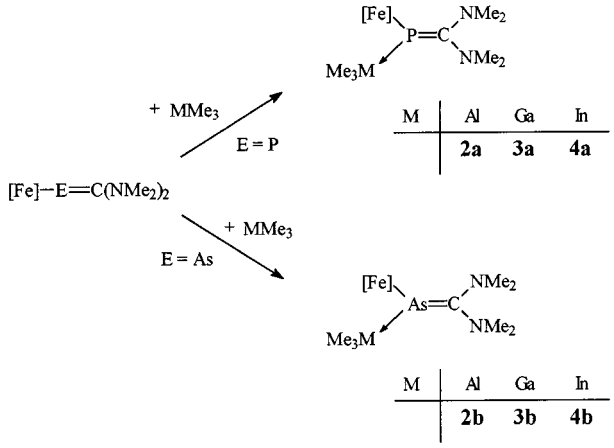
Treatment of **1a** and **1b** with equimolar amounts of $AlMe_3$, $GaMe_3$ and $InMe_3$ in *n*-pentane in the temperature range −78 °C to 20 °C afforded the trimethylmetal adducts **2a,b**, **3a,b** and **4a,b** as air- and moisture sensitive solids, whereas **1a** and **1b** appeared to be inert towards $Al(iPr)_3$. Solutions of compound **2b** in benzene completely decomposed at 20 °C within a few hours. The stability of the remaining adducts in solution was sufficient to provide satisfactory NMR spectra. Purification of the obtained compounds was achieved by recrystallization from *n*-pentane at −28 °C. In the IR spectra (KBr) of adducts **2a**,**b, 3a,b** and

[+] Part 39; part 5: L. Weber, M. H. Scheffer, H.-G. Stammler, B. Neumann, *Inorg. Chim. Acta*, in the press.

[a] Fakultät für Chemie der Universität Bielefeld
Universitätsstraße 25, D-33615 Bielefeld, Germany
Fax: (internat.) +49(0)521/106-6146
E-mail: lothar.weber@uni-bielefeld.de

 © WILEY-VCH Verlag GmbH, D-69451 Weinheim, 1999 1434−1948/99/0909−1607 $ 17.50+.50/0

4a,b intense bands at $\tilde{\nu}$ = 1991−2000 and 1931−1951 cm^{-1} were assigned to the stretching modes of the terminal carbonyls of the $[Fe(CO)_2]$ unit. Hypsochromic shifts of 10−27 cm^{-1} of these bands with respect to **1a** and **1b** indicate a significant withdrawal of electron density from the organophosphorus or the organoarsenic ligand by the Lewis acids.



Scheme 2

The $^{13}C\{^1H\}$-NMR spectra of the phosphaalkene and arsaalkene adducts showed resonances at δ = 219.4−220.8 for the carbonyl carbon atoms, which are only slightly shielded when compared to the starting materials **1a** and **1b**. The resonance for the methylene carbon atom in the phosphaalkene adducts appeared as doublet at δ = 203.0−204.5, and thus is slightly shifted to low-field relative to **1b** (δ = 202.4). Adduct formation was accompanied by a decrease of the $^1J_{PC}$ coupling constant from 97.0 Hz in **1a** to 75.8−80.6 Hz in **2a**-**4a**. In a corresponding $[Ni(CO)_3]$ adduct a similar $^1J_{PC}$ coupling was measured ($^1J_{PC}$ = 77.7 Hz),[4] whereas smaller coupling constants ranging from 59.0 to 67.4 Hz were registered upon protonation, alkylation and silylation of **1a**.[6] The methylene carbon atom of **1b** (δ = 214.8) is shifted upfield to δ = 211.7 (**3b**) and 211.9 (**4b**) upon adduct formation. The $^{31}P\{^1H\}$-NMR spectra of the adducts **2a**, **3a** and **4a** are characterized by singlets at δ = −12.1, 14.5 and 22.2, which are strongly deshielded with respect to **1a** (δ = 135.5).

X-ray Structural Analysis of 2a

To ensure that the metallophosphaalkene is bonded to the metal through the phosphorus atom and to establish the stereochemistry within the ligand an X-ray structural determination of **2a** was undertaken.

An ORTEP drawing of **2a** is shown in Figure 1, also selected bond lengths and angles . The analysis shows that η^1-coordination of the ferriophosphaalkene to trimethylaluminium by virtue of the phosphorus lone pair results in a significant distortion of the organophosphorus ligand. Thus, the phosphorus atom is now trigonal-pyramidally coordinated (sum of angles 340.0°). This value is between those of the corresponding adducts of **1a** to the $[Ni(CO)_3]$ (335.8°)[4] and to the $[Cr(CO)_5]$ units (346.1°).[7] The phosphorus atom forms single bonds to the atoms Fe, Al and C(16). In comparison to **1a** [1.709(5) Å] the PC bond is elongated to 1.779(3) Å, a situation which was also evident in the $[Ni(CO)_3]$ adduct [1.770(5) Å].[4] The iron−phosphorus bond length [2.3174(9) Å] is similar to the one in **1a** [2.325(2) Å].[1] The P−Al bond length of 2.5077(12) Å may be compared to the P−Al distances in the number of adducts of phosphanes and $AlMe_3$ such as $Me_3Al-PH(t\text{-}Bu)CH_2CH_2(t\text{-}Bu)HP-AlMe_3$ [2.533(3) Å],[8] $Me_3Al-P(Ph)_2CH_2CH_2(Ph_2)P-AlMe_3$ [2.544(4) Å][9] and $Me_3Al-P(Ph)_2CH_2CH_2P(Ph)[AlMe_3]CH_2CH_2(Ph)_2P-AlMe_3$ [2.504(6) and 2.535(7) Å].[8]

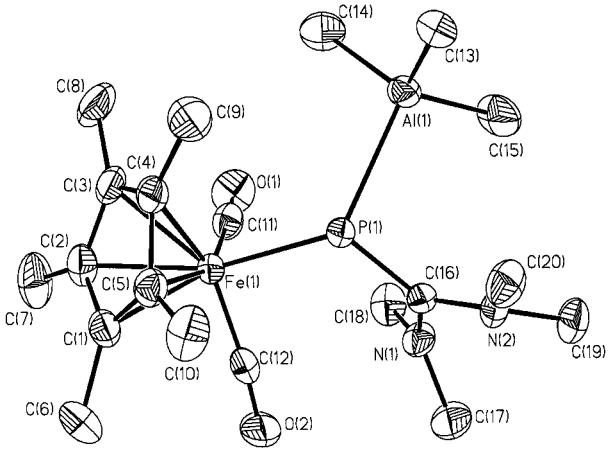


Figure 1. Molecular structure of **2a** in the crystal. Selected bond lengths [Å] and angles [deg]: Fe(1)−C(12) 1.754(3), Fe(1)−C(11) 1.761(3), Fe(1)−P(1) 2.3174(9), Al(1)−C(15) 1.980(4), Al(1)−C(14) 1.984(4), Al(1)−C(13) 1.988(4), Al(1)−P(1) 2.5077(12), P(1)−C(16) 1.779(3), O(1)−C(11) 1.142(4), O(2)−C(12) 1.151(4), N(1)−C(16) 1.358(4), N(1)−C(18) 1.447(4), N(1)−C(17) 1.470(4), N(2)−C(16) 1.363(4), N(2)−C(20) 1.457(4), N(2)−C(19) 1.465(4); C(12)−Fe(1)−C(11) 97.01(16), C(12)−Fe(1)−P(1) 92.08(11), C(11)−Fe(1)−P(1) 92.84(10), C(15)−Al(1)−C(14) 111.87(19), C(15)−Al(1)−C(13) 111.33(18), C(14)−Al(1)−C(13) 112.71(16), C(15)−Al(1)−P(1) 107.58(12), C(14)−Al(1)−P(1) 107.04(12), C(13)−Al(1)−P(1) 105.90(11), C(16)−P(1)−Fe(1) 116.45(10), Fe(1)−P(1)−Al(1) 124.13(4), C(16)−N(1)−C(18) 122.5(3), C(16)−N(1)−C(17) 122.5(3), C(18)−N(1)−C(17) 114.9(3), C(16)−N(2)−C(20) 122.5(3), C(16)−N(2)−C(19) 121.7(3), C(20)−N(2)−C(19) 113.5(3), O(1)−C(11)−Fe(1) 175.6(3), O(2)−C(12)−Fe(1) 174.6(3), N(1)−C(16)−N(2) 115.2(3), N(1)−C(16)−P(1) 126.0(2), N(2)−C(16)−P(1) 118.8(2)

The methylene carbon atom C(16) of **2a** is trigonal planar (sum of angles 360.0°). The same is true for nitrogen atom N(1) (sum of angles 359.9°), whereas atom N(2) slightly deviates from planarity (sum of angles 357.7°). Relatively short carbon−nitrogen bonds C(16)−N(1) [1.358(4) Å] and C(16)−N(2) [1.363(4) Å] indicate effective π-coordination of the lone pair of electrons on the nitrogen atoms with C(16).

In the crystal molecule **2a** adopts a conformation with an orthogonal orientation of the bond P(1)−Al(1) and the vector Cp*−Fe (where Cp* is the centre of the C_5Me_5 ring [torsion angle Cp*−Fe(1)−P(1)−Al(1) = −90.1°]. According to a Newman projection of **2a** (Figure 2) the lone pair at the phosphorus atom is presumably directed towards the

C_5Me_5 ring, leading to a nearly eclipsed position of the vectors Fe(1)−C(12)−O(2) and P(1)−C(16) [torsion angle C(12)−Fe(1)−P(1)−C(16) = 14.5°].

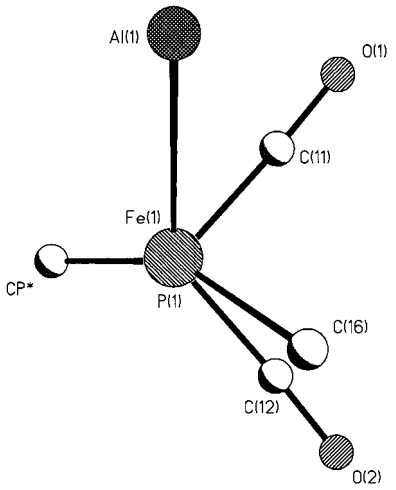


Figure 2. Newman projection of **2a** with view along the P(1)−Fe(1) vector

X-ray Structural Analysis of 3a

The molecular structure in the crystal of the $GaMe_3$ adduct of **1a**, as determined by X-ray diffraction analysis (Figure 3), is closely related to the structure of **2a**. The trigonal-pyramidal phosphorus atom (sum of angles = 340.3°) and the single bond lengths P(1)−C(16) of 1.780(4) Å and Fe(1)−P(1) of 2.3233(17) Å are well comparable in **3a** and **2a**. The Ga−P and Al−P atomic distances are the same within experimental error, which was also observed in the bis-adducts of diphos with $AlMe_3$ and $GaMe_3$. Thus, in $[Me_3GaP(Ph)_2CH_2CH_2P(Ph)_2GaMe_3]$ the Ga−P bond lengths were determined to 2.546(4) Å.[9] Generally, Ga−P bonds in molecules with tetra-coordinate gallium and phosphorus range from 2.347(5) Å in $[(Me_3Si)_3P-GaI_3]$[10] up to 2.683(5) Å in $[Ph_2(H)P\text{-}Ga\{CH_2(t\text{Bu})\}_3]$.[11][12]

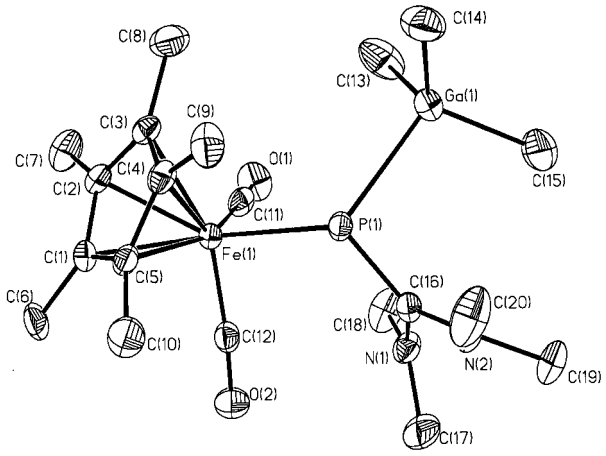


Figure 3. Molecular structure of **3a** in the crystal. Selected bond lengths [Å] and angles [deg]: Ga(1)−C(13) 1.976(6), Ga(1)−C(14) 1.990(5), Ga(1)−C(15) 1.996(5), Ga(1)−P(1) 2.5027(16), Fe(1)−C(12) 1.754(5), Fe(1)−C(11) 1.756(5), Fe(1)−P(1) 2.3233(17), P(1)−C(16) 1.780(4), O(1)−C(11) 1.147(5), O(2)−C(12) 1.151(5), N(1)−C(16) 1.363(5), N(1)−C(18) 1.459(6), N(1)−C(17) 1.462(6), N(2)−C(16) 1.354(5), N(2)−C(20) 1.455(6), N(2)−C(19) 1.473(5); C(13)−Ga(1)−C(14) 112.2(2), C(13)−Ga(1)−C(15) 114.1(3), C(14)−Ga(1)−C(15) 112.6(3), C(13)−Ga(1)−P(1) 107.68(16), C(14)−Ga(1)−P(1) 103.75(17), C(15)−Ga(1)−P(1) 105.67(17), C(12)−Fe(1)−C(11) 97.5(2), C(12)−Fe(1)−P(1) 90.07(15), C(11)−Fe(1)−P(1) 93.83(15), C(16)−P(1)−Fe(1) 117.14(16), C(16)−P(1)−Ga(1) 100.63(15), Fe(1)−P(1)−Ga(1) 122.55(7), C(16)−N(1)−C(18) 122.5(4), C(16)−N(1)−C(17) 122.4(4), C(18)−N(1)−C(17) 115.0(4), C(16)−N(2)−C(20) 123.1(4), C(16)−N(2)−C(19) 122.2(4), C(20)−N(2)−C(19) 113.4(4), O(1)−C(11)−Fe(1) 175.4(4), O(2)−C(12)−Fe(1) 174.7(4), N(2)−C(16)−N(1) 115.0(4), N(2)−C(16)−P(1) 117.9(3), N(1)−C(16)−P(1) 127.1(3)

Experimental Section

All operations were performed under dry, oxygen-free dinitrogen using standard Schlenk techniques. Solvents were dried by standard methods and freshly distilled under argon prior to use. − Infrared spectra were recorded on a Bruker FT-IR IFS66 spectrometer. − ^1H, ^{13}C, and ^{31}P-NMR spectra were recorded at 22 °C by using a Bruker AC 100 (^1H, 100.13 MHz, ^{31}P, 40.53 MHz), Bruker Avance DRX 500 (^1H, 500.13 MHz, ^{13}C, 125.75 MHz, ^{31}P, 202.46 MHz); references: $SiMe_4$ (^1H, ^{13}C) and 85% H_3PO_4 (^{31}P). − Elemental analyses were performed in the microanalytical laboratory of the University of Bielefeld. − The metallophosphaalkene $[\eta^5\text{-}Cp^*(CO)_2Fe-P=C(NMe_2)_2]$ (**1a**)[1] and the metalloarsaalkene $[\eta^5\text{-}Cp^*(CO)_2Fe-As=C(NMe_2)_2]$ (**1b**)[2] were synthesized according to the literature. $AlMe_3$, $GaMe_3$ and $InMe_3$ were purchased commercially (Strem).

$[(\eta^5\text{-}C_5Me_5)(CO)_2FeP\{AlMe_3\}C(NMe_2)_2]$ (2a): A chilled solution (−78 °C) of **1a** (0.39 g, 1.03 mmol) in 50 mL of *n*-pentane was combined with 0.42 mL of a 2.39 M solution of $AlMe_3$ in toluene. Stirring was continued for a period of 1.5 h, during which the mixture was allowed to warm-up to room temp. It was filtered, and the filtrate was diluted with 100 mL of *n*-pentane. Storing at −28 °C for 20 h afforded **2a** (0.19 g, 43%) as a dark brown, air and moisture sensitive solid. − IR (KBr): $\tilde{\nu}$ = 2000 (s, CO), 1951 (s, CO). − ^1H NMR (C_6D_6): δ = −0.14 (s, 9 H, $AlMe_3$), 1.51 (s, 15 H, C_5Me_5), 2.70 (s, br, 12 H, NMe_2). − $^{13}C\{^1H\}$ NMR (C_6D_6): δ = −2.98 (s, $AlCH_3$), 9.31 [s, $C_5(CH_3)_5$], 43.45 (s, NCH_3), 96.25 [s, $C_5(CH_3)_5$], 202.95 (d, $^1J_{PC}$ = 75.8 Hz, PC), 219.38 (s, CO). − $^{31}P\{^1H\}$ NMR (C_6D_6): δ = −12.12 s. − $C_{20}H_{36}AlFeN_2O_2P$ (419.35): calcd. C 53.34, H 8.06, N 6.22; found C 50.89, H 7.91, N 6.03. The C,H,N elemental analysis was repeated several times with crystalline samples, however, no better C-values were obtained.

$[(\eta^5\text{-}C_5Me_5)(CO)_2FeAs\{AlMe_3\}C(NMe_2)_2]$ (2b): To a chilled solution (−78 °C) of **1b** (0.32 g, 0.76 mmol) in *n*-pentane (50 mL) was added 0.33 mL of a 2.39 M solution of $AlMe_3$ (0.79 mmol) in toluene. An orange precipitate spontaneously occurred, which was redissolved upon warming up the mixture to 20 °C. Stirring was continued for 1 h, and then it was filtered. The filtrate was diluted with 50 mL of *n*-pentane and stored at −28 °C to afford 0.15 g (41%) of thermolabile orange-red crystalline **2b**. Solutions in benzene completely decomposed at 20 °C within a few hours which prevented the registration of a reliable $^{13}C\{^1H\}$ NMR spectrum. − ^1H NMR (C_6D_6): δ = −0.09 (s, 9 H, $AlMe_3$), 1.57 (s, 15 H, C_5Me_5), 2.73 (s, br, 12 H, NMe_2). − $C_{20}H_{36}AlAsFeN_2O_2$ (494.26): calcd. C 48.60, H 7.34, N 5.67; found C 48.31, H 6.94, N 5.60.

$[(\eta^5\text{-}C_5Me_5)(CO)_2FeP\{GaMe_3\}C(NMe_2)_2]$ (3a): A *n*-pentane solution (50 mL) of **1a** (0.47 g, 1.24 mmol) was combined at −78 °C with 0.54 g (1.24 mmol) of a 2.3 M solution of $GaMe_3$ in *n*-hexane.

Table 1. Crystallographic data for **2a** and **3a**

	2a	**3a**
empirical formula	$C_{20}H_{36}AlFeN_2O_2P$	$C_{20}H_{36}FeGaN_2O_2P$
mol. mass (g mol^{-1})	450.31	493.05
temp. (K)	173	173
cryst. size (mm)	0.5 × 0.5 × 0.4	0.6 × 0.5 × 0.3
cryst. syst.	monoclinic	monoclinic
space group	$P2_1/c$	$P2_1/n$
a (Å)	15.300(4)	12.392(10)
b (Å)	8.057(2)	15.118(6)
c (Å)	20.221(3)	13.419(8)
α (deg)	90	90
β (deg)	102.36(2)	102.69(5)
γ (deg)	90	90
V (Å^3)	2434.9(9)	2453(3)
Z	4	4
cryst. color	dark-brown	dark-brown
habit	irregular	irregular
d_{calcd} (g cm^{-3})	1.228	1.335
μ Mo K_α (mm^{-1})	0.737	1.771
F(000)	960	1032
θ range (deg)	2.06 to 30.00	2.03 to 27.50
limiting indices	$0 \le h \le 21$	$0 \le h \le 16$
	$0 \le k \le 11$	$0 \le k \le 19$
.	$-28 \le l \le 27$	$-17 \le l \le 17$
no. of reflns. collected	7353	5875
no. of indep. reflns	7113 [$R_{(int)}$ = 0.0587]	5625 [$R_{(int)}$ = 0.0445]
no. of parameters	256	256
absorptions correction	none	semi-empirical from ψ-scans
ρ_{max}, ρ_{min} (e Å^{-3})	0.643, −0.655	0.425, −0.426
goodness of fit on F^2	1.034	1.008
R_F [$I > 2\sigma(I)$]	0.0593 [4650]	0.0576 [3444]
wR_F^2 [$I > 2\sigma(I)$]	0.1236	0.0951
treatment of hydrogen atoms	riding model	riding model

The stirred mixture was allowed to warm to 20 °C within a period of 2 h. Filtration, addition of *n*-pentane (50 mL) to the filtrate and storage at −28 °C for 20 h afforded 0.36 g (59%) of black crystalline **3a**. − IR (KBr): ṽ = 2000 (s, CO), 1947 (s, CO). − ^{1}H NMR (C_6D_6): δ = 0.20 (s, 9 H, $GaMe_3$), 1.51 (s, 15 H, C_5Me_5), 2.71 (s, 12 H, NMe_2). − $^{13}C\{^1H\}$ NMR (C_6D_6): δ = 0.32 (s, $GaCH_3$), 9.24 [s, $C_5(CH_3)_5$], 43.33 (s, NCH_3), 96.23 [s, $C_5(CH_3)_5$], 203.76 (d, $^1J_{PC}$ = 80.6 Hz, PC), 219.62 (s, CO). − $^{31}P\{^1H\}$ NMR (C_6D_6): δ = 14.52 s, br. − $C_{20}H_{36}FeGaN_2O_2P$ (493.06): calcd. C 48.72, H 7.36, N 5.68; found C 47.88, H 6.91, N 5.56.

[(η^5-C$_5$Me$_5$)(CO)$_2$FeAs{GaMe$_3$}C(NMe$_2$)$_2$] (3b): Analogously, the reaction of equimolar amounts of **1b** (0.15 g, 0.36 mmol) and $GaMe_3$ (0.16 g of a 2.3 M solution in *n*-hexane) in *n*-pentane gave 0.10 g (51%) of **3b** as red-black needles. − IR (KBr): ṽ = 1991 (s, CO), 1932 (s, CO). − ^{1}H NMR (C_6D_6): δ = 0.24 (s, 9 H, $GaMe_3$), 1.57 (s, 15 H, C_5Me_5), 2.68 (s, 12 H, NMe_2). − $^{13}C\{^1H\}$ NMR (C_6D_6): δ = −0.46 (s, $GaCH_3$), 9.31 [s, $C_5(CH_3)_5$], 44.50 (s, NCH_3), 95.00 [s, $C_5(CH_3)_5$], 211.7 (s, AsC), 220.8 (s, CO). − $C_{20}H_{36}AsFeGaN_2O_2$ (537.00): calcd. C 44.73, H 6.76, N 5.22; found C 44.30, H 6.50.

[(η^5-C$_5$Me$_5$)(CO)$_2$FeP{InMe$_3$}C(NMe$_2$)$_2$] (4a): A chilled solution (−78 °C) of **1a** (0.53 g, 1.40 mmol) in *n*-pentane (50 mL) was treated with 0.7 mL of a 2 M solution of $InMe_3$ (1.40 mmol) in *n*-pentane. After the usual work up black crystalline **4a** (0.44 g, 58%) was isolated. − IR (KBr): ṽ = 1999 (s, CO), 1946 (s, CO). − ^{1}H NMR (C_6D_6): δ = 0.18 (s, 9 H, $InMe_3$), 1.50 (s, 15 H, C_5Me_5), 2.70 (s, 12 H, NMe_2). − $^{13}C\{^1H\}$ NMR (C_6D_6): δ = −4.56 (s, $InCH_3$), 9.13 [s, $C_5(CH_3)_5$], 43.28 (s, NCH_3), 96.14 [s, $C_5(CH_3)_5$], 204.5 (d, $^1J_{PC}$ = 80.5 Hz, PC), 219.53 (s, CO). − $^{31}P\{^1H\}$ NMR (C_6D_6): δ = 22.2 s, br. − $C_{20}H_{36}FeInN_2O_2P$ (538.16): calcd. C 44.64, H 6.74, N, 5.21; found C 44.64, H 6.80, N 5.12.

[(η^5-C$_5$Me$_5$)(CO)$_2$FeAs{InMe$_3$}C(NMe$_2$)$_2$] (4b): Black crystalline **4b** (0.37 g, 59%) was synthesized analogously from **1b** (0.46 g, 1.09 mmol) and 1.10 mmol (0.55 mL of a 2 M solution in *n*-pentane) of $InMe_3$. − IR (KBr): ṽ = 1993 (s, CO), 1931 (s, CO). − ^{1}H NMR (C_6D_6): δ = 0.21 (s, 9 H, $InMe_3$), 1.54 (s, 15 H, C_5Me_5), 2.66 (s, 12 H, NMe_2). − $^{13}C\{^1H\}$ NMR (C_6D_6): δ = −4.82 (s, $InCH_3$), 9.20 [s, $C_5(CH_3)_5$], 44.20 (s, NCH_3), 95.1 [s, $C_5(CH_3)_5$], 211.9 (s, AsC), 220.5 (s, CO). − $^{31}P\{^1H\}$ NMR (C_6D_6): δ = 14.52 s, br. − $C_{20}H_{36}AsFeInN_2O_2$ (582.10): calcd. C 41.27, H 6.23, N 4.81; found C 41.10, H 6.06, N 4.62.

X-ray Structural Solution and Refinement: The same general procedures were employed to collect the X-ray diffraction data for complexes **2a** and **3a**. Crystal data collection and refinement parameters are given in Table 1. ORTEP drawing of the solid state structure of **2a** and **3a** are shown in Figures 1,2 and 3, respectively.[13] For **2a** and **3a** the data were collected with a Siemens $P2_1$ four-circle diffractometer (Mo-K_α radiation λ = 0.71073 Å). Crystallographic programs used for structure solution and refinement were from SHELXTL PLUS and SHELXL-97. The structure was solved by using Direct Methods and was refined by using full-matrix least squares on F^2 of all unique reflections with anisotropic thermal parameters for all non-hydrogen atoms.

Acknowledgments

This work was generously supported by the Deutsche Forschungsgemeinschaft, Bonn, Germany and the Fonds der Chemischen Industrie, Frankfurt, Germany, which are gratefully acknowledged.

[1] L. Weber, O. Kaminski, H.-G. Stammler, B. Neumann, V. D. Romanenko, *Z. Naturforsch.* **1993**, *48b*, 1784−1794.
[2] L. Weber, O. Kaminski, H.-G. Stammler, B. Neumann, *Chem. Ber.* **1996**, *129*, 223−226.
[3] L. Weber, M. Scheffer, H.-G. Stammler, B. Neumann, *Eur. J. Inorg. Chem.* **1998**, 55−59.
[4] L. Weber, O. Kaminski, B. Quasdorff, H.-G. Stammler, B. Neumann, *J. Organomet. Chem.* **1997**, *529*, 329−341.
[5] L. Weber, M. H. Scheffer, H.-G. Stammler, B. Neumann, *Inorg. Chim. Acta,* in press.
[6] L. Weber, M. H. Scheffer, H.-G. Stammler, B. Neumann, K. K. Laali, *Organometallics*, in press.
[7] B. Quasdorff, Ph.D. Thesis, Universität Bielefeld **1997**, 37−38.
[8] D. A. Atwood, A. H. Cowley, R. A. Jones, R. J. Powell, C. M. Nunn, *Organometallics* **1996**, *15*, 2657−2659.
[9] D. C. Bradley, H. Chudzynska, M. M. Faktor, D. M. Frigo, M. B. Hursthouse, B. Hussain, L. M. Smith, *Polyhedron* **1988**, *7*, 1289−1298.
[10] J. F. Janik, R. A. Baldwin, R. L. Wells, W. T. Pennington, G. L. Schimek, A. L. Rheingold, L. M. Liable-Sands, *Organometallics* **1996**, *15*, 5385−5390.
[11] M. A. Banks, O. T. Beachley, J. D. Maloney, R. D. Rogers, *Polyhedron* **1990**, *9*, 335−342.
[12] For compilations of Ga−P bond lengths see: [a] N. C. Norman, N. L. Pickett, *Coord. Chem. Rev.* **1995**, *145*, 27−54; [b] D. Wiedmann, H.-D. Hausen, J. *Z.* Weidlein, *Anorg. Allg. Chem.* **1995**, *621*, 1351−1357; [c] A. H. Cowley, R. A. Jones, *Angew. Chem.* **1989**, *101*, 1235−1243; *Angew. Chem. Int. Ed. Engl.* **1989**, *28*, 1208.
[13] Crystallographic data (excluding structure factors) for the structures reported in this paper have been deposited with the Cambridge Crystallographic Data Centre as supplementary publication no. CCDC-118723 (**2a**) and CCDC-118724 (**3a**). Copies of the data can be obtained free of charge on application to CCDC, 12 Union Road, Cambridge CB2 1EZ, UK (Fax: +44−1223/336−033; E-mail: deposit@ccdc.cam.ac.uk).

Received February 5, 1999
[I99039]

Two New Carbon-Free Indium(III) Asymmetric Chelates – Synthesis and X-ray Crystal Structures of $[In\{Ph_2P(O)NP(S)Ph_2\text{-}O,S\}_3]\cdot 3/4\ C_6H_6$ and $[InCl\{Ph_2P(S)NP(Se)Ph_2\text{-}S,Se\}_2]$

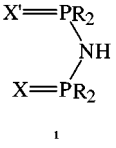
Raymundo Cea-Olivares,[a] Rubén A. Toscano,[a] Simón Hernández-Ortega,[a] Josef Novosad,[b] and Verónica García-Montalvo*[a]

Keywords: Indium / Chalcogens / Chelates / Phosphazenes / Metallacycles

The ligands $[Ph_2(S)PNHP(X)Ph_2]^-$ (X = O, Se) react with $InCl_3$ in a 3:1 ratio to give a tris-chelate $[In\{Ph_2P(O)NP(S)Ph_2\text{-}O,S\}_3]\cdot 0.75\ C_6H_6$ (**2**) and the unexpected pentacoordinate derivative $[InCl\{Ph_2P(Se)NP(S)Ph_2\text{-}Se,S\}_2]$ (**3**). These compounds have been characterized by means of IR, ^1H- and ^{31}P-NMR spectroscopy, positive-ion FAB mass spectrometry and elemental analysis. The molecular structures have been determined by single-crystal X-ray diffraction analysis. The coordination geometry in **2** resembles that observed in the three analogous tris-chelates incorporating the corresponding symmetrical oxygen, sulfur and selenium ligands. Compound **3** exhibits a very distorted trigonal-bipyramidal geometry at indium, where both the selenium and chlorine atoms are in equatorial positions, while the sulfur atoms are in axial positions.

Introduction

Inorganic chelate rings have been the subject of increasing interest in recent years, since they constitute a bridge between traditional inorganic heterocycles (containing mainly non-metallic elements) and classical coordination compounds.[1,2] The anions of the ligands $[R_2(X)PNHP(X')R_2]$ (**1**: R = Ph, Me, *i*-Pr, and OPh, but not all permutations) are excellent chelating agents, which form stable phosphazene metallacycles. They have also found important use as metal extracting agents.[2,3] Compounds containing the symmetric ligands **1a**−**c** have been extensively studied.[4] In contrast, chelate complexes with the asymmetric ligands (**1d**−**f**) have been less well studied, with only few examples known to date.[2,5,6] This is in part due to the long absence of a simple synthetic procedure for such systems. However, more convenient synthetic methods have been reported in the last few years.[2][5]



	X	X′
1a	O	O
1b	S	S
1c	Se	Se
1d	O	S
1e	O	Se
1f	S	Se

In the course of our studies on the coordination chemistry of the imidobis(diphenylphosphanechalcogenide) ligands (**1**) with heavy main group elements, we synthesized some heavier Group 13 complexes [In(III) and Ga(III)] with the symmetric anions **1a**−**c**.[4b−4d] In order to explore possible changes that might be induced by asymmetric ligands (**1d** and **1f**), we decided to synthesize indium(III) derivatives with these ligands.

We report herein on the synthesis and spectroscopic characterization of the indium(III) tris-chelate $[In\{Ph_2P(O)NP(S)Ph_2\text{-}O,S\}_3]$ (**2**) and the unexpected pentacoordinate indium(III) complex $[InCl\{Ph_2P(S)NP(Se)Ph_2\text{-}S,Se\}_2]$ (**3**).

Results and Discussion

The compounds were prepared from $InCl_3$ and the appropriate $K(Ph_2PSNPXPh_2)$ salt (X = O or Se) in a 1:3 molar ratio. In the reaction with the ligand **1f**, only the bis-chelate $[InCl\{Ph_2P(Se)NP(S)Ph_2\text{-}Se,S\}_2]$ (**3**) was obtained, even on employing different molar proportions. There was no evidence for the formation of the expected tris-chelate.

Both complexes were obtained as air-stable, colourless, crystalline solids, and were found to be soluble in some organic solvents (e.g. $CHCl_3$, CH_2Cl_2, benzene, THF), but not in others (hexane, ethanol). They were characterized by partial elemental analyses (C, H, N), IR, ^1H- and ^{31}P-NMR spectroscopy, and positive-ion FAB mass spectrometry. The crystal and molecular structures of both compounds (**2** and **3**) were determined by means of single-crystal X-ray diffraction analysis.

Characteristic infrared bands of the new compounds were assigned by comparison with the spectra of reported compounds containing the $[Ph_2PSNPXPh_2]^-$ ligand.[2, 4−7] The FAB mass spectrum of **2** exhibits a low intensity signal for the molecular ion, but rather intense ion fragments containing ^{115}In, e.g. $[S_2O_2(PPh_2)_4N_2{}^{115}In^+]$ [*m*/*z* (%): 979

[a] Instituto de Química, Universidad Nacional Autónoma de México,
Circuito Exterior, Ciudad Universitaria, México 04510 D.F., México
Fax: (internat.) + 52-5/616-2203
E-mail: vgm@servidor.unam.mx
[b] Inorganic Chemistry Department, Masaryk University, CZ-61137 Brno, Czech Republic

 © WILEY-VCH Verlag GmbH, D-69451 Weinheim, 1999 1434−1948/99/0909−1613 $ 17.50+.50/0

(100)], $[SO(PPh_2)_2N^{115}In^+]$ [*m/z* (%): 546 (45)]. In the case of compound **3**, the base peak corresponds to the expected first fragmentation, i.e. $[M^+ - Cl]$ (*m/z*: 1107). All of the observed signals exhibit the expected isotopic pattern.

The $^{31}P\{^1H\}$-NMR spectra each feature two signals attributable to two non-equivalent phosphorus nuclei P_S and P_X. Upon chelation to In(III), there is a small change in δP and a reduction in ^1J(PSe) for the bonded $[Ph_2P(S)NP(X)Ph_2]^-$ ligand [**2**: δ(P) = 33.6, 23.3; **3**: δ(P) = 40.53, 28.24; ^1J(PSe) = 738 Hz] in comparison to $K[Ph_2P(S)NP(X)Ph_2]$ [X = O: δ(P) = 35.3, 13.9; X = Se: δ(P) = 37.6, 26.7; ^1J(PSe) = 682 Hz].[5]

Structural Description

The structures of the compounds are built-up from discrete $[In\{Ph_2P(O)NP(S)Ph_2\text{-}O,S\}_3]$ (**2**) and $[InCl\{Ph_2P(S)NP(Se)Ph_2\text{-}S,Se\}_2]$ (**3**) molecules. Compound **2** crystallizes with benzene molecules in a 4:3 ratio. The molecular structures of **2** and **3** are shown in Figures 1 and 2, respectively.

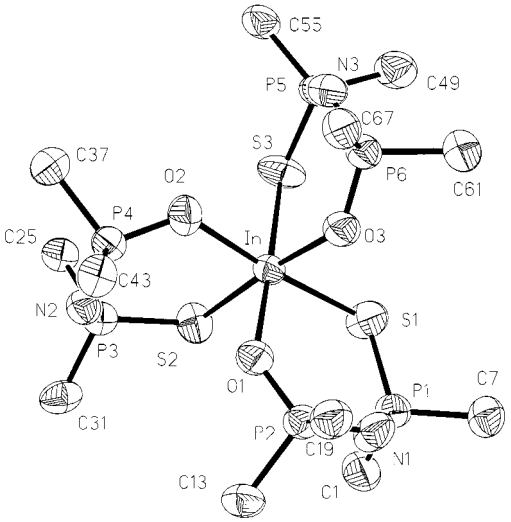


Figure 1. ORTEP view of $[In\{Ph_2P(O)NP(S)Ph_2\text{-}O,S\}_3]\cdot 3/4\ C_6H_6$; **2**; phenyl groups are omitted for clarity; selected bond lengths [Å] and angles [°]: In−O(1) 2.121(4), In−O(2) 2.144(4), In−O(3) 2.125(4), In−S(1) 2.591(1), In−S(2) 2.611(1), In−S(3) 2.595(1), S(1)−P(1) 2.009(3), S(2)−P(3) 2.010(3), S(3)−P(5) 2.021(2), O(1)−P(2) 1.505(5), O(2)−P(4) 1.533(5), O(3)−P(6) 1.507(5), P(1)−N(1) 1.566(6), P(2)−N(1) 1.594(6), P(3)−N(2) 1.582(5), P(4)−N(2) 1.587(5), P(5)−N(3) 1.578(6), P(6)−N(3) 1.592(6); O(1)−In−O(2) 87.8(1), O(1)−In−O(3) 85.4(1), O(1)−In−S(1) 97.2(1), O(1)−In−S(2) 92.1(1), O(1)−In−S(3) 178.3(1), O(2)−In−S(1) 174.6(1), O(2)−In−S(2) 95.9(1), O(2)−In−S(3) 91.1(1), O(3)−In−O(2) 87.8(1), O(3)−In−S(1) 91.0(1), O(3)−In−S(2) 175.4(1), O(3)−In−S(3) 95.9(1), S(1)−In−S(3) 83.73(7), S(1)−In−S(2) 85.45(7), S(3)−In−S(2) 86.60(6), In−S(1)−P(1) 106.42(9), In−S(2)−P(3) 104.61(9), In−S(3)−P(5) 105.69(9), In−O(1)−P(2) 134.3(3), In−O(2)−P(4) 127.7(3), In−O(3)−P(6) 132.1(3), P(1)−N(1)−P(2) 133.6(4), P(3)−N(2)−P(4) 128.8(3), P(5)−N(2)−P(6) 128.8(4), N(1)−P(1)−S(1) 119.7(2), N(2)−P(3)−S(2) 118.5(2), N(3)−P(5)−S(3) 119.7(2), N(1)−P(2)−O(1) 117.9(3), N(2)−P(4)−O(2) 118.1(3), N(3)−P(6)−O(3) 118.2(3)

In **2**, the coordination geometry at indium is similar to that observed in the three analogous compounds incorporating the corresponding symmetrical ligands, $[In\{Ph_2P(X)NP(X')Ph_2\text{-}X,X'\}_3]$ [X = X′ = O (**4**), S (**5**), Se (**6**)].[4b−4d] The indium atom is bonded to three ligands through the sulfur and oxygen atoms, leading to a very distorted octahedron. This may be largely attributed to the asymmetry of the ligand. The molecule corresponds to the facial isomer. The In−X bond lengths [av. In−O 2.13(4), In−S 2.599(2) Å] agree well with the values found for the corresponding bonds in **4** [av. In−O 2.127(9) Å] and **5** [av. In−S 2.63(3) Å],[4a] as well as those found in previous structure determinations.[8−10] The O−In−S bite angles [av. 96.3(2)°] are larger than the corresponding O−In−O [**4**: av. 89.5(7)°] and S−In−S [**5**: av. 91.9(16)°] bite angles observed in the two analogous compounds. The inter-ligand angles fall in the range 83.73(7)° to 92.1(1)°.

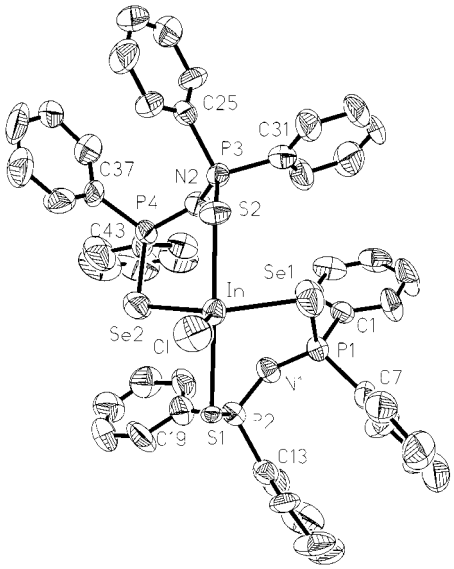


Figure 2. ORTEP view of $[InCl\{Ph_2P(Se)NP(S)Ph_2\text{-}Se,S\}_2]$, **3**; selected bond lengths [Å] and angles [°]: In−Cl 2.422(3), In−Se(1) 2.570(2), In−Se(2) 2.583(2), In−S(1) 2.693(3), In−S(2) 2.642(3), Se(1)−P(1) 2.160(4), Se(2)−P(4) 2.184(4), S(1)−P(2) 2.088(4), S(2)−P(3) 2.048(4), P(1)−N(1) 1.582(10), P(2)−N(1) 1.591(10), P(3)−N(2) 1.597(9), P(4)−N(2) 1.603(10); Cl−In−Se(1) 115.5(1), Cl−In−Se(2) 114.4(1), Cl−In−S(1) 84.0(1), Cl−In−S(2) 84.6(1), Se(1)−In−Se(2) 129.98(7), S(1)−In−S(2) 168.53(8), Se(1)−In−S(2) 85.55(9), Se(2)−In−S(2) 98.37(9), Se(1)−In−S(1) 97.76(7), Se(2)−In−S(1) 87.96(7), In−Se(1)−P(1) 101.8(1), In−Se(2)−P(4) 102.4(1), In−S(1)−P(2) 99.1(1), In−S(2)−P(3) 103.7(1), P(1)−N(1)−P(2) 130.9(6), P(3)−N(2)−P(4) 127.7(6), N(1)−P(1)−Se(1) 116.2(4), N(1)−P(2)−S(1) 115.8(4), N(2)−P(4)−Se(2) 118.0(4), N(2)−P(3)−S(2) 117.4(4)

The pentacoordinate geometry found in $[InCl\{Ph_2P(S)NP(Se)Ph_2\text{-}S,Se\}_2]$ (**3**) was completely unexpected since all of the previously studied indium(III) complexes with the analogous $[R_2(X)PNHP(X')R_2]^-$ ligands are tris-chelates.[4b−4d] This structure is also interesting in view of the fact that many of the known pentacoordinate indium structures result from intermolecular associations[9] and only a few examples correspond to discrete pentacoordinate molecules.[10] In complex **3**, only two of the ligands are attached to the indium atom through the sulfur and selenium atoms. The resulting arrangement can be described as a very distorted trigonal bipyramid (TP), where Se(1), Se(2), and a chlorine atom are equatorially positioned, while S(1) and

S(2) are axially positioned. The diaxial angle is 168.53(8)°, while the average equatorial angle is 119.9(10)°. Four of the remaining In−donor atom angles are less than 90°. The S−In−Se bite angles [98.37(9)° and 97.76(7)°] are larger than the corresponding S−In−S [**5**: av. 91.9(16)°] and Se−In−Se [**6**: av. 96.9(9)°] bite angles in the octahedral compounds with the symmetrical ligands.[4c−e]

The axial In−S bond lengths resemble those found in the analogous sulfur tris-chelate [av. **5**: 2.63(3) Å],[4b] while the In−Se distances [In−S 2.583(2) and 2.570(2) Å] are shorter than the corresponding bonds in the analogous selenium tris-chelate [**6**: av. 2.75(3) Å].[4d] These In−Se lengths are closer to those measured for the less crowded [In{Se(2,4,6-*t*-$Bu_3C_6H_2$)}$_3$] derivative.[8b] The In−Cl bond length [2.422(3) Å] is similar to the equatorial In−Cl distance in the pentacoordinate [$(n$-$C_4H_9)_4N]_2$[InCl{$S_2C_2(CN)_2$}$_2$], 2.418(2) Å,[10a] and the axial In−Cl length in [$Et_4N]_2$[$InCl_5$], 2.415(2) Å.[10b] The average In−Cl equatorial bond length in the trigonal-bipyramidal adduct $InCl_3$·$2PPh_3$ is 2.383(5) ± 0.05 Å.[10d]

In both compounds **2** and **3**, the resulting $InSXP_2N$ (X = O, Se) chelate rings may be considered as having a very distorted boat conformation with the indium and nitrogen atoms at the apices. A similar arrangement was found for asymmetric $PbOSP_2N$ rings[6b] as well as for the symmetric InO_2P_2N rings in **4**, which also exhibit a boat conformation.[4c] The symmetric InS_2P_2N chelate rings adopt a twisted boat conformation (**5**).[4b] In contrast, the $InSe_2P_2N$ ring in **6** displays both conformations (boat and twisted boat), but with the selenium and phosphorus atoms at the apices.[4d] Average P−S [**2**: 2.013(4); **3**: 2.068(4) Å], P−O [**2**: 1.515(5); **3**: 2.172(4) (X = Se) Å], and P−N [**2**: 1.582(6); **3**: 1.586(10) Å] bond lengths are consistent with a delocalized π-bond structure involving the five ligand atoms of the chelate ring, as has been noted for cyclic phosphazene.[11]

The packing in the crystal structures is largely determined by van der Waal′s forces. There are no particularly short intermolecular contacts.

Experimental Section

Chemicals of commercial grade were purchased from Aldrich and were used as supplied. Solvents were distilled prior to use. The asymmetric [R_2(X)PNHP(X′)R_2] ligands **1d** [12] and **1f**[5] were prepared by published methods. They were converted to the corresponding potassium salts by treatment with KO*t*Bu according to a previously described procedure.[13] The ^{1}H- and ^{31}P{^{1}H}-NMR spectra were obtained at room temperature in $CDCl_3$ on a Varian Unity spectrometer operating at 299.94 MHz and 121 MHz, respectively [external references: $Si(CH_3)_4$ and 85% H_3PO_4]. FAB^+ MS (3-nitrobenzyl alcohol matrix) were measured on a Jeol JMS-SX102A instrument. The IR spectrum of **2** (KBr pellet) was recorded on a Nicolet FT-IR Magna 750 spectrometer, while that of **3** (Nujol) was recorded on a Bruker IFS28 spectrometer. Elemental analyses of **2** and **3** were performed with a Galbraith Laboratories (Knoxville, TN) analyzer and a Fison′s Instruments (Italy) EA 1108 apparatus, respectively.

[In{$Ph_2P(O)NP(S)Ph_2$-*O,S*}$_3$] (2): A solution of $InCl_3$ (0.032 g, 0.15 mmol) in water (5 mL) was added to a solution of K[$Ph_2P(S)NP(O)Ph_2$] (0.207 g, 0.44 mmol) in methanol (3 mL). The white solid formed was filtered off, washed with water, and dried in vacuo. Yield: 0.13 g (61%); m.p. > 320°C. − ^{31}P NMR ($CDCl_3$): δ = 33.6 (s), 23.3 (s). − IR (KBr): 1230 cm^{-1} vs [ν(PN)]

Table 1. Crystallographic and structure solution data for **2**·3/4C_6H_6 and **3**

	2·3/4 C_6H_6	**3**
Formula	$C_{72}H_{60}InN_3O_3P_6S_3$·3/4 C_6H_6	$C_{48}H_{40}ClInN_2P_4S_2Se_2$
Formula mass	1470.75	1141.01
Cryst. size [mm]	0.59 × 0.34 × 0.23	0.34 × 0.24 × 0.14
Diffractometer	Siemens P4 PC	Siemens P4 PC
Radiation	Mo-K_α (λ = 0.71073 Å)	Mo-K_α (λ = 0.71073 Å)
Temperature	293(2) K	293(2) K
Crystal system	Triclinic	Monoclinic
Space group	*P*1bar	*Cc*
a [Å]	11.62(2)	20.214(3)
b [Å]	15.47(2)	12.637(2)
c [Å]	22.341(2)	21.162(2)
α [°]	102.97(1)	90.0
β [°]	100.37(1)	115.12(1)
γ [°]	92.77(1)	90.0
V [Å^3]	3836.8(8)	4894.4(12)
Z	2	4
ρ_{calcd} [mg/cm^3]	1.265	1.548
F(000)	1501	1780
μ [mm^{-1}]	0.561	2.272
θ range [°]	1.36 to 25.00	1.96 to 30.00
Reflections collected	15662	13079
Independent reflections	13423 (R_{int} = 0.0502)	7321 (R_{int} = 0.00)
Parameters refined	852	539
R (F_o)	0.0642	0.0585
R_w (F_o)	0.1638	0.1282
Largest diff. peak/hole	1.205/−0.896 eÅ^{-3}	1.331/−0.521 eÅ^{-3}
Goodness-of-fit	1.042	0.80

+ 1176 s [ν(PN)/δ(CH)], 1125 s [ν(PO)], 740 m [γ(CH), Ph], 530 vs [γ(PNP)], 560 m [ν(PS)]. − MS (FAB$^+$) ($CHCl_3$): *m/z*: 1411 [M^+], 1334 [$O_3S_3P_6Ph_{11}N_3{}^{115}In^+$], 979 [$S_2O_2(PPh_2)_4N_2{}^{115}In^+$], 903 [$S_2O_2P_4Ph_7N_2{}^{115}In^+$], 546 [$SO(PPh_2)_2N^{115}In^+$], 514 [$O(PPh_2)_2N^{115}In^+$], 416 [$S(PPh_2)_2N^+$], 400 [$OP_2Ph_4N^+$]. − $C_{72}H_{60}InN_3P_6O_3S_3$ (1412.1): calcd. C 61.24, H 4.28, N 2.98; found C 61.10, H 4.14, N 2.87.

[InCl{$Ph_2P(Se)NP(S)Ph_2$-*Se,S*}$_2$] (3): The synthetic procedure was very similar to that used for **2**, starting from $InCl_3$ (0.044 g, 0.2 mmol) and K[$Ph_2P(Se)NP(S)Ph_2$] (0.32 g, 0.6 mmol). Yield: 0.17 g (77%); m.p. 198 °C. − ^{31}P NMR ($CDCl_3$): δ = 40.53 [s, P(s)], 28.24 [s, ^1J(PSe) = 738 Hz, P(Se)]. − IR (Nujol): 1198 cm^{-1} vs [ν(PN)] + 1174 s [ν(PN)/δ(CH)], 744 m [γ(CH), Ph], 529 vs [γ(PNP)/ν(PSe)], 582 m [γ(PNP)/ν(PS)]. − MS (FAB$^+$) ($CHCl_3$): *m/z*: 1107 [{^{80}SeS$(PPh_2)_2N$}$2^{115}In^+$], 611 [$^{80}SeS(PPh_2)N^{115}In^+$], 496 [$^{80}SeS(PPh_2)_2N^+$], 464 [$^{80}Se(PPh_2)_2N^+$], 416 [$S(PPh_2)_2N^+$], 384 [$(PPh_2)_2N^+$]. − $C_{48}H_{40}ClInN_2P_4S_2Se_2$ (1141.01): calcd. C 50.52, H 3.53, N 2.45, S 5.62; found C 50.41, H 3.39, N 2.35, S 5.15.

X-ray Diffraction Studies: Crystals suitable for X-ray analysis were obtained by slow diffusion of *n*-hexane into benzene (**2**) or chloroform (**3**) solutions of the corresponding compound. Details of the data collections and refinements are summarized in Table 1. The structures were solved by direct methods and refined by full-matrix least-squares calculations using the program system SHELXL-97.[14] Non-hydrogen atoms were refined anisotropically, while H atoms were refined using a riding model (U = 0.06). The Flack parameter for **3** was η = 0.003(19).[15] A semiempirical (ψ scan) absorption correction was applied for **3** (0.92957/0.62808). The crystal structure data (excluding structure factors) have been deposited with the Cambridge Crystallographic Data Centre as supplementary publication nos. CCDC-113996 (**2**) and CCDC-113995 (**3**). Copies of the data can be obtained free of charge on application to CCDC, 12 Union Road, Cambridge CB2 1EZ, U.K. [Fax: (internat.) + 44-1223/336-033; E-mail: deposit@ccdc.cam.ac.uk].

Acknowledgments

This work was supported by CONACYT project grant 0109P-E. We thank R. Gaviño Ramírez and L. Velasco-Ibarra for their work in recording NMR and mass spectra, respectively.

[1] I. Haiduc, I. Silaghi-Dimitrescu, *Coord. Chem. Rev.* **1986**, *74*, 127−270.
[2] A. M. Z. Slawin, M. B. Smith, J. D. Woollins, *J. Chem. Soc., Dalton Trans.* **1996**, 3659.
[3] [3a] O. Novrátil, E. Herrmann, G. Grossmann, J. Teply, *Collect. Czech. Chem. Commun*. **1990**, *55*, 364. − [3b] T. H. Le Quyen, S. Umetani, M. Matsui, *J. Chem. Soc., Dalton Trans.* **1997**, 3835.
[4] See, for example: [4a] R. O. Day, R. R. Holmes, A. Schmidpeter, K. Stoll, L. Howe, *Chem. Ber.* **1991**, *124*, 2443. − [4b] R. Cea-Olivares, R. A. Toscano, G. Carreón, J. Valdés-Martínez, *Monatsh. Chem.* **1992**, *123*, 391. − [4c] V. García-Montalvo, R. Cea-Olivares, D. J. Williams, G. Espinosa-Pérez, *Inorg. Chem*. **1996**, *35*, 3948. − [4d] V. García-Montalvo, R. Cea-Olivares, J. Novosad, J. D. Woollins, R. A. Toscano, G. Espinosa-Pérez, *Chem. Ber*. **1996**, *129*, 919. − [4e] V. García-Montalvo, R. Cea-Olivares, J. Novosad, J. D. Woollins, A. M. Z. Slawin, P. Kilian, M. López-Cardoso, P. García y García, G. Espinosa-Pérez,, *J. Chem. Soc., Dalton Trans.* **1997**, 1025, and references cited therein.
[5] P. Bhattacharyya, A. M. Z. Slawin, M. B. Smith, *J. Chem. Soc., Dalton Trans.* **1998**, 2467.
[6] [6a] O. Siiman, J. Vetuskey, *Inorg. Chem.* **1980**, *19*, 1672. − [6b] V. García-Montalvo, R. Cea-Olivares, G. Espinosa-Pérez, *Polyhedron* **1996**, *15*, 829. − [6c] R. Rösler, J. E. Drake, C. Silvestru, J. Yang, I. Haiduc, *J. Chem. Soc., Dalton Trans.* **1996**, 391. − [6d] P. Z. Zák, M. Fofana, J. Kamenícek, T. Glowiak, *Acta Crystallogr., Sect. C* **1989**, *45*, 1686. − [6e] A. M. Z. Slawin, M. B. Smith, J. D. Woollins, *Polyhedron* **1998**, *17*, 4465.
[7] J. Ellermann, J. Sutter, F. A. Knoch, M. Moll, *Chem. Ber*. **1994**, *127*, 1015.
[8] See, for example: [8a] J. P. Oliver, *J. Organomet. Chem.* **1995**, *500*, 269. − [8b] K. Ruhlandt-Senge, P. P. Power, *Inorg. Chem*. **1993**, *32*, 3478 and references cited therein.
[9] See, for example: [9a] H. M. M. Shearer, J. Twis, K. Wade, *J. Organomet. Chem.* **1980**, *184*, 309. − [9b] K. Mertz, W. Schwartz, F. Zettler, H. D. Hausen, *Z. Naturforsch.* **1975**, *30b*, 159 and references cited therein.
[10] See, for example: [10a] R. O. Day, R. R. Holmes, *Inorg. Chem*. **1982**, *21*, 2379. − [10b] D. S. Brown, F. W. B. Einstein, D. G. Tuck, *Inorg. Chem*. **1969**, *8*, 14. − [10c] M. V. Veidis, G. Palenik, *J. Chem. Soc. D* **1969**, 586. − [10d] S. Dhingra, M. G. Kanatzidis, *Polyhedron* **1991**, *10*, 1069. − [10e] M. Tschinkl, A. Schier, J. Riede, F. P. Gabbai, *Inorg. Chem*. **1998**, *37*, 5097. − [10f] S. Suh, D. M. Hoffman, *Inorg. Chem*. **1998**, *37*, 5823.
[11] R. Allcock, *Phosphorus−Nitrogen Compounds*, Academic Press, New York, **1972**, chapter 3.
[12] A. Schmidpeter, H. Groeger, *Chem. Ber.* **1967**, *100*, 3979.
[13] A. Schmidpeter, H. Groeger, *Z. Anorg. Allg. Chem*. **1966**, *345*, 106.
[14] G. M. Sheldrick *SHELXL-97 − A Program for Crystal Structure Refinement*, Inst. Anorg. Chem., Univ. Göttingen, Germany, **1997**.
[15] H. D. Flack, *Acta Crystallogr.* **1983**, *A39*, 876.

Received February 8, 1999
[I99043]

A Universal Two-Parameter Kratzer-Potential and Its Superiority over Morse's for Calculating and Scaling First-Order Spectroscopic Constants of 300 Diatomic Bonds

Guido Van Hooydonk*[a]

Keywords: Calculations / Bond theory / Electronic structure / Molecular dynamics / Kratzer / Morse / Potential energy curve

After decades of intensive research, the question remains whether or not a universal two- or three-parameter potential exists. For a large number of about 300 bonds, we now critically review the constraints for potentials and asymptotes, involved in three available scaling processes (Varshni, Calder–Ruedenberg, and Graves–Parr). We show that the covalent Sutherland parameter can never be a universal scaling factor. This implies that the usual constraint $U(R) = -D_e$ at $R = \infty$ for potentials is only desirable and that the natural asymptote D_e is not even needed to explain the relations between the constants. We show that ionic potentials of generalized Kratzer-type (Varshni's V^{th} potential) and their ionic Coulomb-like asymptotes Ae^2/R_e (with A close to 1) behave as simple universal two-parameter potentials. For both α_e and $\omega_e x_e$, this potential gives percentage deviations 2 to 3 times smaller than Morse's three parameter potential for hundreds of bonds. We also prove that the Graves–Parr scaling hypothesis is valid, despite these authors' own conclusion. We discuss various new relations between spectroscopic constants.

1. Introduction

Finding a universal two- or three-parameter potential still has considerable theoretical interest not only for molecular spectroscopy and for the theory of the chemical bond but also for a number of practical chemical processes such as metallic adhesion, cohesion and chemisorption, where similar potentials appear.[1]

For decades, considerable efforts were made on scaling potentials and/or spectroscopic constants.[1–15] This ever-continuing search for what Tellinghuisen[10] once called the *Holy Grail of Spectroscopy* remains justified since the spectroscopic constants of a large number of diatomic bonds exhibit an extremely simple, intriguing behavior, not yet accounted for theoretically. Various opinions persist whether or not a universal low parameter function really exists and the matter is certainly not yet solved.[9] Experience shows that even a three-parameter potential cannot be of universal character,[2][3] a thesis we will now reconsider.

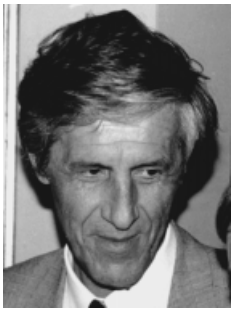
In this review, we use a method devoid of two of the common problems in this kind of research, e.g. finding representative sets for

(a) *molecules (and constants)*: the set used here is beyond doubt representative and also large enough, as we collected all readily available spectroscopic data for about 400 bonds and for

(b) *potentials*: here we confront two completely different low-parameter reduced potentials: a reputed covalent one and a less known ionic one. Both stand for a series of related potentials in their category.

[a] Ghent University, Department of Library Sciences, and Department of Physical and Inorganic Chemistry,
Rozier 9, B-9000 Ghent, Belgium
E-mail: guido.vanhooydonk@rug.ac.be

Supporting information for this article is available on the WWW under http://www.wiley-vch.de/home/eurjoc or from the author.



The author (born 1944) obtained his Ph.D. in 1971 at the University of Ghent (chemistry). He then moved to the University Library, built in 1935 by the famous Bauhaus co-founder, designer and architect Henry Van de Velde. – In 1990 he became professor and chief librarian. He implemented an integrated library system, one of the first in Europe to focus on a dynamic integration of bibliographic sources with the on-line catalog (http://www.lib.rug.ac.be). He published books and articles on different aspects of the library and on a derivative of library sciences, bibliometrics. – Since 1971, he published about 40 articles on many aspects of the theory of the chemical bond, still his main research interest. Numerous spectroscopic data are used to confront bonding theories with experiment. Recent experimental work is on the analysis of pigments in medieval manuscripts by TXRF- and micro-Raman spectrometry. Prof. Van Hooydonk is a referee for many journals and a member of national and international societies in exact and in library sciences.

MICROREVIEWS: This feature introduces the readers to the authors' research through a concise overview of the selected topic. Reference to important work from others in the field is included.

 © WILEY-VCH Verlag GmbH, D-69451 Weinheim, 1999 1434–1948/99/1010–1617 $ 17.50+.50/0

2. Overview of Scaling Spectroscopic Constants and Potentials: Aim of This Work

The most essential (zeroth order) information about chemical bonding is contained in only *three constants*: the dissociation energy D_e (the natural asymptote), the bond length R_e and the force constant k_e. These determine an important *species-dependent* scale factor, the dimensionless Sutherland[11] parameter Δ, defined as

$$\Delta = 1/2\ k_e R_e^2/D_e = a_0/D_e \quad (1)$$

Herein a_0, the first coefficient in the Dunham expansion[12] near the minimum and representing the asymptote in the harmonic oscillator presentation, is scaled by D_e, the atomic dissociation limit or the natural asymptote. By definition, a_0 is determined by the two *zero*th order spectroscopic constants (see below). D_e can be determined experimentally in various ways.

For the two *first order spectroscopic constants*, Varshni[3] introduced two dimensionless parameters F and G also related to the next coefficients a_1 and a_2 in the Dunham expansion. Both F and G derive from the potential and are numerical functions of Δ. From these two theoretical relations $F(\Delta)$ and $G(\Delta)$, a theoretical $G(F)$ relation follows. The experimental $G(F)$ plot is, in general, roughly in line with the theoretical expectations for empirical potentials.[6] Many inconsistencies, almost like a "spectroscopic gap" between different kinds of bonds,[6] are found both in $F(\Delta)$- and $G(\Delta)$ plots, *meaning that something fundamental must be wrong with the Sutherland parameter as a scaling aid in molecular spectroscopy.*[3][6]

Although 30 years after Varhsni's standard analysis[3] of 23 bonds, Graves and Parr[2] analyzed 150 bonds and argued that the square root of the Sutherland parameter is the better species-dependent scale factor, this new scaling operation did not fit the experimental data any better.[10] Both the Varshni and the Graves and Parr analyses are essentially similar and lead to the same conclusions. Scaling by the Sutherland parameter (Δ or even $\Delta^{1/2}$) is not effective, which is correct. Their next conclusion that, therefore, a universal three-parameter potential cannot exist, is probably not correct, as we intend to demonstrate in this study and did so already some time ago on a smaller scale.[6][7]

Later, Jhung and co-workers[9] proved theoretically that a universal three-parameter function exists, but, unfortunately enough, they were unable to identify its analytical form. The best candidate, to their opinion, would be the Morse potential.[13] However, this popular (overworked[3]) potential is known to be bad for ionic bonds, a class of molecules not studied by Jhung.[9] Smith et al.[14] suggested to include an ionic term in the potential, a procedure that gave good results.

Graves and Parr in their analysis of the scaling problem[2] concluded that a three-parameter potential must always make some compromise on D_e, R_e, or k_e. This seems like an invitation to question the universal character of Δ, where these three constants are united, see Equation (1). Looking for such a compromise is one of the challenges of this work. In fact, we suggested some time ago,[6] even before Graves and Parr, that an alternative Sutherland parameter should be used and that a universal potential might be of ionic type, an hypothesis to be reviewed now in the context of scaling on a much larger set of bonds.

This thesis is in line with the alternative scaling (Sutherland-like) parameter t, introduced for ionic bonds by Varshni and Shukla[4] many years ago and used by Van Hooydonk[6] as a universal scaling parameter for both ionic and non-ionic bonds. Ionic potentials[4] use an asymptote D_x, different from D_e, leading to an alternative Sutherland parameter a_0/D_x. This shift in asymptotes seems a solution for the compromise, suggested by Graves and Parr.[2]

Recently, and in line with our earlier work,[6] also Von Szentpaly[15] suggested another alternative asymptote D_x: the valence state energies of the atoms, which refers to a rather classical Atoms In Molecules (AIM) approach. This asymptote consists of two separated atoms, frozen in the same valence state they have at the equilibrium distance. In this terminology, an ionic approach is an IIM (Ions In Molecules) method, which freezes ions instead of atoms. Both our results with the IIM method[6] and Von Szentpaly's with AIM method[15] remove several problems with $F(\Delta)$- and $G(\Delta)$ plots, due to the use of the covalent Sutherland parameter.

Very recently and partly because of these latter two approaches, Freeman, March, and Von Szentpaly[16] argued that an empirical power relation between G and F would be evidence for chaotic/fractal behavior in anharmonicities. As one can never underestimate the impact of (inverse-) power-laws, such as Coulomb's, in chemistry and physics, this problem is now reviewed also.

We now collected constants of 400 diatomic (*inorganic*) molecules, with bonds between zero-, mono-, and polyvalent atoms, of molecular ions, of isotopomers, and of excited states. Scaling based upon alternative asymptotes and simple potentials is critically examined by three related scaling methods available in the literature (Varhsni,[3] Graves−Parr,[2] and Calder−Ruedenberg[5]).

Except for the data collection (section 3), the paper is divided in 4 main sections: (4) theoretical constraints for potentials; (5) extensions and consequences of earlier results on scaling properties of the covalent Sutherland parameter; (6) the search for a universal two-parameter function: theoretical requirements and (7) the search for a universal two-parameter function: testing the theoretical results with the constants.

3. Data Collection

Data for 402 bonds are taken from Huber and Herzberg[17] and Radzig and Smirnov,[18] without checking for accuracy. Different mass units are used (C = 12 in the first and a.m.u. in the second). For 21 bonds, first order constants are not simultaneously available. For 76 bonds, D_e is not available, which leaves about 300 bonds for a one-by-

one comparison between covalent and other scaling approaches.

4. Theoretical Constraints for Potentials

4.1 Universality of Potentials

Two methods can be used to decide whether or not a function is universal: (a) PECs, potential energy curves (RKR method) fall within ± 5%, of the function and/or (b) calculated spectroscopic constants fall ± 5%, of the experimental values. In either case, the number of a variety of bonds must be large. Method (a) can be used in combination with (b). However, since the number of bonds in this study is very large, we can only use method (b). A perfect result for (b) does not warrant the same result for (a) in the complete range $0 \leq R \leq \infty$ (Steele et al.[8]).

4.2 The Dunham Expanion

The Dunham expanion[12] around the minimum is:

$$U(\rho) = a_0\rho^2(1 + a_1\rho + a_2\rho^2 + ...) - D_e \quad (2a)$$

where a_n are constants and where the variable is

$$\rho = (R - R_e)/R_e \quad (2b)$$

The first term is the well-known harmonic oscillator equation and the first constant (the well depth or the Dunham asymptote) is given by [see also Equation (1)]:

$$a_0 = \omega_e^2/4\ B_e \quad (2c)$$

Since a_0 is solely determined by zeroth order spectroscopic constants, the Dunham asymptote is a *mathematical* asymptote. The next Dunham coefficients are related to the first-order constants: a_1 to α_e, the rotation-vibration constant, and a_2 to $\omega_e x_e$, the anharmonicity constant. Dividing all terms in (2a) by D_e shows why the covalent Sutherland parameter is an important scaling aid. Conversely, accounting for the higher Dunham coefficients is also a major test for the universal character of a potential.

4.3 Constraints for Potentials and Asymptotes

Although constraints for potentials can be divided in two classes: necessary and desirable (Varshni[3]), we will restrict ourselves here to some general constraints. As remarked by Von Szentpaly,[15] one global constraint is that an A/R^x-law is preferential for *attraction*

− A should allow for interacting charges: the concept of *valences* (as in the Calder−Ruedenberg Column classification,[5] also used by Graves and Parr[2]), for *charge-transfer* between partially charged atoms, as argued by Smith, Schlosser, Leaf, Ferrante, and Rose[14]

− $1/R^x$ should allow for the idea of forces *getting smaller with distance* (reflected in the Herschbach and Laurie Row classification[19])

(a) with $x = 1$, this is in line with *Coulomb's fundamental law*, and in the next instance, with ionic bonding (see Berzelius,[20] Kossel,[21] Van Hooydonk[6][7]), although also covalent bonding calls for a $1/R$-law (Borkman and Parr,[22] Sanderson[23])

(b) with $x \neq 1$, a number of other possibilities are open (Varshni[3]), among which the idea of (inverse) *power- laws* (see Freeman, March and Von Szentpaly[16]).

For *repulsion*, a large number of solutions are available (see Varshni[3] for a review).

More detailed constraints for potentials are not repeated here (see for instance Varhsni,[3] Calder and Ruedenberg,[5] Jenc[8]). Basic constraints for any potential $U(R)$ are

(i) $U(0) = \infty$ (or very large) *and* $U(\infty) = 0$

(ii) $U(R_e) = -D_e$

(iii) $U'(R_e) = 0$ and

(iv) $U''(R_e) = 4\pi^2\mu\omega_e^2 = k_e$ (the force constant or the curvature at the minimum), where μ is the reduced mass. The force constant and R_e determine the first coefficient in the Dunham expanion a_0, see Equation (1) and (2c). Replacing condition (ii) by $U(R_e) = -D_x$ instead of D_e does not alter any of the next mathematical steps required to arrive at Varhsni's parameters F and G. Scaling the higher derivatives $U'''(R_e)$, $U^{IV}(R_e)$, ... by the force constant $k_e = U''(R_e)$, leads the parameters X and Y, related to F and G and to the next coefficients in the Dunham expansion a_1 and a_2 and to the first order constants. At this stage, Sutherland's parameter comes in as a scaling factor, called so by Varshni[3] to honor Sutherland's work.

The question is whether constraint (ii) is either necessary or only desirable. We know of no simple (low parameter) analytical function that accounts for the atomic dissociation limit, whereas a large number of simple analytic potentials are available, leading to well defined but different asymptotes. Also Von Szentpaly[15] gave arguments for replacing the atomic dissociation limit as a scaling factor and retraced earlier arguments to do so (see also below). We will consider constraint (ii) as *desirable*, since exactly this condition expresses our *desires* and expectations about a perfect universal function. Modifying constraint (ii) is also a way of interpreting the empirical fact that, after decades of intensive research by numerous researchers all over the world, a really universal (low parameter) function has not yet been found.

All other constraints mentioned above *must remain valid* for a universal function (mainly for reasons of *internal* consistency). However, if *any* two or three-parameter function can be found that produces an asymptote D_x with a simple chemical meaning and which scales the Dunham coefficients efficiently, the question of scaling is probably solved. How to reach the atomic dissociation limit with that potential, would lead to a different, more transparent, situation.

The Dunham expansion itself does not require the atomic dissociation limit. It is limited to the situation around the equilibrium internuclear distance in the first place and to a consistent reproduction of the spectroscopic constants by

means of a relatively simple series expansion in terms of an harmonic oscillator model (see below).

5. Previous Results on the Scaling Properties of the Sutherland Parameter

5.1 The Zeroth Order Spectroscopic Constants (the Dunham Asymptote) and Scaling

Scaling has much to do with the relations between the constants determining a_0, as scaling is essentially a two-dimensional operation (Graves and Parr[2]).

The two zeroth order constants (the vibrational constant ω_e and the rotational constant B_e) are known to have a very intimate relationship, which made $1/R$ potentials so popular in the past, since $B_e = 1/(\mu R_e^2)^{1/2}$.

An ω_e (B_e) plot shows two basic characteristics: (a) a Row dependency (Herschbach–Laurie[19]) and (b) a Column dependency (Calder–Ruedenberg[5]).

Figure 1a on the Row dependency and Figure 1b on the Column dependency represent some of the results obtained from our data. The almost parallel lines combining molecules in the same Row have an intercept at the x-axis (B_e), whereas the parallel lines representing the Column classification have an intercept at the y-axis (ω_e). Taking two parallel lines in Figure 1b (Column dependency) together with two parallel lines in Figure 1a (Row dependency) would always result in a (scaled and oblique) replica of the Periodic Table. A similar scattering is observed when a plot (not shown) is made for the two first order constants: $\omega_e x_e$ (or x_e) and α_e. Figure 1c gives the normal (i.e. non-logarithmic) plot between the two zeroth order constants.

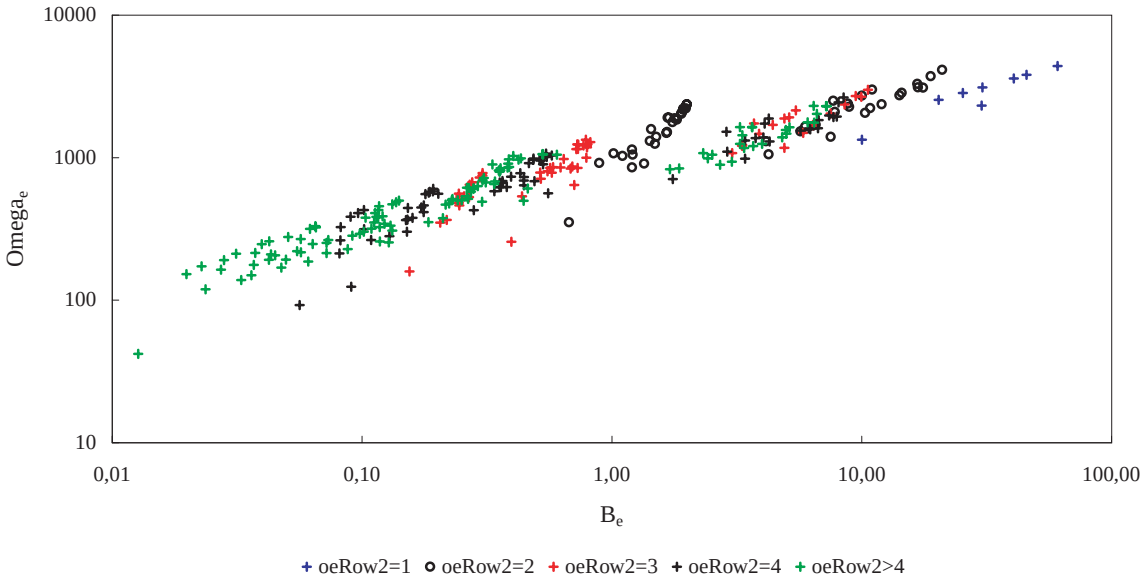


Figure 1a. Omega$_e$ versus B$_e$ for 300 bonds (Row-classification) (log-scale)

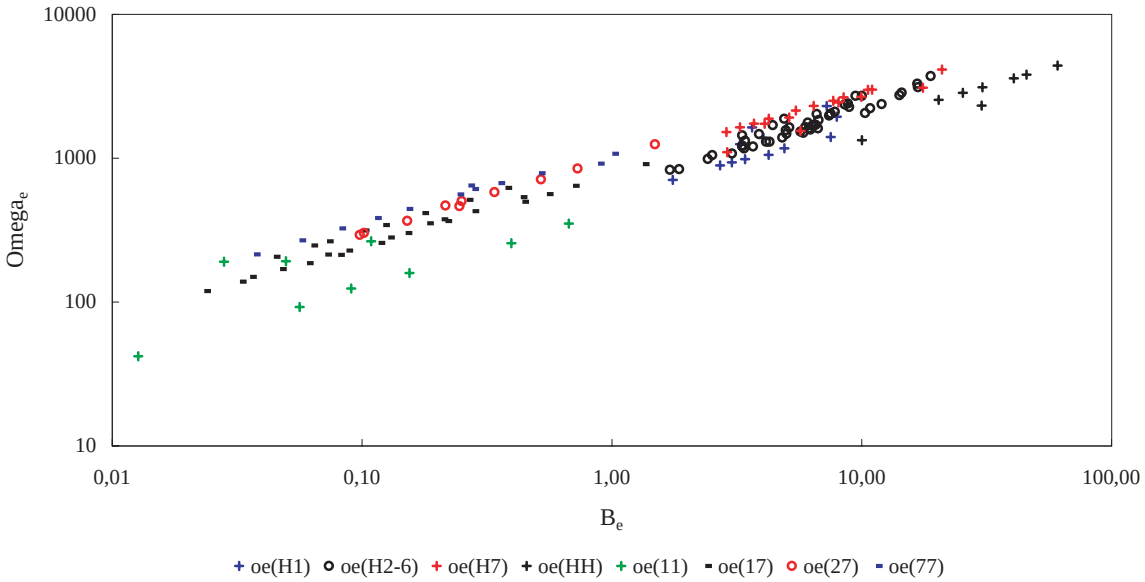


Figure 1b. Omega$_e$ versus B$_e$ for 300 bonds (Column-classification) (log-scale)

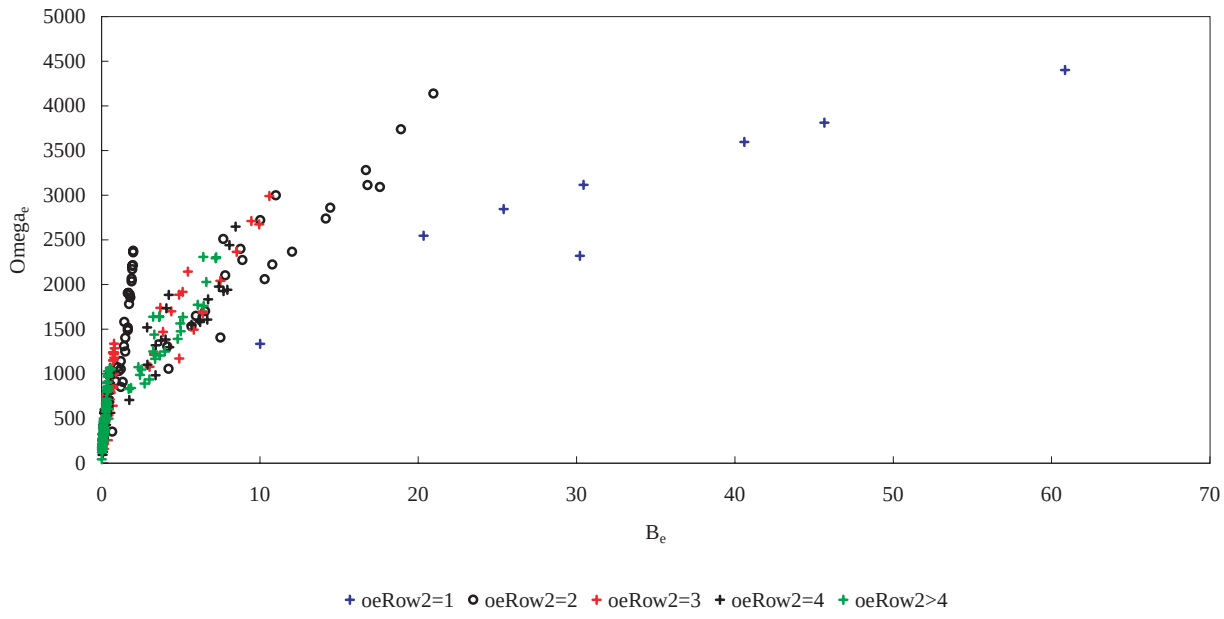


Figure 1c. Omega$_e$ versus B$_e$ (Row-classification) (normal scale)

Perfect scaling seems to consist in reducing these replicas of the two-dimensional table to a one-dimensional version. For *atomic spectroscopy*, this would not be a problem, since either the atomic number Z or the atom mass M can be used (both are rather simply related to one another). The H atom is the prototype in atomic bonding: its energy and its spectroscopic behavior are easily computed from first principles. But, if perfect scaling in *molecular spectroscopy* can be achieved, a similar solution must exist: using first principles, a universal potential will determine the energy and the spectroscopic behavior of a universal bond, which can then be considered as the equivalent of the H atom in atomic spectroscopy. To arrive at a situation analogous to that found in atomic spectroscopy, a scaling system must be found which brings the scattering in the data-points in Figure 1a−c down to almost a single smooth line.

Since the two zeroth order constants completely determine the Dunham asymptote, such a relation would be extremely valuable for scaling this asymptote. In second order, scaling a_0 has immediate consequences for the first order constants also, according to Varshni's analysis[3] and its Graves−Parr variant.[2] Despite the fact that a $1/R$ law seems to interfere with the two constants that determine a_0, scaling the Dunham asymptote is almost invariantly done by means of D_e, the atomic dissociation limit (the covalent Sutherland parameter).

5.2 Relations Between First-Order Constants (Varhsni Functions *F* and *G*) and Scaling by the Covalent Sutherland Parameter: Early Observations

In addition to a re-appraisal of the Sutherland parameter, Varshni[3] showed that two dimensionless parameters F and G relate to the first order spectroscopic constants:

$$F = \alpha_e\omega_e/6\ B_e^2 \quad (3)$$

$$G = \omega_e x_e \mu R_e^2/2.1078\cdot 10^{-10} \quad (4)$$

However, already 40 years ago, Varshni remarked that $F(\Delta)$- and $G(\Delta)$ plots for 23 bonds seemed to generate two sets of different molecules, for which he could hardly give an explanation.[3] Therefore, he *had* to conclude that a universal three-parameter potential probably could not exist. Varshni's early observation was later referred to as a *spectroscopic gap*[6] between different types of bonds as it leads to a conflict between the Morse potential and the covalent Sutherland parameter. In fact, we now made a plot (see Figure 2a) of the Varshni function F (related to a_1) against the square root of the covalent Δ for 91 bonds between monovalent atoms. The theoretical result[3] of a Morse potential is $F = \Delta^{1/2} - 1$ and is represented by a solid line in Figure 2a. If the Morse potential is the most likely candidate for being a universal function (Jhung et al.[9]) and if $\Delta^{1/2}$ is the best scaling factor (Graves and Parr[2]), something very elementary must be wrong: only 22 out of 91 data-points (25%) are on or close to the line theoretically predicted by the Morse potential.

To make things worse, a $G(\Delta)$ plot leads to the same situation (Varshni,[3] Van Hooydonk[6]). In this case,[3] the Morse potential predicts that $G = 8\Delta$. Figure 2b gives the corresponding plot for the same 91 bonds. We can only conclude again either (a) that the Morse potential can never reach the status of a universal potential or (b) that the covalent Sutherland parameter can never be a perfect universal scaling aid.

Strangely enough, most of these discrepancies disappear when G is plotted directly as a function of F, whereby the intermediary step involving the covalent Sutherland parameter Δ is avoided. This illustrates the intriguing relations,

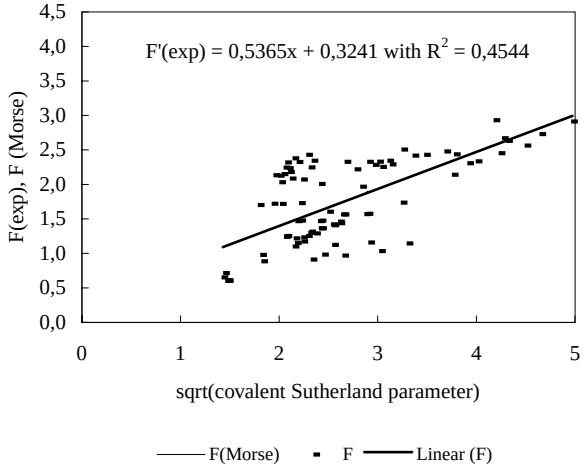


Figure 2a. F(exp) and F(Morse) versus sqrt(covalent Sutherland parameter) for 91 single bonded diatomics

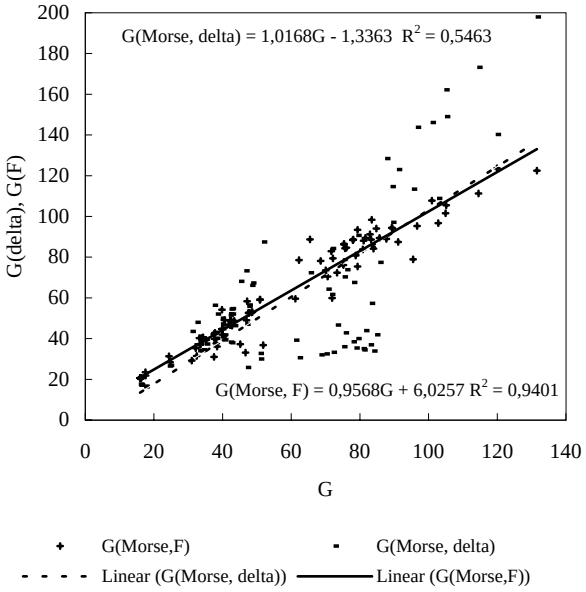


Figure 2b. G(Morse, delta) and G(Morse, F) versus G for 91 single bonded diatomics

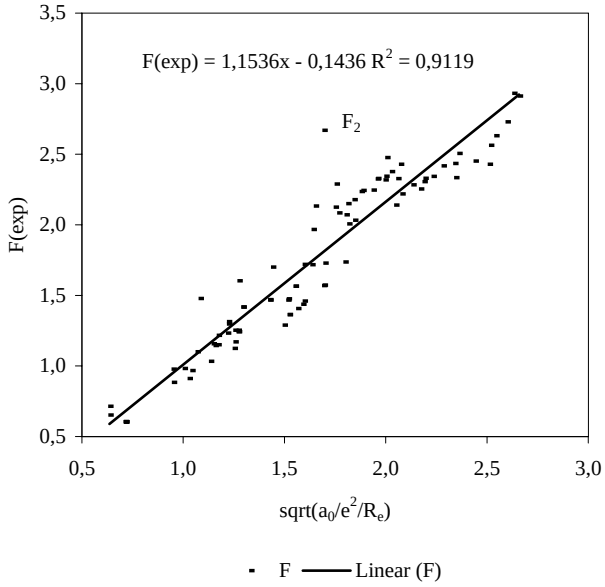


Figure 2c. F(exp) versus sqrt($a_0/e^2/R_e$) for 91 single bonded diatomics

that exist between the spectroscopic constants and shows that, in reality, there is no spectroscopic gap at all.[6]

This effect is also shown in Figure 2b by the data-group G(Morse F). If we use the prediction of the Morse potential that $\Delta = (1 + F)^2$ and calculate G from $G = 8(1+F)^2$, i.e. without the interference of Δ values, the Morse′s three-parameter potential almost behaves like a universal function (Jhung[9]).

Consequently, the covalent Sutherland parameter is not at all a good scaling factor. This answers our dissatisfaction with the last conclusion by Varshni[3] and Graves and Parr[2] that a universal *three*-parameter potential (like Morse′s) does not exist, if this conclusion is based on the fact that scaling with the covalent Sutherland parameter does not work.

We see that things go wrong as soon as an external parameter D_e, not simply related to the zeroth order constants, is introduced as a scaling parameter for a_0, which is completely and solely determined by these zeroth order constants. And although attempts were made to correlate D_e with some constants, such a correlation has no universal validity (probably on account of the very same reason: we refer to the linear Birge−Spooner extrapolation, discussed by Varshni,[3] which is ultimately also based upon the usefulness of a covalent Δ for scaling).

It appears that F and G would both be independent of D_e. The Morse potential is not a universal potential in the whole range of R values (0 to ∞) but appears to be a good approximation to a universal function around R_e. This is not a surprise, when one looks at the analytical form of and the variable in the Morse function: both are very similar to Dunham′s.

5.3 An Alternative Sutherland Parameter

Having to re-scale Δ, the most important species dependent scaling factor in molecular spectroscopy, may seem a drastic measure. We discuss the two asymptotes involved.

5.3.1 The Dunham Asymptote a_0

This mathematical asymptote is determined by the zeroth order constants alone. Hence, only mathematical re-scaling can be allowed. At least theoretically, re-scaling the Dunham asymptote is not that strange after all, since Dunham used the variable $(R - R_e)/R_e$ in his harmonic oscillator model.[12] For small deviations around the equilibrium distance, this variable refers to energies varying with R, which is not in line with observation on the molecular level and in physics and chemistry. The resulting well depth a_0 is difficult to understand in terms of a bonding model and it always leads to a completely wrong and too large a dissociation limit at $R = \infty$. This asymptote is not a natural atomic or molecular state but a mathematical artifact. It results from forcing Hooke′s law to apply to chemical bonding, in an attempt to recover mathematically all lower order spectroscopic constants in the harmonic oscillator

model. However, *this limitation of Dunham's asymptote is at the same time also its major advantage:* it provides us with a true, i.e. mathematical, reflection of the situation at the minimum, without any interference of external or higher order effects.

Now, the very similar variable $(R - R_e)/R$ would almost give the same oscillator behavior around R_e. In addition, this variable refers to an attractive energy varying with $1/R$, much more plausible in physical and chemical processes and the potential would not behave badly at $R = \infty$, as it will always converge to a finite limit (Van Hooydonk;[7] Simons, Parr, and Finlan[24]). This variable is well-known in physics and chemistry and was introduced by Kratzer,[25] more than 10 years before Dunham published his analysis.

The mathematical re-scaling for a_0 consists in a change of variable in Dunham's series. A change in the variable has a consequence for the asymptote, equal to

$D_x = D_{ion} = e^2/R_e$

corresponding with an (ionic) Coulomb energy between two point charges (attraction through a $1/R$-law) and with an ionic bonding model. Experiment shows that very often $D_e < D_x < a_0$, which is important for other reasons (see below). For 40 bonds, the performance of Kratzer potentials is good, even for higher order spectroscopic constants,[6][7] not under review now.

5.3.2 The Atomic Dissociation Limit D_e

Like constraint (ii), this limit seems untouchable, as it is experimentally and consistently reproduced in various ways. Yet, it is not closely bound to the low order constants as is a_0 at $R = R_e$.

Indeed, a number of effects can interfere between R_e and ∞ before the atomic dissociation limit is actually reached (see Varshni[3]). We give two examples. First, if the non-crossing rule interferes between the minimum and ∞, a fundamental change in the potential or in its parameters must have occurred. Consequently, the atomic dissociation limit D_e is then not a true reflection of the bonding situation at R_e (Varshni[3]). Second, if the atoms are *charged* at R_e, as in ionic bonds, a dissociation into *neutral* atoms is not a true reflection of the bonding state either. However, these two disturbing situations can never occur for the (artificial) Dunham-dissociation process, leading to a_0, which is, by definition, always and only, a true reflection of the bonding characteristics at R_e. If in some cases the atomic dissociation limit D_e is an n^{th} order asymptote, it has been subjected to effects, which are not included in the zeroth order potential describing the situation at the minimum. Then, we are in need of another alternative asymptote (and potential) that can be used to scale a_0 accordingly.

5.3.3 Constraints for an Alternative Sutherland Parameter

A possible solution would consist in leaving out the atomic dissociation limit as a scaling energy-level and a change of the variable in the Dunham potential, which entrains a different asymptote automatically (an ionic one in the case of the Kratzer variable).

The *necessary* constraints for an alternative asymptote D_x remain stringent: it should

− have a simple relation with zeroth order spectroscopic constants, very much like a_0

− derive from a two or three parameter universal potential

− have a simple chemical meaning (bonding model)

− reproduce correctly the first order spectroscopic constants (i.e. distinctively better than the results presented in Figure 2a and 2b using the Morse potential) and

− be situated between a_0 and D_e, in order that the non-crossing rule can interfere to obtain the correct dissociation limit D_e. $D_x - D_e$, would then determine the critical distance.

We realize that skipping condition (ii) opens the way for other potentials with possibly universal characteristics.[15] However, using a priori another dissociation limit to account for the observed PE curves, also a priori introduces an apparent error: this should constantly be kept in mind when comparing the performances of different potentials and asymptotes.

5.3.4 Scaling *F* and *G* by Ionic Sutherland Parameters

In principle, one could imagine various potentials with alternative asymptotes. We suggested that the ionic dissociation limit (and an ionic potential) is a good alternative,[6] as it is almost as good a *natural* dissociation limit as the atomic one and, it is usually situated between a_0 and D_e. The alternative (AIM-) asymptote of Von Szentpaly[15] seems to meet these constraints too, although his potential is not that transparent as an ionic one, it is not a reduced potential and the bonding model it relies upon is not that simple either (AIM-approach). A fairly good reason for choosing an ionic asymptote is that most of the aberrations showing in $F(\Delta)$- and $G(\Delta)$ plots, when a covalent Δ is used (see Figure 2a−b), disappear, *in agreement with experiment*, when the covalent bond energy is replaced by the ionic bond energy *for both ionic and non-ionic molecules.*[6][7] But, in general, two kinds of ionic asymptotes can be distinguished, depending on their D_e dependency.

5.3.4.1 Ionic Sutherland Parameter Depending on D_e

Only for dissociation in $A^+ + B^-$, a good approximation for the ionic Sutherland parameter is

$$\Delta_{ion} = 1/2\ k_e R_e^2/D_{ion} = a_0/D_{ion} \quad (5a)$$

where

$$D_{ion} = IE_B - EA_A + D_e \quad (5b)$$

in which IE_X is the ionization energy and EA_X the electron affinity. However, this is a poor approximation for the ionic

asymptote of bonds with intermediate polarity. In addition, it will always depend upon D_e (for a general D_{ion}, valid for all types of bonds, see below).

5.3.4.2 Ionic Sutherland Parameter not depending on D_e

For ionic molecules, with a spectroscopic behavior rationalized by ionic functions, Varhsni and Shukla[4] already suggested another scaling parameter t, defined as

$$t = 2 + k_e R_e^3/e^2 \quad (6)$$

independent of D_e and which relies upon an eigenvalue

$$D_x = e^2/R_e \quad (7a)$$

corresponding with a different ionic (Coulomb) Sutherland parameter

$$\Delta'_{ion} = 1/2\ k_e R_e^2/D'_{ion} = a_0/e^2/R_e \quad (7b)$$

This is the most natural ionic asymptote imaginable in chemistry (Coulomb attraction between two point charges) and it is exactly the asymptote generated by a Kratzer potential. This asymptote can, when generally valid, be extended to all types of bonds without exception (for which R_e is known) and can even be applied to bonds for which D_e is not known, which is the case for many of the 400 bonds, inventoried in the present study.

5.3.5 Results with Ionic Sutherland Parameters − Discussion

For 40 bonds, the constants of non-ionic (i.e. covalent or homonuclear) molecules can be brought in line with ionic bonds just using an ionic Sutherland parameter.[6] In addition, the RKR curves are correctly reproduced for different kinds of bonds.[6] Not only $F(\Delta_{ion})$ and $G(\Delta_{ion})$ plots but also $F(t)$ and $G(t)$ plots show very smooth relations, not too far away from the ones theoretically expected by ionic potentials.[6] Figure 2c illustrates these earlier findings on a larger scale for *91* single bonds, whereby experimental F values are plotted against the *square root* of the ionic Coulomb Sutherland parameter, simply related to the Varshni −Shukla parameter t:

$$\Delta'_{ion} = a_0/e^2/R_e = (1/2)k_e R_e^3/e^2 = t/2 - 1 \quad (8)$$

We cannot but conclude from Figure 2c, in which no *gap* appears at all, that our suggestion to change the variable in the Dunham expansion and to use the alternative asymptote generated for scaling turns out to be very satisfactory. The slope of the trend line is almost *unity*, the intercept is almost *zero* and most data-points are on or very close to the empirical fit. The goodness of fit is over *0.9*, including the data point for F_2, which is the most notable exception. This is also an exception in the Von Szentpaly scheme[15] and in many other instances.

In comparison with Figure 2a, Figure 2c represents a significant improvement, both practically and theoretically. We are now justified to elaborate the theoretical predictions of ionic potentials and to see whether or not they can be considered as universal (low parameter) potentials.

6. Universal Two-Parameter Functions: Theoretical Requirements

6.1 Ionic Potentials

Born,[26] Pauling,[27] and Mulliken[28] all had a special interest for ionic potentials, which remain an important part of the chemical heritage (see Varshni and Shukla′s review[4] for alkali-halides, dissociating nearly into ions, with $D_e \approx D_{ion}$). The choice of empirical ionic potentials is very large[4] and it is impossible to give a full overview here. However, since all ionic potentials are similar, we give two functions, bearing a direct relationship with Coulomb′s law.

6.1.1 The Born−Landé Potential[25]

$$U(R) = -e^2/R + B/R^n \quad (9)$$

is one of the oldest ionic potentials and it is a simplified version of the general Mecke[29]−Sutherland[11] function, used by Grüneisen[30] and Mie[31] in solid state physics. The potential was discussed by Varshni and Shukla.[4] Their results for F and G in function of Δ are given in Table 1 below. Its asymptote equals

$$D_x = e^2(1 - 1/n)/R_e \quad (10)$$

and is, in general, larger than D_e. Values for n are obtained using ionization energies, electron affinities and D_e, which is always needed. In general $n \approx 9$, but $n = 2$ is a special case.

6.1.2 The Kratzer[25]−Fues[32] Potential

With $n = 2$ in (9), a Kratzer-type potential is generated, of the general form

$$U(R) = -2Ae^2/R + B/R^2 \quad (11)$$

which is a very attractive potential[6,7,33,34]. This Coulomb function also generates a simple asymptote, comparable in magnitude with (10), and equal to

$$D_x = Ae^2/R_e \quad (12).$$

The Kratzer variable

$$\lambda = (R_e - R)/R \quad (13)$$

behaves almost exactly as the Dunham variable ρ around R_e (see above). With $A = 1$, this is even a *one parameter potential*.

In reduced form, the potential can be *forced* towards the atomic dissociation limit at infinite separation instead of to its natural asymptote (12), leading to

$$U(R) = D_e(1 - R_e/R)^2 \quad (14)$$

and then becomes a *two parameter potential*. Since we proposed the variable (13) to replace Dunham's ρ, an expansion of (14) in terms of ρ generates (ideal) ionic Dunham coefficients[7]:

$$a_n = (-1)^n (n + 1) \quad (15)$$

Even these simple values are of the correct order of magnitude in a number of cases. With a deviation of ± 25%, these *mathematical* coefficients are obeyed by about 1/5 of 381 bonds:

- for $-a_1 = 2 \pm 0.50$: 108 bonds
- for $a_2 = 3 \pm 0.75$: 76 bonds.

In his analysis of the Kratzer potential, Varshni[3] argued that this *two* parameter potential always gives $\Delta = 1$ (see Table 1), a value reserved exclusively for $D_x = a_0$. He remarked that this Δ value (= 1) did not occur in practice with a_0/D_e values and he had to reject the potential. In our set of over 300 bonds, we found 2.040 as the lowest value for the *covalent* Sutherland parameter (for T_2^+). Applying constraint (ii), Varhsni could not try a different asymptote, although for ionic asymptotes, the situation $\Delta_{ion} < 1$ also occurs. Instead, he introduced a generalization, expected to yield better results, when coupled to D_e (see next section).

Although they did not mention Kratzer's work, Simons, Parr, and Finlan[24] also attempted to remedy the convergence problem of the Dunham series, i.e. its wrong behavior at $R = \infty$, by using the Kratzer variable λ, leading to a function known as the SPF potential. Despite the advantages the SPF potential certainly has, we showed[7] a long time ago that this can never be an appropriate solution. In the SPF theory λ remains coupled with (if not to say forced to) the atomic dissociation energy, which is not its natural eigenvalue.

6.1.3 Generalized Kratzer Potentials

The Varshni-V potential[3]

$$U(R) = D_e[1 - (R_e/R)^m]^2 \quad (16)$$

is a straightforward generalization of the Kratzer potential (14), although the asymptote should be e^2/R_e, and not D_e. The corresponding *reduced* generalized function is

$$U(R)/D_e = [1 - (R_e/R)^m]^2 = (1 - r^{-m})^2 \quad (17)$$

with $R = rR_e$, r being a number, obeying $0 \le r \le \infty$. This potential was applied to a variety of bonds with satisfactory results, only after replacing D_e with D_{ion}.[6][7] This generalization leads to the F and G expressions, collected in Table 1, where the potential is denoted by *Kratzer I-Varshni V*. Reminding Figure 2c, the identity $F = m = \Delta^{1/2}$ is intriguing. We will test here

$$U(R) = Ae^2/R_e[1 - (R_e/R)^m]^2 \quad (18)$$

With $A = 1$, this is a *two parameter (R_e and m) ionic potential:* just two parameters, R_e and k_e, suffice to reach a first order solution for the spectroscopic constants. The third parameter, available for further fitting, is A in Equation (18), as the only practical further scaling element is the Coulomb interaction. Here, parameterization in terms of the Calder−Ruedenberg idea of a Column classification (ionicity, charge-effects, ...) can logically be considered (see Figure 1). Only if the results obtained with $A = 1$ are acceptable for bonds with one or two monovalent atoms, we can allow other A values (for instance for multiple bonds). In cases where $A \neq 1$, we deal with a *three*-parameter potential.

Other generalizations of the Kratzer potential are possible[7]: a ratio $(R_e + a)/(R + a)$ leads to

$$U(R) = D_x [1 - (R_e + a)/(R + a)]^2$$
$$= D_x (1 - R_e/R)^2 [1/(1 + a/R_e)]^2 \quad (19)$$

in which the original Kratzer potential is multiplied by the square of a normalizing or scaling factor $y = 1/(1 + a/R_e)$. Expanding this alternative generalized Kratzer function in ρ, we get $F = 2\Delta^{1/2} - 1$ (see Table 1) as the Dunham coefficients will now be given by[7]

$$a_n = (-\Delta^{1/2})^n (n + 1) \quad (20)$$

These are scaled coefficients with respect to the ideal ionic ones given in Equation (15), where $\Delta^{1/2} = 1$. Results are collected in Table 1 under the potential *Kratzer II*. If D_x is an ionic dissociation limit computed from atomic data or computed directly from R_e, *ionic functions remain two parameter potentials.*

6.2 Ionic Dissociation Energy and the Ground State of Molecules

6.2.1 The Born−Landé Asymptote

To avoid the cumbersome procedure to obtain the n values needed for the Born−Landé asymptote (10), we want to replace it with a simpler variant, also independent of D_e.

Normally, ionic bond energies (asymptotes) are either given by $IE_A - EA_B + D_e$ for dissociation into A^+ and B^- or $IE_B - EA_A + D_e$ for dissociation into A^- and B^+ and, in both cases, D_e is needed. For bonds of intermediate polarity, the situation is less clear. If B has the higher electronegativity and *if both ionic forms are present in the ground state in a ratio* b^2/a^2 with $a^2 + b^2 = 1$, this virtual ionic dissociation energy would not be available experimentally. We can try to calculate it by putting

$$e^2(1 - 1/n)/R_e = a^2[(IE_B - EA_A) + D_e] + b^2[(IE_A - EA_B) + D_e]$$
$$= [IE_A + a^2(IE_B - IE_A)] - (a^2EA_A + b^2EA_B) + D_e \quad (21a)$$
$$\approx IE_A + a^2(IE_B - IE_A) \quad (21b)$$

In going from Equation (21a) to (21b), we used the intermediate result,[34] that, in first approximation,

$$D_e = a^2EA_A + b^2EA_B \quad (22)$$

and this might remove D_e from the ionic bond energies in a systematic way.

With the definition of the bond polarity $I = b^2 - a^2$, this ionic asymptote will further reduce to

$$e^2(1 - 1/n)/R_e \approx IE_A + (1 - I)(IE_B - IE_A)/2 \quad (23)$$

$$\approx 1/2(IE_A + IE_B)(1 - I^2) \quad (24)$$

if $I = (IE_B - IE_A)/(IE_A + IE_B)$ is used as a first order approximation for the bond polarity I.

Strictly spoken, I should depend on electronegativities, according to Wilmshurst.[35] Using IE_X as an approximation for either the Pauling[36] electronegativity χ_P or Mulliken's[37] $\chi_M = (IE_X + EA_X)/2$ is acceptable, especially if Mulliken's definition is taken as a guideline (in general $IE_X >> EA_X$). The only theoretical advantage of these deductions is a simplification of the ionic bond energy (21), which can now be computed from available atomic quantities (ground state ionization energies of atoms), as intended. Using Pauling χ_P values would not alter much to the result for the asymptote (except in a few cases).

The asymptote for a virtual dissociation in $a^2(A^- + B^+) + b^2(A^+ + B^-)$ gives an idea of the bonding situation at R_e, since the bonding partners, isolated at $R = \infty$, are frozen in the same (*charged*) states they had at the equilibrium distance (IIM method).

Developing (23) further shows that

$$e^2(1 - 1/n)/R_e \approx 2\ IE_AIE_B/(IE_A + IE_B) \quad (25)$$

For homonuclear bonds XX, we get

$$e^2(1 - 1/n)/R_e \approx (IE_X - EA_X) + D_e \approx IE_X \quad (26)$$

if the difference between EA_X and D_e is not too large.

Using this approximation would again lead to a *two-parameter* potential, at least for bonds between monovalent atoms, whereby just k_e and R_e will be needed to compute F and G. Additional refinements are possible using valence state ionization energies instead of ground state values, similar an approach as suggested by Von Szentpaly in his AIM approximation.[15]

Rewriting Equation (25) in function of effective charges q_X and covalent radii r_X of atoms X and using $IE_X = q_X e^2/2r_X$, where q_X and r_X are respectively the effective nuclear charge (for the valence electron) and the covalent radius of atom X, we obtain

$$e^2(1 - 1/n)/R_e = e^2(1 - I^2)(q_Ar_B + q_Br_A)/r_Ar_B.$$

If both q_A and q_B are not too different from 1, a standard relation results for the bond length

$$R_e \approx r_A + r_B$$

since the two polarity terms will cancel in first approximation. This brings ionic bond energies in line with the Kratzer asymptote, as intended by eliminating D_e in the Born−Landé asymptote.

6.2.2 The Kratzer Asymptote

Whether or not the Kratzer asymptote e^2/R_e is (or must be) the same as the Born−Landé asymptote is not clear. The predictions of these two ionic potentials will therefore be tested as such. We notice the dependence of the theoretical ionic bond energies upon $(1 - I^2)$ in Equation (23), which also suggests an alternative Kratzer I asymptote equal to

$$D_x = e^2(1 - I^2)/R_e \quad (27)$$

This corresponds with A in (18) equal to $(1 - I^2)$, a correction for charge transfer in the bond. If valid, this means that for two interacting charges at equilibrium the following Equation applies

$$A = q_Aq_B = A'(1 - I)(1 + I) = A'(1 - I^2) \quad (28)$$

if $q_X \approx 1 \pm I$, a strange formula for ionic bonds anyhow ($I = 1$ would mean $A = 0$), to be tested below with the spectroscopic constants. $A' = 1$ in Equation (28) would still give rise to two parameter Kratzer potentials, since I can be calculated from atomic quantities. It must be noticed that A will not only be determined by the atom's partial *charge* ($\pm I$) but also by its *valence* (which is a Column classification effect, as noticed by Calder and Ruedenberg[5]).

6.3 Relations Between the First-Order Parameters *F* and *G* and the Scaling Factor Δ for Some Standard Potentials

According to Varshni's procedure,[3] the higher derivatives of potentials, scaled by the second, result in relations between F and G and the Sutherland parameter Δ, shown in Table 1. Most potentials can be considered as two *or* three parameter functions (see above), only Morse's function is always a *three*-parameter potential. First order-zeroth order relations like $F(\Delta)$ allow a computation of D_x values, the intermediate asymptotes, directly from the spectroscopic constants for each of the potentials mentioned in Table 1.

For the same Δ values, large differences are expected for $F(\Delta)$ and $G(\Delta)$. Leaving out the Kratzer potential, the following F values are respectively obtained for $\Delta = 9$: 6.33, 3.00, 5.00, and 2.00 (difference > 300%). Differences (in%) for $\Delta = 1$ would be larger, as the respective F values are equal to 1.00, 1.00, 1.00, and 0.

Translating this into D_x values gives for $F = 2$ values ranging from $a_0/2.666$ to $a_0/0.41$, a ratio of 1/6.5, which must be clearly visible. Since, in theory, there are no differences between the Δ's in Table 1 (in a standard theory, they all equal the *covalent* Sutherland parameter), this would lead to conflicts, when the relative merits of potentials are to be compared, and universal scaling would become practically impossible (see Figure 2).

The resulting $G(F)$ relations and the G/F ratios, are similar, as they all start with a scaling factor $(1 + F)^2$. This factor relates to $a_1 = -(1 + F)$. Comparing the potentials

Table 1. $F(\Delta)$, $G(\Delta)$, and $G(F)$ relations according to some potentials

Potential	$F =$	$G =$	$G(F)$	G/F value	
				for $F = 1$	$F = 3$
Born−Landé	$2\Delta/3 + 1/3$	$(8\Delta^2 + 38\Delta + 26)/3$	$3 + 15F + 6F^2$ $= 6(1 + F)^2 + 3(F - 1)$	24	34
Kratzer	1	24	24 $(= 6(1 + F)^2)$	24	24
Kratzer I (= Varhsni V)	$\Delta^{1/2}$	$8\Delta + 12\Delta^{1/2} + 4$	$4 + 12F + 8F^2$ $= 8(1 + F)^2 - 4(1 + F)$	28	39
Kratzer II	$2\Delta^{1/2} - 1$	24Δ	$6 + 12F + 6F^2$ $= 6(1 + F)^2$	24	32
Morse	$\Delta^{1/2} - 1$	8Δ	$8 + 16F + 8F^2$ $= 8(1 + F)^2$	32	43

shows that, theoretically, Morse's potential gives the highest G values, followed by Kratzer I, Born−Landé, and Kratzer II in that order.

6.4 The *G*/*F* Ratio

Table 1 shows that theoretical G/F ratios obey equations of the general form

$$G/F = aF + b + c/F \ldots \quad (29)$$

where a, b, and c are constants and where the exponent of F [equal to 1 in Equation (29)] depends on the potential. Predictions about G/F values are roughly comparable with observed values.

In terms of the constants and according to Varshni's definition,[3] the G/F ratio obeys

$$G/F \approx (\omega_e x_e/\omega_e)\,(B_e/\alpha_e)$$
$$\approx (B_e/\omega_e)\,(\omega_e x_e/\alpha_e)$$
$$\approx \omega_e x_e B_e/\alpha_e\omega_e \quad (30)$$

independent of Δ and in which all lower order constants are pair-wise coupled in a symmetrical (vibrational/rotational or first order/zeroth order) or in an anti-symmetrical way. The normalizing factor for G, to distinguish between potentials, should rather be a_1^2 or $(1+F)^2$ (as in the Graves−Parr scheme[2]), but this would destroy part of the relation of the G/F ratio with the four constants in Equation (30). The G/F ratio plays an important role in other scaling schemes, although this is not always apparent in the original publications.

6.4.1 The *G*/*F* Ratio and the Calder−Ruedenberg Constant *C*

In the first large-scale analysis on constants of 160 diatomics, Calder and Ruedenberg[5] concluded 30 years ago that the G/F ratio is a constant C and that it is equal to

$$C = 4(1+a_1)/(a_2 - 5a_1^2/4) \approx 1.39\ (\pm\ 5\%) \quad (31)$$

The reported error of 5% for 160 bonds sounds impressive. They did not mention, however, that this constant C bears an intimate numerical relation with the G/F ratio:

$$G/F = 48/C \quad (32)$$

This follows from the relations between F and G and the lower order Dunham coefficients:

$$a_1 = -(1 + F) \quad (33a)$$
$$a_2 = (5/4)\,a_1^2 - G/12 \quad (33b)$$

since substituting (33a) and (33b) in (31) immediately gives (32). Very unfortunately, Calder and Ruedenberg did not at all discuss *potentials*: they restricted their analysis to the constants.

Translating their analysis to potentials and predicted G/F values [Table 1 and Equation (29)] leads to a contradiction: C can never be a constant as it will always depend upon F in a particular way for each of the potentials in Table 1 (see also Varshni[3] for other examples).

In the case of the Kratzer II potential, $C = 8F/(1 + F)^2$ leads to $C = 0$ for $F = 0$, with a maximum of 2 for $F = 1$ and then gradually decreasing with increasing F to 1.33 for $F = 4$. These predictions are roughly in line with observation, even Calder and Ruedenberg's: C values in general decrease with increasing F (or $-a_1$) values. Even the reputed Morse potential gives a similar result for C. With the ideal ionic coefficients (15), the constant C is equal to 2, of the correct order of magnitude.[7]

We showed some time ago how the difference between the asymptote D_x and the atomic asymptote D_e can influence quantitatively C values,[7] which, if true, might also point towards an external influence on G/F values (see further below).

Calder−Ruedenberg's idea of a constant C arose from classifying molecules in function of the position of the atoms in the columns of the Periodic Table (which might be a very rough intuitive measure for *valence* and for *bond ionicity* too, see above). This classification is justified by relations found between constants, whereby a clustering was observed for bonds between atoms in the same Columns of the Table (as illustrated in Figure 1b). Graves and Parr[2] also used the Column classification. However, these authors concluded that it did not help *significantly* to reveal scaling trends, in clear contradiction with the Calder−Ruedenberg analysis, its claimed accuracy and its conclusion.

The Graves−Parr conclusion is in line with our discussion about scaling given above (see Figure 1a−b) and we

will discuss the matter more fully below in another context. Despite this negative conclusion of Graves and Parr, the idea for a possible grouping of molecules in the spirit of Calder and Ruedenberg remains important in the context of Coulomb attraction

$$q_A q_B e^2/R \tag{34}$$

We refer to the discussion of A values in Equation (28), in terms of *charge* and *valence* effects. Strictly spoken, the Calder−Ruedenberg classification invokes an additional (hidden) parameter, not yet quantified. In line with the remarks by Graves and Parr, we will show that several of the Calder−Ruedenberg groups overlap (see also Figure 1b).

6.4.2 The *G*/*F* Ratio and the Graves−Parr Scaling System

In addition, in the Graves−Parr scaling system, the G/F ratio plays a dominant role, although this is not apparent in their paper.[2] They showed that the Dunham coefficients a_1 and a_2 should both be scaled by the *covalent* Sutherland parameter. With perfect scaling, the ratio of a_1^2/Δ and a_2/Δ should theoretically be a constant. However, statistical effects, not mentioned by Graves and Parr, will also increase the goodness of fit with respect to the unscaled coefficients. Table 2 gives some results.

Table 2. Graves−Parr scaling procedure

Potential	$a_1^2 =$	$a_2 =$	$a_1^2/a_2 =$
Kratzer	4	3	4/3 = 1.333
Kratzer I − Varshni V	$(1+\Delta^{1/2})^2$	$7/12(1 + \Delta^{1/2})^2 + (1/3)(1 + \Delta^{1/2})$	$1.714/(1 + 4/[7(1 + \Delta^{1/2}))]$
Kratzer II	4Δ	3Δ	4/3 = 1.333
Morse	Δ	$(7/12)\Delta$	12/7 = 1.714

The relations between the Dunham coefficients and the Varshni parameters F and G in Equation (33) show that a_1^2/a_2 is also determined by the G/F ratio. Whereas 3 potentials lead to a constant, only the Kratzer-I−Varshni-V function predicts that a_1^2/a_2 should be a function of $\Delta^{1/2}$ (or of F).

6.4.3 The *G*/*F* Ratio: Chaotic/Fractal Behavior

Freeman, March and Von Szentpaly[16] argued that an empirical power $G(F)$ relation exists

$$G = 27.4F^{4/3} \tag{35}$$

This, in their opinion, suggests chaotic/fractal behavior. Equation (35) leads to the ratio

$$G/F = 27.4F^{1/3} \tag{36}$$

resulting in the values 27 and 40 for F equal to 1 and 3, comparable with those in Table 1.

If this relation were reliable, this would probably complicate the search for a universal potential.

7. Universal Two-Parameter Functions: Theory versus Experiment

7.1 Lower-Order Constants

The spectroscopic constants ω_e, $\omega_e x_e$, B_e, and α_e exhibit intriguing relations, some of which were discussed already above and also by Calder and Ruedenberg[5] in order to justify the Column classification and by Herschbach and Laurie[19] for the Row classification. These will not be repeated here, although we discuss 100 bonds containing H, of which only 10 were included in the Calder−Ruedenberg analysis (one relation was extended to H bonds in Figure 1a and 1b).

We first present the results for the last identity in Equation (30) for 381 diatomic molecules in Figure 3. The empirical *power* relation (logarithmic scale), valid for differences of the order of 10^7 in the two axes, combined with a high R^2 value, is not significantly better than the empirical *linear* relation. Since these also determine the G/F ratio, chaotic/fractal behavior[16] may be put in doubt. The accuracy for the computed product of a pair of two constants is 10% for 381 bonds, which illustrates the overall quality of the relations between the constants. Various other relations are found. In some cases, an empirical power relation gives a goodness of fit of (over) 0.9, as can be seen from the results in Table 3. It is not always clear, however, whether or not this is due to large-scale differences or to a basic relation between the constants. We believe this is a matter of further research.

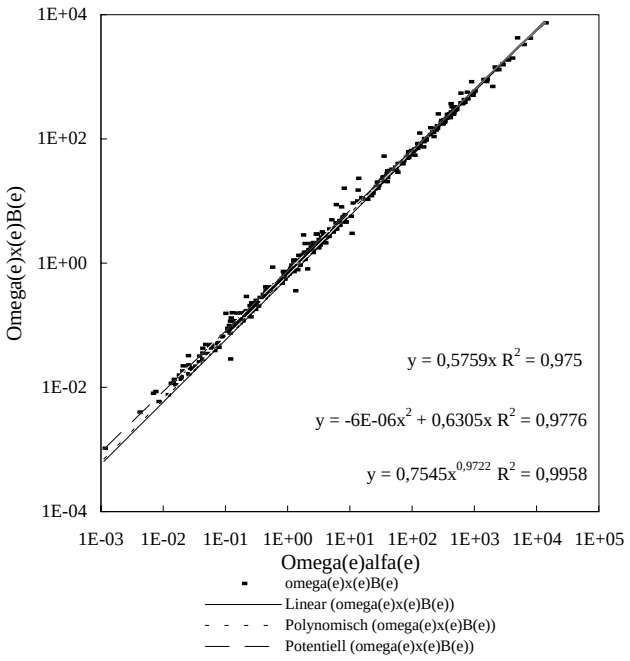


Figure 3. G/F: $\text{omega}_e x_e B_e$ versus $\text{omega}_e\text{alfa}_e$ for 380 bonds

Table 3. Empirical power relations between observed spectroscopic constants ω_e, $\omega_e x_e$, $_{Be}$ and α_e and equivalents for $14.4/R_e$ and a_0 (cm^{-1}) for 381 bonds and D_e(eV) for 300 bonds

$Y(X)$	Empirical $Y(X)$ relation	R^2	Remark
$\omega_e(\alpha_e)$	$3363.4X^{0.2996}$	0.7315	
$\omega_e(\omega_e x_e)$	$304.6\ X^{0.5386}$	0.8086	
$\omega_e(B_e)$	$894.48X^{0.4546}$	0.8336	
$\omega_e x_e(B_e)$	$7.2793X^{0.8044}$	0.9368	important for G, Equation (4)
$\omega_e x_e(\alpha_e)$	$92.138X^{0.5691}$	0.9466	corresponding with a $G(F)$ relation
$B_e(\alpha_e)$	$22.111X^{0.6956}$	0.9769	best fit, important for F, Equation (3)
$\omega_e(14.4/R_e)$	$3.6185X^{2.5694}$	0.8456	
$\omega_e(D_e)$	$391.38X^{0.5584}$	0.2166	for 300 bonds with D_e known
$\omega_e(a_0)$	$41.183X^{0.2372}$	0.0393	

For 381 bonds, the 6 relations between the constants in the upper part of Table 3 are quite reliable, the best being the 6^{th} $B_e(\alpha_e)$ in terms of R^2. This empirical power relation reproduces B_e values from α_e with an average absolute deviation of 10% for most bonds. The 5^{th} corresponds with a $G(F)$ relation (see above). Two other relations with a relative good fit are important for F and G.

The second part of Table 3 gives a confrontation of 3 asymptotes as to their possible relationships with the harmonic frequency, for which the R^2 values are much higher than for the remaining three spectroscopic constants (not shown). For the asymptotes D_e and a_0, there is no significant global relation. The situation is different for the ionic asymptote. However, if the asymptotes (x values) are corrected for reduced masses, the goodness of fit is drastically improved for all asymptotes (for the Kratzer asymptote, even the identity results in the case of B_e). Therefore, the groupings observed in Figure 1a and 1b originate for the larger part from the reduced masses. This is most apparent for H-containing bonds, which seem to form a different spectroscopic group (see Figure 1 and next sections).

7.2 Derived Constants (a_0, k_e, Δ, F, G)

We first confront the asymptotes with the harmonic frequency according to the Column classification (see also Table 3). As remarked by Calder and Ruedenberg,[5] the intuitively sound relation between the two most important constants of a bond, i.e. a_0 and ω_e, can be visualized in the corresponding plot (Figure 4a). Although a_0 depends on the square of ω_e by definition, no straight general relation is observed, except for some classes of bonds. In agreement with the situation in Figure 1a−b, also here we find regularities (Row- or Column classifications). Figure 4a also shows *why* Calder and Ruedenberg excluded most H-containing bonds from their analysis: these distinctly form a different spectroscopic class and the dividing line between H-containing molecules and the other is clearly visible. This line would be situated exactly where a breaking of the symmetry occurs between atom mass M and atom number Z, i.e. at $Z = 1$. Merely using Hooke's law to account for the constants (as in Dunham's oscillator model, where forces depend on masses) is not uniformly applicable throughout the Periodic Table.

Next, substituting a_0 with D_e (Figure 4b) does not improve the picture at all and no new or better global relationship emerges, on the contrary (in agreement with the results in Table 3). The only classes of bonds for which regularities appear (Column-classes 11, 77, and 27) are also grouped or equally regular in Figure 4a. For other groups, the regularities in Figure 4a have disappeared. This seems to justify our suggestion that D_e, the atomic dissociation limit, is only reached in a number of cases, after other effects have been operating between R_e and ∞. Therefore, it seems fair to exclude constraint (ii) in a search for a universal potential (see also Table 3).

Thirdly, substituting a_0 with the ionic dissociation energy (calculated from ionization energies, the Kratzer II asymptote) leads to a better picture (not shown) but which is intermediate with that obtained when one replaces a_0 with the Kratzer I asymptote. Figure 4c gives the plot for e^2/R_e. A similar plot has already been given in Figure 1, since $(B_e)^{1/2}$ can be used as a substitute for e^2/R_e in the x-axis. Figure 1 being an ω_e ($1/\mu R^2$) plot, it is readily concluded that this leads to a completely different picture than the one having a_0 in the x-axis (Figure 4a) both for the H-containing bonds and for other bonds. In fact, and contrary to Figure 4b for D_e, and apart from the scaling and classification effects already discussed above, Figure 4c also shows how well the harmonic frequencies of bonds are correlated with $1/R_e$. This dependence is characteristic for ionic potentials and we remind thereby that multiple bonds were not even excluded from these Figures. As well as the results in Table 3, this strengthens our ideas about the correct variable for the oscillator presentation. Indeed, Figure 4c gives large-scale evidence for the intuitive idea that an ionic Coulomb law seems to govern bond mechanics and that charges and valences are important to account for trends in the harmonic frequencies of bonds.

The details of clustering or classification in Figure 1a and 1b were discussed above. However, we must now remark that, in Figure 1b, the parallel lines are more close to each other and even extend linearly into the H group (points on the right side in Figure 1b). The number of lines that must be drawn in Figure 1b to encompass all data points seems less than in Figure 1a.

In terms of an additional parameter for a potential, it seems that a few values for A in Equation (28) would be sufficient to unify the complete picture in Figure 1b.

Experiment clearly shows, through Figure 4c, that the ionic dissociation limit can indeed be a serious candidate for explaining the relations between the spectroscopic constants. This asymptote seems very suited also for scaling a_0, as it correlates extremely well with the two $zero^{th}$ order constants, which completely determine a_0. These are exactly some of the constraints for the alternative asymptote, given above. The transformation of the Dunham variable into the Kratzer variable for which we gave theoretical arguments

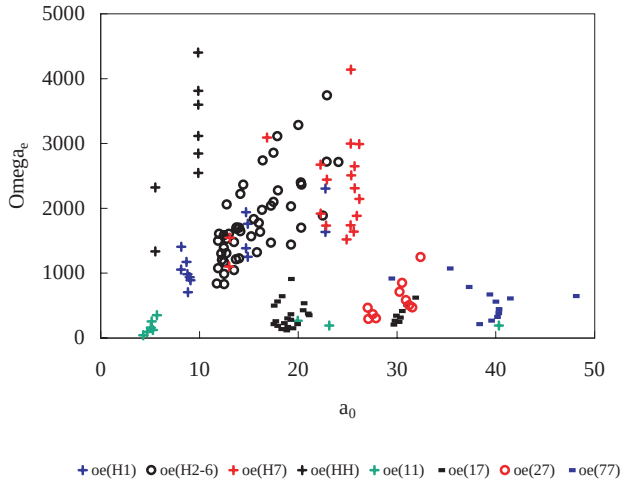


Figure 4a. Omega$_e$ versus a_0 (Column-classification)

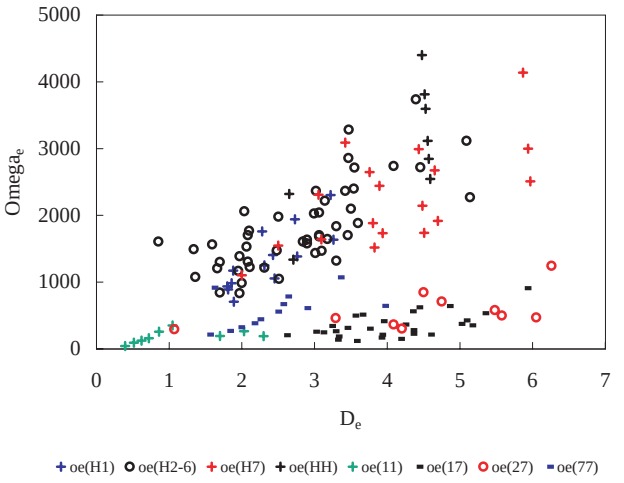


Figure 4b. Omega$_e$ versus D_e (Column-classification)

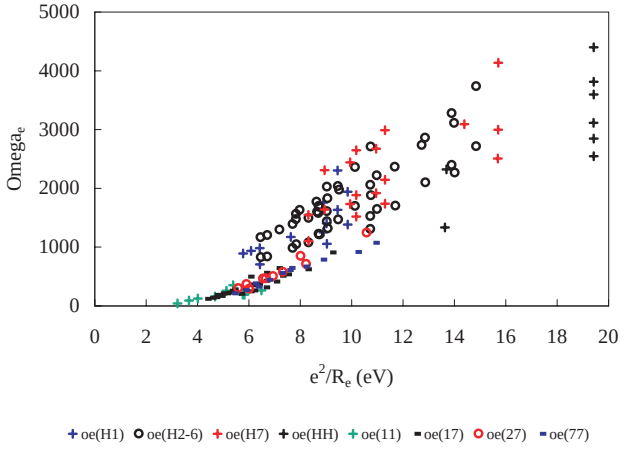


Figure 4c. Omega$_e$ versus e^2/R_e (Column-classification)

above, seems to be very effective indeed and is confirmed by experiment (see Figure 4c and Table 3).

7.3 Atomic Mass-Atomic Charge Symmetry Breaking

If we compare Figure 4c with the corresponding Figure 4a−b, we already notice a significant improvement in the relation between the harmonic frequency and the asymptote. Since Figure 1a and Figure 1b are a justification for the two classification schemes (by Row or by Column), we now find a third effect operating in this correlation: symmetry breaking between atomic masses and atomic charges.

To illustrate this symmetry-breaking effect, we made a plot (Figure 5) of the reduced mass μ versus its equivalent ζ in terms of atom numbers Z, or

$$\zeta = 2Z_AZ_B/(Z_A+Z_B) \quad (37)$$

since, roughly, $M_X = 2Z_X$, especially in the lower part of the Periodic Table ($Z < 50$). Although a linear or a power fit gives R^2 values equal to almost unity, only a log-scale reveals the details of the symmetry-breaking effect at $Z = 1$ (see Figure 5). Only D-containing bonds follow the trend of the general relation. Reduced masses are determined by Rows and by Columns, as well as reduced atomic charges (atom numbers Z).

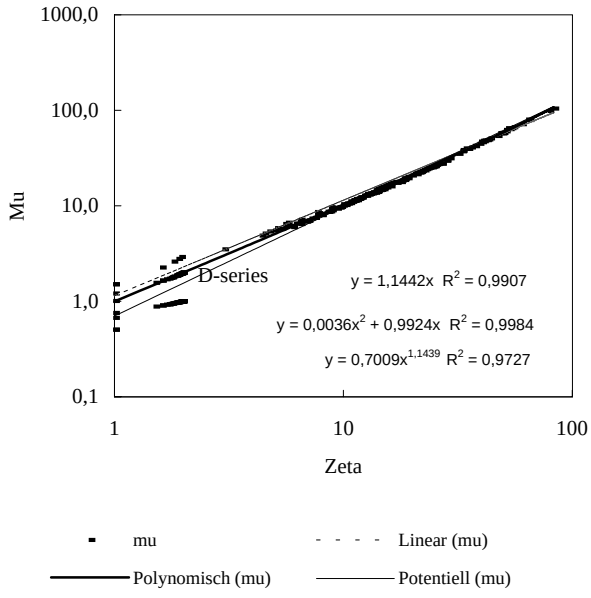


Figure 5. Mu versus Zeta for 300 bonds

In fact, most of the discontinuities between H- and non-H bonds in Figure1a−b disappear if the square root of the harmonic frequency is plotted against an R value, that is corrected for a symmetry breaking effect at $Z = 1$, or

$$R_{corr} = R_e\,(\zeta/\mu)^{1/2} \quad (38)$$

The result is shown in Figure 6a which should be compared with Figure 4c (see above) to notice the global effect. The goodness of fit for a linear relation is 0.93, for a power fit it is 0.95 and for a quadratic one it is over 0.97. This is an improvement over the situation with the Dunham asymptote plotted against the harmonic frequency (Figure 4a) and may even question the validity of the classification schemes, discussed above, as all data-points seem to gather around a *single* line. For instance Row- or Column classifications are hardly visible (see Figure 6b for a log-log plot), and if persistent, hardly quantifiable. A comparison of Fig-

ure 6b with Figure 1 shows the scaling effects we were looking for.

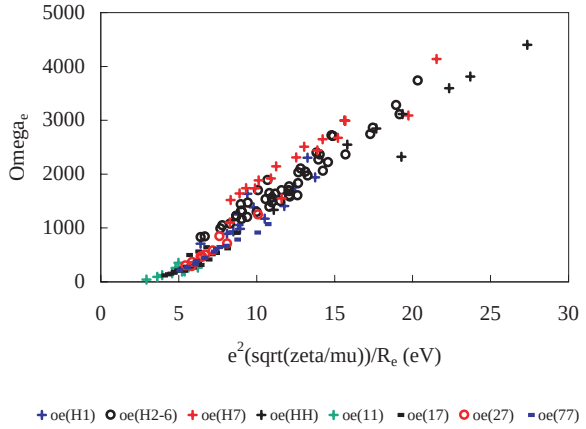


Figure 6a. Omega$_e$ versus e^2(sqrt(zeta/mu))/R$_e$ (Column-classification)

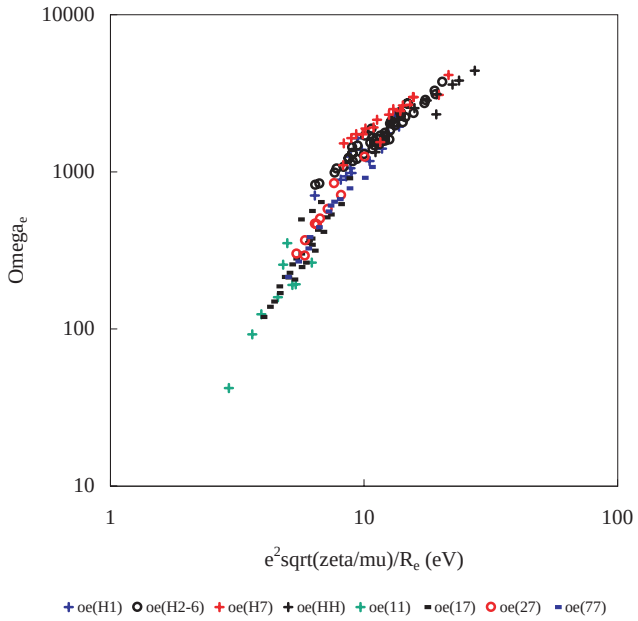


Figure 6b. Omega$_e$ versus e^{2}sqrt(zeta/mu)/R$_e$ (Column-classification) (log-scale)

These results are in agreement with classical dynamics (the dependence of the frequency on the ratio Z/M). This generalization of the ω_e ($1/R_e$) relation provides us with a possibility to achieve universal scaling in terms of charges and Coulomb-like potentials, reminding thereby the spectroscopic definition of a_0, see Equation (2b).

7.4 Experimental and Theoretical $G(F)$ Relations

Unlike the $F(\Delta)$- and $G(\Delta)$ relations (see Figure 2a and 2b), the $G(F)$ relation is completely determined by the spectroscopic constants. This relation represents a challenge for potentials and for scaling (see for instance the $\omega_e x_e$ (α_e) dependence in Table 3). We now confront the experimental $G(F)$ relation with the predictions of the potentials in Table 1.

Figure 7a presents the global view for the 381 diatomics with both G and F available. The best fit of a quadratic relation nearly goes through the origin (intercept −1.38), but the coefficients of F are 7.4 for the quadratic and 21.8 for the linear term (see the Equations in Table 1). The power fit gives $28.974F^{1.2978}$, not too far away from the Freeman fit (see Equation 35). Both empirical relations have the same goodness of fit of $R^2 = 0.843$. We observe that the Morse function is closest to the empirical fit, followed by the Kratzer I potential. The goodness of fit is in agreement with that found for the $\omega_e x_e$ (α_e) relation in Table 3.

Nevertheless, there is a strong bias from exotic molecules (Van der Waals molecules, excited states, ...) with anomalous G/F values. Leaving out all excited states and extreme cases gives Figure 7b for some 300 bonds. The empirical quadratic equation is (only) slightly better than the power relation. This empirical quadratic relation gives G ($\approx \omega_e x_e$) from F ($\approx \alpha_e$) within 9.8% of experiment, which is quite accurate given the number and the different kinds of molecules. The empirical fit lies between the Morse and Kratzer curves, but is closer to Morse's. The coefficients compare well with the theoretical ones given in Table 1.

At this stage (Figure 7a and 7b), the enlargement of the data-sample does not favor the conclusion of Freeman et al.[16] about chaotic/fractal behavior, especially not in terms of the goodness of fit. Further material at high F values, where the empirical approaches diverge (Figure 7a), might be decisive in this respect, although this information will be hard to find.

We notice from Figure 7a and 7b that the Morse potential seems to validate Jhung's hypothesis[9] and that the Kratzer I potential is low (see also our discussion of Table 1).

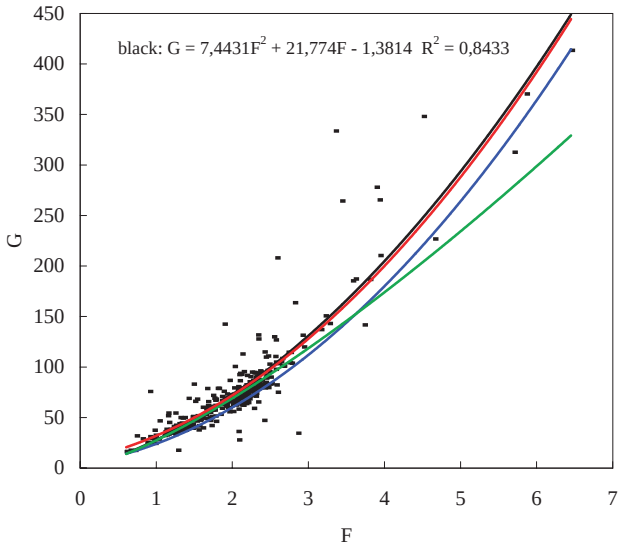
When the set is limited to 91 bonds between monovalent atoms (Figure 7c), different equations are generated. We now have $G = 9.55F^2 + 9.473F + 10.355$ with $R^2 = 0.9439$ and $G = 30.012F^{1.2162}$ with $R^2 = 0.9405$ (not shown), which are again close to the theoretical relations given in Table 1. Comparing the theoretical results of Table 1 with those of empirical quadratic fitting leads us to conclude that the Morse and the Kratzer I potential are the best choices in that order for reproducing the empirical $G(F)$ plot.

A different situation is found, when the theoretical predictions by the potentials are considered for the $G(\Delta)$ relation (see below). For the 91 bonds between monovalent atoms, the Morse results were already given above (Figure 2b), with a goodness of fit of only 0.5786 and a slope of 1.067 for an intercept of −3.57 in the case of a linear fit.

7.5 Predictions for First-Order Constants α_e and $\omega_e x_e$: Comparing the Performance of Kratzer and Morse Potentials

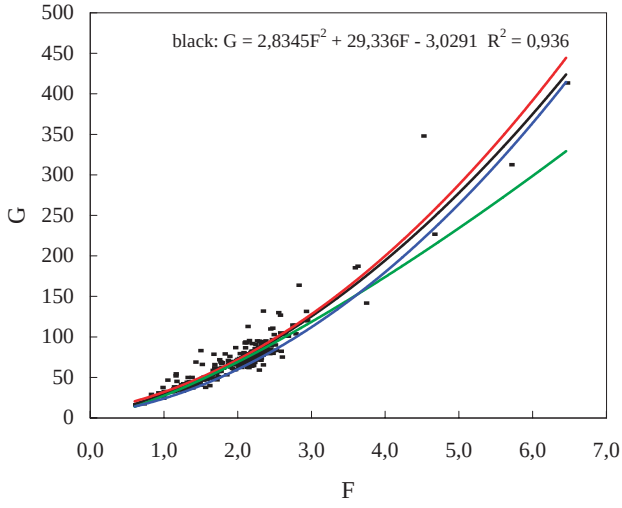
7.5.1 Ionic Sutherland Parameters for 91 Single Bonds and F

Figure 8a gives a plot of the three ionic Sutherland parameters versus F for 91 bonds between monovalent atoms. Even including F_2 (with $F = 2.667$), the goodness of fit for



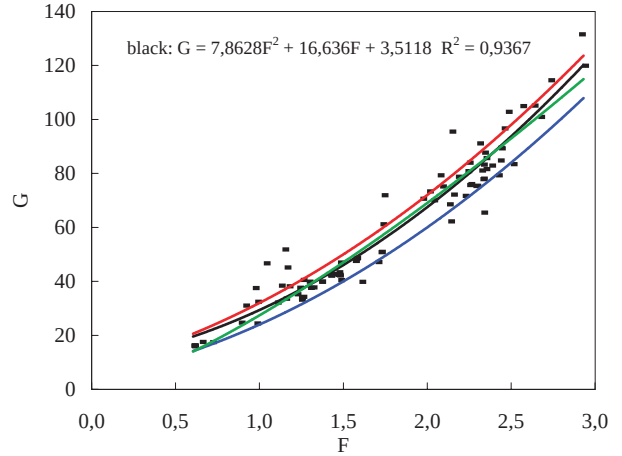
red: Morse; blue KratzerI/Varshni V, green Freeman…, empirical

Figure 7a. Plot of G versus F for 381 bonds



red: Morse; blue: Kratzer I/varshni V; green: Freeman, empirical

Figure 7b. G versus F for 300 bonds



red: Morse; blue: Kratzer I/Varshni V; green: Freeman, empirical

Figure 7c. G versus F for 91 single bonded diatomics

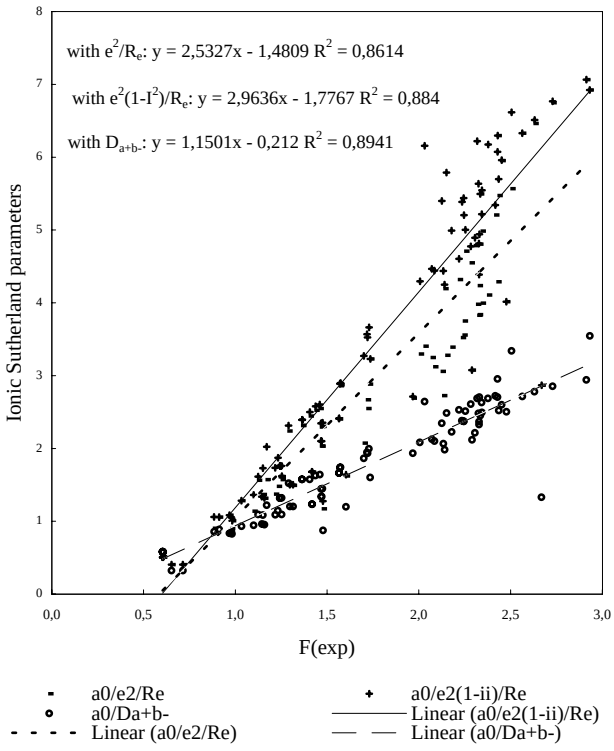


Figure 8a. Plot of 3 ionic Sutherland parameters versus F(exp) for 91 single bonded diatomics

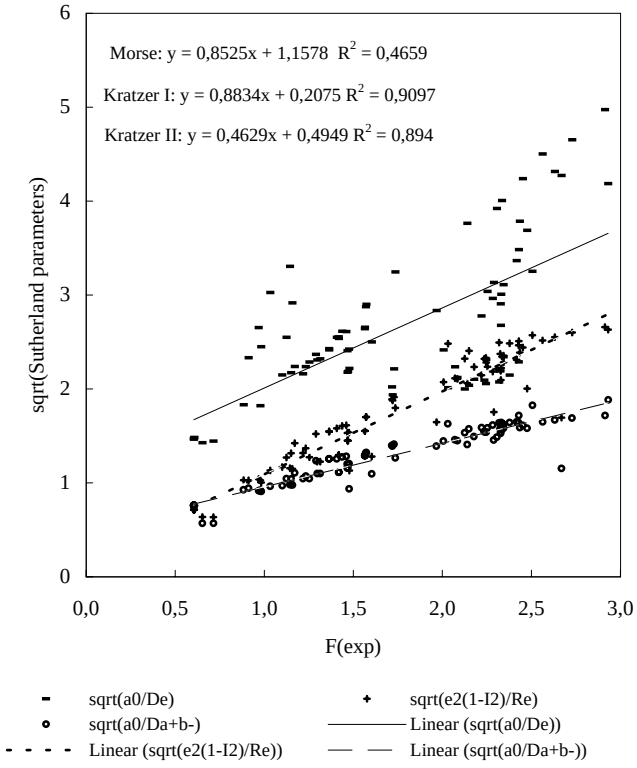


Figure 8b. Square root of different Sutherland parameters versus F for 91 single bonded diatomics

all ionic asymptotes is relatively high. The series, based upon D_{A+B-}, calculated from ionization potentials, has polarity effects ($1 - I^2$) included automatically. The trends observed show that a quadratic dependence might be better (see the Graves−Parr suggestion and see Table 1).

Figure 8b represents the results with $\sqrt{\Delta}$ for the same 91 bonds but now the covalent Sutherland parameter is included for comparison (see also Figure 2). Despite the scale differences, it is readily concluded that *any ionic Sutherland parameter is superior to the covalent one.* Slopes and intercepts are as expected, even for the Morse relation. The covalent Sutherland parameter may be plausible for some (classes of) molecules. About 50 are situated near the theoretical line but 40 are completely out of range (another illustration of Varshni′s earlier observation and of the spectroscopic gap, artificially created by the covalent Sutherland parameter, see above).

The predictions of a Kratzer potential are good. Empirical fitting through the origin yields the theoretically expected coefficient of nearly 1, with a goodness of fit almost identical to a linear fit, with a free intercept (not shown). The other series, based upon D_{A+B-} (also promoting the Born−Landé potential in Figure 8a) practically leads to a relation of the form

$$F = 2\Delta^{1/2} - 1 \text{ or } \Delta^{1/2} = F/2 + 1/2$$

(goodness of fit 0.89). This corresponds with the predictions of the *Kratzer II* potential.

Since the polarity I of the bond is computed from *atomic* quantities, Figure 8b is achieved by means of ionic *two parameter* potentials.

7.5.2 Calculation of α_e and $\omega_e x_e$ for 308 Bonds

A calculation of the constants α_e and $\omega_e x_e$ directly from the potentials gives the results collected in Table 4, given in Supporting Information.

Only for α_e, we tried to present the results graphically (see Figure 9a), using a log scale due to the large differences in α_e values. Two help-lines are drawn at ± 25% of the experimental α_e values. Help-lines at a lower percentage interfere too much with the empirical fittings through the origin (−20% would nearly coincide with the Morse trendline, whereas +10% or +15% would have been too close to the Kratzer trendline). For 308 bonds, the mean deviation for the Kratzer I potential is 18.1% and for Morse′s 20.1% (see also Table 4). This makes the performance of the two comparable but the errors are too large for a universal potential.

We must however divide these 308 bonds in two main series:

– 197 bonds with at least one monovalent atom and a main column element

– 111 other bonds, including bonds between polyvalent atoms, Van der Waals molecules, ...

This distinction is necessary since we can expect that only with A' near or equal to 1, the Kratzer I asymptote can reasonably be calculated without any further assumptions. For these 197 *simple* bonds, it can be expected that also Morse′s function will behave at its best. Part one of Table 4 in the Supporting Information (197 bonds) reveals that the performance of the two parameter Kratzer potential with a *wrong* asymptote is now significantly better than Morse′s three parameter potential, which uses the natural and *correct* asymptote.

Table 5a gives an overview of the spread of the mean deviations (%) in the 197 and 111 series. It is easily verified that the Kratzer potential is superior to Morse′s for pre-

Table 4. Data for 308 bonds (sample for 27 bonds from part one: 197 bonds containing at least one mono-valent atom)[a]

Nr	Bond	Col Class	$\omega_e x_e$ (exp)	$\omega_e x_e$ Kratzer	$\omega_e x_e$ Morse	%$\omega_e x_e$ Kratzer	%$\omega_e x_e$ Morse	α_e (exp)	α_e Kratzer	α_e Morse	% α_e Kratzer	% α_e Morse	*C*	abs% *C*	*F*	*G*
1	Cs_2	1A1A	0.0823	0.05	0.14	−44.9	68.7	0.0000264	0.000027	0.000053	1.0	101.5	1.061	21.6	1.145	51.84
2	K_2	1A1A	0.328	0.20	0.51	−40.3	56.9	0.000212	0.000237	0.000424	11.7	99.9	1.042	22.9	1.034	46.70
3	Li_2	1A1A	2.61	2.08	3.66	−20.1	40.3	0.00704	0.007939	0.010294	12.8	46.2	1.409	4.2	0.911	31.03
4	LiNa	1A1A	1.612	1.20	2.38	−25.7	47.9	0.0036	0.003678	0.005312	2.2	47.6	1.448	7.1	0.983	32.46
5	Na_2	1A1A	0.72547	0.49	1.09	−32.9	50.3	0.0008736	0.000940	0.001493	7.6	70.9	1.239	8.4	0.968	37.50
6	NaK	1A1A	0.511	0.32	0.77	−37.2	50.8	0.0004584	0.000455	0.000759	−0.8	65.6	1.230	9.0	1.158	45.15
7	LiO	1A6	12.5	7.66	6.45	−38.7	−48.4	0.0151	0.018179	0.013383	20.4	−11.4	0.856	36.7	1.483	83.09
8	CsBr	1A7	0.374	0.38	0.17	0.3	−55.5	0.000124012	0.000130	0.000060	4.5	−51.7	1.376	1.8	2.378	82.93
9	CsCl	1A7	0.731	0.75	0.31	3.2	−57.5	0.00033756	0.000363	0.000157	7.6	−53.6	1.372	1.5	2.318	81.10
10	CsF	1A7	1.615	1.91	0.75	18.5	−53.7	0.00117562	0.001435	0.000587	22.1	−50.1	1.392	3.0	2.032	70.06
11	CsI	1A7	0.2505	0.24	0.12	−3.1	−50.6	0.000068263	0.000069	0.000036	1.5	−47.0	1.375	1.7	2.429	84.79
12	KBr	1A7	0.8	0.72	0.36	−10.2	−55.0	0.00040481	0.000415	0.000205	2.6	−49.3	1.327	1.8	2.178	78.78
13	KCl	1A7	1.3	1.21	0.56	−7.3	−56.6	0.0007899	0.000820	0.000386	3.8	−51.1	1.327	1.8	2.236	80.83
14	KF	1A7	2.4	2.63	1.12	9.5	−53.3	0.002335038	0.002552	0.001099	9.3	−52.9	1.488	10.0	2.126	68.57
15	KI	1A7	0.574	0.55	0.32	−3.5	−43.4	0.00026776	0.000272	0.000157	1.6	−41.5	1.429	5.7	2.246	75.68
16	LiBr	1A7	3.53	3.83	2.27	8.6	−35.7	0.0056442	0.006209	0.003358	10.0	−40.5	1.621	19.9	1.717	50.83
17	LiCl	1A7	4.501	4.84	2.65	−7.4	−41.1	0.00800961	0.008741	0.004362	9.1	−45.5	1.620	19.8	1.720	50.95
18	LiF	1A7	7.929	8.72	4.35	10.0	−45.2	0.0202826	0.021569	0.009512	6.3	−53.1	1.731	28.0	1.700	47.14
19	LiI	1A7	3.39	3.12	2.17	−8.0	−35.9	0.00409	0.004528	0.002873	10.7	−29.8	1.356	0.3	1.729	61.18
20	NaBr	1A7	1.5	1.23	0.76	−17.9	−49.6	0.00094095	0.000960	0.000562	2.0	−40.3	1.253	7.3	2.071	79.31
21	NaCl	1A7	2.05	1.77	0.98	−13.8	−52.1	0.00162482	0.001643	0.000874	1.1	−46.2	1.330	1.6	2.084	75.19
22	NaF	1A7	3.4	3.54	1.67	4.1	−50.8	0.00455869	0.004502	0.002042	−1.2	−55.2	1.645	21.7	2.133	62.24
23	NaI	1A7	1.08	0.93	0.69	−13.8	−36.3	0.00064777	0.000669	0.000457	3.3	−29.4	1.314	2.8	2.007	73.32
24	RbBr	1A7	0.463	0.46	0.23	−0.4	−50.7	0.00018596	0.000190	0.000095	2.1	−48.8	1.432	5.9	2.325	77.91
25	RbCl	1A7	0.92	0.83	0.37	−10.1	−59.6	0.00045365	0.000471	0.000214	3.9	−52.9	1.283	5.1	2.244	83.96
26	RbF	1A7	1.9	2.09	0.88	9.8	−53.9	0.00152279	0.001704	0.000736	11.9	−51.6	1.430	5.8	2.150	72.13
27	RbI	1A7	0.335	0.31	0.18	−6.1	−46.2	0.00010946	0.000110	0.000063	0.5	−42.7	1.378	2.0	2.344	81.60

[a] The complete Table 4 is available as "Supporting Information".

Table 5a Number of bonds in groups of mean %-deviations by number of bonds, by constant, by potential, by series (197 or 111)

Constant	Potential	series # bonds	# with 0−5%	# with 5−10%	# with 10−15%	# with 15−20%	# with 20−30%	# with 30−40%	# with 40−50%	# with 50−100%	# with ≥100%
α_e	Kratzer	197	**85**	**41**	**28**	**15**	19	7	1		1
α_e	Morse	197	**31**	**28**	**23**	**17**	37	23	17	20	1
α_e	Kratzer	111	*5*	*14*	*7*	*9*	18	33	6	18	1
α_e	Morse	111	*20*	*30*	*24*	*11*	19	3	3	1	
$\omega_e x_e$	Kratzer	197	**49**	**38**	**25**	**31**	35	10	6	3	
$\omega_e x_e$	Morse	197	**22**	**32**	**24**	**19**	28	24	16	30	2
$\omega_e x_e$	Kratzer	111	*6*	*14*	*14*	*14*	19	17	9	14	4
$\omega_e x_e$	Morse	111	*26*	*12*	*13*	*12*	28	12	5	3	

Table 5b. Column classification of 197 bonds with at least one monovalent atom: mean deviations for calculated α_e and $\omega_e x_e$ values with the Kratzer (I) and the Morse potential

Column 1	Data/Column 2	1	2	3	4	5	6	7	H	Total
1	**Nr**	**9**	**2**	**2**		**1**	**4**	**28**		**46**
	%α_e(Kratzer I)	9.86	3.16	10.02		4.73	15.61	5.39		7.24
	%α_e(Morse)	50.63	4.28	12.07		15.74	7.59	37.45		34.42
	%$\omega_e x_e$(Kratzer I)	33.43	7.47	22.32		33.54	28.20	8.98		16.48
	%$\omega_e x_e$(Morse)	38.00	9.36	10.23		11.47	19.43	38.75		33.81
7	**Nr**		**10**	**22**	**8**	**8**	**4**	**12**		**64**
	%α_e(Kratzer I)		19.11	10.35	10.88	6.68	13.05	6.02		10.68
	%α_e(Morse)		28.72	28.46	13.65	7.61	46.80	26.52		24.83
	%$\omega_e x_e$(Kratzer I)		25.85	9.36	7.81	9.06	26.18	22.95		15.30
	%$\omega_e x_e$(Morse)		26.67	24.57	13.25	16.12	84.03	37.14		28.50
H	**Nr**	**13**	**19**	**9**	**8**	**5**	**7**	**18**	**8**	**87**
	%α_e(Kratzer I)	8.73	17.02	6.70	3.19	5.32	8.15	9.11	15.08	10.24
	%α_e(Morse)	5.36	36.74	8.23	10.64	12.25	17.35	13.10	25.13	17.78
	%$\omega_e x_e$(Kratzer I)	9.95	16.85	16.15	17.90	16.73	19.89	7.33	6.15	13.13
	%$\omega_e x_e$(Morse)	13.25	44.29	13.31	20.95	21.97	16.12	15.23	7.46	21.35
Nr		***22***	***31***	***33***	***16***	***14***	***15***	***58***	***8***	***197***
%α_e(Kratzer I)		9.19	16.80	9.34	7.04	6.06	11.44	6.67	15.08	**9.68**
%α_e(Morse)		23.88	32.06	21.95	12.15	9.85	22.60	27.63	25.13	**23.95**
%$\omega_e x_e$(Kratzer I)		19.56	19.15	11.99	12.85	13.55	23.78	11.36	6.15	**14.62**
%$\omega_e x_e$(Morse)		23.38	36.35	20.63	17.10	17.88	35.11	31.12	7.46	**26.56**

dicting the two constants in 197 series. The number of bonds in the 0−10% range is twice as large for the Kratzer potential, 126 and 86, than for Morse′s, 59 and 54 respectively.

The first row of data in Table 5a shows that up to bond number 85, the average deviation is ±2.38%. Up to number 126, it is ±3.97%, up to 154 ±5.41%, up to 170 ±6.47% and up to 188 ±8.08% (for bond 197 it is 100%). As we pointed out above that an average error of about ±5% can be considered as a reasonable limit for a "universal potential", the Kratzer-I−Varshni-V potential seems to meet this criterion and is certainly superior to Morse′s.

Error ranges derived from the square root of the percentage deviation for α_e times that for $\omega_e x_e$ for the same bond in the same 197 series give

− Kratzer potential deviation ±20% 171 bonds; ±10% 128; ±5% 57

− Morse potential deviation ±20% 109 bonds; ±10% 62; ±5% 20.

With this criterion, Kratzer′s potential is again superior to Morse′s. With Kratzer′s potential, the deviation for 171 bonds (i.e. 87% of 197 bonds) is ±7% for α_e and $\omega_e x_e$ combined.

In order to get an idea of the regularities in these results, we arranged all 308 bonds according to a rough Column classification, e.g. NaK in 11, RbF in 17, BeCl in 27, ... We also computed *C* (the Calder−Ruedenberg constant) and its % deviation from the average value. *F* and *G* values are also given. Table 4 (Supporting Information) gives these additional results for all 308 bonds, divided in the 2 series, ordered by a Column classification and alphabetically by bond.

A global comparison of the performances of the Kratzer and Morse potentials for calculating α_e and $\omega_e x_e$ for the 197 simple bonds is given in Table 5b, using the Column classification as a guideline. The % deviations for the Kratzer potential are smaller than those obtained with the Morse potential. Only rarely, one observes a better score for the Morse potential. The Morse results found here are slightly better than those reported by Varshni, who qualified this potential as not too good.

In the 23 bonds used by Varhsni[3] 17 would belong to the 197 series and his results are ±36.4% for α_e and ±32.9% for $\omega_e x_e$ (for 23 bonds: he found deviations of 33.1% and 31.2% respectively). Varshni′s best results were obtained with an *empirical* potential. The 23-bond set gave errors of ±22.1% for α_e and ±11.1% for $\omega_e x_e$. The figures for the 17 bonds set are nearly the same and comparable with those in Table 5b.

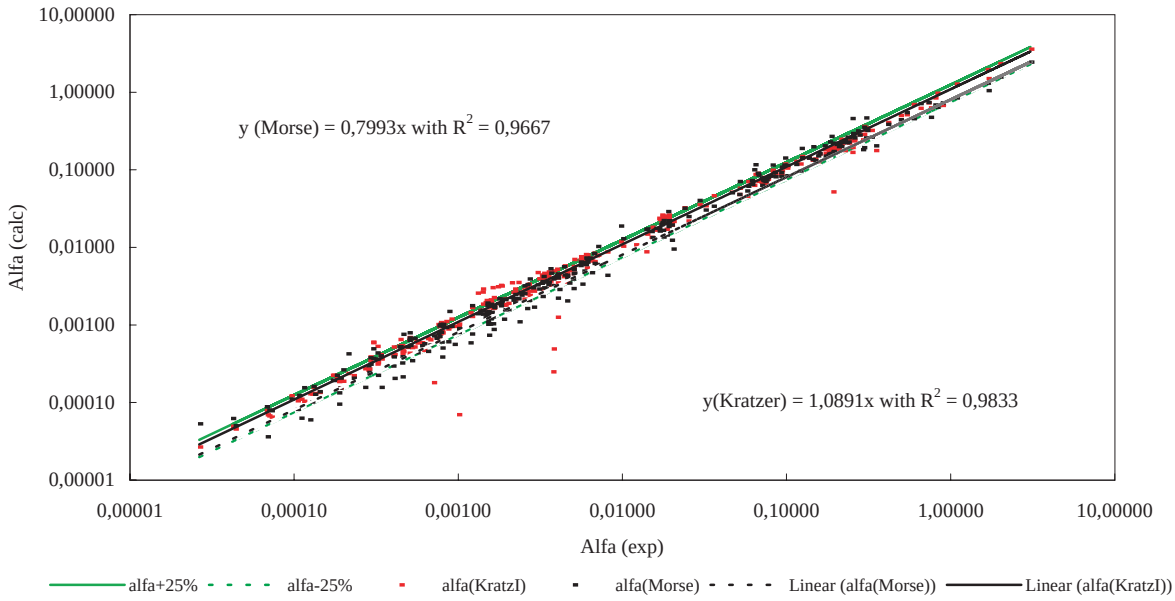


Figure 9a. Alfa for 312 diatomics, computed from Kratzer I/Varshni V and Morse potentials

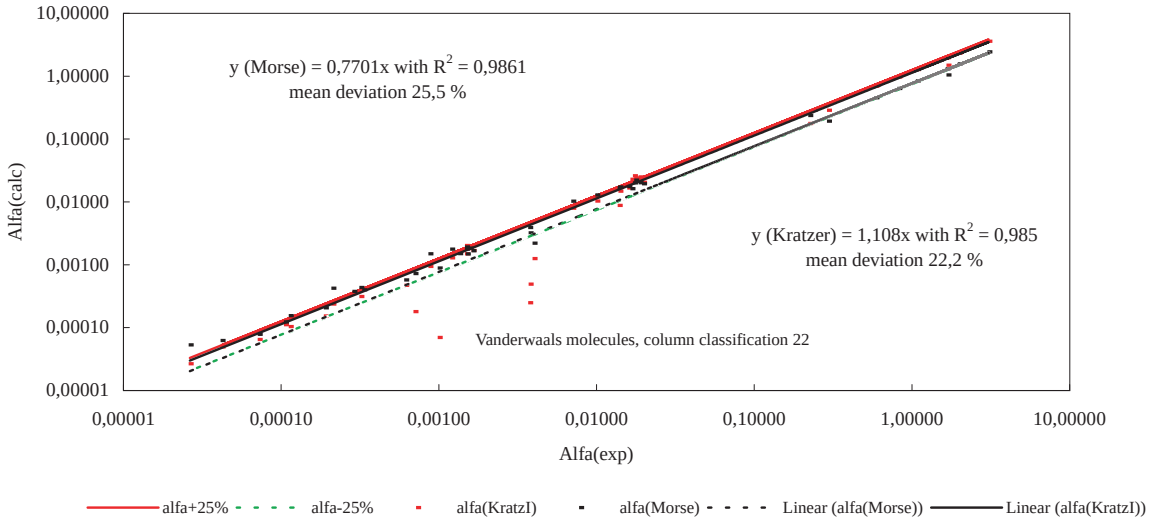


Figure 9b. Alfa for 42 homonuclear bonds, computed from Kratzer I/Varshni V and Morse potentials

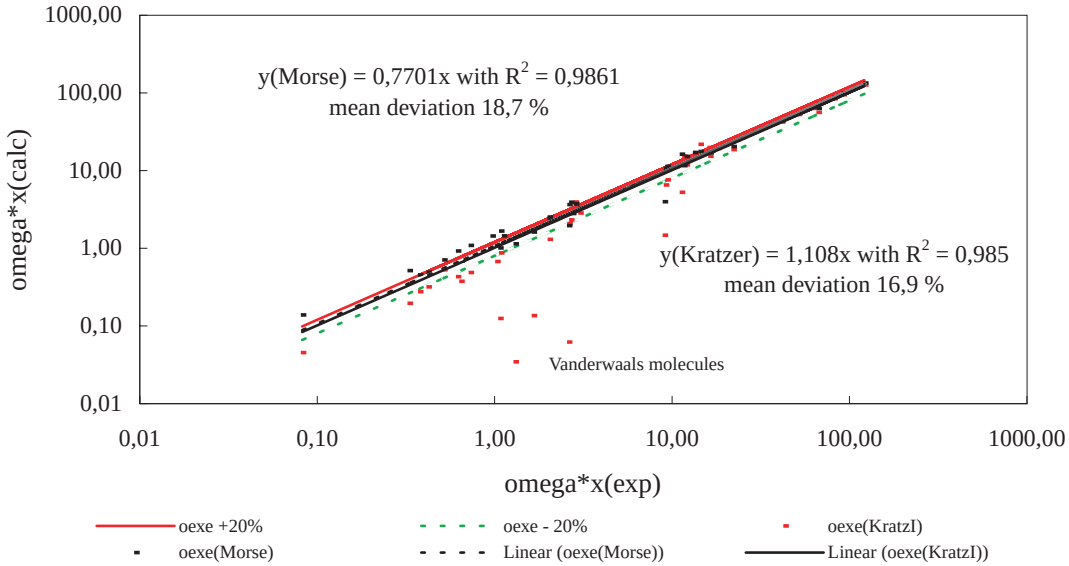


Figure 9c. Omega*x for 42 homonuclear bonds, computed from Kratzer I/Varshni V and Morse potentials

With respect to the Morse results, mean deviations in % are 2 to 3 times smaller for the Kratzer potential (Table 5b). We must keep in mind that many of the compiled constants are uncertain, not all equally accurate and sometimes even in error: the experimental α_e value for YCl (bond Nr. 77 in Table 4) is probably not correct.

Part two of Table 4 reveals interesting further details on this subject. For these 111 bonds, the situation is opposite in terms deviations. Now, Morse′s potential seems superior to Kratzer′s. However, the overall result for the 308 bonds is slightly in favor of the Kratzer potential again. However, this is not straightforward an interpretation.

In fact, the largest deviations for the Kratzer I potential in the 111 bonds set are found

(a) for cases in which $A << 1$ (Van der Waals molecules in group 22 and bonds with noble gas elements in group O): here all deviations are *negative and very large* (between 50 and 100%), meaning that the ionic limit is *overestimated* with an A value around 1

(b) for cases in which $A >> 1$ (multiple bonds): here the opposite situation applies, since all deviations are now *positive and large* (> 20%), as expected. Here the ionic limit is clearly *underestimated*. Numerical results are shown in Tables 4−5.

We did not want an empirical parameterization of the results (for instance using coefficients of empirical trendlines produced in the plots instead of their theoretical values[2][3]). In many cases, this would improve the results empirically (smaller% deviations).

7.5.3 Calculation of α_e and $\omega_e x_e$ for 43 Homonuclear Bonds

With Varshni,[3] we do not understand why the Morse potential has such a good reputation, especially for covalent bonds, as mentioned in many textbooks. Therefore, we selected data for homonuclear diatomics and compared the performances for this type of bond (43 bonds are available, polyvalent atoms, molecular ions, noble gases, ... are all included, see Table 4, Supporting Information).

We present the results in Figure 9b for α_e with the rather surprising conclusion that even here the mean deviations for the ionic Kratzer I potential are smaller than for Morse′s covalent potential. Nevertheless, 5 Van der Waals bonds are included (for which the ionic potential with $A = 1$, $I = 0$, underestimates these asymptotes). These points are indicated in Figure 9a.

In addition, for $\omega_e x_e$ (see Figure 9c) a similar situation applies. Despite the large deviations from $A = 1$ (both > 1 and <1), exactly as in the 111 series and despite the wrong asymptote, the performance of the Kratzer potential is still comparable with that of Morse′s for 43 homonuclear bonds. This is a surprising and unexpected result.

7.5.4 Calculation of α_e and $\omega e x e$ for 91 Single Bonds

For 91 bonds between two monovalent atoms, interesting details show (Table 4, Supporting Information). We refer for this set also to Figure 2, Figure 8, and Figure 7c. The global results are:

− Kratzer potential: mean % deviation for α_e ±8.2, for $\omega_e x_e$ ±13.16%

− Morse potential: mean % deviation for α_e ±25.9, for $\omega_e x_e$ ±26.54%.

These deviations are, as expected, even more pronounced and again in favor of the Kratzer-I−Varshni V potential (see also Tables 5a−b).

7.5.5 Conclusion of This Section

It is difficult to visualize all the results obtained thus far, due to large differences in magnitude, as in Figure 9a−b−c. Nevertheless, we can safely conclude that

(a) an ionic function is better than a covalent one and especially that

(b) the Kratzer-I−Varshni V potential is the most likely candidate, if any, for being a *two-parameter* universal potential.

We will try to illustrate these differences graphically using the Graves−Parr scaling method.[2]

7.6 Scaling 300 Pairs of Dunham Coefficients with an Ionic Sutherland Parameter in the Graves−Parr Scaling Hypothesis

The failure of the Graves−Parr scaling hypothesis led these authors to conclude that this is a deciding step towards the determination of *a four-parameter potential*.[2] Our thesis is to abandon simply the covalent Sutherland parameter as a species dependent scale factor. We can indeed easily demonstrate that the mathematically correct Graves−Parr scaling hypothesis is valid, contrary to their own conclusion, and, hence, that a fourth parameter is not necessary at all.

Let us first give a picture of the unscaled a_1^2 and a_2 values for 381 bonds (Figure 10). Graves and Parr used 150 bonds, leading to a maximum value of the coordinates of 17 for y and 11 for x, considerably lower than those appearing in Figure 10. The empirical fit gives a coefficient of 1.4, within 6% of the coefficient predicted by the Kratzer potentials (Table 2). Even the Kratzer potential, with *ideal* Dunham coefficients (Equation 15), is in line. The most important feature of this Figure 10 is that this scale enlargement to 381 bonds already leads to a rough *clustering*, in agreement with the Graves−Parr scaling hypothesis, and contrary to their own observation, which mentions only *scattering*.[2]

Scaling the coefficients with the covalent Sutherland parameter reduces the number of available data to 303, as D_e must be available. Figure 11 gives the result after scaling with the three parameter Morse potential. The slope is near

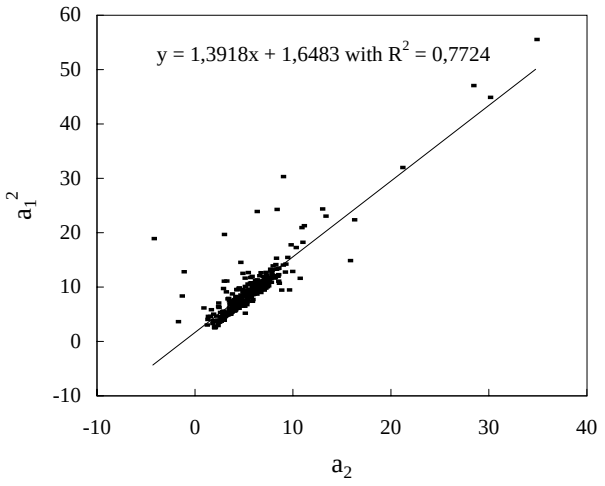


Figure 10. Unscaled a_1^2 versus unscaled a_2 for 381 bonds

unity for a trend line through the origin and the fit of 0.9 is better than in Figure 10 (but this could also be due to a statistical effect, not mentioned by Graves and Parr). Theoretically, at least according to the Graves−Parr[2] scaling hypothesis, the slope should not only be unity but all data points should focus (*cluster*) at a locus near $x = 1$, $y = 1$. This is apparently not the case (see Figure 11).

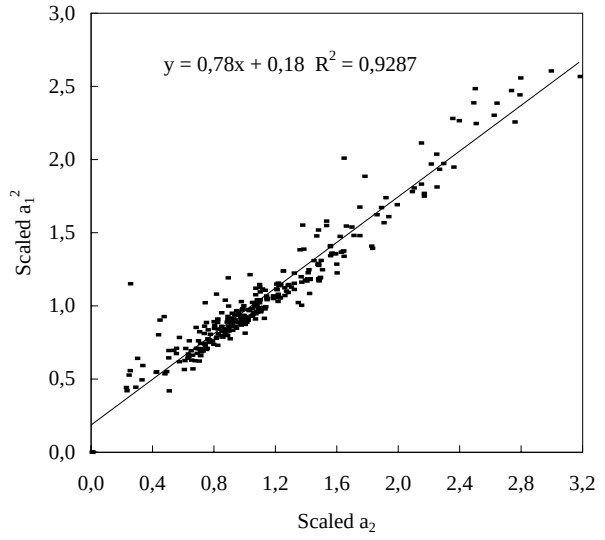


Figure 11. Scaled a_1^2 versus scaled a_2 (covalent Sutherland parameter, D_e) for 312 bonds

We do not show the result for scaling with the Kratzer II potential but immediately give the plot in Figure 12, resulting from scaling with the ionic Sutherland parameter (Kratzer-I−Varshni-V two parameter potential). Since we are no longer dependent on the availability of D_e (just R_e is sufficient), we could at the same time have treated the 381 bonds in Figure 10. However, we wish to compare the two potentials under review by a one by one method. Therefore the same set of 303 bonds is analyzed as in Figure 11 and the same scale is retained to make the differences more pronounced. In comparison with Figure 11, we observe a considerable improvement. This shows above all in the clustering of the data-points in the range $0.8 < x < 1.2$ and $0.8 < y < 1.2$, which is to be expected if the Graves−Parr scaling hypothesis is valid. The slope is near unity but the fit is less than in Figure 11 (which could be a normal consequence of more intensive clustering).

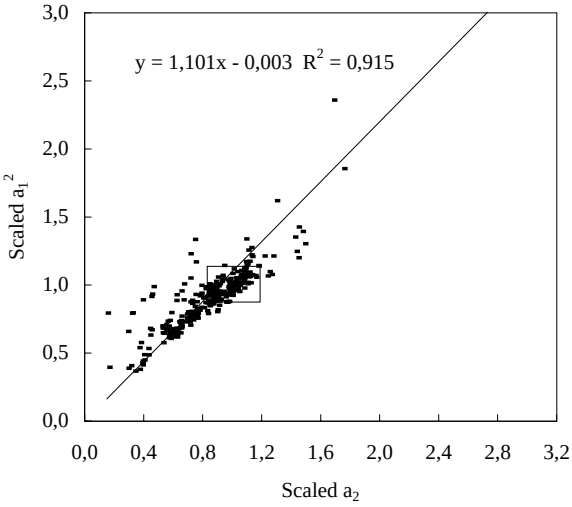


Figure 12. Scaled a_1^2 versus scaled a_2 (ionic Sutherland parameter, e^2/R_e) for 312 bonds

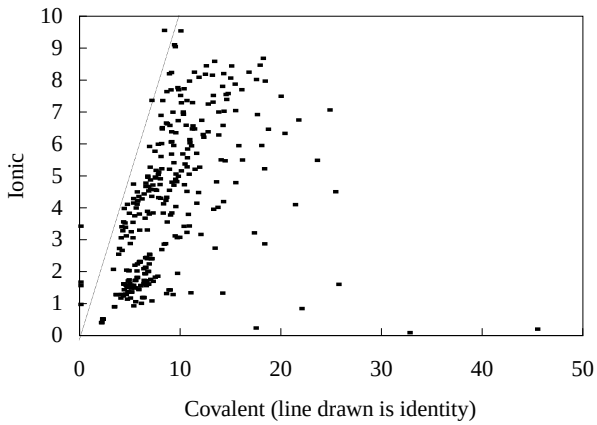


Figure 13. Plot of covalent versus ionic Sutherland parameter for 312 bonds

All this is the more remarkable since the covalent Sutherland parameter values are, on average, *twice as large* than the ionic ones. To illustrate this, we made a plot of the two Sutherland parameters in Figure 13. Scaling by *larger* values should automatically compresses the scaled data to *smaller* values, whereas exactly the opposite effect is observed: the scaling operation is more effective using smaller scaling factors (ionic Sutherland parameters). Considering this shows that the scaling/clustering is even more effective than one could conclude from a simple comparison of the two Figures 11 and 12.

In Figure 14−15, we present the results for the 91 bonds between monovalent atoms. The Morse Graves−Parr plot, Figure 14, does not differ significantly from the general one, Figure 11. For just 22 out of 91 bonds, the data cluster in the critical box. On the contrary for the ionic potential in

Figure 15, the opposite result is obtained: only 21 data points are outside the critical range near $x = 1$, $y = 1$, the most important deviation being found for F_2, indicated in Figure 15. We cannot but conclude that the Graves−Parr scaling hypothesis is indeed valid, contrary to their conclusion. However, this only shows when an alternative asymptote acts as a species dependent scaling factor.

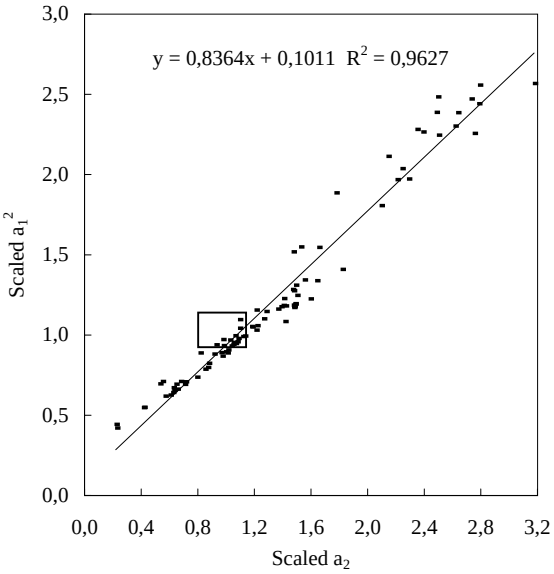


Figure 14. Scaled a_1^2 versus scaled a_2 (covalent Sutherland parameter, D_e) for 91 single bonds

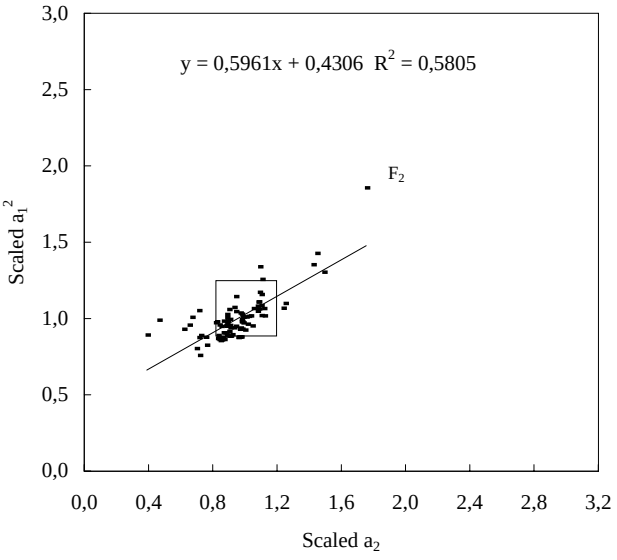


Figure 15. Scaled a_1^2 versus scaled a_2 (ionic Sutherland parameter, e^2/R_e) for 91 single bonds

We had to diverge on this aspect not only for important theoretical but also for practical reasons. Normal graphical procedures are difficult to apply for data, extending to several powers of 10 for a large number of cases (see above, Figure 9a−c and the data in Table 4).

The last figure in this section, Figure 16, represents the scaling results, using the generalized Kratzer-I−Varshni-V potential. This is the only potential giving the theoretical result that $\Delta^{1/2} = F$. This result must be compared with Figure 12.

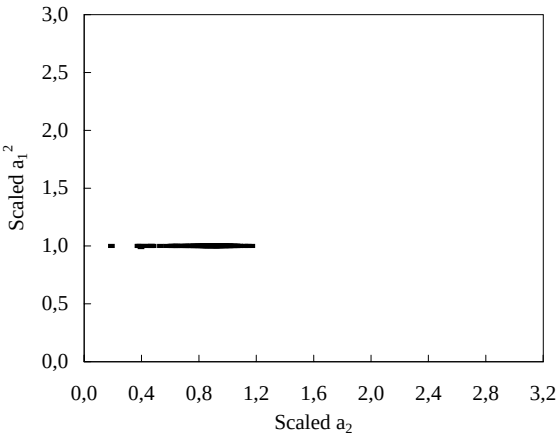


Figure 16. Scaled a_1^2 versus scaled a_2 (Kratzer result, Sutherland parameter = F^2) for 312 bonds

Scaling is now *of course perfect* for a_1^2 but a spread remains for a_2, although 244 data points out of the 303 are still within the critical box (now *line*) near unity. The concentration of 244 data-points in Figure 16 between *0.8 and 1.2 on the x-axis* and an average value for the scaled a_2 of 0.859, i.e. 1 ±14%, for the 303 bonds indicates that the Kratzer-I−Varshni-V potential is quite effective but not completely exact. The spread in the scaled a_2 values is due in the first instance to a scattering in *G*/*F* values. Maybe, the Dunham series is in need of revision (possibly with respect to the truncation of the series for the vibrational energy given the relatively small average deviations on the *x*-axis or, maybe, higher order Dunham coefficients are needed). Maybe also asymptote differences (and hence the critical distance) come into play.[7]

Introducing a third parameter in the Kratzer-I−Varshni-V function might improve the scaling operation and its universal characteristics. Unlike Graves and Parr, we conclude that a four-parameter function is not necessary to obtain better scaling. The large number of data used is an extra argument for this conclusion. Finally, Figure 16 can only be reproduced from ionic potentials as soon as we can show how the identity $F = \Delta^{1/2}$ can be obtained from our scheme for *all* molecules, i.e. those including $A \neq 1$.

7.7 Extension of the Predictions to All Molecules

We now proceed to the necessary, be it totally empirical, extension of the results obtained thus far to all bonds. We can apply a classification scheme (Calder−Ruedenberg[5] or Herschbach−Laurie[19]). A classification in either way is like adding an additional third (but not quantified) parameter. We therefore constructed a pivot table with the Column classification as a guideline and calculated mean *A* factors in Equation (28) using the Kratzer-I−Varshni-V potential and experimental *F* values. We wish to restrict the number of A values to a minimum and require that they should be not too far from 1 in all cases, where at least *one monovalent atom* is present. With two polyvalent atoms in

Table 6. Mean values of F(calc)/F, absolute% deviations and mean C values for 269 bonds with 7 different A values (Column classification) monovalent-monovalent monovalent-polyvalent polyvalent-polyvalent

Groups		H1	H7	H H	11	17	7 7	H2−6	1.2−6	27	37	4 7	5 7	6 7	26	33	3.5−6	44	4.5−6	5 5	5 6	6 6	
A value or Mean																							Total
0.8			*2*		*2*			*5*	*1*														*10*
F(calc)/F			0.956		0.984			1.021	1.014														1.006
abs%F			4.41		2.70			3.37	3.28														3.32
C			1.751		1.302			1.685	1.410														1.560
0.9	#	*4*		*1*	*1*	*2*	*1*	*10*	*3*	*1*		*1*	*3*	*3*			*1*					*1*	*32*
F(calc)/F		1.029		0.989	0.997	1.023	1.014	1.027	1.016	0.959		1.037	1.009	0.998			0.971					1.022	1.015
abs%F		2.92		1.14	0.28	2.39	1.39	2.74	4.38	4.10		3.66	3.08	0.66			2.88					2.20	2.62
C		1.638		1.956	1.173	1.387	1.063	1.579	1.424	0.932		1.530	1.515	1.241			1.848					1.264	1.482
1.0	#	*2*	*5*	*1*	*3*	*18*	*10*	*19*	*3*		*18*	*3*	*3*								*1*	*3*	*89*
F(calc)/F		0.992	1.014	0.975	1.008	1.003	0.987	0.999	1.007		1.005	1.004	0.980								0.971	1.044	1.001
abs%F		0.77	2.51	2.47	1.32	2.66	2.69	2.31	3.17		2.35	1.77	2.03								2.88	4.40	2.45
C		1.578	1.588	1.783	1.246	1.406	1.207	1.597	1.264		1.469	1.437	1.462								1.157	1.371	1.444
1.1	#	*5*	*11*		*3*	*7*		*6*		*3*		*2*	*2*		*2*	*2*	*2*	*1*	*1*		*2*	*2*	*51*
F(calc)/F		0.990	1.000		1.000	0.993		1.003		1.001		0.966	0.999		1.004	0.968	0.966	1.038	1.039		0.962	1.009	0.995
abs%F		2.91	2.38		1.69	1.33		2.40		1.70		3.44	1.32		2.70	3.17	3.44	3.80	3.92		3.82	1.28	2.37
C		1.688	1.627		1.230	1.517		1.486		1.459		1.541	1.482		1.302	1.155	1.231	1.429	1.269		1.258	1.367	1.477
1.2	#	*2*	*1*	*6*		*1*		*5*	*1*	*4*	*1*			*1*	*2*				*4*	*3*	*5*	*4*	*40*
F(calc)/F		0.991	0.983	0.982		1.018		1.017	1.003	0.993	1.003			1.013	1.029				1.009	1.003	0.996	0.994	1.000
abs%F		2.12	1.73	1.78		1.75		1.68	0.32	1.64	0.32			1.29	2.89				2.19	2.18	1.97	2.72	1.93
C		1.595	1.539	1.801		1.392		1.439	0.856	1.525	1.390			1.755	1.302				1.253	1.149	1.310	1.377	1.434
1.3	#									*1*	*1*	*2*			*3*		*1*		*11*	*2*	*1*	*2*	*24*
F(calc)/F										1.003	0.970	1.010			1.005		1.013		1.006	1.016	0.964	0.971	1.001
abs%F										0.31	3.03	1.12			2.14		1.32		1.73	1.60	3.59	2.91	1.87
C										1.366	1.304	1.144			1.222		1.424		1.260	1.301	1.409	1.205	1.264
1.4	#							*3*		*1*	*1*						*2*	*2*	*8*	*4*	*2*		*23*
F(calc)/F								0.977		1.000	0.989						1.014	0.977	0.997	0.977	0.975		0.988
abs%F								2.34		0.02	1.15						1.37	2.31	1.99	2.31	2.53		1.99
C								1.495		1.456	1.417						1.482	1.409	1.403	1.252	1.359		1.395
Total	#	13	18	8	9	28	11	48	9	10	21	8	8	4	7	2	6	3	24	9	11	12	269
F(calc)/F		1.003	1.001	0.982	0.999	1.003	0.990	1.008	1.011	0.994	1.002	1.000	0.995	1.001	1.011	0.968	0.990	0.997	1.005	0.994	0.981	1.007	1.001
abs%F		2.46	2.49	1.79	1.63	2.28	2.57	2.46	3.28	1.61	2.23	2.26	2.25	0.82	2.51	3.17	2.30	2.81	1.98	2.11	2.64	2.89	2.32
C		1.641	1.618	1.818	1.245	1.432	1.194	1.566	1.304	1.423	1.455	1.402	1.487	1.370	1.268	1.155	1.450	1.416	1.307	1.229	1.304	1.336	1.437
Ions	#		5	2			2	11										1	2	2	1	1	27

a bond, larger deviations for A from unity can be expected. These would then have to follow roughly the Calder−Ruedenberg classification,[5] if this makes sense. These authors, with Graves and Parr,[2] used 13 groups (13 values for the additional but hidden parameter) in their analyses of 150 molecules, of which some classes are very similar and nearly coincide (see also *F*igure 1b).

Table 6 gives the results. Only *seven* different (rounded) A values are needed to encompass the results for 269 bonds (in which 27 molecular ions are included, see bottom line of Table 6). The %-deviations of the experimental F values are given, as well as the mean C value for each class. The correlation with the Column classification is roughly followed for polyvalent atoms but we do not discuss the details. We observe that an ionic *three*-parameter potential is largely sufficient. In addition, just 5 A parameters *around unity*, i.e. 0.8; 0.9; 1.0; 1.1, and 1.2 account for more than 220 of the 269 bonds, covering F to within ±3% (and hence also α_e).

Obviously, a three parameter ionic potential is capable of producing Figure 16, which is the best scaling result yet obtainable for the Dunham coefficients a_1 and a_2. This is based upon the identity $F = \Delta^{1/2}$, which is also generated by the generalized Kratzer-I−Varshni-V potential.

7.8 G/F (Calder−Ruedenberg Constant C) and $G/(1 + F)^2$ Values

The C ratio′s in Tables 4−6 reveal that the mean deviation is about the same as for α_e computed with the Kratzer-I−Varshni-V potential. For the corresponding G/F values in function of F, the observed spread (not shown) is 3 times larger than for the $G/(1 + F)^2$ values. This leads us again to conclude that C is far from being constant (see above). However, it is difficult to find any regularity in G/F values (C values) or in $G/(1 + F)_2$ values. This remains the largest stumbling block in achieving a complete picture in the spectroscopic behavior of molecules in terms of ionic potentials or of any kind of potential. The scattering in the G/F ratio is also responsible for the scattering in the scaled a_2 values in Figure 16. Reminding the definition of G/F (or C), in Equation (30), all this must not come as a surprise.

Preliminary analyses point in the direction of a possible relation of the G/F- or similar ratio′s with the critical distance (which corresponds with the asymptote difference). Although this sounds logical[7] and in line with the possible interference of the non-crossing rule (see above), a further discussion of this important question is not given, as more work is needed.

7.9 The Existence of a Universal Two-Parameter Function: Alternative Choices

Against all expectations in the literature, the $F(\Delta)$- and $G(\Delta)$ relations and the scaling effects of an ionic Kratzer-I−Varshni-V potential upon a_1 and a_2 indicate that even a universal ***two***-parameter function does exist for the situation around R_e for a large number and variety of bonds. In addition, its performances for reproducing first order constants are excellent. Using a third parameter for this

function results in an exact fit, as far as F is concerned (see Table 6) and, hence, in almost perfect scaling (as depicted in Figure 16) with a small number (7) of A values for 269 bonds. This corresponds with a really universal three parameter potential.

However, speaking of two or three parameters has become somehow confusing, since we disregarded constraint (ii). But, to put all functions on an equal basis, other functions should be tested upon their relative merits for coping with the constants, using for scaling, instead of D_e, the asymptote generated by the function itself (an example was given by Von Szentpaly[15]).

We cannot predict the outcome of such a review, although we tested here two important *reduced* functions, belonging to two completely different classes of potentials (Morse, exponential and of covalent type versus generalized Kratzer, Coulomb-like and of ionic type). However, a better low parameter potential may appear for scaling purposes. Then, one must review also its capacity (a) to explain chemical bonding (at the minimum) and/or (b) to reproduce the atomic dissociation limit.

In this last respect, any ionic potential will fail by definition as will any other potential with an asymptote $D_x \neq D_e$. In fact, under the rather severe simplifying conditions inherent to ionic potentials and without the condition that D_e should be reproduced, the deviations found in $G(F)$ plots as well as those found in $G/F(F)$ plots indicate that inconsistencies remain with ionic and, most probably, also with a number of other potentials. These can be due either to (a) errors in experimental data (not taken into account), (b) the choice of the potentials (and their analytical form), (c) the Dunham expansion (in which higher order terms in the vibrational part are neglected), (d) higher Dunham coefficients (not considered here[2][24]) or finally to (e) a discontinuous switch between dissociation limits at an R value $\infty > R > R_e$, whereby there is a corresponding shift from one potential to another or from one set of parameters to another in the same potential (non-crossing rule, see next section).

7.10 Obtaining the Correct or Atomic Dissociation Limit, Using an Ionic Two-Parameter Potential

The inconsistencies observed for scaled a_2 values (or in G and in G/F ratios and related ones) indicate that away from the minimum other corrections or additional coefficients are needed for the situation at $R >> R_e$. As the ionic asymptote is situated between a_0 and D_e, the non-crossing rule can interfere.

For large R, interatomic forces are commonly designed as Van der Waals-forces, varying with $1/R^n$, with $n>2$, which are not point charge Coulomb forces[39] as the ones leading to the *ionic* dissociation limit. Very recently, a possible switch from an ionic (Kratzer) potential to a covalent one somewhere between R_e and ∞ was described by Herrick and O′Connor.[40] The problem is not discussed here in detail, as, with Graves and Parr,[2] we remain convinced that the *primary* evidence about the relations between the constants and even about convergence is to be found in the first constants in the Dunham expanion and to the (analytical form of the) potential, wherein R_e, k_e and the asymptote (be it D_e or D_x) will invariantly play a crucial role.

But, these important further details must not distract us from the main conclusion *that a universal two-parameter ionic function exists within reasonable limits.*

7.11 Chaotic/Fractal Behavior

Although we present evidence that Coulomb′s (inverse power) law is important for understanding the relations between the constants of a large number of molecules, this does not fully support fractal/chaotic behavior in anharmonicities.[16] The evidence presented thus far[16] is not yet convincing. We found that power relations in some critical cases are not significantly better than classical linear or quadratic relations. We showed that the use of power laws can be misleading, as fundamental details can get lost (the breaking of the M−Z symmetry). Using log-scales may be an aid when scale differences get large, but they do not change the underlying physical or chemical ideas.

7.12 A Universal Bond, Atomic and Molecular Spectroscopy

Finding a universal function is equivalent to finding a universal bond, a standard for molecular spectroscopy, and the equivalent of H, the standard for atomic spectroscopy.

The Kratzer potential is also applicable in atomic spectroscopy.[34] In molecular spectroscopy, a *one parameter potential* reduces to $U(R) = (e^2/R_e)(1 - R_e/R)^2$ and leads to $\Delta^{1/2} = 1$ (or $F = 1$). Then the most likely candidate for a universal bond should obey almost all of the following constraints to within reasonable limits: $D_x \approx D_{ion} \approx e^2/R_e \approx e^2/2r_X \approx a_0 \approx IE_X$; $F \approx \Delta^{1/2} \approx 1$; $G \approx 24-30$ and, perhaps also $D_{e(XX)} = EA_X$.[34] So we end ultimately with molecules containing Li (with H or other alkali metals), with BeH bonds and, eventually, with the molecule Li_2 (see for instance Table 4). We had, of course, preferred (*desired*) to end with H_2 to make the analogy between atomic and molecular spectroscopy complete, but maybe this is a matter of further scaling (we refer to the breaking of the M−Z symmetry). In addition, the PE curve generated for Li_2 (ground and excited states) computed from a generalized Kratzer potential coincides with the RKR curve.[7] Hence, our search for a simple (two-parameter) potential in molecular spectroscopy, brings us back, at least in a first order approximation around R_e, to atomic spectroscopy and the Bohr-atom model. The fact that ionization potentials appear as the leading term in the global molecular scaling process may contribute to this result. Ionization potentials show a well-known Column and Row dependence, as well as a Z and/or mass dependence, capable of transforming the Periodic Table in a one-dimensional array (see our discussion at Figure 1). This is understandable, when looking

at the analytical form of the Kratzer potential, shaped to be applied in atomic spectroscopy too and used by Fermi[38] in a number of other instances. This now leads to a formal link between atomic and molecular spectroscopy.[34]

The theoretical basis for the universal character of the Kratzer potential is easily recognized. Its quadratic term in R is a generalization of the quantum hypothesis that the angular momentum be constant or that the velocity of a particle varies as $1/R$. The repulsive part in the Kratzer potential corresponds with a kinetic energy term. This secures that, at equilibrium, the ratio between attraction and repulsion terms is always 1/2.

Having in mind that Coulomb′s law is at the hart of this unifying process and that this fundamental law together with a quantum-hypothesis is automatically included in any Kratzer-type potential, it becomes easier to understand

(a) why a universal potential, if it exists in molecular spectroscopy, is also important for a number of other phenomena in *applied* chemistry[1]

(b) that such a potential is very suited for scaling spectroscopic constants and, finally,

(c) that a truly universal potential might indeed have exactly this analytical form.

8. Conclusion

We presented almost conclusive evidence that the Holy Grail of Spectroscopy[10] is an ionic *two-parameter* potential of Kratzer−Varshni-V-type. Bound to a *wrong* asymptote, this simple potential leads to a quantitatively excellent first order approximation for an impressively large number of spectroscopic constants and is superior to a *three-parameter* Morse potential, which uses the *correct* asymptote.

This *wrong* asymptote also gives a smooth picture of the bonding situation at R_e, exactly the only region where Dunham′s analysis (which refers to an asymptote of its own) makes sense. Whether or not the best scaling asymptote is the ionic dissociation limit, could be a matter of further research but the present results reveal that it is certainly a good candidate. Hence, ionic asymptotes can no longer be disregarded in *any* theory of chemical bonding.

Even for homonuclear bonding, the accuracy and consistency of the ionic bonding model, which was the standard by excellence in the early days of theoretical chemistry[6,7,20,21,34] now seems beyond any doubt. Unfortunately, this elementary model was abandoned soon after quantum-mechanical results became available, which led to a new theory of bonding. Ironically enough, exactly the *supposedly poor* performance of ionic potentials in molecular spectroscopy was, at that time, one of the major arguments to abandon the ionic bonding model.[28] Now, our large-scale analysis shows that, on the contrary, ionic potentials are performing very well. Looking at the situation *near the minimum*, we must conclude that covalent or Lewis bonding can be quantitatively rationalized in terms of ionic bonding, which has its roots in Coulomb′s law. The rationale behind the observed simple behavior of spectroscopic constants is that, *at the minimum*, a bond XX is well represented by an equal mixture of two ionic structures $X^+X^- + X^-X^+$. This gives a different but essentially equivalent interpretation of the Lewis concept of valence electron sharing. It appears that we discovered a *trompe l′oeil* in chemistry[41]: the *spectroscopic* behavior of *atoms* in *molecules* is rationalized by the interference of an unobservable (*ionic*) *asymptote*, different from the asymptote we can observe: the *atomic dissociation limit*.

Acknowledgments

Spectroscopic work supported by grant G.0073.96 of the FWO-Vlaanderen (Fund for Scientific Research-Flanders).

[1] J. Ferrante, J. R. Smith, J. H. Rose, *Phys. Rev. Lett.* **1983**, *50*, 1385; J. H. Rose, J. Ferrante, J. R. Smith, *Phys. Rev. Lett.* **1981**, *47*, 675; J. Ferrante, H. Schlosser, J. R. Smith, *Phys. Rev. A*, **1991**, *43*, 3487.
[2] J. L. Graves, R. G. Parr, *Phys. Rev. A* **1985**, *31*, 1 (see also: J. L. Graves, *Int. J. Quant. Chem*. **1997**, *65*, 1).
[3] Y. P. Varshni, *Rev. Mod. Phys.* **1957**, *29*(4), 664.
[4] Y. P. Varshni, R. C. Shukla, *J. Chem. Phys.* **1961**, *35*(2), 582; Y. P. Varshni, R. C. Shukla, *Rev. Mod. Phys.* **1963**, *35*(1), 130; Y. P. Varshni, R. C. Shukla, *J. Molec. Spectr.* **1965**, *16*, 63.
[5] G. V. Calder, K. Ruedenberg, *J. Chem. Phys.* **1968**, *49*(12), 5399.
[6] G. Van Hooydonk, *Z. Naturforsch. A* **1982**, *37*, 710; *Z. Naturforsch. A* **1982**, *37*, 971.
[7] G. Van Hooydonk, *THEOCHEM − J. Mol. Struct.* **1983**, *105*, 69.
[8] F. Jenc, Int. Rev. Phys. Chem. **1996**, *15*(2), 467−523; *Phys. Rev. A.* **1990**, *42*, 403−414; *Adv. At. Mol. Phys.* **1983**, *19*, 265; D. Steele, E. R. Lippincott, J. T. Vanderslice, *Rev. Mod. Phys.* **1968**, *34*, 239.
[9] K. S. Jhung, I. H. Kim, K. B. Hahn, K.-H. Oh, *Phys. Rev. A.* **1989**, *40*, 7409; K. S. Jhung, I. H. Kim, K.-H Oh, K. B. Hahn, K. H. C. Jhung, *Phys. Rev. A.* **1990**, *42*, 6497.
[10] J. Tellinghuisen, S. D. Henderson, D. Austin, K. P. Lawley, R. J. Donovan, *Phys. Rev. A* **1989**, *39*, 925; see also: A. A. Zavitsas, *J. Am. Chem. Soc.* **1991**, *111*, 4755.
[11] G. B. B. M. Sutherland, Proc. *Indian Acad. Sci.* **1938**, *8*, 341.
[12] J. L. Dunham, *Phys. Rev.* **1932**, *41*, 713, 721.
[13] P. M. Morse, *Phys. Rev.* **1929**, *34*, 57.
[14] J. R. Smith, H. Schlosser, W. Leaf, J. Ferrante, J. H. Rose, *Phys. Rev. A* **1989**, *39*, 514.
[15] L. Von Szentpaly, Chem. *Phys. Lett.* **1995**, *245*, 209.
[16] G. R. Freeman N. H. March, L. Von Szentpaly, *THEOCHEM − J. Mol. Struct.* **1997**, *394*, 11.
[17] K. P. Huber, G. Herzberg, *Molecular Spectra and Molecular Structure*, vol. IV (Constants of Diatomic Molecules), Van Nostrand-Reinhold, New York, **1979**.
[18] A. A. Radzig, B. M. Smirnov, *Reference data on atoms, molecules and ions*, Springer Series in Chemical Physics 31, Springer, Berlin, **1985**.
[19] D. H. Herschbach, V. W. Laurie, *J. Chem. Phys.* **1961**, *35*, 458.
[20] J. J. Berzelius, *Lehrbuch der Chemie*, Arnold, Dresden, **1835**.
[21] W. Kossel, *Ann. Phys.* **1916**, *49*, 229; *Z. Phys.* **1924**, *23*, 403.
[22] R. F. Borkman, R. G. Parr, *J. Chem. Phys.* **1968**, *48*, 1116.
[23] R. T. Sanderson, *Chemical Bonds and Bond Energy*, Academic Press, New York, **1976**.
[24] G. Simons, R. G. Parr, J. M. Finlan, *J. Chem. Phys.* **1973**, *59*(6), 3229−3234; G. Simons, J. M. Finlan, *Phys. Rev. Lett*. **1974**, *33*, 131.
[25] A. Kratzer, *Z. Phys.* **1920**, *3*, 289; *Ann. Phys.* **1922**, *67*, 127.
[26] M. Born, A. Landé, *Verh. Dsch. Phys. Ges.* **1918**, *20*, 210.
[27] L. Pauling, Proc. *Nat. Acad. Sci. India* **1956**, *A25*, 1.
[28] R. S. Mulliken, *Phys. Rev.* **1936**, *50*, 1017; *Phys. Rev.* **1936**, *50*, 1028.
[29] R. Mecke, *Z. Phys.* **1927**, *42*, 390.
[30] E. Grüneisen, *Ann. Phys.* **1908**, *26*, 393.
[31] G. Mie, *Ann. Phys.* **1903**, *11*, 657.
[32] E. Fues, *Ann. Phys.* **1926**, *80*, 376.
[33] 33. A. Requena, J. Zuniga, L. M. Fuentes, A. Hidalgo, *J. Chem.*

Phys. **1986**, *85*, 3939; J. M. Frances, J. Zuniga, M. Alacid, A. Requena, *J. Chem. Phys.* **1989**, *90*(10), 5536; A. Bastida, J. Zuniga, M. Alacid, A. Requena, A. Hidalgo, *J. Chem. Phys.* **1990**, *93*(5), 3408; A. Requena, M. Alacid, A. Bastida, J. Zuniga, Int. *J. Quant. Chem*. **1994**, *52*(1), 165; M. Bag, M. M. Panja, R. Dutt, Y. P. Varshni, *J. Chem. Phys.* **1991**, *95*(2), 1139−1143; D. R. Herrick, S. O′Connor, *J. Chem. Phys.* **1998**, *109*(6), 2071; R. L. Hall, N. Saad, *J. Chem. Phys.* **1998**, *109*(8), 2983; D. Secrest, *J. Chem. Phys.* **1988**, *89*, 1017, *J. Phys. Chem*. **1991**, *95*(3), 1058; A. Alijah, G. Duxbury, *Mol. Phys.* **1990**, *70*(4), 605; J. F. Ogilvie, *J. Chem. Phys.* **1988**, *88*(4), 2804; C. Amiot, *J. Chem. Phys.* **1990**, *93*(12), 8591, *J. Mol. Spectr*. **1991**, *147*(2), 370; B. H. Chang, D. Secrest, *J. Chem. Phys.* **1991**, *84*(2), 1196; S. Brajamani, C. A. Singh, *J. Phys. A, Math. Gen*. **1990**, *23*(15), 3421; J. Makarewicz, *J. Phys. B, Atom Mol. Opt. Phys.* **1988**, *21*(22), 3633; R. E. Moss, I. A. Sadler, *Mol. Phys.* **1989**, *68*(5), 1015; M. Molski, J. Konarski, *Phys. Rev. A* **1993**, *47*(1), 711, *Chem. Phys. Lett.* **1992**, *196*(5), 517, *Acta Phys. Pol. A* **1992**, *81*(4−5), 495, *Theor. Chim. Acta* **1993**, *85*(5), 325, *J. Molec. Struct*. **1993**, *297*, 415; J. Konarski, *Bull. Pol. Acad. Sci. Chem*. **1995**, *43*(4), 279; K. Nakagawa, H. Uehara, Chem. *Phys. Lett.* **1990**, *168*(1), 96; K. Nakagawa, M. Akiyama, *Chem. Phys. Lett*. **1992**, *190*(1−2), 91; J. F. Ogilvie, H. O. Mcc, *J. Molec. Struct*. **1991**, *263*, 167; F. M. Fernandez, J. F. Ogilvie, *Chem. Phys. Lett.* **1990**, *169*(4), 292; C. G. Diaz, F. M. Fernandez, E. A. Castro, *Chem. Phys.* **1991**, *157*(1−2), 35; F. M. Fernandez, E. A. Castro, *J. Math. Chem*. **1993**, *12*(1−4), 1; I. L. Cooper, *Chem. Phys*. **1988**, *121*(3), 343, *Int. J. Quant. Chem*. **1994**, *49*(1), 25; T. Hayes, D. Bellert, T. Buthelezi, P. J. Brucat, *Chem. Phys. Lett.* **1998**, *287*(1−2), 22; J. Konarski, *J. Molec. Struct*. **1992**, *270*, 491; J. K. G. Watson, *J. Chem. Phys.* **1989**, *90*(11), 6443; J. Morales, J. J. Pena, G. Ovando, V. Gaftoi, *J. Math. Chem*. **1997**, *21*(3), 273; J. Morales, G. Arreaga, J. J. Pena, V. Gaftoi, G. Ovando, *J. Math. Chem*. **1995**, *18*(2−4), 309; K. Takcz-Smiech, W. S. Ptak, A. Kolezynski, Int. *J. Quant. Chem*. **1996**, *57*(6), 1097; K. Tkacz, W. S. Ptak, *J. Molec. Struct*. **1992**, *275*, 23; K. Tkacz-Smiech, W. S. Ptak, A. Kolezynski, J. Mrugalski, *Int. J. Quant. Chem*. **1994**, *51*(6), 569; K. Tkacz, W. S. Ptak, *THEOCHEM − J. Molec. Struct*. **1989**, *61*, 91; P. Chang, C. S. Hsue, *Phys. Rev. A*. **1994**, *49*(6), 4448; J. Pliva, *J. Molec. Spectr.* **1999**, *193*(1), 7; K. A. Walker, M. C. L. Gerry, *J. Chem. Phys.* **1998**, *109*(13), 5439; J. Dvorak, L. Skala, *Collect. Czech. Chem. Commun*. **1998**, *63*(8), 1161; M. M. Chaudhari, S. H. Behere, *Ind. J. Pure Appl. Phys*. **1996**, *34*(1), 42; A. Aguado, J. J. Camacho, M. Paniagua, *THEOCHEM − J. Molec. Struc*. **1992**, *86*, 135; Y. Ergun, H. O. Pamuk, E. Yurtsever, *Z. Naturforsch. A* **1990**, *45*, 889; C. J. Ballhausen, M. Gajhede, Chem. *Phys. Lett*. **1990**, *165*(5), 449; J. Mehra, *Found. Phys*. **1988**, *18*(2), 107.

[34] G. Van Hooydonk, *THEOCHEM − J. Molec. Struct*. **1984**, *109*, 87.

[35] J. K. Wilmshurst, *J. Chem. Phys.* **1959**, *30*, 561; *J. Phys. Chem*. **1958**, *62*, 631.

[36] L. Pauling, *J. Am. Chem. Soc*. **1932**, *54*, 3570.

[37] R. S. Mulliken, *J. Chem. Phys.* **1934**, *2*, 782.

[38] V. Weisskopf, *Letters in Theoretical Physics*, vol. III, Interscience, New York, **1961**.

[39] C. A. Coulson, *Proc. Roy. Soc. (Edinburgh)*, **1932**, *A135*, 459; L. Pauling, J. Y. Beach, *Phys. Rev.* **1935**, *47*, 686.

[40] D. R. Herrick, S. O′Connor, *J. Chem. Phys.* **1998**, *109*(1), 11.

[41] G. Van Hooydonk, hep-th/9902152 for another application.

Received January 7, 1999
[O99005]

Biomimetic Morphogenesis of Fluorapatite-Gelatin Composites: Fractal Growth, the Question of Intrinsic Electric Fields, Core/Shell Assemblies, Hollow Spheres and Reorganization of Denatured Collagen

Susanne Busch,[a] Hans Dolhaine,[b] Alexander DuChesne,[c] Sven Heinz,[a] Oliver Hochrein,[a] Franco Laeri,[d] Oliver Podebrad,[e] Uwe Vietze,[d] Thomas Weiland,[e] and Rüdiger Kniep,*[a][+]

Keywords: Fractals / Materials science / Fluorapatite / Collagen / Intrinsic electric fields / Core/shell assemblies

The biomimetic growth of fluorapatite in gelatin matrices at ambient temperature (double-diffusion technique) starts with elongated hexagonal-prismatic seeds followed by self-similar branching (fractal growth) and ends up with anisotropic spherical aggregates. The chemical system fluorapatite/gelatin is closely related to in vivo conditions for bone or tooth formation and is well suited to a detailed investigation of the formation of an inorganic solid with complex morphology (morphogenesis). The fractal stage of the morphogenesis leads to the formation of closed spheres with diameters of up to 150 μm. The self-assembled hierarchical growth thereby shows immediate parallels to the topological branching criteria of the macromolecular starburst dendrimers. A second growth stage around the closed spheres of the first stage is characterized by the formation of concentric shells consisting of elongated prismatic fluorapatite units with nearly parallel orientation (maximum diameter of the complete core/shell spheres of 1 mm). The specific structure of the core/shell assembly is similar to the dentin/enamel structure in teeth. Together with the idea of the biological significance of electric fields (pyro-, piezoelectricity) during apatite formation under in vivo or biomimetic conditions the present paper considers the composite character of the material and the mechanisms of fractal growth (branching criteria and architecture, the influence of intrinsic electric fields etc.).



Dr. Susanne Busch studied chemistry at Darmstadt University of Technology and received her Ph.D. degree under the supervision of Prof. Dr. R. Kniep in winter 1998. The thesis is entitled "Self-Organization and Morphogenesis of Apatite-Gelatin-Composites under Biomimetic Conditions." At present she is continuing her research on the topic of biomimetic growth of apatite at the Max-Planck-Institute for Chemical Physics of Solids, Dresden.

Dr. Hans Dolhaine studied chemistry at the Universities of Münster, Dortmund and Düsseldorf. He received his Ph.D. degree in 1977. The thesis entitled "NMR-studies on Phosphonates" was performed in Prof Dr. G. Hägele's laboratories at the University of Düsseldorf, supported by a fellowship from the "Studienstiftung des Deutschen Volkes." Currently he is working on various industrial research projects at the Henkel KGaA, Düsseldorf.

Dr. Alexander DuChesne studied chemistry at the Universities of Mersburg and Sofia. In 1991 he started investigations on block copolymer morphologies at the Max-Planck-Institute for Polymer Research in Mainz under the supervision of Prof. Dr. G. Wegner. After receiving his Ph.D. degree in 1993 he went to University College, Dublin to work on conformational transitions of thermoreversible polymer gels with Prof. Dr. K. Dawson. In 1995 he returned to the Max-Planck-Institute at Mainz. He is a specialist in transmission electron microscopy and his current research interests include water-soluble coatings, latex film characterization, polymer morphology, phase transitions, biomineralization and composites.

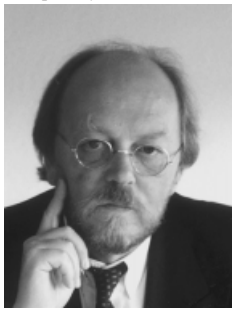
Dipl. Chem. Sven Heinz studied chemistry at the University of Regensburg where he received his diploma under the supervision of Prof. Dr. R. Andreesen (Dept. of Haematology and Oncology, University Hospital, Regensburg). In 1996, he joined the group of Prof. Kniep at Darmstadt University of Technology to work in the field of gelatin matrix-assisted biomineralization. In 1997, he returned to the group of Prof. Andreesen where he is currently working on his Ph.D. thesis characterising new dendritic cell-specific gene products.

Dipl.-Ing. Oliver Hochrein studied chemistry at Darmstadt University of Technology, where he received his diploma degree in 1996. He is currently working on his Ph.D. thesis about the synthesis and characterization of nitridometalates. In September 1998 he followed Prof. Kniep to the Max-Planck-Institute for Chemical Physics of Solids at Dresden where he continues his work. Furthermore he is interested in the visualization and simulation of growth processes in biomimetic systems.

Dr. Franco Laeri studied at the University of Bern. He received his Ph.D. degree in 1984 from the Institute of Applied Physics at Darmstadt University of Technology . He then went to IBM in San Jose, USA, and returned to Darmstadt in 1984. His current research interest is centered around the optical and electronic properties of ordered porous materials and nanocomposites.

Dipl.-Ing. Oliver Podebrad studied electrical engineering at Darmstadt University of Technology and received his diploma degree in 1994. Since 1995, he has worked as a research assistant in the department of Theory of Electromagnetic Fields at Darmstadt University of Technology. His main research interest is the numerical calculation of electromagnetic fields with a subgrid-formulation of the Finite Integration Method.

Dipl. Phys. Uwe Vietze studied physics at the Institute of Applied Physics at Darmstadt University of Technology and is a Ph.D. candidate. He obtained his diploma degree in 1994 and his current work involves the optical and electronical properties of ordered porous materials and nanocomposites.



Prof. Dr.-Ing. Thomas Weiland studied electrical engineering and mathematics at Darmstadt University of Technology and received his Ph.D. degree in 1977. As a fellow at the European Institute for Nuclear Research (CERN, Switzerland) he continued his work on electromagnetic computing. In 1983, at the DESY in Hamburg, he founded an international collaboration for 3-D electromagnetic simulations. Since 1989, he is a full professor at Darmstadt University of Technology, as head of the department of Theory of Electromagnetic Fields. In 1993, he was elected a full member of the Academy of Science and Literature at Mainz. He received the "Leibniz-Prize" from the German Research Association in 1987 and the "Max Planck Research Prize for International Collaboration" in 1995.

Prof. Dr. Rüdiger Kniep studied chemistry and mineralogy at the Technical University of Braunschweig and received his Ph.D. degree under the supervision of Prof. Dr. A. Rabenau (Max Planck Institute for Solid State Research, Stuttgart) at the Technical University of Braunschweig in 1973. After his habilitation at the University of Düsseldorf in 1978 he was made a professor of inorganic chemistry in 1979. In 1987 he moved as a full professor of inorganic chemistry to the Darmstadt University of Technology (Eduard Zintl Institute). Since 1998 he is a scientific member of the Max Planck Society and director at the Max-Planck-Institute for Chemical Physics of Solids, Dresden.

MICROREVIEWS: This feature introduces the readers to the authors' research through a concise overview of the selected topic. Reference to important work from others in the field is included.

 © WILEY-VCH Verlag GmbH, D-69451 Weinheim, 1999 1434−1948/99/1010−1643 $ 17.50+.50/0

1. Introduction

The basic principles of biomimetic growth of inorganic solids[1][2] include distinct cooperative phenomena between organic and inorganic components. The complex systems assume control of the processes of self-organization, self-similarity, hierarchical arrangements, shape-formation (form-selectivity) and transcription of informations from the microscopic level to the macroscopic range. In cases where the time scale of the biomimetic morphogenesis of an inorganic material is similar to that in biological systems, the development of specific shapes and morphologies can be systematically investigated from the nucleation to the final stage.

In a recent paper[3] the biomimetic growth and self-assembly of fluorapatite spheroids by double diffusion in denatured collagen matrices (gelatin) at 25°C was described phenomenologically. The morphogenesis begins with elongated hexagonal-prismatic seeds. Progressive stages of self-assembled (noncrystallographic) upgrowths of needle-shaped prisms at both ends of the seed lead to dumbbell-shaped aggregates, which complete their shapes by successive branchings to end up with spheres that are notched to a greater or lesser extent. A selected sequence of scanning electron microscopy (SEM) pictures representing the morphogenesis from a needlelike seed to a spherocrystal is shown in Figure 1.[3][4] The surface of a just closed sphere also consists of (small) needlelike units following the general principles of self-similarity.

An investigation of numerous SEM pictures at various stages of the morphogenesis has already led to a *fractal model* for the formation of the (anisotropic) fluorapatite spheres.[3][4] Furthermore, according to the previously postulated hypothesis, the fractal branching of successive generations and the overall symmetry of the self-assembled aggregates may be considered as consequences of *intrinsic electric fields*, which take over control of the growth of the aggregates.[3][4] This interpretation of the specific morphogenesis of the fluorapatite aggregates is broadly based on natural phenomena concerning the biological significance of piezoelectricity,[5] as well as on observations concerning the pyroelectric effect in bone.[6] In addition, the influence of electric polarization on acceleration and deceleration of bonelike crystal growth on hydroxyapatite ceramics was also shown in a recent paper[7] which, in fact, supports the idea that "uniform electric fields, rather than the localized charges usually cited, may determine the sites of crystal nucleation and overgrowth."[8]

This paper now makes a careful attempt at a first approach to the interpretation of the following phenomenological observations:

- **First growth stage**: Fractal growth (branching criteria and architecture, see Section 2).
- **Second growth stage:** Core/shell assemblies (formation of concentric shells around the closed spheres of the first stage, see Section 3).
- **Composite character** of the material (see Section 5).
- Formation of **hollow spheres by** "decalcification" of the composite aggregates (see Section 5).
- **Reorganization of denatured collagen** (gelatin) during morphogenesis (see Section 5).

The specific peculiarities of the chemical system under investigation are caused by numerous preceding stages of selection during evolution. This criterion should be kept in mind when studying and assessing the observations and models given in the present paper. It should also be noted at this point that the formation of morphologies similar to that of dumbbell-shaped aggregates or peanut-type particles, which are found in various chemical systems under various chemical growth conditions,[9] are not necessarily generated by the same mechanism of morphogenesis.

2. Fractal Growth and Architecture

The growth of anisotropic fluorapatite spheres[3][4] by double diffusion in denatured collagen matrices (gelatin) begins with elongated hexagonal-prismatic seeds up to 30 μm in length (critical ratio length/diameter ≈ 5:1). Progressive stages of self-assembled (noncrystallographic) upgrowths of needle-shaped prisms at both ends of the seed (fractal branching) lead to dumbbell-shaped aggregates (Figure 1) which complete their shapes by successive and self-similar upgrowths to give notched spheres after about the 10th fractal generation. The morphogenesis from a needle-shaped seed of about 10 μm in length to a spherocrystal of about 60 μm in diameter takes approximately one week. The fractal growth and architecture is controlled by two noncrystallographic parameters, which were derived from SEM images at different growth stages: i) the maximum aperture angle between the long axis of the seed and the needle-axes of the units of the following generation is 45 ± (5)°; ii) subsequent generations scale down in their lengths by a factor of ≈ 0.7. Based on these two limiting conditions the fractal model[10] of a just closed sphere is shown in Figure 2 (2D-simulation with the umbrella-tree model; crossing of individual crystals suppressed). The simulated surface of the spherocrystal consists of very small needlelike units, an observation which is consistent with the SEM images (mean diameter < 0.1 μm for the surface prisms of a just closed sphere). Inside the spherocrystal a torus-shaped cavity is

[a] Eduard-Zintl-Institut der Technischen Universität, Hochschulstraße 10, D-64289 Darmstadt, Germany
[b] Henkel KGaA, TTR-Anorganische Chemie, Henkelstraße 67, D-40191 Düsseldorf, Germany
[c] Max-Planck-Institut für Polymerforschung, Ackermannweg 10, D-55128 Mainz, Germany
[d] Institut für Angewandte Physik der Technischen Universität, Schloßgartenstraße 7, D-64289 Darmstadt, Germany
[e] Fachgebiet Theorie Elektromagnetischer Felder der Technischen Universität, Schloßgartenstraße 8, D-64289 Darmstadt, Germany
[+] New address: Max-Planck-Institut für Chemische Physik fester Stoffe (im VEM Sachsenwerk), Pirnaer Landstraße 176, D-01257 Dresden, Germany

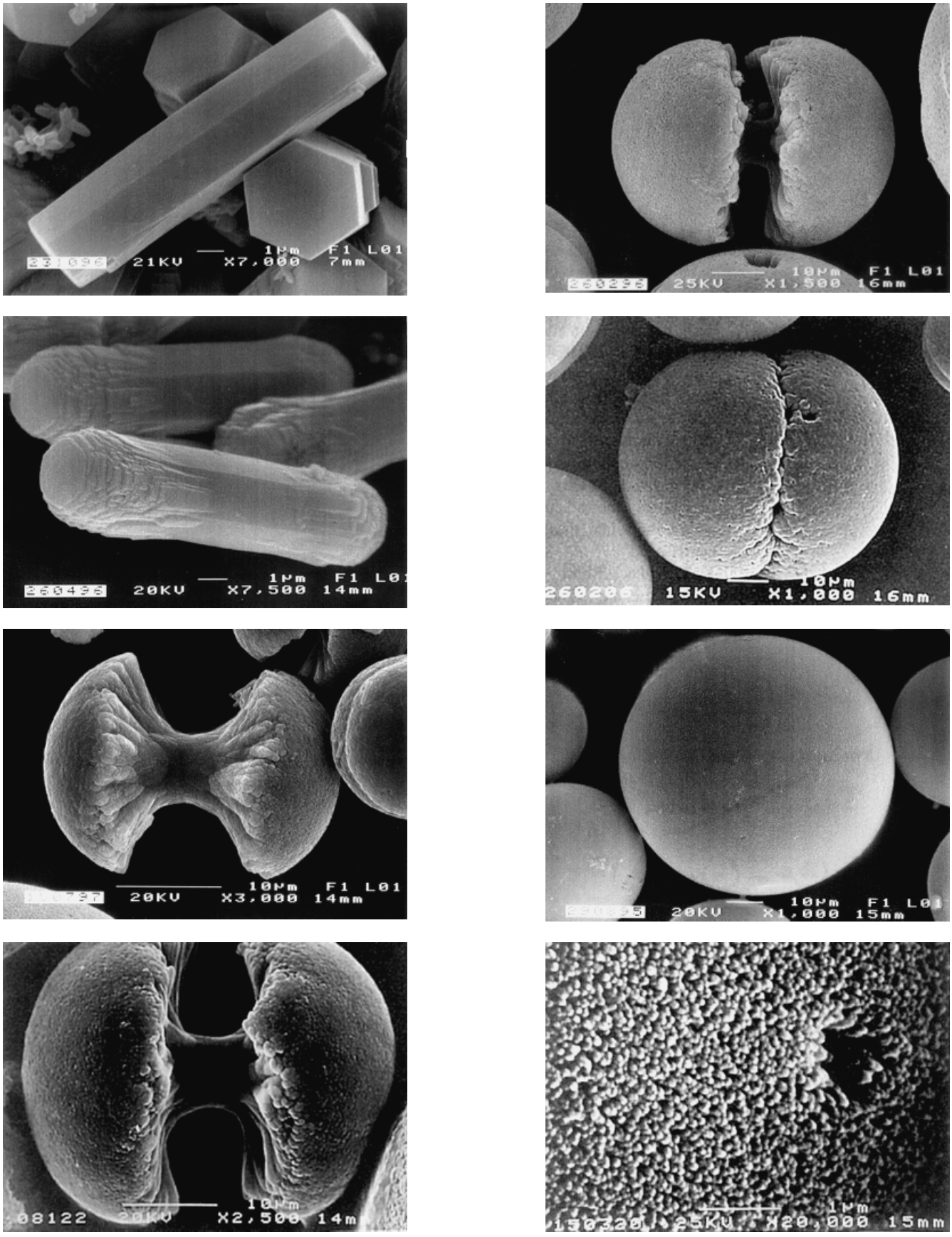


Figure 1. Selected sequence of SEM images of progressive stages of self-assembled (hierarchical) growth of fluorapatite aggregates (morphogenesis): from an elongated hexagonal-prismatic seed (top left) through dumbbell shapes to spheres; the surface of a just closed sphere also consists of needlelike units (bottom right) following the general principles of self-similarity

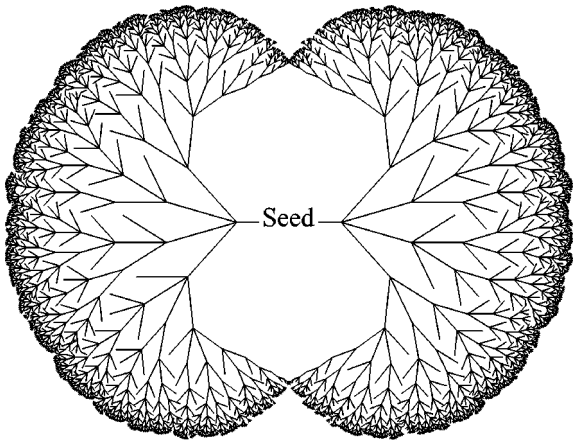


Figure 2. 2D-simulation of a just closed fluorapatite spheroaggregate; fractal model (seed plus 10 generations) assuming a fourfold splitting in each generation (in fact, orders of noncrystallographic branching can be higher); maximum opening angle 48°, scale down factor 0.7; crossing of individuals is suppressed by particular rules following real growth conditions: i. all individuals have the same growing speed; ii. members of higher generations are suppressed, if they cross members of a lower generation; iii. if members of the same generation reach the crossing point at the same time, it is a random decision which one is deleted; if crossing is "nonsymmetric", the individual reaching the crossing point first is favoured; iv. to simulate diffusion-inhibition inside the growing dumbbell area all individuals with an angle greater than 160° relative to the seed are deleted

formed around the elongated seed. A similar architecture is generated by the geometrical model of a splitting needle at constant growth rate and constant splitting rate.[11]

Selected stages of the morphogenesis (SEM images), together with more detailed 3D-simulations,[12] are shown in Figure 3. SEM images of fragments of a spherocrystal are given in Figure 4 and agree very well with the fractal model (Figure 2, Figure 3, Figure 4b). The fragments were produced by breaking spherocrystals perpendicular (Figure 4a) and parallel (in plane; Figure 4d) to the long seed axis. The seed position within a spherocrystal is clearly seen in the centre of the hemisphere (Figure 4a, simulation: Figure 4b). The hexagonal cross-section of the seed and the channel surrounding the seed are shown in Figure 4c. It is interesting to note that the cleavage area of the elongated hexagonal-prismatic seed is characterized by a radial structure starting from the middle, an observation which is in agreement with the idea of nucleation by cylindrical preorientation of macromolecular units ("liquid crystal seed").[13] Figure 4d shows an inner-sphere cross-section parallel to the long seed axis; the two holes represent the torus-shaped cavity around the elongated seed between. The complex but symmetric structure of growth (mirror plane perpendicular to the long seed axis and through the holes) corresponds to the fractal model given in Figures 2−4 and will be discussed in more detail later together with the idea of permanent

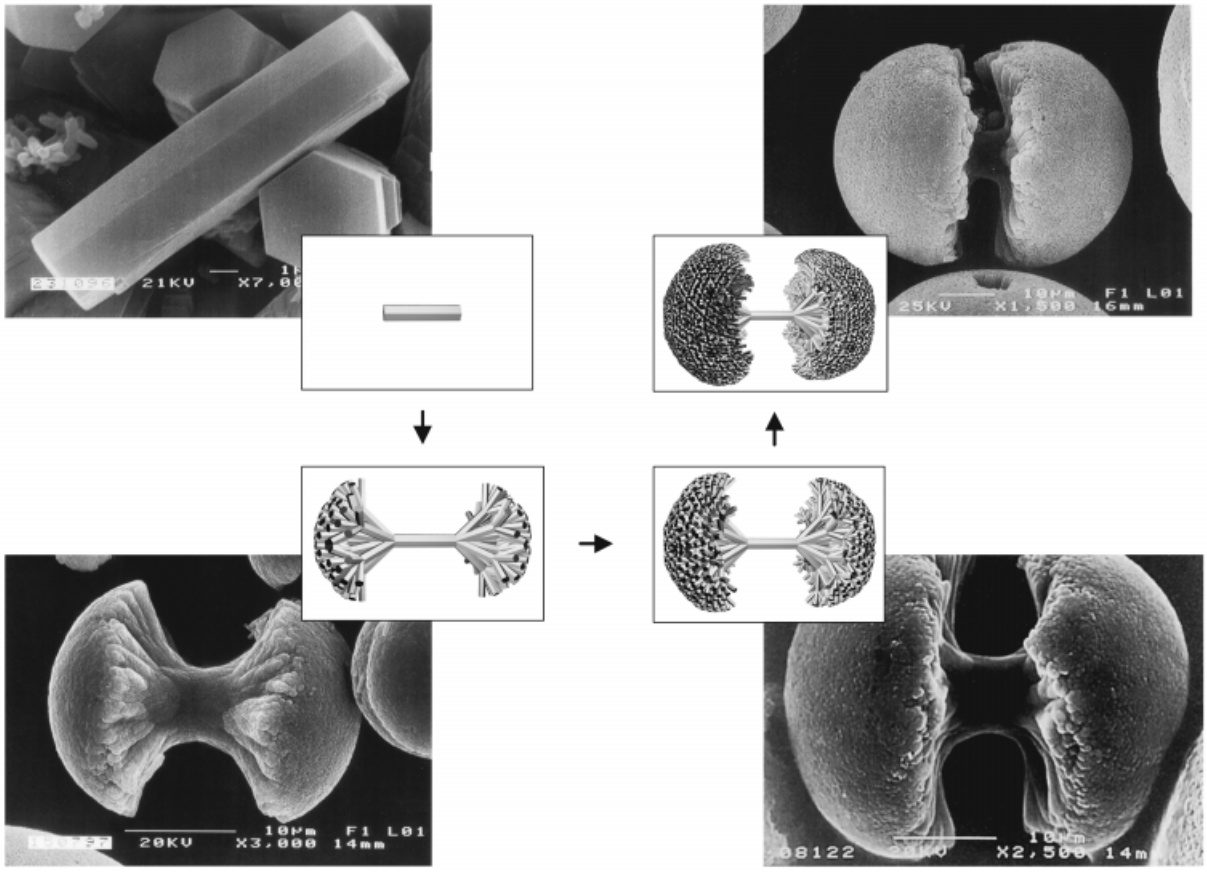


Figure 3. Selected stages of the fractal morphogenesis (SEM images) together with 3D-simulations (from top left anticlockwise: seed, seed + 2, + 3 and + 4 generations)

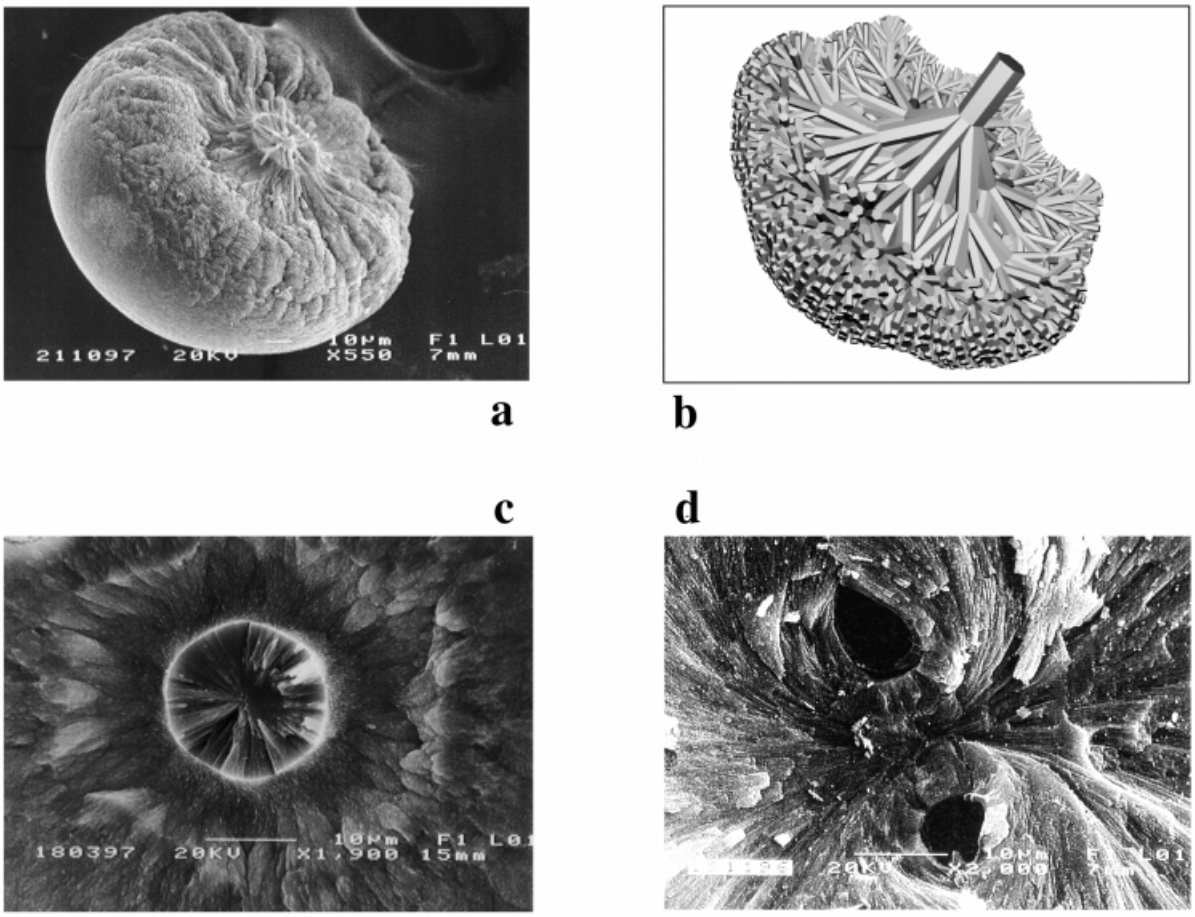


Figure 4. SEM images of specific fragments of a spheroaggregate (fractal model in Figures 2 and 3). **a:** Hemisphere broken perpendicular to the long seed axis; **b:** 3D-simulation[12] of situation **a** (seed + 4 generations); **c:** Hexagonal shaped cross-section of the seed and surrounding channel; **d:** Inner-sphere cross-section parallel (in plane) to the long seed axis

dipoles and their influence on morphogenesis. Here, only a brief comment is given concerning the inner architecture of the spherocrystal (Figure 4d) and the distribution of electric field lines around a given permanent dipole. This situation is demonstrated in Figure 5, in which the growth-orientation within a spherocrystal (section parallel/in plane to the seed) shows a remarkable correspondence to the orientation of electric field lines around a permanent dipole.

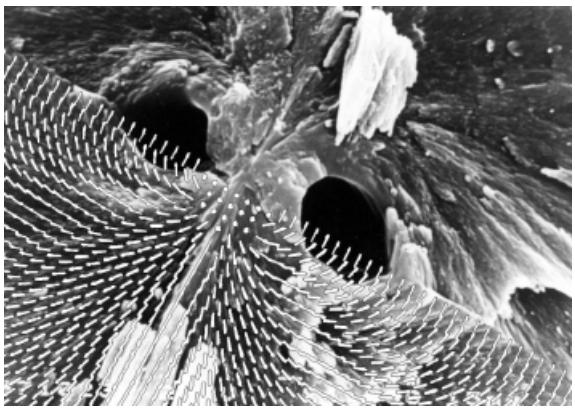


Figure 5. SEM image of a bisectioned spherocrystal broken parallel (in plane) to the long seed axis (Figure 4d) combined with the calculated shape of electric field lines around a permanent dipole (field lines reduced to only one half of the complete area)

3. Core/Shell Assemblies

After the spherocrystals have closed, this special kind of fractal morphogenesis no longer applies and a second, more conventional, growth mechanism by the formation of concentric shells[14] of fluorapatite around the core follows (Figure 6). The shells are built of needle-shaped rods oriented perpendicular to the core-surface and nearly parallel to each other (radial growth). Obviously, the small needle-shaped prisms of the last generation of the fractal core act as nucleation centers for the growing shell. The core/shell interface represents a sphere of decreased stability against thermal and/or mechanical treatment. In fact, the core is easily removed from the shell (Figure 6). Simultaneously, the core and shell assemblies bear a strong resemblance to the complex organisation of teeth (dentin- and enamel).[15] Bundles of needles are combined in bigger assemblies in the same way as the small prisms in enamel are aggregated to enamel rods (Figure 7).

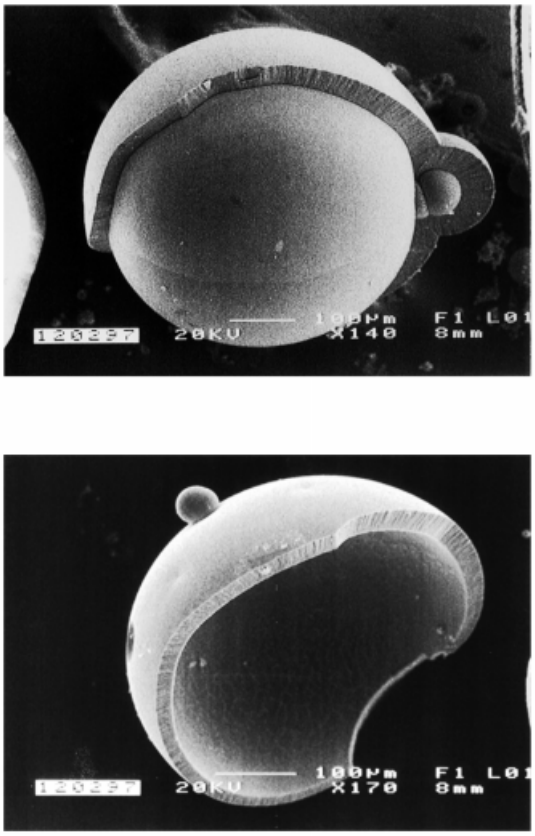


Figure 6. SEM images of a core/shell assembly. **a**: Shell partly removed, free core; **b**: Core removed from the shell

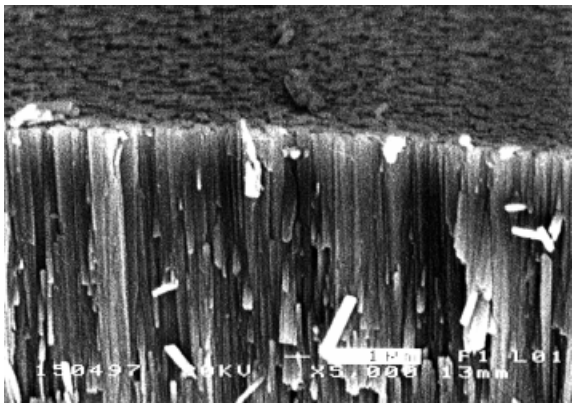


Figure 7. SEM image: Section of a shell area and the surface of a core/shell assembly

4. Intrinsic Electric Fields

Coming back to the core spherocrystal and its architecture, the essential task is to find an interpretation for the noncrystallographic (fractal) splitting of crystal generations and for the overall symmetry ($C_{\infty h}$) of the self-assembled core aggregates. The basic premise in this hypothesis is the presence of intrinsic electric fields which take over control of the growth of the aggregates. This means that the individual "crystals" (actually composite units, see below) − the seeds as well as individuals of the following generations − contain a permanent dipole, an assumption which is consistent with observations on the biological significance of electric fields (pyro-, piezoelectricity) during apatite formation under in vivo or biomimetic conditions.[5−8] The polarity of collagen and the structural peculiarity of the apatite family, varying between centrosymmetric and acentric distribution of the X-species $\{Ca_5(X)[PO_4]_3$, X = F, Cl, OH$\}$[16] support these ideas. We should also bear in mind the extremely mild biomimetic growth conditions, which should favour a high degree of order of the atomic arrangements − partial substitution of F^- by OH^- causes an

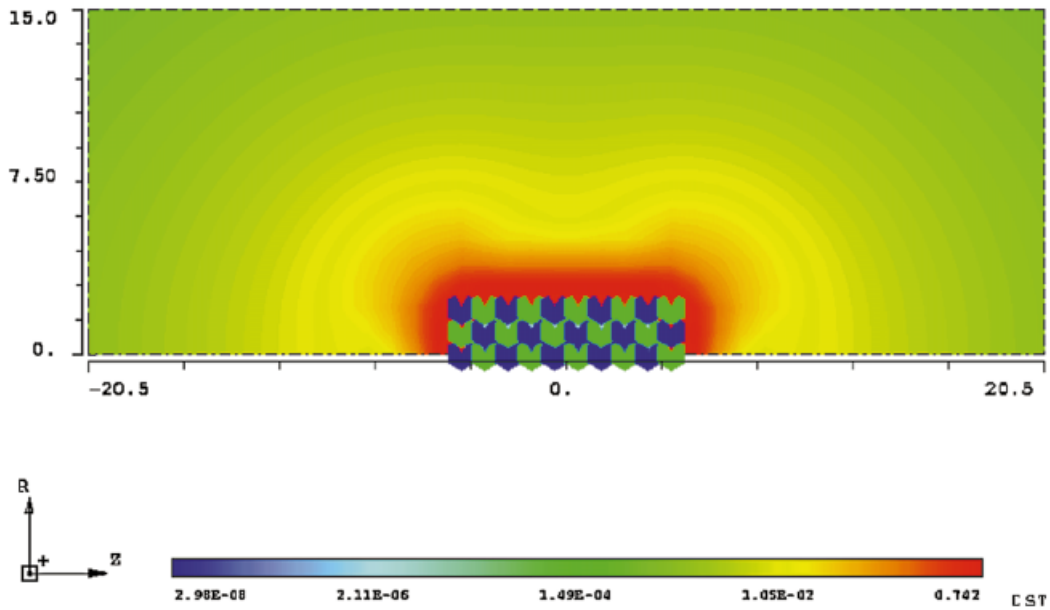


Figure 8. Two-dimensional, logarithmic representation of the distribution of the electric field strengths around an elongated permanent dipole (seed). Elementary dipoles (blue/green graphs = charges +/−; staggered arrangement along the horizontal direction) represent the seed within the coloured area; calculation using the MAFIA program.[19]

asymmetric displacement of the X-species from their "normal" positions (mirror planes)[17] causing a possible reduction of symmetry from the centrosymmetric point group 6/m to the pyroelectric point group 6. Finally, the polar organic component and the inorganic material may act together in the sense of an ordered composite structure, which then gives rise to the formation of a strong (intrinsic) permanent dipole. In this context it is important to note that in vivo nucleation and growth of apatite nanocrystals within a collagen fibril structure leads to an ordered composite system with the *c* axes of the apatite particles oriented parallel to the long axes of the collagen fibrils.[18]

The distribution of the electric field strength around an elongated seed with a permanent dipole (simulation by a set of elementary dipoles; staggered arrangement) was calculated using the MAFIA program[19] and is shown in Figure 8 as a coloured chart of the intensity of the dipole field. Because the field strength is higher at the poles than between them, a bonelike shape results with the maximum field intensities at the edges. The bonelike extension of areas of stronger field strengths starting from the edges of the seed (red/orange in Figure 8) corresponds directly to the self-assembled upgrowths at both ends of the seeds (fractal branching) during progressive growth of the fluorapatite aggregates. Even the maximum aperture angle between the long axis of the seed and the needle axes of prisms of the following generation of about ± 45(5)° is in agreement with the general direction of the extension of higher field strengths around the elongated permanent dipole.

A two-dimensional simulation of the morphogenesis of the overall orientation of electric field lines around a growing spherocrystal is shown in Figure 9 [Permanent dipoles and fractal branching: seed (a); seed + 2 generations (b); seed + 3 generations (c)]. These diagrams give an impression of the possible interactions between the intrinsic electric fields, the charged or polar components in solution, and the growing aggregate within the gelatin matrix. The following points seem to be of significance and, in principle, are consistent with the observed morphogenesis of the fractal solid: i) the transport of ions from the solution to the growing seed (aggregate) and the reorientation of polar organic molecules are influenced by the strength and direction of the electric fields; ii) electric field lines with an orientation between "parallel and perpendicular" to the seed (to the individuals on top of the growing surface of the spherocrystal) do not contribute to a preferred growth rate; iii) the lack of preferred orientation of the electric field lines inside the growing spherocrystal causes reduced growthrates within this area and formation of the torus-shaped cavity.

Experimental indications for the significance of intrinsic electric fields, which assume control of the growth of the fractal spherocrystals, were obtained by using a modified growth-chamber (Figure 10) including an external electric field of 5000 V/1.4 cm (D.C. conditions). The idea was to influence fractal branching of the growing aggregates, and, in fact, splitting of the seeds (area of high field strengths at the edges of an elongated permanent dipole, Figure 8) is predominantly affected by the external field (Figure 11). Instead of similarly shaped polyhedra with definite prism and basal planes, the upgrowing generation under an external

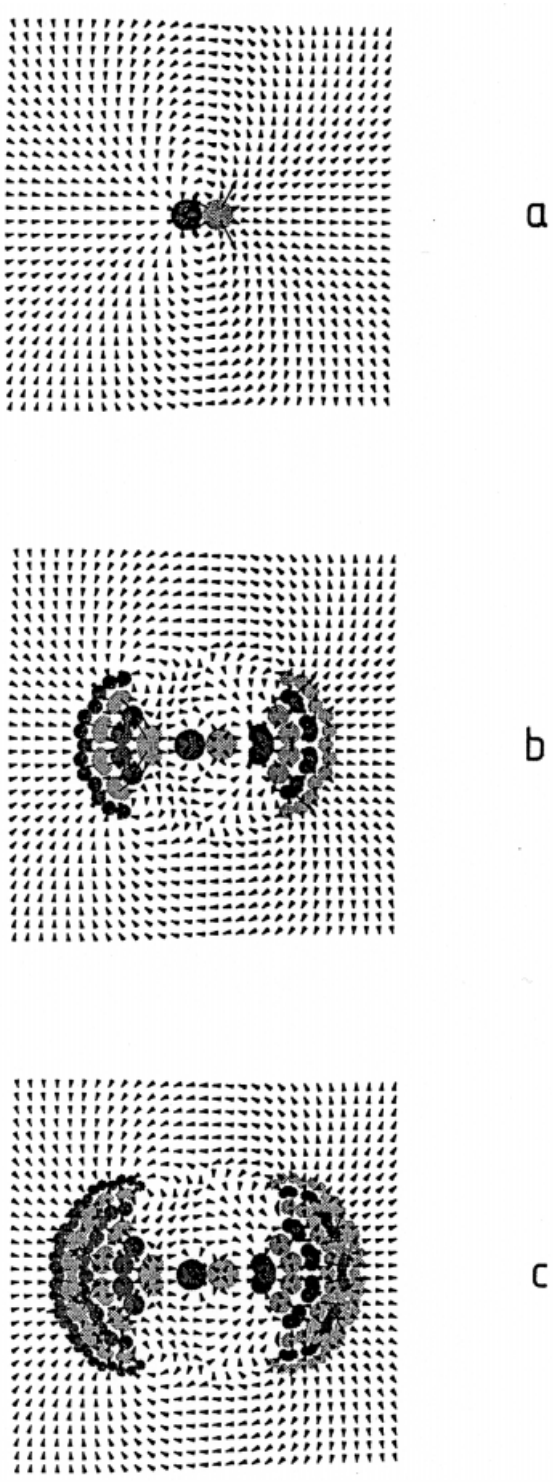


Figure 9. Two-dimensional calculation of the morphogenesis of the overall orientation of electric field lines around a growing spherocrystal; every permanent dipole is represented by a combination of two circles (black/grey circles = charges +/−). a: seed; b: seed + 2 generations; c: seed + 3 generations; arrows show the directions of the electric field lines; no distinction is made for field strengths (see Figure 8)

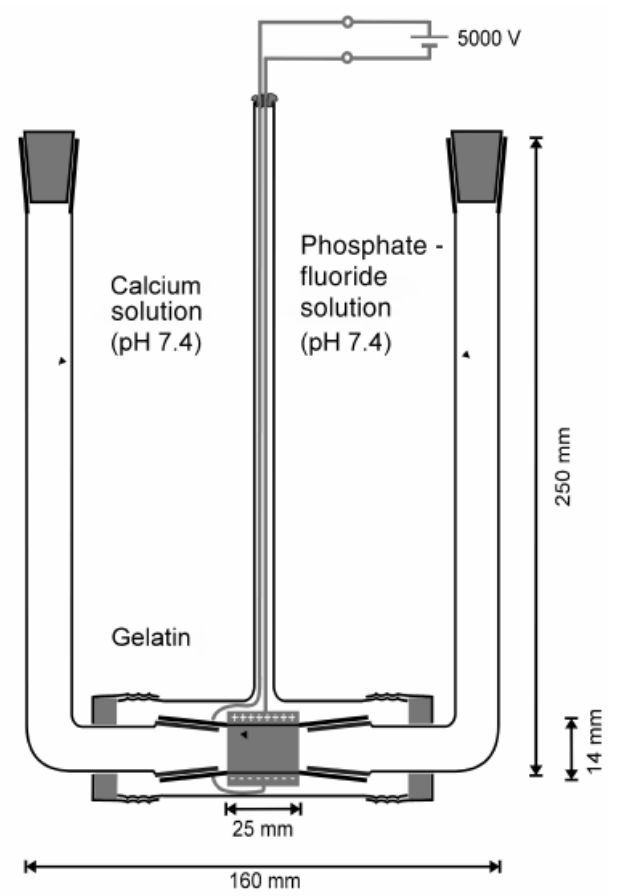


Figure 10. Modified growth chamber (double diffusion technique) including the facility for application of an external electric field (5000 V/1.4 cm; D. C. conditions); the electrodes are placed on opposite sites of the horizontal glass tube which contains the gelatin plug; to prevent contact with moisture the electric circuit is protected by an outer glass envelope; the equipment is suitable for use in thermostats operating with water

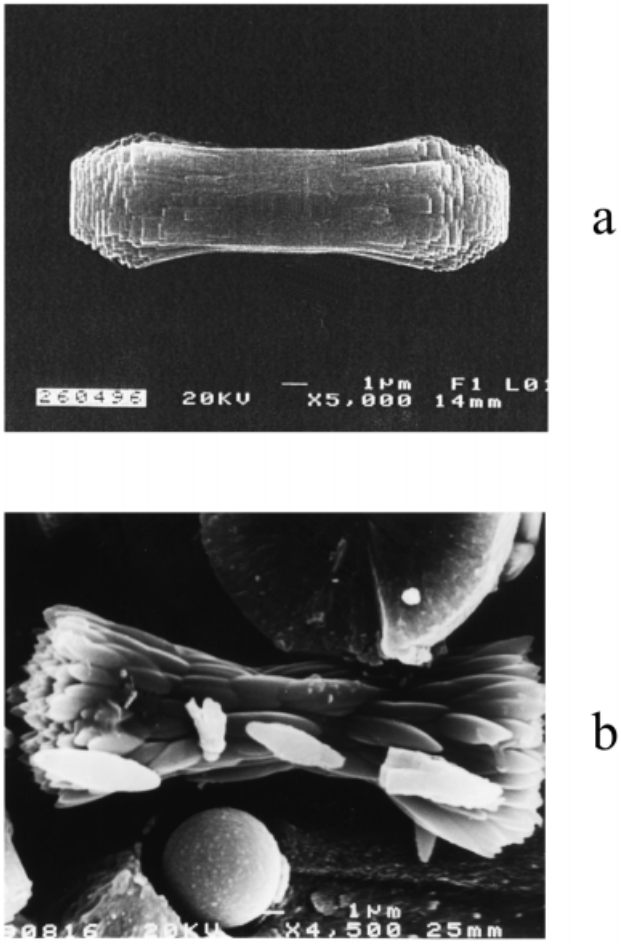


Figure 11. SEM images of fluorapatite seeds together with the first upgrowing generation. a: without external field. b: with applied external field (5000 V/1.4 cm)

field is characterized by sharpened and bent faces. Moreover, the growing rate of fluorapatite aggregates is significantly diminished by using an external field.

If the spherocrystals (fluorapatite-gelatin composites, see below) represent solid aggregates containing a permanent dipole, a pyroelectric effect similar to that observed in bone and other collagen-containing materials[6] should be expected. We therefore developed an experimental setup for measuring the pyroelectric effect of small aggregates (down to 100 μm in size).[20] The sensitivity of the equipment is already suitable for determining the pyroelectric coefficient of small particles of tourmaline (4.3×10^{-10} coul. $cm^{-2}°C^{-1}$); however, the expected order of about $2-4 \times 10^{-13}$ coul. $cm^{-2}°C^{-1}$ for bonelike materials[6] has not yet been attained. On the other hand, we were able to get an experimental indication for the presence of a permanent dipole in the spherocrystals by placing them in a high-voltage field between two condenser plates. As shown in Figure 12 an applied voltage of 5 kV/cm leads to chainlike arrangements of the spherocrystals. The spherocrystals within the chains are mainly oriented in such a way that the elongated seeds of the spheres (in a direction perpendicular to the equatorial grooves) are in a parallel arrangement, a picture which is consistent with the expected orientation of rod-shaped permanent dipoles between condenser plates.

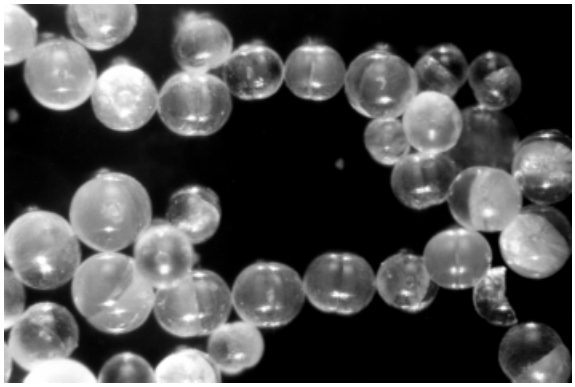


Figure 12. Orientation of fluorapatite spherocrystals exposed to an external high-voltage field of 5 kV/cm (horizontal field); max. sphere-diameter: 400 μm

5. Composite Character, Hollow Spheres and Reorganization of Denatured Collagen during Morphogenesis

The experimental indications for the presence of permanent dipoles and intrinsic electric fields are one of the specific characteristics of the spherocrystals and their morphogenesis. The second essential point is to gain further insight into the composite-nature of the spherocrystals. As already shown by thermogravimetry,[3][4] the biomimetically-grown spherocrystals consist of about 95 wt.-% fluorapatite and about 5 wt.-% organic material and water. A similar ratio of inorganic and organic material is found for human enamel.[21] The composite structure of the spherocrystals is also reflected by dissolution processes in EDTA (0.25 N, pH = 7) as solvent for the inorganic component. Two main observations have been made on treatment of fluorapatite spheres with a neutral EDTA solution at 25°C; they concern firstly the dissolution of the fluorapatite spheres and secondly the structural correlation between apatite and gelatin.

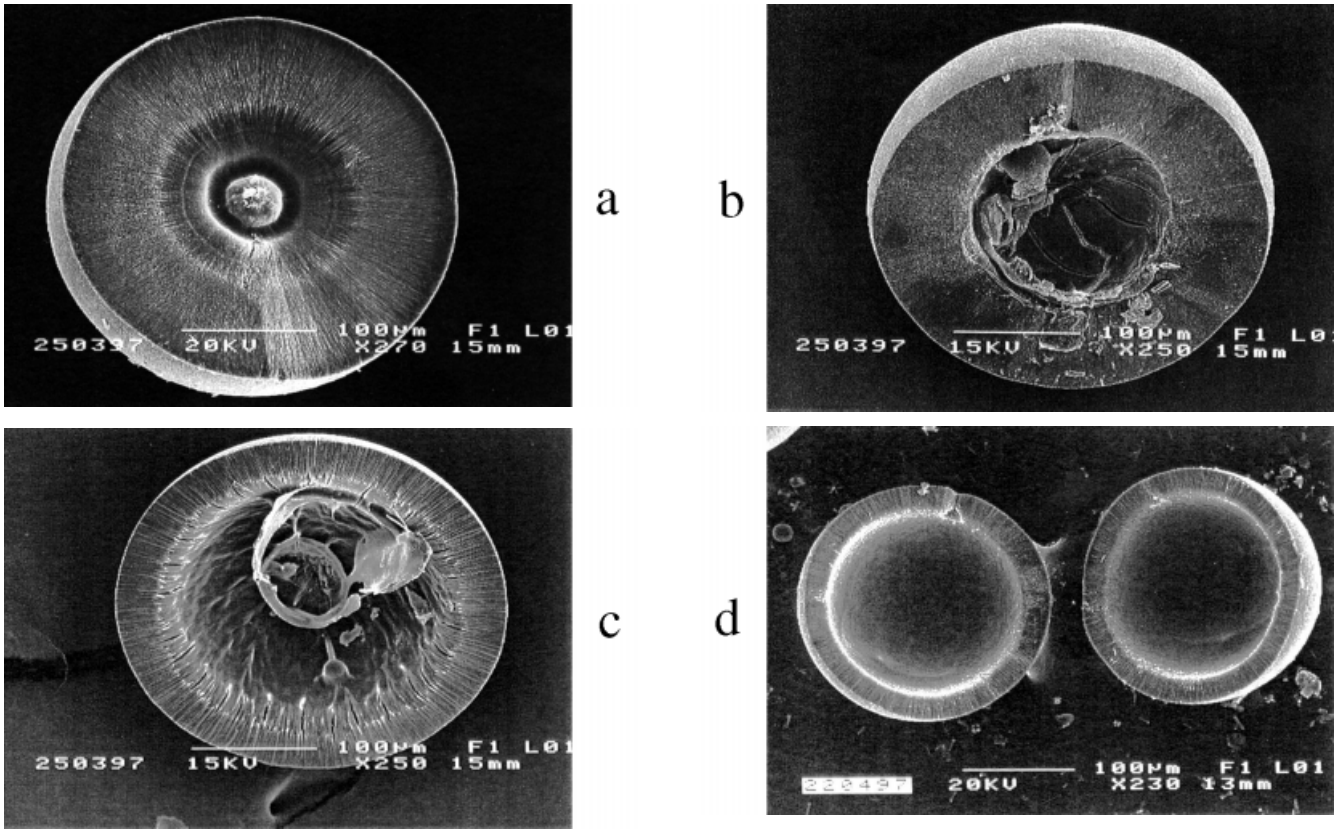


Figure 13. Dissolution of fluorapatite core/shell assemblies in EDTA as solvent; SEM images of hollow hemispheres broken from spheres after treatment with EDTA for 24 h (a), 48 h (b), 72 h (c) and 96 h (d); picture (d) represents the two hollow hemispheres of the same individual; due to shrinking effects during the preparation for SEM investigations (drying) the residual gelatin inside the core loses its original (biomimetic) structure

The first observation is that the dissolution of core/shell assemblies starts within the core and spreads out to the shell, thereby running through continuous stages of apatite hollow-spheres filled with residual gelatin. This situation is shown in Figure 13, which represents hollow hemispheres broken from spheres at different stages of dissolution. In the first stage of the dissolution process the seed within the core is only weakly affected; the later generations of the fractal core spherocrystal are obviously dissolved first (a). After the core has been completely dissolved the attack of the solvent extends to the shell structure and the dissolution progresses leading to a decrease of the wall thickness and an increase of the cavity area (b-d). Decreasing thickness of the "inorganic wall" is consistent with increasing elasticity of the spheres in solution; the consistency of the completely "decalcified" and translucent spheres is similar to that of jellyfish. The early stages of the dissolution process of the fluorapatite core/shell assemblies show close similarities to the early effects of caries:[22] while the surface of a tooth might still be intact, a cavity is formed in the underlying parts. This mechanism occurs in hydroxyapatite-containing teeth as well as in shark teeth (fluorapatite), as was shown by an in vitro study of simulated caries attacks.[23] It was also supposed[24] that the decomposition products of bacteria and their complexing properties are responsible for caries. In the course of these investigations[24] caries-like lesions were obtained by using EDTA as a model reagent.

The second major observation concerning the composite nature of the spherocrystals gives a first answer to the question whether there is a structural correlation between apatite and gelatin. Figure 14 shows images (optical microscope with crossed polarizers) of closed composite core aggregates (a) and of the jellyfish-like spheres (b) obtained

after complete dissolution of the apatite component. The gelatin spheroids show a significant anisotropic optical behaviour (Brewster cross) identical to undissolved spherocystals but without interference colours because of the lack of the inorganic material. Hence there is a strong structural correlation between the orientation of apatite crystallites and the gelatin within the composite spheres, indicating substantial reorganization of the macromolecular matrix within the area of a growing aggregate. Birefringence analyses (λ plate) of partially dissolved and broken specimens show that the directions of the optically denser axes in the apatite crystallites (*c* axes) and the gelatin (chain direction) coincide, as would be expected if the gelatin was preferentially oriented during the process of apatite growth.

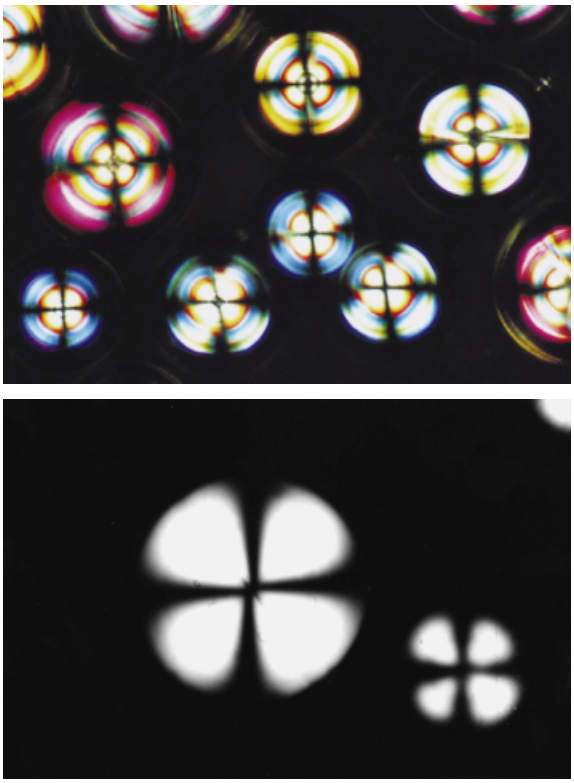


Figure 14. Images from a polarization microscope (crossed polarizers) of just closed composite spheres (apatite/gelatin; a) and of completely "decalcified" spheres (gelatin; b); the gelatin spheroids (b) show significant anisotropic behaviour (Brewster-cross) identical with that of the undissolved spherocrystals (a) but without interference colours because of the lack of inorganic material (apatite); sphere diameters between 100 μm and 150 μm

For transmission electron microscopy (TEM) investigations the composite spherocrystals were first separated from the gelatin matrix by pressing them through a screen and treating them with water. Prior to the dissolution process with EDTA the isolated spheres were immediately fixed with glutardialdehyde and subsequently contrasted with osmium tetraoxide. The water was then extracted by gradual exchange with acetone and the spheres embedded in epoxy resin. Ultrathin sections were prepared at low temperature and subsequently stained with uranyl acetate. In Figure 15 parallel alignments of residual apatite crystallites are visible within a matrix of embedding material and stained gelatin forming a dark network. Within this network stripes are discernible giving the impression of a gelatin structure oriented parallel to the longitudinal axes (*c* axes) of the apatite crystallites. It is thought that the preparation does not change the original gelatin structure of the composite significantly and hence it is assumed that the structure visible in Figure 15 represents the distribution of gelatin within the composite together with apatite. The combination of the TEM observations with the results of optical microscopy leads us to conclude that the stripes (Figure 15) are bundles of gelatin which are stressed and ordered in a parallel orientation together with areas of crystalline apatite. This means that the growth of the aggregates is associated with significant interactions between apatite and gelatin, which cause a reorientation of gelatin from an irregular (amorphous) to an ordered (anisotropic) state.

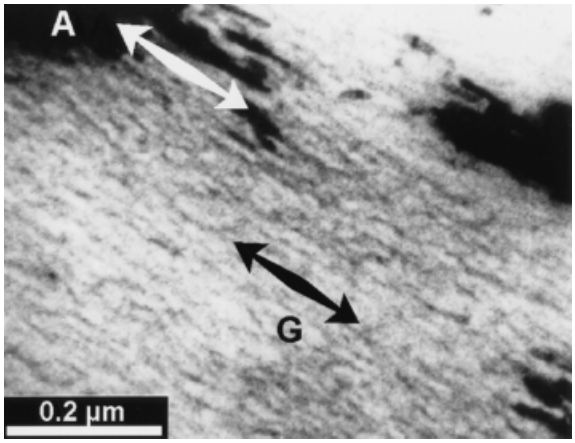


Figure 15. TEM image of an ultrathin section of an apatite/gelatin composite spherocrystal after treatment with EDTA (partial dissolution of the inorganic component, for preparation see text); "A" represents an area of residual apatite crystallites with their longitudinal axes (c axes) parallel to the bright arrow; the stained gelatin region "G" shows an overall orientation (black arrow) parallel to the apatite longitudinal axes

6. Concluding Remarks

In summary, the apatite-gelatin system seems to be well suited for a wide range of interdisciplinary studies to gain further insight into the principles of the morphogenesis of a complex biomimetic material. This story is just beginning and there are still a lot of questions, as can also be seen in the title of the present paper!

Before coming to the end of this contribution only one peculiarity, which may include the key to the deeper understanding of the mechanism of the morphogenesis, should be emphasized in more detail. Though the seed units of the fractal aggregates are formed with a perfect hexagonal-prismatic habit they do not correspond to a single crystal, a fact which is demonstrated by the specific appearance of the fracture area perpendicular to the seed axis (Figure 16). The radial structure of the fracture area indicates that the nucleation of a hexagonal-prismatic unit starts from a central seed which may be formed by fibril-analogous arrange-

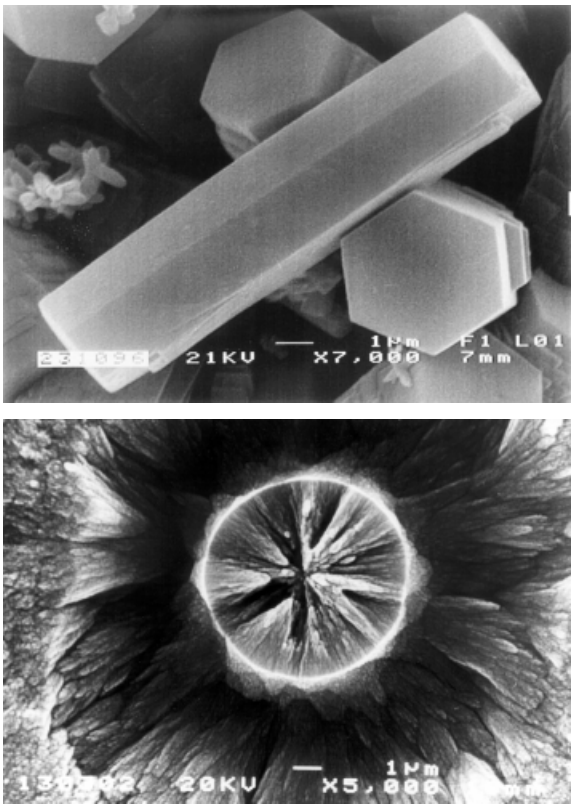


Figure 16. SEM images: Hexagonal prismatic seed (top) and fracture area of a seed (bottom) nearly perpendicular to the seed axis

ments of gelatin molecules able to provide active centres for the nucleation of apatite. The actual size of the apatite crystallites formed is not defined at present and may extend from the nanoscopic to the mesoscopic scale. If this low-scale composite model is valid, the macroscopic hexagonal-prismatic seed is not a single crystal but a hierarchically ordered inorganic/organic composite superstructure. This important question will be the central subject of our future investigations.

Acknowledgments

This work was supported by the Fonds der Chemischen Industrie.

[1] S. Mann, *J. Chem. Soc., Dalton Trans.* **1997**, 3953−3961.
[2] N. Coombs, D. Khushalani, S. Oliver, G. A. Ozin, G. C. Shen, I. Sokolov, H. Yang, *J. Chem. Soc., Dalton Trans.* **1997**, 3941−3952.
[3] R. Kniep, S. Busch, *Angew. Chem.* **1996**, *108*, 2787−2791; *Angew. Chem. Int. Ed. Engl.* **1996**, *35*, 2624−2626.
[4] S. Busch, Ph. D. Thesis, TU Darmstadt 1998.
[5] C. A. L. Basett, *Calc. Tiss. Res.* **1968**, *1*, 273−287.
[6] S. B. Lang, *Nature* **1966**, *12*, 704−705.
[7] K. Yamashita, N. Oikawa, T. Umegaki, *Chem. Mater.* **1996**, *8*, 2697−2700.
[8] P. Calvert, S. Mann, *Nature* **1997**, *386*, 127−129.
[9] *Apatite*: K. Schwarz, M. Epple, *Chem. Eur. J.* **1998**, *4*, 1898−1903; *ZSM-48*: V. J. Hufnagel, P. Behrens, *10th German Zeolite Conference* (Bremen), **1998,** Abstract A6; *a-*Fe_2O_3: N. Sasaki, Y. Murakami, D. Shindo, T. Sugimoto; *J. Coll. Interface Sci.* **1999**, *213*, 121−125; $BaSO_4$: L. Qi, H. Cölfen, M. Antonietti, *Angew. Chem*., in press.
[10] B. B. Mandelbrot: *Die fraktale Geometrie der Natur*, Birkhäuser Verlag, Basel, **1991**.
[11] M. N. Maleev, *Tschermaks Min. Petr. Mitt.* **1972**, *18*, 1−16.
[12] POVRAY 3.1e©, **1991−1999**, The Persistence of Vision Team, http://www.povray.org.
[13] G. A Ozin, H. Yang, I. Sokolov, N. Coombs, *Adv. Mater.* **1997**, *9*, 662−667.
[14] W. J. Schmidt, *Naturwiss.* **1947**, *9*, 273−277.
[15] H. E. Schroeder: *Orale Strukturbiologie*, Thieme Verlag, Stuttgart/New York, **1982**.
[16] M. Bauer, W. E. Klee, *Z. Kristallogr.* **1993**, *206*, 15.
[17] M. Braun, C. Jana, *Chem Phys. Lett.* **1995**, *245*, 19.
[18] *Biomimetic Materials Chemistry* (Ed.: S. Mann), VCH Publishers Incorp., New York, **1996**.
[19] The MAFIA collaboration, User′s Guide MAFIA Version 4.X, CST Gesellschaft für Computer-Simulationstechnik mbH, Lauteschlägerstr. 38, D-64289 Darmstadt.
[20] F. Laeri: Measurement of the pyroelectric effect of small particles, unpublished.
[21] M. Okazaki, J. Tokahashi, H. Kimura, *J. Osaka Univ. Dent. Sch.* **1989**, *29*, 47−52.
[22] N. Schwenzer: *Zahn-, Mund-, Kiefer-Heilkunde*, Bd. 4, Thieme-Verlag, Stuttgart/New York, **1988**.
[23] J. G. Clement, D. J. Langdon, A. Thistleton, *Caries Res.* **1981**, *15*, 451−452.
[24] A. Schatz, J. J. Martin, *Bl. Zahnheilkunde* **1965**, *26*, 191−203.

Received March 28, 1999
[I99160]

Calcium Ions Do Accelerate the DNA Binding of New Antitumor-Active Platinum Aminophosphonate Complexes

Marieke J. Bloemink,[a] Jeroen J. H. Diederen,[a] Jaco P. Dorenbos,[a] Robert J. Heetebrij,[a] Bernhard K. Keppler,[b] and Jan Reedijk*[a]

Keywords: Calcium / Platinum Complexes / Aminophosphonate / Antitumor agents

The presence of Ca^{2+} has a marked effect on the reaction kinetics of platinum phosphonate complexes with d(GpG). Compounds studied are [*cis*-Pt(NH_3)$_2$(bmpaa)] and [Pt(*R*,*S*-dach)(ntmp)]. The formation of GG-*N7*,*N7* chelates and the release of the phosphonate ligand as observed by NMR is significantly accelerated by the presence of Ca^{2+}, which is ascribed to its interaction with the phosphato groups in the ligands.

Introduction

The therapeutic activity of the well-known antitumor drug cisplatin [*cis*-diamminedichloroplatinum(II)] is thought to originate from its interaction with DNA, resulting in inhibition of DNA synthesis.[1] The main reaction product has proven to be the G*N7*,G*N7*-intrastrand crosslink.[2] Numerous analogs of cisplatin have been synthesized and tested in order to improve the therapeutic properties. A rational approach to the development of cytostatics involves the use of carrier functions that cause a specific accumulation of the potential antitumor agents in the target organs or in the target cells. Platinum complexes containing phosphonic acid ligands have been designed for the treatment of bone tumors,[3] since bisphosphonates show a high affinity for bone and other calcified tissues.[4] Four interesting examples of such compounds, i.e. [*cis*-Pt(NH_3)$_2$(bmpaa)] (**a**), [Pt(*R*,*S*-dach)(apmd)] (**b**), [*cis*-Pt(NH_3)$_2$(ntmp)] (**c**), and [Pt(*R*,*S*-dach)(ntmp)] (**d**)[5] are shown in Figure 1, of which [*cis*-Pt(NH_3)$_2$(bmpaa)] (**a**) is expected to enter clinical trials.[6]

Previous work has shown that [*cis*-Pt(NH_3)$_2$(ntmp)] (**c**) and [Pt(*R*,*S*-dach)(ntmp)] (**d**) are capable of forming GG-*N7,N7* chelates (in analogy with cisplatin), concomittant with the release of the phosphonate ligand.[7] Because of the slow reaction kinetics of these platinum complexes, observed at physiological pH, an activation mechanism was supposed to be present in vivo. The principal objective of the work reported here has been to investigate this activation mechanism and, in particular, the influence of the presence of Ca^{2+} on the reaction kinetics.

Results and Discussion

Reaction of [*cis*-Pt(NH_3)$_2$(bmpaa)](**a**) or [Pt(*R*,*S*-dach)(apmd)] (**b**) with d(GpG) [for the structure of d(GpG), see Figure 2] in water, results in the formation of G*N7*,G*N7* chelates, as deduced from the NMR data, in analogy with the Pt phosphonate compounds **c** and **d** (resulting chelates are [*cis*-Pt(NH_3)$_2${d(GpG)-N7(1),N7(2)}] in case of compound **a** and [Pt(*R*,*S*-dach){d(GpG)-N7(1),N7(2)}] in case of compound **b**).[7] In addition free phosphonate ligand is formed. Since the primary amine is a strongly coordinating ligand and usually acts as a non-leaving group it is rather surprising that in the same molecule, i.e. [Pt(*R*,*S*-dach)(apmd)] (**b**), RNH_2 can act as non-leaving group (dach), but also as leaving group (apmd).

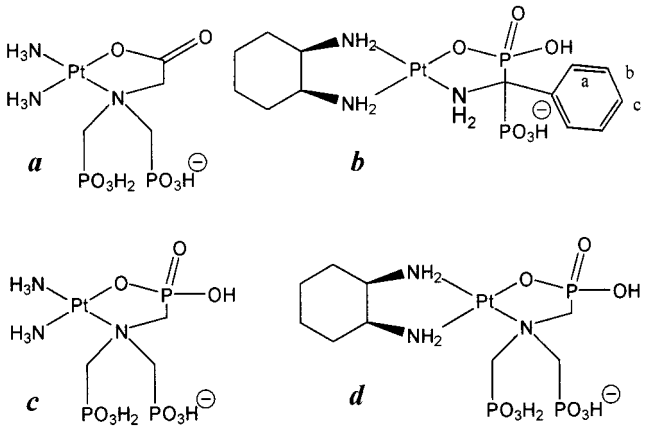


Figure 1. Structures of the platinum phosphonate complexes[*cis*-Pt(NH_3)$_2$(bmpaa)] (**a**), [Pt(*R*,*S*-dach)(apmd)] (**b**), [*cis*-Pt(NH_3)$_2$(ntmp)] (**c**) and [Pt(*R*,*S* dach)(ntmp)] (**d**)

At physiological pH compound **a** is not very reactive towards d(GpG) (see Table 1). The same lack of reactivity towards d(GpG) is observed for compound **d** at physiological pH (see Table 1; see Figure 3). Therefore, an activation mechanism has been proposed to occur in vivo.[7] Initially, it was investigated whether S-containing nucleophiles (cysteine, methionine, gluthatione) could act as activators, because of their known affinity[8] for platinum compounds. However, although initially the reaction of **d** with G bases proceeds faster in the presence of cysteine, methionine or GSH (as determined by UV-Vis spectroscopy), the resulting

[a] Leiden Institute of Chemistry, Gorlaeus Laboratories, Leiden University,
P. O. Box 9502, NL-2300 RA Leiden, The Netherlands
[b] University of Vienna, Institute for Inorganic Chemistry, Währingerstrasse 42, A-1090 Vienna, Austria

 © WILEY-VCH Verlag GmbH, D-69451 Weinheim, 1999 1434–1948/99/1010–1655 $ 17.50+.50/0

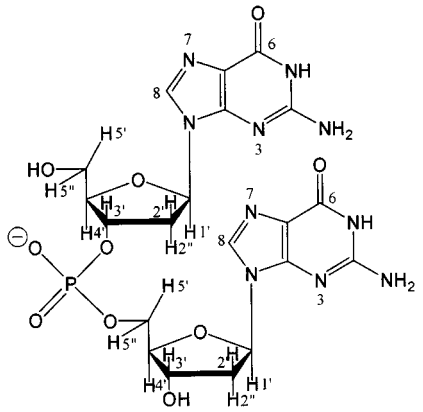


Figure 2. A schematic representation of the dinucleotide anion 2-deoxyguanylyl(3→5′)-2-deoxyguanosine, d(GpG)

product proved to be [Pt(*R*,*S*-dach)(nucl-*S*)(G-*N7*)] (as observed by NMR) and this was found not to be very reactive towards a second G base. Since coordination to a second G base is thought to be necessary for antitumor activity, S-containing nucleophiles are unlikely candidates for an activation mechanism in vivo because they inactivate, rather than activate, platinum phosphonate complexes.

The bmpaa ligand is not released from [*cis*-$Pt(NH_3)_2$(bmpaa)] in the presence of $CaCl_2$, for weeks at 310 K, if no G bases are present. So the above release of bmpaa is not just caused by the $CaCl_2$. Instead the attack of the G base on Pt is significantly enhanced by the presence of Ca^{2+}. The slightly enhanced reactivity in the presence of NaCl could be due to the presence of Na^+ which may also reduce the negative charge on the phosphonate groups, although less pronounced than for Ca^{2+}.

To study the possible effect of (de)protonation, the same experiment has been repeated at slightly acidic pH (pH 6.5) (see Table 1). With these complexes the presence of Ca^{2+} also enhances the reaction, as in the case of pH 7.0. An additional effect, however, must be present under these conditions, since overall the reaction is faster at pH 6.5 than at pH 7. A possible explanation could be that the H^+ ions can also slightly reduce the negative charge on the phosphonate ligand (a similar effect as Na^+, vide supra). Another explanation comes from the known pK_a values of [*cis*-$Pt(NH_3)_2(OH_2)_2$] (pK_{a1} = 5.02, pK_{a2} = 6.93).[9] This implies that at pH 6.5 for the aquated form of cisplatin the predominant species is [*cis*-$Pt(NH_3)_2(OH_2)(OH)]^+$ whereas at pH 7.0 almost all Pt is present as [*cis*-$Pt(NH_3)_2(OH)_2$]

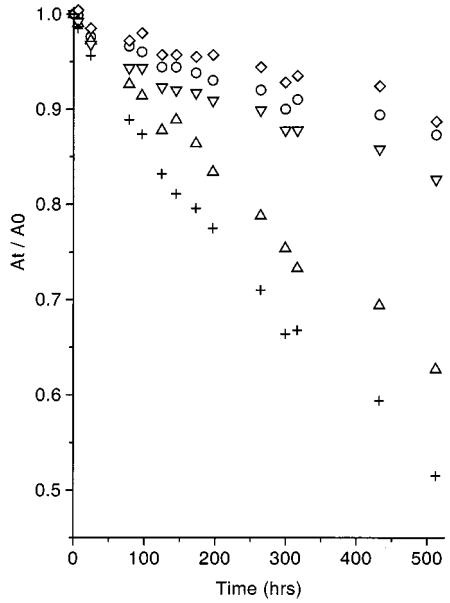


Figure 3. Influence of Ca^{2+} on the reaction of d(GpG) with platinum phosphonate complexes at pH 7 as determined from UV data. ◇ = [Pt(*R*,*S*-dach)(ntmp)]; ○ = [*cis*-$Pt(NH_3)_2$(bmpaa)]; + = [Pt(*R*,*S*-dach)(ntmp)] + Ca^{2+}; ▽ = [*cis*-$Pt(NH_3)_2$(bmpaa)] + Na^+; △ = [*cis*-$Pt(NH_3)_2$(bmpaa)] + Ca^{2+}. A_t/A_o is defined as: $[A_t(\lambda_{max}) - A_t(\lambda_{min})]/[A_o(\lambda_{max}) - A_o(\lambda_{min})]$

which is relatively inert, relative to the aqua species. Although for the Pt phosphonate complexes a direct attack of the G base on the carboxylate is involved (considered to be step 1), it cannot be ruled out that, in case of the subsequent step, the *N*-coordinated phosphonate ligand is hydrolyzed before the second G base will coordinate. This coordination of the second G would occur slower at pH 7.0, due to the presence of coordinated OH, whereas at pH 6.5 relatively more aqua ligand would be present.

The enhanced reactivity of platinum phosphonate complexes in slightly acidic media and in the presence of Ca^{2+} may explain their antitumor properties and selectivity for bone tumors. Since in tumor tissue the pH is known to be (approximately) 0.5 pH units lower than in normal tissues,[10] the reactivity of Pt phosphonates may be enhanced in tumor tissues. In addition, the phenomenon called "bone buffering" may also contribute to the enhanced reactivity of phosphonate compounds in tumors. Bone buffering occurs during prolonged acidosis or other pathological conditions.[11] Calcium phosphate (present as hydroxyapatite in

Table 1. $t_{1/2}$ values (hours) for the several reactions of d(GpG) with [*cis*-$Pt(NH_3)_2$(bmpaa)] and [Pt(*R*,*S*-dach)(ntmp)] (10^{-5} M) as determined from UV data (standard deviations in parentheses)

Compound	pH	$t_{1/2}$	Compound	pH	$t_{1/2}$
[*cis*-$Pt(NH_3)_2$(bmpaa)]	6.5	501 (20)	[Pt(*R*,*S*-dach)(ntmp)]	6.5	479 (20)
+$CaCl_2$	6.5	189 (22)	+ $CaCl_2$	6.5	295 (18)
[*cis*-$Pt(NH_3)_2$(bmpaa)]	7.0	2391 (24)	[Pt(*R*,*S*-dach)(ntmp)]	7.0	2871 (21)
+$CaCl_2$	7.0	685 (7)	+ $CaCl_2$	7.0	521 (10)
+NaCl	7.0	1641(17)			

the inorganic part of the bone) is relatively insoluble; however at lower pH the calcium phosphate can go into solution and the levels of Ca^{2+} and phosphate rise. The increased phosphate concentration is thus able to buffer the H^+ ions, whereas the increased Ca^{2+} level can enhance the reactivity of the platinum phosphonate complexes.

Attack of the G base on Pt does result in release of bmpaa, which is significantly enhanced by the presence of Ca^{2+} The interaction of the calcium ions with the negatively charged phosphonate groups is held responsible for this. This interaction results in less negative charge around the platinum and thus the attack of the incoming G-base is less hindered by electronic repulsion. These observations suggest a possible activation mechanism in vivo induced by calcium and slightly acidic conditions and would nicely explain the antitumor properties of these platinum phosphonate complexes.

Experimental Section

Syntheses: The compounds were synthesized as described elsewhere,[7] and characterized by elemental analysis and IR spectra.

NMR Spectra: The NMR spectra were recorded on a Bruker WM300 spectrometer at 297 K in D_2O (99.95%, Merck). – ^{1}H-NMR data (δ in ppm) were scaled in solution to TMA (tetramethylammonium nitrate, δ = 3.18 downfield TMS), and referenced to TMS and ^{31}P-NMR data were referenced to H_3PO_4 (85%). [*cis*-Pt(NH_3)$_2$(ntmp)] and [Pt(*R*,*S*-dach)(ntmp)] were characterized with ^{1}H- and ^{31}P-NMR spectroscopy as described before.[12] Chemical shift data for the other Pt compounds are: [*cis*-Pt(NH_3)$_2$(bmpaa)]: $\delta H_{CH\text{-}P}$ = 3.56, 3.33; $\delta H_{CH\text{-}COO}$ = 4.30; $\delta^{31}P$ = 10.20. [For comparison: free bmpaa ligand: $\delta H_{CH\text{-}P}$ = 3.60; $\delta H_{CH\text{-}COO}$ = 4.13; $d^{31}P$ = 7.88]. [Pt(*R*,*S*-dach)(apmd)]: δH_a = 7.99, δH_b = 7.43 and δH_c = 7.36; $\delta^{31}P$ = 12.86. [For comparison: free apmd ligand: δH_a = 7.68, δH_b = 7.35 and δH_c = 7.27; $\delta^{31}P$ = 10.55].

Reactions: One equivalent of d(GpG) was allowed to react with one equivalent of complex **a** or complex **d** at 310 K in the dark (10^{-5} M) and the reaction was followed by UV-VIS spectroscopy ((DMS-200 UV-Visible Spectrophotometer, Varian). The pH was kept constant by addition of small amounts (μL) of NaOH (0.1 N) to the reaction mixture. Reactions in the presence of likely activators, such as S-containing nucleophiles, $CaCl_2$ or NaCl, were performed as described above, using the following concentrations: cysteine, methionine, gluthatione, and (*S*)-methylgluthatione ($5\cdot10^{-5}$ M and $5\cdot10^{-6}$ M); $CaCl_2$ ($5\cdot10^{-4}$ M); NaCl (10^{-3} M). After completion of the reaction (no changes in the UV-VIS spectrum can be observed any more) the reaction products were lyophilized and analyzed by NMR. The excess of Ca^{2+} was removed by using oxalic acid and the precipitate was removed by filtration.

Acknowledgments

Support for this work by the Council for Chemical Sciences of the Netherlands Organisation for Scientific Research (CW-NWO) and the foundation of Applied Technical Research (STW) (Grant 349-2293) and a loan of K_2PtCl_4 form Johnson Matthey Ltd. (Reading, England) are greatly appreciated. We acknowledge Pharmachemie BV (Haarlem, the Netherlands) for their financial support. Also support concerted by the COST Actions D1-92/002 (Biocoordination Chemistry) and D8-97/0007 (Chemistry of Metals in Medicine) is kindly acknowledged.

[1] For some reviews see: W. I. Sundquist, S. J. Lippards, *Coord. Chem. Rev.* **1990**, *100*, 293. J. Reedijk, *Inorg. Chim. Acta* **1992**, *198-200*, 873. D. B. Zamble. S. J. Lippard, *Trends Biochem. Sc.* **1995**, *20*, 435. J. Reedijk, *Chem. Comm.* **1996**, 801

[2] A. M. J. Fichtinger-Schepman, J. L. van der Veer, J. H. J. den Hartog, P. H. M. Lohman, J. Reedijk, *Biochemistry* **1985**, *24*, 707. A. M. J. Fichtinger-Schepman, A. T. van Oosterom, P. H. M. Lohman, F. Berends, *Cancer Res.* **1987**, *47*, 3000.

[3] [3a] T. Klenner, P. Valenzuele-Paz, B. K. Keppler, G. Angres, H. R. Scherf, F. Wingen, D. Schmähl, *Cancer Treat. Rev.* **1990**, *17*, 253. – [3b] T. Klenner, F. Wingen, B. K. Keppler, B. Krempien, D. Schmähl, *J. Cancer Res. Clin. Oncol*. **1990**, *116*, 341. – [3c] T. Klenner, B. K. Keppler, F. Amelung, D. Schmähl, *J. Cancer Res. Clin. Oncol*. **1989**, *115*, S54. – [3d] B. K. Keppler, M. R. Berger, T. Klenner, M. E. Heim, *Adv. Drug Res.* **1990**, *19*, 243. – [3e] S. Frühauf, W. J. Zeller, *Cancer Research* **1991**, *51*, 2943.

[4] F. Wingen, D. Schmähl, *Drug Research* **1985**, *35*, 1565.

[5] Abbreviations used: bmpaa = bis(methylphosphate)aminoacetate; dach = diaminocyclohexane; ntmp nitrilotrismethylenephosphonic acid; apmd = 1-amino-1-phenyl-methane-1,1-diphosphonic acid.

[6] T. J. Einhäuser, M. Galanski, B. K. Keppler, *Journal of Analytical Atomic Spectrometry*, **1996**, 11, 747-750.

[7] M. J. Bloemink, J. P. Dorenbos, R. J. Heetebrij, B. K. Keppler, J. Reedijk, H. Zahn, H. *Inorg. Chem.* **1994**, *33*, 1127.

[8] [8a] S. S. G. E. van Boom, J. Reedijk, *J. Chem. Soc. Chem. Commun.* **1993**, 1397. – [8b] K. J. Barnham, M. I. Djuran, P. del S. Murdoch, P. J. Sadler, *J. Chem Soc. Chem. Commun.* **1994**, 721.

[9] M. Green, M. Garner, D. M. Orton, *Transition Met. Chem. Weinheim (Ger.)* **1992**, *17*, 164–176.

[10] J. L. Wike-Hooley, J. Haveman, H. S. Reinhold, *Radiother. Oncol.* **1984**, *2*, 343.

[11] M. L. G. Gardner, in: *Medical acid-base balance; the basic principles*, Bailiere Tindall, London, **1978**, pp. 7–22.

[12] T. Klenner, P. Valenzuele-Paz, F. Amelung, H. Münch, H. Zahn, B. K. Keppler, H. Blum, in: *Metal Complexes in Chemotherapy* (Ed.: B. K. Keppler), VCH Verlagsgesellschaft, Weinheim, **1993**, 85–127.

Received December 2, 1998
[I98414]

Insights into the Staudinger Reaction: Experimental and Theoretical Studies on the Stabilization of *cis*-Phosphazides

Christoph Widauer,[a] Hansjörg Grützmacher,*[a] Igor Shevchenko,*[b] and Volker Gramlich[c]

Dedicated to Prof. Dr. Edgar Niecke on the occasion of his 60th birthday

Keywords: Phosphorus / Iminophosphorane / Staudinger reaction / Heterocycles / Ab initio calculations

The Staudinger-model reaction H_3P (**1**) + HN_3 (**2**) → $H_3P{=}NH$ (**5**) + N_2 (**6**) has been investigated at the CCSD(T)/6-31G**//MP2(Full)/6-31G* level. Primary products formed in this reaction are the phosphazides $H_3P{=}N{-}N{=}NH$ (**3**) which exist as *trans* and *cis* isomers. In contrast to some previous assumptions, ***cis*-3** is 8.2 kcal mol^{-1} more stable than ***trans*-3** but decomposes rather easily into the expected products $H_3P{=}NH$ and N_2. This decomposition can be effectively hampered by intramolecular donor–acceptor interactions as shown by calculations on model compounds as well as by experiments. Thus the reaction of a methylene-σ^3,λ^3-phosphanyl-σ^5,λ^5-phosphorane with PhN_3 led to a new four-membered heterocycle containing a thermally remarkable stable *cis*-phosphazide moiety.

Since 1919 the reaction between azides and phosphanes (Staudinger reaction) has been widely used by phosphorus chemists for the preparation of λ^5-iminophosphoranes (phosphazenes).[1] In the course of the reaction the primary imination products, phosphazides, are formed, which are rarely stable under ambient conditions.[2] In a few cases, where R is strongly electron donating, R′ strongly electron withdrawing, or where both R and R′ are sterically bulky, remarkable stable phosphazides $R_3P{=}N{-}N{=}NR'$ have been isolated.[3][4] Here we wish to report on the first detailed ab initio study of the Staudinger reaction and a new possibility to stabilize phosphazides.

The Staudinger-model reaction H_3P (**1**) + HN_3 (**2**) → $H_3P{=}NH$ (**5**) + N_2 (**6**) has been investigated at the CCSD(T)/6-31G**//MP2(Full)/6-31G* level of theory.[5] In the first step of this reaction the *trans*-configured and *cis*-configured phosphazides ***trans*-3** and ***cis*-3** are formed, respectively. Subsequently, decomposition of these intermediates leads to the phosphazene **5** and dinitrogen (**6**) (Scheme 1).

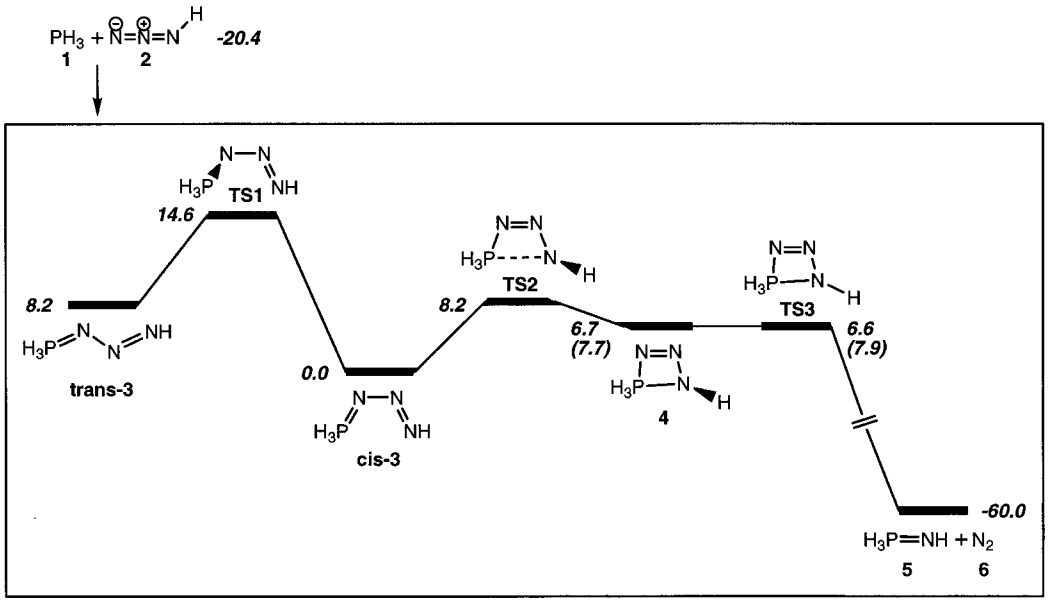
In Figure 1, the geometry-optimized structures of the phosphazides ***trans*-3**, ***cis*-3**, the transition states **TS1**, **TS2**, and **TS3**, the phosphatriazete **4**, and the phosphazene **5** are shown. Calculated total energies of all species are given in Table 1 and atomic charges on P and N of ***trans*-3** and ***cis*-3** obtained by Natural Bond Orbital analyses (NBO) are given in Table 2.

[a] Institute of Inorganic Chemistry, ETH-Zentrum, Universitätsstrasse 6, CH-8092 Zürich, Switzerland
Fax: (internat.) +41 1/632 10 90
E-mail: gruetz@inorg.chem.ethz.ch
[b] Institute of Bioorganic Chemistry
Murmanskaya Street 1, 252660 Kiev 94, Ukraine
[c] Institute of Crystallography, ETH-Zentrum
Sonneggstrasse 5, CH-8092 Zürich, Switzerland

The structures of some phosphazides have been determined experimentally.[3][4] Most of these compounds contain a *trans*-configured phosphazide moiety[3] while the *cis*-conformation[4] has rarely been observed. This led to the assumption that the *trans* conformers are more stable than their corresponding *cis* isomers. However, at least for the parent model system $H_3P{=}N{-}N{=}NH$ our calculations show a different picture: ***cis*-3** is more stable than ***trans*-3** by 8.2 kcal mol^{-1}. The isomerisation of ***trans*-3** to ***cis*-3** proceeds via the transition state **TS1** and requires an activation energy of 6.4 kcal mol^{-1}. Indeed, the *cis* isomer, though thermodynamically more stable, decomposes rather easily into $H_3P{=}NH$ (**5**) and N_2 (**6**). On the reaction coordinate, the transition state **TS2** has to be overcome, which is 8.2 kcal mol^{-1} higher in energy than ***cis*-3**. This reaction can be described as an intramolecular nucleophilic attack of the negatively charged nitrogen centre N3 (−0.55 e) on the positively charged phosphorus centre (+0.95 e). As a result, the P−N3 distance is shortened from 2.402 Å in ***cis*-3** to 1.880 Å in **TS2**. The approach of the N3 centre towards the phosphorus centre is accompanied by a pseudo-rotation at the phosphorus centre. Thereby, the formerly short P=N1 bond (1.673 Å in ***cis*-3**) is lengthened (1.924 Å in **TS2**) and the nitrogen centre N1 takes an axial position within the distorted trigonal-bipyramidal coordination sphere of the phosphorus centre.

The next product encountered on the reaction pathway is the C_1-symmetric λ^5-triazaphosphete **4**. This heterocycle is 6.7 kcal mol^{-1} higher in energy than ***cis*-3**. Molecule **4** is well-prepared for the cycloreversion leading towards the phosphazene **5** and dinitrogen. The P−N1 bond (1.951 Å) and N2−N3 bond (1.434 Å) are even longer than the ones in **TS2** while the N2−N3 bond is shorter. Calculations performed for **4** at higher levels of theory [MP4(Full) and

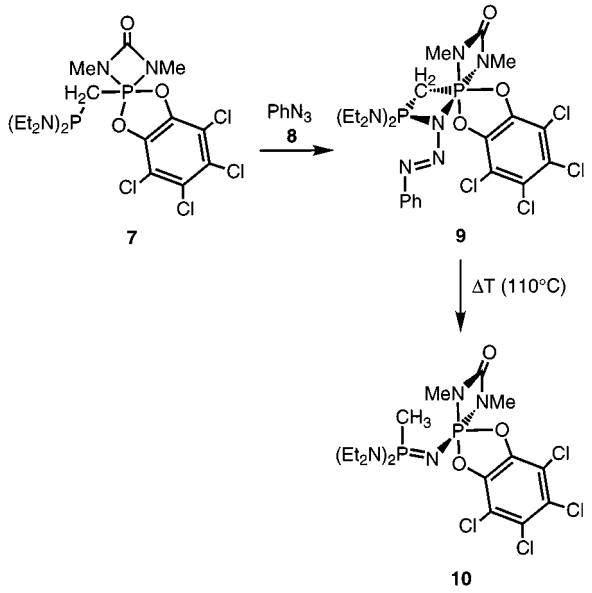
 © WILEY-VCH Verlag GmbH, D-69451 Weinheim, 1999 1434−1948/99/1010−1659 $ 17.50+.50/0



Scheme 1. Schematic representation of the isomerisation and decomposition pathways of ***cis*-3**; the refined and ZPE-corrected relative energies at the CCSD(T)/6-31G**//MP2(Full)/6-31G* level are given in kcal mol^{-1}; for **4** and **TS3** the refined relative energies at the CCSD(T) level without ZPE-correction are additionally given in parentheses

QCISD(Full)] confirm that triazete **4** is a local minimum on the energy hypersurface. However, without ZPE correction, **4** is only 0.2 kcal mol^{-1} lower in energy than **TS3**. Inclusion of zero-point energies reverses this ordering making **TS3** 0.1 kcal mol^{-1} lower in energy than **4**. This means that ordinary transition-state theory cannot be expected to describe this region of the hypersurface accurately. Therefore, we are not able to distinguish between a stepwise or concerted reaction mechanism at this point.[6] However, we can assume that ***cis*-3** decomposes via **TS2** to form phosphazene $H_3P{=}NH$ (**5**) with loss of dinitrogen.

During the decay of ***cis*-3** to **5** under extrusion of N_2 the valence configuration at N1 and N2 changes from sp^2 to sp. This process may be hampered when the lone pair at one of these nitrogen centres is involved in a donor−acceptor interaction. To test this idea we prepared the methylenephosphanyl phosphorane **7**[7] and reacted it with phenyl azide **8** (Scheme 2).



Scheme 2. Synthesis of trisspirocyclic **9**

The compound **7** contains a (λ^3,σ^3)-phosphorus centre, which can undergo a Staudinger reaction with an azide. To this phosphorus centre, a strongly positively charged (λ^5,σ^5)-phosphorus centre is bonded in the β position which can act as electron-pair acceptor. The reaction of **7** with **8** proceeds smoothly in diethyl ether without evolution of dinitrogen. The product **9** was recrystallized from toluene to afford colorless crystals suitable for an X-ray structure analysis. The result is shown in Figure 2, selected bond lengths and angles are given in the figure caption.

In compound **9** the azide moiety, indeed, takes a bridging position between the two phosphorus centres P1 and P2, thereby forming a planar four-membered ring. The P1−N1−N2−N3 unit shows a *cis* configuration. The P1−N3 distance (2.977 Å) is considerably longer than that calculated for ***cis*-3** (2.402 Å). However, apart from this distance, all other P−N and N−N bond lengths are in good agreement with distances and angles observed in ***cis*-3**. The intramolecular interaction between N1 and P2 augments the coordination number of P2 from five to six and the (λ^5,σ^6)-P2−N1 bond (1.812 Å) is, as expected, considerably longer than the P1=N1 bond (1.626 Å). The heterocycle **9** shows unusual thermal behavior when heated to 100−110°C in toluene. No dinitrogen evolution is observed but the iminophopshorane **10** is obtained which was unequivocally characterized by its NMR spectra. The mechanism leading to its formation is still unclear.

At this stage of our investigation, we returned to theoretical studies. Since the parent phosphazides ***trans*-3** and ***cis*-3**

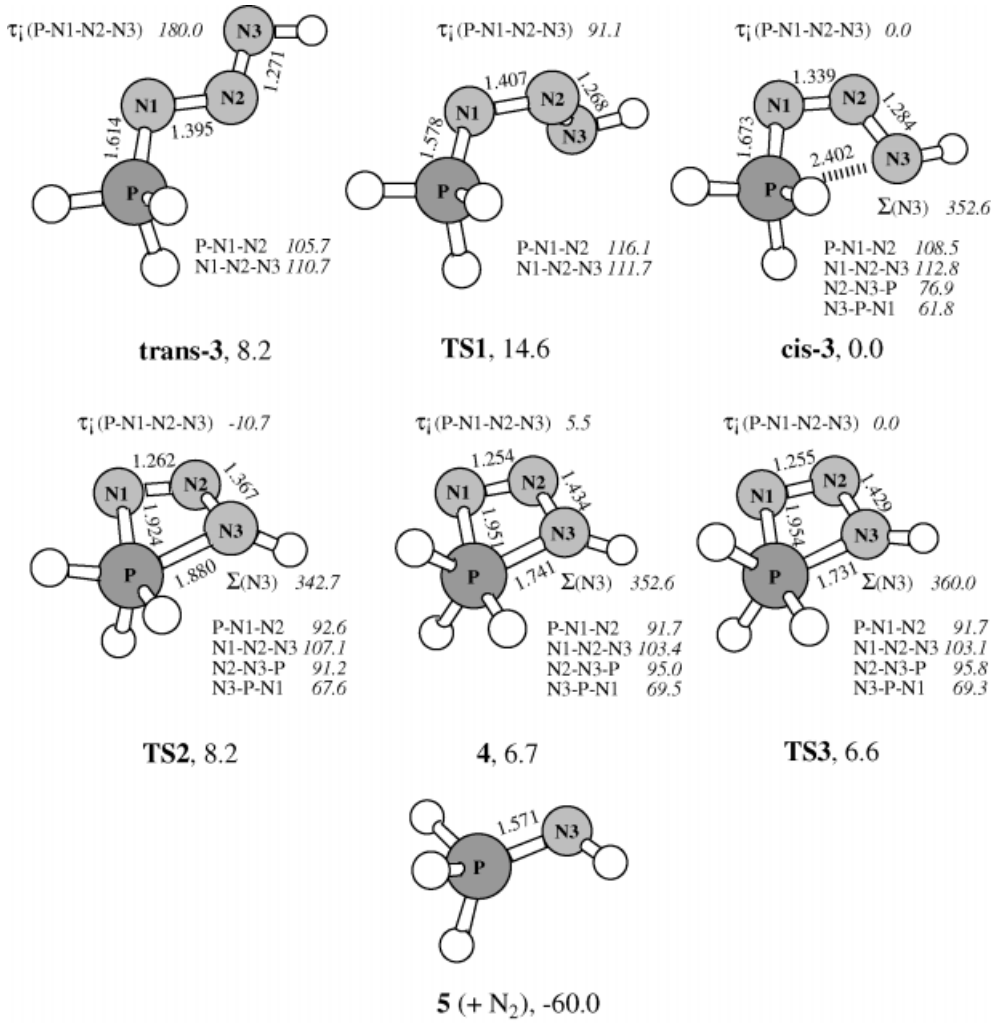


Figure 1. Schematic representation of the fully optimized MP2 structures of the Staudinger model reaction $H_3P + N_3H \rightarrow [H_3P-N=N-NH] \rightarrow H_3P=NH + N_2$ including selected bond lengths [Å], angles [°], and dihedrals τ [°]; relative energies are given in kcal mol^{-1}

Table 1. Energies for reactants, intermediates, transition states, and products of the reactions **1** + **2** → **3** → **5** + **6** and **12** → **13** → **15** + **6** as well as for the phosphazides ***cis*-11** and ***trans*-11**

	CCSD(T)/6-31G**//MP2(FULL)/6-31G*						
	sym	$E_{tot,opt}$	$E_{tot,ref}$	ZPE	N	$E_{rel,opt}$	$E_{rel,ref}$
1 + **2**		–506.913507	–506.977975	29.2	[b]	–23.0	–20.4[c]
***cis*-3**	C_s	–506.884108	–506.952590	33.8	0	0.0	0.0
***trans*-3**	C_s	–506.869078	–506.938648	33.2	0	8.9	8.2
TS1	C_1	–506.858065	–506.928200	33.0	1	15.6	14.6
TS2	C_1	–506.870509	–506.937569	32.5	1	7.3	8.2
4	C_1	–506.872567	–506.940327	32.7	0	6.2	6.7[d]
TS3	C_s	–506.872441	–506.940001	32.5	1	6.0	6.6
5 + **6**		–506.977098	–507.042359	30.1	[b]	–62.0	–60.0[c]
***cis*-11**	C_1	–1395.38109		78.7	0	0	
***trans*-11**	C_1	–1395.37594		78.8	0	3.3	
12	C_1	–571.393729	–571.503381	58.9	0	19.2	18.6
***cis*-13**	C_1	–571.427110	–571.535920	60.7	0	0.0	0.0
***trans*-13**	C_1	–571.418281	–571.527430	60.5	0	5.4	5.2
TS4	C_1	–571.391318	–571.499418	58.5	1	20.3	20.7
14	C_1	–571.497302	–571.600441	58.7	0	–46.0	–42.5
15 + **6**		–571.524975	–571.611543	57.7	[b]	–64.3	–50.4[c]

[a] All structures were optimized at the MP2(Full)/6-31G* level ($E_{tot,opt}$). Refined energies were obtained at the CCSD(T)/6-31G** level ($E_{tot,ref}$), except for ***cis*-11** and ***trans*-11**, respectively. Total energies in Hartrees, zero point energies (ZPE, unscaled) and relative energies ($E_{rel,opt}$, $E_{rel,ref}$, ZPE correction included) in kcal mol^{-1}; N: number of negative frequencies. – [b] Frequency analyses show that **1** and **2**, **5** and **6** as well as **15** are local minima. – [c] No BSSE (basis-set superposition error) correction included. – [d] Calculations at higher levels of theory (MP4, QCISD) confirm that **4** is a local minimum on the hypersurface.

Table 2. Atomic charges of ***trans*-3** and ***cis*-3**

	atomic charges	
	***trans*-3**	***cis*-3**
P	1.090	0.953
N1	–0.830	–0.737
N2	–0.104	–0.002
N3	–0.383	–0.554

[a] Selected atomic charges for the phosphazides ***trans*-3** and ***cis*-3**, respectively, obtained by NBO analysis at the MP2(Full)/6-31G* level.

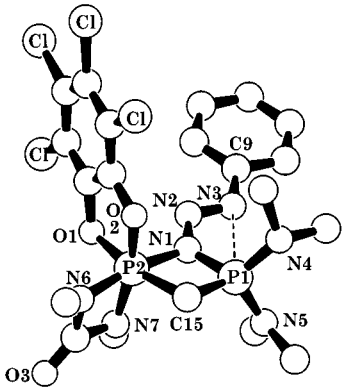


Figure 2. X-ray structure of **9** including selected bond lengths [Å] and angles [°]; H atoms and disordered ethyl groups at N4 and N5 are omitted for clarity: P1–N1 1.626(6), P1–N4 1.622(5), P1–N5 1.612(5), P1–C15 1.770(6), P1–N3 2.928(5), P2–N1 1.812(5), P2–N6 1.754(5), P2–N7 1.761(5), P2–C15 1.865(6), P2–O1 1.758(4), P2–O2 1.754(5), N1–N2 1.361(6), N2–N3 1.254(6); N1–P1–C15 84.0(3), N4–P1–N5 108.0(3), N1–P2–C15 76.4(2), O1–P2–O2 89.1(2), N6–P2–N7 72.9(3), P1–C15–P2 96.0(3), P1–N1–P2 103.4(3), P1–N1–N2 129.3(4), P2–N1–N2 126.9(4), N1–N2–N3 115.1(6), N2–N3–C9 117.8(6)

are rather different from the experimentally obtained structure **9**, we have performed ab initio calculations for ***cis*-11** and ***trans*-11** which are better models. The PF_4 moiety was chosen as substitute for the acceptor group including the hexa-coordinated P2 centre in **9** and the $P(NH_2)_2$ group was chosen to replace the $P1(NEt_2)_2$ unit. The structures of ***cis*-11** and ***trans*-11** were also optimized at the MP2(Full)//6-31G* level and are shown in Figure 3.

The *cis* isomer is again more stable than the *trans* isomer. However, at the MP2(Full)/6-31G* level, the energy difference amounts to only 3.3 kcal mol^{-1} and is 5.6 kcal mol^{-1} smaller than that observed for the parent compounds ***cis*-3** and ***trans*-3**. Thus, the observed *cis*-configuration of the P–N1–N2–N3 unit in **9** might be simply preferred for steric reasons. Generally, the agreement between the calculated structure of ***cis*-11** and that of **9** is acceptable. The four-membered heterocycle which is planar in **9** deviates slightly from planarity in ***cis*-11** and, in an opposite sense, in ***trans*-11**. As was also observed experimentally, the P2–N1 and P2–C bonds pointing away from the hexa-coordinated phosphorus centre P2 are considerably longer than corresponding P1–N1 and P1–C bond lengths. The largest deviation is seen in the intramolecular P1–N3 contact, which is about 0.2 Å longer in ***cis*-11** than the experimental value observed in **9**.

Since the theoretical investigation of the decomposition pathways of **11** is very expensive, we investigated the boromethyl phosphazides **12** and **13**. The decomposition of these compounds is easier to study at the level of theory used throughout this paper and **12** and **13** should serve as reliable models for the study of the effect of intramolecular donor–acceptor interactions. The structures optimized at the MP2(Full)/6-31G* level are shown in Figure 4 including selected bond lengths and angles.

Rotation around the P–C bond interconverts **12** to ***cis*-13**. Intramolecular nucleophilic attack of N1 onto the boron centre leads to the formation of the four-membered B,C,P,N heterocycle. The energy gained by this process amounts to 18.6 kcal mol^{-1} and can be taken as measure of the donor-acceptor stabilization energy of the N1–B interaction. The heterocycle ***cis*-13** is 5.2 kcal mol^{-1} more stable than ***trans*-13**. However, this energy difference is again smaller than that found for the parent compounds ***cis*-3** and ***trans*-3**, respectively (8.2 kcal mol^{-1}). Obviously, the *trans*-isomers become *thermodynamically* more stabilized than the *cis*-isomers by intramolecular donor-acceptor interactions. The latter remain, however, energetically favored. The structure of the *cis*-configured phosphazide moiety P1–N1–N2–N3 does not differ significantly from the one calculated for ***cis*-11** or the one observed in **9**. Note that the P–N3 contact becomes considerably longer (ca. 0.3 Å) in the cyclic compound ***cis*-13** (2.767 Å) while in the acyclic

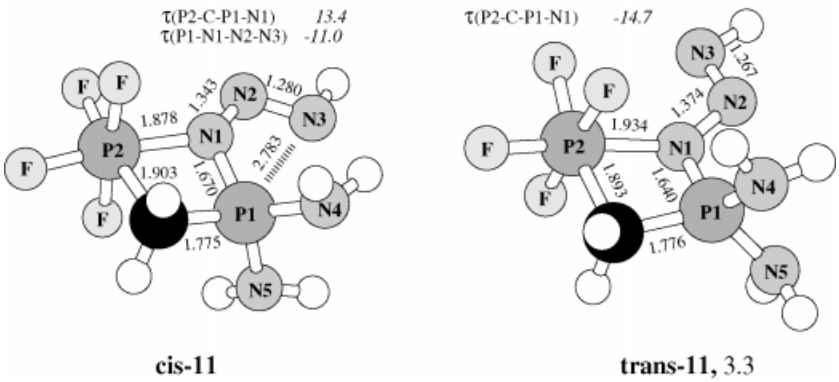


Figure 3. Schematic representation of the isomers ***cis*-11** and ***trans*-11** including bond lengths [Å] and dihedrals τ [°]; the relative energy is given in kcal mol^{-1}

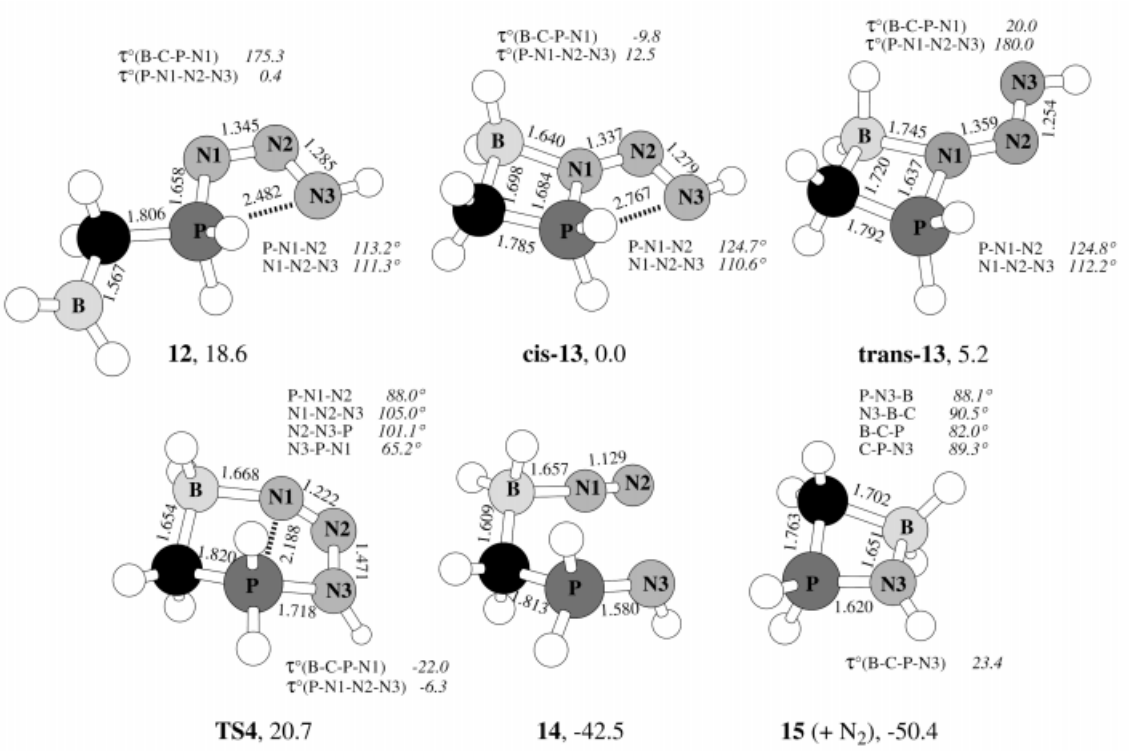


Figure 4. Schematic representation of the fully optimized MP2 structures of the (boromethyl)phosphazides $(H_2BCH_2)H_2P{=}N1{-}N2{=}N_3H$ including selected bond lengths [Å], angles [°], and dihedrals τ [°]; relative energies are given in kcal mol^{-1}

structure **12** this distance (2.482 Å) lies in the same range as has been calculated for the parent compound ***cis*-3** (2.402 Å). The cleavage of dinitrogen from ***cis*-13** proceeds via the bicyclic transition state **TS4** which is 20.7 kcal mol^{-1} higher in energy. This activation barrier is 12.5 kcal mol^{-1} higher than that calculated for the decay of ***cis*-3**. The phosphazene **14** is formed exothermically (−42.5 kcal mol^{-1}) and still contains the dinitrogen N_2 molecule coordinated to the Lewis-acidic boron centre. After dissociation of N_2, the heterocycle **15** is observed as the final product and encloses the thermodynamically highly favored reaction sequence. This example shows that intramolecular donor−acceptor interaction between an electron pair acceptor and the lone pair at the N1 centre may efficiently hamper *kinetically* the decay of *cis*-phosphazides into phosphazenes and dinitrogen.

Experimental Section

Calculations: The calculations were performed with the GAUSSIAN 94 program package.[8] All structures were fully optimized at the MP2(Full) level using the polarized split-valence-shell 6-31G* basis set.[5a,5b] Refined energies were obtained at the CCSD(T) level,[5c−5e] except for ***cis*-11** and ***trans*-11**, in conjunction with the slightly extended basis set 6-31G**,[5b] which also contains p polarization functions on the hydrogen atoms. The vibrational frequency calculations were carried out to characterize all structures as minima or transition states. Relative energies were corrected for zero-point vibrational energy (ZPE) using the unscaled MP2 corrections. Atomic charges were obtained at the MP2(Full)/6-31G* level according to Reed and Weinhold's NBO analysis,[9] which is implemented in GAUSSIAN 94. Selected total and relative energies of all calculated structures are presented in Table 1.

***cis*-Phosphazide 9**: A solution of **7**[7] (150 mg, 0.27 mmol) in 2 mL of diethyl ether was treated with 50 mg (0.42 mmol) of phenylazide and the reaction mixture was allowed to stay at room temperature for 30 min. The bottom of the flask was rubbed by a glass stick to promote the crystallization and after formation of the first crystals the solution was allowed to stay at −18 °C for 12 h. Crystals of **9** were separated and recrystallized from toluene. M.p.: 139−141 °C. Yield 116 mg (64%). − ^{1}H NMR (90 MHz, $CDCl_3$): 1.12 [t, ^3J(H,H) = 7.02 Hz, 12 H, NCH_2CH_3], 2.77 [d, ^3J(P,H) = 14.4 Hz, 6 H, NCH_3], 2.9−3.4 (m, 8 H, NCH_2CH_3), 2.9−3.4 (m, 2 H, PCH_2P), 7.23−7.52 (m, 5 H, C_6H_5). − ^{13}C NMR (22.5 MHz, $CDCl_3$): 13.2 [d, ^3J(P,C) = 2.9 Hz, 4C, Et], 27.9 [d, ^2J(P,C) = 4.9 Hz, 2C, NMe], 38.6 [dd, ^1J(P,C) = 86.8 Hz, ^1J(P,C) = 122.9 Hz, P−C−P], 39.4 [d, ^2J(P,C) = 5.9 Hz, 4C, Et], 113.6 [d, ^2J(P,C) = 16.5 Hz, 2C, Ar], 121.4 (s, 2C, Ar), 121.8 (s, 2C, Ar), 129.1 (s, 1C, Ar), 129.21 (s, 2C, Ar), 143.2 (s, 1C, Ar), 148.2 (s, 2C, Ar), 160.9 [d, ^2J(P,C) = 12.6 Hz, CO]. − $C_{24}H_{33}Cl_4N_7O_3P_2$: calcd. C 42.94, H 4.95, N 14.60; found C 42.47, H 4.98, N 14.82.

Iminophosphorane 10: ^{31}P NMR (C_6D_6): 23.5 [d, ^2J(P,P) = 44 Hz]; −52.1 [d, ^2J(P,P) = 44 Hz]. − ^{1}H NMR (C_6D_6): δ = 0.66 [t, ^3J(H,H) = 7.08 Hz, 12 H, Et], 1.09 [d, ^2J(P,H) = 14.2 Hz, P−CH_3], 2.3−2.7 (m, 8 H, Et), 2.87 [d, ^3J(P,H) = 13.4 Hz, NCH_3].

X-ray Analysis of *cis*-Phosphazide 9: Orthorhombic, space group *Pbca*; a = 18.284(14), b = 17.158(12), c = 20.37(2) Å; V = 6392(8) Å^3; Z = 8, MoK_α-radiation, $2\Theta_{max}$ = 41.4°. 3011 independent reflections; direct methods; full-matrix least-squares refinement based on F^2 with SHELXTL (Version 5.0); R_1 = 4.6%, wR_2 = 9.32% (based on F^2) for 389 parameters and 3010 reflections with $I > 2\sigma(I)$. All non-hydrogen atoms were refined anisotropically. Hydrogen atoms were refined using the riding model. Crystallographic data (excluding structure factors) have been deposited at the Cambridge Crystallographic Data Centre as supplementary publication no. CCDC-101754. Copies of the data can be obtained, free of

charge, on application to CCDC, 12 Union Road, Cambridge CB2 1EZ [Fax: (internat.) +44-1223/336033; E-mail: deposit@chemcrys.cam.ac.uk].

Acknowledgments

This work was supported by the Swiss National Science Foundation.

[1] [1a] H. Staudinger, J. Meyer, *Helv. Chim. Acta* **1919**, *2*, 635. – [1b] Y. G. Gololobov, I. N. Zhmurova, L. F. Kasukhin, *Tetrahedron* **1981**, *37*, 437. – [1c] E. Niecke, D. Gudat in: *Multiple Bonds and Low Coordination in Phosphorus Chemistry* (Eds.: M. Regitz, O. J. Scherer), Thieme, Stuttgart, **1990**, 392. – [1d] E. Niecke, D. Gudat, *Angew. Chem.* **1991**, *103*, 251; *Angew. Chem., Int. Ed. Engl.* **1991**, *30*, 217. –[1e] Y. G. Gololobov, L. F. Kasukhin, *Tetrahedron* **1992**, *48*, 1353. – [1f] W. Johnson, *Ylides and Imines of Phosphorus*, Wiley, New York **1993**, 403.

[2] [2a] G. Wittig, K. Schwarzenbach, *Liebigs Ann. Chem.* **1961**, *650*, 1. – [2b] J. E. Leffler, U. Honsberg, T. Tsuno, I. Forsblad, *J. Org. Chem.* **1961**, *26*, 4810. – [2c] R. W. Saalfrank, E. Ackermann, M. Fischer, U. Wirth, H. Zimmermann, *Chem. Ber.* **1990**, *123*, 115. – [2d] C. K. Lowe-Ma, R. A. Nissan, W. S. Wilson, *J. Org. Chem.* **1990**, *55*, 3755.

[3] [3a] G. L. Hillhouse, G. V. Goeden, B. L. Haymore, *Inorg. Chem.* **1982**, *21*, 2064. – [3b] A. N. Chernega, M. Y. Antipin, Y. T. Struchkov, I. E. Boldeskul, M. P. Ponomarchuk, L. F. Kasukhin, V. P. Kukhar, *Zh. Obshch. Khim.* **1984**, *54*, 1979. – [3c] C. G. Chidester, J. Szmuszkovicz, D. J. Duchamp, L. G. Laurian, J. P. Freeman, *Acta Cryst.* **1988**, *C44*, 1080. – [3d] A. N. Chernega, M. Y. Antipin, Y. T. Struchkov, M. P. Ponomarchuk, L. F. Kasukhin, V. P. Kukhar, *Zh. Obshch. Khim.* **1989**, *59*, 1256. – [3e] A. A. Tolmachev, A. N. Kostyuk, E. S. Kozlov, A. P. Polishchuk, A. N. Chernega, *Zh. Obshch. Khim.* **1992**, *62*, 2675. – [3f] J. R. Goerlich, M. Farkens, A. Fischer, P. Jones, R. Schmutzler, *Z. anorg. allg. Chem.* **1994**, *620*, 707. – [3g] K. Bieger, G. Bouhadir, R. Reau, F. Dahan, G. Bertrand, *J. Am. Chem. Soc.* **1994**, *118*, 8087.

[4] [4a] P. Molina, C. López-Leonardo, J. Llamas-Botía, C. Foces-Foces, C. Fernández-Castaño, *Tetradedron* **1996**, *52*, 9629. – [4b] M. Alajarín, P.Molina, A. López-Lázaro, C. Foces-Foces, *Angew. Chem.* **1997**, *109*, 147.

[5] [5a] C. Møller, M. S. Plesset, *Phys. Rev.* **1934**, *46*, 618. – [5b] J. A. Pople, M. Head-Gordon, K. Raghavachari, *Chem. Phys. Lett.* **1987**, *89*, 7382. – [5c] G. D. Purvis, R. J. Bartlett, *J. Chem. Phys.* **1982**, *76*, 1910. – [5d] G. E. Scuseria, C. L. Janssen, H. F. Schaefer, III, *J. Chem. Phys.* **1988**, *89*, 7382. – [5e] G. E. Scuseria, C. L. Janssen, H. F. Schaefer, III, *J. Chem. Phys.* **1989**, *90*, 3700.

[6] [6a] J.E. Leffler, R.D. Temple, *J. Am. Chem. Soc.* **1967**, *89*, 5235. – [6b] H. Bock, M. Schnöller, *Angew. Chem.* **1968**, *80*, 667. [6c] J. G. Gololobov, L. F. Kasukhin, U. S. Petrenko, *Phosphorus Sulfur* **1987**, *30*, 393.

[7] I.V. Shevchenko, R. Schmutzler, *Heteroat. Chem.* **1992**, *4*, 307.

[8] M. J. Frisch, G. W. Trucks, H. B. Schlegel, P. M. W. Gill, B. G. Johnson, M.A. Robb, J. R. Cheeseman, T. Keith, G. A. Petersson, J. A. Montgomery, K. Raghavachari, M. A. Al-Alaham, V. G. Zakrzewski, J. V. Ortitz, J. B. Foresman, J. Cioslowski, B. B. Stefanov, A. Nanayakkara, M. Challacombe, C. Y. Peng, P. Y. Ayala, W. Chen, M. W. Wong, J. L. Andres, E. S. Replogle, R. Gomperts, R. L. Martin, D. J. Fox, J. S. Binkley, D. J. Defrees, J. Baker, J. J. P. Stewart, M. Head-Gordon, C. Gonzalez, J. A. Pople, *GAUSSIAN 94 Revision D4 Ed.*, Gaussian Inc. Pittsburgh, **1995**.

[9] A.E. Reed, L.A Curtis, F. Wheinhold, Chem. Rev. **1988**, *88*, 899.

Received January 2, 1999
[I99022]

An Unusual Reaction of Hexafluoroacetone with Methylenediphosphanes: Facile Synthesis of Carbodiphosphoranes

Igor Shevchenko,*[a] Rostislav Mikolenko,[a] Sandra Loss,[b] and Hansjörg Grützmacher*[b]

Keywords: Methylenediphosphane / Hexafluoroacetone / Carbodiphosphorane / Ylides / Carbenes

The oxidation of the methylenediphosphanes **3a,b** with hexafluoroacetone does not lead to the expected dioxaphospholane heterocycles, but yields quantitatively the carbodiphosphoranes **5a,b**. Compounds **5a,b** easily add HCl, HF or Cl_2 to the ylidic bonds. The chloro derivative **14b,** and its analogue **17** were used for the synthesis of phosphonium substituted carbenes.

It is well-known that the reaction of phosphanes with two equivalents of hexafluoroacetone (HFA) leads to the formation of phosphoranes in which the phosphorus atom is included in dioxaphospholane heterocycles.[1–4] It turns out that this is not the only possible pathway for this reaction. In one of our previous papers we described the formation of the phosphorus ylide **2** from the reaction of the methylenephosphinophosphorane **1** with one equivalent of HFA.[5] However, we considered this to be an exception to the rule as **1** possesses unique chemical properties due to the ability of the λ^5-phosphorus atom to form zwitterionic structures with tetra- and hexacoordinate phosphorus atoms bearing opposite charges.[6] According to the X-ray data **2** may indeed have the zwitterionic structure **2′**.[5]

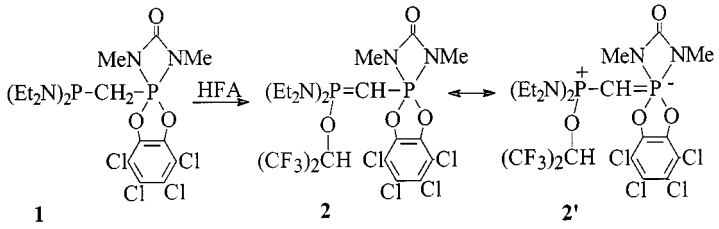
It appears, however, that this reaction is not an exception, but has a more common nature. In our preliminary communication[7] we reported an unusual reaction of the bis[bis(dialkylamino)phosphinyl]methanes **3a,b** with two equivalents of hexafluoroacetone, which quantitatively yields the carbodiphosphoranes **5a,b**. The addition of HFA to **3a,b** is accompanied by the migration of two protons from the $P-CH_2-P$ unit to the carbon atoms of HFA. Thus the presence of a methylene group between the two phosphorus atoms is a necessary condition for this reaction.

Formally, the mechanism of the formation of the carbodiphosphoranes **5a,b** can be considered to be an addition of the tautomeric P–H ylide form **3′a,b** to the carbonyl function of HFA. However, it is more likely that the migration of the proton from the $P-CH_2-P$ unit follows an electrophilic attack by HFA on the phosphorus. This reaction probably consists of two steps with the intermediate formation of the monoylides **4a** or **4b**. However, we could not detect these compounds by NMR spectroscopy. If only one equivalent of HFA was added to methylenediphosphanes **3a,b**, the reaction mixture was found to consist of starting material **3** and reaction product **5** in equal proportions. The reaction proceeds smoothly at room temperature by slow bubbling of gaseous HFA through a solution of **3a** or **3b** in hexane. The $^{31}P\{^1H\}$ NMR spectra of the reaction mixtures show the presence of only one compound **5a** or **5b**, respectively (one singlet at $\delta = 33 - 37$). The location of the two equivalent protons in the α-positions to the CF_3 groups is confirmed by the ^{19}F-NMR spectra: all fluorine atoms are equivalent and appear as a doublet at $\delta = -73.0$ with a $^3J_{HF}$ coupling constant of 6.8 Hz. The $HC(CF_3)_2$ protons display the same coupling constant in the ^1H-NMR spectra, showing a characteristic low field multiplet at $\delta = 6.2$. NMR spectroscopic studies revealed an interesting phenomenon: this multiplet of nine slightly broadened lines is a combination of a septet, caused by $^3J_{FH}$coupling, and a triplet caused by $^3J_{PH}$coupling, with approximately equal coupling constants. The two marginal lines are of very low intensity and can only be distinguished at high signal-to-noise ratio and amplification. This unexpected $^3J_{PH}$ triplet was also found in the ^{31}P-NMR spectrum of **5a** or **5b** when measured with the selective decoupling of the protons of the NR_2 group. This means that the protons of the two $HC(CF_3)_2$ units are equivalent for each of the two phosphorus atoms and vice versa. This unusual P–H coupling is probably accounted for by a rapid exchange between the two protons of the $HC(CF_3)_2$ groups, as in **5′a,b**. Derivatives of **5a,b** – the hydrochloride salts **7a,b**, the tetrafluoroborate **16** and the dichloro- and tetrachloro derivatives **13, 14** – exhibit the same spectroscopic phenomenon (see below). It should be noted that the dimethylamino groups of **5a** appear in the ^1H-NMR spectrum not as a doublet, but as a pseudo-triplet, at $\delta = 2.59$, with a broadened central line which is consistent with the NMR spectroscopic data of known compounds. The analogous carbodiphosphorane, which has chlorine atoms instead of HFA groups at the two phosphorus atoms, shows the same pattern for the NMe_2 groups in its ^1H-NMR spectrum.[8]

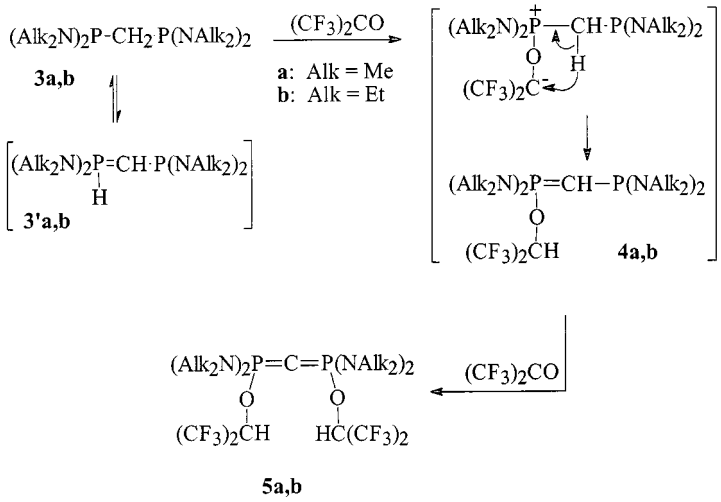
Theoretically, the reaction of **3a**,**b** with HFA can also lead to compounds **6a**,**b**, which are structural isomers of **5a**,**b** and which would have approximately the same spectral

[a] Institute of Bioorganic Chemistry,
Murmanskaya Street 1, 252660 Kiev, Ukraine
Fax: (internat.) + 38-044/573-2552
E-mail: ishev@bpci.kiev.ua; ishev@bioorg.kiev.ua
[b] Laboratorium für Anorganische Chemie,
ETH-Zentrum,
Universitätstrasse 6, CH-8092 Zürich
Fax: (internat.) + 41-1/632-1090
E-mail: gruetz@inorg.chem.ethz.ch

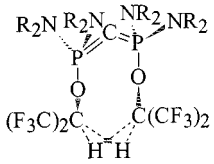
 © WILEY-VCH Verlag GmbH, D-69451 Weinheim, 1999 1434–1948/99/1010–1665 $ 17.50+.50/0



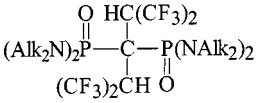
Scheme 1. Reaction of **1** with HFA



Scheme 2. Reaction of **3a,b** with HFA



5'a,b

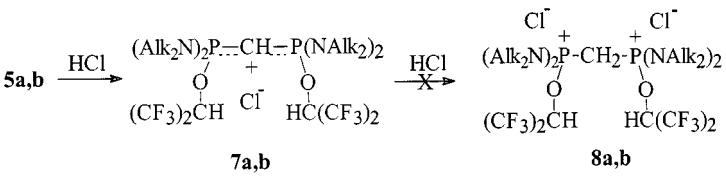


6a,b

data. However, unlike **6a,b**, the carbodiphosphoranes **5a,b** have an ylidic structure which was subsequently confirmed by treating them with HCl to form the stable salts **7a,b**. As strong bases, **5a**,**b** also react with ammonium chlorides. For this reason, small quantities of **7a**,**b** are always formed together with **5a,b** if the starting methylenediphosphanes **3a,b** are contaminated with dialkylammonium chlorides. However, compounds **7a,b** are not soluble in hexane and can easily be separated.

The structures of **7a,b** are entirely consistent with the NMR spectroscopic data obtained. The ^{13}C-NMR spectrum shows a triplet for the P−C−P carbon atom at δ = 7.35. Such an upfield chemical shift is indicative of a carbon atom bearing a negative charge. The ^{1}H-NMR spectrum of **7a** is shown in Figure 1. As in the case for **3a**, the $HC(CF_3)_2$ protons are equivalent towards each phosphorus atom and appear as a multiplet of nine lines at δ = 6.71. This signal, however, is not well resolved due to larger differences between the $^{3}J_{FH}$ and $^{3}J_{PH}$coupling constants. As in **3a,** the NMe_2 units of **7a** appear as pseudo triplets in the ^{1}H- and ^{13}C-NMR spectra. It is important to note that, despite their ylidic character, **7a,b** are very stable towards hydrolysis. With HCl no further reaction occurs and the expected diphosphonium salts **8a,b** cannot be obtained in this way.

The carbodiphosphorane **5a** slowly decomposes in hexane solution at room temperature and its signal in the ^{31}P-NMR spectrum disappears within several hours. Compound **5b,** containing bulkier diethylamino substituents, is more stable and a hexane solution of **5b** can be stored without decomposition for two days. However, subsequent evaporation of the solvent causes **5b** to decompose. The choice of hexane as solvent is very important for the preparation



Scheme 3. Reaction of **5a,b** with HCl

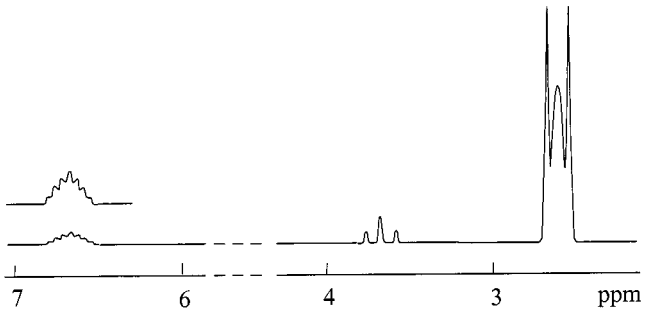


Figure 1. The ^{1}H-NMR spectrum of **7a**

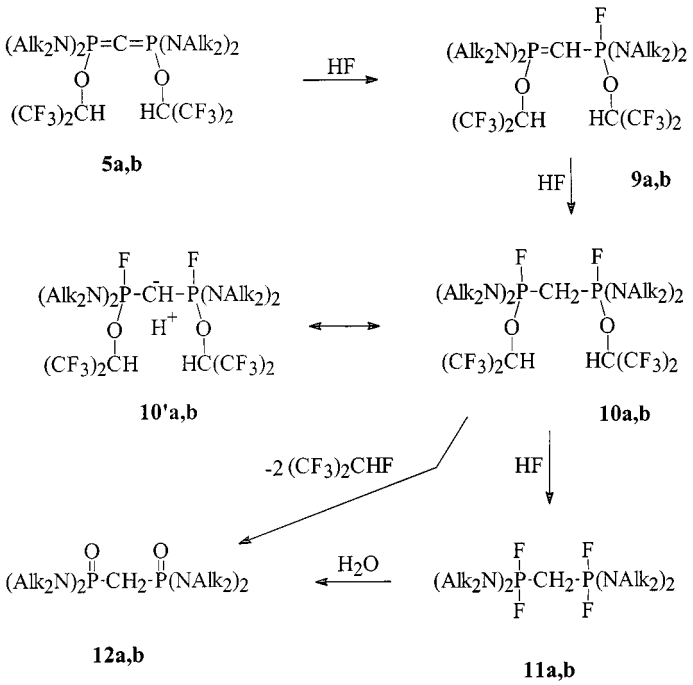
of carbodiphosphoranes **5a,b**. In other solvents they either cannot be obtained (CH_2Cl_2, $CHCl_3$) or are much less stable (C_6H_6, THF).

The decomposition of **5a,b** occurs by several steps (Scheme 4). All the intermediate compounds **9a,b - 12a,b** have been detected in the reaction mixture at different stages of the reaction. Due to the significant basicity of **5a,b** the reaction proceeds by an intermolecular abstraction of HF. In this way, half of the molecules of **5a,b** are used as a source of HF, that is why other compounds are also present in the reaction mixture. For example, small amounts of crystalline diethylammonium hexafluorophosphate (about 1%) can be isolated from the reaction mixture.

The proposed reaction pathway was confirmed by the reaction of **5a,b** with HF. The addition of one equivalent of HF gives the monofluorides **9a,b** which have, unlike their chloride analogues **7a,b,** two inequivalent phosphorus atoms and display two doublets of doublets with characteristic $^2J_{PP}$, $^1J_{FP}$ and $^3J_{FP}$ coupling constants of 45.9 Hz, 950 Hz and 13.7 Hz, respectively, in the ^{31}P-NMR spectra. In contrast to HCl, which does not add to **7a,b,** HF reacts with the monofluorides **9a,b** so readily that it is impossible to obtain **9a,b** without the difluorides **10a,b**. Compounds **10a,b** are also able to react further with HF to give the methylene-bis(difluorophosphoranes) **11a,b**. If a definite amount of HF (2.2 equiv.), or $Et_3N{\cdot}2HF$, is added, the reaction mixture consists only of the difluorides **10** and bis(difluorophosphoranes) **11**, which can easily be separated as compounds **10** are insoluble in hexane and precipitate as a light yellow oil, whereas compounds **11** remain in solution.

The difluorides **10a,b** possess interesting spectral characteristics. Their ^{31}P-NMR spectra display a complex resonance of the AA′XX′ spin system (Figure2) which does not vary in the temperature range from −60 to +60°C. A theoretical calculation of the FPPF system using the experimentally obtained coupling constants gives the same pattern. The carbon atom of the FP−CH_2−PF chain displays the expected triplet of triplets in the ^{13}C-NMR spectra. However, its upfield chemical shift (δ = 10), which is very close to that of the ylides **5a,b** or **7a,b**, shows that it bears a negative charge. The same conclusion can be drawn from the ^{1}H-NMR spectra, as the two acidic methylene protons show a broad signal at δ = 9.5. This indicates that the real structure of these compounds is probably closer to that of **10′a,b**.

The methylenebis(difluorophosphoranes) **11** were isolated as a low-melting crystalline product **11a** or light yellow oil **11b**. Their hydrolysis led to the dioxaderivatives **12a,b**. Interestingly, these compounds were also formed even if the decomposition of the carbodiphosphoranes **5a,b** was carried out under dry conditions. This can probably be explained by the removal of 1,1,1,2,3,3,3-heptafluoropropane from the difluorides **10a,b**. In order to confirm the formation of **12a,b** we tried to obtain them independently



Scheme 4. Reaction of **5a,b** with HF

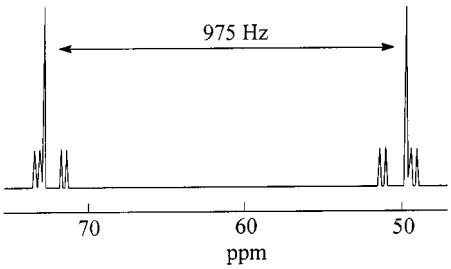


Figure 2. The ^{31}P-NMR spectrum of compounds **10a,b**

by the reaction of **3a,b** with oxygen. However, even after bubbling gaseous oxygen through a solution of **3a** or **3b** in dichloromethane, at room temperature, over long periods of time no reaction occurred, although it was later found that sulfur reacts very readily with **3a,b**.

The carbodiphosphorane structure of **5** is also confirmed by the rection with chlorine. Thus, **5b** very easily adds two equivalents of chlorine at room temperature to give the tetrachloro derivative **14**. The reaction initially forms the dichloro derivative **13** which, however, cannot be obtained in a pure form in this way, as a further reaction with chlorine occurs. This compound can be prepared by the abstraction of two chlorine atoms from **14** with $SnCl_2$ but, on a preparative scale, the use of the reaction between **14** and the starting carbodiphosphorane **5b** is more convenient. Compounds **13** and **14** were isolated as stable crystalline compounds which are insoluble in nonpolar solvents.

We were interested in dichloride **13,** not only for confirmation of the structure of **5,** but also because of its possible application for the synthesis of carbenes. For this purpose we studied the reaction of **13** with silver tetrafluoroborate. The reaction is carried out in boiling chloroform for 2 hours. However, the phosphonium-substituted carbene **15** turned out to be unstable under these conditions and the only product which could be isolated from the reaction mixture was its derivative **16**. This compound is analogous to the salt **7b** and contains a hydrogen atom attached to the P−C−P carbon atom, which was subsequently confirmed by an X-ray structure analysis (Figure 3). The formation of

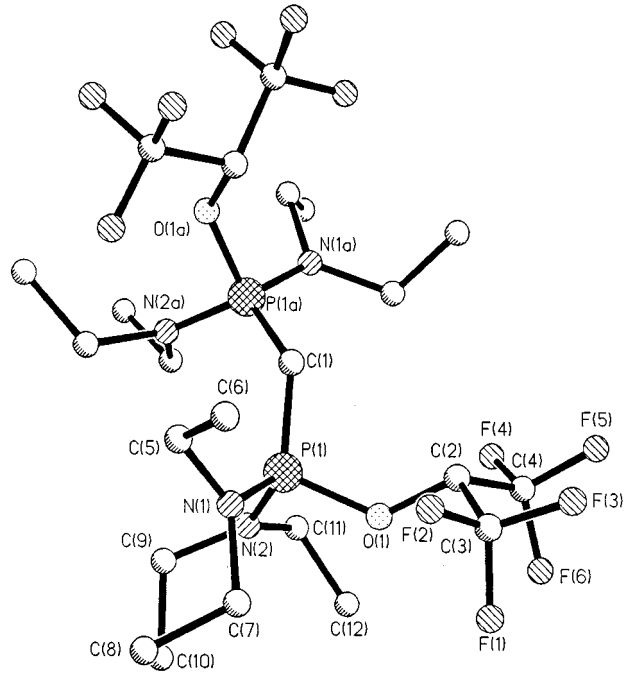
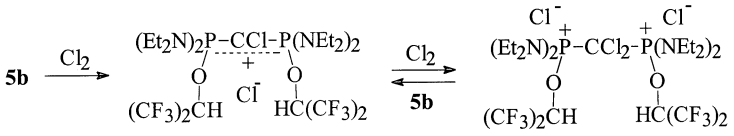


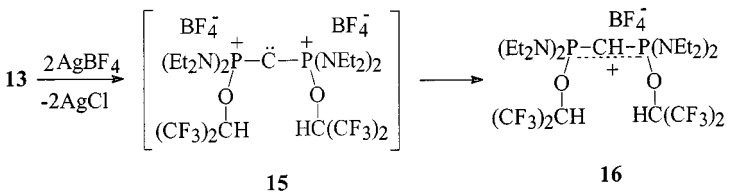
Figure 3. Molecular structure of **16**; selected bond lengths [Å] and angles [°]: P(1)−N(2) 1.618(6), P(1)−N(1) 1.619(6), P(1)−O(1) 1.625(4), P(1)−C(1) 1.681(6), O(1)−C(2) 1.408(6); P(1)#1−C(1)−P(1) 131.5(4); N(2)−P(1)−N(1) 109.27(13), N(2)−P(1)−O(1) 99.4(2), N(1)−P(1)−O(1) 105.5(2), N(2)−P(1)−C(1) 117.6(2), N(1)−P(1)−C(1) 113.66(11), O(1)−P(1)−C(1) 109.9(3), C(2)−O(1)−P(1) 127.5(2)

16 probably confirms the formation of the carbene **15** as an intermediate.

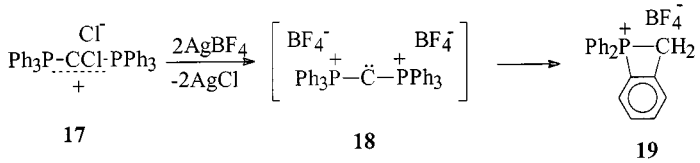
As was pointed out above, the tetrafluoroborate **16,** as well as the original carbodiphosphoranes **5a,b** and their derivatives **7a,b**, **13** and **14**, display an interesting spectroscopic phenomenon: the equivalence of the $HC(CF_3)_2$ protons for each of the two phosphorus atoms. This can be explained by a rapid exchange of the protons in solution on the NMR timescale. The crystal structure of **16** shows that these protons point towards the inside of the molecule and, if a rotation around the P−C−P bonds in solution is possible, they should be situated very close to each other thus



Scheme 5. Reaction of **5b** with Cl_2



Scheme 6. Reaction of **13** with $AgBF_4$



17 **18** **19**

Scheme 7. Reaction of **17** with $AgBF_4$

allowing the exchange process. Obviously, this rotation or flip-flop movement around the P−C−P bonds must be possible, as can be seen from the equivalence of the NMe_2 or NEt_2 protons in the NMR spectra, although in the solid state these groups are inequivalent as the molecule of **16** has C2 symmetry.

In order to study the stability of carbenes in such systems, it was interesting to change the substituents at the phosphorus atoms of the P−C−P triad. We chose the dichloro derivative of hexaphenylcarbodiphosphorane[9] **17** as a suitable starting material. Its properties differ remarkably from those of **13**. For example, the chlorination of **17** does not give the tetrachloride but instead leads to the cleavage of a P−C bond.[10]

The reaction of **17** with $AgBF_4$ (Scheme 7) requires milder conditions and works at room temperature. However, the expected carbene **18** is also unstable. It decomposes with the cleavage of one P−C bond to give the cyclic phosphonium salt **19**, which is the main product in this reaction. Compound **19** has a methylene group in the α position to the phosphorus atom and can only be formed from the carbene **18**. It has already been shown that, when the benzene ring at the phosphorus atom has a suitable *ortho* substituent, carbene intermediates can undergo intramolecular reactions often leading to the formation of cyclic products.[11,12,13] Similar results were obtained with diisopropylamino groups attached to a phosphorus atom near the carbene centre.[14] Comparing these data with those known for stable carbenes,[15] one can postulate that the stabilization of a carbene centre requires substituents with σ-accepting and π-donating abilities. Phosphonium groups do not meet one of these conditions.

Experimental Section

All reactions and manipulations were carried out in a nitrogen atmosphere in a dry box or with standard Schlenk techniques, unless otherwise indicated. Solvents were dried by standard procedures and distilled in a nitrogen atmosphere and either used immediately or stored in the dry box prior to use. Glassware was oven-dried at 100°C overnight prior to use. NMR spectra were recorded on JEOL FX-90Q and Bruker WP-200 multinuclear NMR spectrometers. Chemical shifts were measured relative to residual solvent peaks and referenced to Me_4Si (^1H, ^{13}C) or to external 85% H_3PO_4 (^{31}P). Reagents **3a,b**[16] were prepared by standard methods.

Carbodiphosphorane 5a: Gaseous HFA (29.6 mL, 1.32 mmol) from a syringe was slowly bubbled through a solution of **3a** (0.139 g, 0.55 mmol) in 1 mL of hexane at 20°C. If the starting diphosphane is contaminated with dialkylammonium chloride an appropriate amount of salt **7a** is formed which can be easily separated as it is not soluble in hexane. ^1H NMR (200 MHz, [D_8]toluene):[17] δ = 2.59 (pseudo t, $^3J_{PH}$ = 11.6 Hz, 24 H, NCH_3), 6.25 (t of sept, $^3J_{FH}$ = 6.8 Hz, $^3J_{PH}$ = 6.8 Hz, 2 H, $CHCF_3$). − ^{19}F NMR (84.26 MHz, C_6H_{14}): δ = −73.0 (d, $^3J_{HF}$ = 6.8 Hz, 12 F). − ^{31}P NMR (36.2 MHz, C_6H_{14}): δ = 36.7.

Carbodiphosphorane 5b: This compound was obtained as described above from HFA (29.6 mL, 1.32 mmol) and **3b** (0.20 g, 0.55 mmol). − ^1H NMR (200 MHz, [D_8]toluene):[17] δ = 0.98 (t, $^3J_{HH}$ = 7.1 Hz, 24 H, NCH_2CH_3), 3.00 (m, 16 H, NCH_2CH_3), 6.09 (t of sept, $^3J_{FH}$ = 6.8 Hz, $^3J_{PH}$ = 6.8 Hz, 2 H). − ^{19}F NMR (84.26 MHz, C_6H_{14}): δ = −72.9 (d, $^3J_{HF}$ = 6.8 Hz, 12 F). − ^{31}P NMR (36.2 MHz, C_6H_{14}): δ = 33.6.

Phosphonium Chloride 7a: To a solution of **5a** in hexane 1 equiv. of HCl (as a solution in ether) was added at 20°C. The precipitate of **7a** which formed was separated by filtration and recrystallized from CH_2Cl_2/ether at −15°C. Yield 63%. − M.p. 183−185°C (dec.). − ^1H NMR (200 MHz, $CDCl_3$): δ = 2.71 (pseudo t, $^3J_{PH}$ = 10.7 Hz, 24 H, NCH_3), 3.67 (t, $^2J_{PH}$ = 10.0 Hz, 1 H, PCHP), 6.71 (t of sept, $^3J_{FH}$ = 5.9 Hz, $^3J_{PH}$ = 6.8 Hz, 2 H, $CHCF_3$). − ^{13}C NMR (50.3 MHz, $CDCl_3$): δ = 7.4 (t, $^1J_{PC}$ = 209 Hz, PCP), 37.3 (pseudo t, $^2J_{PC}$ = 4.9 Hz, 8 C, NCH_3), 70.3 [sept, $^2J_{FC}$ = 34 Hz, 2 C, $CH(CF_3)_2$], 120.8 (q, $^1J_{FC}$ = 285 Hz, 4 CF_3). − ^{19}F NMR (84.26 MHz, $CDCl_3$): δ = −73.9 (d, $^3J_{HF}$ = 5.9 Hz, 12 F). − ^{31}P NMR (36.2 MHz, $CDCl_3$): δ = 58.6. − $C_{15}H_{27}ClF_{12}N_4O_2P_2$(620.79): calcd. C 29.02, H 4.38; found C 28.77, H 4.32.

Phosphonium Chloride 7b: This compound was prepared as descibed above. Yield 52%. − M.p. 151−153°C. − ^1H NMR (200 MHz, $CDCl_3$): δ = 1.06 (t, $^3J_{HH}$ = 6.8 Hz, 24 H, NCH_2CH_3), 3.05 (m, 16 H, NCH_2CH_3), 3.23 (t, $^2J_{PH}$ = 13.7 Hz, 1 H, PCHP), 6.75 (t of sept, $^3J_{FH}$ = 5.9 Hz, $^3J_{PH}$ = 6.8 Hz 2 H, $CHCF_3$). − ^{13}C NMR (50.3 MHz, $CDCl_3$): δ = 7.3 (t, $^1J_{PC}$ = 209 Hz, PCP), 13.7 (s, 8 C, NCH_2CH_3), 40.6 (s, 8 C, NCH_2CH_3), 70.4 [sept, $^2J_{FC}$ = 34 Hz, 2 C, $CH(CF_3)_2$], 120.8 (q, $^1J_{FC}$ = 285 Hz, 4 CF_3). − ^{19}F NMR (84.26 MHz, $CDCl_3$): δ = −73.0 (d, $^3J_{HF}$ = 5.9 Hz, 12 F). − ^{31}P NMR (36.2 MHz, $CDCl_3$): δ = 59.1. − $C_{23}H_{43}ClF_{12}N_4O_2P_2$(733.01): calcd. C 37.69, H 5.91; found C 28.77, H 4.32.

Methylenebis[bis(diethylamino)difluoro(1,1,1,3,3,3-hexafluoro-2-propoxy)phosphorane] 10b: To a solution of **5b** in hexane, obtained as described above, one molar equivalent of $Et_3N{\cdot}2HF$ was added. The colourless oil separated from the mixture after stirring for 20 min at room temperature was washed with hexane and dried in vacuo. Yield 26.5%. − ^1H NMR (200 MHz, $CDCl_3$): δ = 1.14 (t, $^3J_{HH}$ = 7.07 Hz, 24 H, NCH_2CH_3), 3.13 (m, 16 H, NCH_2CH_3), 4.38 [sept, $^3J_{FH}$ = 6.8 Hz, 2 H, $HC(CF_3)_2$], 9.2 (broad s, 2 H, P−CH_2−P). − ^{13}C NMR (22.5 MHz, $CDCl_3$): δ = 10.32 (tt, $^1J_{PC}$ = 206.1 Hz, $^2J_{FC}$ = 24.4 Hz, FP−CH_2−PF), 13.3 (s, 8 C, NCH_2CH_3), 40.3 (d, $^2J_{PC}$ = 4.9 Hz, 8 C, NCH_2CH_3), 68.6 [sept, $^2J_{FC}$ = 32.2 Hz, 2 C, $CH(CF_3)_2$], 122.3 [q, $^1J_{FC}$ = 284.2 Hz, 4 C, $CHCF_3)_2$]. − ^{19}F NMR (84.26 MHz, $CDCl_3$): δ = −76.4 (d, $^3J_{HF}$ = 6.8 Hz, 12 F, CF_3), −72.5 (d, $^1J_{PF}$ = 975.6 Hz, 2 F, FP−CH_2−PF). − ^{31}P NMR (36.2 MHz, $CDCl_3$): δ = 63.1 [symmetrical multiplet, (see Figure 1), $^1J_{FP}$ = 975.6 Hz, $^2J_{PP}$ = 44.0 Hz, $^3J_{FP}$ = 7.8 Hz, 2 P, FP−CH_2−PF].

Methylenebis[bis(dimethylamino)difluorophosphorane] 11a: To a solution of carbodiphosphorane **5a**, prepared from **3a** (1.2 mmol) and HFA (2.88 mmol), in 4 mL of hexane, was added $Et_3N{\cdot}2HF$ (353 mg, 2.5 mmol). After stirring at room temperature for 30 min the reaction solution was separated from the residue formed. Evaporation of the solvent in vacuo gave 390 mg of a crude product which gave **11a** after recrystallisation from hexane. Yield 120 mg (30%). − M.p. 47−48°C. − ^{1}H NMR (200 MHz, $CDCl_3$): δ = 2.28 (t of quint, $^2J_{HP}$ = 23.4 Hz, $^3J_{HF}$ = 15.8 Hz, P−CH_2−P), 2.69 (dt, $^3J_{PH}$ = 10.5 Hz, $^4J_{FH}$ = 2.6 Hz, 24 H, NCH_3). − ^{13}C NMR (22.5 MHz, $CDCl_3$): δ = 39.6 (t of quint, $^1J_{PC}$ = 182.4 Hz, $^2J_{FC}$ = 44.9 Hz, $F_2P-CH_2-PF_2$), 39.9 (dt, $^2J_{PC}$ = 10.7 Hz, $^3J_{FC}$ = 6.8 Hz 8 C, NCH_3). − ^{19}F NMR (84.26 MHz, $CDCl_3$): δ = −31.4 (dt, $^1J_{PF}$ = 720.2 Hz, $^3J_{HF}$ = 15.8 Hz, 4F). − ^{31}P NMR (36.2 MHz, $CDCl_3$): δ = −53.2 (t, $^1J_{FP}$ = 720.2 Hz, 2 P). − $C_9H_{26}F_4N_4P_2$ (328.28): calcd. C 32.93; H 7.98. found C 32.43; H 8.47.

Methylenebis[bis(diethylamino)difluorophosphorane] (11b): To a solution of carbodiphosphorane **5b**, prepared from **3b** (1.2 mmol) and HFA (2.88 mmol), in 4 mL of hexane, was added $Et_3N{\cdot}2HF$ (353 mg, 2.5 mmol). After stirring the mixture at room temperature for 30 min the reaction solution was separated from the residue formed. Evaporation of the solvent in vacuo gave 390 mg of a crude product from which **11b** was extracted with 1 mL of cold hexane at −15°C. Evaporation of the hexane in vacuo gave 11b as a light yellow oil of about 90% purity. Yield 180 mg (33%). Compound **11b** is thermally stable and can be purified by low-pressure distillation (0.03 Torr) at 110−115°C if prepared on a large scale. − ^{1}H NMR (200 MHz, $CDCl_3$): δ = 1.06 (t, $^3J_{HH}$ = 7.02 Hz, 24 H, NCH_2CH_3), 2.31 (m, broad, 2 H, P−CH_2−P), 2.97 (m, 16 H, NCH_2CH_3) − ^{13}C NMR (22.5 MHz, $CDCl_3$): δ = 15.73 (s, 8 C, NCH_2CH_3), 44.0 (m, $^2J_{PC}$ = 8.7 Hz, $^3J_{FC}$ = 7.8 Hz, 8 C, NCH_2CH_3), 45.2 (t of quint, $^1J_{PC}$ = 182.4 Hz, $^2J_{FC}$ = 43.9 Hz, $F_2P-CH_2-PF_2$) − ^{19}F NMR (84.26 MHz, $CDCl_3$): δ = −38.0 (dt, $^1J_{PF}$ = 728.1 Hz, $^3J_{HF}$ = 14.0 Hz, 4 F) − ^{31}P NMR (36.2 MHz, $CDCl_3$): δ = −52.2 (t, $^1J_{FP}$ = 728.1 Hz, 2 P).

Methylenebis[bis(diethylamino)phosphane oxide] (12b): A solution of **11b** (115 mg, 0.261 mmol) in 0.5 mL of dichloromethane was added to a solution of sodium carbonate (55 mg, 0.52 mmol) in 0.5 mL of water and the reaction mixture stirred at room temperature for 0.5 h. The organic layer was then separated and volatiles evaporated in vacuo. The residue was extracted with 2 mL of hexane. Evaporation of hexane in vacuo gave 54 mg of pure **12b** as a light yellow oil (yield 52%). Compound **12b** is thermally stable and can be purified by low-pressure distillation (0.03 Torr) at 130−135°C if prepared on a large scale. − ^{1}H NMR (200 MHz, $CDCl_3$): δ = 1.10 (t, $^3J_{HH}$ = 7.07 Hz, 24 H, NCH_2CH_3), 2.24 (t, $^3J_{PH}$ = 16.7 Hz, 2 H, P−CH_2−P), 3.08 (dq, $^3J_{PH}$ = 10.7 Hz, $^3J_{HH}$ = 7.07 Hz, 16 H, NCH_2CH_3) − ^{13}C NMR (22.5 MHz, $CDCl_3$): δ = 14.13 (s, 8 C, NCH_2CH_3), 24.75 (t, J_{PC} = 105.3 Hz, P−C−P), 38.88 (m, 8 C, NCH_2CH_3) − ^{31}P NMR (36.2 MHz, $CDCl_3$): δ = 26.7 (s, 2 P). − MS: M_{calc} = 396.5; M_{exp}(EI) = 396; $M_{exp.}$(CI pos.) = 397.

Dichloro Derivative 13: To a solution of **14** (255 mg, 0.304 mmol) in 4 mL of THF at −20°C was added one molar equivalent of the carbodiphosphorane **5b** in hexane. A ^{31}P-NMR spectrum of the reaction mixture showed only one signal at 59.9 ppm. The mixture was allowed to react at this temperature for 15 min. The fine colourless crystals of **13** formed during this time were separated, washed with hexane and dried in vacuo. Yield 391 mg (84%). The product can be recrystallized from dichloromethane-ether. M.p. 160−162°C. − ^{1}H NMR (200 MHz, $CDCl_3$): δ = 1.18 (t, $^3J_{HH}$ = 7.08 Hz, 24 H, NCH_2CH_3), 3.17 (dq, $^3J_{PH}$ = 11.7, $^3J_{HH}$ = 7.08 Hz, 16 H, NCH_2CH_3), 6.71 [m, 2 H, $CH(CF_3)_2$]. − ^{13}C NMR (22.5 MHz, $CDCl_3$): δ = 6.96 (t, $^1J_{PC}$ = 207.73 Hz, P−CCl_2−P), 13.81 (s, 8 C, NCH_2CH_3), 40.72 (s, 8 C, NCH_2CH_3), 70.24 [sept, $^2J_{FC}$ = 33.2 Hz, 2 C $CH(CF_3)_2$], 120.67 [q, $^1J_{FC}$ = 284.78 Hz, 4 C, $CH(CF_3)_2$]. − ^{19}F NMR (84.26 MHz, $CDCl_3$): δ = −72.8 [d, $^3J_{HF}$ = 5.9 Hz, 12 F, $CH(CF_3)_2$]. − ^{31}P NMR (36.2 MHz, $CDCl_3$): δ = 59.9 (s, 2 P). − $C_{23}H_{42}Cl_2F_{12}N_4O_2P_2$ (767.46): calcd. C 36.00, H 5.52; found C 36.68, H 6.17.

Tetrachloro Derivative 14: To a stirred solution of the carbodiphosphorane **5b**, prepared from **3b** (0.42 mmol) and HFA (1.01 mmol), in 1 mL hexane, chlorine (0.84 mmol, as a solution in CCl_4) was added at room temperature. The precipitated yellow oil (257 mg) was separated and recrystallized from dichloromethane-ether. (NB: If the ^{31}P-NMR spectrum of the oil shows a second signal of the intermediate dichloride at 59.9 ppm, more chlorine solution should be added). Yield 138 mg (38%), colourless crystalline product. M.p. 109−113°C. − ^{1}H NMR (200 MHz, $CDCl_3$): δ = 1.19 (t, $^3J_{HH}$ = 6.82 Hz, 24 H, NCH_2CH_3), 3.19 (dq, $^3J_{PH}$ = 11.7, $^3J_{HH}$ = 6.82 Hz, 16 H, NCH_2CH_3), 5.80 [m, 2 H, $CH(CF_3)_2$]. − ^{13}C NMR (22.5 MHz, $CDCl_3$): δ = 13.05 (s, 8 C, NCH_2CH_3), 30.26 (t, $^1J_{PC}$ = 229.2 Hz, P−CCl_2−P), 40.66 (s, 8 C, NCH_2CH_3), 71.12 [sept, $^2J_{FC}$ = 35.1 Hz, 2 C, $CH(CF_3)_2$], 119.91 [q, $^1J_{FC}$ = 285.7 Hz, 4 C, $CH(CF_3)_2$]. − ^{19}F NMR (84.26 MHz, $CDCl_3$): δ = −71.85 [d, $^3J_{HF}$ = 5.9 Hz, 12 F, $CH(CF_3)_2$]. − ^{31}P NMR (36.2 MHz, $CDCl_3$): δ = 55.0 (s, 2 P). − $C_{23}H_{42}Cl_4F_{12}N_4O_2P_2$ (838.38): calcd. C 32.95, H 5.05; found C 33.83, H 5.72.

Phosphonium Tetrafluoroborate 16: To a solution of **13** (300 mg, 0.391 mmol) in 3 mL of $CHCl_3$ was added $AgBF_4$ (90 mg, 0.469 mmol). After refluxing for 3 h the hot reaction mixture was filtered and kept at room temperature for 24 h. The colourless crystals of **16** formed during this time were separated, washed with hexane and dried in vacuo. Yield 69 mg (21%). − M.p. 192−193°C. − ^{1}H NMR (200 MHz, $CDCl_3$): δ = 1.19 (t, $^3J_{HH}$ = 7.08 Hz, 24 H, NCH_2CH_3), 3.18 (dq, $^3J_{PH}$ = 11.7, $^3J_{HH}$ = 7.08 Hz, 16 H, NCH_2CH_3), 5.30 [m, 2 H, $CH(CF_3)_2$]. − ^{19}F NMR (84.26 MHz, $CDCl_3$): δ = −72.9 [d, $^3J_{HF}$ = 5.86 Hz, 12 F, $CH(CF_3)_2$], −151.3 (s, BF_4). − ^{31}P NMR (36.2 MHz, $CDCl_3$): δ = 58.4 (s, 2 P). − $C_{23}H_{43}BF_{16}N_4O_2P_2$ (784.35): calcd. C 35.22, H 5.53; found C 36.82; H 5.63.

Bicyclic Phosphonium Salt 19: To a solution of **17** (300 mg, 0.494 mmol) in 3 mL of CH_2Cl_2, $AgBF_4$ (385 mg, 1.98 mmol) was added and the reaction mixture stirred at room temperature for 48 h. The liquid phase of the reaction mixture was separated and ether was added until it became turbid. The precipitate formed during 24 h at room temperature was separated and dissolved in 1.5 mL of CH_2Cl_2. This solution was washed with 1 mL of water and then ether was added until it became turbid. The crystalline product formed over 24 h at room temperature was separated and dried in vacuo (0.03 Torr). Yield 85 mg (47%). − M.p. 195−197°C. − ^{1}H NMR (200 MHz, $CDCl_3$): δ = 5.22 (d, $^2J_{PH}$ = 5.9 Hz, 2 H, CH_2), 7.76 (m, 14 H, Ar). − ^{19}F NMR (84.26 MHz, $CDCl_3$): δ = −152.4 (s, BF_4). − ^{31}P NMR (36.2 MHz, $CDCl_3$): δ = 22.95 (s). − $C_{19}H_{16}BF_4P$ (362.11): calcd. C 63.02, H 4.45; found C 59.00, H 4.76. Mass spectrum: $M_{calc.}$ = 362.11; $M(cation^+)_{calc.}$ = 275.3; $M(cation^+)_{exp.}$(EI) = 277.

X-ray Crystal Structure Determination of Compound 16: Crystal data: $C_{23}H_{43}BF_{16}N_4O_2P_2$, M_r = 784.36, d = 1.484 Mg/m^3; μ = 0.24 mm^{-1}, orthorhombic, space group *Pbcn*; a = 9.74(4), b = 317.53(7), c = 20.53(8) Å; V = 350(2) Å^3; Z = 4, rhombic colourless crystal 0.8 × 0.7 × 0.6 mm. Data collection and reduction: Data were collected to $2\Theta_{max}$ = 48.1° with a STOE Image plate system using monochromated (graphite monochromator) Mo-K_α

radiation. 17227 reflections were collected (hemisphere), of which 2717 were independent (R_{int} = 0.0700). The structure was solved by direct methods and subjected to full-matrix least-squares refinement based on F^2 with SHELXTL (Version 5.0). R_1 = 4.06%, wR_2 = 9.57% (based on F^2) for 247 parameters and 1570 reflections with $I > 2\sigma(I)$. All non-hydrogen atoms were refined anisotropically. Hydrogen atoms were refined using the riding model. The fluorine atoms of the BF_4^- anion were split, resulting in positions having reasonable occupancy factors and B−F bond lengths and F−B−F angles. Crystallographic data (excluding structure factors) have been deposited at the Cambridge Crystallographic Data Centre as supplementary publication no. CCDC-112955. Copies of the data can be obtained, free of charge, on application to CCDC, 12 Union Road, Cambridge CB2 1EZ, UK, (Fax: + 44-1223/336033 or E-mail: deposit@ccdc.cam.ac.uk).

Acknowledgments

We are indebted to Ms. D. Döring and Mr. T. Kaschner for their cooperation and to the Swiss National Science Foundation and the DAAD for financial support.

[1] M. Witt, K. S. Dathathreyan, H. W. Roesky, *Adv. Inorg. Chem. Radiochem.* **1986**, *30*, 223−312.
[2] R. Burgada, R. Setton, "Preparation, Properties and Reactions of Phosphoranes", in: *The Chemistry of Organophosphorus Compounds* (Ed.: F. R. Hartley), in *The Chemistry of Functional Groups* (Series Ed.: S. Patai), Wiley, Chichester, New York, Brisbane, Toronto, Singapore, **1994**, vol. 3; ch. 3, p. 185−272.
[3] F. U. Seifert, G.-V. Röschenthaler, *J. Fluorine Chem.* **1995**, *70*, 171−174.
[4] I. Neda, C. Melnicky, A. Vollbrecht, A. Fischer, P. G. Jones, R. Schmutzler, *Z. Anorg. Allg. Chem.* **1996**, *622*, 1047−1059.
[5] I. V. Shevchenko, A. Fischer, P. G. Jones, R. Schmutzler, *Polyhedron* **1993**, *12*, 435−444.
[6] I. V. Shevchenko, *Tetrahedron Lett.* **1995**, *36*, 2021−2024.
[7] I. V. Shevchenko, *Chem Commun.* **1998**, 1203−1204.
[8] A. P. Marchenko, G. N. Koydan, N. A. Oleynik, I. S. Zal′tsman I.S., A. M. Pinchuk, *Zh. Obshch. Khim.* **1988**, *58*, 1665−1666; *Chem. Abstr.* **1989**, *110*, 173342f.
[9] R. Appel, F. Knoll, H. Scholer, H.-D. Wihler, *Angew. Chem.* **1976**, *88*, 769−770.
[10] R. Appel, F. Knoll, W. Michel, W. Morbach, H.-D. Wihler, H. Veltmann, *Chem. Ber.* **1976**, *109*, 58−70.
[11] D. V. Griffith, K. Karim, B. J. Whitehead, *Zh. Obshch. Khim*. **1993**, 63, 2245; *Chem. Abstr.* **1994**, *121*, 205523m.
[12] D.V.Griffiths, P. A. Griffiths, K. Karim, B. J. Whitehead, *J. Chem. Res.* **1996**, 176−177.
[13] D. V. Griffiths, P. A. Griffiths, K. Karim, B. J. Whitehead, *J. Chem. Soc., Perkin Trans., 1* **1996**, 555.
[14] M.-J. Menu, Y. Dartiguenave, M. Dartiguenave, A. Baceiredo, G. Bertrand, *Phosphorus Sulfur Silicon* **1990**, *47,* 327−334.
[15] A. J. Arduengo, III, R. L. Harlow, M. Kline, *J. Am. Chem. Soc.* **1991**, *113*, 361.
[16] Compound **3a** was prepared in 79% yield (bp 68−70°C, 0.03 Torr) in a similar manner to its diethylamino derivative **3b**: M. Fild, J Heinze, W. Krueger, *Chem.-Ztg.* **1977**, *101*, 259.
[17] The ^{1}H-NMR spectra of **5a** and **5b** were recorded in hexane or in [D_8]toluene immediately after HFA had been added to the solution of **3a** or **3b**.

Received February 19, 1999
[I99057]

Syntheses of Chiral Cyclotriphosphazenes and Their Use in Cyclolinear Polymers

Isabelle Dez,[a] Joëlle Levalois-Mitjaville,[b] Hansjörg Grützmacher,*[a] Volker Gramlich,[c] and Roger de Jaeger[b]

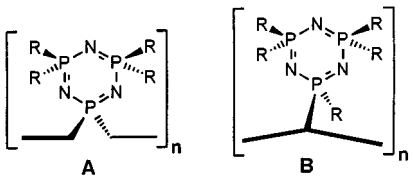
Keywords: Phosphazenes / Polymers / Chirality / Urethanes / TGA / Thermochemistry / Asymmetric synthesis

The reaction of hexachlorocyclotriphosphazene with two equivalents of the chelating diols 2,2′-dioxybiphenyl and 2′,2′′-dioxy-1′,1′′-bi-2-naphthyl was investigated. Although a mixture of different stereoisomers may be expected, only the formation of the *meso*-compounds [(*R,S*)-$(O,O)_2Cl_2P_3N_3$] is found (O,O stands for the diolate). Interestingly, when the remaining PCl_2 group undergoes reaction with hard nucleophiles like 4-methoxy phenolate, a change of configuration at one phosphorus center is observed and racemic mixtures of chiral [(*R,R*)-$(O,O)_2(RO)_2P_3N_3$] and [(*S,S*)-$(O,O)_2(RO)_2P_3N_3$] phosphazenes are observed. Enantiomerically pure cyclotriphosphazenes were obtaines from either the (*R*)- or (*S*)-form of 2′,2′′-dioxy-1′,1′′-bi-2-naphthyl. Soft nucleophiles like amines, however, do not affect the configuration at the phosphorus centers and allow the synthesis of *meso*-[(*R,S*)-$(O,O)_2(R^1RN)_2P_3N_3$] compounds. the bifunctional cyclotriphosphazenes [$(O,O)_2$(4-OH–$C_4H_4O)_2P_3N_3$] and [(*R,S*)-$(O,O)_2(H_2N)_2P_3N_3$] were used in polyaddition reactions with hexymethylene di(isocyanate) to give cyclolinea polymers of different stereochemical compositions corresponding to the stereochemistry of the phosphazene precursor (i.e. either a racemic mixture of homochiral polymer strands, enantiomerically pure polymers, or the *meso*-form of polymers was obtained). The properties of these polymers are discussed and a mechanism for the change of stereochemistry is proposed.

Introduction

Polyurethanes are generally characterized by poor thermal stability due to the thermally labile urethane group. Their thermal decomposition starts in the region of 150−200°C. Several attempts to increase the thermal stability of polyurethanes by introducing thermally stable groups have been reported.[1−2] Phosphazenes are well-known to impart thermal stability and flame-retardant characteristics to polymer systems[3−6] and cyclomatrix phosphazene polymers containing cyclotriphosphazene rings are known for their excellent fire resistance.[7−12] The modification of different polymers such as polyesters, polyimides, etc. by phosphazenes has been reported previously.[10][11] These polymers may be divided into two groups: in cyclolinear polymers of type **A** the phosphorus centers of the cyclophosphazene moieties are incorporated into the polymer backbone, while in polymers of type **B** the phosphazene rings are attached as pendant groups on the backbone (Scheme 1).

Polymers of types **A** and **B** have commonly been prepared by polycondensation of chloro-substituted cyclotriphosphazenes, $Cl_{6-x}R_xP_3N_3$, with bifunctional substrates. However, these polymerizations are complicated by multiple displacements of chlorine atoms and generally lead to random mixtures of polymers, incorporating both geminally and vicinally substituted phosphazenes.[5,11,13−15] In this respect, the synthesis of spirocyclic cyclotriphosphazenes, $(O,O)Cl_4P_3N_3$ or $(O,O)_2Cl_2P_3N_3$, from sterically congested diols HO,OH (where O,O represents a chelating diol) and $Cl_6P_3N_3$ is interesting, since their preparation permits the selective synthesis of phosphazenes with one or two PCl_2 units.[8,16,17] These monomers should prove useful for the preparation of well-defined cyclolinear polymers of type **A**. Indeed, Kumar and Gupta[9] have reported the synthesis of cyclolinear polyphosphazene polyimides starting from a bis(amino)-bis(spiro)-substituted cyclotriphosphazene $(H_2N)_2(O,O)_2P_3N_3$. Recently, we described the synthesis of new cyclolinear phosphazene polyurethanes from diisocyanates and a bis(spiro)cyclotriphosphazene containing a geminal $P(O-C_6H_4-OH)_2$ unit.[8]



Scheme 1. Depiction of cyclolinear (**A**) and pendant (**B**) phosphazene polymers

The diols 2,2′-dioxybiphenyl and 2′,2′′-dioxy-1′,1′′-bis(2-naphthyl) (abbreviated throughout this paper as biphenoxy and binaphthoxy, respectively) have previously been used for the synthesis of spirocyclic phosphazenes.[8−9,16−19] Tris(2,2′-dioxybiphenylyl)cyclotriphos-

[a] Inorganic Chemistry Laboratory, ETH-Zentrum, Universitätstrasse 6, CH-8092 Zürich, Switzerland
Fax: (internat.) +41 1/632 10 90
E-mail: gruetz@inorg.chem.ethz.ch
[b] Laboratoire de Spectrochimie Infrarouge et Raman, CNRS UPR 2631 L, Bât. C5, Université des Sciences et Technologies de Lille, F-59655 Villeneuve d′Ascq, France
[c] Institute of Crystallography, ETH-Zentrum, Sonneggstrasse 5, CH-8092 Zürich, Switzerland

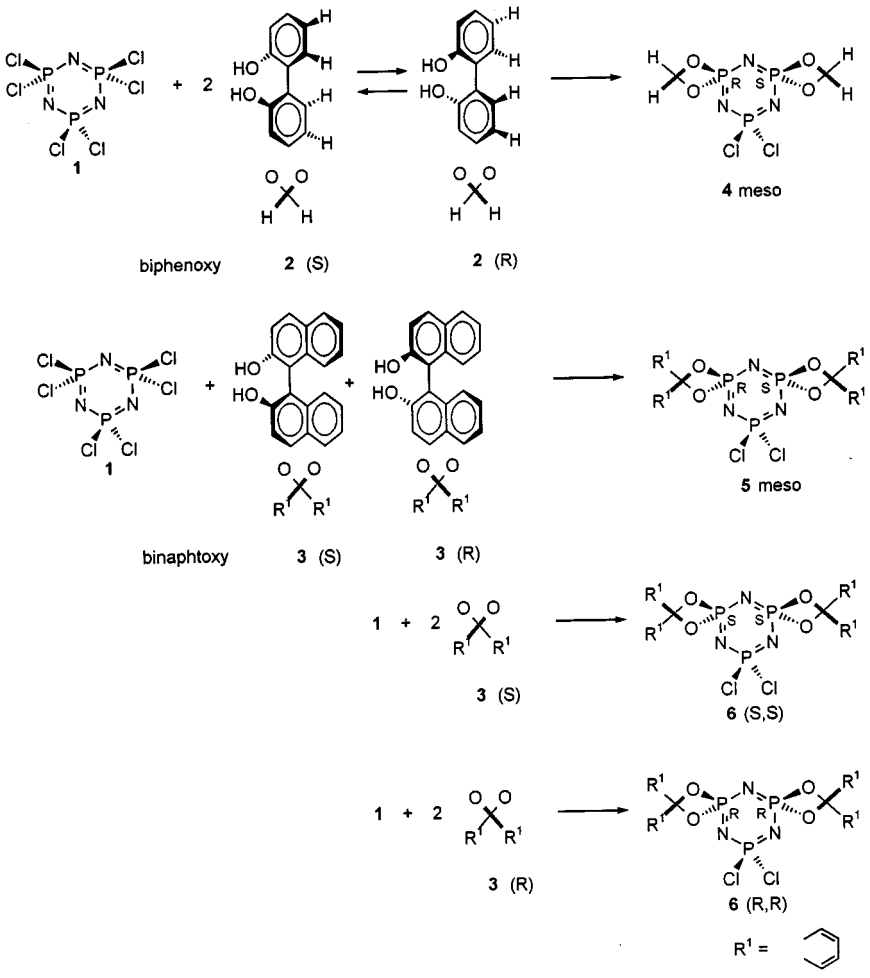
 © WILEY-VCH Verlag GmbH, D-69451 Weinheim, 1999 1434−1948/99/1010−1673 $ 17.50+.50/0

phazene[18] is stable up to at least 350°C and does not undergo polymerization by thermal ring-opening. Hence, increased thermal stability may be expected for polymers incorporating these motifs. Furthermore, binaphthoxy is commercially available in the form of two atropisomers, which do not interconvert at ambient temperature. This offers the possibility of achieving a simple synthesis of enantiomerically pure spirocyclic phosphazenes and hence of chiral polymers. The latter may have interesting properties as supports for catalysts. In this context, it is noteworthy that although the enantiomers of the sterically less hindered biphenoxy rapidly interconvert at ambient temperature, chiral (*R*) or (*S*)-configured phosphorus centers will be formed upon ring-closure by reaction with hexachlorocyclotriphosphazene. In particular, different diastereomers may be formed when racemic mixtures of diols are used and more than one O,O unit is bonded to an oligophosphazene. Thus, cyclotriphosphazenes made up of all (*R*)- or all (*S*)-configured phosphorus centers and/or having different (*R*)- or (*S*)-configured phosphorus centers within one P_3N_3 ring may be anticipated. Remarkably, although multiply-substituted cyclophosphazenes bearing biphenoxy or binaphthoxy groups are known, no particular attention has hitherto been focused on their stereochemistry. We have therefore investigated the synthesis of bis(spirocyclic) phosphazenes of the type $(O,O)_2Cl_2P_3N_3$ in more detail and report here on the somewhat unexpected results obtained. Furthermore, we also describe the incorporation of these phosphazenes into polyurethanes, allowing the synthesis of chiral polymers with improved thermal stabilities.

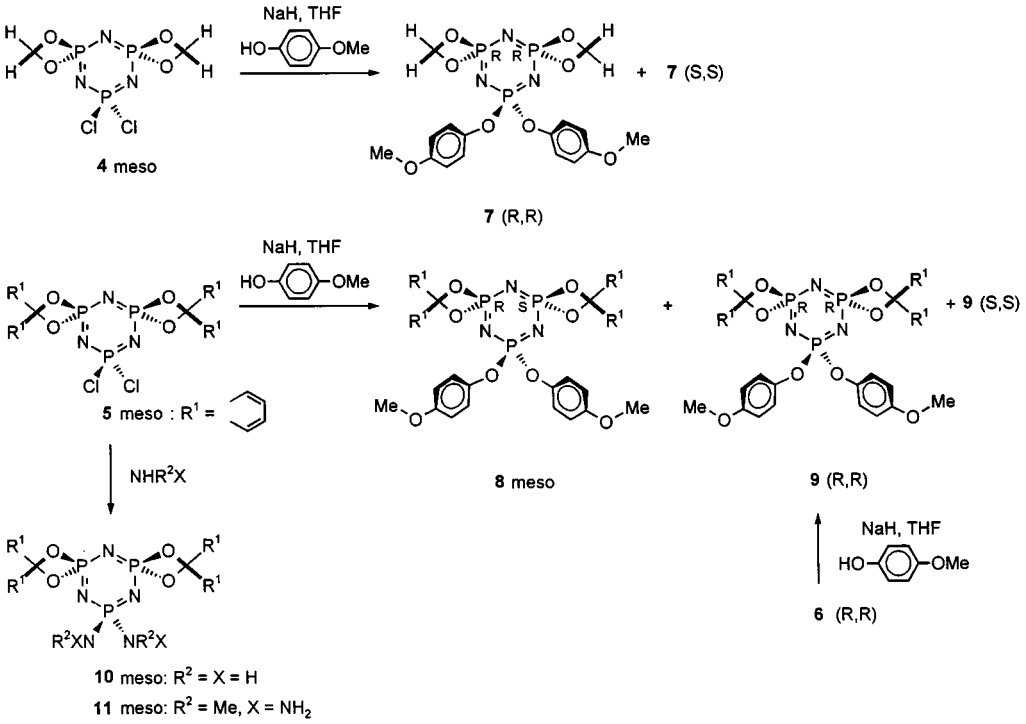
Results

Synthesis of Bis(spirocyclic) Phosphazenes

Starting from hexachlorocyclotriphosphazene **1** and two equivalents of biphenolate **2**, the bis(spirocyclic) cyclotriphosphazene **4** was obtained as described previously (Scheme 2).[8] Since **2** exists in the form of rapidly interconverting (*R*)- and (*S*)-isomers, the formation of three stereoisomers might have been expected, namely a pair of (*R*,*R*)- or (*S*,*S*)-configured enantiomers and the diastereotopic *meso* form. These diastereoisomers may be distinguished by ^{31}P-NMR spectrometry. However, only one diastereoisomer was formed, as evidenced by the observation of a single set of resonances of an AB_2 spin system in the ^{31}P-NMR spectrum of the crude reaction mixture. X-ray analysis (vide infra) showed that this isomer was, in fact, the *meso* diastereomer, [(*R*,*S*)-$(O,O)_2Cl_2P_3N_3$], containing one (*R*)- and one (*S*)-configured phosphorus center.



Scheme 2. Synthesis of bis(spirocyclic) phosphazenes *meso*-**4**, *meso*-**5**, **6**(*S,S*), and **6**(*R,R*)



Scheme 3. Synthesis of bis(spirocyclic) phosphazenes **7**(*R,R*), **7**(*S,S*), *meso*-**8**, **9**(*R,R*), *meso*-**10**, and *meso*-**11**

In a subsequent experiment, **1** was reacted with a racemic mixture of sodium binaphtholate **3**, consisting of one equivalent of **3**(*S*) and one equivalent of **3**(*R*), which do not interconvert at room temperature. Again only one of the possible stereoisomers of **5** was obtained. By subsequent chemical transformation (vide infra), it was unequivocally shown that here too only the *meso* isomer **5** had been formed. When **1** was reacted with two equivalents of either enantiomerically pure **3**(*S*) or **3**(*R*), the respective chiral cyclotriphosphazenes **6**(*S,S*) or **6**(*R,R*) were obtained. The optical rotation angle α of **6**(*R,R*) was determined as $[\alpha]^{25} = -103°$, which is considerably larger than the value found for unbonded binaphthol ($[\alpha]^{25} = -33°$).

The nonchiral bis(biphenoxy)-substituted cyclotriphosphazene *meso*-**4** was treated with two equivalents of sodium 4-methoxyphenolate in THF at room temperature (Scheme 3) and the reaction was followed by ^{31}P-NMR spectrometry. The resonance of the PCl_2 unit in *meso*-**4** (δ = 30.4) disappeared, while a multiplet at δ = 11.2 was observed constituting the A part of a new AB_2 spin system. After 3 h, quantitative conversion into **7** had been achieved.

Surprisingly, in the ^{1}H- and ^{13}C-NMR spectra of **7**, only one signal for the CH_3 group of the methoxy substituents was observed. If we assume that the (*R,S*)-configuration at the phosphorus centers of the starting material *meso*-**4** is retained in the course of the substitution reaction, then the phenolate substituents are placed *within* the mirror plane and hence cannot be interconverted by this symmetry operation. Therefore, the methyl groups of the 4-methoxy substituents become diastereotopic and should give rise to two resonance signals. On the other hand, if the configuration at one phosphorus center is changed under the reaction conditions from (*R*) to (*S*) − or vice versa − chiral cyclotriphosphazenes **7**(*R,R*) or **7**(*S,S*) with (*R,R*)- and (*S,S*)-configured phosphorus centers will be obtained. In these, the methyl groups are related by a C_2 axis of symmetry and one resonance signal is to be expected. Indeed, X-ray analysis revealed that the configuration at one phosphorus center had changed and that the product corresponded to a racemic mixture of **7**(*R,R*) and **7**(*S,S*). Both enantiomers are present in the unit cell (space group $P\bar{1}$). Stimulated by this finding, we next re-investigated the synthesis of tris(biphenoxy)cyclotriphosphazene[18] by reacting *meso*-**4** with one further equivalent of **2**. Indeed, the sparingly soluble product showed only one ^{31}P-NMR resonance at δ = 22.9 in DMF solution. Evidently, a change of configuration at the phosphorus centers also occurred, leading to a racemic mixture of chiral cyclotriphosphazenes having all (*R,R,R*)- or (*S,S,*S)-configured phosphorus centers.

When the binaphthoxy-substituted compound *meso*-**5** was reacted with 4-methoxyphenolate, a mixture of the stereoisomers *meso*-**8**, **9**(*R,R*), and **9**(*S,S*) was obtained, *meso*-**8** being the major product {ratio *meso*-**8**/[**9**(*R,R*) + **9**(*S,S*)] = 70:30}. As expected, in the ^{1}H-NMR spectrum, the *meso* isomer shows two signals for the magnetically inequivalent methoxy substituents (δ = 3.80 and 3.95), while only one signal (δ = 3.87) is seen for the enantiomers **9**(*R,R*) and **9**(*S,S*). The latter was obtained in enantiomerically pure form by reacting **6**(*R,R*) with 4-methoxyphenolate, which led exclusively to **9**(*R,R*). This cyclotriphosphazene was characterized by X-ray structure analysis (vide infra). It is noteworthy that an equimolar mixture of **6**(*R,R*) and **6**(*S,S*) under identical reaction conditions (THF, room temp., 3 h)

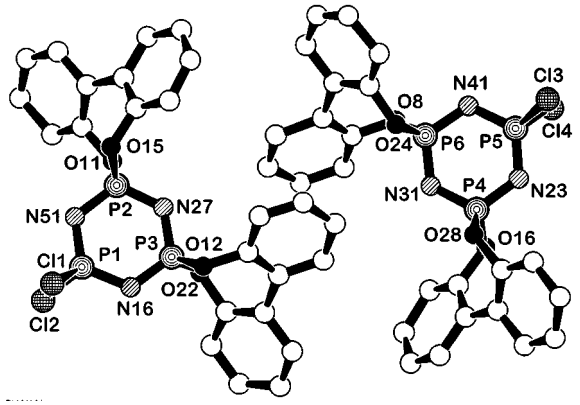


Figure 1. SCHAKAL view of *meso*-**4**

Table 1. Selected bond lengths [Å] and angles [°] in *meso*-**4**

Bond	Length [Å]	Bond	Angle [°]
P(1)−N(51)	1.567(7)	N(51)−P(1)−N(16)	119.8(3)
P(1)−N(16)	1.570(7)	Cl(1)−P(1)−Cl(2)	99.62(14)
P(1)−Cl(1)	2.001(3)	N(51)−P(1)−Cl(1)	109.3(3)
P(1)−Cl(2)	2.002(3)	N(16)−P(1)−Cl(1)	108.8(3)
P(2)−N(27)	1.560(6)	N(51)−P(1)−Cl(2)	108.4(3)
P(2)−N(51)	1.589(7)	N(16)−P(1)−Cl(2)	109.0(3)
P(2)−O(11)	1.567(5)	N(27)−P(2)−N(51)	117.2(3)
P(2)−O(15)	1.591(5)	O(11)−P(2)−O(15)	103.7(3)
P(3)−N(27)	1.567(6)	N(27)−P(2)−O(11)	105.5(3)
P(3)−N(16)	1.580(7)	O(11)−P(2)−N(51)	111.5(3)
P(3)−O(12)	1.564(5)	N(27)−P(2)−O(15)	112.5(3)
P(3)−O(22)	1.586(5)	N(51)−P(2)−O(15)	105.6(3)
		N(27)−P(3)−N(16)	117.4(3)
		O(12)−P(3)−O(22)	103.6(3)
		O(12)−P(3)−N(27)	111.9(3)
		O(12)−P(3)−N(16)	105.5(3)
		N(27)−P(3)−O(22)	105.7(3)
		N(16)−P(3)−O(22)	112.0(3)
		P(1)−N(16)−P(3)	120.8(4)
		P(1)−N(51)−P(2)	120.9(4)
		P(2)−N(27)−P(3)	123.8(4)

led exclusively to a mixture of **9**(*R*,*R*) and **9**(*S*,*S*) and no *meso*-**8** was observed.

Finally, we investigated the reactions of *meso*-**5** with aqueous ammonia[20] and methylhydrazine[21] in THF solution. Under mild reaction conditions, the replacement of both chlorine centers was observed and the products *meso*-**10** and *meso*-**11** were obtained quantitatively. In *meso*-**11**, the more basic methyl-substituted nitrogen center is bonded to the phosphorus center, as was observed previously.[22] Again, the magnetically inequivalent methyl groups in *meso*-**11** give rise to separate signals (δ = 3.11 and 2.86), proving that the configuration at the phosphorus centers is retained. The presence of the amino groups was also confirmed by the IR spectrum, which featured two bands at $\tilde{\nu}$ = 3340 and 3460 cm^{-1}.

X-ray Structure Analyses

In order to unequivocally determine the stereochemistries of compounds *meso*-**4**, **7**(*R*,*R*), and **9**(*R*,*R*), X-ray crystal structure analyses were performed. Details of the data collections are given in Table 4.

The result obtained for *meso*-**4** is shown in Figure 1 and selected bond lengths and angles are listed in Table 1.

In the crystal, two molecules of *meso*-**4** are aligned in a coplanar fashion (the interplanar angle between the two P_3N_3 planes amounts to 8.3°) by intermolecular π-stacking of two arene moieties of the biphenoxy substituents. The P_3N_3 rings are almost planar [deviations (Å) from best planes: P1(−0.003)−P2(0.005)−P3(−0.004)−N16(0.007)−N27(0.002)−N51(−0.003) and P4(−0.029)−P5(−0.004)−P6(−0.052)−N23(0.005)−N31(0.054)−N41(0.026)] and slightly elongated along the axes running through P1−N27 and P5−N31, respectively. Nevertheless, all P−N and P−O distances, P−N−P (121.8°) and N−P−N (118.0°) angles lie within the expected ranges.[23] The Cl−P−Cl angle (99.4°) is slightly smaller than the O−P−O angles (103.7°). There are no unusually short repulsive intramolecular interactions. The (*R*)-(P2,P6) and (*S*)-(P3,P4) configurations of the two biphenoxy-substituted phosphorus centers within one molecule can clearly

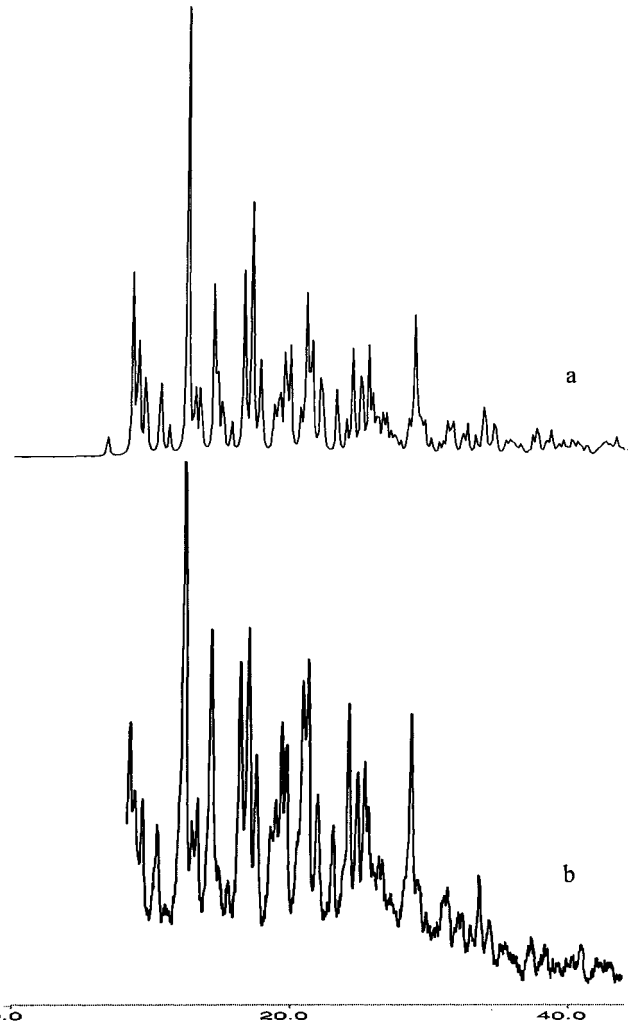


Figure 2. X-ray powder diffraction pattern of *meso*-**4**; a: calculated spectrum; b: experimental spectrum

be seen. In order to verify that the conformer found in the crystal corresponds to that observed in the bulk, we performed a powder diffraction study of microcrystalline material. In Figure 2, the experimental diffraction pattern (bottom) is compared with that calculated using the parameters derived from the single crystal used for the structure determination.

As can be seen, there is an almost perfect fit between the two patterns, which confirms that all synthesized material is of the *meso* form of **4**.

A plot of the molecular structure of the (*R*,*R*)-isomer of **7** is shown in Figure 3. Selected bond lengths and angles are given in Table 2.

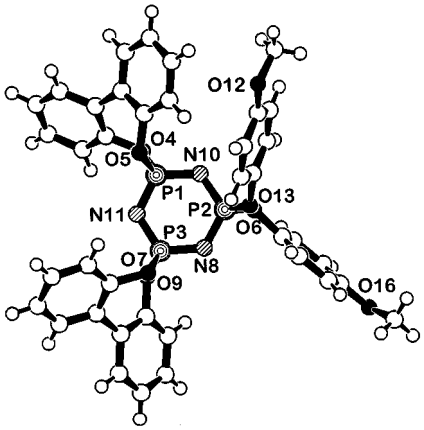


Figure 3. SCHAKAL view of **7**(*R*,*R*)

Table 2. Selected bond lengths [Å] and angles [°] in **7**(*R*,*R*)

Bond	Length [Å]	Bond	Angle [°]
P(1)−N(10)	1.561(3)	N(10)−P(1)−N(11)	117.89(14)
P(1)−N(11)	1.574(3)	O(4)−P(1)−O(5)	102.6(6)
P(1)−O(4)	1.585(2)	N(10)−P(1)−O(4)	105.19(13)
P(1)−O(5)	1.589(2)	N(11)−P(1)−O(4)	112.13(14)
P(2)−N(10)	1.578(3)	N(10)−P(1)−O(5)	112.15(14)
P(2)−N(8)	1.578(3)	N(11)−P(1)−O(5)	105.87(14)
P(2)−O(13)	1.563(3)	N(8)−P(2)−N(10)	117.7(2)
P(2)−O(6)	1.573(2)	O(13)−P(2)−O(6)	103.63(14)
P(3)−N(8)	1.563(3)	N(8)−P(2)−O(13)	108.0(2)
P(3)−N(11)	1.576(3)	O(6)−P(2)−N(8)	109.64(14)
P(3)−O(7)	1.585(3)	N(10)−P(2)−O(13)	111.60(13)
P(3)−O(9)	1.590(2)	N(10)−P(2)−O(6)	105.44(13)
		N(8)−P(3)−N(11)	118.1(2)
		O(7)−P(3)−O(9)	102.87(12)
		O(7)−P(3)−N(8)	112.6(2)
		O(7)−P(3)−N(11)	104.5(2)
		N(8)−P(3)−O(9)	106.3314)
		N(11)−P(3)−O(9)	111.47(14)
		P(1)−N(11)−P(3)	121.7(2)
		P(1)−N(10)−P(2)	121.8(2)
		P(2)−N(8)−P(3)	122.0(2)

The other enantiomer is also found in the unit cell (space group $P\bar{1}$), but is not shown. The P_3N_3 ring is almost planar [deviations (Å) from the best plane: P1(−0.053)−P2(−0.025)−P3(0.006)−N8(−0.005)−N10(0.055)−N11(0.022)] and all P−N distances are almost equal (largest variation 0.017 Å), indicating that no unusual steric interactions are involved. An idealized C_2 axis of symmetry runs through P2−N11 and interconverts the methyl groups bonded to O12 and O16.

The chiral cyclotriphosphazene **9**(*R*,*R*) crystallizes in the axial chiral space group $P_2(1)$. The molecule is shown in such a way that the idealized C_2 axis running through P1−N3 lies horizontal in the plane of the paper (Figure 4); selected bond lengths and angles are listed in Table 3.

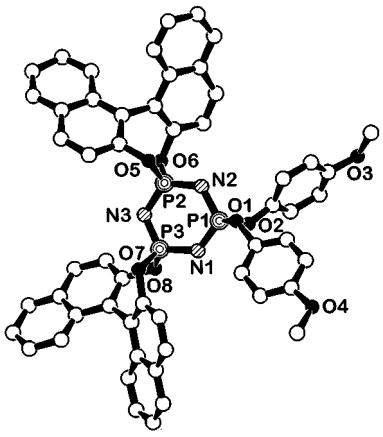


Figure 4. SCHAKAL view of **9**(*R*,*R*)

Table 3. Selected bond lengths [Å] and angles [°] in **9**(*R*,*R*)

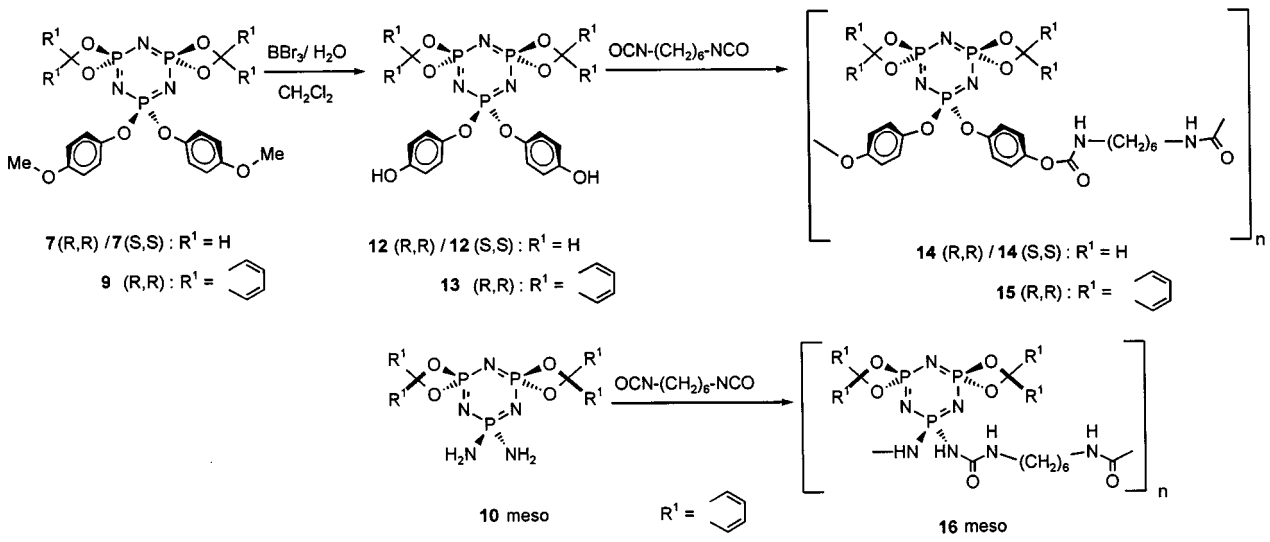
Bond	Length [Å]	Bond	Angle [°]
P(2)−N(3)	1.568(10)	N(3)−P(2)−O(5)	112.4(5)
P(2)−O(5)	1.582(8)	N(3)−P(2)−N(2)	118.7(5)
P(2)−N(2)	1.571(10)	O(5)−P(2)−N(2)	104.7(5)
P(2)−O(6)	1.612(7)	N(3)−P(2)−O(6)	107.6(5)
P(3)−O(7)	1.567(7)	O(5)−P(2)−O(6)	101.8(4)
P(3)−N(3)	1.566(11)	N(2)−P(2)−O(6)	110.3(5)
P(3)−N(1)	1.581(9)	O(7)−P(3)−N(3)	107.7(5)
P(3)−O(8)	1.620(7)	O(7)−P(3)−N(1)	112.3(5)
P(1)−N(1)	1.539(10)	N(3)−P(3)−N(1)	116.0(5)
P(1)−O(1)	1.564(8)	O(7)−P(3)−O(8)	102.7(4)
P(1)−N(2)	1.594(10)	N(3)−P(3)−O(8)	110.6(5)
P(1)−O(2)	1.610(8)	N(1)−P(3)−O(8)	106.7(5)
		N(1)−P(1)−O(1)	114.3(5)
		N(1)−P(1)−N(2)	117.6(3)
		O(1)−P(1)−N(2)	102.9(5)
		N(1)−P(1)−O(2)	104.2(4)
		O(1)−P(1)−O(2)	104.6(4)
		N(2)−P(1)−O(2)	112.7(5)
		P(2)−N(2)−P(1)	120.5(6)
		P(1)−N(1)−P(3)	124.3(6)
		P(2)−N(3)−P(3)	122.6(4)

Among the phosphazenes investigated in this work, **9**(*R*,*R*) is the most sterically encumbered. This is reflected in a larger variation of the bond lengths (P−N 1.539−1.594 Å; P−O 1.564−1.620 Å) and angles (P−N−P 116.0−118.7°; N−P−N 120.5−124.3°), and in a slight puckering of the P_3N_3 ring [deviations (Å) from the best plane: P1(0.022)−P2(0.024)−P3(−0.02)−N2(−0.38)−N1(0.006)−N3(0.005)]. The internal O5−P2−O6 (101.8°) and O7−P−O8 (102.7°) angles are slightly smaller than the rather open O1−P1−O2 (104.6°). Generally, however, no severe steric interactions leading to unusual distortions are observed.

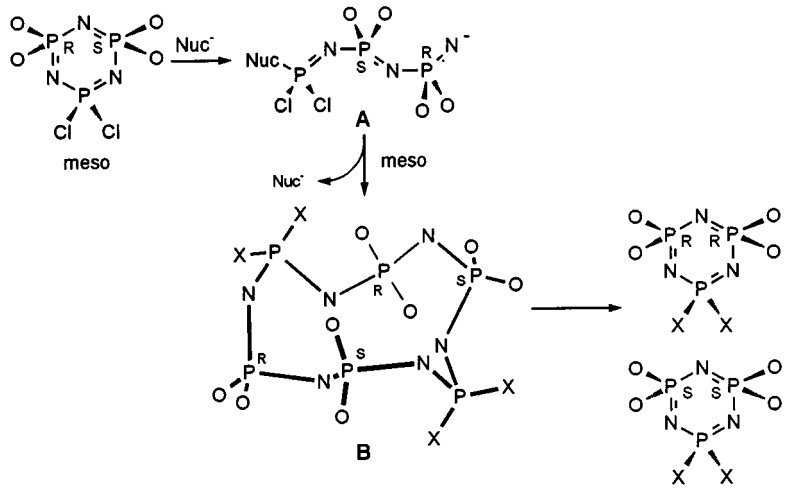
Discussion

Clearly, the *meso* forms of the 1,1-P-dichloro-substituted cyclotriphosphazenes, *meso*-**4** and *meso*-**5**, respectively, seem to be favored when racemic mixtures of the diols **2** and **3** are used. It is quite remarkable that these are formed exclusively and we cannot offer a straightforward explanation as to why the chiral (*R*,*R*) or (*S*,*S*) forms are not found. On the other hand, an anionic nucleophile converts the *meso* forms either quantitatively, as in the case of *meso*-**4**, or at least partially, as is observed for *meso*-**5**, into the axial chiral isomers. This is even more surprising because the sterically more demanding 4-methoxyphenolate groups should give rise to increased steric interactions, which, at first glance, may be smaller in the *meso* isomers. However, just the opposite may be true and attractive interactions, for example between aromatic hydrogen centers and a π-system of a neighboring arene moiety, may determine the relative stabilities. Such an interaction (< 2.8 Å) is seen in the molecular structure of **7**(*R*,*R*) (Figure 3) between one hydrogen center of a biphenoxy group and the π-cloud of a 4-methoxyphenolate residue. In any case, a plausible mechanism for the change of the configuration at the phosphorus centers within one P_3N_3 unit must be found. While one may speculate about pentacoordinated phosphorus centers undergoing Berry rotation when the biphenoxy-substituted cyclotriphosphazene *meso*-**4** is reacted with an anionic nucleophile, such a possibility is highly unlikely for *meso*-**5**. Instead, a complete intermolecular exchange of (*R*)- or (*S*)-configured (O,O)P units must take place and we propose the mechanism outlined in Scheme 4 to explain this observation.

Nucleophilic attack on the electrophilic PCl_2 group leads to ring-opening and formation of intermediate **A**. This may act as a further nucleophile, attacking a second equivalent of *meso*-configured 1,1-dichlorocyclotriphosphazene. A dimer **B** containing a twelve-membered P_6N_6 ring could thus be formed, although higher oligomers cannot be ruled out. The structures of cyclophosphazenes $(R_2PN)_n$ have been comprehensively determined for $n = 3-12$.[23] It is found that the P−N−P angles in particular widen with ring size [e.g. 133° in $(Me_2PN)_6$]. This may increase the steric interactions between substituents on neighboring phosphorus centers and may be particularly unfavorable for (*R*,*S*)-configured pairs (see Figure 1). Finally, the larger ring **B** collapses into the thermodynamically more stable six-membered chiral phosphazenes. While this mechanism is admittedly highly speculative, it would explain why no *meso*-**8** is obtained when **6**(*R*,*R*) is reacted with 4-methoxyphenolate. It is even conceivable that the substitution of the chlorines by phenolate residues occurs at the stage of the larger-ring phosphazenes. It is noteworthy that no further *meso*-**8** is converted into **9**(*R*,*R*) or **9**(*S*,*S*) when the reaction is carried out for an extended period in the presence of excess phenolate after complete conversion has been already achieved. Raising the temperature to about 100°C led to nonspecific degradation of the reaction products. Thus, it seems that a PCl_2 group is necessary in order to observe the stereochemical phenomena. Furthermore, only hard nucleophiles lead to exchange of the (O,O)P groups, since amine bases do not alter the stereochemistry of the starting materials (cf. the synthesis of *meso*-**10** and *meso*-**11** from *meso*-**5**). Finally, we note that the interconversion of rings of different sizes has been described for anionic cyclosilazanes[24] and it is well-known that cyclosiloxanes, which are isoelectronic with phosphazenes, easily undergo a ring-opening polymerization (ROP) in the presence of base.[25] To the best of our knowledge, equilibria between rings of different sizes, as is



Scheme 4. Syntheses of cyclolinear polymers



Scheme 5. Proposed mechanism for exchange of (O,O)P groups

indirectly evidenced here by an exchange of stereochemically different (O,O)P groups, have not previously been described in cyclophosphazene chemistry.

Syntheses of Polymers

In order to obtain cyclolinear polymers, we converted the racemic mixture of 4-methoxy-substituted phosphazenes **7**(*R*,*R*) and **7**(*S*,*S*) as well as enantiomerically pure **9**(*R*,*R*) into the hydroxylated compounds **12** and **13** by reacting them with BBr_3 and then hydrolyzing the intermediate boron compounds[26] (Scheme 5).

These reactions proceeded with complete retention of the stereochemistry at the phosphorus centers. For instance, using the mixture of isomers *meso*-**8**, **9**(*R*,*R*) and **9**(*S*,*S*) obtained according to Scheme 3, two ^{1}H-NMR signals were observed for the OH groups of the *meso* isomer (δ = 4.05 and 4.11) and one (δ = 4.09) for the enantiomers, in the same ratio as the integrals of the methoxy resonances of the starting material. The enantiomerically pure compound **13**(*R*,*R*) exhibited an optical rotation angle of $[\alpha]^{25} = -119°$. The presence of hydroxyl groups in **12**(*R*,*R*)/**12**(*S*,*S*) and **13**(*R*,*R*) was evident from the IR spectra, which featured a broad band located near 3400 cm^{-1} corresponding to the OH stretching vibration. Furthermore, the complete conversion of **7** and **9** into **12** and **13**, respectively, was evident from the ^{1}H- and ^{13}C-NMR spectra owing to the disappearance of the signals attributable to the methoxy functions.

Polyurethanes incorporating cyclotriphosphazene units were prepared by direct polyaddition of either the bifunctional hydroxylated racemic mixture of **12**(*R*,*R*)/**12**(*S*,*S*) or enantiomerically pure **13**(*R*,*R*) or the bis(amino)-substituted *meso* compound *meso*-**10** with hexamethylenediisocyanate (HDI). The reactions were performed in DMF at 80°C and the polymers **14**(*R*,*R*)/**14**(*S*,*S*), **15**(*R*,*R*), and *meso*-**16** were purified by precipitation and repeated extractions with methanol.[27] The ^{31}P-NMR spectra in [D_6]DMSO solution were very similar to the spectra of the monomers.

The ^{1}H-NMR and IR spectra confirmed the formation of polyurethane structures; the IR spectra of **14**(*R*,*R*)/**14**(*S*,*S*), **15**(*R*,*R*), and *meso*-**16** are given in Figure 5.

The spectra show the characteristic absorptions of the cyclotriphosphazene ring and aromatic groups at around $\tilde{\nu}$ = 1250, 1170, and 960 cm^{-1}, attributable to P=N, (P)−C−O and P−O−(C) stretching vibrations, respectively.[28] These results confirmed that the cyclotriphosphazene units remained unaffected when incorporated into the polymers. The urethane groups present in **14**(*R*,*R*)/**14**(*S*,*S*), **15**(*R*,*R*), and *meso*-**16** are characterized by NH stretching vibrations at $\tilde{\nu} \approx 3350$ cm^{-1} and C=O stretching vibrations at $\tilde{\nu} \approx 1700$ cm^{-1}. In the ^{1}H-NMR spectra of the polymers, a resonance at $\delta \approx 9.6$ can be attributed to the NH proton of the urethane linkage. The molecular weight of **14**(*R*,*R*)/**14**(*S*,*S*) was estimated by steric exclusion chromatography in THF to be $\overline{M}_w$bar = 17000 with a molecular weight distribution $\overline{M}_w$bar/$\overline{M}_n$bar = 1.7. The molecular weights of **15**(*R*,*R*) and *meso*-**16** could not be determined because of the poor solubilities of these polymers in THF.

In terms of the stereochemistries at the phosphorus centers, the polyurethanes prepared in this work are representatives of three different polymer types. Thus, **14**(*R*,*R*)/**14**(*S*,*S*) consists of a racemic mixture of homochiral polymer chains, **15**(*R*,*R*) is the first example of an enantiomerically pure cyclolinear phosphazene polymer (optical rotation angle $[\alpha]^{25} = -111°$), while *meso*-**16** contains (*R*)- and (*S*)-configured phosphorus centers within one polymer strand. The thermal behavior of these three polymers was investigated by dynamic thermogravimetric analysis (TGA) in air. Typical TGA curves for **14**(*R*,*R*)/**14**(*S*,*S*), **15**(*R*,*R*), and *meso*-**16** are shown in Figure 6.

It can be seen that the incorporation of cyclotriphosphazene moieties increases the thermal stability of all polyurethanes. Note that simple "organic" polyurethanes show thermooxidative decomposition starting at ca. 200°C. For **14**(*R*,*R*)/**14**(*S*,*S*), the temperature corresponding to 10%

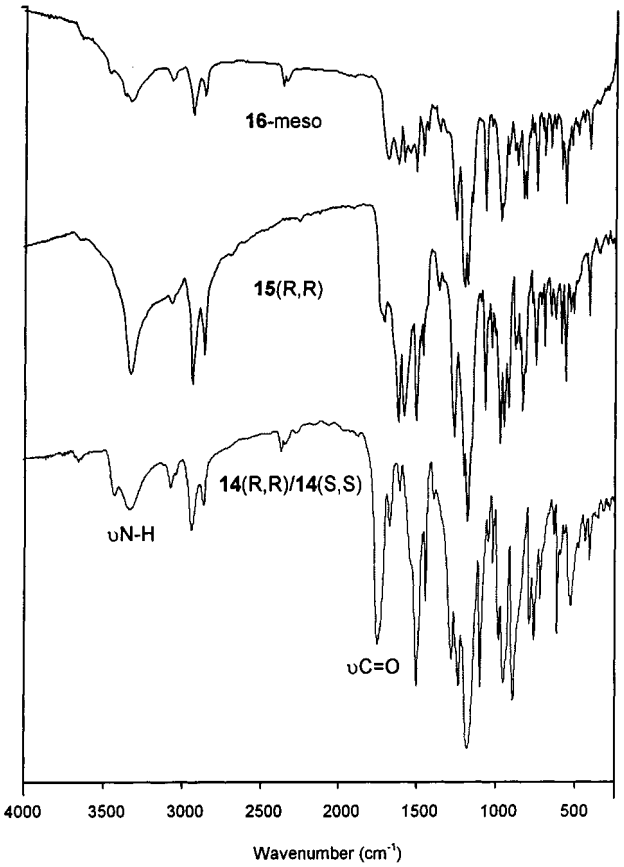


Figure 5. Infrared spectra of polymers **14**(*R*,*R*)/**14**(*S*,*S*), **15**(*R*,*R*), and *meso*-**16**

weight loss (T_{10}) is found to be 325°C. The value of T_{10} is lower for **15**(*R*,*R*) (280°C), but lies in the same range for *meso*-**16** (315°C). At a temperature of 500°C, 72%, 60%, and 70%, respectively, of the original masses of **14**(*R*,*R*)/**14**(*S*,*S*), **15**(*R*,*R*), and *meso*-**16** still remain. This high char yield is characteristic of cyclotriphosphazene-containing polymers[8–10] and accounts for their flame-retardant properties. For comparison, the thermal behavior of a polyurethane synthesized from 1,3-bis(hydroxy)benzene and HDI was investigated. Its T_{10} was found to be low (209°C) and complete decomposition was observed at just 600°C.[3] However, the thermal stability of **15**(*R*,*R*), in which only one stereoisomer of the diol is present, is significantly lower than those of **14**(*R*,*R*)/**14**(*S*,*S*) and *meso*-**16**. In the latter, both atropisomers of the diols are present. As can be deduced from Figure 1, a favorable packing by π-stacking of the arene moieties may be responsible for the enhanced thermal stabilities of these polymers.

Conclusion

Reactions of hexachlorocyclotriphosphazene **1** with two equivalents of the chelating diols 2,2′-dioxybiphenyl, **2**(*S*), **2**(*R*), or 2′,2′′-dioxy-1′,1′′-bis(2-naphthyl), **3**(*S*), **3**(*R*), lead only to the formation of the *meso* compounds [(*R*,*S*)-$(O,O)_2Cl_2P_3N_3$] *meso*-**4** or *meso*-**5**, respectively. Remarkably, when the remaining PCl_2 group is reacted with a hard nucleophile such as 4-methoxyphenolate, either a racemic mixture of chiral [(*R*,*R*)-$(O,O)_2(RO)_2P_3N_3$], **7**(*R*,*R*), and [(*S*,*S*)-$(O,O)_2(RO)_2P_3N_3$], **7**(*S*,*S*), (O,O = 2,2′-dioxybiphenyl) is formed, or at least partial racemization occurs, leading to a mixture of all possible stereoisomers *meso*-**8**, **9**(*R*,*R*) and **9**(*S*,*S*) [O,O = 2′,2′′-dioxy-1′,1′′-bis(2-naphthyl)]. While one may speculate about five-coordinated phosphorus centers undergoing Berry rotation in the case of O,O = biphenoxy, this phenomenon is highly unlikely when O,O = binaphthoxy and does not explain the configurational change at the phosphorus centers. In order to explain the exchange of complete (O,O)P-units within the cycles, we

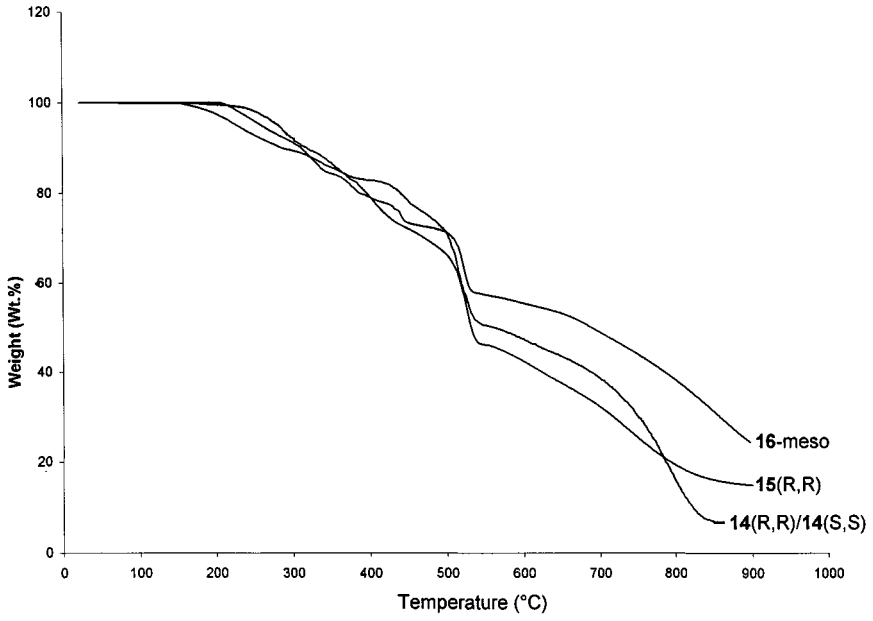


Figure 6. Thermogravimetric analysis of **14**(*R*,*R*)/**14**(*S*,*S*), **15**(*R*,*R*), and *meso*-**16** conducted at a heating rate of 8°C/min in air

Table 4. Crystal data and structure refinement for *meso*-**4**, **7**(*R*,*R*), and **9**(*R*,*R*)

	meso-**4**	**7**(*R*,*R*)	**9**(*R*,*R*)
Empirical formula	$C_{24}H_{16}Cl_2N_3O_4P_3$	$C_{38}H_{30}N_3O_8P_3$	$C_{54}H_{38}N_3O_8P_3$
Formula weight	574.21	749.56	949
Temperature [K]	293(2)	293(2)	293(2)
Wavelength [Å]	1.54178	1.54178	0.71073
Space group	*Cc*	$P\bar{1}$	*P*2(1)
Crystal system	Monoclinic	Triclinic	Monoclinic
Unit cell dimensions [Å][°]	*a* = 11.078(5)	*a* = 11.669(6)	*a* = 9.657(2),
	b = 26.711(13)	*b* = 11.866(10)	*b* = 23.686(5),
	c = 17.403(9)	*c* = 13.919(12)	*c* = 10.487(2)
	α = 90	α = 101.12(6)	α = 90
	β = 101.75(4)	β = 96.88(6)	β = 90.30(3)
	γ = 90	γ = 111.23(5)	–
Volume [Å^3]	5042(4)	1725(2)	2398.7(8)
Z	8	8	2
Density [mg·m^3] (calcd.)	1.513	1.444	1.437
Absorption coefficient [mm^{-1}]	4.447	2.091	0.297
F(000)	2336	776	1074
Crystal size [mm^3]	0.3 × 0.2 × 0.2	0.4 × 0.3 × 0.2	0.4 × 0.3 × 0.3
θ range for data collection [°]	3.31 to 50.01	3.31 to 49.99	1.72 to 20.08
Index ranges	$-10 \le h \le 10$	$-11 \le h \le 11$	$-9 \le h \le 9$
	$0 \le k \le 26$	$-11 \le k \le 11$	$-22 \le k \le 0$
	$0 \le l \le 17$	$0 \le l \le 13$	$-10 \le l \le 10$
Reflections collected	2621	3539	4663
Independent reflections	2621 (R_{int} = 0.0122)	3539 (R_{int} = 0.0000)	2332 (R_{int} = 0.0000)
Absorption correction	None	None	None
Refinement method	Full-matrix least-squares on F^2		
Data/restraints/parameters	2611/0/648	3539/0/470	2332/465/641
Goodness-of-fit on F^2	1.078	1.060	1.038
Final *R* indices [$I>2\sigma(I)$]	*R*1 = 0.0444, *wR*2 = 0.1122	*R*1 = 0.0411, *wR*2 = 0.1162	*R*1 = 0.0355, *wR*2 = 0.0889
R indices (all data)	*R* = 0.0450, *wR*2 = 0.1134	*R*1 = 0.0425, *wR*2 = 0.1179	*R*1 = 0.0374, *wR*2 = 0.0902
Extinction coefficient [mm^{-1}]	0.00023(6)	0.0072(5)	0.0093(15)
Largest diff. peak & hole [e.Å^{-3}]	0.325 and −0.467	0.343 and −0.340	0.391 and −0.212
Absolute structure parameter	−0.01(2)	–	0.50(16)

propose ring-opening and the formation of larger cycles, i.e. cyclohexaphosphazenes, which collapse to reform cyclotriphosphazenes with different stereochemistry. Chiral cyclotriphosphazenes such as **9**(*R*,*R*) and **9**(*S*,*S*) were obtained using either of the enantiomerically pure (*R*)- or (*S*)-forms of 2′,2′′-dioxy-1′,1′′-bis(2-naphthyl) **3** as starting materials. The change of configuration is furthermore related to the presence of a PCl_2 unit in the phosphazene ring, since the stereochemistry of all phenoxy-substituted phosphazenes [$(O,O)_2(RO)_2P_3N_3$] is retained, even when these are reacted with excess phenolate RO^- under harsh conditions. Interestingly, soft nucleophiles such as amines do not affect the configuration at the phosphorus centers and thus allow the synthesis of *meso*-[(*R*,*S*)-$(O,O)_2(R^1RN)_2P_3N_3$] compounds. These observations show that seemingly simple substitution reactions on chloro-substituted phosphazenes are more complex than they might at first appear. The bifunctional cyclotriphosphazenes [(*R*,*R*)-$(O,O)_2$(4-HO−$C_4H_4O)_2P_3N_3$] and/or [(*S*,*S*)-$(O,O)_2$(4-HO−$C_4H_4O)_2P_3N_3$] and [(*R*,*S*)-$(O,O)_2(H_2N)_2P_3N_3$] are suitable monomers for polyaddition reactions with hexamethylenediisocyanate, which furnish cyclolinear polyurethane polymers. Depending on the stereochemistry of the phosphazene precursor, either a racemic mixture of homochiral polymer strands, an enantiomerically pure polymer, or the *meso* form of a polymer was obtained. The latter was found to show the highest thermal stability

Experimental Section

General Methods: ^{31}P-, ^{1}H-, and ^{13}C-NMR spectra were recorded in CD_2Cl_2 and $CDCl_3$ for most compounds, those of *meso*-**10** were recorded in [D_8]THF, while polymers where examined in [D_6]DMSO using Bruker DPX250 and DPX300 NMR spectrometers. Chemical shifts (ppm) are positive in the low-field direction and are quoted relative to external 85% H_3PO_4 (^{31}P) or external TMS (^{1}H, ^{13}C). – Infrared spectra were recorded with a Perkin−Elmer 783 spectrometer. The samples were dispersed in KBr. – Mass spectra were recorded on a Finnigan MAT 8200 spectrometer operating in the EI (70 eV) mode. – Thermogravimetric measurements were performed in air on a Setaram NTB10−8 instrument at a heating rate of 8°C/min. – The optical rotation angles were measured on a Perkin−Elmer 241MC polarimeter [*c* = 1, $CHCl_3$ for **6**(*R*,*R*), **9**(*R*,*R*) and **13**(*R*,*R*); DMF for **15**(*R*,*R*)] using light of the Na D line (λ = 589 nm). – The X-ray powder diffraction pattern of *meso*-**4** was recorded using a Stoe STADIP powder diffractometer equipped with a position-sensitive detector (radiation: Cu-$K_{\alpha1}$).

Tetrahydrofuran (THF), chlorobenzene, dichloromethane, and dimethylformamide (DMF) were obtained from Aldrich. THF, CH_2Cl_2, and DMF were purified by distillation. Sodium hydride, biphenol, binaphthol [(+/−); *R*(+)], sodium hydroxide, 4-methoxyphenol, methylhydrazine, boron tribromide, ammonium hydroxide solution, and 1,6-hexamethylenediisocyanate (HDI) were purchased from Aldrich or Fluka and were used as received. Hexachlorocyclotriphosphazene, $N_3P_3Cl_6$, (Nippon Soda) was

Table 5. Spectroscopic data for intermediate compounds and precursors

Compd.	^{31}P NMR δ [ppm]	^{1}H NMR [$^{-1}$]	^{13}C NMR *m/z*	IR frequency	MS
meso-**4**	20.72, 30.43, J_{AB} = 79.28 Hz	7.31−7.55 (m, Ar)	147.3 (m, Ar), 129.9 (m, Ar), 129.7 (m, Ar), 128.5 (m, Ar), 126.5 (m, Ar), 121.8 (m, Ar)	1226.7 (ν P=N), 1172, 962 (ν P−O−Ar)	574 [M$^+$]
meso-**5**	21.78, 30.44, J_{AB} = 77.65 Hz	7.23−7.55 (m, Ar), 7.65 (d, Ar), 7.75 (d, Ar), 8.00 (t, Ar), 8.09 (t, Ar)		1265 (ν P=N), 1184, 973 (ν P−O−Ar)	773 [M$^+$]
6(*R*,*R*), **6**(*S*,*S*)	21.97, 30.22, J_{AB} = 78.59 Hz	7.28−7.35 (m, Ar), 7.41−7.53 (m, Ar), 7.63 (d, Ar), 7.87 (m, Ar), 7.90 (s, Ar), 7.99 (d, Ar), 8.12 (d, Ar)	121.8 (m, Ar), 126.1 (d, Ar), 127.0 (d, Ar), 127.6 (s, Ar), 128.9 (d, Ar), 131.5 (d, Ar), 132.4 (m, Ar), 136.6 (m, Ar), 147.1 (m, Ar)	1263 (ν P=N), 1188, 973 (ν P−O−Ar)	773 [M$^+$]
7(*R*,*R*), **7**(*S*,*S*)	12.22, 26.59, J_{AB} = 61.99 Hz	3.93 (s, CH_3), 6.80 (d, Ar), 7.42 (d Ar), 6.90−7.31 (m, Ar)	55.5 (s, CH_3), 114.4 (m, Ar), 122.2 (m, Ar), 122.6 (m, Ar), 125.9 (m, Ar), 128 (m, Ar), 129.5 (m, Ar), 129.6 (m, Ar), 146 (m, Ar), 147 (m, Ar), 155.5 (m, Ar)	2836 (ν C−H, OCH_3), 1231 (ν P=N), 1173, 948 (ν P−O−Ar)	749 [M$^+$]
meso-**8**	12.03, 27.56, J_{AB} = 61.36 Hz	3.80, 3.95 (s, OCH_3), 7.15 (d, Ar), 7.28−7.54 (m, Ar), 7.61 (d, Ar), 7.97 (m, Ar), 8.03 (m, Ar), 8.13 (d, Ar)	55.2, 55.5 (s, OCH_3), 114.0 (d, Ar), 114.3 (d, Ar), 120.7 (m, Ar), 120.9 (m, Ar), 121.3 (m, Ar), 121.9 (d, Ar), 122.0 (d, Ar), 125.1 (m, Ar), 126.1 (m, Ar), 126.8 (m, Ar), 128.0 (m, Ar), 130.3 (m, Ar), 131.4 (m, Ar), 132.1 (m, Ar), 147.0 (m, Ar)	2833 (ν C−H,OCH_3), 1268 (ν P=N), 1170, 975 (ν P−O−Ar)	949 [M$^+$]
9(*R*,*R*), **9**(*S*,*S*)	11.76, 27.87, J_{AB} = 61.79 Hz	3.88 (s, OCH_3), 6.96 (d, Ar), 7.06 (d, Ar), 7.28−7.49 (m, Ar), 7.85 (d, Ar), 7.93−7.95 (m, Ar)	55.4 (s, OCH_3), 114.2 (d, Ar), 121.1 (m, Ar), 121.3 (m, Ar), 121.7 (d, Ar), 125.1 (d, Ar), 126.9 (d, Ar), 128.1 (s, Ar), 130.3 (d, Ar), 131.3 (d, Ar), 131.7 (d, Ar), 144.4 (m, Ar), 146.8 (t, Ar), 147.0 (t, Ar)	2830 (ν C−H, OCH_3), 1260 (ν P=N), 1162, 970 (ν P−O−Ar)	949 [M$^+$]
meso-**10**	20.29, 27.43, J_{AB} = 47.63 Hz	7.28−8.15 (m, Ar)	121.5 (m, Ar), 122.6 (m, Ar), 125.7 (m, Ar), 126.5 (m, Ar), 127.8 (m, Ar), 129.7 (d, Ar), 131.3 (m, Ar), 132.0 (m, Ar), 136.0 (m, Ar), 146.9 (m, Ar)	3460, 3340 (ν N−H), 1544 (δ N−H), 1256 (ν P=N), 1176, 969 (ν P−O−Ar)	
meso-**11**	28.31, 29.34, J_{AB} = 58.32 Hz	2.84 (d, CH_3), 3.11 (d, CH_3), 7.25−7.65 (m, Ar), 7.75 (d, Ar), 8.01−8.22 (m, Ar)		3412, 3324 (ν N−H), 2790 (ν C−H), 1566 (δ N−H), 1255 (ν P=N), 1170, 966 (ν P−O−Ar)	791 [M$^+$]
12(*R*,*R*), **12**(*S*,*S*)	12.74, 26.83, J_{AB} = 62.27 Hz	6.79 (d, Ar), 7.60 (d, Ar), 6.88−7.32 (m, Ar), 8.33 (s, OH)	116.8 (m, Ar), 122.7 (m, Ar), 122.8 (m, Ar), 122.9 (m, Ar), 127.1 (m, Ar), 129.4 (m, Ar), 129.4 (m, Ar), 143 (m, Ar), 148.9 (m, Ar), 155.2 (m, Ar)	3358 (ν O−H), 1231 (ν P=N), 1175, 951 (ν P−O−Ar)	721 [M$^+$]
13(*R*,*R*)	12.32, 28.19, J_{AB} = 61.81 Hz	5.18 (s, OH), 6.92 (d, Ar), 7.19−7.54 (m, Ar), 7.90 (d, Ar), 8.04 (m, Ar)	115.6 (m, Ar), 121.1 (m, Ar), 121.5 (m, Ar), 121.8 (d, Ar), 125.0 (d, Ar), 126.9 (d, Ar), 17.0 (d, Ar), 128.1 (s, Ar), 130.4 (d, Ar), 131.4 (d, Ar), 131.9 (d, Ar), 144.3 (d, Ar), 146.8 (m, Ar), 152.5 (m, Ar)	3401 (ν O−H), 1259 (ν P=N), 1166, 973 (ν P−O−Ar)	921 [M$^+$]

purified by vacuum sublimation. All reactions and manipulations were carried out under inert atmosphere.

Compounds *meso*-**4**, **7**(*RR*)/**7**(*S*,*S*), and **12**(*R*,*R*)/**12**(*S*,*S*) were synthesized according to a procedure reported elsewhere.[8]

Crystallographic Analyses of *meso*-4, 7(*R*,*R*), and 9(*R*,*R*): The data sets for the single-crystal X-ray studies were collected on either a Nonius CAD4 or a fully automated Siemens−Stoe AED2 four-circle diffractometer. All calculations were performed on a Digital Corporation VAX system using the SHELXS-86 and SHELXS-93 program suites.[29][30]

Specific data relating to the crystal structures and refinements are collected in Table 4. The structures were solved by direct methods and refined by full-matrix least-squares on F^2.

The graphical representations of the molecular structures were drawn using the SCHAKAL program.[31]

Synthesis of 2,2-Dichloro-4,4,6,6-bisspiro(2′,2′′-dioxy-1′,1′′-binaphthyl)]cyclotriphosphazene [*meso*-5, 6(*R*,*R*), 6(*S*,*S*)]: A three-necked round-bottomed flask was charged with chlorobenzene (12 mL), water (20 mL), $N_3P_3Cl_6$ (1.13 g, 3.25 mmol), 2,2′-dihydroxy-1,1′-binaphthyl (2.16 g, 6.51 mmol), sodium hydroxide (0.52 g, 13.01 mmol), and TBA (0.10 g, 0.324 mmol). The reaction mixture was stirred rapidly at room temperature for 3 h and then heated at 70°C for a further 3 h. The solvents were then removed under reduced pressure to leave a brown residue, which was washed with chlorobenzene and acetone and dried. A white solid was obtained (2.4 g, 85%); m.p. > 250°C. Spectroscopic data are given in Table 5.

Synthesis of 2,2-Bis(4-methoxyphenyloxy)bisspiro(2′,2′′-dioxy-1′,1′′-binaphthyl)]cyclotriphosphazene [*meso*-8, 9(*R*,*R*), 9(*S*,*S*)]: A solution of 4-methoxyphenol (0.73 g, 5.92 mmol) in THF was added dropwise to a solution of *meso*-**5** [or **6**(*R*,*R*) or **6**(*S*,S)] (2.56 g, 2.96 mmol) in THF containing suspended NaH (0.14 g, 20 mmol). The mixture was stirred at room temperature for 3 h and then the THF was removed under reduced pressure. The residue was redissolved in dichloromethane and the resulting solution was extracted twice with 10% aqueous NaOH, washed with water (three times),

Table 6. Spectroscopic data for polymers **14**(*R*,*R*)/**14**(*S*,*S*), **15**(*R*,*R*) and *meso*-**16**

Compd.	^{31}P NMR δ [ppm]	^{1}H NMR δ [ppm]	IR frequency [cm^{-1}]
14(*R*,*R*), **14**(*S*,*S*)	26.13, 12.08, J_{AB} = 62.60 Hz	1.32 (CH_2), 1.47 (CH_2), 3.07 (CH_2-NH-), 7.15−7.80 (m, Ar), 9.65 (s, NH)	3389 (ν N−H), 1745 (ν C=O), 1230 (ν P=N), 1171, 946 [ν (P−O−Ar)]
15(*R*,*R*)	27.32, 12.21, J_{AB} = 60.02 Hz	1.25 (CH_2), 1.50 (CH_2), 3.10 (CH_2-NH-), 6.90−8.20 (m, arom.), 9.61 (s, NH)	3319 (ν N−H), 1731 (ν C=O), 1259 (ν P=N), 1170, 973 [ν (P−O−Ar)]
meso-**16**	27.43, 20.29, J_{AB} = 47.79 Hz	1.23 (CH_2), 1.46 (CH_2), 2.96 (CH_2-NH-), 7.22−8.30 (m, arom.)	3363 (ν N−H), 1545 (δ N−H), 1686 (ν C=O), 1256 (ν P=N), 1181, 969 [ν (P−O−Ar)]

and dried over anhydrous sodium sulfate. After filtration and removal of the solvent under reduced pressure, 2.33 g (83%) of *meso*-**8** [or **9**(*R*,*R*) or **9**(*S*,S)] was obtained; m.p. 199°C. − $C_{54}H_{38}N_3O_8P_3$: calcd. C 67.1, H 4.0, N 4.3; found C 66.8, H 3.8, N 4.3. − Spectroscopic data are given in Table 5.

Synthesis of 2,2-Bis(4-hydroxyphenyloxy)bisspiro(2′,2′′-dioxy-1′,1′′-binaphthyl)]cyclotriphosphazene [13(*R*,*R*)/13(*S*,*S*)]: A solution of 1.07 g (4.26 mmol) of boron tribromide in anhydrous CH_2Cl_2 (10 mL) was added dropwise to a solution of **6**(*R*,*R*) or **6**(*S*,*S*) (2.02 g, 2.13 mmol) in anhydrous CH_2Cl_2 (15 mL). The reaction mixture was stirred at room temperature for 3 h and then poured into water (50 mL). The residue obtained was dissolved in CH_2Cl_2 and the resulting solution was washed with water (three times). The solvent was finally removed under reduced pressure to leave 1.37 g (70%) of **13**(*R*,*R*); m.p. 210°C. − $C_{52}H_{34}N_3O_8P_3$: calcd. C 67.8, H 3.7, N 4.6; found C 67.7, H 3.8, N 4.5. Spectroscopic data are given in Table 5.

Synthesis of 2,2-Bis(amino)-bisspiro(2′,2′′-dioxy-1′,1′′-binaphthyl)]-cyclotriphosphazene (*meso*-10): A solution of 0.605 mL (8.11 mmol) of ammonium hydroxide in THF (10 mL) was added dropwise to a solution of *meso*-**5** (1.57 g, 2.03 mmol) in the same solvent (10 mL). The reaction mixture was stirred at 40°C for 1 h and at room temperature for 2 h and then the THF was removed under reduced pressure. The residue obtained was washed with water (three times) and dried, furnishing 1.16 g (78%) of *meso*-**10**; m.p. >250°C. Spectroscopic data are given in Table 5.

Synthesis of 2,2-Bis(methylhydrazino)bisspiro(2′,2′′-dioxy-1′,1′′-binaphthyl)]cyclotriphosphazene (*meso*-11): To a solution of *meso*-**5** (1.56 g, 2.01 mmol) in THF was added a solution of methylhydrazine (0.43 mL, 8.05 mmol) in THF (4 mL) at 0°C. The resulting mixture was stirred for 2 h at room temperature and then the solvent was evaporated. The residue was taken up in chloroform and the mixture was filtered by passage through Celite. Evaporation of the solvent from the filtrate furnished 1.11 g (70%) of *meso*-**11**. Spectroscopic data are given in Table 5.

Synthesis of Polyurethanes [14(*R*,*R*)/14(*S*,*S*), 15(*R*,*R*), and *meso*-16]: A solution of **12**(*R*,*R*)/**12**(*S*,*S*) or **13**(*R*,*R*) or *meso*-**10** together with HDI (molar ratio, diol or diamine/diisocyanate = 1:1) in DMF was stirred at 80°C for 48 h. The reaction mixture was then poured into cold methanol to precipitate the polymer, which was washed several times with methanol, and finally dried in vacuo at 100°C for 12 h to give a white-yellow solid soluble in DMF and DMSO. − **14**(*R*,*R*)/**14**(*S*,*S*): $C_{44}H_{36}N_5O_{10}P_3$: calcd. C 59.4, H 4.3, N 7.9; found C 58.6, H 4.5, N 8.2. **15**(*R*,*R*): $C_{60}H_{46}N_5O_{10}P_3$: calcd. C 66.1, H 4.2, N 6.4; found C 68.3, H 4.0, N 6.3. *meso*-**16**: $C_{48}H_{40}N_7O_6P_3$: calcd. C 63.8, H 4.4, N 10.8; found C 66.2, H 4.6, N 11.1. Spectroscopic data are given in Table 6.

Acknowledgments

This work was supported by the ETH Zürich.

[1] B. Massiulanis, *J. Appl. Polym. Sci.* **1985**, *30*, 2731.
[2] B. Massiulanis, J. Hrouz, *J. Appl. Polym. Sci.* **1987**, *34*, 1941.
[3] I. Dez, R. De Jaeger, *J. Inorg. Organomet. Polym.* **1996**, *6*, (2), 111.
[4] M. Fukuhara, C. Osawa, Jap. Patent 74,133,470; *Chem. Abs.* **1975**, *83*, 29808.
[5] C. W. Allen, *The Chemistry of Inorganic Homo- and Heterocycles* (Eds.: I. Haiduc, D. B. Sowerby), Academic Press, New York, **1987**, *2*, 501.
[6] P. Radhakrishnan Nair, C. P. Reghunadan Nair, D. J. Francis, *Eur. Polym. J.* **1996**, *32*, 1415.
[7] K. Miyata, K. Muraoka, T. Itaya, T. Tanigaki, K. Inoue, *Eur. Polym. J.* **1996**, *32*, 1257.
[8] I. Dez, R. De Jaeger, *Phosphorus, Sulfur and Silicon* **1998**, *130*, 1.
[9] D. Kumar, A. Gupta, *Macromolecules* **1995**, *28*, 6323.
[10] Y. Ko, S. Cheong, U.S. Patent 5,677,416; *Chem. Abs.* **1997**, *127*, 319406e.
[11] D. Kumar, G. M. Fohlen, J. A. Parker, *Macromolecules* **1983**, *16*, 1250.
[12] M. Kajiwara, H. Saito, *J. Macromol. Sci. Chem.* **1981**, *A16(4)*, 873.
[13] D. Kumar, G. M. Fohlen, J. A. Parker, *J. Polym. Sci.: Polym. Chem. Ed.* **1986**, *24*, 2425.
[14] Y. W. Chen-Yang, J. S. Jiang, Y. W. Ho, S. J. Cheng, *J. Inorg. Organomet. Polym.* **1992**, *2*, 243.
[15] C. W. Allen, *Chem. Rev.* **1991**, *91*, 119.
[16] R. A. Pelc, K. Brandt, Z. Jedlinski, *Phosphorus, Sulfur and Silicon* **1990**, *47*, 375.
[17] G. A. Carriedo. L. Fernandez-Catuxo, F. J. Garcia Alonso, P. Gomez-Elipe, P. A. Gonzalez, *Macromolecules* **1996**, *29*, 5320.
[18] H. R. Allcock, M. T. Stein, J. A. Stanko, *J. Am. Chem. Soc.* **1971**, *93*, 3173.
[19] K. Brandt, Z. Jedlinski, *J. Org. Chem.* **1980**, *45*, 1672.
[20] G. R. Feistel, M. K. Feldt, R. L. Dieck, T. Moeller, *Inorg. Synth.* **1973**, *14*, 24.
[21] R. Kraemer, C. Galliot, J. Mitjaville, A. M. Caminade, J. P. Majoral, *Heteroatom. Chem.* **1996**, *7*, 149.
[22] F. Hochart, Ch. Mouveaux, J. Levalois-Mitjaville, R. De Jaeger, *Tetrahedron Lett.* **1998**, *39*, 6171.
[23] R. T. Oakley, S. J. Rettig, N. L. Paddock, J. Trotter, *J. Am. Chem. Soc.* **1985**, *107*, 6923.
[24] K. Dippel, E. Werner, U. Klingebiel, *Phosphorus, Sulfur and Silicon* **1992**, *64*, 15.
[25] I. Manners, *Angew. Chem.* **1996**, *108*, 1712; *Angew. Chem. Int. Ed. Engl.* **1996**, *35*, 1602.

[26] A. Medici, G. Fantin, P. Pedrini, M. Gleria, F. Minto, *Macromolecules* **1992**, *25*, 2569.
[27] J. B. Lee, T. Kato, S. Ujiie, K. Iimura, T. Uryu, *Macromolecules* **1995**, *28*, 2165.
[28] L. C. Thomas, *Interpretation of the Infrared Spectra of Organophosphorus Compounds*, Heyden, London, New York, and Rheine, **1974**.
[29] G. M. Sheldrick, *SHELXL-93*, *Program for Crystal Structure Determination*, University of Göttingen, **1993**.
[30] G. M. Sheldrick, *SHELXL-86*, University of Göttingen, **1986**.
[31] E. Keller, *SCHAKAL 88B/V16*, Kristallographisches Institut der Universität Freiburg, **1998**.

Received March 5, 1999
[I99087]

Electron-Poor 2,3-Dihydro-1,3-diborolyl Ruthenium Compounds: Synthesis, Complexation, Oxidative Addition, Capping, and Stacking Reactions

Thomas Müller,[a] Michael Kaschke,[a] Melanie Strauch,[a] Achim Ginsberg,[a] Hans Pritzkow,[a] and Walter Siebert*[a]

Dedicated to Professor Helmut Werner on the occasion of his 65th birthday

Keywords: Boranes / Ruthenium / Sandwich Complexes / Diboroles / Triple-decker

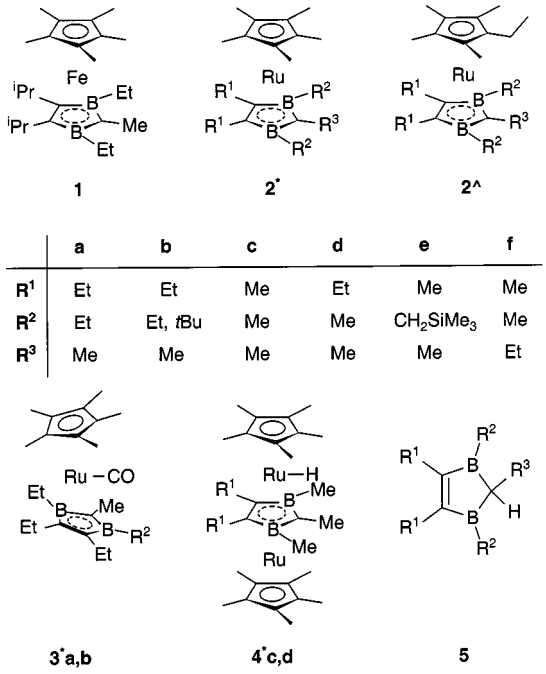
The addition products of lithium alkyls and the pentaalkyl-2,3-dihydro-1,3-diborole derivatives **5a–f** react with $[\{(C_5Me_5)RuCl\}_4]$ and $[\{(C_5Me_4Et)RuCl\}_4]$ to form the violet sandwich compounds **2*c–f** and **2^c**, **f**. These formally 16 VE complexes are in fact electron-poor 18 VE species, because a high-lying combination of σ(B–C) orbitals interacts with the d_{xz} orbital of the Ru atom. Addition of *tert*-butyl isocyanide to **2*a**, or **2*d** leads to the isonitrile complexes **6*a**, and **6*d**, as indicated by the spectroscopic data and X-ray structure analyses. At low temperature the interaction of **2*a**, **c**, or **e** with H_2 yields the classic dihydride complexes **7*a**, **c**, and **e**, respectively, which have been studied by NMR. Oxidative addition of $H_3B{\cdot}THF$ to the ruthenium atom of **2*a** or **c**, followed by a reductive elimination of H_2 and migration of the boranediyl group gives the yellow *closo*-RuC_3B_3 ruthenacarboranes **8*a** and **8*c**, respectively. The reaction of $[(C_2H_4)_2RhCl]_2$ and **2*c** generates the tetranuclear complex **9*c**.

Introduction

Organometallic complexes of the iron triad having less than 18 valence electrons (VE) are of particular interest for catalytic reactions. In the formally 16 VE complexes $[\{(C_5Me_5)Ru(XR)\}_2]$ (X = O, S)[1–3] the Ru atom is coordinatively unsaturated, and the sulfur compounds function as catalysts in the addition of thiols to polar alkynes.[4] Recently, 16 VE $[Ru(C_5Me_5)L_2]^+$ complex cations containing the ligands L_2 = 2,2′-bipyridyl[5a] or a 1,4-diazabutadiene derivative[5b] have been reported.

The formally 16 VE iron complex $[(\eta^5\text{-}C_5Me_5)Fe(\eta^5\text{-}(Ci\text{Pr})_2(BEt)_2CMe)]$ (**1**) has unusual properties.[6] It is thermally stable up to 200°C and shows a folded 1,3-diborolyl ring along the B−B vector by an angle of 41.3°. This unique folding allows a high−lying combination of σ (B−C) orbitals of the 1,3-diborolyl ligand to interact with the empty metal d_{xz} orbital to complete the 18 VE shell.[6] Compound **1** and the isoelectronic Ru complexes **2*a** and **b** are electron-poor, as demonstrated by their reaction with CO. In the case of **1**, a red product of unknown structure is formed, whereas **2*a** and **b** produce the expected monocarbonyl compounds **3*a** and **b**.[6]

Treatment of $[(C_5Me_5)RuCl]_4$ with the less bulky boron heterocycles **5c** and **d** in the presence of an excess of NaH led to the formation of 30 VE triple-decker complexes $[(C_5Me_5)Ru\{\mu,\eta^5\text{-}(CR^1)_2(BR^2)_2CMe\}RuH(C_5Me_5)]$ (**4*c** and **d**) containing a Ru−H bond.[6] The expected sandwich complexes **2*c** and **d** were not obtained. In this paper we describe the synthesis of several ruthenium complexes **2*** (* = pentamethylcyclopentadienyl derivatives) and **2^** (^ = ethyltetramethylcyclopentadienyl derivatives) with less bulky boron heterocycles using lithium methyl as reagent. We report reactions of **2** with *tert*-butylisocyanide, dihydrogen, borane, and the dimer of bisethenerhodium chloride.



	a	b	c	d	e	f
R^1	Et	Et	Me	Et	Me	Me
R^2	Et	Et, *t*Bu	Me	Me	CH_2SiMe_3	Me
R^3	Me	Me	Me	Me	Me	Et

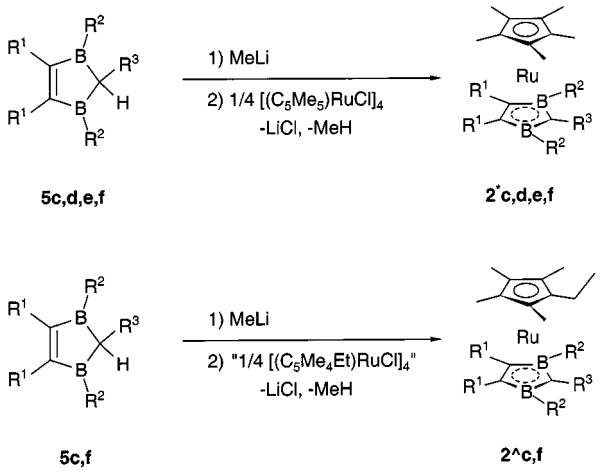
[a] Anorganisch-Chemisches Institut der Universität Heidelberg, Im Neuenheimer Feld 270, D-69120 Heidelberg, Germany
Fax: (internat.) +49 (0)6221/ 54-5609
E-mail: ci5@ix.urz.uni-heidelberg.de

 © WILEY-VCH Verlag GmbH, D-69451 Weinheim, 1999 1434−1948/99/1010−1685 $ 17.50+.50/0

Results and Discussion

Synthesis of Sandwich Complexes 2

The 2,3-dihydro-1,3-diborole derivatives **5c**−**f** are treated with LiMe at −55°C to form addition products, which react with $[(C_5Me_5)RuCl]_4$[7] to give the violet complexes **2*c**, **d**, **e**, and **f** (Scheme 1). In addition to the sandwich compounds **2*c** and **d**, small amounts of the triple-decker compounds **4*c** and **d** are formed, whereas when NaH instead of LiMe is used as base, only the triple-deckers **4*c** and **d** are obtained.[6] The synthesis of the derivatives **2^c** and **f** is achieved by reacting of the boron heterocycle **5c** or **5f** with MeLi and $[(C_5Me_4Et)RuCl]_n$[8] The latter is generated in situ by the reaction of $[(C_5Me_4Et)RuCl_2]_2$ with $[Li(Et_3BH)]$. Isolation and purification of the extremely air-sensitive complexes **2** is achieved by chromatography either on alumina at low temperature or on silica gel at room temperature.

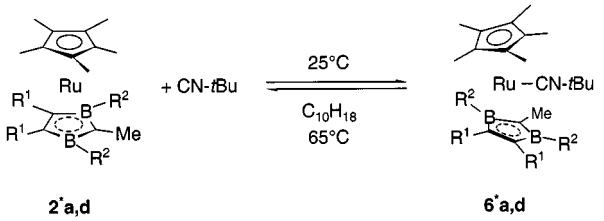


Scheme 1. Formation of complexes **2*** and **2^**

The air-sensitivity of the **2*** and **2** complexes increases with decreasing bulkiness of the ligands. Upon contact with air the color of the complexes changes, and yellow products are formed (see below). Most of the complexes **2*** and **2^** with bulky heterocycle ligands are oily liquids, except for **2*c**, **2*f**, and **2^c**, which are solids. The new compounds are characterized by MS and NMR. In the ^{13}C-NMR spectra, broad signals of the carbon atoms C2 are observed near $\delta = 190$. The following are the C2 shifts for the various complexes: **2*a** $\delta = 191.2$, **2*d** 190.6, **2^f** 190.1, **2^c** 185.8, and **2*c** 185.1. This low-field shift may be the result of a strong interaction between C2 and the ruthenium atom, as it is found in the sandwich **1** [the Fe−C2 distance is 1.899(6) Å, while the Fe−C3,4 distance is 2.116(3) Å][6].

Complexation of 2* with CN*t*Bu

The yellow carbonyl complexes **3*a** and **b** were obtained from the reaction of violet **2*a** and **b** with carbon monoxide.[6] Likewise, with the donor *tert*-butylisocyanide, the yellow complexes **6*a** and **d** are formed (Scheme 2) as crystalline products, which are difficult to purify, because they decompose on a column and during sublimation above 65°C. Their composition was deduced from spectroscopic data and X-ray structure analyses (see below). The ^{13}C-NMR signal for C2 of the isonitrile complex **6*a** appears at $\delta = 70.1$, which is in the range expected for 18 VE compounds. In the ^{11}B-NMR the complexes **6*a**, and **d** exhibit only one signal at $\delta = 29.6$ for **6*a** and 29.4 for **6*d**, whereas **3*b**[6] shows two signals at $\delta = 23.0$ and 36.6. The temperature-dependent ^{11}B-NMR spectra of **6*a** give a relatively sharp signal at 40°C, which gradually broadens at lower temperatures and disappears at −60°C. The ^{1}H- and ^{13}C-NMR spectra of **6*a** and **d** exhibit a double set of signals, which indicates that the isonitrile ligand is not symmetrically bonded with respect to the boron heterocycle, as it is observed for the CO ligand in **3*a** and **b**.[6]

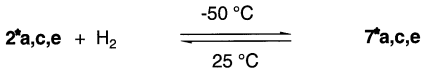


Scheme 2. Addition of CN-*t*Bu to **2*a,d**

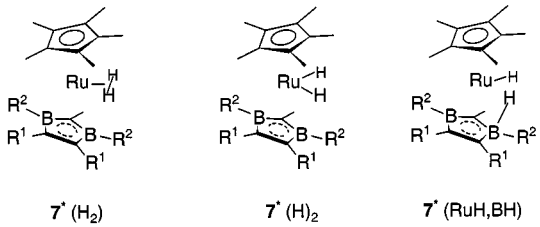
The reactions of CO and CN*t*Bu with **2*a** or **d** occur almost quantitatively. No interaction is observed between **2*** and amines (NH_3, isobutylamine), phosphanes (PEt_3, PPh_3), ethylene, or thiophene. There seems to be a weak interaction between THF and **2***, as indicated by ^{1}H- and ^{11}B-NMR spectra (see Experimental Section).

Oxidative Addition of H_2 to 2*

Addition of hydrogen to **2*a**, **c**, or **e** in hexane, tetrahydrofuran, or toluene, leads to the labile complexes **7*a**, **c**, and **e**, which could not be isolated. The color of the solution is violet at room temperature, but reversibly changes to yellow around −50°C. The weakly bonded hydrogen may be easily removed in vacuum. The complexes decompose after a few hours at room temperature, at −80°C they are stable for days. Three isomers for **7*a**, **c**, and **e** seem possible: the non-classic dihydrogen complex **7***(H_2), the classic dihydride complex **7***$(H)_2$, and the complex **7***(RuH,BH) with one hydrogen at the ruthenium and the other at the boron atom.



Scheme 3. Reaction of **2*** with hydrogen



The solution of the complexes **7*a**, **c**, and **e** have been studied by IR and NMR (^{1}H, ^{11}B, and ^{13}C). IR measurements at 20°C show one strong band after 8 scans: 2977 cm^{-1} for **7*a**, 2975 cm^{-1} for **7*c**, and 2979 cm^{-1} for **7*e**. Unfortunately, the complexes decomposed during the measurements. The ^{1}H-NMR spectra exhibit a high-field signal at $\delta = -12.49$ (**7*a**), -12.24 (**7*c**), and -11.91 (**7*e**), which is in the range for compounds with Ru−H or Ru(H_2) bonds [CpRu(CO)(PCy_3)(H_2)]$^+$: -7.91,[10] $RuH_2(H_2)_2(PCy_3)_2$: -9.1,[11] $Ru_2H_4(H_2)(PCy_3)_4$: -12.5,[11] ($\eta^5C_5Me_5$)Ru(μ-$H)_4$Ru($\eta^5C_5Me_5$): -13.99[12]). A temperature-dependent ^{1}H NMR of **7*c** furnished no information about what happened at −50°C, no shift of the high-field signal at $\delta = -12.24$ occurred (Figure 1).

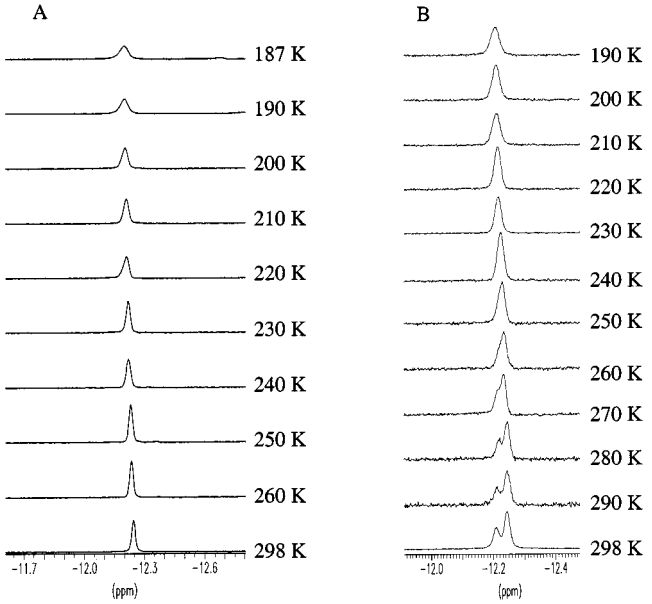


Figure 1. ^{1}H NMR (200.13 MHz, [D_8]THF) at various temperatures after the reaction of **2*c** and H_2 (A) respectively HD (B)

There are two ^{1}H NMR methods to differentiate between the three isomers **7***(H_2), **7***($H)_2$, and **7***(RuH, BH). The first method is the T_1 method, developed by R. H. Crabtree et al.[13] for distinguishing classic hydrides with terminal M−H bonds from non-classic hydrides with H−H as well as M−H bonds. T_1 is a function of the complex structure (dipole−dipole mechanism is the major contributor to this relaxation, a short H−H bond gives small T_1 values down to 3 ms[10]), the magnetic field power, and molecular motion. Molecular motion is dependant on both temperature and solvent, therefore T_1 is measured in dependence of the temperature and a search carried out for the minimum.[14] It is suggested that for $T_{1min} < 40$ ms (250 MHz) a non-classic structure is proposed, and for $T_{1min} > 100$ ms a classic structure is proposed, while values in between are not clearly determinable.[14] Complexes **7*a** and **e** should have small T_{1min} values for a classic and very small T_{1min} values for non-classic structures, because **7*** has a small moment of inertia. In our measurements of **7*a** and **e** no minimum was observed (Figure 2). Unfortunately, the T_1 values (**7*a** = 115 ms and **7*e** = 72) are in the range between a classic and a non-classic complex, therefore we cannot distinguish the two isomers 7*(H_2) and 7*($H)_2$ by this method.

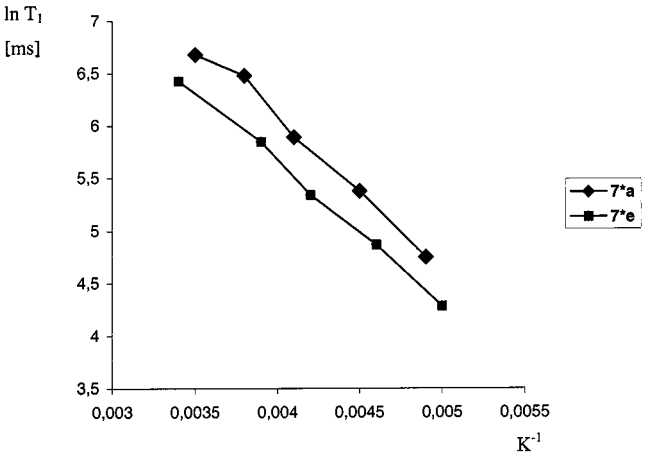


Figure 2. Plot of ln T_1 versus inverse temperature for **7*a**,**e** in [D_8]THF at 200.13 MHz

The second method used to differentiate between classic and non-classic complexes is the H/D exchange. The relationship between the H−D distance and the H−D coupling has been discussed.[15] No coupling is observed when **2*c** is treated with HD (Figure 3, **A**). From this we conclude that no H−D non-classic complex is present. Two signals in **A** of Figure 3 appear at $\delta = -12.21$ and -12.24 in a ratio 1: 1.7. The signal at $\delta = -12.24$ is the same as for **2*c** + H_2 (**C** in Figure 3). When H_2 is bubbled into a solution of **7*c**(HD), the signal at $\delta = -12.21$ decreases and disappears after 10 min (Figure 3).

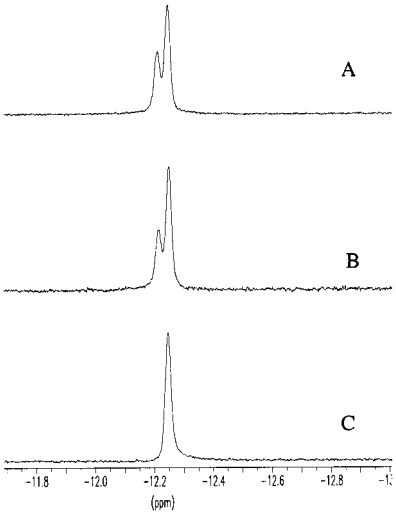


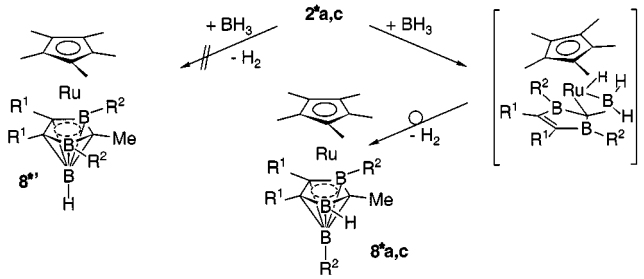
Figure 3. ^{1}H NMR (200.13 MHz, [D_8]THF) of **2*c**, treated with HD and H_2; **A** obtained by bubbling HD into the solution of **2*c**, **B** after H_2 is bubbled for 4 min through the solution of **A**, **C** after H_2 is bubbled for 10 min through the solution of **B**

The temperature-dependent ^{1}H NMR of **2*c** + HD shows that the two signals merge into one another around −50°C (Figure 1) which may parallel the change of the color from violet to yellow. At present we are unable to interpret the findings, in which the compounds **7***(H_2) and

7*(RuH,BH) may be involved. The color change at −50°C is agreement with an adduct formation, as it is observed when complexes **2*** react with a 2e donor such as CO and CN−R. Therefore, we assume that H_2 has added to **2*** to give **7***$(H)_2$ (dihydro complex).

Capping and Stacking Reactions of 2

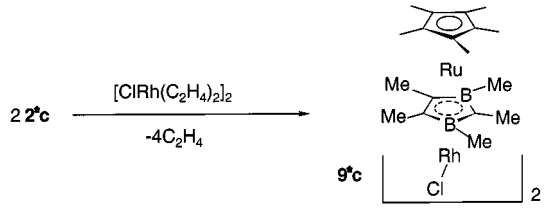
When BH_3·THF is added to **2*a**, or **c** in hexane, the color of the solution changes in a few minutes from violet to yellow, and the tricarbahexaboranyl complexes **8*a** or **8*c** are formed, based on MS, ^{1}H-, ^{11}B-, and ^{13}C-NMR spectra. The isomer **8***′ with BH in the apex position was not detected in the ^{11}B-NMR spectrum as indicated by the absence of a high-field doublet. Three ^{11}B-NMR signals of equal intensity (**8*a**: δ = −0.4, 3.9, 6.6, **8*c**: δ = 1.1, 2.3, 6.0) prove the formation of **8*a** and **8*c**.



Scheme 4. Reaction of **2*a,c** with BH_3

We propose the following mechanism: In the first step an oxidative addition of BH_3 at the ruthenium occurs, followed by the elimination of H_2 to give a transient boranediyl complex, which rearranges with migration of one B−R^2 group into the apex position. Simultaneously, the B−H unit moves into the empty ring position to yield the ruthenacarboranes **8*a** and **c**. According to the cluster rules[16] **8*** has 16 framework electrons and 7 cluster atoms expected for a *closo* structure. Alternatively, **8*** may be described as an 18 VE complex in which the (neutral) 2,3,5-tricarbahexaboranyl ligand supplies 5e for bonding to the metal.[17][18]

When **2*c** is reacted with $[ClRh(C_2H_4)_2]_2$ the diamagnetic tetranuclear complex **9*c** with 56 VE is obtained in 30% yield. The MS and NMR data support the proposed structure of **9*c**, which may be viewed as a pentadecker complex having two bridging chlorine atoms in the central position. It is comparable with the tetranuclear $\{(C_5H_5)Ni[(EtC)_2(BEt)_2CMe]Co(CO)\}_2$ complex having 58 VE.[19]



Scheme 5. Formation of tetranuclear complex **9*c**

Crystal Structures of 6*a, d

The structures of **6*a** and **d** are similar to that of the CO complex **3*b**. The isonitrile group is bonded to the ruthenium, causing a tilt of the Cp* and the 1,3-diborolyl ligands. The best planes through Cp* and 1,3-diborolyl form an angle of 28.6°. The isonitrile is located near one boron atom. The distance B1−C15 is relatively short (2.42 Å) as observed in the CO complex **3*b** (2.41 Å for B1−C17). This weak interaction causes a deviation from linearity of Ru−C≡N*t*Bu (∠ RuCN = 169°), which increases slightly in **3*b** (∠ RuCO = 167°). The 1,3-diborolyl ligand is not planar, but it is less folded along the B1−B3 vector by 16.2° (in **3*a** 19.0°) compared with 41.3° in **1**. The Ru−B distances are significantly larger than those to C, all are in the expected range.

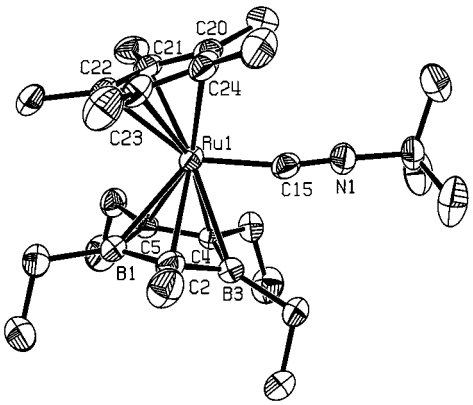


Figure 4. Molecular structure of **6*a** in the crystal

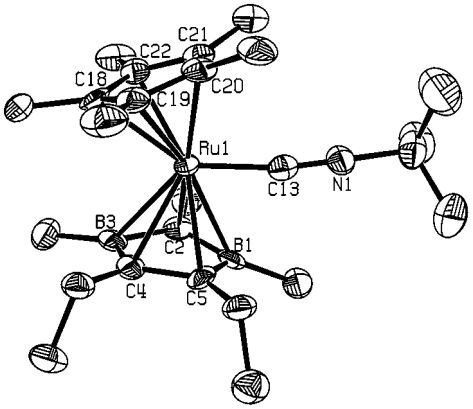


Figure 5. Molecular structure of **6*d** in the crystal

Conclusions

In contrast with our earlier findings,[6] sandwich complexes **2c−f** with less bulky groups may be obtained at low temperature using LiMe instead of NaH as reagent. The electron-poor 18 VE complexes **2*a,** and **c** react with donor ligands such as CO and $CNCMe_3$ to form donor-acceptor compounds, with different stability: CO >> $CNCMe_3$ > H_2 > THF. The complexes **2*a** and **c** activate the B−H bonds

Table 1. Some selected distances [Å] and angles [°] in **6*a**, **d**

Compound	**6*a**	**6*d**
Ru−C(Cp*)	2.215−2.266(2)	2.21−2.27(1)
Ru−C2	2.284(3)	2.29(1)
Ru−C4	2.293(2)	2.33(1)
Ru−C5	2.296(3)	2.27(2)
Ru−B1	2.422(3)	2.40(2)
Ru−B3	2.434(3)	2.44(1)
Ru−C15(C13)	1.944(3)	1.94(1)
B1−C2	1.523(4)	1.51(2)
B3−C2	1.531(3)	1.57(2)
B1−C5	1.559(4)	1.56(2)
B3−C4	1.576(3)	1.54(2)
C4−C5	1.423(3)	1.42(2)
C15(C13)−B1	2.419(3)	2.417(2)
B1−C2−B3	107.4(2)	109.0(13)
C2−B3−C4	105.6(2)	104.0(12)
C2−B1−C5	105.6(2)	104.6(13)
B3−C4−C5	108.6(2)	111(2)
B1−C5−C4	110.1(2)	108.6(13)
Ru−C15(C13)−N1	168.9(2)	168.6(13)
*t*Bu−N1−C15(C13)	170.5(2)	165(2)
γ[a]	28.59(11)	27.5; 29.0(4)
φ[b]	16.7(2)	14.0; 17.1(8)

[a] γ = Angle between the planes C20C21C22C23C24 and B1C5C4B3. − [b] φ = Folding angle between the planes B1B3C4C5 and C2B1B3.

of BH_3 to give with elimination of hydrogen the ruthenacarborane complexes **8*a** and **c**. Reaction of **2*c** $[ClRh(C_2H_4)_2]_2$ leads to the Cl-bridged pentadecker **9*c**

Experimental Section

General: Experiments were carried out under nitrogen or argon, which had been dried and purified before use. Solvents were dried by conventional methods and saturated with nitrogen. − NMR spectra were recorded on Bruker AC-200 (^{1}H: 200.13 MHz, ^{13}C: 50.32 MHz, ^{11}B: 64.21 MHz) and Bruker AC-500 (^{1}H: 500.13 MHz, ^{13}C: 125.76 MHz) in C_6D_6 as solvent. Chemical shifts are relative to that of TMS and $BF_3{\cdot}OEt_2$. − The mass spectra were recorded on Varian MAT CH7, Finnigan MAT 8230, and JEOL. The MS Station JMS 700 (reference for HRMS is perflourated Kerosin). GC mass spectra were recorded on HP-5890 II gas chromatograph with HP-5971 MSD (column HP-3, 12.5m × 0.25 mm × 0.25 μm). − IR spectra were measured on Bruker IFS 28. Neutral alumina or silica gel used for chromatography had been dried and alumina deactivated by addition of 5% water.

2-Ethyl-1,3-diiodo-4,5-dimethyl-2,3-dihydro-1,3-diborole: 2-Butyne (3.24 g, 60 mmol) was slowly added to a solution of 1,1-bisdiiodoborylpropane (33 g, 60 mmol) in 30 mL of pentane at 0°C. The reaction mixture was allowed to warm to 20°C, stirred for 1 h and then the solvent and iodine were removed in vacuum. 2-Ethyl-1,3-diiodo-4,5-dimethyl-2,3-dihydro-1,3-diborole was isolated by distillation as lightly yellow liquid. Yield 18 g (81%) − b. p. 67°C/10^{-3} Torr. − ^{1}H NMR (200.13 MHz, C_6D_6): δ = 1.00 (br, 1 H, B_2CHCH_2), 1.15 (t, 3 H, $^3J_{HH}$ = 7.4 Hz, CH_2CH_3), 1.72 (s, 6 H, = CCH_3), 1.89 (m, 2 H, $CHCH_2CH_3$). − ^{13}C NMR (50.32 MHz, C_6D_6): δ = 15.6 (=CCH_3), 16.9 (CH_2CH_3), 23.2 ($CHCH_2CH_3$), 52.7 (B_2CHCH_2, br), 175.0 (=CCH_3, br). − ^{11}B NMR (64.21 MHz, C_6D_6): δ = 64.8.

2-Ethyl-1,3,4,5-tetramethyl-2,3-dihydro-1,3-diborole (5d): 2-Ethyl-1,3-diiodo-4,5-dimethyl-2,3-dihydro-1,3-diborole (21.5 g, 58 mmol) was dissolved in 40 mL of pentane and cooled to −5°C. 2.78 g (39 mmol) of $AlMe_3$ in 20 mL of pentane were added dropwise within 30 min. After warming to room temp. and stirring over night the solvent was removed in vacuum (80 Torr), and colorless **5d** was distilled. Yield: 6.9 g (79%). − b. p. 20°C/10^{-3} Torr. − ^{1}H NMR (200.13 MHz, C_6D_6): δ = 1.69 (s, 6 H, BCH_3), 2.07 (t, 3 H, $^3J_{HH}$ = 7.1 Hz, CH_2CH_3), 2.42 (t, 1 H, $^3J_{HH}$ = 5.9 Hz, B_2CHCH_2), 2.67 (m, 2 H, $CHCH_2CH_3$), 2.78 (s, 6 H, CCH_3). − ^{13}C NMR (50.32 MHz, C_6D_6): δ = 4.3 (BCH_3, br), 14.3 (=CCH_3), 16.9 (CH_2CH_3), 19.9 ($CHCH_2CH_3$), 51.6 (B_2CHCH_2, br), 173.0 (=CCH_3, br). − ^{11}B NMR (64.21 MHz, C_6D_6): δ = 69.6. − GC-MS: retention time: 2.28 min. − *m/z* (%) = 148 [M^+] (35), 133 [$M^+ - CH_3$] (34), 117 [$M^+ - CH_3, - CH_4$] (33), 41 [$C_3H_5^+$] (100).

2,4,5-Trimethyl-1,3-bis(trimethylsilylmethylene)-2,3-dihydro-1,3-diborole (5e): $LiCH_2SiMe_3$ (40 mL, 1 M in pentane) was added dropwise to a solution of 7.16 g (20 mmol) of 1,3-diiodo-2,4,5-trimethyl-2,3-dihydro-1,3-diborole in 40 mL of pentane at 0°C. The yellow reaction mixture became colorless and a white solid precipitated. After warming to room temp. and stirring over night the precipitate was filtered. The solvent was removed in vacuum (50 Torr) and colorless **5e** was distilled. Yield: 3.5 g (63%). − b. p. 49°C/10^{-3} Torr. − ^{1}H NMR (200.13 MHz, C_6D_6): δ = 0.09 [s, 18, $Si(CH_3)_3$], 1.01 (d, 2 H, $^2J_{HH}$ = 9.5 Hz, BCH_2Si), 1.15 (d, 2 H, $^2J_{HH}$ = 9.5 Hz, BCH_2Si), 1.27 (d, 3 H, $^3J_{HH}$ = 5.2 Hz, $CHCH_3$), 1.32 (q, 1 H, $^3J_{HH}$ = 5.2 Hz, B_2CHCH_3), 1.88 (s, 6 H, =CCH_3). − ^{13}C NMR (50.32 MHz, C_6D_6): δ = 2.4 [$Si(CH_3)_3$], 12.2 (=CCH_3), 15.5 (BCH_2Si, br), 15.9 ($CHCH_3$), 39.2 (B_2CHCH_3, br), 172.0 (=CCH_3, br). − ^{11}B NMR (64.21 MHz, C_6D_6): δ = 68.8. − MS (EI): *m/z* (%) = 278 [M^+] (16), 263 [$M^+ - CH_3$] (7), 190 [$M^+ - CH_2SiMe_3$] (9), 73 [Me_3Si^+] (100). − HRMS calcd. for $C_{14}H_{32}B_2Si_2$: 278.2229, found: 278.2231, Δ*m* = 0.2 mmu.

(η^5-Pentamethyl-2,3-dihydro-1,3-diborolyl)(η^5-pentamethylcyclopentadienyl)ruthenium (2*c): 1.38 mL (2.2 mmol) of 1.6 M LiMe were added dropwise to a solution of 256 mg (2.2 mmol) of **5c** in THF (35 mL) at −55°C. The reaction mixture was allowed to stir for 15 min and then transferred via canula to a flask containing 600 mg (0.55 mmol) of $[Cp^*RuCl]_4$ in 40 mL of THF, cooled to −55°C. After stirring for 12 h the solvent was removed in vacuum. The violet residue was dissolved in 5 mL of hexane and purified by chromatography, either on Al_2O_3 at −20°C or on silica gel at room temp. using hexane as eluant. **2*c** was isolated as a dark violet solid. Yield: 380 mg (47%). − m.p. 138°C (decomp.). − ^{1}H NMR (200.13 MHz, C_6D_6): δ = 0.21 (s, 6 H, BCH_3), 1.46 (s, 15 H, $C_5(CH_3)_5$), 2.23 (s, 6 H, =CCH_3), 2.83 (s, 3 H, B_2CCH_3). − ^{13}C NMR (50.32 MHz, C_6D_6): δ = −1.8 (BCH_3, br), 10.6 [$C_5(CH_3)_5$], 16.4 (=CCH_3), 20.9 (B_2CCH_3), 83.8 [$C_5(CH_3)_5$], 118.8 (=CCH_3, br), 185.8 (B_2CCH_3, br) − ^{11}B NMR (64.21 MHz, C_6D_6): δ = 20.6−^{1}H NMR (200.13 MHz, [D$_8$]THF): δ = −0.01 (s, 6 H, BCH_3), 1.61 [s, 15 H, $C_5(CH_3)_5$], 2.25 (s, 6 H, =CCH_3), 2.59 (s, 3 H, B_2CCH_3). − ^{13}C NMR (50.32 MHz, [D$_8$]THF): δ = 11.1 [$C_5(CH_3)_5$], 16.8 (=CCH_3), 20.8 (B_2CCH_3), 84.8 [$C_5(CH_3)_5$], = CCH_3 and B_2CCH_3 not observed. − ^{11}B NMR (64.21 MHz, [D$_8$]THF): δ = 22.6. − MS (EI): *m/z* (%) = 370 [M^+] (88), 351 [$M^+ - CH_3, - 4$ H] (100), 336 [$M^+ - 2\ CH_3, - 4$ H] (74), 301 [$M^+ - C_3H_8, - BCH_3$] (77), 233 [$Cp^*Ru^+ - 4$ H] (77), 41 [$C_3H_5^+$] (89). − HRMS calcd. for $C_{18}H_{30}B_2Ru$: 370.1571, found 370.1563, Δ*m* = 0.8 mmu.

(η^5-4,5-Diethyl-1,2,3-trimethyl-2,3-dihydro-1,3-diborolyl)(η^5-pentamethylcyclopentadienyl)ruthenium (2*d): Same procedure as for **2*c**. The product, **2*d** was obtained from **5d** (162 mg, 1 mmol), LiMe (0.63 mL, 1 mmol) and $[Cp^*RuCl]_4$ (274 mg, 0.25 mmol) as a dark violet oil. Yield: 147 mg (37%). − b. p. 75°C/10^{-3} Torr. −

^{1}H NMR: δ = 0.26 (s, 6 H, BCH_3), 1.32 (t, 6 H, $^3J_{HH}$ = 7.5 Hz, = CCH_2CH_3), 1.45 [s, 15 H, $C_5(CH_3)_5$], 2.4 (m, 4 H, =CCH_2CH_3), 2.8 (s, 3 H, CCH_3), 3.15 (m, 4 H, =CCH_2CH_3). − ^{13}C NMR: δ = −0.5 (BCH_3, br), 11.7 [$C_5(CH_3)_5$], 15.1 (=CCH_2CH_3), 22.0 (B_2CCH_3), 26.3 (=CCH_2CH_3), 85.1 [$C_5(CH_3)_5$], 123.6 (=CCH_2CH_3, br), 190.6 (B_2CCH_3, br). − ^{11}B NMR: δ = 21. − MS (EI): *m/z* (%) = 397 [M^+ −H] (100), 383 [M^+ − CH_3] (98), 368 [M^+ − C_2H_6] (24), 353 [M^+ − 3 CH_3] (26), 235 [Cp*Ru^+ − H] (60). − HRMS calcd. for $C_{20}H_{34}B_2Ru$: 398.1890, found 398.1889, Δ*m* = 0.1 mmu.

[η^5-2,4,5-Trimethyl-1,3-bis(trimethylsilylmethylene)-2,3-dihydro-1,3-diborolyl](η^5-pentamethylcyclopentadienyl)ruthenium (2*e): Same procedure as for **2*c**. The product, **2*e** was obtained from **5e** (444.6 mg, 1.6 mmol), LiMe (1 mL, 1.6 mmol), and [Cp*RuCl]$_4$ (435 mg, 0.4 mmol) as a dark violet oil. Yield: 334 mg (41%). − b. p. 85°C/10−^{3} Torr. − ^{1}H NMR (200.13 MHz, C_6D_6): δ = 0.01 [s, 18 H. $Si(CH_3)_3$], 0.09 (d, 2 H, $^2J_{HH}$ = 15 Hz, BCH_2Si), 0.43 (d, 2 H, $^2J_{HH}$ = 15 Hz, BCH_2Si), 1.48 [s, 15 H, $C_5(CH_3)_5$], 2.23 (s, 6 H, =CCH_3), 2.74 (s, 3 H, B_2CCH_3). − ^{13}C NMR (50.32 MHz, C_6D_6): δ = 1.2 [$Si(CH_3)_3$], 5.7 [B$CH_2Si(CH_3)_3$, br], 10.7 [$C_5(CH_3)_5$], 16.7 (=CCH_3), 22.1 (B_2CCH_3), 83.4 [$C_5(CH_3)_5$], 118.8 (=CCH_3, br), B_2CCH_3 not observed. − ^{11}B NMR (64.21 MHz, C_6D_6): δ = 21.7. − MS (EI): *m/z* (%) = 514 [M^+] (4), 426 [M^+ − $Si(CH_3)_3$, − CH_3] (4), 233 [Cp*Ru^+ − 4 H] (5), 73 [Me_3Si^+] (100). − HRMS calcd. for $C_{24}H_{46}B_2RuSi_2$: 514.2361, found 514.2357, Δ*m* = 0.4 mmu.

(η^5-2-Ethyl-1,3,4,5-tetramethyl-2,3-dihydro-1,3-diborolyl)(η^5-pentamethylcyclopentadienyl)ruthenium (2*f): Same procedure as for **2*c**. The product, **2*f** was obtained from **5f** (326 mg, 2.2 mmol), LiMe (1.38 mL, 2.2 mmol) and [Cp*RuCl]$_4$ (590 mg, 0.55 mmol) as a dark violet solid. Yield: 160 mg (19%). − m.p. 148°C (decomp.). − ^{1}H NMR (200.13 MHz, C_6D_6): δ = 0.25 (s, 6 H, BCH_3), 1.45 (s, 15 H, C_5CH_3), 1.66 (t, 3 H, $^3J_{HH}$ = 7.6 Hz, $B_2CCH_2CH_3$), 2.20 (s, 6 H, =CCH_3), 3.20 (q, 2 H, $^3J_{HH}$ = 7.6 Hz, $B_2CCH_2CH_3$). − ^{13}C NMR (50.32 MHz, C_6D_6): δ = −1.6 (BCH_3, br), 10.9 [$C_5(CH_3)_5$], 16.4 (=CCH_3), 16.8 ($B_2CCH_2CH_3$), 29.7 ($B_2CCH_2CH_3$), 83.8 [$C_5(CH_3)_5$], 118.4 (=CCH_3, br), $B_2CCH_2CH_3$ not observed. − ^{11}B NMR (64.21 MHz, C_6D_6): δ = 21.5. − MS (EI): *m/z* (%) = 384 [M^+] (40), 368 [M^+ − CH_4] (100), 232 [Cp*Ru^+ − 5 H] (15). − HRMS calcd. for $C_{19}H_{32}B_2Ru$: 384.1727, found 384.1723, Δ*m* = 0.4 mmu.

(η^5-Pentamethyl-2,3-dihydro-1,3-diborolyl)(η^5-1-ethyl-2,3,4,5-tetramethylcyclopentadienyl)ruthenium (2^c): Li(Et_3BH) (1.14 mL, 1 M in THF) was added dropwise to a suspension of (Cp^ $RuCl_2$)$_2$ (365 mg, 0.57 mmol) in 40 mL of THF and then stirred for 45 min. In another flask with a cooled solution (−55°C) of **5c** (189 mg, 1.27 mmol) in 40 mL of THF 1.38 mL (2.2 mmol) of 1.6 M LiMe were added dropwise and allowed to stir for 15 min at −55°C. Subsequently the reaction mixture was transferred via canula to the likewise cooled flask of the ruthenium reaction. After stirring for 12 h the solvent was removed in vacuum. The violet residue was dissolved in 5 mL of hexane and purified by chromatography, either on Al_2O_3 at −20°C or on silica gel at room temp. using hexane as eluant. **2^c** was isolated as a dark violet solid. Yield: 88 mg (20%) − m.p. 145°C (decomp.). − ^{1}H NMR (200.13 MHz, C_6D_6): δ = 0.21 (s, 6 H, BCH_3), 0.84 (t, 3 H, $^3J_{HH}$ = 7.6 Hz, $C_5CH_2CH_3$), 1.43 [s, 6 H, $C_5(CH_3)_4$], 1.50 [s, 6 H, $C_5(CH_3)_4$], 1.89 (q, 2 H, $^3J_{HH}$ = 7.6 Hz, $C_5CH_2CH_3$), 2.23 (s, 6 H, =CCH_3), 2.83 (s, 3 H, B_2CCH_3). − ^{13}C NMR (50.32 MHz, C_6D_6): δ = −2.2 (BCH_3, br), 10.4 and 10.6 [$C_5(CH_3)_4$], 14.8 ($C_5CH_2CH_3$), 16.4 (=CCH_3), 19.1 ($C_5CH_2CH_3$), 21.0 (B_2CCH_3), 83.3, 83.9, and 89,8 ($C_5(CH_3)_4Et$), 118.9 (=CCH_3, br), 185.8 (B_2CCH_3, br). − ^{11}B NMR (64.21 MHz, C_6D_6): δ = 20.7. − MS (EI): *m/z* (%) = 384 [M^+] (39), 243 [Cp Ru^+ − 7 H] (100), 41 [$C_3H_3^+$] (35). − HRMS calcd. for $C_{19}H_{32}B_2Ru$: 384.1727, found 384.1703, Δ*m* = 2.4 mmu.

(η^5-2-Ethyl-1,3,4,5-tetramethyl-2,3-dihydro-1,3-diborolyl)(η^5-1-ethyl-2,3,4,5-tetramethyl cyclopentadienyl)ruthenium (2^f): Same procedure as for **2^c**. The product, **2^f** was obtained from **5f** (250 mg, 1.7 mmol), LiMe (1.06 mL, 1.7 mmol) and [Cp^ $RuCl_2$]$_2$ (543 mg, 0.85 mmol), treated with 1.7 mL (1.7 mmol) of 1 M Li(Et_3BH) as a dark violet oil. Yield: 188 mg (27%). − b.p. 85°C/10^{-3} Torr. − ^{1}H NMR (200.13 MHz, C_6D_6): δ = 0.25 (s, 6 H, BCH_3), 0.83 (t, 3 H, $^3J_{HH}$ = 7.4 Hz, $C_5CH_2CH_3$), 1.44 [s, 6 H, $C_5(CH_3)_4$], 1.49 [s, 6 H, $C_5(CH_3)_4$], 1.65 (t, 3 H, $^3J_{HH}$ = 7.6 Hz, $B_2CCH_2CH_3$), 1.90 (q, 2 H, $^3J_{HH}$ = 7.4 Hz, $C_5CH_2CH_3$), 2.20 (s, 6 H, =CCH_3), 3.21 (q, 2 H, $^3J_{HH}$ = 7.6 Hz, $B_2CCH_2CH_3$). − ^{13}C NMR (50.32 MHz, C_6D_6): δ = −1.2 (BCH_3, br), 10.8 [$C_5(CH_3)_4$], 10.5 [$C_5(CH_3)_4$], 16.4 (=CCH_3), 16.8 ($B_2CCH_2CH_3$), 14.8 ($C_5CH_2CH_3$), 19.1 ($C_5CH_2CH_3$), 29.8 ($B_2CCH_2CH_3$), 83.3, 84.0, and 89.5 [$C_5(CH_3)_4Et$], 118.6 (=CCH_3, br), 190.1 (B_2CCH_2, br). − ^{11}B NMR (64.21 MHz, C_6D_6): δ = 21.8. − MS (EI): *m/z* (%) = 398 [M^+] (52), 382 [M^+ − CH_4] (100), 368 [M^+ − C_2H_6] (22), 243 [Cp Ru^+ − 8 H] (12), 149 [Cp $^+$] (77), 41 [$C_3H_5^+$] (28). − HRMS cald. for $C_{20}H_{34}B_2Ru$: 398.1890, found 398.1881, Δ*m* = 0.9 mmu.

(η^5-1,3,4,5-Tetraethyl-2-methyl-2,3-dihydro-1,3-diborolyl)(η^5-pentamethylcyclopentadienyl)ruthenium *tert*-Butylisocyanide (6*a): Compound **2*a** (100 mg, 0.24 mmol) was dissolved in hexane (15 mL) and CNC_4H_9 (19.5 mg, 24 mmol) was added dropwise. The color changed immediately from violet to yellow. After partial removal of the solvent in vacuum **6*a** crystallized at −20°C. Yield: 80 mg (66%) − m.p. 75°C (diss. to the starting materials). − ^{1}H NMR (200.13 MHz, C_6D_6): δ = 1.17 (t, 3 H, $^3J_{HH}$ = 7.3 Hz, = CCH_2CH_3), 1.24 [s, 9 H, $CNC(CH_3)_3$], 1.34 (t, 3 H, $^3J_{HH}$ = 7.3 Hz, =CCH_2CH_3), 1.38−1.49 (m, 10 H, BCH_2CH_3), 1.51 (s, 3 H, B_2CCH_3), 1.55 [s, 15 H, $C_5(CH_3)_5$], 1.83−2.22 (m, 4 H, = CCH_2CH_3). − ^{13}C NMR (50.32 MHz, C_6D_6): δ = 6.8 (BCH_2CH_3, br), 9.6 [$C_5(CH_3)_5$], 10.5 (BCH_2CH_3, br), 12.2 and 12.9 (BCH_2CH_3), 15.6 (B_2CCH_3), 17.2 and 17.6 (=CCH_2CH_3), 21.5 and 22.6 (=CCH_2CH_3), 31.5 [$CNC(CH_3)_3$], 56.4 [$CNC(CH_3)_3$], 67.5 (B_2CCH_3, br), 90.8 [$C_5(CH_3)_5$], 102.6 and 121.7 (=CCH_2CH_3, br), 166.5 [$CNC(CH_3)_3$]. − ^{11}B NMR (64.21 MHz, C_6D_6): δ = 29.6. − MS (EI): *m/z* (%) = 509 [M^+] (44), 425 [M^+ − $CNC(CH_3)_3$] (53), 396 [M^+ − C_2H_5, − $CNC(CH_3)_3$] (100), 367 [M^+ − 2 C_2H_5, − $CNC(CH_3)_3$] (30), 236 [Cp*Ru^+ − H] (15), 57 [$C_4H_9^+$] (40). − HRMS calcd. for $C_{27}H_{47}B_2NRu$: 509.2938, found 509.2953, Δm = 1.5 mmu. − FT-IR (hexane): $\tilde{\nu}_{CN}$ = 2048 cm^{-1}, 2088 cm^{-1} (weak).

(η^5-4,5-Diethyl-1,2,3-trimethyl-2,3-dihydro-1,3-diborolyl)(η^5-pentamethylcyclopentadienyl)ruthenium *tert*-Butylisocyanide (6*d): Same procedure as for **6*a**. The product, **6*d** was obtained from **2*d** (95.5 mg, 0.24 mmol) in 15 mL of hexane and 19 mg (0.24 mmol) of $CNC(CH_3)_3$ as yellow crystals. Yield: 76.3 mg (66%) − m.p. 65°C (diss. to the starting materials). − ^{1}H NMR (200.13 MHz, C_6D_6): δ = 0.80 (s, 3 H, BCH_3), 0.84 (s, 3 H, BCH_3), 1.16 (t, 3 H, $^3J_{HH}$ = 7.5 Hz, =CCH_2CH_3), 1.25 [s, 9 H, $CNC(CH_3)_3$], 1.30 (t, 3 H, $^3J_{HH}$ = 7.5 Hz, =CCH_2H_3), 1.47 (s, 3 H, B_2CCH_3), 1.55 [s, 15 H, $C_5(CH_3)_5$], 1.85−2.19 (m, 4 H, = CCH_2CH_3). − ^{13}C NMR (50.32 MHz, C_6D_6): δ = −1.6 (BCH_3, br), 1.9 (BCH_3, br), 10.5 [$C_5(CH_3)_5$], 16.4 (B_2CCH_3), 17.7 (= CCH_2CH_3), 18.4 (=CCH_2CH_3), 22.3 (=CCH_2CH_3), 23.5 (= CCH_2CH_3), 32.5 [$CNC(CH_3)_3$], 57.0 [$CNC(CH_3)_3$], 70.1 (B_2CCH_3, br), 91.6 [$C_5(CH_3)_5$], 109.8 (=CCH_2CH_3, br), 121.9 (=CCH_2CH_3, br), 164.4 [$CNC(CH_3)_3$]. − ^{11}B NMR (64.21 MHz, C_6D_6): δ = 29.4 − MS (EI): *m/z* (%) = 481 [M^+] (40), 397 [M^+ − H, − CN*t*Bu]

(30), 382 [$M^+ - H, - CNtBu, - CH_3$] (100). – HRMS calcd. for $C_{25}H_{43}B_2NRu$: 481.2625, found 481.2650, Δm = 2.5 mmu. – FT-IR (hexane): $\tilde{\nu}_{CN}$ = 2084 cm^{-1}, 2031 cm^{-1} (weak).

(η⁵-1,3,4,5-Tetraethyl-2-methyl-2,3-dihydro-1,3-diborolyl)(η⁵-pentamethylcyclopentadienyl)ruthenium Dihydride (7*a): Complex **2*a** (50 mg, 0.12 mmol) was dissolved in 20 mL of hexane, and H_2 gas was bubbled through the solution for 4 min at a flow rate of 10 mLmin^{-1}. The color changed reversibly at −50°C from violet to yellow. For NMR studies, the deuterated solvents were used instead of hexane. – ^{1}H NMR (200.13 MHz, C_6D_6): δ = −12.49 (s, 2 H, Ru−H), 1.21−1.35 (m, 10 H, BCH_2CH_3), 1.43 (t, 6 H, $^3J_{HH}$ = 8.3 Hz, =CCH$_2$CH_3), 1.53 [s, 15 H, C$_5$(CH$_3$)$_5$], 1.66 (s, 3H, B$_2$CCH$_3$), 1.93 and 2.14 (m, 2H, =CCH_2CH$_3$). – ^{13}C NMR (50.32 MHz, C_6D_6): δ = 5.1 (BCH$_2$CH$_3$, br), 9.7 (BCH$_2$CH$_3$), 10.5 [C$_5$(CH$_3$)$_5$], 13.7 (=CCH$_2$CH$_3$), 22.2 (=CCH$_2$CH$_3$), 30.2 (B$_2$CCH$_3$), 94.6 [C$_5$(CH$_3$)$_5$], 114 (=CCH$_2$CH$_3$, br), B$_2$CCH$_3$ not observed. – ^{11}B NMR (64.21 MHz, C_6D_6): δ = 20.1.

(η⁵-1,2,3,4,5-Pentamethyl-2,3-dihydro-1,3-diborolyl)(η⁵-pentamethylcyclopentadienyl)ruthenium Dihydride (7*c): Same procedure as for **7*a**. The product, **7*c** was formed as a yellow solution from **2*c** (40 mg, 0.11 mmol) in 20 mL of hexane and H_2 gas (10 mLmin^{-1}) at −50°C. – ^{1}H NMR (200.13 MHz, [D$_8$]THF): δ = 0.40 (s, 6 H, BCH$_3$), 1.85 [s, 15 H, C$_5$(CH$_3$)$_5$], 1.62 (s, 6 H, =C−CH$_3$), 1.19 (s, 3 H, B$_2$CCH$_3$), −12.25 (s, 2 H, Ru−H). – ^{13}C NMR (50.32 MHz, [D$_8$]THF): δ = −4.9 (BCH$_3$, br), 10.9 [C$_5$(CH$_3$)$_5$], 14.7 (=CCH$_3$), 31.2 (B$_2$CCH$_3$), 96.7 [C$_5$(CH$_3$)$_5$], =CCH$_3$ and B$_2$CCH$_3$ not observed. – ^{11}B NMR (64.21 MHz, [D$_8$]-THF): δ = 22.9.

(η⁵-1,2,3,4,5-Pentamethyl-2,3-dihydro-1,3-diborolyl)(η⁵-pentamethylcyclopentadienyl)ruthenium Hydride Deuteride [7*c(HD)]: It was obtained from **2*c** (40 mg, 0.11 mmol) in 0.6 mL of [D$_8$]THF and HD gas (10 mLmin^{-1} for 4 min) as a yellow solution at −50°C. – ^{1}H NMR (200.13 MHz, [D$_8$]THF): δ = 0.40 (s, 6 H, BCH$_3$), 1.85 [s, 15 H, C$_5$(CH$_3$)$_5$], 1.63 (s, 6 H, =CCH$_3$), 1.18 (s, 3 H, B$_2$CCH$_3$), −12.21 and −12.24 (s, 1 H, Ru−H). – ^{11}B NMR (64.21 MHz, [D$_8$]THF): δ = 22.8.

[η⁵-2,4,5-Trimethyl-1,3-bis(trimethylsilylmethylene)-2,3-dihydro-1,3-diborolyl](η⁵-pentamethylcyclopentadienyl)ruthenium Dihydride (7*e): Same procedure as for **7*a**. The product, **7*e** was obtained as a yellow solution from **2*e** (50 mg, 0.1 mmol) in 20 mL of hexane and H_2 gas (10 mLmin^{-1}) at −50°C. – ^{1}H NMR (200.13 MHz, C_6D_6): δ = −11.91 (s, 2 H, Ru−H), 0.25 [s, 18 H, Si(CH$_3$)$_3$], 0.64 (d, 2 H, $^2J_{HH}$ = 3.1 Hz, BCH$_2$Si), 0.83 (d, 2 H, $^2J_{HH}$ = 3.1 Hz, BCH$_2$Si), 1.42 (s, 3 H, B$_2$CCH$_3$), 1.53 (s, 15 H, C$_5$(CH$_3$)$_5$), 1.76 (s, 6 H, =CCH$_3$). – ^{13}C NMR (50.32 MHz, C_6D_6): δ = 1.5 [Si(CH$_3$)$_3$], 10.3 [C$_5$(CH$_3$)$_5$], 16.5 (=CCH$_3$), 23.0 (B$_2$CCH$_3$), 96.0 [C$_5$(CH$_3$)$_5$], =CCH$_3$ and B$_2$CCH$_3$ not observed. – ^{11}B NMR (64.21 MHz, C_6D_6): δ = 22.5.

(1,2,3,6-Tetraethyl-5-methyl-4-hydrido-2,3,5-tricarbahexaboranyl)-(η⁵-pentamethylcyclopentadienyl)ruthenium (8*a): BH_3 in THF (0.24 mL, 1 M, 0.24 mmol) was added dropwise to a solution of **2*a** (100 mg, 0.24 mmol) in 40 mL of hexane at room temp. After the yellow reaction mixture had been stirred for 15 min, the solvents were removed in vacuum and the yellow solid was sublimed. Yield: 30 mg (29%). – m.p. 130°C. – ^{1}H NMR (500.13 MHz, C_6D_6): 0.07 (m, 1 H, BCH_2CH$_3$), 0.20 (m, 1 H, BCH_2CH$_3$), 0.83 (t, 3 H, $^3J_{HH}$ = 7.9 Hz, BCH$_2$CH_3), 1.02 (t, 3 H, $^3J_{HH}$ = 7.6 Hz, CCH$_2$CH_3), 1.23−1.34 (m, 5 H, BCH_2CH_3), 1.36 (t, 3 H, $^3J_{HH}$ = 7.5 Hz, CCH$_2$CH_3), 1.64 (s, 3 H, B$_2$CCH$_3$), 1.73 [s, 15 H, C$_5$(CH$_3$)$_5$], 1.75−1.89 (m, 3 H, CH_2CH$_3$), 2.14 (m, 1 H, CCH_2CH$_3$). – ^{13}C NMR (125 MHz, C_6D_6): 4.0 (BCH$_2$CH$_3$, br), 8.9 (BCH$_2$CH$_3$, br), 10.6 (B$_2$CCH$_3$), 11.3 [C$_5$(CH$_3$)$_5$], 12.3 (BCH$_2$CH$_3$), 12.7 (BCH$_2$CH$_3$), 14.4 (CCH$_2$CH$_3$), 14.6 (CCH$_2$CH$_3$), 21.0 (CCH$_2$CH$_3$), 21.4 (CCH$_2$CH$_3$), 68.5 (B$_2$CCH$_3$, br), 78.4 (CCH$_2$CH$_3$, br), 80.7 (CCH$_2$CH$_3$, br), 84.4 [C$_5$(CH$_3$)$_5$]. – ^{11}B NMR (64.21 MHz, C_6D_6): −0.4 (1 B, BH, $^1J_{BH}$ = 156 Hz), 3.9 (1 B, BCH$_2$CH$_3$), 6.6 (1 B, BCH$_2$CH$_3$). – MS (EI): *m*/*z* (%) = 438 [M^+] (100), 423 [$M^+ - CH_3$] (10), 235 [Cp*Ru$^+$ − 2 H] (15).

(1,2,3,5,6-Pentamethyl-4-hydrido-2,3,5-tricarbahexaboranyl)(η⁵-pentamethylcyclopentadienyl)ruthenium (8*c): Same procedure as for **8*a**. The complex **8*c** was obtained as a yellow solid from **2*c** (180 mg, 0.49 mmol) in 50 mL of hexane and BH_3 (0.5 mL, 1 M, 0.5 mmol). Yield: 90 mg (48%). – m.p. 110°C. – ^{1}H NMR (200.13 MHz, C_6D_6): δ = −0.55 (s, 3 H, BCH$_3$), 1.44 (s, 3 H, BCH$_3$), 1.73 [s, 15 H, C$_5$(CH$_3$)$_5$], 1.89 (s, 3 H, B$_2$CCH$_3$), 1.99 (s, 3 H, =CCH$_3$), 2.12 (s, 3 H, =CCH$_3$). – ^{13}C NMR (75.46 MHz, C_6D_6): δ = 11.9 [C$_5$(CH$_3$)$_5$], 12.9 (=CCH$_3$), 13.4 (=CCH$_3$), 17.3 (B$_2$CCH$_3$), 83.5 [C$_5$(CH$_3$)$_5$], BCH$_3$, B$_2$CCH$_3$, and =CCH$_3$ not observed. – ^{11}B NMR (64.21 MHz, C_6D_6): δ = 1.1 (1 B, BH, $^1J_{BH}$ = 159 Hz), 2.3 (1 B, BCH$_3$), 6.0 (1 B, BCH$_3$). – MS (EI): *m*/*z* (%) = 382 [M^+] (100), 367 [$M^+ - CH_3$] (20), 233 [Cp*Ru$^+$ − 4 H] (15). – HRMS calcd. for $C_{18}H_{31}B_3Ru$: 381.1761, found 381.1761, Δm = 0.0 mmu.

Dimer of [(η⁵-Pentamethyl-2,3-dihydro-1,3-diborolyl)(η⁵-pentamethylcyclopentadienyl)ruthenium]rhodium Chloride (9*c): To a suspension of μ-dichlorotetraethylenedirhodium (180 mg, 0.46 mmol) in 30 mL of THF 380 mg of **2*c** (1.03 mmol) dissolved in 15 mL of THF was added. After stirring for 12 h the reaction mixture was filtered and the solvent was removed in vacuum. The black residue was purified by chromatography (silica gel, hexane/toluene, 50:50) to give a dark brown solid. Yield: 210 mg (44%). – m.p. 170°C (decomp.). – ^{1}H NMR (200.13 MHz, C_6D_6): δ = 1.28 [s, 15 H, C$_5$(CH$_3$)$_5$], 1.39 (s, 6 H, BCH$_3$), 1.97 (s, 3 H, B$_2$CCH$_3$), 2.23 (s, 6 H, =CCH$_3$). – ^{11}B NMR (64.21 MHz, C_6D_6): δ = 21.8. – MS (EI): *m*/*z* (%) = 1016 [M^+] (100), 779 [M^+ − **2*c**] (4), 509 [M^+ − **2*c** − Rh − Cl] (45), 473 [**2*c**Rh$^+$] (35), 233 [Cp*Ru$^+$ − 4 H] (8).

Table 2. Crystal and collection parameters for compounds **6*a**, **d**

	6*a	**6*d**
Empirical formula	$C_{27}H_{47}B_2NRu$	$C_{25}H_{43}B_2NRu$
Formula weight	508.3	480.3
Crystal system	triclinic	monoclinic
Space group	*P*−1	$P2_1$
Unit cell [Å, °]		
a	9.671(7)	12.035(6)
b	11.115(8)	15.131(8)
c	14.224(10)	14.486(6)
α	72.58(6)	90
β	78.38(6)	95.57(3)
γ	73.13(5)	90
V [Å^3]	1385(2)	2625(2)
Z	2	4
Calcd. density [g/cm^3]	1.22	1.22
Adsorp. coeff. [mm^{-1}]	0.58	0.61
F(000)	540	1016
Crystal size [mm]	0.4 × 0.45 × 0.55	0.2 × 0.25 × 0.45
θ_{max} [°]	25	25
Index range	−11/+11, −12/+13, 0/16	−14/+14, 0/+17, 0/+17
No. of reflections		
unique	4884	4799
observed [$I > 2\sigma(I)$]	4528	3748
Transmission	0.925−1.000	0.763−1.000
Parameters	298	554
Final *R* indices		
*R*1 [$I > 2\sigma(I)$]	0.025	0.063
*wR*2 [all reflections]	0.062	0.165
Largest diff.peak/hole[e/Å^3]	+0.53/−0.53	+1.03/−1.00

Crystal Structure Determinations for 6*a,d: Diffraction data were collected on a Siemens-Stoe AED2 diffractometer (Mo-K_α radiation, graphite monochromator) in the ω-scan mode at −70°C. Crystal data and details of the measurements are summarized in Table 2. The structures were solved by direct methods (SHELXS86)[20] and refined by full-matrix least-squares methods (SHELXL93)[20] based on F^2 with all reflections. Non-hydrogen atoms were refined anisotropically, hydrogen atoms were added in calculated positions. − Crystallographic data (excluding structure factors) for the structures reported in this paper have been deposited with the Cambridge Crystallographic Data Center: CCDC-116376 (**6*a**), CCDC-116377 (**6*d**). Copies of the data can be obtained free of charge by application to CCDC, 12 Union Road, Cambridge CB2 1EZ, UK [Fax: int. code + 44-1223/336-001; E-mail: deposit@ccdc.cam.ac.uk].

Acknowledgments

This work was supported by The German Science Foundation (SFB 247) and BASF AG.

[1] U. Koelle, C. Rietmann, U. Englert, *J. Organomet. Chem.* **1992**, *423*, C20; U. Kölle, B. S. Kang, U. Englert, *J. Organomet. Chem.* **1991**, *420*, 227.
[2] M. Nisho, H. Matsuzaka, Y. Mizohe, M. Hidai, *J. Chem. Soc, Chem. Commun.* **1993**, 375.
[3] H. Matsuzaka, Y. Mizohe, M. Nishio, M. Hidai, *J. Chem. Soc, Chem. Commun*. **1991**, 1011.
[4] U. Koelle, C. Rietmann, J. Tsol, T. Wagner, U. Englert, *J. Organomet. Chem.* **1995**, *14*, 703.
[5] [5a] G. G. A. Balavoine, T. Boyer, *J. Organomet. Chem.* **1992**, *11*, 456 − [5b] B. de Klerk-Engels, J. G. P. Delis, K. Vrieze, K. Goubitz, J. Fraanje, *J. Organomet*. *Chem.* **1994**, *13*, 3269.
[6] W. Siebert, R. Hettrich, M. Kaschke, H. Wadepohl, W. Weinmann, M. Stephan, H. Pritzkow, I. Hyla-Kryspin, R. Gleiter, *Chem. Eur. J.* **1996**, *2*, 487.
[7] P. J. Fagan, M. D. Ward, J. C. Calabrese, *J. Am. Chem. Soc*. **1989**, *111*, 1698.
[8] U. Koelle, B. Kang, U. Englert, *J. Organomet. Chem.* **1991**, *420*, 227−235.
[9] W. Siebert, R. Hettrich, H. Pritzkow, *Angew. Chem.* **1994**, *106*, 215; *Angew. Chem. Int. Ed. Engl.* **1994**, *33*, 203.
[10] M. S. Chinn, D. M. Heinekey, *J. Am. Chem. Soc.* **1987**, *109*, 5865.
[11] G. J. Kubas, *Acc. Chem. Res.* **1988**, *21*, 123−129.
[12] H. Suzuki, H. Omori, D. H. Lee, Y. Yoshida, M. Fukushima, M. Tanaka, Y. Moro-oka, *Organometallics* **1994**, *13*, 1129−1146.
[13] R. H. Crabtree, M. Lavin, L. Bonneviot, *J. Am. Chem. Soc.* **1986**, *108*, 4032−4037.
[14] R. H. Crabtree, *Angew. Chem.* **1993**, *105*, 828−845; *Angew. Chem. Int. Ed. Engl.* **1993**.
[15] D. M. Heinekey, W. J. Oldham, Jr., *Chem. Rev.* **1993**, *93*, 913−926.
[16] K. Wade, *Adv. Inorg. Chem. Radiochem.* **1976**, *18*, 1; D. M. P. Mingos, *Adv. Organomet. Chem.* **1977**, *15*, 1.
[17] W. Siebert, A. Feßenbecker, A. Hergel, R. Hettrich, V. Schäfer, *Chem. Ber.* **1993**, *126*, 2205−2210.
[18] W. Siebert, W. Weinmann, H. Pritzkow, L. G. Sneddon, *Chem. Ber.* **1997**, *130*, 324−333.
[19] M. W. Whiteley, H. Pritzkow, U. Zenneck, W. Siebert, *Angew. Chem.* **1982**, *94*, 464; *Angew. Chem. Int. Ed. Engl.* **1982**, *21*, 453.
[20] G. M. Sheldrick, *SHELXS 86*, Univ. Göttingen **1986**; *SHELXL 97*, Univ. Göttingen **1997**.

Received March 15, 1999
[I99104]

Synthesis of Tetraborylethenes and 1,1,1′,1′-Tetra- and Hexaborylethanes; Electronic Interactions in Tetraborylethenes and 1,1,1′,1′-Tetraborylethanes, and HF-SCF Calculations

Martin Bluhm,[a] Andreas Maderna,[a] Hans Pritzkow,[a] Sabine Bethke,[b] Rolf Gleiter,*[b] and Walter Siebert*[a]

Dedicated to Prof. Wolf-Peter Fehlhammer on the occasion of his 60th birthday

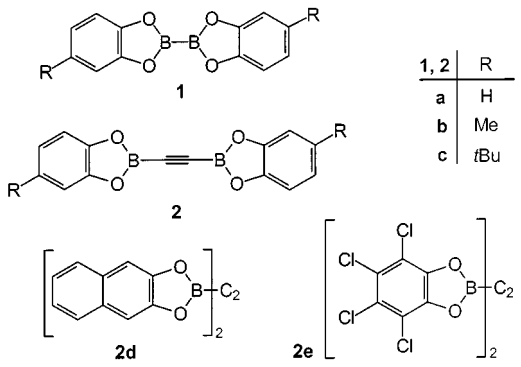
Keywords: Boranes / Homogeneous catalysis / Ab initio calculations / Donor-acceptor systems / X-ray analysis

The catechol-substituted diboranes(4) **1** react with the catechol-substituted diborylacetylenes **2**, in the presence of $[Pt(PPh_3)_2(C_2H_4)]$ or $[Pt(PPh_3)_4]$, to give tetra- and hexaborylethane derivatives. When $[Pt(cod)_2]$ is used as catalyst, the tetraborylethene **5a** is formed exclusively. Catalytic hydrogenation of **5a** affords the 1,1,1′,1′-tetraborylethane **4a**, which has been studied by an X-ray structure analysis. Natural Bond Orbital (NBO) analyses for the RHF/3–21G optimized geometries of **4a** and **5a** reveal intramolecular stabilization of the boron p_z orbital. This covers B–O, B–B, and agostic interactions. The photoelectron spectrum of **5a** is reported

Introduction

The platinum-catalyzed diboration reaction of acetylenes was reported by Suzuki and Miyaura in 1993.[1] Mechanistic studies[2−4] revealed that, in the first step, an oxidative addition of diborane(4) to the platinum occurs followed by the insertion of a π-bonded acetylene into the Pt−B σ bond. Subsequent reductive elimination leads to the 1,2-diborylethene derivatives. Catechol-substituted diboranes(4), which are air-stable and easy to handle, have also been used. The highly reactive tetrachlorodiborane(4) (B_2Cl_4) readily adds, without a catalyst, to acetylene or acetylene derivatives to give (*Z*)-1,2-bis(dichloroboryl)ethenes.[5] Further reaction of $(CH)_2(BCl_2)_2$ with B_2Cl_4 affords tetrakis(dichloroboryl)ethane in excellent yield.[6] Recently a tetraborylethane was proposed as an intermediate in the hydroboration of bis(diethylboryl)acetylene, which rearranges to give carborane clusters.[7] Diboration of ethenes to 1,2-diborylethanes can be achieved by using bis(1,5-cyclooctadiene)platinum[8] $[Pt(cod)_2]$, tris(norbornene) platinum[8] $[Pt(nbe)_3]$ or bis(dibenzylideneacetone)platinum[9] $[Pt(dba)_2]$.

Tetraborylethenes are useful building blocks for the synthesis of new heterocycles, carboranes and for functionalized ethenes. The first example was synthesized in low yields by gas-phase reaction of carbon with B_2F_4.[10] Here we wish to report a detailed investigation into the platinum-catalyzed reactions of catechol-substituted diboranes **1** with the corresponding diborylacetylenes **2,** whereby access to air-stable tetraborylethenes, and tetraboryl- and hexaborylethanes is achieved.



Results and Discussion

Hexaborylethanes 3

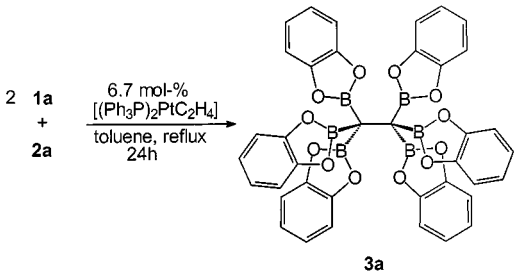
In refluxing toluene, an excess of the diborylacetylene **2a** reacts with the diborane(4) **1a** in the presence of (ethene)-bis(triphenylphosphane)platinum catalyst, and **3a** is isolated in 71% yield.[11] This compound is insoluble in nonprotic solvents but slightly soluble in methanol with slow decomposition. The molecule ion of **3a** can be detected by mass spectrometry (EI, CI and FD). In the ^{11}B NMR spectrum (CD_3OD) a broad signal at δ = 34 for **3a** and a sharp one at δ = 19 for the methanolysis product $C_6H_4O_2BOCD_3$ appear. The boron-bound carbon atom is found as a broad signal at δ = 23 in the ^{13}C NMR spectrum (T = 203 K).

Other hexaborylethane derivatives are obtained from the substituted diborylacetylene **2d**[12] and the diborane(4) **1a**. Due to steric hindrance in the starting compounds, the

[a] Anorganisch-Chemisches Institut der Universität Heidelberg, Im Neuenheimer Feld 270, D-69120 Heidelberg, Germany
Fax: (internat.) + 49-(0)6221/545609
E-mail: ci5@ix.urz.uni-heidelberg.de
[b] Organisch-Chemisches Institut der Universität Heidelberg, Im Neuenheimer Feld 270, D-69120 Heidelberg, Germany
Fax: (internat.) + 49-(0)6221/544205
E-mail: rolf.gleiter@urz.uni-heidelberg.de

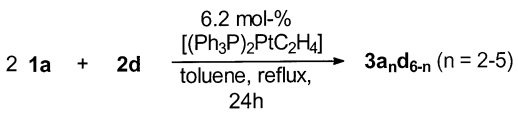
 © WILEY-VCH Verlag GmbH, D-69451 Weinheim, 1999 1434−1948/99/1010−1693 $ 17.50+.50/0

yields of the hexaborylethane derivatives $\mathbf{3a_nd_{6-n}}$ (n = 2−5) are low. During the formation of these compounds an unexpected exchange of the boryl substituents takes place, as indicated by mass spectrometric studies of the products. As shown in Scheme 2, the reaction of **2d** with **1a** in the presence of $[Pt(PPh_3)_2(C_2H_4)]$ leads to a mixture of the derivatives $\mathbf{3a_nd_{6-n}}$ (n = 2−5), in which between five and two boryl substituents of **1a** and between one and four substituents of **2d** are incorporated. It is unknown whether the exchange occurs before or after the formation of the hexaborylethanes.



Scheme 1

These results clearly demonstrate that in refluxing toluene the platinum compounds $[Pt(PPh_3)_2(C_2H_4)]$ or $[Pt(PPh_3)_4]$ catalyze the double diboronation of the diborylacetylene **2a** with the diborane(4) **1a** to give the hexaborylethane **3a**.[11][13] Under these conditions the reaction does not stop at the expected tetraborylethene **5a**,[14] but leads to **3a**. Such a double diboronation of an alkyne in the presence of platinum phosphane catalysts has not previously been described and its formation had been disclaimed on the basis of theoretical calculations.[15] Our findings of a high reactivity of the diborylacetylene **2a** may be due to its flat shape[16] and to the easy formation of catecholboryl platinum compounds[3] relative to that of other derivatives.

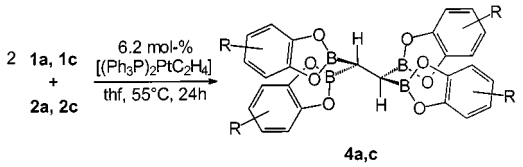


Scheme 2

Tetraborylethanes 4

Surprisingly, the formation of tetraborylethanes[17][18] occurs by catalysis with $[Pt(PPh_3)_2(C_2H_4)]$ or $[Pt(PPh_3)_4]$ under mild conditions (55°C). A 1:1 mixture of **1a** and **2a** reacts in the presence of these platinum complexes to give 1,1,1′,1′-tetra(benzo-1,3-dioxa-2-borol-2-yl)ethane (**4a**) in low yield. The reaction proceeds in tetrahydrofuran and in toluene. Purification of **4a** is achieved by sublimation under high vacuum. Under the same reaction conditions **1c** and **2c** form the tetraborylethane **4c** in very low yield.

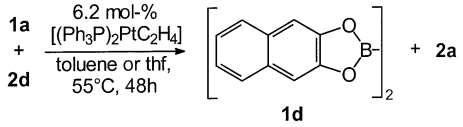
The molecular formula of **4a,c** follows from the molecular ions of **4a** and **4c** found in the EI mass spectrum and from the NMR spectroscopic data. The ^{11}B NMR spectrum (CD_3OD) shows a broad signal at δ = 32.5 for **4a,c** and a



Scheme 3

sharp one at δ = 19 for the methanolysis product. The signal in the ^{13}C NMR spectrum for the boron-bound carbon atoms of **4a** is observed at δ = 10. In the ^1H NMR spectrum, the two hydrogen atoms of the ethane unit appear as a broad singlet at δ = −0.1, which is in the same range for similar compounds.[19]

Attempts have been made to elucidate the origin of the hydrogen atoms in the ethane derivatives **4**. There is no incorporation of deuterium when the reaction is carried out in dry $[D_8]$thf. As the formation of a tetraborylethane also takes place in dry CCl_4 the hydrogen atoms must originate from other sources. Compound **1a** also reacts with the octachloro derivative **2e** to give the tetraborylethane derivative $\mathbf{4a_2e_2}$, which indicates that the hydrogen atoms cannot come from the diborylacetylene **2e**. We assume that a transfer of hydrogen atoms from the aryl substituents of the platinum phosphane catalysts occurs by an *ortho*-metalation reaction. The formation of tetraborylethanes most likely occurs by the intermediate formation[14,18,20,21] of 1,3-benzodioxa-2-borole followed by double hydroboration of the diborylacetylene.



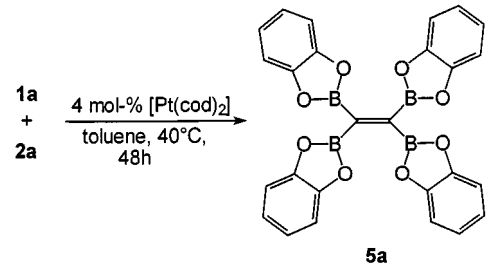
Scheme 4

A different reaction takes place when **1a** and **2d** react in the presence or absence of $[Pt(PPh_3)_2(C_2H_4)]$ at 55°C in tetrahydrofuran, in toluene or in a mixture of both solvents. The expected bis(naphthalene-1,3-dioxa-2-borol-2-yl)-bis(benzo-1,3-dioxa-2-borol-2-yl)ethane does not form but, instead, the new compound 1,1:2,2-bis(2,3-naphthalenedioxy)diborane(4) (**1d**) is formed by an exchange of the boryl groups. The colorless air-stable solid **1d** is obtained in 74% yield. Its mass and NMR spectra prove the formation of the new diborane(4) derivative **1d**, which could not be obtained from the reaction between $B_2(NMe_2)_4$ and naphthalene-1,2-diol.[22] In the ^1H NMR spectrum **1d** shows a multiplet for the naphthol substituents and in the ^{13}C NMR spectrum, five signals for the naphthol carbon atoms. The ^{11}B NMR spectrum of **1d** in CD_3OD exhibits a signal at δ = 31.6 and a sharp one at δ = 19 for the methanolysis product of **1d**.

Tetraborylethene 5a

As outlined above, the attempt to synthesize tetraborylethene derivatives leads to the formation of tetraborylethane

compounds **4** when triphenylphosphane-platinum catalysts are used. The previously elusive tetraborylethene **5a** is obtained, however, from **1a** and **2a** with the base-free platinum catalyst [Pt(cod)$_2$] under mild conditions in toluene. Compound **5a** is formed in 70% yield as a colorless solid which sublimes at 160°C under high vacuum.



Scheme 5

The molecule ion of **5a** is detected in the EI and CI mass spectra whereas the M^+ ion for **4a** is not observed. The boron-bound carbon atoms of the double bond are found as a broad singlet at $\delta = 165$ in the low-temperature ^{13}C NMR spectrum ($T = 203$ K). The ^{11}B NMR spectrum (CD_3OD) shows a broad signal at $\delta = 30$ for **5a** and a sharp one at $\delta = 19$ for the methanolysis product of **5a**. The Raman spectrum of **5a** exhibits a band at 1549 cm^{-1} for the stretching vibration of the double bond. The IR spectrum of **5a** and Raman spectrum of the reference substance **1a** do not contain this band.

At temperatures above 40°C the hexaboryl derivative **3a** forms in toluene, because **1a** adds across the double bond of **5a**. By catalytic hydrogenation of **5a** (palladium/active carbon, 5 bar pressure) **4a** is formed in 35% yield.

Crystal Structure and Geometrical Parameters for 4a

To elucidate the structure of **4a**, an X-ray diffraction study was carried out (crystal data and structure refinement for **4a** are listed in Table 6). A single crystal of **4a**(thf)$_2$ was grown from a tetrahydrofuran solution at 4°C. Table 1 shows some of the structural parameters of **4a** as obtained from the X-ray diffraction structure analysis and the HF/3−21G geometry optimization. The crystal structure determination (Figure 1) shows a staggered conformation for the substituents at the central C−C single bond. The large substituents and the hydrogen atoms adopt the *anti* position. This result is in agreement with ab initio calculations (see Table 1). In the crystal structure, two tetrahydrofuran molecules are coordinated to the boron atoms. The C1−C1′ distance is elongated (1.585 Å, calcd. 1.575 Å), and comparable with that of other characterized tetraborylethane derivatives.[6]

The angles around the carbon atoms of the ethane unit are nearly tetrahedral, the B1−C1−B2 angle being larger (113.30°, calcd. 113.80°) than the H1−C1−B1 angle (107.78°, calcd. 107.15°) and the H1−C1−B2 angle (109.65°, calcd. 107.27°) due to steric reasons. The distances O5−B1 (2.728 Å) and O5−B2 (2.673 Å) confirm a bonding interaction between the tetrahydrofuran molecules and the boron atoms.

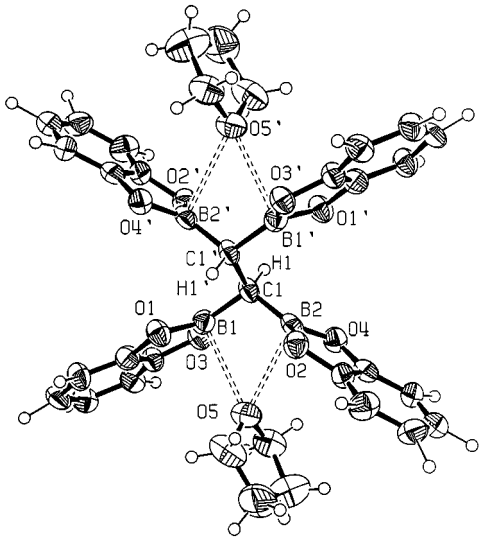


Figure 1. Molecule structure of **4a** in the crystal; selected bond lengths [Å] and angles [°]: C1−C1′ 1.5853(56), C1−B1 1.5511(47), B1−O1 1.3954(38), B2−O5 2.6738(41), B1−O5 2.7283(43), C1−H1 0.9903(287); B1−O5−B2 57.5(15), B1−C1−B2 113.3(16), H1−C1−B1 107.78(1.65), H1−C1−B2 109.65(1.61)

Table 1. Structural parameters for **4a**(thf)$_2$

4a(thf)$_2$	C1−C1′	O5−B1	O5−B2	B1C1B2	H1C1B1	H1C1B2
(exptl.)	1.585	2.728	2.673	113.30	107.78	109.65
(calcd.)	1.575	2.728[a]	2.673[a]	113.80	107.15	107.27

[a] These values remain fixed during the optimization, calcd. = RHF/3−21G//RHF/3−21G-calculations, bond lengths are in Angstrom, angles are in degrees. For the atomic numbering see Figure 1.

Computational Details for 4a and 5a

The geometries of **4a** and **5a** were fully optimized with GAUSSIAN94[23] at the Hartree−Fock level of theory using the split-valence 3−21G basis set. Compound **4a** was optimized in the point group symmetries C_i and C_{2h}, and **5a** in C_{2v}, C_{2h}, D_2 and D_{2h} symmetries. HF/3−21G frequency calculations were performed to verify that the structures are minima on the potential energy hypersurface, i.e. the eigenvectors of the Hessian matrix were all positive. The electronic structures of **4a** and **5a** were analyzed by means of a Natural Bond Orbital (NBO) analysis.[24]

Calculated Geometrical Parameters for 5a

Since there are no structural data available for **5a**, geometry optimizations were computed in several point groups. The global minimum on the HF/3−21G potential energy surface of **5a** belongs to the point group C_{2h} (see Figure 2, conformer **A**). In this structure two diametrically

opposed catechol rings are twisted by 90° out of the molecular plane while the remaining two are located in the molecular plane containing the four boron atoms. Conformation **A** favors an additional interaction between the lone pairs of the oxygen atoms and the boron centers lying opposite them, as shown in Figure 3.

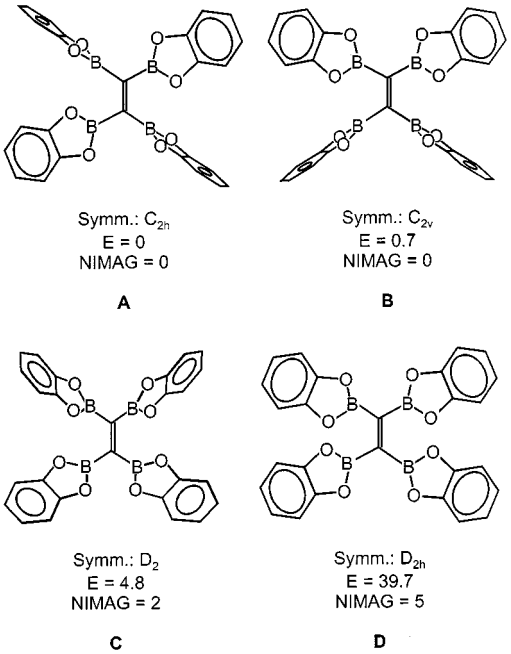


Figure 2. Calculated conformers of **5a**. E: relative energies [kcal/mol] corrected with zero-point energies and thermal enthalpies. NIMAG: number of imaginary frequencies

A conformation which is closely related to that just described belongs to point group C_{2v} (see Figure 2, conformer **B**). It is a local minimum, which is 0.7 kcal/mol less favored than **A**. In **B**, two geminal catechol rings are twisted by 90° to provide a donor-acceptor interaction between two vicinal catechol rings. The other two conformations shown in Figure 2 belong to point groups D_2 (**C**) and D_{2h} (**D**). Both represent higher order saddle points. In conformation **C** all rings are twisted propeller-like 42° out of the molecular plane. This conformation no longer allows donor-acceptor interactions as in the previously discussed conformations. In the case of conformation **D** all four catechol rings are coplanar to the ethylene fragment. This arrangement causes severe steric repulsion between the lone pairs at the oxygen atoms of vicinal catechol rings.

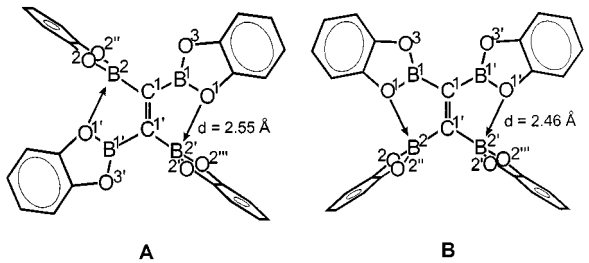


Figure 3. Intramolecular B−O interactions for conformers **A** and **B** (**5a**)

Table 2 summarizes some of the structural parameters of **5a** as obtained from the HF/3-21G geometry optimization in C_{2h}, C_{2v}, D_2 and D_{2h} symmetry. Structure **A** shows two types of boron atoms which are coordinated differently: B1 and B1′ are part of an extensive π system which is delocalized over two catechol moieties connected by the ethylene unit. However, the catechol groups of B2 and B2′ (see Figure 3) are oriented perpendicular to the plane containing the ethylene group and therefore experience a smaller stabilization by π-electron density delocalization from only one catechol group. This is compensated by intramolecular donation of electron density from the oxygen lone pairs of O1 and O1′ to the p_z orbitals of B2 and B2′, which is shown by short B2−O1′ and B2′−O1 interactions for conformers **A** (2.55 Å) and **B** (2.46 Å). The variations in B−O bond lengths in **A** and **B** (1.398−1.415 Å) are in line with electron density being donated from the lone pairs of O1 and O1′thus causing a lengthening of the B1−O1 bond and a shortening of the B1−O3 bond. The length of the B2−O2 bond (of the acceptor boron atom) is slightly longer than the averaged B1−O1 and B1−O3 bond lengths, due to electron donation from O1′ to B2.

Table 2. Calculated structural parameters for **5a**

	C1−C1′[a]	B2−O1′[a]	B2−O3[a]	B1−O1[a]	B1−O3[a]	B2−O2[a]	D1[b]	D2[b]
A	1.347	2.552	3.202	1.409	1.398	1.406	90.0	0.0
B	1.352	2.464	3.353	1.415	1.398	1.405	90.0	0.0
C	1.346	3.000	3.250	1.402	1.406	1.40	139.3	139.3
D	1.366	3.151	2.937	1.402	1.412	1.40	0.0	0.0

[a] Bond lengths in Å. − [b] Dihedral angles D are in degrees; D1 = O2B2C1C1′, D2 = O1B1C1C1′. For the atomic numbering see Figure 3.

To quantify these stabilizing B−O-interactions, a second-order perturbation theory treatment according to the Weinhold Natural Bond Orbital (NBO) localization procedure[23] was performed. As shown in Table 3, there is a stabilization of the empty boron p_z orbital by delocalized π electrons, especially from the neighboring oxygen atoms. The intramolecular donor-acceptor interaction O1−B2′ and O1′−B2 can be clearly seen. Each interaction stabilizes **A** by 15.5 kcal/mol. Although the stabilization is even higher in **B** (21.0 kcal/mol for each interaction) due to shorter O1−B2′ and O1′−B2 distances, this configuration does not represent the global minimum energy structure of **5a** because of repulsive interactions of these geminal catechol rings, which are coplanar with the ethylene fragment. No intramolecular O3−B2 or O3′−B2′ donor-acceptor interactions can be seen, because the distance is too long (3.2 Å in **A**, 3.4 Å in **B**) for an interaction, although the orientation is the same for O3−B2 and O1′−B2. Stabilization by π-electron density from the ethylene fragment can only exist for the boryl groups which are located in this plane (B1 and B1′). Although in close proximity, the

amount of stabilization is not much larger than the amount of intramolecular stabilization. The largest stabilization is due to π-electron density donation from the lone pairs of the neighboring oxygen atoms (Table 3).

Table 3. Second-order perturbation theory energies according to the Weinhold natural bond orbital (NBO) localization procedure[29] for **5a**

	Lp (O1′)[a] ↓ p_Z (B2)	Lp (O3)[a] ↓ p_Z (B2)	Lp (O2)[a] ↓ p_Z (B2)	Lp (C1)[a] ↓ p_Z (B2)	Lp (C1)[a] ↓ p_Z (B1)
A	15.54	0.00	75.06	0.00	29.01
B	21.00	0.00	75.45	0.00	35.09

[a] Lp = lone pair; energy in kcal/mol. For the atomic numbering see Figure 3.

PE Spectrum of 5a

The He^I PE spectrum of **5a** is shown in Figure 4. RHF/3−21G calculations were carried out in order to assign the bands to individual ionization processes. In the range 8.3−9.7 eV there is a broad band of overlapping ionization events (bands 1−3), followed by band 4 at 11.2 eV. The recorded vertical ionization energies agree very well with calculated negative orbital energies, according to Koopmans′ theorem.[25] The bands 1−3 (exp. 8.3−9.7 eV; calcd. 8.8−9.7 eV) are assigned to ionization processes from the eight highest occupied molecular orbitals, which are shown in Figure 5. These orbitals can be described as linear combinations between the π system of the catechol rings and the ethylene π system. The recorded energy differences Δ between band 3 and 4 compare well with the results of the calculations [Δ (exp.) 1.7 eV; Δ (calcd.) 1.5 eV]. Band 4 is assigned to ionization processes from the ethylene π-orbital.

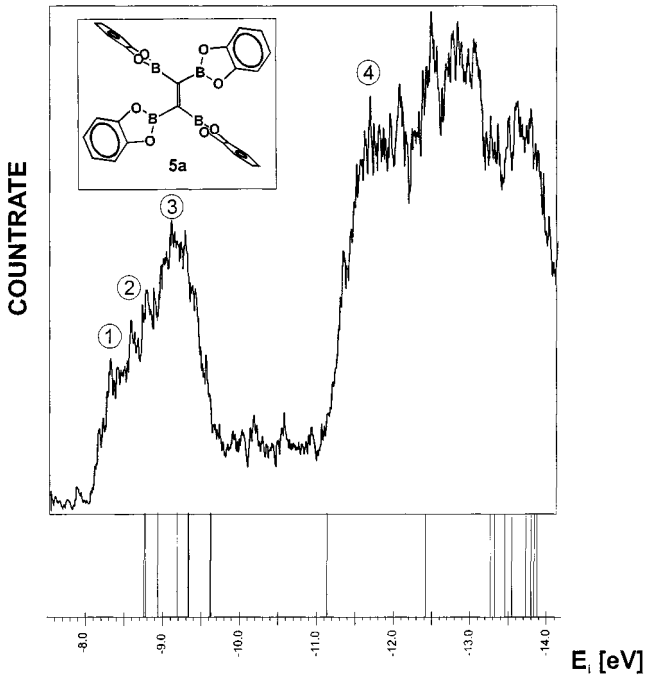


Figure 4. Photoelectron spectrum of **5a**

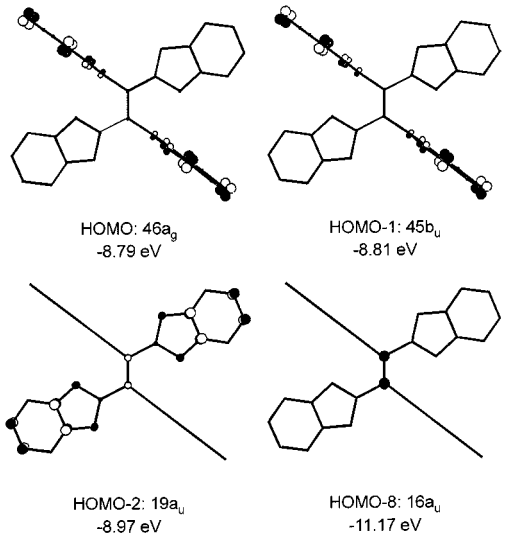


Figure 5. Selected occupied RHF/3−21G orbitals of **A** (**5a**)

Calculated Geometrical Parameters for 4a

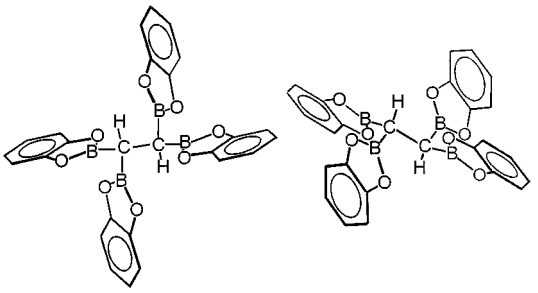
Figure 6 shows the most favorable conformations of **4a**, calculated without the coordinated tetrahydrofuran molecules. The global minimum on the HF/3−21G potential energy surface belongs to point group C_i (conformer **E**). In this structure the geminal catechol rings are twisted by 53° to provide a B−O donor-acceptor interaction between two vicinal catechol rings (Table 4). Additionally, there is a B−B interaction between the boron atoms of two geminal catechol rings and an agostic interaction between one boron p_z orbital and the C−H bond of the ethane fragment. In point group C_{2h} (conformer **F**, Figure 6) there is a mirror plane, spanned by the two C−H bonds of the ethane moiety, which disables donor-acceptor interactions. As a consequence, this structure represents a second-order saddle point, which is disfavored by 4.2 kcal/mol (corrected with zero-point energies and thermal energies) relative to **E**.

Table 4. Calculated structural parameters for **4a** (without coordinated thf)

4a	C1−C1′[a]	B1C1B2[a]	H1C1B1[a]	H1C1B2[a]	C1O1C1′O1′[a]	NIMAG[b]
E	1.582	112.97	107.31	108.02	51.3	0
F	1.573	115.00	106.50	106.50	0.0	2

[a] RHF/3−21G-optimizations, bond lengths are in Å, angles are in degrees. − [b] NIMAG: number of imaginary frequencies. For the atomic numbering see Figure 7.

To quantify these stabilizing B−O, B−B and agostic interactions, a second-order perturbation theory treatment according to the Weinhold Natural Bond Orbital (NBO) localization procedure[24] was performed. The relative orientation of the "empty" boron p_z orbital to the C−H bond of the ethane fragment is nearly coplanar and thus enables a stabilization by an agostic interaction. The acceptor boron p_z orbital has an occupation number of 0.318 and stabilizes the geminal boron p_z orbital, which shows an occupation number of 0.323. The larger occupation number



E F

Figure 6. Calculated conformers of **4a**. E: relative energies corrected with zero-point energies and thermal enthalpies. NIMAG: number of imaginary frequencies

is due to an additional intramolecular donor-acceptor interaction from the σ-type oxygen lone pair of the *cis* vicinal catechol group. As for **5a**, the large stabilization by π-electron density donation from the lone pairs of the neighboring oxygen atoms can also be seen (Table 5).

Table 5. Second-order perturbation theory energies according to the Weinhold Natural Bond Orbital (NBO) localization procedure[23] for **4a**.

	Lp (B1)[a] ↓ p_Z (B2)	Lp (O1′)[a] ↓ p_Z (B2)	σ (C1−H1)[a] ↓ p_Z (B1)	σ (C1−H1)[a] ↓ p_Z (B2)	Lp (O2)[a] ↓ p_Z (B2)
E	12.13	12.11	8.96	1.47	71.81

[a] Lp = lone pair; energy in kcal/mol. For the atomic numbering see Figure 7.

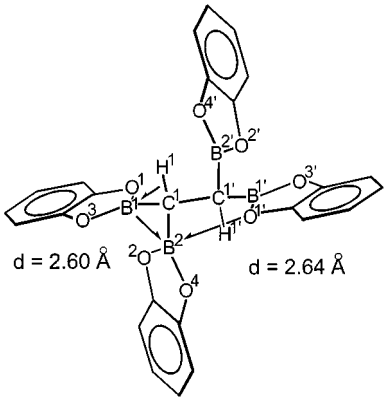


Figure 7. Intramolecular B−O, B−B, and agostic interactions for conformer **E** (**4a**)

Experimental Section

General: Reactions were carried out under dry nitrogen, with standard Schlenk techniques. Solvents were dried, distilled and saturated with nitrogen. Glassware was dried with a heat-gun under high vacuum. ^{1}H, ^{13}C, ^{11}B NMR: Bruker AC 200 and 500 spectrometers; NMR references are $(CH_3)_4Si$ and BF3·Et2O. Mass spectra were obtained on a Finnigan MAT 8200 plus (EI technique) and ZAB-2F VG-Micromass CTD spectrometer (EI and HR-EI techniques) and on a Jeol MS station JMS 700 (EI, HR-EI and CI techniques). − Bis(benzo-1,3-dioxa-2-borol-2-yl)acetylene **2a,**[16] bis(naphthalene-1,3-dioxa-2-borol-2-yl)acetylene **2d,**[12] diborane(4)-compounds **1a−c,**[26] $[Pt(PPh_3)_2(C_2H_4)]$,[27] and $[Pt(cod)_2]$[28] were prepared according to literature procedures.

Bis[(4-*tert*-butylbenzo)-1,3-dioxa-2-borol-2-yl]acetylene (2c): (4-*tert*-Butylbenzo)-2-chloro-1,3-dioxa-2-borole (10 g, 47.6 mmol) in toluene (40 mL) and bis(trimethylstannyl)acetylene (7.6 g, 21.6 mmol) in toluene (40 mL) were simultaneously added dropwise to 200 mL of toluene at −78°C. The mixture was allowed to warm to room temp. and stirred for 24 h. The solvent was removed, the residue was stirred in pentane, filtered and dried in vacuum. Yield: 5.5 g (68%), sbp. 145°C/10^{-3} Torr. − ^{1}H NMR (200.1 MHz, $CDCl_3$): δ = 1.32 (s, 18 H, CH_3), 7.18−7.31 (m, 6 H, H_{ar}). − ^{13}C NMR (50.3 MHz, $CDCl_3$): δ = 31.7 (CH_3), 34.9 [*C*$(CH_3)_3$], 110.1, 111.9, 120.4, 145.2, 147.4, 147.5 (C_6H_3). − ^{11}B NMR (64.2 MHz, $CDCl_3$): δ = 24.1 (s). − EI-MS: *m*/*z* (%) 374 (54) [M^+], 359 (100) [$M^+ - CH_3$], 200 (17) [$M - (C_4H_9)C_6H_3O_2B + H]^+$. − HR-MS: *m*/*z* 374.18655 (M^+), calcd. $^{12}C_{22}{}^1H_{24}{}^{11}B_2{}^{16}O_4$: 374.18607 (Δ = 0.48 mmu).

Bis[(tetrachlorobenzo)-1,3-dioxa-2-borol-2-yl]acetylene (2e): (Tetrachlorobenzo)-2-chloro-1,3-dioxa-2-borole (18.3 g, 63 mmol) in toluene (60 mL) and bis(trimethylstannyl)acetylene (10 g, 29 mmol) in toluene (60 mL) were simultaneously added dropwise to 250 mL of toluene at −78°C. The mixture was allowed to warm to room temp. and stirred for 24 h. The precipitate was filtered and dried in vacuum. Yield: 11.6 g (74%), sbp. 190°C. − ^{13}C NMR (50.3 MHz, [d_4]MeOH): δ = 102 (B*CC*B, br.), 120.4, 123.3, 144.2 (C_6Cl_4). − ^{11}B NMR (64.2 MHz, [d_4]MeOH): δ = 22.1 (s), 19.1 (s, $Cl_4C_6O_2$-$BOCD_3$). − EI-MS: *m*/*z* (%) 538 (18.9) [M^+], 282 (70.0) [$M^+ - Cl_4C_6O_2B$]. − HR-MS: *m*/*z* 537.74298 (M^+), calcd. $^{12}C_{14}{}^{11}B_2{}^{16}O_4{}^{35}Cl_6{}^{37}Cl_2$: 537.74316 (Δ = 0.18 mmu).

Hexa(benzo-1,3-dioxa-2-borol-2-yl)ethane (3a): Compound **2a** (472 mg, 1.8 mmol), **1a** (431 mg, 1.8 mmol) and (ethene)bis(triphenylphosphane)platinum (83 mg, 0.12 mmol, 6.7 mol-%) were refluxed in 15 mL of toluene for 24 h. The precipitate was then filtered and purified by washing several times with THF and CH_2Cl_2. The colorless solid was dried in vacuum. Yield: 522 mg (71%), sbp. 457°C. Under the same conditions the catalyst tetrakis(triphenylphosphane)platinum gives **3a** in 57% yield. − ^{1}H NMR (200.1 MHz, [d_4]MeOH): δ = 6.61−6.77 (m, H_{ar}). − ^{13}C NMR (50.3 MHz, [d_4]MeOH): δ = 146.3, 120.9, 116.4 (C_6H_4). − ^{13}C NMR (125.8 MHz, [d_4]MeOH, 203 K): δ = 23 (B_3C, br.). − ^{11}B NMR (64.2 MHz, [d_4]MeOH): δ = 34 (s), 19 (s, $C_6H_4O_2BOCD_3$). − HR-MS: *m*/*z* 738.1860 (M^+), calcd. $^{12}C_{38}{}^1H_{24}{}^{16}O_{12}{}^{11}B_6$: 738.1826 (Δ = 3.4 mmu). − $C_{38}H_{24}O_{12}B_6$ (737.47): calcd. C 61.88, H 3.28; found C 61.93, H 3.57.

Mixture of Naphthalene- and Benzo-1,3-dioxa-2-borol-2-ylethanes $3a_nd_{6-n}$ (n = 2−5): A solution of **2d** (1.00 g, 2.76 mmol), **1a** (660 mg, 2.76 mmol) and (ethene)bis(triphenylphosphane)platinum (128 mg, 0.17 mmol) in 20 mL of toluene was refluxed for 48 h. The precipitate was filtered and purified by washing several times with THF and CH_2Cl_2. The colorless solid was dried in vacuum. Yield: 428 mg. − ^{1}H NMR (200.1 MHz, [d_4]MeOH): δ = 6.62−6.85 (m, C_6H_4), 7.10−7.63 (m, $C_{10}H_6$). − ^{13}C NMR (50.3 MHz, [d_4]MeOH): δ = 110.5, 116.7, 121.2, 124.4, 127.0, 131.0, 146.5, 147.8. − ^{11}B NMR (64.2 MHz, [d_4]MeOH): δ = 31 (s), 19 (s, $C_6H_4O_2BOCD_3$ and $C_{10}H_6O_2BOCD_3$). − EI-MS *m*/*z* (%) 937 (5.7) [M(**3a$_2$d$_4$**) − H]$^+$, 887 (23.6) [M(**3a$_3$d$_3$**) − H]$^+$, 838 (63.4) [M(**3a$_4$d$_2$**)]$^+$, 787 (68.3) [M(**3a$_5$d$_1$**) − H]$^+$, 720 (28.5) [M(**3a$_4$d$_2$**) −

$C_6H_4O_2B + H]^+$, 670 (27.6) [M(**3a$_4$d$_2$**) − $C_{10}H_6O_2B + H]^+$ and [M(**3a$_5$d$_1$**) − $C_6H_4O_2B + H]^+$.

Tetra(benzo-1,3-dioxa-2-borol-2-yl)ethane (4a). − Method A: Compound **2a** (1.54 g, 5.9 mmol), **1a** (1.29 g, 5.4 mmol) and tetrakis(triphenylphosphane)platinum (330 mg, 0.27 mmol, 5 mol-%) were heated in 35 mL of THF at 55°C for 24 h. The solvent was evaporated in vacuum and the precipitate was stirred in diethyl ether and filtered. Washing with diethyl ether gave a yellowish solid that was dried in vacuum. Further purification was performed by sublimation under high vacuum. Yield: 220 mg (11.5%) colorless solid, sbp. 170°C/10^{-5} Torr. − **Method B:** In a pressure apparatus 300 mg (0.6 mmol) of **5a** was suspended with 70 mg of a palladium/active carbon catalyst in 100 mL of toluene. The apparatus was filled with hydrogen gas (5 bar). After stirring the mixture for 24 h the catalyst was filtered and the solvent was evaporated in vacuum. The remaining solid was dried in vacuum. Yield: 130 mg (43.2%) colorless solid. − ^{1}H NMR (200.1 MHz, [d$_6$]DMSO): δ = 6.36−6.91 (m, 16 H, H_{ar}), −0.11 (s, 2 H, B_2CH). − ^{13}C NMR (50.3 MHz, [d$_4$]MeOH): δ = 116.4, 121.0, 146.3. − ^{13}C NMR (125.8 MHz, [d$_4$]MeOH, T = 203 K): δ = 10 (B_2C, br.). − ^{11}B NMR (64.2 MHz, [d$_4$]MeOH): δ = 32.5 (s), 19 (s, $C_6H_4O_2BOCD_3$). − HR-MS: *m/z* 502.1390 (M^+), calcd. $^{12}C_{26}{}^1H_{18}{}^{16}O_8{}^{11}B_4$: 502.1374 (Δ = 1.6 mmu).

Tetra[(4-*tert*-butylbenzo)-1,3-dioxa-2-borol-2-yl]ethane (4c): 672 mg (1.8 mmol) of **2c**, 630 mg (1.8 mmol) of **1c**, and 82 mg (0.1 mmol, 6.2 mol-%) of (ethene)bis(triphenylphosphane)platinum were heated in 20 mL of thf at 55°C for 40 h. The precipitate was filtered and dried in vacuum. Yield: 33 mg (2.5%). − ^{1}H NMR (200.1 MHz, [d$_4$]MeOH): δ = 6.67−6.82 (m, 12 H_{ar}), 1.24 (s, 36 H, CH_3), 0.10 (s, 2 H, B_2CH). − ^{13}C NMR (50.3 MHz, [d$_4$]MeOH): δ = 32.3 (CH_3), 35.1 ($C(CH_3)_3$), 114.1, 116.1, 117.7, 144.0, 144.5, 145.9 (C_6H_3). − ^{11}B NMR (64.2 MHz, [d$_4$]MeOH): δ = 32.5 (s), 19 (s, $C_6H_4O_2BOCD_3$). − CI-MS: *m/z* (%) 726 (64.7) [M^+], 727 (62.7) [M + H]$^+$, 552 (21.4) [M − $(C_4H_9)C_6H_3O_2B$ + H]$^+$, 377 (38.0) [M − 2 $(C_4H_9)C_6H_3O_2B$ + H]$^+$. − HR-MS: *m/z* 726.3903 (M^+), calcd. $^{12}C_{42}{}^1H_{50}{}^{16}O_8{}^{11}B_4$: 726.3878 (Δ = 2.5 mmu).

Bis(benzo-1,3-dioxa-2-borol-2-yl)-bis[(tetrachlorobenzo)-1,3-dioxa-2-borol-2-yl]ethane (4a$_2$e$_2$): Compound **2e** (1.00 g, 1.86 mmol), **1a** (42 mg, 1.86 mmol) and bis(triphenylphosphane)(ethene)platinum (97 mg (0.12 mmol, 7 mol-%) were refluxed in 20 mL of toluene for 48 h. The precipitate was filtered and dried in vacuum. Yield: 289 mg (20%). − ^{1}H NMR (200.1 MHz, [d$_4$]MeOH): δ = 6.60−6.77 (m, 8 H, H_{ar}), 0.1 (s, 2 H, B_2CH). − ^{13}C NMR (50.3 MHz, [d$_4$]MeOH): δ = 146.3, 121.0, 116.4 (C_6H_4), 144.2, 123.4, 120.5 (C_6Cl_4). − ^{11}B NMR (64.2 MHz, [d$_4$]MeOH): δ = 32.4 (s), 19 (s, $C_6H_4O_2BOCD_3$ and $Cl_4C_6O_2BOCD_3$). − EI-MS: *m/z* (%) 778 (18) [M^+], 254 (100) [$C_{12}H_8O_5B_2{}^+$], 392 (48) [$C_{12}H_4O_5B_2Cl_4{}^+$].

1,1:2,2-bis(2,3-naphthalenedioxy)diborane(4) (1d): Compound **2d** (600 mg, 1.66 mmol), **1a** (394 mg, 1.66 mmol) and bis(triphenylphosphane)(ethene)platinum (77 mg, 0.1 mmol, 6.2 mol-%) were heated in 20 mL of toluene at 50°C for 72 h. The colorless precipitate was filtered, washed with toluene and dried in vacuum. Yield: 416 mg (74%), sbp. 150°C/10^{-3} Torr. − ^{1}H NMR (200.1 MHz, [d$_4$]MeOH): δ = 7.14−7.55 (m, H_{ar}). − ^{13}C NMR (50.3 MHz, [d$_4$]MeOH): δ = 110.8, 124.5, 127.0, 131.1, 147.9 ($C_{10}H_6$). − ^{11}B NMR (64.2 MHz, [d$_4$]MeOH): δ = 31.6 (s), 19 (s, $C_{10}H_6O_2$-$BOCD_3$). − EI-MS: *m/z* (%) 338 (100) [M^+], 169 (12) [M^+ − $C_{10}H_6O_2B$], 355 (6) [$(C_{10}H_6O_2B)_2O^+$]. − HR-MS: *m/z* 338.09237 (M^+), calcd. $^{12}C_{20}{}^1H_{12}{}^{16}O_4{}^{11}B_2$: 338.09216 (Δ = 0.21 mmu). − $C_{20}H_{12}O_4B_2$ (338.09): calcd. C 71.08, H 3.57; found C 69.34, H 3.62.

Tetra(benzo-1,3-dioxa-2-borol-2-yl)ethene (5a): Compound **2a** (3.00 g, 11.5 mmol), 1a (2.725 g, 11.5 mmol) and of bis(1,5-cyclooctadiene)platinum (188 mg, 0.46 mmol, 4 mol-%) were heated in 55 mL of toluene at 40°C for 24 hours. The precipitate was then filtered and washed with CH_2Cl_2 and dried in vacuum. Yield: 4.025 g (70%), sbp. 160°C/10^{-5} Torr. − ^{1}H NMR (200.1 MHz, [d$_4$]MeOH): δ = 6.60−6.79 (m, H_{ar}). − ^{13}C NMR (50.3 MHz, [d$_4$]MeOH): δ = 146.3, 120.9, 116.4 (C_6H_4), 165 (B_2C, br., weak). − ^{13}C NMR (125.8 MHz, [d$_4$]MeOH, T = 203 K): δ = 165 (B_2C, br.). − ^{11}B NMR (64.2 MHz, [d$_4$]MeOH): δ = 29.9 (s), 19 (s, $C_6H_4O_2BOCD_3$). − CI-MS: *m/z* (%) 500 (100) [M^+], 501 (78.4) [M + H]$^+$, 557 (1.8) [M + C_4H_9]$^+$ − HR-MS: *m/z* 500.12158 (M^+), calcd. $^{12}C_{26}{}^1H_{16}{}^{11}B_4{}^{16}O_8$: 500.12173 (Δ = 0.15 mmu). − Raman: $\tilde{\nu}$ = 1549 cm^{-1} (C=C), 1620 cm^{-1} (ar.), 1471, 1330, 1230, 1150, 1002, 818, 611 cm^{-1}, 3066 cm^{-1} (C−H). − $C_{26}H_{16}O_8B_4$ (499.65): calcd. C 62.50, H 3.23; found C 62.33, H 3.65.

X-ray Crystal Structure Determinations of 4a: Crystal data and details of the structure determination are listed in Table 1. Unique sets of intensity data were collected at −70°C with a four-circle diffractometer (Mo-K_α radiation λ = 0.7107 Å, graphite monochromator, ω scan). Empirical absorption corrections (ψ-scans) were applied. The structure was solved by direct methods [SHELXS86][29] and refined by least-squares methods based on F^2 with all measured reflections [SHELXL97].[30] All non-hydrogen atoms were refined anisotropically. Hydrogen atoms were included in calculated positions.

Crystallographic data (excluding structure factors) for the structure reported in this paper have been deposited with the Cambridge Crystallographic Data Centre as supplementary publication no. CCDC-116696. Copies of the data can be obtained free of charge on application to CCDC, 12 Union Road, Cambridge CB2 1EZ, UK; fax: (internat.) + 44-1223/336-001; E-mail: deposit@ccdc.cam.ac.uk

Table 6. Crystal data and structure refinement for **4a**

	4a
Empirical formula	$C_{26}H_{18}O_8B_4{\cdot}2C_4H_8O$
Formula weight	645.9
Crystal system	monoclinic
Space group	$P2_1/c$
Unit cell	
A [Å]	8.600(5)
B [Å]	16.139(8)
C [Å]	12.204(6)
β [deg]	104.18(4)
Volume [Å^3]	1642(2)
Z	2
Calcd. density [g/cm^3]	1.306
Adsorp. coeff. [mm^{-1}]	0.09
F(000)	676
Crystal size [mm]	0.40 × 0.45 × 0.55
Θ-range [deg]	25.0
Index-ranges	−10/+9 0/+19 0/+14
No. of reflections	2894
unique	2894
observed [$I > 2\sigma(I)$]	1548
Parameters	285
Final *R* indices	
*R*1 [$I > 2\sigma(I)$]	0.052
*wR*2	0.146
Largest diff.peak/hole[e/Å]	0.18/−0.22

PE spectrum of 5a: The He^{I} PE spectrum was recorded on a Perkin–Elmer PS18 spectrometer. The recording temperature was 230°C. The calibration was performed with Ar (13.76 and 15.94 eV) and Xe (12.13 and 13.44 eV). A resolution of 20 meV on the $^2P_{3/2}$ Ar line was obtained.

Acknowledgments

We thank A. Flatow for recording the PE spectrum and Dr. S. Lebedkin, Forschungszentrum, Karlsruhe, for the Raman spectrum of **5a**. We are grateful to the Graduiertenkolleg der Universität Heidelberg, the Deutsche Forschungsgemeinschaft (SFB 247) and the Fonds der Chemischen Industrie.

[1] T. Ishiyama, N. Matsuda, N. Miyaura, A. Suzuki, *J. Am. Chem. Soc.* **1993**, *115*, 11018
[2] T. Ishiyama, N. Matsuda, M. Murata, F. Ozawa, A. Suzuki, N. Miyaura, *Organometallics* **1996**, *15*, 713.
[3] G. Lesley, P. Nguyen, N. J. Taylor, T. B. Marder, A. J. Scott, W. Clegg, N. C. Norman, *Organometallics* **1996**, *15*, 5137.
[4] C. N. Iverson, M. R. Smith III, *Organometallics* **1996**, *15*, 5155.
[5] [5a] C. Chambers, A. K. Holliday, S. M. Walker, *Proc. Chem. Soc.* **1964**, 286. – [5b] C. Chambers, A. K. Holliday, *J. Chem. Soc.* **1965**, 3459.
[6] P. Frankhauser, F. Kuhlmann, A. Krämer, H. Pritzkow, W. Siebert, *Chem. Ber.* **1993**, *126*, 1291.
[7] B. Wrackmeyer, H.-J. Schanz, M. Hofmann, P. v. R. Schleyer, *Angew. Chem.* 1998**,** *110*, 1329, *Angew. Chem. Int. Ed. Engl.* **1998**, *37*, 1245.
[8] C. N. Iverson, M. R. Smith III, *Organometallics* **1997**, *16*, 2757.
[9] T. Ishiyama, M. Yamamoto, N. Miyaura, *Chem. Comm.* **1997**, 689.
[10] J. E. Dobson, P. M. Tucker, F. G. A. Stone, R. Schaeffer, *J. Chem. Soc., A* **1969**, *12*, 1882.
[11] M. Bluhm, Diploma thesis, Universität Heidelberg, **1997**.
[12] C. Ester, part of the planned PhD thesis, Universität Heidelberg, **1999**.
[13] M. Goll, Diploma thesis, Universität Heidelberg, **1998**.
[14] A. Maderna, H. Pritzkow, W. Siebert, *Angew. Chem.* **1996**, *108*, 1664, *Angew. Chem. Int. Ed. Engl.* **1996**, *35*, 1501.
[15] Q. Cui, D. G. Musaev, K. Morokuma, *Organometallics* **1997**, *16*, 1355.
[16] H. Schulz, G. Gabbert, H. Pritzkow, W. Siebert, *Chem. Ber.* **1993**, *126*, 1593.
[17] A. Maderna, PhD thesis Universität Heidelberg, **1997**.
[18] M. Bluhm, part of the planned PhD thesis, Universität Heidelberg, **1999**.
[19] W. Siebert, U. Ender, W. Herter, *Z. Naturforsch.* **1985**, *40b*, 326.
[20] C. N. Iverson, M. R. Smith III., *J. Am. Chem. Soc.* **1995**, *117*, 4403.
[21] H. Braunschweig, *Angew. Chem.* **1998**, *110*, 1882, *Angew. Chem. Int. Ed. Engl.* **1998**, *37*, 1786.
[22] W. Clegg, F. J. Lawlor, G. Lesley, T. B. Marder, N. C. Norman, A. G. Orpen, M. J. Quayle, C. R. Rice, A. J. Scott, F. E. S. Souza, *J. of Organometallic Chemistry* **1998**, *550*, 183.
[23] M. J. Frisch, G. W. Trucks, H. B. Schlegel, P. M. W. Gill, B. G. Johnson, M. A. Robb, J. R. Cheeseman, T. Keith, G. A. Petersson, J. A. Montgomery, K. Raghavachari, M. A. Al-Laham, V. G. Zakrzewski, J. V. Ortiz, J. B. Foresman, J. Cioslowski, B. B. Stefanov, A. Nanayakkara, M. Challacombe, C. Y. Peng, P. Y. Ayala, W. Chen, M. W. Wong, J. L. Andres, E. S. Replogle, R. Gomperts, R. L. Martin, D. J. Fox, J. S. Binkley, D. J. Defrees, J. Baker, J. P. Stewart, M. Head-Gordon, C. Gonzalez, and J. A. Pople, *GAUSSIAN94, Revision E.2*, Gaussian Inc., Pittsburgh PA, **1995**.
[24] A. E. Reed, L. A. Curtis, F. Weinhold, *Chem. Rev.*, **1988**, *88*, 899.
[25] T. Koopmans, *Physica* **1934**, *1*, 104.
[26] C. N. Welch, S. G. Shore, *Inorg. Chem.* **1968**, *7*, 225.
[27] C. D. Cook, G. S. Jauhal, *J. Am. Chem. Soc.* **1968**, *90*, 1464.
[28] G. E. Herberich, B. Heßner, *Z. Naturforsch.* **1979**, *84b*, 638.
[29] G.M. Sheldrick, *SHELXS86*, Univ. Göttingen, **1986**.
[30] G.M. Sheldrick, *SHELXS97*, Univ. Göttingen, **1997**.

Received April 9, 1999
[I99127]

Te...Te Interlayer Interactions, Te → Metal Electron Transfer and Electrical Conductivity in the $MM'Te_5$ Phases (M = Nb, M′ = Ni, Pd; M = Ta, M′ = Ni, Pt)

Pere Alemany*[a] and Enric Canadell*[b]

Keywords: Ternary Tellurides / Conductivity / Electronic structure / Layered compounds / Low-dimensional metals.

The layered ternary tellurides $NbNiTe_5$, $TaNiTe_5$, $TaPtTe_5$ and $NbPdTe_5$ are all metallic, but the conductivity of the latter is between one and two orders of magnitude smaller. A tight binding study of the electronic structure of these phases suggests that the large conductivity difference results from the different Te···Te interlayer interactions and the Te → M (M = Nb, Ta) electron transfer that they induce.

Introduction

Several ternary transition metal tellurides are layered materials and exhibit metallic behavior.[1][2] Thus, one could expect that these materials may show the low temperature structural modulations and resistivity anomalies characteristic of many low-dimensional metals.[3][4] However this seems not to be the case.[5] The most likely reason for this unexpected behavior lies in the many short Te...Te interactions which these materials possess. As shown by several theoretical studies,[6–8] such interactions exert a strong control over the electronic structure in the region around the Fermi level. The mechanism by which the interlayer Te...Te interactions control the structural or transport properties of these materials is by raising the top of the tellurium bands which, as a consequence, overlap (or increase the overlap) with the transition metal d-block bands. This has two consequences. First, there is a Te → metal electron transfer so that the transition metal atom is really in an oxidation state somewhat lower than that expected from the stoichiometric formula and usual ideas concerning transition metal and chalcogen oxidation states. For instance, the layered binary telluride $NbTe_2$, in which the Nb atoms are formally d^1, exhibits a structure with double zigzag chains which would be expected if Nb was really $d^{4/3}$.[9] Theoretical calculations have shown that the Te → Nb electron transfer does indeed occur.[6b,9] Second, the density of states at the Fermi level, which has a strong control over the conductivity of these metallic systems, can be significantly affected. We have recently suggested that the large difference in the metallic conductivity (one order of magnitude) of the two structurally related tellurides $Ta_3Pd_3Te_{14}$ and $Ta_4Pd_3Te_{16}$, can be rationalized on the basis of the different density of states at the Fermi level for the two phases, and that such a difference is largely imposed by the interlayer Te...Te interactions.[7]

A series of ternary layered tellurides exhibiting interesting conducting properties is that of the $MM'Te_5$ (M = Nb, M′ = Ni, Pd; M = Ta, M′ = Ni, Pt) phases.[1] All of these systems are metallic but one of them, $NbPdTe_5$, is between one and two orders of magnitude less conducting than the other three. The $NbNiTe_5$, $TaNiTe_5$ and $TaPtTe_5$ phases have similar conductivities. The layers of the four salts are of the same type but, interestingly, the interlayer stacking is the same for the three phases with similar conductivity and differs from that of the less conducting phase.[1] This immediately suggests that the Te...Te interlayer interactions must exert a strong control over the conductivity of these phases also.[1d] Thus, we felt it would be interesting to study the possible relationship between the interlayer Te...Te interactions and the conductivity of the four $MM'Te_5$ phases.

The calculations reported here are of the extended Hückel type[10] with the exponents and parameters summarized in Table 1. The electronic structure of $NbNiTe_5$ and $NbPdTe_5$ was studied by Halet et al[8] some years ago. However, as briefly discussed above, the understanding of the role of the Te...Te interactions in determining the electronic structure of ternary tellurides has considerably progressed in recent years so that we thought it was of interest to reexamine some aspects of the electronic structure of these phases. Here we will concentrate on the possible relationship between the Te...Te interlayer interactions, Te → metal electron transfer and conductivity for this interesting family of solids and refer the reader to the work of Halet et al[8] for a more complete discussion of the relationship between the geometrical and electronic structure of the $MM'Te_5$ layers.

Results and Discussion

Crystal Structure and Te···Te Short Contacts

The electronic structure of these materials is very complex[8] so that it is very important to clearly understand

[a] Departament de Química-Física and
Centre Especial de Recerca en Química Teòrica,
Universitat de Barcelona, Diagonal 647,
08028 Barcelona, Spain.
Fax: (internat.) + 34-93/4021231
E-mail: pere@linus.qui.ub.es
[b] Institut de Ciència de Materials de Barcelona (CSIC),
Campus de la U.A.B., 08193 Bellaterra, Spain.
Fax: (internat.) + 34-93/5805729
E-mail: canadell@icmab.es

 © WILEY-VCH Verlag GmbH, D-69451 Weinheim, 1999 1434–1948/99/1010–1701 $ 17.50+.50/0

Table 1. Exponents and parameters used in the calculations.[a]

atom	orbital	H_{ii} (eV)[b]	ζ_1	ζ_2	c_1[c]	c_2[c]
Nb	5s	−6.71	1.89			
	5p	−3.88	1.85			
	4d	−8.14	4.08	1.64	0.6401	0.5516
Ta	6s	−6.89	2.28			
	6p	−3.94	2.24			
	5d	−8.03	4.76	1.94	0.6597	0.5589
Ni	4s	−8.13	2.10			
	4p	−4.18	2.10			
	3d	−12.40	5.75	2.30	0.5683	0.6292
Pd	5s	−7.55	2.19			
	5p	−4.06	2.15			
	4d	−13.76	5.98	2.613	0.5264	0.6372
Pt	6s	−7.69	2.55			
	6p	−4.13	2.55			
	5d	−13.53	6.01	2.696	0.6334	0.5513
Te	5s	−18.78	2.51			
	5p	−10.16	2.16			

[a] A modified Wolfsberg-Helmholz formula (J. Ammeter, H.-B. Bürgi, J. Thibeault, R. Hoffmann, *J. Am. Chem. Soc*. **1978**, *100*, 3686) was used to calculate the off-diagonal H_{ij} values. – [b] A. Vela, J. L. Gázquez, *J. Phys. Chem*. **1988**, *92*, 5688. – [c] Contraction coefficients used in the double-ζ expansion.

what are the key aspects of the crystal structure on which we must concentrate when trying to understand the band structure calculations to be reported in the next sections. There are different ways to describe the crystal structure of a solid depending on the particular aspect one wishes to examine. Since the conductivity of a metal is dominated by the levels near the Fermi level, the appropriate structural description should be that leading to a qualitative feeling of the nature and structural dependency of such levels. As shown in Figure 1a, the $MM'Te_5$ layers present in the $MM'Te_5$ phases can be considered to result from the condensation of MTe_3 face sharing trigonal prismatic chains and $M'Te_3$ edge sharing octahedral chains. Because of the condensation, the M atoms form two additional bonds with the Te atoms of the adjacent octahedral chains so that they are really in a bicapped trigonal prismatic environment. Consequently, the $MM'Te_5$ layers can be simply described as a series of bicapped trigonal prismatic MTe_5 chains glued by the M′ atoms which reside in the octahedral holes in between them.

The previous description has an important implication. As already discussed,[7] these bicapped trigonal prismatic (btp) chains lead to five chains of direct Te...Te short contacts (see Figure 1a) as well as to four zigzag chains of Te...Te short contacts formed by the capping Te atoms and those of the triangular basis of the prisms (i.e., the four zigzag chains, two of *n* contacts and two of *o* contacts, shown in Figure 1b). The Te p orbitals parallel to these chains (both along the zigzag and direct chains) are very well oriented to make very strong overlaps and lead to very strongly dispersive Te-based bands which cross the Fermi level and are responsible for the above mentioned Te → metal electron transfer. Thus, it is tempting to consider the pentagonal shaped columns of Te atoms glued together by the M and M′ atoms as the essential building blocks that we should use in order to try to understand what happens near the Fermi level.

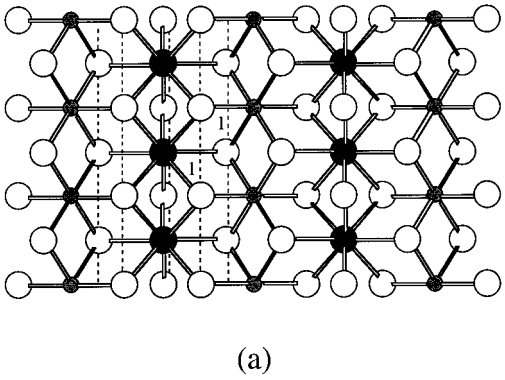


Figure 1a. View of a $MM'Te_5$ layer along a direction perpendicular to the slab.

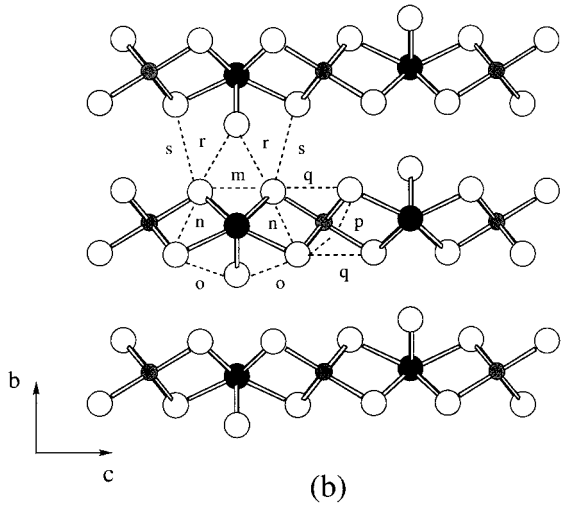


Figure 1b. Projection view of the crystal structure of $NbNiTe_5$, $TaNiTe_5$ and $TaPtTe_5$ along the *a* axis.

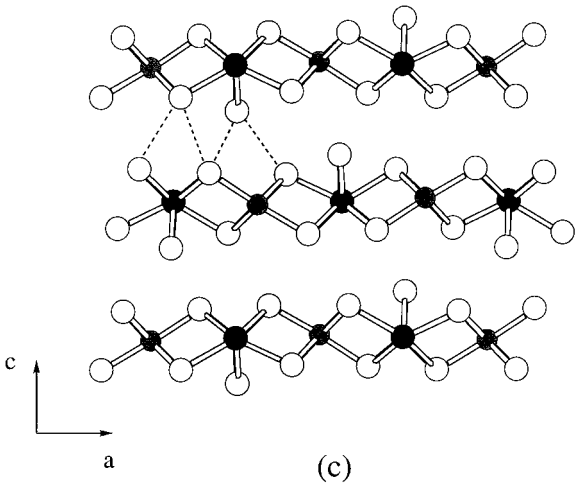


Figure 1c. Projection view of the crystal structure of $NbPdTe_5$ along the *b* axis. Large black circles represent the M atoms (Nb, Ta), large open circles the Te atoms and smaller grey circles the M′ atoms (Ni, Pd, Pt). The Te···Te contacts discussed in the text have been shown as dotted lines.

If we proceed along this line, we should next consider how these Te columnar units interact. Obviously, they interact along the intralayer intercolumn direction through the M′−Te bonds. However, the bonding and antibonding M′−Te levels are far from the Fermi level. The levels of the columnar units crossing the Fermi level must be Te-based so that the intercolumn interactions along the layer must be dominated by the direct Te...Te intercolumn contacts. There are five Te...Te short contacts of this type per formula unit. If for instance we look at the $NbNiTe_5$ structure these contacts are 3.623 Å and 3.788 Å(×4) (see contacts *p* and *q* in Figure 1b, respectively). Of course, these contacts should have a non-negligible but comparatively smaller influence than the intracolumn ones on the dispersion of the above mentioned Te very wide bands. Not only the orbital orientation is much better along the columns but there are more and considerably shorter intracolumn Te...Te contacts: 3.331 Å (×4), 3.460 Å (×4), 3.656 Å (×5) for $NbNiTe_5$ (see contacts *o*, *n* in Figure 1b and *l* in Figure 1a, respectively). There is another very short intracolumn Te...Te contact (3.196 Å in $NbNiTe_5$, see *m* in Figure 1b) which is perpendicular to the chain direction and is going to play an important role in our discussion (see later).

The way in which the layers order relative to each other for $NbNiTe_5/TaNiTe_5/TaPtTe_5$ and $NbPdTe_5$ is shown in Figures 1b and 1c, respectively. The btp chains in one layer are aligned with those in the next layer in Figure 1b ($NbNiTe_5/TaNiTe_5/TaPtTe_5$) whereas this is not the case in Figure 1c ($NbPdTe_5$). Of course, this leads to somewhat different Te...Te contacts, those in $NbPdTe_5$ being shorter. However, at this point, the important aspect we would like to scrutinize is the possible strength of these Te...Te contacts with respect to the intercolumn intralayer ones. In $NbNiTe_5$ there are six interlayer contacts: 3.789 Å (×4) and 3.931 Å (×2) (see contacts *r* and *s* in Figure 1b, respectively). Thus, for the time being, and just on the basis of the crystal structure information, we may suggest that the influence of the Te...Te intralayer and interlayer intercolumn contacts on the dispersion of the Te levels near the Fermi level should not be that different. We conclude that around the Fermi level there should be Te bands with very large dispersion along the direction of the Te columns and only a moderate one along *both* the intralayer and interlayer intercolumn directions.

Can the M and M′ levels be completely neglected as seems to be suggested by the previous discussion? As already mentioned, the M′-based bands (M′ being a very electronegative metal atom) will be far from the Fermi level and thus we can ignore them in our qualitative scheme. However this is not the case for the low-lying M-based ones. The very wide Te-based bands will cross some of the low-lying M-based bands, which would be empty if it were not for the existence of such wide Te bands, and lead to the Te → metal electron transfer. Thus, some of the low-lying *d* levels of the M atoms can play a very important role in understanding the electronic structure of the $MM'Te_5$ phases near the Fermi level and this is why, coming back to the beginning of this section, we propose that the MTe_5 btp chains are the more convenient building blocks to be used in discussing the relationship between the electronic structure and electrical conductivity of the $MM'Te_5$ phases.

Band Structure of the $MM'Te_5$ Phases

The calculated band structures for a single layer and the three dimensional structure of $TaNiTe_5$ are shown in Figures 2a and 2b, respectively. It should be remembered that the unit cell of $TaNiTe_5$ contains two $TaNiTe_5$ layers. Because of the overall similarity of the results we will only discuss here those concerning $TaNiTe_5$, although a similar study has been carried out for all the phases of this family.

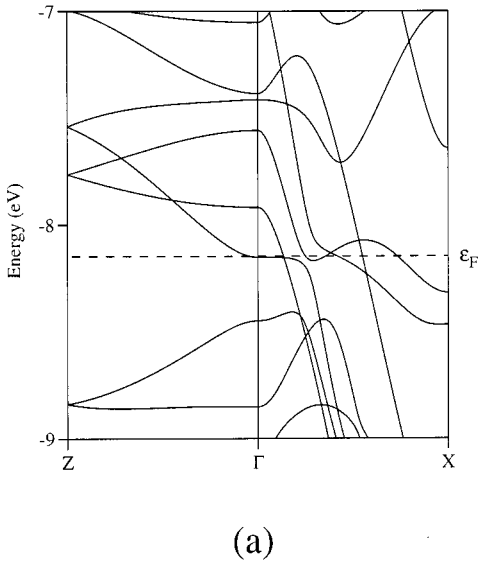


Figure 2a. Calculated dispersion relations for a single layer of $TaNiTe_5$.The Γ, X and Z labels in refer to the wave vector points (0, 0), (*a**/2, 0) and (0, *c**/2), respectively. The dashed line refers to the Fermi level.

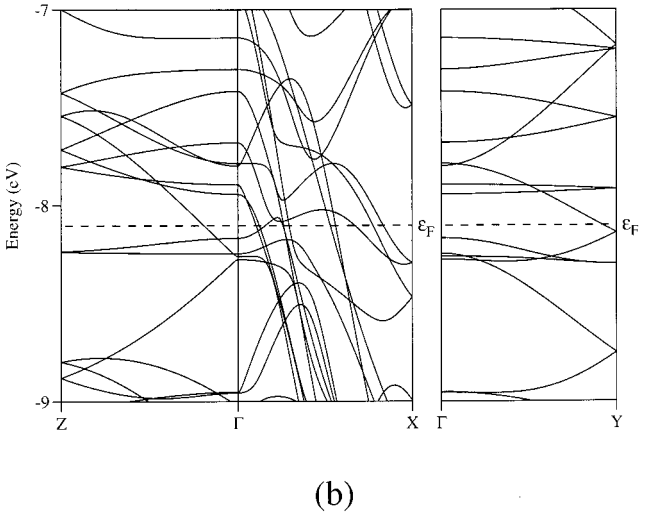


Figure 2b. Calculated dispersion relations for the 3D structure of $TaNiTe_5$, where the dashed lines refer to the Fermi level. The labels Γ, X, Y and Z refer to the wave vector points (0, 0, 0), (*a**/2, 0, 0), (0, *b**/2, 0) and (0, 0, *c**/2), respectively.

The most important observations based on the calculated band structures are the following. First, the 3D band structure is not just the superposition of twice that of a single layer. Indeed, some bands split considerably when introducing the interlayer interactions (compare for instance the two band structures along the $\Gamma \rightarrow Z$ direction). This is also clear when looking at the $\Gamma \rightarrow Y$ direction in Figure 2b (i.e., along the b^*-direction, b being the interlayer direction): some bands which cross or lie near the Fermi level have a quite sizeable dispersion. Thus, it is clear that the interlayer Te...Te interactions cannot be neglected. Second, there are several extremely wide bands along the $\Gamma \rightarrow X$ direction (i.e., along the a^*-direction, a being the propagation direction of the btp chains) which are mainly Te in character and which cross the Fermi level, as expected from the presence in these phases of Te-based btp chains. Third, in the region around the Fermi level these wide bands cross two bands per layer which are much less dispersive and are mainly Ta (or Nb in the $MNbTe_5$ phases) in character. Fourth, the dispersion of most of the bands along the $\Gamma \rightarrow X$ direction is very large but those along the $\Gamma \rightarrow Y$ and $\Gamma \rightarrow Z$ directions (i.e., the interlayer and intralayer interchains directions, respectively) are smaller but non-negligible and of the same order of magnitude along both directions.

The first and fourth observations make the importance of the interlayer Te...Te interactions clear and, maybe more surprisingly, the fact that the interlayer interactions are as strong as the intralayer interchain interactions. The second and third observations clearly show that there is an important electron transfer from Te to Ta (or Nb in the $MNbTe_5$ phases). Of course, this transfer is something inherent to the $MM'Te_5$ layers (see Figure 2a) but it is importantly affected by the interlayer Te...Te interactions. These conclusions are common to the four $MM'Te_5$ phases and completely validate the qualitative discussion of the previous section. From the viewpoint of the electrical conductivity our study suggests that these phases must be 3D metals although with a strong anisotropy, i.e., the conductivity should be much higher along the btp chain direction. The only difference between the $NbPdTe_5$ and the $NbNiTe_5$/$TaNiTe_5$/$TaPtTe_5$ phases is that the Fermi level does not cut bands along the interlayer $\Gamma \rightarrow Y$ direction for $NbPdTe_5$; there is a relatively small band gap along this direction. This fact is probably inherent to the different interlayer stacking and is not a parameter dependent feature because it was also noted by Halet et al[8] who used a different set of parameters in their calculations. Thus, $NbPdTe_5$ should have a weaker 3D metallic character than the other three $MM'Te_5$ phases. However, we should not conclude that the smaller conductivity of $NbPdTe_5$ originates from this fact because the conductivity of these phases is largely dominated by the Te...Te interactions along the btp chain direction. We must look in more detail at the electronic structure before discussing this point.

Our previous work[7] on the ternary tellurides $Ta_3Pd_3Te_{14}$ and $Ta_4Pd_3Te_{16}$ showed how the interlayer Te...Te interactions are responsible for the large difference in the density of states at the Fermi level [$N(\varepsilon_f)$] between the two phases and we proposed that this fact was at the heart of the large difference in conductivity between the two phases. Both the qualitative discussion of section 2 and the band structure calculations, suggest that the interlayer Te...Te interactions must also be very important in determining the conductivity of the $MM'Te_5$ phases whereas the nature of the M′ transition metal atom should not play a major role. That the conductivity and the strength of the Te...Te interlayer interactions should be correlated can be seen in Figure 3a where we have plotted the room temperature conductivity of the four $MM'Te_5$ phases vs the shortest Te...Te interlayer contact (such a correlation has already been noted previously[1a]). The four $MM'Te_5$ phases appear perfectly aligned in this plot and $NbPdTe_5$ is clearly separated from the other three phases, the shorter interlayer Te...Te contacts being associated with the smaller conductivities.

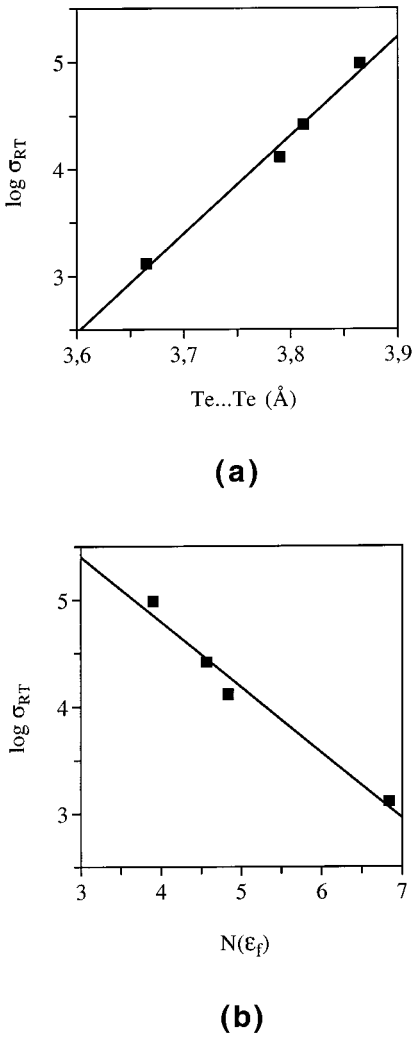


Figure 3. (a) Plot of the log σ_{RT} (σ_{RT}: room temperature conductivity) vs the shortest Te···Te interlayer contact for the $MM'Te_5$ phases. (b) Plot of the log σ_{RT} vs the calculated density of states at the Fermi level $N(\varepsilon_f)$ for the $MM'Te_5$ phases.

Figure 3b shows a plot of the room temperature conductivity versus the calculated $N(\varepsilon_f)$ for the $MM'Te_5$ phases. Contrary to intuitive expectations, the conductivity increases as $N(\varepsilon_f)$ decreases. This result is also obtained when

the $N(\varepsilon_f)$ calculated for a single layer is used. Thus, it is clear that the situation in the $MM'Te_5$ series is very different from that in the $Ta_3Pd_3Te_{14}$ and $Ta_4Pd_3Te_{16}$ phases: the $N(\varepsilon_f)$ cannot be taken as a basis for understanding the conductivity differences in the $MM'Te_5$ phases. In fact, these results should not be that surprising given that there are many bands crossing the Fermi level and that some of them are quite flat for large zones of the Brillouin zone. In other words, with such a complex situation, an increase in $N(\varepsilon_f)$ does not necessarily mean that the conductivity must increase because the mobility of the different types of electrons can be rather different. A fraction of the electrons may be very mobile and delocalized making a strong contribution to the electrical conductivity of the phase and another fraction can behave as localized electrons having a very weak contribution to the electrical conductivity. As a matter of fact, the magnetic susceptibility of the metallic phases $NbNiTe_5$ and $TaNiTe_5$ is temperature dependent[1d] as if there were localized electrons as well as delocalized electrons in these phases. For $TaPtTe_5$ and $NbPdTe_5$ the magnetic susceptibility is temperature independent as expected for a normal metal.[1d] Thus, there seems to be a strong competition between a localized vs delocalized behavior for some of the electrons near the Fermi level in the $MM'Te_5$ phases so that it is not really surprising that there is no correlation between the calculated values of the $N(\varepsilon_f)$ and the conductivity.

Te...Te Interlayer Interactions, Te → M (M = Nb, Ta) Electron Transfer and Conductivity of the $MM'Te_5$ Phases

At this point we would like to have a closer look at the Te → metal electron transfer induced by the Te...Te interlayer interactions mentioned above. As expected, the Te → M′ electron transfer (M′ = Ni, Pd, Pt) is very small (0.014, 0.017, 0.021 and 0.041 electrons per M′ atom for $TaPtTe_5$, $TaNiTe_5$, $NbNiTe_5$ and $NbPdTe_5$, respectively). The Te → M electron transfer (M = Nb, Ta) is quite strong (0.129, 0.157, 0.189 and 0.267 electrons per M atom for $TaPtTe_5$, $TaNiTe_5$, $NbNiTe_5$ and $NbPdTe_5$, respectively). As shown in Figure 4a, there is a clear correlation between the strength of this Te → M electron transfer and the shorter Te...Te interlayer contacts. The transfer increases when the Te...Te interlayer contacts become shorter, i.e., the interlayer Te...Te interactions become stronger. Interestingly, the four $MM'Te_5$ phases appear perfectly aligned in this plot and $NbPdTe_5$ is clearly separated from the other three phases. These results make clear the relationship between the Te...Te interlayer interactions and the very important electron transfer that they induce. Since we noted the excellent correlation between the conductivity and the Te...Te interlayer interactions (see Figure 3a) it is not surprising to find also an excellent correlation between the conductivity and the strength of the Te → M electron transfer (see Figure 4b).

In order to analyze the nature of this electron transfer we carried out calculations in which the Te...Te interlayer

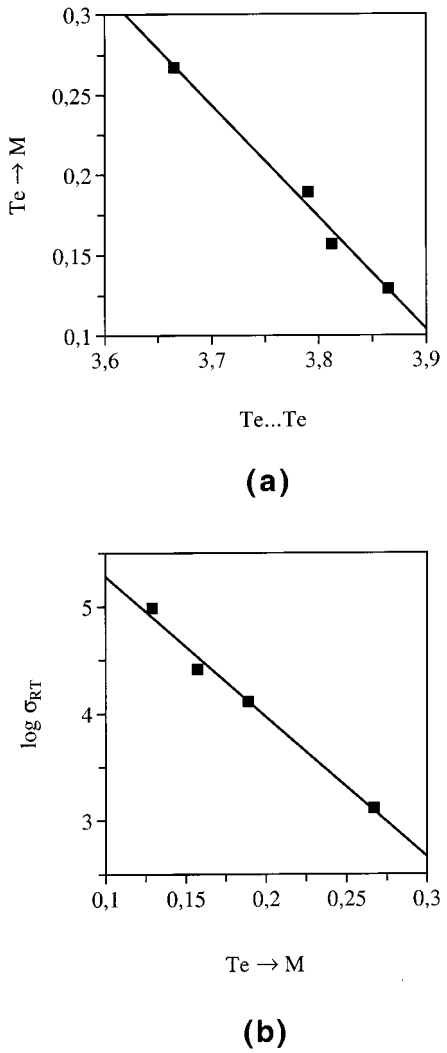


Figure 4. (a) Plot of the Te → M (M = Nb, Ta) electron transfer due to the interlayer Te···Te interactions vs the shortest Te···Te interlayer contact for the $MM'Te_5$ phases. (b) Plot of the log σ_{RT} vs the Te → M (M = Nb, Ta) electron transfer induced by the interlayer Te···Te interactions for the $MM'Te_5$ phases.

overlaps were deleted and we compared the results with those for the full calculations. The electrons are mainly transferred from the two Te atoms forming the shorter side (3.196 Å in $NbNiTe_5$) of the triangular faces of the prisms (see contact *m* in Figure 1b). In fact they are transferred from the bonding combination of the two p orbitals of these atoms perpendicular to the layer, i.e., from a bonding π-type orbital. These Te p orbitals interact very well with the p orbital of the two capping Te atoms which is parallel to the direction of the btp chain. They are also those pointing towards the next layer and implicated in the shorter interlayer Te...Te short contacts. Of course, the overlap population of the shorter Te−Te triangular side decreases when the Te...Te interlayer interactions are switched on. Assuming that the local x, y and z coordinates point approximately towards the *a*, *b* and *c* directions of Figure 1b, the electrons are transferred towards an M orbital which can be described as x^2-y^2 which mixes in some z^2 character, in

other words, an orbital which is in between an x^2-y^2 orbital and a z^2 orbital.

Coming back to our main purpose, we suggest that it is the Te → M electron transfer induced by the interlayer interactions which lies behind the conductivity differences for the $MM'Te_5$ phases. The reason is the following: because of the Te → M electron transfer, the electrons dominating the conductivity of the $MM'Te_5$ phases, i.e., the Te-based electrons near the Fermi level, are less screened from the core attractive forces of the Te atoms engaged in the Te → M electron transfer. Consequently, they are more tightly bound and their contribution to the conductivity is reduced.[11] In chemical terms, the Te atoms engaged in the electron transfer behave as ′more electronegative′ because of the electron transfer and attract more strongly their electrons. This effect will increase with the strength of the Te...Te interlayer interactions making less metallic the $MM'Te_5$ phases with stronger interlayer Te...Te interactions.

Let us remember that the electrons transferred leave a Te−Te bonding orbital located in the shorter side of the triangular faces of the prisms. Thus, the conductivity of the $MM'Te_5$ phases and the length of this Te...Te short contact should be correlated: as the Te → M electron transfer increases, the Te...Te short contact should increase and the conductivity decrease. In fact, this is the case. According to the presently available crystal structures[1] this Te...Te short contact is 3.153 Å for $TaPtTe_5$, 3.183 Å for $TaNiTe_5$, 3.196 Å for $NbNiTe_5$ and 3.242 Å for $NbPdTe_5$. This is in excellent agreement with the conductivity of these phases which decreases in the same order. Thus, we believe that even if our argument is very simple and naive, it grasps the essential feature underlying the conductivity behavior of these phases.

Finally, concerning the two structurally related $Ta_3Pd_3Te_{14}$ and $Ta_4Pd_3Te_{16}$ phases, we would like to point out that the former, which has a conductivity one order of magnitude smaller than the latter, also has a larger Te → M electron transfer and the shortest interlayer Te...Te contacts. Thus, the argument developed here should also work for these phases. However, $Ta_3Pd_3Te_{14}$ also has a considerably smaller density of states at the Fermi level so that it is not clear which of the two effects really leads to the difference in conductivity. Magnetic susceptibility measurements could be helpful in scrutinizing this point.

Conclusions

In summary, we believe that the present work provides a simple explanation for the long standing problem of the conductivity differences in the $MM'Te_5$ phases. It also provides additional evidence for the important role that interlayer Te...Te interactions can play in modulating the conductivity of metallic layered tellurides.

Acknowledgments

This work was supported by the DGES-Spain Projects PB96-0859 and PB95-0848-C02-01 and by Generalitat de Catalunya (1997 SGR 24 and 1997 SGR 072). E. C. would like to thank Dr. J. Fontcuberta (ICMAB) for a very helpful discussion

[1] [1a] E. W. Liimatta, J. A. Ibers, *J. Solid State Chem*. **1987**, *71*, 384. – [1b] E. W. Liimatta, J. A. Ibers, *J. Solid State Chem*. **1988**, *77*, 141. – [1c] E. W. Liimatta, J. A. Ibers, *J. Solid State Chem*. **1989**, *78*, 7. – [1d] A. Mar, J. A. Ibers, *J. Solid State Chem*. **1991**, *92*, 352.

[2] [2a] A. Mar, J. A. Ibers, *J. Chem. Soc. Dalton Trans.* **1991**, 639. – [2b] A. Mar, J. A. Ibers, *J. Solid State Chem*. **1992**, *97*, 366. – [2c] M. F. Mansuetto, P. M. Keane, J. A. Ibers, *J. Solid State Chem*. **1992**, *101*, 257. – [2d] J. F. Mitchell, J. K. Burdett, P. M. Keane, J. A. Ibers, D. C. DeGroot, T. P. Hogan, J. L. Schindler, C. R. Kannewurf, *J. Solid State Chem*. **1992**, *99*, 103. – [2e] A. Mar, J. A. Ibers, *J. Am. Chem. Soc*. **1993**, *115*, 3227. – [2f] J. L. Huang, B. G. Huang, *Acta Crystallogr. A*, **1990**, *46*, C-287. – [2g] B. Huang, B. Shang, J. Huang, *Jiegou Huaxue* **1988**, *7*, 133. – [2h] B. Huang, J. Huang, *Jiegou Huaxue* **1988**, 7, 214. – [2i] B. Huang, J. Huang, S. Liu, *Jiegou Huaxue* **1989**, 8, 145. – [2j] J. Li, M. E. Badding, F. J. DiSalvo, *Inorg. Chem*. **1992**, *31*, 1050. – [2k] J. Li, P. J. Carroll, *Mater. Res. Bull*. **1992**, *27*, 1073. – [2l] Y. Park, D. C. Degroot, J. Schindler, C. R. Kannewurf, M. Kanatzidis, *Angew. Chem. Int. Ed. Engl*. **1991**, *30*, 1325. – [2m] W. Tremel, *Angew. Chem. Int. Ed. Engl*. **1991**, *30*, 840. – [2n] W. Tremel, *J. Chem. Soc., Chem. Commun*. **1991**, 1405. – [2o] W. Tremel, *Angew. Chem. Int. Ed. Engl*. **1992**, *31*, 217. – [2p] J. Neuhausen, W. Tremel, *J. Alloys Comp*. **1994**, *204*, 215. – [2q] J. Neuhausen, W. Finckh, W. Tremel, *Inorg. Chem*. **1995**, *34*, 3823. – [2r] L. Monconduit, M. Evain, F. Boucher, R. Brec, J. Rouxel, *Z, Anorg. Allg. Chemie* **1992**, *616*, 177. – [2s] A. van der Lee, M. Evain, L. Monconduit, R. Brec, V. Petricek, *Inorg. Chem*. **1994**, *33*, 3032. – [2t] M. Evain, L. Monconduit, R. Brec, *J. Solid State Chem*. **1995**, *119*, 394.

[3] J. A. Wilson, F. J. DiSalvo, S. Mahajan, *Adv. Phys.* **1975**, *24*, 117.

[4] E. Canadell, M.-H. Whangbo, *Chem. Rev.* **1991**, *91*, 965.

[5] See for instance the discussion in ref.[2o]

[6] [6a] S. Jobic, P. Deniard, R. Brec, J. Rouxel, A. Jouanneaux, A. Fitsch, *Z. Anorg. Allg. Chem*. **1991**, *598/599*, 199. – [6b] E. Canadell, S. Jobic, R. Brec, J. Rouxel, M.-H. Whangbo, *J. Solid State Chem*. **1992**, *99*, 189. – [6c] E. Canadell, L. Monconduit, M. Evain, R. Brec, J. Rouxel, M.-H. Whangbo, *Inorg. Chem*. **1993**, *32*, 10. – [6d] M. Evain, L. Monconduit, A. van der Lee, R. Brec, J. Rouxel, E. Canadell, *New J. Chem*. **1994**, *18*, 215. – [6e] F. Boucher, V. Zhukov, M. Evain, *Inorg. Chem*. **1996**, *35*, 5050. – [6f] A. Mar, S. Jobic, J. A. Ibers, *J. Am. Chem. Soc*. **1992**, *114*, 8963.

[7] P. Alemany, S. Jobic, R. Brec, E. Canadell, *Inorg. Chem*. **1997**, *36*, 5050.

[8] J.-F. Halet, R. Hoffmann, W. Tremel, E. W. Liimatta, J. A. Ibers, *Chem. Mat*. **1989**, *1*, 451.

[9] M.-H. Whangbo, E. Canadell, *J. Am. Chem. Soc*., **1992**, *114*, 9587.

[10] M.-H. Whangbo, R. Hoffmann, *J. Am. Chem. Soc*. **1978**, *100*, 6093.

[11] J. S. Dugdale, *The Electrical Properties of Metals and Alloys*, Arnold Publ., London, **1977**.

Received March 13, 1999
[I99109]

Hydrido(carbonyl) and Hydrido(carbene) Complexes of Ruthenium

Helmut Werner,*[a] Wolfram Stüer,[a] Birgit Weberndörfer,[a] and Justin Wolf[a]

Dedicated to Professor Dirk Walther on the occasion of his 60th birthday

Keywords: Carbene complexes / Carbonyl complexes / Diazoalkanes / Hydrido complexes / Ruthenium

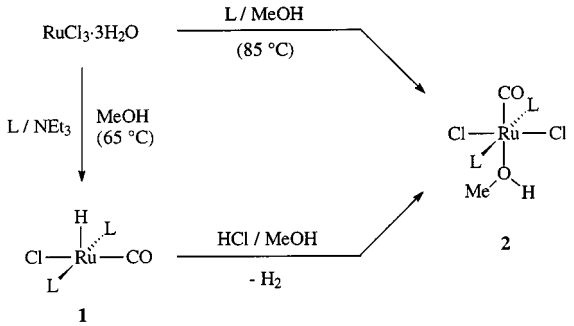
The five-coordinate compound [RuHCl(CO)(P*i*Pr$_2$Ph)$_2$] (**1**), which was prepared from $RuCl_3 \cdot 3\ H_2O$ and P*i*Pr$_2$Ph in methanol in the presence of NEt_3, reacts with CO and with diazoalkanes $RCHN_2$ (R = Ph, H) to give the six-coordinate complexes [RuHCl(CO)$_2$(P*i*Pr$_2$Ph)$_2$] (**4**) and [RuHCl(CO)(=CHR)(P*i*Pr$_2$Ph)$_2$] (**5**, **6**), respectively. If the reaction of **1** with CH_2N_2, which at –78 °C affords **6**, is carried out at room temperature, the ionic compound [MeP*i*Pr$_2$Ph][RuHCl$_2$(CO)(P*i*Pr$_2$Ph)$_2$] (**7**) is formed. The corresponding PPN salt was obtained from **1** and [PPN]Cl. The X-ray crystal structure analysis of **7** revealed, that the anionic species [RuHCl$_2$(CO)(P*i*Pr$_2$Ph)$_2$]$^-$ contains the chloro ligands in *cis* and the phosphanes in *trans* disposition. The Ru=CH$_2$ bond of compound **6** is quite labile and, therefore, the CH$_2$ unit is easily displaced by CO or pyridine. From **1** and pyridine, an isomeric mixture of [RuHCl(CO)(py)(P*i*Pr$_2$Ph)$_2$] (**9a**, **b**) is formed. Treatment of **1** with HC≡CR (R = H, Ph) yields the five-coordinate vinylruthenium(II) complexes [Ru(CH=CHR)Cl(CO)(P*i*Pr$_2$Ph)$_2$] (**12**, **13**) by insertion of the alkyne into the Ru–H bond. The preparation of [RuHX(CO)(P*i*Pr$_2$Ph)$_2$] (X = CF_3CO_2, I) is also reported.

In the search for coordinatively unsaturated complexes with M(P*i*Pr$_3$)$_2$ as a molecular unit, we previously found that treatment of $RuCl_3 \cdot 3\ H_2O$ and $OsCl_3 \cdot 3\ H_2O$ with triisopropylphosphane in methanol leads to the formation of the five-coordinate hydrido(carbonyl)metal compounds [MHCl(CO)(P*i*Pr$_3$)$_2$] (M = Ru, Os) in good to excellent yields.[1] Owing to the free coordination site, these complexes react smoothly with CO, PMe_3, and $P(OMe)_3$ to give the corresponding six-coordinate hydridoruthenium(II) and -osmium derivatives. Further studies revealed that the starting materials [MHCl(CO)(P*i*Pr$_3$)$_2$] are also highly reactive toward terminal acetylenes; however, in this case instead of the anticipated alkyne(hydrido) compounds [MHCl(CO)(HC≡CR)(P*i*Pr$_3$)$_2$] the isomeric insertion products [M(CH=CHR)Cl(CO)(P*i*Pr$_3$)$_2$] are formed.[2]

When we attempted to insert *carbenes* into the M–H bond of the five-coordinate precursors [MHCl(CO)(P*i*Pr$_3$)$_2$], we recently discovered that the complex with M = Os reacts not only with CH_2N_2 but also with substituted diazomethanes $RCHN_2$ by addition of the respective carbene CHR (R = Ph, CO_2Et, $SiMe_3$) to the metal affording the octahedral carbene(hydrido)osmium(II) compounds [OsHCl(CO)(=CHR)(P*i*Pr$_3$)$_2$].[3] In contrast, the ruthenium complex [RuHCl(CO)(P*i*Pr$_3$)$_2$] catalyses the decomposition of diazoalkanes $RCHN_2$ to give olefins RCH=CHR and N_2.[4] Since we knew from our recent work in rhodium chemistry,[5] that both the bulkiness *and* the donor/acceptor capabilities of tertiary phosphanes influences the stability of a carbene-metal bond, we set out to prepare complexes of the general composition [RuHCl(CO)(PR$_3$)$_2$] with phosphanes other than P*i*Pr$_3$. In this paper we report the synthesis of both five-coordinate [RuHCl(CO)(P*i*Pr$_2$Ph)$_2$] and a series of 1:1 adducts including those with CH_2 and CHPh as the additional ligand.

Results and Discussion

Following the procedure used for the preparation of [RuHCl(CO)(P*i*Pr$_3$)$_2$],[1] treatment of a solution of $RuCl_3 \cdot 3\ H_2O$ in methanol with a sixfold excess of P*i*Pr$_2$Ph in the presence of NEt_3 at 65 °C leads to the formation of the analogous chloro(hydrido)ruthenium(II) derivative [RuHCl(CO)(P*i*Pr$_2$Ph)$_2$] (**1**). The yellow, only slightly air-sensitive solid precipitates from the solution in analytically pure form. The ^{1}H-NMR spectrum of **1** displays for each of the four diastereotopic methyl groups of the phosphane ligands a doublet of virtual triplets which is in agreement with the proposed structure. The presence of the hydrido ligand is indicated by the high-field resonance at δ = –24.67 which is split into a triplet due to P-H coupling.



Scheme 1. L = P*i*Pr$_2$Ph

[a] Institut für Anorganische Chemie der Universität Würzburg, Am Hubland, D-97074 Würzburg, Germany

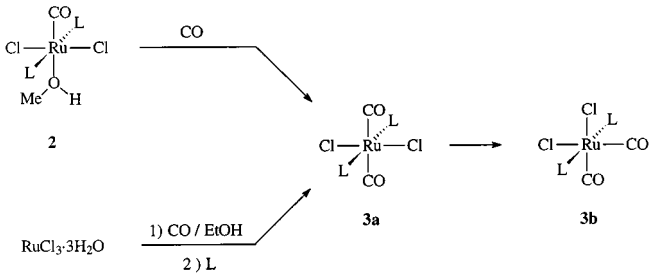
 © WILEY-VCH Verlag GmbH, D-69451 Weinheim, 1999 1434–1948/99/1010–1707 $ 17.50+.50/0

When we changed the reaction conditions in order to increase the yield of compound **1**, we discovered that from $RuCl_3 \cdot 3\,H_2O$, P*i*Pr_2Ph and methanol a by-product is formed besides **1**, which is the six-coordinate dichlororuthenium(II) complex **2** (Scheme 1). After raising the temperature to 85 °C and the time of reaction to 70 h, the isolated yield of **2** was improved to 41%. Moreover, compound **2** is obtained quantitatively upon treatment of the hydrido complex **1** with gaseous HCl in CH_2Cl_2/CH_3OH (1:1). Hereby, the evolution of H_2 is observed. Although it is known that the related hydridoosmium compound $[OsHCl(CO)(P\textit{i}Pr_3)_2]$ reacts with HCl to afford the rather stable dihydrogen complex $[OsCl_2(H_2)(CO)(P\textit{i}Pr_3)_2]$,[6] our attempts to isolate or detect spectroscopically the corresponding 1:1 adduct of **1** and H_2 failed.

With regard to the mechanism of formation of compound **2** from $RuCl_3 \cdot 3\,H_2O$, P*i*Pr_2Ph, and methanol, we assume that initially the chloro(hydrido)ruthenium(II) derivative **1** is generated as an intermediate which, subsequently, reacts with the phosphonium chloride [HP*i*Pr_2Ph]Cl (formed from an excess of P*i*Pr_2Ph) to give **2**. The coordination of methanol to the ruthenium center in **2** is indicated by the appearance of a strong $\tilde{\nu}$(OH) band at 3563 cm^{-1} in the IR spectrum and of a broad singlet (with a relative intensity of 3 H) at $\delta = 2.48$ in the ^{1}H-NMR spectrum. Since the ^{1}H-NMR spectrum of **2** displays only two signals for the PCHC*H*$_3$ protons instead of four as in the case of **1**, we conclude that not only the two phosphanes but also the two chloro ligands are *trans* disposed. A structurally related 1:1 adduct of a dichlororuthenium(II) complex with a weakly bound solvent molecule of the composition $[RuCl_2(H_2O)(CO)(PEt_3)_2]$ was recently isolated by Carty et al. and characterized by an X-ray crystal structure analysis.[7]

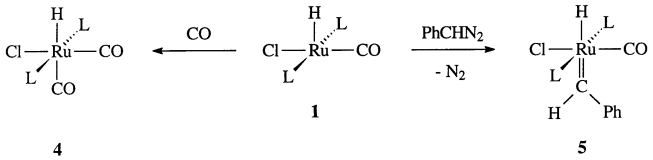
The labile methanol ligand of compound **2** is easily displaced by CO to give the six-coordinate dicarbonyl complex $[RuCl_2(CO)_2(P\textit{i}Pr_2Ph)_2]$ (see Scheme 2). The orange product **3a** initially formed is relatively stable in the solid state but rearranges in solution to the thermodynamically preferred yellow isomer **3b**. An independent synthesis of **3a** consists of the reduction of $RuCl_3 \cdot 3\,H_2O$ by CO in the presence of ethanol, followed by addition of P*i*Pr_2Ph. Since the IR spectrum of **3a** exhibits *one* and that of **3b two** CO stretching frequencies, we assume that **3a** is the *all-trans* and **3b** the *cis,cis,trans* isomer. A similar conclusion was drawn by Nelson et al. who prepared, also from $RuCl_3 \cdot 3\,H_2O$ as the starting material, two isomeric forms of the ruthenium(II) compound $[RuCl_2(CO)_2(PPh_3)_2]$.[8]

The five-coordinate chloro(hydrido) complex **1** is also highly reactive toward CO and affords in the presence of carbonmonoxide in ether the dicarbonyl derivative **4** in quantitative yield (Scheme 3). The open coordination site of the precursor compound **1**, however, cannot only be occupied by CO but also by phenylcarbene. If a solution of **1** in toluene is treated dropwise with a solution of $PhCHN_2$ in hexane, a change of color from yellow to orange occurs and the evolution of gas (N_2) is observed. After removal of the solvent and recrystallization from toluene an orange



Scheme 2. L = P*i*Pr_2Ph

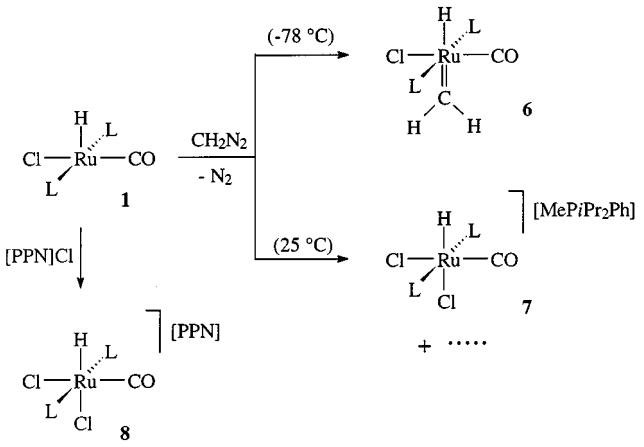
solid is isolated which according to the elemental analysis and the spectroscopic data represents the six-coordinate ruthenium(II) complex **5**. The fact, that the carbene(hydrido) and not the isomeric benzyl compound $[Ru(CH_2Ph)Cl(CO)(P\textit{i}Pr_2Ph)_2]$ is formed, is clearly indicated by the ^{1}H-NMR spectrum, which displays besides the signals for the two phosphanes a doublet of triplets for the hydrido ligand at high field ($\delta = -2.77$) as well as a broadened singlet for the carbene C*H*Ph proton at low field ($\delta = 18.22$). The ^{13}C-NMR spectrum of **5** exhibits resonances at $\delta = 343.4$ and 203.3 which are assigned to the Ru=*C*HPh and Ru-*C*O carbon atoms, respectively.



Scheme 3. L = P*i*Pr_2Ph

The parent diazoalkane CH_2N_2 behaves similarly to $PhCHN_2$ and reacts with the starting material **1** to yield the hydrido(methylene) complex **6** (Scheme 4). However, while the phenylcarbene derivative **5** is thermally stable as a solid up to 138 °C and can be stored under argon at room temperature for weeks, the $RuH(CH_2)$ compound **7** decomposes above −50 °C. Thus it could not be characterized by elemental analysis but only by spectroscopic means. Similarly to **5**, the ^{1}H-NMR spectrum of **6** displays a hydride resonance at $\delta = -2.60$ and two signals for the nonequivalent Ru=CH_2 protons at $\delta = 17.38$ and 16.36. The chemical shifts for these signals differ only slightly to those of the related osmium complex $[OsHCl(=CH_2)(CO)(P\textit{i}Pr_3)_2]$, which is, however, in contrast to **6** significantly more stable.[3]

At room temperature, the reaction of **1** with CH_2N_2 led to a different result. If the solution of the two reacting substrates in toluene/ether is stirred for ca. 12 h, a white precipitate is formed which is easily soluble in dichloromethane but almost insoluble in benzene and ether. These properties, together with the analytical data, indicate that an ionic complex of the composition [MeP*i*Pr_2Ph][$RuHCl_2$(CO)(P*i*Pr_2Ph)$_2$] (**7**) is formed. Based on control measurements (in CD_2Cl_2) in an NMR tube we assume that initially the methylene compound **6** is formed as an intermediate which rapidly decomposes to give inter alia the starting material **1** and [MeP*i*Pr_2Ph]Cl. Both compounds then react to afford



Scheme 4. L = P*i*Pr_2Ph

7. The most typical spectroscopic features of **7** are the two resonances in the ^{31}P-NMR spectrum (in CD_2Cl_2) at δ = 40.6 (sharp singlet) and 47.0 (broad singlet) which are assigned to the phosphorus nuclei of the cation and anion, respectively. Since the hydride signal in the ^{1}H-NMR spectrum at 28 °C is also rather broad (but sharpens in CD_2Cl_2 at −50 °C to a triplet with a P-H coupling of 22.4 Hz), we suppose that at room temperature the anion $[RuHCl_2(CO)(PiPr_2Ph)_2]$ partially dissociates in $[RuHCl(CO)(PiPr_2Ph)_2]$ (**1**) and Cl^-. This proposal is in agreement with the observation that upon cooling at −50 °C the ^{31}P-NMR resonance of the anion of **7**, although still relatively broad, is shifted from δ = 47.0 to 43.5, this process being reversible. A similar phenomenon was observed by measuring the ^{31}P-NMR spectrum of $[OsHCl_2(CO)(PiPr_3)_2]^-$ at different temperatures.[4] We note (see Scheme 4) that the PPN-salt **8** of the anion $[RuHCl_2(CO)(PiPr_2Ph)_2]^-$ is obtained as a white solid from **1** and [PPN]Cl in nearly quantitative yield. The IR as well as the ^{1}H-, ^{13}C-, and ^{31}P-NMR spectra of **8** differ only slightly to those of **7** and thus deserves no further comment.

In order to substantiate the exact composition of **7**, a single-crystal X-ray structure analysis was carried out. As Figure 1 reveals, the coordination geometry around the metal center of the anion is distorted octahedral, with the two phosphanes in *trans* and the two chloro ligands in *cis* disposition. The P1−Ru−P2 axis is considerably bent, the bond angle of 163.49(3)° being comparable to that in the related neutral osmium complex $[OsCl_2(=CHPh)(CO)(PiPr_3)_2]$ [167.5(2)°].[3] The most notable detail of the structure of the anion, however, is the significant difference of the Ru−Cl bond lengths. While the bond length between ruthenium and the chloride *trans* to CO is 2.499(1) Å, that between the metal and the chloride *trans* to hydride is 2.618(1) Å. This difference (which is hard to understand owing to the similar *trans* influence of CO and hydride) could be used as an argument to explain the assumed dissociation of the anion $[RuHCl_2(CO)(PiPr_2Ph)_2]$ into **1** and Cl^-. We note that for the two carbonyl(hydrido)iridium(III) complexes $[IrHCl_2(CO)(PiPr_3)_2]$ and $[IrHCl_2(CO)(PPh_3)\{PPh_2(o\text{-}C_6H_4OH)\}]$, both containing a planar $IrHCl_2(CO)$ unit with *cis*-disposed chloro ligands, a similar difference in the Ir−Cl bond lengths of about 0.10 and 0.18 Å, respectively, has been observed.[9][10]

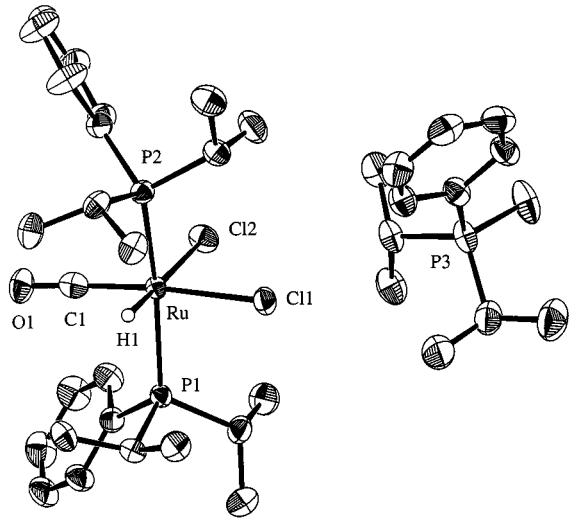
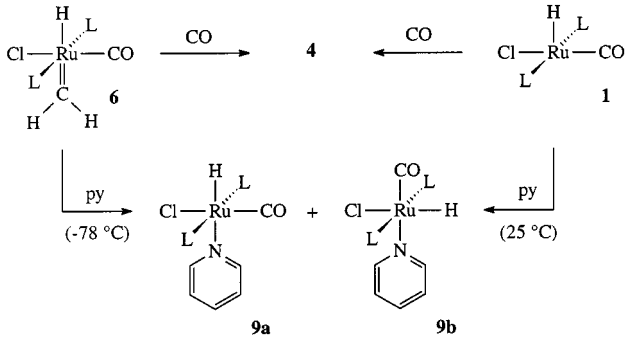


Figure 1. Molecular structure (ORTEP plot) of **7**; the hydrogen atoms besides H1 are omitted for clarity; selected bond lengths [Å] and angles [°]: Ru−P1 2.351(1), Ru−P2 2.358(1), Ru−Cl1 2.499(1), Ru−Cl2 2.618(1), Ru−H1 1.53(2), Ru−C1 1.806(3), C1−O1 1.137(3); P1−Ru−P2 163.49(3), C1−Ru−Cl1 172.71(8), P2−Ru−Cl1 90.81(4), P2−Ru−Cl2 98.41(4), P2−Ru−C1 90.2(1), Cl2−Ru−Cl1 90.31(4), Cl2−Ru−C1 96.67(9), Cl2−Ru−P1 97.97(4), Cl1−Ru−P1 87.04(4), C1−Ru−P1 89.9(1), H1−Ru−P1 84.0(1), H1−Ru−P2 79.5(1), H1−Ru−C1 88.5(1), H1−Ru−Cl1 84.6(1), H1−Ru−Cl2 174.5(1), Ru−C1−O1 176.1(2)

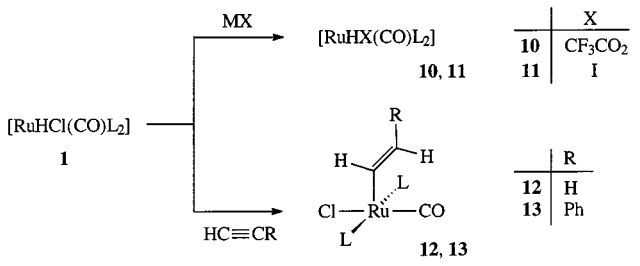
Attempts to initiate an insertion of the carbene ligand into the Ru−H bond of compound **6** by treatment of **6** with Lewis bases such as CO or pyridine led to a displacement of the CH_2 unit. This finding differs with ab initio calculations which predict that for the model system $RuH(=CH_2)Cl$ the conversion into $Ru(CH_3)Cl$ proceeds with a rather low barrier of 11.5 kcal/mol and is exothermic by 7.1 kcal/mol.[11] The model system, however, is coordinatively unsaturated while compound **6** is not. As shown in Scheme 5, the reaction of **6** with CO affords the dicarbonyl complex **4** together with traces of ethene. In contrast, treatment of **6** with pyridine gives a mixture of two isomers **9a** and **9b**, which are also obtained from the five-coordinate starting material **1** and pyridine. Regarding the ligand arrangement of **9a** and **9b**, a plausible assumption is that in one isomer the pyridine is *trans* to hydride and in the other *trans* to CO. The fact, that both the chemical shifts of the hydride signals in the ^{1}H NMR (at δ = −13.54 and −14.41) and of the two resonances in the ^{31}P-NMR spectrum (at δ = 48.9 and 43.8) differ only slightly, seems to be in agreement with this proposal. The alternative, that the hydride and the carbonyl ligands are *trans* to each other, is less likely since in this case, which corresponds to the situation in compound **4**, the hydride signal should be observed at considerably lower field (for **4**: δ = −5.23). In this context we note that Caulton and co-workers recently reported that treatment of $[RuH(OR_F)(CO)(PtBu_2Me)_2]$ (R_F = CH_2CF_3) with pyridine

also produces a mixture of two isomers of the composition $[RuH(OR_F)(CO)(py)(PtBu_2Me)_2]$.[12]



Scheme 5. L = P*i*Pr$_2$Ph

Similarly to $[RuHCl(CO)(PiPr_3)_2]$ and $[OsHCl(CO)(PiPr_3)_2]$, which react with MX by salt metathesis to give the ruthenium(II) and osmium(II) derivatives $[MHX(CO)(PiPr_3)_2]$ (X = Br, I, N_3, OR, SR),[13] the five-coordinate compound **1** can be converted with CF_3CO_2Tl and KJ to the related hydrido(trifluoracetato) and hydrido(iodo) complexes **10** and **11**, respectively (see Scheme 6). While the orange-yellow $RuH(O_2CCF_3)$ species **10**, in analogy to the starting material **1,** is only slightly air-sensitive, the brown hydrido(iodo) compound **11** smoothly decomposes (in solution as well as in the solid state) in the presence of air. Despite the different behavior of **1** and **11** toward O_2, the spectroscopic data of both complexes are quite similar. This is illustrated by the chemical shifts both of the hydride signal (**1**: $\delta = -24.67$; **11**: $\delta = -25.0$) in the ^{1}H-NMR and of the CO resonance (**1**: $\delta = 197.7$; **11**: $\delta = 198.7$) in the ^{13}C-NMR spectra. In contrast, the corresponding NMR spectra of **10** exhibit the signal for the RuH moiety at $\delta = -18.23$ and that for the CO ligand at $\delta = 205.1$. Owing to these data we assume that the CF_3CO_2 unit of **10** is coordinated in a chelating fashion, which increases the coordination number for ruthenium(II) from five (in **1**) to six (in **10**). This structural proposal is supported by the IR spectrum of **10**, in which the symmetrical and the antisymmetrical OCO stretching vibrations appear at 1597 and 1410 cm^{-1}, respectively. According to extensive studies, particularly by Robinson et al.,[14][15] the observed difference of 187 cm^{-1} clearly points to a bidentate, not a monodentate, linkage of the trifluoracetate to the ruthenium center.



Scheme 6. L = P*i*Pr$_2$Ph

As mentioned above, the chloro compound **1** reacts readily with $PhCHN_2$ at room temperature to give the phenylcarbene complex **5** in 42% isolated yield. Contrary to this result, the trifluoracetato and iodo derivatives **10** and **11** are less reactive toward $PhCHN_2$ and upon stirring a solution of the two respective substrates in toluene for 2−4 h a complex mixture of products is formed. We not only failed to separate the mixture but also found no evidence for the presence of a Ru=CHPh species among the various components.

Completely inert toward $PhCHN_2$ are the vinyl complexes **12** and **13**, which have been obtained likewise to the corresponding ruthenium and osmium compounds $[M(CH=CHR)Cl(CO)(PiPr_3)_2]$ (M = Ru, Os; R = H, Ph)[2] from the starting material **1** and acetylene or phenylacetylene, respectively (Scheme 6). Both complexes, **12** and **13**, are moderately air-sensitive solids which are easily soluble in common organic solvents (with the exception of hexane and pentane). The *trans* stereochemistry at the C=C bond of **13** is strongly supported by the large H−H coupling constant for the vinyl protons, which is 14.0 Hz.[16] The ^{13}C-NMR resonances for the $CH=CH_2$ carbon atoms of **12** appear at $\delta = 152.5$ and 120.5, the chemical shifts being quite similar to those of $[Ru(CH=CH_2)Cl(CO)(PiPr_3)_2]$.[2] Attempts to convert compound **12** to the π-allyl complex $[RuCl(\eta^3\text{-}C_3H_5)(CO)(PiPr_2Ph)_2]$ by treatment with CH_2N_2, in analogy to the preparation of $[RuCl(\eta^3\text{-}C_3H_5)(CO)(PPh_3)_2]$ by Hill and co-workers,[17] remained unsuccessful.

In summary, the present investigations have shown that in contrast to $[RuHCl(CO)(PiPr_3)_2]$ the related five-coordinate bis(diisopropylphenylphosphane) complex **1** reacts with CH_2N_2 and $PhCHN_2$ to generate the six-coordinate carbeneruthenium(II) derivatives **5** and **6**. Although theoretical calculations reveal that an insertion of the carbene unit into the Ru−H bond is conceivable, attempts to prepare alkylruthenium compounds from **5** or **6** as a precursor failed. As recent studies by Caulton and Eisenstein indicate,[18] the conversion of a $RuH(CH_2)$ to a $RuCH_3$ unit could be strongly influenced by the phosphane ligands linked to the ruthenium center, the more bulky P*t*Bu$_2$Me being more suitable than P*i*Pr$_3$. We finally note that despite the lability of the carbene−ruthenium bond, which is most obvious in **6,** the complexes **5** and **6** are catalytically inactive in olefin metathesis. Whether this is due to the octahedral geometry, that hinders the addition of an olefin, or to the presence of a Ru−H bond, is open to speculation.

Experimental Section

All operations were carried out under argon using Schlenk techniques. The diazoalkanes CH_2N_2 and $PhCHN_2$[19] were prepared as reported in the literature. All other starting materials were commercial products from Aldrich, Strem and ABCR. − NMR: Bruker AC 200 and AMX 400 [dvt = doublet of virtual triplets; $N = {}^3J(PH) + {}^5J(PH)$ or $^1J(PC) + {}^3J(PC)$, respectively]. − Melting points determined by DTA.

1. Preparation of [RuHCl(CO)(P*i*Pr$_2$Ph)$_2$] (1): A solution of 1.00 g (3.98 mmol) of $RuCl_3 \cdot 3\,H_2O$ in 35 mL of methanol was treated dropwise with 4.63 g (23.8 mmol) of P*i*Pr$_2$Ph. After the solution was stirred for 10 min at room temperature, 1.09 mL (7.88 mmol)

of NEt_3 were added and the mixture was heated for 5 h at 65 °C. After the solution was cooled to room temperature, a yellow precipitate was formed which was filtered, washed twice with 5 mL of methanol, then with 10 mL of pentane and dried in vacuo; yield 1.43 g (65%); m.p. 194 °C (dec.). − IR (KBr): $\tilde{\nu}$ = 2100 cm^{-1} (RuH), 1900 (CO). − ^1H NMR (400 MHz, C_6D_6): δ = 7.72 (m, 4 H, C_6H_5), 7.11 (m, 6 H, C_6H_5), 3.22, 2.62 (both m, 2 H each, PC*H*CH_3), 1.33 [dvt, *N* = 14.4, *J*(HH) = 6.8 Hz, 6 H, PCHC*H*$_3$], 1.25 [dvt, *N* = 16.0, *J*(HH) = 6.8 Hz, 6 H, PCHC*H*$_3$], 1.15 [dvt, *N* = 15.2, *J*(HH) = 7.2 Hz, 6 H, PCHC*H*$_3$], 0.87 [dvt, *N* = 13.2, *J*(HH) = 6.6 Hz, 6 H, PCHC*H*$_3$], −24.67 [t, *J*(PH) = 20 Hz, 1 H, RuH]. − ^{13}C NMR (100.6 MHz, C_6D_6): δ = 197.7 [t, *J*(PC) = 10 Hz, CO], 135.0, 127.9 (both vt, *N* = 11 and 8 Hz, *ortho*- and *meta*-C of C_6H_5), 130.5 (s, *para*-C of C_6H_5), 129.4 (vt, *N* = 35 Hz, *ipso*-C of C_6H_5), 22.5, 20.8 (both vt, *N* = 23 and 22 Hz, P*C*HCH$_3$), 18.5, 18.3, 17.8, 15.5 (all s, PCH*C*H$_3$). − ^{31}P NMR (162.0 MHz, C_6D_6): δ = 55.5 (s). − $C_{25}H_{39}ClOP_2Ru$ (554.1): calcd. C 54.20, H 7.10, Ru 18.24; found C 53.92, H 7.00, Ru 18.45.

2. Preparation of [$RuCl_2$(CO)(MeOH)(P*i*Pr_2Ph)$_2$] (2): a) A solution of 1.00 g (3.98 mmol) of $RuCl_3 \cdot 3\,H_2O$ in 10 mL of methanol was treated dropwise with 1.95 g (10.0 mmol) of P*i*Pr_2Ph and heated for 70 h at 85 °C. After the reaction mixture was cooled to room temperature, the resulting pale yellow precipitate was filtered, washed twice with 10 mL of methanol, and dried in vacuo; yield: 1.01 g (41%). − b) A slow stream of dried HCl was passed through a solution of 83 mg (0.15 mmol) of **1** in 4 mL of dichloromethane-methanol (1:1) for ca. 1 min. The solvent was removed and the resulting yellow solid was dried in vacuo; yield: 92 mg (99%); m.p. 138 °C (dec.). − IR (KBr): $\tilde{\nu}$ = 3563 cm^{-1} (OH), 1918 (CO). − ^1H NMR (400 MHz, C_6D_6): δ = 7.58 (m, 4 H, C_6H_5), 7.20−6.82 (m, 6 H, C_6H_5), 3.50 (m, 4 H, PC*H*CH_3), 2.48 (s, 3 H, C*H*$_3$OH), 1.72 [dvt, *N* = 15.6, *J*(HH) = 7.6 Hz, 12 H, PCHC*H*$_3$], 1.09 [dvt, *N* = 12.8, *J*(HH) = 6.4 Hz, 12 H, PCHC*H*$_3$], signal of CH_3OH not observed. − ^{31}P NMR (162.0 MHz, C_6D_6): δ = 36.7 (s). − $C_{26}H_{42}Cl_2O_2RuP_2$ (620.5): calcd. C 50.32, H 6.82; found C 50.38, H 6.88.

3. Preparation of *trans,trans,trans*-[$RuCl_2$(CO)$_2$(P*i*Pr_2Ph)$_2$] (3a): A solution of 100 mg (0.40 mmol) of $RuCl_3 \cdot 3\,H_2O$ in 5 mL of ethanol was stirred in a pressure bottle under CO atmosphere (1 bar) for 5 h at 65 °C. After the reaction mixture was cooled to 0 °C, it was treated under CO dropwise with a solution of 155 mg (0.80 mmol) of P*i*Pr_2Ph in 1.3 mL of chloroform. The solution was stirred for 15 h at room temperature, the resulting orange precipitate was filtered, washed with 5 mL of ethanol and dried in vacuo; yield: 186 mg (79%). − IR (KBr): $\tilde{\nu}$ = 1975 cm^{-1} (CO). − ^{31}P NMR (81.0 MHz, $CDCl_3$): δ = 32.7 (s).

4. Preparation of *cis,cis,trans*-[$RuCl_2$(CO)$_2$(P*i*Pr_2Ph)$_2$] (3b): A solution of 186 mg (0.30 mmol) of **3a** in 5 mL of chloroform was heated for 15 min at 80 °C. After the reaction mixture was cooled to room temperature, the solvent was removed and the yellow solid was dried in vacuo; yield: 186 mg, (99%); m.p. 69 °C (dec.). − IR (KBr): $\tilde{\nu}$ = 2020 cm^{-1} (CO), 1960 (CO). − ^1H NMR (400 MHz, $CDCl_3$): δ = 8.12 (m, 4 H, C_6H_5), 7.45 (m, 6 H, C_6H_5), 3.25 (m, 4 H, PC*H*CH_3), 1.36 [dvt, *N* = 15.2, *J*(HH) = 7.2 Hz, 12 H, PCHC*H*$_3$], 1.19 [dvt, *N* = 14.4, *J*(HH) = 7.2 Hz, 12 H, PCHC*H*$_3$]. − ^{13}C NMR (100.6 MHz, $CDCl_3$): δ = 195.2 [t, *J*(PC) = 11 Hz, CO], 134.2, 128.1 both vt, *N* = 7 and 8 Hz, *ortho*-C and *meta*-C of C_6H_5), 130.4 (s, *para*-C of C_6H_5), 127.7 (vt, *N* = 36 Hz, *ipso*-C of C_6H_5), 23.4 (vt, *N* = 24 Hz, P*C*HCH$_3$), 18.5, 17.7 (both s, PCH*C*H$_3$). − ^{31}P NMR (162.0 MHz, $CDCl_3$): δ = 30.6 (s). − $C_{26}H_{38}Cl_2O_2RuP_2$ (616.5): calcd. C 50.65, H 6.21; found C 50.56, H 6.01.

5. Preparation of [$RuHCl(CO)_2$(P*i*Pr_2Ph)$_2$] (4): A slow stream of CO was passed at room temperature through a suspension of 124 mg (0.22 mmol) of **1** in 5 mL of ether until a clear, almost colorless solution was formed. The solvent was removed and the remaining white solid was dried in vacuo; yield 130 mg (99%); m.p. 161 °C (dec.). − IR (KBr): $\tilde{\nu}$ = 2010 cm^{-1} (RuH), 1950, 1900 (CO). − ^1H NMR (400 MHz, CD_2Cl_2): δ = 7.85 (m, 4 H, C_6H_5), 7.50 (m, 6 H, C_6H_5), 2.99, 2.89 (both m, 2 H each, PC*H*CH_3), 1.28 [dvt, *N* = 16.1, *J*(HH) = 7.1 Hz, 6 H, PCHC*H*$_3$], 1.22 [dvt, *N* = 16.8, *J*(HH) = 7.2 Hz, 6 H, PCHC*H*$_3$], 1.12 [dvt, *N* = 13.8, *J*(HH) = 7.1 Hz, 6 H, PCHC*H*$_3$], 1.01 [dvt, *N* = 15.9, *J*(HH) = 7.2 Hz, 6 H, PCHC*H*$_3$], −5.23 [t, *J*(PH) = 20 Hz, 1 H, RuH]. − ^{13}C NMR (100.6 MHz, CD_2Cl_2): δ = 200.8, [t, *J*(PC) = 8 Hz, CO], 198.3 [t, *J*(PC) = 11 Hz, CO], 134.9, 128.2 (both vt, *N* = 10 and 9 Hz, *ortho*-C and *meta*-C of C_6H_5), 130.5 (s, *para*-C of C_6H_5), 128.8 (vt, *N* = 35 Hz, *ipso*-C of C_6H_5), 23.3, 22.5 (both vt, *N* = 29 and 23 Hz, P*C*HCH$_3$), 18.3, 17.8, 17.4, 16.8 (all s, PCH*C*H$_3$). − ^{31}P NMR (162.0 MHz, CD_2Cl_2): δ = 59.6 (s). − $C_{26}H_{39}ClO_2P_2Ru$ (582.1): calcd. C 53.65, H 6.75; found C 53.74, H 7.06.

6. Preparation of [RuHCl(CO)(=CHPh)(P*i*Pr_2Ph)$_2$] (5): A solution of 156 mg (0.28 mmol) of **1** in 10 mL of toluene was treated dropwise with 0.27 mL of a 1.5 M solution of $PhCHN_2$ (0.42 mmol) in hexane. A change of color from yellow to orange occurred and the evolution of gas was observed. After the reaction mixture was stirred for 30 min at room temperature, the solvent was removed in vacuo, and pentane was added to the oily residue. Ultrasonic irradiation of this mixture gave an orange precipitate, which was filtered, washed three times with 2 mL of pentane and dried in vacuo. The crude product (yield ca. 80%) still contained ca. 5% of compound **1**. After recrystallization from toluene at −20 °C, a pure orange solid was obtained; yield 76 mg (42%); m.p. 138 °C (dec.). − IR (KBr): $\tilde{\nu}$ = 1930 cm^{-1} (CO). − ^1H NMR (400 MHz, C_6D_6): δ = 18.22 (m, 1 H, Ru=C*H*Ph), 8.22 (m, 2 H, C_6H_5), 7.74 (m, 4 H, C_6H_5), 7.12 (m, 9 H, C_6H_5), 3.14, 2.81 (both m, 2 H each, PC*H*CH_3), 1.49 [dvt, *N* = 16.8, *J*(HH) = 7.2 Hz, 6 H, PCHC*H*$_3$], 0.99 [dvt, *N* = 14.8, *J*(HH) = 7.2 Hz, 6 H, PCHC*H*$_3$], 0.96 [dvt, *N* = 16.8, *J*(HH) = 7.2 Hz, 6 H, PCHC*H*$_3$], 0.95 [dvt, *N* = 14.8, *J*(HH) = 7.2 Hz, 6 H, PCHC*H*$_3$], −2.77 [dt, *J*(PH) = 21, *J*(HH) = 2 Hz, RuH]. − ^{13}C NMR (100.6 MHz, C_6D_6): δ = 343.4 (s, Ru=*C*HPh), 203.3 [t, *J*(PC) = 12 Hz, CO], 154.3 [s, *ipso*-C of Ru=CH(*C*$_6$H$_5$)], 135.0 (vt, *N* = 9 Hz, C_6H_5), 133.2, 132.1, 130.0, 129.6, 127.6, 125.6 (all s, C_6H_5), 23.8, 23.6 (both vt, *N* = 22 and 31 Hz, P*C*HCH$_3$), 18.5, 17.1, 17.0, 16.8 (all s, PCH*C*H$_3$). − ^{31}P NMR (162.0 MHz, C_6D_6): δ = 75.2 (s). − $C_{32}H_{45}ClORuP_2$ (644.2): calcd. C 59.67, H 7.04; found C 59.23, H 6.80.

7. Preparation of [RuHCl(CO)(=CH_2)(P*i*Pr_2Ph)$_2$] (6): A suspension of 123 mg (0.22 mmol) of **1** in 5 mL of toluene was treated dropwise at −78 °C with 1.5 mL of a ca. 0.5 M solution of diazomethane (ca. 0.75 mmol) in ether. Almost instantaneously, a pale yellow solid precipitated, the formation of which was facilitated upon addition of 10 mL of pentane (−78 °C). The mother liquor was removed, the remaining residue washed with 5 mL of pentane (−78 °C) and dried at −78 °C in vacuo. Since the pale yellow solid decomposed at −50 °C, it was characterized spectroscopically. − ^1H NMR (400 MHz, [D_8]THF, −53 °C): δ = 17.36, 16.38 (both br s, 1 H each, Ru=CH_2), −2.60 [t, *J*(PH) = 20 Hz, RuH], signals of C_6H_5 and C_3H_7 protons overlap with those of the solvents used for preparation.

8. Preparation of [MeP*i*Pr_2Ph][$RuHCl_2$(CO)(P*i*Pr_2Ph)$_2$] (7): A solution of 100 mg (0.18 mmol) of **1** in 10 mL of toluene was treated dropwise with 1 mL of a ca. 0.5 M solution of diazomethane in ether (ca. 0.5 mmol) at room temperature. The color of the reaction

mixture changed from yellow to dark red and the evolution of gas was observed. After the reaction mixture was stirred for ca. 15 h, a white precipitate was formed, which was filtered, washed twice with 5 mL of pentane, and dried in vacuo; yield 41 mg (30%); m.p. 138 °C (dec.). – IR (KBr): $\tilde{\nu}$ = 2085 cm^{-1} (RuH), 1940 (CO). – ^{1}H NMR (400 MHz, CD_2Cl_2); signals for $[RuHCl_2(CO)(P$-$i Pr_2Ph)_2]^-$: δ = 8.08 (m, 4 H, C_6H_5), 7.70 (m, 2 H, C_6H_5), 7.38 (m, 4 H, C_6H_5), 2.99, 2.82 (both m, 2 H each, PC*H*CH_3), 1.22 [br d, *J*(HH) = 6.7 Hz, 6 H, PCHC*H*$_3$], 1.17 [br d, *J*(HH) = 6.7 Hz, 6 H, PCHC*H*$_3$], 1.08 [dvt, *N* = 11.6, *J*(HH) = 5.8 Hz, 6 H, PCHC*H*$_3$], 1.01 [dvt, *N* = 13.4, *J*(HH) = 6.7 Hz, 6 H, PCHC*H*$_3$], −17.8 (br s, 1 H, RuH); signals for $[MeP$-$i Pr_2Ph]^+$: δ = 7.84−7.59 (m, 5 H, C_6H_5), 3.18 (m, 2 H, PC*H*CH_3), 2.26 [d, *J*(PH) = 12.4 Hz, 3 H, PC*H*$_3$], 1.29 [dd, *J*(HH) = 7.2, *J*(PH) = 10.8 Hz, 6 H, PCHC*H*$_3$], 1.34 [dd, *J*(HH) = 6.8, *J*(PH) = 10.8 Hz, 6 H, PCHC*H*$_3$]. – ^{13}C NMR (100.6 MHz, CD_2Cl_2); signals for $[RuHCl_2(CO)(Pi Pr_2Ph)_2]^-$: δ = 203.0 [t, *J*(PC) = 13.1 Hz, CO], 135.8, 127.3 (both vt, *N* = 10.0 and 8.0 Hz, *ortho*- and *meta*-C of C_6H_5), 132.4 (vt, *N* = 27.3 Hz, *ipso*-C of C_6H_5) 129.2 (s, *para*-C of C_6H_5), 23.9, 22.7 (both vt, *N* = 26.1 and 20.2 Hz, P*C*HCH$_3$), 19.0, 18.3, 18.1, 17.6 (all s, PCH*C*H$_3$); signals for $[MeP$-$i Pr_2Ph]^+$: δ = 135.0 [d, *J*(PC) = 3 Hz, *para*-C of C_6H_5], 133.0, 130.6 both d, *J*(PC) = 8 Hz and 11 Hz, *meta*- and *ortho*-C of C_6H_5], 115.7 [d, *J*(PC) = 78 Hz, *ipso*-C of C_6H_5], 21.5 [d, *J*(PC) = 47 Hz, P*C*HCH$_3$], 15.9, 15.8 both d, *J*(PC) = 2 Hz, PCH*C*H$_3$], −0.5 [d, *J*(PC) = 52 Hz, P*C*H$_3$]. – ^{31}P NMR (162.0 MHz, CD_2Cl_2): δ = 47.0 (s, PiPr$_2$Ph), 40.6 (s, $[MeP$-$i Pr_2Ph]^+$). – $C_{38}H_{61}Cl_2OP_3Ru$ (798.8): calcd. C 57.14, H 7.70; found C 57.32, H 7.70.

9. Preparation of [PPN][$RuHCl_2(CO)(Pi Pr_2Ph)_2$] (8): A solution of 104 mg (0.19 mmol) of **1** in 10 mL of benzene was treated with 108 mg (0.19 mmol) of [PPN]Cl. The color of the solution changed gradually from yellow to pale yellow. After the reaction mixture was stirred for ca. 18 h at room temperature, a white solid precipitated, which was filtered, washed three times with 5 mL of benzene, and dried in vacuo; yield 187 mg (88%); m.p. 125 °C (dec.). – IR (KBr): $\tilde{\nu}$ = 2062 cm^{-1} (RuH), 1890 (CO). – ^{1}H NMR (200 MHz, CD_2Cl_2): δ = 8.32 (m, 4 H, C_6H_5), 7.66−7.36 (m, 36 H, C_6H_5), 3.11, 2.70 (both m, 2 H each, PC*H*CH_3), 1.33 [dvt, *N* = 14.1, *J*(HH) = 7.0 Hz, 6 H, PCHC*H*$_3$], 1.20 [dvt, *N* = 14.9, *J*(HH) = 7.2 Hz, 6 H, PCHC*H*$_3$], 1.03 (m, 12 H, PCHC*H*$_3$), −16.1 (br s, 1 H, RuH). – ^{13}C NMR (50.3 MHz, CD_2Cl_2): δ = 203.3 [t, *J*(PC) = 15.7 Hz, CO], 135.0 (s, PC_6H_5), 134.1 (s, PPN), 132.9, 128.6 both vt, *N* = 26.2 and 25.7 Hz, PC_6H_5), 132.4, 129.7, 128.4, 126.2 (all m, PPN), 127.1 (s, PC_6H_5), 24.0, 22.3 (both vt, *N* = 26.8 and 19.5 Hz, P*C*HCH$_3$), 18.8, 18.3, 18.0, 17.1 (all s, PCH*C*H$_3$). – ^{31}P NMR (81.0 MHz, CD_2Cl_2): δ = 45.7 (br s, PiPr$_2$Ph), 21.6 (s, PPN). – $C_{61}H_{69}Cl_2NOP_4Ru$ (1128.1): calcd. C 64.95, H 6.17, N 1.24; found C 64.73, H 6.11, N 1.20.

10. Preparation of [$RuHCl(CO)(py)(Pi Pr_2Ph)_2$] (9a, b): A suspension of 82 mg (0.15 mmol) of **1** in 5 mL of hexane was treated with 0.05 mL (0.62 mmol) of pyridine at room temperature. After the reaction mixture was stirred for ca. 3 min, a white solid precipitated, which was filtered, washed three times with 5 mL of pentane and dried in vacuo; yield 89 mg (95%); m.p. 115 °C (dec.). The same compound was formed upon addition of ca. 0.1 mL of pyridine to a solution of 80 mg (0.14 mmol) of **6** in 1 mL of [D_8]THF at −78 °C. After the solution was warmed to room temperature, the ^{1}H-NMR spectrum indicated the complete conversion of **6** to **9a**, **b**. – ^{1}H NMR (400 MHz, C_6D_6); signals for **9a**: δ = 8.20, 7.07, 6.16 (all m, NC_5H_5 and C_6H_5) 3.19, 2.83 (both m, 2 H each, PC*H*CH_3), 1.41 [dvt, *N* = 13.6, *J*(HH) = 6.8 Hz, 6 H, PCHC*H*$_3$], 1.22 [dvt, *N* = 13.2, *J*(HH) = 6.6 Hz, 6 H, PCHC*H*$_3$], 1.10 [dvt, *N* = 14.0, *J*(HH) = 7.0 Hz, 6 H, PCHC*H*$_3$], 0.89 [dvt, *N* = 15.0, *J*(HH) = 7.2 Hz, 6 H, PCHC*H*$_3$], −13.54 [t, *J*(PH) = 22.0 Hz, 1 H, RuH]; signals for **9b**: δ = 7.57, 7.07, 6.51 (all m, NC_5H_5 and C_6H_5), 2.67, 1.81 (both m, 2 H each, PC*H*CH_3), 1.35 [dvt, *N* = 16.4, *J*(HH) = 7.0 Hz, 6 H, PCHC*H*$_3$], 1.29 [dvt, *N* = 13.6, *J*(HH) = 6.8 Hz, 6 H, PCHC*H*$_3$], 1.21 [dvt, *N* = 13.6, *J*(HH) = 6.8 Hz, 6 H, PCHC*H*$_3$], 0.99 [dvt, *N* = 13.4, *J*(HH) = 6.7 Hz, 6 H, PCHC*H*$_3$], −14.41 [t, *J*(PH) = 21.8 Hz, 1 H, RuH]. – ^{31}P NMR (162.0 MHz, CD_2Cl_2): δ = 48.9, 43.8 (both s). – $C_{30}H_{44}ClONP_2Ru$ (633.2): calcd. C 56.91, H 7.00, N 2.21; found C 56.62, H 7.04, N 2.23.

11. Reaction of Compound 6 with CO: A slow stream of CO was passed through a solution of 80 mg (0.14 mmol) of **6** in 1 mL of [D_8]THF at −80 °C. After the solution was warmed to room temperature, the ^{1}H-NMR spectrum indicated the complete conversion of **6** to **4**.

12. Preparation of [$RuH(CF_3CO_2)(CO)(Pi Pr_2Ph)_2$] (10): A solution of 192 mg (0.35 mmol) of **1** in 10 mL of toluene was treated with 111 mg (0.35 mmol) of CF_3CO_2Tl and stirred for 15 h at room temperature. The solution was decanted from the solid residue and then brought to dryness in vacuo. An orange-yellow microcystalline solid was obtained; yield 188 mg (86%); m.p. 177 °C (dec.). – IR (KBr): $\tilde{\nu}$ = 2090 cm^{-1} (RuH), 1910 (CO), 1597 ($OCO_{as.}$), 1410 ($OCO_{sym.}$). – ^{1}H NMR (400 MHz, C_6D_6): δ = 7.89 (m, 4 H, C_6H_5), 7.31−7.17 (m, 6 H, C_6H_5), 2.54 (m, 4 H, PC*H*CH_3), 1.42 [dvt, *N* = 15.9, *J*(HH) = 7.2 Hz, 6 H, PCHC*H*$_3$], 1.33 [dvt, *N* = 15.0, *J*(HH) = 7.2 Hz, 6 H, PCHC*H*$_3$], 1.24 [dvt, *N* = 14.6, *J*(HH) = 7.1 Hz, 6 H, PCHC*H*$_3$], 1.01 [dvt, *N* = 13.3, *J*(HH) = 6.7 Hz, 6 H, PCHC*H*$_3$], −18.23 [t, *J*(PH) = 20 Hz, 1 H, RuH]. – ^{13}C NMR (100.6 MHz, C_6D_6): δ = 205.1 [t, *J*(PC) = 10 Hz, CO], 164.2 [q, *J*(FC) = 38 Hz, CF_3CO_2] 134.7, 128.1 (both vt, *N* = 10 and 14 Hz, *ortho*-C and *meta*-C of C_6H_5), 130.1 (s, *para*-C of C_6H_5], 128.7 (vt, *N* = 34 Hz, *ipso*-C of C_6H_5), 115.0 [q, *J*(FC) = 287 Hz, CF_3CO_2], 24.5, 24.3, (both vt, *N* = 24 and 23 Hz, P*C*HCH$_3$), 19.1, 18.4, 18.1, 17.2, (all s, PCH*C*H$_3$). – ^{19}F NMR (376.4 MHz, C_6H_6): δ = −75.4 (s). – ^{31}P NMR (162.0 MHz, C_6D_6): δ = 53.7 (s). – $C_{27}H_{39}F_3O_3P_2Ru$ (631.6): calcd. C 51.34, H 6.22; found C 51.03, H 5.98.

13. Preparation of [$RuHI(CO)(Pi Pr_2Ph)_2$] (11): A solution of 200 mg (0.36 mmol) of **1** in 10 mL of dichloromethane was treated with 600 mg (3.61 mmol) of KI and stirred for 15 h at room temperature. The reaction mixture was filtered and the filtrate was brought to dryness in vacuo. The brown microcrystalline residue was washed with methanol and dried; yield 116 mg (50%); m.p. 122 °C (dec.). – ^{1}H NMR (400 MHz, C_6D_6): δ = 7.70 (m, 4 H, C_6H_5), 7.46 (m, 6 H, C_6H_5), 3.33, 3.02 (both m, 2 H each, PC*H*CH_3), 1.35 [dvt, *N* = 15.2, *J*(HH) = 7.6 Hz, 6 H, PCHC*H*$_3$], 1.19 [dvt, *N* = 15.2, *J*(HH) = 7.2 Hz, 6 H, PCHC*H*$_3$], 1.14 [dvt, *N* = 16.8, *J*(HH) = 8.0 Hz, 6 H, PCHC*H*$_3$], 1.04 [dvt, *N* = 13.2, *J*(HH) = 6.8 Hz, 6 H, PCHC*H*$_3$], −25.0 (br s, 1 H, RuH). – ^{13}C NMR (100.6 MHz, C_6D_6): δ = 198.7 [t, *J*(PC) = 12 Hz, CO], 134.9, 127.8 (both vt, *N* = 10 and 8 Hz, *ortho*-C and *meta*-C of C_6H_5), 130.1 (s, *para*-C of C_6H_5), 130.3 (vt, *N* = 36 Hz, *ipso*-C of C_6H_5), 25.1, 24.4 (both vt, *N* = 27 and 23 Hz, P*C*HCH$_3$), 19.6, 19.5, 19.1, 17.8 (all s, PCH*C*H$_3$). – ^{31}P NMR (162.0 MHz, C_6D_6): δ = 53.3 (s). – $C_{25}H_{39}IOP_2Ru$ (645.5): calcd. C 46.52, H 6.09; found C 46.13, H 5.67.

14. Preparation of [$Ru(CH{=}CH_2)Cl(CO)(Pi Pr_2Ph)_2$] (12): A slow stream of acetylene was passed through a suspension of 129 mg (0.23 mmol) of **1** in 15 mL of pentane until a change of color from yellow to red occurred. After the suspension was stirred for 30 min at room temperature, a red solid precipitated which was filtered, washed with pentane and dried in vacuo; yield 119 mg (90%); m.p.

124 °C (dec.). – IR (KBr): $\tilde{\nu}$ = 1923 cm^{-1} (CO). – $^1H\{^{31}P\}$NMR (200 MHz, $CDCl_3$): δ = 8.15 [dd, *J*(HH) = 14.0 Hz, *J*(HH) = 6.0 Hz, 1 H, C*H*=CH_2], 7.81 (m, 4 H, C_6H_5), 7.38 (m, 6 H, C_6H_5), 5.22 [d, *J*(HH) = 6.0 Hz, 1 H, one H of =CH_2], 4.89 [d, *J*(HH) = 14.0 Hz, 1 H, one H of =CH_2], 3.24, 2.87 (both m, 2 H each, PC*H*CH_3), 1.26 [d, *J*(HH) = 7.0 Hz, 6 H, PCHC*H*$_3$], 1.16 [d, *J*(HH) = 7.2 Hz, 6 H, PCHC*H*$_3$], 1.08 [d, *J*(HH) = 7.2 Hz, 6 H, PCHC*H*$_3$], 1.01 [d, *J*(HH) = 6.8 Hz, 6 H, PCHC*H*$_3$]. – ^{13}C NMR (50.3 MHz, $CDCl_3$): δ = 200.7 [t, *J*(PC) = 12 Hz, CO], 152.5 [t, *J*(PC) = 10 Hz, *C*H=CH_2], 133.9, 127.0 (both vt, *N* = 13 and 8 Hz, *ortho*-C and *meta*-C of C_6H_5), 129.6 (s, *para*-C of C_6H_5), 129.6 (vt, *N* = 33 Hz, *ipso*-C of C_6H_5), 120.5 (s, CH=*C*H_2), 23.7, 22.4 (both vt, *N* = 23 and 21 Hz, P*C*HCH$_3$), 20.7, 18.9, 18.3, 17.4 (all s, PCH*C*H$_3$). – ^{31}P NMR (81.0 MHz, $CDCl_3$): δ = 35.6 (s). – $C_{27}H_{41}ClORuP_2$ (580.1): calcd. C 55.90, H 7.12; found C 55.60, H 7.12.

15. Preparation of [Ru(CH=CHPh)Cl(CO)(P*i*Pr$_2$Ph)$_2$] (13): A suspension of 100 mg (0.18 mmol) of **1** in 10 mL of hexane was treated with 19 μL (0.18 mmol) of phenylacetylene and stirred for 1 h at room temperature. A violet solid precipitated which was filtered, washed three times with pentane, and dried in vacuo; yield 74 mg (62%); m.p. 148 °C (dec.). – IR (KBr): $\tilde{\nu}$ = 1916 cm^{-1} (CO). – $^1H\{^{31}P\}$ NMR (400 MHz, CD_2Cl_2): δ = 8.83 [d, *J*(HH) = 13.4 Hz, 1 H, C*H*=CHPh], 7.78 (m, 4 H, C_6H_5), 7.44 (m, 6 H, C_6H_5), 7.25 (m, 4 H, C_6H_5), 7.06 (m, 1 H, C_6H_5), 6.15 [d, *J*(HH) = 13.4 Hz, 1 H, CH=C*H*Ph], 3.27, 2.94 (both m, 2 H each, PC*H*CH_3), 1.33 [d, *J*(HH) = 7.0 Hz, 6 H, PCHC*H*$_3$], 1.27 [d, *J*(HH) = 7.1 Hz, 6 H, PCHC*H*$_3$], 1.16 [d, *J*(HH) = 7.0 Hz, 6 H, PCHC*H*$_3$], 1.04 [d, *J*(HH) = 7.0 Hz, 6 H, PCHC*H*$_3$]. – ^{31}P NMR (162.0 MHz, CD_2Cl_2): δ = 35.0 (s). – $C_{33}H_{45}ClORuP_2$ (656.2): calcd. C 60.40, H 6.91, Ru 15.40; found C 60.15, H 6.98, Ru 15.34.

Determination of the X-ray Crystal Structure of 7:[20] Single crystals were grown upon cooling of a saturated solution of **7** in toluene from 25 °C to −20 °C. Crystal data (from 5000 reflections, 1.95° < Θ < 26.20°): triclinic; space group *P*-1 (No. 2); *a* = 12.237(3), *b* = 14.039(6), *c* = 15.697(4) Å, α = 85.96(4), β = 76.94(3), γ = 70.33(4)°; *V* = 2474(1) Å^3, *Z* = 2; $d_{calc.}$ = 1.258 gcm^{-3}; μ(Mo-K_α) = 0.555 mm^{-1}; crystal size 0.2 × 0.2 × 0.1 mm; IPDS (STOE), Mo-K_α radiation (0.71073 Å), graphite monochromator; *T* = 173(2) K; φ-scans, max. 2θ = 52.40°; 18792 reflections measured, 9434 independent ($R_{int.}$ = 0.0557), 7477 with $I > 2\sigma(I)$. Intensity data were corrected for Lorentz and polarization effects. The structure was solved by the Patterson method (SHELXS-86).[21] Atomic coordinates and the anisotropic thermal parameters of non-hydrogen atoms were refined by full-matrix least squares on F^2 (SHELXL-93).[22] The positions of all hydrogen atoms except of H1 were calculated according to ideal geometry and refined by using the riding method. The position of H1 was located in a final difference Fourier synthesis and refined isotropically without restraints. The asymmetric unit includes one and a half molecules of toluene which were refined anisotropically with restraints. The half molecule was located on the inversion center of the space group. The other molecule of toluene was found disordered and two positions were refined with occupancy factors of 0.646 and 0.354. Conventional $R = 0.0339$ [for 7477 reflections with $I > 2\sigma(I)$], and weighted $wR_2 = 0.0953$ for all 9434 located reflections; reflection/parameter ratio 17.31; residual electron density +0.505/−0.916 eÅ^{-3}.

Acknowledgments

This work was supported by the Deutsche Forschungsgemeinschaft (SFB 347) and the Fonds der Chemischen Industrie. We are grateful to the latter in particular for a Kekulé scholarship (to W. S.). Moreover, we thank C. Eichhorn for commited collaboration during an advanced study course. We also thank Dr. W. Buchner and Mrs. M.-L. Schäfer for NMR measurements, Mrs. R. Schedl and Mr. C. P. Kneis for performing the elemental analyses and DTA measurements. Generous support by the BASF AG and the Degussa AG (gifts of chemicals) is also gratefully acknowledged.

[1] M. A. Esteruelas, H. Werner, *J. Organomet. Chem.* **1986**, *303*, 221−231.
[2] H. Werner, M. A. Esteruelas, H. Otto, *Organometallics* **1986**, *5*, 2295−2299.
[3] H. Werner, W. Stüer, M. Laubender, C. Lehmann, R. Herbst-Irmer, *Organometallics* **1997, 16**, 2236−2238.
[4] W. Stüer, Dissertation, Universität Würzburg, **1999**.
[5] [5a] P. Schwab, N. Mahr, J. Wolf, H. Werner, *Angew. Chem.* **1993**, *105*, 1498−1500; *Angew. Chem. Int. Ed. Engl.* **1993**, *32*, 1480−1482. – [5b] H. Werner, *J. Organomet. Chem.* **1995,** *500*, 331−336. – [5c] H. Werner, P. Schwab, E. Bleuel, N. Mahr, P. Steinert, J. Wolf, *Chem. Eur. J.* **1997,** *3*, 1375−1384. – [5d] E. Bleuel, Dissertation, Universität Würzburg, to be submitted.
[6] [6a] M. A. Esteruelas, E. Sola, L. A. Oro, H. Werner, *Angew. Chem.* **1988**, *100*, 1621−1622; *Angew. Chem. Int. Ed. Engl.* **1988**, *27*, 1563−1564. – [6b] M. A. Esteruelas, F. J. Lahoz, E. Ouate, L. A. Oro, C. Valero, B. Zeier, *J. Am. Chem. Soc.* **1995**, *117*, 7935−7942.
[7] Y. Sun, N. J. Taylor, A. J. Carty, *Inorg. Chem.* **1993**, *32*, 4457−4459.
[8] [8a] D. W. Krassowski, J. H. Nelson, K. R. Brower, D. Hauenstein, R. A. Jacobson, *Inorg. Chem.* **1988**, *27*, 4294−4307. – [8b] D. W. Krassowski, K. Reimer, H. E. LeMay, J. H. Nelson, *Inorg. Chem.* **1988**, *27*, 4307−4309.
[9] D. Capitani, P. Mura, *Inorg. Chim. Acta* **1997**, *258*, 169−181.
[10] L. Dahrenburg, K. Herbst, M. Kühnlein, *Z. Anorg. Allg. Chem.* **1997**, *623*, 250−258.
[11] E. A. Carter, W.A. Goddard III, *Organometallics* **1988**, *7*, 675−686.
[12] J. T. Poulton, K. Folting, W. E. Streib, K. G. Caulton, *Inorg. Chem.* **1992**, *31*, 3190−3191.
[13] [13a] M A. Tena, O. Nürnberg, H. Werner, *Chem. Ber.* **1993**, *126*, 1597−1602. – [13b] M. A. Tena, Dissertation, Universität Würzburg, **1993**.
[14] S. D. Robinson, M. F. Uttley, *J. Chem. Soc., Dalton Trans.* **1973,** 1213−1220.
[15] Summarising articles: [15a] G. B. Deacon, R. J. Phillips, *Coord. Chem. Rev.* **1980**, *33*, 227−250. – [15b] C. Oldham in: *Compr. Coord. Chem.* (Eds.: G. Wilkinson, R. D. Gillard, J. A. McCleverty), Bd. 2, Pergamon, Oxford, **1987**, Kap. 15.6.
[16] H. Günther, *NMR-Spektroskopie*, Thieme Verlag, Stuttgart, **1973**.
[17] A. F. Hill, C. T. Ho, J. D. E. T. Wilton-Ely, *J. Chem. Soc., Chem. Commun.* **1997**, 2207−2208.
[18] K. G. Caulton, personal communication.
[19] [19a] D. G. Farnum, *J. Org. Chem.* **1963**, *28*, 870−872. – [19b] Technical Information Bulletin No. Al-180 from Aldrich.
[20] Crystallographic data (excluding structure factors) for the structure of **7** have been deposited with the Cambridge Crystallographic Data Centre as supplementary publication no. CCDC-120117. Copies of the data can be obtained free of charge on application to the Director, CCDC, 12 Union Road, Cambridge CB2 1EZ, UK (Fax: internat. +44 (0)1223/ 336-033; E-mail: deposit@ccdc.cam.ac.uk).
[21] G. M. Sheldrick, *Acta Crystallogr. Sect. A*, *46*, **1990**, 467.
[22] G. M. Sheldrick, a program for crystal structure refinement, University of Göttingen, **1993**.

Received May 4, 1999
[I99152]

Transition Metal Complexes with Sulfur Ligands, 138[+]

Synthesis, Structures, and Reactions of Sulfur-Rich Nickel and Platinum Complexes with [MS_3] and [MNS_2] Cores

Dieter Sellmann,*[a] Daniel Häußinger,[a] and Frank W. Heinemann[a]

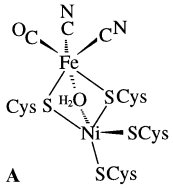
Dedicated to Professor Wolf Peter Fehlhammer on the occasion of his 60th birthday

Keywords: Nickel complexes / Platinum complexes / S ligands / C–S cleavage / Hydride complexes

Nickel and platinum complexes with tridentate ligands, having [S_3] or [NS_2] donor sets were investigated in order to model active sites of enzymes such as hydrogenases or CO dehydrogenases. Starting from diphenyl sulfide, a preparative synthesis was developed for 'S_3'-H_2 ['S_3'-H_2 = bis(2-mercaptophenyl) sulfide]. Reactions of 'S_3'-H_2 or anionic '$S_3'^{2-}$ with nickel and platinum precursors resulted in the formation of binuclear [Ni('S_3')]$_2$ (**1**) and trinuclear [Pt('S_3')]$_3$ (**5**). Complex **1** was cleaved by PMe_3 or CN^- to give the mononuclear complexes [Ni('S_3')(PMe_3)] (**2**) and NMe_4[Ni('S_3')(CN)] (**3**). Attempts to coordinate hydride to the [Ni('S_3')] fragment led to C–S bond cleavage of the ligand and formation of $(NMe_4)_2$[{Ni(μ-SC_6H_5)($S_2C_6H_4$)}$_2$] (**4**). Oxidative addition of Li['S_3'-H] to [Pt(PPh_3)$_4$] afforded the platinum hydride complexes Li[Pt(H)('S_3')] and Li[Pt(H)(PPh_3)('S_3')] which, however, could not be separated from each other and yielded [Pt('S_3')(PPh_3)] (**6**) when treated with MeOH. In order to investigate electronic effects of the donor set, the 'S_3' ligand was modified by alkylation of one thiol group to give 'RS_3'-H derivatives (R = Me, Et, Cy) and by replacing a mercaptophenyl unit by an amine in 'Et_2NS_2'-H ['Et_2NS_2'-H = *N*,*N*-diethyl-2-(2-mercaptothiophenyl)ethylamine]. Reactions of Ni^{II} or Ni^0 compounds with these ligands in a 1:1 ratio yielded the 1:2 complexes [Ni('MeS_3')$_2$] (**7**), [Ni('EtS_3')$_2$] (**9**) and [Ni('CyS_3')$_2$] (**10**), with '$RS_3'^-$ acting as bidentate ligands only. Complex **7** reversibly reacted with PMe_3 to form *cis*-[Ni(PMe_3)$_2$('MeS_3')$_2$] (**8**), exhibiting monodentate 'MeS_3' ligands. [Ni('Et_2HNS_2')$_2$]Br_2 (**11**) reacted reversibly with bases to presumably give octahedral [Ni('Et_2NS_2')$_2$]. Complexes **7**, **9** and **10** also did not yield any [Ni('RS_3')(H)] hydride complex when treated with hydride sources. Oxidative addition of 'CyS_3'-H to [Pt(PPh_3)$_4$] yielded the hydride complexes [Pt(H)('CyS_3')] and [Pt(H)(PPh_3)('CyS_3')] which, however, formed an inseparable mixture and underwent C–S bond cleavage when heated, affording [Pt(*o*-$S_2C_6H_4$)(PPh_3)$_2$]. The molecular structures of **1**, **2**, **3**, **5**, **6**, **7**, and **11** were determined by X-ray crystallography, revealing butterfly-like shapes for the [MS_3L] cores of the complexes.

Introduction

The current interest in nickel thiolate and thioether complexes to a large extent results from the nickel–sulfur moieties that constitute the active centers of enzymes such as hydrogenases[1] or CO dehydrogenases.[2] For example, the X-ray structure analysis of hydrogenase from *D. gigas* has shown that the active site contains nickel surrounded by four cysteine thiolate donors, two of which form bridges to a [Fe(CO)(CN)$_2$] moiety (**A**).[3]



A

The search for hydrogenase model compounds has resulted in a considerable number of new ligands and complexes.[4] However, complexes which model structural *and* functional features of the enzyme centers have remained very rare. These features comprise sulfur coordination of the nickel center *and* catalysis of reactions according to Equations 1a and/or 1b.

$$2\,H^+ + 2\,e^- \rightleftharpoons H_2 \qquad (1a)$$

$$H_2 + D_2O \rightleftharpoons HD + HDO \qquad (1b)$$

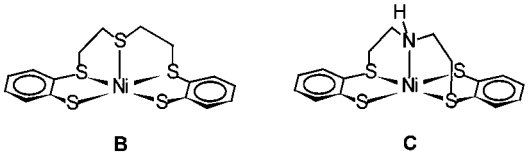
Reaction according to Equation 1b requires the heterolytic cleavage of H_2 into H^+ and H^- ions. When this reaction takes place at the nickel–sulfur site of hydrogenases, nickel–sulfur hydride complexes are likely intermediates. Isolable complexes of this type are extremely rare in spite of the large number of nickel hydride complexes carrying phosphane or carbon coligands. Holm et al. reported five-coordinate complexes of the type [Ni(H)-{$N(C_2H_4SR)_3$}]$^+$,[5] and we have obtained four-coordinate [Ni(H)(PMe_3)($S_2C_6H_4$)]$^-$.[6] However, these complexes proved to be extremely moisture-sensitive and could not yet be shown to catalyze the H_2/D^+ exchange according to Equation 1b. Other nickel complexes, e.g., [Ni('S_5')][7] (**B**) or

[+] Part 137: D. Sellmann, A. Fürsattel, *Angew. Chem.* **1999**, *111*, 2142–2145; *Angew. Chem. Int. Ed. Engl.* **1999**, *38*, 2023–2026.

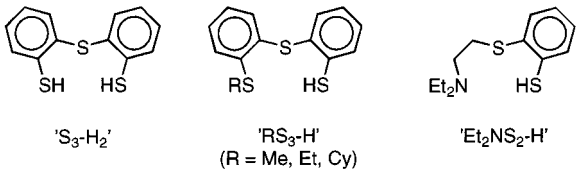
[a] Institut für Anorganische Chemie der Universität, Egerlandstr. 1, D-91058 Erlangen, Germany
Fax: (internat.) + 49-(0)9131/852-7367
E-mail: sellmann@anorganik.chemie.uni-erlangen.de

 © WILEY-VCH Verlag GmbH, D-69451 Weinheim, 1999 1434–1948/99/1010–1715 $ 17.50+.50/0

[Ni('N_HS_4')]$_2$[8] (**C**) readily underwent unwanted S−C(alkyl) cleavage reactions when investigated for the coordination of additional hydride ligands from hydride sources such as $LiAlH_4$, $LiBEt_3H$, or $NaBH_4$.[9]



These unwanted C−S cleavages, leading to destruction of the nickel−sulfur cores, drew our attention to the 'S_3'-H_2 ligand and its 'RS_3'-H and 'Et_2NS_2'-H derivatives.



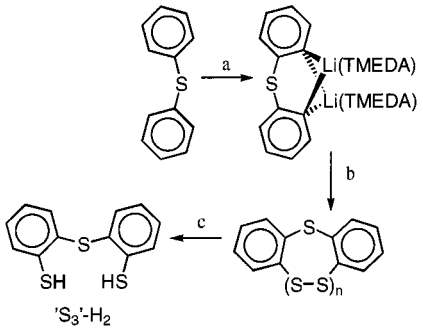
S−C(aryl) bonds are usually more stable than S−C(alkyl) bonds toward reductive S−C cleavage.[10] Furthermore, [Ni('S_3')] fragments formed from Ni^{II} salts and 'S_3'$^{2-}$ were anticipated to provide a readily accessible vacant site for hydride addition. Potential [Ni(H)('S_3')]$^-$ adducts directly compare with [Ni(H)(PMe_3)($S_2C_6H_4$)]$^-$ when the phosphane is exchanged for an isoelectronic thioether ligand. 'S_3'-H_2 is related to the recently described ligands MeN(*o*-$C_6H_4SH)_2$,[11] PhP(*o*-$C_6H_4SH)_2$,[12] PhP($C_2H_4SH)_2$,[13] and P(*o*-$C_6H_4SH)_3$,[14] which also give nickel complexes.

The first synthesis of 'S_3'-H_2, resulting in milligram yields after chromatography, has been reported by Block et al.[15] Therefore, the first goal of our investigations was to find a different approach to this ligand in order to make 'S_3'-H_2 available in preparative gram amounts. Attempts to coordinate 'S_3'$^{2-}$ and biologically relevant coligands such as H^-, H_2, S^{2-}, or CN^- to nickel(II) gave results that prompted us to extend our studies to platinum(II) complexes and the 'S_3' ligand derivatives 'RS_3'-H (R = Me, Et, Cy) and 'Et_2NS_2'-H.

Results and Discussion

Synthesis of 'S_3'-H_2

The target ligand 'S_3'-H_2 formed in a four-step one-pot reaction according to Scheme 1.



Scheme 1. Synthesis of 'S_3'-H_2

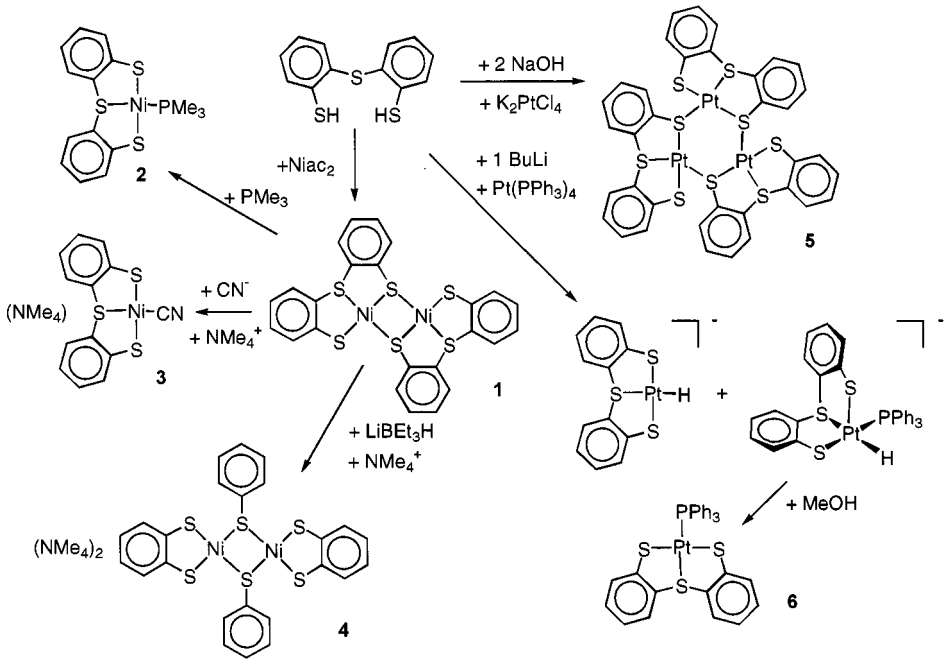
Twofold *ortho*-lithiation of diphenyl sulfide [$S(C_6H_5)_2$] with *n*BuLi in hexanes/TMEDA (tetramethylethylenediamine) at room temperature yielded [{Li(TMEDA)}$_2$S($C_6H_4)_2$] (step a), which has recently been characterized by Kranz et al.[16] Subsequent addition of 1.5 equivalents of elemental sulfur (3/8 S_8) gave a mixture of polysulfides in which the lithiated *ortho*-C atoms are bridged by S-chains (step b). Reduction of the S−S bonds was achieved with an excess of $LiAlH_4$ in THF at elevated temperature (70°C). Final acidification with concentrated hydrochloric acid, extraction and recrystallization from boiling THF/hexanes yielded 'S_3'-H_2 as white microcrystals (step c). By this method, 'S_3'-H_2 could be obtained in amounts of up to 10 g, which totaled ca. 20% yield from $S(C_6H_5)_2$.

Further experiments showed that step b of Scheme 1 is crucial for the overall yield. In this step, species such as thianthrene $C_{12}H_8S_2$ whose reduction cannot yield 'S_3'-H_2, are also formed. Addition of EtBr to the mixture resulting from step a yielded bis(2-ethylphenyl) sulfide in 91% yield, demonstrating that the *ortho*-lithiation of diphenyl sulfide had occurred in nearly quantitative yield. Isolation of the extremely moisture-sensitive [{Li(TMEDA)}$_2$S($C_6H_4)_2$] and its subsequent reaction with elemental sulfur did not improve the overall yield. Treatment of the [{Li(TMEDA)}$_2$S($C_6H_4)_2$] solution with S_2Cl_2 resulted only in traces of 'S_3'-H_2.

Nickel(II) and Platinum(II) Complexes of 'S_3'$^{2-}$

Scheme 2 summarizes complexes and their reactions. The reaction of 'S_3'-H_2 with $Ni(ac)_2{\cdot}4H_2O$ yielded brown-black microcrystals of analytically pure [Ni('S_3')]$_2$ (**1**). Complex **1** is air stable, diamagnetic and so sparingly soluble even in hot DMF or DMSO that no meaningful NMR spectra could be recorded. Recrystallization from hot DMF (175°C) in a sealed ampoule yielded single crystals, whose X-ray crystal structure analysis revealed the dinuclear structure of **1**. The nickel centers exhibit a tetrahedrally distorted planar coordination by four sulfur donors. The fourth coordination site in each [Ni('S_3')] fragment is blocked by a thiolate bridge.

In order to investigate the accessibility of this fourth coordination site, suspensions of [Ni('S_3')]$_2$ (**1**) were treated with nucleophiles such as PMe_3, KCN, Li_2S, and N_2H_4 in mixtures of THF/MeOH, THF/MeOH/H_2O, or MeOH/H_2O, which warranted sufficient solubility of the nucleophiles. Although [Ni('S_3')]$_2$ (**1**) is practically insoluble in these solvent mixtures, in all cases rapid reactions occurred. The resulting PMe_3 and KCN reaction products could be fully characterized. Orange [Ni(PMe_3)('S_3')] (**2**), which was obtained in nearly quantitative yield, is diamagnetic, soluble in common organic solvents except pentane or MeOH, and air-stable for longer periods of time. NMR spectra and X-ray structure determination proved that [Ni(PMe_3)('S_3')] is mononuclear in solution and in solid state. The reaction of [Ni('S_3')]$_2$ (**1**) with KCN in MeOH/H_2O rapidly afforded a yellow solution from which, upon addition of NMe_4Cl,



Scheme 2. Synthesis and reactions of nickel(II) and platinum(II) 'S_3'$^{2-}$ complexes

brown NMe_4[Ni(CN)('S_3')] (**3**) precipitated. Complex **3** too, is diamagnetic and was shown to contain a four-coordinate Ni center by X-ray structure analysis.

The reactions of [Ni('S_3')]$_2$ (**1**) with N_2H_4 or Li_2S/NMe_4Cl yielded products whose elemental analyses, IR and NMR spectra indicated the formation of [Ni(N_2H_4)('S_3')] and $(NMe_4)_2$[μ-S{Ni('S_3')}$_2$], respectively. These species, however, could not be obtained in pure form.

Numerous attempts to cleave [Ni('S_3')]$_2$ (**1**) in an analogous way with hydrides, in order to obtain a [Ni(H)('S_3')]$^-$ species, remained unsuccessful. When [Ni('S_3')]$_2$ (**1**) was treated with $LiBEt_3H$ in THF at various temperatures (−90 to −30 °C) or with $NaBH_4$ in MeOH at room temperature, rapid reactions occurred yielding dark-yellow to brown solutions. Addition of NMe_4Cl in MeOH precipitated red-brown microcrystals whose elemental analyses and spectroscopic data were compatible with the dinuclear complex $(NMe_4)_2$[Ni(SC_6H_5)($S_2C_6H_4$)]$_2$ (**4**). Complex **4** is diamagnetic and soluble in DMF or DMSO. The ^{1}H- and ^{13}C-NMR spectra of **4** revealed that the 'S_3' ligand of **1** had been cleaved into thiophenolate and 1,2-benzenedithiolate ligands. The ESI mass spectrum of **4** showed a peak at *m*/*z* = 306.9 which was assigned to the dinuclear anion of **4** (calculated for $^{12}C_{24}{}^1H_{18}{}^{58}Ni_2{}^{32}S_6$: *m*/*z* = 306.922). The formation of **4** was corroborated by its independent synthesis from Ni^{2+}, $LiSC_6H_5$, $Li_2S_2C_6H_4$, and NMe_4Cl, yielding the identical compound. C−S bond cleavage in the 'S_3' ligand was also observed when mononuclear [Ni(PMe_3)('S_3')] (**2**) was treated with $LiBEt_3H$ or $NaBH_4$. [Ni('S_3')]$_2$ (**1**) did not react with molecular hydrogen at standard pressure or with equimolar amounts of hydrochloric acid. Excess hydrochloric acid hydrolyzed **1** to give $NiCl_2$ and free 'S_3'-H_2.

The synthesis of 'S_3'-H_2 demonstrates that 'S_3'$^{2-}$ is stable for longer periods of time in the presence of $LiAlH_4$ at elevated temperatures. Therefore the C−S bond cleavage by hydride reagents in nickel-coordinated 'S_3'$^{2-}$ is remarkable. It indicates a considerable activation of either the 'S_3' ligand or the hydrides by coordination to nickel(II). Following the tenet of coordination chemistry that the heavier homologues are frequently more stable, we also investigated reactions of 'S_3'-H_2 with platinum(II).

The reaction between K_2PtCl_4 and Na_2-'S_3' in H_2O yielded red [Pt('S_3')]$_3$ (**5**) besides other products. Its trinuclear structure was elucidated by X-ray diffraction. [Pt('S_3')]$_3$ (**5**) could also be obtained from [$PtCl_2$(COD)] and 'S_3'-H_2 in THF.[17] [Pt('S_3')]$_3$ (**5**) is air-stable and slightly more soluble than [Ni('S_3')]$_2$ (**1**), not only in DMF and DMSO, but also in THF and CH_2Cl_2. Treatment of [Pt'S_3']$_3$ (**5**) in THF with $LiBEt_3H$ at room temperature yielded yellow solutions. The ^{1}H-NMR spectra of these solutions indicated that the [Pt('S_3')] fragments had remained intact, but they showed no signals which could be assigned to a [Pt(H)('S_3')]$^-$ species. The viability of such a species, however, could be demonstrated when 'S_3'-H_2 was monodeprotonated with one equivalent of *n*BuLi and the resulting Li['S_3'-H] subsequently reacted with [Pt(PPh_3)$_4$]. By oxidative addition of the remaining SH moiety of Li['S_3'-H] to the Pt^0 center, a mixture of two hydride complexes resulted. They could be isolated in solid state, identified by their ^{1}H-NMR hydride resonances and coupling constants as Li[Pt(H)(PPh_3)('S_3')] [δ(PtH) = −10.65] and Li[Pt(H)('S_3')] [δ(PtH) = −15.72]. The Pt−H bonds were also indicated by the IR spectra showing ν(Pt−H) bands at 2109 cm^{-1} in KBr and 2127 cm^{-1} in dioxane. However these two complexes could not be separated because they exhibit practically identical solubilities. Attempts to separate the two complexes by fractional crystallization from THF/MeOH yielded only very few single orange crystals

of the hydride-free [Pt(PPh_3)('S_3')] (**6**), whose structure was determined by X-ray crystallography.

Synthesis of 'RS_3'-H Ligands (R = Me, Et, Cy) and 'RS_3' Nickel(II) and Platinum(II) Complexes

The 'RS_3'-H ligands were synthesized in order to investigate the influence of different donor sets (thioether vs. thiolate), charge (neutral vs. anionic), and sterical requirements (small vs. large R substituents) on the stability of potential nickel and platinum hydride complexes with S_3 donor sets. Selective monoalkylation of dithiols having equivalent thiol functions is not trivial,[18] and this also became apparent in the 'RS_3'-H synthesis. Alkylation of [Ni('S_3')] complexes was considered the most promising method, because previous alkylations of $[Ni(S_2C_6H_4)_2]^{2-}$ complexes had selectively yielded the monoalkylated 1,2-benzenedithiol derivatives, 1,2-C_6H_4(SH)(SR), in straightforward reactions.[19]

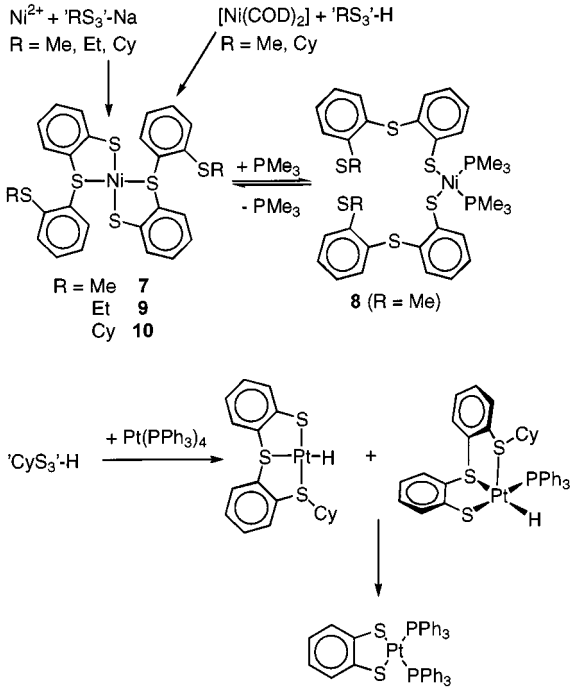
In contrast to these reactions, the alkylation of [Ni('S_3')]$_2$ (**1**) or [Ni(PMe_3)('S_3')] (**2**) with R_3OBF_4 (R = Me, Et) yielded mixtures of complexes that contained not only the monoalkylated target ligand 'RS_3'$^-$ but to a minor extent also dialkylated 'R_2S_3' species as well as the non-alkylated 'S_3'$^{2-}$ starting ligand. However, acidic hydrolysis of the complexes with aqueous HCl and subsequent purification of the resulting mixture of 'RS_3'-H, 'R_2S_3', and 'S_3'-H_2 species by repeated alkaline and acidic extractions yielded 'MeS_3'-H and 'EtS_3'-H in sufficient purity to be unambiguously identified by ^{1}H-NMR spectroscopy and used for the synthesis of complexes.

Alkylation of [Ni('S_3')] complexes by cyclohexyl bromide or tosylate proved impossible, probably due to steric hindrance. The "direct" alkylation of the monolithium salt Li['S_3'-H] with cyclohexyl bromide under drastic conditions (DMF, 125°C, 6 h) and acidic workup gave a mixture of 'CyS_3'-H, 'Cy_2S_3', and 'S_3'-H_2. Repeated extractions of this mixture, similar to those described above, yielded the 'CyS_3'-H target ligand in sufficient purity for identification and synthesis of complexes.

The ligating properties of the 'RS_3'$^-$ and 'S_3'$^{2-}$ ligands towards Ni^{II} differed more than expected. In all structurally characterized complexes, the 'RS_3' ligands acted as bidentate or even monodentate ligands only (Scheme 3).

The 1:1 reaction between Ni^{II} salts and Na['MeS_3'] gave the 1:2 complex [Ni('MeS_3')$_2$] (**7**). The identical complex was obtained in the attempt to coordinate 'MeS_3'-H to [Ni(1,5-cyclooctadiene)$_2$] in a 1:1 oxidative addition reaction. [Ni('MeS_3')$_2$] (**7**) is almost insoluble in all common solvents, but could be characterized by X-ray diffraction.

In an attempt to remove one 'MeS_3' ligand from [Ni('MeS_3')$_2$] (**7**) with PMe_3 in order to achieve a tridentate coordination of the remaining 'MeS_3', an excess of PMe_3 was required to achieve a reaction. However, this reaction did not yield the target complex [Ni(PMe_3)('MeS_3')] but [Ni(PMe_3)$_2$('MeS_3')$_2$] (**8**). The structure of **8** was concluded from elemental analysis and the ^{1}H-NMR spectrum showing one PMe_3 doublet and one set of eight aromatic signals for the



Scheme 3. Synthesis and reactions of nickel and platinum 'RS_3'$^-$ complexes

'MeS_3' ligand. One of the aromatic signals is split into a doublet of pseudotriplets by a long-range coupling to ^{31}P ($^5J_{H,P}$ = 2.6 Hz). This clearly indicates the postulated *cis* isomer of **8**, as strong coupling over five bonds can only take place along a W-shaped backbone, where the phosphane ligand is *trans* to the thiolate. The PMe_3 addition is reversible. Attempts to crystallize **8** from a $CDCl_3$ solution yielded PMe_3-free [Ni('MeS_3')$_2$] (**7**) in the course of three weeks.

'EtS_3'$^-$ was anticipated to give more soluble complexes. Indeed, [Ni('EtS_3')$_2$] (**9**), resulting from the 1:1 reaction between Ni^{II} salts and 'EtS_3'$^{2-}$, proved sufficiently soluble for recording ^{1}H-NMR spectra. They show only one set of 'EtS_3' signals indicating that [Ni('EtS_3')$_2$] (**9**) is structurally analogous to [Ni('MeS_3')$_2$] (**7**).

'CyS_3'$^-$ yielded complexes that were even more soluble. However, also with 'CyS_3'$^-$ only the 1:2 complex [Ni('CyS_3')$_2$] (**10**) could be obtained. It likewise resulted from Ni^{II} salts and 'CyS_3'-H, and oxidative addition reactions of 'CyS_3'-H with [Ni($CO)_4$], [Ni(phen)$_2$], or [Ni(PMe_3)$_4$]. Intermediate nickel hydride species such as [Ni(H)('CyS_3')] could not be detected.

Metal hydride species were observed with platinum, but again only as inseparable mixtures of at least two complexes. The oxidative addition of 'CyS_3'-H to [Pt(PPh_3)$_4$] gave a mixture of [Pt(H)('CyS_3')] and [Pt(H)(PPh_3)('CyS_3')], which were identified by their ^{1}H-NMR hydride signals at δ = −15.74 [$^1J(^{195}Pt-H)$ = 1155 Hz] and δ = −11.38 [$^1J(^{195}Pt-H)$ = 1260 Hz], respectively (Figure 1). The hy-

dride signals of [Pt(H)(PPh_3)('CyS_3')] are split into doublets by coupling to ^{31}P [^2J(H,P) = 20 Hz].

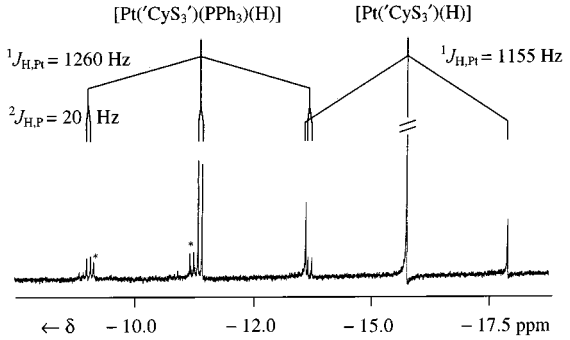
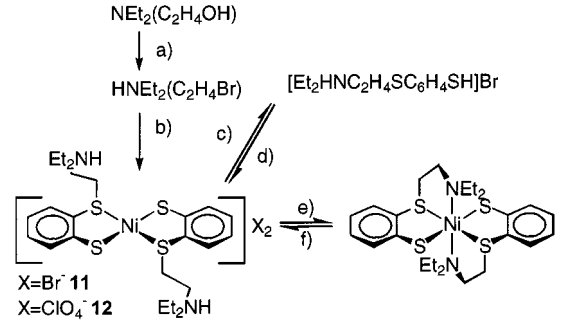


Figure 1. High-field region of the ^{1}H-NMR spectrum (270 MHz, [D_8]THF) of a mixture of [Pt('S_3')(PPh_3)(H)] and [Pt('S_3')(H)] (* denotes impurities)

Heating the mixtures in order to remove the PPh_3 ligand from [Pt(H)(PPh_3)('CyS_3')] resulted in C–S cleavage of the CyS_3 ligand, loss of the hydride ligands and formation of [$Pt(PPh_3)_2(S_2C_6H_4)$], which was characterized by elemental analysis and ^{1}H-NMR spectroscopy.

Synthesis and Reactions of [Ni('Et_2HNS_2')$_2$]$^{2+}$

In order to investigate the influence of amine vs. thioether donors, the tridentate amine–thioether–thiol ligand 'Et_2NS_2'-H was synthesized (Scheme 4).



Scheme 4. Synthesis and reactions of [Ni('Et_2HNS_2')$_2$]$^{2+}$: a) + PBr_3/HBr; b) + [$Ni(S_2C_6H_4)_2$]$^{2-}$; c) + HBr; d) + $Ni(ClO_4)_2 \cdot 6H_2O$; + *n*BuLi; f) + H_2O

Bromination of [$NEt_2(C_2H_4OH)$] with PBr_3 yielded $NEt_2(C_2H_4Br)$ as the ammonium salt [$NHEt_2(C_2H_4Br)$]Br. Subsequent treatment of the benzenedithiolate complex [$Ni(S_2C_6H_4)_2$]$^{2-}$ with [$NHEt_2(C_2H_4Br)$]Br gave [Ni('Et_2HNS_2')$_2$]Br_2 (**11**), which could be hydrolyzed with aqueous HBr to yield the ammonium bromide derivative ['Et_2HNS_2'-H]Br. Twofold deprotonation of ['Et_2HNS_2'-H]Br and reaction with either 0.5 or 1 equivalent of $Ni(ClO_4)_2 \cdot 6H_2O$ in both cases yielded the 1:2 complex [Ni('Et_2HNS_2')$_2$]$(ClO_4)_2$ (**12**). The reaction of [Ni('Et_2HNS_2')$_2$]$(ClO_4)_2$ suspensions in THF with 2 equivalents of strong bases such as BuLi or $LiBEt_3H$ reversibly gave dark-red solutions. They presumably contain [Ni('Et_2NS_2')$_2$] with six-coordinate Ni centers. However, a 1:1 complex containing [Ni('Et_2NS_2')] fragments could not be obtained.

X-ray Structure Determinations

X-ray structural characterizations allowed for the determination of the molecular structure of a considerable number of complexes and to confirm conclusions drawn from spectroscopic data. Figure 2 shows the molecular structures of [Ni('S_3')]$_2$ (**1**), [Ni(PMe_3)('S_3')] (**2**), NMe_4[Ni('S_3')CN)]·$0.5CH_2Cl_2$ (**3**·$0.5CH_2Cl_2$), [Ni('MeS_3')$_2$] (**7**), [Pt('S_3')(PPh_3)] (**6**), [Pt('S_3')]$_3$·2THF·MeOH, (**5**·2THF·MeOH), and [Ni('Et_2HNS_2')$_2$]Br_2 (**11**). Table 1 lists selected distances and angles.

All compounds consist of discrete molecules or ions. The solvate molecules do not interact with the metal complexes. [Ni('S_3')]$_2$ (**1**), [Ni('MeS_3')$_2$] (**7**), and [Ni('Et_2HNS_2')$_2$]Br_2 (**11**) exhibit crystallographically required inversion symmetry. In all complexes, the metal centers are four-coordinate, adopting distorted planar configurations. [Ni('S_3')]$_2$ (**1**), [Ni(PMe_3)('S_3')] (**2**), and [Ni(CN)('S_3')]$^-$ (**3**) exhibit a distinct tetrahedral distortion, whereas the platinum coordination of [Pt('S_3')]$_3$ (**5**) and [Pt(PPh_3)('S_3')] (**6**) is close to ideal square-planar.

The distances and angles are in the usual range found in diamagnetic nickel(II) and platinum(II) thioether–thiolate complexes. It is worth noting, however, that the Ni–S(thioether) distances of [Ni('S_3')]$_2$ (**1**) [210.3(3) pm], [Ni(PMe_3)('S_3')] (**2**) [213.8(2) pm], and [Ni(CN)('S_3')]$^-$ (**3**) [212.4(1) pm] are short and smaller than the respective Ni–S(thiolate) distances. Ni–S(thioether) distances in comparable complexes are usually in the range of ca. 217–218 pm,[20] and Ni–S distances in nickel thioether–thiolate complexes frequently do not differ at all.[21] If they differ, the Ni–S(thioether) distances are longer than the Ni–S(thiolate) distances.[22] It is remarkable that even in [Ni(PMe_3)('S_3')] (**2**) and [Ni(CN)('S_3')]$^-$ (**3**), the Ni–S(thioether) distances are short despite of the coordination *trans* to PMe_3 or CN^-, respectively, which are ligands known to have a strong *trans* influence.[23] The same holds true for the platinum complex [Pt('S_3')(PPh_3)] (**6**).[24] The short M–S(thioether) distances can be rationalized by the topology and rigidity of the 'S_3' ligand leading to rigid annellated five-membered [MSCCS] rings that force the thioether donors close to the metal centers. The rigidity of the 'S_3' ligand and sp^3 hybridization of the thioether donor further lead to the particular geometry of the [M('S_3')] fragments. They all exhibit a butterfly-like shape as illustrated by Figure 3.

In [Ni('S_3')]$_2$ (**1**), two such fragments are bridged by thiolate donors. The resulting four-membered [Ni_2S_2] ring is folded along the [S–S] axis such that the Ni(1)–Ni(1a) distance is 273.2(4) pm, and the molecule adopts a bowl-like shape (Figure 4).

A comparable Ni–Ni distance is found in [$Ni(SC_2H_4SC_2H_4S)]_2$ (273.9 pm).[25] These distances are significantly longer than Ni–Ni distances in nickel metal (249.2 pm)[26] and complexes such as [$Ni_8S(t$BuS$)_9$] (244.4 and 247.1 pm),[27] [$Ni(PhC(O)S)_2]_2$ (249 pm)[28] or [Ni(1,3-diphenyltriazenido)$_4]_2$ (238 pm),[29] for which Ni–Ni bonds

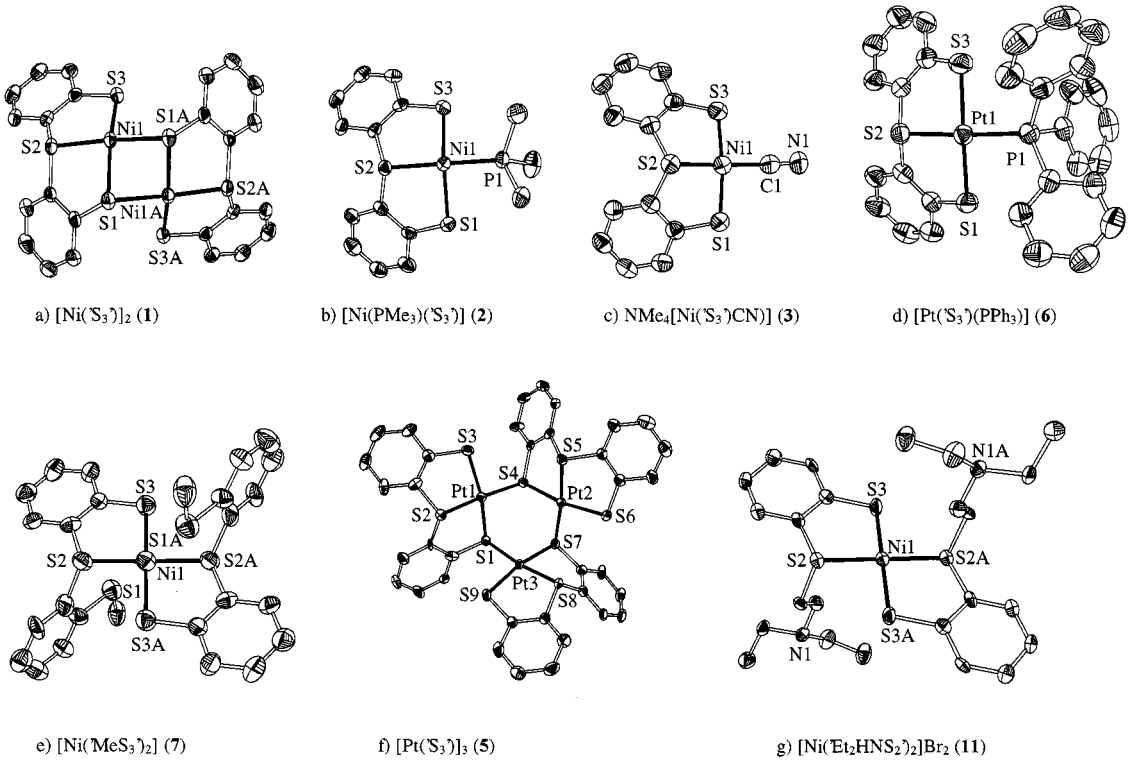


Figure 2. ORTEP Diagrams of a) [Ni('S_3')]$_2$ (**1**), b) [Ni(PMe_3)('S_3')] (**2**), c) NMe_4[Ni('S_3')CN)]·0.5CH_2Cl_2 (**3**·0.5CH_2Cl_2), d) [Pt('S_3')(PPh_3)] (**6**), e) [Ni('MeS_3')$_2$] (**7**), f) [Pt('S_3')]3·2THF·MeOH, (**5**·2THF·MeOH), g) [Ni('Et_2HNS_2')$_2$]Br_2 (**11**) (50% probability ellipsoids; hydrogen atoms, solvent molecules and counter ions omitted)

Table 1. Selected distances [pm] and angles [°] of [Ni('S_3')]$_2$ (**1**), [Ni('S_3')(PMe_3)] (**2**), NMe_4[Ni('S_3')(CN)]·0.5CH_2Cl_2 (**3**·0.5CH_2Cl_2), [Ni('MeS_3')$_2$] (**7**), [Ni('Et_2HNS_2')$_2$]Br_2 (**11**), [Pt('S_3')]3·2THF·MeOH (**5**·2THF·MeOH) and [Pt('S_3')(PPh_3)] (**6**)

Compound	[Ni('S_3')]$_2$	[Ni('S_3')(PMe_3)]	[Ni('S_3')(CN)]$^-$	[Ni('MeS_3')$_2$]	[Ni('Et_2NS_2')$_2$]Br_2		[Pt('S_3')]$_3$[c]		[Pt('S_3')(PPh_3)]
	1	**2**	**3**	**7**	**11**		**5**		**6**
M(1)−S(1)	218.3(1)	216.2(2)	216.2(1)	333.8(3)	477.1(9)[b]	231.2(3)	231.6(3)[d]	232.7(3)[e]	231.2(1)
M(1)−S(2)	210.4(3)	213.8(2)	212.4(1)	215.6(3)	216.1(2)	225.8(4)	225.4(3)	225.1(3)	228.7(1)
M(1)−S(3)	213.7(1)	214.8(2)	215.8(1)	219.0(3)	217.3(2)	230.3(3)	228.5(3)	228.2(4)	231.2(1)
M(1)−L	216.9(3)[a]	215.8(2)	185.7(4)			232.1(4)[f]	232.0(3)[g]	231.1(3)[h]	226.1(1)
M−M	273.2(4)	−	−	−	−	362.0(1)[i]	338.6(1)[k]	351.2(1)[l]	−
S(1)−M(1)−S(2)	87.89(9)	89.81(7)	90.10(4)			89.09(12)	87.28(11)	86.07(12)	87.69(4)
S(1)−M(1)−S(3)	161.80(3)	158.50(7)	160.03(5)			167.31(12)	167.33(13)	168.13(11)	163.92(5)
S(2)−M(1)−S(3)	92.02(7)	91.71(7)	90.80(4)	90.56(11)	91.11(9)	86.47(13)	88.89(12)	89.36(12)	87.08(4)
S(1)−M(1)−L	83.15(8)[a]	90.73(7)	92.76(11)			88.83(12)[f]	88.30(11)[g]	88.27(12)[h]	94.40(4)
S(2)−M(1)−L	165.73(3)[a]	168.08(7)	166.91(12)			175.91(12)[f]	173.52(12)[g]	172.38(11)[h]	177.85(4)
S(3)−M(1)−L	99.95(7)[a]	92.13(8)	90.86(11)			96.27(12)[f]	96.41(12)[g]	97.15(12)[h]	90.76(4)

[a] L = S(1a). − [b] Ni(1)−N(1). − [c] Three independent [PtS_3] units. − [d] Pt(2)−S(4). − [e] Pt(3)−S(7). − [f] L = S(4). − [g] L = S(7). − [h] L = S(1). − [I] Pt(1)−Pt(2). − [k] Pt(2)−Pt(3). − [l] Pt(3)−Pt(1).

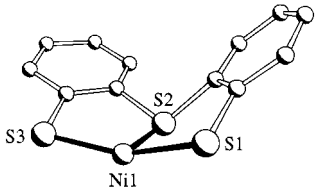


Figure 3. [Ni('S_3')] fragment in [Ni(PMe_3)('S_3')] (**2**)

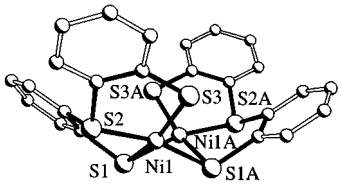


Figure 4. Lateral view of [Ni('S_3')]$_2$ (**1**)

are discussed. However, even Ni−Ni distances of 276.3(3) pm[30] and 279.5(3) pm[31] have been assumed to indicate weak Ni−Ni interactions. The trinuclear [Pt('S_3')]$_3$ (**5**) exhibits a cyclohexane-like [PtS_3]$_3$ six-membered ring with chair conformation. The Pt−S−Pt thiolate bridges are nearly symmetrical. Related structures are found in [$Pd(SC_2H_4SC_2H_4S)$]$_3$,[25b] [Ni('μ-$S_2C_3Me_2$')$_3$],[32] and [Ni('tBuS$_4$')]$_3$.[33]

The structures of [Ni('MeS_3')$_2$] (**7**) and [Ni('Et_2HNS_2')$_2$]Br_2 (**11**) unambiguously show that the potentially tridentate ligands only serve as bidentate ligands. The S(1) and S(1a) thioether donors of [Ni('MeS_3')$_2$] (**7**) occupy approximately apical positions in a distorted octahedron, but the Ni−S(1) and Ni−S(1a) distances [333.8(3) pm] are significantly larger than the sum of the van der Waals radii (310 pm)[26] and exclude Ni−S bonding interactions.

Conclusion

The objective of this work was to find nickel−sulfur ligand complexes that are stable towards reductive C−S cleavage and offer vacant sites for the coordination of hydrogenase-relevant small molecules. To achieve this goal, syntheses of 'S_3'-H_2, 'RS_3'-H (R=Me, Et, Cy), and 'Et_2NS_2'-H have been developed. X-ray structure analyses of the resulting nickel(II) and platinum(II) complexes have established the structural basis for reactivity studies.

Nickel(II) coordination by 'S_3'$^{2-}$ gave binuclear [Ni('S_3')]$_2$ (**1**) and platinum(II) formed trinuclear [Pt('S_3')]$_3$ (**5**). The [Ni('S_3')] fragment is robust and yielded stable [Ni(L)('S_3')] adducts with coligands such as PMe_3 and CN^-. In this respect, the [Ni('S_3')] fragment contrasts with other nickel thioether−thiolate complexes in which the ligands are decoordinated by cyanide.[34] The [Ni('S_3')] fragment probably also adds hydride. However, nickel-coordinated 'S_3'$^{2-}$ is unstable towards hydride reagents such as $LiAlH_4$ or $LiBEt_3H$. They cleaved the 'S_3'$^{2-}$ ligand into thiophenolate and 1,2-benzenedithiolate that formed [{Ni(SC_6H_5)($S_2C_6H_4$)}$_2$]$^{2-}$. This putatively indicates that in the reaction between [Ni('S_3')] fragments and hydride sources, highly reactive [Ni(H)('S_3')]$^-$ species form because 'S_3'$^{2-}$ in the free state is stable towards $LiAlH_4$, even under vigorous reaction conditions. While no [M(H)('S_3')]$^-$ species with M = Ni could be identified, a [Pt(H)('S_3')]$^-$ complex was detected by ^{1}H-NMR spectroscopy and isolated in the solid state. However, it could not be separated from [Pt(H)(PPh_3)('S_3')]$^-$ complexes which were formed concomitantly. Modification of 'S_3'$^{2-}$ by alkylating one thiolate donor gave the new ligands 'RS_3'-H with R = Me, Et, Cy. When coordinated to nickel(II), these ligands act as bidentate ligands only. Under all applied conditions, exclusively 1:2 complexes of the general formula [Ni('RS_3')$_2$] resulted, in which the RS-thioether donors do not coordinate.

[Ni('RS_3')] hydride complexes could not be detected. In contrast, when [Pt(PPh_3)$_4$] was treated with 'CyS_3'-H, ^{1}H-NMR spectroscopy revealed the formation of [Pt(H)('CyS_3')]. The concomitant formation of the equally highly soluble [Pt(H)(PPh_3)('CyS_3')] prevented the isolation in pure form. Additionally, the platinum-bonded hydride appears to be still highly reactive, because at elevated temperatures 'CyS_3' cleavage and formation of [Pt(PPh_3)$_2$($S_2C_6H_4$)] took place.

Modification of the 'RS_3'-H ligands by exchanging the RSC_6H_4 entity for $NEt_2(C_2H_4)$ gave the new ligand 'Et_2NS_2'$^-$. It formed the 1:2 nickel complex [Ni('Et_2HNS_2')$_2$]Br_2 (**11**) in which the two amine N atoms are protonated.

In conclusion, the tridentate sulfur ligand 'S_3'$^{2-}$ forms nickel(II) and platinum(II) complexes whose [M('S_3')] fragments coordinate coligands such as PR_3, CN^-, and H^-. The resulting [M(H)('S_3')]$^-$ species were detectable with platinum(II). The alkylated derivatives 'RS_3' preferably act as bidentate ligands and give the 1:2 complexes [Ni('RS_3')$_2$]. Current studies are probing the interaction of molecular hydrogen with the new complexes.

Experimental Section

General Methods: Unless otherwise noted, all reactions and operations were carried out under nitrogen at room temperature using standard Schlenk techniques. Solvents were dried and distilled before use. As far as possible, reactions were monitored by IR or NMR spectroscopy. − Spectra were recorded with the following instruments: IR (KBr pellets or CaF_2 cuvettes, solvent bands were compensated): Zeiss IMR 25 and Perkin−Elmer 983. − NMR: Jeol JNM-GX 270 and Jeol JNM-EX 270; with the residual protiosolvent signal used as reference for ^{1}H-NMR spectra. $^{13}C\{^1H\}$-NMR spectra were referenced using the solvent peaks, $^{31}P\{^1H\}$-NMR spectra were referenced externally. Chemical shifts are quoted on the δ scale (downfield shifts are positive) related to tetramethylsilane (^{1}H, ^{13}C) or 85% H_3PO_4 (^{31}P). Spectra were recorded at room temperature unless stated otherwise. ^{1}H: 270.0 MHz, $^{13}C\{^1H\}$; 67.8 MHz, $^{31}P\{^1H\}$: 109.4 MHz. − Mass spectra: Varian MAT 212 spectrometer and Jeol M.Station 700. − Elemental analyses: Carlo Erba EA 1106 or 1108 analyzer. − $S(C_6H_5)_2$ and *n*BuLi (2.5 M in hexanes) were purchased from Aldrich. 'S_2'-H_2,[35] [Pt(PPh_3)$_4$],[36] [Pt(PEt_3)$_4$],[37] and [$PtCl_2$(COD)][38] were prepared by literature methods.

'S_3'-H_2: At room temperature, TMEDA (38 mL, 253 mmol), a solution of *n*BuLi in hexanes (2.5 M, 100 mL, 250 mmol) and diphenyl sulfide (20 mL, 118 mmol) were successively added to 200 mL of hexanes. The solution was stirred for 24 h, in the course of which a beige solid precipitated. Under vigorous stirring elemental sulfur (10.8 g, 337 mmol) was added, the resulting yellow suspension was stirred for another 48 h, and concentrated to dryness. The yellow residue was dissolved in THF (200 mL) and $LiAlH_4$ (10.0 g, 264 mmol) was added in small portions. ***Caution:*** *A vigorous reaction takes place and the reaction suspension starts foaming up.* Subsequently, the reddish suspension was heated at reflux for 5 h, in the course of which the color turned to light yellow green. The resulting mixture was cautiously added in small portions to a mixture of crushed ice (400 g) and concentrated hydrochloric acid (200 mL). ***Caution:*** *A vigorous evolution of* H_2 and H_2S occurs, and this reaction must be carried out in a well-ventilated hood. After the vigorous reaction had ceased, a further 50 mL of concentrated HCl was added, and the resulting suspension was extracted with of CH_2Cl_2 (3 × 200 mL). The combined organic phases were washed with dilute aqueous HCl, dried with Na_2SO_4, and concentrated to dryness. The reddish yellow waxy residue was digested with Et_2O (ca. 200 mL) until an ivory solid resulted. It was separated, recrystallized from hot THF/hexanes to give brilliant white 'S_3'-H_2. Yield: 6.5 g [22% from $S(C_6H_5)_2$]. − $C_{12}H_{10}S_3$ (250.41): calcd. C 57.56, H 4.03, S 38.42; found C 57.74, H 4.06, S 38.72. − MS (FD, CCl_4); *m/z*: 250 [M$^+$]. − ^{1}H NMR ($CDCl_3$): δ = 7.45−7.35 (m, 2 H, C_6H_4), 7.25−7.0 (m, 6 H, C_6H_4), 4.10 (s, 2 H, SH). − ^{1}H NMR (C_6D_6): δ = 7.01 (m, 2 H, H6-C_6H_4), 6.96 (m, 2 H, H3-C_6H_4), 6.68 (m, 2 H, H4-C_6H_4), 6.63 (m, 2 H, H5-C_6H_4), 3.81 (m, 2 H, SH).

– $^{13}C\{^1H\}$ NMR ($CDCl_3$): δ = 135.6, 132.9, 130.8, 128.9, 127.2 (C_6H_4). – $^{13}C\{^1H\}$ NMR (C_6D_6): δ = 135.7 (C2-C_6H_4), 132.8 (C1-C_6H_4), 132.5 (C6-C_6H_4), 130.2 (C3-C_6H_4), 128.2 (C4-C_6H_4), 126.5 (C5-C_6H_4). – IR (KBr): $\tilde{\nu}$ = 3052, 2555, 1565, 1445, 1426, 1259, 1035, 745 cm^{-1}.

[Ni('S_3')]$_2$ (1): 'S_3'-H_2 (2.450 g, 9.78 mmol) in THF (30 mL) was added dropwise to a solution of $Ni(ac)_2{\cdot}4H_2O$ (2.435 g, 9.78 mmol) in MeOH (50 mL). A brown precipitate formed which was separated, washed with MeOH (50 mL) and recrystallized from boiling DMF to give black microcrystals of **1**. Yield: 2.73 g (91%). – $C_{24}H_{16}Ni_2S_6$ (614.17): calcd. C 46.94, H 2.63, S 31.33; found C 46.81, H 2.56, S 30.83. – IR (KBr): $\tilde{\nu}$ = 3050, 1561, 1443, 1425, 1093, 759, 747, 740, 729 cm^{-1}.

[Ni('S_3')(PMe_3)] (2): PMe_3 (370 mg, 4.86 mmol) was added to a brown suspension of [Ni('S_3')]$_2$ (**1**) (1.065 g, 1.73 mmol) in THF (5 mL) and a dark brown solution formed. Addition of MeOH (40 mL) precipitated orange microcrystals that were separated, washed with MeOH (40 mL) and dried. Yield: 1.25 g (94%). – $C_{15}H_{17}NiPS_3$ (383.16): calcd. C 47.02, H 4.47, S 25.11; found C 47.11, H 4.46, S 24.57. – ^1H NMR (C_6D_6): δ = 7.55 (d, 2 H, H6-C_6H_4), 7.28 (d, 2 H, H3-C_6H_4), 6.82 (m 2 H, H5-C_6H_4), 6.65 (m, 2 H, H4-C_6H_4), 0.93 [d, $^2J_{H,P}$ = 10.9 Hz, 9 H, $P(CH_3)_3$]. – $^{13}C\{^1H\}$ NMR ($CDCl_3$) δ = 152.5 (d, $^3J_{P,C}$ = 14.0 Hz, C_6H_4) 133.3, 130.5, 129.4, 128.3, 123.5 (C_6H_4), 14.9 [d, $^1J_{P,C}$ = 30.6 Hz, $P(CH_3)_3$]. – $^{13}C\{^1H\}$ NMR (C_6D_6): δ = 153.6 (d, *trans*-$^3J_{P,C}$ = 14.1 Hz, C1-C_6H_4), 133.3 (d, *cis*-$^3J_{P,C}$ = 2.0 Hz, C2-C_6H_4), 130.1 (d, $^4J_{P,C}$ = 1.7 Hz, C6-C_6H_4), 128.7 (s, C5-C_6H_4), 128.1 (d, $^4J_{P,C}$ = 1.2 Hz, C3-C_6H_4), 122.6 (s, C4-C_6H_4), 13.5 [d, $^1J_{P,C}$ = 30.6 Hz, $P(CH_3)_3$]. – $^{31}P\{^1H\}$ NMR ($CDCl_3$) δ = –9.2 [$P(CH_3)_3$]. – IR (KBr): $\tilde{\nu}$ = 3040, 2960, 1564, 1444, 1425, 1096, 950, 735 cm^{-1}.

(NMe_4)[Ni('S_3')(CN)] (3): A solution of KCN (141.5 mg, 2.17 mmol) in a mixture of MeOH (10 mL) and H_2O (1 mL) was added dropwise to a brown suspension of [Ni('S_3')]$_2$ (**1**) (650 mg, 1.06 mmol) in THF (10 mL). The resulting yellow green solution was concentrated to dryness, and the remaining solid was redissolved in MeOH (20 mL) and H_2O (1 mL). The solution was filtered, combined with NMe_4Cl (220 mg, 2.0 mmol) in MeOH (2 mL), and layered with Et_2O (20 mL). Brown crystals precipitated, which were separated after 7 d, washed with Et_2O and dried in vacuo. Yield: 520 mg (60%).– $C_{17}H_{20}N_2NiS_3$ (407.26) calcd. C 50.14, H 4.95, N 6.88; found C 45.58, H 4.36, N 5.98. – ^1H NMR ([D_6]acetone/$CDCl_3$): δ = 7.36 (d, 2 H, C_6H_4), 7.03 (d, 2 H, C_6H_4), 6.78 (m, 2 H, C_6H_4), 6.68 (m, 2 H, C_6H_4), 2.92 [12 H, s, $N(CH_3)_4$]. – IR (KBr): $\tilde{\nu}$ = 3050, 3026, 2110, 1569, 1482, 1441, 1431, 948, 733 cm^{-1}.

(NMe_4)$_2$[{Ni(SC_6H_5)($S_2C_6H_4$)}$_2$] (4). – a) From [Ni('S_3')]$_2$ and $LiBEt_3H$: At –90°C, $LiBEt_3H$ (3 mL of a 1 M THF solution, 3 mmol) was added to a brown suspension of [Ni('S_3')]$_2$ (**1**) (615 mg, 1.0 mmol) in THF (15 mL). When the temperature was slowly raised to –30°C, a yellow–green solution formed. It was layered with a cold solution of NMe_4Cl (0.329 g, 3.0 mmol) in MeOH (15 mL) and kept at –30°C for 3 d. Red-brown microcrystals precipitated which were separated, washed with MeOH, and dried in vacuo. Yield: 340 mg (45%). – **b) From Ni(ac)$_2$·4H$_2$O, $SC_6H_5^-$, and *o*-$S_2C_6H_4^{2-}$:** A solution of thiophenol (1.10 g, 10 mmol) and LiOMe (380 mg, 10 mmol) in MeOH (10 mL) was added to $Ni(ac)_2{\cdot}4H_2O$ (2.48 g, 10 mmol) in MeOH (40 mL). A red-brown suspension resulted, which was combined with a solution of *o*-$C_6H_4(SH)_2$ (1.42 g, 10 mmol) and LiOMe (760 mg, 20 mmol) in MeOH (20 mL), stirred for 2 h and concentrated to dryness. Addition of DMF (40 mL) to the residue and heating the suspension to 100°C for 2 h gave a clear brown solution, which was reduced in volume to 10 mL. Addition of Me_4NCl (1.095 g, 10 mmol) in MeOH (50 mL) at room temperature precipitated red-brown microcrystals which were separated, washed with MeOH (45 mL) and Et_2O (20 mL), and dried in vacuo. Yield: 3.06 g (80%). – $C_{32}H_{42}N_2Ni_2S_6$ (764.51): calcd. C 50.28, H 5.54, N 3.66, S 25.16; found C 47.16, H 5.38, N 3.23, S 23.42. – MS (ESI, MeOH) ([$^{12}C_{24}{}^1H_{18}{}^{58}Ni_2{}^{32}S_6$]$^{2-}$); *m/z*: calcd. 306.922; found 306.9. – ^1H NMR ([D_6]DMSO): δ = 8.22 (m, 4 H, C_6H_5), 7.05 (m, 6 H, C_6H_5), 6.80 (m, 4 H, C_6H_4), 6.40 (m, 4 H, C_6H_4), 3.07 [s, 24 H, $N(CH_3)_4$]. – $^{13}C\{^1H\}$ NMR ([D_6]DMSO): δ = 150.0, 139.8, 134.8, 126.8, 125.5, 124.3, 118.7 (C_6H_5, C_6H_4), 54.35 [t, $^1J_{C,N}$ = 4.2 Hz, $N(CH_3)_4$]. – IR (KBr): $\tilde{\nu}$ = 3045, 3007, 1571, 1542, 1479, 1433, 1282, 1233, 1101, 1021, 948, 743, 692, 665 cm^{-1}.

[Pt('S_3')]$_3$ (5). – a) From K_2PtCl_4 and 'S_3'-H_2: A solution of K_2PtCl_4 (1.06 g, 2.55 mmol) in H_2O (20 mL) was combined with a solution of 'S_3'-H_2 (640 mg, 2.55 mmol) in aqueous NaOH (51 mL of a 0.1 M solution, 5.1 mmol). A yellow suspension resulted which was stirred at 50°C for 2 h. The yellow solid was separated, washed with H_2O (40 mL), dried at 50°C, and extracted with THF (20 mL). The red THF extracts were filtered and layered with MeOH to give yellow-red crystals of [Pt('S_3')]3·2THF·MeOH. – ^1H NMR ([D_8]THF): δ = 7.95–6.40 (m, C_6H_4). – **b) From [$PtCl_2$(COD)] and 'S_3'-H_2:**[17] Solid 'S_3'-H_2 (865 mg, 3.46 mmol) was added to a solution of [$PtCl_2$(COD)] (1.293 g, 3.46 mmol) in THF (20 mL) and the resulting solution was stirred for 12 h. A yellow precipitate formed which was isolated, washed with THF (10 mL) and dried in vacuo. Yield: 1.24 g (81%). – $C_{36}H_{24}S_9Pt_3$ (1330.44): calcd. C 32.50, H 1.82; found C 32.54, H 1.95.

Li[Pt('S_3')(H)], Li[Pt('S_3')(H)(PPh_3)], and [Pt('S_3')(PPh_3)] (6): *n*BuLi (0.4 mL of a 2.5 M solution in hexanes, 1.0 mmol) was added to a solution of 'S_3'-H_2 (250 mg, 1.0 mmol) in THF (10 mL), and a pale yellow solution resulted, which was added dropwise to a suspension of [$Pt(PPh_3)_4$] (1.24 g, 1.0 mmol) in THF (30 mL). A yellow-orange solution resulted and was stirred for 1 h at 70°C and concentrated to dryness. The orange residue was extracted with warm hexanes (120 mL) in several portions and the remaining pale yellow powder was isolated and dried in vacuo. It was characterized by ^1H-NMR spectroscopy to be a mixture of Li[Pt('S_3')(H)], Li[Pt('S_3')(H)(PPh_3)] and some remaining PPh_3. – ^1H NMR ([D_8]THF): δ = 7.93–6.62 (m, C_6H_4/C_6H_5), –10.65 {d + dd, $^1J_{H,Pt}$ = 1274 Hz, $^2J_{H,P}$ = 21 Hz, Pt*H* in Li[Pt('S_3')(*H*)(PPh_3)]}, –15.72 {s + d, $^1J_{H,Pt}$ = 1242 Hz, Pt*H* in Li[Pt('S_3')(*H*)]}. – IR (KBr): $\tilde{\nu}$ = 2109 cm^{-1} (ν_{PtH}); (*p*-dioxane): $\tilde{\nu}$ = 2127 cm^{-1} (ν_{PtH}).

'MeS_3'-H: At –90°C, solid [Ni('S_3')(PMe_3)] (270 mg, 0.71 mmol) was added to a suspension of Me_3OBF_4 (105 mg, 0.71 mmol) in CH_2Cl_2 (15 mL). The suspension was warmed to room temperature and stirred for 4 h to give a yellow-brown solution. Addition of Et_2O (20 mL) precipitated a yellow-green powder that was separated, washed with little Et_2O and redissolved in CH_2Cl_2 (15 mL) to give a yellow-green solution. Addition of half-concentrated hydrochloric acid (20 mL) resulted in decoloration of the CH_2Cl_2 phase. The organic layer was separated and the aqueous phase was extracted with CH_2Cl_2 (15 mL). The combined CH_2Cl_2 extracts were dried with Na_2SO_4 and concentrated to give an oily pale yellow residue. It was dissolved in Et_2O (20 mL) and the resulting solution was extracted with aqueous NaOH (10%, 20 mL). The aqueous phase was separated, washed with Et_2O (10 mL), acidified with aqueous HCl, and extracted with CH_2Cl_2 (30 mL) in several portions. The combined CH_2Cl_2 layers were dried with Na_2SO_4 and concentrated to give 'MeS_3'-H as a colorless oil, which was identified by NMR spectroscopy. Yield: 60 mg (32%). – ^1H NMR ($CDCl_3$): δ = 7.50–6.95 (m, 8 H, C_6H_4), 4.26 (s, 1 H, SH), 2.54

(s, 3 H, CH_3). − $^{13}C\{^1H\}$ NMR ($CDCl_3$): δ = 140.2, 136.9, 134.1, 134.0, 132.6, 131.3, 130.3, 129.1, 128.4, 127.2, 126.9, 126.5 (C_6H_4), 16.8 (CH_3).

NBu_4'EtS_3': $Et_3O{\cdot}BF_4$ (743 mg, 3.91 mmol) in CH_2Cl_2 (5 mL) was added to a stirred brown suspension of [Ni('S_3')]$_2$ (1.20 g, 1.96 mmol) in CH_2Cl_2 (50 mL). In the course of 16 h, a brown solution resulted to which concentrated aqueous HCl (40 mL) was added. After stirring for another 2 h, the CH_2Cl_2 phase had turned colorless. The CH_2Cl_2 phase was separated and the remaining aqueous phase was extracted with CH_2Cl_2 (20 mL). The combined CH_2Cl_2 extracts were concentrated to give a colorless oil, which was dissolved in MeOH (20 mL) and combined with 5 mL of a 1 M MeOH solution of Bu_4NOH (5 mmol). Et_2O (100 mL) was added and the resulting solution cooled to −78°C. Colorless microcrystals precipitated, which were separated at −78°C after 1 d, washed with Et_2O (−78°C) and dried. Yield: 1.20 g (59%).− ^1H NMR ([D$_4$]MeOH): δ = 7.47−7.26 (m, 4 H, C_6H_4), 7.11 (m, 1H, C_6H_4), 6.70 (m, 1H, C_6H_4), 6.56 (m, 1H, C_6H_4), 6.32 (m, 1H, C_6H_4), 3.22 (t, 8 H, NCH_2), 2.92 (q, 2 H, SCH_2), 1.64 (m, 8 H, NCH_2CH_2), 1.39 (m, 8 H, $NCH_2CH_2CH_2$), 1.28 (t, 3 H, SCH_2CH_3), 0.99 (t, 12 H, $NCH_2CH_2CH_2CH_3$). − $^{13}C\{^1H\}$ NMR ([D$_4$]MeOH): δ = 148.5, 144.0, 140.3, 136.9, 135.8, 135.1, 129.5, 127.8, 126.5, 126.2, 125.0, 121.9 (C_6H_4), 59.5 (t, $^1J_{C,N}$ = 5.3 Hz, NCH_2), 27.1 (SCH_2), 24.9 (NCH_2CH_2), 20.8 ($NCH_2CH_2CH_2$), 14.2 (SCH_2CH_3), 14.0 ($NCH_2CH_2CH_2CH_3$).

'EtS_3'-H: [Ni('EtS_3')$_2$] (**9**) (280 mg, 0.46 mmol) was suspended in CH_2Cl_2 (20 mL), concentrated HCl (20 mL) was added and the mixture was stirred for 2 h. The CH_2Cl_2 phase was separated and the aqueous phase was extracted with CH_2Cl_2. The combined organic layers were dried with Na_2SO_4 and concentrated to yield 'EtS_3'-H as a colorless oil. Yield: 230 mg (90%). − MS (FD, CH_2Cl_2); *m*/*z*: 278 [M^+]. − ^1H NMR (CD_2Cl_2): δ = 7.47−7.03 (m, 7 H, C_6H_4), 6.88 (d, 1 H, C_6H_4), 4.28 (s, 1 H, SH), 3.02 (q, 2 H, SCH_2), 1.35 (t, 3 H, SCH_2CH_3).

'CyS_3'-H: At −30°C, 'S_3'-H_2 (5.90 g, 23.6 mmol) in THF (25 mL) was combined with *n*BuLi (10 mL of 2.5 M in hexanes, 25 mmol), and the resulting solution was concentrated to dryness at room temperature. The light yellow residue was dissolved in DMF (50 mL), combined with cyclohexyl bromide (8.00 g, 49.1 mmol) and heated to 125°C for 6 h. All volatile materials were removed at 110°C in vacuo (1 mbar), the remaining oil was dissolved in CH_2Cl_2 (30 mL) and half-concentrated HCl (50 mL) was added. The CH_2Cl_2 phase was separated, and the aqueous phase was extracted with CH_2Cl_2 (60 mL). The combined CH_2Cl_2 phases were washed with dilute aqueous HCl (5 mL), dried with Na_2SO_4, and concentrated. The remaining oil was redissolved in Et_2O (40 mL) and hexanes (10 mL) and filtered. Aqueous NaOH (50 mL, 10%) was added to the filtrate, the mixture was agitated vigorously in a separating funnel and subsequently allowed to separate. In the course of ca. 30 min three phases formed of which the thin middle one displayed a pale red color. This phase was carefully separated, acidified with half-concentrated HCl and extracted with CH_2Cl_2 (60 mL). The CH_2Cl_2 extracts were washed with dilute aqueous HCl (10 mL), dried with Na_2SO_4, and concentrated at 60°C (0.1 mbar). The remaining oil of 'CyS_3'-H was identified by NMR spectroscopy. Yield: 3.27 g (42%). − ^1H NMR ($CDCl_3$): δ = 7.55−7.01 (m, 7 H, C_6H_4), 6.67 (d, 1 H, C_6H_4), 4.33 (s, 1 H, SH), 3.27 [m, 1 H, $SCH(CH_2)_5$], 2.13 [1.15 (m, 10 H, $SCH(CH_2)_5$]. − $^{13}C\{^1H\}$ NMR ($CDCl_3$): δ = 140.0, 139.2, 136.3, 133.7, 133.0, 130.1, 129.5, 129.2, 127.8, 127.1, 126.1, 126.0 (C_6H_4), 46.7 [$SCH(CH_2)_5$], 33.2, 26.0, 25.7 [$SCH(CH_2)_5$].

[Ni('MeS_3')$_2$] (7): 'MeS_3'-H (210 mg, 0.80 mmol) in THF (10 mL) was treated with NaOMe (0.8 mL of a 1 M solution in MeOH, 0.80 mmol) and combined with $NiBr_2{\cdot}3H_2O$ (270 mg, 1.0 mmol) in MeOH (10 mL). A red solution resulted from which an orange to ochreous solid precipitated that was separated after 1 d, washed with MeOH (30 mL), and dried. Yield: 210 mg (90%). − $C_{26}H_{22}NiS_6$ (585.56): calcd. C 53.33, H 3.79; found C 52.18, H 3.86. − IR (KBr): $\tilde{\nu}$ = 3047, 2963, 2924, 1564, 1442, 1423, 1097, 750 cm^{-1}.

[Ni('MeS_3')$_2$(PMe_3)$_2$] (8): PMe_3 (70 mg, 0.92 mmol) was added to a suspension of Ni('MeS_3')$_2$] (**7**) (60 mg, 0.10 mmol) in THF (5 mL), and a deep red solution resulted. Addition of MeOH (8 mL) precipitated an orange solid that was separated, washed with MeOH (5 mL) and Et_2O (15 mL), and dried. Yield: 55 mg (75%). − $C_{32}H_{40}NiP_2S_6$ (737.72): calcd. C 52.10, H 5.47, S 26.08; found C 51.99, H 5.41, S 25.64. − ^1H NMR ($CDCl_3$): δ = 7.80 (d, 2 H, C_6H_4), 7.39 (d, 2 H, C_6H_4), 7.28 (pseudo-t, 2 H, C_6H_4), 7.18 (d, 2 H, C_6H_4), 7.04 (pseudo-t, 2 H, C_6H_4), 6.88 (d pseudo-t, 2 H, $^5J_{H,P}$ = 2.6 Hz, C_6H_4), 6.82−6,69 (m, 4 H, C_6H_4), 2.38 (s, 6 H, CH_3), 1.27 [d, 18 H, $^2J_{H,P}$ = 5 Hz, $P(CH_3)_3$].

[Ni('EtS_3')$_2$] (9): $NiCl_2{\cdot}6H_2O$ (200 mg, 0.85 mmol) in MeOH (5 mL) was added to a stirred solution of NBu_4'EtS_3' (440 mg, 0.85 mmol) in MeOH (10 mL). An orange-brown precipitate formed that was separated after 2 h, washed with MeOH (15 mL) and recrystallized from hot DMF. Yield: 460 mg (88%). − $C_{28}H_{26}NiS_6$ (613.61): calcd. C 54.81, H 4.27, S 31.35; found C 54.51, H 4.29, S 30.18. − ^1H NMR (C_6D_6): δ = 7.92 (m, 2 H, C_6H_4), 7.41 (m, 2 H, C_6H_4), 6.94−6.78 (m, 6 H, C_6H_4), 6.68−6.57 (m, 4 H, C_6H_4), 6.38 (m, 2 H, C_6H_4), 2.57 (q, 4 H, CH_2), 0.99 (t, 6 H, CH_3). − IR (KBr): $\tilde{\nu}$ = 3049, 2965, 2924, 1566, 1444, 1424, 1261, 1246, 1100, 756, 738 cm^{-1}.

[Ni('CyS_3')$_2$] (10): Ni(ac)$_2{\cdot}4H_2O$ (250 mg, 1.0 mmol) in MeOH (10 mL) was added to 'CyS_3'-H (175 mg, 0.53 mmol) in THF (10 mL), yielding a red solution. This solution was reduced in volume to 5 mL, and MeOH (20 mL) was added. An orange-brown solid precipitated which was separated, washed with MeOH (30 mL) and dried. Yield: 170 mg (90%). − $C_{36}H_{38}NiS_6$ (721.80): calcd. C 59.91, H 5.31, S 26.65; found C 60.00, H 5.22, S 26.38. − MS (FD, CH_2Cl_2); *m*/*z*: 720 [M^+]. − ^1H NMR ($CDCl_3$): δ = 7.99−6.69 (m, 8 H, C_6H_4), 3.35 [m, 1 H,$SCH(CH_2)_5$], 2.16−1.08 [m, 10 H, $SCH(CH_2)_5$]. − IR (KBr): $\tilde{\nu}$ = 3048, 2927, 2850, 1565, 1443, 1424, 1099, 745 cm^{-1}.

[Pt(H)('CyS_3')] and [Pt(H)('CyS_3')(PPh_3)]: A solution of 'CyS_3'-H (335 mg, 1.0 mmol) in THF (10 mL) was added to a suspension of [Pt(PPh_3)$_4$] (1.25 g, 1.0 mmol) in THF (30 mL). The yellow suspension was stirred for 20 min upon which an orange solution resulted, which was heated to reflux for 1 h. After allowing to come to room temperature, MeOH (20 mL) was added to precipitate a pale yellow solid. This product was separated and extracted several times with hot hexanes (120 mL). The remaining pale yellow powder was dried in vacuo and was characterized by means of NMR spectroscopy to consist of a mixture of [Pt('CyS_3')(H)], [Pt('CyS_3')(H)(PPh_3)] and PPh_3. − ^1H NMR ([D$_8$]THF): δ = 7.98−6.43 (m, C_6H_4/C_6H_5), 3.15−3.09 [m, $SCH(CH_2)_5$], 2.05−0.97 [m, $SCH(CH_2)_5$], −11.38 {d + dd, $^1J_{H,Pt}$ = 1260 Hz, $^2J_{H,P}$ = 20 Hz, PtH in [Pt('CyS_3')(H)(PPh_3)]}, −15.74 {s + d, $^1J_{H,Pt}$ = 1155 Hz, Pt*H* in [Pt('CyS_3')(H)]}. − $^{31}P\{^1H\}$ NMR ([D$_8$]THF): δ = 23.5 {s + d, $^1J_{P,Pt}$ = 3260 Hz, *P*Ph_3 in [Pt('CyS_3')(H)(PPh_3)]}. − IR (KBr): $\tilde{\nu}$ = 2110 cm^{-1} (ν_{PtH}); (THF): $\tilde{\nu}$ = 2117 cm^{-1} (ν_{PtH}).

[Pt(PPh_3)$_2$($S_2C_6H_4$)]: A solution of 'CyS_3'-H (330 mg, 1.0 mmol) in toluene (5 mL) was combined with a suspension of [Pt(PPh_3)$_4$] (1.240 g, 1.0 mmol) in toluene (25 mL). The resulting orange suspension was heated to 80°C (10 min) and then to 100°C to give a clear yellow-orange solution. After 30 min at 100°C, yellow microc-

rystals of $[Pt(PPh_3)_2(S_2C_6H_4)]$ precipitated, which were isolated at room temperature, washed with toluene (15 mL) and pentanes (15 mL), and dried in vacuo. − $C_{42}H_{34}P_2PtS_2$ (859.90): calcd. C 58.67, H 3.99, S 7.46; found C 58.77, H 4.04, S 7.38. − ^{1}H NMR (CD_2Cl_2): δ = 7.70−7.10 (m, 32 H, C_6H_4, C_6H_5), 6.68 (m, 2 H, C_6H_4).

[$Et_2HNC_2H_4Br$]Br: At 0°C, $Et_2NC_2H_4OH$ (45.1 g, 385 mmol) was cautiously combined with aqueous HBr (100 mL, 47%, 884 mmol) and PBr_3 (86.4 g, 320 mmol). The mixture was sealed in a thick-walled glass ampoule and heated to 140°C for 11 h. From the resulting brown product, all volatile components were removed in vacuo, the residue was redissolved in boiling EtOH (150 mL) and allowed to cool to room temperature. Upon addition of Et_2O (200 mL), colorless microcrystals precipitated, which were separated, washed with Et_2O (100 mL), and dried. Yield: 79.9 g (80%). − $C_6H_{15}Br_2N$ (261.01): calcd. C 27.61, H 5.79, N 5.37; found C 27.20, H 5.99, N 4.88.− ^{1}H NMR ([D$_4$]MeOH): δ = 4.78 (s, 1 H, NH), 3.72 (m, 2 H, NC_2H_4Br), 3.56 (m, 2 H, NC_2H_4Br), 3.25 [q, 4 H, $N(CH_2CH_3)_2$], 1.28 [t, 6 H, $N(CH_2CH_3)_2$]. − ^{13}C{^{1}H} NMR ([D$_4$]MeOH): δ = 54.0 (NCH_2CH_2Br), 48.9 [$N(CH_2CH_3)_2$], 24.4 [$N(CH_2CH_2)Br$], 9.1 [$N(CH_2CH_3)_2$].

[Ni(‘Et_2HNS_2’)$_2$](ClO$_4$)$_2$ (12): ***Caution:*** *Although we did not face any difficulties, the use of perchlorates in the presence of organic material may cause explosions and perchlorates must be treated accordingly (protective shields).* A stirred solution of *o*-$C_6H_4(SH)_2$ (3.685 g, 25.9 mmol) in MeOH (30 mL) was deprotonated with NaOMe (2.81 g, 51.8 mmol) and added to a solution of $Ni(ClO_4)_2{\cdot}6H_2O$ (4.74 g, 13.0 mmol) in MeOH (65 mL). To the resulting brown-yellow solution of $[Ni(S_2C_6H_4)_2]^{2-}$, a solution of $[Et_2HNC_2H_4Br]Br$ (6.76 g, 25.9 mmol) in MeOH (50 mL) was added dropwise within 20 min. The resulting solution was stirred for 24 h at room temperature, subsequently heated at reflux for 4 h, and then allowed to cool to room temperature again. A yellow-red precipitate formed which was separated, washed with MeOH (40 mL) and dried in vacuo for 3 d. Yield: 6.7 g (70%). − $C_{24}H_{38}Cl_2N_2NiO_8S_4$ (740.45): calcd. C 38.93, H 5.17, N 3.78, S 17.32; found C 39.58, H 5.41, N 3.83, S 17.26. − ^{1}H NMR ([D$_4$]MeOH): δ = 7.62 (m, 1 H, C_6H_4), 7.44 (m, 1 H, C_6H_4), 7.26 (m, 1 H, C_6H_4), 7.13 (m, 1 H, C_6H_4), 4.88 (s, NH), 3.71 (br., 2 H, NC_2H_4S), 3.57 (br., 2 H, NC_2H_4S), 3.24 (q, 4 H, NCH_2CH_3), 1.19 (t, 6 H, NCH_2CH_3). − IR (KBr): $\tilde{\nu}$ = 3053, 2971, 2933, 2656, 2470, 1566, 1447, 1419, 1261, 1244, 1097, 741, 624 cm^{-1}.

[‘Et_2HNS_2’-H]Br: [Ni(‘Et_2HNS_2’)$_2$](ClO$_4$)$_2$ (**12**) (500 mg, 0.675 mmol) in $CHCl_3$ (20 mL) was treated with concentrated aqueous HBr (20 mL, 47%, 175 mmol) and stirred vigorously for 2 h. The resulting light-yellow $CHCl_3$ phase was separated, dried with Na_2SO_4 and concentrated to dryness, yielding a white solid of [‘Et_2HNS_2’-H]Br that was identified by NMR spectroscopy. Yield: 270 mg (62%). − ^{1}H NMR ($CDCl_3$): δ = 10.90 (s, 1 H, br., NH), 8.02−6.21 (m, 4 H, C_6H_4), 4.59 (s, 1 H, SH), 4.00−3.19 (m, 8 H, NC_2H_4S, NCH_2CH_3), 1.63 (t, 6 H, NCH_2CH_3).

X-ray Structure Analysis of [Ni(‘S_3’)]$_2$ (1), [Ni(‘S_3’)(PMe$_3$)] (2), NMe$_4$[Ni(‘S_3’)(CN)]·0.5CH_2Cl_2 (3·0.5CH_2Cl_2), [Ni(‘MeS_3’)$_2$] (7), [Ni(‘Et_2HNS_2’)$_2$]Br_2 (11), [Pt(‘S_3’)]$_3$·2THF·MeOH (5·2THF·MeOH) and [Pt(‘S_3’)(PPh$_3$)] (6): Black cubes of [Ni(‘S_3’)]$_2$ (**1**) were obtained by solvothermal crystallization. A suspension of **1** (80 mg) in DMF (2 mL) was sealed in a thick-walled glass ampoule, heated to 175°C for 10 h by means of an electric furnace and slowly cooled to room temperature at a rate of 1°C·h^{-1}. Black prisms of [Ni(‘S_3’)(PMe$_3$)] (**2**) crystallized from a saturated THF solution that was layered with MeOH. Red-black columns of NMe$_4$[Ni(‘S_3’)(CN)]·0.5CH_2Cl_2 (**3**·0.5CH_2Cl_2) were grown from a saturated 1:1 THF/MeOH solution that was layered with Et_2O. In the course of 20 d, red prisms of [Ni(‘MeS_3’)$_2$] (**7**) grew from a $CDCl_3$ solution of [Ni(‘MeS_3’)$_2$(PMe$_3$)$_2$] which had been used for NMR measurements. [Ni(‘Et_2HNS_2’)$_2$]Br_2 (**11**) crystallized as yellow platelets upon cooling of a hot MeOH solution of [Ni(‘Et_2HNS_2’)$_2$](ClO$_4$)$_2$ (**12**) and LiBr to room temperature. Yellow-red plates of [Pt(‘S_3’)]3·2THF·MeOH (**5**·2THF·MeOH) were grown from a THF solution that was layered with MeOH. Orange columns of [Pt(‘S_3’)(PPh$_3$)] (**6**) resulted from a mixture of Li[Pt(‘S_3’)(H)] and Li[Pt(‘S_3’)(H)(PPh$_3$)] in THF that had been layered with MeOH. Suitable single crystals were sealed in glass capillaries under N_2. Data was collected at 293 K (**1**, **3**·0.5CH_2Cl_2, **6**) or 200 K (**2**, **5**·2THF·MeOH, **7**, **11**) with a Siemens P4 diffractometer using Mo-K_α radiation (λ = 71.073 pm), a graphite

Table 2. Selected crystallographic data of [Ni(‘S_3’)]$_2$ (**1**), [Ni(‘S_3’)(PMe$_3$)] (**2**), NMe$_4$[Ni(‘S_3’)(CN)]·0.5CH_2Cl_2 (**3**·0.5CH_2Cl_2), [Ni(‘MeS_3’)$_2$] (**7**), [Ni(‘Et_2HNS_2’)$_2$]Br_2 (**11**), [Pt(‘S_3’)]3·2THF·MeOH (**5**·2THF·MeOH) and [Pt(‘S_3’)(PPh$_3$)] (**6**)

Compound	**1**	**2**	**3**·0.5CH_2Cl_2	**7**	**11**	**5**·2THF·MeOH	**6**
Formula	$C_{24}H_{16}Ni_2S_6$	$C_{15}H_{17}NiPS_3$	$C_{17.5}H_{21}ClN_2NiS_3$	$C_{26}H_{22}NiS_6$	$C_{24}H_{38}Br_2N_2NiS_4$	$C_{45}H_{44}O_3Pt_3S_9$	$C_{30}H_{23}PPtS_3$
M_r [g/mol]	614.1	383.1	449.7	585.5	701.3	1506.6	705.7
Cryst. system	monoclinic	monoclinic	monoclinic	monoclinic	monoclinic	triclinic	monoclinic
Space group	*C*2/*c*	*Cc*	*P*2/*c*	$P2_1/n$	$P2_1/c$	*P*1bar	$P2_1/n$
a [pm]	2131.9(11)	900.4(3)	1686.5(2)	977.1(9)	1374.7(8)	788.5(1)	899.0(1)
b [pm]	876.2(6)	1832.9(7)	994.3(2)	1151.0(14)	1102.8(3)	1721.8(3)	1139.3(3)
c [pm]	1392.8(15)	1051.1(3)	1276.1(2)	1087.3(7)	1012.5(4)	1742.1(3)	2558.7(4)
α [°]						96.94(1)	
β [°]	123.56(8)	106.28(3)	105.04(1)	91.16(6)	108.46(4)	92.61(1)	90.93(1)
γ [°]						100.60(1)	
V [nm^3]	2.168(3)	1.665(1)	2.066(1)	1.223(2)	1.456(1)	2.302(1)	2.620(1)
Z	4	4	4	2	2	2	4
$d_{calcd.}$ [gcm^{-3}]	1.88	1.53	1.45	1.59	1.60	2.17	1.79
μ [cm^{-1}]	23.28	16.24	13.74	13.21	37.14	95.41	56.73
Cryst. size [mm]	0.4 × 0.4 × 0.3	0.4 × 0.4 × 0.3	0.5 × 0.4 × 0.3	0.4 × 0.3 × 0.2	0.4 × 0.4 × 0.2	0.4 × 0.2 × 0.1	1.0 × 0.2 × 0.2
2θ range [°]	4−54	4−54	4−54	5−50	5−52	3−54	3−54
Measd. refl.	4446	3390	6837	2582	3123	11637	10224
Indep. refl.	2397	3272	4550	2152	2724	10077	5771
Obsd. refl.	1857	2717	2452	1024	1356	6110	4295
Ref. parameters	145	179	222	151	151	543	316
*R*1[a]; *wR*2 [%]	2.4; 5.7	4.4; 12.5	3.9; 10.3	7.9; 23.2	6.6; 18.6	5.3; 13.6	2.2; 5.4

[a] [$I > 2\sigma(I)$].

monochromator and ω-scan technique (scan speed 3.0−30° min^{-1}). Due to the experimental setup, ψ-scan absorption correction was not possible, therefore absorption effects have been corrected using ΔF^2 methods (XABS2)[39] in the case of **2**, **5**·2THF·MeOH, **6**, **7**, and **11**. Structures were solved by direct methods (SHELXTL). Full-matrix least-squares refinements on F^2 were carried out with SHELXTL 5.03.[40] Non-hydrogen atoms were refined isotropically. The hydrogen atoms of **1**, **2**, **3**·0.5CH_2Cl_2, **6**, **7**, and **11** were located in Fourier synthesis difference maps. The hydrogen atoms in [Pt('S_3')]3·2THF·MeOH (**5**·2THF·MeOH) were geometrically positioned. For all hydrogen atoms both the positional parameters and a common isotropic displacement parameter were restricted during refinement. In the case of **2**, the absolute structure has been established by refinement of the Flack parameter[41] [$x = -0.02(2)$]. Table 2 contains selected crystallographic data.[42]

Acknowledgments

Support of these investigations by the Deutsche Forschungsgemeinschaft and Fonds der Chemischen Industrie is gratefully acknowledged. We wish to thank Dr. M. Moll for the recording of numerous NMR spectra and Mr. W. Donaubauer for technical assistance in the X-ray diffraction studies.

[1] [1a] J. R. Lancaster, *FEBS Lett.* **1980**, *115*, 285−288. − [1b] E. G. Graf, R. K. Thauer, *FEBS Lett.* **1981**, *136*, 165−169.
[2] [2a] AS. W. Ragsdale, J. E. Clark, L. G. Ljungdahl, L. L. Lundie, H. L. Drake, *J. Biol. Chem.* **1983**, *258*, 2364−2369. − [2b] R. B. Diekert, M. Ritter, *FEBS Lett.* **1983**, *151*, 41−44.
[3] [3a] A. Volbeda, M.-H. Charon, C. Piras, E. C. Hatchikian, M. Frey, J. C. Fontecilla-Camps, *Nature (London)* **1995**, *373*, 580−587. − [3b] R. Cammack, *Nature (London)* **1995**, *373*, 556−557. − [3c] A. Volbeda, E. Garcin, C. Piras, A. L. de Lacey, V. M. Fernandez, E. C. Hatchikian, M. Frey, J. C. Fontecilla-Camps, *J. Am. Chem. Soc.* **1996**, *118*, 12989−12996.
[4] [4a] D. K. Mills, Y. M. Hsioa, P. J. Farmer, E. V. Atnip, J. H. Reibenspies, M. Y. Darensbourg, *J. Am. Chem. Soc.* **1991**, *113*, 1421−1423. − [4b] G. J. Colpas, R. O. Day, M. Maroney, *Inorg. Chem.* **1992**, *31*, 5053−5055.
[5] [5a] P. Stavropoulos, M. Carrìe, M. C. Muetterties, R. H. Holm, *J. Am. Chem. Soc.* **1990**, *112*, 5385−5387. − [5b] P. Stavropoulos, M. C. Muetterties, M. Carrìe, R. H. Holm, *J. Am. Chem. Soc.* **1991**, *113*, 8485−8492.
[6] D. Sellmann, M. Geck, D. Häußinger, J. Käppler, G. Mahr, G. Rackelmann, F. Knoch, M. Moll, *Fourth International Conference on the Molecular Biology of Hydrogenase*, Noordwijkerhout, The Netherlands, August 14th−19th, **1994**, Abstracts.
[7] D. Sellmann, S. Fünfgelder, G. Pöhlmann, F. Knoch, M. Moll, *Inorg. Chem.* **1990**, *29*, 4772−4778.
[8] D. Sellmann, S. Fünfgelder, F. Knoch, *Z. Naturforsch.* **1991**, *46b*, 1593−1600.
[9] D. Sellmann, S. Fünfgelder, F. Knoch, M. Moll, *Z. Naturforsch.* **1991**, *46b*, 1601−1608.
[10] [10a] D. Sellmann, H.-P. Neuner, M. Moll, F. Knoch, *Z. Naturforsch.* **1991**, *46b*, 303−306. − [10b] M. Tiecco, *Synthesis* **1988**, 749−759.
[11] R. Hahn, A. Nakamura, K. Tanaka, Y. Nakayama, *Inorg. Chem.* **1995**, *34*, 6562−6564.
[12] E. Block, M. Gernon, H. Kang, G. Ofori-Okai, J. Zubieta, *Inorg. Chem.* **1991**, *30*, 1736−1747.
[13] [13a] G. Schwarzenbach, *Chem. Zvesti* **1965**, *19*, 200−208; *Chem. Abstr.* **1965**, *63*, 5673e. − [13b] P. J. Blower, J. R. Dilworth, G. J. Leigh, B. D. Neaves, F. B. Normanton, *J. Chem. Soc., Dalton Trans.* **1985**, 2647−2653.
[14] [14a] E. Block, G. Ofori-Okai, J. Zubieta, *J. Am. Chem. Soc.* **1989**, *111*, 2329−2331. − [14b] J. D. Franolic, W. Y. Wang, M. Millar, *J. Am. Chem. Soc.* **1992**, *114*, 6587−6588.
[15] E. Block, V. Eswarakrishnan, M. Gernon, G. Ofori-Okai, C. Saha, K. Tang, J. Zubieta, *J. Am. Chem. Soc.* **1989**, 111, 658−665.
[16] M. Kranz, H. Dietrich, W. Mahdi, G. Müller, F. Hampel, T. Clark, R. Hacker, W. Neugebauer, A. J. Kos, P. v. R. Schleyer, *J. Am. Chem. Soc.* **1993**, *115*, 4698−4704.
[17] D. Sellmann, F. Geipel, unpublished results.
[18] U. T. Mueller-Westerhoff, B. Vance in *Comprehensive Coordination Chemistry*, vol. 2 (Ed.: G. Wilkinson), Pergamon, Oxford, **1987**, p. 602.
[19] D. Sellmann, H. Schillinger, F. Knoch, *Inorg. Chim. Acta* **1992**, *198*, 351−357.
[20] [20a] P. H. Davis, L. K. White, R. L. Belford, *Inorg. Chem.* **1975**, *14*, 1753−1757. − [20b] J. M. Desper, S. H. Gellman, R. E. Wolf, Jr., S. R. Cooper, *J. Am. Chem. Soc.* **1991**, *113*, 8663−8671.
[21] M. A. Halcrow, G. Christou, *Chem. Rev.* **1994**, *94*, 2421−2481.
[22] A. Herman, R. M. Wing, *J. Organomet. Chem.* **1973**, *63*, 441−450.
[23] [23a] F. A. Cotton, G. Wilkinson, *Advanced Inorganic Chemistry*, 5th ed., Wiley, New York, **1988**, p. 1300. − [23b] D. Sellmann, H. Schillinger, F. Knoch, *Z. Naturforsch.* **1992**, *47b*, 748−753. − [23c] D. Sellmann, H. Schillinger, F. Knoch, *Z. Naturforsch.* **1992**, *47b*, 645−655.
[24] [24a] C. A. Ghilardi, S. Midollini, A. Orlandini, G. Scapacci, A. Vacca, *J. Organomet. Chem.* **1993**, *461*, C4−C6. − [24b] N. Hadj-Bagheri, R. J. Puddephatt, L. Manojlovic-Muir, A. Stefanovic, *J. Chem. Soc., Dalton Trans.* **1990**, 535−540.
[25] [25a] J. Harley-Mason, *J. Chem. Soc.* **1952**, 146−149. − [25b] G. A. Barclay, E. M. McPartlin, N. C. Stephenson, *Inorg. Nucl. Chem. Lett.* **1967**, *3*, 397−402.
[26] J. Emsley, *The Elements*, Clarendon, Oxford, **1989**.
[27] T. Krüger, B. Krebs, G. Henkel, *Angew. Chem.* **1989**, *101*, 54−55; *Angew. Chem. Int. Ed. Engl.* **1989**, *28*, 61−62.
[28] M. Bonamico, G. Dessy, V. Fares, *Chem. Commun.* **1969**, 697−698.
[29] M. Corbett, B. F. Hoskins, *Chem. Commun.* **1968**, 1602−1604.
[30] A. C. Villa, A. G. Manfredotti, M. Nardelli, C. Pelizzi, *Chem. Commun.* **1970**, 1322−1323.
[31] J. P. Fackler, Jr., W. J. Zegarski, *J. Am. Chem. Soc.* **1973**, *95*, 8566−8574.
[32] D. Sellmann, D. Häußinger, F. Knoch, M. Moll, *J. Am. Chem. Soc.* **1996**, *118*, 5368−5374.
[33] D. Sellmann, H. Schillinger, F. Knoch, *Z. Naturforsch.* **1992**, *47b*, 645−655.
[34] D. Sellmann, S. Fünfgelder, F. Knoch, *Z. Naturforsch.* **1992**, *47b*, 51−60.
[35] J. Degani, R. Fochi, *Synthesis* **1976**, 471−472.
[36] R. Ugo, F. Cariati, G. La Monica, *Inorg. Synth.* **1968**, *11*, 105−108.
[37] T. Yoshida, T. Matsuda, S. Otsuka, *Inorg. Synth.* **1979**, *19*, 110−111.
[38] G. Brauer, *Handbuch der Präparativen Anorganischen Chemie*, Enke, Stuttgart, **1972**, vol. III.
[39] S. Parkin, B. Moezzi, H. Hope, *J. Appl. Cryst.* **1995**, *28*, 53−56.
[40] *SHELXTL 5.03*, Siemens Analytical X-Ray Instr., Madison, WI, USA, **1995**.
[41] H. D. Flack, *Acta Crystallogr.* **1983**, *A39*, 876−881.
[42] Crystallographic data (excluding structure factors) for the structures reported in this paper have been deposited with the Cambridge Crystallographic Data Centre as supplementary publication no. CCDC-118908 (**1**), -118909 (**2**), -118910 (**3**), -118911 (**5**), -118912 (**6**), -118913 (**7**), -118914 (**11**). Copies of the data can be obtained free of charge on application to CCDC, 12 Union Road, Cambridge CB2 1EZ, UK (Fax: + 44-1223/336-033; E-mail: deposit@ccdc.cam.ac.uk).

Received May 7, 1999
[I99167]

Molybdenum(VI) Bisimidoaryl Phenoxide and Alkoxide Complexes: Molecular Structures of $[Mo(NAr)_2(OCMe_2\text{-}2\text{-}py)(CH_2SiMe_3)]$ and $[\{Mo(NAr)_2Me(OMe)\}_2]$

Jim A. M. Brandts,[a] Jaap Boersma,[a] Anthony L. Spek,[b][+] and Gerard van Koten*[a]

Keywords: Molybdenum / Bisimidoaryl / Alkoxide and phenoxide ligands / Intramolecular coordination / Imido complexes / Chelates

The synthesis and characterisation is reported of new, five-coordinate molybdenum(VI) bisimidoaryl complexes $[Mo(NAr)_2(O\text{-}N)(R)]$ [Ar = $C_6H_3(iPr)_2$-2,6; *O-N* = 2-pyridyldiphenylmethoxide (**a**), 2-pyridyldimethylmethoxide (**b**), 8-quinolinolate (**c**); R = Cl, Me, CH_2SiMe_3] and the corresponding bisalkoxide (**a**, **b**) and bisphenolate [**c**, **d** = $(OC_6H_4CH_2NMe_2\text{-}2)^-$] Mo^{VI} bisimidoaryl complexes $[Mo(NAr)_2(O\text{-}N)_2]$. These complexes can be formed by simple alcoholysis reactions between $[Mo(NAr)_2Cl_2(DME)]$ and the appropriate alcohol in the presence of Et_3N. The remaining chloride can be replaced by a methyl or trimethylsilylmethyl group by transmetallation with MeMgCl or $LiCH_2SiMe_3$. The solid state structure of $[Mo(NAr)_2(OCMe_2\text{-}2\text{-}py)(CH_2SiMe_3)]$ (**5**) has been determined by single-crystal X-ray analysis. A similar synthetic procedure was used to synthesise and characterise $[\{Mo(NAr)_2Me(OMe)\}_2]$ (**7**). The two methoxide ligands bridge between the two molybdenum(VI) nuclei. Compounds in which the ligand can form six-membered chelate rings {like $[Mo(NAr)_2(OC_6H_4CH_2NMe_2\text{-}2)_2]$ (**9**) and analogues} are usually difficult to obtain in a pure form and yields are typically low.

Introduction

Alkoxide and phenoxide ligands play an important role in catalysts developed for classical olefin metathesis polymerisation. The stability, reactivity and selectivity of the catalysts is often determined by the nature of the ancillary alkoxide or phenoxide ligands, as reported by Schrock,[1] Grubbs,[2] Basset[3] and others for $[WCl_{6-x}(OAr)_x]$ (x = 0−4, 6) or $[WOCl_{4-n}(OAr)_n]$ (n = 0−4) catalysts.[4] Van der Schaaf et al. have shown that the use of intramolecularly coordinating alkoxide and phenoxide ligands in tungsten(VI) alkylidene complexes yields complexes with special properties.[5] Enhanced stability, high ring-opening metathesis polymerisation (ROMP) activity (turnover frequency < 1/h at 20°C; > 20000/h at 70°C) and selectivity, and unexpected so-called "latent" behaviour were found.[6] Analogous compounds based on molybdenum as the active metal centre are desirable because molybdenum catalysts appear to tolerate functionalities to a greater degree than the corresponding tungsten catalysts.[7] Therefore, we have prepared and characterised a series of molybdenum(VI) bisimidoaryl phenoxide and alkoxide complexes containing a potentially intramolecularly coordinating amine. The ligands we used, depicted in Figure 1, are all monoanionic, potentially *O,N*-chelating ligands, i.e. $[OCPh_2\text{-}2\text{-pyridyl}]^-$ (**a**),[6][8] $[OCMe_2\text{-}2\text{-pyridyl}]^-$ (**b**),[6] 8-oxyquinolinate (**c**)[6] and $[OC_6H_4CH_2NMe_2\text{-}2]^-$ (**d**).[5]

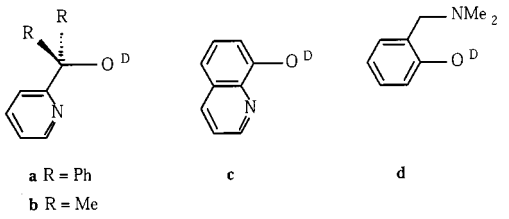


Figure 1. Selected alkoxide and phenoxide ligands with potentially *ortho*-chelating amine donors

At this point we have focused on the synthesis of Mo^{VI} compounds with the general formula $[Mo(NAr)_2(O\text{-}N)(R)]$ (*O-N* = **a**, **b**, **c** or **d**; R = Cl, Me, CH_2SiMe_3; Ar = 2,6-diisopropylphenyl) and the corresponding bisalkoxide (**a**, **b**) and bisphenolate (**c**, **d**) Mo^{VI} complexes $[Mo(NAr)_2(O\text{-}N)_2]$.

Results

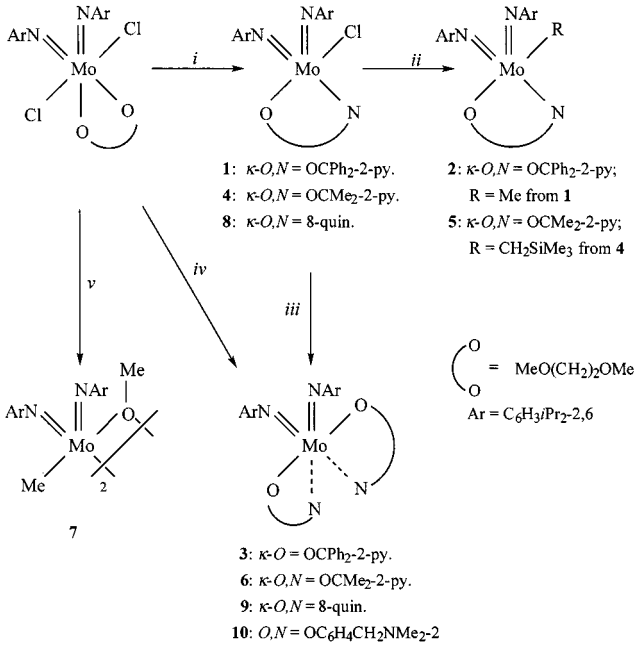
Synthesis of Complexes 1−6

Direct alcoholysis of $[Mo(NAr)_2Cl_2(DME)]$ with $[HOCPh_2\text{-}2\text{-py}]$ in the presence of Et_3N afforded the mono(2-pyridyldiphenylmethoxide) molybdenum(VI) complex $[Mo(NAr)_2(OCPh_2\text{-}2\text{-py})Cl]$ (**1**) in almost quantitative yield. The analogous methylated compound $[Mo(NAr)_2(OCPh_2\text{-}2\text{-py})(Me)]$ (**2**) was obtained by reaction of **1** with MeMgCl. The corresponding bis(2-pyridyldiphenylmethoxide) molybdenum(VI) complex $[Mo(NAr)_2(OCPh_2\text{-}2\text{-py})_2]$ (**3**) was made by either treating **1** with one equivalent of

[a] Debye Institute, Department of Metal-Mediated Synthesis, Utrecht University,
Padualaan 8, NL-3584 CH, Utrecht, The Netherlands
Fax: (internat.) + 31-30/252-3615
E-mail: g.vankoten@chem.uu.nl
[b] Bijvoet Center for Biomolecular Research, Department of Crystal and Structural Chemistry, Utrecht University,
Padualaan 8, NL-3584 CH, Utrecht, The Netherlands
E-mail: spea@chem.uu.nl
[+] X-ray crystallography.

 © WILEY-VCH Verlag GmbH, D-69451 Weinheim, 1999 1434−1948/99/1010−1727 $ 17.50+.50/0

[LiOCPh$_2$-2-py] or by reaction of [Mo(NAr)$_2$Cl$_2$(DME)] with two equivalents of [LiOCPh$_2$-2-py] (see Scheme 1).



Scheme 1: *i*: The appropriate alcohol, Et_3N, $-Et_3NHCl$, −1,2 dimethoxyethane, Et_2O, > 95% yield; *ii*: **2**: MeMgCl, $-MgCl_2$, THF, 92% yield; **5**: $LiCH_2SiMe_3$, Et_2O, −LiCl, 80% yield; *iii* and *iv*: by reaction of lithium phenolates or alcoholysis, see experimental section; *v*: MeOH, Et_3N, $-Et_3NHCl$, MeMgCl, $-MgCl_2$, yield: 68% yield

All these compounds are intensely coloured, e.g. dark red (**1**), orange (**2**) and red/purple (**3**). The solid complexes **1** and **2** are moisture-sensitive but can be handled in air for short periods of time (less than 1 min.) without any noticeable decomposition. Compound **3** is stable in air even at high temperatures (> 200°C). The compounds containing the 2-pyridyldimethylmethoxide ligand [OCMe$_2$-2-py]$^-$ **(b)** (**4**: Cl, **5**: CH_2SiMe_3 and **6**: [OCMe$_2$-2-py]$^-$) can be made in a similar manner (see Scheme 1). NMR spectroscopy and elemental analysis confirmed their composition.

NMR-Spectroscopic Analysis

The ^{1}H NMR spectra of **1**−**6** (C_6D_6) show a septet and two doublet resonances for the *i*Pr *ortho* substituents of the NAr ligands. In the $^{13}C\{^1H\}$ NMR spectra these *i*Pr groups appear as three separate resonances indicating that all four *i*Pr groups are equivalent but that the CMe_2 moieties are diastereotopic. The R-substituents of the *O,N*-ligand (**a**: R = Ph; **b**: R = Me) of **1**, **2**, **4** and **5** show only one set of resonaces and are equivalent over the whole temperature range (220 K − 330 K) studied. These results indicate the presence of a molecular symmetry plane in the complexes, which renders both R-substituents in the *O,N*-ligands equivalent on the NMR time scale, but gives no further information about the actual coordination mode of the *O,N*-ligand. This can only be rationalised either by a structure in which the prochiral OC[1] and py-N centres are found in an apparent molecular symmetry plane in the case of Mo−N coordination, or when the *O,N*-ligand is monodentate O-bonding and the free pyridine substituent undergoes rapid rotation around the O−CR_2 bond.

The chemical shift difference ($\Delta\delta$)[9] between the hydrogen *ortho* to the pyridyl nitrogen in the complexes and that in the free parent ligand suggests that the pyridyl group coordinates intramolecularly in complexes **1** ($\Delta\delta$ = 1.35), **2** ($\Delta\delta$ = 0.59), **4** ($\Delta\delta$ = 1.19) and **5** ($\Delta\delta$ = 0.70). This implies that the apparent molecular symmetry plane in solution arises from fluxional processes involving alternating reversible N−Mo bond breaking and formation, and monodentate O-bonding. Finally, as compounds **1**, **2**, **4** and **5** have similar features in their NMR spectra it can be assumed that these compounds have the same structural characteristics.

The ^{1}H and $^{13}C\{^1H\}$ NMR spectra of compound **3** and **6** (C_6D_6) show two sets of resonances for the R-substituents in the OCR_2 (**3**: R = Ph; **6**: R = Me) moieties of the methoxide ligands. These R-substituents are diastereotopic because only one set of pyridyl carbons appears in the ^{13}C NMR spectrum. The very small chemical shift difference value of py-H^6 in **3** ($\Delta\delta$ = −0.11) suggests the absence of Mo−N bonding, making it a four-coordinate species. This is probably forced by the presence of sterically demanding phenyl substituents. In contrast, the corresponding chemical shift difference in **6** ($\Delta\delta$ = 0.79) does suggest an intramolecular coordination between Mo and N. In this particular case, coordination of the nitrogen atoms in both methoxide ligands would lead to a hexacoordinate molybdenum species in which the two imidoaryl ligands are likely to adopt a *cis* conformation to maximise d-orbital overlap between the π-electrons of the imido ligands and the empty d-orbitals.[10] For the same reason the pyridyl-N-donor ligands will be positioned *trans* with respect to each imidoaryl ligand. This would give hexacoordinate diimidoaryl molybdenum(VI) compounds, with a ligand array similar to that present in the solid-state structure of the analogous dioxo molybdenum(VI) compound found by Schultz et al.[8c]

Solid-State Structure of [Mo(NAr)$_2$(OCMe$_2$-2-py)(CH_2SiMe_3)] (5)

To get further insight into the molecular geometry of this series of molybdenum(VI) compounds, a single crystal X-ray structure determination of **5** was carried out and its molecular structure, with the adopted numbering scheme, is depicted in Figure 2. Selected bond lengths and angles are given in Table 1.

In compound **5** the ligands form a distorted trigonal bipyrimidal geometry around the Mo^{VI} centre (43.7% along the Berry pseudorotation coordinate from trigonal bipyramid to square pyramid) in which the N3-bonded imido ligand and N1 occupy the apical positions. The metal lies in the basal plane defined by O1, N2 and the C_{ipso} (C9) of the neosilyl (= CH_2SiMe_3) group. The *O,N*-ligand is didentate

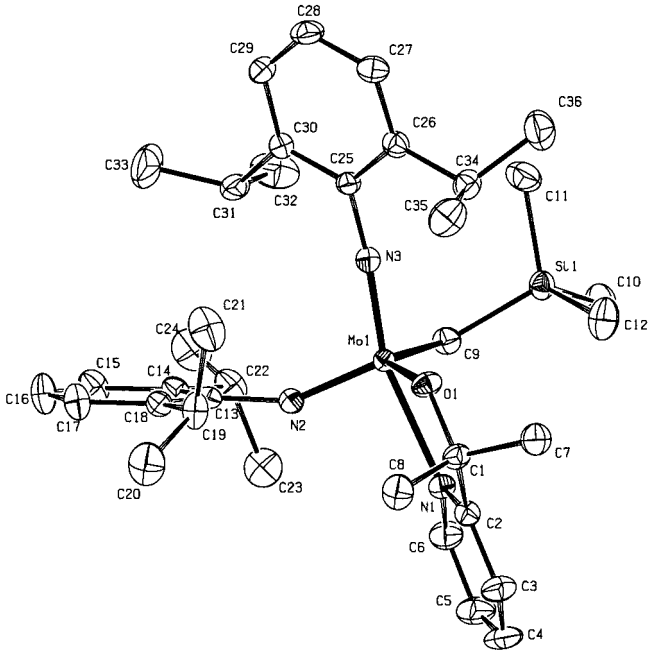


Figure 2. ORTEP drawing (50% probability atomic displacement ellipsoids) of **5**; hydrogen atoms have been omitted for clarity

chelating in the solid state with a Mo1−N1 bond length of 2.346(2) Å, typical for sp^2-nitrogen to molybdenum coordination[8c] and comparable to those found in corresponding tungsten complexes.[6][11] The metal-carbon bond length [Mo1−C9, 2.156(2) Å] observed for compound **5** is rather large (this bond in other molybdenum alkyl complexes lies in the range 2.08−2.20 Å).[12] The bond angle Mo1−C9−Si1 is larger than expected for a sp^3 carbon although similar bond angles have also been found in analogous *O,N*-ligand-containing tungsten neosilyl compounds.[6] No agostic interactions of the α-hydrogens were found (NMR, X-ray).

Table 1. Selected intramolecular distances [Å] and angles [°] of **5**[a]

Bond lengths [Å]		Bond angles [°]	
Mo1−O1	1.9504(19)	Mo1−O1−C1	128.96(13)
Mo1−N1	2.346(2)	Mo1−C9−Si1	116.82(11)
Mo1−N2	1.7686(18)	Mo1−N2−C13	152.52(15)
Mo1−N3	1.7529(19)	Mo1−N3−C25	172.95(18)
Mo1−C9	2.156(2)		
C9−Si1	1.864(2)		
O1−C1	1.406(3)		

[a] The estimated standard deviations of the last significant digits are shown in parentheses.

Formation of [{Mo(NAr)$_2$Me(OMe)}$_2$] (7)

In one attempt to synthesise the methylated derivative [Mo(NAr)$_2$(OCMe$_2$-2-py)(Me)] by reaction of compound **4** with a small excess of MeMgCl in THF, orange crystals of an unknown product (**7**) were obtained. NMR spectroscopy and elemental analysis pointed to the formation of a molybdenum compound containing one methyl, one methoxide and two imidoaryl ligands. However, compound **7** could not be synthesised again by the original synthetic route (**4** + MeMgCl in THF), not even in the presence of deliberately added air, water or methanol. Since the formation of a molybdenum compound such as **7** was unexpected and could not easily be rationalised, a single-crystal X-ray

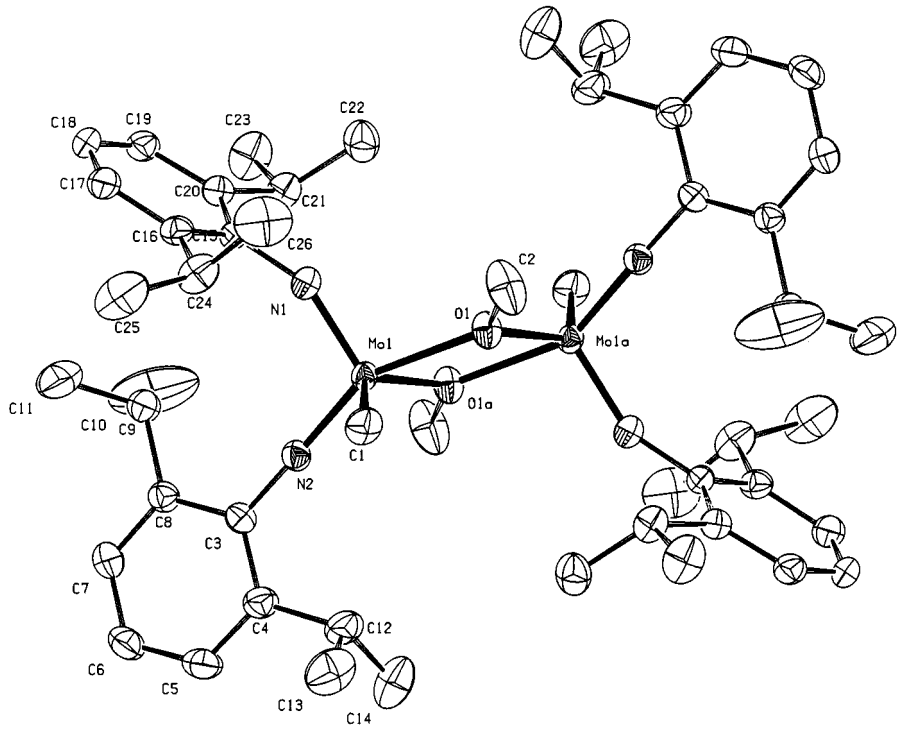


Figure 3. ORTEP drawing (50% probability atomic displacement ellipsoids) of **7**; hydrogen atoms have been omitted for clarity

analysis was carried out. The molecular structure of the orange compound, with the adopted numbering scheme, is depicted in Figure 3 and selected bond lengths and angles are given in Table 2.

Table 2. Selected geometrical details of **7**[a]

Bond lengths [Å]		Bond angles [°]	
Mo1−C1	2.161(4)	Mo1−O1−Mo1a	111.16(9)
Mo1−O1	2.157(2)	O1−Mo1−O1a	68.84(8)
Mo1−N1	1.757(3)	Mo1−N1−C15	153.7(2)
Mo1−N2	1.756(3)	Mo1−N2−C3	177.4(2)
N1−C15	1.388(4)		
N2−C3	1.383((4)		
O1−C2	1.421(5)		

[a] The estimated standard deviations of the last significant digits are shown in parentheses.

The solid state structure shows a dimeric compound in which each molybdenum nucleus indeed contains two imidoaryl ligands, one methyl group and one bridging methoxide ligand: [{Mo(NAr)$_2$Me(OMe)}$_2$] (**7**). Compound **7** has an inversion point positioned at the crossing of the virtual lines Mo1−Mo1a and O1−O1a. Each molybdenum centre has a distorted square-pyramidal coordination sphere (67.9% along the Berry-pseudorotation coordinate from trigonal bipyramid to square pyramid) in which the N1-bonded imido ligand occupies the apical position. The basal plane of the square pyramid is defined by N2, C1, O1 and O1a. Both molybdenum nuclei contain one bent [153.7(2)°] and one almost linear [177.4(2)°] imidoaryl ligand. The formation of bridging alkoxide or phenoxide ligands between two molybdenum (or tungsten) nuclei has previously been reported.[13]

Now that compound **7** had been fully analysed and characterised, a different synthetic route was developed using direct alcoholysis of [Mo(NAr)$_2$Cl$_2$(DME)] with MeOH (in presence of Et$_3$N) and subsequent reaction with MeMgCl. Compound **7** is thermally stable up to 185°C before decomposition takes place and decomposes in air within a few hours. It is soluble in most polar solvents (including CH_2Cl_2 and $CHCl_3$) but is only slightly soluble in benzene and toluene and does not dissolve in pentane or hexanes.

Synthesis and Characterisation of Complexes 8−10

The molybdenum bisimidoaryl phenoxide complexes containing the 8-quinolinolato ligand **c** (**8** and **9**) and the (dimethylamino)methyl phenoxide ligand **d** (**10**) were also synthesised by alcoholysis (see Scheme 1). The ^{1}H NMR spectra of **8** ($\Delta\delta$ = 1.20) and **9** ($\Delta\delta$ = 0.21)[14] suggest the presence of intramolecular coordination between Mo and the quinolinate nitrogen. The ^{1}H NMR spectroscopic data of **10** did not indicate the presence of such a Mo−N coordination since the H^6 proton is not shifted relative to that of the free parent 2-(dimethylamino)methyl phenol. Attempts to alkylate **8** by transmetallation reactions were unsuccessful as mixtures of the desired product and Li-**c** or ClMg-**c** that could not be separated were obtained. Apparently ligand exchange reactions do occur. Compounds in which the ligand can form six-membered chelate rings (like **10** and analogues) are usually difficult to obtain pure (also by transmetallation reactions using the sodium or lithium phenolates) and yields are typically low. Possibly, the formation of six-membered instead of five-membered chelate rings is thermodynamically less favoured.

Reactivity of the Complexes

Molybdenum(VI) complexes such as [Mo(NAr)$_2$(C$_6$H$_4$(CH$_2$NMe$_2$)-2)(Me)] react with *n*BuLi and, in the presence of dimethoxyethane (DME), the corresponding [Li(DME)$_2$Mo(NAr)$_2${C$_6$H$_4$(CH$_2$NMe$_2$)-2}(Me)(*n*Bu)] can be isolated.[15] This lithium molybdate(VI) compound can be thermally activated to give a mixture of paramagnetic Mo^V compounds, [Mo(NAr)$_2${C$_6$H$_4$(CH$_2$NMe$_2$)-2}(Me)] and [Mo(NAr)$_2${C$_6$H$_4$(CH$_2$NMe$_2$)-2}(*n*Bu)]. Small amounts of 1-butene were also detected as a result of β-H elimination reactions. This mixture becomes ROMP-active after dry air is bubbled through the solution. A tentative explanation for this is that dioxygen insertion into a Mo − C bond[16] may facilitate ligand-exchange reactions and alkylidene formation after α-H elimination.

According to their composition and structural features it is unlikely that complexes **1−10** as such can be active as ring-opening metathesis polymerisation (ROMP) catalysts. However, the reaction of compounds **2** and **5** with *n*BuLi gave products that show high ROMP activity with norbornene without activation with dry air. Analysis of these reaction products showed the presence of several Mo^V and Mo^{VI} complexes and [LiOCR$_2$-2-py] (R = Ph **2** and R = Me **5**) as a result of ligand exchange reactions. These unavoidable exchange reactions hamper the isolation of the active molybdenum alkylidene species although high molecular weight polynorbornene was found ($M_n = 1 \times 10^6$ g/mol, 90% *cis* double bonds, PDI = 2.5)

Experimental Section

General: Syntheses were carried out with standard Schlenk techniques under dry, oxygen-free nitrogen. Toluene, benzene, hexane, and pentane were carefully dried and distilled from sodium benzophenone-ketyl prior to use. CH_2Cl_2 was distilled from CaH_2. − NMR Spectra (^{1}H and ^{13}C{^{1}H}) were recorded on Bruker AC200 and Bruker AC300 spectrometers, with chemical shifts referenced to Me$_4$Si. − Elemental analyses were carried out by Dornis und Kolbe, Mikroanalytisches Laboratorium, Mülheim a.d. Ruhr, Germany. − [Mo(NAr)$_2$Cl$_2$(DME)],[17] HOCPh$_2$-2-pyridyl,[6] [LiOCPh$_2$-2-pyridyl],[6] HOCMe$_2$-2-pyridyl,[6] [LiOCMe$_2$-2-pyridyl],[6] LiCH$_2$SiMe$_3$,[18] and 2-[(dimethylamino)methyl]phenol[5] were prepared according to literature procedures.

[Mo(NAr)$_2$(OCPh$_2$-2-py-*κ*-*O,N*)Cl] (1): To a solution of [Mo(NAr)$_2$Cl$_2$(DME)] (2.34 g, 3.85 mmol) in Et$_2$O/benzene (80 mL in a 1:1 ratio) was added Et$_3$N (0.6 mL, 4.3 mmol) and a solution of HOCPh$_2$-2-pyridyl (1.00 g, 3.85 mmol) in Et$_2$O (20 mL) at ambient temperature. After stirring for 2 h, an off-white precipitate was re-

moved by centrifugation. The solid was washed with Et_2O (2 × 40 mL) and the Et_2O washings were combined with the mother liquor. All volatiles were removed in vacuo leaving a red crystalline solid (2.85 g, 100%) which was pure according to NMR spectroscopy and elemental analysis. − M.p.: 168°C − ^{1}H NMR: δ = 9.53 (d, 1, py-H^6), 7.37 (dd, 4, Ph-H), 7.05 (m, 10, ArH), 6.95 (m, 3, ArH) 6.77 (m, 1, py-H) 6.54 (m, 1, py-H), 3.87 (sept, 4, C*H*Me$_2$), 1.24 (d, 12, CH*Me*$_2$), 1.09 (d, 12, CH*Me*$_2$). − ^{13}C NMR: δ = 167.7 (py-C^2), 155.0 (C*ipso* NAr), 149.5, 146.6 (Ar-C), 144.0 (C*para* NAr), 138.1, 128.8, 128.6, 128.3, 126.9, 124.8, 123.1, 122.8 (Ar-C), 95.9 (OC), 28.7 (*C*HMe$_2$), 24.1 (CH*Me*$_2$), 23.3 (CH*Me*$_2$). − $C_{42}H_{48}ClMoN_3O$ (742.26): C 67.96, H 6.52, N 5.66; found C 67.90, H 6.58, N 5.61.

[Mo(NAr)$_2$(OCPh$_2$-2-py-κ-O,N)(Me)] (2): To a solution of **1** (0.44 g, 0.59 mmol) in THF (40 mL) was added 200 μl of a 3 M THF solution of MeMgCl (0.6 mmol). The reaction mixture was allowed to stir overnight. After 18 h all volatiles were removed in vacuo (3 h, 60°C). The remaining red solid was extracted with pentane (2 × 40 mL). The precipitate was removed by centrifugation, the pentane layers were collected, concentrated (30 mL), and stored at −30°C. After one week orange crystals (0.39 g, 0.54 mmol, 92% yield) were isolated that were pure according to NMR spectroscopy and elemental analysis. M.p.: 152°C − ^{1}H NMR: δ = 8.77 (d, 1, py-H^6), 7.47 (m, 4, Ph-H), 7.05 (m, 13, Ar-H), 6.75 (m, 1, py-H) 6.39 (m, 1, py-H), 3.84 (sept, 4, C*H*Me$_2$), 1.67 (s, 3, Mo−Me), 1.21 (d, 12, CH*Me*$_2$), 1.09 (d, 12, CH*Me*$_2$). − ^{13}C NMR: δ = 169.2 (py-C^2), 154.2 (C*ipso* NAr), 149.2, 148.0, 142.9, 137.7, 128.3, 128.1, 127.6, 125.3, 124.7, 123.0, 122.6 (Ar-C), 95.4 (OC), 28.6 (*C*HMe$_2$), 25.3 (Mo−Me), 24.5 (CH*Me*$_2$), 23.5 (CH*Me*$_2$). − $C_{43}H_{51}MoN_3O$ (721.84): C 71.55, H 7.12, N 5.82; found C 71.64, H 7.08, N 5.76.

[Mo(NAr)$_2$(OCPh$_2$-2-py-κ-O)$_2$] (3): To a solution of **1** (0.99 g, 1.34 mmol) in THF (60 mL) was added [Li−OCPh$_2$-2-pyridyl] (0.36 g, 1.34 mmol) as a solid. The reaction mixture was warmed to 50°C. After stirring two hours all volatiles were removed in vacuo (3 h, 60°C). The remaining red solid was extracted with CH_2Cl_2 (3 × 30 mL). The precipitate was removed by centrifugation, the CH_2Cl_2 layers were collected and concentrated to a volume of 10 mL. The remaining suspension was washed with pentane (3 × 20 mL), and the remaining solid dried in vacuo leaving a purple/red, air-stable product (1.23 g, 1.27 mmol, 95% yield). M.p.: > 200°C − ^{1}H NMR: δ = 8.07 (d, 2, py-H^6), 7.86 (d, 4, Ph-H), 7.47 (dd, 2, py-H), 7.26 (m, 4, Ph-H) 7.14−6.83 (m, 18, ArH), 6.58 (m, 2, py-H), 5.86 (m, 2, py-H), 4.31 (sept, 4, C*H*Me$_2$), 1.32 (d, 12, CH*Me*$_2$), 0.96 (d, 12, CH*Me*$_2$). − ^{13}C NMR: d = 164.9 (py-C^2), 155.0 (C*ipso* NAr), 151.3, 149.6, 149.2 (2 x), 141.6, 135.9, 129.6, 128.7, 127.9, 127.6, 127.1, 123.0, 122.9, 122.8, 121.5 (Ar-C), 94.1 (OC), 27.8 (*C*HMe$_2$), 24.9 (CH*Me*$_2$). − $C_{60}H_{62}MoN_4O_2$ (967.12): C 74.52, H 6.46, N 5.79; found C 74.38, H 6.43, N 5.72.

[Mo(NAr)$_2$(OCMe$_2$-2-py-κ-O,N)Cl] (4): An analogous method to that described for the synthesis of **1** was used. The synthesis was typically done on a 4 mmol scale using HOCMe$_2$-2-pyridyl. Yields are quantitative. M.p.: 177°C. − ^{1}H NMR: δ = 9.44 (d, 1, py-H^6), 7.06−6.92 (m, 7, Ar-H), 6.55 (m, 2, py-H), 4.08 (sept, 4, C*H*Me$_2$), 1.47 (s, 6, CMe$_2$), 1.28 (d, 12, CH*Me*$_2$), 1.20 (d, 12, CH*Me*$_2$). − ^{13}C NMR: δ = 171.4 (py-C^2), 154.8 (C*ipso* NAr), 149.2, 143.8, 139.1, 126.7, 122.8 (2 x), 120.1 (Ar-C), 86.4 (O*C*Me$_2$), 30.6 (OC*Me*$_2$), 28.6 (*C*HMe$_2$), 25.1 (CH*Me*$_2$), 23.4 (CH*Me*$_2$). − $C_{31}H_{44}ClMoN_3O$ (606.11): C 61.43, H 7.32, N 6.93; found C 61.49, H 7.29, N 6.82.

[Mo(NAr)$_2$(OCMe$_2$-2-py-κ-O,N)(CH$_2$SiMe$_3$)] (5): To a solution of **3** (0.75 g, 1.24 mmol) in Et_2O (60 mL) was added a solution of LiCH$_2$SiMe$_3$ (0.12 g, 1.24 mmol) in Et_2O (20 mL) at −78°C. The reaction mixture was warmed to room temperature (0.5 h). After two hours the white precipitate was removed by centrifugation and the Et_2O layer was collected and concentrated (10 mL). The orange crystals were collected and dried in vacuo (0.65 g, 0.99 mmol, 80% yield). The crystalline material was pure according to NMR spectroscopy and elemental analysis. M.p.: 154°C. − ^{1}H NMR: δ = 8.95 (dd, 1, py-H^6), 7.07 (m, 7, Ar-H), 7.66 (m, 1, py-H), 6.56 (m, 1, py-H), 4.08 (sept, 4, C*H*Me$_2$), 1.71 (s, 2, Mo−CH$_2$Si), 1.57 (s, 6, OCMe$_2$), 1.32 (d, 12, CH*Me*$_2$), 1.21 (d, 12, CH*Me*$_2$). − ^{13}C NMR: δ = 172.1 (py-C^2), 154.6 (C*ipso* NAr, broad), 148.0, 142.9 (broad), 138.2, 124.8, 122.7, 122.5, 120.4 (Ar-C), 85.0 (O*C*Me$_2$), 32.4 (MoCH$_2$Si), 31.7 (OCMe$_2$), 28.3 (*C*HMe$_2$), 25.3 (CH*Me*$_2$), 23.2 (CH*Me*$_2$), 2.1 (SiMe$_3$). − $C_{36}H_{55}MoN_3OSi$ (669.88): C 64.55, H 8.28, N 6.27; found C 64.68, H 8.35, N 6.27.

[Mo(NAr)$_2$(OCMe$_2$-2-py-κ-O,N)$_2$] (6): An analogous method to that described for the synthesis of **3** was used but **4** was the starting material. The synthesis was typically done on a 2 mmol scale with HOCMe$_2$-2-pyridyl. Yield 91%. M.p.: >200°C. − ^{1}H NMR: δ = 9.04 (m, 2, py-H^6), 7.04 (m, 4, Ar-H), 6.88 (m, 4, Ar-H), 6.55 (m, 4, py-H), 4.35 (sept, 4, C*H*Me$_2$), 1.81 (s, 6, OCMe$_2$), 1.57 (s, 6, OCMe$_2$), 1.42 (d, 12, CH*Me*$_2$), 1.12 (d, 12, CH*Me*$_2$). − ^{13}C NMR: δ = 170.5 (py-C^2), 155.3 (C*ipso* NAr), 146.8, 142.3, 137.6, 123.2, 123.0, 121.5, 119.6 (Ar C), 83.0 (O*C*Me$_2$), 31.7 (OC*Me*$_2$), 27.5 (CH*Me*$_2$), 25.4 (OC*Me*$_2$), 24.3 (CH*Me*$_2$), 24.3 (*C*HMe$_2$). − $C_{38}H_{54}MoN_4O_2$ (694.82): C 65.69, H 7.83, N 8.06; found C 65.58, H 7.86, N 7.95.

[{Mo(NAr)$_2$Me(OMe)}$_2$] (7): To a solution of [Mo(NAr)$_2$Cl$_2$(DME)] (1.45 g, 2.38 mmol) in Et_2O (50 mL) was added Et_3N (0.5 mL, 3.6 mmol) and MeOH (96 μL, 2.38 mmol). After 1 h the precipitate that had formed was removed by centrifugation and the upper layer was collected. All volatiles were removed in vacuo from this upper layer and the remaining solid was dissolved in THF (40 mL). To the solution 0.79 mL of a 3 M THF solution of MeMgCl (2.38 mmol) was added at ambient temperature. After 2 h stirring all volatiles were removed *in vacuo* (3 h, 60°C) and the remaining solids were washed with pentane (2 × 20 mL). The remaining solid was isolated and recrystallised from Et_2O (60 mL). At −30°C red crystals could be isolated after 5 days (0.80 g, 68% yield, 1.62 mmol). M.p. with decomposition.: 185°C. − ^{1}H NMR: δ = 7.07−6.94 (m, 6, Ar-H), 4.36 (s, 3, Mo−CH$_3$), 3.84 (sept, 4, C*H*Me$_2$), 1.44 (s, 3, Mo−CH$_3$), 1.25 (d, 12, CH*Me*$_2$), 1.19 (d, 12, CH*Me*$_2$). − ^{13}C NMR: δ = 152.6 (C*ipso* NAr), 144.3, 126.7, 122.8 (Ar C), 67.7 (Mo−Me) 28.8 (*C*HMe$_2$), 25.5 (Mo−Me), 24.2 (CH*Me*$_2$), 23.7 (CH*Me*$_2$). − [(C$_{26}$H$_{40}$MoN$_2$O)$_2$] (985.12): C 63.40, H 8.19, N 5.69; found C 63.25, H 8.13, N 5.63.

[Mo(NAr)$_2$(8-quin-κ-O,N)Cl] (8): An analogous method to that described for the synthesis of **1** was used. The synthesis was typically done on a 2 mmol scale with 8-quinolinol. Yield: 96%. M.p.: 194°C. − ^{1}H NMR: δ = 9.52 (d, 1, H^1-quin), 7.40 (dd, 1, H-quin), 7.22 (m, 8, Ar-H), 6.82 (dd, 1, H-quin) 6.60 (m, 1, quin-H), 4.03 (sept, 4, C*H*Me$_2$), 1.24 (d, 12, CH*Me*$_2$), 1.10 (d, 12, CH*Me*$_2$). − ^{13}C NMR: δ = 163.2 (C*ipso* quin), 154.4 (C*ipso* NAr), 149.4, 144.9 142.1, 139.1, 129.8, 127.9, 122.7, 122.0, 115.9, 114.6 (Ar C), 28.9 (*C*HMe$_2$), 24.2 (CH*Me*$_2$), 23.8 (CH*Me*$_2$). − $C_{33}H_{40}ClMoN_3O$ (626.10): C 63.31, H 6.44, N 6.71; found C 63.59, H 6.35, N 6.78.

[Mo(NAr)$_2$(8-quin-κ-O,N)$_2$] (9): To a solution of [Mo(NAr)$_2$Cl$_2$(DME)] (1.87 g, 3.08 mmol) in benzene (80 mL) was added Et_3N (1 mL, 7.2 mmol) and a solution of 8-quinolinol (0.89 g, 6.16 mmol) in Et_2O (20 mL) at ambient temperature. After stirring for 18 h, all volatiles were removed in vacuo and the remaining solid was extracted with pentane (5 × 40 mL). The precipitate was removed by centrifugation and the pentane layers were collected

and concentrated leaving a red crystalline solid (2.85 g, 100%) which was pure according to NMR spectroscopy and elemental analysis. NMR spectroscopy and elemental analysis showed the presence of one pentane solvent molecule per molybdenum atom in the crystals. M.p.: 182°C. – ^{1}H NMR: δ = 8.60 (d, 2, quin H[7]), 7.40–6.76 (m, 14, Ar-H), 6.23 (m, 2, quin H), 4.02 (sept, 4, C*H*Me$_2$), 1.35 (d, 12, CH*Me*$_2$), 0.97 (d, 12, CH*Me*$_2$). – ^{13}C NMR: δ = 164.3 (C*ipso* quin), 154.8 (C*ipso* NAr), 145.0, 141.7, 140.9, 137.4, 130.2, 129.9, 124.1, 122.5, 121.7, 114.8, 114.2 (Ar C), 28.5 (*C*HMe$_2$), 24.3 (CH*Me*$_2$), 24.0(CH*Me*$_2$). – $C_{47}H_{58}MoN_4O_2$ (806.95): C 69.96, H 7.25, N 6.94; found C 69.85, H 7.12, N 6.79.

[Mo(NAr)$_2$(OC$_6$H$_4$CH$_2$NMe$_2$-2)$_2$] (10): An analogous method to that described for the synthesis of **8** was used. The synthesis was typically done on a 4 mmol scale with two equivalents of 2-(dimethylamino)methyl phenol and an excess of Et$_3$N. The product was collected as a dark-red crystalline material from a concentrated pentane solution. Yield 28%. M.p.: 108°C. – ^{1}H NMR: δ = 7.17 (m, 4, Ar-H), 6.92 (m, 6, Ar-H), 6.84 (m, 4, ArH), 3.92 (sept, 4, C*H*Me$_2$), 3.74 (CH$_2$), 2.36 (N(CH$_3$)$_2$, 1.11 (d, 24, CH*Me*$_2$). – ^{13}C NMR: δ = 164.0 (C *ipso* OAr), 154.0 (C*ipso* NAr), 143.5, 130.1, 128.8, 126.2, 125.2, 123.0, 120.1, 119.8 (Ar C), 63.8 (CH$_2$), 47.5 (N(CH$_3$)$_2$, 28.0 (*C*HMe$_2$), 24.5 (CH*Me*$_2$). – $C_{42}H_{58}MoN_4O_2$ (746.89): C 67.54, H 7.83, N 7.50; found C 67.68, H 7.79, N 7.42.

Structure Determination and Refinement of 5 and 7: X-ray data were collected on an Enraf–Nonius CAD4T rotating anode diffractometer for a transparent, red/orange (**5**) or red (**7**) crystal glued on top of a glass fibre with inert fluorinated oil. The unit-cell parameters were checked for the presence of higher lattice symmetry. Data were corrected for Lorentz polarisation effects. An empirical absorption correction was applied (PLATON/DELABS).[19] The structures were solved by direct methods and subsequent difference Fourier techniques (SHELXS86).[20] Refinement on F^2 was carried out by full-matrix least-squares techniques (SHELXL93)[21] using no observance criterion. Hydrogen atoms were included on calculated positions, riding on their carrier atoms. All non-hydrogen atoms were refined with anisotropic atomic displacement parameters. All hydrogen atoms were refined with a fixed isotropic atomic displacement parameter related to the value of the equivalent isotropic atomic displacement parameter of their carrier atom. Weights were optimised in the final refinement cycles. Neutral atom scattering factors and anomalous dispersion corrections were taken from the International Tables for Crystallography.[22] Geometrical calculations and illustrations were performed with PLATON.[19] All calculations were performed on a DECstation 5000 cluster. Crystal data and numerical details of the structure determinations and refinements are collected in Table 3. Selected geometrical details of the structures of **5** and **7** are listed in Tables 1 and 2, respectively. Crystallographic data (excluding structure factors) for the structures reported in this paper have been deposited with the Cambridge Crystallographic Data Centre as supplementary publication no. CCDC-106132 (structure **5**) and CCDC-106134 (structure **7**). Copies of the data can be obtained free of charge on application to CCDC, 12 Union Road, Cambridge CB2 1EZ, UK [Fax: (internat). + 44-1223/336-033; E-mail: deposit@ccdc.cam.ac.uk].

Acknowledgments

We gratefully acknowledge Dr. G. J. M. Gruter (DSM Research) and Dr. F. H. van der Steen (Shell, Amsterdam) for fruitful discussions. Financial support was given by the Dutch Technology Foundation (STW) with financial aid from the Council for Chemical Science of the Netherlands/Organization for Scientific Research (NWO/CW).

[1] [1a] R. R. Schrock, *Polyhedron* **1995**, *14*, 3177–3195. – [1b] K. M. Totland, T. J. Boyd, G. G. Lavoie, W. M. Davis, R. R. Schrock, *Macromolecules* **1996**, *29*, 6114–6125.
[2] O. Fujimura, F. J. de la Mata, R. H. Grubbs,*Organometallics* **1996**, *15*, 1865–1871.
[3] [3a] J. Couturier, M. Leconte, J. M. Basset, *J. Organomet. Chem.* **1993**, *451*, C7–C9. – [3b] J. Couturier, C. Paillet, M. Leconte, J. M. Basset, K. Weiss, *Angew. Chem. Int. Ed. Engl.* **1992**, *31*, 628–631.
[4] [4a] N. Calderon, J. P. Lawrence, E. A. Ofstead, *Adv. Organomet. Chem.* **1979**, *17*, 449. – [4b] K. J. Ivin, J. C. Mol, *Olefin Metathesis and Metathesis Polymerization*, Academic Press, London, **1997**. – [4c] H. T. Dodd, K. J. Rut, *J. Mol. Catal.* **1982**, *15*, 103–110. – [4d] H. T. Dodd, K. J. Rut, *J. Mol. Catal.* **1985**, *28*, 33–36. – [4e] F. Quignard, M. Leconte, J. M. Basset, *J. Mol. Catal.* **1985**, *28*, 27–32. – [4f] A. Bell, *Polym. Prepr. (Am. Chem. Soc., Div. Polym. Chem.)* **1991**, 64, 102; **1992**, 67, 39. – [4g] A. Bell, *J. Mol. Catal.* **1992**, *76*, 165–180. – [4h] W. Sjardijn, A. H. Kramer, U.S. Patents 4,729,976, **1986**, and 4,810,762, **1987** (*Chem. Abstr.* **1987**, *107*, 116121x). – [4i] S. M. Beshouri, R. R. Schrock, J. C. Dewan, *Inorg. Chem.* **1989**, *28*, 1243–1248. – [4j] S. M. Beshouri, I. P. Rothwell, *Inorg. Chem.* **1986**, *25*, 1962–1964.
[5] [5a] P. A. van der Schaaf, J. T. B. H. Jastrzebski, M. P. Hogerheide, W. J. J. Smeets, A. L. Spek, J. Boersma, G. van Koten, *Inorg.Chem.* **1993**, *32*, 4111–4118. – [5b] P. A. van der Schaaf, J. Boersma, W. J. J. Smeets, A. L. Spek, G. van Koten, *Inorg.Chem.* **1993**, *32*, 5108–5113.
[6] P. A. van der Schaaf, R. A. T. M. Abbenhuis, W. P. A. van der Noort, R. de Graaf, D. M. Grove, W. J. J. Smeets, A. L. Spek, G. van Koten, *Organometallics* **1994**, *13*, 1433–1444.
[7] J. H. Oskam, H. H. Fox, K. B. Yap, D. H. McConville, R. O′Dell, B. J. Lichtenstein, R. R. Schrock, *J. Organomet. Chem.* **1993**, *459*, 185–198.
[8] [8a] T. Tsukahara, D. C. Swenson, R. F. Jordan, *Organometallics* **1997**, *16*, 3303–3313. – [8b] I. Kim, Y. Nishihara, R. F. Jordan, *Organometallics* **1997**, *16*, 3314–3323. – [8c] B. E. Schultz, S. F. Gheller, M. C. Muetterties, M. J. Scott, R. H. Holm, *J. Am. Chem. Soc.* **1993**, *115*, 2714–2722.
[9] Δδ is defined as δ(py-H^6) metal complex – δ(py-H^6) 2-pyridyl alcohol (py-H^6, **a**: δ = 8.18; **b**: δ = 8.25). NMR spectroscopic data for compounds **1–6** are given in the experimental section.
[10] [10a] D. L. Morrison, P. M. Rodgers, Y.-W. Chao, M. A. Bruck, T. L. Grittini, S. J. Tajima, A. L. Alexander, A. L. Rheingold, D. E. Wigley, *Organometallics* **1995**, *14*, 2435–2446. – [10b] D. L. Morrison, D. E. Wigley, *Inorg. Chem.* **1995**, *34*, 2610–2616.
[11] [11a] I. R. Hanson, D. L. Hughes, *J. Chem. Soc., Dalton Trans.* **1981**, 390–399. – [11b] R. O. Day, W. H. Batschelet, R. D. Archer, *Inorg. Chem.* **1980**, *19*, 2113–2122.
[12] [12a] J. A. M. Brandts, R. A. Gossage, J. Boersma, A. L. Spek, G. van Koten, *Organometallics*, **1999**, *18*, 2642–2648. – [12b] G. L. Casty, T. D. Tilley, G. P. A. Yap, A. L. Rheingold, *Organometallics* **1997**, *16*, 4746–4754. – [12c] A. Bell, W. Clegg, P. W. Dyer, M. R. J. Elsegood, V. C. Gibson, E. L. Marshall, *J. Chem. Soc., Chem. Commun.* **1994**, 2547–2548. – [12d] A. Bell, W. Clegg, P. W. Dyer, M. R. J. Elsegood, V. C. Gibson, E. L. Marshall, *J. Chem. Soc., Chem. Commun.* **1994**, 2247–2248. – [12e] W. M. Vaughan, K. A. Abboud, J. M. Boncella, *J. Organomet. Chem.* **1995**, *485*, 37–43. – [12f] G. C. Green, M. L. H. Green, J. T. James, P. C. Konidaris, G. H. Maunder, P. Mountford, *J. Chem. Soc., Chem Commun.* **1992**, 1361–1365.
[13] For example: [13a] D. E. Barber, R. F. Bryan, M. Sabat, K. S. Bose, B. A. Averill, *Inorg. Chem.* **1996**, *35*, 4635–4642. – [13b] W. Clegg, M. R. J. Elsewood, R. J. Errington, R. Bakri, *Acta Crystallogr. C* **1996**, *52*, 2145. – [13c] V. G. Kessler, A. V. Mironov, N. Y. Turova, A. I. Yanovky, Y. T. Struchkov, *Polyhedron* **1993**, *12*, 1573. – [13d] B. Kamenar, B. Korpar-Colig, M. Penavic, M. Cindric, *Acta Crystallogr. C* **1990**, *46*, 195. – [13e] M. H. Chisholm, K. Folting, M. A. Lynn, W. E. Streib, D. B. Tiedtke, *Angew. Chem. Int. Ed. Engl.* **1997**, *36*, 52–54. – [13f] A. J. Nielson, J. M. Waters, *Polyhedron* **1982**, *1*, 561.

[14] $\Delta\delta$ is defined as δ(quin-H[1]) metal complex − δ(quin-H[1]) 8-quinolinol (quin-H[1]: **c**: δ = 8.39). NMR-spectroscopic data for compounds **8−10** are given in the experimental section.
[15] J. A. M. Brandts, M. van Leur, R. A. Gossage, J. Boersma, A. L. Spek, G. van Koten, *Organometallics*, **1999**, *18*, 2633−2641.
[16] [16a] W. A. Nugent, R. L. Harlow, *J. Am. Chem. Soc.* **1980**, *102*, 1759. − [16b] T. V. Lubben, P. T. Wolczanski, *J. Am. Chem. Soc.* **1987**, *109*, 424.
[17] H. F. Fox, K. B. Yap, J. Robbins, S. Cai, R. R. Schrock, *Inorg. Chem.* **1992**, *32*, 2287−2289.
[18] L. H. Sommer, F. A. Mitch, G. M. Goldberg, *J. Am. Chem. Soc.* **1949**, *71*, 2746−2750.
[19] A. L. Spek, *Acta Crystallogr.* **1990**, *A46*, C34.
[20] G. M. Sheldrick, *SHELXS86, Program for crystal structure determination*, University of Göttingen, Göttingen, Germany, **1986**.
[21] G. M. Sheldrick, *SHELXL93, Program for crystal structure refinement*, University of Göttingen, Göttingen, Germany, **1993**.
[22] *International Tables for Crystallography* (Ed.: A. J. C. Wilson), Kluwer Academic Publishers, Dordrecht, The Netherlands, **1992**, vol. C.

Received December 23, 1998
[I98456]

Structures of Rare Earth Homodinuclear Macrocyclic Complexes with the Polyamine Polycarboxylic Ligand 1,4,7,10,14,17,20,23-Octaazacyclohexacosane-1,4,7,10,14,17,20,23-octaacetic Acid (H_8OHEC) in the Crystal and in Solution

Herbert Schumann,*[a] Ulrike A. Böttger,[a] Hardy Weisshoff,*[b] Burkhard Ziemer,[b] and Adolf Zschunke[b,c]

Dedicated to Professor Dr. Manfred Meisel on the occasion of his 60th birthday

Keywords: Crystal structure / Solution structure / Homodinuclear lanthanide complexes / Lanthanides / Macrocyclic ligands / Polyamine polycarboxylic acid

The solid-state structures of the four homodinuclear chelate complexes, $[Na_2(Y_2OHEC)(H_2O)_2] \cdot 7\ H_2O \cdot C_2H_5OH$ (**1**), $[Na_2(Gd_2OHEC)(H_2O)_2] \cdot 12\ H_2O$ (**2**), $[Na_2(Eu_2OHEC)(H_2O)_2] \cdot 11\ H_2O$ (**3**), and $[Cs_2(La_2OHEC)(H_2O)_2] \cdot 14\ H_2O$ (**4**) (H_8OHEC = 1,4,7,10,14,17,20,23-octaazacyclohexacosane-1,4,7,10,14,17,20,23-octaacetic acid), were determined by X-ray crystal structure analysis. Each lanthanide(III) ion is ninefold coordinated by eight donor atoms of the ligand system and the oxygen atom of one water molecule. The structures are compared with those of DOTA- and TETA-coordinated complexes and the conformation of the OHEC ligand system with that of the parent amine and its dinuclear copper complex. NMR investigations of the diamagnetic complex **1** indicate a very similar environment of the lanthanide cations in solution and in the solid state. Low-temperature and variable-temperature ^{1}H-NMR measurements prove the existence of two isomers of **1** (3.5:1 ratio) which undergo conformational processes. The rate constants of these processes were deduced from a complete line shape analysis and were used to determine the activation parameters.

Introduction

Lanthanide complexes with macrocyclic polyamine polycarboxylate ligand systems have been the subject of many investigations[1] because they are promising substances for biomedical applications in the field of radioimmunotherapy[2] and can be used as contrast-enhancing agents in magnetic resonance imaging.[3] The best investigated compounds of this class are the mononuclear lanthanide(III) chelates of the macrocyclic ligand DOTA (1,4,7,10-tetraazacyclododecane-1,4,7,10-tetraacetate) and of ligands based on the DOTA skeleton.[4,5] The solid state X-ray structures of DOTA complexes of Ln^{III} (Ln= Y,[4d] La,[4f] Eu,[4a] Gd,[4b,c] and Lu[4e]) show the metal ions in a mono-capped square-antiprismatic coordination sphere. The high rigidity of the DOTA complexes allowed the estimation of conformational and coordination equilibria in aqueous solution by NMR spectroscopy.[4e,6]

In contrast, only a few binuclear lanthanide(III) complexes with macrocyclic polyamine ligands are known, e.g. Eu^{III}, Gd^{III}, and Tb^{III} complexes of a branched hexaazacyclododecane ligand containing six 2,2′-bipyridine pendants units,[7] Gd^{III} complexes of DOTA derivatives in which the two metal ions are located between two ligand molecules forming a dimeric unit,[5d] and the complex $[BO\{Gd(DO3A)(H_2O)\}_2]$ in which the two DO3A rings {$BO(DO3A)_2$ = 2,11-dihydroxy-4,9-dioxa-1,12-bis[1,4,7,10-tetraaza-4,7,10-tris(carboxymethyl)cyclododecyl]dodecane} are connected by a dihydroxydioxadodecane chain.[8]

Recently we reported the successful synthesis of two new hexadecadentate macrocyclic polyamine polycarboxylic ligands H_8OTEC (1,4,7,10,13,16,19,22-octaazacyclotetracosane-1,4,7,10,13,16,19,22-octaacetic acid) and H_8OHEC (1,4,7,10,14,17,20,23-octaazacyclohexacosane-1,4,7,10,14,17,20,23-octaacetic acid) and of some of their mono- and dinuclear lanthanide(III) chelate complexes,[9] among them the binuclear OHEC complexes of Y, Gd, and Eu. The acid/base properties of these ligands were characterised by potentiometry and NMR titration techniques.[10]

In this paper we present the crystal structures of the homodinuclear complexes of yttrium(III), gadolinium(III), europium(III), and lanthanum(III) with the ligand H_8OHEC as well as the solution structure and the dynamics of the diamagnetic Y^{III} complex.

[a] Institut für Anorganische und Analytische Chemie, Technische Universität Berlin, Strasse des 17. Juni 135, D-10623 Berlin, Germany
Fax: (internat.) +49 (0)30/3142 2168
E-Mail: schumann@chem.tu-berlin.de
[b] Institut für Angewandte Analytik und Umweltchemie, Humboldt Universität zu Berlin, Hessische Str. 1−2, D-10115 Berlin, Germany
[c] Bundesanstalt für Materialforschung und -prüfung, Rudower Chaussee 5, D-12489 Berlin, Germany
Supporting information for this article is available on the WWW under http://www.wiley-vch.de/home/eurjic or from the author.

 © WILEY-VCH Verlag GmbH, D-69451 Weinheim, 1999 1434−1948/99/1010−1735 $ 17.50+.50/0

Results and Discussion

Synthesis

The homodinuclear lanthanide(III) complexes were synthesised by treating H_8OHEC with the lanthanide oxides Ln_2O_3 (Ln = Eu,[9] Gd,[9] La) in refluxing water. Freshly prepared $Y(OH)_3$[9] was used for the synthesis of the yttrium complex instead of Y_2O_3, because of the faster reaction in that case. The colourless and highly water-soluble complexes were characterised by means of FAB-MS.

$$2\ Y(OH)_3 + H_8OHEC + 2\ NaOH \rightarrow Na_2[Y_2(OHEC)(H_2O)_2] + 6\ H_2O$$
1

$$Ln_2O_3 + H_8OHEC + 2\ MOH \rightarrow M_2[Ln_2(OHEC)(H_2O)_2] + 3\ H_2O$$
2 (Ln/M = Gd/Na),
3 (Ln/M = Eu/Na),
4 (Ln/M = La/Cs)

As known from the synthesis of the DOTA and modified DOTA lanthanide(III) complexes,[6a,11,12] the formation of the compounds **1** to **4** is also slow. A pH value of 8.5 and heating of the aqueous solutions to reflux are essential reaction conditions for the entrance of the lanthanide ions into the tetraaza coordination pockets of the OHEC ligand, which otherwise would be blocked by protonation of the strongly basic ring nitrogens. This is supported by the protonation scheme of H_8OHEC established by potentiometric titration and pH-dependent $^1H/^{13}C$ NMR titration [the four highest protonation constants were assigned to the ring nitrogens: log K = 11.07, 10.21, 9.58, and 8.54 (298 K, 0.1 M KCl)].[10] In neutral or acidic solution, the lanthanide ions are coordinated only weakly to the outer sphere of the cyclic ligand[13] and free lanthanide ions can be detected electrochemically,[14] by ^{89}Y-NMR,[9] and by reaction with xylenol orange.

Molecular Structures

The molecular structures of the complexes **1** to **4** were determined by single crystal X-ray diffraction. Suitable single crystals were obtained from saturated aqueous solutions of the pure complexes either by slow diffusion of ethanol into the solution of **1** or by slow evaporation of the solutions of **2**, **3**, or **4**. The composition of the crystals correspond to the formulas $[Na_2(Y_2OHEC)(H_2O)_2] \cdot C_2H_5OH \cdot 7\ H_2O$ (**1**), $[Na_2(Gd_2OHEC)(H_2O)_2] \cdot 12\ H_2O$ (**2**), $[Na_2(Eu_2OHEC)(H_2O)_2] \cdot 11\ H_2O$ (**3**) or $[Cs_2(La_2OHEC)(H_2O)_2] \cdot 14\ H_2O$ (**4**). All four complexes crystallise in the monoclinic space group $P2_1/n$. The crystal data, the data collection and the refinement parameters are listed in Table 4 (see Experimental Section).

Although only the Gd^{III} complex **2** and the Eu^{III} complex **3** are isostructural, the conformation of the macrocyclic OHEC unit as well as the coordination geometry around the metal ions are the same for all four structures. Figures 1a and 1b show the solid conformation of **1** in two different views for better understanding, Figure 1c shows the conformation in $[Na(YDOTA)(H_2O)]$ to visualise the differences of the acetate and the amine coordination in complexes of lanthanide metals with DOTA and OHEC. Due to the different ionic radii of the metals, the structures differ in the positions of the lanthanide ions with respect to the mean plane of the cyclic ligand. Whereas in the Y^{III} and La^{III} complexes **1** and **4** the inversion centre of the space group P $2_1/n$ corresponds to the centre of gravity of the molecule resulting in a centrosymmetric geometry, the two halves of the molecules **2** and **3** containing the Gd^{III} and Eu^{III} ions are only almost equal to each other.

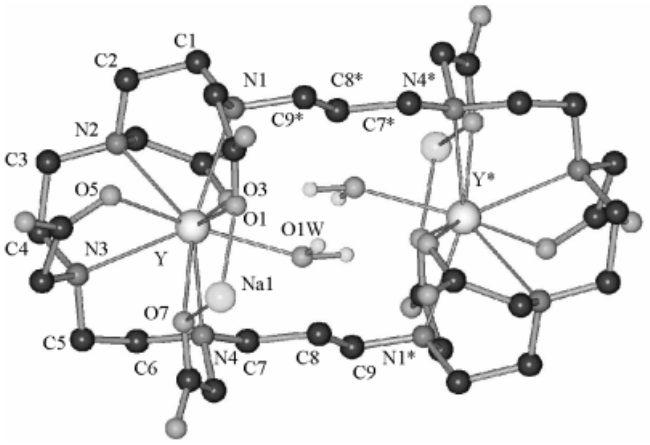


Figure 1a. Solid-state conformation of **1** with numbering scheme; with * designated atoms represent symmetry-equivalent positions ($-x$, $-y$, $-z$); for selected bond length [pm] and angles [°] in **1** see Supporting Information

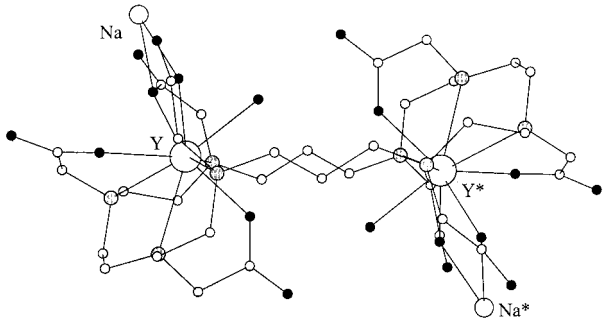


Figure 1b. Solid-state conformation of **1**, side view; carbon atoms contours only, nitrogen atoms filled grey, oxygen atoms filled black

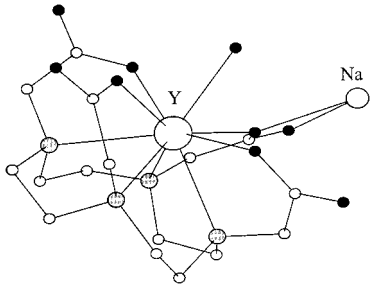
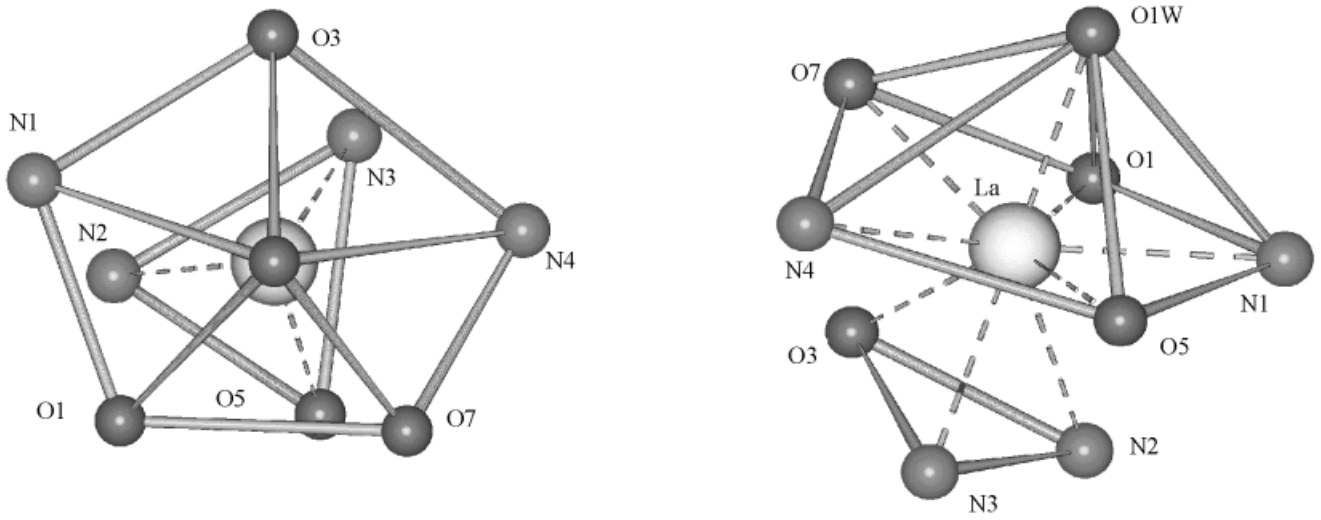


Figure 1c. Solid-state conformation of $[Na(YDOTA)(H_2O)]$; carbon atoms contours only, nitrogen atoms shaded in grey, oxygen atoms black



O1W−La−N4	76.11(19)	O7−La−N4	62.77(18)	N3−La−N2	66.49(2)
O1W−La−N2	144.60(2)	O3−La−N4	70.97(19)	N1−La−N2	66.39(19)
O1W−La−N3	140.30(2)	O3−La−N1	83.43(18)	N3−La−N4	67.47(19)
O1W−La−N1	92.10(2)	O1−La−N1	62.22(18)	O7−La−O1	79.30(18)
O1W−La−O1	68.39(18)	O3−La−N2	62.90(2)	O3−La−O1	136.11(19)
O5−La−O1W	135.07(19)	O7−La−N3	70.30(2)	O5−La−O1	69.48(18)

Figure 2. Coordination polyhedron about the lanthanum ion in **4**, top view (left) and side view (right); angles [°] involving lanthanum(III) and atoms from the coordination sphere

Coordination Geometry of the Lanthanide Ions

As demonstrated for **1** in Figure 1, the two lanthanide ions of each complex are completely encapsulated by the macrocyclic ligand. Each lanthanide ion is coordinated by the four nitrogen and four carboxylic oxygen atoms belonging to one half of the overall hexadecadentate ligand. The ninth coordination site of each lanthanide ion is occupied by the oxygen atom of a water molecule. However, the resulting coordination geometry corresponds neither to a monocapped square antiprism, nor to a tricapped trigonal prism, the two coordination polyhedrons representing the most common geometries of nine-coordinate complexes.[15] It can be best described in terms of an irregular polyhedron built up by a trigonal plane and a monocapped pentagonal plane (Figure 2). Three oxygen atoms and two nitrogen atoms of the ligand form the pentagonal plane [the maximum deviation of the atoms from this plane is observed in **2** (22 pm)], which is capped by the oxygen atom of a water molecule. The donor atoms remaining from this half of the ligand, one carboxylic oxygen and two nitrogen atoms, form the trigonal plane. The lanthanide ion is sandwiched between these two planes with a shorter distance to the centre of the capped pentagonal plane (for Gd^{III} in **2** the distance from the pentagonal plane is 46 pm, that from the trigonal plane is 195 pm). In all complexes, the capping oxygen atom of the water molecule and the lanthanide ion lie on an axis passing through the centres of both planes.

In contrast to the DOTA-like lanthanide complexes, in which all acetate groups are situated on one side of the ring adopting a four-bladed propeller-like conformation (see Figure 1c), three of the four carboxylic groups of the OHEC ligand coordinate each lanthanide(III) ion from one side of the ligand ring and the fourth from the opposite side (see Figure 1b).

A least-square plane of the macrocycle formed from the propylene chains and the four adjacent N atoms was calculated for all four complexes. The displacement of the lanthanides from this plane increases with increasing ionic radius of the lanthanide. For the La^{III} complex **4**, the least-squares equation for this plane, defined by the atoms C7, C8, C9, N4, and N1 and the corresponding symmetry-equivalent atoms, corresponds to $-9.5290x + 8.9063y + 3.1741z - 1.5870 = 0$. The maximum deviation of the carbon atoms from this plane is −38.41 pm, that of the nitrogen atoms −19.76 pm. The La^{III} ions are found ±37.47 pm centrosymmetrically above and below this mean plane. The displacement of the other lanthanide atoms from the corresponding ring mean planes is ±33.06 pm for Y^{III} in **1**, +36.53 pm and −31.76 pm for Gd^{III} in **2** and +35.20 pm and −32.30 pm for Eu^{III} in **3**.

Like the metal ions, the metal-coordinating water molecules are situated centrosymmetrically (**1**, **4**) or nearly centrosymmetrically (**2**, **3**) above and below the mean ring planes with Ln−O(water) distances in the range of the Ln−O(acetate) distances (Table 1). The $Gd^{III}-OH_2$ contacts are similar to those found for mononuclear complexes.[4b,c;5a,e]

The minimum and maximum bond angles and interatomic distances of the OHEC ligand (Table 1) agree quite well with those found for TETA (1,4,8,11-tetraazacyclotetradecane-1,4,8,11-tetraacetate)[4g] and DOTA poly-

aza polycarboxylic complexes.[4] Moreover, the Ln−N and Ln−O contacts are within the range of the values reported for mononuclear structures.[4] The differences between the maximum and minimum interatomic distances are greatest for Ln−O in **1** and for Ln−N in **3**, whereas the smallest differences are found for **4**, but altogether, all these differences are much smaller than those reported for the ion $[Eu(DOTA)(H_2O)]^-$, the complex with the greatest distortions within the series of DOTA lanthanide complexes.[4a]

Conformation of the Ligand

The overall conformation of the OHEC macrocycle in the diyttrium complex **1** is shown in Figure 3, together with the qualitative torsion angles. To accommodate two large lanthanide(III) ions within the ring a centrosymmetric biangular conformation, label {13 13} by Dale,[16] with two genuine corners is adopted, which allows all eight nitrogen atoms to direct their lone electron pair efficiently to the lanthanide ions. The fourfold repetition of *anti* torsion angles in the propylene chains expands the ring. This conformation was found to be essentially the same in all four complexes (for torsion angles of the macrocycle in the dilanthanide(III) OHEC complexes see Supporting Information).

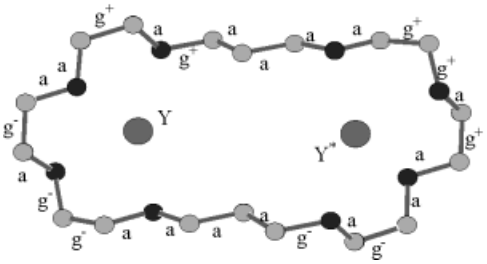


Figure 3. Conformation of the OHEC-ligand in **1**, with corresponding qualitative torsion angles

Surprisingly, the uncomplexed macrocycle of the parent compound OHEC-amine (1,4,7,10,14,17,20,23-octaazacyclohexacosane)[9] shows a highly ordered conformation ruled by a hydrogen-bonding pattern. Its solid state structure reveals a centrosymmetric quadrangular {10 3 10 3} conformation, established by both intramolecular and intermolecular three-centre and two-centre NH···N interactions, thus preventing the enclosure of water molecules into the crystal. This conformation represents a preorganised state for small transition metal ions. In fact, the OHEC-

Table 1. Minimum and maximum interatomic distances [pm] and angles [°] in dilanthanide(III) OHEC complexes and related compounds

	1	**2**	**3**	**4**	**[Eu(DOTA)]$^-$** [4a]	**[Tb(TETA)]$^-$** [4g]
C−C	150.5(6)	150.5(6)	149.4(9)	154.4(10)	162.3(6)	149.4(5)
	152.8(5)	152.5(6)	153.1(9)	150.0(11)	142.6(5)	154.8(6)
C−N	147.9(5)	149.9(5)	146.9(8)	150.8(10)	164.3(6)	147.4(5)
	150.8(5)	146.8(5)	150.1(9)	146.3(10)	137.5(4)	150.9(5)
C−O	128.4(5)	128.9(5)	123.1(10)	127.9(10)	120.2(5)	123.6(5)
	124.9(5)	125.8(5)	125.4(8)	125.6(10)	139.0(5)	124.2(5)
C=O	122.4(5)	125.2(5)	127.8(8)	122.2(10)	116.1(5)	125.4(5)
	125.7(5)	122.3(6)	126.0(8)	125.0(9)	132.5(5)	128.7(5)
C−C−C	106.5(3)	106.0(3)	106.8(5)	106.2(6)		
		108.2(3)	108.4(5)			
C−N−C	103.3(3)	103.6(3)	103.9(5)	103.9(6)	104.6(3)	106.1(3)
	111.0(3)	110.1(3)	110.8(5)	110.9(6)	114.6(3)	110.4(3)
N−C−C	110.7(3)	110.1(3)	111.5(6)	106.2(6)	107.0(3)	110.3(3)
	118.4(3)	118.0(3)	118.3(5)	117.8(6)	117.1(3)	116.2(3)
O−C−O	124.3(4)	123.4(5)	123.0(7)	122.3(8)	116.9(4)	123.5(4)
	125.2(4)	125.4(4)	126.2(6)	125.7(8)	130.5(3)	125.8(4)
O−C−C	116.6(3)	116.9(3)	117.2(6)	117.6(7)	112.4(4)	117.5(4)
	118.9(4)	118.7(4)	118.8(6)	118.4(7)	117.0(3)	118.0(4)
O^M−C−C	115.9(4)	116.6(4)	116.4(6)	117.0(7)	112.5(4)	117.1(3)
	118.2(3)	118.6(4)	118.6(4)	118.4(7)	120.8(3)	117.8(3)
Ln−O	241.2(2)	234.7(3)	236.2(4)	246.4(5)	251.1(3)	230.2(3)
	228.4(3)	246.5(3)	248.2(4)	252.9(5)	238.7(3)	233.0(3)
Ln−N	264.7(3)	262.3(4)	265.4(5)	275.3(6)	290.0(3)	257.5(3)
	276.7(3)	276.7(4)	279.9(5)	286.7(6)	251.0(3)	262.0(3)
Ln−OH_2	236.3(3)	240.6(3)	243.0(5)	252.6(6)	248.0(3)	
		243.8(3)	246.0(5)			
Ln−Ln	665.3	652.1	652.0	636.0		
O−Ln−O	74.46(9)	74.13(15)	73.84(10)	79.30(18)	78.46(9)	74.1(1)
	133.97(9)	134.73(15)	135.11(10)	133.70(18)	147.51(9)	133.46(9)
O−Ln−N	64.93(9)	64.27(15)	64.78(10)	62.22(18)	60.79(9)	66.63(9)
	139.38(9)	138.34(16)	138.56(10)	140.82(18)	143.63(9)	151.50(9)
N−Ln−N	67.43(11)	67.65(17)	67.70(11)	66.40(2)	64.69(9)	70.4(1)
	145.79(9)	149.19(16)	148.26(10)	151.99(19)	107.56(9)	136.74(9)
O−Ln−OW	66.88(10)	67.25(15)	67.16(10)	68.39(18)	68.67(9)	
	135.61(10)	135.19(15)	135.31(11)	135.07(19)	75.58(9)	
N−Ln−OW	76.51(10)	77.92(16)	77.68(11)	76.11(19)	124.5(1)	
	141.55(12)	140.45(17)	40.65(12)	144.6(2)	129.81(9)	

amine ligand of the dinuclear Cu^{II} complex [Cu_2(OHEC-amine)(SO_4)$_2$][9] adopts in the solid state a very similar {5 5 3 5 5 3} conformation (for torsion angles of the macrocycle in the OHEC-amine ligand and in [Cu_2(OHEC-amine)(SO_4)$_2$] see Supporting Information).

Packing Pattern

All four complexes are wrapped in a water matrix. Besides the water molecules coordinated to the metal ions, the complexes **2** to **4** contain 12, 11, or 14 additional water molecules, respectively. In **1**, the position of one water molecule is occupied to 50% by ethanol, with identical positions of the oxygen atoms.

The crystal of **1** is built up from infinite one-dimensional chains of $[Y_2(OHEC)(H_2O)_2]^{2-}$ units, arranged parallel to the *a* axis and linked by a network of $Na^+\cdots O$ contacts, involving the sodium cation, the carboxylate oxygen atoms and the water molecules associated with the cation. In **2** and **3** the chain runs along the *c* axis. The molecular units of **4** are held together by caesium ions and water molecules forming an infinite chain parallel to the *a* axis. In all structures there is an additional three-dimensional framework built up by hydrogen bonds between water molecules and carboxylic oxygen atoms.

NMR Investigations of the Diamagnetic $[Y_2(OHEC)]^{2-}$ Complex

The lanthanide metals in the oxidation state Ln^{3+} are known to form stable but highly fluxional chelates with a variety of ligands.[6d] Their complexes with DOTA or with modified DOTA ligands together with a number of other O- or N-donor polydentate ligands[17] are among the very few examples exhibiting the same structure in the solid state as in solution. They form highly symmetric and extremely rigid structures, since the DOTA 12-membered tetraazacycle prefers to adopt a square {3 3 3 3} geometry offering a high degree of preorganisation.[6a] This is also valid for lanthanide(III) complexes of TETA, in which the cyclic ligand shows a biangular {7 7} conformation.[4g,18]

Also the large macrocyclic ligand H_8OHEC surprisingly forms a dinuclear yttrium(III) complex that is rigid on the NMR time scale. This fact gives the possibility of gaining some insight into the coordination characteristics and the solution structure of the complexes described here, and also to investigate whether conformational isomers possibly slowly equilibrate.

Temperature-dependent solution NMR studies of the diamagnetic dinuclear lanthanum(III) OHEC complex were unrevealing. The ^{1}H-NMR spectra in D_2O at 300 and 600 MHz showed a series of broad overlapping resonances characteristic of fluxional behaviour. A ^{1}H-NMR spectrum at 600 MHz of $[(La_2(OHEC)]^{2-}$ is shown as Supporting Information.

Figure 4 presents the experimental and the simulated ^{1}H-NMR spectra of $[Y_2(OHEC)]^{2-}$ at 278 K. Starting from the

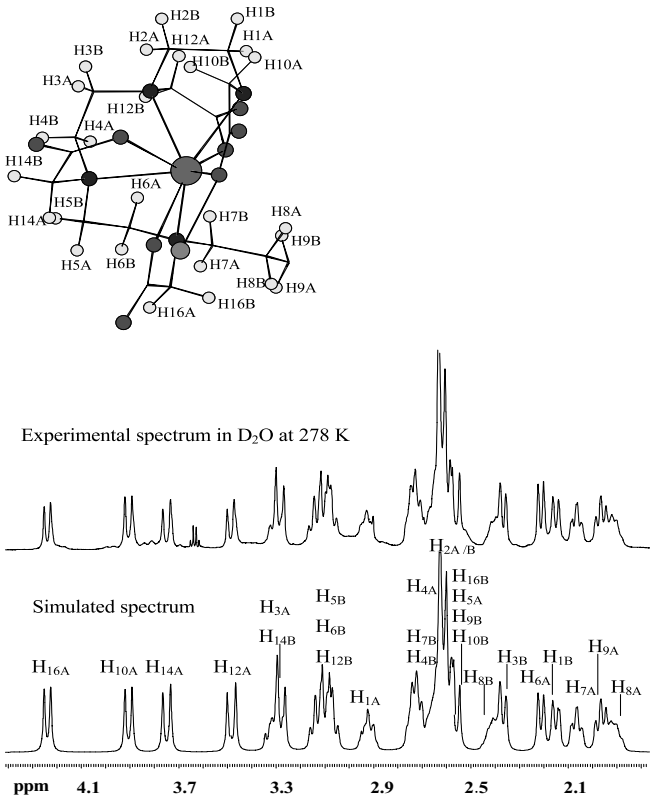


Figure 4. Experimental and simulated ^{1}H-NMR spectra of $[Y_2(OHEC)]^{2-}$ at 278 K in D_2O, pH = 8.5; plot of the asymmetric unit of $[Y_2(OHEC)]^{2-}$ illustrates the designation of atoms in the NMR spectra

Table 2. ^{1}H- and ^{13}C-NMR chemical shifts of $Na_2[Y_2(OHEC)]$

Backbone	protons	δ ^{1}H [ppm] at 278 K	δ ^{1}H [ppm] at 365 K	carbons	δ ^{13}C [ppm] at 278 K
N1	H1A	2.92	2.72	C1	57.4
	H1B	2.16	2.20		
	H2A	2.64	2.60	C2	53.4
	H2B	2.64	2.60		
N2	H3A	3.33	3.14	C3	53.9
	H3B	2.38	2.37		
	H4A	2.63	2.54	C4	52.5
	H4B	2.74	2.78		
N3	H5A	2.60	2.54	C5	54.3
	H5B	3.15	3.10		
	H6A	2.22	2.18	C6	47.5
	H6B	3.09	3.04		
N4	H7A	2.08	2.02	C7	55.7
	H7B	2.76	2.69		
	H8A	1.92	1.84	C8	19.8
	H8B	2.41	2.28		
	H9A	1.97	1.92	C9	55.9
	H9B	2.66	2.71		
side chain					
N1	H10A	3.91	3.78	C10	56.0
	H10B	2.56	2.55		
				C11	178.8
N2	H12A	3.49	3.51	C12	63.5
	H12B	3.11	3.01		
				C13	177.7
N3	H14A	3.26	3.31	C14	57.4
	H14B	3.76	3.53		
				C15	178.6
N4	H16A	4.25	4.15	C16	60.3
	H16B	2.61	2.59		
				C17	177.4

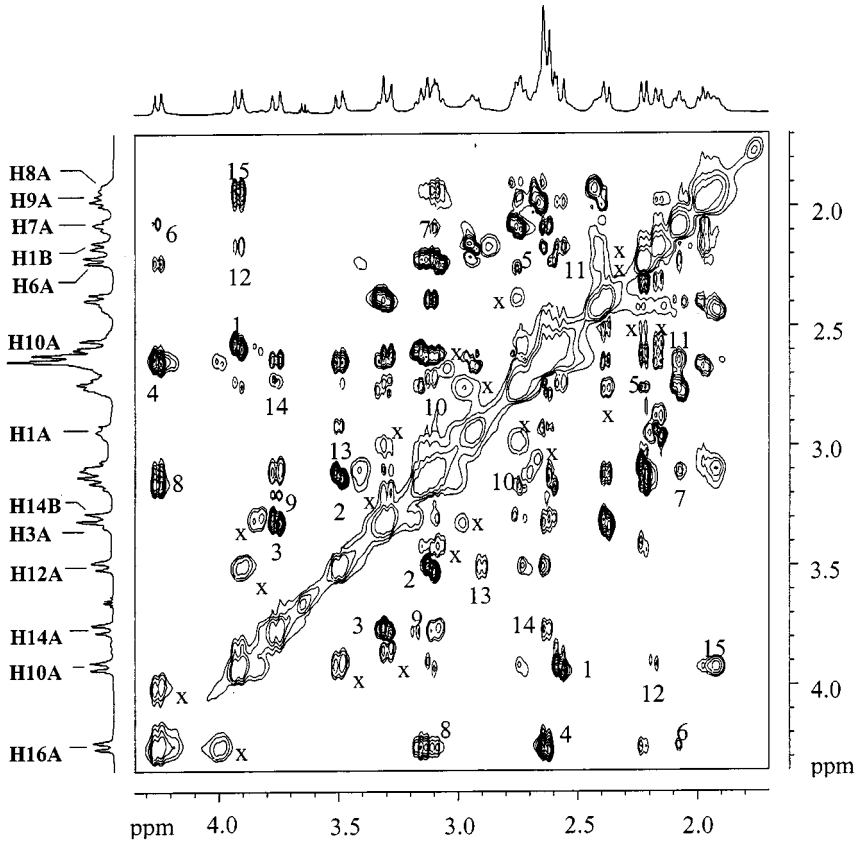


Figure 5. ROESY spectrum of $[Y_2(OHEC)]^{2-}$ at 278 K, mixing time 80 ms; the designation of the peaks is according to Table 3, column 4; exchange peaks are labelled with "x"

methylene proton H16A the step by step assignment was carried out with the HMQC and HMBC spectra and the cross peaks of the ROESY spectra. The ^{1}H- and ^{13}C chemical shift values are listed in Table 2 according to the designation in the solid-state structure.

Two features of these spectra are of particular interest. First, according to the centrosymmetric geometry of the complex in the solid state only half of the carbon and proton signals should appear in the NMR spectra. This is exactly the case for $[Y_2(OHEC)]^{2-}$, the solid-state geometry of which accounts for 26 proton and 17 carbon resonances, which all are observed in the spectra.

The second important feature of the ^{1}H-NMR spectrum (Figure 4) is the fact that the experimental spectrum clearly shows a few low intensity peaks indicating that at least two isomers (3.5:1 ratio) are present in aqueous solution. The minor isomer shows the signal number of an unsymmetric molecule, since temperature increase causes coalescence of each of the signals of the major conformation with two signals of the minor conformation. This loss of centrosymmetry may be caused by independent dynamic processes occurring in the two halves of the originally centrosymmetric molecule. Unfortunately, the NMR data do not allow an unambiguous assignment of the geometry of this minor isomer present in solution.

In order to determine the solution structure of $[Y_2(OHEC)]^{2-}$ a quantitative analysis of the ROESY spectra (Figure 5) measured at different mixing times was carried out. The intensity of the ROE signals was determined by measuring the volume of the ROESY cross peaks. On the basis of the X-ray crystal structure determination, the occurrence of non-sequential ROEs should be limited owing to the relatively large diameter of the complexed ligand. Hence, ROE information was only obtained from geminal

Table 3. Comparison of proton-proton distances derived from crystal structure and ROESY spectra

Proton pair		distance from crystal structur analysis [pm]	distance from ROE [pm]	No. in Figure 5
geminal protons				
H10A	H10B	156	170	1
H12A	H12B	157	170	2
H14A	H14B	156	170	3
H16A	H16B	157	160	4
Nongeminal protons				
H7B	H6A	212	240	5
H7A	H16A	259	270	6
H7A	H6B	226	220	7
H6B	H16A	235	210	8
H5B	H14B	270	270	9
H5B	H4B	240	220	10
H10B	H1B	253	260	11
H10A	H1B	245	270	12
H12A	H1A	246	240	13
H14B	H4B	215	240	14
H10A	H9A	202	190	15

protons and protons in close neighbourhood. Table 3 lists distances derived from the crystal structure and quantitative ROE measurements. The good agreement of the distance information obtained by these two different methods allows a strong resemblance to be claimed between solid and solution structure. The level of convergence of the structures was quantified by root mean square (rms) deviations calculated as the average of all possible pairwise comparisons, giving 50 ± 5 pm for comparisons based on all heavy atoms.

The low-temperature ROESY spectrum in Figure 5 proves the existence of an exchange process between major and minor conformation by the observation of exchange peaks, designated with "x", of protons undergoing mutual chemical exchange. All NMR signals of the major isomer show two exchange peaks at low temperatures.

For the methylene proton 16A of the acetate side arm, which is little disturbed by signal overlapping, variable-temperature ^{1}H-NMR spectra have been recorded and simulated (Figure 6). At 278 K the proton shows a doublet with an intensity of 78% for the major isomer, and two further doublets at higher field each with 11% of intensity for the minor isomer. With increasing temperature broadening and coalescence of the three signals occurs, followed by a sharpening to one doublet around 365 K. The band shapes of the depicted spectra were calculated for a two-site exchange. The kinetic parameters were deduced from the Arrhenius plot (E_A = 51.3 ± 2 kJ/mol) and the Eyring plot ($\Delta H^{\#}$ = 49 ± 2 kJ/mol). The free energy of activation $\Delta G^{\#}$ at 300 K was calculated from the Eyring equation to be 65.0 ± 3 kJ/mol.

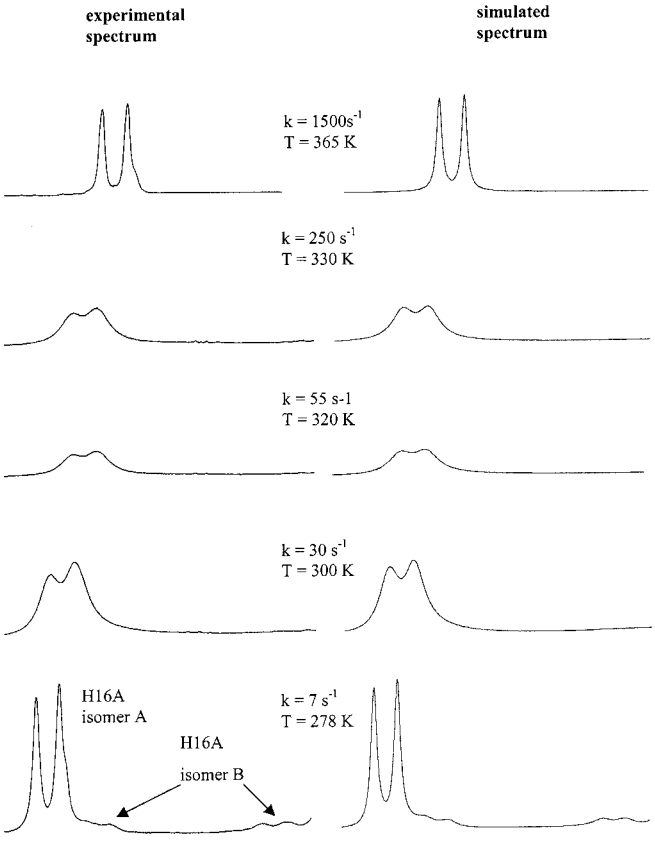


Figure 6. Selected experimental (on the left) and calculated (on the right) ^{1}H-NMR spectra of $[Y_2(OHEC)]^{2-}$ (CH_2 acetate region, proton H16A exchanging between two conformational environments) at different temperatures showing the derived rate constants

By comparison with the solution dynamics of the DOTA lanthanide complexes, two different types of motion should be possible within the $[Y_2(OHEC)]^{2-}$ moiety, one involving the rotation of the acetate arms and the other corresponding to a conformational inversion of the macrocyclic ring. Both processes potentially lead to an interchange between conformational isomers.[6] Although the DOTA and TETA complexes have totally different geometries the similar activation parameters of $[Y_2(OHEC)]^{2-}$ suggest a turning round of acetate groups without releasing the coordinative bonds.[6a,6d,4e,18]

Experimental Section

General Remarks: Materials: All reagents were purchased from Merck or Aldrich and were used without further purification. The ligand H_8OHEC as well as its yttrium(III) and lanthanide(III) complexes (Ln = Gd, Eu) were prepared by the published method.[9] − Elemental analyses and FAB mass spectra confirmed the composition of the compounds. The elemental analyses were recalculated for anhydrous compounds. The complexes contain at least two molecules of water per molecule of complex, dependent of the duration of the drying procedure. − Elemental analysis: Perkin−Elmer 2400 Series CHNS/O Analyzer. − MS: Double-focusing ZAB instrument, VG company (FAB).

H_8OHEC: M.p: 230−235°C. − $C_{34}H_{60}N_8O_{16}$ (836.41): calcd. C 48.80, H 7.23, N 13.39; found C 49.01, H 7.44, N 13.43%. − FAB^+MS (magic bullet/H_2O) *m/e*: 837 $[M + H]^+$, 859 $[M + Na]^+$, 875 $[M + K]^+$. Na^+ and K^+ are from impurities of the water used.

$Na_2[Y_2(OHEC)]$ (1): Dec. > 300°C. − $C_{34}H_{52}N_8Na_2O_{16}Y_2$ (1052.46): calcd. C 38.79, H 4.98, N 10.64; found C 38.60, H 4.69, N 10.38%.

$Na_2[Gd_2(OHEC)]$ (2): Dec. > 300°C. − $C_{34}H_{52}Gd_2N_8Na_2O_{16}$ (1189.25): calcd. C 34.34, H 4.41, N 9.42; found C 34.60, H 4.41, N 9.08%. − FAB^+MS of the complex (thioglycerine/methanol/H_2O) *m/e*: 1185−1196 $[M + H]^+$.

$Na_2[Eu_2(OHEC)]$ (3): Dec. > 300°C. − $C_{34}H_{52}Eu_2N_8Na_2O_{16}$ (1180.17): calcd. C 34.57, H 4.44, N 9.49; found C 34.83, H 4.53, N 10.00%. − FAB^+MS (thioglycerine/methanol/H_2O) *m/e*: 1177−1183 $[M + H]^+$.

$Cs_2[La_2(OHEC)]$ (4): The complex was prepared by treating 0.5 g (0.62 mmol) of H_8OHEC and 404.0 mg (1.24 mmol) of La_2O_3 suspended in 40 mL of distilled water. The mixture was refluxed for 24 h to obtain a clear solution. After cooling to room temperature and adjustment of the pH to 8.5 with 0.1 M Cs_2CO_3, the solution was refluxed for another 2 h and then filtered to remove traces of precipitated $La(OH)_3$. After removal of the solvent, the residue was recrystallised from water/ethanol. The separated colourless crystals were dried in vacuo at 80°C. Yield 76%. − $C_{34}H_{52}Cs_2La_2N_8O_{16}$ (1371.97): calcd. C 29.75, H 3.81, N 8.16; found C 29.53, H 4.01, N 8.08%. − FAB^+MS (thioglycerine/methanol/H_2O) *m/e*: 1394.5−1397.5 $[M + Na]^+$, 1128.8 $[M - 2\,Cs+Na]^-$.

X-ray Crystallographic Study: Suitable crystals of **1** were obtained by slow diffusion of ethanol into a concentrated aqueous solution of the recrystallised diyttrium complex. Suitable crystals of **2**, **3**,

Table 4. Crystal data, details of data collection, and structure refinement for **1**, **2**, **3**, and **4**

	1	**2**	**3**	**4**
Crystal Data				
Empirical formula	$C_{34}H_{52}N_8Na_2O_{16}Y_2 \cdot 7\ H_2O \cdot C_2H_5OH$	$C_{34}H_{52}Gd_2N_8Na_2O_{16} \cdot 12\ H_2O$	$C_{34}H_{52}Eu_2N_8Na_2O_{16} \cdot 11\ H_2O$	$C_{34}H_{52}Cs_2La_2N_8O_{16} \cdot 14\ H_2O$
M_r [amu]	1242.81	1405.49	1412.94	1624.70
Crystal system	monoclinic	monoclinic	monoclinic	monoclinic
Space group	$P\ 2_1/n$ (14)	$P\ 2_1/n$ (14)	$P\ 2_1/n$ (14)	$P\ 2_1/n$ (14)
Crystal size [mm]	0.56 × 0.48 × 0.28	0.40 × 0.32 × 0.20	0.72 × 0.64 × 0.20	0.39 × 0.32 × 0.12
a [pm]	1481.8 (2)	1380.6 (2)	1394.3 (4)	1241.2 (2)
b [pm]	1224.0 (2)	2654.5 (3)	2673.5 (6)	1404.7 (2)
c [pm]	1572.9 (3)	1478.5 (2)	1485.2 (5)	1721.9 (3)
α [°]	90	90	90	90
β [°]	112.42 (2)	107.09 (2)	106.97 (3)	110.70 (2)
γ [°]	90	90	90	90
V [Å ^{3}]	2637.2 (6)	5178.9 (11)	5295 (3)	2808.4 (8)
ρ_{calc} [gcm^{-3}]	1.595	1.849	1.772	1.921
Z	2	4	4	2
F (000) [e]	600	1608	2872	1608
μ (Mo-$K\alpha$) [mm^{-1}]	2.299	2.657	2.46	2.872
Data Collection				
Diffractometer	STOE Ipds	STOE Ipds	STOE Stadi-4	STOE Ipds
Radiation, [Å]		Mo Kα, 0.71071	graphite monochromator	
T [K]	200 (2)	200 (2)	295 (2)	200 (2)
scan mode	φ - rotation	φ - rotation	$2\Theta/\omega = 0.5$	φ - oscillation
h, k, l ranges	±10, ±10, ±13	−16/15, ±31, ± 17	−16/15, 0/31, −16/17	−15/14, ±17, ±20
2Θ range [°]	4.46−47.0	3.86−50.22	3.04−49.98	4.56−50.24
Measured data	11802	34400	10459	18680
unique data (all)	3904	9041	9259	5023
R_{int}	0.1096	0.0920	0.0631	0.1709
data used f. refinement	3904	9040	9235	5011
Absorption correction	refdelf (difabs)	refdelf (difabs)	empirical (ψ -scan)	no
T_{min}/T_{max}	0.447/1.0	0.523/0.998	0.548/0.997	−/−
Refinement				
refined parameters	435	763	674	343
H atoms [found/geom.]	32/0	24/52	24/52	10/26
$R1$[a] [$F_0 > 4\sigma(F_0)$]	0.0300 (2966 refl.)	0.0307 (7482)	0.0432 (7751)	0.0556 (3684)
$wR2$[b] (all)	0.0935	0.0818	0.1188	0.1434
GoF (all)	0.912	0.991	1.141	0.976
Weighting par.a,b[c]	0.0371, 0	0.0381, 0	0.048, 0.0098	0.0597, 0
ρ_{final}(max/min) [e Å $^{-3}$]	0.542/−0.659	2.172/−0.832	2.872/−1.027	3.464/−1.531

[a] $R1 = \Sigma||F_o| - |F_c||/\Sigma|F_o|$. − [b] $wR2 = [\Sigma\ w(F_o^2 - F_c^2)^2/\Sigma\ w(F_o^2)^2]^{1/2}$. − [c] $w = 1/[\sigma^2(F_o^2) + (a\ P)^2 + b\ P]$; $P = (F_o^2 + 2F_c^2)/3$.

and **4** were obtained by slow evaporation of a concentrated aqueous solution of the recrystallised dilanthanide complexes.

The single crystals of compounds **1**, **2**, and **4** were measured on the STOE Ipds one circle diffractometer supplied with an imaging plate area detector at 200 K in nitrogen atmosphere. Intensity correction for Lorentz and polarisation effects and in the case of **1** and **2** also for absorption (Difabs-related)[19] was applied.

A crystal of the compound **3** was measured on a STOE Stadi-4 four circle diffractometer at room temperature in air. Intensity data were corrected for Lorentz, polarisation and absorption (ψ-scan technique).[20]

Structures were solved by direct methods[21] and refined by full-matrix least squares against F^2[22] supported by STOE Xstep software. The thermal motion of all non-hydrogen atoms was treated anisotropically, that of hydrogen atoms isotropically and tied 1.2 times higher than the corresponding attached atom.

In the structure of **1** the positions of all H-atoms of the OHEC unit and six H-positions of water molecules were found in difference electron density maps (difmaps) and successfully refined in least-squares refinement. The H-atoms at the partially occupied water and ethanol sites could not be localised.

For the refinement of **2**, **3**, and **4** the hydrogen atoms of the OHEC units were calculated in their idealised positions and allowed to ride on their attached atoms during the least squares cycles.

In structure **2** two of fourteen water positions have site occupation factors of only 0.8 and 0.5. All H atoms at fully occupied water sites were found in difmaps and their positions could be refined by least squares.

In structure **3**, where either two of fourteen water sites are not fully occupied (0.67 and 0.33 in part, respectively), all H atoms of fully occupied water sites were localised in difmaps, but had to be fixed in the following least squares cycles.

In the crystal structure of **4** all seven water sites are completely occupied, but nevertheless only ten of fourteen water hydrogens could be found in difmaps (obviously the data set of **4** was of poor quality; even the application of difabs failed!). Consequently, all hydrogen atoms had to be restrained or fixed for least-squares refinement.

Further details of the crystal-structure investigations may be obtained from the Fachinformationszentrum Karlsruhe, D-76344 Eggenstein- Leopoldshafen, Germany, on quoting the depository numbers CSD-410446 for **1**, CSD-410447 for **2**, CSD-410444 for **3**, and CSD-410445 for **4**.

NMR: Samples for NMR spectroscopy were prepared by dissolving 50 mg of the complex in 0.75 mL of D_2O in a 5-mm sample tube (Wilmad). NMR spectra were acquired at 600 MHz on a Bruker AMX 600 spectrometer. 2D spectra (DQF-COSY, ROESY, TOCSY, HSQC, and HMBC) were recorded at 278 K with a spec-

tral width of 7200 Hz for protons and 33000 Hz for ^{13}C. The TPPI method of acquisition was used in all cases. The signal due to residual HDO was suppressed by continuous low-power irradiation. Data matrices typically consisted of 2048 complex points in F2 for each of the 512 F1 increments, the data being zero-filled to a 2048 × 1024 complex matrix before transformation. The apodisation functions used in processing were 90° shifted sine-bell squared for all 2D experiments. 2D spectra were processed using the UXNMR program on a Silicon Graphics O2 workstation. ROESY crosspeaks were integrated by the AURELIA[23] software including offset correction according to Bull.[24] The temperature dependence of the proton resonances was determined by recording the 1D spectra at 278 to 373 K with temperature steps of 10 K. The temperature was calibrated against a 100% ethylene glycol insert sample. Rate constants were evaluated by comparing the experimental spectra with those calculated with the program DNMR-SIM.[25] The simulation of one dimensional ^{1}H-NMR spectra were performed with the Bruker Software WIN-DAISY.[26]

Acknowledgments

This work was supported by the *Fonds der Chemischen Industrie* and the *Deutsche Forschungsgemeinschaft* as well as the Sonderforschungsbereich 335 Anisotrope Fluide.

[1] V. Alexander, *Chem. Rev.* **1995**, *95*, 273−342.
[2] [2a] J. P. L. Cox, K. J. Jankowski, R. Kataky, D. Parker, N. R. A. Beeley, B. A. Boyce, M. A. W. Eaton, K. Millar, A. T. Millican, A. Harrison, C. Walker, *J. Chem. Soc., Chem. Commun.* **1989**, 797−798. − [2b] D. Parker, *Crown Compounds Toward Future Applications* (Ed.: S.R. Cooper), VCH Publishers, Inc., New York, **1992**, Chapter 4.
[3] [3a] R. B. Lauffer, *Chem. Rev.* **1987**, *87*, 901−927. − [3b] R. G. Choppin, K. M. Schaab, *Inorg. Chim. Acta* **1996**, *252*, 299−310.
[4] [4a] M.-R. Spirlet, J. Rebizant, J. F. Desreux, M.-F. Loncin, *Inorg. Chem.* **1984**, *23*, 359−363. − [4b] J. P. Dubost, J. M. Legar, M. H. Langlois, D. Meyer, M. C. R. Schaefer, *Acad. Sci. Paris Ser. 2* **1991**, *312*, 349. − [4c] C. A. Chang, L. C. Francesconi, M. F. Malley, K. Kumar, J. Z. Gougoutas, M. F. Tweedle, *Inorg. Chem.* **1993**, 32, 3501−3508. − [4d] D. Parker, K. Pulukkody, F. C. Smith, A. Batsanov, J. A. K. Howard, *J. Chem. Soc. Dalton Trans.* **1994**, 689−693. − [4e] S. Aime, A. Barge, M. Botta, M. Fasano, J. D. Ayala, G. Bombieri, *Inorg. Chim. Acta* **1996**, *246*, 423−429. − [4f] S. Aime, A. Barge, F. Benetello, G. Bombieri, M. Botta, F. Uggeri, *Inorg. Chem.* **1997**, *36*, 4287−4289. − [4g] M.-R. Spirlet, J. Rebizant, M. F. Loncin, J. F. Desreux, *Inorg. Chem.* **1984**, *23*, 4278−4283.
[5] [5a] S. Aime, P. L. Anelli, M. Botta, F. Fedeli, M. Grandi, P. Paoli, F. Uggeri, *Inorg. Chem.* **1992**, *31*, 2422−2428. − [5b] S. Aime, M. Botta, G. Ermondi, F. Fedeli, F. Uggeri, *Inorg. Chem.* **1992**, *31*, 1100−1103. − [5c] D. Dischino, E. J. Delaney, J. E. Emswiler, G. T. Gaughan, J. S. Prasad, S. K. Srivastava, M. F. Tweedle, *Inorg. Chem.* **1991**, *30*, 1265−1269. − [5d] S. I. Kang, R. S. Ranganathan, J. E. Emswiler, K. Kumar, J. Z. Gougoutas, M. F. Malley, M. F. Tweedle, *Inorg. Chem.* **1993**, *32*, 2912−2918. − [5e] K. Kumar, C. A. Chang, L. C. Francesconi, D. D. Dischino, M. F. Malley, M. F. Gougoutas, M. F. Tweedle, *Inorg. Chem.* **1994**, *33*, 3567−3575. − [5f] Z. Kovacs, A. D. Sherry, *J. Chem. Soc., Chem.Commun.* 1995, 185−186. − [5g] J. Huskens, D. A. Torres, Z. Kovacs, J. P. André, C. F. G. C. Geraldes, A. D. Sherry, *Inorg. Chem.* **1997**, *36*, 1495−1503. − [5h] J. Platzek, P. Blaszkiewicz, H. Gries, P. Luger, G. Michl, A. Müller- Fahrnow, B. Radüchel, D. Sülzle, *Inorg. Chem.* **1997**, *36*, 6086−6093.
[6] [6a] J. F. Desreux, *Inorg. Chem.* **1980**, *19*, 1319−1324. − [6b] S. Aime, M. Botta, G. Ermondi, *Inorg. Chem.* **1992**, *31*, 4291−4299. − [6c] K. Roth, S. Hoeft, *Chem. Ber.* **1993**, *126*, 869−873. − [6d] V. Jacques, J. F. Desreux, *Inorg. Chem.* **1994**, *33*, 4048−4053. − [6e] S. Aime, M. Botta, M. Fasano, P. M. Marques, C. F. G. C. Geraldes, D. Pubanz, A. E. Merbach, *Inorg. Chem.* **1997**, *36*, 2059−2068 and references cited therein. − [6f] S. Aime, M. Botta, G. Ermondi, E. Terreno, P. L. Anelli, F. Fedeli, F. Uggeri, *Inorg. Chem.* **1996**, *35*, 2726−2736. − [6g] S. Aime, M. Botta, A. S. De Sousa, D. Parker, *Angew. Chem.* **1998**, *110*, 2819−2820.
[7] R. Ziessel, M. Maestri, L. Pridi, V. Balzani, A. V. Dorsselaer, *Inorg. Chem.* **1993**, *32*, 1237−1241.
[8] E. Tóth, S. Vauthey, D. Pubanz, A. E. Merbach, *Inorg. Chem.* **1996**, *35*, 3375−3379.
[9] U. A. Böttger, H. Gries, F. E. Hahn, H. Hemling, G. Kociok-Köhn, J. Pickardt, J. Platzek, B. Radüchel, B. Schiefner, H. Schumann, K. Zietzke, A. Zschunke, *Chem. Ber.* **1997**, *130*, 267−277.
[10] U. A. Böttger, H. Weisshoff, A. Zschunke, H. Schumann, to be published.
[11] [11a] M. Kodama, T Koike, A. B. Mahatma, E. Kimura, *Inorg. Chem.* **1991**, *30*, 1270−1273. − [11b] S. L. Wu, W. D. Horrocks, Jr., *Inorg. Chem.* **1995**, *34*, 3724−3732.
[12] S. L. Wu, K. A. Johnson, W. D. Horrocks, Jr., *Inorg. Chem.* **1997**, *36*, 1884−1889.
[13] C. Lecomte, V. Dahaoui-Gindrey, H. Chollet, C. Gros, A. K. Mishra, F. Barbette, P. Pullumbi, R. Guilard, *Inorg. Chem.* **1997**, *36*, 3827−3838.
[14] U. Böttger, O. Galin, H. Schumann, M. Michman, *Inorg. Chim. Acta* **1995**, *231*, 29−34.
[15] M. G. B. Drew, *Coord. Chem. Rev.* **1977**, *24*, 179−275 and references cited therein.
[16] J. Dale, *Isr. J. Chem.* **1980**, *20*, 3−11.
[17] [17a] P. M. Lowe, P. Caravan, S. J. Rettig, C. Orvig, *Inorg. Chem.*, **1998**, *37*, 1637−1647. − [17b] F. Renaud, C. Piguet, G. Bernardinelli, J.-C. G. Bünzli, G. Hopfgartner, *Chem. Eur. J.,* **1997**, *3*, 1646−1659.
[18] J. F. Desreux, M. F. Loncin, *Inorg. Chem.* **1986**, *25*, 69−74.
[19] N. Walker, D. Stuart, *Acta Cryst. A39* **1983**, 158−166.
[20] A. C. T. North, D. C. Phillips, F. S. Mathews, *Acta Cryst. A24* **1968**, 351−359.
[21] G. M. Sheldrick, *Acta Cryst. A46* **1990**, 467−473.
[22] G. M. Sheldrick, *Program for Crystal Structure Refinement* **1993**, Universität Göttingen, Germany.
[23] *AURELIA* manual, version 941101.3 Bruker Analytische Messtechnik GmbH, FRG, **1994**.
[24] T. E. J. Bull, *Magn. Reson.***1988**, *80*, 470.
[25] *DNMR-SIM*, version 1.00, G. Haegele, R. Fuhler, Institut für Anorganische und Strukturchemie I, Universität Düsseldorf, FRG, **1996**. This program is available on the Internet: ftp://ftp.uni-duesseldorf.de/pub/msdos/chemie.
[26] WIN-DAISY, version 4.0 Bruker-Franzen Analytik GmbH, FRG, **1997**.

Received March 3, 1999
[I99081]

Novel Concepts in Directed Biaryl Synthesis, 68[+]
Enantioselective Organic Syntheses Using Chiral Transition Metal Complexes, 9[++]
Atropo-Diastereoselective Ring Opening of Biaryl Thionolactones Using [CpRu{(*S*,*S*)-CHIRAPHOS}]$^+$ as a Chiral Auxiliary

Wolfdieter A. Schenk,*[a] Jörg Kümmel,[a] Irene Reuther,[a] Nicolai Burzlaff,[a] Andreas Wuzik,[b] Olaf Schupp,[b] and Gerhard Bringmann*[b]

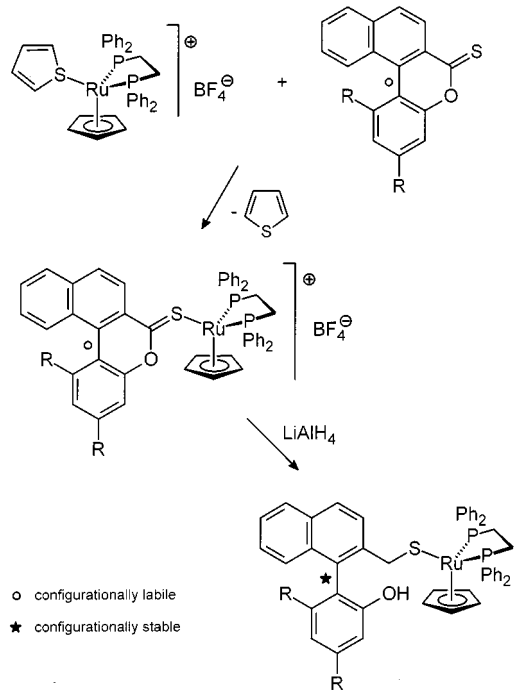
Dedicated to Professor Helmut Werner on the occasion of his 65th birthday

Keywords: Biaryls / Lactones / Nucleophilic additions / Ruthenium / S ligands

The substitution-labile thiophene complex [CpRu{(*S*,*S*)-CHIRAPHOS}(SC_4H_4)]BF_4 (**2**) [(*S*,*S*)-CHIRAPHOS = (2*S*,3*S*)-bis(diphenylphosphanyl)butane], prepared from [CpRu{(*S*,*S*)-CHIRAPHOS}Cl] (**1**), thiophene, and $AgBF_4$, reacted with the biaryl-thionolactones **3a–f** to give the corresponding S-coordinated complexes **4a–f** in high yields. The structure of **4c**, which crystallized as the pure (*S*,*S*,*P*) diastereoisomer, was determined by X-ray crystallography. Coordination of the ruthenium fragment caused an elongation of the C=S bond, a contraction of the C–O bond within the lactone ring and a flattening of that ring. Single hydride transfer with $LiBEt_3H$ converted **4a–f** into the thiolactolate complexes **5a–f** in good yields and diastereoselectivities. An X-ray structure determination of the major isomer of **5a** revealed it to be the (*S*,*S*,*S*,*P*) diastereoisomer. Protonation with NH_4PF_6 converted **5a–f** into the corresponding ring-opened thioaldehyde complexes **6a–f**. Alkylation of **5a** with methyl iodide resulted in Ru–S cleavage to give the oxothioacetal **7a** and [CpRu{(*S*,*S*)-CHIRAPHOS}I] (**8**). Full reduction of **4a–f** with $LiAlH_4$ produced the thiolate complexes **9a–f** in high yields and 6–74% *de*. Methylation at sulfur converted **9a–c** into the corresponding thioether complexes **10a–c**, which were cleaved to **8** and the free methyl thioethers **11a–c** without isomerization of the biaryl axis.

Introduction

Natural products containing a chiral, configurationally stable biaryl axis are attracting considerable attention due to their widespread pharmacological activities.[3][4] Their stereocontrolled synthesis remains a fascinating challenge. One of the most efficient synthetic pathways consists of the preparatively facile formation of a bridged, but still configurationally labile biaryl system followed by an atropo-diastereo- or atropo-enantioselective ring-opening step.[5] The necessary element of chirality may already be present in the molecule,[6] or it may be introduced either by the reagent[7] or by attaching a chiral auxiliary to the bridged biaryl substrate.[8] We have previously demonstrated that configurationally unstable biaryl thionolactones can easily be introduced as ligands into half-sandwich ruthenium complexes. Double nucleophilic addition of hydride converts the coordinated thionolactones into axially chiral racemic thiolates (Scheme 1).[9]



Scheme 1. Coordination and ring opening of biaryl thionolactones

[+] Part 67: Ref.[2]
[++] Part 8: Ref.[1]

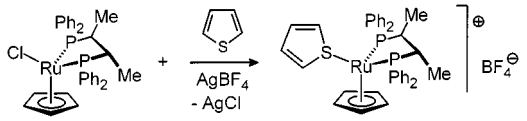
[a] Institut für Anorganische Chemie der Universität, Am Hubland, D-97074 Würzburg, Germany.
Fax: (internat.) + 49-(0)931/888-4605
E-mail: wolfdieter.schenk@mail.uni-wuerzburg.de
[b] Institut für Organische Chemie der Universität, Am Hubland, D-97074 Würzburg, Germany.
Fax: (internat.) + 49-(0)931/888-4755
E-mail: bringman@chemie.uni-wuerzburg.de

 © WILEY-VCH Verlag GmbH, D-69451 Weinheim, 1999 1434–1948/99/1010–1745 $ 17.50+.50/0

By using a similar but chiral, enantiomerically pure complex it should be possible to achieve a diastereoselective ring cleavage of the thionolactone. The coordinatively unsaturated complex fragment [CpRu{(*S*,*S*)-CHIRAPHOS}]$^+$ [(*S*,*S*)-CHIRAPHOS = (2*S*,3*S*)-bis(diphenylphosphanyl)-butane] appeared to be a promising candidate.[10] This chiral auxiliary has previously been employed by us, and with considerable success, in the diastereoselective oxidation of coordinated thioethers.[11–14]

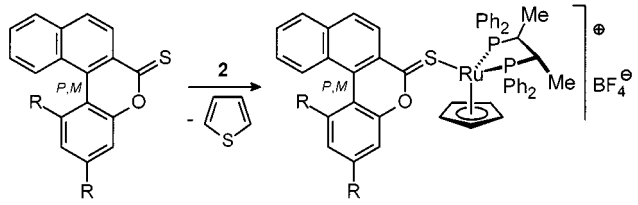
Results

The synthesis of thionolactone complexes by ligand exchange requires a reactive starting material.[9] Thus, [CpRu{(*S*,*S*)CHIRAPHOS}Cl] (**1**) was treated with silver tetrafluoroborate in the presence of thiophene to give the enantiomerically pure thiophene complex **2** in almost quantitative yield (Equation 1).



1 **2** (95%) (1)

Compound **2** is a yellow, crystalline, air-sensitive material. Its ^{1}H-NMR spectrum exhibits, *inter alia*, the typical AA′XX′ pattern at δ = 5.81 and 6.83 indicating the presence of a thiophene ligand. The reaction of **2** with the thionolactones **3a**–**f** at room temperature was accompanied by an immediate color change from yellow to dark purple. The pure thionolactone complexes were readily purified by chromatography and isolated in almost quantitative yields as deep purple crystalline solids (Equation 2).



3a - f **4a - f** (91 - 96%) (2)

R	H	OMe	Me	Et	*i*-Pr	*t*-Bu
	a	**b**	**c**	**d**	**e**	**f**
de (%)		10[a]	10	14	20	6

[a] at 210 K

The ^{31}P-NMR spectra of **4a**–**f** reveal a dynamic process whose rate depends on the size of the substituent R. The limiting cases are marked by **4a** (R = H), which even at 210 K exists as a mixture of rapidly equilibrating diastereoisomers, and **4c**–**f** (R = Me, Et, *i*Pr, *t*Bu), which up to 380 K exhibit two separate sets of signals for the two diastereoisomers. With the exception of R = *t*Bu, the diastereomeric ratio increases slightly with the size of R. Compound **4b** (R = OMe) shows two sets of signals at 210 K in a 55:45 ratio (10% *ee*) which coalesce at 263 K. A standard lineshape analysis yielded an activation barrier for this process of $\Delta G^{\neq}$ = 48 kJ mol^{-1}. ^{1}H-NMR spectra of samples of **4c** and **4d**, if recorded immediately after dissolution at 253 K, gave distinctly higher diastereomeric ratios. This indicates that, for those two compounds, the epimerization of the biaryl axis has a half-life at this temperature in the range of a few minutes. In the ^{13}C-NMR spectra at 295 K the thiocarbonyl function gives rise to one (**4a, b**) or two (**4c**–**e**) signals at δ = 200, which are split into doublets of doublets due to coupling with the nonequivalent phosphorus nuclei. A single crystal of **4c** was subjected to an X-ray structure determination. Figure 1 shows a view of the cation.

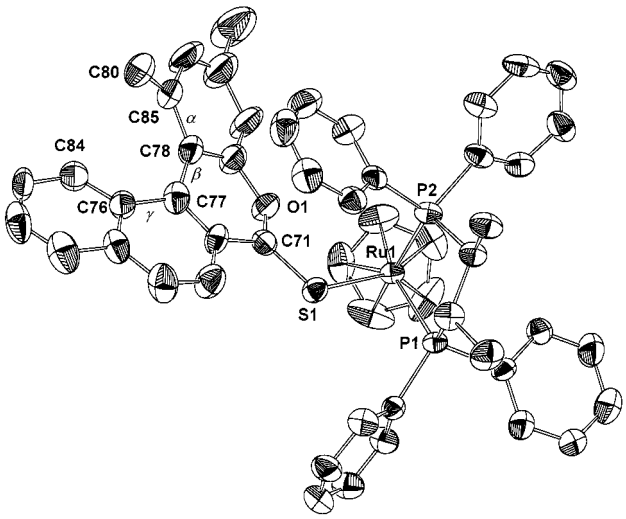
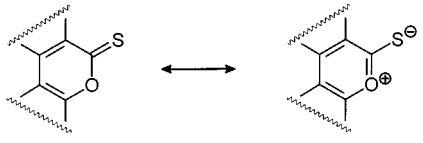


Figure 1. Structure of the Cation of [CpRu{(*S*,*S*)-CHIRAPHOS}($SC_{19}H_{14}O$)]BF_4 (**4c**) (hydrogen atoms omitted); selected bond lengths (pm) and angles (deg): Ru(1)–P(1) 227.8(2), Ru(1)–P(2) 231.2(2), Ru(1)–S(1) 233.1(2), C(71)–S(1) 165.5(8), C(71)–O(1) 134.3(10); P(1)–Ru(1)–P(2) 83.40(7), P(1)–Ru(1)–S(1) 85.42(7), P(2)–Ru(1)–S(1) 89.09(8), C(71)–S(1)–Ru(1) 114.0(3), C(71)–S(1)–Ru(1)–P(1) 169.3(5), C(71)–S(1)–Ru(1)–P(2) 86.0(5), C(80)–C(85)–C(78)–C(77) 15.2(25), C(85)–C(78)–C(77)–C(76) 27.3(23), C(78)–C(77)–C(76)–C(84) 20.0(20)

The coordination geometry around the ruthenium atom is adequately described as octahedral, in which the C_5H_5 ligand occupies three adjacent sites. All bond lengths to ruthenium are similar those in the closely related thioaldehyde complex [CpRu(dppe)(η^1-S=CHC_6H_4OMe)]PF_6.[15] The two angles S–Ru–P(1) and S–Ru–P(2) are markedly different as a result of the fixed configuration of the five-membered Ru{(*S*,*S*)-CHIRAPHOS} chelate ring. The bonding within the thionolactone ring can be described in terms of two canonical forms **A** and **B** (Scheme 2).



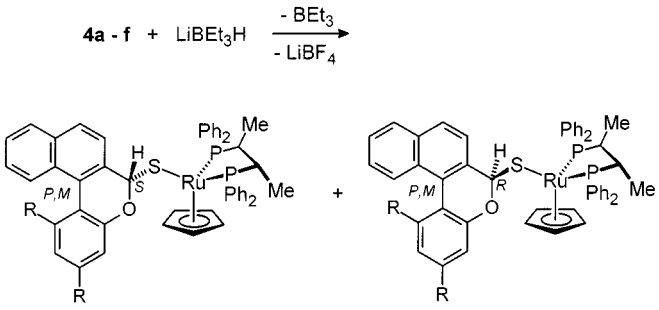
A **B**

Scheme 2. Resonance forms of the thionolactone ring

The coordination of a cationic metal complex at sulfur is expected to increase the contribution of the benzenoid resonance form **B** by dissipating the negative charge. Indeed, the C=S bond in the complex is 2 pm longer than in the uncoordinated thionolactone **3c**,[9] while the C(71)−O bond within the lactone ring of the complex is shorter by 1.6 pm. The two aryl moieties are helically twisted; of the two possible forms, only the *P* diastereoisomer is found in the crystal (see Figure 1). This helical distortion is a result of the steric repulsion between the *ortho* methyl group and the hydrogen atom in the 8-position of the naphthyl part. As seen in other cases,[16] the sum of the dihedral angles α [C(80)−C(85)−C(78)−C(77)], β [C(85)−C(78)−C(77)−C(76)], and γ [C(78)−C(77)−C(76)−C(84)] (Figure 1) can serve as a measure of this distortion. At 62.5°, this sum is only marginally different from the corresponding value for uncoordinated **3c** (63.6°).[9] The individual contributions to this sum, however, differ markedly; β in particular is distinctly smaller in the complex **4c** (27.3°) than in uncoordinated **3c** (33.4°). This flattening of the lactone ring, which has been observed previously for complexes of the analogous oxolactones,[8] hints at some degree of "aromatization" as expressed by the resonance form **B** (Scheme 2). The orientation of the biaryl-thionolactone ligand within the complex is another conspicuous feature of the structure of **4c**. The C=S group and the Ru−P(1) bond are nearly in the same plane, while the Ru−P(2) bond is almost perpendicular to that plane (Figure 1). As a result, one diastereomorphous half space around the thionolactone function is shielded by one of the phenyl groups of the (*S*,*S*)-CHIRAPHOS ligand, while the other half space remains exposed.

Treatment of the thionolactone complexes **4a**−**f** with $LiBEt_3H$ in THF at −70°C followed by slowly warming to 20°C was accompanied by a color change to yellow. Workup by extraction with benzene and freeze-drying gave the yellow, crystalline, slightly air-sensitive thiolactolate complexes **5a**−**f** in very good yields (Equation 3).

The room-temperature NMR spectra of these compounds indicate the presence of two (**5a**, **b**) or four (**5c**−**f**) diastereoisomers. The ^{31}P-NMR spectrum of **5b** consists of two broad signals which, upon cooling to 270 K, decoalesce into two AX spin systems due to a slowed inversion of the biaryl axis. The activation barrier could not be determined precisely but seems to be somewhat higher than that of the helimerization of **4b**. In the ^{13}C-NMR spectra the thioacetal carbon gives rise to a resonance at $\delta = 90$ with a 5 Hz coupling to only one of the phosphorus nuclei. This hints at an unsymmetrical arrangement of the thiolactolate ligand in the coordination sphere of the ruthenium atom, with one dihedral angle C−S−Ru−P close to 90° and the other close to 180°. Interestingly, for the two opposing helimers of the major diastereoisomer, the signals in the ^{1}H-NMR spectrum of the HC(S)O group are separated by up to 1.58 ppm. An inspection of the molecular structure of **5a** (see below) suggests that this may be due to differing anisotropy effects of one of the phenyl groups of the CHIRAPHOS ligand.



R		(*S*,*P*)	(*S*,*M*)	[(*R*,*P*) + (*R*,*M*)] (%)
H	**a**	93		7
OMe	**b**	65	28[a]	7
Me	**c**	52	38	< 10
Et	**d**	53	37	< 10
i-Pr	**e**	55	35	< 10
t-Bu	**f**	45	45	< 10

[a] at 220 K

(3)

An X-ray structure determination was carried out on a crystal of the major diastereoisomer of **5a**, Figure 2 shows a view of the molecule.

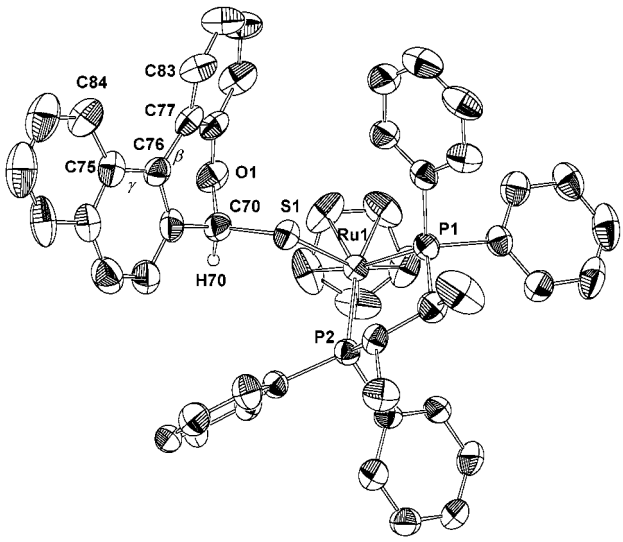


Figure 2. Structure of the Cation of [CpRu{(*S*,*S*)-CHIRAPHOS}($SC_{17}H_{11}O$)] (**5a**) [hydrogen atoms omitted, except for H(70)]; selected bond lengths (pm) and angles (deg): Ru(1)−P(1) 227.0(2), Ru(1)−P(2) 225.7(2), Ru(1)−S(1) 242.2(2), C(70)−S(1) 180.2(7), C(70)−O(1) 144.2(9); P(1)−Ru(1)−P(2) 84.41(7), P(1)−Ru(1)−S(1) 88.37(6), P(2)−Ru(1)−S(1) 81.78(6), C(70)−S(1)−Ru(1) 109.1(3), C(70)−S(1)−Ru(1)−P(1) 167.8(3), C(70)−S(1)−Ru(1)−P(2) 72.4(3). C(83)−C(77)−C(76)−C(75) 26.5(10), C(77)−C(76)−C(75)−C(84) 10.9(10)

The [CpRu{(*S*,*S*)-CHIRAPHOS}] part is almost identical to that of **4c** with the exception of the orientation of one phenyl group of the chiral chelate ligand. The hydride addition has led to an increase of the Ru−S and C−S bond lengths by 9 and 15 pm, respectively. Also, the C−O bond within the former lactone ring is longer by 10 pm. The configuration at the newly formed stereocenter is *S* while the biaryl axis of the crystalline compond has a fixed *P* configuration. The dihedral angles within the biaryl system

(β = 26.5°, γ = 10.9°) still indicate a sizable distortion. These values should, however, not be compared to those of **4c** where the interaction of the *ortho* methyl substituent at the phenyl group greatly contributes to the extent of the helical distortion.[16][17] In order to prove the identity of the single crystal as the bulk material of **5a** unambiguously, a powder diffraction diagram was recorded and compared with the pattern calculated from the single crystal data, which resulted in a perfect match (Figure 3).

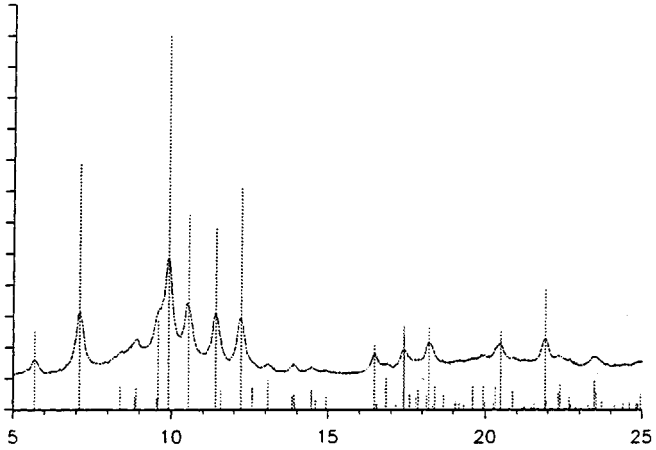
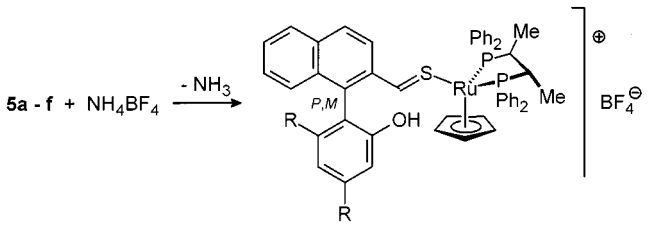


Figure 3. [CpRu{(*S*,*S*)-CHIRAPHOS}($SC_{17}H_{11}O$)] (**5a**), comparison of measured powder diffraction diagram (trace) and calculated diffraction pattern (bars)

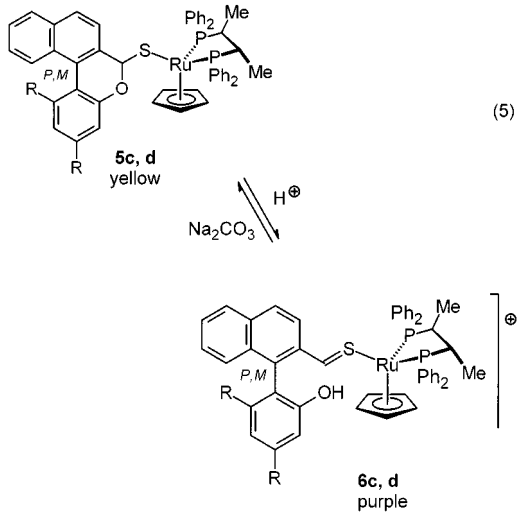
When exposed to traces of moisture or acid, solutions of the thiolactolate complexes **5a**−**f** occasionally turned deep purple, which is the characteristic color of thioaldehyde complexes.[15] Indeed, treatment of **5a**−**f** (as diastereomeric mixtures, Equation 3) with an excess of NH_4BF_4 in acetone (Equation 4) resulted in a quantitative transformation (as judged by NMR spectroscopy) into the corresponding thioaldehyde complexes **6a**−**f**.



6a - f (62 - 75%) (4)

R	H	OMe	Me	Et	*i*-Pr	*t*-Bu
	a	**b**	**c**	**d**	**e**	**f**
de (%)	5	8	12	12	23	0

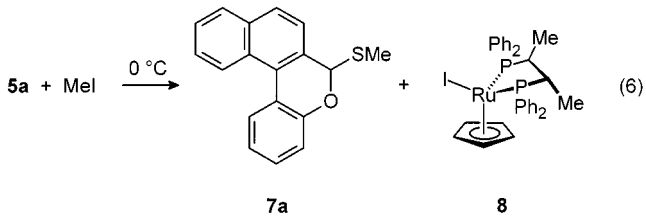
While **6a** was stable only in the presence of NH_4BF_4, the substituted derivatives could be isolated in good yields as deep purple crystalline solids. A similar opening of the thiolactolate could be achieved with various Lewis acids. Thus, when $LiBF_4$ was added to a solution of **5b** in acetone and the solvent removed under reduced pressure, a color change from yellow to purple was observed. According to the ^1H and ^{13}C-NMR spectra complete conversion into the thioaldehyde complex **6b** had taken place with 4% *de.* A similar result was obtained upon treatment of a solution of **5a** in THF with [$ZrCl_4(THF)_2$]. The red reaction mixture was worked up by addition of NH_4BF_4 in acetone and chromatography over silica and yielded **6a** with 20% *de.* Protonation and ring opening are reversible: Stirring suspensions of **6c** or **6d** and sodium carbonate in benzene produced clear yellow solutions, from which **5c** and **5d**, respectively, were isolated in reasonable yields (Equation 5).



(5)

As expected, **6a**−**f** were formed as mixtures of diastereoisomers in these reactions. The diastereomeric excess depends somewhat on the conditions used and increases slightly with increasing size of R; again R = *t*Bu (**6f**) is a conspicuous exception. The presence of a thioaldehyde functionality is unambiguously deduced from the characteristic low field signals in the ^1H (d = 9.7−10.3) and ^{13}C NMR (d = 210−217) spectra. The carbon resonance is split into an apparent triplet caused by roughly equal couplings to the two nonequivalent phosphorus nuclei.

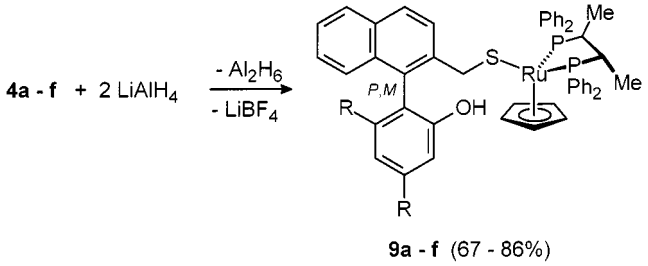
In an attempt to detach the thiolactolate ligand from the metal, **5a** was treated with methyl iodide at 0°C (Equation 6).



(6)

Within a few days complete conversion into the free monothioacetal **7a** and the known iodo complex **8**[12] took place. Chromatographic separation yielded **7a** as an impure yellow oil, which was identified spectroscopically. Full re-

duction of the thionolactone complexes **4a**−**f** was achieved with an excess of $LiAlH_4$ (Equation 7).



9a - f (67 - 86%)

R	H	OMe	Me	Et	*i*-Pr	*t*-Bu
	a	**b**	**c**	**d**	**e**	**f**
de (%)	52	8	74	33	33	6

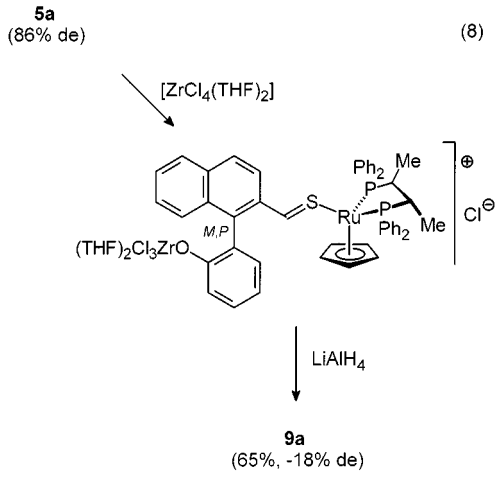
(7)

The highest diastereoselectivities were obtained by combining the reagents at −70°C, keeping the mixtures for 8 h at this temperature, and then allowing them to slowly warm to 20°C. Workup by chromatography over silica gel gave good yields of the yellow crystalline thiolate complexes **9a**−**f**. Their ^{13}C-NMR spectra show a signal at $\delta = 40$ for the benzylic carbon atom, which is split due to coupling with two nonequivalent phosphorus nuclei. The absolute values of the two coupling constants differ considerably, one of them being smaller than 1 Hz in some instances. This again hints at an unsymmetric orientation of the thiolate ligand in the coordination sphere of the ruthenium atom. The chemical shift difference of the diastereotopic benzylic protons is another noteworthy feature. It is consistently small (0.08−0.48 ppm) for the major diastereoisomer and large (0.93−1.46 ppm) for the minor one. Since chemical shift differences in these systems are mainly caused by anisotropy effects of the various aryl groups, we are confident that all major and minor isomers have the same configuration of the biaryl axis.

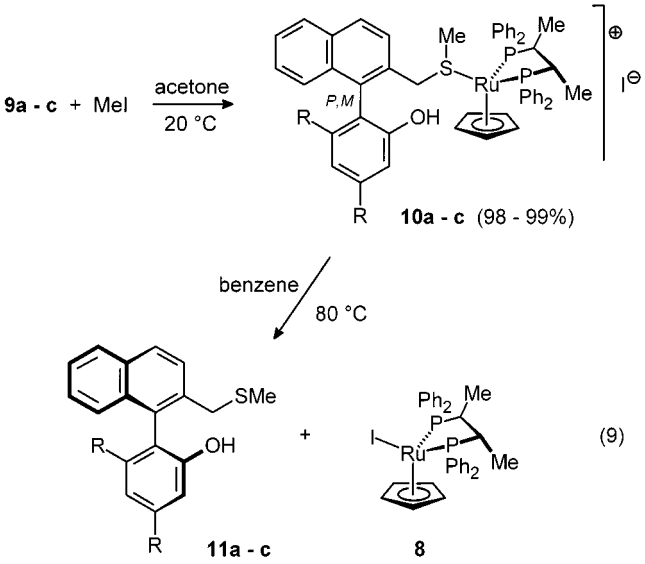
Some experiments aimed at finding ways to influence the diastereoselectivity of the ring-opening reaction were carried out. Thus, reduction of a sample of the thiolactolate **5c** (20% de) at −70°C with $LiAlH_4$ in THF gave the ring-opened thiolate complex **9c** in 61% yield and only 10% *de*. Under the same conditions, $LiBEt_3H$ was much more efficient producing **9c** in 80% yield and 50% *de*. In a similar experiment, a sample of **5a** with 86% *de* was treated at −70°C in THF with $[ZrCl_4(THF)_2]$ whereupon its color changed to red. It was kept at this temperature for 8 h to ensure complete ring opening to the thioaldehyde intermediate, and then $LiAlH_4$ was added (Equation 8).

This time, the thiolate complex **9a** was obtained with 65% yield and 18% *de* but with *opposite diastereoselectivity*, i. e. the minor diastereoisomer of Equation 7 was now the major one (hence the minus sign in Equation 8).

The demetalation of the thiolate complexes was achieved in two steps. Alkylation of **9a**−**c** with methyl iodide gave the thioether complexes **10a**−**c** in quantitative yields as light-yellow crystalline materials. The ionic nature of the



products is apparent from their insolubility in less polar media. The newly introduced methyl group gives resonances in the ^{1}H and ^{13}C-NMR spectra at $\delta = 1$ and 25, respectively. When the salts **10a**−**c** were heated in benzene a smooth ligand substitution took place, giving the iodo complex **8** and the liberated thioethers **11a**−**c** (Equation 9).



(9)

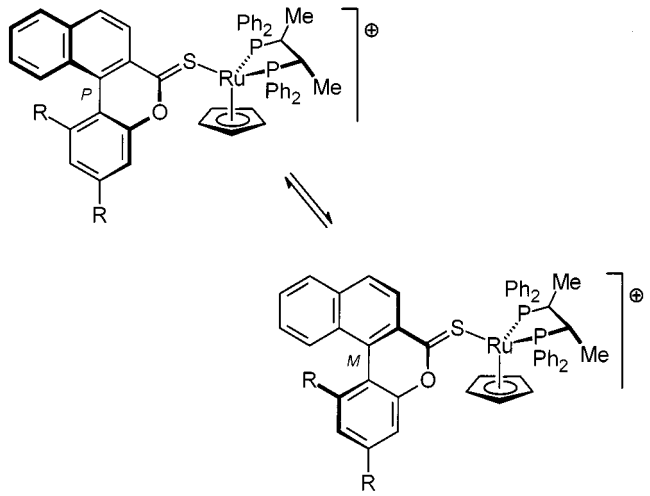
R	H	OMe	Me
	a	**b**	**c**
ee (%)	50 (*P*)	8 (*M*)	74 (*P*)

The latter were isolated after chromatography as slightly yellow oils and their enantiomeric purity checked by HPLC on a chiral phase.[18] The enantiomeric ratios of **11a**−**c** thus obtained were identical to the diastereomeric ratios of the starting complexes **9a**−**c** (Note that the change of the stereochemical descriptor for **11b** is due only to formal reasons, because of the higher priority of the MeO substituent). Finally, a comparison of the CD spectrum of **11c** with that of authentic (*M*)−**11c**[18] showed that the reaction sequence described here had yielded the *P* enantiomer.

Discussion

The work described here is part of an ongoing effort to use chiral transition metal complexes as auxiliaries for various types of enantioselective organic transformations.[19−22] Previously we have shown that double hydride addition to achiral ruthenium complexes of thionolactones leads to a smooth ring-opening reaction.[9] It was expected, therefore, that with the use of similar, but chirally modified, metal templates an atropo-diastereoselective opening of the thionolactone ring could be achieved. The required chiral thionolactone complexes **4a**−**f** are readily accessible by a ligand exchange reaction starting with the highly labile thiophene complex **2,** which in turn was obtained in excellent yield in close analogy to known syntheses.[9][23]

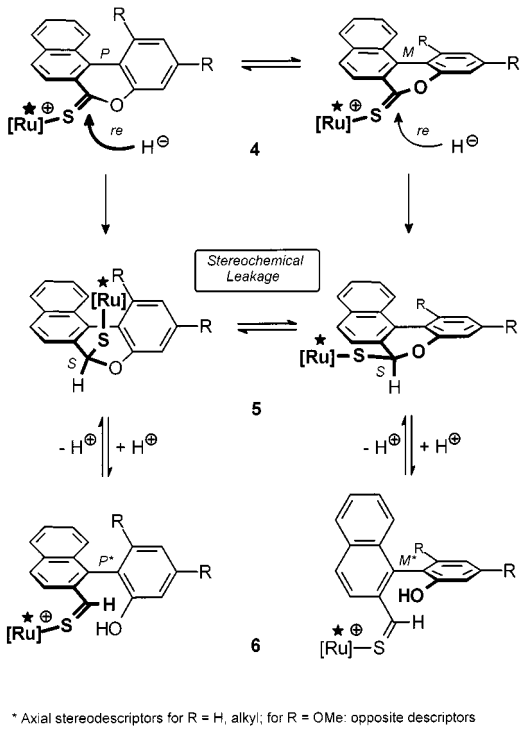
The structure determination of **4c** revealed some interesting aspects. First of all, the compound crystallized as a single diastereoisomer with *P* configuration at the biaryl axis, whereas in solution both diastereoisomers are of almost equal energy. In the solid state, the lactone carbon atom is perfectly shielded from the *si* side by one of the phenyl groups of the (*S*,*S*)-CHIRAPHOS ligand (Figure 1). It is thus tempting to hope that nucleophiles will add from the *re* side with high diastereoselectivity. This, however, is perhaps a too simplistic view. In solution, a dynamic equilibrium between both diastereoisomers [(*S*,*S*,*P*) and (*S*,*S*,*M*)] exists (Scheme 3), whose interconversion rate depends strongly on the size of R.



Scheme 3. Helimerization of the biaryl axis of thionolactone complexes **4a**−**e**

The limiting cases are marked by an immeasurably rapid equilibration, even at low temperature, for R = H (**4a**), and a slow interconversion in the range of several minutes for R = Me, Et, *i*Pr, *t*Bu (**4c**−**f**). This helimerization process is fundamental to an understanding of the stereoselectivity of the hydride addition, which depends on the relative rates of *re* versus *si* attack on both diastereoisomers, as well as the rate of their interconversion. An important clue to the solution structures of the thionolactone complexes comes from the observation of two fairly different ^3J(P,C) couplings of the C=S group for each of the diastereoisomers of **4b**−**f**. This indicates that the two dihedral angles C−S−Ru−P also remain unequal in solution. Furthermore, the (*S*,*S*,*M*) diastereoisomer must have a similar structure with a near coplanar arrangement of C(71), S(1), Ru(1), and P(1). This can be deduced unequivocally from the fact that, in the room temperature NMR spectra of **4a** and **4b**, the ^{13}C signal of the thionolactone group still appears as a doublet of doublets with two unequal couplings. If the inversion of the biaryl axis were accompanied by a rotation of the Ru−S bond such as to expose the *si* side for nucleophilic attack, the couplings ^3J(P,C) of the two diastereoisomers should average out and make the signal at δ = 200 appear as a triplet. The conclusion, therefore, is that for both diastereoisomers of the thionolactone complexes **4a**−**f**, *re* addition is strongly favoured over *si* addition (Equation 3). Molecular models, however, seem to indicate that the (*S*,*S*,*M*) diastereoisomers are, for steric reasons, less accessible and therefore less prone to react with any nucleophiles.

The structure determination of **5a** shows that, as expected, the (*S*,*S*,*S*) diastereoisomer is the major product. From an inspection of Figure 2 we can also see that a *P* configuration of the biaryl axis necessarily implies an axial positioning of the S−Ru unit and an equatorial one of the H substituent at the six-membered thiolactolate ring. It is unlikely that a minor change of the remote substituents R would invert the direction of the hydride addition (see above). Thus it is safe to assume that the major diastereoisomer of **5b** has the (*S*,*S*,*S*) configuration as well. For this compound the helimerization can be slowed down sufficiently to observe separate NMR signals for the (*S*,*S*,*S*,*P*) and (*S*,*S*,*S*,*M*) helimers, which at 253 K are present in a 60: 40 ratio (both helimers of the (*S*,*S*,*R*) diastereoisomer were present in too low a concentration to be assigned with certainty). The *M* helimer has the hydrogen atom in an axial position, which leads to a characteristic[24] high-field shift to δ = 3.72. These results then help to assign the relative (and absolute) configurations of the two major isomers of **5c**−**f** unambiguously. In all cases these are characterized by a large shift difference of the S(O)CH hydrogen atom, which means that the most abundant isomer has this hydrogen atom in an equatorial and the second isomer in an axial position. This implies that the two major isomers must have opposite configurations at the biaryl axis and identical configurations at the tetrahedral carbon atom. Further support for this interpretation is supplied by the stereochemical outcome of the protonation − ring opening reaction (Equation 4). The observed low diastereoselectivity clearly reflects the ratios of the two major isomers of the starting complexes **5a**−**f**. This facile ring opening is driven by the steric strain caused by the *ortho* substituent R, and produces a highly reactive thioaldehyde function which readily takes up a second hydride.[15] On the other hand, by its reversibility under basic conditions (Equation 5), the facile formation of a thioaldehyde intermediate is a serious obstacle in the attempted atropo-enantioselective ring opening reaction since it provides a "stereochemical leakage" (Scheme 4).



Scheme 4. Stereochemical leakage in the hydride addition-ring-opening sequence

As already explained for the oxo analogs[2,5,24,25] the thioaldehyde complexes *P*-**6** can cyclize back to the thiolactolate complexes *S*,*P*-**5**, equilibrate to *S*,*M*-**5**, and then burst open out of both helimeric forms of **5** to eventually give *P*- and *M*-**6**. In favourable cases, this leakage may be overcome as shown by the rapid reaction of **4c** with $LiAlH_4$, which produces **9c** with 74% *de* (Equation 7). A variation of the hydride reagent or a masking of the phenolic oxygen by addition of a strong Lewis acid (Equation 8) does indeed change the stereochemical outcome of the reduction. However, this did as yet not lead to a significant improvement, since the two configurations of the biaryl axis are already present in roughly equal amounts in the intermediates **5a**−**f**.

Conclusions

The work presented here demonstrates that transition metal complexes can be used successfully as chiral auxiliaries in the atropo-diastereoselective ring opening of configurationally unstable biaryllactones. A distinct advantage of the use of stable complexes is the possibility to isolate and structurally characterize important intermediates and thus gain detailed information on their stereochemical properties. The stereochemical leakage, however, provided by the facile helimerization and ring-opening of the thiolactolate intermediates, is still a major obstacle. Nevertheless, a further development of this strategy should be possible by combining the hydride reagent with a bulky, less reactive Lewis acid capable of discriminating between the (*S*,*S*,*S*,*P*) and (*S*,*S*,*S*,*M*) diastereoisomers of the thiolactolate intermediates **5**.

Experimental Section

All experiments were carried out in Schlenk tubes under an atmosphere of nitrogen in suitably purified solvents. Water was distilled under nitrogen immediately before use. − IR: Perkin−Elmer 283, Bruker IFS 25. − ^{1}H NMR: Bruker AMX 400, δ values relative to TMS. − ^{13}C NMR: Bruker AMX 400, δ values relative to TMS. Assignments were routinely checked by DEPT. In some cases the signals in the ^{13}C-NMR spectra for quaternary carbon atoms were too weak to be detected. − ^{31}P NMR: Bruker AMX 400, δ values relative to 85% H_3PO_4. The signals in the ^{1}H- and ^{13}C-NMR spectra of the (*S*,*S*)-CHIRAPHOS ligand are very similar for all compounds and have therefore been omitted from the lists of spectral data. − Elemental analyses: Analytical Laboratory of the Institut für Anorganische Chemie. The following starting materials were obtained as described in the literature: [CpRu{(*S*,*S*)-CHIRAPHOS}Cl] (**1**),[26] thionolactones **3a**−**f**,[9][17] $[ZrCl_4(THF)_2]$.[27] All other reagents were used as purchased.

[CpRu{(*S*,*S*)-CHIRAPHOS}(SC_4H_4)]BF_4 (2): To a solution of **1** (0.40 g, 0.64 mmol) and thiophene (0.50 g, 5.95 mmol) in dichloromethane (50 mL) was added $AgBF_4$ (0.125 g, 0.64 mmol) 0°C and the resulting mixture stirred vigorously for 30 min. The solution was then filtered over Celite, the filtrate evaporated to 2 mL, and the product precipitated by adding diethyl ether. The product thus obtained may still contain traces of silver salts but is usually pure enough for further reactions. An analytical sample was obtained by recrystallization from dichloromethane/ether. Yield 0.29 g (95%), yellow crystalline powder, m.p. 60°C (dec). − ^{1}H NMR (400 MHz, CD_2Cl_2, 20°C): δ = 4.24 (s, 5 H, C_5H_5), 5.81, 6.83 (AA′XX′-system, N = 6.1 Hz, 4 H, SC_4H_4). − ^{31}P NMR (162 MHz, CD_2Cl_2, 20°C): δ = 69.8 [d, ^2J(P,P) = 41 Hz], 81.3 [d, ^2J(P,P) = 41 Hz]. − $C_{37}H_{37}BF_4P_2RuS$ (763.6) calcd C 58.20, H 4.88; found C 57.99, H 5.16.

Synthesis of the Thionolactone Complexes 4a−f: To a solution of **2** (0.15 g, 0.20 mmol) in dichloromethane (8 mL) was added the appropriate thionolactone (0.20 mmol). The color immediately changed to deep purple. The mixture was stirred for 12 h, then evaporated to 2 mL and the product precipitated by adding diethyl ether and pentane. Further purification by chromatography over a short (10 cm) silica column with dichloromethane as an eluent, followed by crystallization from dichloromethane/pentane gave deep purple crystalline powders.

4a: Yield 179 mg (95%), m.p. 176°C (dec). − ^{1}H NMR (400 MHz, $CDCl_3$, 20°C): δ = 4.73 (s, 5 H, C_5H_5). − ^{13}C NMR (100 MHz, $CDCl_3$, 20°C): δ = 84.0 (s, C_5H_5), 199.4 [dd, ^3J(P,C) = 8 Hz, ^3J(P,C) = 5 Hz, C=S] − ^{31}P NMR (162 MHz, $CDCl_3$, 20°C): δ = 69.7 [d, ^2J(P,P) = 38 Hz], 84.1 [d, ^2J(P,P) = 38 Hz]. − $C_{50}H_{43}BF_4OP_2RuS$ (941.8) calcd. C 63.77, H 4.60; found C 62.93, H 5.02.

4b: Yield 188 mg (94%), m.p. 189°C (dec). − ^{1}H NMR (400 MHz, $CDCl_3$, 20°C): δ = 3.77 (s, 3 H, OCH_3), 3.89 (s, 3 H, OCH_3), 4.70 (s, 5 H, C_5H_5). − ^{13}C NMR (100 MHz, $CDCl_3$, 20°C): δ = 55.5 (s, OCH_3), 56.4 (s, OCH_3), 84.1 (s, C_5H_5), 199.2 [dd, ^3J(P,C) = 8 Hz, ^3J(P,C) = 5 Hz, C=S]. − ^{31}P NMR (162 MHz, $CDCl_3$, 20°C): δ = 69.6 [d, ^2J(P,P) = 37 Hz], 84.2 [d, ^2J(P,P) = 37 Hz]. − ^{31}P NMR (162 MHz, $CDCl_3$, −60°C): δ = 65.5 [d, ^2J(P,P) = 37 Hz], 69.1 [d, ^2J(P,P) = 37 Hz], 83.9 [d, ^2J(P,P) = 37 Hz], 84.2 [d, ^2J(P,P) = 37 Hz]. − $C_{52}H_{47}BF_4O_3P_2RuS$ (1001.8) calcd. C 62.34, H 4.73; found C 62.29, H 4.63.

4c: Yield 186 mg (96%), m.p. 186°C (dec). − ^{1}H NMR (400 MHz, $CDCl_3$, 20°C) (both diastereoisomers): δ = 2.08 (s, 6 H, CH_3), 2.43 (s, 3 H, CH_3), 2.47 (s, 3 H, CH_3), 4.72 (s, 5 H, C_5H_5), 4.73 (s, 5 H, C_5H_5). − ^{13}C NMR (100 MHz, $CDCl_3$, 20°C) (both diastereoisomers): δ = 21.3 (s, CH_3), 21.4 (s, CH_3), 23.4 (s, CH_3), 23.5 (s, CH_3), 84.0 [t, ^2J(P,C) = 2 Hz, C_5H_5], 198.3 [dd, ^3J(P,C) = 8 Hz, ^3J(P,C) = 5 Hz, C=S], 199.5 [dd, ^3J(P,C) = 9 Hz, ^3J(P,C) = 5 Hz, C=S]. − ^{31}P NMR (162 MHz, $CDCl_3$, 20°C) (both diastereoisomers): δ = 69.6 [d, ^2J(P,P) = 37 Hz], 71.5 [d, ^2J(P,P) = 38 Hz], 83.9 [d, ^2J(P,P) = 38 Hz], 84.0 [d, ^2J(P,P) = 37 Hz]. − $C_{52}H_{47}BF_4OP_2RuS$ (1001.8) calcd. C 64.40, H 4.88; found C 64.17, H 5.02.

4d: Yield 184 mg (92%), m.p. 141°C (dec). − ^{1}H NMR (400 MHz, $CDCl_3$, 20°C) (both diastereoisomers): δ = 1.36 [t, ^3J(H,H) = 7.6 Hz, 2 × 3 H, CH_3], 1.37 [t, ^3J(H,H) = 7.6 Hz, 2 × 3 H, CH_3], 2.53 −2.37 (m, 4 H, CH_2), 2.79 [q, ^3J(H,H) = 7.5 Hz, 2 H, CH_2], 2.83 [q, ^3J(H,H) = 7.7 Hz, 2 H, CH_2], 4.75 (s, 5 H, C_5H_5), 4.77 (s, 5 H, C_5H_5). − ^{13}C NMR (100 MHz, $CDCl_3$, 20°C (both diastereoisomers): δ = 14.9 (s, CH_3), 15.0 (s, CH_3), 28.60 (s, CH_2), 28.66 (s, CH_2), 28.70 (s, CH_2), 28.73 (s, CH_2), 84.0 (s, C_5H_5), 84.1 (s, C_5H_5), 198.4 (br, C=S), 199.5 [dd, ^3J(P,C) = 9 Hz, ^3J(P,C) = 5 Hz, C=S]. − ^{31}P NMR (161 MHz, $CDCl_3$, 20°C (both diastereoisomers): δ = 69.4 [d, ^3J(P,P) = 37 Hz]. 71.7 [d, ^3J(P,P) = 38 Hz], 83.8 [d, ^3J(P,P) = 38 Hz], 84.2 [d, ^3J(P,P) = 38 Hz]. − $C_{54}H_{51}BF_4OP_2RuS$ (997.9) calcd. C 64.92, H 5.15, S 3.20; found C 64.06, H 5.17, S 3.34.

4e: Yield 187 mg (91%), m.p. 163°C (dec). − ^{1}H NMR (400 MHz, $CDCl_3$, 20°C) (both diastereoisomers): δ = 0.60 [d, ^3J(H,H) = 6.7 Hz, 2 × 3 H, CH_3], 0.84 [d, ^3J(H,H) = 6.7 Hz, 2 × 3 H, CH_3], 1.37 [d, ^3J(H,H) = 6.7 Hz, 3 H, CH_3], 1.39 [d, ^3J(H,H) = 6.7 Hz, 3 H, CH_3], 1.50 [d, ^3J(H,H) = 6.7 Hz, 3 H, CH_3], 1.51 [d, ^3J(H,H) = 6.7 Hz, 3 H, CH_3], 3.03 [sep, ^3J(H,H) = 6.7 Hz, 2 H, CH], 3.11 [sep, ^3J(H,H) = 6.7 Hz, 2 H, CH], 4.72 (s, 5 H, C_5H_5), 4.76 (s, 5 H, C_5H_5). − ^{13}C NMR (100 MHz, $CDCl_3$, 20°C) (both diastereoisomers): δ = 20.6 (s, CH_3), 23.4 (s, CH_2), 23.7 (s, CH_2), 23.7 (s, CH_2), 23.8 (s, CH_2), 27.7 (s, CH_3), 27.7 (s, CH_3), 84.1 (s, C_5H_5), 84.2 (s, C_5H_5), 198.3 [dd, ^3J(P,C) = 8 Hz, ^3J(P,C) = 5 Hz, C=S], 199.4 [dd, ^3J(P,C) = 9 Hz, ^3J(P,C) = 5 Hz, C=S]. − ^{31}P NMR (161 MHz, $CDCl_3$, 20°C) (both diastereoisomers): δ = 69.1 [d, ^3J(P,P) = 38 Hz], 71.7 [d, ^3J(P,P) = 38 Hz], 83.8 [d, ^3J(P,P) = 38 Hz], 84.2 [d, ^3J(P,P) = 37 Hz]. − $C_{56}H_{55}BF_4OP_2RuS$ (1025.9) calcd. C 65.48, H 5.14, S 3.12; found C 64.39, H 5.23, S 2.99.

4f: Yield 203 mg (96%), m.p. 90°C (dec). − ^{1}H NMR (400 MHz, $CDCl_3$, 20°C) (both diastereoisomers): δ = 0.96 (s, 9 H, CH_3), 0.97 (s, 9 H, CH_3), 1.44 (s, 9 H, CH_3), 1.46 (s, 9 H, CH_3), 4.68 (s, 5 H, C_5H_5), 4.74 (s, 5 H, C_5H_5). − ^{13}C NMR (100 MHz, $CDCl_3$, 20°C): δ = 31.1 (s, CH_3), 31.2 (s, CH_3), 32.78 (s, CH_3), 32.81 (s, CH_3), 35.0 [s, C(*t*Bu)], 35.1 [s, C(*t*Bu)], 39.56 [s, C(*t*Bu)], 39.6 [s, C(*t*Bu)], 84.1 (s, C_5H_5), 84.3 (s, C_5H_5), 198.5 [dd, ^3J(P,C) = 8 Hz, ^3J(P,C) = 5 Hz, C=S], 199.5 [dd, ^3J(P,C) = 9 Hz, ^3J(P,C) = 4 Hz, C=S]. − ^{31}P NMR (161 MHz, $CDCl_3$, 20°C): δ = 69.1 [d, ^3J(P,P) = 38 Hz], 71.3 [d, ^3J(P,P) = 38 Hz], 83.8 [d, ^3J(P,P) = 38 Hz], 84.2 [d, ^3J(P,P) = 38 Hz]. − $C_{58}H_{59}BF_4OP_2RuS$ (1054.0) calcd. C 66.02, H 5.64, S 3.03; found C 65.03, H 5.63, S 3.36.

Synthesis of the Thiolactolate Complexes 5a−f: A solution of the lactone complex (0.10 mmol) in THF (10 mL) was treated at −70°C with 0.11 mL of a 1 M solution of $LiBEt_3H$ in the same solvent. Within a few minutes the color of the solution changed from deep purple to brownish-yellow. After allowing the mixture to warm to 20°C the solvent was removed under vacuum and the residue extracted with benzene (8 mL). After filtration over Celite the mixture was evaporated to 2 mL, frozen, and the remaining benzene sublimed off under vacuum. The products were isolated as yellow crystalline powders. Compounds **5d−f** were invariably obtained contaminated with a trace of the corresponding thioaldehyde complex **6d−f**.

5a: Yield 75 mg (88%), m.p. 74°C (dec). − ^{1}H NMR (400 MHz, C_6D_6, 20°C), major diastereoisomer: δ = 4.86 (s, 5 H, C_5H_5), 5.31 [d, 1 H, ^4J(P,H) = 0.8 Hz, S(O)CH]; minor diastereoisomer: δ = 4.71 (s, 5 H, C_5H_5), 6.10 [br, 1 H, S(O)CH]. − ^{13}C NMR (100 MHz, C_6D_6, 20°C), major diastereoisomer: δ = 82.6 (s, C_5H_5), 90.7 [d, ^3J(P,C) = 7 Hz, S(O)CH]; minor diastereoisomer: δ = 83.6 (s, C_5H_5), 92.9 [br, S(O)CH]. − ^{31}P NMR (161 MHz, C_6D_6, 20°C), major diastereoisomer: δ = 77.1 [d, ^3J(P,P) = 32 Hz], 87.7 [d, ^3J(P,P) = 32 Hz]; minor diastereoisomer: δ = 74.8 [d, ^3J(P,P) = 42 Hz], 87.1 [d, ^3J(P,P) = 42 Hz]. − $C_{50}H_{44}OP_2RuS$ (856.0) calcd. C 70.01, H 5.18, S 3.75; found C 69.01, H 5.14, S 3.48.

5b: Yield 79 mg (86%), m.p. 136°C (dec). − ^{1}H NMR (400 MHz, [D_8]toluene, −20°C), major diastereoisomer, both helimers: δ = 3.41 (s, 3 H, OCH_3), 3.28 (s, 3 H, OCH_3), 3.32 (s, 3 H, OCH_3), 3.48 (s, 3 H, OCH_3), 3.72 [s, 1 H, S(O)CH], 4.74 (s, 2 × 5 H, C_5H_5), 5.31 [s, 1 H, S(O)CH]; minor diastereoisomer: δ = 4.62 (s, 5 H, C_5H_5). − ^{13}C NMR (100 MHz, C_6D_6, 20°C), both diastereoisomers: δ = 55.0 (s, OCH_3), 55.3 (s, br, OCH_3), 82.9 (s, br, C_5H_5), 91.3 [s, S(O)CH]. − ^{31}P NMR (162 MHz, [D_8]toluene, −20°C), major diastereoisomer: δ = 72.7 [d, ^3J(P,P) = 34 Hz], 75.5 [d, ^3J(P,P) = 34 Hz], 87.0 [d, ^3J(P,P) = 34 Hz], 87.2 [d, ^3J(P,P) = 34 Hz]. − $C_{52}H_{48}O_3P_2RuS$ (916.0) calcd. C 68.18, H 5.28, S 3.50; gef. C 67.88, H 5.43, S 3.44.

5c: Yield 76 mg (86%), m.p. 68°C (dec). − ^{1}H NMR (400 MHz, C_6D_6, 20°C), major helimer: δ = 2.19 (s, 3 H, CH_3), 2.37 (s, 3 H, CH_3), 4.84 (s, 5 H, C_5H_5), 5.45 [d, 1 H, ^4J(P,H) = 1.2 Hz, S(O)CH]; minor helimer: δ = 2.17 (s, 3 H, CH_3), 2.31 (s, 3 H, CH_3), 3.87 [s, 1 H, S(O)CH], 4.80 (s, 5 H, C_5H_5). − ^{13}C NMR (100 MHz, C_6D_6, 20°C), major helimer: δ = 21.6 (s, CH_3), 23.0 (s, CH_3), 82.4 (s, C_5H_5), 90.6 [d, ^3J(P,C) = 5 Hz, S(O)CH]; minor helimer: δ = 21.5 (s, CH_3), 22.6 (s, CH_3), 83.7 (s, C_5H_5), 94.5 [d, ^3J(P,C) = 6.2 Hz, S(O)CH]. − ^{31}P NMR (162 MHz, C_6D_6, 20°C), major helimer: δ = 75.8 [d, ^3J(P,P) = 34 Hz], 87.5 [d, ^3J(P,P) = 34 Hz]; minor helimer: 74.1 [d, ^3J(P,P) = 37 Hz], 87.2 [d, ^3J(P,P) = 37 Hz]. − $C_{52}H_{48}OP_2RuS$ (884.0) calcd. C 70.65, H 5.47; found C 70.74, H 5.32.

5d: Yield 71 mg (78%), m.p. 91°C (dec). − ^{1}H NMR (400 MHz, C_6D_6, 20°C), both helimers: δ = 1.07 [t, ^3J(H,H) = 7.5 Hz, 2 × 3 H, CH_3], 1.15 [t, ^3J(H,H) = 7.6 Hz, 2 × 3 H, CH_3], 1.32 [t, ^3J(H,H) = 7.6 Hz, 2 × 3 H, CH_3], 2.51 [q, ^3J(H,H) = 7.7 Hz, 4 × 2 H, CH_2], 3.99 [s, 1 H, S(O)CH], 4.82 (s, 5 H, C_5H_5). 4.86 (s, 5 H, C_5H_5), 5.41 [d, ^4J(P,H) = 1.2 Hz, 1 H, S(O)CH]. − ^{13}C NMR (100 MHz, C_6D_6, 20°C), both helimers: δ = 14.3 (s, CH_3), 15.7 (s, CH_3), 15.8 (s, CH_3), 17.1 (s, CH_3), 28.6 (s, CH_2), 29.4 (s, CH_2), 29.4 (s, CH_2), 29.6 (s, CH_2), 82.5 (s, C_5H_5), 83.6 (s, C_5H_5), 94.2 [s, S(O)CH], 94.3 [s, S(O)CH]. − ^{31}P NMR (162 MHz, C_6D_6, 20°C), major helimer: δ = 78.0 [d, ^3J(P,P) = 31 Hz], 87.8 [d, ^3J(P,P) = 32 Hz]; minor helimer: 74.2 [d, ^3J(P,P) = 37 Hz], 86.7 [d, ^3J(P,P) = 37 Hz]. − $C_{54}H_{52}OP_2RuS$ (912.1)calcd. C 71.11, H 5.75, S 3.52; found C 68.91, H 6.42, S 3.42.

5e: Yield 70 mg (74%), m.p. 75°C (dec). − ^{1}H NMR (400 MHz, C_6D_6, 20°C), both helimers: δ = 1.20 [d, ^3J(H,H) = 6.9 Hz, 3 H, CH_3], 1.22 [d, ^3J(H,H) = 7.0 Hz, 3 H, CH_3], 1.30 [d, ^3J(H,H) = 6.9 Hz, 3 H, CH_3], 1.34 [d, ^3J(H,H) = 6.8 Hz, 3 H, CH_3], 1.37 [d, ^3J(H,H) = 6.9 Hz, 3 H, CH_3], 1.44 [d, ^3J(H,H) = 6.9 Hz, 3 H, CH_3], 1.54 [d, ^3J(H,H) = 6.7 Hz, 3 H, CH_3], 1.58 [d, ^3J(H,H) = 6.6 Hz, 3 H, CH_3], 2.79 [q, ^3J(H,H) = 6.8 Hz, 1 H, CH], 3.22 [q, ^3J(H,H) = 6.8 Hz, 1 H, CH], 3.38 [q, ^3J(H,H) = 6.8 Hz, 1 H, CH], 3.58 [q, ^3J(H,H) = 6.8 Hz, 1 H, CH], 4.13 [s, 1 H, S(O)CH], 4.85

(s, 5 H, C_5H_5), 4.88 (s, 5 H, C_5H_5), 5.36 [d, ^4J(P,H) = 1.1 Hz, 1 H, S(O)CH]. − ^{13}C NMR (100 MHz, C_6D_6, 20°C), both helimers: δ = 20.4 (s, CH_3), 24.1 (s, CH_3), 24.3 (s, CH_3), 24.5 (s, CH_3), 31.1 (s, CH), 32.4 (s, CH), 34.6 (s, CH), 34.8 (s, CH), 82.5 (s, C_5H_5), 83.4 (s, C_5H_5). − ^{31}P NMR (162 MHz, C_6D_6, 20°C), major helimer: δ = 79.4 [d, ^3J(P,P) = 31 Hz], 87.9 [d, ^3J(P,P) = 31 Hz]; minor helimer: 73.9 [d, ^3J(P,P) = 38 Hz], 86.3 [d, ^3J(P,P) = 38 Hz]. − $C_{56}H_{56}OP_2RuS$ (940.15) calcd. C 71.54, H 6.00, S 3.41; found C 70.14, H 6.16, S 3.32.

5f: Yield 72 mg (74%), m.p. 110°C (dec). − ^{1}H NMR (400 MHz, C_6D_6, 20°C), both helimers: δ = 1.29 (s, 9 H, CH_3), 1.31 (s, 9 H, CH_3), 1.39 (s, 9 H, CH_3), 1.46 (s, 9 H, CH_3), 4.04 [s, 1 H, S(O)CH], 4.78 (s, 5 H, C_5H_5), 4.80 (s, 5 H, C_5H_5), 5.19 [s, 1 H, S(O)CH]. − ^{13}C NMR (100 MHz, C_6D_6, 20°C): δ = 31.5 (s, CH_3), 31.5 (s, CH_3), 33.1 (s, CH_3), 33.2 (s, CH_3), 34.8 [s, C(*t*Bu)], 38.7 [s, C(*t*Bu)], 39.1 [s, C(*t*Bu)], 82.8 (s, C_5H_5), 83.4 (s, C_5H_5). − ^{31}P NMR (162 MHz, C_6D_6, 20°C): δ = 74.1 [d, ^3J(P,P) = 37 Hz], 78.6 [d, ^3J(P,P) = 32 Hz], 86.2 [d, ^3J(P,P) = 37 Hz], 87.8 [d, ^3J(P,P) = 32 Hz]. − $C_{58}H_{60}OP_2RuS$ (968.20) calcd. C 71.95, H 6.25, S 3.31; found C 69.94, H 6.55, S 3.31.

Synthesis of the Thioaldehyde Complexes 6a−f: To a solution of the lactolate complex (0.10 mmol) in acetone (15 mL) was added an excess of NH_4BF_4, which caused an immediate color change to deep purple. After 1 h the product and the excess of NH_4BF_4 were precipitated by adding pentane. Compounds **6b−f** were purified by chromatography over silica gel with dichloromethane/acetone 10:1 as eluent. Compound **6a** reverted back to **5a** upon chromatography and could be separated only incompletely from the excess ammonium salt. After crystallization from dichloromethane/pentane the products were obtained as deep purple crystalline powders.

6a: Yield 100 mg (ca. 95%), contaminated with NH_4BF_4. − ^{1}H NMR (400 MHz, $CDCl_3$, 20°C), both helimers: δ = 4.48 (s, 5 H, C_5H_5), 4.58 (s, 5 H, C_5H_5), 6.92 (br, 1 H, OH), 9.77 [d, ^4J(P,H) = 1.6 Hz, 1 H, HC=S], 9.96 (br, 1 H, HC=S). − ^{13}C NMR (100 MHz, $CDCl_3$, 20°C), both helimers: δ = 85.7 (s, C_5H_5), 86.0 (s, C_5H_5), 213.3 (br, HC=S), 216.5 [t, ^3J(P,C) = 7 Hz, HC=S]. − ^{31}P NMR (161 MHz, $CDCl_3$, 20°C), both helimers: δ = 76.0 [d, ^3J(P,P) = 38 Hz], 76.2 [d, ^3J(P,P) = 37 Hz], 83.9 [d, ^3J(P,P) = 37 Hz], 84.1 [d, ^3J(P,P) = 38 Hz].

6b: Yield 75 mg (75%). − ^{1}H NMR (400 MHz, $CDCl_3$, 20°C), both helimers: δ = 2.85 (s, 3 H, OCH_3), 3.13 (s, 3 H, OCH_3), 3.25 (s, 3 H, OCH_3), 3.57 (s, 3 H, OCH_3), 4.27 (s, 5 H, C_5H_5), 4.31 (s, 5 H, C_5H_5), 6.50 (br, 1 H, OH), 9.75 (br, 1 H, HC=S), 9.79 (br, 1 H, HC=S). − ^{13}C NMR (100 MHz, $CDCl_3$, 20°C), both helimers: δ = 55.5 (s, OCH_3), 55.7 (s, OCH_3), 55.8 (s, OCH_3), 85.7 (s, C_5H_5), 215.6 (m, br, HC=S). − ^{31}P NMR (161 MHz, $CDCl_3$, 20°C), major helimer: δ = 75.3 [d, ^3J(P,P) = 38 Hz], 83.9 [d, ^3J(P,P) = 38 Hz]; minor helimer: δ = 76.6 [d, ^3J(P,P) = 37 Hz], 83.9 [d, ^3J(P,P) = 37 Hz]. − $C_{52}H_{49}BF_4O_3P_2RuS$ (1003.85) calcd. C 62.22, H 4.92, S 3.19; found C 61.95, H 5.09, S 3.00.

6c: Yield 70 mg (72%), m.p. 147°C (dec). − ^{1}H NMR (400 MHz, $CDCl_3$, 20°C), major helimer: δ = 1.41 (s, 3 H, CH_3), 2.21 (s, 3 H, CH_3), 4.54 (s, 5 H, C_5H_5), 6.24 (s, 1 H, OH), 9.81 [d, ^4J(P,H) = 1.6 Hz, 1 H, HC=S]; minor helimer: δ = 1.34 (s, 3 H, CH_3), 2.28 (s, 3 H, CH_3), 4.32 (s, 5 H, C_5H_5), 6.19 (s, 1 H, OH), 10.04 [d, ^4J(P,H) = 1.6 Hz, 1 H, HC=S]. − ^{13}C NMR (100 MHz, $CDCl_3$, 20°C), both helimers: δ = 19.8 (s, CH_3), 20.2 (s, CH_3), 21.3 (s, CH_3), 21.4 (s, CH_3), 86.1 (s, C_5H_5), 86.4 (s, C_5H_5), 210.7 (br, HC=S), 214.8 [t, ^3J(P,C) = 5.6 Hz, HC=S]. − ^{31}P NMR (161 MHz, $CDCl_3$, 20°C), major helimer: δ = 75.7 [d, ^3J(P,P) = 38 Hz], 88.7 [d, ^3J(P,P) = 38 Hz]; minor helimer: δ = 77.8 [d, ^3J(P,P) = 36 Hz], 82.9 [d, ^3J(P,P) = 36 Hz]. − $C_{52}H_{49}BF_4OP_2RuS$ (971.85) calcd. C 64.27, H 5.08, S 3.30; found C 63.52, H 5.69, S 3.27.

6d: Yield 70 mg (70%), m.p. 106°C (dec). − ^{1}H NMR (400 MHz, $CDCl_3$, 20°C), major helimer: δ = 0.57 [t, ^3J(H,H) = 7.6 Hz, 3 H, CH_3], 1.20 [t, ^3J(H,H) = 7.6 Hz, 3 H, CH_3], 1.62−1.78 (m, 2 H, CH_2), 2.60 [q, ^3J(H,H) = 7.6 Hz, 2 H, CH_2], 4.35 (s, 5 H, C_5H_5), 6.24 (s, 1 H, OH), 10.06 (s, 1 H, HC=S); minor helimer: δ = 0.68 [t, ^3J(H,H) = 7.6 Hz, 3 H, CH_3], 1.17 [t, ^3J(H,H) = 7.6 Hz, 3 H, CH_3], 1.62−1.78 (m, 2 H, CH_2), 2.55 [q, ^3J(H,H) = 7.6 Hz, 2 H, CH_2], 4.48 (s, 5 H, C_5H_5), 5.93 (s, 1 H, OH), 9.93 (s, 1 H, HC=S). − ^{13}C NMR (100 MHz, $CDCl_3$, 20°C), both helimers: δ = 14.6 (s, CH_3), 14.7 (s, CH_3), 15.5 (s, CH_3), 15.7 (s, CH_3), 26.2 (s, CH_2), 26.7 (s, CH_2), 28.8 (s, CH_2), 28.9 (s, CH_2), 86.2 (s, C_5H_5), 86.4 (s, C_5H_5), 211.0 [t, ^3J(P,C) = 6.0 Hz, HC=S], 213.8 [t, ^3J(P,C) = 6.0 Hz, HC=S]. − ^{31}P NMR (161 MHz, $CDCl_3$, 20°C), major helimer: δ = 75.4 [d, ^3J(P,P) = 38 Hz], 83.5 [d, ^3J(P,P) = 38 Hz]; minor helimer: δ = 77.5 [d, ^3J(P,P) = 37 Hz], 82.9 [d, ^3J(P,P) = 37 Hz]. − $C_{54}H_{53}BF_4OP_2RuS$ (999.90) calcd. C 64.87, H 5.34, S 3.21; found C 63.88, H 5.14, S 2.82.

6e: Yield 74 mg (72%), m.p. 120°C (dec). − ^{1}H NMR (400 MHz, $CDCl_3$, 20°C), major helimer: δ = 0.55 [d, ^3J(H,H) = 6.8 Hz, 3 H, CH_3], 0.88 [d, ^3J(H,H) = 6.8 Hz, 3 H, CH_3], 2.03 [sept, ^3J(H,H) = 6.8 Hz, 1 H, CH], 2.88 [sept, ^3J(H,H) = 6.8 Hz, 1 H, CH], 4.37 (s, 5 H, C_5H_5), 6.00 (s, 1 H, OH), 10.28 (s, 1 H, HC=S); minor helimer: δ = 0.74 [d, ^3J(H,H) = 6.8 Hz, 3 H, CH_3], 0.90 [d, ^3J(H,H) = 6.8 Hz, 3 H, CH_3], 2.88 [sept, ^3J(H,H) = 6.8 Hz, 1 H, CH], 2.91 [sept, ^3J(H,H) = 6.8 Hz, 1 H, CH], 4.43 (s, 5 H, C_5H_5), 5.70 (s, 1 H, OH), 10.24 (s, 1 H, HC=S). − ^{13}C NMR (100 MHz, $CDCl_3$, 20°C): δ = 23.4 (s, CH_3), 23.5 (s, CH_3), 24.0 (s, CH_3), 24.1 (s, CH_3), 24.1 (s, CH_3), 24.2 (s, CH_3), 24.6 (s, CH_3),29.7 (s, CH_3), 30.5 (s, CH), 30.5 (s, CH), 34.3 (s, CH), 34.4 (s, CH), 86.5 (s, C_5H_5), 86.6 (s, C_5H_5), 211.9 [t, ^3J(P,C) = 6.3 Hz, HC=S], 212.7 [t, ^3J(P,C) = 6.1 Hz, HC=S]. − ^{31}P NMR (161 MHz, $CDCl_3$, 20°C), major helimer: δ = 75.7 [d, ^3J(P,P) = 39 Hz], 83.3 [d, ^3J(P,P) = 39 Hz], minor helimer: δ = 76.0 [d, ^3J(P,P) = 39 Hz], 83.1 [d, ^3J(P,P) = 39 Hz]. − $C_{56}H_{57}BF_4OP_2RuS$ (1027.96) calcd. C 65.43, H 5.59, S 3.12; found C 64.78, H 5.68, S 3.10.

6f: Yield 65 mg (62%). − ^{1}H NMR (400 MHz, $CDCl_3$, 20°C), both helimers: δ = 0.69 (s, 9 H, CH_3), 0.79 (s, 9 H, CH_3), 1.30 (s, 9 H, CH_3), 1.33 (s, 9 H, CH_3), 4.34 (s, 5 H, C_5H_5), 4.44 (s, 5 H, C_5H_5), 5.22 (s, br, 1 H, OH), 5.43 (s, br, 1 H, OH), 10.22 (s, 1 H, HC=S), 10.28 (s, 1 H, HC=S). − ^{13}C NMR (100 MHz, $CDCl_3$, 20°C), both helimers: δ = 31.4 (s, CH_3), 31.4 (s, CH_3), 32.5 (s, CH_3), 32.7 (s, CH_3), 35.0 [s, C(*t*Bu)], 35.0 [s, C(*t*Bu)], 37.1 [s, C(*t*Bu)], 37.2 [s, C(*t*Bu)], 86.6(s, C_5H_5), 86.8 (s, C_5H_5), 210.3 [t, HC=S, ^3J(P,C) = 7 Hz], 212.2 (br, HC=S). − ^{31}P NMR (161 MHz, $CDCl_3$, 20°C): δ = 75.6 [d, ^3J(P,P) = 48 Hz], 75.9 [d, ^3J(P,P) = 48 Hz], 82.7 [d, ^3J(P,P) = 39 Hz], 82.7 [d, ^3J(P,P) = 39 Hz]. − $C_{58}H_{61}BF_4OP_2RuS$ (1056.01) calcd. C 65.97, H 5.82, S 3.04; found C 64.78, H 5.68, S 3.10.

2-(Methylthio)benzonaphthopyran 7a: A solution of **5a** (50 mg, 0.06 mmol) and methyl iodide (0.5 mL, 8.03 mmol) in toluene was stored for 7 d at − 6°C. The mixture was then evaporated to dryness and the residue chromatographed over silica gel with toluene/acetone 10:1 as an eluent. The first yellow fraction contained the iodo complex **8**.[12] Compound **7a** was isolated from the second yellow band as a pale yellow oil, which was characterized spectroscopically. Yield 7 mg (45%). − ^{1}H NMR (400 MHz, $CDCl_3$, 20°C): δ = 2.21 (s, 3 H, SCH_3), 6.56 [s, 1 H, S(O)CH], 7.18 [d, ^3J(H,H) = 8.0 Hz, 1 H, aryl], 7.25 [d, ^3J(H,H) = 7.6 Hz, 1 H, aryl], 7.36 [d, ^3J(H,H) = 7.9 Hz, 1 H, aryl], 7.38 [d, ^3J(H,H) = 8.4 Hz, 1 H, aryl], 7.54 [d, ^3J(H,H) = 8.2 Hz, 1 H, aryl], 7.57 [d, ^3J(H,H) =

8.0 Hz, 1 H, aryl], 7.81 [d, ^3J(H,H) = 8.2 Hz, 1 H, aryl], 7.90 [d, ^3J(H,H) = 7.8 Hz, 1 H, aryl], 8.10 [d, ^3J(H,H) = 7.7 Hz, 1 H, aryl], 8.61 [d, ^3J(H,H) = 7.9 Hz, 1 H, aryl].

Synthesis of the Thiolate Complexes 9a−f: To a solution of the thiolactone complex (0.20 mmol) in THF (10 mL) was added $LiAlH_4$ (20 mg, 0.50 mmol) at −70°C. Within a few minutes the color of the solution changed from deep purple to yellow. After allowing the mixture to warm to 20°C the solvent was removed under vacuum and the residue extracted with benzene (8 mL). After filtration over Celite the mixture was evaporated to dryness, the residue dissolved in dichloromethane and chromatographed over silica gel. The fraction containing the yellow band was evaporated to dryness and the product crystallized from benzene/pentane and was isolated as a yellow crystalline powder.

9a: Yield 117 mg (68%), m.p. 121°C (dec). − ^{1}H NMR (400 MHz, C_6D_6, 20°C), major helimer: δ = 2.85 [d, ^2J(H,H) = 9.8 Hz, 1 H, SCH_2], 3.22 [d, ^2J(H,H) = 9.8 Hz, 1 H, SCH_2], 4.22 (s, 5 H, C_5H_5), 8.88 (s, 1 H, OH); minor helimer: δ = 1.78 [d, ^2J(H,H) = 9.9 Hz, 1 H, SCH_2], 3.01 [d, ^2J(H,H) = 9.9 Hz, 1 H, SCH_2], 4.30 (s, 5 H, C_5H_5), 9.19 (s, 1 H, OH). − ^{13}C NMR (100 MHz, C_6D_6, 20°C), major helimer: δ = 40.5 [dd, ^3J(P,C) = 6 Hz, ^3J(P,C) = 2 Hz, SCH_2], 84.6 (s, C_5H_5); minor helimer: δ = 36.8 [d, ^3J(P,C) = 5 Hz, SCH_2], 82.1 (s, C_5H_5). − ^{31}P NMR (161 MHz, C_6D_6, 20°C), major helimer: δ = 67.5 [d, ^3J(P,P) = 42 Hz], 90.5 [d, ^3J(P,P) = 42 Hz]; minor helimer: δ = 75.3 [d, ^3J(P,P) = 36 Hz], 86.1 [d, ^3J(P,P) = 36 Hz]. − $C_{50}H_{46}OP_2RuS$ (858.0) calcd. C 69.99, H 5.40; found C 69.76, H 5.76.

9b: Yield 130 mg (71%), m.p. 120°C (dec). − ^{1}H NMR (400 MHz, C_6D_6, 20°C), major helimer: δ = 2.92 (s, OCH_3), 2.93 [d, ^2J(H,H) = 9.9 Hz, 1 H, SCH_2], 3.41 [d, ^2J(H,H) = 9.9 Hz, 1 H, SCH_2], 3.54 (s, OCH_3), 4.38 (s, 5 H, C_5H_5), 9.33 (s, 1 H, OH); minor helimer: δ = 1.79 [d, ^2J(H,H) = 9.8 Hz, 1 H, SCH_2], 2.98 (s, OCH_3), 3.17 [d, ^2J(H,H) = 9.8 Hz, 1 H, SCH_2], 3.47 (s, OCH_3), 4.32 (s, 5 H, C_5H_5), 9.10 (s, 1 H, OH). − ^{13}C NMR (100 MHz, C_6D_6, 20°C), both helimers: δ = 37.1 [d, ^3J(P,C) = 6 Hz, SCH_2], 41.0 [d, ^3J(P,C) = 6 Hz, SCH_2], 54.9 (s, OCH_3), 55.0 (s, OCH_3), 55.0 (s, OCH_3), 55.1 (s, OCH_3), 83.6 (s, C_5H_5), 84.7 (s, C_5H_5). − ^{31}P NMR (161 MHz, C_6D_6, 20°C), major helimer: δ = 66.5 [d, ^3J(P,P) = 42 Hz], 90.8 [d, ^3J(P,P) = 42 Hz]; minor helimer: δ = 74.8 [d, ^3J(P,P) = 36 Hz], 86.1 [d, ^3J(P,P) = 36 Hz]. − $C_{52}H_{50}O_3P_2RuS$ (918.0) calcd. C 68.03, H 5.49; found C 67.80, H 5.49.

9c: Yield 119 mg (67%), m.p. 124°C (dec). − ^{1}H NMR (400 MHz, C_6D_6, 20°C), major helimer: δ = 1.80 (s, CH_3), 2.27 (s, CH_3), 2.93 [d, ^2J(H,H) = 9.8 Hz, 1 H, SCH_2], 3.13 [d, ^2J(H,H) = 9.8 Hz, 1 H, SCH_2], 4.24 (s, 5 H, C_5H_5), 8.32 (s, 1 H, OH); minor helimer: δ = 1.71 (s, CH_3), 2.02 [d, ^2J(H,H) = 10.0 Hz, 1 H, SCH_2], 2.34 (s, CH_3), 2.95 [d, ^2J(H,H) = 10.0 Hz, 1 H, SCH_2], 4.29 (s, 5 H, C_5H_5), 8.60 (s, 1 H, OH). − ^{13}C NMR (100 MHz, C_6D_6, 20°C), major helimer: δ = 20.3 (s, CH_3), 21.4 (s, CH_3), 40.3 [dd, ^3J(P,C) = 6 Hz, ^3J(P,C) = 2 Hz, SCH_2], 84.7 (s, C_5H_5); minor helimer: δ = 19.8 (s, CH_3), 20.2 (s, CH_3), SCH_2 signal superimposed by major helimer, 83.6 (s, C_5H_5) − ^{31}P NMR (161 MHz, C_6D_6, 20°C), major helimer: δ = 67.0 [d, ^3J(P,P) = 41 Hz], 90.4 [d, ^3J(P,P) = 41 Hz]; minor helimer: δ = 75.5 [d, ^3J(P,P) = 36 Hz], 85.9 [d, ^3J(P,P) = 36 Hz]. − $C_{52}H_{50}OP_2RuS$ (886.0) calcd. C 70.49, H 5.69; found C 70.97, H 5.64.

9d: Yield 124 mg (68%). − ^{1}H NMR (400 MHz, C_6D_6, 20°C), major helimer: δ = 0.86 [t, ^3J(H,H) = 7.6 Hz, 3 H, CH_3], 1.26 [t, ^3J(H,H) = 7.6 Hz, 3 H, CH_3], 2.15 [q, ^3J(H,H) = 7.6 Hz, 1 H, CH_2], 2.17 [q, ^3J(H,H) = 7.6 Hz, 1 H, CH_2], 2.63 [q, ^3J(H,H) = 7.6 Hz, 2 H, CH_2], 2.91 [d, ^2J(H,H) = 10.0 Hz, 1 H, SCH_2], 3.16 [d, ^2J(H,H) = 10.0 Hz, 1 H, SCH_2], 4.22 (s, 5 H, C_5H_5); minor helimer: δ = 0.80 [t, ^3J(H,H) = 7.6 Hz, 3 H, CH_3], 1.31 [t, ^3J(H,H) = 7.6 Hz, 3 H, CH_3], 1.79 [d, ^2J(H,H) = 9.6 Hz, 1 H, SCH_2], 2.09 [q, ^3J(H,H) = 7.6 Hz, 1 H, CH_2], 2.10 [q, ^3J(H,H) = 7.6 Hz, 1 H, CH_2], 2.68 [q, ^3J(H,H) = 7.6 Hz, 2 H, CH_2], 2.96 [d, ^2J(H,H) = 9.6 Hz, 1 H, SCH_2], 4.27 (s, 5 H, C_5H_5). − ^{13}C NMR (100 MHz, C_6D_6, 20°C), major helimer: δ = 15.1 (s, CH_3), 16.3 (s, CH_3), 26.9 (s, CH_2), 29.3 (s, CH_2), 40.3 (br, SCH_2), 84.6 (s, C_5H_5); minor helimer: δ = 15.1 (s, CH_3), 16.4 (s, CH_3), 26.9 (s, CH_2), 29.4 (s, CH_2), 37.2 (br, SCH_2), 83.6 (s, C_5H_5). − ^{31}P NMR (161 MHz, C_6D_6, 20°C), major helimer: δ = 67.0 [d, ^3J(P,P) = 41 Hz]. 90.4 [d, ^3J(P,P) = 41 Hz]; minor helimer: δ = 75.7 [d, ^3J(P,P) = 36 Hz], 85.9 [d, ^3J(P,P) = 36 Hz]. − $C_{54}H_{54}OP_2RuS$ (914.1) calcd. C 70.95, H 5.95, S 3.51; found C 70.61, H 5.82, S 3.21.

9e: Yield 124 mg (66%). − ^{1}H NMR (400 MHz, C_6D_6, 20°C), major helimer: δ = 0.95 [d, ^3J(H,H) = 6.8 Hz, 3 H, CH_3], 1.05 [d, ^3J(H,H) = 6.8 Hz, 3 H, CH_3], 1.32 [d, ^3J(H,H) = 6.8 Hz, 3 H, CH_3], 1.32 [d, ^3J(H,H) = 6.8 Hz, 3 H, CH_3], 2.45 [sept, ^3J(H,H) = 6.8 Hz, 1 H, CH], 2.46 [sept, ^3J(H,H) = 6.8 Hz, 1 H, CH], 2.92 [d, ^2J(H,H) = 10.0 Hz, 1 H, SCH_2], 3.19 [d, ^2J(H,H) = 10.0 Hz, 1 H, SCH_2], 4.17 (s, 5 H, C_5H_5); minor helimer: δ = 0.95 [d, ^3J(H,H) = 6.8 Hz, 6 H, CH_3], 1.79 [d, ^2J(H,H) = 9.6 Hz, 1 H, SCH_2], 2.58−2.72 (m, 2 H, CH), 2.96 [d, ^2J(H,H) = 9.6 Hz, 1 H, SCH_2], 3.36 [d, ^3J(H,H) = 7.2 Hz, 3 H, CH_3], 3.38 [d, ^3J(H,H) = 7.2 Hz, 3 H, CH_3], 4.26 (s, 5 H, C_5H_5); − ^{13}C NMR (100 MHz, C_6D_6, 20°C), major helimer: δ = 24.2 (s, CH_3), 24.5 (s, CH_3), 24.7 (s, CH_3), 24.9 (s, CH_3), 30.8 (s, CH), 34.7 (s, CH), 40.7 (br, SCH_2), 84.6 (s, C_5H_5); minor helimer: δ = 24.1 (s, CH_3), 24.5 (s, CH_3), 24.5 (s, CH_3), 24.7 (s, CH_3), 30.8 (s, CH), 34.8 (s, CH), 37.5 [d, ^3J(P,C) = 6 Hz, SCH_2], 83.7 (s, C_5H_5). − ^{31}P NMR (161 MHz, C_6D_6, 20°C), major helimer: δ = 66.9 [d, ^3J(P,P) = 42 Hz], 90.3 [d, ^3J(P,P) = 42 Hz]; minor helimer: δ = 75.8 [d, ^3J(P,P) = 36 Hz], 85.8 [d, ^3J(P,P) = 36 Hz]. − $C_{56}H_{58}OP_2RuS$ (942.2) calcd. C 71.39, H 6.21, S 3.40; found C 71.11, H 6.42, S 3.10.

9f: Yield 167 mg (86%). − ^{1}H NMR (400 MHz, C_6D_6, 20°C), both helimers: δ = 1.06 (s, 9 H, CH_3), 1.07 (s, 9 H, CH_3), 1.40 (s, 9 H, CH_3), 1.45 (s, 9 H, CH_3), 1.77 [d, ^2J(H,H) = 9.9 Hz, 1 H, SCH_2], 2.92 [d, ^2J(H,H) = 9.7 Hz, 1 H, SCH_2], 3.00 [d, ^2J(H,H) = 9.7 Hz, 1 H, SCH_2], 3.23 [d, ^2J(H,H) = 9.9 Hz, 1 H, SCH_2], 4.15 (s, 5 H, C_5H_5),4.24 (s, 5 H, C_5H_5). − ^{13}C NMR (100 MHz, C_6D_6, 20°C), both helimers: δ = 31.8 (s, CH_3), 31.9 (s, CH_3), 32.7 (s, CH_3), 32.9 (s, CH_3), 34.8 [s, C(*t*Bu)], 34.9 [s, C(*t*Bu)], 37.4 [s, C(*t*Bu)], 37.5 [s, C(*t*Bu)], 41.3 [dd, ^3J(P,C) = 7 Hz, ^3J(P,C) = 2 Hz, SCH_2], 83.7 (s, C_5H_5), 84.5 (s, C_5H_5). − ^{31}P NMR (161 MHz, C_6D_6, 20°C), both helimers: δ = 67.2 [d, ^3J(P,P) = 42 Hz], 76.3 [d, ^3J(P,P) = 36 Hz], 85.7 [d, ^3J(P,P) = 36 Hz], 90.0 [d, ^3J(P,P) = 42 Hz]. − $C_{58}H_{62}OP_2RuS$ (970.2) calcd. C 71.80, H 6.44, S 3.30; found C 70.08, H 6.14, S 2.98.

Hydride Reduction of 5c: To a solution of **5c** (80 mg, 0.09 mmol) in THF (5 mL) was added at −70°C an excess (0.25 mmol) of either $LiBEt_3H$ or $LiAlH_4$. After 1 h the mixture was allowed to warm to 20°C. The solvent was then removed under vacuum and the dry residue extracted with benzene. After filtration over Celite and drying under vacuum **9c** was obtained as a yellow powder. Yields and diastereoisomer ratios are given in Equation 7.

Zirconium-assisted Hydride Reduction of 5a: To a solution of **5a** (100 mg, 0.12 mmol) in THF (15 mL) was added $[ZrCl_4(THF)_2]$ (200 mg, 0.53 mmol) at −70°C whereupon the color slowly changed to purple. After 8 h at this temperature the mixture was treated with $LiAlH_4$ (20 mg, 0.50 mmol), which caused an immediate color change to yellow. A few droplets of water were added to quench the excess hydride reagent, and then the mixture was

warmed to 20°C and evaporated under vacuum. The dry residue was extracted with benzene (8 mL), filtered over Celite, and the product isolated by freeze-drying. Yield 67 mg (65%), yellow crystalline powder, identified by ^{1}H and ^{31}P NMR as a mixture of both helimers of **9a** with inverted diastereoisomer ratio.

Alkylation of the Thiolate Complexes 9a−c: To a solution of the thiolate complex (0.10 mmol) in acetone (10 mL) was added methyl iodide (0.05 mL, 0.80 mmol) at 20°C. After 10 min the mixture was evaporated to 1 mL and the product precipitated by adding diethyl ether and pentane. After repeated washings with pentane and drying under vacuum the product was isolated as a pale yellow crystalline powder.

10a: Yield 98 mg (98%), m.p. 87°C (dec). − ^{1}H NMR (400 MHz, $CDCl_3$, 20°C), major helimer: δ = 0.99 (s, 3 H, SCH_3), 4.23 (s, 5 H, C_5H_5), SCH_2 and OH signals obscured by phosphane ligand; minor helimer: δ = 4.19 (s, 5 H, C_5H_5). − ^{13}C NMR (100 MHz, $CDCl_3$, 20°C), both helimers: δ = 25.0 (s, SCH_3), 47.2 (m, br, SCH_2), 85.1 (s, C_5H_5), 85.2 (s, C_5H_5). − ^{31}P NMR (161 MHz, $CDCl_3$, 20°C), major helimer: δ = 65.9 [d, ^3J(P,P) = 39 Hz], 82.7 [d, ^3J(P,P) = 39 Hz]; minor helimer: δ = 64.9 [d, br, ^3J(P,P) = 40 Hz], 83.0 [d, ^3J(P,P) = 40 Hz]. − $C_{51}H_{49}IOP_2RuS$ (1000.0) calcd. C 61.26, H 4.94, S 3.21; found C 61.06, H 4.88, S 3.20.

10b: Yield 104 mg (98%), m.p. 91°C (dec). − ^{1}H NMR (400 MHz, $CDCl_3$, 20°C), major helimer: δ = 1.04 (s, 3 H, SCH_3), 3.39 (s, 3 H, OCH_3), 3.70 (s, 3 H, OCH_3), 4.30 (s, 5 H, C_5H_5), SCH_2 and OH signals obscured by phosphane ligand; minor helimer: δ = 1.04 (s, 3 H, SCH_3), 3.36 (s, 3 H, OCH_3), 3.68 (s, 3 H, OCH_3), 4.25 (s, 5 H, C_5H_5). − ^{13}C NMR (100 MHz, $CDCl_3$, 20°C), both helimers: δ = 24.3 (s, SCH_3), 25.1 (s, SCH_3), 46.9 (m, br, SCH_2), 47.2 (m, br, SCH_2), 55.3 (s, OCH_3), 55.7 (s, OCH_3), 85.0 (s, C_5H_5). − ^{31}P NMR (161 MHz, $CDCl_3$, 20°C), major helimer: δ = 66.2 [d, ^3J(P,P) = 40 Hz], 83.1 [d, ^3J(P,P) = 40 Hz]; minor helimer: δ = 64.9 [d, br, ^3J(P,P) = 40 Hz], 82.6 [d, ^3J(P,P) = 40 Hz]. − $C_{53}H_{53}IO_3P_2RuS$ (1060.0) calcd. C 60.06, H 5.04, S 3.02; found C 59.69, H 4.94, S 2.96.

10c: Yield 102 mg (99%), m.p. 73°C (dec). − ^{1}H NMR (400 MHz, $CDCl_3$, 20°C), both helimers: δ = 1.03 (s, 3 H, SCH_3), 1.47 (s, 3 H, CH_3), 2.18 (s, 3 H, CH_3), 4.27 (s, 5 H, C_5H_5), 4.30 (s, 5 H, C_5H_5), SCH_2 and OH signals obscured by phosphane ligand. − ^{13}C NMR (100 MHz, $CDCl_3$, 20°C), both helimers: δ = 19.7 (s, CH_3), 21.0 (s, CH_3), 25.0 (s, br, SCH_3), 47.2 (m, br, SCH_2), 84.8 (s, C_5H_5). − ^{31}P NMR (161 MHz, $CDCl_3$, 20°C), major helimer: δ = 67.0 [d, ^3J(P,P) = 40 Hz], 83.1 [d, ^3J(P,P) = 40 Hz]; minor helimer: δ = 65.5 [d, br, ^3J(P,P) = 40 Hz], 83.5 [d, ^3J(P,P) = 40 Hz]. − $C_{53}H_{53}IOP_2RuS$ (1028.0) calcd. C 61.92, H 5.20; found C 61.79, H 5.43.

Detachment of the Methyl Thioethers 11a−c: A suspension of the thioether complex (0.1 mmol) in benzene (2 mL) was heated under reflux for 12 h. The mixture was worked up as described for **7a** leaving **11a−c** as pale yellow oils which were characterized by ^{1}H NMR.

11a: − ^{1}H NMR (400 MHz, C_6D_6, 20°C): δ = 1.60 (s, 3 H, SCH_3), 3.47, 3.48 (AB system, ^2J(H,H) = 15.0 Hz, 2 H, SCH_2), 4.59 (s, 1 H, OH), 6.85−8.30 (m, 10 H, aryl).

11b: − ^{1}H NMR (400 MHz, C_6D_6, 20°C): δ = 1.71 (s, 3 H, SCH_3), 3.00 (s, 3 H, OCH_3), 3.39 (s, 3 H, OCH_3), 3.68 (s, 2 H, SCH_2), 4.78 (s, 1 H, OH), 6.22−8.31 (m, 8 H, aryl).

11c: − ^{1}H NMR (400 MHz, C_6D_6, 20°C): δ = 1.65 (s, 3 H, SCH_3), 1.78 (s, 3 H, CH_3), 2.18 (s, 3 H, CH_3), 3.50 (s, 2 H, SCH_2), 4.60 (s, 1 H, OH), 6.66−8.30 (m, 8 H, aryl).

X-ray Structure Determination of [CpRu{(*S,S*)-CHIRAPHOS}-($SC_{19}H_{14}O$)]BF_4 (4c): Black-purple crystals suitable for an X-ray structure determination were obtained by diffusion of hexane into a dichloromethane solution of **4c**. Twenty-five centered reflections from a crystal of the dimensions given in Table 1 gave a rhombohedric unit cell. Data were collected from one fourth of the reflection sphere in the range 2° < Θ < 26° (Enraf−Nonius CAD 4 diffractometer, Mo-K_α radiation, graphite monochromator, filter factor 16.4). No absorption correction was applied (minimum

Table 1. Details of the structure determinations of [CpRu{(*S,S*)-CHIRAPHOS}($SC_{19}H_{14}O$)]BF_4 (**4c**) and [CpRu{(*S,S*)-CHIRAPHOS}($SC_{17}H_{11}O$)] (**5a**)

Compound	**4c**	**5a**
Empirical formula	$C_{52}H_{47}BF_4OP_2RuS{\cdot}CH_2Cl_2$	$C_{50}H_{44}OP_2RuS{\cdot}1.5\ C_6D_6$
Mol. mass	1054.70	982.21
Color	black-purple	orange
Crystal size (mm)	0.18×0.15×0.10	0.18×0.18×0.12
Temperature (K)	293(2)	293(2)
λ (Å)	0.70930	0.70930
Space group	*R*3 (No. 146)	$P22_12_1$ (No. 18)
a (Å)	18.869(2)	9.951(2)
b (Å)	18.869(2)	19.835(4)
c (Å)	36.705(9)	24.803(4)
V (Å^3)	11318(3)	4869(2)
Z	9	4
ρ (calc) (mg mm^{-3})	1.393	1.333
μ (Mo−K_α) (cm^{-1})	5.70	1.73
Θ Range (°)	2.15−25.92	2.04−29.90
Index range *h*	0, 20	0, 13
k	0, 20	0, 27
l	−45, 45	0, 34
Measured reflections	5408	7821
Independent reflections	5408	7821
Observed reflections	3999	3901
Parameters	586	583
R[a]	0.0452	0.0600
wR_2[a]	0.0938	0.0698

[a] $I_o > 2\ \sigma\ (I_o)$.

transmission 97.84%). The structure was solved by Patterson methods (program SHELXS 86)[28] in the space group R3 (Nr. 146). A CH_2Cl_2 molecule was found in the asymmetric unit and refined anisotropically. H atoms were included in idealized positions, coupled to their carbon atoms. The BF_4^- anion was found distributed over three special positions, one of which was slightly disordered. Twenty restraints were introduced to preserve the geometries of BF_4 and CH_2Cl_2. Least-squares cycles of the SHELXL 93 program package[29] led to the R values given in Table 1. The five highest maxima of the final difference Fourier map were all below 0.520 e $Å^{-3}$. Further details of the structure determination may be obtained from the Fachinformationszentrum Karlsruhe, D-76344 Eggenstein-Leopoldshafen, on quoting the depository number CSD 408734.

X-ray Structure Determination of [CpRu{(*S,S*)-CHIRAPHOS}($SC_{17}H_{11}O$)] (5a): Clear orange crystals suitable for an X-ray structure determination grew out of a C_6D_6 solution. Twenty-five centered reflections from a crystal of the dimensions given in Table 1 gave an orthorhombic unit cell. Data were collected from one eighth of the reflection sphere in the range $2° < \Theta < 30°$ (Enraf−Nonius CAD 4 diffractometer, Mo-K_α radiation, graphite monochromator, filter factor 16.4). An empirical absorption correction based on the counts of nine reflections was applied (min. transmission 97.80%). The structure was solved by Patterson methods (program SHELXS 86)[28] in the space group $P22_12_1$ (Nr. 18). The 1.5 molecules of C_6D_6 found in the asymmetric unit were refined anisotropically. H atoms were included in idealized positions, coupled to their carbon atoms. Least-squares cycles of the SHELXL 93 program package[29] led to the R values given in Table 1. The five highest maxima of the final difference Fourier map were below 0.503 e $Å^{-3}$. Further details of the structure determination may be obtained from the Fachinformationszentrum Karlsruhe, D-76344 Eggenstein-Leopoldshafen, on quoting the depository number CSD 408735.

Acknowledgments

This work has been supported by the *Deutsche Forschungsgemeinschaft* (SFB 347 ″Selektive Reaktionen Metall-aktivierter Moleküle″) and the *Fonds der Chemischen Industrie.* We are indebted to Dr. M. Lerch of the Institut für Silikatforschung, Würzburg, for recording the powder diffraction diagram of **5a**.

[1] N. Burzlaff, W. A. Schenk, *Eur. J. Inorg. Chem.* **1999**, 1435−1443.
[2] G. Bringmann, S. Güssregen, D. Vitt, R. Stowasser, *J. Mol. Model.* **1998**, *4*, 165−175.
[3] G. Bringmann, C. Günther, M. Ochse, O. Schupp, S. Tasler, *Prog. Chem. Org. Nat. Prod.* (Eds.: W. Herz, H. Falk, G. W. Kirby, R. E. Moore, Ch. Tamm), submitted for publication.
[4] G. Bringmann, G. François, L. Aké Assi, J. Schlauer, *Chimia* **1998**, *52*, 18−28.
[5] G. Bringmann, M. Breuning, S. Tasler, *Synthesis* **1999**, 525−558.
[6] G. Bringmann, W. Saeb, M. Rübenacker, *Tetrahedron* **1999**, *55*, 423−432.
[7] G. Bringmann, M. Breuning, *Tetrahedron: Asymmetry* **1999**, *10*, 385−390.
[8] G. Bringmann, O. Schupp, K. Peters, L. Walz, H. G. von Schnering, *J. Organomet. Chem.* **1992**, *438*, 117−130.
[9] G. Bringmann, B. Schöner, O. Schupp, W. A. Schenk, I. Reuther, K. Peters, E.-M. Peters, H. G. von Schnering, *J. Organomet. Chem.* **1994**, *472*, 275−284.
[10] G. Consiglio, F. Morandini, *Chem. Rev.* **1987**, *87*, 761−778.
[11] W. A. Schenk, J. Frisch, W. Adam, F. Prechtl, *Angew. Chem.* **1994**, *106*, 1699- 1701; *Angew. Chem. Int. Ed. Engl.* **1994**, *33*, 1609−1611.
[12] W. A. Schenk, J. Frisch, M. Dürr, N. Burzlaff, D. Stalke, R. Fleischer, W. Adam, F. Prechtl, A. K. Smerz, *Inorg. Chem.* **1997**, *36*, 2372−2378.
[13] W. A. Schenk, M. Dürr, *Chem. Eur. J.* **1997**, *3*, 713−716.
[14] W. A. Schenk, B. Steinmetz, M. Hagel, W. Adam, C. R. Saha-Möller, *Z. Naturforsch. B* **1997**, *52*, 1359−1371.
[15] W. A. Schenk, T. Stur, E. Dombrowski, *J. Organomet. Chem.* **1994**, *472*, 257−273.
[16] G. Bringmann, T. Hartung, L. Göbel, O. Schupp, C. L. J. Ewers, B. Schöner, R. Zagst, K. Peters, H. G. von Schnering, *Liebigs Ann. Chem.* **1992**, 225−232.
[17] See also: K. Peters, E.-M. Peters, G. Bringmann, O. Schupp, *Z. Naturforsch. B* **1996**, *51*, 431−432; G. Bringmann, A. Wuzik, O. Schupp, K. Peters, E.-M. Peters, *Z. Naturforsch. B*, **1997**, *52*, 355−358.
[18] G. Bringmann, A. Wuzik, O. Schupp, J. Kümmel, W. A. Schenk, manuscript in preparation.
[19] G. Bringmann, M. Breuning, S. Busemann, J. Hinrichs, T. Pabst, R. Stowasser, S. Tasler, A. Wuzik, W. A. Schenk, J. Kümmel, D. Seebach, G. Jaeschke in *Selective Reactions of Metal-Activated Molecules,* Part 3 (Eds.: H. Werner, P. Schreier), Vieweg, Braunschweig, **1998**, S. 141−145.
[20] W. A. Schenk, N. Burzlaff, M. Hagel in *Selective Reactions of Metal-Activated Molecules,* Part 3 (Eds.: H. Werner, P. Schreier), Vieweg, Braunschweig, **1998**, S. 241−243.
[21] W. A. Schenk, M. Dürr, B. Steinmetz, W. Adam, C. R. Saha-Möller in *Selective Reactions of Metal-Activated Molecules,* Part 3 (Eds.: H. Werner, P. Schreier), Vieweg, Braunschweig, **1998**, S. 245−246.
[22] W. A. Schenk, T. Beucke, J. Kümmel, F. Servatius, N. Sonnhalter, G. Bringmann, A. Wuzik in *Selective Reactions of Metal-Activated Molecules,* Part 3 (Eds.: H. Werner, P. Schreier), Vieweg, Braunschweig, **1998**, S. 247−249.
[23] J. W. Benson, R. J. Angelici, *Organometallics* **1992**, *11*, 922−927.
[24] G. Bringmann, M. Breuning, H. Endress, D. Vitt, K. Peters, E.-M. Peters, *Tetrahedron* **1998**, *54*, 10677−10690.
[25] G. Bringmann, D. Vitt, J. Kraus, M. Breuning, *Tetrahedron* **1998**, *54*, 10691−10698.
[26] G. Consiglio, F. Morandini, F. Bangerter, *Inorg. Chem.* **1982**, *21*, 455−457.
[27] L. E. Manzer, *Inorg. Synth.* **1982**, *21*, 135−140.
[28] G. M. Sheldrick, *SHELXS 86, Program for Crystal Structure Solution*, Universität Göttingen, Germany **1986**.
[29] G. M. Sheldrick, *SHELXL 93, Program for Crystal Structure Refinement*, Universität Göttingen, Germany **1993**.

Received April 1, 1999
[I99113]

Synthesis, Structural Characterization, Electrochemistry, and Reactivities of Heptaosmium Carbonyl Clusters Bearing Thioxane Ligands – Crystal and Molecular Structures of $[Os_7(CO)_{16}\{(\mu\text{-}S(CH_2)_2OCH_2CH_2\}_2]$, $[Os_7(CO)_{17}\{(\mu\text{-}S(CH_2)_2OCH_2CH_2\}\{S(CH_2)_2OCH_2CH_2\}]$, and $[Os_7(CO)_{18}\{(\mu\text{-}S(CH_2)_2OCH_2CH_2\}]$

Kelvin Sze-Yin Leung[a] and Wing-Tak Wong*[a]

Keywords: Osmium / Cluster / Electrochemistry

Reaction of the activated heptaosmium cluster $[Os_7(CO)_{19}(MeCN)_2]$ with 1,4-thioxane in CH_2Cl_2 at ambient temperature led to the isolation of three air-stable clusters $[Os_7(CO)_{16}\{\mu\text{-}S(CH_2)_2OCH_2C^aH_2(S\text{–}C^\alpha)\}_2]$ (**1**), $[Os_7(CO)_{17}\{\mu\text{-}S(CH_2)_2OCH_2C^aH_2(S\text{–}C^\alpha)\}\{S(CH_2)_2OCH_2C^aH_2(S\text{–}C^\alpha)\}]$ (**2**) and $[Os_7(CO)_{18}\{\mu\text{-}S(CH_2)_2OCH_2C^aH_2(S\text{–}C^\alpha)\}]$ (**3**). The metal skeletons of these clusters are in the form of a winding helix made up of four tetrahedra sharing three common faces. From electrochemical studies, the extent of the cathodic shifts of the reduction waves of these clusters were found to differ from that of the parent cluster $[Os_7(CO)_{21}]$. Treatment of **2** with carbon monoxide produced an isomer of **3**, namely compound **4**, which has the same molecular formula as **3**, but a different ligand arrangement.

Introduction

The chemistry of heptaosmium carbonyl clusters is not well explored, probably because reliable synthetic routes are unavailable, unlike the case for the hexaosmium system.[1] Pyrolysis of $[Os_3(CO)_{12}]$ at 210°C leads to a small amount of $[Os_7(CO)_{21}]$ (< 10%) after repeated TLC purification.[2] A more rational synthesis of a heptaosmium cluster is by nucleophilic attack of a mononuclear osmium fragment at a Os_6 cluster core that contains a labile ligand such as MeCN. The heptaosmium dihydrido clusters $[H_2Os_7(CO)_{20}]$, $[H_2Os_7(CO)_{21}]$, and $[H_2Os_7(CO)_{22}]$ have been obtained by this strategy.[3] Subsequent reactions of $[H_2Os_7(CO)_{20}]$ with diphenylacetylene is reported to give $[Os_7(CO)_{15}(\mu_3\text{-}CPh)_4]$ and $[Os_7(CO)_{18}(\mu_3\text{-}CPh)_2]$.[4] A similar reaction with dimethylacetylene as the ligand afforded $[Os_7(CO)_{19}(\mu_3\text{-}\eta^2\text{-}C_2Me_2)]$.[5] Lewis and Braga have shown that treatment of the parent cluster $[Os_7(CO)_{21}]$ with trimethoxyphosphane in the presence of Me_3NO yields the red-brown cluster $[Os_7(CO)_{20}P(OMe)_3]$.[6] Hoping to develop a more accessible synthetic route for higher-nuclearity cluster systems, we previously used the preformed labile species $[Os_6(CO)_{16}(MeCN)_2]$ to synthesize a number of hexaosmium cluster derivatives bearing donor ligands.[7] We extended this approach to the heptanuclear system and prepared the title compounds and studied their reactions. Their molecular structures were determined by single-crystal X-ray crystallography.

[a] Department of Chemistry, The University of Hong Kong, Pokfulam Road, Hong Kong, P. R. China
Fax: (internat.) +852/2547-2933
E-mail: wtwong@hkucc.hku.hk

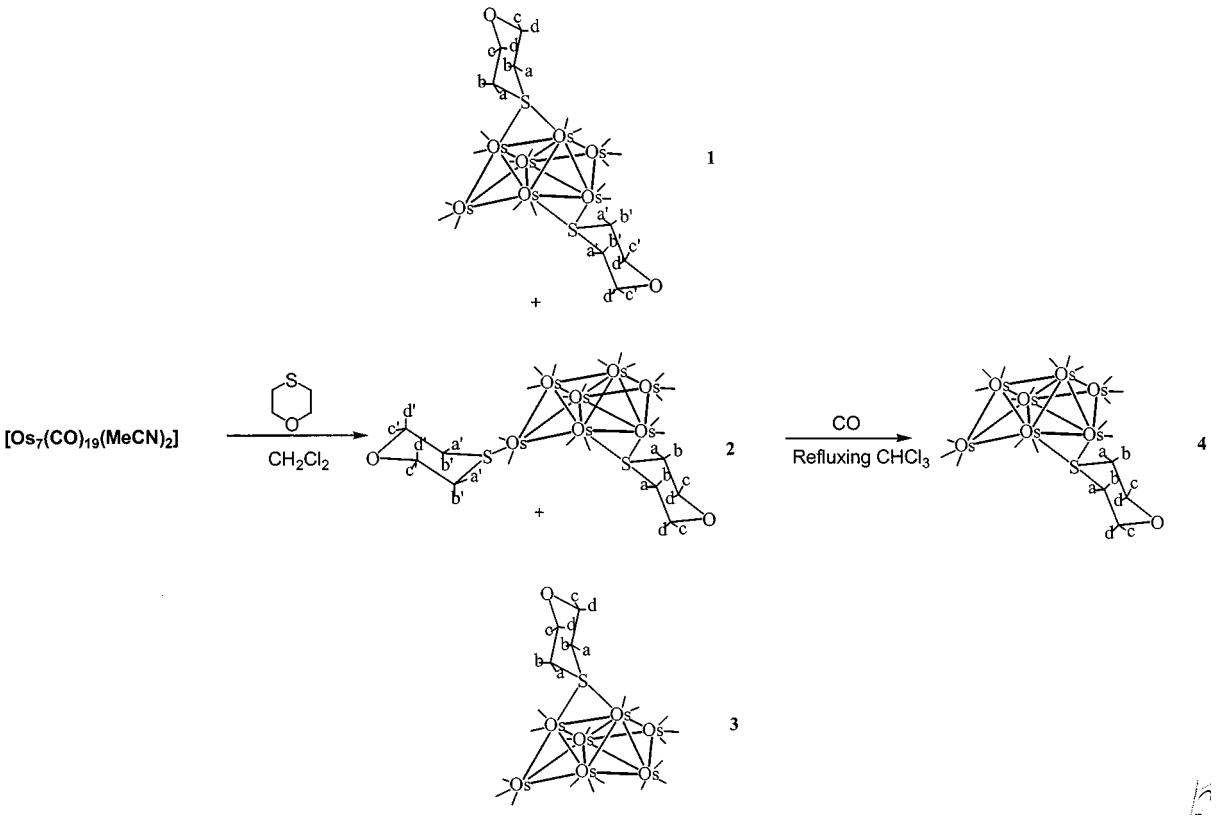
Results and Discussion

Synthesizing a cluster derivative by nucleophilic displacement of a donor ligand with a preformed labile parent carbonyl cluster is a general and effective way to generate new clusters in low-nuclearity systems.[8] The advantage of using such a strategy is not only the mild reaction conditions needed, but also that the reaction is more selective. However, there have been only very few reports of cluster syntheses with this approach in hexa- and heptanuclear systems, such as the preparation of hexanuclear clusters from the reactions with pyridine[7a] and 7-azaindole.[7b] In this article we report the use of $[Os_7(CO)_{19}(MeCN)_2]$, which is generated from the parent cluster $[Os_7(CO)_{21}]$, to synthesize a new family of heptanuclear cluster compounds containing thioxane ligands.

Treatment of the heptanuclear carbonyl cluster $[Os_7(CO)_{21}]$ with 2 equiv. Me_3NO, in acetonitrile at −78°C, led to the formation of an activated cluster precursor $[Os_7(CO)_{19}(MeCN)_2]$. Subsequent reaction of this labile cluster with 1,4-thioxane in CH_2Cl_2, at ambient temperature for 6 h, followed by TLC purification, gave three air-stable clusters $[Os_7(CO)_{16}\{\mu\text{-}S(CH_2)_2OCH_2C^aH_2(S-C^\alpha)\}_2]$ (**1**), $[Os_7(CO)_{17}\{\mu\text{-}S(CH_2)_2OCH_2C^aH_2(S-C^\alpha)\}\{S(CH_2)_2OCH_2C^aH_2(S-C^\alpha)\}]$ (**2**), and $[Os_7(CO)_{18}\{\mu\text{-}S(CH_2)_2OCH_2C^aH_2(S-C^\alpha)\}]$ (**3**) (Scheme 1). Their formulae were first established by FAB MS and ^{1}H-NMR spectroscopy, and were eventually confirmed by X-ray crystallography. All the spectroscopic data are summarized in Table 1.

The metal frameworks of clusters **1**, **2**, and **3** may be described as four fused tetrahedra sharing three common faces, or two fused bicapped trigonal bipyramids sharing a

 © WILEY-VCH Verlag GmbH, D-69451 Weinheim, 1999 1434−1948/99/1010−1757 $ 17.50+.50/0



Scheme 1. Reaction of $[Os_7(CO)_{19}(MeCN)_2]$ with 1,4-thioxane in CH_2Cl_2 at ambient conditions

Table 1. Spectroscopic data for $[Os_7(CO)_{19}(MeCN)_2]$ and clusters **1** to **4**

	IR $\tilde{\nu}$(CO)[a] [cm^{-1}]	^1H NMR δ (J [Hz])[b]	Mass spectrum m/z[c]
$[Os_7(CO)_{19}(MeCN)_2]$	2069(w), 2042(s), 2008(s)	2.86 (s, 6 H)	–
1	2080(w), 2059(s), 2005(vs)	3.87−4.48 (m, 8 H, H_a, H_b, $H_{a'}$, $H_{b'}$), 3.31−3.79 (m, 8 H, H_c, H_d, $H_{c'}$, $H_{d'}$)	1988(1988)
2	2078(s), 2051(vs), 2020(vs), 2010(vs), 1964(w), 1943(w)	4.21−4.53 (m, 8 H, H_a, H_b, $H_{a'}$, $H_{b'}$), 3.82−3.97 (m, 8 H, H_c, H_d, $H_{c'}$, $H_{d'}$)	2108 (2108)
3	2085(vw), 2070(s), 2065(s), 2058(vs), 2037(s), 2011(ms)	4.57−4.69 (m, 4 H, H_a, H_b), 3.81−3.94 (m, 4 H, H_c, H_d)	1940 (1940)
4	2095(w), 2070(vs), 2055(vs), 2018(vs)	4.23−4.47 (m, 4 H, H_a, H_b), 3.52−3.94 (m, 4 H, H_c, H_d)	1940 (1940)

[a] CH_2Cl_2. – [b] CD_2Cl_2. – [c] Simulated values given in parentheses.

common triangular face. This kind of Os_7 architecture differs widely from the parent cluster $[Os_7(CO)_{21}]$, which is a monocapped octahedron.[9] The compound $[Os_7(CO)_{17}(\eta^6\text{-}C_6H_6)]$[10], prepared by Lewis and co-workers, is so far the only structurally characterized homometallic example with this type of metal skeleton. Although the metal framework of some heterometallic clusters such as $[Cp_3W_3Ir_4(\mu\text{-}H)(CO)_{12}]$[11] is similar, complexes $[Fe_4(CO)_{12}\{Au(L)\}_2BH]$ (L = $AsPh_3$ or PPh_3),[12] $[Fe_3(CO)_9P\{Au(PPh_3)\}_3]$,[13] and $[Fe_4(CO)_{12}Au_2\{P(p\text{-}MeC_6H_4)_3\}_2BH]$[14] could be considered similar only if the edge-bridging, rather than face-capping, heteroatoms are regarded as one of the vertices.

The molecular geometry of complex **1** and its atomic labelling scheme is depicted in Figure 1. Some selected interatomic bond lengths and angles are given in Table 2. Compound **1** crystallizes in the monoclinic space group $C2/c$ with half a molecule per asymmetric unit. All the internuclear Os−Os distances are within 2.703(9) to 2.994(4) Å which is comparable to those found in other high-nuclearity clusters. Thioxane ligands bridge the Os(1)−Os(2) and Os(1)*−Os(2)* edges of the metal skeleton. As predicted by the Effective Atomic Number (EAN) rule, there are fifteen metal−metal bonds.[15] The structure of this 96 CVE cluster can be rationalized by the condensed polyhedral approach,[16] but it is not possible to assign 18 electrons to each osmium atom. This is not uncommon for high-nuclearity system, as was suggested by Adams,[17] Kaesz,[18] and Lewis.[19]

The redox properties of cluster **1** were studied by cyclic voltammetry (CV) and controlled potential electrolysis

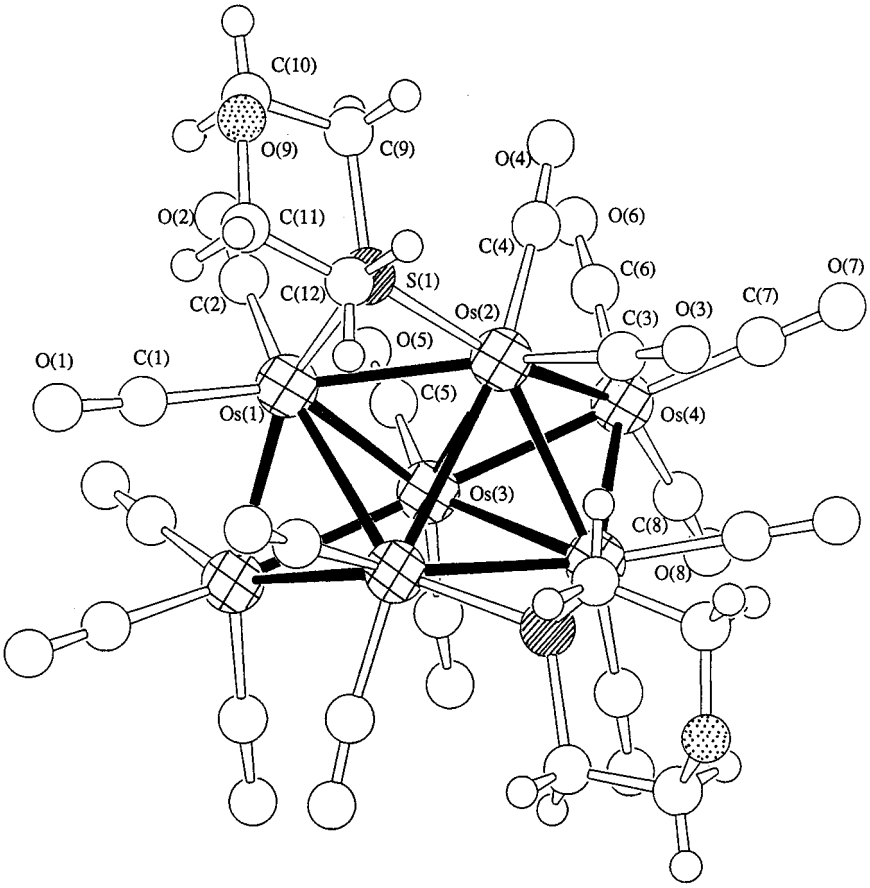


Figure 1. Molecular structure of cluster **1** with atom labels for non-hydrogen atoms

Table 2. Selected bond lengths [Å] and angles [°] for cluster **1**

Os(1)−Os(2)	2.737(1)	Os(3)−Os(4)	2.722(1)
Os(1)−Os(2)*	2.830(1)	Os(1)−S(1)	2.292(4)
Os(1)−Os(3)	2.705(1)	Os(2)−S(1)	2.288(4)
Os(1)−Os(4)*	2.744(1)		
Os(2)−Os(2)*	2.994(1)	Os(1)−S(1)−Os(2)	73.4(1)
Os(2)−Os(3)	2.703(1)	S(1)−Os(1)−Os(2)	53.2(1)
Os(2)−Os(4)	2.877(1)	Os(1)−Os(2)−S(1)	53.4(1)

(CPE) at a platinum disc electrode. The parent cluster $[Os_7(CO)_{21}]$ undergoes a single, irreversible two-electron transfer step with $E_p = -0.10$ V vs Ag/AgCl, to yield the corresponding dianion $[Os_7(CO)_{20}]^{2-}$. We believe that the incorporation of a sulfur heteroatom in the cluster framework should lead to changes in redox behaviour. The cyclic voltammograms of compound **1** in acetonitrile solution contained an irreversible cathodic wave at ca. $E_p = -0.22$ V vs Ag/AgCl. Cyclic voltammetric measurements were obtained at scan rates varying from 50 mV to 10,000 mV s^{-1}, but the ΔE_p values remained virtually unchanged. This observation, together with the findings in CPE, are characteristic of an irreversible two-electron transfer process involving reduction of **1** into its corresponding dianion $[\mathbf{1}]^{2-}$. Because the thioxane groups are better σ-donors than carbonyl ligands are, coordination of such a good σ-donor in **1** would raise the LUMO energy; this in turn would make reduction more difficult, and would therefore lead to a more cathodic potential. For **1**, an additional irreversible anodic wave is located at ca. $E_p = +0.37$ V vs Ag/AgCl. It is likely that this oxidation process, which is absent in the parent cluster, is the consequence of oxidation of the thioxane ligands. Ferrocene was added as an internal reference, and its half-wave potential $E_{1/2} = +0.10$ V vs Ag/AgCl remained practically constant throughout the measurement. The electrochemical data are collected in Table 3.

Table 3. Cyclic voltammetric data for $[Os_7(CO)_{21}]$ and compounds **1**, **2**, and **3** in MeCN (0.1 mol dm^{-3} $^nBu_4NPF_6$) at 298 K

Compound	E_{pa} [V][a] vs $Ag/AgNO_3$	E_{pc} [V][a] vs $Ag/AgNO_3$
$[Os_7(CO)_{21}]$	–	−0.10
1	+0.37	−0.22
2	+0.37	−0.24
4	+0.38	−0.17

[a] E_{pa} and E_{pc} are the anodic and cathodic potentials respectively.

The heptametallic cluster **2** is analogous to **1**, except that one bridging thioxane group is replaced by a terminally bonded ligand. In the solid state, both ligand forms are in the chair conformation, with all the C−C bonds staggered. A perspective drawing of cluster **2** with its atomic numbering is shown in Figure 2. Some important bond parameters are given in Table 4. Compared with their counterparts in compound **1**, all the metal−metal bond lengths are within

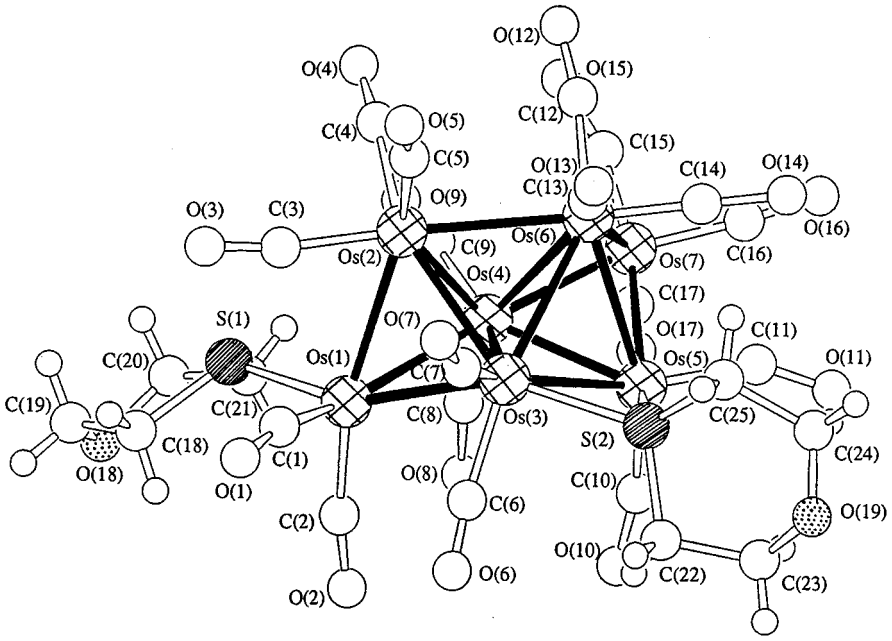


Figure 2. Molecular structure of cluster **2**

the expected ranges. The redox properties of complex **2** were also studied, and all the electrochemical data are presented in Table 3. The cyclic voltammograms of **2** are very similar to those of **1**, with one irreversible reduction wave at ca. $E_p = -0.24$ V and one irreversible oxidation peak at ca. $E_p = +0.37$ V vs Ag/AgCl. The assignment of these two

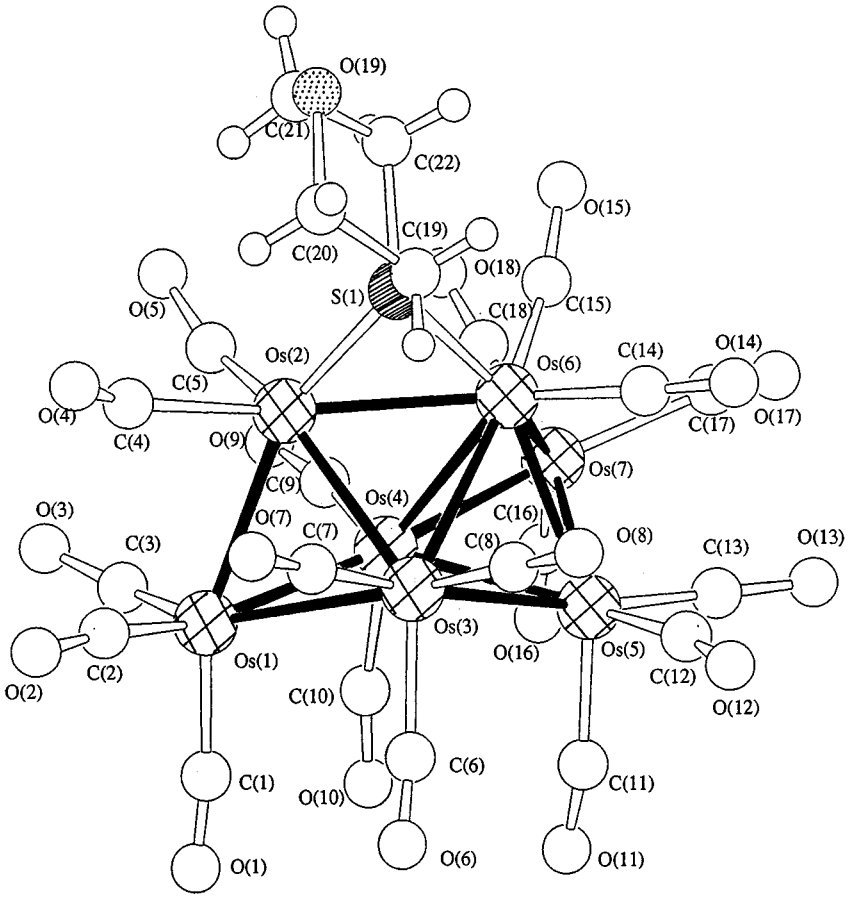


Figure 3. Molecular structure of cluster **3**

Table 4. Selected bond lengths [Å] and angles [°] for cluster **2**

Os(1)−Os(2)	2.830(3)	Os(4)−Os(7)	2.676(3)
Os(1)−Os(3)	2.860(3)	Os(5)−Os(6)	2.853(3)
Os(1)−Os(4)	2.727(3)	Os(5)−Os(7)	2.789(4)
Os(2)−Os(3)	2.812(3)	Os(6)−Os(7)	2.938(3)
Os(2)−Os(4)	2.707(3)	Os(1)−S(1)	2.34(1)
Os(2)−Os(6)	2.875(3)	Os(3)−S(2)	2.32(1)
Os(3)−Os(4)	2.726(3)	Os(5)−S(2)	2.30(1)
Os(3)−Os(5)	2.763(3)		
Os(3)−Os(6)	2.885(3)	Os(3)−S(2)−Os(5)	73.5(5)
Os(4)−Os(5)	2.675(3)	S(2)−Os(5)−Os(3)	53.5(3)
Os(4)−Os(6)	2.780(3)	Os(5)−Os(3)−S(2)	52.9(3)

peaks follow that of **1**, since **1** and **2** are structurally similar.

Carboxylation of **2** in refluxing $CHCl_3$ led to the formation of $[Os_7(CO)_{18}\{\mu\text{-}S(CH_2)_2OCH_2C^aH_2(S-C^\alpha)\}]$ (**4**) which is an isomer of **3**. Spectroscopic data of **4** (FAB MS, ^{1}H-NMR, and IR spectra) suggested that a CO molecule replaced the terminally bonded thioxane ligand. However, prolonged carboxylation of **2** did not recover the starting cluster $[Os_7(CO)_{21}]$. This contrasts with the facile replacement of both thioxane ligands observed for the analogous compound $[Os_6(CO)_{15}\{S(CH_2)_2OCH_2C^aH_2(S-C^\alpha)\}\{\mu\text{-}S(CH_2)_2OCH_2C^aH_2(S-C^\alpha)\}]$.[20] Under similar conditions, **2** did not react with molecular hydrogen.

The metal skeleton of **3** is identical to that of **1** and **2**, with eighteen terminally bonded carbonyl groups and a thioxane ligand bridging Os(2) and Os(6). Its molecular structure is presented in Figure 3 and some selected bond parameters are given in Table 5. Interestingly, the structure can be regarded as a monocapped Os(7) atom on the hexanuclear species $[Os_6(CO)_{16}\{\mu\text{-}S(CH_2)_2OCH_2C^aH_2(S-C^\alpha)\}]$ previously reported by us.[20] The three metal−metal bonds between Os(7) and Os(4), Os(5), and Os(6) differ widely, to range from 2.678(4) to 2.866(4) Å, with a slightly tilted capping as a result. However, this is not observed for both clusters **1** and **2**. Cyclic voltammograms of cluster **3** have the same features found for **1** and **2**, with a pair of cathodic and anodic waves at ca. $E_p = -0.17$ V and $+0.38$ V vs Ag/AgCl, respectively. The reduction wave of compound **3**, however, is less cathodic than that of its disubstituted counterparts, reflecting the reduction in electron donation by a single thioxane, and hence a lower LUMO energy.

Table 5. Selected bond lengths [Å] and angles [°] for cluster **3**

Os(1)−Os(2)	2.757(4)	Os(4)−Os(7)	2.678(4)
Os(1)−Os(3)	2.941(4)	Os(5)−Os(6)	2.792(4)
Os(1)−Os(4)	2.694(4)	Os(5)−Os(7)	2.830(4)
Os(2)−Os(3)	2.845(4)	Os(6)−Os(7)	2.866(4)
Os(2)−Os(4)	2.674(4)	Os(2)−S(1)	2.26(2)
Os(2)−Os(6)	2.760(4)	Os(6)−S(1)	2.32(2)
Os(3)−Os(4)	2.738(4)		
Os(3)−Os(5)	2.867(4)		
Os(3)−Os(6)	2.911(4)	Os(2)−S(1)−Os(6)	74.1(5)
Os(4)−Os(5)	2.723(4)	S(1)−Os(6)−Os(2)	52.0(5)
Os(4)−Os(6)	2.727(4)	Os(6)−Os(2)−S(1)	53.9(5)

Although compounds **1**, **2**, and **3** have identical metal architectures and similar ligand dispositions, there is no evidence for their interconversion. Neither **3** nor **4** could be obtained from prolonged carboxylation of **1** in $CHCl_3$. Similarly, treating **3** with an excess of thioxane did not lead to the isolation of **4**, and vice versa. The change of the metal core in **1**, **2** and **3** from the starting osmium cluster $Os_7(CO)_{21}$ can take place in the preparation of $Os_7(CO)_{19}(MeCN)_2$. However, we have not been able to obtain the structure of $Os_7(CO)_{19}(MeCN)_2$.

Experimental Section

General: All reactions and manipulations were carried out under dry argon with standard Schlenk techniques. All solvents were purified and dried by standard methods prior to use.[21] Chemicals were purchased from Aldrich Chemicals and were used as received. Vacuum pyrolysis of $[Os_3(CO)_{12}]$ gave the heptaosmium cluster $[Os_7(CO)_{21}]$;[2] $[Os_7(CO)_{19}(MeCN)_2]$ was prepared as described below. − Infrared spectra were recorded on a Bio-Rad FTS-7 spectrometer, in 0.5 mm thick calcium fluoride solution cells. − ^{1}H NMR and ^{1}H{^{1}H} COSY spectra were recorded on a Bruker DPX-300 NMR spectrometer, in CD_2Cl_2 with reference to $SiMe_4$ (δ = 0). − Mass spectra were measured on a Finnigan MAT 95 instrument by the fast atom bombardment technique, with *m*-nitrobenzyl alcohol or α-thioglycerol as the matrix solvents. − Elemental analyses were conducted by Butterworth Laboratories, UK. − Routine separation of products in air was performed by thin-layer chromatography (TLC), on plates coated with Merck kieselgel 60 GF_{254}. − All electrochemical measurements were performed under an argon purge, to exclude oxygen, in a conventional two-compartment cell, separated by a sintered glass disc. Acetonitrile was freshly distilled and de-aerated prior to use. The supporting electrode was 0.1 M tetra-*n*-butylammonium tetrafluoroborate in MeCN. Voltammetric experiments were carried out with a Princton Applied Research (PAR) model 273A potentiostat, connected to an interfaced computer. A standard three-electrode cell consisting of an Ag/AgCl reference electrode (Bioanalytical), a platinum wire counter electrode (Aldrich), and a glassy carbon working electrode (Bioanalytical) were employed. The ferrocenium/ferrocene couple ($FeCp_2^{+/0}$) was used as internal reference.

Preparation of $[Os_7(CO)_{19}(MeCN)_2]$: The compound $[Os_7(CO)_{21}]$ (200 mg, 0.104 mmol) was dissolved in a mixture of CH_2Cl_2 (90 cm^3) and MeCN (7.2 cm^3) to give a bright orange solution. The reaction mixture was stirred at −78 °C for 30 min before dropwise addition of a Me_3NO solution (16 mg, 2 mol-equiv) in CH_2Cl_2 from a pressure-equalizing dropping funnel. After all the Me_3NO solution had been added, the reaction mixture was further stirred for 15 min before leaving it to warm up at ambient temperature. Excess Me_3NO was then filtered off and the solvent was removed in vacuo to give a bright brown solid residue. (Yield: 102 mg, 50%)

Preparation of $[Os_7(CO)_{16}\{\mu\text{-}S(CH_2)_2OCH_2C^aH_2(S-C^\alpha)\}_2]$ (1), $[Os_7(CO)_{17}\{\mu\text{-}S(CH_2)_2OCH_2C^aH_2(S-C^\alpha)\}\{S(CH_2)_2OCH_2C^aH_2(S-C^\alpha)\}]$ (2), and $[Os_7(CO)_{18}\{\mu\text{-}S(CH_2)_2OCH_2C^aH_2(S-C^\alpha)\}]$ (3): The cluster $[Os_7(CO)_{19}(MeCN)_2]$ (120 mg, 0.062 mmol) was dissolved in CH_2Cl_2 (40 cm^3) and stirred while a dilute solution of 1,4-thioxane (0.57 cm^3 diluted in 10 cm^3 CH_2Cl_2) was added dropwise over 30 min at ambient conditions. After the reaction continued for a further 6 h, the solution was filtered and the volume was reduced to ca. 5 cm^3 in vacuo. The residue was subsequently purified by TLC using hexane/CH_2Cl_2 (10:20 v/v) as eluent. Three brown bands: **1** (R_f = 0.77, 20 mg, 0.010 mmol, 16%), **2** (R_f = 0.59, 45 mg, 0.022 mmol, 36%), and **3** (R_f = 0.32, 18 mg, 0.016 mmol, 27%), together with several uncharacterized, low-yield products were then eluted consecutively. Brown crystals suitable for diffraction analyses of **1** and **3** were obtained, separately, from $CHCl_3$/

Table 6. Summary of crystal data and data collection parameters for clusters **1**, **2**, and **3**

Compound	**1**	**2** · C_7H_8	**3**
Empirical formula	$C_{24}H_{16}O_{18}Os_7S_2$	$C_{32}H_{24}O_{19}Os_7S_2$	$C_{22}H_8O_{19}Os_7S$
M	1987.90	2108.05	1939.75
Crystal colour, habit	brown, cubic	brown, rod	brown, cubic
Crystal size [mm]	0.21 × 0.25 × 0.19	0.16 × 0.18 × 0.25	0.18 × 0.18 × 0.19
Crystal system	monoclinic	triclinic	monoclinic
Space group	*C*2/*c* (#15)	*P*1bar (#2)	$P2_1/n$ (#14)
a [Å]	21.818(1)	11.302(1)	18.904(1)
b[Å]	10.325(1)	14.639(2)	9.410(1)
c[Å]	18.687(1)	17.050(1)	19.729(1)
α [°]	–	72.05(1)	–
β [°]	118.43(1)	89.59(1)	111.92(1)
γ [°]	–	69.67(1)	–
V [Å^3]	3702.1(5)	2500.7(5)	3255.8(6)
Z	4	2	4
D [g cm^{-3}]	3.566	2.799	3.957
F(000)	3472	1864	3360
μ(Mo-K_α) [cm^{-1}]	240.95	178.46	273.33
No. reflections collected	16211	21001	28739
No. unique reflections	3708	6491	4877
No. observed reflections [$I > 1.50\sigma(I)$]	2776	3620	2205
R	0.049	0.089	0.084
R′	0.057	0.097	0.083
Goodness of fit	1.38	1.49	1.31
Maximum Δ/σ	0.00	0.00	0.00
No. parameters	231	258	237
Maximum, minimum density in (*F* map/e Å^{-3}, close to Os)	3.60, −2.99	3.72, −2.99	3.15, −2.95

toluene solutions (1:8 v/v), at room temperature, after 3 and 6 d, respectively. Compound **2** was obtained, by slow evaporation of a toluene/$CHCl_3$ solution at −10 °C for 4 d, as brown, rod-shaped crystals, as a solvate of stoichiometry **2**·C_7H_8. – **1**: $C_{24}H_{16}S_2O_{18}Os_7$: calcd. C 14.5, H 0.8, S, 3.2; found C 14.2, H 0.8, S 3.2. – **2**: $C_{25}H_{16}S_2O_{19}Os_7$: calcd. C 14.9, H 0.8, S 3.2; found C 15.0, H 0.9, S 3.2. – **3**: $C_{22}H_8SO_{19}Os_7$: calcd. C 13.6, H 0.4, S 1.7; found C 13.4, H 0.4, S 1.7.

Carboxylation and Hydrogenation of 2: Compound **2** (40 mg, 0.020 mmol) was continuously purged with a stream of carbon monoxide, in refluxing $CHCl_3$ (10 cm^3). Reaction progress was monitored by solution infrared and spot TLC over a period of 4 h. The solvent was then removed in vacuo, the residue was redissolved in a minimum amount of CH_2Cl_2 and purified by TLC, with hexane:CH_2Cl_2 (10:20 v/v) as eluent, to give compounds **4** (R_f = 0.66, 11 mg, 0.006 mmol, 29%) and unchanged **2** (R_f = 0.38, 20 mg, 0.010 mmol, 50%). The procedure described was repeated with hydrogen, but no observable changes were detected by either spot TLC or IR monitoring.

Crystallography: Single crystals, suitable for X-ray crystallography, were chosen for clusters **1** and **3.** Compound **3** was mounted on a glass fibre while **2** was mounted in a Lindermann glass capillary with epoxy resin. Diffraction data were collected at ambient temperature on a MAR research imaging plate diffractometer for exposure periods of 300, 600, and 360 s per frame for compounds **1**, **2**, and **3** respectively. All intensity data were corrected for Lorentz and polarization effects. An approximation of absorption correction by inter-image scaling was applied for all compounds. Space groups were determined for all the crystals from a Laue symmetry check, and their systematic absences, and were then confirmed by successful refinement. The structures were solved by direct method SIR92[22] and expanded by difference Fourier technique. For **1**, the solution was refined on *F* by full-matrix least-squares analysis with all atoms refined anisotropically while all the hydrogen atoms in the ligand were generated in their idealized positions (C−H 0.95 Å) and fixed throughout. However, for **2**, attempts to refine all non-hydrogen atoms anisotropically gave unreasonably high thermal parameters for the C and O atoms. Therefore, only the heavy atoms (Os and S) were included in subsequent anisotropic refinement cycles. Initial attempts to refine the toluene solvent in **2** by rigid-group constraint gave high B_{eq} values, indicating considerable disorder. It was then fixed throughout in the subsequent refinement processes to give a significant improvement. As a result of the poor quality of the diffraction data for complex **3**, only heavy atoms such as osmium and sulfur were subjected to anisotropic refinement. A summary of the crystallographic data is given in Table 6. All calculations were performed on a Silicon-Graphics computer using the program package TEXSAN.[23] Crystallographic data (excluding structure factors) for the structures reported in this paper has been deposited with the Cambridge Crystallographic Data Centre as supplementary publication no. CCDC-119664 to 119666. Copies of the data can be obtained free of charge on application to CCDC, 12 Union Road, Cambridge CB2 1EZ, UK [Fax: (int) +44-1223/336 033; E-mail: deposit@ccdc.cam.ac.uk].

Acknowledgments

We gratefully acknowledge financial support from the Hong Kong Research Grants Council and the University of Hong Kong. K. S.-Y. L acknowledges the receipt of a postgraduate studentship and a scholarship, administered by the University of Hong Kong and the Epson Foundation respectively.

[1] [1a] D. F. Shriver, H. D. Kaesz, R. D. Adams, *The Chemistry of Metal Cluster Complexes*, VCH, New York, **1992**. – [1b] G. Gonzale-Moraga, *Cluster Chemistry*, Springer-Verlag, Berlin, **1994**.

[2] C. R. Eady, B. F. G. Johnson, J. Lewis, *J. Chem. Soc., Dalton Trans.* **1975**, 2606.

[3] B. F. G. Johnson, J. Lewis, M. McPartlin, J. Morris, G. L. Powell, P. R. Raithy, M. D. Vargas, *J. Chem. Soc., Chem. Commun*. **1986**, 429.
[4] [4a] B. F. G. Johnson, J. Lewis, J. A. Lunniss, D. Braga, F. Grepioni, *J. Chem. Soc., Chem. Commun*. **1988**, 972. – [4b] D. Braga, F. Grepioni, B. F. G. Johnson, J. Lewis, J. A. Lunniss, *J. Chem. Soc., Dalton Trans.* **1991**, 2223.
[5] D. Braga, F. Grepioni, B. F. G. Johnson, J. Lewis, J. A. Lunniss, *J. Chem. Soc., Dalton Trans.* **1992**, 1101.
[6] B. F. G. Johnson, J. Lewis, J. A. Lunniss, D. Braga, F. Grepioni, *J. Organomet. Chem*. **1991**, *401*, C46.
[7] [7a] K. S.-Y. Leung, W.-T. Wong, *J. Chem. Soc., Dalton Trans.* **1997**, 4357. – [7b] K. S.-Y. Leung, W.-T. Wong, *J. Chem. Soc., Dalton Trans.* **1998**, 1939.
[8] [8a] Y. -K. Au, K. -K. Cheung, W. -T. Wong, *Inorg. Chim. Acta.* **1995**, *238*, 193. – [8b] Y. -K Au, K. -K. Cheung, W. -T. Wong, *J. Chem. Soc., Dalton Trans.* **1995**, 1047. – [8c] Y. -K Au, K. -K. Cheung, W. -T. Wong, *Inorg. Chim. Acta.* **1995**, *228*, 267.
[9] C. R. Eady, B. F. G. Johnson, J. Lewis, R. Mason, P. B. Hitchcock, K. Thomas, *J. Chem. Soc., Chem. Commun*. **1977**, 385.
[10] J. Lewis, C. -K. Li, C. A. Morewood, M. C. R. de. Arellano, P. R. Raithby, W. -T. Wong, *J. Chem. Soc., Dalton Trans.* **1994**, 2159.
[11] S. M. Waterman, M. G. Humphrey, D. C. R. Hockless, *Organometallics* **1996**, *15*, 1745.
[12] [12a] C. E. Housecroft, A. L. Rheingold, *Organometallics* **1987**, *6*, 1332. – [12b] C. E. Housecroft, A. L. Rheingold, P. Zanello, *J. Organomet. Chem*. **1991**, *408*, 7.
[13] D. L. Sunick, P. S. White, C. K. Schauer, *Inorg. Chem*. **1993, 32**, 5665.
[14] C. E. Housecroft, M. S. Shongwe, A. L. Rheingold, *Organometallics* **1989**, *8*, 2651.
[15] B. F. G. Johnson, J. Lewis, *Adv. Inorg. Chem. Radiochem*. **1981**, *24*, 225.
[16] D. M. P. Mingos, *J. Chem. Soc., Chem.Commun*. **1983**, 706.
[17] R. D. Adams, D. F. Foust, P. Mathur, *Organometallics* **1983**, *2*, 990.
[18] Y. C. Lin, C. B. Knobler, H. D. Kaesz, *J. Organomet. Chem*. **1981**, *213*, C41.
[19] G. R. John, B. F. G. Johnson, J. Lewis, *J. Organomet. Chem*., **1979**, *181*, 143.
[20] K. S.-Y. Leung, W.-T. Wong, *J. Chem. Soc., Dalton Trans.*, submitted for publications.
[21] D. D. Perrin, W. L. F. Armarego, *Purification of Laboratory Chemicals,* 3rd ed., Pergamon, Oxford, **1988**.
[22] SIR92, A. Altomare, M.C. Burla, M. Camalli, M. Cascarano, C. Giacovazzo, A. Guagliardi, G. Polidori, *J. Appl. Crystallogr*, **1994**, *27*, 435.
[23] TEXSAN, Crystal Structure Analysis Package, Molecular Structure Corporation, Houston, TX, **1985** and **1992**.

Received May 5, 1999
[I99168]

Synthesis of Boron-Halogenated Diborylamines and Diborylhydrazines by Cleavage of Stannazanes

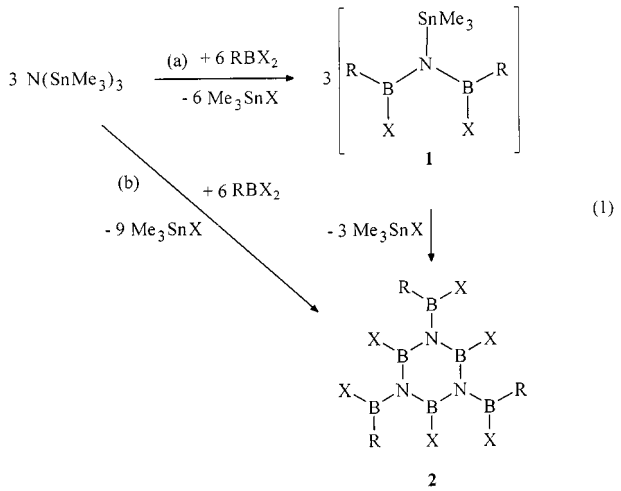
Stefan Diemer,[a] Heinrich Nöth,*[a] and Wolfgang Storch*[a]

Keywords: Diborylamines / Diborylhydrazines / Bis(organohaloboryl)amines / Bis(organohaloboryl)hydrazines / Structure elucidation

The diborylamines R′–N(BRX)$_2$ (**3**; X = Cl, Br) are obtained by stannazane cleavage of distannylorganylamines R′–N(SnMe$_3$)$_2$ (**4**) with alkyldihaloboranes RBX$_2$ in a 1:2 molar ratio. The presence of the sterically demanding substituents R and R′ also causes carbon–tin bond cleavage, resulting in low yields of **3**. However, carbon–tin bond cleavage can be suppressed by the use of bis(dimethylchlorostannyl)-organylamines **5** as the nitrogen source for the synthesis of diborylamines. This results in almost quantitative yields of the compounds **3**. Treatment of the distannylhydrazines R$_2$N–N(SnMe$_3$)$_2$ (**7**) with RBX$_2$ in a 1:2 molar ratio leads to the formation of *N*,*N*-bis(alkylhaloboryl)hydrazines **8** under mild conditions and in good yield. The molecular structures of **3** and **8** were determined by multinuclear magnetic resonance spectra in solution as well as by X-ray structure analysis in the case of **8d**. A typical structural feature of **8d** is the intramolecular BN adduct formation. Support for the constitutions of compounds **8c** comes from MS fragmentation patterns as well as from IR spectra.

Introduction

The synthetic potential of aminostannanes, distannylamines as well as tristannylamines, is due to the easy Sn−N cleavage reactions involving Lewis acids.[1] Diborylamines functionally substituted at the boron atoms of the type Me$_3$SnN(BXR)$_2$ (**1**), obtained by the reaction of (Me$_3$Sn)$_3$N with organyldihaloboranes, are labile for X = Cl, Br. The compounds decompose to borylated borazines **2** by further stannazane bond cleavage[2] according to Equation (1).



(1)

Recently, thermally stable examples of **1,** afforded by replacement of the Me$_3$Sn group by the sterically more demanding *t*Bu group, have been reported.[3] Bis(haloboryl)-amines R′−N(BRX)$_2$ (**3**) with small organyl groups R′ attached to the nitrogen atom, and bulky groups R attached to the boron atoms, are up to this date unknown. Only a few examples of asymmetrically substituted diborylamines with different alkyl groups R and X = Cl at the boron atoms have already been described.[4] Boron-functional diborylamines are, however, useful precursors for the synthesis of B-, N- and Sn-containing heterocycles.[5][6] Two different routes for the synthesis of diborylamines of type **3** have been established in recent years. One route involves the electrophilic addition of dihaloorganoboranes to iminoboranes[6] or to aminoiminoboranes.[7] The other route uses the stannazane bond cleavage of distannylamines with dihaloorganoboranes under kinetically controlled conditions. This route represents a rather convenient method for the synthesis of diborylamines of type **3,** which are not accessible by other routes.[3] Compounds **3** containing electron-withdrawing substituents R′ attached to the nitrogen atoms are hardly known. In particular this concerns *N*,*N*-diborylhydrazines containing the hydrazine moiety, obtained by formal replacement of the R′ group for the R″$_2$N group in diborylamines of type **3**.

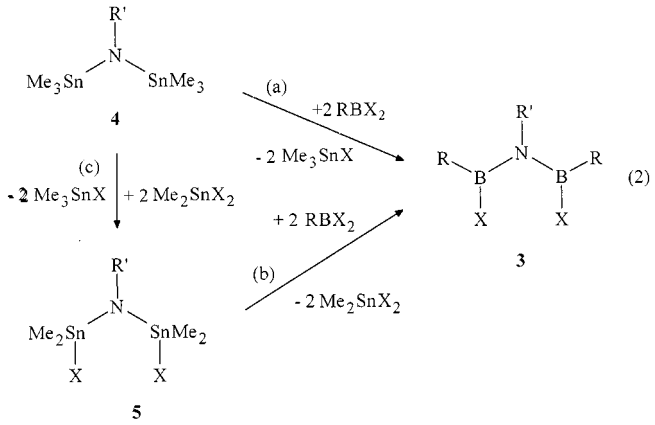
Here we report on the synthesis of boron-halogenated diborylamines and -hydrazines by stannazane cleavage reactions and the spectroscopic properties as well as some structural features.

Bis(organylhaloboryl)organylamines

A series of diborylamines of type **3** (R′ = alkyl) have been reported using bis(trimethylstannyl)organylamines **4** as starting materials according to Equation 2a.[3] However, the synthesis of **3** with sterically more demanding groups R, for example R = *t*Bu, failed, due to the kinetically hindered approach of the organyldihaloborane to the Lewis-basic nitrogen center of **4** (see Formula 2). Therefore, cleavage of carbon−tin bonds predominates over the cleavage of the

[a] Institute of Inorganic Chemistry,
Ludwig-Maximilians-Universität München,
Butenandtstraße 7−13, Haus D, D-81377 München, Germany

 © WILEY-VCH Verlag GmbH, D-69451 Weinheim, 1999 1434−1948/99/1010−1765 $ 17.50+.50/0



3/4/5	a	b	c	d	e	f	g	h	i	k	l	m	n	o	p	q
R	*t*Bu	*t*Bu	Me	Ph	*t*Bu	*t*Bu	*t*Bu	Me	Me	Me	Me	Me	*i*Pr	*t*Bu	Me	Me
R′	Me	Me	Ph	Ph	Ph	Ph	*t*Bu	*t*Bu	Mes	Dipp	Me_3Si	Me_3Si	Me_3Si	Me_3Si	Me_3Si	Mes
X	Cl	Br	Br	Cl	Cl	Br	Cl	Br	Br	Br	Cl	Br	Br	Cl	Cl/Br	Me
Equation	2b	2a/b	2a	2b	2b	2c/2b	2b	2a/2b	–	–	2b	2a	2a	2b	2b	2c,b

nitrogen−tin bonds even under mild conditions. However, Sn−N cleavage is favoured again by treatment of the distannylamines $R'-N(SnMe_3)_2$ (**4**) with small organoboronhalides: For example reaction of **4** (R′ = *t*Bu) with RBX_2 compounds containing the sterically less demanding methyl group yields the diborylamine **3h**.[3] However, the Sn−N bond cleavage of **4** proceeds under mild conditions with $MeBBr_2$, and even with *i*PrBBr$_2$, yielding **3m**[8] and **3n**, in the case of R′ = Me_3Si. However, isolation of the *N*-phenyldiborylamines **3c** and **3d** failed, because they decompose rapidly to the respective borazines and organodihaloboranes (see Equation 1b) on removing the solvent from the reaction mixtures. **3f** could also not be isolated, because the stannylaminoborane, *t*BuBrB−NPh−$SnMe_3$, detected by NMR as an intermediate, decomposes more rapidly with formation of a borazine (see Equation 1) prior to a second Sn−N bond cleavage. In addition, there is a competitive reaction due to the carbon−tin bond cleavage. Obviously, the low basicity of the anilino nitrogen atom prevents the attack of another alkylboron dihalide at the N centre. However, when *N*-methyldistannylamine (**4a**) is used, the Sn−N bond cleavage is favored even when it is treated with *t*BuBBr$_2$. The product obtained is **3b** according to Equation 2a. In this case the ratio of Sn−N to Sn−C bond cleavage is 4:1, estimated on the basis of the ^{11}B-NMR spectrum of the reaction mixture. Contrary to these findings the distannylamines **4i** and **4k,** bearing sterically demanding groups R′, react even with $MeBBr_2$ quantitatively to give Me_2BBr and the bis(bromostannyl)amines **5i** and **5k,** respectively,[9] according to Equation 3.

$$\underset{\textbf{4i,4k}}{R'-N(SnMe_3)_2} \xrightarrow[-\ 2\ Me_2BBr]{+\ 2\ MeBBr_2} \underset{\textbf{5i, 5k}}{R'-N(SnMe_2Br)_2} \qquad (3)$$

Performing the same reaction with **5i**, with the sterically less demanding mesityl group as substituent R′ yields the

$$\underset{\textbf{5i}}{Mes-N(SnMe_2Br)_2} \xrightarrow[-\ 2\ Me_2SnBr_2]{+\ 2\ Me_2BBr} \underset{\textbf{3q}}{Mes-N(BMe_2)_2} \qquad (4)$$

products according to Equation 3 in the first step, but does not prevent further attack of Me_2BBr to immediately form the diborylamine **3q** at room temp. according to Equation 4.

In summary, when distannylamines, $R'-N(SnMe_3)_2$ (**4**) are used as starting materials for the synthesis of *B*-halogen-substituted diborylamines according to Equation 2a, Sn−C bond cleavage reactions can only be suppressed partially. However, almost quantitative Sn−N bond cleavage occurs when distannylamines **5** of type $RN(SnMe_2X)_2$ are treated with organoboron dihalides according to Equation 2b.

Therefore, the whole series of halogenoboron diborylamines **3a**−**3q** can be prepared using a procedure according to Equation 2b, except for **3i** and **3k**. No reaction occurs on treatment of the distannylamines **5i** and **5k** with $MeBBr_2$ even under reflux conditions for several hours. As mentioned above, the steric demands of the mesityl- and the 2,6-diisopropylphenyl group attached to the nitrogen atom of the distannazanes **5i** and **5k** prevents the attack of $RBHal_2$ at the N atom, but not at the Sn atom of the Me_3Sn moiety. Consequently, **5i** and **5k** even react with the strong Lewis acid BCl_3 with formation of the distannazanes $RN(SnMe_2Cl)_2$ by tin−carbon bond cleavage.[9]

Sterically demanding groups R attached to the boron atoms in RBX_2 also hinder the stannazane cleavage reactions, even if the distannylamine bears a sterically less demanding group R′ at the nitrogen atom. Therefore only one of the Sn−N bonds of **5a** is cleaved by treatment with an excess of $MesBCl_2$ after a period of 2 d in boiling $CHCl_3$ according to Equation 5.

Purification of the stannylaminoborane **6a** by distillation or recrystallisation failed due to slow decomposition at

$$[Me\text{-}N(SnMe_2Cl)_2]_2 \xrightarrow[-\,Me_2SnCl_2\ -\,2\,MesBCl_2]{+\,4\,MesBCl_2} 2\ Mes(Cl)B\text{—}NMe\text{—}SnMe_2Cl \qquad (5)$$

(5a)$_2$ **6a**

room temp., as indicated by ^{11}B-NMR spectroscopy. However, the presence of stannylaminoboranes **6** as intermediates en route to diborylamines is shown not only by NMR spectroscopy, but also by the reaction of the distannylamine $PhN(SnMe_2Cl)_2$ (**5d**) with $MesBCl_2$ in a 1:1 molar ratio according to Equation 6b. The stannylaminoborane **6d**, which could not be isolated, subsequently reacts with $MeBBr_2$ in a 1:1 molar ratio with the formation of the asymmetrically substituted diborylamine **3r** according to Equation 6c.

$$PhN(SnMe_3)_2 \xrightarrow[-\,2\,Me_3SnCl]{+\,2\,Me_2SnCl_2} PhN(SnMe_2Cl)_2 \qquad (6a)$$

4c **5d**

$$\mathbf{5d} \xrightarrow[-\,Me_2SnCl_2]{+\,MesBCl_2} \mathbf{6d} \qquad (6b)$$

$$\mathbf{6d} \xrightarrow[-\,Me_2SnBr_2]{+\,MeBBr_2} \mathbf{3r} \qquad (6c)$$

Surprisingly, the diborylamine **3r** can be distilled in vacuo and heated to 90°C without decomposition. In general, the synthesis of a variety of diborylamines of type **3** follows the route shown in the Equations 2c and 2b, and described step by step for **3r** (Equations. 6a–c). The derivatives **3e** and **3f**, which are also not accessible following the route according to Equation 2a, are obtained in good yield using the "one-pot reaction" described in Equations 6a–c. The progress of the reactions described by Equations 2c and 2b, leading to the formation of **3e**, has been monitored by ^{11}B-NMR as a function of time during a period of 145 h; the result is shown in Figure 1. A typical feature of this reaction is the exchange of a bromine atom of *t*BuBBr$_2$ against a chlorine atom of the distannazane **5d** in the initial step. After warming the reaction mixture from −50°C to ambient temp. over a period of 2.5 h the cleavage of the first tin–nitrogen bond of **5d** is completed with formation of the stannylaminoborane PhN(B*t*BuCl)SnMe$_2$Cl. As shown in Figure 1 even after 4 d no further reaction occurs with another equiv. of the alkylhaloborane at room temp.

However, the second Sn–N bond cleavage starts if the reaction mixture is maintained at reflux, and after 2 h the respective diborylamine **3e** is found. It can be isolated (b.p. 50°C/high vac) in good yield, decomposing to yield only trace amounts of the borazine (PhNB*t*Bu)$_3$ under these conditions. Nevertheless, the Cl/Br exchange proceeds selectively as well as quantitatively. This reaction can be used as a convenient method to introduce B–Cl bonds in functionally substituted diborylamines starting with bromoboranes.

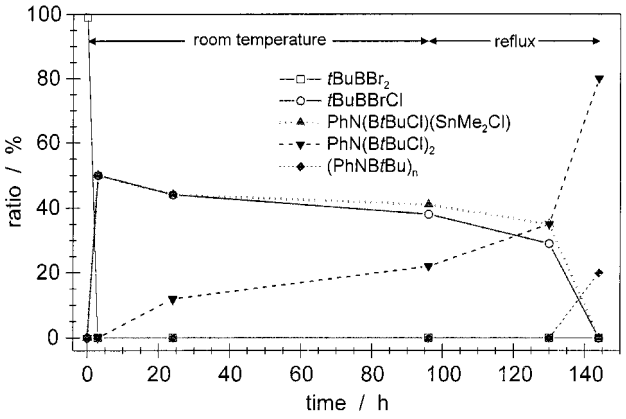


Figure 1. Reaction of $PhN(SnMe_2Cl)_2$ (**5d**) with *t*BuBBr$_2$ in a 1:2 molar ratio monitored by ^{11}B NMR over a period of 145 h

N,*N*-Bis(organylhaloboryl)-*N*′,*N*′-diorganylhydrazines

A variety of cyclic 1,1-diborylhydrazines[10] as well as few examples of noncyclic derivatives[11] are already known. Their chemical properties and structural features, for example the donor property of the diorganylamino group of the hydrazine moiety,[11b] are scarcely investigated. However, functionally boron-substituted diborylhydrazines, are hitherto unknown, although they might be attractive reagents in preparative chemistry. Moreover, they may offer information about structure and bonding, and for that reason we looked for a convenient access to this class of compounds.

The synthesis of *N*,*N*-diorganyl-*N*′,*N*′-dihaloborylhydrazines is achieved under mild conditions by allowing distannylhydrazines **7** to react with RBX_2 in a 1:2 molar ratio according to Equation 7.

$$R'_2N\text{—}N(SnMe_3)_2 \xrightarrow[-\,2\,Me_3SnX]{+\,2\,RBX_2} R'_2N\text{—}N(BRX)_2 \qquad (7)$$

7 **8**

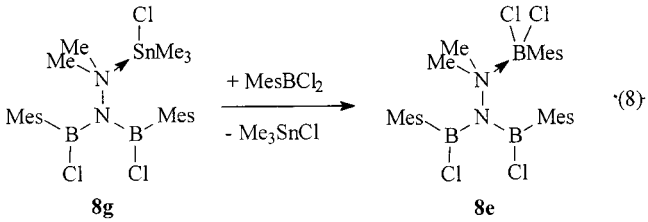
	7a	**7b**
R'	Me	Ph

	8a	**8b**	**8c**	**8d**	**8e**	**8f**
R	Me	*i*Pr	*t*Bu	Mes	Me	*t*Bu
R'	Me	Me	Me	Me	Ph	Ph
X	Br	Br	Br	Cl	Br	Br

Contrary to the Sn–C bond-cleavage reaction occurring with the formation of the diborylamines **3** according to Equation 2a, no such bond cleavage reaction has been observed in case of the distannylhydrazines. The basicity of the tin atoms bearing a nitrogen atom in compounds **7** is obviously high compared to the distannylamines **4**, presumably due to the α-effect of the nitrogen atom of the adjacent R_2N group.[12] Subsequently, the Sn–N bond cleavage proceeds quantitatively according to Equation 7, even in the presence of sterically demanding groups R attached to the boron atoms of RBX_2.

The treatment of the distannylhydrazines **7a** or **7b** with $MeBBr_2$ according to Equation 7 produces only a colorless solid, insoluble in polar and nonpolar solvents, after removal of the volatile components. The ^{11}B- and the ^{119}Sn-NMR spectra recorded from the reaction mixture before removal of the volatile components, however, indicate the formation of the diborylhydrazines **8a** and **8e**. In contrast, the reaction of RBX_2 with bulkier groups R = *i*Pr, *t*Bu, and Mes proceeds slowly with formation of **8b**−**d**. Surprisingly, these compounds show two ^{11}B-NMR signals pointing to the presence of tri- and tetracoordinated boron atoms (see Table 2). The remarkable structural difference between the diborylhydrazines **8** when compared to the diborylamines **3** is the formation of an intramolecular Lewis acid/base adduct, featuring a three-membered B_2N ring unit (see below). The presence of monomeric molecular units is also confirmed by a molecular-mass determination of compounds **8** in solution.

Treatment of the *N*,*N*-diphenyl-*N*′,*N*′-distannylhydrazines **7** with $MeBBr_2$ or $tBuBBr_2$ yields the corresponding diborylhydrazines, which, however, could be detected only in solution. A variety of signals are found in the ^{11}B-NMR spectrum of the reaction mixture [^{11}B NMR: (= 50.2 (**8f** uncertain), 30.3, 22.5, 2.6].[9] The isolation of **8e** and **8f** from the insoluble residue failed, presumably due to the formation of polymeric species by intermolecular B←N interaction, or adduct formation of the R_2N group of **8** with Me_3SnX. The latter can be excluded by controlling the reaction conditions, especially the concentration of the starting materials in the reaction mixture. For example, the diborylhydrazine **8d** formes an adduct only with Me_3SnCl (**8g**) when the concentration of the distannylhydrazine **7a** exceeds 0.13 mol/L in a dichloromethane solution, and the addition time of $MesBCl_2$ is shorter than 60 min (see Experimental Section). In this case the tin halide is only released from **8g** by substitution with an excess of $MesBCl_2$, forming **8h** according to Equation 8.



8g **8e** (8)

NMR Spectra

Diborylamines

Selected ^1H-, ^{11}B-, ^{13}C-, and ^{14}N-NMR data of the *B*-halogen substituted diborylamines **3** and triborylamines are listed in Table 1, and of halogenated diborylhydrazines **8** in Table 2. Both tables also contain NMR data of some other compounds for comparison. For additional data see the Experimental Section.

The shielding of the ^{11}B and ^{14}N nuclei are in accordance with a trigonal-planar environment of both atoms in the diborylamines of type **3**. They are also in agreement with the data of known diborylamines.[3][6] However, compared to aminohaloboranes, for example $Me_2N-B(Me)Cl$ (^{11}B NMR: δ = 38.5),[13] the ^{11}B nuclei of the diborylamines are deshielded by 10−15 ppm, as there is only one pair of electrons at the N atom to be shared by two boron atoms in (pp) π-bonding. Additional deshielding results from the torsion between the planes of the boron and the nitrogen atoms due to the bulky substituents R and R′ attached to these atoms. This causes an additional decrease of the (BN) π-interaction. In contrast to the ^{11}B-NMR data of asymmetrically substituted diborylamines of the type $RN(BR'X)(BR''X)$[6] with two different ^{11}B-NMR signals (see Table 1; **3p**), there is only one signal detected for the two boron nuclei in **3r**. Therefore, the degree of distortion around the BN axis of both of the boryl groups in type **3** compounds, due to sterically induced crowding, is approximately of the same order, featuring a geometry shown in Figure 2c. The structure of a "borylated aminoborane" **b** (see Figure 2) assumed for compounds of type **3p** as well as a planar diborylamine framework **a** (see Figure 2) can be excluded.

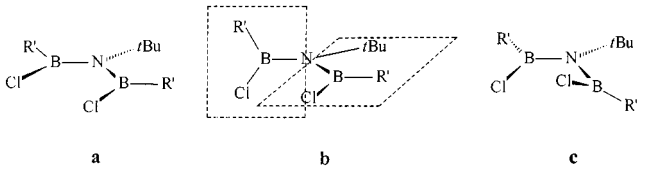


Figure 2. Alternative stereoisomers of diborylamines of type **3**

It is well known that in compounds RR′BX, the exchange of a chlorine for a bromine atom[14] results in a significant deshielding of the boron nucleus. This influence is also detected in the diborylamines of type **3**. Electron-withdrawing substituents (for example R′ = Ph) or sterically demanding groups attached to the nitrogen atom (for example R′ = $SiMe_3$, causing a larger torsion angle between the boron and nitrogen planes) also exhibit a significant downfield shift of the ^{11}B resonance. However, introduction of a third boryl group (R_2B) at the nitrogen atom leads to a larger deshielding of the boron nuclei of ca. 8 ppm, due to the π-acceptor quality of this group. **3t** (see Table 1) represents one of the rare examples of an asymmetrically substituted triborylamine.[15]

The π-acceptor function of the different boryl groups in diborylamines of type **3** is shown by the deshielding of the central nitrogen nucleus. Our NMR study confirms, that a deshielding of the nitrogen nuclei is accompanied by better shielding of the boron nuclei, owing to (BN)π interaction and vice versa. The larger sensitivity of the nitrogen nucleus to changes in (BN)π interaction is demonstrated by comparison of the $\delta^{14}N$ data for the diborylamines **3l**−**3m** as well as that of **3o**−**3n**. Replacement of a chlorine by a bromine atom leads to a significant downfield shift of about 15−16 ppm (^{14}N), as a consequence of less (BX) π-bonding in the B−Br bond. Moreover, the influence of the sterically

Table 1. ^{11}B-, ^{14}N-, ^{1}H- and ^{13}C-NMR data of diborylamines and related compounds

Compound	No.	δ^{11}B (ppm)	$h_{1/2}$ [Hz]	δ^{14}N (ppm)	$h_{1/2}$ [Hz]	^{1}H NMR (δ) *ECH*	BC*H*	BCC*H*	^{13}C NMR (δ) E*C*	B*C*	BC*C*	Remark
Me−N(B*t*BuCl)$_2$	**3a**	49.9	154	−268	178	2.90	–	1.08	33.16	25	28.31	[a]
Me−N(B*t*BuBr)$_2$	**3b**	48.0	174	−259	197	2.88	–	1.09	33.95	26	28.48	[a]
*t*Bu−N(B*t*BuCl)$_2$	**3g**	45.5		−226		–	–	1.11	55.13	27	30.32	[a,b]
Ph−N(BMeBr)$_2$	**3s**	51.0	161			–	1.2	–				[c]
Ph−N(B*t*BuCl)$_2$	**3e**	50.6	253	−234	506	–	–	1.01	141.47	26	28.65	[a]
Ph−N(B*t*BuBr)$_2$	**3f**	49.3	300	−228	488	–	–	0.98	141.39	27	29.24	[a]
Ph−N(BPhCl)$_2$	**3d**	46.9	385			–	–					[c]
Ph−N(B^{1}MeCl)−B^{2}MesCl	**3r**	50.2	600	not measured		–	0.91	–	146.54	10 (B^1)	136.78	[a,d]
Me$_3$Si−N(BMeCl)$_2$	**3l**	50.3	128	−234	84	0.30	0.86	–	1.80	12	–	[e1,f]
Me$_3$Si−N(BMeBr)$_2$	**3m**	49.8	248	−219		0.35	1.09	–			–	[e2,g]
Me$_3$Si−N(B*i*PrCl)$_2$		52.2		−239		0.18	1.03	0.97	1.78	24.2		[e3,h]
Me$_3$Si−N(B*i*PrBr)$_2$	**3n**	52.2	321	−230	109	0.33	1.33	1.05	1.89	25.8	19.12	[e4,h]
Me$_3$Si−N(B*t*BuCl)$_2$	**3o**	53.8	218	−246	271	0.39	–	1.02	4.41	34.3	28.87	[e5,g,i]
*t*Bu−N(B^{1}EtCl)−	B^1	63.6		not measured		–	1.1 m	–	–	9.0	29.2q	[i]
(B^2*t*Bu Cl) (**3s**)	B^2	40.4					–	1.45	55.7			
Me$_2$B^1−N(B^{2}MeBr)$_2$	B^1	68.4		−204		–	1.1	–	–			[h]
	B^2	47.1					–	0.97				
*i*Pr$_2$B^1−N(B^2*i*PrCl)$_2$	B^{1}B^2	72.5		−213		–	1.1 m	1.1 m	–	24.22	19.41	[h]
		47.5					1.0 m	1.0 m		2.4	9.2	
Me$_2$B^1−N(B^2*t*BuCl)$_2$	B^1	62.6	276	−206	180	–	0.71	–	–	14	–	
(**3t**)	B^2	56.6	291				–	1.06		12	28.51	

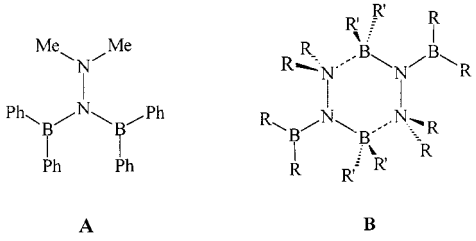
[a] E = N. – [b] Data from ref.[43]; ^{1}H/^{11}B values are largely consistent with the data of Paetzold et al.[6] – [c] Recorded as a sample of the reaction mixture (CH_2Cl_2); isolation failed. – [d] ^{11}B signal accompanied by a high-field shoulder at δ ≈ 48 (B^1 or B^2); assignment not possible. – [e1] E = Si; ^{29}Si NMR: δ = 6.46; [e2] not measured; [e3] 4.6; [e4] 5.61; [e5] 7.56. – [f] ^{11}B-, ^{14}N- and ^{1}H-NMR data in agreement with ref.[44] – [g] Data from ref.[45] and references there. – [h] Data from ref.[3] – [i] ^{11}B, ^{1}H and ^{13}C values largely consistent with those of Paetzold et al.[6]

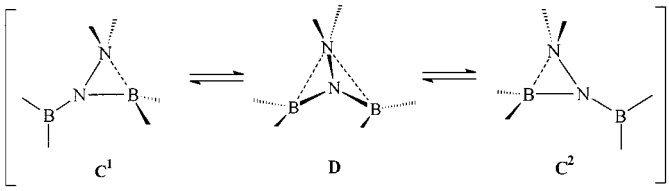
demanding groups R′ on the torsion angle between the nitrogen and the boron planes is demonstrated by a significant deshielding of the nitrogen nuclei as demonstrated by the compound pairs **3n/3o** (ΔN: +12 ppm) and **3m/3n** (ΔN: +11 ppm).

The ^{1}H- and ^{13}C-NMR data also are in accordance with the suggested structures, particularly the monomeric molecular geometry of the species of type **3**. The ^{13}C-NMR signals of the carbon atoms directly linked to the boron atoms can only be detected by cooling the sample between −20°C to −40°C. At ambient temp. the signals vanish due to quadrupolar relaxation of the second kind.[16] The ^{13}C resonances of carbon atoms adjacent to the boron atoms are hardly affected by changes of the shielding at the boron nuclei owing to smaller changes of the polarity of the B−C σ-bonds.

Diborylhydrazines

There is some information available about the structures of fully alkylated *N,N*-diborylhydrazines from NMR data. In particular, the nonassociated nature (^{11}B NMR: δ = 42.0) of compounds of type **A** (Scheme 1) with tricoordinated boron atoms[11] is ascertained. Replacement of both the Ph_2B groups by Me_2B groups in **A** results in only one broad ^{11}B-NMR signal at δ = 23.[17] This shift suggests a weak B−N coordinate bond and points to a fluxional behavior of the boryl groups as delineated in the sequence **C**^{1}/**D**/**C**^{2} (Scheme 1). The molecular-mass determination ascertains the presence of a monomeric unit. These data indicate an equilibrium between the intramolecular adducts **C**^{1} and **C**^{2}, with rapid migration of the Me_2N group. Therefore, only one high-field ^{11}B signal appears, according to the nonclassical constitution **D**, representing the transition state between the two resonance hybrids **C**^{1} and **C**^{2}. Asymmetrically substituted diborylhydrazines show two ^{11}B resonances (^{11}B NMR: δ = 0.7, 43.5), which point to a cyclodimeric structure of type **B**, (Scheme 1), featuring a six-membered ring.[17]





Scheme 1. Structural features of *N,N*-diborylhydrazines

The ^{11}B-NMR and the ^{14}N-NMR spectra of the boron-halogen substituted diborylhydrazines **8b**, **8c** and **8d** show one signal for a tricoordinated and one signal for a tetraco-

Table 2. ^{11}B-, ^{14}N-, ^{1}H- and ^{13}C-NMR data of diborylhydrazines and related compounds

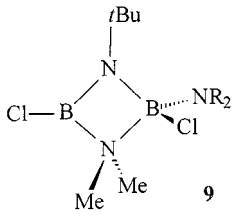
$R_2N-N(BR'X)(BR''Y)$					No.	^{11}B NMR	^{14}N NMR	^{13}C NMR(δ)		^{1}H NMR (δ)		Structure[a]	Remarks
R	R′	R″	X	Y		δ	δ	B(C)*C*	N*C*	B(C)*Me*	N*me*		
Me	*i*Pr	*i*Pr	Br	Br	**8b**	2.1 38.9	−276 −305	19.36	46.8	0.97	3.09	**C**	[b,c]
Me	*t*Bu	*t*Bu	Br	Br	**8c**	2.0 40.3	−263 −328	29.99 30.15	46.57 51.06	1.01 1.04	3.13 3.27	**C**	[b−d]
Me	Mes	Mes	Cl	Cl	**8d**	0.7 38.6	not measured not measured		45.83	−	3.12	**C**	[b]
Ph	Me	Me	Br	Br	**8e**	(48.9) −2.4 40.0					–	**A** **B** or **C**	[b,e]
Ph	*t*Bu	*t*Bu	Br	Br	**8f**	50.2				0.80	–	**A**	[e]
Me	Ph	Ph	Ph	Ph	**8g**	42					2.50	**A**	[f]
Me	Ph	Me	Ph	Me	**8h**	0.7 43.5		4.55 143.4	46.7	0.60	2.60	**B**	[g]
Me	Me	Me	Me	Me	**8i**	23.0	−196 −323	6.8	38.5	0.15	2.70	**C** or **D**	[c,g]

[a] See Scheme 1. − [b] δ^{11}B data: high field: endocyclic B atom; low field: exocyclic B atom. − [c] δ^{14}N data: high field: diorganylamino group; low field: diborylamino group. − [d] Pairs of signals for the alkyl groups: *t*Bu: endo- and exocyclic; NMe_2: above and below the ring plane. − [e] Not isolated; **8e**: mixture of products, composed of the adduct **B** or **C** and the monomer **A** (δ^{11}B in parenthesis) and the borazine. − [f] Data from ref.[11] − [g] Data from ref.[17]

ordinated boron atom. These data are in accordance with both, a dimeric unit **B**, or with a monomeric species **C**, featuring an intramolecular adduct. Molecular-mass determination in solution and subsequently the X-ray structure determination of **8d** (see below) confirm the monomeric structure, derived from type **C**.

The tetracoordinated boron nuclei of compounds **8b−e** are better shielded than those in dimeric aminohaloboranes, for example $[EtClB-NMe_2]_2$ (^{11}B NMR: δ = 10.2), or in amineborane adducts, $Ph_2(Cl)B-NMe_3$ (^{11}B NMR: δ = 10.9),[14] or in the BN heterocycle **9** (^{11}B NMR: δ = 10.8). It is suggested that this indicates higher electron density at the boron nuclei due to the higher basicity of the hydrazine nitrogen atom of the Me_2N group compared to the aminoborane nitrogen atom. Therefore, the deformation of the bond angles in the cycloadduct, featuring a three-membered ring, have no significant influence on the shielding of the boron nuclei. The ^{11}B-NMR data of the exocyclic tricoordinated boron atoms of the diborylhydrazines are in good agreement with those of aminohaloboranes, for example *t*BuClB−NMe_2 (^{11}B NMR: δ = 40.5),[14] *t*BuClB−NHMes (^{11}B NMR: δ = 40.9),[45] indicating marked (BN) π-interaction between the exocyclic boryl group and the central nitrogen atom. A typical diborylamine ^{11}B-NMR shift of 10 ppm downfield compared to the respective aminoboranes (see above), can be measured for the diborylhydrazine **8f** (^{11}B NMR: δ = 50.2). Obviously, the weak basicity of the Ph_2N nitrogen atom, owing to the π-acceptor function of the phenyl substituents as well as their sterical demand, prevents the formation of an intramolecular adduct.

The ^{14}N-NMR data of the diborylhydrazines **8b** and **8c** confirm the proposed structures. From other derivatives no signal could be detected. Two signals are observed, one of these at high field in the range of "ammonia" nitrogen nuclei, and the other one in the range of "aminoborane" nitrogen nuclei. These values and the ^{11}B-NMR data are in good accordance with those measured for asymetrically substituted diborylamines, featuring four-membered rings with formation of an intramolecular BN adduct,[7] as depicted in **9**.



9

Additional information about the structural features is provided by ^{1}H- and ^{13}C-NMR data. As expected, two groups of signals for the methyl groups above and below the plane of the three-membered ring, as well as for the endo- and exocyclic organyl groups attached to the boron atoms, are observed in the NMR spectra of **8b**, **8c** and **8d**. Those of **8b** and **8d** only show a broadening of the ^{1}H- and ^{13}C-NMR signals at room temp., but the doubling of the signals of **8c** is visible even at ambient temperatures.

Mass Spectra

The diborylamines **3** as well as the diborylhydrazines **8** have been studied by mass spectrometry. Fragments with an abundance larger than 2% are listed in the Experimental Section. The fragmentations of **3b**, **3r** and **8b**, which are characteristic for both classes of compounds are summarized in Schemes 2−4. Measured isotope patterns correspond to the calculated ones.

Characteristic for the ionization by electron impact is the low intensity of the molecular ions of the species containing the B−N−B unit, which show the weak stabilization of the

positive charge of the radical cation in the molecular framework. Contrary to these findings the ionization of the diborylamine **3r** and the diborylhydrazine **8d** leads to the formation of the molecular ion as the base peak, certainly due to the better stabilization of the positive charge by delocalization into the π-system of the aromatic rings attached to the boron atoms. Therefore, these molecules show very few secondary fragments. Concerning the fragmentation pattern, the ionization proceeds preferentially at the central nitrogen atom. This is true also for the fragmentation of the diborylhydrazines, although the first ionization energy of the dimethylamino group is approximately 1 eV lower than that of the diborylamine fragment according to the photoelectron spectrum of $Me_2N-N(BMe_2)_2$.[17]

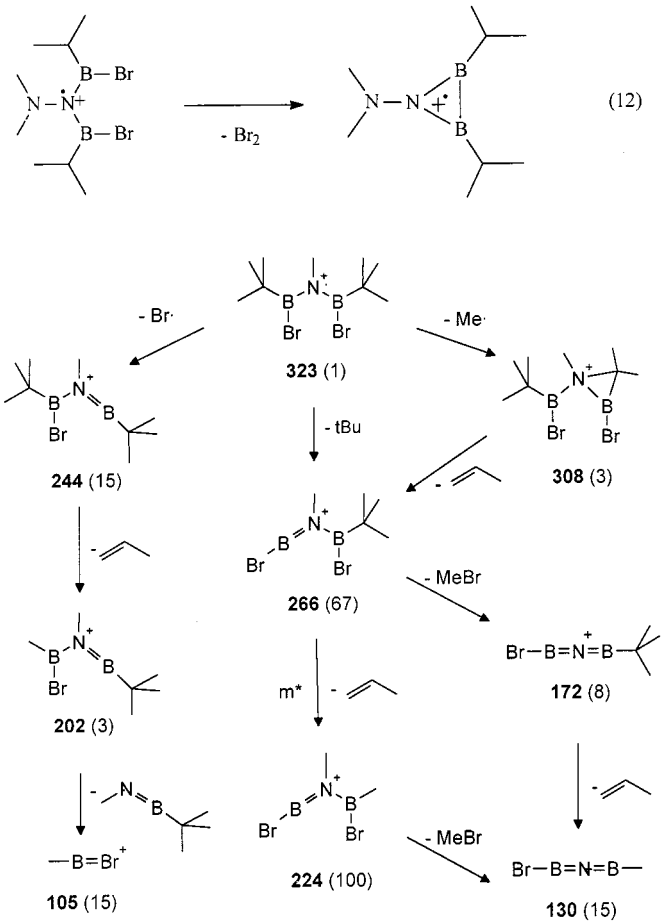
The predominant primary fragmentation is that of α-elimination, demonstrated by the appearence of nitrenium cations $Y-B=N^+R-BR'X$ (Y = alkyl, aryl, hal) in high intensity (see Scheme 2, fragment ion 244; Scheme 3, fragment ion 198). It proceeds by elimination of a substituent in α-position to the ionized centre by homolytic bond cleavage, with the sequence Mes ≈ *t*Bu > *i*Pr > Br > Cl ≈ Me. The ease of α-bond cleavage depends on the stability of the eliminated radical as well as the resulting cation. The mesityl group elimination, however, is facilitated due to the steric relief of the parent ion.

Another important primary fragmentation via neutral particles like R_2BX or RBX_2 can be detected in the mass spectra of **3r** (Scheme 2), **3e**, **8c** and **8d**, all of them showing the molecular ion as the 100% peak.

Characteristic fragments found are bis(boranediyl)iminium ions of the type $[X-B=N=B-Y]^+$; they appear at the end of a fragmentation path with remarkable intensity (Scheme 2). The appropriate ions in the mass spectra of the diborylhydrazines bear the even more stabilizing Me_2N group. Therefore, the fragment *m*/*z* 159 and 95 (Scheme 4), for example, appear as 100 and 41% peaks, respectively.

A McLafferty-type rearrangement with the elimination of propene or isobutene, denoted as "McL" in the fragmentation schemes, can be observed in the fragmentations of **3t**, **8a** and **8b** (see Schemes 2 and 4).

The mass spectra of the diborylhydrazines show no fragment ions with masses larger than the monomeric molecular units. This lends support to the formation of an intramolecular adduct as deduced from NMR data and shown in Figure **C** (Scheme 1). Therefore, all nitrenium ions with an amino group attached to the boron atom may also be drawn as a cyclic fragment ion according to the structure of type **C**. Additionally, the fragmentation patterns of the diborylhydrazines exhibit radical cations of remarkable intensity with an azadiboriridine structure. These fragments are formed by α-elimination of halogen molecules from the parent molecular cation according to Equation 12. The appearance of the azadiboriridine ring unit as a relatively stable radical cation gives rise to the assumption that the heterocycle is not only stable as a species in the exited state, but also as molecular unit in the ground state. Therefore, reactions were performed to obtain heterocycles with the hydrazine moiety, depicted in Equation12, by use of the well-known procedure of the reductive B−B bond formation.

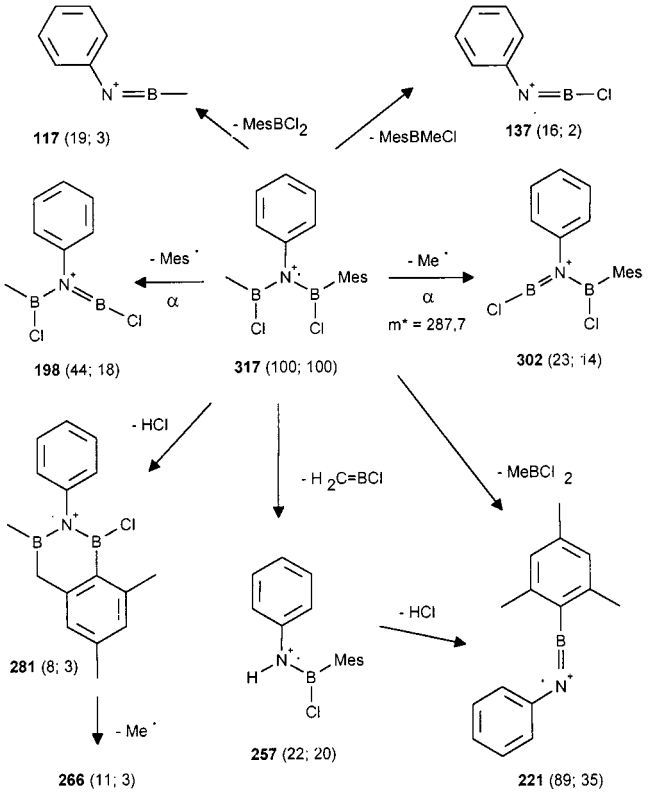


Scheme 2. Fragmentation of the diborylamine **3b**

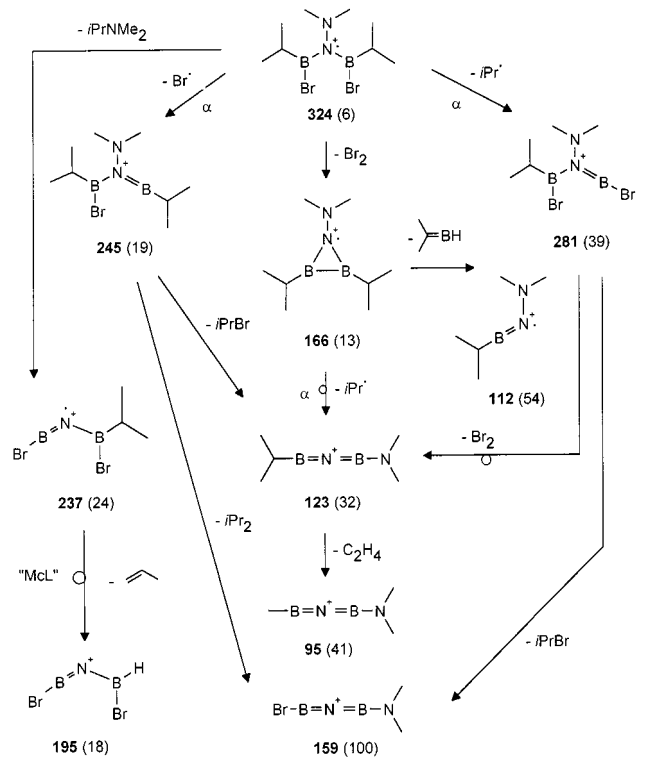
Molecular Structures

The characteristic structural features of the halogenated *N*,*N*-diborylhydrazines, found in solution, are confirmed by the molecular structure of **8d** (Figure 3), determined in the solid-state by X-ray crystallography. Selected bonding parameters are listed in the caption of Figure 3. Compound **8d** crystallizes in the orthorhombic space group $Pca2_1$, $Z = 4$, and serves as a model for the proposed intramolecular donor-acceptor complex **C** (Scheme 1). The endocyclic B1−N1 length of 1.484(5) Å is in the range of a single (sp^2-sp^2) bond length, the exocyclic B2−N1 length [1.381(5) Å] is, however, consistent with a B−N bond order of > 1.5 of a double bond. Moreover, the small torsion angle N2−N1−B2−Cl2 of 3.4° allows effective (BN) π-interaction between the exocyclic boryl group and the N1 atom of the three-membered ring. The molecular geometry of **8d** in the solid state is fully compatible with the NMR data. Thus, the structure of this compound in the solid and in solution do not differ.

The extremely enlarged B1−N1−B2 angle of 163.3(9)° compared to the appropriate N2−N1−B2 angle of



Scheme 3. Fragmentation of the diborylamine **3r**



Scheme 4. Fragmentation of the diborylhydrazine **8b**

129.4(3)° should be noted. This asymmetrical framework can only be rationalized by a steric repulsion between the two mesityl groups. Although the bond angles in the three-membered ring are small, resulting in a weak overlap of the σ-bond orbitals, the B1−N2 length between the tetracoordinated nitrogen atom and boron atom is remarkably short. It is of the same size as that in the borylated hydrazine **10** ($d_{(BN)}$: 1.626 Å).[18] However, the respective B−N bond of the four-membered cycloadduct **11** ($d_{(BN)}$: 1.713 Å)[19] is 0.10 Å longer, probably due to the sterically more demanding tetramethylpiperidino group compared to the Me_2N group. Therefore, steric repulsion of the mesityl groups in **8d** causes the opposite effect and may be responsible for the short B1−N2 bond. As a consequence of the different hybridization of the boron atoms the B1−Cl1 bond is 0.05 Å longer than the B2−Cl2 bond.

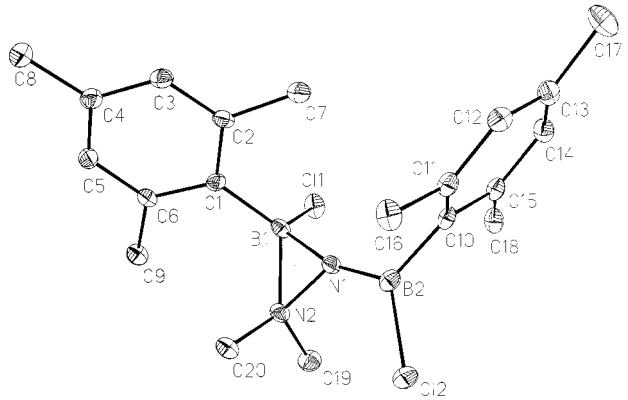
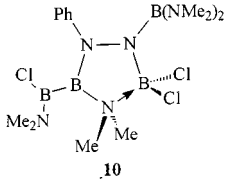
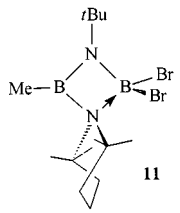


Figure 3. Molecular structure of $Me_2N-N(BMesCl)_2$) (**8d**) in ORTEP-type description; thermal ellipsoids represent a 25% probability; hydrogen atoms are not shown for the sake of clarity; selected bond lengths [Å] (esds are given in parentheses as units in the last digit): B1−N1 1.484(5), B1−N2 1.624(5), B2−N1 1.381(5), N1−N2 1.474(4), B1−Cl1 1.843(4), B2−Cl2 1.796(5), B1−C1 1.575(6), B2−C10 1.562(6), C1−C2 1.423(5), C1−C6 1.432(5), C10−C11 1.405(5), C10−C15 1.412(5); selected bond angles [°]: B1−N1−B2 163.3(9), B1−N1−N2 66.6(2), B2−N1−N2 129.4(3), N1−B2−Cl2 119.5(3), N1−B2−C10 121.8(3), C10−B2−Cl2 118.7(3), N1−B1−C1 124.0(3), N1−B1−Cl1 115.7(3); torsion angle [°]: N2−N1−B2−Cl2 3.4



10



11

Experimental Section

General: All manipulations were performed in dry nitrogen. Glassware was dried prior to use by heating in vacuo. − NMR: Bruker AC P200 (^{11}B, ^{14}N), Jeol GSX 270 (^{119}Sn) or Jeol EX 400 (^{1}H, ^{13}C) instrument; standards: TMS (internal, ^{1}H, ^{13}C), $BF_3{\cdot}OEt_2$ (external, ^{11}B), $NaNO_3$ (aqueous solution, external, ^{14}N), tetramethyltin (external, ^{119}Sn). When the coupling constant is stated as $^{n}J^{119(117)}Sn^{m}X$ = ..., (...), the value in parentheses describes the coupling of the X nucleus with the ^{117}Sn isotopomer. The notation $^{n}J(^{119/117}Sn^{m}X)$ represents the coupling of both isotopomers with X, when the coupling cannot be resolved. A questionmark after a formula or a number means assignment is uncertain. The solvent-

dependent NMR data of the alkylhalostannanes, detected in the reaction mixtures, are quoted here and compared with ref. values. If no deviation is detected, the data are not mentioned again in the procedures. – ^{1}H NMR (CH_2Cl_2): δ = 0.67 [Me_3SnCl, $^2J(^{119}Sn^1H)$ = 58.5 Hz], 0.79 [Me_3SnBr, $^2J(^{119}Sn^1H)$ = 57.8 Hz], 1.21 [Me_2SnCl_2, $^2J(^{119}Sn^1H)$ = 68.5 Hz], 1.40 [Me_2SnBr_2, $^2J(^{119}Sn^1H)$ = 65.5 Hz]. – ^{1}H NMR(ref. values in CCl_4): δ = 0.61[20] [Me_3SnCl, ^2J ($^{119}Sn^1H$) = 58.1 Hz[20]], 0.73[20] [Me_3SnBr, $^2J(^{119}Sn^1H)$ = 57.8 Hz[20]], 1.15[20] [Me_2SnCl_2, $^2J(^{119}Sn^1H)$ = 68.2 Hz[21]], 1.33[20] [Me_2SnBr_2, $^2J(^{119}Sn^1H)$ = 66.7 Hz[20]]. – ^{1}H NMR (Tol): δ = 0.27 (!)[45] (Me_3SnCl), 0.52 (!) (Me_2SnCl_2[45]), 0.52 (!) (Me_2SnBr_2[45]). – IR spectra: Nujol-Hostaflon mulls between CsI plates with a Nicolet SZDX FT-IR spectrometer, data are quoted in cm^{-1}; selected characteristic vibrations are given only. – MS: Varian CH7 instrument with electron impact ionisation at 70 eV, data are given in the sequence: *m*/*z* (%, assignment). The masses found refer to the isotopes ^{1}H, ^{12}C, ^{11}B, ^{14}N, ^{35}Cl, ^{120}Sn. – Elemental analyses: performed at the Microanalytical laboratory of the institute. When marked with * the elemental analysis by combustion suffers from a) the deviation from the calculated values due to the formation of boron carbide and boron oxide melt, and b) difficulties in handling of the samples because of spontaneous inflammability or hydrolysis. – X-ray: Siemens P4 four-circle diffractometer; Mo-K_α radiation, graphite monochromator; single crystals were mounted under argon using glass capillaries. Crystal data were determined and intensity data recorded at 213 K; program X-scan, structure solution by Patterson method and refinement using the SHELX-PLUS PC version package; final refinement was performed using the SHELX-93 programs.[22] All atoms except hydrogen atoms are described with anisotropic temp. factors, all hydrogen positions were geometrically placed [*d*(CH) = 0.96 Å] and included in the refinement by using the riding model and fixed U_i. Details of the crystal structure determination is available on request from the Cambridge Crystallographic Data Center (CCDC) on quoting the depository number CSD-112146, the names of the authors, and the journal citation.

Starting Materials: $N(SnMe_3)_3$[23] was prepared in a modified procedure[15] from $NaNH_2/NH_3/OEt_2/Me_3SnCl$, $(Me_2SnCl)_3N$,[24] Me_2SnCl_2,[25] Me–N($SnMe_3$)$_2$,[26] Ph–N($SnMe_3$)$_2$[26], Mes–N($SnMe_3$)$_2$,[9] Dipp–N($SnMe_3$)$_2$,[9] Me_3Si–N($SnMe_3$)$_2$,[27] *t*Bu–N($SnMe_2Cl$)$_2$,[9] Me_3Si–N($SnMe_2Cl$)$_2$,[9][43] Dipp–N($SnMe_2Cl$)$_2$,[9] Me_2N–N($SnMe_3$)$_2$,[28] $N_2(SnMe_3)_4$,[29] Me_2B–N($SnMe_3$)$_2$,[30] $MeBBr_2$ and Et_2BCl,[31] Me_2BBr,[32] *i*$PrBCl_2$,[33] *t*$BuBBr_2$,[34] $MesBBr_2$.[35]

General Procedure I. – Reaction of Bis(trimethylstannyl)amines with Dihaloorganylboranes RBX_2 with Sterically Less Demanding Groups R and Bis(trimethylstannyl)hydrazines with Dihaloorganylboranes: A solution of the distannylamine $RN(SnMe_3)_2$ in CH_2Cl_2 was slowly added (≥ 60 min) to a stirred solution of the dihaloorganylborane RBX_2 in CH_2Cl_2 at −65°C to −75°C. After allowing the mixture to slowly attain ambient temp., stirring was continued for 12 h at 25°C. A sample of the reaction mixture, checked by ^{1}H and ^{11}B NMR, confirmed quantitative reactions, or in some cases methylation, of the boron atoms. After removal of the solvent at 25°C/12 Torr, the most volatile component was removed either by fractional distillation of the residue using a 10-cm Vigreux column (Me_3SnBr, b.p. ca. 30°C/10^{-2} Torr or 53–55°C/12 Torr), or by sublimation (Me_3SnCl, subl.p. 25°C/10^{-3} Torr). The removal of Me_3SnCl (or Me_2SnCl_2) was completed by repeated dissolution of the residue in CH_2Cl_2, followed by removal of the solvent, and repeated sublimation. Finally, the diborylamine was obtained as the next volatile fraction.

General Procedure II. – Reactions of Bis(halodimethylstannyl)amines with Dihaloorganoboranes RBX_2 with Sterically More Demanding Groups R = *t*Bu, Mes: The bis(halodimethylstannyl)amine $RN(SnMe_2X)_2$ (X = Cl or Br), dissolved in CH_2Cl_2, was slowly added (≥ 60 min) at −60 to −50°C, whilst stirring, to a solution of the dihaloorganoborane RBX_2 in CH_2Cl_2. The mixture was then allowed to slowly attain ambient temp. and the stirring was continued for 12 h at 25°C. A sample was then checked by ^{1}H and ^{11}B NMR which confirmed an almost quantitative reaction. After stripping off the solvent at 25°C/12 Torr, the residue was dissolved in petroleum ether (ca. half of the volume of the previous solvent). The dimethyltin dihalide, which is only sparingly soluble in petroleum ether, crystallized after a period of 4–6 h at −30°C and was then removed by filtration. After removal of the solvent from the filtrate at 25°C/12 Torr the colorless residue, solidifying at ambient temp., was washed with petroleum ether (2 ×) and purified by fractional distillation in vacuo using a 10-cm Vigreux column. If the residue of the reaction mixture is a mobile oil, the Me_2SnX_2 compounds were removed by continually maintaining the product at 25°C/10^{-6} Torr. The alkylhalostannanes Me_3SnX and Me_2SnX_2 (X = Cl, Br), formed by stannazane bond cleavage according to procedure I or II, were identified by their ^{1}H-NMR spectra. Deviations and quantities are given below. The reaction proceeds with Cl/Br exchange, when X equals chlorine in $RN(SnMe_2X)_2$ and bromine in RBX_2.

Bis(bromo-*tert*-butylboryl)methylamine (3b). – Procedure I: Bis(trimethylstannyl)methylamine (**4a**) (5.40 g, 7.1 mmol), dissolved in 10 mL of CH_2Cl_2, was added to a solution of *t*$BuBBr_2$ (3.20 g, 13.9 mmol) in 20 mL of CH_2Cl_2 over 90 min. – ^{11}B NMR (reaction mixture): δ = 48.3 [**3b**, shoulder MeN($SnMe_2Br$)(BMeBr)?], 80.9 [*t*Bu(Me)BBr]; ratio: 8:2. – B.p. 35–38°C/10^{-3} Torr. – Yield: 1.0 g of **3b** (43%); colorless crystals. – M.p. ca. 30°C. – ^{1}H- and ^{11}B-NMR data correspond to another sample of **3b**, prepared according to procedure II (see below).

Attempt to Prepare Bis(bromomethylboryl)phenylamine (3c) from 4c and $MeBBr_2$ (Molar Ratio 1:2). – Procedure I: $PhN(SnMe_3)_2$ (**4c**) (5.40 g, 12.8 mmol), dissolved in 20 mL of CH_2Cl_2, was added over 30 min to a solution of $MeBBr_2$ (4.80 g, 25.9 mmol) in 20 mL of CH_2Cl_2. – ^{11}B NMR (reaction mixture): δ = 51.5 [$PhN(BBrMe)_2$ (**3c**)], 78.7 (Me_2BBr), 62.1 ($MeBBr_2$), 39.8 [$PhN(SnMe_3)(BMeBr)$], 32.3 ($Ph–N=B–Me)_3$; ratio: 10.5:1.5:0.6:1.5:0.7; after 16 h stirring: 12.5:1.5:0:0:0.6 [NMR data of **3c**: ^{1}H NMR: δ = 1.2 (s, 6 H, B*Me*), 6.9–7.5 (m, 5 H, C_6H_5); ^{11}B NMR: δ = 51.0]. During removal of the volatile components at 25°C/13 Torr the ^{11}B-NMR signal of **3c** became weaker and disappeared after the residue was kept at room temp. for 1 d (^{11}B NMR: δ = 62.1, 32.3).

Attempt to Prepare Bis(chlorophenylboryl)phenylamine (3d) by Reaction of 4c with $PhBCl_2$ (Molar Ratio 1:2). – Procedure I: $PhN(SnMe_3)_2$ (**4c**) (4.70 g, 11.3 mmol), dissolved in 25 mL of CH_2Cl_2, was added dropwise over 30 min to a solution of $PhBCl_2$ (3.50 g, 22.2 mmol) in 15 mL of CH_2Cl_2. – ^{11}B NMR (ca. 17 h stirring): δ = 55.0 ($PhBCl_2$), 47 [Ph–N($BPhCl)_2$ (**3d**)], 37.2 [Ph–N(BPhCl)($SnMe_3$)?], signal ratio: 1:0.1:1, after 12 d the ratio had changed to 0.5:9.1:0.4. The solvent and most of the Me_3SnCl was removed at 25°C/12 Torr. – ^{1}H NMR (residue, CH_2Cl_2): δ = 0.65 (Me_3SnCl), 7.30–7.68 (m, C_6H_5, **3d**). – ^{11}B NMR (residue, CH_2Cl_2): d = 46.9 (**3d**). – While Me_3SnCl was sublimed from the residue at ambient temp./10^{-3} Torr, the diborylamine **3d** decomposed slowly with formation of $(Ph–N=B–Ph)_3$ and $PhBCl_2$, the latter two were also detectable in the cold trap (^{11}B NMR: δ = 34 and 55). The borazine $(Ph–N=B–Ph)_3$,[36] separated from a petroleum ether solution of the residue and kept at room temp. for 2 d (0.52 g, 26%), was recrystallized from decane (15 mL), m.p.

124°C. – ^{1}H NMR ($CDCl_3$): δ = 6.71–6.87 (m, 5 H, C_6H_5), 6.91–7.49 (5 H, C_6H_5). – ^{11}B NMR (CH_2Cl_2): δ = 34.2. – MS: 537 (100, M^+), 460 (17, M^+ – Ph), 383 (5.2, M^+ – 2 Ph), 358 [39, $(Ph–N{\equiv}B–Ph)_2^+$], 230 (12, 460^{2+}), 179 (80, $Ph–N{\equiv}B–Ph^+$). – IR: $\tilde{\nu}$ = 3074 cm^{-1} (w), 3055 (w), 3026 (w), 3011 (w), 1599 (m), 1492 (m), 1438 (m), 1384 (s, ν(BN); for comparison ν(BN) = 1368 cm^{-1}[37]), 1369 (vs), 696 (s). – $C_{36}H_{30}B_3N_3$ (537.1)*: calcd. C 80.51, H 5.63, N 7.82; found C 72.18, H 5.65, N 5.91.

Reaction of Bis(trimethylstannyl)phenylamine (4c) with *t*BuBBr$_2$ (Molar Ratio 1:2), Attempt to Prepare Bis(bromo-*tert*-butylboryl)-phenylamine (3f), NMR-Scale reaction. – Procedure I:. A solution of *t*BuBBr$_2$ (0.37 g, 1.6 mmol), dissolved in 2 mL of CH_2Cl_2, was added dropwise to a solution of bis(trimethylstannyl)phenylamine (**4c**) (0.33 g, 0.8 mmol) in 1 mL of CH_2Cl_2 within 15 min at −78°C. – ^{11}B NMR (mixture after a period of ca. 3 d stirring at ambient temp.): δ = 80.5 [*t*Bu(Me)BBr], 66.2 (*t*BuBBr$_2$), 43.1 [PhN(B*t*BuBr)(SnMe$_3$)], signal ratio: 3:4:2. – ^{1}H NMR: δ = 7.1 (PhN), 1.14 (*t*BuBBr$_2$), 1.03 [*t*Bu(Me)BBr], 0.96 [N(B*t*BuBr)], 0.74 (Me_3SnBr), 0.53 ($NSnMe_3$).

Attempt to Prepare Bis(bromomethylboryl)-2,6-diisopropylphenylamine (3k) from 4k and MeBBr$_2$ (Molar Ratio 1:2), NMR-Scale reaction. – Procedure I: A solution of Dipp-N(SnMe$_3$)$_2$ (**4k**) (0.28 g, 0.56 mmol), dissolved in 1 mL of CH_2Cl_2, was added dropwise to a solution of $MeBBr_2$ (0.21 g, 1.1 mmol) in 1 mL of CH_2Cl_2 over a period of 30 min at −78°C. – ^{11}B NMR (mixture after ca. 1 d stirring at ambient temp.): δ = 79.1 (Me_2BBr). – ^{1}H NMR: δ = 0.79 [Sn*Me*$_2$Br, Dipp-N(SnMe$_2$Br)$_2$ (**5k**)], 1.05 (*Me*$_2$BBr), 1.15 (*Me*$_2$CH, **5k**), 3.64 (Me_2CH). – d^{1}H- and d^{11}B-NMR data correspond to an authentic sample of **5k**, prepared according to ref.[9] After 14 d stirring at room temp., no intensity change of the NMR signals in the reaction mixture was detected.

Bis(dimethylboryl)mesitylamine (3q). – Procedure II: MesN(SnMe$_3$)$_2$ (**4i**) (10.70 g, 23.5 mmol), dissolved in 25 mL of CH_2Cl_2, was added to a solution of $MeBBr_2$ (9.15 g, 49.3 mmol) in 10 mL of CH_2Cl_2 within 1 h at −50°C. – ^{1}H NMR (reaction mixture, CH_2Cl_2): δ = 0.78 [N(Sn*Me*$_2$Br)$_2$ of **5i**, ^2J (^{119}Sn^{1}H) = 63.0]. – ^{119}Sn NMR: δ = 77.8 [^2J(^{119}Sn^{117}Sn) = 135 Hz (**5i**)]. – ^{11}B NMR: δ = 78.5 ($h_{1/2}$ = 325 Hz, Me_2BBr). – After 2 d stirring at room temp. and a workup according to procedure II, the distillation yielded 4.1 g of **3q** (81%), b.p. ca. 50°C/10^{-6} Torr, as a colorless liquid. – ^{1}H NMR ($CDCl_3$): δ = 0.43 (s, br., 12 H, B*Me*$_2$), 1.93 (s, 6 H, *o*-*Me*–Ph), 2.25 (s, 3 H, *p*-*Me*–Ph), 6.85 (s, 2 H, $C_6H_2Me_3$). – ^{13}C NMR: δ = 10.38 (br., BMe_2), 19.03 (*o*-*Me*–Ph), 20.84 (*p*-*Me*–Ph), 128.79 (*m*-C), 132.59 (*o*-C), 133.62 (*p*-C), 146.48 (*i*-C). – ^{11}B NMR: δ = 58.1 ($h_{1/2}$ = 229 Hz). – ^{14}N NMR: δ = −210 ($h_{1/2}$ = 371 Hz). – MS: 215 (52, M·$^+$), 200 (100, M^+ – Me, m*), 185 (6, M^+ – C_2H_5), 160 (31, M^+ – H_2C=BMe), etc. – IR [nujol/hostaflone]: $\tilde{\nu}$ = 1314 cm^{-1} [s, $\nu_{as}(B_2N)$,[39] 1251 [s, $\nu_s(B_2N)_s$?], 1263 [s, ν(CN)?], 1000 [w, ν_{as}(BC)], 900 [w, $\nu_s(CB_2)$]. – $C_{13}H_{23}B_2N$ (215.0): calcd. C 72.64, H 10.79, N 6.52; found C 72.29, H 10.78, N 6.41. – Filtration of the residue, insoluble in petroleum ether, yielded Me_2SnBr_2 (14.6 g, 96%). – ^{1}H NMR (CH_2Cl_2: δ = 1.42 [*Me*$_2$SnBr$_2$, ^2J(^{119}Sn^{1}H = 65.5].[23]

Bis(bromomethylboryl)trimethylsilylamine (3m).[38] **– Procedure I:** A solution of $MeBBr_2$ (13.6 g, 73.1 mmol) in 40 mL of CH_2Cl_2 was added dropwise to **4l** (15.2 g, 36.5 mmol), dissolved in 50 mL of CH_2Cl_2, over 60 min at −75°C. – ^{1}H NMR (ambient temp.): δ = 0.35 (Me_3Si), 0.74 (Me_3SnBr), 1.09 (MeB). – ^{11}B NMR: δ = 49.8. – Yield: 6 g of **3m** (55%), b.p. 71–75°C/13 Torr, colorless liquid. – ^{1}H NMR: δ = 0.35 (Me_3Si), 1.1 (MeB). – ^{11}B NMR: δ = 49.5. – ^{14}N NMR: δ = −220. Consistent with the ref. values.[38]

Bis(bromoisopropylboryl)trimethylsilylamine (3n). – Procedure I: Bis(trimethylstannyl)trimethylsilylamine (**4l**) (22.8 g, 55 mmol), dissolved in 60 mL of CH_2Cl_2, was added over 60 min at ca. −78°C, to a solution of *i*PrBBr$_2$ (23.8 g, 111 mmol) in 50 mL of CH_2Cl_2. – ^{11}B NMR (mixture at ambient temp.): δ = 52.2 (**3n**). – Yield: 15.6 g of **3n** (80%) as a colorless liquid, b.p. 59–65°C/5·10^{-2} Torr. – ^{1}H NMR ($CDCl_3$): δ = 0.33 (s, 9 H, Me_3Si), 1.05 [d, 12 H, BCH*Me*$_2$, ^3J(^{1}H^{1}H) = 5.9 Hz], 1.33 (m, 2 H, BC*H*Me$_2$). – ^{13}C NMR: δ = 1.89 [$SiMe_3$, ^1J(^{29}Si^{13}C) = 59 Hz], 19.12 (BCH*Me*$_2$), 25.8 (br., B*C*HMe$_2$). – ^{11}B NMR: δ = 52.2 ($h_{1/2}$: 321 Hz). – ^{14}N NMR: δ = −230 ($h_{1/2}$: 109 Hz). – ^{29}Si NMR: δ = 5.6. – MS: 355 (12, M^+), 340 (18, M^+ – Me), 276 (65, M^+ – Br), etc. – $C_9H_{23}B_2Br_2NSi$ (354.8): calcd. C 30.47, H 6.53, N 3.95; found C 30.66, H 6.66, N 3.89.

Bis(*tert*-butylchloroboryl)trimethylsilylamine (3o).[6a] **– Procedure II:** To a solution of *t*BuBBr$_2$ (30.6 g, 135 mmol) in 90 mL of CH_2Cl_2 was added bis(chlorodimethylstannyl)trimethylsilylamine (**5l**) (30.6 g, 67.2 mmol), dissolved in 50 mL of CH_2Cl_2, within 60 min at ca. −78°C. – ^{11}B NMR (mixture at ambient temp): δ = 54.2 (**3o**). – Yield: 13.6 g of **3o** (69%) as a colorless liquid, b.p. 65–66°C/10^{-1} Torr (or 45–49°C/5·10^{-3} Torr). – ^{1}H NMR ($CDCl_3$): δ = 0.39 (s, 9 H, Me_3Si), 1.02 (s, 18 H, BC*Me*$_3$). – ^{13}C NMR: δ = 4.41 [$SiMe_3$, ^1J(^{29}Si^{13}C) = 59.5 Hz], 28.87 (BC*Me*$_3$), 34.31(B*C*Me$_3$). – ^{11}B NMR: δ = 53.82 ($h_{1/2}$: 218 Hz). – ^{14}N NMR: δ = −246 ($h_{1/2}$: 271 Hz). – ^{29}Si NMR (C_6D_6): δ = 7.56. – MS: 293 (22, M^+), 278 (19, M^+ – Me), 258 (11, M^+ – Cl), etc. – $C_9H_{23}B_2Cl_2NSi$ (294.0): calcd. C 44.95, H 9.26, N 4.76; found C 45.12, H 9.18, N 4.86.

Bis(*tert*-butylchloroboryl)methylamine (3a). – Procedure II: [MeN(SnMe$_2$Cl)$_2$]$_2$ [(**5a**)$_2$] (11.8 g, 14.9 mmol), dissolved in 70 mL of CH_2Cl_2, was added to a solution of *t*BuBBr$_2$ (13.8 g, 59.6 mmol) in 80 mL of CH_2Cl_2 within 2.5 h at −60 to −50°C. A precipitate formed which redissolved. After removal of $Me_2SnBrCl$ [15 g, 95%,^{1}H NMR(CH_2Cl_2): δ = 1.32; ^{119}Sn NMR: δ = 114.1] by crystallization and removal of the solvent at 25°C/12 Torr, compound **3a** (4.1 g, 58%) was obtained by distillation at 29–30°C/10^{-6} Torr as a colorless liquid. – ^{1}H NMR ($CDCl_3$): δ = 1.08 (s, 18 H, BC*Me*$_3$), 2.90 (s, 3 H, *Me*N). – ^{13}C NMR: δ = 25 (br., B*C*Me$_3$), 28.31 (BC*Me*$_3$), 33.16 (N*Me*). – ^{11}B NMR: δ = 50.0 ($h_{1/2}$ = 147 Hz). – ^{14}N NMR: δ = −268 ($h_{1/2}$ = 178 Hz). – MS: 235 (< 1, M^+), 220 (3, M^+ – Me), 200 (3, M^+ – Cl), 178 (49, M^+ – *t*Bu), 162 (6, 178^+ – CH_4, or 220^+ – *t*BuH), 158 (< 1, 200^+ – H_2C=CHMe), 142 (3, 158^+ – CH_4), 136 (100, 178^+ – H_2C=CHMe), 61 (10, 136^+ – MeNBCl). – IR: $\tilde{\nu}$ = 1362 cm^{-1} [vr, $\nu_{as}(B_2N)$[39]], 1283 [s, ν(CN)], 1215 [s, $\nu_s(B_2N)$], 1072 [ν(BC)], 908 [vr, ν(BCl)]. – $C_9H_{21}B_2Cl_2N$ (235.8): calcd. C 45.84, H 8.98, N 94; found C 45.31, H 8.42, N 5.59.

Bis(bromo-*tert*-butylboryl)methylamine (3b). – Procedure II: [MeN(SnMe$_2$Br)$_2$]$_2$ [(**5b**)$_2$] (5.8 g, 6.0 mmol) was added to a solution of *t*BuBBr$_2$ (5.4 g, 23.8 mmol) in 20 mL of CH_2Cl_2, dissolved in 70 mL of CH_2Cl_2, over 1.5 h at −55 to −50°C; a violent reaction with temporary formation of a solid occurred. **3b** (2.50 g, 64%) was obtained by condensation at 25–28°C/10^{-6} Torr into a cooled trap (−78°C); colorless crystals (m.p. ca. 30°C). – ^{1}H NMR ($CDCl_3$): δ = 1.09 (s, 18 H, BC*Me*$_3$), 2.88 (s, 3 H *Me*N). – ^{13}C NMR: δ = 26 (br., B*C*Me$_3$), 28.48 (BC*Me*$_3$), 33.95 (N*Me*). – ^{11}B NMR: δ = 48.0 ($h_{1/2}$ = 174 Hz). – ^{14}N NMR: δ = −259 ($h_{1/2} \approx$ 197 Hz). – MS: 323 (ca. 1, M·$^+$), 308 (3, M^+ – Me), 266 (67, M^+ – *t*Bu), 250 (2, 308^+ – *t*BuH), 244 (15, M^+ – Br), 224 (100, 266^+ – H_2C=CHMe), 202 (3, 244^+ – H_2C=CHMe), 186 (9, 202^+ – CH_4), 172 (8, *t*BuBNBBr$^+$), 160 (14, 202^+ – H_2C=CHMe), 130 (15, MeBNBBr$^+$), 105 (15, $MeBBr^+$), 92 (3, 186^+ – MeBr); – IR: $\tilde{\nu}$ =

1365 [s, $\nu_{as}(B_2N)$[39]] 1277 [m, ν(CN)], 1210 [s, $\nu_s(B_2N)$], 1068 [m, ν(BC)], 883 [vr, ν(BBr)]. − $C_9H_{21}B_2Br_2N$ (324.7): calcd. C 33.29, H 6.52, N 4.31; found C 33.05, H 6.83, N 4.97.

***tert*-Butylbis(chloro-*tert*-butylboryl)amine (3g).**[6] **− Procedure II:** **t**BuN$(SnMe_2Cl)_2$ (**5a**) (3.50 g, 8.0 mmol), dissolved in 10 mL of CH_2Cl_2, was added to a solution of *t*BuBBr_2 (3.60 g, 16 mmol) in 10 mL of CH_2Cl_2 over 0.5 h at −30°C. Yield: 2.16 g of **3g** (97%), as a colorless liquid, b.p. 42°C/10^{-2} Torr. − ^{1}H NMR ($CDCl_3$): δ = 1.11 (s, 18 H, BC*Me*$_3$), 1.28 (s, 9 H, NC*Me*$_3$). − ^{13}C NMR: δ = 27 (br., B*C*Me$_3$), 30.32 (BC*Me*$_3$), 33.24 (NC*Me*$_3$), 55.1 (N*C*Me$_3$). − ^{11}B NMR: δ = 45.5 ($h_{1/2}$ = 179 Hz). − ^{14}N NMR: δ = −226 ($h_{1/2} \approx$ 215 Hz). − MS: 275 (ca. 1, $M^{\cdot+}$), 260 (7, M^+ − Me), 240 (3, M^+ − Cl), 218 (33, M^+ − *t*Bu), 176 (100, 218^+ − H_2C=CHMe), 61 (12, MeBCl). − IR: $\tilde{\nu}$ = 1344 cm^{-1} [s, $\nu_{as}(B_2N)$], 1269 [s, ν(CN)], 1190 [s, $\nu_s(B_2N)$], 1108 [m, ν(BC)], 903 [s, ν(BCl)]. − $C_{12}H_{27}B_2Cl_2N$ (277.9): calcd. C 51.87, H 9.79, N 5.04; found C 52.90, H 10.10, N 5.39.

Bis(bromomethylboryl)-*tert*-butylamine (3h).[3] **− Procedure I:** **t**BuN$(SnMe_3)_2$ (**4g**) (26.8 g, 67.2 mmol) dissolved in 25 mL of CH_2Cl_2 was added dropwise to a solution of $MeBBr_2$ (25.0 g, 135 mmol) in 25 mL of CH_2Cl_2 at −78°C. Yield: 16.1 g of **3h** (85%), as a colorless liquid, b.p. 35°C/10^{-1} Torr. − ^{1}H NMR($CDCl_3$): δ = 1.18 (s, 6 H, B*Me*), 1.44 (s, 9 H, NC*Me*$_3$). − ^{11}B NMR: δ = 47.5 ($h_{1/2}$ = 190 Hz). − ^{14}N NMR: δ = −212, ($h_{1/2} \approx$ 230 Hz). − $C_6H_{15}B_2Br_2N$ (282.6): calcd. C 25.50, H 5.35, B 7.65, Br 56.54, N 4.96; found C 24.44, H 5.23, B 7.38, Br 55.28, N 4.70. − The NMR data are identical with ref. values.[3]

Attempt to Prepare Bis(chloromesitylboryl)methylamine (3t) from Bis(bromodimethylstannyl)methylamine (5b)$_2$ and MesBCl$_2$ (Molar Ratio 1:4): A suspension of (**5b**)$_2$ (2.6 g, 2.7 mmol) in 50 mL of CH_2Cl_2 was added to a solution of $MesBCl_2$ (2.15 g, 10.7 mmol) in 30 mL of CH_2Cl_2 within 1.25 h at −78°C. NMR data of the mixture after 7 d stirring at ambient temp. indicated the formation of the intermediate stannylaminoborane {^{11}B NMR (CH_2Cl_2): δ = 38.3 [Me−N(BMesCl) ($SnMe_2Br$) (?)], 60.4 [$MesBCl_2$, ref.: 61.4 (C_6D_6);[40] 61.1 (CD_2Cl_2)[40]]}. After keeping for 24 h in boiling CH_2Cl_2 and an additional 20 h in boiling $CHCl_3$, no change of signal intensities could be detected in an NMR sample of the reaction mixture. $Me_2Sn(Cl)Br$ (^{1}H NMR: δ = 1.32; ^{119}Sn NMR: δ = 114.1) was removed by crystallization from petroleum ether and the solvent at 25°C/12 Torr. Fractional distillation of the residue gave: (i) $MesBCl_2$ (0.24 g, ca. 85%), b.p. 50°C/10^{-5} Torr [^{11}B NMR (CH_2Cl_2): δ = 60.4]; (ii) 0.66 g of a highly viscous liquid, b.p. 80°C/10^{-5} Torr; ^{11}B NMR (CH_2Cl_2/$CDCl_3$): δ = 37.8; ^{1}H NMR: δ = 1.29 [$SnMe_2$, $^2J(^{117(119)}Sn^1H)$ = 65.2 (68.4) Hz], 2.25 (*o*,*p*-*Me*$_3C_6H_2$−B), 6.81 (*m*-H, Mes); ^{14}N NMR: δ = −282 ($h_{1/2}$ = 473 Hz); (iii) residue: yellow solid. − ^{11}B NMR (CH_2Cl_2): δ = 38.8, 47 (sh, ?). The purification by crystallization from CH_2Cl_2, toluene, or petroleum ether failed according to ^{1}H- and ^{11}B-NMR data.

Bis(*tert*-butylchloroboryl)phenylamine (3e):[45] A suspension of Me_2SnCl_2 (10.1 g, 46.1 mmol) in 40 mL of CH_2Cl_2 was treated with $PhN(SnMe_3)_2$ (**4c**), dissolved in 30 mL of CH_2Cl_2, while stirring at room temp. This mixture was added dropwise, while stirring, to *t*B$uBBr_2$ (10.5 g, 46.0 mmol), dissolved in 50 mL of CH_2Cl_2, within 1.5 h at −50°C. After allowing the reaction mixture to attain ambient temp. within 1.5 h, the progress of the reaction was controlled by NMR (see Figure 1) during a period of 96 h stirring at room temp. followed by a period of 48 h under reflux. ^{1}H- and ^{11}B-NMR data of the mixture as a function of time, given in the sequence time [h]; d^{11}B NMR [ppm], ratio [%]; d^{1}H NMR [ppm]: Measurement 1: 0; 67.5 (*t*B$uBBr_2$); 100; 0.63 (Me_3SnCl), 0.78 ($PhN(SnMe_2Cl)_2$). Measurement 2: ca. 3; 40.4 [PhN(B*t*BuCl)$SnMe_2Cl$], 50; 63.5 (*t*BuBClBr), 50; 0.72 (Me_3SnBr), 0.78 [$PhN(SnMe_2Cl)_2$], 1.33 ($Me_2SnClBr$); [^{1}H-NMR signal of Me_3SnCl and $PhN(SnMe_2Br)_2$ disappeared]. Measurement 3: 24; 42.1 [PhN(B*t*BuCl)$SnMe_2Cl$], 44; 50.4 [PhN(B*t*BuCl)$_2$], 12; 64.0 (*t*BuBClBr), 44; 0.72 (Me_3SnBr), 1.34 ($Me_2SnClBr$), (^{1}H-NMR signal of **4c** vanished completely). Measurement 4: 96; 41.2 [PhN(B*t*BuCl)$SnMe_2Cl$], 41; 49.9 [PhN(B*t*BuCl)$_2$], 22; 64.0 (*t*BuBClBr), 38; 0.73 (Me_3SnBr), 1.35 ($Me_2SnClBr$). Measurement 5: 96 (25°C) + 34 (reflux); 43.3 [PhN(B*t*BuCl)$SnMe_2Cl$], 35; 50.0 [PhN(B*t*BuCl)$_2$], 35; 63.7 (*t*BuBClBr), 29. Measurement 6: 96 (25°C) + 48 (reflux); 50.1 [PhN(B*t*BuCl)$_2$], ca. 80; 38.9 [$(PhNBtBu)_n$?], ca. 20. − After the solvent was removed at 25°C/12 Torr and Me_3SnBr as well as $Me_2SnClBr$ (d^{1}H = 1.35) was condensed into a trap at −78°C, fractional distillation of the residue yielded 3.8 g (55%) of **3e** as a colorless liquid; b.p. 48−51°C/10^{-5} Torr. − ^{1}H NMR ($CDCl_3$): δ = 1.01 (s, 18 H, BC*Me*$_3$), 7.32 (m, 5 H, C_6H_5). − d^{13}C: 26 (br., B*C*Me$_3$, detected after Gauß transformation only), 28.65 (BC*Me*$_3$), 127.03 (*p*-C), 29.02 (*o*-C), 129.02 (*m*-C), 141.47 (*i*-C). − ^{11}B NMR: δ = 50.6 ($h_{1/2}$ = 253 Hz). − ^{14}N NMR: δ = −234 ($h_{1/2}$ = 506 Hz). − MS [% (70 eV, 15 eV), assignment]: 236 (11, 7, M^+ − *t*Bu), 194 (69, 89, M^+ − *t*BuBCl), 180 (18, 16, 236^+ − C_4H_8), 152 (14, 11, 194^+ − C_3H_6). 143 (2, 7, $PhN{\equiv}BC_3H_5^+$), 138 (100, 100, 194^+ − C_4H_8), 137 (40, M^+ − tBu_2BCl), 103 (22, 14, $PhN{\equiv}BH^+$), 77 (40, 2, Ph^+). − IR: $\tilde{\nu}$ = 1365 cm^{-1} [s, $\nu_{as}(B_2N)$[42]], 1278 [s, ν(CN)], 1197 [s, $\nu_s(B_2N)$], 1104 [s, ν(BC)], 907 [s, ν(BCl)]. − $C_{14}H_{23}B_2Cl_2N$ (297.9): calcd. C 56.45, H 7.78, N 4.70; found C 54.08, H 7.52, N 4.60.

Bis(bromo-*tert*-butylboryl)phenylamine (3f): A suspension of Me_2SnBr_2 (16.10 g, 52.1 mmol) in 40 mL of CH_2Cl_2 was treated with $PhN(SnMe_3)_2$ (**4c**) (10.90 g, 26.0 mmol), dissolved in 40 mL of CH_2Cl_2, while stirring at room temp. This reaction mixture was added dropwise, while stirring, to *t*B$uBBr_2$ (11.9 g, 52.1 mmol), dissolved in 40 mL of CH_2Cl_2, within 130 min at −68 to −40°C. After allowing the reaction mixture to attain ambient temp., the solvent was removed at 25°C/12 Torr, Me_3SnBr as well as Me_2SnBr_2 was condensed into a trap at −78°C over a period of 4 d, the fractional distillation of the viscous residue yielded 7.0 g (69%) of **3f** as colorless liquid, b.p. 69−77°C/10^{-5} Torr. − ^{1}H NMR ($CDCl_3$): δ = 0.98 (s, 18 H, BC*Me*$_3$), 7.30 (m, 5 H, C_6H_5). − ^{13}C NMR: δ = 27 (br., B*C*Me$_3$, detected after Gauß transformation only), 29.24 (BC*Me*$_3$), 127.7 (*p*-C), 129.34 (*o*-C), 129.38 (*m*-C), 141.93 (*i*-C). − ^{11}B NMR: δ = 49.3 ($h_{1/2}$ = 300 Hz). − ^{14}N NMR: δ = −228 ($h_{1/2}$ = 488 Hz). − MS: *m*/*z* [% (70 eV, 15 eV), assignment]: 385 (< 1, 3, M^+), 328 (32, 66, M^+ − *t*Bu), 305 (12, 29, M^+ − HBr), 286 (17, 13, 328^+ − C_3H_6),. 263 (12, 29, 305^+ − C_3H_6), 248 (39, 46, 305^+ − *t*Bu), 239 (26, 61, 385^+ − C_4H_8BBr), 183 (100, 100, 239^+ − H_2C=CMe_2), 168 (10, 2, 248^+ − HBr), 128 (17, 0, PhBNBMe), 103 (18, 1, $PhN{\equiv}BH^+$). − IR: $\tilde{\nu}$ = 1359 [s, $\nu_{as}(B_2N)$[42]], 1270 [s, ν(CN)], 1191 [s, $\nu_s(B_2N)$], 1097 [s, ν(BC)], 884 [vr, ν(BBr)]. − $C_{14}H_{23}B_2Br_2N$ (386.8): calcd. C 43.48, H 5.99, N 3.62; found C 44.02, H 5.99, N 3.77.

Attempt to Prepare Bis(chloromesitylboryl)phenylamine (3u) from Bis(chlorodimethylstannyl)phenylamine (5d) and MesBCl$_2$ (Molar Ratio 1:2): A suspension of Me_2SnCl_2 (5.8 g, 26.4 mmol) in 20 mL of CH_2Cl_2 was treated with $PhN(SnMe_3)_2$ (**4c**) (5.54 g, 13.2 mmol), dissolved in 20 mL of CH_2Cl_2, while stirring at room temp. This mixture was added dropwise to a stirred solution of $MesBCl_2$ (5.31 g, 26.4 mmol) in 30 mL of CH_2Cl_2 over 110 min at −68 to −40°C. After the reaction mixture had attained ambient temp., it was kept for 2 d at reflux {^{11}B NMR (CH_2Cl_2): δ = 38.9 [PhN(BMesCl)$SnMe_2Cl$], 59.8 ($MesBCl_2$), ratio: ca. 1:1. − ^{1}H NMR: δ = 1.26 ($SnMe_2Cl$), 1.22 (Me_2SnCl_2), 0.66 (Me_3SnCl), ratio: 1:1:2}. After removal of the solvent at 25°C/12 Torr, the residue

was dissolved in 70 mL of toluene and kept at reflux for another 7 h. No change of signal intensities could be detected in the NMR spectra. After another 7 h at reflux, the solution contained a 1:2 mixture of the diborylamine **3u** (^{11}B NMR: δ = 48.1), the stannylaminoborane (^{11}B NMR: δ = 38.5) and (PhN≡BMes)$_2$ (^{11}B NMR: δ = 40), presumed as the decomposition product. The separation of these products either by fractional crystallization or by fractional sublimation failed. − ^{1}H NMR [CH_2Cl_2, enriched PhN(BMesCl)SnMe$_2$Cl]: δ = 1.29 [s, 6 H, Sn*Me*$_2$Cl, $^2J(^{117(119)}Sn^1H)$ = 66.5 (69) Hz], 2.29 (s, 3 H, *p*-Me), 2.42 (s, 3 H, *o*-Me), 2.93 (s, 3 H, *o*-Me), 5.58−7.30 (m, 7 H, C_6H_x of Ph and Mes). − ^{11}B NMR: δ = 39.5 ($h_{1/2}$ = 406 Hz).

Attempt to Prepare Bis(chloromethylboryl)mesitylamine (3v) from 4i and BCl_3 (Molar Ratio 1:2): BCl_3 (3.5 g, 30 mmol) was condensed into a solution of MesN(SnMe$_3$)$_2$ (**4i**) (7.0 g, 15 mmol) in 40 mL of CH_2Cl_2, cooled to −50°C. After allowing the solution to attain ambient temp., it was stirred for 17 h at room temp. [^{11}B NMR: δ = 61.4 (MeBCl$_2$), 75.9 (Me$_2$BCl), ratio: 10:0.5]. The ^{1}H- and ^{119}Sn-NMR spectra indicated the quantitative formation of MesN(SnMe$_2$Cl)$_2$ (**5i**); the signals are identical with those of an authentic sample of **5i**[9]. Although the reaction mixture was kept under reflux for additional 9 h using a dry ice condensor there was no indication (^{11}B-NMR control) of a further reaction.

(*tert*-Butylchloroboryl)mesitylamine by Reaction of (Bromodimethylstannyl)(*tert*-butylchloroboryl)mesitylamine with H_2O (Molar Ratio 1:1): After purification of **5i**, obtained according to the procedure (for **3v**) described above, by removal of the volatile components at 25°C/12 Torr and dissolution of the residue in 30 mL of toluene, it was treated dropwise while stirring with a solution of *t*BuBBr$_2$ (6.8 g, 30 mmol) in 15 mL of toluene at −60 to −50°C. NMR data of the reaction mixture after allowing to attain ambient temp. − ^{11}B NMR: δ = 66.1 (*t*BuBBr$_2$), 64.6 (*t*BuBBrCl), 62.5 *t*BuBCl$_2$. − The NMR control after additional 36 h under reflux indicated the formation of ca. 50% of MesN(B*t*BuCl)SnMe$_2$Br (^{11}B NMR: δ = 42.8). After hydrolysis with H_2O (30 µL, 1.7 mmol) and keeping the reaction mixture under reflux for72 h, the solvents were removed in vacuo and MesNHB*t*BuCl (1.5 g, 42%) was sublimed at 43−45°C/10^{-6} Torr as colorless crystals, subl. p. 42°C. − NMR data of MesNHB*t*BuCl in $CDCl_3$: ^{1}H NMR: δ = 1.13 (s, 9 H, BC*Me*$_3$), 2.18 (s, 6 H, *o*-Me), 2.29 (s, 3 H, *p*-Me), 5.44 (m, 1 H, N*H*), 6.91 (s, 2 H, *m*-H). − ^{13}C NMR: δ = 18.52 (*o*-Me), 20.90 (*p*-Me), 27.72 (BC*Me*$_3$), 128.70 (*m*-C), 134.49 (*o*-C), 135.49 (*p*-C), 135.57 (*i*-C). − ^{11}B NMR: δ = 40.9 ($h_{1/2}$ = 267 Hz). − ^{14}N NMR: δ = −270 ($h_{1/2}$ = 590 Hz). − MS: 237 (100, M$^+$), 222 (11, M$^+$ − Me), 181 (49, M$^+$ − C_4H_8, m*), 180 (55, M$^+$ − *t*Bu), 179 (100, M$^+$ − *t*BuH or 181$^+$ − H_2, MesNBCl), 145 (16, MesNBH). − IR: $\tilde{\nu}$ = 3356 cm^{-1} (s, NH), 3040 (w), 3020 (w), 3026 (w), 2942 (vs), 2863 (s), 1608 (m), 1489 (s). 1459 (s), 1442 (s), 1400 (m), 1377 (s), 1359 (s), 1280 (m, vs BN), 1250 (s), 961 (vs, νBCl), 854 (s), 651 (s), 603 (s). − $C_{13}H_{21}BClN$ (237.6)*: calcd. C 65.72, H 8.91, N 5.90; found C 64.94, H 9.13, N 5.69.

Bromomethylboryl(chloromethylboryl)(trimethylsilyl)amine (3p): Me$_3$SiN(SnMe$_2$Cl)$_2$ (**5l**) (5.2 g, 11.4 mmol), dissolved in 70 mL of CH_2Cl_2, was added dropwise to a solution of MeBBr$_2$ (4.25 g, 22.9 mmol) in 15 mL of CH_2Cl_2 within 1.5 h at −55 to −50°C. The workup was according to Procedure I; the distillation of the residue yielded **3p** (1.55 g, 65%) at 59−61°C/12 Torr as a colorless liquid. − ^{1}H NMR ($CDCl_3$): δ = 0.30 (s, 9 H, Si*Me*$_3$), 0.89 (br. s, 6 H, B*Me*X). − ^{13}C NMR: δ = 1.80 [q, $^1J(^{13}C^1H)$ = 119.4 Hz, Si*Me*$_3$], 12 [q, v. br., $^1J(^{13}C^1H)$ = 120 Hz, B*Me*Cl]. − ^{11}B NMR: δ = 50.3 ($h_{1/2}$ = 128 Hz). − ^{14}N NMR: δ = −234 ($h_{1/2}$ = 84 Hz). − ^{29}Si NMR: δ = 6.46 (recorded at 218 K). − $C_5H_{15}B_2BrClNSi$ (253.0)*: calcd. C 23.72, H 5.98, N 5.53; found C 22.98, H 5.77, N 5.01; C/H/N ratio: calcd. 5:15:1; found 5.31:15.9:1.

Bis(*tert*-butylchloroboryl)(dimethylboryl)amine (3t).[9] − Procedure II: a) A solution of *t*BuBBr$_2$ (10.85 g, 47.4 mmol) in 50 mL of CH_2Cl_2 was added dropwise to Me$_2$BN(SnMe$_2$Cl)$_2$ (10.0 g, 23.6 mmol), dissolved in 50 mL of CH_2Cl_2, within 90 min at −70°C. The distillation yielded **3t** (2.20 g, 40%), b.p. 28−38°C/10^{-6} Torr, as a colorless liquid. The NMR data are identical with those of an authentic sample of **3t** described below. − $C_{10}H_{24}B_3Cl_2N$ (261.65)*: calcd. C 45.91, H 9.25, Cl 27.10, N 5.35; found C 48.55, H 9.20, Cl 26.70, N 5.28.

b) Me$_2$BBr (5.6 g, 46.1 mmol), dissolved in 25 mL of CH_2Cl_2, was added dropwise to a solution of N(SnMe$_3$)$_3$ (23.30 g, 46.1 mmol) in 35 mL of CH_2Cl_2 while stirring for 2 h at −78 to −60°C. After allowing the mixture to attain ambient temp. and 1 h of stirring at room temp., the ^{1}H- and ^{11}B-NMR spectra recorded from a sample of the reaction mixture indicated quantitative formation of Me$_2$BN(SnMe$_3$)$_2$ (**4r**) and Me$_3$SnBr. − ^{1}H NMR (CH_2Cl_2): δ = 0.30 [s, 18 H, Sn*Me*$_3$, **4r**, $^2J(^{117(119)}Sn^1H)$ = 53 (56) Hz], 0.33 (s, 6 H, B*Me*$_2$), 0.76 (9 H, *Me*$_3$SnBr). − ^{11}B NMR: δ = 52.4 ($h_{1/2}$ = 157 Hz); ref.:[3][42] ^{1}H NMR: δ = 0.26 [s, 18 H, Sn*Me*$_3$, **4r**, $^2J(^{119}Sn^1H)$ = 55 Hz], 0.30 (s, 6 H, B*Me*$_2$). − ^{11}B NMR: δ = 53.4 ($h_{1/2}$ = 230 Hz). − This mixture was added dropwise over 45 min to a solution of Me$_2$SnCl$_2$ (20.3 g, 92.2 mmol) in 150 mL of CH_2Cl_2 at room temp. The quantitative formation of Me$_2$BN(SnMe$_2$Cl)$_2$ (**5r**) and Me$_3$SnCl was checked by NMR (CH_2Cl_2). − ^{1}H NMR: δ = 0.45 (s, 6 H, B*Me*$_2$), 0.64 (18 H, *Me*$_3$SnCl), 0.76 (9 H, *Me*$_3$SnBr), 0.93 [s, 12 H, Sn*Me*$_2$Cl, $^2J(^{117(119)}$ Sn^1 H) = 63(66) Hz]. − ^{11}B NMR: δ = 53.6 ($h_{1/2}$ = 224 Hz). − After removal of ca. 130 mL of CH_2Cl_2, the reaction mixture was added dropwise over 90 min to a solution of *t*BuBBr$_2$ (20.91 g, 91.8 mmol) in 50 mL of CH_2Cl_2 at −78°C. After allowing it to attain ambient temp., 4 d stirring at room temp., removal of the solvent at 25°C/12 Torr and the major part of the volatile components (Me$_3$SnCl, Me$_3$SnBr) at 25°C/10^{-3} Torr, Me$_2$SnBr$_2$ was separated from the solid residue by crystallization at −30°C from 50 mL of petroleum ether according to procedure II. After removal of the solvent of the filtrate at 0°C/12 Torr and sublimation of small amounts of alkylhalostannanes at 0°C/10^{-3} Torr, distillation yielded Me$_2$BN(B*t*BuCl)$_2$ (**3w**) [6.04 g, 50% based on N(SnMe$_3$)$_3$] as colorless liquid, extremly sensitive to moisture and oxygen, b.p. 43−45°C/10^{-3} Torr. − ^{1}H NMR ($CDCl_3$): δ = 0.71 (s, 6 H, B*Me*$_2$), 1.06 (s, 18 H, BC*Me*$_3$Cl). − ^{13}C NMR: δ = 12 (br., B*C*Me$_3$Cl), 14 (br., B*Me*$_2$), 28.51 (BC*Me*$_3$Cl). − ^{11}B NMR ($CDCl_3$): δ = 56.6 (2 B, *Bt*BuCl, $h_{1/2}$ = 291 Hz), 62.6 (1 B, B*Me*$_2$, $h_{1/2}$ = 276 Hz). − ^{14}N NMR: δ = −206 ($h_{1/2}$ = 179 Hz). − MS: *m/z* [% (70 eV), assignment]: 261 (1, M$^+$), 246 (2, M$^+$ − Me), 226 (1, M$^+$ − Cl), 162 (59, 204$^+$ − Me$_2$BH), 150 (40, 226$^+$ − Me$_2$BCl: *t*BuBNB*t*Bu), 148 (39, 204$^+$ − BMe$_3$), 128 (34, 204$^+$ − ClBMe$_2$), 122 (29, 204$^+$ − H$_2$C=B*t*Bu), 108 (81, 246$^+$ − *t*BuBCl$_2$: *t*BuBNBMe), 86 (87, 204$^+$ − *t*BuMeBCl), 66 (100, MeBNBMe). − IR: $\tilde{\nu}$ = 1313 cm^{-1} [s, ν_{as}(B$_3$N)], 1216 [s, ν_s(B$_3$N)], 946 [s, ν(BCl)], further frequences not assigned. − $C_{10}H_{24}B_3Cl_2N$ (261.7): calcd. C 45.91, H 9.25, N 5.35; found C 45.86, H 9.48, N 5.68.

(Chloromesitylboryl)(chloromethylboryl)phenylamine (3r): A solution of Me$_2$SnCl$_2$ (6.6 g, 30.0 mmol) in 30 mL of CH_2Cl_2 was treated with PhN(SnMe$_3$)$_2$ (**4c**) (6.31 g, 15.0 mmol), dissolved in 20 mL of CH_2Cl_2, and the mixture was then added dropwise over 90 min at −50°C, while stirring, to MesBCl$_2$ (3.0 g, 15.0 mmol), dissolved in 20 mL of CH_2Cl_2. − NMR data (after 16 h,CH_2Cl_2): ^{11}B NMR: δ = 38.5 [PhN(BMesCl)SnMe$_2$Cl (**6b**)]. − ^{1}H NMR: δ = 1.28 (SnMe$_2$Cl), 1.24 (Me$_2$SnCl$_2$), 0.69 (Me$_3$SnCl), ratio: 1:1:2.

– After cooling the reaction mixture to −50°C again, a solution of $MeBBr_2$ (2.8 g, 15.0 mmol) in 30 mL of CH_2Cl_2 was added over a period of 90 min. After 2 d stirring at room temp., the solvent was removed at 25°C/12 Torr and the organotin halides (Me_3SnCl, Me_2SnCl_2, $Me_2SnClBr$) at 25°C/10^{-6} Torr. Traces of $Me_2SnClBr$ were sublimed at 25−55°C/10^{-6} Torr and the diborylamine **3r** (1.53 g, 32%) distilled at 87−88°C/10^{-6} Torr solidifying to colorless crystals. – ^{1}H NMR ($CDCl_3$): δ = 0.88 (br. s, 3 H, B*Me*), 2.66 (s, 3 H, *p*-Me), 2.75 (s, 6 H, *o*-Me), 7.21 (s, 2 H, *m*-H, Mes), 7.44 (m, 2 H, *m*-H, Ph), 7.67 (m, 1 H, *p*-H, Ph), 7.77 (m, 2 H, *o*-H, Ph). – ^{13}C NMR: δ = 10 (br., B*Me*), 21.22 (*p*-Me), 21.89 (*o*-Me), 119.60 (*p*-C, Ph), 126.39 (*o*-C, Mes), 127.67 (*o*-C, Ph), 127.83 (*m*-C, Mes), 128.95 (*m*-C, Ph), 136.78 (*p*-C, Mes), 137 (v br., *i*-C, B-*Mes*), 146.54 (*i*-C, N−*Ph*). – ^{11}B NMR: δ = 50.2 (assym., shoulder at ca. 50, *B*Me and *B*Mes, $h_{1/2}$ = 572 Hz). – MS: *m*/*z* [% (70 eV, 20 eV), assignment]: 317 (100, 100, M^+), 302 (23, 14, M^+ − Me, m* = 287.7), 281 (8, 3, M^+ − HCl), 266 (11, 3, 281^+ − Me), 257 (22, 20, M^+ − H_2C=BCl), 221 (89, 35, M^+ − $MesBCl_2$: MesBNPh), 198 (44, 16, M^+ − Mes), 137 [16, 2, M^+ − Mes(Me)BCl], 117 (19, 3, M^+ − $MesBCl_2$). – IR: ṽ = 1368 [vr, $(B_2N)_{as}$], 1289 (s, CN), 1261 (s, CN), 1203 [s, $(B_2N)_s$], 1113 (m, BC), 1029 (m, BC), 956 (m, BCl), 878 (s, BCl). – $C_{16}H_{19}B_2Cl_2N$ (317.86)*: calcd. C 60.46, H 6.03, N 4.10; found C 61.64, H 6.33, N 4.60.

Reaction of 1,1-Dimethyl-2,2-bis(trimethylstannyl)hydrazine (7a) with $MeBBr_2$ (Molar Ratio 1:2). – Attempt to prepare 1,1-Dimethyl-2,2-bis(bromomethylboryl)hydrazine (**8a**). – Procedure I: **7a** (4.9 g, 12.8 mmol), dissolved in 15 mL of CH_2Cl_2, was added dropwise within 80 min to a solution of $MeBBr_2$ (4.6 g, 25 mmol) in 5 mL of CH_2Cl_2 at −70 to −40°C. – NMR data (after 16 h stirring at ambient temp.): ^{1}H NMR: δ = 0.76 (Me_3SnBr). – ^{11}B NMR: δ = 45 [$MeBrB(Me_3Sn)NNMe_2$?], 37, 18 (ratio: ca. 1:1:10), additional signals of very low intensity at δ = 9, −1, −4, −25. No evidence for the formation of $Me_2N-N(BMeBr)_2$ (**8a**) was detected by NMR. – After removal of the volatile components at 25°C/13 Torr and distillation of Me_3SnBr (5 g, 83%) at 25−55°C/10^{-2} Torr, a yellow/brown, viscous residue remained, which was fairly insoluble in petroleum ether and benzene. No pure product could be isolated by crystallization, neither from these solvents nor from CH_2Cl_2.

2,2-Bis(bromoisopropylboryl)-1,1-dimethylhydrazine (8b). – Procedure I: 7a (4.90 g, 12.8 mmol), dissolved in 15 mL of CH_2Cl_2, was added dropwise within 150 min to a solution of *i*$PrBBr_2$ (7.90 g, 36.8 mmol) in 40 mL of CH_2Cl_2 at −78 to −70°C. The workup was carried out after 20 h of stirring at room temp. After removal of the solvent (25°C/13 Torr) and Me_3SnBr (34°C/10^{-3} Torr), the distillation of the remaining oil yielded 2.46 g of **8b** (41%) as colorless, viscous liquid, b.p. 82−86°C/10^{-3} Torr. Redistillation at 40−41°C/10^{-5} Torr yielded 1.4 g of pure **8b** (23%) and a residue. – ^{11}B NMR ($CDCl_3$): d = 36.6 [$(Me_2NN{\equiv}BiPr)_3$?]. – **8b** is spontaneously inflammable in contact with air and turns dark brown when stored at room temp. – ^{1}H NMR ($CDCl_3$): δ = 0.97 (m, not resolved, 14 H, *iPr*B), 3.09 (s, br., not resolved, 6 H, Me_2N). – ^{13}C NMR: δ = 13 (br., B*C*HMe_2), 19.36 (br., BCH*Me*$_2$), 46.84 (br., N*Me*$_2$). – d^{11}B: 2.1 (B_{endo}, 1 B, $h_{1/2}$ = 265 Hz), 38.9 (1 B, B_{exo}, $h_{1/2}$ = 433 Hz). – ^{14}N NMR: δ = −276 (1 N, *N*B_2, $h_{1/2} \approx$ 625 Hz), −305 (*N*Me_2, 1 N, $h_{1/2} \approx$ 625 Hz); $h_{1/2}$ is a crude estimate. – MS: 324 (6, M^+), 281 (39, M^+ &NDASH; *i*Pr), 245 (19, M^+ − Br), 237 (24, M^+ &NDASH; *i*$PrNMe_2$), 195 (18, 237 − H_2C=CH−CH_3), 166 (13, M^+ − Br_2), 159 (100, $BrBNBNMe_2^+$), 130 (17, $BrBNBMe^+$), 123 (32, 166^+ − *i*Pr_2), 116 (14, $BrBNBH^+$), 112 (54, *i*$PrBNNMe_2$), 95 (41, $MeBNBNMe_2^+$). – IR (selected vibrations): ṽ = 1362 cm^{-1} [s, $\nu_{as}(B_2N)$, for comparison (BN) = 1368 cm^{-1}[42]] 1308 [m, ν(CN)], 1197 [m, $\nu_s(B_2N)$], 1058 [s, ν(BC)], 819 (s) and 743 [s, ν(BBr)], 658 [s, ν(N→B)]. – $C_8H_{20}B_2Br_2N_2$ (325.7)*: calcd. C 29.50, H 6.19, N 8.60; found C 32.35, H 6.69, N 9.48; C/H(N ratio calcd. 8:20:2; found 8:19.7:2.

2,2-Bis(bromo-*tert*-butylboryl)-1,1-dimethylhydrazine (8c). – Procedure I: 7a (15.60 g, 40.4 mmol), dissolved in 60 mL of CH_2Cl_2, was added within 3 h to a solution of *t*$BuBBr_2$ (18.40 g, 80.7 mmol) in 50 mL of CH_2Cl_2 at −78°C. After 17 h stirring at room temp., removal of the solvent and Me_3SnBr, the liquid residue was purified twice by distillation. Yield: 8.4 g of **8c** (58%) as a colorless, viscous liquid, b.p. 63−66°C/10^{-5} Torr. The liquid is spontaneously inflammable in contact with air and moisture. In a second experiment **8c** crystallized after distillation, m.p. 36−41°C. – ^{1}H NMR ($CDCl_3$): δ = 1.01 (s, 18 H, *tBu*B_{endo}), 1.04 (s, 18 H, *tBu*B_{exo}), 3.13 (s, 3 H, *Me*$_A$Me$_B$N), 3.27 (s, 3 H, Me$_A$*Me*$_B$N). – ^{13}C NMR: δ = 27.99 (B_{exo}C*Me*$_3$), 30.15 (B_{endo}C*Me*$_3$), 46.57 (N*Me*$_A$Me$_B$), 51.06 (NMe$_A$*Me*$_B$). – ^{11}B NMR: δ 2.0 (1 B, B_{endo}, $h_{1/2}$ = 96 Hz), 40.3 (1 B, B_{exo}, $h_{1/2}$ = 193 Hz) (for B*C*Me$_3$ signal not found). – ^{14}N NMR: δ = −263 (1 N, *N*B_2, $h_{1/2} \approx$ 499 Hz), −328 (1 N, *N*Me_2, $h_{1/2} \approx$ 403 Hz). – MS (70 eV, 20 eV): 352 (2, 6, M^+), 337 (5, 2, M^+ − Me), 295 (56, 100, M^+ − *t*Bu), 273 (38, 48, M^+ − Br), 239 (100, 78, 295^+ − H_2C=CMe_2), 217 (26, 8, 273^+ − H_2C=CMe_2), 194 (8, M^+ − Br_2), 179 (6, 194^+ − Me), 175 (14, 217^+ − H_2C=CH−CH_3), 159 (78, 273^+ − *t*Bu−*t*Bu), 137 (19, *t*$BuBNBNMe_2^+$), 130 (38, $BrBNBMe^+$), 126, (30, 54, *t*$BuBNNMe_2^+$), 116 (74, $BrBNBH^+$), 111 (22, *t*$BuBNNMe^+$), 95 (28, $MeBNBNMe_2^+$), 66 (21, $MeBNBMe^+$). – IR: ṽ = 1361 cm^{-1} [s, $\nu_{as}(B_2N)$], 1265 [s, ν(CN)], 1201 [s, $\nu_s(B_2N)$], 1058 [s, ν(BC)], 851 (s) and 764 [s, ν(BBr)], 651 [s, (N→B)]. – $C_{10}H_{24}B_2Br_2N_2$ (353.76)*: calcd. C 33.95, H 6.84, N 7.92; found C 35.25, H 7.31, N 8.74; C/H(N ratio calcd. 10:24:2; found 9.7:23.2:2.0; mol. mass: found 358.9 (cryoscopically in cyclohexane).

2,2-Bis(chloromesitylboryl)-1,1-dimethylhydrazine (8d). – Procedure I: a) **7a** (1.7 g, 4.4 mmol), dissolved in 20 mL of CH_2Cl_2, was added within 1 h to a solution of $MesBCl_2$ (1.8 g, 9.1 mmol) in 15 mL of CH_2Cl_2 at −70 to −60°C. The work up was carried out after 20 h of stirring at room temp. ^{1}H- and ^{11}B-NMR spectra of the reaction mixture gave no evidence for the formation of the adduct **8d**. After removal of the solvents and sublimation of Me_3SnCl, the residue of crude **8d** was purified by crystallization from CH_2Cl_2. Yield: 0.97 g of **8d** (57%) as a colorless powder, m.p. 136°C, decomp. Single crystals suitable for X-ray structure determination were obtained by recrystallization from CH_2Cl_2 at −18°C. – ^{1}H NMR ($CDCl_3$): δ = 2.23 (m, 18 H, *o*-Me−Ph, *p*-Me−Ph), 3.12 (br. s, 6 H, N*Me*$_2$), 6.78 (br. s, 4 H, *m*-H−Ph). – d^{13}C: 21.13 (*p*-Me−Ph), 29.69 (*o*-Me−Ph), 45.83 (N*Me*$_2$), 126.9 ($C_6H_2Me_3$), 127.6 ($C_6H_2Me_3$), 127.7 (br.), 138 (br, *i*-C_A), 139.5 (br.), 140 (br., *i*-C_B). – ^{11}B NMR: δ = 0.7 (1 B, B_{endo}, $h_{1/2}$ = 482 Hz), 38.6 (1 B, B_{exo}, $h_{1/2}$ = 573 Hz). – MS: 388 (100, M·$^+$), 373 (1, M^+ − Me), 353 (23, M^+ − Cl), 345 (15, M^+ − H_2C=NMe), 344 (20, 345^+ − H), 343 (21, 345^+ − H_2), 318 (8, $M^{+\cdot}$ − 2 Cl), 309 (10, 344^+ − HCl), 274 (16, $MesBNBMes^+$), 269 (75, M^+ − Mes), 225 (35, M^+ − $MesNMe_2$), 224 (39, 225^+ − H), 223 (18, M^+ − ClBMes), 190, (27, $MesBNBCl^+$), 189 (14, 225^+ − HCl), 188 (77, $MesBNNMe_2^+$), 187 (15, 223^+ − HCl), 144 (24, 344^+ − $MesBCl_2$); – IR: ṽ = 1357 cm^{-1} [s, $\nu_{as}(B_2N)$], 1260 [s, ν(CN)], 1225 [s, $\nu_s(B_2N)$], 1050 [s, ν(BC)], 932 (s) and 859 [s, ν(BBr)], 664 [s, (N→B)]. – $C_{20}H_{28}B_2Cl_2N_2$ (389.0)*: calcd. C 61.76, H 7.26, N 7.20; found C 59.69, H 7.58, N 7.36; mol. mass: found 377 (cryoscopically in cyclohexane). – X-ray structure analysis data of **8d**: Formula $C_{20}H_{28}B_2Cl_2N_2$; M_r = 388.96; colourless prism; size 0.3 × 0.2 × 0.1 mm, orthorhombic; space group *Pca*2(1), *a* = 12. 3263(1), *b* = 12.6905(2), *c* = 13.7050(1) Å, *V* = 2143.83(4) Å^3, *Z* = 4, $\rho_{calcd.}$ = 1.205 g cm^{-3}; μ(Mo-K_α) = 0.309 mm^{-1}, *F*(000) = 824. – Data

collection: 11736 reflections in $-15 \le h \le 15$, $-16 \le k \le 9$, $-16 \le l \le 16$, measured in the range $4.60° \le 2\theta \le 58.22°$; 3751 independent reflections; $R_{int} = 0.0492$, 2456 reflections with $F_o > 4\sigma(F_o)$, semi-empirical absorption correction, 243 variables, $R = 0.0376$, $wR^2 = 0.0845$, largest difference peak: 0.178 e/Å^3.

b) A solution of $MesBCl_2$ (2.5 g, 12.5 mmol) in 15 mL of CH_2Cl_2 was added to a solution of **7a** (2.5 g, 6.4 mmol) in 15 mL of CH_2Cl_2 over a period of 60 min at −70 to −60°C. NMR data after a period of 16 h stirring at ambient temp.: ^{1}H NMR: δ = 0.67 [s, 9 H, Me_3SnCl, $^2J(^{117(119)}Sn^1H)$ = 56.2 (58.6) Hz], 0.69 [s, 9 H, Me_3SnCl, $^2J(^{117(119)}Sn^1H)$ = 55.2 (57.6) Hz, $^3J(^{117(119)}Sn^1H)$ = 35.2 (38.6) Hz?], 2.31 [s, br., 6 H, NMe_2, $^3J(^{117(119)}Sn^1H)$ = 36.8 Hz], 2.57 (s, 6 H, *p*-Me−Ph), 2.93 (s, 12 H, *o*-Me), 6.81 (br. s, 4 H, *m*-H−Ph). − ^{11}B NMR: δ = 39.6 ($h_{1/2}$ = 393 Hz). − The workup was according to Procedure I after a period of 17 h. The residue, obtained after removal of the volatile components at 25 to 40°C/12−10^{-5} Torr, was dissolved in CH_2Cl_2 and checked by ^{1}H- and ^{11}B-NMR spectroscopy. The spectra are identical with those of the reaction mixture, but the signal of the noncoordinated Me_3SnCl had disappeared. The latter was detected in the trap. The ^{1}H-NMR signal for Me_3SnCl, forming an adduct with **8d**, was found at δ = 0.70 [$^2J(^{117(119)}Sn^1H)$ = 57.6 Hz]. − Sn−N bond-cleavage experiment: The NMR sample of the residue, dissolved in 5 mL of CH_2Cl_2, was checked by NMR after addition of a drop of $MesBCl_2$: ^{11}B NMR: δ = 39.1 [assignment: $Me_2N-N(BMesCl)_2 \cdot Me_3SnCl$], −0.7 [$Me_2N-N(BMesCl)_2 \cdot MesBCl_2$], ratio: 3:2. − ^{1}H NMR: δ = 0.72 and 0.74 (Me_3SnCl·coordinated and Me_3SnCl in solution). With additional $MesBCl_2$ the signal at δ = 39.1 (^{11}B NMR) lost intensity and the signal at δ = −0.7 gained intensity; the excess of $MesBCl_2$ led to the following NMR data of the reaction mixture: ^{11}B NMR: δ = 59.5 ($MesBCl_2$), 36.6 and −0.9 [assignment: $Me_2N-N(BMesCl)_2 \cdot MesBCl_2$]. − ^{1}H NMR: δ = 0.81 [sharp signal,·dissolved Me_3SnCl, $^2J(^{117(119)}Sn^1H)$ = 56.6 (59.1)]. A mixture of unidentifiable products resulted when keeping the residue at room temp. for a few hours or by heating in vacuo up to 100°C/10^{-5} Torr in order to remove Me_3SnCl coordinated to the Me_2N group.

Attempt to Prepare 2,2-Bis(bromomethylboryl)-1,1-diphenylhydrazine (8e) by Reaction of 7b with $MeBBr_2$ (Molar Ratio 1:2): 7b (5.34 g, 10.5 mmol), dissolved in 15 mL of CH_2Cl_2, was added over 60 min to a solution of $MeBBr_2$ (4.6 g, 24.8 mmol) in 15 mL of CH_2Cl_2 at −75 to −65°C. NMR data after 16 h stirring at ambient temp.: ^{1}H NMR: δ = 0.77 [s, 9 H, Me_3SnBr]. − ^{11}B NMR: δ = 34.5 [$(Ph_2NN{=}BMe)_3$?], 40.0/−2.4 [signal ratio: ca. 1:1, **8e** (intramolecular BN adduct formation?)], 48.9 [$Ph_2N-N(BMeBr)_2$ (**8e**) noncyclic compound?]. − The workup was carried out according to Procedure I after 17 h of stirring. The residue obtained after removal of the volatile components was dissolved in CH_2Cl_2 and checked by ^{1}H- and ^{11}B-NMR spectroscopy. The predominant signal among others in the ^{11}B-NMR spectrum was that at δ = 34.5 [$(Ph_2NN{=}BMe)_3$?]; after 12 h, additional signals (δ = 28.8, 31.9) could be detected in the solution. Attempts to separate the products failed even by fractional recrystallization from toluene at various temperatures. The only volatile compound obtained was Me_3SnBr.

Acknowledgments

We gratefully acknowledge the support of this research by the Deutsche Forschungsgemeinschaft, the Fonds der Chemischen Industrie and the Chemetall GmbH. We also thank Mrs. C. Neumann for support of the synthetic work, Mrs. D. Ewald for recording the mass spectra and Mr. T. Seifert for the X-ray structure determination.

[1] A. Appel, C. Kober, C. Neumann, H. Nöth, M. Schmidt and W. Storch, *Chem. Ber.* **1996**, *129*, 175−189 and refs. therein.
[2] H. Nöth, P. Otto, W. Storch, *Chem. Ber.* **1985**, *118*, 3020−3031.
[3] H. Nöth, P. Otto, W. Storch, *Chem. Ber.* **1986**, *119*, 2517−2530.
[4] P. Paetzold, C. v. Plotho, G. Schmid, R. Schrader, D. Bougeard, U. Pfeiffer, R. Gleiter, W. Schäfer, *Chem. Ber.* **1984**, *117*, 1089−1095.
[5] W. Storch, reported at the *VII. Int. Meeting on Boron Chemistry*, Torun, Poland, **1990**.
[6] [6a] R. Boese, B. Kröckert, P. Paetzold, *Chem. Ber.* **1987**, *120*, 1913−1915. − [6b] P. Paetzold, B. Redenz-Stormanns, R. Boese, *Chem. Ber.* **1991**, *124*, 2435−2441.
[7] H. Nöth, S. Weber, *Z. Naturforsch.* **1983**, *38b*, 1460−1465; F. Dirschl, E. Hanecker, H. Nöth, W. Rattay, W. Wagner, *Z. Naturforsch.* **1986**, *41b*, 32−37.
[8] The diborylamine **3m** has also been obtained in low yield via Si−N cleavage but under comparatively drastic conditions: K. Barlos, H. Christl, H. Nöth, *Liebigs Ann. Chem.* **1976**, 2272−2283.
[9] S. Diemer, H. Nöth, K.Polborn, W. Storch, *Chem. Ber.* **1992**, *125*, 389−400 (details on reactions according to Equation 3)
[10] [10a] D. Nölle, H. Nöth, *Angew. Chem.* **1971**, *83*, 112−113. − [10b] D. Nölle, H. Nöth, W. Winterstein, *Z. Anorg. Allg. Chem.* **1974**, *406*, 235−250. − [10c] K. Niedenzu, B. K. Christmas, *Z. Anorg. Allg. Chem.* **1978**, *439*, 103−111. − [10d] P. C. Bharara, H. Nöth, *Z. Naturforsch.* **1979**, *34b*, 1352−1357. − [10e] W.Pieper, D. Schmitz, P. Paetzold, *Chem. Ber.* **1981**, *114*, 3801−3812. − [10f] A. Meller, M. Armbrecht, *Chem. Ber.* **1986**, *119*, 1−8.
[11] [11a] H. Nöth, W. Regnet, H. Rihl, R. Standfest, *Chem. Ber.* **1971**, *104*, 722−733. − [11b] H. Fußstetter, H. Nöth, *Liebigs Ann. Chem.* **1981**, 633−641.
[12] J. March, *Advanced Organic Chemistry*, 3rd edition, John Wiley & Sons Inc., New York, Chichester, Brisbane, Toronto, Singapore, **1985**, p. 310 and refs. cited therein.
[13] H. Nöth, H. Vahrenkamp, *Chem. Ber.* **1967**, *100*, 3353−3358.
[14] H. Nöth, B. Wrackmeyer, *NMR Spectrocopy on Boron Compounds, Basic Principles and Progress* (Eds.: F. Diehl, E. Fluck, P. Kosfeld), Springer Verlag, Berlin, Heidelberg, New York, **1978**.
[15] P. Otto, Ph. D. Thesis, University of Munich, **1986**.
[16] [16a] D. T. Pegg, D. M. Doddrell, W. M. Brooks, M. R. Bendall, *J. Magn. Reson.* **1981**, *44*, 32−36. − [16b] D. T. Pegg, D. M. Doddrell, M. R. Bendall, *J. Chem. Phys.* **1982**, *77*, 2745−2751.
[17] H. Fußstetter, H. Nöth, *Liebigs Ann. Chem.* **1981**, 633−641.
[18] H. Hommer, Ph. D. Thesis, University of Munich, **1994**.
[19] H. Nöth, S. Weber, *Z. Naturforsch.* **1983**, *38b*, 1460−1465.
[20] V. S. Petrosyan, *NMR Spectra and Structures of Organotin Compounds, Progress in NMR Spectroscopy*, **1977**, *11*, 115−148.
[21] B. Wrackmeyer, *Annual Rep. NMR Spectrosc.* **1985**, *16*, 73−186.
[22] G. M. Sheldrick, *SHELXL-93, Program for the Refinement of Crystal Structures*, University of Göttingen, **1993**.
[23] K. Sisido, S. Kozima, *J. Org. Chem.* **1964**, *29*, 907−909.
[24] C. Kober, J. Kroner, W. Storch, *Angew. Chem.* **1993**, *105*, 1693−1695; *Angew. Chem. Int. Ed. Engl.* **1993**, *32*, 1608−1610.
[25] [25a] W. P. Neumann, *Die organische Chemie des Zinns*, Ferdinand Enke Verlag, Stuttgart, **1967**. − [25b] M. Pereyre, J.-P. Quintarr, A. Rahm, *Tin in Organic Synthesis*, Butterworth & Co. Ltd., London, Boston, **1987** and refs. cited therein.
[26] K. Jones, M. F. Lappert, *J. Chem. Soc.* **1965**, 1944−1951.
[27] H. W. Roesky, H. Wietzer, *Chem. Ber.* **1974**, *107*, 3186−3190.
[28] N. Wiberg, M. Veith, *Chem. Ber.* **1971**, *104*, 3191−3203.
[29] N. Wiberg, M. Veith, *Chem. Ber.* **1971**, *104*, 3176−3190.
[30] W. Storch, H. Nöth, *Chem. Ber.* **1977**, *110*, 1636−1642.
[31] W. Hansen, P. Paetzold, *Z. Anorg. Allg. Chem.* **1966**, *345*, 79−86.
[32] H. Nöth, P. Fritz, *Z. Anorg. Allg. Chem.* **1963**, *322*, 297−309.
[33] From iPr$_3$B and BCl_3 catalysed with BH3·THF: see R. Köster, M. A. Grassberger, *Liebigs Ann. Chem.* **1968**, *719*, 169−172.
[34] Modified procedure, from 2-*t*Bu-1,3,2-dithiaborolane and Br_2 in CH_2Cl_2, see H. Prigge, Ph. D. Thesis, University of Munich, **1983**.
[35] W. Hansen, P. Paetzold, *Z. Anorg. Allg. Chem.* **1966**, *345*, 79−86.

[36] S. J. Groszos, S. F. Stafiej, *J. Am. Chem. Soc.* **1958**, *80*, 1357−1360.
[37] I. Haiduc, *The Chemistry of Inorganic Ring Systems*, Wiley Interscience, London, New York, Sydney, Toronto **1970**, part 1, p. 124−273.
[38] K. Barlos, H. Christl, H. Nöth, *Lieb. Ann. Chem.* **1976**, 2272−2278.
[39] For comparison $\nu_{as}(B_2N)$ = 1310−40 cm^{-1}: H. Vahrenkamp, Ph. D. Thesis, University of Munich, **1967**.
[40] D. Kaufmann, *Chem. Ber.* **1987**, *120*, 901−905.
[41] G. Linti, Ph. D. Thesis, University of Munich, **1990**.
[42] W. Storch, H. Nöth, *Chem. Ber.* **1977**, *110*, 1636−1642. H. Nöth, P. Otto, W. Storch, *Chem. Ber.* **1986**, *119*, 2517−2530.
[43] M. Kaufmann, Staatsexamensarbeit, Universität München, **1988**.
[44] K. Barlos, Ph. D. Thesis, University of Munich, **1977**.
[45] S. Diemer, Ph. D. Thesis, University of Munich, **1993**.

Received November 14, 1998
[I98404]

On the Metal-Ion-Coordinating Properties of the Benzimidazolate Residue in Aqueous Solution – Extent of Acidification of Benzimidazole-(N3)H Sites by (N1)-Coordinated Divalent Metal Ions

Larisa E. Kapinos[a] and Helmut Sigel*[a]

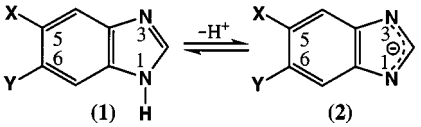
Keywords: Acidity constants / Benzimidazolate complexes / Imidazole-type ligands / Metal ion complexes / Nitrobenzimidazoles / Stability constants

The stability constants of the 1:1 complexes formed between Mg^{2+}, Mn^{2+}, Co^{2+}, Ni^{2+} or Cd^{2+} (= M^{2+}) and the anionic 5(6)-nitrobenzimidazolate [= $(NBI–H)^-$] or 5,6-dinitrobenzimidazolate [= $(DNBI–H)^-$] were determined by potentiometric pH titrations in aqueous solution (25 °C; I = 0.5 M, $NaNO_3$). The acidity constants for the deprotonation of the (N1)H sites in neutral NBI and DNBI (= L) were measured by the same method. The comparison of the stability constants determined for the $M(L–H)^+$ complexes with those calculated from log K^M_{ML} versus pK^H_{HL} straight-line plots, which were established recently for neutral benzimidazole-type ligands, reveals that the stabilities of the $M(L–H)^+$ complexes are significantly enhanced, as one might have expected due to the negative charge present on the ligands. Of course, the electron-withdrawing properties of (N3)-bound metal ions facilitate the release of the proton from the (N1)H site in the $M(NBI)^{2+}$ and $M(DNBI)^{2+}$ complexes, if compared to the situation in the free ligands. The effect of a metal ion bound to a benzimidazolate or imidazolate residue on the coordination tendency toward a further metal ion (giving rise to an imidazolate bridge) was estimated.

1. Introduction

Benzimidazole (1,3-dideazapurine) and its derivatives show biological activity[1–6] and are often employed in drug design.[1][2] For example, nitrobenzimidazoles act as substrates for the two-electron reduction catalyzed by DT-diaphorase,[3] and 5,6-dinitrobenzimidazole and related compounds are substrates for purine nucleoside phosphorylase which allows the synthesis of nucleoside analogues.[4] Other nitrobenzimidazoles are studied for their analgesic and anti-inflammatory activity[5] as well as for their antiproliferative and antiviral activity.[6] Since benzimidazole derivatives act biologically often via their nucleoside[4] and nucleotide[1] analogues, the metal-ion-binding properties of the benzimidazole residue are of general interest because such reactions usually also involve metal ions.[7–9]

In our attempts[10] to increase the understanding of the metal-ion-binding dichotomy[11] of the adenine residue, we have recently correlated[12] the acid-base and metal-ion-binding properties of a series of benzimidazoles by constructing log K^M_{ML} versus pK^H_{HL} plots which result for a given metal ion in a straight line (see Section 2.2). In this study[12] we had included 5(6)-nitrobenzimidazole (NBI) and 5,6-dinitrobenzimidazole (DNBI) because they release the proton from their monoprotonated forms, $H(NBI)^+$ and $H(DNBI)^+$, with a low pK_a, i.e. p$K^H_{H(NBI)}$ = 3.61 and p$K^H_{H(DNBI)}$ = 1.72,[12] which allowed us to extend the indicated correlation far into the acidic pH range. Considering that the deprotonation of monoprotonated benzimidazole, $H(BI)^+$, occurs with p$K^H_{H(BI)}$ = 5.63[12] and the formation of the corresponding anion $(BI–H)^-$ with pK^H_{BI} = 12.8,[13] which means that the two pK_a values are separated by $\Delta pK_a \approx 7$,[13] one may expect that the pK_a values of NBI and DNBI differ by about the same extent, and thus, the formation of their anions is expected to occur in the pK_a range of about 8.5 to 10.5. The acid-base equilibrium for their neutral and anionic forms is depicted in Figure 1.



DNBI: X = Y = NO_2 **(DNBI–H)$^-$**

NBI: X = NO_2; Y = H **(NBI–H)$^-$**

Figure 1. Chemical structures of 5(6)-nitrobenzimidazole (NBI) and 5,6-dinitrobenzimidazole (DNBI) in their neutral (**1**) and anionic forms (**2**)

A pK_a range of 8.5 to 10.5 is easily accessible for potentiometric pH titrations and therefore also suitable for the determination of stability constants. Surprisingly, no systematic study focussing on the stability of metal ion complexes in aqueous solution appears to have been carried out[14–16] for benzimidazolate or imidazolate and related ligands, even though the latter is well known to occur as a bridging residue between two metal ions in Cu,Zn superoxide dismutase[17][18] and also in a number of (low-molecular-weight) complexes studied in solution[19–21] and in the solid state;[21][22] actually quite a number of complexes formed with deprotonated imidazole derivatives and a variety of metal ions have been isolated and their properties studied (e.g.[21–23]). Interestingly, already about 60 years ago the formation of an imidazolate complex was suggested

[a] Institute of Inorganic Chemistry, University of Basel, Spitalstrasse 51, CH-4056 Basel, Switzerland
Fax: (internat.) + 41-61/267-1017
E-mail: Sigel@ubaclu.unibas.ch

 © WILEY-VCH Verlag GmbH, D-69451 Weinheim, 1999 1434–1948/99/1010–1781 $ 17.50+.50/0

to occur with ferrihemoglobin[24] and the possibility to deprotonate the pyrrole nitrogen in imidazole complexes has been confirmed in the years thereafter.[25] However, with the deficit indicated above in mind we endeavored now to measure the stability constants of the complexes formed between Mg^{2+}, Mn^{2+}, Co^{2+}, Ni^{2+}, or Cd^{2+} (M^{2+}) and 5(6)-nitrobenzimidazolate or 5,6-dinitrobenzimidazolate (Figure 1).

2. Results and Discussion

2.1. Definition of Equilibria and Results

Benzimidazole and its derivatives (L) can accept one proton at N3 to give the monoprotonated species HL^+ which gives rise to the deprotonation reaction according to Equilibrium 1a.

$$HL^+ \rightleftharpoons H^+ + L \quad (1a)$$

$$K^H_{HL} = [H^+][L]/[HL^+] \quad (1b)$$

The corresponding acidity constants for $H(NBI)^+$ and $H(DNBI)^+$ have recently been determined: $pK^H_{H(NBI)} = 3.61 \pm 0.02$ and $pK^H_{H(DNBI)} = 1.72 \pm 0.06$.[12] However, as indicated already in Section 1, one expects that the proton present at N1 in the neutral form of NBI and DNBI (Figure 1) can also be ionized according to Equilibrium 2.

$$L \rightleftharpoons (L-H)^- + H^+ \quad (2a)$$

$$K^H_L = [(L-H)^-][H^+]/[L] \quad (2b)$$

Indeed, the experiments carried out now (25°C; $I = 0.5$ M,[26] $NaNO_3$) prove this to be correct; the corresponding acidity constants are $pK^H_{NBI} = 10.58 \pm 0.03$ and $pK^H_{DNBI} = 8.92 \pm 0.03$. The present acidity constant for the deprotonation of NBI is in fair accord with earlier spectrophotometric determinations which gave $pK^H_{NBI} = 10.69$ (25°C)[27] and 10.86 (25°C; $I = 0.1$ M)[13] as well as potentiometric titrations which resulted in $pK^H_{NBI} = 10.31$ (25°C)[28][29] and 11.2.[28][30]

$$\Delta pK_a = pK^H_L - pK^H_{HL} \quad (3)$$

The difference defined in Equation 3 for the NBI and DNBI systems equals $\Delta pK_{a/NBI} = (10.58 \pm 0.03) - (3.61 \pm 0.02) = 6.97 \pm 0.04$ and $\Delta pK_{a/DNBI} = (8.92 \pm 0.03) - (1.72 \pm 0.06) = 7.20 \pm 0.07$. Hence, the acidity constants of the Equilibria 1a and 2a can be determined independently for both ligands because the buffer regions are not overlapping. The ΔpK_a values of about 7 agree with previous observations made for benzimidazole derivatives.[13]

Both, the neutral species L and the deprotonated species $(L-H)^-$ may form complexes with metal ions (M^{2+}) according to Equilibria 4a and 5a.

$$M^{2+} + L \rightleftharpoons ML^{2+} \quad (4a)$$

$$K^M_{ML} = [ML^{2+}]/([M^{2+}][L]) \quad (4b)$$

$$M^{2+} + (L-H)^- \rightleftharpoons M(L-H)^+ \quad (5a)$$

$$K^M_{M(L-H)} = [M(L-H)^+]/([M^{2+}][(L-H)^-]) \quad (5b)$$

The stability constants for the $M(NBI)^{2+}$ complexes have recently been determined by potentiometric pH titrations and those for the $M(DNBI)^{2+}$ complexes by spectrophotometry.[12] These previous results, which are listed in column 2 of Table 1, have been taken into account in the evaluations of the potentiometric pH titrations which were carried out now to determine the stability constants of the $M(NBI-H)^+$ and $M(DNBI-H)^+$ complexes (Equation 5). The corresponding results are given in column 3 of Table 1. No values for the complexes with Cu^{2+} and Zn^{2+} could be determined because of their strong tendency to form hydroxo species.

Equilibria 4a and 5a are connected via Equilibrium 6a and the corresponding acidity constant can be calculated according to Equation 7.

$$ML^{2+} \rightleftharpoons M(L-H)^+ + H^+ \quad (6a)$$

$$K^H_{ML} = [M(L-H)^+][H^+]/[ML^{2+}] \quad (6b)$$

$$pK^H_{ML} = pK^H_L + \log K^M_{ML} - \log K^M_{M(L-H)} \quad (7)$$

These acidity constants are listed in column 4 of Table 1. They allow to quantify the effect of a (N3)-bound metal ion on the deprotonation of the (N1)H site by defining the difference between the two relevant acidity constants according to Equation 8.

$$\Delta pK_{a/ML} = pK^H_L - pK^H_{ML} \quad (8)$$

These differences are given in column 5 of Table 1; they are of the order observed previously for imidazole complexes.[25] Since the error limits for the $\Delta pK_{a/ML}$ values are relatively large, no conclusions can be drawn for the $M(NBI)^{2+}$ and $M(DNBI)^{2+}$ complexes of Mg^{2+}, Mn^{2+} and Ni^{2+} regarding any possible differences in the acidification. However, for Co^{2+} and Cd^{2+} the acidification is clearly more pronounced in the $M(NBI)^{2+}$ complexes. This means that, relatively speaking, the deprotonation at the (N1)H site leads to a more significant stability increase in the case of the NBI complexes compared to the DNBI ones. This conclusion will also be confirmed below (see the final paragraph in Section 2.2).

2.2. Metal-Ion-Binding Properties of the Benzimidazolate Residue

To which extent does the deprotonation of the (N1)H site (see Figure 1) affect the stability of the complexes? An answer to this question may be obtained by applying the recently constructed $\log K^M_{ML}$ versus pK^H_{HL} plots, where L represents a series of benzimidazole-type ligands.[12] Three examples are shown in Figure 2 and the pertinent parameters which define the straight lines are listed in Table 2 for those metal ions considered in the present study.

Table 1. Logarithms of the stability constants of the ML^{2+} (Equation 4) and $M(L-H)^{+}$ complexes (Equation 5), together with the negative logarithms of the acidity constants (Equations 6 and 7) of the corresponding ML^{2+} complexes, where L = NBI or DNBI, as determined by potentiometric pH titrations in aqueous solution at 25°C and I = 0.5 M ($NaNO_3$)[a–c]

M^{2+}	log K^{M}_{ML}	log $K^{M}_{(ML-H)}$	pK^{H}_{ML}	$\Delta pK_{a/ML}$[d]
5(6)-Nitrobenzimidazole (NBI)[a]				
Mg^{2+}	−0.09 ± 0.15	0.41 ± 0.10	10.08 ± 0.18	−0.50 ± 0.18
Mn^{2+}	0.37 ± 0.07	2.22 ± 0.14	8.73 ± 0.16	−1.85 ± 0.16
Co^{2+}	1.25 ± 0.02	3.67 ± 0.17	8.16 ± 0.17	−2.42 ± 0.17
Ni^{2+}	1.63 ± 0.05	4.1 ± 0.4	8.1 ± 0.4	−2.5 ± 0.4
Cd^{2+}	1.51 ± 0.05	4.63 ± 0.16	7.46 ± 0.17	−3.12 ± 0.17
5,6-Dinitrobenzimidazole (DNBI)[a]				
Mg^{2+}	−0.11 ± 0.05[e]	0.62 ± 0.08	8.19 ± 0.10	−0.73 ± 0.10
Mn^{2+}	0.08 ± 0.05[e]	1.85 ± 0.04	7.15 ± 0.07	−1.77 ± 0.08
Co^{2+}	0.84 ± 0.07[f]	2.73 ± 0.06	7.03 ± 0.10	−1.89 ± 0.10
Ni^{2+}	1.23 ± 0.10[f]	3.31 ± 0.16	6.84 ± 0.19	−2.08 ± 0.19
Cd^{2+}	0.96 ± 0.09[f]	3.34 ± 0.17	6.54 ± 0.19	−2.38 ± 0.19

[a] Acidity constants: p$K^{H}_{H(NBI)}$ = 3.61 ± 0.02 (Equation 1; from ref.[12]), pK^{H}_{NBI} = 10.58 ± 0.03 (Equation 2); p$K^{H}_{H(DNBI)}$ = 1.72 ± 0.06 (Equation 1; from ref.[12])[f], pK^{H}_{DNBI} = 8.92 ± 0.03 (Equation 2). – [b] The error limits given are *three times* the standard error of the mean value or the sum of the probable systematic errors, whichever is larger. The error limits of the derived data (in the present case for columns 4 and 5) were calculated according to the error propagation after Gauss. Regarding the reasons why in some instances the errors are rather large, the Experimental Section should be consulted. – [c] The values in the second column are taken from ref.[12] – [d] See Equation 8 in Section 2.1. – [e] These values were experimentally not accessible (see ref.[12]); they were calculated with the straight-line equations defined in Table 2 and the micro acidity constant p$k_{ma/H(DNBI)}$ = 2.02 which follows from p$K^{H}_{H(DNBI)}$ = 1.72; see ref.[12] – [f] These values were measured by spectrophotometry (see ref.[12]).

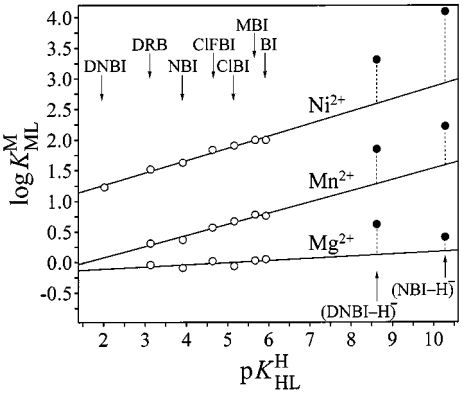


Figure 2. Evidence for an increased stability of several M^{2+} 1:1 complexes of 5,6-dinitrobenzimidazolate, $(DNBI-H)^{-}$, and 5(6)-nitrobenzimidazolate, $(NBI-H)^{-}$, (•) (see structure **2** in Figure 1), based on log K^{M}_{ML} versus pK^{H}_{HL} plots for the 1:1 complexes of Mg^{2+}, Mn^{2+} and Ni^{2+} with the following neutral benzimidazole-type ligands (o): 5,6-dinitrobenzimidazole (DNBI; see **1** in Figure 1), 5,6-dichloro-1-(β-D-ribofuranosyl)benzimidazole (DRB), 5(6)-nitrobenzimidazole (NBI; see **1** in Figure 1), 6-chloro-5-fluorobenzimidazole (ClFBI), 5(6)-chlorobenzimidazole (ClBI), 1-methylbenzimidazole (MBI) and benzimidazole (BI) (from left to right). The corresponding equilibrium constants are taken from ref.[12]; note, where appropriate the micro acidity constants (pk_{am}) were applied (for details see ref.[12]); the parameters for the least-squares lines drawn through these data sets are given in Table 2; the vertical broken lines emphasize the stability differences to the corresponding reference lines (Equation 11); these differences are listed in column 4 of Table 3; the data pairs for the $M(DNBI-H)^{+}$ and $M(NBI-H)^{+}$ complexes are from Table 1 and Equations 9 and 10; all plotted equilibrium constants refer to aqueous solutions at 25°C and I = 0.5 M ($NaNO_3$).

Table 2. Straight-line correlations for M^{2+}-benzimidazole-type complex stabilities and benzimidazole group basicities,[a,b] for aqueous solutions at 25°C and I = 0.5 M ($NaNO_3$)

M^{2+}	m	b	SD
Mg^{2+}	0.035 ± 0.020	−0.179 ± 0.095	0.051
Mn^{2+}	0.182 ± 0.017	−0.287 ± 0.081	0.045
Co^{2+}	0.186 ± 0.011	0.513 ± 0.048	0.042
Ni^{2+}	0.201 ± 0.011	0.860 ± 0.052	0.042
Cd^{2+}	0.293 ± 0.011	0.385 ± 0.050	0.039

[a] The slopes (m) and intercepts (b) for the straight baselines from plots of log K^{M}_{ML} versus pK^{H}_{HL} were calculated[12] from equilibrium constants involving the seven (or six in the case of Mg^{2+} and Mn^{2+}) sterically unhindered ligands (L) which are named in Figure 2 (see also ref.[12]). The fourth column lists *three times* the standard deviations (SD) resulting from the differences between the experimental and calculated values for the seven (or six) ligand systems. – [b] The above data for m, b and SD are abstracted from Tables 3 and 4 in ref.[12] Straight-line equation: $y = mx + b$, where x represents the pK_a value of any monoprotonated benzimidazole-type ligand and y the calculated stability constant (log K) of the corresponding ML complex; the errors given with m and b correspond to one standard deviation (1 σ). The listed SD values (3 σ; column 4) are considered as reasonable error limits for any stability constant calculation in the pK_a range 2–6; for the error limits outside of this range see Section 2.2.

For a comparison of the stability constants determined now with these straight lines, the acid-base properties of NBI and DNBI need to be considered in detail: Once the corresponding anion $(L-H)^{-}$ has formed, there are two equal ways for the formation of the neutral species L (Figure 1). Consequently, the benzimidazolate derivatives appear to be more basic than they actually are. This means, micro acidity constants as defined in Equations 9 and 10 for DNBI and NBI, in which this statistical effect is considered, need to be used in any kind of acid-base comparisons.

$$pk_{ma/DNBI} = pK^{H}_{DNBI} - 0.3 = (8.92 \pm 0.03) - 0.3 = 8.62 \pm 0.03 \quad (9)$$

$$pk_{ma/NBI} = pK^{H}_{NBI} - 0.3 = (10.58 \pm 0.03) - 0.3 = 10.28 \pm 0.03 \quad (10)$$

It may be added that this reasoning is also valid (see section 2.2 of ref.[12]) for 5(6)-nitrobenzimidazole which has non-equivalent substituents at C5 and C6 (Figure 1).

Table 3. Comparison of the logarithms of the stability constants of $M(NBI-H)^+$ and $M(DNBI-H)^+$ complexes (Equation 5) as determined by potentiometric pH titrations (exptl.)[a] in aqueous solution at 25°C and I = 0.5 M ($NaNO_3$) with the calculated (calcd.) stability constants based on the basicity[b] of the benzimidazolate nitrogen atoms and the reference-line equations of Table 2.

M^{2+}	log $K^M_{M(L-H)}$ exptl.[a]	log $K^M_{M(L-H)}$ calcd.[b]	log Δ[c]
5(6)-Nitrobenzimidazolate, $(NBI-H)^-$			
Mg^{2+}	0.41 ± 0.10	0.18 ± 0.27	0.23 ± 0.29
Mn^{2+}	2.22 ± 0.14	1.58 ± 0.23	0.64 ± 0.27
Co^{2+}	3.67 ± 0.17	2.43 ± 0.21	1.24 ± 0.27
Ni^{2+}	4.1 ± 0.4	2.93 ± 0.22	1.2 ± 0.5
Cd^{2+}	4.63 ± 0.16	3.40 ± 0.22	1.23 ± 0.27
5,6-Dinitrobenzimidazolate, $(DNBI-H)^-$			
Mg^{2+}	0.62 ± 0.08	0.12 ± 0.16	0.50 ± 0.18
Mn^{2+}	1.85 ± 0.04	1.28 ± 0.14	0.57 ± 0.15
Co^{2+}	2.73 ± 0.06	2.12 ± 0.12	0.61 ± 0.13
Ni^{2+}	3.31 ± 0.16	2.59 ± 0.14	0.72 ± 0.21
Cd^{2+}	3.34 ± 0.17	2.91 ± 0.13	0.43 ± 0.21

[a] These values are from column 3 in Table 2. – [b] Calculated with the micro acidity constants $pk_{ma/NBI}$ = 10.28 and $pk_{ma/DNBI}$ = 8.62 (see Equations 9 and 10 and text in Section 2.2) and the straight-line equations given in Table 2. These error limits are estimates; see ref.[31] – [c] The error limits for these differences were calculated according to the error propagation after Gauss.

Application of the micro acidity constants of Equations 9 and 10 and of the stability constants of the $M(NBI-H)^+$ and $M(DNBI-H)^+$ complexes leads to the solid data points seen in Figure 2. Their vertical distances to the corresponding reference lines defined for neutral benzimidazole complexes reflect the effect of the negative charge of the benzimidazolates. This stability increase is defined by Equation 11, where log $K^M_{M(L\text{-}H)expt1}$ represents the experimentally measured stability constant and log $K^M_{M(L\text{-}H)calcd}$ the one calculated with the micro acidity constants (Equations 9 and 10) and the straight-line parameters of Table 2. The corresponding results are summarized in Table 3.[31]

$$\log \Delta = \log K^M_{M(L-H)expt1} - \log K^M_{M(L-H)calcd} \quad (11)$$

The stability enhancements log Δ (Equation 11), listed in column 4 of Table 3, indicate that the $M(NBI-H)^+$ and $M(DNBI-H)^+$ complexes are by about 0.2 to 1.2 log units more stable than complexes formed with neutral benzimidazoles of the same pK_a range. Comparison of these log Δ values reveals that in the case of Mg^{2+}, Mn^{2+} and Ni^{2+} the error limits are too large for meaningful conclusions, whereas for the complexes with Co^{2+} and Cd^{2+} it is certain that the stability enhancement for $(NBI-H)^-$ is more pronounced than that for $(DNBI-H)^-$ (see Table 3). Hence, one may conclude that the slopes of log $K^M_{M(L-H)}$ versus pK^H_L plots are somewhat larger than those of log K^M_{ML} versus pK^H_{HL} seen in Figure 2. Based on the stability enhancements observed for the $M(DNBI-H)^+$ complexes, which have relatively low error limits (Table 3, column 4), it appears that the extent of the stability enhancement is relatively independent of the metal ion considered.

3. Conclusions

The present study reveals that a metal ion bound to N3 of a benzimidazole residue acidifies the proton at the (N1)H site by about 0.5 to 3 pK_a units depending on the metal ion considered. The resulting benzimidazolate complexes are more stable than those formed with the corresponding neutral benzimidazoles. Clearly, it is safe to assume that this also holds for imidazole and imidazolate complexes.

How do two metal ions bound to the same imidazolate or benzimidazolate residue affect each other, as, e.g., in Cu,Zn superoxide dismutase[17][18] where an imidazolate residue bridges the two metal ions? Our results show, ignoring the one for $Mg(NBI-H)^+$ (Table 3), that the creation of a negative charge (−1) on the ligand leads on average to a stability enhancement of about 0.5−1.2 log units for the binding of the first metal ion at one of the nitrogens. Thus, in a first approximation one may assume that binding of the second metal ion at the other nitrogen atom is inhibited due to charge repulsion of the now positively (+1) charged liganding unit by approximately the same extent. Hence, an estimation of the stability constant, log $K^M_{M_2(L-H)}$, for $M_2(L-H)^{3+}$ complexes is obtained by subtracting from the stability constants, log K^M_{ML}, valid for the ML^{2+} complexes (Table 1)[12] the mentioned 0.5−1.2 log units. This then means that the stabilities of the $M(L-H)^+$ and $M_2(L-H)^{3+}$ complexes differ overall by about 1 to 2.4 log units. This conclusion also explains why under our experimental conditions no $M_2(L-H)^{3+}$ complexes were observed.

Experimental Section

1. Materials, Apparatus, and Definitions: The same reagents, experimental equipment and computers for the calculation procedures were used as previously.[12] The acidity constants determined are so-called practical, mixed or Brønsted constants.[26] Their negative logarithms given for aqueous solution at I = 0.5 M ($NaNO_3$) and 25 °C may be converted into the corresponding concentration constants by subtracting 0.03 from the pK_a values listed in the tables.[26] The ionic product of water (K_w) does not enter into the calculations because the differences in NaOH consumption between solutions with and without ligand (see below) are evaluated. The stability constants presented are, as usual, concentration constants.

2. Determination of Equilibrium Constants: The acidity constants $K^H_{H(NBI)}$ (see also ref.[12]) and K^H_{NBI} of NBI were determined by titrating 25 mL of 7.2 mM HNO_3 (I = 0.5 M, $NaNO_3$; 25 °C) in the presence and absence of 2.5 mM 5(6)-nitrobenzimidazole with 3 mL of 0.1 M NaOH. In the calculations of the two pK_a values for this ligand (L) the species H^+, HL^+, L and $(L-H)^-$ were considered.[12] Since the solubility of 5,6-dinitrobenzimidazole is low, more diluted solutions had to be used in this case, i.e., the acidity constant K^H_{DNBI} of DNBI was measured by titrating 25 mL of 0.15 mM HNO_3 (I = 0.5 M, $NaNO_3$) in the presence and absence of 0.24 mM DNBI with 1 mL of 0.01 M NaOH and calculated by taking into account the species H^+, L and $(L-H)^-$.[12] The final results for the acidity constants K^H_L of NBI and DNBI are the averages of 34 and 21 pairs of titrations, respectively.

The stability constants $K^{M}_{M(L-H)}$ of the $M(NBI-H)^+$ and $M(DNBI-H)^+$ complexes were determined under the same conditions as the acidity constants, but $NaNO_3$ was partly or fully replaced by $M(NO_3)_2$ (I = 0.5 M; 25 °C). For the systems with NBI the following concentrations of $M(NO_3)_2$ were employed: 0.1667 M (M^{2+}/L = 67:1 for Mg^{2+} and Mn^{2+}), 0.0417 M (M^{2+}/L = 17:1 for Co^{2+} and Ni^{2+}), 0.0333 M (M^{2+}/L = 13:1 for Cd^{2+}), 0.0208 M (M^{2+}/L = 8:1 for Ni^{2+} and Cd^{2+}), and 0.0104 M (M^{2+}/L = 4:1 for Ni^{2+}). Similarly, in the case of DNBI the following $M(NO_3)_2$ concentrations were used: 0.1667 M (M^{2+}/L = 695:1 for Mg^{2+} and Mn^{2+}), 0.0833 M (M^{2+}/L = 347:1 for Mn^{2+}), 0.0208 M (M^{2+}/L = 87:1 for Co^{2+} and Ni^{2+}), 0.0167 M (M^{2+}/L = 70:1 for Co^{2+}), 0.0104 M (M^{2+}/L = 43:1 for Co^{2+}), 0.00667 M (M^{2+}/L = 28:1 for Ni^{2+} and Cd^{2+}), and 0.00333 M (M^{2+}/L = 14:1 for Ni^{2+} and Cd^{2+}). The stability constants $K^{M}_{M(L-H)}$ of the $M(NBI-H)^+$ and $M(DNBI-H)^+$ complexes were calculated by taking into account the equilibrium constants determined previously for the HL^+ and ML^{2+} species[12] and by considering now the species H^+, HL^+, L, $(L-H)^-$, M^{2+}, ML^{2+}, and $M(L-H)^+$ and by collecting the data from the titration pairs every 0.1 pH unit. The pH range from a formation degree of the complexes of about 2% to the beginning of the hydrolysis of $M(aq)^{2+}$, which was evident from the titrations without ligand, was used for the evaluations. The formation degree for the $M(DNBI-H)^+$ complexes reached approximately 20−45%, depending on the metal ion, which is satisfying. However, the $M(NBI-H)^+$ complexes formed only to about 5−14% and with Mg^{2+} even only 3.5% could be reached under the experimental conditions. This results in somewhat larger final error limits for the $M(NBI-H)^+$ complexes (see Table 1, vide supra). However, the results showed no dependence on the excess of M^{2+} used in the experiments; i.e., there was no indication for the formation of $M_2(L-H)^{3+}$ complexes. The final results given for the stability constants $K^{M}_{M(L-H)}$ are always the averages from at least four independent pairs of titrations.

Acknowledgments

Research grants from the Swiss National Science Foundation, the Swiss Federal Office for Education and Science (COST D8), and the Novartis Foundation (formerly Ciba-Geigy-Jubilee Foundation) are gratefully acknowledged.

[1] H.-G. Genieser, E. Winkler, E. Butt, M. Zorn, S. Schulz, F. Iwitzki, R. Störmann, B. Jastorff, S. O. Døskeland, D. Øgreid, S. Ruchaud, M. Lanotte, *Carbohydrate Res.* **1992**, *234*, 217−235.
[2] M. Murray, A. J. Ryan, P. J. Little, *J. Med. Chem.* **1982**, *25*, 887−892.
[3] [3a] Ž. Anusevičius, A. E. M. F. Soffers, N. Čénas, J. Šarlauskas, J. Segura-Aguilar, I. M. C. M. Rietjens, *FEBS Lett.* **1998**, *427*, 325−329. − [3b] J. Šarlauskas, E. Dičkancaité, A. Nemeikaité, Ž. Anusevičius, H. Nivinskas, J. Segura-Aguilar, N. Čénas, *Arch. Biochem. Biophys.* **1997**, *346*, 219−229.
[4] I. A. Mikhailopulo, Z. Kazimierczuk, A. I. Zinchenko, V. N. Barai, V. V. Romanova, L. A. Eroshevskaya, *Nucleosides Nucleotides* **1995**, *14*, 477−480.
[5] S. Ersan, S. Nacak, N. Noyanalpan, E. Yesilada, *Arzneimittelforsch.* **1997**, *47*, 834−836.
[6] L. Garuti, M. Roberti, T. Rossi, C. Cermelli, M. Portolani, M. Malagoli, M. Castelli, *Anticancer Drug Des.* **1998**, *13*, 397−406.
[7] H. Sigel, A. Sigel (Eds.), *Metal Ions in Biological Systems*, vol. 25 ("Interrelations among Metal Ions, Enzymes, and Gene Expression"), M. Dekker, New York, Basel, Hong Kong, **1989**, pp. 1−557.
[8] J. J. R. Fraústo da Silva, R. J. P. Williams, *The Biological Chemistry of the Elements*, Clarendon, Oxford, **1991**, pp. 1−561.
[9] A. Sigel, H. Sigel (Eds.), *Metal Ions in Biological Systems*, vol. 32 ("Interactions of Metal Ions with Nucleotides, Nucleic Acids, and Their Constituents"), M. Dekker, New York, Basel, Hong Kong, **1996**, pp. 1−814.
[10] [10a] H. Sigel, N. A. Corfù, L.-n. Ji, R. B. Martin, *Comments Inorg. Chem.* **1992**, *13*, 35−59. − [10b] L. E. Kapinos, B. Song, A. Holý, H. Sigel, *Chimia* **1996**, *50*, 334. − [10c] L. E. Kapinos, B. Song, A. Holý, M. Bastian, H. Sigel, *Chimia* **1996**, *50*, 373.
[11] [11a] R. B. Martin, *Met. Ions. Biol. Syst.* **1996**, *32*, 61−89, see ref.[9] − [11b] R. B. Martin, *Acc. Chem. Res.* **1985**, *18*, 32−38.
[12] L. E. Kapinos, B. Song, H. Sigel, *Chem. Eur. J.* **1999**, *5*, 1794−1802.
[13] H. Walba, R. Ruiz-Velasco, Jr., *J. Org. Chem.* **1969**, *34*, 3315−3320.
[14] *IUPAC Stability Constants Database*, Version 3.02, compiled by L. D. Pettit, H. K. J. Powell, Academic Software, Timble, Otley, W. Yorks, U.K., **1998**.
[15] *NIST Critically Selected Stability Constants of Metal Complexes*, Reference database 46, Version 5.0, data collected and selected by A. E. Martell, R. M. Smith, U.S. Department of Commerce, National Institute of Standards and Technology, Gaithersburg, MD, USA, **1998**.
[16] *Joint Expert Speciation System (JESS),* Version 5.3, joint venture by K. Murray, P. M. May, Division of Water Technology, CSIR, Pretoria, South Africa, School of Mathematical and Physical Sciences, Murdoch University, Murdoch, Western Australia, **1996**.
[17] [17a] H. A. Azab, L. Banci, M. Bosari, C. Luchinat, M. Sola, M. S. Viezzoli, *Inorg. Chem.* **1992**, *31*, 4649−4655. − [17b] H.-J. Scholl, J. Hüttermann, M.-S. Viezzoli, *Inorg. Chim. Acta* **1998**, *273*, 131−141.
[18] T. J. Lyons, E. B. Gralla, J. S. Valentine, *Met. Ions Biol. Syst.* **1999**, *36*, 125−177.
[19] K. Bernauer, L. Verardo, *Angew. Chem. Int. Ed. Engl.* **1996**, *35*, 1716−1717.
[20] [20a] T. Gajda, B. Henry, J.-J. Delpuech, *J. Chem. Soc., Dalton Trans.* **1992**, 2313−2319. − [20b] T. Gajda, B. Henry, J.-J. Delpuech, *Inorg. Chem.* **1995**, *34*, 2455−2460.
[21] [21a] J.-L. Pierre, P. Chautemps, S. Refaif, C. Beguin, A. E. Marzouki, G. Serratrice, E. Saint-Aman, P. Rey, *J. Am. Chem. Soc.* **1995**, *117*, 1965−1973. − [21b] G. Tabbi, W. L. Driessen, J. Reedijk, R. P. Bonomo, N. Veldman, A. L. Spek, *Inorg. Chem.* **1997**, *36*, 1168−1175.
[22] M. A. M. Lorente, F. Dahan, Y. Sanakis, V. Petrouleas, A. Bousseksou, J.-P. Tuchagues, *Inorg. Chem.* **1995**, *34*, 5346−5357.
[23] [23a] A. W. Addison, S. Burman, C. G. Wahlgren, O. A. Rajan, T. M. Rowe, E. Sinn, *J. Chem. Soc., Dalton Trans.* **1987**, 2621−2630. − [23b] M.-a. Haga, M. M. Ali, R. Arakawa, *Angew. Chem. Int. Ed. Engl.* **1996**, *35*, 76−78. − [23c] R. F. Carina, L. Verzegnassi, G. Bernardinelli, A. F. Williams, *Chem. Commun.* **1998**, 2681−2682.
[24] [24a] C. D. Russell, L. Pauling, *Proc. Nat. Acad. Sci. U. S.* **1939**, *25*, 517−522. − [24b] C. D. Coryell, L. Pauling, *J. Biol. Chem.* **1940**, *132*, 769−779.
[25] [25a] R. J. Sundberg, R. B. Martin, *Chem. Rev.* **1974**, *74*, 471−517. − [25b] H. Sigel, R. B. Martin, *Chem. Rev.* **1982**, *82*, 385−426.
[26] H. Sigel, A. D. Zuberbühler, O. Yamauchi, *Anal. Chim. Acta* **1991**, *255*, 63−72.
[27] J. L. Cohen, K. A. Connors, *J. Pharm. Sci.* **1970**, *59*, 1271−1276.
[28] D. D. Perrin, *Dissociation Constants of Organic Bases in Aqueous Solution*, IUPAC, Butterworths, London, **1965**, p. 267.
[29] V. A. Pavlova, *Zhur. Nauch. i Priklad. Fot. i Kinematog.* **1958**, *3*, 101−111; *Chem. Abstr.* **1958**, *52*, 20135d.
[30] L. S. Efros, B. A. Poraĭ-Koshits, *Zhur. Obshcheĭ Khim.* **1953**, *23*, 697−705; *Chem. Abstr.* **1954**, *48*, 7603h.
[31] The error limits of the calculated stability constants given in column 4 of Table 2 apply to the pK_a range 2−6, yet the data points for the $M(NBI-H)^+$ and $M(DNBI-H)^+$ complexes (Figure 2) are located at considerably higher pK_a values. Therefore, the error limits for the values calculated (calcd.) now were estimated in the following way: The error limits given with the intercepts b in column 3 of Table 2 reflect the error for a calculation based on $pK^{H}_{HL} = 0$; since the last experimental point of the straight line for Mg^{2+} (see Figure 2) is about three pK_a units away from the intercept at $pK^{H}_{HL} = 0$, for each pK_a unit the error limit of b (column 3 in Table 2) divided by 3 results. Considering that $pk_{ma/NBI} = 10.28$ is about 4.3 pK_a units larger than the last experimental point of the straight lines (Figure 2) the

mentioned value needs to be multiplied by 4.3 giving ±(0.095 : 3) × 4.3 = ±0.136 as the error limit for the calculated stability constant of the $Mg(NBI-H)^+$ complex. To be on the safe side, this value is further multiplied by 2 to give the error limit of ±0.27 which is listed in column 3 of Table 3. For the $Mn(NBI-H)^+$ complex exactly the same procedure applies. For Ni^{2+} (see Figure 2), Co^{2+} and Cd^{2+},[12] for which the last experimental point is only about two pK_a units away from the intercept, $pK^H_{HL} = 0$, the analogous calculation gives, e.g., for $Ni(NBI-H)^+$ the error limit ±(0.052 : 2) × 4.3 × 2 = ±0.22, which appears in column 3 of Table 3, and for $Ni(DNBI-H)^+$ ±(0.052 : 2) × 2.6 × 2 = ±0.14. All the other error limits given in column 3 of Table 3 were calculated correspondingly.

Received February 11, 1999
[I99066]

A Simple New Structural Force Field for the Computation of Linear Metallocenes

Peter Comba*[a] and Thomas Gyr[a]

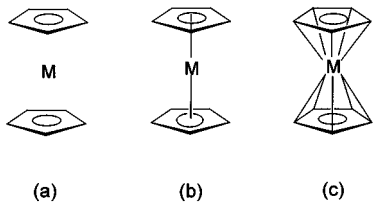
Keywords: Molecular mechanics / Metallocenes / Ferrocene / Points on a sphere / Rotation barrier

A new structural force field for metallocenes is presented, which involves harmonic bonding potentials from the metal center to each of the carbon atoms, no angular potentials around the metal ion, inter-ligand 1,3-non-bonded interactions, and transferable parameters for the ligand backbones. The model has been parameterized for ferrocene, ruthenocene, and osmocene derivatives and the force field has been validated with relevant structures from the CSD files (Fe: 34, Ru: 10, Os: 2). The conformational space [rotation of the Cp (cyclopentadienyl) rings] has been searched with a cartesian stochastic search routine and energy barriers have been computed by scanning the pseudo-torsional angles involving the centroids of the two Cp rings. The computed energy barriers are smaller than those determined experimentally, but the predicted increase in transition energy upon substitution of the Cp rings is in agreement with experiment and the torsional angles for the minimum structures are computed accurately. It is suggested that the underestimated barrier height is due to the neglect of solvation.

Introduction

Molecular mechanics is well established in organic chemistry,[1][2] force-field calculations are becoming increasingly important in biochemistry,[2−5] and there is an increasing number of well-balanced force fields enabling accurate prediction of the structures and properties of transition-metal coordination compounds.[6−8] However, there are still relatively few reports concerning force fields for organometallic compounds.[6][7] One of the reasons for this is that the connectivity and type of bonding is often rather ambiguous, especially for fluxional systems. For metallocenes, for example, the very manner in which these systems are drawn highlights the problem (Scheme 1). It should be borne in mind that, in general, the basis of molecular mechanics is not to use realistic bonding models.[6] However, the computed structures and, in favorable cases, some thermodynamic parameters (isomer distributions, dynamics) and vibrational spectroscopic parameters should reproduce the experimental data.[6] Thus, any of the models represented in Scheme 1 might be used, irrespective of the fact whether any particular metallocene has more ionic or more covalent bonding character, provided that the parameterization allows a reasonable modeling of structural parameters (metal−Cp ring distance, metal−carbon distance, angle between the Cp planes, torsional angle and barrier, i.e. eclipsed or staggered conformation, and the corresponding activation energy for the interconversion). In addition, it should be easy to extend the model to other classes of organometallic compounds, such as cyclopentadienyl−metal compounds with various other donors, transition-metal compounds with other classes of ligands such as benzene or allyl groups, and cyclopentadienyl−main-group element compounds.

The molecular mechanics approaches for dealing with metallocenes used to date[9−21] can be classified according to the structural plots depicted in Scheme 1: (a) purely electrostatic models, i.e. no covalent bonds (no harmonic but electrostatic and/or van der Waals potentials) between the Cp rings and the metal center;[11][16] (b) models in which the metal center is connected to dummy atoms at the centers of the Cp rings;[9−13,15,21] (c) models with covalent bonds between the metal center and either three carbon atoms per Cp ring[21] or each of the carbon atoms (10-coordinate metal center).[19][20]



Scheme 1

The most appealing approach reported to date involves interactionless dummy atoms, where the forces on the dummy atoms at the centroid of the five-membered rings are distributed among the Cp carbon atoms to avoid strain on the Cp rings.[12] This model allowed accurate computation of the structures and vibrational spectra of linear metallocene compounds.[12] The only obvious disadvantage is that this method needs a specific algorithm, which is not generally available in commercial programs. As yet, it has only been used for linear metallocenes and has not been extended to other similar problems such as the computation of metal−allyl compounds.

We now present a new structural force field for linear metallocenes (M = Fe, Ru, Os), which involves bonding of

[a] Anorganisch-Chemisches Institut, Universität Heidelberg, Im Neuenheimer Feld 270, D-69120 Heidelberg, Germany
Fax: (internat.) + 49-(0)6221/54-6617
E-mail: comba@akcomba.oci.uni-heidelberg.de
Supporting information for this article is available on the WWW under http://www.wiley-vch.de/home/eurjic or from the author.

 © WILEY-VCH Verlag GmbH, D-69451 Weinheim, 1999 1434−1948/99/1010−1787 $ 17.50+.50/0

Table 1. Experimentally determined structures considered in this study

Type of ligand	Metal center	Ligand(s)[a]	CCDC No.	Ref.
Unbridged	Fe^{2+}	$(Cp)_2$	FEROC26	[28]
		$(MeCp)_2$	ENTRY'NOYSEZ	[30]
		$(Me_4Cp)_2$	JAROUB	[31]
		$(Me_5Cp)_2$	FODWEZH	[32]
		$(Et_4Cp)_2$	KOPJII	[33]
		$(Et_5Cp)_2$	KIYNIP	[34]
		$[1,2\text{-}(t\text{Bu})_2Cp]_2$	LIBFUX	[35]
		$[1,3\text{-}(t\text{Bu})_2Cp]_2$	TBUFER01	[36]
		$[1,2,4\text{-}(Cyh)_3Cp]_2$	HEZHUB	[37]
	Ru^{2+}	$(Cp)_2$	CYCPRU06	[38]
		$(1,3\text{-}Me_2Cp)_2$	HANYOK	[39]
		$(Me_4Cp)_2$	GIHGUH	[40]
		$(Me_5Cp)_2$	DATHIP	[41]
		$(Me_4EtCp)_2$	HAWPEA	[42]
	Os^{2+}	$(Cp)_2$	SINWER	[43]
		$(Me_5Cp)_2$	GENGUB	[44]
Mono-bridged	Fe^{2+}	$Cp-[1,1,2,2\text{-}(Me)_4Et]-Cp$	METFER	[45]
		$(3\text{-}t\text{BuCp})_2-1,1,2,2\text{-}(Me)_4Et$	TOGFAW	[46]
		$Cp-Prop-Cp$	FICJUW	[47]
		$(Cp-Me)_2-O$	FICKAD	[47]
		$(Cp-Me)_2-S$	FICKEH	[47]
		$Cp-Pent-Cp$	JIWGUR	[48]
	Ru^{2+}	$Cp-Et-Cp$	WEVKIR	[49]
		$Cp-Prop-Cp$	CEJLOS	[50]
		$Me_4Cp-Prop-CpMe_4$	YOSYIO	[51]
		$(Cyp)Cp-Prop-Cp$	DABDIT	[52]
		$Cp-But-Cp$	CEJLUY	[50]
Dibridged (sym.)	Fe^{2+}	$Cp-1,2\text{-}Et_2-Cp$	WICTIL	[53]
		$Cp-1,2\text{-}Prop_2-Cp$	YUMRAZ	[54]
		$Cp-1,2\text{-}Prop_2-Cp$	FICKIL	[47]
		$Cp-1,3\text{-}Prop_2-Cp$	TRMEFE01	[47]
		$(Cyp)Cp-1,2\text{-}Prop_2-Cp(Cyp)$	TTMFER	[55]
		$Cp-1,2\text{-}(Prop)(Me-O-Me)-Cp$	FICKORH	[47]
		$Cp-1,3\text{-}(Prop)(Me-O-Me)-Cp$	FICLAE	[47]
		$Cp-1,2\text{-}Bu_2-Cp$	COBSAN	[56]
		$Cp-1,3\text{-}Bu_2-Cp$	PEFGAI	[57]
Tribridged (sym.)	Fe^{2+}	$Cp-1,2,4\text{-}Prop_3-Cp$	YUMRIH	[54]
		$(Cyp)Cp-1,2,3\text{-}Prop_3-Cp(Cyp)$	PTMFER	[58]
		$Cp-1,2,4\text{-}Bu_3-Cp$	COBSER	[56]
		$Cp-1,2,4\text{-}Pent_3-Cp$	COBSIV	[56]
Tribridged (asym.)	Fe^{2+}	$Cp-1,1'\text{-}Prop-2,4',4,2'\text{-}Bu_2-Cp$	DUBJIT	[59]
Tetrabridged (sym.)	Fe^{2+}	$Cp-Pent_4-Cp$	SACVUN	[60]
Tetrabridged (asym.)	Fe^{2+}	$Cp-2\text{-}Prop-1,3,4\text{-}Bu_3-Cp$	FEROPI	[61]
		$Cp-1,3\text{-}Prop_2-2,4\text{-}Bu_2-Cp$	CEPWOJ	[62]
Pentabridged (sym.)	Fe^{2+}	$Cp-Bu_5-Cp$	DOMLIA10	[63]
Pentabridged (asym.)	Fe^{2+}	$Cp-Prop-Bu_4-Cp$	BETRUN	[64]

[a] Nomenclature: Cp = cyclopentadienyl, substructures in brackets in front of a Cp ring are substituents of the corresponding Cp; substructures between the two Cp rings are bridges; symmetrical bridges are only numbered at one Cp; Me = methylene, Et = ethylene, Prop = propylene, Bu = butylene, *t*Bu = *tert*-butylene, Pent = pentenyl, Cyh = cyclohexyl, Cyp = *n*, *n* + 1 propyl attached to a Cp ring.

all carbon atoms to the metal center (10-coordinate metal atom for MCp_2) and the replacement of valence angle terms around the metal center by inter-ligand 1,3-non-bonded interactions (modified points-on-a-sphere approach). Thus, the Cp rings are free to rotate about the centroid−metal−centroid axis without any need for defining dummy atoms, and there is no restriction in terms of a tilt between the two Cp planes. This approach is in agreement with simple MO considerations, i.e. the system is electronically degenerate with respect to the C_5 axis, which is also apparent from experiment. The points-on-a-sphere molecular mechanics model has been widely used for transition-metal coordination compounds[6,8,22,23] and is implemented in most commercially available programs. The only modification to generally available programs is the exclusion of 1,3-non-bonded interactions between covalently linked carbon atoms (intra-ligand 1,3-interactions), which has been simple to include in our software and force field. A similar but not identical approach to metallocene modeling has recently been developed for cyclopentadienyl−early transition-metal systems.[24]

Experimental Structural Data

The structural data considered in this study included selected X-ray-structural analyses of MCp_2 compounds with M = Fe, Ru, Os, where Cp_2 are two cyclopentadienyl rings or substituted Cp rings or where the two rings are bridged (substituents or bridges incorporating heteroatoms such as sulfur or silicon were not considered). The relevant structures (46 data sets; 34 Fe, 10 Ru, 2 Os), separated into simple and strapped sandwich compounds, are presented in Table 1.

Structural Parameters

The structural parameters considered here (average metal−carbon distance *b*; average distance *d* of the metal ion from the Cp planes; tilt angle α, torsional angle δ) are shown in Figure 1. The experimentally observed and computed parameters are given in Table 2 (the full set of structural data, experimental and computed, of all structures is available as Supporting Information). Note that, for some compounds, various experimental data sets are available. This is particularly true in the case of ferrocene, for which various polymorphic modifications are known and intermolecular interactions, polymorphism, disorder, gas-phase structures, and dynamics have been discussed extensively.[25−28] The fact that the computed and experimentally determined activation energies for the Cp ring rotations of the non-strapped metallocenes are generally small (see be-

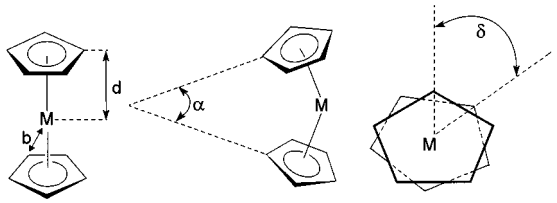


Figure 1. Definition of the structural parameters [torsion angle δ has the periodicity (360/5°), except for unsymmetrically substituted Cp rings; staggered: δ = 36°; eclipsed: δ = 0°]

Table 2. Averages of observed and computed structural parameters of metallocenes[a]

Structure		b[b] [Å]		d [Å]		α [°]		δ [°]	
		Observed	Computed	Observed	Computed	Observed	Computed	Observed	Computed
Fe	$(Cp)_2$	2.02(1)	2.04(0)	1.64	1.66	0.0	0.0	36.0	35.9
Fe	$(MeCp)_2$	2.08(2)	2.04(0)	1.70	1.66	6.1	0.2	1.5	30.6
Fe	$(Me_4Cp)_2$	2.09(1)	2.05(0)	1.71	1.66	0.0	0.1	180.0	172.1[c]
Fe	$(Me_5Cp)_2$	2.10(1)	2.05(0)	1.71	1.66	0.0	0.0	36.0	36.0[c]
Fe	$(Et_4Cp)_2$	2.10(1)	2.05(0)	1.71	1.66	1.8	2.8	76.8	54.0
Fe	$(Et_5Cp)_2$	2.10(0)	2.05(0)	1.71	1.67	1.0	0.1	23.2	23.0
Fe	$[1,2\text{-}(t\text{Bu})_2Cp]_2$	2.06(1)	2.06(1)	1.66	1.67	0.0	0.0	180.0	180.0
Fe	$[1,3\text{-}(t\text{Bu})_2Cp]_2$	2.06(1)	2.06(1)	1.67	1.68	8.9	11.1	88.2	89.6
Fe	$[1,2,4\text{-}(Cyh)_3Cp]_2$	2.06(0)	2.05(1)	1.66	1.67	2.0	1.9	177.9	177.4
Ru	$(Cp)_2$	2.19(0)	2.18(0)	1.81	1.82	0.7	3.5	0.4	30.8
Ru	$(1,3\text{-}Me_2Cp)_2$	2.18(0)	2.18(0)	1.82	1.82	1.6	0.5	2.9	0.5
Ru	$(Me_4Cp)_2$	2.18(0)	2.18(0)	1.81	1.82	1.9	1.0	2.6	34.2
Ru	$(Me_5Cp)_2$	2.18(0)	2.17(0)	1.81	1.82	0.2	0.1	0.8	22.3
Ru	$(Me_4EtCp)_2$	2.18(2)	2.18(0)	1.82	1.82	5.1	0.6	141.7	123.2
Os	$(Cp)_2$	2.19(0)	2.18(0)	1.80	1.82	1.8	0.3	0.6	28.1[c]
Os	$(Me_5Cp)_2$	2.04(2)	2.17(0)	1.69	1.81	0.0	0.0	36.0	36.0[c]
Fe	$\{Cp\text{-}[1,1,2,2\text{-}(Me)_4Et]\text{-}Cp\}$	2.04(2)	2.05(1)	1.64	1.67	23.6	28.3	10.4	11.9
Fe	$[(3\text{-}t\text{BuCp})_2\text{-}1,1,2,2\text{-}(Me)_4Et]$	2.08(3)	2.05(1)	1.69	1.67	29.4	27.3	10.2	12.1
Fe	(Cp−Prop−Cp)	2.03(0)	2.04(0)	1.63	1.66	7.9	12.6	2.2	0.0
Fe	$[(Cp\text{-}Me)_2\text{-}O]$	2.03(1)	2.04(1)	1.63	1.66	11.9	15.5	1.3	0.0
Fe	$[(Cp\text{-}Me)_2\text{-}S]$	2.03(1)	2.04(0)	1.63	1.66	6.0	7.3	2.4	0.1
Fe	(Cp−Pent−Cp)	2.08(4)	2.06(1)	1.74	1.67	13.3	15.9	3.6	21.6
Ru	(Cp−Et−Cp)	2.16(2)	2.20(1)	1.79	1.85	29.6	37.1	8.5	10.0
Ru	(Cp−Prop−Cp)	2.17(1)	2.18(0)	1.81	1.82	14.8	20.6	0.5	0.1
Ru	$(Me_4Cp\text{-}Prop\text{-}CpMe_4)$	2.17(2)	2.18(1)	1.79	1.82	11.2	16.8	0.5	1.2
Ru	[(Cyp)Cp−Prop−Cp]	2.17(1)	2.18(0)	1.80	1.82	15.6	20.5	1.0	0.2
Ru	(Cp−But−Cp)	2.18(0)	2.18(0)	1.82	1.82	1.7	0.2	3.0	14.1
Fe	$(Cp\text{-}1,2\text{-}Et_2\text{-}Cp)$	2.01(2)	2.07(2)	1.61	1.69	28.7	33.2	2.6	3.2
Fe	$(Cp\text{-}1,2\text{-}Prop_2\text{-}Cp)$	2.07(1)	2.04(0)	1.68	1.66	18.4	18.0	0.0	0.0
Fe	$(Cp\text{-}1,2\text{-}Prop_2\text{-}Cp)$	2.03(1)	2.04(0)	1.63	1.66	13.0	17.9	1.2	0.0
Fe	$(Cp\text{-}1,3\text{-}Prop_2\text{-}Cp)$	2.01(1)	2.03(1)	1.60	1.64	9.9	15.4	1.4	0.1
Fe	$[(Cyp)Cp\text{-}1,2\text{-}Prop_2\text{-}Cp(Cyp)]$	2.03(1)	2.04(0)	1.62	1.65	11.0	17.8	2.2	0.7
Fe	[Cp−1,2-(Prop)(Me−O−Me)−Cp]	2.03(1)	2.04(0)	1.62	1.66	15.0	20.0	0.6	0.0
Fe	[Cp−1,3-(Prop)(Me−O−Me)−Cp]	2.02(1)	2.03(2)	1.62	1.64	12.9	17.6	0.8	0.8
Fe	$(Cp\text{-}1,2\text{-}Bu_2\text{-}Cp)$	2.03(1)	2.04(0)	1.65	1.66	6.9	9.0	11.6	17.1
Fe	$(Cp\text{-}1,3\text{-}Bu_2\text{-}Cp)$	2.03(1)	2.02(1)	1.63	1.63	0.0	1.2	36.0	36.1
Fe	$(Cp\text{-}1,2,4\text{-}Prop_3\text{-}Cp)$	2.04(2)	1.99(2)	1.61	1.59	3.7	7.2	2.2	0.1
Fe	$[(Cyp)Cp\text{-}1,2,3\text{-}Prop_3\text{-}Cp(Cyp)]$	2.01(1)	2.03(1)	1.60	1.64	11.2	23.4	1.9	1.0
Fe	$(Cp\text{-}1,2,4\text{-}Bu_3\text{-}Cp)$	2.04(0)	2.03(0)	1.63	1.64	5.5	7.1	15.0	16.3
Fe	$(Cp\text{-}1,2,4\text{-}Pent_3\text{-}Cp)$	2.05(0)	2.05(0)	1.65	1.67	3.1	2.9	0.5	0.1
Fe	$(Cp\text{-}1,1'\text{-}Prop\text{-}2,4',4,2'\text{-}Bu_2\text{-}Cp)$	2.02(0)	2.03(1)	1.62	1.64	5.7	11.0	0.8	2.9
Fe	$(Cp\text{-}Pent_4\text{-}Cp)$	2.06(1)	2.07(1)	1.66	1.69	6.6	11.1	1.1	2.4
Fe	$(Cp\text{-}2\text{-}Prop\text{-}1,3,4\text{-}Bu_3\text{-}Cp)$	2.03(0)	2.03(1)	1.62	1.64	0.2	4.0	1.3	5.7
Fe	$(Cp\text{-}1,3\text{-}Prop_2\text{-}2,4\text{-}Bu_2\text{-}Cp)$	2.02(1)	2.01(2)	1.61	1.62	8.7	12.2	31.5	32.5
Fe	$(Cp\text{-}Bu_5\text{-}Cp)$	2.01(1)	2.00(2)	1.59	1.61	1.0	7.3	1.6	3.9
Fe	$(Cp\text{-}Prop\text{-}Bu_4\text{-}Cp)$	2.02(0)	2.03(0)	1.61	1.64	1.8	1.5	0.9	16.8

[a] For definition of the structural parameters, see Figure 1. − [b] Standard deviation (SD, in%) in brackets; $SD = \sqrt{\frac{n\sum x^2 - (\sum x)^2}{n^2}}$. − [c] Corresponds to a local minimum; see Table 5 for global minimum.

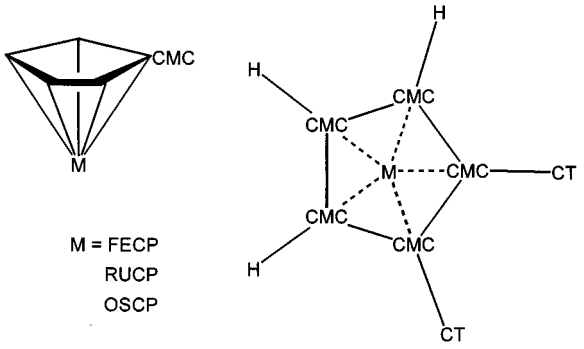


Figure 2. Definition of atom types used in Table 3

low) indicates that an arbitrary selection of test structures is acceptable.

The MOMEC program and force field were used for the calculations.[22] Parameters not previously published[23] are given in Table 3 (the atom-type labels are defined in Figure 2; starting values for the parameters were taken from vibrational spectroscopic data and/or from other force fields[6][12] and refined by fitting to the set of test structures). The conformational space was searched with a cartesian stochastic search routine ("random kick" Monte Carlo method), which has recently been implemented in MOMEC and validated for a series of (amine)cobalt(III) compounds.[29]

Table 3. New MOMEC force-field parameters[a−c]

Bond-stretch parameters				Valence-angle parameters				
Atom 1	Atom 2	k_b [mdyn Å^{-1}]	r_0 [Å]	Atom 1	Atom 2	Atom 3	k_θ [mdyn Å rad^{-2}]	θ_0 [rad]
FECP	CMC	0.750	2.020	FECP	CMC	CMC	0.010	1.222
RUCP	CMC	0.500	2.176	FECP	CMC	CT	0.100	2.217
OSCP	CMC	0.350	2.180	FECP	CMC	H	0.100	2.217
CMC	CMC	7.400	1.400	CMC	FECP	CMC	0.000	3.141
CMC	CT	5.000	1.500	RUCP	CMC	CMC	0.010	1.222
CMC	H	5.000	1.090	RUCP	CMC	CT	0.100	2.217
				RUCP	CMC	H	0.100	2.217
				CMC	RUCP	CMC	0.000	3.141
				OSCP	CMC	CMC	0.010	1.222
				OSCP	CMC	CT	0.100	2.217
				OSCP	CMC	H	0.100	2.217
				CMC	OSCP	CMC	0.000	3.141
				CMC	CMC	CT	0.350	2.199
				CMC	CMC	CMC	0.400	1.885
				CMC	CMC	H	0.350	2.199
				CMC	CT	CT	0.250	1.909
				CMC	CT	H	0.160	1.911

Torsional-angle parameters							Out-of-plane parameters				
Atom	Atom	Atom	Atom	k_ϕ [mdyn Å]	m	ϕ_{offset} [rad]	Atom 1	Atom 2	Atom 3	Atom 4	k_{oop} [mdyn Å rad^{-2}]
H	CMC	CMC	CT	0.015	2	1.571	CMC	CMC	CMC	CT	2
CMC	CMC	CMC	CT	0.015	2	1.571	CMC	CMC	CMC	H	2
H	CMC	CMC	CMC	0.015	2	1.571					
CT	CMC	CMC	CT	0.015	2	1.571					
H	CMC	CMC	H	0.015	2	1.571					

Non-bonded parameters		
Atom	r_{VdW} [Å]	ε
FECP	0.000	0.000
OSCP	0.000	0.000
RUCP	0.000	0.000
CMC	2.100	0.044

[a] All other parameters have been published previously.[23] − [b] For atom-type labels, see Figure 2. − [c] 1 dyn = 10 $^{-5}$ N.

The average observed and computed metal−carbon distances *b* are 2.10 Å and 2.10 Å for iron, 2.18 Å and 2.18 Å for ruthenium, and 2.11 Å and 2.18 Å for osmium (for osmium only two data sets were available, one of which related to a low-temperature structure). A similar degree of accuracy in the computations of the distances *d* of the metal center from the Cp planes is found, and the observed error in the tilt angle α is generally less than 3° and at most 7°. This is especially remarkable for the asymmetrically bridged compounds. The torsional angles δ are, in general, also predicted accurately (to within less than ±10°). Structures with larger differences between the computed and observed torsional angles have freely rotating Cp ligands (non-strapped) and crystal structures with staggered Cp rings. Plots of strain energy along the rotational coordinate indicate that structures similar to that observed are local minima (see below). Details concerning the quality of the computed structures are given in Table 4; full details are available as Supporting Information.

Cp Ring Rotation

Scanning of the strain energy along the rotational mode of the Cp rings is simple in models that use dummy atoms at the centroids of the Cp rings. We use constraints on plane-twist functions (angle between two planes; one of the planes is defined by three carbon atoms of a Cp ring, the other by the metal center and one carbon atom of each of the two Cp rings; from each of the constrained plane-twist angles the corresponding torsional angle δ is calculated). It is possible to apply a force on this rotation to increase the barrier for the Cp ring rotation. However, there does not seem to be an electronic reason for such a potential. The difference between the observed and computed energy barriers might be due to a reorganization of the solvent sheath, which is not considered explicitly in our calculations.[6] The computed energy barriers are mainly due to changes in van der Waals contacts, and it has been suggested previously that this is probably the most important effect.[6][12] It should be borne in mind, however, that our aim was to derive a structural force field for ferrocene, ruthenocene, osmocene and derivatives. Thus, the computation along the ring rotation mode is used here to evaluate local minima and not for the accurate determination of rotational barriers.

As expected, the computed energy barriers (Table 5) are generally underestimated, but the increasing barrier height upon substitution [cf. $Fe(Cp)_2$, $Fe(Me_5Cp)_2$] is of the expected order. A plot of the strain energy along the Me_5Cp rotation for the latter structure indicates that there is a concerted rotation of the methyl groups, which is shown in Figure 3. Here, the structural plots help to visualize the con-

Table 4. Comparison of observed and computed structures of ferrocene, ruthenocene, osmocene and their derivatives

Compound		RMS[a] [Å]	Plane[b] [Å]	
Fe	$(Cp)_2$	0.022	0.00	0.00
Fe	$(MeCp)_2$	0.303 (0.090)	0.00	0.00
Fe	$(Me_4Cp)_2$	0.095	0.01	0.00
Fe	$(Me_5Cp)_2$	0.056	0.00	0.00
Fe	$(Et_4Cp)_2$	0.235 (0.059)	0.00	0.00
Fe	$(Et_5Cp)_2$	0.045	0.00	0.00
Fe	$[1,2\text{-}(t\text{Bu})_2Cp]_2$	0.029	0.01	0.01
Fe	$[1,3\text{-}(t\text{Bu})_2Cp]_2$	0.040	0.02	0.02
Fe	$[1,2,4\text{-}(Cyh)_3Cp]_2$	0.041	0.01	0.01
Ru	$(Cp)_2$	0.312 (0.060)	0.00	0.00
Ru	$(1,3\text{-}Me_2Cp)_2$	0.041	0.00	0.00
Ru	$(Me_4Cp)_2$	0.236 (0.039)	0.00	0.00
Ru	$(Me_5Cp)_2$	0.201 (0.039)	0.00	0.00
Ru	$(Me_4EtCp)_2$	0.191 (0.095)	0.00	0.00
Os	$(Cp)_2$	0.288 (0.087)	0.00	0.00
Os	$(Me_5Cp)_2$	0.162	0.00	0.00
Fe	$(Cp)_2$–[1,1,2,2-$(Me)_4$Et]	0.068	0.04	0.04
Fe	$(3\text{-}t\text{BuCp})_2$–1,1,2,2-$(Me)_4$Et	0.067	0.04	0.04
Fe	(Cp–Prop–Cp)	0.061	0.01	0.01
Fe	[$(Cp–Me)_2$–O]	0.053	0.02	0.02
Fe	[$(Cp–Me)_2$–S]	0.038	0.01	0.01
Fe	(Cp–Pent–Cp)	0.247 (0.131)	0.04	0.00
Ru	(Cp–Et–Cp)	0.091	0.03	0.03
Ru	(Cp–Prop–Cp)	0.069	0.01	0.01
Ru	(Me_4Cp–Prop–$CpMe_4$)	0.113	0.02	0.02
Ru	[(Cyp)Cp–Prop–Cp]	0.070	0.01	0.01
Ru	(Cp–But–Cp)	0.114	0.00	0.00
Fe	(Cp–1,2-Et_2–Cp)	0.106	0.02	0.04
Fe	(Cp–1,2-$Prop_2$–Cp)	0.043	0.01	0.01
Fe	(Cp–1,2-$Prop_2$–Cp)	0.054	0.01	0.01
Fe	(Cp–1,3-$Prop_2$–Cp)	0.067	0.04	0.04
Fe	[(Cyp)Cp–1,2-$Prop_2$–Cp(Cyp)]	0.071	0.01	0.01
Fe	[Cp–1,2-(Prop)(Me–O–Me)–Cp]	0.060	0.01	0.01
Fe	[Cp–1,3-(Prop)(Me–O–Me)–Cp]	0.066	0.05	0.05
Fe	(Cp–1,2-Bu_2–Cp)	0.065	0.01	0.01
Fe	(Cp–1,3-Bu_2–Cp)	0.028	0.02	0.02
Fe	(Cp–1,2,4-$Prop_3$–Cp)	0.105	0.06	0.07
Fe	[(Cyp)Cp–1,2,3-$Prop_3$–Cp(Cyp)]	0.094	0.03	0.04
Fe	(Cp–1,2,4-Bu_3–Cp)	0.034	0.01	0.01
Fe	(Cp–1,2,4-$Pent_3$–Cp)	0.030	0.01	0.01
Fe	(Cp–1,1′-Prop–2,4′,4,2′-Bu_2–Cp)	0.072	0.03	0.02
Fe	(Cp–$Pent_4$–Cp)	0.061	0.01	0.01
Fe	(Cp–2-Prop–1,3,4-Bu_3–Cp)	0.087	0.04	0.01
Fe	(Cp–1,3-$Prop_2$–2,4-Bu_2–Cp)	0.063	0.06	0.05
Fe	(Cp–Bu_5–Cp)	0.082	0.06	0.06
Fe	(Cp–Prop–Bu_4–Cp)	0.170 (0.060)	0.01	0.01

[a] RMS overlay of the computed and the observed (CCDC) structures (metal center and 10 Cp carbon atoms only; values in brackets are the sums of individual RMS values for both M–CP fragments). – [b] RMS deviation of the best plane of the two computed Cp rings; $RMS = \sqrt{\frac{\sum_N (x_a - x_b)^2 + (y_a - y_b)^2 + (z_a - z_b)^2}{N}}$.

Table 5. Comparison of some observed and computed rotational energy barriers for ferrocene, ruthenocene, osmocene and derivatives

Structure		Energy barrier[a] [kJ/mol]		Global minimum[b] [°]	
		Observed	Computed	Observed	Computed
Fe	$(Cp)_2$	3.7[c]	0.2	0.0[c] (e)	35.9
Ru	$(Cp)_2$	33.9[38]	0.5	0.0 (e)	30.8
Os	$(Cp)_2$	–	0.1	–	10.3
Fe	$(Me_4Cp)_2$	–	4.7	–	107.1
Ru	$(Me_4Cp)_2$	–	2.0	–	34.2
Fe	$(Me_5Cp)_2$	4.0[65]	6.4	23.7	22.2
Ru	$(Me_5Cp)_2$	–	3.1	–	22.3
Os	$(Me_5Cp)_2$	–	3.3	–	23.2
Fe	$(MeCp)_2$	–	1.1	–	30.6
Fe	$(Et_4Cp)_2$	–	5.4	–	24.6
Fe	$(Et_5Cp)_2$	–	7.9	–	22.7

[a] Conformational arrangement is indicated in brackets, where *e* = eclipsed, *s* = staggered. – [b] Minima determined by rotating one Cp ring in one direction using a plane-twist function (no force, i.e. $k_\delta = 0.0$); energy scan increment: 1°. – [c] Values obtained by electron diffraction in the gas phase. At low temperature, X-ray and neutron diffraction data indicate that the rings are staggered by about 10°.[66]

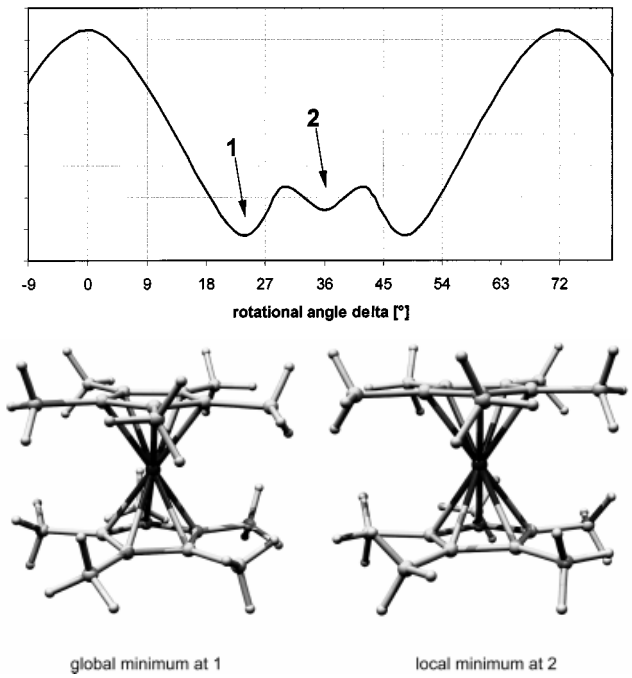


Figure 3. Rotational energy plot of $Fe(Me_5Cp_2)$ (grid: 1 kJ/mol)

certed rotations. The global energy minimum of $Fe(Me_5Cp)_2$ ($\delta = 22.2°$) is in excellent agreement with that computed using an alternative approach ($\delta = 23.7°$).[12] Thus, structural features, including those of the ring rotation, are well reproduced by our new force field, while dynamic properties are not. The approach used here allows the application of a force on the ring rotation; published data relating to other force fields suggest that this might lead to realistic energy barriers when the corresponding force constant is metal-ion-dependent.[12]

In conclusion, we have been able to demonstrate that the simple points-on-a-sphere model leads to an accurate structural force field for linear metallocenes, and that this approach may be extended to a range of other organometallic systems.

Supporting Information

Detailed structural data (comparison of experimentally observed and computed structural parameters) are available: Table S1 (supplementary to Table 2) gives the complete set of carbon-to-metal bond lengths *b* [see Figure 1; the metal center is atom number 1, C(2)–C(6) are carbon atoms of ring 1, and C(7)–C(11) are carbon atoms of ring 2] and rotational angles δ (the values given in parentheses after the rotational angles are RMS deviations of the carbon atoms from the best plane of each Cp ring). Table S2 (sup-

plementary to Table 5) lists the rotational energy barriers for all metallocene compounds discussed in Table 5.

Acknowledgments

Financial support from the Deutsche Forschungsgemeinschaft and the Fonds der Chemischen Industrie is gratefully acknowledged. We also thank Michael Melter and Professor Marc Zimmer for helpful discussions.

[1] U. Burkert, N. L. Allinger, *Molecular Mechanics*, American Chemical Society, New York, **1982**, vol. 177.
[2] A. R. Leach, *Molecular Modelling*, Longman, Edinburgh, **1996**.
[3] A. Warshel, *Computer Modeling of Chemical Reactions in Enzymes and Solution*, John Wiley and Sons, Inc., New York, Chichester, **1991**.
[4] J.-P. Doucet, J. Weber, *Computer-Aided Molecular Design: Theory and Applications*, Academic Press, London, San Diego, New York, **1996**.
[5] L. Banci, P. Comba, *Molecular Modeling and Dynamics of Bioinorganic Systems*, Kluwer, Dordrecht, **1997**.
[6] P. Comba, T. W. Hambley, *Molecular Modeling of Inorganic Compounds*, VCH, Weinheim, **1995**.
[7] C. R. Landis, D. M. Root, T. Cleveland, *Molecular Mechanics Force Field for Modeling Inorganic and Organometallic Compounds*, VCH Verlag, New York, Weinheim, **1995**, vol. 6.
[8] B. P. Hay, *Coord. Chem. Rev.* **1993**, *126*, 177.
[9] K. E. du Plooy, C. F. Marais, L. Carlton, R. Hunter, J. C. A. Boeyens, N. J. Coville, *Inorg. Chem.* **1989**, *28*, 3855.
[10] S. C. Mackie, Y.-S. Park, H. F. Shurvell, M. C. Baird, *Organometallics* **1991**, *10*, 2993.
[11] S. G. Davies, A. E. Derome, J. P. McNally, *J. Am. Chem. Soc.* **1991**, *113*, 2854.
[12] T. N. Doman, C. R. Landis, B. Bosnich, *J. Am. Chem. Soc.* **1992**, *114*, 7264.
[13] A. K. Rappé, K. S. Colwell, C. J. Casewit, *Inorg. Chem.* **1993**, *32*, 3438.
[14] J. C. A. Boeyens, D. C. Levendis, *S. Afr. J. Chem.* **1982**, *35*, 144.
[15] E. S. Shubina, L. M. Epstein, T. V. Timofeeva, Y. T. Struchkov, A. Z. Kreindlin, S. S. Fadeeva, M. I. Rybinskaya, *J. Organomet. Chem.* **1988**, *346*, 56.
[16] F. M. Menger, M. J. Sherrod, *J. Am. Chem. Soc.* **1988**, *110*, 8606.
[17] H.-J. Thiem, M. Brandl, R. Breslow, *J. Am. Chem. Soc.* **1988**, *110*, 8612.
[18] P. D. Beer, E. L. Tite, M. G. B. Drew, A. Ibbotson, *J. Chem. Soc., Dalton Trans.* **1990**, 2543.
[19] J. M. Rudzinski, E. Osawa, *J. Phys. Org. Chem.* **1992**, *5*, 382.
[20] J. M. Rudzinski, E. Osawa, *J. Phys. Org. Chem.* **1993**, *6*, 107.
[21] R. Blom, A. Hammel, A. Haaland, J. T. Weidlein, T. V. Timofeeva, Y. T. Struchkov, *J. Organomet. Chem.* **1993**, *462*, 131.
[22] P. Comba, T. W. Hambley, G. Lauer, N. Okon. *MOMEC97: A Molecular Modeling Package for Inorganic Compounds* (Eds.: P. Comba, T. W. Hambley, G. Lauer, N. Okon), Lauer & Okon Chemische Verfahrens- & Softwareentwicklung, E-mail: cvs-hd@t-online.de, Heidelberg, **1997**.
[23] J. E. Bol, C. Buning, P. Comba, J. Reedijk, M. Ströhle, *J. Comput. Chem.* **1998**, *19*, 512.
[24] H. H. Brintzinger, M. H. Prosenc, F. Schaper, A. Weeber, U. Wieser, *J. Mol. Structure*, in press.
[25] J. D. Dunitz, *Acta Crystallogr.* **1995**, *B51*, 619.
[26] D. Braga, *Chem. Rev.* **1992**, *92*, 633.
[27] D. Braga, F. Greponi, *Organometallics* **1992**, *11*, 711.
[28] C. P. Brock, Y. Fu, *Acta Crystallogr., Sect. B* **1997**, *53*, 928.
[29] J. Bartol, P. Comba, M. Melter, M. Zimmer, *J. Comput. Chem.*, accepted.
[30] K.-F. Tebbe, R. Buchem, *Z. Anorg. Allg. Chem.* **1998**, *624*, 679.
[31] J. S. Miller, D. T. Glatzhofer, D. M. O'Hare, W. M. Reiff, A. Chakraborty, A. J. Epstein, *Inorg. Chem.* **1989**, *28*, 2930.
[32] J. S. Miller, J. H. Zhang, W. M. Reiff, *J. Am. Chem. Soc.* **1987**, *109*, 4584.
[33] D. Stein, H. Sitzmann, R. Boese, *J. Organomet. Chem.* **1991**, *421*, 275.
[34] D. Stein, H. Sitzmann, R. Boese, E. Dormann, H. Winter, *J. Organomet. Chem.* **1991**, *412*, 143.
[35] R. P. Hughes, A. S. Kowalski, J. R. Lomprey, A. L. Rheingold, *Organometallics* **1994**, *13*, 2691.
[36] R. Boese, D. Blaser, N. Kuhn, S. Stubenrauch, *Z. Kristallogr.* **1993**, *205*, 282.
[37] J. A. Burman, M. L. Hays, D. J. Burkey, P. S. Tanner, T. P. Hanusa, *J. Organomet. Chem.* **1994**, *479*, 135.
[38] P. Seiler, J. D. Dunitz, *Acta Crystallogr., Sect. B* **1980**, *36*, 2946.
[39] R. U. Kirss, A. Quazi, C. H. Lake, M. R. Churchill, *Organometallics* **1993**, *12*, 4145.
[40] J. Shimei, L. Li, Y. Guangdi, L. Juzheng, *Jiegou Huaxue (J. Struct. Chem.)* **1988**, *7*, 222.
[41] D. C. Liles, A. Shaver, E. Singleton, M. B. Wiege, *J. Organomet. Chem.* **1985**, *288*, C33.
[42] L.-H. Lai, Z.-Y. Zhang, M.-C. Shao, *Chem. Res. Chin. Univ.* **1992**, *8*, 258.
[43] J. C. A. Boeyens, D. C. Levendis, M. I. Bruce, M. L. Williams, *J. Crystallogr. Spectrosc. Res.* **1986**, *16*, 519.
[44] D. O'Hare, J. C. Green, T. P. Chadwick, J. S. Miller, *Organometallics* **1988**, *7*, 1335.
[45] M. B. Laing, K. N. Trueblood, *Acta Crystallogr.* **1965**, *19*, 373.
[46] M. J. Drewitt, S. Barlow, D. O'Hare, J. M. Nelson, P. Nguyen, I. Manners, *J. Chem. Soc., Chem. Commun.* **1996**, 2153.
[47] M. Hillman, J. D. Austin, *Organometallics* **1987**, *6*, 1737.
[48] T.-Y. Dong, H.-M. Lin, M.-Y. Hwang, T.-Y. Lee, L.-H. Tseng, S.-M. Peng, G.-H. Lee, *J. Organomet. Chem.* **1991**, *414*, 227.
[49] J. M. Nelson, A. J. Lough, I. Manners, *Angew. Chem. Int. Ed. Engl.* **1994**, *33*, 989.
[50] S. Ohba, Y. Saito, S. Kamiyama, A. Kasahara, *Acta Crystallogr., Sect. C: Cryst. Struct. Commun.* **1984**, *40*, 53.
[51] K. Hashidzume, H. Tobita, H. Ogino, *Organometallics* **1995**, *14*, 1187.
[52] S. Ohba, Y. Saito, T. Ishii, S. Kamiyama, A. Kasahara, *Acta Crystallogr., Sect. C: Cryst. Struct. Commun.* **1985**, *41*, 709.
[53] K. Hafner, C. Mink, H. J. Lindner, *Angew. Chem. Int. Ed. Engl.* **1994**, *33*, 1479.
[54] T.-Y. Dong, S.-H. Lee, *J. Organomet. Chem.* **1995**, *487*, 77.
[55] M. Hillman, E. Fujita, *J. Organomet. Chem.* **1978**, *155*, 99.
[56] M. Hillman, E. Fujita, H. Dauplaise, A. Kvick, R. C. Kerber, *Organometallics* **1984**, *3*, 1170.
[57] M. Hisatome, K. Nakanishi, K. Yamakawa, K. Kozawa, T. Uchida, *Bull. Chem. Soc. Jpn.* **1992**, *65*, 3275.
[58] L. D. Spaulding, M. Hillman, G. J. B. Williams, *J. Organomet. Chem.* **1978**, *155*, 109.
[59] M. Hisatome, J. Watanabe, K. Yamakawa, K. Kozawa, T. Uchida, *Nippon Kagaku Kaishi (J. Chem. Soc. Jpn.)* **1985**, 572.
[60] M. Hisatome, R.-I. Yamashita, J. Watanabe, K. Yamakawa, Y. Iitaka, *Bull. Chem. Soc. Jpn.* **1988**, *61*, 1687.
[61] M. Hisatome, Y. Kawaziri, K. Yamakawa, Y. Iitaka, *Tetrahedron Lett.* **1979**, 1777.
[62] M. Hisatome, J. Watanabe, K. Yamakawa, K. Kozawa, T. Uchida, *J. Organomet. Chem.* **1984**, *262*, 365.
[63] M. Hisatome, J. Watanabe, Y. Kawajiri, K. Yamakawa, *Organometallics* **1990**, *9*, 497.
[64] M. Hisatome, Y. Kawajiri, K. Yamakawa, Y. Harada, Y. Iitaka, *Tetrahedron Lett.* **1982**, *23*, 1713.
[65] A. Almenningen, A. Haaland, S. Samdal, J. Brunvoll, J. L. Robbins, J. C. Smart, *J. Organomet. Chem.* **1979**, *173*, 293.
[66] A. Haaland, *Acc. Chem. Res.* **1979**, *12*, 415.

Received March 8, 1999
[I99092]

Cyanide-Bridged Arrays of 2, 3 and 4 Metal Atoms Based on Salene–Iron Complexes – Syntheses, Structures and Metal–Metal Interactions

Andreas Geiß[a] and Heinrich Vahrenkamp*[a]

Dedicated to Professor Wolf-Peter Fehlhammer on the occasion of his 60th birthday

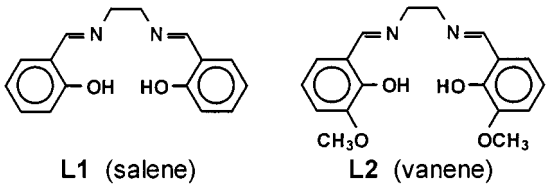
Keywords: Iron complexes / Salene ligands / Cyanide bridging / Electron transfer / Metal–metal interactions

Salene–Fe^{III} complexes of the types LFeCl and $[LFe(CN)_2]^-$ were treated with organometallic reagents to introduce the cyanide-linked units $(CO)_5Cr$, $(CO)_5Mo$, $(CO)_5W$, $Cp(CO)_2Fe$, Cp(dppe)Fe, and $Cp(PPh_3)_2Ru$. IR spectra and structure determinations revealed that all resulting complexes contained M–CN units with N coordination to the salene–Fe units. They were either dinuclear M–CN–Fe(salene), trinuclear M–CN–Fe(salene)–NC–M, or tetranuclear M–CN–Fe(salene)–Fe(salene)–NC–M species. Cyclic voltammetry showed that there are significant electronic interactions between the two outer organometallic units in the trinuclear complexes. UV/Vis spectra indicated a metal–metal charge transfer from the outer Cp(dppe)Fe groups to the central Fe^{III}. The magnetic moments at room temperature of the tri- and tetranuclear complexes are slightly lower than those calculated for isolated high-spin Fe^{III} species.

In the previous papers of this series[1][2] and in a feature article[3] we have outlined our interest in complexes containing cyanide-bridged arrays of redox-active transition metal ions. Our aim is to elucidate the factors determining the extent of electronic interactions between remote metal centers in such arrays. Our preparative approach consists of constructing the arrays from cyanometal complexes L_nM-CN and complexes $L_nM'-X$ containing labile ligands X. This approach allows a wide variation of L, M and X, as well as of the geometrical relation between two cyanide bridges at a central metal ion (*cis*, *trans*, tetrahedral, etc.), and of the orientations of the cyanide bridges (cyanide vs. isocyanide). The techniques used to assess the metal–metal interactions include IR spectroscopy, cyclic voltammetry, preparative redox chemistry, magnetic measurements and NIR spectroscopy. Our main contribution to this area is the design and variation of suitable new compounds, the investigation of which extends the work of previous researchers in the field.[3]

So far we have gained basic knowledge by studying dinuclear M–CN–M′ complexes and then applied this knowledge to include symmetrical trinuclear complexes of the types $M(CN-M')_2$ or $M(NC-M')_2$.[2,4,5] One important finding from these studies is that, as expected, a linear array of M–CN units allows for much better remote interactions than bent arrays. This was verified by finding an interaction between the terminal metal ions in a tetranuclear complex that was obtained accidentally.[6] Accordingly, we focused our preparative efforts on building blocks that only allow a *trans* arrangement of cyanide bridges at a connecting metal center. In essence this means the use of disc-like L_nM units with planar tetradentate ligands L_n as building blocks, as already applied some years ago by Hanack for the synthesis of electrically conducting [(Pc)M–CN] polymers (Pc = phthalocyanine).[7]

For the present investigation we chose salene ligands to ensure square-planar metal coordination of the central metal ions. The advantage of these ligands is their easy accessibility and variability, as well as the fact that they are good coligands for both square-pyramidal L^4M-X and octahedral $X-ML^4-Y$ complexes.[8] Our aim was to construct linear multinuclear arrays by using cyanide for X and Y. This paper describes our results obtained with salene–iron units. Iron was chosen as the central metal because of its redox properties. The tetradentate ligands were either salene itself (**L1**) or its bis(methoxy)-substituted variant vanene (**L2**) (Scheme 1).



L1 (salene) **L2** (vanene)

Scheme 1

Preparations

The starting iron complexes with salene ligands were **1a**,**b**, and **2a**,**b**.[9] We expected the former to lead to CN-bridged arrays with (salene)Fe–N coordination and the latter to maintain their (salene)Fe–C coordination upon attachment of other metals to the cyanide ligands.

(**L1**)Fe–Cl **1a**	K[(**L1**)Fe(CN)$_2$] **2a**
(**L2**)Fe–Cl **1b**	K[(**L2**)Fe(CN)$_2$] **2b**

[a] Institut für Anorganische und Analytische Chemie der Universität Freiburg,
Albertstraße 21, D-79104 Freiburg, Germany
Fax: (internat.) + 49-(0)761/203-6001
E-mail: vahrenka@uni-freiburg.de

 © WILEY-VCH Verlag GmbH, D-69451 Weinheim, 1999 1434–1948/99/1010–1793 $ 17.50+.50/0

Complexes **1** were treated with the monofunctional cyanometal complexes **3**−**8** with the aim of replacing the halide by the cyanometal "ligands" and possibly attaching a second cyanometal unit to form trinuclear species.

$Cp(CO)_2Fe-CN$ **3**

$Na[(CO)_5Cr-CN]$ **6**

$Cp(dppe)Fe-CN$ **4**

$Na[(CO)_5Mo-CN]$ **7**

$Cp(PPh_3)_2Ru-CN$ **5**

$Na[(CO)_5W-CN]$ **8**

Conversely, complexes **2** were reacted with the monofunctional species **9**−**11**, which are the sources of the cationic electrophiles $Cp(L_2)M$ to be attached at the N terminus of the cyanide ligands.

$[Cp(CO)_2Fe(THF)]PF_6$ **9**

$[Cp(dppe)Fe(CH_3CN)]Br$ **10**

$Cp(PPh_3)_2Ru-Cl$ **11**

All 1:1 combinations between complexes **1** and reagents **4**−**8** in methanol led to products with an Fe/M ratio of 1:1. In only one case, however, was such a product isolated as a simple dinuclear complex: The two most volumious partners, **1b** and **5**, yielded **12**, whose constitution was confirmed by a structure determination of its PF_6^- salt.

$[(H_2O)(\mathbf{L2})Fe-NC-Ru(PPh_3)_2Cp]^+$ **12**

In all other cases the 1:1 products were found to be associated with dimeric entities, i.e. tetranuclear complexes, in the solid state. This was ascertained by structure determinations of **[13a]**$(PF_6)_2$ and **[13a]**$(BPh_4)_2$ and deduced from the spectral similarities and solubility properties for the other complexes. This behavior corresponds to that of **1a**, which is also dimeric in the solid state but probably monomeric in polar solvents.[9][10] Complexes **13**−**17** were isolated and, of these, the ionic ones (**13**, **14**) could be crystallized as ClO_4^-, PF_6^-, SbF_6^- or BPh_4^- salts upon addition of the corresponding counterions.

$[(\mathbf{L})Fe-NC-Fe(dppe)Cp]_2^{2+}$ **13a**: L = **L1**; **13b**: L = **L2**

$[(\mathbf{L1})Fe-NC-Ru(PPh_3)_2Cp]_2^{2+}$ **14**

$[(\mathbf{L1})Fe-NC-M(CO)_5]_2$ **15**: M = Cr; **16**: M = Mo; **17**: M = W

Some of the tetranuclear dimers **13**−**17** were also precipitated from solutions containing two equivalents of the cyanometal reagents per equivalent of starting complex **1**. By adjusting the reaction conditions, however, the expected trinuclear complexes with two cyanometal "ligands" could be isolated. Starting from **1a** and **1b** these were **18a**, **18b**, **20a**, **21**, **22**, and **23**. Of these, the cationic compounds (**18**, **20**) could again be precipitated with one or several of the four anions named above, while the anionic ones (**21**−**23**) were precipitated as PPh_4^+ salts. Their trinuclear nature was ascertained by a structure determination of **[20a]**PF_6.

$(\mathbf{L})Fe\{NC-Fe(CO)_2Cp\}_2]^+$ **18a**: L = **L1**; **18b**: L = **L2**

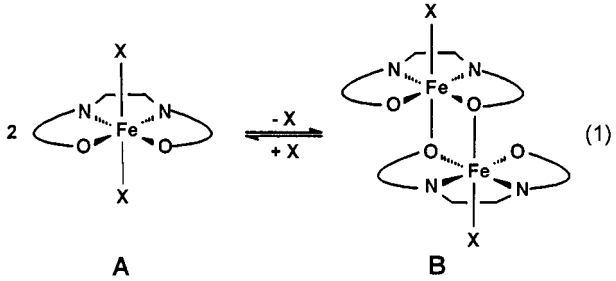
$[(\mathbf{L})Fe\{NC-Fe(dppe)_2Cp\}_2]^+$ **19a**: L = **L1**; **19b**: L = **L2**

$[(\mathbf{L})Fe\{NC-Ru(PPh_3)_2Cp\}_2]^+$ **20a**: L = **L1**; **20b**: L = **L2**

$[(\mathbf{L})Fe\{NC-M(CO)_5\}_2]^-$ **21**: M = Cr; **22**: M = Mo; **23**: M = W

Attempts to obtain complexes like **13**−**21** with an inverted orientation of the bridging cyanide ligands by using **2a** and **2b** as starting materials were unsuccessful. Invariably the Fe^{III}-attached cyanide ligands of **2a** and **2b** were turned around upon attachment of the other organometallic units. Thus **18a**, **19a**, and **20a** were obtained as PF_6^- salts from **2a**, and **9**, **10**, or **11**. Likewise, **19b** and **20b** resulted, though not in a pure form, from **2b** and **10** or **11**.

The formation of the isolated complexes can be understood from the solution behavior of the simple salene−Fe^{III} complexes.[8−11] It is known that **1a** and **1b**, which are molecular dimers in the solid state, are solvated and probably ionized in solution, being engaged in a monomer-dimer equilibrium as shown in Equation 1. This equilibrium should depend on the solvent, on other donor ligands, on the anions present, and on the solubility of the various species. The monomer **A**, with X = CH_3OH, would represent the simplest species in methanol solutions of **1a** or **1b**. For X = CN^- complex **A** would be the intact starting material **2a** or **2b**. Partial replacement of the labile ligands X from **A** or **B** could change the total charge of the solution species and hence their solubility or their preference in the equilibrium.



(1)

Of the isolated complexes, the 1:1 species **13**−**17** show their dimeric nature by their lower solubility compared to the 1:2 species **18**−**23**, which for **13** and **14** also corresponds to a dipositive charge of the complex cations. Steric effects are evident from the fact that the most voluminous cyanometal "ligand" **5** does not want to form a 1:2 complex (**20b**) starting from (**L2**)FeCl, but rather the unique 1:1 complex **12**. Likewise, the least voluminous cyanometal "ligand" **3** could not be incorporated into a 1:1 complex, but easily formed the 1:2 complexes **18a** and **18b**. Electronic effects can also be invoked to explain the lower tendency for the formation of **20b** in comparison to **20a**: The vanene ligand (**L2**) is more electron-rich than the salene ligand (**L1**), and hence the Fe^{III} ion coordinated by it is less prone to bind a sixth donor. The low binding tendency of all (**L1**)Fe−X or (**L2**)Fe−X complexes for a sixth donor ligand also provides

an explanation for the inversion of the cyanide attachment to the Fe^{III} center in **2a** and **2b** upon complexation to the incoming organometallic units. This feature allows the liberation of CN^- in solution, which also makes the crystallization of dimeric (salene)Fe−CN possible.[12]

Structures

One representative example of each structural type was subjected to X-ray analysis. In the case of **13a** the complex salts with either PF_6^- or BPh_4^- as counterions differed so much in their ν(CN) IR data (see below) that it seemed worthwhile to explain this phenomenon in terms of their structures.

Compound [**12**]SbF_6 (see Figure 1) is the only species in this report that is dinuclear in the solid state and that bears a ligand other than cyanide or salene on the central Fe^{III} ion. The coordination geometries in **12** [distorted octahedral at Fe^{III}, piano stool at Ru] are normal. The salene ligand **L2** defines a square-planar environment of the iron center to a good approximation and can itself be described by the "stepped" conformation.[8][11] The Fe−O(water) distance of 2.18 Å is significantly longer than the Fe−O(salene) distances (av. 1.89 Å), while the Fe−N(cyanide) distance (2.05 Å) is a little shorter than the Fe−N(salene) distances (av. 2.08 Å).

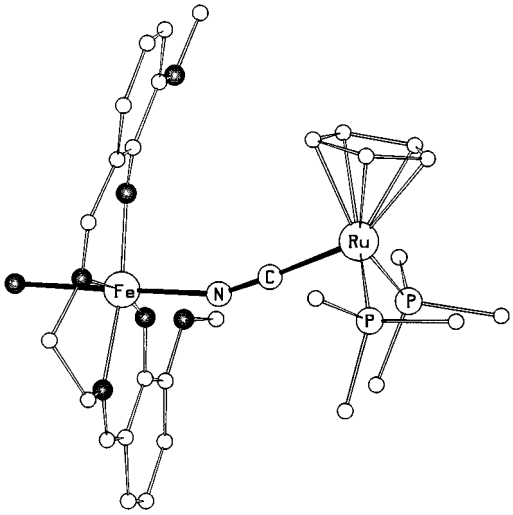


Figure 1. Structure of complex **12** in [**12**]SbF_6; Selected bond lengths [Å] and angles [°]: Fe−O(salene) 1.885(7) and 1.902(7), Fe−N(salene) 2.083(9) and 2.076(9), Fe−O(H_2O) 2.184(6), Fe−N(CN) 2.046(8), C−N(CN) 1.13(1), Ru−C(CN) 1.973(10); Fe−N−C(CN) 160.1(9), R−C−N(CN) 176.4(9)

The bridging cyanide ligand in **12** shows typical features. Its π-acceptor terminus, the C atom, is naturally bound to the electron-rich ruthenium atom as it is the better π donor. This is reflected by the Ru−C distance, which is shorter than the Fe−N distance on the other side. Likewise, the Ru−C−N angle (176°) is much closer to linearity than the Fe−N−C angle (160°). These two indicators of the π-bonding abilities of the C and N atoms of the cyanide ligand, as well as of the metal centers attached to them, have been found to be of good diagnostic value.[1−3]

The two complex salts derived from **13a**, containing PF_6^- and BPh_4^- as counterions, were both found to have the dimeric units of **13a** in the solid state. The structure determination of [**13a**]$(PF_6)_2$ resulted in an unsatisfactory *R* value of 0.119, and only the structure of [**13a**]$(BPh_4)_2$ is discussed in detail here (see Figure 2). The dimer **13a** is centrosymmetrical in both compounds. As usual for such salene complex dimers,[8][11] one each of the salene oxygen atoms is used to bridge the two monomer units resulting in a central Fe_2O_2 square, and the salene ligands once again have the "stepped" conformation.

The bonding characteristics of the bridging cyanide ligands compare closely with those in **12**, both in terms of metal−cyanide bond lengths and of the angles at C and N. There is ample precedence for bridging cyanide coordinated to the iron center at the C and N terminus,[1][2] including Prussian Blue.[13] The Fe′−C distance in **13a** compares well with other Fe−C distances in Cp(dppe)Fe−CN derivatives, but the Fe−N distance in **13a** is larger than other such distances in complexes of low-valent iron. It is, however, comparable to the Fe^{III}−N distance in Prussian Blue.

The two major differences between the shapes of the dimeric units **13a** in [**13a**]$(BPh_4)_2$ and [**13a**]$(PF_6)_2$ lie in the bending of the Fe−CN−Fe bridge and the relative orientation of the Fe(salene) units with respect to the Fe(dppe)Cp units. The latter in [**13a**]$(PF_6)_2$ are rotated by about 30° around the Fe−CN−Fe′ line compared to [**13a**]$(BPh_4)_2$. More significant is the difference in the Fe−N−C angles, which are 152° in [**13a**]$(BPh_4)_2$ and 178° in [**13a**]$(PF_6)_2$. The voluminous tetraphenylborate counterions seem to cause severe bending of the "soft" Fe−N−C angles, which in turn is the reason for the lowering of ν(CN) in [**13a**]$(BPh_4)_2$ (see below).

Compound [**20a**]PF_6 has an approximately linear Ru−CN−Fe−NC−Ru arrangement in the solid state (see Figure 3). Its general features can be compared with those of [**12**]SbF_6: The central Fe^{III} ion has a roughly octahedral coordination, its "stepped" salene ligand comprises a roughly square-planar FeO_2N_2 arrangement, and the attachment of the $Cp(PPh_3)_2Ru$−CN "ligands" is similar. The second $Cp(PPh_3)_2Ru$−CN unit in [**20a**]PF_6 occupies the position of the water ligand in [**12**]SbF_6 but is not symmetry-related to the first one.

The attachment of two cyanometal units to the (salene)-Fe^{III} center leads to different bonding characteristics of the bridging cyanide ligands in **20**. Compared to **12** the central Fe−N bonds are 0.05 Å longer, which may point to a *trans* effect, while the Ru−C(cyanide) bond lengths in both complexes are virtually identical. The bending of the Fe−N−C(cyanide) angles in **20** is less pronounced than in **12**, while the bending of the Ru−C−N(cyanide) angles is more pronounced. However, since all four angles Fe−N−C and Ru−C−N are bent in the same direction, the total deviation of the Fe−N−C−Ru sequences from linearity (18−24°) is the same in both complexes. Indeed, in **20** all

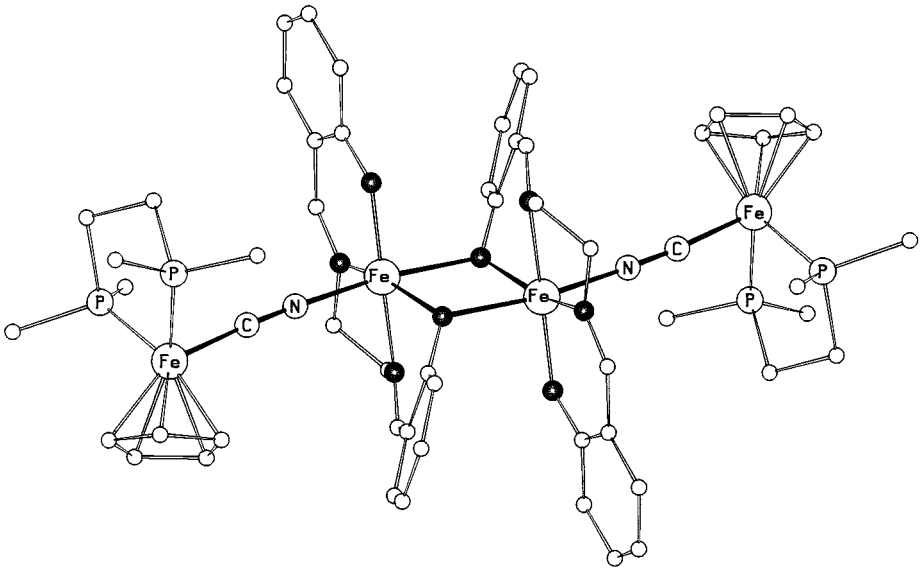


Figure 2. Structure of complex **13a** in [**13a**]$(BPh_4)_2$; selected bond lengths [Å] and angles [°]: Fe−O(unbridged) 1.876(4), Fe−O(bridge) 1.991(4), Fe−O′(bridge) 2.117(4), Fe−N(salene) 2.091(5) and 2.123(5), Fe−N(CN) 2.017(5), C−N(CN) 1.161(7), Fe′−C(CN) 1.817(7), Fe− − −Fe(across bridge) 4.835(2); O−Fe−O(bridge) 78.4(2), Fe−O−Fe(bridge) 101.6(2), Fe−N−C(cyanide) 151.5(5), Fe′−C−N(cyanide) 178.2(6)

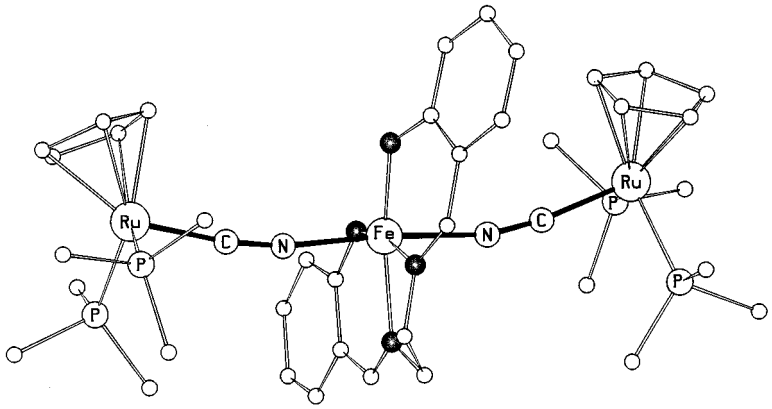


Figure 3. Structure of complex **20** in [**20**]PF_6; selected bond lengths [Å] and angles [°]: Fe−O(salene) 1.902(3) and 1.925(4), Fe−N(salene) 2.128(4) and 2.102(4), Fe−N(CN) 2.092(4) and 2.092(4), C−N(CN) 1.151(5) and 1.162(6), Ru−C(CN) 1.965(4) and 1.961(4); N−Fe−N-(cyanide) 174.3(2), Fe−N−C(cyanide) 166.1(4) and 169.9(4), Ru−C−N(cyanide) 170.5(4) and 172.3(4)

atoms of the Ru−CN−Fe−NC−Ru sequence lie approximately in one plane.

IR Data

The ν(CO) data of the complexes with carbonyl ligands are listed in the Experimental Section. The ν(CN) values are given in Table 1 for the solid state and for solutions.

Based on the accumulated experience with oligonuclear complexes of the cyanometal "ligands" **3**−**8**[1,2,4,5] and on the cross-comparison of the data in Table 1, several unambiguous conclusions can be drawn about the structure and bonding in the complexes described here. The simplest of these can be derived from the observation that, with few exceptions (**18a**,**b**), the ν(CN) values are lower in the bridged complexes than in the free metallocyanides **3**−**8**. This means that the kinematic effect [constraint of CN motion by double attachment, i.e. raising of ν(CN)] is outweighed by an electronic effect. The latter consists in the electron withdrawal at the N terminus of the CN by the electron-poor Fe^{III} center, which in turn causes enhanced π-backdonation from the electron-rich organometallic units at the C terminus into the π* orbitals of the C−N bond, and hence a weakening of this bond. Proof for this is found in the ν(CO) values of the "ligands" **3**, **6**, **7**, and **8**, which are raised upon formation of the oligonuclear complexes.

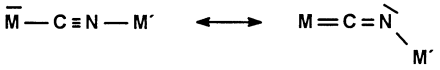
The data for the dimeric 1:1 complexes **13a**, **13b** and **14** indicate that the amount of π-backdonation seems to depend on structural details. The solid-state IR spectra of these complexes show a marked dependence of ν(CN) upon the counterion present. This is most evident for **13a**, which experiences a decrease of 20 cm^{-1} in ν(CN) on going from the smallest (ClO_4^-) to the largest counterion (BPh_4^-). As seen from the structure determinations (see above) this

Table 1. IR data ν(CN) [cm^{-1}]

	L_nM'[a]	In KBr	In solution[b]
3	$Cp(CO)_2Fe$	2116	C: 2119
4	Cp(dppe)Fe	2062	C: 2062
5	$Cp(PPh_3)_2Ru$	2072	C: 2072
6	$(CO)_5Cr$	2108	M: 2103
7	$(CO)_5Mo$	2107	M: 2103
8	$(CO)_5W$	2111	M: 2104
[**12**]PF_6	$Cp(PPh_3)_2Ru$	2063	C: 2061
[**12**]SbF_6	$Cp(PPh_3)_2Ru$	2061	C: 2061
[**13a**]ClO_4	Cp(dppe)Fe	2058	C: 2013
[**13a**]PF_6	Cp(dppe)Fe	2048	C: 2013
[**13a**]SbF_6	Cp(dppe)Fe	2052	C: 2013
[**13a**]BPh_4	Cp(dppe)Fe	2039	C: 2013
[**13b**]PF_6	Cp(dppe)Fe	2058	C: 2014
[**13b**]SbF_6	Cp(dppe)Fe	2056	C: 2014
[**14**]PF_6	$Cp(PPh_3)_2Ru$	2055	C: 2029
[**14**]SbF_6	$Cp(PPh_3)_2Ru$	2054	C: 2029
[**14**]BPh_4	$Cp(PPh_3)_2Ru$	2051	C: 2029
15	$(CO)_5Cr$	2097	M: 2099
16	$(CO)_5Mo$	2102	M: 2104
17	$(CO)_5W$	2104	M: 2106
[**18a**]ClO_4	$Cp(CO)_2Fe$	2134	C: 2137
[**18b**]SbF_6	$Cp(CO)_2Fe$	2132	C: 2133
[**19a**]PF_6	Cp(dppe)Fe	2063	C: 2059
[**19b**]SbF_6	Cp(dppe)Fe	2057	C: 2054
[**20a**]PF_6	$Cp(PPh_3)_2Ru$	2076	C: 2072
[**20b**]SbF_6	$Cp(PPh_3)_2Ru$	2071	C: 2069
[**21**]PPh_4	$(CO)_5Cr$	2114	M: 2102
[**22**]PPh_4	$(CO)_5Mo$	2115	M: 2104
[**23**]PPh_4	$(CO)_5W$	2119	M: 2107

[a] Terminal organometallic unit. − [b] C: dichloromethane, M: methanol.

corresponds to an increased bending of the C−N−Fe^{III} linkage at the nitrogen atom. In accord with similar observations for Fe−CN−Cu systems[14] a simplistic explanation for this may be proposed by formulating an angle-dependent variation between a C−N double bond and a C−N triple bond according to the resonance formula in Scheme 2.



Scheme 2

Complexes **13** and **14** also show significantly different ν(CN) values in the solid state and in solution, and their solution IR data are not dependent on the counterions present. While their tetranuclear nature in the solid state was proved by the structure determinations, this indicates that in solution they are dinuclear, i.e. monomeric. This is in accord with the electrochemical data (see below). It is also supported by the fact that **12**, the only monomeric complex of this type, shows the same ν(CN) values in the solid state and in solution and for both counterions. Unlike **13** and **14**, the uncharged 1:1 complexes **15**−**17** show the same ν(CN) values in the solid state and in solution and, furthermore, in solution their ν(CN) values are virtually identical to those of the free metallocyanides **6**−**8**. In the absence of further indicators (no structures, no good electrochemical data) it cannot be concluded whether they are tetrameric in both the solid state and in solution or dissociate to yield the free metallocyanides in solution.

The ν(CN) data of the trinuclear complexes **19** and **20** are characteristically different from those of their (in solution) dinuclear counterparts **13** and **14**: For the trinuclear systems the ν(CN) values are 40−45 cm^{-1} higher and come close to those of the free metallocyanides **4** and **5**. This demonstrates reduced π-backdonation from the terminal metals to the cyanide ligands, corresponding with the fact that in the trinuclear systems two L_nM−CN "ligands" satisfy the acceptor properties of the central (salene)Fe^{III} units. The validity of this argument is supported by two further observations: Firstly the monomeric dinuclear complex **12** shows its CN band 30 cm^{-1} higher than its water-free counterpart **14**, secondly the dimeric and tetranuclear complexes **13** and **14** show ν(CN) values that are close to those of their trinuclear analogs **19** and **20**. In all these species with clearly octahedral coordination of the central Fe^{III}, the ν(CN) values are high, while for **13** and **14** in solution they are low. A consistent interpretation thus requires that **13a**, **13b** and **14** are five-coordinate in solution, i.e. have only one donor ligand for Fe^{III} in addition to the salene ligand.

Electrochemistry

All new complexes were subjected to cyclic voltammetry in dichloromethane solution. As previously observed, it was found that the species with carbonyl ligands (**15**−**18**, **21**−**23**) do not yield reversible redox waves and lead to electrode coating. All other compounds, however, showed a reversible multistep redox behavior that allowed a consistent interpretation of their electronic nature and of their metal−metal interactions. The corresponding data are listed in Table 2.

Table 2. Cyclic-voltammetry data

	L_nM'[b]	red. Fe^{III}	ox(1) L_nM	ox(2) L_nM
4	Cp(dppe)Fe		0.48	
5	$Cp(PPh_3)_2Ru$		0.79	
[**12**]SbF_6	$Cp(PPh_3)_2Ru$	−0.30	1.08	
[**13a**]PF_6	Cp(dppe)Fe	−0.34	0.86	
[**13b**]PF_6	Cp(dppe)Fe	−0.31	0.82	
[**14**]PF_6	$Cp(PPh_3)_2Ru$	−0.32	1.12	
[**19a**]PF_6	Cp(dppe)Fe	−0.35	0.46	0.86
[**20a**]PF_6	$Cp(PPh_3)_2Ru$	−0.39	0.89	1.12[c]

[a] In dichloromethane, scan speed 100 mV/s, potentials in V vs. Ag/AgCl. − [b] Terminal organometallic unit. − [c] Irreversible.

In all oligonuclear complexes the reduction of the central Fe^{III} ion occurs within the very narrow potential range of −0.32 to −0.39 V. This points to a very good balance of electron acceptance by the central iron and electron donation by its one or two axial ligands. As an example, the water molecule and the Ru−CN ligand in **12** have about the same effect as the single Ru−CN ligand in **14**. This implies that the Ru−CN ligand in **14** must donate more

electron density than that in **12**, which is clearly evident from the IR data and, to a lesser extent, also from the redox potentials of the Ru−CN units in **12** and **14**. The inherent implication that the 1:1 complexes **13** and **14** are monomeric, i.e. dinuclear, in solution is borne out by the simplicity of their cyclic voltammograms, which for the corresponding tetranuclear complexes should show at least one more redox wave due to the stepwise reduction of the two closely spaced, i.e. strongly interacting, central Fe^{III} centers.

The increase of the redox potentials of the cyanometal "ligands" **4** and **5** upon single coordination to the (salene)-Fe^{III} unit amounts to 0.3−0.4 V. This is somewhat larger than observed previously for related dinuclear complexes,[1,2,4,5] and corresponds to the considerable withdrawal of electron density through π-backdonation as diagnosed above from the IR data. In this respect the pair of complexes **13a/13b** provides an internal test for the mutual effects of the shift of electron density between the two redox centers across the cyanide bridge. In **13a** the (salene)Fe^{III} unit is more difficult to reduce (i.e. more electron-rich) and, in addition, the Cp(dppe)Fe unit is more difficult to oxidize (i.e. more electron-poor) than their counterparts in **13b**.

In the trinuclear complexes **19a** and **20a** the Fe^{III} centers are slightly more difficult to reduce than in the dinuclear complexes, corresponding to their higher electron density due to the presence of two cyanometal donors. On the other hand, the first oxidative waves appear at significantly lower potentials than in the dinuclear complexes. This agrees again with the observations from the IR data, which indicate a significantly smaller π-backdonation from the outer organometallic units in **19a** and **20a**. Figure 4 shows the two voltammograms.

The most important feature of the trinuclear complexes **19a** and **20a** is the occurrence of two well-separated oxidative waves in their voltammograms. These must represent the stepwise oxidation of the two outer organometallic units. At first glance the two oxidation potentials in both cases are conspicuously close to those of the dinuclear complexes (**13a**, **14**) plus the two free metallocyanides (**4**, **5**), leading to the suspicion that **19a** and **20a** dissociate into these components in solution. However, these components should be detectable in the IR spectra and (for **4** and **5**) by NMR, which was not the case. Thus, the large separation of the redox waves must be taken as being real and as an indication of a strong electronic interaction between the two outer organometallic units which are ca. 10 Å apart. The extent of this interaction, as measured by the potential separation, is unusually large when compared to that in related trinuclear $(M'-CN)_2M$ complexes investigated by other researchers[15−17] and ourselves.[2][4]

It seemed feasible that the isolation of the mono-oxidized species [**19a**]X_2 or [**20a**]X_2 should be possible after chemical oxidation or controlled potential electrolysis. These species would be valuable for probing the long-range metal−metal interactions by optically induced MMCT as described in the following section. However, various attempts to generate these species chemically or electrolytically, or even to spectroscopically prove their existence in solution, met with failure.

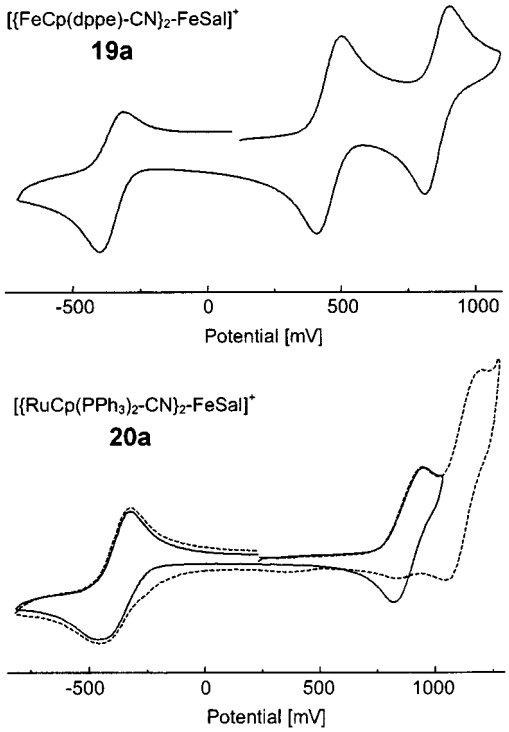


Figure 4. Cyclic voltammograms of **19a** and **20a** (for details see Table 2); for **20a** the solid line corresponds to a scan range of −0.80 to +1.05 V, the dashed line to a scan range of −0.80 to +1.35 V

Metal−Metal Charge Transfer

The phenomenon of optically induced metal−metal charge transfer (MMCT) finds its popular representation in the name Prussian Blue (generally accepted for a class of compounds of approximate composition $M^IFe^{II}Fe^{III}(CN)_6 \cdot x\ H_2O$, corresponding to an MMCT absorption at 680 nm. The practical relevance of this has led to many investigations of the optical properties of coordination compounds containing cyanide-bridged metal centers.[3] Few of those, however, reproduce the electronic situation in Prussian Blue, which contains Fe^{III} as a d^5 high-spin species attached to the N terminus and Fe^{II} as a d^6 low-spin species attached to the C terminus of the cyanide bridge. All complexes described here have just this configuration and thus are simple low-molecular representatives of Prussian Blue.

The optical properties of the complexes yield partial justification for this statement. Table 3 lists the UV/Vis absorption of the analytically pure compounds (except **15**−**17**, which are insoluble in dichloromethane). It is evident that the spectra are dominated by the LMCT absorptions in the visible range, of which those due to the (salene)Fe^{III} units are 5 to 10 times as intense as those due to the organometallic units. For the di- and trinuclear complexes containing carbonyl ligands on the organometallic units (**18**, **21**−**23**) there are no further spectral features, leading to the conclusion that a possible MMCT from the outer metal centers

to the central Fe^{III} is too high in energy to be discernable from the LMCT, in accord with the high redox potentials of these outer organometallic groups.

Table 3. UV/Vis data {in dichloromethane, $\lambda_{max}(\varepsilon_{max})$ [nm(M^{-1} cm^{-1})]}

	L_nM'[a]	LMCT	MMCT
1a	–	474(4300)	
1b	–	453(3800), 512(3600)	
3	$Cp(CO)_2Fe$	348(830)	
4	Cp(dppe)Fe	409(620)	
5	$Cp(PPh_3)_2Ru$	330(300)	
[**12**]SbF_6	$Cp(PPh_3)_2Ru$	494(5800)	
[**13a**]PF_6	Cp(dppe)Fe	416(4900), 504(4950)	741(2200)
[**13b**]PF_6	Cp(dppe)Fe	492(5700), 560(6000)	796(2500)
[**14**]PF_6	$Cp(PPh_3)_2Ru$	430(4600), 497(5000)	
[**18a**]ClO_4	$Cp(CO)_2Fe$	402(4300), 504(3400)	
[**18b**]SbF_6	$Cp(CO)_2Fe$	422(5400), 495(4300)	
[**19a**]PF_6	Cp(dppe)Fe	404(5800), 500(5950)	630(3950)
[**20a**]PF_6	$Cp(PPh_3)_2Ru$	440(4400), 494(5300)	
[**21**]PPh_4	$(CO)_5Cr$	440(2600), 511(3400)	
[**22**]PPh_4	$(CO)_5Mo$	439(2900), 503(3500)	
[**23**]PPh_4	$(CO)_5W$	440(3100), 491(3600)	

[a] Terminal organometallic unit.

At first glance this also seems to be the case for the ruthenium-containing complexes **12**, **14**, and **20a**. However, their absorption intensities for the LMCT are higher and their spectral traces extend by about 100 nm further into the visible range than those of the aforementioned complexes. This situation is represented in Figure 5. It can be interpreted by a hidden MMCT absorption at ca. 550 nm. Again, the high redox potentials of the Ru centers in these complexes can serve as an explanation for the high MMCT energies.

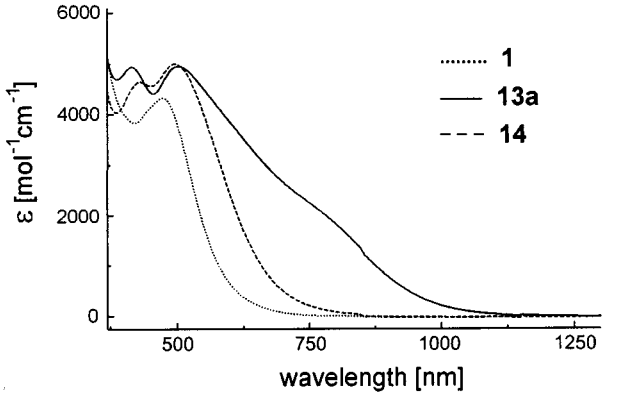


Figure 5. Superposition of the UV/Vis spectra of the reference compound **1a** and its dinuclear $Fe^{III}-NC-Fe^{II}$ and $Fe^{III}-NC-Ru^{II}$ derivatives **13a** and **14** (in CH_2Cl_2)

Only for the di- and trinuclear complexes containing Cp(dppe)Fe as the organometallic unit with the lowest redox potential on the terminal positions (**13a**, **13b**, **19a**) are the MMCT absorptions visible as shoulders in the spectra, cf. Figure 5. Compound **13b** shows the MMCT transition of lowest energy, which can be explained by the observations, mentioned above, that in **13b** both the Fe^{III} center is easier to reduce and the Fe^{II} center easier to oxidize than their counterparts in **13a**. The observation that the trinuclear complex **19a** shows an MMCT of higher energy than its dinuclear counterpart **13a**, despite the lower first redox potential of its Cp(dppe)Fe unit, cannot be explained by the simple arguments used here. It serves, however, as additional proof that **19a** does not dissociate into **13a** and **4** in solution, as suspected above. Altogether the MMCT energies of these three complexes come close enough to that of Prussian Blue to allow the statement that they represent a viable model of its high-spin-$Fe^{III}-NC-$low-spin-Fe^{II} arrangement.

The MMCT transitions observed here correspond to electronic interactions between neighboring metal centers, and in the trinuclear complexes the intramolecular redox process transfers an electron from the terminal metal centers to the central Fe^{III}. Thus, the ability of the tri- and tetranuclear species for long-range metal−metal interactions has not been exploited. This poses the challenge of either obtaining the elusive one-electron oxidation products of **19** or **20** or preparing unsymmetrical (i.e. heterotrimetallic) trinuclear complexes.

Magnetism

All new complexes contain several unpaired electrons located on the salene-bound high-spin Fe^{III} centers. Their magnetic moments were determined at room temperature by the Gouy method in order to find out how the basic magnetic properties of (salene)Fe^{III} complexes are modified by the attachment of the cyanometal "ligands" and to possibly detect new magnetic interactions. The measured values of χ_{mol} were corrected for the diamagnetic contributions,[18] and from the resulting values $c^{corr}{}_{mol}$ the magnetic moments μ_{eff} were calculated using the formula $\mu_{eff} = 2.828(\chi^{corr}{}_{mol} \cdot T)^{1/2}$. The corresponding data are listed in Table 4.

Table 4. Magnetic data at room temperature

	χ_{mol} [10^{-2} $cm^{-3}mol^{-1}$]	$\chi^{corr}mol$ [10^{-2} $cm^{-3}mol^{-1}$]	μ_{eff} [μ_B]
a) reference compounds			
1a			5.19[19]
1b			5.01[19]
b) 1:1 complexes			
[**12**]SbF_6	1.286	1.363	5.65
[**13a**]PF_6	1.168	1.229	5.37
[**13b**]SbF_6	1.119	1.189	5.27
[**14**]PF_6	1.249	1.334	5.59
15	1.141	1.169	5.23
16	1.165	1.196	5.29
17	1.151	1.185	5.27
c) 1:2 complexes			
[**18a**]ClO_4	1.291	1.327	5.58
[**18b**]SbF_6	1.181	1.231	5.37
[**19a**]PF_6	1.310	1.408	5.74
[**20a**]PF_6	1.327	1.444	5.82
[**21**]PPh_4	1.239	1.300	5.52
[**22**]PPh_4	1.263	1.330	5.58
[**23**]PPh_4	1.225	1.298	5.51

It is known that the Fe^{III} ion in salene complexes can be low-spin [e.g. (salene)$Fe(CN)_2$] or high-spin [e.g. (salene)-Fe(imidazole)$_2$][20] and that the dimeric (salene)Fe−X complexes represented by **B** show antiferromagnetic coupling between the two high-spin Fe^{III} ions, amounting, for instance, to $J = -8\ cm^{-1}$ for our reference complex **1a**.[19] Thus, there existed the possibility that the cyanometal "ligands" employed here would induce low-spin behavior or stronger magnetic coupling within the $Fe_2(salene)_2$ cores, as we have observed before for $[Fe_4S_4]^{2+}$ cores ligated by cyanometal units.[21]

As Table 4 shows, all magnetic moments are lower than the spin-only value of 5.92 μ_B for high-spin d^5. For the trinuclear 1:2 complexes this cannot be explained by antiferromagnetic coupling. It is possibly an expression of spin crossover, i. e. the presence of small amounts of low-spin species. Such an equilibrium of high-spin and low-spin Fe^{III} complexes was deduced for [(**L2**)Fe(imidazole)$_2$]BPh_4.[20] Irrespective of this it is evident that the cyanometal "ligands" are not strong enough to induce a real low-spin situation.

The lowering of the magnetic moments for the 1:1 complexes points to antiferromagnetic coupling within the $Fe_2(salene)_2$ units with the same order of magnitude as previously observed for the (salene)Fe−X dimers.[9,12,19,20] Thereby it is another indication that all complexes **13**−**17** exist as tetranuclear dimers in the solid state with structures comparable to that of **13a**. Complex **12**, which has a typically higher magnetic moment close to that of the spin-only value, underlines this, being the only monomeric 1:1 complex in the solid state due to its aqua ligand. Thus a consistent qualitative description of the magnetic properties can be achieved with the room temperature data, while a more detailed description would require low-temperature measurements.

Conclusions

The combination of (salene)Fe^{III} fragments with cyanometal units has yielded three types of arrangements: dinuclear 1:1 complexes, dimers thereof as tetranuclear 2:2 complexes, and linear trinuclear 1:2 complexes. The constitution of the tetranuclear species, which exist only in the solid state, was confirmed by a structure determination, by the IR data and the magnetic measurements. Their existence as dinuclear species in solution was deduced from the electrochemical and IR data and by reference to the structure determination of a related complex. The identity of the trinuclear species in the solid state and in solution was ascertained by the electrochemical, spectroscopic and magnetic measurements, again in combination with a crystal structure analysis.

The electronic interactions between the metal atoms across the cyanide bridges were evaluated by cyclic voltammetry and UV/Vis spectroscopy. The electrochemical measurements revealed a strong interaction between the terminal metal atoms in the linear trinuclear M−CN−Fe−NC−M arrays, the electronic spectra showed an optically induced metal−metal charge transfer from the terminal M^{II} centers to the (salene)Fe^{III} center. The electronic situation and the energy of the MMCT make the complex [(salene)Fe^{III}−NC−Fe^{II}(dppe)Cp]$^+$ (**13**) the simplest molecular analog of Prussian Blue.

In comparison to the di- and trinuclear systems previously reported by us, which were mostly organometallic complexes,[1,2,4] the compounds described here show four characteristic features: (1) They have a compositional (and structural) variability that can only partly be controlled by the synthetic approach. (2) They are labile with respect to the orientation of the CN bridge, resulting in the accessibility of only one of the two orientational isomers. (3) They show an unusually large separation of the two redox waves for the two outer, chemically equivalent, M′ units, indicating a strong electronic interaction between them. (4) They are paramagnetic and of high spin, opening the possibility to study magnetic interactions.

Experimental Section

The general working conditions, the synthesis of the organometallic reagents and the details of the measurement procedures are listed in ref.[1] Complexes **1a**, **1b**, **2a** and **2b** were prepared according to ref.[9] Magnetic susceptibilities were measured with an MSB Auto Balance, which was calibrated with $K_3[Fe(CN)_6]$. Analytical data for the new complexes are given in Table 5.

[12]PF_6: 0.500 g (1.20 mmol) of **1b** and 0.858 g (1.20 mmol) of **5** in 50 mL of methanol were heated to 50°C for 2 h and then filtered hot. After addition of 0.195 g (1.20 mmol) of NH_4PF_6, the mixture was stirred at 50°C for 30 min and again filtered hot. The filtrate was kept in an open beaker until about half of the solvent had evaporated. The precipitate was filtered off, washed with ether and dried in a stream of nitrogen to yield 487 mg (30%) of [**12**]PF_6 as black crystals, m.p. 230°C (dec.).

[12]SbF_6: This compound was obtained in the same way from 0.500 g (1.20 mmol) of **1b**, 0.858 g (1.20 mmol) of **5** and 0.310 g (1.20 mmol) of $NaSbF_6$. Yield 504 mg (31%) of [**12**]SbF_6 as black crystals, m.p. 230°C (dec.).

[13a]ClO_4: 104 mg (0.29 mmol) of **1a** and 159 mg (0.29 mmol) of **4** in 50 mL of methanol were stirred at 50°C for 2 h, filtered hot, treated with 31 mg (0.29 mmol) of $LiClO_4$, stirred at 50°C for 30 min and filtered hot. Slow cooling to room temperature (12 h) led to the precipitation of 126 mg (45%) of [**13a**]ClO_4 as black crystals, m.p. 220°C (dec.), which were washed with ether and dried in a stream of nitrogen.

[13a]PF_6: This compound was obtained in the same way from 204 mg (0.57 mmol) of **1a**, 311 mg (0.57 mmol) of **4** and 93 mg (0.57 mmol) of NH_4PF_6. Yield 192 mg (33%) of [**13a**]PF_6, black crystals, m.p. 220°C (dec.).

[13a]BPh_4: This compound was obtained in the same way from 212 mg (0.59 mmol) of **1a**, 324 mg (0.59 mmol) of **4** and 203 mg (0.59 mmol) of $NaBPh_4$. Yield 312 mg (44%) of [**13a**]BPh_4, black crystals, m.p. 180°C (dec.).

[13a]SbF_6: This compound was obtained in the same way from 195 mg (0.55 mmol) of **1a**, 298 mg (0.55 mmol) of **4** and 141 mg (0.55 mmol) of $NaSbF_6$. Yield 235 mg (39%) of [**13a**]SbF_6, black crystals, m.p. 225°C (dec.).

[13b]PF_6: This compound was prepared in the same way as [**12**]PF_6 from 152 mg (0.36 mmol) of **1b**, 199 mg (0.36 mmol) of **4** and 59 mg (0.36 mmol) of NH_4PF_6 in 70 mL of methanol. Yield 103 mg (26%) of [**13b**]PF_6 as black crystals, m.p. 200°C (dec.).

[13b]SbF_6: This compound was prepared in the same way as described above, from 107 mg (0.26 mmol) of **1b**, 140 mg (0.26 mmol) of **4** and 66 mg (0.26 mmol) of $NaSbF_6$. Yield 89 mg (30%) of [**13b**]SbF_6 as black crystals, m.p. 190°C (dec.).

[14]ClO_4: This compound was prepared in the same way as [**12**]PF_6, from 113 mg (0.32 mmol) of **1a**, 226 mg (0.32 mmol) of **5** and 34 mg (0.32 mmol) of $LiClO_4$. Yield 153 mg (42%) of [**14**]ClO_4, black crystals, m.p. 230°C (dec.).

[14]PF_6: This compound was prepared in the same way as described above, from 154 mg (0.43 mmol) of **1a**, 309 mg (0.43 mmol) of **5** and 35 mg (0.43 mmol) of NH_4PF_6. Yield 253 mg (50%) of [**14**]PF_6, black crystals, m.p. 240°C (dec.).

[14]SbF_6: This compound was prepared in the same way as described above, from 207 mg (0.58 mmol) of **1a**, 415 mg (0.58 mmol) of **5** and 150 mg (0.58 mmol) of $NaSbF_6$. Yield 279 mg (38%) of [**14**]SbF_6, black crystals, m.p. 240°C (dec.).

[14]BPh_4: This compound was prepared in the same way as described above, from 100 mg (0.28 mmol) of **1a**, 200 mg (0.28 mmol) of **5** and 96 mg (0.28 mmol) of $NaBPh_4$. Yield 178 mg (47%) of [**14**]BPh_4, black crystals, m.p. 200°C (dec.).

15: 200 mg (0.56 mmol) of **1a** and 135 mg (0.58 mmol) of **6** in 100 mL of methanol were stirred at 50°C for 2 h. After cooling to room temperature, the mixture was filtered. The precipitate was washed 3 times with 20 mL of cold methanol and then with 20 mL of ether and dried in vacuo, leaving 123 mg (41%) of **15** as a blue-purple powder, m.p. 130°C. − IR (CH_3OH): $\tilde{\nu}$(CO) = 1907 cm^{-1} m, 1934 s, 2053 m.

16: This compound was prepared in the same way as described above, from 296 mg (0.83 mmol) of **1a** and 236 mg (0.83 mmol) of **7**. Yield 164 mg (34%) of **16** as a purple powder, m.p. 140°C. − IR (CH_3OH): $\tilde{\nu}$(CO) = 1910 cm^{-1} m, 1937 s, 2058 m.

17: This compound was prepared in the same way as described above, from 303 mg (0.85 mmol) of **1a** and 316 mg (0.85 mmol) of **8**. Yield 206 mg (36%) of **17** as a red-brown powder, m.p. 145°C. − IR (CH_3OH): $\tilde{\nu}$(CO) = 1902 cm^{-1} m, 1929 s, 2058 m.

[18a]PF_6 from 1a: 149 mg (0.42 mmol) of **1a** and 169 mg (0.83 mmol) of **3** were stirred in 50 mL of methanol at 50°C for 2 h. After a hot filtration, 68 mg (0.42 mmol) of NH_4PF_6 was added and the mixture stirred at 50°C for 30 min. After filtration, the solvent was removed in vacuo, the residue taken up in 30 mL of dichloromethane, the solution filtered and then layered with 60 mL of petroleum ether (b.p. 60−70°C). 161 mg (44%) of [**18a**]PF_6 was separated as brown crystals, m.p. 180°C (dec.), which were filtered off, washed with 20 mL of petroleum ether and dried in a stream of nitrogen. − IR (CH_2Cl_2): $\tilde{\nu}$(CO) = 2024 cm^{-1} s, 2065 s.

[18a]ClO_4: This compound was prepared in the same way as described above, from 101 mg (0.28 mmol) of **1a**, 115 mg (0.57 mmol) of **3** and 30 mg (0.28 mmol) of $LiClO_4$. Yield 122 mg (52%) of [**18a**]ClO_4, brown crystals, m.p. 180°C (dec.). − IR (CH_2Cl_2): $\tilde{\nu}$(CO) = 2024 cm^{-1} s, 2065 s.

[18a]SbF_6: This compound was prepared in the same way as described above, from 150 mg (0.42 mmol) of **1a**, 170 mg (0.84 mmol) of **3** and 109 mg (0.42 mmol) of $NaSbF_6$. Yield 167 mg (41%) of [**18a**]SbF_6, brown crystals, m.p. 180°C (dec.). − IR (CH_2Cl_2): $\tilde{\nu}$(CO) = 2024 cm^{-1} s, 2065 s.

[18a]BPh_4: This compound was prepared in the same way as described above, from 175 mg (0.49 mmol) of **1a**, 199 mg (0.98 mmol) of **3** and 167 mg (0.49 mmol) of $NaBPh_4$. Yield 219 mg (43%) of [**18a**]BPh_4, brown powder, m.p. 165°C (dec.). − IR (CH_2Cl_2): $\tilde{\nu}$(CO) = 2024 cm^{-1} s, 2065 s.

[18a]PF_6 from 2a: 230 mg (0.56 mmol) of **2a** and 41 mg (1.12 mmol) of **9** in 50 mL of methanol were stirred at room temp. for 12 h. 92 mg (0.56 mmol) of NH_4PF_6 was added, the mixture stirred for another 5 h and then filtered. The filtrate was concentrated to dryness, the residue taken up in 20 mL of dichloromethane, the solution filtered and the filtrate layered with 60 mL of petroleum ether (b.p. 60−70°C). The resulting precipitate consisted of **3** and

Table 5. Analytical characterization

	Empirical formula Molecular mass	Analyses calcd./found C	 H	 N
[**12**]PF_6	$C_{60}H_{55}F_6FeN_3O_5P_3Ru$	57.11	4.39	3.33
	1261.94	56.61	4.32	3.28
[**12**]SbF_6	$C_{60}H_{55}F_6FeN_3O_5P_2RuSb$	53.28	4.10	3.11
	1352.71	53.19	4.04	3.14
[**13a**]ClO_4	$C_{48}H_{43}ClFe_2N_3O_6P_2$	59.62	4.48	4.35
	966.98	59.38	4.56	4.36
[**13a**]PF_6	$C_{48}H_{43}F_6Fe_2N_3O_2P_2$	56.94	4.28	4.15
	1012.49	56.66	4.26	4.13
[**13a**]BPh_4	$C_{72}H_{63}BFe_2N_3O_2P_2$	72.87	5.35	3.54
	1186.76	72.66	5.28	3.53
[**13b**]PF_6	$C_{50}H_{47}F_6Fe_2N_3O_4P_3$	55.99	4.42	3.92
	1072.54	55.24	4.47	3.98
[**13b**]SbF_6	$C_{50}H_{47}F_6Fe_2N_3O_4P_2Sb$	51.62	4.07	3.61
	1163.32	50.75	4.07	3.64
[**14**]ClO_4	$C_{58}H_{49}ClFeN_3O_6P_2Ru$	61.20	4.34	3.69
	1138.36	60.38	4.28	3.74
[**14**]PF_6	$C_{58}H_{49}F_6FeN_3O_2P_3Ru$	58.84	4.17	3.55
	1183.87	58.65	4.07	3.51
[**14**]SbF_6	$C_{58}H_{49}F_6FeN_3O_2P_2RuSb$	54.65	3.87	3.30
	1274.65	54.48	3.72	3.22
[**14**]BPh_4	$C_{82}H_{69}BFeN_3O_2P_2Ru$	72.52	5.12	3.09
	1358.14	72.15	5.07	3.09
15	$C_{22}F_{14}CrFeN_3O_7$	48.91	2.61	7.78
	540.21	48.78	2.61	7.62
16	$C_{22}H_{14}FeMoN_3O_7$	45.23	2.42	7.19
	584.16	45.32	2.30	6.44
17	$C_{22}H_{14}FeN_3O_7W$	39.32	2.10	6.25
	672.07	40.30	2.34	6.08
[**18a**]PF_6	$C_{32}H_{24}F_6Fe_3N_4O_6P$	44.02	2.77	6.42
	873.07	44.88	3.05	6.12
[**18a**]ClO_4	$C_{32}H_{24}ClFe_3N_4O_{10}$	46.44	2.92	6.77
	827.56	46.18	2.93	6.53
[**18a**]SbF_6	$C_{32}H_{24}F_6Fe_3N_4O_6Sb$	39.88	2.51	5.81
	963.84	41.60	2.52	5.92
[**18a**]BPh_4	$C_{56}H_{44}BFe_3N_4O_6$	64.22	4.66	5.98
	1047.34	63.20	4.13	6.03
[**18b**]SbF_6	$C_{34}H_{28}F_6Fe_3N_4O_8Sb\cdot$ 1.5 CH_2Cl_2	37.04	2.71	4.87
	1151.30	36.74	2.93	5.77
[**19a**]PF_6	$C_{80}H_{72}F_6Fe_3N_4O_2P_5\cdot$ 2 CH_3OH	60.72	4.97	3.45
	1621.96	59.67	4.73	3.50
[**20a**]PF_6	$C_{100}H_{84}F_6FeN_4O_2P_5Ru_2\cdot$ 1.5 CH_3OH	62.56	4.65	2.88
	1948.70	62.10	4.57	2.91
[**20a**]SbF_6	$C_{100}H_{84}F_6FeN_4O_2P_4Ru_2Sb\cdot$ 1.5 CH_3OH	59.78	4.45	2.75
	2039.47	59.11	4.25	2.76
[**21**]PPh_4	$C_{52}H_{34}Cr_2FeN_4O_{12}P$	56.90	3.12	5.10
	1097.67	55.78	3.30	4.82
[**22**]PPh_4	$C_{52}H_{34}FeMo_2N_4O_{12}P$	52.68	3.89	4.73
	1185.56	52.63	3.11	3.75
[**23**]PPh_4	$C_{52}H_{34}FeN_4O_{12}PW_2$	45.88	2.52	4.12
	1361.38	46.70	2.75	3.81

[**18a**]PF_6. After three crystallizations from dichloromethane/petroleum ether (1:3), 134 mg (55%) of pure [**18a**]PF_6 was obtained.

[18b]SbF_6 from 1b: This compound was prepared in the same way as described above for [**18a**]PF_6, from 155 mg (0.37 mmol) of **1b**, 151 mg (0.74 mmol) of **3** and 96 mg (0.37 mmol) of $NaSbF_6$. Yield 116 mg (27%) of [**18b**]$SbF_6 \cdot 1.5\ CH_2Cl_2$ as a dark brown powder with m.p. 180°C (dec.). − IR (CH_2Cl_2): $\tilde{\nu}$(CO) = 2014 cm^{-1} s, 2060 s.

[18b]SbF_6 from 2b: This compound was prepared in the same way as described above for [**18a**]PF_6, from 235 mg (0.50 mmol) of **2b**, 396 mg (1.01 mmol) of **9** and 130 mg (0.50 mmol) of $NaSbF_6$. Yield 125 mg (43%) of [**18b**]$SbF_6 \cdot 1.5\ CH_2Cl_2$.

[19a]PF_6: This compound was prepared in the same way as described above for [**18a**]PF_6, from 115 mg (0.28 mmol) of **2a**, 358 mg (0.56 mmol) of **10** and 46 mg (0.28 mmol) of NH_4PF_6. Yield 74 mg (33%) of [**19a**]$PF_6 \cdot 2\ CH_3OH$ as black crystals with m.p. 180°C (dec.).

[19b]SbF_6: This compound was prepared in the same way as described above for [**18a**]PF_6, from 225 mg (0.48 mmol) of **2b**, 614 mg (0.96 mmol) of **10** and 124 mg (0.48 mmol) of $NaSbF_6$. The recrystallization procedure yielded 50 mg (15%) of [**19b**]SbF_6 as a black powder that contained ca. 10% of impurities.

[20a]PF_6 from 1a: This compound was prepared in the same way as described above for [**12**]PF_6, from 100 mg (0.28 mmol) of **1a**, 401 mg (0.56 mmol) of **5** and 46 mg (0.28 mmol) of NH_4PF_6. Yield 84 mg (15%) of [**20a**]$PF_6 \cdot 1.5\ CH_3OH$ as black crystals of m.p. 190°C (dec.).

[20a]SbF_6: This compound was prepared in the same way as described above, from 150 mg (0.42 mmol) of **1a**, 601 mg (0.84 mmol) of **5** and 109 mg (0.42 mmol) of $NaSbF_6$. Yield 125 mg (15%) of [**20a**]$SbF_6 \cdot 1.5\ CH_3OH$, black crystals, m.p. 190°C (dec.).

[20a]PF_6 from 2a: 230 mg (0.56 mmol) of **2a** and 813 mg (1.12 mmol) of **11** in 50 mL of methanol were stirred at room temp. for 12 h. 92 mg (0.56 mmol) of NH_4PF_6 was added and the mixture stirred for another 5 h. After filtration, the filtrate was kept in a refrigerator, which led to the precipitation of a small amount of [**14**]PF_6. Slow concentration of the remaining solution yielded 135 mg (25%) of [**20a**]$PF_6 \cdot 1.5\ CH_3OH$, which was filtered off, washed with 20 mL of ether and dried in a stream of nitrogen.

[20b]SbF_6: This compound was prepared in the same way as described above for [**18a**]PF_6, from 225 mg (0.48 mmol) of **2b**, 696 mg (0.96 mmol) of **11** and 124 mg (0.48 mmol) of $NaSbF_6$. Yield 75 mg (14%) of crude [**20b**]SbF_6 as a black powder that contained ca. 15% of impurities.

[21]PPh_4: 200 mg (0.56 mmol) of **1a**, 271 mg (1.13 mmol) of **6** and 50 mL of methanol were stirred at 50°C for 2 h. After cooling to room temperature, the precipitate of **15** was filtered off. The filtrate was treated with 211 mg (0.56 mmol) of PPh_4Cl and stirred for 30 min at 50°C. After filtration, the solution was concentrated to dryness, the residue taken up in 20 mL of dichloromethane and layered with 50 mL of petroleum ether (b.p. 60−70°C). Within a few days, 135 mg (22%) of [**21**]PPh_4 had precipitated as dark purple needles, m.p. 135°C (dec.), which were filtered off, washed with 20 mL of petroleum ether and dried in a stream of nitrogen. − IR (CH_3OH): $\tilde{\nu}$(CO) = 1905 cm^{-1} m, 1935 s, 2058 m.

[22]PPh_4: This compound was prepared in the same way as described above for [**21**]PPh_4, from 200 mg (0.56 mmol) of **1a**, 319 mg (1.12 mmol) of **7** and 210 mg (0.56 mmol) of PPh_4Cl. Yield 175 mg (26%) of [**12**]PPh_4, red-brown needles, m.p. 150°C (dec.). − IR (CH_3OH): $\tilde{\nu}$(CO) = 1910 cm^{-1} m, 1938 s, 2059 m.

[23]PPh_4: This compound was prepared in the same way as described above for [**21**]PPh_4, from 200 mg (0.56 mmol) of **1a**, 417 mg (1.12 mmol) of **8** and 210 mg (0.56 mmol) of PPh_4Cl. Yield 163 mg (21%) of [**23**]PPh_4, brown powder, m.p. 140°C (dec.). − IR (CH_3OH): $\tilde{\nu}$(CO) = 1904 cm^{-1} m, 1930 s, 2057 m.

Structure Determinations:[22] The crystals were obtained directly from the reaction solutions. Diffraction data were recorded at room

Table 6. Crystallographic details

	[**12**]SbF_6	[**13a**]PF_6	[**13a**]BPh_4	[**20a**]PF_6·1.5 MeOH
Empirical formula	$C_{60}H_{55}F_6FeN_3O_5P_2RuSb$	$C_{96}H_{86}F_{12}Fe_4N_6P_4P_6$	$C_{144}H_{126}B_2Fe_4N_6O_4P_4$	$C_{100}H_{84}F_6FeN_4O_2P_5Ru_2$· 1.5 CH_3OH
Molecular mass	1352.7	2024.9	2373.4	1948.7
Crystal size [mm]	0.5 × 0.5 × 0.2	0.8 × 0.4 × 0.2	0.7 × 0.5 × 0.2	0.6 × 0.4 × 0.4
Space group	$P2_1/n$	$P-1$	$P-1$	$P-1$
Z	4	1	1	2
a [Å]	14.128(4)	12.487(3)	12.679(2)	14.458(3)
b [Å]	27.902(3)	13.345(3)	14.676(2)	15.178(3)
c [Å]	14.931(3)	15.029(3)	17.490(2)	22.412(4)
α [°]	90	108.27(2)	101.92(1)	80.24(3)
β [°]	100.74(2)	100.94(2)	90.14(1)	71.08(3)
γ [°]	90	94.07(2)	106.64(1)	89.55(3)
V [$Å^3$]	5783(2)	2312.0(9)	3044.4(7)	4579(1)
d(calcd.) [g cm^{-3}]	1.55	1.45	1.30	1.41
μ(Mo-$K_α$) [mm^{-1}]	1.10	0.80	0.58	0.64
hkl range	h: 0 to 17 k: 0 to 34 l: −18 to 18	h: −14 to 14 k: −15 to 15 l: 0 to 17	h: −14 to 0 k: −17 to 17 l: −20 to 21	h: −18 to 0 k: −18 to 18 l: −27 to 26
Refl. measd.	11903	8342	11349	19349
Indep. refl.	11357	8009	10835	18583
Obs. refl. [$I > 2\ σ(I)$]	6914	2996	5363	12496
Parameters	712	578	739	1117
Refl. refined	11357	8009	10835	18583
R_1 (obs.refl.)	0.079	0.118	0.065	0.048
wR_2 (all refl.)	0.280	0.454	0.167	0.137
Residual el. density [$e/Å^3$]	+1.5 −1.3	+1.1 −0.9	+0.8 −0.4	+1.1 −1.1

temperature using the ω/2θ technique with a Nonius CAD4 diffractometer fitted with a molybdenum tube (K, $\lambda = 0.7107$ Å) and a graphite monochromator. Empirical absorption corrections based on ψ scans were applied. The structures were solved with direct methods and refined anisotropically with the SHELX program suite.[23] Hydrogen atoms were included with fixed distances and isotropic temperature factors 1.2 times those of their attached atoms. Parameters were refined against F^2. The R values are defined as $R_1 = \Sigma|F_o - F_c|/\Sigma F_o$ and $wR_2 = \{\Sigma[w(F_o^2 - F_c^2)^2]\Sigma[w(F_o^2)^2]\}^{1/2}$. Drawings were produced with SCHAKAL.[24] Table 6 lists the crystallographic data.

Acknowledgments

This work was supported by the Deutsche Forschungsgemeinschaft (Graduiertenkolleg "Ungepaarte Elektronen") and by the Fonds der Chemischen Industrie.

[1] N. Zhu, H. Vahrenkamp, *Chem. Ber.* **1997**, *130*, 1241−1252.
[2] G. N. Richardson, U. Brand, H. Vahrenkamp, *Inorg. Chem.* **1999**, *38*, 3070−3079.
[3] H. Vahrenkamp, A. Geiß, G. N. Richardson, *J. Chem. Soc., Dalton Trans.* **1997**, 3643−3651.
[4] N. Zhu, H. Vahrenkamp, *J. Organomet. Chem.* **1999**, *573*, 67−72.
[5] G. N. Richardson, H. Vahrenkamp, *J. Organomet. Chem.*, in print.
[6] A. Geiß, M. Keller, H. Vahrenkamp, *J. Organomet. Chem.* **1997**, *541*, 441−443.
[7] M. Hanack, J. Metz, *J. Am. Chem. Soc.* **1983**, *105*, 828−830.
[8] M. D. Hobday, T. C. Smith, *Coord. Chem. Rev.* **1972**, *9*, 311−337.
[9] M. Gulotti, L. Casella, A. Pasini, R. Ugo, *J. Chem. Soc., Dalton Trans.* **1977**, 339−345.
[10] M. Gerloch, F. E. Mabbs, *J. Chem. Soc.* **A 1967**, 1900−1908.
[11] M. Calligaris, G. Nardin, L. Randaccio, *Coord. Chem. Rev.* **1972**, *7*, 385−403.
[12] Y. Nishida, S. Oshio, S. Kida, *Chem. Lett.* **1975**, 79−80.
[13] H. J. Buser, D. Schwarzenbach, W. Peter, A. Ludi, *Inorg. Chem.* **1977**, *16*, 2704−2710.
[14] M. J. Scott, R. H. Holm, *J. Am. Chem. Soc.* **1994**, *116*, 11357−11367.
[15] F. L. Atkinson, A. Christophides, N. G. Connelly, H. J. Lawson, A. C. Loyns, A. G. Orpen, G. M. Rosair, G. H. Worth, *J. Chem. Soc., Dalton Trans.* **1993**, 1441−1450; N. C. Brown, G. B. Carpenter, N. G. Connelly, J. G. Crossley, A. Martin, A. G. Orpen, L. Rieger, P. H. Rieger, G. Worth, *J. Chem. Soc., Dalton Trans.* **1996**, 3977−3984.
[16] M. Zhou, W. Pfennig, J. Steiger, D. van Egen, A. B. Bocarsly, *Inorg. Chem.* **1990**, *29*, 2456−2466. Y. Wu, C. Cohran, A. B. Bocarsly, *Inorg. Chim. Acta* **1994**, *226*, 251−258.
[17] B. J. Coe, T. J. Meyer, P. S. White, *Inorg. Chem.* **1995**, *34*, 3600−3609.
[18] C. J. O′Connor, *Prog. Inorg. Chem.* **1982**, *29*, 203−283.
[19] W. M. Reiff, G. J. Long, W. A. Baker, *J. Am. Chem. Soc.* **1968**, *90*, 6347−6351.
[20] Y. Nishida, S. Oshio, S. Kida, *Bull. Chem. Soc. Jpn.* **1977**, *50*, 119−122.
[21] N. Zhu, J. Pebler, H. Vahrenkamp, *Angew. Chem.* **1996**, *108*, 984−985; *Angew. Chem. Int. Ed. Engl.* **1996**, *35*, 894−895.
[22] The crystallographic data of the structures described in this paper were deposited with the Cambridge Crystallographic Data Centre as supplementary publication no. CCDC-115536 ([**12**]SbF_6), -115537 ([**13a**]PF_6), -115538 ([**13a**]BPh_4) and 115539 ([**20a**]PF_6)] Copies of these data are available free of charge from CCDC, 12 Union Road, Cambridge CB2 1EZ (Fax: int. + 44-1223/336-033; E-mail: deposit@ccdc.cam.ac.uk).
[23] G. M. Sheldrick, *SHELX-86* and *SHELXL-93*, Programs for Crystal Structure Determination, Universität Göttingen, **1986** and **1993**.
[24] E. Keller, *SCHAKAL for Windows*, Universität Freiburg, **1998**.
Received March 9, 1999
[I99096]

Kinetics and Mechanism of the Outer-Sphere Oxidation of Horse-Heart Cytochrome *c* by an Anionic Chromium(v) Complex – Kinetic Evidence for Precursor Formation and a Late Electron-Transfer Transition State

Manuela Körner[a] and Rudi van Eldik*[a]

Keywords: Cytochrome *c* / Chromium(v) / Saturation kinetics / Separation of K and k_{ET} / Volume profile / Kinetics

The irreversible outer-sphere electron-transfer reaction between *trans*-bis(2-ethyl-2-hydroxybutanoato(2–))oxochromate(v) and cytochrome c^{II} was investigated as a function of pH, concentration, temperature and pressure. The plot of the observed pseudo-first order rate constant as a function of the Cr^{V} concentration shows a clear trend towards saturation at higher Cr^{V} concentrations, from which the precursor formation constant and the electron-transfer rate constant could be separated (K = 37 ± 5 M^{-1} and k_{ET} = 1510 ± 180 s^{-1} at pH 4.8 and 279 K). In the low Cr^{V} concentration range the second-order electron-transfer rate contants were measured as a function of temperature (ΔH^{+} = 20.9 ± 0.6 kJ mol^{-1}; ΔS^{+} = –79.9 ± 2.1 J K^{-1} mol^{-1}; ΔG^{+} (279 K) = 43.2 kJ mol^{-1}). High-pressure experiments were performed at two different pH values. The kinetic (stopped-flow) and thermodynamic (electrochemical) measurements as a function of pressure enabled the construction of a volume profile for the system at 279 K. The activation volumes for the redox process are –9.2 ± 0.2 (pH 5.0) and –11.1 ± 0.8 cm^3 mol^{-1} (pH 4.7), and the overall reaction volumes were estimated to be –7 ± 2 (pH 5.0) and –10 ± 2 cm^3 mol^{-1} (pH 4.7) . The transition state of the redox reaction lies to a large extent on the product side and can be described as "late". The results are discussed in comparison to earlier measurements using cobalt and ruthenium complexes as reaction partners for cytochrome *c*.

Introduction

Cytochrome *c* typically undergoes outer-sphere electron-transfer reactions with metal complexes such as $Co(phen)_3^{2+/3-}$, $Co(terpy)_2^{2+/3+}$, or $Ru(NH_3)_5py^{2+/3+}$ (phen = 1,10-phenanthroline; terpy = 2,2′:6′,2′′-terpyridine).[1–3] This type of mechanism includes the formation of an outer-sphere precursor complex as a result of electrostatic interactions (Equation 1), a subsequent rate-determining electron-transfer step k_{ET} (Equation 2), and the dissociation of the successor complex to the final redox products (Equation 3).

Under pseudo-first-order conditions, i.e. at least a 10-fold excess of one of the reactants (viz. Red), and under the condition that the reaction proceeds to completion, this general mechanism leads to the rate law given by Equation 4.

For most systems K[Red] << 1, since the reactants are of similar charge, such that K is very small. Under these circumstances, the measured second-order rate constants represent $K \cdot k_{ET}$. If K[Red] >> 1, then the observed rate constants become independent of the [Red] at high concentrations of Red and the limiting rate constant k_{ET} is reached. In the case of highly negatively charged $Fe(CN)_6^{4-/3-}$ ions, saturation kinetics for the reaction with cytochrome were reported.[4] However, in later work it was demonstrated that the interpretation of the observed saturation kinetics was complicated by the fact that the reaction is reversible.[5] This led to a significant intercept in the plots of k_{obs} versus concentration, such that the saturation in k_{obs} at high concentrations could not be observed anymore.

$$Ox + Red \underset{}{\overset{K}{\rightleftharpoons}} Ox/Red \quad (1)$$

$$Ox/Red \xrightarrow{k_{ET}} Ox^{-}/Red^{+} \quad (2)$$

$$Ox^{-}/Red^{+} \overset{K_{Diss}}{\rightleftharpoons} Ox^{-} + Red^{+} \quad (3)$$

$$k_{obs} = \frac{K \cdot k_{ET}[Red]}{1 + K[Red]} \quad (4)$$

In principle, it should be possible to tune the extent of precursor formation by selecting reactants of high and opposite charge. This has been attempted in a number of cases,[5–7] but to our knowledge real rate saturation has only been found in studies of the reduction of cytochrome *c* by chromous ion and dithionite.[8][9] In all other cases, the observed second-order rate constant for the outer-sphere mechanism represents the product $K \cdot k_{ET}$, and values of K and k_{ET} can only be separated by using a theoretical approach. With the aid of the Fuoss Equation,[10][11] a precursor formation constant of 3 M^{-1} for the reaction of cytochrome *c* with positively charged metal complexes such as $Ru(NH_3)_5py^{2+/3+}$, and a value of 200 M^{-1} for the reaction with $Fe(CN)_6^{4-/3-}$ was calculated.

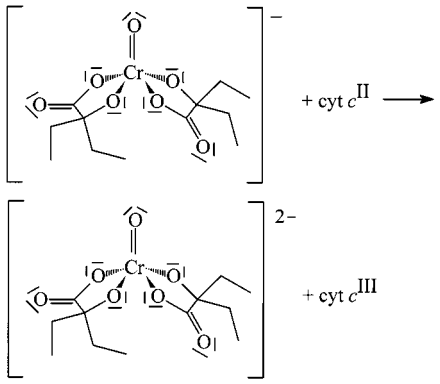
In our earlier work we have studied the outer-sphere electron-transfer reactions between cytochrome *c* and complexes of the type $Ru(NH_3)_5X^{2+/3+}$ (X = ammonia, pyridine, 4-ethyl-pyridine, isonicotinamide and 3,5-lutidine), as well as a series of chelated Co(II/III) diimine complexes.[12–14] In these systems precursor formation was so weak that K and k_{ET} could not be separated kinetically.

[a] Institute for Inorganic Chemistry, University of Erlangen-Nürnberg,
Egerlandstraße 1, D-91058 Erlangen, Germany
Fax: (internat.) +49(0)9131/85–27387
E-mail: vaneldik@chemie.uni-erlangen.de

 © WILEY-VCH Verlag GmbH, D-69451 Weinheim, 1999 1434–1948/99/1010–1805 $ 17.50+.50/0

However, the driving force of these reactions was so low that the kinetics of these redox reactions could be studied in both directions. This enabled us to construct volume profiles from high-pressure kinetic and thermodynamic data for the reversible electron-transfer processes, from which information on the location of the transition state in terms of volume changes along the reaction coordinate could be obtained. The volume profiles turned out to be highly symmetrical with the transition state located approximately halfway between the reactant and product states. The overall volume changes could be shown to be mainly due to intrinsic and solvational volume changes on the redox partner of cytochrome *c*, since cytochrome *c* itself undergoes almost no volume change during the electron-transfer process.[15]

In the present study we have selected an anionic Cr(v) complex, *trans*-bis(2-ethyl-2-hydroxybutanoato(2−))oxochromate(v), as the redox partner for cytochrome *c*. This complex has several negatively charged donor centers that could interact in a specific way with the positive charges on the surface of cytochrome *c* in order to enhance precursor formation. In solution, Cr^{V} species are often intermediates in Cr^{vi} oxidations of organic and biological substrates, e.g. they react rapidly with DNA. There is evidence for implicating Cr^{V} species as carcinogens in biosystems featering interactions of ribonucleotides with added chromate.[16−19] The isolation of relatively stable Cr^{V} complexes enabled detailed studies into the structures and chemistry of Cr(v).[20−23] Cr^{IV} has an even more rare oxidation state. In aqueous media alkoxo and porphyrinato complexes of Cr^{IV} are generally unstable, while diperoxo triamines $[Cr^{IV}(O_2)_2(NR_3)_3]$ are stable in water for several hours in acidic media.[24−26] To stabilize the complex used in this study in aqueous solution, the ligand 2-ethyl-2-hydroxybutyric acid was used in excess.[27] The overall redox reaction is given in Scheme 1.



Scheme 1. Reaction between *trans*-bis(2-ethyl-2-hydroxybutanoato(2−))oxochromate(V) and horse heart cytochrome c^{II}

Higher-valent metallo-oxoporphyrins of iron, manganese and chromium are essential for understanding the mechanisms of enzymatic pathways, e.g. dealing with the oxidation of metalloporphyrins by hydroperoxides in aqueous solution, and with the alkene epoxidation by higher-valent metallo-oxoporphyrins.[28] The driving force for studying metalloporphyrin-catalyzed reactions is to develop synthetic species which are able to reproduce and mimick the different heme enzyme-mediated reactions like oxygenation, oxidation, oxidative chlorination, and dismutation.[29] The result of ligand-exchange chemistry in water[30][31] and with quinic acid in methanol[32] showed that 2-hydroxy acids are preferred strongly to 1,2-diols for binding to Cr^{V}. Since 2-hydroxy acids, such as citrate and lactate, are present in cells, they may bind to the Cr^{V} that is produced intracellularly by reduction of carcinogenic Cr^{VI}. They even may show preference for binding to Cr^{V}, with respect to 1,2-diol ligands, such as ascorbate, sugars and their derivatives. The biologically relevant analogues to *trans*-bis(2-ethyl-2-hydroxybutanoato(2−))oxochromate(v) are likely to be one type of the Cr^{V} species present in the cells that are transformed genetically by exposure to Cr^{VI}. This justifies the need to study the reactions of well-characterized model 2-hydroxy acid complexes with DNA.[18][20]

Indeed the outer-sphere interaction of the redox partners turned out to be significant and could be accounted for theoretically. In addition, the volume profile constructed for the electron-transfer process clearly reveals a nonsymmetrical nature with respect to the location of the transition state, from which it can be concluded that the process is characterized by a "late" (product-like) transition state. This can be accounted for in terms of the effective precursor complex-formation found for the present system, as compared to the absence of such precursor formation in the case of the ruthenium and cobalt complexes studied before.[12−14]

Results

Kinetic Studies

The redox reaction was studied under pseudo-first order conditions. The cytochrome concentration was throughout 0.025 mM and the chromium complex in at least a 10-fold excess. A typical absorbance-time trace is shown in Figure 1.

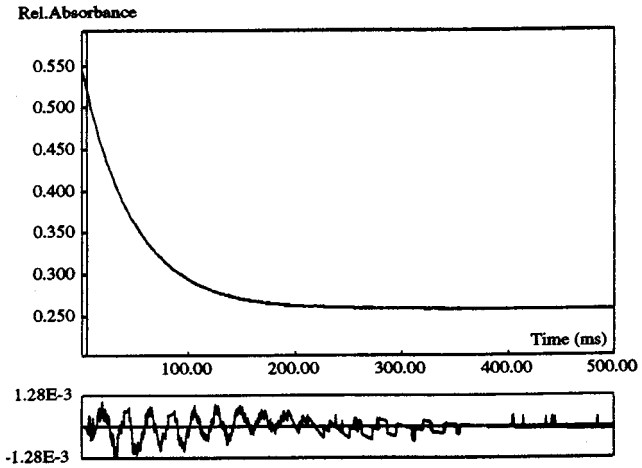


Figure 1. Typical absorbance-time trace fitted with one-exponential decay (k_{obs} = 20.9 ± 0.009 s^{-1}) for [Cr^{V}] = 0.30 mM, pH = 4.8, [L] = 0.0054 M, T = 15°C, λ = 550 nm

Aqueous acetate buffer solutions in the pH range 3.9 to 5.2 were used for the pH-dependence study reported in

Table 1. Between pH 4.6 and 5.0 the rate remains constant, whereas at pH 4.3 the reaction is accelerated by a factor of 1.5. The concentration dependence (Figure 2) was investigated at pH 4.8, and up to a 400-fold excess of Cr^V was used. In order to guarantee the stability of the chromium complex an excess of free ligand was added to the reaction medium. The free ligand concentration was increased even more in another experiment (Figure 2) to check whether there might be some aquation of the chromium complex accompanied by direct binding to cytochrome. These measured points did not differ at all from the former experiments and therefore an inner-sphere mechanism can be excluded.

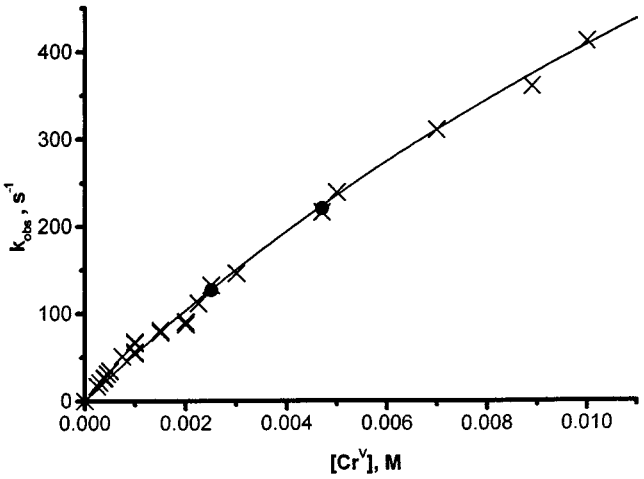


Figure 2. Observed pseudo-first-order rate constant as a function of chromium complex concentration; (×) measured data, except for the one-fold weighted point (0; 0); conditions: pH 4.8; [HAc] = 0.12 M, [KAc] = 0.20 M, [L] = 0.0054 M, $[LiNO_3]_{max}$ = 0.40 M, I = 0.6 M; 15°C; curve results from the best fit based on the kinetic saturation model, Equation 4; influence of increased free ligand concentration on the rate constant was checked (•) (personal suggestion by P. A. Lay to ensure an outer sphere mechanism and to exclude possible direct binding of the chromium complex to cytochrome); conditions: pH 4.8; [HAc] = 0.12 M, [KAc] = 0.20 M, [L] = 0.10 M, $[LiNO_3]_{max}$ = 0.30 M, I = 0.6 M; 15°C

The observed rate constants clearly show a trend toward saturation at higher Cr^V concentrations. A nonlinear least-square fit of the data according to Equation (4) resulted in $K = 37 \pm 5\ M^{-1}$ and $k_{ET} = 1510 \pm 170\ s^{-1}$ at 288 K. The temperature dependence of the reaction was studied at very low Cr^V concentration, i.e. where a linear correlation between k_{obs} and Cr^V concentration exists. The Eyring plot for the second-order rate constants is given in Figure 3, and the calculated activation parameters are $\Delta H^{\neq} = 20.9 \pm 0.1$ kJ mol^{-1} and $\Delta S^{\neq} = -79.9 \pm 0.2$ J K^{-1} mol^{-1}. All ambient pressure measurements were performed in acetate buffer mostly at pH 4.8.

Measurements at elevated pressure (up to 150 MPa) were performed at two pH values, above and below pH 4.8, in order to check the possible influence of a shift to lower pH values at higher pressure caused by an increase in the dissociation constant of acetic acid with increasing pressure.[45] As a result the pH is not constant during a pressure run. The plots of $\ln k_{obs}$ versus pressure are shown in Figure 4, from which it follows that $\Delta V^{\neq} = -9.2 \pm 0.6$ and -11.1 ± 0.8 cm^3 mol^{-1} at 279 K and pH 5.0 and 4.7, respectively. The more negative number at the lower pH is consistent with our observation mentioned above that the reaction is accelerated in more acidic solutions, as a result of the increased acid strength of the buffer at elevated pressures.

Cytochrome $c^{II/III}$ exhibits a much smaller pressure dependence, and a reaction volume of $+5$ cm^3 mol^{-1} was estimated.[15] Therefore, the observed volume of activation mainly results from volume changes on the chromium complex when it changes its overall charge from -1 to -2 during the reduction by cytochrome c^{II}. This is also demonstrated by the significantly negative activation entropy, which is in line with a significant increase in electrostriction during the electron-transfer process.

Electrochemical Studies

In order to construct a volume profile for an irreversible reaction, the activation volume for the reaction and the overall reaction volume, i.e. the difference between the par-

Table 1. Kinetic data for the electron-ransfer reaction between $O{=}CrL_2^{1-}$ and horse-heart cytochrome c^{II}

T [°C]	pH	p [MPa]	c(Cr^V) [mM]	k_{obs} [s^{-1}]	k_f [M^{-1} s^{-1}]
25.0	5.2	0.1	0.25	$O{=}CrL_2^{1-}$ decomposes	
	5.0			21.28 ± 0.08	85100
	4.8			22.43 ± 0.05	89700
	4.6			21.40 ± 0.09	85600
	4.3			31.4 ± 0.2	125500
	3.9			cytochrome c^{II} oxidizes	
15.0	4.8	0.1	0.25	17.21 ± 0.05	68800
				16.54 ± 0.12	66200
			0.30	21.38 ± 0.07	71300
				21.33 ± 0.05	71100
			0.38	26.32 ± 0.05	69300
			0.40	26.69 ± 0.05	66700
				26.19 ± 0.09	65500
			0.45	31.2 ± 0.2	69300
			0.50	34.20 ± 0.09	68400
				34.52 ± 0.08	69000
				35.90 ± 0.08	70200
			0.75	51.5 ± 0.1	68700
			1.00	54.69 ± 0.09	54700
				56.3 ± 0.1	54700
				68.02 ± 0.12	68000
				66.6 ± 0.2	66600
				66.5 ± 0.2	66500
			1.50	81.0 ± 0.2	54000
				78.7 ± 0.2	52500
			2.00	90.1 ± 0.2	45000
				87.9 ± 0.2	44000
				90.9 ± 0.3	45500
				88.9 ± 0.2	44000
			2.25	112.3 ± 0.4	49900
			2.50	133.0 ± 0.1	53200
			2.50*	127.2 ± 0.2	50800
			3.00	146.6 ± 0.3	48900
			4.70	216.3 ± 1.0	46000
			4.70*	220.6 ± 1.0	46900
			5.00	238.7 ± 1.0	47700
			7.00	310.9 ± 1.3	44400
			8.90	360.7 ± 1.0	40500
			10.0	411.8 ± 2.5	41200
5.0	4.8	0.1	0.25	11.05 ± 0.03	44200
15.0				16.54 ± 0.12	66100
25.0				22.36 ± 0.08	89400
35.0				29.87 ± 0.09	119500

Table 2. Kinetic data for the electron-transfer-reaction between $O{=}CrL_2^{1-}$ and horse heart cytochrome c^{II} (continued)

T [°C]	pH	p [MPa]	C(Cr^V) [mM]	k_{obs} [s^{-1}]	k_f [M^{-1} s^{-1}]
5.0	4.8	0.1	0.40	18.3 ± 0.1	45700
15.0				26.2 ± 0.1	65500
25.0				36.1 ± 0.3	90300
35.0				49.3 ± 0.2	123300
5.5	5.0	6.5	0.25	12.3 ± 0.03	
		25		13.6 ± 0.2	
		35		14.1 ± 0.2	
		60		15.4 ± 0.3	
		95		16.6 ± 0.3	
		125		20.0 ± 0.1	
5.5	4.7	21	0.25	12.9 ± 0.3	
		57		14.1 ± 0.2	
		80		17.5 ± 0.1	
		105		19.2 ± 0.3	
		130		21.1 ± 0.4	
		150		23.9 ± 0.5	

Experimental conditions: [cyt c^{II}] = $2.5 \cdot 10^{-5}$ M: λ = 550 nm. − pH = 5.2; [HAc] = 0.04 M, [KAc] = 0.20 M, [L] = 0.005 M, [$LiNO_3$] = 0.40 M, I = 0.6 M; pH = 5.0; [HAc] = 0.08 M, [KAc] = 0.27 M, [L] = 0.0082 M, $[LiNO_3]_{max}$ = 0.32 M, I = 0.6 M; pH = 4.8; [HAc] = 0.12 M, [KAc] = 0.20 M, [L] = 0.0054 M, $[LiNO_3]_{max}$ = 0.40 M, I = 0.6 M;* pH = 4.8; [HAc] = 0.12 M, [KAc] = 0.20 M, [L] = 0.10 M, $[LiNO_3]_{max}$ = 0.30 M, I = 0.6 M; pH = 4.7; [HAc] = 0.20 M, [KAc] = 0.30 M, [L] = 0.017 M, $[LiNO_3]_{max}$ = 0.31 M, I = 0.6 M; pH = 4.6; [HAc] = 0.20 M, [KAc] = 0.27 M, [L] = 0.017 M, [$LiNO_3$] = 0.31 M, I = 0.6 M; pH = 4.3; [HAc] = 0.40 M, [KAc] = 0.20 M, [L] = 0.012 M, [$LiNO_3$] = 0.39 M, I = 0.6 M; pH = 3.9; [HAc] = 0.40 M, [KAc] = 0.08 M, [L] = 0.011 M, [$LiNO_3$] = 0.51 M, I = 0.6 M;Calculated activation parameters for k_f: $\Delta H^{\neq}$ = 20.9 ± 0.6 kJ mol^{-1}; $\Delta S^{\neq}$ = −79.9 ± 2.1 J K^{-1} mol^{-1}; $\Delta G^{\neq}$ (279 K) = 43.2 kJ mol^{-1}; $\Delta V^{\neq}$ (pH 5.0 and 279 K) = −9.2 ± 0.6 cm^3 mol^{-1}; $\Delta V^{\neq}$ (pH 4.7 and 279 K) = −11.1 ± 0.8 cm^3 mol^{-1}; intercept −(0.1 ± 0.9) s^{-1}, resulting from linear fit in the low-concentration range (0.25−0.50 mM Cr^V); slope (55350 ± 2290) M^{-1} s^{-1}.

Table 3. High-pressure electrochemistry

pH	p [MPa]	E (vs. NHE) [mV]
5.0	0.1	430 ± 1
	22.0	438 ± 1
	49.8	444 ± 1
	75.2	450 ± 1
	95.7	454 ± 1
	125.0	462 ± 1
4.7	14.8	435 ± 1
	24.5	439 ± 1
	49.2	445 ± 1
	73.5	449 ± 1
	95.0	461 ± 1
	123.0	465 ± 1
	146.0	471 ± 1
	165.0	477 ± 1

[Cr^V] = 5.0 mM, T = 5.5°C, reference electrode (Ag/ 0.01 M $AgNO_3$, 1.0 M KNO_3), scan rate 2 mV s^{-1}, $\Delta V_{corr.}$(Ag/Ag+) = −11.9 ± 0.5 cm^3 mol^{-1} (25°C, I = 1.0 M KNO_3).[52]

tial molar volumes of reactant and product species, are required. For the cytochrome $c^{II/III}$ system the partial molar volume difference has already been studied.[15] The difference in partial molar volume for the $Cr^{V/IV}$ system was investigated electrochemically under the same reaction conditions as those selected for the high-pressure stopped-flow experiments. For the electrochemical measurements at

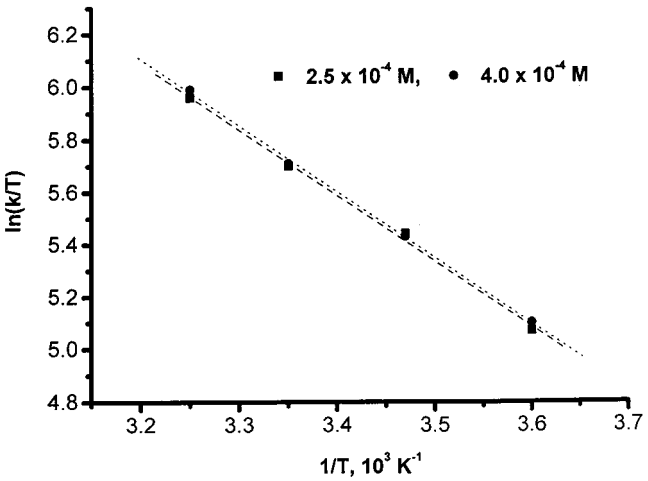


Figure 3. Temperature dependence for 0.25 and 0.40 mM Cr^V complex concentrations at pH 4.8; [HAc] = 0.12 M, [KAc] = 0.20 M, [L] = 0.0054 M, [$LiNO_3$] = 0.40 M, I = 0.6 M

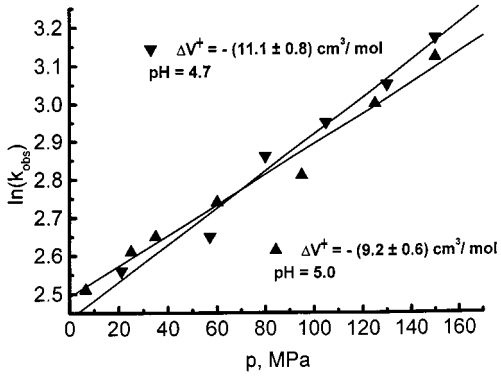


Figure 4. Plot of lnk_{obs} versus pressure. − Conditions: [Cr^V] = 0.25 mM, 279 K; pH = 5.0; [HAc] = 0.08 M, [KAc] = 0.27 M, [L] = 0.0082 M, $[LiNO_3]_{max}$ = 0.32 M, I = 0.6 M; pH = 4.7; [HAc] = 0.20 M, [KAc] = 0.30 M, [L] = 0.017 M, $[LiNO_3]_{max}$ = 0.31 M, I = 0.6 M

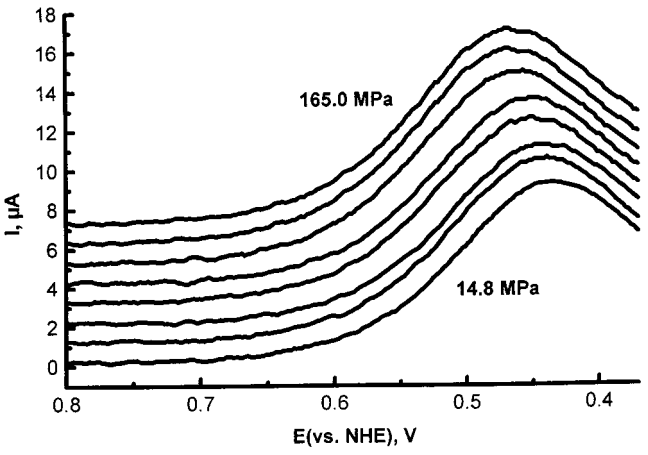


Figure 5. Differential pulse voltammograms of the $Cr^{V/IV}$ couple at pH 4.7 as a function of pressure, recorded at 14.8, 24.5, 49.2, 73.5, 95.0, 146.0 and 165.0 MPa; the traces are offset by arbitrary amounts on the current scale to improve legibility

pressures up to 165 MPa, experiments with CV and DPV were performed. Both techniques are in general comp-

lementary, but DPV showed more reproducible data in the present case.[46,47,48] Figure 5 reports the recorded DPVs as a function of pressure.

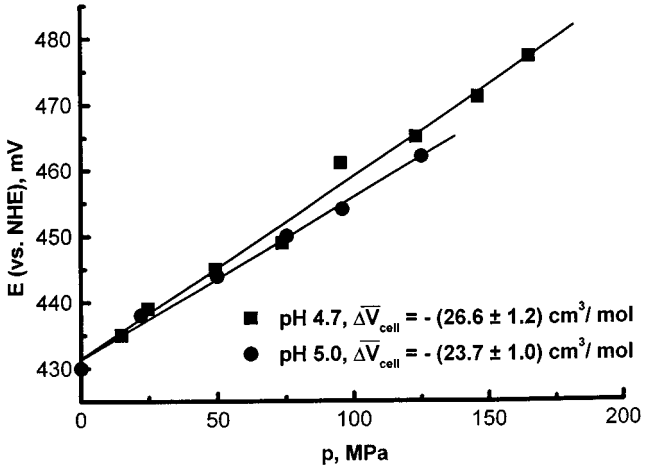


Figure 6. Plot of the redox potential for the $Cr^{V/IV}$ system at pH 5.0 and 4.7 as a function of pressure

The change in redox potential with increasing pressure is moderate, as expected for an overall charge increase from −1 to −2. The volume change associated with the overall cell reaction was estimated from the plot of the measured redox potential as a function of pressure (Figure 6). The measured $E_{1/2}$ value for the redox couple at ambient pressure is in good agreement with data reported by other authors.[49−51] The reaction volume associated with the $Cr^{V/IV}$ redox couple can now be calculated from the cell reaction volume by substracting the volume contribution of the reference electrode $Ag/AgNO_3$ which was shown to be −11.9 ± 0.5 $cm^3\ mol^{-1}$.[52] The resulting reaction volumes are −11.8 ± 0.5 (pH 5.0) and −14.7 ± 0.7 $cm^3\ mol^{-1}$ (pH 4.7), and reflect the overall volume changes arising from the reduction of Cr^V to Cr^{IV}, as well as that caused by a change in the overall charge from −1 to −2. The solvational effects in terms of a significant increase in electrostriction obviously overrule the intrinsic volume changes in order to account for the overall negative reaction volumes.

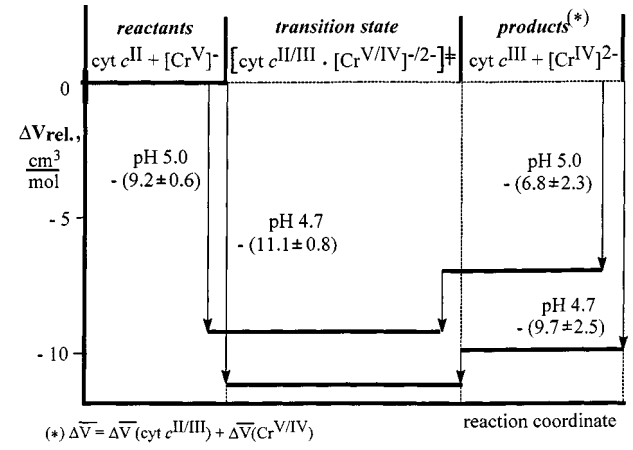


Figure 7. Volume profile for the irreversible reaction of cytochrome c^{II} with *trans*-bis(2-ethyl-2-hydroxybutanoato(2−))oxochromate(V)

The employed complex $[O{=}Cr^V(Lig)_2]^-$ was crystallographically characterized as a five-coordinate oxo compound with a distorted trigonal-bipyramidal geometry.[53] At pH 2.5 to 4.0 in the presence of ligand and buffer, Cr^{IV} solutions suffer perceptible loss within a few minutes due to disproportionation, $2Cr^{IV} \rightarrow Cr^{III} + Cr^V$, and reduction by the parent ligand, $2Cr^{IV}\ Et_2C(OH)COO^- \rightarrow 2Cr^{III} + Et_2C{=}O + CO_2 + H^+$.[25][38] Electrochemical studies have shown that major structural rearrangement follows the electron-transfer process in the Cr^{IV}/Cr^{III} system, but not in the Cr^V/Cr^{IV} couple.[51] The suggestion that a third ligand will enter the coordination sphere at the vacant site on Cr^V was disgarded later on.[35] The formation of six-coordinate forms is much less likely for complexes with the more bulky ligands. The Cr^V complex has a distorted trigonal-bipyramidal geometry, whereas the Cr^{IV} complexes are likely to remain as five-coordinate oxo complexes, like their Cr^V/Cr^V analogues. There is no evidence for Cr^V complexes containing three chelate ligands and such complexes are not expected to form for steric reasons. The redox potential for $Cr^{IV/III}$ is more positive, which means that it is a stronger oxidizing agent than $Cr^{V/IV}$. The quasi-reversible one-electron redox process (corresponding to $Cr^V + e^- \rightleftharpoons Cr^{IV}$) can only be observed at the electrode surface because there is a lack of conversion of Cr^{IV} to Cr^{III} due to an extremely slow electrokinetic process for the reduction of the Cr^{IV} intermediates.[24] Cr^{IV} exists mainly in the form of bis-chelated complexes. The stability of Cr^{IV} complexes exhibits a bell-shaped pH dependence. The region of maximum stability and the corresponding half-life ($[Cr^{IV}]_0$ = 0.1 mM; 25°C) is 30 min at pH ≈ 3. Half-lives were determined from the absorbance changes at 550 nm, where the absorbances of Cr^{III} and Cr^V complexes were negligible in comparison with that of Cr^{IV}.[25] The important difference in the chemical properties of Cr^{IV} and Cr^V is that 2-hydroxy carboxylates are much poorer ligands for Cr^{IV} than for Cr^V. This is probably the result of the lower acidity of the ROH groups bound to Cr^{IV}. Thus, the ROH groups remain largely protonated at pH 2 to 4, whereas those of the corresponding Cr^V complexes are fully deprotonated under these conditions.[25]

Saturation Kinetics

In order to account for the experimentally observed rate constants as a function of the Cr^V concentration, the Fuoss theory was applied.[10] The reaction conditions are water as solvent at 279 K and 0.6 M ionic strength. Even at high ionic strength, the acetate shows no specific binding ability for cytochrome.[74] This should be the same for the ligand, which is added in excess in order to stabilize the complex and is very similar in structure. In addition, the number of protein-bound nitrates, two in the reduced and one in the oxidized form, is independent of the anion concentration.[74] The adopted permittivity leads to a reciprocal Debye-Hückel radius of 2.52 nm.[54] There are three possible positions for negative charges on the Cr^V complex,

viz. the oxo group, the ring carboxylate oxygen, and the carboxylate oxygen, which are all exposed to solvent water. The ring hydroxo group is sterically hindered by the bulky ethyl groups. For the evaluation of the contact radius for the chromium complex, the X-ray structure and different van der Waals radii for oxygen are available.[55,56−58] The contact radius for cytochrome *c* was estimated to be 1.66 nm.[59] A combination of these values result in a contact distance in the range between 1.82 and 2.21 nm. The outer-sphere preequilibrium constant *K* and the associated rate constant k_{ET} were now calculated by varying the possible ionic charge on the cytochrome center. Since the chromium reactant carries an overall charge of −1, and the enzyme has a net charge of +6.5,[59] the product of the ionic charges can adapt theoretical values between −1 and −6.5, depending on to what extent charge is neutralized by the presence of counter ions and local charge effects influence the electron-transfer process. Both *K* and k_{ET} increase more on increasing the contact radius of the chromium complex than on changing the effective ionic charge. On the basis of a 75% agreement between the values calculated with the Fuoss Equation and those obtained in the kinetic measurements, the product of the ionic charges should be at least 1.5 for Cr...C=O, 6.5 for Cr−O and 7.0 for Cr=O. However, the following aspects should also be considered: electrostatic interactions in the precursor complex are assigned to a larger extent to charge localized at the haem crevice than to the sum of all charges;[60][61] lysine 13, 72, 86 and Histidin 33 (at pH values below its pK_a of 6.4) show kinetic relevance for anionic redox partners and a local charge of +3 to +4 on the cytochrome surface was estimated from kinetic measurements as a function of ionic strength.[62−66] Based on this information, conclusions can be reached with respect to the three possible contact radii. The most probable position for charge localization on the chromium complex is the Cr...C=O group, which is more likely than the Cr−O group and in turn much better than the Cr=O position. This is in agreement with some classical explanations.[67] In summary, the results from the kinetic studies are consistent with predictions on the basis of the Fuoss postulations.

The thermal and pressure activation parameters were determined at low Cr^{V} concentrations due to the time resolution of the kinetic equipment, with the result that the observed second-order rate constant is a composite function and represents $K{\cdot}k_{ET}$. The observed entropy and volume of activation are both significantly negative and indicate a highly-structured transition state. More mechanistic insight can be gained from an analysis of the volume profile for the overall process.

Volume Profile

The molar volume change associated with the redox couple cytochrome $c^{II/III}$ was estimated to be +(5.0 ± 0.8) cm^3 mol^{-1}.[15] This value indicates that there is a slight increase in the partial molar volume of cytochrome c^{II} during the oxidation process, even though the overall charge increases from +6.5 to +7.5, which is expected to cause a solvational volume collapse due to an increase in electrostriction. A number of reports in the literature report a more compact structure for the reduced protein as compared to cytochrome c^{III}.[59,68−71] However, the increase in the size of the protein results in the partial accommodation of water molecules from the bulk in the protein framework. A small overall volume increase is therefore obtained.[65] It is assumed that the volume change on cytochrome *c* is the same at pH 5 and 7. Cytochrome does not show any pH dependence in this pH range; deviations only occur at pH ≥ 8.0.[6,12,73] In order to calculate the overall reaction volume, the contribution arising from the $Cr^{V/IV}$ complex has to be added (see Figure 7). We found that a significant volume collapse accompanies this reduction process (see electrochemical studies).

Detailed electrochemical measurements as a function of pressure resulted in a good correlation between the volume changes associated with changes in electrostriction and the change in the overall charge on the complex.[52] As a useful working rule the electrostrictive volume changes by ca. 4 cm^3 mol^{-1} per unit difference in the square of the charge on the oxidized and reduced forms of the complex. In the present case this difference is 3, from which an electrostritive volume collapse of ca. 12 cm^3 mol^{-1} can be predicted. By way of comparison, the experimental values reported for the couples $Fe(phen)(CN)_4^{1-/2-}$ and $Fe(bpy)(CN)_4^{1-/2-}$ are −13.6 and −13.8 cm^3 mol^{-1}, respectively.[52] From this it follows that the solvational volume changes due to a significant increase in electrostriction, represent the major contribution toward the overall negative reaction volumes found in this study. The oxidation of cytochrome c^{II} by the Cr^{v} oxo species is therefore associated with a moderate overall volume decrease of −7 and −10 cm^3 mol^{-1} (see Figure 7). The location of the transition state can be described as "late" in terms of the overall volume change and is close to the product state. This can at present only be related to the efficient precursor formation occurring in the system.

In contrast, the investigated $Co^{III/II}$ and $Ru^{III/II}$ systems referred to in the Introduction show no kinetic evidence for precursor formation and exhibit very similar volume changes for both the forward and reverse electron-transfer reactions.[12−14] The ruthenium complexes exhibit negligible intrinsic volume changes and therefore mainly solvational effects account for the observed volume changes.[12] In the case of the $Co^{III/II}$ systems, there is a volume increase due to a decrease in solvent electrostriction and an intrinsic contribution.[14] Both these systems involve large volume changes, and the transition state lies almost exactly halfway between the partial molar volumes of the reactants and products in the reported volume profiles. This means that the reorganisation in the transition state is very similar for both the forward and back reactions in the reversible electron-transfer process in the absence of significant precursor formation. The nonsymmetrical nature of the volume profile found in the present study must therefore be related to

the effective formation of a precursor species. A similar situation was recently encountered in the volume profiles for a series of intramolecular electron-transfer reactions of ruthenated cytochrome *c* sytems.[72] In that case different possible explanations for the nonsymmetric appearance of the volume profiles were presented. It is our objective in future work to search for redox systems involving cytochrome *c* that will exhibit an even more efficient precursor formation in order to be able to determine a volume profile for the electron-transfer reaction within the precursor species, i.e. under conditions of saturation kinetics where electron transfer is the rate determining step, something that was not possible in the present study.

Conclusions

The outer-sphere electron-transfer reaction between horse-heart cytochrome *c* and anionic trans-bis(2-ethyl-2-hydroxybutanoato(2−))oxochromate showed a clear trend towards rate saturation, which is rather unusual for cytochrome and its interaction with small reaction partners. The precursor formation constant and the electron-transfer rate constant could be separated kinetically. In order to account for the experimentally observed rate constants as a function of the Cr^V concentration, the Fuoss theory was applied. It revealed additional information that the contact between both reactants occurs most probable with the solvent exposed carboxylate oxygen on chromium. Measured activation and reaction volumes at two pH values enabled the construction of a volume profile for the reaction which differs significantly from the symmetric volume profiles reported for outer-sphere electron-transfer reactions of cobalt and ruthenium complexes. Information regarding the location of the reaction coordinate could be obtained.

Experimental Section

Methods: UV/vis spectra were recorded on either a Hewlett−Packard HP8452 or a Shimadzu UV-2101PC spectrophotometer. − IR spectra were measured in KBr disks on a Mattson Polaris 10410R FT-IR spectrometer. − A Bruker ESP 300E X-band spectrometer operating at about 9.5 GHz was used for recording EPR spectra of solutions contained in a quartz flat cell. EPR spectrometer settings were as follows: central field, 3480 G; sweep width, 100 G; microwave power, 10.1 mW; modulation frequency, 100 kHz; modulation amplitude, 0.974 G; receiver gain, 1.25×10^3; conversion time, 20.48 ms; time constant, 10.24 ms; number of scans, 1; temperature 298 K. − The pH of the solutions was measured on a Metrohm 716 DMS Titrino pH-meter. The kinetic traces for the reduction of cytochrome *c* were recorded at 550 nm. The reactions at ambient pressure were followed using an Applied Photophysics SX-18 MV stopped-flow instruments (Leatherhead, UK), to which an online data acquisition system was connected. The kinetic traces, consisting of 1000 points per trace, were collected, stored and fitted on an Acorn 5000 computer using Applied Photophysics software (Leatherhead, UK). In order to observe the progress of the overall reaction, time resolved spectra were recorded on an Applied Photophysics SX-18 MV stopped-flow instrument (Leatherhead, UK) equipped with a J&M TIDAS 16−500 diode array detector (Aalen, Germany). A homemade high-pressure stopped-flow system was used for the high pressure kinetic measurements.[39][40] The kinetic traces consisting of 1000 points per trace, were collected and stored on an IBM-compatible computer using Biologic (Claix, France) software. The rate constants were calculated using the OLIS KINFIT program (Olis, Bogart, Georgia, USA). All Instruments were thermostated to ± 0.1 °C. The kinetic traces showed exellent first-order behavior over 5 half-lives. − In general, all solutions were prepared under nitrogen to avoid complications with dissolved oxygen. All test solutions were protected from light to avoid photoinduced decomposition.[41] The freshly prepared solutions were transferred into the stopped-flow unit using gastight Optima Graf Fortuna glass syringes (Roth). All experiments were performed in acetate buffer of different pH values. − Electrochemical measurements were performed with an EG&G Princeton Applied Research 263 System; the data were stored and fitted using Model 270/250 Research Electrochemistry Software 4.00. For electrochemical measurements at elevated pressure, a homemade, high-pressure cell similar to that described in the literature[42] and thermostated to ± 0.1 °C, was employed. Prior to use, the glassy carbon electrode surface was polished with an aqueous suspension of 3 micron followed by 1 micron alumina (Alfa) on a polishing cloth, followed by rinsing with distilled water and further cleaning with a dry tissue. The Pt plate auxiliary electrode was cleaned in 5 M aqueous HNO_3, rinsed with distilled water and dried with a tissue. The reference electrode consisted of a Ag wire in 0.01 M $AgNO_3$ and 1.0 M KNO_3 solution. The chromium solutions were filled into the electrochemical cell under nitrogen. Nitrogen was passed through the solution for another few minutes to assure that oxygen is absent. The potassium hexacyanoferrate couple was used as external standard. All Differential Pulse Voltammetric (DPV) measurements were performed under the following conditions: pulse height 25 mV, pulse weight 50 ms, scan rate 2 (pH 5.0) and 4 mV s^{-1} (pH 4.7). Voltammograms were scanned in the negative direction. For all analyses and plots, Excel[43] and Origin[44] software was used except when otherwyise stated.

Caution: Cr^V complexes are mutagenic, cleave DNA rapidly *in vitro*, and are potentially carcinogenic.[18][33] Contact with skin and inhalation must be avoided.

Reagents: Horse-heart cytochrome *c* (type VI, Sigma) was purified and reduced as reported before.[13] The concentrations of the cytochrome solutions were determined by UV/vis spectroscopy. Sodium bis(2-ethyl-2-hydroxybutanoato(2−))oxochromate(V) was synthesized following the method of Krumpolc and Rocek and was recrystallized from acetone-chloroform.[34][35] − Anal. calcd for $C_{12}H_{22}CrNaO_8$: C 39.03; H 6.01; found: C 39.58; H 6.44). − The IR spectra shows $\tilde{\nu}$(Cr=O) (cm^{-1}) = 996 (ref. 998, 1000) and $\tilde{\nu}$(C=O) = 1677 (s) (ref. 1660, 1683).[20,36,37] In the UV/vis range the complex exhibited a maximum at 510 nm with an extinction coefficient of 165 M^1 cm^{-1} in aqueous solution, which is in agreement with literature data.[34][35] The X-band EPR spectra of the sample (ca. 0.002 M) in buffer solution of pH 5.0 shows a single main peak g = 1.984 (^{52}Cr, $I = 0$) with four small lines due to the hyperfine coupling with ^{53}Cr ($I = {}^3/_2$, 9.54% natural abundance; hyperfine coupling constant 18.3 Gauss).[20,35,38] − The following chemicals were used in the preparation of the reaction solutions: 2-ethyl-2-hydroxybutyric acid (99%), potassium acetate (KAc) and acetic acid (HAc) (Aldrich), and lithium nitrate (Fluka). All commercial reagents were of analytical grade and were used without further purification. Solutions of Cr^V were prepared by dissolving the synthesized sodium salt of the complex in the buffer solutions under nitrogen directly before use.

Acknowledgments

The authors are gratefull to the Deutsche Forschungsgemeinschaft (Gratuierten Kolleg "Homogener und Heterogener Elektronentransfer") for support of this project.

[1] S. Wherland, H. B. Gray, *Biological Aspects of Inorganic Chemistry*, John Wiley, New York, **1977**, p 289.
[2] G. R. Moore, E. G. S. Eley, G. Williams, *Advances in Inorganic and Bioinorganic Mechanisms* (Ed.: A. G. Sykes), Academic Press, London, **1984**, vol. 3, p 1.
[3] P. L. Drake, R. T. Hartshorn, J. M. McGinnis, A. G. Sykes, *Inorg. Chem.* **1989**, *28*, 1361−1366.
[4] W. G. Miller, M. A. Cusanovitch, *Biophys. Struct. Mech.* **1975**, *1*, 97−111.
[5] J. Butler, D. M. Davies, A. G. Sykes, *J. Inorg. Biochem.* **1981**, *15*, 41−53.
[6] H. L. Hodges, R. A. Holwerda, H. B. Gray, *J. Am. Chem. Soc.* **1974**, 3132−3137.
[7] S. Speh, Ph. D. Thesis, Technical University of Darmstadt, Germany, **1993**.
[8] J. K. Yandell, D. P. Fay, N. Sutin, *J. Am. Chem. Soc.* **1973**, *95*, 1131−1137.
[9] [9a] C. Creutz, N. Sutin, *Proc. Nat. Acad. Sci. U.S.* **1973**, *70*, 1701−1703. [9b] D. O. Lambeth, G. Palmer, *J. Biol. Chem.* **1973**, *248*, 6095−6103.
[10] R. M. Fuoss, *J. Am. Chem. Soc.* **1958**, *80*, 5059−5061.
[11] R. D. Cannon, *Electron Transfer Reactions*, Butterworth,London, **1980**, chapter 4.2.
[12] M. Meier, J. Sun, J. F. Wishart, R. van Eldik, *Inorg. Chem.* **1996**, *35*, 1564−1570.
[13] B. Bänsch, M. Meier, P. Martinez, R. van Eldik, C. Su, J. Sun, S. S. Isied, *Inorg. Chem.* **1994**, *33*, 4744−4749.
[14] M. Meier, R. van Eldik, *Chem. Eur. J.* **1997**, *3*, 39−46.
[15] J. Sun, J. F. Wishart, R. van Eldik, R. D. Shalders, T. W. Swaddle, *J. Am. Chem. Soc.* **1995**, *117*, 2600−2605.
[16] D. M. Goodgame, P. B. Hayman, D. F. Hathaway, *Polyhedron* **1982**, *1*, 497−499.
[17] S. Kawanishi, S. Inove, S. Sand, *J. Biol. Chem.* **1986**, *261*, 5952−5958.
[18] R. P. Farrell, R. J. Judd, P. A. Lay, N. E. Dixon, R. S. U. Baker, A. M. Bonin, *Chem. Res. Toxicol.* **1989**, *2*, 227−229.
[19] R. N. Bose, S. Moghaddas, E. Gelerinter, *Inorg. Chem.* **1992**, *31*, 1987−1994.
[20] R. P. Farrell, P. A. Lay, *Comments Inorg. Chem.* **1992**, *13*, 133−175.
[21] R. Colton, *Coord. Chem. Rev.* **1985**, *62*, 85−130.
[22] M. Mitewa, P. R. Bontchev, *Coord. Chem. Rev.* **1985**, *61*, 241−272.
[23] J. K. Beattie, G. P. Haight, Jr., *Prog. Inorg. Chem.* **1972**, *17*, 93−145.
[24] R. N. Bose, B. Fonkeng, G. Barr-David, R. P. Farrell, R. J. Judd, P. A. Lay, D. F. Sangster, *J. Am. Chem. Soc.* **1996**, *118*, 7139−7144.
[25] R. Codd, P. A. Lay, A. Levina, *Inorg. Chem.* **1997**, *36*, 5440−5448.
[26] E. S. Gould, *Coord. Chem. Rev.* **1994**, *135/136*, 651−684.
[27] N. Rajasekar, R. Subramaniam, E. S. Gould, *Inorg. Chem.* **1983**, *22*, 971−975.
[28] R. D. Arasasingham, T. C. Bruice, *The Activation of Dioxygen and Homogeneous Catalytic Oxidation* (Ed.: D. H. R. Barton), Plenum Press, New York, **1993**, p. 147−169.
[29] B. Meunier, *Chem. Rev.* **1992**, *92*, 1411−1456.
[30] R. Bramley, J.-Y. Ji, P. A. Lay, *Inorg. Chem.* **1991**, *30*, 1557−1569.
[31] M. Charara, B. Sc. Thesis, University of Sydney, Australia, **1988**.
[32] G. Barr-David, M. Charara, R. Codd, R. P. Farrell, J. A. Irwin, P. A. Lay, R. Bramley, S. Brumby, J.-Y. Ji, G. R. Hanson, *J. Chem. Soc., Faraday Trans.* **1995**, *91*, 1207−1216.
[33] C. T. Dillon, P. A. Lay, A. M. Bonin, N. E. Dixon, T. J. Collins, K. L. Kostka, *Carcinogenesis* **1993**, *14*, 1875−1880.
[34] M. Krumpolc, J. Rocek, *J. Am. Chem. Soc.* **1979**, *101*, 3206−3209.
[35] Y.-T. Fanchiang, R. N. Bose, E. Gerinter, E. S. Gould, *Inorg. Chem.* **1985**, *24*, 4679−4684.
[36] R. Bramley, R. P. Farrell, J.-Y. Ji, P. A. Lay, *Aust. J. Chem.* **1990**, *43*, 263−279.
[37] M. Krumpolc, B. G. DeBoer, J. Rocek, *J. Am. Chem. Soc.* **1978**, *100*, 145−153.
[38] M. C. Ghosh, E. Gelerinter, E. S. Gould, *Inorg. Chem.* **1992**, *31*, 702−705.
[39] vanR. Eldik, D. A. Palmer, R. Schmidt, H. Kelm, *Inorg. Chim. Acta* **1981**, *50*, 131−135.
[40] vanR. Eldik, W. Gaede, S. Wieland, J. Kraft, M. Spitzer, D. A. Palmer, *Rev. Sci. Instrum.* **1993**, *64*, 1355−1357.
[41] M. Krumpolc, J. Rocek, *Inorg. Chem.* **1985**, *24*, 617−621.
[42] H. Doine, T. W. Whitcombe, T. W. Swaddle, *Can. J. Chem.* **1992**, *70*, 81−88.
[43] *Excel*, Version 5.0, Microsoft Software, **1993**.
[44] *Origin. Technical Graphics and Data Analysis for Windows*, *Version 4.1*, Microcal Software, Inc., Northampton, MA, **1996**.
[45] Y. Kitamura, T. Itoh, *J. Solution Chem.* **1987**, *16*, 715−725.
[46] J. Osteryoung, *J. Chem. Educ.* **1983**, *60*, 296.
[47] G. A. Mabott, *J. Chem. Educ.* **1983**, *60*, 697.
[48] K. K. Rodgers, S. G. Sligar, *J. Am. Chem. Soc.* **1991**, *113*, 9419−9421.
[49] R. N. Bose, V. D. Neff, E. S. Gould, *Inorg. Chem.* **1986**, *25*, 165−168.
[50] J. M. Eckert, R. J. Judd, P. A. Lay, *Inorg. Chem.* **1987**, *26*, 2189−2191.
[51] R. N. Bose, B. Fonkeng, G. Barr-David, R. P. Farrell, R. J. Judd, P. A. Lay, D. F. Sangster, *J. Am. Chem. Soc.* **1996**, *118*, 7139−7144.
[52] J. I. Sachanidis, R. D. Shalders, P. A. Tregloan, *Inorg. Chem.* **1994**, *33*, 6180−6186.
[53] R. J. Judd, T. W. Hambley, P. A. Lay, *J. Chem. Soc., Dalton Trans.* **1989**, 2205−2210.
[54] H. Landolt, R. Börnstein, A. Eucken, *Zahlenwerte und Fakten aus Physik, Chemie, Astronomie, Geophysik, Technik*, Springer-Verlag; Berlin, **1959**, *II. Band, 6. Teil Elektrische Eigenschaften I*, p 767.
[55] For the carboxylate oxygen the Cr...C=O distance was calculated by using the available bond distances and angles, and assuming that the five-membered chelate ring is planar. Distortion at the ring is negligible.
[56] F. A. Cotton, G. Wilkinson, P. L. Gaus, *Grundlagen der Anorganischen Chemie*, VCH, Weinheim, **1990**, p 97.
[57] R. A. Marcus, *J. Chem. Phys.* **1957**, *26*, 867−871.
[58] A. Bondi, *J. Phys. Chem.* **1964**, *68*, 441−451.
[59] K. Heremanns, M. Bormans, J. Snauwaert, H. Vandersypen, *Faraday Discuss. Chem. Soc.* **1982**, *74*, 343−348.
[60] T. E. Meyer, J. A. Watkins, C. T. Przysiecki, G. Tollin, M. A. Cusanovich, *Biochem.* **1984**, *23*, 4761.
[61] S. K. Chapman, J. D. Sinclair-Day, A.G. Sykes, S. C. Tam, R. J. P. Williams, *J. Chem. Soc. Chem. Commun.* **1983**, 1152−1154.
[62] J. Butler, S. K. Chapman, D. M. Davies, A. G. Sykes, S. H. Speck, N. Osheroff, E. Margoliash, *J. Biol. Chem.*, **1983**, *258*, 6400−6404.
[63] J. Butler, D. M. Davies, A. G. Sykes, W. H. Koppenol, N. Osheroff, E. Margoliash, *J. Am. Chem. Soc.* **1981**, *103*, 469−471.
[64] C. G. S. Eley, G. R. Moore, G. Williams, R. J. P. Williams, *Eur. J. Biochem.* **1982**, *124*, 295−303.
[65] R. Margalit, A. Schejter, *Eur. J. Biochem.* **1973**, *32*, 492−499.
[66] T. Goldkorn, A. Schejter, *J. Biol. Chem.* **1979**, *254*, 12562.
[67] The oxo group shifts electron density to the chromium center (weak back bonding from Cr). The ethyl groups increase the electron density on the carboxylate group (inductive effect).
[68] A. M. Berghuis, G. D. Bryer, *J. Mol. Biol.* **1992**, *223*, 959−976.
[69] Y. Feng, H. Roder, S. W. Englander, *Biochemistry* **1990**, *29*, 3494−3504.
[70] G. Liu, C. A. Grygon, T. G. Spiro, *Biochemistry* **1989**, *28*, 5046−5050.
[71] J. Trewhella, V. A. P. Carlson, E. H. Curtis, D. B. Heidorn, *Biochemistry* **1988**, *27*, 1121−1125.
[72] J. Sun, C. Su, M. Meier, S. S. Isied, J. F. Wishart, R. van Eldik, *Inorg. Chem.*, in press.
[73] T. Ikeshoji, K. Taniguchi, F.M. Hawkridge, *J. Electroanal. Chem.* **1989**, 270, 297−308.
[74] G. Battistuzzi, M. Borsari, D. Dallari, I. Lancelloti, M. Sola, *Eur. J. Biochem.* **1996**, *241*, 208−214.
Received March 31, 1999

Received March 31, 1999
[I99112]

Preparation, Characterization, and Properties of Various Novel Ionic Derivatives of Pentacarbonyltungsten

Wolfram Palitzsch,[a] Christian Beyer,[a] Uwe Böhme,*[a] Ben Rittmeister,[a] and Gerhard Roewer[a]

Keywords: Tungsten / Carbonyl complexes / Undecamethylcyclohexasilyl / Transition metal silicon compounds / Anions / Tungsten silicide / Silicon

The complexes $[Li(DIME)_2][W(CO)_5L]$ [L = OCN **2**, NCS **3a**, PPh_2 **4**, $SiMe_2Ph$ **8**, $N(SiMe_3)_2$ **9**, CH_2Ph **10**, Si_6Me_{11} **11**; DIME = diethylene glycol dimethyl ether] have been prepared by reaction of $[Li(DIME)_2][W(CO)_5I]$ (**1**) with KOCN, KSCN, $NaPPh_2$, $LiSiMe_2Ph$, $LiN(SiMe_3)_2$, $PhCH_2MgCl$, and KSi_6Me_{11}, respectively. Photochemical ligand substitution in $W(CO)_6$ has been used as an alternative method for the preparation of pentacarbonyl tungstates; $[K(DIME)_2][W(CO)_5NCS]$ (**3b**), $[Na(DIME)_2][W(CO)_5N_3]$ (**5**), $[Li(DIME)_2][W_2(CO)_{10}(\mu\text{-}H)]$ (**6**), and $[K(DIME)_2][W_2(CO)_{10}(\mu\text{-}CN)]$ (**7**) were synthesized in this manner. The molecular structure of $[Li(DIME)_2][W(CO)_5Si_6Me_{11}]$ (**11**) has been determined by X-ray diffraction analysis. The spectral and chemical properties of **2–11** are discussed. Pyrolysis of **11** leads to tungsten silicide and tungsten carbide.

Introduction

For a long time, chemists have been interested in $[M^0(CO)_5X]^-$ anions of the Group VIA elements.[1] The fact that they could easily be prepared from $M(CO)_6$ and $R_4N^+X^-$[2] and their role as starting materials in the synthesis of derivatives of the relevant transition metals attracted considerable attention. In 1963, Abel and co-workers reported the synthesis of pentacarbonylhalometallate anions.[2] They were able to isolate $R_4N^+[M(CO)_5X]^-$ species from reactions of tetraalkylammonium halides with metal hexacarbonyls, but the products were characterized only by infrared spectroscopy. The authors indicated that the goal of isolating and purifying these compounds was frustrated by decomposition. In a recent communication, we described a cation design that should offer improved thermal stability.[3]

Because transition metal silicon compounds are useful precursors for metal silicides, the design of suitable compounds fulfilling this role is very important.[4] The chemistry of ionic transition metal silyl derivatives remains largely unexplored. Only a few compounds of this type derived from monosilanes have been reported.[5]

In our laboratory, compounds of the type $[Li(DIME)_2][M(CO)_5I]$ [M = W (**1**), Mo] have been synthesized with a modification of the method described by Abel and co-workers. It is very easy to substitute the iodine while retaining the d^6-character of the tungsten, and hence the $[W(CO)_5I]^-$ anion represents an interesting and versatile building block. Silyllithium or Grignard reagents react with complexes such as the $[W(CO)_5I]^-$ anion. In the present work, we describe the preparation and properties of new compounds including pseudohalide derivatives in order to further development in this field.

Accordingly, we decided to introduce the Si_6Me_{11} group into this anionic complex of tungsten. Some transition metal compounds of undecamethylcyclohexasilane have been described in the last few years,[6] but as far as we are aware, only one X-ray structure analysis of a cyclohexasilyl transition metal compound has hitherto been published.[7] We report herein on the synthesis and characterization of $[Li(DIME)_2][W(CO)_5Si_6Me_{11}]$ (**11**), for which single-crystal structural data could be obtained.

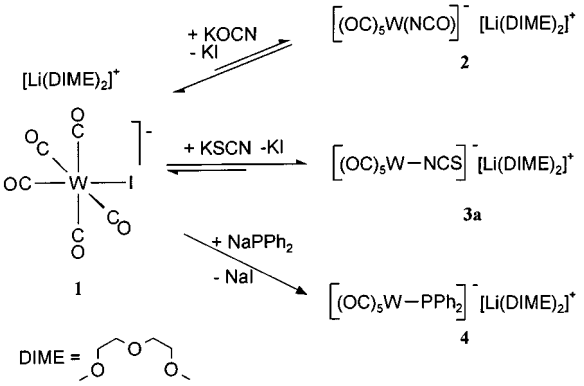
Among the transition metal silicides, those of tungsten offer excellent oxidation resistance. Consequently, they are being considered as potential high-temperature structural materials, capable of operating well beyond the stable temperature limits possible with superalloys. WSi_2 has a high melting temperature of 2165°C.[8] The fabrication and characterization of W−Si−C phases is a challenge in materials science. It would be very desirable if such high-temperature resistant materials could be prepared from potential precursors such as **11**.

Results and Discussion

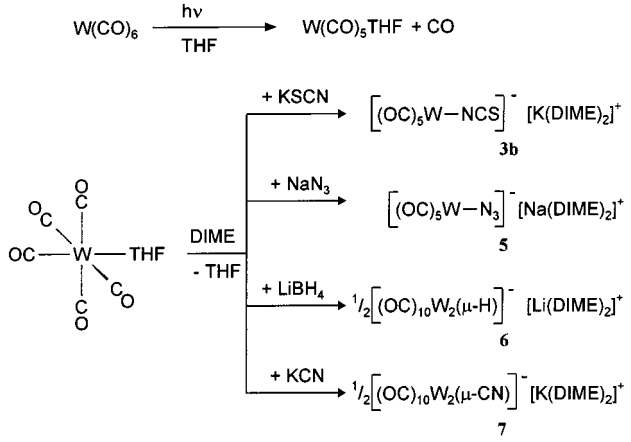
The iodide complex **1** was chosen as the starting compound for the synthesis of further $[W(CO)_5L]^-$ anions. It was generated by the reaction of $W(CO)_6$ with anhydrous lithium iodide diethyl ether complex ($LiI \cdot OEt_2$) in DIME (diethylene glycol dimethyl ether). Complex **1** reacts with a variety of reagents under substitution of the iodide by the incoming nucleophile (see Schemes 1 and 3). Reactions with potassium cyanate and potassium thiocyanate were performed in DME at room temperature. However, these reactions provide the pseudohalide pentacarbonyltungstates **2** and **3a** only as mixtures with the starting material **1**.

[a] Technische Universität Bergakademie Freiberg, Institut für Anorganische Chemie,
Leipziger Straße 29, D-09596 Freiberg, Germany
E-mail: boehme@silicium.aoch.tu-freiberg.de

 © WILEY-VCH Verlag GmbH, D-69451 Weinheim, 1999 1434−1948/99/1010−1813 $ 17.50+.50/0



Scheme 1. Substitution of iodide by pseudohalide ions



Scheme 2. Anionic derivatives starting from $W(CO)_5THF$

The infrared spectra of **2** and **3a** feature four bands in the carbonyl stretching region.[9] While only three infrared bands are to be expected for rigorous C_{4v} symmetry, the rather weak band at 1960 cm^{-1} in **3a** can be assigned to the formally infrared inactive B_1 mode.[10] The characteristic modes of the pseudohalides are found at 2245 cm^{-1} (ν_{NCO} in **2**) and 2090 cm^{-1} (ν_{NCS} in **3a**). All attempts to separate **2** and **3a** from the starting compound **1** by recrystallization were unsuccessful. As the product mixture contained **1** as the major and **2** as the minor component, we were unable to obtain a full spectroscopic characterization of **2**. Specifically, it could not be established whether the cyanate ion is coordinated through nitrogen or oxygen at the tungsten atom.

Reaction of **1** with sodium diphenylphosphide in THF/dioxane yielded a red oil, the NMR and IR spectroscopic data of which were consistent with the formula $[Li(DIME)_2][W(CO)_5PPh_2]$. The infrared spectrum features four bands attributable to the $W(CO)_5$ fragment at 2045, 1964, 1936, and 1880 cm^{-1}. In the ^{13}C-NMR spectrum, the signals of the CO carbon atoms are split into doublets due to coupling with the phosphorus atom bound to the $W(CO)_5$ fragment.

The reaction of the tungsten pentacarbonyl THF adduct with pseudohalides represents an alternative route for preparing substitution products of the type $[(OC)_5W{-}X]^-$ (see Scheme 2). Donor adducts of $W(CO)_5$ have been used previously as reactive intermediates.[11] It is easy to prepare $W(CO)_5THF$ from $W(CO)_6$ by photochemical ligand substitution in THF solution.

Reaction of $W(CO)_5THF$ with KSCN in DIME yields **3b** as a yellow microcrystalline powder. The ^{13}C-NMR spectrum features one signal due to the thiocyanate carbon atom at $\delta = 135.1$ and three signals due to the DIME ligand coordinated at the potassium ion. The signals of the CO carbon atoms are found at $\delta = 197.6$ and 201.6, with an intensity ratio of 1:4. The $^1J(^{13}C,^{183}W)$ coupling constant, which is well resolved in the spectrum of this compound, has a value of 129.2 Hz. The spectroscopic data of compound **3b** correspond well with the data of $[NEt_4][W(CO)_5NCS]$, which was described by Buchner and Schenk.[12] The infrared spectrum of **3b** features four bands in the carbonyl stretching region and one characteristic band for the stretching mode of the NCS ligand as described above. Generally, the thiocyanate ion is able to coordinate to metals through either the nitrogen or the sulfur atom. The high frequency ν_{CN} band indicates that in this case the thiocyanate is coordinated to the tungsten through the nitrogen atom.[13] As mentioned above, the product **3a** formed by nucleophilic substitution of iodide by SCN^- was found to be contaminated with the starting compound **1**; however, the product of the photochemical reaction sequence was free from impurities.

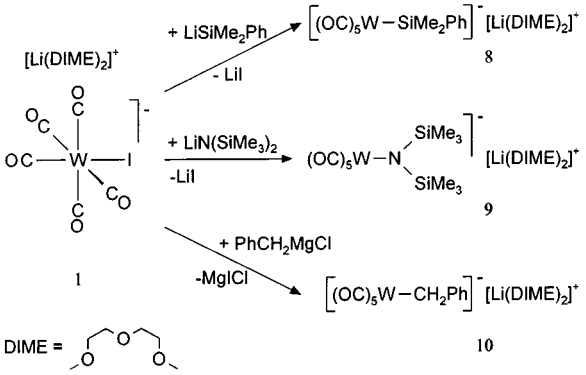
Reaction of potassium selenocyanate (KSeCN) with $W(CO)_5THF$ in DIME failed to give the desired product $[K(DIME)_2][W(CO)_5NCSe]$ in all cases, even at low temperatures. Instead, a finely divided black precipitate was formed, which was identified as elemental selenium by flame photometry and its melting point (215−217°C).

Sodium azide decomposes in solution if it is exposed to strong light. Therefore, the synthesis of $[Na(DIME)_2][W(CO)_5N_3]$ **5** was performed in a two-step sequence. The $W(CO)_5THF$ adduct was prepared photochemically as above. The solution of $W(CO)_5THF$ thus formed was then added dropwise to a solution of sodium azide protected from bright light. The product **5** was found to be air- and light-sensitive and was characterized by its ^{13}C-NMR and IR spectra. The ^{13}C-NMR spectrum features the characteristic 1:4 peak intensity ratio due to the CO carbon atoms at low field, as well as additional signals due to the DIME ligand (for details, see the Experimental Section). Four IR bands are seen in the carbonyl stretching region. One additional weak band at 2080 cm^{-1} can be assigned to the asymmetric stretching mode of the azide group. To assess the stability of compound **5** in solution, the NMR sample was stored for one week at room temperature. When an NMR spectrum was recorded after this period, the ^{13}C-NMR signals of the $[W(CO)_5N_3]^-$ ion could no longer be detected. New signals were seen, which corresponded to $W(CO)_6$ and $[W(CO)_5NCO]^-$. The mechanism of decomposition of $[W(CO)_5N_3]^-$ might be analogous to the Curtius rearrangement.[14] Reactions of metal carbonyls with N_3^- have been studied extensively.[15]

Because the tetrahydroborate ion is isoelectronic with the fluoride, hydroxide, amide, and methyl ions, we were also interested in carrying out reactions of $W(CO)_5THF$ with lithium tetrahydroborate. The ^{13}C-NMR data of **6** reveal the presence of a $W(CO)_5$ unit, since two signals for carbonyl carbon atoms are seen, with an intensity ratio of 1:4. One signal at $\delta = -12.55$ is seen in the ^1H-NMR spectrum of **6**. It is split into a triplet due to coupling with two tungsten atoms [$^1J(^1H,^{183}W) = 42.0$ Hz]. The chemical shift and coupling constant of this proton are characteristic features of such μ-hydrogen-bridged ditungsten complexes. A few examples have been described previously, which showed very similar chemical shifts and coupling constants as those found for **6**.[16] In addition, we observed signals due to a BH_4-containing side-product in the NMR spectra of **6**, which are most probably attributable to a small amount of $[Li(DIME)_2][W(CO)_4(\mu^2\text{-}BH_4)]$. It was not possible to remove this impurity by recrystallization.

Reaction of $W(CO)_5THF$ with potassium cyanide in THF in the presence of DIME yielded a yellow microcrystalline powder. The ^{13}C-NMR spectrum of this substance reveals the presence of two different $W(CO)_5$ units, since two sets of carbonyl carbon atom signals with an intensity ratio of 1:4 are seen. This pattern is suggestive of the formation of a dimeric CN-bridged complex. The carbon atom signal of the CN group is found at $\delta = 152.5$. Five bands are seen in the carbonyl stretching region of the IR spectrum (see Experimental Section). There is probably a superposition of the absorptions of the two different $W(CO)_5$ fragments. The stretching mode of the cyanide group is observed at 2124 cm^{-1}. Comparable compounds, such as the bridged complex $[PPN][W_2(CO)_{10}(\mu\text{-}CN)]$ and $[NEt_4][W(CO)_5CN]$, show absorptions at 2121 cm^{-1} and 2104 cm^{-1}, respectively.[17] The high wavenumber shift of the ν_{CN} mode, together with the aforementioned NMR data, lead us to the conclusion that the bridged complex $[K(DIME)_2][(OC)_5W(\mu\text{-}CN)W(CO)_5]$ **7** was formed in this reaction.

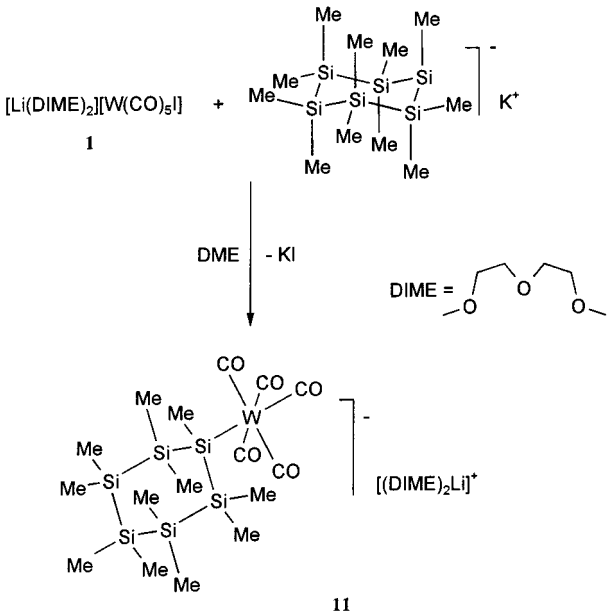
Reaction of $[Li(DIME)_2][W(CO)_5I]$ (**1**) with 1 molar equivalent of lithium bis(trimethylsilyl)amide $Li[N(SiMe_3)_2]$ in tetrahydrofuran gave $[Li(DIME)_2][W(CO)_5N(SiMe_3)_2]$ (**9**). Treatment of **1** with the Grignard reagent $PhCH_2MgCl$ in diethyl ether solution afforded complex **10** (Scheme 3). Complex **8** was prepared by adding a solution of $[Li(DIME)_2][W(CO)_5I]$ (**1**) in DME to an excess of $LiSiMe_2Ph$.



Scheme 3. Syntheses of compounds **8**–**10** by nucleophilic substitution

Complexes **8**, **9**, and **10** were isolated and purified by extraction with pentane. Subsequent recrystallization from dichloromethane gave yellowish solids. Compounds **8**–**11** can be safely dried in vacuo at room temperature without loss of the DIME ligands. Complex **9** proved to be more air-sensitive than compounds **8**, **10**, and **11**. The IR spectra of compounds **8**, **9**, and **10** exhibit three ν_{CO} bands ($2A_1$ and E). These stretching modes are in agreement with data found for the corresponding neutral $M(CO)_5X$ species.[18] The ^1H-NMR spectra are indicative of the presence of the DIME ligand (3 signals) and also feature characteristic signals for the substituents at the tungsten atom: $\delta = 7.54$ (m, SiPh), 0.58 ($SiMe_2$) for **8**; $\delta = 0.0$ ($SiMe_3$) for **9**; $\delta = 7.26$ (m, Ph), 1.25 (CH_2) for **10**. The ^{13}C-NMR data of **9** and **10** confirm the presence of the DIME ligand (3 signals) and of the substituents at the tungsten atom (see Experimental Section). The ^{29}Si-NMR peak of **8** at $\delta = -6.13$ gives evidence that one silicon atom is present.

Undecamethylcyclohexasilyl potassium (KSi_6Me_{11}) is well-established as a useful reagent for the synthesis of a variety of transition metal silyl complexes. $[Li(DIME)_2][W(CO)_5Si_6Me_{11}]$ (**11**) was prepared according to Scheme 4. The reaction of one equivalent of $[Li(DIME)_2][W(CO)_5I]$ with KSi_6Me_{11} in DME at ambient temperature resulted in the novel substance $[Li(DIME)_2][W(CO)_5Si_6Me_{11}]$ (**11**).



Scheme 4. Synthesis of compound **11**

The cyclohexasilyl derivative **11** was found to be more stable than complexes **8**–**10**. In the solid state, **11** is prone to very slow decomposition in air. It decomposes thermally between 160 and 250°C (TG). It is quite soluble in protic solvents, for example, wet methanol, with no evidence of decomposition in solution detectable in the NMR spectrum. Recrystallization from dichloromethane/pentane at −20°C gave analytically pure yellow crystals of **11** suitable for an X-ray crystallographic study. The structure was solved and refined in space group $P2_1/n$. **11** crystallizes in discrete ionic pairs; the structure of the cation is shown in

Figure 1. The lithium atom is coordinated by two DIME molecules in a distorted octahedral coordination geometry. The tridentate ether molecules chelate the lithium atom with meridional coordination. The Li−O bond lengths in **11** of 2.009 to 2.285 Å are in the same range as the Li−O distances reported for **1**.[3] The structures of these cations are isotypic.

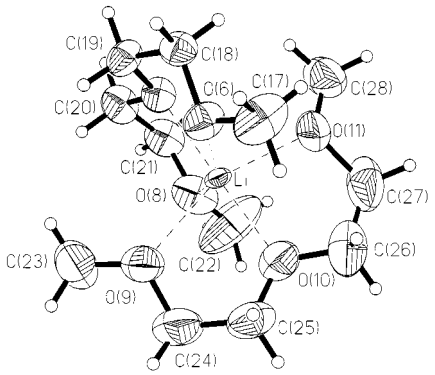


Figure 1. Structure of the $[Li(DIME)_2]^+$ cation in **11**

The structure of the undecamethylcyclohexasilylpentacarbonyltungsten anion is shown in Figure 2. The $[W(CO)_5Si_6Me_{11}]^-$ anion has approximately C_{4v} symmetry with a W−Si bond length of 2.670(2) Å, which is slightly longer than the corresponding distance of 2.614(2) Å in $[PPN][W(CO)_5SiMe_3]$.[19] The tungsten atom resides in an almost regular octahedron with $CO_{eq}-W-CO_{eq}$ angles very close to 90° and a $CO_{ax}-W-Si_{ax}$ angle of 175.3(2)°. The W−C distances for the four equatorial CO ligands range from 2.011 to 2.044 Å, while the W−C bond to the axial CO ligand measures only 1.966(6) Å. This is possibly a reflection of a greater π-back-bonding to the CO ligand situated *trans* to the silyl group. Two of the four equatorial CO′s are bent towards the Si_6Me_{11} ligand, resulting in Si(1)−W−C(4) and Si(1)−W−C(5) angles of 84.6(2) and 80.2(2)°, respectively. The cyclohexasilyl ligand adopts a chair conformation with the $W(CO)_5$ group in an equatorial position.

Crystallographic data and data collection parameters are listed in Table 3. Salient bond lengths and angles are listed in Table 1.

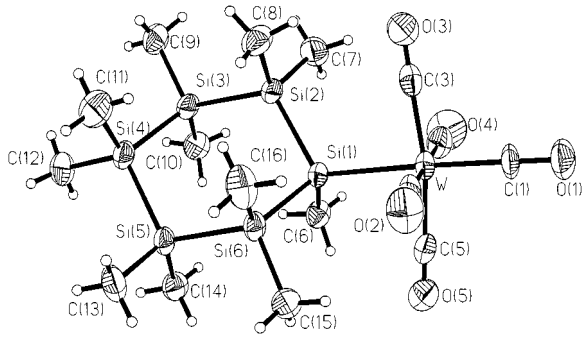


Figure 2. Structure of the $[W(CO)_5Si_6Me_{11}]^-$ anion in **11**

Table 1. Selected bond lengths [Å] and bond angles [°] in **11**

W−C(1)	1.966(6)	Li−O(6)	2.285(10)
W−C(2)	2.017(8)	Li−O(7)	2.046(9)
W−C(3)	2.011(7)	Li−O(8)	2.138(10)
W−C(4)	2.044(8)	Li−O(9)	2.274(11)
W−C(5)	2.016(8)	Li−O(10)	2.009(10)
W−Si(1)	2.670(2)	Li−O(11)	2.118(11)
C(1)−O(1)	1.176(8)	O(10)−Li−O(7)	177.9(6)
C(2)−O(2)	1.151(9)	O(7)−Li−O(8)	79.4(4)
C(3)−O(3)	1.163(9)	O(7)−Li−O(6)	75.5(3)
C(4)−O(4)	1.122(9)	O(7)−Li−O(11)	98.1(4)
C(5)−O(5)	1.162(9)	O(7)−Li−O(9)	105.2(4)
C(4)−W−C(3)	90.2(3)		
C(4)−W−C(5)	89.7(3)		
C(2)−W−C(3)	90.4(3)		
C(2)−W−C(5)	89.8(3)		
C(1)−W−Si(1)	175.3(2)		

In the infrared spectrum of **11**, four metal carbonyl bands at 2020 (w), 1915 (m), 1890 (s), and 1860 (m) cm^{-1} are observed, which are characteristic of a metal pentacarbonyl anion.[2] The IR bands can be assigned to the three IR-active fundamental vibrations ($2A_1 + E$) expected for a C_{4v} metal pentacarbonyl species and to the B_1 vibration, although this is IR inactive for rigorous C_{4v} geometry. This assessment is in agreement with those for the corresponding $M(CO)_5X$ species by Casey.[9a] The ^{1}H-NMR signals of the DIME ligands are observed at δ = 3.40 (s, CH_3) and δ = 3.56 and 3.65 (m, CH_2CH_2). The ^{1}H-NMR resonances for the methyl groups bonded to the silicon appear in the typical range with δ values near to zero (see Table 2).

Table 2. ^{1}H-, ^{13}C-, and ^{29}Si-NMR data of compound **11**[a]

δ^{1}H DIME	Me−Si	δ^{13}C DIME	CO	Si−Me	δ^{29}Si
3.65, 3.56 (CH_2), 3.40 (CH_3)	0.49, 0.22, 0.15, 0.14, 0.11, 0.10	70.75, 69.30 (CH_2), 59.31 (CH_3)	212.16, 207.67	−2.14, −3.18, −3.79, −4.19, −4.85, −5.95, −6.79	−75.7, −42.0, −40.7, −30.7

[a] Recorded in $CDCl_3$ at 25°C; data in ppm are relative to Me_4Si at δ = 0.0.

The fact that six signals are observed indicates that the silicon ring adopts a chair conformation. Single-crystal structure analysis confirms this assumption. The ^{29}Si-NMR spectrum of compound **11** features four resonances for the *cyclo*-silyl ligand bonded at the metal atom (Table 2). The ^{29}Si-NMR chemical shifts for the anion $[W(CO)_5Si_6Me_{11}]^-$ move progressively to higher field relative to the shifts for the analogous $[Mo(CO)_5Si_6Me_{11}]$,[7] which is the expected trend for complexes of this type.[20] The ^{13}C-NMR data of **11** are in agreement with the proposed structure (Table 2).

Pyrolysis of $[Li(DIME)_2][W(CO)_5Si_6Me_{11}]$ (11)

Thermogravimetry (TG) and differential thermal analysis (DTA) were performed using a MOM Budapest Derivato-

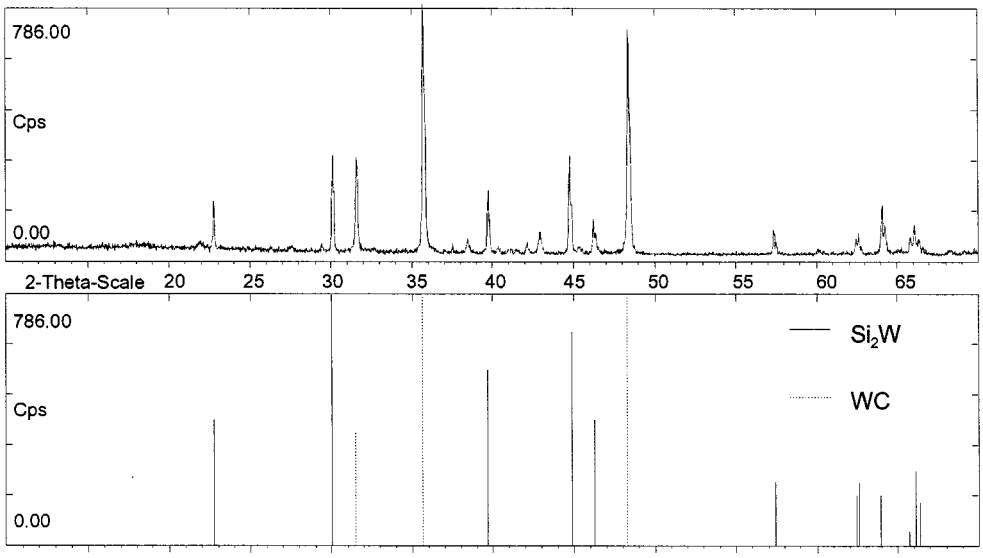


Figure 3. Comparison of the XRD pattern of the pyrolyzed sample of $[Li(DIME)_2][W(CO)_5Si_6Me_{11}]$ (**11**) (top) with powder diffraction files: 11−0195 WSi_2, 25−1047 WC (bottom)

graph. An atmosphere of Ar (at a flow rate of 200 mL/min^{-1}) and a corund open pan were used for the experiment. A sample of **11** was heated at a rate of 5 °C min^{-1} up to 1400°C. Decomposition started at 160°C and reached a maximum rate at 230°C. The mass lost amounted to 29% of the sample mass at 250°C, which corresponds to the loss of 2 DIME molecules per formula unit. The following substances could be detected by GC analysis: CO at 400−1000°C, CH_4 at 500−800°C, and H_2 < 1200°C. X-ray analysis after the pyrolysis indicated that the product was mainly a mixture of WSi_2 and WC (Figure 3).

Conclusions

In conclusion, $[Li(DIME)_2][W(CO)_5I]$ (**1**) reacts readily with nucleophilic reagents such as alkyls and organoamides, -phosphides, and -silyls. The preferred site of reactivity is the W−I bond. Thus, it is evident that **1** is a highly useful reagent for preparing a wide variety of $W(CO)_5$ derivatives. Reaction of **1** with pseudohalides leads to mixtures of starting material and product. This is probably due to the weak nucleophilicity of the pseudohalides. Therefore, the salt elimination route is not suitable for preparing pure pseudohalide−pentacarbonyltungstate derivatives. However, it is possible to obtain these derivatives by using the photochemical reaction sequence via $W(CO)_5THF$. The X-ray crystal structure of **11** confirms that the cyclohexasilyl ring is bound to the tungsten. The production of pure tungsten silicide is a challenging task with potential applications in materials science; thus it is noteworthy that thermolysis of **11** produces WSi_2 together with WC. Further investigations concerning the synthesis and thermal decomposition pathways of metal−silicon compounds are currently under way.

Experimental Section

All preparative work and sample handling was carried out under Ar with dry glassware and in dry solvents. Diethylene glycol dimethyl ether (DIME) was repeatedly distilled from freshly cut Na until effervescence was no longer observed. It was distilled once more and then stored in a sealed flask in a drybox prior to use. Starting materials $W(CO)_6$ and $Li[N(SiMe_3)_2]$ were purchased from Fluka Chemie AG. $W(CO)_6$ was vacuum-sublimed prior to use. All alkaline pseudohalides were dried in vacuo for 4 h prior to use. The syntheses of $PhCH_2MgCl$,[21] $LiSiMe_2Ph$,[22] and KSi_6Me_{11}[23] were carried out according to established procedures.

NMR spectra were recorded on a Bruker MSL 200 spectrometer. − Elemental analyses were performed on a CHN-O-Rapid (Heraeus). The carbon values recorded were systematically lower due to carbide formation. − Infrared spectra were recorded on a Specord 75 IR instrument in the range 4000 to 400 cm^{-1} for samples pressed into a KBr disc. − X-ray powder diffraction patterns were obtained using a Siemens D5000 diffractometer with Cu-K_α radiation.

Synthesis of $[Li(DIME)_2][W(CO)_5I]$ (1): A sample of $W(CO)_6$ (5.0 g, 0.014 mol) was added to a solution of $LiI{\cdot}Et_2O$ (3.0 g, ≈ 0.014 mol) in diethylene glycol dimethyl ether (20 mL). The mixture was heated at 80°C for 2 days, during which it became bright yellow. IR monitoring showed the formation of a species with a ν(CO) pattern typical for $[W(CO)_5L]$ species: $\tilde{\nu}$ = 1950, 1915, 1850 cm^{-1}. The solvent was removed in vacuo to leave a yellow residue. This was redissolved in dichloromethane and then treated with *n*-pentane to give yellow crystals of **1** (isolated yield 93.7%). − ^{1}H NMR ($CDCl_3$/TMS): δ = 3.75, 3.64, 3.45 (DIME). − ^{13}C NMR ($CDCl_3$/TMS): δ = 202.62, 197.18 (CO), 70.58, 69.37, 59.54 (DIME). − $C_{17}H_{28}ILiO_{11}W$ (697.8): calcd. C 21.88, H 3.02; found C 21.74, H 3.10.

Synthesis of $[Li(DIME)_2][W(CO)_5NCO]$ (2) and $[Li(DIME)_2][W(CO)_5NCS]$ (3a): $[Li(DIME)_2][W(CO)_5I]$ (**1**) (0.003 mol) and an equimolar amount of KOCN or KSCN, respectively, were suspended in DME and the mixture was stirred for 24 h at room tem-

perature. The solvent was then evaporated in vacuo, and the remaining solid was washed with *n*-pentane and taken up in dichloromethane. The resulting suspension was filtered to remove insoluble alkaline halides. Addition of *n*-pentane to the clear solution and cooling to 5°C led to the deposition of **3a** as a yellow solid. – ^{1}H NMR ($CDCl_3$/TMS): δ = 3.74, 3.63, 3.46 (DIME). – ^{13}C NMR ($CDCl_3$/TMS): δ = 201.4 (CO_{ax}), 197.6 (CO_{eq}), 135.4 (NCS), 70.7, 69.3 (DIME). – IR (KBr): ν_{CO} = 2060 (w), 1960 (w, sh), 1910 (s), 1860 (m) cm^{-1}; ν_{NCS} = 2090 (w) cm^{-1}. The spectra of **3a** prepared by this method show additional signals attributable to **1**.

Synthesis of [K(DIME)$_2$][W(CO)$_5$NCS] (3b): $W(CO)_5THF$ was prepared immediately prior to use by irradiating a solution of $W(CO)_6$ (2.5 g, 0.0071 mol) in dry THF (concentration about 0.1 mol/L) under Ar for 4 h with a high-pressure Hg lamp (160 W).[24] Meanwhile, a solution of potassium thiocyanate (0.69 g, 0.0071 mol) in DIME (15 mL) was prepared. The synthesized tungsten pentacarbonyl THF adduct was then added to this solution over a period of 10 min. The resulting mixture was stirred for 24 h at room temperature. The solvent and excess $W(CO)_6$ were then removed in vacuo. Pentane was added, the product was isolated by filtration, washed with *n*-pentane, and dried in vacuo to afford **3b** as a yellow microcrystalline powder. – ^{1}H NMR ($CDCl_3$/TMS): δ = 3.66, 3.59, 3.42 (DIME). – ^{13}C NMR ($CDCl_3$/TMS): δ = 201.6 (CO_{ax}), 197.6 [$^1J(^{13}C,^{183}W)$ = 129.2 Hz (CO_{eq})], 135.1 (NCS), 71.5, 69.9, 59.0 (DIME). – IR (KBr): ν_{CO} = 2066 (w), 1975 (w, sh), 1918 (s), 1864 (m) cm^{-1}; ν_{NCS} = 2093 (w) cm^{-1}.

Synthesis of [Li(DIME)$_2$][W(CO)$_5$PPh$_2$] (4): [Na(dioxane)$_n$][PPh_2] was prepared according to the method of Issleib.[25] [Li(DIME)$_2$][W(CO)$_5$I] (2.54 g, 0.0035 mol) was dissolved in THF (40 mL) and a solution of [Na(dioxane)$_n$][PPh_2] (ca. 0.01 mol) in THF/dioxane (23 mL) was added at −76°C. The resulting mixture was stirred for a period of 10 h, during which the colour changed from yellow/orange to red. DIME (20 mL) was then added to the reaction mixture. The resulting suspension was filtered and the solvents were evaporated in vacuo. All attempts at crystallization led only to a clear red oil **4**. – ^{1}H NMR ($CDCl_3$/TMS): δ = 7.73, 7.23, 7.04 (Ph), 3.75, 1.86 (THF), 3.72, 3.62, 3.44 (DIME). – ^{13}C NMR ($CDCl_3$/TMS): δ = 204.7 [$^2J(^{13}C,^{31}P)$ = 12.9 Hz (CO_{ax})], 201.2 [$^1J(^{13}C,^{183}W)$ = 123.9 Hz (CO_{eq})], 151.2 [$^1J(^{13}C,^{31}P)$ = 12.3 Hz (C_{ipso})], 133.4 [$^2J(^{13}C,^{31}P)$ = 10.9 Hz (C_{ortho})], 126.8 [$^3J(^{13}C,^{31}P)$ = 7.7 Hz (C_{meta})], 125.5 (C_{para}), 71.0, 69.7, 59.4 (DIME), 68.0, 25.6 (THF). – IR (THF): ν_{CO} = 2045 (w), 1964 (w, sh), 1936 (s), 1880 (m) cm^{-1}.

Synthesis of [Na(DIME)$_2$][W(CO)$_5$N$_3$] (5): $W(CO)_5THF$ was prepared as described above. Sodium azide (0.46 g, 0.0071 mol) was dissolved in methanol (60 mL) and THF (80 mL) and then DIME (20 mL) was added to the solution. The tungsten pentacarbonyl THF adduct was added dropwise to this mixture with stirring. After stirring for 10 h, the solvents were evaporated in vacuo and excess *n*-pentane was added to the yellow residue. The resulting yellow solid was collected by filtration and washed with *n*-pentane. The solid residue was redissolved in THF, the resulting solution was filtered, and *n*-pentane was added to the filtrate to crystallize the product. The product was found to be sensitive to light and air. It decomposes in CH_2Cl_2 and $CHCl_3$. In solution, the product converts into $W(CO)_6$ and [Na(DIME)$_2$][W(CO)$_5$NCO]. – ^{1}H NMR (CD_3OD/TMS): δ = 3.62, 3.54, 3.36 (DIME). – ^{13}C NMR (CD_3OD/TMS): δ = 203.4 (CO_{ax} N_3), 199.8 [$^1J(^{13}C,^{183}W)$ = 129.3 Hz (CO_{eq} N_3)], 202.2 (CO_{ax} OCN), 199.4 (CO_{eq} OCN), 192.4 [$W(CO)_6$], 72.9, 71.3, 59.1 (DIME). – IR (THF): ν_{CO} = 2040 (w), 1965 (s), 1910 (s), 1865 (m) cm^{-1}, ν_{N3} = 2080 (w) cm^{-1}; ν_{OCN} = 2245 (w) cm^{-1}.

Synthesis of [Li(DIME)$_2$][W$_2$(CO)$_{10}$(μ-H)] (6): $W(CO)_5THF$ was prepared as described above. $LiBH_4$ (0.185 g, 0.0085 mol) was dissolved in a mixture of THF (60 mL) and DIME (20 mL). The tungsten pentacarbonyl THF adduct was added dropwise to the $LiBH_4$ solution over a period of 15 min. at 0°C and the reaction mixture was stirred for 8 h. After evaporation of the solvent, the residue was redissolved in THF, the resulting solution was filtered, and *n*-pentane was added to the filtrate. The clear solution was cooled to −20°C to crystallize the product. – ^{1}H NMR (CD_3CN/TMS): δ = 3.61, 3.52, 3.35 (DIME), −12.55 [$^1J(^1H,^{183}W)$ = 42.0 Hz (WH)]. – ^{13}C NMR (CD_3CN/TMS): δ = 202.0 (CO_{ax}), 199.7 [$^1J(^{13}C,^{183}W)$ = 124.2 Hz (CO_{eq})], 71.7, 70.2, 59.1 (DIME); impurities: $LiBH_4$: ^{1}H NMR (CD_3CN/TMS): δ = −0.46 [quadruplet, $^1J(^1H,^{11}B)$ = 83.2 Hz]. – ^{11}B NMR ($CD_3CN/BF_3{\cdot}Et_2O$): δ = −39.43; [Li(DIME)$_2$][W(CO)$_4$(μ^2-BH_4)]: ^{1}H NMR (CD_3CN/TMS): δ = −11.84 (weak). – ^{13}C NMR (CD_3CN/TMS): δ = 201.4, 200.8 (CO, weak). – IR (KBr): ν_{CO} = 2071 (w), 2041 (m), 2014 (w), 1966 (m, sh), 1936 (s), 1873 (s, br), 1839 (m), 1802 (w, sh) cm^{-1}; ν_{BH} = 2246 (s, br) cm^{-1}.

Synthesis of [K(DIME)$_2$][W$_2$(CO)$_{10}$(μ-CN)] (7): $W(CO)_5THF$ was prepared as described above. Potassium cyanide (0.55 g, 0.0085 mol) was dissolved in a mixture of THF (40 mL) and DIME (20 mL). The tungsten pentacarbonyl THF adduct was then added dropwise to the potassium cyanide solution over a period of 15 min. at 0°C. The resulting mixture was stirred for 4 h and then the remaining traces of KCN were filtered off. The solvent was removed under reduced pressure, *n*-pentane was added to the residue, and the precipitate was collected by filtration. The green-yellow solid was taken up in THF and filtered, and the collected solid was washed with *n*-pentane and dried in vacuo to afford a yellow microcrystalline powder **7**. The product was found to be sensitive to light and air. – ^{1}H NMR ($CDCl_3$/TMS): δ = 3.65, 3.59, 3.42 (DIME). – ^{13}C NMR ($CDCl_3$/TMS): δ = 202.3 (CO_{ax} NC), 197.9 [$^1J(^{13}C,^{183}W)$ = 129.0 Hz (CO_{eq} NC)], 200.2 (CO_{ax} CN), 196.9 [$^1J(^{13}C,^{183}W)$ = 125.0 Hz (CO_{eq} CN)], 152.5 (CN), 71.5, 70.0, 59.0 (DIME). – IR (THF): ν_{CO} = 2057 (w), 1971 (sh), 1934 (s), 1900 (m), 1880 (m); ν_{CN} = 2124 (w). – UV/vis (EtOH): λ_{max} (ε/l·mol^{-1}·cm^{-1}) = 230 (80870), 248 (54515), 338 (3947), 362 (4021), 384 (2740) nm.

Synthesis of [Li(DIME)$_2$][W(CO)$_5$SiMe$_2$Ph] (8): A solution of **1** (0.005 mol, 3.49 g) in DME (20 mL) was added slowly, over a period of 4 h, to an excess of $LiSiMe_2Ph$ (0.006 mol) in THF. The mixture was stirred for further 3 h and then the solvents were removed in vacuo. The remaining orange solid was redissolved in dichloromethane (20 mL) and this solution was filtered. Pentane (50 mL) was added to the clear yellow filtrate and complex **8** crystallized on cooling. The mother liquor was removed by means of a cannula. The residue was washed with pentane, dried in a stream of argon, and then at oil-pump vacuum to afford 2.8 g (79%) of **8** as a yellow solid. – ^{1}H NMR ($CDCl_3$/TMS): δ = 7.54 (SiPh), 3.68, 3.59, 3.43 (DIME), 0.58 ($SiMe_2$). – ^{29}Si NMR (dichloromethane/D_2O): δ = −6.13. – IR ($CHCl_3$): ν_{CO} = 1925, 1887, 1815 cm^{-1}. – $C_{25}H_{39}LiO_{11}SiW$ (706.1): calcd. C 42.52, H 5.51; found C 41.86, H 5.53.

Synthesis of [Li(DIME)$_2$][W(CO)$_5$N(SiMe$_2$)$_2$] (9): A solution of **1** (0.005 mol, 3.49 g) in THF was cooled to −76°C, whereupon 5 mL (0.005 mol) of a 1 M solution of Li[$N(SiMe_3)_2$] in THF was added. The mixture was stirred for 2 h while being allowed to warm to room temperature. After evaporation of the solvent, the residue was redissolved in DME (20 mL) and the resulting solution was filtered. Pentane was added to the clear yellow solution to start the crystalli-

zation. After cooling, the yield of **9** was 1.4 g (38.3%). The product was recrystallized from dichloromethane/pentane to afford an orange solid. – ^{1}H NMR ($CDCl_3$): δ = 3.71, 3.60, 3.40 (DIME), 0.00 ($SiMe_3$). – ^{13}C NMR ($CDCl_3$): δ = 205.67, 197.04 (CO), 70.43, 69.19, 59.45 (DIME), 2.39 ($SiMe_3$). – IR ($CDCl_3$): ν_{CO} = 1928, 1874, 1855 cm^{-1}. – $C_{19}H_{46}LiO_{11}Si_2W$ (731.32): calcd. C 31.20, H 6.28; found C 30.76, H 6.22.

Synthesis of [Li(DIME)$_2$][W(CO)$_5$CH$_2$Ph] (10): $PhCH_2MgCl$ (0.005 mol, 12.8 mL of a 0.4 M Grignard solution) was treated with a solution of 0.005 mol (3.49 g) of **1** in DME (20 mL) and the resulting mixture was stirred for 2 h at room temperature. Subsequent evaporation of the solvents left a yellow solid, which was taken up in dichloromethane (30 mL) under cooling. This mixture was then filtered and the filtrate was concentrated to dryness to afford 1.7 g (51.4%) of **10**. – ^{1}H NMR ($CDCl_3$/TMS): δ = 7.26 (Ph), 3.74, 3.64, 3.44 (DIME), 1.25 (CH_2). – ^{13}C NMR ($CDCl_3$/TMS): δ = 138.78, 130.68, 128.73, 126.48 (Ph), 70.85, 69.58, 59.49 (DIME), 45.58 (CH_2). – IR ($CDCl_3$): ν_{CO} = 1934, 1916, 1885 cm^{-1}. – $C_{24}H_{35}LiO_{11}W$ (662.04): calcd. C 43.54, H 5.28; found C 43.45, H 5.24.

Synthesis of [Li(DIME)$_2$][W(CO)$_5$Si$_6$Me$_{11}$] (11): KSi_6Me_{11} was prepared from *cyclo*-Si_6Me_{12} (2.6 g, 0.007 mol) and $KOC(CH_3)_3$ (0.78 g, 0.007 mol) in DME (10 mL) and then added dropwise at room temperature over a period of 15 min. to a stirred solution of **1** (5.08 g, 0.007 mol) in DME (20 mL). After stirring the mixture at room temperature for 12 h, the solvent was removed under reduced pressure. Then, a mixture of *n*-pentane/dichloromethane (1:1, 20 mL) was added to the residue and the precipitate was filtered off. The filtrate was concentrated to dryness under reduced pressure and *n*-pentane (20 mL) was added to the residue to produce a slightly yellow suspension. An orange oil separated from the mixture after addition of approximately 10 drops of dichloromethane. Yellow crystals of **11** deposited from the oil after 1 d at −20°C. Yield: 4.82 g (74%). The NMR data are shown in Table 2. – IR (nujol): ν_{CO} = 2020 (w), 1915 (m), 1890 (s), 1860 (m). – $C_{28}H_{61}LiO_{11}Si_6W$: calcd. C 36.04, H 6.58; found C 35.91, H 6.74.

Experimental Procedure for X-ray Crystallography: A suitable single crystal of **11** was mounted on a glass fibre under paraffin oil and transferred to the diffractometer. Diffraction measurements were made on an Enraf−Nonius CAD-4 diffractometer at −83°C using graphite-monochromated Cu-K_α radiation (λ = 1.5418 Å) with ω−2θ scans. The structure was solved by direct methods and refined by full-matrix least-squares on F^2 with anisotropic thermal parameters. Hydrogen atoms were placed in calculated positions and allowed to ride on their corresponding carbon atoms. An empirical absorption correction was performed on the basis of ψ scans. Crystallographic data and the results of the refinements are summarized in Table 3. Full crystallographic data (excluding structure factors) for the structure reported in this paper have been deposited with the Cambridge Crystallographic Data Centre as supplementary publication no. CCDC-100623. Copies of the data can be obtained free of charge on application to the CCDC, 12 Union Road, Cambridge CB2 1EZ, U.K. [Fax: (internat.) + 44-1223/336-033; E-mail: deposit@ccdc.cam.ac.uk].

Table 3. Crystal data and structure refinement for [Li(DIME)$_2$][W(CO)$_5$Si$_6$Me$_{11}$] (**11**)

	11
Empirical formula	$C_{28}H_{61}LiO_{11}Si_6W$
Formula weight	933.10
Temperature	190(2) K
Wavelength	1.54180 Å
Crystal system	monoclinic
Space group	$P2_1/n$
Unit cell dimensions	a = 19.116(2) Å, α = 90° b = 14.308(2) Å, β = 96.810(10)° c = 20.264(3) Å, γ = 90°
Volume	4639.7(11) Å^3
Z	4
Density (calculated)	1.336 Mg/m^3
Absorption coefficient	6.468 mm^{-1}
F(000)	1912
Crystal size	0.4 × 0.3 × 0.15 mm
θ range for data collection	3.32−74.77°
Index ranges	$-20 \le h \le 20$, $0 \le k \le 17$, $-25 \le l \le 9$
Reflections collected	14335
Independent reflections	9517 [R(int) = 0.0944]
Refinement method	Full-matrix least squares on F^2
Data/restraints/parameters	9517/0/439
Goodness-of-fit on F^2	1.038
Final R indices [$I > 2\sigma(I)$]	R_1 = 0.0575, wR_2 = 0.1453
R indices (all data)	R_1 = 0.0787, wR_2 = 0.1609
min. transmission	0.6843
max transmission	0.9998
Largest diff. peak and hole	2.051 and −3.071 e·Å^{-3}

Acknowledgments

Financial support for this work from the Deutsche Forschungsgemeinschaft and the Fonds der Chemischen Industrie is gratefully acknowledged.

[1] J. L. Atwood, S. G. Bott, P. C. Junk, M. T. May, *J. Organomet. Chem.* **1995**, *487*, 7 and references cited therein.
[2] E. W. Abel, I. S. Butler, J. G. Reid, *J. Chem. Soc.* **1963**, 2068.
[3] W. Palitzsch, U. Böhme, G. Roewer, *J. Chem. Soc., Chem. Commun*. **1997**, 803.
[4] A. Zechmann, E. Hengge, Organosilicon Chemistry II, *From Molecules to Materials* (Eds.: N. Auner, J. Weis), VCH Verlagsgesellschaft, Weinheim, **1994**, p. 585.
[5] [5a] E. E. Isaacs, W. A. G. Graham, *Can. J. Chem.* **1975**, *53*, 467. – [5b] R. H. Heyn, T. D. Tilley, *Inorg. Chem.* **1990**, *29*, 4051.
[6] [6a] E. Hengge, E. Pinter, M. Eibl, F. Uhlig, *Bull. Soc. Chim. Fr.* **1995**, *132*, 509. – [6b] E. Hengge, M. Eibl, F. Schrank, *J. Organomet. Chem.* **1989**, *369*, C23.
[7] W. Palitzsch, U. Böhme, C. Beyer, G. Roewer, *Organometallics* **1998**, *17*, 2965.
[8] R. Kiefer, F. Benesovsky, E. Gallistl, *Z. Metallkunde* **1952**, *43*, 284.
[9] [9a] C. P. Casey, S. W. Polichnowski, *J. Am. Chem. Soc.* **1978**, *100*, 7565. – [9b] J. E. Ellis, G. P. Hagen, *Inorg. Chem.* **1977**, *16*, 1357. – [9c] D. J. Darensbourg, R. K. Hanckel, C. G. Bauch, M. Pala, D. Simmons, J. N. White, *J. Am. Chem. Soc.* **1985**, *107*, 7463.
[10] [10a] F. A. Cotton, C. S. Kraihanzel, *J. Am. Chem. Soc.* **1962**, *84*, 4432. – [10b] C. S. Kraihanzel, F. A. Cotton, *Inorg. Chem.* **1963**, *2*, 533.
[11] [11a] W. Strohmeier, K. Gerlach, *Chem. Ber.* **1961**, *94*, 398. – [11b] W. Strohmeier, G. Schönauer, *Chem.Ber.* **1961**, *94*, 1346.
[12] W. Buchner, A. Schenk, *Inorg. Chem.* **1984**, *23*, 132.
[13] M. H. Quick, R. J. Angelici, *Inorg. Chem.* **1976**, *15*, 160.
[14] D. Barton, W. D. Ollis (Eds.), *Comprehensive Organic Chemistry*, Pergamon Press, Oxford, **1979**, vol. 2, 258.
[15] [15a] I. M. Lorkovic, M. S. Wrighton, W. M. Davis, *J. Am. Chem. Soc.* **1994**, *116*, 6220 and references cited therein. – [15b] W. Beck, H. Werner, H. Engelmann, H. S. Smedal, *Chem. Ber.* **1968**, *101*, 2143.
[16] [16a] U. Anders, W. A. G. Graham, *J. Chem. Soc., Chem. Commun.* **1965**, 499. – [16b] R. G. Hayter, *J. Am. Chem. Soc*. **1966**, *88*, 4376. – [16c] L. Arndt, T. Delord, M. Y. Darensbourg, *J. Am. Chem. Soc*. **1984**, *106*, 456.

[17] J. K. Ruff, *Inorg. Chem.* **1969**, *8*, 86.
[18] L. E. Orgel, *Inorg. Chem.* **1962**, *1*, 25.
[19] D. J. Darensbourg, C. G. Bauch, J. H. Reibenspies, A. L. Rheingold, *Inorg. Chem.* **1988**, *27*, 4203.
[20] R. Krentz, R. K. Pomeroy, *Inorg. Chem.* **1985**, *24*, 2976.
[21] H. G. O. Becker (Ed.), *Organikum*, VEB Deutscher Verlag der Wissenschaften, Berlin, **1984**, p. 623.
[22] W. A. Herrmann (Ed.), *Synthetic Methods of Organometallic and Inorganic Chemistry*, G. Thieme Verlag, Stuttgart, New York, **1996**, vol. 2, p. 167.
[23] F. Uhlig, P. Gspaltl, M. Trabi, E. Hengge, *J. Organomet. Chem.* **1995**, *493*, 33.
[24] K. Maeyama, N. Iwasawa, *J. Am. Chem. Soc.* **1998**, *120*, 1928.
[25] K. Issleib, A. Tzschach, *Chem. Ber.* **1959**, *92*, 1118.

Received February 16, 1999
[I99052]

Mono- and 1,1′-Disubstituted Aza Ferrocenyl Compounds: Evidence for an Original Electroactive Fluorescent Species

Béatrice Delavaux-Nicot*[a] and Suzanne Fery-Forgues[b]

Keywords: Ferrocenyl ligands / Electrochemistry / Fluorescence / Azaalkyl compounds / Crown compounds

New azaalkyl or azacrown ferrocenyl compounds containing a C_5H_4COCC- linkage are accessible from mono- or diacetylferrocene upon treatment with the appropriate aldehydes ($CHOC_6H_4$-*p*-R, R = NEt_2, N-aza-15-crown-5). Preliminary results concerning the electrochemical behaviour of complexes $[(C_5H_5)Fe(C_5H_4COCH{=}CHC_6H_4NEt_2)]$ (**3a**), $[Fe(C_5H_4COCH{=}CHC_6H_4NEt_2)_2]$ (**5a**), the novel ferrocenophane $[Fe(C_5H_4COCH_2)_2CHC_6H_4NEt_2]$ (**6a**) and its protonated species $[Fe(C_5H_4COCH_2)_2CHC_6H_4NHEt_2][BF_4]$ (**7a**), are reported. The ferrocenyl ligand **5a** is a rare example of a molecule which is both electroactive and fluorescent.

Introduction

The design of ferrocene-based ion sensors constitutes an area of active research,[1] especially for property-directed synthesis.[2] Of special interest are novel functionalised molecules which are able to change an easily measurable physical property by coordination or interaction with a target molecule. Among these new molecules are redox-functionalised receptors which are able to display a shift of the redox potential upon addition of particular substrates, and we have recently been involved in the synthesis of electroactive ferrocenyl receptors for the electrochemical recognition of cations and anions.[3] Studies concerning ion recognition by fluorescent sensors are also well documented and offer a wide range of applications.[4] Despite the development of these two areas, to the best of our knowledge, few examples of fluorescent ferrocenyl ion sensors have been described[5] probably because ferrocene derivatives are known to be efficient fluorescence quenchers.[6] It is noteworthy that Beer et al. have developed two particularly interesting polymetallic [Ru-Fe] systems where anion binding induces a luminescence revival.[5] In the compounds described by Beer et al.[5], luminescence arises from organometallic ruthenium(II) and osmium(II) bipyridyl moieties and the ferrocene residue acts as a quencher. As a complementary part of our research, a *purely organic* fluorescent ion sensor subunit containing an R-aza complexing moiety (−COCH=CHC_6H_4-*p*-R, R = NEt_2 or aza-15-crown-5)[7] was combined with a redox ferrocenyl fragment to give rise to a new type of ion-sensing device. This choice was mainly made for the following reasons: i) It has recently been shown for a dibenzylideneacetone containing these aza fragments that the photophysical properties of the fluorescent group can be modified upon complexation of the nitrogen atom.[7] ii) Redox active ionophores based on covalently linked crown ether-metallocene systems have received much attention in recent years and give a good selective electrochemical response to the presence of a guest cation.[8] It is worth noting that in our simple ligands, the ferrocenyl moiety is involved in the conjugated π system, and a physical response for ion recognition either by electrochemistry and/or by fluorescence methods can be expected.

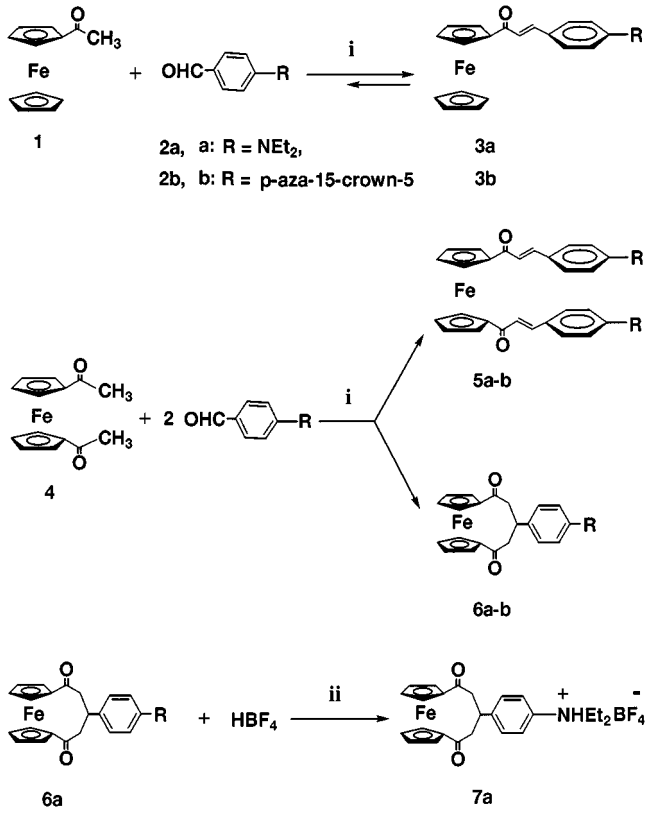
In this paper we report the characterization of novel electroactive ferrocenyl ligands presenting a rare C_5H_4COCC linkage[9] (Scheme 1) and preliminary results concerning the physical properties of the original fluorescent electroactive molecule $[Fe(C_5H_4COCH{=}CHC_6H_4NEt_2)_2]$ (**5a**).

Results and discussion

In order to test the efficiency of the synthesis of easily isolable products presenting the desired properties, a reaction was performed between the monosubstituted ferrocenyl compound $[(C_5H_5)Fe(C_5H_4COCH_3)]$ (**1**) and *p*-diethylaminobenzaldehyde (**2a**) or crown aldehyde [N-(4-formylphenyl)aza-15-crown-5] (**2b**) in basic solution (1:1 ethanol/10% aqueous NaOH). With **2a**, the expected compound $[(C_5H_5)Fe(C_5H_4COCH{=}CHC_6H_4NEt_2)]$ (**3a**) formed in 40% yield (by NMR spectroscopy), after stirring for 6 hours. It was isolated as a red powder after purification and identified by DCI-NH_3 mass spectroscopy ($[M + H]^+$ = 388). The ^1H NMR spectroscopic data were consistent with a *trans* geometry of the ethylenic protons ($^3J_{H-H}$ = 15.4 Hz)[10a] and our spectroscopic assignment was in agreement with the literature data for related compounds.[11][12] The isolated yield of **3a** was not improved under different experimental conditions, probably because of a reverse aldol condensation. The compound $[(C_5H_5)Fe(C_5H_4COCH{=}CHC_6H_4$-*p*-aza-15-crown-5)] (**3b**) was obtained, after 31 h of reaction with **2b**, in 50% yield (by NMR spectroscopy) and characterized after isolation as a red oil.

[a] Laboratoire de Chimie de Coordination du CNRS,
UPR 8241 lié par conventions à l′Université Paul Sabatier et à l′Institut National Polytechnique de Toulouse,
205, route de Narbonne, F-31077 Toulouse Cedex 04, France
[b] Laboratoire des Interactions Moléculaires et Réactivité Chimique et Photochimique,
UMR 5623 au CNRS, 118 route de Narbonne, F-31062 Toulouse Cedex
E-mail: delavaux@lcc-toulouse.fr

 © WILEY-VCH Verlag GmbH, D-69451 Weinheim, 1999 1434−1948/99/1010−1821 $ 17.50+.50/0



Scheme 1. *Reagents and conditions*: i) 1:1 ethanol/10% aqueous NaOH, room temp; ii) CH_3CN, 20°C.

An identical procedure was carried out to obtain the disubstituted ferrocenyl derivative [Fe(C_5H_4COCH=$CHC_6H_4NEt_2)_2$] (**5a**). The analogous compound [Fe(C_5H_4-$COCH$=$CHC_6H_4NMe_2)_2$][13] has been proposed in the literature for photographic use though no characterization or yield have yet been reported. Two equivalents of **2a** were reacted with one equivalent of [Fe($C_5H_4COCH_3)_2$] (**4**) to give, after stirring for 4 h at 20°C, a mixture (50%, NMR) of compound **5a** and the ferrocenophane [Fe(C_5H_4-$COCH_2)_2CHC_6H_4NEt_2$] (**6a**) in a 2/3 ratio. A two-step chromatography workup allowed the separation of pure **5a** as a light-sensitive powder and **6a** as an orange powder with 7% and 9% yield, respectively. Attempts to improve the synthesis of **5a**, as reported in the patent in ref.,[12] or in excess of **2a** according to another published procedure,[14a] failed. The yield of ferrocenophane **6a** was increased (40%) by stirring the reagents for 18 hours (4 equivalents of aldehyde) and performing several diffusions in a toluene/pentane mixture of the red fraction obtained after simple chromatography on alumina. According to the literature, **6a** can be formed either by an aldol condensation in a 1/1 stoichiometry followed by an intramolecular Michael addition[14] or by a reverse aldol condensation in basic medium starting from **5a**.[15] This explains why **6a** is the major compound in solution.

For the disubstituted compound **5a**, DCI-NH_3 mass spectroscopy showed a $[M + H]^+$ molecular peak at the expected value of 589. The IR spectrum exhibited a $\tilde{\nu}$(C=O) vibration at 1644 cm^{-1}, this low value being due to the conjugation of the CO group in the molecule.[10b] The proposed structure was first deduced from NMR spectroscopic data, which revealed high symmetry. The protons of the CH groups, as for the monosubstituted compound **3a**, are in *trans* positions. In the $^{13}C\{^1H\}$-NMR spectrum, a singlet observed at $\delta = 192.4$ in $CDCl_3$ was attributed to the CO groups. 2D NMR experiments were carried out and clearly verified our assignments.

In the case of **6a**, the number and the multiplicity of the signals observed for the cyclopentadienyl protons in the ^1H-NMR spectrum showed the asymmetry of the molecule. In the $^{13}C\{^1H\}$-NMR spectrum a lone singlet was detected for the CO groups ($\delta = 199.5$, $CDCl_3$). Analysis of the ^1H-^{13}C HMBC spectra supported the existence of a bridge linkage between the Cp ring, in which the CO carbon atoms are strongly coupled to the H atom of the CH group and to each proton of the CH_2 groups. The bridge between the Cp rings may force them out of coplanarity and staggers them by less than 36°. It probably also pushes the CO groups out of the Cp ring planes and in the same direction.[16] Selective decoupling ^1H-NMR experiments (400 MHz, 223 K, $CDCl_3$) indicated that the CH_2 protons of the ferrocenophane chain are diastereotopic (at 293 K, a broad singlet at $\delta = 2.50$ and a triplet at $\delta = 2.90$ were detected for both CH_2 groups). X-ray structures of [5]-ferrocenophane are not common but it has been previously reported that the ferrocenophane molecules have conformational mobility in solution: the Cp rings can undergo small torsional vibrations with respect to each other around the axis passing through the center of the rings and the iron atom.[17]

The analogous reaction of **4** with the crown aldehyde **2b** produced, after stirring for 17 h, [Fe(C_5H_4COCH=CHC_6H_4-*p*-aza-15-crown-5)$_2$] (**5b**) and [Fe(C_5H_4-$COCH_2)_2CHC_6H_4$-*p*-aza-15-crown-5)] (**6b**) in a 3:7 ratio. These compounds were identified by DCI-NH_3 mass spectroscopy ($[M + H]^+ = 881$ and 576, respectively). The NMR spectroscopic data of a pure sample of **6b** were very similar to those obtained for **6a** when considering the same basic cyclic structure for both compounds. 2D NMR experiments allowed a clear assignment of the ^{13}C-NMR chemical shifts, in particular for the carbons of the Cp and crown rings whose signals appeared in the same region of the spectra.

Compound **6a** was protonated to provide useful data concerning the analysis of its electrochemical behaviour. When treated with one equivalent of $HBF_4 \cdot Et_2O$ in CH_3CN, **6a** afforded [Fe($C_5H_4COCH_2)_2CHC_6H_4$-$NHEt_2$][BF_4] (**7a**) (95% NMR, MS (FAB): 430 [M − $BF_4]^+$). The ^1H-^1H COSY NMR spectrum clearly confirmed the nature of the protonation site (nitrogen): a correlation between the NH^+ proton[3e] (broad singlet, $\delta = 8.60$) and the NCH_2 protons (complex multiplet, $\delta = 3.65$) was observed (CD_3CN, 300 MHz).

The electrochemical behaviour of compounds **3a**, **5a** and **6a** (R = NEt_2) was investigated. For compounds **3a** and **5a** two redox waves were observed by cyclic voltammetry (CV). The oxidation peak potentials (Epa) of the amine moieties (0.88 V and 0.78 V vs SCE for **3a** and **5a**, respectively) are

in the expected range of values.[18] It is to be noted that $CH_3COCH{=}CHC_6H_4NEt_2$ (**8**) was oxidized at Epa = 0.74 V in CH_2Cl_2. For the Fe(II)/Fe(III) couple, the Epa values, 0.65 V and 1.15 V for **3a** and **5a**, respectively, depend on the number of CO substituents, which are strong electron-withdrawing groups.[11b] This was confirmed by the data obtained for **1** and **4** under the same experimental conditions. Stepwise addition of $HBF_4{\cdot}Et_2O$ to a solution of compound **3a** in CH_3CN resulted in a clear evolution of the ferrocene wave from $E_{1/2}$ = 0.61 to 0.67 V, associated with the disappearance of the second wave (Figure 1, top). The solution turned pink and the new species were oxidized (Fe^{III}) and recovered by electrolysis at 0.75 and 0.30 V, respectively, although some decomposition occurred.

The electrochemical oxidation of compound **6a** resulted in the observation of quasi-reversible redox waves of equal intensity at 0.77 and 0.99 V (Epa vs SCE), assigned to the amine and ferrocene parts, respectively (Figure 1, bottom). This was verified by a two-step electrolysis at controlled potential (0.90 and 1.10 V, respectively), coupled with cyclic and linear voltammetry measurements. The stepwise addition of 1 equivalent of $HBF_4{\cdot}Et_2O$ in CH_3CN to compound **6a** induced the disappearance of the first wave, whereas there was no effect on the second. Moreover, the new species formed had the same electrochemical characteristics and behaviour towards electrochemical oxidation (at 1V) as compound **7a** under the same conditions.

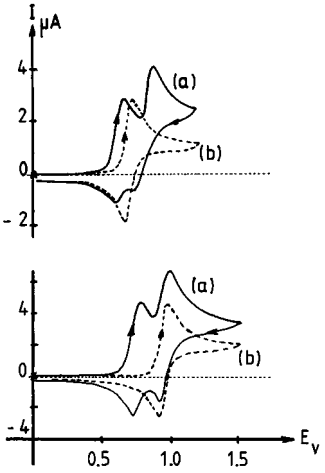


Figure 1. Cyclic voltammograms of (a) **3a**, (b) **3a** + 1 equiv. of $HBF_4{\cdot}Et_2O$ (top); cyclic voltammograms of (a) **6a**, (b) **6a** + 1 equiv. of $HBF_4{\cdot}Et_2O$, at 0.1 V s^{-1} in CH_3CN (bottom); experimental conditions: Pt electrode (1 mm) in 0.1 mol L^{-1} solution of Bu_4NPF_6 in CH_3CN, complex concentration 10^{-3} M

It has been shown that in a molecule with a saturated spacer such as **6a**, the protonation of the nitrogen atom may induce an anodic shift of the oxidation potential of the Fe^{II}/Fe^{III} couple.[3e,19] However, the nitrogen-iron distance is too long in **6a** for such an effect to be detected.[19] Interposition of a conjugated spacer between the ionophore and the ferrocene unit produces a noticeably different electrochemical response towards H^+ addition for **3a**. Electronic communication becomes possible through the spacer between the redox center and the protonated site, inducing an anodic shift of $\Delta E_{1/2}$ = 60 mV for this couple. This property is of real importance and suggests that molecules such as **3a**,**b** and **5a**,**b** could be electrochemical cation sensors.

The spectroscopic properties of compounds **3a** and **5a** were investigated in CH_3CN. The absorption spectra of these compounds (Figure 2) can be interpreted in accordance with the literature data.[6b,20] The broad low-intensity band located above 460 nm and well visible in the case of **3a** can be assigned to the d-d transition of iron in ferrocene. The intense band at 408 nm for **3a** and 416 nm for **5a** can similarly be attributed to charge transfer (CT) between the donor amino group and the acceptor carbonyl group. This band was strongly red-shifted with respect to the CT band of chalcone **8** (λ_{abs} = 382 nm in CH_3CN), which is in agreement with the extension of the conjugated system. The absorption spectrum of crown compounds **3b** and **5b** is similar in shape to that of **3a** and **5a**, respectively. Molar absorption coefficients were also found to be very close (for example ε_{404} = 28 600 and 30 000 L mol^{-1} cm^{-1} for **3a** and **3b**, respectively). The absorption spectrum of **6a** in CH_2Cl_2 displays a strong absorption band peaking around 264 nm and two weak bands between 300 and 360 nm, the latter two being assigned to the ferrocenyl moiety. It was checked that the protonated compound **7a** did not exhibit the long wavelength absorption band characteristic of the ferrocenium ion.

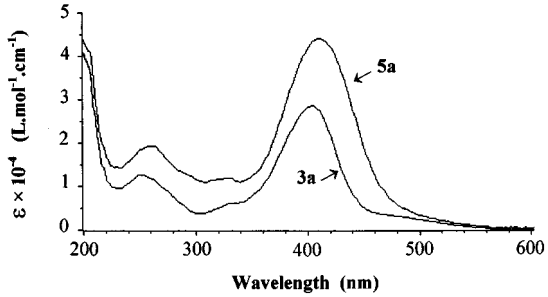


Figure 2. Absorption spectra of **3a** and **5a** in CH_3CN, ε = molar absorption coefficient

Very weak emission could be expected for compounds **3a** and **5a**, since ferrocenyl residues are known to quench luminescence. Indeed, when excited at the absorption band maximum, **3a** displays a very weak ($\Phi = 1 \times 10^{-4}$) fluorescence signal around 560 nm at room temperature. In contrast, an intense unresolved emission band was observed for compound **5a** (Figure 3). Absorption or excitation spectra of compound **5a** were similar. The quantum yield reached 7.7×10^{-2}, i.e. around ten times higher than that of **8** and only two times lower than that of diaminodibenzylidenacetone (**9**) in the same solvent.[7] This shows that in **5a** the ferrocenyl moiety, far from acting as a simple fluorescence quencher, behaves essentially as an auxochrome. Compound **5a** was studied in different solvents (Table 1). A strong positive solvatochromic effect was observed both in the absorption and emission spectra, which is also reminiscent of the behaviour of **9**.[21] This trend was accompanied by a drastic increase of the fluorescence quantum yield in polar media, which generally indicates the in-

volvement of an emissive intramolecular CT in the excited state.

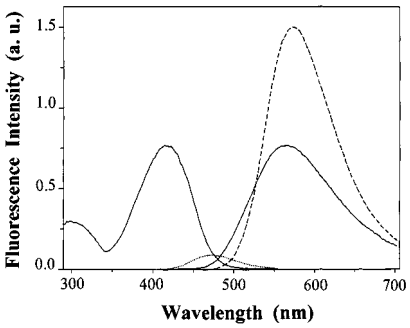


Figure 3. Excitation (λ_{em} = 560 nm) and emission (λ_{ex} = 416 nm) spectra of **5a** in CH_3CN (full line); emission spectra of **8** (λ_{ex} = 382 nm, dotted line) and **9** (λ_{ex} = 444 nm, broken line); the emission spectra are normalized according to the fluorescence quantum yield

Table 1. Spectroscopic data for **5a** in different solvents: absorption wavelength (λ_{abs}), emission wavelength (λ_{em}), fluorescence quantum yield (Φ_F) and Lippert polarity parameter (Δ_f)

Solvent	λ_{abs} (nm)	λ_{em} (nm)	Φ_F[a]	Δ_f
Cyclohexane	386	–	$<10^{-4}$	−0.001
Toluene	404	487	1.3×10^{-3}	0.013
Dioxane	404	495	4.3×10^{-3}	0.021
Ethyl acetate	404	516	1.4×10^{-2}	0.202
Tetrahydrofuran	412	523	2.1×10^{-2}	0.210
Acetone	410	541	2.4×10^{-2}	0.287
Acetonitrile	416	560	7.7×10^{-2}	0.306

[a] $\lambda_{ex} = \lambda_{abs}$.

Preliminary studies showed that crown compound **5b** was also fluorescent and could therefore find interesting applications as a fluoroionophore.

Conclusion

These results clearly indicate that new electroactive and fluorescent species containing only ferrocene as a metallic moiety can be obtained. Work is in progress to understand the electrochemical and unusual photophysical properties of **5a−b** better, and to test their potential ability for cation recognition by both techniques.

Experimental Section

Physical Methods: NMR, electrochemical and photophysical measurements were made as previously reported.[3e,7] The fluorescence spectra were corrected. The fluorescence quantum yield was determined relative to coumarin 6 in ethanol as the standard (Φ_F = 0.78).[22] Fast atom bombardment (FAB^+) or desorption chemical ionization (DCI) mass spectrometry were performed on a Nermag R 10 at the Service Commun de Spectrométrie de Masse de l'Université Paul Sabatier et du CNRS, Toulouse.

Complex 3b: To 20 mL of a basic solution (1:1 ethanol/10% aqueous NaOH) was added dropwise a mixture of 1 equiv. of **1** (315 mg, 1.38 mmol) and 1.1 equiv. of **2b** (490 mg, 1.52 mmol) dissolved in 10 mL ethanol. The light-protected mixture was stirred for 31 h at room temperature and the solvent evaporated to dryness. The organic phase was extracted with dichloromethane. The solution was filtered with a cannula under nitrogen, the solvent was evaporated off and the residue washed with pentane. The product was purified by column chromatography on alumina (eluent: pentane/CH_2Cl_2) and collected as a red fraction. After evaporation of the solvent, the product was washed with pentane and dried under vacuum for several hours to afford a red oil (240 mg, 33% yield). – ^{1}H NMR (300 MHz, $CDCl_3$, 293 K): δ = 3.67 (m, 16 H), 3.80 (m, 4 H) (CH_2 Crown), 4.22 (s, 5 H, C_5H_5), 4.56, 4.92 (each t, J_{HH} = 1.9 Hz, 4 H, C_5H_4), 6.70 (*CH*−CN), 7.55 (*CH*−CH−CN) (each d, J_{HH} = 8.9 Hz, 4 H, C_6H_4), 6.96 (CH=*CH*−CO), 7.76 (*CH*=CH−CO) (each d, J_{HH} = 15.5 Hz, 2 H). – ^{13}C{^{1}H} NMR (75.47 MHz, $CDCl_3$, 293 K): δ = 53.13, 68.69, 70.49, 70.66, 71.75 (s, CH_2 Crown), 69.99, 72.65, 81.69 (C_5H_4), 70.41 (C_5H_5), 111.93 (*CH*−CN), 123.08 (C_{ipso}−C=C), 130.65 (*CH*−CH−CN), 149.69 (C_{ipso}−N) (C_6H_4), 118.30 (CH=*CH*−CO), 141.92 (*CH*=CH−CO), 193.46 (CO), each s. MS (FAB); *m*/*z*: 533 $[M]^+$. – $C_{29}H_{35}FeNO_5$: calcd. C 65.27, H 6.62, N 2.63; found C 64.95, H 6.41, N 2.64.

Complex 5a and 6a: A mixture of 1 equiv. of **4** (400 mg, 1.48 mmol) and 2 equiv. of **2a** (524 mg, 2.96 mmol) in 20 mL ethanol was added dropwise to 20 mL of a basic solution (1:1 ethanol/10% aqueous NaOH). After stirring for 4 h at 20°C, the organic phase was extracted with dichloromethane, the solution filtered and the solvent evaporated to dryness. After column chromatography on alumina (eluent: CH_2Cl_2 then THF) a red fraction was collected and protected from light. Compounds **5a** and **6a** were separated by thin layer chromatography on silica gel (eluent: ethyl acetate/toluene: 1:2.5) in the dark. The products were rapidly extracted with acetone. Compound **5a** (red band) was purified by diethyl ether extraction and washing with pentane, and dried under vacuum to afford a red powder (61 mg, 7% yield). Compound **6a** (orange band) was washed with pentane, dried under vacuum and obtained as an orange powder (57 mg, 9% yield). Complex **5a**. – ^{1}H NMR (400 MHz, $CDCl_3$, 293 K): δ = 1.20 (t, J_{HH} = 7.1 Hz, 12 H, CH_3), 3.41 (q, J_{HH} = 7.1 Hz, 8 H, CH_2N), 4.53, 4.91 (each t, J_{HH} = 1.9 Hz, 8 H, C_5H_4), 6.62 (*CH*−CN), 7.51 (*CH*−CH−CN) (each d, J_{HH} = 8.9 Hz, 8 H, C_6H_4), 6.90 (CH=*CH*−CO), 7.75 (*CH*=CH−CO) (each d, J_{HH} = 15.4 Hz, 4 H). – ^{13}C{^{1}H} NMR (100.62 MHz, $CDCl_3$, 293 K): δ = 12.59 (CH_3), 44.47 (CH_2N), 70.99, 74.03, 82.47 (C_5H_4), 111.16 (*CH*−CN), 121.69 (C_{ipso}−C=C), 130.65 (*CH*−CH−CN), 149.37 (C_{ipso}−N) (C_6H_4), 116.87 (CH=*CH*−CO), 142.70 (*CH*=CH−CO), 192.38 (CO), each s. – MS (DCI): 589 $[M + H]^+$. – $C_{36}H_{40}N_2O_2Fe$: calcd. C 73.45, H 6.85, N 4.76; found C 73.07, H 6.97, N 4.64. Complex **6a.** – NMR: See text, close to **6b** (vide infra). MS (DCI): 430 $[M + H]^+$. – $C_{25}H_{27}FeNO_2$: calcd. C 69.91, H 6.34, N 3.26; found C 69.72, H 6.20, N 3.11.

Selected data for **6b:** ^{1}H NMR (400 MHz, $CDCl_3$, 223 K): δ = 2.41 (br d, J_{HH} = 12.0 Hz, 2 H, CH_2CO), 2.87 (br t, J_{HH} = 12.5 Hz, 2 H, CH_2CO), 3.66 (m, 20 H, CH_2 Crown), 4.25 (br t, J_{HH} = 11.5 Hz, 1 H, CH), 4.63, 4.66, 4.87, 4.91 (each br s, 8 H, C_5H_4), 6.61 (*CH*−CN), 7.21 (*CH*−CH−CN) (each d, J_{HH} = 8.5 Hz, 4 H, C_6H_4). – ^{13}C{^{1}H} NMR, (100.62 MHz, $CDCl_3$, 223 K): δ = 45.39 (CH), 46.61 (CH_2), 52.75, 67.84, 69.88, 71.57 (CH_2, crown), 68.84, 72.47, 74.25, 75.05, 81.81 (C_5H_4), 110.70 (*CH*−CN), 127.74 (*CH*−CH−CN), 131.64 (C_{ipso}−CH), 145.58 (C_{ipso}−N) (C_6H_4), 199.44 (CO), each s.

Selected data for **7a:** ^{1}H NMR (300 MHz, CD_3CN, 293 K): δ = 1.08 (t, J_{HH} = 7.1 Hz, 6 H, CH_3), 2.29 (m, 2 H, CH_2CO), 3.09 (br

t, J_{HH} = 12.4 Hz, 2 H, CH_2CO), 3.65 (m, 4 H, CH_2N), 4.15 (br t, J_{HH} = 11.4 Hz, 1 H, CH), 4.65, 5.07 (m, 8 H, C_5H_4), 7.46 (CH−CN), 7.65 (*CH*−CH−CN) (each d, J_{HH} = 8.6 Hz, 4 H, C_6H_4), 8.60 (br s, 1 H, NH). − $^{13}C\{^1H\}$ NMR (75.47 MHz, $CDCl_3$, 223 K): δ = 10.03 (CH_3), 46.14 (*CH*$_2$,CO, CH), 54.62 (CH_2N), 68.79, 72.83, 74.44, 74.94, 82.61 (C_5H_4), 122.87 (*CH*−CN), 129.60 (*CH*−CH−CN), 135.47 (C_{ipso}−N) 148.89 (C_{ipso}−CH) (C_6H_4), 179.78 (CO), each s.

Acknowledgments

We gratefully acknowledge Dominique de Montauzon (Service d′Electrochimie du LCC, Toulouse, CNRS) for expert technical assistance and fruitful discussions.

[1] For example: [1a] M. C. Grossel, M. R. Goldspink, J. A. Hriljac and S. C. Weston, *Organometallics* **1991**, *10*, 851−860 and references therein. − [1b] E. C. Constable, *Angew. Chem. Int. Ed. Engl.* **1991**, *30*, 407−408 and references therein. − [1c] P. D. Beer, *Chem. Soc. Rev.* **1989**, *18*, 409−450. − [1d] P. D. Beer, *Adv. Inorg. Chem.* **1992**, *39*, 79−157. − [1e] J. C. Medina, T. T. Goodnow, M. T. Rojas, J. L. Atwood, B. C. Lynn, A. E. Kaifer and G. W. Gokel, *J. Am. Chem. Soc.* **1992**, *114*, 10583−10595.

[2] H. Plenio and C. Aberle, *Organometallics* **1997**, *16*, 5950−5957 and references therein.

[3] [3a] B. Delavaux-Nicot, N. Lugan, R. Mathieu and J.-P. Majoral, *Inorg. Chem*. **1992**, *31*, 334−336. − [3b] B. Delavaux-Nicot, R. Mathieu, D. de Montauzon, G. Lavigne and J.-P. Majoral, *Inorg. Chem*. **1994**, *33*, 434−443. − [3c] B. Delavaux-Nicot, B. Douziech, R. Mathieu and G. Lavigne, *Inorg. Chem*. **1995**, *34*, 4256−4261. − [3d] B. Delavaux-Nicot, Y. Guari, B. Douziech and R. Mathieu, *J. Chem. Soc., Chem. Commun.* **1995**, 585−587. − [3e] B. Delavaux-Nicot, A. Bigeard, A. Bousseksou, B. Donnadieu and G. Commenges, *Inorg. Chem*. **1997**, *36*, 4789−4797.

[4] For example: [4a] A. Prasanna de Silva, H. Q. N. Gunaratne, T. Gunnlaugsson, A. J. M. Huxley, C. P. McCoy, J. T. Rademacher and T. E. Rice, *Chem. Rev.* **1997**, *97*, 1515−1566. − [4b] *Fluorescent Chemosensors for Ion and Molecule Recognition*; A.W. Czarnik, ACS Symposium Ser. 538: Washington DC, **1993**.

[5] [5a] P. D. Beer, A. R. Graydon and L. R. Sutton, *Polyhedron* **1996**, *15*, 2457−2461. − [5b] P. D. Beer, F. Szemes, V. Balzani, C. M. Salà, M. G. B. Drew, S. W. Dent and M. Maestri, *J. Am. Chem. Soc*. **1997**, *119*, 11864−11875.

[6] [6a] G. L. Geoffroy and M. S. Wrighton, *Organometallic photochemistry*, Academic Press, New York, **1979**, chapter 5, 230−257. − [6b] P. D. Harvey, L. Gan and C. Aubry, *Can. J. Chem*. **1990**, *68*, 2278−2288. − [6c] P. D. Harvey and L. Gan, *Inorg. Chem*. **1991**, *30*, 3239−3241.

[7] N. Marcotte, S. Fery-Forgues, D. Lavabre, S. Marguet and V. G. Pivovarenko, *J. Phys., Chem.* **1999**, *103*, 3163−3170.

[8] M. C. Grossel, D. G. Hamilton, J. I. Fuller and E. Millan-Barios, *J. Chem. Soc., Dalton. Trans.* **1997**, 3471−3477.

[9] For example: *Ferrocenes* A. Togni and T. Hayashi ed., VCH, New York, **1995**.

[10] [10a] R. M. Silverstein, G. C. Bassler and T. C. Morril, in *Spectrometric Identification of Organic Compounds*, Fourth Edition, J. Wiley and Sons, New York, **1981**, Chapter 4, 205. − [10b] R. M. Silverstein, G. C. Bassler and T. C. Morril, in *Spectrometric Identification of Organic Compounds*, Fourth Edition, J. Wiley and Sons, New York, **1981**, Chapter 3, 117−118.

[11] [11a] A. N. Nesmeyanov, G. B. Shulp′in, L. V. Rybin, N. T. Gubenko, M. I., Rybinskaya, P. V. Petrovskii and V. I. Robas, *J. Gener. Chem. USSR*, **1974**, *44*, 1994−2001. − [11b] A. G. Nagy and S. Tomas, *J. Org. Chem*. **1984**, *266*, 257−268.

[12] A. G. Nagy, *J. Org. Chem*. **1985**, *291*, 335−340.

[13] J. P. C. G. Dubosc, U.S. Patent 1967, 3,335,008.

[14] [14a] T. A. Mashburn Jr., C. E. Cain and C. R. Hauser, *J. Org. Chem*. **1960**, *25*, 1982−1986. − [14b] T. H. Barr and W. E. Watts, *Tetrahedron* **1968**, *24*, 3219−3235.

[15] J. A. Winstead, *J. Org. Chem*. **1972**, *37*, 1271−1272.

[16] E. Gyepes, T. Glowiack and S. Toma, *J. Organomet. Chem*. **1986**, *316*, 163−168.

[17] T. N. Sal′nikova, V. G. Andrianov, M. Y. Antipin and Y. T. Struchkov, *Sov. J. Coord. Chem.* **1977**, *3*, 732−737.

[18] P. D. Beer, C. Blackburn, J. F. McAleer and H. Sikanyika, *Inorg. Chem.* **1990**, *29*, 378−381.

[19] H. Plenio, J. Yang, R. Diodone and J. Heinze, *Inorg. Chem*. **1994**, *33*, 4098−4104.

[20] [20a] S. Toma, A. Gaplovsky and I. Pavlik, *Monatsh. Chem*. **1985**, *116*, 479−486. − [20b] P. D. Harvey and J. G. Sharma, *Can. J. Chem.* **1990**, *68*, 223−227.

[21] [21a] A. A. Khalaf, S. H. Etaiw, R. M. Issa and A. K. El-Shafei, *Rev. Roum. Chim.* **1977**, *22*, 1251−1259. − [21b] J. M. Eisenhart and A. B. Ellis, *J. Org. Chem.* **1985**, *50*, 4108−4113. − [21c] R. J. De Voe, M. R. V. Sahyun, E. Schmidt, M. Sadrai, N. Serpone and D. K. Sharma, *Can. J. Chem*. **1989**, *67*, 1565−1575.

[22] G. A. Reynolds and K. H. Drexhage, *Opt. Commun.* **1975**, *13*, 222−225.

Received January 18, 1999
[I99013]

Mono(cyclooctatetraenyl)samarium Complexes: the Return of the Normally "Inaccessible" Bis(trimethylsilyl)amido Derivative

M. Visseaux,*[a] A. Dormond,[a] and D. Barbier-Baudry[a]

Keywords: Samarium / Early organolanthanides / Bis(trimethylsilyl)amido / Cyclooctatetraenyl / Lanthanides

The complexes [(COT)Ln{N(SiMe$_3$)$_2$}(THF)] (Ln = late lanthanide metal) are readily accessible but, until now, the samarium analogue has proved elusive. The latter can be formed in solution but is easily desolvated during the isolation process, leading to a highly associated complex which is only soluble in coordinating solvents or in the presence of ancillary ligands.

Introduction

There is now a growing interest in the cyclooctatetraenyl derivatives of the metals of groups 3 and 4. As an alternative to traditional cyclopentadienyl chemistry, this ligand provides original structural features,[1a,1b] and, due to their potential for olefin[2] and lactone polymerization,[3] cyclooctatetraenyl complexes are often protected by patents. Our research has recently turned towards diene polymerization catalysed by early lanthanide metal complexes[4] and we envisaged the use of monocyclooctatetraenyl derivatives as possible starting materials for convenient catalyst precursors. During our first investigations into lanthanide chemistry, we had observed the formation of [(COT)Sm{N(SiMe$_3$)$_2$}(THF)], (COT = C_8H_8) in polar (deuterated THF) and nonpolar (deuterated benzene) solvents.[5] Therefore we were surprised when it was reported that the amido complexes [(COT)Ln{N(SiMe$_3$)$_2$}(THF)] could only be isolated for yttrium and the late lanthanide metals.[6a] For samarium, this compound could not be isolated, an unusual inverse half-sandwich complex being formed instead.[6b] Because [(COT)Sm{N(SiMe$_3$)$_2$}(THF)] could provide a good precursor for catalytically active cationic cyclooctatetraenyl species (see ref.[7] for recent results in this field), we decided to look again at the reaction of Na[N(SiMe$_3$)$_2$] with [(COT)SmCl(THF)]$_2$. In this communication we report new data leading to a better understanding of these apparently contradictory data.

Results and Discussion

All syntheses were first performed in an NMR tube and then scaled up. In a typical reaction, [(COT)SmCl(THF)]$_2$, **1** and NaN(SiMe$_3$)$_2$ were mixed in a 1/1 molar ratio in an NMR tube and C_6D_6 was added. The violet complex **1** is not soluble in benzene but, after vigorously stirring for a short time, a purple solution and a grey-brown precipitate were obtained. A set of signals clearly indicative of the presence of a mono(bistrimethylsilyl)amido complex was observed {δ = 9.17 (8 H, COT), and −2.37 [18 H, N(SiMe$_3$)$_2$]}.

Because the same compound had previously been obtained by mixing the reactants in deuterated THF and then changing the solvent for deuterated benzene,[8] the bulk synthesis of [(COT)Sm{N(SiMe$_3$)$_2$}(THF)], **2**, was performed in THF with 1/1 stoichiometric amounts of the reactants. After 16 hours stirring at room temperature, the solvent was removed and the crude product extracted with toluene. The reddish solution was slowly concentrated leaving a small crop of deep red crystals (unsuitable for X-ray analysis) and a mother liquor which, after separation of the crystals, was evaporated to dryness. Both fractions were analysed by NMR spectroscopy. The crystals were insoluble in benzene: when C_6D_6 was added to a sample of ca 5−6 mg, after smooth heating and ultrasonic stirring, a pale orange solution was obtained and a brown precipitate deposited. NMR spectroscopic analysis of the solution showed virtually only one component − the known complex Sm[N(SiMe$_3$)$_2$]$_3$ (δ = −1.57 ppm).[9] The NMR tube was then connected to a vacuum line, degassed and THF added. The precipitate immediately dissolved giving a pink-purple solution and only the signals previously observed for **2** were present.

The red solid which was obtained from the mother liquor was found, by elemental analysis, to correspond to the partially desolvated complex [(COT)Sm{N(SiMe$_3$)$_2$}(THF)$_{0.5}$]. It was only sparingly soluble in deuterated benzene and, as well as a reddish precipitate, a pale purple solution of **2** was obtained {δ (C_6D_6) = 9.19 (8 H, COT), 5.95 (4 H, THF), 2.17 (4 H, THF), −2.37 [18 H, N(SiMe$_3$)$_2$]}.

A sample of analytically pure unsolvated [(COT)SmN(SiMe$_3$)$_2$]$_n$ **3**, was obtained (see experimental) by the slow evaporation of a toluene solution of **2**. The IR spectrum confirmed the absence of coordinated THF[10a,b] (no absorption in the range 1010 − 1030 cm^{-1}), and the presence of the COT^{2-} ligand (C−H bending at 719, 869 cm^{-1}).[10b,11]

[a] Laboratoire de Synthèse et d'Electrosynthèse Organométalliques (L.S.E.O.-U.M.R. 5632),
Faculté des Sciences Gabriel, Université de Bourgogne,
6 bd Gabriel, F-21000 Dijon, France.
E-mail: mvisseau@u-bourgogne.fr

 © WILEY-VCH Verlag GmbH, D-69451 Weinheim, 1999 1434−1948/99/1010−1827 $ 17.50+.50/0

Crystals of **2** could be obtained at low temperature, as thin foliated plates, during the concentration of a THF solution but they rapidly redissolved when the temperature was raised. Simultaneously, a colour change from pink to red, corresponding to the desolvation, was observed.

By using a nearly 1:2 molar ratio of **1** and Na[N(-$SiMe_3)_2$], the formation of an anionic compound, [(COT)Sm{$N(SiMe_3)_2$}$_2$Na], **4**, was observed. This anionic complex is soluble in benzene and can be extracted with pentane. An analogous anionic compound containing two sterically demanding ligands, [(COT)Ln{$CH(SiMe_3)_2$}$_2$-$Li(THF)_2$], has also been described as being soluble in hexane.[12]

Complex **4** was not formed alone: in the benzene solution, the presence of **2** (30%) and $Sm[N(SiMe_3)_2]_3$ **(5)** (15%) was also observed {percentages estimated by integration of the (COT) and $N(SiMe_3)_2$ signals in the ^1H NMR spectrum}. In deuterated THF as solvent, the composition of the mixture was different − the presence of the less soluble [$(COT)_2$SmNa], (δ = 13.21)[10b] (10%), was also observed. The mixture contained **4** as major component (65%) and **2** (25%). The solvent was removed in vacuo and the remaining traces of coordinated solvent were eliminated by three cycles of toluene condensation and evaporation. The residue was extracted with pentane, the pentane solution transferred to another tube and pentane removed in vacuo. After addition of C_6D_6, the NMR spectrum was recorded. Signals corresponding to the half-sandwich complex[6b] were observed (10%), as well as those of **2** (25%), **4** (45%) and **5** (20%). After addition of THF, the signals of the half-sandwich complex decreased and disappeared within 12 hours.

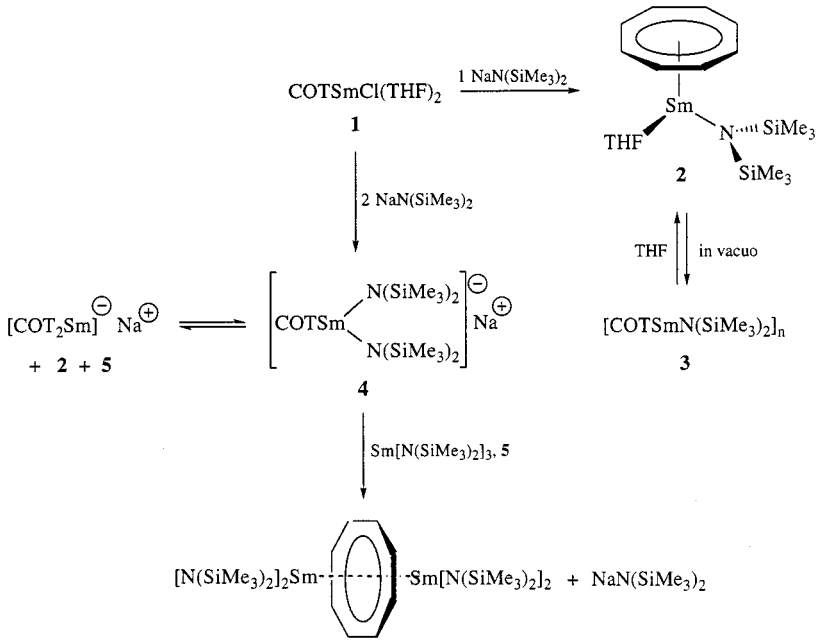
In summary, we could observe the formation of the expected [(COT)Sm{$N(SiMe_3)_2$}(THF)] **(2)** when performing the reaction without an excess of amido reagent. This complex was easily desolvated, leading to an insoluble, highly associated compound [(COT)Sm{$N(SiMe_3)_2$}]$_n$ **(3)** isolated as deep red microcrystals, whose IR data are very close to those of unsolvated uranium and thorium analogues.[13] After addition of the required quantity of THF the soluble complex **2** is recovered. For the desolvated complex **3**, the saturation of the coordination sphere of the samarium ought to be completed by bridging $N(SiMe_3)_2$ groups, as commonly observed for main group derivatives,[14] or more seldom for transition metal organometallic complexes.[15] The previously described half-sandwich complex [{$N(SiMe_3)_2$}$_2$Sm(COT)Sm{$N(SiMe_3)_2$}$_2$] can be obtained with a 1:2.6 molar ratio of the reactants.[6b] We could also observe the formation of this compound, in a lower yield, with a 1:2 molar ratio of the reactants. It was not stable in the presence of THF. Conproportionation-disproportionation reactions have been observed in the uranium series between an associated monocyclooctatretraenyl complex and an unsolvated homoleptic borohydride (Scheme 1).[16]

$$[(C_8H_8)U(BH_4)_2]_n + U(BH_4)_4 \longrightarrow (BH_4)_3U(C_8H_8)U(BH_4)_3$$

$$(BH_4)_3U(C_8H_8)U(BH_4)_3 \xrightarrow{THF} [(C_8H_8)U(BH_4)_2](THF) + U(BH_4)_4(THF)_2$$

Scheme 1

Nevertheless, in the samarium series, by mixing **3** and $Sm[N(SiMe_3)_2]_3$ no such reaction occurred. It was consequently postulated that the formation of the half sandwich could occur in the alkane phase, from **4** and **5**, with elimination of $Na[N(SiMe_3)_2]$ (Scheme 2). In fact, after heating a (deuterated) benzene solution containing **4** and **5**, the half-sandwich complex was found to be the major component of the mixture.



Scheme 2. Formation of cyclooctatetraenylsilylamido derivatives

Conclusions

These experiments emphasize the great importance of the ionic strength or the polarity of the reaction medium for organolanthanide syntheses, dominated by the exchange ligand reactions. They also show the interest of using paramagnetic lanthanides for these studies: even for an element inducing a relatively small paramagnetic shift, the NMR spectra allow us to observe the different equilibria established in neutral or polar media.

Experimental Section

General: All experiments were performed with rigorous exclusion of oxygen and moisture, using a JACOMEX glovebox and vacuum line techniques. Solvents were stored over sodium-benzophenone and vacuum-transferred to reaction vessels. Deuterated solvents were distilled over Na/K alloy. NMR spectra were recorded on a Bruker AC 200 spectrometer (297 K). IR spectra were recorded in nujol mulls with a Bruker IFS/66V Spectrometer. Elemental analyses were performed with a Fisons EA 1108 CHONS apparatus. $[(COT)SmCl(THF)]_2$ **1** was prepared as previously described[10b] but with solid $K_2(COT)$ as reagent.[13] $Na[N(SiMe_3)_2]$ was purchased from Aldrich and used without further purification.

$[(COT)SmN(SiMe_3)_2(THF)]$ (2): *NMR scale*: $[(COT)SmCl(THF)]_2$ (8 mg) and $Na[N(SiMe_3)_2]$ (3 mg) were placed in an NMR tube, 0.5 mL of C_6D_6 was added and the mixture was stirred by sonication until the two solids dissolved. A purple solution of **2** and a grey-brown precipitate were obtained. *Bulk synthesis*: $[(COT)SmCl(THF)]_2$ (280 mg), and $Na[N(SiMe_3)_2]$ (118 mg), were placed in a flask connected to the vacuum line and THF (20 mL) was added by condensation. After 4 hours stirring the deep violet solution became purple. The solvent was then removed and toluene added. After filtration, the solution was condensed and red crystals deposited. They were separated, washed with toluene and dried. NMR(C_6D_6): soluble after addition of THF, exhibiting the set of signals for **2**.The mother liquor was transferred into another flask and the solvent removed in vacuo, giving a dark red solid. – ^{1}H NMR(C_6D_6), only partially soluble, signals of **2**: δ (C_6D_6) = 9.19 (8 H, COT), 5.95 (4 H, THF), 2.17 (4 H, THF), −2.37 [18 H, $N(SiMe_3)_2$]. – $C_{14}H_{26}NSi_2Sm(THF)_{0.5}$ (451): calcd. C 42.61, H 6.70, N 3.11; found C 42.84, H 6.31, N 3.08.

$[(COT)Sm[N(SiMe_3)_2]_n$ (3): $[(COT)SmCl(THF)]_2$ **1** (240 mg) and $Na[N(SiMe_3)_2]$ (101 mg) were placed in a flask connected to the vacuum line and THF (20 mL) was added by condensation. After 20 minutes stirring at ambient temperature, the mixture was heated at reflux for 5 minutes to give a deep purple solution, with some remaining violet crystals of **1** and a greyish precipitate. The volatiles were then removed in vacuo and toluene(20 mL) was added. After stirring for a short time, the mixture was allowed to stand overnight to allow the precipitation of the sodium salt and other insolubles. After filtration the solution was very slowly evaporated to dryness, at ambient temperature, leaving **3** as deep red microcrystals. Yield ca 65%. – IR (nujol): $\tilde{\nu}$ = 1254 (s) cm^{-1}, 1241(s), 986 (vs), 869 (s), 840 (s), 822 (s), 770 (m), 719 (s), 663 (m). – $C_{14}H_{26}NSi_2Sm$ (414.9): calcd. C 40.53, H 6.32, N 3.38; found C 40.37, H 6.17, N 3.39. No melting point was observed up to 210 °C. A slow decomposition occurred, shown by the formation of a colourless solid.

Formation of Adducts

THF Adduct: In the glove box 6 mg of **3** were introduced into an NMR tube and C_6D_6 added. No colour developed in solution after vigorous shaking. The solvent was frozen, the tube connected to the vacuum line, evacuated, and then THF was added at ambient temperature. The purple colour of **2** appeared on melting of the solvent and no precipitate was observed.

Nitrile Adduct: 6 mg of **3** were introduced into an NMR tube and C_6D_6 added. After addition of 7 mg (3 eq) of 2,4,6,trimethylbenzonitrile an orange solution was obtained. – ^{1}H NMR: δ = 9.13 (8 H, COT), −2.24 {(18 H, $N(SiMe_3)_2$}, 6.32, 2.31 and 1.78 (nitrile).

$(COT)Sm[N(SiMe_3)_2]_2Na$ (4) and Half-Sandwich Complex: In an NMR tube were placed 8 mg of **1** and 7 mg of $NaN(SiMe_3)_2$. C_6D_6 (0.5 mL) was added and after a few minutes of gentle heating, the ^{1}H NMR spectrum of the resulting orange solution was recorded. – ^{1}H NMR (C_6D_6) **4**: δ = 8.47 (8 H, COT), 3.75 (4 H, THF), 1.48 (4 H, THF), −1.56 [36 H, $N(SiMe_3)_2$] (the integration of the $N(SiMe_3)_2$ signal indicated the presence of overlapped **5**); **2**: δ = 9.19 (8 H, COT) −2.41 [18 H, $N(SiMe_3)_2$]; δ = 9.25 (8 H) and −2.23 (72 H) (traces < 3%), tentatively attributed to the half-sandwich complex The latter signals disappeared after 12 h. After changing the solvent, **4**: δ (C_4D_8O) = 8.63 (8 H) −1.75 (36 H); **2**: δ = 9.57 (8 H) −1.21(18 H); δ = 13.2 $(COT)_2SmNa$. – The tube was then pumped dry, toluene added by condensation and then removed, and pentane (1 mL) added. After stirring for five minutes and decanting, the pentane solution was transferred into another tube, the volatiles were evacuated and C_6D_6 was added: δ(C_6D_6) = 9.27 (4 H, COT), −2.24 [36 H, $N(SiMe_3)_2$], half-sandwich complex; **2**: δ = 9.06 (8 H, COT) −2.50 [18 H, $N(SiMe_3)_2$]; **4**: δ = 8.35 (8 H) and −1.64 [36 H, $N(SiMe_3)_2$]; **5**: δ = −1.56. After addition of a tenfold excess of THF, an NMR spectrum was immediately recorded. The intensities of the signals of **2** and of the half-sandwich complex had significantly decreased (by 50%). C_6D_6 was added to the pentane-insoluble residue, which was sparingly soluble in benzene. The NMR spectrum was identical to the earlier one except that **2** was present only in trace amounts (<1%). – **3** (8 mg), **5** (8 mg) and 0.5 mL of C_6D_6 were added to an NMR tube. The tube was vigorously stirred then subjected to sonication. Only **5** was present in the solution. After addition of $NaN(SiMe_3)_2$, **3** disappeared and the solution was found to contain **4** and **5**. After a few minutes of gentle heating, the ^{1}H NMR spectrum of the orange solution was recorded. Compounds **4**, **5** and the half-sandwich complex (27, 17 and 56%, respectively) were present.

[1] [1a] W. J. Evans, R. D. Clark, M. A. Ansari, J. W. Ziller, *J. Am. Chem. Soc.* **1998**, *120,* 9555−9563. – [1b] P. Poremba, F. T. Edelmann, *J. Organomet. Chem.* **1998**, *553*, 393−395.

[2] T. Sakai, Pat. **1997,** JP 09328510 A2, F. G. N. Cloke, D. Peron, Pat. **1997**, WO 9746567 A1, L. Gila; A. Proto, E. Ballato, D. Vigliarolo, G. Lugli, Pat. **1997**, EP 757996 A1.

[3] S. Agarwal, M. Karl, S. Anfang, K. Dehnicke, A. Greiner, *Polymer Preprints* **1998**, *39*, 361−362.

[4] D. Baudry-Barbier, N. Andre, A. Dormond, C. Pardes, P. Richard, M. Visseaux, *Eur. J. Inorg. Chem.* **1998**, 1721−1727.

[5] M. Visseaux, *These* S027, Dijon, France, **1992**.

[6] [6a] F. T. Edelmann, *Angew. Chem. Int. Ed. Eng.* **1995**, *34*, 2466−2488. – [6b] H. Schumann, J. Winterfeld, L. Esser, G. Kociok-Köhn, *Angew. Chem. Int. Ed. Eng.* **1993**, *32*, 1208−1210.

[7] S. Cendrowski-Guillaume, M. Nierlich, M. Lance, M. Ephritikhine, *Organometallics* **1998**, *17*, 786−788.

[8] ^{1}H NMR (80 MHz, C_4D_8O): δ = 9.58 (8 H, COT), −1.49 {18 H, $N(SiMe_3)_2$}. After solvent evaporation and addition of C_6D_6, δ = 9.31 and −2.29.

[9] D. C. Bradley, J. S. Ghotra, F. A. Hart, *J. Chem. Soc. Dalton* **1973**, 1021−1023.
[10] [10a] A. L. Wayda, *Organometallics* **1983**, *5*, 565−566. − [10b] K. O. Hodgson, F. Mares, D. F. Starks, A. Streitwieser, *J. Am. Chem. Soc.* **1973**, *95*, 8650−8658.
[11] P. Bruin, M. Booij, J. H. Teuben, *J. Organomet. Chem*. **1988**, *350*, 17−23.
[12] H. Schumann, J. Winterfeld, F. H. Görlitz, J. Pickard, *Chem. Commun*. **1993**, 623−625.
[13] T. M. Gilbert, R. R. Ryan, A. P. Sattelberger, *Organometallics* **1988**, *7*, 2514−18.
[14] M. F. Lappert, M. J. Slade, A. Singh, J. L. Atwood, R. D. Rodgers, R. Shahir, *J. Am. Chem. Soc.* **1983**, *105*, 302−304.
[15] C. Cummins, R. R. Schrock, W. M. Davis, *Organometallics* **1991**, *10*, 3781−3785.
[16] D. Baudry, E. Bulot, M. Ephritikhine, M. Nierlich, M. Lance, J. Vigner, *J. Organomet. Chem.* **1990**, *388*, 279−287.

Received March 1, 1999
[I99072]

The Hexahydro-*closo*-hexaborate Dianion $[B_6H_6]^{2-}$ and Its Derivatives

Wilhelm Preetz*[a] and Gerhard Peters[a]

Keywords: Hexahydro-*closo*-hexaborate / Syntheses / Protonation / Non-rigidity / Substitution reactions / Derivatives / Kinetics / Degradation and expansion products / Crystal structure data /NMR data / IR and Raman data / Normal coordinate analyses / ESR and electrochemical data / Ab initio results

$[B_6H_6]^{2-}$ as the smallest known hydro-*closo*-borate is only moderately stable, and therefore its reaction chemistry remained unexplored for quite a long time. Since the mid 1980s some progress has been made in this field, and a considerable number of derivatives has been prepared. The provided structural and spectroscopic data together with the results of more sophisticated theoretical investigations by high level ab initio methods are a good basis for a systematic review on this class of compounds, and may encourage further synthetic and theoretical work. This is the aim of the present article giving a comprehensive survey up to the beginning of 1999.

Introduction

The story of the polyhedral *closo*-borates is characterized as an interplay of theoretical and synthetic progress. Based on theoretical studies of the valence structures of boron hydrides the existence of closed-shell hydro-*closo*-borate anions of the type $[B_nH_n]^{2-}$, $n = 5-12$, had been predicted in 1954.[1−3] Even some years later, in 1959 and 1960 salts of the exceptionally stable species $[B_{10}H_{10}]^{2-}$ [4] and $[B_{12}H_{12}]^{2-}$ [5] could be synthesized. The until now smallest known member of this series $[B_6H_6]^{2-}$, which is merely moderately stable, evaded preparation until 1964[6] − a decade after its prediction.

While for $[B_{10}H_{10}]^{2-}$ and $[B_{12}H_{12}]^{2-}$ an extensive derivative chemistry had been established very soon after their discovery,[7][8] for $[B_6H_6]^{2-}$ until 1984 the unique descendant remained $[B_6Br_6]^{2-}$, which only has been mentioned in a footnote.[9] The reason for this hiatus may lie in the initially complicated synthesis using the dangerous diborane, the small yield, and the instability of $[B_6H_6]^{2-}$ in acidic media. Therefore, a more vigorous study of its reaction chemistry was difficult, and demanded better synthetic routes to

[a] Institut für Anorganische Chemie, Christian-Albrechts-Universität Kiel,
Otto-Hahn-Platz 6/7, D-24098 Kiel, Germany
Fax: (internat.) + 49-(0)431/880-1520
E-mail: preetz@ac.uni-kiel.de



Wilhelm Preetz, born in 1934, received his Ph.D. degree in 1963 under supervision of Professor Dr. E. Blasius at the Technical University of Berlin. After his habilitation at the University of Saarland, Saarbrücken, he became Full Professor of Inorganic Chemistry at the Christian-Albrechts-University of Kiel in 1971. His main fields of research are the preparation, separation, structural, and spectroscopic characterization of octahedral mixed-ligand complexes with investigations on the trans effect and trans influence, of transition metal complexes and clusters with multiple metal−metal bonds, and since 1980 of closo-borate clusters, especially the chemistry of the little investigated $[B_6H_6]^{2-}$.



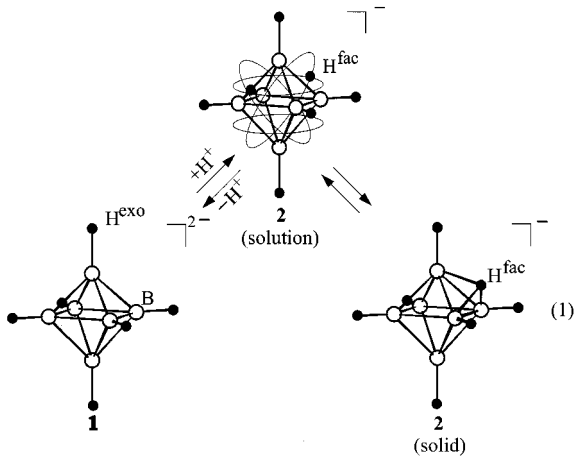
Gerhard Peters studied chemistry at the Christian-Albrechts-University of Kiel. He joined the group of Prof. Dr. W. Preetz with a thesis on thiocyanato linkage isomers of osmium and on new complexes of Re and Tc with multiple metal−metal bonds, and received his Ph.D. in 1982. Currently, he is engaged in multinuclear high-resolution NMR spectroscopy on solutions and solids at the Department of Inorganic Chemistry of the Christian-Albrechts-University of Kiel. Besides, he is an instructor for advanced students and an adviser of scientific co-workers in the fields of inorganic chemistry, radiochemistry and electrochemistry.

MICROREVIEWS: This feature introduces the readers to the authors' research through a concise overview of the selected topic. Reference to important work from others in the field is included.

 © WILEY-VCH Verlag GmbH, D-69451 Weinheim, 1999 1434−1948/99/1111−1831 $ 17.50+.50/0

its preparation. Stimulated by our findings in the fields of classical octahedral mixed-ligand complexes of the transition metals and of the hexanuclear clusters of Mo, W, Nb, and Ta[10] with respect to the interrelation between symmetry and structural and spectroscopic properties, the octahedral B_6 cage with its terminally bonded or *exopolyhedral* substituents seemed to be a worthwhile investigation object, in order to study these interrelations in this field, too.

In this review we report on the parent compound $[B_6H_6]^{2-}$ (**1**) and its derivatives resulting by replacement of the *exopolyhedral* H atoms against inorganic and organic substituents. The cluster anion is a regular octahedral cage of 6 B atoms surrounded by a larger octahedron of 6 radially disposed *exopolyhedral* H atoms. Special attention is drawn to the property of $[B_6H_6]^{2-}$ to react as a Brønsted base, and to attach an additional proton H^{fac} giving $[B_6H_6H^{fac}]^-$ (**2**). In solution in a nonrigid structure H^{fac} fluctuates across the octahedron′s surface via the edges, and in the solid state it is fixed above one of the octahedron′s facets, as is shown in Equation 1.



(1)

The protolysis equilibrium in Equation 1 is exemplary, and it will be of crucial importance for the chemistry of the *closo*-hexaborates and their substitution processes. Furthermore, $[B_6H_6]^{2-}$ is discussed as a ligand in metal complexes, and some reactions modifying the B_6 core are included, while the carbaboranes are excluded. The literature for the title subject is covered up to the beginning of 1999.

The structures of most of the compounds have been solved by single-crystal X-ray structure analyses, and, in general, ^{11}B-NMR spectroscopy is used for the characterization of the derivatives, accompanied by the respective hetero-nucleus NMR spectroscopy in case of suitable substituent nuclei such as ^{1}H, ^{13}C, ^{19}F, ^{29}Si, ^{77}Se, ^{113}Cd, and ^{199}Hg. Further, the vibrational spectra, IR and Raman, have been measured and for sure assignment accompanied by normal coordinate analyses.

The influence of the different substituents on the kinetics, the molecular parameters and the spectral properties is discussed in detail. In some special cases ab initio calculations have been performed to obtain insight into the electronic and molecular structures, and to affirm the assignment of spectral data by frequency analysis and by calculated NMR chemical shifts.

Whenever possible, the pK_a values of the protolysis equilibria determined by potentiometric titration are reported, and for redox active species electrochemical data are added. UV/Vis and ESR spectroscopy have been applied to the colored radical anions obtained by oxidation processes.

Syntheses, Structure, and Properties of $[B_6H_6]^{2-}$

Starting with commercially available materials diborane is generated in a first step as formulated in Equation 2.

$$3\ NaBH_4 + 4\ BF_3 \cdot O(C_2H_5)_2 \xrightarrow{20\ °C,\ Diglyme} 2\ B_2H_6\uparrow + 3\ NaBF_4 + 4\ (C_2H_5)_2O \quad (2)$$

B_2H_6 is passed through a diglyme solution of tetrahydroborate, and octahydrotriborate $[B_3H_8]^-$ is formed as an intermediate product according to Equation 3.

$$B_2H_6 + NaBH_4 \xrightarrow{90\ °C,\ Diglyme} Na[B_3H_8] + H_2\uparrow \quad (3)$$

On boiling, the colorless reaction mixture turns to yellow, and in parallel reactions the following clusters are produced as given in Equations 4−6.

$$2\ Na[B_3H_8] \xrightarrow{162\ °C,\ Diglyme} Na_2[B_6H_6] + 5\ H_2\uparrow \quad (4)$$

$$4\ Na[B_3H_8] \xrightarrow{162\ °C,\ Diglyme} Na_2[B_{10}H_{10}] + 2\ NaBH_4 + 7\ H_2\uparrow \quad (5)$$

$$5\ Na[B_3H_8] \xrightarrow{162\ °C,\ Diglyme} Na_2[B_{12}H_{12}] + 3\ NaBH_4 + 8\ H_2\uparrow \quad (6)$$

The ratio of $[B_6H_6]^{2-}/[B_{10}H_{10}]^{2-}/[B_{12}H_{12}]^{2-}$ is 2:1:15, and the total amount of $[B_6H_6]^{2-}$ is 5% at most. In a recently published one-pot synthesis[11] the liberation of large and dangerous amounts of B_2H_6 is avoided, and yield of $[B_6H_6]^{2-}$ is raised to 25%. Boron trifluoride−diethyl ether is treated in diglyme at 100° C with an excess of tetrahydroborate according to Equation 7 to give $Na[B_3H_8]$,[12] which is transformed by subsequent refluxing for 36 h into a mixture of the *closo*-borate clusters.[11]

$$5\ NaBH_4 + 4\ BF_3 \cdot O(C_2H_5)_2 \xrightarrow{100\ °C,\ Diglyme} 2\ Na[B_3H_8] + 2\ H_2\uparrow + 3\ NaBF_4 + 4\ (C_2H_5)_2O \quad (7)$$

Fortunately, from the always resulting product mixtures of all synthetic routes a crude separation of $[B_6H_6]^{2-}$ from $[B_{10}H_{10}]^{2-}$ and $[B_{12}H_{12}]^{2-}$ is possible on the basis of the protolysis equilibrium of $[B_6H_6]^{2-}$ and the pH dependence of the solubility of the tetra-*n*-butylammonium $[nBu_4N]^+$ salts in water.[13][14] While $[B_{10}H_{10}]^{2-}$ and $[B_{12}H_{12}]^{2-}$ are precipitated in basic media, $[B_6H_6]^{2-}$ remains in solution, from which after separation and following cautious acidification $[nBu_4N][B_6H_6H^{fac}]$ is obtained as a scarcely soluble compound. Dissolution in dichloromethane and addition of an aliquot amount of $[nBu_4N]OH$ yields the deprotonated $[nBu_4N]_2[B_6H_6]$, which in aqueous solution is converted into the scarcely soluble Cs salt according to Equation 8.

$$[n\mathrm{Bu_4N}]_2[B_6H_6] + 2\ CsOH \rightarrow Cs_2[B_6H_6]\downarrow + 2\ [n\mathrm{Bu_4N}]OH \quad (8)$$

Protonation to the well-soluble $Cs[B_6H_6H^{fac}]$ is accomplished by addition of an aliquot amount of hydrochloric acid.

As another synthetic route, however with small yields only, the reaction of iodine with tetrahydroborate may be mentioned as described by Equation 9.[15–17]

$$6\ NaBH_4 + 2\ I_2 \rightarrow Na_2[B_6H_6] + 4\ NaI + 9\ H_2\uparrow \quad (9)$$

As in the preceding reactions the intermediate formation of $[B_3H_8]^-$ as formulated in Equations 3 and 7 is decisive, and also in the solid small amounts of $[B_6H_6]^{2-}$ are produced from salts of $[B_3H_8]^-$ on tempering them above 200° C.[18] Anhydrous $Na_2[B_6H_6]$ is conveniently prepared by reaction of $Na[B(C_5H_6)_4]$ and $[n\mathrm{Bu_4N}]_2[B_6H_6]$ in methanol.[19]

$[B_6H_6]^{2-}$ (**1**) has a regular octahedral cage of 6 B atoms surrounded by a larger octahedron of 6 radially disposed *exopolyhedral* H atoms. This octahedral structure of $[B_6H_6]^{2-}$ had been postulated already in 1954,[1][3] and could be confirmed for the solid state by X-ray structure analyses on the $[Me_4N]^+$,[20] K^+ and Cs^+ salts,[21] and for the solution state by NMR spectroscopy.[22][23] The B–B and B–H distances are 169, 172.1, 172.2 pm and 111, 107, 109 pm, respectively. On polycrystalline $Cs_2[B_6H_6]$ a solid-state ^{11}B-, ^{133}Cs-, and ^{1}H-NMR study at 1.88 T has been performed revealing fine structure due to ^{11}B-^{1}H and ^{10}B-^{1}H quadrupolar and dipolar interactions, which has allowed the calculation of the B–H distance to 119 pm. The accuracy of the determination of distances by NMR spectroscopy, X-ray, and neutron diffraction has been discussed.[24]

As the Brønsted base $[B_6H_6]^{2-}$ has a pK_a value of 7 the protonated form $[B_6H_6H^{fac}]^-$ (**2**) is present already in weak acidic solutions.[14] The localization of H^{fac} above one of the facets of the octahedron in a face-capped structure had been predicted on the basis of theoretical calculations,[25–29] and was confirmed by X-ray analyses on $[Ph_4P][B_6H_6H^{fac}]$, $[Ni(bipy)_3][B_6H_6H^{fac}]_2$, and $[Ni(phen)_3][B_6H_6H^{fac}]_2$.[30] The observed decomposition of $[B_6H_6H^{fac}]^-$ in stronger acidic media is explained by the instability of the twofold protonated species, the hypothetical *closo*-borane $[B_6H_8]$, which should better be written as $[B_6H_6(H^{fac})_2]$. This also follows from theoretical investigations, and corresponds to experimental results on $[H_2Os_6(CO)_{18}]$.[25,28,31,32]

A more profound understanding of the Brønsted base behavior of $[B_6H_6]^{2-}$ is provided by calculations of the electron density. An instructive idea is given by the electron localization function (ELF)[33][34] of the three-center, two-electron (3c2e) bonds of the B_3 faces. The maxima of electron density are centered above the eight faces resulting in the geometrical arrangement of a cube, the dual polyhedron to the octahedron. For this reason the faces of the octahedron are the favored regions for the addition of H^{fac} or the attack of other electrophilic reactants, and because of their Lewis basicity they can act as donating centers to Lewis acidic metal ions.

In principle, ^{1}H-NMR solution spectroscopy as the quick method of choice allows the reliable identification of H^{fac}, and provides slightly solvent- and cation-dependent high-field signals with unresolved ^{11}B couplings at $\delta(^1H) = -5.6$ for H^{fac}, while the signal of the *exopolyhedral* protons is a quadruplet with the typical pattern due to quadrupolar coupling to ^{11}B ($I = 3/2$) at $\delta(^1H) = 1.2$. The ^{1}H-coupled ^{11}B spectra of both $[B_6H_6]^{2-}$ and $[B_6H_6H^{fac}]^-$ show markedly solvent- and cation-dependent single doublets, each, with coupling constants $^1J(^{11}B,^1H^{exo}) = 140-150$ Hz. Table 1 gives an overview of the solvent and cation dependence.

In solutions of both $[B_6H_6]^{2-}$ and $[B_6H_6H^{fac}]^-$ the 6 B core atoms as well as the 6 terminal H atoms are chemically and magnetically equivalent at room temperature, and therefore H^{fac} must fluctuate across all faces with the same residence time. The migration is intramolecular, and takes place chiefly via the edges across the surface of the octahedron with a migration barrier in the order of 10 kcal·mol^{-1}.[22] This way is favored energetically in comparison to that across the vertices by 21 kcal·mol^{-1}.[36] From studies on different salts a cation–anion interaction must be taken into consideration,[22][36] and from relaxation considerations with respect to quadrupolar coupling and electric field gradient interactions $^1J(^{11}B,^1H^{fac})$ scalar coupling constants of 13 and 16 Hz for $[n\mathrm{Bu_4N}][B_6H_6H^{fac}]$ and $[Ni(bipy)_3][B_6H_6H^{fac}]_2$ in acetone have been derived, respectively.[22] Only after cooling of solutions containing $[B_6H_6H^{fac}]^-$ below the coalescence temperature the ^{11}B resonance is split into two signals with $\delta(^{11}B)$ shifted downfield for the uncapped facet and upfield for the facet capped by H^{fac} [22] (see Table 1). The coalescence points have been determined to 196 K at 1.88 T for $[Ni(bipy)_3][B_6H_6H^{fac}]_2$ in acetone[22] and to 227 K at 9.35 T for $[Ph_4As][B_6H_6H^{fac}]$ in CD_2Cl_2.[35] Because of the great interest in the fluxional behavior of the additional proton H^{fac} different calculations with regard to the barrier of movement across the octahedron facets have been done. From the temperature dependence of the ^{11}B-NMR spectra of $[n\mathrm{Bu_4N}][B_6H_6H^{fac}]$ and $[Ni(bipy)_3][B_6H_6H^{fac}]_2$ in acetone values of 10 and 11.5 kcal·mol^{-1} have been determined,[22] which are in good agreement with theoretical investigations resulting in 10.4 kcal·mol^{-1} with an SCF/DEHD approach,[36] 12.1 kcal·mol^{-1} at the MP2/6-31G* level,[37] and in 8.3 kcal·mol^{-1} at the B3LYP/6-311+G** level.[38] This low energetic barrier is attributed to the three-dimensional aromaticity[39][40] of *closo*-borates, which may be described as the tendency of the molecule anions to realize equal electronic conditions at all boron atoms by a "cluster current". In several theoretical studies the migration barrier of H^{fac} in $[B_6H_6H^{fac}]^-$ has been compared to those in $[B_{10}H_{10}H^{fac}]^-$ [41] and $[B_7H_7H^{fac}]^-$, $[B_9H_9H^{fac}]^-$, $[B_{12}H_{12}H^{fac}]^-$.[38,42–44] The cluster bond enthalpies have been calculated for $[B_nH_n]^{2-}$, $n = 6, 8-10$.[45]

$[B_6H_6]^{2-}$ can be deuteriated completely by treatment with D_2O.[46] Kinetic investigations have shown, that the reaction rate is proportional to the ratio of the protonated form, so that the deuteriation proceeds very fast in neutral or acidic media, while in basic media it runs not at all or very

Table 1. Chemical shifts $\delta(^1H)$ and $\delta(^{11}B)$ [ppm] and coupling constants $^1J(^1H,^{11}B)$ [Hz] of $[B_6H_6]^{2-}$ (a) and $[B_6H_6H^{fac}]^-$ (b) in different solvents, at different temperatures and with different cations and of $[B_6D_6D^{fac}]^-$ (c)

Cation		T [K]	Solvent	$\delta(^1H)$ *exo*	*fac*	$\delta(^{11}B)$	$^1J(^1H,^{11}B)$ *exo*	*fac*	Ref.
$[Ni(bipy)_3]^{2+}$	b	190	acetone	1.2	−5.6	−6.7, −15.3	150	13	[22]
	b	300	acetone	1.2	−5.6	−14.7	146	–	
$[nBu_4N]^+$	b	190	acetone	–	−5.6	−9.9, −17.8	146	16	[22]
	b	300	acetone	–	−5.6	−14.2	144	–	
$[nBu_4N]^+$	b	297	CD_3CN	–	–	−13.6	147	–	[23]
	a	297	CD_3CN	–	–	−13.2	133	–	
$[nBu_4N]^+$	c	297	CD_3CN	–	–	−13.9	–	–	[23]
$[nBu_4N]^+$	b	297	CD_3CN[a]	–	−5.6	−14.6	145	–	[35]
	a	297	CD_3CN[b]	–	–	−14.8	133	–	
$[nBu_4N]^+$	b	297	CD_2Cl_2	–	−5.4	−18.0	145	–	[35]
	a	297	CD_2Cl_2[b]	–	–	−18.0	132	–	
$[Ph_4As]^+$	b	297	CD_2Cl_2	1.1	−5.5	−18.0	147	–	[35]
	b	223	CD_2Cl_2	1.1	−5.5	−14.1, −21.7	–	–	
	a	297	CD_2Cl_2	1.1	–	−18.0	133	–	
Cs^+	b	297	H_2O	1.2	−3.9	−17.7	146	–	[35]
	a	297	H_2O[c]	1.2	–	−18.1	123	–	
Cs^+	c	297	D_2O[d]	–	–	−17.9	–	–	[35]
$[Me_4N]^+$	a	not reported	–	–	−13.0	122	–	–	[6]

[a] = + citric acid. − [b] = + DBU. − [c] = + OH^-. − [d] = + NaH_2PO_4.

slow.[14] Although the movement of H^{fac} across the octahedral surface proceeds from face to face via the edges and not via the corners, the decisive step is the intramolecular exchange of H^{fac} or D^{fac} respectively against one of the terminally bonded H atoms. The activation energy of this process has been determined to be 18 kcal·mol^{-1}.[14]

As $[B_6H_6]^{2-}$ may serve as a paradigm of the class of doubly octahedral structured systems, its vibrational spectra have been examined and interpreted repeatedly.[47−49] The octahedral structure of $[B_6H_6]^{2-}$, which has been proven by X-ray structure analysis and by NMR spectroscopy, is clearly derived from the vibrational spectra, too. For a 12-atomic *homoleptic* molecule $[B_6X_6]^{2-}$ with point group O_h the normal modes of vibration transform as given by Equation 10.

$$\Gamma_{\tilde{\nu}} = 2\,A_{1g} + 2\,E_g + T_{1g} + 3\,T_{1u} + 2\,T_{2g} + 2\,T_{2u} \quad (10)$$

For systems with a center of symmetry the rule of mutual exclusion is valid, and according to the group-theoretical selection rules the vibrations with symmetries A_{1g}, E_g, and T_{2g} are Raman-active, those with symmetry T_{1u} are IR-active and those with T_{1g} and T_{2u} are inactive. The B_6 cage and the X_6 octahedra, put into each other, perform coherent vibrations, which are subdivided in two groups[50]:

1. Vibrations with equidirectional movement of the two spheres (in phase) transform as given in Equation 11.

$$\Gamma_{\text{in phase}} = A_{1g} + E_g + T_{1u} + T_{2g} + T_{2u} \quad (11)$$

2. Vibrations with a counter-directional movement of the two spheres (anti phase) transform as given in Equation 12.

$$\Gamma_{\text{anti phase}} = A_{1g} + E_g + T_{1g} + 2T_{1u} + T_{2g} + T_{2u} \quad (12)$$

The normal vibrations are presented in Figure 1. The highest spectral resolution on the parent compound has been achieved by measurement at low temperature.[51] As the isotopic ratio of boron at natural abundance is 80.22% ^{11}B and 19.78% ^{10}B, $[B_6H_6]^{2-}$ is in fact an isotopomeric series $[^{11}B_n{}^{10}B_{(6-n)}H_6]^{2-}$, $n = 0-6$, and this is observed in the 10 K Raman spectra with very sharp lines for the respective isotopomers having a half-width of 1.5 cm^{-1}, only. An unambiguous assignment of the normal vibrations has become possible by measurement of the final members $[^{11}B_6H_6]^{2-}$ (96% ^{11}B) and $[^{10}B_6H_6]^{2-}$ (92% ^{10}B), which have been prepared in high isotopic enrichment.[52] The Raman-active cage vibrations $\tilde{\nu}_1$, $\tilde{\nu}_2$, and $\tilde{\nu}_3$ are shifting with increasing n in steps of 7 cm^{-1} to lower frequencies. From the fine-structure of the signals even the geometrical isomers of the isotopomers, existing for $n = 2$, 3, and 4, are recognizable. Normal coordinate analysis has been carried out on the basis of a modified valence force field with the Wilson GF matrix method utilizing a set of 6 force constants (Table 2), and an excellent adaptation of the computed values to the observed frequencies has been achieved (Table 3).[50] This is true also for the deuteriated compounds $Cs_2[^{11}B_6D_6]$ and $Cs_2[^{10}B_6D_6]$.[50] Due to the markedly different masses of the boron isotopes ^{10}B and ^{11}B the isotopic effect on the degeneracy is observed.[53] Only for the pure final members of the series with $n = 0$ and $n = 6$ O_h point symmetry is valid. For the members with $n = 1-5$ symmetry is descending to D_{4h}, C_{4v}, C_{3v}, and C_{2v}, with the result that normal vibrations derived from the degenerate modes with symmetry T and E become less or nondegenerate, and the corresponding lines are split. By restriction of the rule of mutual exclusion certain lines of the IR spectrum are recognizable with weak intensity also in the Raman spectrum.[50] Calculations of the potential energy distribution (PED) show that $\tilde{\nu}_1$ and $\tilde{\nu}_3$ with PED values of 98% are nearly genuine modes of the B_6 core, while the same is right for the B−H fundamentals $\tilde{\nu}_2$ and $\tilde{\nu}_4$. The other vibrations exhibit with 10% and 90%, respectively, pronounced couplings between the core modes and the boron-substituent

modes.[50] The influence of protonation has been studied by vibrational spectroscopy on the pair $Cs_2[B_6H_6]$ and $Cs[B_6H_6H^{fac}]$.[14] The symmetric and antisymmetric vibrations of H^{fac} against the B_3 facet could not be observed, but have been calculated to lie in the range of 1800 and 1280 cm^{-1}, respectively.[54] A characteristic shift of B−H stretching modes by about 100 cm^{-1} to higher frequencies is observed on protonation, viz. the Raman lines at 2414 and 2460 cm^{-1} to 2522 and 2574 cm^{-1}, and the broad IR band at 2432 cm^{-1} to 2518−2545 cm^{-1}. In the range of the skeletal vibrations beyond 1100 cm^{-1} many additional bands are exhibited for the protonated compound if compared to the deprotonated one.[14] These observed higher B−H frequencies of the protonated cluster in comparison to the deprotonated could be verified by ab initio frequency analyses.[54]

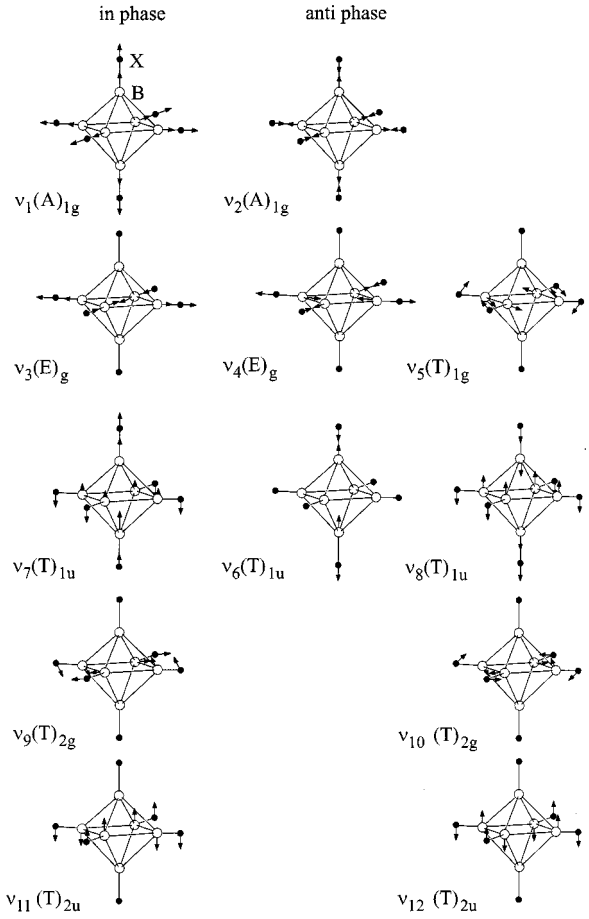


Figure 1. In-phase and anti-phase normal vibrations of a $[B_6X_6]^{2-}$ molecule

Concerning the fluxional behavior of H^{fac} the monosubstitution products of $[B_6H_6]^{2-}$ are particularly interesting, because as a consequence of substitution the octahedron is built up from two energetically different square pyramids: an upper one topped by the substituted boron atom, which is called the *ipso* boron atom, and a lower one topped by the *antipodal* boron atom. Accordingly, protonation may happen either in the *antipodal* or the *ipso* sphere (see Figure 2), and this may be influenced by the nature of the substituent. Therefore, systematic efforts have been made in preparing and characterizing such $[B_6H_5H^{fac}X]^-/[B_6H_5H^{fac}R]^-$ species. Details on this subject will be discussed in the derivatives section beyond.

Table 2. Averaged bond lengths d [pm] and calculated force constants f [10^2 N·m^{-1}] of the cluster anions $[B_6X_6]^{n-}$ (X = H, Cl, Br, I; n = 1, 2)

	n	X=H	Cl	Br	I
d_1(B−B)	1		173	173	173
	2	172	172	168	165
d_2(B−X)	1		176	191	212
	2	109	182	199	219
f_d(BB)	1		1.17	1.18	1.18
	2	1.78	1.40	1.43	1.49
f_d(BX)	1		4.17	3.34	2.60
	2	3.19	3.99	3.28	2.35
$d_1^2 f_\alpha$(BBB)	1		0.15	0.17	0.25
	2	0.64	0.29	0.27	0.29
$d_1 d_2 f_\alpha$(BBX)	1		0.39	0.34	0.51
	2	0.18	0.49	0.51	0.54
$f_{dd'}$(BB/BB)	1		0.30	0.24	0.40
	2	0	0.10	0.15	0.15
f_{dd}(BB/BB)	1		−0.08	−0.02	−0.03
	2	0	−0.07	−0.05	−0.02
f_{dd}(BB/BX)	1		0.05	−0.03	0
	2	0	0.03	0	0
$d_1 f_{d\alpha}$(BX/BBB)[a]	1		−0.39	−0.32	−0.41
	2	−0.21	−0.61	−0.45	−0.31
$d_1 f_{d\alpha}$(BX/BBB)[b]	1		0	0	0
	2	0.08	0	0	0
$d_2 f_{d\alpha}$(BX/BBX)	1		0	0	0.20
	2	0	0.25	0.18	0.08
$d_1^2 f_{\alpha\alpha}$(BBB/BBB)	1		0.20	0.30	0
	2	0	0	0	0

[a] X at the middle B atom. − [b] Bond as part of the angle.

Derivatives

Halogeno Substituents

The derivative chemistry of $[B_6H_6]^{2-}$ started in 1984 with the syntheses of the hexahalo-*closo*-hexaborates $[B_6X_6]^{2-}$, X = Cl, Br, and I,[55], and their characterization by ^{11}B-NMR[56] and vibrational spectroscopy.[57] They are formed in a series of substitution steps by reaction of $[B_6H_6]^{2-}$ with the free halogens in strong basic aqueous solution according to Equation 13.

$$[B_6H_6]^{2-} + n\,X_2 + n\,OH^- \rightarrow [B_6H_{(6-n)}X_n]^{2-} + n\,X^- + n\,H_2O \quad (n = 1-6) \qquad (13)$$

The pH dependence of the reaction of $[B_6H_6]^{2-}$ with iodine in aqueous solution has been studied by potentiometry showing an almost instantaneous stoichiometric course without gas evolution.[58] The partially halogenated derivatives are obtained as intermediates by moderate application of the halogens,[59] or better by reaction with the *N*-halosuccinimides NXS, X = Cl, Br, and I.[60] However, mixtures with several components always result. As the rate of halogenation is very fast for the first steps, the mono- and the disubstituted products are accessible in small yields only, while the 3- to 5-fold substituted species are produced in

Table 3. Assignment of calculated (c) and observed (o) frequencies [cm^{-1}] of the cluster anions $[^{11}B_6X_6]^{n-}$ (X = H, Cl, Br, I; n = 1, 2); i.a. = inactive, n. o. = not observed

$\tilde{\nu}_i$	N	$[^{11}B_6H_6]^{n-}$		$[^{11}B_6Cl_6]^{n-}$		$[^{11}B_6Br_6]^{n-}$		$[^{11}B_6I_6]^{n-}$	
		o	c	o	c	o	c	o	c
$\tilde{\nu}_1$	1			1206	1206	1206	1204	1162	1163
	2	988	989	1217	1219	1202	1202	1165	1167
$\tilde{\nu}_2$	1			334	334	201	204	156	159
	2	2455	2453	333	329	209	210	151	153
$\tilde{\nu}_3$	1			n.o.	981	961	960	895	894
	2	816	816	979	981	945	944	901	901
$\tilde{\nu}_4$	1			324	324	211	212	152	152
	2	2414	2410	319	320	206	207	152	151
$\tilde{\nu}_5$	1			i.a.	493	i.a.	442	i.a.	516
	2	i.a.	838	i.a.	547	i.a.	536	i.a.	537
$\tilde{\nu}_6$	1			950	954	916	909	943	940
	2	2421	2421	1125	1125	1090	1091	1058	1060
$\tilde{\nu}_7$	1			521	518	425	432	364	367
	2	1044	1039	536	536	439	439	386	385
$\tilde{\nu}_8$	1			n.o.	127	n.o.	73	n.o.	69
	2	729	729	141	139	96	96	74	73
$\tilde{\nu}_9$	1			738	737	686	689	736	737
	2	763	767	744	743	749	747	744	746
$\tilde{\nu}_{10}$	1			n.o.	105	n.o.	55	n.o.	53
	2	697	695	111	114	74	71	53	58
$\tilde{\nu}_{11}$	1			i.a.	540	i.a.	482	i.a.	545
	2	i.a.	538	i.a.	634	i.a.	624	i.a.	633
$\tilde{\nu}_{12}$	1			i.a.	82	i.a.	46	i.a.	42
	i.a.	813	i.a.	95	i.a.	59	i.a.	45	

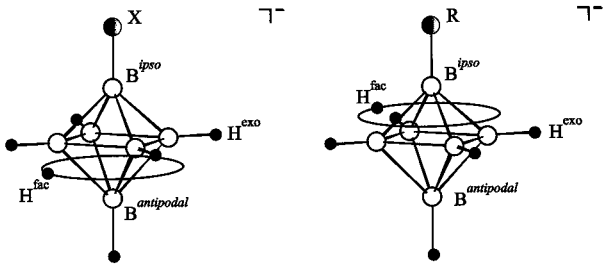


Figure 2. Fluctuation of H^{fac} in monosubstituted $[B_6H_5H^{fac}X]^-$ and$[B_6H_5H^{fac}R]^-$

high concentrations. For the isolation of pure compounds on a preparative scale ion exchange column chromatography with diethylaminoethylcellulose as a stationary phase and molar aqueous salt solutions as mobile phases has proven a well-tried method.[59−61] The rate of elution decreases strongly in the series Cl > Br > I, and additionally with increasing degree of halogenation. While the differences in mobility for higher halogenated compounds are more than 100%, those within the pairs of geometrical isomers are merely 5−15%. Therefore, their separation is very difficult, and can be overcome only by repeated ion exchange procedures with careful work up of the separated front and final sections of the corresponding chromatographic zones.

The tendency towards formation of the *cis*/*fac* isomers decreases within the series Cl, Br, I, and with increasing degree of halogenation. While in the Cl and Br series for n = 2, 3, and 4 the pairs of geometrical isomers are formed in different ratios, in the I series the pure *trans* and *mer* isomers are found exclusively. As a result *trans*-$[B_6H_4I_2]^{2-}$, *mer*-$[B_6H_3I_3]^{2-}$, and *trans*-$[B_6H_2I_4]^{2-}$ are prepared in a stereomeric pure form very easily and with highest yields.[59] Unlike compounds with a low degree of halogenation the tetra-, penta-, and hexahalohydro-*closo*-hexaborates are stable against dilute mineral acids for reasonably long times. With respect to Equation 1 only the monohalo derivatives can be protonated without difficulties, and a crystal structure of $[Ph_4P][B_6H_5H^{fac}I]$ may serve as an example.[62] Utilizing a glass electrode for potentiometric titration with 0.1 N NaOH the pk_a values have been determined for the acid-base pairs $[B_6H_5H^{fac}X]^-/[B_6H_5X]^{2-}$ to be 5.35, 5.00, and 4.65 for X = Cl, Br, and I, respectively.[14] Because of their decomposition in stronger acidic media the protonation of the dihalo derivatives and even more of the compounds with higher degree of halogenation is no longer measurable by titration. The pk_a values are < 2.5, decreasing with increasing degree of halogenation. On the protonated monosubstituted derivatives $[B_6H_5H^{fac}X]^-$ and $[B_6H_5H^{fac}R]^-$, X = Cl, Br, I, SCN, R = CH_3, C_2H_5, n-C_3H_7, n-C_4H_9,

n-C_8H_{17}, variable-temperature ^{11}B-NMR studies have been performed, and revealed the migration of H^{fac} to occur in the *ipso* sphere of the B_6 octahedron for the alkyl derivatives and in the *antipodal* sphere in case of the halogens and SCN in these series[63] (see Figure 2).

Studies on the deuteriation of the halohydro-*closo*-hexaborates have shown that the H/D exchange rate decreases in agreement with their increasing basic character in the series Cl > Br > I, and in particular with increasing degree of halogenation. Accordingly, the H/D exchange must occur via the protonated forms. Since protonation is strongly impeded with increasing degree of substitution, and further is limited by decomposition on increasing acidification, the iodo-*closo*-hexaborates with 3 or more I substituents cannot be deuteriated. Thus, to obtain the species $[B_6D_nI_{(6-n)}]^{2-}$ ($n = 1-3$) iodination of $[B_6D_6]^{2-}$ is the exclusive synthetic route.[14]

A special feature of the kinetics of deuteriation is that the H atoms are exchanged at different rates with respect to the geometrical arrangement of the substituents. For example, the H atoms in *antipodal* position to the halogen substituents in $[B_6ClH_5]^{2-}$ and $[B_6Cl_3H_3]^{2-}$ are exchanged at about the 100-fold rate in comparison to the other *exopolyhedral* H atoms. This *antipodal effect*[64] may be regarded as an analogue to the *trans effect* of the coordination compounds.[10] An impressive example of the *antipodal influence* is discussed below on the series of mixed hexahalo-*closo*-hexaborates.

The preparation of the bis-*heteroleptic* halo derivatives $[B_6X_nY_{(6-n)}]^{2-}$ ($n = 1-5$, X ≠ Y = Cl, Br, I) is achieved by reaction of the pure partially halogenated $[B_6H_nY_{(6-n)}]^{2-}$ with the corresponding halogen or *N*-halosuccinimide in aqueous basic solution.[60][65] However, in each case successive halogenation is only possible with the respective heavier halogen, in other words: in a synthetic route the more electronegative substituent must be introduced at first, and then the less electronegative substituent as the second. The reaction Equations 14a−14c are valid.

$$[B_6Cl_nH_{(6-n)}]^{2-} + (6-n)\ Br_2 \rightarrow [B_6Cl_nBr_{(6-n)}]^{2-} + (6-n)\ HBr\ (n = 1-5) \quad (14a)$$

$$[B_6Cl_nH_{(6-n)}]^{2-} + (6-n)\ I_2 \rightarrow [B_6Cl_nI_{(6-n)}]^{2-} + (6-n)\ HI\ (n = 1-5) \quad (14b)$$

$$[B_6Br_nH_{(6-n)}]^{2-} + (6-n)\ I_2 \rightarrow [B_6Br_nI_{(6-n)}]^{2-} + (6-n)\ HI\ (n = 1-5) \quad (14c)$$

The course of substitution in these series cannot be influenced by any changes in the reaction conditions, and it is impossible to unlink halogen atoms attached to the B_6 cluster, at least, if the B_6 core has to be retained. Therefore, the possibility of chlorinating or brominating some readily available partially iodinated geometric isomers in order to synthesize the respective chloro- or bromohydro-*closo*-hexaborates from the iodohydro-*closo*-hexaborates is ruled out.

On treatment of dichloromethane solutions of the hexahalo-*closo*-hexaborates with Br_2, $(SCN)_2$, BrF_3, or $K[BrF_4]$ intense colors can be observed due to the formation of the radical anions $[B_6X_6]^{\bullet-}$. The half-wave potentials $E_{1/2}$ were determined by cyclic voltammetry to be 0.58, 0.77, and 0.88 V for X = Cl, Br, I, respectively.[66][67] In case of the partially halogenated compounds $E_{1/2}$ is shifted to less positive potentials without exception, for example to 0.28 V for *fac*- and *mer*-$[B_6Cl_3H_3]^{2-}$, 0.29 V for $[B_6BrH_5]^{2-}$, and 0.19 V for $[B_6H_5I]^{2-}$. The parent compound $[B_6H_6]^{2-}$ is oxidized at a half-wave potential $E_{1/2} = 0.86$ V, however, under the experimental conditions (CH_3CN, $[nBu_4N]ClO_4$, Pt working electrode, Pt auxiliary electrode vs. Ag/AgCl/LiCl sat. in EtOH) the electrochemical process is irreversible.[66] For $Cs_2[B_6H_6]$ in water at a Pt electrode vs. saturated calomel electrode a value of −0.3 V has been reported.[68] On the preparative scale chemical oxidation with Ce^{IV} according to Equation 15 is suitable.

$$[nBu_4N]_2[B_6X_6] + [NH_4]_2[Ce(NO_3)_6] \rightarrow [nBu_4N][B_6X_6] + [nBu_4N]NO_3 + 2\ [NH_4]NO_3 + Ce(NO_3)_3\ (X = Cl, Br, I) \quad (15)$$

In this way deep blue $[B_6I_6]^{\bullet-}$, orange $[B_6Br_6]^{\bullet-}$and yellowish-green $[B_6Cl_6]^{\bullet-}$ are generated. The X-ray structures of the $[nBu_4N]^+$ and the bis(triphenylphosphanyl)imminium $[Ph_3P{=}N{=}PPh_3]^+$ salts have been solved.[66][67] Because of the paramagnetism ^{11}B-NMR spectra could not be recorded. The characteristic transitions in the UV/Vis spectra with extinction coefficients in the order of 1000−6000 $cm^2 \cdot mol^{-1}$ are shifted systematically to lower energies in the series Cl, Br, I. The radical anions and some mixed congeners of the type $[B_6X_nY_{(6-n)}]^{\bullet-}$ (X ≠ Y = Cl, Br, I), dissolved in dichloromethane, exhibit intense ESR signals in the X-band spectra, which in some cases are observable only on frozen solutions down to 4 K. The expected hyperfine couplings due to the isotopes ^{11}B and ^{10}B could not be resolved. A strongly increasing *g* anisotropy on replacing Cl by Br and especially by I with $g_1 = 2.04$, $g_2 = 1.66$, $g_3 = 1.15$ is interpreted by increasing participation of the halide orbitals in the singly occupied molecular orbitals (SOMOs) of the clusters.[69] The 10 K IR and Raman spectra of $[B_6X_6]^{2-}$, like the parent compound $[B_6H_6]^{2-}$, exhibit patterns of sharp lines reflecting the isotopomeric series $[^{10}B_n{}^{11}B_{(6-n)}X_6]^{2-}$ (X = Cl, Br, I, H; $n = 0-6$). Using the molecular parameters of X-ray structure analyses the vibrations of $[B_6X_6]^{2-}$ and the radical anions $[B_6X_6]^{\bullet-}$ have been assigned by normal coordinate analyses.[70][71] With sets of 8 force constants (Table 2) a good agreement of observed and calculated frequencies has been achieved (Table 3).

On the chemical shifts $\delta(^{11}B)$ of the series of mixed hexahalo-*closo*-hexaborates $[B_6X_nY_{(6-n)}]^{2-}$ (X ≠ Y =Cl, Br, I; $n = 5-2$) a linear regression analysis has been performed. Depending on the geometric position of the substituents in symmetric X−B···B−X and Y−B···B−Y and asymmetric X−B···B−Y arrangements of the cluster anions and their mutual influences on the electron density at the substituted ^{11}B nuclei the *antipodal influence* AI has been calculated as the difference between the ^{11}B shifts of the corresponding asymmetric and the symmetric arrangements for a given *n* according to Equation 16a.

$$AI = \delta(^{11}B)_{asym} - \delta(^{11}B)_{sym} \quad (16a)$$

The *antipodal shift constant* ASC[10] of a series is obtained as the difference of the *antipodal influences* of two successive compounds according to Equation 16b. The results are given in Table 4.

$$ASC = AI_{(n+1)} - AI_{(n)} \quad (16b)$$

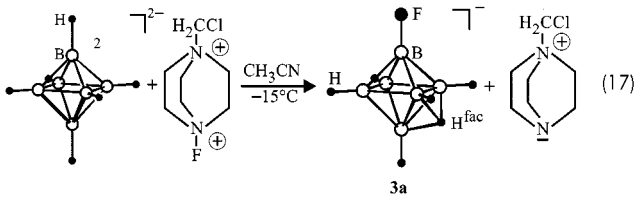
Table 4. *Antipodal Influence* AI [ppm] and *Antipodal Shift Constants* ASC [ppm] of the series *closo*-$[B_6X_nY_{(6-n)}]^{2-}$ (X ≠ Y = Cl, Br, I; n = 5−2), derived from the chemical shifts δ(^{11}B) [ppm] for symmetric X−B···B−X or Y−B···B−Y and asymmetric X−B···B−Y arrangements

Compounds[a]	δ(^{11}B) sym.	asym	AI	ASC
$[B_6\mathbf{Cl}_5Br]^{2-}$	−17.00	−17.18	−0.18	+0.34
$[B_6\mathbf{Cl}_4Br_2]^{2-}$	−16.54	−16.38	+0.16	+0.34
$[B_6\mathbf{Cl}_3Br_3]^{2-}$	−16.08	−15.58	+0.50	+0.34
$[B_6\mathbf{Cl}_2Br_4]^{2-}$	−15.62	−14.78	+0.84	
$[B_6Cl\mathbf{Br}_5]^{2-}$	−19.31	−19.42	−0.11	+0.03
$[B_6Cl_2\mathbf{Br}_4]^{2-}$	−19.96	−20.04	−0.08	+0.03
$[B_6Cl_3\mathbf{Br}_3]^{2-}$	−20.61	−20.66	−0.05	+0.03
$[B_6Cl_4\mathbf{Br}_2]^{2-}$	−21.26	−21.28	−0.02	
$[B_6\mathbf{Cl}_5I]^{2-}$	−15.97	−13.82	+2.15	+0.36
$[B_6\mathbf{Cl}_4I_2]^{2-}$	−14.50	−11.99	+2.51	+0.36
$[B_6\mathbf{Cl}_3I_3]^{2-}$	−13.03	−10.16	+2.87	+0.36
$[B_6\mathbf{Cl}_2I_4]^{2-}$	−11.57	−8.33	+3.24	
$[B_6Cl\mathbf{I}_5]^{2-}$	−26.57	−27.28	−0.71	−0.02
$[B_6Cl_2\mathbf{I}_4]^{2-}$	−28.58	−29.31	−0.73	−0.02
$[B_6Cl_3\mathbf{I}_3]^{2-}$	−30.59	−31.34	−0.75	−0.02
$[B_6Cl_4\mathbf{I}_2]^{2-}$	−32.60	−33.37	−0.77	
$[B_6\mathbf{Br}_5I]^{2-}$	−17.50	−16.78	+0.72	−0.53
$[B_6\mathbf{Br}_4I_2]^{2-}$	−16.57	−16.38	+0.19	−0.52
$[B_6\mathbf{Br}_3I_3]^{2-}$	−15.65	−15.98	−0.33	−0.53
$[B_6\mathbf{Br}_2I_4]^{2-}$	−14.72	−15.58	−0.86	
$[B_6Br\mathbf{I}_5]^{2-}$	−26.00	−25.86	+0.14	−0.22
$[B_6Br_2\mathbf{I}_4]^{2-}$	−27.26	−27.34	−0.08	−0.22
$[B_6Br_3\mathbf{I}_3]^{2-}$	−28.52	−28.82	−0.30	−0.22
$[B_6Br_4\mathbf{I}_2]^{2-}$	−29.78	−30.30	−0.52	

[a] The respective ^{11}B nuclei under consideration are bonded to the substituents typed with bold letters.

The synthesis of the up to now unique fluoro compounds $[B_6FH_5H^{fac}]^-$ and $[B_6FH_5]^{2-}$ has succeeded only recently. Various experiments with the common fluorination agents had failed because of their acidic character or their too strong oxidation power. However, the desired fluorination product is formed with XeF_2 in dichloromethane at −60° C, even if yield is very low. Decisive progress was made with the commercially available 1-(chloromethyl)-4-fluoro-1,4-diazabicyclo[2.2.2]octane bis(tetrafluoroborate) (abbr.: F-TEDA-$[BF_4]_2$),[72] which has tailor-made properties for this application, and thus enables synthesis of $[B_6FH_5H^{fac}]^-$ (**3a**) (see Figure 3) in 50% yield according to Equation 17. This synthesis concept has successfully applied to prepare fluorine derivatives of $[B_{10}H_{10}]^{2-}$ [73][74] and $[B_{12}H_{12}]^{2-}$.[72]

$[n\mathrm{Bu}_4N][B_6FH_5H^{fac}]$, dissolved in dichloromethane, is deprotonated by $[n\mathrm{Bu}_4N]OH$, and upon addition of cesium acetate $Cs_2[B_6FH_5]$ is precipitated. The ^{19}F resonances are observed as typical quadrupolar coupled quadruplets due to I = 3/2 of ^{11}B with δ(^{19}F) = −212.8, $^1J(^{19}F,^{11}B)$ = 63 Hz and δ = −209.5 for the protonated and deprotonated compound, respectively.[72] $^1J(^{11}B,^{19}F)$ coupling is not resolved in the ^{11}B spectra, but is attained from the ^{19}F spectra in the order of 60 Hz. The X-ray structure determination on single crystals of $K_2[B_6FH_5]$ failed because of the orientation disorder of the nearly spherical cluster anions in the unit cell. Therefore, the structural parameters of *closo*-$[B_6FH_5]^{2-}$ have been derived from ab initio calculations on the basis of C_{4v} symmetry at the MP2/6-31G* level revealing B−F and B−B bond lengths of 143.4 and 172.5−173.9 pm, respectively. The results of the ab initio frequency analysis correspond with the assignments and values obtained from normal coordinate analysis, and a good agreement of observed and calculated frequencies is achieved. The valence force constants are $f_d(BB) = 1.92\cdot10^2$ and $f_d(BF) = 5.25\cdot10^2$ N·m^{-1}.[75]



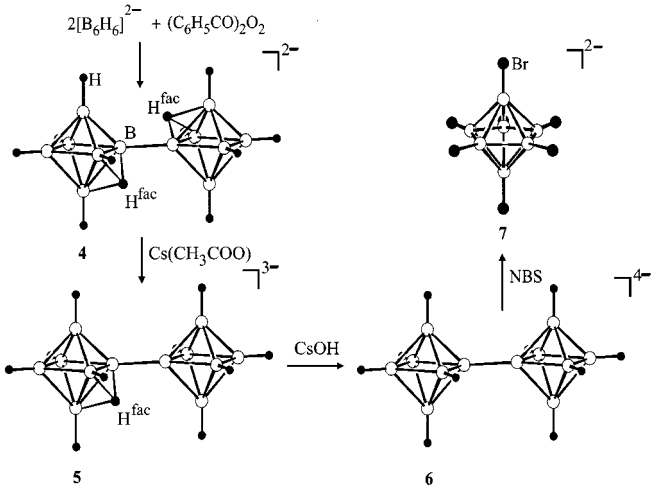
(17)

In resemblance to the iodination reactions (Equations 14b and 14c) $[B_6FH_5]^-$, prepared according to Equation 17, reacts with I_2 in aqueous solution at pH = 9 to give $[B_6FI_5]^{2-}$ {δ(^{11}B) = +3.8 (*ipso*), −30.1 (equatorial), −33.3 (*antipodal*); δ(^{19}F) = −247.6, $^1J(^{19}F,^{11}B)$ = 54 Hz} as described by Equation 18.[76]

$$[B_6FH_5]^{2-} + 5\ I_2 \rightarrow [B_6FI_5]^{2-} + 5\ HI \quad (18)$$

In contrast to the perhalogenated *closo*-hexaborates oxidation of $[B_6H_6]^{2-}$ takes a surprising course. In dichloromethane with dibenzoyl peroxide two cluster units are joined by a σ bond with a B−B distance of 170 pm to the novel *conjuncto*-cluster $[H^{fac}H_5B_6-B_6H_5H^{fac}]^{2-}$ (**4**). The deprotonation of the dianion proceeds in two steps, first with cesium acetate to the trivalent $[H^{fac}H_5B_6-B_6H_5]^{3-}$ (**5**) with pK_a = 9.6, and secondly with CsOH to $Cs_4[H_5B_6-B_6H_5]^{4-}$ (**6**).[77] By single-crystal structure analysis of $[Ph_4P]_2[H^{fac}H_5B_6-B_6H_5H^{fac}]$ the H^{fac} atoms could not be refined, but their location above the *ipso* spheres is clearly indicated by a 6% expansion of the respective faces adjacent to the B−B bridge. Based on averaged crystallographic data and adopting idealized D_{4h} symmetry a normal coordinate analysis has been performed. With a set of eleven force constants [e.g. $f_d(BB)_{conjuncto} = 2.9\cdot10^2$ and $f_d(BB)_{cage} = 1.6\cdot10^2$ N·m^{-1}] a very good agreement of observed and calculated frequencies has been achieved.[77] Even more surprising oxidation of **6** with *N*-bromosuccinimide at pH > 9 takes place under expansion of the octahedral core, and heptabromo-*closo*-heptaborate $[B_7Br_7]^{2-}$ (**7**)[78] as the first structurally secured derivative of the parent heptahydro-*closo*-heptaborate $[B_7H_7]^{2-}$ [68][79] is obtained. A single-crystal structure determination has succeeded on its $[(C_5H_5N)_2CH_2]^{2+}$ salt revealing the pen-

tagonal-bipyramidal arrangement of 7 boron atoms.[78] An illustration of these reactions is presented by Scheme 1.



Scheme 1. Oxidation of $[B_6H_6]^{2-}$

Pseudohalo and Chalcogeno Substituents

During reaction of $[B_6H_6]^{2-}$ with the pseudohalogens $(SCN)_2$ or $(SeCN)_2$ in dichloromethane the protonated compounds $[B_6H_5H^{fac}(SCN)]^-$ and $[B_6H_5H^{fac}(SeCN)]^-$ are formed, respectively,[80][81] which can be precipitated on addition of an ethanol solution of cesium acetate as the deprotonated salts $Cs_2[B_6H_5(SCN)]$ and $Cs_2[B_6H_5(SeCN)]$. A crystal structure of $Cs_2[B_6H_5(SCN)]$ with a B−S−C angle of 99.8° clearly indicates S bonding of the thiocyanate.[82] Reaction of $[B_6H_5(SCN)]^{2-}$ with Na in liquid NH_3 yields $[B_6H_5S]^{3-}$, while the analogous Se compound $[B_6H_5Se]^{3-}$ is prepared from $[B_6H_5(SeCN)]^{2-}$ already by treatment with CsOH in dichloromethane/methanol, indicating the less stability of the SeCN group. On $[Ph_4P][B_6H_5H^{fac}(SH)]$ a crystal structure determination has been performed.[83] The protonation of $[B_6H_5S]^{3-}$ is especially interesting, because the following compounds are to be assumed: $[B_6H_5H^{fac}S]^{2-}$, $[B_6H_5(SH)]^{2-}$, $[B_6H_5H^{fac}(SH)]^-$, and $[B_6H_5(SH_2)]^-$. $[B_6H_6(H^{fac})_2S]^-$, $[B_6H_5H^{fac}(SH)_2]$, and $[B_6H_6(H^{fac})_2(SH)]$ are not very likely because of their too strong acidity. Up to now the protolysis equilibria according to Eqations 19a, 19b have been established.[83]

$$[B_6H_5S]^{3-} + H^+ \rightleftharpoons [B_6H_5H^{fac}S]^{2-} \quad (19a)$$

$$[B_6H_5H^{fac}S]^{2-} + H^+ \rightleftharpoons [B_6H_5H^{fac}(SH)]^- \quad (19b)$$

The expected reaction to completely substituted derivatives in analogy to Equation 13 with an excess of $(SCN)_2$ or $(SeCN)_2$ in the presence of a base has been proven to be false.[84] Virtually, the cluster is degraded, and beside the long-known $[B(NCS)_4]^-$ [85] as a main product the novel compound $[B_2(NCS)_6]^{2-}$ is formed.[86] NCS stands for *N*-bonded thiocyanate, while SCN has the meaning of *S*-bonded thiocyanate. In contrast to the well-known boron trihalides this boron tripseudohalide is dimerized. By X-ray structure analysis on the $[Ph_3P{=}N{=}PPh_3]^+$ salt the B−B bond length has been determined to be 173 pm. An extensive vibrational spectroscopic study including ^{10}B and ^{11}B isotopic labeling accompanied by normal coordinate analysis has been performed resulting in the remarkably high force constant $f_d(BB) = 3.62{\cdot}10^2\ N{\cdot}m^{-1}$.[86] As an interesting feature *N*-bonding has been clearly confirmed by X-ray structure determination for these compounds in contrast to the *closo* clusters, where *S*-bonding prevails without exceptions up to now. The same is found in case of the SeCN compounds $[BH_n(NCSe)_{(4-n)}]^-$ ($n = 0-4$),[87] which has been proven by crystal structures on $[BH(NCSe)_3]^-$ and $[B_3H_7(NCSe)]^-$ [88] in comparison to $[B_6H_5(SeCN)]^{2-}$.[81] Here ^{77}Se-NMR spectroscopy is a valuable tool to distinguish the bonding mode of the selenocyanate: Signals of *N*-bonded substituents are found in the high-field region around $\delta(^{77}Se) = -300$, while *Se*-bonded species resonate in the downfield region between $\delta = 0$ and -100, viz. at $\delta = -72.8$ for $[B_6H_5(SeCN)]^{2-}$, at $\delta = -68.2$ for $[B_{10}H_9(SeCN)]^{2-}$, and even more deshielded at $\delta = -22.6$ for $[B_{12}H_{11}(SeCN)]^{2-}$.[81] During reaction of $[B_6H_6]^{2-}$ with cyanogen $(CN)_2$, which is generated from KCN and $CuSO_4$ in aqueous basic medium, the cyano derivatives $[B_6(CN)H_5]^{2-}$ and *cis*-$[B_6(CN)_2H_4]^{2-}$ are formed, and confirmed by X-ray structure determination.[89]

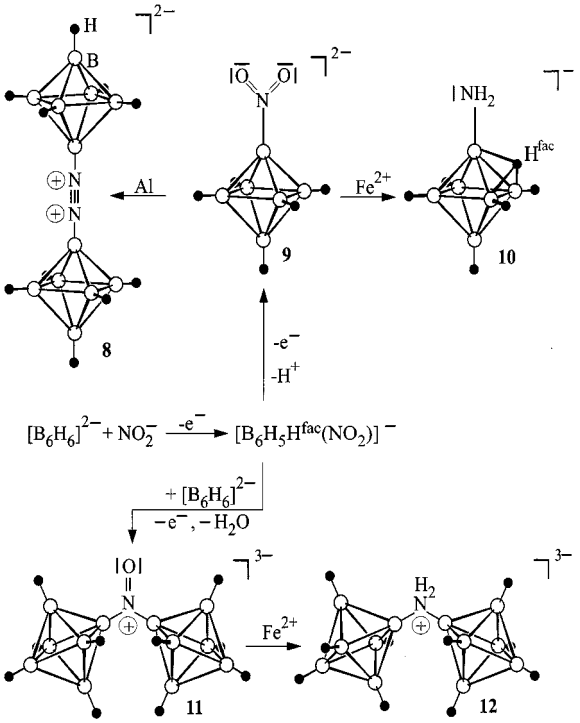
N-Bonded Substituents

On irradiation of an aqueous alkaline solution of $[B_6H_6]^{2-}$ and nitrite ions with a mercury vapor lamp the color turns to intense blue. From this solution a blue and a yellow product have been isolated by ion exchange chromatography on diethylaminoethylcellulose. On the basis of spectroscopic data these compounds have been assigned erroneously.[90] Both species are also obtainable, however in very low yields, from $[nBu_4N]_2[B_6H_6]$ in acetonitrile by addition of isopentyl nitrite. The highest yields of 8% for both of the compounds are attained during electrolysis of a dichloromethane solution containing $[nBu_4N][B_6H_6H^{fac}]$, $[nBu_4N]NO_2$, and 8-diazabicyclo[5.4.0]undec-7-ene (abbr.: DBU) as a base at a platinum electrode in the separated anodic room of an electrolysis cell with a carbon cathode. The single-crystal X-ray analysis revealed, that the yellow compound is the mononitro derivative $[B_6H_5(NO_2)]^{2-}$ (**9**),[91] and the blue compound is the dimeric bridged species $[H_5B_6-(NO)-B_6H_5]^{3-}$ (**11**).[92] *Caution! Both compounds are stable as Cs salts, however, they explode if only are touched. By anodic oxidation of* $[B_6H_5(NO_2)]^{2-}$*, the yellow, highly explosive cis-*$[B_6H_4(NO_2)_2]^{2-}$ *has become feasible.*[93] The mononitro compound $[B_6H_5(NO_2)]^{2-}$ (**9**) is reduced with Fe^{2+} in aqueous alkaline solution to the amine derivative $[B_6H_5H^{fac}(NH_2)]^-$ (**10**) analogous to aniline. Although H^{fac} could not be refined by X-ray structure analysis, it is likely positioned between a B_3 facet and the free electron pair of the NH_2 group.[94] If aluminum is used as a reducing agent in place of Fe^{2+}, the reduction process is ceased at the state of zero-valent nitrogen, and two cluster

units are bridged by a triply bonded dinitrogen molecule according to Equation 20.

$$2\,[B_6H_5(NO_2)]^{2-} + 2\,Al + 4\,H_2O \rightarrow [H_5B_6{-}N{\equiv}N{-}B_6H_5]^{2-} + 2\,[Al(OH)_4]^- \quad (20)$$

The X-ray structure analysis of μ-dinitrogenbis(pentahydro-*closo*-hexaborate) (**8**) succeeded on single crystals of the tetraphenylarsonium $[Ph_4As]^+$ salt.[95] In the same way as for $[B_6H_5(NO_2)]^{2-}$ reduction with Fe^{2+} in alkaline solution is applicable to $[H_5B_6{-}(NO){-}B_6H_5]^{3-}$ (**11**), and yields the amido-bridged derivative $[H_5B_6{-}(NH_2){-}B_6H_5]^{3-}$ (**12**).[96] According to its Brønsted base character two protons are added in neutral aqueous solution to give $[H^{fac}H_5B_6{-}(NH_2){-}B_6H_5H^{fac}]^-$, and the X-ray structure has been solved, however without refinement of H^{fac}.[96] The reactions and connections between the derivatives with N-substituents are shown in Scheme 2. Furthermore *cis*-$[B_6(CN)H_4(NO_2)]^{2-}$ and *cis*-$[(CN)H_4B_6{-}(NO){-}B_6H_4(CN)]^{3-}$ have been prepared and structurally characterized.[97] A highly interesting arrangement of B_6 in a cyclic structure has been found for hexakis(diethylamino)-*cyclo*-hexaborane $[B_6\{N(C_2H_5)_2\}_6]$,[98] however, the claimed interconversion of the *cyclo* structure to the octahedral structure could not be verified by X-ray structure determination.



Scheme 2. Derivatives of $[B_6H_6]^{2-}$ with N substituents

Organic Substituents

As already discussed in detail *closo*-$[B_6H_6]^{2-}$ is a Brønsted base with a pk_a value of 7.0. This fact will be of crucial importance during the following substitution reactions, because all protonated *closo*-hexaborates are inaccessible to substitution. This subject has already been discussed in the sections on the halogens and *pseudo*-halogens, and the same is true for the alkylation reactions. It is also the reason for the quite different alkylation conditions observed for the *closo*-borates. While the higher members $[B_{10}H_{10}]^{2-}$ and $[B_{12}H_{12}]^{2-}$ react under acidic conditions,[99] $[B_6H_6]^{2-}$ demands at least neutral solutions for the first substitution step and strong basic media for subsequent substitutions. In this way *mono*-, *di*-, and *tri*-alkyl-*closo*-hexaborates have been synthesized utilizing alkyl halides as alkylation agents.[100][101] On principle, all organic solvents must be dried accurately prior to use in order to maintain $[B_6H_6]^{2-}$ really in its deprotonated state.

For introduction of alkyl substituents $[n\mathrm{Bu}_4\mathrm{N}]_2[B_6H_6]$ is dissolved in dichloromethane or acetonitrile and treated with alkyl halides.[101] According to common organic concepts the alkyl carbon atom attached to the halogen atom is more positive through the −I effect of the halogen according to $R{-}C^{\delta+}{-}X^{\delta-}$, and an electrophilic attack on the region of maximum electron density above the octahedron facets is to be assumed. The resulting transitory state with a four-center, two-electron (4c2e) $C^{\delta+}{-}B_3$ interaction is stabilized by displacement of an *exopolyhedral* H atom from a vertex onto a facet of the B_6 cluster giving a more favorable 4c2e $H^{fac}{-}B_3$ bond and a common 2c2e B−C σ-bond under liberation of the respective halide ion. The course of alkylation reactions is exemplified by Equation 21.

$$[n\mathrm{Bu}_4\mathrm{N}]_2[B_6H_6] + RX \rightarrow [n\mathrm{Bu}_4\mathrm{N}][B_6H_5H^{fac}R] + [n\mathrm{Bu}_4\mathrm{N}]X\ (R = CH_3, C_2H_5, n\text{-}C_3H_7, n\text{-}C_4H_9, n\text{-}C_8H_{17}) \quad (21)$$

Alkyl iodides have proven as the most suitable agents, but as reactivity generally decreases with increasing chain length, *n*-octyl iodide, for example, must be applied in large excess and at 80° C to obtain $[B_6(n\text{-}C_8H_{17})H_5H^{fac}]^-$.[80] In the series of alkyl derivatives the Brønsted base character increases with increasing chain length, as is demonstrated by the pk_a values: 8.85 for CH_3, 9.50 for C_2H_5, 9.55 for *n*-C_3H_7 and 9.60 for both *n*-C_4H_9 and *n*-C_8H_{17}.[80] Deprotonation and precipitation as Cs salts is accomplished by addition of CsOH, dissolved in ethanol, to the dichloromethane solutions of $[n\mathrm{Bu}_4\mathrm{N}][B_6H_5H^{fac}R]$ as given by Equation 22.

$$[n\mathrm{Bu}_4\mathrm{N}][B_6H_5H^{fac}R] + 2\,CsOH \rightarrow Cs_2[B_6H_5R] + [n\mathrm{Bu}_4\mathrm{N}]OH + H_2O \quad (22)$$

The Cs salts are soluble in water, but show markedly basic reactions due to protolysis according to Equation 23.

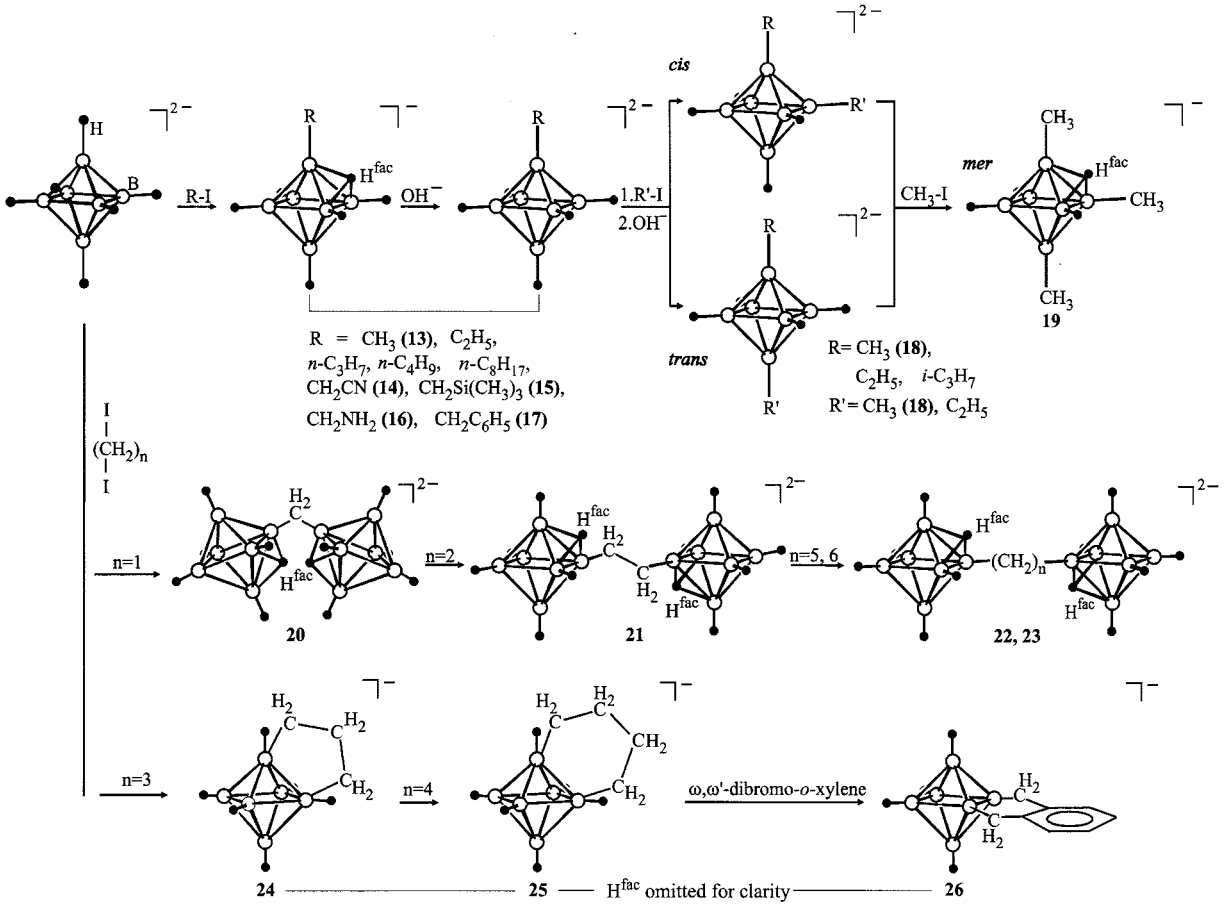
$$[B_6H_5R]^{2-} + H_2O \rightleftharpoons [B_6H_5H^{fac}R]^- + OH^- \quad (23)$$

As to be seen from Equation 21 the formation of the protonated compounds is unavoidable, and reaction is stopped at the monosubstituted state. For further substitution well-considered deprotonation procedures are required, which may be exemplified in the following substitution series: The $[Ph_4As]^+$ salt of the protonated com-

pound of choice is suspended in strong basic aqueous solution. In this way colorless $[Ph_4As][B_6H_5H^{fac}R]$ (**13**–**17**) is transformed to yellow $[Ph_4As]_2[B_6H_5R]$. The isolated deprotonated monoalkyl derivative is treated with the neat alkyl iodide of choice, whereupon the solid is decolorized. The colorless product $[Ph_4As][B_6H_4H^{fac}RR']$ (**18**) is dissolved in acetonitrile, and on addition of CsOH in 2-propanol *cis*- and *trans*-$Cs_2[B_6H_4RR']$ are obtained (R = CH_3, C_2H_5, *i*-C_3H_7; R′ = CH_3, C_2H_5).[102] With the up to now highest degree of alkylation the threefold methylated compound *mer*-$[B_6(CH_3)_3H_3H^{fac}]^-$ (**19**) has been synthesized, which refuses deprotonation, and thus further substitution. It is prepared from *cis*- or *trans*-$[Ph_4As]_2[B_6(CH_3)_2H_4]$ (**18**), which is obtained in the manner described above, on digestion with CH_3I (see Scheme 3, 1st row).

up from two protonated cluster anions bridged by methylene or a methylene chain. $[H^{fac}H_5B_6-(CH_2)-B_6H_5H^{fac}]^-$ (**20**) has a bent structure and two ionizable protons with pk_{a1} = 6.0 and pk_{a2} = 10.9[107]. For $[H^{fac}H_5B_6-(CH_2)_2-B_6H_5H^{fac}]^-$ (**21**)[108] only a single pk_a value = 10.9 has been found, and the same applies to the μ-pentamethylene (**22**) and μ-hexamethylene (**23**) derivatives with pk_a = 8.8 and pk_a = 9.1,[109] respectively. (see Scheme 3, 2nd row).

Interestingly, alkylation with 1,3-diiodopropane or 1,4-diiodobutane prefers an intramolecular route, and the two boron atoms of an edge of the octahedron are substituted resulting in *ansa*-like species with five- or six-membered anellated rings, respectively.[100] Both compounds are isolated in their protonated form $[B_6(-CH_2-CH_2-$



Scheme 3. Alkylation of $[B_6H_6]^{2-}$

Additionally, the derivatives $[B_6(CH_2CN)H_5H^{fac}]^-$ (**14**) pk_a = 5.85,[103] $[B_6\{CH_2-Si(CH_3)_3\}H_5H^{fac}]^-$ (**15**), $\delta(^{29}Si)$ = 2.25,[104] $[B_6(CH_2NH_2)H_5H^{fac}]^-$ (**16**),[105] and $[B_6\{CH_2(C_6H_5)\}H_5H^{fac}]^-$ (**17**)[106] are to be mentioned for the sake of completeness, which have been synthesized from $[nBu_4N]_2[B_6H_6]$ by reaction with chloroacetonitrile, trimethyliodomethylsilane, *N*-(chloromethyl)phthalimide, and benzyl bromide, respectively.

By reaction of $[B_6H_6]^{2-}$ with ω,ω′-diiodoalkanes $I-(CH_2)_n-I$ (*n* = 1, 2, 5, and 6) dicluster anions $[H^{fac}H_5B_6-(CH_2)_n-B_6H_5H^{fac}]^-$ are formed, which are built $H_2C-)H_4H^{fac}]^-$ (**24**) and $[B_6(-CH_2-CH_2-CH_2-H_2C-)H_4H^{fac}]^-$ (**25**) (see Scheme 3, 3rd row). Although H^{fac} could not be refined during X-ray structure analysis, its location is clearly indicated by markedly expanded B_3 facets.[100] Another six-membered anellated ring system featuring the interesting connection of a two- and a three-dimensional aromatic system is provided by *cis*-$[B_6(o$-xylene$)H_4H^{fac}]^-$ (**26**, see Scheme 3, 3rd row), which is obtained with ω,ω′-dibromo-*ortho*-xylene as alkylating agent. Structures have been solved of single crystals of the tetraphenylphosphonium $[Ph_4P]^+$ salt and the $[nBu_4N]^+$ salt.

Refinement of H^{fac} failed in the former case, but succeeded in the latter with $B-H^{fac}$ distances ranging from 111 pm to 148 pm and an expansion of the corresponding B_3 facet by about 7%.[110] A selection of the essentials of alkylation reactions is given by Scheme 3.

Very recently, the first aryl derivative the $[B_6(p\text{-}C_6H_4-NO_2)H_5H^{fac}]^-$ has been obtained by reaction of $[B_6H_6]^{2-}$ with *para*-bromonitrobenzene in acetonitrile and isolated in its deprotonated form as the red salt $Cs_2[B_6(p\text{-}C_6H_4-NO_2)H_5H^{fac}]$. After complete chlorination with *N*-chlorosuccinimide an X-ray structure determination succeeded on single crystals of $[(C_5H_5N)_2CH_2][B_6(p\text{-}C_6H_4-NO_2)Cl_5]$.[111] The reduction of $[B_6(p\text{-}C_6H_4-NO_2)H_5H^{fac}]^-$ with Fe^{II}, Al, and Raney-Ni in the presence of N_2H_4 results in a deep blue compound, which in all probability is the diazo compound $[H_5B_6-C_6H_4-N{\equiv}N-C_6H_4-B_6H_5]^{2-}$, as derived from ^{11}B- and ^{14}N-NMR data.[112]

Additionally, the following explosive alkylnitro derivatives have been synthesized and characterized by X-ray structure determination: *cis*-$[B_6(CH_3)H_4(NO_2)]^{2-}$, *fac*- and *mer*-$[B_6(CH_3)H_3(NO_2)_2]^{2-}$,[113] and *cis*-$[B_6(C_2H_5)H_4(NO_2)]^{2-}$.[114] From the structural data is to be seen, that the B_6 cage is expanded in direction towards the substituents in case of alkyl,[101][102] while it is compressed in case of cyano,[89] nitro,[91] and halo[62][115] substituents with shortening of the cage B···B diagonal distances in the order of 5−10%.

In an effort to obtain more insight into the influence of the localization of H^{fac}, and to calculate the energetic barrier of movement of H^{fac}, ab initio calculations have been performed with the GAUSSIAN 94[116] program. Structure optimization has been done according to standard methods on HF/6-31G*-basis, and the hyper face minimum has been confirmed by analytical frequency analysis.[117] The refinement of geometry and the calculation of the total energies is performed on MP2/6-31G* level assuming C_{4v} symmetry for $[B_6FH_5]^{2-}$ (**3**) and $[B_6(CH_3)H_5]^{2-}$ (**13**) and their respective protonated derivatives both for localization of H^{fac} above an *antipodal* facet (**3a** and **13a**) and an *ipso* facet (**3b** and **13b**) (see Figure 3). Similar to $[B_6H_6]^{2-}$ an energy of approx. 450 kcal·mol^{-1} is gained by protonation. This corresponds to the property of the monosubstituted derivatives to act as Brønsted bases. The relative energetic differences between *ipso* and *antipodal* protonation are indeed small, however, they are in agreement with the results of the ^{11}B-NMR investigations.[54] The fluorine compound is more stable by about 1 kcal·mol^{-1} in case of *antipodal* protonation (**3a**) as compared to *ipso* protonation (**3b**). For the methyl compound the opposite behavior is observed, and an even smaller gain in stability of merely 0.06 kcal·mol^{-1} results with *ipso* protonation (**13c**) in comparison to *antipodal* protonation (**13a**). However, the *ipso* localization of H^{fac} (**13b**) is affirmed by NMR investigations[54] and X-ray structure analysis.[101]

Between H^{fac} and the H atoms of the methyl group in $[B_6H_5H^{fac}(CH_3)]^-$ distances of 258, 279, and 320 pm have been obtained from X-ray structure. As a consequence an

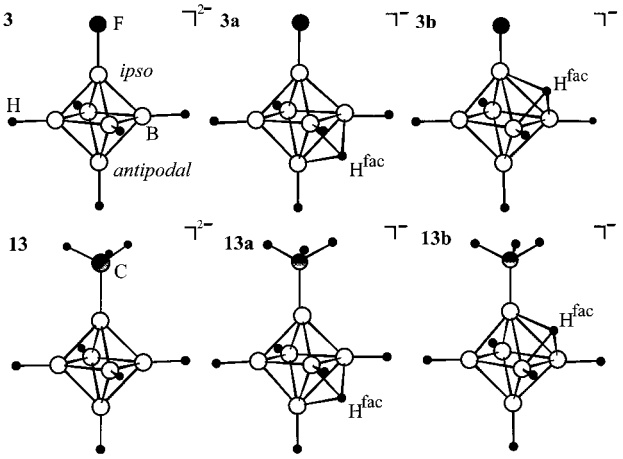


Figure 3. Localization of H^{fac} in monosubstituted $[B_6H_6]^{2-}$

assumed nuclear Overhauser interaction could be proven by 2D-^{1}H-NOESY NMR spectroscopy. This may be the reason for the decreased tendency of $[B_6H_5H^{fac}(CH_3)]^-$ with $pK_a = 8.85$[80] to dissociate in comparison to $[B_6H_6H^{fac}]^-$ with $pK_a = 7$[14] and $[B_6H_5H^{fac}F]^-$ with $pK_a = 5$.[72] Further, the obtained structure parameters served as a basis for calculation of the NMR shifts making use of the RHF/GIAO method[118] with an Ahlrichs tzp basis set.[119] In order to eliminate the solvent influence on the chemical shift referencing was done by use of signals of the respective deprotonated parent compounds in the same solvent as secondary standards. The ^{1}H-, ^{11}B-, ^{13}C-, and ^{19}F-NMR shifts have been calculated and found in good agreement with experimental data.[120] Furthermore, former results of vibrational spectroscopic assignments and the results of normal coordinate analyses could be verified by the ab initio frequency analyses. In good agreement with the experimental data[14] the ab initio calculations result in shifts of the terminal B−H valence modes by about 100 to 200 cm^{-1} to higher frequencies for the protonated cluster anions. This is consistent with the calculated shortening of the B−H distances. An effect of the protonation is also observed on the vibrational frequencies of polyatomic substituents. Accordingly, the C−H valence vibration of $[B_6(CH_3)H_5H^{fac}]^-$ is shifted to higher energy by about 150 cm^{-1} in comparison to $[B_6(CH_3)H_5]^{2-}$.[54] The symmetric and antisymmetric vibration of H^{fac} against the B_3 facet have not been observed, but are calculated to 1820 and 1295 cm^{-1} for *antipodal*-localized H^{fac}, and to 1791 and 1275 cm^{-1} for *ipso*-localized H^{fac}, respectively.[54]

The chemical shift of the nonequivalent ^{11}B nuclei in monosubstituted derivatives of $[B_6H_6]^{2-}$ and the mutual influence of substitution on the *ipso* and the *antipodal* B atoms depends on the electronegativity, the polarizability, and the spin orbit coupling of that atom bound to the cluster. While the signals of the equatorial B atoms are found nearly uninfluenced around $\delta = -15$, the resonances of the *ipso*- and *antipodal*-B are shifted increasingly with decreasing electronegativity or with increasing polarizability and spin orbit coupling, namely to high field for the *ipso*-B and

downfield for the *antipodal*-B. These qualitative trends are visualized by Figure 4.

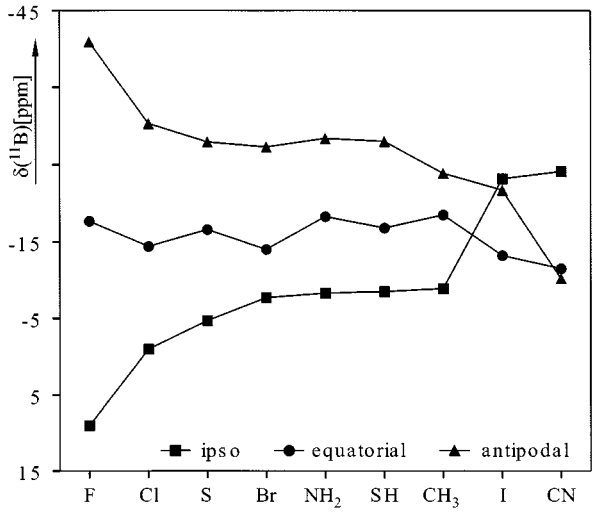


Figure 4. ^{11}B-NMR shifts of monosubstituted derivatives $[B_6H_6]^{2-}$

$[B_6H_6]^{2-}$ as a Ligand in Metal Complexes

In contrast to the higher *closo*-borates only a few metal derivatives are known for *closo*-$[B_6H_6]^{2-}$. By reaction of the nucleophilic nickelocene with $[B_6H_6]^{2-}$ two electrons are donated to the boron cluster, reducing it to the hypothetical $[B_6H_6]^{4-}$,[11] and induce cage opening. By elimination of a cyclopentadienyl ligand from Ni and oxidative addition of the borate moiety Ni atoms are built into the boron core, and under expansion of the octahedron the *closo*-metallaborates $[(\eta^5\text{-}C_5H_5)NiB_6H_6]^-$ [11][121] and $[(\eta^5\text{-}C_5H_5)_3Ni_3B_6H_6]^-$ [122] are formed, which correspond to the parent *closo*-borates $[B_7H_7]^{2-}$ [68][79] and $[B_9H_9]^{2-}$.[123] In contrast to the reaction of nickelocene with $[B_6H_6]^{2-}$ from cobaltocene and $[B_6H_6H^{fac}]^-$ the molecule compound $[(\eta^5\text{-}C_5H_5)Co(\eta^5\text{-}C_5H_4)B_6H_5H^{fac}]$ is formed with a normal σ(B−C) bond from one of the cyclopentadienyl groups C atoms to a vertex of the B_6 cluster having a bond length of 157.5 pm.[124]

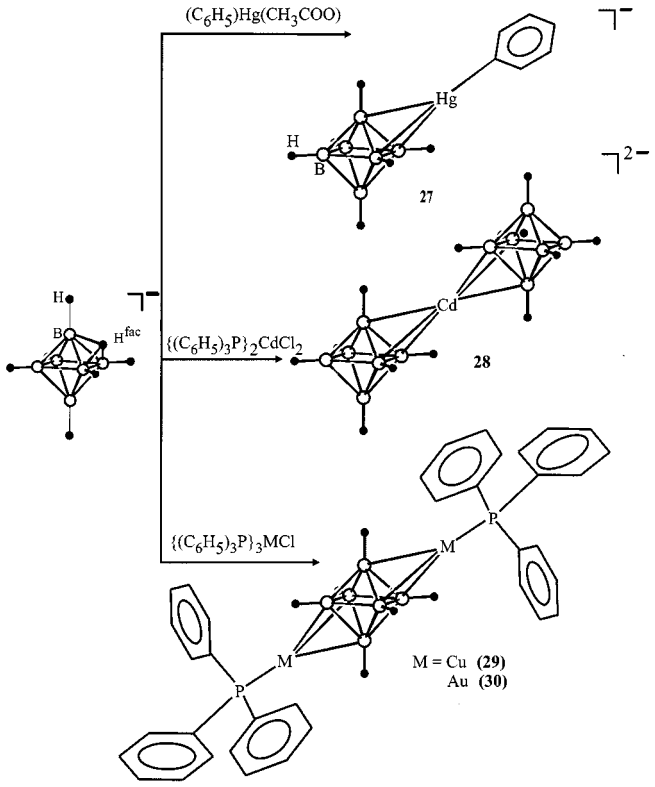
In accordance with the high electron density above the octahedral B_3 facets $[B_6H_6]^{2-}$ can act as a Lewis base and coordinate in a 4c2e bond to the metal atom of a complex. In this way $[(C_6H_5)Hg(\eta^3\text{-}B_6H_6)]^-$ (**27**) was synthesized from phenylmercury acetate, and its structure was solved on the $[Ph_4P]^+$ salt with B−Hg distances from 240 to 243 pm indicating the localization above one facet, the edges of which are markedly elongated to 183 pm.[125] In CD_2Cl_2 at 263 K a singlet has been recorded with $\delta(^{199}Hg) = -74$ vs. $Hg_2(NO_3)_2$ saturated in D_2O. However, the *hapticity* of $[B_6H_6]^{2-}$ must not be inevitably three, but may be two. This has been found in [(2,2′-bipyridine)Pb($\eta^{2,3}$-B_6H_6)], in which $[B_6H_6]^{2-}$ is coordinated via an η^2-B_2 edge as well as via an η^3-B_3 facet,[126] although considerable long Pb−B_3 distances of about 280 pm resulted for the η^3 coordination.

Two η^3-$[B_6H_6]^{2-}$ ligands, which are symmetrically arranged with distances of 218 pm from the Cd^{2+} center to the B_3 planes, are found in $[Cd(\eta^3\text{-}B_6H_6)_2]^{2-}$ (**28**),[127] which has been prepared from $[B_6H_6]^{2-}$ and $[\{(C_6H_5)_3P\}_2CdCl_2]$. The ^{113}Cd resonance of **28** in CD_2Cl_2 is found in the low-field region at $\delta(^{113}Cd) = 117$ vs. 3 M $Cd(NO_3)_2$ in D_2O at $\delta = -692.1$. From a view on the structure the term of a Cd^{2+} sandwich complex with the two B_6 clusters as three-dimensional aromatic systems seems to be justified.

During the reactions of $[\{(C_6H_5)_3P\}_3MCl]$, M = Cu and Au, with $[B_6H_6]^{2-}$ the binuclear complexes $[\{(C_6H_5)_3P\}_2M_2(\mu\text{-bis-}\eta^3\text{-}B_6H_6)]$ (**29**, **30**) are formed, containing $[B_6H_6]^{2-}$ as a bridging ligand in a bis(tri-*hapto*) mode of two opposite B_3 facets.[128] The metal centers in **29** and **30** are found in remarkably short distances of about 210 pm above the B_3 planes. The Au compound **30** has been obtained in two polymorphous forms in dependence of the crystallization conditions. While from dichloromethane solutions on slow diffusion of methylbutane, isopentane, or petroleum ether large cubic crystals (form A, space group *Pa*3bar) are precipitated, the same procedure with diethyl ether or *n*-pentane yields needles (form B, space group *Pccn*).[129] The coordinating B_3 facets are markedly expanded in both cases, viz. by 6% in A and 8% in B. However, packing in the elementary cells is different. The molecules in A are stacked loosely against one another, whereas in form B compact infinite stacking is to be seen. Therefore, the difference of about 40% in the calculated densities ρ(A) = 1.326 and ρ(B) = 1.885 g·cm^{-3} (B) is surprising. In analogy to the reactions of Cu and Au $[\{(C_6H_5)_3P\}_3AgCl]$ forms with $[B_6H_6]^{2-}$ in a first step $[\{(C_6H_5)_3P\}_2Ag_2\{\mu\text{-bis}(\eta^3\text{-}B_6H_6)\}]$. However, this complex is very instable, and due to the lack of suitable single crystals structural proof by X-ray analysis has not yet been done. The ^{11}B-NMR spectra agree with those of the respective Cu and Au complexes. During decomposition of the initial product metallic silver is precipitated, and from the remnants a dichloromethane adduct of *hypho*-decahydrohexaborane $[\{(C_6H_5)_3P\}_2B_6H_{10}] \cdot CH_2Cl_2$ could be crystallized, and its structure could be solved.[130] This is the first documented example for the opening of a *closo*-B_6 cluster to a *hypho*-hexaborane. An illustration of the versatile ligating capabilities of $[B_6H_6]^{2-}$ is given in Scheme 4.

Concluding Remarks

Systematically synthesized derivatives of the hexahydro-*closo*-hexaborate $[B_6H_6]^{2-}$ with classical inorganic and organic substituents were characterized structurally and spectroscopically. In this way, a better insight into the chemical and physical properties of this class of compounds was gained, and strong mutual support of the ab initio results and the experimental data could be achieved. As a central point of the reaction chemistry the protolysis behavior and its special importance during substitution reactions was discussed. The localization of the additional proton H^{fac}, bound in the solid state above one of the facets of the octa-



Scheme 4. $[B_6H_6]^{2-}$ as a tri-*hapto* ligand in metal complexes

hedron via a 4c2e bond, could be refined in several X-ray structures. In the solution state clear evidence of H^{fac} was given by ^{1}H-NMR spectroscopy. The dynamic behavior due to the fluctuation of H^{fac} across the octahedron facets in the parent compound $[B_6H_6H^{fac}]^-$ and the $[B_6H_5H^{fac}X]^-$ species was elucidated by variable-temperature ^{11}B-NMR spectroscopy and determination of the coalescence points. The interrelations between symmetry, electronic and geometrical structure, and spectroscopic properties could be demonstrated by the monosubstituted derivatives as instructive examples for the energetic difference between the *ipso* and the *antipodal* sphere arising through substitution. The effect of this imbalance depends on the nature of the substituent. This has been proven by single-crystal X-ray structure determinations and different NMR-spectroscopic techniques, and has been affirmed by ab initio calculations with the GAUSSIAN 94 program on the MP2/6-31G* level resulting in a consistent discussion of the experimental and theoretical data with strong mutual support. From the empirical data the following facts could be manifested:

- $pK_a < 7$ for X = halogen, pseudohalogen or NO_2, $pK_a > 7$ for X = alkyl
- In solid salts and in solution below the coalescence temperature H^{fac} is fixed above one of the *antipodal* facets in the case of halogen and pseudohalogen substituents, while it resides above one of the *ipso* facets in the case of alkyl substituents. The B_3 facets capped by H^{fac} are generally expanded by 5−8%.
- On substitution the octahedral B_6 cage is deformed with changes of the diagonal cage B···B distances up to 5−10%. It is compressed in direction towards the substituents in the case of halogen, pseudohalogen or N-substituents and expanded in direction towards substituents in the case of alkyl.
- The synthesis of bis(heteroleptic) derivatives $[B_6X_nY_{(6-n)}]^{2-}$ ($n = 1-5$, X ≠ Y = Cl, Br, I) requires that in a synthetic route the more electronegative substituent must be introduced at first, and then the less electronegative substituent as the second.
- During repeated substitution further substituents are directed in *trans*/*mer* position by I^- and in *cis* positions by NO_2^- and CN^-.
- A systematic *antipodal* influence within the complete series of persubstituted mixed halo-*closo*-hexaborates $[B_6Cl_nBr_{(6-n)}]^{2-}$, $[B_6Cl_nI_{(6-n)}]^{2-}$, and $[B_6Br_nI_{(6-n)}]^{2-}$ ($n = 1-5$) has been found, and therefrom for each series a characteristic *antipodal* shift constant (ASC) has been derived.

Besides this subsumption of the results of systematic synthetic work, which is already a good justification to pursue derivative chemistry, some reactions of the *closo*-B_6 parent compound have led unintentionally into new directions: Under formation of a B−B bond the *conjuncto* compounds $[H^{fac}H_5B_6-B_6H_5H^{fac}]^{2-}$ and $[H_5B_6-B_6H_5]^{4-}$ were formed, and therefrom by expansion the first structurally characterized *closo*-heptaborate $[B_7Br_7]^{2-}$ was established. Another new field of research is the introduction of $[B_6H_6]^{2-}$ as a ligand in coordination compounds, bound in an η^3 fashion to metal centers like Pb^{2+}, Cd^{2+}, Hg^+, Cu^+, Ag^+, and Au^+. For the first time opening to a *hypho*-borane of a ligated $[B_6H_6]^{2-}$ to Ag^+, the decahydrohexaborane B_6H_{10}, has been realized. Last, but not least the planned expansion of the octahedral cage by metal atoms to form hydro-*closo*-metallaborates with some examples of Ni is in its beginning, and promises interesting new pathways.

[1] W. H. Eberhardt, B. Crawford, W. N. Lipscomb, *J. Chem. Phys.* **1954**, *22*, 989.
[2] H. C. Longuet-Higgins, M. de V. Roberts, *Proc. R. Soc.* **1954**, *A224*, 336.
[3] H. C. Longuet-Higgins, M. de V. Roberts, *Proc. R. Soc.* **1955**, *A230*, 110.
[4] M. A. Hawthorne, A. R. Pitochelli, *J. Am. Chem. Soc*. **1955**, *81*, 5519.
[5] A. R. Pitochelli, M. A. Hawthorne, *J. Am. Chem. Soc*. **1960**, *82*, 3228.
[6] J. L. Boone, *J. Am. Chem. Soc.* **1964**, *86*, 5036.
[7] W. H. Knoth, U. S. P. 3390966, **1968**; *Chem. Abstr.* **1968**, *69*, 44973y.
[8] W. H. Knoth, H. C. Miller, J. C. Sauer, J. H. Balties, Y. T. China, E. L. Muetterties, *Inorg. Chem*. **1964**, *3,* 1955.
[9] W. R. Hertler according to F. Klanberg, E. L. Muetterties, *Inorg. Chem.* **1966**, *5*, 1955, footnote 17.
[10] W. Preetz, G. Peters, D. Bublitz, *Chem. Rev.* **1996**, *96*, 977.
[11] R. M. Kabbani, *Polyhedron* **1996**, *15*, 1951.
[12] W. J. Dewkett, M. Grace, H. Beall, *Inorg. Synth.* **1974**, *15*, 111.
[13] D. M. Vinitskii, V. L. Lagun, K. A. Solntsev, N. T. Kuznetsov, *Russ. J. Inorg. Chem.* **1984**, *29*, 1079.
[14] W. Preetz, A. Heinrich, J. Thesing, *Z. Naturforsch.* **1988**, *43b*, 1319.
[15] A. V. Agafonov, K. A. Solntsev, N. T. Kuznetsov, *Koord. Khim.* **1980**, *6*, 1767; *Chem. Abstr.* **1980**, *94*, 24248d.
[16] L. V. Titov, M. B. Levicheva, S. B. Psikka, *Russ. J. Inorg. Chem.* **1984**, *29*, 386.

[17] D. M. Vinitskii, T. V. Rezvova, K. A. Solntsev, N. T. Kuznetsov, *Russ. J. Inorg. Chem.* **1988**, *33*, 450.
[18] A. V. Agafanov, K. A. Solntsev, D. M. Vinitskii, N. T. Kuznetsov, *Russ. J. Inorg. Chem.* **1982**, *27*, 1697.
[19] D. M. Vinitskii, V. L. Lagun, K. A. Solntsev, N. T. Kuznetsov, *Russ. J. Inorg. Chem.* **1985**, *30*, 1089.
[20] R. Schaeffer, Q. Johnson, G. S. Smith, *Inorg. Chem.* **1965**, *4*, 917.
[21] I. Yu. Kuznetsov, D. N. Vinitskii, K. A. Solntsev, N. T. Kuznetsov, L. A. Butman, *Russ. J. Inorg. Chem.* **1987**, *32*, 1803.
[22] K. A. Solntsev, Yu. A. Buslaev, N. T. Kuznetsov, *Russ. J. Inorg. Chem.* **1986**, *31*, 633.
[23] N. T. Kuznetsov, K. A. Solntsev, *Chemistry of Inorganic Hydrides*, Nauka Publ., Moscow, **1990**.
[24] V. I. Privalov, V. P. Tarasov, M. A. Meladze, D. M. Vinitskii, K. A. Solntsev, N. T. Kuznetsov, *Russ. J. Inorg. Chem.* **1989**, *34*, 630.
[25] J. Evans, *J. Chem. Soc., Dalton Trans.* **1978**, 25.
[26] P. Brint, E. F. Healy, T. R. Spalding, T. Whelan, *J. Chem. Soc., Dalton Trans.* **1981**, 2512.
[27] R. L. DeKock, C. P. Jasperse, *Inorg. Chem.* **1983**, *22*, 3843.
[28] M. A. Cavanough, T. P. Fehlner, R. Stramel, M. E. O′Neill, K. Wade, *Polyhedron* **1985**, *4*, 687.
[29] T. Whelan, P. Brint, *J. Chem. Soc., Faraday Trans.* **1985**, *81*, 267.
[30] I. Yu. Kuznetsov, D. N. Vinitskii, K. A. Solntsev, N. T. Kuznetsov, L. A.Butman, *Dokl. Akad. Nauk. SSR* **1985**, *283*, 873; *Chem. Abstr.* **1986**, *104*, 27821w.
[31] D. R. Armstrong, P. G. Perkins, J. P. Stewart, *J. Chem. Soc., Dalton Trans.* **1973**, 627.
[32] M. McPartlin, C. R. Eady, B. F. G. Johnson, J. Lewis, *J. Chem. Soc., Chem. Comm.* **1976**, 883.
[33] A. D. Becke, K. E. Edgecombe, *J. Chem. Phys.* **1990**, *92*, 5397.
[34] A. Burkhard, U. Wedig, H. G. v. Schnering, *Z. Anorg. Allg. Chem.* **1993**, *619*, 437.
[35] B. Steuer, G. Peters, W. Preetz, unpublished results.
[36] A. M. Mebel, O. P. Charkin, K. A. Solntsev, N. T. Kuznetsov, *Russ. J. Inorg. Chem.* **1988**, *33*, 958.
[37] M. L. McKee, M. Bühl, O. P. Charkin, P. v. R. Schleyer, *Inorg. Chem.* **1993**, *32*, 4549.
[38] A. M. Mebel, P. v. R. Schleyer, K. Najafian, O. P. Charkin, *Inorg. Chem.* **1998**, *37*, 1693.
[39] J. Aihara, *J. Am. Chem. Soc.* **1978**, *100*, 3339.
[40] R. B. King, *J. Math. Chem.* **1990**, *4*, 69.
[41] A. M. Mebel, O. P. Charkin, K. A. Solntsev, N. T. Kuznetsov, *Russ. J. Inorg. Chem.* **1988**, *33*, 1292.
[42] M. Bühl, A. M. Mebel, O. P. Charkin, P .v. R. Schleyer, *Inorg. Chem.* **1992**, *31*, 3769.
[43] A. M. Mebel, O. P. Charkin, M. Bühl, P. v. R. Schleyer, *Inorg. Chem.* **1993**, *32*, 463.
[44] A. M. Mebel, O. P. Charkin, P. v. R. Schleyer, *Inorg. Chem.* **1993**, *32*, 469.
[45] C. E. Housecroft, R. Snaith, K. Moos, R. E. Mulvey, M. E. O′Neill, K. Wade, *Polyhedron* **1985**, *4*, 1875.
[46] D. M. Vinitskii, T. V. Rezvova, K. A. Solntsev, N. T. Kuznetsov, *Russ. J. Inorg. Chem.* **1987**, *32*, 1347.
[47] J. Bragin, D. S. Urevig, M. Diem, *J. Raman Spectrosc.* **1982**, *82*, 86.
[48] P. Brint, B. Sangchakr, P. W. Fowler, V. J. Weldon, *J. Chem. Soc., Dalton Trans.* **1989**, 2253.
[49] B. E. Douglas, C. A. Hollingsworth, *Symmetry in Bonding and Spectra*, Academic Press, Orlando, San Diego, New York, London, Toronto, Montreal, Sidney, Tokyo, **1985**, p. 343.
[50] J. Thesing, W. Preetz, *Z. Naturforsch.* **1990,** *45b*, 641.
[51] W. Preetz, E. Parzich, *Z. Naturforsch.* **1993**, *48b*, 1737.
[52] W. Preetz, J. Thesing, *Z. Naturforsch.* **1989**, *44b*, 121.
[53] G. Herzberg, *Molecular Spectra and Molecular Structure, II* ("Infrared and Raman Spectra of Polyatomic Molecules"), Van Nostrand Reinhold Company, New York, **1945,** p. 236ff, p. 309ff.
[54] B. Steuer, G. Peters, W. Preetz, *Z. Naturforsch.* **1998**, *53b*, 991.
[55] W. Preetz, J. Fritze, *Z. Naturforsch.* **1984**, *39b*, 1472.
[56] J. Fritze, W. Preetz, H. C. Marsmann, *Z. Naturforsch.* **1987**, *42b*, 287.
[57] J. Fritze, W. Preetz, *Z. Naturforsch.* **1987**, *42b*, 293.
[58] V. S. Khain, A. A. Volkov, E. N. Pletyukhina, I. V. Malyk, *Russ. J. Inorg. Chem.* **1991**, *36*, 917.
[59] W. Preetz, J. Fritze, *Z. Naturforsch.* **1987**, *42b*, 282.
[60] W. Preetz, M. Stallbaum, *Z. Naturforsch.* **1990,** *45b*, 1113.
[61] W. Preetz, H.-G. Srebny, H. C. Marsmann, *Z. Naturforsch.* **1984**, *39b*, 6, 189.
[62] W. Preetz, D. Sonnak, *Z. Naturforsch.* **1994**, *49b*, 1809.
[63] A. Heinrich, W. Preetz, H. C. Marsmann, *Z. Naturforsch.* **1988,** *43b*, 1647.
[64] S. Hermanek, *Chem. Rev.* **1992**, *92*, 325.
[65] J. Thesing, M. Stallbaum, W. Preetz, *Z. Naturforsch*. **1991,** *46b*, 602.
[66] A. Heinrich, H.-L. Keller, W. Preetz, *Z. Naturforsch.* **1990**, *45b*, 184.
[67] V. Lorenzen W. Preetz, *Z. Naturforsch.* **1997**, *52b*, 565.
[68] F. Klanberg, D. R. Eaton, L. J. Guggenberger, E. L. Muetterties, *Inorg. Chem*. **1967**, *6*, 1271.
[69] V. Lorenzen, W. Preetz, F. Baumann, W. Kaim, *Inorg. Chem*. **1998**, *37*, 4011.
[70] J. Thesing, W. Preetz, J. Baurmeister, *Z. Naturforsch*. **1991,** *46b*, 19.
[71] J. Thesing, J. Baurmeister, W. Preetz, D. Thiery, H. G. von Schnering, *Z. Naturforsch.* **1991,** *46b*, 800.
[72] H. Thomsen, O. Haeckel, U. Krause, W. Preetz, *Z. Anorg. Allg. Chem.* **1996**, *622*, 2061.
[73] S. V. Ivanov, S. M. Ivanova, S. M. Miller, O. P. Anderson, K. A. Solntsev, S. H. Strauss, *Inorg. Chem.* **1996**, *35*, 6914.
[74] S. V. Ivanov, A. J. Lupinetti, K. A. Solntsev, S. H. Strauss, *J. Fluorine Chem.* **1998**, *89*, 65.
[75] B. Steuer, H. Thomsen, W. Preetz, *Z. Naturforsch.* **1997**, *52b*, 443.
[76] H. Thomsen, W. Preetz, *Z. Naturforsch.* **1998**, *53b*, 829.
[77] D. Bublitz, A. Franken, W. Preetz, H. Thomsen, *Z. Naturforsch.* **1996**, *51b*, 609.
[78] A. Franken, H. Thomsen, W. Preetz, *Z. Naturforsch*. **1996**, *51b*, 744.
[79] E. L. Muetterties, E. L. Hoel, C. G. Salentine, M. F. Hawthorne, *Inorg. Chem*. **1975**, *14*, 950.
[80] A. Heinrich, W. Preetz, *Z. Naturforsch.* **1988**, *43b*, 1327.
[81] C. Nachtigal, B. Steuer, W. Preetz, *Chem. Ber.* **1996**, *129*, 1531.
[82] W. Preetz, S. Zander, C. Bruhn, *Z. Naturforsch.* **1998**, *53b*, 816.
[83] B. Steuer, S. Zander, W. Preetz, *Z. Anorg. Allg. Chem.* **1998**, *624,* 1829.
[84] W. Preetz, M. G. Hake, *Z. Naturforsch.* **1992**, *47b*, 1119.
[85] F. Klanberg, *Z. Anorg. Allg. Chem.* **1962**, *316*, 14.
[86] W. Preetz, B. Steuer, *Z. Naturforsch.* **1996**, *51b*, 551.
[87] S. J. Andrews, J. A. Welch, *Inorg. Chim. Acta* **1984**, *88*, 153.
[88] B. Steuer, W. Preetz, *Z. Naturforsch.* **1998**, *53b*, 271.
[89] W. Preetz, A. Franken, M. Rath, *Z. Naturforsch.* **1993**, *48b*, 598.
[90] M. G. Hake, W. Preetz, *Z. Naturforsch.* **1992**, *47b*, 1347.
[91] A. Franken, W. Preetz, M. Rath, K.-F. Hesse, *Z. Naturforsch.* **1993**, *48b*, 1727.
[92] A. Franken, W. Preetz, *Z. Naturforsch.* **1994**, *49b*, 1263.
[93] A. Franken, W. Preetz, *Z. Naturforsch.* **1995**, *50b*, 1030.
[94] A. Franken, W. Preetz, *Z. Naturforsch.* **1995**, *50b*, 11.
[95] A. Franken, W. Preetz, *Z. Naturforsch.* **1995**, *50b*, 781.
[96] A. Franken, W. Preetz, *Z. Naturforsch.* **1995**, *50b*, 767.
[97] A. Franken, W. Preetz, *Z. Naturforsch.* **1995**, *50b*, 1362.
[98] M. Baudler, K. Rockstein, W. Oehlert, *Chem. Ber.* **1991**, *124*, 1149.
[99] I. B. Sivaev, K. A. Solntsev, N. T. Kuznetsov, *Koord. Khim.* **1991**, *17*, 881; *Chem. Abstr.* **1991**, *115*, 159210h.
[100] W. Lübbe, A. Franken, W. Preetz, *Z. Naturforsch.* **1994**, *49b*, 1115.
[101] J. Baurmeister, A. Franken, W. Preetz, *Z. Naturforsch.* **1995**, *50b*, 623.
[102] J. Baurmeister, A. Franken, W. Preetz, *Z. Naturforsch.* **1995**, *50b*, 772.
[103] A. Franken, W. Preetz, *Z. Naturforsch.* **1994**, *49b*, 471.
[104] J. Baurmeister, A. Franken, W. Preetz, *Z. Naturforsch.* **1995**, *50b*, 1025.
[105] A. Franken, W. Preetz, *Z. Naturforsch.* **1994**, *49b*, 1267.
[106] B. Steuer, G. Peters, W. Preetz, *Inorg. Chim. Acta* **1999**, *289*, 70.
[107] W. Lübbe, W. Preetz, *Z. Naturforsch.* **1996**, *51b*, 545.
[108] W. Lübbe, W. Preetz, *Z. Naturforsch.* **1996**, *51b*, 363.
[109] W. Lübbe, W. Preetz, *Z. Naturforsch.* **1996**, *51b*, 359.
[110] W. Lübbe, W. Preetz, *Z. Naturforsch.* **1996**, *51b*, 691.
[111] S. Zander, C. Drewes, W. Preetz, 10th IMEBORON, PA-05, Durham, **1999**.

[112] S. Zander, W. Preetz, in preparation.
[113] C. Drewes, W. Preetz, *Z. Naturforsch.* **1999**, *54b*, 349.
[114] C. Drewes, W. Preetz, *Z. Naturforsch.* **1999**, *54b*, 772.
[115] D. Sonnak, W. Preetz, *Z. Naturforsch.* **1998**, *53b*, 206.
[116] M. J. Frisch, G. W. Trucks, H. B. Schlegel, P. M. W. Gill, B. G. Johnson, M. A. Robb, J. R. Cheeseman, T. A. Keith, G. A. Petersson, J. A. Montgomery, K. Raghavachari, M. A. Al-Laham, V. G. Zakrzewski, J. V. Ortiz, J. B. Foresman, J. Cioslowski, B. B. Stefanov, A. Nanayakkara, M. Challacombe, C. Y. Peng, P. Y.Ayala, W. Chen, M. W. Wong, J. L. Andres, E. S. Replogle, R. Gomperts, R. L. Martin, D. J. Fox, J. S. Brinkley, D. J. Defrees, J. Baker, J. P. Stewart, M. Head- Gordon, C. Gonzalez, J. A. Pople, *GAUSSIAN 94* (Revision D.2), Gaussian Inc., Pittsburgh, PA, **1995**.
[117] J. Hehre, L. Radom, P. v. R. Schleyer, J. A. Pople, *Ab initio Molecular Orbital Theory*, Wiley, New York, **1986**.
[118] K. Wolinski, J. F. Hilton, P. Pulay, *J. Am. Chem. Soc*. **1990**, *112*, 8251.
[119] A. Schäfer, H. Horn, R. Ahlrichs, *J. Chem. Phys.* **1992**, *97*, 2571.
[120] B. Steuer, Dissertation, Christian-Albrechts-Universität Kiel, **1997**.
[121] D. M. Vinitskii, V. L. Lagun, K. A. Solntsev, N. T. Kuznetsov, K. N. Marushkin, Z. Yanoušek, K. Baše, B. Štibr, *Russ. J. Inorg. Chem.* **1984**, *29*, 1714.
[122] V. L. Lagun, K. A. Solntsev, V. I. Ponomarev, A. I. Prokhorov, A. M. Orlova, N. T. Kuznetsov, *Russ. J. Inorg. Chem.* **1994**, *39*, 505.
[123] H. Binder, R. Kellner, K. Vass, M. Hein, F. Baumann, M. Wanner, R. Winter, W. Kaim, W. Hönle, Y. Grin, H. Wedig, M. Schultheiss, R. K. Kremer, H. G. von Schnering, O. Groeger, G. Engelhardt, *Z. Anorg. Allg. Chem.* **1999**, *625*, 1059.
[124] T. Schaper, W. Preetz, *Z. Naturforsch.* **1998**, *53b*, 819.
[125] T. Schaper, W. Preetz, *Z. Naturforsch.* **1997**, *52b*, 57.
[126] V. L. Lagun, S. B. Katser, A. M. Orlova, T. V. Rezvova, L. V. Goeva, K. A. Solntsev, N. T. Kuznetsov, *Russ. J. Inorg. Chem.* **1992**, *18*, 312.
[127] T. Schaper, W. Preetz, *Inorg. Chem.* **1998**, *37*, 363.
[128] T. Schaper, W. Preetz, *Chem. Ber.* **1997**, *130*, 405.
[129] T. Schaper, C. Näther, W. Preetz, *Z. Naturforsch.* **1999**, *54b*, 345.
[130] T. Schaper, W. Preetz, *Z. Naturforsch.* **1998**, *53b*, 1326.

Received April 27, 1999
[I99156]

Formation and Structural Characterisation of an Unusual Cyclic Hexameric Oxotitanium Complex

Tim Kemmitt,*[a] Najeh I. Al-Salim,[a] and Graeme J. Gainsford[a]

Keywords: Titanium / Amino alcohols / Metal alkoxide / Oxo alkoxide / Metallacycles

$Ti_6O_6(MDEA)_6 \cdot 2CH_2Cl_2$ (MDEA = *N*-methyldiethoxoamine) was obtained by the controlled hydrolysis of the $Ti(MDEA)_2$ complex and analysed by X-ray diffraction. The compound consists of a ring of six [TiO_5N] octahedra, edge bridged by μ_2-oxide and a μ_2-alkoxide arm of the aminoalkoxide ligand.

Introduction

Modification of metal alkoxides is a common technique in the formation of sol-gel materials, and is used to control the hydrolysis rate and condensation pathways of the oxo-alkoxide fragments. The modification involves the introduction of bi- or multidentate anionic ligands, such that the reactivity of the resulting compound is lower than the parent alkoxide thus allowing size control of the primarily formed oxo-particles. Examples of titanium oxo-complexes include oxo-alkoxides,[1−5] β-diketonates,[6−8] carboxylates,[9−15] and related complexes.[16−22] These exhibit a rich variation in structural types characterised by different coordination modes of the ligands, variations in linkages of the coordination polyhedra, degree of hydrolysis, and coordination number of the central atom. The titanium oxo-alkoxides exhibit degrees of condensation {defined as z/x for $[Ti_xO_z](OR)_{4x-2z}$} from 0.33 to 1.33,[3] while the degree of condensation accessible to the titanium carboxylates and other derivatives is more limited due to the increased coordination requirement of the modifying ligands. Mixed-metal complexes have been reported which further extend the range of structural features available.[23,24]

The coordination number for titanium is commonly 6, although ligand constraints have resulted in complexes with coordination numbers of 5[8,25−27] and 7.[25,26,28,29] Di- and polynuclear titanium complexes are generally characterised by vertex- and edge-sharing polyhedra, although a diolato-alkoxide containing a rare face-sharing linkage was recently reported.[25]

Amino alcohols have been applied as modifiers, and have been demonstrated to exhibit favourable properties for application in titanium sol-gel chemistry[30,31] and MOCVD.[32] Several derivatives of triethanolamine have been reported,[26,27,29,33−35] two of which contain oxo- linkages,[26,34] but crystalline derivatives of other amino alcohols are rare[28,36] and none of these are oxo-complexes.

[a] Industrial Research Ltd,
P.O. Box 31−310, Lower Hutt, New Zealand
Fax: (internat.) + 64-4/569-0142
E-mail: T.Kemmitt@irl.cri.nz

Results and Discussion

We have isolated a crystalline derivative of *N*-methyldiethanolamine (MDEA), of composition $Ti_6O_6(MDEA)_6 \cdot 2CH_2Cl_2$. This compound was obtained by the hydrolysis and condensation of $Ti(MDEA)_2$ **(2)** prepared from the reaction of $Ti(OPr)_4$ with two equivalents of $MDEAH_2$. It is difficult to be definitive about the sequence of substitution and hydrolysis reactions occurring, but it seems necessary to first form the bis MDEA complex from $Ti(OPr)_4$, which can then be carefully hydrolysed to form **1**. Although **1** contains a single equivalent of MDEA per titanium, we have been unsuccessful in our attempts to prepare and isolate this product using this reactant ratio. The hexameric oxo complex **1** is much more hydrolytically stable than the parent bis complex which is highly hydrophilic. Crystals of **1** retained their integrity for several hours in the open air, degrading only due to the loss of dichloromethane molecules of crystallisation. This also occurred if the crystals were stored in sealed containers in the absence of dichloromethane vapour. In contrast, crystals of **2** became soft and waxy almost immediately on exposure to atmospheric moisture. The preparation and isolation of **2** will be reported later in a full paper, together with data on other related complexes.

Compound **1** consists of a ring of six [TiO_5N] edge-linked octahedra (Figure 1). This contrasts with titanium oxo-carboxylates which include a high proportion of corner-shared octahedra. Each titanium is coordinated to a single MDEA ligand incorporating one terminal alkoxide, one μ_2-bridging alkoxide, and one terminal amine (Figure 2). The six μ_2-oxide bridges are located on the inside edge of the ring, alternating above and below the plane of the ring. The methylamine groups similarly appear on alternating faces of the ring, but are located on the outside edge of the ring. Each of these methyl groups is involved in a C−H···O interaction with the terminal alkoxide oxygen of an adjacent diethoxomethylamino group {C(25)−H(25A)···O(14), H···O = 233 pm}. Two molecules of dichloromethane are co-crystallised with each macrocycle, and are located one on each face of the ring, with their

 © WILEY-VCH Verlag GmbH, D-69451 Weinheim, 1999 1434−1948/99/1111−1847 $ 17.50+.50/0

hydrogen atoms pointing towards the plane of the ring and their chlorine atoms pointing away from the ring. Significant hydrogen bonding occurs between these dichloromethane protons and the closest μ_2-oxide bridges {C(120)−H(12C)···O(10), H···O = 229 pm, C···H···O = 154°}. The total assembly is pseudo-centrosymmetric.

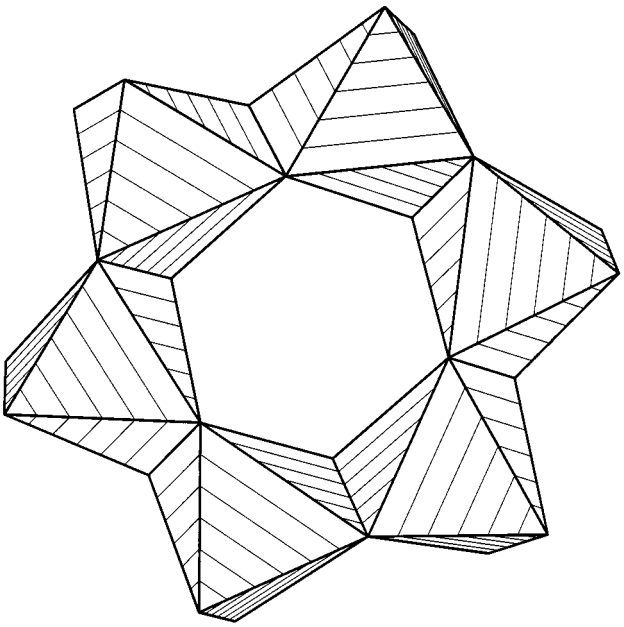


Figure 1. Molecular geometry of the coordination polyhedra in $[Ti_6(\mu_2\text{-}O_6)(\mu_2\text{-}OCH_2CH_2NCH_3{\cdot}CH_2CH_2O)_6{\cdot}2CH_2Cl_2$

The narrow bite angles (74, 76 and 79°) made by the coordinated MDEA, and the long Ti−N bond (av. = 235 pm), result in a coordination geometry around titanium that is extremely distorted from an ideal octahedron. The Ti−O bond lengths of the oxo bridges alternate long and short around the ring, with the shorter distances (av. = 175.7 pm) being *trans* to the long Ti−N bonds, and the longer distances (av. = 196.3 pm) being *trans* to the shorter terminal alkoxy arm of the MDEA.

The MDEA ligand coordinated to Ti(6) exhibits conformational disorder. Conformational rigidity may be preserved in the other MDEA ligands by the proximity of the dichloromethane to the ligands coordinated to Ti(1), Ti(2), Ti(4) and Ti(5). The MDEA coordinated to Ti(3) {which is pseudosymmetrically related to Ti(6)} is also held in one conformation by hydrogen bonding with a molecule of dichloromethane {C(31)−H(31A)···Cl(2), H···Cl = 270 pm} and weak intermolecular hydrogen bonding with a bridging oxygen from an adjacent macrocycle {C(32)−H(32B)···O(24), H···O = 258 pm}.

The macrocycle hole size, measured between opposite oxygens (less 140 pm for oxygen van der Waals radii), is 451, 447 and 480 pm for O(10)···O(40), O(30)···O(60) and O(20)···O(50) respectively. Related six- and eight-membered "coronate" complexes of Fe have been prepared with MDEA and triethanolamine ligands.[37] Bridging in these complexes is solely via the μ_2-alkoxo groups of the amino alcohols as the complexes do not include oxo ligands.

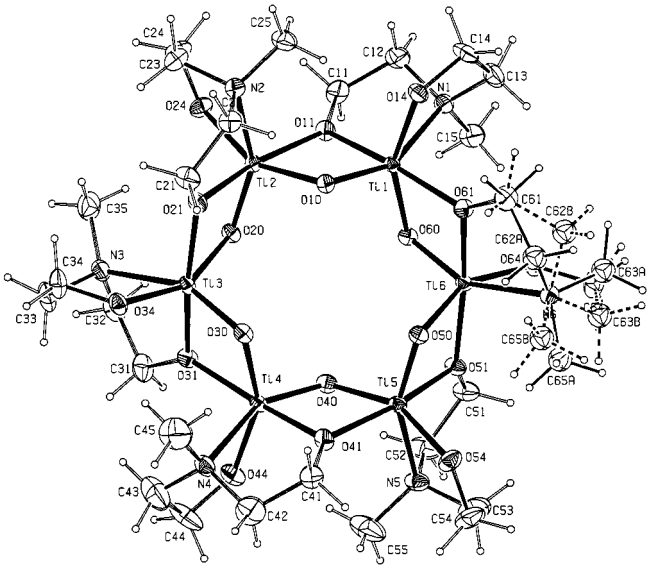


Figure 2. X-ray crystal structure of the hexameric assembly **1** (ORTEP drawing) showing the conformational disorder in the ligand attached to Ti(6)

Experimental Section

Hexakis[titanium(μ_2-oxo)(*N*-methyldiethoxoamine)] (1): A sample of $Ti(MDEA)_2$ (0.1 g) was dissolved in dry dichloromethane (5.0 mL). A layer of moist diethyl ether (10 cm^3) was carefully added and left to diffuse slowly into the the dichloromethane solution over 4 days. The crystalline product precipitated from solution, and X-ray quality crystals were removed from the side of the flask. Yield 0.06 g.

X-ray Crystallographic Study:[38] $C_{32}H_{70}{\cdot}Cl_4N_6O_{18}Ti_6$, Fw = 1256.14. Monoclinic, space group $P\ 2_1/c$, a = 1101.63(2), b = 2238.60(5), c = 2108.43(5) pm, β = 100.203(1)°, V = 5117.4(2)·10^6 pm^3, d_{calc} = 1.63 $Mg{\cdot}m^{-3}$ for Z = 4, μ = 1.171 mm^{-1}, λ(Mo-K_α) = 71.073 pm, T = 158 K. A tabular crystal 0.80 × 0.50 × 0.40 mm was cut from a larger block immersed in mounting oil and rapidly mounted under a nitrogen stream on a Siemens P4 SMART diffractometer with a Siemens CCD area detector. The data collection nominally covered a hemisphere of reciprocal space, by a combination of two sets of exposures (14322 reflections). Each exposure took 15 s, the first at 0.3° intervals over a total of 52.8° in ω; the second covered 360° in ϕ (the mounting axis). Crystal decay was monitored by repeating the initial 10 frames at the end of the data collection and analyzing the duplicate reflections. The data (θ = 2.62 to 26.08°) were corrected for Lorentz and polarization factors and crystal decay (SAINT) and an empirical absorption correction (SADABS) was applied giving 7184 unique data.

The structure was solved by direct methods (SHELXS-97)[38] and successive difference-Fourier syntheses. Refinement was by full matrix least-squares based on wF_o^2 using $w = 1/[\sigma^2(F_o^2) + (0.0635*P)^2 + 0.34*P]$ where $P = (F_o^2 + 2F_c^2)/3$ and F_o and F_c are the observed and calculated structure factor amplitudes from SHELXL-97.[39] The disorder found for the ligand bound to Ti(6) was modelled using two conformations which refined to occupancies of 0.680(4) and 0.320(4) (see Figure 2). All hydrogen atoms were refined as riding atoms with isotropic thermal parameters set at 1.2 times the atom to which they were bound. All other atoms were refined with anisotropic thermal parameters. Refinement converged at R_1 = 0.0454, [for 5723 reflections with $I > 2\sigma(I)$], 588 parameters, wR_2 = 0.1320; final GOF = 1.008. The final difference map

showed no peak larger than 1.047 eA^{-3} and no hole larger than -0.604 eA^{-3}, and these were < 120 pm from Ti and C atoms.[40]

[1] V. W. Day, T. A. Eberspacher, W. G. Klemperer, C. W. Park, *J. Am. Chem. Soc.* **1993**, *115,* 8469.
[2] R. Schmid, A. Mosset, J. Galy, *J. Chem. Soc., Dalton Trans.* **1991**, 1999.
[3] V. W. Day, T. A. Eberspacher, Y. Chen, J. Hao, W. G. Klemperer, *Inorg. Chim. Acta* **1995**, *229,* 391.
[4] T. J. Boyle, T. M. Alam, E. R. Mechenbier, B. L. Scott, J. W. Ziller, *Inorg. Chem.* **1997**, *36,* 3293.
[5] C. F. Campana, Y. Chen, V. W. Day, W. G. Klemperer, R. A. Sparks, *J. Chem. Soc., Dalton Trans.* **1996**, 691.
[6] G. D. Smith, C. N. Caughlan, J. A. Campbell, *Inorg. Chem.* **1972**, *11,* 2989.
[7] P. Toledano, M. In, C. Sanchez, *C. R. Acad. Sci. Paris* **1990**, *311,* 1161.
[8] P. D. Moran, C. E. F. Rickard, G. A. Bowmaker, R. P. Cooney, J. R. Bartlett, J. L. Woolfrey, *Inorg. Chem.* **1998**, *37,* 1417.
[9] R. Papiernik, L. G. Hubert-Pfalzgraph, J. Vaissermann, M. C. H. B. Goncalves, *J. Chem. Soc., Dalton Trans.* **1998**, 2285.
[10] S. Doeuff, Y. Dromzee, C. Sanchez, *C. R. Acad. Sci. Paris* **1989**, *308,* 1409.
[11] P. Toledano, M. In, C. Sanchez, *C. R. Acad. Sci. Paris* **1991**, *313,* 1247.
[12] T. M. Alam, T. J. Boyle, C. D. Buchheit, R. W. Schwartz, J. W. Ziller, *Mat. Res. Soc Symp. Proc.* **1994**, *346,* 35.
[13] G. Kickelbick, U. Schubert, *Eur. J. Inorg. Chem.* **1998**, 159.
[14] I. Gautier-Luneau, A. Mosset, J. Galy, *Z. Kristallogr.* **1987**, *180,* 83.
[15] S. Doeuff, Y. Dromzee, F. Taulelle, C. Sanchez, *Inorg. Chem.* **1989**, *28,* 4439.
[16] U. Schubert, E. Arpac, W. Glaubitt, A. Helmerich, C. Chau, *Chem. Mater.* **1992**, *4,* 291.
[17] U. Schubert, S. Tewinkel, F. Moller, *Inorg. Chem.* **1995**, *34,* 995.
[18] K. Wieghardt, U. Quilitzsch, J. Weiss, B. Nuber, *Inorg. Chem.* **1980**, *19,* 2514.
[19] N. W. Eilerts, J. A. Heppert, M. L. Kennedy, F. Takusagawa, *Inorg. Chem.* **1994**, *33,* 4813.
[20] J. V. Barkley, J. C. Cannadine, I. Hannaford, M. M. Harding, A. Steiner, J. Tallon, R. Whyman, *Chem. Commun.* **1997**, 1653.
[21] T. J. Boyle, R. W. Schwartz, R. J. Doedens, J. W. Ziller, *Inorg. Chem.* **1995**, *34,* 1110.
[22] R. Fleischer, H. Wunderlich, M. Braun, *Eur. J. Org. Chem.* **1998**, 1063.
[23] K. G. Caulton, L. G. Hubert-Pfalzgraph, *Chem. Rev.* **1990**, *90,* 969.
[24] C. D. Chandler, C. Roger, M.J. Hampden-Smith, *Chem. Rev.* **1993**, *93,* 1205.
[25] N. Pajot, R. Papiernik, L. G. Hubert-Pfalzgraph, J. Vaissermann, S. Parraud, *J. Chem. Soc., Chem. Commun.* **1995**, 1817.
[26] W. M. P. B. Menge, J. G. Verkade, *Inorg. Chem.* **1991**, *30,* 4628.
[27] A. A. Naiini, S. L. Ringrose, Y. Su, R. A. Jacobson, J. G. Verkade, *Inorg. Chem.* **1993**, *32,* 1290.
[28] D.F. Evans, J. Parr, S. Rahman, A. M. Z. Slawin, D. J. Williams, C. Y. Wong, J. D. Woollins, *Polyhedron* **1993**, *12,* 337.
[29] G. Boche, K. Mobus, K. Harms, M. Marsch, *J. Am. Chem. Soc.* **1996**, *118,* 2770.
[30] Y. Takahashi, Y. Matsuoka, *J. Mater. Sci.* **1988**, *23,* 2259.
[31] N. Tohge, E. Fujii, T. Minami, *J. Mater. Sci. Materials in Electronics* **1994**, *5*, 356.
[32] A. C. Jones, T. J. Leedham, P. J. Wright, M. J. Crosbie, K. A. Fleeting, D. J. Otway, P. O′Brien, M. E. Pemble, *J. Mater. Chem.* **1998**, *8,* 1773.
[33] A. A. Naiini, W. M. P. B. Menge, J. G. Verkade, *Inorg. Chem.* **1991**, *30,* 5009.
[34] H. J. Cohen, *J. Organomet. Chem.* **1966**, *5,* 413.
[35] R. L. Harlow, *Acta Cryst.* **1983**, *C39,* 1344.
[36] D. M. Puri, R. C. Mehrotra, *J. Indian Chem. Soc.* **1962**, *39,* 447.
[37] R. W. Saalfrank, I. Bernt, E. Uller, F. Hampel, *Angew. Chem. Int. Ed. Engl.* **1997**, *36,* 2482.
[38] G.M. Sheldrick, *Acta Cryst.* **1990**, *A46,* 467.
[39] G. M. Sheldrick, University of Göttingen, Germany **1997**.
[40] Crystallographic data (excluding structure factors) for the structure reported in this paper have been deposited with the Cambridge Crystallographic Data Centre as supplementary publication no. CCDC-127303. Copies of the data can be obtained free of charge on application to CCDC, 12 Union Road, Cambridge CB2 1EZ, UK [Fax: (internat.) + 44-1223/336-033; E-mail: deposit@ccdc.cam.ac.uk].

Received June 22, 1999
[I99228]

Novel μ_3-Coordination of Urea at a Nickel(II) Site: Structure, Reactivity and Ferromagnetic Superexchange

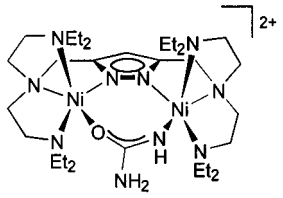
Franc Meyer,*[a] Matthias Konrad,[a] and Elisabeth Kaifer[a]

Keywords: Urea / Nickel / Coordination modes / Cooperative effects / Magnetic properties

A tetranuclear mixed-spin nickel(II) complex featuring two urea molecules in an unprecedented μ_3-κN:κN′:κO coordination mode has been structurally characterized. The two central high-spin nickel(II) ions exhibit ferromagnetic coupling (J = +3.4 cm^{-1}) mediated by the NH_2–C–O linkages of the bridging urea. In solution the temperature dependence of the UV/Vis optical absorption and of the magnetic moment indicate that, upon cooling, additional solvent molecules bind to the terminal low-spin metal ions and a concomitant spin change occurs. In the solid state the coordinated urea ligands can be thermally degraded to cyanate within the grip of the multimetallic nickel(II) site.

The coordination and conversion of urea at transition metal complexes,[1] in particular at dinuclear nickel(II) systems,[2−5] has received considerable attention in recent years. The main incentive for this arises from the endeavor to understand and mimic the unique properties of the natural metalloenzyme urease, which contains two cooperating nickel(II) ions within its active site, and which achieves at least a 10^{14}-fold rate enhancement for the biological hydrolysis of urea.[6][7] According to the initially proposed mechanism[8] of urease activity, the urea substrate is activated by O-coordination to one nickel(II) ion in conjunction with extensive hydrogen bonding within the active site pocket, and is attacked by a nucleophilic hydroxide bound to the adjacent second metal ion. Subsequent structural findings for both native and inhibited urease, however, together with structure-based molecular modeling of the catalytic mechanism, led to the alternative suggestion of a bridging coordination mode of both urea and hydroxide at the bimetallic core.[9] The most recent reactivity studies of urea derivatives coordinated to mononuclear metal centers have indicated that a cyanate NCO intermediate might be involved in the urease mechanism.[10] Evidently, the precise details of urea binding within the enzyme active site, as well as the key steps of its catalytic conversion, are still far from being fully understood.

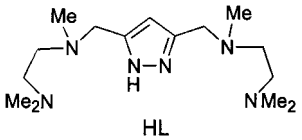
This situation, therefore, stimulates the synthesis and investigation of small nickel(II) coordination compounds in order to elucidate possible coordination modes of urea − also in a more general sense − and to probe their relevance to the metal-assisted hydrolytic degradation of this fundamental and ubiquitous substrate at multimetallic sites. Whereas several dinickel(II) complexes with η^1(O)-coordinated urea have hitherto been prepared and studied,[3][4] only recently have we reported the pyrazolate-based complex **1** which represents the first structurally characterized example of a μ_2-κN:κO bridging coordination mode of (deprotonated urea at a dinickel(II) site (Scheme 1).[5]



1

Scheme 1. Urea-bridged dinickel(II) complex **1**[5]

This system enabled a thermal decomposition of the substrate within the tight grip of the bimetallic pincer to yield a N,O-bridging cyanate, but no substantial activation towards hydrolytic degradation (tested by attempting ethanolytic cleavage to yield ethyl carbamate) could be observed. We considered the absence of any additional docking site for the alcohol nucleophile as one likely reason for the lack of hydrolytic reactivity of **1**, in accordance with the idea of a requisite activation of both the urea substrate and the nucleophile at the bimetallic core. To avoid this drawback, we have now employed a different dinucleating ligand matrix L (Scheme 2),[11] which bears fewer N-donors within the chelating side arms attached to the heterocycle, and which was thus expected to provide accessible coordination sites at both metal centers.



HL

Scheme 2. Ligand HL employed in this work[11]

Treatment of HL with two equivalents of base and [Ni(H$_2$O)$_6$](ClO$_4$)$_2$ in the presence of an excess of urea affords the red compound **2**, which is moderately soluble in polar solvents such as a mixture of methanol/acetone (1:1). Its mass spectrum shows signals corresponding to

[a] Anorganisch-Chemisches Institut, Universität Heidelberg, Im Neuenheimer Feld 270, D-69120 Heidelberg, Germany
Fax: (internat.) + 49-(0)6221/545707
E-mail: Franc@sun0.urz.uni-heidelberg.de

 © WILEY-VCH Verlag GmbH, D-69451 Weinheim, 1999 1434−1948/99/1111−1851 $ 17.50+.50/0

$[LNi_2(OCN_2H_3)]^+$ and $[LNi_2(OCN_2H_3)(ClO_4)]^+$, confirming the formation of a dinickel(II) complex containing deprotonated urea. The presence of the latter is further corroborated by strong IR absorptions at 1636 cm^{-1} [$\tilde{\nu}$(C=O)] as well as in the range 3100−3460 cm^{-1} [$\tilde{\nu}$(N−H)]. Small crystals of **2** could be obtained by layering a solution in methanol/acetone (1:1) with Et_2O, and an X-ray crystallographic analysis was performed (Figure 1).[12]

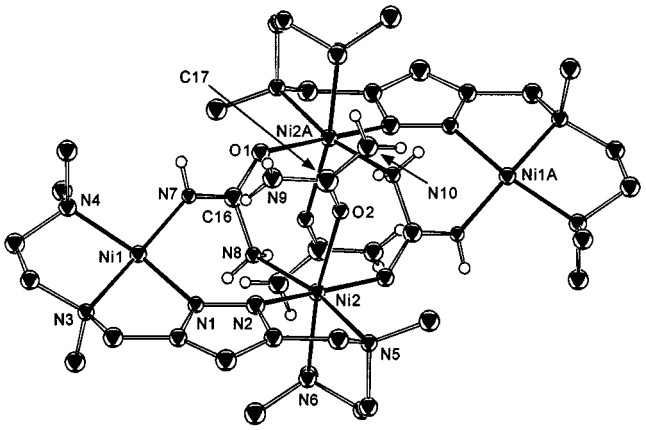
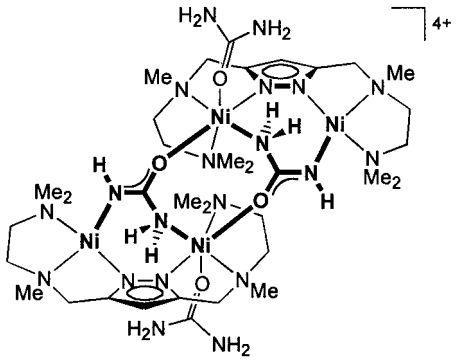


Figure 1. Molecular Structure of the cation of **2**; for clarity most of the hydrogen atoms have been omitted; selected atom distances (Å) and angles (°): Ni1−N1 1.886(3), Ni1−N3 1.897(4), Ni1−N4 1.975(3), Ni1−N7 1.897(4), Ni2−O1A 2.070(3), Ni2−O2 2.151(3), Ni2−N2 2.014(4), Ni2−N5 2.143(4), Ni2−N6 2.176(4), Ni2−N8 2.108(4), N1−N2 1.372(5), O1−C16 1.254(5), N7−C16 1.311(6), N8−C16 1.427(5), O2−C17 1.249(5), N9−C17 1.339(6), N10−C17 1.357(6), Ni1···Ni2 4.232, Ni2···Ni2A 4.349; O1−C16−N7 125.7(4), O1−C16−N8 117.8(4), N7−C16−N8 116.5(4), O2−C17−N9 123.6(5), O2−C17−N10 120.5(4), N9−C17−N10 115.9(4)

The solid-state structure of **2** reveals that pyrazolate-based bimetallic moieties containing urea as secondary bridging units have indeed been formed. Unexpectedly however, two of these moieties are found to be linked by an unprecedented μ_3-κN:κN′:κO coordination of the urea substrate. The central feature of the tetranuclear framework is an eight-membered ring system which is composed of two nickel atoms spanned by two N,O-bound urea molecules (Scheme 3), and which is situated on a crystallographic center of symmetry. The remaining deprotonated urea NH-groups are coordinated to the additional outer nickel centers.

An unambiguous distinction between the O, NH, and NH_2 donors of the μ_3-bridging, planar urea ligand (sum of angles around C16: 360.0°) is primarily based on the characteristic order of bond lengths *d*(C16−O1) = 1.254(4) Å, *d*[C16−N7(NH)] = 1.311(6) Å and *d*[C16−N8(NH_2)] = 1.427(5) Å, where the two C−N bonds are significantly shortened or lengthened, respectively, in comparison to the C−N bonds of purely η^1(O)-bound urea [1.339(6)/1.357(6) Å, see below]. Further corroboration stems from the assignment of the N-bound H atoms which were located in the difference fourier map and refined. Thus the sum of bond



Scheme 3. Schematic structure of the cation of **2**; the central core featuring the μ_3-bridging urea is set off in bold

angles around the trigonal-planar amide−N7 amounts to 359.4°, while the angles around the tetrahedral amine center N8 are found in the expected range of 105−114°.

A further urea molecule is η^1(O)-bound to the central Ni2 and Ni2A ions, thereby completing their distorted octahedral (OC-6) coordination spheres. In contrast, the outer Ni1 and Ni1A atoms are nested in square-planar (SP-4) environments, which can be attributed to the stronger σ-donor capacity of the anionic NH(amide) donor compared to the neutral NH_2(amine) and O donor sites of the μ_3-bridging urea ligand. The predicted low-spin d^8-configuration for such SP-4 nickel(II) ions is confirmed by magnetic measurements performed on powdered samples of solid **2**, which are in accordance with the presence of a mixed-spin complex having only two paramagnetic high-spin d^8 centers per tetranuclear complex (μ_{eff} = 3.21 μ_B at 288 K per paramagnetic Ni^{II}).

Upon cooling a solution of **2** in methanol/acetone (1:1) a color change from red to greenish-blue is observed. Following this process by UV/Vis spectroscopy (Figure 2) confirms the gradual disappearance of the major optical absorption of **2** at λ_{max} = 480 nm and a slight shift and rise of the low intensity absorption bands at around 380 and 625 nm.

These changes suggest an increase in coordination number of the SP-4 nickel ions and the formation of five- or even six-coordinate metal centers caused by the additional binding of extra solvent molecules at lower temperatures. However, the absence of any isosbestic points is indicative of a more complex process which is possibly due to a sequential coordination of the solvent ligands to the two terminal metal ions in **2**, or to a concurrent break-up of the tetranuclear system into bimetallic entities. The solution magnetic moment (determined by the Evans method)[15] rises from 3.5(±0.1) μ_B at 303 K to 4.1(±0.1) μ_B at 223 K per pyrazolate-based bimetallic unit (Figure 3), where the maximum value is close to the spin-only value expected for two high-spin nickel(II) ions (the slight decrease of μ_{eff} at even lower temperatures might be due to antiferromagnetic coupling within the pyrazolate-based bimetallic units). This corroborates the assumed transformation of the low-spin

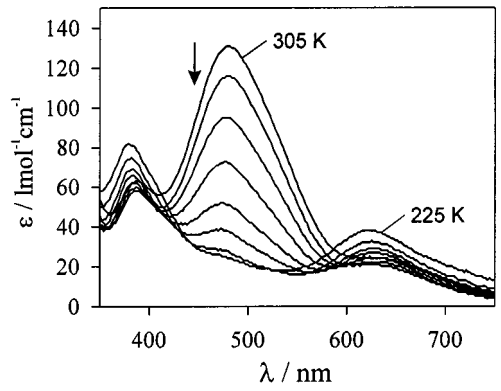


Figure 2. Temperature dependence of the UV/Vis spectrum of **2**; spectra at 225 K and in the range 245−305 K (steps of 10 K) are shown

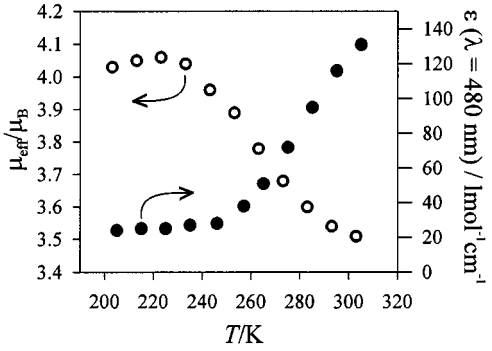


Figure 3. Temperature dependence of the molar optical absorption at 480 nm for **2** (solid circles) and of the solution magnetic moment per pyrazolate-based bimetallic fragment of **2** (open circles)

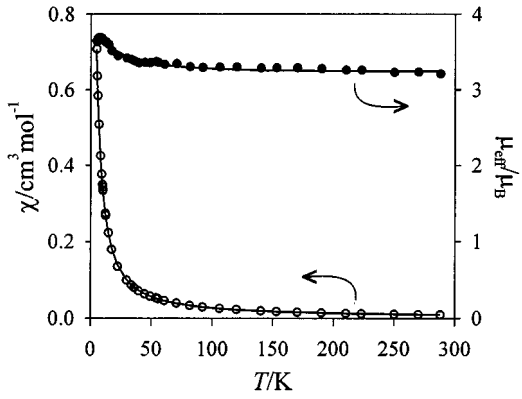


Figure 4. Temperature dependence of the molar magnetic susceptibility (open circles) and magnetic moment (solid circles) per pyrazolate-based bimetallic fragment of **2**. The solid lines represent the calculated fit (see text)

SP-4 nickel(II) ions to five- or six-coordinate high-spin nickel(II) centers upon cooling.

The temperature dependence of both the UV/Vis data as well as of the solution magnetic moment (Figure 3) reveals that conversion of the greenish-blue species to the red complex **2** is still incomplete at temperatures up to 305 K. It is pivotal in the present context, that activation of a potential nucleophile by coordination to the terminal nickel(II) ions is apparently feasible in **2**; this is assumed to be required for a subsequent nucleophilic attack on either the bridging urea or on the η^1(O)-bound urea substrate at the proximate central site. Still, the activity of **2** for the ethanolysis of urea (determined by a method described previously[3d]) is low, amounting to a conversion of only 1.2 equivalents of the substrate after five days refluxing in ethanol. It appears reasonable to ascribe this to the anionic character of the deprotonated μ_3-urea ligand, which obviously prevents it from being susceptible to nucleophilic attack. On the other hand, heating of solid **2** to elevated temperatures (140°C) causes conversion of coordinated urea to cyanate, as evidenced by the gradual appearance of the characteristic IR absorption for the ν_{asym}(NCO) stretch[5b] at 2193 cm^{-1} and a dominant mass spectrometric signal at m/z = 552 corresponding to $[LNi_2(NCO)(ClO_4)]^+$. This finding again shows that urea can be thermally degraded to cyanate within the clamp of an appropriate arrangement of nickel(II) ions.[3c,5]

The magnetic properties of powdered samples of solid **2** have been studied over the temperature range 4.8−288 K, as major structural changes of the tetranuclear framework (as observed in solution) are not expected to occur in the solid state. Data for the magnetic susceptibility and μ_{eff} are depicted in Figure 4. The rise of μ_{eff} with decreasing temperature − reaching a maximum of 3.69 μ_B per pyrazolate-based dinickel(II) entity at 7.0 K − is indicative of ferromagnetic coupling between the two central OC-6 metal centers.

At even lower temperatures the magnetic moment tends to drop, which is probably due to zero-field splitting effects or additional intermolecular antiferromagnetic interactions. The experimental data were simulated by a modified expression based on the isotropic Heisenberg model ($\boldsymbol{H} = -2J \times \boldsymbol{S}_1 \times \boldsymbol{S}_2$ with $S_1 = S_2 = 1$) {Equation (1)} where p is the molar fraction of paramagnetic impurities and θ is a Weiss constant that was included to describe phenomenologically the decrease of $\mu_{eff}(T)$ at low temperatures.[16] The best fit parameters obtained are g = 2.25, J = +3.4 cm^{-1}, $p < 0.01$ and θ = −0.62 [$R = \Sigma(\chi^{calc} - \chi^{obs})^2/\Sigma(\chi^{obs})^2 = 6.0 \times 10^{-5}$].

Considering the large separation of the two high-spin nickel(II) ions in **2** (4.349 Å), the surprising ferromagnetic exchange interaction is expected to be ligand-mediated and is evidently transmitted by a σ-bond pathway. These combined abilities of deprotonated urea to (i) mediate ferromagnetic superexchange and (ii) to bind three metal ions in a bridging fashion, make this component a promising candidate for the design of higher-dimensional coordination networks with interesting magnetic properties. Insight into the geometric requirements and the underlying mechanisms of the exchange coupling will be the subject of future studies.

In conclusion, we have shown that urea can simultaneously bind to three different metal ions, and that it can be thermally degraded to cyanate within such grip of a multimetallic nickel(II) site. Furthermore, urea is able to bring

$$\chi_m = (1-p)\{[Ng^2\mu_B{}^2/k(T-\theta)][2\exp(2J/kT) + 10\exp(6J/kT)]/[1 + 3\exp(2J/kT) + 5\exp(6J/kT)]\} + 2p(2Ng^2\mu_B{}^2/3kT) + 2N_\alpha \quad (1)$$

about ferromagnetic exchange coupling in the novel μ_3-κN:κN′:κO-coordination mode. These findings should offer new perspectives with respect to the use of the simple urea molecule as a building block for extended coordination networks, as well as with respect to the metal-mediated activation and transformation of this ubiquitous substrate.

Experimental Section

Caution! Although no problems were encountered in this work, transition metal perchlorate complexes are potentially explosive and should be handled with proper precautions.

Complex 2: A solution of the ligand HL[11] (0.25 g, 0.84 mmol) in thf (20 mL) and MeOH (1 mL) was treated with two equivalents of *n*BuLi (2.5 M in hexane) at 0°C and stirred for 5 min. $[Ni(H_2O)_6](ClO_4)_2$ (0.62 g, 1.69 mmol) and additional MeOH (20 mL) were then added and the red solution stirred at room temperature for 1 h. After the addition of urea (0.15 g, 2.50 mmol) stirring was continued for a further 2 h. All volatile material was then removed under reduced pressure and the residue taken up in MeOH/acetone (1:1, 60 mL) and layered with Et_2O. Red crystalline material of the product **2**·2(acetone) gradually formed (0.51 g, 0.32 mmol, 77%). − IR (KBr): $\tilde{\nu}$ = 3456 (s), 3346 (s), 3115 (m), 2915 (w), 1689 (m, $C{=}O_{acetone}$), 1636 (vs), 1571(m), 1463 (s), 1096 (vs) cm^{-1}. − $C_{34}H_{76}Cl_4N_{20}Ni_4O_{20}$·2(acetone) (1577.84): calcd C 30.45, H 5.62, N 17.75; found C 30.08, H 5.63, N 17.37.

Acknowledgments

We sincerely thank Prof. Dr. G. Huttner for his generous and continuous support of our work. Grants from the Deutsche Forschungsgemeinschaft (Habilitandenstipendium for F. M.) and the Fonds der Chemischen Industrie are gratefully acknowledged.

[1] [1a] P. Maslak, J. J. Sczepanski, M. Parvez, *J. Am. Chem. Soc.* **1991**, *113*, 1062−1063. − [1b] A. W. Watson, D. P. Fairlie, *Inorg. Chem.* **1995**, *34*, 3087−3092. − [1c] N. V. Kaminskaia, N. M. Kostic, *Inorg. Chem.* **1997**, *36*, 5917−5926. − [1d] N. V. Kaminskaia, N. M. Kostic, *Inorg. Chem.* **1998**, *37*, 4302−4312; and references cited therein.

[2] [2a] R. M. Buchanan, M. S. Mashuta, K. J. Oberhausen, J. F. Richardson, *J. Am. Chem. Soc.* **1989**, *111*, 4497−4498. − [2b] D. Volkmer, A. Hörstmann, K. Griesar, W. Haase, B. Krebs, *Inorg. Chem.* **1996**, *35*, 1132−1135. − [2c] D. Volkmer, B. Hommerich, K. Griesar, W. Haase, B. Krebs, *Inorg. Chem.* **1996**, *35*, 3792−3803. − [2d] F. Meyer, A. Jacobi, B. Nuber, P. Rutsch, L. Zsolnai, *Inorg. Chem.* **1998**, *37*, 1213−1218. − [2e] B. Hommerich, H. Schwöppe, D. Volkmer, B. Krebs, *Z. Anorg. Allg. Chem.* **1999**, *625*, 75−82.

[3] [3a] H. E. Wages, K. L. Taft, S. J. Lippard, *Inorg. Chem.* **1993**, *32*, 4985−4987. − [3b] T. Koga, H. Furutachi, T. Nakamura, N. Fukita, M. Ohba, K. Takahashi, H. Okawa, *Inorg. Chem.* **1998**, *37*, 989−996. − [3c] S. Uozumi, H. Furutachi, M. Ohba, H. Okawa, D. E. Fenton, K. Shindo, S. Murata, D. J. Kitko, *Inorg. Chem.* **1998**, *37*, 6281−6287. − [3d] M. Konrad, F. Meyer, A. Jacobi, P. Kircher, P. Rutsch, L. Zsolnai, *Inorg. Chem.* **1999**, in press.

[4] K. Yamaguchi, S. Koshino, F. Akagi, M. Suzuki, A. Uehara, S. Suzuki, *J. Am. Chem. Soc.* **1997**, *119*, 5752−5753.

[5] [5a] F. Meyer, H. Pritzkow, *Chem. Commun.* **1998**, 1555−1556. − [5b] F. Meyer, E. Kaifer, P. Kircher, K. Heinze, H. Pritzkow, *Chem. Eur. J.* **1999**, *5*, 1617−1630.

[6] P. A. Karplus, M. A. Pearson, R. P. Hausinger, *Acc. Chem. Res.* **1997**, *30*, 330−337.

[7] E. Jabri, M. B. Carr, R. P. Hausinger, P. A. Karplus, *Science* **1995**, *268*, 998−1002.

[8] [8a] N. E. Dixon, P. W. Riddles, C. Gazzola, R. L. Blakeley, B. Zerner, *Can. J. Biochem.* **1980**, *58*, 1335−1344. − [8b] S. J. Lippard, *Science* **1995**, *268*, 996−997.

[9] [9a] S. Benini, W. R. Rypniewski, K. S. Wilson, S. Mangani, S. Ciurli *J. Biol. Inorg. Chem.* **1998**, *3*, 268−273. − [9b] S. Benini, W. R. Rypniewski, K. S. Wilson, S. Miletti, S. Ciurli, S. Mangani *Structure* **1999**, *7*, 205−216.

[10] L. Roecker, J. Akande, L. N. Elam, I. Gauga, B. W. Helton, M. C. Prewitt, A. M. Sargeson, J. H. Swango, A. C. Willis, T. Xin, J. Xu, *Inorg. Chem.* **1999**, *38*, 1269−1275.

[11] F. Meyer, U. Ruschewitz, P. Schober, B. Antelmann, L. Zsolnai, *J. Chem. Soc., Dalton Trans.* **1998**, 1181−1186.

[12] Crystallographic analysis of **2** ($C_{17}H_{38}Cl_2N_{10}Ni_2O_{10}$·acetone): M = 789.0, monoclinic, crystal size 0.05 × 0.04 × 0.03 mm, space group $P2_1/c$, a = 11.984(2), b = 18.535(4), c = 14.426(3) Å, β = 92.14(3)°, V = 3202(1) $Å^3$, Z = 4, ρ_{calc} = 1.637 g cm^{-3}, μ(Mo-K_α) = 1.412 mm^{-1}, T = 200 K, F(000) = 1648. The measurement was carried out on a Siemens CCD diffractometer with graphite-monochromated Mo-K_α radiation. All calculations were performed using the SHELXT PLUS software package. Structures were solved by direct methods with the SHELXS-97 and refined with the SHELXL-97 program.[13] The program XPMA[14] was used for graphical handling of the data. Atomic coordinates and thermal parameters of the non-hydrogen atoms were refined in anisotropic models by full-matrix least-squares calculation based on F^2. In general the hydrogen atoms were placed at calculated positions and allowed to ride on the atoms they are attached to, except for the hydrogen atoms of the urea molecules which were located in the difference fourier map and refined. 49935 measured reflections (6220 independent), $R1$ = 0.054 and $wR2$ = 0.1071 for 3626 observed reflections [$I > 2\sigma(I)$] and 438 parameters. Largest residual electron density 0.463/-0.437 e $Å^{-3}$. Crystallographic data (excluding structure factors) for the structure reported in this paper have been deposited with the Cambridge Crystallographic Data Centre as supplementary publication no. CCDC 127485. Copies of the data can be obtained free of charge on application to CCDC, 12 Union Road, Cambridge CB2 1EZ, UK {fax: (internat.) + 44-1223/336-033; E-mail: deposit@ccdc.cam.ac.uk}.

[13] G. M. Sheldrick, SHELXL-97, Program for Crystal Structure Refinement, Universität Göttingen, 1997; SHELXS-97, Program for Crystal Structure Solution, Universität Göttingen, 1997.

[14] L. Zsolnai, G. Huttner, *XPMA*, Universität Heidelberg, 1998; http://www.rzuser.uni-heidelberg.de/v54/xpm.html.

[15] [15a] D. F. Evans, *J. Chem. Soc.* **1959**, 2003−2005. − [15b] D. F. Evans, T. A. James, *J. Chem. Soc., Dalton Trans.* **1979**, 723−726.

[16] [16a] C. J. O′Connor, *Progr. Inorg. Chem.* **1982**, *29*, 203−283. − [16b] O. Kahn, *Molecular Magnetism*, VCH Publishers, New York, **1993**; N_α refers to the temperature-independent paramagnetism [100 × 10^{-6} cm^3/mol per nickel(II) ion]; all other parameters have their usual meaning. Experimental data have been corrected for the underlying diamagnetism.

Received July 5, 1999
[I99238]

Synthesis and Structure of the First Fullerene Complex of Titanium $Cp_2Ti(\eta^2\text{-}C_{60})$

V. V. Burlakov,[a] A. V. Usatov,[a] K. A. Lyssenko,[a] M. Yu. Antipin,[a] Yu. N. Novikov,[a] and V. B. Shur*[a]

Keywords: Fullerenes / Titanium / Complexes / X-ray analysis

The first fullerene complex of titanium $Cp_2Ti(\eta^2\text{-}C_{60})$ has been synthesized by reaction of the bis(trimethylsilyl)-acetylene complex of titanocene $Cp_2Ti(\eta^2\text{-}Me_3SiC_2SiMe_3)$ with an equimolar amount of fullerene-60 in toluene at room temperature under argon. An X-ray diffraction study of the complex has shown that it has the structure of a titanacyclopropane derivative.

Recent studies have revealed the ability of fullerenes to form complexes with transition metal compounds.[1,2] The majority of studies in this exciting area have been conducted on C_{60} for which a large number of complexes with different transition metals have been prepared and structurally characterized. Among fullerene complexes, the least studied ones are those of the Group IVB metals. Thus, for zirconium, the only available data on complexation with fullerenes concern the work on the hydrozirconation of C_{60} with Cp_2ZrHCl.[3,4] For titanium and hafnium, no fullerene complexes have previously been described.

In the present communication, we wish to report on the synthesis and structure of the first fullerene complex of titanium $Cp_2Ti(\eta^2\text{-}C_{60})$ **(1)**, which is readily obtained from the reaction of the bis(trimethylsilyl)acetylene complex of titanocene $Cp_2Ti(\eta^2\text{-}Me_3SiC_2SiMe_3)$ with an equimolar amount of fullerene-60 in toluene at room temperature under argon.

The isolated complex is a black crystalline solid which is poorly soluble in aromatic hydrocarbons. According to elemental analysis and X-ray diffraction data (see below), crystals of the complex contain one molecule of toluene per molecule of **1**. The molecular structure of $\mathbf{1}\cdot C_6H_5CH_3$ is shown in Figure 1. Selected bond lengths and angles for $\mathbf{1}\cdot C_6H_5CH_3$ are given in Table 1. The complex is a bis(η^5-cyclopentadienyl)titanium derivative in which the $(\eta^5\text{-}C_5H_5)_2Ti$ unit is bound to the olefinic C(1)−C(2) bond at the 6:6 ring junction of the fullerene core in an η^2-fashion. Such a mode of bonding is typical of fullerene complexes with transition metal compounds.

The coordination to titanium results in a significant elongation of the fullerene C(1)−C(2) bond. The length of this bond in **1** is 1.507(6) Å which is considerably greater than the corresponding C−C distance in free C_{60} (1.38 Å)[1] and is close to the values characteristic of the endocyclic C−C single bonds of cyclopropane [1.510(2) Å][7] and its heteroanalogues [e. g. 1.484(3) Å in thiirane,[8,9] 1.502(5) Å in phosphirane[8,10]]. Thus, complex **1** has the structure of a titanacyclopropane derivative.

A similar η^2-coordination of the olefin molecule with a titanium atom has been found in the previously described ethylene complex of permethyltitanocene $Cp^*_2Ti(\eta^2\text{-}C_2H_4)$.[8] However, the length of the coordinated C−C bond of the olefin ligand in this complex [1.438(5) Å] is noticeably smaller than that in complex **1**.

The influence of the complexation to titanium on the geometry of the C_{60} moiety is manifested not only in the elongation of the C(1)−C(2) bond but also in the lengthening of the other C−C bonds formed by the C(1) and C(2) atoms. As can be seen from Table 1, the C(1)−C(6), C(1)−C(9), C(2)−C(3) and C(2)−C(12) bond lengths in the molecule of **1** span the range of 1.478(6)−1.492(6) Å (av. 1.486 Å) while the average C−C distance at the other 5:6 ring junctions is 1.467 Å (1.45 Å in free fullerene[1]). The average C−C bond length at the 6:6 ring junctions in complex **1** [excluding the C(1)−C(2) bond] is 1.393 Å which is close to that in free C_{60} (1.38 Å[1]). Due to coordination by the Cp_2Ti unit, the C(1) and C(2) atoms of the fullerene ligand deviate from the planes of the corresponding 5- and 6-membered rings (by ca. 0.19 Å), as a result of which these rings acquire an envelope and a flattened sofa conformation, respectively. The other 5- and 6-membered cycles in the C_{60} moiety are planar within 0.005 Å. The distortion of the fullerene core in **1** can also be demonstrated by the comparison of its "radii" in different directions. Thus, the distances from the centroid of the C_{60} ligand[11] to the C(1) and C(2) atoms bonded to titanium are 3.75 Å whereas the corresponding average distance to the other carbon atoms of C_{60} is significantly shorter (3.540 Å).

The geometry of the bent sandwich in **1** is not exceptional. The planes of the $\eta^5\text{-}C_5H_5$ rings form a dihedral angle of 48.2°. The titanium atom and the coordinated C(1)−C(2) bond of the fullerene are located in the bisector plane of this dihedral angle. The distance from the titanium to the centroids of the $\eta^5\text{-}C_5H_5$ ligands is 2.06 Å. The Ti(1)−C(1) and Ti(1)−C(2) bond lengths are virtually identical [2.304(4) and 2.295(5) Å]. The Ti(1)−C(1)−C(2)

[a] A.N. Nesmeyanov Institute of Organoelement Compounds, Russian Academy of Sciences,
Vavilov St. 28, Moscow 117813, Russia
Fax: (internat.) + 7-095/135-5085
E-mail: vbshur@ineos.ac.ru

 © WILEY-VCH Verlag GmbH, D-69451 Weinheim, 1999 1434−1948/99/1111−1855 $ 17.50+.50/0

$$Cp_2Ti(\eta^2\text{-}Me_3SiC_2SiMe_3) + C_{60} \longrightarrow Cp_2Ti(\eta^2\text{-}C_{60}) + Me_3SiC_2SiMe_3$$

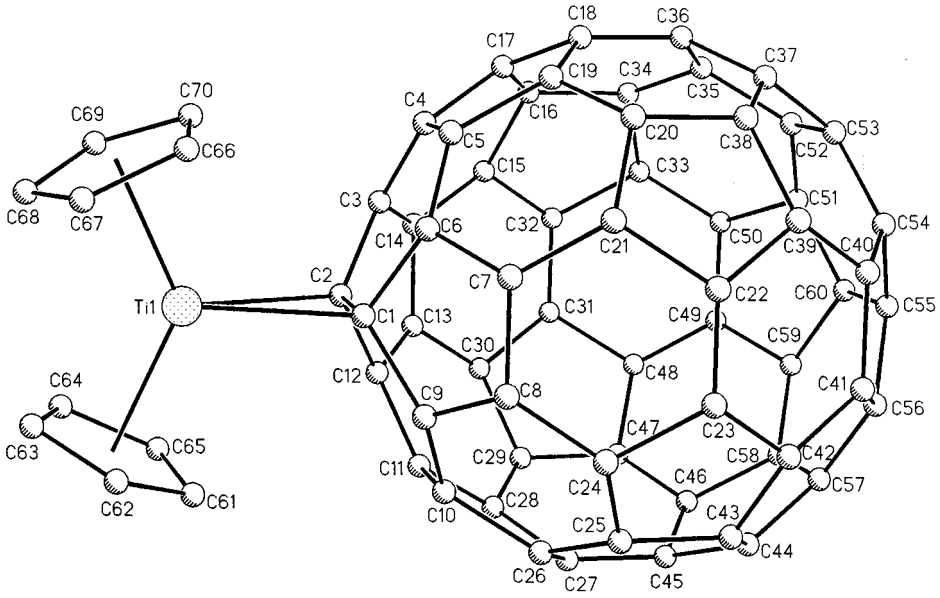


Figure 1. Molecular structure of complex **1** in the solid state

Table 1. Selected bond lengths [Å] and angles [°] for **1**·$C_6H_5CH_3$

Bond lengths			
Ti(1)−C(1)	2.304(4)	Ti(1)−C(68)	2.404(5)
Ti(1)−C(2)	2.295(5)	Ti(1)−C(69)	2.395(5)
Ti(1)−C(61)	2.367(6)	Ti(1)−C(70)	2.380(5)
Ti(1)−C(62)	2.384(6)	C(1)−C(2)	1.507(6)
Ti(1)−C(63)	2.378(6)	C(1)−C(6)	1.492(6)
Ti(1)−C(64)	2.349(6)	C(1)−C(9)	1.485(6)
Ti(1)−C(65)	2.352(5)	C(2)−C(3)	1.478(6)
Ti(1)−C(66)	2.361(5)	C(2)−C(12)	1.488(6)
Ti(1)−C(67)	2.345(5)		
Bond angles			
C(1)−Ti(1)−C(2)	38.3(2)	Cp(1)−Ti(1)−C(2)	114.4(7)
Ti(1)−C(1)−C(2)	70.5(2)	Cp(2)−Ti(1)−C(1)	111.6(7)
Ti(1)−C(2)−C(1)	71.2(2)	Cp(2)−Ti(1)−C(2)	115.3(7)
Ti(1)−C(1)−C(6)	123.1(3)	C(2)−C(1)−C(6)	115.5(4)
Ti(1)−C(1)−C(9)	125.0(3)	C(2)−C(1)−C(9)	117.8(4)
Ti(1)−C(2)−C(3)	123.9(3)	C(6)−C(1)−C(9)	102.6(4)
Ti(1)−C(2)−C(12)	124.1(3)	C(1)−C(2)−C(3)	117.3(4)
Cp(1)−Ti(1)−Cp(2)[a]	130.9(7)	C(1)−C(2)−C(12)	115.3(4)
Cp(1)−Ti(1)−C(1)	111.2(7)	C(3)−C(2)−C(12)	102.8(4)

[a] Cp(1) and Cp(2) are the centroids of Cp rings C(61)−C(65) and C(66)−C(70), respectively.

and Ti(1)−C(2)−C(1) bond angles are 70.5(2) and 71.2(2)°, respectively. The mutual orientation of the η^5-C_5H_5 rings closely corresponds to a staggered conformation. The average C−C bond length in the η^5-C_5H_5 groups is 1.386 Å.

Analysis of the atomic anisotropic displacement parameters of **1** was performed using the THMA-11 program.[12] The agreement between the experimental U_{ij} values and those calculated from the rigid-body LTS model[13] is characterized by a high value of the R_u factor (0.25), while the same value calculated in the segmented-rigid approximation for the (η^2-C_{60})Ti moiety was found to be rather low (0.095). Thus, the metallofullerene fragment in **1** can be correctly analyzed in terms of the LTS approximation and the high value of R_u for the whole molecule is probably caused by the significant libration motion of the η^5-C_5H_5 ligands. Analysis of the rigid-body LTS tensors for the (η^2-C_{60})Ti unit revealed that its libration motion is highly anisotropic. The eigenvalues of the libration tensor (L) are 17.3, 6.0 and 4.8 deg^2 and its maximum eigenvalue (L_1) is observed along the axis with the minimum moment of inertia, which coincides with the C_2 symmetry axis of the molecule. Taking into account that the L_1 value is rather low we can conclude that the barrier of the rotation for the C_{60} moiety in the crystal structure of **1**·$C_6H_5CH_3$ is high.

The crystal packing of **1** can be described as corrugated layers parallel to the *bc* crystallographic plane with the solvate toluene molecules between the layers. The shortest distance between the centroids of the C_{60} cores within the layers is 9.816 Å, while the corresponding distance between the layers is 10.29 Å. It is noteworthy that the distance within the layers is considerably shorter than in the crystal structure of free fullerene-60 (10.02 Å)[14] and the Van der Waal's radius of C_{60} (10.18 Å).[15]

Experimental Section

Experiments were carried out under argon with careful exclusion of air and moisture. Toluene was purified in the usual manner and freshly distilled before use over sodium under an atmosphere of

argon. The starting acetylene complex $Cp_2Ti(\eta^2\text{-}Me_3SiC_2SiMe_3)$ was prepared by the method described in refs.[5,6]

Synthesis of $Cp_2Ti(\eta^2\text{-}C_{60})$ (1): Fullerene-60 (0.101 g, 0.14 mmol) was dissolved in 50 mL of toluene and to the resulting violet solution was added a solution of $Cp_2Ti(\eta^2\text{-}Me_3SiC_2SiMe_3)$ (0.055 g, 0.16 mmol) in toluene (5 mL). The reaction mixture was filtered and then kept overnight at room temperature under argon. During the course of the reaction, the colour of the mixture turned dark brown/green and within 24 h black crystals of $\mathbf{1}\cdot C_6H_5CH_3$ were precipitated. The solution was decanted, the crystals were washed with a small amount of toluene and dried at 20°C in a stream of argon. The yield of $\mathbf{1}\cdot C_6H_5CH_3$ was 0.04 g (29%). – $C_{77}H_{18}Ti$ (990.81): calcd. C 93.34, H 1.83; found C 93.34, H 1.75.

X-ray Structure Determination of 1: Crystals of $\mathbf{1}\cdot C_6H_5CH_3$ are monoclinic, space group $P2_1/c$, a = 15.951(5) Å, b = 13.678(4) Å, c = 19.313(6) Å, β = 108.11(2)°, V = 4005(2) Å^3, $d_{calc.}$ = 1.643 g·cm^{-3}, Z = 4. Intensities of 6329 reflections (R_{int} = 0.0174) were measured at 150 K on a Siemens P3 automated diffractometer using Mo-K_α radiation (λ = 0.71073 Å, balanced filter, $\theta - 2\theta$ scan, $\theta \leq 24°$). The structure was solved by direct methods and refined by full-matrix least squares against F^2 in the anisotropic (H-atoms isotropic) approximation. All hydrogen atoms were located from the electron density difference synthesis and were included in the refinement using the rigid motion model. The refinement converged to wR_2 = 0.2254 and GOF = 1.115 for 6329 independent reflections {R_1 = 0.0757 was calculated against F for 4699 observed reflections with $I > 2\sigma(I)$}. The number of refined parameters was 706. The final difference electron density map showed a maximum of 0.368 and a minimum of −0.642 eÅ^{-3}. All calculations were performed using SHELXTL PLUS 5.0 on an IBM PC/AT. Crystallographic data (excluding structure factors) for the structure reported in this paper have been deposited with the Cambridge Crystallographic Data Centre as supplementary no. CCDC-127616. Copies of the data can be obtained free of charge on application to CCDC, 12 Union Road, Cambridge CB2 1EZ UK [Fax: (internat.) + 44-1223/336-033; E-mail: deposit@ccdc.cam.ac.uk].

Acknowledgments

This work was supported by grants from the Russian Foundation for Basic Research (Project codes 99−03−33008, 99−03−32893, 97−03−33783) and the Russian State Research Programme "Fullerenes and Atomic Clusters" (Project code 4-1-98).

[1] A. L. Balch, M. M. Olmstead, *Chem. Rev.* **1998**, *98*, 2123−2165.
[2] V. I. Sokolov, V. V. Bashilov, *Platinum Metals Rev.* **1998**, *42*, 18−24.
[3] S. Ballenweg, R. Gleiter, W. Krätschmer, *Tetrahedron Lett.* **1993**, *34*, 3737−3739.
[4] S. Ballenweg, R. Gleiter, W. Krätschmer, *J. Chem. Soc., Chem. Commun.* **1994**, 2269−2270.
[5] V. V. Burlakov, U. Rosenthal, P. V. Petrovskii, V. B. Shur, M. E. Vol′pin, *Metalloorg. Khim*. **1988**, *1*, 953−954 [*Organomet. Chem. USSR* **1988**, *1*, 526−527 (Engl. Transl.)].
[6] V. V. Burlakov, A. V. Polyakov, A. I. Yanovsky, Yu. T. Struchkov, V. B. Shur, M. E. Vol′pin, U. Rosenthal, H. Görls, *J. Organomet. Chem*. **1994**, *476*, 197−206.
[7] L. V. Vilkov, V. S. Mastryukov, N. I.Sadova, *Determination of the Geometrical Structure of Free Molecules*, Mir Publishers, Moscow, **1983**.
[8] S. A. Cohen, P. R. Auburn, J. E. Bercaw, *J. Am. Chem. Soc*. **1983**, *105*, 1136−1143.
[9] K. Okiye, C. Hirose, D. G. Lister, J. Sheridan, *J. Chem. Phys. Lett*. **1974**, *24*, 111.
[10] M. T. Bowers, R. A. Beaudet, H. Goldwhite, R. Tang, *J. Am. Chem. Soc*. **1969**, *91*, 17−20.
[11] The position of the centroid of the fullerene ligand in **1** was calculated without taking the C(1)−C(2) and the opposite C(55)−C(60) bonds into account.
[12] T. Maverick, K. N. Tueblood, *Thermal motion analysis program THMA-11*, Zurich, **1987**.
[13] T. Maverick, J. D. Dunitz, *Mol. Phys.* **1987**, *62*, 451−459.
[14] P. W. Stephens, D. Cox, J. W. Lauher, L. Mihaly, J. B. Wiley, P. Allemand, A. Hirsch, K. Holczer, Q. Li, J. D. Tompson, F. Wudl, *Nature*, **1992**, *355*, 4145−4147.
[15] Yu. L. Slovokhotov, I. V. Moskaleva, V. I. Shil′nikov, E. F. Valeev, Yu. N. Novikov, A. I. Yanovsky, Yu. T. Struchkov, *Mol. Mat*. **1996**, *8*, 117−124.

Received July 5, 1999
[I99239]

Coordination Polymers, 14[+]

1D- and 2D-Coordination Polymers from Self-Complementary Building Blocks: Co-Crystallization of (*P*)- and (*M*)-Single-Stranded Diastereoisomers

Rolf W. Saalfrank,*[a] Harald Maid,[a] Frank Hampel,[a] and Karl Peters[b]

Dedicated to Prof. Dr. W.-P. Fehlhammer on the occasion of his 60th birthday

Keywords: Coordination polymers / Helical structures / Copper / Self-assembly / Supramolecular chemistry

Reaction of methanolic copper(II) acetate solution with oxazolidine **21** (HL^7) led to the formation of the one-dimensional coordination polymer 1D-$^1_\infty[CuL^7_2]$ **23**. On the contrary, reaction of copper(II) acetate in methanol with pyrrolidine **24** (HL^8) yielded the two-dimensional coordination polymer 2D-$^2_\infty[CuL^8_2]$ **26**. A common feature of **23** and **26** are the C_{2h}-symmetric coordinatively unsaturated building blocks **22** and **25**. In 1D-$^1_\infty[CuL^7_2]$ **23**, the cyano groups are linked to copper in a *side-on* fashion and the monomers **22** are oriented parallel to one another, whereas in 2D-$^2_\infty[CuL^8_2]$ **26** the cyano groups are bound to copper in the *end-on* mode and the monomers **25** are oriented at an angle of 117° to one another. In both 1D-**23** and 2D-**26**, copper has a distorted octahedral coordination sphere. On the other hand, reaction of methanolic copper(II) acetate solution with enantiomerically pure (5*S*)-pyrrolidine **27** ($HL^{9(S)}$) led to the formation of the diastereomeric helical strands (*M*)-/(*P*)-1D-$^1_\infty[CuL^{9(S)}_2]$ **29**. (*M*)- and (*P*)-**29** are present in pairs in the infinite unit cell. In helical 1D-**29**, copper is tetragonal-pyramidally coordinated and the C_2-symmetric monomers **28** ($CuL^{9(S)}_2$) are linked through only one cyano group. Moreover, it has been shown that the reaction of chiral racemic pyrrolidine **30** ($HL^{10(R,S)}$) with copper(II) acetate via the intermediate C_i-symmetric building blocks **31** ($CuL^{10(R)}L^{10(S)}$) furnishes one-dimensional 1D-$^1_\infty[CuL^{10(R)}$-$L^{10(S)}]$ **32**. Single-crystal X-ray diffraction analyses of the supramolecular species **23**, **26**, **29**, and **32** unequivocally establish the structures of these coordination polymers.

Introduction

With the growing understanding of supramolecular chemistry,[1] it might ultimately become feasible to routinely design and control solid-state architectures and therefore function.[2] Increasingly, solid structures are being invented and created rather than discovered. Realisation of such macromolecular targets requires the ability to assemble small supramolecular units that can be further aggregated in a controlled fashion. In order to construct such assemblies, we have developed coordinatively unsaturated building blocks of copper(II) and iron(II) with two additional ligating sites that do not interfere with the monomer assembly process but facilitate controlled aggregation.

We have recently shown that reaction of methanolic copper(II) acetate solution with tetrazole **8** (HL^1) leads to the formation of the three-dimensional coordination polymer 3D-$^3_\infty[CuL^1_2]$ **1**,[3] whereas under exactly the same conditions pyrrolidine **9** (HL^2) forms the two-dimensional coordination polymer 2D-$^2_\infty[CuL^2_2]$ **2**.[4] A prerequisite for the formation of 3D-**1** and 2D-**2** is the intermediate generation of the coordinatively unsaturated copper(II) building blocks **14** ($L = L^1$) and **15** ($L = L^2$). The monomers **14** and **15** are bidentate and coordinate through the two cyano groups. This leads to *perpendicular* linking of the monomers and to coordinative saturation at the copper(II) centers of **14** and **15** with formation of the corresponding three- and two-dimensional coordination polymers **1** and **2**. Thus, during the crystallization of the polymers **1** and **2**, the role of the building blocks **14** and **15** is twofold. They react both as metals and as ligands.[5] The exact structures of **1** and **2** were established by single-crystal X-ray analyses. In both polymers, the coordination sphere about the copper(II) atoms is a slightly distorted tetragonal bipyramid.

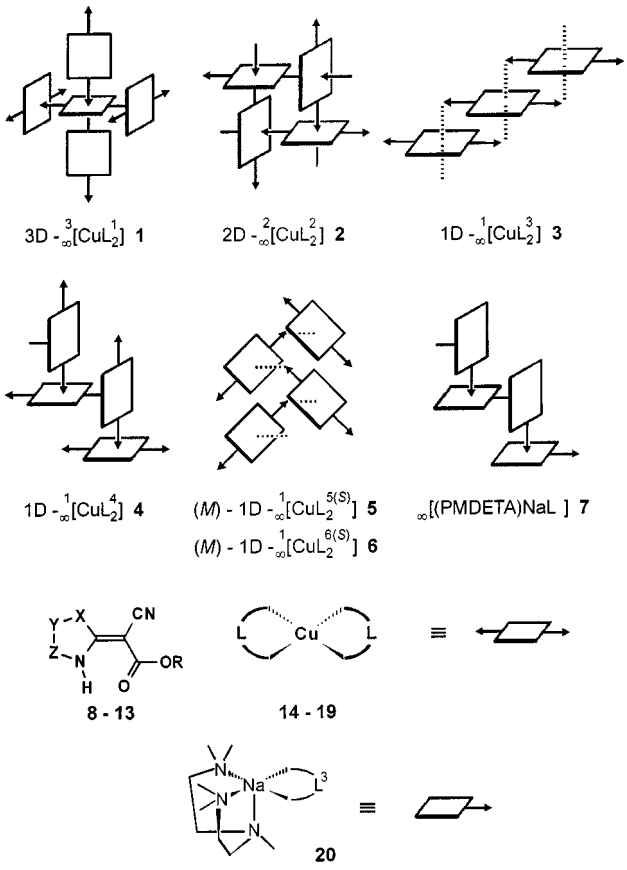
Unexpectedly, reaction of methanolic copper(II) acetate solution with tetrazole **10** (HL^3) furnished the coordination polymer 1D-$^1_\infty[CuL^2_2]$ **3**. In the case of **3**, a *parallel* rather than a *perpendicular* orientation of the building blocks **16** ($L = L^3$) leads to one-dimensionality.[6] A one-dimensional zigzag coordination polymer 1D-$^1_\infty[CuL^4_2]$ **4** was also obtained starting from benzoxazolidine **11** (HL^4). The reduced dimensionality of **4** allows **17** ($L = L^4$) to coordinate to copper(II) through one cyano group only.[7]

In contrast to the C_{2h}-symmetric monomers **14**–**17**, the C_2-symmetric building block (*S*,*S*)-**18** ($L = L^{5(S)}$), generated from (*S*)-methoxycarbonylpyrrolidine **12** ($HL^{5(S)}$), is sterically shielded at one side and thus couples only through

[+] Part 13: Ref.[12]

[a] Institut für Organische Chemie der Universität Erlangen-Nürnberg,
Henkestraße 42, D-91054 Erlangen, Germany
Fax: (internat.) +49-(0)9131/852-1165
E-mail: saalfrank@organik.uni-erlangen.de
[b] Max-Planck Institut für Festkörperforschung,
Heisenbergstraße 1, D-70506 Stuttgart, Germany

 © WILEY-VCH Verlag GmbH, D-69451 Weinheim, 1999 1434–1948/99/1111–1859 $ 17.50+.50/0



8 (HL^{1}) : X = $NCMe_3$; Y–Z = N=N , R = CMe_3

9 (HL^{2}) : X, Y, Z = CH_2 ; R = Me

10 (HL^{3}) : X = NCH_2CHMe_2 ; Y–Z = N=N , R = M

11 (HL^{4}) : X = O; Y–Z = C_6H_4 ; R = Me

12 ($HL^{5(S)}$) : X, Y = CH_2 ; Z = (*S*)-$CHCO_2Me$; R = M

13 ($HL^{6(R/S)}$) : X = O; Y = CH_2 ; Z = (*R*/*S*)-CHEt; R = M

14: L = L^{1}

15: L = L^{2}

16: L = L^{3}

17: L = L^{4}

18: L = $L^{5(S)}$

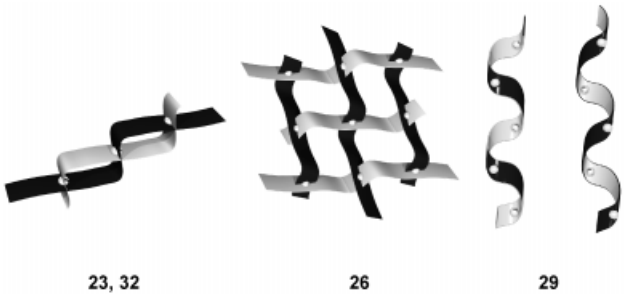
19: L = $L^{6(R/S)}$

one cyano group. This leads to the helical one-dimensional coordination polymer 1D-$^{1}_{\infty}$[$CuL^{5(S)}_{2}$] **5**. According to the X-ray diffraction analysis, the crystal is composed of two almost identical helix strands, (*P*)-1D-$^{1}_{\infty}$[$CuL^{5(S)}_{2}$] **5** and (*M*)-1D-$^{1}_{\infty}$[$CuL^{5(S)}_{2}$] **5**,[8] which generate pairs of diastereoisomers.[9] It is noteworthy that the stereogenic centers in (*S*,*S*)-**18** do not lead to asymmetric induction. Racemic mixtures of single-stranded coordination polymers with (*P*)- and (*M*)-helicity were also obtained with achiral ligands and copper(I).[10]

To date, only a few examples of chiral, non-racemic helical coordination polymers have been reported, where the chirality is induced by a stereogenic center.[11][12] For example, reaction of a methanolic solution of enantiomerically pure oxazolidines **13** ($HL^{6(R/S)}$) with copper(II) acetate and crystallization from chloroform afforded single-crystals suitable for X-ray diffraction analysis. This analysis showed the crystals to be composed of identical, palindromic one-dimensional strands (*P*)-1D-$^{1}_{\infty}$[$CuL^{6(R)}_{2}$] **6** and (*M*)-1D-$^{1}_{\infty}$[$CuL^{6(R)}_{2}$] **6**.[8][13] Each cylindrical strand is formed by a set of C_2-symmetric copper(II) building blocks (*R*,*R*)-**19** (L = $L^{6(R)}$) and (*S*,*S*)-**19** (L = $L^{6(S)}$).

Regardless of steric considerations, by using a Group 1 metal, the zigzag one-dimensional coordination polymer 1D-$^{1}_{\infty}$[(PMDETA)NaL^{3}] **7** was formed. The polymer **7** is generated from the coordinatively unsaturated building block [(PMDETA)NaL^{3}] **20**.[14]

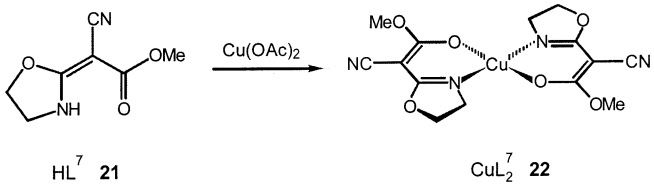
We report here on the synthesis of the one-dimensional coordination polymers 1D-$^{1}_{\infty}$[CuL^{7}_{2}] **23** and 1D-$^{1}_{\infty}$[$CuL^{10(R)}$-$L^{10(S)}$] **32**, the two-dimensional coordination polymer 2D-$^{2}_{\infty}$[CuL^{8}_{2}] **26**, and the helical coordination polymer strands (*P*)-/(*M*)-1D-$^{1}_{\infty}$[$CuL^{9(S)}_{2}$] **29**, which generate pairs of diastereoisomers in the infinite unit cell.[15]



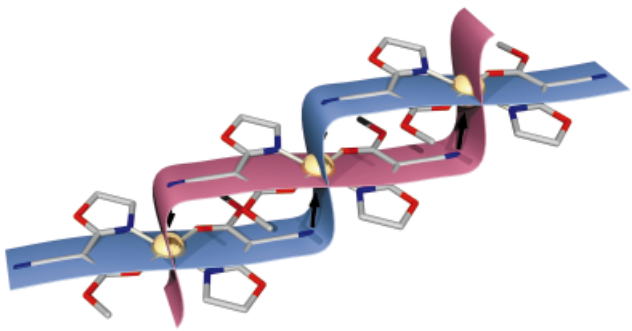
Results and Discussion

One-Dimensional Coordination Polymer 1D-$^{1}_{\infty}$[CuL^{7}_{2}] (23)

Reaction of a solution of NH-acidic oxazolidine **21** (HL^{7})[16][17] with copper(II) acetate in methanol yielded dark-green microcrystals.



HL^{7} **21** CuL^{7}_{2} **22**



1D - $^{1}_{\infty}$[CuL^{7}_{2}] **23**

On the basis of elemental analysis data and an X-ray diffraction study, the product was identified as the one-dimensional coordination polymer 1D-$^{1}_{\infty}$[CuL^{7}_{2}] **23**. The construc-

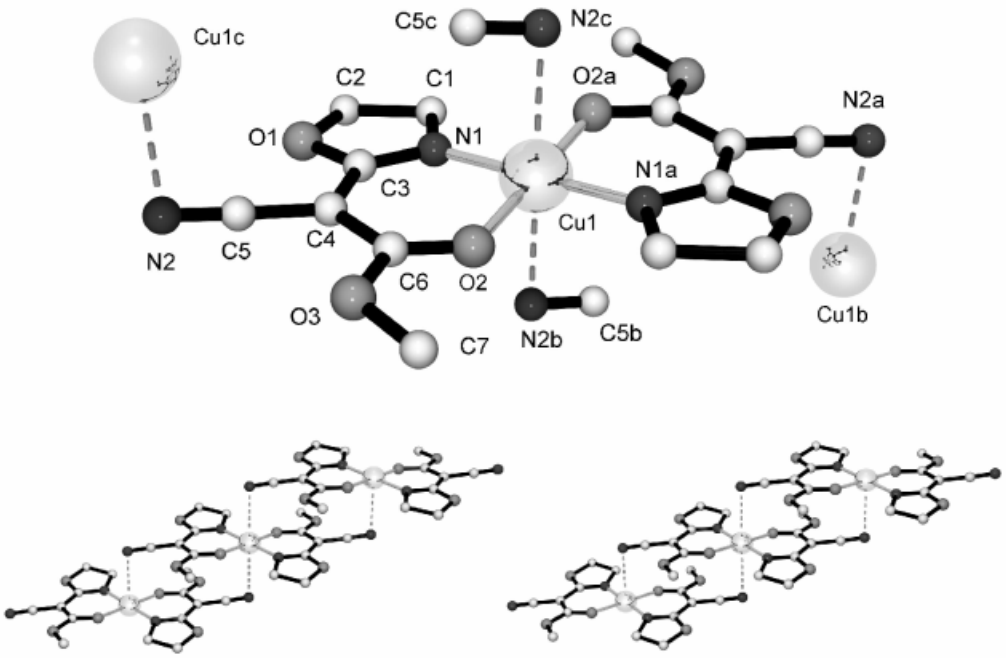
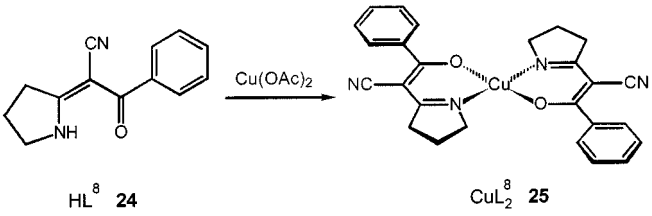
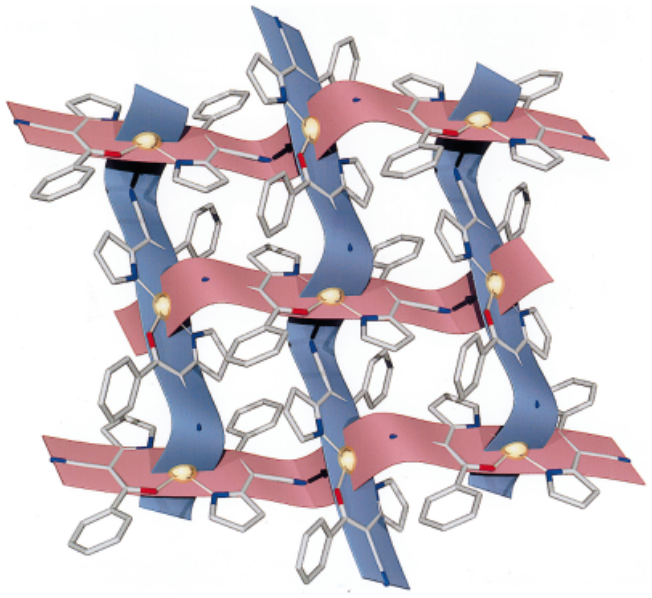


Figure 1. Top: structure of monomeric unit **22** of one-dimensional coordination polymer 1D-$^{1}_{\infty}$[CuL$^{7}_{2}$] **23** showing atomic numbering; H atoms omitted for clarity; bottom: stereoview of **23** in the infinite unit cell

tion of **23** becomes clear if one assumes the formation and linkage of the self-complementary building blocks **22** (Cu L$^{7}_{2}$). Intermediate **22** is coordinatively unsaturated and is also bis-monodentate with respect to the two CN groups. Specifically, the C_{2h}-symmetric monomers **22** are aligned parallel to one another. The equatorial cyano groups are coupled to copper in a *side-on* fashion with a Cu(1c)−N(2)−C(5) angle of 99.84° (Figure 1). The d^{9}-Cu^{II} ions are six-fold coordinated and are located in the center of a square-planar bipyramid. The Cu(1c)−N(2) distance amounts to 291.0 pm.



HL^{8} **24** CuL$^{8}_{2}$ **25**



2D -$^{2}_{\infty}$[CuL$^{8}_{2}$] **26**

Two-Dimensional Coordination Polymer 2D-$^{2}_{\infty}$[CuL$^{8}_{2}$] (26)

In order to study the effect of the ligands on the dimensionality of the coordination polymers, we treated a methanolic solution of pyrrolidine **24** (HL^{8})[16][18] with copper(II) acetate and isolated a green precipitate, which dissolved most readily in coordinating solvents. According to the microanalytical data and a single-crystal X-ray diffraction analysis, the two-dimensional coordination polymer 2D-$^{2}_{\infty}$[CuL$^{8}_{2}$] **26** was formed.

Polymer **26** is generated from the coordinatively unsaturated C_{2h}-symmetric building blocks **25** (CuL$^{8}_{2}$) along the two cyano groups. This leads to coordinative saturation at the copper(II) centers through distorted tetragonal bipyramids (Figure 2). The Cu(a)−N(10) distance measures 277.1 pm. The cyano groups of monomer **25** are bound to copper with a Cu(a)−N(10)−C(9) angle of 117.0°. The Cu−Cu distances amount to 759.9 pm (coplanar) and 992.3 pm (interplanar).

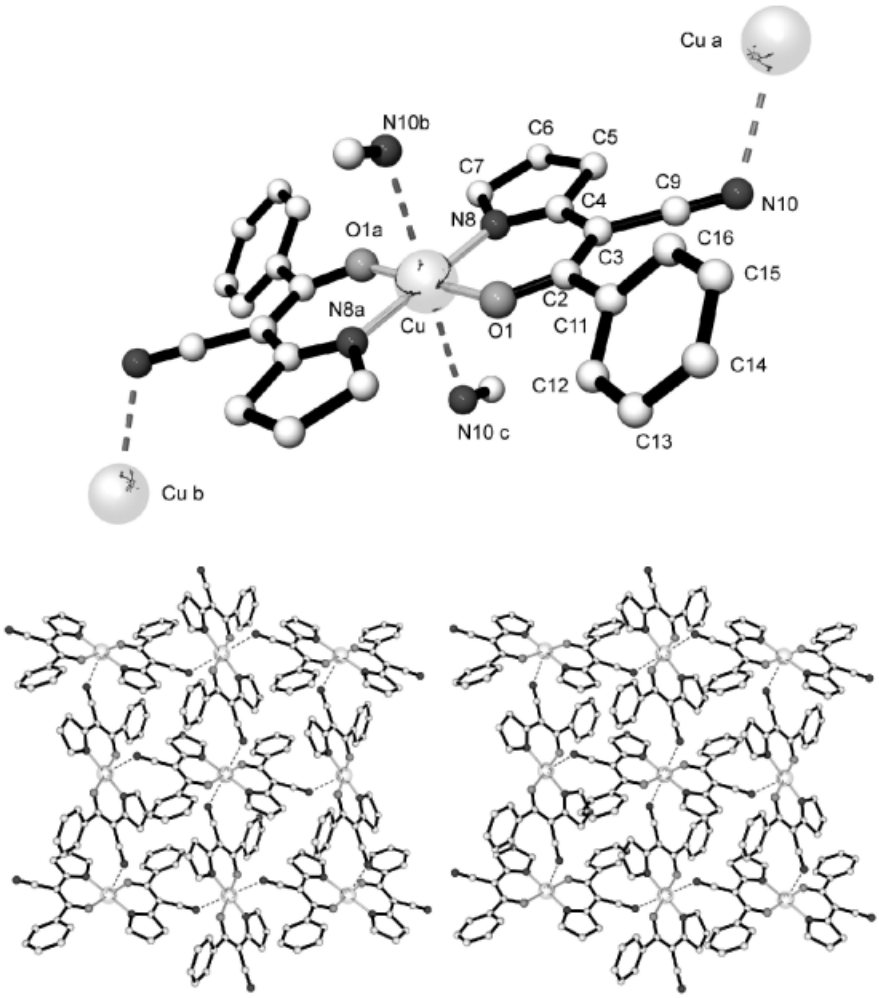
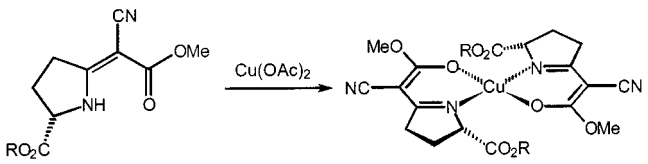


Figure 2. Top: structure of monomeric unit **25** of two-dimensional coordination polymer 2D-$^{2}_{\infty}$[CuL^{8}_{2}] **26** showing atomic numbering; H atoms omitted for clarity; bottom: stereoview of **26** in the infinite unit cell

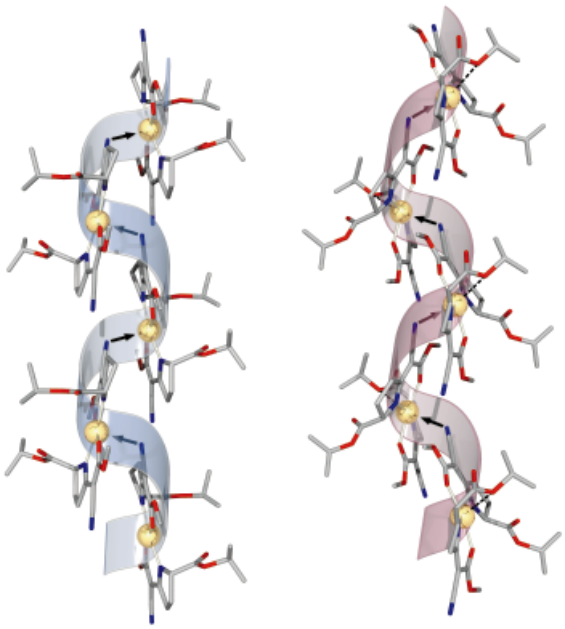
Helical Strands (M)-/(P)-1D-$^{1}_{\infty}$[$CuL^{9(S)}_{2}$] (29)

Reaction of a methanolic copper(II) acetate solution and (*S*)-isopropyloxycarbonylpyrrolidine **27** ($HL^{9(S)}$)[16] in the presence of triethylamine furnished light-green needles. According to the stoichiometric composition and an X-ray crystal structure analysis, the product obtained consisted of the helical coordination polymer (*M*)-/(*P*)-1D-$^{1}_{\infty}$[$CuL^{9(S)}_{2}$] **29**.[19]

The formation of the one-dimensional coordination polymer **29** can be rationalized if one assumes the intermediate generation of the coordinatively unsaturated C_2-symmetric building block [$CuL^{9(S)}_{2}$] **28**, which is sterically shielded at one side by two isopropyloxycarbonyl groups. Therefore, in



$HL^{9(S)}$ **27** R = $CHMe_2$ $CuL^{9(S)}_{2}$ **28**



(*M*)-/(*P*) -1D-$^{1}_{\infty}$[$CuL^{9(S)}_{2}$] **29**

contrast to 1D-$^{1}_{\infty}$[CuL$^{7}_{2}$] **23**, where copper displays tetragonal-bipyramidal coordination, attack of **28** through only one cyano group is possible. This leads to tetragonal-pyramidal coordination at the copper(II) centers with formation of **29**. The infinite unit cell is composed of helix strands made up of pairs of the diastereoisomers (*M*)-/(*P*)-1D-$^{1}_{\infty}$[CuL$^{9(S)}_{2}$] **29**.

It is noteworthy that the stereogenic centers of the chiral C_2-symmetric monomers [CuL$^{9(S)}_{2}$] **28** did not induce asymmetry in favour of either an (*M*)- or a (*P*)-helix. Each strand is composed of a set of identical monomeric building blocks **28**, which differ considerably in their bond lengths and angles. The available structural data for the monomeric units (*M*)-**28** [Figure 3 (a)] and (*P*)-**28** [Figure 3 (b)] reveal that each of the Cu atoms of the helical diastereoisomers (*M*)-**29** [Figure 3 (c)] and (*P*)-**29** [Figure 3 (d)] is linked through the nitrogen atom of only one neighbouring cyano group of the monomers. The central Cu atoms in (*M*)-**29** and (*P*)-**29** are almost tetragonal-pyramidally coordinated, with the planes of the two ligands L$^{9(S)}$ (HL$^{9(S)}$ = **27**) twisted with respect to one another to form angles of 7.97° and 13.64° [torsion angles: angles between the perpendiculars of the planes O(1)−Cu(1)−N(1), O(5)−Cu(1)−N(3), and O(9)−Cu(1)−N(5), O(13)−Cu(1)−N(7), respectively]. The distances Cu(1)−N(2a) and Cu(2)−N(8a) are 259.3 pm in (*M*)-**29** and 265.3 pm in (*P*)-**29**. The bond angles C(3Aa)−N(2a)−Cu(1) and C(301a)−N(8a)−Cu(2) are found to be 114.0° in (*M*)-**29** and 127.4° in (*P*)-**29**, respectively. The main difference between (*M*)-**28** and (*P*)-**28** is the short distance of 301.8 pm between Cu(2) and O(12) in (*P*)-**28**.

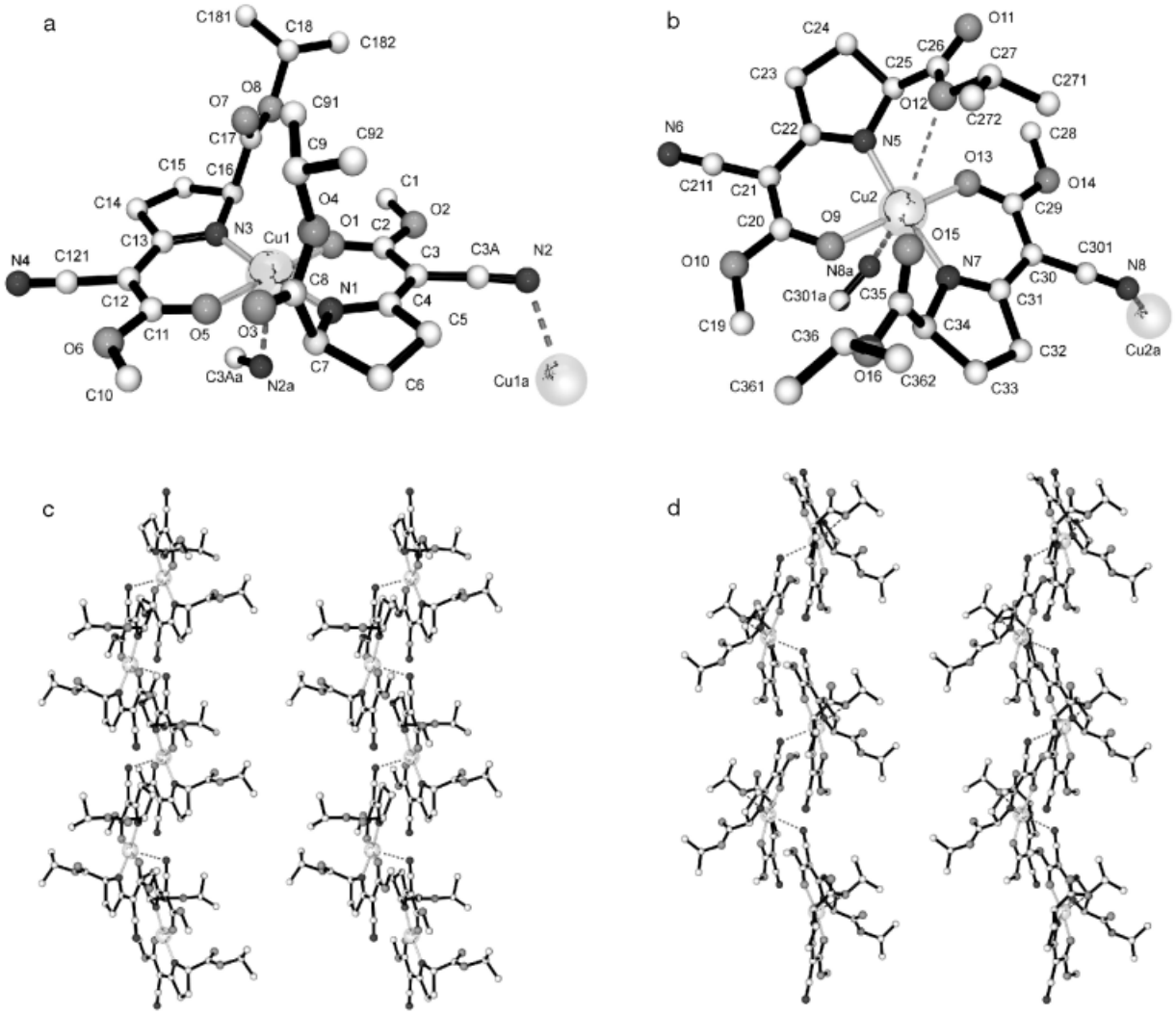
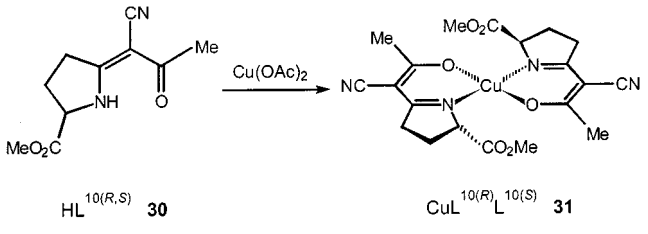


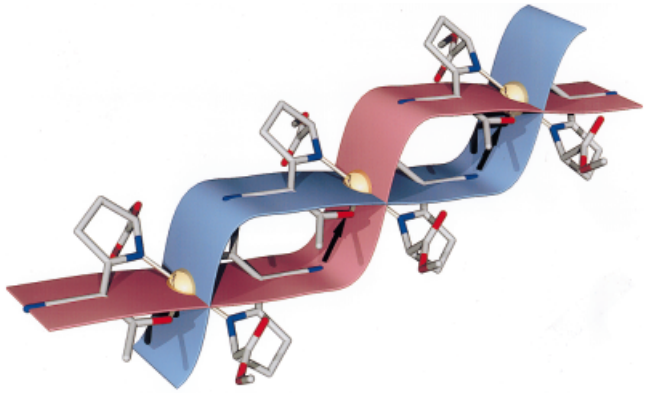
Figure 3. Top: structure of the monomeric units (*M*)-**28** (a) and (*P*)-**28** (b) showing atomic numbering of the helical diastereoisomers (*M*)-/(*P*)-1D-$^{1}_{\infty}$[CuL$^{9(S)}_{2}$] **29**; H atoms omitted for clarity; bottom: stereoview of **29** in the infinite unit cell (c) (*M*)-**29**, (d) (*P*)-**29**

One-Dimensional Coordination Polymer 1D-$^{1}_{\infty}$[CuL$^{10(R)}$L$^{10(S)}$] (32)

In contrast to enantiomerically pure pyrrolidine **27** (HL$^{9(S)}$), which led via the C_2-symmetric intermediate **28** to the helical strands (*M*)-/(*P*)-1D-$^{1}_{\infty}$[CuL$^{9(S)}_2$] **29**, reaction of a methanolic solution of NH-acidic, chiral, racemic pyrrolidine **30** (HL$^{10(R,S)}$) with copper(II) acetate afforded the C_i-symmetric coordinatively unsaturated building block (CuL$^{10(R)}$L$^{10(S)}$) **31**. Dipole−cation interaction between the CN groups and the copper(II) centers of the key intermediates **31** yielded the one-dimensional coordination polymer 1D-$^{1}_{\infty}$[CuL$^{10(R)}$L$^{10(S)}$] **32**.



HL$^{10(R,S)}$ **30** CuL$^{10(R)}$L$^{10(S)}$ **31**



1D -$^{1}_{\infty}$[CuL$^{10(R)}$L$^{10(S)}$] **32**

The monomers **31** are aligned parallel to one another and the equatorial cyano groups of **31** are directed towards the copper in a *side-on* fashion with a Cu(1a)−N(2)−C(4) angle of 111.6° (Figure 4). The d^9-Cu(II) ions are six-fold coordinated and are located in the center of a square plane. The Cu(1)−N(2b) distance of 354.6 pm in **32** is rather long compared with that of 291.0 pm in **23** (Figure 1).

Conclusions

The high degree of symmetry of the coordination polymers obtained through spontaneous organization of the self-complementary building blocks **22** and **25** (C_{2h}), **28** (C_2), and **31** (C_i) is surprising. However, we are far from being able to foresee structures such as the one-dimensional coordination polymers 1D-$^{1}_{\infty}$[CuL$^{7}_2$] **23** and 1D-$^{1}_{\infty}$[CuL$^{10(R)}$L$^{10(S)}$] **32**, the two-dimensional sheets 2D-$^{2}_{\infty}$[CuL$^{8}_2$] **26**, or the helical strands (*M*)-/(*P*)-1D-$^{1}_{\infty}$[CuL$^{9(S)}_2$] **29**, which generate pairs of diastereoisomers in the infinite unit cell. The present study on the use of self-complementary building blocks for the construction of coordination polymers suggests that more experimental endeavour is necessary in order to be able to predict the dimensionality of these potential materials.

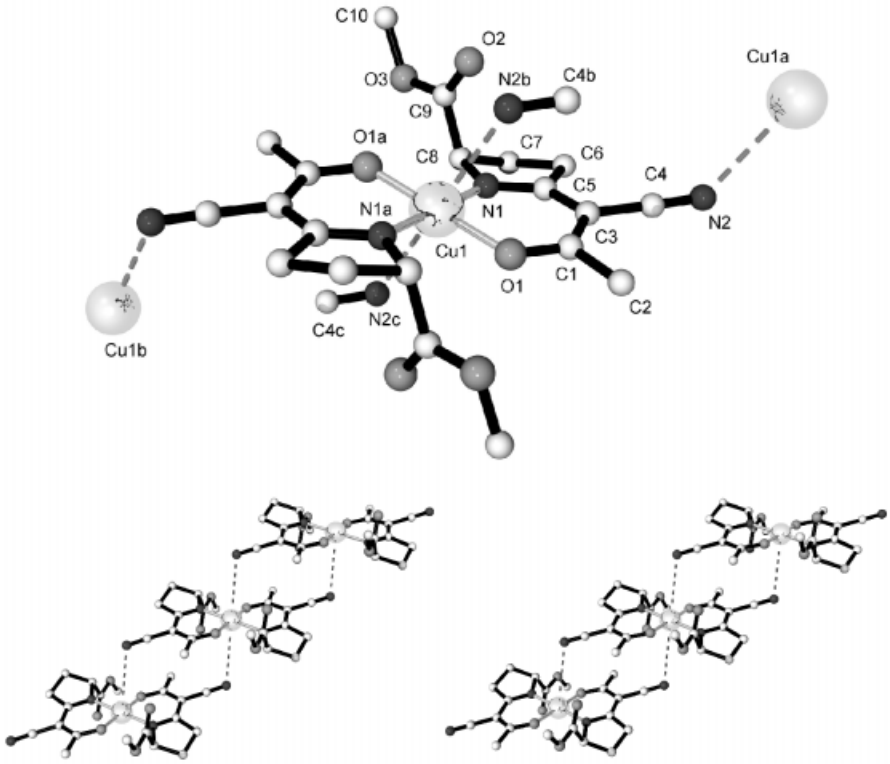


Figure 4. Top: structure of monomeric unit **31** of one-dimensional coordination polymer 1D-$^{1}_{\infty}$[CuL$^{10(R)}$L$^{10(S)}$] **32** showing atomic numbering; H atoms omitted for clarity; bottom: stereoview of **32** in the infinite unit cell

Experimental Section

Materials and Methods: All common reagents and solvents were purchased from commercial suppliers and were used without further purification unless otherwise indicated. − Melting points were determined on a Wagner−Munz apparatus and are uncorrected. − Infrared spectra were recorded on a Beckman Acculab or on a Perkin−Elmer 1420 ratio recording infrared spectrophotometer. − ^{1}H- and ^{13}C-NMR spectra were recorded on a JEOL JNM-GX-400 spectrometer at 400 and 100.5 MHz, respectively. The carbon atoms were assigned with the aid of the DEPT technique. All chemical shifts are based on the δ scale, referenced to TMS as an internal standard. − Mass spectra were recorded on a Varian MAT311 A (EIMS) or on a micromass ZabSpec (ion-desorption from a *m*-nitrobenzyl alcohol matrix: 8 keV, caesium atoms FAB-MS).

General Procedure for the Synthesis of the Vinylogous Amide Ligands 21, 24, 27, and 30:[16] A stirred mixture of a cyclic imino ether and the corresponding β-oxo nitrile (for quantitative proportions, refer to specific cases) was heated for 24 h at 100°C. Ethanol, formed during the reaction, was distilled off (in a stream of nitrogen in the case of **27** and **30**). The hot reaction mixture was then filtered, cooled to 20°C, and the excess starting materials were recovered by distillation under reduced pressure. The brownish crude product was washed with cold methanol. Colourless crystals were obtained from methanol.

Methyl (*E*)-2-Cyano-2-(oxazolidine-2-ylidene)acetate (21): Prepared from 4,5-dihydro-2-ethyloxyoxazole[16] (4.6 g, 40 mmol) and methyl cyanoacetate (15.8 g, 160 mmol). Yield: 4.2 g (62%); m.p. 144°C. − ^{1}H NMR (400 MHz, $CDCl_3$/[D$_6$]DMSO, 5:1, 25°C): δ = 3.75 (s, 3 H, CH_3), 3.93 [t, ^3J(H,H) = 8.3 Hz, 2 H, $C_{(4)}H_2$], 4.72 [t, ^3J(H,H) = 8.3 Hz, 2 H, $C_{(5)}H_2$], 8.72 (br. s, 1 H, NH). − ^{13}C NMR (100.5 MHz, $CDCl_3$/[D$_6$]DMSO, 5:1, 25°C): δ = 43.67 ($C_{(4)}$), 51.56 (CH_3), 55.92 (=*C*−CN), 69.50 ($C_{(5)}$), 116.67 (CN), 168.34, 172.07 (C=O or $C_{(2)}$). − IR ($CHBr_3$): $\tilde{\nu}$ = 3320 (NH), 2940 (CH), 2200 (C≡N), 1670 (C=O), 1590 cm^{-1} (C=C). − MS (70 eV, EI): *m*/*z* (%): 168 [M$^+$] (30).

(*Z*)-2-Cyano-2-(pyrrolidine-2-ylidene)-1-phenylethanone (24):[18] Prepared from 5-ethyloxy-3,4-dihydro-2*H*-pyrrole[16] (4.1 g, 36 mmol) and benzoylacetonitrile (1.3 g, 9 mmol). Yield: 1.7 g (89%); m.p. 145°C. − ^{1}H NMR (400 MHz, $CDCl_3$, 25°C): δ = 2.09 (br. q, 2 H, $C_{(4)}H_2$), 3.02 (br. t, 2 H, $C_{(3)}H_2$), 3.72 (br. t, 2 H, $C_{(5)}H_2$), 7.40−7.49 (m, 3 H, Ar $C_{(3,4,5)}$H), 7.79−7.87 (m, 2 H, Ar $C_{(2,6)}$H), 10.89 (br. s, 1 H, NH). − ^{13}C NMR (100.5 MHz, $CDCl_3$, 25°C): δ = 20.23 ($C_{(4)}$), 34.13 ($C_{(3)}$), 49.80 ($C_{(5)}$), 77.63 (=*C*−CN), 121.00 (C≡N), 127.78, 128.09 (Ar $C_{(3,4,5)}$), 131.25 (Ar $C_{(2,6)}$), 138.91 (Ar $C_{(1)}$), 176.03 ($C_{(2)}$), 190.88 (C=O). − IR (KBr): $\tilde{\nu}$ = 3280 (NH), 3030 (CH), 2190 (C≡N), 1620 (C=O), 1585, 1490 cm^{-1} (C=C). − MS (70 eV, EI): *m*/*z* (%): 212 [M$^+$] (50).

Methyl (*Z*)-2-Cyano-2-[(2*S*)-2-isopropyloxycarbonylpyrrolidine-5-ylidene]acetate (27): Prepared from (2*S*)-5-ethyloxy-2-isopropyloxycarbonyl-3,4-dihydro-2*H*-pyrrole (15 g, 75 mmol) and methyl cyanoacetate (30 g, 300 mmol). Yield: 15.6 g (82%); m.p. 130°C. − ^{1}H NMR (400 MHz, $CDCl_3$, 25°C): δ = 1.28, 1.29 [d, ^3J(H,H) = 6.0 Hz, 3 H, CH_3], 2.18−2.27 (m, 1 H, $C_{(3)}H_A$), 2.43−2.52 (m, 1 H, $C_{(3)}H_B$), 2.93−3.08 (m, 2 H, $C_{(4)}H_2$), 3.77 (s, 3 H, OCH_3), 4.54 [dd, ^3J(H,H) = 8.8 Hz, ^3J(H,H) = 5.5 Hz, 1 H, $C_{(2)}$H], 5.07 [sept., ^3J(H,H) = 6.1 Hz, 1 H, CH], 9.16 (br. s, 1 H, NH). − ^{13}C NMR (100.5 MHz, $CDCl_3$, 25°C): δ = 21.81 (2 CH_3), 25.44 ($C_{(3)}$), 32.60 ($C_{(4)}$), 51.77 (OCH_3), 62.60 ($C_{(2)}$), 68.83 (=*C*−CN), 70.15 (OCH), 118.27 (C≡N), 167.93, 170.01, 173.63 (2 C=O or $C_{(5)}$). − IR ($CHBr_3$): $\tilde{\nu}$ = 3332 (NH), 2980, 2950 (CH), 2207 (C≡N), 1736, 1677 (C=O), 1592 cm^{-1} (C=C). − MS (70 eV, EI): *m*/*z* (%): 252 [M$^+$] (12).

(*Z*)-1-Cyano-1-(2-methoxycarbonylpyrrolidine-5-ylidene)propan-2-one (30): Prepared from β-oxobutyronitrile[20] (7.1 g, 86 mmol) and (2*S*)-5-ethyloxy-2-methoxycarbonyl-3,4-dihydro-2*H*-pyrrole (29.6 g, 173 mmol). Yield: 2.8 g (16%); m.p. 117°C. − ^{1}H NMR (400 MHz, $CDCl_3$, 25°C): δ = 2.22−2.32 (m, 1 H, $C_{(3)}H_A$), 2.41−2.51 (m, 1 H, $C_{(3)}H_B$), 2.33 (s, 3 H, CH_3), 2.94−3.10 (m, 2 H, $C_{(4)}H_2$), 3.78 (s, 3 H, OCH_3), 4.63 [dd, ^3J(H,H) = 8.9 Hz, ^3J(H,H) = 5.3 Hz, 1 H, CH], 10.61 (br. s, 1 H, NH). − ^{13}C NMR (100.5 MHz, $CDCl_3$, 25°C): δ = 24.60 ($C_{(3)}$), 27.80 (CH_3), 32.59 ($C_{(4)}$), 52.87 (OCH_3), 62.53 ($C_{(2)}$), 80.09 (=*C*−CN), 119.79 (C≡N), 170.38, 173.32 (O−C=O or $C_{(5)}$), 195.12 (C=O). − IR ($CHBr_3$): $\tilde{\nu}$ = 3230 (NH), 2990, 2940 (CH), 2180 (C≡N), 1750, 1640 (C=O), 1580 cm^{-1} (C=C). − MS (70 eV, EI): *m*/*z* (%): 208 [M$^+$] (28).

General Procedure for the Synthesis of the Coordination Polymers 23 and 26: A solution of vinylogous amide ligand **21** (336 mg, 2 mmol) or **24** (442 mg, 2 mmol) in 40 mL methanol was added to a stirred solution of 1 mmol copper(II) acetate monohydrate in 50 mL methanol. After 1 h, the analytically pure precipitate was filtered off, dried in vacuo (oil pump), and crystallized.

1D-$^1_\infty$[CuL$^7_2$] (23): Yield: 397 mg (100%) as dark-green crystals from chloroform/diethyl ether; m.p. > 250 °C. − IR ($CHBr_3$): $\tilde{\nu}$ = 2960 (CH), 2190 (C≡N), 1625 (C=N), 1535 cm^{-1} (C=C). − MS (FAB): *m*/*z* (%): 628 [$Cu_2L_3^+$] (17), 460 [$Cu_2L_2^+$] (16), 398 [CuL_2^+] (11).

1D-$^1_\infty$[CuL$^8_2$] (26): Yield: 422 mg (97%) as turquoise-green crystals from chloroform/diethyl ether; m.p. > 250°C (dec.). − IR ($CHBr_3$): $\tilde{\nu}$ = 2940, 2870 (CH), 2190 (C≡N), 1590 (C=N), 1490, 1480 (C=C). − MS (70 eV, EI): *m*/*z* (%): 485 [CuL_2^+] (56).

General Procedure for the Synthesis of the Coordination Polymers 29 and 32: A solution of vinylogous amide ligand **27** (336 mg, 2 mmol) or **30** (442 mg, 2 mmol) in 40 mL methanol was added to a stirred solution of copper(II) acetate monohydrate (200 mg, 1 mmol) in 50 mL methanol. Triethylamine (0.27 mL, 2 mmol) was then added and after 15 min the solvent was removed in vacuo. The residue was dissolved in 100 mL chloroform and the resulting solution was washed with water (3 × 50 mL) and dried with magnesium sulfate. The solvent was then removed and the product was crystallized. In the case of coordination polymer **29** it proved important to carry out all reaction steps at room temperature and to adhere strictly to the reaction time in order to prevent partial racemization.

(*P*)-/(*M*)-1D-$^1_\infty$[CuL$^{9(S)}_2$] (29): Yield: 380 mg (67%) as light-green crystals from chloroform/diethyl ether; m.p. 213°C (dec.). − IR ($CHBr_3$): $\tilde{\nu}$ = 2980, 2880 (CH), 2200 (C≡N), 1730, (C=O), 1605 (C=N), 1510 cm^{-1} (C=C). − MS (FAB): *m*/*z* (%): 1510 [$Cu_4L_5^+$] (1), 1258 [$Cu_4L_4^+$] (25), 1195 [$Cu_3L_4^+$] (68), 944 [$Cu_3L_3^+$] (44), 881 [$Cu_2L_3^+$] (47), 630 [$Cu_2L_2^+$] (17), 566 [CuL_2^+] (100).

1D-$^1_\infty$[CuL$^{10(R)}$L$^{10(S)}$] (32): Yield: 233 mg (49%) as dark-green crystals from chloroform/diethyl ether; m.p. 209°C (dec.). − IR ($CHBr_3$): $\tilde{\nu}$ = 2990, 2920 (CH), 2190 (C≡N), 1740 (C=O), 1590 (C=N), 1480 cm^{-1} (C=C). − MS (FAB): *m*/*z* (%): 1019 [$Cu_3L_4^+$] (6), 957 [$Cu_2L_4^+$] (0.3), 812 [$Cu_3L_3^+$] (1), 749 [$Cu_2L_3^+$] (15), 540 [$Cu_2L_2^+$] (6), 478 [CuL_2^+] (100).

Crystal Structure Determination of Compound 23: $C_{14}H_{14}CuN_4O_6$, M_r = 397.83, monoclinic space group $P2_1/n$, a = 674.53(8) pm, b = 898.31(24) pm, c = 1312.53(10) pm, β = 96.182(8)°, V = 0.7907(2) nm^3, Z = 2, ρ_{calcd} = 1.671 Mgm^{-3}, F(000) = 406, λ =

71.073 pm, T = 293(2) K, μ(Mo-K_α) = 1.422 mm^{-1}, crystal dimensions 0.40×0.040×0.30 mm, 5.5° ≤ 2Θ ≤ 52.6°; 1671 measured reflections, of which 1603 were independent (R_{int} = 0.0221) and were employed in the structure refinement (116 parameters, 0 restraints). The R values are $R1 = \Sigma |F_o - F_c|/|F_o|$ = 0.0306 [$I > 2\sigma(I)$] and $wR2 = [\Sigma W(F_o^2 - F_c^2)/\Sigma wF_o^4]^{1/2}$ = 0.0897 (all data); residual electron density (peak/hole): 391/−415 e/nm^3.

Crystal Structure Determination of Compound 26: $C_{26}H_{22}CuN_4O_2$, M_r = 486.05, monoclinic space group $P2_1/a$, a = 1054.0(2) pm, b = 1094.8(1) pm, c = 992.2(2) pm, β = 102.57(1)°, V = 1.1176(3) nm^3, Z = 2, ρ_{calcd} = 1.444 Mg m^{-3}, λ = 71.073 pm, μ(Mo-K_α) = 1.01 mm^{-1}, crystal dimensions 0.5×0.55×0.1 mm, θ range: 1.75° to 27.5°; 2563 measured reflections, of which 2316 were independent; data/parameter ratio 12.50. The final reliability indices based on 1888 reflections with $F > 3\sigma(F)$ were R = 0.039 and wR = 0.037 using the weighting scheme $w = 1/\sigma^2(F)$; min./max. residual electron density: 370/460 e/nm^3.

Crystal Structure Determination of Compound 29: $C_{24}H_{30}CuN_4O_8$, M_r = 566.06, monoclinic space group $P2_1$, a = 1241.2(3) pm, b = 1181.6(2) pm, c = 1905.7(4) pm, β = 105.28(3)°, V = 2.6962(9) nm^3, Z = 4, ρ_{calcd} = 1.394 Mg m^{-3}, F(000) = 1180, λ = 71.073 pm, T = 293(2) K, μ(Mo-K_α) = 0.862 mm^{-1}, crystal dimensions 0.50×0.30×0.20 mm, 5.6° ≤ 2Θ ≤ 49.2°; 7900 measured reflections, of which 4791 were independent (R_{int} = 0.0406) and were employed in the structure refinement (667 parameters, 1 restraint). The R values are $R1$ = 0.0369 [$I > 2\sigma(I)$] and $wR2$ = 0.1039 (all data); residual electron density (peak/hole): 300/−424 e/nm^3.

Crystal Structure Determination of Compound 32: $C_{20}H_{22}CuN_4O_6$, M_r = 477.96, triclinic, space group $P\bar{1}$; a = 767.00(5) pm, b = 871.04(11) pm, c = 858.66(6) pm, α = 108.142(7)°, β = 94.301(6)°, γ = 103.008(8)°, V = 0.52459(8) nm^3, Z = 1, ρ_{calcd} = 1.513 Mg m^{-3}, F(000) = 247, λ = 71.073 pm, T = 293(2) K, μ(Mo-K_α) = 1.086 mm^{-1}, crystal dimensions 0.30×0.30×0.10 mm, 5.1° ≤ 2Θ ≤ 48.1°; 1775 measured reflections, of which 1636 were independent (R_{int} = 0.0234) and were employed in the structure refinement (143 parameters, 0 restraints). The R values are $R1$ = 0.0373 [$I > 2\sigma(I)$] and $wR2$ = 0.1084 (all data); residual electron density (peak/hole): 643/−655 e/nm^3. − Crystallographic data for **23**, **29** and **32** were collected on Nonius CAD-MACH3 diffractometers equipped with graphite-monochromated Mo-K_α radiation by use of θ and ω scans. The structures were solved by direct methods (SHELX-86) and refined by full-matrix least-squares treatment against F^2 using the SHELXL-93 program system.[22] All non-hydrogen atoms were refined anisotropically. The positions of the hydrogen atoms were fixed in ideal positions (riding model) and were included without refinement and with fixed isotropic U. − Crystallographic data for **26** were collected on a Siemens R3m/V diffractometer equipped with graphite-monochromated Mo-K_α radiation using the Wyckoff-scan technique. The structure was solved by direct phase determination and refined by full-matrix least-squares treatment using the SHELXTL-PLUS program system. The positions of the hydrogen atoms were included as a riding model without refinement and with fixed isotropic U. − Two-dimensional 2D-$^2_\infty$[CuL_2^{12}] **33** and 2D-$^2_\infty$[CuL_2^{12}] **34** were also obtained with ethyl (*Z*)-2-cyano-2-(pyrrolidine-2-ylidene)acetate (HL^{11}) and (*E*)-2-cyano-2-(oxazolidine-2-ylidene)-1-phenylethanone (HL^{12}). − Crystallographic data (excluding structure factors) for all structures reported in this paper have been deposited with the Cambridge Crystallographic Data Centre as supplementary publication nos. CCDC-111706 (**23**), CCDC-111831 (**26**), CCDC-111702 (**29**), CCDC-111703 (**32**), CCDC-111704 (**33**), and CCDC-111705 (**34**). Copies of the data can be obtained free of charge on application to the CCDC, 12 Union Road, Cambridge CB2 1EZ, U.K. [Fax: (internat.) +44 (0)1223/336033; E-mail: deposit@ccdc.cam.ac.uk].

Acknowledgments

This work was supported by the Deutsche Forschungsgemeinschaft, the Fonds der Chemischen Industrie, and the Volkswagen-Stiftung.

[1] J.-M. Lehn, *Supramolecular Chemistry − Concepts and Perspectives*, VCH, Weinheim, **1995**; D. Philp, J. F. Stoddart, *Angew. Chem.* **1996**, *108*, 1243−1286; *Angew. Chem. Int. Ed. Engl.* **1996**, *35*, 1154−1196.

[2] S. R. Batten, R. Robson, *Angew. Chem.* **1998**, *110*, 1558−1595; *Angew. Chem. Int. Ed. Engl.* **1998**, *37*, 1460−1494; R. Robson in: *Comprehensive Supramolecular Chemistry, Vol. 6* (Eds.: D. D. Manicol, F. Toda, R. Bishop), Pergamon, Oxford, **1996**, p. 733; C. Kaes, M. W. Hosseini, C. E. F. Rickard, B. W. Skelton, A. H. White, *Angew. Chem.* **1998**, *110*, 970−972; *Angew. Chem. Int. Ed. Engl.* **1998**, *37*, 920−922; M. J. Zaworotko, *Chem. Soc. Rev.* **1994**, 283−288; A. J. Blake, N. R. Champness, S. S. Chung, W.-S. Li, M. Schröder, *J. Chem. Soc., Chem. Commun.* **1997**, 1005−1006; K. A. Hirsch, D. Venkataraman, S. R. Wilson, J. S. Moore, S. Lee, *J. Chem. Soc., Chem. Commun.* **1995**, 2199−2200; L. Carlucci, G. Ciani, D. M. Proserpio, *J. Chem. Soc., Chem. Commun.* **1994**, 2755−2756.

[3] R. W. Saalfrank, C.-J. Lurz, K. Schobert, O. Struck, E. Bill, A. X. Trautwein, *Angew. Chem.* **1991**, *103*, 1499−1501; *Angew. Chem. Int. Ed. Engl.* **1991**, *30*, 1494−1496; R. W. Saalfrank, O. Struck, K. Nunn, C.-J. Lurz, R. Harbig, K. Peters, H. G. von Schnering, E. Bill, A. X. Trautwein, *Chem. Ber.* **1992**, *125*, 2331−2335.

[4] R. W. Saalfrank, R. Harbig, O. Struck, E.-M. Peters, K. Peters, H. G. von Schnering, *Z. Naturforsch.* **1996**, *51b*, 399−408; R. W. Saalfrank, O. Struck, K. Peters, H. G. von Schnering, *Chem. Ber.* **1993**, *126*, 837−840. See also: R. W. Saalfrank, O. Struck, D. Danion, J. Hassa, L. Toupet, *Chem. Mater.* **1994**, *6*, 1432−1436.

[5] G. Denti, S. Serroni, S. Campagna, A. Juris, M. Ciano, V. Balzani in: *Perspectives in Coordination Chemistry* (Eds.: A. F. Williams, C. Floriani, A. E. Merbach), VCH, Weinheim, **1992**, p. 153.

[6] R. W. Saalfrank, R. Harbig, O. Struck, F. Hampel, E.-M. Peters, K. Peters, H. G. von Schnering, *Z. Naturforsch.* **1997**, *52b*, 125−134. See also: R. W. Saalfrank, D. Danion, F. Hampel, J. Hassa, O. Struck, L. Toupet, *Chem. Ber.* **1994**, *127*, 1283−1286; R. W. Saalfrank, K. Schobert, S. Trummer, A. Wolski, *Z. Naturforsch.* **1995**, *50b*, 642−648; M. J. Hannon, C. L. Painting, W. Errington, *J. Chem. Soc., Chem. Commun.* **1997**, 1805−1806.

[7] M. Decker, Ph. D. Thesis, Univ. Erlangen-Nürnberg, Germany, **1997**.

[8] The diagram only shows the (*M*)-helix.

[9] R. W. Saalfrank, O. Struck, K. Peters, H. G. von Schnering, *Inorg. Chim. Acta* **1994**, *222*, 5−11.

[10] O. J. Gelling, F. van Bolhuis, B. L. Feringa, *J. Chem. Soc., Chem. Commun.* **1991**, 917−919.

[11] D. A. Evans, K. A. Woerpel, M. J. Scott, *Angew. Chem.* **1992**, *104*, 439−441; *Angew. Chem. Int. Ed. Engl.* **1992**, *31*, 430−433; J. F. Modder, G. van Koten, K. Vrieze, A. L. Spek, *Angew. Chem.* **1989**, *101*, 1723−1725; *Angew. Chem. Int. Ed. Engl.* **1989**, *28*, 1698−1700.

[12] R. W. Saalfrank, M. Decker, F. Hampel, K. Peters, H. G. von Schnering, *Chem. Ber./Recueil* **1997**, *130*, 1309−1313.

[13] In contrast to (*M*)-1D-$^1_\infty$[$CuL_2^{5(S)}$] **5**, (*P*)-1D-$^1_\infty$[$CuL_2^{6(R)}$] **6** and (*M*)-1D-$^1_\infty$[$CuL_2^{6(R)}$] **6** are generated in chloroform from the stable, less hindered, methanol precursors (*R*,*R*)-**19**(HOMe) and (*S*,*S*)-**19**(HOMe) by repetitive backside attack by one cyano group of a second molecule and loss of methanol according to an S_N2-type mechanism.[12]

[14] R. W. Saalfrank, O. Struck, M. G. Davidson, R. Snaith, *Chem. Ber.* **1994**, *127*, 2489−2492.

[15] The diagrams were created with the program MOLMOL and were rendered with the Persistence of Vision Raytracer, R. Koradi, M. Billeter, K. Wüthrich, *J. Mol. Graphics* **1996**, *14*, 51−55.

[16] The starting materials **21**, **24**, **27**, and **30** were prepared according to ref.[17]
[17] Y. Yamada, D. Milijkovic, P. Wehrli, B. Golding, P. Lölinger, R. Keese, K. Müller, A. Eschenmoser, *Angew. Chem.* **1969**, *81*, 301−306; *Angew. Chem. Int. Ed. Engl.* **1969**, *8*, 343-348; H. Fritschi, U. Leutenegger, K. Siegmann, A. Pfaltz, W. Keller, C. Kratky, *Helv. Chim. Acta* **1988**, *71*, 1541−1552.
[18] G. M. Coppola, R. Damon, A. D. Kahle, M. J. Shapiro, *J. Org. Chem.* **1981**, *46*, 1221−1222.
[19] The helicity is defined with respect to the order of the copper(II) ions.
[20] B. F. Becker, H. P. Fritz, *Liebigs Ann. Chem.* **1976**, *6*, 1015−1022; B. Prager, P. Jacobson, *Beilsteins Handbuch der Organischen Chemie* **1921**, *H 3*, 658.
[21] G. M. Sheldrick, *SHELXL-93, Programm für die Kristallstrukturverfeinerung*/Program for Crystal Structure Refinement, Universität Göttingen, **1993**.

Received April 16, 1999
[I99136]

Structural and Energetical Characterization of the Methylbutadiene–$Fe(CO)_3$ Isomers and Related Reactive Intermediates with Quantum Chemical Methods

Anja Pfletschinger,[a] Hans-Günther Schmalz,*[a] and Wolfram Koch*[a][+]

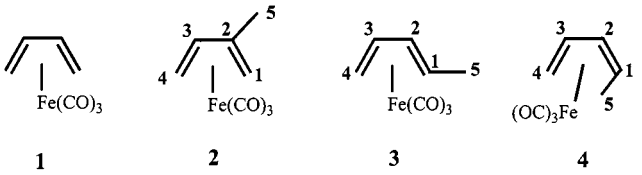
Keywords: Density functional calculations / 1,3-Diene–$Fe(CO)_3$ / Conformational analysis / Iron / Organometallic chemistry / Reactive intermediates

A theoretical investigation of isoprene–$Fe(CO)_3$ (**2**), (*E*)-1,3-pentadiene–$Fe(CO)_3$ (**3**), (*Z*)-1,3-pentadiene–$Fe(CO)_3$ (**4**), and reactive intermediates derived from these complexes was undertaken, employing the HF/DFT hybrid functional Becke3LYP, and the results are presented. Special emphasis is placed on cationic, anionic, and radical intermediates formally derived by abstraction of a hydride, a proton, or a hydrogen atom from the methyl group of the parent complexes. The geometry, energy, and electronic situation of the calculated species are discussed in the context of experimental facts. This leads to a better mechanistic understanding of the chemistry of acyclic butadiene–$Fe(CO)_3$ complexes, provides insights into structural details of the intermediates involved, and allows the evaluation of possible resonance formulae. The calculation of transition states of isomerization (or racemization) processes even permits a quantitative description of energy profiles. In this way, the configurational stability of relevant cationic, anionic and radical intermediates can be estimated.

Introduction

Acyclic 1,3-diene−$Fe(CO)_3$ complexes are well established as valuable intermediates in organic synthesis.[1] Besides the use of the $Fe(CO)_3$ fragment as a protecting group for the 1,3-diene unit, many synthetic applications are based on transformations that exploit the ability of the $Fe(CO)_3$ unit to stabilize positive[2] or negative[3] charge in a position adjacent to the complexed diene. Due to the steric bulk of the metal fragment, many reactions of such complexes additionally proceed with a high level of stereocontrol.[4]

While crystal structures of the parent η^4-butadiene−$Fe(CO)_3$ complex **1** and quite a large number of other neutral 1,3-diene−$Fe(CO)_3$ complexes are available,[5] very little is definitely known about the structure of the anionic and cationic intermediates.[6] In order to develop a deeper understanding of these systems and to improve the predictability of the chemistry of acyclic butadiene−$Fe(CO)_3$ complexes, it would be highly desirable to obtain information about structural and energetical details of reactive intermediates involved in this chemistry. As a follow-up to our previous theoretical investigation employing density functional theory of cationic, anionic, and radical reactive intermediates derived from toluene−$Cr(CO)_3$,[7] we provide in this paper a detailed and comprehensive picture of the computed structural and energetical features of η^4-methylbutadiene−$Fe(CO)_3$ isomers **2**, **3**, and **4**, as well as the corresponding cationic, anionic, and even radical species of type $(C_5H_7)Fe(CO)_3^{+/-/\bullet}$ derived from **2**, **3**, and **4** by formal abstraction of a proton, a hydride, or an H radical from the methyl group.



1 **2** **3** **4**

Scheme 1. The parent systems: 1,3-butadiene−$Fe(CO)_3$ (**1**), isoprene−$Fe(CO)_3$ (**2**) and the pentadiene−$Fe(CO)_3$ complexes **3** and **4**; please note the numbering system which is uniformly applied in this paper

Computational Details

In the work described in this paper we used the same computational strategy that we successfully applied in our previous work on reactive intermediates derived from η^6-toluene−$Cr(CO)_3$.[7] Therefore, a brief description of the computational strategy will suffice at this point. For further details the reader is referred to ref.[7] All calculations were carried out using the popular Becke3LYP hybrid density functional.[8] An all electron basis set, described by Wachters,[9] was extended by a set of f-functions for the iron atom and was applied while the standard D95* split valence basis set was chosen for C, H, and O. All calculations were performed employing Gaussian94[10] as implemented on our own IBM RS/6000 workstations and the CRAY J90 computer of the Konrad-Zuse-Zentrum für Informationstechnik Berlin. The electron density was analyzed through the *Natural Bond Orbital* (NBO) scheme introduced by Weinhold and co-workers.[11] The harmonic frequencies were calculated for all molecules considered in order to identify

[a] Institut für Organische Chemie der Technischen Universität Berlin,
Straße des 17. Juni 135, D-10623 Berlin
Fax: (internat.) + 49-(0)30/ 314-21105
E-mail: w.koch@gdch.de
schmalz@wap0109.chem.tu-berlin.de
[+] Present address: Gesellschaft Deutscher Chemiker, Postfach 900440, D-60444 Frankfurt a. M., Germany
Supporting information for this article is available on the WWW under http://www.wiley-vch.de/home/eurjoc or from the author.

 © WILEY-VCH Verlag GmbH, D-69451 Weinheim, 1999 1434−1948/99/1111−1869 $ 17.50+.50/0

stationary points as minima or transition states and to estimate the zero point energies (ZPE) for which all energies are corrected. The calculations of the radical complexes all resulted in the expected S^2 value of 0.75 for a doublet.

Results and Discussion

The Neutral $C_5H_8-Fe(CO)_3$ Complexes

We began our study with the neutral complexes **2**, **3**, and **4**, which are shown in Figure 1. These three neutral isomers serve as reference systems for the investigation of the related cationic, anionic, and radical intermediates discussed below. The complexes **3** and **4** can be considered as configurational isomers, which formally can be converted into each other by a simple rotation around the C1−C2 bond. The theoretically predicted structures of complexes **2**, **3**, and **4** are depicted in Figure 1.[12]

The neutral isoprene tricarbonyl iron complex **2** shows a regular arrangement of the η^4-diene ligand with a slightly shorter internal C2−C3 bond (1.423 Å) compared to the C1−C2 and the C3−C4 bonds (1.436 Å and 1.434 Å, respectively). The iron atom is positioned symmetrically below the plane of the butadiene fragment and the $Fe(CO)_3$-tripod assumes a conformation with one CO pointing towards the open side of the diene ligand. As in the case of previous theoretical studies on **1**,[13] the structure calculated for **2** is in good general accordance with X-ray crystal structures[5] of such complexes and with a microwave structure for **1**.[14] The barrier for the rotation of the $Fe(CO)_3$ moiety in **2** was computed to be 11.1 kcal mol^{-1}, which is considerably closer to the experimentally determined barrier (10.6 kcal mol^{-1}) than values from previous calculations.[15] It is interesting to note that this barrier is significantly higher than, for instance, that of the metal fragment in the neutral toluene $Cr(CO)_3$ complex, which amounts to only 0.8 kcal mol^{-1}.[7] In the rotational transition state **2′** (Figure 2), the C2−C3 bond is now *longer* than the bond lengths of the terminal C−C bonds by 0.017 Å. The calculation of the harmonic vibrational frequencies confirms that structure **2′** is indeed the transition state of the $Fe(CO)_3$ rotation and is characterized by an imaginary frequency of 82.4 cm^{-1}, connected to the expected transition mode.

In the other two isomers, **3** and **4** (Figure 1), the iron is also η^4 bonded to the organic ligand with Fe−C bond lengths of about 2.0 Å. The structures show that the methyl substituents do not visibly disturb the preferred geometry of the parent η^4-butadiene−$Fe(CO)_3$ substructure. Compound **3** is energetically more stable than its stereoisomer **4** by 8.9 kcal mol^{-1}. In all three complexes the $C-CH_3$ bond appears as a normal σ-bond with a typical bond length between 1.51 and 1.53 Å.

A view of the NBO analysis (see Figure 1) reveals a negative partial charge on the iron atom (≈ −0.32 |e|) in all three neutral complexes. The CO groups have positive charges of +0.125 |e| to +0.155 |e| (sum of the partial

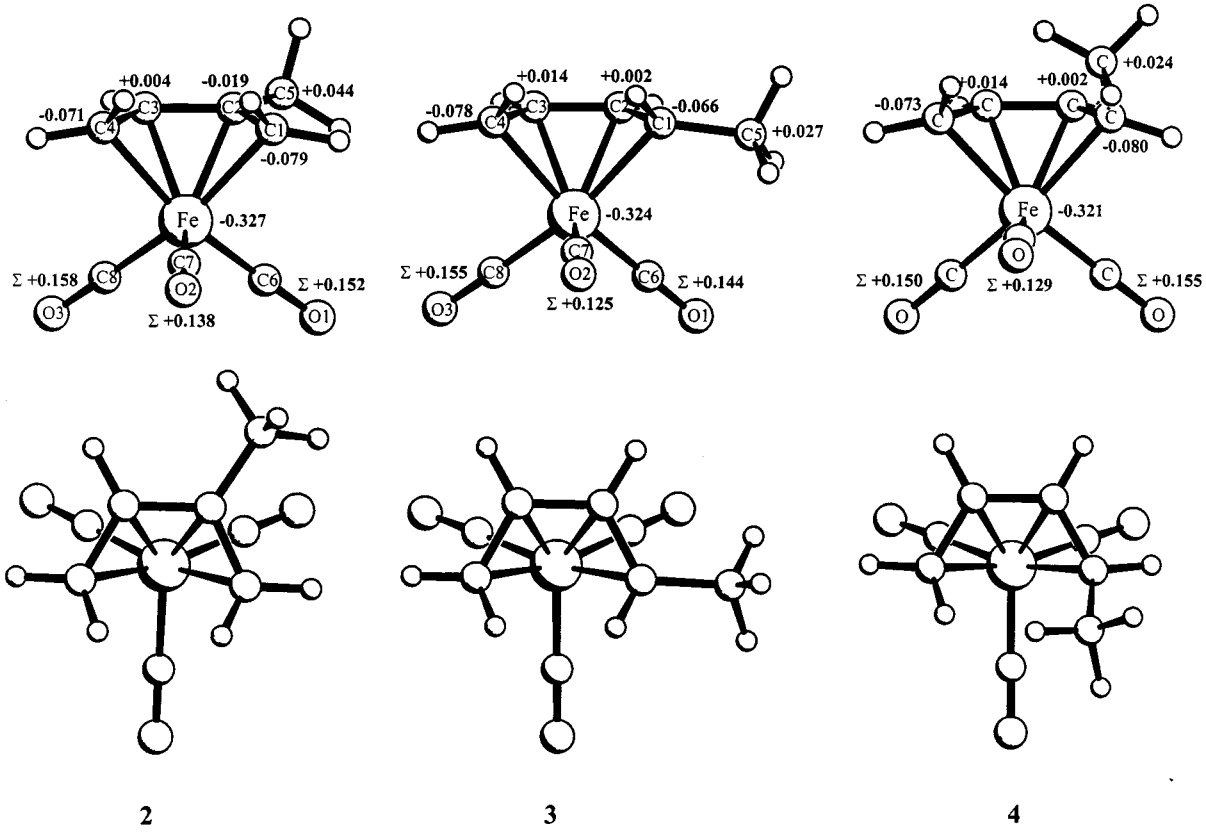


Figure 1. Ground-state structures of the neutral methylbutadiene complexes **2**, **3** and **4**; the charges of the hydrogen atoms are summed into the carbon atoms

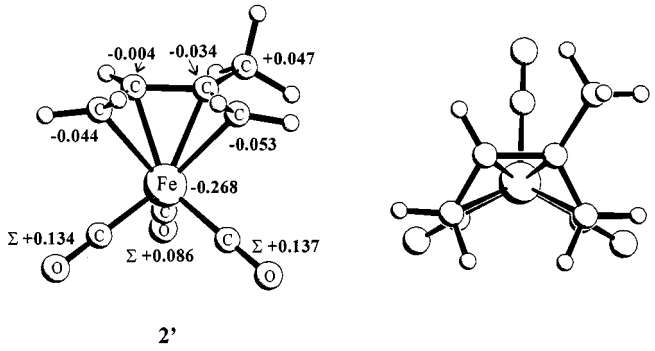
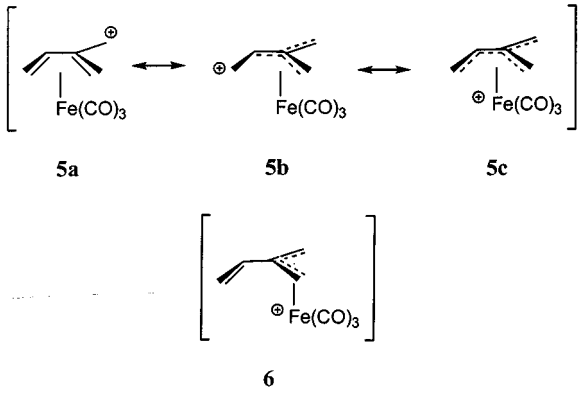


Figure 2. Calculated structure of the transition state (**2'**) for the rotation of the $Fe(CO)_3$ moiety in **2**



Scheme 2. Mesomeric structure of the cationic intermediates derived from the isoprene−$Fe(CO)_3$ complex **2**

charges of C and O). In all cases the CO group, which is pointing towards the open side of the butadiene ligand, carries the smallest positive charge. Therefore, the $Fe(CO)_3$ unit, which is characterized by total charges of at least +0.1 |e|, cannot be regarded as an electron-withdrawing group, in contrast to the metal fragment in arene−$Cr(CO)_3$ complexes,[7] where the $Cr(CO)_3$ moiety was negatively charged. Compared to C1 and C4, the inner carbon atoms (C2 and C3) have a slightly more positive partial charge. This is in accord with the experimental observation that under kinetic control the attack of nucleophiles occurs regioselectively at the inner carbon atoms.[16]

The geometrical parameters of the neutral complexes **2**, **3**, and **4** serve as a good indicator for the intepretation of the data obtained for the cationic, anionic and radical intermediates (see Table 1). The total energies and the zero point corrections for all calculated structures are collected in Table 2.

The Cationic C_5H_7−$Fe(CO)_3$ Complexes

Transformations of 1,3-diene−$Fe(CO)_3$ derivatives involving metal-stabilized cationic intermediates have been known for many years and have gained particular importance in organic syntheses.[1,2,17] Although some of the cationic intermediates have been characterized by spectroscopic methods,[18] data concerning structural and energetic features of these intermediates are very rare. At this point, modern theoretical methods open an ideal complementary avenue for obtaining far reaching insights into structural, energetical and, finally, mechanistic details of such species.

We commenced our investigation by first characterizing the cationic C_5H_7−$Fe(CO)_3^+$ complexes **5** and **6**, which were formally generated by abstraction of a hydride from the methyl group of the isoprene complex **2** (Scheme 2).

Our calculations suggest that only two minimum structures can be distinguished and these differ in the hapticity of the metal coordination. In the energetically most stable structure the metal coordinates to the ligand in an η^5 mode. This structure, which obeys the 18-valence electron (VE) rule, may be represented by the three mesomeric forms **5a**, **5b** and **5c** depicted in Scheme 2. The second structure, a formal 16 VE species that is energetically less favored by 7.4 kcal mol^{-1}, is perfectly described by formula **6**. In contrast to a previous picture based on a Frontier Orbital Analysis,[19] it is not possible to treat the two structures **5a** and **5b** as separate species. The calculated structures of species **5** and **6** are depicted in Figure 3 while the theoretically predicted bond lengths are collected in Table 1.

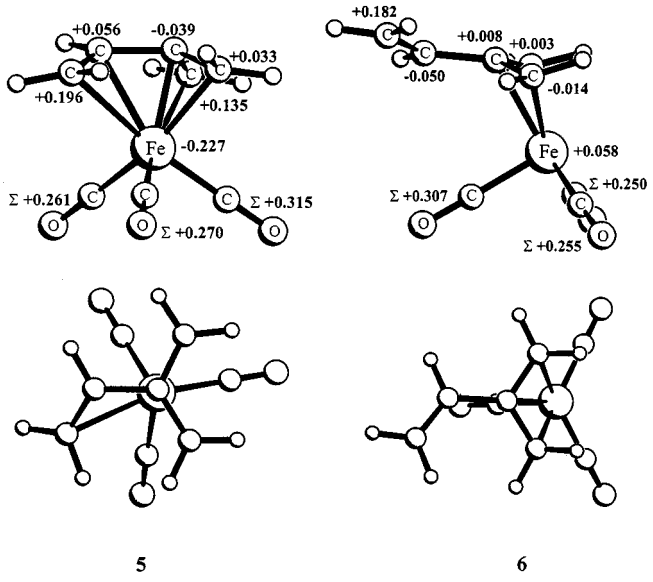


Figure 3. Structures of the two cationic complexes **5** and **6**

Compared to the neutral complex **2**, in structure **5** the iron tricarbonyl tripod has moved more closely to C2. This leads to a trimethylenemethane−$Fe(CO)_3$-type substructure involving the carbon atoms C1, C2, C3, and C5. As a result, the bond between Fe and C2 is shortened to 1.991 Å from 2.107 Å in **2** while C1, C3, and C4 have similar bond lengths to the iron (2.145, 2.197, and 2.266 Å, respectively). Whereas about 50% of the positive charge is localized on the metal carbonyl unit, in the organic ligand positive partial charges are mainly found at C4 (+0.196 |e|) and C5 (+0.135 |e|), a situation that is in accord with the mesomeric structures **5a** and **5b**. Taken together, all three meso-

meric structures seem to contribute, but **5c** is probably the best formal representation of the calculated structure. In the η^3-isomer **6** the iron is bonded to C1, C2, and C5. This structure can be considered as a cationic η^3-allyl−$Fe(CO)_3$ complex bearing a vinyl side-chain. Two features of this structure are especially remarkable: Firstly, about 80% of the positive charge is now transferred to the iron carbonyl moiety. Secondly, the most electron deficient carbon atom is C4 (+0.182 |e|), which has no interaction with the $Fe(CO)_3$ group. It is further worth noting that the preferred conformation of the $Fe(CO)_3$ tripod has changed from fully staggered in **5** to eclipsed in **6** (Figure 3). Because the C2−C3 bond (1.48 Å) in **6** is a single bond, rotation around this bond should be possible. This would lead to a racemization of the planar chiral structure (**6** → *ent*-**6**). Calculation of the transition state of this process resulted in a barrier of $\Delta H^{\#} = 5.4$ kcal mol^{-1}. As **6** is energetically only 7.4 kcal mol^{-1} above **5**, the overall energy barrier for the racemization of the η^5 structure **5** amounts to 12.8 kcal mol^{-1}. This translates into a half life for **5** of ca. 10^{-3} s at 0°C and of ca. 14 s at −78°C.[20] The energy profile of the racemization of **5** is depicted in Figure 4.

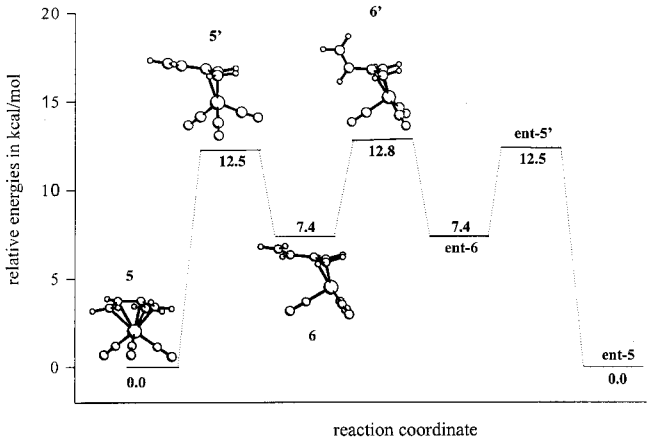
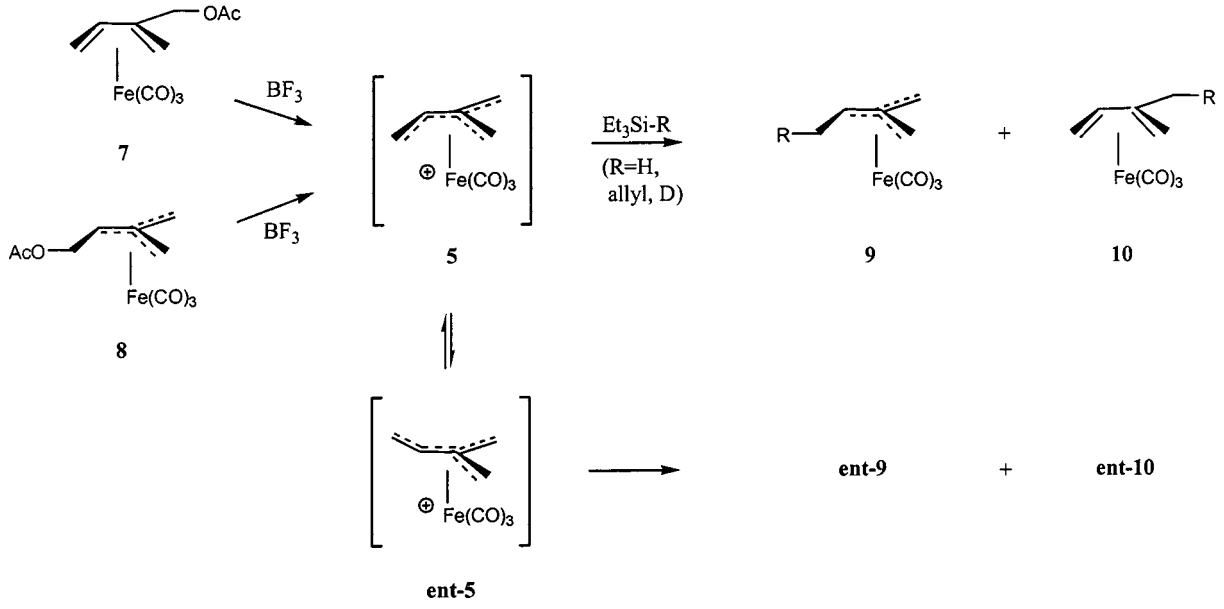


Figure 4. Energy profile of the racemization of **5** to *ent*-**5**

These results are in very good agreement with the qualitative picture that was derived by Gerlach,[21] Donaldson,[22] and Franck-Neumann[23] from experimental studies. These authors had shown that the intermediate cations **5**, generated from precursors **7** or **8** in the presence of Lewis acids, undergo reaction with (soft) nucleophiles to afford mixtures of products **9** and **10** (Scheme 3). The predominant formation of trimethylenemethane complexes **9** under kinetically-controlled conditions shows that the nucleophilic attack occurs preferentially at C4. This regioselectivity correlates nicely with the calculated partial charges in the intermediate **5** (Figure 3). The rather low barrier of racemization discussed above is also in good agreement with the experimental fact that a high degree of stereospecificity (retention of absolute stereochemical information) is only achieved when the reactions are performed at low temperatures (−78°C).[21]

The chemistry discussed above is often complicated by facile proton-catalyzed isomerization of **9** to **10**.[19−21] It was therefore interesting to calculate the relative energies of these two species (for R = H). The calculated structure (Figure 5) of the parent methyl-substituted trimethylenemethane (TMM)[24] complex **9** (R = H) reveals the expected coordination mode of the iron fragment to the ligand. This structure is in excellent agreement with X-ray crystal structures of TMM−$Fe(CO)_3$ derivatives. The maximum deviation of the bond lengths amounts to 0.03 Å and, in particular, the distances between iron and the TMM ligand are very well represented with deviations less than 0.02 Å.[25] In order to achieve a stronger coordination to the metal, the central carbon atom (C2) of the ligand is no longer planar but significantly pyramidalized ("umbrella-like").



Scheme 3. S_N1 reaction of substituted isoprene−$Fe(CO)_3$ complexes involving intermediates of type **5**

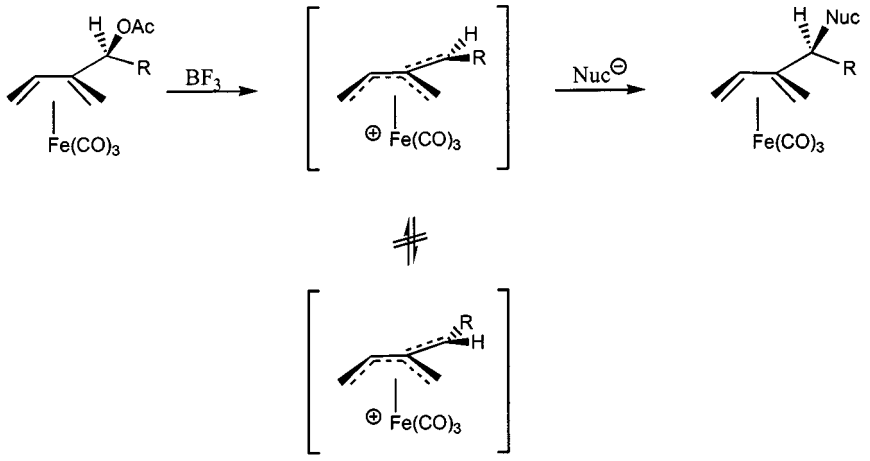
Table 1. Bond lengths for the complexes **2**–**24** in Å

	2	**2′**	**3**	**4**	**5**	**5ts**	**6**	**9**	**11**	**12**	**13**	**14**	**15**
C1–C2	1.436	1.423	1.428	1.442	1.428	1.475	1.437	1.436	1.476	1.430	1.493	1.496	1.437
C2–C3	1.423	1.439	1.422	1.420	1.474	1.427	1.478	1.438	1.411	1.430	1.412	1.475	1.468
C3–C4	1.434	1.421	1.433	1.433	1.377	1.411	1.353	1.514	1.430	1.408	1.425	1.432	1.354
C1–C5	–	–	1.515	1.525	–	–	1.432	–	1.367	1.407	1.345	–	–
C2–C5	1.511	1.511	–	–	1.414	1.425	–	1.439	–	–	–	1.359	1.442
Fe–C1	2.119	2.176	2.167	2.150	2.145	2.159	2.095	2.138	2.257	2.161	2.358	2.122	2.119
Fe–C2	2.107	2.108	2.093	2.082	1.991	2.029	2.203	1.957	2.088	2.155	2.082	2.537	2.023
Fe–C3	2.083	2.084	2.075	2.090	2.197	2.114	3.287	2.171	2.141	2.161	2.125	2.097	3.006
Fe–C4	2.112	2.170	2.121	2.125	2.467	2.166	4.256	3.239	2.150	2.228	2.136	2.090	4.042
Fe–C5	3.249	3.241	3.276	3.234	2.266	2.200	2.096	2.123	2.712	2.228	3.604	3.751	2.097
Fe–C6	1.798	1.793	1.797	1.798	1.818	1.830	1.837	1.798	1.852	1.839	1.865	1.777	1.775
Fe–C7	1.788	1.771	1.786	1.803	1.831	1.744	1.786	1.797	1.836	1.817	1.846	1.771	1.766
Fe–C8	1.799	1.772	1.797	1.784	1.854	1.657	1.840	1.797	1.813	1.838	1.805	1.776	1.769
C6–O1	1.159	1.160	1.159	1.158	1.144	1.147	1.163	1.157	1.146	1.144	1.143	1.173	1.177
C7–O2	1.158	1.162	1.159	1.158	1.145	1.146	1.164	1.157	1.145	1.145	1.143	1.174	1.177
C8–O3	1.158	1.162	1.158	1.159	1.144	1.145	1.163	1.157	1.145	1.144	1.144	1.174	1.176

	16	**17**	**18**	**19**	**20**	**21**	**22**	**23**	**24**
C1–C2	1.491	1.463	1.477	1.432	1.462	1.423	1.472	1.414	1.481
C2–C3	1.402	1.434	1.437	1.468	1.450	1.483	1.415	1.476	1.419
C3–C4	1.359	1.432	1.430	1.354	1.411	1.347	1.422	1.347	1.417
C1–C5	–	1.356	1.354	1.429	–	–	1.351	1.414	1.349
C2–C5	1.364	–	–	–	1.407	1.421	–	–	–
Fe–C1	2.088	3.048	3.091	2.033	2.089	2.150	2.889	2.115	2.911
Fe–C2	2.828	2.186	2.150	2.187	2.189	2.081	2.204	2.182	2.172
Fe–C3	3.369	2.023	2.032	3.248	2.122	2.939	2.094	3.272	2.100
Fe–C4	3.396	2.122	2.130	4.056	2.184	3.911	2.126	4.205	2.144
Fe–C5	3.775	4.184	4.014	2.124	3.223	2.160	3.932	2.132	3.738
Fe–C6	1.759	1.764	1.765	1.780	1.807	1.845	1.801	1.800	1.801
Fe–C7	1.754	1.777	1.761	1.756	1.798	1.807	1.808	1.860	1.858
Fe–C8	1.765	1.760	1.781	1.779	1.809	1.805	1.847	1.804	1.804
C6–O1	1.180	1.177	1.179	1.178	1.157	1.157	1.158	1.159	1.159
C7–O2	1.182	1.177	1.179	1.179	1.158	1.158	1.159	1.157	1.158
C8–O3	1.177	1.179	1.176	1.176	1.158	1.159	1.158	1.159	1.158

The $Fe(CO)_3$ tripod prefers the fully staggered conformation. Compared to **10** (R = H; i.e. **2**), the isomer **9** (R = H) is less stable by 4.5 kcal mol^{-1}. This explains the almost complete disappearance of **9** in the equilibrium.

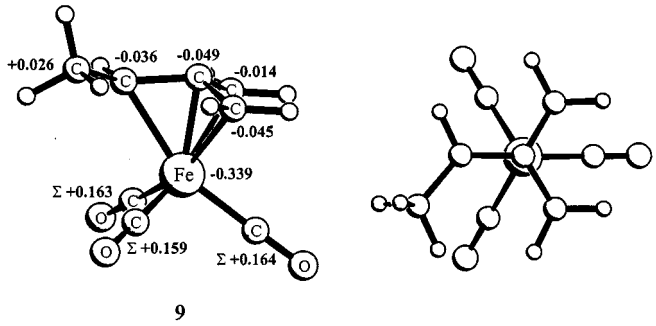
Another important point is the configurational stability of the intermediates of type **5** during S_N1-type transformations at C5 in the case of substituted substrates, which proceed with retention of configuration (Scheme 4).[21] This is reflected by our quantum chemical calculations, which predict a very high barrier of 44.2 kcal mol^{-1} for the rotation around the C2–C5 bond in the parent model compound **5**. In the transition structure **5ts** the positive charge is mostly localized at C5 and cannot be stabilized by interaction with the iron atom due to the orthogonal orientation of the formally empty p-orbital and the correspondingly vanishing overlap of C5 with potential donor orbitals from the metal.



Scheme 4. Retention of configuration in S_N1 transformations

Table 2. Total energies and zero point energy correction (ZPE) for structures **2**−**24**

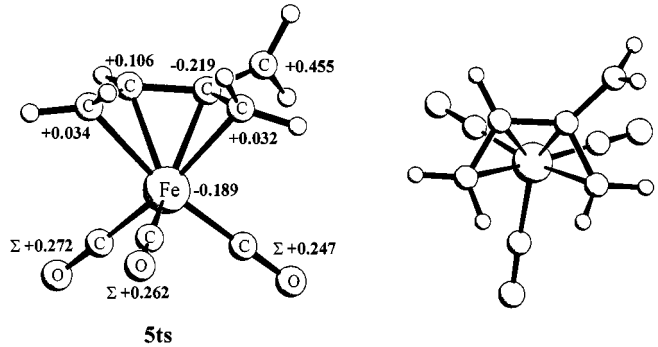
	Total energies [Hartree]	ZPE [kcal mol^{-1}]
2	−1799.16467	89.3
2′	−1799.14649	89.0
3	−1799.16123	89.4
4	−1799.15141	89.5
5	−1798.28055	82.6
5′	−1798.08107	81.0
5ts	−1798.20612	80.1
6	−1798.26669	81.3
6′	−1798.07915	80.8
9	−1799.15757	89.4
11	−1798.27904	82.4
11ts	−1798.20070	79.1
12	−1798.29514	83.3
13	−1798.25954	81.1
14	−1798.57893	80.3
14ts	−1798.51141	78.1
15	−1798.59358	80.4
16	−1798.553277	79.7
17	−1798.59183	80.4
17ts	−1798.50744	78.7
18	−1798.58556	80.4
19	−1798.58831	80.2
20	−1798.51056	80.5
20ts	−1798.45038	76.8
21	−1798.52934	80.8
22	−1798.53662	80.9
22ts	−1798.48923	79.8
23	−1798.52441	81.0
24	−1798.52695	80.7



9

Figure 5. Structure of the neutral trimethylenemethane complex **9**

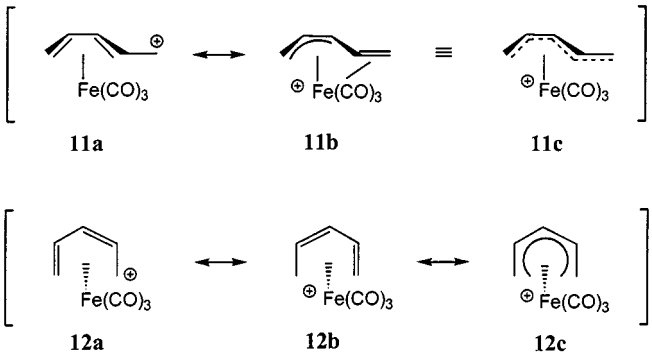
Because of this lack of interaction between the iron and the positive center C5, the transition structure **5ts** contains an almost undistorted diene−$Fe(CO)_3$ unit.



5ts

Figure 6. Transition state (**5ts**) for the rotation of the $C5H_2$ group around the bond between C2 and C5

A second system, namely the cationic pentadienyl $Fe(CO)_3$ complexes, was also investigated. These species (**11** and **12**) formally result from abstraction of a hydride ion (H^-) from the methyl group of the neutral diene−$Fe(CO)_3$ complexes **3** and **4**, respectively (Scheme 5). Possible representations of the two configurational isomers **11** and **12** are shown in Scheme 5.



Scheme 5. Mesomeric forms of the cationic intermediates **11** and **12**

Our computational investigation of **11** and **12** led to the two minimum structures shown in Figure 7.[12] The calculated geometry of **11** indicates an η^4 coordination mode with an additional attractive interaction between Fe and C5. This becomes evident in a strong bending of C5 towards the metal. The clear double bond character of the C1−C5 bond (1.37 Å) emphasizes the contribution of the mesomeric form **11b**. About 50% of the positive charge is transferred to the $Fe(CO)_3$ group as expressed by formulae **11b** and **11c**. On the other hand, structure **11a** mirrors the charge distribution of the ligand. As expected, the calculated structure of complex **12** exhibits C_s symmetry with the organic ligand forming a totally delocalized π-system. The C−C bond lengths in the pentadienyl ligand are all in the same range of ca. 1.4 Å, which fits well with the experimental data of an X-ray diffraction analysis of [(2,4-dimethylpentadienyl)$Fe(CO)_3$]BF_4.[6] The $Fe(CO)_3$ tripod interacts with the pentadienyl ligand in an η^5-manner, which is also in full agreement with NMR spectroscopic results.[18a] All carbon atoms of the ligand in **12** have a similar, slightly positive, partial charge. Structure **12** is computed to be more stable than **11** by 9.2 kcal mol^{-1}.

The facile (reversible) isomerization of intermediates of type **11** to the more stable horseshoe isomers of type **12** is a well established experimental fact that has often been exploited in selective synthesis.[26] In this case an experimental value for the barrier of isomerization was available[27] and we therefore considered this system as being an ideal touchstone for the accuracy of our computational methodology. The isomerization of **11** to **12** can formally be regarded as a rotation around the C2−C3 bond. Our calculations predict an activation energy for this process, connected with the transition structure **13**, of 11.0 kcal mol^{-1} above that of **11**. In Figure 8 the energy profile for this process is displayed. The experimental value of 13 kcal mol^{-1} found by Sorensen et al. for the barrier of isomeriz-

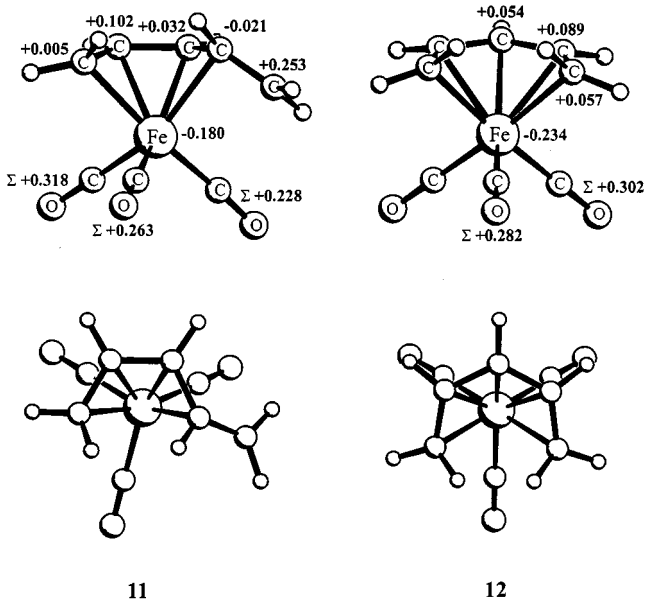


Figure 7. Structures of the cationic pentadienyl−Fe(CO)$_3$ complexes **11** and **12**

ation is therefore in very good agreement with the computed barrier.[27]

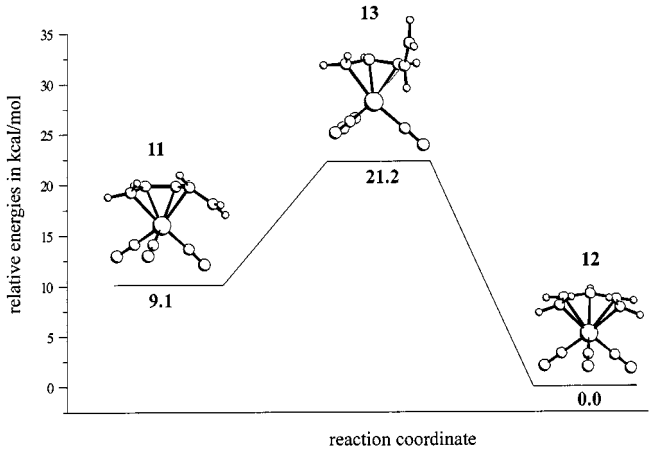


Figure 8. Energy profile for the isomerization of complexes **11** and **12**

Analysis of the transition state structure **13** clearly shows only an η^3 coordination of the iron fragment to the ligand. This structure is a 16 VE cationic η^3 allyl complex in which the vinyl substituent is turned to the opposite side of the metal fragment by about 90° around the C2−C3 bond. It is interesting to note that all our attempts failed to locate the transition state structure for this rotation in the neutral complexes **3** and **4**. The reason for the much higher rotational barrier for the interconversion of these isomers is probably that any η^3 bonded intermediate (transition state) would correspond to a disfavored zwitterionic or diradical species.

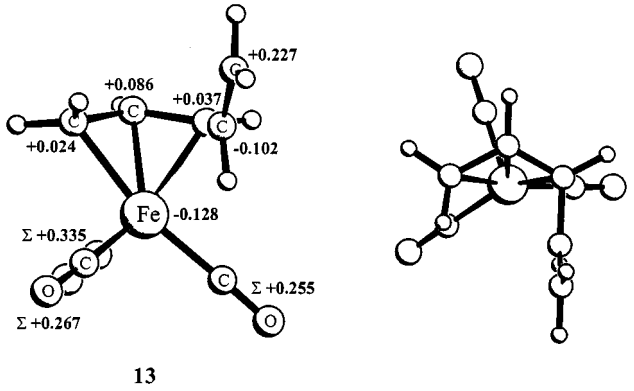
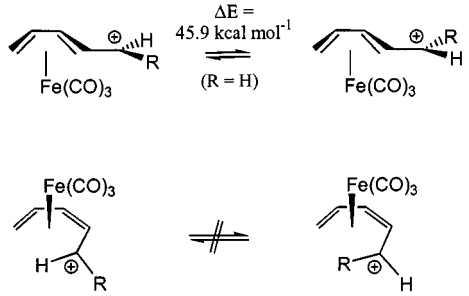


Figure 9. Structure of the transition state **13**, which is passed during the isomerization process shown in Figure 8

From the point of view of the synthetic chemist it is highly useful that S_N1-type reactions in the allylic position (at C5) of 1,3-pentadiene−Fe(CO)$_3$ complexes proceed with virtually complete retention of configuration.[28] We were interested to see if our calculations could quantify the obvious configurational stability of the cationic intermediates. In the case of the pentadienyl cation **11** we were able to determine a rotational barrier of 45.9 kcal mol^{-1} (Scheme 6). The corresponding transition structure **11ts** is depicted in Figure 10. In contrast, the transition state for the corresponding isomerization of **12** could not be localized. This indicates a very strong stabilization of the U-shaped pentadienyl cation by η^5-coordination to the metal. Therefore, the energy barrier for the rotation of a terminal CH_2 group in **12** should be extremely high and isomerization is not likely to take place.



Scheme 6. Rotation of the C5H$_2$ group around the bond between C1 and C2 of the cationic complexes **11** and **12**

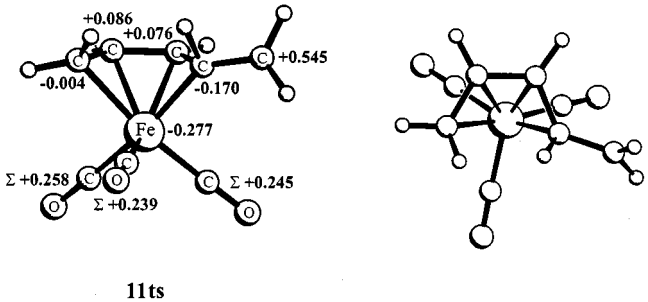


Figure 10. Transition structure **11ts** for the rotation of the C5H$_2$ group around the bond between C1 and C2 of the cationic complex **11**

The Anionic $C_5H_7-Fe(CO)_3$ Complexes

Compared to the cationic complexes discussed above, very little has been reported about the corresponding anionic iron complexes. While a few reactions involving such intermediates have been described,[3] virtually nothing is known about their geometry and electronic structures.

Firstly, we will present our results concerning the anionic system arising from proton abstraction from the methyl group of the isoprene complex **2**. The calculations revealed the two minimum structures **14** and **15** depicted in Figure 11. Both species formally count 18 VE and may be represented by two resonance formulae according to Scheme 7.

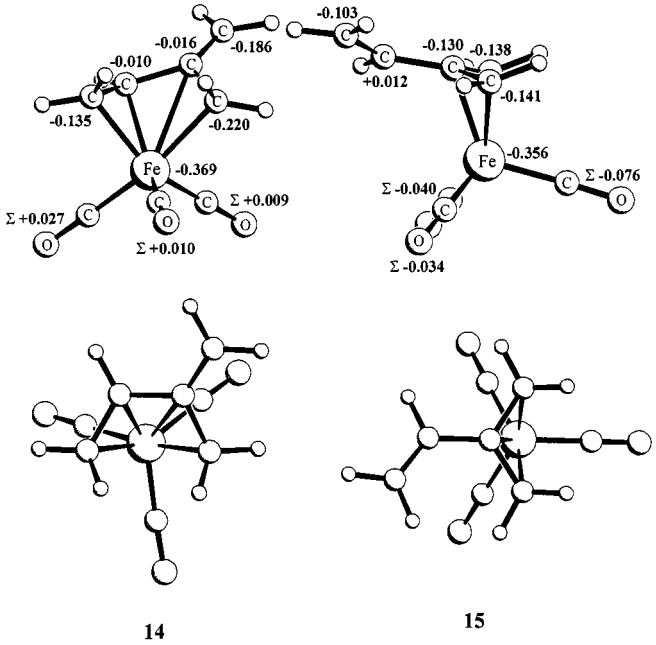
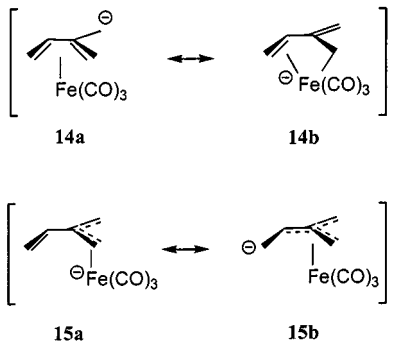


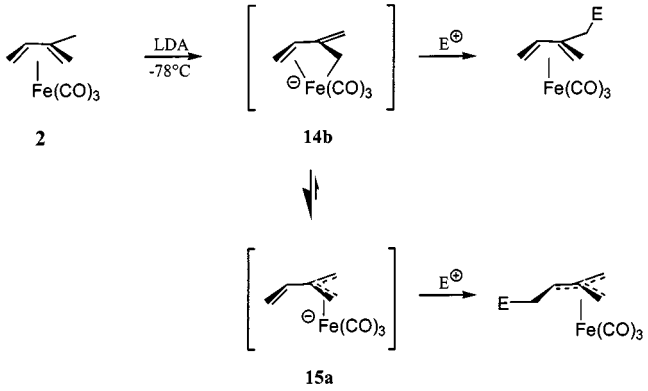
Figure 11. Structures of the anionic complexes **14** and **15**



Scheme 7. Mesomeric forms of the anionic complexes **14** and **15** derived from the isoprene−$Fe(CO)_3$ complex **2**

In structure **14** the deprotonated center (C5) has no contact with the iron. The C2−C5 bond has clear double bond character (bond length 1.36 Å) and is bent away to the opposite side of the $Fe(CO)_3$ moiety. The short Fe−C1 distance (2.12 Å) and a negative partial charge of −0.323 |e| of the $Fe(CO)_3$ fragment also indicate that **14b** is a better representation of this species than **14a**. In contrast to **14**, in the isomeric species **15** there is a strong interaction between the iron and C5. In fact, **15** is best regarded as a vinyl-substituted η^3-allyl complex as expressed by formula **15a**. Here the iron tricarbonyl group takes over 50% of the negative charge. It is interesting to note that this isomer is more stable than **14** by 9.2 kcal mol^{-1}. It is clear that the anionic intermediate prefers an η^3-allyl coordination mode (**15**) where more negative charge can be transferred to the metal fragment than in the mixed π/σ bonding in **14**. This is in accordance with the experimental observation that species **14**, which is initially formed through deprotonation of **2** at low temperatures, rearranges to a more stable isomer (**15**) on warming. While **14** gives 2-substituted butadiene−$Fe(CO)_3$ derivatives on reaction with electrophiles, **15** gives rise to TMM-type products (Scheme 8).[3a]

One should note that this situation is contrary to the one found for the cationic complexes **5** and **6**, where structure **5** is energetically more favored. However, this can easily be understood in terms of the 18-electron rule.



Scheme 8. Deprotonation reaction of the isoprene−$Fe(CO)_3$ complex **2** involving the anionic intermediates **14** and **15**, respectively

In order to gain a better understanding of this chemistry, the transition state for the interconversion of **14** to **15** was calculated. The relative energy of the resulting transition structure **16** was found to lie 15.4 kcal mol^{-1} above **14** and 24.6 kcal mol^{-1} above **15**. The energy profile for this process is shown in Figure 12.

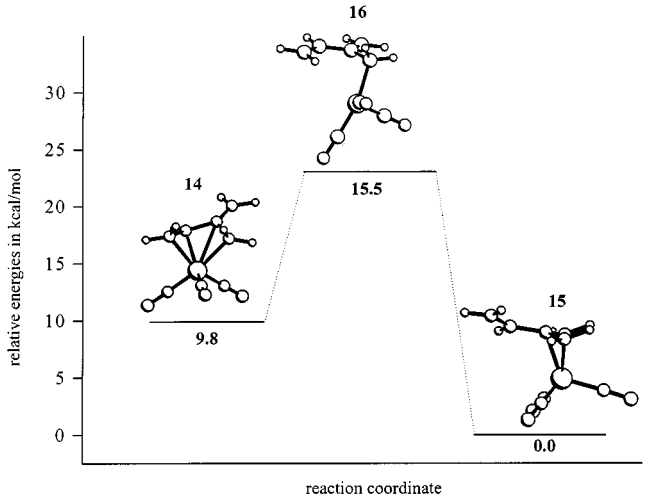
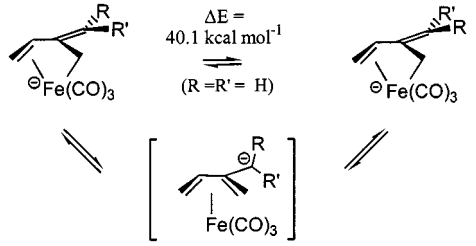


Figure 12. Energy profile for the isomerization of **14** and **15**

We further addressed the question as to whether a deprotonation/alkylation sequence at C5 of 5-substituted derivatives of **2** would proceed with stereochemical retention or not. In order to estimate the configurational stability of the corresponding intermediates, the barrier for the rotation around the C2−C5 bond in **14** was computed. A value of 40.1 kcal mol^{-1} was obtained and this shows that no isomerization should occur under common reaction conditions (Scheme 9). The high rotational barrier results from the fact that in the transition state the negative partial charge is not delocalized and is mainly located at C5 (−0.64 |e|) while the butadiene−$Fe(CO)_3$ substructure remains almost undisturbed.



Scheme 9. Rotation of the $C5H_2$ group around the bond between C2 and C5 of the anionic complex **14**

Very little has been reported about the generation and reactivity of the anionic pentadienyl $Fe(CO)_3$ complexes **17** and **18**.[29] Therefore, it is particularly interesting to look at the results of the optimized structures of these species (Figure 13).

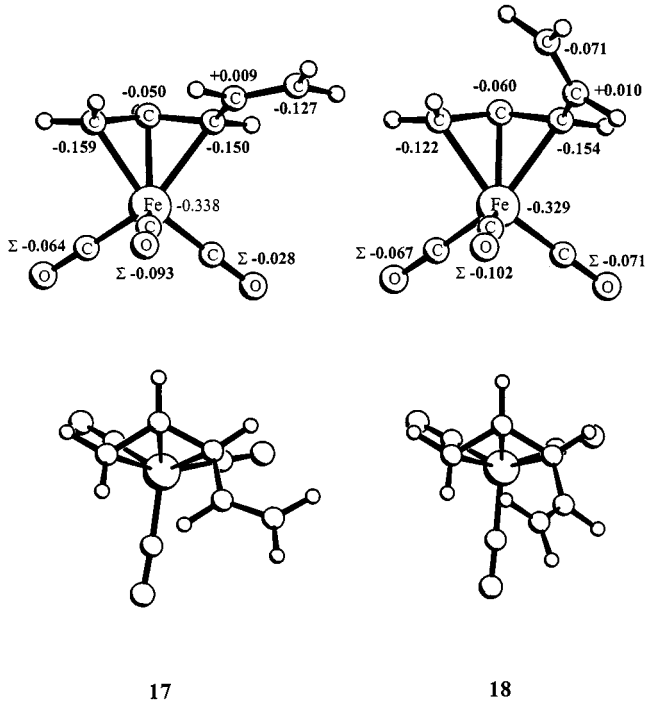
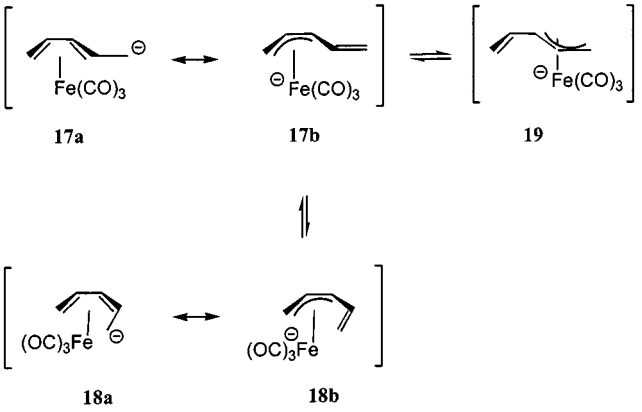


Figure 13. Structures of the anionic complexes **17** and **18**

In both isomers, **17** and **18**, the bond between C1 and C5 is characterized as a double bond with bond lengths of 1.356 Å and 1.354 Å, respectively. The iron is η^3-bonded to the pentadienyl ligand and the C_3H_4−$Fe(CO)_3$ substructure has a local mirror symmetry with one CO group, the iron atom and C3 lying in the mirror plane. The three carbon atoms C2, C3, and C4 assume a delocalized π-allyl system with C−C bond lengths of 1.43 Å. The two anionic complexes **17** and **18** can be considered as being conformers by rotation around the C1−C2 single bond. It is important to note that **17** is more stable than the sterically congested isomer **18** by 5.6 kcal mol^{-1}. These results can be described in terms of the mesomeric structures depicted in Scheme 10.



Scheme 10. Mesomeric forms of the anionic pentadienyl−$Fe(CO)_3$ complexes **17** and **18**

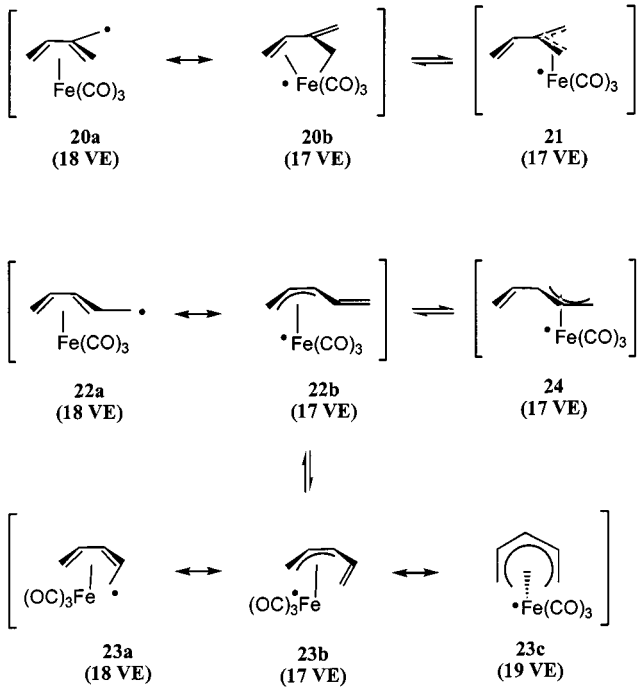
In accordance with the structural features discussed above, formulae **17b** and **18b** are unambiguously the better representations of these anionic intermediates. This becomes especially apparent by looking at the geometrical details (η^3 bonding mode) and the electron density distribution that is characterized by accumulating more than one half of the negative charge at the $Fe(CO)_3$ group. It should be briefly mentioned that the configurational stability at the deprotonated center in **17** is very high ($\Delta E^{\ddagger} = 52.9$ kcal mol^{-1}) due to similar reasons as in the case of **14**. We also investigated the isomer **19**, a species that could possibly arise from **17** by haptotropic rearrangement of the metal fragment (Scheme 10). It was found that **19** is disfavored energetically by 3.7 kcal mol^{-1} compared to **17**. This suggests that, if anyone were to succeed in selectively deprotonating **3** at C5, the products of a subsequent reaction with an electrophile will be governed by the reactivity of the (most stable) anionic intermediate **17**. From the theoretical point of view there is no reason why this kind of transformation should not be feasible.

The Radical C_5H_7−$Fe(CO)_3$ Complex

To the best of our knowledge, very few radical reactions of butadiene $Fe(CO)_3$ complexes have ever been described.[30] Therefore, the investigation of possible radical intermediates with theoretical methods could help to evaluate potential preparative opportunities.

We will begin with a discussion of the radical complex **20**, which is formally derived by abstracting a hydrogen

atom ($H^{\bullet}$) from the isoprene complex **2**. It is of interest to assess whether the unpaired electron is mainly located at C5 or delocalized to the $Fe(CO)_3$ moiety, corresponding to the mesomeric formulae **20a** and **20b**, respectively (Scheme 11). The calculated structure of this species (Figure 14) indicates that one third of the spin density is located at the iron and two thirds at C5. Regarding the geometry (the iron shows an η^4 bonding mode to the butadiene) as well as the fact that the main part of the spin density is located at C5, the mesomeric structure **20a** seems to be the better representation of this complex. On the other hand, the bond between C2 and C5 is shortened (1.407 Å) and part of the spin density is located at Fe, indicating a contribution of **20b** and suggesting an energetical barrier for the rotation around the C2−C5 bond. Indeed, a barrier of 11.3 kcal mol^{-1} was determined for this process.



Scheme 11. Mesomeric forms of the radical intermediates **20**−**24**

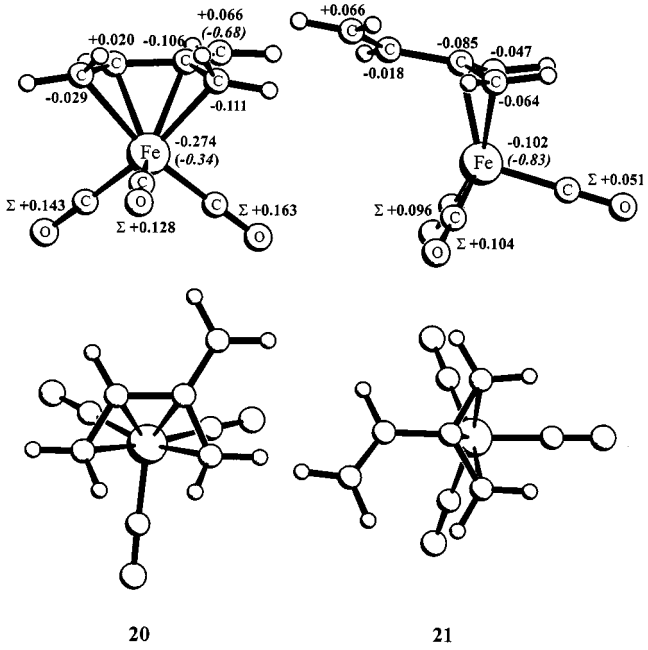


Figure 14. Structures of the radical complexes **20** and **21** formally derived by abstraction of a hydrogen atom from the neutral isoprene−$Fe(CO)_3$ complex **2**

Calculation of the isomeric structure **21** (Scheme 11) revealed that this isomer is energetically favored by 11.6 kcal mol^{-1} in comparison with **20**. In isomer **21** more than 80% of the spin density is localized at the iron center. Thus, it is not unlikely that trimethylenemethane derivatives with a substituent at C4 will be formed in reactions of such intermediates. The energetical difference between **20** and **21** is about 2 kcal mol^{-1} larger than that between the corresponding anionic complexes **14** and **15**, and it is therefore not improbable that a rapid isomerization of **20** to the more stable intermediate **21** will occur.

Finally, the radical pentadienyl complexes **22** and **23**, formally derived from **3** and **4**, respectively, will be discussed. These two species both show an η^3 bonding mode of the metal to the organic ligand (Figure 15) and a geometry akin to that of the anionic pentadienyl complexes **17** and **18**. In both complexes (**22** and **23**) the spin density is almost completely localized at the iron atom (−0.83 |e| and −0.86 |e|, respectively). Therefore, the mesomeric formulae **22b** and **23b** (Scheme 11) perfectly describe the calculated structures. These species can thus be considered as conformers. The calculations revealed an energetical difference of 7.7 kcal mol^{-1} with **22** being the more stable conformer. The interconversion of **22** and **23** by rotation of the vinyl group can easily take place as it is associated with only a small barrier (11.7 kcal mol^{-1} from **22** to **23** and 4.0 kcal mol^{-1} from **23** to **22**). For complex **22** another isomer (**24**) must be considered that, according to our calculations, is energetically 6.4 kcal mol^{-1} disfavored in comparison with **22**. One can expect that the haptotropic isomerization of **22** to **24** should easily take place. It is interesting to note that all these open shell systems prefer a 17 VE configuration at the iron. The (formal) 18 VE structures **22a/23a** and especially the (η^5) 19 VE structure **23c**[30b] do not describe these complexes well.

These results nicely reflect the experimental observation that radicals of type **22/23** react with CBr_4 at the iron to form η^3-allyl−$Fe(CO)_3Br$ complexes.[30b] On the other hand, the small contribution of the mesomeric formulae **22a/23a** provides some spin density at C5, which explains the formation of C5−C5 dimers.[30b,c] Calculation of the transition state for the rotation of the $C5H_2$ group in **22** predicts an energy barrier of 28.6 kcal mol^{-1} for this process. Although this barrier is not as high as in the corresponding cationic or anionic complexes (**11** and **17**, respectively), the configurational stability at C5 should be sufficiently high to allow stereospecific transformations in the case of C5-substituted derivatives.

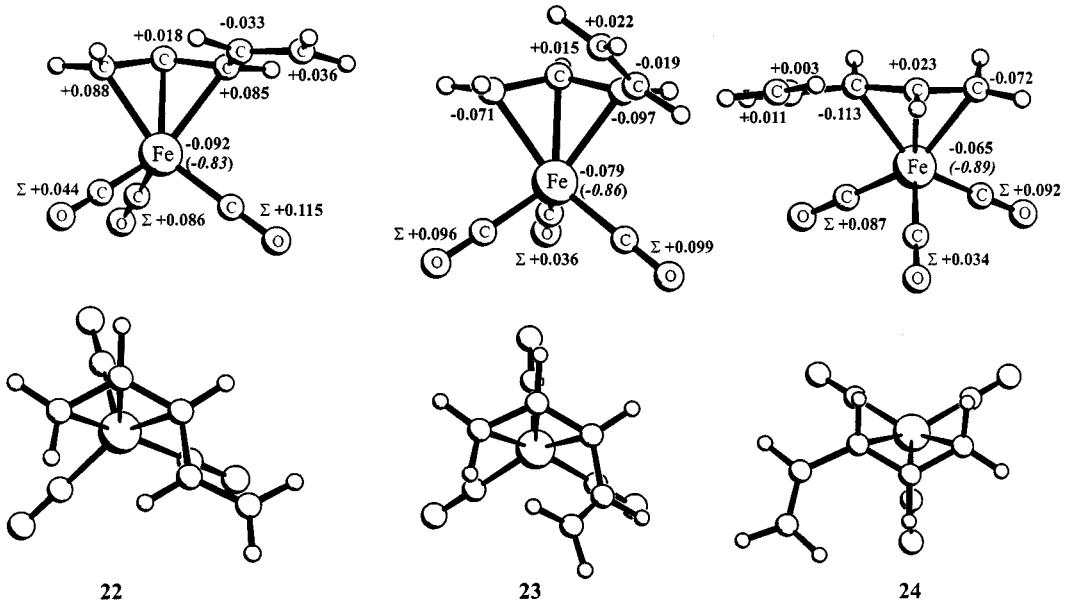


Figure 15. Structures of the radical complexes **22**, **23** and **24** formally derived by abstraction of an hydrogen atom from the neutral pentadiene−Fe(CO)$_3$ complexes **3** and **4**, respectively

Conclusions

The quantum chemical investigation of acyclic 1,3-diene−Fe(CO)$_3$ complexes and their cationic, anionic, and radical intermediates with density functional methods gives a very clear and precise picture of the structures and the reactivity of such species. The high accuracy of the calculations becomes obvious in the few cases where the comparison with experimental data is possible. The calculated structures are used as a reliable basis for the evaluation of possible resonance formulae and for the subtle interpretation of the electronic and conformational situation in the various intermediates. Furthermore, the calculation of energy barriers even permits the rationalization of dynamic phenomena such as isomerization (and racemization) processes. In particular, the calculations predict a pronounced configurational stability of the different intermediates, challenging experimental exploitation. All in all, our computational study provides new insights into the chemistry of acylic 1,3-diene−Fe(CO)$_3$ complexes and experimental facts now appear in a much more lucid light.

Supporting Information available: Lists with the *x*,*y*,*z* coordinates for all calculated structures reported in this paper.

Acknowledgments

This work was financially supported by the Deutsche Forschungsgemeinschaft and the Fonds der Chemischen Industrie. A generous amount of computer time and excellent service was provided by the Konrad-Zuse-Zentrum für Informationstechnik Berlin (Dr. T. Steinke) and the Zentraleinrichtung Rechenzentrum der TU Berlin.

[1] For selected recent reviews, see: [1a] R. Grée, *Synthesis* **1989**, 341. − [1b] A. J. Pearson, *Iron Compounds in Organic Synthesis*, Academic Press, London, **1994**. − [1c] R. Grée, J. P. Lellouche in: *Advances in Metal-Organic Chemistry*, vol. 4 (Ed.: L. S. Liebeskind), JAI Press, Greenwich, **1995**, pp. 129−273. − [1d] H.-J. Knölker in: *Transition Metals for Organic Synthesis*, vol. 1 (Eds.: M. Beller, C. Bolm), Wiley-VCH, Weinheim, **1998**, pp. 534−549.

[2] [2a] E. O. Fischer, R. D. Fischer, *Angew. Chem.* **1960**, *72*, 919. − [2b] N. A. Clinton, C. P. Lillya, *J. Am. Chem. Soc.* **1970**, *92*, 3065; for an excellent compilation of the literature on cationic dienyl−Fe(CO)$_3$ complexes, see ref.[1c]; see also refs.[18,19,21−28]

[3] [3a] M. F. Semmelhack, E. J. Fewkes, *Tetrahedron Lett.* **1987**, *28*, 1497. − [3b] M. Franck-Neumann, D. Martina, M.-P. Heitz, *J. Organomet. Chem.* **1986**, *315*, 59.

[4] For some recent applications in stereoselective total synthesis, see: [4a] W. R. Roush, C. K. Wada, *J. Am. Chem. Soc.* **1994**, *116*, 2151. − [4b] C. Iwata, Y. Takemoto, *J. Chem. Soc., Chem. Commun.* **1996**, 2497. − [4c] T. J. Benvegnu, R. Grée, *Tetrahedron* **1996**, *52*, 11821. − [4d] V. Prahlad, W. A. Donaldson, *Tetrahedron Lett.* **1996**, *37*, 9169. − [4e] J. T. Wasicak, R. A. Craig, R. Henry, B. Dasgupta, H. Li, W. A. Donaldson, *Tetrahedron* **1997**, *53*, 4185.

[5] For the X-ray crystallographic investigation of **1**, see: O. S. Mills, G. Robinson, *Acta Crystallogr.* **1963**, *16*, 758; for many other crystal structures of diene−Fe(CO)$_3$ complexes, see the Cambridge Structural Database.

[6] Even though a number of cationic pentadienyl−Fe(CO)$_3$ complexes have been isolated as crystalline solids (see ref.[2]), to the best of our knowledge only one X-ray crystal structure has been reported: A. L. Rheingold, B. S. Haggerty, H. Ma, R. D. Ernst, *Acta Crystallogr.* **1996**, *C52*, 1110.

[7] A. Pfletschinger, T. K. Dargel, J. W. Bats, H.-G. Schmalz, W. Koch, *Chem. Eur. J.* **1999**, *5*, 537.

[8] [8a] A. D. Becke, *J. Chem. Phys.* **1993**, *98*, 5648. − [8b] A. D. Becke, *J. Chem. Phys.* **1993**, *98*, 1372. − [8c] P. J. Stephens, F. J. Devlin, C. F. Chabalowski, M. J. Frisch, *J. Phys. Chem.* **1994**, *98*, 11623.

[9] A. J. H. Wachters, *J. Chem. Phys.* **1970**, *52*, 1033.

[10] *Gaussian 94*, Revision B.3: M. J. Frisch, G. W. Trucks, H. B. Schlegel, P. M. W. Gill, B. G. Johnson, M. A. Robb, J. R. Cheeseman, T. Keith, G. A. Peterson, J. A. Montgomery, K. Raghavachari, M. A. Al-Laham, V. G. Zakrzewski, J. V. Ortiz, J. B. Foresman, C. Y. Peng, P. Y. Ayala, W. Chen, M. W. Wong, J. L.

Andres, E. S. Replogle, R. Gomperts, R. L. Martin, D. J. Fox, J. S. Binkley, D. J. Defrees, J. Baker, J. P. Stewart, M. Head-Gordon, C. Gonzalez, J. A. Pople, Gaussian, Inc., Pittsburgh, PA, **1995**.

[11] [11a] A. E. Reed, L. A. Curtiss, F. Weinhold, *Chem. Rev.* **1988**, *88*, 899. – [11b] E. D. Glendening, A. E. Reed, J. E. Carpenter, F. Weinhold, *NBO Version 3.1*.

[12] For a list of bond lengths, see Table 1; for further structural details, see supporting information.

[13] [13a] M. Bühl, O. L. Malkina, V. G. Malkin, *Helv. Chim. Acta.* **1996**, *79*, 742. – [13b] O. Gonzales-Blanco, V. Branchadell, *Organometallics* **1997**, *16*, 475; for a recent DFT study on some neutral substituted butadiene–$Fe(CO)_3$ complexes, see: O. Gonzales-Blanco, V. Branchadell, R. Grée, *Chem. Eur. J.* **1999**, *5*, 1722.

[14] S. G. Kukolich, M. A. Roehrig, D. W. Wallace, G. L. Henderson, *J. Am. Chem. Soc.* **1993**, *115*, 2021.

[15] [15a] The calculation of the rotanional barrier of **1** using the same computational approach gave a comparable value (11.1 kcal mol^{-1}), which is also significantly higher than that found by Gonzales-Blanco and Branchadell[13b] (9.6 kcal mol^{-1}) and that (7.2 kcal mol^{-1}) obtained by: T. A. Albright, R. Hoffmann, P. Hoffmann, *J. Am. Chem. Soc.* **1977**, *99*, 7546. – [15b] For an experimental value, see: D. Leibfritz, H. tom Dieck, *J. Organomet. Chem.* **1976**, *105*, 255.

[16] [16a] M. F. Semmelhack, J. W. Herndon, *Organometallics* **1983**, *2*, 363. – [16b] M. F. Semmelhack, J. W. Herndon, J. K. Liu, *Organometallics* **1983**, *2*, 1885. – [16c] M. F. Semmelhack, H. T. M. Le, *J. Am. Chem. Soc.* **1984**, *106*, 2715. – [16d] M. F. Semmelhack, H. T. M. Le, *J. Am. Chem. Soc.* **1985**, *107*, 1455. – [16e] M.-C. P. Yeh, B.-A. Sheu, H.-W. Fu, S.-I. Tau, L.-W. Chuang, *J. Am. Chem. Soc.* **1993**, *157*, 5941.

[17] See, for instance: C. Quirosa-Guillou, J.-P. Lellouche, *J. Org. Chem.* **1994**, *59*, 4693.

[18] [18a] J. E. Mahler, R. Pettit, *J. Am. Chem. Soc.* **1963**, 85, 3955. – [18b] J. E. Mahler, R. Pettit, *J. Am. Chem. Soc.* **1963**, 85, 3959. – [18c] P. A. Dobosh, D. G. Gresham, D. J. Kowalski, C. P. Lillya, E. S. Magyar, *Inorg. Chem.* **1978**, *17*, 1775.

[19] B. R. Bonazza, C. P. Lillya, *J. Am. Chem. Soc.* **1974**, 96, 2298.

[20] E. L. Eliel, S. H. Wilen, *Stereochemistry of Organic Compounds*, Wiley, New York **1994**, p. 426.

[21] [21a] D. Kappes, H. Gerlach, P. Zbinden, M. Dobler, W. A. König, R. Krebber, G. Wenz, *Angew. Chem.* **1989**, *101*, 1744; *ibid. Int. Ed. Engl.* **1989**, *28*, 1657. – [21b] D. Kappes, H. Gerlach, P. Zbinden, M. Dobler, *Helv. Chim. Acta* **1990**, *73*, 2136.

[22] W. A. Donaldson, M. A. Hossain, *Tetrahedron Lett.* **1991**, *32*, 7047.

[23] M. Franck-Neumann, A. Kastler, P.-J. Colson, *Tetrahedron Lett.* **1991**, *32*, 7051.

[24] [24a] G. F. Emerson, K. Ehrlich, W. P. Giering, P. C. Lauterbur, *J. Am. Chem. Soc.* **1966**, *88*, 3172. – [24b] K. Ehrlich, G. F. Emerson, *J. Am. Chem. Soc.* **1972**, *94*, 2464; for a review, see: [24c] M. D. Jones, R. D. W. Kemmit, *Adv. Organomet. Chem.* **1987**, *27*, 279.

[25] [25a] M. R. Churchill, K. Gold, *Inorg. Chem.* **1969**, *8*, 401. – [25b] A. Allmenninghen, A. Haaland, K. Wahl, *Act. Chem. Scand.* **1969**, *23*, 1145.

[26] [26a] C. Tao, W. A. Donaldson, *J. Org. Chem.* **1993**, *58*, 2134. – [26b] W. A. Donaldson, M.-J. Jin, P. T. Bell, *Organometallics* **1993**, *12*, 1174. – [26c] W. A. Donaldson, L. Shang, R. D. Rogers, *Organometallics* **1994**, *13*, 6.

[27] One should, however, be aware that the barrier of isomerization has been determined only for 1,5,5-trimethyl-substituted derivatives of **11** and **12**: T. S. Sorenson, C. R. Jablonski, *J. Organomet. Chem.* **1970**, *25*, C62.

[28] [28a] M. Uemura, T. Minami, Y. Yamashita, K.-i. Hiyoshi, Y. Hayashi, *Tetrahedron Lett.* **1987**, *28*, 641. – [28b] E. Heßler, H.-G. Schmalz, G. Dürner, *Tetrahedron Lett.* **1994**, *35*, 4547.

[29] Only some cases where the anions are stabilized by additional functional groups have been reported: [29a] A. Salzer, A. Hafner, *Helv. Chim. Acta* **1983**, *66*, 1774. – [29b] A. Hafner, W. von Philipsborn, A. Salzer, *Angew. Chem.* **1985**, *97*, 136; *Angew. Chem. Int. Ed. Engl.* **1985**, *24*, 126.

[30] [30a] D. Astruc, *Electron Transfer and Radical Processes in Transition Metal Chemistry*, VCH, Weinheim, **1995**. – [30b] R. E. Lehmann, J. K. Kochi, *Organometallics* **1991**, *10*, 190. – [30c] C. Zou, K. J. Ahmed, M. S. Wrighton, *J. Am. Chem. Soc.* **1989**, *111*, 1133.

Received April 26, 1999
[I99146]

Organometallic Complexes of Multianionic Phosphazenates

Gavin T. Lawson,[a] Chacko Jacob,[a] and Alexander Steiner*[a]

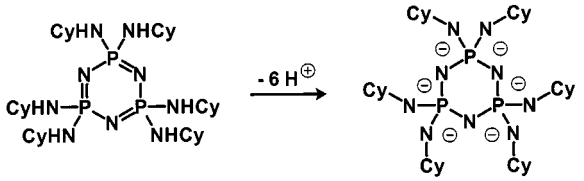
Keywords: Phosphazenes / Phosphazenates / Aluminium / Zinc / Multianionic ligands

The amino-substituted phosphazene $P_3N_3(NHCy)_6$ **1** reacts as a multiprotic acid undergoing full deprotonation in the presence of Me_3Al and Et_2Zn, respectively, which results in the formation of multinuclear metal phosphazenates: Trimethyl aluminium deprotonates **1** with evolution of six equivalents of methane to give the pentanuclear organoaluminium complex $[(thfMeAl)(Me_2Al)_4\{P_3N_3(NCy)_6\}]$ **2**. Diethylzinc deprotonates **1** yielding the hexanuclear zinc complex $[(EtZn)_6\{P_3N_3(NCy)_6\}]$ **3**. The higher homologue $P_4N_4(NHCy)_8$ **4** reacts with diethylzinc undergoing sixfold deprotonation giving the hexanuclear complex $[(EtZn)_6\{P_4N_4(NHCy)_2(NCy)_6\}]$ **5**, where two NH functions remain protonated. All three metal complexes **2**, **3** and **5** are soluble in aprotic organic solvents. The highly charged phosphazenate ligands contain three and four PN_4 tetrahedra which are fused in a corner-sharing manner forming P_3N_3 and P_4N_4 ring structures, respectively. These are isoelectronic with *meta*-silicate anions, but in addition equiped with organic groups at terminally arranged N atoms. Both phosphazenate ligands contain various coordination sites and show a high flexibility of their central P–N ring conformation toward the complexed organometallic framework.

Introduction

Metal complexes of multianionic ligand systems (X^{n-}, $n \geq 4$), which are soluble in aprotic organic solvents, are very rare, due to the high polarity of their salt-like structures. Deprotonated calixarenes[1] and porphyrinogens[2] as well as two examples of carbanionic derivatives[3][4] are among the few systems reported so far. Nevertheless, multianionic ligands of high solubility in aprotic organic solvents such as hydrocarbons or aliphatic ethers promise interesting applications in organometallic chemistry, in particular they facilitate multinuclear metal arrangements.

Recently we have shown that cyclic phosphazenes, which are substituted with primary amino groups, can act as multiprotic acids in the presence of strong organometallic bases yielding multianionic phosphazenates, a novel class of highly charged ligand systems (Scheme 1).[5] *n*-Butyllithium deprotonates $P_3N_3\{N(H)Cy\}_6$ (**1**) six times generating the dimeric complex $[(thf)_4Li_{12}\{P_3N_3(NCy)_6\}_2]$ (**1a**).[5a]



Scheme 1. Multiple deprotonation leading to the phosphazenate hexaanion $[P_3N_3(NCy)_6]^{6-}$

Although **1a** contains two phosphazenate hexaanions $[P_3N_3(NCy)_6]^{6-}$ and twelve lithium cations, it is soluble in hydrocarbons. In fact, $[P_3N_3(NCy)_6]^{6-}$ is the most highly charged anion reported so far, which forms an alkaline metal complex of high solubility in hydrocarbon solvents. Lithium cations are tightly bonded via N atoms to the central P_3N_9 core in **1a**. The peripherally arranged organic groups cover the complex with a lipophilic surface and provide solubility in nonpolar solvents. The central P_3N_3 ring in **1a** is puckered. In contrast, planar ring conformations are usually observed in neutral cyclotriphosphazenes.[6] P−N bond lengths are similar throughout the P_3N_9 core, whereas ring P−N bonds in neutral amino-substituted phosphazenes are usually considerably shorter than P−N bonds involving amino substituents, due to different bond order. Thus it can be assumed that in phosphazenates such as **1a** the negative charge is spread more or less equally over all nitrogen atoms. This is also indicated by the coordination behaviour of $[P_3N_3(NCy)_6]^{6-}$, where all N atoms are involved in coordination to metal centers. Phosphazenate anions are electronically related to silicate anions, which are well-known anionic frameworks in solid-state chemistry. The central P_3N_9 core in $[P_3N_3(NCy)_6]^{6-}$ is isoelectronic to the trimeric *meta*-silicate ion $[Si_3O_9]^{6-}$. In addition it is equiped with organic groups providing solubility in nonpolar media and thus facilitating organometallic chemistry in solution. In particular the generation of multinuclear metal complexes looks very promising due to the number of possible coordination sites and the formally multianionic nature of the ligands. In this paper we present our investigations regarding the coordination behaviour of phosphazenates in multinuclear organometallic complexes of aluminium and zinc.

Results and Discussion

We have treated $P_3N_3(NHCy)_6$ (**1**) with trimethylaluminium or diethylzinc. Both reactions were carried out in refluxing toluene and organometallic reagents were applied

[a] Department of Chemistry, University of Liverpool,
Crown Street, Liverpool L69 7ZD, UK
Fax: (internat.) + 44-151/794-3588
E-mail: A.Steiner@liv.ac.uk

 © WILEY-VCH Verlag GmbH, D-69451 Weinheim, 1999 1434−1948/99/1111−1881 $ 17.50+.50/0

in excess (1.2 equiv. per deprotonation step) to ensure high metalation grades. Gas evolution was observed in all cases and clear reaction solutions were obtained. Evaporation of the solvent gave colourless microcrystalline solids, which are thermally stable and show no sign of decomposition below 200°C. However, all obtained metal complexes are air and moisture sensitive and require handling in an inert gas atmosphere.

[(thfMeAl)(Me$_2$Al)$_4${P$_3$N$_3$(NCy)$_6$}] (2)

Complete deprotonation of **1** occurs in the presence of excess Me_3Al in toluene. The crude product of the reaction of **1** with Me_3Al was crystallised from a mixture of THF/n-hexane. X-ray structure analysis reveals the formation of the pentanuclear aluminium complex [(thfMeAl)(Me$_2$Al)$_4$-{P$_3$N$_3$(NCy)$_6$}] (**2**) (Figure 1).

$$\underset{\mathbf{1}}{P_3N_3(NHCy)_6} + 5\,Me_3Al \rightarrow \underset{\mathbf{2}}{[(thfMeAl)(Me_2Al)_4\{P_3N_3(NCy)_6\}]} + 6\,CH_4 \quad (1)$$

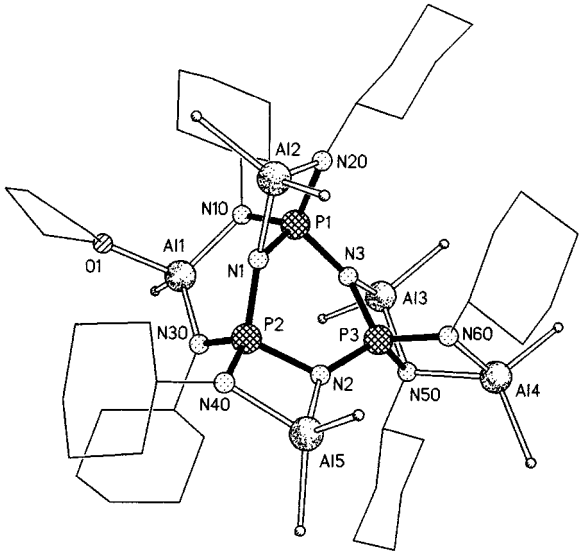


Figure 1. Crystal structure of **2**

Complex **2** contains four Me_2Al units and one MeAl unit which is further coordinated by one thf molecule. All five Al atoms have tetrahedral environments and are accommodated in bidentate chelating coordination sites at the centrally arranged phosphazenate core. Al atoms of Me_2Al units are coordinated by N−P−N chelates and thus part of four-membered Al−N−P−N ring systems, whereas the aluminium atom of the thfMeAl unit is part of a six-membered Al−N−P−N−P−N ring system. Al−N bond lengths to Me_2Al units are slightly longer (av. 1.95 Å) than Al−N lengths to the monomethyl-substituted Al atom (av. 1.86 Å) reflecting the relatively strong Al−N-bonds between the ligand and the formally dicationic MeAl unit. The N−Al−N angle at the AlMe unit is considerably wider [109.4(3)°] than at the Me_2Al units [av. 77.0(3)°] (see Table 1). All nitrogen atoms of the phosphazenate core are involved in coordination towards metal centers. Altogether

Table 1. Selected bond lengths [Å] and angles [°] for **2**

	bond length [Å]		bond length [Å]
P1−N3	1.665(6)	Al1−N10	1.857(6)
P1−N1	1.642(6)	Al1−N30	1.862(7)
P2−N1	1.630(6)	Al1−O1	1.917(6)
P2−N2	1.680(6)	Al2−N20	1.915(7)
P3−N2	1.621(6)	Al2−N1	1.974(6)
P3−N3	1.650(6)	Al3−N3	1.927(6)
P1−N10	1.640(7)	Al3−N50	2.014(7)
P1−N20	1.616(6)	Al4−N60	1.888(6)
P2−N30	1.654(6)	Al4−N50	2.041(7)
P2−N40	1.600(6)	Al5−N40	1.900(6)
P3−N50	1.708(6)	Al5−N2	1.969(6)
P3−N60	1.602(6)		
	bond angle [°]		
N3−P1−N1	106.8(3)		
N1−P2−N2	108.2(3)		
N2−P3−N3	107.5(3)		
N10−P1−N20	118.6(3)		
N30−P2−N40	116.2(3)		
N50−P3−N60	94.8(3)		
P1−N1−P2	116.6(3)		
P2−N2−P3	121.5(4)		
P3−N3−P1	127.0(4)		

the ligand shows three different coordination pattern in **2**, which are the bidentate chelates **A**, **B** and **C** referring to Scheme 2. Similar coordination pattern have been observed in other aluminium complexes containing P−N ligands, but in contrast to the pentanuclear complex **2**, they exclusively accommodate only one or two metal centers.[7]

The six-membered P−N ring system of the phosphazenate core shows a distorted boat conformation. As already observed in the structure of **1a** there is no marked distinction between terminal and ring P−N-bond lengths in **2** (see Table 1), with the exception of the rather long bond between P-3 and N-50 which is coordinating to two aluminium atoms. The P−N-stretching frequency of the phosphazenate ring in **2** (1079 cm^{-1}) is red-shifted compared to corresponding bands in IR spectra of neutral amino-substituted phosphazenes (1200 cm^{-1})[6] indicating a decrease in bond order between ring atoms from the neutral to the metalated species as well as strong interactions between metal centers and ligand N atoms.

Three signals are present in the ^{31}P NMR spectrum of **2** due to the three nonequivalent phosphorus atoms, thus dynamic behaviour at room temperature can be excluded. As expected each ^{31}P signal shows a dd pattern. However coupling constants differ markedly between ^{31}P nuclei. Whereas two coupling constants are relatively large (J = 12.4 and 16.3 Hz, respectively), the third one amounts only to 2.5 Hz, indicating low electronic interactions across one P−N−P unit within the P_3N_3 ring. The ^{1}H spectrum of **2** is rather complex, due to nonequivalent substituents. Me_2Al protons appear between $\delta = -0.1$ and $-\delta = 0.4$, whereas the protons of the MeAl unit show a chemical shift of $\delta = 0.61$.

[(EtZn)$_6${P$_3$N$_3$(NCy)$_6$}] (3)

Treatment of **1** with excess Et_2Zn in toluene leads to complete deprotonation of the hexaprotic phosphazene precur-

sor, which results in the formation of the hexanuclear zinc complex $[(EtZn)_6\{P_3N_3(NCy)_6\}]$ (**3**) (Figure 2).

$$\underset{\mathbf{1}}{P_3N_3(NHCy)_6} + 6\,Et_2Zn \rightarrow \underset{\mathbf{3}}{[(EtZn)_6\{P_3N_3(NCy)_6\}]} + 6\,C_2H_6 \quad (2)$$

Six metal atoms occupy bi- and tridentate coordination sites in **3** encapsulating the centrally arranged multidentate ligand. Four ethylzinc moieties are accommodated in tripodal sites, two of type **D** (Zn-2, Zn-3) and two of type **E** (Zn-1, Zn-4), resulting in a cage structure comprising the phosphazenate ring atoms, the four terminal N atoms N-10, N-20, N-40, N-60 and the aforementioned four Zn atoms. The other two ethylzinc units (Zn-5, Zn-6) are chelated in the bidentate fashion **B**. All nitrogen functions are involved in coordination toward metal atoms. Zn−N distances vary widely and depend mainly on coordination numbers of participating atoms. These correspond to those found in zinc phosphazene complexes containing related coordination sites.[8] The shortest distances are observed between the tri-coordinate zinc atoms and the terminally arranged N atoms [av. 1.90 Å]. Distances of Zn-5 and Zn-6 to the ring−N-functions are considerably longer [av. 2.31 Å]. Within tripodal sites of the cage each zinc atom has two shorter [av. 2.12 Å] and one longer Zn−N-bond [av. 2.43 Å]. An interesting feature of **3** is the substantial involvement of N_{ring} atoms in coordination toward metal centers. Each one interacts with two zinc atoms, resulting in a distorted tetrahedral environment at N-2 (av. Zn−N−Zn 99°) and in an almost linear Zn−N−Zn arrangement at N1 and N3 (av. 157°). P−N lengths of ring- and terminally located P−N-bonds in **3** are in the same range [av. 1.64 Å] indicating equal charge distribution over all N-functions (see Table 2). The six-membered phosphazenate ring system in **3** adopts a *twist* conformation.

NMR-spectra of **3** are in correspondence with the crystal structure (Table 4). ^{31}P NMR of **3** shows a triplet (P-1) and a doublet (P-2/P-3) in the intensity ratio 1:2 reflecting the molecular C_2-symmetry of **3**, where P-1 and N-2 are located on a noncrystallographic C_2-axis. The ^1H NMR shows two distinct environments for zinc-bonded ethyl groups, which can be assigned to bidentate and tripodal coordination sites, respectively. The very strong P−N-stretch band appears at 1055 cm^{-1} and is, as in **2**, markedly red-shifted compared to corresponding bands of neutral phosphazenes.

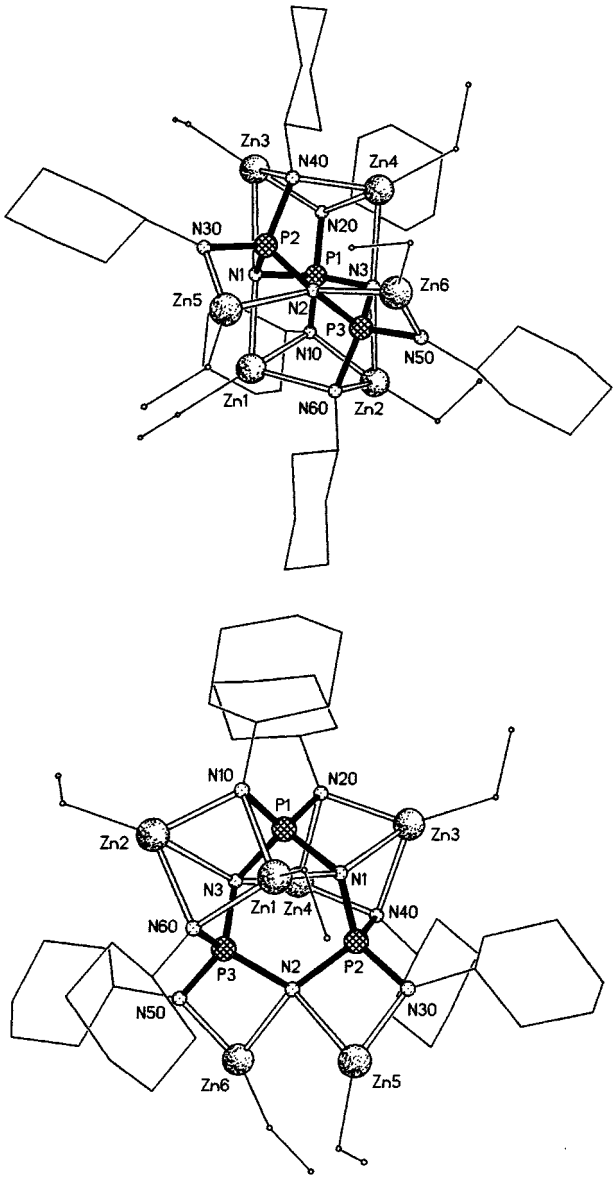


Figure 2. Crystal structure of **3** showing two views from different angles. Only one of two independent complexes in the asymmetric is shown

Coordination Pattern of the Hexaanionic Ligand System $[P_3N_3(NCy)_6]^{6-}$

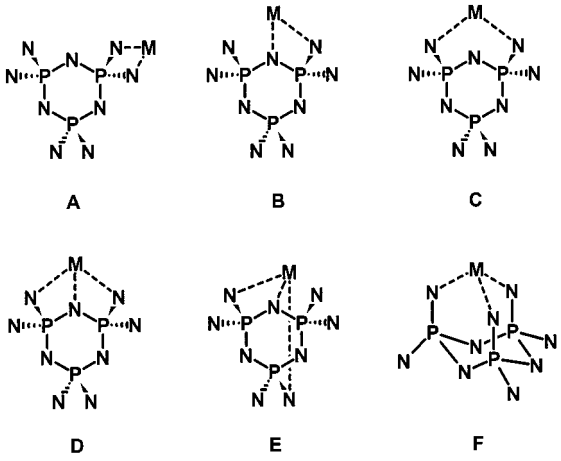
Scheme 2 illustrates the coordination modes which we have observed so far in complexes containing the hexaanionic ligand system $[P_3N_3(NCy)_6]^{6-}$. Both terminal and ring N atoms can take part in coordination to metal centers via bidentate (**A**, **B** and **C**) as well tripodal sites (**D**, **E** and **F**). Exclusively bidentate coordination sites of type **A**, **B** and **C** are present in the aluminium complex **2**, resulting in four (**A** and **B**) and six-membered (**C**) metallo heterocycles. Ethylzinc moieties in **3**, occupy in addition to the bidentate site **B**, tripodal sites of type **D** and **E**. Another tripodal coordination mode, which involves exclusively terminal N atoms of one ligand face resulting in a hetero-adamantane cage (**F**), has been observed in the lithium complex **1a**.[5a]

Six-membered phosphazenate ring systems in **2** and **3** are puckered as in the lithium complex **1a**, which is in contrast to the usually planar arrangement of six-membered rings in neutral cyclotriphosphazenes.[6] This reflects the high flexibility of the phosphazenate backbone in the presence of cooordinated metal centers. The complexed metal array determines the conformation of the central P_3N_3 ring, resulting in a *chair* conformation in the presence of lithium cations in **1a**, a *boat* conformation in the organo aluminium complex **2** and a *twist* conformation in the organozinc derivative **3**.

Table 2. Selected bond lengths [Å] and angles [°] for **3**

	bond length [Å]			bond length [Å]	
P1−N3	1.664(12)	1.661(13)	Zn1−N1	2.157(12)	2.190(11)
P1−N1	1.677(12)	1.663(12)	Zn1−N10	2.307(12)	2.314(12)
P2−N1	1.651(13)	1.648(12)	Zn1−N60	2.160(12)	2.105(12)
P2−N2	1.662(12)	1.678(13)	Zn2−N3	2.548(12)	2.433(13)
P3−N2	1.671(12)	1.670(13)	Zn2−N10	2.026(12)	2.028(12)
P3−N3	1.622(12)	1.647(13)	Zn2−N60	2.147(12)	2.148(12)
P1−N10	1.625(12)	1.631(13)	Zn3−N1	2.531(12)	2.480(11)
P1−N20	1.616(13)	1.617(13)	Zn3−N20	2.012(13)	2.042(12)
P2−N30	1.619(12)	1.612(13)	Zn3−N40	2.128(12)	2.147(11)
P2−N40	1.647(12)	1.664(12)	Zn4−N3	2.201(12)	2.220(13)
P3−N50	1.637(12)	1.587(13)	Zn4−N20	2.358(13)	2.318(12)
P3−N60	1.650(12)	1.672(13)	Zn4−N40	2.110(12)	2.126(11)
			Zn5−N2	2.313(12)	2.293(13)
			Zn5−N30	1.889(12)	1.904(12)
			Zn6−N2	2.313(12)	2.245(13)
			Zn6−N50	1.885(12)	1.903(13)

	bond angle [°]	
N3−P1−N1	105.8(6)	106.7(6)
N1−P2−N2	110.2(6)	109.6(6)
N2−P3−N3	108.8(6)	107.8(6)
N10−P1−N20	122.7(7)	122.1(7)
N30−P2−N40	116.3(6)	117.3(6)
N50−P3−N60	114.1(7)	116.8(6)
P1−N1−P2	114.3(7)	115.7(7)
P2−N2−P3	112.6(7)	114.3(8)
P3−N3−P1	116.5(7)	116.6(8)



Scheme 2. Coordination pattern of the hexaanionic ligand system $[P_3N_3(NCy)_6]^{6-}$

$[(EtZn)_6\{P_4N_4(N(H)Cy)_2(NCy)_6\}]$ (5)

Having studied the coordination behaviour of the six-membered ring phosphazenate $[P_3N_3(NCy)_6]^{6-}$ in the presence of various metal environments we were interested what type of coordination modes its higher homologue $[P_4N_4(NCy)_8]^{8-}$ might adopt. So far we have succeeded in determining the structure of the product gained from the reaction of $P_4N_4(NHCy)_8$ (**4**) with diethylzinc: Although an excess of Et_2Zn has been used only six of the eight NH functions in **4** have been deprotonated, even after refluxing the reaction mixture for 12 h in toluene. The hexanuclear zinc complex **5** has been isolated which contains the hexaanionic ligand system $[P_4N_4(NHCy)_2(NCy)_6]^{6-}$ (Figure 3)

$$\underset{\mathbf{4}}{P_4N_4(NHCy)_8} + 6\,Et_2Zn \rightarrow \underset{\mathbf{5}}{[(EtZn)_6\{P_4N_4(NHCy)_2(NCy_6\}]} + 6\,C_2H_6 \quad (3)$$

The structure of **5** is closely related to that of **3**: The six zinc atoms occupy bi- and tridentate coordination sites around the centrally arranged multidentate ligand. Four EtZn units are accommodated in tripodal sites (Zn-1, Zn-2, Zn-3 and Zn-4), resulting in cage structure assembled of phosphazenate ring atoms, four terminal N-functions and the four Zn atoms. Zn-5 and Zn-6 are chelated in bidentate ligand sites. The complex exhibits noncrystallographic C_2-symmetry. Structural parameters involving metal centers correspond largely to those observed in **3** (see Table 3) and coordination modes around the P_4N_{12} core of **5** resemble types **B**, **D** and **E** of the P_3N_9 core (Scheme 2). It is worth mentioning that both complexes **3** and **5** are the only ones which have been structurally characterised so far, where one single ligand accommodates such a large number of Zn atoms.

Two N functions in **5** remain protonated, even if excess of the strong organozinc base is used. This is also indicated by the appearance of a weak N−H-band at 3400cm^{-1} in the IR spectrum of **5**. The incomplete deprotonation of **4** in the presence of Et_2Zn can be rationalised by the increased number of sterically demanding cyclohexyl groups covering the surface of the complexes (from six in **3** to eight in **5**), which is accompanied by only modest expansion of the ligand core. With the exception of the two protonated N atoms, all nitrogen-functions are involved in coordination toward metal-centers. The P_4N_4 ring is puckered and has a similar conformation to that in the tetraanionic ligand system $[N_4\{P(Ph)(NCy)\}_4]^{4-}$.[5b]

Two signals in the ^{31}P NMR of **5** reveal two pairs of chemically equivalent phosphorus nuclei: P-1 and P-3 are carrying exclusively deprotonated substituents, whereas both P-2 and P-4 are bonded to one deprotonated and one protonated nitrogen atom. Surprisingly both ^{31}P NMR signals in **5** exist of doublets, where one would anticipate a set of two triplets in case the four ^{31}P nuclei act as a A_2B_2-system. Temperature dependent measurements (−80°C to 40°C) indicate no sign of fluctuation within the complexes. The $^3J_{P-P}$ coupling constants across two P−N−P units located opposite to each other in the P_4N_4 ring might be too small to be observed. A similar observation was made in **2**, where one P−N−P unit gave a considerably lower coupling constant as the other two P−N−P units. The ^1H NMR spectrum resembles that of **3**. There are two distinct sets of signals for zinc-bonded ethyl groups, which can be assigned to tripodal and bidentate coordination sites, respectively. However, evidence for both protonated NH groups cannot be drawn from the ^1H NMR spectrum, due to overlap of the NH-signal with the complex pattern of cyclohexyl groups.

Conclusion

Organometallic complexes of multianionic phosphazenates have been generated by deprotonation reactions of

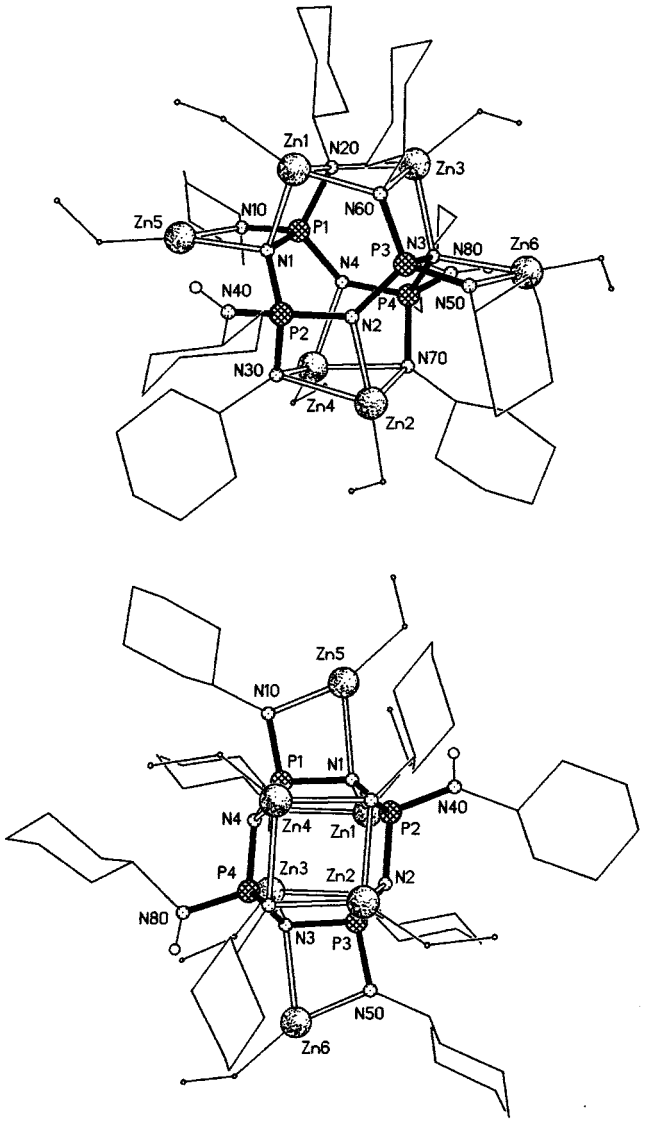


Figure 3. Crystal structure of **5** showing two views from different angles

amino-substituted phosphazenes with strong organometallic bases. The high charge of these new ligands facilitates the accommodation of a large number of metal cations per ligand molecule. The lipophilic character of these systems provides synthetic applications in aprotic organic solvents. We are focussing on transition metal complexes and extending our investigations to polymeric derivatives based on polyphosphazenates. Metal complexes of polyphosphazenates promise novel hybrid materials with unusual electronic or magnetic properties depending on the accommodated metal species. The organic substituent determines the appearance and flexibility of the material (e.g. films, fibres, glasses). Small molecular derivatives, such as the cyclic phosphazenates presented in this paper, can act as useful model compounds mimicking the microscopic behaviour of the corresponding polymer.

Table 3. Selected bond lengths [Å] and angles [°] for **5**

	bond length [Å]		bond length [Å]
P1−N1	1.670(11)	Zn1−N1	2.132(11)
P1−N4	1.613(11)	Zn1−N20	2.319(12)
P1−N10	1.626(9)	Zn1−N60	2.001(10)
P1−N20	1.646(11)	Zn2−N3	2.138(11)
P2−N1	1.644(11)	Zn2−N20	2.025(11)
P2−N2	1.617(10)	Zn2−N60	2.363(11)
P2−N30	1.642(11)	Zn3−N2	2.098(11)
P2−N40	1.609(13)	Zn3−N30	2.314(10)
P3−N2	1.626(11)	Zn3−N70	2.101(13)
P3−N3	1.660(11)	Zn4−N4	2.132(13)
P3−N50	1.611(9)	Zn4−N30	2.085(13)
P3−N60	1.648(10)	Zn4−N70	2.252(11)
P4−N3	1.639(11)	Zn5−N1	2.272(9)
P4−N4	1.635(10)	Zn5−N10	1.888(11)
P4−N70	1.639(11)	Zn6−N3	2.276(10)
P4−N80	1.623(13)	Zn6−N50	1.888(10)
	bond angle[°]		
N4−P1−N1	110.2(6)		
N10−P1−N20	115.2(6)		
N2−P2−N1	114.4(6)		
N40−P2−N30	113.7(7)		
N2−P3−N3	107.9(6)		
N50−P3−N60	116.4(5)		
N4−P4−N3	111.9(5)		
N80−P4−N70	112.4(7)		
P1−N1−P2	122.4(6)		
P2−N2−P3	129.4(7)		
P3−N3−P4	124.4(7)		
P1−N4−P4	130.8(7)		

Experimental Section

General Remarks: All manipulations were performed under dry nitrogen atmosphere in standard Schlenk-glassware or in a glove box. − Solvents were dried over sodium (toluene) and potassium (hexane, THF), respectively. − Precursors **1** and **4** were prepared according to literature methods.[9] Organometallic reagents were applied as standard solutions: Me_3Al, 2.0 M in hexane (Aldrich); Et_2Zn, 1.0 M in hexane (Aldrich). − FT-IR spectra were recorded on a Perkin−Elmer Paragon 1000 spectrometer in nujol between CsI plates. − NMR spectra were recorded on a Bruker AMX 400 spectrometer.

Preparation of [(thfMeAl)(Me$_2$Al)$_4${P$_3$N$_3$(NCy)$_6$}] (2): Me_3Al (5 mL of a 2.0 M solution in hexane, 10 mmol) was added to a solution of **1** (1 g, 1.38 mmol) in toluene (20 mL). The reaction mixture was refluxed for 1 h, then stirred for 30 min at room temperature and subsequently filtered through Celite. The solvent was evaporated and the residue recrystallised from of THF/hexane solution. After storage at room temperature for several days, colourless crystals of the solvate **2**·THF·hexane were obtained. Lattice solvent could be removed in vacuum. Yield of lattice solvent free product: 1.07 g, 1.01 mmol (73%). − ^{1}H NMR (400 MHz, $CDCl_3$, 25°C, TMS): δ = −0.4 to −0.1 [b, 24 H, $(CH_3)_2$Al], 0.61 (b, 3 H, CH_3Al), 1.40 (m, 4 H, thf), 1.5−2.4 [m, 60 H, CH(CH_2)$_5$], 2.56 (m, 4 H, thf), 3.42 [m, 6 H, CH(CH_2)$_5$]. − ^{31}P NMR (162 MHz, $CDCl_3$, 25°C, 85% H_3PO_4): δ = 9.55 (dd, $^2J_{P-P}$ = 2.5, 16.3 Hz), 12.5 (dd, $^2J_{P-P}$ = 12.4, 16.3 Hz), 16.4 (dd, $^2J_{P-P}$ = 2.5, 12.4 Hz). − IR (Nujol): $\tilde{\nu}$ [cm^{-1}] = 1413, 1293, 1260, 1216, 1190, 1124, 1079 (vs, P−N stretch), 1029, 956, 890. 849, 816, 630. − $C_{49}H_{101}Al_5N_9OP_3$ (1060.23): calcd. C 55.51, H 9.60, N 11.89; found C 54.89, H 9.51, N 11.64.

Preparation of [(EtZn)$_6${P$_3$N$_3$(NCy)$_6$}] (3): Et_2Zn (10 mL of a 1.0 M solution in hexane, 10 mmol) was added to a solution of **1** (1 g, 1.38 mmol) in toluene (20 mL). The reaction mixture was refluxed

Table 4. Crystal data of **2**, **3** and **5**

	2 × THF × hexane	**3**	**5** × hexane
Empirical formula	$C_{59}H_{123}Al_5N_9O_2P_3$	$C_{48}H_{96}N_9P_3Zn_6$	$C_{66}H_{134}N_{12}P_4Zn_6$
Molecular mass	1218.47	1284.47	1611.95
a [Å]	13.082(4)	21.919(12)	12.681(6)
b [Å]	23.821(4)	22.085(6)	14.858(6)
c [Å]	23.327(3)	13.544(5)	22.153(8)
α [°]	90	99.90(3)	86.64(7)
β [°]	98.30(2)	105.27(5)	82.71(6)
γ [°]	90	102.44(4)	69.43(6)
V [Å^3]	7139(3)	5992(4)	3876(3)
Crystal system	Monoclinic	Triclinic	Triclinic
Space group	$P2_1/n$	$P\bar{1}$	$P\bar{1}$
Crystal size [mm^3]	0.25 × 0.25 × 0.20	0.30 × 0.30 × 0.25	0.40 × 0.35 × 0.15
Z	4	4	2
ρ_{calc} [g cm^{-3}]	1.125	1.424	1.381
μ (Mo-K_α) [mm^{-1}]	0.187	2.482	1.955
F(000)	2664	2688	1708
Transmission$_{max/min}$	1.000/0.932	0.967/0.562	0.988/0.549
Refl. collected	9738	16175	10586
Refl. unique (R_{int})	9344 (0.063)	15690 (0.074)	10125 (0.078)
Data/parameter	9344/703	15690/645	10125/709
$R1$ [$I > 2\sigma(I)$]	0.089 (6618 refl.)	0.081 (8517 refl.)	0.096 (5167 refl.)
$WR2$ (all data)	0.258	0.223	0.287
Final diff map [eÅ^{-3}]	0.62/−0.61	1.13/−1.10	1.23/−1.33

for 1 h, then stirred for 30 min at room temperature and subsequently filtered through Celite. The solvent was evaporated and the residue recrystallised from of THF/hexane solution. After storage at room temperature for several days, colourless crystals of **3** were obtained. Yield: 1.17 g, 0.91 mmol (66%). − ^{1}H NMR (400 MHz, $CDCl_3$, 25°C, TMS): δ = 0.25 (q, 4 H, CH_3CH_2Zn), 0.34 (q, 8H CH_3CH_2Zn), 0.91 (t, 6 H, CH_3CH_2Zn), 1.10 (t, 12 H, CH_3CH_2Zn), 1.1−2.2 [m, 60 H, $CH(CH_2)_5$], 2.97 [m, 6 H, $CH(CH_2)_5$]. − ^{31}P NMR (162 MHz, $CDCl_3$, 25°C, 85% H_3PO_4): δ = 31.2 (d, $^2J_{P-P}$ = 11 Hz), 33.5 (t, $^2J_{P-P}$ = 11 Hz). − IR (Nujol): $\tilde{\nu}$ [cm^{-1}] = 1409, 1290, 1261, 1229, 1200, 1145, 1079, 1055 (vs, P−N stretch), 1023, 994, 944, 886, 846, 804, 609. − $C_{48}H_{96}N_9P_3Zn_6$ (1284.47): calcd. C 44.88, H 7.53, N 9.81; found C 44.54, H 7.44, N 9.58.

Preparation of [(EtZn)$_6${P$_4$N$_4$(N(H)Cy)$_2$(NCy)$_6$}] (5): Et_2Zn (10 mL of a 1.0 M solution in hexane, 10 mmol) was added to a solution of **4** (1 g, 1.04 mmol) in toluene (20 mL). The reaction mixture was refluxed for 1 h, then stirred for 30 min at room temperature and subsequently filtered through Celite. The solvent was evaporated and the residue recrystallised from of thf/hexane solution. After storage at room temperature for several days, colourless crystals of the solvate **5**·hexane were obtained. Lattice solvent could be removed in vacuum. Yield of solvent free product: 0.84 g, 0.55 mmol (53%). − ^{1}H NMR (400 MHz, $CDCl_3$, 25°C, TMS): δ = 0.21 (q, 4 H, CH_3CH_2Zn), 0.28 (q, 8 H, CH_3CH_2Zn), 0.50 (t, 6 H, CH_3CH_2Zn), 0.93 (t, 12 H, CH_3CH_2Zn), 1.1−2.2 [m, 80 H, $CH(CH_2)_5$], 3.04 [m, 8 H, $CH(CH_2)_5$]. − ^{31}P NMR (162 MHz, $CDCl_3$, 25°C, 85% H_3PO_4): δ = 21.3 (d, $^2J_{P-P}$ = 10 Hz), 26.4 (d, $^2J_{P-P}$ = 10 Hz). − IR (Nujol): $\tilde{\nu}$ [cm^{-1}] = 3400 (w, N−H stretch), 1579, 1261, 1071 (vs, P−N stretch), 1021, 930, 887, 798, 666; $C_{60}H_{120}N_{12}P_4Zn_6$ (1525.87): calcd. C 47.23, H 7.93, N 11.02; found C 46.84, H 7.94, N 10.78.

X-ray Structure Determination of 2, 3 and 5: Crystal data were recorded on a Rigaku-AFC6S diffractometer, Mo-K_α radiation (λ = 0.71073 Å), T = 153 K, $2\theta_{max.}$ = 45°, 2θ/ω-scan mode, absorption corrections based on ψ-scans, structures were solved by direct methods and refined by full-matrix least squares against F^2 using all data.[10] The asymmetric unit of the crystal structure of **3** contains two crystallographically independent complexes. Crystals of **2** and **5** crystallise as solvates: Asymmetric unit content: **2**·THF·hexane, **3** and **5**·hexane, respectively. Lattice solvents in both structures are disordered as well as part of ethyl groups in **3** and **5** and cyclohexyl groups in **5**. Disordered groups were split on two positions and refined using geometrical restraints. All nonhydrogen groups were refined anisotropically with the exception of lattice solvent molecules, C and N positions in **3** and disordered C positions in **5**, which were refined isotropically. H positions were fixed geometrically. Crystallographic data (excluding structure factors) for the structures reported in this paper have been deposited with the Cambridge Crystallographic Data Centre as supplementary publications no. CCDC-118485 (**2**), CCDC-118486 (**3**) and CCDC-118487 (**5**). Copies of the data can be obtained free of charge on application to CCDC, 12 Union Road, Cambridge CB2 1EZ, UK (Fax: (internat.) + 44-1223/336−033; E-mail: deposit@ccdc.cam.ac.uk

Acknowledgments

This work was supported by the EPSRC, the Royal Society, the Nuffield Foundation and the Research Development Fund, University of Liverpool.

[1] J. M. Smith, S. G. Bott, *Chem. Commun.* **1996**, 377.
[2] [2a] S. De Angelis, E. Solari, C. Floriani, A. Chiesi-Villa, C. Rizzoli, *J. Chem. Soc., Dalton Trans.* **1994**, 2467. − [2b] C. Floriani, *Chem. Commun.* **1996**, 1257.
[3] M. Winkler, M. Lutz, G. Müller, *Angew. Chem. Int. Ed. Engl.* **1994**, *33*, 2279.
[4] H. Bock, K. Gharagozloo-Hubmann, C. Näther, N. Nagel, Z. Havlas, *Angew. Chem. Int. Ed. Engl.* **1996**, *35*, 631.
[5] [5a] A. Steiner, D. S. Wright, *Angew. Chem. Int. Ed. Engl.* **1996**, *35*, 636. − [5b] A. Steiner, D. S. Wright, *Chem. Commun.* **1997**, 283.
[6] [6a] H. R. Allcock, *Chem. Rev.* **1972**, *72*, 315. − [6b] S. S. Krishnamurthy, A. C. Sau, M. Woods, *Adv. Inorg. Chem.* **1978**, *21*, 41.
[7] [7a] A. N. Chernega, M. Yu Antipin, Yu. T. Struchkov, I. E. Boldeskul, V. F. Shul′gin, V. D. Romanenko, *Zh. Strukt. Khim.* **1985**, *26*, 120. − [7b] V. D. Romanenko, V. F. Shul′kin, V. V. Skopenko, A. N. Chernega, M. Yu Antipin, Yu. T. Struchkov,

I. E. Boldeskul, L. N. Markovskii, *Zh. Obshch. Khim.* **1985**, *55*, 282. – [7c] M. Veith, M. Kross, J.-F. Labarre, *J. Mol. Struct.* **1991**, *248*, 345. – [7d] P. Braunstein, R. Hasselbring, D. Stalke, *New J. Chem.* **1996**, *20*, 337. – [7e] R. Hasselbring, H. W. Roesky, A. Heine, D. Stalke, G. M. Sheldrick, *Z. Naturforsch.* **1993**, *B48*, 43. For reviews on metal phosphazene complexes see: – [7f] M. Witt, H. W. Roesky, *Chem. Rev.* **1994**, *94*, 1163; [7g] H. R. Allcock, J. L. Desorcie, G. H. Riding, *Polyhedron* **1987**, *6*, 119.

[8] [8a] A. N. Chernega, M. Yu. Antipin, Yu. T. Struchkov, V. D. Romanenko, *Koord. Khim.* **1989**, *15*, 849. – [8b] S. K. Pandey, A. Steiner, H. W. Roesky, D. Stalke, *Inorg. Chem.* **1993**, *32*, 5444. – [8c] M. Krieger, R. O. Gould, K. Harms, S. Parsons, K. Dehnicke, *Chem. Ber.* **1996**, *129*, 1621. – [8d] D. Min, Y. Do, *Chem. Lett.* **1994,** 1989. – [8e] Y. Byun, D. Min, J. Do, H. Yun, Y. Do, *Inorg. Chem.* **1996**, *35*, 3981.

[9] [9a] S. K. Ray, R. A. Shaw, *J. Chem. Soc.* **1961**, 872. – [9b] V. Chandrasekhar, K. Vivekanandan, S. Nagendran, G. T. Senthil Andavan, N. R. Weathers, J. C. Yarbrough, A. W. Cordes, *Inorg. Chem.* **1998**, *37*, 6192.

[10] G. M. Sheldrick, *SHELX-97*, *X-ray structure determination programme*, Universität Göttingen, **1997**.

Received May 31, 1999
[I99189]

Hydrido(carbene), Hydrido(diazoalkane), Aqua(carbene), and Vinyl(carbene) Complexes of Osmium(II)

Helmut Werner,*[a] Wolfram Stüer,[a] Justin Wolf,[a] Matthias Laubender,[a] Birgit Weberndörfer,[a] Regine Herbst-Irmer,[b] and Christopher Lehmann[b]

Dedicated to Professor Alberto Ceccon on the occasion of his 65th birthday

Keywords: Osmium / Carbene complexes / Hydrido complexes / Diazoalkane complexes / Vinyl complexes

The five-coordinate compound [OsHCl(CO)(P*i*Pr$_3$)$_2$] (**1**) reacts with CH_2N_2 and other diazoalkanes $RCHN_2$ (R = Ph, CO_2Et, $SiMe_3$) in ether or toluene at 25 °C to give instead of the expected insertion products [Os(CH_2R)Cl(CO)(P*i*Pr$_3$)$_2$] the isomeric hydrido(carbene)osmium(II) complexes [OsHCl(=CHR)(CO)(P*i*Pr$_3$)$_2$] (**2–5**) in excellent yields. With Me_3SiCHN_2 as the substrate, the 1:1 adduct [OsHCl(N_2CHSiMe_3)(CO)(P*i*Pr$_3$)$_2$] (**6**) was detected at low temperature as an intermediate. The reactions of **1** with Ph_2CN_2 and $Cl_4C_5N_2$ afford the hydrido(diazoalkane)compounds [OsHCl(N_2CR_2)(CO)(P*i*Pr$_3$)$_2$] (**7**, **8**), which are quite stable and do not eliminate N_2 to give the corresponding hydrido(carbene)metal derivatives. Treatment of **3** (R = Ph) with either HCl or HBF_4/H_2O leads to the cleavage of the Os-H bond and results in the formation of [$OsCl_2$(=CHPh)(CO)(P*i*Pr$_3$)$_2$] (**10**) and [OsCl(=CHPh)(OH_2)(CO)(P*i*Pr$_3$)$_2$]BF_4 (**11**), respectively. The vinyl compound [OsCl(CH=CHPh)(CO)(P*i*Pr$_3$)$_2$] (**12**) behaves similarly to **1** and affords the carbene complex [OsCl(CH=CHPh)(=CHPh)(CO)(P*i*Pr$_3$)$_2$] (**13**) upon treatment with $PhCHN_2$. Compound **13** rearranges in solution at room temperature to give the π-allyl complex [Os(η^3-PhCHCHCHPh)Cl(CO)(P*i*Pr$_3$)$_2$] (**14**) as the dominating species. The crystal and molecular structures of **4**, **5**, **10**, and **11** have been determined by X-ray crystallography.

After we found that the four- and five-coordinate iridium complexes containing [IrCl(P*i*Pr$_3$)$_2$] as a building block offer a rich chemistry, including various routes to C−H activation,[1] we started a search for related osmium compounds with a 14- or 16-electron configuration at the metal center. Attempts to prepare either [$OsCl_2$(P*i*Pr$_3$)$_2$] or [$OsCl_2$(P*i*Pr$_3$)$_3$] by treatment of $OsCl_3 \cdot 3\,H_2O$ with triisopropylphosphane in methanol led instead to the five-coordinate hydrido(carbonyl) compound [OsHCl(CO)(P*i*Pr$_3$)$_2$] (**1**) supposedly with a square-pyramidal configuration.[2] This compound reacts with a variety of small molecules such as H_2, O_2, CO, CH_2=CHCN, and acetone to give 1:1 adducts in which the entering ligand occupies the free coordination site *trans* to hydride.[2][3] However, when we used terminal alkynes HC≡CR as the substrate we observed that compound **1** does not produce the expected six-coordinate hydrido(alkyne) complexes [OsHCl(CO)(η^2-HC≡CR)(P*i*Pr$_3$)$_2$] but gives the five-coordinate vinylosmium(II) derivates [OsCl(CH=CHR)(CO)(P*i*Pr$_3$)$_2$] in excellent yields.[4]

This unexpected insertion prompted us to study also the reactivity of **1** towards CH_2N_2 and other diazoalkanes with the hope that on this route, via OsH(CHR) species as intermediates, coordinatively unsaturated alkyl(carbonyl)osmium(II) compounds could be formed. From previous studies in our laboratory we knew that, by using [OsH(η^2-BH_4)(CO)(P*i*Pr$_3$)$_2$] as the starting material, alkylosmium(II) complexes of the general composition [OsH(CH_2R)(CO)$_2$-(P*i*Pr$_3$)$_2$] are accessible but due to the 18-electron configuration of the metal center these compounds are quite inert.[5] After Roper reported that the reaction of diazomethane with [OsCl(*o*-Tol)(CO)(PPh_3)$_2$] gave the η^2-acyl compound [OsCl{η^2-C(O)*o*-Tol}(=CH_2)(PPh_3)$_2$] by migration of the aryl ligand to CO,[6] it seemed also conceivable that from **1** and CH_2N_2 even a formylosmium species [OsCl{η^2-C(O)H}(=CH_2)(P*i*Pr$_3$)$_2$] could be obtained.

In this paper we describe the preparation of a series of hydrido(carbene)osmium(II) complexes from CH_2N_2 and $RCHN_2$ as the carbene source, the spectroscopic characterization of a labile OsH(N_2CHR) intermediate as well as the isolation of stable hydrido(diazoalkane) compounds with Ph_2CN_2 and $N_2C_5Cl_4$ as ligands, the reactivity of the hydrido(carbene)metal derivatives toward Broensted acids, and the synthesis of a vinyl(carbene)osmium compound that rearranges to an isomeric η^3-allyl complex by C−C coupling. Parts of these studies have already been communicated.[7]

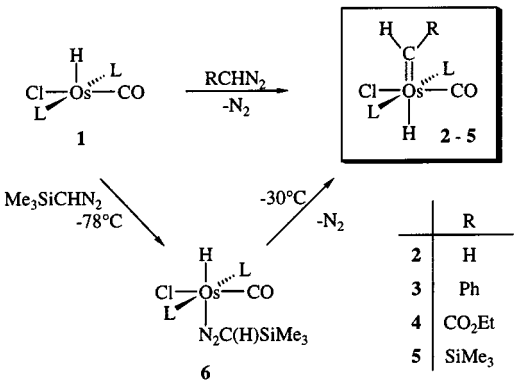
Results and Dicussion

The reaction of the starting material **1** with a freshly prepared solution of diazomethane in ether proceeds quite rapidly at room temperature and furnishes, after removal of the solvent, the hydrido(carbene) complex **2** in almost quantitative yield (Scheme 1). The fact, that compound **2** and not the isomeric methyl derivate [OsCl(CH_3)(CO)(P-*i*Pr$_3$)$_2$] is formed, is confirmed by the ^{1}H-NMR spectrum

[a] Institut für Anorganische Chemie der Universität Würzburg, Am Hubland, D-97074 Würzburg, Germany
[b] Institut für Anorganische Chemie der Universität Göttingen, Tammannstr. 4, D-37077 Göttingen, Germany

 © WILEY-VCH Verlag GmbH, D-69451 Weinheim, 1999 1434−1948/99/1111−1889 $ 17.50+.50/0

which displays besides the signals for the two phosphane ligands a triplet of triplets for the OsH proton at high field (δ −4.48) and two broadened singlets for the $OsCH_2$ protons at low field (δ 17.90 and 16.88). The ^{13}C-NMR spectrum of **2** exhibits resonances at δ = 285.0 and 182.0, which are assigned to the $OsCH_2$ and OsCO carbon atoms, respectively.



Scheme 1. L = P*i*Pr$_3$

Substituted diazomethanes such as $PhCHN_2$, EtO_2CCHN_2 and Me_3SiCHN_2 behave similarly to CH_2N_2 and react with the hydrido compound **1** to produce the corresponding carbene complexes **3**−**5** in excellent yields. The reaction of **1** with Me_3SiCHN_2 is relatively slow and needs ca. 15 h for completion at room temperature. We found that the octahedral compound $[OsHCl(CO)(PPh_3)_3]$[8] equally reacts with CH_2N_2 and $PhCHN_2$ quite smoothly but in this case the diazoalkane is converted into N_2 and the respective olefin without changing the composition of the osmium(II) derivative.

The new hydrido(carbene) complexes **3**−**5** are orange to yellow microcrystalline solids which are only moderately air-sensitive and which, in contrast to **2**, can be stored under argon at room temperature for weeks. The $OsCH_2$ compound **2** is more labile and, particularly in solution, decomposes slowly to give a mixture of products among which ethene was detected. The most characteristic features of the spectroscopic data of **3**−**5** are the hydride resonances at δ −4.5 to −5.6 in the ^1H NMR and the signal of the carbene carbon atom at δ 267−327 in the ^{13}C-NMR spectra. It should be emphasized that the signal of the OsH proton of compounds **2**−**5** experiences a significant downfield shift by ca. 27 ppm compared to the starting material **1**, which presumably is due to the strong influence of the carbene ligand *trans* to the hydride. The IR spectra of **2**−**5** (in KBr) exhibit a strong ν(CO) bond at ca. 1880−1940 cm^{-1} as well as a weaker absorption at ca. 1830−1865 cm^{-1}, which is assigned to the Os−H stretching frequency.

The molecular structures of **4** and **5** are shown in Figures 1 and 2. In both cases, the coordination geometry arround the metal center is distorted octahedral with the two phosphanes, the CO and the chloride, and the hydride and the carbene ligand occupying *trans* positions. The most noteworthy detail is the strong bending of the P−Os−P axis [144.88(2)° for **4** and 141.38(4)° for **5**] toward the (not exactly localized) position of the hydride ligand. This bending is much more pronounced than in *cis*,*cis*,*trans*-$[OsH(CH_3)(CO)_2(PiPr_3)_2]$ [165.6(1)°][5] and in the five-coordinate compound $[OsCl(CH{=}CHPh)(CO)(PiPr_3)_2]$ (**12**, see below) where the P−Os−P angle is 167.4(1)°.[4] The Os−C(carbene) distances in **4** and **5** are in the range of that of other carbene(chloro)osmium(II) complexes such as $[OsCl(=CH_2)(NO)(PPh_3)_2]$ [1.92(1) Å] and $[OsCl(=CF_2)(NO)(PPh_3)_2]$ [1.967(4) Å] containing NO as an additional ligand.[9]

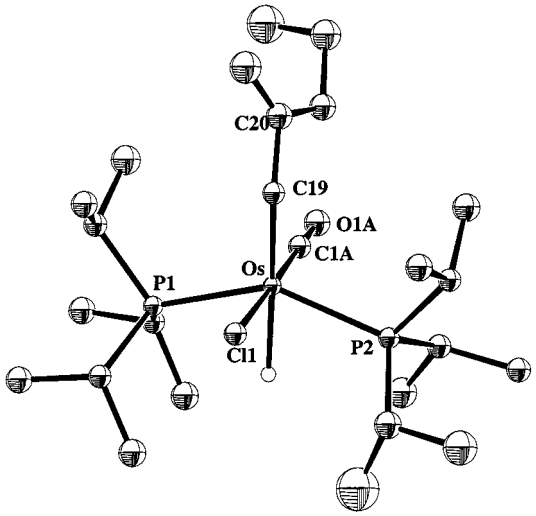


Figure 1. Molecular structure of **4**; the metal-bonded hydrogen is not exactly located, the other hydrogen atoms are omitted for clarity; selected bond lengths [Å] and angles [°]: Os−Cl 2.475(1), Os−P1 2.392(1), Os−P2 2.394(1), Os−C1A 1.840(3), Os−C19 1.949(2), C1A−O1A 1.153(3), C19−C20 1.489(3); P1−Os−P2 144.88(2), P1−Os−Cl 90.47(2), P1−Os−C1A 90.2(1), P1−Os−C19 108.3(1), P2−Os−Cl 89.82(2), P2−Os−C1A 90.9(1), P2−Os−C19 106.6(1), Cl−Os−C1A 177.7(1), Cl−Os−C19 83.6(1), C1A−Os−C19 94.1(1), Os−C1A−O1A 178.9(3), Os−C19−C20 133.7(2)

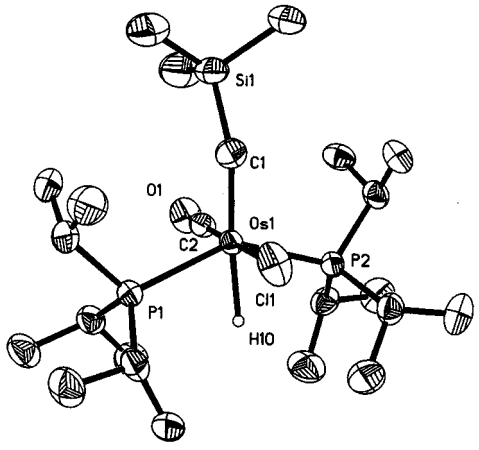
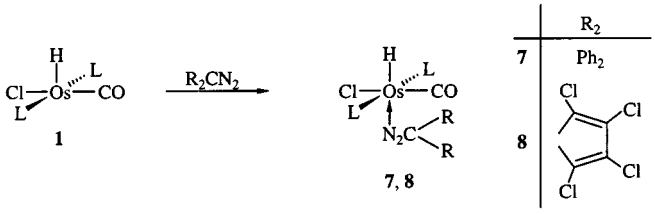


Figure 2. Molecular structure of **5**; the metal-bonded hydrogen is not exactly located, the other hydrogen atoms are omitted for clarity; selected bond lengths [Å] and angles [°]: Os−Cl 2.514(1), Os−P1 2.403(1), Os−P2 2.396(1), Os−C1 1.965(5), Os−C2 1.830(5), O1−C2 1.166(5), C1−Si 1.878(5); P1−Os−P2 141.38(4), P1−Os−Cl 89.88(4), P1−Os−C1 110.4(2), P1−Os−C2 90.4(1), P2−Os−Cl 89.93(4), P2−Os−C1 107.8(2), P2−Os−C2 91.5(2), Cl−Os−C1 82.1(2), Cl−Os−C2 177.3(1), C1−Os−C2 95.3(2), Os−C1−Si 144.9(3), Os−C2−O 179.4(4)

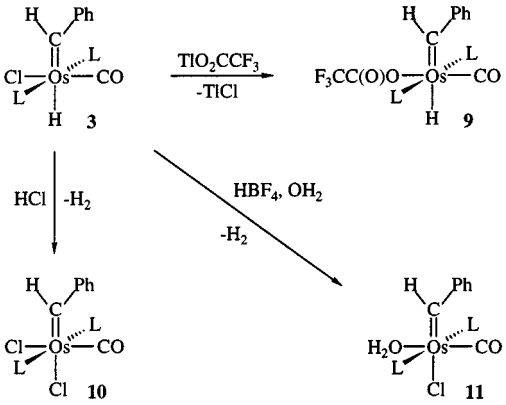
Following the observation that compound **1** reacts much more slowly with Me_3SiCHN_2 than with the other diazoalkanes, attempts were made to detect or even isolate an $Os(N_2CHR)$ species as an intermediate. Therefore, we carried out the reaction of **1** with Me_3SiCHN_2 in toluene at −78°C and found that under these conditions a product is formed that is stable at −78°C for several days. Evaporation of the solvent led to a slow evolution of gas (N_2) and to partial formation of the hydrido(carbene) complex **5**. This compound is formed nearly quantitatively upon warming the toluene solution to ca. −20°C. The ^{1}H-NMR spectrum of the low-temperature product **6** displays a hydride signal at δ = −13.70 (broadened singlet) and a resonance for the Me_3SiCHN_2 proton at δ = 2.80. Owing to these data, we assume that the intermediate is an $OsH(N_2CH\text{-}SiMe_3)$ derivative in which the trimethylsilyldiazomethane occupies the coordination position *trans* to hydride (see Scheme 1). The ^{13}C-NMR spectrum of **6** exhibits a signal for the $N_2CHSiMe_3$ carbon atom at δ = 33.4 and the IR spectrum, apart from the ν(CO) bond at 1890 cm^{-1}, an absorption at 1933 cm^{-1} which can be assigned either to the Os-H or the N≡N stretching frequency.

If compound **1** is not treated with CH_2N_2 or a monosubstituted derivative $RCHN_2$ but with Ph_2CN_2 or $Cl_4C_5N_2$ in toluene (see Scheme 2), a reaction takes place which is not accompanied by the evolution of gas. After removal of the solvent, off-white or light brown solids are isolated which in agreement with the elemental analyses are the hydrido(diazoalkane)osmium complexes **7** and **8**. At room temperature under argon, the compounds are stable for weeks and in solution even on warming to 40°C do not eliminate N_2 to give the corresponding hydrido(carbene) derivatives $[OsHCl(=CPh_2)(CO)(P\textit{i}Pr_3)_2]$ and $[OsHCl(=C_5Cl_4)(CO)(P\textit{i}Pr_3)_2]$, respectively. While the ^{1}H-NMR spectrum of **8** displays the hydride resonance at δ = −7.06 as a triplet with ^2J(P,H) = 22 Hz, the corresponding Os−H signal of **7** appears at δ = −11.44 as a broad singlet at room temperature. However, upon cooling the solution of **7** in $CDCl_3$ to −10°C the broadening disappears and a sharp triplet is observed. Since the pattern of the phosphane resonances of **7** does not change at different temperatures, we assume that the broadening of the hydride signal at 25°C is due to the mobility of the diphenyldiazomethane ligand which could coordinate either via the terminal nitrogen atom or via the N=N bond.[10][11] Based on the IR data of **7**, it is difficult to decide whether an $Os(\eta^1\text{-}N_2CPh_2)$ or an $Os(\eta^2\text{-}N_2CPh_2)$ bonding mode exists.



Scheme 2. L = P*i*Pr$_3$

The hydrido(carbene) complexes **3**−**5** are thermally as well as photochemically rather inert and do not react either in the absence or in the presence of Lewis bases such as CO or CN*t*Bu to afford the corresponding five- or six-coordinate alkylosmium(II) derivatives by migratory insertion. Some other reactions aimed to displace one of the anionic ligands of compound **3** are illustrated in Scheme 3. Treatment of a solution of **3** in toluene with an equimolar amount of TlO_2CCF_3 led to the formation of the related trifluoroacetato compound **9** which is isolated as an orange, almost air-stable solid in 89% yield. A comparison of the IR data of **9** with those of other carboxylato transition-metal complexes[12] indicates that the $CF_3CO_2^-$ ligand of **9** is coordinated in a κ^1- and not in a κ^2-fashion. It should be mentioned that compound **9** like the related chloro derivative **3** does not react upon warming to 60°C in benzene to give the corresponding isomer $[Os(CH_2Ph)(O_2CCF_3)(CO)(P\textit{i}Pr_3)_2]$.



Scheme 3. L = P*i*Pr$_3$

While the reaction of **2** with a solution of HCl in toluene yields a mixture of products, among which the dihydrogen adduct $[OsCl_2(H_2)(CO)(P\textit{i}Pr_3)_2]$ could be observed by ^{1}H- and ^{31}P-NMR spectroscopy,[13] the single component **10** is obtained on treatment of **3** with HCl in toluene. The isolated yield of the dark red, air-stable solid is 98%. The ^{1}H- and ^{13}C-NMR spectra of **10** both exhibit a low-field signal for the Os*CH* proton at δ = 19.04 and the Os*C*H carbon atom at δ = 278.0, respectively, and therefore confirm that a derivative of **3** still containing the carbene ligand is formed.

The structural proposal for **10** has been substantiated by X-ray crystallography. There are two independent molecules **A** and **B** in the asymmetric unit which slightly differ in the conformation of the phosphane ligands with respect to the carbene unit. As shown in Figure 3 for molecule **A**, the osmium center of compound **10** is octahedrally coordinated with the two chloro ligands in *cis* and the two triisopropylphosphanes in *trans* disposition. In contrast to the hydrido(carbene) complexes **4** and **5**, the axis P−Os−P of **10** is much less bent, the bond angle P−Os−P being 167.5(2)° for **A** and 166.3(2)° for **B**, respectively. While the Os−CO distances of **4**, **5** and **10** are almost the same, the bond length Os−C(carbene) of **10** is slightly shorter than that of

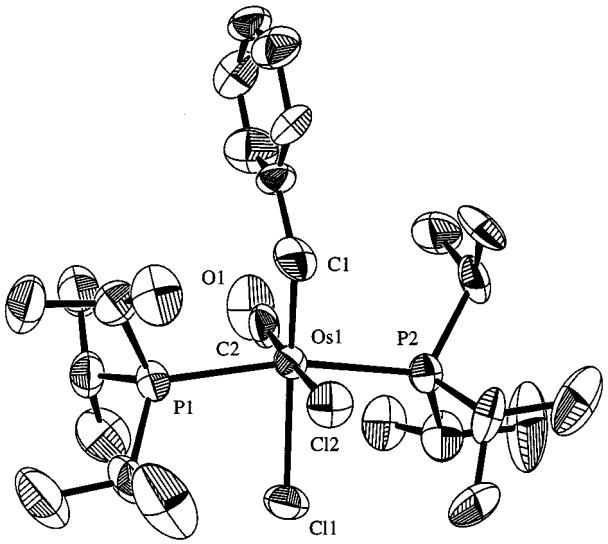


Figure 3. Molecular structure of **10**; there are two independent molecules **A** and **B** in the asymetric unit; hydrogen atoms apart from H1 are omitted for clarity; selected bond lengths [A] and angles [°]: Molecule **A**: Os1−Cl1 2.484(4), Os1−Cl2 2.487(5), Os1−P1 2.469(5), Os1−P2 2.466(5), Os1−C1 1.95(2), Os1−C2 1.85(2), C1−C50 1.46(2), O1−C2 1.13(2); P1−Os1−P2 167.5(2), P1−Os1−Cl1 84.6(2), P1−Os1−Cl2 90.7(2), P1−Os1−C1 93.3(5), P1−Os1−C2 91.3(5), P2−Os1−Cl1 82.9(2), P2−Os1−Cl2 90.7(2), P2−Os1−C1 99.0(5), P2−Os1−C2 89.9(5), Cl1−Os1−Cl2 86.8(2), Cl1−Os1−C1 169.3(2), Cl1−Os1−C2 95.9(6), Cl2−Os1−C1 82.7(6), Cl2−Os1−C2 176.8(2), C1−Os1−C2 94.6(8), Os1−C1−C50 139(2), Os1−C2−O1 176(2), Molecule **B**: Os2−Cl3 2.489(5), Os2−Cl4 2.478(4), Os2−P3 2.466(5); Os2−P4 2.476(5), Os2−C3 1.89(2), Os2−C4 1.83(2), C3−C60 1.49(2), O3−C4 1.16(2); P3−Os2−P4 166.3(2), P3−Os2−Cl3 82.1(2), P3−Os2−Cl4 88.8(2), P3−Os2−C3 98.0(5), P3−Os2−C4 89.6(6), P4−Os2−Cl3 84.2(2), P4−Os2−Cl4 90.3(2), P4−Os2−C3 95.5(5), P4−Os2−C4 91.7(6), Cl3−Os2−Cl4 88.1(2), Cl3−Os2−C3 171.4(5), Cl3−Os2−C4 93.5(6), Cl4−Os2−C3 93.5(6), Cl4−Os2−C4 177.5(5), C3−Os2−C4 95.0(8), Os2−C3−C60 142(1), Os2−C4−O2 179(2)

5. The distance Os−C1 in molecule **A** is nearly identical with the Os−C(carbene) bond length in the related bis(triphenylphosphane)osmium(II) derivative *cis,cis,trans*-$[OsCl_2(=CHPh)(CO)(PPh_3)_2]$ [1.94(1) Å],[14] whereas the distance Os−C3 in molecule **B** [1.89(2) Å] corresponds precisely to the Os−C(carbene) distance of *cis,cis,trans*-$[OsCl_2(=CHCH_2Ph)(CO)(P\mathit{i}Pr_3)_2]$ [1.887(9) Å].[13] There is no difference in the Os−Cl bond lengths in **10** (in neither **A** nor **B**), indicating that the *trans* influences of the carbonyl and carbene ligands are virtually the same. We note in this context that the formation of **10** from **3** and HCl is uncommon insofar as analogous reactions of carbeneosmium(II) and -ruthenium(II) compounds with Broensted acids mainly proceed by attack of the proton at the carbene carbon atom to give alkylmetal derivatives.[9,14,15]

Similarly to the reaction of **3** with HCl, treatment of the starting material **3** with HBF_4 in the presence of water leads to the cleavage of the Os−H bond and affords the cationic aqua(carbene) complex **11** in 68% isolated yield. Instead of HBF_4, the carbenium salt $[CPh_3]BF_4$ can also be used as the electrophilic substrate. The composition of **11** (which is an orange, slightly air-sensitive solid) has been confirmed both by elemental analysis and conductivity measurements. The presence of the coordinated water molecule is clearly indicated in the IR spectrum by the strong ν(OH) bond at 3373 cm^{-1}. The ^{1}H-NMR spectrum of **11** (in CD_2Cl_2) is temperature-dependent. While at 290 K and slightly below (see Figure 4) the resonance for the OH_2 protons cannot be observed, at 266 K a relative broad signal appears which sharpens at 243 K to a singlet. This change of pattern is accompanied by a distinct separation of two resonances in the region between δ = 8.0−8.8 which are assigned to the *ortho*-hydrogen atoms of the phenyl ring. Brookhart[16] and Grubbs[17] both reported about similar observations in the case of cationic carbeneiron and -ruthenium complexes and attributed the observed effects to the interaction between the phenyl substituent and the positively charged carbene carbon atom. For **11** an analogous explanation could also be reasonable, in particular since in the ^{1}H-NMR spectrum of the related, but neutral, precursor **3** even at 213 K only one broadened resonance for the *ortho*-CH protons of the phenyl ring appears. We note that an aqua(carbene)osmium-

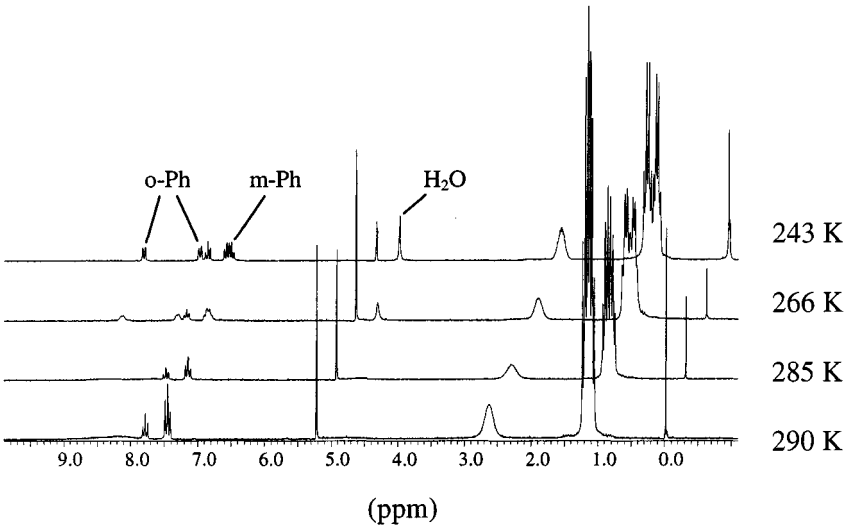


Figure 4. ^{1}H-NMR spectra of compound **11** in CD_2Cl_2 at different temperatures

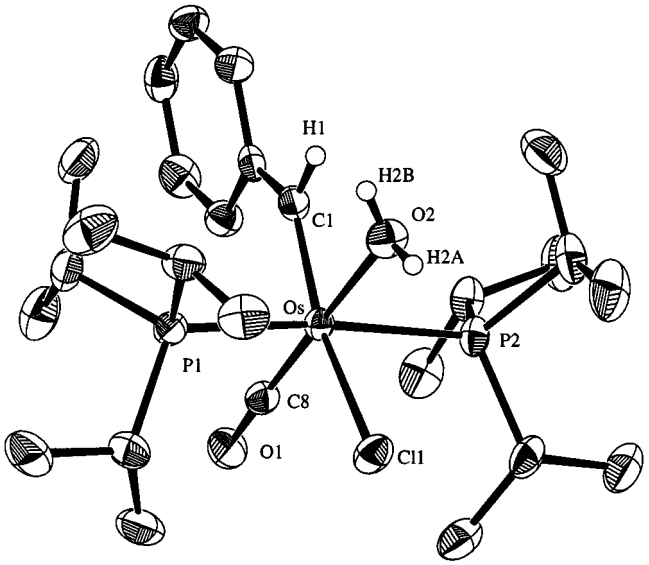


Figure 5. Molecular structure of the cation of **11**; hydrogen atoms apart from H1, H2A, and H2B are omitted for clarity; selected bond lengths [Å] and angles [°]: Os−P1 2.476(2), Os−P2 2.477(2), Os−Cl1 2.477(2), Os−C1 1.915(7), Os−C8 1.823(7), Os−O2 2.182(5), C1−C2 1.449(9), C8−O1 1.159(8); P1−Os−P2 172.90(6), P1−Os−Cl1 85.42(6), P1−Os−C1 95.3(2), P1−Os−C8 89.5(2), P1−Os−O2 89.9(2), P2−Os−Cl1 87.49(6), P2−Os−C1 91.6(2), P2−Os−C8 91.1(2), P2−Os−O2 89.3(2), Cl1−Os−C1 165.3(2), Cl1−Os−C8 98.0(2), Cl1−Os−O2 80.5(2), C1−Os−C8 96.7(3), C1−Os−O2 84.9(3), C8−Os−O2 178.4(2), Os−C8−O1 177.3(6), Os−C1−C2 140.9(5)

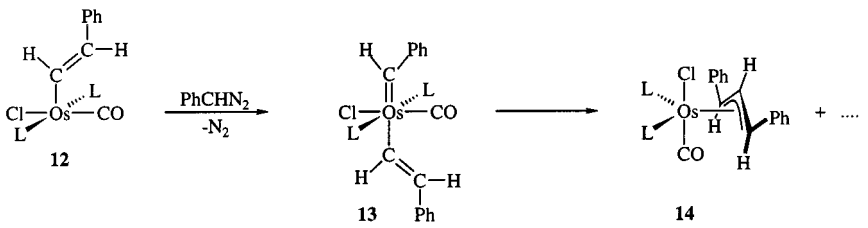
(II) compound similar to **11** with the composition $[OsCl(=CHCH=CH_2)(H_2O)(CO)(P\mathit{i}Pr_3)_2]BF_4$ has been described by Esteruelas et al. but due to the lability of this species neither NMR-spectroscopic nor structural data have been reported.[18]

The molecular structure of the cation of **11** is shown in Figure 5. Although in analogy to the other carbeneosmium(II) complexes **4**, **5**, and **10** the coordination geometry around the metal center is not perfectly octahedral, the bending of the three main axes P1−Os−P2, C8−Os−O2, and C1−Os−Cl1 is less pronounced than in the related neutral compounds with an Os−CHPh bond. The most noteworthy structural feature is that in contrast to **4**, **5**, and **10** the chloro ligand in **11** is mutually *cis* and not *trans* to the CO group. The conclusion is that in the course of the reaction of **3** with HBF_4/H_2O a rearrangement of the ligand sphere occurs. The bond length Os−C1 in **11** is slightly shorter than in the hydrido(carbene) derivatives **4** and **5**, but corresponds almost exactly to the average of the metal−carbene distances found for molecules **A** and **B** in the dichloro complex **10**.

The five-coordinate vinylosmium(II) compound **12**, which (as mentioned above) was prepared from **1** and phenylacetylene,[4] also reacts with $PhCHN_2$ to give the expected six-coordinate carbene complex **13** in 82% yield (Scheme 4). Attempts to prepare **13** on an alternative route failed because in contrast to **1** the hydrido(carbene) derivative **3** does not react with PhC≡CH by insertion of the alkyne into the Os−H bond. The ^{1}H- and ^{31}P-NMR spectra of **13** in ($CDCl_3$) reveal that in solution two isomeric species in the ratio of 2:1 are present which probably differ in the orientation of the carbene unit to the vinyl ligand. Although due to the preliminary results of an X-ray structure analysis of **13**[19] there is no doubt that in the crystal the CHPh and the CH=CHPh groups are *trans* to each other, we cannot exclude that in solution a mixture of both the *cis* and the *trans* isomer exists. With regard to the stereochemistry of the OsCH=CHPh moiety, the large H−H coupling of ca. 19 Hz between the vinyl protons indicates that the metal and the phenyl group are *trans*-disposed.

In benzene or toluene, the carbene(vinyl)osmium(II) derivative **13** is somewhat labile and rearranges slowly to a product which probably is the π-allyl complex **14**. The same reaction in chloroform leads to a mixture of at least two compounds which could not be separated by fractional crystallization or chromatographic techniques. Attempts to obtain **14** in analytically pure form also failed since during column chromatography of a solution of **14** in benzene decomposition occurred. The most typical features of the ^{1}H-NMR spectrum of **14** are the sharp triplet at δ = 6.09 for the central CH proton of the allyl moiety and the doublet of doublet resonance at δ = 4.14 (with the relative intensity of 2 H) which is assigned to the two equivalent terminal protons of the PhCHCHCHPh group. The relatively large H−H coupling constant (11.6 Hz) for these two signals indicate that the terminal protons are in *anti* position. A related compound to **14** with the composition $[OsH(\eta^3\text{-}C_3H_5)(CO)(P\mathit{i}Pr_3)_2]$ exists and has been prepared in our laboratory from **1** and C_3H_5MgBr.[20]

With regard to the mechanism of formation of **14** from compound **13** we note that in rhodium and ruthenium chemistry work by Maitlis and us has already demonstrated that coupling between a vinyl group and a carbene ligand in the coordination sphere of a transition-metal occurs leading to an allyl unit.[21][22] Moreover, Hill and co-work-



Scheme 4. L = P*i*Pr$_3$

ers recently reported that the five-coordinate vinyl complex $[Ru(CH=CH_2)Cl(CO)(PPh_3)_2]$ reacts with excess diazomethane to afford the corresponding π-allyl species $[RuCl(\eta^3\text{-}C_3H_5)(CO)(PPh_3)_2]$ via a carbeneruthenium compound as an observed intermediate.[23]

Conclusion

The work presented in this paper has shown that treatment of the five-coordinate starting material **1** with CH_2N_2 and substituted diazoalkanes $RCHN_2$ does not lead to the insertion of the respective carbene into the Os−H bond and, therefore, does not afford the alkylosmium(II) complexes $[Os(CH_2R)Cl(CO)(P\textit{i}Pr_3)_2]$. Instead, the isomeric hydrido(carbene) derivatives **2−5** are formed in excellent yields. The X-ray crystal structure analyses of two representatives **4** and **5** have confirmed that in the hydrido(carbene)osmium(II) compounds the hydride and the carbene ligand are in *trans* disposition. The same stereochemistry has been found for the related ruthenium(II) complexes $[RuHCl(=CHR)(CO)(P\textit{i}Pr_2Ph)_2]$ where R is H or Ph.[24] Recently, Caulton and co-workers reported that the reaction of $[MHCl(CO)(P\textit{t}Bu_2Me)_2]$ (M = Os, Ru) with diazomethane yields at low temperature also the corresponding hydrido(methylidene) derivatives $[MHCl(=CH_2)(CO)(P\textit{t}Bu_2Me)_2]$ which, however, isomerize at 25°C or below to $[M(CH_3)Cl(CO)(P\textit{t}Bu_2Me)_2]$.[25] In agreement with our studies, these authors equally observed that the osmium complex **2** decomposes unselectively to a mixture of products among which **1** and ethene could be detected. Caulton et al. assume that the remarkable ligand dependence ($P\textit{t}Bu_2Me$ vs. $P\textit{i}Pr_3$) is attributed to the fact that the $MH(=CH_2)$ to $M(CH_3)$ isomerization of the six-coordinate compounds require phosphane dissociation and that the smaller $P\textit{i}Pr_3$ (compared to $P\textit{t}Bu_2Me$) fails to dissociate at a rate competitive with alternative decomposition reactions.[25] Recent ab initio MP2 calculations by Eisenstein et al.[26] are in agreement with these results. The theoretical work also reveals that for $[OsHCl(=CH_2)(CO)(P\textit{i}Pr_3)_2]$ the isomer, in which H and CH_2 are mutually *cis*, is more stable than that in which these ligands are mutually *trans*.[26] Therefore, the final conclusion is that the isolated hydrido(carbene) complex **2** and probably also the analogous derivatives **3−5** are kinetically protected by a high barrier for site exchange which seems to be a prerequisite for an insertion reaction

Experimental Section

All operations were carried out under argon using Schlenk techniques. The starting materials **1**[2] and **12**[4] were prepared as described in the literature. − NMR: Bruker AC 200 and AMX 400 [dvt = doublet of virtual triplets; $N = {}^3J(PH) + {}^5J(PH)$ or ${}^2J(PC) + {}^4J(PC)$, respectively]. − Melting points determined by DTA.

1. Preparation of $[OsHCl(=CH_2)(CO)(P\textit{i}Pr_3)_2]$ (2): A suspension of 84 mg (0.15 mmol) of **1** in 10 mL of diethyl ether was treated at room temperature with 0.80 mL of a freshly prepared 0.3 M solution of diazomethane in OEt_2. An evolution of gas (N_2) occurred. After the reaction mixture was stirred for 2 min, the solvent was removed and the yellow microcrystalline solid dried in vacuo; yield 86 mg (99%); m.p. 95°C (dec.). − IR (KBr): $\tilde{\nu}$ = 1910 cm^{-1} (CO), 1857 (OsH). − ^1H NMR (400 MHz, C_6D_6): δ = 17.90, 16.88 (both br s, 1 H each, $OsCH_2$), 2.46 (m, 6 H, $PCHCH_3$), 1.10 [dvt, N = 14.4, ${}^3J(H,H)$ = 7.2 Hz, 18 H, $PCHCH_3$], 1.02 [dvt, N = 14.6, ${}^3J(H,H)$ = 7.2 Hz, 18 H, $PCHCH_3$], −4.48 [tt, ${}^2J(P,H)$ = 30, ${}^3J(H,H)$ = 2 Hz, 1 H, OsH]. − ^{13}C NMR (100.6 MHz, C_6D_6): δ = 285.0 (br s, $Os=CH_2$), 182.0 [t, ${}^2J(P,C)$ = 8.0 Hz, CO], 25.0 (vt, N = 28.6 Hz, $PCHCH_3$), 19.1, 18.5 (both s, $PCHCH_3$). − ^{31}P NMR (162.0 MHz, C_6D_6): δ = 56.5 [s, ${}^1J(^{187}Os,^{31}P)$ = 168 Hz]. − $C_{20}H_{45}ClOOsP_2$ (589.2): calcd. C 40.77, H 7.70; found C 40.50, H 8.01.

2. Preparation of $[OsHCl(=CHPh)(CO)(P\textit{i}Pr_3)_2]$ (3): A solution of 200 mg (0.35 mmol) of **1** in 10 mL of toluene was treated dropwise with 0.30 mL of a 1.4 M solution of $PhCHN_2$ in hexane at room temperature. An evolution of gas (N_2) occurred which was accompanied by a change of color from orange to dark yellow and finally to red (indicating excess of $PhCHN_2$). After the reaction mixture was stirred for 30 min, it was worked up as described for **2**. Orange crystals; yield 230 mg (99%); m.p. 117°C (dec.). − IR (KBr): $\tilde{\nu}$ = 1878 cm^{-1} (CO), 1830 (OsH). − ^1H NMR (400 MHz, $CDCl_3$): δ = 17.45 (m, 1 H, Os=CH), 8.20 (m, 2 H, C_6H_5), 7.51 (m, 1 H, C_6H_5), 7.29 (m, 2 H, C_6H_5), 2.61 (m, 6 H, $PCHCH_3$), 1.10 [dvt, N = 14.0, ${}^3J(H,H)$ = 6.8 Hz, 36 H, $PCHCH_3$)], −4.50 [dt, ${}^2J(P,H)$ = 29.5, ${}^3J(H,H)$ = 4.5 Hz, 1 H, OsH]. − ^{13}C NMR (100.6 MHz, $CDCl_3$): δ = 296.8 (br s, Os=*C*HPh), 183.4 [t, ${}^2J(P,C)$ = 8.0 Hz, CO], 157.2 (s, *i*-C_6H_5), 132.1, 129.8, 129.6 (all s, C_6H_5), 25.9 (vt, N = 27.8 Hz, $PCHCH_3$), 18.8, 18.7 (both s, $PCHCH_3$). − ^{31}P NMR (162.0 MHz, $CDCl_3$): δ = 47.9 [s, ${}^1J(^{187}Os,^{31}P)$ = 168 Hz]. − $C_{26}H_{49}ClOOsP_2$ (665.3): calcd. C 46.94, H 7.42; found C 47.34, H 7.42.

3. Preparation of $[OsHCl(=CHCO_2Et)(CO)(P\textit{i}Pr_3)_2]$ (4): A solution of 105 mg (0.18 mmol) of **1** in 5 mL of toluene was treated with 0.04 mL of N_2CHCO_2Et at room temperature. An evolution of gas (N_2) occurred which was accompanied by a change of color from orange to dark brown. After the reaction mixture was stirred for 30 min, the solvent was removed in vacuo and the residue was extracted with a mixture of 10 mL of hexane and 0.5 mL of toluene. The extract was filtered and the filtrate was concentrated in vacuo to give an orange solid; yield 98 mg (81%); m.p. 133°C (dec.). − IR (KBr): $\tilde{\nu}$ = 1923 cm^{-1} (CO), 1863 (OsH), 1650 (CO_2Et). − ^1H NMR (400 MHz, C_6D_6): δ = 17.22 [dt, ${}^3J(H,H)$ = ${}^3J(P,H)$ = 3.0 Hz, 1 H, Os=CH]; 4.23 [q, ${}^3J(H,H)$ = 7.5 Hz, 2 H, CH_2CH_3], 2.60 (m, 6 H, $PCHCH_3$), 1.17 [t, ${}^3J(H,H)$ = 7.5 Hz, 3 H, CH_2CH_3], 1.14, 1.06 [both dvt, N = 14.7, ${}^3J(H,H)$ = 7.5 Hz, 18 H each, $PCHCH_3$], −4.95 [dt, ${}^3J(H,H)$ = 3.0, ${}^2J(P,H)$ = 31.6 Hz, 1 H, OsH]. − ^{13}C NMR (50.3 MHz, $CDCl_3$): δ = 267.7 (br s, Os=*C*HCO_2Et), 181.5 [t, ${}^3J(P,C)$ = 2.5 Hz, *C*O_2Et], 179.3 [t, ${}^2J(P,C)$ = 8.9 Hz, CO], 59.6 (s, *C*H_2CH_3), 29.9 (vt, N = 28.8 Hz, $PCHCH_3$), 18.7 (s, $PCHCH_3$), 14.4 (s, CH_2CH_3). − ^{31}P NMR (81.0 MHz, $CDCl_3$): δ = 56.6 [s, ${}^1J(^{187}Os,^{31}P)$ = 165 Hz]. − $C_{23}H_{49}ClO_3OsP_2$ (661.3): calcd. C 41.78, H 4.79; found C 41.51, H 7.19.

4. Preparation of $[OsHCl(=CHSiMe_3)(CO)(P\textit{i}Pr_3)_2]$ (5): A solution of 100 mg (0.17 mmol) of **1** in 5 mL of toluene was treated with 0.15 mL of a 2.0 M solution of Me_3SiCHN_2 in hexane and stirred for 15 h at room temperature. The solvent was evaporated in vacuo, the remaining yellow microcrystalline solid washed twice with 2 mL of hexane and dried in vacuo; yield 91 mg (79%); m.p. 132°C (dec.). − IR (KBr): $\tilde{\nu}$ = 1938 cm^{-1} (CO). − ^1H NMR (200 MHz, $CDCl_3$): δ = 19.85 [dt, ${}^3J(P,H)$ = ${}^3J(H,H)$ = 2 Hz, 1 H, Os=C*H*$SiMe_3$], 2.53 (m, 6 H, $PCHCH_3$) 1.20 [dvt, N = 14.2, ${}^3J(H,H)$ = 7.2 Hz,

18 H, PCHCH_3], 1.08 [dvt, N = 14.7, ^3J(H,H) = 7.3 Hz, 18 H, PCHCH_3], 0.16 (s, 9 H, $SiCH_3$), −5.62 [dt, ^2J(P,H) = 28.6, ^3J(H,H) = 2 Hz, 1 H, OsH]. − ^{13}C NMR (100.6 MHz, $CDCl_3$): δ = 327.3 (s, Os=*C*HSiMe$_3$), 182.6 [t, ^2J(P,C) = 8.0 Hz, CO], 25.2 (vt, N = 28.6 Hz, P*C*HCH$_3$), 19.2, 18.8 (both s, PCH*C*H$_3$), 0.5 (s, $SiCH_3$). − ^{31}P NMR (162.0 MHz, $CDCl_3$): δ = 56.5 [s, J(^{187}Os,^{31}P) = 170 Hz]. − $C_{23}H_{53}ClOOsP_2Si$ (661.4): calcd.C 41.77, H 8.08; found C 41.32, H 8.26.

5. Generation of [OsHCl(N$_2$CHSiMe$_3$)(CO)(P*i*Pr$_3$)$_2$] (6): A solution of 35 mg (0.06 mmol) of **1** in 5 mL of toluene was treated at −78°C with 0.05 mL of a 2.0 M solution of Me_3SiCHN_2 in hexane. An instant change of color from orange to light yellow occurred which is not accompanied by an evolution of gas. Attempts to isolate the product by low-temperature evaporation of the solvent led always to a mixture of **5** and **6**. Spectroscopic data for **6**: IR (KBr): $\tilde{\nu}$ = 1890 cm^{-1} (CO), 1933 (OsH or N_2). − ^{1}H NMR (400 MHz, $CDCl_3$): δ = 2.80 (s, 1 H, Me$_3$SiC*H*N$_2$), 2.62 (m, 6 H, PC*H*CH$_3$), 1.26 [dvt, N = 13.2, ^3J(H,H) = 6.7 Hz, 18 H, PCHCH_3], 1.23 [dvt, N = 13.6, ^3J(H,H) = 7.0 Hz, 18 H, PCHCH_3], 0.13 (s, 9 H, $SiCH_3$), −13.70 (br s, 1 H, OsH). − ^{13}C NMR (100.6 MHz, $CDCl_3$): δ = 178.8 [t, ^2J(P,C) = 8.3 Hz, CO], 33.4 (s, Me$_3$Si*C*HN$_2$), 24.5 (vt, N = 26.0 Hz, P*C*HCH$_3$), 19.2, 19.0 (both s, PCH*C*H$_3$), 0.3 (s, $SiCH_3$). − ^{31}P NMR (162.0 MHz, $CDCl_3$): δ = 28.3 [s, J(^{187}Os,^{31}P) = 176 Hz].

6. Preparation of [OsHCl(N$_2$CPh$_2$)(CO)(P*i*Pr$_3$)$_2$] (7): A solution of 51.0 mg (0.09 mmol) of **1** in 2 mL of toluene was treated dropwise at room temperature with a solution of 18.1 mg (0.09 mmol) of Ph_2CN_2 in 5 mL of toluene. After the reaction mixture was stirred for 2 min, the solvent was removed in vacuo and the residue washed twice with 3 mL of hexane. An off-white solid was obtained which was dried in vacuo; yield 51 mg (75%); m.p. 69°C (dec.). − IR (KBr): $\tilde{\nu}$ = 1890 cm^{-1} (CO), 1952 (OsH or N_2). − ^{1}H NMR (400 MHz, $CDCl_3$): δ = 7.32 (m, 8 H, C_6H_5), 7.15 (m, 2 H, C_6H_5), 2.60 (m, 6 H, PC*H*CH$_3$), 1.22 [dvt, N = 13.7, ^3J(H,H) = 6.6 Hz, 18 H, PCHCH_3], 1.15 [dvt, N = 13.8, ^3J(H,H) = 6.8 Hz, 18 H, PCHCH_3], -11.44 (br s, 1 H, OsH). − ^{13}C NMR (100.6 MHz, $CDCl_3$): δ = 179.2 [t, ^2J(P,C) = 9.1 Hz, CO], 129.2, 128.6, 127.7, 126.5 (all s, C_6H_5), 24.6 (vt, N = 25.8 Hz, P*C*HCH$_3$), 19.4, 19.3 (both s, PCH*C*H$_3$), signal of Ph_2CN_2 not observed. − ^{31}P NMR (162.0 MHz, $CDCl_3$): δ = 28.0 [s, J(^{187}Os,^{31}P) = 180 Hz]. − $C_{32}H_{53}ClN_2OOsP_2$ (769.4): calcd. C 49.95, H 6.94, N 3.64; found C 49.66, H 6.78, N 3.55.

7. Preparation of [OsHCl(N$_2$C$_5$Cl$_4$)(CO)(P*i*Pr$_3$)$_2$] (8): This compound was prepared analogously as described for **7**, using 50.0 mg (0.09 mmol) of **1** and 23.8 mg (0.10 mmol) of $N_2C_5Cl_4$ as starting materials. Light brown solid; yield 53 mg (75%); m.p. 73°C (dec.). − IR (hexane): $\tilde{\nu}$ = 1904 cm^{-1} (CO), 1941 (OsH or N_2). − ^{1}H NMR (400 MHz, C_6D_6): δ = 2.55 (m, 6 H, PC*H*CH$_3$), 1.15−1.08 (br m, 36 H, PCH*C*H$_3$), −7.06 [t, ^2J(P,H) = 22 Hz, 1 H, OsH]. − ^{13}C NMR (100.6 MHz, C_6D_6): δ = 177.3 [t, ^2J(P,C) = 7.8 Hz, CO], 113.3, 108.0 (both s, CCl), 82.2 (br s, N_2C), 24.9 (vt, N = 27.4 Hz, P*C*HCH$_3$), 19.9, 19.0 (both s, PCH*C*H$_3$). − ^{31}P NMR (162.0 MHz, C_6D_6): δ = 26.3 [s, J(^{187}Os,^{31}P) = 170 Hz]. − $C_{24}H_{43}Cl_5N_2OOsP_2$ (805.1): calcd. C 35.81, H 5.38, N 3.48; found C 35.37, H 5.62, N 3.36.

8. Preparation of [OsH(O$_2$CCF$_3$)(=CHPh)(CO)(P*i*Pr$_3$)$_2$] (9): A solution of 120 mg (0.18 mmol) of **3** in 10 mL of toluene was treated with 58 mg (0.18 mmol) of CF_3CO_2Tl and stirred for 15 h at room temperature. A white solid (TlCl) slowly precipitated. The solution was filtered, the filtrate was concentrated in vacuo and the remaining orange solid dried; yield 121 mg (89%); m.p. 106°C (dec.). − IR (KBr): $\tilde{\nu}$ = 1885 cm^{-1} (CO), 1680 (OCO asym), 1425 (OCO sym). − ^{1}H NMR (400 MHz, $CDCl_3$): δ = 17.16 [m, d after ^{31}P decoupling, ^3J(H,H) = 4.4 Hz, 1 H, Os=C*H*Ph], 8.15 (m, 2 H, C_6H_5), 7.54 (m, 1 H; C_6H_5), 7.35 (m, 2 H, C_6H_5), 2.43 (m, 6 H, PC*H*CH$_3$), 1.15 [dvt, N = 14.0, ^3J(H,H) = 7.0 Hz, 18 H, PCHCH_3], 1.12 [dvt, N = 13.6, ^3J(H,H) = 6.8 Hz, 18 H, PCHCH_3], −2.93 [dt, ^2J(P,H) = 29.7, ^3J(H,H) = 4.4 Hz, 1 H, OsH]. − ^{13}C NMR (100.6 MHz, $CDCl_3$): δ = 295.5 (s, Os=*C*HPh), 185.4 [t, ^2J(P,C) = 9.0 Hz, CO], 160.5 [q, ^2J(C,F) = 36 Hz, O$_2$*C*CF$_3$], 156.6 (s, *i*-C_6H_5), 132.5, 130.4, 129.6 (all s, C_6H_5), 115.1 [q, ^1J(C,F) = 293 Hz, O$_2$C*C*F$_3$], 26.4 (br vt, P*C*HCH$_3$], 18.9, 18.8 (both s, PCH*C*H$_3$). − ^{31}P NMR (162.0 MHz, $CDCl_3$): δ = 53.0 [s, J(^{187}Os,^{31}P) = 170 Hz]. − ^{19}F NMR (188.0 MHz, CD_2Cl_2): δ = −75.0 (s). − $C_{28}H_{49}F_3O_3OsP_2$ (742.3): calcd. C 45.27, H 6.65; found C 45.04, H 6.32.

9. Preparation of [OsCl$_2$(=CHPh)(CO)(P*i*Pr$_3$)$_2$] (10): A solution of 100 mg (0.15 mmol) of **3** in 5 mL of toluene was treated with 1.80 mL of a ca. 1.0 M solution of HCl in toluene. A rapid change of color from orange to red occurred which was accompanied by the evolution of gas (H_2). The solvent was removed, the red air-stable solid was washed twice with 5 mL of pentane and dried; yield 102 mg (98%); m.p. 155°C. − IR (KBr): $\tilde{\nu}$ = 1915 cm^{-1} (CO). − ^{1}H NMR (400 MHz, C_6D_6): δ = 19.04 (s, 1 H, Os=C*H*Ph), 8.28 (br s, 2 H, C_6H_5), 7.07 (m, 3 H, C_6H_5), 2.72 (m, 6 H, PC*H*CH$_3$), 1.25 [dvt, N = 14.0, ^3J(H,H) = 7.0 Hz, 18 H, PCHCH_3], 1.08 [dvt, N = 13.6, ^3J(H,H) = 6.8 Hz, 18 H, PCHCH_3]. − ^{13}C NMR (100.6 MHz, C_6D_6): δ = 278.0 (s, Os=*C*HPh), 181.0 [t, ^2J(P,C) = 7.6 Hz, CO], 157.2 (s, *i*-C_6H_5), 132.9, 132.0, 130.3 (all s, C_6H_5), 25.6 (vt, N = 28.8 Hz, P*C*HCH$_3$), 20.1, 19.4 (both s, PCH*C*H$_3$). − ^{31}P NMR (162.0 MHz, C_6D_6): δ = 9.3 [s, J(^{187}Os,^{31}P) = 154 Hz]. − $C_{26}H_{48}Cl_2OOsP_2$ (699.8): calcd. C 44.63, H 6.91; found C 44.35, H 6.67.

10. Preparation of [OsCl(=CHPh)(CO)(H$_2$O)(P*i*Pr$_3$)$_2$]BF$_4$ (11): a) A solution of 234 mg (0.35 mmol) of **3** in 5 mL of benzene was treated with 1.0 mL of a 48% solution of HBF_4 in water (7.65 mmol) and vigorously stirred for 3 min at room temperature. The aqueous phase was separated and washed four times with 5 mL of benzene each. The organic phase and the benzene washings were combined, and the solution was concentrated to ca. 10 mL in vacuo. Upon standing for 3 h, an orange solid precipitated which was seperated from the mother liquor. The solid was then dissolved in 10 mL of ether and the solution stored for 10 h at −20°C. Orange-yellow crystals were formed which were filtered, washed twice with 2 mL of ether (0°C) and dried; yield 184 mg (68%). − b) A solution of 60 mg (0.09 mmol) of **3** in 5 mL of toluene was treated with 30 mg (0.09 mmol) of $[CPh_3]BF_4$ and stirred for 15 h at room temperature. The solvent was removed, the orange-yellow solid washed four times with 3 mL of hexane each and dried; yield 44 mg (64%); m.p. 109°C (dec.). − Λ = 65 cm$^2\Omega^{-1}$mol^{-1} (in CH_3NO_2). − IR (KBr): $\tilde{\nu}$ = 3375 cm^{-1} (OH), 1936 (CO). − ^{1}H NMR (200 MHz, CD_2Cl_2, −30°C): δ = 17.18 (s, 1 H, Os=C*H*Ph), 8.80, 7.97, 7.85 (all m, 1 H each, C_6H_5), 7.53 (m, 2 H, C_6H_5), 4.98 (s, 2 H, H_2O), 2.55 (m, 6 H, PC*H*CH$_3$), 1.26 [dvt, N = 14.7, ^3J(H,H) = 7.3 Hz, 18 H, PCHCH_3], 1.11 [dvt, N = 13.7, ^3J(H,H) = 6.9 Hz, 18 H, PCHCH_3]. − ^{13}C NMR (50.3 MHz, CD_2Cl_2, −30°C): δ = 274.2 [t, ^2J(P,C) ca. 15 Hz, Os=*C*HPh], 181.2 [t, ^2J(P,C) ca. 9 Hz, CO], 134.8, 134.6, 132.5, 130.7, 130.6 (all s, C_6H_5), 24.1 (vt, N = 25.5 Hz, P*C*HCH$_3$), 19.2, 18.0 (both s, PCH*C*H$_3$). − ^{19}F NMR (188.0 MHz, CD_2Cl_2, −30°C): δ = −148.7 (s). − ^{31}P NMR (81.0 MHz, CD_2Cl_2, −30°C): δ = 19.6 (s). − $C_{26}H_{51}BClF_4O_2OsP_2$ (770.1): calcd. C 40.55, H 6.68; found C 41.01, H 6.97.

11. Preparation of [Os(CH=CHPh)Cl(=CHPh)(CO)(P*i*Pr$_3$)$_2$] (13): A suspension of 112 mg (0.17 mmol) of **12** in 5 mL of hexane was

treated dropwise with 0.30 mL of a 1.4 M solution of $PhCHN_2$ in hexane at room temperature. A red solution was formed from which after stirring for 20 min a red solid precipitated. The mother liquor was decanted, the remaining red solid was washed three times with 3 mL of hexane (0°C) and dried; yield 104 mg (82%); m.p. 68°C (dec.). – IR (C_6H_6): $\tilde{\nu}$ = 1890 cm^{-1} (CO). – ^1H NMR (400 MHz, C_6D_6): δ = 19.08 (s, 1 H, Os=C*H*Ph), 9.92 [d, ^3J(H,H) = 19.0 Hz, 1 H, CH=C*H*Ph], 8.42, 7.59 (both br s, 2 H each, C_6H_5), 7.38 [dt, ^3J(H,H) = 19.0, ^3J(P,H) ≈ 2 Hz, 1 H, C*H*=CHPh], 7.27, 7.04 (both m, 3 H each, C_6H_5), 2.49 (m, 6 H, PC*H*CH_3), 1.14 [dvt, *N* = 14.0, ^3J(H,H) = 7.1 Hz, 18 H, PCHC*H*$_3$], 1.10 [dvt, *N* = 13.6, ^3J(H,H) = 6.8 Hz, 18 H, PCHC*H*$_3$]. – ^1H NMR (400 MHz, $CDCl_3$), isomer **A**: δ = 19.31 (s, 1 H, Os=C*H*Ph), 9.15 [d, ^3J(H,H) = 18.7 Hz, 1 H, CH=C*H*Ph], 8.35, 7.59 (both m, 2 H each, C_6H_5), 7.26 (m, C_6H_5), 6.99 (m, 1 H, C*H*=CHPh), 2.49 (m, 6 H, PC*H*CH_3), 1.11 [dvt, *N* = 14.0, ^3J(H,H) = 7.1 Hz, 36 H, PCHC*H*$_3$]; isomer **B**: δ = 18.66 (s, 1 H, Os=C*H*Ph), 9.38 [d, ^3J(H,H) = 18.9 Hz, 1 H, CH=C*H*Ph], 8.27, 7.59 (both m, 2 H each, C_6H_5), 7.26 (m, C_6H_5), 6.90 [d, ^3J(H,H) = 18.9 Hz, 1 H, C*H*=CHPh], 2.49 (m, 6 H, PC*H*CH_3), 0.99 [dvt, *N* = 14.0, ^3J(H,H) = 7.1 Hz, 36 H, PCHC*H*$_3$]. – ^{13}C NMR (100.6 MHz, C_6D_6): δ = 302.8 (m, Os=*C*HPh), 184.6 [t, ^2J(P,C) = 9 Hz, CO], 158.3 (s, *i*-C_6H_5), 147.4 [t, ^2J(P,C) = 6 Hz, *C*H=CHPh], 142.5 [t, ^2J(P,C) = 3 Hz, CH=*C*HPh], 133.4, 131.5, 130.2, 125.6, 125.5, 125.4 (all s, C_6H_5), 27.0 (vt, *N* = 28 Hz, P*C*HCH_3), 19.9, 19.7 (both s, PCH*C*H$_3$). – ^{31}P NMR (162.0 MHz, C_6D_6): δ = 2.1 [s, J(^{187}Os,^{31}P) = 154 Hz]. – ^{31}P NMR (162.0 MHz, $CDCl_3$), isomer **A**: δ = 3.5 (s); isomer **B**: δ = 2.6 (s). – $C_{34}H_{56}ClOOsP_2$ (768.5): calcd. C 53.14, H 7.35; found C 52.73, H 7.16.

12. Generation of [OsCl(η^3-PhCHCHCHPh)(CO)(P*i*Pr$_3$)$_2$] (14): A solution of 80 mg (0.10 mmol) of **13** in 2 mL of benzene was stirred for 24 h at room temperature. After the solvent was evaporated, a red oil was obtained. The ^1H-NMR spectrum of this material revealed that apart from small amounts of **13** and some unidentified by-products the dominating species (ca. 90%) is compound **14**. Attempts to seperate the by-products from the wanted complex **14** by fractional crystallisation or chromatographic techniques failed. Characteristic NMR data for **14**: ^1H NMR (400 MHz, C_6D_6): δ = 7.63 (br s, 4 H, C_6H_5), 7.20 (m, 6 H, C_6H_5), 6.09 [t, ^3J(H,H) = 11.6 Hz, 1 H, PhCHC*H*CHPh], 4.14 [dd, ^3J(H,H) = 11.6, ^2J(P,H) = 4.8 Hz, 2 H, PhC*H*CHC*H*Ph], 2.47 (m, 6 H, PC*H*CH_3), 1.40, 1.31 (both br m, 36 H, PCHC*H*$_3$). – ^{13}C NMR (100.6 MHz, C_6D_6): δ = 180.8 [t, ^2J(P,C) = 10.0 Hz, CO), 96.8 (br s, Ph*C*HCH*C*HPh), 67.0 (br s, PhCH*C*HCHPh), 31.0 (br s, PCH*C*H$_3$), 21.1 (br s, PCH*C*H$_3$), signals of phenyl carbon atoms are very broad and could not be exactly assigned. – ^{31}P NMR (162.0 MHz, C_6D_6): δ = −8.5 (br s).

13. Determination of the X-ray Crystal Structures of Compounds 4, 5, 10, and 11: Single crystals of **4** and **10** were obtained from toluene/hexane at −20°C, crystals of **5** from hexane at −20°C, and crystals of **11** from benzene/ether at −20°C. Data of **4** and **5** were collected on a Stoe–Siemens–Huber diffractometer with CCD area detector, those of **10** and **11** on an Enraf–Nonius CAD4 diffractometer using monochromated $Mo_{K\alpha}$ radiation (λ = 0.71073 Å). Intensity data were corrected for LP effects. Multi-scan absorption correction was applied for **4** and **5** and a semi-empirical absorption correction was applied for **10** and **11**. The structures of **4**, **10**, and **11** were solved by direct methods and the structure of **5** by Patterson and Fourier methods..[27] All non-hydrogen atoms were refined anisotropically by full-matrix least squares on F^2,[28] and a riding model was employed in the refinement of the hydrogen atom positions. The hydrogen atoms H19 and H20 of **4** and H10 of **5** were refined freely; H1 of **5** was refined with a distance restraint and by setting the displacement parameter to 120% of the equivalent isotropic U value of C1; H1, H2A, and H2B of **11** were refinded by setting the displacement parameter to 120% of the equivalent isotropic U value of C1 and O2. Two independent molecules (**A** and **B**) of **10** were found in the asymmetric unit. In Figure 3 only molecule **A** is shown. Table 1 contains crystallographic data of the whole asymmetric unit (the chemical formula belongs to one molecule). In the asymmetric unit of **11,** one benzene molecule and two half benzene molecules were found and refined anisotropically with restraints. Crystallographic data (excluding structure factors) for the structures reported in this paper have been deposited with the Cambridge Crystallographic Data Centre as supplementary publication no. CCDC-128215 (**4**), -128216 (**5**), -128217 (**10**), and -128218 (**11**). Copies of the data can be obtained free of charge on application to CCDC, 12 Union Road, Cambridge CB2 1EZ, UK (Fax: internat. + 44-1223/336–033; E-mail: deposit@ccdc.cam.ac.uk).

[1] [1a] H. Werner, A. Höhn, M. Dziallas, *Angew. Chem.* **1986**, *98*, 1112–1114; *Angew. Chem. Int. Ed. Engl.* **1986**, *25*, 1090–1092. – [1b] M. Dziallas, H. Werner, *J. Organomet. Chem.* **1987**, *333*, C29–C32. – [1c] H. Werner, T. Dirnberger, M. Schulz, *Angew. Chem.* **1988**, *100*, 993–994; *Angew. Chem. Int. Ed. Engl.* **1988**, *27*, 948–950. – [1d] A. Höhn, H. Werner, *J. Organomet. Chem.* **1990**, *382*, 255–272. – [1e] H. Werner, A. Höhn, M. Schulz, *J. Chem. Soc., Dalton Trans.* **1991**, 777–781. – [1f] M. Schulz, H. Werner, *Organometallics* **1992**, *11*, 2790–2795.

[2] M. A. Esteruelas, H. Werner, *J. Organomet. Chem.* **1986**, *303*, 221–231.

[3] [3a] M. A. Esteruelas, E. Sola, L. A. Oro, U. Meyer, H. Werner, *Angew. Chem.* **1988**, *100*, 1621–1622; *Angew. Chem. Int. Ed. Engl.* **1988**, *27*, 1563–1564. – [3b] A. Andriollo, M. A. Esteruelas, U. Meyer, L. A. Oro, R. A. Sanchez-Delgado, E. Sola, C. Valero, H. Werner, *J. Am. Chem. Soc.* **1989**, *111*, 7431–7437. – [3c] M. A. Esteruelas, C. Valero, L. A. Oro, U. Meyer, H. Werner, *Inorg. Chem.* **1991**, *30*, 1159–1160.

[4] H. Werner, M. A. Esteruelas, H. Otto, *Organometallics* **1986**, *5*, 2295–2299.

[5] M. A. Esteruelas, F. J. Lahoz, J. A. Lopez, L. A. Oro, C. Schlünken, C. Valero, H. Werner, *Organometallics* **1992**, *11*, 2034–2043.

[6] [6a] D. S. Bohle, G. R. Clark, C. E. F. Rickard, W. R. Roper, W. E. Shepard, L. J. Wright, *J. Chem. Soc., Chem. Commun.* **1987**, 563–565. – [6b] D. S. Bohle, G. R. Clark, C. E. F. Rickard, W. R. Roper, L. J. Wright, *J. Organomet.Chem.* **1988**, *358*, 411–447.

[7] H. Werner, W. Stüer, M. Laubender, C. Lehmann, R. Herbst-Irmer, *Organometallics* **1997**,*16*, 2236–2238.

[8] [8a] L.Vaska, *J. Am. Chem. Soc.* **1964**, *86*, 1943–1950. – [8b] T. J. Collins, K. R. Grundy, W. R. Roper, *J. Organomet. Chem.* **1982**, *231*, 161–172.

[9] [9a] A. F. Hill, W. R. Roper, J. M. Waters, A. H. Wright, *J. Am. Chem. Soc.* **1983**, *105*, 5939–5940. – [9b] P. J. Brothers, W. R. Roper, *Chem. Rev.* **1988**, *88*, 1293–1326.

[10] [10a] A. Nakamura, T. Yoshida, M. Cowie, S. Otsuka, J. A. Ibers, *J. Am. Chem. Soc.* **1977**, *99*, 2108–2117. – [10b] K. D. Schramm, J. A. Ibers, *Inorg. Chem.* **1980**, *19*, 2441–2448. – [10c] S. Gambarotta, C. Floriani, A. Chiesi-Villa, C. Guastini, *J. Am. Chem. Soc.* **1982**, *104*, 1918–1924. – [10d] L. Brandt, J. Wolf, H. Werner, *J. Organomet. Chem.* **1993**, *444*, 235–244. – [10e] L. B. Kool, M. D. Rausch, H. G. Alt, M. Herberhold, A. F. Hill, U. Thewalt, B. Wolf, *J. Chem. Soc., Chem. Commun.* **1986**, 408–409. – [10f] J. L. Polse, R. A. Andersen, R. G. Bergman, *J. Am. Chem. Soc.* **1996**, *118*, 8737–8738.

[11] Summarizing articles: [11a] W. A. Herrmann, *J. Organomet. Chem.* **1983**, *250*, 319–343. – [11b] D. Sutton, *Chem. Rev.* **1993**, *93*, 995–1022. – [11c] M. Putala, D. A. Lemenovskii, *Russ. Chem. Rev.* **1994**, *63*, 197–216.

[12] [12a] S. D. Robinson, M. F. Uttley, *J. Chem. Soc., Dalton Trans.* **1973**, 1213–1220. – [12b] G. B. Deacon, R. J. Phillips, *Coord. Chem. Rev.* **1980**, *33*, 227–250.

[13] M. A. Esteruelas, F. J. Lahoz, E. Onate, L. A. Oro, C. Valero, B. Zeier, *J. Am. Chem. Soc.* **1995**, *117*, 7935−7942.
[14] M. A. Gallop, W. R. Roper, *Adv. Organomet. Chem.* **1986**, *25*, 121−198.
[15] W. R. Roper, *J. Organomet. Chem.* **1986**, *300*, 167−190.
[16] [16a] M. Brookhart, G. O. Nelson, *J. Am. Chem. Soc.* **1977**, *99*, 6099−6100. − [16b] M. Brookhart, J. R. Tucker, G. R. Husk, *J. Organomet. Chem.* **1980**, *193*, C23−C26.
[17] M. S. Sanford, L. M. Henling, R. H. Grubbs, *Organometallics* **1998**, *17*, 5384−5389.
[18] M. A. Esteruelas, F. J. Lahoz, E. Onate, L. A. Oro, B. Zeier, *Organometallics* **1994**, *13*, 4258−4265.
[19] O. Gevert, unpublished results.
[20] C. Schlünken, H. Werner, *J. Organomet. Chem.* **1993**, *454*, 243−246.
[21] P. M. Maitlis, H. C. Long, R. Quyoum, M. L. Turner, Z.-Q. Wang, *J. Chem. Soc., Chem.Commun.***1996**, 1−8.
[22] [22a] R. Wiedemann, P. Steinert, M. Schäfer, H. Werner, *J. Am. Chem. Soc*. **1993**, *115*, 9864−9865. − [22b] R. Wiedemann, J. Wolf, H. Werner, *Angew. Chem*. **1995**, *107*, 1359−1361; *Angew. Chem. Int. Ed. Engl*. **1995**, *34*, 1244−1246. − [22c] H. Werner, R. Wiedemann, P. Steinert, J. Wolf, *Chem. Eur. J.* **1997**, *3*, 127−137.
[23] A. F. Hill, C. T. Ho, J. D. E. T. Wilton-Ely, *J. Chem. Soc., Chem.Commun.* **1997**, 2207−2208.
[24] H. Werner, W. Stüer, B. Weberndörfer, J. Wolf, *Eur. J. Inorg. Chem.* **1999**, in press.
[25] D. Huang, G. J. Spivak, K. G. Caulton, *New J. Chem.* **1998**, *22*, 1023−1025.
[26] H. Gerard, E. Clot, O. Eisenstein, *New J. Chem.* **1999**, *23*, 495−498.
[27] **4**: G. M. Sheldrick, *SHELXS-97*, University of Göttingen, Göttingen, Germany, **1990**; **5**: G. M. Sheldrick, *SHELXS-96*, University of Göttingen, Göttingen, Germany, **1990**; **10**, **11**: G. M. Sheldrick, *SHELXS-86*, University of Göttingen, Göttingen, Germany, **1986**.
[28] **4**: G. M. Sheldrick, *SHELXL-97*, University of Göttingen, Göttingen, Germany, **1997**; **5**: G. M. Sheldrick, *SHELXL-96*, University of Göttingen, Göttingen, Germany, **1996**; **10**, **11**: G. M. Sheldrick, *SHELXL-93*, University of Göttingen, Göttingen, Germany, **1993**.

Received June 29, 1999
[I99233]

Synthesis and Structure of [1]Borametallocenophanes of Titanium, Zirconium, and Hafnium

Holger Braunschweig,*[a] Carsten von Koblinski,[a] Maliya Mamuti,[a] Ulli Englert,[a] and Ruimin Wang[a]

Keywords: Boron / Titanium / Zirconium / Hafnium / Metallocenophanes / Metallocenophanes

Various [1]borametallocenophane complexes of all the group IV metals were obtained in high yield by a very efficient multistep, one-pot synthesis. By this method not only the biscyclopentadienyl and diindenyl complexes [{$R_2NB(\eta^5$-$C_5H_4)_2$}MCl_2] (M = Zr, R = Me, $SiMe_3$, **4a**, **b**; M = Hf, R = $SiMe_3$, **5**) and [{$(Me_3Si_2)NB(\eta^5$-$C_9H_6)_2$}MCl_2] (M = Ti, **6**; M = Zr, **7**) were obtained, but also complexes with two different η^5-coordinated ligands such as [{$i Pr_2NB(\eta^5$-$C_5H_4)(\eta^5$-$C_9H_6)$}MCl_2] (M = Zr, **8**; M = Hf, **9**). Some of compounds **4–9** were chosen to investigate their catalytic properties with respect to Ziegler-Natta-type polymerisation of olefins, and proved to be highly efficient for the preparation of polyethylene.

Introduction

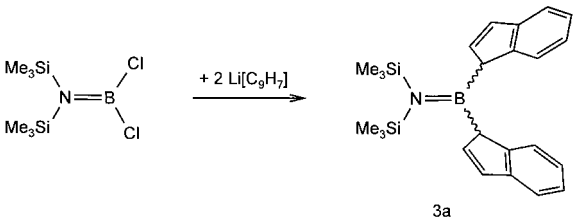
In the course of our investigations on both strained[1a,1b] and unstrained[2a,2b] [1]borametallocenophanes, we recently reported the first [1]boratitanocenophanes, which were obtained in high yields from a convenient one-pot synthesis. Metallocenophanes of group IV elements are of special interest due to their remarkable qualities as highly active Ziegler-Natta-type catalysts for olefin polymerisation.[3] Such catalytic processes could be accelerated by a bridging Lewis acidic centre such as boron.[4] Structurally authenticated boron-bridged metallocenophanes of group IV metals are restricted to a very few examples, including [{$(Me_2S)PhB(\eta^5$-$C_5H_4)_2$}$ZrCl_2$] (**1**) which has a four-coordinate boron atom in the bridge.[5] During the preparation of this paper, further zirconium complexes with three- and four-coordinate boron atoms [{$i Pr_2NB(\eta^5$-$C_5H_4)_2$}$ZrCl_2$] (**2a**), [{$i Pr_2NB(\eta^5$-$C_9H_6)_2$}$ZrCl_2$] (**2b**), [{(L)$PhB(\eta^5$-$C_9H_6)_2$}$ZrCl_2$] (L = PMe_3, thf, OEt_2; **2c**), obtained by an analogous method to that described for the synthesis of [{$(Me_3Si)_2NB(\eta^5$-$C_5H_4)_2$}$TiCl_2$],[2a,2b] were reported by Ashe and Reetz.[6a,6b]

In the present paper we report on the synthesis, structure and catalytic properties of several [1]borametallocenophanes of Ti, Zr, and Hf, which were obtained by convenient reactions in high yields.

Results and Discussion

Synthesis and Structure of $(Me_3Si)_2NB(C_9H_7)_2$ (3a, b)

As already reported for $(Me_3Si)_2NB(C_5H_5)_2$[2a] the corresponding diindenylborane $(Me_3Si)_2NB(C_9H_7)_2$ (**3a**) is obtained in almost quantitative yields as a colourless solid from the reaction of $(Me_3Si)_2NBCl_2$ with $Li[C_9H_7]$ according to Equation 1.



(1)

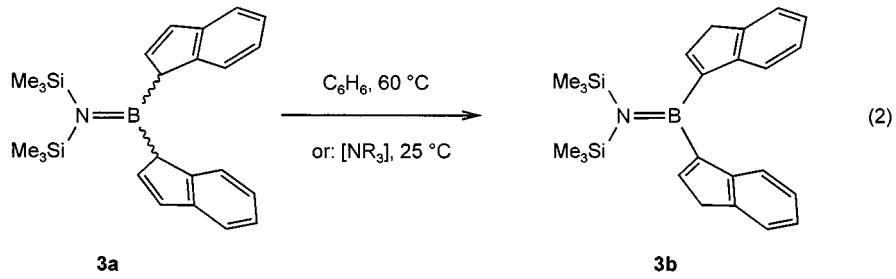
3a

The 1-indenyl isomer **3a**, in which boron is bound to a saturated carbon atom and thus adopts an allylic position, represents the kinetically controlled product of this reaction. A quantitative rearrangement yielding the thermodynamically more stable vinylic isomer **3b** is achieved by either heating **3a** for 2 h to 60°C in benzene or by treating **3a** with catalytic amounts of NEt_3 in benzene at room temperature (Equation 2). The spectroscopic data of **3a, b**, such as the distinct low-field shift in the ^{11}B NMR spectrum for the allylic isomer with respect to the vinylic isomer [δ = 57.6 (**3a**) and 50.6 (**3b**)], resemble those of corresponding diindenyl(organyl)boranes,[6b] diorganyl(indenyl)boranes[7a,b] and 1,2-diindenyldiboranes(4),[8] which were reported very recently to undergo the same type of rearrangement. Compound **3a**, with two stereocentres, is expected to form a mixture of a C_2-symmetrical *rac* and a C_S-symmetrical *meso* isomer. The presence of both isomers is evident from the double set of signals in the ^{13}C NMR spectra.

Single crystals of **3b** suitable for an X-ray structure analysis were obtained from hexane at −30°C. The compound crystallises in the monoclinic space group *C*2/*c* and the molecule adopts almost C_2 symmetry in the solid state (Figure 1). Both the boron and nitrogen atoms are in a trigonal-planar environment, and due to the steric demand of the bulky Me_3Si groups, the Si1−N−Si2 plane is twisted with respect to the C11−B−C21 plane. The corresponding torsion angles are −51.28° (Si1−N−B−C21) and −50.73° (Si2−N−B−C11). Hence, together with an extended B−N

[a] Institut für Anorganische Chemie der Technischen Hochschule, Templergraben 55, D-52056 Aachen, Germany
E-mail: holger.braunschweig@ac.rwth-aachen.de

 © WILEY-VCH Verlag GmbH, D-69451 Weinheim, 1999 1434−1948/99/1111−1899 $ 17.50+.50/0



bond length of 144.3(5) pm a less effective backbonding from nitrogen to boron can be assumed. Both B−C and C−C bond lengths are in the expected range and resemble the data known for the corresponding 1,2-diindenyldiborane(4) derivative.[8]

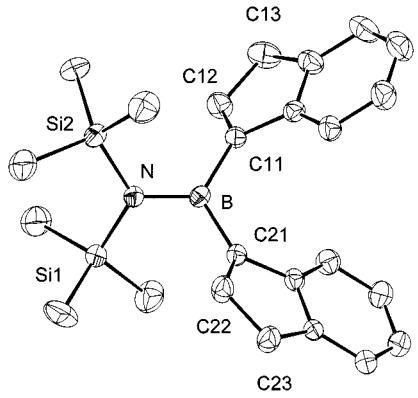


Figure 1. Structure of **3b** in the crystal (ellipsoids at 30% probability); selected distances (pm) and angles (°): B−N 144.3(5), B−C11 157.5(5), C11−C12 133.8(6), C12−C13 150.3(5); Si1−N−B 118.3(3); N−B−C11 120.1(4), C11−B−C21 118.9(3)

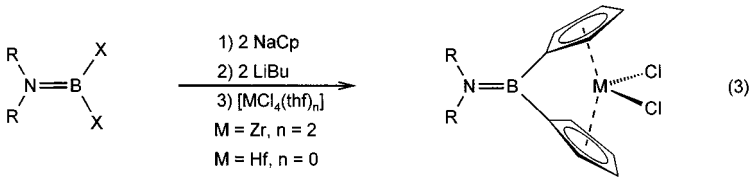
Synthesis and Structure of the [1]Borametallocenophanes

In analogy to the synthesis of [{$(SiMe_3)_2NB(\eta^5$-$C_5H_4)_2$}$TiCl_2$][2a,2b] the [1]borametallocenophanes [{$R_2NB(\eta^5$-$C_5H_4)_2$}MCl_2] (M = Zr, R = Me, $SiMe_3$, **4a**, **b**; M = Hf, R = $SiMe_3$, **5**) were obtained in three-step, one-pot syntheses according to Equation 3.[2b] In the case of **4a** the dibromoborane Me_2NBBr_2 served as starting material, whereas **4b** and **5** were obtained from the dichloro derivative $(Me_3Si)_2NBCl_2$. Although being sterically rather demanding, the latter aminodihaloborane is known to undergo substitutions of both chloride ligands more easily than the much smaller Me_2NBCl_2.[9a,9b] This is due to the electron-withdrawing effect of the silyl ligands, which enhances the electrophilicity of the boron centre. All products were isolated as yellow crystalline solids in high yields (**4a,** 91%; **4b,** 96%; **5,** 85%). These zirconium and hafnium complexes are readily soluble in CH_2Cl_2 and proved to be more stable towards decomposition in solution than the corresponding titanium derivative [{$(SiMe_3)_2NB(\eta^5$-$C_5H_4)_2$}-$TiCl_2$].[2a]

The structure of **4a**, **b** and **5** in solution was derived from multinuclear NMR spectra, showing the expected two pseudo triplets in the ^{1}H NMR spectra for the AA′BB′ spin system of the cyclopentadienyl protons at δ = 5.28, 6.62 (**4a**), 5.16, 6.61 (**4b**), and 5.54, 6.68 (**5**). The resonances in the ^{11}B NMR spectrum of **4b** and **5** at about δ = 47 resemble the signal of the uncoordinated ligand[2a] and show the expected low-field shift with respect to the signal of the dimethylamino derivative **4a** at δ = 38.7.

Suitable single crystals of **4a** were obtained by recrystallisation from a 70:30 mixture of CH_2Cl_2 and Et_2O at −30°C. The compound crystallises in the space group $P2_1/n$, and the molecule exhibits a slight deviation from the C_{2v} symmetry, which was assumed from its structure in solution (Figure 2). The B−N distance was found to be 138.4(4) pm, thus indicating a B−N double bond. As expected the two cyclopentadienyl ligands adopt an eclipsed orientation, and the geometry of **4a** is very similar to that of [{$(SiMe_3)_2NB(\eta^5$-$C_5H_4)_2$}$TiCl_2$],[2a] and to the corresponding zirconium complex [{iPr$_2$NB(η^5-$C_5H_4)_2$}$ZrCl_2$] (**2a**), the structure of which was described very recently.[6a]

The boron-bridged diindenyl complexes [{(Me_3Si_2)-$NB(\eta^5$-$C_9H_6)_2$}MCl_2] (M = Ti, **6**; M = Zr, **7**) were obtained according to the procedures described in Equations 4a and 4b. $(Me_3Si_2)NBCl_2$ was treated with two equivalents of Li[C_9H_7] in hexane, LiCl was removed by filtration, and after addition of Et_2O, the filtrate was treated with two equivalents of BuLi. The obtained slurry was subsequently reacted with [$TiCl_3(thf)_3$] or [$ZrCl_4(thf)_2$] at low tempera-



4a, b; M = Zr, R = Me, X = Br; R = Me_3Si, X = Cl
5; M = Hf, R = Me_3Si, X = Cl

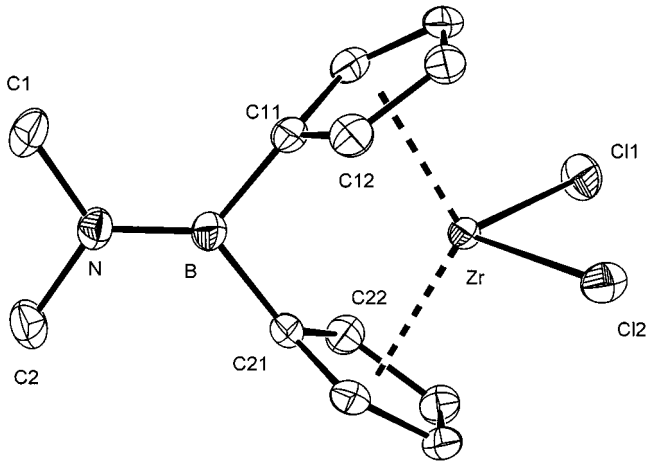


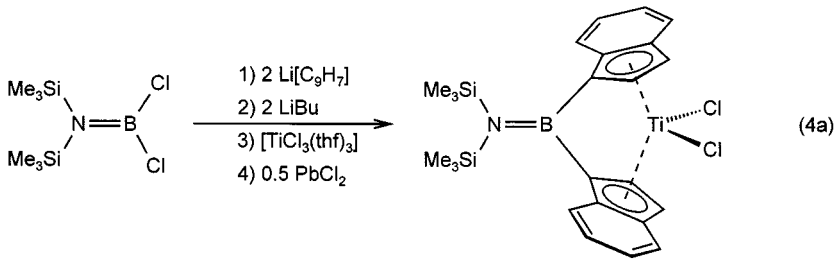
Figure 2. Structure of **4a** in the crystal (ellipsoids at 30% probability); selected distances (pm) and angles (°): Zr−Cl1 242.92(8), Zr−Cl2 245.79(9), B−N 138.4(4); Cl1−Zr−Cl2 100.87(3), C11−B−C21 105.9(3), C11−B−N 127.5(3), C21−B−N 126.5(3)

tures. In the case of the titanium complex **6** the intermediate Ti^{III} species was oxidised with $PbCl_2$.[10] The two complexes were isolated as dark red or orange crystalline materials, respectively, in yields of 71% (**6**) and 82% (**7**) and their constitutions in solution deduced from multinuclear NMR spectra. Although the general formation of a mixture of both *rac* (C_2 symmetry) and *meso* (C_s symmetry) isomers was reported for related element-bridged diindenyl complexes,[6a,6b,11] single sets of signals in the ^{13}C NMR spectra of **6** and **7** reveal the presence of only one isomer in our case. After reaction of **7** with two equivalents of LiMe, the corresponding complex $[\{(Me_3Si_2)NB(\eta^5\text{-}C_9H_6)_2\}ZrMe_2]$ was obtained,[12] and a single resonance for both metal-coordinated methyl groups in the NMR spectra indicates the presence of the *rac* isomer. This is further demonstrated by the formation of predominantly isotactic polypropylene (M.p. 116°C, triad ratio mm/mr/rr = 86:7:7 determined by ^{13}C NMR spectroscopy[13]) from **7** as a catalyst for the polymerisation of propene.

The preparation of [1]borametallocenophanes by the present method can be extended to the corresponding boron-bridged complexes with two different η^5-coordinated ligands, which have not previously been reported. This is demonstrated by the synthesis of $[\{i Pr_2NB(\eta^5\text{-}C_5H_4)(\eta^5\text{-}C_9H_6)\}MCl_2]$ (M = Zr, **8**; M = Hf, **9**) according to Equation 5. Stepwise treatment of iPr_2NBCl_2 with $Na[C_5H_5]$ and $Li[C_9H_7]$, subsequent reaction with two equivalents of BuLi, and addition of $[MCl_4(thf)_n]$ (M = Zr, n = 2; M = Hf, n = 0) afforded the mixed [1]borametallocenophanes **8**, **9** in 82% and 74% yield, respectively, as orange, crystalline solids. The spectroscopic data of both compounds, such as the ^{11}B NMR signals at about δ = 40, together with the expected patterns for η^5-cyclopentadienyl and η^5-indenyl ligands in the ^1H and ^{13}C NMR spectra prove their constitution in solution. A restricted rotation with respect to the boron−nitrogen double bond is indicated by double sets of signals for the isopropyl groups in both the ^1H and ^{13}C NMR spectra.

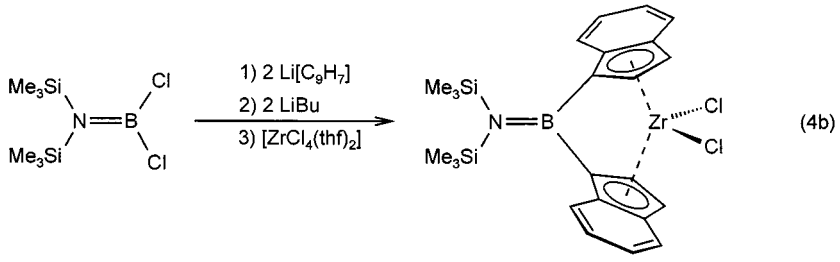
Conclusion

The synthetic method described in this paper and previously reported for $[\{(Me_3Si)_2NB(\eta^5\text{-}C_5H_4)_2\}TiCl_2]$ provides a convenient and general route to group IV [1]borametallocenophanes showing either η^5-cyclopentadienyl or η^5-indenyl ligands such as $[\{R_2NB(\eta^5\text{-}C_5H_4)_2\}MCl_2]$ (M = Zr, R = Me, $SiMe_3$, **4a**, **b**; M = Hf, R = $SiMe_3$, **5**) and $[\{(Me_3Si_2)NB(\eta^5\text{-}C_9H_6)_2\}MCl_2]$ (M = Ti, **6**; M = Zr, **7**). The novel complexes $[\{iPr_2NB(\eta^5\text{-}C_5H_4)(\eta^5\text{-}C_9H_6)\}MCl_2]$



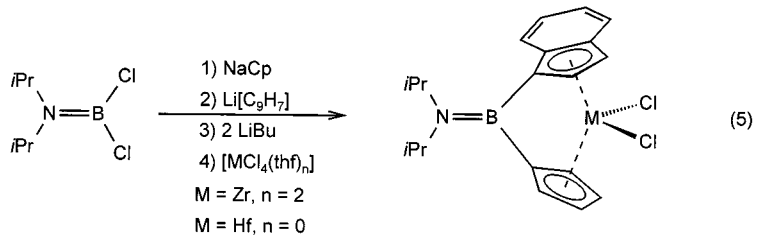
(4a)

6



(4b)

7



8; M = Zr
9; M = Hf

(M = Zr, **8**; M = Hf, **9**) showing two different η^5-coordinated ligands are obtained in a similar manner. Further studies will focus on the catalytic properties of these [1]Borametallocenophanes. Preliminary investigations have already shown them to be highly efficient catalysts for the Ziegler-Natta-type polymerisation of olefins, showing, for example, activities of 5258 kg PE·mol[catalyst]$^{-1}$h^{-1} (**6**) and 8905 kg PE·mol[catalyst]$^{-1}$h^{-1} (**4a**)

Experimental Section

All manipulations were carried out under a dry nitrogen atmosphere with common Schlenk techniques. Solvents and reagents were dried by standard procedures, distilled, and stored under nitrogen over molecular sieves. $(Me_3Si)_2NBCl_2$,[14] iPr_2NBCl_2,[15] $Na[C_5H_5]$,[16] $[ZrCl_4(thf)_2]$,[17] $[TiCl_3(thf)_3]$[17] and Me_2NBBr_2[18] were obtained according to literature procedures. NMR: Varian Unity 500 at 499.843 MHz (^{1}H, internal standard TMS), 150.364 MHz (^{11}B, BF3·OEt2 in C_6D_6 as external standard), 125.639 MHz (^{13}C{^{1}H}, APT, internal standard TMS); all NMR spectra were recorded in CD_2Cl_2 as solvent unless otherwise stated. Mass spectra were recorded on a Finnigan MAT 95 (70 eV) and elemental analyses (C, H, N) were obtained from a Carlo−Erba elemental analyzer, model 1106.

$(Me_3Si)_2NB(1\text{-}C_9H_7)_2$ (3a): $Li[C_9H_7]$ (7.38 g, 60.41 mmol) was suspended in 100 mL hexane, and a solution of $(Me_3Si)_2NBCl_2$ (7.31 g, 30.20 mmol) in 20 mL hexane was added at 0°C. The yellow suspension was allowed to warm to ambient temperature and stirred for 2 h. All volatiles were removed in high vacuum, and the remaining solid was extracted with 50 mL of hexane. After filtration **3a** was obtained as a white crystalline solid by cooling to −30°C (11.64 g, 96%). − ^{1}H NMR (C_6D_6): δ = 0.24 (s, 18 H, $SiMe_3$), 3.61 (m, 2 H, B−CH_{ind}), 6.06−7.43 (m, 12 H, CH_{ind}) − ^{11}B NMR: δ = 57.6 (s). − ^{13}C NMR: δ = 3.75 (isomer 1), 4.83 (isomer 2) ($SiMe_3$), 54.8 (br, B−C_{ind}), 120.8 (1), 121.0 (2), 123.6 (1), 123.9 (2), 124.8 (1), 125.4 (2), 125.9 (1), 126.4 (2), 131.3 (1), 131.9 (2), 135.0 (1), 136.3 (2) (CH_{ind}), 144.1 (1), 144.3 (2), 146.3 (1), 146.7 (2) (C_{ind}). − MS; *m/z* (%): 401 (90) [M$^+$], 386 (25) [M$^+$ − Me], 286 (40) [M$^+$ − ind]. − $C_{24}H_{32}BNSi_2$ (401.51): calcd. C 71.80, H 8.03, N 3.49; found C 71.69, H 8.21, N 3.25.

$(Me_3Si)_2NB(3\text{-}C_9H_7)_2$ (3b): Compound **3b** was quantitatively obtained by a) refluxing a solution of **3a** (2.00 g, 4.98 mmol) in 50 mL benzene for 3 h, or by b) treatment of **3a** (1.50 g, 3.74 mmol) with a catalytic amount of NEt_3 (0.1 mL) in 40 mL benzene for 2 h at ambient temperature. Suitable single crystals of **3b** were obtained by recrystallisation from hexane at −30°C. − ^{1}H NMR (C_6D_6): δ = 0.23 (s, 18 H, $SiMe_3$), 3.22 (m, 4 H, CH_{2ind}), 6.70−7.29 (m, 10 H, CH_{ind}) − ^{11}B NMR: δ = 50.6 (s). − ^{13}C NMR: δ = 4.66 ($SiMe_3$), 40.18 (CH_{2ind}), 122.97, 123.78, 124.74, 126.42, 128.29, 142.70, 144.29 (C_{ind}).

[{$Me_2NB(\eta^5\text{-}C_5H_4)_2$}$ZrCl_2$] (4a): $Na[C_5H_5]$ (1.69 g, 19.20 mmol) was suspended in 40 mL hexane and a solution of Me_2NBBr_2 (2.05 g, 9.55 mmol) in 10 mL hexane was added dropwise at 0°C. After warming to ambient temperature, the yellow suspension was stirred for 2 h. NaBr was removed by filtration, and the residue was washed with 15 mL of diethyl ether. The filtrate was cooled to 0°C and 13.00 mL (20.80 mmol) of 1.6 M BuLi in hexane was slowly added . A white precipitate was formed immediately, the suspension was allowed to come to ambient temperature and stirred for 16 h. The yellow suspension was cooled to −70°C and $[ZrCl_4(thf)_2]$ (3.62 g, 9.60 mmol) and 15 mL of diethyl ether was added. After warming to ambient temperature and stirring for an additional 2 h, the yellow suspension was filtered. The filtrate was stored overnight at −30°C to yield **4a** as a yellow, crystalline solid (3.02 g, 91%). − ^{1}H NMR ([D$_8$]toluene): δ = 2.49 (s, 6 H, NMe_2), 5.28 (m, 4 H, C_5H_4), 6.62 (m, 4 H, C_5H_4). − ^{11}B NMR: δ = 38.7 (s). − ^{13}C NMR: δ = 39.43 (NMe_2), 111.58, 125.69 (C_5H_4), 137.52 (C_{ipso}). − MS; *m/z* (%): 345 (60) [M$^+$], 330 (5) [M$^+$ − Me], 301 (20) [M$^+$ − NMe_2]. − $C_{12}H_{14}BCl_2NZr$ (345.19): calcd. C 41.75, H 4.09, N 4.06; found C 41.45, H 3.80, N 3.87.

[{$(Me_3Si)_2NB(\eta^5\text{-}C_5H_4)_2$}$ZrCl_2$] (4b): As described for **4a** $Na[C_5H_5]$ (1.94 g, 22.00 mmol) was treated with $(Me_3Si)_2NBCl_2$ (2.66 g, 11.00 mmol) and subsequently with 1.6 M BuLi (13.75 mL, 22.00 mmol) and $[ZrCl_4(thf)_2]$ (4.15 g, 11.00 mmol). Compound **4b** was obtained as a yellow crystalline material (4.87 g, 96%). − ^{1}H NMR (C_6D_6): δ = 0.11 (s, 18 H, $SiMe_3$), 5.16 (m, 4 H, C_5H_4), 6.61 (m, 4 H, C_5H_4). − ^{11}B NMR: δ = 47.4 (s). − ^{13}C NMR: δ = 5.05 ($SiMe_3$), 109.63, 124.95 (C_5H_4). − MS; *m/z* (%): 461 (100) [M$^+$], 446 (50) [M$^+$ − Me], 315 (45) [M$^+$ − 2($SiMe_3$)$_2$]. − $C_{16}H_{26}BCl_2NSi_2Zr$ (461.50): calcd. C 41.64, H 5.68, N 3.04; found C 41.50, H 5.80, N 3.09.

[{$(Me_3Si)_2NB(\eta^5\text{-}C_5H_4)_2$}$HfCl_2$] (5): As described for **4a** $Na[C_5H_5]$ (1.96 g, 22.23 mmol) was treated with $(Me_3Si)_2NBCl_2$ (2.69 g, 11.10 mmol) and subsequently with 1.6 M BuLi (13.94 mL, 22.30 mmol) and $HfCl_4$ (3.56 g, 11.10 mmol). Compound **5** was obtained as a yellow crystalline material (5.18 g, 85%). − ^{1}H NMR (CD_2Cl_2): δ = 0.30 (s, 18 H, $SiMe_3$), 5.54 (m, 4 H, C_5H_4), 6.68 (m, 4 H, C_5H_4). − ^{11}B NMR: δ = 46.7 (s). − ^{13}C NMR: δ = 4.91 ($SiMe_3$), 108.38, 123.96 (C_5H_4), 140.09 (C_{ipso}). − MS; *m/z* (%): 549 (35) [M$^+$], 534 (50) [M$^+$ − Me], 441 (20) [M$^+$ − $SiMe_3$ − Cl]. − $C_{16}H_{26}BCl_2HfNSi_2$ (548.77): calcd. C 35.02, H 4.78, N 2.55; found C 34.78, H 4.81, N 2.45.

[{$(Me_3Si)_2NB(\eta^5\text{-}C_9H_6)_2$}$TiCl_2$] (6): $Li[C_9H_7]$ (3.48 g, 28.50 mmol) was suspended in 40 mL hexane and a solution of $(Me_3Si)_2NBCl_2$ (3.44 g, 14.20 mmol) in 20 mL hexane was added dropwise at 0°C. After warming to ambient temperature, the yellow suspension was

stirred for 2 h. LiCl was removed by filtration and the residue washed with 15 mL of diethyl ether. The filtrate was cooled to 0°C and 17.81 mL (28.50 mmol) 1.6 M BuLi in hexane was slowly added. A white precipitate was formed immediately, the suspension was allowed to come to ambient temperature and stirred for 16 h. The orange suspension was cooled to −100°C and $[TiCl_3(thf)_3]$ (5.26 g, 14.20 mmol) was added. Whilst warming to ambient temperature the colour changed to dark violet. The suspension was stirred for 2 h and then treated with $PbCl_2$ (1.97 g, 7.10 mmol). After stirring for 16 h, all volatiles were removed in high vacuum, the remaining solid was extracted with 40 mL of CH_2Cl_2, and filtered. The filtrate was stored overnight at −30°C to yield **6** as a dark violet, crystalline solid (5.23 g, 71%). − ^{1}H NMR (CD_2Cl_2): δ = 0.29 (s, 18 H, $SiMe_3$), 6.84−7.52 (m, 12 H, CH_{ind}). − ^{11}B NMR: δ = 48.6 (s). − ^{13}C NMR: δ = 4.81 ($SiMe_3$), 115.83, 123.52, 124.82, 126.40, 127.62, 129.51 (CH_{ind}). − MS; *m*/*z* (%): 518 (10) [M^+], 503 (25) [M^+ − Me], 468 (50) [M^+ − Me − Cl]. − $C_{24}H_{30}BCl_2NSi_2Ti$ (518.30): calcd. C 55.62, H 5.83, N 2.70; found C 55.31, H 5.76, N 2.58.

[{$(Me_3Si)_2$NB(η^5-C_9H_6)$_2$}ZrCl$_2$] (7): As described for **4a** Li[C_9H_7] (2.76 g, 22.60 mmol) was treated with $(Me_3Si)_2NBCl_2$ (2.74 g, 11.30 mmol) and subsequently with 1.6 M BuLi (14.13 mL, 22.60 mmol) and $[ZrCl_4(thf)_2]$ (4.26 g, 11.30 mmol). Compound **7** was obtained as an orange crystalline material (5.20 g, 82%). − ^{1}H NMR (CD_2Cl_2): δ = 0.37 (s, 18 H, $SiMe_3$), 6.71−7.53 (m, 12 H, CH_{ind}). − ^{11}B NMR: δ = 48.5 (s). − ^{13}C NMR: δ = 5.18 ($SiMe_3$), 112.81, 113.32, 123.90, 125.94, 126.80, 127.54 (CH_{ind}). − MS; *m*/*z* (%): 561 (35) [M^+], 546 (5) [M^+ − Me], 399 (40) [M^+ − Zr − 2Cl], 285 (100) [M^+ − Zr − C_9H_6 − 2Cl]. $C_{24}H_{30}BCl_2NSi_2Zr$ (561.62): calcd. C 51.33, H 5.38, N 2.49; found C 51.02, H 5.45, N 2.28.

[{*i*Pr_2NB(η^5-C_5H_4)(η^5-C_9H_6)}ZrCl$_2$] (8): Na[C_5H_5] (1.51 g, 17.20 mmol) was suspended in 40 mL hexane and a solution of *i*Pr_2NBCl_2 (3.13 g, 17.20 mmol) in 5 mL hexane was added dropwise at 0°C. After warming to ambient temperature, the suspension was stirred for 2 h. NaCl was removed by filtration, the residue was washed with 5 mL hexane and the filtrate added dropwise to a suspension of Li[C_9H_7] (2.10 g, 17.20 mmol) in 20 mL hexane at 0°C. After stirring for 4 h at ambient temperature the LiCl was removed by filtration, washed with 5 mL hexane, and 10 mL of diethyl ether was added to the filtrate. The filtrate was cooled to 0°C and 21.50 mL (34.40 mmol) 1.6 M BuLi in hexane was added slowly. A white precipitate was formed immediately, the suspension was allowed to come to ambient temperature and stirred for 16 h. The suspension was cooled to −70°C and $[ZrCl_4(thf)_2]$ (6.49 g, 17.20 mmol) was added. After warming to ambient temperature and stirring for an additional 4 h, the orange suspension was filtered, evaporated to dryness, and the remaining solid was extracted with 30 mL CH_2Cl_2. After filtration compound **8** was obtained as an orange crystalline solid at −30°C (6.37 g, 82%). − ^{1}H NMR (CD_2Cl_2): δ = 1.18 (d, 6 H, Me), 1.39 (d, 6 H, Me), 3.50 (m, 1 H, C*H*Me_2), 4.08 (m, 1 H, C*H*Me_2), 6.21 (m, 1 H, CH_{ind}), 6.53 (m, 1 H, CH_{ind}), 6.46, 6.71 (2m, 4 H, C_5H_4), 7.28 (m, 2 H, CH_{ind}), 7.60 (m, 2 H, CH_{ind}). − ^{11}B NMR: δ = 40.0 (s). − ^{13}C NMR: δ = 23.42, 26.16 (Me), 40.07, 44.34 (*C*HMe_2), 116.23, 122.09, 122.96, 125.10 (C_5H_4), 126.19, 126.74, 127.65, 127.90, 133.61, 134.28 (CH_{ind}). − MS; *m*/*z* (%): 451 (5) [M^+], 436 (20) [M^+ − Me], 115 (100) [$C_9H_6^+$]. − $C_{20}H_{24}BCl_2NZr$ (451.36): calcd. C 53.22, H 5.36, N 3.10; found C 52.97, H 5.44, N 2.91.

[{*i*Pr_2NB(η^5-C_5H_4)(η^5-C_9H_6)}HfCl$_2$] (9): As described for **8** Na[C_5H_5] (0.30 g, 3.41 mmol) and Li[C_9H_7] (0.42 g, 3.41 mmol) were treated with *i*Pr_2NBCl_2 (0.62 g, 3.41 mmol) and subsequently 1.6 M BuLi with (4.26 mL, 6.82 mmol) in hexane and $HfCl_4$ (1.09 g, 3.41 mmol). Compound **9** was obtained as an orange, crystalline solid (1.36 g, 74%). − ^{1}H NMR (CD_2Cl_2): δ = 1.18 (d, 6 H, Me), 1.40 (d, 6 H, Me), 3.51 (m, 1 H, C*H*Me_2), 4.06 (m, 1 H, C*H*Me_2), 6.05, (m, 2 H, C_5H_4) 6.36 (m, 1 H, CH_{ind}), 6.48 (m, 2 H, C_5H_4), 6.55 (m, 1 H, CH_{ind}), 7.28 (m, 2 H, CH_{ind}), 7.61 (m, 2 H, CH_{ind}). − ^{11}B NMR: δ = 39.6 (s). − ^{13}C NMR: δ = 22.40, 25.56 (Me), 39.47, 46.34 (*C*HMe_2), 117.63, 121.19, 121.86, 124.00 (C_5H_4), 124.89, 125.64, 126.40, 126.60, 132.21, 134.18 (CH_{ind}). − MS; *m*/*z* (%): 539 (15) [M^+], 524 (40) [M^+ − Me], 504 (25) [M^+ − Cl], 115 (100) [$C_9H_6^+$]. − $C_{20}H_{24}BCl_2HfN$ (538.63): calcd. C 44.60, H 4.49, N 2.60; found C 43.95, H 4.44, N 2.31.

X-ray Structure Determination of 3b: $C_{24}H_{32}BNSi_2$; formula mass 401.51 g·mol^{-1}, monoclinic spacegroup *C*2/*c* (No. 15); *a* = 33.283(6), *b* = 7.069(2), *c* = 23.734(5) Å, β = 120.08(3)°, *V* = 4832(5) Å^3, *Z* = 8, ρ_{calcd} = 1.10 g·cm^{-3}, μL_{in} = 1.38 mm^{-1}. ENRAF-Nonius CAD4 diffractometer; CuK_α-radiation (λ = 1.54184 Å); graphite monochromator. Data collection at 293 K on a colourless crystal of about 0.44 × 0.22 × 0.16 mm^3 using ω scans in the diffraction range 3 < 2Θ < 65° yielded 8368 reflections. The data were corrected for Lorentz and polarization effects, and a numerical absorption correction by Gaussian integration[19] (min. trans. 0.669, max. trans. 0.817) was applied. After merging symmetry-equivalent data 4159 unique reflections remained for structure solution by direct methods[20] and subsequent Fourier difference syntheses. Least-squares refinement on structure factors[21] was performed with anisotropic displacement parameters for all non-hydrogen atoms and hydrogen atoms in calculated positions {C−H = 0.98 Å, U_{iso}(H) = 1.3 U_{eq}(C)}. Convergence was obtained for 253 variables, 2382 unique observations with $I > 1.0\,\sigma(I)$ and R = 0.064, R_w = 0.069, GOF = 1.145. A final difference Fourier map showed fluctuations of less than 0.65 eÅ^{-3}.

X-ray Structure Determination of 4a: $C_{12}H_{14}BCl_2NZr$; formula mass 345.19 g·mol^{-1}, monoclinic spacegroup $P2_1/n$ (No. 14); *a* = 11.532(3), *b* = 10.099(4), *c* = 12.179(4) Å, β = 104.70(2)°, *V* = 1372(1) Å^3, *Z* = 4, ρ_{calcd} = 1.67 g·cm^{-3}, μL_{in} = 2.67 mm^{-1}. ENRAF-Nonius CAD4 diffractometer; AgK_α-radiation (λ = 0.56087 Å); graphite monochromator. Data collection at 293 K on a colourless rod of about 0.40 × 0.20 × 0.15 mm^3 using ω−2Θ scans in the diffraction range 1 < Θ < 24° resulted in 9114 reflections. The data were corrected for Lorentz and polarization effects. After merging symmetry-equivalent data 4368 unique reflections remained for structure solution by direct methods;[20] the structure model was completed by Fourier difference syntheses. Least-squares refinement on structure factors[21] was performed with anisotropic displacement parameters for all non-hydrogen atoms and hydrogen atoms in calculated positions {C−H = 0.98 Å, U_{iso}(H) = 1.3 U_{eq}(C)}. Convergence was obtained for 168 variables, 3408 observed data with $I > 1.0\,\sigma(I)$ and R = 0.041, R_w = 0.039, GOF = 0.964. A final difference Fourier map showed fluctuations of less than 0.96 eÅ^{-3}.

Crystallographic data (excluding structure factors) for the structures) reported in this paper have been deposited with the Cambridge Crystallographic Data Centre as supplementary publication nos. CCDC-127944 (**3b**) and CCDC-127945 (**4a**). Copies of the data can be obtained free of charge on application to CCDC, 12 Union Road, Cambridge CB2 1EZ, UK [Fax: (internat.) +1223/336−033; E-mail: deposit@ccdc.cam.ac.uk].

Acknowledgments

We thank the Deutsche Forschungsgemeinschaft, Fonds der Chemischen Industrie and BASF AG, Ludwigshafen for support.

[1] [1a] H. Braunschweig, R. Dirk, M. Müller, P. Nguyen, D. P. Gates, I. Manners, *Angew. Chem.* **1997**, *109*, 2433−2435, *Angew. Chem. Int. Ed. Engl.* **1997**, *36*, 2338−2340. − [1b] H. Braunschweig, R. Dirk, U. Englert, A. Berenbaum, F. Jäkle, A. J. Lough, I. Manners, *J. Am. Chem. Soc.* **1999**, submitted.
[2] [2a] H. Braunschweig, C. von Koblinski, R. Wang, *Eur. J. Inorg. Chem.* **1999**, 69−73. − [2b] H. Braunschweig, C. von Koblinski, M. O. Kristen, Patentschrift, O.Z.0050/49643, **1998**, submitted.
[3] W. Kaminski, *J. Chem. Soc., Dalton Trans.* **1998**, 1413−1418, and references herein.
[4] J. A. Klang, D. B. Collum, *Organometallics* **1988**, *7*, 1532−1537.
[5] D. S. Stelck, P. J. Shapiro, N. Basickes, *Organometallics* **1997**, *16*, 4546−4550.
[6] [6a] A. J. Ashe, III, X. Fang, J. W. Kampf, *Organometallics* **1999**, *18*, 2288−2290. − [6b] M. T. Reetz, M. Willuhn, C. Psiorz, R. Goddard, *Chem. Commun.* **1999**, 1105−1106.
[7] [7a] I. D. Gridnev, A. Meller, *Main Group Metal Chemistry* **1998**, *21*, 271−277. − [7b] E. Barday, B. Frange, B. Hanquet, G. E. Herberich, *J. Organomet. Chem.* **1999**, *169*, 225−232.
[8] J. Knizek, I. Krossing, H. Nöth, W. Ponikwar, *Eur. J. Inorg. Chem.* **1998**, 505−509.
[9] [9a] H. Braunschweig, C. Kollann, U. Englert, Eur. J. Inorg. Chem. 1998, 465−468. − [9b] H. Braunschweig, C. Kollann, K. W. Klinkhammer, *Eur. J. Inorg. Chem.* **1999**, in press.
[10] J. Okuda, T. Eberle, T. P. Spaniol, *Chem. Ber.* **1997**, *130*, 209−215.
[11] R. L. Halterman, *Chem. Rev.* **1992**, *92*, 965−994.
[12] E. Samuel, M. D. Rausch, *J. Am. Chem. Soc.* **1973**, *95*, 6263−6269.
[13] [13a] F. A. Bovey, in: *NMR − Basic Principles and Progress*, *Vol. 4* (Eds.: P. Diehl, E. Fluck, R. Kosfeld), Springer-Verlag Berlin, **1971**. − [13b] H. H. Brintzinger, D. Fischer, R. Mühlhaupt, B. Rieger, R. Waymouth, *Angew. Chem.* **1995**, 1255−1283, *Angew. Chem. Int. Ed. Engl.* **1995**, *34*, 1143−1169.
[14] P. Geymayer, E. G. Rochow, U. Wannegat, *Angew. Chem.* **1964**, *76*, 499−500, *Angew. Chem. Int. Ed. Engl.* **1964**, *3*, 633.
[15] W. Gerrard, H. R. Hudson, E. F. Mooney, *J. Chem. Soc.* **1960**, 5168.
[16] K. Ziegler, H. Froitzheim-Kühlhorn, K. Hafner, *Chem Ber.* **1956**, *89*, 434.
[17] L. E. Manzer, *Inorg. Synth.* **1982**, *21*, 135−136.
[18] A. J. Banister, N. N. Greenwood, B. P. Straughan, J. Walker, *J. Chem. Soc.* **1964**, 995−1000.
[19] P. Coppens, L. Leiserowitz, D. Rabinovich, *Acta Crystallogr.* **1965**, *18*, 1035−1038.
[20] G. M. Sheldrick, "SHELXS86, Program for Structure Solution", University of Göttingen, Germany, **1986**.
[21] ENRAF-Nonius, "SDP Version 5.0", Delft, The Netherlands, **1989**.

Received July 1, 1999
[I99236]

Intramolecular Carbyne–Isocyanide Coupling to an Alkyne Ligand at a d^4 Tungsten Center

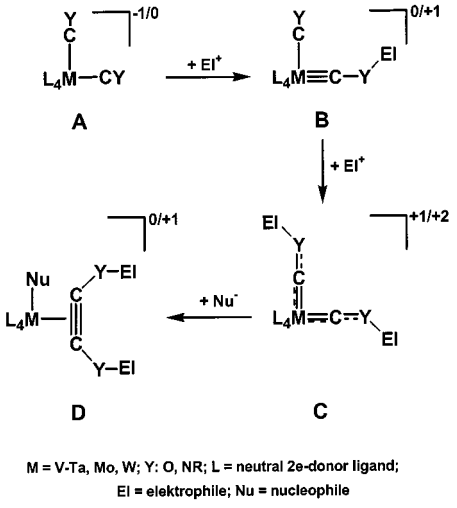
Alexander C. Filippou,*[a] Bernhard Lungwitz[a] and Gabriele Kociok-Köhn[a]

Keywords: Carbyne complexes / Carbene complexes / Alkyne complexes / C_1 building blocks / C–C coupling

Oxidative decarbonylation of $Cp^*(CO)_2W{\equiv}CNEt_2$ (**1**) with $PhICl_2$ affords the aminocarbyne complex *cis*-$Cp^*(Cl)_2(CO)W{\equiv}CNEt_2$ (**2**), which reacts with *t*BuNC to give the CO substitution product *cis*-$Cp^*(Cl)_2(t\text{BuNC})W{\equiv}CNEt_2$ (**3**) ($Cp^* = C_5Me_5$). Complex **3** undergoes a carbyne–isocyanide coupling reaction with HCl to yield the alkyne complex $Cp^*(Cl)_3W[\eta^2\text{-}t\text{Bu(H)NC}{\equiv}CNEt_2]$ (**4**). In comparison, the reaction of *cis*-$Cp^*(Cl)_2[P(OMe)_3]W{\equiv}CNEt_2$ (**5**) with HCl affords the 16e carbene complex $Cp^*(Cl)_3W{=}C(H)NEt_2$ (**6**) after elimination of $P(OMe)_3$. Complex **5** was obtained from the CO ligand-exchange reaction of **2** with $P(OMe)_3$. Treatment of **6** with *t*BuNC yields the cationic 18e carbene complex $[Cp^*(Cl)_2(t\text{BuNC})_2W{=}C(H)NEt_2]Cl$ (**7**). The mechanism of the C–C coupling reaction of **3** to give **4** is discussed and the crystal structures of **4** and **6** are described.

Introduction

The transition-metal-mediated conversion of carbon monoxide and related C_1 building blocks to organic compounds is a major goal in organometallic chemistry.[1] In this context a class of metal-centered C−C bond-forming reactions involving the coupling of two carbonyl or isocyanide ligands to an alkyne unit has attracted the attention of several research groups (Scheme 1).[2]



Scheme 1. Mechanism of the carbonyl/isocyanide coupling reactions of Group V and VI transition metal complexes; first ionic charge: M = V−Ta, second ionic charge: M = Mo, W

In the first two steps of these reactions successive addition of an electrophile occurs to the O/N atom of the carbonyl/isocyanide ligand leading initially to the carbyne complex **B** and then to the bis-carbyne complex **C**.[3] In the last step a carbyne−carbyne coupling reaction of **C** affords the alkyne complex **D** (Scheme 1).[3g,3k−3m,3o−3q] The carbonyl or isocyanide ligands in **A** and **B** are activated for an electrophilic addition at the heteroatom. This activation occurs upon coordination of these ligands to an octahedral, "electron-rich" d^6 metal center, which is known to form strong metal−carbon triple bonds.[3,4] It was therefore interesting to elucidate whether such ligand-coupling reactions could also occur at transition-metal centers with a different d electron configuration. This has prompted us to carry out the following work reporting on the intramolecular coupling of a carbyne with an isocyanide ligand at a d^4 tungsten center.

Results and Discussion

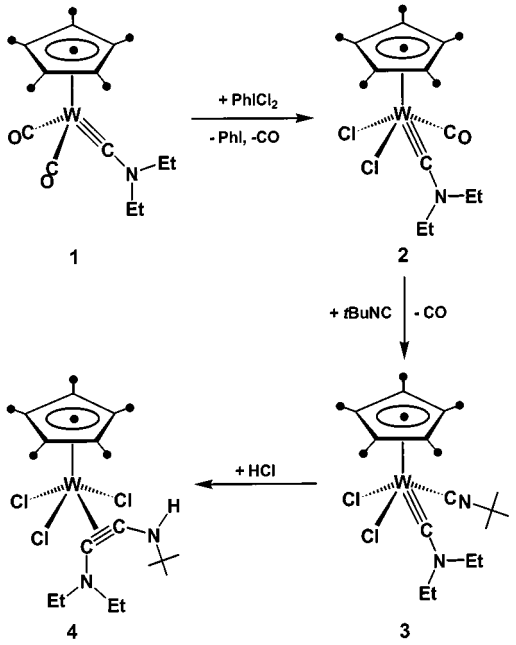
Starting material for the reactions described below was the W^{II} aminocarbyne complex **2**,[4] which was prepared upon oxidative decarbonylation of **1**[5] with one equivalent of $PhICl_2$ in dichloromethane and isolated as a violet solid in 88% yield (Scheme 2). Complex **2** is readily soluble in CH_2Cl_2 and THF, poorly soluble in Et_2O, insoluble in pentane and decomposes upon heating at 176°C.

Treatment of **2** with *t*BuNC in refluxing toluene yielded the CO substitution product **3**. Complex **3** was isolated in 76% yield as a rose-colored, thermally stable solid, which melts at 105°C (Scheme 2). **3** undergoes a selective and fast carbyne−isocyanide coupling reaction with HCl in diethyl ether to afford the violet W^{IV} alkyne complex **4** in 92% yield (Scheme 2). Complex **4** is thermally stable in the solid state and decomposes upon heating at 157°C.

Complexes **2**−**4** were fully characterized (see Experimental Section). The IR spectra of **2** and **3** in CH_2Cl_2 show an intense absorption for the $\nu(C_{carbyne}{\equiv}N)$ stretching vibration at $\tilde{\nu}$ = 1600 and 1571 cm^{-1}, which indicates the strong π conjugation of the amino group with the tungsten−carbon triple bond.[5] The ^1H- and $^{13}C\{^1H\}$-NMR

[a] Fachinstitut für Anorganische und Allgemeine Chemie der Humboldt-Universität zu Berlin,
Hessische Straße 1−2, D-10115 Berlin
Fax: (internat.) +49 (0)30/20936939
E-mail: filippou@chemie.hu-berlin.de

 © WILEY-VCH Verlag GmbH, D-69451 Weinheim, 1999 1434−1948/99/1111−1905 $ 17.50+.50/0



Scheme 2. Syntheses of the complexes **2**, **3** and **4**

spectra of **2** and **3** at 293 K display one set of resonances for the methyl and methylene protons of the aminocarbyne ligand indicating a fast rotation of the diethylamino group around the $C_{carbyne}-N$ bond. The methylene protons of each ethyl group are diastereotopic because of the C_1 symmetry of **2** and **3**. However, they are isochronous by accident and give rise to one quadruplet resonance in the ^{1}H-NMR spectra of **2** and **3** at 293 K. Variable-temperature ^{1}H-NMR spectra (300 MHz) of **2** in CD_2Cl_2 show this complex to be fluxional due to hindered rotation of the amino group about the $C_{carbyne}-N$ bond. The free energy of activation, $\Delta G^{\neq}(T_c)$, for the site exchange of the ethyl groups was calculated at the coalescence temperature T_c of the methyl proton resonances (T_c = 191 K, 300 MHz) to be 39.8 kJ mol^{-1}. The activation barrier is smaller than that of *cis*-Cp(Cl)$_2$(CO)W≡CN*i*Pr$_2$ [$\Delta G^{\neq}$ = 50.5 kJ mol^{-1}] and *cis*-Cp*(Cl)$_2$(CO)W≡CN*i*Pr$_2$ [$\Delta G^{\neq}$ = 47.4 kJ mol^{-1}], but similar to that of *cis*-Cp*(Br)$_2$(CO)W≡CNEt$_2$ [$\Delta G^{\neq}$ = 39.6 kJ mol^{-1}].[5c,6] Further support for the structures of **2** and **3** was given by the ^{13}C{^{1}H}-NMR spectra, which display a carbyne−carbon resonance at low field (**2**: δ = 310.0; **3**: δ = 306.4). This resonance is accompanied by tungsten satellites due to coupling with the ^{183}W nucleus. The ^1J(W,C) coupling constant of 210.0 (**2**) and 223.3 Hz (**3**) is typical of 18e W^{II} aminocarbyne complexes.[4,5c] In comparison, two low-field resonances are observed in the ^{13}C{^{1}H}-NMR spectrum of **4** (δ = 218.5, 219.3) indicating the presence of a 4e-donor alkyne ligand.[3c,3g,3k,7] Furthermore, an intense absorption band is observed in the IR spectrum of **4** in CH_2Cl_2 at 1667 cm^{-1}, which can be assigned to the ν(N=C=C=N) stretching vibration of the diaminoacetylene ligand and suggests an extensive delocalization of the amino-nitrogen lone-pair electrons in the alkyne ligand.[3c,3g,3k] Further evidence for this was given by the NMR spectra of **4** revealing a "frozen" rotation of the diethylamino group about the $C_{alkyne}-N$ bond (see Experimental Section) and the single-crystal X-ray diffraction study of **4**, which shows rather short $C_{alkyne}-N$ bonds [1.301(5) and 1.347(5) Å] and $W-C_{alkyne}$ bonds [2.008(4) and 2.043(4) Å], a long $(C-C)_{alkyne}$ bond of 1.366(6) Å and planar amino groups (Figure 1).[3g,3k,7] Planarity of the amino groups is indicated by the sum of bond angles at the atoms N1 and N2 of 359.3 and 354.6°, respectively. Other features of the molecular structure of **4** are the near orthogonality of the alkyne-ligand plane defined by the atoms W,C6,C7 and the Cp* ring plane (dihedral angle = 80.9°), as well as the *trans* position of the *t*Bu substituent.[8]

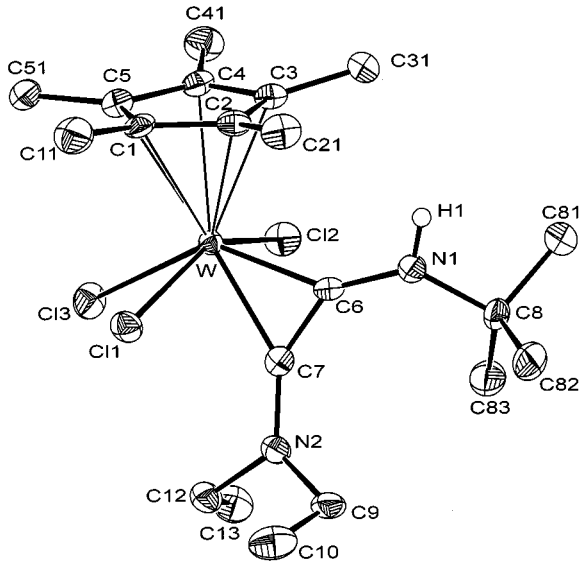
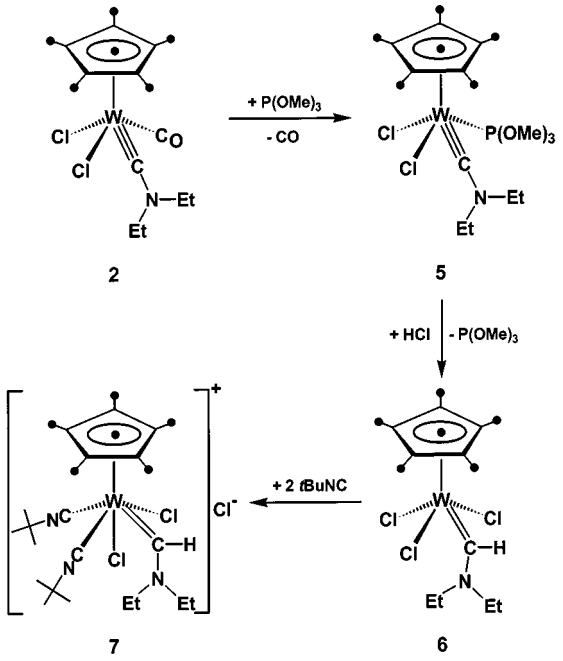


Figure 1. ZORTEP plot of the molecular structure of **4** with the thermal ellipsoids drawn at the 50% probability level; hydrogen atoms are omitted for clarity reasons except that bonded to the nitrogen atom N1; selected bond lengths [Å] and angles [°]: W−C6 2.008(4), W−C7 2.043(4), W−Cl1 2.4457(13), W−Cl2 2.4817(12), W−Cl3 2.4477(12), C6−C7 1.366(6), C6−N1 1.347(5), C7−N2 1.301(5), W−C_g 2.089, (C_g denotes the center of gravity of the Cp* ring), Cl1−W−Cl2 149.04(4), Cl1−W−Cl3 80.92(4), Cl2−W−Cl3 79.21(4), N1−C6−C7 140.5(4), N2−C7−C6 142.4(4), C6−W−C7 39.4(2), W−C6−N1 147.4(3), W−C7−N2 146.8(3), C6−N1−C8 129.4(4), C7−N2−C9 123.5(4), C7−N2−C12 119.5(4), C9−N2−C12 116.3(4)

We were interested to elucidate the mechanism of the acid-promoted carbyne−isocyanide coupling reaction of **3** (Scheme 2) and therefore prepared the aminocarbyne complex **5** from **2** and P(OMe)$_3$ by thermal CO ligand exchange in THF (Scheme 3).

Complex **5** was isolated after purification by column chromatography on silanized silica as an orange solid in 77% yield. It is readily soluble in CH_2Cl_2 and THF, sparingly soluble in Et_2O and decomposes upon heating at 98°C. Treatment of **5** with one equivalent of HCl afforded, after elimination of P(OMe)$_3$, the 16e tungsten(IV) aminocarbene complex **6** as a red, water-sensitive solid in 64% yield (Scheme 3).[4] Complex **6** is very soluble in CH_2Cl_2, sparingly soluble in Et_2O and decomposes upon heating at 135°C.



Scheme 3. Syntheses of the complexes **5**, **6** and **7**

The reaction of complex **6** with *t*BuNC was studied. Addition of the isocyanide to the Lewis acidic tungsten center of **6** would be expected to give the 18e carbene complex $Cp^*(Cl)_3(tBuNC)W{=}C(H)NEt_2$, which would rearrange to afford the alkyne complex **4**, if addition of HCl to the tungsten–carbon triple bond of **3** is the first step of the carbyne–isocyanide coupling reaction of **3** to give **4** (Scheme 2). However, treatment of **6** with *t*BuNC in CH_2Cl_2 afforded the cationic 18e tungsten(IV) aminocarbene complex **7** selectively,[4] which was isolated as a yellow solid in 82% yield (Scheme 3). The outcome of this reaction was independent of the molar ratio of the reactants, half of the starting material **6** being converted into **7**, when only one equivalent of *t*BuNC was used. These results suggest that carbene complex intermediates are not formed during the reaction of **3** with HCl.[3f,3p,9] Instead of this, they indicate a reaction pathway involving protonation of **3** at the isocyanide nitrogen atom followed by spontaneous carbyne–carbyne ligand coupling to afford the alkyne complex **4**. This suggestion is supported by earlier work showing that the 2e-oxidation of W^{II} bis(aminocarbyne) complexes is accompanied by C–C coupling of the carbyne ligands.[3g]

Complexes **5**–**7** were also fully characterized (Experimental Section). The IR spectrum of the aminocarbyne complex **5** in CH_2Cl_2 displays an intense absorption for the $\nu(C_{carbyne}{\equiv}N)$ stretching vibration at 1547 cm^{-1}. This absorption appears at lower wavenumbers than that of **2** and **3** indicating stronger metal–carbyne back bonding.[5] The ^{1}H-NMR spectrum of **5** at 293 K shows one triplet resonance for the methyl protons and two doublets of quadruplets for the diastereotopic methylene protons of the aminocarbyne ligand due to fast rotation of the diethylamino group about the $C_{carbyne}$–N bond and the presence of only the C_1-symmetric *cis* stereoisomer in solution.[5c] The

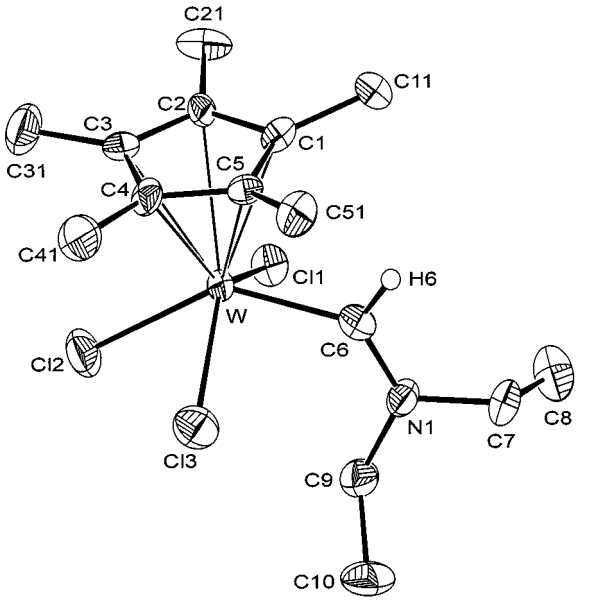


Figure 2. ZORTEP plot of the molecular structure of **6** with the thermal ellipsoids drawn at the 50% probability level; hydrogen atoms are omitted for clarity reasons except that bonded to the carbon atom C6; selected bond lengths [Å] and angles [°]: W–C6 2.065(7), W–Cl1 2.413(2), W–Cl2 2.418(2), W–Cl3 2.382(2), W–C_g 1.979 (C_g denotes the center of gravity of the Cp* ring), C6–N1 1.300(9), Cl1–W–Cl2 81.93(7), Cl1–W–Cl3 133.49(7), Cl2–W–Cl3 81.08(8), Cl1–W–C6 81.8(2), Cl2–W–C6 138.5(3), Cl3–W–C6 83.0(2), W–C6–N1 129.2(6), C6–N1–C7 120.6(7), C6–N1–C9 123.2(6), C7–N1–C9 116.1(6)

$^{13}C\{^1H\}$ spectrum of **5** diplays a doublet resonance for the carbyne–carbon nucleus at $\delta = 306.5$ [^2J(P,C) = 37.8 Hz]. The aminocarbene complexes **6** and **7** are distinguished by an IR absorption band of medium intensity at 1508 and 1579 cm^{-1}, which is assigned to the $\nu(C_{carbene}{\equiv}N)$ stretching vibration. The position of this band indicates the strong π interaction of the amino group with the metal–carbon double bond. This is supported by the temperature-dependent ^{1}H-NMR spectra of **6** (400 MHz) in the range of 233–293 K revealing a hindered rotation of the diethylamino group about the $C_{carbene}$–N bond. The free energy of activation for the site exchange of the inequivalent ethyl groups was found to be 57.3 kJ mol^{-1}. Furthermore, the ^{1}H-NMR spectrum of **7** (400 MHz) in CD_2Cl_2 at 293 K displays two sets of resonances for the methyl and methylene groups indicating that rotation of the diethylamino group around the $C_{carbene}$–N bond is slow on the NMR time scale. The ^{1}H-NMR spectra of **6** and **7** show a singlet resonance at low field (**6**: $\delta = 10.56$; $\delta = 9.95$) for the proton bound to the carbene carbon atom. Accordingly, the carbene carbon resonances of **6** and **7** at $\delta = 248.7$ and 230.9 are split into doublets in the proton-coupled ^{13}C-NMR spectra. The ^1J(C,H) coupling constant of the 16e complex **6** is, at 140.1 Hz, of similar magnitude to that of the 18e complex **7** (144.2 Hz) and excludes any agostic interaction of the C–H bond with the metal center in **6**.[9,10] This is verified by the solid-state structure of **6** showing a W–$C_{carbene}$–N bond angle [W–C6–N1 = 129.2(6)°] in the range found for nondistorted carbene ligands (Figure

2).[10,11] The W−$C_{Carbene}$ bond of 2.065(7) Å is shorter than that of structurally related W^{II} aminocarbene complexes {e.g. [*cis*-Cp*$(CO)_2$(Cl)W=C(H)NEt_2]: W−C = 2.141(3) Å} due to the smaller covalent radius of tungsten(IV). The short $C_{carbene}$−N bond of 1.300(9) Å reflects the double-bond character of this bond in full agreement with the spectroscopic data of **6**. The plane of the aminocarbene ligand passing through the atoms W, C6, and N1 is almost perpendicular to the Cp* ring plane (dihedral angle between the best planes = 88.5°).

Conclusion

The carbyne−isocyanide coupling reaction of *cis*-Cp*$(Cl)_2$(*t*BuNC)W≡$CNEt_2$ (**3**) with HCl to give the alkyne complex Cp*$(Cl)_3$W[η^2-*t*Bu(H)NC≡$CNEt_2$] (**4**) shows that electrophilic activation of C_1 ligands related to carbon monoxide, is also possible at a metal center in high oxidation state and induces C−C bond formation. In comparison, the aminocarbyne complex *cis*-Cp*$(Cl)_2$[$P(OMe)_3$]W≡$CNEt_2$ (**5**) adds HCl to the metal−carbon triple bond to afford the 16e aminocarbene complex Cp*$(Cl)_3$W=C(H)NEt_2 (**6**) after elimination of $P(OMe)_3$. The reaction of **6** with *t*BuNC to give the 18e carbene complex [Cp*$(Cl)_2$(*t*BuNC)W=C(H)NEt_2]Cl (**7**) suggests that electrophilic activation of **3** occurs upon protonation of the isocyanide ligand at the nitrogen atom.

Experimental Section

General: Standard inert-atmosphere techniques were used for all syntheses and sample manipulations. The solvents were dried by standard methods (pentane with CaH_2, diethyl ether, THF and toluene with Na/benzophenone, CH_2Cl_2 with P_2O_5 and Na/Pb alloy) and distilled under argon prior to use. Column chromatography was carried out on a silanized silica support (Merck 7719; 0063−0.200 mm) as the stationary phase in a thermostated column of 15-cm length and 2-cm diameter. The silanized silica was dried in vacuo at 150°C prior to use. Complex **1**,[5b] $PhICl_2$,[12] and *t*BuNC[13] were prepared according to literature procedures. $P(OMe)_3$ was distilled under argon prior to use. All other chemicals were commercially available. − Elemental analyses were obtained from the Central Analytical Group of the Department of Chemistry of the Humboldt-Universität zu Berlin and the Microanalytical Laboratory of the Institute of Inorganic Chemistry of the Technische Universität München. − Solution IR spectra were recorded on a Bruker IFS-55 spectrometer using a NaCl cell. ^{1}H-, $^{13}C\{^1H\}$-, and $^{31}P\{^1H\}$-NMR spectra were recorded on a Bruker AM-300 or a Jeol GX-400 spectrometer in dry, deoxygenated [D_2]dichloromethane. The ^{1}H- and $^{13}C\{^1H\}$-NMR spectra were calibrated against the internal residual proton and natural-abundance ^{13}C resonances of the deuterated solvent ([D_2]dichloromethane, δ_H = 5.32 and δ_C = 53.8) and the $^{31}P\{^1H\}$-NMR spectra against an external 85% H_3PO_4 aqueous solution. − Mass spectra were obtained with a Hewlett−Packard 5995A or a Varian MAT 311 A spectrometer; *m*/*z* values are given relative to the ^{184}W and ^{35}Cl isotopes. − Melting points were determined using a Büchi 530 melting point apparatus and are not corrected. The samples were sealed under argon in capillary tubes and heated with a rate of 1 K min^{-1}. − IR spectra of the heated samples were recorded and compared with those of authentic samples to determine whether the compounds had decomposed.

***cis*-Cp*$(Cl)_2(CO)$W≡$CNEt_2$ (2):** A solution of **1** (0.46 g, 1.00 mmol) in 20 mL of CH_2Cl_2 was cooled to −78°C and treated with a solution of freshly prepared $PhICl_2$ (0.275 g, 1.00 mmol) in 10 mL of CH_2Cl_2. The reaction mixture was allowed to warm to room temperature and stirred for 2 h. Evolution of gas was observed and the color of the solution changed from intense yellow to violet. The complete conversion of **1** to **2** was confirmed by IR spectroscopy in the region of 2200−1500 cm^{-1}. The purple solution was concentrated in vacuo to a few milliliters and a diethyl ether/pentane mixture (1:1) was added to precipitate complex **2**. The supernatant solution was discarded and the residue was washed twice with 10 mL of a diethyl ether/pentane mixture (1:1) and dried in vacuo. Yield 0.44 g (88%), violet, microcrystalline solid, m.p. 176°C (decomp.). − IR (CH_2Cl_2): $\tilde{\nu}$ = 1986 cm^{-1}, vs [ν(CO)], 1600 s [$\nu(C_{carbyne}\cdots N)$]. − ^{1}H NMR (400 MHz, CD_2Cl_2, 293 K): δ = 1.32 [t, ^3J(H,H) = 7.3 Hz, 6 H, $N(CH_2CH_3)_2$], 2.05 (s, 15 H, C_5Me_5), 3.50 [q, ^3J(H,H) = 7.3 Hz, 4 H, $N(CH_2CH_3)_2$]. − $^{13}C\{^1H\}$ NMR: (100.6 MHz, CD_2Cl_2, 293 K): δ = 11.8 (C_5Me_5), 14.9 [$N(CH_2CH_3)_2$], 50.6 [$N(CH_2CH_3)_2$], 109.3 (C_5Me_5), 228.2 [CO, ^1J(W,C) = 135.6 Hz], 310.0 [W≡C, ^1J(W,C) = 210.0 Hz]. − EI-MS (70 eV): *m*/*z* = 473 [M^+ − CO], 444 [M^+ − CO − Et], 389 [M^+ − CO − Et − EtNC]. − $C_{16}H_{25}Cl_2NOW$ (502.14): calcd. C 38.27, H 5.02, Cl 14.12, N 2.79, O 3.19, W 36.61; found C 38.17, H 4.85, Cl 14.52, N 3.05, O 3.75, W 36.99%.

***cis*-Cp*$(Cl)_2$(*t*BuNC)W≡$CNEt_2$ (3):** A suspension of **2** (1.02 g, 2.03 mmol) in 50 mL of toluene was treated at ambient temperature with *t*BuNC (0.253 mL, 2.23 mmol) and then refluxed for 2 h. The color of the solution changed from violet to bright-red. An IR spectrum of the solution was recorded to confirm the complete conversion of **2** to **3**. The solution was then evaporated to dryness, the residue dissolved in a minimum amount of CH_2Cl_2 and the solution treated at −78°C with 10 mL of diethyl ether and 20 mL of pentane to precipitate complex **3**. This procedure was repeated once to afford **3** as a rose-colored, microcrystalline solid. − Yield 0.86 g (76%), m.p. 105°C. − IR (CH_2Cl_2): $\tilde{\nu}$ = 2135 cm^{-1}, vs [ν(*t*BuN≡C)], 1571 s [$\nu(C_{carbyne}\cdots N)$]. IR (toluene): $\tilde{\nu}$ = 2129 cm^{-1}, vs [ν(*t*BuN≡C)], 1577 s [$\nu(C_{carbyne}\cdots N)$]. − ^{1}H NMR (300 MHz, CD_2Cl_2, 293 K): δ = 1.29 [t, ^3J(H,H) = 7.2 Hz, 6 H, $N(CH_2CH_3)_2$], 1.56 (s, 9 H, Me_3C), 1.98 (s, 15 H, C_5Me_5), 3.46 [q, ^3J(H,H) = 7.2 Hz, 4 H, $N(CH_2CH_3)_2$]. − $^{13}C\{^1H\}$ NMR: (75.5 MHz, CD_2Cl_2, 293 K): δ = 11.9 (C_5Me_5), 15.4 [$N(CH_2CH_3)_2$], 31.2 (Me_3C), 49.5 [$N(CH_2CH_3)_2$], 58.5 (Me_3C), 107.2 (C_5Me_5), 166.7 (Me_3CNC), 306.4 [W≡C, ^1J(W,C) = 223.3 Hz]. − $C_{20}H_{34}Cl_2N_2W$ (557.26): calcd. C 43.11, H 6.15, N 5.03; found C 43.32, H 6.35, N 5.13%.

Cp*$(Cl)_3$W[η^2-*t*Bu(H)NC≡$CNEt_2$] (4): A solution of **3** (0.129 g, 0.23 mmol) in 30 mL of diethyl ether was treated at −78°C with a 1 M solution of HCl in diethyl ether (0.23 mL, 0.23 mmol). The reaction mixture was allowed to warm to room temperature and stirred for 1 h. During this time precipititation of a violet solid was observed. The supernatant solution was decanted off and the precipitate washed twice with 10 mL of cold diethyl ether (−78°C) and dried in vacuo. Yield 0.126 g (92%), violet solid, m.p. 157°C (decomp.). − IR (CH_2Cl_2): $\tilde{\nu}$ = 3435 cm^{-1}, m [ν(NH)], 1667 s [$\nu(N\cdots C\cdots C\cdots N)$]. − ^{1}H NMR (300 MHz, CD_2Cl_2, 258 K): δ = 1.22 (t, 3 H, CH_2CH_3), 1.30 (t, 3 H, CH_2CH_3), 1.34 (s, 9 H, CMe_3), 1.97 (s, 15 H, C_5Me_5), 4.01 (q, 2 H, CH_2CH_3), 4.32 (q, 2 H, CH_2CH_3), 5.77 (s, 1H, NH). − $^{13}C\{^1H\}$ NMR (75.5 MHz, CD_2Cl_2, 258 K): δ = 11.0 (C_5Me_5), 15.1 (CH_2CH_3), 15.6 (CH_2CH_3), 31.4 (CMe_3), 51.3 (CH_2CH_3), 51.9 (CH_2CH_3), 58.2 (CMe_3), 117.7 (C_5Me_5), 218.5, 219.3 (C_{alkyne}). − EI-MS (70 eV):

m/z = 557 [M⁺ − Cl], 501 [M⁺ − Cl − $Me_2C{=}CH_2$], 473 [M⁺ − Cl − $Me_2C{=}CH_2$ − CNH_2], 444 [M⁺ − Cl −$Me_2C{=}CH_2$ − CNH_2 − Et], 389 [M⁺ − Cl − $Me_2C{=}CH_2$ − CNH_2 − Et −EtNC], 353 [M⁺ − Cl − $Me_2C{=}CH_2$ − CNH_2 − Et − EtNC − HCl]. − $C_{20}H_{35}Cl_3N_2W$ (593.72): calcd. C 40.46, H 5.94, N 4.72, Cl 17.91; found C 40.32, H 6.12, N 4.75, Cl 17.85%.

***cis*-Cp*(Cl)₂[P(OMe)₃]W≡CNEt₂ (5):** A solution of **2** (0.12 g, 0.24 mmol) in 30 mL of THF was treated with $P(OMe)_3$ (0.034 mL, 0.29 mmol) and refluxed for 5 h. An IR spectrum of the reaction solution was recorded in the region 2200−1500 cm^{-1} to ensure the complete conversion of **2** to **5**. Afterwards the solution was evaporated to dryness and the residue was purified by column chromatography on silanized silica at −20°C. Elution with diethyl ether afforded an orange fraction, which was evaporated to dryness to give **5** as an orange, microcrystalline solid. Yield 0.11 g (77%), m.p. 98°C (decomp.). − IR (CH_2Cl_2): $\tilde{\nu}$ = 1547 cm^{-1}, s [$\nu(C_{carbyne}{\cdots}N)$]. IR (THF): $\tilde{\nu}$ = 1544 cm^{-1}, s [$\nu(C_{carbyne}{\cdots}N)$]. − ^{1}H NMR (400 MHz, CD_2Cl_2, 293 K): δ = 1.26 [t, ^3J(H,H) = 7.3 Hz, 6 H, $N(CH_2CH_3)_2$], 1.96 (s, 15 H, C_5Me_5), 3.38 [dq, ^2J(H,H) = 13.7 Hz, ^3J(H,H) = 7.3 Hz, 2 H, $N(CH_AH_BCH_3)_2$], 3.54 [dq, ^2J(H,H) = 13.7 Hz, ^3J(H,H) = 7.3 Hz, 2 H, $N(CH_AH_BCH_3)_2$], 3.78 [d, ^3J(P,H) = 10.4 Hz, 9 H, OCH_3]. − $^{13}C\{^1H\}$ NMR: (100.6 MHz, CD_2Cl_2, 293 K): δ = 11.8 (C_5Me_5), 15.4 [$N(CH_2CH_3)_2$], 48.2 [d, ^4J(P,C) = 3.4 Hz, $N(CH_2CH_3)_2$], 54.8 [d, ^2J(P,C) = 7.9 Hz, OMe], 108.6 (C_5Me_5), 306.5 [d, ^2J(P,C) = 37.8 Hz, W≡C]. $^{31}P\{^1H\}$ NMR (162.1 MHz, CD_2Cl_2, 293 K): δ = 133.3 [^1J(W,P) = 435.1 Hz]. CI-MS: *m/z* = 473 [M⁺ − $P(OMe)_3$]. − $C_{18}H_{34}Cl_2NO_3PW$ (598.20): calcd. C 36.14, H 5.73, Cl 11.85, N 2.34, W 30.73; found C 36.08, H 5.75, Cl 11.90, N 2.36, W 30.80%.

Cp*(Cl)₃W=C(H)NEt₂ (6): A sample of **5** (0.11 g, 0.18 mmol) was suspended in 40 mL of diethyl ether and treated at −78°C with a 1 M solution of HCl in diethyl ether (0.18 mL, 0.18 mmol). The reaction mixture was warmed to room temperature and stirred for 2.5 h. During this time the color of the suspension changed from orange to red. The resulting red precipitate was then allowed to settle, the supernatant solution was decanted and the precipitate washed three times with 10 mL of cold diethyl ether (−78°C) and dried in vacuo. Yield 0.06 g (64%), red solid, m.p. 135°C (decomp.). − IR (CH_2Cl_2): $\tilde{\nu}$ = 1508 cm^{-1}, m [$\nu(C_{carbene}{\cdots}N)$]. − ^{1}H NMR (400 MHz, CD_2Cl_2, 233 K): δ = 1.24 [t, ^3J(H,H) = 7.3 Hz, 3 H, CH_2CH_3], 1.29 [t, ^3J(H,H) = 7.3 Hz, 3 H, CH_2CH_3], 2.31 (s, 15 H, C_5Me_5), 3.65 [q, ^3J(H,H) = 7.3 Hz, 2 H, CH_2CH_3], 3.81 [q, ^3J(H,H) = 7.3 Hz, 2H, CH_2CH_3], 10.56 (s, 1H, W=C*H*). − ^{13}C NMR (100.6 MHz, CD_2Cl_2, 233 K): 13.5 (C_5Me_5), 16.5 (CH_2CH_3), 16.7 (CH_2CH_3), 50.9 (CH_2CH_3), 54.2 (CH_2CH_3), 107.3 (C_5Me_5), 248.7 [W=*C*, ^1J(W,C) = 103.8 Hz; ^1J(C,H) = 140.1 Hz]. − FD-MS (CH_2Cl_2): *m/z* = 509 [M⁺]. − $C_{15}H_{26}Cl_3NW$ (510.59): calcd. C 35.29, H 5.13, Cl 20.83, N 2.74, W 36.01; found C 34.60, H 5.04, Cl 20.87, N 2.76, W 35.99%.

[Cp*(Cl)₂(*t*BuNC)₂W=C(H)NEt₂]Cl (7): A solution of **6** (0.125 g, 0.24 mmol) in 10 mL of CH_2Cl_2 was treated at room temperature with *t*BuNC (0.058 mL, 0.51 mmol). The color of the solution changed from red over green to orange. After 1 h stirring at room temperature the solution was evaporated to dryness, the residue dissolved in a minimum amount of THF and the product precipitated by addition of diethyl ether. Yield 0.136 g (82%), yellow solid, m.p. 102°C. − IR (CH_2Cl_2): $\tilde{\nu}$ = 2188 cm^{-1}, s, 2132 m [ν(*t*BuN≡C)], 1579 w [$\nu(C_{carbene}{\cdots}N)$]. − ^{1}H NMR (300 MHz, CD_2Cl_2, 293 K): δ = 1.32 [t, 3 H, ^3J(H,H) = 7.3 Hz, CH_2CH_3], 1.40 [t, ^3J(H,H) = 7.3 Hz, 3 H, CH_2CH_3], 1.56 (s, 18 H, 2 × CMe_3), 2.13 (s, 15 H, C_5Me_5), 3.84 (q, ^3J(H,H) = 7.3 Hz, 2 H, CH_2CH_3), 4.15 (m, 2H, CH_2CH_3), 9.95 (s, 1H, W=C*H*). − ^{13}C NMR (75.5 MHz, CD_2Cl_2, 293 K): 11.8 (C_5Me_5), 14.2 (CH_2CH_3), 14.5 (CH_2CH_3), 30.4 (CMe_3), 30.9 (CMe_3), 53.6 (CH_2CH_3), 58.4 (CH_2CH_3), 59.0 (CMe_3), 59.9 (CMe_3), 103.7 (C_5Me_5), 146.4 (*t*BuN*C*), 154.6 (*t*BuN*C*), 230.9 [W=*C*, ^1J(W,C) = 84.4 Hz; ^1J(C,H) = 144.2 Hz]. − $C_{25}H_{44}Cl_3N_3W$ (676.85): calcd. C 44.36, H 6.55, Cl 15.71, N 6.21; found C 44.40, H 6.61, Cl 15.59, N 5.83%.

X-ray Crystal-Structure Determination of 4 and 6: Data collection for **4** was performed on a CAD4-Enraf−Nonius and for **6** on a STOE STADI4 four-circle diffractometer with graphite monochromated Mo-K_α radiation (λ = 0.71073 Å). After data reduction and LP correction the structures were solved with Patterson Methods (SHELXS-86)[14] and subsequent difference-Fourier synthesis (SHELXL-93).[15] Refinement on F^2 was carried out by full-matrix least-squares techniques (SHELXL-93). Non-hydrogen atoms were refined anisotropically, the atoms H1 in **4** and H6 in **6** were refined isotropically. All other hydrogen atoms were calculated using a riding model. Geometrical calculations were performed with PLATON[16] and illustrations with ZORTEP.[17]

Single crystals of **4** were obtained upon diffusion of diethyl ether into a solution of **4** in CH_2Cl_2 at −30°C; $C_{20}H_{35}Cl_3N_2W$ (593.70); crystal dimensions 0.6 × 0.3 × 0.2 mm; orthorhombic, space group $P2_12_12_1$ (Nr. 19), *a* = 9.460(2), *b* = 13.868(4), *c* = 17.056(3) Å, *V* = 2237.7(9) $Å^3$, *Z* = 4, $\rho_{calcd.}$ = 1.762 g cm^{-3}; *T* = 166 K, μ = 5.327 mm^{-1}, *F*(000) = 1176, ω-2Θ scan, 4° ≤ 2Θ ≤ 50°; 2321 total reflections, 2168 unique and 2161 with $I > 2\sigma(I)$, which were used for refinement; empirical absorption correction DIFABS (min. 0.876, max. 1.112);[18] residual electron density, min/max −0.359/0.389 e$Å^{-3}$; refinement of the 239 parameters resulted in R_1 = 0.0142, $wR_2(F^2)$ = 0.0312, GOF = 1.088.

Single crystals of **6** were obtained upon diffusion of diethyl ether into a solution of **6** in CH_2Cl_2 at −30°C; $C_{15}H_{26}Cl_3NW$ (510.57); crystal dimensions 0.5 × 0.4 × 0.3 mm; orthorhombic, space group *Pbca* (Nr. 61), *a* = 12.551(9), *b* = 15.487(10), *c* = 18.663(2) Å, *V* = 3628(4) $Å^3$, *Z* = 8, $\rho_{calcd.}$ = 1.870 g cm^{-3}; *T* = 190 K, μ = 6.553 mm^{-1}, *F*(000) = 1984, ω−2Θ −scan, 4° ≤ 2Θ ≤ 50°; 1984 total reflections, 1754 unique and 1745 with $I > 2\sigma(I)$, which were used for refinement; empirical absorption correction DIFABS (min. 0.906, max. 1.337); residual electron density, min/max −0.722/0.609 e$Å^{-3}$; refinement of the 185 parameters resulted in R_1 = 0.0269, $wR_2(F^2)$ = 0.0586, GOF = 1.134.[19]

Acknowledgments

We thank the Deutsche Forschungsgemeinschaft, the Fonds der Chemischen Industrie and the Humboldt-Universität zu Berlin for financial support, M. Barth, Dr. U. Hartmann, and U. Kursawe for the elemental analyses and Dr. M. von Löwis, A. Woyda, Prof. Dr. F. R. Kreißl, and R. Dumitrescu for recording the mass spectra.

[1] B. Cornils, W. A. Herrmann, *Applied Homogeneous Catalysis with Organometallic Compounds*, *Vol. 1,* VCH, Weinheim, **1996**, pp. 29−200.

[2] [2a] R. N. Vrtis, S. J. Lippard, *Isr. J. Chem.* **1990**, *30*, 331−341. − [2b] A. Mayr, C. M. Bastos, *Prog. Inorg. Chem.* **1992**, *40*, 1−98. − [2c] E. M. Carnahan, J. D. Protasiewicz, S. J. Lippard, *Acc. Chem. Res.* **1993**, *26*, 90−97. − [2d] A. C. Filippou in: *Organic Synthesis via Organometallics*, (Eds.: G. Helmchen, J. Dibo, D. Flubacher, B. Wiese), F. Vieweg & Sohn Verlagsgesellschaft, Braunschweig, **1997**, pp. 97−119.

[3] [3a] J. Chatt, A. J. L. Pombeiro, R. L. Richards, *J. Chem. Soc., Dalton Trans.* **1980**, 492−498. − [3b] R. N. Vrtis, Ch. P. Rao, S. Warner, S. J. Lippard, *J. Am. Chem. Soc.* **1988**, *110*, 2669−2670. − [3c] A. C. Filippou, W. Grünleitner, *Z. Naturforsch. B* **1989**,

44, 1023−1034; *Z. Naturforsch. B* **1991**, *46*, 216−230. − [3d] A. C. Filippou, W. Grünleitner, *J. Organomet. Chem.* **1990**, *393*, C10−C16; *J. Organomet. Chem.* **1990**, *398*, 99−115. − [3e] A. J. L. Pombeiro, R. L. Richards, *Coord. Chem. Rev.* **1990**, *104*, 13−38. − [3f] A. Mayr, C. M. Bastos, *J. Am. Chem. Soc.* **1990**, *112*, 7797−7799. − [3g] A. C. Filippou, W. Grünleitner, C. Völkl, P. Kiprof, *Angew. Chem.* **1991**, *103*, 1188−1191; *Angew. Chem., Int. Ed. Engl.* **1991**, *30*, 1167−1169. − [3h] R. N. Vrtis, S. Liu, Ch. P. Rao, S. G. Bott, S. J. Lippard, *Organometallics* **1991**, *10*, 275−285. − [3i] J. D. Protasiewicz, S. J. Lippard, *J. Am. Chem. Soc.* **1991**, *113*, 6564−6570. − [3j] E. M. Carnahan, S. J. Lippard, *J. Chem. Soc., Dalton Trans.* **1991**, 699−706. − [3k] A. C. Filippou, C. Völkl, W. Grünleitner, P. Kiprof, *J. Organomet. Chem.* **1992**, *434*, 201−223. − [3l] A. Mayr, C. M. Bastos, N. Daubenspeck, G. A. McDermott, *Chem. Ber.* **1992**, *125*, 1583−1588. − [3m] J. D. Protasiewicz, A. Masschelein, S. J. Lippard, *J. Am. Chem. Soc.* **1993**, *115*, 808−810. − [3n] J. J. R. Fraústo da Silva, M. A. Pellinghelli, A. J. L. Pombeiro, R. L. Richards, A. Tiripicchio, Y. Wang, *J. Organomet. Chem.* **1993**, *454*, C8−C10. − [3o] A. C. Filippou, P. Hofmann, P. Kiprof, H. R. Schmidt, C. Wagner, *J. Organomet. Chem.* **1993**, *459*, 233−247. − [3p] C. M. Bastos, N. Daubenspeck, A. Mayr, *Angew. Chem.* **1993**, *105*, 793−795; *Angew. Chem., Int. Ed. Engl.* **1993**, *32*, 743−745. − [3q] J. A. Acho, S. J. Lippard, *Organometallics* **1994**, *13*, 1294−1299. − [3r] R. H. Henderson, A. J. L. Pombeiro, R. L. Richards, J. J. R. Fraústo da Silva, Y. Wang, *J. Chem. Soc., Dalton Trans.* **1995**, 1193−1199.

[4] The carbyne ligand is considered formally as a cationic 2e-donor ligand bearing a pair of empty orthogonal acceptor orbitals of π symmetry, the carbene ligand as a neutral 2e-donor ligand bearing an empty π-acceptor orbital, and the cyclopentadienyl group as an anionic 6e-donor ligand. Given this formalism, the metal center has in complexes **B**, **C**, and **1** a d^6, in complexes **2**, **3**, and **5** a d^4 and in complexes **6** and **7** a d^2 electron configuration.

[5] [5a] A. C. Filippou, E. O. Fischer, *J. Organomet. Chem.* **1988**, *349*, 367−374. − [5b] A. C. Filippou, W. Grünleitner, *Z. Naturforsch B* **1989**, *44*, 1572−1580. − [5c] B. Lungwitz, A. C. Filippou, *J. Organomet. Chem.* **1995**, *498*, 91−107.

[6] B. Lungwitz, Dissertation, Humboldt-Universität zu Berlin, Cuviller Verlag, Göttingen, **1995**.

[7] J. L. Templeton, *Adv. Organomet. Chem.* ***1989****, 29, 1−100.*

[8] The stereodescriptor *trans* is used here to specify the configuration of the C6−N1 "quasi-double bond": E. Juaristi, *Introduction to Stereochemistry and Conformational Analysis*, J. Wiley & Sons, New York, **1991**, p. 43.

[9] C. M. Bastos, K. S. Lee, M. H. Kjelsberg, A. Mayr, D. van Engen, S. A. Koch, J. D. Franolic, W. T. Klooster, T. F. Kloetzle, *Inorg. Chim. Acta* **1998**, *279*, 7−23.

[10] W. A. Nugent, J. M. Mayer, *Metal-Ligand Multiple Bonds*, J. Wiley & Sons, New York, **1988**, pp. 132−134.

[11] A. C. Filippou, D. Wössner, B. Lungwitz, G. Kociok-Köhn, *Angew. Chem.* **1996**, *108*, 981−983; *Angew. Chem., Int. Ed. Engl.* **1996**, *35*, 876−878.

[12] H. J. Lucas, E. R. Kennedy, *Org. Synth. Collect. Index* **1976**, *Vol. 3*, 482−483.

[13] R. E. Schuster, J. E. Scott, J. Casanova, Jr., *Org. Synth.* **1966**, *46*, 75−77.

[14] G. M. Sheldrick, SHELXS-86, Program for Crystal Structure Solution, University of Göttingen, Germany, **1986**.

[15] G. M. Sheldrick, SHELXL-93, Program for Crystal Structure Determination, University of Göttingen, Germany, **1993**.

[16] [16a] A. L. Spek, PLUTON-92, PLATON-93, graphics program, University of Utrecht, Netherlands, **1992** and **1993**. − [16b] A. L. Spek, *Acta Crystallogr. A* **1990**, *46*, C34.

[17] L. Zsolnai, H. Pritzkow, ZORTEP, ORTEP program for PC, University of Heidelberg, Germany, **1994**.

[18] N. Walker, D. Stewart, DIFABS, *Acta Crystallogr. A* **1983**, *39*, 158.

[19] Crystallographic data (excluding structure factors) for the structures reported in this paper have been deposited with the Cambridge Crystallographic Data Centre as supplementary publication no. CCDC-121964 and -121965. Copies of the data can be obtained free of charge on application to CCDC, 12 Union Road, Cambridge CB2 1EZ, UK [Fax: (internat.) + 44-1223/336033, E-mail: deposit@ccdc.cam.ac.uk].

Received July 6, 1999
[I99240]

Macrocyclic Polyamines Containing Phenanthroline Moieties – Fluorescent Chemosensors for H^+ and Zn^{2+} Ions

Andrea Bencini,*[a] M. Alexandra Bernardo,[b] Antonio Bianchi,*[a] Vieri Fusi,[c] Claudia Giorgi,[c] Fernando Pina,*[b] and Barbara Valtancoli[a]

Keywords: Macrocycles / Photochemistry / Fluorescence spectroscopy / Coordination chemistry / Zinc

The macrocyclic ligands **L2** and **L3**, containing a triethylenetetraamine and a tetraethylenepentaamine moiety linked to the methyl groups of 2,9-dimethyl-1,10-phenanthroline, bind H^+ and Zn^{2+} ions giving rise to modulation of the fluorescence emission intensity. The equilibrium constants and the enthalpy changes for ligand protonation were determined by means of pH-metric and microcalorimetric methods in 0.1 M Me_4NCl solutions at 298.1±0.1 K. Also the stability constants of the Zn^{2+} complexes were determined under the same experimental conditions. **L2** forms only mononuclear complexes, while **L3** also forms dizinc(II) species. The phenanthroline group has fluorescence emission properties, but interaction with the lone pairs of benzylic nitrogen atoms produces an efficient quenching of the emission. Such a quenching effect can be avoided by deactivation of the benzylic nitrogen atoms by means of protonation or Zn^{2+} complexation. Hence, **L2** and **L3** behave as chemosensor for H^+ and Zn^{2+}, the photochemical properties of the ligands being modulated by the formation of different protonated and complexed species. In the case of **L3**, the fluorescence emission is also controlled by the metal to ligand molar ratio, because of the formation of an emissive binuclear complex.

Introduction

One of the most attractive methods to detect the presence of a chemical species in solution lies in the use of fluorescent receptors whose fluorescence emission is sensitive to the binding of the target substrate.[1−9] Either enhancement or quenching of the fluorescence emission signals can be observed upon substrate coordination, and can be used to quantify the receptor−substrate interaction.

Such *chemosensors*, namely molecules capable of binding substrates and at the same time signaling their presence, contain binding and signaling functions. Phenanthroline, for instance, is characterised by an intense fluorescence emission and contains two amine groups, which can act as binding sites for H^+ and metal cations, producing important modifications of the emission properties.[10] For this reason phenanthroline has attracted a great deal of interest in the last year for the preparation of efficient chemosensors. Nevertheless, this chelating ligand does not form stable complexes with a large number of metal cations and consequently its applicability as chemosensor is strongly reduced.

A convenient approach to prepare efficient chemosensors for metal cations consists in the association of the fluorescence emission properties of phenanthroline with the high stability conferred to metal complexes by macrocyclic ligands. For this purpose, we have synthesised the three macrocyclic ligands **L1**−**L3** containing a phenanthroline moiety and a polyaminic chain of increasing length and increasing number of nitrogen donor atoms.

In recent studies,[11−13] macrocyclic polyamines with similar structures but containing *p*-phenylene spacers instead of phenanthroline, have been used as chemosensors for binding H^+ and metal ions in solution. These ligands exhibit pH dependence of the fluorescence emission at room temperature, showing an increase in emission with increasing ligand protonation, and chelation enhancement of fluorescence (CHEF effect) in the presence of Zn^{2+}.

In the present paper we report the results of a thermodynamic and photochemical study of the binding of H^+ and Zn^{2+} cations by the phenanthroline derivatives **L1**−**L3**, showing that the insertion of different aromatic spacers in cyclic polyamines produces chemosensors characterised by significantly different photochemical properties. The results obtained with **L1** were published in a previous paper.[14]

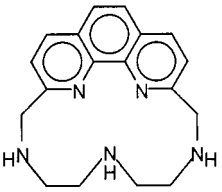
Results and Discussion

Ligand Proton Transfer Properties

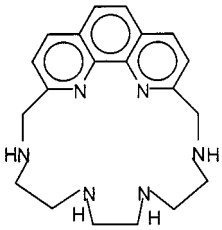
Table 1 lists the thermodynamic parameters (log*K*, $\Delta H°$, $T\Delta S°$) experimentally determined for the protonation reactions involving **L1**−**L3**. These data follow the trend found for the analogous polyazamacrocycles containing only secondary amine groups, characterised by decreasing protonation constants with increasing protonation degree, and largely favourable ($\Delta H° < 0$) enthalpic contributions to li-

[a] Department of Chemistry, University of Florence,
Via Maragliano 75/77, I-50144 Florence, Italy
Fax: (internat.) + 39-055/354845
E-mail: bianchi@chim1.unifi.it
[b] Departamento de Química, Centro de Química-Fina e Biotecnologia, Universidade Nova de Lisboa,
Quinta da Torre 2825, Monte de Caparica, Portugal
Fax: (internat.) + 351-11/2948550
E-mail: fjp@dq.fct.unl.pt
[c] Institute of Chemical Sciences, University of Urbino,
Piazza Rinascimento 6, I-61029 Urbino, Italy
Fax: (internat.) + 39-0722/350032
E-mail: vieri@chim.uniurb.it

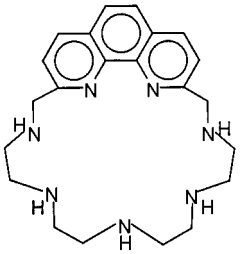
 © WILEY-VCH Verlag GmbH, D-69451 Weinheim, 1999 1434−1948/99/1111−1911 $ 17.50+.50/0



L1



L2



L3

gand protonation.[15] In particular the enthalpy changes found in each protonation step are significantly higher than the analogous values reported for the protonation of 2,9-dimethyl-1,10-phenanthroline (20 kJ mol^{-1}),[16] which can be considered the most appropriate reference compounds for the phenanthroline moiety of **L1**−**L3**, suggesting that such a moiety is not directly involved in the protonation processes, despite the fact they should be at least capable of assisting protonation of the secondary amine groups by means of hydrogen bonding, as observed in the crystal structure of the $[H_3\mathbf{L1}]Br{\cdot}H_2O$ salt.[14] The distribution of the protonated species formed at the different pH values by **L2** and **L3** is shown in Figure 1.

In order to ascertain the role played by the phenanthroline nitrogen atoms in the protonation of the present ligands, we have investigated the microscopic protonation sequence of **L1**−**L3** by recording their ^{1}H- and ^{13}C-NMR spectra in aqueous solutions at various pH values. All the assignments were made on the basis of ^{1}H-^{1}H homonuclear and ^{1}H-^{13}C heteronuclear correlation experiments at the different pH values studied. The results obtained for **L1** were presented in a recent report.[14] Accordingly, it was shown that the first proton binding of **L1** involved the central amine group of the ligand, while the second protonation produced a reorganisation of the proton distribution with localisation of the two H^+ ions on the benzylic nitrogens, and all three secondary amine groups are protonated in $[H_3\mathbf{L1}]^{3+}$.

Table 1. Thermodynamic parameters for the protonation of **L1**, **L2** and **L3** in 0.1 M Me_4NCl at 298.1 K[a,b]

Reaction	**L1**	**L2**	**L3**
		log *K*	
$L + H^+ = LH^+$	9.93(1)	9.72(1)	9.38(1)
$LH^+ + H^+ = LH_2^{2+}$	7.68(3)	8.71(1)	8.74(1)
$LH_2^{2+} + H^+ = LH_3^{3+}$	4.07(3)	6.18(3)	7.18(2)
$LH_3^{3+} + H^+ = LH_4^{4+}$		2.18(4)	3.85(3)
$LH_4^{4+} + H^+ = LH_5^{5+}$			1.80(5)
		$-\Delta H°$ [kJmol^{-1}]	
$L + H^+ = LH^+$	35.9(1)	35.19(7)	33.98(6)
$LH^+ + H^+ = LH_2^{2+}$	38.5(1)	41.13(6)	41.55(4)
$LH_2^{2+} + H^+ = LH_3^{3+}$	38.0(1)	36.45(7)	39.63(5)
$LH_3^{3+} + H^+ = LH_4^{4+}$			28.47(6)
$LH_4^{4+} + H^+ = LH_5^{5+}$			24.2(1)
		$T\Delta S°$ [kJmol^{-1}]	
$L + H^+ = LH^+$	20.5(1)	20.1(1)	19.3(1)
$LH^+ + H^+ = LH_2^{2+}$	5.2(1)	8.4(1)	8.1(1)
$LH_2^{2+} + H^+ = LH_3^{3+}$	−14.9(1)	−1.3(1)	1.2(1)
$LH_3^{3+} + H^+ = LH_4^{4+}$			−6.6(1)
$LH_4^{4+} + H^+ = LH_5^{5+}$			−14.0(1)

[a] Values in parentheses are standard deviations in the last significant figure. − [b] Values for **L1** are taken from ref.[14]

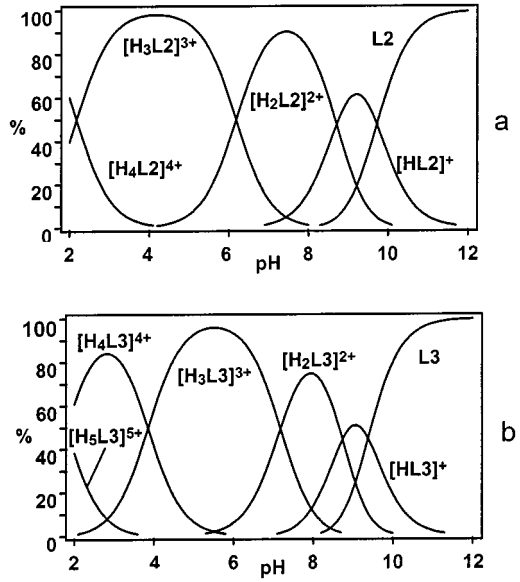


Figure 1. Distribution diagrams of the protonated species formed by **L2** and **L3** as a function of pH ([L] = 1×10^{-3} M, 0.1 M Me_4NCl, 298.1 K)

Figure 2a shows the ^{1}H-NMR spectra recorded at various pH values and Figure 2b reports ^{13}C-NMR chemical shifts of **L2** as a function of the pH value. The ^{13}C-NMR spectrum of **L2** at pH = 12.0, where the unprotonated amine predominates in solution (Figure 1), exhibited four peaks for the aliphatic carbons C1−C4, and six peaks for

the aromatic carbon atoms C5−C10. The ^{1}H-NMR spectrum of **L2** at this pH value showed a singlet at δ = 2.72 (integrating for four protons and assigned to the hydrogen atoms of the ethylenic chain H1), a multiplet at δ = 2.82 (eight protons, the hydrogen atom H2 and H3) and a singlet at δ = 4.03 (4 protons, H4). Also evident were a singlet at δ = 7.42 and two doublets at δ = 7.49 and δ = 8.04 for the aromatic protons H10, H6 and H7, respectively. These spectral features indicate a time-averaged C_{2v} symmetry. This symmetry is preserved throughout all the pH range investigated.

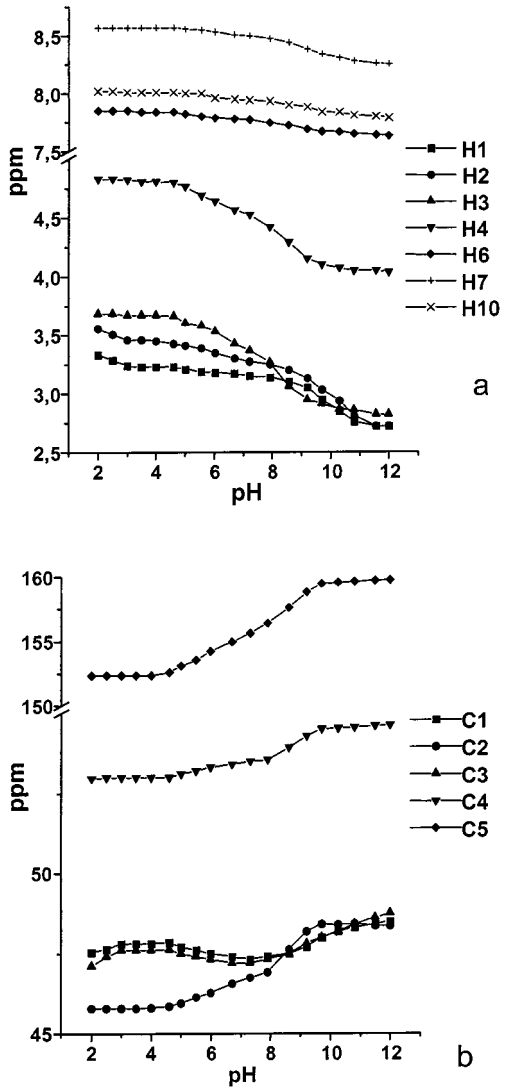


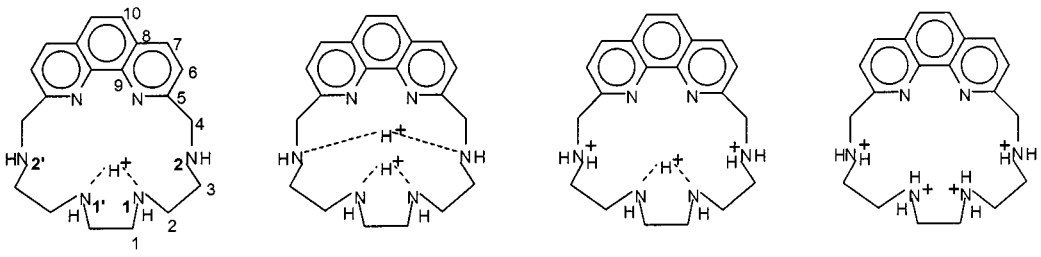
Figure 2. pH dependence of ^{1}H-NMR (a) and ^{13}C-NMR (b) chemical shifts of significant **L2** signals; for the sake of simplicity, the remaining ^{13}C-NMR signals are not reported since they do not shift significantly over the considered pH range 12−2: C6: δ = 124.3−124.4; C7: δ = 138.8−140.4; C8: δ = 128.8−130.2; C9: δ = 144.9−145.1; C10: δ = 127.0−128.3

In the pH range 11−9, where the first proton binds to the ligand (Figure 1), the signal of the hydrogen atoms H1 and H2 in the α-position with respect to N1 exhibits a downfield shift, while the other signals do not shift appreciably. This suggests that the first protonation step involves the nitrogen atoms N1 and N1′ (Scheme 1). This hypothesis is confirmed by the ^{13}C-NMR spectra recorded in the same pH range which show that the resonances of the carbon atoms C3 and C1, in the β-position with respect to N1 and N1′, respectively, shift upfield (Figure 2b), in good agreement with the β-shift reported for the protonation of polyamines.[15] This higher proton affinity of the nitrogen atoms N1 and N1′ in comparison with N2 and N2′ can be ascribed to the inductive effects of the heteroaromatic moiety on the adjacent N2 and N2′ amine groups.

In the pH range 9−7, the macrocycle binds a second proton, giving the $[H_2\mathbf{L2}]^{2+}$ species (Figure 1). The formation of this diprotonated form markedly affects the pattern of the ^{1}H- and ^{13}C-NMR spectra. In particular, the signals of H3 and H4 show a remarkable downfield shift (Figure 2a). On the other hand, the signals of H1 and H2 do not shift appreciably in this pH range. Considering the ^{13}C-NMR spectra (Figure 2b), the resonances of C2 and C5 in the β-position with respect to N2 exhibit a marked upfield shift. It is noteworthy that the β-shifts observed for signals of aromatic carbon atoms are more pronounced than those for aliphatic ones.[15] The same effect will be observed for **L3**. These spectral features indicate that the second protonation step takes place on the benzylic nitrogen atoms N2 and N2′, as shown in Scheme 1. As can be seen in Figure 1, **L2** is mainly in its triprotonated form in the pH range 6−2. The formation of the triprotonated species is accompanied by a marked downfield shift of the signals of H3 and H4 in the ^{1}H-NMR spectra, and by an upfield displacement of the resonances of C2 and C5 in the ^{13}C-NMR spectra. These observations indicate that the third protonation step occurs once again on the benzylic nitrogen atoms N2 and N2′. Therefore in the $[H_3\mathbf{L2}]^{3+}$ species both the benzylic nitrogen atoms are protonated and a proton is shared between the N1 and N1′ nitrogen atoms. The fourth protonation step takes place on the N2 and N2′ amine groups, as evidenced by the downfield shift of the signals of H1 and H2 at pH < 3.

It is interesting to note that the signals of the aromatic protons H7 and H10 undergo a small, but significant, downfield shift from alkaline to acidic pH. A similar, although less evident behaviour of the ^{1}H-NMR signals of aromatic protons was observed for **L1**,[14] and ascribed to the involvement of phenanthroline nitrogen atoms in stabilising the protonated forms by means of hydrogen bonding and/or partial delocalisation of the acidic protons, which are expected to increase with decreasing pH value. The same explanation applies for **L2**.

L3 shows a similar protonation mechanism. In this case, the macrocycle also presents a time-averaged C_{2v} symmetry in aqueous solution, throughout all the pH ranges investigated. Figures 3a and 3b show the ^{1}H- and ^{13}C-NMR spectra, respectively, recorded at various pH values. In the pH range 10−8, where the first two protons bind to the ligand (Figure 1), the signals of the hydrogen H1 in the α-position with respect to N1, as well as those of H2 and H3, in the α-position with respect to N2, exhibit a downfield shift,



$[HL2]^{+}$ $[H_2L2]^{2+}$ $[H_3L2]^{3+}$ $[H_4L2]^{4+}$

Scheme 1

while the other signals do not shift appreciably, indicating that the first two protonation steps involve the nitrogen atoms N1, N2 and N2′ (Scheme 2). This hypothesis is confirmed by the ^{13}C-NMR spectrum recorded in the same pH range, which shows that the resonances of the carbon atom C2, in the β-position with respect to N1, as well as the signals of C1 and C4, in the β-position with respect to N2, shift upfield (Figure 3).

In the pH range 8−5, the macrocycle binds a third proton, giving the $[H_3\mathbf{L3}]^{3+}$ species (Figure 1). The most significant effect in the ^{1}H-NMR spectrum is the remarkable downfield shift of the signal of H5 (Figure 3a). Considering the ^{13}C-NMR spectrum (Figure 3b), the resonance of C2 in the β-position with respect to N1, as well as the signals of C3 and C6, in the β-position with respect to N3 exhibit a marked upfield shift. On the contrary, the signals of C1 and C4, in the β-position with respect to N2, shift downfield. These spectral features indicate that in the $[H_3\mathbf{L3}]^{3+}$ species the acidic protons are located on the N1, N3 and N3′ nitrogen atoms. Since the protons occupy alternate positions, separated by either the aromatic moiety or the unprotonated N2 and N2′ amine groups, such a disposition would mean a minimum in electrostatic repulsion, resulting in a stabilisation of the $[H_3\mathbf{L3}]^{3+}$ species, which is prevalent in aqueous solution in a wide pH range (pH = 7.5−4). At pH < 5, the macrocycle binds a fourth proton. As shown in Figure 3b, in the pH range 5−2, a remarkable upfield shift of the signals of the carbon atoms C4 and C1in the β-position with respect to N2 is observed. On the contrary, the resonance of C2 shifts downfield. These data indicate that in the $[H_4\mathbf{L3}]^{4+}$ species, the four acidic protons are positioned on the N2, N2′, N3 and N3′ nitrogen atoms.

On the other hand, in the case of **L3**, the signals of the aromatic protons (H7, H8, H10) in the ^{1}H-NMR spectrum shift downfield on lowering the solution pH. Such a shift, although more pronounced than for **L2**, is rather modest when compared to the shifts experienced by the aliphatic protons, but is indicative, as observed for **L1** and **L2**, of some involvement of phenanthroline nitrogen atoms in stabilising the protonated forms by means of hydrogen bonding and/or partial delocalisation of the acidic protons. As shown below, such modest involvement of phenanthroline nitrogen−proton binding contributes significantly to the luminescent behaviour of these ligands.

Actually, the fluorescence emission is very sensitive to the protonation state of these molecules. The shape and the position of the fluorescence emission spectra of **L2** and **L3** are identical to those of phenanthroline but, as previously observed for **L1**,[14] the intensity of the emission increases with decreasing pH, decreasing again in very acidic solutions (Figure 4). The position of the spectra are maintained over all the pH ranges. In other words, for these types of macrocyclic polyamines, protonation increases the emission intensity, but the fully protonated species are not the most emissive forms, as otherwise observed for polyazacyclophanes.[11−13] As a matter of fact, the decrease in intensity of fluorescence emission in very acidic solution coincides with the formation of the $[H_4\mathbf{L2}]^{4+}$ and $[H_5\mathbf{L3}]^{5+}$.

This quenching effect found at low pH values is more marked for **L3** than for **L2** (Figure 4), while it is less evident for **L1**. To explain these features, we must consider that quenching of fluorescence emission in these molecules can be achieved by: i) interaction of the phenanthroline nitrogen atoms with positively charged species, such as H^+, leading to a relative stabilisation of the weak emissive $n\pi^*\rightarrow$gs state in comparison with the strong emissive $\pi\pi^*\rightarrow$gs one; as already found for **L1**,[14][17] this interaction can explain the quenching observed at very acidic pH values; ii) electron-transfer processes from the lone pairs of the amine groups to the excited state of phenanthroline, a phenomenon that can account for the quenching owing to the deprotonation of polyamines. In the case of **L1**, it was suggested that the amine groups responsible for type-ii quenching are the benzylic ones. This hypothesis is confirmed by the pH dependence of the fluorescence emission of **L2** and **L3**. As can be seen in Figure 4, where the intensity of the emission is superimposed on the species distribution diagram of the protonated species formed as a function of pH, the most emissive species are $[H_3\mathbf{L2}]^{3+}$, $[H_3\mathbf{L3}]^{3+}$ and $[H_4\mathbf{L3}]^{4+}$, in agreement with the NMR-spectroscopic results indicating that the benzylic nitrogen atoms are protonated in these species. However, in the fully protonated forms the benzylic

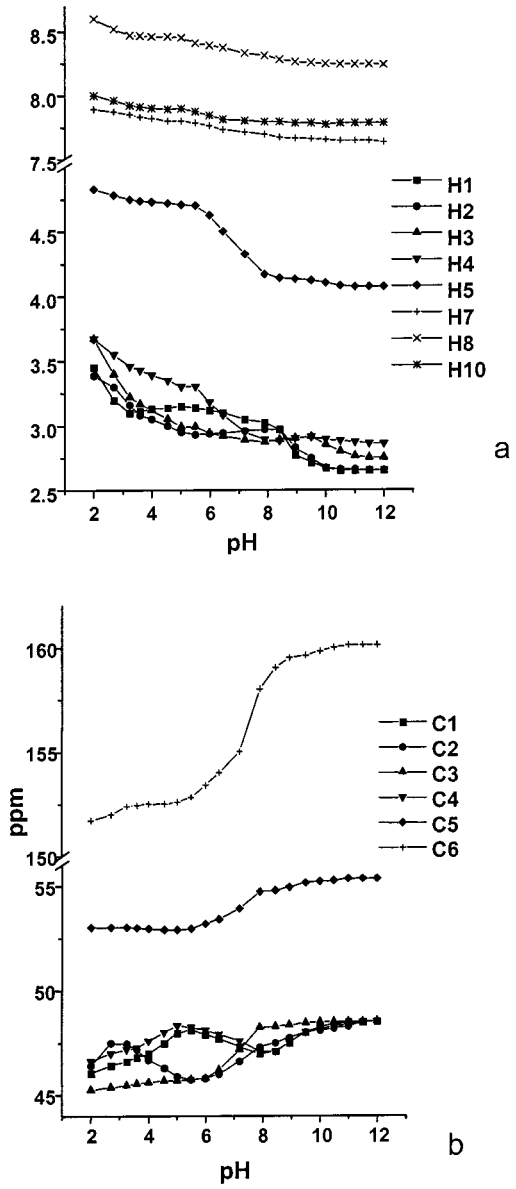


Figure 3. pH dependence of ^{1}H-NMR (a) and ^{13}C-NMR (b) chemical shifts of significant **L3** signals; for the sake of simplicity, the remaining ^{13}C-NMR signals are not reported since they do not shift significantly over the considered pH range 12−2: C7: δ = 124.6−124.3; C8: δ = 138.9−140.2; C9: δ = 128.8−130.2; C10: δ = 145.1−145.1; C11: δ = 127.2−128.4

nitrogen atoms are also protonated, but the increasing involvement of the phenanthroline nitrogen atoms in stabilising the protonated forms by means of hydrogen bonding and/or delocalisation of H^+ ions quench the fluorescence emission. This quenching effect (type i) increases in the order **L1** < **L2** < **L3** along with the overall number of H^+ ions binding the receptors. Such behaviour is also in accordance with the shifts observed in the absorption spectra; as already observed for **L1**, by increasing the pH value, a red shift is observed, except for very acidic solutions where the opposite effect occurs. Similar two-valley one-peak profiles of the fluorescence intensity were recently observed for the protonated species of acyclic amines containing pyridyl and anthracene frangments.[4a]

Zn^{2+} Complexation in Solution

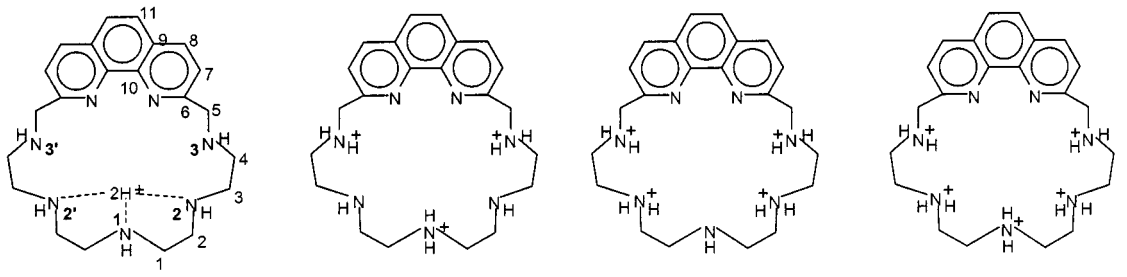
The stability constants of the complexes formed by **L2** and **L3** with Zn^{2+} are listed in Table 2, together with the analogous data[14] previously reported for **L1**, while the distribution diagrams of the complexes formed as a function of the pH value for equimolar concentrations (1×10^{-3} M) of ligands and metal ion are shown in Figure 5. From these data it is evident that increasing the dimensions of the ligand from **L1** to **L3** by inserting additional amine groups gives rise to: i) decreasing stability of the $[ZnL]^{2+}$ complex; ii) increasing ability to form protonated complexes; and iii) formation of binuclear complexes.

Comparison of the stability constant of $[Zn\mathbf{L1}]^{2+}$ with the stability constant of the analogous complex with the pentaazamacrocycle 1,4,7,10,13-pentaazacyclopentadecane suggested[14] that the lower stability of the **L1** complex could be explained by considering that some donor atoms of the **L1** complex are not involved, or are weakly involved, in the coordination to the metal ion. This suggestion was supported by the crystal structure of the $[Zn\mathbf{L1}H_2O]^{2+}$ complex which showed the metal ion in a distorted tetrahedral coordination environment defined by the phenanthroline nitrogen atoms, the central aliphatic nitrogen atom and a water molecule, the two benzylic nitrogen atoms interacting weakly at a large distance (ca. 2.5Å).[14]

The decreasing stability trend observed for the $[ZnL]^{2+}$ complexes with **L1**−**L3** indicates that the presence of a larger number of donor atoms does not enhance the binding ability of such ligands toward Zn^{II}, suggesting that the number of donor atoms participating in the coordination does not parallel the increasing number of donors in the ligands. Hence, a larger number of donors not involved in the coordination determines the formation of larger, less stable chelate rings, which reduce the complex stability. On the other hand, an increasing number of uncoordinated amine groups favours the formation of protonated complex species, as actually observed, and allows the complex of the larger ligand **L3** to have enough free donor atoms to bind a further metal ion.

Notwithstanding that, **L3** does not exhibit a marked tendency to bind the second metal ion, as revealed by the value of the relevant equilibrium constant {$\log K = 4.39(6)$ for $[ZnL]^{2+} + Zn^{2+} = [Zn_2L]^{4+}$; Table 2} and displayed in Figure 5b by the low percentage of $[Zn_2\mathbf{L3}]^{4+}$ (maximum 15%) formed in the presence of equimolar concentrations (1×10^{-3} M) of ligands and metal ion. The three ligands also seem to have different characteristics in the formation of hydroxylated complexes (Table 2), but positive conclusions on this aspect cannot be drawn, considering the restricted pH range (2.5−8) in which it was possible to study complexation with **L3** (see Experimental Section).

Information concerning the donor atoms involved in the coordination to Zn^{2+} are furnished by the emission properties of these complexes. Figure 6 displays the fluorescence emission behaviour of the Zn^{2+}/**L2** system in the pH range 2−8; the emission curve in this Figure is superimposed on the species distribution diagram of the system. The emis-



$[H_2L3]^{2+}$ $[H_3L3]^{3+}$ $[H_4L3]^{4+}$ $[H_5L3]^{5+}$

Scheme 2

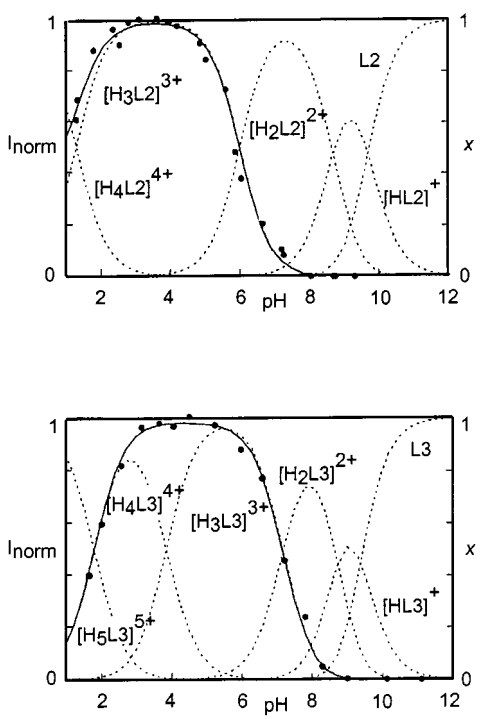


Figure 4. Fluorescence emission profile (•) of **L2** and **L3** as a function of pH and molar fractions of the protonated species formed in the examined solution ([L] = 2×10^{-5} M, 0.1 M Me_4NCl, 298.1K)

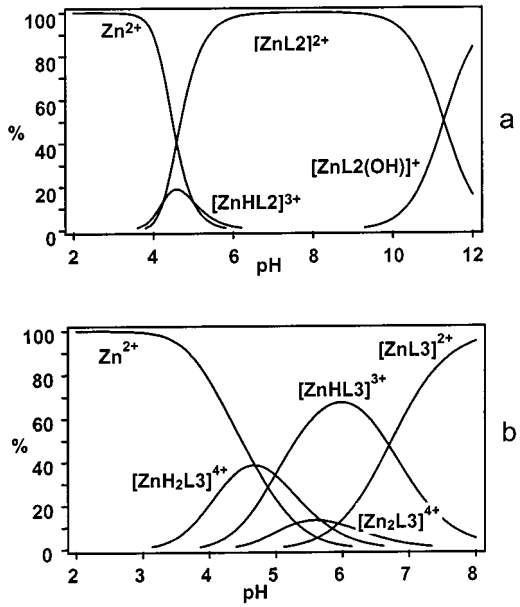


Figure 5. Distribution diagrams of the complexed species formed by **L2** and **L3** as a function of pH ([L] = $[Zn^{2+}] = 1\times10^{-3}$ M, 0.1 M Me_4NCl, 298.1 K)

Table 2. Stability constants of the Zn^{2+} complexes formed by **L1**, **L2** and **L3** in 0.1 M Me_4NCl at 298.1 K[a,b]

Reaction	**L1**	**L2** log *K*	**L3**
$Zn^{2+} + L = [ZnL]^{2+}$	16.15	14.29(1)	12.38(6)
$[ZnL]^{2+} + H^+ = [ZnLH]^{3+}$		4.24(1)	6.70(3)
$[ZnLH]^{3+} + H^+ = [ZnLH_2]^{4+}$			4.99(4)
$[ZnL]^{2+} + OH^- = [ZnLOH]^+$	4.44	2.55(7)	
$[ZnLOH]^+ + OH^- = [ZnL(OH)_2]$	2.75		
$[ZnL]^{2+} + Zn^{2+} = [Zn_2L]^{4+}$			4.39(6)

[a] Values in parentheses are standard deviations in the last significant figure. – [b] Values for **L1** are taken from ref.[14]

sion in the pH range in which no complex formation occurs (pH = 2–3.5) is determined by the emission properties of the free ligand protonated species previously described. Taking into account such emission properties of the ligand protonated species, the emission curve in Figure 6 can be fitted, considering all uncomplexed and complexed species, showing that the $[ZnH\mathbf{L2}]^{3+}$ complex is an emissive species, the quantum yield being slightly lower than for $[H_3\mathbf{L2}]^{3+}$, while $[Zn\mathbf{L2}]^{2+}$ determines a quenching effect. The same characteristic was observed for $[Zn\mathbf{L1}]^{2+}$.[14] In that case it was verified that the quenching effect is independent of the coordination of the phenanthroline nitrogen atoms to Zn^{2+}, but it is determined by electron transfer from the lone pairs of the benzylic amine groups to the excited state of phenantroline. Hence, quenching of the fluorescence emission can be prevented by "neutralisation" of the lone pairs of the benzylic nitrogen atoms, which can be attained by both protonation, as discussed above, and Zn^{2+} complexation. Tak-

ing into account these considerations, we deduce that in the not-emissive $[ZnL2]^{2+}$ species the benzylic nitrogens are not involved, or not fully involved, in metal ion coordination, while in the emissive $[ZnHL2]^{3+}$ complex these nitrogen atoms are involved in the binding of H^+ and Zn^{2+}.

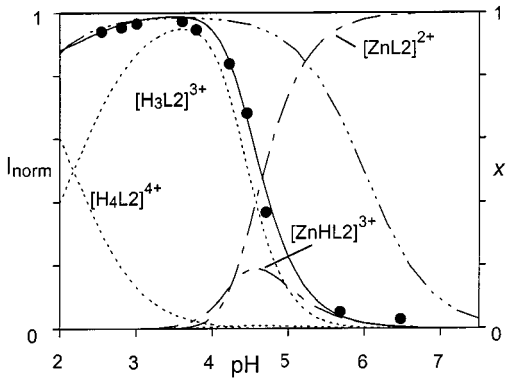


Figure 6. Fluorescence emission profile (•) of the system **L2**/Zn^{2+} as a function of pH and molar fractions of the species formed in the examined solution ([L] = $[Zn^{2+}]$ = 2×10^{-5} M, 0.1 M Me_4NCl, 298.1 K); the dotted-dashed line is the fluorescence profile in the absence of a metal ion

Similar considerations can be used to explain the fluorescence emission properties of the Zn^{2+}/**L3** system (Figure 7). In this case, the formation of both mono- and binuclear complexes must be considered. Spectrofluorimetric measurements performed with a solution containing Zn^{2+} and **L3** in 1:1 and 2:1 molar ratios, at different pH values, showed that $[ZnH_2L3]^{4+}$ and $[Zn_2L3]^{4+}$ are emissive species, the second one being significantly less efficient. Fitting of the fluorescence emission curves in Figure 7 was achieved taking into account the contributions deriving from the protonated forms of **L3** determined in the absence of a metal ion. The nonemissive character of the $[ZnL3]^{2+}$ complex reveals that, as already observed for the analogous complexes with **L1** and **L2**, the benzylic nitrogen atoms of the ligand are not involved, or at most are partially involved, in the coordination, in agreement with the conclusion previously drawn on the basis of the equilibrium data. In this case, even protonation of the complex leading to the $[ZnHL3]^{3+}$ species does not deactivate the quenching properties of the benzylic nitrogen atoms, and fluorescence emission is observed only when the diprotonated complex $[ZnH_2L3]^{4+}$ is formed. The quantum yield of this species is almost identical to that found for $[H_3L3]^{3+}$ in which the benzylic nitrogen atoms are protonated. On the other hand, the quantum yield of the binuclear complex $[Zn_2L3]^{4+}$ is about fivefold lower, indicating that the deactivation of the benzylic nitrogen atoms determined by the two metal ions is not complete. Considering the particular reluctance of benzylic nitrogen atoms to participate in the formation of mononuclear complexes, resulting from the molecular rigidity around the phenanthroline moiety, we can also expect that in the formation of the binuclear $[Zn_2L3]^{4+}$ species, the ligand suffers serious strain preventing the full involvement of benzylic nitrogen lone pairs in coordination.

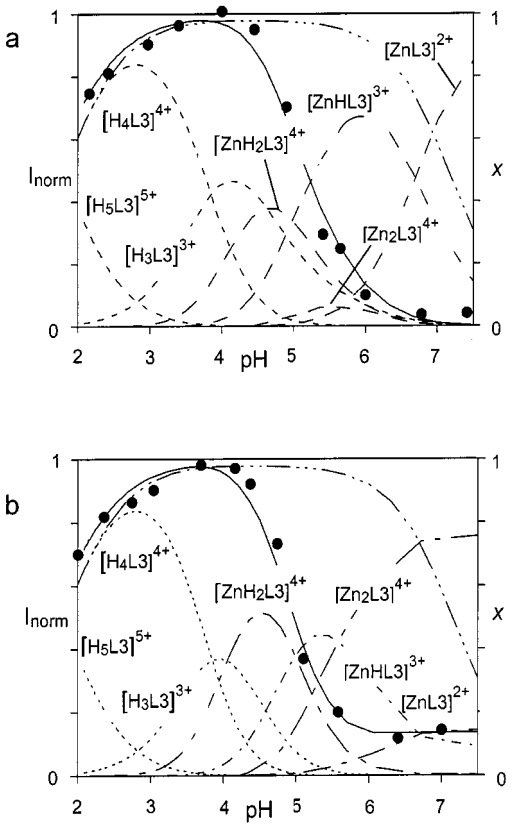


Figure 7. Fluorescence emission profile (•) of the system **L3**/Zn^{2+} as a function of pH and molar fractions of the species formed in the examined solutions; a: [L] = $[Zn^{2+}]$ = 2×10^{-5} M; b: [L] = 2×10^{-5} M, $[Zn^{2+}]$ = 4×10^{-5} M; 0.1 M Me_4NCl, 298.1 K; the dotted-dashed line is the fluorescence profile in absence of metal ion

Conclusion

Insertion of the large and rigid phenanthroline unit into macrocyclic structures leads to strained ligands, such as **L1**−**L3**, in which the simultaneous coordination of all donor atoms to a single metal ion is precluded. In the case of **L1**−**L3**, the benzylic nitrogen atoms in close proximity to the phenanthroline unit are not involved in the coordination to the metal ion in the $[ZnL]^{2+}$ complexes, independently of the number of donor atoms and ligand size.

The phenanthroline groups have fluorescence emission properties, but interaction with the lone pairs of benzylic nitrogen atoms produces an efficient quenching of the emission. To avoid such a quenching effect, the benzylic nitrogen atoms can be deactivated by protonation or Zn^{2+} complexation. Hence, **L1**−**L3** behave as chemosensors for H^+ and Zn^{2+}, the emissive properties of the ligands being modulated by the formation of different protonated and complexed species. The ability of Zn^{2+} to form nonemissive species (chelation enhancement of quenching, CHEQ) is a peculiarity of these ligands. The opposite effect (chelation enhancement of fluorescence, CHEF) is commonly ob-

served[11−13] with other families of polyamine ligands. In the case of the larger **L3** ligand, the fluorescence emission is also controlled by the molar metal-to-ligand ratio, because of the formation of the emissive $[Zn_2\mathbf{L3}]^{4+}$ species.

Experimental Section

General Procedures and Materials: Ligands **L1**−**L3** were synthesised as reported[18] and used in the form of their hydrobromic salts. All pH-metric measurements (pH = −log [H^+]) employed for the determination of ligand protonation constants and Zn^{2+} complexation constants were carried out in 0.1 M Me_4NCl solutions at 298.1±0.1 K, by using the equipment and the methodology that has been already described.[19] The combined Ingold 405 S7/120 electrode was calibrated as a hydrogen concentration probe by titrating known amounts of HCl with CO_2-free NaOH solutions and determining the equivalent point by Gran's method[20] which allows one to determine the standard potential $E°$ and the ionic product of water [pK_w = 13.83(1) at 298.1±0.1 K in 0.1 M Me_4NCl]. At least three measurements (about 100 data points each) were performed for each system in the pH ranges 2.5−10.5 (2.5−8 for Zn^{2+}/**L3** owing to precipitation occurring at higher pH values). In all experiments the ligand concentration [L] was about 1×10^{-3} M, while in the complexation experiments, the Zn^{2+} concentration was varied in the range 0.8[L] < [Zn^{2+}] < 1.5[L]. The computer program HYPERQUAD[21] was used to calculate both protonation and complexation constants from emf data. The enthalpies of ligand protonation were determined in 0.1 M Me_4NCl solution by means of an automated system composed of a Thermometric AB thermal activity monitor (model 2277) equipped with a perfusion-titration device and a Hamilton Pump (model Microlab M) coupled with a 0.250-mL gas-tight Hamilton syringe (model 1750 LT). The measuring vessel was housed in a 25-L water thermostat which was maintained at the chosen temperature within $\pm2\times10^{-4}$ K. The microcalorimeter was checked by determining the enthalpy of reaction of strong base (NaOH) with strong acid (HCl) solutions. The value obtained, −13.55(5) kcal mol^{-1} was in agreement with the literature value.[16] − In a typical experiment, an Me_4NOH solution (0.1 M, addition volumes 15 μL) was added to acidic solutions of the ligands (5×10^{-3} M, 1.5 mL). − Corrections for the heats of dilution were applied. The corresponding enthalpies of reaction were determined from the calorimetric data by means of the AAAL program.[22] At least three titrations (about 120 data points) were performed for each system. − 200.0-MHz ^{1}H- and 50.32-MHz ^{13}C-NMR spectra in D_2O solutions at different pH values were recorded at 298 K with a Bruker AC-200 spectrometer. In ^{1}H-NMR spectra, peak positions are reported relative to HOD at δ = 4.75. Dioxane was used as reference standard in ^{13}C-NMR spectra (δ = 67.4). ^{1}H-^{1}H and ^{1}H-^{13}C 2D correlation experiments were performed to assign the signals. Small amounts of 0.01 M NaOD or DCl solutions were added to a solution of the ligand to adjust the pD value. The pH value was calculated from the measured pD values using the following relationship:[23] pH = pD − 0.40. Spectrophotometric and spectrofluorimetric titrations were performed in 0.1 M Me_4NCl solutions at 298.1±0.1 K with a Perkin−Elmer Lambda-6 spectrophotometer and with a SPEX F111 Fluorolog spectrofluorimeter, respectively. The sample-pH values, measured by means of a Metrohm 713 pH-meter, were adjusted by appropriate additions of $HClO_4$ and NaOH solutions.

Acknowledgments

Financial support from the Italian Ministero dell'Università e della Ricerca Scientifica e Tecnologica (MURST) is gratefully acknowledged.

[1] [1a] R. A. Bissel, A. P. De Silva, H. Q. N. Gunaratne, P. L. M. Lynch, G. E. M. Maguire, K. R. A. S. Sandanayake, *Chem. Soc. Rev.* **1992**, *21*, 187−195. − [1b] R. A. Bissel, A. P. De Silva, H. Q. N. Gunaratne, P. L. M. Lynch, C. P. McCoy, G. E. M. Maguire, K. R. A. S. Sandanayake, *Top. Curr. Chem.* **1993**, *168*, 223. − [1c] A. P. De Silva, H. Q. N. Gunaratne, T. Gunnlaugsson, A. J. Huxley, C. P. McCoy, J. T. Rademacher, T. E. Rice, *Chem. Rev.* **1997**, *97*, 1515−1566.
[2] V. Balzani, F. Scandola, *Supramolecular Photochemistry*, Ellis Horwood, Chichester, **1991**.
[3] [3a] A. W. Czarnik, *ACS Symp. Ser.* **1992**, *538* ("Fluorescent Chemosensors for Ion and Molecule Recognition"). − [3b] M. E. Huston, K. W. Haider, A. W. Czarnik, *J. Am. Chem. Soc.* **1988**, *110*, 4460−4462.
[4] [4a] V. Amendola, L. Fabbrizzi, P. Pallavicini, A. Perotti, *J. Chem. Soc., Dalton Trans.* **1998**, 2053−2057. − [4b] L. Fabrizzi, M. Licchelli, P. Pallavicini, A. Perotti, A. Taglietti, D. Sacchi, *Chem. Eur. J.* **1996**, *1*, 75−82. − [4c] L. Fabrizzi, M. Licchelli, P. Pallavicini, A. Taglietti, *Inorg. Chem.* **1996**, *35*, 1733−1736.
[5] [5a] L. R. Sousa, J. M. Larson, *J. Am. Chem. Soc.* **1977**, *99*, 307−310. − [5b] J. M. Larson, L. R. Sousa, *J. Am. Chem. Soc.* **1978**, *100*, 1943−1944.
[6] H. Shizuka, K. Takada, T. Morita, *J. Phys. Chem.* **1980**, *84*, 994.
[7] H. Bouas-Laurent, A. Castellan, M. Daney, J.-P. Desvergne, G. Guinand, P. Marsau, M.-H. Riffaud, *J. Am. Chem. Soc.* **1986**, *108*, 315−317.
[8] B. Valeur, J. Bourson, J. Pouget, M. Kaschke, N. P. Nernsting, *J. Phys. Chem*. **1992**, *96*, 6545.
[9] [9a] M. B. Inoue, E. F. Velazquez, F. Medrano, K. L. Ochoa, J. C. Galvez, M. Inoue, Q. Fernando, *Inorg. Chem.* **1998**, *37*, 4070−4075. − [9b] M. B. Inoue, F. Medrano, M. Inoue, A. Raitsimring, Q. Fernando, *Inorg. Chem.* **1997**, *36*, 2335−2340.
[10] P. G. Sammes, G. Yahioglu, *Chem. Soc. Rev.* **1994**, 23, 327, and references therein.
[11] M. A. Bernardo, A. J. Parola, F. Pina, E. García-España, V. Marcelino, S. V. Luís, J F. Miravet, *J. Chem. Soc. Dalton Trans.* **1995**, 993−997.
[12] M. A. Bernardo, J. A. Guerrero, E. García-España, S. V. Luis, J. M. Llinares, F. Pina, J. A. Ramírez, C. Soriano, *J. Chem. Soc., Perkin Trans 2* **1996**, 2335.
[13] M. A. Bernardo, F. Pina, E. Gracía-España, J. LaTorre, S. V. Luis, J. M. Llinares, J. A. Ramírez. C. Soriano, *Inorg. Chem.* **1998**, *37*, 3835−3942.
[14] C. Bazzicalupi, A. Bencini, A. Bianchi, C. Giorgi, V. Fusi, B. Valtancoli, M. A. Bernardo, F. Pina, *Inorg. Chem.*, in press.
[15] A. Bencini, A. Bianchi, E. Gracía-España, M. Micheloni, J. A. Ramírez, *Coord. Chem. Rev.* **1999**, *188*, 97−156.
[16] R. M. Smith, A. E. Martell, *NIST Critical Stability Constants Database*, version 2, **1995**.
[17] [17a] N. Armaroli, L. De Cola, V. Balzani, J.-P. Sauvage, C. O. Dietrich-Buchecker, J. M. Kern, *J. Chem. Soc., Faraday Trans.* **1992**, *88*, 553−556. − [17b] J. M. Kern, J.-P. Sauvage, J. L. Weidmann, N. Armaroli, L. Flamigni, P. Ceroni, V. Balzani, *Inorg. Chem.* **1997**, *36*, 5329−5338.
[18] [18a] C. Bazzicalupi, A. Bencini, V. Fusi, C. Giorgi, P. Paoletti, B. Valtancoli, *Inorg. Chem.* **1998**, *37*, 941−947. − [18b] C. Bazzicalupi, A. Bencini, V. Fusi, C. Giorgi, P. Paoletti, B. Valtancoli, *J. Chem. Soc., Dalton Trans.* **1999**, 393−399.
[19] A. Bianchi, L. Bologni, P. Dapporto, M. Micheloni, P. Paoletti, *Inorg. Chem.* **1984**, *23*, 1201−1205.
[20] G. Gran, *Analyst (London)* **1952**, *77*, 661−671.
[21] P. Gans, A. Sabatini A. Vacca, *Talanta* **1996**, *43*, 1739−1753.
[22] A. Vacca, *AAAL Program*, University of Florence, **1997**.
[23] A. K. Covington, M. Paabo, R. A. Robinson, R. G. Bates, *Anal. Chem.* **1968**, *40*, 700.

Received March 16, 1999
[I99101]

Synthesis and Properties of Chiral Ruthenium Complexes Containing *O*-, *S*- and *P*-Functionalized Cp-Ligands

Adolphus A. H. van der Zeijden,*[a] Jhonny Jimenez,[a] Chris Mattheis,[a] Christoph Wagner,[b] and Kurt Merzweiler[b]

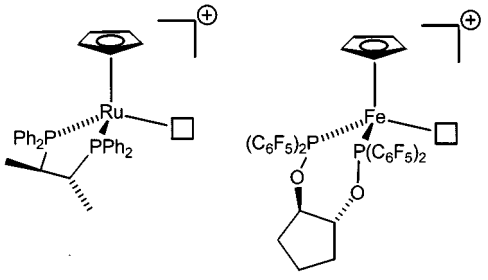
Keywords: Ruthenium / Chirality / Cyclopentadienyl complexes / Kinetics / Asymmetric catalysis

Novel, functionalized, chiral Cp-ligands with S- and P-donor atoms were designed. Together with known analogues containing ether side-chains they were complexed to ruthenium for use as chiral Lewis-acid catalysts. In the ether complexes [RuCl(η^5-$C_5H_4CH_2CH_2OR$)(PPh_3)$_2$] {R = Me, (1*S*)-isobornyl, (1*R*)-menthyl, (1*R*)-fenchyl} the Cp-ligand is only η^5-coordinated; all attempts to provoke a bidentate, Cp/O coordination were unsuccessful. The sulfide complex [Ru{η^5:η^1-$C_5H_4CH_2CH_2S$[(1*R*)-neomenthyl]}(PPh_3)$_2$][OTf] contains a bidentate Cp/S-coordinated ligand, but it is unstable. The stable phosphane complex [RuCl(η^5:η^1-$C_5H_4CH_2CH$(Me)-PPh_2)(PPh_3)] exists as a 77:23 mixture of diastereomers containing a strongly bidentate Cp/P ligand. The diastereomers interchange, with Ru–Cl bond cleavage as the rate-determining step.

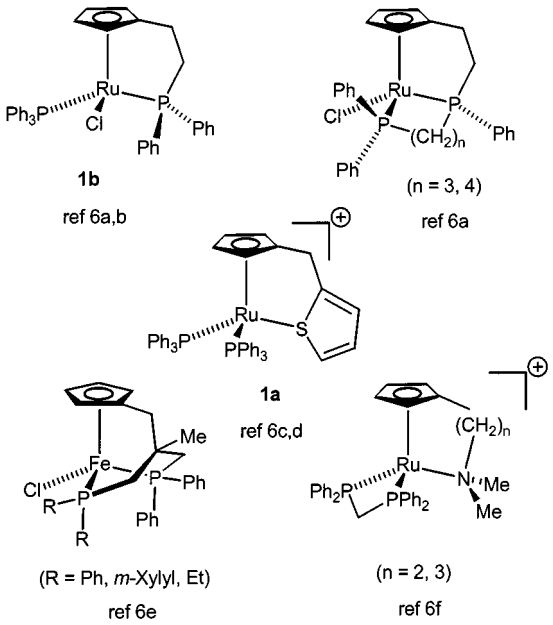
Introduction

The use of chiral Lewis acids in organic transformations is mainly confined to derivatives of the elements aluminium, boron, and titanium.[1] The use of other transition metals is very limited mainly because of their reduced Lewis acidity.[2] However, with a proper choice of ligands (notably π-acceptor ligands like NO and CO) and a positive charge, complexes can be obtained with quite high Lewis-acidities {e.g. $Cp(CO)_2Fe^+$}.[3] Moreover, the use of transition metals offers a greater choice of ligands, and therefore more possibilities for (chiral) modifications, than the classical main group and d^0-metal complexes. Last but not least, transition metal Lewis acids are generally much less sensitive to water. The 16-electron half-sandwich complexes of type $CpM(L)_2^+$ (M = Fe, Ru; L = CO, phosphane) have been thoroughly studied as Lewis-acid catalysts especially for the Diels–Alder reaction.[3c,f] Chiral modifications have been synthesized using bidentate diphosphane ligands.[4]

We pursue another strategy, in that we connect a Cp-ring with a chiral functional group capable of intramolecular coordination.[5] Examples of group 8 metal complexes containing Cp-ligands with phosphorous (**1b**), sulfur (**1a**) and amine side-chains are known.[6]



ref 4a ref 4b

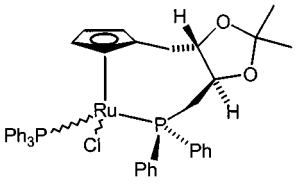


Until recently, only two examples of enantiopure systems were known.[7a,b]

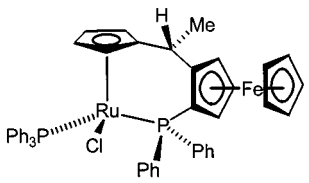
A very recent paper by Trost describes the design of a whole range of chiral, functionalized Cp-ligands as well as the synthesis of their ruthenium derivatives.[7c] In an extension of this work we present our efforts on the synthesis and use of chiral ruthenium complexes using the known ether ligands $C_5H_5CH_2CH_2OR$ {R = Me (**2a**), isobornyl (**2b**), menthyl (**2c**), fenchyl (**2d**)},[5c,d] the newly developed

[a] Institut für Anorganische Chemie, Martin-Luther-Universität Halle-Wittenberg,
Geusaer Strasse, D-06217 Merseburg, Germany
Fax: (internat.) + 49−3461/462002
E-mail: zeijden@chemie.uni-halle.de
[b] Institut für Anorganische Chemie, Martin-Luther-Universität Halle-Wittenberg,
Kurt-Mothes Strasse 2, D-06099 Halle, Germany
Supporting information for this article is available on the WWW under http://www.wiley-vch.de/home/eurjoc or from the author.

 © WILEY-VCH Verlag GmbH, D-69451 Weinheim, 1999 1434−1948/99/1111−1919 $ 17.50+.50/0



(2 diastereomers in 59:41 ratio)
ref 7a



(1 diastereomer)
ref 7b

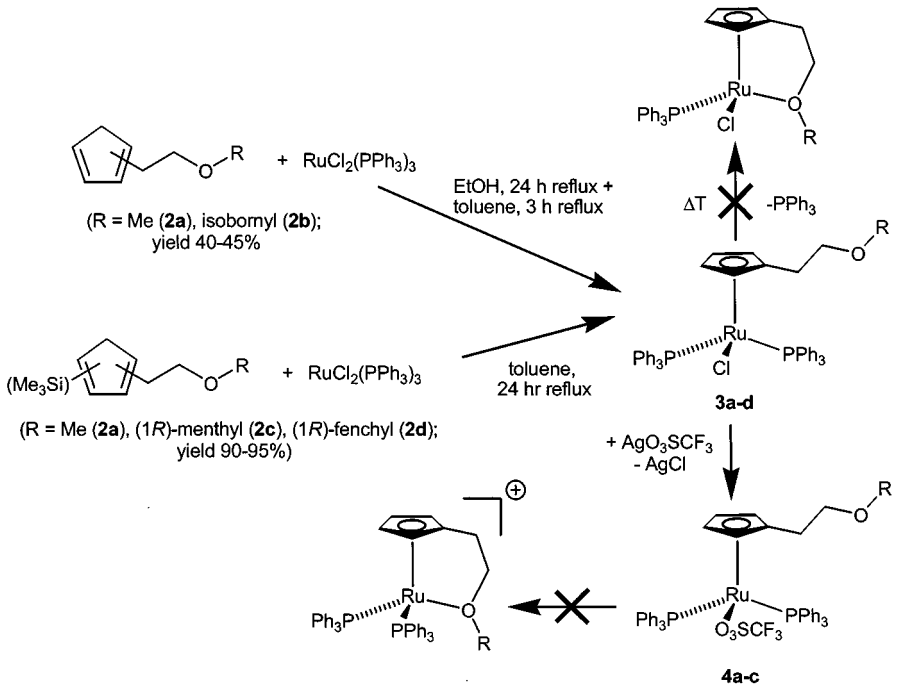
chiral sulfur ligand $C_5H_5CH_2CH_2S$[(*1R*)-neomenthyl] and the phosphorous ligand *(S)*-$C_5H_5CH_2CH(Me)PPh_2$. Special interest is also focused on the stereochemical rigidity of the ruthenium center.

Results and Discussion

According to the procedure of Kauffmann the ether ligands $C_5H_5CH_2CH_2OR$ {R = Me (**2a**), (1*S*)-isobornyl (**2b**)} were reacted with $RuCl_2(PPh_3)_3$ (Scheme 1),[6a] affording $[RuCl(\eta^5\text{-}C_5H_4CH_2CH_2OR)(PPh_3)_2]$ (**3a**, **3b**) in moderate yield. Much better yields were obtained when using the Me_3Si-derivative of the Cp-ligand affording **3a** (R = Me), **3c** {R = (1*R*)-menthyl} and **3d** {R = (1*R*)-fenchyl}. The complexes were characterized by their elementary analyses and their ^1H, ^{31}P and ^{13}C NMR spectra (see supplementary material).

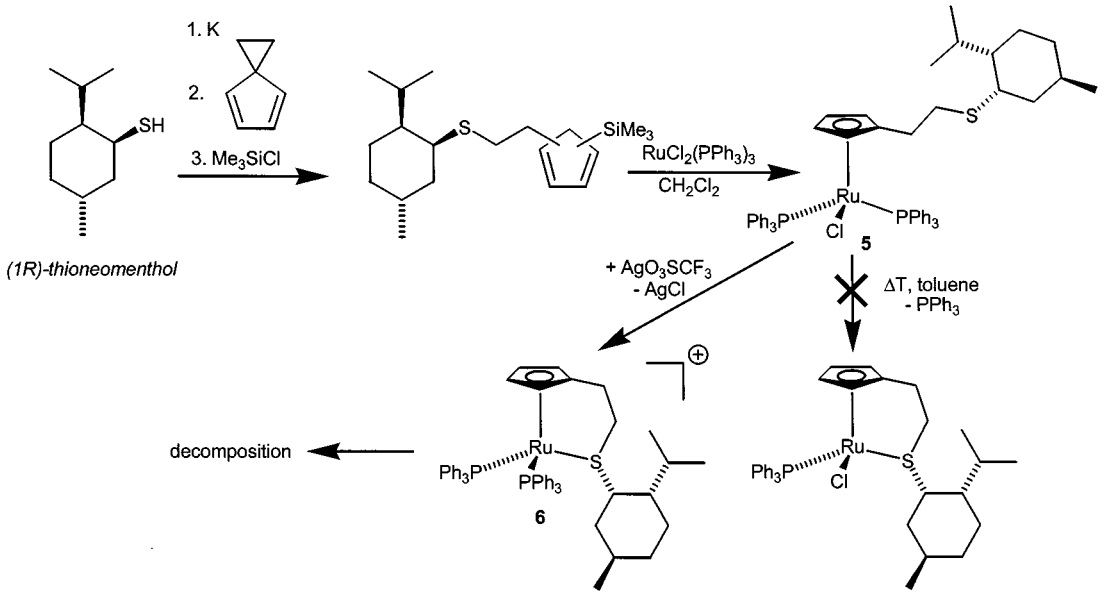
Coordination of the ether-moiety should be revealed by low-field shifts in the ^1H and ^{13}C NMR spectra of the CH_2OCH moieties,[5d] and this is not the case.[9] Moreover, *O*-coordination in the isobornyl derivative **3b** is expected to result in ether cleavage with formation of camphene, and this is also not observed.[5d] The problem is not steric in nature, since the small, achiral methyl ether ligand in **3a** and **4a** doesn't coordinate either. There is obviously a reluctance of the "hard" ether moieties to coordinate to the 'soft' ruthenium center. We therefore concentrated further efforts on the design of Cp-ligands with the "soft" donor atoms sulfur and phosphorous.

A new Cp-ligand with a chiral sulfide side-chain was prepared as outlined in Scheme 2. Its synthesis is based on a method developed by Kauffmann involving a nucleophilic ring-opening reaction of spiro[2.4]hepta-4,6-diene.[10a,b] The potassium salt of (1*R*)-neomenthanethiol[10c,d] was used as the nucleophile. The resulting potassium cyclopentadienide was directly converted into the trimethylsilyl derivative and reacted with $RuCl_2(PPh_3)_3$ affording $[RuCl\{\eta^5\text{-}C_5H_4CH_2CH_2S[(1R)\text{-neomenthyl}]\}\{PPh_3)_2]$ (**5**) in good yield. The chiral ruthenium complex was characterized by its elemental analysis and ^1H, ^{13}C and ^{31}P NMR spectra. As for the ether analogues **3**, the side-chain is not coordinated to the ruthenium center. In this case also prolonged heating in toluene does not result in substitution of one of



Scheme 1. Ruthenium chemistry of the ether-derived Cp ligands

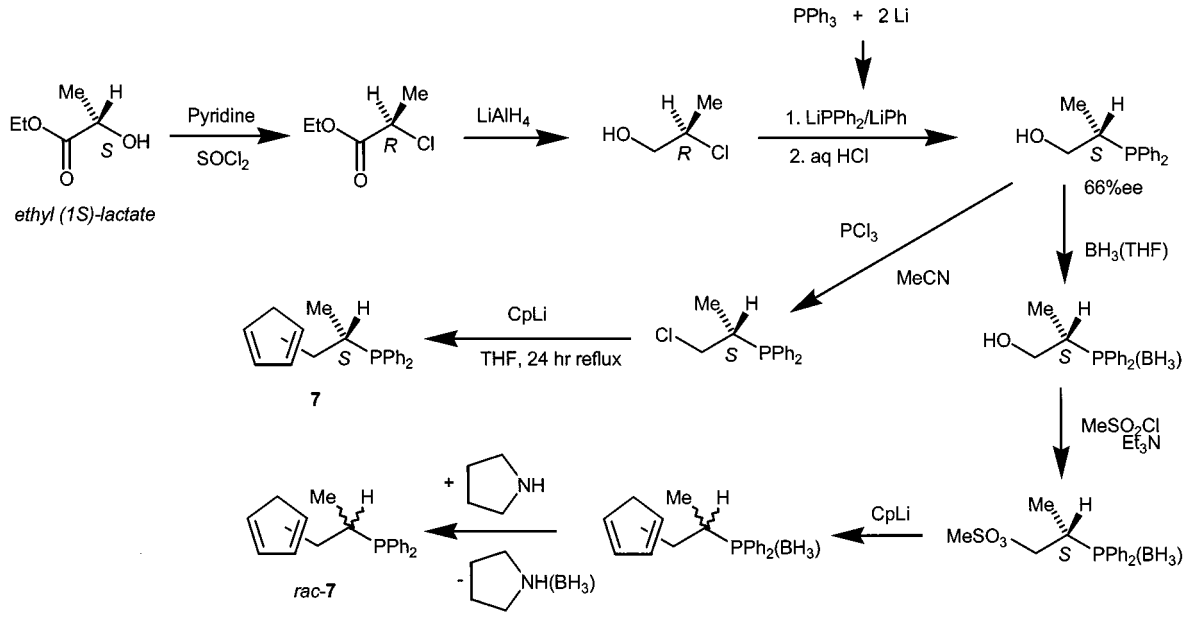
The analytical data indicate that the ether handle in **3** is not coordinated. Prolonged heating of **3** in toluene does not result in expulsion of one of the coordinated PPh_3 ligands (Scheme 1) and subsequent coordination of the ether handle. In another attempt to coordinate the ether handles, and in view of the existence of $[CpRu(PPh_3)_2(THF)][PF_6]$[8], the triflate complexes **4a–c** were synthesized (Scheme 2). the phosphane ligands by the sulfide moiety. Reaction of **5** with AgOTf yields the triflate complex $[Ru\{\eta^5\text{:}\eta^1\text{-}C_5H_4CH_2CH_2S[(1R)\text{-neomenthyl}]\}\{PPh_3)_2][OTf]$ **6**. In contrast to the ether homologues **4**, there is clear evidence for intramolecular coordination of the sulfide side-chain in **6**, and a cationic structure similar to **1a** is proposed.[6c] In comparison to the signals of **5**, low-field shifts are observed



Scheme 2. Synthesis of a chiral sulfur-based Cp ligand and its ruthenium complexes

for the nuclei of the SCH_2-moiety in **6** (^{1}H NMR: from 2.5−2.7 to 3.6−3.9 ppm. ^{13}C NMR: from 31.8 to 53.9 ppm). There is also a smaller low-field shift in the ^{13}C NMR spectrum for the adjacent SCH moiety from 46.5 to 49.9 ppm, whereas the signal shifts to *high*-field in the ^{1}H NMR spectrum (from 3.14 to 2.53 ppm). This contrasting observation may be due to the proximity of the phenyl rings of the PPh_3 ligands causing ring-current shielding. Further evidence for intramolecular coordination of the sulfide moiety comes from the ^{31}P NMR spectrum of **6**, in which the proximity of the chiral neomenthyl moiety causes a clear diastereotopic splitting of the signals of the two PPh_3 ligands ($^2J_{PP}$ = 36 Hz). Unfortunately, complex **6** is unstable and decomposes within a few hours at room temperature, possibly by S−C bond scission. We were therefore unable to use **5** or **6** as an asymmetric Lewis acid catalyst, and therefore concentrated our further efforts on the design of chiral phosphorous ligands.

A novel chiral Cp/phosphane ligand *(S)*-$C_5H_5CH_2CH(Me)PPh_2$ (**7**) was synthesized by the pathway outlined in Scheme 3. The starting material, (*S*)-ethyl lactate, was first converted into (*R*)-$HOCH_2CH(Me)Cl$ according to the literature.[11] The reaction with a mixture of Ph_2PLi and PhLi (prepared in situ from PPh_3 and lithium), after the method developed by Pringle,[12] afforded (*S*)-$HOCH_2CH(Me)PPh_2$ in excellent yield.[13][14] The crude material had an *ee* of 60% by optical rotation {the actual *ee* was 66% (*S*/R = 83:17), vide supra}. As the reaction



Scheme 3. Synthesis of a chiral lactic acid based Cp/phosphane ligand

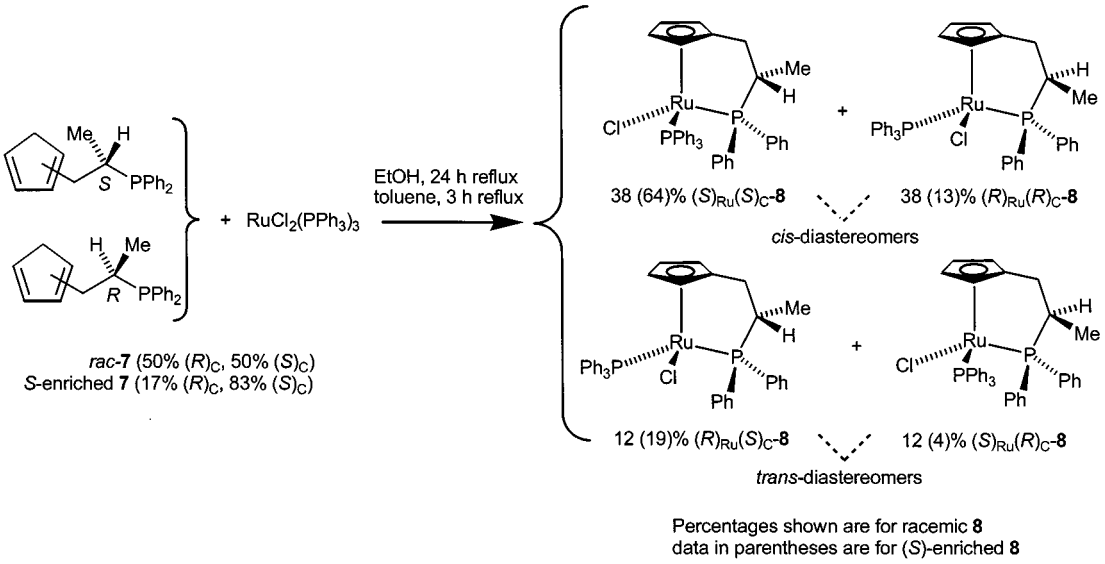
pathway involves two S_N2 reactions (Scheme 3), at least one of them apparently did not proceed with complete inversion at the stereogenic carbon center.

The conversion of the hydroxy functionality into a leaving group (in order to react it with CpLi) without oxidation of the phosphane is quite difficult.[15] Therefore, the phosphane moiety was protected through coordination with borane.[15] The alcohol could then be converted into the mesylate ester. Subsequent reaction with CpLi {curiously, CpNa mainly results in elimination and formation of $H_3BP(allyl)Ph_2$} and decomplexation of borane with pyrrolidine affords $C_5H_5CH_2CH(Me)PPh_2$ (**7**). However, this substance is a racemate, which we discovered after its complexation with ruthenium (vide infra). Racemization probably occurred during the reaction with CpLi by (reversible) deprotonation of the stereogenic carbon which is activated by complexation of BH_3.[16]

Fortunately, we found a method to chlorinate (*S*)-$HOCH_2CH(Me)PPh_2$ without oxidation of the phosphane. The reagent of choice was PCl_3 and, in the presence of excess Et_3NHCl and using acetonitrile as a solvent, (*S*)-$ClCH_2CH(Me)PPh_2$ is obtained in 60−70% yield. The reaction with CpLi afforded **7** in moderate yield, but with 66% *ee*. Reaction of *rac*-**7** or *S*-enriched **7** with $RuCl_2(PPh_3)_3$ according to Kauffmann's method,[6a] afforded $[RuCl\{\eta^5:\eta^1\text{-}C_5H_4CH_2CH(Me)PPh_2\}(PPh_3)]$ (**8**) in low yield {8% based on (*S*)-$HOCH_2CH(Me)PPh_2$, Scheme 4} after isolation by chromatography.

whereas the minor set contains the $(S)_{Ru}(R)_C/(R)_{Ru}(S)_C$ enantiomers (*trans*-diastereomer). Discrimination and assignment was based on an X-ray crystal structure determination of the latter (vide infra). The $(S)_C$ enantiomerically-enriched material contains a total of 83% (64 + 19) $(S)_C$ diastereomers (see Scheme 4). The minor *trans*-diastereomer is much more soluble than the major *cis*-diastereomer, and therefore the former can be selectively extracted and crystallized out of a saturated diethyl ether solution within a few days (interconversion of diastereomers is slow in this solvent, vide infra). Curiously, *rac, trans*-**8** crystallizes in both a monoclinic and a triclinic space group. The X-ray structure determinations show that both unit cells contain enantiomeric pairs of the *trans*-diastereomer (Figure 1). The geometrical data (Tables 3−4) are very similar and also closely resemble those of **1b**.[6b] Minor differences between the three crystal structures are found in the puckering of the chelate ring and in the orientation of some of the phenyl groups, especially those of C(31)−C(36) and C(41)−C(46) of the PPh_3 ligand.

The conformation of the chelate ring of solid **8** is largely maintained in solution (Figure 2). The methyl group in the ring is fixed in an *anti* position with respect to the Cp-ring. Consequently, in the CH_2-moiety one of the hydrogens is in an *anti*-position with respect to the PPh_2-group and the other is *gauche*. This is clearly seen from the $^3J_{HP}$ coupling constants of 48.9 and 8.7 Hz, respectively, for the major *cis*-diastereomer of **8**. The minor *trans*-diastereomer has a simi-



Scheme 4. Ruthenium complexes with ligand **7**

The orange compound was characterized by elementary analysis, mass spectrometry, and ^1H, ^{13}C and ^{31}P NMR spectroscopy (Table 1 and 2). The NMR spectroscopic data are very similar to those of the achiral analogue **1b**, and are in agreement with a bidentate coordination of the Cp/phosphorous ligand. The ruthenium center is chiral, and therefore **8** is composed of two sets of diastereomers in about 77:23 ratio. The major set contains the $(R)_{Ru}(R)_C/(S)_{Ru}(S)_C$ pair of enantiomers (*cis*-diastereomer),[21] lar *anti*-coupling of 45.8 Hz and a *gauche*-coupling of 2.8 Hz.

Another spectroscopic feature of **8** is the extreme upfield chemical shift in the ^1H NMR spectrum of one of the Cp hydrogens (2.35 ppm for the *cis*-diastereomer and 2.98 ppm for the *trans*-diastereomer in $CDCl_3$). This phenomenon has also been observed for **1b** (2.45 ppm) and was ascribed to shielding by one of the phenyl rings of the PPh_3 ligand.[6b] The chemical shifts of the nuclei of the Cp-ring of

Table 1. Selected ^1H and ^{31}P NMR Data of $[RuX\{\eta^5:\eta^1\text{-}C_5H_4CH_2CH(Me)PPh_2\}(PPh_3)]$;[a] (*J*, Hz)

X	Nr	Isomer	C*H*$_3$	C*H*$_2$	PC*H*	C$_5$*H*$_4$	C*P*Ph$_2$	*P*Ph$_3$
Cl	**8**	*cis*-diastereomer (77%) $[(R)_{Ru}(R)_C$ and $(S)_{Ru}(S)_C]$	0.92 (dd, 6.9 and *11.7*)	1.75 (td, 13.0 and *8.7*) 2.08 (ddd, 5.3, 13.0 and *48.9*)	3.12 (m)	2.35, 4.42 5.05, 5.13	67.1 (d, *35*)	42.3 (d, *35*)
		trans-diastereomer (23%) $[(S)_{Ru}(R)_C$ and $(R)_{Ru}(S)_C]$	1.01 (dd, 7.0 and *11.8*)	1.97 (td, 13.5 and *2.8*) 2.42 (ddd, 7.6, 13.8 and *45.8*)	3.68 (m)	2.98, 4.54 5.01 (2 H)	65.3 (d, *37*)	46.2 (d, *37*)
Br	**11**	*cis*-diastereomer (76%) $[(R)_{Ru}(R)_C$ and $(S)_{Ru}(S)_C]$	0.90 (dd, 7.3 and *9.9*)	1.75 (m)* 2.10 (ddd, 5.5, 13.8 and *49.5*)	3.16 (m)	2.42, 4.40 5.08, 5.12	65.7 (d, *34*)	41.1 (d, *34*)
		trans-diastereomer (24%) $[(S)_{Ru}(R)_C$ and $(R)_{Ru}(S)_C]$	0.93*	1.75 (m)* 2.36 (ddd, 6.9, 13.8 and *48.1*)	3.72 (m)	3.40, 4.58 4.95, 5.03	66.5 (d, *37*)	45.0 (d, *37*)
I	**12**	*cis*-diastereomer (74%) $[(R)_{Ru}(R)_C$ and $(S)_{Ru}(S)_C]$	0.86 (dd, 6.7 and *10.8*)	1.71 (td,13.3 and *6.2*) 2.10 (ddd, 5.4, 13.8 and *51.5*)	3.23 (m)	2.60, 4.33 5.10, 5.16	63.3 (d, *33*)	40.3 (d, *33*)
		trans-diastereomer (26%) $[(S)_{Ru}(R)_C$ and $(R)_{Ru}(S)_C]$	0.86*	1.56 (td, 13.7 and *4.7*) 2.27 (m)*	3.65 (m)	3.99, 4.60 4.90, 5.09	67.2 (d, *37*)	44.5 (d, *37*)

[a] In $CDCl_3$; J_{HP} in italics; PPh signals 6.7−8.0 ppm (m, 25 H); signals marked with an asterisk were poorly resolved due to overlap with other signals.

Table 2. Selected ^{13}C NMR Data of $RuX[\eta^5:\eta^1\text{-}C_5H_4CH_2CH(Me)PPh_2](PPh_3)$[a]

X	Nr	Isomer	C*H*$_3$	C*H*$_2$	PC*H*	C$_5$*H*$_4$				
Cl	**8**	*cis*-diastereomer	16.2 (d, 5)	29.6 (d, 6)	52.8 (d, 30)	61.5 (s)	77(d, 12?)*	83.0 (d, 9)	86.1 (d, 4)	110.0 (s, br)
		trans-diastereomer	15.3 (d, 8)	30.8 (d, 6)	60.6 (dd, 27 and 5)	64.9 (s)	75.7 (d, 13)	82.6 (d, 6)	85.1 (d, 9)	112.4 (s, br)
Br	**11**	*cis*-diastereomer	16.1 (d, 5)	29.4 (d, 6)	52.7 (d, 29)	63.3 (s)	76.5 (d?)*	82.7 (d, 9)	85.6 (d, 5)	109.7 (s, br)
		trans-diastereomer	15.5 (d, 7)	29.8 (d, 6)	58.5 (dd, 27 and 5)	66.5 (s)	75.9 (d, 11)	82.6 (d?)*	84.1 (d, 8)	111.5 (s, br)
I	**12**	*cis*-diastereomer	16.4 (d, 5)	29.3 (d, 7)	52.8 (d, 29)	67.9 (s)	75.6 (d, 11)	82.0 (d, 9)	85.2 (d, 4)	109.6 (s, br)
		trans-diastereomer	15.9 (d, 7)	29.2 (d, 7)	56.3 (dd, 28 and 5)	70.4 (s)	75.4 (d, 11)	82.5*	82.6*	110.3 (s, br)

[a] In $CDCl_3$; J_{CP} (Hz) in parentheses; PPh signals 125−137 ppm; signals marked with an asterisk were poorly resolved due to overlap with other signals.

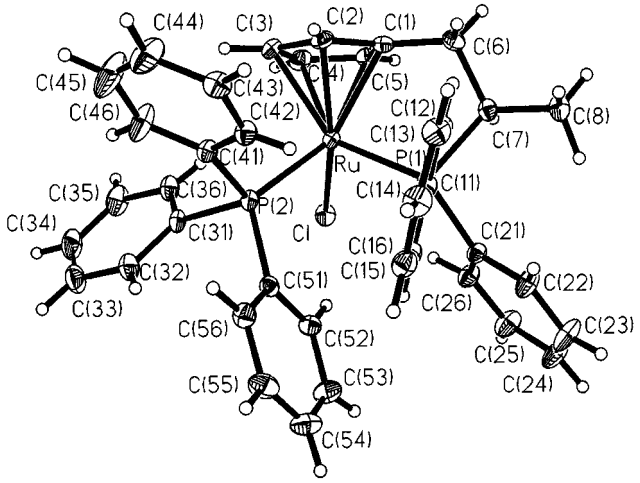


Figure 1. X-ray structure of *racemic, trans*-**8** (monoclinic modification)

cis- and *trans*-**8** could be assigned with help of COSY and $^1H,^{13}C$-HETCOR experiments (see *supplementary material*).

Reaction of **1b** (as a pair of enantiomers) with $AgBF_4$ in the presence of (*R*)-$H_2NCH(Me)Ph$ yields the cationic complex $[Ru(\eta^5:\eta^1\text{-}C_5H_4CH_2CH_2PPh_2)(PPh_3)\{(R)\text{-}H_2NCH(Me)Ph)\}][BF_4]$ as a 50:50 mixture of diastereomers.[6b] A similar reaction conducted with *rac*-**8** (using AgO_3SCF_3 and (*S*)-$H_2NCH(Me)Ph$) affords the salt $\{RuCl[\eta^5:\eta^1\text{-}C_5H_4CH_2CH(Me)PPh_2](PPh_3)[(S)\text{-}H_2NCH(Me)Ph)]\}(O_3SCF_3)$ (**9**) as a mixture of four diastereomers in the ratio of 38:38:12:12 (Scheme 5). The reaction is assumed to proceed with retention of configuration at the metal, as is usual for substitutions on $CpML_2X$ systems.[17] If the same reaction is conducted with $(S)_C$-enriched **8**, the four diastereomers of **9** are obtained in a 64:13:19:4 ratio. Identification of the diastereomers by NMR spectroscopy (Table 5) was possible due to differences in the intensity of the signals. It was assumed that the starting compound (*S*)-$HOCH_2CH(Me)PPh_2$ {having an estimated (*S*)-enrichment of 60% by optical rotation}, did not change its configuration during the synthesis of **7**−**9**. Therefore, from the pair of diastereomers with $(S)_{Ru}(S)_C$ and $(R)_{Ru}(R)_C$ configuration (64 + 13%), the major diastereomer (64%) has configuration $(S)_{Ru}(S)_C$ and the minor one (13%) has $(R)_{Ru}(R)_C$. Consequently, the diastereomer with 19% abundance has configuration $(R)_{Ru}(S)_C$, and that with 4% abundance has $(S)_{Ru}(R)_C$. Finally, the enantiopurity of $(S)_C$-enriched **8** and of the starting compound (*S*)-$HOCH_2CH(Me)PPh_2$ is now more accurately determined as being 66% (64 + 19−13−4). The product mixture of **9** is unstable. Some of the $(S)_{Ru}$ isomers are converted into the $(R)_{Ru}$ isomers within a few days in solution, thereby maintaining the ratio of the $(S)_C$ and $(R)_C$ isomers (83:17). Longer standing times lead to decomposition of the reaction mixture.

Table 3. Crystal data and structure refinement for *rac, trans*-**8**

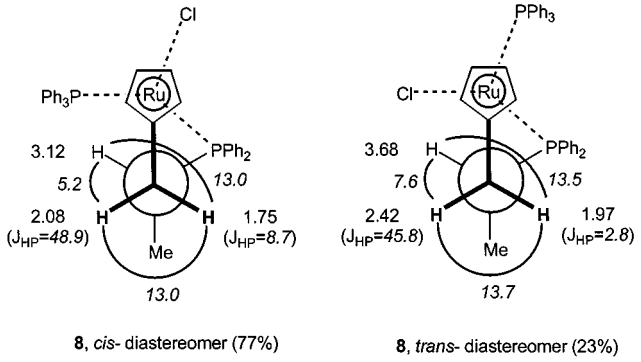
Empirical formula		$C_{38}H_{35}ClP_2Ru$	
Formula weight		690.12	
Measurement device		STOE-STADI IV	STOE-IPDS
Temperature [K]		293	220
Wavelength [Å]		0.71073	
Crystal size [mm]		0.20 × 0.25 × 0.30	0.30 × 0.25 × 0.15
Crystal system		triclinic	monoclinic
Space group		$P\bar{1}$	$P2_1/c$
Unit cell dimensions	a [Å]	10.565(2)	9.269(2)
	b	12.317(6)	36.712(6)
	c	14.632(4)	10.051(2)
	α [°]	67.79(3)	90
	β	89.16(4)	109.68(3)
	γ	68.07(3)	90
Volume [Å^3], Z		1617.3(9), 2	3220.6(12), 4
Calculated density [Mg/m^3]		1.417	1.423
Absorption coefficient [mm^{-1}]		0.692	0.695
F(000)		708	1416
2Θ range [°]		1.04−51.96	4.44−52.14
Limiting indices		$-12 \le h \le 13$, $-15 \le k \le 15$, $-18 \le l \le 18$	$-11 \le h \le 11$, $-44 \le k \le 43$, $-12 \le l \le 12$
Reflections, measured		12811	19977
Reflections, unique		6325 [R(int) = 0.0596]	6236 [R(int) = 0.1525]
No. of refined parameters		516	483
Goodness-of-fit on F^2		1.146	0.822
Final R indices [$I>2\sigma(I)$]		$R1$ = 0.0433, $wR2$ = 0.0730	$R1$ = 0.0573, $wR2$ = 0.1043
R indices (all data)		$R1$ = 0.0768, $wR2$ = 0.0896	$R1$ = 0.1688, $wR2$ = 0.1331
Largest diff. peak and hole [eÅ^{-3}]		0.614 and −0.365	0.711 and −0.522

Table 4. Selected bond lengths [Å] and angles (°) for *rac, trans*-**8** (triclinic/monoclinic)

Ru−Cl	2.4653(12)	2.462(2)	Ru−P(1)	2.3274(18)	2.319(2)
Ru−P(2)	2.3107(13)	2.308(2)	Ru−C(1)	2.177(4)	2.168(9)
Ru−C(2)	2.164(4)	2.177(9)	Ru−C(3)	2.213(4)	2.208(8)
Ru−C(4)	2.231(5)	2.216(8)	Ru−C(5)	2.212(5)	2.193(11)
P(1)−C(7)	1.879(4)	1.868(9)	P(1)−C(11)	1.843(4)	1.826(7)
P(1)−C(21)	1.847(4)	1.833(8)	P(2)−C(31)	1.840(4)	1.856(8)
P(2)−C(41)	1.838(4)	1.833(7)	P(2)−C(51)	1.831(4)	1.843(7)
C(1)−C(2)	1.434(6)	1.399(13)	C(1)−C(5)	1.408(6)	1.423(14)
C(1)−C(6)	1.500(6)	1.496(14)	C(2)−C(3)	1.429(6)	1.446(13)
C(3)−C(4)	1.399(7)	1.388(12)	C(4)−C(5)	1.425(7)	1.396(16)
C(6)−C(7)	1.532(6)	1.545(12)	C(7)−C(8)	1.520(6)	1.553(13)
Cl−Ru−P(1)	100.89(5)	102.42(7)	Cl−Ru−P(2)	89.98(5)	89.77(8)
P(1)−Ru−P(2)	99.59(6)	99.73(7)	Ru−P(1)−C(7)	100.90(15)	102.8(3)
Ru−P(1)−C(11)	117.95(13)	118.8(2)	Ru−P(1)−C(21)	128.34(13)	126.0(3)
C(7)−P(1)−C(11)	106.60(19)	105.0(4)	C(7)−P(1)−C(21)	99.31(19)	101.2(4)
C(11)−P(1)−C(21)	100.57(19)	100.2(3)	Ru−P(2)−C(31)	116.80(16)	116.3(3)
Ru−P(2)−C(41)	111.92(14)	111.9(2)	Ru−P(2)−C(51)	119.19(15)	120.2(3)
C(31)−P(2)−C(41)	100.73(19)	100.4(3)	C(31)−P(2)−C(51)	100.45(19)	100.9(3)
C(41)−P(2)−C(51)	105.5(2)	104.6(3)	C(2)−C(1)−C(5)	108.2(4)	107.1(10)
C(2)−C(1)−C(6)	127.1(4)	126.7(10)	C(5)−C(1)−C(6)	124.5(4)	126.2(11)
C(1)−C(2)−C(3)	106.5(4)	108.6(9)	C(2)−C(3)−C(4)	109.1(4)	106.2(10)
C(3)−C(4)−C(5)	107.8(4)	110.0(10)	C(1)−C(5)−C(4)	108.3(5)	108.0(11)
C(1)−C(6)−C(7)	112.6(3)	111.6(8)	P(1)−C(7)−C(6)	109.7(3)	108.6(7)
P(1)−C(7)−C(8)	119.1(4)	118.3(6)	C(6)−C(7)−C(8)	112.0(4)	113.7(8)

The presumable reaction product of $(S)_C$-enriched **8** with AgOTf, $[Ru(\eta^5{:}\eta^1\text{-}C_5H_4CH_2CH(Me)PPh_2)(PPh_3)][OTf]$ (**10**), is a poor Lewis acid, since for instance it does not catalyse the Diels−Alder reaction between cyclopentadiene and methacrolein. In agreement with this is the fact that the related complex $[RuCp(S,S\text{-chiraphos})(C_2H_4)]^+$ doesn't catalyse this reaction either.[2b] NMR spectra of **10** only show broad signals that are not very diagnostic. Without adding a Lewis base, **10** is unstable and fully decomposes within a few hours at room temperature, presumably by reaction with the solvent. The immediate reaction with Lewis bases like (S)-$H_2NCH(Me)Ph$ (vide supra) appears to be stereoselective, with retention of configuration at ruthenium. The reaction of a freshly prepared solution of **10** with Cl^- (as Et_3NHCl) after 10 min affords **8** with the original diastereomer ratio of 77:23.

It was found that the diastereomers of **8** exchange in solution. When crystals of the *trans*-diastereomer are dissolved, one observes the gradual formation of the *cis*-diastereomer until an equilibrium is reached having the original 77:23 ratio (Figure 3). The ruthenium diphosphane complex $[RuCl(\eta^5\text{-}Cp)\{(R)\text{-}Ph_2PCH(Me)CH_2PPh_2\}]$ shows similar

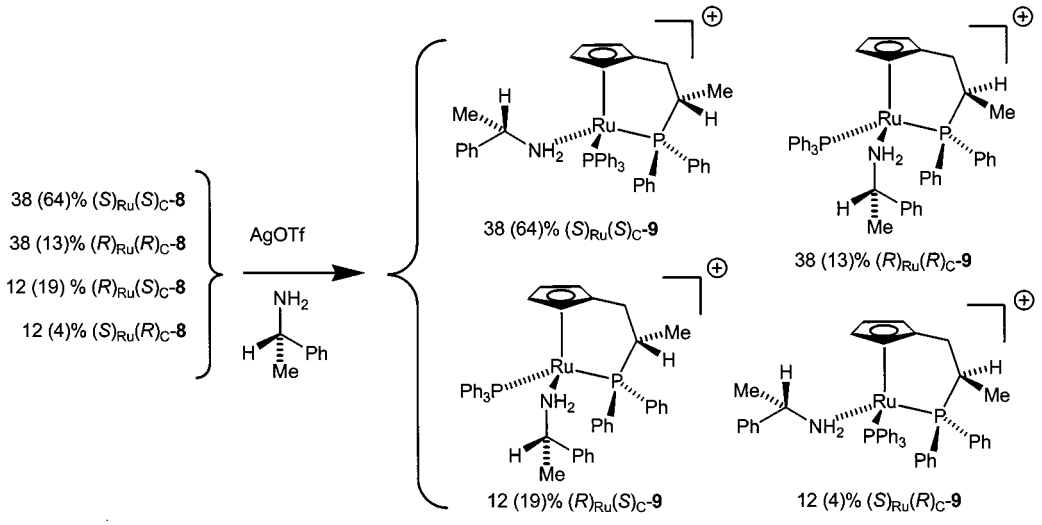


8, *cis*- diastereomer (77%) **8**, *trans*- diastereomer (23%)

Figure 2. Selected ^{1}H NMR data of **8**; the $^2J_{HH}$ coupling of 13.7 Hz in *trans*-**8** is averaged from the measured data (13.5, 13.8 Hz)

behaviour although exchange between the two diastereomers takes several days in chlorobenzene.[18] It was found that the rate of the isomerisation is very solvent-dependent, consistent with dissociation of Cl^- being the rate-determining step (pathway A in Scheme 6) and not decomplexation of the PPh_3 ligand (pathway B in Scheme 6). It also suggests that interconversion of the *cis*- and *trans*-diastereomers of the intermediate cations $[Ru]^+$ is faster than Ru−Cl bond dissociation. It was further found that the presence of extra PPh_3 did not slow down the reaction rate of the *trans-cis* interconversion of **8** in $CDCl_3$, confirming that phosphane dissociation does not trigger the conversion (Figure 4). Despite this, dissociation of PPh_3 in **8** probably does occur. In the related compound $[RuCl(\eta^5\text{-Cp})(PPh_3)_2]$ dissociation of PPh_3 occurs with a rate constant of 5×10^{-6} s^{-1} (thf, 21°C), which is of the same magnitude as chloride dissociation in **8** (4.8×10^{-6} s^{-1}, thf, 23°C).[19] If phosphane dissociation in **8** occurs with a similar rate, then this means that the interconversion of the *cis*- and *trans*- isomers (i.e. site exchange of the chloride) of the intermediate $[RuCl(\eta^5{:}\eta^1\text{-}C_5H_4CH_2CH(Me)PPh_2)]$ is very slow.

In another experiment the *trans-cis* interconversion of **8** was monitored in $CDCl_3$ in the presence of Et_3NHCl (Figure 4). It was expected that when Ru−Cl dissociation is rate-determining for the conversion, then adding Cl^- should slow down the conversion. Actually, the presence of



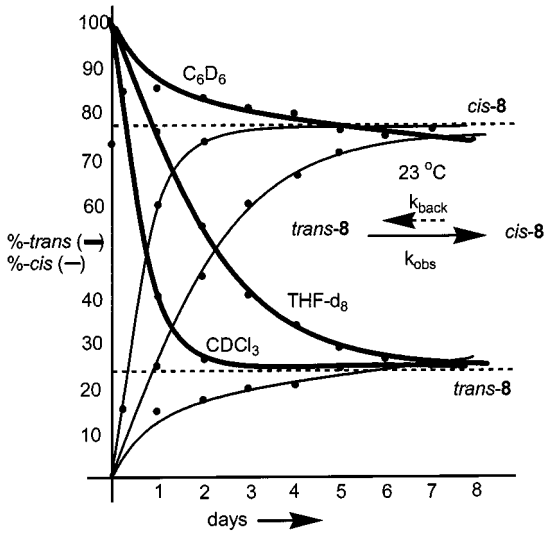
Scheme 5. Preparation of the amine complex **9** as a mixture of 4 diastereomers

Table 5. Selected ^{1}H, ^{13}C and ^{31}P NMR data for the four diastereomers of $\{Ru[\eta^5{:}\eta^1\text{-}C_5H_4CH_2CH(Me)PPh_2](PPh_3)[(R)\text{-}H_2NCH(Me)Ph)]\}\{O_3SCF_3\}$ (**9**)[a]

Isomer	C_5H_4	PCCH_3	CHPPh$_2$	PPh$_3$
$(S)_{Ru}(S)_C$	4.20, 4.37, 4.71, 5.67	0.96 (dd, 6.8 and 13.4 Hz)	72.8 (d, 29 Hz)	49.6 (d, 29 Hz)
$(R_{Ru}(R)_C$	4.20, 4.50,..	0.96?	78.7 (d, 29 Hz)	51.8 (d?)
$(R)_{Ru}(S)_C$	3.85, 4.47, 4.61, 5.09	0.77 (dd, 6.6 and 13.1 Hz)	74.2 (d, 28 Hz)	52.2 (d, 28 Hz)
$(S)_{Ru}(R)_C$	3.85, 4.62, 5.09?, 5.44	0.79?	76.1 (d, 28 Hz)	53.6 (d, 28 Hz)

Isomer	PCCH_3	CH_2	PCH	C_5H_4	C_5H_4	C_5H_4	C_5H_4	CNH_2	$NCCH_3$
$(S)_{Ru}(S)_C$	14.3 (d, 7 Hz)	30.2 (d, 4 Hz)	56.9 (d, 30 Hz)	61.4 (s)	74.7 (d, 9 Hz)	81.9 (d, 9 Hz)	89.2 (s)	58.6	25.8
$(R)_{Ru}(R)_C$	14.1 (d, 7 Hz)	30.2 (d, 4 Hz)	58.1 (d, 30 Hz)	60.7 (s)	74.8 (d, 9 Hz)	80.2 (d, 9 Hz)	88.2 (s)	59.0	26.6
$(R)_{Ru}(S)_C$	16.0 (d, 7 Hz)	28.8 (d, 7 Hz)	53.5 (dd, 30 and 4 Hz)	65.0 (s)	72.2 (d, 10 Hz)	82.5 (d, 6 Hz)	83.2 (d, 4 Hz)	59.6	27.3
$(S)_{Ru}(R)_C$	15.9 (d, 7 Hz)	29.2 (d, 7 Hz)	51.0 (dd, 29 and 4 Hz)	65.6 (s)	71.5 (d, 10 Hz)	80.9 (d, 6 Hz)	84.1 (d, 6 Hz)	61.8	27.3?

[a] In $CDCl_3$; coupling to phosphorous in parentheses.



solvent	polarity (E_t-value)	k_{obs}	k_{back}
$CDCl_3$	39.1	13×10^{-6}	3.6×10^{-6}
thf-d_8	37.4	4.8×10^{-6}	1.4×10^{-6}
C_6D_6	34.8	0.3×10^{-6}	0.08×10^{-6}

($K = 77/23 = 3.35 = k_{obs}/k_{back}$)

Figure 3. Equilibration of the *trans*- and *cis*-diastereomers of **8** in different solvents

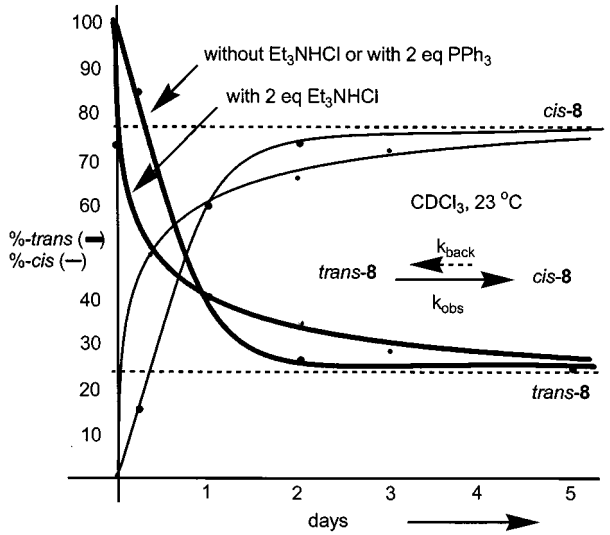
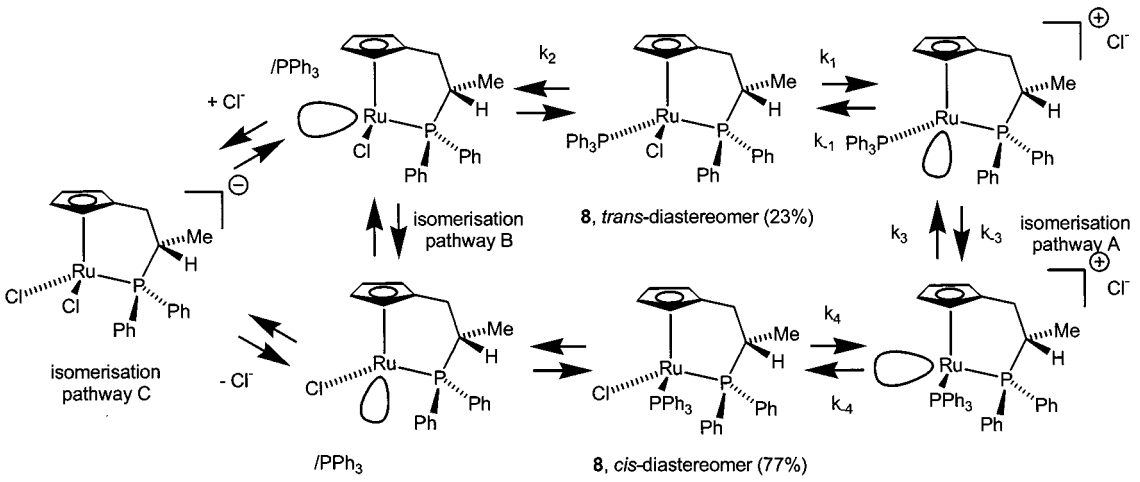


Figure 4. Equilibration of the *trans*- and *cis*-diastereomers of **8** in $CDCl_3$ in the presence of either PPh_3 or Et_3NHCl

other diastereotopic site. This, however, would imply that $Ru-PPh_3$ dissociation becomes rate-determining, and that this dissociation is in fact faster than Ru−Cl dissociation.

In order to study the relative reactivity of *cis*- and *trans*-**8** in more detail we investigated the substitution reactions of **8** with NaBr or NaI. This reaction results in quantitative formation of [RuBr{η^5:η^1-$C_5H_4CH_2CH(Me)PPh_2$}(PPh_3)] (**11**) or [RuI{η^5:η^1-$C_5H_4CH_2CH(Me)PPh_2$}(PPh_3)] (**12**) (see Tables 1 and 2). The reaction was monitored by NMR spec-



Scheme 6. Interconversion of the *trans* and *cis* diastereomers of **8**

Et_3NHCl *enhances* the rate. One reason might be that the slowing down due to the presence of extra Cl^- is counterbalanced by the enhanced polarity of the solvent (a salt effect). It is also possible that Et_3NH^+ labilizes the Ru−Cl bond by forming a hydrogen bond. Another explanation is that a third mechanism is operative for the conversion (pathway C in Scheme 6): after dissociation of PPh_3 from **8** the intermediate [RuCl(η^5:η^1-$C_5H_4CH_2CH(Me)PPh_2$] is trapped by Cl^- forming the anion [$RuCl_2$(η^5:η^1-$C_5H_4CH_2CH(Me)PPh_2$]$^-$ which than loses Cl^- from the troscopy in $CDCl_3$ (Figure 5 and 6). After the reaction was complete, the *cis*/*trans* ratio of **11** and **12** is about the same as in **8**. The presence of 3 equivalents of PPh_3 during the reaction with NaI does not change the reaction profile so that, again, $Ru-PPh_3$ dissociation is not expected to play a role in these substitution reactions. The rate of reaction of **8** is about the same for both substitutions, and is also of a similar magnitude as the *cis*/*trans* conversion of **8**. Although the reactions are heterogenic, it again suggests that Cl^- dissociation is the rate-determining step. For both substi-

tutions the minor *trans*-diastereomer of **8** reacts about three times as fast as the *cis*-diastereomer. This is also in agreement with the rate constants for Cl^- dissociation in *cis*- and *trans*-**8** (Figure 3). As the *cis*-diastereomer has about three times the abundance of the *trans*-isomer, at the beginning of the reaction the *cis*- and *trans*-diastereomers of the cation $[Ru]^+$ should have about equal abundance. As a result, a relatively large proportion of the *trans*-diastereomers of **11** and **12** is formed (Figure 5 and 6). For the reaction with NaI the amount of *trans*-**12** after 2 days is even larger (42%) than the initial amount of *trans*-**8** (23%). This is probably due to the fact that, as *trans*-**8** reacts and disappears about three times faster than *cis*-**8**, the *cis*/*trans* equilibrium of **8** is out of balance and *cis*-$[Ru]^+$ will convert into *trans*-$[Ru]^+$. Then, after both *cis*- and *trans*-**8** have been consumed, the *cis*/*trans* ratio of **12** changes until equilibrium has been reached after about a week. From the profile in Figure 6 it is estimated that I^- dissociation in *trans*- and *cis*-**12** in $CDCl_3$ is about three times as slow ($k_1 = 4.3 \times 10^{-6}$, $k_{-1} = 1.5 \times 10^{-6}$ s^{-1}) as Cl^- dissociation in **8** (see Figure 3). This "peaking" of the abundance of the *trans*-diastereomer is not observed during the reaction of **8** with NaBr. We think that exchange between the *cis*/*trans* diastereomers in **11** is faster than for **12**, and that equilibrium is reached before **8** has completely reacted.

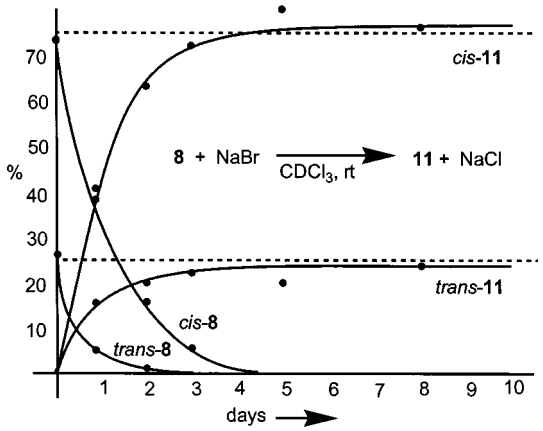


Figure 5. Reaction of **8** with NaBr in $CDCl_3$

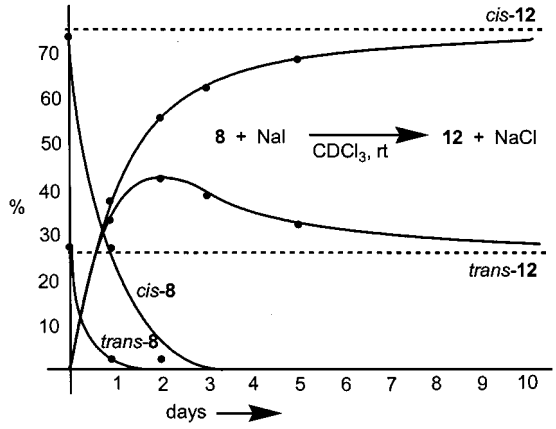


Figure 6. Reaction of **8** with NaI in $CDCl_3$

Conclusions

The experiments presented above confirm that the *cis*- and *trans*-diastereomers of the Cp/phosphane complex **8** (and **11**, **12**) exchange through Cl^- dissociation with intermediate formation of the cations *cis*- and *trans*-**[Ru]**$^+$. The rate of Cl^- dissociation in *trans*-**8** is about 3 times as large as in *cis*-**8**. Furthermore, the cations **[Ru]**$^+$ are too electron rich to develop significant Lewis acidity for asymmetric catalysis. Further modifications of the functionalized Cp-ligands should lead to the formation of only one diastereomer upon coordination, as in the ferrocene-based Cp/phosphane ligand designed by Hidai, mentioned earlier.[7b] Thus, the presence of two, possibly counteracting, diastereotopic sites on the catalyst is not very promising for obtaining high enantioselectivity. Another solution might be the separation of the diastereomers. However, this is only meaningful when the ruthenium complexes are configurationally stable at the metal center. The situation may be improved by using π-acceptor ligands which at the same time would increase the Lewis acidity. In future work, we will concentrate on other coordination environments and transition metals to avoid the diastereomer problem.

Experimental Section

General: All manipulations were carried out under an atmosphere of argon using Schlenk techniques. Solvents were dried and degassed by conventional procedures prior to use. − ^1H and ^{13}C NMR: Varian Gemini 300. − The ^1H and ^{13}C NMR spectra were measured in $CDCl_3$ unless stated otherwise ($CHCl_3$: $\delta_H = 7.24$; $CDCl_3$: $\delta_C = 77.0$) − Mass spectra: AMD Intectra 402, EI-MS, 70 eV; only the primary signal of a mixture of isotopes is given. − Combustion analyses (C,H): CHNS-932 LECO analyzer. The Cp/ether ligands were prepared according to ref.[5c] and their Me_3Si-derivatives according to ref.[5d]

[RuCl{η^5-$C_5H_4CH_2CH_2O$[(1*R*)-fenchyl]}$(PPh_3)_2$] (3d): A suspension of $RuCl_2(PPh_3)_3$ (2.00 g, 2.1 mmol) and {C_5H_4-(CH_2CH_2Ofenchyl)($SiMe_3$)} (1.1 g, 3.5 mmol) in 100 mL of toluene was refluxed for 5 h. After cooling to room temperature the mixture was concentrated and chromatographed (Fluka: silica gel 60, toluene/THF, 9:1). Concentration of the extracts afforded a yellow-orange air stable powder that was washed once with a little pentane. Yield: 1.60 g (1.92 mmol, 91%). − $C_{53}H_{55}ClOP_2Ru$ (906.5): calcd. C 70.2, H 6.1; found C 68.9, H 6.5. − (EI) MS for **3d**, and also for **3a**−**c**, do not show fragments for M; main fragments are due to PPh_3 (262, 183, 108, 78); a fragment with low abundance was recognized as the metallocene Cp'_2Ru (for **3d**: *m*/*z* = 592), obviously a result of rearrangement.

[RuCl{η^5-$C_5H_4CH_2CH_2O$[(1*R*)-menthyl]}{$PPh_3)_2$] (3c): As for **3d**. Yield: 95%. − $C_{53}H_{57}ClOP_2Ru$ (908.5): calcd. C 70.0, H 6.3; found C 70.0, H 5.8.

[RuCl[η^5-$C_5H_4CH_2CH_2OMe$](PPh$_3$)$_2$] (3a). − Method 1: A suspension of $RuCl_2(PPh_3)_3$ (1.0 g, 1.1 mmol) and 0.3 $C_5H_5CH_2CH_2OMe$ (0.3 g, 2.5 mmol) in degassed ethanol was refluxed overnight under argon. The solvent was then replaced by toluene and the mixture heated to reflux for a few hours. Concentration and chromatograpy (Fluka: silica gel 60, toluene/THF, 15:1) afforded a yellow-orange powder (0.4 g, 45%). − **Method 2:** As for **3d**. Yield: 90%. − $C_{44}H_{41}ClOP_2Ru$ (784.3): calcd. C 67.4, H 5.3; found C 67.1, H 5.4.

[RuCl{η^5-$C_5H_4CH_2CH_2O$[(1*S*)-isobornyl]}$(PPh_3)_2$]: As for **3a**, method 1. Yield: 40%. $C_{53}H_{55}ClOP_2Ru$ (906.5): calcd. C 70.2, H 6.1; found C 68.4, H 5.9.

[Ru(O_3SCF_3){η^5-$C_5H_4CH_2CH_2OR$}$(PPh_3)_2$] {R = Me (4a), isobornyl (4b) or menthyl (4c)}: In a typical experiment 0.10 g of **3** was reacted with a slight excess of AgO_3SCF_3 in 10 mL of CH_2Cl_2. After stirring for 10 min at room temperature the solution was filtered over Celite, and evaporated to dryness. The triflates were unstable in solution, and were therefore characterized by their ^{1}H, ^{13}C, and ^{31}P NMR spectra measured immediately after their preparation.

C_5H_4{CH_2CH_2S[(1*R*)-neomenthyl]}($SiMe_3$): A solution of (*S*)-(+)-neomenthanethiol[10b,c] (8.6 g, 50 mmol) in 50 mL of THF was stirred in the presence of excess potassium metal at room temperature overnight. The solution of the resulting potassium thiolate was decanted and spiro[2.4]hepta-4,6-diene[10d] (4.6 g, 50 mmol) was added at 0°C. After stirring for 5 h at 45°C, the reaction mixture was cooled to −78°C and 6 mL (excess) of $ClSiMe_3$ was added. After stirring for 2 h, solvent was evaporated and the residue extracted with a mixture of water and pentane. The pentane extracts were collected, dried over Na_2SO_4, filtered and evaporated to dryness affording the oily title compound in quantitative yield and high purity. − $C_{20}H_{36}SSi$ (336.7): calcd. C 71.4, H 10.8, S 9.5; found C 70.5, H 10.3, S 9.1.

[RuCl{η^5-$C_5H_4CH_2CH_2S$[(1*R*)-neomenthyl]}$(PPh_3)_2$] (5): A mixture of $RuCl_2(PPh_3)_3$ (4.79 g, 5.0 mmol) and C_5H_4{CH_2CH_2S[(1*R*)-neomenthyl]}($SiMe_3$) (1.68 g, 5.0 mmol) in CH_2Cl_2 was stirred overnight at room temperature. The solvent was then evaporated and the residue washed once with pentane. The orange product was isolated by exhaustive extraction with diethyl ether. Yield: 2.96 g (64%). − $C_{53}H_{57}ClP_2RuS$ (924.6): calcd. C 68.9, H 6.2, S 3.5; found C 67.6, H 6.6, S 3.3. − ^{1}H NMR: δ = 0.85, 0.87, 0.91 (all d, 3 × 3 H, neomenthyl), 2.5−2.7 (m, 4 H, CCH_2CH_2S), 3.14 (1 H, SC*H*), 3.27, 3.31, 3.99, 4.01 (C_5H_4). − ^{13}C NMR: δ = 20.9, 21.1, 22.2 ($C_{7,9,10}$), 25.9 (CCH_2), 26.3 (C_8), 27.3 (C_5), 29.9 (C_1), 31.8 (SCH_2), 35.4 (C_6), 40.7 (C_2), 46.5 (C_3), 48.9 (C_4), 76.4, 76.9, 80.0(br), 80.3(br) (C_5H_4).^{31}P NMR: δ = 40.0.

[Ru(O_3SCF_3){η^5-$C_5H_4CH_2CH_2S$[(1*R*)-neomenthyl]}$(PPh_3)_2$] (6): A solution of **6** was generated from **5** as described for **4**. Complex **6** decomposes within a few hours at room temperature in $CDCl_3$ and was therefore only characterized by NMR spectroscopy. Selected NMR spectroscopic data: ^{1}H NMR: δ = 0.61, 0.88, 0.98 (all d, 3 × 3 H, neomenthyl), 2.17, 2.44 (m, 2 × 1 H, CCH_2), 2.53 (1 H, SC*H*), 3.59, 3.97 (m, 2 × 1 H, SCH_2), 4.04, 4.19, 4.50, 4.55 (C_5H_4). − ^{13}C NMR: δ = 20.4, 21.2, 23.7 ($C_{7,9,10}$), 23.9 (CCH_2), 26.4 (C_5), 28.6, 29.1 ($C_{1,8}$), 31.8 (C_6), 36.6 (C_2), 47.2 (C_4), 49.9 (C_3), 53.9 (SCH_2), 76.0, 76.8, 79.8, 82.7 (C_5H_4). − ^{31}P NMR: δ = 33.1 (d, *J* = 36 Hz), 42.8 (d, *J* = 36 Hz).

(*S*)-$HOCH_2CH(Me)PPh_2$: A solution of Ph_2PLi and PhLi was prepared by reacting PPh_3 (29.95 g, 114 mmol) and lithium shavings (3.0 g, 430 mmol) in 200 mL of THF at room temperature overnight. The bright orange solution was then filtered and cooled to −70°C upon which *(R)*-$HOCH_2CH(Me)Cl$ (9.9 g, 105 mmol) was added. The solution was slowly raised to room temperature and stirred overnight. The resulting colorless solution was evaporated to dryness. Water and 100 mL of CH_2Cl_2 were added (in air), and 3 M HCl was added until the mixture was just neutral (ca 40 mL). The organic layer was separated, dried over Na_2SO_4 and evaporated to dryness affording 27.2 g (100%) of a very viscous colorless oil. Except for some trace amounts of $Ph_2P(O)H$, this material was virtually pure. − $C_{15}H_{17}OP$ (244.3): calcd. C 73.8, H 7.0; found C 72.7, H 7.0. − $[\alpha]_D$ (*c* = 3.2, CH_2Cl_2) +4.5° (*ee* ≈ 60%; *S*/*R* ≈ 80:20). Actually, the optical purity is 66% as was found after complexation to ruthenium (vide infra). − ^{1}H NMR: δ = 1.09 (dd, $^3J_{HH}$ = 6.9 Hz, $^3J_{HP}$ = 13.9 Hz, 3 H, CH_3), 2.61 (m, 1 H, C*H*CH_3), 3.54 (ddd, $^2J_{HH}$ = 10.9 Hz, $^3J_{HH}$ = 7.6 Hz, $^3J_{HP}$ = 7.6 Hz, 1 H, OCH_2), 3.70 (ddd, $^2J_{HH}$ = 10.9 Hz, $^3J_{HH}$ = 4.6 Hz, $^3J_{HP}$ = 8.9 Hz, 1 H, OCH_2), 7.32 (m, 6 H, Ph), 7.50 (m, 4 H, Ph). − ^{13}C NMR ($CDCl_3$): δ = 13.71 (d, $^2J_{CP}$ = 13.1 Hz, *C*H_3), 33.64 (s, *C*CH_3), 65.16 (d, $^2J_{CP}$ = 19.8 Hz, O*C*H_2), 128.7, 129.6, 133.7 (m, Ph). − ^{31}P NMR: δ = −9.2.

[RuCl{η^5:η^1-$C_5H_4CH_2CH(Me)PPh_2$}(PPh_3)] (racemic) (8): To a solution of (*S*)-$HOCH_2CH(Me)PPh_2$ (22.4 g, 92 mmol) was added 100 mL of a 1 M solution of BH_3 in THF at −30°C. After stirring for 1 h at room temperature the solvent was removed affording crude (*S*)-$HOCH_2CH(Me)PPh_2(BH_3)$ as a very viscous colorlous oil (23.3 g, ≈ 100%). − ^{1}H NMR: δ = 1.15 (dd, $^3J_{HH}$ = 7.0 Hz, $^3J_{HP}$ = 15.7 Hz, 3 H, CH_3), 2.82 (m, 1 H, C*H*CH_3), 3.6−3.8 (m, 2 H, OCH_2), 7.42 (m, 6 H, Ph), 7.73 (m, 4 H, Ph). − ^{13}C NMR ($CDCl_3$): δ = 11.88 (sbr, *C*H_3), 31.61 (d, $^1J_{CP}$ = 34.9 Hz, *C*CH_3), 63.17 (d, $^2J_{CP}$ = 6.6 Hz, O*C*H_2), 128.7, 131.3, 132.5 (m, Ph). − ^{31}P NMR: δ = 19.8. − A solution of the borane-adduct (6.85 g, 26.6 mmol) and Et_3N (6.0 mL, 43 mmol) in 80 mL of CH_2Cl_2 was cooled to −30°C upon which $MeSO_2Cl$ (3.0 mL, 39 mmol) was added. The thick suspension was stirred for a few hours at room temperature. Addition of water resulted in the formation of two clear layers. The CH_2Cl_2 layer was washed with water several times, then separated, dried over Na_2SO_4 and evaporated to dryness affording 8.77 g (26.1 mmol, ca 98%) of (*S*)-$MeSO_3CH_2CH(Me)PPh_3(BH_3)$ as a light-brown viscous oil. − ^{1}H NMR: δ = 1.20 (dd, $^3J_{HH}$ = 6.9 Hz, $^3J_{HP}$ = 15.4 Hz, 3 H, CCH_3), 2.84 (s, 3 H, SCH_3), 3.10 (m, 1 H, C*H*CH_3), 4.21 (ddd, $^2J_{HH}$ = 10.2 Hz, $^3J_{HH}$ = 6.8 Hz, $^3J_{HP}$ = 9.6 Hz, 1 H, OCH_2), 4.35 (ddd, $^2J_{HH}$ = 10.2 Hz, $^3J_{HH}$ = 4.7 Hz, $^3J_{HP}$ = 6.6 Hz, 1 H, OCH_2), 7.46 (m, 6 H, Ph), 7.65−7.85 (m, 4 H, Ph). − ^{13}C NMR ($CDCl_3$): δ = 11.79 (sbr, *C*H_3), 29.50 (d, $^1J_{CP}$ = 34.9 Hz, *C*CH_3), 37.26 (s, S*C*H_3), 70.24 (d, $^2J_{CP}$ = 11.8 Hz, O*C*H_2), 129.0, 131.7, 132.4 (m, Ph). − ^{31}P NMR: δ = 20.0. − A solution of CpLi was generated by adding 26 mL of a 1.61 M solution of *n*BuLi (42 mmol) in hexane to a solution of 3.5 mL (42 mmol) of freshly cracked CpH in 60 mL of THF with ice-cooling. Then, the above mentioned mesylate (26.1 mmol) was added at −20°C and the dark brown reaction mixture was stirred overnight at room temperature. Solvents were removed and the residue was extracted into CH_2Cl_2. Filtration and removal of solvent afforded 7.91 g of a dark brown oil, mainly containing (*S*)-$C_5H_5CH_2CH(Me)PPh_2(BH_3)$ as a mixture of two regioisomers. − ^{1}H NMR: δ = 1.06 (dd, $^3J_{HH}$ = 7.0 Hz, $^3J_{HP}$ = 16.4 Hz, 3 H, CH_3), 2.3−3.0 {m, C*H*CH_3, CCH_2, Cp(aliphatic), 5 H}, 6.01 (s), 6.17 (s), 6.23 (d, *J* = 5.4 Hz), 6.31−6.40 {m, Cp(olefinic), 3H in total}, 7.41 (m, 6 H, Ph), 7.74 (m, 4 H, Ph). − ^{13}C NMR: δ = 13.23/13.33 (sbr, *C*H_3), 28.03 (d, $^1J_{CP}$ = 36.0 Hz)/28.70 (d, $^1J_{CP}$ = 35.6 Hz, *C*CH_3), 30.56 (d, $^2J_{CP}$ = 3.7 Hz)/31.41 (d, $^2J_{CP}$ = 4.1 Hz, *C*H_2CP), 41.09/42.91 {Cp(aliphatic)}, 133.60/134.03 {Cp(olefinic CH)}, 143.58 (d, $^3J_{CP}$ = 13.6 Hz)/145.63 {d, $^3J_{CP}$ = 14.2 Hz, Cp(olefinic)}, other Cp signals hidden by Ph signals, 128.4 (m), 130.8 (m), 132.2 (m, all Ph). − ^{31}P NMR: δ = 24.8. − This oil was dissolved in 30 mL of degassed pyrrolidine and heated at 70−80°C for 30 min. After removal of solvent the residue was extracted with warm pentane (ca 150 mL in total), and filtered over Celite. Removal of solvent afforded 3.95 g (ca 13 mmol) of (*S*)-$C_5H_5CH_2CH(Me)PPh_2$ as a yellow oil. This material could not be distilled without decomposition and was therefore used without further purification. − ^{1}H NMR: δ = 0.99 (dd, $^3J_{HH}$ = 6.8 Hz, $^3J_{HP}$ = 15.0 Hz, 3 H, CH_3), 2.0−2.9 (m, C*H*CH_3, CCH_2, 3 H), 2.94 {s, Cp(aliphatic), 2 H}, 6.02 (s), 6.18 (s), 6.25 (d, *J* = 4.2 Hz),

6.40 {s, Cp(olefinic), 3H in total}, 7.32 (m, 6 H, Ph), 7.51 (m, 4 H, Ph). – ^{13}C NMR: δ = 16.16 (d, $^2J_{CP}$ = 16.3 Hz)/16.28 (d, $^2J_{CP}$ = 16.4 Hz, *C*H$_3$), 29.87 (d, $^2J_{CP}$ = 10.3 Hz)/30.67 (d, $^2J_{CP}$ = 10.3 Hz, *C*H$_2$CP), 33.59 (d, $^1J_{CP}$ = 19.0 Hz)/34.49 (d, $^1J_{CP}$ = 19.3 Hz, *C*CH$_3$), 41.26/43.48 {Cp(aliphatic)}, other Cp signals hidden by Ph signals, 128.3 (m), 128.7 (m), 133.6 (m, all Ph). – ^{31}P NMR: δ = −0.4. – A suspension of $RuCl_2(PPh_3)_3$ (3.1 g, 3.2 mmol) and 1.83 g of the above oil in 50 mL of degassed ethanol was refluxed overnight. Then, ethanol was replaced by toluene and the mixture was heated to reflux for another few hours. Workup by chromatography (see above) afforded 0.68 g {1.0 mmol, 8% based on $HOCH_2CH(Me)PPh_3$} of racemic [RuCl{η^5:η^1-$C_5H_4CH_2CH(Me)PPh_2$}(PPh_3)] as a 77:23 mixture of diastereomers (NMR) as an orange powder. – $C_{38}H_{35}ClP_2Ru$ (689.6): calcd. C 66.1, H 5.1; found C 64.3, H 5.3. – MS; *m*/*z*(%): 690 (30) [M$^+$], 428 (100) [M$^+$ – PPh_3], 393 (100), [M$^+$ – Cl – PPh_3], 315 (5) [M$^+$ – Cl – PPh_3 – Ph].

Determination of the Enantiopurity of [RuCl{η^5:η^1-C_5H_4-$CH_2CH(Me)PPh_2$}(PPh_3)]. Formation of {Ru[η^5:η^1-$C_5H_4CH_2CH$-$(Me)PPh_2$][(***S*****)-H$_2$**NCH(Me)Ph](PPh_3)}{O_3SCF_3} (9): A solution of **8** (0.10 g, 0.14 mmol) in 2.0 mL of dry $CDCl_3$ was treated with AgO_3SCF_3 (0.04 g, 0.16 mmol) and (*S*)-$H_2NCH(Me)Ph$ (0.12 g, 1 mmol). After stirring for 30 min the silver salts were removed by filtration and the resulting yellow-green solution was analyzed by NMR spectroscopy. The salt **9** is present as a 38:38:12:12 mixture of isomers and is therefore completely racemic.

[RuCl{η^5:η^1-$C_5H_4CH_2CH(Me)PPh_2$}(PPh_3)] (*S* enriched) (8): A mixture of (*S*)-$HOCH_2CH(Me)PPh_2$ (*S*/R ≈ 80:20, see above, 6.0 g, 24.7 mmol) and Et_3NHCl (6.3 g, 46 mmol) in 150 mL of degassed acetonitrile was cooled to −30°C, upon which PCl_3 (4.0 mL, 46 mmol) was added. The resulting bright yellow suspension was stirred for 2 days at 50−60°C. Solvent was removed in vacuo and CH_2Cl_2 and degassed water were added. The CH_2Cl_2 layer was washed with water, filtered and dried over $CaCl_2$. Filtration and removal of solvent afforded 6.24 g of an oily substance mainly containing (*S*)-$ClCH_2CH(Me)PPh_2$ (up to 30% of $Ph_2P(O)H$ may be present due to the partial formation of Ph_2PCl during the chlorination procedure and subsequent hydrolysis). – ^{1}H NMR: δ = 1.18 (dd, $^3J_{HH}$ = 6.8 Hz, $^3J_{HP}$ = 14.6 Hz, 3 H, C*H*$_3$), 2.69 (m, 1 H, C*H*CH$_3$), 3.32 (ddd, $^2J_{HH}$ = 10.4 Hz, $^3J_{HH}$ = 3.1 Hz, $^3J_{HP}$ = 10.4 Hz, 1 H, OC*H*$_2$), 3.68 (ddd, $^2J_{HH}$ = 10.4 Hz, $^3J_{HH}$ = 4.6 Hz, $^3J_{HP}$ = 8.9 Hz, 1 H, OC*H*$_2$), 7.32 (m, 6 H, Ph), 7.50 (m, 4 H, Ph). – ^{13}C NMR ($CDCl_3$): δ = 15.09 (d, $^2J_{CP}$ = 16.2 Hz, *C*H$_3$), 33.72 (d, $^1J_{CP}$ = 13.8 Hz, *C*CH$_3$), 49.07 (d, $^2J_{CP}$ = 26.9 Hz, O*C*H$_2$), 128.8, 130.6, 132.5 (m, Ph). – ^{31}P NMR: δ = −5.1. – This oil was added to a solution of CpLi generated from mixing 21 mL of a 1.61 M solution of *n*BuLi (34 mmol) in hexane and a solution of 3.0 mL (36 mmol) of CpH in 50 mL of THF. This mixture was refluxed for 2 days. Then, 1 mL of water was added and the mixture was evaporated to dyness. Extraction with pentane afforded 2.17 g (ca 7 mmol) of (*S*)-$C_5H_5CH_2CH(Me)PPh_2$ as a yellow oil. Reaction with $RuCl_2(PPh_3)_3$ (3.3 g, 3.4 mmol) and workup as described above afforded 1.17 g of **8** {1.7 mmol, 8% based on $HOCH_2CH(Me)PPh_2$}. The reaction with AgO_3SCF_3 and (*S*)-$H_2NCH(Me)Ph$ (vide supra) afforded a 64:13:19:4 mixture of isomers of **9** and therefore the enantiomeric excess of the Cp-Ligand was 66% (64 + 19−13−4; *S*/*R* = 83:17) which is an agreement with the estimated enantiopurity of the starting product $HOCH_2CH(Me)PPh_2$ of 60% (vide supra).

X-ray Structure Determination of *rac*, *trans*-8: Orange crystals suitable for an X-ray diffraction study were grown within a few days from a saturated ether solution at room temperature. There were two crystal forms. Crystallographic and experimental details are summarized in Table 3. No absorption corrections were made. The structures were solved by direct methods (SHELXS-86)[20a] and refined by full-matrix least squares against F^2 (SHELXL-97).[20b] All non-hydrogen atoms were refined anisotropically, hydrogen atoms isotropically. Crystallographic data (excluding structure factors) for the structures reported in this paper have been deposited with the Cambridge Crystallographic Data Centre as supplementary publication no. CCDC-117007 (triclinic *rac, trans*-**8**) and 117006 (monoclinic *rac, trans*-**8**). Copies of the data can be obtained free of charge on application to CCDC, 12 Union Road, Cambridge CB2 1EZ {fax: (internat.) + 44-1223/336-033, E-mail: deposit@ccdc.cam.ac.uk}.

Reaction of Racemic 8 with NaBr: A solution of **8** (0.08 g, 0.12 mmol) in 1.0 mL of dry $CDCl_3$ was treated with NaBr (0.10 g, 1.0 mmol) of and stirred at room temperature. The reaction was monitored by NMR spectroscopy. After 1 week the reaction was complete. The solution was filtered and evaporated to dryness affording orange-brown RuBr[η^5:η^1-$C_5H_4CH_2CH(Me)PPh_2$](PPh_3) (**11**) as a 76:24 mixture of diastereomers. MS; *m*/*z*(%): 736 (20) [M$^+$], 474 (90) [M$^+$ – PPh_3], 393 (100), [M$^+$ – Br – PPh_3], 315 (5) [M$^+$ – Br – PPh_3 – Ph].

Reaction of Racemic 8 with NaI: The reaction with NaI was performed analogously. The reaction was complete after about 2 weeks. The brown RuI[η^5:η^1-$C_5H_4CH_2CH(Me)PPh_2$](PPh_3) (**12**) was obtained as a 73:27 mixture of diastereomers. MS; *m*/*z*(%): 782 (20) [M$^+$], 520 (100) [M$^+$ – PPh_3], 393 (95), [M$^+$ – I – PPh_3], 315 (5) [M$^+$ – I – PPh_3 – Ph]. Neither the rate of the reaction nor the product formation was changed when the reaction was conducted in the presence of 3 equiv. of added PPh_3 per Ru (NMR monitoring).

Catalysis. Diels−Alder reaction: To a solution of *S*-enriched **8** (0.08 g, 13 μmol) in 10 mL of CH_2Cl_2 was added an excess of AgO_3SCF_3 (0.18 g). After stirring for 10 min the resulting red-brown suspension was filtered over Celite and cooled to −60°C. Then, *i*Pr_2NEt (9 μL, 50 μmol), cyclopentadiene (1.8 mL, 22 mmol) and methacrolein (1.0 mL, 12.2 mmol) were added. The clear yellow solution was stirred at −4°C. Samples were taken regularly over a period of a few days. They were quenched by flash chromatography over silica gel. Volatiles were removed in vacuo (without heating) and the residue was analyzed by ^{1}H NMR spectroscopy. The Diels−Alder product 2-formyl-2-methyl-bicyclo[2.2.1]hept-5-ene could not be found;[5b] instead the gradual formation of dicyclopentadiene was observed.

Supporting Information: ^{1}H, ^{13}C and ^{31}P NMR spectroscopic data for **3** and **4**. A drawing of the assignment of the ^{1}H and ^{13}C NMR spectroscopic data of **8**.

Acknowledgments

Financial support by the Deutsche Forschungsgemeinschaft, the Alexander von Humboldt Stiftung and the Bundesland Sachsen-Anhalt (HSP III program) is gratefully acknowledged.

[1] [1a] K. Narasaka, *Synthesis* **1991**, 1−11. – [1b] H. B. Kagan, O. Riant, *Chem. Rev.* **1992**, *92*, 1007−1019. – [1c] *Catalytic Asymmetric Synthesis* (Ed.: I. Ojima), VCH, New York, **1993**.
[2] [2a] W. Beck, K. Sünkel, *Chem. Rev.* **1988**, *88*, 1405−1421. – [2b] T. K. Hollis, W. Odenkirk, N. P. Robinson, J. Whelan, B. Bosnich, *Tetrahedron* **1993**, *49*, 5415−5430.

[3] [3a] W. H. Hersch, *J. Am. Chem. Soc.* **1985**, *107*, 4599−4601. − [3b] R. V. Honeychuck, P. V. Bonnesen, J. Farahi, W. H. Hersch, *J. Org. Chem.* **1987**, *52*, 5293−5296. − [3c] P. V. Bonnesen, C. L. Puckett, R. V. Honeychuck, W. H. Hersch, *J. Am. Chem. Soc.* **1989**, *111*, 6070−6081. − [3d] R. V. Honeychuck, W. H. Hersh, *Inorg. Chem.* **1989**, *28*, 2869−2886. − [3e] J. W. Faller, Y. Ma, *J. Am. Chem. Soc.* **1991**, *113*, 1579−1586. − [3f] A. S. Olson, W. J. Seitz, M. M. Hossain, *Tetrahedron Lett.* **1991**, *32*, 5299−5302. − [3g] A. A. H. van der Zeijden, V. Shklover, H. Berke, *Inorg. Chem.* **1991**, *30*, 4393−4396.

[4] [4a] J. W. Faller, C. J. Smart, *Tetrahedron Lett.* **1989**, *30*, 1189−1192. − [4b] E. P. Kündig, B. Bourdin, G. Bernardinelli, *Angew. Chem.* **1994**, *106*, 1931−1933.

[5] [5a] A. A. H. van der Zeijden, *Tetrahedron: Asymmetry* **1995**, *6*, 913−918. − [5b] A. A. H. van der Zeijden, *J. Organomet. Chem.* **1996**, *518*, 147−153. − [5c] A. A. H. van der Zeijden, C. Mattheis, *Synthesis* **1996**, 847−850. − [5d] A. A. H. van der Zeijden, C. Mattheis, R. Fröhlich, *Organometallics* **1997**, *16*, 2651−2658. − [5e] A. A. H. van der Zeijden, C. Mattheis, *J. Organomet. Chem.* **1998**, *555*, 5−15.

[6] [6a] T. Kauffmann, J. Olbrich, *Tetrahedron Lett.* **1984**, *25*, 1967−1970. − [6b] A. M. Z. Slawin, D. J. Williams, J. A. Ramsden, C. White, *J. Chem. Soc., Dalton Trans.* **1988**, 2491−2494. − [6c] M. Draganjac, J. Ruffing, T. B. Rauchfuss, *Organometallics* **1985**, *4*, 1909−1911. − [6d] J. Amarasekera, T. B. Rauchfuss, *Inorg. Chem.* **1989**, *28*, 3875−3883. − [6e] B. Antelmann, G. Huttner, J. Vogelgesang, O. Walter, U. Winterhalter, *J. Organomet. Chem.* **1997**, *549*, 139−148. − [6f] H. S. Chu, C. P. Lau, K. Y. Wong, W. T. Wong, *Organometallics* **1998**, *17*, 2768−2777.

[7] [7a] Y. Kataoka, Y. Saito, K. Nagata, K. Kitamura, A. Shibahara, K. Tani, *Chem. Lett.* **1995**, 833−834. − [7b] Y. Nishibayashi, I. Takei, M. Hidai, *Organometallics* **1997**, *16*, 3091−3093. − [7c] B. M. Trost, B. Vidal, M. Thommen, *Chem. Eur. J.* **1999**, *5*, 1055−1069.

[8] M. I. Bruce, P. Hinterding, E. R. T. Tiekink, B. W. Skelton, A. H. White, *J. Organomet. Chem.* **1993**, *450*, 209−218.

[9] The structure of **4** is more complicated than might be expected (J. Amarasekera, T. B. Rauchfuss, S. R. Wilson, *J. Am. Chem. Soc.* **1988**, *110*, 2332−2334). We have evidence that our triflates are in equilibrium with $[Cp^{R}Ru(\eta^6\text{-}PhPPh_2]^+$, PPh_3 and an excess AgO_3SCF_3 if present {complexing with freed PPh_3: ^{31}P NMR ($CDCl_3$): $\delta = 14$}. This is deduced from the persistent "poisoning" of our NMR spectra by signals due to an η^6-coordinated PPh_3 ligand [^1H NMR ($CDCl_3$): $\delta = 6.2$. − ^{13}C NMR: $\delta = 87.4$ (d, $J_{CP} = 6$ Hz), 89.8 (d, $J_{CP} = 16$ Hz), 95.1 (d, $J_{CP} = 24$ Hz)]. See also: T. Wilczewski, *J. Organomet. Chem.* **1985**, *297*, 331−340 and P. J. Fagan, M. D. Ward, J. C. Calabrese, *J. Am. Chem. Soc.* **1989**, *111*, 1698−1719.

[10] [10a] T. Kauffmann, J. Ennen, H. Lhotak, A. Rensing, F. Steinseifer, A. Woltermann, *Angew. Chem.* **1980**, *92*, 321−323. − [10b] C. F. Wilcox Jr., R. R. Craig, *J. Am. Chem. Soc.* **1961**, *83*, 3866−3870. − [10c] B. Strijtveen, R. M. Kellogg, *J. Org. Chem.* **1986**, *51*, 3664−3671. − [10d] M. Mikolajczyk, W. Perlikowska, J. Omelanczuk, *Synthesis* **1987**, 1009−1011.

[11] [11a] C. Altermark, M. Nilsson, B. Otterholm, *Mol. Cryst. Liq. Cryst.* **1987**, *150b*, 277−287. − [11b] B. Koppenhoefer, V. Schurig, *Org. Synth.* **1988**, *66*, 160−172.

[12] N. W. Alcock, A. W. G. Platt, P. Pringle, *J. Chem. Soc., Dalton Trans.* **1987**, 2273−2280.

[13] (*R*)-$HOCH_2CH(Me)PPh_2$ has recently been synthesized in small quantities by a more elaborate procedure but with higher enantioselectivity (>96%): D. Enders, T. Berg, *Synlett* **1996**, 796−798.

[14] A similar reaction using (*S*)-$HOCH_2CH(Me)O_3S$-*p*-tol (B. D. Johnston, K. N. Slessor, *Can. J. Chem.* **1979**, *57*, 233−235) not only affords $HOCH_2CH(Me)PPh_2$, but also about equal amounts of its regioisomer $HOCH(Me)CH_2PPh_2$. Apparently, in this case the reaction proceeds through the intermediacy of propenoxide from which it is known that attack of Ph_2P^- takes place at both carbons of the oxirane ring: K. L. Marsi, M. E. Co-Sarno, *J. Org. Chem.* **1977**, *42*, 778−781.

[15] B. Antelmann, U. Winterhalter, G. Huttner, B. C. Janssen, J. Vogelgesang, *J. Organomet. Chem.* **1997**, *545−546*, 407−420.

[16] T. Imamoto, T. Oshiki, T. Onozawa, T. Kusumoto, K. Sato, *J. Am. Chem. Soc.* **1990**, *112*, 5244−5252.

[17] G. Consiglio, F. Morandini, *Chem. Rev.* **1987**, *87*, 761−778.

[18] [18a] F. Morandini, G. Consiglio, B. Straub, G. Ciani, A. Sironi, *J. Chem. Soc., Dalton Trans.* **1983**, 2293−2298. − [18b] G. Consiglio, F. Morandini, *J. Organomet. Chem.* **1986**, *310*, C66−68.

[19] M. P. Gamasa, J. Gimeno, C. Gonzalez-Bernardo, B. M. Martin-Vaca, D. Monti, M. Bassetti, *Organometallics* **1996**, *15*, 302−308.

[20] [20a] G. M. Sheldrick, SHELXS-86, *Program for Structure Solution*, University of Göttingen, Germany, **1986**. − [20b] G. M. Sheldrick, SHELXL-97, *Program for Crystal Structure Refinement*, University of Göttingen, Germany, **1997**.

[21] *Cis* or *trans* in these compounds refers to the relative positions of the substituents on the two stereogenic centers; at the chiral carbon center Me has higher priority than H and on ruthenium Cl has higher priority than PPh_3. Priority sequence around ruthenium is $C_5H_4R > Cl > PPh_3 > Ph_2PR$.

Received April 8, 1999
[I99126]

Contribution to the Chemistry of Boron, 245[+] A Boron–Boron Double Bond in the Dianions of Tetra(amino)diborates

Heinrich Nöth,*[a] Jörg Knizek,[a] and Werner Ponikwar[a]

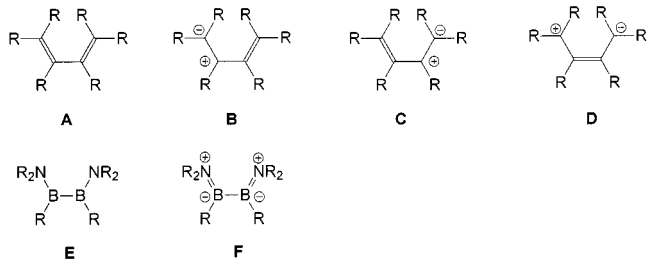
Dedicated to Prof. Dr. Wolfgang Steglich on the occasion of his 65th birthday

Keywords: Diboron compounds / B–B double bond / Dilithium tetra(amino)diborates(2–) / Structure elucidation

A series of mixed tetraaminodiborane(4) compounds bearing pyrrolyl, indolyl, and carbazolyl substituents besides dimethylamino groups has been prepared and subjected to reduction with elemental Li in the presence of diethyl ether. Tetraaminodiborates(2–) are formed, which feature a boron–boron double bond. The diborate anion acts as a double bidentate ligand coordinating pairwise through two of its nitrogen atoms to an Li center, which is tricoordinated by one O and the two N atoms. The new diborates are isoelectronic with tetraaminoethylenes and are expected to be electron-transfer reagents.

Introduction

One of the foremost principles in inorganic and metalorganic chemistry is that of isoelectronic or isolobal systems.[2] One of the systems where this concept first came to prominence was that of boron−nitrogen compounds since the BN atom pair is isoelectronic and isolobal with a pair of carbon atoms. The consequences of isoelectronic systems have been delineated in two classical papers by Wiberg,[3] in which physical properties and structural relationships for pairs of isoelectronic compounds were correlated. As the amount of structural information and our knowledge of the reactivity of boron−nitrogen compounds progressed, it became apparent that fundamental differences exist due to the more polar electron distribution in BN systems compared to that in CC systems. For instance, although the bis(amino)diboranes $R_2N(R)B-B(R)NR_2$[4] are isoelectronic with the 1,3-butadienes $R_2C=(R)C-C(R)=CR_2$, the bonding in the latter is best described by the canonical formulae **A** to **D**, while formulae **E** and **F** describe the bonding situation in the diborane(4) derivative.

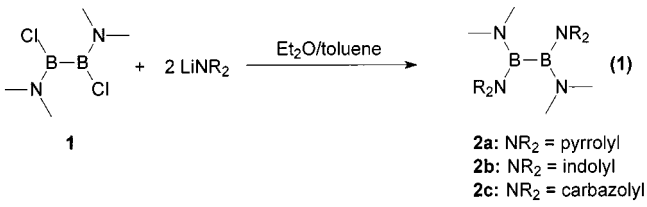


Typical for the diborane(4) derivative is the absence of a double-bond contribution to the boron−boron core, and this is reflected not only in the bond lengths (1.74 Å), but also in the fact that the two $(R_2N)RB$ units adopt interplanar angles between 60 and 90°, depending on the nature of the substituents.[4,5,6]

The majority of tetraaminodiboranes(4), $(R_2N)_4B_2$, are obtained by dehalogenation of bis(amino)boron halides $(R_2N)_2BHal$.[7][8] Yields of the resulting diborane species range from >70% to <1% in very unfavorable cases depending on conditions as well as on experimental skills. Dehalogenation by sodium metal is often the method of choice compared to the use of Na/K alloy, even though longer reaction times are required. One of the possible reasons for the low yields may be a further reaction of the $B_2(NR_2)_4$ formed with excess metal. We report here on this perspective.

Tetraaminodiboranes(4)

For the present study, a number of new tetraaminodiboranes(4) **2a**−**2c** were prepared by allowing bis(dimethylamino)diboron(4) dichloride **1**[9] to react with lithio amides as shown in Equation 1.



The results of X-ray crystal structure determinations of **2a** and **2b** are depicted in Figures 1 and 2 (see also Table 1). The BN bonds to the dimethylamino groups measure 1.390(3) and 1.396(2) Å, respectively. They form interplanar angles with the $B_2(N_A)_2$ plane (the subscript A indicates the amino N atoms) of just 4° and 9° and thus can be considered as being almost coplanar. This allows the formation of strong BN_A π-bonds with a bond order close to 2, as

[+] Part 244: Ref.[1]

[a] Institute of Inorganic Chemistry, University of Munich
Butenandtstraße 5−13, Haus D, D-81377 München, Germany

 © WILEY-VCH Verlag GmbH, D-69451 Weinheim, 1999 1434−1948/99/1111−1931 $ 17.50+.50/0

reflected in the short BN_A bond lengths. In contrast, the BN_H bonds (the subscript H indicates the heterocyclic N atoms) to the indolyl and pyrrolyl ligands are much longer, with an average length of 1.48 Å. The torsion angles between the indolyl and pyrrolyl rings and the BN_AN_H units are 32° and 35°, respectively, which would still allow for a non-negligible BN_H π-interaction. On the other hand, both heterocyclic groups are electronegative substituents, which tend to avoid π-bonding through their N_H atoms. Considering its NMR data, the same holds for compound **2c**.

The dihedral angles N3−B2−B1−N4 and N2−B2−B1−N1 are 75° and 72° in **2a** and 59° and 55° in **2b**. Thus, the twisting about the B−B bond is larger in **2a** than in **2b**, which is remarkable considering the greater steric requirement of the indolyl group. Finally, the boron−boron bond lengths amount to 1.716(2) Å in **2a** and 1.723(4) Å in **2b**, which are appropriate values for B−B single bonds.[10] Therefore, the structural parameters are consistent with a significant contribution from formulae **E** and **F** to the ground states of these molecules.

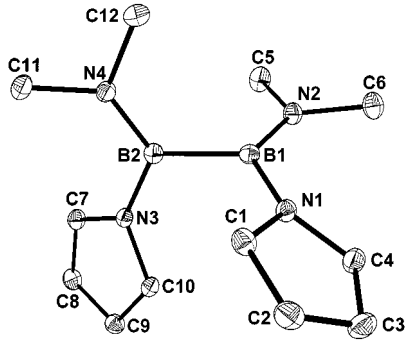


Figure 1. Molecular structure of the diborane(4) **2a** in the crystal; thermal ellipsoids are shown at a 25% probability level

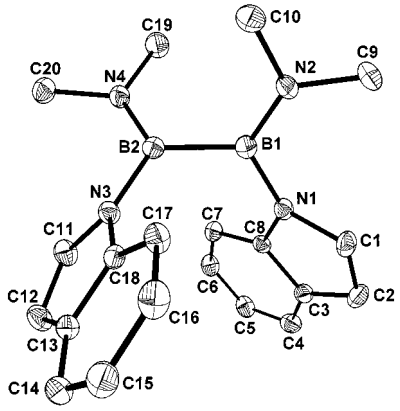


Figure 2. Molecular structure of the diborane(4) **2b** in the crystal; thermal ellipsoids are shown at a 25% probability level

Reduction to Tetraaminodiborates(2−)

Treating solutions of the $B_2(NR_2)_4$ compounds **2a**−**2c** with elemental Li (in finely dispersed form) in toluene leads to a very slow reaction of the metal. The reaction is accompanied by a slight color change of the solution and eventually the ^{11}B-NMR signal disappears, indicating that an insoluble boron-containing precipitate is formed. By carrying out these reactions of **2a** and **2c** in diethyl ether/toluene, yellow and red solutions are formed, respectively. However, for the reduction of **2b**, neat diethyl ether is required as the solvent; in this case the solution turns orange. These reactions proceed according to Equation 2.

From the red solutions of the reduced $B_2(NR_2)_4$ compounds **2a**−**2c**, yellow crystals of **3a**, orange crystals of **3b**, and red crystals of **3c** were isolated. All were found to be extremely air- and moisture-sensitive.[19] Preliminary studies of their chemical behaviour have demonstrated that they can be considered as strong reducing agents. This will be reported in a separate paper.

NMR Spectra

The shielding at the boron atoms of the tetraaminodiboranes(4) (δ^{11}B = 37.0 for **2a**; 36.7 for **2b**; 37.9 for **2c**) corresponds to that found for $B_2(NMe_2)_4$ (δ^{11}B = 36.6) or $B_2(NMe_2)_2Cl_2$ (δ^{11}B = 37.5). Two signals for the NMe_2 groups, both in the ^{1}H- and the ^{13}C-NMR spectra, are indicative of hindered rotation about the B−NMe_2 bond. Considering the ^{1}H-NMR data, the shift differences between these two signals are 0.12 ppm for **2a**, 0.18 ppm for **2b**, and 0.04 ppm for **2c**. The small difference found for **2c** may indicate a greater twisting of the NMe_2 groups in relation to the N_2BB planes, while for **2a** and **2b** the twisting does not exceed 10°.

On anion formation, the boron centers become more shielded by 4.0−9.6 ppm. While the NMR signals for the NMe_2 groups are slightly upfield shifted in **3a** and **3b**, a deshielding of 0.1 ppm is observed for **3c**. These observations are in accord with the trend in the ^{11}B shieldings shown by compounds $Ph(Me_2N)B-B(NMe_2)Ph$[14] and $[Ph(Me_2N)B=B(NMe_2)Ph](LiOEt_2)_2$,[14] where δ^{11}B changes from 49.3 to 33. Since in the anions **3** the amino groups are almost perpendicularly oriented in relation to the B_2N_4 plane, all effects of B−N π-bonding can be neglected and the increased shielding, as well as the decrease in the line width, indicates higher electron density at the boron atoms. This is of course due to the strong B−B π-bonding, which also has the effect that the two BN_2 planes tend to become mutually planar, in contrast to the 57−70° torsion angle found in the neutral compounds. Moreover, the much simpler ^{1}H- and ^{13}C-NMR spectra of the "anions" **3a**−**3c** compared to those of **2a**−**2c** suggest a higher symmetry for the anions (see X-ray structure analysis).

X-ray Structure Analysis

The molecular structures of the dilithium tetraaminodiborates are depicted in Figures 3−5. The structural parameters of the compounds **2a**, **2b**, **3a**−**3c** are summarized in Table 1.

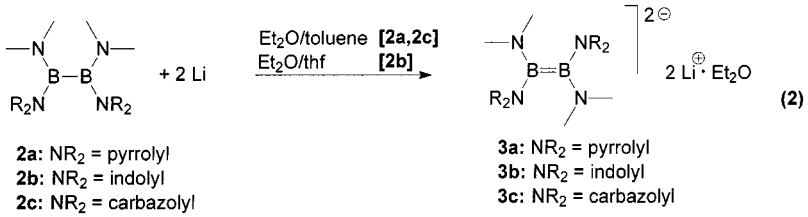


Table 1. Selected bonding parameters; bond lengths in Å, bond angles, and angles between planes in degrees

	2a	**2b**	**3a**[a]	**3b**[b]		**3c**[c]	
B1−B2	1.718(2)	1.723(4)	1.59(1)	1.584(4)	1.578(3)	1.566(9)	1.571(8)
B1−N1	1.487(6)	1.477(3)	1.562(5)	1.564(2)	1.560(2)	1.573(5)	1.564(5)
B1−N2	1.394(2)	1.387(3)	1.537(7)	1.534(3)	1.527(3)	1.540(6)	1.544(5)
B2−N3	1.489(2)	1.480(3)	–	–	1.568(2)	–	–
B2−N4	1.392(3)	1.389(3)	–	–	1.531(3)	–	–
N1−B1−N2	120.7(2)	119.3(2)	114.5(3)	114.0(2)	114.6(2)	112.6(3)	–
N1−B1−B2	116.9(1)	117.4(2)	120.8(6)	121.3(2)	120.9(2)	122.8(5)	–
N2−B1−B2	122.3(2)	123.3(2)	124.7(5)	124.3(2)	123.9(2)	124.1(5)	–
N3−B2−N4	121.1(1)	118.3(2)	–	–	113.8(2)	–	112.9(3)
N3−B2−B1	116.3(2)	118.4(2)	–	–	121.2(2)	–	122.3(4)
N4−B2−B1	122.6(2)	123.2(2)	–	–	124.5(2)	–	124.4(4)
$C_2N1-N1-B1-N2$	32	35	67	68	68	77	–
$C_2N2-N2-B1-N1$	7	10	64	62	57	62	–
$C_2N3-N3-B2-N1$	35	66	–	–	72	–	78
$C_2N4-N4-B2-N3$	3	7	–	–	64	–	63
N_2B1/N_2B2	73	57	0	0	3	0	0

[a] The molecule is centrosymmetric, therefore B2 corresponds with the symmetry-equivalent atom B1A. – [b] Of the two independent molecules of **3b** in the asymmetric unit, one is centrosymmetric (related data given as B1N1N2), while the other is non-centrosymmetric. The core of the molecule has been labelled B2N3N4 and B4N5N6. In the columns, B1 refers to B3, B2 to B4, etc. – [c] There are two independent centrosymmetric molecules in the asymmetric unit. The first molecule is labelled B1N1N2/B1AN1AN2A, the second B2N3N4/B2BN3BN4BA.

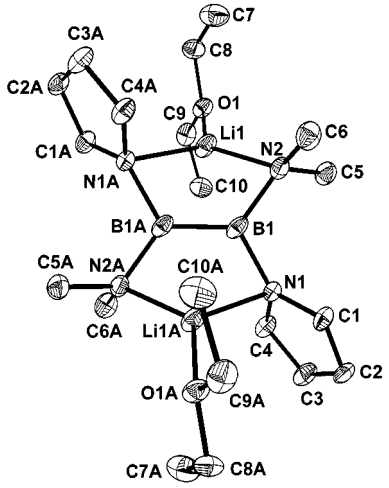


Figure 3. Molecular structure of the diborate **3a** in the crystal; thermal ellipsoids are shown at a 25% probability level

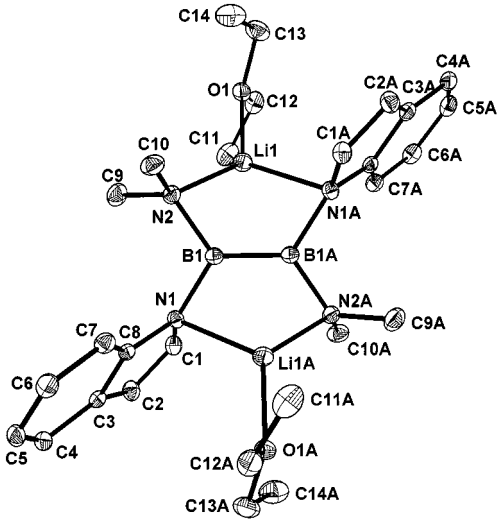


Figure 4. Molecular structure of the diborate **3b** in the crystal; thermal ellipsoids are shown at a 25% probability level

There are two independent molecules in the asymmetric unit for compounds **3b** and **3c**. One of the two molecules of **3b** lies on a crystallographic inversion center, and this also holds true for compound **3a**.

In contrast to the neutral diborane(4) compounds **2**, a planar B_2N_4 moiety is present in the anions of **3**. More importantly, the B−B bond lengths are 0.12 Å shorter than those in the corresponding tetraaminodiboranes. This, as well as the planarity of the B_2N_4 skeleton, gives an excellent indication for the presence of B=B double bonds.

Another structural feature to be noted is that the Me_2N groups are perpendicularly arranged in relation to the B_2N_4 planes, their N atoms being pyramidal, with an average BN_A distance of 1.54 Å. BN_A π-bonding is therefore absent. Moreover, the BN_H bond lengths to the *N*-heterocycles are longer: 1.564(6) Å in **3a**, on average 1.56 Å in **3b**, and 1.562(6) Å and 1.572(6) Å in **3c**, respectively. The rings themselves are twisted in relation to the B_2N_4 plane by 64°,

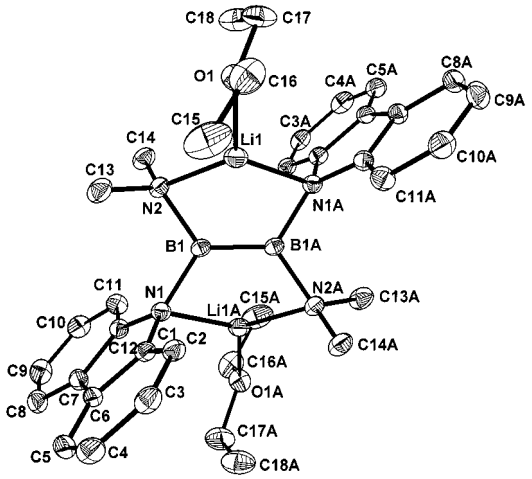


Figure 5. Molecular structure of the diborate **3c** in the crystal; thermal ellipsoids are shown at a 25% probability level

67°, and 74°; BN_H π-bonding can, therefore, also be excluded.[11]

However, the orientation of the amino groups is essential for the coordination of the lithium cations, which are surrounded in a trigonal-pyramidal geometry by two nitrogen atoms and an oxygen atom of an ether molecule. Thus, the tetraaminodiborate(4) unit acts as a bis-bidentate ligand. We assume that this feature of the molecular structure of the diborate can be considered as one reason for the ease of reduction of the tetraaminodiborane to the diborate. The LiN atom distances lie in the range 1.98 Å to 2.25 Å, and compare well with those found in many other LiN compounds.[12][13] Rather wide N−Li−N bond angles are responsible for the comparatively short Li−B distances (2.3−2.2 Å). An even more important reason for the ease of reduction of the tetraaminodiboranes to diborates seems to be that the starting material must bear an aromatic substituent. Considering literature data and our own investigations, there would seem to be no known reductions of diboranes(4) where there is not at least one aromatic ring system connected to the B_2 moiety.[14][15] This leads to the supposition that, in the mechanism of these reactions, the aromatic substituent may act as the primary electron acceptor.

MO Calculations

In order to support the experimental results and to obtain information on the bonding situation and the possibilities of delocalization of the B−B π-bond, geometry optimized MO calculations,[16] including an NBO analysis,[17] were performed on the model compound $(H_2OLi)_2(Me_2N)_2B_2(NC_4H_4)_2$ **4**. Figure 6 shows the geometry of the calculated compound. Some results are summarized in Table 2.

The NBO analysis shows that the B−B σ-bonding orbital and a B−B π orbital are strongly occupied, with each boron $2p_z$ orbital holding 0.9404 e. These orbitals are perpendicular to the B_2N_4 plane and therefore represent a typically

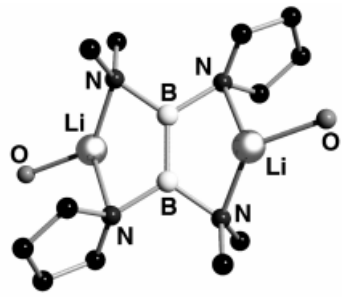


Figure 6. Calculated structure of **4**, Becke 3LYP/6-31G* optimized, NIMAG 0; H atoms have been omitted for clarity

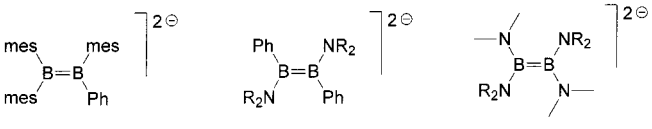
Table 2. Geometrical data for model compound **4** based on Becke 3LYP/6-31G* calculations compared with experimental data for compounds **3a**−**3c**

	Theor. $d_{(E-E)}$ [pm]	Exp. $d_{(E-E)}$ [pm]	Theor. ϕ [°]	Exp. ϕ [°]
B=B	160	157−159	0	0
$B-N_{arom}$	157	156−157	58	64−74
$B-NMe_2$	154	154	69	62−67

localized π-bond. The "second-order pertubation analysis" shows that there is no significant donor−acceptor interaction of the B−B π-bond with orbitals of other atoms. Delocalization of the π-electron density through the BN bonds can therefore be excluded.

Discussion

The first two-electron reduction of a diboron(4) compound was discovered by Power et al. in 1992 using tris(mesityl)phenyldiborane(4) as the diborane(4) source.[15] Shortly afterwards, the reduction of 1,2-bis(dimethylamino)-1,2-diphenyldiborane(4) by lithium in the presence of diethyl ether gave access to the dianion $[Ph(Me_2N)B=B(NMe_2)Ph]^{2-}$.[14] Dianions of the type $[R_2N(Me_2N)B=B(NMe_2)NR_2]^{2-}$ (R_2N = pyrrolyl, indolyl, carbazolyl) now complete a series of tetraaminodiborates(4). Proceeding along this series from the dianion **4a** through **4b** to **4c**, one notes that the differences in the chemical shifts $\delta^{11}B$ become increasingly smaller.



4a **4b** **4c**

For the tetraaryldiborate(4) dianion $\Delta\delta^{11}B$ is 74.3 ppm, for the bis(dimethylamino)bis(phenyl)diborate(4) $\Delta\delta^{11}B$ is 16.3 ppm, while for the tetraaminodiborates(4) described here $\Delta\delta^{11}B$ is only 9.0−9.6 ppm. This is due to the increasing B−N π-bonding effects on the shielding of the B atoms in the neutral diboranes, as demonstrated by the short Me_2N bonds in compounds **2a** and **2b**, which are coplanar

with the N_2BB plane. Therefore, the gain in electron density at the boron atoms in the dianions is largest in compound **4a**, because there is little if any B−C π-bonding in the starting material [it should be noted that the boron atoms in $tBu_3(Me_3Si)B_2$ are even more strongly deshielded; $\delta^{11}B$ = 120], and is obviously smallest in $(R_2N)(Me_2N)B-B(NMe_2)(NR_2)$, which bears four amino groups.

On the other hand, the decrease in the B−B bond lengths on reduction is largest for the tetraaminodiboron moiety (ca. 0.12 Å), while for **4a** Δd(B−B) is 0.08 Å and for **4b** it is 0.07 Å. This cannot be exclusively attributed to the fact that the B−B bond lengths are shorter in $mes_2B-BmesPh$ [1.71(1) Å][15] and $Ph(Me_2N)B-B(NMe_2)Ph$ [1.714(4) Å][14] as compared to those in the new tetraaminodiboranes [1.718(2) Å, 1.723(4) Å]. One reason for the greater contraction of the B−B bond lengths in compounds **3** may lie in the fact that the dianion acts as a chelating ligand forming two five-membered heterocycles with the Li atoms. The lone pairs of the Li-coordinating N atoms are all orientated towards the Li atoms, which precludes delocalization of the boron π-electrons.

While there is normally an atom distance difference of 0.2 Å if a single-bonded system becomes doubly bonded (e.g. the C−C bonds in ethane and ethene, respectively), the B−B bond length difference is smaller. This is to be expected because in the diborate dianions the boron atoms do not change their coordination number and remain sp^2 hybridized. In addition, the two-electron reduction imparts to the boron atom a charge of −0.94 e, which should result in a repulsion between the two boron atoms and hence a counteractive effect on the B=B double bond length. However, the planarity of the B_2N_4 units in the new diborates(4), in addition to all the other discussed geometrical and electronic features and the results of the MO calculations, provide strong evidence for the presence of a truly localized B=B double bond.

Based on the present result, one might envisage that even the simplest tetraaminodiborane(4), $B_2(NMe_2)_4$, might be reducible by lithium. However, experiments carried out in analogy to those described here did not produce a $B_2(NMe_2)_4^{2-}$ anion. Therefore, we suggest that an "aromatic" moiety must be present to allow the electron transfer from lithium (metal) to boron [of the diborane(4)].

Experimental Section

General: All experimental manipulations were conducted under anhydrous conditions employing Schlenk techniques using argon as a protecting blanket. Solvents were dried by conventional methods. Boron-containing starting materials were prepared by literature methods.[7][8] − NMR: Jeol 270 and 400 spectrometers [standards: TMS (^1H, ^{13}C), external $BF_3{\cdot}OEt_2$ (^{11}B)]. − X-ray structure determination: Siemens P4 with CCD area detector, Mo-K_α radiation, graphite monochromator, LT device.

Bis(dimethylamino)bis(pyrrolyl)diborane(4) (2a): To a vigorously stirred suspension of pyrrolyllithium (2.35 g, 29 mmol) in toluene (40 mL) at −78°C was added a solution of dichlorobis(dimethylamino)diborane(4) (2.35 g, 13 mmol) in toluene (15 mL). The suspension was allowed to warm to ambient temperature and stirring was continued for a further 23 h. Then, THF (0.25 mL) was added and, after stirring for an additional 1 h, the insoluble material was removed by centrifugation (15 min at 15000 rpm). The solid was washed with toluene (10 mL). All volatiles were then removed from the solution in vacuo. A greenish colored oil remained, which solidified within a few minutes. Pure **2a** was obtained by sublimation (90°C/9·10^{-3} Torr) in large colorless prisms.[18] Yield: 2.54 g of **2a** (81%), m.p. 48−51°C. − ^{11}B NMR (64 MHz, C_6D_6): δ = 37.0 [$h_{1/2}$ = 320 Hz, $B_2(NMe_2)_2(pyrrolyl)_2$]. − ^1H NMR (270 MHz, C_6D_6): δ = 6.93 (dd, 4 H, $H^{1,4}$), 6.49 (dd, 4 H, $H^{2,3}$), 2.56 [s, 6 H, $N(CH_3)_2$], 2.44 [s, 6 H, $N(CH_3)_2$]. − ^{13}C NMR (68 MHz, C_6D_6): δ = 124.6 (pyrrolyl $C^{1,4}$), 111.6 (pyrrolyl $C^{2,3}$), 42.6 [$N(CH_3)_2$], 39.3 [$N(CH_3)_2$]. − $C_{12}H_{20}B_2N_4$ (241.94): calcd. C 59.57, H 8.33, N 23.16; found C 59.12, H 8.35, N 22.29.

Bis(dimethylamino)bis(indolyl)diborane(4) (2b): Prepared in analogy to **2a** from indolyllithium (7.39 g, 60.0 mmol) in toluene (60 mL) and $B_2(NMe_2)_2Cl_2$ (5.42 g, 30.0 mmol) in toluene (25 mL) with stirring for 18 h. Addition of THF (1 mL), reducing the volume of the solution by ca. 50% and storage for 4 days at −20°C gave crystalline **2b**.[18] Yield: 8.80 g of **2b** (89%), m.p. 63−67°C. − ^{11}B NMR (64 MHz, C_6D_6): δ = 36.7 [$h_{1/2}$ = 400 Hz, $B_2(NMe_2)_2(indolyl)_2$]. − ^1H NMR (400 MHz, C_6D_6): δ = 7.72 (dd, 2 H, H^4), 7.49 (dd, 2 H, H^7), 7.19 (dd, 2 H, H^6), 7.12 (dd, 2 H, H^5), 7.03 (d, 2 H, $^3J_{HH}$ = 2.7 Hz, H^1), 6.67 (d, 2 H, $^3J_{HH}$ = 2.7 Hz, H^2), 2.45 [s, 6 H, $N(CH_3)_2$], 2.27 [s, 6 H, $N(CH_3)_2$]. − ^{13}C NMR (100 MHz, C_6D_6): δ = 139.8 (indolyl C^8), 131.4 (indolyl C^3), 129.5 (indolyl C^1), 122.2 (indolyl C^5), 120.9 (indolyl C^4), 120.7 (indolyl C^6), 113.1 (indolyl C^7), 106.0 (indolyl C^2), 41.2 [$N(CH_3)_2$], 39.9 [$N(CH_3)_2$]. − $C_{20}H_{24}B_2N_4$ (342.05): calcd. C 70.23, H 7.09, N 16.38; found C 69.84, H 7.06, N 16.26.

Bis(carbazolyl)bis(dimethylamino)diborane(4) (2c): Prepared in analogy to **2a** from carbazolyllithium (1.60 g, 9.2 mmol) in toluene (40 mL) and $B_2(NMe_2)_2Cl_2$ (0.83 g, 4.6 mmol) in toluene (20 mL) with stirring for 18 h. THF (0.3 mL) was added, all volatiles were removed from the solution, and then the residue (2.92 g) was dissolved in hot toluene (60 mL). Removal of some insoluble material and cooling to −20°C afforded small crystals. Yield: 1.95 g of **2c** (95%), m.p. 113−117°C. − ^{11}B NMR (64 MHz, toluene): δ = 37.9 [$h_{1/2}$ = 780 Hz, $B_2(NMe_2)_2(Cbz)_2$]. − ^1H NMR (400 MHz, C_6D_6): δ = 8.01 (d, 4 H, $^3J_{HH}$ = 7.8 Hz, $H^{6,9}$), 7.35 (d, 4 H, $^3J_{HH}$ = 8.3 Hz, $H^{3,12}$), 7.29 (ps. t, 4 H, $^3J_{HH}$ = 7.6 Hz, $H^{4,11}$), 7.17 (ps. t, 4 H, $^3J_{HH}$ = 7.3 Hz, $H^{5,10}$), 2.70 [s, 6 H, $N(CH_3)_2$], 2.66 [s, 6 H, $N(CH_3)_2$]. − ^{13}C NMR (100 MHz, C_6D_6): δ = 142.2 (Cbz $C^{7,8}$), 125.6 (Cbz $C^{2,13}$), 125.5 (Cbz $C^{4,11}$), 119.9 (Cbz $C^{6,9}$), 112.6 (Cbz $C^{3,12}$), 41.3 [$N(CH_3)_2$], 41.2 [$N(CH_3)_2$]. − $C_{28}H_{28}B_2N_4$ (442.18): calcd. C 76.06, H 6.38, N 12.67; found C 75.74, H 6.82, N 12.60.

Dilithium Bis(dimethylamino)bis(pyrrolyl)diborate(4) (3a): A suspension of Li powder (40 mg, 13 mmol) in diethyl ether (20 mL) was cooled to −78°C. A solution of **2a** (1.54 g, 6.4 mmol) in toluene (20 mL) was then added under stirring and the suspension was allowed to warm to ambient temperature. After 18 h, the solution was yellow-green in color. The excess Li was then removed and the solution was concentrated in vacuo to a volume of ca. 30 mL. Cooling to −20°C for ca. 12 h led to the deposition of light-yellow crystals.[18] Yield: 1.89 g of **3a** · 2 EtO_2 (73%). **3a** was found to decompose rapidly at 73°C, and within 10 d at ambient temperature. − ^{11}B NMR (64 MHz, C_6D_6): δ = 27.4 [$h_{1/2}$ = 140 Hz, $Li_2B_2(NMe_2)_2(pyrrolyl)_2$]. − ^1H NMR (270 MHz, C_6D_6): δ = 7.13 (m, 4 H, $H^{2,3}$), 7.02 (dd, 4 H, $H^{1,4}$), 3.26 [q, 8 H, ^3J(H,H) = 3.8 Hz, $(OCH_2CH_3)_2$], 2.10 [s, 12 H, $N(CH_3)_2$], 1.10 [t, 12 H, ^3J(H,H) =

3.8 Hz, $(OCH_2CH_3)_2$]. – ^{13}C NMR (68 MHz, C_6D_6): δ = 124.2 (pyrrolyl $C^{1,4}$), 111.7 (pyrrolyl $C^{2,3}$), 65.9 [$(OCH_2CH_3)_2$], 39.5 [$N(CH_3)_2$], 15.5 [$(OCH_2CH_3)_2$].

Dilithium Bis(dimethylamino)bis(indolyl)diborate(4) (3b): Prepared in analogy to **3a** from Li (50 mg, 7.2 mmol) in diethyl ether (15 mL) and **2b** (1.37 g, 4.0 mmol) in diethyl ether (25 mL). Following the addition of **2b** to the Li suspension, an orange-coloured solid separated at −10°C. It was isolated and redissolved in THF (15 mL), then the excess Li was removed by filtration. On leaving the solution to stand overnight at 4°C, orange crystals separated.[18] Yield: 1.73 g (86%). **3b** was found to decompose within 1 d at ambient temperature and within 3 d at 4°C. – ^{11}B NMR (64 MHz, C_6D_6): δ = 27.9 [$h_{1/2}$ = 130 Hz, $Li_2B_2(NMe_2)_2(indolyl)_2$]. – ^{1}H NMR (400 MHz, [D_8]toluene): δ = 8.28 (br. d, 2 H, H^1), 8.02 (br. d, 2 H, H^2), 7.76 (m, 2 H, H^4), 7.44 (m, 2 H, H^7), 7.20 (m, 4 H, $H^{5,6}$), 3.25 [q, 8 H, ^3J(H,H) = 3.8 Hz, $(OCH_2CH_3)_2$], 2.21 [s, 12 H, $N(CH_3)_2$], 1.10 [t, 12 H, ^3J(H,H) = 3.8 Hz, $(OCH_2CH_3)_2$]. – ^{13}C NMR (100 MHz, [D_8]toluene): δ = 140.7 (indolyl C^8), 137.8 (indolyl C^1), 134.8 (indolyl C^3), 122.4 (indolyl C^5), 121.2 (indolyl C^4), 120.1 (indolyl C^6), 113.8 (indolyl C^7), 110.4 (indolyl C^2), 65.9 [$(OCH_2CH_3)_2$], 41.5 [$N(CH_3)_2$], 15.2 [$(OCH_2CH_3)_2$].

Dilithium Bis(dimethylamino)bis(carbazolyl)diborate(4) (3c): To a stirred suspension of Li powder (50 mg, 7.2 mmol) in diethyl ether (20 mL) at 0°C was added a warm solution of **2c** (640 mg, 1.5 mmol) in toluene (25 mL). The solution rapidly turned reddish brown. After stirring for 3 days, the excess Li was removed by filtration and washed with diethyl ether (20 mL). The combined filtrate and washings were then kept at 4°C until some red-brown crystals separated.[18] – ^{11}B NMR (64 MHz, toluene/Et_2O): δ = 28.9 ($h_{1/2}$ = 200 Hz). – ^{1}H NMR (270 MHz, C_6D_6): δ = 7.73 (m, 8 H, H_{arom}), 7.21 (m, 8 H, H_{arom}), 3.14 [q, ^3J(H,H) = 7.0 Hz, $(OCH_2CH_3)_2$], 2.96 [s, 12 H, $N(CH_3)_2$], 1.02 [t, ^3J(H,H) = 7.0 Hz, $(OCH_2CH_3)_2$]. – ^{13}C NMR (68 MHz, C_6D_6): δ = 144.3 (Cbz $C^{7,8}$), 129.1 (Cbz $C^{2,13}$), 126.1 (Cbz $C^{4,11}$), 120.1 (Cbz $C^{6,9}$), 119.5 (Cbz $C^{5,10}$), 116.2 (Cbz $C^{3,12}$), 67.2 [$(OCH_2CH_3)_2$], 43.2 [$N(CH_3)_2$], 15.8 [$(OCH_2CH_3)_2$].

X-ray Structure Determinations: Crystals were covered with perfluoropolyether oil at −40°C and suitable specimens were selected and mounted on a glass fibre. Cell dimensions were determined from the reflections on 15 frames each at four different χ and ψ settings by changing ψ by 0.3° per frame at 193 K. Data collection was performed in the hemisphere mode of the SMART program at 193 K by collecting a total of 1300 frames. Data reduction was performed using the program SAINT; no absorption correction was applied. The structures were solved by direct methods (SHELXTL-97). Non-hydrogen atoms were refined anisotropically (SHELX-97) and hydrogens were placed in calculated positions by applying a riding model. Crystallographic data and selected data relating to the data collection and refinement are summarized in Table 3.

Acknowledgments

We thank the Fonds der Chemischen Industrie, Chemetall AG, and the Leibniz Rechenzentrum München for support, and Mr. P. Mayer and Mr. W. Linscheid for recording the many spectra.

Table 3. Crystallographic data and data referring to data collection and refinement of compounds **2a**, **2b**, **2c**, **3a**, **3b**, and **3c**

Compound	**2a**	**2b**	**3a**	**3b**	**3c**
Chem. formula	$C_{12}H_{20}B_2N_4$	$C_{20}H_{24}B_2N_4$	$C_{20}H_{40}B_2Li_2N_4O_2$	$C_{28}H_{44}B_2Li_2N_4O_2$	$C_{36}H_{48}B_2Li_2N_4O_2$
Form. wght.	241.94	342.05	404.06	504.17	604.28
Cryst. size [mm]	0.2×0.3×0.3	0.2×0.3×0.3	0.15×0.15×0.2	0.15×0.2×0.4	0.15×0.2×0.3
Cryst. system	Monoclinic	Monoclinic	Monoclinic	Monoclinic	Monoclinic
Space group	*P*2(1)/*c*	*P*2(1)/*n*	*P*2(1)/*c*	*P*2(1)/*n*	*P*2(1)/*c*
a [Å]	7.6127(4)	9.220(4)	9.1015(5)	7833(3)	17.6037(5)
b [Å]	15.6592(8)	14.901(5)	8.7833(5)	14.531(4)	13.81160(10)
c [Å]	12.0229(6)	14.428(7)	16.1059(8)	39.826(13)	16.2832(4)
α [°]	90	90	90	90	90
β [°]	94.957(1)	105.497(7)	92.569(1)	90.94(1)	115.034(1)
γ [°]	90	90	90	90	90
V [Å^3]	1427.87(13)	1910.2(14)	1286.23(12)	4533(2)	3587.10(14)
Z	4	4	2	6	4
ρ(calcd.), [Mg/m^3]	1.125	1.189	1.043	1.108	1.119
μ [mm^{-1}]	0.068	0.070	0.065	0.068	0067
F(000)	520	728	440	1632	1296
Index range	$-8 \le h \le 6$, $-18 \le k \le 18$, $-14 \le l \le 14$	$-10 \le h \le 10$, $-14 \le k \le 17$ $-16 \le l \le 16$	$-10 \le h \le 10$ $-9 \le k \le 9$ $-17 \le l \le 12$	$-9 \le h \le 9$ $-16 \le k \le 15$ $-46 \le l \le 46$	$-20 \le h \le 15$ $-16 \le k \le 5$ $-17 \le l \le 17$
2θ [°]	49.42	4820	46.50	49.42	49.42
Temp. [K]	183(2)	193(2)	163(2)	173(2)	183(2)
Refl. collected	7015	8857	5400	22085	6864
Refl. unique	2103	2782	1583	7383	4944
Refl. observed (4σ)	1861	2505	1335	5326	3311
R (int.)	0.0319	0.0350	0.0590	0.0305	0.0466
No. variabies	167	240	141	526	423
Weighting scheme[a] *x*/*y*	0.0390/0.6830	0.0343/1.1067	0.0723/2.4569	0.0448/1.2757	0.0205/5.2607
GOOF	1.101	1.256	1.189	1.032	1.174
Final *R* (4σ)	0.0408	0.0565	0.0713	0.0465	0.0796
Final *wR*2	0.0968	0.1202	0.1693	0.0994	0.1380
Larg. res. peak [e/Å^3]	0.282	0.269	0.298	0.226	0.329

[a] $w^{-1} = \sigma^2F_o^2 + (xP)^2 + \gamma P$; $P = (F_o^2 + 2F_c^2)/3$.

[1] W. Lippert, H. Nöth, W. Ponikwar, T. Seifert, *Eur. J. Inorg. Chem.* **1999**, 817−823.
[2] R. Hoffmann, *Angew. Chem.* **1982**, *94*, 725−739; *Angew. Chem. Int. Ed. Engl.* **1982**, *21*, 711
[3] E. Wiberg, *Naturwissenschaften* **1948**, *35*, 182−212.
[4] H. Nöth, P. W. Fritz, *Angew. Chem.* **1961**, *73*, 408−410; *Z. Anorg. Allg. Chem.* **1963**, *324*, 129−145.
[5] H. Hommer, H. Nöth, J. Knizek, W. Ponikwar, H. Schwenk-Kircher, *Eur. J. Inorg. Chem.* **1998**, 1519−1527.
[6] A. Moezzi, M. M. Olmstead, P. P. Power, *J. Chem. Soc., Dalton Trans.* **1992**, 2429−2434.
[7] R. J. Brotherton, A. L. McCloskey, L. L. Petterson, H. Steinberg, *J. Am. Chem. Soc.* **1960**, *82*, 6242−6248.
[8] H. Nöth, W. Meister, *Chem. Ber.* **1961**, *94*, 509−514.
[9] H. Nöth, W. Meister, *Z. Naturforsch.* **1962**, *17B*, 714−718.
[10] For a compilation of data on B−B bond lengths, see ref.[6]
[11] It has been shown that practically no BN π-bonding is present in $B(NR_2)_3$ compounds when NR_2 = pyrrolyl, indolyl; B. Wrackmeyer, B. Schwarzer, W. Milius, *Inorg. Chim. Acta* **1996**, *241*, 87.
[12] F. Pauer, P. P. Power in: *Lithium Chemistry: A Theoretical and Experimental Overview* (Eds.: A.-M. Sapse, P. von R. Schleyer), John Wiley and Sons, New York, Chichester, Brisbane, Toronto, Singapore, **1995**, chapter 9.
[13] R. E. Mulvey, *Chem. Soc. Rev.* **1998**, *27*, 339−346.
[14] A. Moezzi, R. A. Barlett, P. P. Power, *Angew. Chem.* **1992**, *104*, 1075−1076; *Angew. Chem. Int. Ed. Engl.* **1992**, *31*, 1082.
[15] A. Moezzi, M. M. Olmstead, P. P. Power, *J. Am. Chem. Soc.* **1992**, *114*, 2715−2717.
[16] *Gaussian 94, Revision C.3*: M. J. Frisch, G. W. Trucks, H. B. Schlegel, P. M. W. Gill, B. G. Johnson, M. A. Robb, J. R. Cheeseman, T. Keith, G. A. Petersson, J. A. Montgomery, K. Raghavachari, M. A. Al-Laham, V. G. Zakrewski, J. V. Ortiz, J. B. Foresman, J. Cioslowski, B. B. Stefanov, A. Nanayakkara, M. Challacombe, C. Y. Peng, P. Y. Ayala, W. Chen, M. W. Wong, J. L. Andres, E. S. Replogle, R. Gomperts, R. L. Martin, D. J. Fox, J. S. Binkley, D. J. Defrees, J. Baker, J. P. Stewart, M. Head-Gordon, C. Gonzalez, J. A. Pople, Gaussian, Inc., Pittsburgh PA, **1995**.
[17] *NBO 3.1*: E. D. Geldening, J. K. Badenshoop, A. E. Reed, J. E. Carpenter, F. Weinhold, Theoretical Chemistry Institute, University of Wisconsin, Madison, **1992**. A. E. Reed, R. B. Weinstock, F. Weinhold, *Chem. Rev.* **1988**, *88*, 899−926.
[18] Crystallographic data (excluding structure factors) for the structures reported in this paper have been deposited with the Cambridge Crystallographic Data Centre as supplementary publication nos. CCDC-118113/118114/118115/118116/118117. Copies of the data can be obtained free of charge on application to the CCDC, 12 Union Road, Cambridge CB2 1EZ, U.K. [Fax: (internat.) +44 (0)1223 336033; E-mail: deposit@ccdc.cam.ac.uk].
[19] The stabilities of the tetraaminodiborates(4) **3** decrease rapidly if a stronger donor than diethyl ether is used for coordination of the lithium atoms. Thus, the preparation of the THF-coordinated dilithium tetraaminodiborate(4) **3a** by reduction of the corresponding tetraaminodiborane(4) **2a** in THF or via ligand exchange leads to the desired THF-coordinated dianionic species, which decomposes rapidly above −30°C. In the presence of crown ether ligands, however, the decomposition temperature decreases to less than −78°C. On the other hand, the lithium atoms are not necessary for the stability of all the diborate species: substitution of the NMe_2 groups in the diborane(4) **2a** with mesityl groups leads to the compound mes(pyrrolyl)BB(pyrrolyl)mes **2d**. By reduction of **2d** with lithium in diethyl ether or THF, dilithium tetraaminodiborates(4) can be obtained, which are stable at room temperature. These and other results will be reported shortly.

Received April 12, 1999
[I99128]

[Pd(N,N-chelate)(olefin)] Complexes Containing Chiral Nitrogen Chelates Based on Carbohydrates – Enantioselectivity of Olefin Coordination

Maria L. Ferrara,[a] Federico Giordano,[a] Ida Orabona,[a] Achille Panunzi,[b] and Francesco Ruffo*[a]

Dedicated to Prof. Fausto Calderazzo on the occasion of his 70th birthday

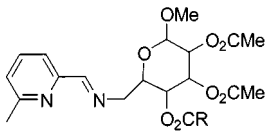
Keywords: Palladium / Bidentate nitrogen ligands / Carbohydrates / Alkenes / Enantioselectivity

Chiral N,N-chelates of formula 6-Me-pyridine–2-CH=N–R (**1**) and R–N=CH–CH=N–R (**2**) (R = 6-deoxy-α-D-glucoside or 6-deoxy-α-D-mannoside residue) and their palladium(0) complexes [Pd(N,N-chelate)(olefin)] (**I**) were prepared. Symmetrical type **2** ligands induced higher enantioselectivity in the coordination of prochiral olefins. The ability of a type **1** chelate to promote a stereoselective process was also assessed, i.e. dimethylfumarate inserted into the Pd–Me bond formed upon methylation of a type **I** complex with 50% ee. Finally, a water-soluble Pd^0 complex was also prepared by deprotecting the alcoholic functions on the sugar residue, and its molecular structure determined through X-ray diffractometry.

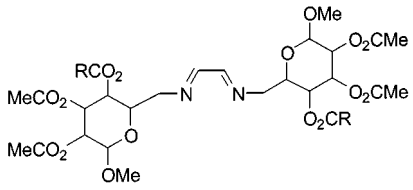
Introduction

An important challenge that chemical sciences must meet in the forthcoming third millenium is that of making available chiral products by means of environmentally friendly processes. Organometallic chemistry may be able to fulfill this demand,[1] since metal-assisted enantioselective syntheses can often reduce the consumption of resources. To date, the best results have been achieved by using phosphanes as chiral auxiliaries of active transition metals.[2] However, nitrogen ligands are attracting increasing interest.[3] Aiming to contribute to this growing field of research, we investigated the feasibility of using new chiral N,N-chelates based on carbohydrates[4] (Figure 1), with the assumptions that (i) these natural products can be a convenient source of chiral auxiliaries, and (ii) both a lypophylic and a hydrophilic form of the ligands can be available depending on whether or not the alcoholic functions are protected. In the latter case the environmental and economic benefits of using the ligands in aqueos media would be added.

In a previous report[5] we described type **1** and **2** ligands derived from α-D-mannose, and their alkene−Pt^0 complexes. A preliminarly investigation of the ability of the ligands to induce stereoselective coordination of prochiral olefins yielded encouraging results. Therefore, our studies have been extended to the synthesis of related chelates based on α-D-glucose. Olefin−Pd^0 species containing nitrogen ligands are currently receiving a lot of attention,[6] so [Pd(N,N-chelate)(olefin)] complexes **I** were prepared. In this paper we describe the synthesis of the ligands, and the preparation and the solution behaviour of the complexes. The ability of the chelates to induce enantioselective coordination of prochiral olefins is also discussed. Furthermore, the ability of one chelate to promote a stereoselective stoichiometric process is assessed, i.e. insertion of dimethylfumarate into the Pd−Me bond formed upon oxidative addition of Me_3OBF_4 to a complex of type **I**. Finally, preparation of a water-soluble compound of type **I** by deprotecting the alcoholic functions on the sugar residue is reported, along with its structure as determined through X-ray crystallography.



1



2

Figure 1. General formula of type **1** and **2** ligands

[Pd(N,N-chelate)(olefin)]
I

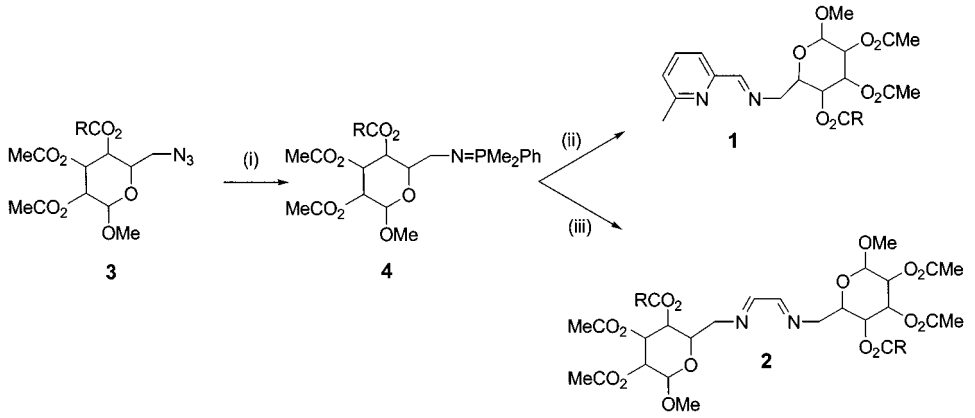
[a] Dipartimento di Chimica, Università di Napoli "Federico II"
Via Mezzocannone 4, I-80134 Napoli, Italia
Fax: (internat.) + 39-081/5527771
E-mail: ruffo@chemna.dichi.unina.it
[b] Facoltà di Agraria and Dipartimento di Chimica, Università di Napoli "Federico II"
Via Mezzocannone 4, I-80134 Napoli, Italia

 © WILEY-VCH Verlag GmbH, D-69451 Weinheim, 1999 1434−1948/99/1111−1939 $ 17.50+.50/0

Results and Discussion

Synthesis and Characterization of the Ligands

The synthesis of the N,N-chelates is depicted in Scheme 1. The compounds are identified by a number followed by a capital letter, which indicates the sugar (M = mannose or G = glucose), and by the specification of the R substituent (Me or Ph). The symmetry of ligands of type **1** and **2** is C_1 and C_2, respectively. For both types three different derivatives were obtained. Among derivatives of type **1**, **1G-Ph** and **1M-Ph** differ by the nature of the carbohydrate (respectively glucose and mannose), substituents being equal. **1G-Me** and **1G-Ph** are both based on glucose, while the R substituent in position 4 is different. Analogous considerations hold true for ligands of type **2**.



Scheme 1

Known procedures allowed the synthesis of methyl-2,3,4-tri-*O*-acetyl-6-azido-6-deoxy-α-D-glucoside (**3G-Me**),[7] methyl-2,3-di-*O*-acetyl-4-*O*-benzoyl-6-azido-6-deoxy-α-D-glucoside (**3G-Ph**),[8][9] methyl-2,3-di-*O*-acetyl-4-*O*-benzoyl-6-azido-6-deoxy-α-D-mannoside (**3M-Ph**)[9] by starting from the corresponding commercial methyl-α-D-piranosides. Reaction of these azides with $PMePh_2$ afforded the iminophosphoranes **4**,[10] which were converted in situ into type **1** or type **2** ligands by condensation with, respectively, 6-methyl-2-pyridinecarboxaldehyde or glyoxal. The ligands were obtained in pure form as white powders by column chromatography. Their characterization was performed through NMR spectroscopy, elemental analysis and optical activity measurements (see Experimental Section).

Synthesis of [Pd(N,N-chelate)(olefin)] Complexes (I)

It is known[11] that the metal−alkene bond can be described in terms of a σ donation from the filled alkene π orbital to an empty metal orbital, and a π back donation from a filled metal orbital to the empty π* orbital of the alkene. The latter contribution plays a prominent role in Pd^0- and Pt^0-olefin complexes, and, for this reason, their stability increases as the electron-acceptor properties of the alkene grow.[6a,6d,6e]

In the presence of good donor ligands,[6e,12] such as type **1** or **2** diimines, a satisfactory electronic balance within the complex is met only if the alkene is able to withdraw effectively electron density from the metal centre through π back donation. Hence, stable type **I** complexes could be obtained only with olefins bearing good electron-acceptor substituents. Dimethylfumarate (dmf), fumarodinitrile (fdn), and maleic anhydride (ma) were effectively used. The synthesis of the complexes was performed by reacting $[Pd(dba)_2]$[13] (dba = dibenzylideneacetone) with the chelate and the olefin in dry toluene (Equation 1). The products were obtained in pure form after column chromatography as yellow to orange microcrystalline powders.

$$[Pd(dba)_2] + \text{N,N-chelate} + \text{olefin} \rightarrow \mathbf{I} + 2\ \text{dba} \quad (1)$$

Alternatively, fdn or ma derivatives could be synthetized by substituting dmf in **I** according to Equation 2.

$$[Pd(\text{N,N-chelate})(\text{dmf})] + \text{ma} \rightarrow [Pd(\text{N,N-chelate})(\text{ma})] + \text{dmf} \quad (2)$$

Only with ligands **1** was it possible to obtain dmf complexes of type **I** in acceptable yields, while in the presence of chelates **2** dmf complexes displayed little stability. These results probably reflect the electronic features of both the alkenes and the N,N-chelates. Actually, fdn and ma show similar electron-withdrawing abilities, both more pronounced than that displayed by dmf.[6d,14] Furthermore, according to previous studies,[12] ligands **2** are expected to be better σ donors than ligands **1** where one nitrogen atom belongs to a pyridine ring. Therefore, it seems reasonable that the above-mentioned good electronic balance within the complex can be achieved only in the presence of fdn or ma.

Type **I** complexes can be handled in air and were stored for long time at 233 K without appreciable decomposition.

They were fairly soluble in chlorinated solvents or toluene, but were poorly soluble in ether and insoluble in hexane. Complexes of type **1** ligands were stable in solution, while a slow decomposition process (days to completion) leading to Pd, N,N-chelate and free olefin was monitored for type **I** complexes containing ligands **2**.

NMR Spectroscopy

Large high-field shift [$\Delta\delta(^1H) \geqslant 3$ ppm, $\Delta\delta(^{13}C) \geqslant 90$ ppm] of both olefin protons and carbons was observed in the NMR spectra (Tables 1 and 2) according to a remarkable π back donation contribution to the Pd−alkene bond. As expected, the shift[15] was more pronounced for maleic anhydride and fumarodinitrile, which display the better electron-acceptor properties.

NMR spectra also allowed information to be gained on the solution behaviour of species of type **I**. Previous studies[6d,6e] disclosed that [Pd(N,N-chelate)(olefin)] complexes can be involved in dynamic processes in solution, i.e. olefin dissociation/association and olefin rotation around the metal−alkene axis. The rate of both processes decreases as the bulkiness of the N,N-ligand and/or the electron-accepting properties of the alkene grow.

For a given complex of type **I** the number of possible isomers and their symmetry depend on the geometry of both the alkene and the N,N-chelate. Prochiral olefins (dmf or fdn, C_{2h} symmetry) can afford two diastereomers depending on whether the alkene coordinates *re* or *si*. They can interconvert by dissociation of the alkene and its reassociation (with the opposite enantioface) to Pd. Spectra recorded at 298 K displayed separated signals for the diastereomers, which indicates that their interconversion, and hence olefin dissociation, is slow[16] at room temperature. At 328 K the spectra showed little difference with respect to those recorded at room temperature, but for variation of the olefin patterns due to the increased rate of alkene rotation. However, when an excess of olefin was added, the signals broadened even at room temperature. Two exceptions were [Pd(**2G-Me**)(fdn)], for which it was necessary to raise the temperature in order to observe broad olefin signals, and [Pd(**1G-Me**)(dmf)], whose spectrum at 328 K displayed averaged signals for the diastereomers even in the absence of free dmf. This spectral evidence indicates that the rate of alkene dissociation−reassociation is increased by the presence of free unsaturated ligand, according to an associative mechanism.[6d,6e]

The two halves of dmf or fdn in each one of the diastereomers containing either **1M-Ph** or **1G-Me** appeared not to be equivalent at 298 K, i.e. olefin protons gave rise to doublets or AB quartets and/or the corresponding carbons resonated separately. This result indicates that at room temperature olefin rotation is also slow, since a fast rotation would exchange the two halves of the unsaturated ligand. As expected, olefin resonances broadened in the spectra at 328 K, due to a fastened olefin rotation.

On the other hand, the room-temperature NMR spectra of [Pd(**1G-Ph**)(fdn)] showed a symmetrical olefin in one of the two diastereomers. This suggests that olefin rotation may or may not be hindered, according to which enantioface is coordinated. At 328 K olefin rotation also becomes

Table 1. Selected ^{1}H-NMR data[a] for [Pd(N,N-chelate)(olefin)] complexes

Complex	N=CH	HC=CH	6-*Me*-py	$MeCO_2$
[Pd(**1M-Ph**)(dmf)] isomer, 55%	8.32 (1 H)	3.84 (ABq, 2 H)	2.71 (3 H)	2.18 (3 H), 1.88 (3 H)
[Pd(**1M-Ph**)(dmf)] isomer, 45%	8.40 (1 H)	3.84 (ABq, 2 H)	2.73 (3 H)	2.18 (3 H), 1.88 (3 H)
[Pd(**1M-Ph**)(ma)] isomer, 60%	8.29 (1 H)	4.1−3.8 (m, 2 H)	2.66 (3 H)	2.18 (3 H), 1.88 (3 H)
[Pd(**1M-Ph**)(ma)] isomer, 40%	8.34 (1 H)	4.1−3.8 (m, 2 H)	2.68 (3 H)	2.18 (3 H), 1.89 (3 H)
[Pd(**1M-Ph**)(fdn)] isomer, 55%	8.42 (1 H)	[b,c]	2.87 (3 H)	2.18 (3 H), 1.90 (3 H)
[Pd(**1M-Ph**)(fdn)] isomer, 45%	8.30 (1 H)	[b,c]	2.67 (3 H)	2.18 (3 H), 1.87 (3 H)
[Pd(**1G-Ph**)(dmf)] isomer, 55%	8.29 (1 H)	[d]	2.71 (3 H)	2.07 (3 H), 1.90 (3 H)
[Pd(**1G-Ph**)(dmf)] isomer, 45%	8.32 (1 H)	[d]	2.72 (3 H)	2.09 (3 H), 1.90 (3 H)
[Pd(**1G-Ph**)(fdn)] isomer, 55%	8.38 (1 H)	[e,c]	2.85 (3 H)	2.09 (3 H), 1.91 (3 H)
[Pd(**1G-Ph**)(fdn)] isomer, 45%	8.29 (1 H)	[e,c]	2.63 (3 H)	2.09 (3 H), 1.88 (3 H)
[Pd(**1G-Me**)(dmf)] isomer, 55%	8.32 (1 H)	[f,c]	2.79 (3 H)	2.14 (3 H), 2.06 (3 H), 2.02 (3 H)
[Pd(**1G-Me**)(dmf)] isomer, 45%	8.27 (1 H)	[f,c]	2.82 (3 H)	2.14 (3 H), 2.05 (3 H), 2.03 (3 H)
[Pd(**1G-Me**)(fdn)] isomer, 85%	8.38 (1 H)	2.91 (2 H)	2.90 (3 H)	2.16 (3 H), 2.07 (3 H), 2.02 (3 H)
[Pd(**1G-Me**)(fdn)] isomer, 15%	8.33 (1 H)	[d]	2.90 (3 H)	2.05 (3 H), 2.02 (3 H), 1.99 (3 H)
[Pd(**2M-Ph**)(fdn)] isomer, 70%	8.06 (2 H)	2.93 (2 H)		2.16 (6 H), 1.90 (6 H)
[Pd(**2M-Ph**)(fdn)] isomer, 30%	8.03 (2 H)	2.86 (2 H)		2.15 (6 H), 1.86 (6 H)
[Pd(**2M-Ph**)(ma)]	7.92 (2 H)	3.93 (d, 1 H), 3.78 (d, 1 H)		2.18 (6 H), 1.90 (6 H)
[Pd(**2G-Ph**)(fdn)] isomer, 75%	8.05 (2 H)	2.93 (2 H)		2.08 (6 H), 1.90 (6 H)
[Pd(**2G-Ph**)(fdn)] isomer, 25%	[d]	2.86 (2 H)		2.08 (6 H), 1.87 (6 H)
[Pd(**2G-Me**)(fdn)] isomer, 97%	8.10 (2 H)	2.89 (2 H)		2.11 (6 H), 2.05 (6 H), 2.01 (6 H)
[Pd(**1M***)(fdn)] isomer, 55%[g]	8.74 (1 H)	[h]	2.88 (3 H)	
[Pd(**1M***)(fdn)] isomer, 45%[g]	8.71 (1 H)	[h]	2.91 (3 H)	

[a] At 298 K and 250 MHz. In $CDCl_3$, $CHCl_3$ (δ = 7.26) as internal standard. The following abbreviations are used for describing NMR multiplicities: app, apparent; no attribute, singlet; d, doublet; ABq, AB quartet; m, multiplet. − [b] The olefin protons resonate at δ = 2.91 (ABq, 2 H) and 2.89 (app d, 2 H). − [c] Due to the similar abundance of the diastereomers the signals cannot be attributed unequivocally. − [d] Hidden by other signals. − [e] The olefin protons resonate at δ = 2.87 (2 H) and 2.91 (ABq, 2 H). − [f] The olefin protons resonate at δ = 3.82 (2 H) and 3.63 (m, 2 H). − [g] In D_2O, HDO (δ = 4.80) as internal standard. − [h] The olefin protons resonate at δ = 3.24 (app d, 2 H) and 3.18 (ABq, 2 H).

Table 2. Selected ^{13}C-NMR data[a] for [Pd(N,N-chelate)(olefin)] complexes

Complex	N=CH	OCH(OMe)	NCH_2	HC=CH
[Pd(**1M-Ph**)(dmf)] isomer, 55%	165.2 (1 C)	98.3 (1 C)	64.9 (1 C)	41.6 (1 C), 41.3 (1 C)
[Pd(**1M-Ph**)(dmf)] isomer, 45%	165.4 (1 C)	98.5 (1 C)	63.9 (1 C)	42.1 (1 C), 41.2 (1 C)
[Pd(**1M-Ph**)(ma)] isomer, 60%	165.4 (1 C)	98.5 (1 C)	64.9 (1 C)	[b,c]
[Pd(**1M-Ph**)(ma)] isomer, 40%	165.6 (1 C)	98.6 (1 C)	64.1 (1 C)	[b,c]
[Pd(**1M-Ph**)(fdn)] isomer, 55%	165.7 (1 C)	98.5 (1 C)	63.4 (1 C)	[d,c]
[Pd(**1M-Ph**)(fdn)] isomer, 45%	165.3 (1 C)	98.8 (1 C)	65.1 (1 C)	[d,c]
[Pd(**1G-Ph**)(dmf)] isomer, 55%	170.4 (1 C)	96.3 (1 C)	64.8 (1 C)	[e,c]
[Pd(**1G-Ph**)(dmf)] isomer, 45%	170.4 (1 C)	96.3 (1 C)	63.9 (1 C)	[e,c]
[Pd(**1G-Ph**)(fdn)] isomer, 55%	165.8 (1 C)	96.8 (1 C)	63.2 (1 C)	[f,c]
[Pd(**1G-Ph**)(fdn)] isomer, 45%	165.4 (1 C)	96.7 (1 C)	65.0 (1 C)	[f,c]
[Pd(**1G-Me**)(dmf)] isomer, 55%	162.3 (1 C)	96.4 (1 C)	63.0 (1 C)	42.0 (1 C), 41.5 (1 C)
[Pd(**1G-Me**)(dmf)] isomer, 45%	165.4 (1 C)	96.0 (1 C)	64.4 (1 C)	42.4 (1 C), 41.2 (1 C)
[Pd(**1G-Me**)(fdn)] isomer, 85%	165.5 (1 C)	96.5 (1 C)	62.9 (1 C)	18.4 (1 C), 18.2 (1 C)
[Pd(**2M-Ph**)(fdn)] isomer, 70%	161.5 (2 C)	98.7 (2 C)	63.3 (2 C)	19.4 (2 C)
[Pd(**2M-Ph**)(fdn)] isomer, 30%	160.4 (2 C)	98.5 (2 C)	64.7 (2 C)	19.1 (2 C)
[Pd(**2M-Ph**)(ma)]	161.3 (2 C)	98.6 (1 C), 98.4 (1 C)	65.0 (1 C), 63.9 (1 C)	42.4 (1 C), 42.0 (1 C)
[Pd(**2G-Ph**)(fdn)] isomer, 75%	161.7 (2 C)	96.8 (2 C)	63.4 (2 C)	19.5 (2 C)
[Pd(**2G-Ph**)(fdn)] isomer, 25%	160.5 (2 C)	96.7 (2 C)	64.6 (2 C)	19.2 (2 C)
[Pd(**2G-Me**)(fdn)] isomer, 97%	161.6 (2 C)	96.6 (2 C)	63.4 (2 C)	19.4 (2 C)
[Pd(**1M***)(fdn)] isomer, 55%	161.5 (1 C)	101.1 (1 C)	63.3 (1 C)	[g,c]
[Pd(**1M***)(fdn)] isomer, 45%	161.5 (1 C)	100.7 (1 C)	64.7 (1 C)	[g,c]

[a] At 298 K and 62.9 MHz. In $CDCl_3$, $^{13}CDCl_3$ (δ = 77.0) as internal standard. – [b] The olefin carbon atoms resonate at δ = 41.4 (1 C), 41.0 (2 C), 40.7 (1 C). – [c] Due to the similar abundance of the diastereomers the signals cannot be attributed unequivocally. – [d] The olefin carbon atoms resonate at δ = 18.3 (3 C), 17.7 (1 C). – [e] The olefin carbon atoms resonate at δ = 42.1 (1 C), 41.6 (1 C), 41.2 (2 C). – [f] The olefin carbon atoms resonate at δ = 18.3 (2 C), 18.1 (1 C), 17.6 (1 C). – [g] The olefin carbon atoms resonate at δ = 17.4 (3 C), 17.1 (1 C).

fast in the more stereochemically rigid isomer. A similar situation holds true for [Pd(**1G-Ph**)(dmf)].

No information concerning olefin rotation was available from NMR spectra of dmf or fdn derivatives containing ligands of type **2**. Actually, since the complexes display C_2 symmetry, all the nuclei related by the twofold axis are expected to be equivalent.

Maleic anhydride (C_{2v} symmetry) affords complex [Pd(**1M-Ph**)(ma)] in two isomeric forms, which can interconvert by either olefin rotation or dissociation/reassociation of the alkene. Since the isomers are separately observed in both spectra, it can be inferred that both motions are hindered at room temperature. At 328 K the proton spectrum consists of a unique broad pattern due to fast interconversion of the diastereomers. Conversely, complex [Pd(**2M-Ph**)(ma)] exists as a unique isomer. Both ^{1}H- and ^{13}C-NMR spectra show an unsymmetrical olefin, thus demonstrating that dissociation/reassociation of the alkene is slow at 298 K. Also the rotation of the alkene is hindered at room temperature, as suggested by the nonequivalence of the two halves of the N,N-ligand in the carbon spectrum. On raising the temperature to 328 K olefin rotation becomes fast, as suggested by the presence of a symmetric and sharp proton pattern for the N,N-chelate.

Enantioselectivity of Olefin Coordination

As mentioned above, the coordination of prochiral olefins to the [Pd(N,N-chelate)] moiety gives rise to two diastereomers according to which enanantioface is bound to the metal centre. Fresh solutions of complexes of type **I** displayed the presence of both diastereomers, whose ratio could be measured by integrating suitable peaks (Table 3). The ratio was neither affected by prolonged standing in solution nor by the presence of free olefin, which merely increased the rate of interconversion of the diastereomers (see above). These observations indicate that equilibrium is reached within a few seconds from dissolution of the samples. Analogous platinum compounds[5] require several minutes before equilibrium is attained.

Table 3. Diastereomeric equilibrium composition[a] for complexes of type **I** with prochiral olefins

Complex	Composition
[Pd(**1M-Ph**)(dmf)]	55:45
[Pd(**1M-Ph**)(fdn)]	55:45
[Pd(**1G-Ph**)(dmf)]	55:45
[Pd(**1G-Ph**)(fdn)]	55:45
[Pd(**1G-Me**)(dmf)]	55:45
[Pd(**1G-Me**)(fdn)]	85:15
[Pd(**2M-Ph**)(fdn)]	70:30
[Pd(**2G-Ph**)(fdn)]	75:25
[Pd(**2G-Me**)(fdn)]	97:3
[Pd(**1M***)(fdn)][b]	55:45

[a] In $CDCl_3$ at 298 K. – [b] In D_2O at 298 K.

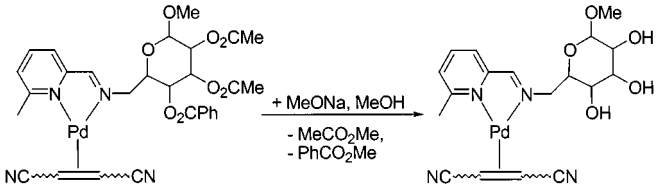
An inspection of Table 3 reveals that the most relevant result concerning enantioselectivity was obtained in the case of [Pd(**2G-Me**)(fdn)]. The ratio between the diastereomers was estimated to be 97:3, indicating a strong preference for the coordination of one enantioface. Discrimination was also observed for the same olefin in the presence of either **2G-Ph** or **2M-Ph**, although to a lesser extent, affording diastereomeric ratios of 75:25 and 70:30, respectively. These results reveal that changing the 4-substituent on the glucoside residue (**2G-Me** vs **2G-Ph**) plays a more important role

than variation of the carbohydrate residue itself (**2G-Ph** vs **2M-Ph**). Among ligands **1**, only **1G-Me** competes with the symmetrical chelates, giving rise to a diastereomeric ratio of 85:15 in the presence of fdn. Conversely, the other ligands of type **1** induce little preference for one enantioface of dmf or fdn. It is also noteworthy that the values of diastereomeric excesses reported in Table 3 are very close to those measured for corresponding Pt^0 complexes containing the same ligands,[5][17] as observed for other related M^0 compounds.[6e,18]

These findings indicate that type **2** ligands prompt more effectively enantioselective coordination of *trans*-olefins. It is also observed that **1G-Me** and **2G-Me**, both based on a glucoside having acetyl groups as substituents, display the better discriminating properties within the corresponding class. However, the complexity of the ligands in terms of both steric and electronic features does not allow an easy rationalization of the factors which determine these results.

Synthesis and X-ray Structure of the Water-Soluble Complex [Pd(1M*)(fdn)]

Water-soluble Pd^0 complexes have recently attracted attention due to their possible use as catalysts in aqueous media.[19] During this work we successfully attempted the synthesis of a water-soluble type **I** complex by deprotecting the alcoholic functions in the sugar residue of the ligand. Treatment of [Pd(**1M-Ph**)(fdn)] with a catalytic amount of sodium methoxide in methanol resulted in quantitative hydrolysis of the ester groups of the carbohydrate residue (Scheme 2).



Scheme 2

The corresponding product [Pd(**1M***)(fdn)] could be isolated in high yield by adding diethyl ether to the reaction mixture. The most prominent feature of the complex is its solubility in both lypophilic (e.g. chloroform) and hydrophylic (e.g. water or methanol) solvents. Analogous to its parent derivative, the complex exists in solution as an equilibrium mixture of two diastereomers in 55:45 ratio.

The X-ray solid-state structure of the complex was determined. Crystallization from methanol/diethyl ether yielded

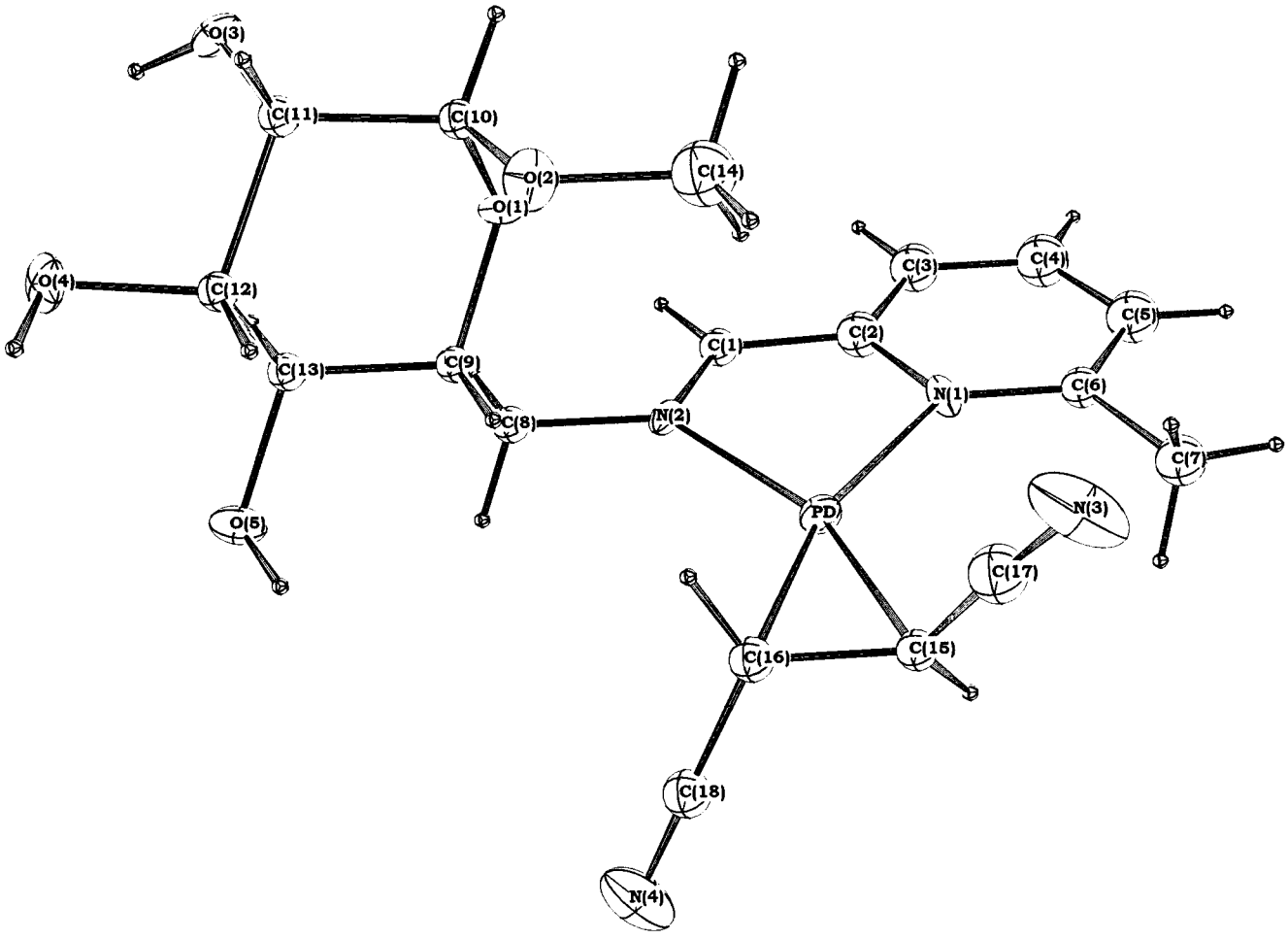


Figure 2. ORTEP view of [Pd(**1M***)fdn] showing the atom labelling scheme

single crystals only for one of the two diastereomers. An ORTEP drawing of this molecule with the atom labelling scheme is shown in Figure 2. Relevant geometric parameters are given in Table 4.

Table 4. Selected geometrical parameters for [Pd(**1M***)-(fdn)]·MeOH[a]

Bond lengths [Å]	
Pd−N(2)	2.11(1)
Pd−N(1)	2.17(1)
Pd−C(15)	2.05(2)
Pd−C(16)	2.04(2)
C(15)−C(17)	1.38(3)
C(15)−C(16)	1.46(3)
C(1)−C(2)	1.43(2)
C(17)−N(3)	1.19(3)
C(16)−C(18)	1.40(3)
N(1)−C(2)	1.37(2)
C(18)−N(4)	1.17(3)
N(2)−C(1)	1.27(2)
N(1)−C(6)	1.34(2)
C(8)−C(9)	1.53(2)
N(2)−C(8)	1.46(2)
Bond angles [°]	
N(1)−Pd−N(2)	77.5(5)
C(15)−Pd−C(16)	41.8(7)
N(1)−Pd−C(15)	122.3(6)
N(2)−Pd−C(16)	118.3(6)
Pd−C(15)−C(16)	69(1)
Pd−C(16)−C(15)	69(1)
C(16)−C(15)−C(17)	113(2)
C(15)−C(16)−C(18)	114(2)
N(3)−C(17)−C(15)	173(3)
N(4)−C(18)−C(16)	179(2)
Pd−N(1)−C(2)	112(1)
Pd−N(2)−C(1)	114(1)
N(2)−C(1)−C(2)	122(1)
Pd−N(2)−C(8)	126(1)
C(1)−N(2)−C(8)	120(1)
N(2)−C(8)−C(9)	110(1)
Torsional angles [°]	
Pd−C(16)−C(15)−C(17)	110(1)
Pd−C(15)−C(16)−C(18)	105(1)
Pd−N(2)−C(8)−C(9)	56(2)
N(2)−C(8)−C(9)−O(1)	62(1)
C(17)−C(15)−C(16)−C(18)	−145(2)

[a] ESDs in parentheses.

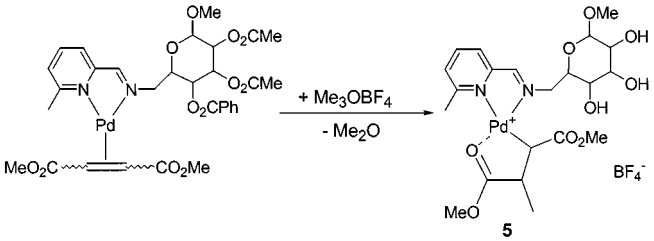
As expected[6e] for zerovalent [Pd(N,N-chelate)(olefin)] complexes the coordination geometry at Pd is trigonal planar. The coordination plane includes the pyridine ring. In fact, the atoms Pd, N(1), N(2), C(15), C(16), C(1), C(2), C(3), C(4), C(5), C(6), C(7), C(8) are coplanar within 0.06(2) Å. The sugar residue adopts the expected chair conformation and its mean plane is almost orthogonal to the coordination plane. As a consequence of the chemical non-equivalence, the bond lengths Pd−N(1) [2.17(1) Å] and Pd−N(2) [2.11(1) Å] are slightly, but significantly, different, and lie at the extremes of the range commonly found in Pd/α-diimine complexes,[6a,6c,6e] the shorter bond being adjacent to the double bond C(1)−N(2). The bite angle N(1)−Pd−N(2) [77.5(5)°] is very close to that found for most bidentate nitrogen ligands.[6c,6e] The olefin is bound to the metal in a regular arrangement. The two Pd−C bond lengths are equal, within the experimental error [average value 2.045(20) Å], and compare well with the values found in Pd complexes of α-diimines with electron-poor olefins.[6c,6e] The lengthening of the olefinic bond [C(15)−C(16) 1.46(3) Å], and the large out-of-plane displacements of the cyano groups [the torsion angle C(17)−C(15)−C(16)−C(18) being 145(2)°] compared with the value of 1.34 Å for the free alkene provide clear evidence of a rehybridization towards sp^3 of the olefinic carbon atoms upon coordination, in keeping with the substantial π back donation from the metal (see above).

Addition of Me_3OBF_4 to [Pd(1G-Ph)(dmf)]

Use in catalysis of type **I** complexes seems plausible.[6f] As organic processes promoted by Pd^0 species often involve oxidative addition to Pd^{II} and/or (stereoselective) insertion of unsaturated substrates into Pd^{II}−alkyl bonds, a preliminarly investigation of the feasibility of stoichiometric reactions of this kind in the coordination environment provided by a chelate of type **1** was made.

We previously reported[20] that [Pd(1,10-phen)(dmf)] reacts with Me_3OBF_4 affording the cyclometallated Pd^{II} product [Pd{CH(CO_2Me)CHMe(CO^aOMe)}(1,10-phen)-(*Pd*−O^a)]BF_4. The process proceeds in two steps, i.e. (i) oxidative addition of the oxonium salt to the Pd^0 complex affording the Pd^{II}−Me bond, and (ii) olefin insertion with attainment of a stereogenic carbon atom bound to Pd.

The analogous reaction was performed on [Pd(**1G-Ph**)(dmf)] (Scheme 3). The process was monitored through NMR spectroscopy and was complete within 24 hours at room temperature affording **5**. The *trans* arrangement of the carbonyl group with respect to the *N*-imino atom was assigned, taking into account the well-established geometry of a closely related Pt^{II} species.[5] The presence of two diastereomers in 75:25 ratio indicates that the reaction had occurred with significant stereoselectivity.



Scheme 3

Conclusion

This work demonstrated the reasonable feasibility of synthesising chiral diimino ligands based on carbohydrates. Results of preliminary investigations into their ability in inducing enantioselective processes were promising results, with Pd^0 complexes with prochiral olefins being prepared

stereoselectively and achievement of a stoichiometric asymmetric insertion process. A rare example of a chiral Pd^0 water-soluble complex was also provided by deprotecting the alcoholic groups of the carbohydrate residue in one ligand, and its structure determined through X-ray diffractometry.

Experimental Section

General: NMR spectra were recorded with a 250-MHz spectrometer (Bruker Model AC-250). The solvents were $CDCl_3$ [$CHCl_3$ (δ = 7.26) and $CDCl_3$ (δ = 77.0) as standards for ^1H and ^{13}C spectra, respectively] and CD_3NO_2 [CD_2HNO_2 (δ = 4.33) and $^{13}CD_2HNO_2$ (d = 62.9) as standards for ^1H and ^{13}C spectra, respectively]. Optical activity measurements were performed with a Perkin−Elmer Polarimeter (Model 141). The following abbreviations are used for describing NMR multiplicities: d, doublet; dd, double doublet; dt, double triplet; m, multiplet; no attribute, singlet; t, triplet. − Compounds **3G-Me**,[7] methyl-2,3-di-*O*-acetyl-4-*O*-benzoyl-6-bromo-6-deoxy-α-D-glucoside,[8] **1M-Ph**,[5] **2M-Ph**[5] and $[Pd(dba)_2]$[13] were prepared according to published methods. Toluene was distilled from sodium, dichloromethane from calcium hydride, and methanol from magnesium immediately before use. − Elemental analysis for the new compounds are collected in Table 5.

3G-Ph: The compound was prepared in 80% yield as described for **3M-Ph**[9] by starting from methyl-2,3-di-*O*-acetyl-4-*O*-benzoyl-6-bromo-6-deoxy-α-D-glucoside.[8] − ^1H-NMR resonances (in $CDCl_3$, at 250 MHz): δ = 7.97 (d, 2 H), 7.57 (t, 1 H), 7.45 (t, 2 H), 5.68 (t, 1 H), 5.22 (t, 1 H), 5.02 (d, 1 H), 4.95 (dd, 1 H), 4.08 (m, 1 H), 3.48 (3 H, OMe), 3.40 (m, 2 H), 2.09 (3 H, $MeCO_2$), 1.89 (3 H, $MeCO_2$). − Selected ^{13}C-NMR resonances (in $CDCl_3$, at 62.9 MHz): δ = 96.7 (1 C, C1 of glucoside), 70.9, 70.2, 69. 4, 68.9 (4 C, C2−C5 of glucoside), 55.6 (1 C, OMe), 51.1 (1 C, NCH_2), 20.7 (1 C, *Me*CO_2), 20.6 (1 C, *Me*CO_2).

1G-Ph, 1G-Me, 2G-Ph, and 2G-Me: To a stirred solution of $PPhMe_2$ (0.14 g, 1.0 mmol) in 5 mL of dry dichloromethane kept in an ice bath was added dropwise a solution of the appropriate azide **3** (1.0 mmol) in 5 mL of dry dichloromethane. After the addition was complete, the ice bath was removed and formation of nitrogen was observed. Progression of the reaction was monitored by TLC analysis on silica of the reacting mixture with ethyl acetate/petroleum ether, 1:1. The reaction affording the corresponding imino-phosphorane **4** was complete within 3 hours. In the case of **1G-Ph** and **1G-Me** the solvent was removed under vacuum and the residue was dissolved in 5 mL of dry toluene containing 4-Å molecular sieves. To the solution was added 6-methyl-2-pyridinecarboxaldehyde (0.12 g, 1.0 mmol), and after 1 h of stirring at 363 K the solvent was removed under vacuum. In the case of **2G-Ph** and **2G-Me**, after formation of **4** was complete, glyoxal (40% w/w in water, 0.5 mmol) was added to the dichloromethane solution, followed by sodium sulphate. After 15 minutes the reaction mixture was filtered and the solvent removed under vacuum. In all cases, the crude reaction products were filtered through a column of Florisil (15 × 1.5 cm) with ethyl acetate/petroleum ether, 1:1 to give the products as white glassy solids (yield: 60−70%). − Selected ^1H-NMR resonances (in $CDCl_3$, at 250 MHz): **1G-Ph**: δ = 8.32 (1 H, CH=N), 5.75 (t, 1 H), 5.35 (t, 1 H), 5.00 (m, 1 H), 4.93 (1 H), 4.29 (m, 1 H), 3.90 (d, 1 H), 3.75 (dd, 1 H), 3.36 (3 H, OMe), 2.55 (3 H, Me-py), 2.07 (3 H, $MeCO_2$), 1.90 (3 H, $MeCO_2$); **1G-Me**: δ = 8.32 (1 H, CH=N), 5.50 (m, 1 H), 5.10 (t, 1 H), 4.88 (m, 2 H), 4.15 (m, 1 H), 3.84 (d, 1 H), 3.66 (dd, 1 H), 3.33 (3 H, OMe), 2.56 (3 H, Me-py), 2.05 (3 H, $MeCO_2$), 2.02 (3 H, $MeCO_2$), 2.00 (3 H, $MeCO_2$); **2G-Ph**: δ = 7.78 (2 H, CH=N), 5.70 (t, 2 H), 5.27 (t, 2 H), 4.95 (m, 4 H), 4.23 (m, 2 H), 3.77 (dd, 2 H), 3.59 (dd, 2 H), 3.40 (6 H, OMe), 2.08 (6 H, $MeCO_2$), 1.89 (6 H, $MeCO_2$); **2G-Me**: δ = 7.88 (2 H, CH=N), 5.47 (t, 2 H), 5.05 (t, 2 H), 4.87 (m, 4 H), 4.08 (m, 2 H), 3.75 (dd, 2 H), 3.57 (dd, 2 H), 3.35 (6 H, OMe), 2.05 (6 H, $MeCO_2$), 2.01 (6 H, $MeCO_2$), 1.98 (6 H, $MeCO_2$). − Selected ^{13}C-NMR resonances (in $CDCl_3$, at 62.9 MHz): **1G-Ph**: δ = 164.8 (1 C, CH=N), 96.4 (1 C, C1 of glucoside), 71.1, 71.0, 70.0 and 68.4 (4 C, C2-C5 of glucoside), 61.2 (1 C, NCH_2), 55.1 (1 C, OMe), 24.2 (1 C, *Me*-py), 20.7 (1 C, *Me*CO_2), 20.6 (1 C, *Me*CO_2); **1G-Me**: δ = 164.9 (1 C, CH=N), 96.4 (1 C, C1 of glucoside), 71.0, 70.4 and 68.1 (4 C, C2-C5 of glucoside), 60.9 (1 C, NCH_2), 55.1 (1 C, OMe), 24.1 (1 C, *Me*-py), 20.7 (3 C, *Me*CO_2); **2G-Ph**: δ = 164.2 (2 C, CH=N), 96.6 (2 C, C1 of glucosides), 71.1, 70.9, 69.9, 68.3 (8C, C2-C5 of glucosides), 61.2 (2 C, NCH_2), 55.3 (2 C, OMe), 20.8 (2 C, *Me*CO_2), 20.6 (2 C, *Me*CO_2); **2G-Me**: δ = 164.3 (2 C, CH=N), 96.5 (2 C, C1 of glucosides), 70.9, 70.3, 67.9 (8C, C2-C5 of glucosides), 60.8 (2 C, NCH_2), 55.2 (2 C, OMe), 20.7 (6 C, *Me*CO_2). − $[\alpha]_D^{25}$ (0.050 M in dichloromethane): **1G-Ph**: +100; **1G-Me**: +100; **2G-Ph**: +85; **2G-Me**: +110.

[Pd(N,N-chelate)(olefin)]: To a suspension of $[Pd(dba)_2]$ (0.58 g, 1.0 mmol) in 5 mL of dry toluene were added the N,N-chelate (1.5 mmol) and the olefin (1.5 mmol). After 1 h of stirring (12 h when olefin = dmf) the solvent was removed under vacuum from the resulting mixture. The residue was separated by chromatography on silica gel with dichloromethane (to remove dba) and then

Table 5. Elemental analyses for all new compounds

Compound	Formula	C found (calcd.)	H found (calcd.)	N found (calcd.)
1G-Me	$C_{20}H_{26}N_2O_8$	56.59 (56.87)	6.31 (6.20)	6.55 (6.63)
1G-Ph	$C_{25}H_{28}N_2O_8$	62.21 (61.98)	5.89 (5.82)	5.93 (5.78)
2G-Me	$C_{28}H_{40}N_2O_{16}$	50.87 (50.91)	6.22 (6.10)	4.32 (4.24)
2G-Ph	$C_{38}H_{44}N_2O_{16}$	57.98 (58.16)	5.59 (5.65)	3.51 (3.57)
[Pd(**1M-Ph**)(dmf)]	$C_{31}H_{36}N_2O_{12}Pd$	50.85 (50.66)	4.87 (4.94)	3.93 (3.81)
[Pd(**1M-Ph**)(ma)]	$C_{29}H_{30}N_2O_{11}Pd$	50.89 (50.56)	4.44 (4.39)	4.10 (4.07)
[Pd(**1M-Ph**)(fdn)]	$C_{29}H_{30}N_4O_8Pd$	51.90 (52.07)	4.41 (4.52)	8.30 (8.37)
[Pd(**1G-Ph**)(dmf)]	$C_{31}H_{36}N_2O_{12}Pd$	50.62 (50.66)	5.05 (4.94)	3.65 (3.81)
[Pd(**1G-Ph**)(fdn)]	$C_{29}H_{30}N_4O_8Pd$	52.23 (52.07)	4.43 (4.52)	8.61 (8.37)
[Pd(**1G-Me**)(dmf)]	$C_{26}H_{34}N_2O_{12}Pd$	46.24 (46.40)	5.21 (5.09)	4.27 (4.16)
[Pd(**1G-Me**)(fdn)]	$C_{24}H_{28}N_4O_8Pd$	47.63 (47.50)	4.60 (4.65)	9.04 (9.23)
[Pd(**2M-Ph**)(fdn)]	$C_{42}H_{46}N_4O_{16}Pd$	51.88 (52.05)	4.86 (4.78)	5.65 (5.78)
[Pd(**2M-Ph**)(ma)]	$C_{42}H_{46}N_2O_{19}Pd$	50.91 (51.00)	4.60 (4.69)	2.89 (2.83)
[Pd(**2G-Ph**)(fdn)]	$C_{42}H_{46}N_4O_{16}Pd$	52.28 (52.05)	4.66 (4.78)	5.86 (5.78)
[Pd(**2G-Me**)(fdn)]	$C_{32}H_{42}N_4O_{16}Pd$	45.60 (45.48)	5.08 (5.01)	6.81 (6.63)

with dichloromethane/methanol, 40:1. The solvents were removed under vacuum from the collected yellow-orange fractions affording the product as a yellow microcrystalline solid (yield: 75−85%). Alternatively, fdn or ma complexes could be prepared by starting from the corresponding dmf complexes, according to the following example: To a solution of [Pd(**1M-Ph**)(dmf)] (0.074 g, 0.10 mmol) in 1 mL of dichloromethane was added fumarodinitrile (0.012 g, 0.15 mmol). The resulting solution was chromatographed as described above affording pure [Pd(**1M-Ph**)(fdn)] (yield 80−85%).

[Pd(1M*)(fdn)]: To a stirred solution of [Pd(**1M-Ph**)(fdn)] (0.067 g, 0.10 mmol) in 2.5 mL of dry methanol was added a catalytic amount of sodium methoxide in the same solvent. After 30 min of reaction, separation of the yellow product was observed. After a further 16 h of stirring, the precipitation of the product was enhanced by addtion of diethyl ether. The complex was separated, washed with diethyl ether (3 × 3 mL) and dried under vacuum (0.040 g, yield: 83%).

Addition of Me_3OBF_4 to [Pd(1G-Ph)(dmf)] with Formation of 5: A solution of the complex (0.022 g, 0.030 mmol) in 0.5 mL of deuterionitromethane was added to solid Me_3OBF_4 (0.005 g, 0.033 mmol). The resulting solution was transferred into an NMR tube and spectra were recorded until no more chemical changes were detected. − Selected ^{1}H-NMR resonances (in CD_3NO_2, at 250 MHz): **5** (diastereomer, 75%): δ = 8.41 (1 H, CH=N), 4.09 (3 H, OMe), 3.50 (3 H, OMe), 3.40 (3 H, OMe), 2.70 (3 H, *Me*-py), 1.07 (d, 3 H, CH*Me*); (diastereomer, 25%): 8.42 (1 H, CH=N), 4.10 (3 H, OMe), 2.62 (3 H, *Me*-py), 1.00 (d, 3 H, CH*Me*).

X-ray Crystal-Structure Determination of [Pd(1M*)(fdn)]: Crystals suitable for X-ray analysis were grown from methanol/diethyl ether. The crystal, collection, and refinement data are presented in Table 6. Data collection was performed at room temperature with an Enraf−Nonius MACH3 diffractometer with graphite-monochromated Mo-K_α radiation using the ω/θ scan technique. The unit-cell parameters and orientation matrix were obtained from a least-squares fitting of the setting values of 25 strong reflections in the range $13° \leq \theta \leq 14°$. Three monitoring reflections, measured every 500, showed no intensity decrease. Corrections for Lorentz-polarization effects were applied but not for absorption. The structure was solved by routinary application of Patterson and Fourier techniques. Refinement on *F* was carried out by full-matrix least squares minimizing the quantity $\Sigma w(\Delta F)^2$ with $w^{-1} = [\sigma^2(F_o) + (0.02F_o)^2 + 1]$, where σ is derived from counting statistics. Owing to the insufficient number of observed reflections of high values of θ, the final refinement was carried out with anisotropic thermal parameters for Pd, O and N, and isotropic for C and the non-hydrogen atoms of the solvent molecule MeOH. H atoms at calculated positions were added as riding atoms with isotropic thermal parameters 1.3 times larger than that of the carrier atoms. The H atoms of the solvent molecule were neglected. The final Fourier difference map was within ±0.6 e/Å^3. All calculations were performed with the Enraf−Nonius (SDP) set of programs.[21] Crystallographic data (excluding structure factors) for the structure reported in this paper have been deposited with the Cambridge Crystallographic Data Centre as supplementary publication no CCDC-133171. Copies of the data can be obtained free of charge on application to CCDC, 12 Union Road, Cambridge CB2 1EZ, UK [Fax: (internat.) + 44-1223/336-033; E-mail: deposit@ccdc.cam.ac.uk].

Table 6. Crystallographic data for [Pd(**1M***)(fdn)] · MeOH

Crystal size [mm]	0.02 × 0.20 × 0.30
Empirical formula	$C_{18}H_{22}N_4O_5Pd{\cdot}CH_3OH$
Molecular mass	512.8
Crystal system	orthorhombic
Space group	$P2_12_12_1$
a [Å]	7.8370 (1)
b [Å]	27.5000 (3)
c [Å]	10.3280 (2)
V [Å^3]	2225.8
Z	4
F(000)	1048
$D_{calcd.}$ [gcm^{-3}]	1.53
$D_{measd.}$ [gcm^{-3}]	1.50
λ (Mo-K_α) [Å]	0.71073
θ_{max} [°]	27
μ [cm^{-1}]	8.61
No. of reflections measured	2837
No. of independent reflections	2774
No. of reflections above 3σ(*I*)	1167
No. of refined parameters	171
Goodness of fit	1.10
R	0.048
Rw	0.053

Acknowledgments

We thank the Consiglio Nazionale delle Ricerche, the MURST and the Centro Interdipartimentale Ricerhe: Ambiente (CIRAM), Università di Napoli "Federico II" for financial support, and the Centro Interdipartimentale di Metodologie Chimico-Fisiche, Università di Napoli "Federico II" for NMR and X-ray facilities.

[1] See, for example: S. Otto, G. Boccaletti, J. B. F. N. Engberts, *J. Am. Chem. Soc.* **1998**, *120*, 4238.
[2] For examples of organic processes of industrial relevance catalyzed by metal/phosphane complexes see: [2a] W. S. Knowles, *Acc. Chem. Res.* **1983**, *16*, 106. − [2b] S. Akutagawa, *Appl. Catal. A* **1995**, *128*, 171. − [2c] H. Kumobayashi, *Recl. Trav. Chim. Pays-Bas* **1996**, *115*, 201.
[3] [3a] A. Togni, L. M. Venanzi, *Angew. Chem. Int. Ed. Engl.* **1994**, *33*, 497. − [3b] H. Brunner, R. Störiko, *Eur. J. Inorg. Chem.* **1998**, 783 and refs. therein.
[4] Other types of ligands based on carbohydrates are known. For recent examples, see: [4a] T. Tanase, Y. Yasuda, T. Onaka, S. Yano, *J. Chem. Soc., Dalton Trans.* **1998**, 345. − [4b] R. Kadyrov, D. Heller, R. Selke, *Tetrahedron: Asymmetry* **1998**, *9*, 329. − [4c] J. Costamagna, N. P. Barroso, B. Matsuhiro, M. Villagràn, *Inorg. Chim. Acta* **1998**, *273*, 191. − [4d] M. Stolmàr, C. Floriani, G. Gervasio, D. Viterbo, *J. Chem. Soc., Dalton Trans.* **1997**, 1119. − [4e] M. Tschoerner, G. Trabesinger, A. Albinati, P. S. Pregosin, *Organometallics* **1997**, *16*, 347.
[5] M. L. Ferrara, M. Funicello, I. Orabona, A. Panunzi, F. Ruffo, *Organometallics* **1998**, *17*, 3832.
[6] [6a] R. A. Klein, P. Witte, R. van Belzen, J. Fraanje, K. Goubitz, M. Numan, H. Schenk, J. M. Ernsting, C. J. Elsevier, *Eur. J. Inorg. Chem.* **1998**, 319. − [6b] B. Milani, A. Anzilutti, L. Vicentini, A. Sessanta o Santi, E. Zangrando, S. Geremia, G. Mestroni, *Organometallics* **1997**, *16*, 5064. − [6c] M. Kranenburg, J. G. P. Delis, P. C. J. Kramer, P. W. N. M. van Leewen, K. Vrieze, N. Veldman, A. L. Spek, K. Goubitz, J. Fraanje, *J. Chem. Soc., Dalton Trans.* **1997**, 1839. − [6d] L. Canovese, F. Visentin, P. Uguagliati, B. Crociani, *J. Chem. Soc., Dalton Trans.* **1996**, 1921. − [6e] R. van Asselt, C. J. Elsevier, W. J. J. Smeets, A. L. Spek, *Inorg. Chem.* **1994**, *33*, 1521. − [6f] R. van Asselt, C. J. Elsevier, *Organometallics* **1992**, *11*, 1999.
[7] S. Hanessian, D. Ducharme, R. Massé, M. L. Capmau, *Carbohydr. Res.* **1978**, *63*, 265.
[8] P. Deslongchamps, C. Moreau, D. Frèhel, R. Chênevert, *Can. J. Chem.* **1975**, *53*, 1204.
[9] D. Horton, A. E. Luetzow, *Carbohydr. Res.* **1968**, *7*, 101.
[10] Compounds similar to **4** are known. For a recent example, see: J. M. Garcia Fernàndez, C. Mellet Ortiz, V. M. Diaz Pèrez, J. Fuentes, J. Kovàcs, I. Pintèr, *Tetrahedron Lett.* **1997**, *38*, 4161.
[11] [11a] J. Chatt, L. A. Duncanson, *J. Chem. Soc.* **1953**, 2939. − [11b] M. J. S. Dewar, *Bull. Soc. Chim. Fr.* **1951**, *18*, C71.
[12] K. J. Cavell, D. J. Stufkens, K. Vrieze, *Inorg. Chim. Acta* **1980**, *47*, 67.

[13] M. F. Rettig, P. M. Maitlis, *Inorg. Synth.* **1990**, *28*, 110.
[14] Ts. Ito, S. Hasegawa, Y. Takahashi, Y. Ishii, *J. Organomet. Chem.* **1974**, *73*, 401.
[15] Average ^{1}H- (^{13}C-)NMR $\Delta\delta$ values for the olefin nuclei are: fdn: ca. 3.4 (100); ma: 3.2 (95); dmf: 3.0 (90).
[16] Henceforth, a process which is *slow* (or *fast*) *in the NMR time scale* will be simply indicated as *slow* (or *fast*).
[17] F. Ruffo, unpublished results.
[18] B. Jedlicka, R. E. Rülke, W. Wasseinsteiner, R. Fernández-Galán, F. A. Jalón, B. R. Manzano, J. Rodríguez-de La Fuente, N. Veldman, H. Kooijman, A. L. Spek, *J. Organomet. Chem.* **1996**, *516*, 97.
[19] [19a] D. J. Darensbourg, T. J. Decuir, N. W. Stafford, J. R. Robertson, J. D. Draper, J. H. Reibenspies, A. Kathó, F. Joó, *Inorg. Chem.* **1997**, *36*, 4218. – [19b] J. W. Ellis, K. N. Harrison, P. A. T Hoye, A. G. Orpen, P. G. Pringle, M. B. Smith, *Inorg. Chem.* **1992**, *31*, 3026.
[20] A. De Renzi, I. Orabona, F. Ruffo, *Inorg. Chim. Acta* **1997**, *258*, 105.
[21] B. Frenz, *Crystallographic Computing 5*, Oxford University Press, **1991**, *11*, 126.

Received April 19, 1999
[I99137]

Physicochemical Characterization of MS-325, a New Gadolinium Complex, by Multinuclear Relaxometry[+]

Robert N. Muller,*[a] Bernd Radüchel,[b] Sophie Laurent,[a] Johannes Platzek,[b] Corinne Piérart,[a] Peter Mareski,[b] and Luce Vander Elst[a]

Keywords: MS-325 / Angiography / MRI contrast agent / NMR spectroscopy / Interaction with HSA / Gadolimium

The physicochemical characterization of MS-325 [trisodium {4-(*R*)-[(4,4-diphenylcyclohexyl)phosphanooxymethyl]-3,6,9-triaza-3,6,9-tris(methoxycarbonyl)undecanedioato}gadolinium-(III)], a new derivative of Gd-DTPA {Magnevist®: dimeglumin [{3,6,9-triaza3,6,9-tris(methoxycarbonyl)undecanedioato}gadolinium(III)], presented as a potentially useful angiographic contrast agent, was carried out in various media. Water solution, protein-containing solution, phosphorylated metabolites solution, and Zn^{2+}-containing solution were investigated using different NMR techniques such as water ^{1}H nuclear magnetic relaxation rates, water ^{17}O transverse relaxation rates, and ^{31}P longitudinal relaxation rates of phosphorylated metabolites. The proton relaxivity of MS-325 in water was found to be higher than that of the parent compound Gd-DTPA; this can be attributed to the longer rotational correlation time (τ_R) of the hydrated complex, and possibly to an apparently shorter mean distance (r) between the protons of the coordinated water molecule and the gadolinium ion. The kinetic and thermodynamic stability of MS-325 in solutions containing phosphorylated metabolites (ATP, phosphocreatine and inorganic phosphate) were measured by ^{31}P relaxation rate analysis and found to be higher than for Gd-DTPA. Similarly, the Zn^{2+} transmetallation process studied by proton relaxometry is slower than for the same reference compound. Finally, an analysis of the noncovalent binding of MS-325 to serum proteins by proton relaxometry showed that MS-325 interacts with human serum albumin (HSA) and that the association constant of this interaction is equal to 6100 ± 2130 M^{-1}. A peak relaxivity of approx. 50 $s^{-1}mM^{-1}$ was determined at 25 MHz for the protein-bound paramagnetic complex. This value is lower than the maximal relaxivity predicted for a paramagnetic center totally immobilized at the surface of the protein.

Introduction

Small gadolinium complexes, which can interact with high molecular weight molecules through covalent or noncovalent bonds, are potential intravascular Magnetic Resonance Imaging (MRI) contrast agents. A noncovalent binding to endogenous proteins can exist in vivo; this results in a reduced extravasation of the paramagnetic complex, and therefore in a subsequent increase of its persistence in blood, but does not preclude a fairly rapid and selective renal excretion. On the other hand, binding to macromolecules decreases the molecular mobility and thus enhances the relaxivity of the paramagnetic center, i.e. its ability to increase the relaxation rate of the protons of water molecules. Contrast agents that are likely to interact with serum proteins, are therefore attracting a great deal of interest.

MS-325 [trisodium {4-(*R*)-[(4,4-diphenylcyclohexyl)phosphonooxymethyl]-3,6,9-triaza-3,6,9-tris(methoxycarbonyl)-undecanedioato}gadolinium(III)] (Figure 1) is a new MRI contrast agent which has been reported to exhibit a remarkable affinity for serum proteins.[1][2] This derivative of Gd-DTPA [Magnevist®: dimeglumin {3,6,9-triaza-3,6,9-tris-(methoxycarbonyl)undecanedioato}gadolinium(III)] has a diphenylcyclohexyl group attached to one of the ethylene bridges of the backbone by means of a phosphodiester linkage.[1][2] The presence of this substituent is responsible for the noncovalent binding to plasma proteins which, as expected, leads to a reduction in the rate of molecular tumbling and, consequently, to an enhanced efficacy as a relaxing agent in blood.[1] In addition, the interaction with blood macromolecules produces a marked increase in the plasma half-life relative to hydrophilic contrast agents such as Gd-DTPA, the parent compound, or Gd-DOTA {Dotarem®: meglumin [1,4,7,10-tetrakis(methoxycarbonyl)-1,4,7,10-tetraazacyclododecane]gadolinium(III)}.[3] MS-325 has been shown to provide very good and persistent enhancement of blood vessels on MRI angiographic evaluations.[3–8]

So far, few physicochemical data are available concerning a comprehensive description and understanding of the properties of this molecule. The aim of this work is to extend the in vitro physicochemical characterization of MS-325 by quantitatively evaluating and interpreting: 1) the proton relaxivity (r_1) in water at various magnetic fields and temperatures; 2) the exchange time of the coordinated water molecule (τ_M) estimated through the analysis of the temperature-dependence of the ^{17}O transverse relaxation rate of water in MS-325 aqueous solution; 3) the rotational correlation time (τ_R) calculated from ^{2}H longitudinal relaxation rate of the deuterated ligand complexed to lantha-

[+] Part of this work has been presented at the 7th Meeting of the International Society of Magnetic Resonance in Medicine.

[a] NMR Laboratory, Department of Organic Chemistry, University of Mons-Hainaut,
B-7000 Mons, Belgium
Fax: (internat.) + 32-65/373520
E-mail: robert.muller@umh.ac.be
[b] Schering AG, Research Laboratories,
D-13342 Berlin, Germany

 © WILEY-VCH Verlag GmbH, D-69451 Weinheim, 1999 1434–1948/99/1111–1949 $ 17.50+.50/0

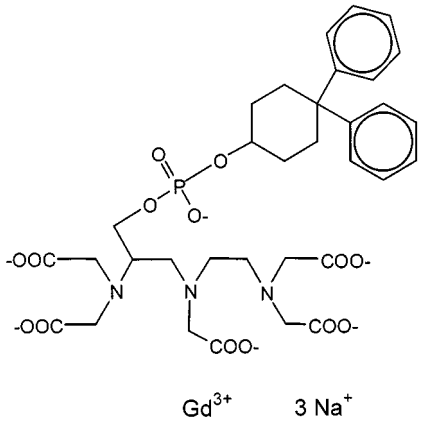


Figure 1. Structure of MS-325 [trisodium {4-(*R*)-[(4,4-diphenylcyclohexyl) phosphonooxymethyl]-3,6,9-triaza-3,6,9-tris(methoxycarbonyl)undecanedioato}gadolinium(III)]

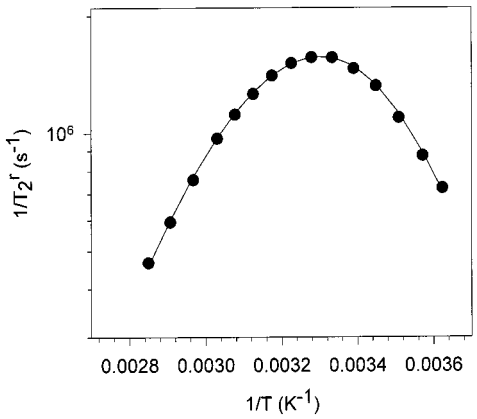


Figure 2. Reduced transverse relaxation rate of oxygen-17 ($1/T_2^r$) as a function of the reciprocal of the temperature for an aqueous solution containing 12.5 mM of MS-325 (B_o = 7.05 T)

num, a diamagnetic lanthanide ion; 4) the noncovalent interaction with human serum albumin studied by proton and deuterium relaxometry; 5) the transmetallation by Zn^{2+} ions using proton relaxometry; and 6) the kinetic and thermodynamic stability of the gadolinium complex in solutions containing phosphorylated metabolites which are potential competitors for the complexation of the lanthanide ions {ATP, phosphocreatine (PCr), and inorganic phosphate (Pi)}. This study will be carried out through the evolution of the ^{31}P longitudinal relaxation rates.

Considering the clinical context of this kind of study, most of the data are reported at 310 K, the physiological body temperature, as well as at the standard temperature of 298 K.

Results and Discussion

Water Solution

The residence time of water molecules in the first coordination sphere of the complex (τ_M) was obtained from the analysis of the temperature-dependence of the ^{17}O transverse relaxation rate of water in MS-325 solution. This procedure allows for the determination of: i) the hyperfine coupling constant ($A/\hbar$) between the ^{17}O nucleus and the electron spin; ii) the parameters defining the rate of exchange of the coordinated water molecule {enthalpy ($\Delta H^{\neq}$) and entropy ($\Delta S^{\neq}$) of activation}; and iii) the parameters related to the electronic relaxation time [the correlation time of the modulation of the zero-field splitting τ_V, the activation energy for this process E_V, and B which depends on the trace of the square of the zero-field splitting tensor (Δ^2) and on the electron spin S ($B = \Delta^2\{4S(S + 1) - 3\}/25$)].[9][10]

The theoretical fitting of the reduced transverse relaxation rates ($1/T_2^r = [H_2O]/\{[\text{Gd-complex}] \cdot T_2^P\}$) obtained over a temperature range extending from 276 to 351 K (Figure 2) gives a τ_M^{298} value of 195 ± 32 ns similar to that of 200 ± 51 ns reported for another C-substituted Gd-DTPA derivative (*S*)-Gd-EOB-DTPA [disodium {4-(*S*)-3,6,9-tris(methoxycarbonyl)-4-(4-ethoxybenzyl)-3,6,9-triazaundecanedioato}gadolinium(III)].[9] These τ_M values are however shorter than those observed for Gd-DTPA (τ_M^{298} = 331 ± 60 ns,[11] 303 ns[12]). In our fitting, the number of coordinated water molecules (q) was assumed to be equal to 1 as in Gd-DTPA and (*S*)-Gd-EOB-DTPA complexes. The other parameters of the fitting are given in Table 1.

Table 1. Parameters obtained from the fitting of the reduced transverse relaxation rate of oxygen-17 in MS-325 solution ([MS-325] = 12.5 mM)

	MS-325	Gd-DTPA[a]	(*S*) Gd-EOB-DTPA[b]
τ_M^{298} [ns]	195±32	331±60	200±51 (201)
τ_V^{298} [ps]	18.7 ±0.9	12.3±0.3	15.3±1.94 (2.4)
B [10^{20} s^{-2}]	5.22 ±0.24	2.60±0.30	2.51±0.28 (0.49)
E_V [kJ/mol]	6.4±2.7	4.5±4.2	7.1±5.9 (12.0)
$A/\hbar$ [10^6 rad s^{-1}]	−4.1±0.06	−3.41±0.11	−4.07±0.45 (−4.24)
$\Delta H^{\neq}$ [kJ/mol]	51.3 ±0.3	51.5±0.3	53.5±0.3 (54.3)
$\Delta S^{\neq}$ [J/mol K]	55.8±0.4	52.1±0.6	63.0±12.9 (65.7)

[a] From ref.[11] – [b] the values reported in this table were obtained by improving the fitting of the data of ref.[9]; the values in parentheses are from ref.[9]

The proton relaxivity (r_1), defined as the increase of the solvent relaxation rate induced by 1 mmol·l^{-1} of the paramagnetic complex, is the sum of two contributions arising from short-distance interactions (innersphere mechanism) and from longer-distance interactions (outersphere mechanism). The influence of τ_M on proton relaxivity is well understood. When this exchange time is short relative to the relaxation time of the protons of the coordinated water molecules, the overall proton relaxivity is enhanced by a temperature decrease. On the contrary, when the exchange time is long, the global relaxivity is levelled off or even decreased by a reduction of the temperature. This latter behavior has been observed for bisamide derivatives of Gd-DTPA.[11,13–15] The τ_M values found for MS-325 by ^{17}O-NMR spectroscopy over the temperature range explored are characteristic of a nonlimiting exchange. This is con-

firmed by the increase of the relaxivities when the temperature is decreased (Figure 3).

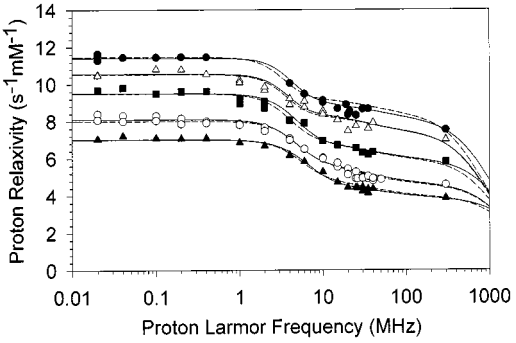


Figure 3. ^{1}H NMRD relaxivity profiles of MS-325 in water at different temperatures ([MS-325] = 1 mM): 278 K: closed circles, 288 K: open triangles, 298 K: closed squares, 310 K: open circles, 318 K: closed triangles. The lines correspond to the theoretical fittings of the data points (solid lines: r = 0.295 nm, dashed lines: r = 0.31 nm)

As compared to Gd-DTPA,[9][16] the proton relaxivity of MS-325 at 310 K is higher over the whole proton Larmor frequency range and, in this respect, behaves like that of (*S*)-Gd-EOB-DTPA. For this last compound, the increased relaxivity was mainly attributed to a shorter mean distance of interaction between the protons of the coordinated water molecule and the gadolinium ion (0.281 nm for (*S*)-Gd-EOB-DTPA and 0.31 nm for Gd-DTPA).[9]

The fittings of the proton Nuclear Magnetic Relaxation Dispersion (NMRD) profiles were performed as described in the experimental section according to the classical paramagnetic relaxation formalisms.[17−19] The following strategy was adopted: after subtraction of the diamagnetic relaxation rate of the solvent, the outersphere and the innersphere contributions were simultaneously fitted after attribution of fixed or calculated values to the various parameters. The relative diffusion constant D was fixed to the diffusion constant of water,[20] d, the distance of closest approach for the outer sphere contribution was set at 0.36 nm,[14][21] τ_M values were those obtained by ^{17}O NMR, and q, the number of water molecules in the first coordination sphere of Gd^{3+}, was given a value of one. The parameters describing the electronic relaxation times, τ_V and τ_{SO} (the electronic relaxation time at zero field), were optimized for the outersphere and the innersphere contributions simultaneously. It is well-known that parallel and accurate determination of both τ_R, the rotational correlation time of the hydrated complex, and r, the distance between the protons of the coordinated water molecules and the gadolinium ion, can be ambiguous, unless independent information about τ_R and/or r is available. For instance, good fits of the 310 K experimental data can be achieved with pairs of values of r and τ_R ranging from 0.285 to 0.31 nm for the former and from 68 to 110 ps for the latter (Table 2).

Assuming that τ_R can be estimated by the Stokes−Einstein law and that the molecular volume is roughly proportional to the molecular weight, the τ_R of MS-325 should be approximately 1.6 times larger than that of Gd-DTPA.

Table 2. Values of τ_R obtained from the fitting of the proton NMRD profiles at 310 K using different r values

r [nm]	τ_R [ps]
0.285	68
0.290	76
0.295	84
0.3	91
0.31	110

At 310 K, τ_R values of MS-325 should thus be around 90−95 ps and correspond to a distance r of 0.3 nm. If (*S*)-Gd-EOB-DTPA is taken as a reference, τ_R should be around 80−85 ps at 310 K and r should be 0.295 nm. The τ_R value obtained by the analysis of the deuterium longitudinal relaxation rate of the deuterated ligand complexed to the diamagnetic La^{3+} ion is however markedly longer (τ_R = 117±12 ps at 310 K) and corresponds to a distance of 0.31 nm. Two values of r (0.295 and 0.31 nm) were thus used for the fittings performed at 278, 288, 298, 310, and 318 K (Figure 3 and Table 3).

As for other C-substituted derivatives of Gd-DTPA,[9,11,21] the proton relaxivity enhancement observed for MS-325, as compared to the unsubstituted Gd-DTPA, can thus be related to a longer rotational correlation time τ_R and possibly to a shorter apparent H−Gd distance r.

Solutions Containing Phosphorylated Metabolites

In an earlier study, adenosine triphosphate (ATP) was shown to efficiently compete with open-chain chelates for the complexation of gadolinium ions.[22] This metabolite thus appears to be a good probe to assess the kinetics as well as the thermodynamic stability of the complex. The decrease of the T_1 of the phosphorus nuclei of ATP in solutions containing Gd-DTPA has indeed been reported to result from the formation of a complex between ATP and Gd^{3+} whose characteristics have been described elsewhere.[23] The same protocol was applied to MS-325 in ATP-containing solutions and the results were compared to those previously obtained for Gd-DTPA[22] and (*S*)-Gd-EOB-DTPA[9] (Figure 4).

Immediately after addition of the gadolinium complex, ^{31}P relaxation rates increase and reach a plateau after a delay which depends on the structure of the Gd complex. The equilibrium value of the P-31 relaxation rates is reached more quickly for Gd-DTPA (ca. 30 min) than for (*S*)-Gd-EOB-DTPA (ca. 6 h) or for MS-325 (ca. 24 h). The kinetic stability of MS-325 is thus increased as compared to (*S*)-Gd-EOB-DTPA which itself is more stable than Gd-DTPA. The thermodynamic stability was then tested at equilibrium on solutions containing various amounts of contrast agents. The measurements were performed after the steady state was reached for each solution (24 h, 8 h and 1 h after mixing the phosphorylated metabolite solution and MS-325, (*S*)-Gd-EOB-DTPA and Gd-DTPA, respectively) (Figure 5).

Table 3. Values of τ_R, τ_{SO}, τ_V, and τ_M obtained from the fitting of the proton NMRD profiles at different temperatures (d = 0.36 nm)

T [K]	D [10^{-5} cm^{2}s^{-1}]	τ_{so} [ps][a]	τ_v [ps][a]	τ_R [ps][a]	τ_M [ns][b]
278	1.42	91 or 110	30 or 39	165 or 241	930
288	1.96	86 or 101	30 or 38	140 or 189	415
298	2.62	78 or 101	22 or 33	110 or 142	195
310	3.5	72 or 93	18 or 32	84 or 108	83
318	4.1	66 or 83	13 or 25	69 or 92	50

[a] The first values correspond to the results of the fitting performed with r set to 0.295 nm, the second ones correspond to r = 0.31 nm. – [b] These values were obtained from ^{17}O NMR spectroscopy and fixed during the proton NMRD fitting.

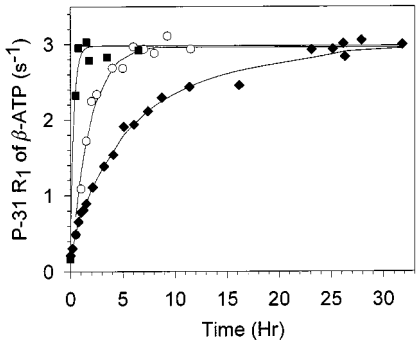


Figure 4. ^{31}P longitudinal relaxation rates of β-ATP peak in a buffered solution (Krebs–Henseleit, pH = 7.2 to 7.4) containing 20 mM of ATP, PCr, and Pi and 0.124 mM of MS-325 (closed diamonds), (*S*)-Gd-EOB-DTPA (open circles) or Gd-DTPA (closed squares) as a function of the time elapsed after addition of the contrast agent

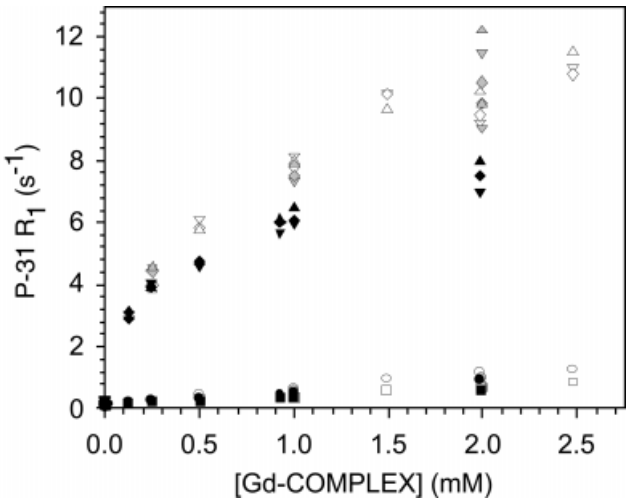


Figure 5. ^{31}P longitudinal relaxation rates of ATP, PCr, and Pi peaks in a buffered solution (Krebs-Henseleit, pH = 7.2 to 7.4) containing 20 mM of ATP, PCr, and Pi and increasing amounts of MS-325, (*S*)-Gd-EOB-DTPA or Gd-DTPA; the measurements were performed at the equilibrium of the reaction between the Gd complex and phosphorylated metabolites (24 h, 8 h or 1 h, respectively after mixing of the phosphorylated metabolites and the complex); MS-325 (black closed symbols), (*S*)-Gd-EOB-DTPA (open symbols), Gd-DTPA (gray closed symbols), Pi (circles), PCr (squares), α-ATP (reversed triangles), β-ATP (diamonds), γ-ATP (triangles)

The slightly lower P-31 relaxation rate enhancements obtained with MS-325 indicate that the concentration of the complex formed between Gd and ATP is lower. Consequently, the thermodynamic stability of MS-325 appears to be high as compared to Gd-DTPA or (*S*)-Gd-EOB-DTPA.

Transmetallation by Zn^{2+} Ions

Transmetallation of the complex by Zn^{2+} results in the release of gadolinium ions in solutions. In the presence of phosphate ions, with which they form an insoluble phosphate complex, these released lanthanide ions precipitate and no longer contribute to the proton paramagnetic relaxation rate of the solution. Consequently, the water proton relaxation rate decreases during the transmetallation process and its evolution can be used to quantitatively monitor the evolution of the system. In identical experimental conditions (B_0 = 0.47 T, T = 310 K, 2.5 mM of gadolinium complex, 2.5 mM of Zn^{2+} ions and phosphate buffer pH 7) no significant change of the paramagnetic relaxation rate was noticed for the macrocyclic gadolinium complexes Gd-DOTA and Gd-HPDO3A [{10-(2-hydroxypropyl)-1,4,7-tris(methoxycarbonyl)-1,4,7,10-tetraazacyclododecane}-gadolinium(III)] (Figure 6). This observation is in good agreement with the well-known very high kinetic and thermodynamic stabilities of these complexes.[24][25] On the contrary, R_1^P decreased to about 50% of its initial value for Gd-DTPA after 5000 minutes, showing that a significant transmetallation takes place for this open-chain gadolinium complex (Figure 6). Comparatively, the results obtained

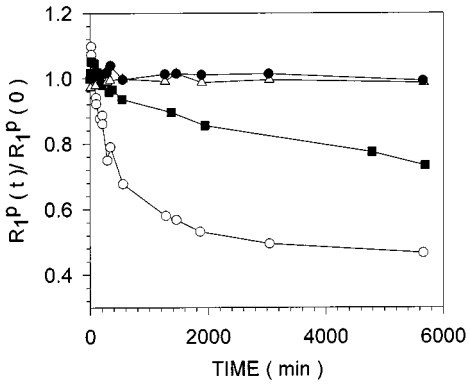


Figure 6. Time evolution of the normalized water proton paramagnetic relaxation rate (T = 310 K, ν_o = 20 MHz) in solution containing 2.5 mM of gadolinium complex and 2.5 mM of Zn^{2+} (MS-325: closed squares, Gd-DTPA: open circles, Gd-HPDO3A: closed circles, Gd-DOTA: open triangles)

with MS-325 indicate a relatively slower and limited evolution of the proton paramagnetic longitudinal relaxation rate (about 75% of its initial value after 5000 minutes).

These results demonstrate that MS-325 is more stable towards transmetallation by Zn^{II} than Gd-DTPA.

Serum and Other Protein-Containing Solutions

The high "apparent" proton relaxivity of MS-325 in serum has been related to its binding to serum proteins as studied by ultrafiltration methods.[3][6] Binding to macromolecules results in a significant τ_R increase which in turn usually induces a hump in the high field part of the ^1H NMRD profile. The NMRD profiles recorded in a reconstituted lyophylized serum (Kontrollogen) or in human serum albumin (HSA) are characteristic of such interactions with macromolecules (Figure 7).

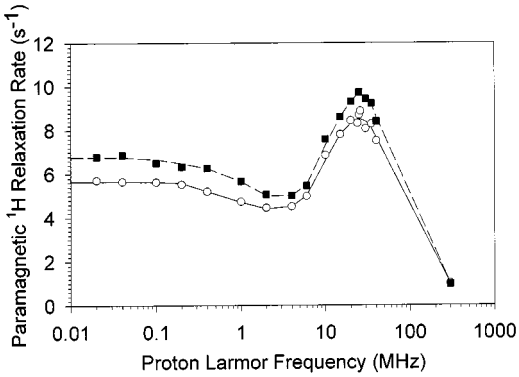


Figure 7. Proton paramagnetic relaxation rate of solutions containing 0.25 mM of MS-325 and 4% of HSA (open circles) or serum Kontrollogen (closed squares) at 310 K

The non-linear increase of the proton paramagnetic relaxation rate measured at 20 MHz on solutions containing 4% of HSA ([HSA] = $p°$ = 0.6 mM) and various concentrations of MS-325 ($s°$ = 0−2.08 mM) (Figure 8) agrees with a strong binding. At this magnetic field, the paramagnetic relaxation rate of a solution containing 1 mM of MS-325 and 4% of HSA is 4.6 times larger than in pure water.

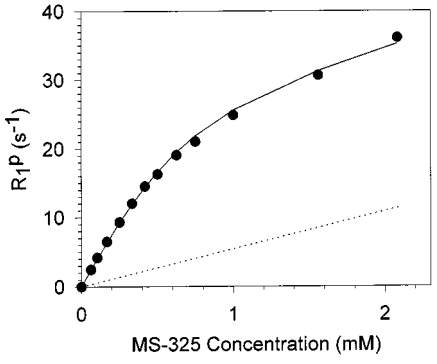


Figure 8. Proton longitudinal paramagnetic relaxation rate in solutions containing 4% of HSA and increasing amounts of MS-325 (closed circles) (ν_o = 20 MHz, T = 310 K); the plain line corresponds to the fitting of the data and the dashed line represents R_1^P in a water solution free of albumin

The "apparent" relaxivity calculated for each MS-325 concentration decreases from about 40 $s^{-1}mM^{-1}$ at low concentrations to 17 $s^{-1}mM^{-1}$ for the maximum concentration of 2.08 mM. Fitting of the data according to Equation 1 provides, on the one hand, an estimation of the association constant (Ka) characterizing the interaction between HSA and MS-325 and, on the other hand, a value of the relaxivity of the noncovalently bound complex (r_1^c). The relaxivity of the free contrast agent is r_1^f. The fitted Ka and r_1^c values are 6100±2130 M^{-1} and 48.9±3.5 $s^{-1}mM^{-1}$, respectively [the number of equivalent and independent interaction sites (N) was set to 1]. Consequently, in solutions containing 4% of HSA and less than 0.3 mM of MS-325, more than 70% of MS-325 interacts with the protein. These results are in good agreement with the ultrafiltration data of Lauffer et al. who reported that the association constant of the strongest site(s) is in the order of 10^4 M^{-1}.[6]

In the experimental conditions of the NMRD study (Figure 7, 0.25 mm of MS-325 and 4% of HSA), 0.18 mM of MS-325 are bound to the protein. The proton paramagnetic relaxation rate profiles (Figure 7) thus represent the combined contributions of the free and the bound Gd complex. Knowing the proton NMRD profile of the free MS-325 as well as the concentration of free and bound Gd complex obtained from the equilibrium study (see above), the proton NMRD profile of the HSA-MS-325 complex can be calculated (Figure 9).

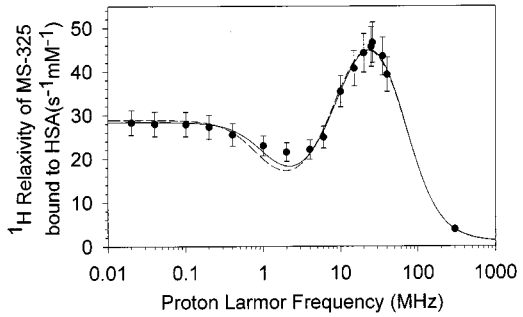


Figure 9. Calculated theoretical ^1H NMRD profile of the complex HSA-MS-325 at 310 K (closed circles) and its fittings (plain line: r = 0.295 nm, dashed line: r = 0.31 nm)

The fitting of this profile was then performed using the equations usually adopted for the description of small gadolinium complexes in aqueous solutions for the two distances r used previously (see Experimental Section). These equations, however, are known to be unappropriate to describe the low field range of the profile for slow-rotating systems, especially regarding the electron spin system.[26] Depending on the distance r used for the fittings, the values of τ_V and τ_{SO} are 38 or 41 ps and 287 or 351 ps. These values are thus recognized as inaccurate but the values of τ_R (3.3 or 4.4 ns), which are mainly determined from the high field range, are acceptable. In separate experiments run on the deuterated lanthanum analog of MS-325, the increase of the deuterium linewidths measured in solutions containing 4% of HSA and decreasing concentrations of the complex was analyzed as described in reference 9. The fitted value of K_a and R_2 of the complex (R_2^c) were 5590

M^{-1} and 1210 s^{-1} respectively. This R_2^c value corresponds to a τ_R of the order of 6 to 7 ns. All these values of τ_R are lower than the value of 14 ns calculated for HSA at 310 K using Stokes's law.[27] This difference indicates that the mobility of the paramagnetic center is higher than expected for a complex fully immobilized on the surface of the protein and agrees with the picture of the ligand interacting with the protein through the [(4,4-diphenylcyclohexyl)phosphonooxymethyl] chain and leaving some mobility freedom to the rest of the bound molecule. The longer τ_M obtained by the fitting (171 or 252 ns as compared to 83±13 ns in aqueous solution free of protein) might result from interactions at the surface of the protein, although this hypothesis seems to be contradicted by the previous discussion about molecular mobility.

In serum Kontrollogen, the paramagnetic relaxation rates are slightly higher than in albumin solution (Figure 7). For other paramagnetic complexes like Gd-DTPA, Gd-DOTA, or Gd-HPDO3A which do not interact with blood macromolecules, 10 to 25% higher water proton relaxation rates were also observed in serum as compared to HSA solutions (unpublished data). This can be explained by the higher viscosity of serum as compared to a 4% HSA solution (at 310 K, the viscosity of serum Kontrollogen is equal to 1.18 cp as compared to 0.84 cp for a 4% HSA solution). From the above, it is thus clear that the increase of the paramagnetic relaxation rate in serum mostly results from the noncovalent interaction of MS-325 with albumin. These results are in good agreement with the high performance liquid chromatography experiments of Lauffer et al.[6]

Conclusion

The multinuclear magnetic resonance approach used in this work shows that, compared to its parent compound Gd-DTPA, MS-325 exhibits a higher proton relaxivity which can be attributed to a slower tumbling resulting from a higher molecular weight and possibly to an apparently shorter mean distance between the hydrogen atoms of the water molecules and the gadolinium ions. The exchange time of the coordinated water molecule τ_M does not limit the proton relaxivity as demonstrated by the ^{17}O and proton relaxometric studies performed between 278 to 318 K.

In solutions containing ATP, a partial decomplexation of MS-325 occurs but the rate and the extent of this process are smaller than for the parent compound. The kinetic and the thermodynamic stabilities of this C-substituted derivative are thus increased. Similarly, the transmetallation process by Zn^{2+} ions is reduced as compared to Gd-DTPA. These results confirm a previously reported hypothesis regarding the favorable role of C-substitution.[9]

The proton relaxometric study of the noncovalent interaction with serum proteins, and more particularly with HSA, shows that the association constant characterizing the equilibrium between HSA and MS-325 is about 6100±2130 M^{-1} for a number of interaction sites equal to 1. As shown by the parameters calculated from the ^1H and ^2H relaxometry data, the paramagnetic center of the noncovalently bound complex is not fully immobilized at the surface of the protein and consequently does not develop the maximum relaxivity allowed by the rate of the water exchange. If the paramagnetic complex would experience the rotational correlation time of albumin (τ_R = 14 ns[27]), its relaxivity calculated with the parameters reported above should be maximal around 20−25 MHz and reach 59 $s^{-1}mM^{-1}$.

Experimental Section

General: MS-325 was synthesized as described by McMurry et al.[2] and Sajiki et al.[28] − Gd-DTPA (Magnevist®) was provided by Schering AG (Berlin, Germany), Gd-DOTA (Dotarem®) by Guerbet (Aulnay-sous-Bois, France), Gd-HPDO3A (ProHance®) by Bracco (Milano, Italy), and (*S*)-Gd-EOB-DTPA (Eovist®) by Schering AG (Berlin, Germany). D_2O (99.9%) was obtained from Aldrich (Bornem, Belgium), serum (Kontrollogen L) from Behring (Marburg, Germany), and nondefatted human albumin (fraction V) from Sigma (Bornem, Belgium). ATP disodium salt (Janssen Chimica, Geel, Belgium), phosphocreatine disodium salt (Sigma, Bornem, Belgium), Na_2HPO_4 (Merck, Overijse, Belgium), and NaN_3 (Aldrich, Bornem, Belgium) were used for ^{31}P NMR measurements. Phosphate buffer pH 7 (Merck, Overijse, Belgium) and $ZnCl_2$ (Fluka, Bornem, Belgium) were used for the transmetallation studies. − The lanthanum complex was synthesized by reaction of La_2O_3 with the ligand in water and was precipitated by addition of acetone. Deuteration of the lanthanum complex at the α position of the carboxylic groups was performed by the procedure described by Wheeler and Legg:[29] 200 mg of lanthanum complex were dissolved in 20 mL of D_2O, the pD was adjusted to 10.6 by addition of K_2CO_3 and the mixture was heated at reflux with stirring for 24 h. The pD was then adjusted to 7 with concentrated hydrochloric acid, the solution was evaporated to a final volume of 10 mL and the solid KCl was removed by filtration. Acetone was added to induce precipitation of the deuterated compound, which was isolated by filtration, dissolved in 10 mL of H_2O, dialyzed, and isolated after lyophilization. The deuteration was confirmed by ^1H-NMR spectroscopy. The sodium and potassium contents were controlled by ion-selective electrodes. The final product was labelled with 10 deuterium atoms and contained 2 Na^+ and 1 K^+ counterions. − ^1H NMR (D_2O): La-complex: δ = 7.5−7.15 (10 H); 4.3−1.7 (29 H); La-deuterated complex: δ = 7.5−7.15 (10 H); 4.3−1.7 (19 H)

NMR Spectroscopy: Proton Nuclear Magnetic Relaxation Dispersion (NMRD) profiles were recorded on a Field Cycling Relaxometer (Field Cycling Systems, Oradell, New Jersey, USA) working between 0.24 mT and 1.2 T. The samples (0.6 mL) were contained in 10 mm o.d. tubes. Proton relaxation rates were also measured at 0.47 T on a Minispec PC-20 (Bruker, Karlsruhe, Germany). The temperature was controlled by a perchlorinated liquid flow. T_1 shorter than 50 ms were measured on this system using a specially-designed pulse sequence to overcome the limitations of the standard Minispec microprocessor. The data points were then fitted with a three-parameter minimization routine. The additional relaxation rates at 7.05 T were obtained on a Bruker AMX-300 (Bruker, Karlsruhe, Germany) spectrometer. − ^1H NMRD curves were fitted according to the theoretical innersphere model described by Solomon[17] and Bloembergen[18] and to the outersphere contribution described by Freed.[19] Calculations were performed with previously described software.[30][31] − The proton data ob-

$$R_1^{p\,obs} = 1000 \times \left\{ \left(r_1^{f} \times s^\circ \right) + \frac{1}{2}\left(r_1^{c} - r_1^{f} \right) \left(\left(N \times p^\circ \right) + s^\circ + Ka^{-1} - \sqrt{\left(\left(N \times p^\circ \right) + s^\circ + Ka^{-1} \right)^2 - 4 \times N \times s^\circ \times p^\circ} \right) \right\} \quad (1)$$

tained in HSA solution were fitted using Equation 1,[32] where *Ka* is the association constant, p° is the protein concentration, s° is the concentration of the paramagnetic complex, *N* is the number of independent interaction sites, and r_1^c and r_1^f are the relaxivities of the complex HSA-contrast agent and of the free contrast agent, respectively.

^{31}P-NMR T_1 measurements were performed on 2 mL samples contained in 10 mm o.d. tubes on a Bruker MSL-200-15 spectrometer (Bruker, Karlsruhe, Germany) fitted with a broadband probe. The temperature was regulated by air or nitrogen flow controlled by a BVT 1000 unit. The solutions contained 20 mM of ATP, phosphocreatine (PCr) and inorganic phosphate (Pi) dissolved in Krebs Henseleit buffer (pH = 7.2−7.4) with 2 mM of NaN_3 added to prevent degradation of ATP and PCr by bacteria. The 90° and 180° pulse lengths were 7 μs and 14 μs, respectively. − Transmetallation by Zn^{II} ions was evaluated by the decrease of the water proton longitudinal relaxation rate at 310 K and 20 MHz (Bruker Minispec PC 20) of buffered solutions (pH 7, phosphate buffer) containing 2.5 mM of the gadolinium complex and 2.5 mM of Zn^{II}. − ^{17}O- and ^{2}H-NMR spectra were recorded on 2 mL samples (10 mm o.d. tubes) on a Bruker AMX-300 spectrometer (Bruker, Karlsruhe, Germany) using a broadband probe and a Bruker BVT-2000 unit for temperature control. ^{17}O transverse relaxation times of distilled water (pH = 6.5) were measured using a CPMG sequence and a subsequent two-parameter fit of the data points. The 90° and 180° pulse lengths were 25 μs and 50 μs, respectively. ^{17}O T_2 of water in MS-325 solution ([MS-325] = 12.5 mM, pH = 6.0−7.0) was obtained from linewidth measurement. Checks were performed so that for this paramagnetic solution, the T_2 obtained from linewidth measurement and from CPMG sequence were similar. All ^{17}O spectra were proton decoupled. The concentration of MS-325 was 12.5 mM. The analysis of the ^{17}O and ^{2}H data is described elsewhere.[9] − All T_1 measurements at 4.7 T and 7.05 T (^{1}H, ^{2}H, ^{31}P) were performed with the inversion recovery or fast inversion recovery Fourier transform technique and a subsequent three-parameter fit of the peak heights.

Acknowledgments

The authors thank Mrs Patricia de Francisco for her help in preparing the manuscript. This work was supported by the ARC Program 95/00-194 of the French Community of Belgium, the Biomed II MACE Program of the Commission of the European Communities (contract BMH4-CT-96-0051; DG12-SSMA) and the Fonds National de la Recherche Scientifique (FNRS) of Belgium.

[1] R. B. Lauffer, D. J. Parmelee, H. S. Ouellet, R. P. Dolan, H. Sajiki, D. M. Scott, P. J. Bernard, E. M. Buchanan, K. Y. Ong, Z. Tyeklar, K. S. Midelfort, T. J. Mc Murry, R. C. Walovitch, *Acad. Radiol.* **1996**, *3*, S356−S358.
[2] T. J. Mc Murry, H. Sajiki, D. M. Scott, R. B. Lauffer, *US Patent WO 96/23526.*
[3] D. J. Parmelee, R. C. Walovitch, H. S. Ouellet, R. B. Lauffer, *Invest. Radiol.* **1997**, *32*, 741−747.
[4] W. Lin, D. R. Abendschein, E. M. Haacke, *J. Magn. Reson. Imaging* **1997**, *7,* 183−190.
[5] W. Lin, D. R. Abendschein, A. Celik, R. P. Dolan, R. B. Lauffer, R. C. Walovitch, E. M. Haacke, *J. Magn. Reson. Imaging* **1997**, *7*, 963−971.
[6] R. B. Lauffer, D. J. Parmelee, S. U. Dunham, H. S. Ouellet, R. P. Dolan, S. Witte, T. J. McMurry, R. C. Walovitch, *Radiology* **1998**, *207*, 529−538.
[7] T. M. Grist, F. R. Korosec, D. C. Peters, S. Witte, R. C. Walowitch, R. P. Dolan, W. E. Bridson, E. K. Yucel, C. A. Mistretta, *Radiology* **1998**, *207*, 539−544.
[8] P. V. Prasad, J. Cannillo, D. R. Chavez, W. Li, E. S. Pinchasin, R. P. Dolan, R. Walovitch, R. R. Edelman, *Acad. Radiol.* **1998**, *5*, S219−222.
[9] L. Vander Elst, F. Maton, S. Laurent, F. Seghi, F. Chapelle, R. N. Muller, *Magn. Reson. Med.* **1997**, *38*, 604−614.
[10] K. Micskei, L. Helm, E. Brücher, A. E. Merbach, *Inorg. Chem.* **1993**, *32*, 3844−3850.
[11] S. Laurent, L. Vander Elst, S. Houzé, N. Guérit, R. N. Muller, manuscript in preparation.
[12] D. H. Powell, O. M. Ni Dhubhghaill, D. Pubanz, L. Helm, Y. S. Lebedev, W. Schlaepfer, A. E. Merbach, *J. Am. Chem. Soc.* **1996**, *118*, 9333−9346.
[13] F. Maton, Ph.D. Dissertation, Univ. of Mons-Hainaut, Belgium **1993**.
[14] S. Aime, M. Botta, M. Fasano, S. Paoletti, P. L. Anelli, F. Uggeri, M. Virtuani, *Inorg. Chem.* **1994**, *33*, 4707−4711.
[15] S. Aime, M. Botta, M. Fasano, S. Paoletti, C.Terreno, *Chem. Eur. J.* **1997**, *3*, 1499−1504.
[16] S. H. Koenig, R. D. Brown, III, in *NMR Spectroscopy of Cells and Organisms* (Ed.: R.K. Gupta), CRC Press, Boca Raton, **1987**, vol II, p 75−114.
[17] I. Solomon, *Phys. Rev.* **1955**, *99*, 559−565.
[18] N. Bloembergen, *J. Chem. Phys.* **1957**, *27*, 572−573.
[19] J. H. Freed, *J. Chem. Phys.* **1978**, *68*, 4034−4037.
[20] H. R. Pruppacher, *J. Chem. Phys.* **1972**, *56*, 101−107.
[21] F. Uggeri, S. Aime, P. L. Anelli, M. Botta, M. Brocchetta, C. de Haën, G. Ermondi, M. Grandi, P. Paoli, *Inorg. Chem.* **1995**, *34,* 633−642.
[22] L. Vander Elst, Y. Van Haverbeke, J.-F. Goudemant, R. N. Muller, *Magn. Reson. Med.* **1994**, *31*, 437−444.
[23] L. Vander Elst, R. N. Muller, *Inorg. Chim. Acta* **1998**, *273*, 92−100.
[24] X. Wang, T. Jin, V. Comblin, A. Lopez-Mut, E. Merciny, J. F. Desreux, *Inorg. Chem.* **1992**, *31,* 1095−1099.
[25] M. F. Tweedle, J. J. Hagan, K. Kumar, S. Mantha, C.A. Chang, *Magn. Reson. Imaging* **1991**, *9*, 409−415.
[26] I. Bertini, O. Galas, C. Luchinat, G. Parigi, *J. Magn. Reson. Ser. A* **1995**, *113*, 151−158.
[27] H. F. Bennett, R. D. Brown III, S. H. Koenig, H. M. Swartz, *Magn. Reson. Med.* **1987**, *4*, 93−111.
[28] H. Sajiki, K. Y. Ong, S. T. Nadler, H. E. Wages, T. J. McMurry, *Synth. Commun.* **1996**, *26*, 2511−2522.
[29] W. D. Wheeler, J. I. Legg, *Inorg. Chem.* **1985**, *24*, 1292.
[30] R. N. Muller, D. Declercq, P. Vallet, F. Giberto, B. Daminet, H. W. Fischer, F. Maton, Y. Van Haverbeke, Proc., ESMRMB, 7th Annual Congress, Strasbourg, France, **1990**, p. 394.
[31] P. Vallet, Ph. D. Dissertation, Univ. of Mons-Hainaut, Belgium **1992**.
[32] L. Vander Elst, S. Laurent, F. Botteman, R. N. Muller, *Magn. Reson. Materials Phys. Biol. Med.* **1998**, *6 (suppl 1)*, 84.

Received April 29, 1999
[I99150]

The Interpretation of the Terminal ν(CO) Spectra of Some Tetranuclear Carbonyl Clusters

Sidney F. A. Kettle,*[a] Eliano Diana,[b] Enrico Boccaleri,[b] and Pier Luigi Stanghellini*[c]

Keywords: Cluster compounds / Vibrational spectroscopy / Spherical harmonics / Carbonyl complexes

The recently suggested spherical (SHM) and tensor (THM) harmonic models are applied to the interpretation of the terminal ν(CO) spectra of twenty six tetrahedral transition metal clusters containing between four and twelve terminal carbonyl groups. Although the SHM is perhaps the more generally relevant, there are species for which the THM is appropriate as a first approximation. The distinction between the two appears to be associated with a disruption of the band structure of the cluster either by the introduction of heterometal atoms or by the presence of a group – acetate ester, halide or hydride – presumably acting as an electronegative substituent.

Introduction

In a recent communication we explored the application of a novel, spherical harmonic, model (SHM) to the interpretation of the terminal ν(CO) vibrational spectra of transition metal cluster carbonyls.[1] The model, which in its simplest form ignores the cluster structure and geometry, was found to be of general applicability. It is the only extant model which successfully explains how a large, low-symmetry molecule with a large number of terminal CO groups can show only a single peak in the solution infrared. The model in its simplest form carries out a spherical harmonic expansion of the ν(CO) modes, considering the CO groups as radially attached to the spherical cluster surface. The spherical harmonic analysis of the vibrational problem shows that, of the harmonic subtended (S + P + D + F +....), only the P mode is infrared active and only the S and D modes are Raman active. So the simple model predicts two Raman bands, noncoincident with the single infrared. When the model is extended to take account of the molecular symmetry, splitting of the single degenerate feature is expected, together with intensity transfer between the spherical harmonic descendants of the same symmetry. More complex spectra can arise, yet there are very few clusters containing a three-dimensional array of metal atoms for which the SHM fails to give a convincing spectral interpretation.[2]

A limited group of clusters, all with a tetrahedral metal core, was found to exhibit a different spectral pattern. This pattern was susceptible to interpretation by a tensor harmonic formalism (the tensor harmonic model, THM), which requires the introduction of strong tangential (to the surface of the sphere) dipolar-active modes. This model predicts several strong and well-separated peaks. This point is illustrated in Figure 1, where we give the expected qualitative diagrammatic spectra for C_{3v} tetranuclear clusters with nine terminal CO groups (the most common structure − vide infra), following the SHM or THM, respectively.

The two models can be related to the recently proposed "metal cluster selection rule",[3] which is a cluster-equivalent to the well-known "surface selection rule" of metals.[4] A dipole moment change in an adsorbed molecule (or in a CO bonded to a cluster) induces an image dipole moment change in the metal bulk (or in the metal cluster). The dipole moment changes perpendicular to the metal surface reinforce and those parallel to it cancel, leading to the rule "only dipole moment changes perpendicular to the surface are spectrally dipole active". The clusters following the SHM are able to sustain image dipole and so behave as metals. The clusters following the THM are not able to do this and so approximate to insulators.

Some tetrahedral clusters required the SHM for the interpretation of their spectra and others the THM. Those that required the latter model were those in which the metal atoms were separated by electronegative bridging ligands.[5] The interpretation placed on this observation is that the presence of these ligands gave clusters which lacked the transition-dipole induced metallic conductivity. However, it was recognised that the matter was not so simple: "...it can be a delicate matter. So, although a sulfur bridged Re_4 species is [one that follows the THM] the reported data indicate that corresponding iron compound [does not]".[2] Related to this is the fact that it appears to be the case that it is only for tetrahedral species that the duality of model applicability occurs with such clarity. In that the tetrahedron is the simplest of all three-dimensional arrangements of metal atoms, this itself is perhaps not too surprising − the larger the metal cluster the more applicable the SHM, or so it seems.

Given the "delicate" nature of the choice of applicability of the SHM or the THM to tetrahedral clusters we felt the matter worthy of a more detailed study. All the evidence indicates that, in reality, there is continuity between the SHM and the THM, an aspect which, as the above dis-

[a] School of Chemical Sciences, University of East Anglia, Norwich NR4 7TJ, Great Britain
[b] Dipartimento di Chimica IFM, Università di Torino, via Pietro Giuria 7, I-10125 Torino, Italy
[c] Dipartimento di Scienze e Tecnologie avanzate, Università del Piemonte Orientale "A. Avogadro", Corso T. Borsalino 54, I-15100 Alessandria, Italy

 © WILEY-VCH Verlag GmbH, D-69451 Weinheim, 1999 1434−1948/99/1111−1957 $ 17.50+.50/0

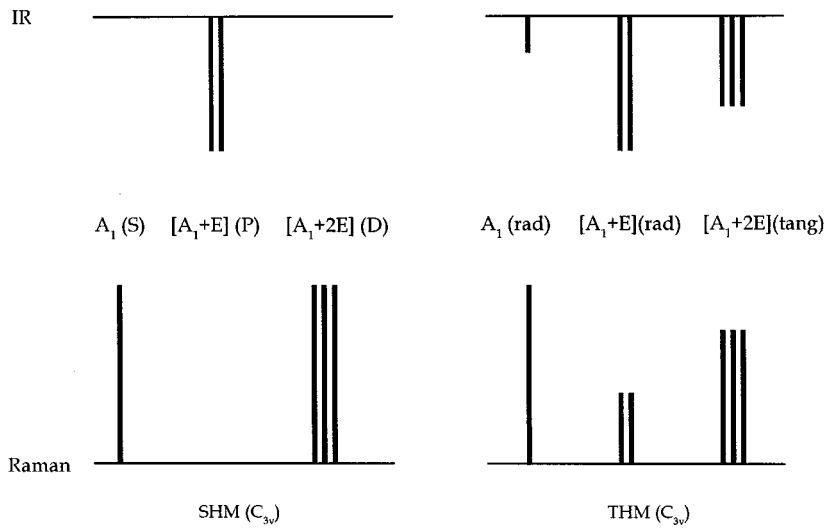


Figure 1. Schematic representation of the prediction of the SHM and of the THM for a $M_4(CO)_9$ system in C_{3v} symmetry; the order of the splitting within any one harmonic is molecule-dependent and so no indication of relative intensities within a set is given

cussion shows, seems particularly important for tetrahedral clusters. What of tetrahedral clusters which have no electronegative bridge atoms? Is there evidence that they may show at least putative THM behaviour? The present work is devoted to a study of this question and does so by a review of the infrared and, wherever data are available, the Raman spectra of some tetrahedral transition metal cluster carbonyls.

Results

Table 1 details the tetrahedral metal carbonyl clusters that we have reviewed. They were selected from those references that include figures which show the infrared spectra and do not merely give frequency data.

The Raman spectra were recorded by us whenever possible. It is convenient to start by a study of the spectra of

Table 1. The spectral behaviour of the (CO) features of some tetrahedral metal carbonyl clusters

N[a]	Complex	Symmetry[b]		P splitting[c] (cm^{-1})	Vibr. Model	Spectra	
		CO′s	molecule			infrared	Raman
1a	$Co_4(CO)_{12}$	C_{3v}	C_{3v}	8	SHM	this paper and ref.[6]	this paper
1b	$Rh_4(CO)_{12}$	C_{3v}	C_{3v}	5	SHM	this paper and ref.[6]	this paper
1c	$Co_3FeH(CO)_{12}$	C_{3v}	C_{3v}	9	borderline	this paper and ref.[6]	this paper
1d	$[Fe_3RhH(CO)_{12}]^{2-}$	C_{3v}	C_s	22	THM	this paper and ref.[7]	this paper
1e	$[Fe_2Ir_2(CO)_{12}]^{2-}$	C_{3v}	C_s	ca. 28	THM	ref.[8]	ref.[9]
1f	$[FeIr_3(CO)_{12}]^-$	C_{3v}	C_s	ca. 35	THM	ref.[8]	ref.[9]
1g	$[Fe_2Ir_2(CO)_{12}AuPPh_3]^-$	C_{3v}	C_s	35	THM	this paper and ref.[8]	this paper
1h	$[Ir_4(CO)_{11}H]^-$	C_{3v}	C_s	10	SHM	ref.[10]	n.a.
1i	$[Ru_2Rh_2(CO)_{12}H]^-$	C_{3v}	C_s	20	borderline	ref.[11]	n.a.
1j	$Co_3Rh(CO)_{12}$	C_{3v}	C_s	ca. 10	SHM	ref.[12]	n.a.
1k	$Rh_3Ir(CO)_{12}$	C_{3v}	C_{3v}	3	SHM	ref.[12]	n.a.
1l	$Co_2Rh_2(CO)_{12}$	C_{3v}	C_s	15	borderline	ref.[12]	n.a.
1m	$Rh_2Ir_2(CO)_{12}$	C_{3v}	C_s	0	SHM	ref.[12]	n.a.
1n	$Co_2Ir_2(CO)_{12}$	C_{3v}	C_s	17	borderline	ref.[12][13]	n.a.
2a	$Co_4(CO)_{11}PPh_3$	C_s	C_s	ca. 15	SHM	this paper and ref.[14]	this paper
2b	$[Ir_4(CO)_{11}COOMe]^-$	C_s	C_s	ca. 30	THM	ref.[15]	n.a.
2c	$[Co_4(CO)_{11}COOMe]^-$	C_s	C_s	20	borderline	ref.[16][17]	n.a.
2d	$[Rh_4(CO)_{11}COOMe]^-$	C_s	C_s	35	THM	ref.[16][17]	n.a.
2e	$[Co_4(CO)_{11}I]^-$	C_s	C_s	20	borderline	ref.[17][18]	n.a.
3a	$[Rh_3Ru(CO)_{12}]^{2-}$	C_s	C_s	ca. 20	borderline	ref.[19]	n.a.
3b	$[Ir_4(CO)_{10}H_2]^{2-}$	C_s	C_s	20	borderline	ref.[20]	n.a.
3c	$[Ru_2Rh_2(CO)_{12}]^{2-}$	C_s	C_s	ca. 30	THM	ref.[11]	n.a.
3d	$[Ru_2Rh_2(CO)_{12}AuPPh_3]^-$	C_s	C_s	18	borderline	ref.[11]	n.a.
4a	$[RhRu_3(CO)_{13}]^-$	C_3	C_3	0	SHM	ref.[19]	n.a.
5a	$Ir_4(CO)_{12}$	T_d	T_d	0	SHM	ref.[21]	ref.[22]
6a	$[Rh_4(CO)_{12}]^-$	C_s	C_s	0	SHM	ref.[16]	n.a.

[a] The numbers refer to the number and to the arrangement of the terminal CO′s, irrespective of the presence of bridging CO′s, other ligands or different metal atoms; **1**: (9 CO′s), $[M(CO)_3][M(CO)_2]_3$; **2**: (8 CO′s), $[M(CO)_3][M(CO)_2]_2[M(CO)]$ (**2e** is $[M(CO)_2]_4$); **3**: (7 CO′s), $[M(CO)_3][M(CO)_2][M(CO)]_2$; **4**: (10 CO′s), $[M(CO)_3]_3[M(CO)]$; **5**: (12 CO′s), $[M(CO)_3]_4$; **6**: (4 CO′s), $[M(CO)]_4$. – [b] The symmetry relates to the terminal CO groups and to the whole molecule, respectively. – [c] Applicable as a first approximation.

three structurally closely related species, **1a, 1b** and **1c**, all of C_{3v} symmetry, symmetry shared, of course, by the arrangement of the terminal CO groups. The group-theoretically predicted features are $3A_1 + 3E$, all modes being both infrared and Raman active. Their infrared and Raman spectra are shown in Figures 2, 3 and 4.

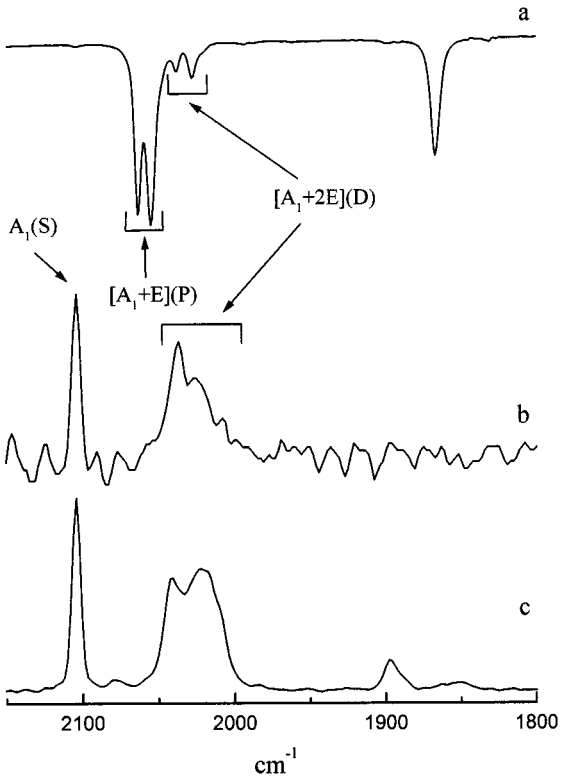


Figure 2. Solution infrared (a) and Raman (b: solution; c: crystals) spectra in the CO stretching region; complex: $Co_4(CO)_{12}$ (**1a**); solvents: (a) *n*-hexane, (b) CCl_4.

In these figures we also give the Raman spectra of crystalline samples; comparison of these with those from solutions gives confidence that the Raman spectrum of a crystalline compound, where this is the only one available, is not far removed from that of the dissolved species. All species show a high frequency A_1 mode, strong in the Raman spectrum and weak but coincident in the infrared spectrum; we shall have little to say concerning this mode beyond noting that it is the S mode of the SHM.

The complex $Co_4(CO)_{12}$ provides a good starting point for the study of the other modes because its spectra conform to the SHM predictions rather well. Consider the infrared spectrum, with two intense peaks, one approximately twice the intensity of the other, separated by ca. 8 cm^{-1}. Assignment as an $A_1 + E$ splitting of the P mode of the SHM by the molecular C_{3v} symmetry is clear. Equally clear is that very little mixing occurs between functions originating in the P and D harmonics; the $2E + A_1$ peaks at lower frequency, D in origin, are relatively weak in the infrared. The absence of any significant Raman intensity at the positions of the two strong infrared peaks is in accordance with the occurrence of little mixing. Conversely, the Raman D-originating peaks are split into a strong Raman peak, corre-

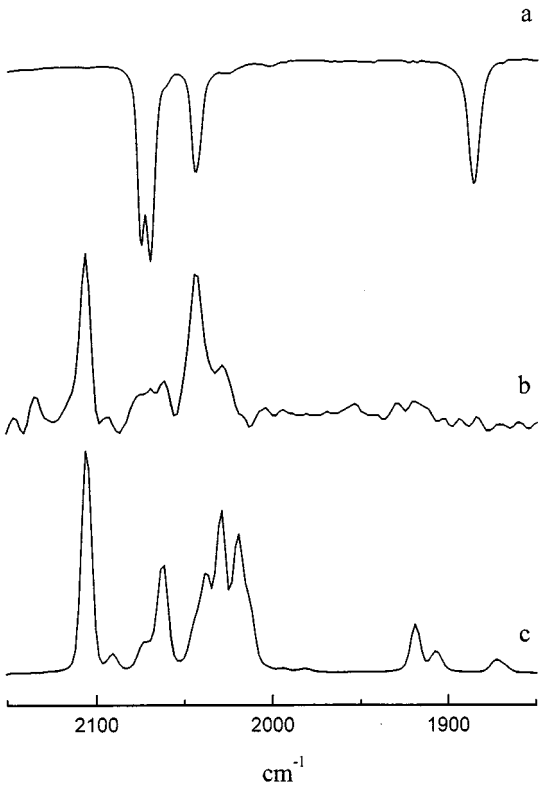


Figure 3. (see Figure 2); complex: $Rh_4(CO)_{12}$ (**1b**); solvents: (a) *n*-hexane, (b) CCl_4.

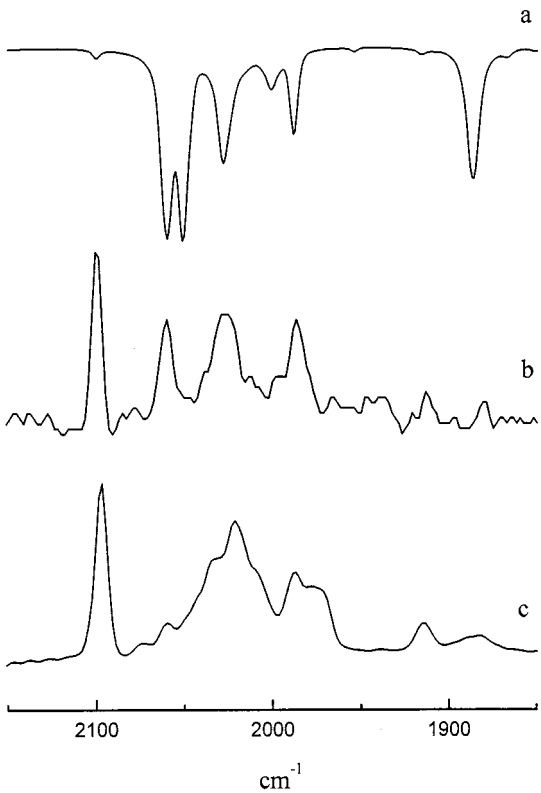


Figure 4. (see Figure 2); complex: $Co_3FeH(CO)_{12}$ (**1c**); solvents: (a) *n*-hexane, (b) CCl_4.

sponding to a weak infrared band, and a medium-broad peak largely coincident with another weak infrared absorption. There is another very weak and broad infrared peak at longest wavelength. As we shall see, a consistent pattern emerges if it is the lower frequency E modes which are most effective at stealing infrared intensity from the higher E mode. The Raman intensities, therefore, suggest that the assignment of these three infrared peaks is E, E and A_1 in that order, rather than E, A_1, E as previously suggested on the basis of the infrared spectrum alone.[4] The general explanation of the spectra seems clear, as is the conclusion arising from them: the SHM provides a convincing interpretation of the vibrational spectra. With this interpretation established, that of **1b** is also clear; it is basically the same. However, there is one significant difference: although the splitting of the individual spherical harmonics is less, the mixing between P and D functions is greater. The evidence for this assertion is that in the infrared the higher of the two E (D) is (relatively) stronger than in the cobalt species. Conversely, and as required by the SHM, the Raman E (P) is (relatively) stronger than in **1a** (the solid state spectra help to remove any ambiguity on this point). The spectra of **1c**, although significantly different, are related to the pattern set by **1a** and **1b**. However, the splitting of the (infrared active) P mode seems reversed. The E mode infrared intensity is distributed amongst all of the infrared-active E modes so that the E (P) is now weakened such that it is of about the same intensity as the A_1 (P), a considerable intensity having been transferred to both of the E (D) s, this transfer serving to identify them. The A_1/E (P) interchange is indicated by the infrared-Raman coincidence, which for this species occurs for the higher frequency P-derived mode (cf. **1b**). The infrared intensities indicate clearly that the zeroth-order SHM functions are significantly mixed in this species. The Raman is in complete agreement with this, the correspondences being just those expected. However, the reversed pattern of splitting in the P mode of the SHM (and, probably, changes in the D mode splitting too, vide infra), show that the substitution of a Co by FeH has had a significant disruptive effect and induced a significant move towards THM behaviour. A limiting THM behaviour would be characterised by an A_1 (S) and [A_1 + E](P) splitting of the radial modes and a [A_1 + 2E] splitting of the tangential modes. In particular, the tangential modes will have significant infrared intensity, a feature that serves to characterise the THM; it is to be noted that a P mode splitting occurs in both the SHM and the THM, although it seems to be larger in the latter.

In summary, through the series **1a**−**c** we see a progression from almost pure SHM behaviour through to something that shows characteristics which surely indicate a transition to something closer to the THM limit. For this reason we do not regard the evident E, A_1, E splitting of the lower infrared set in **1c** as requiring the same pattern for **1a**.

The effect of metal-atom substitution in tetrahedral clusters can be further explored in the complex **1d**. It has a (solid state) Raman spectrum which very closely resembles that of **1b** and which surely must be interpreted similarly (Figure 5).

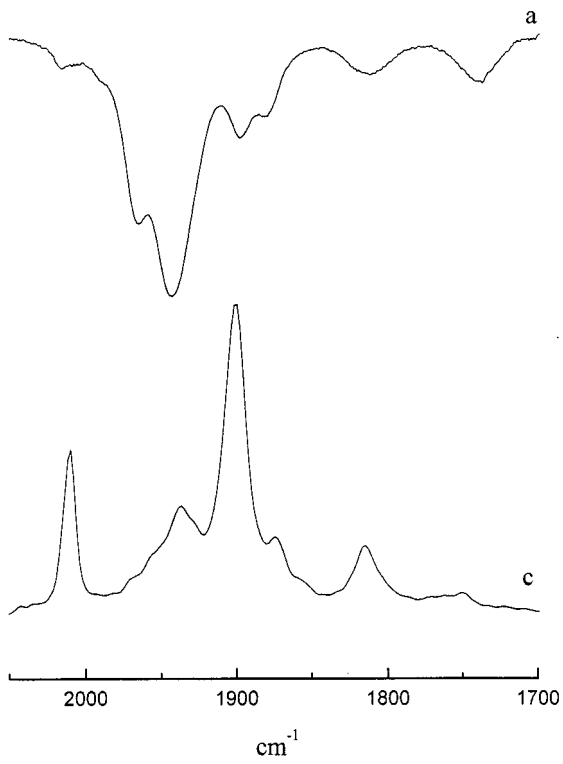


Figure 5. (see Figure 2); complex: $[Fe_3RhH(CO)_{12}]^{2-}$ (**1d**); solvents: (a) CH_3CN.

The intermolecular CO coupling (factor group effects) in anionic metal carbonyl clusters is minimised by the dilution effect caused by the presence of a large counterion. This is relevant to complex **1d** which has C_s symmetry, as the rhodium atom lies in the basal triangle.[7] Notwithstanding its lower symmetry and the presence of a "hetero" metal atom, the similarity of its spectra with those of **1b** is remarkable. As we have pointed out, such an indifference to metal atom heterogeneity is not unusual in clusters and the fact that the indifference is implicit within the SHM has been claimed[2] as a strength of the model. Other complexes sustain this assessment. Consider the pair **1e** and **1f**, whose spectra have already been reported.[8] The similarity of the spectra of **1e** with those of the C_{3v} complexes is clearly evident. The spectra of **1f** suffer from the poor quality of the Raman spectrum and of the broadness of the infrared; however, the patterns seem similar and so too, presumably, are the explanations. Moreover, the complex **1g**, structurally derived from **1e** with an $AuPPh_3$ unit bridging the basal $FeIr_2$ triangle,[8] does not show any significant changes in the spectra (Figure 6) − the splitting of the P and D modes is simply more evident.

Finally, we have considered seven other species, **1h**−**1n**. Like all of the molecules considered so far, they have nine terminal CO groups and C_s symmetry. Immediately evident is the overall similarity between comparable spectra, both

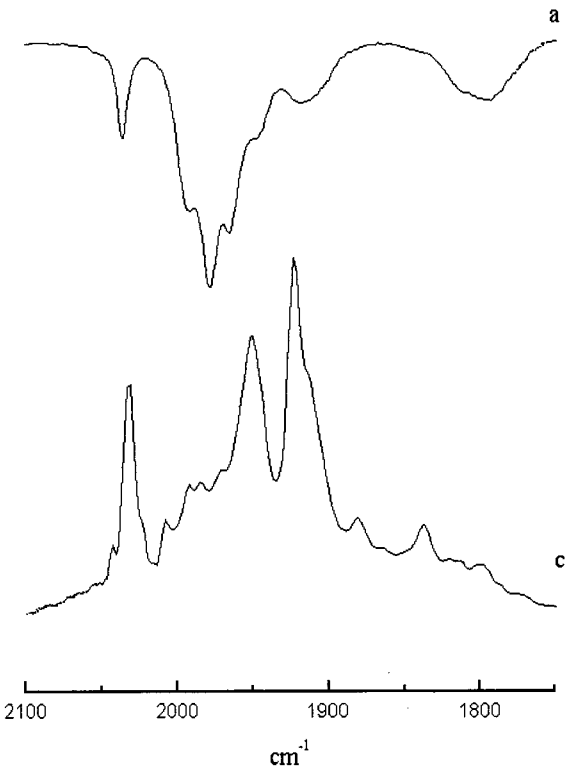


Figure 6. (see Figure 2); complex: $[Fe_2Ir_2(CO)_{12}AuPPh_3]^-$ (**1g**); solvents: (a) CH_2Cl_2.

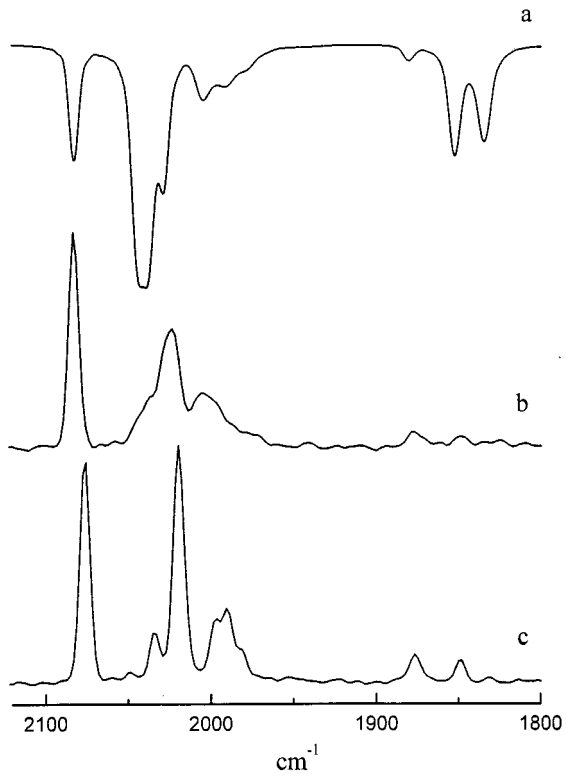


Figure 7. (see Figure 2); complex: $Co_4(CO)_{11}PPh_3$ (**2a**); solvents: (a) CCl_4, (b) CCl_4.

between these species and those of Figures 2−6, notwithstanding the fact that two of these species contain H as a bridging ligand and that one has a M_4, two a MM'_3 and the other four a $M_2M'_2$ core. It is clear that the general pattern established for the first three molecules, of C_{3v} symmetry, is applicable to others of C_s. This is helpful because the low symmetry of the latter means that group theory, unaided, offers few insights.

Figure 7 shows the ir and Raman spectra of **2a**, a species derived from **1a** by substitution of a basal CO by a phosphane.[14] Consequently, it has eight terminal carbonyl groups with the structural form $M(CO)_3[M(CO)_2]_2M(CO)$. Like the molecules **1d−1n**, the molecular symmetry is C_s, but whereas for these latter the idealised CO group arrangements are all C_{3v}, this arrangement now has only C_s symmetry. Despite this change, and that of the number of terminal CO ligands, the spectra of Figure 7 are qualitatively very similar to those of Figures 2−6; the S + P + D pattern is clearly recognisable. The only change that seems evident is that the highest frequency, totally symmetric, A′ mode has an increased infrared activity. This is not surprising in view of the reduction in CO group symmetry. The literature reports a set of $[M_4(CO)_{11}COOR]^-$ (M = Co, Rh, Ir) complexes,[15−17] all having the same number and arrangement of the CO groups. Raman spectra are not available but the infrared spectra exhibit a behaviour very close to that just discussed. A general comment which may be made at this point is that, as Table 1 shows, neither metal atom nor terminal carbonyl symmetries have any apparent influence on the spectral behaviour observed.

The compounds **2b−2d** are very interesting in that they all contain a single acetate-derived substituent. As a first approximation, the second and third row transition element examples conform to the THM whilst the first row example lies somewhere between the two extremes. Whilst they conform to the pattern that the introduction of electronegative substituents leads to near THM behaviour, they provide the first examples in which the presence of a single electronegative substituent is sufficient to bring about this transition. The compound **2e**, with a single iodide anion, is borderline, as are a number of other species with H as a ligand. It should be recognised that the species which have been the subject of the present paragraph serve to remove a possible ambiguity concerning the THM. This concerns the matter of Mν(CO)−M′ν(CO) coupling. In that it does not invoke the (additional) coupling via an induced-dipole mechanism of the SHM, could it be that the THM is only appropriate to species in which Mν(CO)−M′ν(CO), or perhaps just $[M\nu(CO)_n]-[M'\nu(CO)_m]$, (with no constraints on M, M′, n or m as long as they refer to different units) coupling is negligible? The present series seem to make it quite clear that the existence of coupling is entirely consistent with the applicability of the THM.

The final set which we review is a series of four tetranuclear species (**3a−d**) containing just seven terminal carbonyl groups. They comprise one M_4, one M_3M' and two $M_2M'_2$ compounds. Their infrared spectra, again of variable quality, are illustrated in the Figures of the relevant papers (Table 1). Yet again, the general impression is one of similarity with the other spectra given in this paper. The essen-

tial indifference of the spectra to the number of terminal carbonyl groups is an indicator of the applicability of a common model and this seems to be that of a borderline between the SHM and THM, with a bias towards the latter.

Finally, we group together three more complexes with different numbers of CO groups and different symmetries. The anion **4a**, of C_3 symmetry but now with ten terminal CO groups has recently bee reported. The carbonyl groups in this complex are arranged as $[M(CO)][M(CO)_3]_3$.[19] In this discussion, this is grouped with the well-known $Ir_4(CO)_{12}$ (**5a**) and $[Rh_4(CO)_{12}]^-$ (**6a**) complexes, with $[M(CO)_3]_4$ and $[M(CO)]_4$ carbonyl arrangements, respectively. What is remarkable is the fact that their infrared spectra differ very little from each other and are even simpler than those reported in Figures 1 and 2, despite the considerable difference in number of terminal CO groups in, and different symmetries of, the relevant molecules. The SHM is applicable to all of them, explaining the spectral observations.

Discussion

The most evident conclusion to be drawn from the spectra discussed above is that they are all related and show little sensitivity to the detailed molecular geometry or, indeed, to the number of terminal carbonyl groups in the molecule. The formal charge on the carbonyl species affects the mean frequency of the band pattern but not its general characteristics. As a starting point, the SHM is clearly appropriate. However, as we suspected when the present work commenced, there seem to be some species that show at least some aspects of a move towards the applicability of the THM. Although we recognise that distinctions are arbitrary − there can be conflicting indications − we incline to the view that when the (commonly observed) splitting of the P mode is less than, say, 10 cm^{-1}, then the SHM is applicable. This applicability is also manifest in the fact that whilst there is infrared intensity in the Raman-active D modes and Raman intensity in the infrared-active P modes, this transfer is less than in the species about to be discussed. When the splitting of the P mode features is greater than, say, 25 cm^{-1}, there is a significant movement towards the applicability of the THM (although the limiting characteristics of this model are rarely encountered). Another indicator of the move towards THM behaviour is an increase in infrared-Raman intensity transfer. So, clusters **1a**, **1b**, **1h**, **1j**, **1k**, **1m**, **2a**, **4a**, **5a** and **6a** show SHM-type behaviour whilst clusters **1d**, **1e**, **1f**, **1g**, **2b**, **2d** and **3c** show a significant move towards THM-type behaviour. Others, **1c**, **1i**, **1l**, **1n**, **2c**, **2e**, **3a**, **3b** and **3d** are rather borderline, emphasising the existence of continuity between the SHM and THM. To further explore this point, we can go back to Figure 1.

The pattern can be reinterpreted in terms of the basic model behind the SHM/THM distinction. Pure SHM has been interpreted as the metal cluster core behaving as a perfect conductor; it can sustain an image dipole, presumably because of a dipole-induced mixing with low-lying excited states. Conversely, pure THM behaviour is associated with the cluster behaving like a perfect insulator. So, the data that we have presented above indicate that the Co_4 cluster is more "metallic" than is the Rh_4. Further, the replacement of a Co by an FeH in the Co_3Fe unit is sufficient to disrupt the band pattern of Co_4 and to give a much less metallic unit. At the present it only seems possible to make such comments post hoc. We have previously commented on the fact that, very often, replacement of a metal atom with a quite different one in a cluster has little, if any, effect on the vibrational spectra. Given the discussion at the beginning of this paper, we would expect that any metal-atom substitutional effect would be particularly evident for tetrahedral clusters and this expectation seem justified, although it does not mean that all tetrahedral mixed-metal species conform to the THM.

In the present work we have reviewed the terminal ν(CO) vibrational spectra of some twenty six tetrahedral cluster carbonyls. The details of the reviews have decreased throughout the paper, for two reasons. First, the spectral similarities observed means that there would otherwise have been much repetition. Second, for many of the later species either no Raman data were available or only relatively poor quality spectra. For the examples discussed at the beginning of the paper, good quality Raman data provided important corroborative evidence for conclusions reached from the infrared. Nonetheless, the general conclusion to be reached is clear. Tetrahedral cluster carbonyls seem to show sensitivity to the molecular composition greater than that revealed for comparable species of a higher nuclearity in a recent survey. In retrospect, this is not a surprising conclusion since the "cluster selection rule" that seems to control cluster spectral activities is related to the surface selection rule of metal surfaces. Tetrahedral clusters are those clusters most removed from the surface of bulk metal. Not surprisingly, therefore, some of the tetrahedral clusters reviewed in the present work seem to show a significant tendency to exhibit vibrational spectroscopic characteristics indicative of a move towards the THM. That the presence of electronegative ligands can make the THM that which is applicable is therefore entirely consistent. Overall, this suggests that other examples of THM applicability will only be found in low-nuclearity clusters.

Conclusions

In the present paper we have addressed the problem of the relative applicability of the SHM and the THM to the terminal ν(CO) vibrations of tetrahedral transition metal carbonyl clusters. For the species, which we surveyed − which were as broadly based as the data available in the literature would allow − they were found to be roughly equally applicable. This pattern explains a confusion apparent in the literature, that there are some tetrahedral species for which the available data are such as to make a normal coordinate analysis possible and others for which the data are not. The former are those that follow the THM. Over-

all, the pattern revealed is one that strongly supports the interpretation of the SHM in terms of a cluster selection rule, akin to the surface selection rule. Substitution of a metal atom of a homometallic cluster by a different metal or the addition of a highly electronegative group or atom to a molecule both have the effect of making the THM more applicable. Equally, they will have the effect of disrupting, at least to some extent, the band structure associated with the metal atoms in the cluster. This connection between band-structure disruption and THM applicability is just that expected on the basis of the cluster selection rule. This conclusion leads to a useful prediction, that THM behaviour should become increasingly rare as the cluster size increases and, as our recent survey has shown, this seems to be the case. In the other direction, there are trimetallic clusters (and, indeed, a whole family of clusters in which all of the metal atoms are located in the same plane) but these clearly merit a separate discussion concerning the applicability of the SHM and THM (vibrations located in the molecular plane may well behave rather differently from displacements perpendicular to it)

Experimental Section

$Co_4(CO)_{12}$[23] (**1a**), $Co_3FeH(CO)_{12}$[24] (**1c**) and $Co_4(CO)_{11}PPh_3$[14] (**2a**) were prepared as previously reported. $Rh_4(CO)_{12}$ (**1b**) was purchased from Sigma Aldrich and used after recrystallisation from *n*-hexane under CO. $[Fe_3RhH(CO)_{12}]^{2-}$ (**1d**) and $[Fe_2Ir_2(CO)_{12}AuPPh_3]^-$ (**1g**) were kindly donated by Professor R. Dalla Pergola, University of Milan.

IR spectra were recorded on a Bruker Equinox 55 FT-IR spectrophotometer at a resolution of 2 cm^{-1} in *n*-hexane for neutral complexes, and in CH_2Cl_2 for anionic systems, both in a NaCl cell. Raman spectra were recorded on a Bruker RFS 100 spectrophotometer equipped with an Nd^{3+}:YAG laser and Ge-diode detector at a resolution of 4 cm^{-1}. Measurements on crystalline samples were performed in capillary vials sealed under inert gas. Due to the risk of heating and decomposition, low laser powers (10−30 mW) were used and several scan-packets (of 50−100 scans each), interleaved by a recovery time and then averaged, were made. Solution spectra were recorded in CCl_4, a solvent that proved to have a very low background in the carbonyl stretching spectral region. Solutions were prepared by stirring the sample in a flask under a nitrogen flow and then filtering off the insoluble excess (highly concentrated solutions are required). Solutions were put into a quartz cuvette, which was sealed under inert gas. Laser powers of about 200 mW and about 3000 scans were used.

Acknowledgments

We are indebted to the Italian MURST (Ministero della Università e della Ricerca Scientifica e Tecnologica) for financial support (40% funding).

[1] S. F. A. Kettle, E. Diana, R. Rossetti, P. L. Stanghellini, *J. Am. Chem. Soc*. **1997,** *119*, 8228.
[2] S. F. A. Kettle, E. Diana, R. Rossetti, P. L. Stanghellini, *Inorg. Chem*. **1998**, *37*, 6502.
[3] S. F. A. Kettle, *Spectrochimica Acta A*, **1998,** *54A*, 1639.
[4] N. A. Pierce, N. Sheppard *Surf. Sci.* **1976**, *59*, 205; N. Sheppard, J. Erkelens *Appl. Spectrosc.* **1984**, *38,* 471;Y. J. Chabal *Surf. Sci. Rep.* **1988**, *8,* 214; S. F. A. Kettle *Theochem* **1995,** *341,* 25.
[5] D. Bright, *J. Chem. Soc., Chem. Commun.* **1970** 1169; U. A. Jayasooria, C.E. Anson, *J. Am. Chem. Soc.* **1986,** *108,* 2894; E. Horn, M. R. Snow, *Aust. J. Chem.* **1981**, *34*, 737; E. W. Abel, P. J. Hendra, R. A. N. McLean, M. M. Qurashi, *Inorg. Chim. Acta* **1969**, *3*, 77; C. Marshall, R. D. Peacock, D. R. Russel, I. L. Wilson, *J. Chem. Soc., Chem. Comm.* **1970,** 1643; E. Horn, M. R. Snow, P. C. Zeleny, *Aust. J. Chem.* **1980**, *33*, 1659; D. J. Darensbourg, K. K. Klausmeyer, J. D. Draper, J. A. Chojnacki, J. H. Reibenspies, *Inorg. Chim. Acta* **1998**, *270*, 405.
[6] G. Bor, G. Sbrignadello, K. Noack, *Helv. Chim. Acta* **1975**, *58*, 815.
[7] R. Della Pergola, L. Garlaschelli, F. Demartin, M. Manassero, N. Masciocchi, G. Longoni, *J. Organomet. Chem.* **1988**, *352*, C59.
[8] R. Della Pergola, L. Garlaschelli, F. Demartin, M. Manassero, N. Masciocchi, M. Sansoni, *J. Chem. Soc., Dalton Trans.* **1990**, 127.
[9] S. F. A. Kettle, E. Diana, P. L. Stanghellini, R. Della Pergola,. *Inorg. Chim. Acta* **1993**, *212*, 75.
[10] R. Bau, M. Y. Chiang, C. Y. Wei, L. Garlaschelli, S. Martinengo, T. F. Koetzle, *Inorg. Chem.* **1984**, *23*, 4758.
[11] A. Fumagalli, D. Italia, M. C. Malatesta, G. Ciani, M. Moret, A. Sironi, *Inorg. Chem.* **1996**, *35*, 1765.
[12] S. Martinengo, P. Chini, V. G. Albano, F. Cariati, T. Salvatori, *J. Organomet. Chem.* **1973**, *59*, 379.
[13] V. G. Albano, G. Ciani, S. Martinengo, *J. Organomet. Chem.* **1974**, *78*, 265.
[14] G. Cetini, O. Gambino, R. Rossetti, P. L. Stanghellini, *Inorg. Chem.*, **1968**, *7*, 609; D.J. Darensbourg, B. Scott Peterson, R. E. Schmidt, *Organometallics* **1982**, *1*, 306
[15] L. Garlaschelli, S. Martinengo, P. Chini, F. Canziani, R. Bau, *J. Organomet. Chem.* **1981**, *213*, 379.
[16] S. Martinengo, A. Fumagalli, P. Chini, V. G. Albano, G. Ciani *J. Organomet. Chem.* **1976**, *116*, 333.
[17] G. Longoni, S. Campanella, A. Ceriotti, P. Chini, V. G. Albano, D. Braga, *J. Chem. Soc., Dalton Trans.* **1980,** 1816.
[18] V. G. Albano, D. Braga, G. Longoni, S. Campanella, A. Ceriotti, P. Chini, *J. Chem. Soc., Dalton Trans.* **1980,** 1820.
[19] A. Fumagalli, M. Bianchi, M. C. Malatesta, G. Ciani, M. Moret, A. Sironi, *Inorg. Chem.* **1998**, *37*, 1324.
[20] G. Ciani, M. Manassero, V. G. Albano, F. Canziani, G. Giordano, S. Martinengo, P. Chini, *J. Organomet. Chem.* **1978**, *150*, C17.
[21] D. Roberto, L. Garlaschelli, M. Pizzotti, *Inorg. Chem.*, **1995**, *34*, 3555.
[22] F. Cariati, V. Valenti, G. Zerbi, *Inorg. Chim. Acta* **1969**, *3*, 378.
[23] R. A. Friedel, I. Wender, S. L. Shufler, H. W. Sternberg, *J. Am. Chem. Soc.* **1955,** *77,* 3951.
[24] P. Chini, L. Colli, M. Peraldo, *Gazz. Chim. Ital.* **1960**, *90*, 1005.
Received May 21, 1999
[I99180]

Synthesis, Characterization and Dynamic Behavior of Mono- and Dinuclear Palladium(II) Carbene Complexes Derived From 1,1′-Methylenebis(4-alkyl-1,2,4-triazolium) Diiodides

Guy Bertrand,[b] Enrique Díez-Barra,*[a] Juan Fernández-Baeza,[a] Heinz Gornitzka,[b] Andrés Moreno,[a] Antonio Otero,[a] René Ignacio Rodríguez-Curiel,[c,d] and Juan Tejeda[a]

Keywords: Palladium / Carbenes / Metallacycles / 1,2,4-Triazole / Coordination modes

Mononuclear palladium carbene complexes **2a–c** and **3** derived from 1,1′-methylenebis(4-alkyl-4,5-dihydro-1*H*-1,2,4-triazole-5-ylidene) have been obtained by the reaction of 1,1′-methylenebis(4-alkyl-1,2,4-triazolium) diiodides **1a–d** with palladium acetate under mild conditions. The mononuclear complexes **2a–c** have been transformed into their corresponding *trans*-binuclear complexes **4a–c**. All compounds were characterized by spectroscopic techniques and the dynamic behavior of **2a–c** and **4a–c** has been studied. The X-ray structures of **2a** and **4c** are reported.

Introduction

A large number of palladium(II) complexes with bidentate ligands (L−L) are known, with this kind of ligand acting predominantly as a chelate to form mononuclear *cis*-[PdX_2(L−L)] complexes. Although some examples of chelate complexes with a *trans*-configuration are known, they are rare; normally, bidentate ligands act as bridges when they form palladium(II) complexes with a *trans*-configuration, but there are relatively few examples of *trans*-binuclear palladium(II) complexes (*trans*-[PdX_2(μ-L−L)]$_2$).[1,2]

In recent years, heterocyclic carbenes have generated a great deal of interest and a large number of reports covering theoretical aspects,[3] synthetic approaches,[4] coordination[4b,4c,4e,5] and catalytic[5g,5k,6] applications have been published. Imidazole and imidazoline rings with different substitution patterns have been extensively studied, several free carbenes and a great number of complexes derived from 2,3-dihydro-1*H*-imidazole-2-ylidene have been obtained.[4] However, carbenes based on the 1,2,4-triazole ring, where an additional nitrogen atom is present in the ring, have received little attention. As far as we know 1,3,4-triphenyl-4,5-dihydro-1*H*-1,2,4-triazole-5-ylidene is the only example of a free carbene isolated.[7] Several rhodium,[6c,6e] and *cis*- and *trans*-palladium[8] complexes derived from 4,5-dihydro-1*H*-1,2,4-triazole-5-ylidene have been prepared, a tungsten compound, with a similar structure to the chelate carbene complex, derived from 1,1′-methylenebis(4-methyl-4,5-dihydro-1*H*-1,2,4-triazole-5-ylidene)[9] and 1,1′-methylenebis(4-methyl-4,5-dihydro-1*H*-1,2,4-triazole-5-ylidene)-1,1′-methylenebis(3-methyl-4,5-dihydro-1*H*-imidazole-5-ylidene)palladium(II) diiodide[5q] have also been reported.

In this paper we report the preparation of mononuclear palladium(II) complexes derived from 1,1′-methylenebis(4-methyl-4,5-dihydro-1*H*-1,2,4-triazole-5-ylidene) (mbmdty), 1,1′-methylenebis(4-isopropyl-4,5-dihydro-1*H*-1,2,4-triazole-5-ylidene) (mbidty), 1,1′-methylenebis(4-butyl-4,5-dihydro-1*H*-1,2,4-triazole-5-ylidene) (mbbdty) and 1,1′-methylenebis(4-octyl-4,5-dihydro-1*H*-1,2,4-triazole-5-ylidene) (mbodty), and their transformation into the corresponding *trans*-binuclear complexes.

Results and Discussion

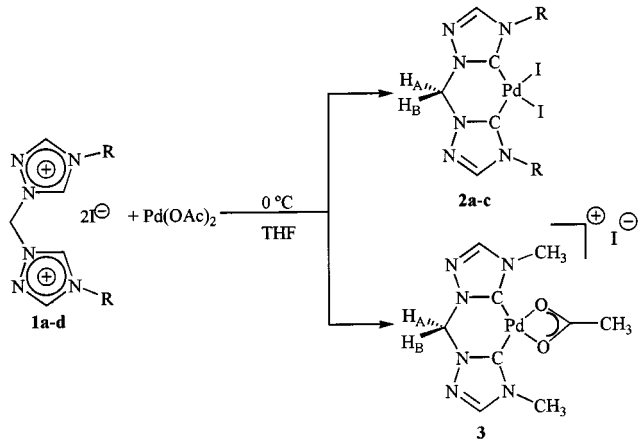
Synthesis of [PdI_2(mbidty)] (2a), [PdI_2(mbbdty)] (2b) and [PdI_2(mbodty)] (2c)

Carbene complexes were prepared by a modification of the palladium(II) acetate route reported by Herrmann for the synthesis of similar compounds.[5g,6a] The reaction of the 1,1′-methylenebis(4-alkyl-1,2,4-triazolium) diiodides[10] (**1a−c**) with palladium(II) acetate in THF at 0°C led exclusively to the mononuclear species **2a−c**, as outlined in Scheme 1. The acidity of the H5 protons of the 1,2,4-triazole ring is higher than that of the H2 imidazole protons. This fact permits very mild reaction conditions in comparison with the usual procedures described for the synthesis of imidazole carbene complexes.[5g,6a]

Compounds **2a−c** present the same patterns in the ^{1}H- and ^{13}C{^{1}H} NMR spectra in [D_6]DMSO, except for the signals of the alkyl substituents. At room temperature an

[a] Departamento de Química Inorgánica, Orgánica y Bioquímica, Facultad de Química,
Universidad de Castilla-La Mancha, Campus Universitario, 13071-Ciudad Real, Spain
Fax: (internat.) + 34-926/295318
E-mail: ediez@qino-cr.uclm.es
[b] Laboratoire Hétérochimie Fondamentale et Appliquée, Bat. 2R1,
Université Paul Sabatier, 118, Route de Narbonne, 31062-Toulouse Cedex, France
Fax: (internat.) + 33-561/558204
[c] Departamento de Química Inorgánica, Orgánica y Bioquímica, Facultad de Química,
Universidad de Castilla-La Mancha, Campus Universitario, 13071-Ciudad Real, Spain
Fax: (internat.) + 34-926/295318
[d] Laboratorio de Síntesis Orgánica. Facultad de Química, Universidad de La Habana,
Zapata e/ Mazón y G, 10400-Ciudad de La Habana, Cuba
Fax: (internat.) + 537/333502

 © WILEY-VCH Verlag GmbH, D-69451 Weinheim, 1999 1434−1948/99/1111−1965 $ 17.50+.50/0



Scheme 1. Summary of reactions leading to the preparation of **2a**−**c** and **3**

AB system was observed for the two methylene bridge protons (H_A and H_B) at about 6.53 and 6.95 ppm. Their coupling constants are in agreement with a geminal coupling. This assignment has been confirmed by NOE difference and HETCOR experiments; NOE intensities of 26% (**2a**), 13% (**2b**), and 14% (**2c**) between the methylene bridge protons have been observed and, in addition, HETCOR experiments show a correlation between each of the signals of the AB system in the ^{1}H NMR spectrum with only one signal in the $^{13}C\{^1H\}$ NMR spectrum (δ = 66.6, 66.7 and 66.7, respectively).

Each compound (**2a**−**c**) showed only one set of signals in the ^{1}H- and $^{13}C\{^1H\}$ NMR spectra for the alkyl substituents (the assignment was confirmed by HETCOR and NOE experiments).[12] These results indicate the equivalence of the alkyl groups, which is in agreement with a symmetric structure. However, in the ^{1}H NMR spectra two doublets of triplets were observed for **2b** and **2c** − one for each proton of N4−CH_2 (δ = 4.18 and 4.80 for **2b** and δ = 4.18 and 4.78 for **2c**) − due to a vicinal coupling (J = 7.1 Hz for both compounds) and a geminal coupling (J = 13.4 Hz for **2b** and 13.6 Hz for **2c**), which show the nonequivalence of the these two protons. In the ^{1}H NMR spectrum the isopropyl groups (**2a**) showed two doublets (δ = 1.33 and 1.53) for the CH_3 protons, which indicates that the methyl groups are nonequivalent, although these nonequivalent methyl groups are from the same isopropyl group because only one signal (δ = 5.41, sep) was observed for N4−CH, which indicates that the two isopropyl groups are equivalent. The equivalence of the isopropyl groups and the nonequivalence of the methyl groups was confirmed by $^{13}C\{^1H\}$ NMR spectroscopy, in which only one signal for N4−CH (δ = 52.7) and two signals for CH_3 (δ = 21.0 and 23.4) were observed.

The patterns in the ^{1}H- and $^{13}C\{^1H\}$ NMR spectra for compounds **2a**−**c** indicate that the two triazole rings are equivalent. We observed only one signal at lower field for H3 in the ^{1}H NMR spectrum (δ = 9.12, **2a**; 8.92, **2b**; 8.90, **2c**), which integrated for two protons, one for each heterocycle. In the $^{13}C\{^1H\}$ NMR spectra of all three compounds two signals appeared at lower field, one for C3 at 142.3 ppm (**2a**), 144.7 ppm (**2b**) or 144.8 ppm (**2c**) and the other for C5 at 166.7 ppm (**2a**), 166.3 ppm (**2b**) or 166.3 ppm (**2c**). The chemical shifts of C5 are in agreement with a coordinated heterocyclic carbenic carbon.[8b] This assignment has also been confirmed by HETCOR experiments.

The NMR spectroscopic and microanalytical data are in accordance with a 1,1′-methylenebis(4-alkyl-4,5-dihydro-1*H*-1,2,4-triazole-5-ylidene) system, although it is not possible to distinguish between mononuclear or binuclear palladium(II) complexes. The FAB-MS for compounds **2a**−**c** showed a peak at an *m*/*z* value double that expected for the mononuclear complexes. Nevertheless, by CI-MS with direct sample introduction the appropriate molecular peak for the mononuclear species was observed. This behavior may be explained by the formation of dimmeric species in solution, a phenomenon that has been observed previously in other systems.[11]

On the basis of the spectroscopic data a square-planar structure for palladium is proposed. Two coordination sites are occupied by two carbenes forming a rigid six-membered metallacyclic structure with a boat-conformation, and the other two coordination sites are occupied by the two iodine atoms (Figure 1). In our complexes the alkyl groups probably create sufficient steric hindrance to prevent boat-to-boat inversion.

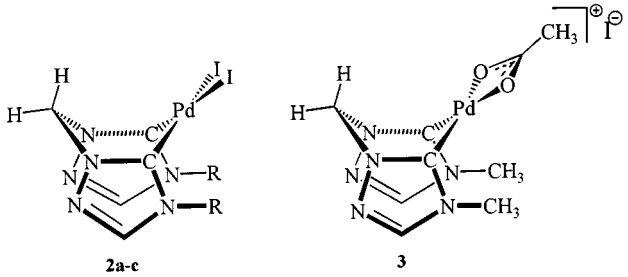


Figure 1. Proposed structures for **2a**−**c** and **3**

In order to confirm this proposal an X-ray crystal structure determination for **2a** was carried out. The solid state structure of this compound is shown in Figure 2. Compound **2a** is mononuclear in the solid state. The coordination sphere of the palladium atom shows a square planar geometry with the two iodide atoms in *cis*-positions.

Synthesis of [Pd(OAc)(mbmdty)]I (3)

Reaction of 1,1′-methylenebis(4-methyl-1,2,4-triazolium) diiodide[12] (**1d**) with palladium(II) acetate under the same conditions as for compounds **2a**−**c** (THF, 0°C) yielded an unexpected carbenic species, **3**, as shown in Scheme 1. This cationic palladium(II) dicarbene complex was characterized by IR, ^{1}H- and $^{13}C\{^1H\}$ NMR spectroscopy and mass spectrometry. The IR spectrum showed characteristic bands at 1408 and 1540 cm^{-1}, which correspond to $\nu_s(CO_2^-)$ and $\nu_a(CO_2^-)$, respectively. The ^{1}H NMR signals for the two

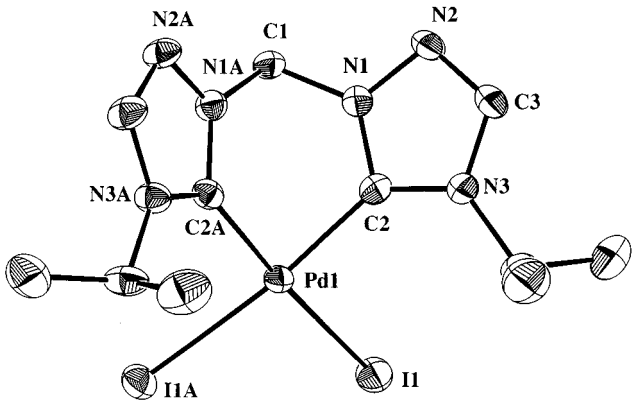


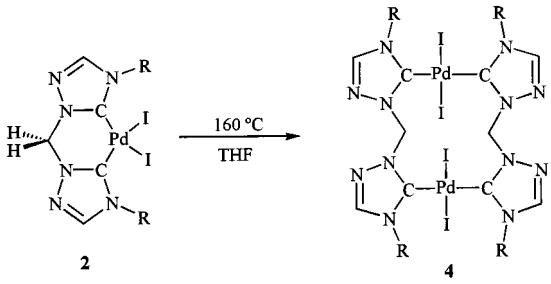
Figure 2. Solid state structure of **2a**; hydrogen atoms and a non-coordinated THF molecule are omitted for clarity; selected bond lengths [pm] and angles [°]: Pd1−C2 1.996(4), Pd1−I1 2.634(1); C2−Pd1−C2A 84.3(2), I1−Pd1−I1A 90.7(1), C2−Pd1−I1 92.2(1), C2−Pd1−I1A 173.2(1).

protons of the methylene bridge form an AB system with signals at 6.94 and 7.56 ppm, with a geminal coupling constant of 14.6 Hz. Moreover, H3 appears as a singlet at 8.95 ppm and we observed two other high-field singlets: one at 3.89 ppm for N4−CH_3 and the other at 1.87 ppm for the methyl group of the acetate. The $^{13}C\{^1H\}$ NMR spectrum showed three signals at lower field: 147.0, 152.0 and 181.7 ppm for C3, the carbenic carbon and COO, respectively. The carbon of the methylene bridge was observed as one signal at 65.0 ppm and two signals appeared at higher field: one at 23.6 ppm for the methyl of the acetate group and the other at 35.8 ppm for N4−CH_3.

CI-MS with direct sample introduction and FAB-MS of compound **3** showed mass peaks corresponding to the mononuclear complex (*m*/*z*: 343 D, $[M - I]^+$; 411 D, $[M - OAc]^+$) but with very low intensity. However, electrospray-MS showed these peaks with intensity of 100% and 66%, respectively. In a similar way to complexes **2a**−**c**, all spectroscopic data obtained for **3** are consistent with a rigid six-membered metallacyclic structure in the boat conformation, as shown in Figure 1.

Synthesis of $[PdI_2(\mu\text{-mbidty})]_2$ (4a), $[PdI_2(\mu\text{-mbbdty})]_2$ (4b) and $[PdI_2(\mu\text{-mbodty})]_2$ (4c)

Heating the carbene complexes **2a**−**c** in THF at 160°C in a Fisher−Porter bottle gave the new *trans*-binuclear palladium(II) species **4a**−**c** as the only products (Scheme 2). Compounds **4** show similar patterns in the ^1H- and $^{13}C\{^1H\}$ NMR spectra ([D_6]DMSO), except for the typical signals of the alkyl substituents. The NMR spectra of **4** were found to be different to those of the mononuclear complexes **2**: The ^1H NMR spectrum shows a very broad singlet at about 7.10 ppm (**4a**), 7.30 ppm (**4b** and **4c**) for the methylene bridges, a broad singlet due to N4−CH_2 for **4b** (δ = 4.40−4.60) and **4c** (δ = 4.30−4.50), and only one doublet (δ = 1.55) for all the methyl groups of the isopropyl units (**4a**). These facts indicate that the structure of the binuclear complexes **4a**−**c** is nonrigid and symmetrical at room temperature. This assignment is in agreement with the $^{13}C\{^1H\}$ NMR spectra, with one signal for the methylene bridges at δ = 67.0 (**4a**); 67.2 (**4b**); 67.3 (**4c**), one signal for N4−CH_2 (δ = 48.8, **4b**; 49.1, **4c**) and one signal for the CH_3 of the isopropyl groups (δ = 25.1, **4a**). The other signals in the ^1H- and $^{13}C\{^1H\}$ NMR spectra are typical for alkyl substituents.[12] In the ^1H NMR spectra only one signal appeared at low field (δ = 9.26, 9.03 and 9.02 for **4a**−**c**, respectively) for H3 of the heterocyclic rings, and these were correlated with only one signal in the $^{13}C\{^1H\}$ NMR spectra (δ = 143.5, **4a**; 145.7, **4b**; 145.8, **4c**). In the $^{13}C\{^1H\}$ NMR spectra we observed one signal of low intensity at lower field, corresponding to the carbenic carbon C5 (δ = 172.0, **4a**; 171.3, **4b**; 171.5, **4c**). This evidence corroborates the symmetrical structure indicated above.



a: R = Isopropyl, **b**: R = Butyl, **c**: R = Octyl

Scheme 2. Summary of reactions leading to the preparation of **4a**−**c**

In a similar way to compounds **2a**−**c**, both the spectroscopic and microanalytical data are in agreement with the structure of the 1,1′-methylenebis(4-alkyl-4,5-dihydro-1*H*-1,2,4-triazole-5-ylidene) system. However, these compounds could have either a mono- or binuclear structure. CI-MS with direct sample introduction, and FAB-MS, for compounds **4a**−**c** showed, without doubt, peaks corresponding to binuclear compounds.[12]

In order to ascertain whether the complexes exist in the *cis*- or *trans*-configuration in the solid state an X-ray crystal structure determination for **4c** was carried out. The solid state structure (Figure 3) shows a binuclear structure in which two dicarbene ligands act as a bridge between two palladium atoms with a *trans*-square planar geometry about the metal centers.

When the mononuclear compounds were transformed into the binuclear complexes a change in their configuration was observed; while the former showed a *cis*-configuration the latter presented a *trans*-configuration. This is reminiscent of the *cis*/*trans* isomerization observed by Herrmann for diiodobis(1,4-dimethyl-4,5-dihydro-1*H*-1,2,4-triazole-5-ylidene)-palladium(II),[8b] in which the rearrangement took place without dissociation of the ligand. However, our results are not consistent with this model because it is not possible to prepare *trans*-chelate complexes with our biscarbenes. − they should act as bridges to form complexes with a *trans*-configuration and, therefore, dissociation of the ligand is necessary.

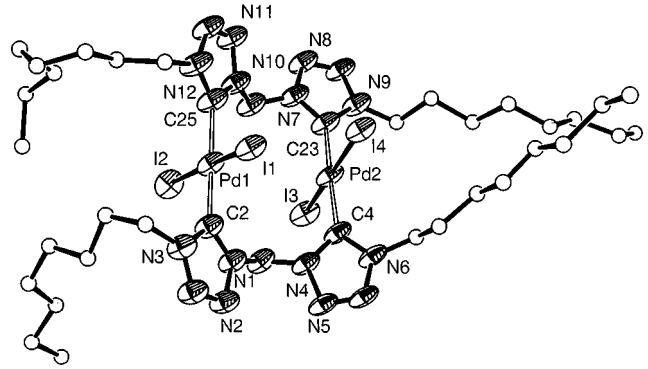
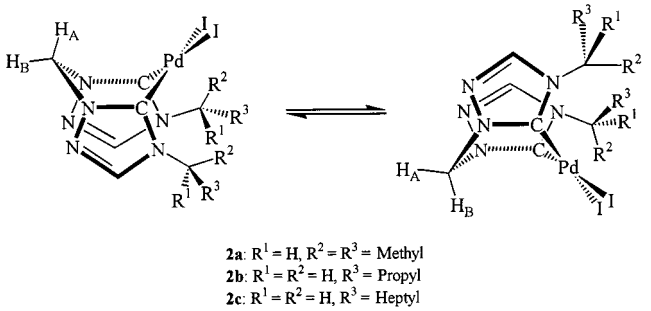


Figure 3. Solid state structure of **4c**; for clarity, the hydrogen atoms and a toluene molecule are omitted, and the octyl substituents are presented in a ball and stick style; selected bond lengths [pm] and angles [°]: Pd1−C2 1.970(17), Pd1−C25 2.018(17), Pd1−I1 2.619(2), Pd1−I2 2.600(2), Pd2−C4 2.017(16), Pd2−C23 1.973(16), Pd2−I3 2.595(2), Pd2−I4 2.599(2); C2−Pd1−C25 177.3(8), I1−Pd1−I2 174.2(1), C2−Pd1−I2 90.0(7), C25−Pd1−I2 92.2(7), C2−Pd1−I1 85.5(7), C25−Pd1−I1 92.3(7), C4−Pd2−C23 176.4(8), I3−Pd2−I4 173.9(1), C23−Pd2−I3 87.5(7), C4−Pd2−I3 90.9(6), C23−Pd2−I4 87.3(7), C4−Pd2−I4 94.1(6)



Scheme 3. Boat-to-boat inversion of **2a**−**c**

Study of the Dynamic Behavior of the Mononuclear and Binuclear Complexes

We have mentioned above that the structures of the mononuclear complexes **2a**−**c** are rigid at room temperature. However, when solutions of these compounds were heated some dynamic behavior was observed. The signals in the ^{1}H NMR spectra of the methylene bridge, N4-methylene for **2b** and **2c,** and methyl (isopropyl) groups for **2a** were observed during the dynamic study. When the ^{1}H NMR spectra of **2a**−**c** were recorded at high temperature, the AB systems corresponding to the diastereotopic protons of the methylene bridges coalesce. This indicates that boat-to-boat inversion takes place at high temperature as shown in Scheme 3.

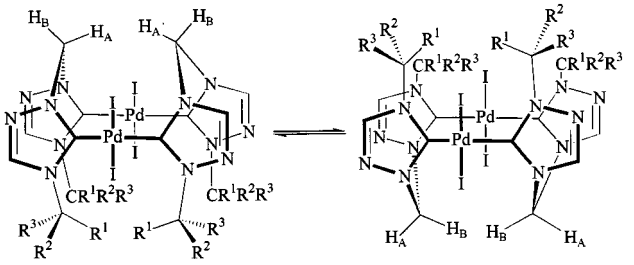
In addition, at high temperature the two doublets due to the methyl protons of the isopropyl groups (**2a**) coalesce, becoming a doublet, and the doublet of triplets due to N4−CH_2 (**2b** and **2c**) also coalesce, to give a triplet. Coalescence temperatures and free energy values[13] ($\Delta G^{\neq}$) are summarized in Table 1.

The similar free energy values obtained for each compound for the methylene bridge protons and from the substituent (N4−R) indicate that the rigid structure exhibited by the mononuclear compounds is responsible for the nonequivalence of the methylene bridge protons, the methylene protons bonded to N4 (**2b** and **2c**), and the methyl groups of the isopropyl substituents (**2a**). Therefore boat-to-boat inversion must be responsible for the equivalence of these sets of protons at higher temperatures.

The binuclear compounds **4a**−**c** also showed a dynamic behavior. In the ^{1}H NMR spectra ([D_8]THF) the methylene bridge protons give rise to a very broad singlet at room temperature which becomes sharper at high temperature and resolves into an AB system at low temperature. This is in agreement with a structure that shows a boat-to-boat-like inversion at room temperature, as outlined in Scheme 4; this inversion could be stopped at low temperature. Moreover, the broad singlet for the N4−CH_2 group of **4b** and **4c** (δ = 4.50 and 4.40, respectively) appeared as two broad signals at low temperature (two doublets of triplets were expected, but broad signals were observed probably due to a loss of resolution in the NMR apparatus at this temperature). In addition, an AB system appeared for the N4−CH_2 group in **4b** and **4c** upon irradiation, at low temperature, at the frequencies of the methylene protons in the 2-position of the chain (N4$CH_2C\mathit{H}_2$) for butyl (**4b**, δ = 2.13) and octyl (**4c**, δ = 2.15) substituents. On the other hand, it was not possible to study the dynamic behavior of **4a** by studying the methyl groups due to the fact that the two doublets expected at low temperature were not observed, again probably because of a loss of resolution in the

Table 1. Coalescence temperatures and free energy values[13] ($\Delta G^{\neq}$)

	AB System		N4−CH_2 or N4−CH_3	
Compound	Coalesc. T (K)	$\Delta G^{\neq}$ (kcal/mol)	Coalesc. T (K)	$\Delta G^{\neq}$ (kcal/mol)
2a	413	19.69	393	19.31
2b	393	18.69	398	18.70
2c	398	18.94	403	18.95
4a	288	12.54	–	–
4b	298	12.99	278	12.69
4c	293	12.78	273	12.42



2a: R^1 = H, R^2 = R^3 = Methyl
2b: R^1 = R^2 = H, R^3 = Propyl
2c: R^1 = R^2 = H, R^3 = Heptyl

Scheme 4. Conformational inversion of **4a**−**c**

NMR apparatus. Coalescence temperatures and free energy values[13] ($\Delta G^{\neq}$) are summarized in Table 1.

We can draw similar conclusions for the binuclear compounds **4a**−**c**. Free energy values indicate that the rigid structure at low temperature is responsible for the nonequivalence of the methylene bridge protons, the nonequivalence of the methylene protons bonded to N4 (**4b** and **4c**), and therefore the inversion at room temperature makes them equivalent.

Experimental Section

General considerations: All operations were performed under an inert atmosphere using standard vacuum line techniques. Solvents were purified by distillation from appropriate drying reagents before use. Melting points were determined in capillary tubes on a Gallenkamp apparatus and are uncorrected. Elemental analyses were performed on a Perkin−Elmer 2400 CHN microanalyzer. IR spectra were recorded (in the region between 4000 and 200 cm^{-1}) on a Perkin−Elmer PE 883 IR spectrophotometer in KBr. NMR spectra were recorded on a Varian Unity 300. Chemical shifts are expressed in parts per million (δ) relative to TMS as internal standard in [D_6]DMSO. FAB-MS were recorded on a VG Autospect instrument using *m*-nitrobenzylalcohol as matrix. CI-MS were recorded on a NERNAG R10−10H instrument in NH_3 or CH_4. The 1,1′-Methylenebis(4-alkyl-1,2,4-triazolium) diiodides (**1a**−**c**) were prepared as previously reported.[10]

Preparation of 1,1′-methylenebis(4-methyl-1,2,4-triazolium) diiodide (1d): A mixture of 1,1′-methylenebis(1,2,4-triazole)[10] (100 mg, 0.67 mmol) and an excess of methyl iodide (15 mL) was stirred and heated at 130°C for 10 h in a 50 mL Fisher−Porter bottle. After cooling, the suspended solid was isolated by filtration, washed with ethyl acetate and recrystallized from ethanol. Yield: 87%; m.p. 211−213°C (decomposition). − ^{1}H NMR: δ = 3.97 (s, 6 H, CH_3), 7.17 (s, 2 H, CH_2), 9.29 (s, 2 H) and 10.39 (s, 2 H) (H3 and H5). − ^{13}C{1H} NMR: δ = 34.6 (CH_3), 62.2 (CH_2), 145.5, 146.4 (C3 and C5). − $C_7H_{12}I_2N_6$ (434.02): calcd C 19.37, H 2.79, N 19.36; found C 18.95, H 3.09, N 19.41.

General Procedure for Preparation of Mononuclear Complexes (2a−c, 3): A suspension of the corresponding 1,1′-methylenebis(4-alkyl-1,2,4-triazolium) diiodide (**1a**−**d**) (0.44 mmol) and palladium acetate (89.7 mg, 0.40 mmol) in THF (250 mL) in an 1 L Schlenk tube was stirred at 0°C for between 4 and 48 h. The crude mixture was filtered and the solvent was evaporated under vacuum. Pure products were isolated as indicated in each case.

Preparation of [PdI_2(mbidty)] (2a): The general procedure for mononuclear complexes was followed. Reaction time was 24 h. The pure product was obtained as a yellow solid after washing with chloroform. Yield: 97%; m.p. 318−320°C (decomposition). − ^{1}H NMR: δ = 1.33 (d, *J* = 6.7 Hz, 6 H, CH_3), 1.53 (d, *J* = 6.7 Hz, 6 H, CH_3), 5.41 (sep, *J* = 6.7 Hz, 2 H, C*H*Me_2), 6.50 and 6.92 (AB system, *J* = 13.9 Hz, 2 H, NCH_2N), 9.12 (s, 2 H, H3). − ^{13}C{^{1}H} NMR: δ = 21.0 (CH_3), 23.4 (CH_3), 52.7 (*C*HMe_2), 66.6 (NCH_2N), 142.3 (C3), 166.7 (C5). − MS (FAB$^+$); *m*/*z* (%): 467 (37) [M + 1 − HI]$^+$, 594 (10) [M]$^+$, 701 (5) [2M − Pd − 3I]$^+$, 1060 (8) [2M − HI]$^+$. − MS (CI, NH_3); *m*/*z* (%): 251 (100) [M + 1 + NH_4 − Pd − 2HI]$^+$, 467 (18) [M + 1 − HI]$^+$, 484 (8) [M + NH_4 − HI]$^+$, 612 (44) [M + NH_4]$^+$. − $C_{11}H_{18}I_2N_6Pd$ (594.53): calcd C 22.22, H 3.05, N 14.14; found C 22.21, H 3.03, N 13.86.

Preparation of [PdI_2(mbbdty)] (2b): The general procedure for mononuclear complexes was followed. Reaction time was 4 h. The pure product was obtained as an orange solid after recrystallization from dichloromethane/diethyl ether. Yield: 95%; m.p. 295−297°C (decomposition). − ^{1}H NMR: δ = 0.87 (t, *J* = 7.3 Hz, 6 H, CH_3), 1.20 (sxt, *J* = 7.3 Hz, 4 H, $NCH_2CH_2CH_2CH_3$), 1.79 (m, *J* = 6.9 Hz, 4 H, $NCH_2CH_2CH_2CH_3$), 4.18 (dt, *J* = 13.4 Hz, *J* = 7.1 Hz, 2 H, one H from each $NCH_2CH_2CH_2CH_3$), 4.80 (dt, *J* = 13.4 Hz, *J* = 7.1 Hz, 2 H, one H from each $NCH_2CH_2CH_2CH_3$), 6.55 and 6.96 (AB system, *J* = 14.0 Hz, 2 H, NCH_2N), 8.92 (s, 2 H, H3). − ^{13}C{^{1}H} NMR: δ = 13.3 (CH_3), 18.7 ($NCH_2CH_2CH_2CH_3$), 31.8 ($NCH_2CH_2CH_2CH_3$), 48.9 ($NCH_2CH_2CH_2CH_3$), 66.7 (NCH_2N), 144.7 (C3), 166.3 (C5). − MS (FAB$^+$); *m*/*z* (%): 495 (100) [M + 1 − HI]$^+$, 621 (15) [M − 1]$^+$, 757 (11) [2M − Pd − 3I]$^+$, 1118 (40) [2M + 2 − HI]$^+$. − MS (CI, NH_3); *m*/*z* (%): 278 (11) [M + NH_4 − Pd − 2HI]$^+$, 512 (3) [M + NH_4 − HI]$^+$, 640 (100) [M + NH_4]$^+$. − $C_{13}H_{22}I_2N_6Pd$ (622.59): calcd C 25.08, H 3.56, N 13.50; found C 24.67, H 3.44, N 13.54.

Preparation of [PdI_2(mbodty)] (2c): The general procedure for mononuclear complexes was followed. Reaction time was 4 h. The pure product was obtained as an orange solid after recrystallization from diethyl ether and washing with cold diethyl ether. Yield: 100%; m.p. 304−306°C (decomposition). − ^{1}H NMR: δ = 0.84 (t, *J* = 6.6 Hz, 6 H, CH_3), 1.12−1.34 [m, 20 H, $NCH_2CH_2(CH_2)_5CH_3$], 1.70−1.92 [m, 4 H, $NCH_2CH_2(CH_2)_5CH_3$], 4.18 [dt, *J* = 13.6 Hz, *J* = 7.1 Hz, 2 H, one H from each $NCH_2CH_2(CH_2)_5CH_3$], 4.78 [dt, *J* = 13.6 Hz, *J* = 7.1 Hz, 2 H, one H from each $NCH_2CH_2(CH_2)_5CH_3$], 6.53 and 6.95 (AB system, *J* = 14.0 Hz, 2 H, NCH_2N), 8.90 (s, 2 H, H3). − ^{13}C{^{1}H} NMR: δ = 13.9 (CH_3), 22.0, 25.6, 28.4, 28.5, 29.9, 31.2 [$NCH_2(CH_2)_6CH_3$], 49.2 [$NCH_2(CH_2)_6CH_3$], 66.7 (NCH_2N), 144.8 (C3), 166.3 (C5). − MS (FAB$^+$); *m*/*z* (%): 607 (100) [M + 1 − HI]$^+$, 735 (15) [M + 1]$^+$, 981 (59) [2M − Pd − 3I]$^+$, 1342 (93) [2M + 2 − HI]$^+$, 1470 (18) [2M + 2]$^+$. − MS (CI, NH_3); *m*/*z* (%): 607 (2) [M + 1 − HI]$^+$, 626 (3) [M + 2 + NH_4 − HI]$^+$, 734 (2) [M]$^+$, 752 (100) [M + NH_4]$^+$. − $C_{21}H_{38}I_2N_6Pd$ (734.80): calcd C 34.33, H 5.21, N 11.44; found C 33.97, H 5.37, N 11.74.

Preparation of [Pd(OAc)(mbmdty)]I (3): The general procedure for mononuclear complexes was followed. Reaction time was 48 h. The crude mixture was extracted with dichloromethane and was filtered, the solvent was evaporated under vacuum and an oil was obtained. The product was isolated as a brown solid after washing with cold chloroform and crystallized together with one molecule of palladium(II) iodide. Yield: 45%; m.p. 309−311°C. − IR: $\tilde{\nu}$ = 1408 cm^{-1} (ν_s CO_2^-), 1540 cm^{-1} (ν_a CO_2^-). − ^{1}H NMR: δ = 1.87 (s, 3 H, CH_3COO), 3.89 (s, 6 H, NCH_3), 6.94 and 7.56 (AB system, *J* = 14.6 Hz, 2 H, NCH_2N), 8.95 (s, 2 H, H3). − ^{13}C{^{1}H} NMR:

δ = 23.6 (CH_3COO), 35.8 (NCH_3), 65.0 (NCH_2N), 147.0 (C3), 152.0 (C5), 181.7 (CH_3COO). − MS (FAB^+); *m/z* (%): 343 (18) [M − I]$^+$, 411 (5) [M − OAc]$^+$. − MS (CI, CH_4); *m/z* (%): 343 (5) [M − I]$^+$, 411 (10) [M − OAc]$^+$. − MS (Electrospray); *m/z* (%): 284 (17) [M − I − OAc]$^+$, 343 (100) [M − I]$^+$, 411 (66) [M − OAc]$^+$. − $C_9H_{13}IN_6O_2Pd{\cdot}PdI_2$ (470.57): calcd C 13.01, H 1.58, N 10.12; found C 13.31, H 1.43, N 10.19.

General Procedure for the Preparation of Binuclear Complexes (4a−c): A THF (15 mL) solution of the mononuclear complex (**2a−c**) (0.20 mmol) was stirred and heated at 160°C in a 50 mL Fisher−Porter bottle for between 24 and 72 h. After cooling, the solution was filtered and solvent was evaporated under vacuum to give an oil. Pure products were isolated as indicated in each case.

Preparation of $[PdI_2(\mu\text{-mbidty})]_2$ (4a): The general procedure for binuclear complexes was followed. The reaction time was 24 h. The crude material was extracted with dichloromethane, filtered, the solvent was evaporated under vacuum and an oil was obtained. The pure product was isolated as a yellow solid after washing with diethyl ether. Yield: 90%; m.p. 321−323°C (decomposition). − ^{1}H NMR: δ = 1.55 (d, *J* = 6.8 Hz, 24 H, CH_3), 5.31 (sep, *J* = 6.8 Hz, 4 H, NC*H*Me_2), 6.60−7.60 (br s, 4 H, NCH_2N), 9.26 (s, 4 H, H3). − ^{13}C{^{1}H} NMR: δ = 25.1 (CH_3), 52.6 (*C*HMe_2), 67.0 (NCH_2N), 143.5 (C3), 172.0 (C5). − MS (FAB^+); *m/z* (%): 809 (25) [M + 1−3I]$^+$, 935 (24) [M-2I]$^+$, 1063 (68) [M + 1−I]$^+$, 1191 (10) [M + 2]$^+$. − MS (CI, NH_3); *m/z* (%): 706 (100) [M + 4 − Pd − 3I]$^+$, 1063 (28) [M + 1 − I]$^+$. − $C_{22}H_{36}I_4N_{12}Pd_2$ (1189.06): calcd C 22.22, H 3.05, N 14.14; found C 22.52, H 3.38, N 14.03.

Preparation of $[PdI_2(\mu\text{-mbbdty})]_2$ (4b): The general procedure for binuclear complexes was followed. The reaction was complete after 24 h. The pure product was isolated as a yellow solid after washing with cold dichloromethane. Yield: 100%; m.p. 302−304°C (decomposition). − ^{1}H NMR: δ = 0.91 (t, *J* = 7.2 Hz, 12 H, CH_3), 1.30 (sxt, *J* = 7.4 Hz, 8 H, $NCH_2CH_2CH_2CH_3$), 2.02 (qui, *J* = 7.4 Hz, 8 H, $NCH_2CH_2CH_2CH_3$), 4.40−4.60 (br s, 8 H, $NCH_2CH_2CH_2CH_3$), 6.80−7.80 (br s, 4 H, NCH_2N), 9.03 (s, 4 H, H3). − ^{13}C{^{1}H} NMR: δ = 13.3 (CH_3), 19.0 ($NCH_2CH_2CH_2CH_3$), 31.1 ($NCH_2CH_2CH_2CH_3$), 48.8 ($NCH_2CH_2CH_2CH_3$), 67.2 (NCH_2N), 145.7 (C3), 171.3 (C5). − MS (FAB^+); *m/z* (%): 367 (13) [(M/2) − 1 − 2I]$^+$, 867 (11) [M + 3 − 3I]$^+$, 992 (18) [M + 1 − 2I]$^+$, 1119 (100) [M + 1 − I]$^+$. − MS (CI, NH_3); *m/z* (%): 1119 (100) [M + 1 − I]$^+$, 1264 (4) [M + 1 + NH_4]$^+$. − $C_{26}H_{44}I_4N_{12}Pd_2$ (1245.17): calcd C 25.08, H 3.56, N 13.50; found C 25.43, H 3.42, N 13.30.

Preparation of $[PdI_2(\mu\text{-mbodty})]_2$ (4c): The general procedure for binuclear complexes was followed. Reaction time was 72 h. The crude material was extracted with dichloromethane, the solvent was evaporated under vacuum and an oil was obtained. The pure product was isolated as a yellow solid after crystallization from cold diethyl ether. Yield: 90%; m.p. 268−270°C. − ^{1}H NMR: δ = 0.83 (t, *J* = 6.3 Hz, 12 H, CH_3), 1.10−1.30 [m, 40 H, $NCH_2CH_2(CH_2)_5CH_3$], 1.90−2.10 [br s, 8 H, NCH_2CH_2-$(CH_2)_5CH_3$], 4.30−4.50 [br s, 8 H, $NCH_2CH_2(CH_2)_5CH_3$], 6.80−7.80 (br s, 4 H, NCH_2N), 9.02 (s, 4 H, H3). − ^{13}C{^{1}H} NMR: δ = 13.9 (CH_3), 22.0, 26.0, 28.6, 29.3, 31.2 [$NCH_2(CH_2)_6CH_3$], 49.1 [$NCH_2(CH_2)_6CH_3$], 67.3 (NCH_2N), 145.8 (C3), 171.5 (C5). − MS (FAB^+); *m/z* (%): 477 (73) [(M/2)-3−2I]$^+$, 981 (20) [M − 1 − Pd − 3I]$^+$, 1089 (29) [M + 1 − 3I]$^+$, 1215 (8) [M − 2I]$^+$, 1343 (100) [M + 1 − I]$^+$, 1469 (6) [M]$^+$. − MS (CI, CH_4); *m/z* (%): 608 (100) [(M/2) − I]$^+$, 735 (16) [(M/2) + 1]$^+$, 1344 (7) [M + 2 − I]$^+$, 1470 (1) [M + 1]$^+$. − $C_{42}H_{76}I_4N_{12}Pd_2$ (1469.60): calcd C 34.33, H 5.21, N 11.44; found C 34.20, H 5.61, N 11.69.

X-ray Crystal Structure Determination for 2a: $C_{15}H_{26}I_2N_6OPd$, M = 666.62, orthorhombic, Pnma, *a* = 14.347(2) Å, *b* = 13.029(1) Å, *c* = 11.482(2) Å, *V* = 2146.3(5) Å^3, *Z* = 4, ρ_c 2.063 Mg m^{-3}, *F(000)* = 1272, λ = 0.71073 Å, T = 173(2) K, μ (Mo Kα) = 3.757 mm^{-1}, crystal size 0.7 × 0.6 × 0.5 mm, 2.84° < &*Theta;* < 24.28°, 16230 reflections (1778 independent, R_{int} = 0.0394) were collected at low temperatures using an oil-coated shock-cooled crystal[14] on a STOE-IPDS diffractometer. A numerical absorption correction was employed and the min./max. transmissions are 0.4539 and 0.5424. The structure was solved by direct methods (SHELXS-97)[15] and 144 parameters using 13 restraints were refined using the least-squares method on F^2.[16] Largest electron density residue: 0.558 e Å^{-3}, R_1 [for $F>2\sigma(F)$] = 0.025 and wR_2 = 0.060 (all data) with $R_1 = \Sigma||F_o|-|F_c||/\Sigma|F_o|$ and $wR_2 = [\Sigma w(F_o^2 - F_c^2)^2/\Sigma w(F_o^2)^2]^{0.5}$. A mirror plane leads to the disorder of a noncoordinated molecule of THF, which is refined anisotropically by ignoring the symmetry (PART-1) using ADP and distance restraints.

X-ray Crystal Structure Determination for 4c: $C_{49}H_{80}I_4N_{12}Pd_2$, M = 1557.65, monoclinic, I2/a, *a* = 17.410(3) Å, *b* = 18.417(3) Å, *c* = 38.870(9) Å, β = 93.74(2)°, *V* = 12437(4) Å^3, *Z* = 8, ρ_c = 1.664 Mg m^{-3}, *F(000)* = 6096, λ = 0.71073 Å, T = 173(2) K, μ(Mo-K_α) = 2.604 mm^{-1}, crystal size 0.2 × 0.2 × 0.02 mm, 1.88° < θ < 21.26°, 50565 reflections (6913 independent, R_{int} = 0.2406) were collected at low temperatures using an oil-coated shock-cooled crystal[14] on a STOE-IPDS diffractometer. The structure was solved by direct methods (SHELXS-97)[15] and 607 parameters using 640 restraints were refined using the least-squares method on F^2.[16] Largest electron density residue: 2.142 e Å^{-3}, R_1 [for $F>2\sigma(F)$] = 0.101 and wR_2 = 0.285 (all data) with $R_1 = \Sigma||F_o|-|F_c||/\Sigma|F_o|$ and $wR_2 = [\Sigma w(F_o^2 - F_c^2)^2/\Sigma w(F_o^2)^2]^{0.5}$. The high freedom of movement of the octyl substituents combined with the poor quality and small size of the crystals led to some problems with the refinement of **4c**. An absorption correction was not possible. The heart of the molecule is very clear and easy to refine, but it is very difficult to localize the positions of the carbon atoms of the chains. For this reason the values of *R*, R_1 and wR_2 are poor.

Crystallographic data (excluding structure factors) for the structures reported in this paper have been deposited with the Cambridge Crystallographic Data Centre as supplementary publication no. CCDC-117654 (**2a**) and CCDC-117655 (**4c**). Copies of the data can be obtained free of charge on application to CCDC, 12 Union Road, Cambridge CB2 1EZ, UK [Fax: (internat.) + 44-1223/336-033; E-mail: deposit@ccdc.cam.ac.uk].

Acknowledgments

Thanks are due to Prof. A. de la Hoz for helpful discussions, to the Spanish DGICYT (PB97−0425) for financial support, and to Agencia Española de Cooperación Iberoamericana for a grant to R. I. R. C.

[1] [1a] M. J. H. Russell, C. F. J. Barnard, *Comprehensive Coordination Chemistry* (Eds.: G. Wilkinson, R. Gillard, J. A. McCleverty), *Vol. 5*, 1st ed., Pergamon Press, Oxford, **1987**, p. 1099. − [1b] A. T. Hutton, *Comprehensive Coordination Chemistry* (Eds.: G. Wilkinson, R. Gillard, J. A. McCleverty), *Vol. 5*, 1st ed., Pergamon Press, Oxford, **1987**, p. 1131. − [1c] A. T. Hutton, C. P. Morley, *Comprehensive Coordination Chemistry* (Eds.: G. Wilkinson, R. Gillard, J. A. McCleverty), *Vol. 5*, 1st ed., Pergamon Press, Oxford, **1987**, p. 1157.

[2] [2a] K. R. Dixon, A. C. Dixon, *Comprehensive Organometallic Chemistry* (Eds.: E. W. Abel, F. G. A. Stone, G. Wilkinson, R. J. Puddephatt), *Vol. 9*, 1st ed., Pergamon Press, Oxford, **1995**, p. 193. − [2b] A. J. Canty, *Comprehensive Organometallic Chem-*

istry (Eds.: E. W. Abel, F. G. A. Stone, G. Wilkinson, R. J. Puddephatt), *Vol. 9*, 1st ed., Pergamon Press, Oxford, **1995**, p. 225. – [2c] J. A. Davies, *Comprehensive Organometallic Chemistry* (Eds.: E. W. Abel, F. G. A. Stone, G. Wilkinson, R. J. Puddephatt), *Vol. 9*, 1st ed., Pergamon Press, Oxford, **1995**, p. 291.

[3] [3a] R. R. Sauers, *Tetrahedron Lett.* **1996**, *37*, 149. – [3b] C. Boehme, G. Frenking, *J. Am. Chem. Soc.* **1996**, *118*, 2039. – [3c] C. Heinemann, T. Müller, Y. Apeloig, H. Schwarz, *J. Am. Chem. Soc.* **1996**, *118*, 2023. – [3d] O. Guerret, S. Solé, H. Gornitzka, M. Teichert, G. Trinquier, G. Bertrand, *J. Am. Chem. Soc.* **1997**, *119*, 6668. – [3e] C. Boehme, G. Frenking, *Organometallics* **1998**, *17*, 5801.

[4] [4a] A. J. Arduengo, III, J. R. Goerlich, W. J. Marshall, *J. Am. Chem. Soc.* **1995**, *117*, 11027. – [4b] W. A. Herrmann, C. Köcher, L. J. Gooβen, G. R. J. Artus, *Chem. Eur. J.* **1996**, *2*, 1627. – [4c] U. Kernbach, M. Ramm, P. Luger, W. P. Fehlhammer, *Angew. Chem. Int. Ed. Engl.* **1996**, *35*, 310. – [4d] M. Regitz, *Angew. Chem. Int. Ed. Engl.* **1996**, *35*, 725. – [4e] W. A. Herrmann, C. Köcher, *Angew. Chem. Int. Ed. Engl.* **1997**, *36*, 2162. – [4f] A. J. Arduengo, III, F. Davidson, H. V. R. Dias, J. R. Goerlich, D. Khasnis, W. J. Marshall, T. K. Prakasha, *J. Am. Chem. Soc.* **1997**, *119*, 12742. – [4g] A. J. Arduengo, III, J. R. Goerlich, R. Krafczyk, W. J. Marshall, *Angew. Chem. Int. Ed. Engl.* **1998**, *37*, 1963.

[5] [5a] R.-Z. Ku, D.-Y. Chen, G.-H. Lee, S.-M. Peng, S.-T. Liu, *Angew. Chem. Int. Ed. Engl.* **1997**, *36*, 2631. – [5b] A. J. Arduengo, III, F. Davidson, R. Krafczyk, W. J. Marshall, M. Tamm, *Organometallics* **1998**, *17*, 3375. – [5c] W. A. Herrmann, G. M. Lobmaier, M. Elison, *J. Organomet. Chem.* **1996**, *520*, 231. – [5d] W. A. Herrmann, M. Elison, J. Fischer, C. Köcher, G. R. J. Artus, *Chem. Eur. J.* **1996**, *2*, 772. – [5e] W. A. Herrmann, F. C. Munck, G. R. J. Artus, O. Runte, R. Anwander, *Organometallics* **1997**, *16*, 682. – [5f] K. M. Lee, C. K. Lee, I. J. B. Lin, *Angew. Chem. Int. Ed. Engl.* **1997**, *36*, 1850. – [5g] W. A. Herrmann, C.-P. Reisinger, M. Spiegler, *J. Organomet. Chem.* **1998**, *557(1–2)*, 93. – [5h] W. A. Herrmann, L. J. Goossen, M. Spiegler, *Organometallics* **1998**, *17*, 2162. – [5i] C. Köcher, W. A. Herrmann, *J. Organomet. Chem.* **1997**, *532*, 261. – [5j] W. A. Herrmann, L. J. Gooβen, M. Spiegler, *J. Organomet. Chem.* **1997**, *547*, 357. – [5k] D. S. McGuinness, M. J. Green, K. J. Cavell, B. W. Skelton, A. H. White, *J. Organomet. Chem.* **1998**, *565*, 165. – [5l] D. E. Hibbs, M. B. Hursthouse, C. Jones, A. Smithies, *Chem. Commun.* **1998**, 869. – [5m] B. Bildstein, M. Malaun, H. Kopacka, K.-H. Ongania, K. Wurst, *J. Organomet. Chem.* **1998**, *552*, 45. – [5n] B. Bildstein, M. Malaun, H. Kopacka, K.-H. Ongania, K. Wurst, *J. Organomet. Chem.* **1999**, *572*, 177. – [5o] M. H. Voges, C. Rømming, M. Tilset, *Organometallics* **1999**, *18*, 529. – [5p] R. W. Alder, M. E. Blake, C. Bortolotti, S. Bufali, C. P. Butts, E. Linehan, J. M. Oliva, A. G. Orpen, M. J. Quayle, *Chem. Commun.* **1999**, 241. – [5q] W. A. Herrmann, J. Schwarz, M. G. Gardiner, M. Spiegler, *J. Organomet. Chem.* **1999**, *575*, 80.

[6] [6a] W. A. Herrmann, M. Elison, J. Fischer, C. Köcher, G. R. J. Artus, *Angew. Chem. Int. Ed. Engl.* **1995**, *34*, 2371. – [6b] C. D. Frohning, C. W. Kohlpaintner, *Applied Homogeneous Catalysis with Organometallic Compounds* (Eds.: B. Cornils, W. A. Herrmann), *Vol. 1*, VCH, Weinheim, **1996**, p. 90. – [6c] D. Enders, H. Gielen, K. Breuer, *Tetrahedron: Asymmetry* **1997**, *8*, 3571. – [6d] W. A. Herrmann, L. J. Goossen, C. Köcher, G. R. J. Artus, *Angew. Chem. Int. Ed. Engl.* **1996**, *35*, 2805. – [6e] D. Enders, H. Gielen, J. Runsink, K. Breuer, S. Brode, K. Boehn, *Eur. J. Inorg. Chem.* **1998**, 913. – [6f] M. G. Gardiner, W. A. Herrmann, C.-P. Reisinger, J. Schwarz, M. Spiegler, *J. Organomet. Chem.* **1999**, *572*, 239. – [6g] C. Zhang, J. Huang, M. L. Trudell, S. P. Nolan, *J. Org. Chem.* **1999**, *64*, 3804.

[7] D. Enders, K. Breuer, G. Raabe, J. Runsink, J. H. Teles, J.-P. Melder, K. Ebel, S. Brode, *Angew. Chem. Int. Ed. Engl.* **1995**, *34*, 1021.

[8] [8a] Y. Fuchita, K. Hidaka, S. Morinaga, K. Hiraki, *Bull. Chem. Soc. Jpn.* **1981**, *54*, 800. – [8b] W. A. Herrmann, J. Fischer, K. Öfele, G. R. J. Artus, *J. Organomet. Chem.* **1997**, *530*, 259.

[9] K. Öfele, W. A. Herrmann, D. Mihalios, M. Elison, E. Herdtweck, W. Scherer, J. Mink, *J. Organomet. Chem.* **1993**, *459*, 177.

[10] E. Díez-Barra, A. De la Hoz, R. I. Rodríguez-Curiel, J. Tejeda, *Tetrahedron* **1997**, *53*, 2253.

[11] [11a] M. Contel, J. Garrido, M. C. Gimeno, P. G. Jones, A. Laguna, M. Laguna, *Organometallics* **1996**, *15*, 4939. – [11b] R. Usón, J. Forniés, J. Fernández Sanz, M. A. Usón, I. Usón, S. Herrero, *Inorg. Chem.* **1997**, *36*, 1912.

[12] See experimental section.

[13] R. J. Abraham, P. Loftus, *Introduction to NMR Spectroscopy*, John Wiley & Sons, **1988**, p. 196.

[14] D. Stalke, *Chem. Soc. Rev.* **1998**, *27*, 171.

[15] G. M. Sheldrick, *Acta Crystallogr.* **1990**, *A46*, 467.

[16] G. M. Sheldrick, SHELXL-97, *Program for Crystal Structure Refinement*, University of Göttingen **1997**.

Received June 20, 1999
[I99234]

A Novel Route to the 5-[2-(Diphenylphosphanyl)ethyl]-1,2,3,4-tetramethylcyclopentadienyl Ligand – Synthesis and Crystal Structure of $[\eta^5:\eta^1\text{-}C_5(CH_3)_4CH_2CH_2PPh_2]ZrCl_3\cdot THF$

Dmitrii P. Krut'ko,*[a] Maxim V. Borzov,[a] Eduard N. Veksler,[a] Roman S. Kirsanov,[a] and Andrei V. Churakov[b]

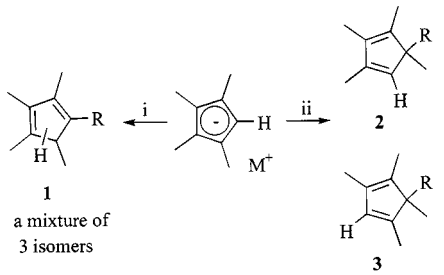
Keywords: Phosphanylethyl-functionalized cyclopentadienyl ligands / Intramolecular coordination / Spiro compounds / Zirconium

The five-step synthesis of the first transition metal complex with the $C_5(CH_3)_4CH_2CH_2PPh_2$ ligand $[\eta^5:\eta^1\text{-}C_5(CH_3)_4CH_2CH_2PPh_2]ZrCl_3\cdot THF$ (**11**), starting from the known compound [2-(dimethylamino)ethyl]tetramethylcyclopentadiene (**4**) via 4,5,6,7-tetramethylspiro[2,4]hepta-4,6-diene (**7**), is reported. Lithium cyclopentadienide $LiC_5(CH_3)_4CH_2CH_2PPh_2$ (**9**), silylated cyclopentadiene $(CH_3)_3SiC_5(CH_3)_4CH_2CH_2PPh_2$ (**10**) and cyclopentadiene $HC_5(CH_3)_4CH_2CH_2PPh_2$ (**12**) were isolated and characterised as pure substances. The crystal structure of the zirconium complex **11** was established by X-ray diffraction analysis.

Introduction

Despite the attractiveness of [2-(diorganophosphanyl)ethyl]tetramethylcyclopentadienes as novel prospective ligands for organometallic synthesis, these side-chain-functionalized cyclopentadienes are relatively unavailable and complexes derived from them are still unknown. Direct alkylation of 1,2,3,4-tetramethylcyclopentadienides with alkyl halides or alkyl toluenesulfonates seems to be of little use in the preparation of 5-alkyl-1,2,3,4-tetramethylcyclopentadienes (**1**), and the question of the regioselectivity of this reaction remains unclear. Both the products of 5-alkylation (**1**)[1][2] and those of 1- and 2-alkylation (**2** and **3**, *gem*-dialkyl-subsituted cyclopentadienes)[3][4] were reported to dominate in the resultant mixtures of alkyltetramethylcyclopentadienes (see Scheme 1).

Nowadays, the synthesis of cyclopentadienes **1** is usually performed by treating 2,3,4,5-tetramethylcyclopenten-2-one with various Grignard or organolithium reagents, followed by dehydration.[5] Unfortunately, this approach is not applicable for the 2-heteroatom-functionalized ethyltetramethylcyclopentadienes **1** ($R = CH_2CH_2ER'_n$; $ER'_n = OR'$, SR', PR'_2, NR'_2, etc.) due to the known instability of 2-heteroatom-functionalized alkylmagnesium or lithium compounds.[6] To overcome this difficulty, preparation procedures for $HC_5(CH_3)_4CH_2CH_2ER'_n$ involving double *sec*-butenylation of esters of 2-heteroatom-substituted propanoic acids $R''O(O)CCH_2CH_2ER'_n$ [$ER'_n = OCH_3$,[3][7] $N(CH_3)_2$,[3] SCH_3[8]], followed by dehydration and cyclization, were developed and shown to give good results. However, synthesis of tetramethyl(2-phosphanylethyl)cyclopentadienes by this latter method has not been reported.



route i dominates:

R-X = $ClCH_2CH_2$-OTs, $M^+ = Li^+$, THF, -10 - 0 °C (ref.[1])

R-X = $ClCH_2CH_2$-Br, $M^+ = K^+$, ether, r.t. (ref.[2])

route ii dominates:

R-X = $ClCH_2CH_2$-OTs, $M^+ = Li^+$, THF, -10 - 0 °C (refs.[3][4])

R-X = $(CH_3)_2NCH_2CH_2$-Cl, $M^+ = K^+$, THF, reflux (ref.[3])

Scheme 1. Direct alkylation of the tetramethylcyclopentadienide

Fortunately, the known cyclopropane ring cleavage reaction of spiro[2,4]hepta-4,6-diene with lithium dialkyl- or diarylphosphides[9] was recently shown for the novel 4,5,6,7-tetramethylspiro[2,4]hepta-4,6-diene (**7**),[2][4] and provided a straightforward route to $LiC_5(CH_3)_4CH_2CH_2PR_2$ (R = alkyl, aryl). In this way, the spiroheptadiene **7** could be, in principle, considered as a key compound in the synthesis of a variety of transition metal complexes derived from tetramethyl(2-phosphanylethyl)cyclopentadienes. However, the availability of the spirane **7** seemed to be rather doubtful. In this paper a convenient preparation procedure for **7**, and synthesis of the first example of a transition metal complex derived from the $C_5(CH_3)_4CH_2CH_2PPh_2$ ligand, are presented.

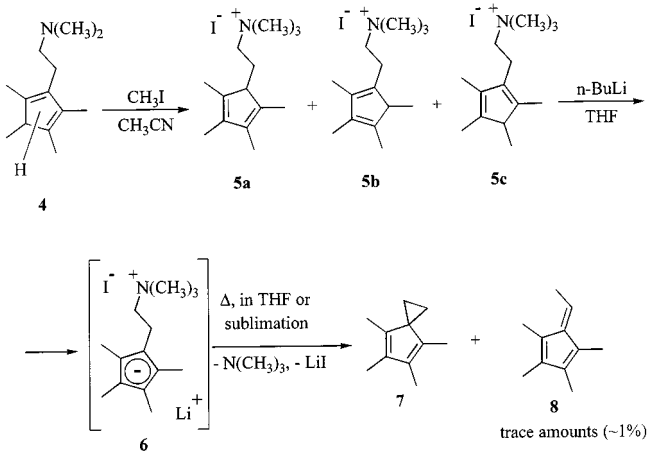
[a] Department of Chemistry, Moscow State University, Leninskie Gory, Moscow, 119899, Russian Federation
Fax: (internat.) + 7-95/932-8846
E-mail: kdp@org.chem.msu.su
[b] N. S. Kurnakov Institute of General and Inorganic Chemistry, Russian Academy of Science,
Leninskii prospect 31, Moscow, 117907, Russian Federation
Fax: (internat.) + 7-95/954-1279
E-mail: churakov@ionchran.rinet.ru

 © WILEY-VCH Verlag GmbH, D-69451 Weinheim, 1999 1434–1948/99/1111–1973 $ 17.50+.50/0

Results and Discussion

The Synthesis of Tetramethylspiroheptadiene 7

5-[2-(Dimethylamino)ethyl]-1,2,3,4-tetramethylcyclopentadiene (**4**) is a well-known and widely used ligand in organometallic chemistry.[10] However, it can also serve as a convenient synthetic precursor of the tetramethylspiroheptadiene **7**. Thus, quaternation of the amine **4** with iodomethane, followed by treatment of the ammonium salt **5** with *n*-butyllithium, leads to the spirane **7** in a good overall yield (see Scheme 2). The isolated product **7** is obtained as an orange/pale yellow liquid (m.p. −7°C). The coloration of **7** is caused by small amounts (ca. 1%) of 1,2,3,4,6-pentamethylfulvene (**8**),[11] which are detectable by ^{1}H-NMR spectroscopy. Probably, the fulvene **8** is formed from the traces of tetramethyl(vinyl)cyclopentadiene which can be expected in the reaction mixture as the "normal" product of a destruction of the quaternary ammonium salt **5** with strong bases.



Scheme 2. Synthesis of the tetramethylspiroheptadiene **7**

The quaternary ammonium salt **5** was isolated as a white crystalline powder with > 95% purity (NMR-spectroscopy data). The dominant identifiable impurity is CH_2=$CHC(O)C(CH_3)$=$CH(CH_3)$. Supposedly, this admixture is formed from $(H_3C)_2NCH_2CH_2C(O)C(CH_3)$=$CH(CH_3)$ which is a typical pollutant of the starting aminoethylcyclopentadiene **4**. It is worth mentioning here that in contrast to the majority of quaternary ammonium iodides, the compound **5** is rather sensitive to air, especially when in a solution, and prolonged operations with it should be carried out either in a dry oxygen-free inert atmosphere or in vacuo.

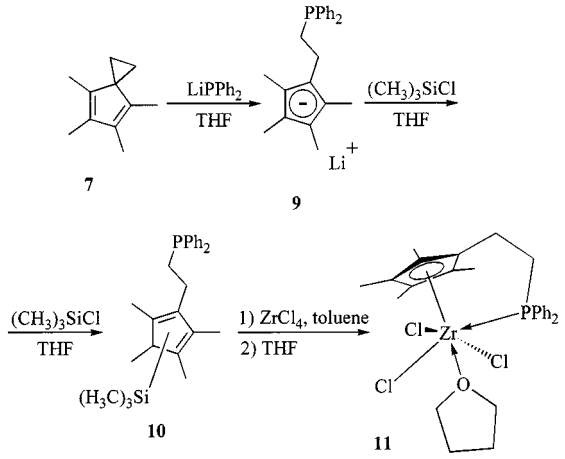
In general, ammonium salts are not typical synthetic precursors of cyclopropanes. In instances where examples of such quaternary salts producing cyclopropanes on treatement with strong bases are known,[12] there are hydrogen atoms at the γ-position to the ammonium group, which possess distinct C−H acidity. Following on from such work,[12] the formation of spiroheptadiene **7** from **5** might be supposed to proceed in at least two steps: deprotonation of cyclopentadiene **5** and the subsequent elimination of $N(CH_3)_3$ (see Scheme 2). In fact in practice, on adding *n*BuLi to a suspension of **5** in THF at −50°C and gradual warming the mixture up to −20°C, the consistency of the initial slurry changes and the precipitate becomes more voluminous. Vigorous evolution of $N(CH_3)_3$ begins only at temperatures exceeding 40−50°C, and to complete the reaction, which is indicated by the dissappearance of the solid phase and no further evolution of $N(CH_3)_3$, it is necessary to heat the reaction mixture under reflux for at least 30 min.

To clarify the reaction pathway, the stepwise conversion of the salt **5** into the spiroheptadiene **7** was attempted. It was found that the reaction of the ammonium salt **5** with *n*BuLi leads first to a solid product **6**, a snow-white powder which is extremely sensitive to air and moisture. Characterisation of the intermediate **6** by means of NMR spectroscopy proved impossible. When attempting to record the ^{1}H-NMR spectrum only signals attributable to the spirane **7** and $N(CH_3)_3$ [NMR (30°C, [D$_8$]THF): δ_H = 2.11 (s), δ_C = 47.94 (s), molar ratio 1:1] were observed; indicative of the thermal instability of **6** in the solvating medium. Moreover, compound **6** is thermally unstable, not only in the presence of THF, but also when dry, and decomposes at a detectable rate when stored at −18°C (evacuated vessel). Thermolysis of dry **6** in vacuo (1.3×10^{-3} mbar) leads to the spirane **7**, $N(CH_3)_3$ (both trapped at −196°C) and LiI (residue) in a molar ratio 1:1:1. Despite the difficulties of characterising **6** by the usual techniques, the authors believe, however, that this deprotonation product possesses the structure suggested in Scheme 2.

Preparation of $LiC_5(CH_3)_4CH_2CH_2PPh_2$ (9) and $[\eta^5{:}\eta^1\text{-}C_5(CH_3)_4CH_2CH_2PPh_2]ZrCl_3\cdot THF$ (11)

The complete synthesis of $[\eta^5{:}\eta^1\text{-}C_5(CH_3)_4CH_2CH_2PPh_2]ZrCl_3\cdot$THF (**11**) is presented in Scheme 3. The three-membered ring cleavage reaction for the spirane **7** with $LiPPh_2$ was performed as described previously,[4] but the excess of $LiPPh_2$ employed was decreased. In comparison with the considerably exothermic reaction of spiro[2,4]heptadiene-4,6 with $LiPPh_2$, which proceeds vigorously even at 10−15°C, in the case of **7** heating at 80−100°C for at least 8 h was required. It is suggested that this is a result of a lower thermodynamic preference for the formation of the pentaalkylcyclopentadienide anion compared to that of the monoalkylcyclopentadienide anion. The elevated temperature required also complicates the reaction due to the process of THF ring cleavage with phosphides,[13] and makes it necessary to apply a considerable excess of $LiPPh_2$.

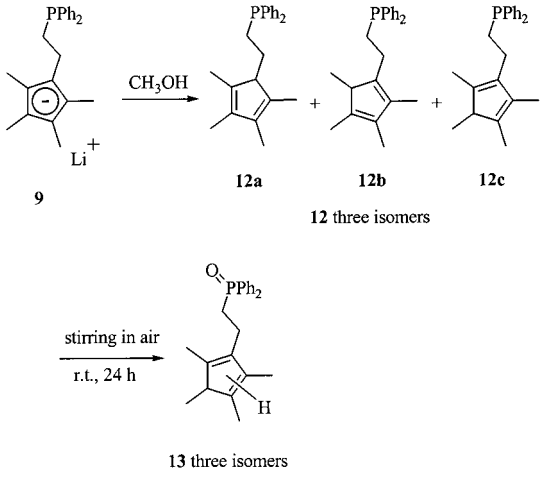
In its pure state the lithium salt **9** is a white crystalline powder, which is extremely sensitive to air and moisture. It is moderately soluble in THF at room or lower temperature. However, the solubility of **9** grows rapidly within the range 80−100°C (sealed vessel), and on cooling a stable supersaturated solution is formed. Previously, we observed that in contrast to the practically insoluble $LiC_5(CH_3)_5$ or $LiC_5(CH_3)_4H$, lithium cyclopentadienides $LiC_5(CH_3)_4CH_2CH_2ECH_3$ (E = O[7], S[8]) and $LiC_5H_4CH_2CH_2PPh_2$,[14]



Scheme 3. Synthesis of the halfsandwich complex **11**

with *n*-donor heteroatom functionalities in side chains, exhibit very good solublities in THF. Thus, from this viewpoint, the cyclopentadienide **9** presents an intermediate case. In the ^{1}H-, ^{13}C{^{1}H}- and ^{31}P{^{1}H}-NMR spectra of **9** ([D$_8$]THF, 30°C) the signals are broadened, probably due to the inter- and/or intramolecular processes of coordination of Li^+ to PPh_2 groups. At the same time no signals due to [H$_8$]THF are present and, thus, one can conclude that the lithium salt **9** contains no solvated THF in the solid state. Taking all these facts into account, it is supposed that in the solid state **9** possesses a "multidecker polymer" structure, which is characteristic for C_5H_5Li,[15] while in a THF solution the cyclopentadienide **9** exists as mono-, or at least oligomeric, species with PPh_2 groups coordinated to Li^+.

As mentioned above, the preparation of $HC_5(CH_3)_4CH_2CH_2PPh_2$ (**12**) was reported previously by other workers.[1] In order to compare the present results with those given in this previous work dry cyclopentadienide **9** was quenched with methanol and the ligand of interest isolated in its C−H form, **12**, as a viscous pale yellow oil sensitive to air (see Scheme 4).



Scheme 4. Preparation and oxidation of the [2-diphenylphosphanyl)-ethylcyclopentadiene **12**

The assignment of the signals in the NMR spectra was performed on the basis of homo- and heteronuclear correlation spectroscopy experiments and coupled ^{13}C spectra. The assignment of the signals to each of the isomers was additionally confirmed by homonuclear NOE experiments (difference spectra), with the relative intensities of the signals also taken into account. As was expected, it was found that **12** is a mixture of three (not two, as reported in ref.[1]) isomers, **12a−c**, in a molar ratio of 1:1.4:1.7, which is close to that observed previously for the three analogous isomers of $HC_5(CH_3)_4CH_2CH_2SCH_3$ (molar ratio ca. 3:4:5).[8] It must be noted here that, in general, the ^{1}H-, ^{31}P{^{1}H}-, and especially ^{13}C{^{1}H}-NMR data for **12** in C_6D_6 solution presented in this work are in poor agreement with that reported by J. Szymoniak et al. for **12** in the same solvent.[1]

When a pentane solution of **12** is exposed to air, the precipitation of the corresponding phosphane oxides, **13a−c** (white amorphous powder), begins after several minutes. However, to complete the oxidation it is neccesary to stir the pentane solution for at least 24 h in air {NMR-spectroscopy monitoring of the reaction mixture; δ_P = 30.0 [s, (**13b**)], 30.1 [s, (**13c**)], 31.7 [s, (**13a**)]}.

In the ^{1}H- and ^{13}C-NMR spectra the isomers **12a−c**, **5a−c**[16] and the previously reported $HC_5(CH_3)_4CH_2CH_2SCH_3$[8] exhibit some significant common features which are worth mentioning here. In both these cases the side-chain protons H^6 and H^7 in the symmetric **a** isomers are markedly shielded (up to 0.5−0.6 ppm) with respect to the same protons in the **b** and **c** isomers. A similar high-field shift (up to 4−8 ppm) is also observed for the signals of C^7 in the **a** isomers. In contrast, the C^6 carbon atoms in the **a** isomers are deshielded (up to ca. 2 ppm) relative to the C^6 carbon atoms in the **b** and **c** isomers. These particularities of the ^{1}H- and ^{13}C{^{1}H}-NMR spectra also seem to be characteristic of a broad variety of 2-heteroatom-functionalized ethyltetramethylcyclopentadienes $HC_5(CH_3)_4CH_2CH_2X$ (X = O, S, N, P heteroatom functionality).

Lithium pentaalkylcyclopentadienides are the most usual and widely used direct precursors of the corresponding cyclpentadienyltrihalozirconium compounds. Undoubtedly, if treated with $ZrCl_4$ in either ether or toluene, the lithium salt **9** would give the desired half-sandwich **11**. However, in this work it was preferred to introduce an additional step and prepare the complex **11** via the intermediate trimethylsilyl-substituted cyclopentadiene **10**.

Cyclopentadienyltrimethylsilanes can be considered as one of the most convenient precursors of the monocyclopentadienyl trihalides of the Group IV metals $C_5H_5MCl_3$ (M = Ti, Zr and Hf).[17] Not long ago this method proved to be useful in the preparation of their ring-permethylated analogues, $C_5(CH_3)_5MCl_3$ (M = Ti, Zr and Hf).[18] In comparison with the route via lithium cyclopentadienides, application of silylated cyclopentadienes affords a number of advantages arising from the fact that the presence of LiCl as a co-product is initially excluded. It is known that LiCl can interact with the target half-sandwiches and form stable ionic products.[19] This complicates the isolation procedure,

and in some cases high-vacuum sublimation is necessary for the final purification of a metal complex.[7,8,20]

Treatment of **9** with $(CH_3)_3SiCl$ in THF followed by removal of the solvent and high-vacuum distillation gives the silane **10** as an air-sensitive pale yellow viscous oil, in an almost quantitative yield. It is an interesting fact that in contrast to the reaction between $(CH_3)_3SnCl$ and $C_5(CH_3)_5Li$ silylation of **9** does not proceed in ether, even at elevated temperatures (80−90°C, 7 h), and the initial cyclopentadienide **9** can be regenerated quantitatively. As expected, the broadened exchange signals in the ^1H- and $^{31}P\{^1H\}$-NMR spectra of **10** indicate that it exists as an equilibrium mixture of three isomers [isomeric with respect to the position of the $(CH_3)_3Si$ group].

The zirconium complex **11** was obtained in a similar fashion to its ring nonmethylated analogue [η^5:η^1-$C_5H_4CH_2CH_2PPh_2$]$ZrCl_3$·THF (**14**),[14] and isolated as an adduct with one molecule of THF (well-formed pale yellow crystals moderately sensitive to air and moisture). The half-sandwich compound **11** was characterised by elemental analysis, mass spectrometry, ^1H-, $^{13}C\{^1H\}$- and $^{31}P\{^1H\}$-NMR spectroscopy and X-ray diffraction analysis (see below). In the NMR spectra, apart from the evident changes caused by replacement of CH_3 groups for hydrogen atoms, the parameters of **11** and **14** are rather similar. The ^{31}P shift of the PPh_2 group in CD_2Cl_2 for the compound **11** (δ_P = 5.8) indicates that in a solution this group remains coordinated to the metal centre [compare with δ_P = 6.1 for **14** (in CD_2Cl_2)[14] and $\delta_P \approx -14$ for non-coordinated PPh_2 groups of (η^5-$C_5H_4CH_2CH_2PPh_2$)(η^5-C_5H_5)$ZrCl_2$[14] and compounds **9**, **10** and **12**].[21]

It is also notable that intramolecular coordination of the PPh_2 group to the Zr centre inverts the order of the absolute $^1J_{C-P}$ and $^2J_{C-P}$ values in the $Ph_2PCH_2CH_2$ fragment. Thus, both for **11** and **14** direct $|^1J_{C-P}|$ exceeds geminal $|^2J_{C-P}|$, while for all other previously studied compounds possessing the non-coordinated $Ph_2PCH_2CH_2$ moiety $|^1J_{C-P}| < |^2J_{C-P}|$.[14]

X-ray Crystal Structure Analysis of the Complex 11

The crystal structure of **11** is shown in Figure 1. The central Zr atom possesses a distorted octahedral coordination, if one assumes that the cyclopentadienyl ligand occupies one coordination site. The cyclopentadienyl ring and the THF molecule lie in the apical positions while the phosphanyl group and three chlorine atoms occupy equatorial positions. The deviation of the Zr atom from the equatorial plane towards the cyclopentadienyl ligand is 0.53 Å. Analysis of the Cambridge Structural Database (Release: April 1998)[22] shows that the Zr−Cl distances [2.4619(10)−2.4921(8) Å] in **11** are within the range of normal values for terminal Zr^{IV}−Cl bonds in monocyclopentadienyl complexes (2.385−2.561 Å). The Zr−P bond [2.8906(11) Å] is significantly longer than was found for both crystalline modifications of the closely related complex **14** [2.8474(5)−2.8729(11) Å].[14] The latter fact can be explained by the influence of the electron-donating effect of four methyl groups at the cyclopentadienyl ring. The Zr−O(THF) bond [2.419(2) Å] in the structure of **11** is also much longer than was observed for the same apical bonds in $(C_5H_4R)ZrCl_3$·2THF [R = H, 2.393(3) Å; R = Me, 2.377(2) Å],[23] and in both modifications of **14** [2.350(3)−2.3613(12) Å].[14]

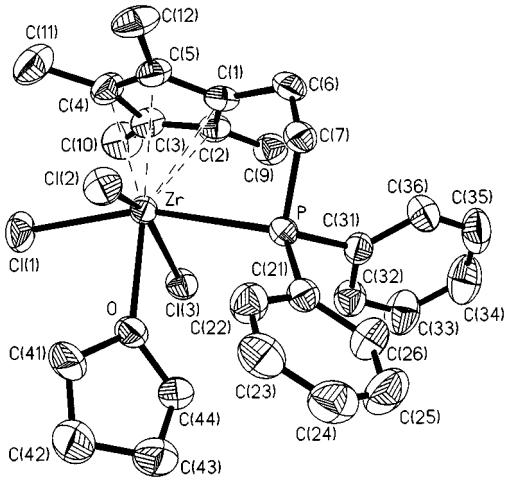


Figure 1. Molecular structure of complex **11**; displacement ellipsoids are shown at 50% probability level; hydrogen atoms are omitted for clarity; selected bond lengths [Å] and angles [°]: Zr−O 2.419(2), Zr−Cl(1) 2.4619(10), Zr−Cl(2) 2.4647(9), Zr−Cl(3) 2.4921(8), Zr−P 2.8906(11), Zr−PL, 2.256(1), P−C(31) 1.828(3), P−C(7) 1.829(3), P−C(21) 1.835(3); O−Zr−Cl(1) 81.72(5), O−Zr−Cl(2) 76.64(5), O−Zr−Cl(3) 76.76(5), Cl(1)−Zr−Cl(2) 89.69(3), Cl(1)−Zr−Cl(3) 90.06(3), Cl(2)−Zr−Cl(3) 153.15(3), O−Zr−P 77.30(5), Cl(1)−Zr−P 158.55(3), Cl(2)−Zr−P 81.23(3), Cl(3)−Zr−P 89.45(3), C(31)−P−C(7) 104.62(14), C(31)−P−C(21) 102.52(12), C(7)−P−C(21) 104.29(13), C(7)−P−Zr 98.59(11), C(21)−P−Zr 123.59(9), C(31)−P−Zr 120.43(9), C(1)−C(6)−C(7) 113.6(2), C(6)−C(7)−P 108.9(2); PL means the least-squares plane of the cyclopentadienyl ring

The cyclopentadienyl ring C(1) through C(5) is planar to within 0.009 Å. All four methyl substituents deviate slightly from the least-squares plane of the ring in the direction opposite to the Zr atom (0.111−0.241 Å). The maximum deviation was found for C(12), which is probably caused by the short intramolecular contact with the Cl(2) atom (3.116 Å).

The coordination environment of the phosphorus atom represents a distorted tetrahedron with approximately equal C−P−C angles [102.52(12)−104.62(14)°]. However, the exocyclic C(Ph)−P−Zr angles [120.43(9)° and 123.59(9)°] are much larger than the endocyclic C(7)−P−Zr angle [98.59(11)°]. Thus, the (Zr−)C(1)−C(6)−C(7)−P−Zr pseudo-metallacycle is significantly strained.

Conclusion

It is evident, that the zirconium half-sandwich **11** may be considered as only the first "model" example of a transition metal complex derived from tetramethyl(2-phosphanylethyl)cyclopentadienyl ligands. Moreover, the authors are convinced that the availability of the key tetramethylspiroheptadiene **7** by the method reported herein opens a facile pathway to a broad variety of transition metal complexes,

not only with the $C_5(CH_3)_4CH_2CH_2PR_2$ ligands but also, probably, with their 2-arsanylethyl analogues.

Experimental Section

General Remarks: All procedures were performed using either conventional glassware in dry oxygen-free argon or in sealed evacuated glass vessels. The solvents employed (and their perdeuterated analogues) were dried with, and distilled from, conventional agents {namely: diethyl ether and THF (sodium benzophenone ketyl); toluene, heptane and pentane (Na/K alloy); CH_2Cl_2 (P_2O_5 and then CaH_2); acetonitrile (a minimal amount of P_2O_5)]; CD_3CN [stirred with and distilled from CaH_2 via a high-vacuum line (1.3×10^{-3} mbar) at 0−10°C]}. When performing procedures in evacuated vessels, the degassed solvents were stored in evacuated reservoirs over the corresponding drying agent, and then transferred via a high-vacuum line directly into reaction vessels by trapping with liq. N_2. Iodomethane (Fluka) was distilled from CaH_2; chlorotrimethylsilane (Fluka) was refluxed with and distilled from aluminium powder (high-vacuum line); diphenylphosphane and zirconium tetrachloride (Fluka) were used without additional purification. $(CH_3)_2NCH_2CH_2C_5(CH_3)_5H$ (**4**) was prepared according to the modified procedure.[3] Thus, for the dehydration and cyclization of $[(CH_3)_2NCH_2CH_2]C(OH)[(CH_3)CH{=}CH(CH_3)]_2$ anhydrous TsOH and DME were used instead of $TsOH{\cdot}H_2O$ and diethyl ether. Lithium diphenylphosphide was obtained by the reaction of Ph_2PH with *n*-butyllithium in pentane, washed with the same solvent on a glass filter and dried in vacuo. − ^1H, ^{13}C, and $^{31}P\{^1H\}$ NMR: Varian VXR-400 spectrometer at 400, 100, and 162 MHz, respectively, internal reference standards CD_3CN (δ_H = 1.93 and δ_C = 1.3), $CDCl_3$(δ_H = 7.24 and δ_C = 77.0), C_6D_6 (δ_H = 7.15 and δ_C = 128.0), CD_2Cl_2 (δ_H = 5.32 and δ_C = 53.8), [D_8]THF (δ_H = 1.73 and δ_C = 25.3), external reference 85% H_3PO_4 ($^{31}P\{^1H\}$). − Elemental analyses: Carlo−Erba automated analyser. − Mass spectra: Kratos-MS-890 and Varian MAT CH7a Fa spectrometers.

Ammonium Salt 5: 25 mL (57.11 g, 402.4 mmol) of CH_3I was added dropwise, at a rate sufficient to maintain gentle reflux, to a stirred solution of cyclopentadiene **4** (38.90 g, 201.2 mmol) in 100 mL of CH_3CN. The reaction mixture was stirred under reflux for an additional 1 h and left overnight at room temp. The crystalline precipitate was filtered off, washed on a glass filter with an ice-cold mixture of CH_3CN/Et_2O (1:1, 2 × 20 mL) and with ether (3 × 20 mL) and dried in vacuo. The mother liquor and washings were combined, concentrated to ca. 50 mL and cooled to −18°C. The precipitated crystals were separated and washed as described above. The mother liquor and washings were worked up once more to give an additional portion of the product. The total amount of quaternary ammonium salt **5** was 47.30 g (70%). Decomposition at ca. 120°C without melting. − ^1H NMR (30°C, CD_3CN): δ = 0.98, 1.00 (each d, $^3J_{HH}$ = 7.6 Hz, $CHC\mathit{H}_3$), 1.69, 1.74, 1.75, 1.78, 1.80, 1.81, 1.86 (each br. s, CCH_3), 2.12 (m, $CHC\mathit{H}_2CH_2N$), 2.54 (m, $C\mathit{H}CH_3$, $CC\mathit{H}_2CH_2N$), 2.66 (m, $C\mathit{H}CH_3$, $CHCH_2C\mathit{H}_2N$), 2.80 (m, $C\mathit{H}CH_2CH_2N$, $CC\mathit{H}_2CH_2N$), 3.04, 3.17, 3.20 (each s, NCH_3), 3.25, 3.43 (each m, $CCH_2C\mathit{H}_2N$). − ^{13}C NMR (30°C, CD_3CN): δ = 10.96, 11.23, 11.56, 11.68, 11.81, 11.97 (each q, $^1J_{CH}$ = 125 Hz, $C\mathit{C}H_3$), 14.19, 14.34 (each q, $^1J_{CH}$ = 126 Hz, $CH\mathit{C}H_3$), 20.35, 20.79 (each t, $^1J_{CH}$ = 129 Hz, $C\mathit{C}H_2CH_2N$), 20.93 (t, $^1J_{CH}$ = 129 Hz, $CH\mathit{C}H_2CH_2N$), 50.17, 52.51 (each d, $^1J_{CH}$ = 123 Hz, $\mathit{C}HCH_3$), 53.51 (d, $^1J_{CH}$ = 123 Hz, $\mathit{C}HCH_2CH_2N$), 53.68 (br. q, $^1J_{CH}$ = 143 Hz, NCH_3), 62.84 (t, $^1J_{CH}$ = 144 Hz, $CHCH_2\mathit{C}H_2N$), 65.71, 66.20 (each t, $^1J_{CH}$ = 144 Hz, $CCH_2\mathit{C}H_2N$), 132.46, 132.96, 133.96, 134.69, 135.23, 138.10, 139.41, 140.02, 140.89, 143.55 (each s, $\mathit{C}CH_3$, $\mathit{C}CH_2CH_2N$). − EI MS (250°C, 70 eV); *m/z* (%): 149 (8) $[HC_5(CH_3)_4CH_2CH_2^+]$, 148 (55) $[HC_5(CH_3)_4CH{=}CH_2^+]$, 147 (8) $[C_7H_3(CH_3)_4^+]$, 142 (5) $[CH_3I^+]$, 134 (5) $[(CH_3)_4C_5{=}CH_2^+]$, 133 (100) $[C_7H_4(CH_3)_3^+]$, 128 (12) $[HI^+]$, 127 (10) $[I^+]$, 119 (21) $[C_7H_5(CH_3)_2^+]$, 105 (41) $[C_7H_6(CH_3)^+]$, 91 (42) $[C_7H_7^+]$, 59 (27) $[(CH_3)_3N^+]$, 58 (61) $[(CH_3)_2N{=}CH_2^+]$. − Compound **5** presents a material of > 95% purity (^1H-NMR data). The dominant admixture is $CH_2{=}CHC(O)C(CH_3){=}CH(CH_3)$. − ^1H NMR (30°C, CD_3CN): δ = 1.41 (dq, 3 H, $^3J_{HH}$ = 6.8 Hz, $^4J_{HH}$ = 1.6 Hz, $=CHC\mathit{H}_3$), 1.77 [quint, 3 H, $^4J_{HH}$ = $^5J_{HH}$ = 1.6 Hz, $=C(CH_3)-$], 5.21 (dd, 1 H, $^2J_{HH}$ = 1.6 Hz, $^3J_{HH}$ = 11.0 Hz, *cis*-$CH_2{=}$), 5.35 (dd, 1 H, $^2J_{HH}$ = 1.6 Hz, $^3J_{HH}$ = 17.1 Hz, *trans*-$CH_2{=}$), 5.43 (qq, 1 H, $^3J_{HH}$ = 6.8 Hz, $^4J_{HH}$ = 1.6 Hz, $=C\mathit{H}CH_3$), 6.87 (dd, 1 H, $^3J_{HH}$ = 17.1 Hz, $^3J_{HH}$ = 11.0 Hz, $C\mathit{H}{=}CH_2$).

4,5,6,7-Tetramethylspiro[2,4]hepta-4,6-diene (7): 57 mL of a 2.16 M hexane solution of *n*-butyllithium (124.0 mmol) was added to a stirred suspension of the ammonium salt **5** (41.53 g, 123.9 mmol) in 250 mL of THF at −60°C. The reaction mixture was allowed to warm gradually to room temp. under continued stirring. Scarlet coloration of the solution appeared and deepened while the white precipitate became more voluminous (ca. −20°C). The mixture was then heated for 30 min under reflux. Vigorous evolution of $N(CH_3)_3$ began at 40−50°C. The colour of the solution changed slowly from dark scarlet to pale orange and the precipitate dissolved. The resultant solution was cooled down to 0°C and poured into an approximately equal volume of ice-cold water. The organic layer was separated, the aqueous layer extracted with Et_2O (3 × 50 mL) and the combined extracts dried with $MgSO_4$. On removing the solvents in a rotary evaporator the product was isolated by distillation as a yellow oil moderately sensitive to air, b.p. 47−48°C at 1.5 mbar. M.p. −7°C. Yield 15.57 g (85%). Compound **7** exhibited a pronounced tendency to undergo polymerisation and was stored at −18°C. − ^1H NMR (30°C, $CDCl_3$): δ = 1.23 (s, 4 H, CH_2), 1.64 (s, 6 H, CH_3), 1.94 (s, 6 H, CH_3). − ^{13}C NMR (30°C, $CDCl_3$): δ = 8.76 (q, $^1J_{CH}$ = 125 Hz, CH_3), 11.21 (t, $^1J_{CH}$ = 164 Hz, CH_2), 11.53 (q, $^1J_{CH}$ = 125 Hz, CH_3), 37.44 (s, C-3), 133.99, 134.39 (each s, $\mathit{C}CH_3$). − EI MS (25°C, 70 eV); *m/z* (%): 148 $[M]^+$ (3), 147 $[C_7H_3(CH_3)_4]^+$ (100), 133 $[C_7H_4(CH_3)_3]^+$ (33), 119 $[C_7H_5(CH_3)_2]^+$ (11), 105 $[C_7H_6(CH_3)]^+$ (10), 91 $[C_7H_7]^+$ (16), 28 $[C_2H_4]^+$ (15). − $C_{11}H_{16}$ (148.25): calcd. C 89.12, H 10.88; found C 88.73, H 11.11.

Deprotonation Product 6:[24] 0.33 mL of a 2.18 M solution of *n*BuLi in hexane (0.72 mmol) was added to a stirred suspension of **5** (0.23 g, 0.69 mmol) in 20 mL of THF at −60°C, and the reaction mixture allowed to warm up to ca. 0°C. The voluminous snow-white precipitate was separated by filtration, washed rapidly on a glass filter with THF (3 × 5 mL) and dried in vacuo to give 0.22 g of **6** as an extremely air- and moisture-sensitive powder. The product was not stable thermally and decomposed noticeably even when stored in an evacuated vessel at −18°C (and considerably faster when stored under THF).

Thermolysis of Deprotonation Product 6:[24] A small portion (41.5 mg, 0.12 mmol) of **6** was placed into a glass tube connected via a liq. N_2 cooled trap to a high-vacuum line. The tube was heated for 20 min at 80°C and then for 20 min at 120°C. The pale yellow liquid (24.0 mg) in the trap presented an equimolar mixture of $N(CH_3)_3$ (0.12 mmol) and spirane **7** (0.12 mmol) (^1H-NMR data). The pale yellow solid residue in the tube (16.5 mg) was found to be LiI (0.12 mmol).

Lithium Cyclopentadienide (9):[24] Solutions of spiroheptadiene **7** (2.46 g, 16.6 mmol) and lithium diphenylphosphide (4.00 g, 22.6 mmol) in THF (total volume 75 mL) were mixed at room

temp. and heated at 90−100°C for 10 h. The solvent was removed by distillation from a hot water bath and the residual brown/red oil allowed to cool down to room temp. In 1 d formation of a white precipitate began. After introducing 15 mL of THF and stirring at room temp. for 5 h, the precipitate was filtered off, washed with 10 mL of cold THF and then with 15 mL of ether. On drying in vacuo 4.50 g (80%) of **9** was obtained as a white powder which was extremely sensitive to air and moisture. − ^{1}H NMR (30°C, [D$_8$]THF): δ = 1.70 (br., 12 H, CH_3), 1.99 (br., 2 H, CH_2P), 2.32 (br., 2 H, CH_2CH_2P), 7.26 (m, 6 H, *meta*-, *para*-C_6H_5), 7.41 (m, 4 H, *ortho*-C_6H_5). − ^{13}C{^{1}H} NMR (30°C, [D$_8$]THF): δ = 11.1 (br. s, CH_3), 23.4 (br. d, $^2J_{CP}$ = 18 Hz, CH_2CH_2P), 32.2 (br. d, $^1J_{CP}$ = 14 Hz, CH_2P), 105.9, 106.7 (each br. s, CCH_3), 112.5 (br. d, $^3J_{CP}$ = 14 Hz, CCH_2CH_2P), 128.65 (s, *para*-C_6H_5), 128.82 (d, $^3J_{CP}$ = 6.0 Hz, *meta*-C_6H_5), 133.61 (d, $^2J_{CP}$ = 18.0 Hz, *ortho*-C_6H_5), 141.2 (br. d, $^1J_{CP}$ = 15 Hz, *ipso*-C_6H_5). − ^{31}P{^{1}H} NMR (30°C [D$_8$]THF): δ = −14.6 (br.).

(2-Diphenylphosphanylethyl)tetramethylcyclopentadiene (Mixture of Isomers) (12):[24] 10 mL of dry degassed methanol [from over $Mg(OCH_3)_2$] was condensed via a high-vacuum line directly onto 0.67 g (1.97 mmol) of lithium cyclopentadienide **9** by trapping with liq. N_2 and the mixture allowed to warm up to room temp. On trapping methanol with liq. N_2 product **12** was isolated by distillation in vacuo as a pale yellow viscous oil (0.65 g, 99%). − ^{1}H NMR (30°C, C_6D_6): δ = 0.90 [d, $^3J_{HH}$ = 7.6 Hz, $CHCH_3$ (**12c**)], 0.95 [d, $^3J_{HH}$ = 7.6 Hz, $CHCH_3$ (**12b**)], 1.65, 1.68, 1.71, 1.76, 1.78 (each br. s, CCH_3), 1.68 [obscured m, CH_2P (**12a**)], 1.85 [m, CH_2CH_2P (**12a**)], 2.06−2.19 [m, CH_2P (**12b**, **12c**)], 2.37 [m, CH (**12b**)], 2.42 [m, CH_2CH_2P (**12b**, **12c**)], 2.52 [m, CH (**12a**)], 2.57 [m, CH (**12c**)], 7.01−7.13 (m, *meta*-, *para*-C_6H_5), 7.40−7.50 (m, *ortho*-C_6H_5). − ^{13}C NMR (30°C, C_6D_6): δ = 11.17, 11.20, 11.27, 11.31, 11.76, 11.80, 11.85 (each q, $^1J_{CH}$ = 126 Hz, CCH_3), 14.16 [q, $^1J_{CH}$ = 128 Hz, $CHCH_3$ (**12c**)], 14.25 [q, $^1J_{CH}$ = 128 Hz, $CHCH_3$ (**12b**)], 21.86 [dt, $^1J_{CH}$ = 128 Hz, $^1J_{CP}$ = 11.8 Hz, CH_2P (**12a**)], 22.61 [dt, $^1J_{CH}$ = 128 Hz, $^2J_{CP}$ = 18.4 Hz, CH_2CH_2P (**12b**)], 22.92 [dt, $^1J_{CH}$ = 128 Hz, $^2J_{CP}$ = 17.7 Hz, CH_2CH_2P (**12c**)], 24.10 [dt, $^1J_{CH}$ = 128 Hz, $^2J_{CP}$ = 19.7 Hz, CH_2CH_2P (**12a**)], 29.20 [dt, $^1J_{CH}$ = 128 Hz, $^1J_{CP}$ = 14.7 Hz, CH_2P (**12b**)], 29.91 [dt, $^1J_{CH}$ = 128 Hz, $^1J_{CP}$ = 14.3 Hz, CH_2P (**12c**)], 49.41 [d, $^1J_{CH}$ = 123 Hz, CH (**12c**)], 51.76 [d, $^1J_{CH}$ = 123 Hz, CH (**12b**)], 56.86 [dd, $^1J_{CH}$ = 123 Hz, $^3J_{CP}$ = 13.4 Hz, CH (**12a**)], 128.60 [dm, $^1J_{CH}$ = 158 Hz, *meta*-, *para*-C_6H_5], 133.17 [dm, $^1J_{CH}$ = 158 Hz, *ortho*-C_6H_5], 133.58, 134.22, 134.54, 135.02, 136.42, 138.21, 138.25, 138.26 (each s, CCH_3), 139.46 [d, $^3J_{CP}$ = 12.5 Hz, CCH_2CH_2P (**12b**)], 139.79 [d, $^1J_{CP}$ = 14.6 Hz, *ipso*-C_6H_5], 139.83 [d, $^1J_{CP}$ = 14.0 Hz, *ipso*-C_6H_5], 139.94 (d, $^1J_{CP}$ = 14.7 Hz, *ipso*-C_6H_5), 142.46 [d, $^3J_{CP}$ = 12.3 Hz, CCH_2CH_2P (**12c**)]. − ^{31}P{^{1}H} NMR (30°C, C_6D_6): δ = −14.4 [s, (**12c**)], −13.9 [s, (**12b**)], −12.6 [s, (**12a**)]. − ^{1}H NMR (30°C, CD_2Cl_2): δ = 1.00 [d, $^3J_{HH}$ = 7.6 Hz, $CHCH_3$ (**12c**)], 1.04 [d, $^3J_{HH}$ = 7.6 Hz, $CHCH_3$ (**12b**)], 1.56 [m, CH_2P (**12a**)], 1.74, 1.78, 1.82, 1.84, 1.86, 1.87 (each br. s, CCH_3), 1.84 [obscured m, CH_2CH_2P (**12a**)], 2.14−2.31 [m, CH_2P (**12b**, **12c**)], 2.37 [m, CH_2CH_2P (**12b**, **12c**)], 2.50 [m, CH (**12b**)], 2.71 [m, CH (**12a**, **12c**)], 7.34−7.45 (m, *meta*-, *para*-C_6H_5), 7.49−7.54 (m, *ortho*-C_6H_5). − EI MS (250°C, 70 eV); *m*/*z* (%): 334 (88) [M$^+$], 319 (85) [M$^+$ − CH_3], 306 (69) [M$^+$ − CH_3−CH_3], 291 (25) [M$^+$ − CH_3−CH_3−CH_3], 199 (100) [$(C_6H_5)_2PCH_2^+$], 121 (99) [M$^+$ − $(C_6H_5)_2PCH_2CH_2$]. − $C_{23}H_{27}P$ (334.45): calcd. C 82.60, H 8.14; found C 83.04, H 8.27.

[2-(Diphenylphosphanyl)ethyl]tetramethyl(trimethylsilyl)cyclopentadiene (10):[24] 1 mL (0.86 g, 7.92 mmol) of $(CH_3)_3SiCl$ was added at room temp. to a suspension of cyclopentadienide **9** (2.51 g, 7.37 mmol) in 20 mL of THF. The stirred reaction mixture was heated at 80°C for 30 min and the solvent removed into a trap cooled with liq. N_2. The product was isolated by distillation in vacuo as a viscous pale yellow oil sensitive to air. Yield 2.98 g (99%). − ^{1}H NMR (30°C, C_6D_6): δ = −0.20 [br., $Si(CH_3)_3$], −0.10 [br., $Si(CH_3)_3$], 1.15 [br., $CH_3CSi(CH_3)_3$], 1.74, 1.79 (each br., CCH_3,), 2.19 (br., CH_2P), 2.49(br., CH_2CH_2P), 7.00−7.12 (br. m, *meta*-, *para*-C_6H_5), 7.42−7.52 (br. m, *ortho*-C_6H_5). − ^{31}P{^{1}H} NMR (30°C, C_6D_6): δ = −13.8 (br.), −13.0 (br.). − EI MS (25°C, 70 eV); *m*/*z* (%): 406 (9) [M$^+$], 391 (8) [M$^+$ − CH_3], 334 (33) [M$^+$ − $CH_2Si(CH_3)_2$], 333 (85) [M$^+$ − $Si(CH_3)_3$], 221 (23) [M$^+$ − $(C_6H_5)_2P$], 220 (84) [M$^+$ − $(C_6H_5)_2PH$], 199 (46) [$(C_6H_5)_2PCH_2^+$], 185 (22) [$(C_6H_5)_2P^+$], 147 (62) [$C_7H_3(CH_3)_4^+$], 146 (87) [M$^+$ − $(C_6H_5)_2PH$−$HSi(CH_3)_3$], 134 (57) [$C_5(CH_3)_4$=CH_2^+], 133 (80) [$C_7H_4(CH_3)_3^+$], 119 (47) [$C_7H_5(CH_3)_2^+$], 105 (47) [$C_7H_6(CH_3)^+$], 91 (60) [$C_7H_7^+$], 73 (100) [$Si(CH_3)_3^+$]. − $C_{26}H_{35}PSi$ (406.63): calcd. C 76.80, H 8.68; found C 77.02, H 8.94.

Zirconium Complex 11:[24] A suspension of 1.28 g (5.49 mmol) of $ZrCl_4$ in 10 mL of toluene and a solution of 2.23 g (5.48 mmol) of silane **10** in 30 mL of the same solvent were mixed at room temp. and the reaction mixture heated at 90−100°C under vigorous stirring for 3 h. On cooling down to room temp., the reaction mixture consisted of a bright yellow solution and a small amount of a brown viscous oil. The solution was decanted and the oil extracted with hot toluene (2 × 5 mL). Removal of all of the volatile components from the combined extracts gave 2.54 g (87%) of crude THF-free **11** as a viscous lemon yellow oil. Addition of 10 mL of THF led to complete dissolution of crude **11**. In less than 1 min fast crystallization began. On removing approximately one-half of the initial amount of THF the mixture was kept overnight. The crystalline product **11** was filtered off, washed on a filter with ether (2 × 5 mL) and dried in vacuo. Yield 1.11 g (34%). The product decomposed at 143°C with foaming (elimination of THF). Single crystals suitable for X-ray analysis were obtained by crystallization from hot THF. − ^{1}H NMR (30°C, CD_2Cl_2): δ = 1.75 (m, 4 H, CH_2CH_2O in THF), 1.98, 2.18 (each s, 6 H, CH_3), 2.97 (dt, 2 H, $^3J_{HH}$ = 7.0 Hz, $^3J_{HP}$ = 21.0 Hz, CH_2CH_2P), 3.09 (q, 2 H, $^3J_{HH}$ = 7.0 Hz, $^2J_{HP}$ = 7.0 Hz, CH_2P), 3.77 (m, 4 H, CH_2O in THF), 7.40 (m, 6 H, *meta*-, *para*-C_6H_5), 7.70 (m, 4 H, *ortho*-C_6H_5). − ^{13}C NMR (30°C, CD_2Cl_2): δ = 13.24, 13.41 (each q, $^1J_{CH}$ = 127 Hz, CH_3), 21.18 (dt, $^1J_{CH}$ = 131 Hz, $^2J_{CP}$ = 11.0 Hz, CH_2CH_2P), 25.77 (t, $^1J_{CH}$ = 133 Hz, CH_2CH_2O in THF), 29.84 (dt, $^1J_{CH}$ = 134 Hz, $^1J_{CP}$ = 21.4 Hz, CH_2P), 69.10 (t, $^1J_{CH}$ = 145 Hz, CH_2O in THF), 128.32, 128.38 (each s, CCH_3), 129.53 (dd, $^1J_{CH}$ = 160 Hz, $^3J_{CP}$ = 8.4 Hz, *meta*-C_6H_5), 130.60 (d, $^1J_{CH}$ = 160 Hz, *para*-C_6H_5), 132.64 (d, $^1J_{CP}$ = 27.5 Hz, *ipso*-C_6H_5), 132.69 (dd, $^1J_{CH}$ = 160 Hz, $^2J_{CP}$ = 9.5 Hz, *ortho*-C_6H_5), 134.06 (d, $^3J_{CP}$ = 4.0 Hz, CCH_2CH_2P). − ^{31}P{^{1}H} NMR (30°C, CD_2Cl_2): δ = 5.8 (s). − EI MS (250°C, 70 eV); *m*/*z* (%): 528 (13) [M$^+$ − THF], 513 (1) [M$^+$ − THF−CH_3], 493 (3) [M$^+$ − THF−Cl], 333 (23) [M$^+$ − THF−$ZrCl_3$], 308 (6) [M$^+$ −THF−$(C_6H_5)_2PCl$], 199 (100) [$(C_6H_5)_2PCH_2^+$], 185 (90) [$(C_6H_5)_2P^+$], 147 (14) [$C_7H_3(CH_3)_4^+$], 133 (24) [$C_7H_4(CH_3)_3^+$], 121 (48) [$C_9H_{13}^+$], 108 (59) [$C_8H_{12}^+$], 91 (21) [$C_7H_7^+$]. − $C_{27}H_{34}Cl_3OPZr$ (603.12): calcd. C 53.77, H 5.68; found C 53.27, H 5.75.

X-ray Crystallographic Study of Complex 11:[25] Crystal data: $C_{27}H_{34}Cl_3OPZr$, M = 603.12, monoclinic, a = 8.336(2), b = 33.943(10), c = 9.863(3) Å, β = 101.90(2)°, V = 2730.8(13) Å^3, space group $P2_1/c$, Z = 4, D_c = 1.467 g/cm^3, F(000) = 1240, μ(Mo-K_α) = 0.773 mm^{-1}. Data collection, structure solution and refinement. A crystal of approximate dimensions 0.4 × 0.3 × 0.3 was used for data collection. A total of 6093 reflections (4470 unique, R_{int} = 0.0244) were measured with an Enraf−Nonius CAD4 diffractometer (graphite-monochromatized Mo-K_α radiation, λ =

0.71073 Å) at room temp. Data was collected in the range $2.19° < \theta < 24.99°$ ($-9 \le h \le 9$, $-40 \le k \le 40$, $0 \le l \le 11$) using the ω scan mode. The structure was solved by direct methods[26] and refined by full-matrix least squares on F^2[27] with anisotropic thermal parameters for all non-hydrogen atoms. All H atoms were placed in calculated positions. Both coordinates and isotropic thermal parameters for H atoms at side-chain carbon atoms C(6) and C(7) and at Ph groups were refined. All other hydrogen atoms were refined using a riding model (U_{iso} were taken as $1.5 \times U_{eq}$ of parent C atoms). The methyl group at C(2) was found to be rotationally disordered over two positions with equal occupancies. The weighting scheme was $w^{-1} = \sigma^2(F^2) + (0.0483P)^2 + 0.5400P$, where $P = (2F_c^2 + F_o^2)/3$. The final residuals were: $R_1 = 0.0285$, $wR_2 = 0.0750$ for 3543 reflections with $I > 2\sigma(I)$ and 0.0463, 0.0802 for all data and 359 parameters. Goof: 1.086, maximum shift/e.s.d.: 0.001, maximum $\Delta\rho = 0.638$ e × Å^{-3}.

Acknowledgments

Financial support from the Russian Foundation for Basic Research (projects No. 98−03−33057a and No. 98−03−33142a) is gratefully acknowledged.

[1] J. Szymoniak, J. Besançon, A. Dormond, C. Moïse, *J. Org. Chem.* **1990**, *55*, 1429−1432.
[2] G. J. M. Gruter, J. A. M. van Beek, H. J. Arts (DSM N. V.), PCT Int. Appl. WO 97/42201, **1997**.
[3] P. Jutzi, J. Dahlhaus, *Synthesis* **1993**, 684−686.
[4] D. P. Krut′ko, M. V. Borzov, E. N. Veksler, E. M. Myshakin, D. A. Lemenovskii, *Izv. Akad. Nauk, ser. khim.* **1998**, 986−989; *Russ. Chem. Bull.* **1998**, *47*, 956−959.
[5] [5a] J. Okuda, K. H. Zimmermann, *J. Organometal. Chem.* **1988**, *344*, C1−C4. − [5b] D. M. Jr. Bensley, E. A. Mintz, S. J. Sussangkarn, *J. Org. Chem.* **1988**, *53*, 4417−4419. − [5c] C. Fendrick, L. D. Schertz, E. A. Mintz, T. J. Marks, *Inorg. Synth.* **1992**, *29*, 193−198.
[6] [6a] J. L. Wardell in *Comprehensive Organometallic Chemistry* (Ed.: G. Wilkinson), Pergamon Press, **1982**, chapter 2. − [6b] W. E. Lindsell in *Comprehensive Organometallic Chemistry* (Ed.: G. Wilkinson), Pergamon Press, **1982**, chapter 4. − [6c] H. Normant, *Bull. Soc. Chim. Fr.* **1972**, 2161−2175.
[7] D. P. Krut′ko, M. V. Borzov, V. S. Petrosyan, A. V. Churakov, L. G. Kuz′mina, *Izv. Akad. Nauk, Ser. Khim.* **1996**, 1828−1832; *Russ. Chem. Bull.* **1996**, *45*, 1740−1744.
[8] D. P. Krut′ko, M. V. Borzov, V. S. Petrosyan, A. V. Churakov, L. G. Kuz′mina, *Izv. Akad. Nauk, Ser. Khim.* **1996**, 984−992; *Russ. Chem. Bull.* **1996**, *45*, 940−949.
[9] [9a] R. T. Kettenbach, W. Bonrath, H. Butenschön, *Chem. Ber.* **1993**, *126*, 1657−1669. − [9b] H. H. Karsch, V. Graf, M. Reisky, E. Witt, *Eur. J. Inorg. Chem.* **1998**, 1403−1406.
[10] [10a] P. Jutzi, U. Siemeling, *J. Organometal. Chem.* **1995**, *500*, 175−185. − [10b] P. Jutzi, T. Redeker, *Eur. J. Inorg. Chem.* **1998**, 663−674.
[11] D. M. Jr. Bensley, E. A. Mintz, *J. Organomet. Chem.* **1988**, *353*, 93−102.
[12] [12a] C. L. Bumgardner, *Chem. Ind. (London)* **1958**, 1555−1156. − [12b] C. L. Bumgardner, *J. Am. Chem. Soc.* **1961**, *83*, 4420−4423.
[13] [13a] S. O. Grim, R. P. Molenda, *Phosphorous* **1974**, *4*, 189−193. − [13b] R. E. Goldsberry, D. E. Lewis, K. Kohn, *J. Organomet. Chem.* **1968**, *15*, 491−493. − [13c] K. B. Mallion, F. G. Mann, *Chem. Ind. (London)* **1963**, 654.
[14] D. P. Krut′ko, M. V. Borzov, E. N. Veksler, A. V. Churakov, J. A. K. Howard, *Polyhedron* **1998**, *17*, 3889−3901.
[15] R. E. Dinnebier, U. Behrens, F. Olbrich, *Organometallics* **1997**, *16*, 3885−3858.
[16] The unambiguous assignment of the signals was made only for **5a** isomer (see Experimental Section).
[17] [17a] K. W . Krebs, H. Engelhard, G. E. Nischk (Farbenfabriken Bayer A. G.), Ger. Offen. 1959322, 29.07.**1971**, Appl. 26.11.**1969**; *Chem. Abstr.* **1971**, *75*, 88768p. − [17b] A. Martin, M. Mena, F. Palacios, *J. Organometal. Chem.* **1994**, *480*, C10−C11. − [17c] C. H. Winter, X. X. Zhou, D. A. Dobbs, M. J. Heeg, *Organometallics* **1991**, *10*, 210−214.
[18] G. H. Llinas, M. Mena, F. Palacios, P. Royo, R. Serrano, *J. Organometal. Chem.* **1988**, *340*, 37−40.
[19] K. A. Butakoff, D. A. Lemenovskii, P. Mountford, L. G. Kuz′mina, A. V. Churakov, *Polyhedron* **1996**, *15*, 489−499.
[20] P. T. Wolczanski, J. E. Bercaw, *Organometallics* **1982**, *1*, 793−799.
[21] The dynamic behaviour of compound **11** in solutions in comparison with that of its analogues is now under investigation and will present a matter of our next publication.
[22] F. Allen, and O. Kennard, *Chem. Design Automation News* **1993**, *8*, 1.
[23] G. Erker, C. Sarter, M. Albrecht, S. Dehnike, C. Kruger, E. Raabe, R. Schlund, R. Benn, A. Rufinska, and R. Mynott, *J. Organometal. Chem.* **1990**, *382*, 89.
[24] The procedure was performed in evacuated sealed glass vessels.
[25] Crystallographic data (excluding structure factors) for the structure reported in this paper have been deposited with the Cambridge Crystallographic Data Centre as supplementary publication no. CCDC-109436. Copies of the data can be obtained free of charge on application to CCDC, 12 Union Road, Cambridge CB2 1EZ, UK [Fax: int. code + 44-1223/336-033; E-mail: deposit@ccdc.cam.ac.uk].
[26] G. M. Sheldrick, *Acta Crystallogr. A* **1990**, *A46*, 467−473.
[27] G. M. Sheldrick, *SHELXL-93*, Universität Göttingen, **1993**.

Received December 17, 1998
[I98439]

Self-Assembly of Pyrazolyl Based Ligands and Silver Cation into Metallamacrocycles and Tubular Coordination Networks

Marielle Loï,[a] Mir Wais Hosseini,*[a] Abdelaziz Jouaiti,[a] André De Cian,[b] and Jean Fischer[b]

Keywords: Pyrazole / Silver / Metallacycles / Macrocycles / Self-assembly

The 2,6-bis(pyrazolyl)pyrazine ligand **1** forms a 2,2-metallamacrocycle **3**, composed of two ligands and two cations, in the presence of the Ag^+ cation. In the crystalline phase, the 1,3,5-tris(pyrazolyl)benzene ligand **2** leads to an infinite metallatubular network in the presence of the Ag^+ cation, composed of the 2,2-metallamacrocycle **4**, which is formed from two molecules of **2** and two cations. This infinite network is formed by double interconnection of consecutive metallamacrocycles through binding of Ag^+ centers by the free pyrazolyl moieties.

For the last decade, much attention has been focused on the formation of metallamacrocycles,[1] and many bis-monodentate ligands such as 4,4′-bipyridine, pyrimidine, bipyrazine, 4,7-phenanthroline or bis-pyridines interconnected by rigid or flexible spacers have been shown to form a variety of metallamacrocycles.[2] Recently, we have reported the formation of silver and palladium 2,2-metallamacrocycles using ligands based on two *p*-dialkylaminopyridine units connected by aliphatic chains of variable length.[3]

A further development in this area could be the formation, using self-assembly processes, of coordination molecular networks based on the interconnection of metallamacrocycles by coordination bonds. As schematically represented in Figure 1, one can design tridentate ligands in which two coordination sites are positioned in such a manner that, in the presence of divalent metal cations, they form 2,2-metallacycles composed of two metals and two ligands; the remaining coordination site would then serve as a connecting center allowing binding to another divalent metal cation and the formation of infinite 1-D networks. This strategy has been demonstrated by using terpyridine ligands bearing a thioether group.[4]

In order to investigate this possibility, ligand **1** was designed, synthesized and structurally characterized in the crystalline phase by X-ray diffraction on a single crystal. Indeed, ligand **1**, based on a pyrazine moiety bearing two pyrazolyl groups at the 2 and 6 positions, may fulfil the above criteria if the two pyrazolyl units and the N4 nitrogen atom of the pyrazine unit participate in the binding of linearly coordinated metal centers. However, **1** can also act either as a tridentate chelating ligand if the N1 nitrogen atom of the pyrazine ring was acting as coordination site in conjunction with the two pyrazolyl groups, or as a tetradentate ligand if, in addition to the two pyrazolyl moieties, both nitrogen atoms of the pyrazine ring were participating in the bonding of metal centers.

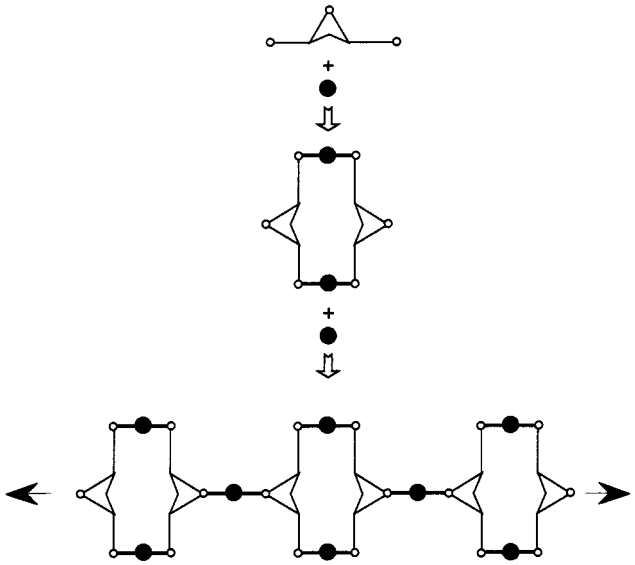


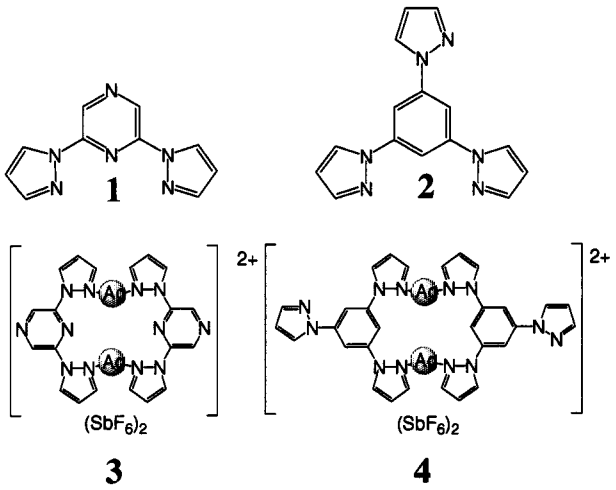
Figure 1. Schematic representation of an infinite coordination network based on interconnection of 2,2-metallamacrocycles by bridging metal centers

Ligand **1** was prepared in 77% yield upon coupling the sodium salt of pyrazole with 2,6-dichloropyrazine in DMF. The pyridine analogue of **1** and its Ru(II)[5] and Cu(II)[6] complexes have previously been reported. The solid state structure of **1** (Figure 2) was determined by an X-ray diffraction study which revealed the following features. In the solid state, the free ligand **1** possesses a plane of symmetry and adopts an almost planar conformation with an N1−N2−C5−N3 dihedral angle of 171.6°. Both the N1 and N1′ atoms are in a trans configuration with respect to N3. Whereas the C5−N2 bond length is 1.4000 Å, the C5−N3 bond is much shorter (1.324 Å), as expected; the N1−N2 bond length is 1.362 Å.

In an attempt to form infinite 1-D networks based on the interconnection of metallamacrocycles, the binding of the

[a] Laboratoire de Chimie de Coordination Organique,
Université Louis Pasteur,
UMR CNRS 7513, F-67000 Strasbourg, France
E-mail: hosseini@chimie.u-strasbg.fr
[b] Laboratoire de Cristallochimie et Chimie Structurale,
Université Louis Pasteur,
F-67000 Strasbourg, France, UMR CNRS 7513

 © WILEY-VCH Verlag GmbH, D-69451 Weinheim, 1999 1434−1948/99/1111−1981 $ 17.50+.50/0



Scheme 1

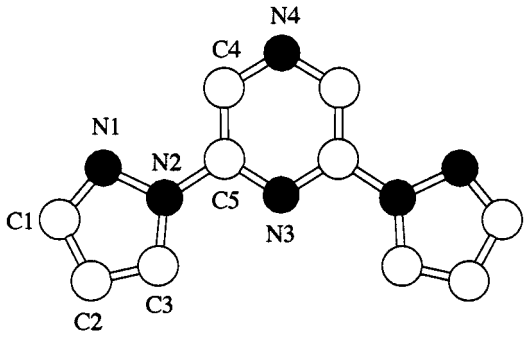


Figure 2. X-ray structure of the free ligand **1** (Table 1); hydrogen atoms omitted for clarity; for bond lengths and angles see text

Ag^+ cation by the ligand **1** was investigated. The Ag^+ cation was selected because, firstly, it forms kinetically labile complexes with nitrogen-containing ligands and, secondly, it may adopt a linear coordination geometry. Indeed, we have previously obtained a silver 2,2-metallamacrocycle in which the Ag^+ cation is linearly coordinated to two nitrogen atoms.[3] However, other types of coordination geometry, in particular trigonal or tetrahedral, are commonly observed. In this case, infinite 1-D linear[7] or helical[8] silver coordination networks in which the cation acts as a tetrahedrally connecting center, were obtained.

Upon reacting equimolar amounts of ligand **1** and $AgSbF_6$in $CHCl_3$/EtOH (1:3) at room temperature, the binuclear silver metallamacrocycle **3** was obtained in 70% yield (Scheme 1). The structure of **3** was investigated by an X-ray diffraction study (Table 1) on a single crystal (see Figure 3). The crystal is exclusively composed of discrete 2,2-metallamacrocycles **3** and SbF_6^- anions; the cationic part is a binuclear silver complex composed of two ligands and two Ag^+ cations forming a 2,2-metallamacrocycle. The latter is formed by the bridging of two pyrazolyl moieties of the ligand by two silver atoms, implying that **1** behaves as a bidentate unit. For ligand **1**, the pyrazolyl and the pyrazine units are tilted by −21.6°. The two ligands are not coplanar but twisted, thus leading to a rather short Ag−Ag distance of 2.911 Å. Both silver cations are almost linearly coordinated (N−Ag−N angle of 178.2°) to two pyrazolyl nitrogen atoms with a N−Ag distance of 2.160 Å. The SbF_6^- anions are neither disordered nor in specific interactions with the cationic units. The formation of such a metallamacrocycle is not unprecedented, analogous structures were obtained from Cu^I and benzimidazole-based ligands,[9] and bis-pyridine and Ag^I.[10] Attempts to generate the desired infinite coordination network by increasing the Ag^+/**1** stoichiometry and by varying the crystallization conditions have so far been unsuccessful.

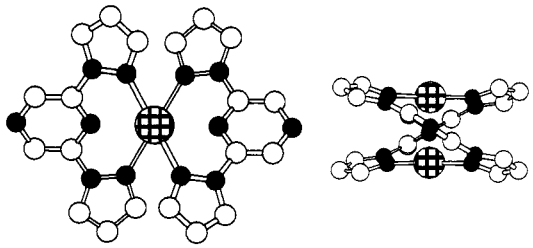


Figure 3. X-ray structure of the metallamacrocycle **3** {projection along the Ag-Ag axis (left) and lateral view (right)} obtained under self-assembly conditions between **1** and the Ag^+ cation (Table 1); hydrogen atoms and anions omitted for clarity; for bond lengths and angles see text

Tubular structures are interesting architectures, in particular with respect to their ability to transport ions or molecules. In principle, such structures may be obtained either from nonreversible covalent bonds, or other types of reversible interactions such as H-bonding or stacking processes. It has been shown that tubular systems may be formed by 1-D chains adopting a helical structure, as observed for polypeptides in natural systems,[11][12] or for helical coordination polymers;[8][13] by interconnection of ring modules as, for example, for cyclic peptides;[11][12] by stacks of cyclic units in the liquid crystalline phase;[14] by poly-[15] or oligomeric[16] structures bearing ring systems; or by rolling up 2-D sheets such as graphite leading to carbon nanotubes.[17] Following the above strategy for the formation of 1-D coordination networks based on the interconnection of metallamacrocyclic units, we reasoned that, by an appropriate choice of ligands, it should be possible to generate tubular coordination networks using the self-assembly strategy based on the formation of reversible coordination bonds. Indeed, the appropriate interconnection of metallamacrocycles may lead to a variety of tubular systems. An example of such an architecture, based on the mutual interconnection of metallamacrocycles, is schematically represented in Figure 4. The formation of such a structure requires a ligand and metal-cation pair allowing the reversible formation of metallamacrocycles and their mutual interconnection (Figure 4). This strategy was demonstrated using terpyridine ligands bearing a thioether group.[9]

We believed that the tridentate ligand **2** composed of three pyrazolyl moieties located in the 1, 3 and 5 positions of a benzene ring might be an interesting unit for the formation of a metallatubular 1-D coordination network. Compound **2**[18] and its 1,3,5-triazine[19] and 1,3,5-(pyrazolyl-1-methyl)[20] analogues have previously been reported. With

Table 1. Single crystal X-ray data for ligand **1** and the silver complexes **2** and **3**[a]

	1	**3**	**4**
Formula	$C_{10}H_8N_6$	$C_{10}H_8AgN_6{\cdot}SbF_6$	$C_{15}H_{12}AgN_6{\cdot}SbF_6$
Molecular weight	212.22	555.83	619.91
Crystal system	Monoclinic	Orthorhombic	monoclinic
Space group	*P*nma	*C*cca	*C*12/*c*1
a(Å)	11.8450(4)	10.3373(2)	22.873(1)
b(Å)	21.3300(9)	14.0278(3)	12.8220(5)
c(Å)	3.8290(4)	21.6100(4)	16.867(1)
β(deg)	89.972(2)	3133.7(2)	128.256(1)
V(Å^3)	967.4(2)		3884.4(6)
Z	4	8	8
Color	colorless	colorless	colorless
Crystal dim. (mm)	0.17 × 0.13 × 0.10	0.20 × 0.15 × 0.08	0.20 × 0.20 × 0.10
D(calc) (g cm^{-3})	1.46	2.36	2.12
F(000)	440	2096	2368
μ(mm^{-1})	0.098	3.045	2.469
Temperature (K)	173	294	294
h/*k*/*l* limits	0,4/−16,16/−30,30	0,14/0,19/0,29	0,35/0,15/−25,20
Theta limits(deg)	2.5/30.55	2.5/29.56	2.5/34.35
Number of data measured	6478	13952	14796
Number of data with $I > 3\ \sigma(I)$	1285	1604	3569
R	0.041	0.050	0.046
R_w	0.053	0.064	0.071
GOF	1.042	1.008	1.355

[a] Radiation: Mo-K_α graphite monochromated; wavelength (Å): 0.71073; diffractometer: KappaCCD; scan mode: phi scans

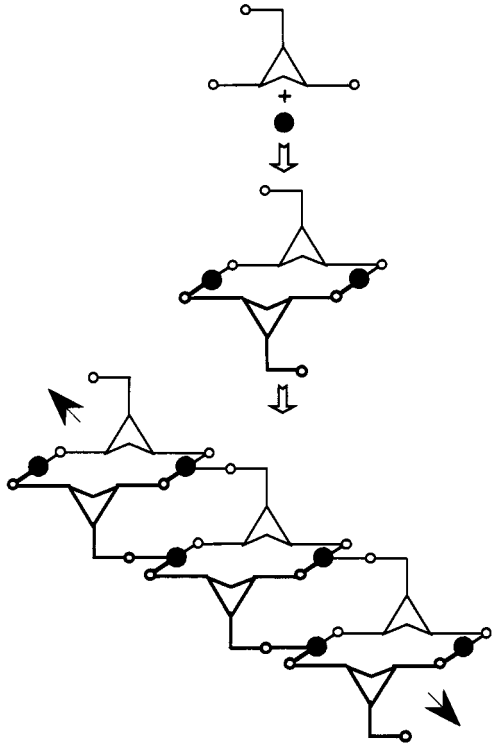


Figure 4. Schematic representation of an infinite coordination tubular network based on mutual interconnection through coordination bonds of consecutive 2,2-metallamacrocycles

respect to the bridging metallic center, the above mentioned strategy requires a tricoordinated metal adopting a T-type coordination geometry. Again, we believed that the Ag^+ cation was the best candidate.

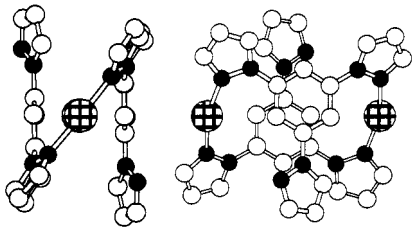


Figure 5. The X-ray structure of the metallamacrocycle **4** composed of **2** and the Ag^+ cation (Table 1). Projection along the Ag-Ag axis (left) and lateral view (right). H atoms and anions are not presented for clarity. For bond lengths and angles see text

Upon slow diffusion in the dark and at room temp. of a solution of **2** in $CHCl_3$ into an EtOH solution of $AgSbF_6$, colorless crystals were obtained after three days which were studied by X-ray diffraction (Table 1). The crystal (Figures 5 and 6), consisting exclusively of ligand **2**, Ag^+ cations and SbF_6^- anions, is composed of parallel cationic metallatubular coordination networks and the SbF_6^- anion. The formation of the tubular structure results from the mutual bridging of the binuclear silver 2,2-metallamacrocycles **4**, (Scheme 1), composed of two Ag^+ cations and two ligands **2** and analogous to the metallamacrocycle **3** obtained with ligand **1**. For the formation of the metallamacrocyclic unit **4** (Figure 5) within each of the two tridentate ligands **2**, two out of three pyrazolyl units are bridged by two Ag^+ cations, the remaining two pyrazolyl units, located at each end of the cyclic structure and pointing in opposite directions with respect to the plane defined by the metallamacrocycle, serve to interconnect consecutive cyclic units (Figure 6). Dealing

with the ligand **2**, the three pyrazolyl moieties are tilted by −41.2°, 32.4° and 23.0° with respect to the phenyl ring, respectively. For the metallamacrocycle **4**, the N−Ag and Ag−Ag distances are 2.150 Å, 2.154 Å and 7.785 Å, respectively. As stated above, the metallamacrocycles are mutually and doubly interconnected (Figure 6) by the third pyrazolyl on each ligand **2** with a rather long N−Ag distance of 2.620 Å; thus the overall coordination geometry around the Ag^+ cation may be described as severely distorted trigonal (T-type) with N−Ag−N angles of 162.4°, 99.0° and 98.6°. As in the case of **3** mentioned above, the SbF_6^- anions were neither disordered nor in specific interactions with the cationic units. Although in terms of topology the network formed may be described as tubular, due to the size of the metallamacrocyclic unit, the internal space within each tubular network is exceedingly small.

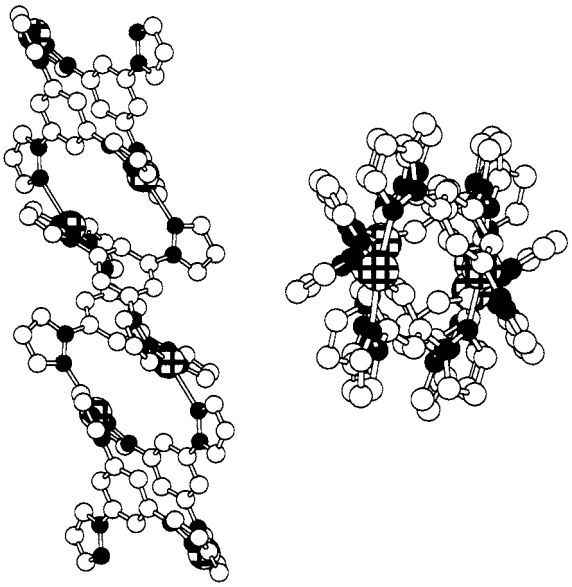


Figure 6. A portion of the X-ray structure showing the formation of the metallatube {parallel (left) and perpendicular (right) views} between the tridentate ligand **2** and Ag^+ cations; hydrogen atoms and anions omitted for clarity

In conclusion, from ligand **1**, bearing two pyrazolyl units, and the Ag^+ cation, both in solution and in the solid state, the formation of a binuclear silver 2,2-metallamacrocycle was achieved and its solid structure was elucidated by X-ray diffraction on a single crystal. With the Ag^+ cation and ligand **2** containing three pyrazolyl, units, the formation of a 1-D tubular coordination network was observed in the solid state by X-ray diffraction on a single crystal. The tubular coordination network results from the mutual interconnection of metallamacrocycles through N−Ag coordination bonds. Due to the size of the metallamacrocyclic unit, the internal size of the tubular architecture obtained was exceedingly small, thus precluding any possible application in terms of its use as a channel. However, increasing the size of the metallamacrocycle by using larger ligands such as 1,3,5-tris(phenylpyrazol)ylbenzene, one might be able to generate tubular networks with sufficient internal space. This type of architecture, due to its cationic nature, may be of interest for the transport of anions, which remains a challenge. Work along these lines is currently in progress

Experimental Section

Synthesis of Ligand 1: To a suspension of pyrazole (274 mg, 4 mmol) in DMF (35 mL) was added NaH (168 mg, 4.22 mmol) and the mixture stirred under argon at 50°C for 20 minutes. To this suspension was added 2,6-dichloropyrazine (300 mg, 2 mmol) and the resulting yellow mixture was heated to 90°C under argon and stirred for a further 12 hours before it was allowed to cool to room temperature. Upon pouring the suspension into cold water, the desired compound **1** was obtained in 77% yield (330 mg) as a white solid which was filtered and further washed with water. m.p. 180−181°C. − ^{1}H NMR (300 MHz, 25°C, [D$_6$]acetone): δ = 6.66 (dd, *J* = 1.3, 2.7 Hz, 2 H, pyrazole), 7.89 (d, *J* = 1.5 Hz, 2 H, pyrazol), 8.84 (d, *J* = 1.5 Hz, 2 H, pyrazole), 9.14 (s, 2 H, pyrazine). − ^{13}C NMR (75.46 MHz, 25°C, $CDCl_3$): δ = 108.8, 127.3, 131.5, 143.3, 144.8. − UV (25°C, $CHCl_3$) λ_{max} (ε mol^{-1}lcm^{-1}): 270 (18400), 327 (29200) nm. − FAB$^{+\ m/z}$ (%) = 212.1 (100%).

Synthesis of the Binuclear Silver Complex 3: Stirring an equimolar mixture of **1** and $AgSbF_6$ (0.23 mmol) in $CHCl_3$/EtOH (1:3) for 5 hours at room temperature in the dark under argon, gave the binuclear silver complex **3** in 80% yield as a white powder which was filtered, washed with CH_2Cl_2 and EtOH and dried. m.p. 240°C (decomposition). − ^{1}H NMR (300 MHz, 25°C, [D$_6$]acetone): δ = 6.83 (dd, *J* = 2.0, 2.7 Hz, 2 H, pyrazole), 7.87 (d, *J* = 1.9 Hz, 2 H, pyrazole), 8.96 (d, *J* = 3.0 Hz, 2 H, pyrazole), 9.40 (s, 2 H, pyrazine). − ^{13}C NMR (75.46 MHz, 25°C, $CDCl_3$): δ = 111.1, 131.2, 134.1, 143.8, 145.2. − FAB$^{+\ m/z}$ (%) = 874.9 (100%, **3**-SbF_6).

Acknowledgments

We thank the Université Louis Pasteur, the CNRS and the Institut Universitaire de France for financial support.

[1] M. Fujita in *Comprehensive Supramolecular Chemistry* (Eds.: J. L. Atwood, J. E. D. Davies, D. D. MacNicol, F. Vögtle), Pergamon, **1996**, *Vol. 9* (Eds. J. P. Sauvage, M. W. Hosseini), p. 253; J. K. M. Sanders, in *Comprehensive Supramolecular Chemistry* (Eds.: J. L. Atwood, J. E. D. Davies, D. D. MacNicol, F. Vögtle, Pergamon, **1996**, *Vol. 9* (Eds. J. P. Sauvage, M. W. Hosseini), p. 131; R. W. Saalfrank, A. Stark, K. Peters, H.-G. von Schnering, *Angew. Chem. Int. Ed. Engl.* **1988**, *27*, 851; P. J. Stang, B. Olenyuk, *Acc. Chem. Res.* **1997**, *30*, 502; C. M. Drain, J.-M. Lehn, *J. Chem. Soc., Chem. Commun*. **1994**, 2313; T. Beissel, R. E. Powers, K. N. Raymond, *Angew. Chem. Int. Ed. Engl.* **1996**, *35*, 1084.

[2] C. V. Krishnamohan Sarma, S. T. Griffin, R. D. Rogers, *Chem. Commun*. **1998**, 215; R.-D. Schnebeck, L. Randaccio, E. Zangrando, B. Lippert, *Angew. Chem. Int. Ed.* **1998**, *37* 119; J. R. Hall, S. J. Loeb, G. K. H. Shimizu, G. P. A. Yap, *Angew. Chem. Int. Ed.* **1998**, *37*, 121.

[3] R. Schneider, M. W. Hosseini, J.-M. Planeix, A. De Cian, J. Fischer, *Chem. Commun*. **1998**,1625.

[4] M. J. Hannon, C. L. Painting, W. Errington, *Chem. Commun*. **1997**, 307; M. J. Hannon, C. L. Painting, W. Errington, *Chem. Commun*. **1997**, 1805.

[5] D. J. Jameson, J. K. Blaho, K. T. Kruger, K. A. Goldsby, *Inorg. Chem*., **1989**, *28*, 4314.

[6] N. K. Solanki, E. J. L. McInnes, F. E. Mabbs, S. Radojevic, M. McPartlin, N. Feeder, J. E. Davies, M. A. Halcrow, *Angew. Chem. Int. Ed*. **1998**, *37*, 2221.

[7] G. Mislin, E. Graf, M. W. Hosseini, A. De Cian, N. Kyritsakas, J. Fischer, *Chem. Commun*. **1998**, 2545.

[8] C. Kaes, M. W. Hosseini, C. E. F. Rickard, B. W. Skelton, A. White, *Angew. Chem. Int. Ed.* **1998**, *37*, 920.

[9] C. Piguet, G. Bernadinelli, A. F. Williams, *Inorg. Chem*. **1989**, *28*, 2920, S. Rüttimann, C. Piguet, G. Bernardinelli, B. Bocquet, A. F. Williams, *J. Am. Chem. Soc*. **1992**, *114*, 4230.
[10] C. M. Hartshorn, P. J. Steel, *Inorg. Chem*. **1996**, *35*, 6902.
[11] D. H. Lee, M. R. Ghadiri in *Comprehensive Supramolecular Chemistry* (Eds: J. L. Atwood, J. E. D. Davies, D. D. Macnicol, F. Vögtle), Pergamon, **1996**, *Vol. 9* (Eds. J.-P. Sauvage, M. W. Hosseini), p. 451; J. D. Lear, Z. R. Wasserman, W. F. DeGrado, *Science* **1988**, *240*, 1177.
[12] P. De Santis, S. Morosetti, R. Rizzo, *Macromolecules* **1974**, *7*, 52; M. R. Ghadiri, J. R. Granja, R. A. Milligan, D. E. McRee, N. Khazanovich, *Nature* **1993**, *366*, 324.
[13] O. J. Gelling, F. van Bolhuis, B. L. Feringa, *J. Chem. Soc., Chem. Commun*. **1991**, 917, Y. Dai, T. J. Katz, D. A. Nichols, *Angew. Chem. Int. Ed. Engl*., **1996**, *35*, 2109; B. Wu, W.-J. Zhang, S.-Y. Yu, X.-T. Wu, *Chem. Commun*. **1997**, 1795.
[14] J.-M. Lehn, J. Malthête, A.-M. Levelut, *J. Chem. Soc., Chem. Commun*. **1985**, 1794; V. Percec, G. Johansson, J. A. Heck, G. Ungar, S. V. Betty, *J. Chem. Soc., Perkin Trans 1* **1993**, 1411, T. Komori, S. Shinkai, *Chem. Lett*. **1993**, 1455.
[15] U. F. Kragten, M. F. M. Roks, R. J. M. Nolte, *J. Chem. Soc., Chem. Commun*. **1985**, 1275; C. Mertesdorf, H. Ringsdorf, *Mol. Cryst. Liq. Cryst*. **1989**, *5*, 1757.
[16] J.-P. Behr, C. J. Burrows, R. J. Heng, J.-M. Lehn, *Tetrahedron Lett*. **1985**, *26*, 215; A. Nakano, Q. Xie, J. V. Mallen, L. Echegoyen, G. W. Gokel, *J. Am. Chem. Soc*. **1990**, *112*, 1287.
[17] S. Iijima, *Nature* **1991**, *354*, 56.
[18] H. Lexy, T. Kauffmann, *Chem. Ber*. **1980**, *113*, 2755.
[19] H. Reimlinger, A. Noels, J. Jadot, A. Van Overstraeten, *Chem. Ber*. **1970**, *103*, 1954.
[20] C. M. Hartshorn, P. J. Steel, *Chem. Commun*. **1997**, 541.

Received February 2, 1999
[I99029]

Synthesis, Structure, Electrochemistry and Reactivity of the Bis(μ-σ-stannanediyl)dinickel Butterfly Cluster $[\{\{(SiMe_3)_2CH\}_2Sn–Ni(\eta^5\text{-}Cp)\}_2]$(*$Ni_2$–$Sn_2$)*

Jörg J. Schneider,*[a] Jörg Hagen,[a] Dieter Bläser,[a] Roland Boese,[a] Fabrizia Fabrizi de Biani,[b] Piero Zanello,[b] and Carl Krüger[c]

Keywords: Cluster / Nickel / Tin / Bimetallic complexes / Electrochemistry

Addition of stannylene $[\{(SiMe_3)_2CH\}_2Sn\mathbf{:}]$ (**2**) to the unbridged homobimetallic Ni–Ni bond of $[\{PEt_3Ni(\eta^5\text{-}Cp)\}_2]$ (**1**) gives the heterobimetallic, tetranuclear compound $[\{\{(SiMe_3)_2CH\}_2Sn–Ni(\eta^5\text{-}Cp)\}_2]$ (**3**) with a butterfly arrangement and leaves the Ni–Ni bond of **1** intact. Elimination of both PEt_3 ligands from the starting material **1** is observed, probably due to steric restraints. Compound **3** is formally related to the hypothetical *closo*-borane $B_4H_4^{2-}$. The Ni–Ni bond in **3** is only slightly elongated [2.454(3) Å] when compared to the starting material **1** [2.41(1) Å]. Compound **3** displays a butterfly arrangement with a hinge angle of 62.5°. An alternative route to **3** is by a direct reaction between nickelocene (**5**) and Lappert's stannylene $[\{(SiMe_3)_2CH\}_2Sn\mathbf{:}]$ in 63% yield. Treating **3** with water results in the cleavage of an Ni–Sn bond and subsequent opening of the cluster cage of **3** to form the trinuclear compound $[(\eta^5\text{-}Cp)Ni\{Sn(CH(SiMe_3)_2\}_2OH]$ (**6**) having an Sn–OH–Sn bridge. The hydroxy proton in **6** can be exchanged by deuterium within a few minutes, as determined by ^{1}H-NMR spectroscopy, giving the monodeuterio product, $[D_1]$-**6**. Compound **6** is reactive towards acetonitrile, leading to cleavage of one Ni–Sn bond, elimination of one $[\{(SiMe_3)_2CH\}_2Sn\mathbf{:}]$ unit, and formation of the organotin hydroxo complex $[\{(SiMe_3)_2CH\}_2(OH)Sn–Ni(\eta^5\text{-}Cp)(CH_3CN)]$ (**7**). In this complex, acetonitrile is coordinated to Ni via its σ lone pair, bearing the OH ligand in a terminal bonding mode to tin.

Introduction

Unbridged transition metal bonds (M−M) exhibit a high reactivity towards insertion and addition reactions of metal ligand fragments, especially when the M−M bond is polarized.[1] For complexes containing homo-metallic M−M bonds as in L_xM-ML_x-type dimers, usually little or no electronic polarization effects are available to enhance the reactivity of the particular M−M bond. Drastic reaction conditions are therefore often necessary to enhance the reactivity of these M−M bonds towards insertion or addition reactions. A unique way to activate homometallic M−M bonds and to increase their reactivity towards further reaction is to sterically overcrowd the ligand periphery L at each L_xM fragment. This results in a substantial weakening of M−M bonding, an increased reactivity, and consequently an easy homolytic scission of the M−M bond in such complexes.

We are interested in the reactivity of the dimer $[\{(\eta^5\text{-}Cp)Ni(PEt_3)\}_2]$ (**1**) containing an unbridged Ni−Ni bond.[2] Although the M−M bond in **1** is in the usual range for an Ni−Ni single bond and shows no significant elongation, **1** displays an unusually high reactivity with respect to a scission of its unbridged Ni−Ni bond.[2][3] This is a result of the sterically crowded situation at both Ni atoms of **1**, as revealed by X-ray crystallography and by ^{1}H-NMR spectroscopy in solution.[2] Rotation of the PEt_3 ligand around the Ni−Ni bond vector is restricted, even in solution, due to steric hindrance. This sterically encumbered ligand situation in **1** gives rise to cleavage of the Ni−Ni bond and insertion of a variety of low-valent main-group-element compounds.[2][3] For example, group-14 chloride $SnCl_2$, displaying carbenoid character, inserts into the Ni−Ni bond of **1** giving $[\{(\eta^5\text{-}Cp)Ni(PEt_3)\}_2SnCl_2]$. Subsequent dehalogention leads to the stannio(IV) monochloride complex $[\{(\eta^5\text{-}Cp)Ni(PEt_3)\}_3SnCl]$.[2] In our work reported here, we set out to find new synthetic entries into Ni/Sn organometallics by direct insertion routes into the M−M bond of **1**. Such Ni/Sn organometallics might be valuable single-source target compounds in MOCVD processes for the preparation of Ni/Sn intermetallics, which recently gained interest with respect to the nature of intermetallic phases like NiSn and Ni_3Sn_2.[4] Further interest is in their use as single-source precursors in bimetallic silica-supported catalysts based on a combination of Ni−Sn, Pd−Sn and Pt−Sn, which up to now are only accessible from a mixture of Sn and M (M = Ni, Pd, Pt) molecular precursors.[5a] Such bimetallics have potential in CO oxidation reactions.[5a] In addition, Ni/Sn intermetallics have proven their catalytic properties as cyclohexane dehydrogenation catalyst.[5b]

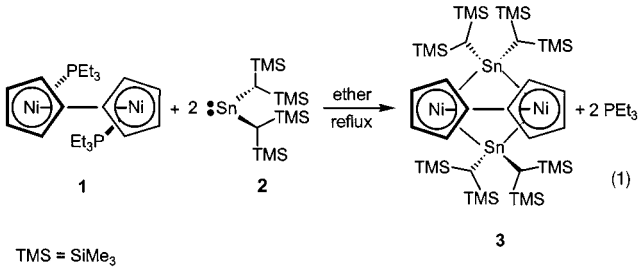
A number of transition metal complexes of stannanediyls $\mathbf{:}SnR_2$ are known so far, and have proven their versatility for coordination of transition metals.[6] We have choosen Lappert's bis{bis(trimethylsilylmethyl)tin} $[\{\{(SiMe_3)_2CH\}_2Sn\}_2]$ (**2**),[7] as candidate for introducing an organic

[a] Institut für Anorganische Chemie der Universität, Universitätsstraße 5−7, D-45117 Essen, Germany
Fax: (internat.) + 49-(0)208/183-4195.
E-mail: joerg.schneider@uni-essen.de
[b] Dipartimento di Chimica, University of Siena, Pian dei Mantellini 44, I-53100 Siena, Italy
[c] Max-Planck-Institut für Kohlenforschung, Kaiser-Wilhelm-Platz 1, D-45470 Mülheim a. d. Ruhr, Germany

 © WILEY-VCH Verlag GmbH, D-69451 Weinheim, 1999 1434−1948/99/1111−1987 $ 17.50+.50/0

SnR_2 group into transition metal compounds under mild conditions. We have recently shown that addition of elemental Se and Te towards the unbridged Co−Sn bond of $[\{(SiMe_3)_2CH\}_2Sn-Co(\eta^2\text{-ethene})(\eta^5\text{-Cp})]$, derived from reaction of **2** with $[(Cp)Co(ethene)_2]$, leads to unique ternary Co/Sn/E organometallics.[8]

We describe here, our studies on the reactivity of Lappert's bis(stannanediyl) **2** towards the Ni−Ni bond of **1**, leading to the formation of a bimetallic Ni−Sn complex **3** with a *closo* cage structure; **3** is formed by the addition of subvalent SnR_2 fragments to the Ni−Ni bond of **1**. The electrochemistry of **3** and of its cage-opened product **6** is reported. In addition, the reactivity of **1** towards cage opening with water as a nucleophile and subsequent further reactivity of this product with acetonitrile is studied.



Results and Discussion

Reaction of $[\{(\eta^5\text{-Cp})Ni(PEt_3)\}_2]$ (1) with $[\{\{(SiMe_3)_2CH\}_2Sn\}_2]$ (2)

Over the course of several days, **1** does not react with **2** at ambient temperature in diethyl ether. However, reflux conditions in diethyl ether for 12 h led to a color change of the initially deep green reaction solution to brown. Workup by crystallization (from ether) gave brown-green crystals of **3** in 50% yield (Equation 1).

According to ^1H and ^{13}C NMR, **3** is diamagnetic and does not contain any signals corresponding to the PEt_3 ligands originally present in the starting complex **1**. This result is confirmed by mass-spectrometric studies which show the molecular peak of **3** at m/z = 1122, with a correct isotropic pattern corresponding to the composition Ni_2Sn_2 (Figure 1). Figure 1 clearly indicates that **3** is thermally robust, propably leaving the Ni_2Sn_2 metal core intact upon vaporization. This is of significance for further MOCVD applications of this compound.

Definitive proof of the spectroscopic data, especially the loss of the PEt_3 ligand came from a single-crystal X-ray investigation, which showed **3** to be indeed a dinickel complex (Figure 2).[9] Two $\{CH(SiMe_3)\}_2Sn$ fragments bridge two 15e-$\{(\eta^5\text{-Cp})Ni\}$ fragments, resulting in a tetrameric Ni_2Sn_2 metal core. The metal atoms show a butterfly arrangement with a hinge angle of 62.5(4)°. The two tin atoms display a distorted tetrahedral geometry with significantly compressed bond angles $\{Si(CH_3)_3\}_2HC-Sn-CH\{Si(CH_3)_3\}_2$, e.g. C6−Sn−C7 102.9(2)°. A characteristic feature of the structure of **3** is the Ni−Ni bond, which is only slightly elongated when compared to the Ni−Ni bond in the starting material **1**. [2.41(1) Å[2] vs. 2.454(3) Å]. Obviously, the steric repulsion upon addition of two **:**SnR_2 stannylene fragments to the Ni−Ni bond has only a minor impact on the geometry of **3**. The Ni−Sn bond length is well in accord with the Ni−Sn bond in $[(\eta^5\text{-Cp})Ni)\{(\mu\text{-}\eta^1\text{:}\eta^1\text{-}$

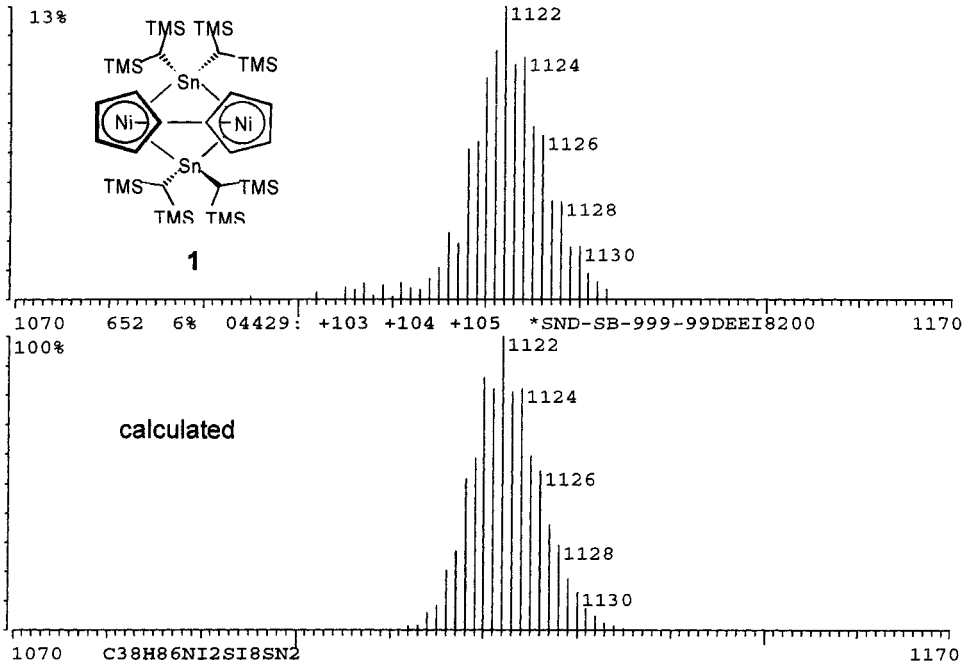


Figure 1. Top: experimental isotopic pattern of the molecular ion peak of **3**; bottom: calculated isotopic pattern for the molecular ion of composition $C_{38}H_{86}Ni_2Si_8Sn_2$

Cp){Sn(*N*(*t*Bu))$_2$SiMe$_3$}$_2$}] (**4**)[12] (Figure 3), containing a somewhat similar {(η^5-Cp)Ni−SnR$_3$} unit with a tetracoordinated Sn atom. The distance between the two tin atoms in **3** is 3.72 Å.

ether, under reflux conditions, to give brown crystals of **3** in 65% (Equation 2).

In contrast to Equation 1, formation of **3** here proceeds by addition of two electronically unsaturated 15e-{CpNi}

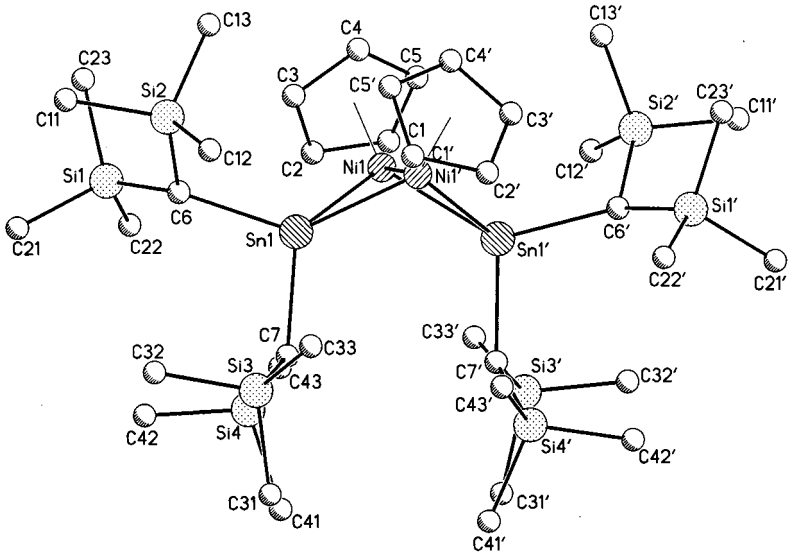


Figure 2. Molecular structure of **3** in the solid state; selected bond lengths [Å] and angles [°]: Sn−Ni 2.502, Ni−Ni 2.454, Sn−C7 2.208(6), Sn−C6 2.230(6), Ni−X1A (1B) 1.74; C6−Sn−C7 102.9(2), Ni−Sn−Ni′ 58.7(1), Sn−Ni−Sn′ 96.2(1)

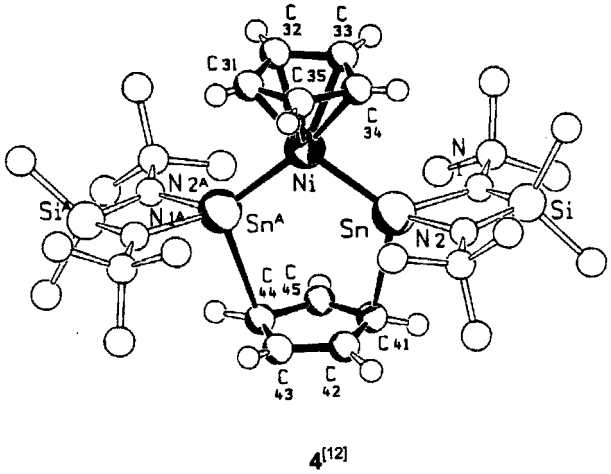


Figure 3. Molecular structure of **4** (reproduced from ref.[12] with permission)

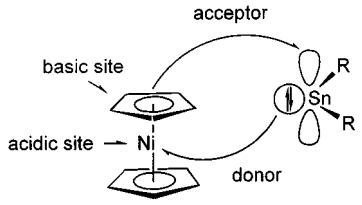
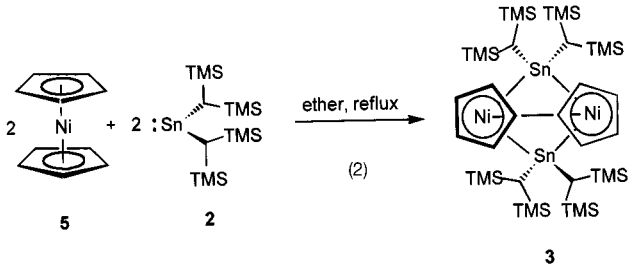


Figure 4. Different reaction sites of nickelocene with an amphiphilic Lewis acid/base stannylene ligand :SnR$_2$



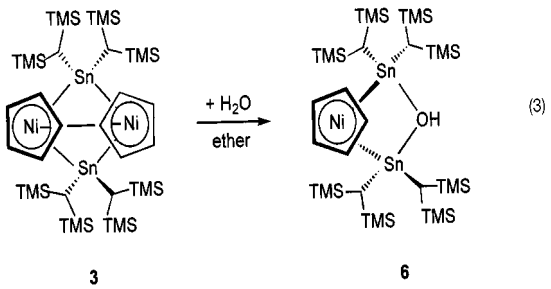
Equation 1 represents a rare case of addition of stannylene fragments SnR$_2$ towards an unbridged M−M bond.[13][14] For electron bookkeeping sake, **3** formally represents a hetero-*closo* structure according to Wade's rules.[15] Taking into account that **3** does not contain any PEt$_3$ ligands (originally present in the starting material **1**), finding a direct synthesis to **3** was challenging. Stannylenes :SnR$_2$ are either able to react as donor or acceptor molecules due to their carbenoid character and the electron-accepting empty π orbitals on tin. Electron-rich metallocenes like nickelocene (**5**) offer either acidic metal sites or basic ligand sites, at which substitution chemistry may proceed (Figure 4). We therefore found that **5** reacts with **2** in fragments, generated thermally from nickelocene, to give the tetranuclear Ni$_2$Sn$_2$ cluster **3**. Veith and Stahl reported a similar reaction of nickelocene with the N-donor-substituted, but more basic, stannylene [Sn(N*t*Bu)$_2$SiMe$_2$}] to yield **4**.[12] Consequently, this reaction resulted in an attack of this stannylene at the acidic Ni center and formal insertion of a stannanediyl fragment into the nickelocene sandwich structure. Obviously, the bis(silyl)stannylene [:Sn{CH(SiMe$_3$)$_2$}$_2$] (**2**) is basic enough to follow this reaction pathway.

With respect to the reactivity of **3**, we observed that if a mixture of **1** and **2** (Equation1) containing **3** is not directly

crystallized from the initial reaction mixture, but still further purified by column chromatography (SiO_2, pentane), aside from **3**, a second compound **6** can be isolated in varying yields. The yield of **6** depends on the chromatography time and age of the stationary SiO_2 phase used. Older charges of SiO_2 containing higher water contents, consequently gave higher yields of **6**. Compound **6** was characterized by spectroscopic data (NMR, MS, and IR). In the mass spectrum, the molecular base-peak for **6** is found at $m/z = 1016$, showing a characteristic Sn/Ni atom isotopic ratio of 2:1 and an initial mass loss of $m/z = [1016 - 17]$, owing to the loss of an OH unit. The OH grouping shows up in the IR spectrum with a sharp OH stretching absorption at $\tilde{\nu} = 3623\ cm^{-1}$.

The ^{1}H-NMR spectrum of **6** gives a characteristic broad OH proton resonance at $\delta = 1.46$ with a $^{119}J_{Sn-H}$ coupling of 12 Hz, which characterizes the Sn−OH−Sn bridge in **6**. Unambigous proof of this assignment and the existence of such a bridging μ-OH ligand came from a deuterium exchange experiment.

Addition of N_2-saturated D_2O to a freshly prepared NMR sample of **3** in N_2-saturated C_6D_6 resulted in a substantial broadening of the initially very sharp OH signal after 5 min contact time, and complete disappearance of the OH proton resonance signal after 30 min, indicating the formation of **5**[OD] by H/D exchange. The remaining proton signals in the ^{1}H-NMR spectrum broaden significantly but do not change their chemical shifts and relative intensity ratios.



To prove the assumption that **6** is not a direct reaction product of **1** and **2**, but is indeed formed by reaction of **3** with water, which must then be responsible for the Ni−Sn bond cleavage of the *closo* cluster **3**, a direct reaction of **3** with H_2O was conducted (Equation 3).

Stirring of an ethereal solution of **3** with a fourfold excess of N_2-saturated H_2O resulted in a color change from brown to red-brown within a few minutes. Workup furnished **6** as brown crystals in 63% yield. All spectroscopic data of **6** obtained by this independent route are in accord with the material obtained by chromatography of **3** on wet SiO_2 as described before. As a result of these experiments it is obvious that **3** is prone to the opening of the butterfly structure by oxidative addition of water. We found that **6** is also formed in a one-pot reaction by addition of excess water to a reaction mixture of **5** and **2** under reflux conditions, followed by subsequent crystallization of the crude material from ether.

A preliminary X-ray crystallographic study of **6** confirms the connectivity of the heavy-atom skeleton containing Sn and Ni, as well as the complete silicon/carbon framework. However, the μ-OH bridge could not be unambigously pinpointed due to the poor crystal quality of **6** obtained so far.[16]

Electrochemistry of 3 and 6

Figure 5 shows the cyclic voltammetric profiles exhibited by complexes **3** and **6** in dichloromethane solution. The dinickel complex **3** displays a rather complicated oxidation pathway (Figure 5, upper trace), in which only the first anodic step exhibits features of transient chemical reversibility (Figure 5, lower trace left). In contrast, the mononickel complex **6** undergoes a single oxidation process, chemically reversible in character on the cyclic voltammetric timescale (Figure 5, right trace).

Controlled potential coulometry ($E_w = +0.5$ V) showed that the oxidation of **6** involves the removal of one electron/molecule. The solution resulting from exhaustive oxidation

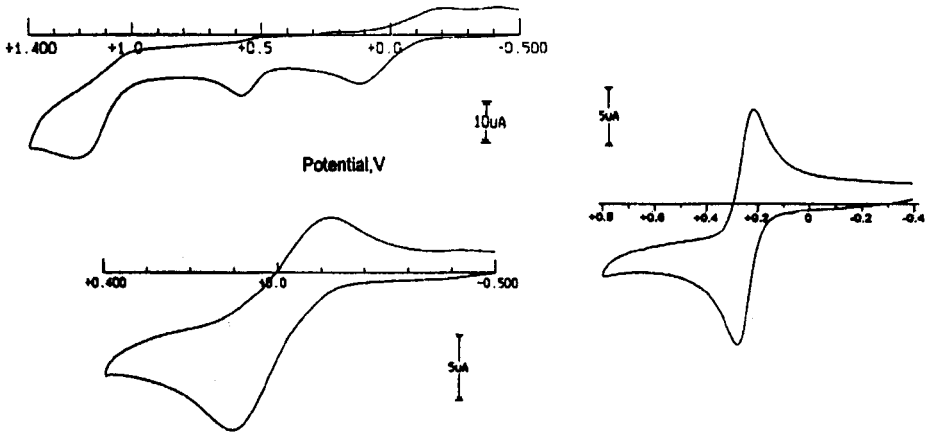


Figure 5. Cyclic voltammetric responses recorded at a platinum electrode in CH_2Cl_2 solutions containing $[Bu_4N][PF_6]$ (0.2 mol dm^{-3}) and **3** (9×10^{-4} mol dm^{-3}) (upper and lower left trace) or **6** (7×10^{-4} mol dm^{-3}) (right trace)

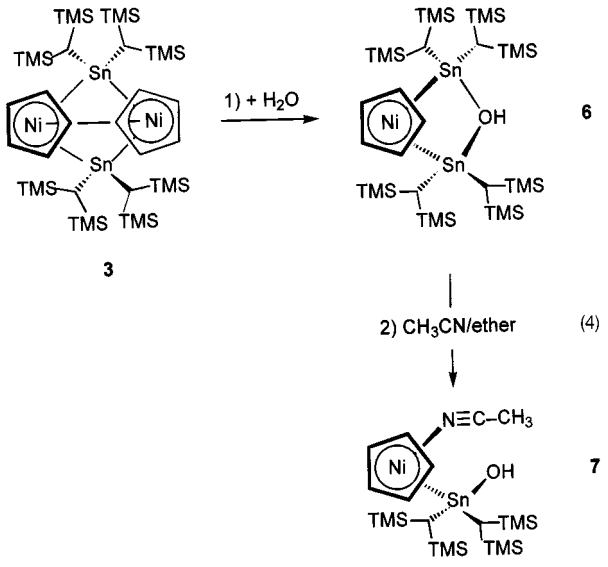
exhibits a cyclic voltammetric profile quite complementary to the original one, thus testifying the chemical reversibility of the redox change **6/6**$^+$ ($E^{\circ\prime}$ = +0.25 V) also during the long times of macroelectrolysis.

The analysis of the cyclic voltammograms of **6** with the scan rate varying from 0.02 Vs^{-1} to 1.00 Vs^{-1} indicates that the anodic step is substantially reversible also from the electrochemical viewpoint, in that the peak-to-peak separation, particularly at slow scan rates, deviates slightly from the theoretical value of 60 mV.[17] For instance, at 0.05 Vs^{-1} it is equal to 70 mV, quite paralleling the value we obtain for the one-electron oxidation of ferrocene under the same experimental conditions ($E^{\circ\prime}$ = +0.38 V). In this picture, the electrochemical reversibility suggests that no significant structural reorganization should accompany the electron removal from **6**.

As far as complex **3** is concerned, we limited our study to the first, partially reversible anodic step (at 0.05 Vs^{-1}, i_{pc}/i_{pa} = 0.7; $E^{\circ\prime}$ = −0.01 V). Controlled potential coulometry (E_w = +0.2 V), even if affected by severe electrode-poisoning phenomena which required repeated cleaning of the electrode surface, seems to involve one electron/molecule. It is important to take into account that after completion of electrolysis a number of new waves appear, which testify the occurrence of framework-destroying processes, but none of this was attributable to the **6/6**$^+$ system. This means that the redox-induced cleavage of the cage of **3**, in spite of the unavoidable presence of traces of water in solution, follows a path different from that illustrated in Equation 3.

Reactivity of 6 Towards CH_3CN

The Sn−OH−Sn bridge in **6** is reactive, and can be opened by a nucleophilic attack, e.g. by acetonitrile. Addition of a large excess of CH_3CN to an ethereal solution of **6** results in a color change from brown-red to blood-red. Prolonged cooling (weeks) of this solution eventually results in brick-red rectangular-shaped crystals of **7** containing a terminal *Ni*-bonded {Sn{CH(TMS)$_2$}$_2$}OH ligand, and a CH_3CN ligand according to spectral data (see Experimental Section) (Equation 4). The OH stretching frequency of **7** at $\tilde{\nu}$ = 3624 cm^{-1} is well in accord with the one observed for **6**.



The molecular structure of **7** in the solid state was determined by X-ray crystallography[9] and displays a two-legged piano-stool geometry at the Ni center (Figure 6), with a trigonal planar structure at Ni as its most prominent feature. The tin atom is coordinated in a strongly distorted tetrahedral environment. The Sn−O bond length [2.017(2) Å] points towards an Sn=O π-bond contribution as it is discussed for [{SnR$_2$(OH)}$_2$(μ-O)] containing a μ-Sn−O−Sn bridge, and two terminal Sn−OH groups [2.032(5) Å].[18] In contrast to **7**, organotin hydroxides often have a bridging OH as in **6** or [Sn(μ-OH)(phenyl)$_3$]$_\infty$.[19] Besides [{SnR$_2$(OH)}$_2$(μ-O)],[18] tris(tropolone)tin hydroxide[20] and [{CH(SiMe$_3$)$_2$}$_2$Sn(H)(OH)],[21] **7** represents another rare case of a compound having a terminal OH functionality.

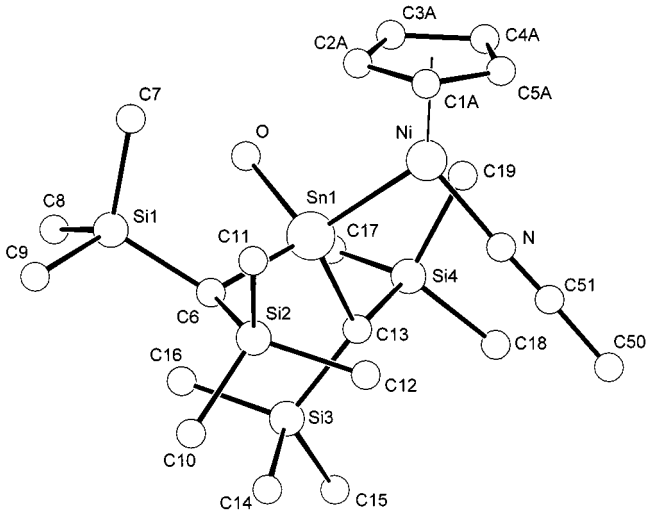


Figure 6. Molecular structure of **7** in the solid state; selected bond lengths [Å] and angles [°]: Ni−Sn 2.472(1), Ni−N 1.829(3), Sn−C13 2.209(3), Sn−C6 2.203(3), Sn−O 2.017, N−C51 1.138(5); C13−Sn−C6 109.3, O−Sn−Ni 109.6(1), C13−Sn−O 102.0(1), O−Sn−C6 102.5(2), C13−Sn−Ni 112.0(2), C6−Sn−Ni 119.6(1), N−Ni−Sn 93.7(1)

Conclusion

Bulky SnR_2 fragments are able to add to the Ni−Ni bond of **2**, forming the tetranuclear Ni_2Sn_2 cluster **3** with a *closo* cage structure. However, steric demands require that both PEt_3 ligands are eliminated in this addition/elimination-type reaction. A novel feature in this complex is the bulky R_2Sn-bridged Ni−Ni bond which is without precedent so far. Compound **3** displays reactivity towards cage opening with H_2O, leading to the trinuclear μ-OH bridged complex **6**. SnR_2 elimination and cleavage of the μ-OH bridge in **3** can be achieved by reaction with acetonitrile. The free coordination site generated by this cleavage is occupied by a σ-donor N→Ni dative bond of the CH_3CN

ligand to the Ni atom. The fact that **3** can be obtained in high yield under mild conditions and is prone to cage opening of its Ni_2Sn_2 skeleton offers some useful features for further studies. It can be envisaged that addition of various nucleophiles other than H_2O are also able to open a synthetic useful pathway into new Ni−Sn organometallics by the cage-opening reaction route of **3**.

The 1:1 Ni/Sn stoichiometry of **3**, as well as its promising evaporation characterictics (10^{-2} Torr/100°C, without decomposition) make **3** an outstanding candidate as single-source precursor to intermetallic nanostructured binary Ni/Sn phases[4][22] by MOCVD techniques. Very recently we have shown that the presence of the bulky mixed hydrocarbyl/organosilyl ligand $\{CH(SiMe_3)_2\}$ in volatile organo-bimetallic main-group complexes is in no way detrimental towards a succesful MOCVD application of organometallic complexes containing this ligand.[23]

Experimental Section

General: All reactions were carried out under dry nitrogen with standard Schlenk techniques. Compounds **1** and **2** were prepared according to published procedures.[2][6] − Microanalyses were performed by the microanalytical laboratory of the Chemistry Department of the University−GH Essen. − All solvents were dried appropriately and were stored under nitrogen. − The NMR spectra were recorded with a Bruker AC 300 spectrometer (300 MHz for ^1H, 75 MHz for ^{13}C) and referenced against the remaining protons of the deuterated solvent. NMR samples were prepared by vacuum transfer of solvents onto the appropriate amount of solid sample, followed by flame sealing of the NMR tube. − MS spectra were recorded with a MAT 8200 instrument using standard conditions (EI, 70 eV) and the fractional sublimation technique for compound inlet. − Materials and apparatus for electrochemistry and coupled EPR spectroscopy have been described elsewhere.[24] − Either a BAS 100 A or a BAS 100 W were used in cyclic voltammetric measurements. The potential values reported refer to the saturated calomel electrode (SCE).

Synthesis of $[\{(SiMe_3)_2CH\}_2Sn-Ni(\eta^5\text{-}Cp)\}_2]$ (3)

A: By Reaction of 1 and 2: To a solution of 700 mg (1.44 mmol) of **1**, dissolved in 100 mL of diethyl ether, was added 1.26 g (1.44 mmol) of dimeric stannanediyl $[\{Sn\{CH(SiMe_3)_2\}_2\}_2]$ (**2**). This solution was refluxed for 24 h resulting in a color change from green-brown to brown. After removal of all volatiles in vacuum, the remaining solid was dissolved in pentane and this solution was filtered. Crystallization at −30°C during the course of several days gave brown crystals of **3** (0.73 mmol, 51%). − MS (EI, 70 eV, T_{vap} = 140°C); *m/z* (%): 1122 (40) [M^+], 963 (30), [M^+ − $CH(SiMe_3)_2$], 685 (15) [M^+ − $Sn\{CH(SiMe_3)_2\}_2$]. − ^1H NMR ([D_6]benzene): δ = 5.30 (s, Cp, 10 H), 2.46 (s, CH, 4 H), 0.32 [s, ^1J(Si,H) = 6.0 Hz, $SiMe_3$, 72 H]. − $\{^1H\}^{13}C$ NMR ([D_6]benzene): δ = 89.12 (s, Cp), 7.91 (s, CH), 5.95 (s, $SiMe_3$) − $C_{38}H_{86}Ni_2Si_8Sn_2$ (1122.58): calcd. C 40.64, H 7.70; found C 40.90, H 7.65.

B: By Reaction of 4 and 2: To a solution of **4** (1.0 g, 5.30 mmol), dissolved in 150 mL of ether, was added 2.32 (2.65 mmol) of $[\{Sn\{CH(SiMe_3)_2\}_2\}_2]$ (**2**). This solution was refluxed for 3 d. Evaporation of all volatiles in vacuum and recrystallisation of the crude residue from pentane gave 1.94 g (1.73 mmol, 64%) of brown crystals of **3**.

Synthesis of $[(\eta^5\text{-}Cp)Ni(\mu\text{-}OH)\{Sn(CH(Si(CH_3)_3)_2)_2\}_2]$ (6): A fourfold excess of N_2-saturated H_2O was added a solution of **3** in diethyl ether {prepared from 0.571 mmol of $[\{Sn\{CH(SiMe_3)_2\}_2\}_2]$ (**2**) and 1.14 mmol of **4**}. After stirring the initial brown solution for about 5 min, a color change to bright red was observed. Additional stirring for 2 h, followed by vacuum removal of all volatiles and recrystallization of the crude residue from diethyl ether at −30°C, gave 368 mg (0.363 mmol, 64%) of **6**. − MS (EI, 70 eV, T_{vap} = 130°C); *m/z* (%): 1016 (20) [M^+], 999 (10) [M^+ − OH] 857(30), [M^+ − $CH(SiMe_3)_2$], 697(100), [M^+ − $[CH(SiMe_3)_2]_2$]. − IR (KBr): $\tilde{\nu}$ = 3623 cm^{-1} (s) (OH), 2949 (s), 2898 (s), 1402 (s), 1250 (s), 839 (br.), 784 (br.) (all tms), 1348 (s), 1315 (s), 1294 (s), 1139 (s), 959 (s) [all Cp]. − ^1H NMR ([D_6]benzene): δ = 5.23(s, Cp, 5 H), 1.46 [br. s, $^2J(^{119}Sn,H)$ = 12 Hz, OH, 1 H], 0.67 (s, CH, 4 H), 0.42 (s, $SiMe_3$, 36 H), 0.24 (s, $SiMe_3$, 36 H). − $\{^1H\}^{13}C$ NMR ([D_6]benzene): δ = 88.4 [s, $^2J(^{119}Sn,C)$ = 19 Hz, Cp], 20.66 (s, CH), 5.17 [s, ^3J(Sn,C) = 15 Hz, $SiMe_3$], 4.29 [s, $^3J(^{119}Sn,C)$ = 15 Hz, $SiMe_3$]. − $C_{33}H_{82}NiOSi_8Sn_2$ (1015.79): calcd. C 39.00, H 8.14, found C 39.06, H 8.15.

Synthesis of $[(\eta^5\text{-}Cp)(CH_3CN)Ni-Sn(OH)\{CH(Si(CH_3)_3)_2\}_2]$ (7): A fourfold excess of N_2-saturated H_2O was added to a solution of **3** in 50 mL of diethyl ether {prepared from 0.571 mmol of $[\{Sn\{CH(SiMe_3)_2\}_2\}_2]$ (**2**) and 1.14 mmol of **4**}. After stirring of the initial brown solution for about 5 min, a color change to bright red was observed. After additional stirring for 2 h, 25 mL of ether was removed under vacuum and replaced by 20 mL of acetonitrile. This solution was filtered and stored for two weeks at −20°C whereupon 730 mg (0.72 mmol, 79%) of brick-red crystals of **7** could be isolated, co-crystallized with 220 mg (0.25 mmol) of **1**. These two compounds were then separated mechanically. − ^1H NMR ([D_6]benzene): δ = 5.29 (s, Cp, 5 H), 1.48 (br. s, *J* = 24 Hz, OH, 1 H), 0.78 (s, C−CH_3, 3 H), 0.43 (s, $SiMe_3$, 36 H). − $\{^1H\}^{13}C$ NMR ([D_6]benzene): δ = 94.48 (s, C_{Sp}), 88.58 [s, Cp, ^2J(Sn,C) = 14.3 Hz], 20.88 [s, CH, $^1J(^{119}Sn,C)$ = 117 Hz, ^1J(Si,C) = 39.0 Hz], 5.36 [s, $SiMe_3$, ^3J(Sn,C) = 16 Hz]. − IR (KBr): $\tilde{\nu}$ = 3624 cm^{-1} (OH), 3220, 2271, 1371 (CH_3CN), 2947, 2923, 2894, 1249, 1015, 841, 663, 608, 521 (all tms), 3088, 2961, 2835, 1400, 1346, 1292, 1242, 1108, 779 (all Cp).

Acknowledgments

This work was supported by the DFG (Heisenberg fellowship to J. J. S. and Sachbeihilfe grant SCHN 375/3−1) and the Fonds der Chemischen Industrie. We thank Dr. D. Stöckigt and Dr. K. Seevogel and co-workers (MPI für Kohlenforschung, Mülheim) for recording mass and infrared spectra.

[1] [1a] D. W. Stephan, *Coord. Chem. Rev.* **1989**, *95*, 41. − [1b] S. Friedrich, H. Memmler, L. H. Gade, W.-S. Li, M. McPartlin, *Angew. Chem.* **1994**, *106*, 705; *Angew. Chem. Int. Ed. Engl.* **1994**, *33*, 676. − [1c] S. Friedrich, L. H. Gade, I. J. Scowen, M. McPartlin, *Angew. Chem.* **1996**, *108*, 1440; *Angew. Chem. Int. Ed. Engl.* **1996**, *35*, 1338. − [1d] S. Friedrich, L. H. Gade, I. S. Scowen, M. McPartlin, *Organometallics* **1995**, *14*, 5344. − [1e] D. Selent, R. Beckhaus, J. Pickart, *Organometallics* **1993**, *12*, 2857. − [1f] L. H. Gade, *Angew. Chem.* **1996**, *108*, 2226; *Angew. Chem. Int. Ed. Engl.* **1996**, *35*, 2089. − [1g] G. Jansen, M. Schubert, B. Findeis, L. H. Gade, I. J. Scowen, M. Mc. Partlin, *J. Am. Chem. Soc.* **1998**, *120*, 7239.
[2] U. Denninger, J. J. Schneider, G. Wilke, R. Goddard, C. Krüger, *Inorg. Chim. Acta* **1993**, *213*, 129.
[3] J. J. Schneider, U. Denninger, J. Hagen, C. Krüger, D. Bläser, R. Boese, *Chem. Ber.* **1997**, *130*, 1433.
[4] G. Schwitzgebel, R. Mildenberger, *Ber. Bunsenges. Phys. Chem.* **1997**, *101*, 1742.

[5] [5a] J. Arana, P. Ramirez de la Piscina, J. Llorca, J. Sales, N. Homs, *Chem. Mater.* **1998**, *10*, 1333. – [5b] A. Onda, T. Komatsu, T. Yashima, *J. Chem. Soc., Chem. Commun.* **1998**, 1507.

[6] [6a] J. D. Cotton, P. J. Davidson, D. E Goldberg, M. F. Lappert, K. M. Thomas, *J. Chem. Soc., Chem. Commun*. **1974**, 893. – [6b] J. D. Cotton, P. J. Davidson, M. F. Lappert, *J. Chem. Soc., Dalton. Trans.* **1976**, 2275. – [6c] C. Pluta, K. R. Pörschke, R. Mynott, P. Betz, C. Krüger, *Chem. Ber.* **1991**, *124*, 1321. – [6d] W. E. Piers, R. M. Whittal, G. Ferguson, J. F. Gallagher, R. D. J. Froese, *Organometallics* **1992**, *11*, 4015. – [6e] J. Krause, K. H. Haack, K.-R. Pörschke, B. Gabor, R. Goddard, C. Pluta, K. Seevogel, *J. Am. Chem. Soc.* **1996**, *118*, 804. – [6f] F. Schager, K. Seevogel, K.-R. Pörschke, M. Kessler, C. Krüger, *J. Am. Chem. Soc*. **1996**, *118*, 13075. – [6g] M. F. Lappert, R. S. Rowe, Coord. *Chem. Rev.* **1990**, *100*, 267. – [6h] P. B. Hitchcock, M. F. Lappert, S. A. Thomas, A. J. Thorne, *J. Organomet. Chem.* **1986**, *315*, 27. – [6i] P. B. Hitchcock, M. F. Lappert, M. C. Misra, *J. Chem. Soc., Chem. Commun.* **1985**, 863. – [6j] P. B. Hitchcock, M. F. Lappert, S. A. Thomas, A. J. Thorne, A. J. Carthy, N. J. Taylor, *J. Organomet. Chem*. **1986**, *315*, 27. – [6k] M. Weidenbruch, A. Stilter, K. Peters, H. G. von Schnering, *Chem. Ber*. **1996**, *129*, 1565. – [6l] M. Weidenbruch, A. Stilter, K. Peters, H. G. von Schnering, *Z. Anorg. Allg. Chem.* **1996**, *14*, 365. – [6m] M. Weidenbruch, A. Stilter, W. Saack, K. Peters, H. G. von Schnering, *J. Organomet. Chem.* **1998**, *560*, 125. – [6n] D. E. Goldberg, D. H. Harris, M. F. Lappert, K. M. Thomas, *J. Chem. Soc., Chem. Commun.* **1976**, 261. – [6o] M. Weidenbruch, H. Kilian, K. Peters, H. G. von Schnering, H. Marsmann, *Chem. Ber.* **1995**, *128*, 983. – [6p] M. Veith, L. Stahl, V. Huch, *J. Chem. Soc., Chem. Commun.* **1990**, 359. – [6q] M. Veith, *Angew. Chem.* **1975**, *87*, 287; *Angew. Chem. Int. Ed. Engl*. **1975**, *14*, 263; *Z. Naturforsch, Teil B,* **1978**, *33*, 7.

[7] [7] P. J. Davidson, M. F. Lappert, *J. Chem. Soc., Chem. Commun.* **1973**, 317. – [7b] P. J. Davidson, D. H. Harris, M. F. Lappert, *J. Chem. Soc., Dalton Trans.* **1976**, 2268. – [7c] J. D. Cotton, P. J. Davidson, M. F. Lappert, *J. Chem. Soc., Dalton. Trans.* **1976**, 2275.

[8] J. J. Schneider, J. Hagen, D. Bläser, C. Krüger, R. Boese, *Angew. Chem*. **1997**, *109*, 771; *Angew. Chem. Int. Ed. Engl.* **1997**, *36*, 739.

[9] **Crystal Structure Analysis of 3:** Nicolet-Siemens R3 four-circle diffractometer with Mo-K_α radiation at 293 K. $C_{38}H_{86}Ni_2Si_8Sn_2 \cdot 1/2C_4H_{10}O$ (1159.65), crystal dimensions 0.47 × 0.38 × 0.31 mm, cell dimensions of the monoclinic system a = 15.327(8), b = 15.989(8), c = 24.631(3) Å, β = 94.56(4)°, V = 6017(5) Å^3, space group $C2/c$ with Z = 4, D_x = 1.280 g m^{-3}, μ = 1.620 mm^{-1}, empirical absorption correction on ψ scans with Siemens-XEMP programme (V.4.20.2), min/max transmission 0.628/0.966, R_{int} before/after correction 0.0699/0.0206, 5461 intensities collected ($2\Theta_{max}$ = 55°), 5315 unique [$R_{int}(F^2)$ = 0.0433], 3907 observed [$F_o^2 \geq 2\sigma(F^2)$], structure solution (direct methods) with Siemens-SHELXS-86[10] and refinement (240 parameters, H atoms as riding groups, 1.2-fold isotropic U values, 1.5-fold for methyl groups of the corresponding C atoms) with SHELXL-97−1, $R1$ = 0.0465, $wR2$ (all data) = 0.1250, GoF = 1.046, $w^{-1} = \sigma^2(F_o^2) + (0.0718\ P)^2 + 0.1022\ P$, where $P = (F_{o,max}^2 + 2F_c^2)/3$, residual electron density 0.656 eÅ^{-3}. The atoms of a diethyl ether molecule C51, C52 and O50 are disordered around the cell origin, and were treated with half occupancy. – **Crystal Structure Analysis of 7:** Siemens SMART diffractometer (Mo-K_α radiation), T = 293 K; structure solution by heavy-atom method (SHELXS-86[10]) and structure refinement by SHELXL-93;[11] monoclinic, space group $P2_1/c$; lattice constants a = 13.8547(14), b = 12.0522(8); c = 19.132(3) Å, β = 99.350(8)°, V = 3152.2(6) Å^3, Z = 4, μ(Mo-K_α) = 1.554 mm^{-1}, crystal size 0.70 × 0.67 × 0.53 mm; θ_{max} = 27.46°; 7203 independent reflections, 7768 measured of which 5942 were considered observed with $I > 2\sigma(I)$; residual electronic density 0.614 and −1.266 e/Å^3. 257 parameters (C, N, Ni, O and Si anisotropic). The Cp ring (C1a−C5a) is disordered. Individual positions could be resolved with occupancy factors of 1/2 (50%). Positions of the H atoms were calculated for idealized positions (d_{C-H} = 0.980 Å); R_1 = 0.0398; wR^2 = 0.1245. – Crystallographic data (excluding structure factors) for the structure(s) reported in this paper have been deposited with the Cambridge Crystallographic Data Centre as supplementary publication no. CCDC-102667 (**7**) and -114509 (**3**). Copies of the data can be obtained free of charge on application to CCDC, 12 Union Road, Cambridge CB2 1EZ, UK [Fax: (internat.) + 44-1223/336-033, E-mail: deposit@ccdc.cam.ac.uk].

[10] G. M. Sheldrick, *SHELXS-86, Program for Crystal Structure Solution*, Universität Göttingen, **1986**.

[11] G. M. Sheldrick, *SHELXL-93, Program for Crystal Structure Refinement*, Universität Göttingen, **1993**.

[12] M. Veith, L. Stahl, *Angew. Chem*. **1993**, *105*, 123; *Angew. Chem. Int. Ed. Engl*. **1993**, *33*, 1731.

[13] C. J. Cardin, D. J. Cardin, H. E. Page, J. M. Power, *J. Chem. Soc., Chem. Commun*. **1984**, 609.

[14] [14a] Addition of stannanediyls **:**SnR_2 to unbridged M−M bonds is reported in: D. E. Westerberg, B. R. Sutherland, J. C. Huffmann, K. G. Caulton, *J. Am. Chem. Soc.* **1988**, *110*, 1642. – [14b] For an example of two $Sn\{CH(SiMe_3)_2\}_2$ fragments bridging two transition metal centers see: W. E. Piers, R. M. Whittal, G. Ferguson, J. F. Gallagher, R. D. J. Froese, *Organometallics* **1992**, *11*, 4015.

[15] K. F. Purcell, J. C. Kotz, *Inorganic Chemistry* W. B. Saunders, Philadelphia, **1977**.

[16] R. Boese, D. Bläser, J. J. Schneider, unpublished results, Universität Essen **1997**.

[17] E. R. Brown, J. R. Sandifer in *Physical Methods of Chemistry, Electrochemical Methods* (Eds.: B. W. Rossiter, J. F. Hamilton), Wiley, New York, **1986**, vol. 2, chapter 4.

[18] M. A. Edelman, P. B. Hitchcock, M. F. Lappert*, J. Chem. Soc., Chem. Commun.* **1990**, 1116.

[19] C. Glidewell, D. C. Lilles, *Acta Crystallogr., Sect. B* **1978**, *34*, 129.

[20] J. J. Park, D. M. Collins, J. C. Hoard, *J. Am. Chem. Soc*. **1970**, *92*, 3636.

[21] F. Schager, R. Goddard, K. Seevogel, K. R. Pörschke, *Organometallics* **1998**, *17*, 1546.

[22] T. T. Kodas, M. Hampden-Smith in *The Chemistry of Metal CVD* (Eds.: T. T. Kodas, M. J. Hampden-Smith), VCH, Weinheim, **1994**.

[23] [23a] J. J. Schneider, J. Hagen, G. Heinemann, J. Bruckmann, C. Krüger, *Thin Solid Films* **1997**, *304*, 144. – [23b] I. S. Chuprakov, K. H. Dahmen, J. J. Schneider, J. Hagen, *Chem. Mater*. **1998**, *10*, 3467.

[24] P. Barbaro, C. Bianchini, F. Laschi, S. Midollini, S. Moneti, G. Scapacci, P. Zanello, *Inorg. Chem*. **1994**, *33*, 1622.

Received February 23, 1999
[I99063]

Density Functional Derived Structures and Molecular Properties of Nickel Dithiolenes and Related Complexes

Christa Lauterbach[a] and Jürgen Fabian*[a]

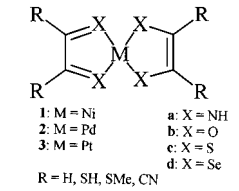
Keywords: Metal dichalcogenolene / Density functional calculations / Cyclic π-electron delocalization / Nickel

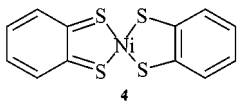
The molecular and electronic structure of the planar nickel dithiolene (**1c**, R = H) and of related complexes derived from nickel dithiolene by replacement of Ni by Pd (palladium dithiolene, **2c**, R = H) or by Pt (platinum dithiolene, **3c**, R = H), or by replacement of S by NH (nickel diiminolene, **1a**, R = H), O (nickel dioxylene, **1b**, R = H) or Se (nickel diselenolene, **1d**, R = H), were studied by density functional theory using the B3LYP functional and the valence triple-zeta basis set 6-311+G* for all atoms except Pd and Pt. For the latter atoms the quasirelativistic effective core potentials of the Stuttgart group were employed. The molecular structure of nickel dithiolene (**1c**, R = H) is satisfactorily reproduced by DFT calculations. The geometry of the corresponding platinum complexes **3a–3d** is more sensitive to relativistic effects, resulting in the contraction of the X–Pt bonds. As shown with the metal dithiolenes, the two ligands are structurally related to mononegative ions of open shell structure. The C–C bond lengths of the complexes are close to those of aromatic and chain-type polymethine structures (about 1.4 Å). The nickel dithiolene (**1c**, R = H) and related complexes have D_{2h} symmetry and are 14 π-electron systems with 10 π-electrons at the ligands and 4 π-electrons at the metal center. The natural population analysis has confirmed that metal M^{++} does accept electrons from the ligands but to a lesser extent than expected. The empty d-orbitals of M^{++} are only partly occupied in the molecular ground state. The positive charge of the metal decreases in the order Ni > Pd > Pt. The ^{1}H chemical shifts and the nucleus-independent chemical shifts (NICSs) of the ring moieties calculated by GIAO-DFT display a pronounced electron delocalization. In agreement with the calculated C–C bond lengths the ^{1}H chemical shifts and the NICS values show a marked bond delocalization. The NICS values show a change of the aromatic delocalization in the order Ni > Pd < Pt and NH > O < S < Se. The wave numbers of the IR spectra of the complexes calculated by DFT are grouped in separate frequency regions. The very intense absorption of **1c** (R = H) in the visible region of the spectrum is surprisingly well reproduced by ab initio single-only configuration interaction calculations. While the color band of the palladium complex is predicted to be red-shifted relative to the nickel complex, a blue shift is calculated on passing from the palladium to the platinum complex. The blue shift is, in part, due to the relativistic contraction of bond lengths in the Pt complexes.

Introduction

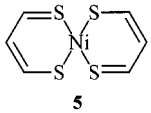
The complexes **1**−**4** (henceforth called metal diheterolenes) are 16-electron metal complexes. In the formal oxidation state of +2 they have a square-planar coordination and two planar bidentate ligand systems. In contrast to porphyrin-based complexes with a metal ion within the cyclic ligand and metallocene-type complexes with a metal ion intercalated between two planar ligands, diheterolenes contain the metal ion as a link between two planar ligands, forming a coplanar compound with five-membered conjugated rings. The metal ion is part of a delocalized π-electron system.

Nickel dithiolenes were first synthesized in the 1960s and the results of the subsequent extensive research were reviewed by Schrauzer,[1][2] Eisenberg,[3] Hoyer,[4][5] Burns[6] and Mueller-Westerhoff[7] and co-workers. Early semiempirical quantum chemical studies revealed the ground-state configuration of the parent nickel dithiolene with the highest occupied (HOMO) and lowest unoccupied molecular orbital (LUMO) of π-type character.[1][2] The lowest unoccupied molecular orbital is mainly located at the ligand. Nickel dithiolene (**1c**, R = H) is a 14 π-electron system with five π-electrons at each ligand and four π-electrons at the nickel center.[8] This complex is clearly distinguished from the bis(3-thioxopropene-1-thiolato)nickel complex **5**, which is a 16-π system with six π-electrons at each ligand.





4



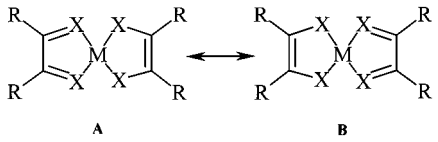
5

Scheme 1

[a] Institut für Organische Chemie der Technischen Universität Dresden,
Mommsenstraße 13, D-01162 Dresden, Germany
Fax: (internat.) + 49(0)351/463-7030
E-mail: fabian@coch01.chm.tu-dresden.de

 © WILEY-VCH Verlag GmbH, D-69451 Weinheim, 1999 1434−1948/99/1111−1995 $ 17.50+.50/0

Viewed in terms of building units of appropriate oxidation states, the dithiolene complexes are derived from M^{2+} and two dimethine radical anions that are terminated by sulfur atoms. These components constitute the neutral complex. Such a ligand system is a member of a series of vinylogous $[N + 1]\pi$ polymethines (polymethine violenes) with $N = 4$.[9] In the composite complex the spins of the radical fragments are paired. This composition of the complex may suggest some biradical character and therefore a nonclassical fragment structure. In fact, to avoid nonsymmetrical formulae, nickel dithiolenes were first represented as resonance hybrids of two Lewis−Kekulé-type structures[1][2] **A** and **B**.



Scheme 2

Complexes related to nickel dithiolene (**1c**, R = H) contain metal atoms M, such as Pd (**2**) and Pt (**3**) in place of Ni (**1**), and hetero atoms X such as NH (**a**), O (**b**) or Se (**d**) in place of S (**c**). Nickel complexes are the most extensively studied so far in this field,[1−8,10] and knowledge about the Pd[11−13] and Pt complexes[14−17] is mainly restricted to compounds with more complex ligands or to metal−metal-bonded dimers.[18][19] The nickel complexes are unique in their electronic, optical and photophysical properties. The facile and reversible electron transfer of **1c**-type complexes has been taken as a model in the study of the function of nickel-containing enzymes.[4,5,20] Nickel dithiolenes may also serve as catalysts.[4][5] These compounds form stacks in the solid state or segregated stacks with donor molecules such as tetrathiofulvalene (TTF) and TTF-type compounds and are electric semiconductors or conductors ("1D metals").[21−27] Complexes with 2-thioxo-1,3-dithiole-4,5-dithiolate and related ligands have attracted particular attention. On the other hand, nickel dithiolenes are chromophores that exhibit intense long-wavelength absorptions in the visible or in the near infrared region of the spectrum[10,12,28−32] up to wavelengths of 1400 nm and with absorption coefficients as large as 80000 $cm^2 \cdot mmol^{-1}$. Given their ability to inhibit photofading of organic dyes they were studied in optical data storage systems[12] and, more recently, as near infrared laser dyes.[10][28] Nickel dithiolenes are versatile building blocks for the design of functional supramolecular arrays and polymer systems[33] and in the search for materials for the emerging optoelectronic technology. Conducting nickel dithiolenes and crown ethers form ion channels in the solid that are potential switches.[34] Efficient second-order NLO chromophores have been recently inserted in a layer of a nickel dithiolene derivative.[27]

We are aware of only a few high-level quantum chemical calculations on metal diheterolenes. These calculations were performed on particular complexes. The parent nickel dithiolene (**1c**, R = H) was calculated by Hartree−Fock,[35−37] by post-Hartree−Fock second-order perturbation theory[38] and by density functional theory.[12] The spin densities of a substituted nickel dithiolene[20] (**1c**, R = CN) were also studied by the latter method. The INDO-type semiempirical CIS approach was used in a basic study of structure and electronic excitation of nickel dithiolene.[8] Nickel dithiolene was first studied by extended Hückel[37] and Pariser−Parr−Pople calculations.[39]

The availability today of low-cost methods for density functional theory (DFT) and of well-defined quasirelativistic effective core potentials of transition metals enables more extended series of compounds to be studied. The purpose of this study is to calculate structure and structure-property relationships of the parent complexes **1**−**3** and of compounds derived from these by substitution of R (R = SH, SMe, CN) by density functional theory (DFT). For the sake of comparison, compounds **4** and **5** were also calculated. The question has been asked as to what extent electron excitation energies are satisfactorily predicted by ab initio calculations based on DFT optimum geometries.

Computational

DFT quantum chemical calculations were carried out using the 1994 release of the GAUSSIAN suite of programs.[40] The functional used throughout this study consists of a nonlocal hybrid HF/DF exchange functional as defined by Becke's three-parameter-equation[41] in conjunction with the nonlocal Lee−Yang−Parr correlation functional[42] (B3LYP for short). In numerous recent calculations DFT provided results that are comparable with those of post-Hartree−Fock ab initio quantum chemistry. For the sake of comparison, MP2 calculations were also performed with the inner electrons kept frozen. Open-shell structures were calculated by the unrestricted Kohn−Sham method. The eigenvalues of the S^2 operator, calculated as 0.76 and 2.03 at maximum, differ only slightly from the exact values (0.75 and 2.0, respectively) thus indicating low-spin contamination. The ground-state geometries were obtained by full geometry optimization. The optimum structures were confirmed by the Hessians. The second derivatives provided the harmonic vibrational frequencies, which were not corrected in this paper for anharmonicity and additional correlation effect by scaling. The calculations were performed by the valence triple-zeta basis set 6-311G augmented by a set of polarization and a set of diffuse functions at the nonhydrogen atoms. The basis set 6-311+G* was used throughout this study. Effective core potentials (ECP) were employed for complexes with Pd and Pt but not for the majority of calculations of complexes with Ni. Central to the concept of effective core potentials is the idea that electrons of the atomic inner shells are chemically inactive and can be substituted by an effective core potential instead being treated explicitly.[43][44] Furthermore, relativistic effects can be incorporated in full-relativistic or quasi-relativistic ECPs .[43−45] Calculations of Pt- and Pd-containing complexes were performed using the beyond Hartree−

Fock quasirelativistic effective core potentials ECP28MWB and ECP60MWB, respectively, which were developed by Stoll and Preuß.[46] The valence basis set is (8s7p6d)/[6s5p3d] in these cases[46] with an additional p-type polarization function for each of the two metals.[47] Since well-known relativistic effects may play an essential role in describing structure and properties of higher row transition-metal compounds,[43−45] the nonrelativistic effective core potential ECP60MHF[48] of Pt was also used for the sake of comparison. The calculations of ^{1}H chemical shifts and of the nucleus-independent chemical shifts (NICSs) were performed by the gauge-including atomic orbital procedure, designated by GIAO-DFT. Because of computational problems in calculating NICSs of complexes containing transition metals by hybrid HF/DF functionals using GAUSSIAN 94, $\delta(^1H)$ chemical shifts and NICS values were calculated by the BLYP functional.[49] NICS values are probes for the extent of "aromatic" electron delocalization in cyclic conjugated systems. These values were defined by von Ragué-Schleyer et al.[50] as the negative values of the isotropic magnetic shieldings in ppm calculated at the center of the rings. NICS1 values refer to the location 1 Å above the center. In the NICS1 values local contributions of the σ-bonds are reduced in favor of the π-effects.[51]

Electronic transition energies were calculated at DFT optimum geometries by full single configuration interactions (CIS) at the ab initio level of theory[52] using the 6-311+G* basis set. Atomic charges were derived by Weinhold's natural population analysis (NPA) using the natural orbital (NBO) partitioning scheme.[53][54] Along these lines the electron population of the π-type orbitals was evaluated in terms of the p_π and d_π contributions of the nonhydrogen atoms.

Results and Discussion

Structure

Selected structural data of the compounds 1−5, optimized by DFT, are collected in Table 1 along with the available experimental data. Experimental parameters were determined by X-ray structure analyses. The experimental data of the Pd complex refer to a substituted Pd dithiolene with monomeric subunits. Experimental M−X bond lengths were found to be shorter in the crystal than those of gas-phase structures.[55] In addition, DFT bond lengths of second and higher row main-group elements are systematically too large.[56] C−S bond lengths, for instance, are overestimated by about 0.03 Å. Given these limitations the agreement between theory and experiment is satisfactory.

Inspection of the data collected in Table 1 shows that the bond lengths are sensitive to the nature of the metal, M, as well as to the hetero atoms, X. As one would expect, the M−S bond lengths in the series of metal dithiolenes increase on passing from Ni−S (2.178 Å) to Pd−S (2.310 Å) and Pt−S (2.314 Å). Thus, the bonds of Pd−S and Pt−S are nearly equal in length. The Pt−S bond length is overestimated if relativistic effects are neglected (ECP60MHF of Pt). The Pt−S bond is contracted by 0.09 Å on replacing the nonrelativistic by the quasirelativistic effective core po-

Table 1. DFT-calculated bond lengths [Å] and angles [°] for complexes **1−5** and experimental data available (in italics)

	R	C−X	X−M	C−C	C−R	CXM	CCX	XMX	XMX′
1a	H	1.340	1.849	1.396	1.085	115.0	113.3	83.3	96.7
1b	H	1.295	1.839	1.396	1.088	111.3	115.6	86.2	93.8
1c	H	1.705	2.178	1.374	1.08	102.9	121.1	92.1	87.9
		1.687[a]	*2.100*	*1.357*	*0.950*	*107.8*	*117.9*	*88.5*	
		1.71[b]	*2.15*		*1.08*	*103*		*88*	*92*
1c	SH	1.715	2.177	1.396	1.775	104.2	120.1	91.4	88.6
1c	SMe	1.718	2.177	1.404	1.770	104.5	119.9	91.3	88.7
		1.70[c]	*2.13*	*1.40*	*1.74*	*105*	*119*	*92*	*88*
1c	CN	1.711	2.171	1.399	1.422	103.7	120.3	92.1	87.9
		1.72[b]	*2.15*		*1.37*	*107*		*91*	*89*
1d	H	1.854	2.296	1.363	1.086	101.4	122.1	93.0	87.0
2a	H	1.342	1.995	1.394	1.084	115.3	115.2	78.9	101.1
2b	H	1.296	2.002	1.396	1.086	111.6	117.8	81.2	98.8
2c	H	1.707	2.310	1.373	1.086	102.6	122.9	88.7	91.3
2c[d]		*1.690*	*2.295*	*1.397*		*99.2*	*124.6*	*92.5*	*87.5*
2d	H	1.855	2.423	1.363	1.086	101.0	123.9	90.2	89.8
3a	H	1.341	2.084	1.395	1.086	115.3	116.3	76.7	103.3
3a[e]	H	1.347	1.997	1.389	1.084	116.6	114.6	77.8	102.2
3b	H	1.294	2.098	1.398	1.089	111.5	119.2	78.7	101.3
3b[e]	H	1.304	2.005	1.387	1.086	112.9	117.1	79.9	100.1
3c	H	1.707	2.406	1.374	1.087	102.4	124.3	86.6	93.4
3c[e]	H	1.709	2.314	1.369	1.086	103.2	122.8	88.1	91.9
3d	H	1.857	2.515	1.364	1.087	100.7	125.1	88.2	91.8
3d[e]	H	1.859	2.429	1.359	1.086	101.5	123.7	89.6	90.4
4		1.728	2.173	1.424		104.3	119.6	92.2	87.8
5	H	1.681	2.226	1.388	1.088	116.6	131.6	97.1	82.9

[a] Ref.[8] – [b] Ref.[3] – [c] Ref.[37] – [d] Experimental data from averaged bond lengths of a substituted palladium dithiolene, see ref.[12] – [e] ECP60MWB of Pt instead of the ECP60MHF.

tential. The C−C bond lengths of the Pt complexes are only slightly shortened and the C−X bonds slightly lengthened. In the series **1c**−**3c** (R = H) the C−S bond lengths are nearly constant (1.71 Å). The lengths of these bonds are practically unaffected by the choice of the effective core potentials. According to the DFT calculations, substitution of the hydrogen atoms of nickel dithiolene by CN (**1c**, R = CN) results in a slight increase in the C−S and C−C bond lengths, whereas the Ni−S bond lengths are slightly shortened. The extension of the C−S bond length is confirmed by the X-ray data. However, the extension in the bond length of the C−C bond with donor and acceptor substitution is noticeable. The bond lengths increase from 1.374 Å (H) to 1.399 Å (CN) and 1.404 Å (SMe).

The C−C bond lengths of the complexes should be an indicator of the cyclic electron delocalization. The calculated C−C bond lengths are mostly affected by the hetero atom X and are in the range between 1.36 Å (X = Se) and 1.40 Å (X = NH). The latter value corresponds to the bond lengths of benzene. According to the C−C bond lengths the degree of bond delocalization decreases in the order NH = O > S > Se. The conjugated electronic system of the complexes appears more or less delocalized. As would be expected, the C−C bond lengths of the dithiolene **4** are more benzenoid if the C−C bonds are simultaneously part of an annulated benzenoid ring. These compounds seem to be only known as anions,[57] a situation that is in contrast to the analogous nitrogen-containing hetero compounds.[58]

In the case of nickel dithiolene (**1c**, R = H) the geometrical parameters were calculated both by DFT and ab initio MP2 with the same basis set 6-311+G* for all main atoms. The most interesting bond lengths are compared in Figure 1.

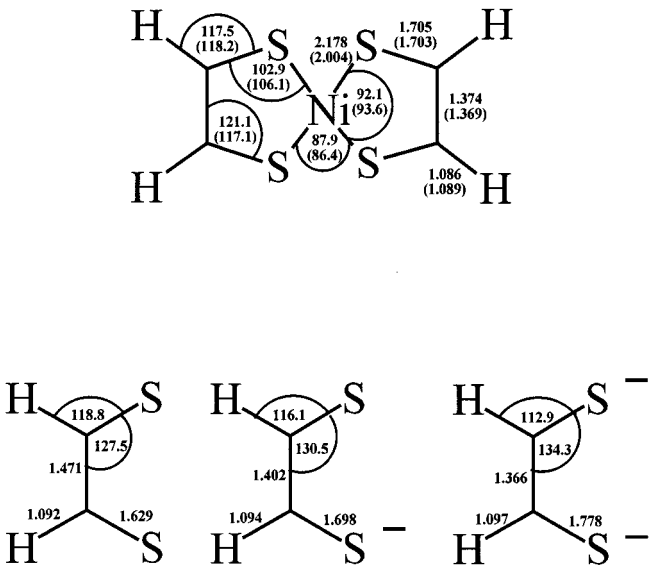


Figure 1. Comparison of selected bond lengths [Å] and bond angles [°] of nickel dithiolene (**1c**, R = H) calculated by DFT (B3LYP/6-311+G*) and by ab initio MP2/6-311+G* calculations (MP2 in parentheses) and the neutral, mononegative and dinegative ligand molecules

Except for the S−Ni bond the differences in the bond lengths calculated by the two theoretical models are remarkably small and confirm the good performance of DFT with respect to ab initio calculations. Because experimental geometries of **1c** (R = H)[3] do not refer to free molecules, the S−Ni bond length does not allow more detailed evaluation of the two methods. It should be mentioned that replacement of the all-electron treatment of Ni by the full-relativistic effective core potential ECP10MDF gives essentially the same bond lengths. The MP2 S−Ni bond length of nickel dithiolene (**1c**, R = H) reported in the literature[38] is between those found in this paper by the different theoretical models. This calculation was performed with a minimal basis set and the LANL1DZ effective core potential of Ni and S atoms.

The C−C bond lengths of the ligands in the complex differ greatly from those of the dithial and ethene-1,2-dithiolate ligand systems, which are the precursor compounds in the synthesis of the complex using reductive and oxidative conditions, respectively. However, the most closely related ligand is the sulfur-terminated dimethine radical. The C−C and C−S bond lengths of this radical are 1.402 and 1.698 Å, respectively, compared with 1.374 and 1.705 Å in the nickel dithiolene complex (see Figure 1).

Electron Distribution and Bonding

The total atomic charges and the population of π-type orbitals are determined by NBO analysis and are listed in Tables 2 and 3, respectively.

Table 2. Total atomic charges of the complexes **1**−**5** calculated by natural orbital population analysis (NPA)

	R	X	M	H_X	C	R
1a	H	−0.753	0.977	0.369	−0.035	0.184
1b	H	−0.624	1.167	−	0.159	0.173
1c	H	0.046	0.463	−	−0.384	0.221
1c	SH	0.030	0.489	−	−0.414	0.261
1c	CN	0.149	0.465	−	−0.284	0.019
1d	H	0.133	0.351	−	−0.443	0.222
2a	H	−0.727	0.837	0.369	−0.037	0.186
2b	H	−0.589	1.009	−	0.163	0.173
2c	H	0.079	0.334	−	−0.384	0.221
2d	H	0.163	0.239	−	−0.444	0.221
3a	H	−0.728	0.849	0.365	−0.034	0.184
3a[a]	H	−0.726	0.848	0.369	−0.045	0.188
3b	H	−0.592	1.015	−	0.167	0.171
3b[a]	H	−0.587	1.026	−	0.151	0.179
3c	H	0.074	0.351	−	−0.382	0.221
3c[a]	H	0.096	0.278	−	−0.389	0.224
3d	H	0.156	0.257	−	−0.442	0.221
3d[a]	H	0.181	0.172	−	−0.447	0.223
4		0.045	0.492	−	−0.211	0.085
5	H	0.006	0.466	−	−0.343[b]/ −0.273	0.216[b]/ 0.213

[a] ECP60MWB of Pt instead of the ECP60MHF. − [b] Non-adjacent to sulfur.

All parts of the molecules, viz. the metal M, the hetero atom X and the substituents R, affect the electron population markedly. M^{++} is an acceptor of electrons. The posi-

Table 3. Selected natural atomic orbital occupancies of π-type orbitals of the complexes **1**−**5** calculated by natural orbital population analysis (NPA)

	R	p_π(X)	p_π(M)	d_{yz}(M)	d_{xz}(M)	π_{total}(M)	p_π(C)	π_{total}[a]
1a	H	1.518	0.019	1.979	1.824	3.822	1.027	14
1b	H	1.601	0.022	1.984	1.838	3.844	0.938	14
1c	H	1.500	0.027	1.981	1.810	3.818	1.045	14
1c	SH	1.571	0.022	1.982	1.859	3.863	1.119	14.6
1c	CN	1.464	0.026	1.975	1.801	3.802	1.081	14
1d	H	1.498	0.024	1.987	1.798	3.809	1.049	14
2a	H	1.518	0.021	1.979	1.811	3.811	1.028	14
2b	H	1.601	0.018	1.987	1.847	3.852	0.936	14
2c	H	1.497	0.023	1.981	1.816	3.820	1.048	14
2d	H	1.493	0.020	1.985	1.814	3.819	1.052	14
3a	H	1.517	0.021	1.981	1.829	3.831	1.019	14
3a[b]	H	1.531	0.025	1.871	1.808	3.704	1.043	14
3b	H	1.599	0.016	1.989	1.871	3.876	0.932	14
3b[b]	H	1.612	0.021	1.979	1.739	3.739	0.953	14
3c	H	1.496	0.021	1.983	1.835	3.839	1.044	14
3c[b]	H	1.505	0.029	1.972	1.742	3.743	1.058	14
3d	H	1.492	0.018	1.986	1.834	3.838	1.049	14
3d[b]	H	1.503	0.025	1.979	1.743	3.747	1.060	14
4		1.531	0.024	1.984	1.773	3.781	1.041	14.1
5	H	1.525	0.014	1.913	1.989	3.916	0.946[c]/1.099	16

[a] Total population of π-type orbitals at the parent complexes. − [b] ECP60MWB of Pt instead of the ECP60MHF. − [c] Non-adjacent to sulfur.

tive charges alter in the order: Ni > Pd < Pt. The atomic charge of Ni in nickel dithiolene is +0.46. In other words, 1.54 electrons are transferred from the two ligands to Ni^{++}. The charge at the Ni increases to a maximum value of about +1 when S is replaced by N or O. Thus, the charge of the Ni is less than expected given the oxidation number of Ni^{II}. The negative charge at the hetero atoms, X, decrease in the order NH > O and becomes positive with S and Se. The carbon atoms adjacent to the chalcogen atoms are also negatively charged. As expected, substituents R may act as donors (SMe) or as acceptors (CN) relative to hydrogen. The effect of the CN acceptor group is characterized by the considerably reduced electron population at the hetero atoms X.

According to the NBO analysis, the occupation of the p_π orbitals of the metal center is negligibly small while the two d_π orbitals are occupied by about 3.8 electrons (see Table 3). The d_π orbital population of the carbon and the hetero atoms is less than 0.005 and, therefore, not listed in Table 3. The populations of the p_π orbitals of nickel dithiolene (**1c**, R = H) at the sulfur and carbon atoms (1.500 and 1.045, respectively) are reminiscent of those in the dimethine ligand system with values of 1.437 and 1.058, respectively. The highly delocalized π-system of the dimethine radical is essentially retained in the complex. The electron populations of the hetero atoms X shows that their donor strength in the π-system is in the order (NH, O) < (S, Se). Clearly, the more polarizable atoms are more strongly involved in the delocalization. Inspection of the electron occupation shows that the 4s and 4p orbitals of the metal center are hardly occupied. This clearly conflicts with the dsp^2-hybridisation model. According to the NBO analysis the d^8 element Ni is occupied by 9.54 electrons ($3d^{9.01}\ 4s^{0.45}\ 4p^{0.07}$) in the nickel dithiolene parent complex. The occupation of the metal 4p orbital is very low. There is an increasing doubt[59] as to whether NBO analysis provides an adequate occupation of (n + 1)p orbitals of transition metals. The occupation is considerably larger if p orbitals are enclosed in the valence shell.[60]

In agreement with Zerner et al.[8] the complex **1c** (R = H) is a 14π-electron system. According to the DFT calculations this conclusion holds for the whole series **1**−**3**. As expected, the metal complex **5** is a 16π-electron system. The electron structure of **5** differs slightly from **1c** (R = H) in the population of π-type orbitals of metal and hetero atoms and in the total amount of electrons that occupy π-type orbitals due to the presence of two more π-type orbitals at the two additional carbon atoms (see Table 3).

Spectral Properties

Because of their intense long-wavelength light absorption, nickel dithiolene and related compounds are well characterized by UV/Vis spectroscopy. For the whole series of compounds considered, one intense low energy electron transition appears in the visible or near infrared region. The calculated absorption wavelength of 623 nm (vertical transition) of nickel dithiolene (**1c**, R = H) has to be compared with the value of 719 nm measured in hexane.[8] Thus, the calculated absorption is about 100 nm in error, a deviation that corresponds to 0.27 eV in units of energy. In general, the error of CIS transition energies is larger.[61] According to CIS calculations of **1**−**3**, the color-determining π→π* ($A_g - B_{3u}$) transition is allowed and of large intensity. This finding is in agreement with previous semiempirical calculations on nickel dithiolenes.[1,2,8] The electronic transition is essentially determined by the HOMO−LUMO one-electron transition. The HOMO (b_{1u}) and LUMO (b_{2g}) are essentially localized over the two ligands (intra-ligand tran-

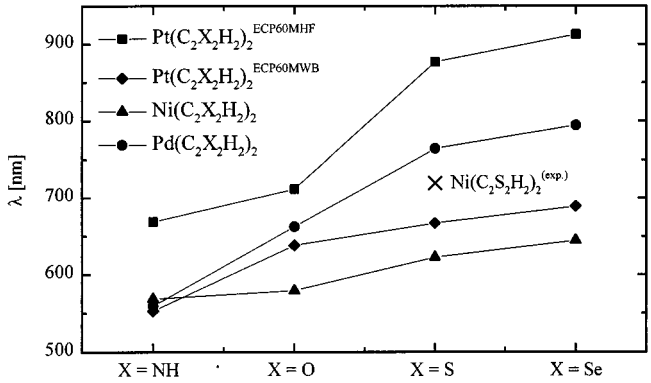


Figure 2. Absorption wavelengths [λ] of the complexes **1**−**3** (R = H) of the first intense electronic transition π→π* in the visible region of the spectrum (experimental value λ_{max} in hexane see ref.[6])

sition). A $3d_{\pi}$-type orbital of the metal ion contributes to the LUMO to a minor extent only. Due to the HF-based single-only approximation the calculated oscillator strengths are too large. In accordance with the predominant localized nature of the frontier orbitals, the ligand-to-metal CT character of the color-determining transition is small and amounts only to 0.01 electrons. As long as the nonrelativistic effective core potential of Pt was used (ECP60MHF) for the CIS calculations the absorption wavelengths of the color band λ_{max} are predicted to increase in the order Ni < Pd < Pt and NH < O < S < Se for nickel dithiolene complexes (see Figure 2 and Table 4). However, the calculated absorption wavelength of the platinum complex is lower than that of the palladium complex if the quasirelativistic ECP60MWB for Pt is taken into account (see Figure 2 and Table 4). The spectral shift is clearly due to the relativistic Pt−S bond contraction that naturally results in an increased energy gap as well as the relativistic destabilization of the LUMO, which includes $5d_{\pi}$-type orbitals.[45] This conclusion was supported by additional calculations: The CIS absorption wavelengths were calculated by using both nonrelativistic and quasirelativistic ECPs for **3c**, whose geometry was optimized without consideration of any relativistic effects. The quasirelativistically calculated absorption wavelength is nearly 100 nm blue-shifted in comparison with that calculated nonrelativistically. If the absorption energy of **3c** is calculated with quasirelativistic ECPs and with the molecular geometry optimized in the same quasirelativistic approximation, then the absorption wavelength is nearly 200 nm blue-shifted.

Thus, the absorption wavelength is predicted to increase on passing from the Ni to the Pd complexes and to decrease from the Pd to the Pt complexes.

HOMO−LUMO energy gaps calculated by RHF ab initio methods are, in general, not used to estimate electron-excitation energies and the calculated energies are much to high. This is not the case with the corresponding Kohn−Sham orbital gap (see Table 4). Encouraged by a recent study,[62] DFT energy gaps were also calculated. The results are listed in Table 4. As can be seen, both the energy differences of the Kohn−Sham frontier orbitals and the CIS excitation energies are nearly of the same order of magnitude and in the correct order: Ni < Pd ≥ Pt (see ref.[21]). Finer details, however, are not reproduced. Whereas the effect of the different metal ion is correctly calculated, the effect of the hetero atoms is at variance with the results of the CIS calculations.

It should be mentioned that the recently tested and very promising time-dependent density functional theory (TD-DFT) methods[63] predict the color band in the visible region at nearly the same absorption wavelength (656 nm) as CIS (623 nm) for nickel dithiolene (**1c**, R = H) based on

Table 4. Comparison of the energy differences of the Kohn−Sham frontier orbitals and CIS excitation energies

	R	ε_{HOMO}[a] [a.u.]	ε_{LUMO}[a] [a.u.]	$\Delta\varepsilon$[a] [a.u.]	ΔE [eV]	[nm]	ΔE_{CIS}[b] [eV]	[nm]
1a	H	−0.15037	−0.08315	0.06722	1.829	678	2.182	568
1b	H	−0.20313	−0.15266	0.05047	1.373	903	2.141	579
1c	H	−0.22805	−0.15912	0.06893	1.876	661	1.991	623
1c	SH	−0.20737	−0.15672	0.05065	1.378	900	1.619	766
1c	SMe	−0.18519	−0.13753	0.04766	1.297	956	1.546	802
1c	CN	−0.28825	−0.22461	0.06364	1.732	716	1.829	678
1d	H	−0.22971	−0.15967	0.07004	1.906	651	1.924	645
2a	H	−0.15019	−0.08835	0.06184	1.683	737	2.217	559
2b	H	−0.20223	−0.15734	0.04489	1.222	1015	1.872	662
2c	H	−0.22391	−0.16302	0.06089	1.657	748	1.623	764
2d	H	−0.22477	−0.16310	0.06167	1.678	739	1.561	794
3a	H	−0.14576	−0.08928	0.05648	1.537	807	1.854	669
3a[c]	H	−0.15440	−0.08106	0.07334	1.996	621	2.243	553
3b	H	−0.19993	−0.15966	0.04027	1.096	1131	1.743	711
3b[c]	H	−0.20899	−0.15573	0.05326	1.449	856	1.943	638
3c	H	−0.22022	−0.16608	0.05414	1.473	842	1.414	877
3c[c]	H	−0.22653	−0.15795	0.06858	1.866	664	1.858	667
3d	H	−0.22104	−0.16602	0.05502	1.497	828	1.358	913
3d[c]	H	−0.22664	−0.15812	0.06852	1.865	665	1.797	689
4		−0.22888	−0.16522	0.06366	1.732	716	1.734	715
5	H	−0.21786	−0.11090	0.10696	2.910	426	[d]	[d]

[a] HOMO and LUMO energies obtained by DFT. − [b] CIS excitation energies based on DFT optimum geometries. − [c] ECP60MWB of Pt instead of the ECP60MHF. − [d] More than one intense absorption between 200 and 300 nm (3.5 and 6 eV).

the DFT optimum geometry using the 6-311+G* basis. The TD-DFT calculation with the smaller basis set (6−31+G*) provides nearly the same absorption wavelength (655 nm) and is more economical.

Biradicaloid chromophoric ylides may have exceptional behavior in that the visible absorption features are well predicted.[64][65] Therefore, the question has been asked as to whether the complexes **1a**−**1d** may be biradicaloid as well. The biradicaloid character should be indicated by the S_0/T_1 splitting energy. The adiabatic S_0/T_1 energy gaps were therefore calculated by an energy-difference method by (U)DFT after optimization of the singlet and triplet molecules (see Figure 3). U in (U)DFT stands for unrestricted Kohn−Sham used in the calculation of the triplet molecule.

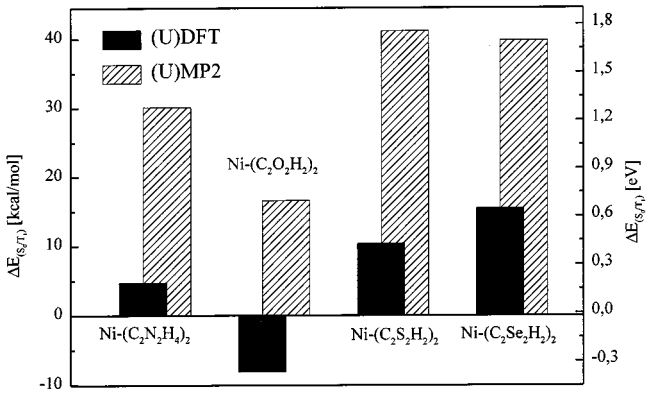


Figure 3. The adiabatic singlet/triplet (S_0/T_1) splitting energies of the complexes **1a**−**1d** (R = H) calculated by (U)DFT (B3LYP/6-311+G*) and (U)MP2 (B3LYP/6-311+G*)

Except for the oxygen-containing complex **1b** (R = H) all molecules are calculated with singlet multiplicity in the ground state. The adiabatic S_0/T_1 energy gap of nickel dithiolene (**1c**, R = H) calculated by (U)DFT is low (10.4 kcal/mol). Because (U)DFT seems to underestimate the singlet-triplet gap, the calculations were repeated on the (U)MP2 level of theory. In this approximation the energy gap amounts to 41.2 kcal/mol for nickel dithiolene. This splitting energy is clearly outside of the range of typical singlet biradicaloid organic compounds (about 25 kcal/mol[66]). In contrast to the (U)DFT calculations, (U)MP2 predicts the oxygen-containing complex **1b** (R = H) as a biradicaloid singlet molecule with an S_0/T_1 splitting energy of about 16 kcal/mol (see Figure 3).

The vibrational spectra of the parent structures **1a** (R = H), **2a** (R = H) and **3a** (R = H) have 45 normal modes, and all the other parent structures of the series **1**−**3** have 33 modes. Because of the D_{2h} symmetry the vibration belongs to 8 representations. Only vibrations due to the representations B_{1u} (out of plane), B_{2u} and B_{3u} (in plane) are allowed in the infrared spectrum and are considered in the following discussion. The calculated wave numbers are hardly dependent on the metal. The line spectra presented in relative intensity in Figure 4 are well grouped in few frequency regions.

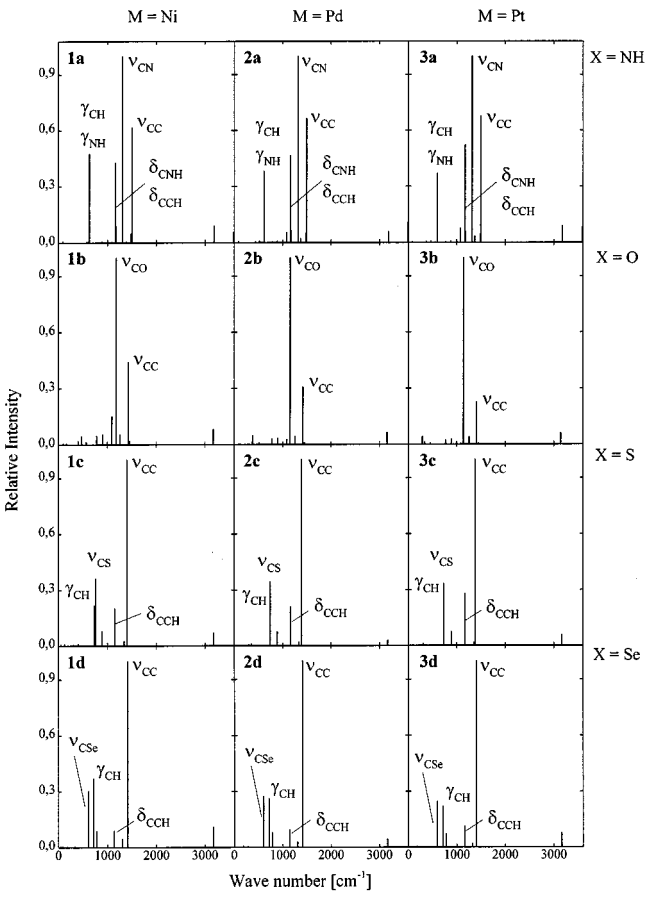


Figure 4. Line spectra of the allowed vibrations of **1**−**3** and assignments of the most intense transitions (relative intensity with respect to the most intense vibrational transitions)

As already documented in some cases, vibrations including the metal center are of small energy. The frequencies are lower than 500 cm^{-1} and of low intensity. However, the intensity of the whole spectrum seems to be greatly dependent on the hetero atoms X. The most intense IR vibrations are ν_{CN}, ν_{CO} and ν_{CC}.

The allowed vibrational frequencies of nickel dithiolene (**1c**, R = H) are compared with data of three experimental studies[67−69] in Table 5. In order to facilitate comparison of the frequencies they are classified according to the symmetry. This classification was also undertaken in two of the experimental studies.[67][68] As far as possible the assignments were given with the same descriptors. The assignments in refs.[67][68] were based on normal coordinate analyses and, in part,[67] on nickel isotope substitution.

The best agreement between the data predicted by DFT and experimental findings was reported by Schläpfer[67] et al. The assignment of the vibration for the systems reported in this paper is fully confirmed. The most intense calculated frequencies deviate by 40 cm^{-1} at maximum without scaling. Some vibrations, such as C−H, C−S and C=C, appear twice in the experimental spectrum.[67] Higher frequencies are overestimated because of the fact that anhar-

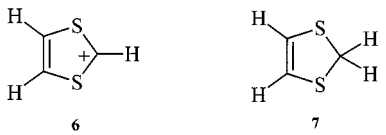
Table 5. Comparison of the allowed, calculated vibrational frequencies of nickel dithiolene (**1c**, R = H) with results of experimental studies (s = strong, vs = very strong)

	Descriptor	$\tilde{\nu}$ [cm^{-1}][a]	$\tilde{\nu}$ [cm^{-1}][b]	$\tilde{\nu}$ [cm^{-1}][c]	$\tilde{\nu}$ [cm^{-1}][d]
B_{2u}					
	δ_{SNiS}	311	237		
	ν_{Ni-S}	417	428	420	422
	ν_{C-S}	760 (s)	798	790	872
	ν_{C-S}				1099 (vs)
	δ_{CCH}	1151 (s)	1098 (s)	1092	
	δ_{CCH}		1110	1104	
	$\nu_{C=C}$, δ_{CCH}	1397 (vs)	1350 (s)	1340	1331 (vs)
	$\nu_{C=C}$, δ_{CCH}		1358		1346 (vs)
	ν_{C-H}				2933
	ν_{C-H}	3176	3018		3012
B_{3u}					
	$\delta_{SNiS'}$	127	76		
					132 (s) in-plane def_{ring}
					233 δ_{NiSC}, def_{ring}
	ν_{Ni-S}				309 (s)
	ν_{Ni-S}	410	398	420	311 (s)
	δ_{CCS}	637	735 (s)		
	ν_{C-S}, δ_{CCS}	892	865	714	
			878 (s)		
				874 δ_{C-H}, ν_{C-S}	
	δ_{CCH}		1260	1253	1258
	δ_{CCH}	1344	1295	1288	1296
	ν_{C-H}	3158	3030		3027
B_{1u}					
	out-of-$plane_{ring}$	52	131		85
	out-of-$plane_{ring}$	252	307		
	out-of-$plane_{C-H}$	738 (s)	760 (s)	754	718 (s)
					727
					747 (s)
					798

[a]Assigned by animation of the calculated vibrations (program: GAUSSIAN94, GAUSSVIEW). – [b] Ref.[67] – [c] Ref.[68] – [d] Ref.[69], no classification of the representations was given.

monicity has been neglected and insufficient consideration has been given to the electron correlation. The assignment in this study does not correspond with that of ref.[68] in the region between 700 and 800 cm^{-1} (see Table 5). The intense vibrations in the region 50 to 500 cm^{-1} found by Adams[69] et al. are also not confirmed.

The C=C frequency of the experimental and theoretical studies is remarkably low. For comparison, the IR spectrum of 2*H*-1,3-dithiole **7** was calculated. The metal of the five-membered ring is now replaced by CH_2. Whereas the C=C vibration of **7** was calculated at 1598 cm^{-1}, the C=C frequency of nickel dithiolene (**1c**, R = H) appears at 1397 cm^{-1}. The assignment of this vibration is more complicated, with the CCH bending also being involved in the vibration.



6 **7**

Scheme 3

The NMR chemical shifts may provide information regarding the electronic structure of the complexes. The paramagnetic ^{1}H chemical shift is a probe for cyclic electronic delocalization.[70] The results of the calculations are gathered in Table 6. The calculated ^{1}H chemical shifts are compared with experimental data of ref.[7] in the cases of **1c**, **2c**, **3c** and **5**. The theoretical ^{1}H chemical shifts of these compounds are slightly underestimated by our calculations compared to the experimental values.

For the sake of comparison the corresponding ^{1}H chemical shifts of 1,3-dithiolylium (δ = 8.95) (**6**) and 2*H*-1,3-dithiol (δ = 5.58) (**7**) were also calculated. Compound **6** is a prototype for a delocalized 6π-electron system with two sulfur atoms, while the bond system is fully localized in **7**. The proton shifts of the complexes **1**–**5** are strongly low-field shifted with respect to the shift in **7** and approach that of the cationic system **6**. Thus, all calculated compounds **1**–**3** seem to have a cyclic electron delocalization, which is in the order NH < O < S < Se and Ni ≈ Pd ≈ Pt.

Finally, Schleyer′s nucleus-independent chemical shifts (NICSs)[50] are considered as a probe of "aromatic" delocalization (see Table 6). NICS values of less than about δ = −3 indicate aromatic delocalization in organic compounds.[71] For nickel dithiolene the calculated NICS values are lower than δ = −8 and indicate aromatic delocalization. According to NICSs the complex **5**, with two six-membered rings, appears to be less delocalized. Electron delocalization is also supported in the five-membered rings of the annulated aromatic rings of **4**. The NICS values of the benzene rings of **4** are about δ = −6.6. The NICS values decrease in the order Ni > Pd > Pt if the Pt complexes were calcu-

Table 6. ^{1}H-NMR chemical shifts and nucleus-independent chemical shifts (NICS) [ppm] calculated by GIAO BLYP/6-311+G*, based on the B3LYP/6-311+G* optimum geometries

		X = NH	X = O	X = S[a]	X = Se
δ (^{1}H)	**1**	6.80	7.81	8.83 (9.14)	9.53
	2	6.92	7.72	8.80 (9.01)	9.72
	3	7.47	7.65	8.33 (8.77)	9.06
	3[b]	6.70	7.91	8.50 (8.77)	9.18
	5			8.49 (8.73)	
				6.98[c] (7.40)	
NICS/NICS1[d]	**1**	−9.73/−6.69	−8.78/−6.12	−8.09/−8.54	−9.09/−9.28
	2	−5.21/−5.03	−2.29/−4.05	−4.62/−5.76	−5.79/−6.30
	3	−4.12/−4.74	−0.09/−2.77	−2.89/−4.34	−4.09/−4.97
	3[b]	−6.28/−5.50	−4.53/−5.01	−5.76/−6.26	−6.90/−6.94
	4			−7.98/−8.54[e]	
				−6.64/−8.51[f]	
	5			−1.37/−1.54	

[a] Experimental value from ref.[7] in parenthesis, measured in $CDCl_3$. − [b] ECP60MWB of Pt instead of ECP60MHF. − [c] The larger value of the ^{1}H-chemical shift belongs to the carbon atom adjacent to the sulfur atom. − [d] NICS/NICS1 of benzene: −7.7/−9.9, calculated by GIAO BLYP/6-311+G*; NICS/NICS1 of benzene: −9.7/−11.5, calculated by HF/6−31+G* (Schleyer et al.[50]). − [e] NICS/NICS1 of the five-membered ring. − [f] NICS/NICS1 of the annelated aromatic ring.

lated with the nonrelativistic effective core potential ECP60MHF. Thus, the aromatic delocalization of Pt-containing complexes appears low in this classification scheme. If relativistic effects for platinum are taken into account, the NICS values alter in the order Ni > Pd < Pt, and the Pt complexes seem to be more aromatic. NICS1 values confirm these conclusions. Less is known of specific effects of the metal on NICS values.

Conclusions

A series of iso-π-electronic metal complexes of the same topology was considered and calculated by the Hohenberg−Kohn−Sham density functional theory. Valence triple-zeta basis sets augmented by two sets of polarization functions and quasirelativistic effective core potentials for transition metals were used. As shown with nickel dithiolene, experimental bond lengths and bond angles are satisfactorily reproduced by DFT calculations. A remarkable relativistic M−X bond length contraction is calculated for platinum complexes. The calculated C−C bond lengths of all Ni, Pd and Pt complexes are in the range between 1.36 Å and 1.40 Å. The strong bond delocalization is supported by the proton chemical shift calculated by GIAO. The chemical shifts are low-field shifted with respect to protons at the double bond in a nonconjugated system. The aromatic delocalization is also supported by Schleyer′s nucleus-independent chemical shift. Ab initio CIS calculations predict satisfactorily an intense absorption in the visible region. The transition is essentially a π→π* transition between HOMO and LUMO and is mainly located at the ligand. According to CIS calculations the wavelengths of the color band λ_{max} increases in the order NH < O < S < Se and Ni < Pd > Pt. The singlet/triplet (S_0/T_1) splitting energies of the complexes **1a**−**1d** (R = H) calculated by the energy difference method by (U)DFT is relatively small. The larger values obtained by (U)MP2 are more reliable. The biradicaloid character of nickel diheterolenes suggested by the formula representation with 5 π-electrons at each ligand is therefore not supported in general, except for the oxygen-containing complex. The electrons clearly interact strongly through the metal center

Acknowledgments

The study was supported by the "Deutsche Forschungsgemeinschaft" (Graduiertenkolleg: Struktur-Eigenschafts-Beziehungen bei Heterocyclen) and by the "Fonds der Chemischen Industrie".

[1] G. N. Schrauzer, V. P. Mayweg, *J. Am. Chem. Soc.* **1965**, *87*, 3585−3592.
[2] G. N. Schrauzer, *Acc. Chem. Res.* **1969**, *2*, 72−80.
[3] R. Eisenberg, *Prog. Inorg. Chem*. **1970**, *12*, 295−369.
[4] E. Hoyer, W. Dietzsch, W. Schroth, *Z. Chem.* **1971**, *11*, 41−53.
[5] R.-M. Olk, B. Olk, W. Dietzsch, R. Kirmse, E. Hoyer, *Coord. Chem. Rev.* **1992**, *117*, 99−131.
[6] R. P. Burns, C. A. McAuliffe, *Adv. Inorg. Chem. Radiochem.* **1979**, *22*, 303−348.
[7] U. T. Mueller-Westerhoff, B. Vance, *Comprehensive Coordination Chemistry* (Ed.: G. Wilkinson), Pergamon, Oxford **1987**, vol 2, chapter 16.5, pp. 595−631 and references therein.
[8] Z. S. Herman, R. F. Kirchner, G. H. Loew, U. T. Mueller-Westerhoff, A. Nazzal, M. Zerner, *Inorg. Chem.* **1982**, *21*, 46−56.
[9] N. Tyutyulkov, J. Fabian, A. Mehlhorn, F. Dietz, A. Tadjer, *Polymethine Dyes, Structure and Properties*, St. Kliment Ohridski, University Press, Sofia, **1991**.
[10] U. T. Mueller-Westerhoff, B. Vance, D. I. Yoon, *Tetrahedron* **1991**, *47*, 909−932.
[11] M. Bonamico, V. Fares, L. Petrilli, F. Tarli, G. Chiozzini, C. Riccucci, *J. Chem. Soc., Dalton Trans.* **1994**, 3349−3354.
[12] M. Arca, F. Demartin, F. A. Devillanova, A. Garau, F. Isai, F. Lelj, V. Lippols, S. Pedraglio, G. Verani, *J. Chem. Soc., Dalton Trans.* **1998**, 3731−3736.
[13] E. Möller, R. Kirmse, *Inorg. Chim. Acta* **1997**, *257*, 273−276.
[14] M. Bonamico, V. Fares, P. Imperatori, L. Suber, F. Tarli, *J. Chem. Soc., Dalton Trans.* **1990**, 931−934 and references therein.
[15] S. D. Cummings, R. Eisenberg, *J. Am. Chem. Soc.* **1996**, *118*, 1949−1960.
[16] S. D. Cummings, R. Eisenberg, *Inorg. Chim. Acta* **1996**, *242*, 225−231.

[17] L. Petrilli, F. Tarli, G. Chiozzini, C. Riccucci, *Polyhedron* **1997**, *16*, 275−279.
[18] K. W. Browall, L. V. Interrante, J. S. Kasper, *J. Am. Chem. Soc.* **1971**, *93*, 6289−6290.
[19] K. W. Browall, T. Bursh, L. V. Interrante, J. S. Kasper, *Inorg. Chem.* **1972**, *8*, 1800−1806.
[20] J. E. Huyett, S. B. Choudhury, D. M. Eichhorn, P. A. Bryngelson, M. J. Maroney, B. M. Hoffman, *Inorg. Chem*. **1998**, *37*, 1361−1367 and references therein.
[21] M. M. Ahmad, A. E. Underhill, *J. Chem. Soc., Dalton Trans.* **1983**, 165−167.
[22] G. C. Papavassilion, A. Terzis, P. Delhaes, *Handbook of Organic Conductors* (Ed. M. S. Nalwa), J. Wiley, Chichester **1997**, vol. 1, chapter 3, pp. 151−227; A. Kobaysho, H. Kobayashi, *Handbook of Organic Conductors* (Ed. M. S. Nalwa), J. Wiley, Chichester **1997**, vol. 1, chapter 5, pp. 249−291.
[23] S. Alvarez, R. Vicente, R. Hoffmann, *J. Am. Chem. Soc.* **1985**, *107*, 6253−6277.
[24] Y. S. J. Veldhuizen, N. Veldam, A. L. Spek, P. Cassoux, R. Carlier, M. M. Mulder, J. G. Haasnoot, J. Reedijk, *J. Chem. Soc., Dalton Trans.* **1988**, 2989−2994.
[25] P. Cassoux, L. Valade, H. Kobayashi, R. A. Clark, A. E. Underhill, *Coord. Chem. Rev.* **1991**, *110*, 115−160.
[26] S. Suu, P. Wu, D. Zhu, Z. Ma, N. Shu, *Inorg. Chim. Acta* **1998**, *268*, 103−108.
[27] I. Malfant, R. Andreu, P. G. Lacroix, C. Faulmann, P. Cassoux, *Inorg. Chem.* **1998**, *37*, 3361−3370.
[28] J. Fabian, H. Nakazumi, M. Masuoka, *Chem. Rev.* **1992**, *92*, 1197−1226.
[29] I. Tabushi, K. Yamamura, H. Nonoguchi, *Chem. Lett*. **1987**, 1373−1376.
[30] F. Bigoli, P. Deplano, F. A. Devillanova, V. Lippolis, P. J. Lukes, M. L. Mercuri, M. A. Pellinghelli, E. F. Trogu, *J. Chem. Soc., Chem. Commun*. **1995**, 371−372.
[31] F. Bigoli, P. Deplano, F. A. Devillanova, J. R. Ferraro, V. Lippolis, P. J. Lukes, M. L. Mercuri, M. A. Pellinghelli, E. F. Trogu, J. M. Williams, *Inorg. Chem.* **1997**, *36*, 1218−1226.
[32] F. Bigoli, P. Deplano, M. L. Mercuri, M. A. Pellinghelli, G. Pintus, E. F. Trogu, G. Zonnedda, H. H. Wang, J. M. Williams, *Inorg. Chim. Acta* **1998**, *273*, 175−183.
[33] Th. F. Bauman, A. G. Barrett, B. M. Hoffman, *Inorg. Chem.* **1997**, *36*, 5661−5665.
[34] T. Nakamura, T. Akutagawa, K. Honda, A. E. Underhill, A. T. Coomber, R. H. Friend, *Nature* **1998**, *394*, 159−161.
[35] M. R. A. Blomberg, U. Wahlgren, *Chem. Phys.* **1980**, *49*, 117−126.
[36] I. Fischer Hjalmars, A. Henrickson-Enflo, *Int. J. Quantum Chem.* **1980**, *18*, 409−419.
[37] C. Kraffert, D. Walther, K. Peters, O. Lindqvist, V. Langer, J. Sieler, J. Reinhold, E. Hoyer, *Z. Anorg. Allg. Chem.* **1990**, *588*, 167−180.
[38] I. I. Zakharov, A. N. Startsev, I. V. Yudanov, G. M. Zhidomirov, *J. Struct. Chem*. **1996**, *37*, 201−205.
[39] H. Shiozaki, H. Nakazumi, T. Kitao, *J. Jpn. Soc. Col. Mat.* **1987**, *60*, 415−419.
[40] M. J. Frisch, G. W. Trucks, H. B. Schlegel, P. M. W. Gill, B. G. Johnson, M. A. Robb, J. R. Cheeseman, T. Keith, G. A. Petersson, J. A. Montgomery, K. Raghavachari, M. A. Al-Laham, V. G. Zakrzewski, J. V. Ortiz, J. B. Foresman, J. Cioslowski, B. B. Stefanov, A. Nanayakkara, M. Challacombe, C. Y. Peng, P. Y. Ayala, W. Chen, M. W. Wong, J. L. Andres, E. S. Replogle, R. Gomperts, R. L. Martin, D. J. Fox, J. S. Binkley, D. J. Defrees, J. Baker, J. P. Stewart, M. Head-Gordon, C. Gonzalez and J. A. Pople, *Gaussian 94 (Revision B.2)*, Gaussian Inc., Pittsburgh PA, USA, **1995**.
[41] A. D. Becke, *J. Chem. Phys.* **1993**, *98*, 5648−5652.
[42] C. Lee, W. Yang, R. G. Parr, *Phys. Rev. B* **1988**, *37*, 785−789.
[43] G. Frenking, I. Antes, M. Böhme, S. Dapprich, A. W. Ehlers, V. Jonas, A. Neuhaus, M. Otto, R. Stegman, A. Veldkamp, S. F. Vyboishchikov, *Rev. Comput. Chem.* **1996**, *8*, 63−144.
[44] Th. R. Cunduri, M. T. Benson, M. L. Lutz, S. O. Sommer, *Rev. Comput. Chem.* **1996**, *8*, 145−202.
[45] P. Pyykkö, *Chem. Rev.* **1988**, *88*, 563−594.
[46] D. Andrae, U. Haeussermann, M. Dolg, H. Stoll, H. Preuß, *Theor. Chim. Acta* **1990**, *77*, 123−141 and references therein.
[47] J. Andzelm, M. Klobukowski, E. Radzio-Andzelm, Y. Sakai, H. Tatewaki, *Physical Sciences Data: Gaussian Basis Sets for Molecular Calculations* (Ed.: S. Huzinaga), Elsevier, Amsterdam **1984**, vol. 16, p. 24.
[48] U. Haeussermann, Internet, http://www.theochem.uni-stuttgart.de.
[49] A. D. Becke, *Phys. Rev. A* **1988**, *38*, 3098−3100.
[50] P. von Ragué Schleyer, C. Maerker, A. Dransfeld, H. Jiao, N. J. R. van Eikema Hommes, *J. Am. Chem. Soc.* **1996**, *118*, 6317−6318.
[51] G. Subramanian, P. von Ragué-Schleyer, H. Jiao, *Organometallics* **1997**, *16*, 2362−2369.
[52] J. B. Foresman, M. Head-Gordon, J. A. Pople, M. J. Frisch, *J. Phys. Chem*. **1992**, *96*, 135−149.
[53] A. E. Reed, L. A. Curtiss, F. Weinhold, *Chem. Rev.* **1988**, *88*, 899−926.
[54] E. D. Glendening, J. K. Badenhoop, A. A. Reed, J. E. Carpenter, F. Weinhold, *Program Package NBO 4.0*, Theoret. Chem. Inst., University of Wisconsin, Madison, **1996**.
[55] G. Frenking, private communication, **1999**; see V. Jonas, G. Frenking, T. Reetz, *J. Am. Chem. Soc.* **1994**, *116*, 8741−8753.
[56] B. Ma, J.-H. Lii, H. F. Schaefer III, N. L. Allinger, *J. Phys. Chem.* **1996**, *100*, 8763−8769.
[57] M. J. Baker-Hawkes, E. Billig, H. B. Gray, *J. Am. Chem. Soc.* **1966**, *88*, 4870−4875.
[58] A. L. Balch, R. H. Holm, *J. Am. Chem. Soc.* **1966**, *88*, 5201−5209.
[59] F. Maseras, K. Morokuma, *Chem. Phys. Lett.* **1992**, 195, 500−504.
[60] C. A. Bayse, M. B. Hall, *J. Am. Chem. Soc.* **1999**, *121*, 1348−1358.
[61] J. F. Stanton, J. Gauss, N. Ishikava, M. Head-Gordon, *J. Chem. Phys.* **1995**, *103*, 4160−4174.
[62] U. Salzner, J. B. Lagowski, P. G. Pickup, R. A. Poirier, *J. Comput. Chem.* **1997**, *18*, 1943−1953.
[63] R. E. Stratman, G. E. Scuseria, M. J. Frisch, *J. Chem. Phys.* **1998**, *109*, 8218−8224.
[64] J. Fabian, *Sulfur Lett*. **1995**, *19*, 93−100.
[65] J. Fabian, Th. Wolff, *J. Photochem. Photobiol. A* **1996**, *96*, 1−5.
[66] J. Wirz, *Pure Appl. Chem.* **1984**, *56*, 1289−1300.
[67] C. W. Schläpfer, K. Nakamoto, *Inorg. Chem.* **1975**, *14*, 1338−1344.
[68] O. Siimann, J. Fresco, *Inorg. Chem.* **1971**, *10*, 297−302.
[69] D. M. Adams, J. B. Cornell, *J. Chem. Soc., A* **1968**, 1299−1303.
[70] P. von Ragué-Schleyer, H. Jiao, *Pure Appl. Chem*. **1996**, *68*, 209−218; and references cited therein.
[71] H. Jiao (research group of P. von Ragué-Schleyer), private communication, **1997**.

Received March 4, 1999
[I99085]

Synthesis of the Uranium Triflates $U(OTf)_3$ and $U(OTf)_4$ – Crystal Structure of $[U(OTf)_2(OPPh_3)_4][OTf]$

Jean Claude Berthet,[a] Monique Lance,[b] Martine Nierlich,[b] and Michel Ephritikhine*[a]

Keywords: Uranium(III) and uranium(IV) complexes / Uranium metal / Hydrides / Chlorides / Triflate complexes / X-ray crystal structure

Reactions of pure triflic acid (TfOH) with UH_3 at 20 °C and with U or UCl_3 at 120 °C afforded $U(OTf)_3$ (**1**), which was transformed into $U(OTf)_4$ (**2**) by reaction with TfOH at 180 °C; **2** was also synthesized by treating UCl_4 with TfOH at 120 °C. The yields were in excess of 90%. The crystal structure of $[U(OTf)_2(OPPh_3)_4][OTf]$ (**3**) was determined, which revealed a seven-coordinate uranium(III) centre bound by monodentate and bidentate triflate ligands.

The widespread interest in metal triflates in both organic and inorganic chemistry[1] prompted us to consider the potential of such complexes of uranium. We recently reported on the first uranium(IV) triflates, $U(OTf)_4(NC_5H_5)$ (OTf = OSO_2CF_3), as well as on some organometallic derivatives. These were prepared by a novel synthetic route, namely the protonolysis of alkyl and amide precursors with pyridinium triflate.[2] Following these first results, it soon became apparent that further studies of uranium triflates would be considerably expedited if we had at our disposal sufficient quantities of the base-free complexes $U(OTf)_3$ (**1**) and $U(OTf)_4$ (**2**). Here, we present simple, large-scale syntheses of **1** and **2** from classical starting materials; Lewis base adducts of **1** and **2** have also been prepared and the crystal structure of one of the first uranium(III) triflates, $[U(OTf)_2(OPPh_3)_4][OTf]$ (**3**), has been determined.

Syntheses of the U^{III} and U^{IV} triflates are summarized in Scheme 1. **1** and **2** were prepared by treating triflic acid (TfOH) with either U, UH_3 or UCl_3 in the absence of solvent; **2** was also synthesized from UCl_4. It was essential that the acid was freshly distilled in order to achieve a clean and straightforward reaction. Treatment of UH_3 with excess TfOH at 20°C afforded **1** as an ochre powder within a few minutes, the reaction being accompanied by the vigorous evolution of dihydrogen gas. Reactions of activated uranium turnings or uranium trichloride were much slower, requiring 3 d at 120°C to reach completion. After evaporation of the excess TfOH and drying in vacuo, **1** was obtained in almost quantitative yield as a very fine green powder. Uranium(III) triflate (**1**) proved to be remarkably stable at 120°C in suspension in pure TfOH and its oxidation, signified by a colour change from ochre to pale green-blue, occurred only when the temperature was raised to 170−180°C; after 10 h, the acid was evaporated and **2** was isolated in quantitative yield. Of course, **2** could be prepared directly, without isolating **1**, by heating U, UH_3 or UCl_3 in TfOH at 180°C. To the best of our knowledge, these reactions of U or UH_3 with TfOH represent the first syntheses of metal triflates from the metal or metal hydride.[1a,3] Alternatively, compound **2** could be synthesized by reaction of TfOH with UCl_4 at 120°C; rapid HCl evolution occurred and the pale green-blue powder of **2** was recovered in 91% yield after evaporation of the excess TfOH.

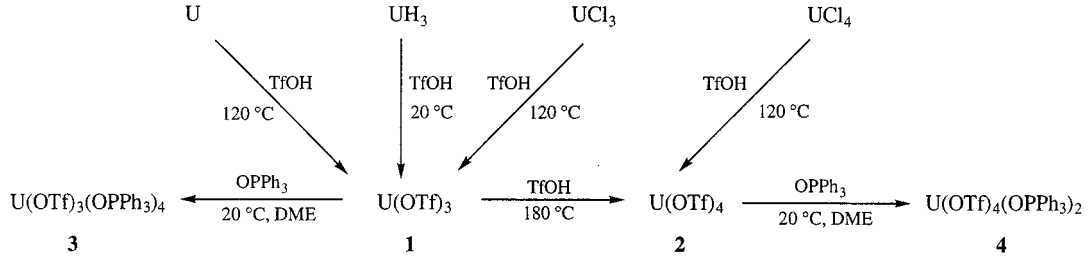
Irrespective of their mode of preparation, compounds **1** and **2** were obtained in a pure state, as established from their elemental analyses. However, the samples retained a trace of triflic acid, even if they were thoroughly dried in vacuo at 150°C for several days; this was evidenced by the formation of pyridinium triflate (< 1%) upon their dissolution in pyridine. The strong Lewis acids **1** and **2** were found to be quite soluble in coordinating solvents such as pyridine and dimethoxyethane (DME), giving stable adducts. Use of tetrahydrofuran (THF) as a solvent was not practical since it was readily polymerized at ambient temperature.

Addition of stoichiometric amounts of $OPPh_3$ to solutions of **1** and **2** in DME led to the immediate formation of $U(OTf)_3(OPPh_3)_4$ (**3**) and $U(OTf)_4(OPPh_3)_2$ (**4**), which were isolated in yields of 85% as red and pale-green powders, respectively. These $OPPh_3$ adducts, as well as the pyridine adducts of **1** and **2**, were found to be soluble in THF and no polymerization of the solvent was observed.

X-ray analysis showed the crystals of **3** to be composed of discrete pairs of OTf anions and $U(OTf)_2(OPPh_3)_4$ cations; such a dissociation of OTf ligands has frequently been encountered, in particular from lanthanide triflates.[4] The structure of **3** is shown in Figure 1, together with selected bond lengths and angles. The uranium atom is surrounded by seven oxygen atoms, which form a distorted pentagonal bipyramid. The apical positions are occupied by two $OPPh_3$ ligands [O(1) and O(4)], while the equatorial positions are occupied by two $OPPh_3$ ligands [O(2) and O(3)], a bidentate triflate group [O(5) and O(6)], and a monodentate triflate group [O(8)]; the U and the five equatorial O atoms are

[a] Laboratoire de Chimie de l'Uranium, Service de Chimie Moléculaire, DSM, DRECAM, CNRS URA 331, CEA Saclay, F-91191 Gif-sur-Yvette, France
Fax: (internat.) + 33-1/69086640
E-mail: ephri@drecam.saclay.cea.fr
[b] Laboratoire de Cristallochimie, Service de Chimie Moléculaire, DSM, DRECAM, CNRS URA 331, CEA Saclay, F-91191 Gif-sur-Yvette, France

 © WILEY-VCH Verlag GmbH, D-69451 Weinheim, 1999 1434−1948/99/1111−2005 $ 17.50+.50/0



Scheme 1. Syntheses of the uranium triflates **1**–**4**

coplanar within ± 0.13 Å. The $OPPh_3$ ligands are arranged such that the steric interactions are minimized. The lengths of the U–O($OPPh_3$) bonds are unexceptional, with an average value of 2.36(2) Å. The U–O(8) bond length to the monodentate OTf ligand [2.446(4) Å] may be compared with those measured in $U(C_5Me_5)_2(OTf)_2(OH_2)$ [2.36(1) and 2.40(1) Å] and $U(C_5H_5)_3(OTf)(CN\mathit{t}Bu)$ [2.485(9) Å].[2] This length is longer than those of typical U–O σ bonds (2.0–2.2 Å) and is even longer than the U–O($OPPh_3$) bond lengths, confirming the weak nucleophilic character of the OTf group. More interestingly, **3** is the first structurally characterized f-block element compound containing an η^2-*O*,*O*′-bonded triflate ligand. Such examples of a bidentate triflate ligand have previously been encountered in d-transition metal complexes, but remain very rare.[5] The U–O(5) and U–O(6) lengths are 0.2 Å longer than the U–O(8) length; such a difference between the metal–oxygen bond lengths of mono- and bidentate OTf ligands has previously been observed, most notably in the titanium compound Ti(NCN)(O*i*Pr)$(OTf)_2$ [NCN = C_6H_3-$(CH_2NMe_2)_2$-2,6].[5a]

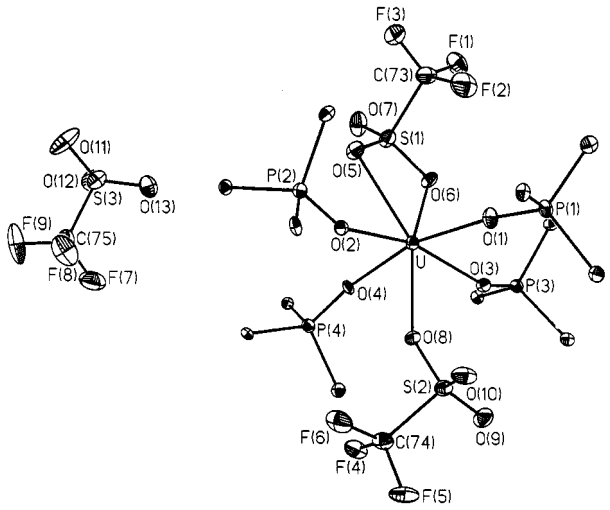


Figure 1. X-ray crystal structure of $[U(OTf)_2(OPPh_3)_4][OTf]$ (**3**) with thermal ellipsoids drawn at the 30% probability level; for the sake of clarity, only the *ipso* carbon atoms (not labelled) of the phenyl rings are represented; selected bond lengths [Å] and angles [°]: U–O(1) 2.370(4), U–O(2) 2.352(4), U–O(3) 2.389(4), U–O(4) 2.348(4), U–O(5) 2.645(5), U–O(6) 2.614(4), U–O(8) 2.446(4); O(1)–U–O(4) 166.2(2), O(3)–U–O(6) 72.45(13), O(5)–U–O(6) 53.80(14), O(2)–U–O(5) 72.88(13), O(2)–U–O(8) 77.95(14), O(3)–U–O(8) 83.12(14)

In conclusion, the new uranium triflates **1** and **2** have been synthesized by treating triflic acid with the corresponding chlorides in a classical manner, or by two novel routes from uranium metal or its hydride. The reactions were easy to perform and, by adjusting the temperature, **1** and **2** were obtained selectively in good yields. The crystal structure of **3** revealed three distinct triflate groups, one being dissociated and the other two coordinating in monodentate and bidentate ligation modes

Experimental Section

All preparations were carried out under argon (less than 2 ppm oxygen and water). Activated uranium turnings were prepared according to ref.[6] except that HgI_2 was replaced by iodine. UH_3,[7] UCl_3,[8] and UCl_4[9] were prepared by published methods. Triflic acid (99%; Aldrich) was freshly distilled prior to use.

Uranium(III) Triflate (1). – From UH_3: Triflic acid (1 mL) was added to UH_3 (250 mg, 1.04 mmol) in a 50-mL round-bottomed flask. The black powder of the hydride was rapidly transformed into an ochre powder, which was accompanied by the vigorous evolution of H_2 gas (***CAUTION!***). In order to ensure that the reaction had reached completion, the mixture was further heated at 100°C for 15 h. The excess TfOH was then distilled off and **1** was obtained as a green powder after drying in vacuo at 120°C for 24 h (687 mg, 96%). – $C_3F_9O_9S_3U$ (685): calcd. F 24.95, S 14.04; found F 24.73, S 13.85. – **From U or UCl_3:** A 200-mL flask was charged with activated uranium turnings (1050 mg, 4.41 mmol) and triflic acid (3 mL) and the mixture was heated for 3 d at 120°C. The excess TfOH was then distilled off and **1** was dried in vacuum at 120°C for 30 h (2840 mg, 94%). – $C_3F_9O_9S_3U$ (685): calcd. F 24.95, S 14.04; found F 24.80, S 14.32. – According to the same procedure, **1** was obtained in 96% yield from UCl_3 (250 mg, 0.72 mmol) and TfOH (3 mL). – $C_3F_9O_9S_3U$ (685): calcd. F 24.95, S 14.04; found F 24.68, S 13.80.

Uranium(IV) Triflate (2). – From UCl_4: A 100-mL flask was charged with UCl_4 (4.0 g, 10.5 mmol) and TfOH (8.5 mL) and the mixture was heated at 120°C. The colour of the powder rapidly turned from green to pale green-blue, which was accompanied by the evolution of HCl vapour. The HCl was pumped off to avoid a build-up of pressure (***CAUTION!***). After 10 h, the excess TfOH was distilled off and the green-blue powder **2** was dried in vacuo at 150°C for 60 h (8.0 g, 91%). – $C_4F_{12}O_{12}S_4U$ (834): calcd. F 27.32, S 15.37; found F 27.10, S 15.25, Cl < 0.1%. – **From U, UH_3 or UCl_3:** The procedure was identical to that used for the preparation of **1** except that the reaction mixture was heated at 180°C for 15 h (UH_3) or 3 d (U or UCl_3). The yields were almost quantitative and the samples were found to be analytically pure.

Tetrakis(triphenylphosphane oxide)uranium(III) Triflate (3): A mixture of **1** (250 mg, 0.36 mmol) and $OPPh_3$ (406 mg, 1.46 mmol) was dissolved in DME (30 mL). After 30 min, the red solution was

concentrated to a volume of 5 mL and diethyl ether (30 mL) was added, whereupon **3** precipitated as a red powder. The product was collected by filtration, washed with toluene, and dried in vacuo (556 mg, 85%). – $C_{75}H_{60}F_9O_{13}P_4S_3U$ (1798): calcd. C 50.09, H 3.36, S 5.35; found C 49.92, H 3.20, S 5.51.

Bis(triphenylphosphane oxide)uranium(IV) Triflate (4): A mixture of **2** (250 mg, 0.30 mmol) and $OPPh_3$ (167 mg, 0.60 mmol) was dissolved in DME (30 mL). After 30 min, the pale-green solution was concentrated to a volume of 5 mL and diethyl ether (40 mL) was added. The green oily material was transformed into a fine powder after stirring for 12 h; the green product **4** was then filtered off, washed with diethyl ether and toluene, and dried in vacuo for 12 h at 20°C (350 mg, 84%). – $C_{40}H_{30}F_{12}O_{14}P_2S_4U$ (1390): calcd. C 34.54, H 2.17, S 9.22; found C 34.71, H 2.30, S 9.08.

X-ray Crystallography of 3: Single crystals were obtained from a mixture of the DME adduct of **1** and excess $OPPh_3$ in THF/diethyl ether. A red crystal of approximate dimensions $0.18 \times 0.12 \times 0.12$ mm was selected. Diffraction data were collected with a Nonius diffractometer equipped with a CCD detector. The lattice parameters were determined from ten images recorded with 1° Φ scans and later refined on all data. The data were recorded at 123 K. A 180° Φ range was scanned in 2° increments with the crystal-to-detector distance fixed at 26 mm. Data were corrected for Lorentz polarization and absorption[10] effects. The structure was solved by the heavy-atom method and refined by full-matrix least squares on F^2 with anisotropic thermal parameters for all non-H atoms. H atoms were introduced at calculated positions and constrained to ride on their parent C atom. $C_{75}H_{60}F_9O_{13}P_4S_3U$ (1798.32), triclinic, space group $P-1$, $a = 13.694(1)$, $b = 14.734(1)$, $c = 19.420(1)$ Å, $\alpha = 92.143(4)$, $\beta = 108.393(4)$, $\gamma = 91.460(4)°$, $V = 3713(3)$ Å^3, $Z = 2$, $D_c = 1.609$ g cm^{-1}, Mo-K_α ($\lambda = 0.71073$ Å), $\mu_{Mo} = 2.441$ mm^{-1}, $F(000) = 1790$, total reflections = 19977, independent reflections = 10109 ($R_{int} = 0.076$), observed reflections [$I > 2\sigma(I)$] = 7023, $R_1 = 0.044$, $wR_2 = 0.077$. All calculations were performed with an O2 Silicon Graphics Station using the SHELXTL package.[11] Crystallographic data (excluding structure factors) for the structure reported in this paper have been deposited with the Cambridge Crystallographic Data Centre as supplementary publication no. CCDC-115885. Copies of the data can be obtained free of charge on application to the CCDC, 12 Union Road, Cambridge CB2 1EZ, U.K. [Fax: (internat.) + 44-1223/336-033; E-mail: deposit@ccdc.cam.ac.uk].

[1] [1a] G. A. Lawrance, *Chem. Rev.* **1986**, 86, 17. – [1b] S. Kobayashi, *Synlett* **1994**, 689.
[2] J. C. Berthet, M. Lance, M. Nierlich, M. Ephritikhine, *J. Chem. Soc., Chem. Commun.* **1998**, 1373.
[3] M. Labrouillère, C. Le Roux, H. Gaspard, A. Laporterie, J. Dubac, J. R. Desmurs, *Tetrahedron Lett.* **1999**, *40*, 285.
[4] [4a] H. C. Aspinall, J. L. M. Dwyer, N. Greeves, E. G. McIver, J. C. Woolley, *Organometallics* **1998**, *17*, 1884. – [4b] P. H. Smith, K. N. Raymond, *Inorg. Chem.* **1985**, *24*, 3469.
[5] [5a] J. G. Donkervoort, J. T. B. Jastrzebski, B. J. Deelman, H. Kooijman, N. Veldman, A. L. Spek, G. van Koten, *Organometallics* **1997**, *16*, 4174. – [5b] L. Giannini, A. Caselli, E. Solari, C. Floriani, A. Chiesi-Villa, C. Rizzoli, N. Re, A. Sgamellotti, *J. Am. Chem. Soc*. **1997**, *119*, 9198.
[6] L. R. Avens, S. G. Bott, D. L. Clark, A. P. Sattelberger, J. G. Watkin, B. D. Zwick, *Inorg. Chem*. **1994**, *33*, 2248.
[7] R. E. Rundle, *J. Am. Chem. Soc*. **1951**, *73*, 4172.
[8] J. J. Katz, I. Sheft, *Adv. Inorg. Chem. Radiochem*. **1960**, *2*, 195.
[9] J. A. Hermann, J. F. Suttle, *Inorg. Synth*. **1957**, *5*, 143.
[10] A. L. Spek, *MULABS PLATON*, University of Utrecht, The Netherlands, **1997**.
[11] G. M. Sheldrick, *SHELXTL-93: Program for the Refinement of Crystal Structures*, University of Gottingen, Germany, **1993**.

Received March 15, 1999
[I99099]

Hexakis(alcohol)zinc Complexes

Claas Sudbrake,[a] Bodo Müller,[a] and Heinrich Vahrenkamp*[a]

Dedicated to Professor Lawrence F. Dahl on the occasion of his 70th birthday

Keywords: Zinc complexes / Alcohol ligands / Structure and bonding

Hexakis(methanol) and hexakis(ethanol) complexes of zinc were prepared under strictly anhydrous conditions and crystallized as perchlorate or hexafluorosilicate salts in space groups of high symmetry. All their OH functions are engaged in hydrogen-bonded cation–anion networks. Their Zn–O distances correspond to those in $[Zn(H_2O)_6]^{2+}$. Their water sensitivity can be explained by a gain in entropy and by a gain in polar interactions upon replacement of alcohol by water ligands.

Hexaaqua transition-metal cations are commonplace and serve as reference points for the discussion of structures, spectra or ligand-field effects as well as being the natural starting materials in preparative coordination chemistry. In contrast, their simplest organic analogues, the hexakis(alcohol) complexes, are so uncommon that they are normally not mentioned in textbooks or even in comprehensive handbooks.[1] The reason for this is their extremely labile nature which does not allow them to be exposed to even traces of the "better" ligand water.

When it comes to synthetic usefulness this lability becomes favourable. Accordingly, hexakis(methanol) or hexakis(ethanol) complexes have been proposed as starting materials for other complexes with weakly coordinating ligands, and for this purpose a number of them have been prepared as salts of the divalent transition metals.[2][3] They were fully characterized by analyses and spectra. From their UV/Vis spectra it could be concluded that the simple alcohols have about the same position in the spectrochemical series as water. So far, only one hexakis(methanol)vanadium(II) complex[4] and two hexakis(ethanol)cobalt(II) complexes[5] have been subjected to crystal structure determinations.

Our interest in these complexes arose from our attempts at modelling the zinc enzyme alcohol dehydrogenase.[6] These studies required the investigation of zinc−alcohol, zinc−alkoxide, and zinc−aldehyde complexes. It turned out that some of the latter are accessible starting from hexakis(ethanol)zinc salts.[7] This fact, together with the limited knowledge about hexakis(alcohol)zinc complexes,[2][3] prompted us to re-investigate their chemistry and to gather information on their structures.

[a] Institut für Anorganische und Analytische Chemie, Universität Freiburg,
Albertstraße 21, D-79104 Freiburg, Germany
Fax: (internat.) + 49-(0)761/203-6001
E-mail: vahrenka@uni-freiburg.de

Preparation and Identification

The extreme sensitivity of the isolated complexes toward water required them to be handled with more than the usual precautions. In contrast, at the beginning of the preparations moisture posed no problems as the zinc reagents were the hexahydrates of the zinc salts. Their dehydration was performed with trimethyl or triethyl orthoformate in the corresponding alcohol, which produces the alcohol itself as the hydrolysis product. This procedure, which was applied by van Leeuwen for compounds **1** and **2**,[2][3] was found to be useful for all three types of hexakis(alcohol)zinc salts prepared here. Thus, from solutions of the hexahydrates of zinc perchlorate, tetrafluoroborate, and hexafluorosilicate in methanol or ethanol, after treatment with a large excess of the corresponding trialkyl orthoformate (10−20 fold), the known perchlorate **1b**, the known tetrafluoroborates **2a**, **b**, and the new hexafluorosilicates **3a**, **b** were obtained {$[(ROH)_6Zn](ClO_4)_2$: **1a**: R = Me; **1b**: R = Et; $[(ROH)_6Zn](BF_4)_2$: **2a**: R = Me; **2b**: R = Et; $[(ROH)_6Zn](SiF_6)$: **3a**: R = Me; **3b**: R = Et}. They are colourless crystalline solids. Their hygroscopicity does not allow them to persist for more than a few seconds in the normal atmosphere.

Unambiguous characterizations of **1b**, **3a** and **3b** were achieved with the structure determinations described below. NMR spectra in deuterioacetone showed that the alcohol ligands stay attached to the zinc ion in this solvent, see Table 1. The observed chemical shifts referred to those of the free alcohols in the same solvent are small, yet significant. Typical dependencies of the chemical shifts upon the nature of the counterions point to cation−anion interactions in solution. The wide spread of the OH NMR resonances indicates the presence of hydrogen bonding. The latter can also be concluded from the IR absorptions in a KBr matrix (see Table 2), which for **1** and **2** roughly resemble those in nujol mulls.[2][3] The $\tilde{\nu}$(OH) bands around

 © WILEY-VCH Verlag GmbH, D-69451 Weinheim, 1999 1434−1948/99/1111−2009 $ 17.50+.50/0

3500 cm^{-1} are quite broad and of relatively low energy. Other noticeable features in the IR spectra include the OH bending vibrations around 1630 cm^{-1} and the typical intense absorptions of the anions in the 1000−1100 cm^{-1} range for ClO_4^- and BF_4^- and around 750 cm^{-1} for SiF_6^{2-}.

Table 1. ^{1}H-NMR data ([D$_6$]acetone), δ [ppm]

	CH_3[a]	CH_2[a]	OH
1b[2]	1.18	3.72	5.39
2a	3.32		2.97
2b	0.97	3.48	4.72
3a	3.20		2.95
3b	0.98	3.43	3.66

[a] ^3J values for the ethyl groups 6.9−7.0 Hz.

Table 2. IR data (KBr), [cm^{-1}]

	ν̃(OH)	δ(OH)	ν̃(anion)
1b[2]	3460m	1620m	1088s
2a	3530s	1629m	1054s
2b	3510s	1636m	1031s
3a	3520s	1635m	765s
3b	3510s	1600m	738s

Solid-State Structures

Crystals of **1b**, **3a** and **3b** were found suitable for an X-ray data collection at ca. −100 °C. All three compounds crystallize in rhombohedral or hexagonal space groups with the zinc ions located on threefold axes in positions with sixfold point symmetry. Thus, there is only one alcohol ligand each in the asymmetric unit, and one Zn−O bond length and two O−Zn−O angles define the coordination sphere. In the case of **3b** a disorder problem of both the coordinated and a co-crystallized ethanol molecule affects the precision of the molecular details which therefore are not discussed here. The general features of the complex cation of **3b**, however, are the same as those of **1b**.

Figures 1 and 2 are combined views of the complex cations, showing both the ball-and-stick and the space-filling displays. The symmetry of the complexes is close to ideally octahedral. The Zn−O bond lengths (average 2.08 Å) are virtually identical to those in the $Zn(H_2O)_6^{2+}$ cation (average 2.09 Å).[8] Hence, there is no lengthening due to steric crowding of the six alcohol molecules, and the lability of the zinc−alcohol complexes cannot be explained by a weakness of the Zn−O bonds.

While the ball-and-stick models in Figures 1 and 2 emphasize the symmetry of the complexes and their similarity to the aqua complexes, their peculiarities can better be visualized by space-filling models. Figure 1 shows that the methanol complex has an ellipsoid-like shape. The separation of hydrophilic and hydrophobic parts therein is noticeable from the orientations of the O−H bonds which

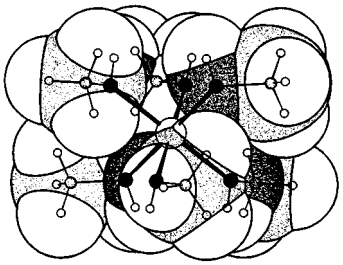


Figure 1. Cation of the methanol complex **3a**; code: Zn and H white, C light grey, O dark grey; bond lengths [Å] and angles [°]: Zn−O 2.086(1), O−C 1.430(2); O−Zn−O 180.0, 87.26(3), and 92.74(3), Zn−O−C 125.5(1)

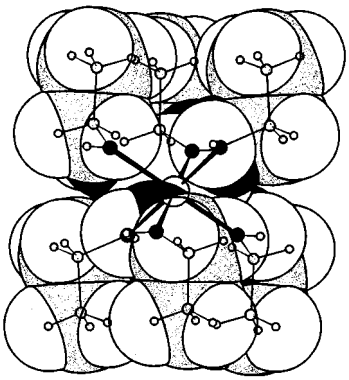


Figure 2. Cation of the ethanol complex **1b** (and similarly **3b**); code: Zn and H white, C light grey, O dark grey; bond lengths [Å] and angles [°] for **1b**: Zn−O 2.078(2), O−H 0.82(6), O−C 1.445(4), C−C 1.483(7); O−Zn−O 180.0, 86.9(1) and 93.1(1), Zn−O−C 130.2(2), O−C−C 110.9(4)

cause the O−H hydrogen atoms to occur in two groups of three on opposite sides of the ellipsoid, cf. the top center of Figure 1. Figure 2 shows that in both ethanol complexes the C−C bonds of the ethyl groups are oriented similarly and roughly parallel to the threefold crystallographic axis, arranging the ethanol ligands in two groups of three. The van der Waals contacts of the ethanol ligands are maximized in this arrangement, forming two hydrophobic islands separated from the polar center of the complex comprised of the Zn−O and O−H bonds. The resulting and characteristic barrel shape of the ethanol complex cations is also verified for the hexakis(ethanol)cobalt(II) complex.[5] It is reminiscent of the layered arrangement of the two *cis*-1,3,5-cyclohexanetriol ligands in their ZnL_2 complex.[9]

The separation of the hydrophilic and hydrophobic regions in the complexes also has the consequence that the alcoholic O−H bonds are exposed to the exterior of the cations. For instance in Figure 2 the white ball to the top right of the zinc ion represents an OH hydrogen atom. This in turn means that these quite acidic hydrogen atoms are within contact distance of the anions in the lattice, facilitating hydrogen bonding between cations and anions. It turns out that this is the case in all three compounds. Each OH group is engaged in a reasonably strong (< 2.8 Å) hydrogen bond. For **1b** this means that three oxygen atoms of each perchlorate anion are hydrogen-bonded. For **3a** and **3b** the number of fluorine atoms matches that of the OH

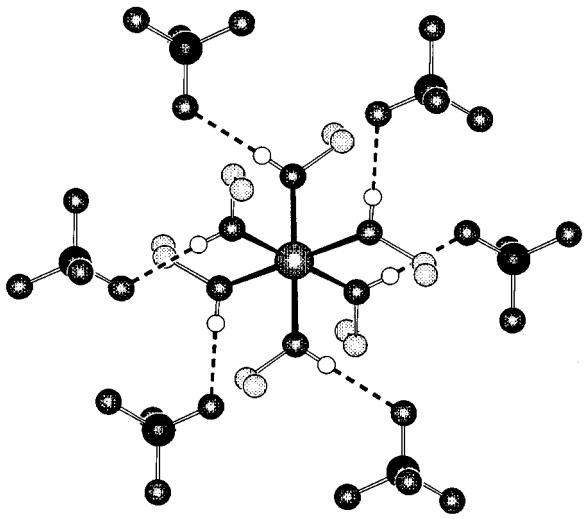


Figure 3. Hydrogen-bonded cation−anion contacts of one $Zn(EtOH)_6$ unit in **1b** (O···O = 2.79 Å)

groups implying that there are also six hydrogen-bonding interactions per SiF_6^{2-} anion. The resulting networks are different in all three cases, see Figures 3−5. Complex **3a** displays a one-dimensional array of hydrogen-bonded cations and anions with triple junctions, complex **3b** a single-layered two-dimensional array with double junctions, and complex **1b** a double-layered two-dimensional array with single junctions.

Discussion

In an alcoholic or water-free environment the hexakis(alcohol) complexes of zinc are stable as salts with noncoordinating anions. Even traces of water, however, lead to their hydrolysis. The alcohols are weaker ligands for zinc than acetone, as can be seen from the persistence of the complexes in acetone solution. They compete with aromatic al-

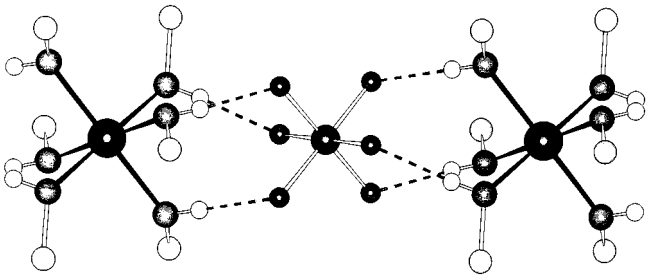


Figure 4. Hydrogen-bonded cation−anion contacts of one SiF_6 unit in **3a** (O···F = 2.66 Å)

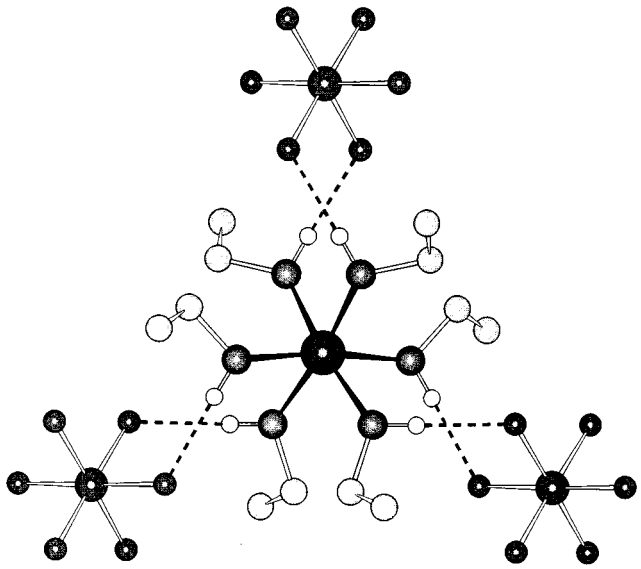


Figure 5. Hydrogen-bonded cation−anion contacts of one $Zn(EtOH)_6$ unit in **3b** (O···F = 2.75 Å)

Table 3. Crystallographic details

	1b	**3a**	**3b**
Empirical formula	$C_{12}H_{36}Cl_2O_{14}Zn$	$C_6H_{24}F_6O_6SiZn$	$C_{12}H_{36}F_6O_6SiZn\cdot C_2H_5OH$
Molecular mass	540.7	399.7	529.9
Crystal size [mm]	0.2 × 0.2 × 0.1	1.2 × 1.0 × 0.9	0.6 × 0.4 × 0.4
Space group	$P-3$	$R-3$	$P-31c$
Z	1	3	2
a [Å]	8.720(3)	11.850(3)	8.650(1)
b [Å]	8.720(3)	11.850(3)	8.650(1)
c [Å]	9.359(1)	9.383(2)	17.450(3)
V [Å^3]	616.3(2)	1141.1(5)	1130.7(3)
$d_{calcd.}$ [g cm^{-3}]	1.46	1.75	1.56
μ(Mo-K_α) [mm^{-1}]	1.27	1.78	1.22
hkl range	h: −9 to 0	h: −10 to 15	h: 0 to 11
	k: −9 to 0	k: −17 to 6	k: −9 to 0
	l: −12 to 12	l: −13 to 12	l: −23 to 23
Measured reflections	1185	1452	2059
Independent reflections	995	878	915
Observed reflections [$I > 2\sigma(I)$]	913	871	555
Parameters	49	32	67
Refined reflections	995	878	915
R_1 (obs. refl.)	0.059	0.022	0.093
wR_2 (all refl.)	0.163	0.061	0.286
Residual electron density [e/Å^3]	+1.0	+0.3	+0.9
	−1.5	−0.6	−1.4

dehydes, as evident from the synthesis of mixed alcohol/aldehyde complexes of zinc.[7] Thus, the alcohol complexes should be valuable as starting materials for other complexes of zinc with weakly coordinating ligands.

The solid-state structures of the alcohol complexes reveal a contrast between the polar environment of the zinc ion as well as the O−H bonds and the hydrophobic nature of the alkyl groups. The former results in hydrogen-bonded cation−anion networks in which all OH functions are engaged. The latter gives rise to a typical barrel shape of the hexakis(ethanol)zinc cations.

The Zn−O bonds in the complexes are as long as the Zn−O bonds in the $Zn(H_2O)_6^{2+}$ ion which indicates that they are equally strong. Hence, the lability toward hydrolysis cannot be explained by bond-strength arguments. However, the structures of the hexakis(ethanol) complexes offer two arguments for the water sensitivity. One of them is a gain of entropy upon release of the alcohol ligands which experience a high degree of order in the complexes. The other is a gain of polar and hydrogen-bonded interactions upon replacement of alcohol by water ligands, both between cations and anions in the solid state and between complex cations or the released alcohols and the solvent molecules in aqueous solution

Experimental Section

General: General working and measuring procedures, see ref.[10]. The zinc salts were obtained commercially. The alcohols were obtained water-free and further dried with magnesium. [D_6]Acetone and petroleum ether (b.p. 50−70°C) were distilled from and kept over 4-Å molecular sieves. Nitrogen (99.999%) as inert gas was dried with BTS catalyst. Reaction vessels, gas pipes etc. were heated in vacuum before use. − Complexes **1b**, **2a**, and **2b** were prepared according to the published procedures.[2][3] The hygroscopicity of the complexes did not allow for C/H determinations.

Hexakis(methanol)zinc Hexafluorosilicate (3a): 6.00 g (19.02 mmol) of $Zn(H_2O)_6(SiF_6)$ in 25 mL of methanol was treated with 40 mL (38.8 g, 366 mmol) of trimethyl orthoformate which caused heating of the mixture and complete dissolution. After stirring for 24 h at room temp. and filtration, all volatiles were removed in vacuo. The residue was taken up in methanol and layered with petroleum ether to yield 5.80 g (76%) of **3a** which was freed from solvent by a syringe and dried in vacuo. − $C_6H_{24}F_6O_6SiZn$ (399.7): calcd. Zn 16.36; found Zn 16.23.

Hexakis(ethanol)zinc Hexafluorosilicate (3b): Like **3a** from 6.00 g (19.02 mmol) of $Zn(H_2O)_6(SiF_6)$ and 40 mL (35.6 g, 240 mmol) of triethyl orthoformate in 25 mL of ethanol with 48 h of stirring. Yield 4.20 g (46%) of **3b**. − $C_{12}H_{36}F_6O_6SiZn$ (483.9): calcd. Zn 13.51; found Zn 13.75.

Structure Determinations:[11] The crystals were obtained directly from the reaction solutions and used without drying in vacuo. They were immersed in fluorinated polyether oil and immediately placed in the nitrogen stream of the diffractometer's cooling system. Diffraction data were recorded at ca. −100°C with the ω/2θ technique on a Nonius CAD4 diffractometer fitted with a molybdenum tube (K_α, λ = 0.7107 Å) and a graphite monochromator. Empirical absorption corrections based on ψ scans were applied. The structures were solved with direct methods and refined anisotropically with the SHELX program suite.[12] Hydrogen atoms were included with fixed distances and isotropic temperature factors 1.5 times those of their attached atoms. The OH hydrogen atom of **1b** was located and refined freely. Parameters were refined against F^2. The R values are defined as $R_1 = \Sigma|F_o - F_c|/\Sigma F_o$ and $wR_2 = [\Sigma[w(F_o^2 - F_c^2)^2]\Sigma[w(F_o^2)^2]]^{1/2}$. Drawings were produced with SCHAKAL.[13] Table 3 lists the crystallographic data.

Acknowledgments

This work was supported by the Deutsche Forschungsgemeinschaft.

[1] See *Comprehensive Coordination Chemistry* (Eds.: G. Wilkinson, R. D. Gillard, J. A. McCleverty), Pergamon Press, Oxford, **1988**, vol. 2 ("Ligands").
[2] P. W. N. M van Leeuwen, *Recl. Trav. Chim. Pays Bas* **1967**, *86*, 247−253.
[3] A. D. van Ingen Schenau, W. L. Groeneveld, J. Reedijk, *Recl. Trav. Chim. Pays Bas* **1972**, *91*, 88−94, and references cited therein.
[4] F. A. Cotton, S. A. Duraj, L. E. Manzer, W. J. Roth, *J. Am. Chem. Soc.* **1985**, *107*, 3850−3855.
[5] I. Bkouche-Waksman, P. L'Haridon, *Acta Crystallogr., Sect. B* **1977**, *33*, 11−21; *Bull. Soc. Chim. Fr.* **1979**, *Partie I*, 50−53.
[6] B. Müller, A. Schneider, M. Tesmer, H. Vahrenkamp, *Inorg. Chem.* **1999**, *38*, 1900−1907, and references cited therein.
[7] B. Müller, H. Vahrenkamp, *Eur. J. Inorg. Chem.* **1999**, 117−127.
[8] The Cambridge Crystallographic Data File contains 7 structures of compounds containing $Zn(H_2O)_6^{2+}$, the Inorganic Crystal Structure Base 15 such structures. The Zn−O(H_2O) distances vary by about ±0.05 Å around the average value of 2.09 Å.
[9] J. Bebendorf, H. B. Bürgi, E. Gamp, M. A. Hitchman, A. Murphy, D. Reinen, M. J. Riley, H. Stratemeier, *Inorg. Chem.* **1996**, *35*, 7419−7429.
[10] M. Förster, R. Burth, A. K. Powell, T. Eiche, H. Vahrenkamp, *Chem. Ber.* **1993**, *126*, 2643−2648.
[11] The crystallographic data of the structures described in this paper were deposited with the Cambridge Crystallographic Data Centre as supplementary publication no. CCDC-115889 (for **1b**), -115887 (for **3a**), and -115888 (for **3b**). Copies of these data are available free of charge from CCDC, 12 Union Road, Cambridge, CB2 1EZ, U.K. [Fax: (internat.) + 44-1223/336-033; E-mail: deposit@ccdc.cam.ac.uk].
[12] G. M. Sheldrick, *SHELX-86* and *SHELXL-93*, *Programs for Crystal Structure Determination*, Universität Göttingen, **1986** and **1993**.
[13] E. Keller, *SCHAKAL for Windows*, Universität Freiburg, **1998**.
Received March 15, 1999
[I99103]

Difluorosilanethione $F_2Si{=}S$ by Flash Vacuum Thermolysis of $(F_3Si)_2S$ and by Reaction of SiS with F_2 – Matrix Studies and Ab initio Calculations

Helmut Beckers,[a] Jürgen Breidung,[b] Hans Bürger,*[a] Ralf Köppe,[c] Carsten Kötting,[d] Wolfram Sander,[d] Hansgeorg Schnöckel,[c] and Walter Thiel[b]

Keywords: Ab initio calculations / Flash pyrolysis / Matrix isolation / Silicon / Multiple bonds / IR spectroscopy

Difluorosilanethione $F_2Si{=}S$ (**1**) has been synthesized by Flash Vacuum Pyrolysis of $(F_3Si)_2S$ at ≥ 500 °C and trapped in an Ar matrix. Furthermore, **1** has been obtained by co-deposition of SiS and F_2/Ar and by pyrolysis of a matrix-isolated SiS_2–XeF_2 complex under cryogenic conditions. All six vibrational fundamentals of **1** have been observed in the matrix IR spectrum. Ab initio calculations at the MP2 and CCSD(T) levels using large basis sets have been performed. These calculations have guided the detection of **1** and the vibrational assignment. The best estimate of the structure of **1** with C_{2v} symmetry is: r(Si=S) 191.1(1) pm, r(SiF) 156.1(1) pm, ∠(FSiF) 103.3(2)°.

Our knowledge of molecular species exhibiting multiple bonds to silicon has expanded greatly over the past 20 years due to both experimental progress and improvements in theoretical methods. Above all, kinetic stabilization by bulky substituents at both sites of Si=Si,[1] Si=C,[2] and Si=Pn (Pn = N, P, As) linkages[3] has enabled the synthesis and isolation of numerous compounds that are thermally stable up to, and even above, room temperature and possess "formally" double bonded silicon atoms. However, chalcogeno derivatives $R^1R^2Si{=}Ch$, with Ch = O, S, etc., provide only the silicon site to accommodate bulky substituents, and it is not surprising that the first kinetically stabilized thioxosilane (silanethione[4]) that is stable at ambient temperature was made only recently.[5]

Monomeric silanones and silanethiones with trigonal planar geometry at silicon are kinetically unstable due to the lack of stabilization by bulky ligands. They have been frequently postulated as intermediates, mostly on the evidence of trapping experiments.[6] Only very few of these short-lived intermediates were, however, directly and unambiguously detected by spectroscopic methods, either in the gas phase, or in cryogenic matrices. Silanones $X_2Si{=}O$ with X = H,[7] F,[8] Cl,[9] and CH_3[10] have been the subject of quite a few successful experimental studies, and numerous theoretical studies have guided and confirmed experimental work.

Photolysis of matrix-isolated SiS in the presence of Cl_2[11] and HCl[12] has provided the first silanethiones, $Cl_2Si{=}S$ and Cl(H)Si=S, with trigonal Si coordination. Monomeric $(CH_3)_2Si{=}S$ (**3**), which was detected by photoelectron spectroscopy, has been generated in the gas phase by flash vacuum thermolysis (FVT) of the cyclotrimer (**4**) and of other organosilicon precursors.[13] However, attempts to synthesize the unsubstituted parent species $H_2Si{=}S$ by FVT of different precursors failed, and only the dehydrogenation product SiS has been observed.[14]

The present investigation adds to the limited list of unstabilized monomeric, four-atom silanethiones by describing $F_2Si{=}S$ (**1**). We report on the synthesis of this species by FVT of $(F_3Si)_2S$ (**2**). The unambiguous synthesis of the latter is also reported here for the first time. Alternatively, **1** can be made in analogy to $Cl_2Si{=}S$[11] by the action of F_2 on SiS under cryogenic conditions. High-level ab initio calculations, which guided the detection and support the characterization of **1** by matrix IR spectroscopy, will also be presented.

$F_2Si{=}S$	$(F_3Si)_2S$	$(CH_3)_2Si{=}S$	$[(CH_3)_2SiS]_3$
1	**2**	**3**	**4**

Experimental Results

It has been shown that at elevated temperature the cyclodimer of **3**, $[(CH_3)_2SiS]_2$ (**5**), is in equilibrium with the cyclotrimer **4**.[15] The photoelectron spectroscopic detection of **3** in the FVT of **4** proved that this equilibrium involves the monomer as an intermediate[13a] although it was not possible to trap **3** in an Ar matrix.[16]

$[(CH_3)_2SiS]_2$

5

We chose **1** as our target molecule because reactions analogous to the dehydrogenation of $H_2Si{=}S$,[14] or its isomerisation to yield the silylene HSi−SH, are unlikely to occur for **1** for thermodynamic reasons, the Si−F bond being particularly strong. It was therefore obvious to examine the thermal decomposition of $(F_2SiS)_2$ (**6**), which has been reported in the literature.[17] This promising precursor **6** was first mentioned by Gutmann et al.,[17a] who passed SiF_4

[a] Anorganische Chemie, FB9, Universität-GH, D-42097 Wuppertal, Germany
E-mail: buerger1@uni-wuppertal.de
[b] Organisch-Chemisches Institut der Universität, CH-8057 Zürich, Switzerland
[c] Institut für Anorganische Chemie der Universität, D-76128 Karlsruhe, Germany
[d] Lehrstuhl für Organische Chemie II der Ruhr-Universität, D-44780 Bochum, Germany

 © WILEY-VCH Verlag GmbH, D-69451 Weinheim, 1999 1434−1948/99/1111−2013 $ 17.50+.50/0

over SiS_2 at 1000°C in a quartz tube. Later, Aylett et al.[17b] claimed to have synthesized **6** by reaction of SiF_2I_2 with red HgS at room temperature.

$(F_2SiS)_2$
6

We have reexamined both reactions[18] and, although we were able to reproduce their general courses and the sparse spectroscopic data quoted, the products claimed to be **6** were in fact identified as $(F_3Si)_2O$[17a] and **2**,[17b] respectively. Our attempts to prepare **6** or other perfluorocyclosilthianes by reaction of the high temperature species SiF_2[19] with OCS or SPF_3 were unsuccessful in spite of the usefulness of OCS to transfer S onto matrix-isolated $SiCl_2$.[11]

Thermolysis of $F_3SiSSiF_3$

The thermolysis of noncyclic silthianes, which might be useful precursors for silanethiones, has not yet been investigated. We have found that in the condensed phase at room temperature **2** decomposes slowly to give SiF_4 and the trisildithiane $F_8Si_3S_2$ (**7**).[18] Upon prolonged storage at 20°C, decomposition of **2** proceeds further to yield more SiF_4 and a solid deposit. The formation of **7** can be rationalized if **1** is considered to be an intermediate (Equations 1 and 2).

$$\mathbf{2} \rightarrow \mathbf{1} + SiF_4 \quad (1)$$

$$\mathbf{2} + \mathbf{1} \rightarrow \underset{\mathbf{7}}{(F_3SiS)_2SiF_2} \quad (2)$$

In order to detect any **1**, which is presumed to be formed according to Equation 1, we pyrolyzed 0.2% **2** seeded in Ar as a carrier gas at ≥ 500°C in a quartz tube of 20 mm length and 10 mm inner diameter. The thermolysis products were condensed onto a cold window mounted at a distance of ca. 20 mm from the port of the oven. The deposit was first studied by infrared spectroscopy with a resolution of 0.5 cm^{-1} in the 400−4000 cm^{-1} region. The spectrum is displayed in Figure 1A.

Evidently the decomposition of **2** is almost quantitative. The spectrum is dominated by the very intense absorption of $^{28}SiF_4$ at 1023.3 cm^{-1}, accompanied by satellites of $^{29}SiF_4$ at 1014.4 cm^{-1} (4.7%) and of $^{30}SiF_4$ at 1006.2 cm^{-1} (3.1%). In addition there are two sharp absorptions at 995.7 and 969.1 cm^{-1} with an intensity ratio of ca. 2:1 (Figure 1A). These absorptions are assigned to a hitherto unknown product. Both the wavenumbers of these two absorptions and their relative intensities agree perfectly with the ab initio predictions for the ν_1 and ν_4 absorption bands, respectively, of $F_2Si{=}S$ (**1**), Table 3.

Although lying in the recorded spectral region, the Si=S stretching vibration ν_2, expected near 640 cm^{-1}, was not found in this particular mid-infrared experiment (Figure 1A) with its predicted intensity being only 0.4% of ν_1.

In order to gather more information on the vibrational spectrum of **1** we have also investigated the matrix in the Far-IR range. Along with bands arising from the ν_4 vibration of SiF_4 and from F_3SiSH (**8**)[18] owing to some hydrolysis or minor contamination of **2**, we eventually detected absorptions at 337, 296, and 247 cm^{-1} with relative intensities of 2.5:4.5:1 (Figure 1B). These absorptions were assigned to **1**. The intensities of these absorptions decreased uniformly on annealing the matrix to 42 K, while absorp-

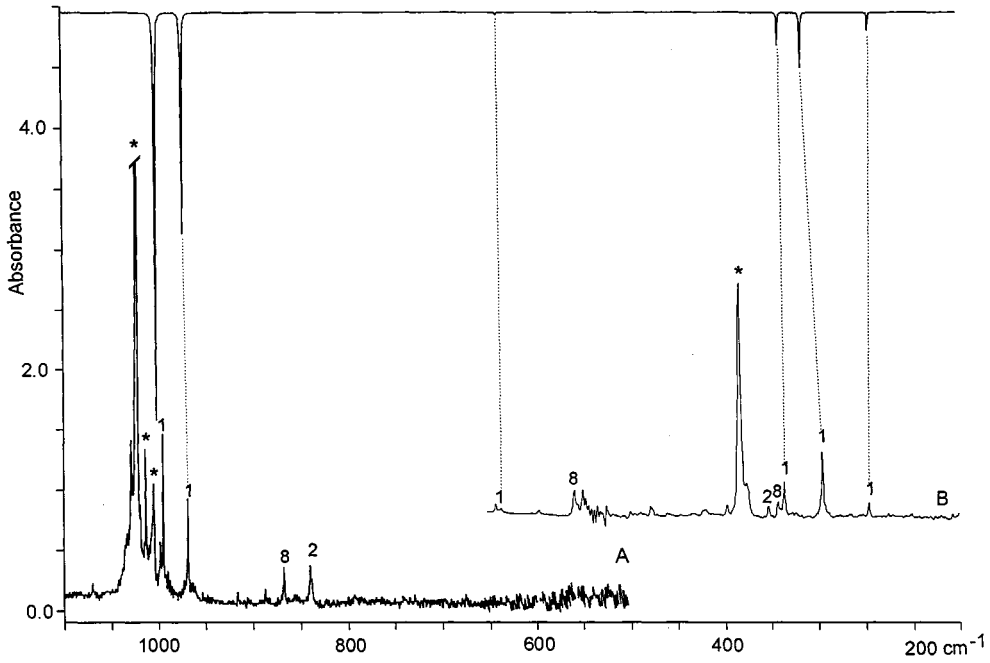


Figure 1. Matrix IR spectra of a deposit obtained by FVP of $(F_3Si)_2S$; A: 500−1100 cm^{-1}; B: 150−650 cm^{-1}; on top, pointing downwards, the ab initio predicted spectrum is shown; the labelling of the absorptions is: **1**: $F_2Si{=}S$; **2**: $(F_3Si)_2S$; **8**: F_3SiSH; SiF_4 peaks are marked by an asterisk

tions of the stable products persisted. UV irradiation of 193 and 248 nm did not change the spectrum.

F_3SiSH

8

The assignment in the 200−360 cm^{-1} range is not as straightforward as in the SiF stretching region because of partial overlap with bands arising from the precursor **2** and the hydrolysis product **8**. Matrix absorptions at 354.1 cm^{-1} (**2**) and 343.1 cm^{-1} (**8**) did not disappear upon annealing the matrix; they correspond to strong gas phase absorptions at 358 and 346 cm^{-1}, respectively, and are assigned to δ_s SiF_3.[18] The corresponding asymmetric deformations observed in the gas phase at 335 and 326 cm^{-1} (**2**) and 325 cm^{-1} (**8**) are weaker and occur in the matrix spectrum at 335.6 cm^{-1} and 322 cm^{-1} (broad, Figure 1). There is a coincidence of the 335.6 cm^{-1} band with that of **1** at 336.5, hence upon annealing of the matrix the band at 337 cm^{-1} is only weakened while those at 296 and 247 cm^{-1} disappear entirely.

Comparison of the matrix spectra before and after annealing reveals a weak feature at 638 cm^{-1} (Figure 1B) that must be due to an unstable intermediate. On the basis of the ab initio calculations (Table 3; see below) we definitely assign this feature to the Si=S stretching vibration. On the other hand, new weak absorptions at 1004, 981.5, 862.2, and 858.0 cm^{-1} (ν SiF) and 561 and 557 cm^{-1} (ν SiS) appear in the annealed spectrum; these have not yet been assigned but might be due to oligomers of **1**.

Reaction of Matrix-Isolated SiS with F_2

In analogy to the synthesis of Cl_2SiS from SiS and Cl_2[11] co-condensation of SiS with F_2 and Ar promises access to **1**. IR spectra of these deposits (Figure 2) revealed, in addition to absorptions of SiS (739 cm^{-1}) and its dimer and its trimer, some red-shifted bands at 728 cm^{-1}, which are assigned to association products of molecular SiS with F_2.

Furthermore, three additional absorptions at 995.6, 969.1, and 296.5 cm^{-1} were observed that, owing to their invariant relative intensities, were assigned to the same, novel short-lived species. Of these, the two strong absorptions > 900 cm^{-1} are likely to be due to SiF stretching vibrations of tetravalent silicon bonded to two or more fluorine atoms. Respective absorptions of Si^{II} fluorides should occur at lower wavenumbers, 840−869 cm^{-1}.[21] One further band at 903 cm^{-1} (Figure 2) has not yet been assigned.

Both the wavenumbers and intensities of the three absorptions mentioned above are in perfect agreement with those that had been assigned in the pyrolysis experiment to **1** on the basis of ab initio calculations. Once again the SiS stretching vibration of **1**, predicted to be near 640 cm^{-1} with very low IR intensity and observed in the spectrum shown in Figure 1B, was too weak to be detected. In addition to the bands of **1**, SiF stretching absorptions of the stable product **8** (986.6 and 865.2 cm^{-1}) and SiF_4 (1023 and 386.7 cm^{-1}) were also observed.

In order to support the assignment of the absorptions of **1** we condensed gaseous SiS with XeF_2 and Ar and photolyzed the resulting deposit with radiation from a high pressure Hg lamp. This experiment was performed by passing Ar over crystalline XeF_2 at −40°C and co-condensing this mixture with SiS. The IR spectrum of this deposit revealed only the presence of SiS, XeF_2 and a band at 725 cm^{-1} assigned to a $SiS{-}XeF_2$ complex. After photolysis, absorptions similar to those observed with a SiS/F_2 mixture appeared and were assigned to **1**. We did not find the SiS stretching vibration of **1** in this experiment. In order to confirm our observation of this vibration (Figure 1B) we plan to study the $SiS{-}Ar/F_2$ system by Raman spectroscopy.

Ab initio Calculations

Theoretical Methods

Quantum-chemical calculations were carried out at the correlated levels of second-order Møller−Plesset perturbation theory (MP2)[22] and coupled cluster theory with single and double excitations[23] augmented by a perturbational estimate of the effects of connected triple excitations [CCSD(T)].[24] These calculations were performed with GAUSSIAN94[25] and MOLPRO94.[26][27]

The correlation-consistent polarized valence basis sets (cc-pVXZ)[28][29] were used throughout, supplemented as suggested recently[30] to take into account core polarization effects in the case of second-row atoms. Specifically, three different basis sets were employed: the first one denoted as VTZ+1 is derived from the triple-zeta cc-pVTZ basis[28][29] by adding a single set of d functions for Si and S[30] whose exponents equal the highest d exponent in the corresponding cc-pV5Z basis.[31] Analogously, the second basis (VQZ+1) is obtained from the quadruple-zeta cc-pVQZ basis set[28][29] by adding the same high-exponent d functions for Si and S.[30][31] Replacement of the cc-pVQZ functions for F and S by the corresponding augmented sets (aug-cc-pVQZ)[29][32] generates the third basis (AVQZ+1), which contains low-exponent diffuse functions to account for the electronegative character of F and S.

Spherical harmonics were used throughout. Unless stated otherwise, the fluorine 1s-like and the silicon and sulfur 1s2s2p-like core molecular orbitals were always required to remain doubly occupied (frozen core approximation). Nondynamical electron correlation is not overly important in F_2SiS, as judged from the coupled cluster T_1 diagnostic,[33][34] which is 0.013 for all three basis sets at the corresponding CCSD(T) minimum energy structures. Therefore, **1** is expected to be well described by single reference coupled cluster wavefunctions. The molecules SiS and SiF_2 were also treated (see below). The T_1 diagnostic for SiF_2 is about 0.014, i.e. similar to the value of F_2SiS, and 0.021 for SiS. Although this latter value is already critical in the sense that results from single-reference electron correlation methods limited to single and double excitations (e.g. MP2, CCSD) should be viewed with caution, CCSD(T) still performs reasonably well.[34]

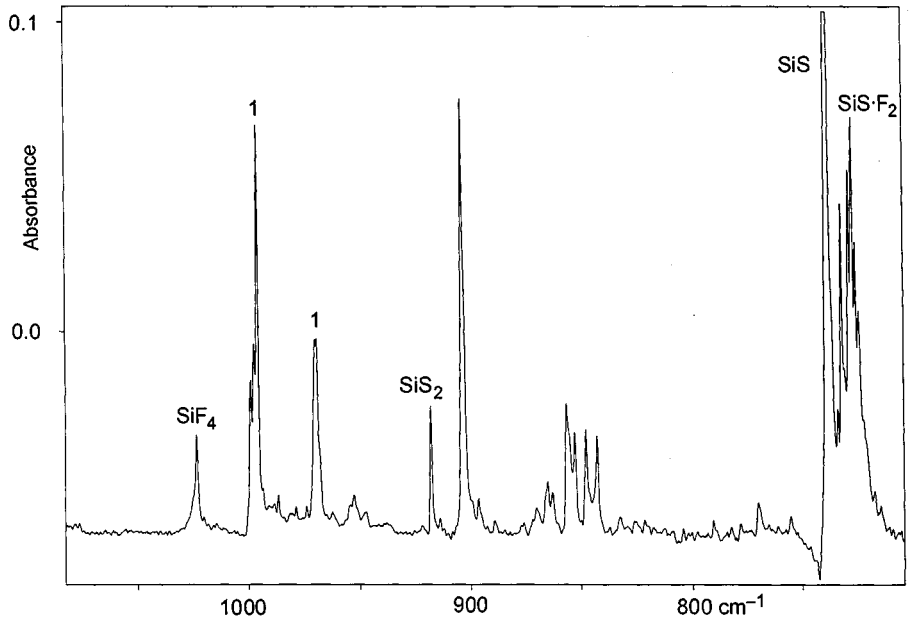


Figure 2. IR spectrum in the 700−1200 cm^{-1} range of the deposit formed by co-deposition of SiS and F_2/Ar; **1**: $F_2Si{=}S$

The molecular geometry of **1** was optimized within the constraint of C_{2v} point group symmetry. For the purpose of comparison, the molecular structures of SiS ($C_{\infty v}$) and SiF_2 (C_{2v}) were also optimized. Analytic energy gradients, as implemented in the GAUSSIAN94 program,[25] were used at the MP2 level of theory, and numerical gradients were employed at the CCSD(T) level with MOLPRO94.[26][27] The largest internal gradient components at the stationary points did not exceed $3{\cdot}10^{-5}$ au.

At the computed equilibrium geometries, harmonic force fields were evaluated either analytically in Cartesian coordinates (MP2/VTZ+1)[25] or numerically in symmetry-adapted internal coordinates from energies[26] (step sizes 0.02 Bohr for bond lengths and 1° for bond angles). The normal modes and the harmonic vibrational frequencies were obtained in the usual manner.[35][36] At the CCSD(T) level, electric dipole moments were determined as numerical derivatives of the potential energy with respect to a finite field component (0.003 au) using the MOLPRO94 program.[26]

The following symmetry coordinates were chosen to represent the quadratic CCSD(T)/VQZ+1 force field:

$S_1(a_1) = 2^{-1/2}\,(r_1 + r_2)$
$S_2(a_1) = R$
$S_3(a_1) = 6^{-1/2}\,(2\alpha - \beta_1 - \beta_2)$
$S_4(b_1) = 2^{-1/2}\,(r_1 - r_2)$
$S_5(b_1) = 2^{-1/2}\,(\beta_1 - \beta_2)$
$S_6(b_2) = \gamma$

where r_1 and r_2 are the two SiF bond lengths, R is the Si−S bond length, α is the F−Si−F bond angle, β_1 and β_2 are the two F−Si−S bond angles, and γ is the out-of-plane angle between the Si−S bond and the SiF_2 plane.

For comparison with the present experimental data, the cubic and quartic force fields of **1** are required to deduce theoretical values for the fundamental vibrational frequencies. The MP2/VTZ+1 cubic and quartic normal coordinate force constants that are not reported explicitly were determined with the use of a finite difference procedure[37] involving displacements along reduced normal coordinates (step size $\Delta q = 0.05$) and the calculation of analytic second derivatives (relative precision $\varepsilon < 10^{-7}$) at these displaced geometries. At the MP2/VTZ+1 equilibrium geometry of **1**, the Cartesian gradient components did not exceed $5{\cdot}10^{-7}$ au. The anharmonicity corrections to the harmonic vibrational wavenumbers were computed from the theoretical anharmonicity constants using standard formulas based on second-order rovibrational perturbation theory.[38][39]

Results and Discussion

Table 1 shows the computed equilibrium geometries, electric dipole moments and atomic charges from a natural population analysis[25] of F_2SiS. As expected, the enlargement of the basis set from VTZ+1 to VQZ+1 shortens the SiF bonds slightly (0.13−0.18 pm) and the SiS bond somewhat more (0.34−0.49 pm) while the FSiF bond angle increases by 0.12−0.15°. The addition of diffuse functions at F and S (AVQZ+1) leads to almost negligible changes in the structural parameters: the bond lengths increase by less than 0.1 pm and the FSiF bond angle decreases by less than 0.05°. For a given basis, CCSD(T) predicts a longer SiS bond and shorter SiF bonds than MP2, but the differences remain small (0.23−0.38 pm), and the computed bond angles are almost identical. Correlating all electrons at the CCSD(T)/VQZ+1 level shortens the SiS and SiF bonds considerably, viz. by 0.85 pm and 0.83 pm, respectively, whereas the FSiF bond angle is only slightly affected (+0.07°). The computed values for the electric dipole moment of **1** are close to 1.2 Debye (see Table 1). The present

Table 1. Computed equilibrium geometries and electric dipole moments of F_2SiS[a]

Constant	MP2 VTZ+1	VQZ+1	AVQZ+1	CCSD(T) VTZ+1	VQZ+1	VQZ+1(ae)[b]	AVQZ+1	Best estimate[c]
SiS	192.25	191.91	191.96	192.63	192.14	191.29	192.20	191.1(1)
SiF	157.28	157.15	157.22	157.02	156.84	156.01	156.90	156.1(1)
FSiF	103.17	103.29	103.26	103.12	103.27	103.34	103.23	103.3(2)
μ_e	1.275	1.222	1.194	1.205	1.181	1.178	1.150	1.19(10)[d]

[a] Bond lengths in pm, bond angles in degrees, dipole moments in Debye. – [b] ae = all electrons correlated. – [c] See text. Estimated errors in parentheses. – [d] CCSD(T)/AVQZ+1 value at the best estimated molecular geometry. The dipole vector is directed from S to Si. A natural population analysis (MP2/VTZ+1)[25] revealed the following atomic charges (atomic units): Si +1.903, S −0.678, F −0.613.

best value [CCSD(T)/AVQZ+1] is believed to be accurate to about 0.1 Debye.

The calculated geometrical data of F_2SiS may be improved by taking into account the errors that appear in analogous calculations for the related molecules SiS and SiF_2, where accurate experimental equilibrium geometries are known.[40][41] For this purpose Table 2 presents computed and experimental equilibrium structures for both species. It is seen that CCSD(T)/VQZ+1 overestimates the bond lengths in SiS and SiF_2 by as much as 0.97 pm and 0.69 pm, respectively, if inner-shell contributions to the electron correlation are neglected. As in the case of **1**, taking core correlation into account [CCSD(T)/VQZ+1(ae)] leads to a considerable contraction of the bond lengths in SiS (−0.69 pm) and SiF_2 (−0.76 pm) while the bond angle in SiF_2 changes only moderately (+0.12°). Consequently, the all-electron bond lengths in SiS and SiF_2 are much closer to the experimental values than those obtained by correlating only the valence electrons (see Table 2). If the errors in the calculated bond lengths of these two molecules (with and without the frozen core approximation) are used to correct the corresponding data for the target molecule **1**, we arrive at three consistent estimates for the equilibrium distances in F_2SiS. The best estimate (see Table 1) is the average of these three individual estimates, which lie within the quoted uncertainty. Since the calculated FSiF bond angles in **1** are quite similar at all levels, we have adopted the CCSD(T)/VQZ+1 value (103.3°) as our best estimate and have assigned an error bar (0.2°) that covers all theoretical values of this angle (see Table 1).

Table 3 reports theoretical results for the fundamental vibrational wavenumbers of F_2SiS and compares them with their experimental counterparts determined in this work. The theoretical values were derived from the corresponding harmonic wavenumbers obtained at a given level, by adding the anharmonicity corrections from MP2/VTZ+1 calculations. At this level there are no complications due to anharmonic resonances, except for $\nu_2/2\nu_6$ where perturbationally and variationally determined Fermi shifts due to this cubic interaction differ by about 4 cm^{-1}. Consequently, all theoretical Fermi shifts of ν_2 (ranging from 3.5−6.4 cm^{-1}) were obtained by matrix diagonalization using harmonic wavenumbers from the given level of theory and the coupling element W_{266} = 10.2 cm^{-1} from MP2/VTZ+1. The calculated fundamental wavenumbers are quite stable with respect to the employed basis sets, i.e. the corresponding data differ at most by 5 cm^{-1}. Comparing CCSD(T) with the associated MP2 data, the differences do not exceed 9 cm^{-1} in absolute value. Generally, the calculated wavenumbers agree with experiment to within 9 cm^{-1}, with the exception of the out-of-plane vibrational mode where the differences range from 11−20 cm^{-1}. From a theoretical point of view, our best data are those from CCSD(T)/VQZ+1 where the rms deviation from experiment is 7 cm^{-1}. This agreement between theory and experiment is as good as can be expected,[34] especially when taking into account that the experimental vibrational wavenumbers have been measured in an argon matrix (15 K) and not in the gas phase. Therefore, our calculations are fully consistent with the assignment of the measured bands to F_2SiS. Further support for this assignment comes from the theoretical (MP2/VTZ+1) intensity pattern of the infrared absorptions, which is in very good agreement with the experimental relative intensities (see Table 3).

In Table 4 the CCSD(T)/VQZ+1 harmonic symmetry force constants of **1** are listed. Not surprisingly, this force field is dominated by the diagonal stretching constants F_{11} (SiF_2 sym. str.), F_{44} (SiF_2 asym. str.), and F_{22} (SiS str.). The associated potential energy distribution (PED) matrix reveals a significant coupling only between the symmetric SiF_2 (S_1) and the SiS (S_2) stretching coordinates (ν_1: 68% SiF_2, 28% SiS; ν_2: 28% SiF_2, 69% SiS), whereas the other

Table 2. Computed and experimental equilibrium geometries[a] of SiS and SiF_2

Molecule	Constant	CCSD(T) VQZ+1	CCSD(T) VQZ+1(ae)[b]	CCSD(T) AVQZ+1	Exp.[c]
SiS	SiS	193.90	193.21	193.96	192.9264(2)
SiF_2	SiF	159.70	158.94	159.85	159.01(1)
	FSiF	100.86	100.98	100.66	100.77(2)

[a] Bond lengths in pm, bond angles in degrees. – [b] ae = all electrons correlated. – [c] Refs.[40][41] for SiS and SiF_2, respectively.

Table 3. Fundamental vibrational wavenumbers (cm^{-1}) of F_2SiS

Mode	Exp.[a]	MP2 VTZ+1[b]	VQZ+1[c]	AVQZ+1[c]	CCSD(T) VTZ+1[c]	VQZ+1[c,d]
a_1 $\nu_s(SiF_2)$	996 (2.60)	1003 (262)	1004	1000	1001	1005 (1015)
ν(SiS)	638 (0.02)	647[e] (1)	647[e]	646[e]	638[e]	641[e] (643)
$\delta(SiF_2)$	337 (0.30)	339 (25)	338	336	340	339 (340)
b_1 $\nu_{as}(SiF_2)$	969 (1.30)	967 (142)	970	965	972	977 (988)
$\rho(SiF_2)$	247 (0.12)	247 (10)	248	247	245	247 (248)
b_2 $\gamma(SiF_2)$	296 (0.54)	316 (33)	313	312	309	307 (308)

[a] Extinction in parentheses. – [b] Infrared band intensities (km/mol) in parentheses (double harmonic approximation). – [c] Anharmonicity corrections from MP2/VTZ+1. – [d] Harmonic wavenumbers in parentheses. – [e] Including the shift due to the $\nu_2/2\nu_6$ Fermi interaction. These shifts have been calculated variationally using harmonic wavenumbers from the indicated level of theory and the interaction constant $W_{266} = 10.2\ cm^{-1}$ (MP2/VTZ+1).

Table 4. Computed[a] harmonic symmetry force constants F_{ij}[b] of F_2SiS

	i	j	F_{ij}		i	j	F_{ij}
a_1	1	1	6.437	b_1	4	4	5.973
	1	2	0.170		4	5	0.152
	1	3	0.263		5	5	0.511
	2	2	5.167				
	2	3	−0.123	b_2	6	6	0.460
	3	3	0.833				

[a] CCSD(T)/VQZ+1. – [b] Units are consistent with energies in aJ, bond lengths in 100 pm, and angles in radians.

normal modes correspond to almost pure symmetry coordinates (dominant PED contributions to $\nu_3 - \nu_6$: above 95%).

Discussion

The present study establishes the existence of hitherto unknown **1** under cryogenic conditions. We have been able to synthesize **1** by FVT of **2**, by reaction of SiS with F_2 in an Ar matrix, and by photolysis of a matrix isolated $SiS{-}XeF_2$ complex. All vibrational fundamentals of **1** were observed. These fundamentals were assigned on the basis of high-level ab initio calculations.

Owing to the strong mixing of the S_1 and S_2 coordinates, the vibration with predominantly Si=S stretching character at $638\ cm^{-1}$ is much lower than those of $Cl_2Si{=}S$ ($805.6\ cm^{-1}$)[11] and Cl(H)Si=S ($775\ cm^{-1}$)[12]. In matrix-isolated Si=S this vibration lies at $739.1\ cm^{-1}$.[42] The Si=S stretching force constant of **1** obtained by quantum chemical calculations, 5.167 Ncm^{-1} (Table 4), exceeds that of $Cl_2Si{=}S$ (4.90 Ncm^{-1})[11] and Cl(H)Si=S (4.83 Ncm^{-1})[12] as well as those of SiS and SiS_2, 4.9 Ncm^{-1}.[43] The C=S stretching force constants of related CS (8.5 Ncm^{-1}), CS_2 (7.7 Ncm^{-1}) and F_2CS (6.7 Ncm^{-1})[44] vary much more.

Difluorosilanethione has the shortest SiS bond and largest SiS stretching force constant so far determined. The "best" prediction of the SiS bond length in **1**, 191.1 pm (Table 1), is significantly shorter than those of the two independent 2,4,6-$[(Me_3Si)_2CH]_3C_6H_2$[2,4,6-$(Me_2CH)_3$-C_6H_2]Si=S molecules as determined by single crystal X-ray diffraction, 194.8(4) and 195.2(4) pm.[5] It is also shorter than in SiS 192.9264(2) pm.[40] The SiS single bond length in $H_3SiSSiH_3$ is considerably longer, 213.6(2) pm.[45]

Experimental Section

Synthesis of $(F_3Si)_2S$ (2):[18] 8.6 g (39.2 mmol) of SiF_3I and 16 g (69 mmol) of HgS were sealed together in a pyrex tube with a volume of 13.3 mL and allowed to react for 7 d at room temperature. Volatile products were purified by fractionated distillation using a low temperature column to yield 0.7 g (6.7 mmol) of SiF_4, 1.7 g (7.9 mmol) of SiF_3I, 2.1 g (10.7 mmol) of **2**, and 0.5 g of less volatile products containing Si and S. The purity of **2**, b.p. −3°C, was checked by IR and ^{19}F-NMR spectroscopy.

Thermolysis of 2: Matrix isolation experiments were performed using standard techniques with an APD CSW-202 Displex closed-cycle He cryostat. Matrices were produced by deposition of Ar (Messer Griesheim, 99.9999%) at a rate of 1.5 sccm/min on a CsI window at 15−20 K. Infrared spectra were recorded with a resolution of $0.5\ cm^{-1}$ employing a Bruker IFS 66 FTIR spectrometer equipped with a KBr beam splitter and a MCT detector. The Far IR experiments were performed using polyethylene windows, a Mylar beam splitter and a DTGS detector. Irradiations were carried out with an Excimer Laser (Lambda Physics COMPex 100, ArF 193 nm, KrF 248 nm).

Reaction of Matrix-Isolated SiS with F_2 or with XeF_2: Experiments were carried out using a Leybold RGD 510 closed cycle cryostat. Matrices were condensed onto a cold copper mirror. Spectra were recorded in absorption by means of a reflection unit using a Bruker IFS 113v FTIR spectrometer. A constant flow of molecular SiS was produced by passing H_2S over solid silicon resistively heated to 1200°C in an alumina tube. Fluorine was stored and mixed with Ar in passivated stainless steel containers. Photolysis (310 nm interference filter) was performed with a high pressure Hg lamp (Osram HBO 200).

Acknowledgments

We thank the Deutsche Forschungsgemeinschaft, the Fonds der Chemischen Industrie, and the Schweizerischer Nationalfonds for financial support. Professor H. Willner, Hannover, is thanked for supplying fluorine.

[1] R. Okazaki, R. West, *Adv. Organomet. Chem.* **1996**, *39*, 231−273.
[2] A. G. Brook, M. A. Brook, *Adv. Organomet. Chem.* **1996**, *39*, 71−158.
[3] M. Driess, *Adv. Organomet. Chem.* **1996**, *39*, 193−229.
[4] According to IUPAC nomenclature compounds with Si=S double bonds are named "thioxosilanes" or "silylidenesulfanes". However, in the relevant literature the name "silanethiones" is common.
[5] [5a] H. Suzuki, N. Tokitoh, R. Okazaki, S. Nagase, M. Goto, *J. Am. Chem. Soc.* **1998**, *120*, 11096−11105. − [5b] H. Suzuki, N. Tokitoh, S. Nagase, R. Okazaki, *J. Am. Chem. Soc.* **1994**, *116*, 11578−11579.
[6] [6a] G. Raabe, J. Michl in *The Chemistry of Organic Silicon Compounds*, Part 2 (Eds.: S. Patai, Z. Rappoport), John Wiley, New York, **1989**, pp. 1015−1142. − [6b] P. Lu, J. K. Paulasaari, W. P. Weber, *Organometallics* **1996**, *15*, 4649−4652. − [6c] J. Chojnowski, W. Stanczyk, *Adv. Organomet. Chem.* **1990**, *30*, 243−307. − [6d] N. C. Norman, *Polyhedron* **1993**, *12*, 2431−2446.
[7] [7a] S. Bailleux, M. Bogey, C. Demuynck, J.-L. Destombes, A. Walters, *J. Chem. Phys.* **1994**, *101*, 2729−2733. − [7b] R. J. Glinski, J. L. Gole, D. A. Dixon, *J. Am. Chem. Soc.* **1985**, *107*, 5891−5894. − [7c] R. Whithnall, L. Andrews, *J. Am. Chem. Soc.* **1985**, *107*, 2567−2568. − [7d] R. Whithnall, L. Andrews, *J. Phys. Chem.* **1985**, *89*, 3261−3268. − [7e] R. Srinivas, D. K. Böhme, D. Sülzle, H. Schwarz, *J. Phys. Chem.* **1991**, *95*, 9836−9841.
[8] H. Schnöckel, *J. Mol. Struct.* **1980**, *65*, 115−123.
[9] H. Schnöckel, *Angew. Chem*. **1978**, *90*, 638−639.
[10] V. N. Khabashesku, Z. A. Kerzina, E. G. Baskir, A. K. Maltsev, O. M. Nefedov, *J. Organomet. Chem*. **1988**, *347*, 277−293.
[11] H. Schnöckel, H.-J. Göcke, R. Köppe, *Z. Anorg. Allg. Chem*. **1989**, *578*, 159−165.
[12] R. Köppe, H. Schnöckel, *Z. Anorg. Allg. Chem.* **1992**, *607*, 41−44.
[13] [13a] C. Guimon, G. Pfister-Guillouzo, H. Lavayssière, G. Dousse, J. Barrau, J. Satgé, *J. Organomet. Chem*. **1983**, *249*, C17−C20. − [13b] V. Lefevre, J.-L. Ripoll, *Phosphorus Sulfur Silicon* **1997**, *120*/*121*, 371−372.
[14] A. Chivé, V. Lefevre, A. Systermans, J. L. Ripoll, M. Bogey, A. Walters, *Phosphorus Sulfur Silicon* **1994**, *91*, 281−284.
[15] [15a] A. Haas, *Angew. Chem*. **1965**, *77*, 1066−1075. − [15b] K. Moedritzer, *J. Organomet. Chem*. **1970**, *21*, 315−320.
[16] L. G. Gusel′nikov, V. V. Volkova, V. G. Avakyan, N. S. Nametkin, M. G. Voronkov, S. V. Kirpichenko, E. N. Suslova, *J. Organomet. Chem*. **1983**, *254*, 173−187.
[17] [17a] V. Gutmann, P. Heilmeyer, K. Utvary, *Monatsh. Chem.* **1961**, *92*, 942−943. − [17b] B. J. Aylett, I. A. Ellis, J. R. Richmond, *J. Chem. Soc., Dalton Trans.* **1973**, 981−987.
[18] H. Beckers, H. Bürger, to be published.
[19] J. L. Margrave, P. W. Wilson, *Acc. Chem. Res.* **1971**, 145−151.
[20] D. W. Kohn, H. Clausenberg, P. Chen, *Rev. Sci. Instrum.* **1972**, *63*, 4003−4005.
[21] J. W. Hastie, R. H. Hauge, J. L. Margrave, *J. Am. Chem. Soc.* **1969**, *91*, 2536−2538.
[22] C. Møller, M. S. Plesset, *Phys. Rev.* **1934**, *46*, 618−622.
[23] G. D. Purvis III, R. J. Bartlett, *J. Chem. Phys.* **1982**, *76*, 1910−1918.
[24] K. Raghavachari, G. W. Trucks, J. A. Pople, M. Head-Gordon, *Chem. Phys. Lett.* **1989**, *157*, 479−483.
[25] M. J. Frisch, G. W. Trucks, H. B. Schlegel, P. M. W. Gill, B. G. Johnson, M. A. Robb, J. R. Cheeseman, T. Keith, G. A. Petersson, J. A. Montgomery, K. Raghavachari, M. A. Al-Laham, V. G. Zakrzewski, J. V. Ortiz, J. B. Foresman, J. Cioslowski, B. B. Stefanov, A. Nanayakkara, M. Challacombe, C. Y. Peng, P. Y. Ayala, W. Chen, M. W. Wong, J. L. Andres, E. S. Replogle, R. Gomperts, R. L. Martin, D. J. Fox, J. S. Binkley, D. J. Defrees, J. Baker, J. P. Stewart, M. Head-Gordon, C. Gonzalez, J. A. Pople, *GAUSSIAN94*, Revisions D.4 and E.2, Gaussian Inc., Pittsburgh, **1995**.
[26] *MOLPRO94* is a package of ab initio programs written by H.-J. Werner and P. J. Knowles, with contributions from J. Almlöf, R. D. Amos, M. J. O. Deegan, S. T. Elbert, C. Hampel, W. Meyer, K. A. Peterson, R. M. Pitzer, A. J. Stone, and P. R. Taylor.
[27] C. Hampel, K. A. Peterson, H.-J. Werner, *Chem. Phys. Lett.* **1992**, *190*, 1−12.
[28] T. H. Dunning, Jr., *J. Chem. Phys.* **1989**, *90*, 1007−1023.
[29] D. E. Woon, T. H. Dunning, Jr., *J. Chem. Phys.* **1993**, *98*, 1358−1371.
[30] J. M. L. Martin, O. Uzan, *Chem. Phys. Lett*. **1998**, *282*, 16−24.
[31] D. E. Woon, T. H. Dunning, Jr., *J. Chem. Phys.* **1995**, *103*, 4572−4585.
[32] R. A. Kendall, T. H. Dunning, Jr., R. J. Harrison, *J. Chem. Phys.* **1992**, *96,* 6796−6806.
[33] T. J. Lee, P. R. Taylor, *Int. J. Quantum Chem. Symp*. **1989**, *23*, 199−207.
[34] T. J. Lee, G. E. Scuseria in *Quantum Mechanical Electronic Structure Calculations with Chemical Accuracy* (Ed.: S. R. Langhoff), Kluwer, Dordrecht, **1995**, pp. 47−108.
[35] E. B. Wilson, Jr., J. C. Decius, P. C. Cross, *Molecular Vibrations*, McGraw-Hill, New York, **1955**.
[36] S. Califano, *Vibrational States*, Wiley, New York, **1976**.
[37] W. Schneider, W. Thiel, *Chem. Phys. Lett*. **1989**, *157*, 367−373.
[38] I. M. Mills in *Molecular Spectroscopy: Modern Research* (Eds.: K. N. Rao, C. W. Mathews), vol. 1, Academic, New York, **1972**, pp. 115−140.
[39] D. A. Clabo, Jr., W. D. Allen, R. B. Remington, Y. Yamaguchi, H. F. Schaefer III, *Chem. Phys.* **1988**, *123*, 187−239.
[40] E. Tiemann, H. Arnst, W. U. Stieda, T. Törring, J. Hoeft, *Chem. Phys.* **1982**, *67*, 133−138.
[41] H. Shoji, T. Tanaka, E. Hirota, *J. Mol. Spectrosc*. **1973**, *47*, 268−274.
[42] R. M. Atkins, P. L. Timms, *Spectrochim. Acta A* **1977**, *33*, 853−857.
[43] H. Schnöckel, R. Köppe in *Organosilicon Chemistry: From Molecule to Materials*, vol. I (Eds.: P. Weis, N. Auner), Verlag Chemie, **1994**, p. 147−153.
[44] A. Haas, H. Willner, H. Bürger, G. Pawelke, *Spectrochim. Acta A* **1977**, *33*, 937−945.
[45] A. Almenningen, L. Fernholt, H. M. Seip, *Acta Chem. Scand.* **1968**, *22*, 51−58.

Received March 29, 1999
[I99111]

Aluminium Hydrazides: Reactions of *tert*-Butylaluminium Chlorides with Dilithium Bis(trimethylsilyl)hydrazide – Formation of Iminoalanes and their Hydrazido Adducts

Werner Uhl,*[a] Jens Molter,[a] and Rainer Koch[a]

Keywords: Aluminium / Hydrazides / Alanes / Lithium / Imino compounds

Di(*tert*-butyl)aluminium chloride reacted with dilithium bis(trimethylsilyl)hydrazide with the formation of a novel $Al_2Li_2N_4$ cage compound **1**. Its structure consists of a dimeric iminoalane $RAl(\mu N–SiMe_3)_2AlR$ (R = CMe_3), which is bridged by a dilithiumhydrazido ligand with an intact N–N bond. A heterocubane-type molecule is formed, in which two vertices are occupied by Al atoms, two by Li atoms and four by N atoms. One face of the cube is strongly distorted due to the short N–N distance of the hydrazido group. A similar compound, **3**, was formed with bis(neopentyl)aluminium chloride but it was isolated in very poor yield. The reaction of $Li_2N_2(SiMe_3)_2$ with $(Me_3C)_2AlCl$ in the presence of THF yielded an adduct **2**, in which each Li atom of the cage is additionally coordinated via Li–Cl–Al bridges to the ligand $(Me_3Al)_2Cl·THF$. The reaction of dilithium bis(trimethylsilyl)hydrazide with *tert*-butylaluminium dichloride gave, by complete cleavage of the hydrazido groups, a dimeric iminoalane $[Me_3C(THF)AlNSiMe_3]_2$ (**4**), in which each aluminium atom is coordinated to one THF molecule. Its uncoordinated, solvent-free form **5** was obtained by heating solid **4** to 150 °C in vacuo for several hours. It was identified as the tetrameric iminoalane $(Me_3CAlNSiMe_3)_4$, which does not adopt the expected heterocubane-type structure, but consists of three anellated four-membered Al_2N_2 heterocycles in a kind of ladder structure. Remarkably, the cage compound **1** could not be obtained by the reaction of an excess of lithium hydrazide with the iminoalanes **4** and **5**. All compounds **1**–**5** were characterized by crystal structure determinations.

Introduction

In contrast to boron hydrazides,[1] which form a well-established class of compounds, only a few hydrazides of the heavier group three elements aluminium to thallium are known in the literature.[2–7] Recently, such compounds have found an increased interest as they are potentially useful as precursors for the formation of ceramic materials like aluminium and gallium nitride.[4–6] Boron hydrazides are easily accessible by the reaction of boron halides with silylhydrazines and the release of chlorosilanes.[1] As recently shown by our group,[8] this method cannot be applied to the synthesis of aluminium hydrazides. Bis(trimethylsilyl)hydrazine, for instance, did not react with dialkylaluminium chlorides with the expected formation of trimethylchlorosilane, but a dismutation reaction occurred and adducts of the aluminium halides with the thermally unstable mono(trimethylsilyl)hydrazine were isolated. The few aluminium or gallium hydrazides known in the literature were obtained by four different methods: (i) the reaction of trialkyl derivatives with the N–H protons of hydrazines with the elimination of alkanes; (ii) the reaction of monolithiated hydrazides with the corresponding aluminium or gallium chlorides; (iii) the treatment of $LiAlH_4$ with hydrazines and the release of elemental hydrogen; (iv) the hydroalumination reaction of azobenzene with an arylaluminium dihydride, which gave elemental hydrogen and an iminoalane as by-products.[2–7] Recently, Nöth et al. synthesized a series of aluminium hydrazides using methods (ii) and (iii).[3] Beside the synthesis of monoaluminium derivatives, we are also very interested in the synthesis of polyaluminium or polygallium hydrazides which contain more than one aluminium or gallium atom coordinated to each N–N group, and we report here on the reaction of *tert*-butylaluminium chlorides with dilithium bis(trimethylsilyl)hydrazide.

[a] Fachbereich Chemie der Universität,
Postfach 2503, D-26111 Oldenburg, Germany
Fax: (internat.) + 49-(0)441/798-3352

Results and Discussion

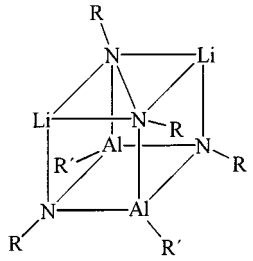
Reaction of Dilithium Bis(trimethylsilyl)hydrazide with $(Me_3C)_2AlCl$

In order to obtain a hydrazido group attached to two aluminium atoms we treated the dilithium hydrazide $Li_2N_2(SiMe_3)_2$[9] with two equivalents of di(*tert*-butyl)aluminium chloride[10] in toluene at room temperature for 36 hours. A complicated mixture of products was formed, from which one component (**1**, Equation 1) was isolated in a pure form after a three-step recrystallization from toluene/*n*-hexane in a yield of 34%. The NMR spectroscopic characterization showed that the desired dialuminiumhydrazide could not have been formed. Three singlets were observed in the ^1H-NMR spectrum with equal intensities, of which two were in the characteristic range for trimethylsilyl groups (δ = 0.38 and −0.05). The other one was assigned to a *tert*-butyl group attached to an aluminium atom (δ = 1.42). Thus, a compound must have been formed which has two chemi-

 © WILEY-VCH Verlag GmbH, D-69451 Weinheim, 1999 1434–1948/99/1111–2021 $ 17.50+.50/0

cally different $SiMe_3$ groups and one type of *tert*-butyl group. The constitution of **1** was established by an X-ray crystal structure determination.

$$2\ ClAl(CMe_3)_2 + Li_2N_2(SiMe_3)_2 \xrightarrow{-\ LiCl}$$



(1)

1 (R = $SiMe_3$; R′ = CMe_3)

The molecular structure of **1** is depicted in Figure 1. A remarkable cage compound was formed, which comprises a four-membered Al_2N_2 heterocycle with each aluminium atom further attached to one *tert*-butyl group and each nitrogen atom to a trimethylsilyl group. Each aluminium atom becomes coordinatively saturated by an interaction with one nitrogen atom of a hydrazido dianion, which bridges the iminoalane heterocycle and has an intact N−N bond. The cage is completed by two lithium atoms, each of which is coordinated by both nitrogen atoms of the hydrazido ligand and one nitrogen atom of the iminoalane moiety. Thus, the structure resembles that of a heterocubane type molecule although it is strongly distorted due to the N−N single bond across one of its faces. The Al_2N_2 heterocycle is not planar, but folded across the N−N axis by 31.2°. Owing to a coordination number of four at the aluminium atoms the Al−N bond lengths (189.2 pm on average) are longer than in some dimeric iminoalanes known from the literature with three-coordinate Al and N atoms (180 to 182 pm),[11] and also longer than the bond lengths calculated by ab-initio methods for $(HAl{-}NH)_2$.[12] A remarkably short transannular Al−Al distance of 248.5(2) pm is observed, which is shorter than in dimeric trimethylaluminium with a 2e-3c AlCAl bond (262 pm)[13] or in dialanes(4) with Al−Al single bonds (264 to 275 pm).[14] Similar short transannular distances have been observed before in other dimeric iminoalanes[11] and in many other heterocyclic main-group compounds.

This iminoalane heterocycle is bridged by a hydrazido group, where each nitrogen atom is attached to one aluminium atom. The Al−N distances (201.1 pm) are longer than those of the Al_2N_2 heterocycle and are in the typical range for dative N→Al bonds.[15] The N−N single bond length [158.9(5) pm] is longer than those usually observed in hydrazine derivatives[8][16] or in the related dimetalated hydrazide $Li_2N_2(SiMe_3)_2$,[9] which has a side-on coordination of the N−N group by both lithium atoms similar to **1**. The Li−N distances are significantly different, those to the imino nitrogen atoms and to one atom of the hydrazido group are short (198.4 pm on average), whilst the distance to the second hydrazido nitrogen is lengthened (215.5 pm).

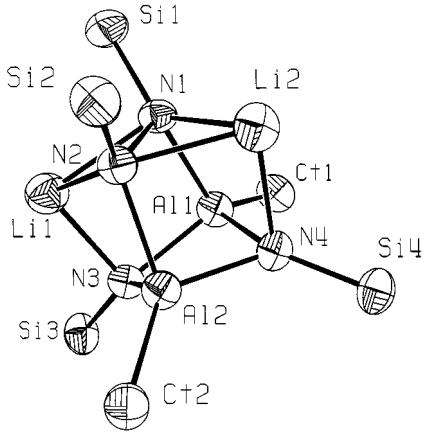


Figure 1. Molecular structure and numbering scheme of compound **1**; thermal ellipsoids are drawn at the 40% probability level (methyl groups omitted for clarity); selected bond lengths [pm] and angles [°]: Al1−N3 187.6(4), Al1−N4 191.4(4), Al2−N3 189.4(4), Al2−N4 188.3(4), N3−Si3 169.9(4), N4−Si4 168.3(4), Al1−Ct1 200.4(5), Al2−Ct2 200.9(5), Al1−N1 201.3(4), Al2−N2 200.8(4), Li1−N1 215.3(10), Li1−N2 196.8(9), Li1−N3 197.3(10), Li2−N1 197.8(9), Li2−N2 215.6(10), Li2−N4 201.8(10), N1−N2 158.9(5), N1−Si1 173.6(4), N2−Si2 174.0(4); N3−Al1−N4 93.8(2), Al1−N3−Al2 82.5(2), N3−Al2−N4 94.2(2), Al1−N4−Al2 81.8(2), Al1−N3−Li1 93.6(3), Al2−N3−Li1 86.2(3), Al1−N4−Li2 85.8(3), Al2−N4−Li2 93.7(3), N1−Al1−N3 92.6(2), N1−Al1−N4 91.3(2), N2−Al2−N3 91.2(2), N2−Al2−N4 92.3(2), N1−Li1−N2 45.1(2), N1−Li1−N3 85.8(4), N2−Li1−N3 90.1(4), N1−Li2−N2 45.0(2), N1−Li2−N4 89.3(4), N2−Li2−N4 84.5(4), Li1−N1−Li2 129.5(4), Li1−N2−Li2 129.9(4), Li1−N1−N2 61.3(3), Li1−N2−N1 73.6(3), Li2−N1−N2 73.5(3), Li2−N2−N1 61.6(3)

At first sight the Li atoms seem to be coordinatively unsaturated, with short contacts to only three nitrogen atoms, but each one also interacts with one methyl group of a trimethylsilyl substituent (Li1−C11 251.0 pm and Li2−C21 248.1 pm). Similar Li−C interactions have been observed in methyllithium[17] and in some lithium bis(trimethylsilyl)methylaluminates.[18]

We have also carried out quantum chemical calculations of the model compound $Li_2(H_3CAlNSiH_3)_2(H_3SiNNSiH_3)$ (**1a**), in which the *tert*-butyl and trimethylsiyl groups of **1** were replaced by CH_3 and SiH_3, respectively. The optimization of the molecular structure of **1a** resulted in a very good agreement between the experimental and calculated structural parameters. Some selected distances and bond angles are summarized in the Experimental Section, where it can be seen that the method chosen is suitable for the description of compound **1**. The largest deviations were observed for the Li−N separations (up to 5 pm) and for the N−N distance of the hydrazido group (151.3 pm instead of 158.9 pm), which may be partially caused by the smaller CH_3 and SiH_3 substituents employed in the calculated molecule **1a**. As clearly shown by NBO analysis, the short Al−Al distance (**1a**: 250.7 pm) must not be interpreted in terms of an Al−Al bonding interaction, and no two- or three-center interactions between the aluminium atoms can be found. The Al−Al bond order is close to zero, and no significant additional interaction between Al orbitals is observed similar to the four-membered heterocycles with short transannular E-E contacts reported previously.

Donor solvents like THF or diethyl ether had a strong influence on the course of this reaction (Equation 1). In diethyl ether no reaction was observed at all over a period of several days at room temperature, and in boiling ether decomposition occurred and only traces of the ether adduct $(Me_3C)_2AlCl{\cdot}OEt_2$ were isolated after recrystallization. Similar observations were made in THF as a solvent. Treatment of dilithium bis(trimethylsilyl)hydrazide with THF gave, after thorough evaporation of the obtained solid, a solvate which, from the integration of its ^1H NMR spectrum, contained half a molecule of THF for each formula unit of the hydrazide. The reaction of this solvate with di(*tert*-butyl)aluminium chloride in hexane gave another cage compound **2** in low yield and a complicated mixture of unknown products (Equation 2). The molecular structure of **2** in the solid state (Figure 2) can be derived from the cage of **1**, but each lithium atom is additionally coordinated via Li−Cl−Al bridges to a THF adduct of the starting chloroalane. The structural parameters of the cage are very similar to those of **1** and are not discussed here in detail. The chloro bridges are almost linear (Cl1 173.9°; Cl2 167.5°), which is in accordance with the steric shielding of the Li atom by the substituents of the cage and the high ionic character of the Li−Cl interaction. Li−Cl (240.1 pm) and Al−Cl distances (219.3 pm) are in the expected range.[19]

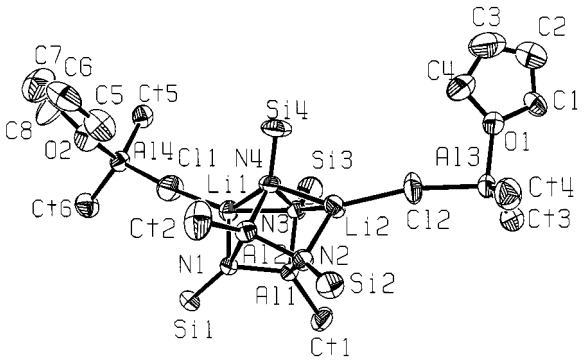


Figure 2. Molecular structure and numbering scheme of compound **2**; thermal ellipsoids are drawn at the 40% probability level (methyl groups omitted for clarity); selected bond lengths [pm] and angles [°]: Al1−N1 187.9(2), Al1−N2 188.8(3), Al2−N1 188.1(3), Al2−N2 188.5(3), N1−Si1 169.6(2), N2−Si2 168.9(2), Al1−Ct1 200.1(3), Al2−Ct2 201.7(4), Al1−N3 199.5(2), Al2−N4 200.0(3), Li1−N1 199.5(6), Li1−N3 212.4(5), Li1−N4 201.6(6), Li2−N2 198.8(5), Li2−N3 203.2(6), Li2−N4 216.4(6), N3−N4 156.1(4), N3−Si3 173.2(2), N4−Si4 172.3(3), Li1−Cl1 237.9(5), Li2−Cl2 242.2(5), Al3−Cl2 219.4(1), Al4−Cl1 219.3(1), Al3−O1 190.6(2), Al4−O2 189.3(3); N1−Al1−N2 93.5(1), Al1−N1−Al2 82.1(1), N1−Al2−N2 93.5(1), Al1−N2−Al2 81.7(1), Al1−N1−Li1 92.0(2), Al2−N1−Li1 86.8(2), Al1−N2−Li2 86.6(2), Al2−N2−Li2 93.6(2), N1−Al1−N3 92.9(1), N2−Al1−N3 92.6(1), N1−Al2−N4 92.6(1), N2−Al2−N4 92.4(1), N3−Li1−N4 44.2(1), N1−Li1−N3 85.9(2), N1−Li1−N4 88.8(2), N3−Li2−N4 43.5(1), N2−Li2−N3 88.6(2), N2−Li2−N4 84.9(2), Li1−N3−Li2 131.0(2), Li1−N4−Li2 129.5(2), Li1−N3−N4 64.3(2), Li1−N4−N3 71.6(2), Li2−N3−N4 72.7(2), Li2−N4−N3 63.7(2), Li1−Cl1−Al4 173.9(1), Li2−Cl2−Al3 167.5(1)

The reaction of dimethylaluminium chloride or di(*tert*-butyl)aluminium bromide with $Li_2N_2(SiMe_3)_2$ gave only mixtures of unknown products, from which no single component could be isolated by recrystallization. A further cage compound **3**) was obtained from the reaction with di(neopentyl)aluminium chloride, and was isolated in a very poor, but reproducible, yield of only 10% after recrystallization from diethyl ether/hexane (Equation 3). Compound **3** decomposes slowly in the reaction mixture, so that the reaction must be stopped after six hours at room temperature. The molecular structure of **3** (Figure 3) is quite similar to that of **1** and need not be discussed in detail. One of the Li atoms (Li2) is coordinated to an ether molecule. As a result the cage is slightly more distorted and the Li−N bonds to Li2 are longer (204.0 and 216.1 pm) than those to Li1 (197.5 and 210.2 pm).

$$2\ ClAl(CH_2CMe_3)_2 + Li_2N_2(SiMe_3)_2 \xrightarrow[-\ LiCl]{Et_2O} \quad (3)$$

$$Li_2(Al\text{-}CH_2CMe_3)_2(Me_3SiN\text{-}NSiMe_3)(N\text{-}SiMe_3)_2 \cdot OEt_2$$

3

Reaction of Dilithium Bis(trimethylsilyl)hydrazide with $(Me_3C)AlCl_2$

The mechanism of the formation of the cage compounds is not well understood. We supposed that a dismutation reaction might play an important role although, in this case, the corresponding trialkylaluminium compound should be formed. However, these trialkylaluminium derivatives could not be unambiguously identified in the NMR spectra of the reaction mixtures. Nevertheless, *tert*-butylaluminium dichloride as a possible intermediate in a dismutation reaction seemed to be an appropriate starting compound for the synthesis of such derivatives in a higher yield. The imido group may be formed by a disproportionation of $[N_2(SiMe_3)_2]^{2-}$, which could yield dilithium or dialuminium trimethylsilylamide and a reactive nitrene or diimine intermediate which could be consumed by the formation of unknown secondary products.

Treatment of $Me_3C-AlCl_2$ with $Li_2N_2(SiMe_3)_2$ in an equimolar ratio without a coordinating solvent gave only decomposition products. Only with the THF solvate of the Li compound and reaction at low temperature was a pure product isolated after recrystallization in a yield of 31%. This compound was subsequently identified as the THF adduct of the corresponding dimeric iminoalane (**4**, Equation 4). Once again, the N−N bond of the hydrazido group was cleaved by the reaction with a chloroalane, and only half of the nitrogen atoms were transferred to the product. The other components of the reaction mixture, which should give more insight into the mechanism of the reaction and the fate of the missing NR groups, could neither be isolated nor identified by NMR spectroscopy. As expected, singlets of equal intensity were observed in the NMR spectra of **4** for the CMe_3 and $SiMe_3$ groups, and broad multiplets were detected for the protons of the coordinated THF molecules. The crystal structure of **4** (Figure 4) reveals two, crystallographically independent, planar Al_2N_2 heterocycles. One is

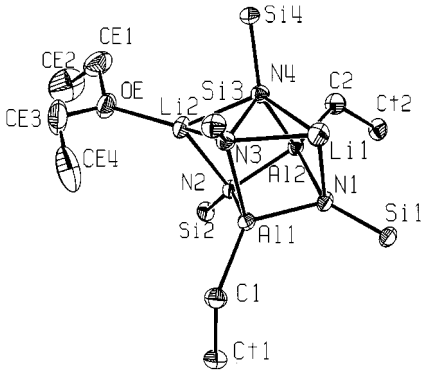
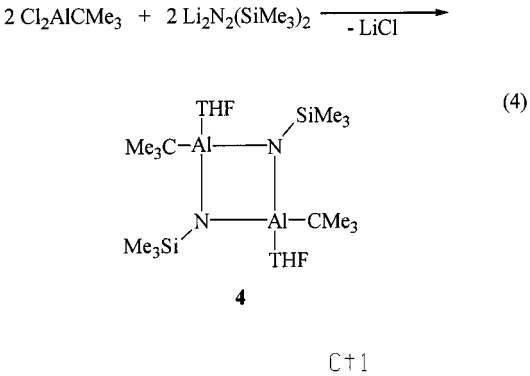


Figure 3. Molecular structure and numbering scheme of compound **3**; thermal ellipsoids are drawn at the 40% probability level (methyl groups omitted for clarity); selected bond lengths [pm] and angles [°]: Al1−N1 188.7(2), Al1−N2 187.2(2), Al2−N1 188.5(2), Al2−N2 188.9(2), N1−Si1 169.0(2), N2−Si2 169.8(2), Al1−C1 198.4(2), Al2−C2 197.9(2), Al1−N3 203.3(2), Al2−N4 200.9(2), Li1−N1 197.7(4), Li1−N3 210.2(4), Li1−N4 197.3(4), Li2−N2 203.9(4), Li2−N3 204.1(3), Li2−N4 216.1(4), N3−N4 157.1(2), N3−Si3 173.2(2), N4−Si4 174.9(2), Li2−OE 196.5(3); N1−Al1−N2 93.18(7), Al1−N1−Al2 82.46(6), N1−Al2−N2 92.67(7), Al1−N2−Al2 82.75(6), Al1−N1−Li1 91.5(1), Al2−N1−Li1 85.9(1), Al1−N2−Li2 88.4(1), Al2−N2−Li2 92.1(1), N1−Al1−N3 92.42(7), N2−Al1−N3 91.95(7), N1−Al2−N4 92.47(7), N2−Al2−N4 92.91(7), N3−Li1−N4 45.20(9), N1−Li1−N3 87.9(1), N1−Li1−N4 90.8(2), N3−Li2−N4 43.78(8), N2−Li2−N3 87.1(1), N2−Li2−N4 84.5(1), Li1−N3−Li2 129.4(2), Li1−N4−Li2 129.9(2), Li1−N3−N4 63.1(1), Li1−N4−N3 71.7(1), Li2−N3−N4 72.2(1), Li2−N4−N3 64.1(1)

located on a crystallographic inversion center, and the other shows a maximum deviation of any atom from the plane of 1 pm. Each Al atom is further coordinated to one *tert*-butyl group and one THF molecule in a distorted tetrahedral environment, while the nitrogen atoms are attached to only one silyl group besides the aluminium atoms of the ring. The nitrogen atoms are almost ideally planar-coordinated with the sum of the angles between 359.4 and 360.0°. The heterocycles deviate slightly from an ideal square geometry and have angles of 87.3° at the nitrogen atom and 92.7° at the aluminium atom. The Al−N distances (183.4 pm on average) are shorter than in the cage compounds described above, which may be due to less steric crowding in the molecules. They are similar to the solvent free iminoalanes reported in the literature.[11] The transannular Al−Al contacts are very small (252.7 pm). As predicted by theory (see above), they do not indicate any bonding interactions between the metal atoms.

The solvent free compound **5** was obtained by heating the THF adduct to 150°C under vacuum for several hours (Equation 5). Compound **5** is almost insoluble in noncoordinating solvents like pentane or toluene and was purified by extraction with boiling toluene in a Soxhlet apparatus. Therefore, we were not able to determine its molar mass in solution by cryoscopy. Two singlets were observed in the ^{1}H NMR spectrum for the $SiMe_3$ and CMe_3 groups with equal intensity, which remained unchanged upon cooling solutions in toluene to −90°C. In the solid state, **5** reveals a unique molecular structure of a tetrameric iminoalane (Figure 5), which comprises three annelated planar four-membered heterocycles. Usually, iminoalanes give cage molecules with up to eight formula units,[20] while very large substituents give dimers or trimers with four- or six-membered heterocycles.[11] No cage compound is formed here, instead a kind of a ladder structure results with angles between the normals of the planes of 63.7°. Different Al−N bond lengths are observed. The shortest one is found between the coordinatively unsaturated atoms Al2 and N2 (180.2 pm), intermediate are the distances between the tri- and tetracoordinated atoms (188.8 pm) and the longest is the separation between the tetracoordinated atoms (Al1−N1 200.6 and Al1−N1′ 193.8 pm). The Al−Al distances are longer than described before (Al1−Al2 262.4 pm, Al1−Al1′ 278.3 pm). As expected, the N−Si bond lengths depend on the coordination number of the nitrogen atom, a short bond is observed to N2 (172.5 pm) and a longer one to N1 (177.4 pm). A similar structure has been observed in a tetraaluminium tetraoxo compound.[21]



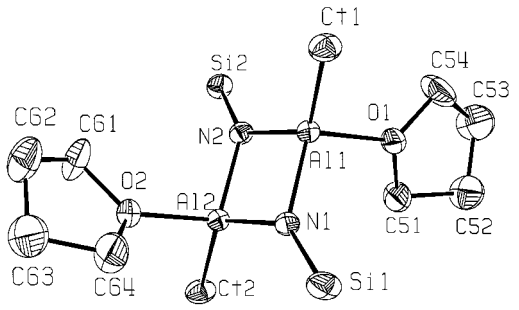
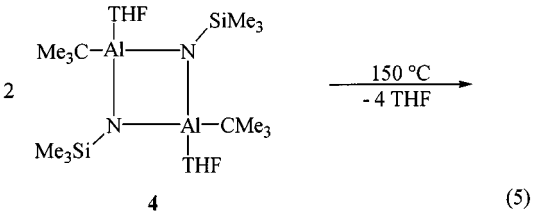
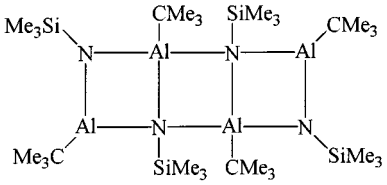


Figure 4. Molecular structure and numbering scheme of compound **4**; thermal ellipsoids are drawn at the 40% probability level (methyl groups omitted for clarity); selected bond lengths [pm] and angles [°]: Al1−N1 184.5(2), Al2−N1 183.0(2), Al1−N2 183.0(2), Al2−N2 183.8(2), Al1−O1 192.8(2), Al1−Ct1 200.5(3), Al2−O2 192.9(2), Al2−Ct2 200.5(3), N1−Si1 167.7(2), N2−Si2 168.5(2); Al1−N1−Al2 87.34(8), Al1−N2−Al2 87.51(8), N1−Al1−N2 92.45(9), N1−Al2−N2 92.67(9), Al1−N1−Si1 133.9(1), Al2−N1−Si1 138.7(1), Al1−N2−Si2 137.1(1), Al2−N2−Si2 134.8(1)

In agreement with the NMR spectroscopic data described above, the structure of **5** in solution may be quite different from that in the solid state. A dimeric iminoalane may be formed by dissociation, or a heterocubane or larger aggregate may exist as the most stable form. Remarkably, the reaction according to Equation 5 is irreversible, and treatment of **5** with a large excess of THF did not yield the THF adduct **4**. Also, the formation of the cage compound **1** was not achieved by the reaction of the solvent-free iminoalane **5** with $Li_2N_2(SiMe_3)_2$ under various conditions,



4 (5)



5

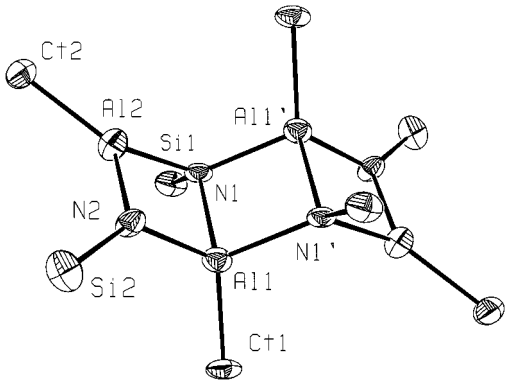


Figure 5. Molecular structure and numbering scheme of compound **5**; thermal ellipsoids are drawn at the 40% probability level (methyl groups omitted for clarity); selected bond lengths [pm] and angles [°]: Al1−N1 200.6(4), Al1−N1′ 193.8(3), Al1−N2 186.6(4), Al1−Ct1 200.8(5), Al2−N1 191.0(4), Al2−N2 180.2(4), Al2−Ct2 196.2(4), N1−Si1 177.4(4), N2−Si2 172.5(3); N1−Al1−N1′ 90.3(1), N1−Al1−N2 89.7(2), Al1−N1−Al1′ 89.7(1), Al1−N1−Al2 84.1(1), Al1′−N1−Al2 117.2(2), N1−Al2−N2 94.8(2), Al1−N2−Al2 91.3(2); Al1′ and N1′ generated by $-x + 1$, $-y$, $-z + 1$

and even the THF adduct did not react with an excess of the lithium hydrazide to form **1**. Obviously, the mechanism of the formation of such cages is very complicated and seems to be determined by several factors, which must remain unclear as long as we have no information concerning the constitution of the by-products

Experimental Section

General: All procedures were carried out under purified argon in dried solvents (THF, diethyl ether and toluene over Na/benzophenone; *n*-hexane and cyclopentane over $LiAlH_4$; pentafluorobenzene over molecular sieves). $Li_2N_2(SiMe_3)_2$,[9] di(*tert*-butyl)aluminium chloride[10] and *tert*-butyl aluminiumdichloride[18] (similar to the bromo derivative) were synthesized according to literature procedures.

Synthesis of 1: A suspension of dilithium bis(trimethylsilyl)hydrazide (0.788 g, 4.19 mmol) in 50 mL of toluene was treated at room temperature with a solution of di(*tert*-butyl)aluminium chloride (1.48 g, 8.38 mmol) in 50 mL of toluene. The mixture was stirred for 36 h, then filtered and evaporated to dryness. Colorless **1** was purified by threefold recrystallization from a toluene/hexane mixture. Yield: 0.38 g (34% based on hydrazide). − M. p. (argon, sealed capillary): 152°C (dec). − ^{1}H NMR (C_6D_6, 300 MHz): δ = 1.42 (s, 18 H, CMe_3), 0.38 (s, 18 H, $Al_2N-SiMe_3$), −0.05 [s, 18 H, $N_2(SiMe_3)_2$]. − ^{13}C NMR (C_6D_6, 75 MHz): δ = 31.2 (CMe_3), 7.7 and 2.8 ($N-SiMe_3$), AlC not detected. − IR (CsBr, paraffin): $\tilde{\nu}$ = 1302 vw, 1252 s, 1223 w δ(CH_3), 1182 vw, 1169 vw, 1152 vw, 1063 w, 997 m, 978 m, 937 m, 889 m ν(CC), ν(NN); 837 vs, 748 s, 723 m ρ(CH_3); 658 w, 635 m, 619 w, 602 w ν(SiC), ν(SiN); 515 m, 457 w, 438 w ν(AlC), ν(AlN); 351 vw δ(SiC). − $C_{20}H_{54}Al_2Li_2N_4Si_4$ (530.9): calcd. Al 10.2; found Al 10.1. − Mol. mass: 522 (cryoscopically in benzene).

Synthesis of 2: Dilithium bis(trimethylsilyl)hydrazide (0.602 g, 3.20 mmol) was dissolved in THF. The solvent was then removed in vacuo and an NMR spectroscopic characterization showed that the adduct $Li_2N_2(SiMe_3)2{\cdot}0.5THF$ had formed. This compound was suspended in 50 mL of *n*-hexane and cooled to −30°C. A solution of di(*tert*-butyl)aluminium chloride (1.132 g, 6.41 mmol) in 50 mL of *n*-hexane was then added dropwise, and the mixture was stirred at room temperature for 16 h. After filtration and evaporation the product was purified by recrystallizing twice from *n*-hexane. Yield: 0.170 g (10% based on hydrazide). − M. p. (argon, sealed capillary): 133°C (dec). − ^{1}H NMR (C_6D_6, 133 MHz): δ = 3.61 (m, 8 H, $O-CH_2$ of THF), 1.46 (s, 18 H, CMe_3 of iminoalane), 1.19 (s, 36 H, CMe_3 of chloroalane ligand), 0.97 (m, 8 H, CH_2 of THF), 0.42 (s, 18 H, $Al_2N-SiMe_3$), 0.15 [s, br., 18 H, $N_2(SiMe_3)_2$]. − ^{13}C NMR (C_6D_6, 75 MHz): δ = 73.4 ($O-CH_2$ of THF), 31.5 (CMe_3 of iminoalane), 30.5 (CMe_3 of chloroalane), 24.6 (CH_2 of THF), 7.8 and 3.7 ($N-SiMe_3$); AlC not detected. − IR (CsBr, paraffin): $\tilde{\nu}$ = 1300 vw cm^{-1}, 1250 s δCH_3; 1182 w, 1138 vw, 1109 vw, 1040 m, 1003 m, 968 s, 934 s ν(CC), ν(CO), ν(NN); 883 m, 839 vs ρ(CH_3); 814 s ν(C_3C); 754 s, 723 w ρ(CH_3); 664 w $\nu_{as}(SiC_3)$; 638 m, 621 m, 598 m $\nu_s(SiC_3)$, ν(SiN); 546 w, 523 w, 463 w ν(AlC); 434 m, 403 m ν(AlCl); 382 vw, 361 w δ(SiC_3). − $C_{44}H_{106}Al_4Cl_2Li_2N_4O_2Si_4$ (1028.4): calcd. Al 10.5; found Al 10.3.

Synthesis of 3: A solution of dineopentylaluminium chloride (0.826 g, 4.04 mmol) in 25 mL of toluene was added at −40°C to a suspension of dilithium bis(trimethylsilyl)hydrazide (0.381 g, 2.02 mmol) in 25 mL of toluene. The mixture was allowed to warm slowly to room temperature. After stirring for 6 h LiCl was filtered off, and the solvent was removed in vacuo. The residue was recrystallized from diethyl ether/*n*-hexane. Yield: 0.130 g (10% based on hydrazide). − M. p. (argon, sealed capillary): 141°C (dec). − ^{1}H NMR (C_6D_6, 300 MHz): δ = 3.20 (q, 4 H, $O-CH_2$), 1.43 (s, 18 H, CMe_3), 0.98 (t, 6 H, CH_3 of diethyl ether), 0.75 (s, 4 H, $Al-CH_2$), 0.43 (s, 18 H, $Al_2N-SiMe_3$), 0.11 [s, 18 H, $N_2(SiMe_3)_2$]. − ^{13}C NMR (C_6D_6, 75 MHz): δ = 65.5 ($O-CH_2$), 36.0 (CMe_3), 14.8 (CH_3 of diethyl ether), 7.4 and 4.1 ($N-SiMe_3$); AlC not detected. − IR (CsBr, paraffin): $\tilde{\nu}$ = 1304 w cm^{-1}, 1250 s δ(CH_3); 1182 w 1167 w, 1152 w, 1125 m, 1096 m, 1065 m, 1005 m, 970 m, 934 s ν(CO), ν(CC), ν(NN); 889 s, 837 vs, 756 s, 721 m ρ(CH_3); 667 m, 662 sh, 621 w, 604 w ν(SiC), ν(SiN); 563 w, 525 m, 463 m ν(AlC); 425 w ν(AlCl). − $C_{22}H_{58}Al_2Li_2N_4Si_4{\cdot}OC_4H_{10}$ (633.0): calcd. Al 8.5; found Al 8.2.

Synthesis of 4: Dilithium bis(trimethylsilyl)hydrazide (1.52 g, 8.07 mmol) was dissolved in THF and the solvent removed in vacuo to give a solid containing half a molecule of THF per formula unit of the hydrazide. This solid was treated with 50 mL of *n*-hexane and cooled to −50°C. *tert*-Butylaluminium dichloride (1.26 g, 8.07 mmol) in 50 mL of *n*-hexane was then added, and the mixture

was slowly warmed to room temperature in 8 h. Colorless crystals of **4** were obtained after filtration, evaporation and recrystallization (twice) from a mixture of hexane and toluene. Yield: 1.21 g (31%). − M. p. (argon, sealed capillary): 255°C (dec). − ^{1}H NMR (C_6D_6, 300 MHz): δ = 3.95 (m, 8 H, O−CH_2), 1.30 (s, 18 H, CMe_3), 1.23 (m, 8 H, CH_2 of THF), 0.30 ppm (s, 18 H, N−$SiMe_3$). − ^{13}C NMR (C_6D_6, 75 MHz): δ = 71.6 (O−CH_2), 31.6 (CMe_3), 25.0 (CH_2 of THF), 7.0 (N−$SiMe_3$), Al−C not detected. − IR (CsBr, paraffin): $\tilde{\nu}$ = 1298 w cm^{-1}, 1246 m, 1235 m δ(CH_3); 1181 w, 1074 m, 1017 vs, 934 w, 922 w ν(CC), ν(CO); 845 s ρ(CH_3); 822 s ν_{C3C}; 760 m, 754 m, 721 w δ(CH_3); 681 m, 658 m, 629 w ν(SiC), ν(SiN); 544 w 519 w, 492 w, 463 w, 434 m ν(AlC), ν(AlN), ν(AlO); 397 vw, 374 vw, 351 vw, 328 vw δ(C_3C), δ(SiC). − $C_{22}H_{52}Al_2N_2O_2Si_2$ (486.8): calcd. Al 11.1; found Al 11.1. − Mol. mass: 455 (cryoscopically in benzene).

Synthesis of 5: Compound **4** (1.0 g, 2.05 mmol) was heated in vacuo to 150°C for 5 h. Product **5** was extracted from the almost insoluble residue by treating with boiling toluene. It can be recrystallized from toluene. Yield: 0.25 g (36%), colorless crystals, sparingly soluble in organic solvents. − M. p. (argon, sealed capillary): >400°C. − ^{1}H NMR (C_6D_6, 300 MHz): δ = 1.31 (s, 9 H, CMe_3), 0.42 (s, 9 H, N−$SiMe_3$). − ^{13}C NMR (C_6D_6, 75 MHz): δ = 32.3 (CMe_3), 8.0 ($SiMe_3$), Al−C not detected. − IR (CsBr, paraffin): $\tilde{\nu}$ = 1312 w, 1252 vs δ(CH_3); 1167 w, 1155 w, 1086 w, 1030 w, 1003 m, 936 s ν(CC); 876 vs, 837 vs ρ(CH_3); 808 vs ν(C_3C); 754 vs, 725 s ρ(CH_3); 679 w, 621 vs ν(SiC), ν(SiN); 552 vs, 465 m ν(AlC). − $C_{28}H_{72}Al_4N_4Si_4$ (685.2): calcd. Al 15.8; found Al 15.7.

X-ray Crystal Structure Determinations: Single crystals were obtained upon cooling solutions of the compounds in hexane/toluene (**1** and **4**), hexane (**2**), hexane/diethyl ether (**3**) or toluene (**5**). Crystal data and structure refinement parameters are given in Table 1.[24] In compound **2**, the trimethylsilyl groups of Si3 and Si4 are disordered. The carbon atoms were refined with occupancy factors of 0.6 and 0.4. The THF carbon atoms C1 and C8 were refined on split positions with occupancy ratios of 0.5 to 0.5 and 0.4 to 0.6, respectively. In compound **4**, the THF molecules of the heterocycle in general position were disordered, and the atoms C11, C12, C14, C21 and C24 were refined in split positions. The molecule located on a crystallographic inversion center was completely disordered and refined in two positions with occupancy factors of 0.68 and 0.32.

Quantum Chemical Calculations: Standard ab initio molecular orbital calculations[25] were carried out with the GAUSSIAN 94 set of programs.[26] The structure of **1a** was optimized at the HF level by using the 6−31G* basis set. Population analysis was performed by employing the NBO program[27] within GAUSSIAN. Bond lengths [pm] and angles [°] of **1a** (average values, experimental values in brackets): Al−N(1,2) 201.6 (201.1), Al−N3 189.5 (188.5), Al−N4 190.2 (189.9), Li−N(3,4) 193.9 (199.6), Li−N(1,2) 198.3 and 219.3 (197.3 and 215.5), N−N 151.3 (158.9), Al−C 197.1 (200.7), N−Si(1,2) 172.8 (173.8), N−Si(3,4) 170.2 (169.1), Al···Al 250.7 (248.5), Li···Al 266.3 and 277.8 (265.9 and 282.8), Al−N−Al 82.7 (82.2), N−Al−N 93.0 (94.0), Li−N−Li 130.2 (129.7), N1−Li−N2 42.1 (45.1), Li−N−N 61.5 and 76.3 (61.5 and 73.6).

Acknowledgments

We are grateful to the *Fonds der Chemischen Industrie* for generous financial support.

Table 1. Crystal data, data collection parameters and structure refinement of compounds **1**−**5**[a]

	1	**2**	**3**	**4**	**5**
Formula	$C_{20}H_{54}Al_2Li_2N_4Si_4$	$C_{44}H_{106}Al_4Cl_2Li_2N_4O_2Si_4$	$C_{26}H_{68}Al_2Li_2N_4OSi_4$	$C_{22}H_{52}Al_2N_2O_2Si_2$	$C_{28}H_{72}Al_4N_4Si_4$
Crystal system	monoclinic	monoclinic	orthorhombic	monoclinic	triclinic
Space group	*C*2/c; No. 15[22]	$P2_1/c$; No. 14[22]	$P2_12_12_1$; Nr. 19[22]	$P2_1/c$; No. 14[22]	*P*−1; No. 2[22]
Z	8	4	4	6	1
Temperature [K]	293	213	213	213	213
$d_{calc.}$ [g/cm^3]	1.039	1.050	1.057	1.067	1.078
a [pm]	1943.2(4)	1618.9(1)	1200.2(2)	992.33(5)	1049.0(2)
b [pm]	1260.6(3)	1963.16(8)	1500.3(3)	1620.04(8)	1080.6(1)
c [pm]	2883.0(6)	2048.5(1)	2209.7(4)	2849.0(2)	1087.8(2)
α [°]	90	90	90	90	68.24(1)
β [°]	106.03(3)	91.845(7)	90	96.738(8)	78.81(2)
γ [°]	90	90	90	90	67.44(1)
V [10^{-30} m^3]	6788(3)	6507.0(6)	3979(1)	4548.4(5)	1055.6(3)
μ [mm^{-1}]	0.241	0.221[b]	0.217[b]	0.157[b]	0.246[b]
Crystal size [mm]	0.49 × 0.38 × 0.30	0.45 × 0.30 × 0.25	0.90 × 0.66 × 0.35	0.72 × 0.50 × 0.44	0.35 × 0.32 × 0.30
Diffractometer	AED-2	Stoe-IPDS	Stoe-IPDS	Stoe-IPDS	Stoe-IPDS
Radiation	Mo-K_α; graphite monochromator				
2Θ range [°]	3.90 ≤ 2Θ ≤ 45.94	4.14 ≤ 2Θ ≤ 52.1	4.72 ≤ 2Θ ≤ 52.02	4.84 ≤ 2Θ ≤ 52.18	4.22 ≤ 2Θ ≤ 52.24
Index ranges	−21 ≤ h ≤ 20 0 ≤ k ≤ 13 0 ≤ l ≤ 31	−20 ≤ h ≤ 19 −24 ≤ k ≤ 24 −25 ≤ l ≤ 25	−14 ≤ h ≤ 14 −18 ≤ k ≤ 18 −24 ≤ l ≤ 24	−11 ≤ h ≤ 11 −19 ≤ k ≤ 19 −35 ≤ l ≤ 34	−12 ≤ h ≤ 12 −12 ≤ k ≤ 12 −13 ≤ l ≤ 13
Independent reflections	4710	12722	7355	8339	3795
Reflections $F > 4\sigma(F)$	3018	6960	6739	6306	2491
Parameters	307	657	372	563	193
$R = \Sigma\|\|F_o\| - \|F_c\|\|/\Sigma\|F_o\|$ ($F > 4\sigma(F)$)	0.0780	0.0569	0.0338	0.0582	0.0726
$wR^2 = \{\Sigma w(F_o^2 - F_c^2)^2/\Sigma w(F_o^2)^2\}^{1/2}$ (all data)	0.1107	0.1520	0.0982	0.1835	0.1259
Max./min. residual [10^{30} e/m^3]	0.34/−0.33	0.53/−0.38	0.49/−0.22	0.54/−0.64	0.85/−0.39

[a]Program: SHELXTL, SHELXL-93;[23] solutions by direct methods; full matrix refinement with all independent structure factors. − [b]Numerical absorption correction.

[1] K. Niedenzu, P. Fritz, W. Weber, *Z. Naturforsch., B Chem. Sci.* **1967**, *22*, 225; J. C. Huffman, H. Fusstetter, H. Nöth, *Z. Naturforsch., B Chem. Sci.* **1976**, *31*, 289−293; P. C. Bharara, H. Nöth, *Z. Naturforsch., B Chem. Sci.* **1979**, *34*, 1352−1357; H. Hommer, H. Nöth, H. Sachdev, M. Schmidt, H. Schwenk, *Chem. Ber.* **1995**, *128*, 1187−1194; D. C. Pestana, P. P. Power, *Inorg. Chem.* **1991**, *30*, 528−535.

[2] N. R. Fetter, B. Bartocha, *Can. J. Chem.* **1961**, *39*, 2001−2008.

[3] H. Nöth, T. Seifert, *Eur. J. Inorg. Chem.* **1998**, 1931−1938.

[4] D. A. Neumayer, A. H. Cowley, A. Decken, R. A. Jones, V. Lakhotia, J. G. Ekerdt, *Inorg. Chem.* **1995**, *34*, 4698−4700.

[5] D. W. Peters, M. P. Power, E. D. Bourret, J. Arnold, *Chem. Commun.* **1998**, 753−754.

[6] Y. Kim, J. H. Kim, J. E. Park, H. Song, J. T. Park, *J. Organomet. Chem.* **1997**, *545−546*, 99−103.

[7] R. J. Wehmschulte, P. P. Power, *Inorg. Chem.* **1996**, *35*, 2717−2718; quantum chemical calculations: L. Nyulaszi, *J. Chem. Soc., Dalton Trans.* **1997**, 2373−2375.

[8] W. Uhl, J. Molter, W. Saak, *Z. Anorg. Allg. Chem.* **1999**, *625*, 321−328.

[9] K. Bode, C. Drost, C. Jäger, U. Klingebiel, M. Noltemeyer, Z. Zak, *J. Organomet. Chem.* **1994**, *482*, 285−292; C. Drost, C. Jäger, S. Freitag, U. Klingebiel, M. Noltemeyer, G. M. Sheldrick, *Chem. Ber.* **1994**, *127*, 845−847.

[10] W. Uhl, J. Wagner, D. Fenske, G. Baum, *Z. Anorg. Allg. Chem.* **1992**, *612*, 25−34; another route: H. Lehmkuhl, O. Olbrysch, H. Nehl, *Liebigs Ann. Chem.* **1973**, 708−714.

[11] R. J. Wehmschulte, P. P. Power, *J. Am. Chem. Soc.* **1996**, *118*, 791−797; *Inorg. Chem.* **1998**, *37*, 6907−6911; K. J. L. Paciorek, J. H. Nakahara, S. R. Masuda, *Inorg. Chem.* **1990**, *29*, 4252−4255; J. D. Fischer, P. J. Shapiro, G. P. A. Yap, A. L. Rheingold, *Inorg. Chem.* **1996**, *35*, 271−272; S. Schulz, L. Häming, R. Herbst-Irmer, H. W. Roesky. G. M. Sheldrick, *Angew. Chem.* **1994**, *106*, 1052−1054; *Angew. Chem. Int. Ed. Engl.* **1994**, *33*, 969−971; S. Schulz, A. Voigt, H. W. Roesky, L. Häming, R. Herbst-Irmer, *Organometallics* **1996**, *15*, 5252−5253; trimeric iminoalanes: K. M. Waggoner, H. Hope, P. P. Power, *Angew. Chem.* **1988**, *100*, 1765−1766; *Angew. Chem. Int. Ed. Engl.* **1988**, *27*, 1699−1670; K. M. Waggoner, P. P. Power, *J. Am. Chem. Soc.* **1991**, *113*, 3385−3393.

[12] R. D. Davy, H. F. Schaefer (III), *Inorg. Chem.* **1998**, *37*, 2291−2295; T. P. Hamilton, A. W. Shaikh, *Inorg. Chem.* **1997**, *36*, 754−755.

[13] R. G. Vranka, E. L. Amma, *J. Am. Chem. Soc.* **1967**, *89*, 3121−3126; J. C. Huffman, W. E. Streib, *J. Chem. Soc., Chem. Commun.* **1971**, 911−912.

[14] W. Uhl, *Z. Naturforsch, B. Chem. Sci.* **1988**, *43*, 1113−1118; R. J. Wehmschulte, K. Ruhlandt-Senge, M. M. Olmstead, H. Hope, B. E. Sturgeon, P. P. Power, *Inorg. Chem.* **1993**, *32*, 2983−2984; N. Wiberg, K. Amelunxen, T. Blank, H. Nöth, J. Knizek, *Organometallics* **1998**, *17*, 5431−5433.

[15] A. Haaland, in *Coordination Chemistry of Aluminum*, (Ed.: G. H. Robinson), VCH, Weinheim, **1993**.

[16] K. Bode, U. Klingebiel, *Adv. Organomet. Chem.* **1996**, *40*, 1−43; S. Dielkus, C. Drost, R. Herbst-Irmer, U. Klingebiel, *Angew. Chem.* **1993**, *105*, 1689−1690; *Angew. Chem. Int. Ed. Engl.* **1993**, *32*, 1625−1626; C. Glidewell, D. W. H. Rankin, A. G. Robiette, G. M. Sheldrick, *J. Chem. Soc., A* **1970**, 318−320; Y. Morino, T. Iijima, Y. Murata, *Bull. Chem. Soc. Japan* **1960**, *33*, 46−48.

[17] E. Weiss, T. Lambertsen, B. Schubert, J. K. Cockroft, A. Wiedenmann, *Chem. Ber.* **1990**, *123*, 79−81.

[18] W. Uhl, J. E. O. Schnepf, *Z. Anorg. Allg. Chem.* **1991**, *595*, 225−238; W. Uhl, M. Layh, W. Massa, *Chem. Ber.* **1991**, *124*, 1511−1516.

[19] H. H. Karsch, K. Zellner, G. Müller, *J. Chem. Soc., Chem. Commun.* **1991**, 466−468; *Organometallics* **1991**, *10*, 2884−2890; F. Schaller, W. Schwarz, H.-D. Hausen, K. W. Klinkhammer, J. Weidlein, *Z. Anorg. Allg. Chem.* **1997**, *623*, 1455−1466.

[20] D. M. Choquette, M. J. Timm, J. L. Hobbs, T. M. Nicholson, M. M. Olmstead, R. P. Planalp, *Inorg. Chem.* **1993**, *32*, 2600−2603; C. Schnitter, S. D. Waezsada, H. W. Roesky, M. Teichert, I. Uson, E. Parisini, *Organometallics* **1997**, *16*, 1197−1202; C. J. Harlan, S. G. Bott, A. R. Barron, *J. Chem. Soc., Dalton Trans.* **1997**, 637−641; A. A. I. Al-Wassil, P. B. Hitchcock, S. Sarisaban, J. D. Smith, C. L. Wilson, *J. Chem. Soc., Dalton Trans.* **1985**, 1929−1934; K. J. Alford, K. Gosling, J. D. Smith, *J. Chem. Soc., Dalton Trans.* **1972**, 2203−2208; S. Amirkhalili, P. B. Hitchcock, J. D. Smith, *J. Chem. Soc., Dalton Trans.* **1979**, 1206−1212; G. Perego, M. Cesari, G. Del Piero, A. Balducci, E. Cernia, *J. Organomet. Chem.* **1975**, *87*, 33−41; S. Cucinella, T. Salvatori, C. Busetto, M. Cesari, *J. Organomet. Chem.* **1976**, *121*, 137−147; P. B. Hitchcock, G. M. McLaughlin, J. D. Smith, K. M. Thomas, *J. Chem. Soc., Chem. Commun.* **1973**, 934−935; an octameric and higher iminoalanes were postulated: H. Nöth, P. Wolfgardt, *Z. Naturforsch. B Chem. Sci.* **1976**, *31*, 697−708; Review: M. Veith, *Chem. Rev.* **1990**, *90*, 3−16.

[21] R. J. Wehmschulte, P. P. Power, *J. Am. Chem. Soc.* **1997**, *119*, 8387−8388.

[22] *International Tables for Crystallography, Space Group Symmetry* (Ed.: T. Hahn), Kluwer Academic Publishers, Dordrecht-Boston-London, **1989**, vol. A.

[23] *SHELXTL-Plus REL. 4.1*, Siemens Analytical X-RAY Instruments Inc., Madison, USA, **1990**; G. M. Sheldrick *SHELXL-93, Program for the Refinement of Structures*, Universität Göttingen, **1993**.

[24] The crystallographic data of compounds **1** to **5** (excluding structure factors) have been deposited with the Cambridge Crystallographic Data Centre as supplementary publication no. CCDC-116986 (**1**), -116985 (**2**), -116987 (**3**), -116988 (**4**), -116989 (**5**). Copies of the data can be obtained free of charge on application to The Director, CCDC, 12 Union Road, Cambridge CB2 1EZ, UK [fax: (internat.) + 44-(1223)/336033; E-mail: deposit@ccdc.cam.ac.uk].

[25] W. J. Hehre, L. Radom, P. v. R. Schleyer, J. A. Pople, *Ab Initio Molecular Orbital Theory*, Wiley, New York, **1986**.

[26] M. J. Frisch, G. W. Trucks, H. B. Schlegel, P. M. W. Gill, B. G. Johnson, M. A. Robb, J. R. Cheeseman, T. A. Keith, G. A. Petersson, J. A. Montgomery, K. Raghavachari, M. A. Al-Laham, V. G. Zakrzewski, J. V. Ortiz, J. B. Foresman, J. Cioslowski, B. B. Stefanov, A. Nanayakkara, M. Challacombe, C. Y. Peng, P. Y. Ayala, W. Chen, M. W. Wong, J. L. Andres, E. S. Replogle, R. Gomperts, R. L. Martin, D. J. Fox, J. S. Binkley, D. J. DeFrees, J. Baker, J. J. P. Stewart, M. Head-Gordon, C. Gonzalez, J. A. Pople, *Gaussian 94*, Gaussian Inc., Pittsburgh PA, **1995**.

[27] J. P. Foster, F. Weinhold, *J. Am. Chem. Soc.* **1980**, *102*, 7211−7218; A. E. Reed, F. Weinhold, *J. Chem. Phys.* **1983**, *78*, 4066−4073; A. E. Reed, R. B. Weinstock, F. Weinhold, *J. Chem. Phys.* **1985**, *83*, 735−746; A. E. Reed, F. Weinhold, *J. Chem. Phys.* **1985**, *83*, 1736−1740; A. E. Reed, L. A. Curtius, F. Weinhold, *Chem. Rev.* **1988**, *88*, 899−926.

Received April 7, 1999
[I99121]

Photochemical Synthesis and Reactivity of New Chloro-Bridged Complexes with Tungstenocene (η^5-C_5H_5)(η^5-$C_5H_4PPh_2$)WClX (X = H, Cl) and Tetracarbonylmetal (Cr, W) Units

Virginie Comte,[a] Marek M. Kubicki,*[a] and Claude Moïse*[a]

Keywords: Tungsten / Sandwich complexes / Bimetallic compounds / Carbonyl complexes

Chloro-bridged bimetallic complexes (η^5-C_5H_5)[η^5-$C_5H_4PPh_2M'(CO)_4$]W(μ-Cl)X [X = Cl (**3**), X = H (**4**); M′ = Cr, W] were prepared by photochemical irradiation of (η^5-C_5H_5)[η^5-$C_5H_4PPh_2M'(CO)_5$]WClX [X = Cl (**1**), X = H (**2**); M′ = Cr, W]. The reactivity of the chloro-bridged complexes towards Lewis bases was studied; by exposure to CO or phosphanes, a facile cleavage of the chloro bridge accompanied by regio- and stereospecific coordination at M′ occurs. The X-ray structure of complex **3** (M′ = W) is reported.

Introduction

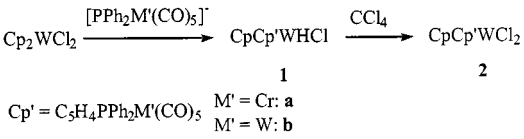
We have recently reported that on treatment of the bent molybdocene and tungstenocene dichlorides with the metallophosphide anions $[PPh_2M'(CO)_x]^-$ (M′ = Cr, Mo, W), nucleophilic S_N2' substitution on one cyclopentadienyl Cp ring occurs.[1] This unexpected reaction offers the possibility of synthesizing various heterobimetallic systems by changing either the metal of the metallophosphide anion (M′) or that of the metallocene dichloride (M = Mo, W). Also in this field, we have observed that compounds with some interesting structures may be obtained by linking the two metallic units by an orthometallation reaction or by the formation of a hydride bridge.[2] The latter μ-H bimetallic cyclic complexes are prepared by UV irradiation of the corresponding terminal dihydrido precursors. They react with CO and phosphanes with concomitant cleavage of the hydride bridge.[3] Our ongoing interest in this area has led us to investigate the behavior of related chloro-hydrido complexes, with emphasis on the nature of the products obtained upon their photolysis. The present paper deals with the tungstenocene derivatives.

Results and Discussion

Chloro-Bridged Complexes

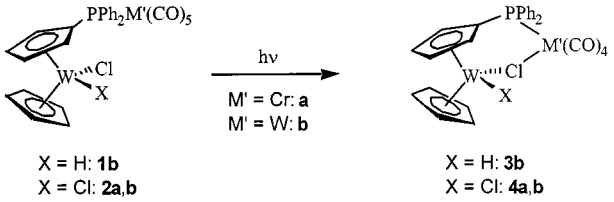
The two starting complexes **1** and **2** (Scheme 1) were prepared as reported previously.[2a] Thus, **1a**,**b** were prepared from Cp_2WCl_2 and $[PPh_2M'(CO)_5]^-$ (M′ = Cr, W) while the corresponding dichloro derivatives **2** were obtained by treatment of **1** with CCl_4.

UV irradiation of **1b** results in the formation of the chloro-bridged complex **3b** (Scheme 2). However, analogous



Scheme 1

treatment of the chromium derivative **1a** does not allow the isolation of defined products.



Scheme 2

Spectroscopic data for the tungsten complex are supportive of the μ-chloro structure **3b**. The CO absorption pattern is typical of an $M'(CO)_4$ fragment (four CO stretching bands), while the ^{1}H-NMR spectrum features a hydride resonance at δ = −12.3 (the signal is found at δ = −10.7 in the precursor **1b**). This suggests that the tungstenocene hydride does not interact with the $W(CO)_4$ fragment and therefore behaves as a terminal ligand. The ^{31}P resonance is shifted downfield with respect to that in **1b** (Δδ = 43 ppm). Such a deshielding may indicate some steric strain on the phosphorus atom due to the formation of the cyclic structure.[4]

Dichlorides **2** may also be transformed to chloro-bridged species by photochemical means (**4**). In contrast to compounds **1**, this reaction works for both M′ = Cr and W. The CO absorption pattern is consistent with an $M'(CO)_4$ chromophore with approximate C_{2v} symmetry. The absorptions are observed at nearly the same frequencies for **3b** and **4b** (mean values are only 5 cm^{-1} lower for **3b** than for **4b**), indicating that the substitution of the terminal H by Cl has little or no effect on the electron density within the $W(CO)_4$ fragment. It is worth noting that ν̃(CO) frequencies re-

[a] Laboratoire de Synthèse et d'Electrosynthèse Organométalliques, UMR CNRS 5632, Université de Bourgogne,
6, Boulevard Gabriel, F-21000 Dijon, France
Fax: (internat.) + 33-3/80396076
E-mail: marek.kubicki@u-bourgogne.fr
claude.moise@u-bourgogne.fr

 © WILEY-VCH Verlag GmbH, D-69451 Weinheim, 1999 1434−1948/99/1111−2029 $ 17.50+.50/0

corded for our (P)(Cl)W(CO)$_4$ units are lower than those reported for diphosphane derivatives (P)$_2$W(CO)$_4$.[5] In particular, the lowest energy B_2 band (assuming C_{2v} symmetry) is shifted by 40−50 cm^{-1}. This indicates that the chloride bridge behaves as a weaker π-acceptor than the phosphane ligand. Note, however, that the values observed for **3b** and **4b** are close to those reported for dibridged complexes Cp$_2$M(μ-PPh$_2$,H)M′(CO)$_4$ (MPPh$_2$ instead of a CpPPh$_2$ bridge),[6] but are higher than those reported for a trinuclear complex with mono-bridged bimetallic units [Cp$_2$MoH(μ-PMe$_2$)]$_2$W(CO)$_4$ (1976, 1901, 1859, and 1811 cm^{-1})[7] or for an electron-rich anion [W(CO)$_4$(PPh*i*Pr$_2$)Cl]$^-$ (1997, 1869, 1857, and 1812 cm^{-1}).[8] ^{31}P resonances for **4a** and **4b** are shifted to lower fields with respect to those of the parent compounds (Δδ = 30 ppm, M′ = Cr; Δδ = 48 ppm, M′ = W). Once again, the observed deshieldings can be attributed to steric strain on the phosphorus atom.

In order to unambiguously establish that complex **3b** contains a chloride bridge, its molecular structure was determined by X-ray diffraction analysis. Suitable crystals for this study were grown from acetone solution. The crystal structure of **3b** is built up by dinuclear organometallic molecules, in which each metal center retains its typical pseudo-tetrahedral (W2) and pseudo-octahedral (W1) geometry (Figure 1). The two metallic fragments are linked through C$_5$H$_4$PPh$_2$ and Cl bridges without direct metal−metal interaction, thus forming a formally five-membered ring. The W1−W2 separation amounts to 4.2611(8) Å (Table 1). Such a separation roughly corresponds to the metal−metal distances observed in mono-bridged one-atom μ-phosphido complexes, e.g. 4.39 Å in Cp$_2$MoH(μ-PPh$_2$)Mn(CO)$_2$Cp[9] and 4.56 Å in [Cp$_2$MoH(μ-PMe$_2$)]$_2$W(CO)$_4$,[7] but is ca. 1 Å longer than the W−W distance (3.27 Å) reported for a dibridged Cp$_2$W(μ-PPh$_2$,μ-H)W(CO)$_4$ complex containing a four-membered central ring.[6] The longest metal−metal distance (4.78 Å) in complexes with a metallocene fragment has been reported for the dibridged compound Cp$_2$Nb(μ-PPh$_2$,dmpm)Mo(CO)$_4$, which has a six-membered central ring.[10] Consequently, the size of the central bridging ring determines the metal−metal distance for complexes without a metal−metal bond.

The refined terminal hydride is found at a typical distance of 1.8(1) Å from the W2 atom. The W1−P bond length of 2.527(3) Å is of little diagnostic value as the W−P distances in W(CO)$_4$P fragments fall in a rather large range from 2.49 to 2.60 Å.[11] The most similar W−P distances are found in the pentacarbonyl compounds W(CO)$_5$PMe$_3$ (2.52 Å)[12] and W(CO)$_5$PPh$_3$ (2.54 Å),[13] the tetracarbonyl compound [W(CO)$_4$PEt$_3$]$_2$(μ-NCC$_6$H$_4$CN) (2.53 Å),[14] as well as in the tetracarbonyl anions [W(CO)$_4$(PR$_3$)X]$^-$ (X = Cl, OAc, OPh and Me) where the W−P bond lengths are close to 2.53−2.54 Å.[15] It can be noted (Table 1) that the W1^0−Cl bond [2.593(3) Å] is longer than the W2^{IV}−Cl one [2.484(3) Å], a difference which is a priori due to the different covalent radii of W^0 and W^{IV}. The tungstenocene−chloride bond length is close to that reported for Cp$_2$MoCl$_2$ (2.47 Å),[16] but is larger than the values reported for the terminal M−Cl bonds in the related [CpPPh$_2$Cr(CO)$_5$]$_2$W(H)Cl [structural model Cp$_2$W(H)Cl, W−Cl = 2.408(4) Å][3] and in *ortho*-metallated Cp[CpPPh$_2$Cr(CO)$_5$]Mo(Cl) [structural model Cp$_2$Mo(C)Cl, Mo−Cl = 2.476(2) Å].[2c] Thus, the W2−Cl bond in **3b** may be considered as remaining strong with little perturbation resulting from coordination to the second W1 atom. Consequently, the W1−Cl bond [2.593(3) Å] has to be regarded as being rather long and weak. A search of the Cambridge Structural Database for W(CO)$_4$Cl structures yielded only 8 entries. The structures of (CO)$_4$W(μ-Cl)$_3$W(CO)$_3$SnCl$_3$ (heptacoordinated W, bridging chlorides) (W−Cl = 2.52 Å, W−Cl−W = 89°)[17] and Cl(CO)$_4$WC(C$_6$H$_5$)Cr(CO)$_3$ (W−Cl = 2.48 Å),[18] as well as those of the anionic species [W(CO)$_5$Cl]$^-$ (W−Cl = 2.56 Å)[19] and [W(CO)$_4$(PMePh$_2$)Cl]$^-$ (W−Cl = 2.58 Å)[15a] are indicative of a weak W1−Cl bond.

Table 1. Selected bond lengths [Å] and angles [°] for **3b**

	Bond length [Å]		Bond angle [°]
W(1)−W(2)	4.2611(8)	CP1−W(2)−CP2[a]	143.5
W(2)−Cl	2.484(3)	H−W(2)−Cl	79(5)
W(2)−H	1.78(15)	W(2)−Cl−W(1)	114.1(1)
W(2)−CP1	1.942	C(1)−W(1)−C(2)	87.2(6)
W(2)−CP2	1.950	C(1)−W(1)−C(4)	88.0(7)
W(1)−P	2.527(3)	C(2)−W(1)−C(4)	88.4(5)
W(1)−Cl	2.593(3)	C(1)−W(1)−C(3)	90.3(5)
W(1)−C(1)	1.919(13)	C(2)−W(1)−C(3)	87.7(5)
W(1)−C(2)	1.983(13)	C(4)−W(1)−C(3)	175.9(5)
W(1)−C(3)	2.036(12)	C(1)−W(1)−P	96.5(4)
W(1)−C(4)	2.004(14)	C(2)−W(1)−P	174.1(4)
P−C(5)	1.793(11)	C(4)−W(1)−P	96.3(4)
P−C(21)	1.832(10)	C(3)−W(1)−P	87.6(3)
P−C(15)	1.846(10)	C(1)−W(1)−Cl	176.2(4)
C(1)−O(1)	1.16(2)	C(2)−W(1)−Cl	89.0(4)
C(2)−O(2)	1.14(2)	C(4)−W(1)−Cl	92.4(5)
C(3)−O(3)	1.135(14)	C(3)−W(1)−Cl	89.0(3)
C(4)−O(4)	1.15(2)	P−W(1)−Cl	87.17(9)

[a] CP1 and CP2 are the centroïds of the C(5)−C(9) and C(10)−C(14) rings.

Reactions of Bridged Complexes with CO and Phosphanes

We have examined the reactivity of the two kinds of chloro-bridged compounds **3** and **4** towards CO and phosphanes, and, for a comparative study, we also carried out similar experiments with the previously reported μ-hydrido complex **5**.[2a] Addition of Lewis bases is regiospecific and occurs in all cases at the M′ metal center. Bubbling of CO through a THF solution of **3b**, **4b** or **5b** leads to the recovery of their precursors **1b**, **2b** and **6b** in high yields (Scheme 3).

Reactions of phosphanes with the chloro derivatives **3b** and **4b** proceed rapidly. With PMe$_3$ and PPhH, only the *cis* isomer is formed, whereas a *cis*/*trans* mixture (ratio 30:70) is obtained when the bulkier triphenylphosphane is used. Thus, the stereochemical course of the ring-opening reaction depends on steric hindrance to the incoming ligands (the cone angles for PMe$_3$, PPh$_2$H and PPh$_3$ are 118°, 126°

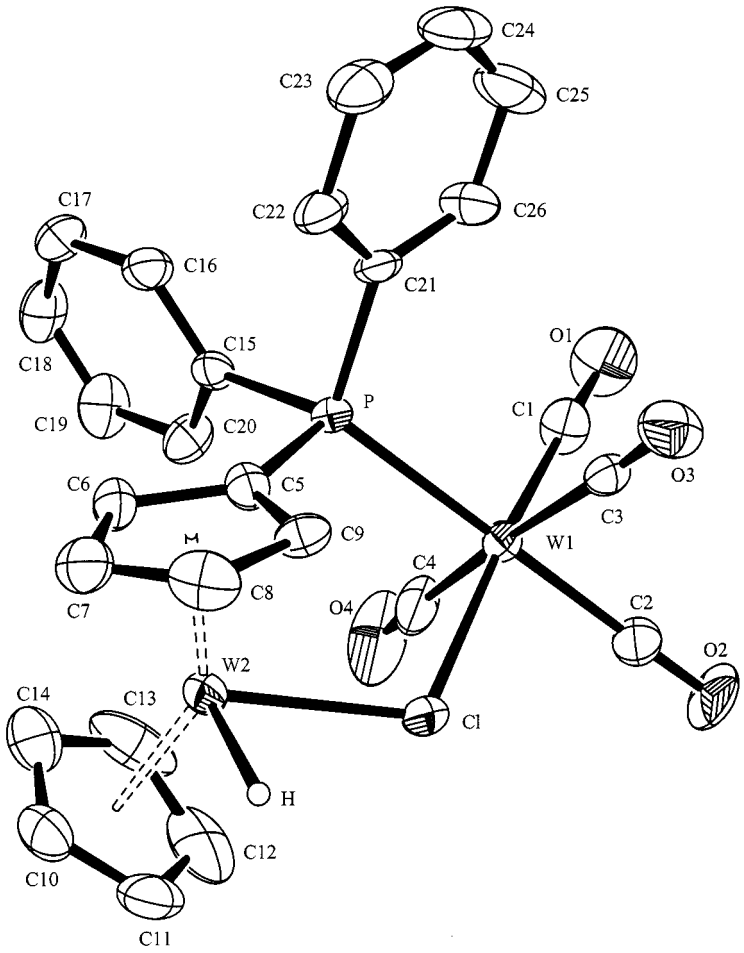
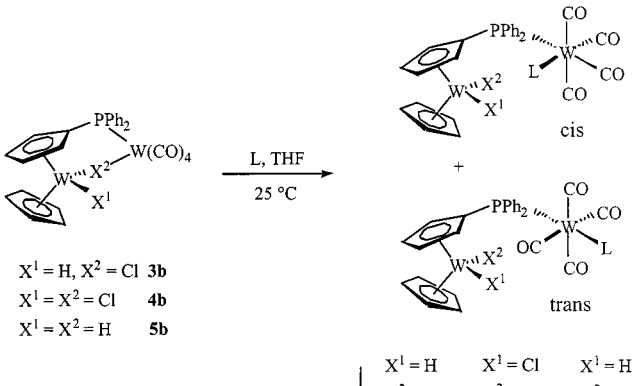


Figure 1. ORTEP view of **3b** (30% probability level)



$X^1 = H, X^2 = Cl$ **3b**
$X^1 = X^2 = Cl$ **4b**
$X^1 = X^2 = H$ **5b**

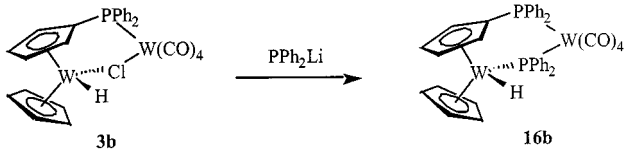
	$X^1 = H$ $X^2 = Cl$	$X^1 = Cl$ $X^2 = Cl$	$X^1 = H$ $X^2 = H$
CO	**1b**	**2b**	**6b**
PMe_3	**7b**	**10b**	**13b**
PPh_2H	**8b**	**11b**	**14b**
PPh_3	**9b**	**12b**	**15b**

Scheme 3

and 145°, respectively).[20] Moreover, the size of the M′ metal ion also seems to play a crucial role in determining the coordination site. The tungsten derivative **3b** furnishes exclusively the *cis* isomer when treated with PMe_3, whereas we have mentioned in a previous paper[3] that its chromium analogue **5a** gives a mixture of *trans* and *cis* isomers in an 80:20 ratio. We have also observed that a longer reaction time or heating is needed in order to achieve cleavage of the hydride bridge in **5b**. The more severe conditions required indicate a greater stability of the M−H−M′ linkage (stronger H−M′ bond) in the μ-H bridged compound **5b** compared to the M−Cl−M′ linkage (weaker Cl−M′ bond). The rather long W1−Cl bond found for **3b** (vide supra) supports this idea. The kinetic nature of the *cis* stereoisomer[21] is confirmed by the isomerization that occurs upon prolonged standing in solution. Thus, the *cis* complex **7b** gives a 70:30 *trans*/*cis* mixture, for example, after 4 h in THF solution. The *cis* and *trans* assignments were made on the basis of IR and ^{31}P-NMR data. Thus, the presence of one or four CO absorptions characterizes a *trans* (D_{4h}) or a *cis* (C_{2v}) arrangement about the M′ metal center. In ^{31}P-NMR spectroscopy, both the chemical shifts and the *J* values are indicative of the mutual position of the two phosphane ligands. A *cis* configuration results in a more shielded resonance of the bridging phosphido group, together with the observation of a smaller $^2J_{pp}$ value (*cis* $^2J_{pp} = 20$ Hz vs. *trans* $^2J_{pp} = 50$ Hz).[22]

Reactions of μ-Chloro Complexes with PPh_2^-

We envisaged that the bridge-opening reaction described above might allow a chloride substitution reaction by treating the μ-chloro complexes with the anionic species $[PPh_2]^-$. The reaction did not proceed starting from the dichloro compound **4b**, but proceeded as expected from the monochloride monohydride **3b** affording the diphosphido complex **16b** together with a small amount of **8b**. Chromatographic purification led to the isolation of **16b** in pure form (Scheme 4).



3b 16b

Scheme 4

The hydride resonance for **16b** is seen as a double doublet ($^2J_{PH}$ = 18.5 Hz and $^4J_{PH}$ = 5 Hz) at δ = −10.3, while the ^{31}P-NMR spectrum displays two well-defined doublets ($^2J_{PP}$ = 20 Hz) located at δ = 38.5 and −27.2, respectively. The *J* value is indicative of the *cis* configuration (vide supra) and the shielded resonance corresponds to the nucleus of a W−P−W phosphido bridge.

We have already discussed the dependence of the ^{31}P chemical shifts in phosphido-bridged bimetallic systems on the M−P−M′ angle.[6] The chemical shift observed for **16b** can be compared with those of related phosphido-bridged complexes, in particular with those displayed by mono-bridged M(μ-P)M′ and by dibridged M(μ-P, μ-H)M′ and M(μ-P, μ-Cl)M′ structures.[23] The former are structures with relatively open M−P−M′ angles (about 125°) and the ^{31}P resonance signals lie at high field in the range δ = −60 to −65 for tungsten compounds. The latter contain a bimetallic cyclic framework with a small M−P−M′ angle value (about 80°), which results in a ^{31}P resonance deshielding by more than 100 ppm.[24] In the complex **16b**, the W−P−W linkage forms part of a pseudo five-membered ring with relatively little angle strain, which accounts for the smaller deshielding compared to those seen in four-membered M(μ-P, μ-H)M′ or M(μ-P, μ-Cl)M′ cyclic frameworks.

Conclusion

In conclusion, chloro-bridged bimetallic complexes **3** and **4** have been synthesized by photochemical irradiation. It is interesting to note that the reaction proceeds equally well when dichloro compound **1** or monochloro-monohydrido compound **2** are used. We have also shown that the chloro bridges are cleaved in a regio- and stereospecific manner when the μ-chloro complexes are exposed to two-electron donor ligands.

Experimental Section

General Comments: All reactions were carried out under purified argon. The solvents and eluents were dried by appropriate procedures and distilled under argon from sodium/benzophenone immediately prior to use. Standard Schlenk techniques and conventional glass vessels were employed. − Column chromatography was performed under argon on silica gel (70−230 mesh). − Elemental analyses were carried out with a Fisons Instruments EA 1108 CHNS-O apparatus. − Electron ionization mass spectra were recorded with a Kratos Concept 32S spectrometer. − ^{1}H- and ^{31}P-NMR spectra were recorded with a Bruker AC 200 spectrometer. Chemical shifts are quoted relative to internal TMS (^{1}H) or external H_3PO_4 (^{31}P). − IR spectra were recorded with a Nicolet 205 FT-IR spectrometer. − The complexes (η^5-C_5H_5)[η^5-C_5H_4-$PPh_2M'(CO)_5$]W(H)(Cl) (**1**), (η^5-C_5H_5)[η^5-C_5H_4-$PPh_2M'(CO)_5$]-WCl_2 (**2**), and (η^5-C_5H_5)[η^5-C_5H_4-$PPh_2M'(CO)_4$]W(H)(μ-H) (**5**) (M′ = Cr, W) were prepared according to literature procedures;[2a,3] PMe_3 and PPh_3 (Strem) were used as received. PPh_2H was prepared according to a literature method[25] and PPh_2Li was prepared from PPh_2H and butyllithium.

(η^5-C_5H_5)[η^5-C_5H_4−$PPh_2W(CO)_4$]W(H)(μ-Cl) (3b): A solution of (η^5-C_5H_5)[η^5-C_5H_4−$PPh_2W(CO)_5$]W(H)(Cl) (**1b**) (1.7 g, 2 mmol) in THF (100 mL) was irradiated with a Hanau TQ 150 lamp for 2 h at room temperature. The solvent was then removed in vacuo, and the residue was washed with 40 mL of pentane and chromatographed (toluene/THF, 1:1). **3b** was obtained as red crystals by recrystallization from acetone; yield 1.0 g (60%). − IR (THF): $\tilde{\nu}_{CO}$ = 2013 (m), 1901 (s), 1882 (s), 1844 (s) cm^{-1}. − ^{1}H NMR ($CDCl_3$): δ = −12.35 (br., 1 H, W−H), 4.28 (m, 1 H, C_5H_4), 4.38 (m, 1 H, C_5H_4), 4.61 (m, 1 H, C_5H_4), 4.90 (s, 5 H, C_5H_5), 6.42 (m, 1 H, C_5H_4), 7.39−7.50 (m, 6 H, C_6H_5), 7.71−7.92 (m, 4 H, C_6H_5). − ^{31}P{^{1}H} NMR ($CDCl_3$): δ = 55.5 (br.). − $C_{26}H_{20}ClO_4PW_2$ (830.6): calcd. C 37.60, H 2.43; found C 37.33, H 2.29.

(η^5-C_5H_5)[η^5-C_5H_4−$PPh_2M'(CO)_4$]W(Cl)(μ-Cl) (4): Complexes **4a** and **4b** were obtained according to the same procedure as described above for **3b**, except that (η^5-C_5H_5)[η^5-C_5H_4−$PPh_2M'(CO)_5$]WCl_2 **2** (0.5 mmol) was used. The crude product was chromatographed on silanized silica (chloroform) to afford **4a** (220 mg, 60%) and **4b** (215 mg, 50%) as green crystals after recrystallization from chloroform. − (η^5-C_5H_5)[η^5-C_5H_4−$PPh_2Cr(CO)_4$]W(Cl)(μ-Cl) (4a): IR (THF): ($\tilde{\nu}_{CO}$ = 2011 (m), 1913 (s), 1888 (s), 1854 (s) cm^{-1}. − ^{1}H NMR ($CDCl_3$): δ = 4.07 (m, 1 H, C_5H_4), 5.45 (s, 5 H, C_5H_5), 5.51 (m, 2 H, C_5H_4), 6.61 (m, 1 H, C_5H_4), 7.35−7.50 (m, 6 H, C_6H_5), 7.56−7.88 (m, 4 H, C_6H_5). − ^{31}P{^{1}H} NMR ($CDCl_3$): δ = 82 (s). − $C_{26}H_{19}Cl_2CrO_4PW$ (733.2): calcd. C 42.59, H 2.61; found C 42.14, H 2.73. − (η^5-C_5H_5)[η^5-C_5H_4−$PPh_2W(CO)_4$]W(Cl)(μ-Cl) (4b): IR (THF): $\tilde{\nu}_{CO}$ = 2015 (m), 1909 (s), 1885 (s), 1849 (s) cm^{-1}. − ^{1}H NMR ($CDCl_3$): δ = 3.99 (m, 1 H, C_5H_4), 5.43 (s, 5 H, C_5H_5), 5.51 (m, 1 H, C_5H_4), 5.87 (m, 1 H, C_5H_4), 6.63 (m, 1 H, C_5H_4), 7.41−7.64 (m, 6 H, C_6H_5), 7.70−7.88 (m, 4 H, C_6H_5). − ^{31}P{^{1}H} NMR ($CDCl_3$): δ = 62.08 (s + d, J_{WP} = 262 Hz). − $C_{26}H_{19}Cl_2O_4PW_2$ (865.02): calcd. C 36.10, H 2.21; found C 36.01, H 2.22.

Synthesis of (η^5-C_5H_5)[η^5-C_5H_4−$PPh_2W(CO)_5$]W(X^1)(X^2) (X^1 = H, X^2 = H, Cl; X^1 = X^2 = Cl): At 50°C, 0.5 mmol of (η^5-C_5H_5)[η^5-C_5H_4−$PPh_2W(CO)_4$]W(X^1)(μ-X^2) (**3b**, **4b** or **5b**) was stirred in THF (20 mL) under carbon monoxide for 2 h. The solvent was then removed under reduced pressure, and the mono-bridged complex (η^5-C_5H_5)[η^5-C_5H_4−$PPh_2W(CO)_5$]W(X_1)(X_2) (**1b**, **2b** or **6b**)[2a] was isolated.

Synthesis of (η^5-C_5H_5)[η^5-C_5H_4−$PPh_2W(CO)_4$(L)]W(H)(Cl) (L = PMe_3, PPh_2H, PPh_3): To a solution of **3b** (200 mg, 0.25 mmol) in THF (20 mL) was added 1 equiv. of the appropriate phosphane and the resulting mixture was stirred at room temperature for 2 h. The solvent was then removed, and the crude product was washed

with pentane (3 × 20 mL). All attempts to recrystallize the complexes resulted in their decomposition.

(η^5-C_5H_5)[η^5-C_5H_4−$PPh_2W(CO)_4(PMe_3)$]W(H)(Cl) (7b): The reaction afforded purely the *cis* isomer **7b**, which was obtained as an orange powder in 60% yield (140 mg). After redissolution of this product in THF and stirring at room temperature, small amounts of the *trans* isomer could be detected. − ***cis* Isomer 7b:** IR (THF): $\tilde{\nu}_{CO}$ = 2013 (m), 1906 (s), 1892 (s), 1872 (s) cm^{-1}. − ^1H NMR ($CDCl_3$): δ = −10.68 (s + d, $^1J_{WH}$ = 60 Hz, 1 H, W−H), 1.16 (d, $^2J_{PH}$ = 7.4 Hz, 9 H, Me), 4.19 (m, 1 H, C_5H_4), 4.58 (m, 1 H, C_5H_4), 4.79 (s, 5 H, C_5H_5), 5.09 (m, 1 H, C_5H_4), 5.75 (m, 1 H, C_5H_4), 7.29−7.43 (m, 6 H, C_6H_5), 7.53−7.62 (m, 4 H, C_6H_5). − $^{31}P\{^1H\}$ NMR ($CDCl_3$): δ = −41.9 (d + dd, $^2J_{PP}$ = 20 Hz, $^1J_{WP}$ = 216 Hz, PMe_3), 16.30 (d + dd, $^2J_{PP}$ = 20 Hz, $^1J_{WP}$ = 246 Hz, PPh_2). − $C_{29}H_{29}ClO_4P_2W_2$ (906.65): calcd. C 38.42, H 3.22; found C 38.86, H 3.60. − ***trans* Isomer 7b:** IR (THF): $\tilde{\nu}_{CO}$ = 1882 (s) cm^{-1}. − ^1H NMR ($CDCl_3$): δ = −10.66 (s + d, $^1J_{WH}$ = 60 Hz, 1 H, W−H), 1.27 (d, $^2J_{PH}$ = 7.4 Hz, 9 H, PMe), 3.25 (m, 1 H, C_5H_4), 4.15 (m, 1 H, C_5H_4), 4.72 (s, 5 H, C_5H_5), 5.19 (m, 1 H, C_5H_4), 6.03 (m, 1 H, C_5H_4), 7.20−7.60 (m, 10 H, C_6H_5). − $^{31}P\{^1H\}$ NMR ($CDCl_3$): δ = −34.1 (d + dd, $^2J_{PP}$ = 50 Hz, $^1J_{WP}$ masked, PMe_3), 16.30 (d + dd, $^2J_{PP}$ = 50 Hz, $^1J_{WP}$ masked, PPh_2).

(η^5-C_5H_5)[η^5-C_5H_4−$PPh_2W(CO)_4(PPh_2H)$]W(H)(Cl) (8b): The *cis* isomer **8b** was obtained as an orange powder in 50% yield (125 mg). When this product was redissolved in THF and stirred at room temperature, decomposition occurred. − IR (THF): $\tilde{\nu}_{CO}$ = 2019 (m), 1918 (s), 1904 (s), 1882 (s) cm^{-1}. − ^1H NMR ($CDCl_3$): δ = −10.75 (s + d, $^1J_{WH}$ = 59 Hz, 1 H, W−H), 4.26 (m, 1 H, C_5H_4), 4.55 (m, 1 H, C_5H_4), 4.77 (s, 5 H, C_5H_5), 5.05 (m, 1 H, C_5H_4), 5.58 (m, 1 H, C_5H_4), 5.49 (dd, $^3J_{PH}$ = 7.4 Hz, $^1J_{PH}$ = 327 Hz, 1 H, P−H), 7.26−7.57 (m, 20 H, C_6H_5). − ^{31}P NMR ($CDCl_3$): δ = 0.75 (d, $^1J_{PH}$ = 326 Hz, $^1J_{WP}$ = 261 Hz, $^2J_{PP}$ masked, PPhH). − $^{31}P\{^1H\}$ NMR ($CDCl_3$): δ = 16.30 (d + dd, $^2J_{PP}$ = 15 Hz, $^1J_{WP}$ = 241 Hz, PPh_2). − MS; *m/z*: 1016 [M^+].

(η^5-C_5H_5)[η^5-C_5H_4−$PPh_2W(CO)_4(PPh_3)$]W(H)(Cl) (9b): The NMR spectra of the product indicated the presence of the *cis* and *trans* isomers in a 30:70 ratio; yield 160 mg (60%). − ***cis*/*trans* Mixture:** IR (THF): $\tilde{\nu}_{CO}$ = 2014 (m), 1913 (s), 1895 (s), 1890 (s), 1869 (s) cm^{-1}. − $C_{44}H_{35}ClO_4P_2W_2$ (1092.87): calcd. C 48.36, H 3.23; found C 48.80, H 3.58. − ***cis* Isomer 9b:** ^1H NMR ($CDCl_3$): δ = −10.97 (s + d, $^1J_{WH}$ = 60 Hz, 1 H, W−H), 4.19 (m, 1 H, C_5H_4), 4.22 (m, 1 H, C_5H_4), 4.61 (s, 5 H, C_5H_5), 4.98 (m, 1 H, C_5H_4), 5.5 (m, 1 H, C_5H_4), 7.19−7.61 (m, 25 H, C_6H_5). − $^{31}P\{^1H\}$ NMR ($CDCl_3$): δ = 13.7 (d + dd, $^2J_{PP}$ = 25 Hz, $^1J_{WP}$ = 236 Hz, PPh_3), 19.9 (d + dd, $^2J_{PP}$ = 25 Hz, $^1J_{WP}$ masked, PPh_2). − ***trans* Isomer 9b:** ^1H NMR ($CDCl_3$): δ = −10.67 (s + d, $^1J_{WH}$ = 61 Hz, 1 H, W−H), 4.43 (m, 1 H, C_5H_4), 4.60 (m, 1 H, C_5H_4), 4.69 (s, 5 H, C_5H_5), 5.03 (m, 1 H, C_5H_4), 5.86 (m, 1 H, C_5H_4), 7.19−7.61 (m, 25 H, C_6H_5). − $^{31}P\{^1H\}$ NMR ($CDCl_3$): δ = 19.20 (d + dd, $^2J_{PP}$ = 60 Hz, $^1J_{WP}$ = 291 Hz, PPh_3), 24.5 (d + dd, $^2J_{PP}$ = 60 Hz, $^1J_{WP}$ = 271 Hz, PPh_2).

Synthesis of (η^5-C_5H_5)[η^5-C_5H_4−$PPh_2W(CO)_4$(L)]WCl_2 (L = PMe_3, PPh_2H, PPh_3): "Open" structures could be isolated using the same procedure as above. All attempts to recrystallize the complexes resulted in their decomposition.

(η^5-C_5H_5)[η^5-C_5H_4−$PPh_2W(CO)_4(PMe_3)$]WCl_2 (10b): The *cis* isomer **10b** was obtained in 60% yield as a grey powder (140 mg). When this product was redissolved in THF and stirred at room temperature, decomposition occurred. − IR (THF): $\tilde{\nu}_{CO}$ = 2013 (m), 1911 (s), 1892 (s), 1876 (s) cm^{-1}. − ^1H NMR ($CDCl_3$): δ = 1.16 (d, $^2J_{PH}$ = 7.4 Hz, 9 H, PMe), 5.12 (m, 2 H, C_5H_4), 5.20 (s, 5 H, C_5H_5), 6.02 (m, 2 H, C_5H_4), 7.39−7.47 (m, 6 H, C_6H_5), 7.59−7.69 (m, 4 H, C_6H_5). − $^{31}P\{^1H\}$ NMR ($CDCl_3$): δ = −41.7 (d + dd, $^2J_{PP}$ = 20 Hz, $^1J_{WP}$ masked, PMe_3), 18.7 (d + dd, $^2J_{PP}$ = 20 Hz, $^1J_{WP}$ masked, PPh_2). − MS; *m/z*: 940 [M^+]. − $C_{29}H_{28}Cl_2O_4P_2W_2$ (941.09): calcd. C 37.01, H 3.00; found C 37.45, H 3.09.

(η^5-C_5H_5)[η^5-C_5H_4−$PPh_2W(CO)_4(PPh_2H)$]WCl_2 (11b): The reaction afforded purely the *cis* isomer **11b**, which was obtained as a grey powder in 60% yield (160 mg). When this product was redissolved in THF and stirred at room temperature, decomposition occurred. − IR (THF): $\tilde{\nu}_{CO}$ = 2020 (m), 1920 (s), 1905 (s), 1884 (s) cm^{-1}. − ^1H NMR ($CDCl_3$): δ = 5.08 (m, 2 H, C_5H_4), 5.20 (s, 5 H, C_5H_5), 5.99 (m, 2 H, C_5H_4), 5.38 (dd, $^4J_{PH}$ = 6.6 Hz, $^1J_{PH}$ = 338 Hz, 1 H, P−H), 7.29−7.55 (m, 20 H, C_6H_5). − ^{31}P NMR ($CDCl_3$): δ = 0.44 (d + dd, $^2J_{PP}$ masked, $^1J_{PH}$ = 338 Hz, $^1J_{WP}$ = 256 Hz, PPhH). − $^{31}P\{^1H\}$ NMR ($CDCl_3$): δ = 18.90 (d + dd, $^2J_{PP}$ = 20 Hz, $^1J_{WP}$ = 230 Hz, PPh_2). − MS; *m/z*: 1050 [M^+]. − $C_{38}H_{30}Cl_2O_4P_2W_2$ (1051.21): calcd. C 43.42, H 2.88; found C 44.85, H 3.16.

(η^5-C_5H_5)[η^5-C_5H_4−$PPh_2W(CO)_4(PPh_3)$]WCl_2 (12b): The NMR spectra of the product indicated the presence of the *cis* and *trans* isomers of **12b** in a 70:30 ratio; yield 200 mg (70%). − ***cis*/*trans* Mixture:** IR (THF): $\tilde{\nu}_{CO}$ = 2015 (m), 1907 (s), 1890 (s), 1885 (s), 1850 (s) cm^{-1}. − $C_{44}H_{34}Cl_2O_4P_2W_2$ (1127.31): calcd. C 46.88, H 3.04; found C 47.14, H 3.56. − ***cis* Isomer 12b:** ^1H NMR ($CDCl_3$): δ = 4.81 (m, 2 H, C_5H_4), 4.95 (s, 5 H, C_5H_5), 5.88 (m, 2 H, C_5H_4), 7.28−7.60 (m, 25 H, C_6H_5). − $^{31}P\{^1H\}$ NMR ($CDCl_3$): δ = 17.42 (d + dd, $^2J_{PP}$ = 20 Hz, $^1J_{WP}$ = 236 Hz, PPh_3), 20.5 (d + dd, $^2J_{PP}$ = 20 Hz, $^1J_{WP}$ masked, PPh_2). − ***trans* Isomer 12b:** ^1H NMR ($CDCl_3$): δ = 5.08 (s, 5 H, C_5H_5), 5.28 (m, 2 H, C_5H_4), 5.58 (m, 2 H, C_5H_4), 7.30−7.61 (m, 25 H, C_6H_5). − $^{31}P\{^1H\}$ NMR ($CDCl_3$): δ = 21.0 (d + dd, $^2J_{PP}$ = 60 Hz, $^1J_{WP}$ masked, PPh_3), 24.4 (d + dd, $^2J_{PP}$ = 60 Hz, $^1J_{WP}$ masked, PPh_2).

Synthesis of (η^5-C_5H_5)[η^5-C_5H_4−$PPh_2W(CO)_4$(L)]WH_2 (L = PMe_3, PPhH, PPh_3): These complexes were isolated following the same procedure as above. All attempts to recrystallize the complexes resulted in their decomposition.

(η^5-C_5H_5)[η^5-C_5H_4−$PPh_2W(CO)_4$(PMe_3)]WH_2 (13b): The *cis* isomer **13b** was obtained in 60% yield as an orange powder (200 mg). − IR (THF): $\tilde{\nu}_{CO}$ = 2010 (m), 1904 (s), 1889 (s), 1870 (s) cm^{-1}. − ^1H NMR ($CDCl_3$): δ = −12.18 (s + d, $^1J_{WH}$ = 71 Hz, 2 H, W−H), 1.12 (d, $^2J_{PH}$ = 7.4 Hz, 9 H, Me), 4.09 (m, 2 H, C_5H_4), 4.44 (s, 5 H, C_5H_5), 5.00 (m, 2 H, C_5H_4), 7.24−7.41 (m, 6 H, C_6H_5), 7.48−7.58 (m, 4 H, C_6H_5). − $^{31}P\{^1H\}$ NMR ($CDCl_3$): δ = −41.7 (d + dd, $^2J_{PP}$ = 20 Hz, $^1J_{WP}$ = 220 Hz, PMe_3), 14.9 (d + dd, $^2J_{PP}$ = 20 Hz, $^1J_{WP}$ = 241 Hz, PPh_2). − MS; *m/z*: 872 [M^+]. − $C_{29}H_{30}O_4P_2W_2$ (872.2): calcd. C 39.94, H 3.47; found C 40.60, H 3.58.

(η^5-C_5H_5)[η^5-C_5H_4−$PPh_2W(CO)_4(PPh_2H)$]WH_2 (14b): After stirring for 24 h, the pure *cis* isomer **14b** was obtained as an orange powder; yield 160 mg (40%). When this product was redissolved in THF and stirred at room temperature, decomposition occurred. −IR (THF): $\tilde{\nu}_{CO}$ = 2017 (m), 1914 (s), 1902 (s), 1877 (s) cm^{-1}. − ^1H NMR ($CDCl_3$): δ = −12.16 (s + d, $^1J_{WH}$ = 73 Hz, 2 H, W−H), 4.10 (m, 2 H, C_5H_4), 4.39 (s, 5 H, C_5H_5), 4.97 (m, 2 H, C_5H_4), 5.48 (dd, $^3J_{PH}$ = 6.6 Hz, $^1J_{PH}$ = 336 Hz, 1 H, P−H), 7.26−7.74 (m, 20 H, C_6H_5). − ^{31}P NMR ($CDCl_3$): δ = 1.44 (d, $^1J_{PH}$ = 336 Hz, $^1J_{WP}$ = 256 Hz, $^2J_{PP}$ masked, PPhH). − $^{31}P\{^1H\}$ NMR ($CDCl_3$): δ = 15.4 (d + dd, $^2J_{PP}$ = 15 Hz, $^1J_{WP}$ = 236 Hz, PPh_2). − MS (*m/z*): 982 [M^+]. − $C_{38}H_{32}O_4P_2W_2$ (982.32): calcd. C 46.46, H 3.28; found C 47.95, H 3.96.

(η^5-C_5H_5)[η^5-C_5H_4−$PPh_2W(CO)_4(PPh_3)$]WH_2 (15b): A mixture of the *cis* and *trans* isomers of **15b** (*cis*/*trans* = 30:70) was obtained after stirring for 48 h at 50°C. The isomers were invariably obtained accompanied by small amounts of the μ-hydrido complex **6b**. − ***cis*/*trans* Mixture:** IR (THF): $\tilde{\nu}_{CO}$ = 2017 (m), 1914 (s), 1889 (s), 1845 (s) cm^{-1}. − ***cis* Isomer 15b:** ^1H NMR ($CDCl_3$): δ = −12.29 (s + d, $^1J_{WH}$ = 71 Hz, 2 H, W−H), 4.03 (m, 2 H, C_5H_4), 4.39 (s, 5 H, C_5H_5), 4.96 (m, 2 H, C_5H_4), 7.26−7.82 (m, 25 H, C_6H_5). − $^{31}P\{^1H\}$ NMR ($CDCl_3$): δ = 12.15 (d + dd, $^2J_{PP}$ = 25 Hz, $^1J_{WP}$ masked, PPh_3), 20.10 (d + dd, $^2J_{PP}$ = 25 Hz, $^1J_{WP}$ masked, PPh_2). − ***trans* Isomer 15b:** ^1H NMR ($CDCl_3$): δ = −12.19 (s + d, $^1J_{WH}$ = 72 Hz, 2 H, W−H), 4.24 (m, 2 H, C_5H_4), 4.32 (s, 5 H, C_5H_5), 5.00 (m, 2 H, C_5H_4), 7.25−7.82 (m, 25 H, C_6H_5). − $^{31}P\{^1H\}$ NMR ($CDCl_3$): δ = 18.70 (d + dd, $^2J_{PP}$ = 60 Hz, $^1J_{WP}$ masked, PPh_3), 25.10 (d + dd, $^2J_{PP}$ = 60 Hz, $^1J_{WP}$ masked, PPh_2).

Synthesis of (η^5-C_5H_5)[η^5-C_5H_4−$PPh_2W(CO)_4$]W(H)(μ−PPh_2) (16b): A solution of PPh_2Li (100 mg, 0.5 mmol) in THF (5 mL) was added dropwise to a stirred solution of **3b** (400 mg, 0.5 mmol) in THF (20 mL) at −78°C. The resulting mixture was allowed to warm to room temperature and then stirred for 3 h. Removal of the solvent afforded an orange residue. NMR spectra indicated the presence of two products, namely the complexes **8b** and **16b**. The crude residue was chromatographed (toluene/THF, 1:1). The first orange band contained **8b**, while **16b** was isolated in ca. 40% yield from the second yellow band (200 mg) as a yellow powder after recrystallization from acetone. − IR (THF): $\tilde{\nu}_{CO}$ = 2004 (m), 1905 (s), 1876 (s), 1860 (s) cm^{-1}. − ^1H NMR ($CDCl_3$): δ = −10.36 (dd + ddd, $^4J_{PH}$ = 5 Hz, $^2J_{PH}$ = 18.5 Hz, $^1J_{WH}$ masked, 1 H, W−H), 4.28 (s, 5 H, C_5H_5), 4.66 (m, 1 H, C_5H_4), 5.04 (m, 1 H, C_5H_4), 5.19 (m, 1 H, C_5H_4), 5.67 (m, 1 H, C_5H_4), 7.18−7.81 (m, 20 H, C_6H_5). − $^{31}P\{^1H\}$ NMR ($CDCl_3$): δ = −27.2 (d + dd, $^2J_{PP}$ = 20 Hz, $^1J_{WP}$ = 211 Hz, $^1J_{WP}$ masked, μ-PPh_2), 38.5 (d + dd, $^2J_{PP}$ = 20 Hz, $^1J_{WP}$ masked, PPh_2). − MS; *m*/*z*: 979 [M^+]. − $C_{38}H_{30}O_4P_2W_2$ (980.3): calcd. C 45.13, H 2.99; found C 45.99, H 3.16.

X-ray Crystallographic Study of 3b: An orange crystal of approximate dimensions 0.35 × 0.35 × 0.10 mm was used for unit cell measurements and intensity data collection, carried out at 296 K with an Enraf−Nonius CAD4 diffractometer with Mo-K_α radiation (λ = 0.71073 Å). The pertinent crystallographic data are given in Table 2. The unit cell was determined from 25 randomly selected reflections (CAD4-EXPRESS).[26] Intensity data were reduced with PROCESS as implemented in the MolEN package[27] with neutral-atom scattering factors taken from the usual source. An empirical absorption correction (ψ scan) was applied. The structure was solved by direct methods (SHELXS-97)[28] and refined by using the SHELXL-97 library.[29] The hydride ligand was located from a difference Fourier map. Crystallographic data (excluding structure factors) for the structure reported in this paper have been deposited with the Cambridge Crystallographic Data Centre as supplementary publication no. CCDC-117399. Copies of the data can be obtained free of charge on application to CCDC, 12 Union Road, Cambridge CB2 1EZ, U.K. [Fax: (internat.) + 44-1223/336-033; E-mail: deposit@ccdc.cam.ac.uk].

Table 2. Crystal data and structure refinement for **3b**

Empirical formula	$C_{26}H_{20}ClO_4PW_2$
Molecular mass	830.54
T [K]	293(2)
Wavelength [Å]	0.71073
Crystal system, space group	monoclinic, $P2_1/c$
Unit cell dimensions	*a* = 16.048(3) Å, *b* = 10.148(2) Å, *c* = 15.728(2) Å, β = 102.14(1)°
V [Å^3]	2504.1(8)
Z	4
Calculated density [Mg/m^3]	2.203
Absorption coefficient [mm^{-1}]	9.381
F(000)	1552
Crystal size [mm]	0.35 × 0.35 × 0.10
Theta range for data collection [°]	2.39 to 24.97
hkl range	0/19, 0/12, −18/18
Reflections collected/unique	4836/3562
EAC, ψ scan, min./max. transm.	25.54/99.99
Refinement method	Full-matrix least squares on F^2
Data/restraints/parameters	3562/0/311
Goodness-of-fit on F^2	1.094
Final *R* indices [$I > 2\sigma(I)$]	*R*1 = 0.0426, *wR*2 = 0.1278
Largest diff. peak and hole [eÅ^{-3}]	2.850 and −2.457

[1] S. Rigny, J.-C. Leblanc, C. Moïse, *New J. Chem.* **1995**, *19*, 145−147.
[2] [2a] S. Rigny, V. I. Bakhmutov, B. Nuber, J.-C. Leblanc, C. Moïse, *Inorg. Chem.* **1996**, *35*, 3202−3209. − [2b] V. Comte, S. Rigny, C. Moïse, *Bull. Soc. Chim. Fr.* **1997**, *134*, 609−614. − [2c] S. Rigny, J.-C. Leblanc, C. Moïse, B. Nuber, *J. Chem. Soc., Chem. Commun.* **1995**, 45−46. − [2d] S. Rigny, J.-C. Leblanc, B. Nuber, C. Moïse, *J. Chem. Soc., Dalton Trans.* **1997**, 1187−1193.
[3] S. Rigny, J.-C. Leblanc, C. Moïse, B. Nuber, *New J. Chem.* **1997**, *21*, 469−476.
[4] C. Barré, M. M. Kubicki, C. Moïse, *Phosphorus Sulfur Silicon* **1993**, *77*, 49−52.
[5] [5a] S. O. Grim, D. A. Wheatland, *Inorg. Chem*. **1969**, *8*, 1716. − [5b] S. O. Grim, J. Del Gaudio, R. P. Molenda, C. A. Tolman, J. P. Jesson, *J. Am. Chem. Soc*. **1974**, *96*, 3416. − [5c] G. Parkin, *Rev. Inorg. Chem*. **1985**, *7*, 251.
[6] C. Barré, P. Boudot, M. M. Kubicki, C. Moïse, *Inorg. Chem.* **1995**, *34*, 284−291.
[7] C. Barré, Thesis, Université de Bourgogne, **1992**.
[8] W. A. Schenk, *J. Organomet. Chem*. **1979**, *179*, 253.
[9] C. Barré, M. M. Kubicki, J.-C. Leblanc, C. Moïse, *Inorg. Chem.* **1990**, *29*, 5244.
[10] G. Boni, M. M. Kubicki, C. Moïse, *Bull. Soc. Chim. Fr*. **1994**, *131*, 895.
[11] 3D Search and Research using the Cambridge Structural Database, F. H. Allen, O. Kennard, *Chemical Design Automation News* **1993**, *8*, 31. Latest version: October **1998**.
[12] F. A. Cotton, D. J. Darensburg, B. W. S. Kolthammer, *Inorg. Chem.* **1981**, *20*, 4440.
[13] M. J. Aronay, I. E. Buys, M. S. Davis, T. W. Hambley, *J. Chem. Soc., Dalton Trans.* **1994**, 2827.
[14] J. S. Rommel, J. B. Weinvach, D. S. Grubisha, D. W. Bennett, *Inorg. Synth.* **1976**, *16*, 162.
[15] [15a] J. Pietsch, A. Wolski, L. Dahlenburg, M. Moll, H. Berke, D. Veghini, I. L. Eremenko, *J. Organomet. Chem*. **1994**, *472*, 55. − [15b] F. A. Cotton, D. J. Darensburg, B. W. S. Kolthammer, R. Kudaroski, *Inorg. Chem.* **1982**, *21*, 1656. − [15c] D. J. Darensburg, B. L. Mueller, C. J. Bischoff, S. S. Chojnacki, J. H. Reibenspiess, *Inorg. Chem.* **1991**, *30*, 2418. − [15d] D. J. Darensburg, R. Kudaroski Hanckel, C. G. Bauch, M. Pala, D. Simmons, J. N. White, *J. Am. Chem. Soc*. **1985**, *107*, 7463.
[16] K. Prout, T. S. Cameron, A. Forder, S. R. Critchley, B. Denton, G. V. Rees, *Acta Crystallogr., Sect. B* **1974**, *B30*, 2290.
[17] T. Szymanska-Buzar, T. Glowiak, *J. Organomet. Chem*. **1995**, *489*, 207.
[18] E. O. Fischer, F. J. Gammel, D. Neugebauer, *Chem. Ber*. **1980**, *113*, 1010.
[19] C. Burschka, W. A. Schenk, *Z. Anorg. Allg. Chem*. **1981**, *477*, 149.
[20] [20a] C. A. Tolman, *Chem. Rev.* **1977**, 77, 313−348. − [20b] T. L. Brown, *Inorg. Chem.* **1992**, *31*, 1286−1294.

[21] [21a] L. T. Phang, K. S. Gan, H. K. Lee, T. S. A. Hor, *J. Chem. Soc., Dalton Trans.* **1993**, 2697−2702. − [21b] D. J. Darensburg, *Inorg. Chem.* **1979**, *18*, 14−17.
[22] [22a] G. Boni, P. Sauvageot, C. Moïse, *J. Organomet. Chem.* **1995**, *489*, C32−C34 and references cited therein. − [22b] G. Boni, P. Sauvageot, E. Marpeaux, C. Moïse, *Organometallics* **1995**, *14*, 5652−5656.
[23] V. Comte, O. Blacque, M. M. Kubicki, C. Moïse, *Organometallics* **1997**, *16*, 5763−5769.
[24] G. Boni, M. M. Kubicki, C. Moïse in *Metal Clusters in Chemistry* (Eds.: P. Braunstein, L. A. Otero, P. R. Raithby), VCH, Weinheim, **1999**, vol. 1, p. 110.
[25] V. D. Bianco, S. Doronzo, *Inorg. Synth.* **1976**, *16*, 162.
[26] Enraf−Nonius, *CAD4 EXPRESS (Version 5.1)*, Delft, The Netherlands, **1992**.
[27] C. K. Fair, *MolEN*, *An Interactive Intelligent System for Crystal Structure Analysis*, Enraf−Nonius, Delft, The Netherlands, **1990**.
[28] G. M. Sheldrick, *SHELXS-97*, *Program for the Solution of Crystal Structures*, University of Göttingen, Germany, **1997**.
[29] G. M. Sheldrick, SHELXL-97, *Program for the Refinement of Crystal Structures*, University of Göttingen, Germany, **1997**.

Received April 8, 1999
[I99123]

Theoretical Studies of Inorganic Compounds, IX[+]

The Lewis Basicity of Diaminocarbene – A Theoretical Study of Donor–Acceptor Complexes of $C(NH_2)_2$, NH_3 and CO with the Lewis Acids EF_3, ECl_3 (E = B, Al, Ga, In), TiF_4 and $TiCl_4$

Ariana Beste,[a] Oliver Krämer,[a] Anja Gerhard,[a] and Gernot Frenking*[a]

Keywords: Diaminocarbenes / Lewis basicity / Ab initio calculations / Donor–acceptor complexes

Quantum chemical calculations at the MP2 level using large valence basis sets up to TZ+2P quality have been carried out in order to predict the geometries and bond energies of the title compounds. The nature of the donor–acceptor bond has also been investigated. The calculations show clearly that diaminocarbenes are much stronger Lewis bases than amines. The complexation energies of $C(NH_2)_2$ have been calculated to be 14–27 kcal/mol higher than those of NH_3. The most strongly bonded complex is $Cl_3Al–C(NH_2)_2$, which has a theoretically predicted Al–C bond energy D_o = 59.1 kcal/mol. In all the complexes, the strength of the Lewis bases is $C(NH_2)_2 > NH_3 > CO$, but the ordering of Lewis acid strength of EX_3 depends on the coordinated Lewis base. TiF_4 and $TiCl_4$ have similar Lewis acidities as BF_3, but the titanium tetrahalides may bind one or two donor molecules with almost the same bond strength. The investigated donor–acceptor bonds have a high degree of ionic character. The largest covalent contributions are found for the diaminocarbene complexes. The covalent character of the $X_3E–CO$ bond increases on going from E = boron to the heavier Group 13 elements, while the opposite order is found for the $X_3E–NH_3$ and $X_3E–C(NH_2)_2$ bonds.

Introduction

The concept of "dative" or "semipolar" bonds between an electron-pair donor and an acceptor introduced by Lewis[1] has become very useful for understanding the structures, bond strengths, and reactivities of donor−acceptor complexes. Chemical bonding in main group chemistry is usually discussed in terms of covalent or ionic interactions and the model of donor−acceptor bonds plays only a minor role. In contrast, it is customary to consider chemical bonding in transition metal compounds as arising from closed-shell interactions between the metal M and the donor ligand D, even when formal cleavage of the M−D bond yields charged fragments M^+ and D^-. This is because coordination compounds are much more common in transition metal chemistry than in main group element chemistry. Nevertheless, it has been shown that the donor−acceptor model is a very useful device for many main group compounds as well.[2]

The strength of a donor−acceptor bond depends on the Lewis acidity and basicity of the binding partners. A given set of Lewis acids or bases can be classified in order of ascending acidity/basicity, but this order may only be valid with respect to a particular binding partner. For example, the π-donor ability of the halogens in BX_3 increases regularly on going from X = fluorine to iodine,[3] but the Lewis acid strength of BX_3 either increases or decreases on going from BF_3 to BI_3, depending on whether the donor−acceptor bond in the complex has more ionic or covalent character. This is the well-known basis of the model of hard and soft acids and bases.[4]

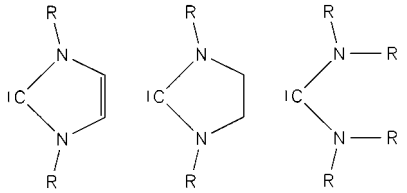
A Lewis base is characterized by having an energetically high-lying electron pair, which serves as the donor moiety. This can either be an atom-centered electron lone-pair, or the π-electrons of a multiple bond. Compounds that have neither lone-pair electrons nor multiple bonds[5] are usually weak Lewis bases. The strongest donor−acceptor bond of a main group complex that has been determined experimentally is that between NMe_3 and $AlCl_3$.[2] The measured dissociation energy of $Cl_3Al−NMe_3$ in the gas phase is D_o = 47.5 ± 2.0 kcal/mol.[6] Even stronger bonds have been predicted theoretically for donor−acceptor complexes of the strong Lewis acid BeO, but this has not yet been experimentally verified.[7]

It is generally the case that the Lewis basicity of lone-pair donor molecules increases on going from right to left across the periodic system of the elements. Thus, the trend in the donor strengths is Ne < FH < OH_2 < NH_3. The next member of this series would be ($^1A_1$) CH_2. Indeed, carbenes are well-known ligands in transition metal chemistry[8] and many transition metal carbene complexes have been synthesized and characterized since Fischer isolated the first example of such a species.[9] Main group carbene complexes have only been known following the isolation by Arduengo of the first stable carbene, i.e. the 1,3-bis(adamantyl) derivative of imidazol-2-ylidene **A** (Scheme 1).[10] Several complexes of substituted analogues of **A** with BH_3, BF_3, AlH_3, and other Lewis acids have since been synthesized.[11][12]

[+] Part VIII: J. Uddin, C. Boehme, G. Frenking, *J. Am. Chem. Soc.*, manuscript submitted.

[a] Fachbereich Chemie, Philipps-Universität Marburg, Hans-Meerwein-Straße, D-35032 Marburg, Germany
E-mail: frenking@chemie.uni-marburg.de

 © WILEY-VCH Verlag GmbH, D-69451 Weinheim, 1999 1434−1948/99/1111−2037 $ 17.50+.50/0



A B C

Scheme 1. Examples of diaminocarbenes that have been synthesized

The chemistry of *N*-heterocyclic carbenes has become one of the most extensively investigated areas of organic and organometallic chemistry in the last decade. Milestones were the isolation of stable saturated diaminocarbenes **B**,[13] the synthesis of stable noncyclic diaminocarbenes **C**,[14] and reports on stable heterocyclic carbenes with other neighbouring atoms such as sulfur[15][16] and oxygen.[16] The interest in metal complexes of *N*-heterocyclic carbenes increased considerably after it was reported that carbene complexes exhibit catalytic properties which might be comparable with those of phosphane complexes.[12][17] In spite of numerous experimental studies, there has been no report concerning the measurement of the bond strength of a donor−acceptor bond between a metal and an *N*-heterocyclic carbene ligand. Experimental observations indicate that the bonds are quite strong, and that the donor−acceptor bonds show mainly carbene→metal σ-donation but little carbene←metal π-back-donation.[12] This assumption is supported by two recent theoretical studies of carbene complexes with beryllium[18] and Group 11 transition metal halides (CuCl, AgCl, AuCl).[19]

The focus of the present paper is the trend in the donor strengths of Lewis bases on going from nitrogen to carbon, i.e. the difference between the donor−acceptor bond strengths of amines and *N*-heterocyclic carbenes when they are bonded to Lewis acids of main group elements or early transition metals. We have chosen the parent compounds NH_3 as the amine and $C(NH_2)_2$ as the carbene. CO has also been included in order to highlight the different donor abilities of carbon lone-pair electrons in sp- and sp^2-hybridized orbitals. The difference between the Lewis basicities of NH_3 and substituted amines is known from experimental[20] and theoretical work.[21] $C(NH_2)_2$ should be a good model for studying the donor strength of *N*-heterocyclic carbenes since substituents at nitrogen influence the carbene center only indirectly. The different donor abilities of $C(NH_2)_2$ and substituted analogues thereof is the subject of another ongoing study in our group. The chosen Lewis acids were the main group compounds EF_3, ECl_3 (E = B, Al, Ga, In) and the titanium tetrahalides TiF_4 and $TiCl_4$. We report here the equilibrium geometries and bond energies calculated at the MP2 level using polarized valence basis sets of up to TZ+2P quality. The electronic structures of the molecules were analyzed with the help of the natural bond orbital (NBO) partitioning scheme developed by Weinhold.[22] This work is part of our ongoing systematic investigation of the structures and stabilities of donor−acceptor complexes of main group and transition metal elements.[23]

Theoretical Methods

The geometry optimizations were carried out using Møller−Plesset perturbation theory terminated at second order (MP2)[24] in conjunction with our standard basis set II,[25] which has a relativistic effective core potential (ECP)[26] with a (441/2111/41) valence basis set for Ti, 6−31G(d)[27] all-electron basis sets for H, B, C, N, O, and F, and ECPs with a (31/31/1) valence basis set for the heavier main-group elements Al, Ga, In, Cl.[28] Improved energy calculations were carried out at the MP2 level using the larger basis set II+. The latter has an additional f-type polarization function at Ti (ζ = 1.506),[29] 6−311G(2d,p)[30] all-electron basis sets for H, B, C, N, O, F, Al, and Cl, and ECPs with a TZ+2P valence basis set (311/311/11)[28] for Ga and In. The harmonic vibrational frequencies and zero-point vibrational energies (*ZPE*) were calculated at the MP2/II level. All structures reported here are minima on the potential energy surface (only positive eigenvalues of the Hessian matrix). The calculations were carried out using the Gaussian-94 program package.[31]

Bond Energies and Geometries

Figure 1 shows the optimized structures and the most important geometrical parameters predicted at the MP2/II level of theory for the complexes **1a**−**10cc** comprising the Lewis acids **1**−**10** and the Lewis bases **a**−**c**. Table 1 gives the energies calculated at the MP2/II+ level using the MP2/II optimized geometries.

The calculated bond dissociation energies of the main group and transition metal complexes containing $C(NH_2)_2$ are very high, showing that the diaminocarbene ligand is a very strong Lewis base. The largest value is calculated for $Cl_3Al-C(NH_2)_2$ (**6c**) (D_e = 61.6 kcal/mol; D_o = 59.1 kcal/mol), while the lowest is predicted for $F_4Ti-C(NH_2)_2$ (**9c**) (D_e = 38.5 kcal/mol). Thus, diaminocarbenes are not only stronger Lewis bases than NH_3, but are even stronger than $N(CH_3)_3$, for which a bond dissociation energy of D_e = 50.2 kcal/mol (D_o = 47.6 kcal/mol, experimental value D_o = 47.5 ± 2 kcal/mol)[6] has been predicted at the MP2/II level for the complex $Cl_3Al-N(CH_3)_3$.[23b] It can thus be foreseen that complexes between *N*-heterocyclic carbenes and $AlCl_3$ will soon replace $Cl_3Al-N(CH_3)_3$ as the most strongly bonded donor−acceptor complexes of main group elements known experimentally.

The Lewis basicity of NH_3 is also high, but is clearly lower than that of $C(NH_2)_2$. The bond dissociation energies of the ammonia complexes are calculated to be between D_e = 44.1 kcal/mol (Cl_3Al-NH_3, **6a**) and D_e = 24.1 kcal/mol (F_4Ti-NH_3 **9a**) for complexes with one Lewis base. The second ammonia ligand in $F_4Ti(NH_3)_2$ (**9aa**) has the lowest bond energy among the NH_3 complexes (D_e = 21.6

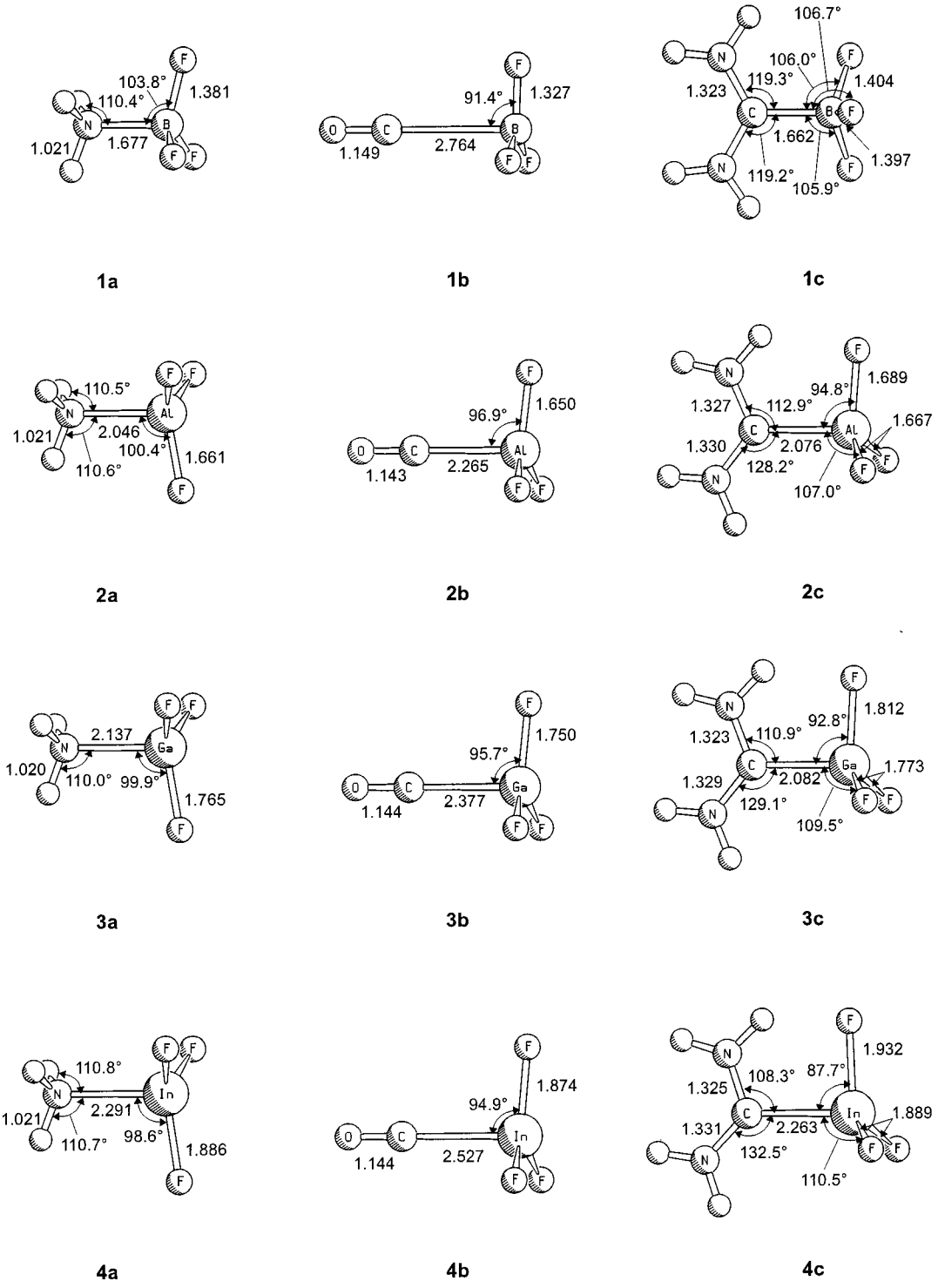


Figure 1. Optimized geometries of the complexes and fragments at the MP2/II level; bond lengths in Å, angles in degrees

kcal/mol). For all the complexes, the calculations show a clear trend in the Lewis basicities CO < NH_3 < $C(NH_2)_2$. CO is always significantly less strongly bonded (by 17−30 kcal/mol) in the complexes than NH_3, while $C(NH_2)_2$ is more strongly bonded (by 14−27 kcal/mol) than NH_3. The most strongly bonded CO complex is predicted to be F_3Al−CO (**2b**) (D_e = 15.1 kcal/mol). Note that CO forms particularly weak bonds with boron halides (D_e = 3.2 kcal/mol in **1b**, 2.3 kcal/mol in **5b**).

The calculated trends in the bond strengths of the Lewis acid adducts depend both on the nature of the Lewis base D and on the halogen atom. For the F_3E−D species, it is found that the complexes with E = Al, Ga, In, and the same ligand D have similar bond dissociation energies,

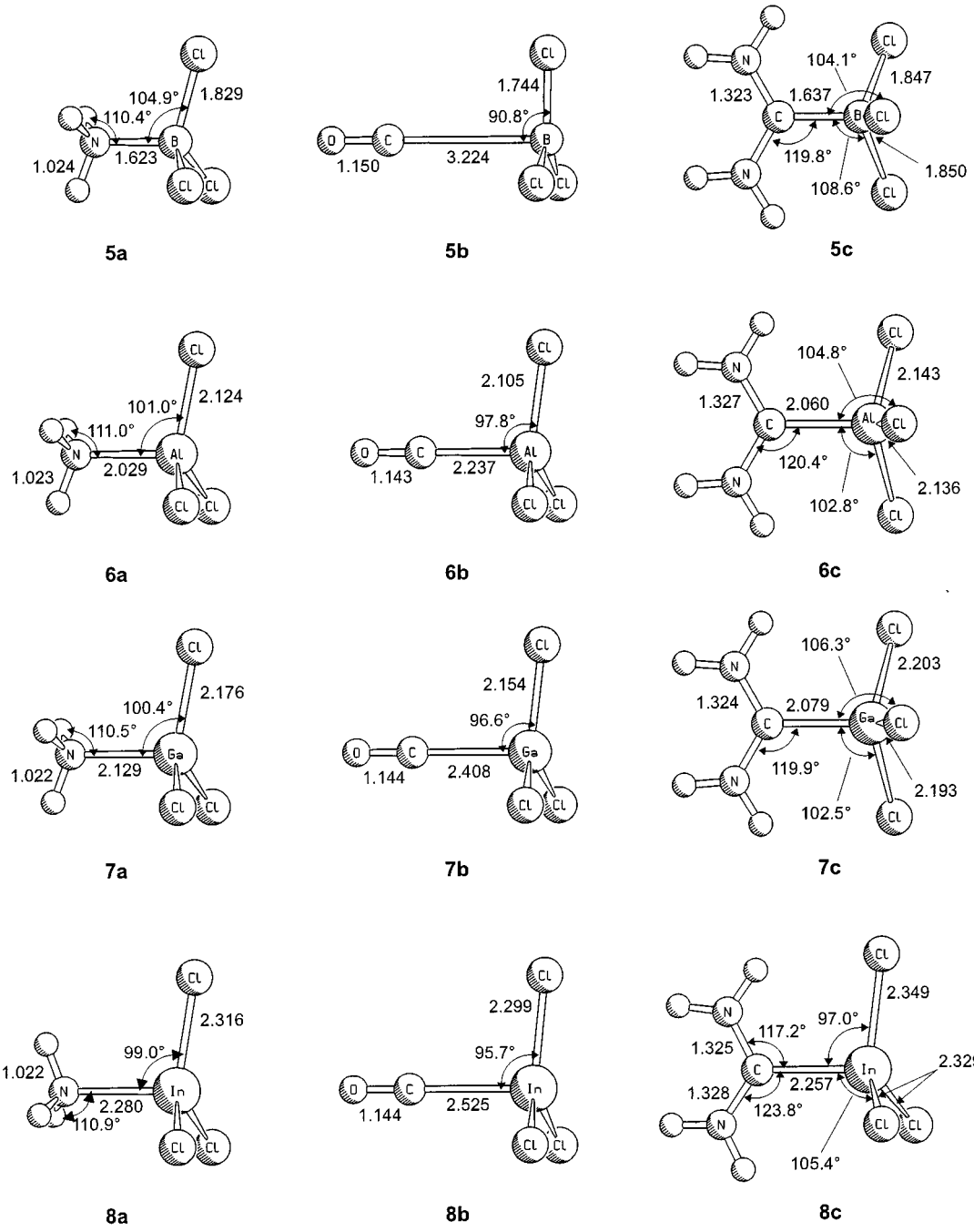


Figure 1. *(Continued)*

while the F_3B-D complexes are clearly less strongly bonded. The situation with the Cl_3E-D complexes is somewhat different. $Cl_3B-C(NH_2)_2$ (**5c**) has a higher bond dissociation energy (D_e = 59.7 kcal/mol) than the gallium complex **7c** (D_e = 57.5 kcal/mol) or the indium complex **8c** (D_e = 57.6 kcal/mol), and it is only slightly less strongly bonded than $Cl_3Al-C(NH_2)_2$ (**6c**) (D_e = 61.6 kcal/mol). NH_3, and particularly CO, form weaker bonds with BCl_3 than with the heavier analogues $AlCl_3$, $GaCl_3$, and $InCl_3$.

A comparison of the donor–acceptor bond strengths of the main group complexes with those of the transition metal compounds shows that for the three donor ligands D, TiF_4 and $TiCl_4$ have similar Lewis acidities as BF_3. The difference between the two groups of complexes is that TiF_4 and $TiCl_4$ can strongly bind *two* ligands D with almost the same bond strength, thereby yielding TiX_4D and TiX_4D_2, while main group Lewis acids show only weak affinities for binding more than one Lewis base.[2] Table 1 shows that in most cases the theoretical bond strengths of the first and second Ti–D bonds are similar. The second Ti–D bond may even be stronger than the first. For example, the energies required for dissociation of the first and second $C(NH_2)_2$ ligands from $Cl_4Ti[C(NH_2)_2]_2$ are 45.8 kcal/mol and 41.2 kcal/mol, respectively. The first and second am-

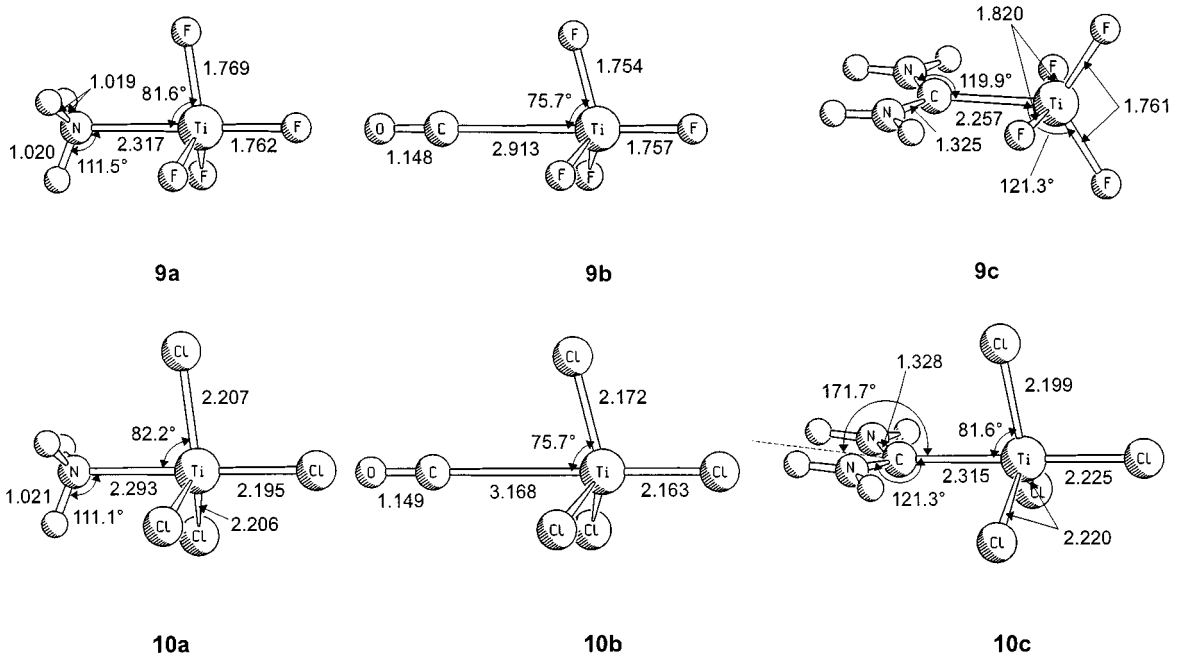


Figure 1. *(Continued)*

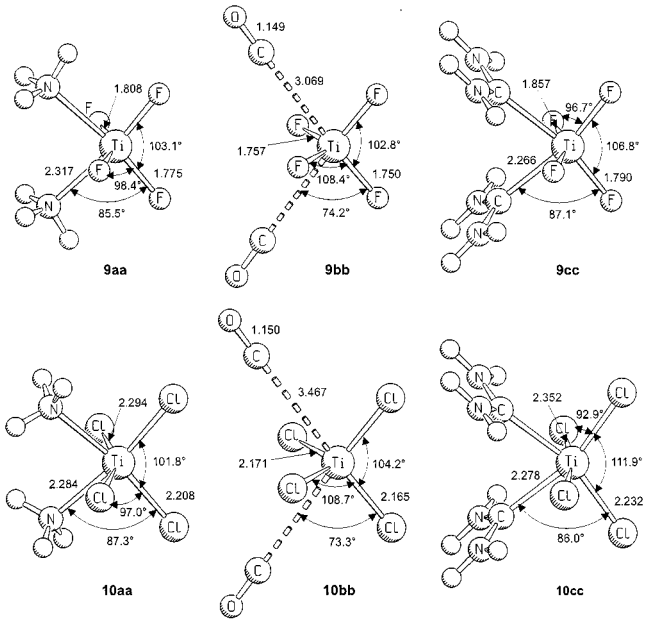


Figure 1. *(Continued)*

monia ligands of $Cl_4Ti(NH_3)_2$ are bound with similar bond strengths (D_e = 24.3 and 23.8 kcal/mol, Table 1). This is in contrast to the relative bond strengths in $OsO_4(NH_3)_2$, where the second NH_3 is clearly more weakly bound (D_e = 7.0 kcal/mol) than the first (D_e = 13.9 kcal/mol).[23b]

The theoretically predicted strong bonding of the first and second carbene ligands in $Cl_4Ti[C(NH_2)_2]_2$ is consistent with the experimental observation that the reaction of $MCl_4(THF)_2$ (M = Ti, Zr, Hf) with 1,3-dialkyl derivatives of imidazol-2-ylidene **A** may yield the respective monocarbene complex Cl_4TiD[32] or the dicarbene complex Cl_4TiD_2,[33] depending on the stoichiometry of the starting materials.

Experimental values for the bond energies are not available, but previous work on other donor−acceptor complexes carried out at the same level of theory showed that the theoretical values deviated by less than 3 kcal/mol from the experimental data.[23b] We believe the present values to have a similar degree of accuracy.

The geometries shown in Figure 1 reveal interesting aspects of the donor−acceptor interactions. We begin the discussion with the main group complexes **1a**−**8c**. It has previously been found that the B−F bond length in BF_3 becomes longer in donor−acceptor complexes F_3B−D, and that this extension of the B−F distance increases with increasing strength of the F_3B−D bond.[23b] The data in Figure 1 and Table 1 show that this also holds true for the BF_3 complexes investigated here, i.e. the B−F bond length increases in the order BF_3 < **1b** < **1a** < **1c**. The same trend is calculated for the other E−F and E−Cl bond lengths. The carbonyl complexes invariably have the shortest E−X bonds, while the longest are found for the diaminocarbene complexes. A correlation of the X_3E−D bond energies with the pyramidalization of the EX_3 moiety of **1a**−**8c** is also found. The angle D−E−X becomes larger in the order D = CO < NH_3 < $C(NH_2)_2$. Some D−E−X bond angles with D = $C(NH_2)_2$ become acute because of hydrogen bonding between one X atom and a proton of the amino group. In particular, the F_3E−$C(NH_2)_2$ complexes show an increased asymmetry about the E−C bond in the order **1c** < **2c** < **3c** < **4c**. Note the significant lengthening of the in-plane E−F

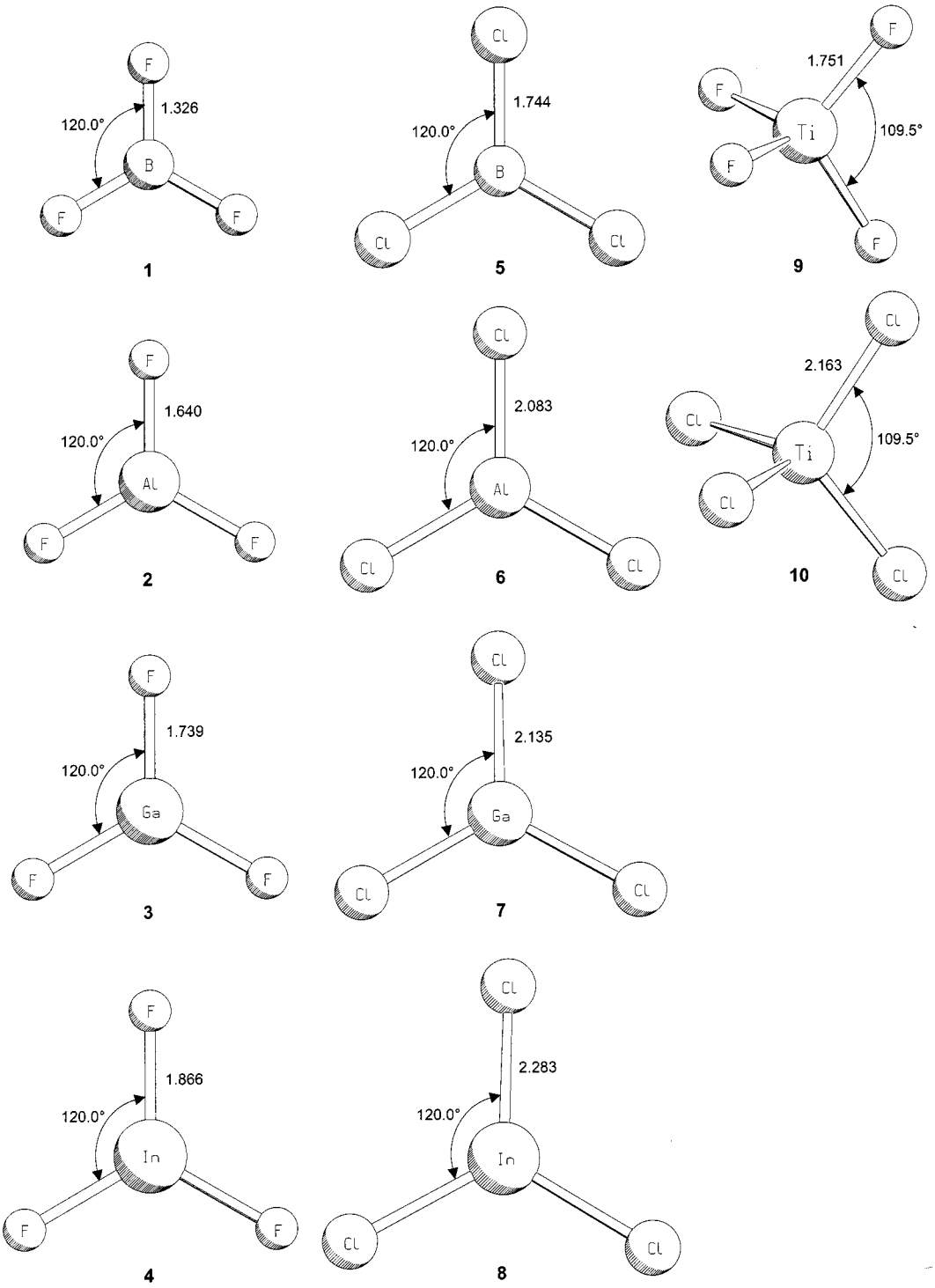


Figure 1. *(Continued)*

bond and the tilt of one amino group towards the in-plane fluorine atom in the complexes. Among the chlorine analogues, the same effect is found only for the indium complex **8c** (Figure 1).

The donor moieties in the pentacoordinated transition metal complexes X_4TiD have the ligand D *trans* to X, except in **9c**, where hydrogen bonding between fluorine and the amino group protons enforces an equatorial position of the carbene ligand. The diaminocarbene ligand in **10c** is slightly tilted from the N_2CTi plane (Figure 1). The hexacoordinated complexes X_4TiD_2 have the ligands D *cis* to one another. The *trans* forms (not shown here) are clearly higher in energy. This is in agreement with experimental evidence.[34]

We did not systematically calculate the activation barriers for rotation about the D−E bonds. However, some test cal-

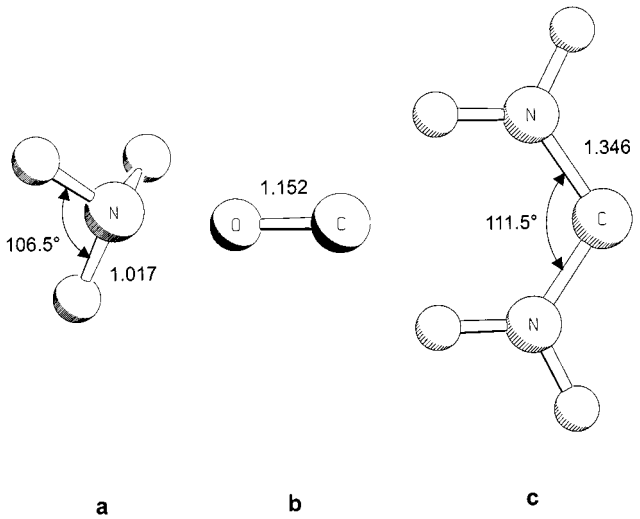


Figure 1. *(Continued)*

Table 1. Calculated total energies E_{tot} [Hartree] and zero-point vibrational energies *ZPE* [kcal/mol] at MP2/II+//MP2/II; theoretically predicted binding energies D_e [kcal/mol] and *ZPE* corrected values D_0 [kcal/mol]

Molecule	No.	Sym.	E_{tot}	ZPE	D_e	D_0
F_3B-NH_3	**1a**	C_{3v}	–380.51466	33.6	23.5	19.9
F_3B-CO	**1b**	C_{3v}	–437.15892	11.6	3.2	2.5
$F_3B-C(NH_2)_2$	**1c**	C_1	–473.73154	47.3	42.5	39.8
F_3Al-NH_3	**2a**	C_{3v}	–597.80920	30.2	43.4	40.4
F_3Al-CO	**2b**	C_{3v}	–654.44088	9.5	15.1	13.7
$F_3Al-C(NH_2)_2$	**2c**	C_S	–691.01919	44.3	58.0	55.5
F_3Ga-NH_3	**3a**	C_{3v}	–357.72434	29.0	38.5	35.6
F_3Ga-CO	**3b**	C_{3v}	–414.35976	8.2	12.5	11.3
$F_3Ga-C(NH_2)_2$	**3c**	C_1	–450.94453	43.4	59.5	56.8
F_3In-NH_3	**4a**	C_{3v}	–357.56041	28.4	40.9	38.2
F_3In-CO	**4b**	C_{3v}	–414.19446	7.8	14.2	13.0
$F_3In-C(NH_2)_2$	**4c**	C_S	–450.77772	42.9	60.1	57.5
Cl_3B-NH_3	**5a**	C_{3v}	–1460.36428	31.3	32.0	27.8
Cl_3B-CO	**5b**	C_{3v}	–1516.99364	8.5	2.3	1.8
$Cl_3B-C(NH_2)_2$	**5c**	C_1	–1553.59516	44.7	59.7	56.7
Cl_3Al-NH_3	**6a**	C_{3v}	–1677.68893	28.3	44.1	41.0
Cl_3Al-CO	**6b**	C_{3v}	–1734.31799	7.5	14.2	12.8
$Cl_3Al-C(NH_2)_2$	**6c**	C_1	–1770.90338	42.3	61.6	59.1
Cl_3Ga-NH_3	**7a**	C_{3v}	–1437.66573	27.4	35.4	32.6
Cl_3Ga-CO	**7b**	C_{3v}	–1494.30137	6.6	9.7	8.6
$Cl_3Ga-C(NH_2)_2$	**7c**	C_1	–1530.88756	41.6	57.5	55.1
Cl_3In-NH_3	**8a**	C_{3v}	–1437.49855	27.0	38.7	36.0
Cl_3In-CO	**8b**	C_{3v}	–1494.13263	6.3	12.0	10.9
$Cl_3In-C(NH_2)_2$	**8c**	C_S	–1530.71538	41.1	57.6	55.4
F_4Ti-NH_3	**9a**	C_1	–513.41667	31.3	24.1	21.3
F_4Ti-CO	**9b**	C_{3v}	–570.06356	10.3	5.4	4.5
$F_4Ti-C(NH_2)_2$	**9c**	C_1	–606.62625	45.9	38.5	35.7
Cl_4Ti-NH_3	**10a**	C_1	–1953.25375	29.0	24.3	21.2
Cl_4Ti-CO	**10b**	C_{3v}	–2009.89740	7.5	3.6	2.9
$Cl_4Ti-C(NH_2)_2$	**10c**	C_1	–2046.46737	42.7	41.2	39.0
$H_3N-F_4Ti-NH_3$	**9aa**	C_1	–569.86748	–	21.6	–
$OC-F_4Ti-CO$	**9bb**	C_S	–683.17536	–	7.3	–
$(NH_2)_2C-F_4Ti-C(NH_2)_2$	**9cc**	C_1	–756.29779	–	39.4	–
$H_3N-Cl_4Ti-NH_3$	**10aa**	C_1	–2009.71145	–	23.8	–
$OC-Cl_4Ti-CO$	**10bb**	C_S	–2123.00973	–	6.5	–
$(NH_2)_2C-Cl_4Ti-C(NH_2)_2$	**10cc**	C_1	–2196.15495	–	45.8	–
BF_3	**1**	D_{3h}	–324.05660	7.9	–	–
AlF_3	**2**	D_{3h}	–541.31953	5.1	–	–
GaF_3	**3**	D_{3h}	–301.24252	4.0	–	–
InF_3	**4**	D_{3h}	–301.07466	3.6	–	–
BCl_3	**5**	D_{3h}	–1403.89274	5.0	–	–
$AlCl_3$	**6**	D_{3h}	–1621.19804	3.1	–	–
$GaCl_3$	**7**	C_S	–1381.18872	2.5	–	–
$InCl_3$	**8**	C_S	–1381.01631	2.2	–	–
TiF_4	**9**	T_d	–456.95767	6.4	–	–
$TiCl_4$	**10**	T_d	–1896.79448	3.8	–	–
NH_3	**a**	C_{3v}	–56.42054	22.1	–	–
CO	**b**	$C_{\infty v}$	–113.09725	3.0	–	–
$C(NH_2)_2$	**c**	C_{2v}	–149.60721	36.7	–	–

culations showed that the rotational barriers appear to be very low, e.g. < 2 kcal/mol.

Analysis of the Bonding Situation

Table 2 shows the results of NBO analyses of the complexes. The data reveal some unexpected features concerning the bonding situations in the molecules.

The calculated D→EX_3 charge donations in complexes of the Group 13 elements E show a marked difference between the boron halides and the heavier analogues. The charge donation OC→BX_3 is negligible, while the charge donations H_3N→BX_3 and $(NH_2)_2C$→BX_3 are rather large. The OC→EX_3 charge donation is greater for the heavier elements E = Al, Ga, In, while the H_3N→EX_3 and $(NH_2)_2C$→EX_3 charge transfer is less than that in the boron complexes. In fact, OC→EX_3 and H_3N→EX_3 charge donations are rather similar for the heavier Group 13 elements (Table 2). The calculated charge transfers in the Group 13 complexes suggest that the covalent character of the OC−EX_3 bond becomes stronger on going from E = boron (where it is practically nil) to E = Al, Ga, In, while the covalency of the H_3N−EX_3 and $(NH_2)_2C$−EX_3 bonds decreases on going from E = boron to E = Al, Ga, In.[35] This surprising result is supported by the calculated bond orders, which are clearly higher for the OC−EX_3 bonds of the heavier Group 13 elements than for boron, while the opposite order is calculated for the H_3N−EX_3 and $(NH_2)_2C$−EX_3 bonds (Table 2). The same conclusion can be drawn from the trend in the polarities of the D−EX_3 bonds. The donor−acceptor bond orbital is invariably polarized towards the donor atom. The polarization is higher for the OC−BX_3 bond (which is a pure carbon lone pair orbital) than for the heavier OC−EX_3 analogues, while the polarizations of the H_3N−EX_3 and $(NH_2)_2C$−EX_3 bonds show the opposite trend. However, in all cases, the donor−acceptor bonds of $C(NH_2)_2$ retain the highest covalent character of the three Lewis bases. The calculated charge donation Δq(D→A), the polarization, and the bond order of the D−A bonds indicate that the covalent character increases in the order X_3B−CO < X_3B−NH_3 < X_3B−$C(NH_2)_2$, while for the other Group 13 Lewis acids the trend is X_3E−CO ≈ X_3E−NH_3 < X_3E−$C(NH_2)_2$.

The Ti−D bonds in the transition metal complexes have less covalent character than those in the Group 13 complexes. The NBO method finds a Ti−D bond orbital only for diaminocarbene complexes, while the TiX_4 complexes with CO and NH_3 as donor ligands have lone-pair orbitals at their donor atoms. The Ti−D bonds are mainly held together by the charge attraction between the large positive charge at the titanium atom and the negative charge of the lone-pair electrons. The calculated partial atomic charges do not reveal the extent of the charge interaction, which is strongly influenced by the topography of the anisotropic charge distribution.

An important feature is highlighted by the calculated hybridization at the Ti end of the X_4Ti−$C(NH_2)_2$ bonds.

Table 2. Results of the NBO analysis at the MP2/II level[a]

Molecule	No.	$\Delta q(D \rightarrow A)$	$q_{D(x)}$	$q_{A(y)}$	$D(x)-A(y)$							BO
					%x	%s(x)	%p(x)	%d(x)	%s(y)	%p(y)	%d(y)	
F_3B-NH_3	**1a**	0.29	–1.03	+1.34	84.71	31.08	68.91	0.02	19.97	79.40	0.62	0.46
F_3B-CO	**1b**	0.03	+0.44	+1.47	100.00	76.44	23.54	0.02	–	–	–	0.05
$F_3B-C(NH_2)_2$	**1c**	0.44	+0.27	+1.20	74.85	39.22	60.76	0.03	25.22	74.38	0.40	0.65
F_3Al-NH_3	**2a**	0.13	–1.19	+1.99	93.80	23.01	76.99	0.00	19.11	79.92	0.97	0.22
F_3Al-CO	**2b**	0.13	+0.44	+1.97	92.83	64.30	35.70	0.01	13.49	84.87	1.65	0.24
$F_3Al-C(NH_2)_2$	**2c**	0.19	+0.06	+1.92	88.95	34.15	65.85	0.00	21.77	76.41	1.82	0.34
F_3Ga-NH_3	**3a**	0.15	–1.16	+1.87	93.10	20.24	79.76	0.00	18.50	81.18	0.31	0.24
F_3Ga-CO	**3b**	0.12	+0.45	+1.86	93.45	63.44	36.55	0.01	12.16	87.12	0.72	0.22
$F_3Ga-C(NH_2)_2$	**3c**	0.23	+0.08	+1.79	86.78	33.25	66.75	0.00	23.39	75.57	1.04	0.40
F_3In-NH_3	**4a**	0.12	–1.18	+1.98	94.24	20.13	79.87	0.00	17.70	81.97	0.33	0.20
F_3In-CO	**4b**	0.10	+0.43	+1.97	94.50	63.12	36.86	0.01	12.26	87.72	0.02	0.19
$F_3In-C(NH_2)_2$	**4c**	0.19	+0.06	+1.91	88.58	32.32	67.67	0.00	22.77	77.16	0.08	0.35
Cl_3B-NH_3	**5a**	0.38	–1.01	+0.23	80.17	35.41	64.57	0.03	20.79	78.84	0.37	0.56
Cl_3B-CO	**5b**	0.01	+0.43	+0.29	100.00	76.91	23.06	0.02	–	–	–	0.02
$Cl_3B-C(NH_2)_2$	**5c**	0.50	+0.28	+0.11	69.63	40.94	59.02	0.04	25.50	74.30	0.20	0.73
Cl_3Al-NH_3	**6a**	0.16	–1.18	+1.47	92.20	28.81	71.18	0.00	19.30	79.59	1.10	0.26
Cl_3Al-CO	**6b**	0.18	+0.48	+1.35	89.08	65.87	34.13	0.00	13.68	84.70	1.62	0.34
$Cl_3Al-C(NH_2)_2$	**6c**	0.26	+0.08	+1.39	85.87	36.85	63.15	0.00	22.12	76.50	1.38	0.53
Cl_3Ga-NH_3	**7a**	0.18	–1.15	+1.38	91.54	26.30	73.70	0.00	18.04	81.73	0.23	0.27
Cl_3Ga-CO	**7b**	0.17	+0.49	+1.29	90.55	65.51	34.48	0.00	10.82	88.60	0.59	0.29
$Cl_3Ga-C(NH_2)_2$	**7c**	0.30	+0.12	+1.30	84.14	35.98	64.02	0.00	23.08	76.40	0.52	0.45
Cl_3In-NH_3	**8a**	0.16	–1.16	+1.60	92.42	24.20	75.80	0.00	17.13	82.79	0.08	0.25
Cl_3In-CO	**8b**	0.15	+0.47	+1.53	91.81	64.37	35.62	0.01	11.34	88.52	0.14	0.26
$Cl_3In-C(NH_2)_2$	**8c**	0.28	+0.12	+1.50	85.37	34.43	65.57	0.00	21.93	78.00	0.06	0.42
F_4Ti-NH_3	**9a**	0.12	–1.14	+2.02	100.0	39.66	60.34	0.00	–	–	–	0.20
F_4Ti-CO	**9b**	0.05	+0.44	+2.06	100.0	73.22	26.77	0.01	–	–	–	0.02
$F_4Ti-C(NH_2)_2$	**9c**	0.25	+0.11	+1.95	86.20	35.28	64.72	0.01	19.42	0.35	80.23	0.42
Cl_4Ti-NH_3	**10a**	0.20	–1.10	+0.61	100.0	40.86	59.14	0.00	–	–	–	0.26
Cl_4Ti-CO	**10b**	0.05	+0.44	+0.62	100.0	74.15	25.84	0.01	–	–	–	0.08
$Cl_4Ti-C(NH_2)_2$	**10c**	0.31	+0.20	+0.58	81.05	37.01	62.99	0.00	35.48	0.61	63.91	0.39
$H_3N-F_4Ti-NH_3$	**9aa**	0.14	–1.12	+1.89	100.0	36.33	63.66	0.01	–	–	–	0.22
$OC-F_4Ti-CO$	**9bb**	0.04	+0.44	+2.02	100.0	76.25	23.73	0.02	–	–	–	0.08
$(NH_2)_2C-F_4Ti-C(NH_2)_2$	**9cc**	0.23	+0.17	+1.74	100.0	36.29	63.70	0.01	–	–	–	0.39
$H_3N-Cl_4Ti-NH_3$	**10aa**	0.21	–1.08	+0.52	100.0	36.59	63.41	0.00	–	–	–	0.28
$OC-Cl_4Ti-CO$	**10bb**	0.02	+0.43	+0.63	100.0	76.93	23.05	0.02	–	–	–	0.04
$(NH_2)_2C-Cl_4Ti-C(NH_2)_2$	**10cc**	0.33	+0.24	+0.46	79.25	36.98	63.02	0.00	23.47	6.41	70.12	0.44

[a] Donor→acceptor charge donation Δq(D→A); partial atomic charges q of the donor atoms D(x) and acceptor atoms A(y); polarization of the donor−acceptor bond D(x)−A(y) in%x, hybridization of the D(x)−A(y) bond, Wiberg bond orders BO of the D(x)−A(y) bond.

Table 2 shows that the contribution from the 3d orbitals to the titanium−carbon bond is much greater than the 4s contribution. It has been suggested that the covalent bonds of the 3d elements are mainly formed by the 4s orbital and that the 3d orbitals are negligible.[36] However, the results presented here and elsewhere[37] show that this bonding model is not in agreement with quantum chemical calculations.

Finally, we would like to mention the NBO results concerning the bonding situation in the free diaminocarbene ligand. The calculations show that the formally vacant p(π) AO of the carbon atom in free $C(NH_2)_2$ is significantly populated by 0.67 e through N→C π-donation. This shows the importance of the allyl-anion-type delocalization in determining the stability of the diamino-substituted carbenes. The same conclusion was drawn from earlier theoretical studies.[38]

Summary and Conclusion

The calculations clearly show that diaminocarbene is a much stronger Lewis base than amines. This has been proven for donor−acceptor interactions with Group 13 trihalides and titanium tetrahalides, and probably holds true for complexes with other Lewis acids as well. The complexation energies of $C(NH_2)_2$ have been calculated to be 14−27 kcal/mol higher than those of NH_3. The most strongly bonded complex is $Cl_3Al-C(NH_2)_2$, which has a theoretically predicted Al−C bond energy D_o = 59.1 kcal/mol. BX_3 is clearly the weakest Lewis acid among the Group 13 trihalides. TiF_4 and $TiCl_4$ have similar Lewis acidities as BF_3, but the titanium tetrahalides may bind one or two donor molecules with almost the same bond strength. The donor−acceptor bonds have a high degree of ionic character. The greatest covalent contributions are found for the diaminocarbene complexes. The covalent character of the X_3E-CO bond becomes higher on going from E = boron to the heavier elements, while the opposite order is found for the X_3E-NH_3 and $X_3E-C(NH_2)_2$ bonds.

Acknowledgments

This study was supported by the Deutsche Forschungsgemeinschaft and the Fonds der Chemischen Industrie. Excellent service was offered by the Hochschulrechenzentrum of the Philipps-Universität Marburg. Additional computer time was provided by the HHLRZ Darmstadt and the HLRZ Stuttgart.

[1] G. N. Lewis, *Valence and the Structure of Atoms and Molecules*, The Chemical Catalog Co., Inc., New York, **1923**.

[2] A. Haaland, *Angew. Chem.* **1989**, *101*, 1017; *Angew. Chem. Int. Ed. Engl.* **1989**, *28*, 992.

[3] G. Frenking, S. Fau, C. M. Marchand, H. Grützmacher, *J. Am. Chem. Soc.* **1997**, *119*, 6648.

[4] R. G. Pearson, *J. Am. Chem. Soc.* **1963**, *85*, 3533. R. G. Pearson, *Hard and Soft Acids and Bases*, Dowden, Hutchinson and Ross, Stroudsburg, PA, **1973**.

[5] Molecules having mirror symmetry may have π orbitals, but not necessarily multiple bonds; π electrons in saturated compounds are energetically much lower lying than in unsaturated compounds and are thus poor donors.

[6] G. A. Andersen, F. R. Forgaard, A. Haaland, *Acta Chem. Scand.* **1972**, *26*, 1947.

[7] [7a] G. Frenking, W. Koch, J. Gauss, D. Cremer, *J. Am. Chem. Soc.* **1988**, *110*, 8007. – [7b] G. Frenking, D. Cremer, *Structure and Bonding*, Springer, Heidelberg, **1990**, vol. 73, p. 17–95. – [7c] W. Koch, J. R. Collins, G. Frenking, *Chem. Phys. Lett.* **1986**, *132*, 330. – [7d] W. Koch, G. Frenking, J. Gauss, D. Cremer, J. R. Collins, *J. Am. Chem. Soc.* **1987**, *109*, 5917. – [7e] G. Frenking, W. Koch, J. R. Collins, *J. Chem. Soc., Chem. Commun.* **1988**, 1147. – [7f] W. Koch, G. Frenking, *Molecules in Natural Science and Medicine – An Encomium for Linus Pauling* (Eds.: Z. B. Maksic, M. Eckert-Maksic), Ellis Horwood, New York, **1991**, p. 225–238.

[8] [8a] K. H. Dötz, H. Fischer, P. Hofmann, F. R. Kreissl, U. Schubert, K. Weiss, *Transition Metal Carbene Complexes*, Verlag Chemie, Weinheim, **1983**. – [8b] K. H. Dötz, *Pure Appl. Chem.* **1983**, *55*, 1689. [8c] K. H. Dötz, *Angew. Chem.* **1984**, *96*, 573; *Angew. Chem. Int. Ed. Engl.* **1984**, *23*, 587. – [8d] L. S. Hegedus, *Pure Appl. Chem.* **1990**, *62*, 691.

[9] A. Maasböl, E. O. Fischer, *Angew. Chem.* **1964**, *76*, 645; *Angew. Chem. Int. Ed. Engl.* **1964**, *3*, 580.

[10] [10a] A. J. Arduengo III, R. L. Harlow, M. Kline, *J. Am. Chem. Soc.* **1991**, *113*, 361. – [10b] A. J. Arduengo III, H. V. R. Dias, R. L. Harlow, M. Kline, *J. Am. Chem. Soc.* **1992**, *114*, 5530.

[11] N. Kuhn, G. Henkel, T. Kratz, J. Kreutzberg, R. Boese, A. H. Maulitz, *Chem. Ber.* **1993**, *126*, 204. A. J. Arduengo III, H. V. R. Dias, J. C. Calabrese, F. Davidson, *J. Am. Chem. Soc.* **1992**, *114*, 9724.

[12] W. A. Herrmann, C. Köcher, *Angew. Chem.* **1997**, *109*, 2257; *Angew. Chem. Int. Ed. Engl.* **1997**, *36*, 2162.

[13] A. J. Arduengo III, J. R. Goerlich, W. J. Marshall, *J. Am. Chem. Soc.* **1995**, *117*, 11027.

[14] R. W. Alder, P. R. Allen, M. Murray, A. G. Orpen, *Angew. Chem.* **1996**, *108*, 1211; *Angew. Chem. Int. Ed. Engl.* **1996**, *35*, 1121.

[15] A. J. Arduengo III, J. R. Goerlich, W. J. Marshall, *Liebigs Ann./Recueil* **1997**, 365.

[16] R. W. Alder, C. P. Butts, A. G. Orpen, *J. Am. Chem. Soc.* **1998**, *120*, 11526.

[17] [17a] J. E. Hill, T. A. Nile, *J. Organomet. Chem.* **1977**, *137*, 293. – [17b] W. A. Herrmann, M. Elison, J. Fischer, C. Köcher, G. R. J. Artus, *Angew. Chem.* **1995**, *107*, 2602; *Angew. Chem. Int. Ed. Engl.* **1995**, *34*, 2371. – [17c] B. Cetinkaya, I. Özdemir, C. Bruenau, P. H. Dixneuf, *J. Mol. Catal. A* **1997**, *L1*, 118. – [17d] W. A. Herrmann, L. J. Gooßen, C. Köcher, G. R. J. Artus, *Angew. Chem.* **1996**, *108*, 2980; *Angew. Chem. Int. Ed. Engl.* **1996**, *35*, 2805.

[18] N. Fröhlich, U. Pidun, M. Stahl, G. Frenking, *Organometallics* **1997**, *16*, 442.

[19] C. Boehme, G. Frenking, *Organometallics* **1998**, *17*, 5801.

[20] D. H. Aue, M. T. Bowers, *Gas-Phase Ion Chemistry* (Ed.: M. T. Bowers), Academic Press, New York, **1979**, Vol. 2, p. 2–52.

[21] J. L. Ozment, A. M. Schmiedekamp, *Int. J. Quantum Chem.* **1992**, *43*, 783.

[22] A. E. Reed, L. A. Curtiss, F. Weinhold, *Chem. Rev.* **1988**, *88*, 899.

[23] [23a] A. W. Ehlers, G. Frenking, *J. Am. Chem. Soc*. **1994**, *116*, 1514. – [23b] V. Jonas, G. Frenking, M. T. Reetz, *J. Am. Chem. Soc.* **1994**, *116*, 8741. – [23c] A. W. Ehlers, G. Frenking, *Organometallics* **1995**, *14*, 423. – [23d] S. Dapprich, G. Frenking, *Angew. Chem.* **1995**, *107*, 383; *Angew. Chem. Int. Ed. Engl.* **1995**, *34*, 354. – [23e] S. Dapprich, G. Frenking, *J. Phys. Chem.* **1995**, *99*, 9352. – [23f] A. W. Ehlers, S. Dapprich, S. F. Vyboishchikov, G. Frenking, *Organometallics* **1996**, *15*, 105. – [23g] G. Frenking, U. Pidun, *J. Chem. Soc., Dalton Trans.* **1997**, 1653. – [23h] R. K. Szilagyi, G. Frenking, *Organometallics* **1997**, *16*, 4807. – [23i] S. F. Vyboishchikov, G. Frenking, *Chem. Eur. J.* **1998**, *4*, 1428.

[24] [24a] C. Møller, M. S. Plesset, *Phys. Rev.* **1934**, *46*, 618. – [24b] J. S. Binkley, J. A. Pople, *Int. J. Quantum Chem.* **1975**, *9S*, 229.

[25] G. Frenking, I. Antes, M. Böhme, S. Dapprich, A. W. Ehlers, V. Jonas, A. Neuhaus, M. Otto, R. Stegmann, A. Veldkamp, S. F. Vyboishchikov, *Reviews in Computational Chemistry,* Vol. 8 (Eds.: K. B. Lipkowitz, D. B. Boyd), VCH Verlagsgesellschaft, New York, p. 63–144.

[26] P. J. Hay, W. R. Wadt, *J. Chem. Phys.* **1985**, *82*, 299.

[27] [27a] R. Ditchfield, W. J. Hehre, J. A. Pople, *J. Chem. Phys.* **1971**, *54*, 724. – [27b] W. J. Hehre, R. Ditchfield, J. A. Pople, *J. Chem. Phys.* **1972**, *56*, 2257. – [27c] P. C. Hariharan, J. A. Pople, *Mol. Phys.* **1974**, *27*, 209. – [27d] P. C. Hariharan, J. A. Pople, *Theor. Chim. Acta* **1973**, *28*, 213. – [27e] M. S. Gordon, *Chem. Phys. Lett.* **1980**, *76*, 163.

[28] A. Bergner, M. Dolg, W. Küchle, H. Stoll, H. Preuß, *Mol. Phys.* **1993**, *80*, 1431.

[29] A. W. Ehlers, M. Böhme, S. Dapprich, A. Gobbi, A. Höllwarth, V. Jonas, K. F. Köhler, R. Stegmann, A. Veldkamp, G. Frenking, *Chem. Phys. Lett.* **1993**, *208*, 111.

[30] [30a] A. D. McLean, G. S. Chandler, *J. Chem. Phys.* **1980**, *72*, 5639. – [30b] R. Krishnan, J. S. Binkley, R. Seeger, J. A. Pople, *J. Chem. Phys.* **1980**, *72*, 650.

[31] Gaussian 94: M. J. Frisch, G. W. Trucks, H. B. Schlegel, P. M. W. Gill, B. G. Johnson, M. A. Robb, J. R. Cheeseman, T. A. Keith, G. A. Petersson, J. A. Montgomery, K. Raghavachari, M. A. Al-Laham, V. G. Zakrzewski, J. V. Ortiz, J. B. Foresman, J. Cioslowski, B. B. Stefanov, A. Nanayakkara, M. Challacombe, C. Y. Peng, P. Y. Ayala, W. Chen, M. W. Wong, J. L. Andres, E. S. Replogle, R. Gomberts, R. L. Martin, D. J. Fox, J. S. Binkley, D. J. Defrees, I. Baker, J. J. P. Stewart, M. Head-Gordon, C. Gonzalez, J. A. Pople, Gaussian Inc., Pittsburgh, PA 1995.

[32] N. Kuhn, T. Kratz, D. Bläser, R. Boese, *Inorg. Chim. Acta* **1995**, *238*, 179.

[33] W. A. Herrmann, K. Öfele, M. Elison, F. E. Kühn, P. W. Roesky, *J. Organomet. Chem.* **1994**, *480*, C7.

[34] T. Carofiglio, C. Floriani, A. Chiesi-Villa, C. Guastini, *Inorg. Chem.* **1989**, *28*, 4417.

[35] A change in the nature of the donor–acceptor interactions between $Cl_3B-N(CH_3)_3$ and $Cl_3Al-N(CH_3)_3$ has previously been reported: V. Jonas, G. Frenking, *Naturwissenschaften* **1994**, *81*, 311.

[36] [36a] M. Gerloch, E. C. Constable, *Transition Metal Chemistry*, VCH Verlagsgesellschaft, Weinheim, **1994**. – [36b] M. Gerloch, *Coord. Chem. Rev.* **1990**, *99*, 199.

[37] [37a] S. Berger, W. Bock, G. Frenking, V. Jonas, F. Müller, *J. Am. Chem. Soc.* **1995**, *117*, 3820. – [37b] V. Jonas, C. Boehme, G. Frenking, *Inorg. Chem.* **1996**, 2097.

[38] [38a] C. Heinemann, T. Müller, Y. Apeloig, H. Schwarz, *J. Am. Chem. Soc.* **1996**, *118*, 2032. – [38b] C. Boehme, G. Frenking, *J. Am. Chem. Soc.* **1996**, *118*, 2039.

Received April 26, 1999
[I99147]

New *Early* Zirconium-Sulfido Metallaligands for *Late* Transition Metals; Synthesis and Reactivity of $[Cp^{tt}_2Zr(SH)_2]$ and $[Cp^{tt}_2Zr(SH)(OTf)]$

Marc A. F. Hernandez-Gruel,[a] Jesús J. Pérez-Torrente,[a] Miguel A. Ciriano,*[a] José A. López,[a] Fernando J. Lahoz,[a] and Luis A. Oro*[a]

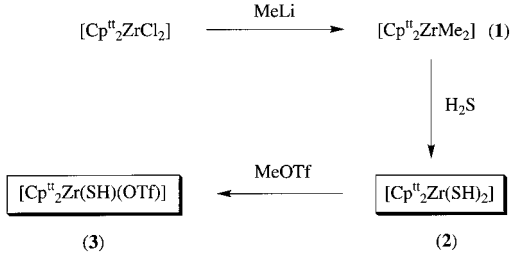
Keywords: Zirconium / Metallocenes / Triflate / Hydrosulfido / Rhodium / Early-late complex

The bishydrosulfido zirconium metallocene compound $[Cp^{tt}_2Zr(SH)_2]$ (**2**) containing the bulky η^5-1,3-di-*tert*-butylcyclopentadienyl (Cp^{tt}) ligand is readily accessible from $[Cp^{tt}_2Zr(CH_3)_2]$ (**1**) upon treatment with H_2S. Reaction of **2** with methyltriflate gives the monohydrosulfido complex $[Cp^{tt}_2Zr(SH)(OSO_2CF_3)]$ (**3**) which exists as two isomers in solution, and has been characterized by X-ray diffraction methods. Complex **2** is an effective metallaligand for the controlled synthesis of new trinuclear *early-late* heterobimetallic complexes (ELHB) with a $ZrRh_2$ core such as $[Cp^{tt}_2Zr(\mu_3\text{-}S)_2\{Rh(CO)_2\}_2]$ (**4**).

Interest in *early-late* heterobimetallic complexes (ELHB) stems in part from the potential new reactivity patterns associated with the presence of two widely divergent transition metals.[1] The combination of both an electron-deficient *early* transition metal and an electron-rich *late* transition metal in a single molecule provides a bifunctional environment which should allow the cooperative activation of organic substrates in both catalytic[2] and stoichiometric reactions.[3] A useful synthetic approach for ELHB complexes involves the use of *early* transition metal complexes as metallaligands for *late* transition metal species.[4] Following this approach we have recently described the use of the titanium bishydrosulfido compound $Cp_2Ti(SH)_2$ for the construction of unusual *early-late* titanium-rhodium tetranuclear complexes and hexanuclear clusters such as $[CpTi(\mu_3\text{-}S_3)\{Rh(tfbb)\}_3]$[5] and $[\{CpTi\}_2(\mu_4\text{-}O)(\mu_3\text{-}S)_4\{Rh_4(CO)_4(PR_3)_2\}]$,[6] respectively.

As part of our general interest in this chemistry we have extended this synthetic methodology to the preparation of zirconium-rhodium ELHB complexes. Mononuclear metallocene zirconium sulfido and hydrosulfido derivatives are rare and usually undergo the loss of H_2S to give sulfido-bridged dimers.[7] Thus, we have attempted to synthesize stable mononuclear zirconium-metallocene hydrosulfido compounds suitable for the synthesis of ELHB complexes. This paper describes the synthesis of such zirconium hydrosulfido complexes containing the bulky Cp^{tt} ligand (Cp^{tt} = η^5-1,3-di-*tert*-butylcyclopentadienyl) and their use as metallaligands for the construction of heterotrinuclear Zr-Rh complexes.

The bishydrosulfido complex $[Cp^{tt}_2Zr(SH)_2]$ (**2**) is obtained in two steps starting from the corresponding metallocene dichloride (Scheme 1). Thus, reaction of $[Cp^{tt}_2ZrCl_2]$ with a slight excess of MeLi in diethyl ether at −78°C gives the dimethyl complex $[Cp^{tt}_2Zr(CH_3)_2]$ (**1**) which can be isolated as off-white crystals,[8] in 96% yield, after removal of LiCl by extraction of the product with hexane. Reaction of **1** with an excess of H_2S(g), in toluene at 95°C in a Pyrex bomb under pressure for 14 h, affords a bright yellow solution from which the complex $[Cp^{tt}_2Zr(SH)_2]$ (**2**) can be obtained as pale yellow crystals, in 87% yield, after recrystallisation from diethyl ether. The ^{1}H NMR spectrum of **2** shows the expected resonances for the protons of the two equivalent Cp^{tt} rings (C_{2v} symmetry) and a singlet at δ = 2.11 ppm for the SH groups. The complex $[Cp^{tt}_2Zr(SH)_2]$ (**2**) reacts with a threefold excess of methyltriflate (CF_3SO_3Me) in dichloromethane to give the monohydrosulfido complex $[Cp^{tt}_2Zr(SH)(OSO_2CF_3)]$ (**3**). This complex is isolated as moisture-sensitive yellow crystals in 81% yield after recrystallisation from diethyl ether.



Scheme 1. The synthesis of hydrosulfido zirconium complexes

The crystal structure of **3** consists of discrete monomers (Figure 1). The metal centre exhibits a *pseudo*-tetrahedral geometry with the sulfur atom of the hydrosulfido ligand, the oxygen of the coordinated triflate anion and the two Cp^{tt} ring centroids at the apices. The Zr−Cp^{tt} ring-centroid distances {2.237(4) and 2.239(5) Å} are identical to those observed in the related complex $[Cp^{tt}_2ZrI_2]$ (2.248 and 2.251 Å)[8a] although the Cp^{tt}−Zr−Cp^{tt} angle is slightly smaller in **3** {129.78(15)°} than in the latter compound (133.0°). The relative disposition of the Cp^{tt} rings along the G(1)···G(2) direction is staggered with a dihedral angle C(2)···G(1)···G(2)···C(15) of 52.4(5)°, thereby reducing the

[a] Departamento de Química Inorgánica, Instituto de Ciencia de Materiales de Aragón,
Universidad de Zaragoza-C.S.I.C., 50009-Zaragoza, Spain
Fax: (internat.) + 34-976/761143
E-mails: mciriano@posta.unizar.es; oro@posta.unizar.es

 © WILEY-VCH Verlag GmbH, D-69451 Weinheim, 1999 1434−1948/99/1111−2047 $ 17.50+.50/0

steric hindrance of the bulky *tert*-butyl substituents. The Zr−O(1) bond length {2.199(3) Å} is similar to other Zr−O(triflate) bond lengths, such as that reported in $[Cp_2Zr(OSO_2CF_3)(\mu\text{-}H)]_2$ {2.205(2) Å};[9] the rather large Zr−O(1)−S(2) angle, 136.59(15)°, compares well with the values described in other triflate complexes (range: 100−164°).[10]

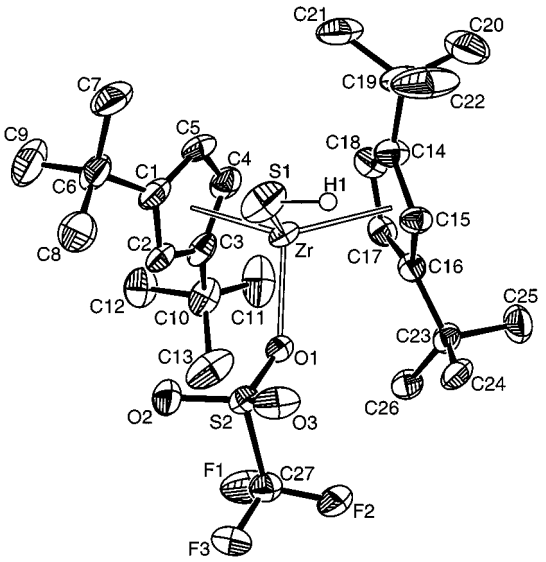
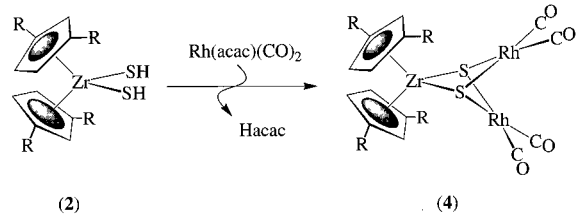


Figure 1. Molecular drawing of $[Cp^{tt}_2Zr(SH)(OSO_2CF_3)]$ (**3**) (hydrogen atoms, except H1, have been omitted for clarity); selected bond lengths [Å] and angles [°]: Zr−S(1) 2.4586(15), Zr−O(1) 2.199(3), Zr−G(1) 2.237(4), Zr−G(2) 2.239(5); S(1)−Zr−O(1) 92.61(7), S(1)−Zr−G(1) 106.74(12), S(1)−Zr−G(2) 105.99(12), O(1)−Zr−G(1) 107.69(13), O(1)−Zr−G(2) 107.74(14), G(1)−Zr−G(2) 129.78(15) [G(1) and G(2) represent the midpoints of the C(1)−C(5) and C(14)−C(18) rings, respectively]

The complex $[Cp^{tt}_2Zr(SH)(OSO_2CF_3)]$ (**3**) exists in solution as two isomers (3:1 ratio in C_6D_6, isomers **3a** and **3b**) as evidenced by ^1H, ^{19}F and ^{13}C NMR spectroscopy. These isomers do not arise from a dissociation of the triflate ligand nor from association of mononuclear complexes, since **3** is a nonconductor in dichloromethane and the molecular weight measured in chloroform is in agreement with a mononuclear formulation. Both isomers show three triplets for the protons of the two equivalent Cp^{tt} rings in the ^1H NMR spectrum in C_6D_6 in accordance with the lower symmetry of **3** compared to its precursor **2**. The main difference between **3a** and **3b** concerns the SH ligand. The major isomer **3a** possesses the structure found in the solid state, since an NOE effect (10%) is observed between the proton of SH ligand at δ = 4.04 ppm and one of the protons of the Cp^{tt} ring {the H(1)···H(C15) distance is 2.526 Å in the solid state}. The minor isomer **3b** shows an unusually low-field-shifted resonance for the proton of the hydrosulfido ligand at δ = 6.27 ppm. In addition, no NOE effect is observed between the SH group and any of the protons of the Cp^{tt} ligands. A reasonable explanation for these observations in **3b** could be the existence of an intramolecular hydrogen bonding between the SH proton and one of the unbound oxygen atoms of the triflate ligand forming a six-membered metallacycle. In fact, a rotation of the hydrosulfido ligand around the Zr−S bond in a molecular model based on the solid state structure of **3** can bring the hydrogen atom to a distance from O(3) of less than 2.55 Å. It should be noted that a similar intramolecular interaction has been observed in the solid state structure of the aquo-complex $[(CH_3)_2Au(\text{-}H_2O)(OSO_2CF_3)]$.[11] Interestingly, the related complex $[Cp^*_2Zr(OH)(OSO_2CF_3)]$ ($Cp^* = \eta^5\text{-}C_5Me_5$), obtained by reaction of $[Cp^*_2Zr(OH)Cl]$ with silver triflate, exits as a single compound in solution.[12]

Additive-deprotonation of $[Cp^{tt}_2Zr(SH)_2]$ (**2**) with appropriate rhodium complexes results in the clean formation of trinuclear d^0-d^8 ELHB compounds with a $ZrRh_2$ core. In contrast, additive-deprotonation reactions of $[Cp^{tt}_2Zr(SH)(OSO_2CF_3)]$ (**3**) are much more complex since the transfer of the sulfido ligands to the d^8 metal centres is observed. Thus, reaction of **2** with two molar equiv. of $[Rh(acac)(CO)_2]$, in diethyl ether, gives the complex $[Cp^{tt}_2Zr(\mu_3\text{-}S)_2\{Rh(CO)_2\}_2]$ (**4**) as a sparingly soluble, emerald-green microcrystalline powder in 93% yield (Scheme 2). The structure of **4** has a triangular $ZrRh_2$ core capped by two symmetrical μ_3-sulfido ligands in accordance with the high symmetry (C_{2v}) observed by NMR spectroscopy. In particular, the ^1H NMR spectrum shows only two resonances for the protons of the Cp^{tt} rings, and a unique doublet for the carbonyl ligands is observed in the $^{13}C\{^1H\}$ NMR spectrum. Reaction of **3** with one molar equiv. of $[Rh(acac)(CO)_2]$ in diethyl ether does not afford the desired *early-late* heterodinuclear complex since a ligand redistribution process takes place. The known anion[13] $[Rh_3(\mu_3\text{-}S)_2(CO)_6]^-$ and the new cation[14] $[Cp^{tt}_2Zr(acac)]^+$ are detected in the reaction mixture. Both species are formed by the transference of the sulfido ligands from zirconium to rhodium, probably through a heterobimetallic intermediate. However, the formation of the ion-pair compound $[Cp^{tt}_2Zr(acac)][Rh_3(\mu_3\text{-}S)_2(CO)_6]$[15] is not clean since the trinuclear ELHB complex **4** and free HCp^{tt} are also observed spectroscopically.

In conclusion, we have synthesized new zirconium hydrosulfido metallocenes containing the bulky Cp^{tt} ligand and shown the ability of the bishydrosulfido complex **2** to build unusual $ZrRh_2$ ELHB complexes in a controlled way. Further work concerning both the scope of this synthetic methodology and the potential reactivity of the monosulfido complex **3** is in progress.



Scheme 2. The synthesis of a trinuclear *early-late* complex with a $ZrRh_2$ core; R denotes the *tert*-butyl group

Experimental Section

General: All manipulations were performed under a dry argon atmosphere using standard Schlenk techniques. Solvents were dried

by standard methods and distilled under argon immediately prior to use. $[Cp^{tt}_2ZrCl_2]$[16] and $[Rh(acac)(CO)_2]$[17] were prepared according to reported methods. NMR spectra were recorded at 20°C on Varian Gemini 2000 (^1H: 300.08, ^{19}F: 282.33 and $^{13}C\{^1H\}$: 75.47 MHz) or Varian UNITY 300 (^1H cyclenOe experiments) spectrometers. Chemical shifts δ are reported in ppm and referenced to Me_4Si using the signal of the deuterated solvent (^1H and ^{13}C). ^{19}F chemical shifts are relative to $CFCl_3$. Coupling constants are given in Hz. IR spectra were recorded on a Nicolet 550 spectrometer. Elemental analyses were performed with a Perkin−Elmer 2400 analyzer. Conductivities were measured in ca. 5×10^{-4} M dichloromethane solutions with a Philips PW 9509 conductimeter. Molecular weights were determined with a Knauer osmometer from chloroform solutions of the complexes. Mass spectra were recorded on a VG Autospec double-focusing mass spectrometer operating in both FAB^+ and FAB^- modes. Ions were produced with the standard Cs^+ gun at ca. 30 kV, 3-nitrobenzyl alcohol (NBA) was used as matrix.

$[Cp^{tt}_2Zr(CH_3)_2]$ (1): $[Cp^{tt}_2ZrCl_2]$ (5 g, 9.68 mmol) was slurried in 100 mL of diethyl ether at −78°C and reacted with a 1.5 M diethyl ether solution of methyllithium (14 mL, 21 mmol). The reaction mixture was allowed to warm to room temperature and then stirred for a further 12 h. The mixture was again cooled to −78°C and 1 mL of methanol was added to destroy the unchanged methyllithium. Solvents were removed under vacuum and the residue was extracted with 70 mL of n-hexane and filtered over dry celite. The resulting solution was concentrated under reduced pressure to ca. 20 mL and stored at −25°C overnight to give off-white crystals. The crystals were collected by filtration and dried in vacuo. Concentration and cooling of the mother liquor gave a second crop of crystals. Overall yield: 4.4 g (96%). − ^1H NMR ($CDCl_3$): δ = 6.47 [t, ^4J(H,H) = 2.7 Hz, 2 H, H_2], 5.38 (d, ^4J(H,H) = 2.7 Hz, 4 H, H_4 and H_5), 1.21 (s, 36 H, CMe_3) (Cp^{tt}), −0.28 (s, 6 H, Zr−CH_3). − $^{13}C\{^1H\}$ NMR ($CDCl_3$): δ = 138.6 (C_1 and C_3), 115.7 (C_2), 100.5 (C_4 and C_5), 33.4 (*C*Me$_3$), 31.4 (C*Me*$_3$) (Cp^{tt}), 31.0 (Zr−*C*H$_3$). − $C_{28}H_{48}Zr$ (475.91): calcd. C 70.67, H 10.17; found C 70.00, H 9.33.

$[Cp^{tt}_2Zr(SH)_2]$ (2): A solution of $[Cp^{tt}_2Zr(CH_3)_2]$ (**1**) (2 g, 4.202 mmol) in toluene (10 mL) was placed in a Pyrex bomb. The reaction vessel was evacuated and charged to a pressure of *ca.* 2.5 atm. with H_2S. The solution was stirred at 95°C for 14 h. The reaction vessel was depressurised and the resulting bright yellow solution flushed with argon. The volatiles were removed under reduced pressure and the residue was dissolved in 55 mL of diethyl ether. The solution was filtered and concentrated under vaccum to the point of crystallisation. Cooling of the solution to −25°C overnight gave the compound as pale yellow crystals which were collected and dried in vacuo. Concentration and cooling of the mother liquor gave a second crop of crystals. Overall yield: 1.876 g (87%). − ^1H NMR ($CDCl_3$): δ = 6.46 [t, ^4J(H,H) = 2.7 Hz, 2 H, H_2], 5.71 [d, ^4J(H,H) = 2.7 Hz, 4 H, H_4 and H_5 of Cp^{tt}], 2.11 (s, 2 H, Zr−S*H*), 1.31 (s, 36 H, C*Me*$_3$). − $^{13}C\{^1H\}$ NMR ($CDCl_3$): δ = 140.6 (C_1 and C_3), 119.8 (C_2), 102.2 (C_4 and C_5), 33.8 (*C*Me$_3$), 31.7 (C*Me*$_3$). − MS (CH_2Cl_2, *m*/*z*,%); FAB^+: 477 (100) $[Cp^{tt}_2Zr(SH)^+]$; FAB^-: 509 (90) $[Cp^{tt}_2Zr(SH)(S)^-]$, 331 (100) $[Cp^{tt}Zr{=}S(S)^-]$. − $C_{26}H_{44}S_2Zr$ (511.98): calcd. C 61.00, H 8.66, S 12.53; found C 60.95, H 8.07, S 12.61.

$[Cp^{tt}_2Zr(SH)(OSO_2CF_3)]$ (3): A solution of $[Cp^{tt}_2Zr(SH)_2]$ (**2**) (0.2 g, 0.391 mmol) in dichloromethane (5 mL) was reacted with methyltriflate (130 μL, 1.185 mmol) to give a bright yellow solution which was stirred for 15 min at room temperature. The volatiles were removed under vacuum and the residue was extracted with 10 mL of diethyl ether. The solution was then filtered and cooled to −25°C to give yellow crystals of the complex which were isolated by filtration and dried under reduced pressure. Yield: 0.1985 g (81%). − ^1H NMR ([D$_6$]benzene); isomer **3a**: δ = 6.92, 5.83 and 5.68 [t, J(H,H) = 2.7 Hz, 2 H each, H_2, H_4 and H_5 of Cp^{tt}], 4.04 (s, 1 H, Zr−S*H*), 1.22 and 1.21 (s, 18 H each, C*Me*$_3$); isomer **3b**: δ = 6.49, 5.95 and 5.76 [t, J(H,H) = 2.7 Hz, 2 H each, H_2, H_4 and H_5 of Cp^{tt}], 6.27 (s, 1 H, Zr−S*H*) 1.21 and 1.13 (s, 18 H each, C*Me*$_3$). − ^{19}F ([D$_6$]benzene): δ = −76.1 and −76.7 (Zr−OSO_2CF_3, isomers **3a** and **3b**, respectively). − $^{13}C\{^1H\}$ NMR ([D$_6$]benzene); isomer **3a**: δ = 144.9 and 144.7 (C_1 and C_3 of Cp^{tt}), 120.0 [q, J(C,F) = 320 Hz, Zr−OSO_2CF_3], 119.1, 105.5 and 104.9 (C_2, C_4 and C_5 of Cp^{tt}), 34.2 and 33.6 (*C*Me$_3$), 31.3 and 31.1 (C*Me*$_3$); isomer **3b**: δ = 148.9 and 147.3 (C_1 and C_3 of Cp^{tt}), 120.2 [q, J(C,F) = 320 Hz, Zr−OSO_2CF_3], 111.6, 107.1 and 104.2 (C_2, C_4 and C_5 of Cp^{tt}), 33.7 and 33.5 (*C*Me$_3$), 31.0 and 30.5 (C*Me*$_3$). − MS (CH_2Cl_2, *m*/*z*,%); FAB^+: 477 (11) $[Cp^{tt}_2Zr(SH)^+]$; FAB^-: 149 (100) $[CF_3SO_3^-]$. − Molecular weight ($CHCl_3$, g mol^{-1}): 622 (calcd. 628). − Conductivity Λ_M (CH_2Cl_2, $4.97.10^{-4}$ M, Ω^{-1} cm^{2}mol^{-1}): 0.22. − $C_{27}H_{43}F_3O_3S_2Zr$ (627.98): calcd. C 51.64, H 6.90, S 10.21; found C 51.55, H 7.17, S 9.14.

$[Cp^{tt}_2Zr(\mu_3\text{-}S)_2\{Rh(CO)_2\}_2]$ (4): $[Rh(acac)(CO)_2]$ (0.504 g, 1.953 mmol) was added to a yellow solution of $[Cp^{tt}_2Zr(SH)_2]$ (**2**) (0.5 g, 0.977 mmol) in diethyl ether (20 mL). The solution immediately turned dark green and a solid crystallized out while stirring for 10 min at room temperature. Filtration of the resulting suspension gave the title compound as an emerald-green microcrystalline powder after washing with n-hexane (2×10 mL) and drying in vacuo. Yield: 0.7535 g (93%). − ^1H NMR ($CDCl_3$): δ = 6.56 [t, ^4J(H,H) = 2.6 Hz, 2 H, H_2], 6.03 [d, ^4J(H,H) = 2.6 Hz, 4 H, H_4 and H_5 of Cp^{tt}], 1.31 (s, 36 H, C*Me*$_3$). − $^{13}C\{^1H\}$ NMR ($CDCl_3$): δ = 185.3 [d, J(C,Rh) = 73 Hz, Rh−*C*O], 148.6 (C_1 and C_3), 121.3 (C_2), 109.0 (C_4 and C_5), 34.6 (*C*Me$_3$), 32.3 (s, C*Me*$_3$). − MS (FAB^+, CH_2Cl_2, *m*/*z*,%): 826 (29) $[M^+]$, 770 (39) $[M^+ - 2CO]$, 742 (34) $[M^+ - 3CO]$, 714 (100) $[M^+ - 4CO]$, 649 (30) $[M^+ - Cp^{tt}]$, 565 (29) $[M^+ - Cp^{tt} - 3CO]$. − IR (CH_2Cl_2) $\tilde{\nu}_{(CO)}$: 2066 (s), 2041 (s), 1994 (s) cm^{-1}. − $C_{30}H_{42}O_4Rh_2S_2Zr$ (827.82): calcd. C 43.53, H 5.11, S 7.75; found C 43.60, H 5.12, S 7.82.

X-ray Structure Analysis of 3: X-ray quality crystals were obtained from a satured solution of **3** in diethyl ether at −25°C. Crystal data for **3**: $C_{27}H_{43}F_3O_3S_2Zr$, M = 627.95, monoclinic, space group $P2_1/n$, a = 12.1680(16), b = 16.594(3), c = 15.184(2) Å, β = 91.260(14)°, V = 3065.1(9) Å^3, T = 173 K, Z = 4, D_c = 1.361 g cm^{-3}, μ(Mo-K_α) = 0.538 mm^{-1}, graphite-monochromated Mo-K_α radiation (λ = 0.71073 Å). Data collected on a Siemens-Stoe AED-2 diffractometer. 8504 ref. collected, 5491 unique and used in the refinement. A ψ-scan absorption correction was applied (min. and max. transmission factors: 0.773, 0.862). The structure was solved by direct methods (SIR92) and refined by full-matrix least-squares on F^2 (SHELXL97). Anisotropic displacement parameters used for all non-hydrogen atoms. Hydrogens were refined riding on the corresponding atoms and included in the model in calculated positions, except that of the hydrosulfido ligand which has been located in a difference-Fourier map. Final R_1 = 0.0456 (4239 ref., $F_o > 4\sigma(F_o)$) and wR_2 = 0.1110 (all data). Crystallographic data for the reported structure have been deposited with the Cambridge Crystallographic Data Centre as supplementary publication no. CCDC-124105 Copies of the data can be obtained free of charge on application to CCDC, 12 Union Road, Cambridge CB2 1EZ, UK [Fax: (internat.) + 44-1223/336-033; E-mail: deposit@ccdc.cam.ac.uk].

Acknowledgments

Financial support from Dirección General de Enseñanza Superior (DGES) (Projects PB95−221−C1 and PB94−1186) and a fellowship from the Ministerio de Educación y Cultura (Dr. M. A. F. Hernandez-Gruel) are gratefully acknowledged.

[1] [1a] D. Zhang, D. B. McConville, J. M. Hrabusa, C. A. Tessier, W. J. Youngs, *J. Am. Chem. Soc.* **1998**, *120*, 3506. − [1b] A. Spannenberg, M. Oberthür, H. Noss, A. Tillack, P. Arndt, R. Kempe, *Angew. Chem.* **1998**, *110*, 2190; *Angew. Chem. Int. Ed.* **1998**, *37*, 2079. − [1c] L. M. Slaughter, P. T. Wolczanski, *Chem. Commun.* **1997**, 2109. − [1d] P. Desmurs, M. Visseaux, D. Baudry, A. Dormond, F. Nief, L. Ricard, *Organometallics* **1996**, *15*, 4178.

[2] [2a] Y. Yamaguchi, N. Suzuki, T. Mise, Y. Wakatsuki, *Organometallics* **1999**, *18*, 996. − [2b] W. A. Herrmann, B. Cornils, *Angew. Chem.* **1997**, *109*, 1074; *Angew. Chem. Int. Ed. Engl.* **1997**, *36*, 1049. − [2c] Ph. Kalck, C. Serra, C. Machet, R. Broussier, B. Gautheron, G. Delmas, G. Trouvé, M. Kubicki, *Organometallics* **1993**, *12*, 1021.

[3] [3a] A. Schneider, L. H. Gade, M. Breuning, G. Bringmann, I. J. Scowen, M. McPartlin, *Organometallics* **1998**, *17*, 1643. − [3b] V. I. Bakhmutov, M. Visseaux, D. Baudry, A. Dormond, Ph. Richard, *Inorg. Chem.* **1996**, *35*, 7316. − [3c] A. M. Baranger, T. A. Hanna, R. G. Bergman, *J. Am. Chem. Soc.* **1995**, *117*, 10041.

[4] [4a] D. W. Stephan, *Coord. Chem. Rev.* **1989**, *95*, 41. − [4b] D. W. Stephan, T. T. Nadasdi, *Coord. Chem. Rev.* **1996**, *147*, 147. − [4c] T. Ikada, S. Kuwata, Y. Mizobe, M. Hidai, *Inorg. Chem.* **1999**, *38*, 64.

[5] R. Atencio, M. A. Casado, M. A. Ciriano, F. J. Lahoz, J. J. Pérez-Torrente, A. Tiripicchio, L. A. Oro, *J. Organomet. Chem.* **1996**, *514*, 103.

[6] M. A. Casado, M. A. Ciriano, A. J. Edwards, F. J. Lahoz, J. J. Pérez-Torrente, L. A. Oro, *Organometallics* **1998**, *17*, 3414.

[7] G. Parkin, *Progr. Inorg. Chem.* **1998**, *47*, 1.

[8] The complex $[Cp^{tt}_2Zr(CH_3)_2]$ was described while this work was in progress:

[8a] W. A. King, S. Di Bella, A. Gulino, G. Lanza, I. L. Fragalà, C. L. Stern, T. J. Marks, *J. Am. Chem. Soc.* **1999**, *121*, 355. − [8b] P. J. Chirik, M. W. Day, J.E. Bercaw, *Organometallics* **1999**, *18*, 1873.

[9] G. A. Luinstra, U. Rief, M. H. Prosenc, *Organometallics* **1995**, *14*, 1551.

[10] 3D Search and Research Using the Cambridge Structural Database, F. H. Allen, O. Kennard, *Chemical Design Automation News* **1993**, *8 (1)*, pp 1 & 31−37.

[11] S. Komiya, J. C. Huffman, J. K. Kochi, *Inorg. Chem.* **1977**, *16*, 2138.

[12] M. J. Carney, P. J. Walsh, F. J. Hollander, R. G. Bergman, *Organometallics* **1992**, *11*, 761.

[13] D. Galli, L. Garlaschelli, G. Ciani, A. Fumagalli, S. Martinengo, A. Sironi, *J. Chem. Soc., Dalton Trans.* **1984**, 55.

[14] $[Cp^{tt}_2Zr(acac)]^+$: ^{1}H NMR ($CDCl_3$): δ = 7.07 (d, ^4J(H,H) = 2.7 Hz, 4 H, H_4 and H_5 Cp^{tt}), 6.27 (s, 1 H, C*H* acac), 6.01 (t, ^4J(H,H) = 2.7 Hz, 2 H, H_2 Cp^{tt}), 2.27 (s, 6 H, CH_3 acac), 1.11 (s, 36 H, CMe_3 Cp^{tt}). − ^{13}C{^{1}H} NMR ($CDCl_3$): δ = 195.6 (*C*O acac), 152.8 (C_1 and C_3), 112.9 (C_2), 111.7 (C_4 and C_5) (Cp^{tt}), 106.7 (*C*H acac) 34.1 (*C*Me$_3$), 30.6 (C*Me*$_3$) (Cp^{tt}), 26.6 (*C*H$_3$ acac). − MS (FAB$^+$, CH_2Cl_2, *m*/*z*,%): 543 (100) $[Cp^{tt}_2Zr(acac)^+]$.

[15] M. A. Casado, Ph.D. Thesis, University of Zaragoza, **1997**.

[16] I. F. Urazowski, V. I. Ponomaryev, I. E. Nifant′ev, D. A. Lemenovskii, *J. Organomet. Chem.* **1989**, *368*, 287.

[17] Yu. S. Varshavskii, T. G. Cherkasova, *Russ. J. Inorg. Chem.* **1967**, *12*, 899.

Received May 31, 1999
[I99191]

Clusters on Clusters: *closo*-Dodecaborate as a Ligand for Au_{55} Clusters

Günter Schmid,*[a] Raphaël Pugin,[a] Wolfgang Meyer-Zaika,[a] and Ulrich Simon[a]

Dedicated to Professor Gerhard Fritz on the occasion of his 80th birthday

Keywords: Gold clusters / *closo*-Dodecaborate / Conductivity / Charging energy

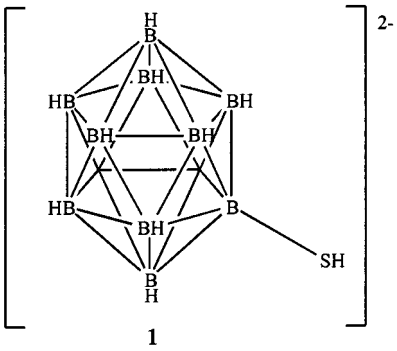
The exchange of PPh_3 in $Au_{55}(PPh_3)_{12}Cl_6$ by $Na_2[B_{12}H_{11}SH]$ using a phase-transfer reaction from CH_2Cl_2 to water needs 6 weeks for reaction, but finally results in the quantitative formation of $Au_{55}[(B_{12}H_{11}SH)Na_2]_{12}Cl_6$ (**2**). Cluster **2**, which is of considerable stability in aqueous solution, has been characterized by ^{1}H-NMR, ^{11}B-NMR, and IR spectroscopy as well as by transmission electron microscopy (TEM). The Na^+ cations can be exchanged by $(octyl)_4N^+$ making the resulting cluster **4** soluble in polar organic solvents. The electrical properties of **2** and **4** are compared with those of $Au_{55}[Ph_2PC_6H_4SO_3N(octyl)_4]_{12}Cl_6$ (**3**), the ammonium derivative of the sodium salt. Cluster **3** shows the expected increase of activation energy in the temperature range of 130–250 K owing to the increase of cluster spacing compared with the sodium derivative. However, clusters **2** and **4**, show electromigration in the electric field, caused by the huge amount of ionic charges in the ligand shell.

Introduction

Over the past decade, the effect of particle size on the electronic properties of ligand-protected metal clusters and colloids has been discussed as one of their most exciting physical properties.[1−6] Since the two-shell cluster $Au_{55}(PPh_3)_{12}Cl_6$[7] has a metal core diameter of 1.4 nm, which is of the order of characteristic length scales such as the de Broglie wavelength, the mean free path or the phase relaxation length, this cluster can be considered as a zero-dimensional quantum dot containing just a few metallic electrons.[4−6,8] Moreover, physical investigations such as impedance[4−6] or charge-transport measurements,[9] as well as scanning tunnelling spectroscopy,[10,11] have clearly indicated the existence of size effects for this cluster, where the protective ligand shell acts as a well-defined insulating barrier around the clusters. A protective ligand shell is an essential condition for control of the growth of the metal particles to prevent them from coalescence or Ostwald ripening. It is of fundamental interest to modify the nature and the thickness of this ligand shell in order to study its influence on the electronic properties. Understanding of this will allow the control of a specific size−property relationship of these solid-state nanomaterials enabling building blocks to be tailored for nanoelectronic devices.[4−6]

In the present work we report the use of disodium mercaptoundecahydro-*closo*-dodecaborate $Na_2[B_{12}H_{11}SH]$ (**1**) (BSH, see Figure 1) as a protective ligand to stabilize Au_{55} clusters for two main reasons: to elaborate new highly stable Au_{55} clusters with Au−S bonds by the use of different bulky ligands, and to follow our prospective work concerning the correlation between cluster spacing and charging energy determined by electronic intercluster tunnelling processes.

[a] Institut für Anorganische Chemie, Universität Essen
Universitätsstraße 5−7, D-45117 Essen, Germany
E-mail: guenter.schmid@uni-essen.de



1

Figure 1. Formal structure of the BSH ligand

A secondary aspect concerns the use of BSH in Boron Neutron Capture Therapy (BNCT).[12] This therapy is a binary treatment modality that can selectively irradiate tumour tissues. BNCT uses drugs containing the ^{10}B isotope that are capable of preferentially accumulating in the tumour which is then irradiated with low-energy neutrons. The interactions of the ^{10}B nucleus with a thermal neutron (neutron capture) causes it to split releasing a lithium nucleus and an alpha particle, so damaging the tumour cells. $Au_{55}[(B_{12}H_{11}SH)Na_2]_{12}Cl_6$ (**2**), described in the following, is highly soluble in water and contains 144 boron atoms per molecule, perhaps enabling a drastic increase of the boron concentration in tumour tissues.

Results and Discussion

In a previous work[13] we described the exchange of the PPh_3 ligands in $Au_{55}(PPh_3)_{12}Cl_6$ by $Ph_2PC_6H_4SO_3Na$ in a phase-transfer reaction to give the water-soluble gold cluster $Au_{55}(Ph_2PC_6H_4SO_3Na)_{12}Cl_6$. More recently, owing to the lability of the triphenylphosphane coordinated to the surface gold atoms and to the well-known affinity of thiol

 © WILEY-VCH Verlag GmbH, D-69451 Weinheim, 1999 1434−1948/99/1111−2051 $ 17.50+.50/0

$$\underset{CH_2Cl_2}{Au_{55}(PPh_3)_{12}Cl_6} + 12\ \underset{\substack{\mathbf{1}\\ water}}{(B_{12}H_{11}SH)Na_2} \xrightarrow[r.t.,\ 6\ weeks]{} \underset{\substack{\mathbf{2}\\ water}}{Au_{55}[(B_{12}H_{11}SH)_{12}Cl_6} + \underset{CH_2Cl_2}{PPh_3} \quad (1)$$

functions to gold atoms, we reported the synthesis of a new Au_{55} cluster protected by a thiol-functionalized oligosilsesquioxane ($T_8-OSS-SH$) ligand, causing excellent solubility in nonpolar hydrocarbons, such as pentane.[14]

Combining these two methods, we have now succeeded in synthesizing a novel *closo*-borate stabilized Au_{55} cluster by a phase-transfer reaction.

The phase-transfer reaction, which in the past has allowed us to substitute PPh_3 by $Ph_2PC_6H_4SO_3Na$, took two days,[13] whereas only two hours were necessary for the synthesis of the thiol-functionalized oligosilsesquioxane gold cluster in organic solvents.[14] Two reasons may be responsible for the extraordinary long reaction time to prepare **2**. First, in contrast to $T_8-OSS-SH$ where a propyl chain separates the thiol function from the bulky oligosilsesquioxane cage, the thiol group in **2** is directly coordinated to the *closo*-borane cluster, so that all bulky protective ligands are very close to the metal core. Second, electrostatic interactions should play a decisive role. Since each *closo*-borate ligand is doubly charged, the observed rapid exchange of half of the PPh_3 molecules by six $[BSH]^{2-}$ anions generates a twelve-fold negatively charged, water-soluble gold cluster. Repulsive electrostatic forces make it progressively more difficult to add additional $[BSH]^{2-}$ ligands. This last point is supported by the ^{1}H-NMR signals and by elementary analyses after different reaction times. Actually, both show that the first six PPh_3 ligands were substituted after a couple of days, one week more being necessary for the next three ones and a further five weeks more for the three last ones. Nevertheless, the expected $Au_{55}[(B_{12}H_{11}SH)Na_2]_{12}Cl_6$ cluster with a total of twenty four negative charges is formed in almost quantitative yield.

After the reaction time of six weeks the $^{13}C\{^1H\}$-NMR, as well as the $^{31}P\{^1H\}$-NMR, spectra of the product do not give any signal and so indicate the absence of PPh_3. This is supported by the ^{1}H-NMR spectrum, where signals for aromatic protons cannot be detected. Elementary analyses indicate only traces of carbon. On the other hand, the presence of BSH is clearly indicated by a broad multiplet in the ^{1}H-NMR spectrum between $\delta = 0.2$ and 2.8 and by the $^{11}B\{^1H\}$-NMR spectrum showing a broad signal between $\delta = -20$ and -11 and a singlet at $\delta = -7.8$. Compared with the spectrum of free BSH the multiplicity is lost due to the coordination to a large metal cluster. The broad ^{11}B-NMR signal can be attributed to the three initial doublets of the free BSH (see Experimental Section). The singlet at $\delta = -7.8$ is caused by the B atom directly bound to the thiol function. In contrast to the corresponding singlet for free BSH ($\delta = -9.6$), it is low-field shifted owing to the coordination of the thiol group to gold. Infrared investigations resulted in bands at $\tilde{\nu} = 2500.6$ (ν B−H), 1061.7 (ν asym. B−S), 973.2 and 947.9 (δ asym. B−S), 836.5 and 723 cm^{-1} (ν B−B). The signals of $Au_{55}(PPh_3)_{12}Cl_6$ at 1584.9 and 1478.7 (ν C=C arom.), 1434.7 and 1097.9 (ν P−Ph), 1328.5, 1026.4, and 690.3 cm^{-1} (δ C−H) could not be observed.

Practical advantages of the new cluster **2** are the solubility and the improved stability. It is soluble in numerous polar solvents like acetone, ethanol, acetonitrile, or methanol, but also in water which allows us to expect possible clinical applications. Transmission electron microscopy (TEM) investigations showed exclusively 1.4 nm particles (Figure 2). Figure 3 shows a model of the relevant cluster part $[Au_{55}(B_{12}H_{11}SH)_{12}]^{24-}$.

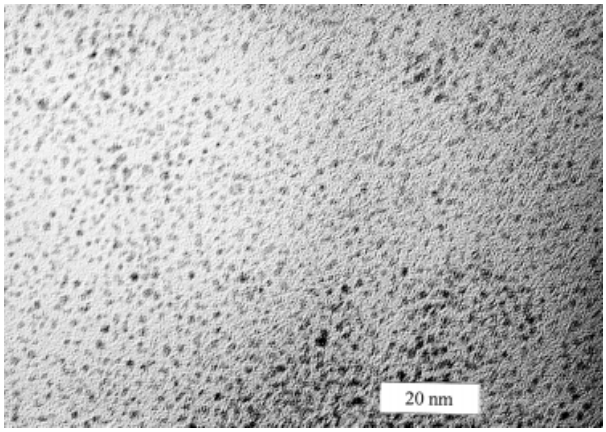


Figure 2. TEM image of $Au_{55}[(B_{12}H_{11}SH)Na_2]_{12}Cl_6$ clusters indicating the monodispersity

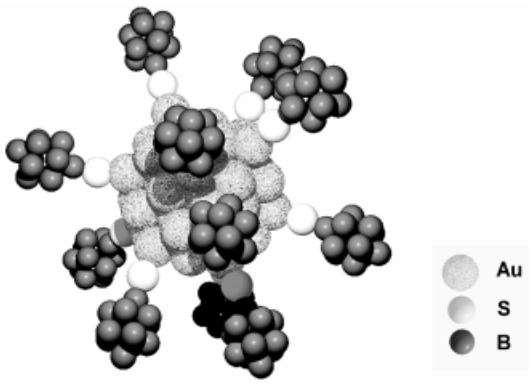


Figure 3. Computer model of the cluster part $[Au_{55}(B_{12}H_{11}SH)_{12}]^{24-}$; the H atoms are omitted

No aggregation was observed in cluster solutions over several months. Compared to the very labile $Au_{55}(PPh_3)_{12}Cl_6$, which aggregates in solution after a couple of hours, this most remarkable change allows reliable investigations not only in the solid state, but also in solutions. Thus, by UV measurements the characteristic plasmon resonance between 500−600 nm of colloids could be excluded.

The unusual stability of **2** compared with $Au_{55}(PPh_3)_{12}Cl_6$ is explained by the greater affinity of thiol func-

$$Au_{55}(Ph_2PC_6H_4SO_3Na)_{12}Cl_6 + 12\ BrN(octyl)_4 \rightarrow Au_{55}[Ph_2PC_6H_4SO_3N(octyl)_4]_{12}Cl_6 + 12\ NaBr \quad (2)$$

water — CH_2Cl_2 — **3** CH_2Cl_2 — water

$$Au_{55}[(B_{12}H_{11}SH)Na_2]_{12}Cl_6 + 24\ BrN(octyl)_4 \rightarrow Au_{55}[(B_{12}H_{11}SH)\{N(octyl)_4\}_2]_{12}Cl_6 + 24\ NaBr \quad (3)$$

water — CH_2Cl_2 — **4** CH_2Cl_2 — water

tions to bind surface gold atoms compared with phosphanes and in particular it is the repulsive electrostatic forces between the 24-fold negatively charged clusters. This is probably the main reason why coalescence between clusters is efficiently suppressed since approaches of two clusters are prevented. Similar explanations allowed us in previous works to compare the stability of $Au_{55}(PPh_3)_{12}Cl_6$ to those of the water soluble $Au_{55}(Ph_2PC_6H_4SO_3Na)_{12}Cl_6$.[13] Actually, although $Au_{55}(PPh_3)_{12}Cl_6$ degrades after two hours if dissolved, the water-soluble cluster stays stable in solution without significant aggregation over weeks. Comparison with cluster **2** suggests that this is probably due to the combination of strong and bulky ligands and of repulsive Coulomb forces.

To investigate the chemical properties and to see if the size of the ligand shell could still be increased, we tried to exchange Na^+ by the bulkier tetraoctylammonium cation. For comparison, this was first realized with the water-soluble cluster $Au_{55}(Ph_2PC_6H_4SO_3Na)_{12}Cl_6$.

This phase-transfer reaction was completed after 3 h and cluster **3** was isolated in almost quantitative yield as a dark-brown solid. The integration of the aryl and alkyl ^{1}H-NMR signals gave a 1:1 ratio of $Ph_2PC_6H_4SO_3^-$ and $[(octyl)_4N]^+$. Moreover, the elementary analyses agreed well with the expected values. Based on these promising results the corresponding phase-transfer reaction was attempted with $Au_{55}[(B_{12}H_{11}SH)Na_2]_{12}Cl_6$ (**2**). The reaction worked as well as that in Equation 2. Cluster **4** was obtained in good yield and was characterized by ^{1}H NMR and TEM. This cation-exchange reaction did not induce any aggregation of the particles and the size distribution of **4** was found by TEM to be as good as that of **2**.

The availability of these new compounds raised the question of how the charge-transport properties are affected by the modified ligand shell as compared to $Au_{55}(PPh_3)_{12}Cl_6$. As described earlier,[4–6,15] single-electron charging effects occur in three-dimensional dense packings of ligand-stabilized metal clusters. The charging energy, involving a thermally activated tunnelling process through the insulating ligand shell, corresponds to the activation energy E_A of the conductivity of the cluster arrangements and therefore depends on the cluster size, as well as on the cluster spacing. While the size is determined by the number of the metal atoms forming the cluster, i.e. 55 in the materials discussed here, the cluster spacing corresponds to the thickness of the ligand shell. Therefore, by modifying the thickness of the ligand shell, a correlation between cluster spacing and charging energy could be established. Actually, a charging energy of 0.15 eV was observed for $Au_{55}(PPh_3)_{12}Cl_6$, having a 0.35 nm thick ligand shell, i.e. a cluster spacing of 0.7 nm. This value increases linearly with the spatial separation of the metallic cores up to 0.26 eV for the previously described $Au_{55}(T_8{-}OSS{-}SH)_{12}Cl_6$, which corresponds to a cluster spacing of 2.8 nm.[16]

This shows that the charging energy in three-dimensional cluster arrangements can be tailored chemically by varying the cluster spacing due to incorporation of bulky ligands or by introduction of spacer molecules. In this context the electrical properties of the clusters **2**, **3**, and **4** are of considerable interest. In contrast to the materials we have examined before, it was not possible to obtain mechanically stable pellets with dense cluster packing. Therefore the clusters were dissolved and then deposited on interdigital microelectrodes (see Experimental Section). Whilst an optically homogeneous layer of **2** with an average thickness of 50–100 μm was formed, **3** and **4** remained as highly viscous films on the microelectrode structure. The temperature dependence of the conductivity was determined in a temperature range of 130–293 K.

According to earlier measurements a temperature dependence $\sigma(T) \sim (T_0/T)^\gamma$ was expected (Mott's conductivity law). At low temperature $\gamma = 1/d + 1$, where d is the dimensionality of the system, reflecting a variable-range hopping process. Going to higher temperatures up to room temperature, the charge transport is dominated by nearest neighbour hops of single electrons instead of hops of variable range, thus being simply activated with $\gamma = 1$ (Arrhenius behaviour). Here the activation energy E_A ($= k_B T_0$) is the energy to transfer one electron from an initially neutral cluster to a next neighbouring neutral cluster via the insulating ligand shell.[15][17] Thus, E_A represents the charging energy, or chemically speaking, the disproportionation energy, which is size and distance dependent.

All samples show significant conductivity at room temperature and thermally activated behaviour. No evaluable results could, however, be obtained from samples **2** and **4** due to pronounced conductance fluctuations during the measurements. This, at a first glance, might be attributed to the huge amount of ionic charges provided by the 12 two-fold negatively charged borate ligands on each cluster. This may lead to electromigration of the clusters in the electric field during the measurements, leading to a fluctuating degree of disorder in the samples. A detailed analysis of this problem will be subject of our future works.

In contrast, the measurements on cluster **3**, which has just 12 instead of 24 charges on its ligand shell, showed a reliable temperature dependence. However, neither a $\sigma(T) \approx 1/T$ nor a $\sigma(T) \approx 1/T^{1/4}$ behaviour could be observed over

the whole temperature range. As displayed in Figure 4, it seems to be possible to divide the temperature range tentatively into a high-temperature and a low-temperature part; in the low-temperature part, which ranges from 130 K up to approx. 250 K an E_A of 0.16 eV could be deduced, while

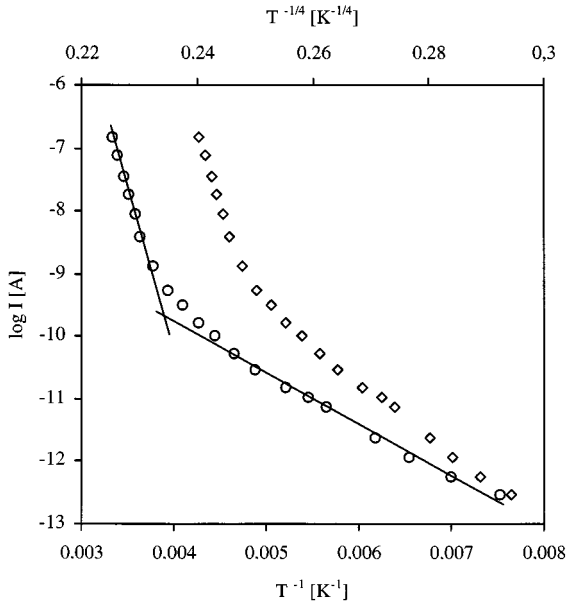


Figure 4. Temperature-dependent current I at a constant voltage U = 5 V of **3** according to the Arrhenius relation (circles) and according to Mott's conductivity law (rhombs); below 250 K E_A = 0.16 eV and above E_A = 0.95 eV

the high-temperature part above displays an E_A of 0.95 eV.

Although it is difficult to determine the exact size of the highly flexible ammonium octyl chains, a cluster spacing of 2.90 ± 0.01 nm might be derived from geometrical considerations if the alkyl chains are stretched. With respect to the previously described linear dependence of the E_A of the cluster spacing, an E_A of 0.24 ± 0.02 eV is expected, which is significantly higher than the 0.16 eV determined here. Thus it seems evident that the alkyl chains are folded and lie close to the central nitrogen atom to give an effective cluster spacing, which is comparable to that in the sodium derivative, even though Na^+ is considerably smaller than $N(octyl)_4^+$. It may also be that the ammonium ions interact strongly with the phenyl rings by hydrophobic−hydrophobic interactions, whereas the Na^+ ion in **2** occupies a position at the periphery of the ligand shell. The rapid increase of E_A above 250 K might originate from an electromigration process during the measurements resulting in disorder, with an increased cluster to cluster and an increased cluster to electrode spacing. Structural deviations from ideal arrangements induce huge effects in the electrical response, especially in the nanometre size range.[18,19,20] Keeping in mind that cluster **3** is a highly viscous liquid instead of a solid, like the Na^+ analogue, it seems to be consistent that this kind of field-induced disorder appears in the octyl ammonium form **3** and not in the Na^+ form.

Conclusions

The series of known Au_{55} clusters bearing 12 $B_{12}H_{11}SH^{2-}$ ions as ligands has been extended by the synthesis of a very special example: the cluster $Au_{55}[(B_{12}H_{11}SH)Na_2]_{12}Cl_6$ (**2**) and its tetraoctylammonium derivative consisting of a 24-fold negatively charged anion with 144 B atoms per molecule. This high concentration of B atoms and the very good solubility in water, accompanied by a remarkable stability, makes this cluster a promising candidate for boron neutron capture therapy. The synthesis succeeds via the exchange of PPh_3 in $Au_{55}(PPh_3)_{12}Cl_6$ by the borate, based on a phase-transfer reaction from dichloromethane to water. The bulkiness of the thiols and especially its two-fold negative charge result in a six-week reaction time. Nevertheless, the reaction is quantitative. ^{1}H- and ^{11}B-NMR spectra, elementary analyses, and transmission electron microscopy have been used to prove the composition and size of the clusters. The sodium cations can be exchanged by tetraoctylammonium making the cluster **4** oily, but also soluble in polar solvents like acetone or alcohols.

In addition to the novel clusters **2** and **4** we synthesized the cluster $Au_{55}[Ph_2PC_6H_4SO_3N(octyl)_4]_{12}Cl_6$ (**3**) to enable a comparison of its electrical properties with those of **2** and **4**. Cluster **3** consists of a twelve-fold negatively charged anion, whereas **2** and **4** have the extreme charge of −24.

The electrical properties of the new compounds **2** and **4** are significantly different from the properties of the clusters investigated previously. While cluster **3** shows an activation energy in the temperature range of 130−250 K which is comparable to the corresponding Na^+ form, above that temperature the microstructure of the samples seems to be affected by the electric field due to electromigration. The latter is also assumed to be the reason for the extraordinary behaviour of **2** and **4**. Although this is just a tentative explanation for the properties observed, it may hint to a principle limit of modifiability of the ligand shell with respect to the possible application in nanoelectronic devices, since the huge amount of ionic charges in the ligand shell seems to induce structural instabilities in the samples under test

Experimental Section

General: $(B_{12}H_{11}SH)Na_2$ (BSH) was commercially available from BORON BIOLOGICALS. As it is highly hygroscopic all reactions were performed using standard Schlenk techniques. Before use it was characterized by NMR spectroscopy: ^{1}H NMR (D_2O): δ = 0.25−1.92 (br. m, 12 H, BH and SH). ^{11}B{^{1}H} NMR (D_2O): δ = −19.55 (d, 1 B, −BH), ^1J(BH) = 125.2 Hz, −16.00 (d, 5 B, −BH), ^1J(BH) = 134.8 Hz, −14.00 (d, 5 B, −BH), ^1J(BH) = 135.0 Hz, −9.6 (s, 1 B, B−SH). − The solvents were dried and purified by standard procedures. − NMR spectra were recorded with a Bruker DPX working at 300 MHz for ^{1}H, 75.5 MHz for ^{13}C{^{1}H}, 121.5 MHz for ^{31}P{^{1}H} and 96.3 MHz for ^{11}B{^{1}H}. − Infrared spectra were recorded on a BIO-RAD FTS-175 spectrometer. − TEM images were obtained using a Philips CM 200 FEG microscope working with 200 kV accelerating voltage and to confirm the absence of colloidal particles, electronic spectra of cluster solutions

were measured on a Varian Cary-1 UV/Vis spectrometer. − Elementary analyses were carried out by the Analytical Laboratory of the Fachbereich Chemie of the University of Essen. − For electrical measurements the samples were deposited from solvent on gold interdigital microelectrodes (structural width = 10 μm) on a quartz substrate.[21,22] After drying the samples in vacuum they were kept under argon during the measurements. Current measurements were performed in a voltage range of ± 5 V using a Keithley 6517 electrometer with an integrated voltage source in a low-temperature measuring cell.

$Au_{55}(PPh_3)_{12}Cl_6$ and $Au_{55}(Ph_2PC_6H_4SO_3Na)_{12}Cl_6$ were synthesized according to described procedures.[7][13]

$Au_{55}[(B_{12}H_{11}SH)Na_2]_{12}Cl_6$ (2): To a solution of 16.7 mg (76.09 μmol) of $[(B_{12}H_{11}SH)Na_2]$ (**1**), dissolved in 125 mL of distilled water and placed in a 250-mL flask, a solution of 80 mg (5.64 μmol) of $Au_{55}(PPh_3)_{12}Cl_6$, dissolved in 60 mL of CH_2Cl_2, was added under vigorous stirring. After 4−6 days the water phase showed a dark brown colour. After a total reaction time of 6 weeks, the emulsion was placed in a separating funnel to separate the water phase carefully from the colourless organic phase and to wash it 4 times with 30 mL of CH_2Cl_2 to remove PPh_3. The solvent was removed under vacuum at room temperature. The brown product was then dissolved in 25 mL of distilled water and filtered through an ANOTOPE® filter (Merck, 20 nm porous diameter) and was precipitated by CH_2Cl_2 and separated. The filtration pad was washed with copious amounts of CH_2Cl_2 and the fine microcrystalline black powder dried overnight under vacuum. Yield: 52 mg (68%). − IR (KBr): $\tilde{\nu}$ = 2500.6 cm^{-1}, vs (ν B−H), 1061.7, m (ν asym B−S), 973.2, w and 947.9, w (δ asym B−S), 836.5, m and 723, w (ν B−B). − ^1H NMR (D_2O): δ = 0.20−2.80 (br. m, 12 H, BH and SH). $^{11}B\{^1H\}$ NMR (D_2O) (10 mm ∅ NMR tube): δ = −20 to −11 (br. m., 11B, *o*-, *m*-, *p*- BH), −7.8 (s, 1 B, B−SH). − ^{31}P- and ^{13}C-NMR signals could not be observed. $Au_{55}B_{144}Cl_6H_{144}Na_{24}S_{12}$ (13683.26 g mol^{-1}): calcd. C 0.00, H 1.05, S 2.81, Na 4.10, Au 79.17; found C 1.30, H 1.26, S 2.72, Na 5.16, Au 77.01.

$Au_{55}[Ph_2PC_6H_4SO_3N(octyl)_4]_{12}Cl_6$ (3): To a solution of 50.0 mg (3.24 μmol) of $Au_{55}(Ph_2PC_6H_4SO_3Na)_{12}Cl_6$, dissolved in 50 mL of distilled water and placed in a 200-mL flask, a solution of 21.5 mg (39.32 μmol) of $[(octyl)_4N]Br$, dissolved in 50 mL of CH_2Cl_2, was added under vigorous stirring. After 3 h the water phase was colourless whereas the organic phase was dark brown. The emulsion was placed in a separating funnel, the organic phase was carefully separated from the colourless water phase and washed 4 times with 30 mL of distilled H_2O to remove NaBr. The solvent was removed at room temperature under vacuum. The brown product was then dissolved in 20 mL of CH_2Cl_2 and filtered through an ANOTOPE® filter (Merck, 20 nm porous diameter). The solvent was evaporated under vacuum and the gold cluster **3** was precipitated by pentane and separated. The filtration pad was washed with copious amounts of pentane, the black microcrystalline powder was dried overnight under vacuum. Yield: 57 mg (85%). This cluster is slightly soluble in benzene and soluble in polar solvents like CH_2Cl_2, $CHCl_3$, acetone, or acetonitrile. − IR (KBr): $\tilde{\nu}$ = 3000−2850 cm^{-1}, s (ν C−H), 1584.7, m and 1478.5, m (ν C=C arom), 1434.8, s and 1097.9, s (ν P−Ph), 1370.0, m (δ C−H), 1328.5, w 1026.6, w and 690.4, vs (δ C−H). − ^1H NMR ($CDCl_3$): δ = 0.85 (t, 12 H, $N[(CH_2)_7CH_3]_4$), 1.26−1.62 (br, 48 H, $N[CH_2(CH_2)_6CH_3]_4$), 3.27 (br, 8 H, $N[CH_2(CH_2)_6CH_3]_4$), 7.30−8.30 (m, 14 H, $Ph_2PC_6H_4SO_3$). − $^{31}P\{^1H\}$ NMR ($CDCl_3$): δ = 35.90 (s, $Ph_2PC_6H_4SO_3$). − $C_{600}H_{984}Au_{55}Cl_6N_{12}O_{36}P_{12}S_{12}$ (20737.3 g mol^{-1}): calcd. C 34.75, H 4.75, N 0.8, S 1.84, Na 0.00, Au 52.24; found C 34.40, H 4.78, N 0.9, S 1.44, Na 0.19, Au 50.32.

$Au_{55}[(B_{12}H_{11}SH)(N(octyl)_4)_2]_{12}Cl_6$ (4): To a solution of 40.0 mg (2.92 μmol) of $Au_{55}[(B_{12}H_{11}SH)Na_2]_{12}Cl_6$ (**2**) dissolved in 40 mL of distilled water and placed in a 200-mL flask, a solution of 40 mg (70.16 μmol) of $[(octyl)_4N]Br$, dissolved in 40 mL of CH_2Cl_2, was added under vigorous stirring. After 3 h reaction, the water phase was colourless, the organic phase presented a dark brown colour. Then, the emulsion was placed in a separating funnel, the organic phase was carefully separated from the colourless water phase and washed 4 times with 30 mL of distilled H_2O in order to remove NaBr. The solvent was removed at room temperature under vacuum. The brown product was dissolved in 20 mL of CH_2Cl_2 and filtered through an ANOTOPE® filter (Merck, 20 nm porous diameter). After removing the solvent under vacuum, **4** was precipitated by pentane but could not be isolated as a powder. A dark-brown oil was obtained which was washed several times with a few mL of pentane and dried overnight under vacuum. This cluster was slightly soluble in benzene and soluble in polar solvents like CH_2Cl_2, $CHCl_3$, acetone, or acetonitrile. − IR (KBr): $\tilde{\nu}$ = 3000−2850 cm^{-1}, s (ν C−H), 2500.0, vs (ν B−H), 1375.0, m (δ C−H), 1060.5, m (ν asym B−S), 972.1, w and 946.5, w (δ asym B−S), 836.0, m and 723, w (ν B−B). ^1H NMR ($CDCl_3$): δ = 0.10−2.25 (br, 132 H, BH and SH, $N[(CH_2)_7CH_3]_4$, $N[CH_2(CH_2)_6CH_3]_4$), 3.30 (br, 16 H, $N[CH_2(CH_2)_6CH_3]_4$). Due to its viscous nature elemental analyses could no be performed.

Acknowledgments

Financial support by the Deutsche Forschungsgemeinschaft (Sonderforschungsbereich 452) and the Fonds der Chemischen Industrie is gratefully acknowledged.

[1] G. Schmid (Ed.), *Clusters and Colloids − From Theory to Applications*, VCH, Weinheim, **1994**.
[2] L. J. de Jongh (Ed.) in *Physics and Chemistry of Metal Cluster Compounds*, Kluwer Academic Publ., Dordrecht, **1994**.
[3] Y. Volokitin, J. Sinzig, L. J. de Jongh, G. Schmid, I. I. Moiseev, *Nature* **1996**, *384*, 621.
[4] G. Schön, U. Simon, *Colloid Polym. Sci.* **1995**, *273*, 101.
[5] G. Schön, U. Simon, *Colloid Polym. Sci.* **1995**, *273*, 202.
[6] U. Simon, *Adv. Mater.* **1998**, *10*, 1487.
[7] G. Schmid, R. Boese, R. Pfeil, F. Bandermann, S. Meyer, G. H. M. Calis, J. W. A. van der Velden, *Chem. Ber.* **1981**, *114*, 3634.
[8] U. Simon, G. Schmid, G. Schön, *Angew. Chem., Int. Ed. Engl.* **1993**, *32*, 250.
[9] R. P. Andres, Th. Bein, M. Dorogi, S. Feng, J. I. Henderson, C. P. Kubiak, W. Mahoney, R. G. Osifchin, R. Reifenberger, *Science*, **1996**, *272*.
[10] R. Houbertz, T. Feigenspan, F. Mielke, U. Memmert, U. Hartmann, U. Simon, G. Schön, G. Schmid, *Europhys. Lett.* **1994**, *28, 9*, 641.
[11] L. F. Chi, M. Hartig, T. Drechsler, Th. Schaak, C. Seidel, H. Fuchs, G. Schmid, *Appl. Phys. Lett. A* **1998**, *66*, 187.
[12] A. H. Soloway, W. Tjarks, B. A. Barnum, F.-G. Rong, R. F. Barth, I. M Codogni, J. G. Wilson, *Chem. Rev.* **1998**, *98*, 1515.
[13] G. Schmid, N. Klein, L. Korste, U. Kreibig, D. Schönauer, *Polyhedron* **1988**, *7*, 605.
[14] G. Schmid, R. Pugin, J.-O. Malm, J.-O. Bovin, *Eur. J. Inorg. Chem.* **1998**, *6*, 813.
[15] M. P. J. van Staveren, H. B. Brom, L. J. de Jongh, *Physics Reports* **1991**, *208*, 1.
[16] G. Schmid, *J. Chem. Soc., Dalton Trans.* **1998**, 1077.
[17] U. Simon, R. Flesch, H. Wiggers, G. Schön, G. Schmid, *J. Mater. Chem.* **1998**, *8*, 517.
[18] V. Gasparian, U. Simon, *Physica B* **1997**, *249*, 289.
[19] U. Simon, V. Gasparian, *Phys. Stat. Sol. B* **1998**, *205*, 223.
[20] R. Pelster, U. Simon, *Colloid Polym. Sci.* **1999**, *277*, 2.
[21] C. Plog, W. Maunz, P. Kurzweil, E. Obermeier and C. Scheibe, *Sensors and Actuators, B* **1995**, *24*, 584.
[22] U. Simon, U. Flesch, W. Maunz, R. Müller, C. Plog, *Microporous Mesoporous Mater.* **1998**, *21*, 111.

Received May 31, 1999
[I99199]

Sulfur Compounds, 209[+]
The Gas Phase Acidities of the Sulfanes H_2S_n (n = 1–4)

André H. Otto[a] and Ralf Steudel*[a]

Keywords: Sulfur / Sulfanes / Acidity / Ab initio MO calculations / Hyperconjugation

The gas-phase acidities ΔG_{acid}(298 K) of the sulfanes H_2S_n (n = 1–4) have been calculated by ab initio molecular orbital theory using the G2 and G2(MP2) methods, which were applied to the geometries of lowest energy. The results show that the higher sulfanes are surprisingly strong proton donors. The acidities (in kJ mol^{-1}) are as follows: H_2S (1444), H_2S_2 (1406), H_2S_3 (1370), H_2S_4 (1347). The latter three values may be compared to those of other strong Brønsted acids like gaseous HNO_2 (1396), HCl (1371), and HBr (1332). The monoanions HS_n^- exhibit an interesting bond length distribution as a consequence of the charge delocalization by hyperconjugation, which in turn may be responsible for the high acidities of the sulfanes.

Introduction

The hydrogen polysulfides or sulfanes H_2S_n ($n > 1$) form a long series of homologous chain-like molecules since the number of sulfur atoms can practically assume any value. Only the lower members with $n = 2-6$ have been prepared as pure compounds.[1] Under standard conditions they form colorless to light yellow liquids. H_2S_2, H_2S_3, and H_2S_4 can be distilled in vacuo. However, all members with n values up to 35 have been detected by ^{1}H-NMR spectroscopy in so-called crude sulfane.[2] These higher members of the series are often called polysulfanes.

For a long time these species were considered to be of academic interest only until it was suspected that H_2S_2 is present in certain "sour gases"[3] while the higher members were detected in the elemental sulfur produced from sour gas. Sour gas is a natural gas that contains substantial concentrations of H_2S (up to 50%). It is produced in large quantities, for instance, in Northern Germany, in Alberta (Canada), and in The United States. If the underground reservoir of the gas also contains elemental sulfur, the following equilibrium will be established (Equation 1).

$$H_2S\,(g.) + 1/8\ S_8\,(s.) \rightleftharpoons H_2S_2\,(l.) \qquad (1)$$

The very high pressure in the underground gas bearing deposits shifts this equilibrium to the right. Since H_2S_2 is a volatile compound, the gas seems to transport elemental sulfur when it is produced.[4] However, during production the gas is partly decompressed and cools down resulting in decomposition of any sulfanes H_2S_n with precipitation of elemental sulfur. This process sometimes causes severe plugging of pipes and valves by solid sulfur. Before such a natural gas can be used as a fuel or as a reagent in the chemical industry the H_2S must be extracted by treatment with ethanolamine or similar solvents, which on heating liberate the H_2S again. This almost pure H_2S is then oxidized by the Claus process to elemental sulfur (Equation 2).

$$H_2S + 1/2\ O_2 \rightarrow 1/n\ S_m + H_2O \qquad (2)$$

The sulfur (S_m) produced by this method is obtained in the liquid form. It consists mainly of S_8 molecules but other homocycles, like S_7, S_6, and larger rings, are also present.[5] However, since reaction (2) will never be complete the liquid sulfur produced also contains some H_2S, which is present mainly as a mixture of long-chain polysulfanes H_2S_n.[6]

$$H_2S\,(g.) + x\ S_m\,(l.) \rightleftharpoons H_2S_n\,(l.) \qquad (3)$$

Due to the high toxicity of H_2S and to the danger of explosions, both the polysulfanes and the H_2S must be removed almost quantitatively from the liquid sulfur, a goal that is achieved by purging with air.[7]

The gas phase structures of the first three members of the sulfane series are well-known from either microwave spectra (H_2S_2,[8] H_2S_3[9]) or high-level ab initio MO calculations (H_2S_4[10]). While H_2S_2 adopts a conformation of C_2 symmetry similar to that of H_2O_2, the higher members H_2S_3 and H_2S_4 exist as equilibrium mixtures of several conformational isomers of almost identical energy. All sulfane molecules are characterized by torsional angles at the S–S bonds of 90°(±10°), but these angles may be positive or negative resulting in the aforementioned conformational variety. The signs of the torsional angles define the so-called motif, which characterizes each conformational isomer. For H_2S_2 the two isomers with $\tau = \pm 90°$ are enantiomers. In the case of H_2S_3 the motif may be either + + (symmetry C_2; the enantiomer has the motif − −) or + − (identical to motif − +; both are of C_s symmetry). In the case of H_2S_4 the motif may be + + + (or − − −; these are enantiomers and of C_2 symmetry), + + − (or − − +; C_1) or +

[+] Part 208: R. Steudel, K. Hassenberg, J. Pickard, *Organometallics,* in press.

[a] Institut für Anorganische und Analytische Chemie, Sekr. C2, Technische Universität Berlin, D-10623 Berlin, Germany
E-mail: steudel@schwefel.chem.tu-berlin.de

 © WILEY-VCH Verlag GmbH, D-69451 Weinheim, 1999 1434–1948/99/1111–2057 $ 17.50+.50/0

− + (identical to − + −; C_s); these conformational isomers are shown in Figure 1.

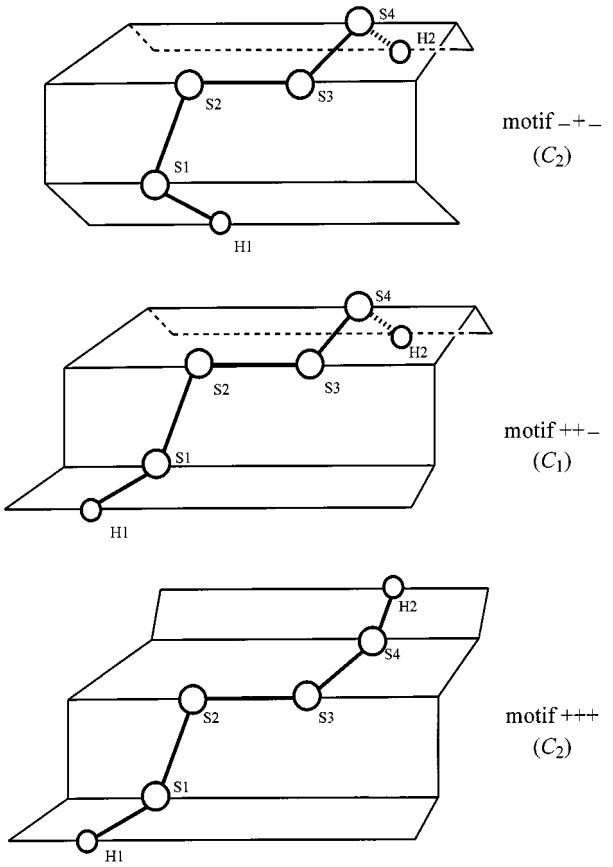


Figure 1. Conformational isomers of H_2S_4 according to a high-level ab initio MO calculation (ref.[10]); the isomer of C_1 symmetry is of lowest energy at 0 K

Hydrogen sulfide, H_2S, is a weak acid in water with pK_a values of 7 and 17 for the first and second dissociation steps (Equations 4, 5).[11]

$$H_2S + H_2O \rightleftharpoons H_3O^+ + HS^- \qquad pK_a = 7 \qquad (4)$$

$$HS^- + H_2O \rightleftharpoons H_3O^+ + S^{2-} \qquad pK_a = 17 \qquad (5)$$

The corresponding pK_a values of the higher sulfanes are not known with certainty. The only related information available comes from the investigation of aqueous polysulfide solutions, which formally contain the dianions of the polysulfanes. In 1960 Schwarzenbach and Fischer[12] titrated aqueous solutions of pure alkali polysulfides (Na_2S_n and K_2S_n with $n = 2-5$) with hydrochloric acid in a flow system and measured the pH value of the mixtures obtained. From these data they derived the following pK_a values for the first and second deprotonation reactions of H_2S_4 and H_2S_5.

		pK$_a$(1)	pK$_a$(2)
$H_2S_4 + H_2O \rightleftharpoons H_3O^+ + HS_4^-$		3.8	
$HS_4^- + H_2O \rightleftharpoons H_3O^+ + S_4^{2-}$			6.3
$H_2S_5 + H_2O \rightleftharpoons H_3O^+ + HS_5^-$		3.5	
$HS_5^- + H_2O \rightleftharpoons H_3O^+ + S_5^{2-}$			5.7

These authors assumed that their starting solutions did not contain any other anions besides HS^-, S_4^{2-}, and S_5^{2-}. Today it is known that this assumption is a crude approximation.[13][14] Therefore, the results obtained by these authors must be considered as approximate. Nevertheless, it became clear that the acidity of the H_2S_n species increases markedly with increasing number of sulfur atoms.

The gas phase acidity of sulfanes is defined as the Gibbs free energy of the dissociation reaction (Equation 6).

$$H_2S_n \rightarrow HS_n^- + H^+ \qquad (6)$$

In the vapor phase the acidity of H_2S has been determined experimentally as $\Delta G_{acid}(298\ K) = 1443 \pm 8$ kJ mol^{-1}.[15] Similar values[16] have been obtained by ab initio MO calculations.[17,18,19]

In the case of H_2S_2 the mass spectrometric investigation of the reaction of the anion HS_2^- with a number of proton donors of known acidity has resulted in a value of ΔG_{acid} of 1418±13 kJ mol^{-1} at 298 K.[20] No experimental or theoretical data are available for the gas phase acidities of H_2S_3 and H_2S_4.

We have studied the gas phase acidities of H_2S, H_2S_2, H_2S_3, and H_2S_4 by theoretical methods. Such data are of significance for studying the problem of corrosion of steel by sour gas containing these species.

Computational Methods

Ab initio molecular orbital calculations were performed at the G2[21] and G2(MP2)[22] levels of theory using the GAUSSIAN program system.[23] The G2 method essentially implies an energy calculation at the QCISD(T)/6-311+G(3df,2p) level of geometries optimized at the

Table 1. Gibbs free energies (hartrees) at 298 K of the species H_2S_n and HS_n^- ($n = 1-4$)

System	Symmetry	G2(MP2)	G2
H_2S	C_{2v}	−398.943608	−398.950239
HS^-	$C_{\infty v}$	−398.382201	−398.389429
H_2S_2	C_2	−796.684079	−796.696107
HS_2^-	C_s	−796.137611	−796.150449
H_2S_3	C_2	−1194.434343	−1194.451534
HS_3^-	C_1	−1193.901631	−1193.919657
H_2S_4 (+ − +)	C_2	−1592.186658	−1592.208909
H_2S_4 (+ − −)	C_1	−1592.186948	−1592.209235
HS_4^- (+ −)	C_1	−1591.662292	−1591.685518

Table 2. Bond distances [pm], bond angles [°] and torsion angles [°] of the species H_2S_n and HS_n^- ($n = 2-4$)

Parameter	H_2S_2 (C_2)	HS_2^- (C_s)	H_2S_3 (C_2)	HS_3^- (C_1)	H_2S_4 (C_2)	H_2S_4 (C_1)	HS_4^- (C_1)
S(1)−S(2)	206.9	210.9	206.8	213.6	206.7	206.5	210.8
S(2)−S(3)			206.8	204.1	206.5	206.7	207.6
S(3)−S(4)					206.7	206.8	204.0
S−H	134.4	135.1	134.5	134.9	134.5	134.5	134.6
S(1)−S(2)−S(3)			107.5	111.1	107.0	107.2	108.2
S(2)−S(3)−S(4)					107.0	106.9	109.9
H(1)−S(1)−S(2)	99.0	102.9	99.0	100.1	98.4	98.4	97.7
H(2)−S(4)−S(3)					98.4	99.0	
H(1)−S(1)−S(2)−H(2)	99.4						
H(1)−S(1)−S(2)−S(3)			85.4	76.1	93.3	89.7	73.4
H(2)−S(4)−S(3)−S(2)			85.4		93.2	−83.6	
S−S−S−S					−82.1	−81.4	−75.7

MP2(full)/6-31G(d) level. Harmonic vibrational wavenumbers were obtained at the HF/6-31G(d) level and were scaled by a factor of 0.8929. The G2(MP2) method is a modified version of G2 but uses the second order Møller−Plesset perturbation theory (MP2) for the basis set extension correction instead of the fourth order (MP4). G2(MP2) is nearly as accurate as the full G2 method at a substantially reduced computational expense. The excellent performance of these methods in predicting gas phase acidities of small molecules is well established.[24]

In order to calculate the atomic charges in the anions HS_n^- ($n = 1-4$) a natural bond orbital (NBO) analysis was carried out at the MP2(fu)/6-31G(d) level of theory.

For details of the quantum chemical methods see ref.[25] All calculations were carried out on a Cray J90 or on a Linux workstation.

In order to allow for the thermal corrections to the Gibbs free energy of the proton a value of −0.010654 Hartree (−28 kJ mol^{-1}) was used.

Results and Discussion

The Gibbs free energies at 298 K of the species H_2S_n and HS_n^- for $n = 1-4$ are given in Table 1. In the case of H_2S_3 the most stable conformation with the motif + + (helical chain) was calculated. For H_2S_4 there are two entries: one for the most stable conformer (motif + + −) and one for the helical isomer of C_2 symmetry, which is slightly less stable.

The geometrical parameters of the sulfanes and of their monoanions are presented in Table 2.

The structures of the neutral sulfanes have been discussed several times by previous authors. However, the monoanions HS_n^- with more than one sulfur atom have neither been calculated nor observed before (excepting HS_2^- by mass spectrometry[20]). These species show an interesting bond length pattern in so far as the S−S bond adjacent to the S−H bond is the longest in the anion (210.8−213.6 pm) and much longer than the single bond length as calculated, for example, for H_2S_2 (206.9 pm). On the other hand, the terminal S−S bonds in HS_3^- and HS_4^- are shorter (204 pm) than the single bond while the central S−S bond in HS_4^- is of intermediate length (207.6 pm). Since the torsion angles at all S−S bonds are in the normal range of 73−100° the differing S−S bond lengths must be caused by the delocalization of the additional negative charge within the anion. An explanation is provided by the concept of hyperconjugation between the lone pair in the 3*p* orbital at an atom S(x) and the antibonding σ* molecular orbital of the bond between atoms S($x + 1$) and S($x + 2$) (Figure 2).

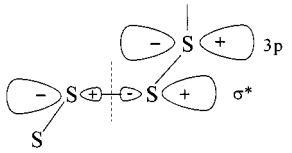


Figure 2. Interaction of the lone pair orbital of sulfur atom S(x) with the empty antibonding σ* molecular orbital of the bond between atoms S($x + 1$) and S($x + 2$) (hyperconjugation); as a consequence the bond S(x)−S($x + 1$) is strengthened while bond S($x + 1$)−S($x + 2$) is weakened

This type of interaction is well-known in sulfur chemistry.[26] It results in a π bond between atoms S(x) and S($x + 1$) (shortened bond) but in a weakening of the bond between atoms S($x + 1$) and S($x + 2$). In HS_4^- two such interactions have to be assumed since the lone pair at S(4) will be delocalized into the σ* MO between S(3) and S(2) and the lone pair at S(3) will be delocalized into the σ* MO at bond S(2)−S(1). In this way the steady increase in the S−S bond lengths from the terminal S atom towards the SH group can be understood.

Table 3. Natural charges (NBO analysis) of the atoms in the anions HS_n^- ($n = 1-4$)

n	H	S(1)	S(2)	S(3)	S(ω)
1	0.05322				−1.05322
2	0.07353	−0.30214			−0.77139
3	0.09949	−0.27652	−0.09775		−0.72522
4	0.13539	−0.23008	−0.09715	−0.07954	−0.72863

The calculated NBO atomic charges of the four anions are presented in Table 3. All sulfur atoms are negatively charged and the hydrogen atoms are always positively charged. This positive charge slightly increases with increasing number of sulfur atoms from +0.05 for HS^- through 0.07 in HS_2^- to 0.10 in HS_3^- and 0.14 in HS_4^-. The ter-

minal sulfur atom is always the most negatively charged atom but its charge decreases from −1.05 in HS^- through −0.77 in HS_2^- to −0.73 in HS_3^- and HS_4^-. The second most negatively charged atom is always the one linked to the hydrogen atom; its charge decreases from −0.30 in HS_2^- through −0.28 in HS_3^- to −0.23 in HS_4^-. The other atoms carry a charge of less than −0.1.

In the case of HS_2^- the geometry and the NBO charges were also calculated at the MP2/6-311++G(d,p) level. While the S−S bond length was calculated as 212.6 pm (0.8% longer than above) the charge of the terminal atom was practically identical (−0.766) as that calculated with the smaller basis set (−0.771).

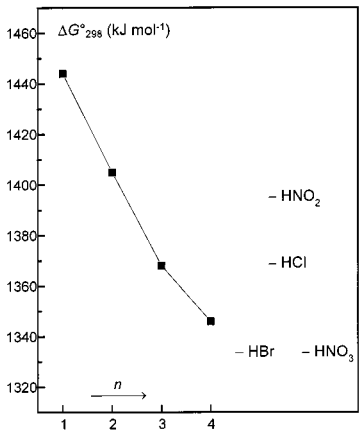


Figure 3. Dependence of the gas phase acidities of the sulfanes H_2S_n (n = 1−4) on the number of sulfur atoms (n) and comparison with the gas phase acidities of HNO_2, HCl, HBr, and HNO_3

The gas phase acidities derived from the data in Table 1 are given in Table 4 and are depicted in Figure 3.

Table 4. Gas phase acidities $\Delta G°_{298}$ [kJ mol^{-1}] of the species H_2S_n (n = 1−4) calculated by the G2(MP2) and G2 methods

System	Symmetry	G2(MP2)	G2
H_2S	C_{2v}	1446	1444
H_2S_2	C_2	1407	1405
H_2S_3	C_2	1371	1368
H_2S_4 (+ − +)	C_2	1349	1346
H_2S_4 (+ − −)	C_1	1350	1347

The acidities calculated for H_2S by the G2 and G2(MP2) methods of 1446 and 1444 kJ mol^{-1}, respectively, are in excellent agreement with the experimental value of 1443 kJ mol^{-1} quoted above. This demonstrates once more that these methods yield reliable data for sulfur compounds.

The dissociation of di-, tri-, and tetrasulfane requires much less Gibbs free energy (free enthalpy) than that of H_2S. There is a drop in ΔG_{acid}(298 K) by 40 kJ mol^{-1} from H_2S to H_2S_2 and of 37 kJ mol^{-1} from H_2S_2 to H_2S_3. Even the addition of another sulfur atom, as in H_2S_4, reduces ΔG_{acid}(298 K) by another 22 kJ mol^{-1}. In other words, the gas phase acidities of di-, tri-, and tetrasulfane are much higher than that of H_2S. The value obtained for disulfane (1406 kJ mol^{-1}) is in excellent agreement with the experimental value of 1418 ± 13 kJ mol^{-1}[20] and comparable to the gas phase acidity[27] of nitrous acid HNO_2 (1396 kJ mol^{-1}). Trisulfane (1370 kJ mol^{-1}) is as strong a proton donor as hydrogen chloride HCl (1371 kJ mol^{-1}), while the acidity of tetrasulfane (1347 kJ mol^{-1}) comes close to that of hydrogen bromide HBr (1332 kJ mol^{-1}) and of nitric acid HNO_3 (1330 kJ mol^{-1})! Since the increase in acidity from H_2S_3 to H_2S_4 is still considerable it can be assumed that H_2S_5 and H_2S_6 will be even stronger acids. A rational explanation for the increase of the acidities with increasing number of sulfur atoms can be given on the basis of the charge capacity of the HS_n fragments, which can obviously accommodate an additional electron more easily the more sulfur atoms they contain since the charge is delocalized onto all sulfur atoms, as discussed above. Therefore, the dissociation of H_2S_2 requires much less Gibbs free energy than that of H_2S and the dissociation of H_2S_3 requires less than that of H_2S_2 and so forth. Since the charge delocalization in the monoanions will also occur in aqueous solution, one would expect the acidity of the aqueous sulfanes to be much higher than that of aqueous H_2S, which is in agreement with the measurements by Schwarzenbach and Fischer.

Derivatives of the sulfanes like the sulfane oxides H−S−S−OH[28] and H−S−S(O)−S−H[29] will probably be similarly strong acids in the vapor phase. These molecules have been proposed as intermediates in the aforementioned Claus process.[29]

In the presence of water vapor the high acidity of gaseous H_2S_2, for example, will result in the formation of hydrated ion pairs like $H_3O^+(H_2O)_x \cdot HS_2^-$ as has been demonstrated in the case of other acids.[30] Since the sour gas always contains water vapor, such ion pairs will be formed and these may be the species responsible for the severe corrosion of steel pipes that has been observed in cases where the sour gas deposit contains both elemental sulfur and H_2S resulting in the formation of H_2S_2.

Acknowledgments

This work has been supported by the Deutsche Forschungsgemeinschaft, by the Verband der Chemischen Industrie and by the Konrad-Zuse-Zentrum für Informationstechnik Berlin.

[1] F. Fehér in *Handbuch der Präparativen Anorganischen Chemie*, 3rd ed., vol. I (Ed.: G. Brauer), F. Enke, Stuttgart, **1975**, p. 356.
[2] J. Hahn, *Z. Naturforsch., B* **1985**, *40*, 263.
[3] J. B. Hyne, G. D. Derdall, *World Oil* Oct. **1980**, 111.
[4] E. Brunner, M. C. Place, W. H. Woll, *Proc. Ann. Conf. Soc. Petr. Engrs.* (Las Vegas, **1985**) SPE 14265.
[5] R. Steudel, R. Strauss, L. Koch, *Angew. Chem. Int. Ed.* **1985**, *24*, 59.
[6] J. B. Hyne, E. Muller, T. K. Wiewiorowski, *J. Phys. Chem.* **1966**, *70*, 3733.
[7] Anonymous, *Sulphur* **1994**, *233* (July/August), 35.
[8] J. Hahn, P. Schmidt, K. Reinartz, J. Behrend, G. Winnewisser, K. M. T. Yamada, *Z. Naturforsch., B* **1991**, *46*, 1338.
[9] M. Liedke, K. M. T. Yamada, G. Winnewisser, J. Hahn, *J. Mol. Struct.* **1997**, *413−414*, 265.
[10] Y. Drozdova, K. Miaskiewicz, R. Steudel, *Z. Naturforsch., B* **1995**, *50*, 889.
[11] W. Giggenbach, *Inorg. Chem.* **1971**, *10*, 1333.
[12] G. Schwarzenbach, A. Fischer, *Helv. Chim. Acta* **1960**, *169*, 1365.

[13] W. Giggenbach, *Inorg. Chem.* **1972**, *11*, 1201.
[14] E. McCampbell Hamilton, Ph. D. Thesis, University of Minnesota, USA, **1991**.
[15] J. E. Bartmess, "Negative Ion Energetics Data" in *NIST Chemistry WebBook* (Eds.: W. G. Mallard, P. J. Linstrom), NIST Standard Reference Database Number 69, November **1998**, National Institute of Standards and Technology, Gaithersburg, MD, USA (http://webbook.nist.gov/chemistry).
[16] Some authors define the gas phase acidity as the energy change or as the enthalpy change of reaction (6).
[17] M. S. Gordon, L. P. Davis, L. W. Burggraf, R. Damrauer, *J. Am. Chem. Soc.* **1986**, *108*, 7889.
[18] J. E. Del Bene, I. Shavitt, *J. Phys. Chem.* **1990**, *94*, 5514.
[19] B. J. Smith, L. Radom, *Chem. Phys. Lett.* **1995**, *245*, 123.
[20] R. A. J. O′Hair, Ch. H. DePuy, V. M. Bierbaum, *J. Phys. Chem.* **1993**, *97*, 7955.
[21] L. A. Curtiss, K. Raghavachari, G. W. Trucks, J. A. Pople, *J. Chem. Phys.* **1991**, *94*, 7221.
[22] L. A. Curtiss, K. Raghavachari, J. A. Pople, *J. Chem. Phys.* **1993**, *98*, 1293.
[23] M. J. Frisch, G. W. Trucks, H. B. Schlegel, P. M. W. Gill, B. G. Johnson, M. A. Robb, J. R. Cheeseman, T. A. Keith, G. A. Petersson, J. A. Montgomery, K. Raghavachari, M. A. Al-Laham, V. G. Zakrzewski, J. V. Ortiz, J. B. Foresman, J. Cioslowski, B. B. Stefanov, A. Nanayakkara, M. Challacombe, C. Y. Peng, P. Y. Ayala, W. Chen, M. W. Wong, J. L. Andres, E. S. Replogle, R. Gomperts, R. L. Martin, D. J. Fox, J. S. Binkley, D. J. Defrees, J. Baker, J. P. Stewart, M. Head-Gordon, C. Gonzalez, J. A. Pople, *GAUSSIAN 94 Revisions D.2* (Cray) and *E.1* (workstation), Gaussian, Inc., Pittsburgh, PA, **1995**.
[24] J. W. Ochterski, G. A. Petersson, K. B. Wiberg, *J. Am. Chem. Soc.* **1995**, *117*, 11299.
[25] J. B. Foresman, A. E. Frisch, *Exploring Chemistry with Electronic Structure Methods*, 2nd ed., Gaussian, Inc., Pittsburgh, PA, **1996**.
[26] R. Steudel, F. Schuster, *J. Mol. Struct.* **1978**, *44*, 143.
[27] Gas phase acidities of HCl, HBr, HNO_2 and HNO_3 were taken from or calculated from the data in ref.[15]
[28] R. Steudel, Y. Drozdova, R. H. Hertwig, W. Koch, *J. Phys. Chem.* **1995**, *99*, 5319.
[29] Y. Drozdova, R. Steudel, *Chem. Eur. J.* **1995**, *1*, 193.
[30] A. Smith, M. A. Vincent, I. H. Hiller, *J. Phys. Chem. A* **1999**, *103*, 1132.

Received July 5, 1999
[I99237]

Structural Analyses of Borane and Chloroborane Adducts of 1,3,5-Dithiaza-, -Dioxaza-, -Thiadiaza-, and -Triazacyclohexanes and Their Rearrangement Products, Boracyclohexanes

Angelina Flores-Parra,*[a] Sonia A. Sánchez-Ruíz,[a] and Carlos Guadarrama-Pérez[a]

Keywords: Borane adducts / Triazacyclohexanes / Thiadiazacyclohexanes / Dioxazacyclohexanes / Boracyclohexanes / Rearrangements

Structural and conformational studies performed by ^{1}H-, ^{11}B-, ^{13}C-, two-dimensional, and variable-temperature NMR spectroscopy of borane and chloroborane adducts of 1,3,5-heterocyclohexanes and their rearrangement products, boracyclohexanes, are reported. *N*-Methyl derivatives gave equatorial *N*-borane adducts whereas the *N*-isopropyl derivatives produced the axial borane compounds. Rearrangement reactions of the adducts gave the first examples of chloroboracyclohexanes bearing boron and nitrogen atoms as stable stereogenic centers. $BClH_2$ and BCl_2H adducts were found to be more stable towards ring rearrangement than the corresponding *N*-BH_3 analogs.

Introduction

We have been systematically studying the synthesis and particularly the coordination behavior of 1,3,5-heterocyclohexanes bearing heteroatoms such as O, S, and N, which are rich in lone pairs and good ligands for Lewis acids.[1] Reactions with boron[1a,1b,1e−1f] and lithium[1g] compounds were investigated because these reagents function as coordination probes conveniently studied by NMR techniques.

Herein, we report extended studies of chloroboranes, which are more acidic reagents which could give stronger coordination bonds and more stable adducts, and of new families of heterocycles: 1,3,5-thiadiazacyclohexanes and 1,3,5-dioxazacyclohexanes. Because these heterocycles are difficult to prepare, few examples of them were known,[2] but fortunately we have recently established suitable reaction conditions for their preparation.[1h]

Results and Discussion

Herein, we present the study of the reactions of BH_3·THF and various chloroborane·DMS with the heterocycles 3,5-dialkyl-1,3,5-thiadiazacyclohexane (**1**, **2**,[1h,2] and **3**[1h]), 5-alkyl-1,3,5-dioxazacyclohexane (**4** and **5**[1h]), 5-alkyl-1,3,5-dithiazacyclohexane (**6**, **7**,[1d] and **8**[1g]), and 1,3,5-trimethyl-1,3,5-triazacyclohexane[1f] (**9**) (Figure 1).

Acid−base studies with BH_3 as the Lewis acid partner, showed that the potential basicity decreases in the order N > S > O. Therefore, we would expect mono(*N*-BX_3) derivatives to form from the reactions of **1**−**9** with BH_3 or chloroborane compounds, and that two or even three borane molecules would coordinate to heterocycles **1**−**3** and **9**. Also,

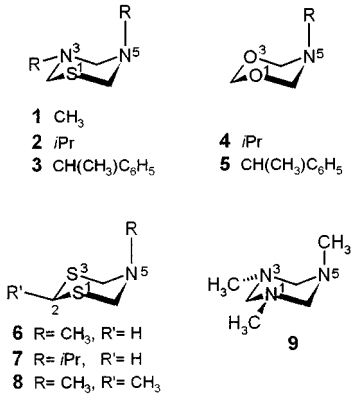


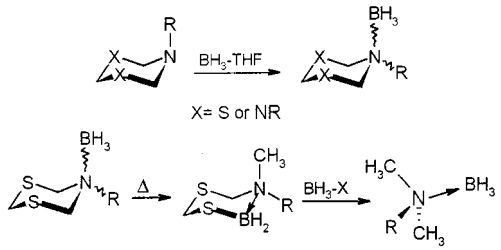
Figure 1

we were interested to find out if coordination would freeze the conformations of the heterocycles. NMR studies of heterocycles **1**−**7** and **9** showed that they are in ring- and nitrogen-conformational equilibrium at room temp. (400-MHz ^{1}H NMR), whereas compound **8** has a preferred chair conformation with the 2-methyl group in the equatorial and the *N*-methyl group in the axial position.[1g]

When heated, *N*-BH_3 adducts of 1,3,5-dithiazacyclohexanes rearrange into boracyclohexanes by exchange of boron and carbon atoms[1b] (Scheme 1). The stability of these boraheterocycles depends on the size of the *N*-alkyl group: Those with bulky groups are rapidly converted into *N*-(BH_3)-dimethylalkylamine complexes.[1b] This rearrangement was not found for 1,3,5-triazacyclohexanes. Therefore, we wanted to investigate if these rearrangements occur for other heterocyclohexanes or with the more reactive chloroboranes, if the more acidic boron atom in the resulting chloroborate allows better coordination and a more stable ring, if the chlorine atom could have a preferred position in a frozen ring and thus result, stereoselectively, in a stereogenic boron atom. In addition, we wanted to study the influence of the chlorine atom on the reactivity and NMR data and on the conformational behavior.

[a] Chemistry Department, Centro de Investigación y de Estudios Avanzados del I.P.N.
A. P. 14-740, C. P. 07000, México D.F., México
Fax: (internat.) + 52-5/747-7113
E-mail: aflores@mail.cinvestav.mx

 © WILEY-VCH Verlag GmbH, D-69451 Weinheim, 1999 1434−1948/99/1111−2063 $ 17.50+.50/0



Scheme 1. Rearrangement of the BH_3 adducts

Borane Adducts

NMR spectroscopy showed that the equimolar reaction of thiadiazacyclohexane **1** with BH_3·THF resulted in monoadduct **10**, whereas an excess of borane led to bis(borane) **11** (Figure 2). The ^{13}C-NMR spectrum of compound **1**, at −90°C in [D_8]THF (100.53 MHz), did not indicate a preferred conformation, as the CH_3 and SCH_2N resonances were averaged, indicating that $\Delta G^{\neq}$ for the ring inversion is very low. In contrast, **10** and **11** are present in frozen conformations, because the CH_2 groups have geminal coupling patterns. Their *N*-BH_3 groups are in equatorial positions as shown by the position of the *N*-CH_3 group in the ^{13}C spectrum at δ ≈ 45;[1e] this conformation is also supported by an X-ray diffraction structure.[1i] The bis(borane) **11** is an analog of the reported compound **12**.[1f] In solution, adduct **10** is slowly transformed into **11** and the free heterocycle. ^{1}H-NMR data are summarized in Table 1.

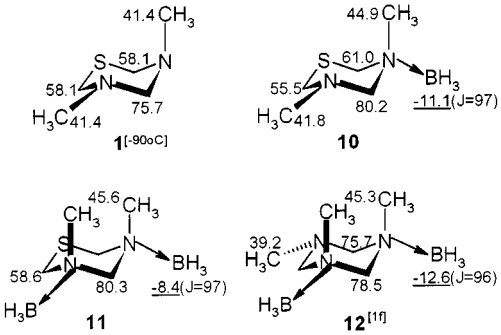


Figure 2. ^{11}B- and ^{13}C-NMR chemical shifts of **10**−**12**

The reaction of equimolar amounts of BH_3·THF and 3,5-diisopropyl-1,3,5-thiadiazacyclohexane (**2**) afforded the stable *N*-borane **13** with the two isopropyl groups in equatorial positions and the BH_3 group in the axial position (Figure 3). Compound **13** is more stable than **14**,[1b] which could be observed only at low temperature. In the presence of an excess of BH_3·THF, **13** rapidly rearranged into **31** (vide infra, Figure 8), whereas the triisopropyltriazacyclohexane **15**[1f] gave a small amount of the bisadduct **16**.[1f] The reaction of BH_3·THF with the dioxazacyclohexane **4** also yielded an *N*-borane, **17**, as shown by NMR spectroscopy at room temp. The stability of the borane adducts is shown by the order of the ease of rearrangemen: **14** > **17** > **13** > **15**.

The room-temp. NMR spectra of **13**−**17** (Figure 3) show that the ring conformation is preferentially that of a chair with the bulky isopropyl groups in equatorial positions, as shown by the ^{13}C-δ values for CH (δ ≈ 54; for the axial position δ ≈ 46).[1e] These heterocycles provide examples of axial BH_3 groups. The frozen conformation of **13** that results from BH_3 addition makes the N atoms stereogenic centers and the C−CH_3 groups diasterotopic. The signal of CH_3 groups of the isopropyl group attached to the coordinated nitrogen atom appear at δ = 15.9 and 15.7, whereas those of the ones attached to the free nitrogen atom appear at δ = 18.8 and 18.4. In the free ligand **2** the signals of all the CH_3 groups appear at δ = 20.1.

Chloroborane Adducts

We prepared the chloroborane adducts of 1,3,5-heterocyclohexanes **18**−**22** and **24**−**29**. The reaction of a commercial mixture of BH_2Cl, $BHCl_2$, and BH_3 (in the ratio 90:8:2, respectively), in DMS, with compounds **6** and **8** produced, in the same ratio, the corresponding adducts **18**−**21** (Figure 4). Upon coordination, the ring of adducts **18**−**21** adopted a preferred conformation with the *N*-methyl group in the axial position as indicated by their ^{13}C-δ values in the range δ = 37.7−40.2 (Table 2). To analyze the trends in the NMR spectra, the data of compounds **18**−**21** were compared to those of the BCl_3 (**22**) and BH_3 (**23**[1b]) adducts of **6**. In the ^{1}H as well as the ^{11}B spectra, the resonances of the CH_2 groups close to the N−B bond are systematically shifted to higher frequencies with an increasing number of chlorine atoms. The coupling constants ^1J(B−H) increase in the same order.

We found that chloroborane adducts are more stable to ring rearrangement than the corresponding *N*-BH_3 analogs, making them useful for the observation and study of coordination compounds of heterocycles with bulky groups. For example, we obtained adduct **24**, derived from 3-isopropyl-1,3,5-dioxazacyclohexane (Table 1, Figure 5). It is moderately stable and could be observed by NMR, but we were not able to detect the corresponding BCl_2H adduct. The *N*-BH_3 adducts of **3** and **5** could not be observed because they are rapidly reduced to the corresponding dimethylamineborane.

Heterocycle **1** has two N sites for borane coordination and readily formed monoadduct **25** and bis(monochloroborane) adduct **26**. Both are stable compounds with the *N*-chloroborane group in the equatorial position as the preferred conformation. In contrast, only one example of an *N*-BCl_3 adduct of a 1,3,5-thiadiazacyclohexane was prepared, **27**, which is a weak complex that decomposes on vacuum evaporation of the solvent. According to its ^{13}C-NMR spectrum, the BCl_3 adopts an axial position (Figure 5). An interesting observation was that BCl_3 adducts of the studied heterocycles are less stable than adducts with at least one B−H bond. This can be explained by the stabilization resulting from interaction between the hydrides on B and the protons on C, as discussed in the next paper.[1i]

The *N*-BH_2Cl monoadduct **28** and bisadduct **29** of 1,3,5-triazacyclohexane (**9**) were obtained. The BH_2Cl groups oc-

Table 1. ^{1}H-NMR data (400 MHz in $CDCl_3$ at 25°C or in [D_8]THF at low temperature; for atomic numbering see Figure 1)

Compd.	R^2 or 2-H_{eq}/2-H_{ax}	4-H_{eq}/4-H_{ax}	6-H_{eq}/6-H_{ax}	N^1−R	N^3-R	N^5-R
1 (−90°C)	3.82/4.57	3.53/3.93	3.82/4.57		2.56	2.56
2 (−95°C)	3.92/4.15	4.76/4.24	3.92/4.15		3.13	3.13
3	4.20/4.58	4.21/4.04	4.20/4.58		3.73	3.73
4 (−80°C)	5.12/5.04	4.68	4.68			3.42
5 (−60°C)	5.11/5.16	4.13/4.59	4.98/4.83			4.63
6 (−80°C)	3.56/4.60	3.93/4.95	3.93/4.95			2.59
7 (−90°C)	3.68/4.65	4.29/4.80	4.29/4.80			3.73
8 (27°C)	1.46/4.24	4.09/4.67	4.09/4.67			2.56
9 (−90°C)	3.86/3.18	3.86/3.18	3.86/3.18	2.83	2.83	2.83
10	3.60/4.14	3.55/4.23	3.66/3.81		2.65	2.61
11	3.54/3.85	3.97/3.71	3.54/3.85		2.47	2.47
12[1f]	3.69/2.59	3.54/3.12	3.54/3.12	2.30	2.79	2.79
13	4.14	4.08/3.51	3.82/3.96		2.99	4.33
15[1f]	3.75/3.07	4.02/3.16	4.02/3.16	2.81	2.81	4.19
16[1f]	4.25/3.64	4.43/4.08	4.43/4.08	3.02	3.89	3.89
17	5.16/4.88	4.80/4.44	4.80/4.44			4.06
24	4.93	4.53/4.28	4.53/4.28			4.37
25	3.66/4.22	3.34/4.32	3.73/4.00		2.61	2.73
28	2.90/2.76	3.74/3.33	3.74/3.33	2.37	2.37	2.92
30[1f]	3.65/3.36	3.73/4.03	3.65/3.36	2.30	2.30	2.47
33	1.39/4.41	3.45/4.94		2.79	2.72	
34	1.40/4.22	3.73/5.12		3.10	2.95	
38 (25°C)	2.65/4.05	3.93/4.30		2.80		2.71

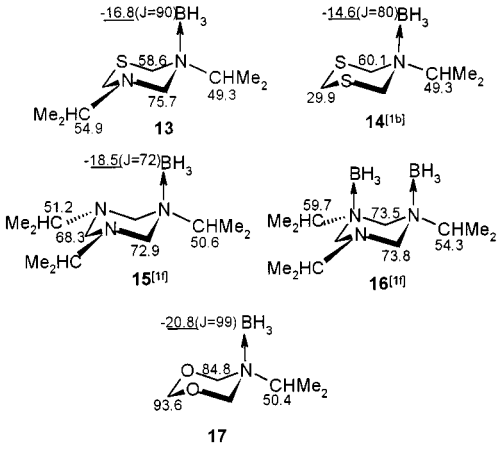


Figure 3. Borane adducts of *N*-isopropyl heterocycles; ^{11}B-NMR data are shown, the boron signal of **16** is masked by that of **15**

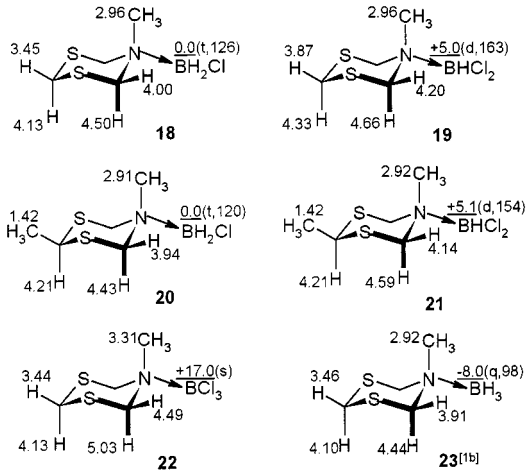


Figure 4. ^{11}B- and ^{1}H-NMR data of **18**−**23**

Table 2. ^{13}C-NMR data (100.5 MHz, in $CDCl_3$ at 25°C or [D_8]THF at low temperature; for atomic numbering see Figure 1; * = quaternary nitrogen atom)

Compd.	C-2	C-4	C-6	N^*−R
1 (−90°C)	58.1	75.7	58.1	41.4
2 (−95°C)	54.1	69.3	54.1	50.3
3	59.2	70.1	59.6	54.6
4 (−20°C)	95.4	81.3	81.3	50.5
5 (−60°C)	95.2	80.2	81.3	56.0
6 (−90°C)	34.3	59.9	59.9	37.5
7 (−80°C)	34.3	56.9	56.9	45.8
8	44.3	60.3	60.3	37.0
9 (−100°C)	80.7	75.9	75.9	39.7,[b] 41.4[a]
18	30.9	60.0	60.0	40.2
19	30.7	59.1	59.1	38.3
20	42.5	61.0	61.0	39.5
21	42.0	59.7	59.7	37.7
22	30.3	58.9	58.9	38.6
23	30.2	62.2	62.2	42.9
32eq (−65°C)	30.2	62.2		44.5*,[a] 47.7*[b]
32ax (−65°C)	29.9	63.9		43.8*,[a] 52.6*[b]
37 (−55°C)	32.0	64.6		44.3*,[a] 53.1*[b]

[a] Axial position. − [b] Equatorial position.

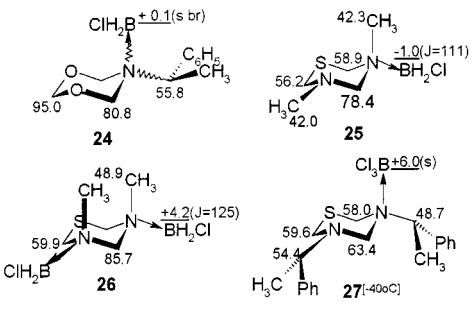


Figure 5. ^{11}B- and ^{13}C-NMR chemical shifts and the preferred conformations of **24**, **25**, **26**, and **27**

cupy equatorial positions and the ring is not fluxional. The ^{13}C chemical shifts of **28** and **30**[1f] were similar, and those of **29** and **12** were also similar[1f] (Figures 2, 6).

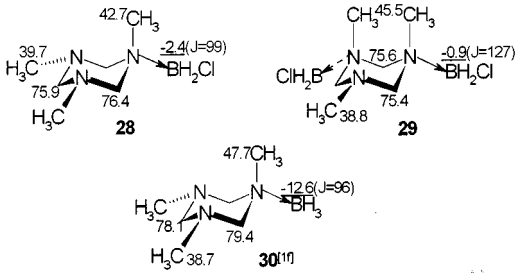


Figure 6. ^{11}B- and ^{13}C-NMR data and the preferred conformations of **28**, **29**, and **30**

1,3,5,6-Thiadiazaboracyclohexane (31)

Herein, we report the first example of a 1,3,5,6-thiadiazaboracyclohexane (**31**), quantitatively formed by reaction of 1,3,5-thiadiazacyclohexane (**2**) and an excess of BH_3·THF in $CHCl_3$ at room temp. The ^{11}B-NMR spectrum of **31** shows a triplet at $\delta = -5.3$, characteristic of an $S-BH_2\leftarrow N$ group. The ring appears nondynamic on the time scale of the ^1H-NMR spectrum at room temp (Figure 7).

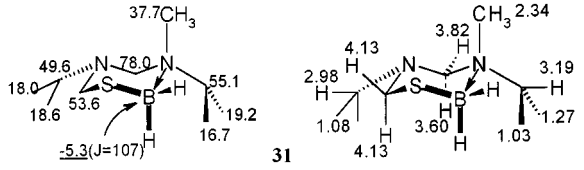


Figure 7. ^{13}C-, ^{11}B-, and ^1H-NMR chemical shifts of **31** at 25°C

1,3,5,6-Dithiazaboracyclohexanes 32−36

2-Chlorobora-1,3,5-dithiazacyclohexanes **32−36** were formed by allowing the 1,3,5-dithiazacyclohexanes **6−8** to react with excess BH_2Cl·DMS in $CHCl_3$. The resulting structures were assigned by HETCOR, COSY, and APT NMR experiments. The positions of the chlorine atoms were determined by their effects on the ^1H resonances of the neighboring protons and by comparison with the analogous BH_2 compounds. The boron atom becomes a stereogenic center and two isomers were indeed observed. At room temp. compound **32** is an equilibrium mixture of the two conformers shown in Figure 8. At −65°C, both conformers were observed in the ^{13}C- (Table 2) and ^{11}B-NMR spectra, for assignment a comparison with **37** was helpful. The conformer with the Cl atom in axial position was present in 70% abundance. At this temperature the $^1J(B-H)$ values of the two isomers differed significantly, with 161 Hz for equatorial B−H and 127 Hz for axial B−H, indicating frozen conformations.

Compound **8** with an excess of BH_2Cl produced the two diasteromers **33** and **34** in a 1:1 ratio (Figure 9). The ^1H- and ^{13}C-NMR data indicate that the chair conformation is the preferred one for both molecules at room temp., and the $C-CH_3$ group anchors the molecule. Here, the boron atom and C-2 are stereogenic centers.

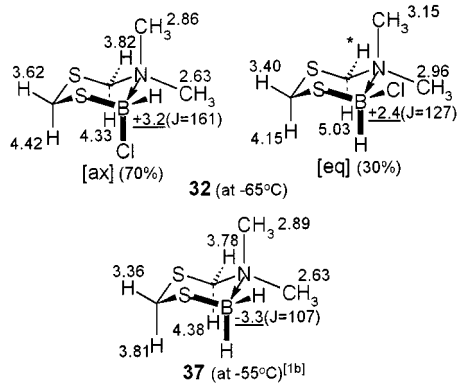


Figure 8. ^1H- and ^{11}B-NMR data of **32** and **37**

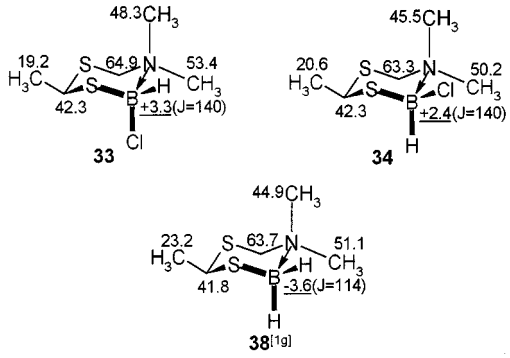


Figure 9. ^{13}C-NMR data of **33**, **34**, and **38** at 25°C

To see if a more bulky *N*-substituent will also function as an anchor for ring inversion, we treated the 1,3,5-dithiazacyclohexane **7** in equimolar amounts with the mixture of chloroboranes for 5 h at room temp. The reaction products were the cyclohexanes **35** (60%) and **36** (40%) (Figure 10). Both compounds were shown by their ^1H-NMR spectra to be nonfluxional, and their boron and nitrogen atoms are stereogenic centers. The equatorial position of the isopropyl groups was found by ^{13}C-NMR spectroscopy (CH at $\delta =$ 59.4 and 54.7 in **35** and **36**, respectively). An anomeric effect produced by the axial chlorine atom on the axial *N*-methyl group (which is deshielded) was observed for **33** and **35**.

Conclusions

The 1,3,5-heterocyclohexanes and borane or chloroborane form stable adducts which have frozen conformations as shown by the geminal coupling pattern of the CH_2 groups. The values of the coupling constants in the frozen free heterocycles vary according to the nature of the heteroatom (OCH_2O: 5.9; SCH_2S: ca. 13.3; NCH_2N: 8.0; SCH_2N: 10.5−13.5). The corresponding values in the adducts do not show systematic trends except for the triazacy-

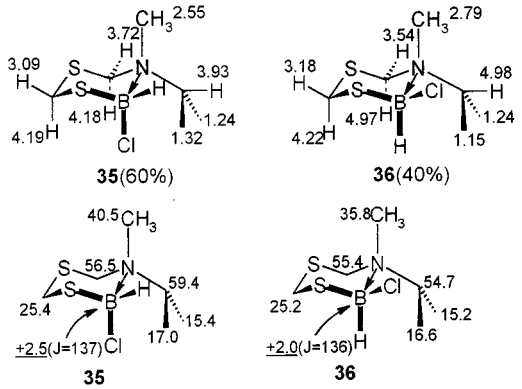


Figure 10. ^{13}C-, ^{11}B-, and ^{1}H-NMR chemical shifts of **35** and **36**

clohexanes and dithiazacyclohexanes where these values increase upon coordination [e.g., in **9** it increases from 8 Hz to 9.1 and 11.7 Hz, and in **6** (SCH_2N) it increases from 12.6 to 13.9−14.3 Hz, Table 3]. The frozen conformations are also deduced from the ^4J_w couplings between the equatorial protons, the values of which vary between 1.2 to 2.6 Hz. In **37** this coupling occurs between the equatorial C−H and B−H, with J = 2.0 Hz.

The configuration of the nitrogen atoms in borane and chloroborane adducts of triaza-, thiadiaza-, dithiaza-, and dioxazacyclohexanes is determined by the size of the *N*-substituents. The bulky isopropyl groups direct the borane units into the axial positions, while the methyl groups direct the boranes to the equatorial positions. ^1J(B−H) constants for axial BH_3 are smaller that the corresponding values for equatorial BH_3, which could be attributed to a weaker coordination of axial borane.

That the formation of adducts resulted in frozen ring conformations indicate that there is a hydride−proton interaction.[1i] This is supported by the result that BCl_3 did not give stable adducts. The use of excess borane and chloroboranes led to new boracyclohexanes. The chloroborata compounds are more stable because SBHCl is more acidic than the SBH_2 group.

Experimental Section

^{1}H-, ^{13}C-, and ^{11}B-NMR spectra were recorded with Jeol spectrometers at frequencies of 270 and 400 MHz for protons; δ values are referenced to TMS, and to $BF_3{\cdot}OEt_2$ for ^{11}B-NMR spectra. − $BH_3{\cdot}$THF was prepared as described.[3] The $BH_{3-n}Cl_n{\cdot}S(CH_3)_2$ mixture was purchased from Aldrich Co. Anhydrous solvents were prepared according to usual laboratory methods. − All reactions were carried out in inert atmosphere with oven-dried glassware. − Adducts **10**, **11, 13**, **17**−**21**, **24**−**29**, and boracyclohexanes **31**−**36** were analyzed only by variable-temperature, and two-dimensional ^{1}H-, ^{13}C-, ^{11}B-NMR spectroscopy. Our attempts to isolate them from the mixture of adducts were unsuccessful because they are unstable. Therefore, we could not perform elemental analyses. However, their structures were derived by comparison to fully characterized similar compounds.[1]

Preparation of Mono-*N*-BH_3 Adducts 10, 13, and 17. − General Procedure: To a solution of the corresponding heterocyclohexane (0.25 g) in 20 mL of dry THF, was added a solution of $BH_3{\cdot}$THF (1.2 mmol) at −78°C. The mixture was stirred for 5 min, and then the solvent was removed under vacuum leaving behind a mixture of adducts as white solids which were analyzed by NMR spectroscopy (**10**, 80%; **13**, 85% and **17**, 80%).

Preparation of 3,5-Bis(borane)-3,5-dimethyl-1,3,5-thiadiazacyclohexane (11): To a stirred solution of **1** (0.25 g, 1.9 mmol) in 20 mL of dry THF, was added a solution of $BH_3{\cdot}$THF (2.0 mmol) at 25°C. After 10 min, more $BH_3{\cdot}$THF (4.1 mmol) was added and the reaction mixture was kept for 30 min at 50°C. The solvent was then removed under vacuum to give the adduct as a white solid. Compound **11** (80%, 0.24 g) was crystallized from $CHCl_3$. m.p. 40°C. − $C_5H_{18}B_2N_2S$ (132.23): calcd. C 37.56, H 11.34, N 17.52; found C 37.51, H 11.46, N 17.36.

Preparation of *N*-$BHCl_2$ and *N*-BH_2Cl Adducts 18−21, 24−26, 28, and 29. − General Procedure: To a stirred solution of the corresponding heterocyclohexane (**1**, **5**, **6**, **8**, or **9**) (0.25 g) in 20 mL of dry $CHCl_3$, was added at −60°C a solution of 1 or 2 equiv. of $BH_{3-n}Cl_n\ SMe_2$. The reaction mixture was stirred for 5 min. The solvents were then removed under vacuum to afford the *N*-$BHCl_2$ and *N*-BH_2Cl adducts: **19** and **21** (8%); **24** (50%); **25** (95%); **26** (85%); **28** (40%), and **29** (95%). − Adduct **18** was crystallized from $CHCl_3$ and obtained in 80% yield (0.27 g). − $C_4H_{11}BClNS_2$ (183.53): calcd. C 26.18, H 6.04, Cl 34.94, N 7.63; found C 26.69,

Table 3. ^2J(H−H) geminal coupling constants for CH_2 and ^4J_w(H−H) for equatorial CH groups; for atomic numbering see Figure 1

Compd.	2-H	4-H	6-H	^4J_w(H−H)	Compd.	2-H	4-H	6-H	^4J_w(H−H)
1 (−90°C)	12.4	13.5	12.4		**20**		12.1	12.1	
2 (−95°C)	10.5	13.5	10.5		**21**		14.1	14.1	
3	13.5	12.1	13.5		**22**	14.0	14.3	14.3	
4 (−80°C)	5.9				**23**	13.9	13.9	13.9	2.0
5 (−60°C)	5.9	10.6	11.4		**24**		11.0	11.0	
6 (−80°C)	13.3	12.7	12.7	2.6	**25**	13.2	13.2	13.2	2.6
7 (−90°C)	13.2	13.2	13.2		**28**	9.8	10.8	10.8	
8 (27°C)		12.6	12.6		**30**[1f]	11.6	13.8	13.8	1.8
9 (−90°C)	8.0	8.0	8.0		**31** (25°C)		7.0		
10	12.6	13.3	12.6	2.5	**32eq** (−65°C)	13.2	12.8		
11	14.1	13.6	14.1		**32ax** (−65°C)	13.5	12.1		
12[1f]	9.1	11.0	11.0	1.7	**33**		12.8		
13		12.5	11.5		**34**		13.1		
15[1f]	7.8	11.0	11.0	1.7	**35**	13.1	13.2		
16[1f]	12.8	14.7	14.7	1.6	**36**	13.0	12.4		
17	5.9	10.6	10.6	1.2	**37** (−55°C)	12.9	12.5		2.0
18	14.0	14.0	14.0	2.1	**38** (25°C)		12.7		
19	14.0	14.0	14.0	2.1					

H 6.09, Cl 34.83, N 6.62. − Adduct **20** was obtained in 85% yield (0.28 g). − $C_5H_{13}BClNS_2{\cdot}CH_2Cl_2$ (282.49): calcd. C 25.51, H 5.35, N 4.96; found C 25.05, H 5.47, N 5.11.

Preparation of 3,5-Diisopropyl-1,3,5,6-thiadiazaboracyclohexane (31): To a solution of **1** (0.25 g, 1.33 mmol) in 20 mL of dry THF, was added a solution of $BH_3{\cdot}$THF (1.2 mmol) at −78°C; the resultant mixture was stirred for 5 min. It was then warmed to 25°C, stirred for 5 min, and the solvent was removed under vacuum. The adduct was obtained as a white solid (70%, 0.19 g). − ^{15}N NMR ($CDCl_3$, 25°C, 270 MHz): δ = −238.

Preparation of 6-Chloro-5-methyl-1,3,5,6-dithiazaboracyclohexanes 32−36. − General Procedure: To a solution of the corresponding heterocyclohexane (0.25 g) in 20 mL of dry CH_2Cl_2, was added 3 equiv. of a mixture of $BHCl_2$, BH_2Cl, and BH_3 in $S(CH_3)_2$ (90:8:2). The reaction mixture was stirred at 40°C for 8 h, and the solvents were subsequently removed by evaporation to afford the dithiazaboracyclohexane **32−36** which were characterized by NMR spectroscopy.

Acknowledgments

We thank Conacyt-Mexico and TWAS (grant 97−337 RG/CHE/LA) for financial support. C. G.-P. is grateful to Conacyt-Mexico for a scholarship and Professor H. Nöth for helpful discussions.

[1] [1a] A. Flores-Parra, N. Farfan, A. I. Hernádez-Bautista, L Fernández-Sánchez, R. Contreras, *Tetrahedron* **1991**, *47*, 6903−6914. − [1b] A. Flores-Parra, G. Cadenas-Pliego, L. M. R. Martínez-Aguilera, M. L. García-Nares, R. Contreras, *Chem. Ber.* **1993**, *126*, 863−867. − [1c] G. Cardenas-Pliego, R. Contreras, J. C. Daran, S. Halut, A. Flores-Parra, *Phosphorus Sulfur Silicon* **1993**, *84*, 9−15. − [1d] G. Cadenas-Pliego, L. M. R. Martínez-Aguilera, A. M. Bello-Ramírez, M.-J. Rosales-Hoz, R. Contreras, J. C. Daran, S. Halut, A. Flores-Parra, *Phosphorus Sulfur Silicon* **1993**, *81*, 111−123. − [1e] G. Cadenas-Pliego, M.-J. Rosales-Hoz, R. Contreras A. Flores-Parra, *Tetrahedron: Asymmetry* **1994**, *5*, 633−640. − [1f] L. M. R. Martínez-Aguilera, G. Cadenas-Pliego, R. Contreras, A. Flores-Parra, *Tetrahedron Asymmetry* **1995**, *6*, 1585−1592. − [1g] C. Guadarrama-Pérez, G. Cadenas-Pliego, L. M. R. Martínez-Aguilera, A. Flores-Parra, *Chem. Ber.* **1997**, *130*, 813−817. − [1h] A. Flores-Parra, S. A. Sanchez-Ruiz, *Heterocycles*, in press. − [1i] A. Flores-Parra, S. A. Sánchez-Ruiz, C. Guadarrama-Pérez, H. Nöth, R. Contreras, *Eur. J. Inorg. Chem.* **1999**, 2069−2073, following paper.

[2] [2a] L. Angiolini, R. P. Duke, R. A. Jones, A. R. Katritzky, *J. Chem. Soc., Perkin Trans. 2* **1972**, 674−680. − [2b] E. R. Braithwaite, J. Graymore, *J. Chem. Soc.* **1953**, 143−145. − [2c] E. R. Braithwaite, J. Graymore, *J. Chem. Soc.* **1950**, 208−210.

[3] H. C. Brown, C. W. Kramer, A. B. Levy, M. M. Midland, *Organic Syntheses via Boranes*, John Wiley and Sons, New York, **1975**, p. 18−25.

Received December 14, 1999
[I98427]

$BH^{\delta-}$–$^{\delta+}HC$ Interactions in *N*-Borane and *N*-Chloroborane Adducts Derived from 1,3,5-Heterocyclohexanes

Angelina Flores-Parra,*[a] Sonia A. Sánchez-Ruiz,[a] Carlos Guadarrama,[a] Heinrich Nöth,[b] and Rosalinda Contreras[a]

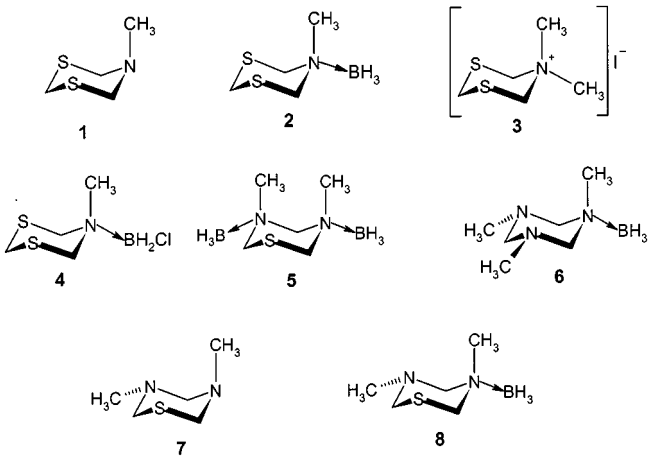
Keywords: Hydridic–protic hydrogen interactions / Amine boranes / 1,3,5-Heterocyclohexanes

The molecular structures of 5-methyl-1,3-dithia-5-azinium-cyclohexane iodide, 5-chloroborane-5-methyl-1,3-dithia-5-azacyclohexane, 3,5-bis(borane)-3,5-dimethyl-1-thia-3,5-diazacyclohexane, and 1-borane-1,3,5-trimethyl-1,3,5-triazacyclohexane were determined by X-ray diffraction studies. Interactions between hydridic and protic hydrogen atoms are present when the distances between hydridic and protic hydrogen atoms are shorter than 265 pm and angles for B–N–C bonds are smaller than 107.6(3)°. These interactions explain the conformation of the borane adducts in the solid state.

Introduction

Six-membered 1,3,5-triheterocyclohexanes bearing N and O and/or S atoms are rich in lone pairs and are therefore expected to be versatile ligands.[1] We have been systematically studying the synthesis of 1,3,5-heterocyclohexanes bearing at least one nitrogen atom[1c,1d,2] and the coordination of these heterocyclohexanes to boranes.[1a–1c,1e–1h]

The *N*-borane adduct **2**, derived from *N*-methyldithiazacyclohexane (**1**), was shown by NMR methods to have a fixed conformation at room temp. in $CDCl_3$ or [D_8]THF. Its NMR spectrum at room temp. is similar to that of the free heterocycle **1** at −65°C (270-MHz ^1H), which, at room temp., in ring-conformational equilibrium, has its CH_3 group in the axial position ($\Delta G^{\geq} = 46.0 \pm 0.8$ kJ/mol). The remarkably static behavior of **2** needs to be explained because the BH_3 and CH_3 groups are expected to behave similarly with regard to ring inversion, and **2** would therefore be expected to be a fluxional cyclohexane like its isolobal compound 5,5-dimethyldithiazoniumcyclohexane iodide (**3**). To find an explanation, the solid-state molecular structures of **1**–**6** and the conformational behavior of **1**,[1a] **2**,[1a,1b] **3**,[1g] **4**,[1h] **5**,[1h] and **6**[1f] were studied. The conformations of **2** and **4**–**6** were shown by NMR spectroscopy to be fixed at room temp. and in solution. A dipolar interaction between the hydridic B–H and protic C–H groups, previously reported for some aminoboron hydrides,[3] could explain these frozen conformations. This possibility was confirmed by the results of the structure analyses of compounds **1**–**6**. The structure of **1** has already been reported,[1c] but is important for comparison with the data of **3** and **4**.



Syntheses

Compound **3** was obtained by conventional methods from **1** and CH_3I, and was crystallized from H_2O. The 1:1 reaction of a commercial mixture of BH_2Cl, $BHCl_2$, and BH_3 in DMS (in a ratio of 90:8:2, respectively) with **1** produced the adducts in the same ratio.[1h] Compound **4** was isolated from this mixture by crystallization from $CHCl_3$ and was characterized by NMR spectroscopy. Its ^{13}C-NMR chemical-shift data indicate that the *N*-methyl group (δ = 39.2) is present in an axial position.[1h]

The N–BH_3 adduct **6** was prepared from the reaction between BH_3·THF and 1,3,5-trimethyl-1,3,5-triazacyclohexane.[1f] It was also a byproduct of the reaction of the same heterocycle with $LiBH_4$ in boiling hexane, and it was isolated by sublimation and recrystallization from the same solvent.

[a] Chemistry Department, Centro de Investigación y de Estudios Avanzados del I.P.N.,
A. P. 14-740, C. P. 07000, México D.F., México
Fax: (internat.) + 52-5/747-7113
E-mail: aflores@mail.cinvestav.mx
[b] Institut für Anorganische Chemie Ludwig-Maximilians-Universität,
Butenandt-Straße 5–13 (Haus D), D-81377 München, Germany

 © WILEY-VCH Verlag GmbH, D-69451 Weinheim, 1999 1434–1948/99/1111–2069 $ 17.50+.50/0

The reaction of 3,5-dimethyl-1-thia-3,5-diazacyclohexane (**7**) with 1 or 2 equiv. of BH_3·THF gave the monoadduct **8** and the bisadduct **5**, as deduced from their NMR spectra.[1h] In both compounds, the $N-BH_3$ groups are in the equatorial positions, as indicated by the ^{13}C-NMR chemical shifts of the $N-CH_3$ groups (close to $\delta = 45$).[1a]

Molecular Structures

The molecular structure of compound **3** is depicted in Figure 1. Crystallographic data and bonding parameters are summarized in Tables 1−2. The formation of the cation is accompanied by a shortening of the S−C bonds (on average 0.03 Å) compared with those of compound **1**. There are intermolecular S···S contacts (2.99 Å) as well as four comparatively short C−H···I contacts ranging from 3.04 to 3.28 Å.

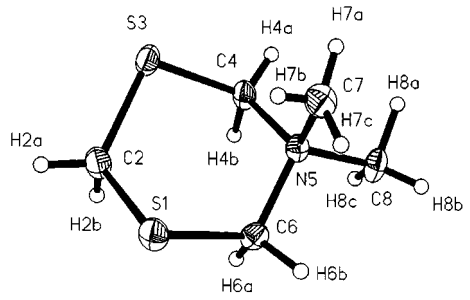


Figure 1. Molecular structure of the cation of **3**

The ring of **4** is also in the chair conformation (Figure 2). The methyl groups are in axial positions and the BH_2Cl moiety is in an equatorial position. The chlorine atom stands antiperiplanar to the methyl group. The molecular structure of **4** compared with that of the free heterocycle **1**[1d] (Table 2) has C−S bonds that are on average shorter by 0.015 Å, a consequence of the ammonium-type N atom in **4**. The BH_3 coordination changes the bond lengths in the ring: The N−C4 [1.502(5) Å], N−C6 [1.496(5) Å], and N−C7 [1.495(5) Å] bonds are expectedly longer in the adduct than in **1** [N−C4: 1.428(4); N−C6: 1.433(4); N−C7: 1.466(5) Å]. On the other hand, in the adduct, the angles C7−N5−C4 [111.0(3)°], C7−N5−C6 [111.0(3)°], and C6−N5−C4 [110.3(3)°] are closer to the angles in the free 1,3,5-dithiazacyclohexane [C7−N5−C4: 114.6(3)°; C7−N5−C6: 114.2(3)°; C6−N5−C4: 113.1(3)°], in accordance with the increased sp^3 character of the nitrogen atom. It is interesting to note the narrow angle C7−N5−B [105.4(3)°] which allows the hydridic atom to be closer to the CH hydrogen atom. Steric repulsion instead of an attractive force between the borane and the methyl group would have resulted in a wider angle.

Single crystals of **5** were obtained from a chloroform solution of **8**. The crystals were obviously formed by disproportionation of the monoborane **8** into **7** and bisborane adduct **5**. The molecular structure of **5** is shown in Figure 3, and its bonding parameters are summarized in Table 2. The C−S bond lengths in **5** match the average C−S bond

Table 1. Crystallographic data for compounds **3**−**6**

Compound	**3**	**4**	**5**	**6**
Empirical formula	$C_5H_{12}INS_2$	$C_4H_{11}BClNS_2$	$C_5H_{18}B_2N_2S$	$C_6H_{18}BN_3$
Molecular mass	277.18	183.52	159.89	143.04
Crystal size [mm]	0.45 × 0.21 × 0.16	0.3 × 0.2 × 0.1	0.4 × 0.2 × 0.1	0.1 × 0.1 × 0.10
Crystal color	colourless	colourless	colourless	colourless
Crystal system	triclinic	monoclinic	orthorhombic	orthorhombic
Space group	*P*−1	*Cc*	*Pca*2(1)	*Aba*2
a [Å]	7.211(1)	5.948(1)	10.366(2)	22.014(9)
b [Å]	7.368(1)	14.618(3)	9.966(2)	15.135(6)
c [Å]	9.248(2)	9.862(2)	9.818(2)	5.552(1)
α [°]	89.23(3)	90	90	90
β [°]	77.58(3)	102.22(3)	90	90
γ [°]	80.56(3)	90	90	90
V [Å^3]	473.2(1)	838.1(3)	1014.3(3)	1850(1)
Z	2	4	4	8
ρ (calcd.) [mg/m^3]	1.945	1.455	1.047	1.027
μ [mm^{-1}]	3.752	0.869	0.258	0.063
F(000)	268	384	352	640
Temperature [K]	293(2)	204	204	183(2)
2θ range for data collection	4.52 to 53.92	5.58 to 43.96°	5.68 to 49.96	3.70 to 55.10
Index ranges	$-9 \le h \le 0$	$0 \le h \le 6$	$-12 \le h \le 12$	$-27 \le h \le 27$
	$-9 \le k \le 9$	$-15 \le k \le 15$	$0 \le k \le 11$	$-18 \le k \le 18$
	$-11 \le l \le 11$	$-10 \le l \le 10$	$0 \le l \le 11$	$-3 \le l \le 3$
Reflections collected	2225	1125	1835	4987
Reflections unique	2057	578	949	1348
Reflections observed (4σ)	1912	571	866	1228
R(int)	0.0108	0.0366	0.0452	0.0346
Number of variables	131	82	91	106
Weighting scheme[a] x/y	0.1365/0.1030	0.0573/0.3046	0.1312/0.000	0.0373/0.6919
GOOF	1.118	0.982	0.985	1.138
Final *R* (4σ)	0.0676	0.0280	0.0529	0.0352
Final *R* *wR*2	0.1592	0.0692	0.1335	0.0816
Largest residual peak [e/Å^3]	4.290	0.334	0.320	0.141

[a] $w^{-1} = \sigma^2 F_o^2 + (xP)^2 + yP$; $P = (F_o^2 + 2F_c^2)/3$.

Table 2. Bond lengths [Å] and bond angles [°] for **1**−**6**

Compd.	**1**[1d]	**3** (X = C8)	**4** (X = B9)	Compd. **5**		Compd. **6**	
S1-C6	1.836(4)	1.790(5)	1.810(4)	S1-C2	1.792(3)	B1-N3	1.623(3)
S1-C2	1.794(4)	1.797(6)	1.810(5)	S1-C6	1.792(4)	N1-C6	1.447(2)
S3-C4	1.836(3)	1.786(5)	1.800(4)	N5-C7	1.492(4)	N1-C4	1.456(2)
S3-C2	1.803(4)	1.792(6)	1.785(4)	N5-C4	1.494(4)	N1-C1	1.465(2)
N5-C7	1.466(5)	1.494(7)	1.496(5)	N5-C6	1.509(4)	N2-C4	1.451(2)
N5-C4	1.428(4)	1.517(6)	1.502(5)	N5-B9	1.644(5)	N2-C5	1.452(2)
N5-C6	1.433(4)	1.519(6)	1.493(5)	N3-C2	1.485(4)	N2-C2	1.462(3)
N5-X	−	1.512(6)	1.627(6)	N3-C4	1.492(4)	N3-C5	1.487(2)
Cl-B9	−	−	1.868(5)	N3-C8	1.495(5)	N3-C6	1.492(2)
		N3-B10	1.640(5)	N3-C3	1.492(3)		
Compd.	**1**[1d]	**3** (X = C8)	**4** (X = B9)	Compd. **5**		Compd. **6**	
C2−S3−C4	97.3(2)	98.6(3)	97.9(2)	C2−S1−C6	94.8(2)	C6−N1−C4	109.9(2)
C2−S1−C6	97.8(2)	99.0(2)	97.1(2)	C7−N5−C4	114.9(3)	C6−N1−C1	109.7(1)
N5−C4−S3	115.7(2)	114.4(3)	115.6(3)	C7−N5−C6	110.4(2)	C4−N1−C1	111.2(1)
N5−C6−S1	116.0(2)	114.4(3)	116.1(3)	C4−N5−C6	110.6(2)	C4−N2−C5	109.5(1)
C6−N5−C7	114.2(3)	112.6(3)	111.6(3)	C7−N5−B9	107.7(3)	C4−N2−C2	111.1(1)
C6−N5−C4	113.1(3)	109.6(4)	110.5(3)	C4−N5−B9	106.0(3)	C5−N2−C2	110.0(2)
C7−N5−C4	114.6(3)	112.5(4)	110.9(3)	C6−N5−B9	106.8(3)	C5−N3−C3	110.1(1)
S3−C2−S1	113.7(2)	113.0(3)	112.7(2)	C2−N3−C4	110.0(3)	C6−N3−C3	110.0(2)
C6−N5−X	−	106.6(4)	109.1(3)	C2−N3−C8	111.3(3)	C5−N3−C6	108.0(1)
C7−N5−X	−	109.0(4)	105.0(3)	C4−N3−C8	114.3(3)	C5−N3−B1	109.3(2)
C4−N5−X	−	106.2(4)	109.6(3)	C2−N3−B10	107.2(3)	C6−N3−B1	109.7(1)
N5−X−Cl	−	−	109.6(3)	C4−N3−B10	106.1(2)	C3−N3−B1	109.7(1)
				C8−N3−B10	107.6(3)	N2−C4−N1	109.2(1)
				N5−C6−S1	113.2(2)		
				N3−C2−S1	113.0(2)		
				N3−C4−N5	118.9(3)		

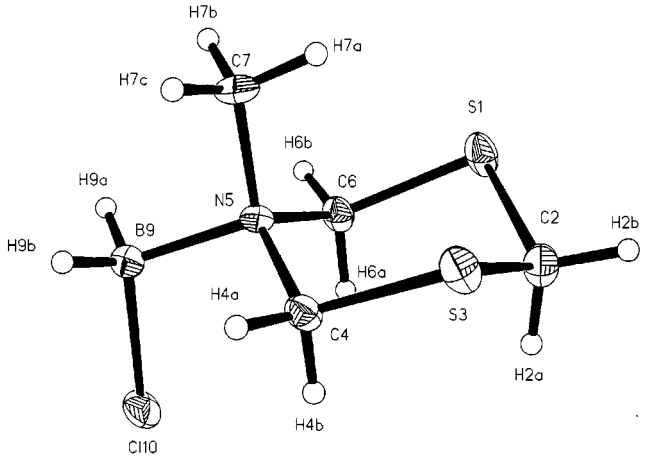


Figure 2. Molecular structure of **4**

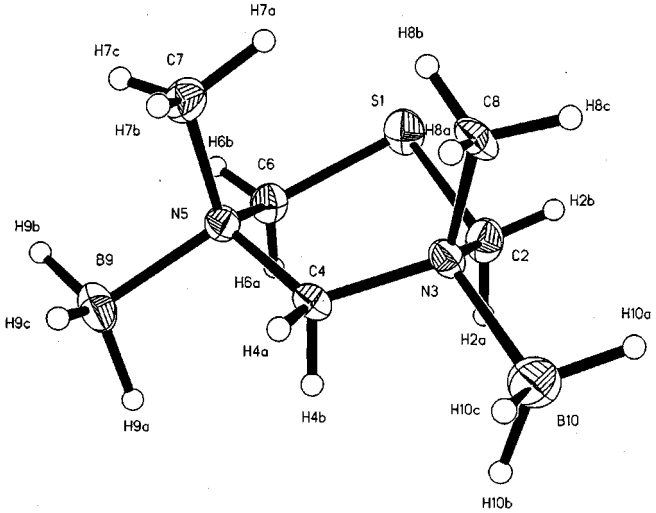


Figure 3. Molecular structure of **5**

lengths of **4**, therefore the two CH_3NBH_3 units must have the same inductive effect on the C−S bond as the ammonium character of the N atom in **4**. Moreover, the N−B bond lengths in **5** are longer than the N−B bond length in **4**. We explain this by the missing inductive effect of the chlorine atom. Compound **5** shows a chair conformation (Figure 3). The two BH_3 groups are in equatorial positions and the two CH_3 groups are in axial positions; the open angles C8−N3−C4 114.6(3)° and C7−N5−C4 114.8(3)° indicate the steric compression suffered by the methyl groups.

The molecular structure of **6** is depicted in Figure 4 and its crystallographic data are presented in Tables 1−3. The heterocycle adopts a chair conformation. The angles around N1, N2, and N3 indicate sp^3 hybridization of these atoms. Two CH_3 groups and BH_3 occupy equatorial positions, and the N3−CH_3 group occupies an axial position.

Interactions between Hydridic and Protic Hydrogen Atoms

The van der Waals radius for the hydrogen atom in a methyl group is reported to be 120 pm.[3] Larger radii have been calculated (145 and 165 pm).[4] In metallic hydrides,

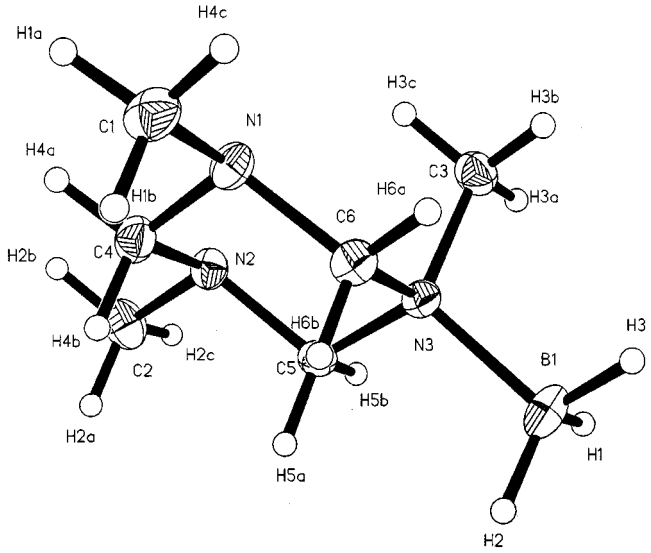


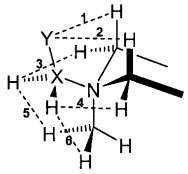
Figure 4. Molecular structure of **6**

the hydrogen ionic radii were found to range from 137 to 154 pm.[5] If an average of 145 pm is assumed, the sum of the van der Waals radii of a protic and an ionic hydridic hydrogen atom is 265 pm. Since the van der Waals radius of the C−H species is 90 pm larger than the hydrogen atomic radius one can estimate that the van der Waals radius of a hydridic hydrogen atom is 145 + 90 = 235 pm. The sum of these van der Waals radii is therefore even larger than that assumed for *r*(H) (van der Waals) + *r*(H^-).

The C−H···H−B atomic distances for **3**−**6** are summarized in Table 3. The distances that are shorter than 265 pm are considered to be the sum of the van der Waals radii, and indicate a strong stabilizing H^+-H^- interaction.[6] The distances in the *N*-methyldithiazinium iodide are all larger than 265 pm.

Hydridic and protic hydrogen atoms have been found to deform the angles of their molecular backbones.[6] $H^{\delta-}-H^{\delta+}$ interactions can therefore also be deduced from the angles between the methyl and the borane groups. For

Table 3. Non-bonding distances $H^{\delta+}-^{\delta-}H$ for **3**−**6**



3: X = C, Y= H; **5**: X = B, Y= H
4: X = B, Y= Cl; **6**: X = B, Y= H

Compd.		1	2	3	4	5	6
3		2.858	2.858	3.514	3.533	2.972	2.352
4		2.730	2.730	2.509	2.448	2.417	2.461
5	N^3	2.563	2.212	2.508	2.523	2.420	2.499
	N^5	2.584	2.311	2.470	2.493	2.313	2.617
6		2.464	2.486	2.544	2.537	2.524	2.445

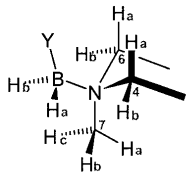
example, B9−N5−C7 [105.0(3)°] in **4**, and B9−N5−C7 and B10−N3−C8 [107.6(3)°] in **5** are smaller than the angle C7−N5−C8 [109.0(4)°] in **3**, thus allowing the close approach of the hydridic and the protic hydrogen atoms as expected for dipolar forces. The torsional angles C5−H5A−H2−B1 (−3.1°), C6−H6B−H2−B1 (4.9°), C5−H5B−H1−B1 (2.2°), and C6−H6A−H3−B1 (−0.5°) are close to 0°, showing that the H^+-H^- interaction is almost at an optimum.

In conclusion, we propose that this kind of intramolecular H^+-H^- interaction[6] is a dominating factor in stabilizing the conformation of boron hydride adducts of azacyclohexanes. It seems to be as important as the intermolecular N−H···H−B interactions that are characteristic for amine−boranes in the solid state, which has recently been pointed out by Crabtree et al.[7]

Experimental Section

The X-ray diffraction studies of **3**−5 were performed with an Enraf−Nonius CAD4 diffractometer (Mo-K_α = 71.069 pm, monochromator: graphite, ω-2θ scan). Cell parameters were determined

Table 4. Torsion angles $C-H^{\delta+}-^{\delta-}H-B$ for **4**−**6**



3, **5** and **6**: Y= H; **4**: Y= Cl

Compd.		$BY-H_aC^6(C^2)$	$BY-H_bC^4$	$BH_b-H_bC^6(C^2)$	$BH_a-H_bC^4$	$BH_b-H_cC^7$	$BH_a-H_bC^7(C^8)$
3		8.42	18.61	9.12	14.79	28.63	7.64
4		3.82	8.51	3.71	1.23	7.78	0.71
5	N^3	20.97	8.51	6.31	36.86	15.08	12.24
	N^5	13.33	12.36	2.66	35.68	10.40	7.73
6		4.92	3.15	0.53	2.18	2.44	3.85

by least-squares refinement of diffractometer angles for 24 automatically centered reflections. Absorption corrections were not necessary; corrections were made for Lorentz and polarization effects. Solution and refinement: direct methods (SHELXS-86) for structure solution. The SHELXL[8] software package was used for refinement and data output. All hydrogen atoms in structures were found in the difference Fourier map. Data was collected for compound **6** with a Siemens P4 instrument with a CCD area detector and a low-temperature device LTP2. The unit cell was determined from the data on 75 frames and data collection was performed in the hemisphere mode with $\Delta\varphi = 0.3°$ and 10 s/frame exposures. Data reduction used the program SAINT. The structure was solved by direct methods (SHELXL-86). Experimental parameters are listed in Table 1. Crystallographic data (excluding structure factors) for the structures reported in this paper have been deposited with the Cambridge Crystallographic Data as supplementary publications nos. CCDC-133313 (**3**), -133314 (**4**), -133315 (**5**) and -133316 (**6**). Copies of the data can be obtained free of charge on application to CCDC, 12 Union Road, Cambridge CB2 1EZ, UK [Fax: (internat). + 44-1223/336-033; E-mail: deposit@ccdc.cam.ac.uk].

5-Methyl-1,3,5-dithiazoniacyclohexane Iodide (3): To a solution of 5-methyl-1,3,5-dithiazacyclohexane (**1**) (1 mmol) in 20 mL of dry THF, CH_3I (1.2 mmol) was added at room temp. The mixture was stirred for 3 h; compound **3** precipitated from the solution. It was filtered and crystallized from H_2O.

Acknowledgments

We thank Conacyt-Mexico and TWAS (grant 97−337 RG/CHE/LA) for financial support and Marco Leyva for the X-ray diffraction structure of **3**. C. G. is grateful to Conacyt-Mexico for a scholarship.

[1] [1a] A. Flores-Parra, N. Farfán, A. I. Hernández-Bautista, L Fernández-Sánchez, R. Contreras, *Tetrahedron* **1991**, *47*, 6903−6914. − [1b] A. Flores-Parra, G. Cadenas-Pliego, L. M. R. Martínez-Aguilera, M. L. García-Nares, R. Contreras, *Chem. Ber.* **1993**, *126*, 863−867. − [1c] G. Cadenas-Pliego, R. Contreras, J. C. Daran, S. Halut, A. Flores-Parra, *Phosphorus Sulfur Silicon* **1993**, *84*, 9−15. − [1d] G. Cadenas-Pliego, L. M. R. Martínez-Aguilera, A. M. Bello-Ramírez, M.-J. Rosales-Hoz, R. Contreras, J. C. Daran, S. Halut, A. Flores-Parra, *Phosphorus Sulfur Silicon* **1993**, *81*, 111−123. − [1e] G. Cadenas-Pliego, M.-J. Rosales-Hoz, R. Contreras, A. Flores-Parra, *Tetrahedron: Asymmetry* **1994**, *5*, 633−640. − [1f] L. M. R. Martínez-Aguilera, G. Cadenas-Pliego, R. Contreras, A. Flores-Parra, *Tetrahedron: Asymmetry* **1995**, *6*, 1585−1592. − [1g] C. Guadarrama-Pérez, G. Cadenas-Pliego, L. M. R. Martínez-Aguilera, A. Flores-Parra, *Chem. Ber.* **1997**, *130*, 813−817. − [1h] A. Flores-Parra, S. A. Sánchez-Ruíz, C. Guadarrama-Pérez, *Eur. J. Inorg. Chem.* **1999**, 2063−2068, preceding paper.

[2] A. Flores-Parra, S. A. Sanchez-Ruíz, *Heterocycles*, in print.

[3] A. Bondi, *J. Phys. Chem.* **1964**, 68, 441−451.

[4] N. L. Allinger, J. A. Hirsch, M. A. Miller, I. J. Tyminski, F. A. Van Catledge, *J. Am. Chem. Soc.* **1968**, *90*, 1199−1210; N. L. Allinger, Y. H. Yuh, J. H. Lii, *J. Am. Chem. Soc.* **1989**, *111*, 8551−8565; 8566−8575; 8576−8582.

[5] K. M. Mackay in *Comprehensive Inorganic Chemistry* (Eds.: J. C. Bailar, H. J. Emeléus, R. Nyholm, A. F. Trotman-Dickenson), Pergamon Press, New York, **1993**, vol. 1. p. 30.

[6] I. I. Padilla-Martínez, M. J. Rosales-Hoz, H. Tlahuext, C. Camacho-Camacho, A. Ariza-Castolo, R. Contreras, *Chem. Ber.* **1996**, *129*, 441−449.

[7] T. B. Richardsson, S. de Gala, R. H. Crabtree, P. E. M. Siegbahn, *J. Am. Chem. Soc.* **1995**, *117*, 12875−12876; R. H. Crabtree, *Science* **1998**, *282*, 2000−2001.

[8] G. W. Sheldrick, *SHELXTL-93 and 97*, University of Göttingen, **1993** and **1997**.

Received October 27, 1999
[I98372]

Porphyrazines with Annulated Diazepine Rings, 1 Synthesis and Characterization of Tetrakis-2,3-(5,7-diphenyl-6*H*-1,4-diazepino)porphyrazine and Its Mg^{II}, Cu^{II}, and Zn^{II} Complexes – X-ray Crystal Structure of 2,3-Dicyano-5,7-diphenyl-6*H*-1,4-diazepine

Maria Pia Donzello,[a] Claudio Ercolani,*[a] Pavel A. Stuzhin,*[b] Angiola Chiesi-Villa,[c] and Corrado Rizzoli[c]

Keywords: Porphyrazines / Diazepines / Tetrakis(diazepino)porphyrazines / Metal complexes / Macrocyclic ligands / Magnesium / Copper / Zinc

A new class of porphyrazine macrocycles carrying peripheral diazepine rings, i.e. tetrakis-2,3-(5,7-diphenyl-6*H*-1,4-diazepino)porphyrazine $[Ph_2DzPzH_2](H_2O)_4$, and its metal derivatives of formula $[Ph_2DzPzM](H_2O)_{x=2-7}$ [M = Mg^{II}-(H_2O), Cu^{II}, Zn^{II}] have been prepared and characterized. Single crystal X-ray work on the monomeric precursor 5,7-diphenyl-2,3-dicyano-6*H*-1,4-diazepine, $Ph_2(CN)_2Dz$, and NMR spectra ($CDCl_3$, $(CD_3)_2SO$) and UV/Vis spectra in solution of different media (basic, neutral, acid) of the monomer and its macrocyclic derivatives have provided information on the conformational flexibility of the diazepine ring as well as on the structural and electronic features of the entire porphyrazine skeleton.

Introduction

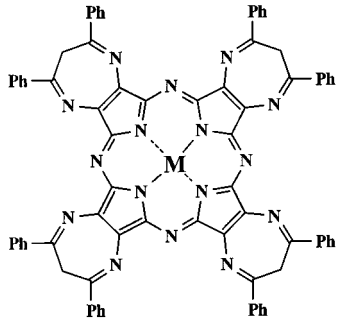
Tetrapyrrolic macrocycles such as porphyrins[1] and phthalocyanines (tetrabenzoporphyrazines), substituted phthalocyanines or their aza analogues,[2] object of extensive studies and practical applications for several decades, have been even more intensively investigated during the last 10−20 years. Comparatively, porphyrazines without annulated six-membered aromatic rings (commonly named also as tetraazaporphyrins), a distinct class of novel macrocycles, have been little studied, although the object of recent increasing attention.[3] Very recently, we have reported on the synthesis and characterization of new classes of porphyrazines carrying five-membered S- and Se-containing heterocycles annulated to the pyrrole rings of the central porphyrazine core, namely tetrakis-3,4-(1,2,5-thiadiazole)-[4] and tetrakis-3,4-(1,2,5-selenodiazole)porphyrazines.[5] Definitely, these new macrocycles can be seen as phthalocyanine-like systems in terms of the square-planar molecular geometry, number of π-electrons, and physical properties (low-solubility, high thermal stability, vaporizability). Nevertheless, the presence in the macrocyclic ring of N atoms and of soft atoms such as S and Se certainly determines a different electronic distribution within the skeletal ring. In addition, S and Se can play an important role in affecting the solid state interunit contacts, which are presently deepfully investigated, this probably opening promising perspectives for the new molecular materials in the field of practical applications (electrical conductivity, electrochromism, nonlinear optical properties, etc.).

We have now extended our attention to the synthesis and characterization of porphyrazine macrocycles having peripheral heptaatomic heterocyclic rings, and report here on the X-ray crystal structure of 5,7-diphenyl-2,3-dicyano-6*H*-1,4-diazepine, $Ph_2(CN)_2Dz$, and on the use of this dicyano species as a monomeric precursor for the synthesis of a new class of porphyrazine macrocycles, i.e. tetrakis-2,3-(5,7-diphenyl-6*H*-1,4-diazepino)porphyrazine, Ph_8DzPzH_2, and its complexes with Mg^{II}, Cu^{II}, and Zn^{II} (see Scheme 1). These tetrapyrrolic species, owing to the structural features of the annulated diazepine rings (see below), markedly differ from the S- and Se-porphyrazines mentioned above, and from the phthalocyanines as well, in many respects. First, they are far from being entirely planar, and, hence, the problem is faced of how the central essentially flat porphyrazine core and the peripheral non planar diazepine rings will reciprocally interfere both structurally and electronically. In addition, the presence of the eight peripheral phenyl groups contribute to infer to the new materials specific physical properties, among them solubility, which may diversify the spectrum of the possible practical applications. Special account should be taken of the fact that the physical properties of this new class of complexes can be modulated by operating appropriate substitutions, presumably possible, in the 5, 6, and 7 positions of the external diazepine rings.

[a] Dipartimento di Chimica, Università degli Studi di Roma "La Sapienza",
P.le A. Moro 5, Roma, I-00185, Italy
Fax: (internat.) + 39-06/49913332
E-mail: ercolani@axrma.uniroma1.it
[b] Department of Organic Chemistry, Ivanovo State University of Chemical Technology,
Friedrich Engels Pr-t 7, Ivanovo, RF-153460, Russia
Fax: (internat.) + 7-932/377743
E-mail: stuzhin@pstu.icti.ivanovo.su
[c] Dipartimento di Chimica Generale ed Inorganica, Università di Parma,
Viale delle Scienze, I-43100 Parma, Italy
Fax: (internat.) + 39-0521/905556
E-mail: angiola@ipruniv.cce.unipr.it

 © WILEY-VCH Verlag GmbH, D-69451 Weinheim, 1999 1434−1948/99/1111−2075 $ 17.50+.50/0

Finally, the N···N···N external cavities can probably be used as the sites for exocyclic metal coordination and formation of multimetallic systems with novel electronic, optical, and redox properties.



Scheme 1

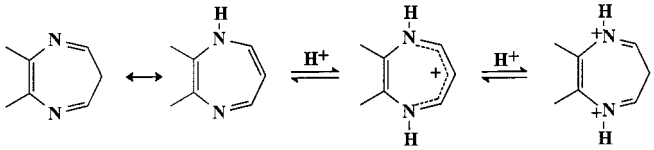
	2	3	4	5
M	Mg	2H	Cu	Zn
Abbreviation	$Ph_8DzPzMg$	Ph_8DzPzH_2	$Ph_8DzPzCu$	$Ph_8DzPzZn$

Results and Discussion

First, we briefly illustrate the structure of the monomeric precursor **1**, and then report on the synthesis and characterization of the macrocycles **2**−**5**.

X-ray Crystal Structure of 5,7-Diphenyl-2,3-dicyano-6*H*-1,4-diazepine, $Ph_2(CN)_2Dz$ (1)

The crystal structure of $Ph_2(CN)_2Dz$ consists of discrete molecules and the crystal packing is determined by van der Waals interactions. Crystal data and details associated with data collection are given in Table 1. The side and front views of the molecule are given in Figure 1 (A, B). Selected bond lengths and angles are quoted in Table 2. The diazepine ring exhibits a boat conformation flattened at the stern, as indicated by the displacements of the C(6), C(2), C(3) atoms from the N(1)−N(4)−C(5)−C(7) mean plane, which are 0.837(2), 0.572(2), 0.588(2) Å, respectively. The dihedral angles formed by the C(5)−C(6)−C(7) and N(1)−C(2)−C(3)−N(4) mean planes with the N(1)−N(4)−C(5)−C(7) mean plane are 119.0 and 148.4°, respectively. The diazepine ring possesses a pseudosymmetry plane running through C(6) and the midpoint of the C(2)−C(3) bond, as indicated by the asymmetry parameter ΔC_s (C4) = 0.011(1). Considering the sequence N(1)−C(2)−C(3)−N(4)−C(5)−C(6)−C(7) the puckering parameters are as follows: q_2 = 0.830(2); q_3 = 0.308(2); Q_T = 0.886(2); φ_2 = 24.3(2); φ_3 = 128.3(4); θ_2 = 69.6(1). The N−C and C−C bond lengths within the diazepine ring appear to be intermediate between those expected for single and double bonds. In fact N(1)−C(2) and N(4)−C(5) lengths are shorter (ca. 1.36 Å) than those in a single bond, while N(1)−C(7) and N(4)−C(5) both 1.301(2) Å], and C(2)−C(3) [1.378(2) Å] are longer than those in a double bond. This indicates that π conjugation permeates the fragment C(7)−N(1)−C(2)−C(3)−N(4)−C(5) internal to the diazepine ring, despite of the fact that the latter is considerably displaced from planarity. The C(51)...C(56) and C(71)...C(76) phenyl rings, which form a dihedral angle of 75.8(1)°, are tilted with respect to the N(1)−N(4)−C(5)−C(7) mean plane by 126.7(1) and 129.0(1)°, respectively.



I II III IV

Scheme 2

Table 1. Experimental data for the X-ray diffraction studies on crystalline compound **1**

	1
Empirical formula	$C_{19}H_{12}N_4$
Formula mass	296.3
Space group	$P2_1/n$ (#14)
a [Å]	9.595(2)
b [Å]	10.828(2)
c [Å]	14.843(3)
α,γ [°]	90
β [°]	95.07
V [Å^3]	1536.1(5)
Z	4
T [°C]	22
λ(Mo-K_α) [Å]	1.54178
$D_{calcd.}$ [g cm^{-3}]	1.281
μ [cm^{-1}]	5.91
Transmission coefficient	0.974−1.000
Unique total data [$I > 0$]	2862
Unique observed data [$I > 2(I)$]	2492
R	0.055
$wR2$	0.176
GOF	1.162

$R = \Sigma|\Delta F|/\Sigma|F_o|$ calculated on the unique observed data [$I > 2(I)$]; $wR2 = [\Sigma w|F^2|^2/w|F_o{}^2|^2]^{1/2}$ calculated on the unique total data with $I > 0$; $GOF = [\Sigma w|F^2|^2/(NO - NV)]^{1/2}$.

As can be well seen from Figure 1A, two hydrogen atoms of the $-CH_2-$ group are inequivalent: One of them is in the equatorial position while another one, being in the quasi-axial position, is located over the diazepine ring. Thus, in the solid state, **1** exists as 6*H* tautomer of type **I** (Scheme 2).

Macrocycles 2−5: Synthetic and General Aspects

Although 2,3-dicyano-6*H*-1,4-diazepines have been known for a long time[6][7] no attempt, to our knowledge, has so far been made to use them as precursors for the preparation of porphyrazines. We have attempted the template tetramerization in presence of magnesium propylate of both 5,7-dimethyl-2,3-dicyano-6*H*-1,4-diazepine, $Me_2(CN)_2Dz$, and 5,7-diphenyl-2,3-dicyano-6*H*-1,4-diazep-

Table 2. Selected bond lengths [Å] and angles [°] for **1**[a]

Bond lengths			
N(1)−C(2)	1.363(3)	C(2)−C(21)	1.445(2)
N(1)−C(7)	1.301(2)	C(3)−C(31)	1.439(3)
N(4)−C(3)	1.360(2)	C(5)−C(6)	1.505(3)
N(4)−C(5)	1.301(2)	C(5)−C(51)	1.468(2)
N(22)−C(21)	1.140(2)	C(6)−C(7)	1.503(3)
N(32)−C(31)	1.138(3)	C(7)−C(71)	1.468(3)
C(2)−C(3)	1.378(2)		
Bond angles			
C(2)−N(1)−C(7)	120.8(2)	N(4)−C(5)−C(6)	119.3(2)
C(3)−N(4)−C(5)	121.3(2)	C(6)−C(5)−C(51)	121.8(2)
N(1)−C(2)−C(21)	113.8(2)	C(5)−C(6)−C(7)	101.0(2)
N(1)−C(2)−C(3)	126.8(2)	N(1)−C(7)−C(6)	119.8(2)
C(3)−C(2)−C(21)	118.5(2)	C(6)−C(7)−C(71)	121.7(1)
N(4)−C(3)−C(2)	125.5(2)	N(1)−C(7)−C(71)	118.5(2)
C(2)−C(3)−C(31)	119.0(2)	N(22)−C(21)−C(2)	178.3(2)
N(4)−C(3)−C(31)	114.9(1)	N(32)−C(31)−C(3)	177.7(2)
N(4)−C(5)−C(51)	118.8(2)		

[a] Atom numbering corresponds to that shown in Figure 1.

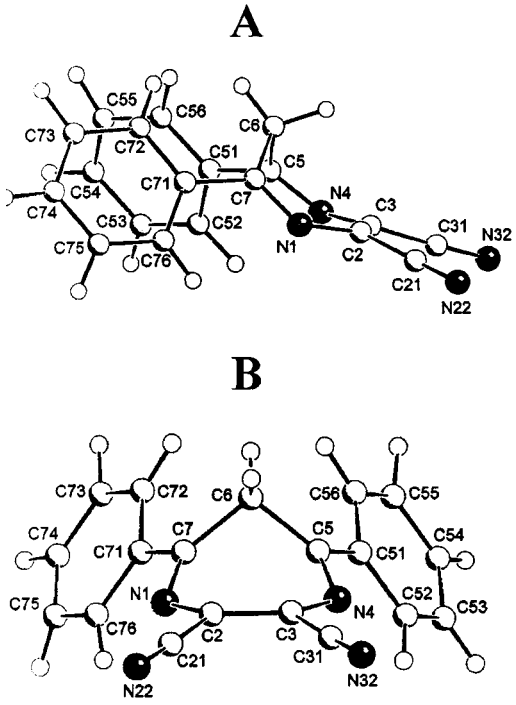


Figure 1. SCHAKAL side (A) and front-top (B) views of $Ph_2(CN)_2Dz$ (**1**)

ine [$Ph_2(CN)_2Dz$, **1**], but only with **1** cyclotetramerization takes place and the Mg^{II} complex $Ph_8DzPzMg$ (**2**) is formed in a high yield as a hydrated bluish-green material.

The Mg complex **2** can be demetallated to the metal-free macrocycle Ph_8DzPzH_2 (**3**) in boiling glacial acetic acid. The use of stronger acids such as CF_3COOH or 96% H_2SO_4 immediately determines demetallation of **2** upon dissolution even at room temperature, as can be evidenced by the UV/Vis spectra (see below). However, these strong acids cannot be used for preparative purposes; in fact, although **3** is stable in 96% H_2SO_4 for days, its precipitation by pouring the solution on ice gives an impure material with low yields, and solutions of **3** in CF_3COOH appear to be not stable enough, and, after even a rapid evaporation of the solvent, an unidentified brown product is obtained (molecular peak in the FAB spectrum at *m*/*z* 1084) instead of the green Ph_8DzPzH_2 (M^+ at 1187.5). A similar brown material, which is presently the object of further investigation, is obtained when non glacial acetic acid is used for preparation of **3** from **2**.

Refluxing of the Mg^{II} complex **2** in glacial acetic acid in the presence of excess of copper acetate results in the formation of the Cu^{II} complex $Ph_8DzPzCu$ (**4**). This latter, and the Zn^{II} complex as well, can be obtained by reaction of the metal-free macrocycle **3** with the pertinent metal acetate in dimethyl sulfoxide (DMSO). All samples of the compounds **2**−**5** were obtained as hydrated materials with slightly variable amounts of water molecules depending on the particular samples, as is evidenced by elemental analysis (C,H,N), thermogravimetric measurements, and IR spectra (see Experimental Section). These water molecules can be completely removed by mild heating under vacuum, exception made for one water molecule retained by the Mg complex. It is assumed that such a water molecule is directly and fairly strongly ligated to the metal center, as observed for several similar Mg^{II}−porphyrazines.[4,5,8]

The macrocyclic structure given in Scheme 1 for the present species is confirmed by FAB measurements (see Experimental Section), and is further supported by NMR, IR, and UV/Vis data. The presence of the peripheral 1,4-diazepine rings in this kind of macrocycles requires examination, developed below, of specific problems concerning their structural and conformational flexibility as well as chemical behaviour, since it is known that 1,4-diazepines can exist, depending on substituents, as 6*H* or 1*H* tautomers **I** and **II**, and in acid media they can be protonated forming successively monocations (diazepinium salts) **III** and dications **IV**[9] (Scheme 2).

^{1}H-NMR Spectra of $Ph_2(CN)_2Dz$ (1) and of the Zn^{II} Complex $Ph_8DzPzZn$ (5)

$Ph_2(CN)_2Dz$ (1) in Solution of $CDCl_3$ and $(CD_3)_2SO$

The ^{1}H-NMR spectrum of **1** (Figure 2, Table 3) definitely confirms that its structure in solution of a nonacidic solvent (chloroform, dimethyl sulfoxide) is similar to that found in the solid state. In fact, in addition to the multiplets of the phenyl protons in the low field region (δ = 7.93, 7.50, and 7.41 for *o*-Ph, *p*-Ph and *m*-Ph, respectively), two doublets for the $-CH_2-$ protons are observed at δ = 1.98 and 5.74 in $CDCl_3$ at 293 K (AB system, ^2J = 11.23 Hz). Such a ^{1}H-NMR pattern for **1** is fully consistent with the tautomeric structure **I** (6*H* tautomer). According to the available ^{1}H-NMR data the 6*H* tautomer **I** is also preferred for the dimethyl derivative $Me_2(CN)_2Dz$,[6] and for 5,7-disubstituted 2,3-benzo-1,4-diazepines (R_2BzDz; R = Me, Ph),[10] whilst the 1*H* tautomer **II** is present in 2,3-dihydro-1,4-diazepines.[9c]

An interesting aspect of the observed ^{1}H-NMR spectrum of **1**, worth to be discussed, is that the CH_2 protons appear,

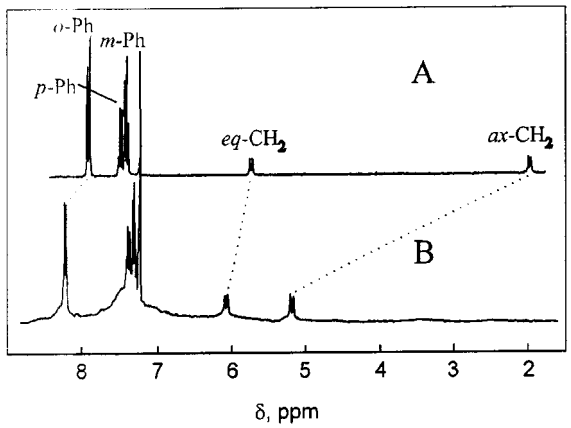


Figure 2. ^{1}H-NMR spectra of (A) $Ph_2(CN)_2Dz$ (**1**) and (B) $Ph_8DzPzZn$ (**5**) in $CDCl_3$

boiling $(CD_3)_2SO$ allowed to explore a wider range of temperatures up to 363 K. As shown in Figure 3 (spectra A−D), the two AB doublets of the CH_2 protons located at δ = 2.32 and 6.19 at 303 K (spectrum A), progressively broaden, completely disappearing at 363 K, thus giving a rough estimation of the coalescence temperature T_c. The high T_c value observed suggests that the ring inversion process for $Ph_2(CN)_2Dz$ is markedly hindered, very likely because of the presence of the two phenyl rings in the 5- and 7-positions.

As far as the position of the CH_2 signals of **1** is concerned, the quasi-axial proton (*ax*-CH_2) is shielded, being located over the plane of the C=N double bonds (Figure 1). Accordingly, the signal is found at higher field than is usual for CH_2 protons adjacent to two sp^2 carbon atoms. The substituents in the diazepine ring appear to have little influence on the resonance position of the *ax*-CH_2 proton

Table 3. Positions of the CH_2 proton signals in the ^{1}H-NMR spectra of compounds containing 1,4-diazepine rings

Compound	Solvent	δ [ppm] *ax*-CH_2	*eq*-CH_2	Splitting ^2J [Hz]	T [°C]
$Ph_2(CN)_2Dz$	$CDCl_3$	1.98	5.74	11.23	293
		1.99	5.73	11.2	313
		2.01	5.70	–	333
	$(CD_3)_2SO$	2.32	6.19	11.18	303
		2.32	6.15	–	323
		2.33	6.14	–	343
		not observed			363 ≈ T_c
$Me_2(CN)_2Dz$[a]	CD_3CN	1.94	4.41	10	243
		singlet		–	T_c ca. room temp.
Ph_2BzDz[b]	C_5D_5N	2.18	5.66	12	223
			3.80	–	353 (T_c = 273±10)
MePhBzDz[b]	CD_3OD	1.97	4.50	12	213
		3.3		–	307 (T_c = 261±7)
Me_2BzDz[b]	CD_3OD	2.04	3.74	11	213
		2.90		–	309 (T_c = 247±8)
$Ph_8DzPzZn$	$CDCl_3$	5.18	6.08	12.6	293
	$(CD_3)_2SO$	5.03	5.99	11.72	373
$Ph_8DzPzMg$	$(CD_3)_2SO$	5.06	5.99	12.10	373

[a] From ref.[6] – [b] From ref.[10]

even at room temperature, as two sharp doublets (again depicted here as an AB system,[9][14] although, owing to their large inequivalence, they might alternatively be considered as an AX system). This means that the inversion of the diazepine ring in this species is slow under these conditions. A different situation is observed in the case of the dimethyl derivative $Me_2(CN)_2Dz$[6] and of 2,3-benzo-1,4-diazepines (R_2BzDz; R = Me, Ph)[10] (Table 3), since for these species the CH_2 protons give a singlet resonance peak at room temperature and only at lower temperatures the peak splits into two doublets (the coalescence temperature T_c is close to room temp. or below, Table 3). Variable temperature ^{1}H-NMR measurements for $Ph_2(CN)_2Dz$ in solution of $CDCl_3$ show that the gradual raising of the temperature from 293 K causes the broadening of the two sharp doublets of the CH_2 protons, and at 333 K two broad unsplit signals are still observed at δ = 2.01 and 5.70 for the axial and equatorial protons, respectively, although clearly the coalescence temperature is not definitely reached. The higher

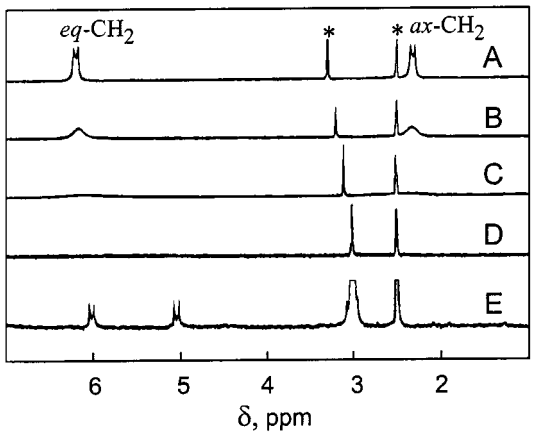


Figure 3. ^{1}H-NMR spectra of $Ph_2(CN)_2Dz$ (**1**) (A−D) and $Ph_8DzPzZn$ (**5**) (E) in $(CD_3)_2SO$ at 313 K (A), 333 K (B), 353 K (C), and 373 K (D, E); signals of nondeuterated solvent and water traces are marked with an asterisk

(Table 3). As to the equatorial proton (*eq*-CH_2), the substituents (especially in 5- and 7-positions) strongly affect the position of its resonance. In $Ph_2(CN)_2Dz$ the *eq*-CH_2 proton is deshielded by the adjacent C=N double bonds and, additionally, by the π-electron ring current of the phenyl rings. Hence, its resonance shifts downfield as compared with that of $Me_2(CN)_2Dz$.

$Ph_8DzPzZn$ (5) in Solution of $CDCl_3$, $(CD_3)_2SO$, CF_3COOH, and H_2SO_4

The ^{1}H-NMR spectrum of $Ph_8DzPzZn$ (**5**) in $CDCl_3$ shows general features similar to those of the monomeric compound $Ph_2(CN)_2Dz$ (compare A and B, Figure 2). At 293 K the phenyl protons give resonances at δ = 8.23, 7.32, and 7.37 for *o*-Ph, *m*-Ph and *p*-Ph, respectively. As to the CH_2 protons, two doublets appear at δ = 5.18 and 6.08 (^2J = 12.5 Hz), which means that in $CDCl_3$ and in $(CD_3)_2SO$ as well (Table 3), all diazepine rings of the Zn^{II} complex **5** are present in the form of the 6*H* tautomer **I**. It can be seen from Figure 2 that in going from $Ph_2(CN)_2Dz$ (**1**) to $Ph_8DzPzZn$ (**5**) a downfield shift is observed for the resonances of the *o*-Ph and CH_2 protons, due to their close position to the porphyrazine macrocycle. These downfield shifts are probably the result of combined structural and electronic effects, since annulation of the diazepine rings very likely implies an increased planarity of the C(7)−N(1)−C(2)−C(3)−N(4)−C(5) moiety, thus allowing an extension of the π-electron conjugation and this, in turn, the deshielding effect of the strong π-electron ring current of the formed porphyrazine macrocycle to which the diazepine rings are attached in this case. The unusually large downfield shift of the axial methylene proton (δ = 3.2) to the new position of δ = 5.18 is especially remarkable and indicates its proximity to the macrocycle. In fact, the distance of this axial methylene hydrogen atom from the center of the porphyrazine macrocycle (ca. 5.3 Å, as can be estimated from the MM+ geometry optimization procedure of the Hyperchem[11]), is 1.7 Å shorter than that of the equatorial hydrogen. Furthermore, such distance is comparable with that of the aromatic pyrrole protons for the Zn complex of unsubstituted porphyrazine (ca. 5.1 Å, singlet at δ = 9.4 in its ^{1}H-NMR spectrum[12]). It is remarkable that in the ^{1}H-NMR spectrum of $Ph_8DzPzZn$ in $(CD_3)_2SO$ even at 373 K (Figure 3, spectrum E) the CH_2 protons give two sharp doublets of the AB system, whilst approximately at the same temperature the monomeric precursor **1** showed coalescence. This means that annulation to the porphyrazine macrocycle very strongly reduces the conformational flexibility of the diazepine ring.

The ^{1}H-NMR spectra of $Ph_8DzPzZn$ in trifluoroacetic and sulfuric acids (Figure 4) differ from those taken in $CDCl_3$ or $(CD_3)_2SO$. This is not surprising, because it is known[9] that 1,4-diazepines exhibit strong basic properties, forming easily (e.g. in CF_3COOH) monocations **III** of diazepinium salts ($pK_{a1} \approx 9$ and 13 for 2,3-benzo- and for 2,3-dihydro-1,4-diazepines, respectively), and, under much more severe conditions (conc. H_2SO_4), diprotonated forms **IV** ($pK_{a2} \approx -1$ and −3 for 2,3-benzo- and for 2,3-dihydro-1,4-diazepines, respectively). The signals of the *m*-Ph and *p*-Ph protons are shifted downfield in CF_3COOH (δ = 8.03 and ca. 8.25, respectively) as compared to their position in the $CDCl_3$ solution. Whilst no AB doublets attributable to the CH_2 protons are observed, two singlets of equal intensity (4 H each) are found present at δ = 4.90 and 8.32.[13] These two resonances can be assigned to the −CH= and NH protons. Their position and relative intensity prove that diazepine rings of $Ph_8DzPzZn$ in the CF_3COOH solution are present in the form of the 1*H* tautomer **II**, rather than in the form of a type-**III** cation. In support of this: a) the olefinic −CH= and NH protons of the 1*H* tautomer **II** of 2,3-dihydro-5,7-dimethyl-1*H*-1,4-diazepine give, similarly, resonances of equal intensity at δ = 4.40 and 7.76 for solution in CCl_4;[9c] b) for the corresponding cation of type **III** in the case of 2,3-dihydro-5,7-diphenyl-1,4-diazepine occurring in CF_3COOH, signals of the −CH= and NH protons are observed at lower fields and have intensity ratio 1:2 [δ = 5.95 (1 H) and 8.1 (2 H)[14]]. Hence, if the tetracation $[Ph_8(DzH)PzZn]^{4+}$ with diazepine rings in form **III** were the case, the −CH= and especially NH resonances should appear at lower fields (due to the influence of the macrocyclic π-electron ring current) and have relative intensity 1:2. Transformation of the diazepine rings of $Ph_8DzPzZn$ from 6*H* tautomer **I** in neutral $CDCl_3$ solution to the 1*H* tautomer **II** in CF_3COOH occurs evidently because of the specific acid solvation of the second nitrogen atom of the diazepine rings and *meso*-nitrogen atoms of the porphyrazine macrocycle by molecules of trifluoroacetic acid. Unlike

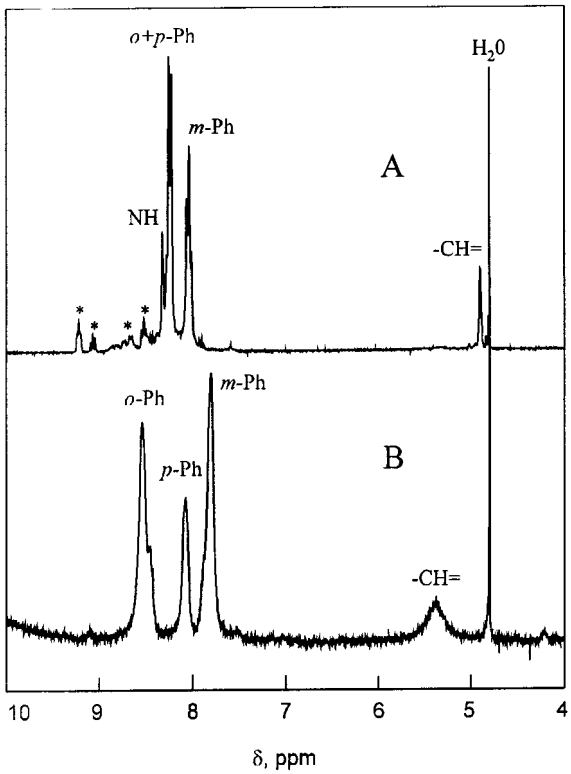


Figure 4. ^{1}H-NMR spectra of $Ph_8DzPzZn$ (**5**) in CF_3COOH (A) and in H_2SO_4 (B); signals of decomposition products are marked with an asterisk

monomeric 1,4-diazepine derivatives, protonation of the diazepine rings in the macrocyclic complex **5** with formation of the tetracation $[Ph_8(DzH)PzZn]^{4+}$ is not favourable under these conditions. Noteworthy, in the case of monomer **1**, due to two electron-withdrawing CN groups present and strongly reducing its basicity, the diazepinium salt $Ph_2(CN)_2DzH^+$ of type **III** is also not formed in CF_3COOH. Accordingly, the ^{1}H-NMR spectral pattern remains characteristic for the 6*H* tautomer **I**, although all signals, because of the acidic solvation, appear at lower fields [multiplets at δ = 8.35, 8.02, 7.87 for *o*-, *p*- and *m*-Ph and two AB doublets (^2J = 11 Hz) at δ = 2.77 and 6.51 for the axial and equatorial CH_2 protons].

The ^{1}H-NMR spectrum of the Zn^{II} complex **5** in H_2SO_4 contains nonresolved multiplets of the phenyl protons (δ = 8.54, 8.07, 7.80 for *o*-, *p*- and *m*-Ph, respectively) and one broad signal at δ = 5.39. The intensity ratio of this signal to the signals of the phenyl protons is 1:10, which allows us to assign it to the olefinic −CH= proton of the monoprotonated diazepine rings in form **III**. For a structure containing doubly protonated diazepine rings **IV** this ratio should be 1:5. Resonances of the NH protons which should be present for both possible structures **III** and **IV** have not been observed. The NH groups located close to the aromatic porphyrazine macrocycle should be strongly deshielded by its π-electron ring current and give resonances downfield with respect to their position in mono- and diprotonated 2,3-dihydro- or 2,3-dibenzo-1,4-diazepines (for 2,3-dihydro-1,4-diazepinium salts **III** δ_{NH} = 8.5−9.5[14][15] and for form **IV** of Me_2BzDz in H_2SO_4 δ_{NH} = 13.4[9c]). No signals are present in the lowfield region (δ > 12.6), where resonances of the NH protons for the structure with doubly protonated diazepine rings **IV** could be expected. Therefore, the octacationic structure $Ph_8(DzH_2)PzZn^{8+}$ can be excluded for the H_2SO_4 solution. For the tetracation $Ph_8(DzH)PzZn^{4+}$ with monoprotonated diazepine rings (form **III**), the NH resonances, expected in the region δ = 9−12, are very likely underneath the intense absorption of H_2SO_4 at δ = 9.3−12.6. In the spectrum taken in deuterated sulfuric acid, the signal of the −CH= proton is not present. This is easily explained by deuterio exchange which is facilitated by the quasi-aromatic properties of the diazepinium salt **III** and hence its reactivity in electrophylic substitution.[16][17]

Although *meso*-nitrogen atoms of the porphyrazine macrocycle can also take part in the acid-base interaction processes,[18] no signal attributable to the $^+N_{meso}$−H resonance was found either in CF_3COOH or in H_2SO_4. It is not surprising that the ^{1}H-NMR spectra provide no evidence of protonation of *meso*-nitrogen atoms. Low relative intensity and broadness (due to the rapid exchange with media) make difficult the detection of these signals, expected in the low field region (possibly nearby the OH absorption of the solvent). UV/Vis spectroscopy in some cases can provide more definite information about acid-base interaction of *meso*-nitrogen atoms.[18]

The ^{1}H-NMR spectra of the Mg^{II} complex **2** in weakly donor solvents show features strictly similar to those observed for the Zn^{II} complex [see data in Table 3 for $(CD_3)_2SO$)]. Similar spectra are also obtained for the free ligand as to the presence of the Ph and CH_2 groups, although the spectra are of poor quality because of low solubility. In strong acids such as H_2SO_4 (96%) complex **2** undergoes demetallation to the free ligand, whose spectra did not allow identification of the central NH groups.

UV/Vis Spectra

UV/Vis spectra of the macrocyclic compounds **2**−**5**, which show strong absorptions in the ranges 250−410 (Soret region) and 600−700 nm (*Q*-band region), deserve some detailed discussion.

Spectra in Basic, Neutral, and Slightly Acidic Solvents

Remarkably, the UV/Vis spectra of the metal-free ligand **3** and the metal complexes **2**, **4**, and **5** in basic, neutral and slightly acidic solvents [pyridine (Table 4), $CHCl_3$, $(CH_3)_2SO$, alcohols, acetic acid] show two well distinct bands in the *Q*-band region (see Figure 5A, B, C for the free ligand, and Figure 5F, G, H for the Cu^{II} complex), i.e. an intense sharp short-wave band with $\lambda_{max} \approx 630-640$ nm (split for the free ligand **3** because of its lower symmetry, i.e. D_{2h}) accompanied by a slightly broader less intense well separated satellite with $\lambda_{max} \approx 660-680$ nm (ca. 800−1000 cm^{-1}).

These two bands cannot be considered as two components of the split *Q*-band originating from considerable lowering of the symmetry of the molecule, since annulation of the four nonplanar diazepine rings cannot significantly disturb the overall D_{4h} symmetry of the chromophore. A split *Q*-band could alternatively originate from dimer formation caused by strong π-interaction,[19] and, indeed, such type of splitting (800−1000 cm^{-1}) has been observed for macrocyclic units brought very close to one another and firmly held together, as occurs, for instance, for the diphthalocyanine systems $(PcRh)_2$,[20] $(PcFe)_2(-C)$ and $(PcRu)_2(-C)$.[21] This is not, however, the case for the present species, for which, noteworthy, the ^{1}H-NMR spectra in $CDCl_3$ give no indication of molecular association even at high concentrations of the species. Clearly, then, the two peaks in the *Q*-band region have a different origin. We suggest that the sharp more intense band at 630−640 nm is associated with the lowest π→π* transition ("normal" *Q*-band), and the less intense long-wave band at 660−680 nm is due to the low lying n→π* transition (Q_n-band), as it is further discussed below.

The φ_n orbitals of the *meso*-nitrogen atoms of the porphyrazine macrocycle and the pyridine-type nitrogen atoms of the annulated heterocyclic rings (e.g. in tetrapyrazinoporphyrazines) have a lower energy than the HOMO, and corresponding n→π* transitions are observed in the Soret band region.[22] The lone pairs of these nitrogen atoms are located in the plane of the porphyrazine skeleton. Differently, the lone pairs of the imido nitrogen atoms in the diazepine rings of compounds **2**−**5** are not coplanar with the macrocycle forming an angle with its mean plane of about

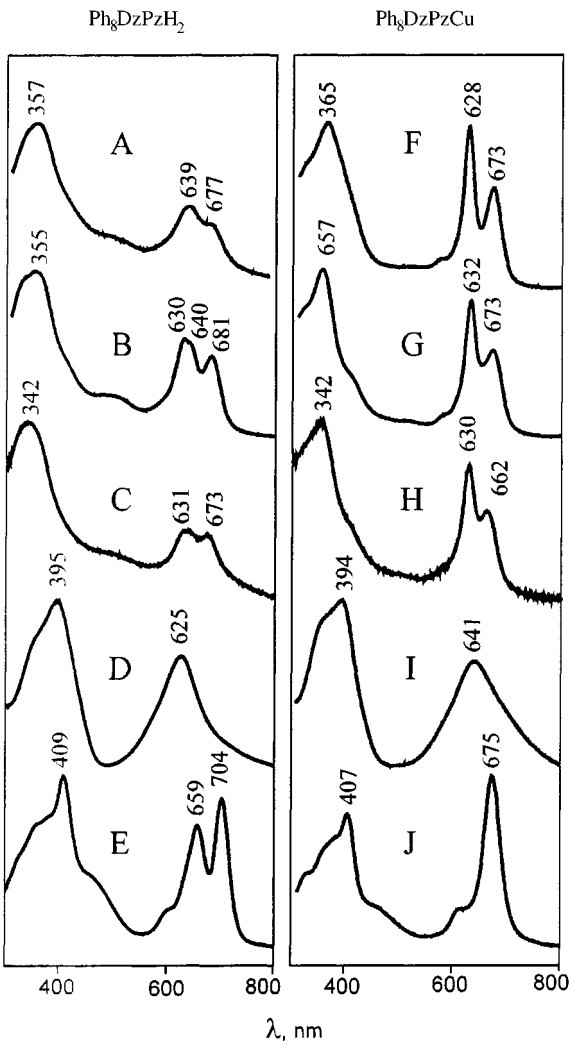


Figure 5. UV/Vis spectra of Ph_8DzPzH_2 (A−E) and $Ph_8DzPzCu$ (F−J) in pyridine (A, F), $CHCl_3$ (B, G), CH_3COOH (C, H), CF_3COOH (D, I) and H_2SO_4 (E, J)

only negligibly affected. This is clear for our species looking at Figure 5 (see spectra B and C, and also F, G, and H).

Spectra in Strong Acids (CF_3COOH, H_2SO_4)

The UV/Vis spectra in CF_3COOH (Figures 5, D and I) show a Soret band at λ_{max} = 394−401 nm, and a broad *Q*-band at λ_{max} = 625−664 nm. No distinct Q_n-band is observed. This type of spectrum is consistent with diazepine rings being present in the 1*H*-tautomeric form **II** as was concluded on the basis of the ^{1}H-NMR data. Strong acidic solvation of the diazepine imido and amino nitrogen atoms and *meso*-nitrogen atoms of the porphyrazine macrocycle is responsible for the diffuse character of the *Q*-band envelope.

The spectra of the Cu and Zn complexes **4** and **5** and of the metal-free macrocycle **3** in solution of conc. H_2SO_4 (96%) are very similar to the spectra of the corresponding unsubstituted, alkyl- or aryl-substituted, and benzo-annulated porphyrazines in neutral solvents[18][19] in that they show a single *Q*-band for complexes **4** and **5** ($\lambda_{max} \approx$ 675−690 nm), and two well-resolved Q_x and Q_y components (659 and 704 nm) for the metal-free ligand **3**. The main maximum in the Soret band envelope is considerably moved towards higher wavelengths (Figure 5, E and J). Such spectra are in full agreement with the symmetrical structure of the macrocycle containing protonated diazepine rings in form **III,** as was also suggested on the basis of the ^{1}H-NMR data. In this structure there is no lone pair on the nitrogen atoms of the diazepine rings and hence the Q_n-band is absent in the spectra. Usually at least one of the *meso*-nitrogen atoms of metalloporphyrazines is protonated in H_2SO_4, which results in a bathochromic shift of the *Q*-band and its observed splitting (in case of interaction with one, two or three *meso*-nitrogen atoms).[18] For our metal complexes, although the maximum of the *Q*-band is shifted bathochromically as compared with neutral solvents by ca. 1000 cm^{-1}, there is no splitting observed due to nonsym-

Table 4. UV/Vis data for Ph_8DzPzH_2, and its Mg^{II}, Cu^{II} and Zn^{II} derivatives in pyridine solution

Compound		λ [nm] (lg ε)					
		Soret region			Q-band region		
Ph_8DzPzH_2	**3**		339sh (4.83)	357 (4.86)	484sh	639 (4.55)	677sh (4.44)
$Ph_8DzPzMg$	**2**		351sh (5.01)	374 (5.05)	589 (4.22)	639 (5.12)	680 (4.83)
$Ph_8DzPzCu$	**4**		323sh (4.82)	365 (4.94)	577 (4.24)	628 (4.93)	673 (4.73)
$Ph_8DzPzZn$	**5**	348sh (4.96)	367 (5.02)	384sh (5.01)	585 (4.20)	637 (5.07)	678 (4.80)

35−40° (as can be estimated from the X-ray data on **1**, and MM+ geometry optimization of Ph_8DzPz^{2-}). As a result the φ_n orbitals of the diazepine imido nitrogen atoms should rise in their energy over HOMO, thus causing the corresponding n→π* electronic transition to appear as a Q_n-band in the long-wave region, as indeed it occurs. The solvatochromic effect is normally large on the peak position of the n→π* transitions, whereas the π→π* transitions are metrical protonation. Symmetrical acid-base interaction with all four *meso*-nitrogen atoms which should give a single bathochromically shifted *Q*-band (e.g. by more than 2500 cm^{-1} for metallophthalocyanines in H_2SO_4)[18] is also impossible. In fact, four positively charged diazepine rings acting as strong electron acceptors should decrease the basicity of the *meso*-nitrogen atoms as compared with unsubstituted porphyrazines in which only two *meso*-nitrogen

atoms can be protonated in H_2SO_4. Thus, in tetra(2,3-pyridino)porphyrazines only one *meso*-nitrogen atom can be protonated in addition to four pyridinium rings.[18] The observed strong bathochromic shift of the Soret band maximum allows to discard protonation of *meso*-nitrogen atoms in H_2SO_4 (and in CF_3COOH as well), because the *B*-band ($a_{2u} \rightarrow e_g$ transition), which is the strongest in the Soret envelope, should be hypsochromically shifted upon protonation.[23]

Conclusion

A new class of porphyrazine macrocycles carrying seven-membered diazepine rings annulated at the periphery of the "internal" tetrapyrrolic macrocycle is reported. This new class of complexes shows specific structural (displacement from planarity of the external diazepine rings, presence of peripherally attached phenyl rings) and UV/Vis spectral features in the *Q*-band region. Further synthetic work is presently being extended to other metal derivatives. Alternative peripheral substitution is possible on the diazepine rings and attempts are in due course for the preparation of new macrocyclic diazepine materials showing better solubility, either in donor or nondonor solvents, and original chemical and physical properties.

Experimental Section

Solvents and Chemicals: Solvents (1-propanol, $CHCl_3$, CH_3COOH, CF_3COOH, pyridine, ethyl alcohol, dimethyl sulfoxide (DMSO), ethyl acetate, acetonitrile, 96% H_2SO_4) and reagents [diaminomaleodinitrile, dibenzoylmethane, P_2O_5, Mg turnings, $Cu(OCOCH_3)_2 \cdot H_2O$, $Zn(OCOCH_3)_2 \cdot 2H_2O$] were pure chemicals (Carlo Erba, Aldrich, Merck).

Chemical Physical Measurements: IR spectra were taken with a Perkin−Elmer 783 spectrophotometer in the range 4000−200 cm^{-1} by using Nujol mulls between CsI disks or KBr pellets. − UV/Vis solution spectra were taken with a Varian Cary 5E spectrometer. − Thermogravimetric analyses were carried out with a Stanton Re Model STA-781 analyzer in N_2 (0.5 L/min). − FAB experiments were carried out with a multiple quadrupole instrument (VG quattro). − Elemental analyses (C, H, N) were provided by the "Servizio di Microanalisi" at the Dipartimento di Chimica, Università "La Sapienza" (Rome).

2,3-Dicyano-5,7-dimethyl-6*H*-1,4-diazepine, $Me_2(CN)_2Dz$: This species has been prepared from diaminomaleodinitrile and acetylacetone according to a known procedure.[6]

2,3-Dicyano-5,7-diphenyl-6*H*-1,4-diazepine, $Ph_2(CN)_2Dz$ (1): Diaminomaleodinitrile (2.4 g, 20 mmol) and dibenzoylmethane (5.0 g, 20 mmol) were condensed in absolute ethanol (80 mL) in the presence of P_2O_5 following closely the procedure reported in the literature.[7] Yield 88%. This material was used for the synthesis of the macrocyclic compounds without further purification. − $Ph_2(CN)_2Dz$ (**1**): $C_{19}H_{12}N_4$ (296.3): calcd. C 77.01, H 4.08, N 18.91; found C 76.94, H 3.88, N 18.80. − ^1H NMR ($CDCl_3$): δ = 1.98 (d, *J* = 11.27 Hz, 1 H, *ax*-CH_2), 5.74 (d, *J* = 11.18 Hz, 1 H, *eq*-CH_2), 7.41 (m, 4 H, *m*-Ph), 7.50 (m, 2 H, *p*-Ph), 7.93 (m, 4 H, *o*-Ph). − ^{13}C NMR ($CDCl_3$): δ = 39.22 (CH_2), 115.04 (CN), 123.68 ($C_{2,3}$), 129.13 (*o*-Ph), 129.82 (*m*-Ph), 133.13 (*p*-Ph), 133.40 (*ipso*-Ph), 149.20 ($C_{5,7}$).

Substituted Porphyrazinatomagnesium Pentahydrate, $[Ph_8DzPzMg(H_2O)] \cdot 4H_2O$ (2): Magnesium metal (0.54 g, 22.2 mmol) was suspended, with stirring, in propyl alcohol (25 mL) in the presence of a small amount of I_2 and the mixture was refluxed for 10 h to complete the conversion of Mg into its corresponding propylate. $Ph_2(CN)_2Dz$ (**1**) (1.5 g, 5.06 mmol) was then added and the mixture kept refluxing for further 8 h. During the reaction the gray mixture changed to dark green, and then to dark blue. At the end of the reaction, propanol was evaporated under reduced pressure and the solid material was suspended in 50% aqueous acetic acid and stirred for 3 h to dissolve the residual unchanged magnesium propylate. The dark bluish-green solid, separated by filtration, was washed with water to neutrality, then with 3 portions of methanol, and brought to constant weight in a vacuum dessicator. Yield 1.42 g (93%). The product can be recrystallized from pyridine/ethyl acetate. All samples obtained from different preparations contained variable amounts of weakly ligated water molecules (4−7). − Representative sample of formula $[Ph_8DzPzMg(H_2O)] \cdot 4H_2O$: $C_{76}H_{58}MgN_{16}O_5$ (1299.71): calcd. C 70.23, H 4.50, N 17.24; found C 69.68, H 4.68, N 16.82. − Thermogravimetric analysis revealed a featureless loss of four water molecules for this sample in the temperature range 25−200°C (found 5.76%, calculated for 4 molecules of H_2O 5.54%), whereas the fifth molecule is more strongly retained, being most likely directly ligated to the central metal. − MS (FAB); *m*/*z* (%): 1210.5 (100) $[M - 5H_2O]^+$, 1227.9 (7) $[M - 4H_2O]^+$, 2418.9 (20) $[M - 5H_2O]_2^+$. − UV/Vis (pyridine): λ_{max} (lg ε) = 351 nm sh, 374 (5.05), 589 (4.22), 639 (5.12), 680 (4.83). − IR (KBr): $\tilde{\nu}$ = 3060 cm^{-1} w, 1645 m, 1600 w, 1580 w, 1527 vs, 1498 w, 1470 w, 1448 s, 1395 w, 1320 m, 1305 w, 1277 m, 1175 s, 1120 s, 1043 m, 1027 w, 1003 w, 983 m, 952 w, 925 vw, 875 w, 840 w, 782 vw, 760 s, 740 w, 710 vs, 690 s, 420 w. − ^1H NMR [$(CD_3)_2SO$ 373 K]: δ = 5.06 (d, *J* = 12.21 Hz, 4 H, *ax*-CH_2), 5.99 (d, *J* = 11.99 Hz, 4 H, *eq*-CH_2), 7.41 (m, 16 H, *m*-Ph), 7.49 (m, 8 H, *p*-Ph), 8.13 (d, *J* = 7.92 Hz, 16 H, *o*-Ph).

Substituted Porphyrazine Tetrahydrate, $[Ph_8DzPzH_2] \cdot 4H_2O$ (3): Solvated magnesium complex **2** (310 mg, 0.24 mmol) was suspended in glacial acetic acid (15 mL) and the mixture refluxed for 16 h. After cooling, the reaction mixture was poured into water. The precipitated dark green solid formed was separated by filtration, washed with H_2O, then with acetone, and brought to constant weight in a vacuum dessicator. Yield 233 mg (77%). − $[Ph_8DzPzH_2] \cdot 4H_2O$: $C_{76}H_{58}N_{16}O_4$ (1259.40): calcd. C 72.48, H 4.64, N 17.79; found C 72.22, H 4.21, N 17.74. − MS (FAB); *m*/*z* (%): 1187.5 (100) $[M - 4H_2O]^+$. − UV/Vis (pyridine): λ_{max} (lg ε) = 339 nm sh, 357 (4.86), 490 sh, 639 (4.55), 677 (4.44). − IR (KBr): $\tilde{\nu}$ = 3298 cm^{-1} w (NH), 3060 m, 1650 m, 1600 vw, 1535 vs, 1498 w, 1480 vw, 1448 s, 1390 vw, 1320 m, 1306 vw, 1285 m, 1187 m, 1120 s, 1080 w, 1040 vw, 1025 m, 1000 w, 975 m, 945 w, 845 w, 790 w, 753 m, 688 vs, 660w, 610 vw, 415 w.

Substituted Porphyrazinatocopper Dihydrate, $[Ph_8DzPzCu] \cdot 2H_2O$ (4): A mixture of $[Ph_8DzPzH_2] \cdot 4H_2O$ (**3**) (250 mg, 0.20 mmol) and anhydrous copper acetate (463 mg, 2.55 mmol) in pyridine (10 mL) was kept refluxing for 6 h. After cooling, the solid separated by centrifugation was washed with water to remove the unchanged Cu^{II} acetate, and dried in a vacuum dessicator. Yield 111 mg (44%). − $[Ph_8DzPzCu] \cdot 2H_2O$: $C_{76}H_{52}CuN_{16}O_2$ (1284.90): calcd. C 71.04, H 4.08, Cu 4.94, N 17.44; found C 70.77, H 4.11, Cu 4.68, N 17.64. − UV/Vis (pyridine): λ_{max} (lg ε) = 323 nm sh, 365 (4.94), 577 (4.24), 628 (4.93), 674 (4.73). − IR (KBr): $\tilde{\nu}$ = 3060 w, *1645 s*, 1600 w, 1585 w, 1530 vs, 1500 m, 1485 m, 1447 s, 1410 w, 1319 m, 1304 m, 1280 m, 1188 s, 1128 vs, 1080 vw, 1050 m, 1028 m, 1000 w, 980m, 952 m, 880 w, 840 vw, 782 vw, 758 s, 737 w, 712 vs, 688 s, 652 w, 622 w, 592 vw, 558 vw, 468 w, 418 m. − Alternatively, the

Cu complex can be prepared by refluxing a mixture of the corresponding Mg^{II} complex (160 mg, 0.125 mmol) and anhydrous copper acetate (176 mg, 0.97 mmol) in glacial acetic acid (10 mL) for 5 h. Yield 83 mg (52%). − $[Ph_8DzPzCu]\cdot 4H_2O$: $C_{76}H_{56}CuN_{16}O_4$ (1320.93): calcd. C 69.11, H 4.27, Cu 4.81, N 16.97; found C 68.14, H 3.62, Cu 5.39, N 17.13.

Substituted Porphyrazinatozinc Heptahydrate, $[Ph_8DzPzZn]\cdot 7H_2O$ (5): A mixture of $[Ph_8DzPzH_2]\cdot 4H_2O$ (**3**) (274 mg, 0.22 mmol) and zinc acetate (380 mg, 1.73 mmol) in pyridine (10 mL) was refluxed for 6 h. After cooling, water (10 mL) was added, and the solid material, separated by centrifugation, was washed with water to remove the excess of the unchanged Zn^{II} salt, and dried in a vacuum dessicator. Yield 192 mg (67%). − $[Ph_8DzPzZn]\cdot 7H_2O$: $C_{76}H_{62}N_{16}ZnO_7$ (1376.80): calcd. C 66.30, H 4.54, N 16.29; found C 65.70, H 4.00, N 16.02. − MS (FAB); *m/z*: 1252 $[M - 7H_2O]^+$. − UV/Vis (pyridine): λ_{max} (lg ε) = 348 nm sh, 367 (5.02), 384 sh, 585 (4.20), 637 (5.07), 678 (4.80). − IR (KBr): $\tilde{\nu}$ = 3055 cm^{-1} w, *1645 s*, 1600 vw, 1582 vw, 1527 vs, 1498 w, 1473 w, 1447 s, 1400 w, 1320 m, 1305 w, 1278 m, 1220 vw, 1178 s, 1127 vs, 1080 vw, 1062 vw, 1043 m, 1027 w, 1002 w, 982 m, 952 w, 872 w, 842 w, 782 wv, 760 s, 748 w, 710 vs, 690 s, 652 w, 623 w, 422 m. − ^1H NMR ($CDCl_3$, 293 K): δ = 5.18 (d, *J* = 12.7 Hz, 4 H, *ax*-CH_2), 6.08 (d, *J* = 12.5 Hz, 4 H, *eq*-CH_2), 7.31 (m, 16 H, *m*-Ph), 7.39 (m, 8 H, *p*-Ph), 8.23 (d, *J* = 7.4 Hz, 16 H, *o*-Ph); [$(CD_3)_2SO$ 373 K]: δ = 5.03 (d, *J* = 12.2 Hz, 4 H, *ax*-CH_2), 5.99 (d, *J* = 12.23 Hz, 4 H, *eq*-CH_2), 7.42 (m, 16 H, *m*-Ph), 7.50 (m, 8 H, *p*-Ph), 8.13 (d, *J* = 7.33 Hz, 16 H, *o*-Ph).

X-ray Crystal Structure Determination of $Ph_2(CN)_2Dz$ (1): Single crystals of **1** were obtained as light-yellow hexagonal prisms during recrystallization of $Ph_2(CN)_2Dz$ from hot acetonitrile. A suitable colorless crystal with the approximate dimensions 0.31×0.34×0.55 mm was mounted on a glass fiber. The reduced cell was obtained with use of TRACER.[24] Data were collected at 295 K with a Siemens AED single-crystal diffractometer. For intensities and background the individual reflection profiles were analyzed.[25] The structure amplitudes were obtained after the usual Lorentz and polarization corrections[26] and the absolute scale was established by the Wilson method.[27] The crystal quality was tested by ψ scans showing that crystal absorption effects could be neglected. The function minimized during the least-square refinements was $\Sigma w(\Delta F^2)^2$. Anomalous scattering corrections were included in all structure factor calculations.[28b] Scattering factors for neutral atoms were taken from ref.[28a] for nonhydrogen atoms and from ref.[29] for H. Structure solution was based on the observed reflections [$I > 2(I)$] while the refinement was based on the unique reflections having $I > 0$. The structure was solved by the direct methods using SIR92.[30] Refinement was done by full-matrix least-squares first isotropically and then anisotropically for all non-H atoms using SHELX93.[31] The hydrogen atoms were located from a difference Fourier map and introduced in the refinements as fixed atoms contributions (U_{iso} = 0.10 $Å^2$). In the last stage of refinement the weighting scheme $w = 1/[\sigma^2(F_o^2) + (aP)^2]$ [with $P = (F_o^2 + 2F_c^2)/3$] was applied with *a* resulting in the value of 0.1001. The final difference map showed no unusual features, with no significant peaks above the general background.[32]

Acknowledgments

C. E. acknowledges financial support by the Ministero Università e Ricerca Scientifica (40%). P. A. S. thanks the Dipartimento di Chimica, Università "La Sapienza" for kind hospitality. Gratitude is expressed to Mr. G. D′Arcangelo [University of "Tor Vergata" (Rome)] for the FAB measurements, to F. Piccioni for taking NMR spectra, and to Dr. P. Galli (University of "La Sapienza") and Dr. R. Dragone (Centro SACSO) for elemental analyses and additional support and collaboration.

[1] *The Porphyrins* (Ed.: D. Dolphin), Acadademic Press, Inc., New York, **1979**, vol. I−VII (a new edition of this series is in preparation and will probably be published in **1999**).
[2] *Phthalocyanines: Properties and Applications* (Eds.: C. C. Leznoff, A. B. P. Lever), VCH Publishers, Inc., New York, **1989−1996**, vol. 1−4.
[3] [3a] J. Fitzgerald, W. Taylor, H. Owen, *Synthesis* **1991**, 686−688. − [3b] P. A. Stuzhin, I. S. Migalova, B. D. Berezin, A. V. Lyubimov, *Koord. Khim*. **1994**, *20*, 444−448; *Chem. Abstr.* **1994**, *121*, 147717g. − [3c] N. S. Mani, L. S. Beall, T. Miller, O. P. Anderson, H. Hope, S. R. Parkin, D. J. Williams, A. G. M. Barrett, B. M. Hoffman, *J. Chem. Soc., Chem. Commun.* **1994**, 2095−2096. − [3d] J. W. Sibert, S. J. Lange, C. L. Stern, A. G. M. Barrett, B. M. Hoffman, *Angew. Chem. Int. Ed. Engl.* **1995**, *34*, 2020−2022. − [3e] C. S. Velazquez, G. A. Fox, W. E. Broderick, K. A. Andersen, O. P. Anderson, A. G. M. Barrett, B. M. Hoffman, *J. Am. Chem. Soc.* **1992**, *114*, 7416−7424. − [3f] T. F. Baumann, M. S. Nasir, J. W. Sibert, A. J. P. White, M. M. Olmstead, D. J. Williams, A. G. M. Barrett, B. M. Hoffman, *J. Am. Chem. Soc.* **1996**, *118*, 10479−10486. − [3g] J. W. Sibert, T. F. Baumann, D. J. Williams, A. J. P. White, A. G. M. Barrett, B. M. Hoffman, *J. Am. Chem. Soc*. **1996**, *118*, 10487−10493.
[4] P. A. Stuzhin, E. M. Bauer, C. Ercolani, *Inorg. Chem.* **1998**, *37*, 1533−1539.
[5] E. M. Bauer, C. Ercolani, P. Galli, I. A. Popkova, P. A. Stuzhin, *J. Porph. Phthal*. **1999**, *3*, 371−380.
[6] R. W. Begland, D. R. Hartter, F. N. Jones, D. J. Sam, W. A. Sheppard, O. W. Webster, F. J. Weigert, *J. Org. Chem.* **1974**, *39*, 2341−2350.
[7] Y. Otsuka, *J. Org. Chem*. **1976**, *141*, 629−633.
[8] M. S. Fischer, D. H. Templeton, A. Zalkin, M. Calvin, *J. Am. Chem. Soc.* **1971**, *93*, 2622−2628.
[9] [9a] I. L. Finar, *J. Chem. Soc*. **1958**, 4094−4097. − [9b] D. Lloyd, R. H. McDougall, D. R. Marshall, *J. Chem. Soc*. **1965**, 3785−3792. − [9c] H. A. Staab, F. Vögtle, *Chem. Ber*. **1965**, *98*, 2701−2714. − [9d] W. J. Barry., I. L. Finar., E. F. Mooney, *Spectrochim. Acta* **1965**, *21*, 1095−1099.
[10] A. Mannschreck, G. Rissman, F. Vögtle, D. Wild, *Chem. Ber.* **1967**, *100*, 335−346. − In order to retain the numbering of the atoms in the diazepine ring we used the name 2,3-benzo-1,4-diazepines instead of somewhat more common 1,5-benzodiazepines. See also ref.[9]
[11] *Hyperchem: A molecular modeling system*, Release 3.0, Hypercube and Autodesk, **1993**.
[12] P. A. Stuzhin, *Khim. Geterotsikl. Soedin*. **1997**, 1364−1370; *Chem. Abstr.* **1998**, *129*, 161437v.
[13] Additional minor signals in the region δ = 8.4−9.3 are due to the products of the decomposition occurring slowly with porphyrazines **2−5** in CF_3COOH.
[14] A. M. Gorringe, D. Lloyd, D. R. Marshall, *J. Chem. Soc. C* **1969**, 1081−1084.
[15] D. Lloyd, R. K. Mackie, H. McNab, D. R. Marshall, *J. Chem. Soc., Perkin Trans. 2* **1973**, 1729−1732.
[16] A. Gorringe, D. Lloyd, D. R. Marshall, L. A. Mulligan, *Chem. Ind.* **1968**, 130−131.
[17] A. R. Butler, D. Lloyd, D. R. Marshall, *J. Chem. Soc. B* **1971**, 795−797.
[18] P. A. Stuzhin, O. G. Khelevina, B. D. Berezin, ref.[1], vol. 4, pp. 19−79.
[19] M. J. Stillman, T. Nyokong, ref.[1], vol. 1, pp. 133−289.
[20] H. Hückstädt, C. Bruhn, H. Homborg, *J. Porphyrins Phthalocyanines* **1997**, *1*, 367−378.
[21] A. Kienast, L. Galich, K. S. Murray, B. Moubaraki, G. Lazarev, J. D. Cashion, H.Homborg, *J. Porphyrins Phthalocyanines* **1997**, *1*, 141−157.
[22] S. S. Dvornikov, V. N. Knyukshto, V. A. Kuzmitski, A. M. Shulga, K. N. Solovyov, *J. Lumin.* **1981**, *23*, 373−392.
[23] P. A. Stuzhin, O. G. Khelevina, *Koord. Khim*. **1998**, *24*, 783−793; *Russ. J. Coord. Chem.* **1998**, *24*, 734−743.

[24] S. L. Lawton, R. A. Jacobson, *TRACER, a cell reduction program*, Ames Laboratory, Iowa State University of Science and Technology, **1965**.
[25] M. S. Lehmann, F. K. Larsen, *Acta Crystallogr., Sect. A: Cryst. Phys., Diffr., Theor. Gen. Crystallogr.* **1974, A30**, 580−584.
[26] Data reduction, structure solution, and refinement were carried out with a *QUANSAN* personal computer equipped with an INTEL PENTIUM processor.
[27] A. J. C. Wilson, *Nature (London)* **1942**, *150*, 151.
[28] *International Tables for X-ray Crystallography*, Kynoch Press, Birmingham, England, **1974**, vol. IV, [28a] p. 99; [28b] p. 149.
[29] R. F. Stewart, E. R. Davidson, W. T. Simpson, *J. Chem. Phys.* **1965**, *42*, 3175−3187.
[30] A. Altomare, M. C. Burla, M. Camalli, G. Cascarano, C. Giacovazzo, A. Guagliardi, G. Polidori, *Acta Crystallogr.* **1994**, *C52*, 2793−2795.
[31] G. M. Sheldrick, *SHELXL-93, Program for the Refinement of Crystal Structures*, University of Göttingen, Germany, **1993**.
[32] Crystallographic data for the structure reported in this paper have been deposited with Cambridge Crystallographic Data Centre as supplementary material no. CCDC-119480. Copies of the data can be obtained free of charge on application to CCDC, 12 Union Road, Cambridge CB2,1EZ, UK [Fax: (internat.) + 44-1223/336-033; E-mail: deposit@ccdc.cam.ac.uk].

Received December 29, 1998
[I98446]

Crystal Structure and Dynamic Behavior of a New Class of Monocationic Organometallic Pd^{II} Compounds with Two Molecules of Bidentate Ligands: $[Pd(L–L)(N–N)(CH_2NO_2)][PF_6]$ (L–L = N–N, dppp)

Barbara Milani,*[a] Gianni Corso,[a] Ennio Zangrando,[a] Lucio Randaccio,[a] and Giovanni Mestroni[a]

Keywords: Palladium / N ligand / P ligand / Copolymerization

Two new classes of organometallic palladium(II) compounds, namely $[Pd(N–N)(CH_2NO_2)_2]$ and $[Pd(L–L)(N–N)(CH_2NO_2)][PF_6]$ [N–N = 2,2′-bipyridine, 1,10-phenanthroline and their substituted derivatives; L–L = 1,3-bis(diphenylphosphino)-propane or N–N] have been synthesized and fully characterized both in the solid state and in solution. The crystal structures of $[Pd(phen)_2(CH_2NO_2)][PF_6]$ and of $[Pd(dppp)(tmphen)(CH_2NO_2)][PF_6]$ show a square-planar coordination geometry for the palladium atom and an unexpected monodentate coordination for the N–N ligand. The behavior in solution, investigated by NMR spectroscopy, shows the presence of dynamic processes involving only the N–N molecules. This fluxional behavior is different for $[Pd(N–N)_2(CH_2NO_2)][PF_6]$ and $[Pd(dppp)(N–N)(CH_2NO_2)][PF_6]$: in the former it most likely involves the substitution of the nitrogen atom *trans* to the CH_2NO_2 moiety by the uncoordinated nitrogen atom of the other N–N ligand; in the latter it may involve the exchange of the two nitrogen atoms at the same coordination site (flipping).

Introduction

Recent developments in homogeneous catalysis show an increasing interest in the use of nitrogen-donor molecules as ancillary ligands.[1] Among the wide variety of nitrogen compounds, ligands containing sp^2-hybridized nitrogen atoms, especially when the N-atom is part of an aromatic ring, like 2,2′-bipyridine (bipy), 1,10-phenanthroline (phen) and bis-oxazoline, have been applied to two reactions of high industrial interest: the reductive carbonylation of nitroaromatic compounds to urethanes[2–4] and the CO/olefin co- and terpolymerization reactions.[5–8]

For several years we have been studying bis(chelate) palladium(II) compounds of general formula $[Pd(N–N)_2][PF_6]_2$ (**I**) and $[Pd(dppp)(N–N)][PF_6]_2$ (**II**) {dppp = 1,3-bis(diphenylphosphino)propane; N–N = bipy, 4,4′-dimethyl-2,2′-bipyridine (dmbipy), phen, 4,7-dimethyl-1,10-phenanthroline (dmphen), 3,4,7,8-tetramethyl-1,10-phenanthroline (tmphen)}, which were found to be efficient catalyst precursors for the above-mentioned reductive carbonylation (compounds of class **I**)[9][10] and copolymerization (compounds of class **I** and **II**)[11–13] reactions. In particular, in the CO/olefin copolymerization reaction the influence of the nitrogen ligand has been investigated in detail with monocationic Pd^{II} compounds which have only one molecule of chelating ligand (N–N) bound to the metal center. The effect of N–N on the stereochemistry of the resulting polyketones was studied by Brookhart,[8] while the influence of N–N in the first and successive insertion steps of CO and alkenes in the copolymerization mechanism was reported by Elsevier and Vrieze.[14] To the best of our knowledge, we are the only group to use Pd^{II} compounds with two molecules of chelating ligand (N–N and/or P–P) as precatalysts for the CO/olefin copolymerization. In this catalytic system the second molecule of chelating ligand, N–N in both classes of complexes, plays an important role, which has been partially examined[12,13,15] although some aspects still remain unclear.

In this paper we report the synthesis and characterization, both in the solid state and in solution, of two new series of stable organometallic Pd^{II} compounds of general formula $[Pd(N–N)(CH_2NO_2)_2]$ and $[Pd(L–L)(N–N)(CH_2NO_2)][PF_6]$ (L–L = dppp, N–N) (Figure 1).

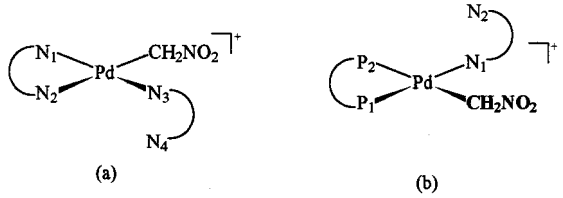


Figure 1. Schematic drawing of complexes $[Pd(N–N)_2(CH_2NO_2)][PF_6]$ and $[Pd(dppp)(N–N)(CH_2NO_2)][PF_6]$

Results and Discussion

Synthesis of the Complexes $[Pd(N–N)(CH_2NO_2)_2]$ (1–5) and $[Pd(L–L)(N–N)(CH_2NO_2)][PF_6]$ (6–11)

The synthesis of the new series of organometallic Pd^{II} compounds, $[Pd(N–N)(CH_2NO_2)_2]$, is achieved by the treatment of a methanolic suspension of the bischelated complexes $[Pd(N–N)_2][PF_6]_2$ with nitromethane in the

[a] Dipartimento di Scienze Chimiche, Università di Trieste, Via Licio Giorgieri 1, I-34127 Trieste, Italy
Fax: (internat.) +39 040 6763903
E-mail: milani@dsch.univ.trieste.it

 © WILEY-VCH Verlag GmbH, D-69451 Weinheim, 1999 1434–1948/99/1111–2085 $ 17.50+.50/0

presence of a strong base, at room temperature. Depending on the nature of the nitrogen-donor chelating ligand the obtained solid has a different composition. When N−N is 2,2′-bipyridine, or its substituted derivatives, only $[Pd(N-N)(CH_2NO_2)_2]$ is obtained as a yellow solid (Scheme 1). On the other hand, when N−N is 1,10-phenanthroline, or its substituted derivatives, we obtain a mixture of compounds containing $[Pd(N-N)(CH_2NO_2)_2]$, as expected, and a new species formulated as $[Pd(N-N)_2(CH_2NO_2)][PF_6]$.

$$[Pd(N\text{-}N)_2][PF_6]_2 \xrightarrow[NaOH,\ MeOH]{CH_3NO_2} [Pd(N\text{-}N)(CH_2NO_2)_2] + 2NaPF_6$$

N-N = bipy and its substituted derivatives

$$[Pd(N\text{-}N)_2][CF_3COO]_2 \xrightarrow[NaOH,\ MeOH]{CH_3NO_2} [Pd(N\text{-}N)(CH_2NO_2)_2] + 2CF_3COONa$$

N-N = phen and its substituted derivatives

Scheme 1. Synthesis of complexes $[Pd(N-N)(CH_2NO_2)_2]$ (**1−5**)

The bis(nitromethyl) compounds with N−N = phen, dmphen and tmphen can easily be synthesized in high yield starting from the more soluble $[Pd(N-N)_2][CF_3COO]_2$, rather than from the corresponding hexafluorophosphate derivatives (Scheme 1).[16] The related monosubstituted derivatives $[Pd(N-N)_2(CH_2NO_2)][PF_6]$ are obtained in pure form as orange solids starting from $[Pd(N-N)_2][PF_6]_2$ and separating the solid from the reaction mixture as soon as the colour turns from yellow to orange, followed by recrystallization of the solid (see Experimental Section). Starting from $[Pd(N-N)_2][PF_6]_2$ the formation of $[Pd(N-N)_2(CH_2NO_2)][PF_6]$ (N−N = phen, dmphen, tmphen) was followed by recording the ^{1}H NMR spectrum of the solid isolated from the reaction mixture at different reaction times. In all cases the solid isolated after 15 min does not contain the starting material and is found to be a mixture of the monosubstituted derivative $[Pd(N-N)_2(CH_2NO_2)][PF_6]$ and the disubstituted derivative $[Pd(N-N)(CH_2NO_2)_2]$ in different ratios depending on the nature of N−N. This ratio increases on going from phen to tmphen.

Therefore, the synthesis of the complexes $[Pd(N-N)(CH_2NO_2)_2]$ is a two-step nucleophilic substitution reaction: the first step, which is very fast, is the attack of the $CH_2NO_2^-$ with formation of the addition product $[Pd(N-N)_2(CH_2NO_2)][PF_6]$; the second step requires dissociation of one of the two chelating ligands and coordination of the second molecule of nucleophile. The second step is slower than the first one, and its rate depends on the nature of the chelating ligand, being fast for unsubstituted phen and slow for tmphen. In the case of bipy as ligand the addition product was never isolated, but the transient orange colour of the synthetic solution of the bis(nitromethyl) derivatives suggests its formation, followed by a very fast reaction to give the final product.

In the case of the mixed-ligand complexes, $[Pd(dppp)(N-N)][PF_6]_2$, the addition product $[Pd(dppp)(N-N)(CH_2NO_2)][PF_6]$ (**9−11**) is synthesized following two different procedures: (i) a direct reaction of $[Pd(dppp)(N-N)][PF_6]_2$ with nitromethane, as for the $[Pd(N-N)_2][PF_6]_2$ complexes (Scheme 2a); (ii) a ligand exchange reaction of one N−N molecule with a molecule of dppp starting from the complexes $[Pd(N-N)_2(CH_2NO_2)][PF_6]$ (Scheme 2b).

$$[Pd(dppp)(N\text{-}N)][PF_6]_2 \xrightarrow[NaOH,\ MeOH]{CH_3NO_2} [Pd(dppp)(N\text{-}N)(CH_2NO_2)][PF_6] + NaPF_6 \quad (a)$$

$$[Pd(N\text{-}N)_2(CH_2NO_2)][PF_6] \xrightarrow[MeOH]{dppp} [Pd(dppp)(N\text{-}N)(CH_2NO_2)][PF_6] + N\text{-}N \quad (b)$$

Scheme 2. Synthesis of complexes $[Pd(dppp)(N-N)(CH_2NO_2)][PF_6]$ (**9−11**)

Characterization of Complexes $[Pd(N-N)(CH_2NO_2)_2]$ (1−5)

The solid-state infrared spectra show two strong bands, one in the range 1481−1457 cm^{-1} and the other between 1348 and 1345 cm^{-1}, which are assigned to the asymmetric and symmetric nitrogen-oxygen stretching frequency, respectively.

The characterization in solution was done by ^{1}H NMR spectroscopy in [D$_6$]DMSO (Table 1). The spectra of all the complexes show a series of signals equal to half the number of chemically equivalent groups for the nitrogen ligand protons, indicating the equivalence of the two halves of the complex. All signals are downfield-shifted with respect to those of the free ligand. The assignments were made as previously reported.[17] The signal due to the two methylenic protons of $CH_2NO_2^-$ appears as a singlet between 5.06 and 4.88 ppm, depending on the nature of N−N (Table 1).

As has already been pointed out,[17a] the signals in the ^{1}H NMR spectrum of H^{2,9} in the phenanthroline series, and

Table 1. ^{1}H-NMR data for complexes **1−8** compared to those of free N−N[a]

Compound/ Ligand	N−N protons H^{2,9}	H^{4,7}	H^{5,6}	H^{3,8}	CH_2NO_2
phen	9.11 (dd)	8.50 (dd)	8.00 (s)	7.79 (dd)	
1	9.48 (dd)	8.93 (dd)	8.25 (s)	8.20 (dd)	5.06 (s)
6	8.96 (d)	8.92 (d)	8.32 (s)	8.00 (dd)	4.97 (s)
dmphen	8.94 (d)		8.16 (s)	7.61 (d)	
2	9.37 (d)		8.38 (s)	8.06 (d)	5.03 (s)
7	8.77 (d)		8.41 (s)	7.82 (d)	4.90 (s)
tmphen[b]	8.83 (s)		8.16 (s)		
8	8.68 (s)		8.42 (s)		4.87 (s)
	N−N protons H$^{6,6'}$	H$^{3,3'}$	H$^{4,4'}$	H$^{5,5'}$	CH_2NO_2
bipy	8.69 (m)	8.39 (m)	7.95 (m)	7.46 (m)	
4	9.16 (d)	8.64 (d)	8.33 (t)	7.89 (t)	4.91 (s)
dmbipy	8.53 (d)	8.23 (s)		7.27 (dd)	
5	8.97 (d)	8.52 (s)		7.70 (d)	4.88 (s)

[a] In [D$_6$]DMSO at room temperature: region of aromatic and $CH_2NO_2^-$ protons. − [b] Compound **3** is not soluble in [D$_6$]DMSO at room temperature. − s = singlet, d = doublet, t = triplet, m = multiplet, dd = doublet of doublets.

of $H^{6,6'}$ in the bipyridine series, are excellent probes for the evaluation of the coordination environment of the palladium atom. Their chemical shifts and bandshape are highly sensitive to the nature of the other ligands bound to the metal and to the presence of dynamic phenomena in solution.

A comparison of the NMR spectra of bis(nitromethyl) complexes $[Pd(N-N)(CH_2NO_2)_2]$ and of monochelated carboxylato derivatives $[Pd(N-N)(CF_3COO)_2]$[17a] shows that, in the first series, the frequencies of the "probe-protons" are downfield shifted with respect to the free ligand, while in the second one they are upfield shifted (Table 2). This observation, together with a lower CIS value (CIS = coordination induced shift; $\Delta\delta$) (Table 2) for the bis(nitromethyl) derivatives with respect to that of the trifluoroacetato compounds, suggests a weaker Pd-N bond in the former, in agreement with the *trans* influence of the $CH_2NO_2^-$ fragment.

Table 2. CIS value ($\Delta\delta$)[a] for the "probe protons" in the two series of complexes $[Pd(N-N)(CF_3COO)_2]$ and $[Pd(N-N)(CH_2NO_2)_2]$

N−N	$[Pd(N-N)(CH_2NO_2)_2]$ $\Delta\delta$ (ppm)	$[Pd(N-N)(CF_3COO)_2]$ $\Delta\delta$ (ppm)
phen	0.37	−0.68
dmphen	0.43	−0.74
bipy	0.47	−0.60
dmbipy	0.44	−0.63

[a] CIS values are positive when shifted downfield with respect to free ligand and negative when shifted upfield.

Characterization of the Complexes $[Pd(L-L)(N-N)(CH_2NO_2)][PF_6]$ (6−11)

The solid-state infrared spectra show the familiar bands of the asymmetric and symmetric nitrogen-oxygen stretching frequency, together with those of the hexafluorophosphate anion.

The molecular structures of the complex cations in **6** and **11** are shown in Figures 2 and 3, respectively, and relevant geometrical parameters are reported in Table 3.

In the $[Pd(phen)_2(CH_2NO_2)]^+$ cation, **6**, the Pd atom exhibits a distorted square planar coordination geometry with one phen molecule acting as a monodentate ligand[18] and the other as a bidentate one (Figure 2), with the metal displaced out of the plane of the four donors by 0.037(2) Å towards N(2).

The chelating phen ligand and the unidentate one are planar within ±0.033(4) and ±0.077(4) Å, respectively, and their mean planes are nearly perpendicular to each other {dihedral angle of 88.91(5)°}. Because of the *trans* influence exerted by the CH_2NO_2 moiety, the Pd-N(5) distance {2.076(3) Å} is longer by 0.035 Å than the Pd-N(4) one {2.042(3) Å}. The latter distance has a value slightly longer than those of about 2.00 Å reported for $[Pd(phen)X_2]$ species,[17a] where X is a weak *trans* influencing ligand and very close to those of about 2.04 Å in the bischelating

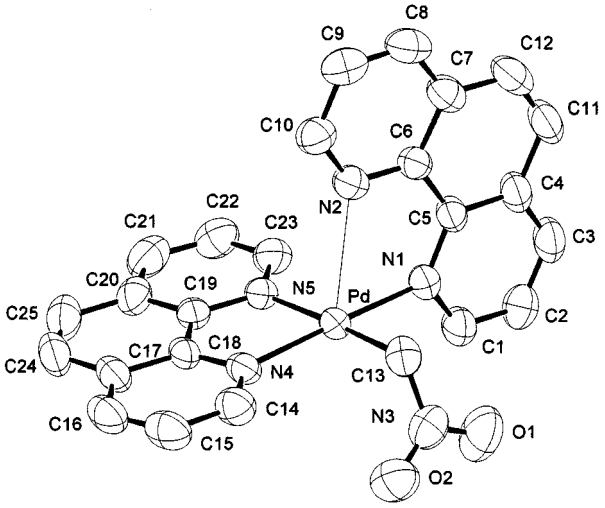


Figure 2. An ORTEP drawing (40% probability thermal ellipsoids) with atom numbering scheme of the cation of **6**

$[Pd(phen)_2]^{2+}$ cations,[17a] which suggests greater steric crowding in the cation of **6** than in $[Pd(phen)X_2]$ complexes. The monodentate phen ligand is bonded to Pd through N(1) {2.065(3) Å}, the other nitrogen being at a distance of 2.674(3) Å.

Table 3. Selected bond lengths [Å] and angles [°]

6:			
Pd−N(1)	2.065(3)	Pd−C(13)	2.052(5)
Pd−N(4)	2.042(3)	Pd−N(2)	2.674(3)
Pd−N(5)	2.076(3)	N(3)−C(13)	1.414(6)
N(1)−Pd−N(4)	174.36(12)	N(4)−Pd−N(2)	112.91(10)
N(1)−Pd−N(2)	70.74(11)	N(5)−Pd−N(2)	88.74(11)
N(1)−Pd−C(13)	88.4(2)	N(4)−Pd−N(5)	80.81(12)
N(1)−Pd−N(5)	95.16(12)	N(3)−C(13)−Pd	108.8(3)
C(13)−Pd−N(2)	92.7(2)	C(1)−N(1)−Pd	117.2(3)
C(13)−Pd−N(4)	95.7(2)	C(5)−N(1)−Pd	123.6(2)
C(13)−Pd−N(5)	176.47(14)	C(6)−N(2)−Pd	104.9(2)
		C(10)−N(2)−Pd	135.5(3)
11:			
Pd−N(1)	2.104(5)	Pd−C(13)	2.157(8)
Pd−P(1)	2.245(2)	Pd−N(2)	2.562(6)
Pd−P(2)	2.333(2)	N(3)−C(13)	1.417(12)
N(1)−Pd−P(1)	179.2(2)	P(1)−Pd−N(2)	109.21(14)
N(1)−Pd−N(2)	71.5(2)	P(1)−Pd−P(2)	90.69(7)
N(1)−Pd−C(13)	88.2(3)	P(2)−Pd−N(2)	88.0(2)
N(1)−Pd−P(2)	89.0(2)	N(3)−C(13)−Pd	112.9(6)
C(13)−Pd−N(2)	102.9(3)	C(1)−N(1)−Pd	119.3(5)
C(13)−Pd−P(1)	91.9(2)	C(5)−N(1)−Pd	122.2(4)
C(13)−Pd−P(2)	167.3(2)	C(6)−N(2)−Pd	107.6(5)
		C(10)−N(2)−Pd	133.9(5)

The CH_2NO_2 group, characterized by the Pd−C(13) distance and the N(3)−C(13)−Pd bond angle of 2.052(5) Å and 108.8(3)°, respectively, is oriented in such a way that NO_2 points to the less "crowded" side of the coordination plane (Figure 2), i.e. towards the coordinated side of the unidentate phen.

In the $[Pd(dppp)(tmphen)(CH_2NO_2)]^+$ cation, **11**, the metal shows a distorted square planar geometry with the tmphen ligand binding in a monodentate fashion through N(1), the other positions being occupied by the diphos-

phine and the CH_2NO_2 group (Figure 3). The metal ion is displaced by 0.129(3) Å out of the plane of the four donors, towards the N(2) atom of tmphen, resulting in a slightly disphenoidal distorsion[19] of the Pd, C(13), N(1), P(1) and P(2) atoms.

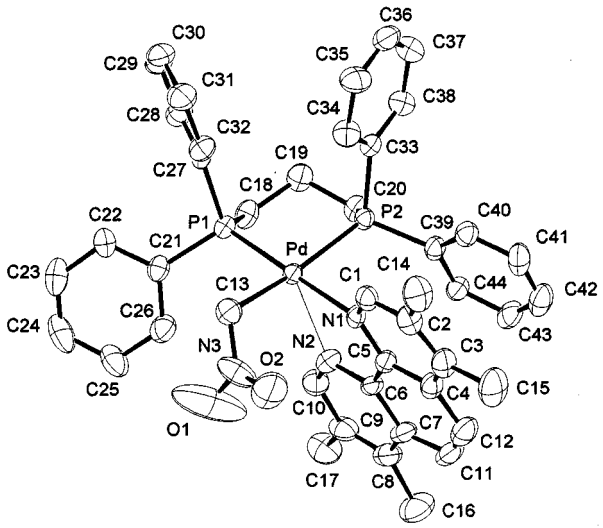


Figure 3. An ORTEP drawing (40% probability thermal ellipsoids) with atom numbering scheme of the cation of **11**

The tmphen ligand is planar within ±0.063(7) Å and makes an angle of 78.9(1)° with the mean coordination plane. It binds with a Pd−N(1) bond length of 2.104(5) Å, longer than that found in **6**, in agreement with the greater *trans* influence of P with respect to that of N. It is worthwhile to note in Figure 3 the stacking of the tmphen ligand with one of the phenyl rings at P(2). The corresponding mean planes make a dihedral angle of 11.5(1)°, with the shortest non-bonding distance N(1)···C(39) of 3.10 Å.

The Pd−P distances are significantly different {2.245(2) and 2.333(2) Å}, the longer one, Pd−P(2), reflecting the *trans* influence of the CH_2NO_2 ligand. The Pd−P(1) distance is similar to those of 2.244(1) and 2.249(2) Å detected in $[Pd(dppp)Cl_2]$[20] and does not significantly differ from the values of 2.262(3) Å found for both the phosphorus atoms in the $[Pd(dppp)(bipy)]^{2+}$ cation.[12] Likewise, steric strains are evidenced in the diphosphine ligand by the large deviations from ideality of the bond angles in the propylenic bridge {from 111.7(5) to 117.4(5)°}.

The Pd−CH_2NO_2 fragment is characterized by a Pd−C(13) distance and a N(3)−C(13)−Pd angle of 2.157(8) Å and 112.9(6)°, respectively. Comparison with the analogous fragment of the cation of **6** shows that in **11** the metal-donor distance is increased by ≈ 0.1 Å and the angle by ≈ 4°. This observation, together with the orientation of the CH_2NO_2 group (towards the uncoordinated side of tmphen), suggests that the latter undergoes more strained interactions with respect to those in the cation of **6**. However, it cannot be excluded that, at least partially, the elongation of the Pd−C(13) bond can be ascribed to the *trans* influence of the P atom as compared to that exerted in **6** by N(5).

The shorter Pd−N(2) distance in the cation of **11** {2.562(6) Å} relative to that found in **6** (2.674(3) Å) is probably due to to the greater coordinating capability of tmphen with respect to that of phen.

These structural results prompted us to indicate for Pd^{II} a strong tendency to be square planar. Very recently the closely related complex $[Pd(phen)_2(COOMe)][PF_6]$ has been reported together with its crystal structure.[21] Although the authors described the complex to be pentacoordinate, the Pd−N distance {2.637(4) Å}, rather longer than normal,[17] and the ratio of the axial/equatorial bond lengths of 1.29 are distinctive of a square planar coordination geometry rather than of a square pyramidal one, as recently reported by Vrieze et al.[18] However, the displacement of the Pd atom towards the uncoordinated nitrogen of the phen (or tmphen) base is indicative of a weak Pd−N interaction both in the present complexes and in the one mentioned above.

The chemical behavior in solution for the $[Pd(N-N)_2(CH_2NO_2)][PF_6]$ compounds (**6-8**) was studied by ^1H NMR spectroscopy in $[D_6]$DMSO (Table 1). The spectra of $[Pd(N-N)_2(CH_2NO_2)][PF_6]$ show, for the nitrogen ligands, four signals integrating for a quarter of the number of chemically equivalent groups, indicating the equivalence of the two ligands bound to palladium and of the two halves of each ligand. In these complexes the signal attributed to the "probe-protons" is shifted upfield with respect to the same signal in the free ligand. The singlet due to the methylenic protons of CH_2NO_2 moiety falls in the range between 4.97 and 4.87 ppm. Its chemical shift is upfield-shifted on going from phen to dmphen and to tmphen. This trend might be related to the electron-donor properties of the ligands. Moreover in the complex $[Pd(tmphen)_2(CH_2NO_2)][PF_6]$ it is possible to unambiguously distinguish the singlet due to the $H^{2,9}$ protons from that of $H^{5,6}$ on the basis of their positive NOE effect with the protons of CH_2NO_2.

For the $[Pd(dppp)(N-N)(CH_2NO_2)][PF_6]$ derivatives (**9-11**) in the ^1H NMR spectra (Table 4), recorded in CD_2Cl_2 at room temperature, three different groups of signals are present: that of the aromatic protons, where the resonances due to the N−N ligand are separated from those of the dppp allowing a clear assignment; that of the $CH_2NO_2^-$, and that of the protons of the propylenic bridge of dppp. The protons of the N−N ligand generate four signals of equal intensity indicating, again, the equivalence of the two halves of this ligand (Table 4a). All signals are shifted with respect to those of the free ligand and, in particular, that due to $H^{2,9}$ is downfield shifted. No signal due to free ligand is present.

The protons of coordinated 1,3-bis(diphenylphosphino)-propane give the same pattern for all complexes: three broad multiplets at high field for the propylenic bridge and four multiplets at low field for the phenyl rings (Table 4b). The number of signals, and their integration, indicates the non-equivalence of the two halves of the diphosphine ligand, as can also be seen from the X-ray structure.

Table 4. ^1H- and $^{31}P\{^1H\}$-NMR data of complexes **9**−**11** in CD_2Cl_2

a)

Compound/Ligand	N−N protons $H^{2,9}$	$H^{4,7}$	$H^{5,6}$	$H^{3,8}$	CH_2NO_2 [^3J(P−H)][a]
phen	9.13 (dd)	8.27 (dd)	7.82 (s)	7.63 (dd)	
9	9.36 (d)	8.31 (d)	7.70 (s)	7.87 (dd)	4.16 (dd) [3.91, 8.79]
dmphen	8.94 (d)		8.04 (s)	7.45 (d)	
10	9.17 (d)		7.87 (s)	7.68 (d)	4.17 (dd) [3.91, 8.79]
tmphen	8.86 (s)		8.06 (s)		
11	8.99 (s)		7.87 (s)		4.18 (dd) [3.91, 8.78]

b)

Compound/Ligand	dppp protons						
	o	*m* + *p*			CH_2 (α)		CH_2 (β)
dppp	7.36 (m)	7.30 (m)			2.19 (t)		1.56 (m)
	o[b]	*p* + *m*[b]	*p*[c]	*o* + *m*[c]	CH_2 (α)[b]	CH_2 (α)[c]	CH_2 (β)
9	7.89 (m)	7.63 (m)	6.97 (m)	6.72 (m)	2.81 (br.)	2.56 (br.)	2.03 (br.)
10	7.79 (m)	7.62 (m)	6.97 (m)	6.70 (m)	2.78 (br.)	2.53 (br.)	2.01 (br.)
11	7.82 (m)	7.64 (m)	6.99 (m)	6.71 (m)	2.78 (br.)	2.53 (br.)	2.03 (br.)

c)[d]

Compound	$^{31}P_1$	$^{31}P_2$	^2J(P−P)[a]
9	15.22(d)	3.84(d)	21.5
10	15.25(d)	3.73(d)	21.5
11	15.03(d)	3.80(d)	21.4

[a] In Hz. − [b] Protons of groups bonded to P_1 (Figure 1b). − [c] Protons of groups bonded to P_2 (Figure 1b). − [d] ^{31}P NMR of free dppp: $\delta = -17.6$.

On the basis of the chemical shift (Table 4b), the four multiplets of the protons of the aromatic rings of dppp can be divided into two sets of two multiplets each: one set is formed by the two multiplets which are upfield shifted with respect to the signals of free dppp (hereafter referred to as the *upfield set*), and the other one by the two multiplets which are shifted downfield (the *downfield set*). The cross peaks in the COSY spectrum correlate the two multiplets inside each set and no cross peak between the *upfield set* and the *downfield* one is present. Therefore, each set is generated by protons belonging to the same phenyl group. The total integration of each set is for ten protons, accounting for two phenyl rings. The comparison of the ^1H NMR spectra of these compounds and those of the $[Pd(dppp)(N-N)][PF_6]_2$ series[12] allows us to assign the *downfield set* to the protons of the two phenyl rings bound to the phosphorus atom *trans* to the Pd−N bond (P_1 in Figure 1b). This assignment is also in agreement with the upfield shift of the resonances of the other two phenyl rings. Indeed, due to the stacking interactions observed in the X-ray structure, their protons are affected by the shielding anisotropy of the tmphen ligand. A similar situation has previously been reported by Natile et al. for the compound *trans*-$[Pt(2,9\text{-dmphen})Br(PPh_3)_2][Br]$.[22]

In the ^1H NMR spectra, the signal due to the methylenic protons of the CH_2NO_2 moiety appears as a doublet of doublets centered at 4.17 ppm (Table 4a). Its chemical shift is practically unaffected by the nature of N−N. Its fine structure is due to a $^1H-^{31}P$ coupling with the two different phosphorus atoms of dppp with coupling constants $^3J(P-H)_{cis} = 3.9$ Hz and $^3J(P-H)_{trans} = 8.8$ Hz.

The $^{31}P\{^1H\}$ NMR spectra present, at room temperature, two sharp doublets, in agreement with the different coordination environment of the phosphorus atoms (Table 4c). The doublet at lowest frequency is attributed to the phosphorus *trans* to the organic fragment (P_2 in Figure 1b).[23] Both of them are at higher frequencies than the signal of free dppp.

Fluxional Behavior of Complexes 6−11

The most important feature in the spectra of the compounds $[Pd(N-N)_2(CH_2NO_2)][PF_6]$ and $[Pd(dppp)(N-N)(CH_2NO_2)][PF_6]$ is the equivalence of the bidentate nitrogen ligand. The presence of a dynamic process has been demonstrated by recording the spectra at low temperature in CD_2Cl_2.

For the complexes $[Pd(N-N)_2(CH_2NO_2)][PF_6]$ at room temperature all signals are sharp. The decrease of temperature causes a progressive broadening of the aromatic frequencies which is particularly evident in the case of $H^{2,9}$ signals. For these protons the signal disappears at T = 193 K. At the lowest temperature we reached, T = 163 K, at least eight signals can be detected (Figure 4). Unfortunately they are still too broad to allow a clear assignment. On the contrary, the signal due to the CH_2NO_2 protons is unaffected by the variation of temperature.

These experiments indicate that at room temperature the dynamic process, which makes the two N−N ligands equivalent, is fast on the ^1H NMR time scale. When one equivalent of the N−N ligand is added to a solution of the com-

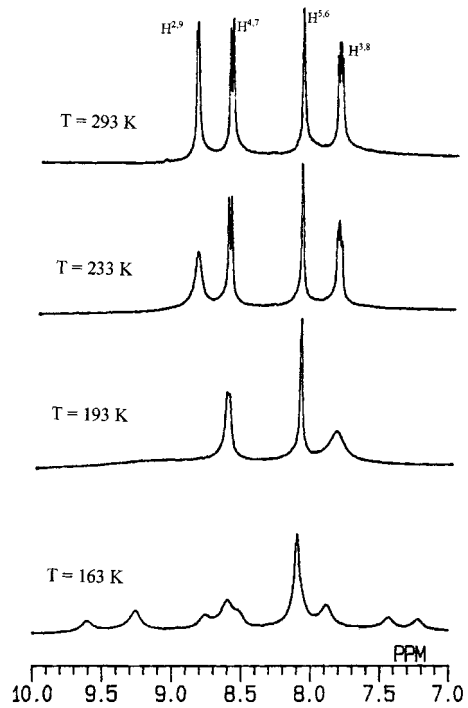
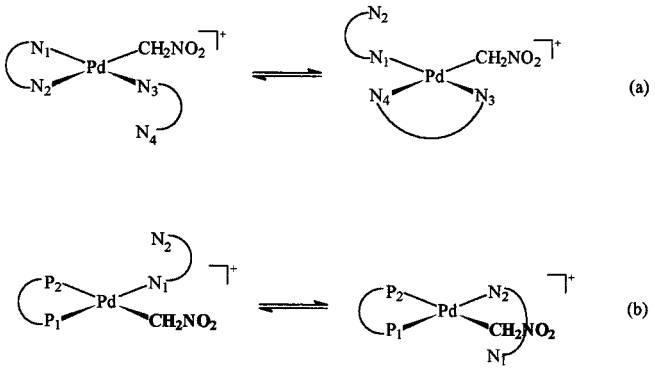


Figure 4. ^{1}H-NMR spectra of $[Pd(phen)_2(CH_2NO_2)][PF_6]$ in CD_2Cl_2: variation with temperature; region of signals of aromatic protons

plex $[Pd(N-N)_2(CH_2NO_2)][PF_6]$, the spectrum measured at room temperature, also shows slightly broadened signals due to free ligand. Therefore, the dynamic process also involves an exchange with the free ligand, which is slower than the intramolecular one. On the basis of these results, one of the possible fluxional processes is the exchange between the unbound nitrogen of the monocoordinated phen (N_4) and one of the two bound nitrogens of the chelated phen, probably the one *trans* to the CH_2NO_2 fragment (N_2) (Scheme 3a).



Scheme 3. Schematic representation of the intramolecular dynamic process of compounds **6**–**11**

For the complexes $[Pd(dppp)(N-N)(CH_2NO_2)][PF_6]$ the signals due to the protons of N–N are sharper than those of the dppp phenyl rings, at room temperature. However, by lowering the temperature all of them broaden. In this case, the $H^{2,9}$ signal disappears at T = 173 K. As already observed for the compounds $[Pd(N-N)_2(CH_2NO_2)][PF_6]$, the decoalescence starts at T = 163 K and again no signal assignment could be performed (Figure 5).

In the compounds $[Pd(dppp)(N-N)(CH_2NO_2)][PF_6]$ the signal of the CH_2NO_2 protons also broadens when lowering the temperature and at T = 163 K it is split into two signals (Figure 5).

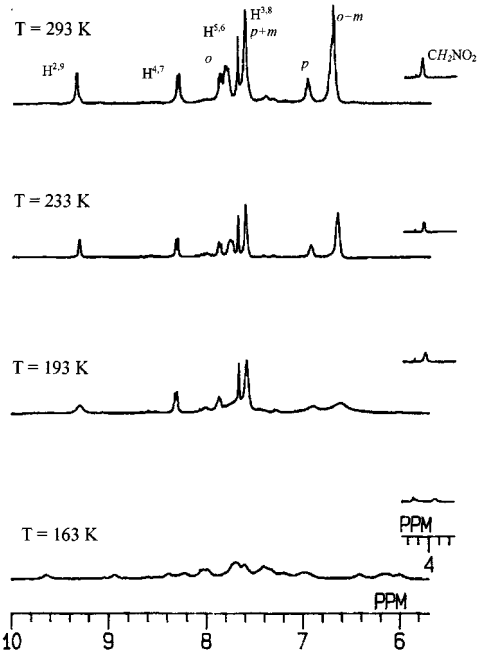


Figure 5. ^{1}H-NMR spectra of $[Pd(dppp)(phen)(CH_2NO_2)][PF_6]$ in CD_2Cl_2: variation with temperature; region of signals of aromatic protons and of CH_2NO_2 moiety

It should be noted that in the $^{31}P\{^1H\}$ NMR spectrum no variation with temperature is observed, suggesting that the two phosphorus atoms are fixed on palladium.

As already observed for the $[Pd(N-N)_2(CH_2NO_2)][PF_6]$ compounds, after addition of one equivalent of N–N to a solution of $[Pd(dppp)(N-N)(CH_2NO_2)][PF_6]$ the spectrum at room temperature also exhibits the signals of free N–N ligand, indicating that the exchange between coordinated and free ligand is slow on the ^{1}H NMR time scale. Therefore, as regards the fluxional behavior of the compounds $[Pd(dppp)(N-N)(CH_2NO_2)][PF_6]$, at least three intramolecular dynamic processes can be involved: (i) the movement of the dppp propylenic bridge, whose rate, at room temperature, is intermediate on the ^{1}H NMR time scale; (ii) the rotation of the phenyl rings of dppp around the P-C_{ipso} bond; (iii) the flipping of the N–N ligand, which exchanges the two nitrogen atoms (N_1 and N_2) at the same coordination site (Scheme 3b). This flipping might be responsible for the equivalence of the two phenyl rings bound to the phosphorus atom *cis* to N–N (P_2 in Figure 1b), one of which exhibits a stacking interaction in the solid state (see above). At room temperature the movements (ii) and (iii) are fast on the ^{1}H NMR time scale.

At the lowest temperature we reached, the CH_2NO_2 protons generate two different signals (Figure 5), because they

are diastereotopic as the palladium atom becomes a stereogenic center. Indeed, the pseudo-symmetry plane present for the complex at room temperature disappears at T = 163 K.

A comparison of the spectra of $[Pd(phen)_2(CH_2NO_2)][PF_6]$ and of $[Pd(dppp)(phen)(CH_2NO_2)][PF_6]$ at T = 163 K shows that the signal at lowest field (9.61 ppm and 9.64 ppm, respectively) has practically the same chemical shift, therefore it may be tentatively attributed to the proton in the *ortho* position with respect to the phen uncoordinated nitrogen atom (N_4 in Figure 1a and N_2 in Figure 1b).

Conclusion

The Pd complexes described above represent one of the first examples of monodentate phen-type ligands with no alkyl substituents at the 2 and 9 positions.

The X-ray structural characterization of these complexes strongly indicates the tendency of palladium(II) to assume a square planar coordination. This is in support of our previous studies on bischelated species where this geometry is ensured by bowing the N−N ligand,[24] and of more recent examples where one of the two molecules of N−N is forced to act as a monodentate ligand.[18][21]

A detailed NMR investigation shows the presence of different dynamic processes in solution: (i) an exchange between coordinated and free N−N ligand; (ii) an intramolecular competition of the unbound nitrogen towards a coordination site at the expense of one N atom of the chelated phen in the $[Pd(N-N)_2(CH_2NO_2)][PF_6]$ complexes; (iii) a flipping of the N−N ligand, in the $[Pd(dppp)(N-N)(CH_2NO_2)][PF_6]$ derivatives, that exchanges the two nitrogen atoms at the same coordination site. The rate of these dynamic processes increases on going from the first to the last one, altough a complete decoalescence could not be reached.

Experimental Section

General Remarks: The nitrogen-donor chelating ligands and dppp (Aldrich) together with the analytical grade solvents (Baker) were used without further purification for synthetic and spectroscopic purposes. IR spectra were recorded on a Perkin Elmer 983G spectrometer in KBr pellets. ^1H NMR spectra were recorded at 400 MHz on a JEOL EX 400 spectrometer operating in Fourier-transform mode, with tetramethylsilane (TMS) as internal standard. Two-dimensional homonuclear correlated spectra (COSY) were obtained with the automatic program of the instrument. ^{31}P NMR spectra were recorded at 161.86 MHz with H_3PO_4 as external reference, where positive shifts are at high frequency.

Syntheses: The compounds $[(N-N)H][PF_6]$, as well as the complexes $[Pd(N-N)_2][PF_6]_2$ and $[Pd(dppp)(N-N)][PF_6]_2$ were synthesized according to the procedures reported in the literature.[11][12] Elemental analyses (C, H, N), performed by Dr. E. Cebulec (Dipartimento di Scienze Chimiche, Trieste, Italy), were in perfect agreement with the proposed stoichiometry (Tables 5 and 6).

Compounds $[(N-N)H][CF_3COO]$: The dinitrogen ligand N−N (5.0 mmol) was dissolved in acetone (15 mL) at room temperature, and trifluoroacetic acid 99% was added (0.47 mL, N−N/CF_3COOH = 1:1.2). Concentration of the solution to approximately a third of the original volume and addition of diethyl ether (15 mL) induced precipitation of the product as a white solid. The solid was removed by filtration and dried under vacuum. Average yield: 70%.

Complexes $[Pd(N-N)_2][CF_3COO]_2$: $Pd(MeCOO)_2$ (0.9 mmol) was dissolved in acetone (10 mL) at room temperature. After 30 min, $[(N-N)H][CF_3COO]$ (2.0 mmol; Pd/$[(N-N)H][CF_3COO]$ = 1:2.2) was added as a solid to the filtered red solution. The product readily precipitated as a yellow solid. After 30 min, it was isolated by filtration, washed with cold acetone and dried under vacuum. Average yield: 75%.

Table 5. Elemental analyses for $[(N-N)H][CF_3COO]$ and $[Pd(N-N)_2][CF_3COO]_2$[a]

Compound	C	H	N
$[(phen)H][CF_3COO]$	57.1 (57.2)	3.05 (3.08)	9.55 (9.52)
$[Pd(phen)_2][CF_3COO]_2$	47.8 (48.5)	2.40 (2.33)	7.90 (8.09)
$[(dmphen)H][CF_3COO]$	59.4 (59.6)	4.02 (4.07)	8.60 (8.69)
$[Pd(dmphen)_2][CF_3COO]_2$	50.5 (51.3)	3.55 (3.60)	9.55 (9.62)
$[(tmphen)H][CF_3COO]$	60.8 (61.7)	4.98 (4.89)	7.96 (8.00)
$[Pd(tmphen)_2][CF_3COO]_2$	49.9 (50.6)	4.54 (4.68)	8.88 (8.93)

[a] Calculated values are reported in parentheses.

$[Pd(N-N)(CH_2NO_2)_2]$ (1−5): The complex $[Pd(N-N)_2][X]_2$ (X = PF_6^- for N−N = bipy and dmbipy; X = CF_3COO^- for N−N = phen, dmphen and tmphen) (0.2 mmol) was suspended in nitromethane (10 mL). A solution of NaOH 0.2 M in methanol was added (3.5 mL; Pd/OH^- = 1:4), obtaining a solution from which the product precipitated as a yellow solid. After 30 min, the solid was removed by filtration, washed with methanol and vacuum dried. Average yield: 70%.

$[Pd(N-N)_2(CH_2NO_2)][PF_6]$ (6−7): The complex $[Pd(N-N)_2][PF_6]_2$ (N−N = phen, dmphen; 0.5 mmol) was added with vigorous stirring to a solution of NaOH in methanol in the presence of nitromethane (4.2 mmol of NaOH in 20 mL CH_3OH and 1.2 mL of CH_3NO_2; Pd/OH^- = 1:8; Pd/CH_3NO_2 = 1:30). The colour of the solid rapidly turned from yellow to orange. The solid was rapidly isolated by filtration, washed with cold methanol and vacuum dried. Average yield: 70%.

Recrystallization: The solid was dissolved in a minimal amount of CH_2Cl_2. From the filtered solution the product precipitated upon addition of diethyl ether.

$[Pd(tmphen)_2(CH_2NO_2)][PF_6]$ (8): The complex $[Pd(tmphen)_2][PF_6]_2$ (0.2 mmol) was suspended in methanol (20 mL). To the suspension a solution of NaOH 0.2 M in methanol (5.0 mL; Pd/OH^- = 1:4) and nitromethane (0.6 mL) were added; the colour turned from yellow to orange. After stirring for 1 h at room temperature the solid was removed by filtration, washed with methanol and vacuum dried. Yield: 80%.

$[Pd(dppp)(N-N)(CH_2NO_2)][PF_6]$ (9−11): The complexes $[Pd(dppp)(N-N)(CH_2NO_2)][PF_6]_2$ can be synthesized following two different procedures: the first slightly differs depending on the nature of N−N (method A), while the second is the same with all the series (method B).

Method A. − $[Pd(dppp)(phen)(CH_2NO_2)][PF_6]$ (9): A solution of NaOH (0.4 mmol; NaOH/Pd = 1.05:1) in methanol (3 mL) in the presence of nitromethane (0.2 mL) was added to a suspension of $[Pd(dppp)(phen)][PF_6]_2$ (0.4 mmol) in methanol (4 mL). The colour of the suspension immediately turned bright yellow and part of the

Table 6. Elemental analyses for the complexes **1**−**11**[a]

Complex	C	H	N
1 [Pd(phen)(CH_2NO_2)$_2$]	40.9 (41.3)	2.90 (2.97)	13.6 (13.8)
2 [Pd(dmphen)(CH_2NO_2)$_2$]	43.9 (44.2)	3.64 (3.71)	12.7 (12.9)
3 [Pd(tmphen)(CH_2NO_2)$_2$]	46.4 (46.7)	4.24 (4.35)	12.0 (12.1)
4 [Pd(bipy)(CH_2NO_2)$_2$]	37.8 (37.7)	3.13 (3.16)	14.2 (14.6)
5 [Pd(dmbipy)(CH_2NO_2)$_2$]	40.8 (40.9)	3.89 (3.93)	13.7 (13.6)
6 [Pd(phen)$_2$(CH_2NO_2)][PF_6]	43.5 (44.7)	2.56 (2.70)	10.2 (10.4)
7 [Pd(dmphen)$_2$(CH_2NO_2)][PF_6]	47.0 (47.8)	3.50 (3.60)	9.50 (9.62)
8 [Pd(tmphen)$_2$(CH_2NO_2)][PF_6]	49.9 (50.6)	4.53 (4.68)	8.86 (8.93)
9 [Pd(dppp)(phen)(CH_2NO_2)][PF_6]	52.7 (53.1)	3.90 (4.01)	4.59 (4.65)
10 [Pd(dppp)(dmphen)(CH_2NO_2)][PF_6]	53.9 (54.1)	4.33 (4.33)	4.38 (4.51)
11 [Pd(dppp)(tmphen)(CH_2NO_2)][PF_6]·CH_2Cl_2	51.8 (51.7)	4.48 (4.44)	4.05 (4.02)

[a] Calculated values are reported in parentheses.

solid was dissolved. After 1 h diethyl ether (50 mL) was added and the mixture was filtered, the solid was washed with cold methanol and vacuum dried. Yield: 85%.

[Pd(dppp)(dmphen)(CH_2NO_2)][PF_6] (10): A solution of NaOH (0.1 mmol; NaOH/Pd = 1.2:1) in methanol (1 mL) in the presence of nitromethane (50 μL) was added to a suspension of [Pd(dppp)(dmphen)][PF_6]$_2$ (0.1 mmol) in methanol (3 mL). The colour of the suspension immediately turned bright yellow and part of the solid was dissolved. Concentration to approximately half of the original volume induced more precipitation of the product as a yellow solid. The solid was removed by filtration, washed with cold methanol and dried under vacuum. Yield: 90%.

[Pd(dppp)(tmphen)(CH_2NO_2)][PF_6] (11): A solution of NaOH (0.4 mmol; NaOH/Pd = 4:1) in methanol (2.5 mL) in the presence of nitromethane (0.25 mL) was added to a suspension of [Pd(dppp)(tmphen)][PF_6]$_2$ (0.1 mmol) in methanol (1 mL). The colour of the suspension immediately turned bright yellow. After 1 min the mixture was filtered, the solid was washed with cold methanol and vacuum dried. Yield: 90%.

Recrystallization: Complex **10** (0.03 g) was recrystallized by dissolving it in methanol (10 mL), yielding a yellow solution from which the product precipitated upon addition of diethyl ether. Complex **11** was recrystallised from a minimal amount of dichloromethane. The solid precipitated upon addition of diethyl ether.

Method B: To a supension of [Pd(N−N)$_2$(CH_2NO_2)][PF_6]$_2$ (0.2 mmol) in methanol (2.5 mL) was added dppp (dppp/Pd = 1:1) together with a minimal amount of dichloromethane (0.15 mL). The mixture was stirred at room temperature for 2 h yielding a bright yellow suspension. The solid was removed by filtration, washed with cold methanol and vacuum dried. Yield: **9** 30%; **10** 70%; **11** 77%.

X-ray Analysis. − X-ray Structure Determination of 6 and 11: Single crystals of [Pd(phen)$_2$(CH_2NO_2)][PF_6] (**6**) and of [Pd(dppp)-

Table 7. Crystal data and details of structure refinements for compounds **6** and **11**

	6	**11**
Empirical formula	$C_{28}H_{24}F_6N_5O_3PPd$	$C_{47}H_{50}F_6N_3O_3P_3Pd$
Molecular mass	729.89	1018.21
Crystal system	triclinic	monoclinic
Space group	$P\bar{1}$ (No.2)	$P2_1$ (No.4)
a [Å]	10.757(1)	11.760(2)
b [Å]	12.042(2)	16.667(2)
c [Å]	12.487(2)	12.119(2)
α [°]	62.46(1)	
β [°]	82.61(1)	106.76(1)
γ [°]	86.48(1)	
V [Å^3]	1422.3(4)	2274.5(6)
Z	2	2
$D_{calcd.}$ [g cm^{-3}]	1.704	1.487
μ (Mo-K_α) [mm^{-1}]	0.789	0.583
F(000)	732	1044
Colour	orange	yellow
θ range	2.50−26.98	2.13−27.96
Octants collected	$-13 \le h \le 13$	$-15 \le h \le 14$
	$-13 \le k \le 15$	$0 \le k \le 21$
	$0 \le l \le 15$	$0 \le l \le 15$
No. of reflections collected	6477	5898
No. of independent reflections	6185 [R(int) = 0.0205]	5648 [R(int) = 0.0277]
Refinement method	Full-matrix least squares on F^2	
No. of reflections with $I > 2\sigma$ (I)	4772	4298
No. of parameters	434	572
Goodness-of-fit	1.050	0.986
$R1$ (F_o)	0.0427	0.0467
$wR2$ (F_o^2)	0.1180	0.1091
Residuals [e Å^{-3}]	0.589, −0.445	0.794, −0.469

(tmphen)(CH_2NO_2)][PF_6] (**11**) suitable for X-ray analysis were obtained with the double-layer method by dissolving the complex in a minimal amount of acetone. Double the volume of diethyl ether was stratified on the filtered yellow solution. The crystals were obtained overnight.

Details of crystal parameters, data collection and refinements of compounds **6** and **11** are summarized in Table 7. Diffraction data were carried out at room temperature using the $\omega-2\theta$ scan technique on a CAD4 Enraf-Nonius single-crystal diffractometer equipped with graphite monochromator and Mo−K_α radiation (λ = 0.7107 Å). Three standard reflections, measured at regular intervals throughout the data collections, showed no noticeable variation in intensity for either crystal. An absorption correction based on ψ-scan method was applied to both the data sets.

The structures were solved by conventional Patterson[25] and Fourier analyses and refined on F^2 by the full-matrix anisotropic least-squares method using the SHELXL-93 package.[26] In both the crystals, a difference Fourier synthesis revealed the presence of a molecule of acetone. In compound **6** this molecule was disordered over two positions with refined site occupancies that complement to 1.0. The final cycles with the fixed contribution of hydrogen atoms, except those of the solvent molecule, converged to final $R1$ and $wR2$ factors reported in Table 3. Refined weighting schemes were $1/[\sigma^2 (Fo^2) + (0.0805P)^2 + 0.07P]$ and $1/[\sigma^2 (Fo^2) + (0.0746P)^2]$ for compound **6** and **11**, respectively, where $P = \{\text{Max}(Fo^2, 0) + 2Fc^2\}/3$. The Flack x parameter[27] of 0.01(4) is indicative of the correct absolute configuration for compound **11**. Crystallographic data (excluding structure factors) for the structures reported in this paper have deposited with the Cambridge Crystallographic Data Center as supplementary publication n. CCDC-113500/113501. Copies of the data can be obtained free of charge on application to CCDC, 12 Union Road, Cambridge CB2 1EZ, UK (Fax: + 44-1223/336-033; E-mail:deposit@ccdc.cam.ac.uk).

Acknowledgments

This work was supported by Ministero dell'Università e della Ricerca Scientifica e Tecnologica (MURST 60%; Rome). We thank Johnson Matthey for a generous loan of $Pd(MeCOO)_2$.

[1] A. Togni, L. M. Venanzi, *Angew. Chem. Int. Ed. Engl.* **1994**, *33*, 497−526.
[2] [2a] P. Wehman, G. C. Dol, E. R. Moorman, P. C. J. Kamer, P. W. N. M. van Leeuwen, J. Fraanje, K. Goubitz, *Organometallics* **1994**, *13*, 4856−4869. − [2b] P. Wehman, V. E. Kaasjager, W. G. J. de Lange, F. Hartl, P. C. J. Kamer, P. W. N. M. van Leeuwen, J. Fraanje, K. Goubitz, *Organometallics* **1995**, *14*, 3751−3761. − [2c] P. Wehman, P. C. J. Kamer, P. W. N. M. van Leeuwen, *Chem. Commun.* **1996**, 217−218. − [2d] J. G. P. Delis, P. G. Aubel, P. W. N. M. van Leeuwen, K. Vrieze, N. Veldman, A. L. Spek, *J. Chem. Soc., Chem. Commun.* **1995**, 2233−2234.
[3] N. Masciocchi, F. Ragaini, S. Cenini, A. Sironi, *Organometallics* **1998**, *17*, 1052−1057.
[4] F. Paul, J. Fischer, P. Ochsenbein, J. A. Osborn, *Organometallics* **1998**, *17*, 2199−2206.
[5] [5a] A. Sen, T. W. Lai, *J. Am. Chem. Soc.* **1982**, *104*, 3520. − [5b] W. T. Lai, A. Sen, *Organometallics* **1984**, *3*, 866. − [5c] A. Sen, Z. Jiang, *Macromolecules* **1993**, *26*, 911−915.
[6] [6a] E. Drent, J. A. M. van Broekhoven, M. J. Doyle, *J. Organomet. Chem.* **1991**, *417*, 235−251. − [6b] E. Drent, P. H. M. Budzelaar, *Chem. Rev.* **1996**, *96*, 663−681.
[7] [7a] M. Barsacchi, G. Consiglio, L. Medici, G. Petrucci, U. W. Suter, *Angew. Chem. Int. Ed. Engl.* **1991**, *30*, 989−991. − [7b] C. Pisano, A. Mezzetti, G. Consiglio, *Organometallics* **1992**, *11*, 20−22. − [7c] M. Barsacchi, A. Batistini, G. Consiglio, U. W. Suter, *Macromolecules* **1992**, *25*, 3604−3606. − [7d] A. Batistini, G. Consiglio, U. W. Suter, *Angew. Chem. Int. Ed. Engl.* **1992**, *31*, 303−305. − [7e] A. Batistini, G. Consiglio, *Organometallics* **1992**, *11*, 1766−1769.
[8] [8a] M. Brookhart, F. C. Rix, J. M. De Simone, J. C. Barborak, *J. Am. Chem. Soc.* **1992**,*114*, 5894−5895. − [8b] M. Brookhart, M. I. Wagner, G. G. A. Balavoine, H. A. Haddou, *J. Am. Chem. Soc.* **1994**, *116*, 3641−3642. − [8c] M. Brookhart, M. L. Wagner, *J. Am. Chem. Soc.* **1996**, *118*, 7219−7220.
[9] [9a] A. Bontempi, E. Alessio, G. Chanos, G. Mestroni, *J. Mol. Catal.* **1987**, *42*, 67−80. − [9b] A. Sessanta o Santi, B. Milani, E. Zangrando, L. Randaccio, G. Mestroni, *J. Organomet. Chem.* **1997**, *545-546*, 89−91.
[10] [10a] R. Santi, A.M. Romano, F. Panella, G. Mestroni, A. Sessanta o Santi, It. Pat. N. MI96A002071, **1996**. − [10b] R. Santi, A.M. Romano, F. Panella, G. Mestroni, A. Sessanta o Santi, It. Pat. N. MI96A002072, **1996**.
[11] B. Milani, A. Anzilutti, L. Vicentini, A. Sessanta o Santi, E. Zangrando, S. Geremia, G. Mestroni, *Organometallics* **1997**, *16*, 5064−5075.
[12] B. Milani, L. Vicentini, A. Sommazzi, F. Garbassi, E. Chiarparin, E. Zangrando, G. Mestroni, *J. Chem. Soc., Dalton Trans.* **1996**, 3139−3144.
[13] [13a] A. Sommazzi, F. Garbassi, G. Mestroni, B. Milani, U.S. Pat. N. 5,310,871, **1994**; *Chem. Abstr.* **1995**, *122*, P266287e. − [13b] A. Sommazzi, F. Garbassi, G. Mestroni, B. Milani, Eur. Pat. N. 97104955.6-2102, **1997**; *Chem. Abstr.* **1997**, *127*, P346797q.
[14] [14a] R. van Asselt, E. E. C. G. Gielens, R. E. Rülke, C. J. Elsevier, *J. Chem. Soc., Chem. Commun.* **1993**, 1203−1205. − [14b] R. van Asselt, E. E. C. G.; Gielens, R. E. Rülke, K. Vrieze, C. J. Elsevier, *J. Am. Chem. Soc.* **1994**, *116*, 977−985. − [14c] B. A. Markies, D. Kruis, M. H. P. Rietveld, K. A. N. Verkerk, J. Boersma, H. Kooijman, M. T. Lakin, A. L. Spek, G. van Koten, *J.Am. Chem. Soc.* **1995**, *117*, 5263−5274. − [14d] J. H. Groen, C. J. Elsevier, K. Vrieze, W. J. J. Smeets, A. L. Spek, *Organometallics* **1996**, *15*, 3445−3455. − [14e] J. H. Groen, J. G. P. Delis, P. W. N. M. van Leeuwen, K. Vrieze, *Organometallics* **1997**, *16*, 68−77. − [14f] J. G. P. Delis, J. H. Groen, K. Vrieze, P. W. N. M. van Leeuwen, N. Veldman, A. L. Spek, *Organometallics* **1997**, *16*, 551−562.
[15] A. Sommazzi, F. Garbassi, G. Mestroni, B. Milani, L. Vicentini, Eur. Pat. N. 96117237.6-2102, **1996**; *Chem. Abstr.* **1997**, *127*, P51110j.
[16] When the synthesis is performed starting from the corresponding monochelated derivatives [Pd(N−N)($RCOO)_2$] (R = Me, CF_3) only brown solids are obtained.
[17] [17a] B. Milani, E. Alessio, G. Mestroni, A. Sommazzi, F. Garbassi, E. Zangrando, N. Bresciani-Pahor, L. Randaccio, *J. Chem. Soc., Dalton Trans.* **1994**, 1903−1911. − [17b] B. Milani, E. Alessio, G. Mestroni, E. Zangrando, L. Randaccio, G. Consiglio, *J. Chem. Soc., Dalton Trans.* **1996**, 1021−1029.
[18] Very recently two examples of palladium(II) compounds with dinitrogen ligands bonded in a monodentate fashion have been structurally characterized either with a flexible bidentate nitrogen ligand, 8-(2-pyridyl)quinoline[14e] or with a more rigid one, bis(anisylimino)acenaphthene: J. H. Groen, B. J. de Jong, J. M. Ernsting, P. W. N. M. van Leeuwen, K. Vrieze, W. J. J. Smeets, A. L. Spek, *J. Organomet. Chem.* **1999**, *573*, 3−13.
[19] R. J. Gillespie, I. Hargittai, *The VSEPR Model of Molecular Geometry*, Allyn and Bacon, Boston, **1991**.
[20] W. L. Steffen, G. J. Palenik, *Inorg. Chem.* **1976**, *15*, 2432−2438.
[21] [21a] R. Garrone, A. M. Romano, R. Santi, R. Millini, *Organometallics* **1998**, *17*, 4519−4522. − [21b] R. Santi, A. M. Romano, R. Garrone, L. Abbondanza, M. Scalabrini, G. Bacchilega, *Macromol. Chem. Phys.* **1999**, *20*, 25−30.
[22] F. P. Fanizzi, M. Lanfranchi, G. Natile, A. Tiripicchio, *Inorg. Chem.* **1994**, *33*, 3331−3339.
[23] G. P. C. M. Dekker, C. J. Elsevier, K. Vrieze, P. W. N. M. van Leeuwen, *Organometallics* **1992**, *11*, 1598−1603.
[24] S. Geremia, L. Randaccio, G. Mestroni, B. Milani, *J. Chem. Soc., Dalton Trans.* **1992**, 2117−2118.
[25] G.M. Sheldrick, "SHELXS-86, program for structure solution" in *Acta Crystallogr., Sect. A* **1990**, *46*, 467−473.
[26] G. M. Sheldrick, *SHELXL-93, Program for crystal structure refinement*, University of Göttingen, Germany, **1993**.
[27] H. D. Flack, *Acta Crystallogr., Sect. A* **1983**, *39*, 876−881.

Received February 1, 1999
[I99028]

Crystallographic and Spectroscopic Characterization of Tetrakis(μ-*N*,*N*′-diarylformamidinato)dichlorodirhenium(III,III) Compounds

Judith L. Eglin,*[a] Chun Lin,[b] Tong Ren,[b] Laura Smith,[a] Richard J. Staples,[c] and David O. Wipf[a]

Keywords: Metal−metal bonds / Rhenium / Formamidinate / UV/Vis spectroscopy / Electrochemistry

Through a variation in the aryl substituents of the formamidinate ligand, a variety of dirhenium compounds has been synthesized with $[XArNC(H)NArX]^-$ where Ar is a substituted C_6H_5 or C_6H_4 aryl ring and X is *p*-MeO (**1**), H (**3**), *m*-MeO (**4**), *p*-Cl (**5**), *m*-Cl (**6**), *m*-CF_3 (**7**), *p*-CF_3 (**8**), 3,4-Cl_2 (**9**), and 3,5-Cl_2 (**10a**, **10b**). UV/Vis and NMR spectroscopy and electrochemical data for **1** and **3–10** have been obtained. X-ray crystallographic analysis of $Re_2Cl_2(\mu\text{-form})_4$ with four different diarylformamidinate ligands and one analog with two different interstitial solvents are presented; $Re_2Cl_2[(p\text{-}MeOC_6H_4)NCHN(p\text{-}MeOC_6H_4)]_4$ (**1**), $Re_2Cl_2[(m\text{-}MeOC_6H_4)NCHN(m\text{-}MeOC_6H_4)]_4 \cdot 2\ CH_2Cl_2$ (**4**), $Re_2Cl_2[(3,4\text{-}Cl_2C_6H_3)NCHN(3,4\text{-}Cl_2C_6H_3)]_4 \cdot 2\ CH_2Cl_2$ (**9**), $Re_2Cl_2[(3,5\text{-}Cl_2C_6H_3)NCHN(3,5\text{-}Cl_2C_6H_3)]_4 \cdot 4\ CH_2Cl_2$ (**10a**), and $Re_2Cl_2[(3,5\text{-}Cl_2C_6H_3)NCHN(3,5\text{-}Cl_2C_6H_3)]_4 \cdot OC_4H_8$ (**10b**).

Introduction

Amidine and amidinate ligands are adaptable ligands in the synthesis of dinuclear transition metal compounds that span the periodic table.[1] Dinuclear transition metal complexes include Ti_2,[2−4] Zr_2,[5] V_2,[6][7] Ta_2,[8−10] Cr_2,[11−13] Mo_2,[11,13−18] W_2[12], Tc_2,[19] Re_2,[20][21] Fe_2,[22−25] Ru_2,[26−32] Os_2,[33] Co_2,[25,34−37] Rh_2,[34,38−41] Ni_2,[42−44] Pd_2,[44][45] Pt_2,[46][47] Cu_2,[48] Ag_2,[48][49] In_2,[50] and Sn_2,[51] and the diversity of dinuclear complexes demonstrates the versatility of the ligand to form both metal−metal bonded and non-bonded systems. Recently, the systematic study of the tunability of the electronic and spectroscopic properties of the resultant complexes with variations in the ligand periphery has become a focus area.[14,15,26−28,43,52,53]

Redox tuning of dinuclear compounds by varying the remote substituents on the aryl ring of diarylformamidinate ligands (form) has been studied in a series of dichromium(II,II),[52] dimolybdenum(II,II),[14][15] and dinickel(II,II)[43] complexes. In the previously studied dinickel systems, metal−metal bonding is absent with a long Ni−Ni separation of 2.462(2) Å observed for $Ni_2[(3,5\text{-}Cl_2C_6H_3)NCHN(3,5\text{-}Cl_2C_6H_3)]_4$.[43] In contrast, the $Cr_2(\mu\text{-form})_4$ and $Mo_2(\mu\text{-form})_4$ systems contain metal−metal quadruple bonds, $\sigma^2\pi^4\delta^2$, with much shorter Cr−Cr and Mo−Mo mean bond lengths of 1.911 and 2.096 Å.[15][52] The study is extended to correlate structural, spectroscopic, and electrochemical properties of $Cr_2^{II,II}$, $Mo_2^{II,II}$, and $Re_2^{III,III}$ quadruply-bonded complexes with the inclusion of the $Re_2Cl_2(\mu\text{-form})_4$ series.[20,21,52] The addition of the $Re_2Cl_2(\mu\text{-form})_4$ complexes allows the comparison of compounds with axially coordinated chlorides and the relativistic effects associated with 5d orbitals to the $Cr_2(\mu\text{-form})_4$ and $Mo_2(\mu\text{-form})_4$ systems previously studied.[20,21,52] A series of dirhenium compounds of the general type $Re_2Cl_2(\mu\text{-form})_4$ has been synthesized with the ligand $[XArNC(H)NArX]^-$, where Ar is a substituted C_6H_5 or C_6H_4 ring and X is *p*-MeO (**1**), H (**3**), *m*-MeO (**4**), *p*-Cl (**5**), *m*-Cl (**6**), *m*-CF_3 (**7**), *p*-CF_3 (**8**), 3,4-Cl_2 (**9**), and 3,5-Cl_2 (**10a**, **10b**). UV/Vis, ^{1}H-NMR, and ^{13}C-NMR spectroscopy are reported for the series in addition to the structural characterization of **1**, **4**, **9**, and **10a**, **b**. A linear free energy relationship is determined from electrochemical studies of the $Re_2Cl_2(\mu\text{-form})_4$ complexes by varying the remote substituents on the aryl ring of the diarylformamidinate ligands.

Results and Discussion

Synthesis

Synthesis of compounds **1** and **3−10** with the general formula $Re_2Cl_2(\mu\text{-form})_4$ proceeds as previously described.[21] Molten reactions of $Re_2Cl_2(\mu\text{-}O_2CCH_3)_4$ with the respective substituted diarylformamidine ligands were performed using a minimum four fold excess of the ligand (Hform) at reaction temperatures between 150° to 180° for 1.5 to 18 hours. Reactions times are dependent on the melting point of the diarylformamidine ligands. A short reaction time results in incomplete ligand substitution and an elevated reaction temperature leads to thermal decomposition of the diarylformamidine ligand.

Molecular Structures

^{1}H-NMR spectra were recorded for compounds **1** and **3−10** to confirm the expected diamagnetic ground state for

[a] Department of Chemistry, Box 9573, Mississippi State University, Mississippi State, MS 39762, USA
[b] Department of Chemistry, Florida Institute of Technology, Melbourne, FL 32901, USA
[c] Department of Chemistry and Chemical Biology, Harvard University, Cambridge, MA 02138, USA

 © WILEY-VCH Verlag GmbH, D-69451 Weinheim, 1999 1434−1948/99/1111−2095 $ 17.50+.50/0

all of the compounds, $\sigma^2\pi^4\delta^2$. The simplicity of the ^{1}H-NMR spectra reflects the high symmetry of the Re_2Cl_2(μ-form)$_4$ complexes and confirms both the bulk purity of the compounds and the general structure of the compounds where X-ray crystallographic data were not obtained.[21] The downfield shift of the singlet for the methine proton (−NC*H*N−) is a distinct feature in the ^{1}H-NMR spectra of the Re_2Cl_2(μ-form)$_4$ series and ^{1}H-NMR data combined with structural data for **1**, **4**, **9**, and **10a**, **b** allowed the calculation of the value of the diamagnetic anisotropy of the Re-Re bond. ^{13}C-NMR spectra were recorded for all of the compounds except **3** and **9** where the solubility of the compounds in CH_2Cl_2 is limited. As a result of poor solubility in most common solvents, the ^{13}C-NMR spectrum of **1** and **4** do not have -O*C*H$_3$ peaks tabulated due to an overlap of the methoxy carbon peak of the compound with the carbon peak of the CH_2Cl_2 solvent which dominates the spectrum.

Crystal structures have been determined for Re_2Cl_2[(*p*-MeOC$_6$H$_4$)NCHN(*p*-MeOC$_6$H$_4$)]$_4$ (**1**), Re_2Cl_2[(*m*-MeOC$_6$H$_4$)NCHN(*m*-MeOC$_6$H$_4$)]$_4$ · 2 CH_2Cl_2 (**4**), Re_2Cl_2[(3,4-Cl$_2$C$_6$H$_3$)NCHN(3,4-Cl$_2$C$_6$H$_3$)]$_4$ · 2 CH_2Cl_2 (**9**), Re_2Cl_2-[(3,5-Cl$_2$C$_6$H$_3$)NCHN(3,5-Cl$_2$C$_6$H$_3$)]$_4$ · 4 CH_2Cl_2 (**10a**), and Re_2Cl_2[(3,5-Cl$_2$C$_6$H$_3$)NCHN(3,5-Cl$_2$C$_6$H$_3$)]$_4$ · OC$_4$H$_8$ (**10b**), with **10a** and **10b** containing the same diarylformamidinate ligand with two different interstitial solvent molecules. Structures of **1**, **4**, **9**, and **10a**, **b** are shown in Figures 1−5, and reflect the D_4 geometry adopted by the dirhenium core ($Re_2N_8Cl_2$) in the molecules.

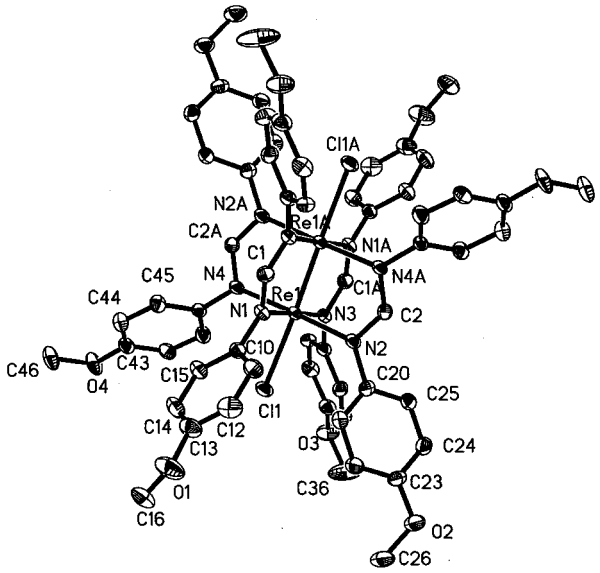


Figure 1. The ORTEP plot of compound **1**; hydrogen atoms are omitted for clarity

A comparison of the Hammett constant of the ligand versus the Re−Re and Re−Cl bond lengths of **1**, **4**, **9**, and **10a**, **b** and Re_2Cl_2[(*p*-tolylC$_6$H$_4$)NCHN(*p*-tolylC$_6$H$_4$)]$_4$ (**2**)[21] indicates the electron donating or withdrawing ability of the ligand has no substantial influence on the bond lengths or angles in the structure (Table 1). The most significant deviation in the Re−Re bond lengths within the series occurs as a result of a change in the interstitial solvent, as in the case of Re_2Cl_2[(3,5-Cl$_2$C$_6$H$_3$)NCHN(3,5-Cl$_2$C$_6$H$_3$)]$_4$ with Re−Re bond lengths of 2.2734(3) Å (4 CH_2Cl_2) and 2.2840(5) Å (OC$_4$H$_8$). More dramatic changes in the structure of the amidinate ligand result in more significant changes in the observed bond lengths and angles.[20] For Re_2Cl_2[(CH$_3$N)$_2$CPh]$_4$ with the *N,N′*-dimethylbenzamidinate ligand and Re−Re and Re−Cl bond lengths of 2.208(2) and 2.654(6) Å, the Re−Cl bond length is significantly elongated in comparison to the diarylformamidinate derivatives due to steric repulsions.[20] As observed in the Re_2Cl_2(μ-form)$_4$ series, only minor variations in the core bond lengths with changes in the substituents on the diarylformamidinate ligands occur for Cr_2(μ-form)$_4$, Mo_2(μ-form)$_4$, and Ni_2(μ-form)$_4$ complexes.[14,15,43,52,54−57]

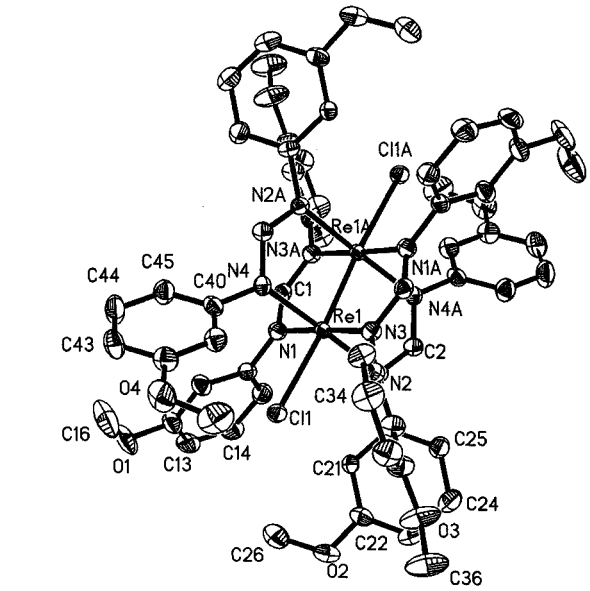


Figure 2. The ORTEP plot of compound **4**; hydrogen atoms and the dichloromethane solvent molecules are omitted for clarity

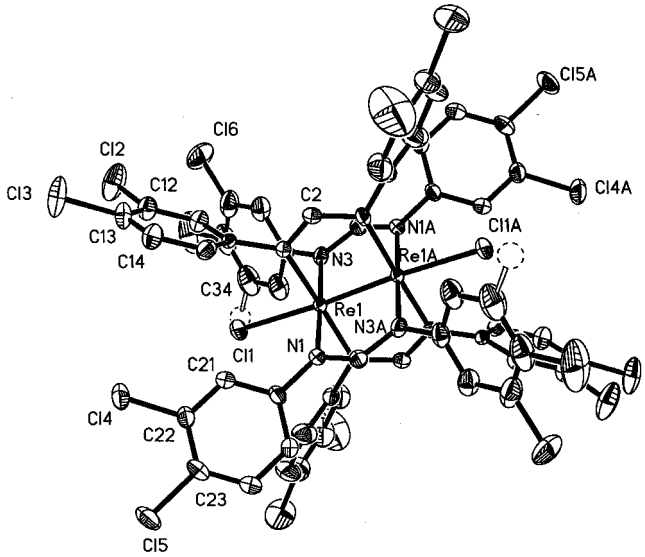


Figure 3. The ORTEP plot of compound **9**; hydrogen atoms and the dichloromethane solvent molecules are omitted for clarity

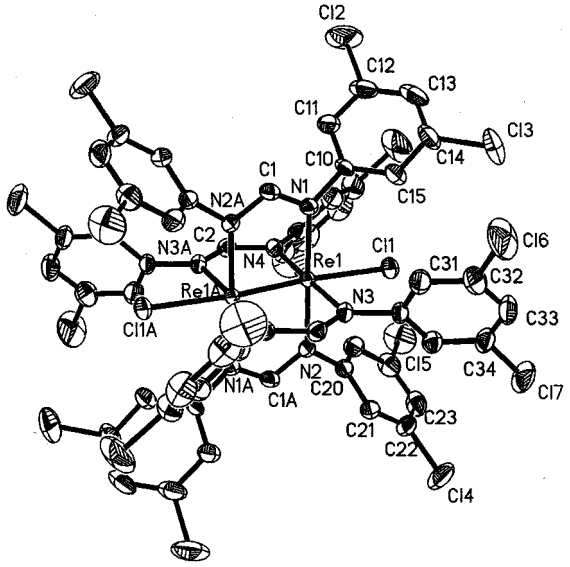


Figure 4. The ORTEP plot of compound **10a**; hydrogen atoms and the dichloromethane solvent molecules are omitted for clarity

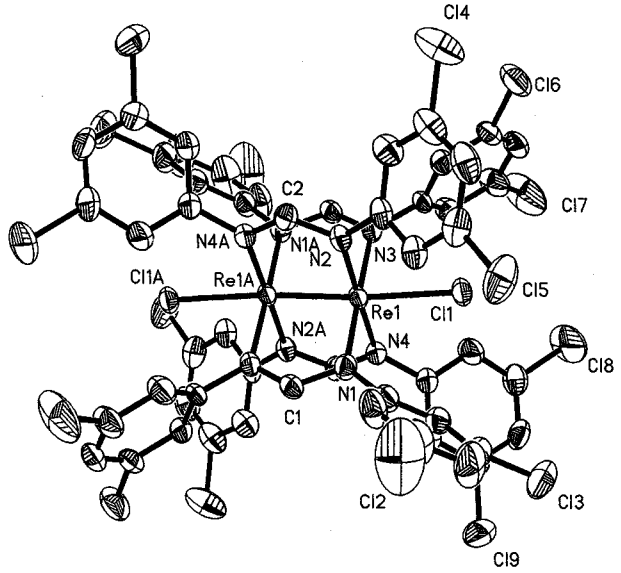


Figure 5. The ORTEP plot of compound **10b**; hydrogen atoms and the THF solvent molecule are omitted for clarity

In order to include relativistic effects of the 5d orbitals and the influence of axially coordinated chlorides in the comparison of the metal−metal bond lengths, the "formal shortness ratio" (FSR) is used to minimize changes in the bond length due to the size of the metal atoms. To determine the FSR for a bond A−B, Equation 1 is applied where D_{A-B} is the distance between the atoms, R_1^A is the radius of atom A, and R_1^B is the radius of atom B.[58] The FSR has been calculated for the Cr_2(μ-form)$_4$ [0.806], Mo_2(μ-form)$_4$ [0.809], and W_2(μ-form)$_4$ [0.839] complexes using the average M−M bond lengths for the diarylformamidinate analogs.[12,43,52,59] Using the average Re−Re bond length (2.2776 Å) in the Re_2Cl_2(μ-form)$_4$ series and a radius of 1.283 Å for the Re atom,[21][60] the FSR of the Re−Re bond [0.888] is significantly larger than the FSR for the group 6 M_2(μ-form)$_4$ series due to coulombic repulsion between the Re^{III} centers[21] and larger than the FSR for $[Re_2Cl_8]^{2-}$ [0.869] due to the presence of two axial chlorides.[58][61]

Table 1. Selected bond lengths [Å] and angles [°] for **1**, **4**, **9**, and **10a**, **b**

Compound	**1**	**4**	**9**	**10a**	**10b**
Re−Re	2.2777(3)	2.2765(6)	2.2783(4)	2.2734(3)	2.2840(5)
Re−N	2.093(3)	2.089(4)	2.095(4)	2.095(3)	2.081(5)
	2.097(3)	2.096(4)	2.096(4)	2.097(3)	2.095(5)
	2.098(3)	2.104(4)	2.102(4)	2.101(3)	2.104(5)
	2.101(3)	2.115(4)	2.119(4)	2.113(3)	2.104(5)
Re−Cl	2.5212(9)	2.486(1)	2.500(1)	2.4897(9)	2.492(2)
Re−Re−Cl	176.63(2)	175.60(3)	173.55(4)	175.39(3)	174.47(4)
N−Re−N	90.0(1)	89.9(2)	89.4(2)	89.3(1)	89.7(2)
	89.9(1)	88.8(2)	89.6(2)	90.0(1)	90.5(2)
	89.9(1)	89.9(2)	90.6(2)	90.6(1)	89.6(2)
	90.2(1)	91.4(2)	90.4(2)	90.1(1)	90.1(2)
	178.6(1)	178.3(2)	178.6(2)	178.5(1)	178.7(2)
	178.5(1)	178.8(2)	178.7(2)	178.7(1)	178.6(2)
N−Re−Re	91.49(8)	91.0(1)	90.5(1)	91.96(8)	92.7(1)
	91.25(8)	92.1(1)	92.5(1)	91.68(9)	90.6(1)
	89.86(8)	90.1(1)	90.7(1)	89.70(9)	88.5(1)
	90.30(8)	89.1(1)	88.7(1)	89.35(8)	90.6(1)
N−Re−Cl	91.24(8)	89.3(1)	90.0(1)	91.39(9)	92.8(1)
	90.72(8)	92.3(1)	93.9(1)	91.53(9)	89.9(1)
	87.41(8)	89.7(1)	89.1(1)	87.14(9)	86.0(1)
	87.73(8)	86.5(1)	84.8(1)	87.30(9)	88.9(1)
N−C−N	123.5(3)	123.0(5)	122.6(5)	121.8(3)	122.8(6)
	123.4(3)	123.1(5)	122.4(5)	122.1(3)	121.2(6)

$$FSR_{AB} = D_{A-B}/(R_1^A + R_1^B) \quad (1)$$

Electrochemistry

Electrochemical studies of the compounds in the Re_2Cl_2(μ-form)$_4$ series were performed in CH_2Cl_2 under nitrogen. Data were obtained at scan rates of 20, 50, 100, and 200 mV/s to determine the values of the first [$E_{1/2}^1$] and second [$E_{1/2}^2$] quasireversible one-electron reduction potentials of compounds **1**−**4** (Table 2). Prior electrochemical studies of **2**, abbreviated Re_2Cl_2(μ-DFM)$_4$,[21] were repeated in order to compare electrochemical data performed under the same experimental conditions. As shown in Scheme 1, successive reduction of Re_2Cl_2(μ-form)$_4$ produces $[Re_2Cl_2$(μ-form)$_4]^-$ and subsequently $[Re_2Cl_2$(μ-form)$_4]^{2-}$.

Table 2. Hammett constant (σ) of the remote substituents of the formamidinate ligands, $E_{1/2}^1$, and $E_{1/2}^2$ values for electrochemical studies of the Re_2Cl_2(μ-form)$_4$ compounds, **1**−**4**, with two one-electron quasireversible reductions

Compound	Hammett constant	$E_{1/2}^1$	$E_{1/2}^2$
1	−0.27	−1.41	−1.68
2	−0.17	−1.39	−1.67
3	0.00	−1.28	−1.55
4	0.12	−1.25	−1.53

A least-squares fit of the $E_{1/2}$ values versus 8σ according to Equation 2 is linear with a slope of ρ, the reactivity constant, period The Hammett constant, σ, is multiplied by eight to account for all of the remote substituents on aryl

Two Successive One-Electron Reductions
for Electron Donating Substituents on the Formamidinate Ligands

$$Re_2Cl_2(\mu\text{-form})_4 \underset{-e^-}{\overset{+e^-}{\rightleftharpoons}} [Re_2Cl_2(\mu\text{-form})_4]^- \underset{-e^-}{\overset{+e^-}{\rightleftharpoons}} [Re_2Cl_2(\mu\text{-form})_4]^{2-}$$

Two-Electron Reduction Resulting in Decomposition
for Electron Withdrawing Substituents on the Formamidinate Ligands

$$Re_2Cl_2(\mu\text{-form})_4 \xrightarrow{+2e^-} [Re_2Cl_2(\mu\text{-form})_4]^{2-}$$

Scheme 1

rings of the diarylformamidinate ligands. An anodic shift of the reduction with an increase in the value of the Hammett constants for the diarylformamidinate ligands is observed for **1**−**4** for both successive one-electron reductions of the dirhenium(III,III) core. At a scan rate of 100 mV/s, the correlation coefficient of the least squares fit of the plot of 8σ versus the $E_{1/2}{}^1$ value for $Re_2Cl_2(\mu\text{-form})_4$ series is 0.990 with ρ equal to 61 mV. When the average of the quasireversible reduction potentials observed at all scan rates is used, as shown in Figure 6, the correlation coefficient of the least squares fit to 8σ versus $E_{1/2}{}^1$ decreases [0.982] with a slight decrease in ρ, 56 mV.

$$\Delta E_{1/2} = E_{1/2}(X) - E_{1/2}(H) = \rho 8\sigma_X \quad (2)$$

where X is the substituent on the formamidinate ligand and H is a hydrogen atom

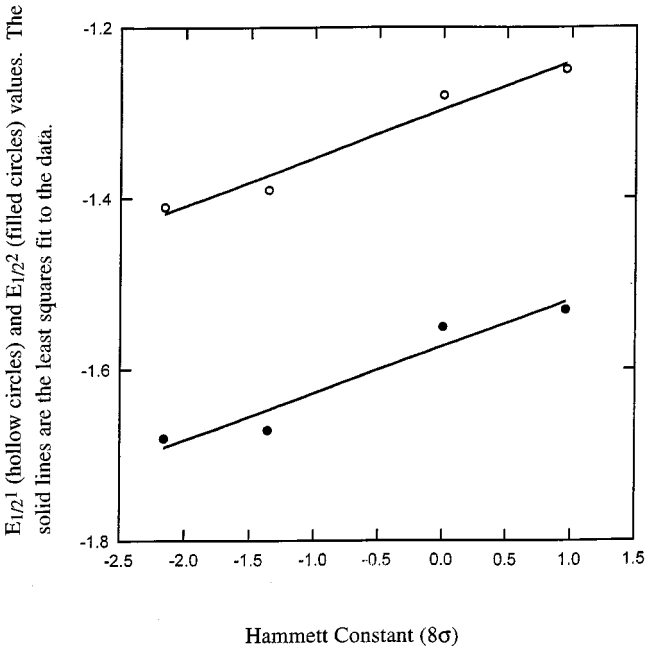


Figure 6. Dependence of $E_{1/2}{}^1$(hollow circles) and $E_{1/2}{}^2$(filled circles) values using the average of all scan rates on the Hammett constant (8σ) for the $Re_2Cl_2(\mu\text{-form})_4$ series. The circles represent the experimental data and the solid lines are the least squares fit to the data

For the $E_{1/2}{}^2$ values, correlation coefficients of the linear least squares fit of the data of 0.968 and 0.966 with ρ values of 51 mV (100 mV/s) and 55 mV (all scan rates, as shown in Figure 6) are observed. The $E_{1/2}{}^1$ values for the $Re_2Cl_2(\mu\text{-form})_4$ series varied over 160 mV and $E_{1/2}{}^2$ values over 150 mV for **1**−**4** (Table 2) and reflect the ability to use remote substituents to fine tune the electrochemical properties at a dinuclear core.[15,43,52,62] A similar trend is observed for $Re_2Cl_2(\mu\text{-}O_2CR)_4$ complexes with alkyl carboxylates. Plots of $E_{1/2}$ values versus the Taft σ* parameter, an indicator of the electron donating or withdrawing ability of the carboxylates, are linear.[62] The anodic shift of the oxidation with increasing values of the Hammett constant of the form ligand is also observed in the $Ni_2(\mu\text{-form})_4$,[43] $Cr_2(\mu\text{-form})_4$,[52] and $Mo_2(\mu\text{-form})_4$[15] series.

Studies of the $M_2(mhp)_4$ series where M_2 is Cr_2, CrMo, Mo_2, MoW, and W_2 and mhp is the 2-oxo-6-methylpyridine ion have demonstrated the first oxidation half potential correlates with the energy of the highest occupied molecular orbital as determined by photoelectron spectroscopy [PES].[63] For the series $Ni_2(\mu\text{-form})_4$ [ρ = 114 mV],[43] $Cr_2(\mu\text{-form})_4$ [ρ = 52.8 mV],[52] $Mo_2(\mu\text{-form})_4$ [ρ = 87.2 mV],[15] and $Re_2Cl_2(\mu\text{-form})_4$ [56 mV ($E_{1/2}{}^1$), 55 mV ($E_{1/2}{}^2$)], the magnitude of the value of ρ correlates to the ligand character of the orbital where the loss of the electron (oxidation) or gain of the electron (reduction) occurs. For the $Ni_2(\mu\text{-form})_4$ series with a large reactivity constant, the HOMO involved in the oxidation is the $6b_1$ orbital with 58% Ni and 42% N character.[44] A smaller reactivity constant is observed for the oxidation of the $Mo_2(\mu\text{-form})_4$ series[15] with a $2b_{2g}$ HOMO orbital with 87% Mo and 4% N character.[18]

The reactivity constants calculated for the $Re_2Cl_2(\mu\text{-form})_4$ complexes **1**−**4** are lower than either the dinickel or dimolybdenum series and similar for both reductions. Since a reduction is occurring, the orbital of interest in the determination of the value of ρ for both $E_{1/2}{}^1$ and $E_{1/2}{}^2$ is the LUMO, $6e_g$, with 91% Re and 1% N character. Very little change in the ligand character of the electrochemically active orbital is observed upon reduction to $Re_2(HNC(H)NH)_4$ with 97% Re and 2% N character for the $5e_g$ orbital.[21] The general trend observed in the $M_2(\mu\text{-form})_4$ complexes is a dependence of the reactivity constant on the ligand character of the orbital involved in either the reduction (LUMO) or oxidation (HOMO). With an increase in the ligand character of the electrochemically active orbital, the $E_{1/2}$ value is more strongly dependent on changes in the remote substituents of the ligand.

In contrast to the two one-electron reductions observed for **1**−**4**, studies of compounds **5**−**10** (Table 3) with more electron-withdrawing substituents on the diarylformamidinate ligands resulted in an irreversible two-electron reduction of the compound, as demonstrated by a ratio of peak currents of 2.48 (a ratio of 2.83 is predicted for compounds **5**−**10** versus **1**−**4** based on no change in diffusion coefficients and concentrations[64]). Two-electron reductions result when the loss of a second electron occurs more easily than the first electron due to an inversion of the reduction potentials[65] and are the result of a structural change.[65−69] For example, the electrochemistry of $[Mo_2Cp_2(CO)_4\{\mu\text{-}$

η^2:η^3-HCC−C(R1)(R2)}]$^+$ complexes is controlled by the R1 and R2 substituents as a result of changes in the energy of the LUMO orbital.[66]

To explain the change in the redox behavior of the Re_2Cl_2(μ-form)$_4$ complexes[57] with more electron-withdrawing substituents, the relative energies of the orbitals involved in the reduction were investigated. Fenske−Hall calculations performed on the Mo_2(μ-form)$_4$ series indicate the δ* orbital (LUMO) with approximately 76% metal character increases in energy by 1.18 eV upon a change in the remote substituent of the formamidinate ligand from 3,5-dichloro to *p*-MeO.[15] In contrast, the σ* orbital with approximately 87% metal character increases in energy by only 0.83 eV with the same variation in the remote substituents.[15] The Fenske−Hall calculations[15] demonstrate that, with increasing ligand character of a particular orbital, a more significant change in the orbital energy occurs with a change in the ligand substituents.

The orbitals of predominantly metal character for Re_2Cl_2(μ-DFM)$_4$ are, in order of increasing energy, $5a_{1g}$ (σ, −14.22 eV), $5e_u$ (π, −11.225 eV), $2b_{2g}$ (δ, −8.804 eV), $6e_g$ (π*, LUMO, −7.174 eV), $2b_{1u}$ (δ*, −6.912 eV), and $6a_{2u}$ (σ*, −3.295 eV). Only a −0.262 eV difference in energy is predicted between the two lowest unoccupied orbitals (π* and δ*) with Re characters of 91% and 59%, respectively.[21] Based on the trend observed in the previous studies of Mo_2(form)$_4$,[15][21] the energy of the δ* orbital decreases more rapidly than the π* orbital with an increase in the electron-withdrawing ability (σ) of the remote substituent on the aryl group of the formamidinate ligand in Re_2Cl_2(μ-form)$_4$ complexes. The energy difference between the π* and δ* orbitals diminishes or even becomes negative with increasing σ, as shown in Figure 7. As a result of the change in the orbital manifold across the series of Re_2Cl_2(μ-form)$_4$ complexes, two quasireversible one-electron reductions occur for the electron donating substituents and an irreversible two-electron reduction occurs for the electron-withdrawing substituents. Although the same general trend in reduction potentials is observed for both the one-electron quasireversible and two-electron irreversible reduction of the Re_2Cl_2(μ-form)$_4$ complexes as shown in Tables 2 and 3, a linear least squares fit of the Hammett constant versus the two-electron irreversible reduction at 100 mV [Table 3] is poor with a correlation coefficient of 0.832 and a ρ value of 44 mV. The electrochemical decomposition product is subsequently oxidized but has not been structurally or spectroscopically characterized.

Electronic Spectra

The electronic spectra of **1** and **3−10** consist of an intense peak between 386 to 418 nm. The transition at 403 nm for Re_2Cl_2[(*p*-tolylC$_6$H$_4$)NCHN(*p*-tolylC$_6$H$_4$)]$_4$[21] is assigned to the δ to δ* transition. The intense peak occurring between 386 and 418 nm in the Re_2Cl_2(μ-form)$_4$ series is assigned to the same transition with no correlation between the Hammett constants of the remote substituents and the energy of the δ to δ* transition observed.[15,54−57]

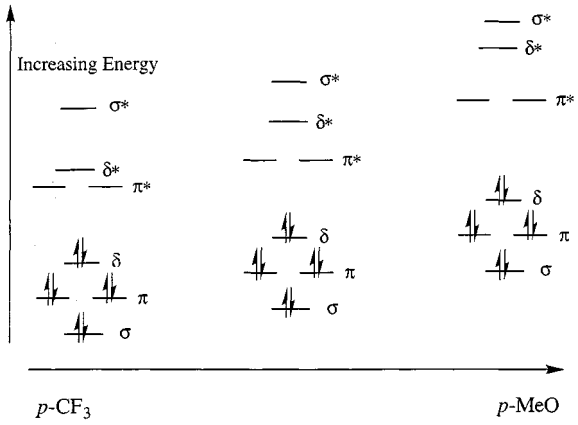


Figure 7. The predicted change in the orbital manifold across the series of Re_2Cl_2(μ-form)$_4$ complexes with changes in the Hammett constant of the remote substituent of the formamidinate ligand

Table 3. Hammett constant (σ) of the remote substituents of the formamidinate ligands and E_{pc} values for electrochemical studies of the Re_2Cl_2(μ-form)$_4$ compounds, **5−10**, with two-electron irreversible reductions

Compound	Hammett constant	E_{pc}
5	0.23	−1.52
6	0.37	−1.53
7	0.43	−1.48
8	0.54	−1.50
9	0.60	−1.36
10a, **10b**	0.74	−1.37

Diamagnetic Anisotropy of the Re−Re Bond

An induced field from circulating electrons results in the diamagnetic anisotropy in transition metal complexes containing metal-metal multiple bonds. In the Re_2Cl_2(μ-form)$_4$ series, the methine proton (−NC*H*N−) of the bridging diarylformamidinate ligand is affected by the induced field caused by the circulating electrons of the Re−Re quadruple bond. As a result, the methine proton is deshielded and a downfield chemical shift is observed. From the chemical shift difference of the methine proton [Δδ = δ(−NC*H*N−Re_2) − δ (−NC*H*N−Ni_2)][43] and structural parameters of these protons (r and θ) extracted from the crystallographic data, the diamagnetic anisotropy for the Re−Re bond is calculated from Equation 3 shown below.[70]

$$\Delta\delta = \frac{\Delta\chi}{4\pi}\left[\frac{1-3\cos^2\theta}{3r^3}\right]$$

The Δχ values calculated based on crystallographic and ^{1}H spectroscopic data for Re_2Cl_2(μ-form)$_4$ with the substituents *p*-MeO, *m*-MeO, 3,5-Cl_2, and 3,4-Cl_2 are 4034, 3890, 3940, and $4154\cdot10^{-36}$ m^3 molecule^{-1}, respectively or $4004\cdot10^{-36}$ m^3 molecule^{-1} on average. Since the chemical shift of the methine proton of Ni_2[(3,4-$Cl_2C_6H_3$)NCHN(3,4-$Cl_2C_6H_3$)]$_4$ is not available, the chemical shift was estimated (δ = 6.185) based on the average

change in the methine proton chemical shift upon coordination to the Ni_2 core from values of nine reported Ni_2(μ-form)$_4$ complexes and the corresponding free ligands.[43] The values are somewhat smaller than $\Delta\chi$ value of $4430 \cdot 10^{-36}$ m^3 $molecule^{-1}$ reported previously for Re_2Cl_2(μ-DFM)$_4$.[12] The correlation of the diamagnetic anisotropy to the Hammett constant of the remote substituents on the diarylformamidinate ligands for the Re_2Cl_2(μ-form)$_4$ series is extremely poor.

Conclusions

With the synthesis of a series of Re_2Cl_2(μ-form)$_4$ compounds incorporating a variety of electron donating and withdrawing remote substituents on the diarylformamidinate ligands, the comparison of structural and spectroscopic properties of M_2(μ-form)$_4$ complexes is extended to include dirhenium(III,III) compounds with axially coordinated chlorides. In the metal−metal bonded, Cr_2(μ-form)$_4$, Mo_2(μ-form)$_4$, and Re_2Cl_2(μ-form)$_4$, and non-bonded systems, Ni_2(μ-form)$_4$, which have variations in the Hammett constant of the remote substituents on the diarylformamidinate ligands, no correlation between the metal−metal bond lengths or metal−nitrogen bond lengths and σ is observed.[14,15,43,52]

The two quasireversible one-electron reductions for **1**−**4** and the two-electron irreversible reductions observed for **5**−**10** reflect the ability to tune the reduction potential over a 150 mV range (**1**−**4**) via the remote substituents on the diarylformamidinate ligand.[14,15,43,52,66] The reactivity constants of the Re_2Cl_2(μ-form)$_4$ series (**1**−**4**) are similar in magnitude to the Cr_2(μ-form)$_4$ series and significantly smaller than either the Mo_2(μ-form)$_4$ or Ni_2(μ-form)$_4$ series.[14,15,43,52] Based on systems where both electrochemical and theoretical data are available, the $E_{1/2}$ value becomes more strongly dependent on changes in the remote substituents on the diarylformamidinate ligand with increasing ligand character of the electrochemically active orbital.[15,18,21,43,44,52] Studies of a series of W_2(μ-form)$_4$ complexes with a variety of substituents on the diarylformamidinate ligands are in progress to determine the effect of the Hammett constant of the ligand substituents on the electrochemical process.

Experimental Section

Starting Materials: The starting materials $[N(n\text{-}Bu)_4]_2[Re_2Cl_8]$,[71] Re_2(μ-$O_2CCH_3)_4Cl_2$,[72] and **2**[21] were synthesized by the standard literature methods. All the diarylformamidine ligands were synthesized according to literature methods, washed under an argon atmosphere with freshly distilled hexanes, and transferred to the drybox.[15][73] The solvents ethanol (EtOH), methanol (MeOH), CH_2Cl_2, ethyl acetate, and hexanes for the synthesis of the Re_2Cl_2(μ-form)$_4$ complexes were used as received without distillation.

Preparation of the Complexes: $Re_2Cl_2[(p\text{-}MeOC_6H_4)NCHN(p\text{-}MeOC_6H_4)]_4$ (**1**). Re_2Cl_2(μ-$O_2CCH_3)_4$ (0.090 g, 0.13 mmol) was heated at 140°C with (p-$MeOC_6H_4$)NHCHN(p-$MeOC_6H_4$) (3 g, 11.7 mmol) under argon for 5 hours. EtOH (40 mL) was added to the molten reaction mixture while hot, and the mixture was vigorously stirred for 1 hour. The orange-yellow solid was collected by filtration and dried under dynamic vacuum. ^{1}H-NMR spectroscopy revealed the presence of free ligand, and the crude product was further purified by chromatography. Yield: 0.093 g (48.8%). − ^{1}H NMR: δ = 8.30 (*s*, 4 H), 6.66 (*m*, 32 H), 3.75 (*s*, 24 H). − ^{13}C NMR δ: 171.1 (*s*), 158.1 (*s*), 145.6 (*s*), 129.2 (*s*), 127.7 (*s*), 113.2 (*s*), 111.8 (*s*). − UV/Vis: λ_{max} (nm) = 278, 418.

$Re_2Cl_2[(C_6H_5)NCHN(C_6H_5)]_4$ (3): Re_2Cl_2(μ-$O_2CCH_3)_4$ (0.110 mg, 0.16 mmol) was heated at 150°C with (C_6H_5)NHCHN(C_6H_5) (2.94 g, 15.0 mmol) under argon for 8 hours. Upon completion of the reaction, the product was extracted with hot ethanol (80 mL), but a clean separation was not achieved. The filtrate and solid were combined and dried on a rotovap. Ethyl acetate (50 mL) was added and the mixture was heated to reflux and the resultant mixture was cold filtered to remove the bulk of the free ligand. The crude product was suspended in 6 mL of CH_2Cl_2 and heated to reflux. Following addition of 30 mL of ethyl acetate and an additional reflux period of 10 minutes, vigorous stirring of the reaction mixture during cooling to room temperature yielded golden flakes of **3**. The solid product was collected by filtration and dried under dynamic vacuum. Yield: 0.142 g (72.5%). − ^{1}H NMR: δ = 8.40 (*s*, 4 H), 7.13 (*d*, 16 H, ^3J = 1.6 Hz), 7.11 (*d*, 8 H), 6.76 (*dd*, 16 H). − ^{13}C NMR: δ = 152.2 (*s*), 128.4 (*s*), 127.0 (*s*). − UV/Vis: λ_{max} (nm) = 278, 396.

$Re_2Cl_2[(m\text{-}MeOC_6H_4)NCHN(m\text{-}MeOC_6H^4)]_4$ (4): Re_2Cl_2(μ-$O_2CCH_3)_4$ (0.110 g, 0.16 mmol) was heated at 140°C with (m-$MeOC_6H_4$)NHCHN(m-$MeOC_6H_4$) (3 g, 11.7 mmol) under argon overnight. Ethyl acetate (35 mL) was added to the molten reaction mixture and the solution refluxed for an hour. The orange-yellow solid was collected by filtration and dried under vacuum. Since TLC indicated incomplete purification, another 35 mL of ethyl acetate was added to the crude product and the mixture refluxed. The purified solid product was collected by filtration and dried under dynamic vacuum. Yield: 0.210 g (89.6%). − ^{1}H NMR: δ = 8.40 (*s*, 4 H), 7.12 (*t*, 8 H, ^3J = 8.0 Hz), 6.66 (*dd*, 8 H, ^3J = 8.3 Hz, ^4J = 1.9 Hz), 6.60 (*d*, 8 H, ^3J = 7.6 Hz), 6.34 (*s*, 8 H), 3.29 (*s*, 24 H). − ^{13}C NMR: δ = 171.3 (*s*), 169. 9 (*s*), 158.7 (*s*), 153.5 (*s*), 128.9 (*s*), 127.5 (*s*), 119.7 (*s*), 118.2 (*s*), 114.5 (*s*), 113.1 (*s*). − UV/Vis: λ_{max} (nm) = 286, 400.

$Re_2Cl_2[(p\text{-}ClC_6H_4)NCHN(p\text{-}ClC_6H_4)]_4$ (5): Re_2Cl_2(μ-$O_2CCH_3)_4$ (0.17 g, 0.25 mmol) was heated at 180°C with (p-ClC_6H_4)NHCHN(p-ClC_6H_4) (2.12 g, 8.0 mmol) under argon for 3 hours. The solid product was dissolved in CH_2Cl_2 and precipitated from solution with EtOH. The orange solid was collected by filtration and dried under dynamic vacuum. Yield: 0.262 g (69.9%). − ^{1}H NMR: δ = 8.32 (*s*, 4 H), 7.14 (*d*, 16 H, ^3J = 8.6 Hz), 6.63 (*d*, 16 H, ^3J = 8.7 Hz). − ^{13}C NMR: δ = 171.3 (*s*), 150.1 (*s*), 132.6 (*s*), 129.3 (*s*), 128.6 (*s*), 128.0 (*s*), 127.2 (*s*). − UV/Vis: λ_{max} (nm) = 274, 398.

$Re_2Cl_2[(m\text{-}ClC_6H_4)NCHN(m\text{-}ClC_6H_4)]_4$ (6): Re_2Cl_2(μ-$O_2CCH_3)_4$ (0.11 g, 0.16 mmol) was heated at 180°C with (m-ClC_6H_4)NHCHN(m-ClC_6H_4) (2.12 g, 8.0 mmol) under argon for 3 hours. Ethyl acetate (15 mL) was added while the molten reaction mixture was still hot. The crude solid product was collected by filtration. The residual free ligand was removed by redissolving the crude product in CH_2Cl_2 and precipitating **6** with hexanes. The orange-yellow solid was collected by filtration and dried under dynamic vacuum. Yield: 0.130 g (54.2%). − ^{1}H NMR: δ = 8.48 (*s*, 4 H), 7.12−7.21 (*m*, 16 H), 6.74 (*d*, 8 H, ^4J = 1.9 Hz), 6.73 (*s*, 8 H). − ^{13}C NMR: δ = 171.7 (*s*), 170.1 (*s*), 152.5 (*s*), 133.2 (*s*), 129.6 (*s*),

128.6 (*s*), 128.2 (*s*), 127.7 (*s*), 127.3 (*s*), 126.3 (*s*), 126.1 (*s*), 124.7 (*s*). − UV/Vis: λ_{max} (nm) = 278, 390.

$Re_2Cl_2[(m\text{-}CF_3C_6H_4)NCHN(m\text{-}CF_3C_6H_4)]_4$ (7): $Re_2Cl_2(\mu\text{-}O_2CCH_3)_4$ (0.17 g, 0.25 mmol) was heated at 156°C with (*m*-$CF_3C_6H_4$)NHCHN(*m*-$CF_3C_6H_4$) (3.1 g, 9.3 mmol) for 15 hours. EtOH (40 mL) was added to the reaction mixture while hot. The mixture stirred vigorously for 1 hour. The solid was collected by filtration, washed with 20 mL of EtOH and 10 mL of hexanes, and dried under vacuum. Yield: 0.39 g (88%). − ^{1}H NMR: δ = 8.57 (*s*, 4 H), 7.46 (*d*, 8 H, ^3J = 7.6 Hz), 7.36 (*t*, 8 H, ^3J = 7.9 Hz), 7.08 (*d*, 8 H, ^3J = 7.4 Hz), 6.85 (*s*, 8 H). − ^{13}C NMR δ: 171.3 (*s*), 151.45 (*s*), 130.12 (*s*), 128.77 (*s*), 124.83 (*s*), 123.93 (*s*). − UV/Vis: λ_{max} (nm) = 294, 386.

$Re_2Cl_2[(p\text{-}CF_3C_6H_4)NCHN(p\text{-}CF_3C_6H_4)]_4$ (8): $Re_2Cl_2(\mu\text{-}O_2CCH_3)_4$ (0.20 g, 0.30 mmol) was heated at 170°C with (*p*-$CF_3C_6H_4$)NHCHN(*p*-$CF_3C_6H_4$) (2.0 g, 6.0 mmol) for 1.5 hours. After cooling, acetone (20 mL) was added to the reaction mixture and the red-orange supernatant solution transferred from the unchanged ligand. Slow evaporation of the acetone resulted in red-orange crystals. The crystals were washed with 10 mL of hexanes, and dried under vacuum. Yield: 0.305 g (57.5%). − ^{1}H NMR: δ = 8.47 (*s*, 4 H), 7.45 (*d*, 16 H, ^3J = 3.9 Hz), 6.81 (*d*, 16 H, ^3J = 3.9 Hz). − ^{13}C NMR: δ = 171.22 (*s*), 154.38 (*s*), 129.44 (*q*, $^1J_{C-F}$ = 33.8 Hz), 127.94 (*d*, $^2J_{C-F}$ = 14.1 Hz), 126.68 (*s*), 125.51 (*s*), 122.91 (*s*), 120.21 (*s*). − UV/Vis: λ_{max} (nm) = 386.

$Re_2Cl_2[(3,4\text{-}Cl_2C_6H_3)NCHN(3,4\text{-}Cl_2C_6H_3)]_4$ (9): $Re_2Cl_2(\mu\text{-}O_2CCH_3)_4$ (0.100 g, 0.15 mmol) was heated at 170°C with (3,4-$Cl_2C_6H_3$)NHCHN(3,4-$Cl_2C_6H_3$) (2.0 g, 6.0 mmol) under dynamic vacuum for 7 hours. Ethanol (30 mL) was added to the orange-brown solid while the reaction mixture was warm. After stirring the solution overnight to dissolve excess ligand, the solution was filtered and the yellow-orange solid collected on the frit. The purified solid product was dried under dynamic vacuum. Yield: 0.132 g (49.6%). − ^{1}H NMR: δ = 8.398 (*s*, 4 H), 7.244 (*d*, 4 H, ^3J = 8.5 Hz), 6.699 (*d*, 4 H, ^4J = 2.4 Hz), 6.603 (*dd*, 4 H, ^3J = 8.5 Hz, ^4J = 2.4 Hz). − UV/Vis: λ_{max} (nm) = 282, 398.

$Re_2Cl_2[(3,5\text{-}Cl_2C_6H_3)NCHN(3,5\text{-}Cl_2C_6H_3)]_4$ (10a, 10b): $Re_2Cl_2(\mu\text{-}O_2CCH_3)_4$ (0.550 g, 0.81 mmol) was heated at 170°C with (3,5-$Cl_2C_6H_3$)NHCHN(3,5-$Cl_2C_6H_3$) (2.0 g, 6.0 mmol) under dynamic vacuum for 7 hours. The orange-brown solid was loaded on a column of chromatographic Silica Gel of 200 to 425 mesh and eluted with CH_2Cl_2. The yellow solution was collected and dried under dynamic vacuum. The addition of ethanol dissolves the excess ligand and the yellow-orange product was collected by filtration of the ethanol suspension. The purified solid product was dried under dynamic vacuum. Yield: 0.302 g (21.0%). − ^{1}H NMR: δ = 8.50 (*s*, 4 H), 7.20 (*s*, 8 H), 6.6 (*d*, H, ^4J = 1.8 Hz). − ^{13}C NMR: δ = 171.3 (*s*), 152.3 (*s*), 134.4 (*s*), 127.4 (*s*), 125.9 (*s*). − UV/Vis: λ_{max} (nm) = 278, 314, 388.

Physical Measurements: The spectroscopy, UV/Vis and ^{13}C-NMR, was performed using CH_2Cl_2 dried over P_2O_5 and freshly distilled under argon prior to use. ^{1}H-NMR spectra were recorded on either a Bruker AMX-360 NMR spectrometer or a General Electric Omega 400 MHz NMR spectrometer with chemical shifts (δ) referenced to the residual $CHCl_3$ (δ = 7.27) in the $CDCl_3$ solvent. ^{13}C-NMR spectra were recorded on a General Electric Omega 400 MHz NMR spectrometer with a 10 mm broad band probe with chemical shifts (δ) referenced to CH_2Cl_2 (δ = 54.2). 10-mm NMR tubes for ^{13}C-NMR spectra were prepared by dissolving the respective $Re_2Cl_2(\mu\text{-form})_4$ complexes in CH_2Cl_2 with a 4 mm NMR insert of either $CDCl_3$ or CD_3CD_2OD to lock. ^{13}C-NMR spectra required 4 to 24 hours of data collection to obtain reasonable signal

Table 4. Crystallographic data for **1**, **4**, **9**, and **10a**, **b**

	1	**4**	**9**	**10a**	**10 b**
Empirical formula	$C_{60}H_{60}Cl_2N_8O_8Re_2$	$C_{61}H_{70}Cl_4N_8O_8Re_2$	$C_{54}H_{31}Cl_{22}N_8Re_2$	$C_{56}H_{36}Cl_{26}N_8Re_2$	$C_{52}H_{28}Cl_{18}N_8ORe_2$
Formula mass	1464.46	1557.45	1944.17	2115.03	1791.32
temp [K]	213(2)	213(2)	213(2)	213(2)	213(2)
wavelength [Å]	0.71073	0.71073	0.71073	0.71073	0.71073
crystal system	monoclinic	monoclinic	orthorhombic	monoclinic	monoclinic
space group	*P*2(1)/*n*, [#14]	*P*2(1)/*c*, [#14]	*Pbca*, [#61]	*P*2(1)/*n*, [#14]	*P*2(1)/*n*, [#14]
a [Å]	14.822(3)	11.145(3)	21.2457(3)	12.4590(2)	11.2331(2)
b [Å]	12.776(2)	19.654(4)	14.3471(2)	19.7205(3)	17.1592(1)
c [Å]	15.263(2)	14.310(3)	22.0263(1)	16.3497(1)	18.4167(3)
β [deg]	91.452(9)	92.19(1)		110.560(1)	94.731(1)
V [Å^3]	2889.3(8)	3132(1)	6713.9(1)	3761.21(9)	3537.74(9)
Z	2	2	4	2	2
d_{calc} [Mg/m^3]	1.683	1.651	1.923	1.868	1.682
absorption coefficient [mm^{-1}]	4.340	4.091	4.523	4.182	4.139
crystal size [mm]	0.15 × 0.2 × 0.2	0.25 × 0.25 × 0.25	0.05 × 0.05 × 0.05	0.25 × 0.20 × 0.15	0.10 × 0.10 × 0.10
theta range for data collection [deg]	1.89 to 27.70	1.76 to 28.32	1.85 to 25.00	1.68 to 28.28	1.62 to 24.69
index ranges	$-18 \le h \le 19$, $-13 \le k \le 16$, $-13 \le l \le 18$	$-13 \le h \le 14$, $-24 \le k \le 17$, $-13 \le l \le 18$	$-25 \le h \le 15$, $-17 \le k \le 17$, $-25 \le l \le 25$	$-15 \le h \le 16$, $-26 \le k \le 26$, $-14 \le l \le 21$	$-13 \le h \le 12$, $-11 \le k \le 20$, $-18 \le l \le 21$
reflections collected	11983	15944	27192	22199	17925
independant reflections	5891 [*R*(int) = 0.0229]	6775 [*R*(int) = 0.0282]	5800 [*R*(int) = 0.0416]	9095 [*R*(int) = 0.0308]	5996 [*R*(int) = 0.0425]
refinement method	full-matrix least-squares on F^2	full-matrix least-squares on F^2	full-matrix least-squares on F^2	full-matrix least-squares on F^2	full-matrix least-squares on F^2
data/restraints/parameters	5891 / 0 / 362	6775/3/388	5800/0/398	9095/0 /415	5996/0/406
$R^{[a]}$ [$I>2\sigma(I)$]	0.0264	0.0393	0.0322	0.0325	0.0550
$R_w^{[b]}$ [$I>2\sigma(I)$]	0.0593	0.1008	0.0733	0.0706	0.0778

[a] $R = \Sigma||F_o| - |F_c||/\Sigma|F_o|$. − [b] $wR = \{\Sigma[w(F_o^2 - F_c^2)^2]/\Sigma[w(F_o^2)^2]\}^{1/2}$.

to noise levels. Data could not be obtained for **3** or **9** due to poor solubility of the compounds in CH_2Cl_2. The UV/Vis spectra were recorded on a Hewlett Packard model 8452 diode array spectrophotometer from 250 to 820 nm. Cyclic voltammetry measurements of compounds **1**−**10** were performed using a Solartron S1 1287 Electrochemical Interface in 0.1 M (nBu$_4$N)PF$_6$ electrolyte and 0.6 mM Re_2Cl_2(μ-form)$_4$ solutions with a 1.6-mm diameter Pt disk working electrode and a Ag wire quasi-reference electrode. The CH_2Cl_2 solutions of the respective complexes were purged for 20 minutes with nitrogen before data were recorded. The nitrogen was presaturated with CH_2Cl_2 to minimize solution evaporation. All electrode potentials are reported versus the ferrocene/ferrocenium $E_{1/2}$ value [0 V].

X-ray Crystallographic Study:[74] Crystals of **1**, **4**, **9**, and **10a**, **b** were grown by slow diffusion of CH_2Cl_2 (**1**, **4**, **9**, and **10a**) or THF (**10b**) solutions of the respective compounds with hexanes. Data were collected for **1**, **4**, **9**, and **10a**, **b** using a Siemens SMART CCD based diffractometer equipped with a LT-2 low-temperature apparatus operating at 213 K. Suitable crystals were mounted on a glass fiber using grease. Data were measured using omega scans of 0.3° per frame for 30 seconds such that a hemisphere was collected. A total of 1271 frames were collected with a final resolution of 0.75 Å (**1**, **4**, and **10a**) and 0.85 Å (**9** and **10b**). The first 50 frames were recollected at the end of data collection for each of the crystals to monitor for decay, but no decomposition during data collection was observed. Cell parameters for **1**, **4**, **9**, and **10a**, **b** were retrieved using SMART[75] software and refined using SAINT on all observed reflections. Data reductions were performed using SAINT[76] software which corrects for decay and Lorentz and polarization effects. Absorption corrections were applied using SADABS[77] supplied by George Sheldrick. The structures were solved by direct methods using the SHELXL-90[78] program and refined by least squares method on F^2, SHELXL-93,[79] incorporated in SHELXTL.PC V 5.03.[80] All non-hydrogen atoms are refined anisotropically. The positions of the hydrogen atoms were determined by difference Fourier methods and refined in **9** and **10a** and were calculated geometrically and refined as a riding model for **1**, **4**, and **10b**. One of the ligands in **9** showed a disorder of the ring to result in a disorder of two of the chloride positions with an occupany of 50% each. Although the dichloromethane solvent molecules of **4** could not be modeled successfully as disordered, the remaining electron density in the structure resides within the solvent molecule. Selected bond lengths and angles for **1**, **4**, **9**, and **10a**, **b** are listed in Table 1 and pertinent crystallographic parameters are summarized in Table 4.

Acknowledgments

J. L. E. and L. S. would like to acknowledge the support of the National Science Foundation EPSCoR program (Grant # EHR 9108767) and the ARI Program (Grant # CHE-92−14521). T. R. would like to acknowledge the partial support from the Petroleum Research Fund/ACS.

[1] J. Barker, M. Kilner, *Coord. Chem. Rev.* **1994**, *133*, 219−300.
[2] P. J. Stewart, A. J. Blake, P. Mountford, *Inorg. Chem.* **1997**, *36*, 3616−3622.
[3] J. R. Hagadorn, J. Arnold, *Inorg. Chem.* **1997**, *36*, 2928−2929.
[4] S. Hao, K. Feghali, S. Gambarotta, *Inorg. Chem.* **1997**, *36*, 1745−1748.
[5] A. Horton, J. deWith, *Organometallics* **1997**, *16*, 5424−5436.
[6] F. A. Cotton, L. M. Daniels, C. A. Murillo, *Inorg. Chem.* **1993**, *32*, 2881−2885.
[7] F. A. Cotton, R. Poli, *Inorg. Chim. Acta* **1988**, *141*, 91−98.
[8] F. A. Cotton, L. M. Daniels, C. A. Murillo, X. Wang, *J. Am. Chem. Soc.* **1996**, *118*, 4830−4833.
[9] F. A. Cotton, L. M. Daniels, J. H. Matonic, X. Wang, C. A. Murillo, *Polyhedron* **1997**, *16*, 1177−1191.
[10] F. A. Cotton, L. M. Daniels, C. A. Murillo, X. Wang, *Inorg. Chem.* **1997**, *36*, 896−901.
[11] F. A. Cotton, D. J. Maloney, J. Su, *Inorg. Chim. Acta* **1995**, *236*, 21−29.
[12] F. A. Cotton, T. Ren, *J. Am. Chem. Soc.* **1992**, *114*, 2237−2242.
[13] W. H. DeRoode, K.Vrieze, *J. Organomet. Chem.* **1977**, *135*, 183−193.
[14] C. Lin, J. D. Protasiewicz, E. T. Smith, T. Ren, *J. Chem. Soc., Chem. Commun.* **1995**, 2257−2258.
[15] C. Lin, J. D. Protasiewicz, E. T. Smith, T. Ren, *Inorg. Chem.* **1996**, *35*, 6422−6428.
[16] F. A. Cotton, T. Inglis, M. Kilner, T. R. Webb, *Inorg. Chem.* **1975**, *14*, 2023−2026.
[17] F. A. Cotton, L. M. Daniels, C. A. Murillo, D. J. Timmons, *Chem. Commun.* **1997**, 1449−1450.
[18] F. A. Cotton, X. Feng, M. Matusz, *Inorg. Chem.* **1989**, *28*, 594−601.
[19] F. A. Cotton, S. C. Haefner, A. P. Sattelberger, *Inorg. Chem.* **1996**, *35*, 7350−7357.
[20] F. A. Cotton, W. H. Ilsley, W. Kaim, *Inorg. Chem.* **1980**, *19*, 2360−2364.
[21] F. A. Cotton, T. Ren, *J. Am. Chem. Soc.* **1992**, *114*, 2495−2502.
[22] F. A. Cotton, L. M. Daniels, J. H. Matonic, C. A. Murillo, *Inorg. Chim. Acta* **1997**, *256*, 277−282.
[23] F. A. Cotton, L. M. Daniels, L. R. Falvello, J. H. Matonic, C. A. Murillo, *Inorg. Chim. Acta* 1997, *256*, 269−275.
[24] F. A. Cotton, L. M. Daniels, C. A. Murillo, *Inorg. Chim. Acta* **1994**, *224*, 5−9.
[25] F. A. Cotton, X. Feng, C. A. Murillo, *Inorg. Chim. Acta* **1997**, *256*, 303−308.
[26] C. Lin, T. Ren, E. J. Valente, J. D. Zubkowski, E. T. Smith, *Chem. Lett.* **1997**, 753−754.
[27] C. Lin, T. Ren, E. J. Valente, J. D. Zubkowski, *J. Chem. Soc., Dalton Trans.* **1998**, 571−576.
[28] C. Lin, T. Ren, E. J. Valente, J. D. Zubkowski, *J. Organomet. Chem.* **1999**, *579*, 114−121.
[29] F. A. Cotton, T. Ren, *Inorg. Chem.* **1991**, *30*, 3675−3679.
[30] J. Bear, B. Han, S. Huang, K. Kadish, *Inorg. Chem.* **1996**, *35*, 3012−3021.
[31] F. A. Cotton, T. Ren, *Inorg. Chem.* **1995**, *34*, 3190−3193.
[32] Y. Li, B. Han, K. Kadish, J. L. Bear, *Inorg. Chem.* **1993**, *32*, 4175−4176.
[33] F. A. Cotton, T. Ren, J. L. Eglin, *Inorg. Chem.* **1991**, *30*, 2559−2563.
[34] L. P. He, C. L. Yao, M. Naris, J. C. Lee, J. D. Korp, J. L. Bear, *Inorg. Chem.* **1992**, *31*, 620−625.
[35] F. A. Cotton, L. M. Daniels, D. J. Maloney, J. H. Matonic, C. A. Murillo, *Inorg. Chim. Acta* **1997**, *256*, 283−289.
[36] F. A. Cotton, L. M. Daniels, X. Feng, D. J. Maloney, J. H. Matonic, C. A. Murillo, *Inorg. Chim. Acta* **1997**, *256*, 291−301.
[37] F. A. Cotton, L. M. Daniels, D. J. Maloney, C. A. Murillo, *Inorg. Chim. Acta* **1996**, *249*, 9−11.
[38] J. C. Le, M. Y. Chavan, L. K. Chau, J. L. Bear, K. M. Kadish, *J. Am. Chem. Soc.* **1985**, *107*, 7195−7197.
[39] S. L. Schiavo, G. Bruno, P. Zanello, F. Laschi, P. Piraino, *Inorg. Chem.* **1997**, *36*, 1004−1012.
[40] P. Piraino, G. Bruno, S. L. Schiavo, F. Laschi, P. Zanello, *Inorg. Chem.* **1987**, *26*, 2205−2211.
[41] J. L. Bear, C. L. Yao, R. S. Lifsey, J. D. Korp, K. M. Kadish, *Inorg. Chem.* **1991**, *30*, 336−340.
[42] D. I. Arnold, F. A. Cotton, D. J. Maloney, J. H. Matonic, C. A. Murillo, *Polyhedron* **1997**, *16*, 133−141.
[43] C. Lin, J. D. Protasiewicz, T. Ren, *Inorg. Chem.* **1996**, *35*, 7455−7458.
[44] F. A. Cotton, M. Matusz, R. Poli, X. Feng, *J. Am. Chem. Soc.* **1988**, *110*, 1144−1154.
[45] C. L. Yao, L. P. He, J. D. Korp, J. L. Bear, *Inorg. Chem.* **1988**, *27*, 4389−4395.
[46] F. A. Cotton, J. H. Matonic, C. A. Murillo, *Inorg. Chem.* **1996**, *35*, 498−503.
[47] F. A. Cotton, J. H. Matonic, C. A. Murillo, *Inorg. Chim. Acta* **1997**, *264*, 61−65.
[48] F. A. Cotton, X. Feng, M. Matusz, R. Poli, *J. Am. Chem. Soc.* **1988**, *110*, 7077−7083.

[49] T. Ren, C. Lin, P. Amalberti, D. Macikenas, J. D. Protasiewicz, J. C. Baum, T. L. Gibson, *Inorg. Chem. Commun.* **1998**, *1*, 23−26.
[50] Y. Zhou, D. S. Richeson, *Inorg. Chem.* **1996**, *35*, 1423−1424.
[51] Y. Zhou, D. S. Richeson, *J. Am. Chem. Soc.* **1996**, *118*, 10850−10852.
[52] K. M. Carlson-Day, J. L. Eglin, C. Lin, L. T. Smith, R. J. Staples, D. O. Wipf, *Polyhedron* **1999**, *18*, 817−824.
[53] T. Ren, *Coord. Chem. Rev.* **1998**, *175*, 43−58.
[54] P. Zuman, *The Elucidation of Organic Electrode Processes*; Academic Press, New York **1969**.
[55] L. P. Hammett, *Physical Organic Chemistry*; McGraw-Hill, New York **1970**.
[56] J. Shorter, *Correlation Analysis in Organic Chemistry*; Clarendon Press, Oxford **1973**.
[57] J. E. Leffler, E. Grunwald, *Rates and Equilibria of Organic Reactions*; John Wiley and Sons, New York **1963**.
[58] F. A. Cotton, R. A. Walton, *Multiple Bonds between Metal Atoms*, 2nd edition; Oxford University Press, Oxford **1993**.
[59] K. M. Carlson-Day, Judith L. Eglin, L. T. Smith, R. J. Staples, *Inorg. Chem.* **1999**, *38*, 2216−2220.
[60] L. Pauling, *The Nature of the Chemical Bond*; Cornell University Press, Ithaca, New York **1960**.
[61] K. M. Carlson-Day, J. L. Eglin, C. Lin, T. Ren, E. J. Valente, J. D. Zubkowski., *Inorg. Chem.* **1996**, *35*, 4727−4732.
[62] V. Srinivasan, R. A. Walton, *Inorg. Chem.* **1980**, *19*, 1635−1640.
[63] B. E. Bursten, F. A. Cotton, A. H. Cowley, B. E. Hanson, M. Lattman, G. G. Stanley, *J. Am. Chem. Soc.* **1979**, *101*, 6244−6249.
[64] A. J. Bard, L. R. Faulkner, *Electrochemical Methods.;* John Wiley and Sons, New York **1980**.
[65] D. H. Evans, K. Hu, *J. Chem. Soc., Faraday Trans.* **1996**, *92*, 3983−3990.
[66] J.-F. Capon, R. Kergoat, N. L. Berre-Cosquer, S. Peron, J.-Y. Saillard, J. Talarmin, *Organometallics* **1997**, *16*, 4645−4656.
[67] K. Hu, D. H. Evans, *J. Phy. Chem.* **1996**, *100*, 3030−3036.
[68] G. J. Wagner, J. Q. Chambers, *Langmuir* **1997**, *13*, 3529−3541.
[69] D. T. Pierce, W. E. Geiger, *J. Am. Chem. Soc.* **1992**, *114*, 6063−6073.
[70] F. A. Cotton, C. A. James, *Inorg. Chem.* **1992**, *31*, 5298−5307.
[71] T. J. Barder, R. A. Walton, *Inorg. Chem.* **1982**, *21*, 2510−2511.
[72] F. A. Cotton, N. F. Curtis, B. F. G. Johnson, W. R. Robinson, *Inorg. Chem.* **1965**, *4*, 326−330.
[73] W. Bradley, I. Wright, *J. Chem. Soc.* **1956**, 640−648.
[74] Crystallographic data (excluding structure factors) for the structures reported in this paper have been deposited with the Cambridge Crystallographic Data Center as supplementary publication nos. CCDC-116605 (**1**), -116606 (**2**), -116609 (**9**), -116607 (**10a**), and -116605 (**10b**). Copies of the data may be obtained free of charge on application to CCDC, 12 Union Road, Cambridge CB2 1EZ, UK [Fax: (internat.) + 44-1223/336-033; E-mail: deposit@ccdc.cam.ac.uk].
[75] *SMART V 4.043 Software for the CCD Detector System*, Siemens Analytical Instruments Division, Madison, WI, **1996**.
[76] *SAINT V 4.035 Software for the CCD Detector System*, Siemens Analytical Instruments Division, Madison, WI, **1995**.
[77] "SADABS, Program for Absorption corrections using Siemens CCD based on the method of Bob Blessing", *Acta Crystallogr.* **1995**, *A51*, 33.
[78] G. M. Sheldrick, *SHELXL-90, Program for the Solution of Crystal Structures*, University of Göttingen, Germany, **1986**.
[79] G. M. Sheldrick, *SHELXL-93, Program for the Refinement of Crystal Structures*, University of Göttingen, Germany, **1993**.
[80] *SHELXTL 5.03 (PC Version), Program Library for Structure Solution and Molecular Graphics*, Siemens Analytical Instruments Division, Madison, WI, **1995**.

Received April 6, 1999
[I99116]

Structure, Properties and Reactivity of the $Fe^{II}Fe^{III}$ and $Zn^{II}Fe^{III}$ Purple Acid Phosphatases

Mark B. Twitchett[a] and A. Geoffrey Sykes*[a]

Keywords: Metalloenzymes / Purple Acid Phosphatases / Phosphate Ester Hydrolysis / Dinuclear metal active sites

This microreview describes the structure, properties and mechanisms of the purple acid phosphatases (PAP). The enzyme is isolated from mammalian, plant and bacterial sources. X-ray structural information is now available for the enzyme from pig (uteroferrin), rat and kidney beans. Features of the mechanism are the concerted action of a labile M^{II} centre (Fe^{II} or Zn^{II}) alongside a more inert Fe^{III}. The latter is effective as a conjugate-base $FeOH^{2+}$, which initiates hydrolysis at the M^{II}-bound phosphate ester by a process involving OH^- replacement of OR^- at the P^V. Histidine residues near to the active site help bind the phosphate and are involved in the release of OR^-. Effects of replacement of the Fe^{II} by Mn^{II}, Co^{II}, Ni^{II}, Cu^{II} and Zn^{II}, and of Fe^{III} by Ga^{III},Al^{III} and In^{III} have been studied. The mechanistic role of the $Zn^{II}Zn^{II}$ combination in alkaline phosphatases, and other related dinuclear centres is also considered.

Introduction

Proteins having dinuclear iron centres are a well characterised category with wide-ranging biological functions.[1−3] They include ribonucleotide reductase,[4][5] methane monooxygenase,[6][7] as well as the O_2-transport/storage protein hemerythrin,[8] and Δ^9 desaturase.[9] In addition the mammalian $Fe^{II}Fe^{III}$ active site in purple acid phosphatase (PAP) is able to catalyse the hydrolysis of phosphate esters written here as $(RO)PO_3H^-$ (Equation 1) where R is an organic group.[1−3,10−13]

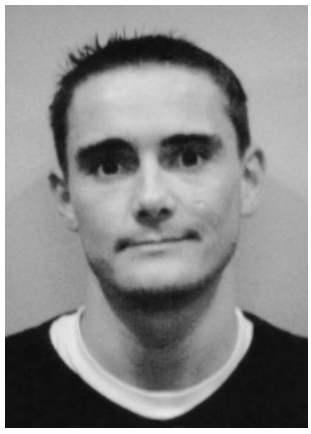
$$(RO)PO_3H^- + H_2O \rightarrow H_2PO_4^- + ROH \quad (1)$$

However, such phosphatase action is not restricted to dinuclear Fe centres, with plant phosphatases using the dinuclear $Zn^{II}Fe^{III}$ combination.[14] Also alkaline phosphatases have $Zn^{II}Zn^{II}$ active centres, and zinc has a prominent role in both phosphatase and phosphoryl-transfer reactions.[1] Interestingly in the case of many zinc enzymes, X-ray structures of reactant, intermediate and product states have provided a lead in determining the mechanism. How-

[a] Department of Chemistry, University of Newcastle, Newcastle upon Tyne, NE1 7RU, UK



Professor A. G. Sykes FRS has BSc., Ph.D., and DSc. degrees in chemistry from the University of Manchester where he researched under the supervision of Professor W.C.E. Higginson. After post-doctoral work in Princeton and Adelaide, he was appointed a Lecturer at the University of Leeds, became a Reader in 1970 and moved to the Chair of Inorganic Chemistry at the University of Newcastle upon Tyne in 1980. His research is primarily in kinetic/mechanistic studies on both inorganic and bioinorganic (metalloprotein) reactions, with purple acid phosphatases a relatively recent interest.



Mark Twitchett received his undergraduate education at the University of East Anglia and University of California Santa Barbara, obtaining his BSc. in Chemistry in 1992. He remained at the University of East Anglia for a further year to obtain his MSc in Spectroscopic and Physical Methods, and then researched with Professor A.G. Mauk on biological electron transfer at the University of British Columbia where he received his Ph.D. in Biochemistry and Molecular Biology in 1998. He has just completed a UK BBSRC Postdoctoral Research Assistantship with Professor Sykes in Newcastle.

MICROREVIEWS: This feature introduces the reader to the authors' research through a concise overview of the selected topic. Reference to important work from others in the field is also included.

 © WILEY-VCH Verlag GmbH, D-69451 Weinheim, 1999 1434−1948/99/1212−2105 $ 17.50+.50/0

	Motif A						Motif B			
	*		* *		*		*		* *	
10	VAV**GDW**GGVPN	26	ILSL**GDN**F**Y**FTG	28	VL**AGNH**DHLG	84	V**AGH**Y**P**VW	26	YLC**GH**D**H**NLQ
9	VAV**GDW**GGVPN	26	VXSX**GDN**F**Y**FSX	28	XX**AGNH**DHXG	74	V**AGH**Y**P**VW	26	YXC**GH**D**H**NXQ
10	VAV**GDW**GGVPN	26	ILSL**GDN**F**Y**FTG	28	VL**AGNH**DHLG	84	V**AGH**Y**P**VW	26	YLC**GH**D**H**NLQ
131	GLI**GDL**GQSFD	17	VLFV**GDL**SYADR	26	WT**AGNH**EIEF	76	V**L**MH**SP**LY	28	VFA**GH**V**H**AYE
164	AVLN**DMG**YTNA	17	AWHG**GDL**SYADD	78	VLP**GNH**EASC	147	V**M**SH**RP**MY	26	YLS**GH**I**H**WYE

Figure 1. Sequence alignment of the purple acid phosphatases: Uteroferrin (Uf), beef spleen, human, kidney bean (*Phaseolus vulgaris*), and *Aspergillus ficuum*; conserved residues are indicated in bold and amino acids coordinating the dinuclear metal site are indicated by *[13]

ever, the intense colour stemming from the Fe^{III} component of mammalian and plant PAP′s has made possible kinetic/mechanistic studies using UV/Vis spectrophotometry.[15−18] Such studies are a major contribution to this review.

Function

Purple acid phosphates are nonspecific phosphomonoesterases which can be isolated from mammalian,[19−23] plant,[24−27] and microbial sources.[28][29] They are distinguished from other acid phosphatases by their purple colours. Mammalian PAP′s are highly conserved dinuclear metal-containing enzymes produced by the osteoclasts i.e. cells that reabsorb bone. The mammalian enzymes are distinguished from lysosomal and prostatic acid phosphatases by their resistance to inhibition by L(+)tartrate, and hence are known as tartrate-resistant acid phosphatases (TRAP′s).[30−32] In the osteoclast the enzyme is believed to be involved in dephosphorylation of phosphoproteins in the bone matrix, namely osteopontin and bone sialoprotein.[33] There have also been reports of low molecular weight phosphatase activity and removal of tyrosine-linked phosphates from the epidermal growth-factor receptor.[34] A role for PAP in the spleen involving degradation of aged red blood cells has also been proposed.[35] The degradation process may correlate to the generation of O_2-related free-radicals from redox changes at the Fe^{II} centre.[36] It has also been suggested that in Alzheimer patients there is a reduction in phosphatase activity in the brain due to a decrease in protein levels. In the case of plant PAP′s a physiological function appears to be the liberation of phosphate from organophosphates, which is important following phosphate starvation.[37]

Physical Properties of PAP

Purple acid phosphatases require acidic conditions for optimum activity and are characterised by an intense purple colour. The latter is brought about by a tyrosine phenolate to iron(III) ligand to metal charge-transfer (LMCT) process, which is observed for both the $Fe^{II}Fe^{III}$ and $Fe^{III}Fe^{III}$ states.[38−41] The PAP enzymes most extensively studied are those from the porcine uterus (known as uteroferrin, Uf, or pig PAP), bovine spleen (BSPAP), and from kidney beans (KBPAP). Complete amino acid sequences for a number of mammalian PAP′s are available (Uf,[42] bovine spleen,[42] human,[43] rat,[44] and mouse PAP.[45]) These have a dinuclear $Fe^{II}Fe^{III}$ active site ($M_r \approx 38$ kDa) and greater than 80% sequence homology. The plant PAP′s have less homology with only 60% identical residues for the enzymes from kidney bean (*Phaseolus vulgaris*) and *Arabidopis thaliana*,[46] and in the former the active site is known to be the $Zn^{II}Fe^{III}$ combination.[14]

Mammalian, plant, and bacterial sequences have revealed five regions of sequence homology which have been further grouped into two signature motifs (A and B)[47] (Figure 1). Thus despite differences in overall amino acid sequences, as well as molecular mass and subunit arrangement, the enzymes have structurally similar active site regions. The mammalian PAP active sites in Uf and BSPAP are spectroscopically well characterised. The dinuclear iron site can exist in two oxidation states, $Fe^{II}Fe^{III}$ (pink) and $Fe^{III}Fe^{III}$ (purple). Of these only the $Fe^{II}Fe^{III}$ combination peak at 515 nm ($\varepsilon = 4450 M^{-1}cm^{-1}$), has significant phosphatase activity.[48][49] The $Fe^{II}Fe^{II}$ state generated by dithionite (0.5 mM) reduction (30 min) has no long term stability, and has not been studied in a similar way. Loss of Fe^{II} occurs, and after 30 min only 40% recovery of the higher oxidation states is possible.[17] The purple $Fe^{III}Fe^{III}$ form is EPR silent and gives a characteristic UV/Vis peak at 550 nm ($\varepsilon = 4300 M^{-1}cm^{-1}$). Recently magnetic susceptibility measurements on protein in the $Fe^{II}Fe^{III}$ states have indicated exchange coupling constants, J values between -5 and $-15 cm^{-1}$ for KBPAP and BSPAP in both states,[50] with the main contribution to antiferromagnetic coupling from the μ-hydroxo bridge.[51][52] Analysis of iron K-edge EXAFS data has suggested that a μ-hydroxo or alkoxy group may be present.[53] Recent CD/MCD studies on this redox state provide confirmation of antiferromagnetic coupling and suggest a μ-hydroxo group.[54] The EPR spectrum of the $Fe^{II}Fe^{III}$ enzyme, with g values at 1.94, 1.76 and 1.56 is consistent with coupling between the high-spin Fe^{II} and Fe^{III} ions.[50,55,56]

In addition to the bridging hydroxo group the existence of a coordinated aqua/hydroxo group to each Fe has been demonstrated by ESEEM (electron spin echo envelope modulation),[57] ENDOR (electron nuclear double resonance),[58] and is consistent with electrochemical studies.[59] Furthermore the remaining endogenous ligands have been

identified by a variety of spectroscopic methods. The intense purple/pink absorbance at 500−600 nm is assigned to a tyrosine phenolate to Fe^{III} charge-transfer band.[60−63] The presence of the tyrosine accounts for the retention of one Fe in the +3 state. The $Fe^{III}Fe^{III}/Fe^{II}Fe^{III}$ reduction potential (E°) is 367mV vs. NHE, whereas that required for the further reduction of $Fe^{II}Fe^{III}$ is negative.[59] Tyrosine is also a ligand in transferrin, active-site coordination $[Fe(Tyr)_2(His)(Asp)(CO_3)]$, where E° for the Fe^{III}/Fe^{II} couple is −520mV,[64] a measure of the difficulty of bringing about the reduction of a tyrosine-coordinated Fe^{III}. Additional evidence from Resonance Raman and ^1H NMR spectroscopy confirms that a tyrosine is bound to the Fe^{III} in PAP.[60−63] Coordination of imidazole and of carboxylate groups have been confirmed by ^1H NMR spectroscopy.[61][62] Pulse EPR[65] and Mossbauer[51,66,67] studies have also been carried out. A demonstration that both Fe atoms are six coordinate comes from CD/MCD investigations,[54] and all information obtained is consistent with the active site structure indicated in Figure 2. It should be noted however that the ^1H NMR studies provide no evidence for a second His coordinated to the Fe^{II}. Fast exchange of the Nε proton with bulk solvent is a possible explanation of effects observed. Studies on plant KBPAP have also been carried out.[48] Acid dissociation pK_a′s for KBPAP determined by UV/Vis absorption spectrophotometry of 4.8 and 9.5 have been assigned to H_2O ligands to the Fe^{III} and Zn^{II} respectively.[11] For BSPAP the first pK_a is also at 4.8,[48] whereas for Uf a smaller value of 3.8 is found.[16]

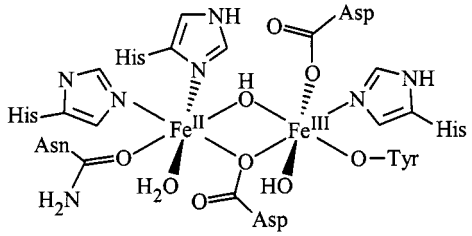


Figure 2. Structure of the $Fe^{II}Fe^{III}$ active sites of mammalian purple acid phosphatases

X-ray Structures

X-ray crystal structures of the 111 kDa homodimeric $Zn^{II}Fe^{III}$ KBPAP enzyme (resolution 2.65Å), the same protein with μ-phosphate coordinated (2.7Å), and the product with μ-tungstate(VI) inhibitor coordinated (3.0Å) have been reported.[11] More recently the structures of μ-phosphato derivatives of two mammalian PAP′s from Uf (1.55Å),[68] and from rat (2.7Å),[69] both believed to be in the $Fe^{III}Fe^{III}$ state, have been determined. The mammalian PAP enzymes are monomeric glycoproteins of ≈ 38 kDa, whereas the two monomer units of KBPAP are connected by a disulfide bridge. Sequence homologies between the monomer unit of the homodimeric KBPAP and mammalian PAP′s have been investigated.[47] With the *N*-terminal domain of KBPAP removed the two enzymes can be aligned. The C-terminal domain incorporates two sandwich βαβαβ motifs. All the ligands to the dimetal site are found within these two motifs.

The high resolution Uf structure confirms octahedral coordination at both metals.[68] The $Fe^{III}-Fe^{III}$ separation is 3.31Å and the phosphate bridges the two metals in a symmetrical manner. Strong electron density is observed consistent with the presence of a μ-hydroxo group, and there is no evidence for phosphate displacing this group. The two metals are also bridged in a monodentate manner by one of the aspartate residues, and there is confirmation that the tyrosine phenolate O-atom is bound to the Fe. The spacial arrangement of the metal ligands are very similar to those in KBPAP, and the α-carbon atoms of all seven coordinated amino acid residues superimpose. The active site is readily accessed from the surrounding solvent. The protein fold of Uf resembles that of KBPAP and some serine/threonine proton phosphatases, despite the <15% homologies.

The KBPAP structure has a $Zn^{II}Fe^{III}$ active site,[11] and unlike the $Fe^{III}Fe^{III}$ Uf and rat structures, is the only one for which the dimetal site is in the active form. The Zn^{II} is ligated to the Nε atom of His-286, the Nδ atom of His-323 and the carbonyl oxygen of Asn-201 (Figure 3). The Fe^{III} is ligated to the Nε atom of His-325, to Tyr-167 and the carboxylate of Asp-135. The Zn−Fe separation is 3.26Å. Three exogenous H_2O/OH^- ligands were modelled into the active site. These are a terminal hydroxo ligand to the Fe^{III}, a terminal H_2O to the Zn^{II}, and a μ-hydroxo bridge between the two metals. From sequence homologies and spectroscopic studies a high degree of conformity with the mammalian active site is indicated (Figures 2 and 3). The similarity of the dimetallic ligation with those of the serine/threonine protein phosphatases, calcineurin (PP2B) and PPI is noted.[70−73]

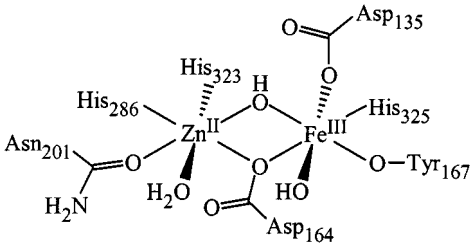


Figure 3. Structure of the $Zn^{II}Fe^{III}$ active site of kidney bean purple acid phosphatase (KBPAP) from X-ray crystallography[11]

In addition three histidine (His 202, 295 and 296) are located near to the dimetallic centre of KBPAP (Figure 4), and are in positions where they can interact with phosphate.[11] It has been proposed that the His-296 protonates the leaving alcohol group. The counterparts of these residues are His-92, Glu-194 and His-195 in the mammalian PAP′s.[68][69] In the two mammalian structures the His-92 and His-195 residues are hydrogen-bonded to the phosphate.[68] The side chain of Glu-194 is not in close contact with the phosphate, and appears to have no similar role to that of His-295 in KBPAP. The conservation of two of the

histidines (His-202 and 296), and their superposition in the different structures, suggests a mechanistic role.

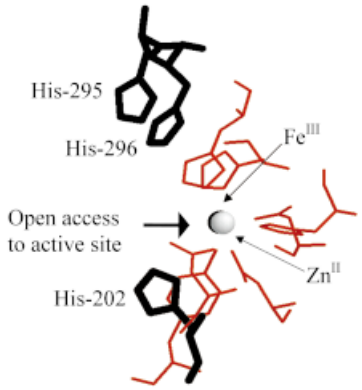


Figure 4. Structure of KBPAP illustrating the close proximity of residues His-202, -295 and -296 to the dinuclear metal active site

Structures of Other Phosphatases

The PAP′s are members of a much larger family of phosphatases recently reviewed.[1] Two other categories, the alkaline phosphatases (AP),[1][74] and the serine/theonine protein phosphatases (PP),[70−73] are mentioned here. The alkaline phosphatases are colourless and have a linear arrangement of two Zn^{II} atoms 4.1Å apart, and a Mg^{II} at 4.8Å. The structure of the native enzyme with phosphate bound (2.0Å resolution) has provided most information. The phosphate substrate bridges Zn1 and Zn2, which have no other bridging ligands, whereas Asp-51 bridges bidentately Zn2 to Mg3 (the third metal atom) (Figure 5).

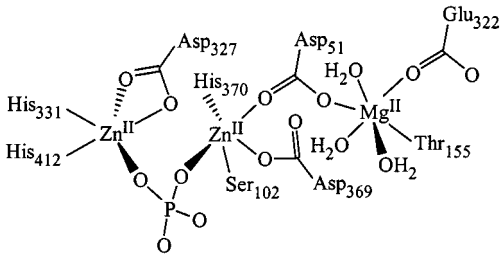


Figure 5. Structure of the $Zn^{II}Zn^{II}Mg^{II}$ active site of alkaline phosphatase with phosphate bound[1]

The Zn1 centre is pentacoordinated by bidentate Asp-327, His-331, His-412 and the O-atom of the phosphate group. The Zn2 is tetrahedral and coordinated by Asp-51, Asp-369, His-370 and phosphate. The Mg3 is ooctahedral with all O-donors, Asp-51, Thr-135, Glu-322 and three H_2O′s. The remaining two O-atoms of the phosphate are tightly held by hydrogen-bonds with the guanidinium group of Arg-166. A particular feature of the mechanism is the incorporation of $(RO)PO_3^{2-}$ into a serine phosphate-ester intermediate (Figure 6) which has been identified by X-ray crystallography.[1]

Coordination of the Ser-102 O-atom to the Zn2 facilitates deprotonation of the side chain, and the serinate nucleophile attacks the phosphate and replaces the OR^- group. The intermediate so formed reacts further with H_2O to give the hydrolysed product. AP appears unique amongst these enzymes in reacting by a two-stage mechanism. The Mg3 ion appears to have a minor role only.

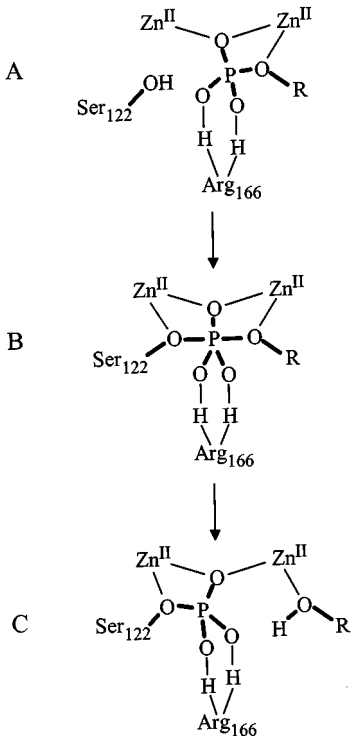


Figure 6. Schematic illustration of the conversion of $(RO)PO_3H^-$ (A) into a serine phosphate ester intermediate (C) by alkaline phosphatase

PP proteins are activated by several metal ions, and probably contain the Fe−Zn combination in the native form. The X-ray crystal structure of the phosphate bound rabbit muscle PP (PP-1) has been determined to 2.1Å resolution,[72] and the dinuclear metal site superimposes well with KBPAP, particularly with respect to the bridging ligands. The metals are both five-coordinate and are 3.3Å apart. They are bridged by an oxygen of Asp-92 and a water (very likely hydroxide). One metal has a distorted trigonal-bipyramidal geometry and additional coordination to Nε of His-173, Nδ of His-248 and the carbonyl oxygen of Asn-124. The other metal ion has a square-pyramidal geometry and additional coordination to Nε of His-66, Asp-64 and another solvent molecule (Figure 7). A notable difference is the substitution of a solvent H_2O for the tyrosine in PAP, and no purple colour is therefore observed.

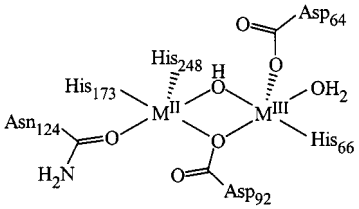


Figure 7. Structure of the active site of rabbit muscle protein phosphatase (PP-1)[72]

Activity of PAP

With the further elucidation of PAP active-site structures it is possible to consider in more detail the mechanism by which these proteins hydrolyse phosphate esters in acidic conditions. Such mechanistic studies have featured prominently in work carried out at Newcastle, with particular emphasis on kinetic analysis of UV/Vis spectrophotometric changes for the interaction of oxyanions with the enzyme.[16][18] Activity measurements are carried out by monitoring UV/Vis changes for the release of nitrophenol from *p*-nitrophenol phosphate, or α-naphthol from α-naphthyl phosphate. The initial slope of a plot of α-naphthol released against time gives the activity in nmol·min^{-1}. In previous studies unit enzyme activity was defined as the amount of enzyme catalysing the hydrolysis of 1 μmol of α-naphthyl phosphate per min. Following observations that the activity of BSPAP exhibits a bell-shaped pH dependence, Witzel and colleagues[48] proposed that two single proton equilibria were involved. One of these for the upward part of the bell-shape curve gives a pK_a of 4.8 and is catalytic, and the second for the downward part gives a pK_a of 6.9 which inhibits reaction. The lower pK_a is also observed in EPR and UV/Vis studies,[48] and has been attributed to deprotonation of the solvent H_2O coordinated to the Fe^{III}. Based on evidence that no nucleophilic residue on the enzyme appears to be involved in the catalytic reaction, and that no covalent bound intermediate is formed as in the case of the phosphotransferases, it has been concluded that a hydroxo ligand bound to the Fe^{III} induces the ester hydrolysis reaction.[16][48] Results obtained from the reaction of labelled adenosine 5′-triphosphate (ATP) with $Fe^{II}Fe^{III}$ PAP have demonstrated that there is transfer of phosphate to an H_2O position on the PAP with overall inversion at the phosphate.[75]

Reaction of Phosphate ($H_2PO_4^-$) With Uf PAP

Although reactions of the $Fe^{II}Fe^{III}$ protein with a number of oxyanions had been studied quite extensively,[19,51,54,61,65,76,77] there has until recently been no clear understanding of the precise function of the Fe^{II} and Fe^{III} combination. At 25°C acid dissociation pK_a values for H_3PO_4 are 2.1 for the formation of $H_2PO_4^-$, and 6.7−7.0 for the formation of HPO_4^{2-}. On addition of excess of phosphate ($H_2PO_4^-$) to $Fe^{II}Fe^{III}$ rapid stopped-flow formation of a phosphato product is observed. Spectrophotometric changes gave a shift in UV/Vis peaks from 515 nm for $Fe^{II}Fe^{III}$ to 535−560 nm (pH dependent) for the phosphato product. Surprisingly first-order rate constants k_{obs} obtained by monitoring absorbance changes at 620 nm indicate that the reaction is independent of $[H_2PO_4^-]$ in the range 10−50 mM (Figure 8).[16] The reactions with phenyl phosphate, pyrophosphate, tripolyphosphate and ATP (adenosine 5′-triphosphate), referred to collectively as PO_4, in which ester hydrolysis occurs, are also independent of $[PO_4]$.[16] Significantly, with $(MeO)_3PO$ no absorbance changes are observed indicating the need for two strongly nucleophilic oxo groups (and/or hydrophilic groups) for attachment to the Fe^{III} chromophore to occur. The latter does however inhibit the reaction of $H_2PO_4^-$, suggesting that an interaction of $(MeO)_3PO$ with Fe^{II} is occurring.

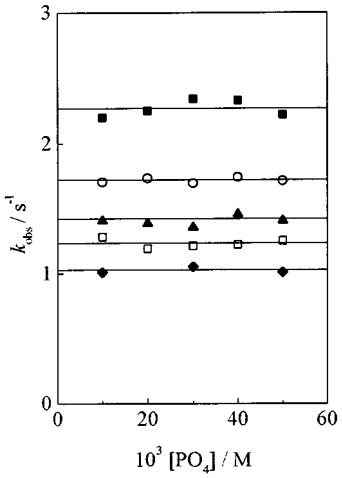


Figure 8. The phosphate concentration independence of first-order rate constants k_{obs} (25°) for the reaction of $Fe^{II}Fe^{III}$ Uf with different phosphates: $H_2PO_4^-$ (○), phenyl phosphate (□), pyrophosphate (■), tripolyphosphate (▲) and ATP (◆) at pH 4.6, I = 0.01M (NaCl)[16]

The mechanism proposed in the case of $H_2PO_4^-$ involves binding first to the Fe^{II}, in a relatively rapid process which does not contribute appreciably to changes in visible absorbance. Bridging to the strongly chromophoric Fe^{III} then occurs. Such a mechanism is consistent with general properties of high-spin Fe^{II} and Fe^{III} ions, the hexaaqua ions of which have water-exchange rate constants close to $10^6 s^{-1}$, and $10^3-10^4 s^{-1}$, respectively.[78][79] Accordingly the reaction sequence can be expressed as in Equation (2).

$$PO_4 + M^{II}\ldots Fe^{III} \underset{}{\overset{K_1.}{\rightleftharpoons}} M^{II}\ Fe^{III} \quad (2)$$
$$\quad\ |\ \ | \qquad\qquad\quad |\ \ |$$
$$\quad H_2O\ OH \qquad\qquad PO_4\ OH$$

followed by bridging to the strongly chromophoric Fe^{III}, (3).

$$M^{II}\ldots Fe^{III} \underset{k_b}{\overset{k_f}{\rightleftharpoons}} M^{II}\ldots Fe^{III} \quad (3)$$
$$|\ \ \ | \qquad\qquad\quad \backslash\ \ / \qquad\qquad$$
$$PO_4\ OH \qquad\qquad\quad PO_4$$

Assuming (2) to be relatively rapid, mass balance can be used to give (4)

$$k_{obs} = \frac{k_f K_1 [PO_4]}{K_1 [PO_4] + 1} + k_b \quad (4)$$

However the first term on the right-hand side suggests that a $[PO_4]$ dependence should be observed. Only if k_b is

dominant, or $K[PO_4] >> 1$ is this equation consistent with the observed $[PO_4]$ independence. There is no evidence for k_b being dominant, and the second possibility is therefore considered. Determination of the overall stability constant K by titration of Uf PAP with $H_2PO_4^-$ at pH 4.9 (40 mM acetate) gives a value of $165M^{-1}$,[80] in agreement with an earlier value of $151M^{-1}$ in 100 mM acetate buffer.[80] No dependence of thermodynamic and kinetic parameters on acetate in the range 25−55 mM, has been observed.[15] The overall K can be written as $K_1\ k_f/k_b$, or K_1K_2 on replacing k_f/k_b with K_2. For the 10−50 mM range of $[PO_4]$ studied no dependence on $[PO_4]$ is observed, and it is concluded that $K_1[PO_4] >> 1$, or alternatively $K_1[PO_4]$ is say > 5, which gives $K_1 > 500\ M^{-1}$. Since K has been determined as $165M^{-1}$, K_2 for the intramolecular step (3) is <0.32. It should be noted that K and K_2 have different units, and that K_1 may benefit from association at the His residues previously indicated, e.g. Figure 8.

It is not clear how the HPO_4^{2-} bridge dissociates. There are two possibilities to consider: (a) by cleavage of the $Fe^{II}-PO_4$ bond, or (b) cleavage of $Fe^{III}-PO_4$. If the first of these applies then dissociation follows a different route to formation. Two of the residues His-202, His-295 and His-296 found in KBPAP are conserved as His-92 and His-195 in mammalian forms, and may help bind the $H_2PO_4^-$ in (2). The mechanism of ester hydrolysis is considered below after sections on the reactions with other oxyanions and redox studies.

Reactions With Other Oxyanions

Further insight into the mechanism of oxyanion binding has been provided by studies on the binding of arsenate(V), molybdate(VI) and tungstate(VI) to $Fe^{II}Fe^{III}$ Uf.[18] Both phosphate and arsenate function as weak competitive inhibitors for phosphate ester hydrolysis by acting as bridging ligands between the two metal centres.[16,19,53,80−83] These oxoanions lower the protein reduction potential and increase the susceptibility of the active site to air oxidation.[58][59] Conversely, tungstate(VI) and molybdate(VI) are reported to be strong noncompetitive inhibitors which increase the reduction potential and stabilise the active site.[18,57,59] It has been suggested that the latter two oxoanions bind in a different manner to the phosphate and arsenate(V), producing a change in the active site EPR spectrum from rhombic to axial, and a change in the UV/Vis spectrum (molybdate). A low resolution structure is available for tungstate(VI) bound to KBPAP.[11] Recent CD/MCD studies on protein having bound phosphate or molybdate have led to the proposal that bound phosphate, unlike molybdate, interacts with the active site μ-OH bridge thus increasing the bond strength between the μ-OH bridge and the Fe^{II}, and producing a more rhombic Fe^{II} centre.[54] EXAFS results have also been reported on $Zn^{II}Fe^{III}$ Uf.[77] A number of anomalies remain, and further work is required in this area.

As far as the kinetics of the reactions of $Fe^{II}Fe^{III}$ Uf with oxyanions XO_4 (molybdate, tungstate and vanadate) are concerned, rate laws independent of $[XO_4]$ are similar to those obtained with $H_2PO_4^-$ phosphate.[18]

Redox Studies on Uf PAP

Two inorganic reagents, $[Fe(CN)_6]^{3-}$ (E° = 410mV) and $[Co(phen)_3]^{3+}$ (E° = 370mV) have been used as oxidants (25°C) for $Fe^{II}Fe^{III}$ Uf PAP, at pH 5.0, I = 0.10M (NaCl), overall Equations (5) and (6).[17]

$$Fe^{II}Fe^{III} + [Co(phen)_3]^{3+} \rightarrow Fe^{III}Fe^{III} + [Co(phen)_3]^{2+} \quad (5)$$

$$Fe^{II}Fe^{III} + [Fe(CN)_6]^{3-} \rightarrow Fe^{III}Fe^{III} + [Fe(CN)_6]^{4-} \quad (6)$$

With $[Co(phen)_3]^{3+}$ as oxidant first-order dependencies on both reactants are observed, giving second-order rate constants k_{Co} of $1.26M^{-1}s^{-1}$. In contrast the reaction with $[Fe(CN)_6]^{3-}$ gives saturation kinetics (Figure 9). This behaviour can be explained by the reaction sequences (7) and (8).

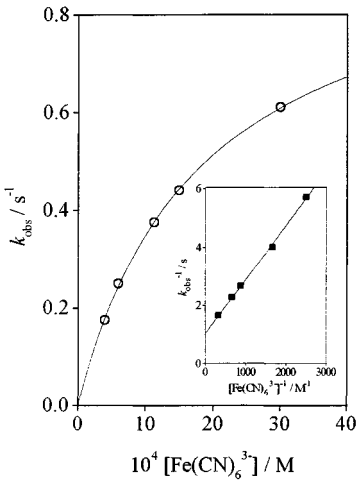


Figure 9. Saturation kinetic behaviour of first-order rate constants k_{obs} (25°C) for the reaction of $Fe^{II}Fe^{III}$ Uf with $[Fe(CN)_6]^{3-}$ at pH 5.0, I = 0.10M (NaCl). The inset shows the reciprocal plot[17]

$$Fe^{II}Fe^{III} + [Fe(CN)_6]^{3-} \overset{K_{Fe}}{\rightleftharpoons} Fe^{II}Fe^{III}\ldots[Fe(CN)_6]^{3-} \quad (7)$$

$$Fe^{II}Fe^{III}\ldots[Fe(CN)_6]^{3-} \overset{k_{Fe}}{\rightarrow} Fe^{III}Fe^{III} + [Fe(CN)_6]^{4-} \quad (8)$$

The part played in phosphate ester hydrolysis by the positive patch of His-202, His-295 and His-296 near to the active of KBPAP (Figure 4) has been discussed.[11] Two of these histidines, His-92 and His-195, are conserved in Uf. Association of $[Fe(CN)_6]^{3-}$ at this site (7), prior to electron transfer (8) is proposed therefore. For such a sequence (9) is derived,

$$k_{obs} = \frac{k_{Fe}\,K_{Fe}\,[Fe(CN)_6^{3-}]}{1 + K_{Fe}\,[Fe(CN)_6^{3-}]} \quad (9)$$

and a graph of $1/k_{obs}$ against $1/[Fe(CN)_6^{3-}]$ is linear. The slope and intercept give K_{Fe} and k_{Fe} values of $540M^{-1}$ and

$1.00s^{-1}$ respectively. Moreover competitive inhibition of the $[Fe(CN)_6]^{3-}$ oxidation by nonredox active $[Cr(CN)_6]^{3-}$ and $[Mo(CN)_8]^{4-}$ is also observed with association constants as defined in (7) of $K_{Cr} = 550M^{-1}$ and $K_{Mo} = 1580M^{-1}$. Together these studies provide support for an electrostatically controlled interaction. The magnitude of the association constants suggests an effective local protein charge as high as +4,[84] which could arise from two $HisH^+$ groups along with some contribution from the active site charge. We note that although the positively charged region on PAP favours anionic reagents, substrates which are cationic also retain an appreciable reactivity. Thus the reaction of $Fe^{III}Fe^{III}$ Uf PAP with the positively charged reductant $[Ru(NH_3)_5H_2O]^{2+}$ ($E° = 67mV$) (10),

$$Fe^{III}Fe^{III} + [Ru(NH_3)_5H_2O]^{2+} \rightarrow Fe^{II}Fe^{III} + [Ru(NH_3)_5H_2O]^{3+} \quad (10)$$

gives a second-order rate constant k_{Ru} of $2.2 \times 10^5 M^{-1}s^{-1}$. The magnitude of the rate constants k_{Co} and k_{Ru} suggest a dependence on thermodynamic driving force.

Effects of pH on PAP Reactivity

Rate constants for the reactions of $H_2PO_4^-$ and phosphate esters $(RO)PO_3H^-$ with $Fe^{II}Fe^{III}$ Uf are dependent on pH in the range 2.6−6.5 (Figure 10).[16]

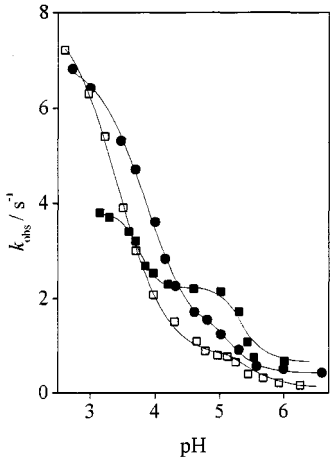


Figure 10. Variation of first-order rate constants k_{obs} (25°C) with pH for the reaction of $Fe^{II}Fe^{III}$ Uf with $H_2PO_4^-$ (●), phenyl phosphate (□), and pyrophosphate (■), $I = 0.10M$ (NaCl)[16]

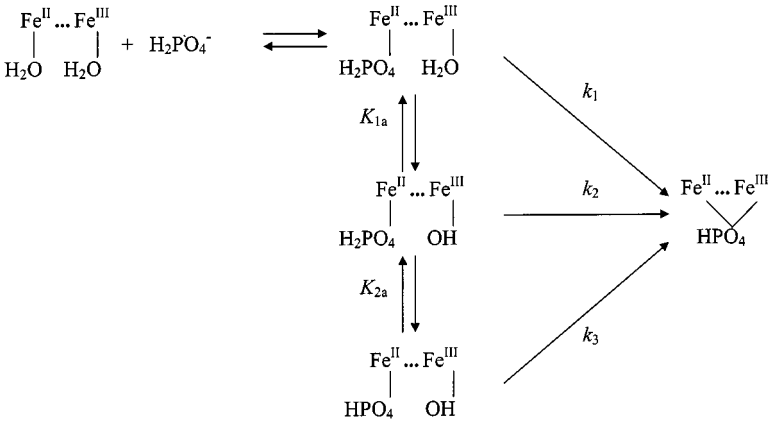
Contributions to pH effects can stem from acid-base effects involving aqua ligands, nearby protein amino acids, and/or free and monodentate phosphate species. In the reaction of $H_2PO_4^-$ rate constants k_{obs} provide evidence for a Uf pK_{1a} of 3.9, which is assigned to acid dissociation at the Fe^{III}.[16] There is some evidence (the inflection at pH ≈ 5) for a second process pK_{2a}. In all other cases (phenyl phosphate, pyrophosphate, tripolyphosphate and ATP) two pK_a values (pK_{1a} and pK_{2a}) are clearly apparent, and rate constants k_1, k_2 and k_3 can be defined for the reactions of different protonated/deprotonated forms of the adduct formed in the first step of Scheme 1.

From the mechanism proposed the rate law (11) can be derived.

$$k_{obs} = k_1 + \frac{(k_3\text{-}k_1)\,K_{1a}K_{2a} + (k_2\text{-}k_1)\,K_{1a}[H^+]}{[H^+]^2 + K_{1a}[H^+] + K_{1a}K_{2a}} \quad (11)$$

From fits to (11) values of K_{1a}, K_{2a}, k_1, k_2 and k_3 are obtained (Table 1). The pK_{1a} values determined are in the range 3.4−3.9 (average 3.8), and are attributed to deprotonation of the Fe^{III} bound H_2O. The same pK_a is obtained from the effects of pH on the UV/Vis absorbance of Uf. As a guide the first acid dissociation constant of $[Fe(H_2O)_6]^{3+}$ is 3.0, whereas $[Fe(H_2O)_6]^{2+}$ remains in the aqua form until >7.[85] The second deprotonation effect (pK_{2a}) suggests that acid dissociation at the phosphate group attached to the Fe^{II} is contributing (Figure 10). As is to be expected shifts are observed in pK_{2a} values, as compared to literature values for the free phosphate reactant (which are 0.4−0.7 pH units higher), as a result of complexing to Fe^{II} and changes in the immediate environment. In the case of $H_2PO_4^-$ this would require that the pK_a of 6.7−7.0 is shifted to 5.1 on attachment to Fe^{II}. For a full treatment the further effect of deprotonation of nearby His residues also needs to be considered.

The effects of pH on activity have been studied to higher pH′s with α-naphthyl phosphate, as illustrated in Figure 11. Maximum activity for Uf is observed at pH 4.9 whereas in the case of KBPAP and BSPAP a shift to the range pH ≈ 5.9 is observed. Earlier studies on Uf with *p*-nitrophenyl phosphate have also indicated maximum activity at pH



Scheme 1

Table 1. Summary of data obtained for the reactions (25°C) of $H_2PO_4^-$, phenylphosphate, pyrophosphate with active $Fe^{II}Fe^{III}$ PAP (Uf) at pH 2.6−6.5, I = 0.10M (NaCl)[16]

	$H_2PO_4^-$	Phenylphosphate	Pyrophosphate
pK_{1a}[a]	3.9	3.4	3.8
pK_{2a}[a]	5.1	5.0	5.4
pK_{1a}[b]	4.0		
pK_{2a}[b]	5.3		
pK_a[c]	6.9	5.6	6.0
k_1/s^{-1}	7.1	8.4	4.7
k_2/s^{-1}	1.8	1.0	2.3
k_3/s^{-1}	0.4	<0.1	0.1

[a] Recomputed using Microcal Origin 5 fitting program. − [b] Data for $Zn^{II}Fe^{III}$ Uf. − [c] Range of pK_a values for $H_2PO_4^-$ 6.7−7.0.

4.9.[86] As yet no explanation for this different behaviour of Uf as compared to BS and KBPAP has been forthcoming, although as already noted the pK_a′s assigned to $Fe^{III}-H_2O$ acid dissociation are smaller (3.9) for Uf than for BSPAP and KBPAP (4.9).

The acid dissociation process pK_{1a} giving the conjugate-base $Fe^{III}-OH$ slows down the substitution of $H_2PO_4^-$ at the Fe^{III}, but has a quite different effect on ester hydrolysis.

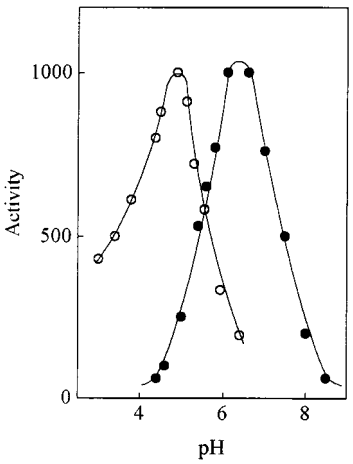
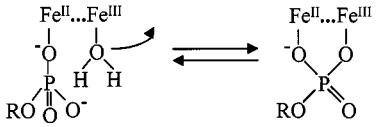


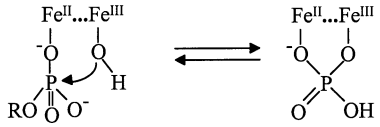
Figure 11. Variation of PAP phosphatase activity with pH, (a) for Uf (○) with 10 mM α-naphthyl phosphate (25°C) using 40 mM buffer;[16][80] and (b) for BSPAP (●), 50 mM *p*-nitrophenyl phosphate (22°C), using 100 mM buffer[100]

Phosphate Ester Hydrolysis

From the above considerations it is likely that the $Fe^{III}-OH$ conjugate-base induces phosphate ester hydrolysis. The suggestion that the μ-OH bridge might alternatively be involved,[87] seems less likely because of its less favourable nucleophilic properties. The $Fe^{III}-OH$ involvement is supported by the KBPAP catalysis of ^{18}O exchange between phosphate and solvent.[88] Rate constants k_{obs} for μ-phosphato formation are maximum at pH 3 when $Fe^{III}-H_2O$ is present exclusively. Under these conditions bridge closure can occur with displacement of the H_2O, but little or no phosphate ester hydrolysis is observed (Scheme 2). At higher pH formation and participation of $Fe^{III}-OH$ becomes more extensive, and k_{obs} decreases as the OH^- is more difficult to substitute than H_2O. However the $Fe^{III}-OH$ participates in ester hydrolysis by substitution into the P^V coordination sphere of $(RO)PO_3H^-$, with displacement of RO^- (Scheme 3). The activity plots as in Figure 11 now become relevant. The increase in activity of Uf at the lower pH′s is due to increased amounts of $Fe^{III}-OH$, which maximises at pH 4.9. The decrease in activity at the higher pH′s may relate to deprotonation of the positive patch histidines, making the binding of phosphate less effective.



Scheme 2



Scheme 3

The mechanism that emerges for PAP is thus one of repeated bridge formation and cleavage with ester hydrolysis taking place on a subsequent if not the first cycle. The reaction sequence has a number of features in common with the intramolecular phosphate hydrolysis occurring in the case of $[Co(en)_2(H_2O)\{PO_3(OC_6H_4NO_2)\}]^+$ (en = ethylenediamine), and involving the conjugate-base $[Co(en)_2(OH)\{PO_3\ (OC_6H_4NO_2\}]$.[89]

Metal Substituted PAP Derivatives

In order to clarify the role of individual metals as components of the dinuclear active site, the reactivity of metal substituted PAP′s has been studied. Work by Zerner and colleagues has shown that the Fe^{II} of active BSPAP is labile and amenable to substitution by various divalent metals (including Co^{II}, Cu^{II}, Zn^{II}, Cd^{II} and Hg^{II}).[41,76,83,90,91] The procedure used involves the reaction of PAP with dithionite for ≈ 5 minutes to remove the labile Fe^{II}, followed by reconstitution using an excess of the M^{II} salt. The effect of substitution of the Fe^{II} in Uf by Mn^{II}, Co^{II}, Ni^{II}, Cu^{II} and Zn^{II} on UV/Vis spectra and kinetic properties has been studied. In some cases (Figure 12) substantial catalytic activity is retained by the $M^{II}Fe^{III}$ product.

The Zn^{II} substituted form of Uf is of particular interest because it resembles the KBPAP active site (Figure 13). Previous studies have shown that the properties of the $Zn^{II}Fe^{III}$ form of the BSPAP enzyme are similar to those of KBPAP.[14,40,83] In a similar manner the Zn^{II} of KBPAP can be substituted by Fe^{II} to form a catalytically active $Fe^{II}Fe^{III}$. Again the properties of the $Fe^{II}Fe^{III}$ form of the KBPAP are similar to those of native $Fe^{II}Fe^{III}$ PAP forms,[92][93] and

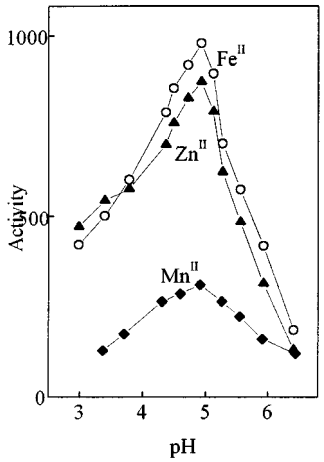


Figure 12. The variation of $M^{II}Fe^{III}$ Uf phosphatase activity (25°C) with pH (40 mM buffer) using α-naphthyl phosphate 10 mM), with M^{II} in turn Fe^{II} (○), Zn^{II} (▲), and Mn^{II} (◆)

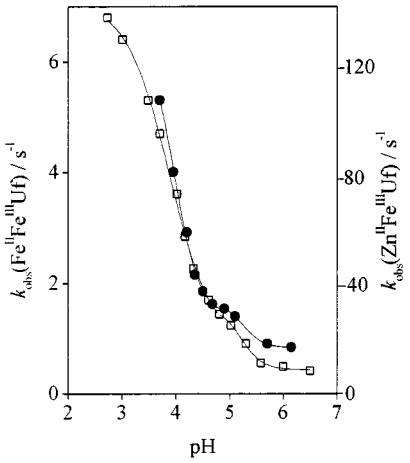


Figure 13 Variation of first-order rate constants k_{obs} (25°C) with pH for the reaction of $H_2PO_4^-$, with $Fe^{II}Fe^{III}$ Uf (□) and $Zn^{II}Fe^{III}$ Uf (●), I = 0.10M (NaCl)

vice versa for $Zn^{II}Fe^{III}$ Uf, although the reaction with $H_2PO_4^-$ is some 35 times more rapid than with $Fe^{II}Fe^{III}$ Uf at pH 4.9.[18] The $Mn^{II}Fe^{III}$ product is also of interest because Mn has been suggested as a component of sweet potato and soya bean PAP′s.[32,33,94–96] We note however that evidence for an $Fe^{II}Fe^{III}$ active site in sweet potatoes has also been reported.[97] It is unlikely that the active site contains $Mn^{II}Mn^{III}$ (as seems to be suggested), since Mn^{III}–Tyr charge transfer bands are not expected to give the same characteristic purple/pink colour as for Fe^{III} PAP′s. An appreciable blue-shift of ≈ 35 nm in phenolate to metal LMCT bands is for example observed for the Mn^{III} substituted transferrin (a lactoferrin form) as compared to the Fe^{III} form.[98]

From details of UV/Vis spectra (Table 2) it can be seen that the replacement of Fe^{II} with other divalent metals produces small but significant changes in peak positions (λ) and absorption coefficients (ε), where the products are different shades of purple. The greatest change in the peak position (λ) is for $Cu^{II}Fe^{III}$ Uf, and may indicate a different coordination of the Cu^{II}, which is known to have an affinity for *N*-donor ligands. The coupling of Fe^{II} to the Fe^{III},[45,50,51] appears to enhance ε values as compared to those for other M^{II} ions. The metal content and spectroscopic characterisation of PAP from sweet potato *Ipomea batatas* PAP has recently been carried out and establishes this as another example of a plant $Zn^{II}Fe^{III}$ protein.[99]

Table 2. UV/Vis peak positions (λ) and absorption coefficients (ε) for M^{II} substituted $M^{II}Fe^{III}$ PAP_r (Uf) (25°C), in sodium acetate buffer pH 4.9, I = 0.10M (NaCl)[80]

M^{II}	λ_{max}/nm	ε/M^{-1}cm^{-1}
Fe^{II}	510	4450[a]
Mn^{II}	514	3350
Co^{II}	518	3370
Ni^{II}	510	3260
Cu^{II}	545	3400
Zn^{II}	525	3580

Until recently metal substitution of M^{II} only was possible. In recent studies however the Fe^{III} centre has been replaced by Ga^{III} to produce $Fe^{II}Ga^{III}$ BSPAP and Zn^{II} Ga^{III} BSPAP.[100] Both forms exhibit catalytic activity similar to that of the native $Fe^{II}Fe^{III}$ BSPAP, providing evidence that diamagnetic Ga^{III} is acting as a functional analogue of Fe^{III}. Not surprisingly the gallium containing enzymes are colourless having lost the purple colour due to the tyrosine to Fe^{III} charge-transfer band. This work also provides kinetic data on the effect of substituting Fe^{II} with Zn^{II}. Thus the $Zn^{II}Fe^{III}$ BSPAP displays a 2–3 fold increase in K_M (the Michaelis constant), and nearly a twofold increase in k_{cat} relative to $Fe^{II}Fe^{III}$ BSPAP. The replacement of Fe^{II} and Fe^{III} of BSPAP to give $Zn^{II}Al^{III}$ and $Zn^{II}In^{III}$ has also been carried out.[101] There is as yet no explanation as to why the $Zn^{II}In^{III}$ form should be inactive.

Conclusions

The naturally occurring dinuclear $Fe^{II}Fe^{III}$ and $Zn^{II}Fe^{III}$ active sites of mammalian and plant purple acid phosphatases respectively make use of the M^{II} and Fe^{III} metal combination in a very subtle way to bring about phosphate ester hydrolysis. X-ray crystallographic studies on the enzyme from three different sources provides evidence for a single aqua or hydroxo ligand on each metal. The M^{II} ions are more labile, whereas Fe^{III} more readily forms conjugate-base (Fe^{III}–OH). The key roles are therefore binding of the phosphate ester to M^{II}, and the nucleophilic action of the OH^- of the Fe^{III} in bringing about phosphate ester hydrolysis. The $Fe^{III}Fe^{III}$ form of PAP has no similar enzymic action even though it does bind phosphate more strongly. The single tyrosine ligand serves to stabilise the Fe^{III} state and prevent its reduction. It also gives the enzyme its attractive colour. Other synthetic metal combinations can bring about phosphatase action although not always with the same efficiency. An essential part of the catalytic cycle is the release

of the μ-phosphate product after hydrolysis, a process which requires further investigation

[1] N. Sträter, W. N. Lipscomb, T. Klabunde, B. Krebs, *Angew. Chem. Int. Ed. Engl.* **1996**, *35*, 2024−2055.
[2] E. Wilcox *Chem. Rev.* **1996**, *96*, 2435−2458.
[3] J. B. Vincent, G. L. Olivier-Lilley, B. A. Averill, *Chem. Rev.* **1990**, *90*, 1447−1467.
[4] J. A. Stubbe, *J. Biol. Chem*. **1990**, *265*. 5329−5332.
[5] P. Nordlund, H. Eklund, *J. Mol. Biol*. **1993**, *232*, 123−164.
[6] J. D. Lipscomb, *Annu. Rev. Microbiol*. **1994**, *48*, 371−399.
[7] K. K Andersson, A. Graslund, *Adv. Inorg. Chem.*, **1995**, 43, 359−408.
[8] P. C. Wilkins, R. G. Wilkins, *Coord. Chem. Rev.* **1987**, *79*, 195−214.
[9] B. G. Fox, J. Shanklin, C. Somerville, E. Münck, *Proc. Natl. Acad. Sci., U. S. A.* **1993**, *90*, 2486−2490.
[10] N. Sträter, T. Klabunde, P. Tucker, H. Witzel, B. Krebs, *Science* **1995**, *268*, 1489−1492.
[11] T. Klabunde, N. Sträter, R. Fröhlich, H. Witzel, B. Krebs, *J. Mol. Biol*. **1996**, *259*, 737−748.
[12] J. B. Vincent, B. A. Averill, *FASEB J.* **1990**, *4*, 3009−3014.
[13] T. Klabunde, B. Krebs, *Structure and Bonding* **1997**, *89*, 177−198.
[14] J. L. Beck, L. A. McConachie, A. C. Summers, W. N. Arnold, J. De Jersey, B. Zerner, *Biochim. Bophys. Acta* **1986**, *869*, 61−68.
[15] M. A. S. Aquino, J.-S. Lim, A. G. Sykes, *J. Chem. Soc., Dalton. Trans.* **1992**, *13*, 2135−2136.
[16] M. A. S. Aquino, J.-S. Lim, A. G. Sykes, *J. Chem. Soc., Dalton. Trans.* **1994**, *15*, 429−436.
[17] M. A. S. Aquino, A. G. Sykes, *J. Chem. Soc., Dalton. Trans.* **1994**, *15*, 683−687.
[18] J.-S. Lim, M. A. S. Aquino, A. G. Sykes, *Inorg. Chem*. **1996**, *35*, 614−618.
[19] T. T. Chen, F. W. Baser, J. J. Cetorelli, W. E. Pollard, R. M. Roberts, *J. Biol. Chem*. **1973**, *248*, 8560−8566.
[20] H. D. Campbell, B. Zerner, *Biochem. Biophys. Res. Commun*. **1973**, *54*, 1498−1 1502.
[21] B. S. Allen, P. R. Nuttleman, C. M. Ketcham, R. M. Roberts, *J. Bone Miner. Res.* **1989**, *4*, 47−50.
[22] T. Efstratiadis, D. W. Moss, *Enzyme* **1985**, *33*, 34−40.
[23] K.-H. W. Lau, T. K. Freeman, D. J. Baylink, *J. Biol. Chem*. **1987**, *262*, 1389−1397.
[24] J. L. Beck, L. A. McConachie, A. C. Summers, W. N. Arnold, J. De Jersey, B. Zerner, *Biochim. Bophys. Acta* **1986**, *869*, 61−68.
[25] S. Fujimoto, T. Nakagawa, A. Ohara, *Agric. Biol. Chem.* **1977**, *41*, 599−600.
[26] K. Uehara, S. Fujimoto, T. Taniguchi, *J. Biochem.* **1974**, *75*, 627−628.
[27] S. Fujimoto, T. Nakagawa, S. Ishimitsu, A. Ohara, *Chem. Pharm. Bul*. **1977**, *25*, 1459−1464.
[28] A. H. J. Ullah, E. M. Mullaney, H. C. Dischinger Jr, *Biochem. Biophy. Res. Commun*. **1994**, *203*, 182−189.
[29] M. M. Jacobs, J. F. Nyc, D. M. Brown, *J. Biol. Chem*. **1971**, *246*, 1419−1425.
[30] C. Y. Li, L. T. Lam, *J. Histochem. Cytochem*. **1970**, *18*, 473−475.
[31] C. M. Ketcham, R. M. Roberts, R. C. M. Simmen, H. S. Nick, *J. Biol. Chem*. **1989**, *264*, 557−563.
[32] C. M. Roberts, G. A. Baumbach, F. W. Bazer, R. M. Roberts, *J. Biol. Chem*. **1985**, *260*, 5768−5776.
[33] J. Schinddelmeiser, D. Münstermann, H. Witzel, *Histochemistry* **1987**, *87*, 13−19.
[34] A. R. Hayman, T. M. Cox, *J. Biol. Chem*. **1994**, *269*, 1294−1300.
[35] B. Ek-Rylander, M. Flores, M. Wendel, D. Heinegård, G. Andersson, *J. Biol. Chem*. **1994**, *269*, 14853−14856.
[36] S. Shimohara, S. Fujimoto, M. Chachin, T. Taniguchi, G. Perry, P. J. Whitehouse, J. Kimura, *Brain Research* **1995**, *699*, 125−129.
[37] K. S. Patel, S. W. Lockless, B. Thomas, T. D. McKnight, *Plant Physiology* **1996**, *111*, 271.
[38] J. W. Pyrz, J. T. Sage, D. G. Debrunner, L. Que Jr, *J. Biol. Chem*. **1986**, *261*, 11015−11020.
[39] R. G. Wilkins, *Chem. Soc. Rev.* **1992**, *21*, 171−178.
[40] J. C. Davis, B. A. Averill, *Proc. Natl. Acad. Sci., U. S. A*. **1982**, *79*, 4623−4627.
[41] J. L. Beck, D. T. Keough, J. De Jersey, B. Zerner, *Biochim. Biophys. Acta*. **1984**, *791*, 357−363.
[42] D. F. Hunt, J. R. Yates III, J. Shabanowitx, N.-Z. Zhu, T. Zirino, B. A. Averill, S. T. Daurat-Larroque, J. G. Shewale, R. M. Roberts, K. Brew, *BioChem. Biophys. Res. Commun*. **1987**, *144*, 1154−1160.
[43] D. K. Lord, N. C. P. Cross, M. A. Bevilacque, S. H. Rider, P. A. Gorman, A. V. Groves, D. W. Moss, D. Sheer, T. M. Cox, *Eur. J. Biochem*. **1990**, *189*, 287−293.
[44] B. Ek-Rylander, P. Bill, M. Norgård, S. Nilsson, G. Andersson, *J. Biol. Chem*. **1991**, *266*, 24684−24689.
[45] A. I. Cassady, A. G. King, N. C. P. Cross, D. A. Hume, *Gene* **1993**, *130*, 201−207.
[46] T. Klabunde, B. Stahl, H. Suerbaum, S. Hahner, M. Karas, F. Hillenkamp, B. Krebs, H. Witzel, *Eur. J. Biochem*. **1994**, *226*, 369−375.
[47] T Klabunde, N. Sträter, B. Krebs, H. Witzel, *FEBS Lett*. **1995**, *267*, 56−60.
[48] M. Dietrich, D. Münstermann, H. Suerbaum, H. Witzel, *Eur. J. Biochem*. **1991**, *199*, 105−113.
[49] M. Merkx, B. A. Averill, *Biochemistry* **1998**, *37*, 11223−11231.
[50] B. A. Averill, J. C. Davis, S. Burman, T. Zirino, J. Sanders-Loehr, T. M. Loehr, J. T. Sage, P. G. Debrunner, *J. Am. Chem. Soc*. **1987**, *109*, 3760−3767.
[51] R. B. Lauffer, B. C. Antanaitis, P. Aisen, L. Que Jr., *J. Biol. Chem*. **1983**, *258*, 14212−14218.
[52] E. Sinn, C. J. O′Connor, J. De Jersey, B. Zerner, *Inorg. Chim. Acta*. **1983**, *78*, L13-L15.
[53] A. E. True, R. C. Scarrow, C. R. Randall, R. C. Holz, L. Que Jr., *J. Am. Chem. Soc*. **1993**, *115*, 4246−4255.
[54] Y.-S. Yang, J. M. McCormick, E. I. Solomon, *J. Am. Chem. Soc*. **1997**, *119*, 11832−11842.
[55] B. C. Antanaitis, P. Aisen, H. R. Lilienthal, *J. Biol. Chem*. **1983**, *4258*, 3166−3172.
[56] P. G. DeBrunner, M. P. Hendrich, J. De Jersey, D. T. Keough, J. T. Sage, B. Zerner, *Biochim. Biophys. Acta*. **1983**, *745*, 103−106.
[57] K. Doi, J. McCracken, J. Peisach, P. Aisen, *J. Biol. Chem*. **1988**, *26*, 5757−5763.
[58] B. C. Antanaitis, P. Aisen, *J. Biol. Chem*. **1985**, *260*, 751−756.
[59] D. L. Wang, R. C. H. Holz, S. S. David, L. Que Jr., M. T. Stankovich, *Biochemistry* **1991**, *30*, 8187−8194.
[60] B. C. Antanaitis, T. Strekas, P. Aisen, *J. Biol. Chem*. **1982**, *257*, 3766−3770.
[61] R. C Scarrow, J. W. Pyrz, L. Que Jr., *J. Am. Chem. Soc*. **1990**, *112*, 657−665.
[62] Z. Wang, L.-J. Ming, L. Que Jr., J. B. Vincent, M. W. Crowder, B. A. Averill, *Biochemistry* **1992**, *31*, 5263−5268.
[63] B. P. Gaber, J. P. Sheridan, F. W. Bazer, R. M. Roberts, *J. Biol. Chem*. **1979**, *254*, 8340−8342.
[64] S. A. Kretchmar, Z. E. Reyes, K. N. Raymond, *Biochim. Biophys. Res. Commun.* **1988**, *108*, 1643−1648.
[65] B. C. Antanaitis, J. Peisach, W. B. Mims, P. Aisen, *J. Biol. Chem.* **1985**, *260*, 4572−4574.
[66] J. T. Sage, Y.-M. Xia P. G. Debrunner, D. T. Keough, J. De Jersey, B. Zerner, *J. Am. Chem. Soc*. **1989**, *111*, 7239−7247.
[67] J. H. Rodriguez, H. N. Ok, Y.-M. Xia, P. G. Debrummer, B. E. Hinrichs, T. Meyer, N. H. Packard, *J. Phys. Chem*. **1996**, *100*, 6849−6862.
[68] L. W. Guddat, A. S. McAlpine, D. Hume, S. Hamilton, J. de Jersey, J. L. Martin, *Structure* **1999**, *7*, 757−767.
[69] J. Uppenberg, F. Lindqvist, C. Svensson, B. Ek-Rylander, G. Andersson, *J. Mol. Biol.* **1999**, *290*, 201−211.
[70] J. P. Griffith, J. L. Kim, E. E. Kim, M. D. Sintchak, J. A. Thomson, M. J. Fitzgibbon, M. A. Fleming, P. R. Caron, K. Hsiao, M. A. Navia, *Cell* **1995**, *82*, 507−522.
[71] C. R. Kissinger, H. E. Parge, D. R. Knighton, C. T. Lewis, L. A. Pelletier, A. Tempcyzk, V. J. Kalish, K. D. Tucker, R. E. Showalter, E. W. Moomaw, L. N. Gastinel, N. Habuka, X. Chen, F. Maldonado, J. E. Baker, R. Bacquet, J. E. Villafranca, *Nature* **1995**, *378*, 641−644.
[72] J. Goldberg, H.-B. Huang, Y.-G. Kwon, P. Greengard, A. C. Nairn, J. Kuriyan, *Nature* **1995**, *376*, 745−753.
[73] M. P. Egloff, P. T. W. Cohen, P. Reinemer, D. Barford, *J. Mol. Biol*. **1995**, *254*, 942−959.
[74] J. E. Coleman, *Annu. Rev. Biophys. Biomol. Struct.* **1992**, *21*, 441−483.

[75] E. G. Mueller, M. W. Crowder, B. A. Averill, J. R. Knowles, *J. Am. Chem. Soc*. **1993**, *115*, 2974−2975.
[76] R. C. Holz, L. Que Jr., L.-J. Ming, *J. Am. Chem. Soc*. **1992**, *119*, 4434−4436.
[77] X. Wang, L. Que Jr., *Biochemistry* **1998**, *37*, 7813−7821.
[78] T. W. Swaddle, A. E. Merbach, *Inorg. Chem*. **1981**, *20*, 4212−4216.
[79] See, for example, R. G. Wilkins in *Kinetics and Mechanism of Reactions of Transition Metal Complexes*, VCH, Weinheim, **1991**.
[80] M. B. Twitchett, A. G. Sykes, unpublished work.
[81] D. T. Keough, J. L. Beck, J. De Jersey, B. Zerner, *Biochem. Biophys. Res. Commun*. **1982**, *108*, 1643−1648.
[82] K. Doi, R. Gupta, P. Aisen, *J. Biol. Chem*. **1987**, *262*, 6982−6985.
[83] S. S. David, L. Que Jr., *J. Am. Chem. Soc*. **1990**, *112*, 6455−6463.
[84] S. K. Chapman, J. D. Sinclair-Day, A. G. Sykes, S.-C. Tam, R. J. P. Williams, *J. Chem. Soc., Chem. Commun.* **1983**, *20*, 1152−1154.
[85] C. F. Baes, E. Mesmer, *The Hydrolysis of Cations*, Wiley-Interscience, New York, **1976**.
[86] D. C. Schlosnagle, F. W. Bazer, J. C. M. Tsibris, R. M. Roberts, *J. Biol. Chem*. **1974**, *249*, 7574−7579.
[87] X. Wang, C. R. Randall, A. E. True, L. Que Jr., *Biochemistry* **1996**, *35*, 13946−13954.
[88] C. J. Wynne, S. E. Hamilton, D. A. Dianysius, J. L. Beck, J. De Jersey, *Arch. Biochem. Biophys.* **1995**, *319*, 133−141.
[89] P. Hendry, A. M. Sargeson, *Prog. Inorg. Chem*. **1990**, *38*, 201−258.
[90] D. L. Keough, D. A. Dionysius, J. De Jersey, B. Zerner, *Biochem. Biophys. Res. Commun*. **1980**, *94*, 600−605.
[91] J. L. Beck, M. J. McArthur, J. De Jersy, B. Zerner, *Inorg. Chim. Acta*. **1988**, *153*, 39−44.
[92] J. L. Beck, J. De Jersey, B. Zerner, M. P. Hendrich, P. G. Debrunner, *J. Am. Chem. Soc*. **1988**, *110*, 3317−3318.
[93] H. Sauerbaum, M. Körner, H. Witzel, E. Althaus, B.-D. Mosel W. Müller-Warmuth, *Eur. J. Biochem*. **1993**, *214*, 313−321.
[94] K. Uehara, S. Fugimoto, T. Taniguchi, *J. Biochem*. **1971**, *70*, 183−185.
[95] S. Fujimoto, A. Ohara, K. Uehara, *Agric. Biol. Chem*. **1980**, *44*, 1659−1660.
[96] S. Fujimoto, T. Nakagawa, A. Ohara, *Chem. Pharm. Bull*. **1977**, *425*, 3283−3288.
[97] S. K. Hefler, B. A. Averill, *Biochem. Biophys. Res. Commun*. **1987**, *146*, 1173−1177.
[98] R. M. C. Dawson, D. C. Elliott, W. H. Elliot, K. M. Jones, In *Data for Biochemical Research*, Oxford Sci. Pubs.
[99] A. Durmus, C. Eiken, B. H. Sift, A. Kratel, R. Kappl, J. Hüttermann, B. Krebs, *E. J. Biochem.* **1999**, *260*, 709−716.
[100] M. Merkx, B. A. Averill, Biochemistry **1998**, *37*, 8490−8497.
[101] M. Merkx, B. A. Averill, *J. Am. Chem. Soc* **1999**, *121*, 6683−6689.

Received February 9, 1999
[I99040]

First Evidence of a Photoinduced Spin Change in an Fe^{III} Complex Using Visible Light at Room Temperature

Angélique Sour,*[a] Marie-Laure Boillot,[a] Eric Rivière,[a] and Philippe Lesot[b]

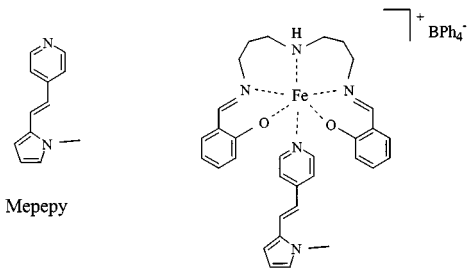
Keywords: Spin crossover / Light-induced spin change / *cis-trans* Isomerization / Visible light irradiation / Iron(III)

An iron(III) complex [Fe(salten)(Mepepy)]BPh_4 containing only one photoisomerizable ligand (Mepepy) has been synthesized, it exhibits a thermally-induced spin crossover in the solid state and in solution {H_2salten = 4-azaheptamethylene-1,7-bis(salicylideneiminate); Mepepy = 1-(pyridin-4-yl)-2-(*N*-methylpyrrol-2-yl)ethene}. The photoisomerizations of both the free and coordinated Mepepy ligand have been observed at room temperature with visible-light irradiation and monitored by UV/Vis and ^{1}H NMR spectrometries. *trans-to-cis* isomerization of only one photosensitive ligand in the iron(III) complex is sufficient to detect a partial spin change of the iron(III) ion. This photoinduced spin change is seen for the first time from a high-spin state to a low-spin state.

Spin crossover phenomena exhibited by transition metal complexes are the subject of intensive studies.[1][2] In this field, the ligand-driven light-induced spin change (LD-LISC) concept first described by our group[3] has opened up new perspectives for the purpose of optical information storage on the molecular scale. For this it is necessary to synthesize complexes in which a photoinduced modification of one or several ligands would result in a ligand field change and trigger the metal ion spin conversion.

The feasibility of the LD-LISC process was first demonstrated[3][4] at 140 K on an iron(II) complex containing four photosensitive ligands. Ultra-violet irradiation of this compound induced a *trans* ↔ *cis* isomerization of the four ligands and a subsequent low-spin (LS) ↔ high-spin (HS) conversion. More recently, the LD-LISC effect has been observed at room temperature[5] on an iron(II) complex containing two photoisomerizable ligands. A *trans* to *cis* photoconversion in this compound induced a low-spin towards high-spin change. We now want to show that the isomerization of only one photosensitive ligand is sufficient to induce a spin change. We will also show that the LD-LISC effect can be observed in an iron(III) compound. For this purpose, we present a study of an iron(III) complex containing only one photoisomerizable ligand which has the distinctive feature of absorbing visible light.

Our strategy was to coordinate an iron(III) ion to a pentadentate salten^{2-} ligand {H_2salten = 4-azaheptamethylene-1,7-bis(salicylideneiminate)}, the sixth position being occupied by a potentially photosensitive Mepepy ligand {Mepepy = 1-(pyridin-4-yl)-2-(*N*-methylpyrrol-2-yl)-ethene}.[6] The H_2salten ligand has been employed because several complexes based on this ligand are known to exhibit thermally-induced spin crossovers.[7][8] The behavior under irradiation of the Mepepy ligand has not yet been explored but the *trans* and *cis* isomers are expected to be stable and interconvertible by visible light. We report here the synthesis of [Fe(salten)(Mepepy)]BPh_4 **(1)**, its electronic and magnetic properties, and the observation of the LD-LISC effect at room temperature by suitable NMR spectroscopic experiments.



Scheme 1. The photosensitive ligand and complex made and studied

The elemental analysis, IR characterizations and the magnetic behavior allow us to propose the structure presented in Scheme 1 for [Fe(salten)(Mepepy)][BPh_4]. The magnetic susceptibility of a powdered sample of **1** was measured in the temperature range 10−320 K. The temperature dependence of the χ_M T product (χ_M = molar magnetic susceptibility) shows a gradual S = 1/2 ↔ S = 5/2 crossover of iron(III) ions (Figure 1) as expected for complexes of this family.[7][8] No thermal hysteresis was observed. The crossover taking place between 150 K and 320 K is obviously incomplete at 320 K however, due to the low thermal stability under partial vacuum, measurements at higher temperatures were not possible. The low temperature plateau around χ_M T = 0.53 $cm^3 \cdot mol^{-1} \cdot K$ indicates that nearly all molecules are in the low-spin state. In contrast, the χ_M T value at 320 K (2.68 $cm^3 \cdot mol^{-1} \cdot K$) indicates that about 55% of the molecules are in the high-spin state (assuming that χ_M T= S(S+1)/2 = 4.4 $cm^3 \cdot mol^{-1} \cdot K$ for S = 5/2).

[a] Laboratoire de Chimie Inorganique, UMR CNRS 8613, Université Paris-Sud, F-91405 Orsay, France
E-mail: angesour@icmo.u-psud.fr
[b] Laboratoire de Chimie Structurale Organique, ESA CNRS 8074, Université Paris-Sud, F-91405 Orsay, France

 © WILEY-VCH Verlag GmbH, D-69451 Weinheim, 1999 1434−1948/99/1212−2117 $ 17.50+.50/0

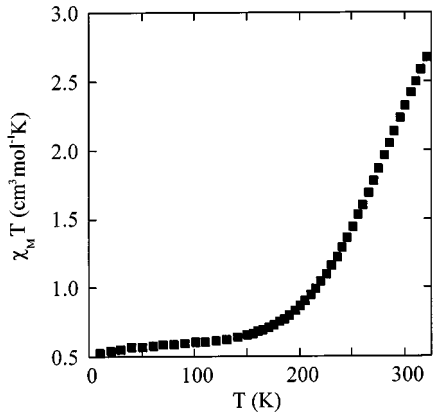


Figure 1. Temperature dependence of χ_M T of [Fe(salten)(Mepepy)]BPh_4 as a powder

Irradiation of the uncoordinated Mepepy ligand was carried out first. The experiments were performed at $\lambda = 405 \pm 5$ nm on acetonitrile solutions at room temperature and monitored by UV/Vis and NMR spectrometry. The UV/Vis spectrum of the free Mepepy ligand shows two $\pi-\pi^*$ transition bands (Figure 2a). Upon irradiation, the strongest effect is observed on the band at $\lambda_{max} = 353$ nm ($\varepsilon = 22800$ M^{-1}·cm^{-1}) which is slightly blue-shifted and decreases to about half its intensity. The band at $\lambda_{max} = 241$ nm ($\varepsilon = 7800$ M^{-1}·cm^{-1}) is less affected. An isosbestic point is observed at 300 nm. Irradiation of the ligand in an NMR tube in deuterated acetonitrile (10^{-3} M) leads to a photostationary state which is composed of 66% of the *cis* isomer and 34% of the *trans* isomer.[9] From these results it is possible to compute the absorption band for the pure *cis* isomer, which is represented in Figure 2a.

We then studied the effect of light on the complex [Fe(salten)(Mepepy)]BPh_4 under the same conditions of solvent and temperature. Irradiation of solutions at wavelengths in the range 320−405 nm leads to very similar evolutions of the UV spectra and the photostationary states are reached within a few minutes. We chose to investigate the effect of visible light at $\lambda = 405 \pm 5$ nm, as for Mepepy. The UV/Vis absorption spectrum of **1** in a 1.87×10^{-5} M acetonitrile solution (Figure 2b) shows a strong band ($\lambda_{max} = 351$ nm, $\varepsilon = 62000$ M^{-1}·cm^{-1}) which can be assigned to a "Mepepy"-centered $\pi-\pi^*$ transition and a weaker band ($\lambda_{max} = 480$ nm, $\varepsilon = 6900$ M^{-1}·cm^{-1}) arising from a ligand-to-metal charge transfer (LMCT). Irradiation of this solution (Figure 2b) leads both to a slight blue-shift of the Mepepy-centered $\pi-\pi^*$ band (from 351 to 345 nm) and to a pronounced decrease of its intensity (from $\varepsilon = 62000$ to $\varepsilon = 39000$ M^{-1}·cm^{-1} at 351 nm). In contrast, the LMCT band at 480 nm is essentially unaffected. The presence of a well defined isosbestic point at 301 nm shows the coexistence of only two molecular species upon irradiation. The parallel evolution upon irradiation of the $\pi-\pi^*$ band of uncoordinated and coordinated Mepepy strongly suggests that irradiation of **1** also causes a *trans* to *cis* photoisomerization of the coordinated Mepepy.

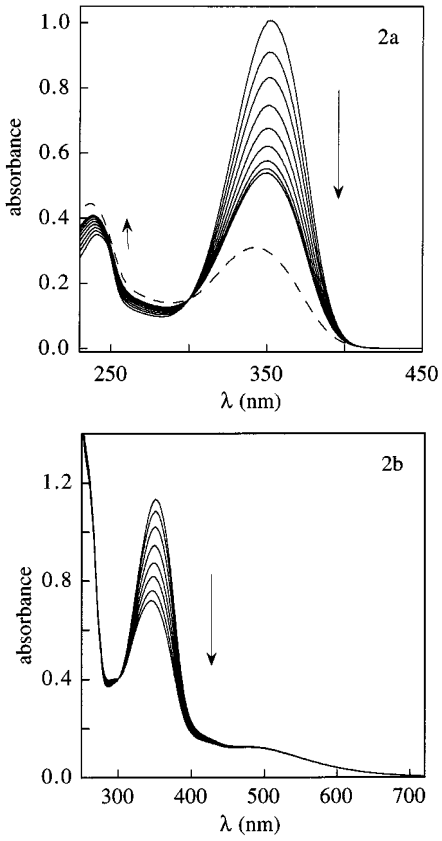


Figure 2. UV/Visible absorption spectra and evolutions upon irradiation at 405 nm of acetonitrile solutions of Mepepy (10^{-5} M) (2a) and of [Fe(salten)(Mepepy)]BPh_4 (1.87×10^{-5} M) (2b); the spectrum in dashed lines in 2a represents the calculated spectrum of pure *cis*-Mepepy

The magnetic susceptibility, and its variation under irradiation, of acetonitrile solutions of **1** were measured by the Evans method (^{1}H NMR spectrometry).[10][11] The temperature dependence of χ_M T has been obtained between 243 K and 333 K for a 10^{-2} M CD_3CN solution of **1** before irradiation. Figure 3 reveals a thermal spin-crossover behavior with χ_M T increasing from 1.48 cm^3·mol^{-1}·K at 243 K to 3.61 cm^3·mol^{-1}·K at 333 K.

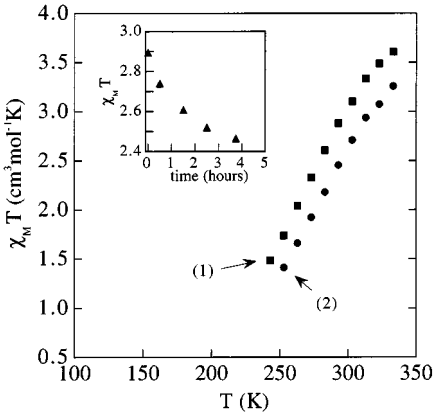


Figure 3. Temperature dependence of χ_M T of a CD_3CN solution (10^{-2} M) of [Fe(salten)(Mepepy)]BPh_4 before irradiation (1) and of a 10^{-3} M CD_3CN solution of the steady state (2); inset: time dependence of χ_M T of a 10^{-3} M CD_3CN solution of [Fe(salten)(Mepepy)]BPh_4

A 10^{-3} M CD_3CN solution of **1** in a capillary has been irradiated at room temperature. The irradiation induces a small decrease (inset of Figure 3) of χ_M T at 294 K from 2.89 to 2.46 $cm^3 \cdot mol^{-1} \cdot K$. This allows us to infer that **1** undergoes a partial HS ↔ LS change under irradiation. The temperature dependence of χ_M T of the steady state (Figure 3) reveals a thermal spin-crossover behavior with χ_M T increasing from 1.41 $cm^3 \cdot mol^{-1} \cdot K$ at 253 K to 3.26 $cm^3 \cdot mol^{-1} \cdot K$ at 333 K. The thermal spin crossovers before as well as after irradiation are reversible. Furthermore, it should be noted that solutions before and after irradiation are stable in the dark.

It is worth pointing out that the photoisomerization of a *trans* to *cis* styryl-pyridine group in an iron(II) complex[4][5] results in a spin change from a low-spin state to a high-spin state. We report here the first example where light irradiation leads to a spin change in the opposite direction. This apparent discrepancy can be explained: as the methylpyrrole moiety of the Mepepy ligand is a strong π-donor group,[6] the conversion of the *trans* isomer into the *cis* isomer results in a decrease of the π-donor character of the ligand and thus increases the ligand field strength and induces the HS ↔ LS change.

In conclusion, we have described the first Fe^{III} complex able to present a "Ligand-Driven Light-Induced Spin Change" behavior at room temperature. The complex contains only one photosensitive ligand which can be effectively photoisomerized by visible light. We have characterized the *trans* to *cis* photoisomerizations of the uncoordinated and coordinated Mepepy ligand and demonstrated that the *trans* to *cis* isomerization in complex **1** is accompanied by a small, but significant, decrease of χ_M T, which shows an unusual high-spin to low-spin change.

Attempts are currently underway to cast thin films of **1** in order to study the effect of light in the solid state.

Experimental Section

General: Starting materials were purchased from Acros. Solvents were purchased from Merck. Acetonitrile was distilled from CaH_2. The photosensitive ligand and its complexe were prepared and handled under darkness to prevent photoisomerization. Magnetic Measurements: Quantum Design SQUID Magnetometer (MPMS5S model). UV/Vis: Varian Cary 5E or Cary 300. IR: Perkin−Elmer Spectrum 1000. NMR: Bruker AM 400 (400 MHz). Evans NMR: the NMR tube is equipped with a special stem coaxial insert (Wilmad, WGS − 5BL). Irradiation: 200 W Hg (Xe) lamp (Oriel) with a standard bandpass filter 405 FS10−25 (Andover Corporation).

The ligand Mepepy[6] was prepared according to the published procedure. − ^{1}H NMR (CD_3CN, 400 MHz): δ = 8.47 (d, J = 5.9 Hz, 2 H), 7.40 (d, J = 5.9 Hz, 2 H), 7.35 (d, J = 16.2 Hz, 1 H), 6.84 (d, J = 16.2 Hz, 1 H), 6.76 (m, 1 H), 6.59 (m, 1 H), 6.11 (m, 1 H), 3.72 (s, 3 H). − IR (KBr): $\tilde{\nu}$ = 955, 965 (C=C *trans*), 1590 (pyridine) cm^{-1}.

[Fe(salten)Cl][7] was prepared according to the published procedure.

[Fe(salten)(Mepepy)][BPh_4] 1: To a solution of [Fe(salten)Cl] (360 mg, 0.84 mmol) in MeOH (16 mL) was added a solution of Mepepy (201 mg, 1.09 mmol) in MeOH (2 mL). The mixture was warmed at 60°C for 1 hour, then filtered. To the filtrate was added a solution of sodium tetraphenylborate (288 mg, 0.84 mmol) in MeOH (4 mL). The mixture was then warmed for a further 5 minutes at 60°C and allowed to stand overnight. The precipitate was filtered off, washed with cold MeOH (3 mL), water (3 × 10 mL), Et_2O (2 × 15 mL) and dried in vacuo for 2 hours to give 466 mg of a black microcrystalline powder (yield 62%). − $C_{56}H_{55}BFeN_5O_2$ (896.7): calcd. C 74.97, H 6.18, N 7.81, Fe 6.24; found C 75.01, H 6.27, N 7.82, Fe 6.00. − IR (KBr): $\tilde{\nu}$ = 3231, 3214 (N−H), 1600 (pyridine), 950 (C=C *trans*), 732, 706, 611 (BPh_4) cm^{-1}.

Acknowledgments

This work was supported by the CNRS (France) and the research fund TMR of the European Community (contract ERB − FMRX − CT 98−0199). We thank Prof. R. Clément for fruitful discussions during the preparation of this manuscript.

[1] P. Gütlich, A. Hauser, H. Spiering, *Angew. Chem.* **1994**, *106*, 2109−2139; *Angew. Chem. Chem. Int. Ed. Engl.* **1994**, 33, 2024−2054.
[2] H. Toftlund, *Coord. Chem. Rev.* **1989**, 94, 67−108; A. Hauser, *Coord. Chem. Rev.* **1991**, 111, 275−290.
[3] C. Roux, J. Zarembowitch, B. Gallois, T. Granier, R. Claude, *Inorg. Chem.* **1994**, 33, 2273−2279.
[4] M. L. Boillot, C. Roux, J. P. Audière, A. Dausse, J. Zarembowitch, *Inorg. Chem.* **1996**, 35, 3975−3980.
[5] M. L. Boillot, S. Chantraine, J. Zarembowitch, J. Y. Lallemand, J. Prunet, *New J. Chem.* **1999**, 179−183.
[6] S. Bradamante, A. Facchatti, G. A. Pagani, *J. Phys. Org. Chem.* **1997**, 10, 514−524.
[7] N. Matsumoto, S. Ohta, C. Yoshimura, A. Ohyoshi, S. Kohata, H. Okawa, Y. Maeda, *J. Chem. Soc., Dalton Trans* **1985**, 2575−2583.
[8] A. Ohyoshi, J. Honbo, N. Matsumoto, S. Ohta, S. Sakamoto, *Bull. Chem. Soc. Jpn.* **1986**, 59, 1611−1613. S. Ohta, C. Yoshimura, N. Matsumoto, H. Okawa, A. Oyoshi, *Bull. Chem. Soc. Jpn.* **1986**, 59, 155−159.
[9] For *cis*-Mepepy: ^{1}H NMR (400 MHz, CD_3CN): δ = 6.61 (d, J = 12.2 Hz, 1 H, C=C *cis*), 6.36 (d, J = 12.2 Hz, 1 H, C=C *cis*), 3.57 (s, 3 H, CH_3).
[10] D. F. Evans, *J. Chem. Soc.* **1959**, 2003−2005.
[11] S. K. Sur, *J. Magn. Reson.* **1989**, 82, 169−173.

Received May 18, 1999
[I99193]

The First Thioallenylidene Complexes from Ruthenium-Butatrienylidene Intermediates

Rainer F. Winter*[a]

Keywords: Ruthenium / Allenylidene complexes / Butadiyne / Electrochemistry / Thio-Claisen rearrangements

Ruthenium-butatrienylidene cations *trans*-[Cl(L$_2$)$_2$Ru=C=C=C=CH$_2$]$^+$ are key intermediates in the synthesis of the first thioallenylidene complexes *trans*-[Cl(L$_2$)$_2$Ru=C=C=C(SR)R′]$^+$ (L$_2$ = dppm, R = Et, R′ = Me: **3a**, L$_2$ = dppm, R = Me, R′ = C$_4$H$_7$: **3b**, L$_2$ = dppe, R = C$_3$H$_5$, R′ = C$_4$H$_7$: **3c**). Spectroscopic and electrochemical data for **3a–c** are presented and are compared with those of their aminoallenylidene analogues. Aminoallenylidene complexes are best represented by the iminiumalkynyl resonance form, while a true cumulene description is much more appropriate for thioallenylidene complexes **3a–c**. Based on a combination of spectroscopic and electrochemical data, we present evidence that the NMR shifts of the carbon atoms of the unsaturated ligand in these allenylidene complexes are correlated to the HOMO–LUMO gap. In situ EPR-, UV/Vis-, and IR-spectro-electrochemistry reveals that the one-electron oxidation occurs at the metal center, while reduction occurs at the carbon–heteroatom terminus.

Introduction

Despite considerable progress in the field of higher homologues of carbene complexes,[1] as yet no stable mononuclear butatrienylidene complex has been reported.[2] There are, however, a growing number of instances where iron or ruthenium butatrienylidene compounds are invoked as key intermediates. Following Selegue′s initial report on the generation of such a species from a coordinated alkynyl ketone,[3] we and others have elaborated a more direct access route starting from substitutionally labile iron or ruthenium precursors [Cp*Fe(dppe)Cl], [CpRu(PPh$_3$)$_2$Cl], or *cis*-[Cl$_2$Ru(L$_2$)$_2$] (L$_2$ = dppm, depe) and butadiyne. The reactivity of the C$_4$H$_2$ ligand is dominated by the alternation of electrophilic and nucleophilic carbon centers and the easy access to the sterically unprotected terminal C=C bond. Apart from remarkable cycloaddition−cycloreversion sequences with aromatic imines,[4] two major reaction types have been identified so far: (i) regioselective addition of protic nucleophiles to the terminal C$_\gamma$=C$_\delta$ bond to give methyl-substituted allenylidene complexes,[5] and (ii) regioselective addition of aprotic nucleophiles to the electron-deficient C$_\gamma$, C$_\alpha$ being sterically protected by the bulky phosphane coligands on ruthenium.[5−7] The initial addition step may be followed by tautomerization,[5a,b] Cope-type rearrangements of quaternary vinylammonium salts resulting from the addition of allylic amines,[6a] or by a shift of the resonance stabilized ferrocenylmethyl cation to the neighbouring nucleophilic C$_\delta$ to give an aminoallenylidene complex with an appended redox-active substituent.[7] We report herein on the successful synthesis of the first thioallenylidene complexes [{Ru}=C=C=C(SR)R′]$^+$ from butatrienylidene intermediates.

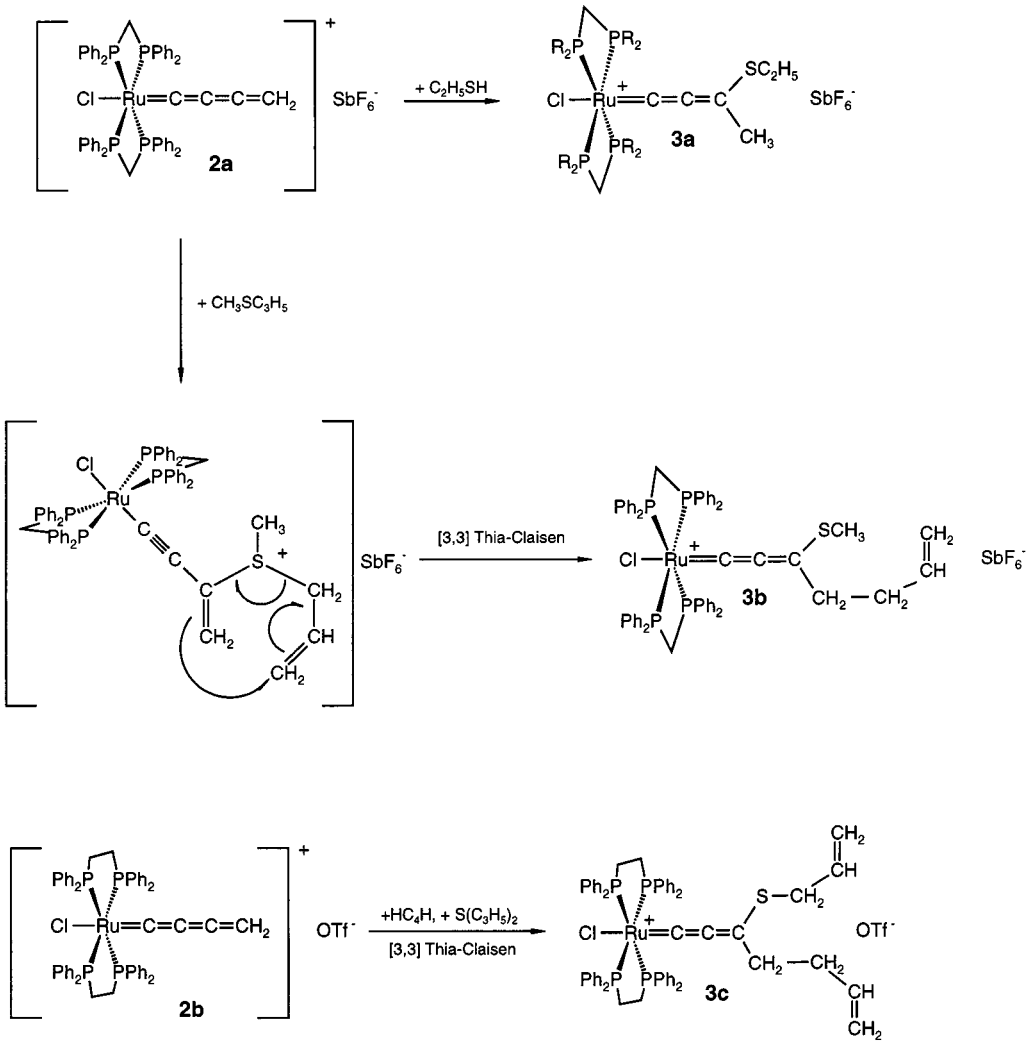
[a] Institut für Anorganische Chemie der Universität Stuttgart, Pfaffenwaldring 55, D-70569 Stuttgart, Germany
E-mail: winter@iac.uni-stuttgart.de

Results and Discussion

We have successfully employed both fundamental strategies, i.e. the regioselective addition of a protic nucleophile (a thiol) and the addition of aprotic nucleophiles (allylic thioethers) with subsequent [3,3] thio-Claisen rearrangement, to effect the synthesis of *trans*-[Cl(L$_2$)$_2$Ru=C=C=C(SR)R′]$^+$ X$^-$ (**3a−c**, L$_2$ = dppm, dppe, X$^-$ = SbF$_6^-$, OTf$^-$, Scheme 1), the first examples of thioallenylidene complexes. Their identities have been unequivocally established by spectroscopic means. The *trans* arrangement of the chloride and allenylidene ligands follows directly from the observation of two ABX$_2$X′$_2$ spin systems for the methylene groups of the dppm ligand and single sharp singlets in the respective ^{31}P-NMR spectra. Our spectroscopic data place the intense yellow-green (**3a**,**b**) or red (**3c**) thioallenylidene complexes close to "conventional" allenylidene analogues without a heteroatom substituent attached to C$_\gamma$. This is exemplified by the intense IR stretch of the C=C=C unit, which is found at ca. 1940 cm^{-1} for **3a−c**, at 1995 cm^{-1} for aminoallenylidene complexes,[6,7] at 1955 cm^{-1} for alkyloxy-substituted allenylidene complexes,[8] and at ca. 1920 to 1950 cm^{-1} for aryl- or alkyl-substituted allenylidene complexes of the same metal fragment.[9]

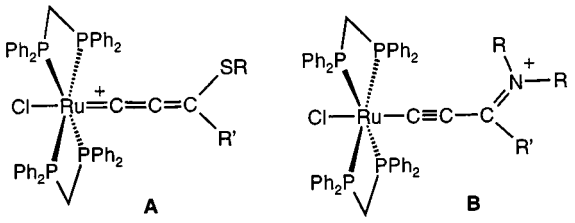
There is ample precedent that aminoallenylidene complexes are best represented by the iminiumalkynyl resonance form **B**.[6,10,11] This is not only evident from the position of the C=C=C stretch in the IR spectrum and the ^{13}C data (vide infra), but also from the two separate resonance signals seen for the identical substituents on the iminium nitrogen atom. High-temperature NMR studies on *trans*-[Cl(dppm)$_2$Ru−C≡C−C(=NMe$_2$)C$_2$H$_4$CH=CH$_2$]$^+$ PF$_6^-$ (**4a**) and its depe-substituted counterpart **4b** reveal that even at 368 K in CD$_3$NO$_2$ the two NMe resonances remain separate and sharp. From this, the barrier to rotation about this C=N bond can be estimated to be well above 71 and 76 kJ mol^{-1}, respectively. On the other hand, thioallenylidene

 © WILEY-VCH Verlag GmbH, D-69451 Weinheim, 1999 1434−1948/99/1212−2121 $ 17.50+.50/0



Scheme 1. Synthesis of the thioallenylidene complexes **3a−c**

complexes **3a−c** are adequately described by the true allenylidene resonance form **A**.



The ^{13}C-NMR signals of the carbon atoms of the unsaturated ligands in **3a−c** are readily discernible and may be assigned by virtue of the P−C coupling constants and the chemical shift values. For other *heteroatom-substituted* allenylidene complexes, both are known to decrease with increasing distance from the metal center.[5−8] ^{13}C-NMR data for a variety of allenylidene complexes containing the *trans*-$[ClRu(dppm)_2]^+$ fragment are collected in Table 1. The following trends emerge: (i) All three carbon atom signals of the cumulene chain are subject to a progressive downfield shift in the order $NR_2 < OR < SR < CR_3$. (ii) The influence of the heteroatom on the shift values *decreases* with *increasing distance* from the *metal center*, with the substituted C_γ being rather insensitive to the nature of the atom attached to it. Thus, the shift differences $\Delta\delta$ for equivalent carbon atoms in all-carbon and amino-substituted allenylidene complexes, which constitute the two extremes in Table 1, amount to ca. 120 ppm for C_α, 90 ppm for C_β, but less than 20 ppm for C_γ.

It has long been known that the characteristic low-field shifts of metal-bound carbene, vinylidene, and cumulenylidene carbon atoms (and obviously also to a lesser degree of C_β) are induced by the paramagnetic term, which itself is related to the HOMO−LUMO gap.[12] We observe a clear manifestation of this trend upon comparison of the electrochemical and optical data for the novel thioallenylidene complexes **3a−c** and those for our aminoallenylidene cations *trans*-$[Cl(dppm)_2Ru{-}C{\equiv}C{-}C(=NMe_2)C_2H_4R]^+$ [R = $CH{=}CH_2$: **4a**, R = $(\eta^5\text{-}C_5H_4)Fe(\eta^5\text{-}C_5H_5)$, Fc: **4c**, Table 2].[6,7] All the complexes undergo well-defined one-electron oxidations and one-electron reductions at potentials that are clearly dependent on the heteroatom attached

Table 1. ^{13}C-NMR data for the allenylidene carbon atoms of complexes $[\{Ru\}=C=C=C(ER_n)R']^+$ [{Ru} = *trans*-{ClRu(dppm)$_2$}$^+$]

ER_n	R′	δ (C_α) ($^2J_{P-C}$)[a]	δ (C_β) ($^3J_{P-C}$)	δ (C_γ) ($^4J_{P-C}$)	ref.
$N(CH_3)_2$	$C_2H_4CH=CH_2$	202.09 (13.9)	118.73 (2.2)	156.91 (−)	[6]
$N(CH_3)_2$	C_2H_4Fc[b]	201.8 (13.6)	119.4 (2.4)	156.7 (−)	[7]
OCH_3	$CH=C(C_6H_5)_2$	252.8 (13.6)	150.2 (2.2)	155.7 (−)	[9]
SCH_3	$C_2H_4CH=CH_2$	283.5 (13.4)	169.5 (2.4)	171.1 (1.5)	this work
SC_2H_5	CH_3	286.2 (13.6)	172.1 (2.3)	168.3 (1.65)	this work
CH_3	CH_3	322.69 (13.9)	199.85 (2.3)	173.33 (−)	[10]
C_6H_5	C_6H_5	307.33 (14.3)	208.94 (2.5)	161.88 (−)	[10]

[a] δ [ppm], *J* [Hz]. − [b] Fc = (η^5-C_5H_4)Fe(η^5-C_5H_5).

to C_γ (Table 2). As is evident from a comparison of the CV traces shown in Figure 1, replacing NR_2 by SR substituents induces significant cathodic shifts in the oxidation and reduction potentials of 0.3 and 0.8 V, respectively. As one may infer from these data, the LUMO is preferentially lowered with respect to the HOMO which, of course, reduces the HOMO−LUMO gap. As a consequence, the energies of the intense optical absorptions in the visible part of the spectra decrease considerably in this series. For aminoallenylidene complexes, this band apparently has some metal-to-ligand charge-transfer (MLCT) character, as indicated by the negative solvatochromism of the order of some 450 to 720 cm^{-1}. In contrast, no such effect is apparent for thioallenylidene complexes **3a−c**. Optical transition energies consistently exceed those measured by electrochemical methods. This is due to the vertical excitation involved in the optical transition (Franck−Condon principle) as compared to the "true" energy difference between the vibrationally relaxed ground and excited states determined by electrochemical methods. The energy difference $\Delta E_{op} - \Delta E_{ec}$ provides a measure of the vibrational excitation associated with the optical transition and therefore of the degree of structural reorganization required upon excitation, and is parameterized as the structural factor $\Delta\chi$ (Equation 1).[13]

$$\Delta E_{op} = \Delta E_{ec} + \Delta\chi \quad (1)$$

In our heteroatom-substituted allenylidene complexes of the dppm ligand, $\Delta\chi$ amounts to 0.46 to 0.47 eV, indicating a moderate degree of structural rearrangement on going from the ground to the excited states. The fact that other values of $\Delta\chi$ are found for complexes with diphosphane chelate ligands other than dppm suggests that the predominant structural change occurs at the metal fragment. Unfortunately, no UV/Vis data have been reported for any other allenylidene complexes containing the *trans*-

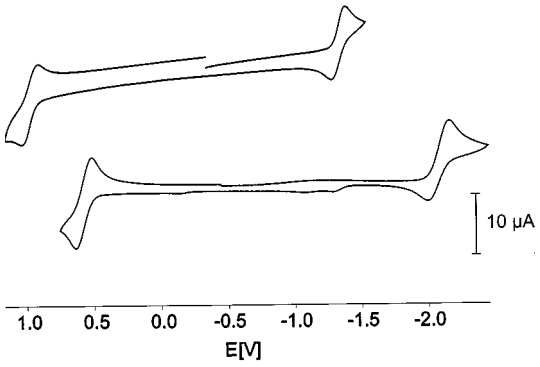


Figure 1. CV traces of *trans*-[Cl(dppm)$_2$Ru−C≡C−C=(NMe_2)C_4H_7]$^+$ (**4a**) at 231 K and *v* = 1 V/s (lower trace) and *trans*-[Cl(dppm)$_2$Ru=C=C=C=(SMe)C_4H_7]$^+$ (**3b**) at 273 K and *v* = 0.2 V/s (upper trace) in CH_3CN

[Cl(dppm)$_2$Ru]$^+$ fragment. Judging, however, from the colours (alkyloxy-substituted allenylidene complexes are orange, while all-carbon substituted analogues are violet to purple)[8,9] and the optical data for the closely related [CpRu(PPh_3)$_2$]$^+$ derivatives,[14] we conclude that the HOMO−LUMO gap decreases in the series NR_2 > OR > SR > CR_3, thus providing a rationale for the observed trends in the ^{13}C-NMR data.

The differences in redox potentials also have a bearing on the chemical stabilities of the oxidation and reduction products (see Figure 1). For the aminoallenylidene complexes **4a**, **c** and the depe derivative *trans*-[Cl(depe)$_2$-Ru−C≡C−C(=NMe_2)$C_2H_4CH=CH_2$]$^+$ (**4b**), the oxidation process is fully reversible, while for the reduction low temperature and sweep rates of about 1 V/s are required to allow the observation of an associated return peak.[7] For thioallenylidene complexes **3a−c**, on the other hand, just the opposite order of stabilities is observed. This makes the oxidation products of **4a−c** and the reduction products of

Table 2. UV/Vis and electrochemical data for amino- and thio-substituted allenylidene cations *trans*-[ClRu(L)$_2$C=C=C(ER_n)R′]$^+$

ER_n	R′	L	ν_{max} [cm^{-1}] (log ε_{max})	$E_{1/2}^{+/2+}$ [V]	$E_{1/2}^{+/0}$ [V]	ΔE_{op} [eV]	ΔE_{ec} [V]	$\Delta\chi$ [eV]
NMe_2	C_4H_7	dppm	25575 (4.230)	+0.57	−2.14	3.17	2.71	0.46
NMe_2	C_2H_4Fc	dppm	25900 (4.361)	+0.62	−2.13	3.21	2.75	0.46
NMe_2	C_4H_7	depe	25060 (4.380)	+0.42	< −2.20	3.11	> 2.62	< 0.49
SEt	Me	dppm	21740 (3.919)	+0.850	−1.375	2.695	2.225	0.47
SMe	C_4H_7	dppm	21505 (4.209)	+0.865	−1.355	2.665	2.220	0.465
SAllyl	C_4H_7	dppe	21230 (4.230)	+0.985	−1.275	2.63	2.26	0.37

3a−c amenable to spectroscopic characterization. Such investigations can be expected to provide information on the oxidation and reduction sites within these allenylidene complexes. In their EPR spectra at 110 K and 4 K, electrochemically oxidized samples of **4c** exhibit an axial pattern at $g_{\parallel} = 2.400$ and $g_{\perp} = 2.067$, respectively. No EPR signals were observed for **4a**. The rather low intensity of the EPR signals and the considerable spread of g values are both supportive of an assignment to an Ru-based radical, such that the oxidation may be viewed as essentially involving a ruthenium(II/III) redox couple. This is also in accord with our observation that fully oxidized *trans*-$[Cl(dppm)_2Ru-C\equiv C-C(=NMe_2)C_2H_4Fc]^{3+}$ (**4c**) displays an intense triplet signal at $g = 2.0064$ arising from coupling of the ferrocinium subunit to a paramagnetic Ru(III) center, giving too weak a signal to be observed directly. The same conclusion has already been reached from UV/Vis and IR spectro-electrochemical studies of this complex.[7]

In the frozen state, the reduced form of the thio-substituted allenylidene complex **3b** exhibits a broadened isotropic signal at $g = 2.0031$, i.e. in a region characteristic of organic radicals. On warming to 295 K, the spectrum gradually resolves into a quintet of triplets, which we successfully simulated assuming coupling constants of 9.86 and 6.60 Gauss (Figure 2). This coupling pattern points to the reduction occurring at the heteroatom-substituted terminus of the allenylidene ligand. The triplet splitting then arises from coupling to the neighbouring methylene group, and the quintet from coupling to the four equivalent phosphorus nuclei across the cumulene bridge. From the resonance form for reduced **3b** shown in Figure 2, one would expect an increase in bond order of the $C_\alpha-C_\beta$ bond from C=C to C≡C upon reduction. On following this process by IR spectro-electrochemistry, the intense allenylidene band does indeed gradually disappear, which is accompanied by the concomitant formation of a new, much weaker feature at 2048 cm^{-1} (Figure 3). The position of this band is characteristic of alkynyl complexes of the *trans*-$[Cl(dppm)_2Ru]^+$ fragment.[8] A severe reduction in absorptivity on going from allenylidene to alkynyl[8] and from cationic to neutral complexes[15] has already been described in the literature. We should state that even in our best runs the reduction was accompanied by some decomposition, as indicated by the fact that only 60% of the initial band intensity was regained upon reoxidation. Nevertheless, we are certain that the observed band at 2048 cm^{-1} originates from the reduced counterpart of **3b** since, upon reoxidation, this band gradually disappears while the original band is partly restored.

In situ UV/Vis spectro-electrochemical experiments require lower concentrations and therefore shorter electrolysis times. Thus, the reduction/reoxidation cycle of **3b** proceeded with more than 90% recovery of the starting material. Upon reduction, the intense allenylidene band at $\lambda = 465$ nm disappears and is replaced by a less intense absorption (log $\varepsilon = 3.980$) at ca. 306 nm, a region characteristic for Ru(II)−alkynyl complexes (Figure 4). We have observed bands with similar positions and intensities for the related

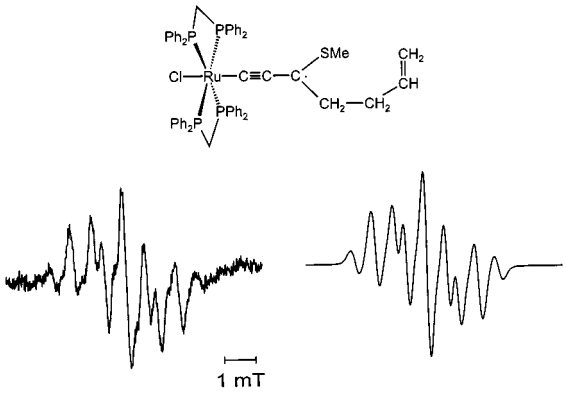


Figure 2. Experimental and simulated EPR spectra of in situ generated *trans*-$[Cl(dppm)_2Ru-C\equiv C-C=(SMe)C_4H_7]^{\bullet}$ at 295 K

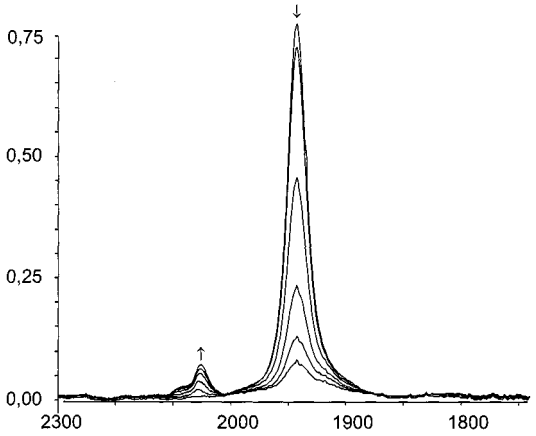


Figure 3. IR spectroscopic changes during the reduction of *trans*-$[Cl(dppm)_2Ru=C=C=C=(SMe)C_4H_7]^+$ (**3b**)

ammoniobutenynyl complexes *trans*-$[ClRu(dppm)_2-C\equiv C-C-(NR_2R')=CH_2]^+$ that result from the trapping of butatrienylidene complexes with tertiary aliphatic or benzylic amines.[6b] Furthermore, the n-π* type transition originating from the dppm ligand is shifted from 271 nm to 263 nm while largely retaining its absorptivity. All this points to reduction of thioallenylidene complexes **3a−c** occurring at the C-heteroatom terminus of the unsaturated ligand, with accompanying changes in the CCC bonding mode.

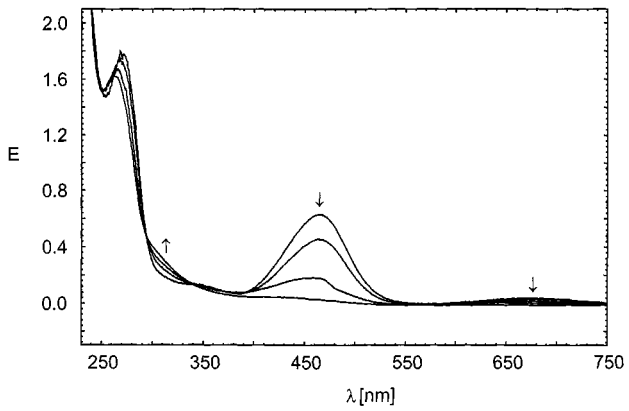


Figure 4. UV/Vis spectroscopic changes during the reduction of *trans*-$[Cl(dppm)_2Ru=C=C=C=(SMe)C_4H_7]^+$ (**3b**)

In summary, we have described the first thio-substituted allenylidene complexes. They are formed by the trapping of Ru-butatrienylidene intermediates by thiols or allylic thioethers. This provides a further example of the utilization of such intermediates in the synthesis of highly unsaturated and functionalized, yet stable ligands. A comparison of the optical, ^{13}C-NMR, and electrochemical data of a series of allenylidene complexes provides a rationale for the observed trend in the ^{13}C-NMR shifts (NR_2 < OR < SR < CR_3) as arising from the decreasing HOMO−LUMO gap within this series. In situ spectro-electrochemical investigations of the oxidized forms of amino-substituted complexes **4b**, **c** and the reduced form of the thioallenylidene complex **3b** have allowed identification of the oxidation and reduction sites within these complexes. Oxidation occurs at the metal center, while the reduction occurs at the *C*-heteroatom terminus and thus at the opposite end of the cumulenic chain. Our findings are in full agreement with EHMO calculations on the cationic allenylidene complexes $[\eta^5\text{-}C_5H_5Ru(CO)(PH_3)=C=C=CH_2]^+$[16a] and $[\eta^5\text{-}C_9H_7Ru(PH_3)_2=C=C=CH_2]^+$.[16b] Both indicate that the HOMO is dominated by contributions from the Ru d-orbitals, while the LUMO is mainly localized on the unsaturated ligand. We now aim to extend our investigations to differently substituted allenylidene complexes in order to probe the general validity of our conclusions.

Experimental Section

All manipulations were performed by standard Schlenk techniques under argon atmosphere. Dichloromethane, hexanes, and acetonitrile were dried by distillation from CaH_2. All solvents were deoxygenated either by at least three freeze-pump-thaw cycles or by saturating with argon prior to use. $[RuCl_2(dmso)_4]$[17] and *cis*-$[RuCl_2(dppm)_2]$ (**1**)[18] were obtained according to literature methods. Butadiyne was prepared from 1,4-dichlorobut-2-yne (Lancaster) on a 4 mmol scale by a slight modification of a published procedure[19] and was isolated at 195 K as a white crystalline solid. ***CAUTION:*** Butadiyne should be handled and stored under rigorous exclusion of air and at temperatures below 230 K. Prior to use, it was thawed in an ice/$CaCl_2$ cooling bath and the required amount (ca. 600 μL) was transferred via a precooled pipette. − NMR: Bruker AC 250. − IR: Elmer Paragon 1000 PC. − UV/Vis: Shimadzu UV-160 or Omega 10 from Bruins Instruments. − EPR: Bruker ESP 3000, HP frequency counter 5350 B, Bruker NMR gaussmeter ER 035 M, with a continuous flow cryostat ESR 900 from Oxford Instruments for low-temperature work. Electrochemistry was performed as described in an earlier publication.[20]

Preparation of *trans*-$[ClRu(dppm)_2=C=C=C(SEt)Me]^+$ SbF_6^- (3a): To a suspension of 171 mg (0.18 mmol) of *cis*-$[RuCl_2(dppm)_2]$ (**1**) and 379 mg (1.46 mmol) of $NaSbF_6$ in 40 mL of CH_2Cl_2, excess butadiyne (ca. 600 μL) was added by syringe. After the colour of the suspension had changed to green, 160 μL (2.16 mmol) of EtSH was added by syringe. The resulting solution was stirred under ambient conditions for 23 h, then filtered, and concentrated to dryness. The residue was thoroughly washed with hexanes. The crude product was then redissolved in chloroform and this solution was stirred at 50°C for 3 days. After evaporation of the solvent, the crude material was chromatographed on silica gel (4% H_2O, column 14 × 3 cm). The product was eluted with CH_2Cl_2/CH_3CN, 8:1, as a yellow-green band. The solvents were removed in vacuo and the remaining green solid was washed with hexanes and dried in vacuo; 72 mg (32%). − ^{1}H NMR ($CDCl_3$): δ = 0.73 [t, 3 H, SCH_2CH_3, ^3J(HH) = 7.54 Hz], 1.10 (s, 3 H, CH_3), 1.62 [q, 2 H, SCH_2, ^3J(HH) = 7.54 Hz], 5.00 [dquint, 2 H, CH_2(dppm), J(HH) = 15.46 Hz, ^2J(PH) = ^4J(P′H) = 4.10 Hz], 5.26 [dquint, 2 H, CH_2(dppm), J(HH) = 15.46 Hz, ^2J(PH) = ^4J(P′H) = 5.00 Hz], 7.13 [t, 8 H, aryl(dppm), ^3J(H-H) = 7.52 Hz], 7.29 [m, 8 H, aryl(dppm)], 7.29 [t, 16 H, aryl(dppm), ^3J(HH) = 7.47 Hz], 7.38 [m, 8 H, aryl(dppm)]. − ^{13}C{^{1}H} NMR (62.9 MHz, CD_3COCD_3): δ = 12.5 (s, SCH_2CH_3), 29.4 (s, SCH_2), 32.8 (s, CH_3), 46.1 [quint, CH_2(dppm), J(PC) = 12.05 Hz], 128.9, 129.5 (quint, *p*-C_6H_5, N = 2.5 Hz), 131.1, 131.8 (s, *m*-C_6H_5), 132.6 (quint, *ipso*-C_6H_5, N = 12.6 Hz), 133.2 (quint, *ipso*-C_6H_5, N = 11.5 Hz), 133.7 (quint, *o*-C_6H_5, N = 3.1 Hz), 134.0 (quint, *o*-C_6H_5, N = 2.9 Hz), 168.3 [quint, C_γ, ^4J(PC) = 1.65 Hz], 172.1 [quint, C_β, ^3J(PC) = 2.3 Hz], 286.2 [quint, C_α, ^2J(PC) = 13.6 Hz]. − ^{31}P{^{1}H} NMR (101.3 MHz): δ = −12.5 [s, P(dppm)]. − IR (KBr): $\tilde{\nu}$ = 1943 (vs, CCC). − UV/Vis (CH_3CN): λ_{max} (log ε) = 232 nm (4.643), 261 (4.556), 320 (sh, 3.908), 460 (3.892), 633 (sh, 3.410), 675 (3.505). (CH_2Cl_2): λ_{max} (log ε) = 238 nm (4.544), 266 (4.653), 462 (3.924), 635 (sh, 3.360), 686 (3.467). − $C_{56}H_{52}ClF_6P_4RuSSb$ (1253.2): calcd. C 53.67, H 4.18; found C 53.83, H 4.33.

Preparation of *trans*-$[ClRu(dppm)_2=C=C=C(SMe)C_4H_7]^+$ SbF_6^- (3b): To a suspension of 172 mg (0.18 mmol) of **1** and 204 mg (0.79 mmol) of $NaSbF_6$ in 40 mL of CH_2Cl_2, excess butadiyne (ca. 600 μL) was added by syringe. After the colour of the suspension had changed to green, 120 μL (1.09 mmol) of $MeSC_3H_5$ was added by syringe. The solution was stirred at room temperature for 17 h, filtered through a cannula, and the solvent was removed in vacuo. The crude product was dissolved in the minimum volume of CH_2Cl_2 and this solution was slowly added to 30 mL of vigorously stirred hexanes. After stirring for 20 min, the solvent was removed by filter cannula and the green precipitate was washed with a further 20 mL of hexanes and dried in vacuo; yield 188 mg (89%). − ^{1}H NMR ($CDCl_3$): δ = 1.16 (s, 3 H, SMe), 1.47 [t, 2 H, CH_2, J(HH) = 7.92 Hz], 1.74 (m, 2 H, CH_2), 4.84 [ddt, 1 H, =CH, ^3J(HH-*trans*) = 17.04 Hz, ^2J(HH) = ^4J(HH) = 1.6 Hz], 4.97 [dd, 1 H, =CH, ^3J(HH-*cis*) = 10.34 Hz, ^2J(HH) = 1.6 Hz], 4.98 [dquint, 2 H, CH_2(dppm), J(HH) = 15.23 Hz, ^2J(PH) = ^4J(P′H) = 4.22 Hz], 5.28 [dquint, 2 H, CH_2(dppm), J(HH) = 15.23 Hz, ^2J(PH) = ^4J(P′H) = 4.87 Hz], 5.43 [ddt, 1 H, =CH, ^3J(HH-*trans*) = 17.04 Hz, ^3J(HH-*cis*) = 10.34 Hz, ^2J(HH) = 7.92 Hz], 7.11 [t, 8 H, aryl(dppm), ^3J(HH) = 7.50 Hz], 7.20 [br, 8 H, aryl(dppm)], 7.29−7.40 [m, 16 H, aryl(dppm)], 7.43 [m, 8 H, aryl(dppm)]. − ^{13}C{^{1}H} NMR (62.9 MHz, CD_3COCD_3): δ = 16.8 (s, SCH_3), 32.2 (s, SCH_2), 45.0 (s, CH_2), 47.1 [quint, CH_2 (dppm), J(PC) = 12.0 Hz], 116.2 (s, $=CH_2$), 128.2, 128.8 (quint, *p*-C_6H_5, N = 2.5 Hz), 130.5, 131.1 (s, *m*-C_6H_5), 131.2 (quint, *ipso*-C_6H_5, N = 12.5 Hz), 132.4 (quint, *ipso*-C_6H_5, N = 11.5 Hz), 132.9 (quint, *o*-C_6H_5, N = 3.1 Hz), 133.2 (quint, *o*-C_6H_5, N = 2.8 Hz), 135.4 (s, =CH), 169.5 [quint, C_β, ^3J(PC) = 2.2 Hz], 171.1 [quint, C_γ, ^4J(PC) = 1.5 Hz], 283.5 [quint, C_α, ^2J(PC) = 13.4 Hz]. − ^{31}P{^{1}H} NMR (101.3 MHz): δ = −12.5 [s, P(dppm)]. − IR (KBr): $\tilde{\nu}$ = 1940 (vs, CCC). − UV/Vis (CH_3CN): λ_{max} (log ε) = 232 nm (4.806), 270 (4.628), 465 (4.210), 663 (3.025); (CH_2Cl_2): λ_{max} (log ε) = 236 nm (4.681), 272 (4.623), 345 (sh, 3.544), 466 (4.211), 670 (2.653). − $C_{58}H_{54}ClF_6P_4RuSSb$ (1279.3): calcd. C 54.46, H 4.25; found C 54.74, H 4.28.

Preparation of *trans*-$[ClRu(dppe)_2=C=C=C(SC_3H_5)C_4H_7]^+$ $CF_3SO_3^-$ (3c): A solution of 42 mg (41 μmol) of $[ClRu(dppe)_2]^+$ $CF_3SO_3^-$[21] in $CDCl_3$ was treated with excess butadiyne. After

30 min, 25 μL of $S(C_3H_5)_2$ (0.19 mmol) was added by means of a syringe. The progress of the reaction was monitored by ^{31}P-NMR spectroscopy. After a further 30 min, **3c** was the only identifiable product. The solution was transferred to a Schlenk tube and the solvent was removed in vacuo. Recrystallization from CH_2Cl_2/Et_2O afforded deep-red crystals. A further crop of microcrystals was obtained by concentration of the mother liquor; total yield 41 mg (84%). – ^1H NMR ($CDCl_3$): δ = 1.97 [br. d, 2 H, SCH_2, J(HH) = 6.44 Hz], 2.21 [br. t, 2 H, CH_2, J(HH) = 7.83 Hz], 2.33 (m, 2 H, CH_2), 2.76 [br. t, 2 H, CH_2 (dppe)], 3.00 [br. m, 2 H, CH_2 (dppe)], 4.76 [ddt, 1 H, =CH, ^3J(HH-*trans*) = 16.52 Hz, ^2J(HH) = ^4J(HH) = 1.4 Hz], 4.93 [ddt, 1 H, =CH, ^3J(HH-*cis*) = 9.92 Hz, ^2J(HH) = ^4J(HH) = 1.5 Hz], 4.98–5.11 (m, 3 H, =CH), 5.75 (m, 1 H, =CH), 6.92 [t, 8 H, aryl(dppe), ^3J(H-H) = 7.55 Hz], 7.04–7.14 [m, 24 H, aryl(dppe)], 7.22 [t, 8 H, aryl(dppe), ^3J(H-H) = 7.23 Hz], 7.32 [m, 8 H, aryl(dppe)]. – $^{13}C\{^1H\}$ NMR (62.9 MHz, $CDCl_3$): δ = 29.8 [quint, CH_2 (dppe), N(PC) = 11.6 Hz], 32.3, 36.5, 45.1 (s, CH_2), 116.8, 120.6 (s, $=CH_2$), 127.7, 128.6 (quint, *p*-C_6H_5, N = 2.4 Hz), 129.4 (=CH), 130.2, 131.0 (*m*-C_6H_5), 132.5 (quint, *ipso*-C_6H_5, N = 11.6 Hz), 133.1 (quint, *ipso*-C_6H_5, N = 11.0 Hz), 132.3 (quint, *o*-C_6H_5, N = 3.0 Hz), 133.8 (quint, *o*-C_6H_5, N = 2.6 Hz), 136.0 (s, =CH), 169.8, 170.2 (C_β, C_γ) 285.1 [quint, C_α, ^2J(PC) = 13.2 Hz]. – $^{31}P\{^1H\}$ NMR (101.3 MHz): δ = 42.5 [s, P(dppm)]. – IR (KBr): $\tilde{\nu}$ = 1939 (vs, CCC). – UV/Vis (CH_3CN) λ_{max} (log ε) = 231 nm (4.706), 265 (4.628), 368 (3.455), 471 (4.230), 681 (2.332); (CH_2Cl_2): λ_{max} (log ε) = 267 (4.623), 370 (3.470), 475 (4.230), 695 (2.380). – $C_{63}H_{60}ClF_3O_3P_4RuS_2$ (1246.7): calcd. C 60.70, H 4.85; found C 60.76, H 4.88.

Acknowledgments

This work was supported by the Deutsche Forschungsgemeinschaft, the Fonds der Chemischen Industrie, Prof. Dr. W. Kaim, and the Institut für Anorganische Chemie der Universität Stuttgart. I also wish to thank Mr. cand. chem. Matthias Wanner for the recording of the EPR spectra and Mr. Dirk Weber for his contributions as part of an advanced laboratory course.

[1] M. I. Bruce, *Chem. Rev.* **1998**, *98*, 2599.
[2] A butatrienylidene six-electron donor ligand in a cluster compound has been communicated: C. J. Adams, M. I. Bruce, B. W. Skelton, A. H. White, *Chem. Commun.* **1996**, 2663.
[3] J. P. Selegue, *Organometallics* **1982**, *1*, 217.
[4] M. I. Bruce, P. Hinterding, M. Ke, P. J. Low, B. W. Skelton, A. H. White, *Chem. Commun.* **1997**, 715.
[5] [5a] M. I. Bruce, P. Hinterding, P. J. Low, B. W. Skelton, A. H. White, *Chem. Commun.* **1996**, 1009. – [5b] M. I. Bruce, P. Hinterding, P. J. Low, B. W. Skelton, A. H. White, *J. Chem. Soc., Dalton Trans.* **1998**, 467. – [5c] V. Guillaume, P. Thominot, F. Coat, A. Mari, C. Lapinte, *J. Organomet. Chem.* **1998**, *565*, 75.
[6] [6a] R. F. Winter, F. M. Hornung, *Organometallics* **1997**, *16*, 4248. – [6b] R. F. Winter, F. M. Hornung, to be published in *Organometallics*.
[7] R. F. Winter, *Chem. Commun.* **1998**, 2209.
[8] D. Touchard, N. Pirio, L. Toupet, M. Fettouhi, L. Ouahab, P. H. Dixneuf, *Organometallics* **1995**, *14*, 5263.
[9] D. Touchard, N. Pirio, P. H. Dixneuf, *Organometallics* **1995**, *14*, 4920.
[10] E. O. Fischer, H. J. Kalder, A. Frank, F. H. Köhler, G. Huttner, *Angew. Chem.* **1976**, *88,* 683; *Angew. Chem. Int. Ed. Engl.* **1976**, *33*, 1360.
[11] [11a] R. Aumann, B. Jasper, R. Fröhlich, *Organometallics* **1995**, *14*, 3173. – [11b] G. Roth, H. Fischer, *Organometallics* **1996**, *15*, 1139.
[12] P. T. Czech, X.-Q. Ye, R. F. Fenske, *Organometallics* **1990**, *9*, 2016.
[13] O. J. Scherer, J. Schwalb, H. Swarowsky, G. Wolmershäuser, W. Kaim, R. Gross, *Chem. Ber.* **1988**, *121*, 443.
[14] M. Tamm, T. Jentzsch, W. Werncke, *Organometallics* **1997**, *16*, 1418.
[15] K. J. Harlow, A. F. Hill, J. D. E. T. Wilton-Ely, *J. Chem. Soc., Dalton Trans.* **1999**, 285.
[16] [16a] M. A. Esteruelas, A. V. Gómez, A. M. López, J. Modrego, E. Oñate, *Organometallics* **1997**, *16*, 5826. – [16b] V. Cadierno, M. P. Gamasa, J. Gimeno, M. González-Cueva, E. Lastra, J. Borge, S. García-Granda, E. Pérez-Carreño, *Organometallics* **1997**, *16*, 2137.
[17] I. P. Evans, A. Spencer, G. Wilkinson, *J. Chem. Soc.*, *Dalton Trans.* **1973**, 204.
[18] B. Chaudret, G. Commenges, R. Poilblanc, *J. Chem. Soc.*, *Dalton Trans.* **1984**, 1635.
[19] K. K. Georgieff, Y. Richard, *Can. J. Chem.* **1958**, *36*, 1280.
[20] R. F. Winter, G. Wolmershäuser, *J. Organomet. Chem.* **1998**, *570*, 201.
[21] J. R. Polam, L. C. Porter, *J. Coord. Chem.* **1993**, 109.

Received May 19, 1999
[I99176]

Molecular Precursors to Group 13 Nitrides, 14 [+]

Synthesis and Structures of $(N_3)_2Ga[(CH_2)_3NMe_2]$, $(N_3)Ga[(CH_2)_3NMe_2]_2$ and $(N_3)_3Ga(NR_3)$ (R = CH_3, C_2H_5)

Anjana Devi,[a] Harald Sussek,[a] Hans Pritzkow,[b] Manuela Winter,[a] and Roland A. Fischer*[a]

Keywords: Gallium / Azides / Chemical vapour deposition / Gallium nitride / Single source precursors

The synthesis, properties and X-ray single crystal structure analysis of the intramolecularly adduct-stabilised organogallium bisazide $(N_3)_2Ga[(CH_2)_3NMe_2]$ (**1**), the mono azide $(N_3)Ga[(CH_2)_3NMe_2]_2$ (**2**) and the trialkylamine adducts of triazidogallium of the type $(N_3)_3Ga(NR_3)$ (**3a**–**d**; R = alkyl) are reported. An unusual isomer **1b** of compound **1** is described, which was obtained by slow cooling of the analytically pure neat liquid compound **1** to 0 °C. The new and unusual structure **1b** can be regarded as a weak associate of dimers linked together by head-to-tail azide bridges. In contrast, compounds **2** and **3a**–**b** (R = CH_3, C_2H_5) are monomeric in the solid state. The suitability of the volatile compounds **1** and **2** as single source precursors to grow GaN thin films by chemical vapour deposition is compared, showing that preferentially oriented crystalline films can be obtained from compound **2** on sapphire substrates at 600–700 °C in vacuo (0.1 Pa). However the films have a grey rather than a transparent appearance, which is presumably due to N-deficiency owing to the lower N-content of the single molecule precursor **2** relative to **1**.

Introduction

The binary group 13 nitride GaN, and its ternary mixed phases with Al and In, are very promising materials for advanced microelectronic and optoelectronic devices such as light emitting diodes and lasers, high temperature and high power devices, as well as chemical sensors, acoustic surface-wave conductors and passivation layers (AlN) for GaAs[1–4] Organometallic vapour phase epitaxy (OMVPE) of these materials is currently achieved by the co-pyrolysis of ER_3 (E = Al, Ga, In; R = alkyl) with a large excess of ammonia (> 1000:1) at very high temperatures (> 1000 °C).[5–7] In order to avoid a large, background n-type carrier concentration due to nitrogen deficiencies, low temperature deposition techniques (< 850 °C) are interesting.[8][9] However, in this situation, the crystal quality of the layers, especially the concentration of point, line and planar defects which are likely to be electrically active, may be a problem. Considerable effort is currently being directed to the development of alternative molecular routes for the synthesis of group 13 nitride materials in the form of thin epitaxial films, disperse powders or nanocrystals embedded into various matrices. Recent examples include the growth of GaN single crystals (2 mm) by a solid-state reaction from sodium azide and gallium metal, the pyrolysis of various gallium amides, hydrazides or gallium azides yielding nanodisperse GaN materials.[11–19] Novel *volatile* single source precursors for use in OMVPE have also increasingly been studied.[17–19] Preformed E–N bonds in the precursor molecule lower the activation energies for the chemical vapour deposition (CVD) growth process. This could be advantageous even in the presence of ammonia as the typical (additional) nitrogen source. Azide derivatives of the group 13 metals are especially promising in this respect because the azide unit constitutes an almost ideal source for the N-component avoiding the nonselective formation of undesired side products upon fragmentation of the hydrocarbon ligands of the precursor during the growth process.[20] We are currently studying a series of adduct-stabilised organo group 13 azides of the general formula $(N_3)_{3-a}E(R)_a(L)_b$ (E = Al, Ga or In; a = 0, 1, 2; R = alkyl; L = py, b = 3; L = NR_3, b = 1), as single molecular sources for OMVPE of the group 13 nitride thin films in the absence of ammonia.[14–16] Other related works deal with the compounds $[R_2GaN_3]_3$ (R = H, CH_3, C_2H_5), $[(CH_3)_2N]_2GaN_3$ and $[X_2Ga(N_3)]_n$ (X = H, Cl.[21–24] Here we wish to report in detail on the improved synthesis and structural properties of the compounds $(N_3)_2Ga[(CH_2)_3NMe_2]$ (**1**), $(N_3)Ga[(CH_2)_3NMe_2]_2$ (**2**) and $(N_3)_3Ga(NR_3)$ (**3a**: R = CH_3; **3b**: C_2H_5) all of which have been successfully used to produce GaN materials. The results of these studies have been published elsewhere, except for the new compound **2** discussed here.[16,19,20]

[+] Part 7: Ref.[31]
[a] Lehrstuhl für Anorganische Chemie II,
Ruhr-Universität Bochum,
D-44780 Bochum, Germany
E-mail: rfischer@aci.ruhr-uni-bochum.de
[b] Anorganisch-chemisches Institut der
Ruprecht-Karls-Universität,
Im Neuenheimer Feld 270, D-69120 Heidelberg, Germany

Results and Discussion

Synthesis and Properties

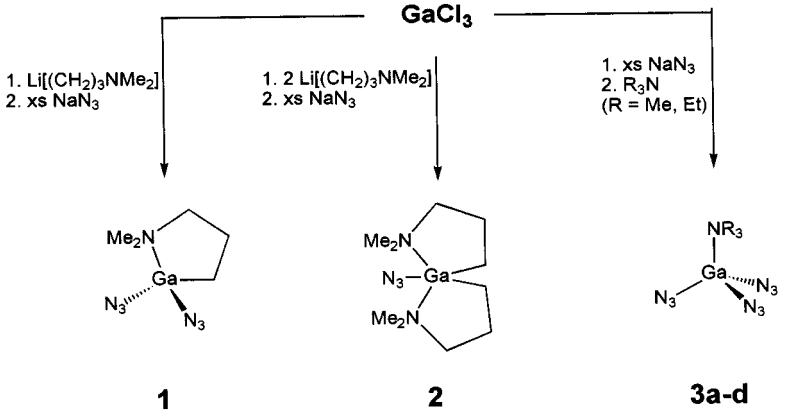
Molecular precursors of the materials used in electronic devices need to be very pure therefore their chemical syn-

thesis needs to be optimised for ultra high purification; a straightforward and high yield synthesis, very pure starting materials, easy scaling-up for larger quantities (multi-gram to kilogram) and very clean, e. g. oxygen and moisture-free, conditions (dry-box) are required. In the case of azide-type precursors for GaN, the compounds $GaCl_3$ and NaN_3 are the natural starting materials and are easily available in very pure forms. Furthermore, traces of chloride impurities are not a serious problem since Cl is electronically inactive in GaN. Adduct formation at the group 13 centre has also been successfully employed to reduce the incorporation of O-impurities arising from the solvents used for synthesis (e.g. ethers) or traces of moisture.[25][26] The title compounds (**1**−**3**) were thus synthesised from $GaCl_3$, NaN_3, $Li[(CH_2)_3NMe_2]$ and NR_3 (R = alkyl) according to Scheme 1. The previously reported synthesis of the bisazido derivative **1** has been significantly improved, indicated by a much higher melting point of +36(±0.1)°C (by DSC) rather than −28°C obtained earlier.[14] At temperatures above 40°C the pure compound **1** is a colourless liquid which can be repeatedly distilled in a dynamic vacuum without decomposition at 150°C (10^{-5} Torr base pressure of the turbo molecular pump system; equilibrium vapour pressure of **1** see below). Transparent single crystals suitable for X-ray crystallography were grown by slow cooling of the neat compound to 0°C. Total elemental analysis gave perfect results within the resolution of the method. NMR and mass spectrometry proved the chemical identity and the absence of any detectable trace impurities, such as Ga−O or Ga−Cl species (isotope pattern). The new monoazido compound **2** was synthesised in a similar manner (Scheme 1). Neither compound **1** nor compound **2** is pyrophoric or explosive when exposed to sudden heating (>10 K/min) or mechanical shock. Compound **2** is almost insensitive to hydrolysis, but prolonged exposure to moist air of **1** and **2** leads to decomposition and, eventually, traces of (explosive) HN_3 are formed. The synthesis of **3a**−**b** had been described previously starting from isolated $[Ga(N_3)_3]_\infty$.[14] However this is dangerous, because of the explosive nature of the polymeric triazidogallium. A one-pot synthesis of **3a**−**b** was thus developed which avoids the isolation of explosive intermediates. The treatment of a toluene suspension of the intermediately formed compound $Na[Ga(N_3)_4]$ with tertiary alkyl amines as donors is a safe way to yield the triazido congeners of type **3** (Scheme 1).[14][27]

Crystal Structures

The X-ray crystallographic data of **1** revealed that a different isomer **1b** had been obtained. The previously reported crystal data for compound **1** were obtained by zone-melting/crystallisation of a sample in a sealed Lindemann capillary mounted on the goniometer of the diffractometer and the data collection were performed at 150 K.[14] This was necessary because crystals of **1** could not be obtained by other techniques at that time, probably because of some unknown trace impurities lowering the melting point of the sample. This isomer **1a** crystallises in the triclinic space group *P*1bar and consists of centrosymmetric dimers exhibiting two asymmetric head bridging azide groups and two terminal azide units (Figure 1a).

The structure of the new isomer **1b** is rather different (Figure 1b). It crystallises from the neat liquid or concentrated toluene solutions (ice cold conditions) in the monoclinic space group *P*2(1)/*n* with four molecules attached together by loose head-to-tail azide bridges (Figure 1c). This tetramer can best be described as a dimer of dimers. Two molecules with the gallium centres Ga and Ga(A) are linked together by one single head-to-tail azide bridge {Ga(A)−N(3B) = 2.814(5) Å} and these dimers are attached to each other by rather long head-to-tail azide bridges of 3.069(6) Å. Figure 1d shows the molecular packing of **1b** in the crystal lattice. No further Ga−N distances shorter than 4.11 Å are present in the crystal lattice. The whole complex is centrosymmetric: for example, the positions of Ga and Ga(B) as well as Ga(A) and Ga(AA) are symmetrically related. All other N_{azide}−Ga contacts are well above the van-der-Waals limit of about 3.50 Å. The two (symmetry related) pairs of terminal azide groups at Ga(A) and Ga(AA), as well as the pairs of bridging azide units at Ga and Ga(B), show the typical features of covalently bonded azides: one longer N_a-N_b bond of about 1.16−1.18 Å and one shorter $N_\beta-N_\gamma$ bond of about



Scheme 1

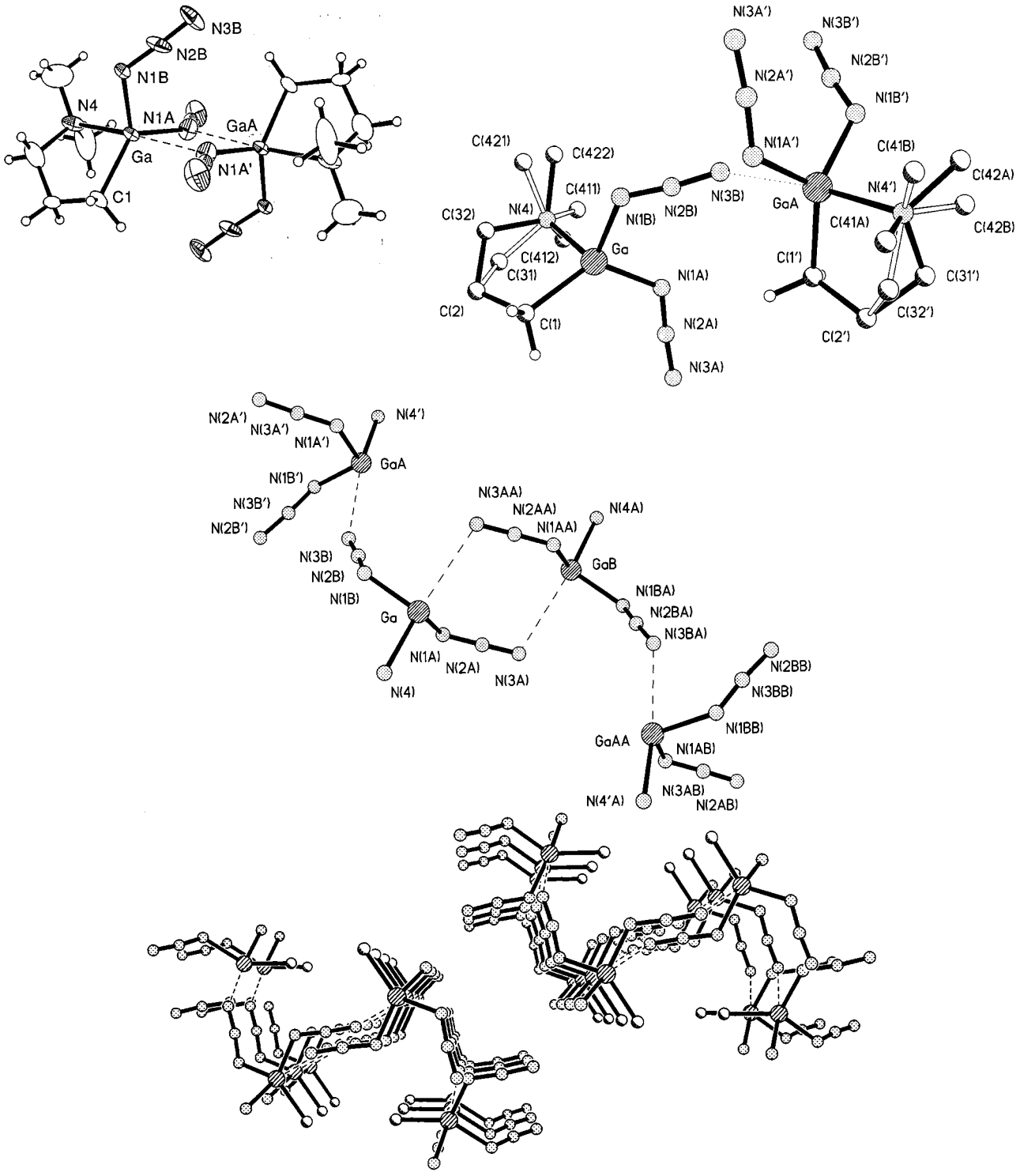


Figure 1. Molecular Structure of **1** in the solid state (ORTEP drawings, the thermal ellipsoids are at the 50% level): (a) compound **1a**;[14] (b) the two crystallographically independent centres Ga and Ga(a) of compound **1b** showing the disordering of the five-membered heterocyclic chelate rings (view of the molecular packing in the cell); (c) the characteristic tetramer (centrosymmetric dimer of dimers); (d) molecular packing of **1b** in the crystal lattice; selected bond lengths [A] and bond angles [deg] around the coordination centre Ga (the respective values for GaA are quite similar) for compound **1b**: Ga−N(1b) 188.5(4), Ga−N(1a) 190.5(4), Ga−N(4) 204.7(4), Ga−C(1) 193.8(4), N(1a)−N(2a) 116.2(5), N(2a)−N(3a) 113.9(5), N(1b)−N(2b) 118.0(5), N(2b)−N(3b) 113.8(5), N(3b)−GaA 281.4(5), Ga−N(3aa) 306.9(6); N(1b)−Ga−N(1a) 105.9(2), N(1b)−Ga−C(1) 123.2(2), N(1a)−Ga−C(1) 123.7(2), N(1b)−Ga−N(4) 101.7(2), N(1a)−Ga−N(4) 105.7(2), C(1)−Ga−N(4) 90.7, N(2a)−N(1a)−Ga 123.5(3), N(3a)−N(2a)−N(1a) 176.0(5), N(2b)−N(1b)−Ga 127.6(3), N(3b)−N(2b)−N(1b) 173.7(4)

1.14−1.15 Å; the angles Ga−N_α−N_β range around 126−129° as a consequence of the sp^2 hybridisation mode at N_α; the angles N_α−N_β−N_γ are close to 180°. There is no significant difference in the structural characteristics be-

tween terminal and bridging azide groups, again indicating the very weak interaction. On including the longer distances of 3.069(6) Å of Ga−N(3AA) compared to 2.814(5) Å for Ga(A)−N(3b), the coordination spheres of Ga and Ga(A) can be described as distorted trigonal bipyramidal. The trigonal bipyramidal coordination sphere of Ga is more distorted than that of Ga(A) as can be judged by the respective sums of their equatorial angles (356.9° vs. 352.8°). The five-membered heterocyclic chelate rings show a typical disorder because of the facile envelope flip due to intramolecular adduct formation. The positions of the involved atoms, C(31), C(32) and C(31′), C(32′) as well as the $N-CH_3$ groups are disordered (site occupation factor of 0.5). The dative Ga−N bonds, e. g. Ga−N(4) of 2.047(4) Å, are within the usual range.

Compound **2** (Figure 2a) crystallises in the monoclinic space group $P2_1$ with only one enantiomer in the asymmetric unit. In contrast to **1,** intermolecular contacts via azide bridges are absent. The structural parameters of monomeric **2** compare with the largely isostructural aluminium homologue.[20][28] Interestingly the respective indium homologue crystallises as a coordination polymer with *symmetric* head-to-tail bridging azide groups and hexa coordinated indium centres.[19] Compound **2** adopts a distorted trigonal bypyramidal structure with the two dimethylamino donor groups at the apical positions with an angle N(1)−Ga−N(2) of 178.0(8)°. The structural parameters of the equatorially coordinated azide are essentially similar to **1a** and **1b** exhibiting a somewhat more pronounced alternation of the N−N bond lengths and a longer $Ga-N_\alpha$ distance of 2.005(5) Å because of the larger covalent radius of the pentacoordinated Ga-centre. The conformational requirements of the chelating aminoalkyl groups cause an enlarged angle C1−Ga−C6 of 144.1(4)° and consequently smaller angles C6−Ga−N3 and C1−Ga−N3 of 107.6(4)° and 108.3(3)°, respectively. The Ga−C bonds are normal and the Ga−N1 and Ga−N2 dative bonds are within the usual range for related structures with penta-oordinated Ga centres, e.g. the chloro analogue of **2**.[25] Figure 2b shows the packing of compound **2** in the elementary cell.

In contrast to **1**, the compounds **3a** and **3b** crystallise as monomeric units, with no short intramolecular contacts, in the triclinic space group *P*1bar (**3a**) or in the monoclinic space group $P2_1/n$ (**3b**). Figure 3 shows the molecular structure of **3a**, which is essentially the same as for **3b** (see Experimental Section). The discussion therefore concentrates on **3a**. The only other structurally characterised compound with a triazido gallium unit is the hexacoordinated pyridine adduct $py_3Ga(N_3)_3$.[14][29] Due to the increased steric bulk of the tertiary amines only one amine ligand binds to the $Ga(N_3)_3$ moiety, rather than three (flat) pyridine ligands, yielding a trigonal pyramidal structure. Consequently the $Ga-N_{azide}$ bond lengths of **3a** and **3b** are somewhat shorter than the values obtained for the pyridine adduct (Figure 3). The short dative $Ga-NR_3$ bond of about 2.00 Å indicates a rather strong donor−acceptor bond to the $Ga(N_3)_3$ unit similar to **1** or $R_3N-GaCl_3$.[14] The structural parameters of the azide groups for **3a** and **3b** are similar to **1** and **2**.

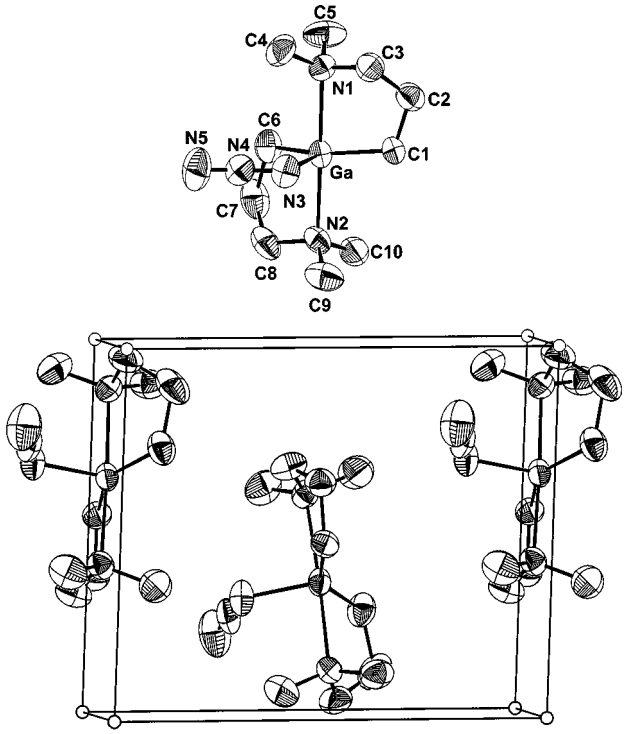


Figure. 2. Molecular Structure of **2** in the solid state (ORTEP drawings, the thermal ellipsoids are at the 50% level); (a) the monomeric unit of **2**; (b) the packing in the elementary cell; selected bond lengths [Å] and bond angles [deg]: Ga−N1 234.5(5), Ga−N2 231.1(5), Ga−N3 200.5(5), Ga−C3 197.3(5), Ga−C8 197.7(7), N3−N4 120.7(8), N4−N5 132.2(9); C3−Ga−C8 144.1(4), C3−Ga−N3 107.6(4), C8−Ga−N3 108.3, C3−Ga−N2 96.8(2), C8−Ga−N2 84.3(3), N3−Ga−N2 89.3(3), C3−Ga−N1 83.4(2), C8−Ga−N1 97.1(2), N3−Ga−N1 88.3(2), N2−Ga−N1 177.5(3), N3−N4−N5 178.0(8), N4−N3−Ga 118.7(5)

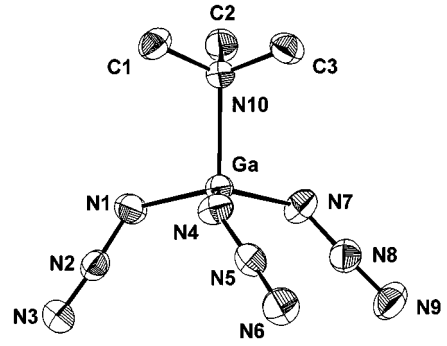


Figure 3. Molecular Structure of **3a** in the solid state (ORTEP drawings, the thermal ellipsoids are at the 50% level); selected bond lengths [Å] and bond angles [deg]: Ga−N1 188.8(2), Ga−N4 188.7(3), Ga−N7 189.2(2), Ga−N10 200.5(2), N1−N2 121.5(3), N2−N3 114.0(3); N1−Ga−N4 124.3(1), N1−Ga−N7 113.0(19, N1−Ga−N10 101.2(1), N4−Ga−N7 112.5(1), N4−Ga−N10 99.5(1), N7−Ga−N10 101.7(1), Ga−N1−N2 122.7(2), N1−N2−N3 175.5(3)

Materials Chemistry

Transparent, smooth (rms of 16 nm by AFM), epitaxial [full width at half maximum (FWHM) of the GaN(002) reflection of 0.72°] and stoichiometric films of GaN were grown by OMCVD on sapphire (0001) substrates at tem-

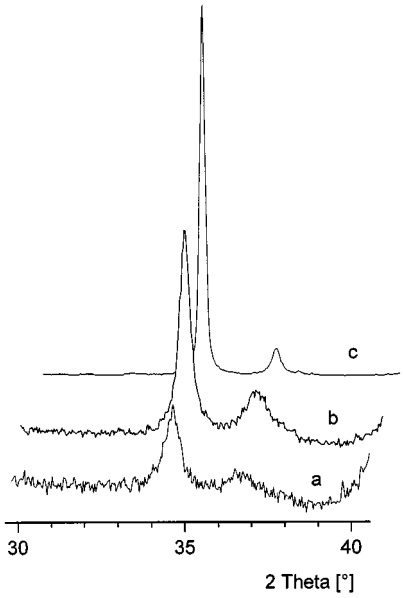


Figure 4. XRD patterns of GaN layers grown on $Al_2O_3(0001)$ using compound **2** in an isothermal horizontal hot wall tube reactor in vacuo (10^{-3} Torr) in the absence of carrier gases and additional sources of nitrogen (i.e. in the absence of ammonia) at substrate temperatures of (a) T = 600°C; (b) T = 650°C; (c) T = 750°C

peratures as low as 1070 K with growth rates up to 3−4 μm/hr from **1** with no additional source of nitrogen (ammonia) either employing an isothermal hot walled or a non-isothermal cold wall reactor system.[16] The vapour pressure of **1** between 25 (2.5 mPa) and 160°C (16 Pa) was determined by standard methods employing a Netzsch VP433 vapour pressure balance by the condensation or the impulse method.[16b] Thus, the vapour pressure of **1** can be calculated according to Equation 1. Compound **2** exhibits a vapour pressure which is an order of magnitude lower. These results show that increasing the coordinative shielding of the Ga centre by sacrificing one azide group does not improve the volatility as one might have expected on the basis of the *monomeric* structure of **2** when contrasted with the *associated* structure of **1**.

$$\ln[p(T)] = 23.7–8840/T\ [Pa] \qquad (1)$$

With a special reactor design the concentration of the fragments $HGaN_x$ and GaN_x (x = 1−6) in the boundary layer above the substrate were measured as a function of the substrate temperature showing a correlation with the growth rate of GaN.[30] We were interested in comparing the properties of the bisazido gallium compound **1** with a closely related compound with only one azide group and thus a lower nitrogen content. Compound **2** proved suitable to grow GaN films by CVD techniques employing similar hot wall conditions as for precursor **1**. The XRD pattern (Figure 4) of the films grown from **2** reveals a small shoulder for the (101) peak besides the dominant (002) reflection. The identity of the bulk material as GaN was independently established by RAMAN spectroscopy (Figure 5). The GaN thin film obtained from **2**, is only preferentially oriented on the sapphire substrate. Due to the lower nitrogen content of the monoazido precursor **2** the quality of the deposited GaN material was poor as judged by the grey appearance of the layers (Ga droplets were not detected by XRD). Also, because of the lower vapour pressure of **2** the growth rates of less than 1 μm/hr obtained were significantly lower than the growth rates obtained from precursor **1** at the same settings of the vaporiser (temperature of 80−100°C). The idea to have fewer Ga−C bonds and as many $Ga-N_3$ moieties as possible in the precursor is nicely underlined by the comparison of the films grown from **1** and **2**. Thus compound **1** seems still to be the best choice

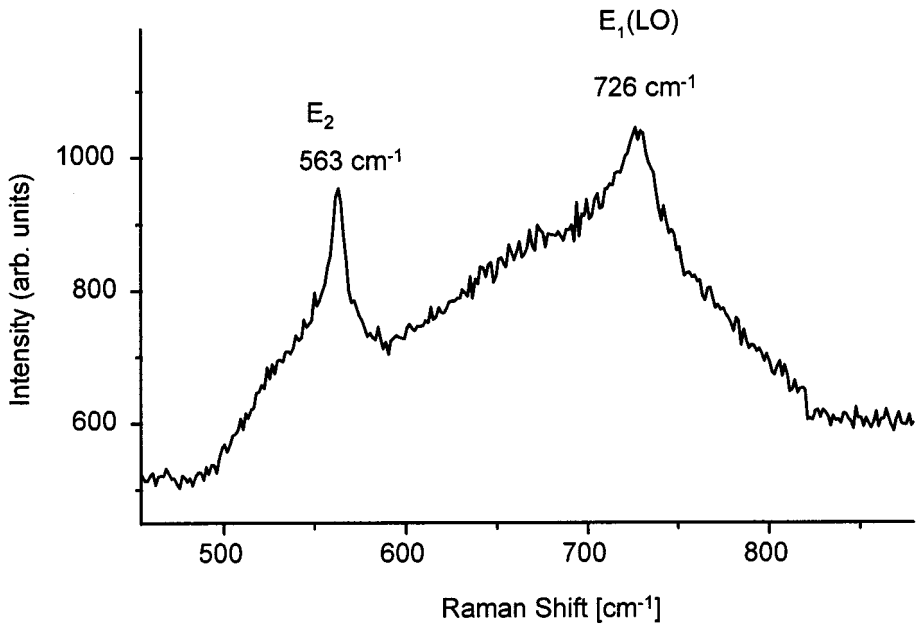


Figure 5. Raman data obtained from the GaN layer of Figure 4c; the characteristic E_2 and E_1 modes at 563 cm^{-1} and 726 cm^{-1} respectively of the GaN lattice vibrations are detected

to derive a nitrogen rich organometallic GaN precursor with an acceptable volatility for technical applications.

In contrast to **1** and **2** the triazido compounds of type **3** cannot be sublimed or volatilised at reasonable rates without the severe danger of explosion of the sample. This is probably because of the gradual loss of the volatile protecting donor ligand NR_3 and the formation of the parent compound $Ga(N_3)_3$ which is highly explosive. TG/DTA measurements were undertaken but have not yet given good quality data because of the detonation of the samples (1−2 mg). However, by taking advantage of this particular property, nanocrystalline GaN was obtained by controlled detonation of **3a** and **3b** contained in a suitable sealed stainless steel autoclave.[27,31,32] Other related adducts of long chain amines, e.g. **3c−e** were also pyrolysed under similar conditions to yield nanocrystalline GaN samples. However, it proved difficult to obtain very pure nano-GaN samples from **3a−b** due to the much higher hydrocarbon content of these precursors.[32]

Conclusions

Molecular precursors of the type $(N_3)_2Ga[(CH_2)_3NMe_2)]$ and $(N_3)Ga[(CH_2)_3NMe_2)]_2$ are single source precursors suitable for the growth of crystalline GaN films by CVD. Compound **2** is monomeric in the solid state while compound **1b** is basically a tetramer (dimer of dimers) with four molecules attached together by loose head to tail azide bridges. The testing of these compounds by CVD has demonstrated the feasibility of depositing GaN films at low temperatures (600−750°C) without any additional source of nitrogen. With respect to the accessible growth rate and thin film properties, films grown from compound **1** were of higher quality than those obtained from compound **2**.

Experimental Section

General procedures: All manipulations were performed utilising carefully oven-dried reaction vessels and Schlenk techniques under an inert atmosphere of purified argon or in a glove box. Solvents were dried under N_2 by standard methods and stored over 4 Å molecular sieves (residual water < 3 ppm, Karl-Fischer). Starting materials not available from commercial sources were synthesised according to the literature or by modified procedures, i. e. Cl_a-$Ga[(CH_2)_3NMe_2]_{3-a}$ (a = 1, 2).[25] The ^1H and ^{13}C NMR spectra were recorded on a Bruker EM 200 spectrometer and were referenced to residual protic impurities of the internal solvent and corrected to tetramethylsilane. The IR spectra were obtained in solution (toluene, pyridine) using 0.1 mm CaF_2 and NaCl cells on a Perkin−Elmer 1650 FT IR or a Bruker IFS 66. Elemental analysis were provided by the Microanalytic Laboratory of the Chemical Institute of the University of Heidelberg and the Service centre of the Faculty of Chemistry at the Ruhr-University of Bochum.

Bisazido[3-(dimethylamino)propyl]gallium (1): $Li[(CH_2)_3NMe_2]$[33] (4.2 g, 45.4 mmol) was suspended in dry ether (75 mL) and was added dropwise to a Schlenk vessel containing $GaCl_3$ (8 g, 45.4 mmol) in dry diethyl ether (75 mL) placed in a dry ice bath. After the addition was completed, the reaction mixture was allowed to stir at room temperature for 15 hours and the bis chloro[3-dimethylamino propyl] gallium formed was sublimed at 100°C to separate it from LiCl. The sublimed product (9.16 g, 40.38 mmol) was then treated with excess NaN_3 (9.72 g, 120 mmol) in toluene and refluxed at 115°C for another 15 hours. After filtration from the white residue, the solvent was removed by vacuum distillation. The product was purified by flask to flask distillation at reduced pressure using a turbomolecular pump (150°C, 10^{-5} mbar). Yield: 5.75 g (90%). − ^1H NMR (C_6D_6, 20°C): δ = 0.38 (t, 2 H, Ga−CH_2), 1.08 (m, 2 H, CH_2), 1.49 (t, 2 H, N−CH_2), 1.71 {s, 6 H, $N(CH_3)_2$}. − ^{13}C NMR (C_6D_6, 20°C): δ = 3.29 (Ga−CH_2), 21.10 (CH_2), 44.57 {$N(CH_3)_2$}, 61.70 (N−CH_2). − MS (EI, 70 eV) *m/z* = 239 [$(N_3)_2Ga\{(CH_2)_3NMe_2\}$]. − IR (toluene): $\tilde{\nu}$ = 2103 vs (N_3) cm^{-1}. − $C_5H_{12}GaN_7$: calcd. C. 25.03, H 5.04, N 40.87, Ga 29.06; found C 24.76, H 5.09, N 40.15, Ga 29.07.

Azidobis[3-(dimethylamino)propyl]gallium (2): Chlorobis[3-(dimethylamino)propyl]gallium[25] (2 g, 7.20 mmol) was dissolved in toluene (10 mL), added to a suspension of sodium azide (2.50 g, 38.45 mmol) in toluene and cooled to −78°C. The mixture was allowed to warm to room temperature after the addition and was subsequently heated to reflux for 15 h. After filtration from the white residue the solvent was removed by vacuum distillation at 25°C. The product was recrystallised from concentrated toluene solution at 5°C. Yield 1.98 g (6.99 mmol, 97.1%) as colourless needles, m.p. 40.3°C. − ^1H NMR (C_6D_6, 20°C): δ = 0.38 (m, 4 H, Ga−CH_2), 1.54 (m, 4 H, CH_2), 1.88 {s, 6 H, $N(CH_3)_2$}, 1.98 (t, 4 H, NCH_2). − ^{13}C NMR (C_6D_6, 20°C): δ = 4.86 (Ga−CH_2), 22.53 (CH_2), 44.58 {$N(CH_3)_2$)}, 61.35 (NCH_2). − MS (EI, 70 eV) *m/z* (%) = 282 (20) [M − H^+], 241 (100) [$Ga\{(CH_2)_3N(CH_3)_2\}_2^+$], 197 (8) [$(N_3)Ga\{(CH_2)_3N(CH_3)_2\}^+$]. − IR (toluene): $\tilde{\nu}$ = 2080 vs (N_3) cm^{-1}. − $C_{10}H_{24}GaN_5$ (284.05): calcd. C 42.28, H 8.51, N 24.65, Ga 24.54; found C 42.41, H 8.45, N 24.44, Ga 25.28.

General One-Pot Synthesis for Alkylamine Adducts of $Ga(N_3)_3$ of the Formula $(R_3N)Ga(N_3)_3$ (3a−d): A sample of freshly sublimed $GaCl_3$ (5.00 g, 28.40 mmol) was treated with a sample of sodium azide (9.23 g, 142.00 mmol) in 20 mL of toluene at −78°C. To this mixture 100 mL of THF was added with stirring. The suspension was allowed to warm to room temperature and was stirred for an additional 24 h. After filtration from the white residue the solution was concentrated by vacuum distillation at 25°C (removal of most of the THF) and 100 mL of toluene was added. At −78°C a sample of the respective alkylamine (113.6 mmol) was added and the mixture warmed to room temperature whilst stirring for 12 h. The reaction mixture was filtered and the solvent removed by vacuum distillation at 25°C. Compounds **3a−b** were recrystallised from concentrated toluene solutions at −30°C. The long chain alkylamine adducts **3a−d** were obtained as viscous, slightly yellow oils, which were thoroughly washed with *n*-pentane to remove excess alkylamine.

$[\{(CH_3)_3N\}Ga(N_3)_3]$ (3a): yield 6.88 g (27 mmol, 95%) m.p. 42.5°C. − ^1H NMR ([D_8]THF, 20°C) δ = 2.49 (s, CH_3) . − ^{13}C NMR ([D_8]THF, 20°C) δ = 47.30 (CH_3). − IR (toluene) $\tilde{\nu}$ = 2132 (vs), 2104 (vs), 1351 (s), 1293 (s) (N_3) cm^{-1}. − $C_3H_9GaN_{10}$ (254.86): calcd. C 14.14, H 3.56, N 54.96, Ga 27.36; found C 14.35, H 3.45, N 54.72, Ga 27.12.

$[\{(C_2H_5)_3N\}Ga(N_3)_3]$ (3b): yield 8.21 g (27.63 mmol, 97.3%) m.p. 47.5°C. − ^1H NMR (C_6D_6, 20°C) δ = 2.98 (q, 2 H, NCH_2), 1.15 (t, 3 H, CH_3). − ^{13}C NMR (C_6D_6, 20°C) δ = 49.1 (NCH_2), 10.1 (CH_3). − IR (toluene) $\tilde{\nu}$ = 2131 (vs), 2105 (vs), 1344 (s), 1291 (s) (N_3) cm^{-1}. − $C_6H_{15}GaN_{10}$ (296.97): calcd. C 24.27, H 5.09, N 47.17, Ga 23.48; found C 24.60, H 5.02, N 47.53, Ga 24.12.

Table 1. Crystal data and structure refinement for **1b**, **2** and **3a**

	1b	**2**	**3a**
Empirical Formula	$C_5H_{12}GaN_7$	$C_{10}H_{24}GaN_5$	$C_3H_9GaN_{10}$
Formula weight	239.94	284.06	254.92
Crystal size [mm]	0.58 × 0.52 × 0.40	0.50 × 0.40 × 0.20	0.5 × 0.3 × 0.2
T, K	203(2)	203(2)	203(2)
Crystal system	Monoclinic	monoclinic	triclinic
Space group (#)	$P2_1/n$ (14)	$P2_1$ (4)	P(-1) (2)
a, Å	6.974(4)	7.275(4)	6.076(3)
b, Å	11.964(4)	10.821(5)	7.546(4)
c, Å	23.916(7)	9.622(5)	11.182(6)
α, °	90	90	79.57(2)
β, °	92.92(4)	106.93(3)	82.76(2)
γ, °	90	90	81.95(2)
V, Å^3	1992.9(14)	724.6(6)	496.6(4)
Z	8	2	2
Calcd. density [Mg/m^3]	1.599	1.302	1.705
m (Mo-K_a)mm^{-1}	2.731	1.885	2.753
F(000)	976	300	256
$\theta_{min} - \theta_{max}$ [°]	2.41−27.49	27	28
Index range	$0 \le h \le 9$, $0 \le k \le 15$, $-31 \le l \le 30$	$-10 \le h \le 9$, $-10 \le k \le 13$, $-11 \le l \le 13$	$-7 \le h \le 8$, $-9 \le k \le 9$, $0 \le l \le 14$
No. of reflection	4856	2966	2387
Unique	4527	2816	2387
Observed [$I > 2\sigma(I)$]	2992	2359	2387
Transmission min/max	0.245/1.000	0.802/0.996	0.653/1.000
No. of Parameters	229	251	164
Largest diff. peak/hole [eÅ^{-3}]	0.908/−0.625	0.984/−0.900	0.569/−0.516
*R*1, *wR*2 [$I > 2\sigma(I)$]	0.0454/0.1409	0.0506/0.1216	0.0313/0.0779
Goodness of fit	0.904	1.069	1.052

$R1 = \Sigma(||F_o|-|F_c||)/\Sigma|F_o|$; $wR2 = [\Sigma_w(F_o^2-F_c^2)^2/\Sigma_w(F_o^2)^2]^{1/2}$; GOF $= [\Sigma_w(F_o^2-F_c^2)^2/(NO-NV)]^{1/2}$.

[{(CH$_3$)$_2$N(C$_8$H$_{17}$)}Ga(N$_3$)$_3$] (3c): yield 9.01 g(25.53 mmol, 93.4%) m.p. 57°C. − ^{1}H NMR (C$_6$D$_6$, 20°C) δ = 1.86 (t, 2 H, NCH$_2$), 1.56 (s, 6 H, NCH$_2$), 1.26−0.80 (m, 12 H, CH$_2$), 0.9 (t, 3 H, CH$_2$C*H*$_3$) − ^{13}C NMR (C$_6$D$_6$, 20°C) δ = 60.12 (NCH$_2$), 44.31 (NCH$_3$), 31.99, 29.22, 26.85, 24.10, 23.00 (5 × CH$_2$), 14.29 (CH$_2$*C*H$_3$). − IR (toluene) $\tilde{\nu}$ = 2130 (vs), 2100 (vs), 1344 (s), 1290 (s) (N$_3$) cm^{-1}. − C$_{10}$H$_{23}$GaN$_{10}$ (353.08): calcd. C 34.02, H 6.47, N 39.67, Ga 19.75; found C 34.27, H 6.84, N 39.17, Ga 19.51.

[{(CH$_3$)$_2$N(C$_{10}$H$_{21}$)}Ga(N$_3$)$_3$] (3d): yield 9.95 g(26.13 mmol, 92%). − ^{1}H NMR (C$_6$D$_6$, 20°C) δ = 2.00 (t, 2 H, NCH$_2$), 1.80 (s, 6 H, NCH$_2$), 1.30−1.00 (m, 16 H, CH$_2$), 0.9 (t, 3 H, CH$_3$). − ^{13}C NMR (C$_6$D$_6$, 20°C) δ = 59.0 (NCH$_2$), 43.5 (NCH$_3$), 31.8−24.6 (8 × CH$_2$), 13.8 (CH$_2$*C*H$_3$). − IR(toluene) $\tilde{\nu}$ = 2130 (vs), 2105 (vs), 1348 (s), 1300 (s) (N$_3$) cm^{-1}. − C$_{12}$H$_{27}$GaN$_{10}$ (381.13): calcd. C 37.79, H 7.09, N 36.74, Ga 18.38; found C 37.91, H 7.50, N 36.82, Ga 17.54.

X-ray Crystal Structure Determination: Crystal data and details of the structure determination of **1**, **2** and **3a** are compiled in Table 1. The data of compound **3b** are available as supplementary publication (see below). Unique sets of intensity data were collected with a four-circle diffractometer (Mo-K_α radiation, λ = 0.71073 Å), graphite monochromator, ω-scan). Empirical absorption corrections (ψ-scans) were applied. The structures were solved by direct methods[34a] and refined by least squares methods based on F^2 with all observed reflections.[34b] All non-hydrogen atoms were refined anisotropically. Crystals of **1**, **2** and **3a,b** were mounted on the goniometer using the perfluoro ether technique with cooling. Data collection were performed with a STOE-AED2 four circle instrument (University of Heidelberg, Mo-K_α radiation λ = 0.71073 Å, graphite monochromator, ω-scan). Empirical absorption correction (ψ-scans) were applied. Correction for absorption was done on the basis of ψ-scans. The structure solution was done with direct methods[34a] and the structure refinement (full matrix least squares against F^2) was undertaken with anisotropic structural parameters for all nonhydrogen atoms employing the program.[34c] The absolute structure of **2** was assigned on the basis of its Flack parameter × of −0.003(29).[36] The structure **1b** shows a disorder at the position C(31), C(32) and C(31′) and C(32′) respectively due to the facile envelope-flip of the five-membered heterocyclus defined by the atoms Ga, C(1), C(2), C(3), N(4). This disorder was fully resolved (Figure 1b). Crystallographic data (excluding structure factors) for the structures reported in this paper have been deposited with the Cambridge Crystallographic Data Centre: CCDC-119479 (**1b**), 119673 (**2**), 119672 (**3a**) and 119671 (**3b**). Copies of the data can be obtained free of charge by application to CCDC, 12 Union Road, Cambridge CB2, 1EZ, UK [Fax: (internat.) + 44−1223/336−033; E-mail: deposit@ccdc.cam.ac.uk].

MOCVD of GaN Thin Films With Compound 2 as Precursor: The MOCVD experiments were conducted employing a simple horizontal hot wall reactor (heated quartz tube) described elsewhere.[35] The system was loaded with degreased single crystalline sapphire substrates (0001) heated to 450°C and evacuated to 10^{-6} mbar for several hours. After filling the reactor with argon the precursor vessel containing a sample of 0.5 g of compound **2** was attached to the quartz tube of the reactor and cooled to −30°C. The system was again evacuated down to a base pressure of 10^{-5} mbar and the oven was set to the desired temperature (600−750°C). Then the precursor reservoir was heated to vaporise the precursor. The pressure during the deposition was about 10^{-3} mbar. No carrier gas was used for the deposition. The obtained films (almost transparent to grey in appearance) were characterised by XRD using a Bruker AXS D8 ADVANCE diffractometer. RAMAN spectra of the films were recorded using a DILOR SPECTRALAB instrument equipped with a microscope using an argon ion laser operating at 514 nm.

Acknowledgments

The authors wish to thank the Deutsche Forschungsgemeinschaft for generous support and Prof. Dr. W. S. Sheldrick for his generous help rendered in solving the crystal structure of compound **1b**. A. D. is grateful to the Alexander von Humboldt Foundation for a fellowship.

[1] S. Fujieda, M. Mitzuta, Y. Matsumoto, *Adv. Mater. Opt. Elec.* **1996**, *6*, 127- 134.
[2] H. Morkoc, S. Strite, G. B. Gao, M. E. Lin, B. Sverdlov, M. Burns, *J. Appl. Phys.* **1994**, *76*, 1363−1398.
[3] H. Okano, N. Tanaka, Y. Takahashi, T. Tanaka, K. Shibata, S. Nakano, *Appl. Phys. Lett.* **1994**, *64*, 166−168.
[4] J. I. Pankove, *Mater. Res. Soc. Symp. Proc.* **1990**, *162*, 515−522.
[5] M. A. Khan, J. N. Kuznia, J. M. V. Hovea, D. T. Olson, *Appl. Phys. Lett.* **1991**, *58*, 526−527.
[6] T. Detchprohm, K. Hiramatsu, N. Sawaki, I. Akasaki, *J. Cryst. Growth* **1994**, *137*, 171−174.
[7] S. Nakamura, N. Iwasa, T. Mukai, *Jpn. J. Appl. Phys.* **1992**, *31*, 1258−1266.
[8] S. D. Lester, F. A. Ponce, M. G. Crawford, D. A. Steigerwald, *Appl. Phys. Lett.* **1995**, *66*, 1249−1251.
[9] D. J. Smith, D. Chandrasakher, B. Sverdolv, A. Botchkarev, A. Salvador, H. Morcoc, *Appl. Phys. Lett.* **1995**, *67*, 1830−1832.
[10] H. Yamane, M. Shimada, S. J. Clarke, F. J. DiSalvo, *Chem. Mater.* **1997**, *9*, 413−416.
[11] M. I. Baraton, X. Chen, K. E. Gonsalves, *J. Mater. Chem*. **1996**, *6*, 1407−1412.
[12] [12a] O. T. Beachley, Jr., J. C. Pazik, M. J. Noble, *Organometallics*, **1998**, *17*, 2121 2123. − [12b] D. K. Gaskill, N. Bottka, M. C. Lin, *Appl. Phys. Lett*., **1986**, 48, 1449. − [12c] S. Miyoshi, K. Onabe, N. Ohkouchi, H. Yaguchi, R. ito, S. Fukatsu, Shirak, S. Yoshida, *J. Cryst. Growth*, **1992**, 124, 439.
[13] A. C. Jones, C. R. Whitehouse, J.S. Roberts, *Chem. Vap. Dep.* **1995**, *1*, 63−78.
[14] R. A. Fischer, A. Miehr, E. Herdtweck, M. R. Mattner, O. Ambacher, T. Metzger, E. Born, S. Weinkauf, C. R. Pulham, S. Parsons, *Chem. Eur. J.* **1996**, *2*, 1353−1358.
[15] R. A. Fischer, A. Miehr, O. Ambacher, T. Metzger, E. Born, *J. Cryst. Growth* **1997**, *170*, 139−143.
[16] [16a] A. Miehr, O. Ambacher, T. Metzger, E. Born, R. A. Fischer, *Chem. Vap. Dep.* **1996**, *2*, 51−55. − [16b] A. Devi, W. Rogge, A. Wohlfart, G. Becker, R. A. Fischer, *Chem. Vap. Dep.* **1999** to be submitted.
[17] J. Kouvetakis, D. Beach, *Chem. Mater.* **1989**, *1*, 476−478.
[18] J. Kouvetakis, J. McMurran, P. Matsunaga, M. O′Keeffe, J. L. Hubbard, *Inorg. Chem.* **1997**, *36*, 1792−1797.
[19] R. A. Fischer, H. Sussek, A. Miehr, H. Pritzkow, E. Herdtweck, *J. Organomet. Chem.* **1997**, 548, 73−82.
[20] R. A. Fischer, A. Miehr, H. Sussek, H. Pritzkow, E. Herdtweck, J. Müller, O. Ambacher, T. Metzger, *J. Chem. Soc., Chem. Commun.* **1996**, 2685−2686.
[21] H. S. Park, S. D: Waezsada, A. H. Cowley, H. W. Roesky, *Chem. Mater*., **1998**, 10, 2251−2257.
[22] V. Lakhotia, D. A. Neumayer, A. H. Cowley, R. A. Jones, J. G. Eckerdt, *Chem. Mater*., **1995**, 7, 546−552.
[23] K. −L. Ho, K. F. Jensen, J. W. Hwang, W. L. Gladfelter, J. F. Evans, *J. Cryst. Growth*, **1991**, 107, 376−380.
[24] J. McMurran, D. Dai, K. Balasubramanian, C. Steffek, J. Kouvetakis, J. L. Hubbard, *Inorg.Chem*. **1998**, 37, 6638−6644.
[25] H. Schuhmann, T. D. Seuss, O. Just, R. Weimann, H. Hemling, F. H. Goerlitz, *J. Organomet. Chem*., **1994**, 479, 171−186.
[26] A. C. Jones, *Chem. Soc. Rev*., **1997**, 101−110.
[27] A. C. Frank, F. Stowasser, H. Sussek, H. Pritzkow, C. R. Miskys, O. Ambacher, M. Giersig, R. A. Fischer, *J. Am. Chem. Soc*., **1998**, *120*, 3512−3513.
[28] J. Mueller, R. A. Fischer, H. Sussek, P. Pilgram, R. Wang, H. Pritzkow, E. Herdtweck, *Organometallics*, **1998**, *17*, 161−166.
[29] D. A. Neumayer, A. H. Cowley, A. H. Decken, R.A. Jones, L. Lakhotia, J. G. Eckerdt, *J. Am. Chem. Soc*. **1995**, *117*, 5893−5895.
[30] J. Schaefer, J. Wolfrum, R. A. Fischer, H. Sussek, *Chem. Phys. Lett*, **1999**, *300*, 152−156.
[31] R. A. Fischer, A. C. Frank, F. Stowasser, O. Stark, H. T. Kwak, H. Sussek, A. Rupp, H. Prtizkow, O. Ambacher, M. Geirsig, *Adv. Mater. Opt. Electron*. **1998**, *8*, 135−146.
[32] A. Rupp, Dipl. Thesis, Heidelberg, **1997**.
[33] K. H. Thiele, E. Langguth, G. E. Mueller, *Z. Anorg. Allg. Chem*. **1980**, *462*, 152.
[34] [34a] G. M. Sheldrick, *SHELX86*, Univ. Göttingen, 1986. − [34b] G. M. Sheldrick, *SHELXL97*, Univ. Göttingen, 1997. − [34c] G. M. Sheldrick, *SHELXL93*, Univ. Göttingen, 1993.
[35] R. A. Fischer, A. Miehr, *Chem. Mater.* **1996**, *8*, 1356−1359.
[36] G. Bernardinelli, H. D. Flack, *Acta Crystallogr*. **1982**, B38, 907.

Received May 25, 1999
[I99188]

Activity of Peroxo and Hydroperoxo Complexes of Ti^{IV} in Olefin Epoxidation: A Density Functional Model Study of Energetics and Mechanism

Ilya V. Yudanov,[a,b] Philip Gisdakis,[a] Cristiana Di Valentin,[a,c] and Notker Rösch*[a]

Keywords: Density functional calculations / Epoxidation / Peroxo complexes / Titanium / Transition states

Epoxidation of olefins by Ti^{IV} peroxo and hydroperoxo (alkylperoxo) complexes was investigated using a hybrid DFT method (B3LYP). Reaction energies and activation barriers for direct oxygen transfer to ethylene as a model olefin were computed for various model complexes to compare the epoxidation activity of Ti(η^2-O_2) and TiOOR (R = H, CH_3) moieties. The activity of complexes with a Ti(O_2) peroxo group is shown to be essentially quenched when the coordination sphere of the complex is saturated by strongly basic (σ-donor) ligands. In contrast, the activity of a TiOOH functional group depends only weakly on the saturation of the coordination sphere of the Ti center. Substitution of methyl for hydrogen in a TiOOH group is found to slightly increase the activation barrier of epoxidation. The computational results give preference to reaction paths that involve TiOOR species. The factors governing the activity of Ti(O_2) and TiOOR groups, in particular the effects of donor ligands, are discussed on the basis of a molecular orbital analysis.

Introduction

Titanium(IV) peroxo species represent an active component in a number of homogeneous and heterogeneous oxidation reactions of organic substrates by hydrogen or alkyl peroxides.[1] Important examples of catalytic processes of this type are the homogeneous stereoselective epoxidation of allylic alcohols by alkyl peroxides catalyzed by Ti^{IV} alkoxides (Sharpless epoxidation)[2] and the heterogeneous epoxidation of olefins on titanium silicates (or silicalites) with amorphous[3] or zeolite-like structures.[4] Despite intense experimental work, the precise structure of the oxidizing active site is still a matter of controversy in most of cases, especially for heterogeneous catalytic processes on titanium silicates.[4–6]

In the known epoxidation reactions, titanium hydroperoxo or alkylperoxo groups, TiOOR (R = H, alkyl), are generally accepted as oxygen donors, while peroxo groups, Ti(η^2-O_2), with two symmetrically coordinated oxygen centers at Ti are considered inert in this reaction. For instance, a TiOO-*t*Bu species is assumed to be responsible for epoxidation in the Sharpless process,[7] and a TiOOH species for epoxidation on Ti silicalite.[4] In early reports active Ti(O_2) species have also been suggested for the latter system.[8][9] Actually, a number of stable and experimentally well-characterized Ti^{IV} η^2-peroxo complexes are not active in olefin epoxidation, e.g. (TPP)Ti(O_2)[10] (TPP = tetraphenylporphyrin) and Ti(O_2)(pic)$_2$·HMPA[11] (HMPA = hexamethylphosphoric triamide; pic = picolinato). However, there is evidence[10] that (TPP)Ti(O_2) becomes active in the epoxidation of cyclohexene once it is transformed to the *cis*-hydroxo(alkylperoxo) complex (TPP)Ti(OH)(OOR), although the latter has never been isolated.

On the other hand, the η^2-peroxo or bis-peroxo d^0 complexes of Mo, W, and Re, which are structurally similar to Ti(O_2) species, are known to epoxidize alkenes.[1,12,13] Thus far, no clear rationalization has been presented as to why η^2-peroxo complexes of Ti are not active in epoxidation. The inactivity of (TPP)Ti(O_2) has been rationalized by steric repulsion between the alkene and the porphyrin ring.[1] However, electronic effects of the porphyrin ring on the properties of the peroxo group might provide a different reason, by analogy with the inhibiting effect of strong coordinating solvents on the epoxidation activity of the bis-peroxo molybdenum complex $MoO(O_2)_2 \cdot HMPA$.[14] Here, the reactivity decrease of the peroxo group under coordination of a seventh ligand to the metal center has been attributed[15][16] to electronic effects rather than to the possibility that the reacting alkene may be prevented from coordinating to the Mo center. An inhibiting electronic effect of basic ligands on the activity of Re and Mo bis-peroxo complexes has also recently been demonstrated computationally.[17–19]

Several theoretical investigations on ethylene epoxidation catalyzed by Ti^{IV} species have been reported.[20–24] These studies presented structures of possible intermediates as well as activation energies for oxygen transfer. Most of them dealt with models of hydroperoxo complexes like $(HO)_3$-TiOOH[20–22] or closely related clusters that partially account for a silicate surrounding, e.g. $(H_3SiO)_2(HO)$-TiOOH[24] and $(H_3SiO)_3(CH_3OH)$TiOOH.[23] The activity

[a] Institut für Physikalische und Theoretische Chemie, Technische Universität München,
D-85747 Garching, Germany
Fax: (internat.) +49 (0)89/289 13622
E-mail: roesch@ch.tum.de
[b] Permanent address: Boreskov Institute of Catalysis, Siberian Branch of Russian Academy of Sciences,
630090 Novosibirsk, Russia
[c] Permanent address: Dipartimento di Chimica Organica, Università degli Studi di Pavia,
V. le Taramelli 10, I-27100 Pavia, Italy

 © WILEY-VCH Verlag GmbH, D-69451 Weinheim, 1999 1434–1948/99/1212–2135 $ 17.50+.50/0

of $Ti(O_2)$ species was investigated only with the model peroxo complex $(HO)_2(H_2O)Ti(O_2)$.[22] Note that the Ti center of most models studied is five-coordinated. This is lower than the typical coordination (six or seven) of the experimentally characterized Ti^{IV} peroxo and alkylperoxo complexes,[11,25–27] i.e. the coordination sphere of these Ti model complexes is not saturated. Under reaction conditions the coordination of Ti centers in titanium silicalites expands beyond the initial tetrahedral structure.[28] Despite there being a number of particular cases that have been considered, a comprehensive computational comparison of properties of $Ti(O_2)$ and TiOOR species and their epoxidation activity is still lacking.

With the present work on Ti^{IV} complexes we continue our series of density functional (DF) investigations on olefin epoxidation in which we have so far studied Re, Cr, Mo, and W d^0 peroxo complexes.[17–19] Here, we compare the epoxidation activity of a number of Ti^{IV} model complexes that contain either peroxo or hydroperoxo (alkylperoxo) functional groups. For this purpose we have calculated the reaction energies and the activation barriers for direct oxygen transfer from both types of peroxo groups, $Ti(\eta^2\text{-}O_2)$ and TiOOR, to the model olefin ethylene. In addition, we pay special attention to the coordination number of the Ti center. The model study presented here will also shed light on the mechanism of epoxidation on titanium silicates.

The goals of the present study are (i) to investigate the mechanism of olefin (ethylene) epoxidation by Ti complexes with peroxo and hydroperoxo (alkylperoxo) functional groups; (ii) to determine factors that govern the reactivity of these groups and, in particular, to study the dependence of the activity on the saturation of the coordination sphere of central Ti ion; and (iii) to consider the effect of an alkyl substituent of the TiOOR moiety on the activation barrier of epoxidation.

Results and Discussion

We intend to focus on the electronic effects of ligands on the properties of the moieties $Ti(O_2)$ and TiOOR, but we want to leave aside steric effects. Therefore, we start with simple monodentate ligands like hydroxyl groups as anionic ligands and ammonia or water as (neutral) σ donors. In this way, we are able to relate the models under study to different types of titanium peroxo compounds: either to complexes with more complicated polydentate organic ligands or to Ti species incorporated in silicate structures. In order to make this relation more realistic we consider at the end models where some hydroxide ligands are replaced by either methoxide or siloxide ligands. We shall take solvent effects into account only through the coordination of additional ligands to the Ti center; no other environment effects are included. However, from studies on Re and Mo peroxo complexes it is known[17][29] that long-range solvent effects and zero-point energy corrections hardly influence reaction energies and activation barriers of oxygen transfer to olefins.

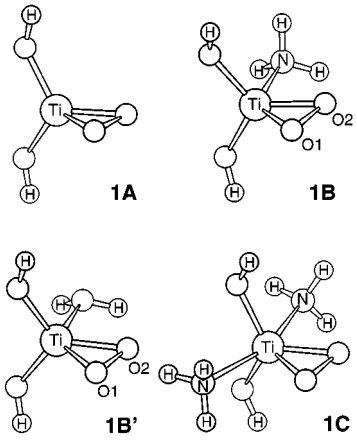


Figure 1. Model complexes with a $Ti(\eta^2\text{-}O_2)$ functional group

Model Complexes

We start by considering model η^2-peroxo complexes of Ti^{IV}. The simplest such model is $(HO)_2Ti(O_2)$, **1A** (Figure 1), with the peroxo group coordinated to Ti in a symmetric η^2 ("side-on") fashion; two hydroxyl ligands provide the oxidation state IV and electro-neutrality of the complex. The coordination sphere of complex **1A** is far from saturated and thus **1A** exhibits significant affinity to basic ligands. The binding energy of further ligands is −32.3 kcal/mol for NH_3 (complex **1B**, Figure 1) and −25.9 for H_2O (**1B′**). Addition of a second NH_3 molecule to **1B** leads to a further energy gain of −16.5 kcal/mol. The resulting complex, **1C** (Figure 1), can be considered as a model of the complex $Ti(TPP)(O_2)$ with the porphyrin ring of the latter substituted by two NH_3 and two hydroxide ligands. Geometry optimizations of the complexes **1A** and **1C** converged to structures with effective C_{2v} symmetry; thus in these complexes the two oxygen centers of the peroxo group are essentially equivalent. In complexes with one basic ligand, **1B** and **1B′**, the symmetry of the peroxo group is slightly distorted with the Ti−O distances differing by 0.02 Å (see Table 1). The calculated structural parameters of the titanium peroxo group (Table 1) are in very good agreement with X-ray data of known Ti^{IV} peroxo complexes.[11,25,26] For instance, the calculated Ti−O and O−O distances of 1.86 and 1.46 Å, respectively, in the peroxo group of complex **1C** are very close to the corresponding experimental values of 1.83 and 1.45 Å, respectively, of the complex $(OEP)Ti(O_2)$ (OEP = octaethylporphyrinato),[26] where Ti also exhibits coordination number 6.

Models of Ti hydroperoxo (alkylperoxo) complexes are shown in Figure 2. Complex **2A** has previously been used for modeling active intermediates of the Sharpless epoxidation[20] and epoxidation centers of Ti-silicalites.[21][22] Model **2B** is derived from **2A** by adding an NH_3 ligand; the calculated ligand binding energy is −13.2 kcal/mol. Model **3A** differs from **2A** by a methyl substituent in place of the hydrogen center of the peroxo group. The fact that no local symmetry in the Ti(OOR) moiety is preserved does not come as a surprise (Table 2). However, the hydroperoxo (alkylperoxo) ligand is still coordinated to Ti by both oxy-

Table 1. Calculated properties of Ti peroxo complexes: intermediates and oxygen transfer transition states. For the designation of the various structures see Figure 1

	1A	**1B**		**1B′**	**1C**
Geometry of peroxo group, Å					
r(O−O)	1.487	1.472		1.472	1.460
r(Ti−O1)	1.823	1.837		1.836	1.861
r(Ti−O2)	1.823	1.859		1.857	1.861
NBO atomic charges, e					
q(O1 front)	−0.45	−0.45		−0.44	−0.48
q(O2 back)	−0.45	−0.49		−0.50	−0.48
total *q*(OO)	−0.90	−0.94		−0.94	−0.96
q(Ti)	1.89	1.72		1.75	1.60
Core level energies, eV					
1s(O1)	−522.0	−520.9		−521.1	−520.2
1s(O2)	−522.0	−520.8		−521.0	−520.2
3s(Ti)[a]	−67.1	−66.0		−66.3	−65.3
Geometry of transition state, Å		front	back	front	
r(O−O)	1.856	1.863	1.854	1.860	1.847
r(Ti−O1)	1.875	1.929	1.731	1.913	2.001
r(Ti−O2)	1.741	1.748	1.965	1.752	1.739
r(O−C1)	2.211	2.110	2.064	2.108	2.020
r(O−C2)	2.211	2.109	2.070	2.141	2.027
Activation barrier, kcal/mol	11.0	19.0	22.3	17.4	27.4

[a] The 1s and 2s eigenvalues of Ti are not available because of the ECP description.

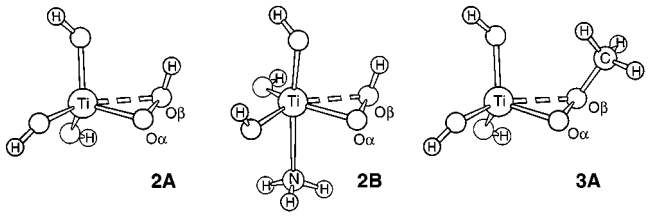


Figure 2. Model complexes with a TiOOR functional group (R = H, CH_3)

gen centers with Ti−Oα and Ti−Oβ distances (Figure 2) of about 1.89 and 2.27 Å, respectively. The plane OOR of the TiOOR group is almost orthogonal to the plane TiOO. The O−O distance is about 1.47 Å. The calculated structure of the TiOOR group agrees very well with recently reported data for {[(η^2-*tert*-butylperoxo)titanatrane]$_2$ · 3 dichloromethane}: *r*(Ti−Oα) = 1.913 Å, *r*(Ti−Oβ) = 2.267 Å, and *r*(O−O) = 1.469 Å.[27] This is the only alkylperoxo complex of Ti reported to date for which an X-ray crystal structure is available. Although the authors[27] chose to designate this structure as η^2, we will not use this notation for TiOOR complexes in the following discussion in order to distinguish them from Ti(O_2) complexes that do exhibit almost ideal η^2 coordination. Models **1B′** and **2A** have the same stoichiometry; a formal proton transfer from the water ligand of **1B′** to the peroxo group leads to **2A**. This transfer is calculated to be exothermic by −7.0 kcal/mol; thus, the hydroperoxo complex **2A** is more stable.

Epoxidation Transition States

In the study of the epoxidation activity of the various intermediates described above we calculated in each case the transition states of oxygen transfer to the model olefin ethylene. The corresponding species will be referred to by a prefix **TS**, e.g. **TS-1A** designates the transition state of ethylene epoxidation by complex **1A**. We focus on the oxygen transfer mechanism where the ethylene double bond directly attacks an oxygen center of the peroxo (hydroperoxo) group. The activation barriers are calculated with respect to the corresponding "free" complexes and an ethylene molecule. We shall neglect the physical interaction between ethylene and a peroxo group of the reaction intermediate in the ground state; this interaction is about 2 kcal/mol.[21]

In the following text we will not discuss the insertion mechanism of Mimoun, which implies that an olefin substrate first binds to the metal center and then inserts into the peroxo-metal bond in a [2 + 2] fashion to form a metallocycle intermediate.[12][14] For **1B** this metallocycle intermediate is calculated to lie 9.7 kcal/mol higher than the reactants and the corresponding activation barrier is 27.3 kcal/mol, while a direct attack requires only 19.0 kcal/mol for activation (Table 1). These findings are very similar to those for d^0 peroxo complexes of Re[17] and Mo[19] where, at the same level of computation, [2 + 2] insertion was shown to exhibit significantly higher activation barriers than a direct transfer.

The calculated transition states of the Ti(O_2) and TiOOR (R = H, CH_3) moieties have a number of features in common and, in general, resemble the structures of transition states of direct oxygen transfer for Re, Mo, and W.[17][19] All transition structures exhibit a spiro orientation of the ethylene unit (Figures 3 and 4), i.e. the plane CCO is almost orthogonal to the plane TiOO. The structure of the ethylene moiety is only slightly distorted from the gas phase structure: the C−C bond in the transition state is elongated by 0.04 Å at most. All these transition states represent a synchronous approach of ethylene to the peroxo moiety with almost equal distances between the carbon atoms and the attacked oxygen center. The largest difference between

Table 2. Calculated properties of Ti hydroperoxo (alkylperoxo) complexes: intermediates and oxygen transfer transition states. Structures **2A**, **2B**, and **3A** are shown in Figure 2. The models **4A/4B** and **5A/5B** are obtained after replacing equatorial OH groups in the models **2A/2B** by OCH_3 (Figure 9) and $OSiH_3$ groups, respectively

	2A	**2B**	**3A**	**4A**	**4B**	**5A**	**5B**
Geometry of peroxo group, Å							
r(O−O)	1.468	1.469	1.466	1.470	1.470	1.468	1.469
r(Ti−Oα)	1.891	1.918	1.888	1.899	1.926	1.892	1.923
r(Ti−Oβ)	2.262	2.276	2.265	2.256	2.268	2.237	2.243
NBO atomic charges, e							
q(Oα)	−0.46	−0.46	−0.46	−0.47	−0.47	−0.45	−0.45
q(Oβ)	−0.46	−0.47	−0.47	−0.46	−0.48	−0.45	−0.47
Total q(OO)	−0.92	−0.93	−0.93	−0.93	−0.95	−0.90	−0.92
q(Ti)	1.77	1.65	1.78	1.80	1.72	1.81	1.69
Core level energies, eV							
1s(Oα)	−521.8	−521.1	−521.6	−521.5	−520.9	−521.9	−521.3
1s(Oβ)	−522.8	−522.4	−522.7	−522.5	−522.2	−522.9	−522.6
3s(Ti)[a]	−66.7	−66.2	−66.6	−66.4	−65.9	−67.0	−66.6
Geometry of transition state, Å							
r(O−O)	1.790	1.768	1.820	1.794	1.802	1.800	1.783
r(Ti−O1)	1.954	2.013	1.957	1.966	2.001	1.969	1.998
r(Ti−O2)	2.061	2.064	2.032	2.059	2.095	2.042	2.067
r(O−C1)	2.202	2.165	2.170	2.187	2.079	2.170	2.117
r(O−C2)	2.120	2.160	2.071	2.111	2.187	2.111	2.186
Activation barrier, kcal/mol	12.7	12.4	15.8	14.5	13.6	15.0	13.7

[a] The 1s and 2s eigenvalues of Ti are not available because of the ECP description.

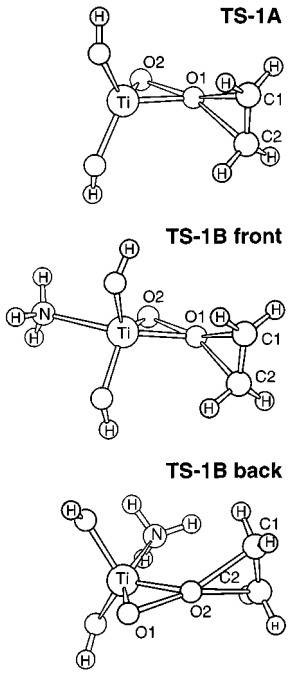


Figure 3. Transition states for direct oxygen transfer from various Ti peroxo complexes to an ethylene molecule

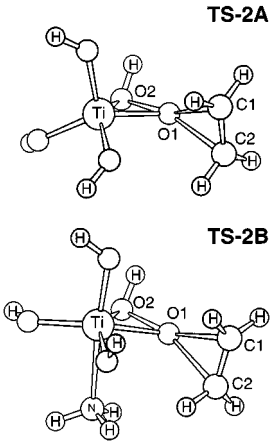


Figure 4. Transition states for direct oxygen transfer from the Ti hydroperoxo intermediates **2A** and **2B** to an ethylene molecule (α attack)

the O−C distances, about 0.03 Å, is found for **TS-1B′** (Table 1). The O−C distances of hydroperoxo complexes differ to a somewhat greater extent, at most by about 0.1 Å in **TS-3A** (Table 2). Similar synchronous transition states were calculated at the same level of computation (B3LYP) for the epoxidation of 1-pentene[30] and allyl alcohol[31] by peroxyformic acid. In the transition states of $Ti(O_2)$ intermediates, one of the Ti−O distances has increased by 0.05−0.14 Å whereas the other Ti−O distance has decreased by about 0.08 Å compared to the corresponding intermediates (Table 1). In the transition states of the TiOOR intermediates, the distance Ti−Oα has increased by 0.07−0.09 Å while the distance Ti−Oβ has decreased by about 0.16−0.21 Å (Table 2). The distances between the metal center and the attacked oxygen in peroxo and hydroperoxo transition states (Ti−O1 and Ti−Oα, respectively) are quite comparable and have values of about 1.9−2.0 Å (Tables 1 and 2). The most dramatic changes on the way to the transition state occur in the structure of the peroxo moiety: the O−O distance increases from about 1.47 Å in the intermediates to 1.82−1.86 Å in the peroxo transition states (Table 1) and to 1.89−1.92 Å in the hydroperoxo transition states (Table 2). A full vibrational analysis was performed for the transition state structures **TS-1B** (Figure 3) and **TS-2A** (Figure 4) as representatives of the two types of intermediates, $Ti(O_2)$ and TiOOR. Each of these structures was found to exhibit a single imaginary frequency; this confirms

the nature of the transition states as first-order saddle points on the corresponding potential energy hypersurfaces.

Oxygen transfer by epoxidation reaction involving d^0 metal peroxo complexes is generally accepted to exhibit electrophilic character.[1][12] This view is based on the fact that peroxo and alkylperoxo complexes react faster with electron-rich alkenes, e.g. with highly alkyl-substituted species. In a recent experimental study with peroxo compounds of V, Mo, and W the electrophilic nature of peroxo oxygen centers was also probed by sulfoxidation of thianthrene 5-oxide, in which an oxygen center of a peroxo complex attacks the electron-rich sulfide group rather than the electron-poor sulfoxide group.[32] In the present calculations, the electrophilic character of the oxygen transfer is manifested through the electron density transfer in the transition state, about 0.2 e, from ethylene to the peroxo (hydroperoxo) complex.

For $Ti(O_2)$ complexes the calculated activation barriers increase strongly in the sequence **1A**, **1B**, **1C**, from 11.0 to 27.4 kcal/mol (Table 1). The first complex of this family, **1A**, exhibits the lowest activation barrier, 11.0 kcal/mol, of all species considered in present work. An additional basic ligand significantly decreases the activity of the peroxo group, as deduced from the activation barriers of the complexes **1B** and **1B′**, which are 19.0 and 17.4 kcal/mol, respectively. It was found that the stronger the basic character of the ligand (ammonia vs. water), the higher the barrier. Note that in the models **1B** and **1B′** the oxygen centers of the peroxide group are not equivalent and, therefore, attacks of both centers have to be considered. We refer to attacks of the oxygen centers O1/O2, i.e. distant from/close to the NH_3 ligand (Figure 3), as "front" or "back" transition states.[17] In Table 1 we report the pertinent parameters of both transition states starting from complex **1B**. The back transition state corresponds to an attack of the more negative center O2, with the olefin in spatial proximity to the base. This situation leads to a somewhat higher barrier of 22.3 kcal/mol, which is in line with previous findings for Re, Mo, and W complexes.[17][19] The highest activation barrier of the peroxo series, 27.4 kcal/mol, is calculated for **1C** with two NH_3 ligands. Thus, saturation of the coordination sphere of the Ti center completely quenches the epoxidation activity of titanium peroxo group.

Analogous trends of increased activation energies concomitant with an increased number of basic ligands have been obtained in calculations on Re, Cr, Mo, and W mono- and bis-peroxo complexes.[17][19] A joint experimental and theoretical study[18] on different base adducts of the bis-peroxo complex $(O_2)_2(H_3C)Re{=}O$ revealed that coordination of a base to the complex induces, mediated by the metal center, additional electron density on the peroxo group; this pushes the *anti*-bonding $\sigma^*(O-O)$ level upward and results in a higher activation barrier (see below). Coordinatively saturated complexes of Re, Mo and W still exhibit moderate activation barriers ranging from 16 to 20 kcal/mol;[17–19] only Cr, which like Ti is a first row transition element, exhibits very high barriers for ethylene epoxidation. For example a barrier of about 40 kcal/mol is calculated for the model complex $(O_2)Cr(=O)_2 \cdot (NH_3)_2$,[19] which is structurally similar to our model **1C** but features oxo instead of hydroxide ligands. Experimental studies on the epoxidation activity of the bis-peroxo molybdenum complex $MoO(O_2)_2 \cdot HMPA$ have also rationalized the inhibiting effect of strongly coordinating solvents as an electronic effect of the additional (seventh) ligand on the properties of the peroxo group.[15][16] However, seven-coordinated $(L\text{-}L)MoO(O_2)_2$ complexes with bidentate L-L basic ligands were recently shown to catalyze epoxidation with *tert*-butyl hydroperoxide as an oxidant, and the formation of an MoOO*t*Bu group as an active center was proposed.[33]

For the TiOOR complexes we consider the α-attack to a peroxo group, i.e. transfer of the oxygen atom that is (closely) bound to the Ti center (Oα in Figure 2). β-attack, i.e. attack of the other oxygen center (with a substituent attached; Oβ in Figure 2), results in a higher activation energy; during this process the O−O bond breaks, accompanied by a proton transfer from Oβ to Oα. For instance, the activation barrier of ethylene epoxidation by **2A** via β-attack is calculated to be 25.7 kcal/mol, compared to 12.7 kcal/mol for α-attack. Similar differences in the barrier heights between α- and β-attack have also been found for hydroperoxo derivatives of Re and Mo.[17][19] At variance with the $Ti(O_2)$ complexes, the reaction barrier of TiOOR intermediates hardly changes upon addition of a donor ligand. Both transition states **TS-2A** and **TS-2B** feature relatively low activation energies of 12.7 and 12.4 kcal/mol, respectively. Thus, despite the additional NH_3 ligand, the activation barrier of **2B** is calculated to be slightly lower than the barrier of **2A**. This small decrease of the barrier height, by 0.3 kcal/mol, is in line with the change of the O−O distance (Table 2), although such minor changes are at the edge of computational accuracy.

Comparison to Other Computational Studies

Next, we shall comment on the absolute values of the calculated activation barriers and on the accuracy of our results. From MP2 calculations,[22] activation barriers have been reported for the front attack of **1B′**, 13.2 kcal/mol, and for the α-attack of **2A**, 14.4 kcal/mol, which are similar to the corresponding values of the present study, 17.4 and 12.7 kcal/mol, respectively. However, these MP2 values have been obtained under C_s symmetry constraints.[22] Two rather different values of the activation barrier of **2A**, 9 (with C_s symmetry constraints)[20] and 21[21] kcal/mol, have been determined in DF calculations where the gradient-corrected BLYP exchange-correlation functional was employed. Significant differences of structural parameters are also worth noting. The C_s symmetry constraints enforce a planar structure of the TiOOH moiety (Figure 2) with a significantly elongated Ti−Oβ distance, 2.6−2.7 Å[20–22] (compared to about 2.27 Å calculated in the present study; Table 1). On the other hand, when used without symmetry constraints the BLYP approach yields too short a value for

Ti−Oβ, 2.1 Å.[21] To check the effect of a C_s symmetry restriction for the present B3LYP investigations, we also calculated **1B′** and **2A** as well as the corresponding transition states **TS-1B′** (front) and **TS-2A** in this way; the resulting activation barriers are 16.1 and 13.8 kcal/mol, respectively. The differences from the corresponding values of full geometry optimizations are only about 1 kcal/mol, but are of opposite sign; thus, the selectivity between the two transition state structures is reduced.

To check for possible basis set effects and to justify the use of ECPs we also performed calculations with an all-electron TZV(f) basis for Ti. Single-point calculations with the geometry optimized in the standard approach (see Computational Details) yield activation barriers of 17.9 and 13.8 kcal/mol for **TS-1B′** (front) and **TS-2A**, respectively. Further optimization of the intermediate **1B′** and the transition state **TS-1B′** (front) leads to a uniform lowering of the total energy values by 0.5 kcal/mol for both structures with almost no effect on the height of the barrier; for **2A** the barrier changes by 0.1 kcal/mol only. These results show that the computational strategy used in the present study is quite accurate. As a further supporting argument, one notes that the structure of the TiOOH group calculated here is in very good agreement with available experimental data,[27] at variance with some earlier quantum chemical investigations.[20−22] The absolute accuracy of the B3LYP approach for activation barriers is another question altogether. However, a critical comparison shows that, at least for barrier heights of organic reactions, B3LYP performs significantly better than BLYP or MP2.[34][35]

Reaction Energies

For both types of species, $Ti(O_2)$ and TiOOR, ethylene epoxidation is an exothermic reaction. By this reaction, $Ti(O_2)$ species transform into complexes with a titanyl Ti=O functional group, while TiOOH species form a TiOH group after loss of one oxygen unit. The reaction energies are computed with respect to isolated products, namely the metal complex and ethylene oxide. The calculated reaction energies for $Ti(O_2)$ species increase from −23.8 kcal/mol for **1A** to −30.7, −31.2, and −34.1 kcal/mol for **1B′**, **1B**, and **1C**, respectively. Obviously, the higher reaction energy for highly coordinated species is due to higher stabilization of Ti=O product by basic ligands compared to initial $Ti(O_2)$ intermediate, since the coordination number of Ti is lower in the product complex due to the loss of one oxygen center. The complexes **2A** and **2B** exhibit significantly higher epoxidation reaction energies of −43.2 and −44.8 kcal/mol, respectively. The reaction profiles of the various $Ti(O_2)$ and TiOOH intermediates are represented in Figure 5 where the energy of the lowest intermediate **1C** + C_2H_4 is taken as reference. Inspection of Figure 5 reveals that the intermediates **1C** and **2B** feature the lowest energies and similar thermodynamic stability. However, epoxidation by **2B** is favored for both thermodymamic (higher reaction energy) and kinetic reasons (lower activation barrier). Evidently, the kinetic argument plays the key role here: epoxidation by the $Ti(O_2)$ intermediate **1C** can be ruled out since the corresponding transition state exhibits an activation barrier of more than 27 kcal/mol; this is more than twice as high as the activation barrier for the TiOOH intermediate **2B**.

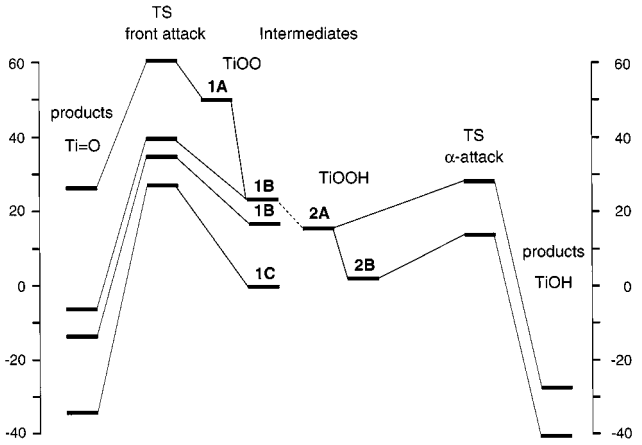


Figure 5. Total energies of intermediates with $Ti(O_2)$ or TiOOR groups and the corresponding transition states and products of ethylene epoxidation, relative to the energy of **1C** + C_2H_4. The activation barrier of proton transfer (dashed line) between the isomers **1B′** and **2A** is not shown

Molecular Orbital Analysis and Discussion

We turn to an analysis of the electronic structure of both types of the reaction intermediates, $Ti(O_2)$ and TiOOH, to rationalize the calculated activity trends. For this purpose, we consider a $Ti(O_2)$ moiety formally as an O_2^{2-} ligand coordinated to a Ti^{4+} d^0 center. The interaction between ligand and metal center can be considered as a donation from the peroxo group to the vacant d orbitals of Ti.

The energy of the unoccupied *anti*-bonding σ*(O−O) level is one of the most important of the factors that determine the activity of peroxo complex in oxygen transfer.[18] The activation of the O−O bond in the transition state is due to the interaction of this orbital in the LUMO group of the metal moiety with the HOMO π(C−C) of ethylene. The σ*(O−O) level is not the true LUMO of the complex; it lies slightly above the manifold of vacant d-levels of the metal center. The energy position of the σ*(O−O) level is expected to reflect the ability of peroxo group to accept additional electron density, which leads to breaking of O−O bond. This is indeed the case: the lower the energy of the σ*(O−O) level, the smaller is the calculated barrier for oxygen transfer. This is demonstrated in Figure 6a where the dependence of the activation barrier on the σ*(O−O) − π(C−C) gap is shown.

Coordination of a basic (σ-donor) ligand to **1A**, e.g. NH_3 in **1B**, increases the electron density at the peroxo group: the charge of the peroxo group given by a natural bond orbital analysis (NBO)[36] changes from −0.90 e in **1A** to −0.94 e in **1B** (and to −0.96 e in **1C** with two NH_3 ligands, Table 1). Concomitantly, the 1s(O) core level energies are shifted upward in **1B** by about 1.1 eV compared to **1A** (by

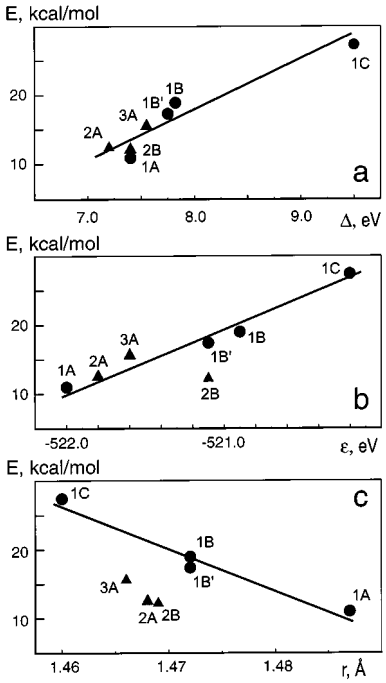


Figure 6. Calculated activation energy $\Delta E^{\#}$ (in kcal/mol) as function of (a) the HOMO−LUMO energy gap $\Delta = \sigma^*(O-O) - \pi(C-C)$ (in eV); (b) the energy ε (in eV) of the 1s(O) core level as a measure of negative charge located on the attacked oxygen center; (c) the O−O bond length (in Å). Data of peroxo group of $Ti(O_2)$ (circles) and TiOOR (triangles) complexes. Lines of linear regression on the data of the $Ti(O_2)$ complexes are also shown

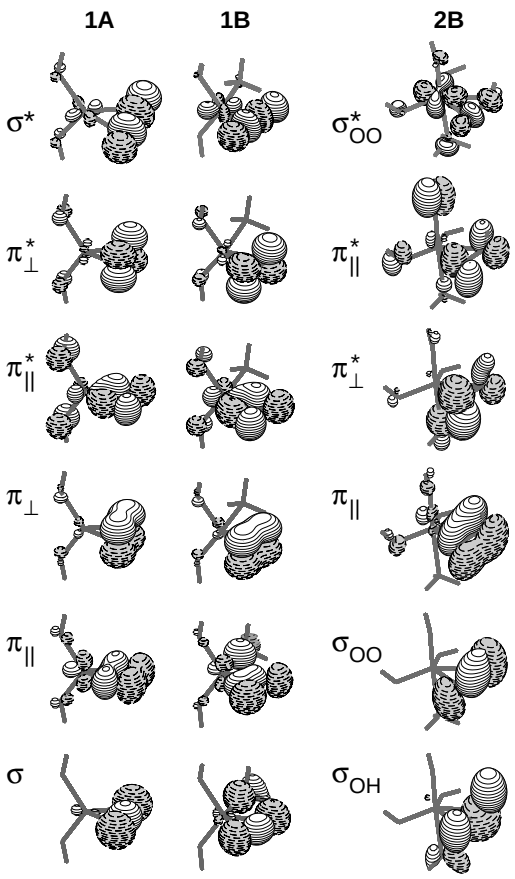


Figure 7. Structure of molecular orbitals of the intermediates **1A** (left), **1B** (center), and **2B** (right) with dominant contributions of the peroxo or hydroperoxo group

about 2.0 eV in **1C**); this is also indicative for an increase of electron density on the peroxo ligand. Thus, additional basic ligands reduce the donation from the peroxo ligand to the metal center; the electrophilic character that controls olefin epoxidation is also reduced.[1][12] Figure 6b shows how the 1s(O) core level energy as an indicator for the electron charge density of the peroxo or hydroperoxo moiety correlates with the calculated barrier of oxygen transfer.

Another factor determining the activation barrier of oxygen transfer is the strength of the O−O bond in the absence of an olefin substrate. When gauging changes in the O−O bonding based on the metal populations of the different O−O derived levels of the peroxo complex, one has to take into account their nature as O−O bonding and *anti*-bonding, respectively. Molecular orbitals of **1A** with important contributions of the peroxide group are shown in Figure 7, right-hand column. It is convenient to classify these orbitals according to the dominant σ and π character with respect to their peroxo contribution. The role of the unoccupied σ* (O−O) level has already been discussed above; let us now consider the occupied O−O orbitals. Since the peroxo group coordinates side-on to the Ti center, each pair of O−O bonding π and *anti*-bonding π* orbitals splits. We shall designate the orbitals with a dominant contribution in the TiOO plane by $\pi_{||}$ or $\pi_{||}$* and those with a dominant contribution perpendicular to that plane by π* or π*. Based on energy considerations, donation from the *anti*-bonding $\pi_{||}$* and π* orbitals of the O_2^{2-} ligand to the vacant d-orbitals of the Ti d^0 center is expected to be strongest; in particular the $\pi_{||}$* orbital exhibits a strong overlap with the d_{yz} orbital of Ti (Figure 7). There is also considerable donation from the lower lying level $\pi_{||}$ (Figure 7). The contributions of the σ(O−O) and π* orbitals to the metal-peroxide interaction are less important for overlap reasons. This analysis is corroborated by an NBO calculation of the moiety TiO_2^{2+} in the geometry of **1A**. This model, which is free of hydroxide ligand contributions, allows a facile separation of the metal-π(O−O) interaction channels according to the various irreducible representations of the point group C_{2v}; however, metal populations may be too large since the ligand sphere is incomplete. The Ti d populations due to donation from $\pi_{||}$* and π* are 0.63 and 0.60 e, respectively; donation from the in-plane $\pi_{||}$* orbital is slightly larger for overlap reasons. Donation from the bonding O−O levels is smaller: 0.20 e from π* and 0.26 e compounded from $\pi_{||}$ and σ. The (stronger) donation from the $\pi_{||}$* and π* orbitals reduces the population of these O−O *anti*-bonding levels in the complex and thus leads to a strengthening of the peroxo bond, while donation from O−O bonding levels has a weakening effect.

This analysis helps to rationalize the changes in the structure of the peroxide group; in **1A**, the O−O bond is elongated by coordination to a Ti center, 1.487 Å (Table 1), compared to a gas phase H_2O_2 molecule (calc. 1.454 Å; exp. 1.452 Å[37]). Upon addition of base the O−O bond short-

ens to 1.47 Å in **1B** and 1.46 in **1C** while the activation barrier for oxygen transfer rises significantly, by 16 kcal/mol in **1C** compared to **1A** (Table 1, Figure 6c). These indicators are consistent with the interpretation that coordination of additional bases to the complex results in a stronger O−O bond with a concomitant increase in the electronic charge of the peroxide group. The question arises as to which of the peroxide orbitals discussed above gains more population as a consequence of the additional basic ligand: the O−O bonding or *anti*-bonding orbitals. Inspection of the orbital structure of **1B** (Figure 7, center column) helps to answer this question: donation to the d-orbital of Ti significantly stabilizes the lone pair of the NH_3 ligand in the complex (Figure 8): in **1B** the energy level that represents the lone pair of NH_3 appears in the same energy region as the bonding levels of the peroxide ligand and thus partially mixes with σ and $\pi_{||}$ levels (Figure 7). Mixing with the orbitals π and π* is essentially forbidden because these orbitals have a node in the TiOO plane where the NH_3 ligand approaches the complex. However, as can be seen from Figure 7, there is also almost no interaction between the NH_3 lone pair and the peroxide *anti*-bonding $\pi_{||}$* level. This may in part be rationalized by the much higher energy of the $\pi_{||}$* level, but also the nodal structure does not favor mixing with the NH_3 lone pair. One is therefore led to conclude that a basic ligand reduces donation from the O−O bonding $\pi_{||}$ orbital more strongly than from the O−O *anti*-bonding $\pi_{||}$* orbital.

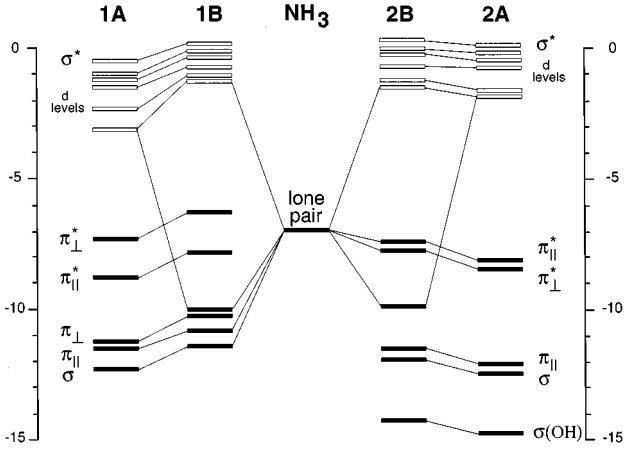


Figure 8. Orbital energy correlation diagram for peroxo and hydroperoxo derivatives

The above analysis shows that the bond between the metal center and the peroxo group plays an important role in the determination of the charge distribution over the orbitals of the peroxo moiety. This statement may be quantified with the help of an NBO charge analysis. The Ti contributions in the Ti−O σ interaction (in the TiOO plane) are 10% and 15% per bond for **1B** and **1C**, respectively. The corresponding contributions to the Ti−O π interaction (orthogonal to the TiOO plane) are 9% and 8% per bond for **1B** and **1C**, respectively. These small contributions of the metal center justify our idealized analysis focusing on the O−O derived orbitals. The increased Ti contributions in **1C** compared to **1B** indicate a strengthening of the Ti−O1 bond, in line with the calculated increase of the barrier for ethylene epoxidation. The elongation of the Ti−O1 bond from 1.84 Å in **1B** to 1.86 Å in **1C** (Table 1) may be due to stronger ligand-ligand repulsion in the highly coordinated **1C** species. However, the direct contribution of this bond to the activation energy should be considered as a second-order effect compared to the properties of the O−O bond. The main role of the Ti−O bond seems to be indirect: it influences the charge redistribution between the metal center and the peroxo group.

Figure 6 reveals that the hydroperoxo complexes follow similar general trends as the $Ti(O_2)$ complexes; however, they yield barriers of a similar height as complex **1A** despite their considerably shorter O−O bonds (Figure 6c). The orbital structure of the TiOOH species exhibits some peculiarities, which will be considered in the following discussion. When a proton is attached to the peroxo group, as in **2A** and **2B**, the electronic structure is significantly changed and a strong asymmetry is induced in the TiOO moiety (Figure 7, right-hand side). An idealized representation of the metal-ligand interaction in terms of OO orbitals has to be used with care for such species. The optimal position of the proton is in the plane almost orthogonal to the TiOO plane. Therefore, the strongest changes occur in the orbitals π and π*. The π contribution to O−O bonding is reduced and the nature of the resulting MO is better described as σ(OH) bonding; this level is the lowest in the orbital diagram of complex **2A** shown in Figure 7. In turn, the MO π* represents the lone pair of the center Oα of the hydroperoxo group (Figure 7). The other orbitals of the peroxo moiety (σ, $\pi_{||}$, and $\pi_{||}$*) remain more or less unchanged. The splitting of *anti*-bonding MOs π* and $\pi_{||}$*, with $\pi_{||}$* now being the HOMO, is significantly smaller, 0.3 eV for **2A**, than for $Ti(O_2)$ complexes where it amounts to more than 1 eV. The NBO analysis shows an almost equal charge distribution between the oxygen centers of the hydroperoxo group. The lower energy of the level 1s(Oβ) (Table 2) can be rationalized by the stabilization due to the electrostatic field of the attached proton.

As in the $Ti(O_2)$ complexes, addition of a donor ligand decreases the positive charge of the metal center, but its influence on the charge of the peroxo group is negligible (cf. the NBO charges and the core level energies of **2A** and **2B**; Table 2). At variance with the findings for "side-on" η^2-peroxo complexes, the additional ligand of the metal center has only a moderate effect on the activity of the hydroperoxo group. The calculated activation barrier of the intermediate **2B** even decreases slightly compared to **2A**. The negative charge of the peroxo group is higher in **2B** than in **2A** (Table 2) and, as a consequence, all pertinent valence levels are shifted upwards (Figure 8); however, this shift is smaller than that calculated when a ligand is introduced in **1A** to form **1B**. In particular, the vacant σ*(O−O) level shifts upwards by only 0.2 eV and its position is still rather low compared to $Ti(O_2)$ intermediates **1B** and **1C**,

which exhibit high barriers (Figure 6a). The apparently small effect of a basic ligand on the properties of the hydroperoxo complexes **2A/2B**, in particular on the oxygen transfer barrier, can be rationalized by the weaker metal-peroxo interaction in these "end-on" complexes. This follows, first of all, from the fact that only one oxygen atom, Oα, is involved in a strong interaction with the Ti center because the distance Ti−Oβ is much longer, by more than 0.3 Å (Table 2). Moreover, the Ti−Oα interaction is weaker than the corresponding interaction in the peroxo species. This can be inferred from the Ti−Oα distances in **2A** and **2B**, 1.89−1.92 Å, which are longer than the corresponding distances Ti−O of the peroxo complexes, 1.82−1.86 Å (Tables 1 and 2). Furthermore, the splitting of levels π* and $\pi_{||}$* is smaller in the hydroperoxo complexes due to reduced overlap with the orbitals of the metal center (Figure 7). The NBO analysis indicates a contribution of Ti to the Ti−Oα σ bond of 10% and 13% for **2A** and **2B**, respectively; this is slightly smaller than in the $Ti(O_2)$ complexes. However, at variance with the bonding of the $Ti(O_2)$ complexes, the π channel of the Ti−Oα interaction almost vanishes and the NBO analysis assigns the π* orbital to a lone pair located at the center Oα.

Coordination of the basic ligand NH_3 to **2A** and formation of species **2B** results in a slight decrease of the calculated activation barrier for the epoxidation of ethylene. This may be due to the fact that the lone pair of the NH_3 ligand of **2B** is stabilized in the gap between bonding and *anti*-bonding orbitals of the "peroxo" moiety. The bonding O−O levels of **2B** are lower in energy than the corresponding levels of the $Ti(O_2)$ intermediate **1B** while the NH_3 lone pair level is slightly higher (Figure 8). Inspection of the orbital structure of **2B** (Figure 7) shows that, in contrast to **1B**, this lone pair orbital of **2B** does not mix with the bonding O−O levels. In fact, this orbital even provides small contributions to the *anti*-bonding orbitals π*(OO) and $\pi_{||}$* (OO) that lie higher in energy. Thus, introduction of the additional basic ligand seems to affect the *anti*-bonding O−O levels of **2B** more than the bonding O−O levels. The resulting increased population of *anti*-bonding O−O levels leads to a weakening of the O−O bond and thus provides a rationalization for the small decrease in the barrier of the O−O bond activation in the epoxidation reaction.

Methyl Substitution of the Hydroperoxo Group

An important question is how a substituent R of the TiOOR moiety affects the epoxidation activity given that alkylhydroperoxides like *t*BuOOH are often used as oxidants.[1][3] To study this effect, we compare the epoxidation activity of the hydroperoxo complex **2A** with its methylperoxo derivative **3A** (Figure 2). Formation of **3A** according to the formal reaction **2A** + CH_3OH → **3A** + H_2O is exothermic by −4.9 kcal/mol. The calculated activation barrier for the complex **3A**, 15.8 kcal/mol, is 3 kcal/mol higher than that of **2A** (Table 2). The small increase of the negative charge on oxygen centers of the group $OOCH_3$ is in line with the weak electron-donating character of the methyl substituent; this inductive effect can also be detected from the small upward shift of 1s(O) levels (Table 2). Concomitantly, the σ*(O−O) level shifts upwards, correlating with an increase in the activation barrier (Figure 6a). The changes in the geometry of the peroxo moiety due to methyl substitution are minor.

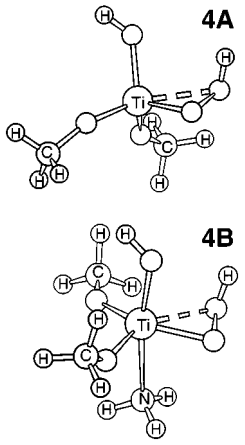


Figure 9. Model Ti hydroperoxo complexes, **4A** and **4B**, with equatorial hydroxide ligands replaced by methyloxide ligands

Methoxide and Siloxide in Comparison with Hydroxide Ligands

Finally, we consider the effects when hydroxide ligands of the model complexes are replaced by either methoxide or siloxide ligands. The methoxide derivatives **4A** and **4B** (Figure 9) are obtained from **2A** and **2B**, respectively, by formally exchanging two equatorial hydroxyl moieties by methoxide ligands. Analogous models with two $OSiH_3$ ligands will be referred to as **5A** and **5B**. These types of ligands are of interest since various titanium alkoxides, $Ti(OR)_4$, as well as titanium silicalites, are used as catalysts in epoxidation processes.[1]

In general, introduction of methoxide or siloxide ligands does not induce large structural changes in the TiOOH group (Table 2). The O−O bond length remains almost unchanged; the Ti−Oα distance becomes slightly shorter, while the Ti−Oβ distance increases somewhat. According to the NBO populations and the core level analysis, methoxide and siloxide ligands attract slightly more electron density from the Ti center than the hydroxide ligands. Thus, the electron density on the peroxo oxygen centers of the complexes **4A** and **4B** is higher (by 0.02 and 0.01 e) than on those of **2A** and **2B**, respectively; concomitantly, the 1s(O) levels shift to less negative energies by 0.2−0.3 eV. On the other hand, in complexes **5A** and **5B** there is somewhat less electron density on the peroxo group (compared to **2A** and **2B**, respectively), although for **5B** it can be detected only from the negative shift, −0.2 eV, of 1s(O) levels. Both types of ligands lead to slightly increased barriers of ethylene epoxidation. As in **2B**, the additional basic ligand NH_3 in **4B** and **5B** reduces the activation barriers by 0.9 and 1.3

kcal/mol compared to **4A** and **5A**, respectively. The corresponding transition states do not exhibit any noteworthy structural differences. Addition of NH_3 to **4A** and **5A** is exothermic by −11.0 and −12.1 kcal/mol, respectively. Based on the experience with the TiOOH models we expect similarly minor changes in the properties of the TiOO moieties due to substitution of hydroxide ligands by methoxide or siloxide.

A recent computational study of Ti silicalites[24] by Sinclair and Catlow also included a DF-BP86 calculation of ethylene epoxidation by the complex $(H_3SiO)_2Ti(OH)OOH$, which is essentially the same as the present model **5A**. For that model an activation barrier of 10.3 kcal/mol was calculated,[24] which is lower than the present result of the hybrid B3LYP, but is in agreement with the trend[34][35] of "pure" DF functionals like BLYP and BP86 in yielding lower barriers than the B3LYP hybrid method, which partially accounts for exact exchange. Sinclair and Catlow also considered the transformation of the structure $(H_3SiO)_2Ti(OH)OOH$ to $(H_3SiO)_2Ti(OH_2)(O_2)$ by an internal proton transfer, which is analogous to the transformation of **1B′** to **2A**.[24] In that study, contrary to the present results for **1B′** and **2A**, the $Ti(O_2)$ species was found to be more stable than the TiOOH analogue by about −10 kcal/mol. This difference may be due either to the different exchange-correlation potentials used or the influence of the $OSiH_3$ ligands. Sinclair and Catlow considered the structure $(H_3SiO)_2Ti(OH_2)(O_2)$ as a poisoned form of the catalyst, but they did not prove its inertness in the epoxidation process by calculating the corresponding transition state.[24] Under reaction conditions, a further base will coordinate to the Ti center; comparison with our models **1B** and **1B′** shows that adding one more basic ligand to $(H_3SiO)_2Ti(OH_2)(O_2)$ will render the activation barrier even higher.

Conclusions

We have studied the epoxidation of ethylene by model Ti^{IV} peroxo complexes with both "side-on" peroxo $Ti(\eta^2-O_2)$ and "end-on" hydroperoxo (or alkylperoxo) TiOOR (R = H, CH_3) moieties by means of hybrid B3LYP density functional calculations. The low coordinated intermediate $(HO)_2Ti(O_2)$ was found to exhibit a relatively low barrier of oxygen transfer, however it is not thermodynamically stable since it readily forms base adducts (Figure 5). Coordination of additional donor ligands to the Ti center (**1B**, **1C**) significantly increases the activation energy of a $Ti(O_2)$ group. Participation of the most stable intermediate **1C**, with its saturated coordination sphere, in the epoxidation process is ruled out for kinetic reasons since the corresponding transition state exhibits a high barrier, above 27 kcal/mol. The inhibiting effect of donor ligands was rationalized with the help of a molecular orbital analysis. Two effects were distinguished: (i) additional basic ligands reduce the electrophilicity of the peroxo group and push the σ*(O−O) orbital responsible for breaking the O−O bond to higher energies; (ii) concomitantly, the populations of the bonding levels of the peroxo group increase and strengthen the O−O bond, as deduced from shorter O−O distances in model complexes with higher coordination numbers. The high activation barrier for coordinatively saturated $Ti(O_2)$ species is in agreement with the experimentally observed chemical stability of known Ti^{IV} peroxo complexes.[10][11]

At variance with $Ti(O_2)$ moieties, the activity of a TiOOH functional group depends only very weakly on the saturation of the Ti coordination sphere. The hydroperoxo group is less sensitive to the coordination of the Ti center since there are less channels for metal-peroxo interaction for such "end-on" structures than in the case of symmetric "side-on" structures $Ti(O_2)$. Calculated reaction energies and activation barriers show that Ti hydroperoxo species are very favorable for thermodynamic *and* kinetic reasons. The hydroperoxo complex **2B**, with one basic ligand, is only slightly less stable than the η^2-peroxo complex **1C** with two basic ligands. Due to its low activation barrier, it exhibits by far the lowest lying transition state (by absolute energy, Figure 5). Substitution of hydrogen by methyl in the TiOOR group (**2A** vs. **3A**) was found to increase the activation barrier for epoxidation by 3 kcal/mol. Substitution of hydroxide anionic ligands in TiOOH model complexes by alkyloxide and siloxide increases the activation barrier by 1−2 kcal/mol. The activation barriers of oxygen transfer from a TiOOR group to an ethylene molecule are calculated in the range of 13−16 kcal/mol, thus are comparable, if not lower, than the barriers calculated at the same level of computation for various Re peroxo species.[17]

In summary, the computational results favor reaction paths that involve hydroperoxo (or alkylperoxo) titanium species over $Ti(O_2)$ species. Thus, the results of the present computational study support the interpretation of experimental and theoretical studies[4,7,10,15] that hydroperoxo intermediates are responsible for the epoxidation reactions by Ti complexes and Ti-silicalites, while the corresponding peroxo species appear (if at all) as a chemically inert structures of side reactions only.

Computational Details

In the density functional calculations[38] we employed the hybrid B3LYP exchange-correlation scheme.[39] The 1s, 2s, and 2p core shells of Ti were replaced by a LANL2 effective core potential (ECP).[40] The corresponding basis set[40] of Ti, which describes the outermost core (3s and 3p) and the valence shells, was used in the contraction (441/2111/41). For main group elements we employed a 6-311G(d,p) basis set.[33] Geometry optimizations of intermediates and transition states were performed without any symmetry constraints. Transition state structures were searched by numerically estimating the matrix of second-order energy derivatives at every optimization step and by requiring exactly one eigenvalue of this matrix to be negative. We checked typical transition state structures by performing a full vibrational analysis, using a TZV basis set for Ti (see below). Reaction energies and barrier heights were evaluated in single-point fashion with the Ti basis set augmented by a polarization f-exponent (1.506).[42]

To check how results depend on the quality of basis set and to validate the ECP for the present study, some model complexes and the corresponding transition states (including a full vibrational analysis) were re-calculated using an all-electron valence triple-ζ (TZV) basis set for Ti (842111/6311/411). Reaction energies and barrier heights were evaluated in single-point calculations with an augmented Ti basis, using the above polarization f-exponent [TZV(f)].

In preceding studies of Re and Mo oxo and peroxo complexes[17][29] zero-point energy corrections were shown to uniformly shift the calculated reaction energies and reaction barriers by small positive values. However, in no case did they change the qualitative picture when reactivity of different intermediates was compared. Therefore, in the present study we refrained from applying zero-point energy corrections to reaction energies and barrier heights.

Acknowledgments

We thank P. Hofmann, H. Rothfuss, J. H. Teles, and G. N. Vayssilov for helpful discussions. This work was supported by the Deutsche Forschungsgemeinschaft, the German Bundesministerium für Bildung, Wissenschaft, Forschung und Technologie (grant no. 03D0050B), INTAS-RFBR (IR-97−1071), and the Fonds der Chemischen Industrie.

[1] K. A. Jørgensen, *Chem. Rev.* **1989**, *89*, 431−458.
[2] T. Katsuki, K. B. Sharpless, *J. Am. Chem. Soc.* **1980**, *102*, 5974−5976.
[3] R. A. Sheldon, *J. Mol. Catal.* **1980**, *7*, 107−126.
[4] M. G. Clerici, P. Ingallina, *J. Catal.* **1993**, *140*, 71−83.
[5] G. Tozzola, M. A. Mantegazza, G. Ranghino, G. Petrini, S. Bordiga, G. Ricchiardi, C. Lamberti, R. Zulian, A. Zecchina, *J. Catal.* **1998**, *179*, 64−71.
[6] G. N. Vayssilov, *Catal. Rev. Sci. Eng.* **1997**, *39*, 209−251.
[7] M. G. Finn, K. B. Sharpless, *J. Am. Chem. Soc.* **1991**, *113*, 113−126.
[8] B. Notari, *Stud. Surf. Sci. Catal.* **1988**, *37*, 413−425.
[9] D. R. C. Huybrechts, L. De Bruycker, P. A. Jacobs, *Nature* **1990**, *345*, 240−242.
[10] H. J. Ledon, F. Varescon, *Inorg. Chem.* **1984**, *23*, 2735−2737.
[11] H. Mimoun, M. Postel, F. Casabianca, J. Fischer, A. Mitschler, *Inorg. Chem.* **1982**, *21*, 1303−1306.
[12] H. Mimoun, in: *Chemistry of Peroxides*, (Ed.: S. Patai), Wiley, Chichester, **1983**, Chapter 15, pp. 463−482.
[13] C. C. Romão, F. E. Kühn, W. A. Herrmann, *Chem. Rev.* **1997**, *97*, 3197−3246.
[14] H. Mimoun, I. S. de Roch, L. Sajus, *Tetrahedron* **1970**, *26*, 37−50.
[15] G. Amato, A. Arcoria, F. P. Ballistreri, G. A. Tomasseli, O. Bortolini, V. Conte, F. Di Furia, G. Modena, G. Valle, *J. Mol. Catal.* **1986**, *37*, 165−175.
[16] E. P. Talsi, K. V. Shalyaev, K. I. Zamaraev, *J. Mol. Catal.* **1993**, *83*, 347−366.
[17] P. Gisdakis, S. Antonczak, S. Köstlmeier, W. A. Herrmann, N. Rösch, *Angew. Chem.* **1998**, *110*, 2333−2336; *Angew. Chem. Int. Ed.* **1998**, *37*, 2211−2214.
[18] F. E. Kühn, A. M. Santos, P. W. Roesky, E. Herdtweck, W. Scherer, P. Gisdakis, I. V. Yudanov, C. Di Valentin, N. Rösch, *Chem. Eur. J.* **1999**, in press.
[19] C. Di Valentin, P. Gisdakis, I. V. Yudanov, N. Rösch, in preparation.
[20] Y. D. Wu, D. K. W. Lai, *J. Org. Chem.* **1995**, *60*, 673−680.
[21] E. Karlsen, K. Schöffel, *Catal. Today* **1996**, *32*, 107−114.
[22] [22a] G. M. Zhidomirov, A. L. Yakovlev, M. A. Milov, N. A. Kachurovskaya, I. V. Yudanov, *Catal. Today* **1999**, *51*, 1−14. − [22b] I. V. Yudanov, Ph. D. Dissertation, Boreskov Institute of Catalysis, Novosibirsk, **1997**.
[23] D. Tantanak, M. A. Vincent, I. H. Hillier, *Chem. Commun.* **1998**, 1031−1032.
[24] P. E. Sinclair, C. R. A. Catlow, *J. Phys. Chem.* **1999**, *103*, 1084−1095.
[25] H. Manohar, D. Schwarzenbach, *Helv. Chim. Acta* **1974**, *57*, 1086−1095.
[26] R. Guilard, J.-M. Latour, C. Lecomte, J.-C. Marchon, J. Protas, D. Ripoll, *Inorg. Chem.* **1978**, *17*, 1228−1237.
[27] G. Boche, K. Möbus, K. K. Harms, M. Marsch, *J. Am. Chem. Soc.* **1996**, *118*, 2770−2771.
[28] A. Zecchina, S. Bordiga, C. Lamberti, G. Ricchiardi, D. Scarano, G. Petrini, G. Leofanti, M. Mantegazza, *Catal. Today* **1996**, *32*, 97−106.
[29] P. Gisdakis, S. Antonczak, N. Rösch, *Organometallics*, in press.
[30] D. A. Singleton, S. R. Merrigan, J. Liu, K. N. Houk, *J. Am. Chem. Soc.* **1997**, *119*, 3385−3386.
[31] R. D. Bach, C. M. Estévez, J. E. Winter, M. N. Glukhovtsev, *J. Am. Chem. Soc.* **1998**, *120*, 680−685.
[32] W. Adam, D. Golsch, J. Sundermeyer, G. Wahl, *Chem. Ber.* **1996**, *129*, 1177−1182.
[33] W. R. Thiel, T. Priermeier, *Angew. Chem.* **1995**, *107*, 1870−1871; *Angew. Chem. Int. Ed. Engl.* **1995**, *34*, 1737−1738.
[34] J. Baker, M. Muir, J. Andzelm, *J. Chem. Phys.* **1995**, *102*, 2063−2079.
[35] A. Görling, S. B. Trickey, P. Gisdakis, N. Rösch, in: *Topics in Organometallic Chemistry*, Vol. 4, (Eds.: J. Brown, P. Hofmann), Springer, Berlin, **1999**, p. 109.
[36] A. E. Reed, L. A. Curtiss, F. Weinhold, *Chem. Rev.* **1988**, *88*, 899−926.
[37] *CRC Handbook of Chemistry and Physics*, 73rd Ed., CRC Press, Boca Raton, FL, **1993**.
[38] *Gaussian 94*, Revision D.4, M. J. Frisch, G. W. Trucks, H. B. Schlegel, P. M. W. Gill, B. G. Johnson, M. A. Robb, J. R. Cheeseman, T. Keith, G. A. Petersson, J. A. Montgomery, K. Raghavachari, M. A. Al-Laham, V. G. Zakrzewski, J. V. Ortiz, J. B. Foresman, J. Cioslowski, B. B. Stefanov, A. Nanayakkara, M. Challacombe, C. Y. Peng, P. Y. Ayala, W. Chen, M. W. Wong, J. L. Andres, E. S. Replogle, R. Gomperts, R. L. Martin, D. J. Fox, J. S. Binkley, D. J. Defrees, J. Baker, J. P. Stewart, M. Head-Gordon, C. Gonzalez, J. A. Pople, Gaussian, Inc., Pittsburgh PA, **1995**.
[39] [39a] A. D. Becke, *J. Chem. Phys.* **1993**, *98*, 5648−5651. − [39b] C. Lee, W. Yang, R. G. Parr, *Phys. Rev. B* **1988**, *37*, 785−789.
[40] P. J. Hay, W. R. Wadt, *J. Chem. Phys.* **1985**, *82*, 299−310.
[41] R. Krishnan, J. Binkley, R. Seeger, J. Pople, *J. Chem. Phys.* **1980**, *72*, 650−654.
[42] A. W. Ehlers, M. Böhme, S. Dapprich, A. Gobbi, A. Höllwarth, V. Jonas, K. F. Köhler, R. Stegmann, A. Veldkamp, G. Frenking, *Chem. Phys. Lett.* **1993**, *208*, 111−114.
[43] A. Schäfer, C. Huber, R. Ahlrichs, *J. Chem. Phys.* **1994**, *100*, 5829−5835.

Received June 18, 1999
[I99226]

"Embroidered" Square Pyramidal Coordination Caps for Nickel(II): Mono-, Di- and Tetrafunctionalisation of a Tetrapodal Pentadentate Ligand with an NN_4 Donor Set

Christian Dietz,[a] Frank W. Heinemann,[a] and Andreas Grohmann*[a]

Dedicated to Professor Hubert Schmidbaur on the occasion of his 65th birthday

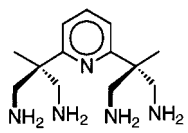
Keywords: Tetrapodal pentadentate ligand / Ligand periphery / Polydentate amine complex / Nickel / Podand / Schiff base

The tetrapodal pentaamine ligand 2,6-bis(1′,3′-diamino-2′-methylprop-2′-yl)pyridine **(1)**, which contains four equivalent primary amino groups, can be derivatised partly or completely by Schiff base condensation with suitable carbonyl compounds. The new ligands thus obtained are mononucleating, as shown by the X-ray crystal structures of their respective nickel(II) complexes. Reaction of **1** with 1 equiv. of salicylaldehyde and subsequent reduction allows the selective modification of one of the four sidearms. The resulting ligand **2** is hexadentate and uninegative in its nickel(II) complex {[(**2**)Ni]PF_6} **(3)** with both the secondary amine and the phenoxide functionalities coordinated to the metal centre. The unreduced Schiff base form of the ligand, **4**, does not form a complex with nickel(II) as readily, and only a small quantity of the mixed salt {[(**4**)Ni][(**1**)Ni(H_2O)]($Br)_2(PF_6)$} **(5)** has been obtained. While the overall coordination of **4** resembles that of **2**, there is considerably more strain in the appended chelate ring, due to the presence of the C=N double bond. Modification of one arm in **1** can also be achieved by condensation with 1 equiv. of acetylacetone, to give the new ligand **6** which, likewise, is hexadentate in its Ni^{II} complex {[(**6**)Ni]$(PF_6)_2$} **(7)**. In this case, however, the *N*/*O*-functional sidearm is not deprotonated. Rather, it is coordinated as the keto-imine tautomer, making **7** a rare example of a metal complex containing this structural fragment. Two-fold functionalisation of **1** is observed upon reaction with acetone, regardless of whether the ketone is present in stoichiometric amounts or in excess, to give the pentadentate ligand **8** with two diagonally juxtaposed isopropylidene-imine units. The complex isolated with this ligand {[(**8**)Ni]$(PF_6)_2$} **(9)** contains pentacoordinate Ni^{II}, the sixth coordination site being blocked by the rigidly positioned isopropylidene groups. When reacted with 4 equiv. of *trans*-cinnamaldehyde, all the primary amino groups in **1** condense to give the four-fold Schiff base **10**, which acts as a pentadentate podand towards nickel(II). In this complex, {[(**10**)Ni(OH_2)]Br_2} **(11),** an aqua ligand completes the coordination octahedron. All ligands are stable towards hydrolysis when coordinated to the metal, despite the presence of *alkyl*-imine groups in some cases.

Introduction

Simple tetrapodal pentadentate ligands which act as square pyramidal coordination caps towards octahedrally coordinating transition metal ions were unknown until recently.[1−5] The ligands are required to have a donor atom in the apical position of the pyramid, whose lone pair is directed towards the centre of the octahedron, as well as four donor arms pointing toward the basal positions. This leaves a sixth site on the metal ion for the coordination of a small monodentate ligand.

A prototypical pentadentate ligand with this topology is the pyridine-derived polyamine **1**, which has been shown to be mononucleating in a series of complexes of nickel(II),[4] cobalt(III),[1,6,7] copper(II)[8] and iron(II).[9] Variation of the basal functional groups to include donors other than primary amines is possible in principle. Such ligands are of basic interest in coordination chemistry, and we have set out to study this class of compounds with a view to using them as head groups in functional metal complexes. All basal donor groups are *terminal* with respect to the ligand framework. Further derivatisation aims to append a "pocket" to the tetrapodal ligand, encircling the sixth coordination site of the metal ion. Depending on the nature of the functional groups present in this pocket, we wish to explore whether the sixth ligand can engage in a two-point interaction with the complex fragment, through a combination of dative bonding to the metal and secondary bonding interactions with the ligand periphery (e.g. hydrogen bonding or π-stacking interactions). Such interactions with the sixth ligand are expected to modulate the thermodynamics and kinetics of its binding, as well as its reactivity.



1

In the case of **1**, the presence of four equivalent primary amino groups makes the molecule an attractive substrate for Schiff base condensations. The present work describes a

[a] Institut für Anorganische Chemie,
Universität Erlangen-Nürnberg,
Egerlandstraße 1, D-91058 Erlangen, Germany
E-mail: grohmann@anorganik.chemie.uni-erlangen.de

 © WILEY-VCH Verlag GmbH, D-69451 Weinheim, 1999 1434−1948/99/1212−2147 $ 17.50+.50/0

series of ligands in which one, two or all four basal amino groups have been derivatised in this manner, and the full characterisation of the Ni^{II} complexes of these "embroidered" square pyramidal coordination caps. Nickel(II) was chosen as the central metal ion as it usually gives complexes that are readily purified (crystallisation, ion exchange chromatography), thus facilitating access to the pure ligands and to complexes of a wider range of metals. This contribution presents results pertaining to Schiff base derivatives of **1** that maintain a mononuclear coordination mode.

Results and Discussion

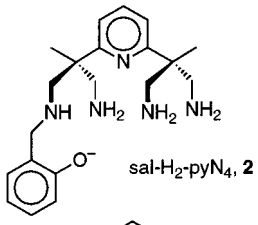
In all condensation reactions reported here, the pentaamine **1** was employed as its tetrakis(hydrobromide) salt/methanol solvate, **1**·4HBr·MeOH.[10] Methanol solutions of **1** were prepared in most cases by neutralisation of HBr with NaOMe, which was generated in situ by dissolving the appropriate amount of sodium metal. NaBr does not precipitate from methanol under the given conditions, and was not removed from solution before attempting the subsequent reactions.

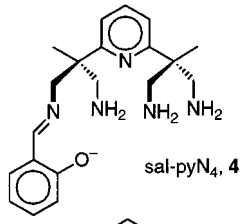
Preliminary experiments showed that the pentaamine **1** reacts readily with 4 equivalents of salicylaldehyde in methanol to give the four-fold Schiff base condensation product, and that reduction of the C=N double bonds with sodium borohydride is similarly straightforward. The Schiff base and the secondary amine derivatives are both potentially nonadentate ligands with NN_4O_4 donor sets, but the presence of four 2-hydroxy substituents in the periphery of the NN_4 pyramid is expected to induce considerable steric crowding with respect to the formation of mononuclear complexes of "small" transition metal ions such as nickel(II), utilizing only the NN_4 donor set. Indeed, we have so far not been able to isolate complexes of the type $[Ni^{II}(NN_4O_4)]$.

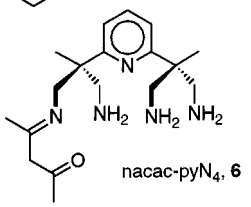
sal-H_2-pyN_4 (2), sal-pyN_4 (4) and Their Complexes With Ni^{II}

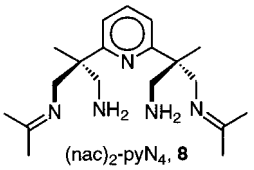
In light of the above observation we attempted the condensation of **1** with only one equivalent of salicylaldehyde, in the hope of obtaining asymmetric ligands of type **2** (after reduction) or **4**. These potentially hexadentate ligands may block all the coordination sites of the metal centre, but their synthesis appears to be a reasonable point of entry into the coordination chemistry of mononucleating derivatives of **1**. In accordance with the terminology used for monosubstituted diamines (so-called "half-units", which are of current interest for their potential in asymmetric catalysis), ligands such as **2** or **4** would represent "quarter-units".[11–13]

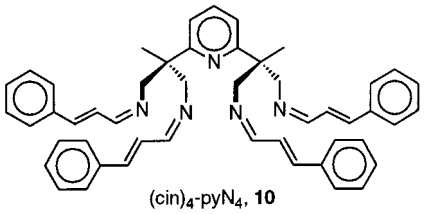
For the preparation of sal-H_2-pyN_4 (formula **2** shows its deprotonated form), one equivalent each of **1** and salicylaldehyde are reacted in methanolic solution at room temperature. The reaction is rapid, as judged by the appearance of a yellow colour which is characteristic of the Schiff base. Reduction of the condensation product in situ with sodium











borohydride gives a solution containing the ligand sal-H_2-pyN_4 (cf. **2**). After workup and addition of a suitable nickel(II) salt, followed by hexafluorophosphate anion, the desired mononuclear metal complex **3** precipitates as a purple crystalline material, in which the ligand is deprotonated and carries a negative charge. No attempt has as yet been made to optimise the yield (30% after recrystallisation). While the 1:1 condensation may not go to completion (see **4** and **5**, below), it is possibly not fully specific either, so that more highly substituted side products (sal:pyN_4 > 1:1) may form which, upon reduction, do not give the respective metal complexes as readily. In any case, nickel complexation should provide a convenient means of isolating pure **2**.

The spectroscopic characteristics of **3** (see Experimental Section) resemble those determined for a series of octahedral nickel(II) complexes of the polyamine ligand **1**, in which a monodentate ligand occupies the sixth coordination site.[4] In the UV/Vis spectrum, an absorption attributable to a d–d transition occurs at λ = 509 nm and thus at higher energy than in the aqua complex [(**1**)Ni(H_2O)]I_2 (λ = 543 nm),[4] indicating that the NN_4O ligand **2** generates a stronger ligand field than the parent NN_4 ligand **1**. The compound is paramagnetic, with shifted and broadened resonances in the ^1H NMR spectrum, as ex-

pected for a complex of octahedrally coordinated high-spin nickel(II).

Compound **3** crystallises with one molecule of water and one molecule of methanol per formula unit. The molecular structure of the cation, which has C_1 symmetry, is shown in Figure 1. The nickel(II) ion is coordinated by the NN_4 part of the ligand donor set in a pyramidal fashion, and the phenoxide oxygen atom of the peripheral arm occupies the coordination site remaining on the metal centre, the overall coordination geometry of Ni^{II} thus being octahedral. All chelate rings are six-membered. The nickel atom is displaced by 0.0397(5) Å towards the phenoxide oxygen atom, relative to the plane defined by the four equatorial amino nitrogen atoms. While the arrangement of donor atoms along the main axes of the octahedron is close to linear {176.4(1) − 177.8(1)°, see Table 1}, the NN_4 donor cap shows a slight distortion similar to that observed for a series of complexes of the type $[(\mathbf{1})Ni(X)]^{n+}$, where X is a neutral or anionic monodentate ligand.[4] The pyridine ring, itself a regular hexagon, is tilted to one side of the NN_4Ni pyramid so that the heterocycle and the aliphatic carbon atoms C18, C19, C22 and C23 are no longer coplanar {interplanar angle = 17.0(2)°}. The acute angle subtended by the lines N11−C13 and N11−Ni1 at N11 is 11.9(1)° (instead of 0°). At the same time, the nonbonded distance C16···C21 is lengthened to 5.370(5) Å, while the corresponding distance C17···C20 is shortened to 4.752(5) Å. As a consequence, the least-squares planes defined by the four methylene carbon atoms C16, C17, C20, and C21, and the four equatorial amino nitrogen atoms N12, N13, N14, and N15, are not parallel but at an angle of 8.0(1)° (Table 2). Since this kind of distortion is also observed in the parent complexes $[(\mathbf{1})Ni(X)]^{n+}$, where it has been attributed to crystal packing effects,[4] it is not necessarily caused by the presence of an additional chelating group in the ligand periphery, viz. the salicylaldehyde-derived side-arm. The accommodation of the latter into the ligand framework does not induce significant changes in any of the $Ni^{II}-N$ bond lengths ($Ni1-N_{eq}$: 2.080(3)−2.129(3) Å; $Ni1-N_{py}$: 2.075(2) Å), as compared to the range of values observed in $[(\mathbf{1})Ni(X)]^{n+}$. In particular, the bond length between Ni1 and the secondary amino nitrogen atom N15 does not differ markedly from the other values for d(Ni−N) in this structure.[14] Apparently, the only structural effect of the chelating sidearm on the NN_4 coordination cap in **3** when compared to that in $[(\mathbf{1})Ni(X)]^{n+}$ is that there are no longer matching pairs of opposite bite angles in the equatorial plane, these angles all being different and spanning the range 85.2(1)−95.3(1)° (Table 1).

The chelate ring formed by the phenoxide sidearm is a folded hexagon, the fold being along the vector O1···C30. Defining the side of the benzene ring facing the equatorial nitrogen atoms as positive, the phenoxide oxygen and methylene carbon atoms (O1 and C30) are displaced from this plane by +0.061(3) Å and −0.139(4) Å, respectively. The secondary amino nitrogen atom N15 is outside the benzene ring plane by +1.026(6) Å. The latter observation supports the notion that free rotation around the bond N15−C30 (i.e. reduction of the imine precursor) greatly facilitates the phenoxide sidearm to become a chelating group (cf. the related discussion for the Schiff base complex **5**, below). The value for d(Ni1−O1) is 2.066(2) Å and thus lies in the range observed for this type of bond in other octahedral Ni^{II} complexes.[15][16]

A nickel(II) complex of the salicylaldimine ligand **4** does not form as readily. Condensation of **1** and salicylaldehyde as described above, followed by addition of suitable Ni^{II} salts, has so far yielded only a small amount of the mixed salt $\{[(\mathbf{4})Ni][(\mathbf{1})Ni(H_2O)](Br)_2(PF_6)\}$ **(5)** the composition of which shows incomplete condensation (cf. the discussion of **2** and **3**, above.) Ligand **4** may be sluggish to form a complex with Ni^{II} because of the unfavourable conformation of the incipient chelate ring due to the presence of a C=N double bond. This ring is expected to be planar (conjugation of the aldimine and aromatic systems) and hence considerably strained. Alternatively, the phenol oxygen atom may remain an uncoordinated spectator group in the ligand periphery (see Introduction). For clarification, **5** has been characterised by X-ray crystallography.

The molecular structure of the cation $[(\mathbf{4})Ni]^+$, in which the ligand is deprotonated to the phenoxide, is shown in Figure 1. The overall coordination of **4** resembles that of **2** (see Figure 1; note the labelling schemes for $[(\mathbf{4})Ni]^+$ and $[(\mathbf{2})Ni]^+$, which reflect similar tilts of the pyridine rings, leading to different labels for the substituted equatorial nitrogen atoms). Some relevant structural parameters of the NN_4 part of the ligand are as follows; while the bond lengths $Ni-N_{py}$ and $Ni-N_{primary}$ are similar in the structures of **3** and **5** (Table 1), the Ni−N bond to the nitrogen atom carrying the appended chelate arm is significantly shorter in **5** {2.018(7) Å} than in **3** {2.119(3) Å}, as expected for an sp^2-hybridised nitrogen atom in the case of **5**. In contrast, the nickel−phenoxide bond is longer in **5** {2.115(5) Å} than in **3** {2.066(2) Å}, which is probably a manifestation of the strain imposed by the C=N double bond. The distortion of the ligand cap is of the same degree as in **3** (Table 2).

The chelate ring formed by the phenoxide sidearm is essentially planar. The maximum deviation from the best plane defined by all six ring atoms is 0.207(4) Å for O1. Selected angles in the ring are C30−N14−Ni1 127.8(7)°, C31−C30−N14 125.2(9)° and Ni1−O1−C32 123.9(5)°. The deviations from the ideal values of 120° and 109.5°, respectively, further attest to the strain in the ring. As manifest in the molecular structure of **3**, this strain is considerably relieved upon reduction of the C=N double bond. It may thus be concluded that, if the incipient chelate ring is six-membered, unsaturation does not altogether prevent its formation. For a donor group appended to the NN_4 cap to remain uncoordinated, and thus set up for interactions with a substrate coordinated to the metal (see Introduction), the donor atom should be attached to the β-, not the γ-carbon atom of the sidearm. The other cation in the structure, $[(\mathbf{1})Ni(H_2O)]^{2+}$, has parameters similar to those previously described for $[(\mathbf{1})Ni(H_2O)]I_2$.[4]

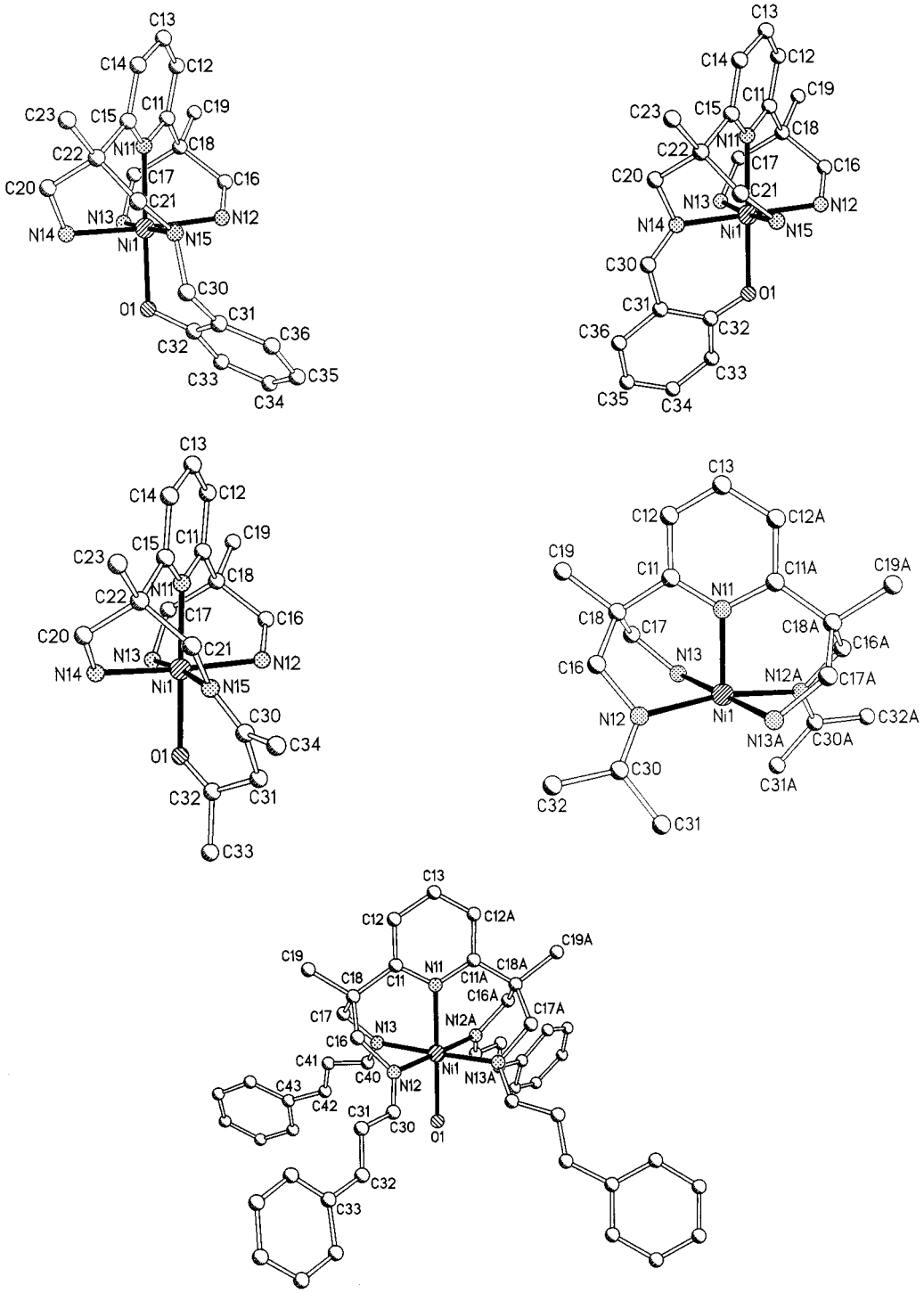


Figure 1. Molecular structures of the cations in **3** (top left), **5** (top right), **7** (middle left), **9** (middle right), and **11** (bottom); for clarity, ball-and-stick representations have been chosen, and hydrogen atoms have been omitted, the atom labelling is based on like orientations of the distortion of the NN_4 ligand cap, where applicable (see text)

nacac-pyN_4 (6), and [(6)Ni]$(PF_6)_2$ (7)

The difficulties in isolating a complex of the salicylaldimine quarter-unit **4** led us to study the condensation reaction of **1** with 1 equiv. of a related carbonyl substrate, acetylacetone (2,4-pentanedione). The expected condensation product is a β-ketoamine. While Schiff bases of salicylaldehyde can only exist as the phenol-imine tautomers, three distinct tautomeric forms are possible for β-ketoamines (enol-imine **A**, keto-enamine **B**, and keto-imine **C**).[17][18] Therefore, whereas salicylaldimines usually lose a proton upon metal complexation to become uninegative ligands, β-ketoamines may be either uninegative or neutral in their complexes, depending on whether the "central" carbon

Table 1. Selected bond lengths [Å] and angles [°] for **3**, **5**, **7**, **9** and **11** with estimated standard deviations in parentheses; the atom numbering is dictated by the tilt of the pyridine ring (see Figures and text)

Bond or Angle	**3**·H_2O·MeOH	**5**·H_2O	**7**	**9**	**11**·2MeOH
Ni1−N11	2.075(2)	2.074(7)	2.043(5)	1.991(4)	2.076(7)
Ni1−N12	2.129(3)	2.106(6)	2.114(5)	2.041(3)	2.106(6)
Ni1−N13	2.084(3)	2.086(6)	2.082(5)	2.080(3)	2.085(5)
Ni1−N14	2.080(3)	2.018(7)	2.100(5)	−	−
Ni1−N15	2.119(3)	2.127(6)	2.049(5)	−	−
Ni1−O1	2.066(2)	2.115(5)	2.105(4)	−	2.167(6)
N12−C30	−	−	−	1.266(4)	1.283(8)
N14−C30	−	1.26(1)	−	−	−
N15−C30	1.489(4)	−	1.276(7)	−	−
C30−C31	1.517(5)	1.48(1)	1.521(9)	1.486(6)	1.45(1)
C31−C32	1.407(5)	1.44(1)	1.506(10)	−	1.34(1)
C32−O1	1.320(4)	1.237(9)	1.208(8)	−	−
C32−C33	1.412(5)	1.44(1)	1.499(9)	−	1.48(1)
C30−C32	−	−	−	1.497(6)	−
N11−Ni1−N12	85.8(1)	86.0(3)	86.5(2)	95.89(9)	89.8(2)
N11−Ni1−N13	91.8(1)	88.2(3)	92.5(2)	90.4(1)	88.9(2)
N11−Ni1−N14	90.6(1)	92.9(3)	89.5(2)	−	−
N11−Ni1−N15	87.2(1)	85.5(2)	93.0(2)	−	−
N12−Ni1−N13	85.2(1)	89.9(2)	87.3(2)	84.8(1)	84.3(2)
N14−Ni1−N15	87.9(1)	84.9(3)	85.1(2)	−	−
N13−Ni1−N14	95.3(1)	94.2(3)	94.5(2)	−	−
N12−Ni1−N15	91.5(1)	90.9(2)	93.5(2)	−	−
N12−Ni1−N13A	−	−	−	95.1(1)	95.7(2)
N12−Ni1−N14	176.4(1)	175.8(3)	175.7(2)	−	−
N13−Ni1−N15	176.6(1)	173.5(3)	174.4(2)	−	−
N12−Ni1−N12A	−	−	−	168.2(2)	179.6(3)
N13−Ni1−N13A	−	−	−	179.3(2)	177.9(3)
N11−Ni1−O1	177.75(10)	178.7(3)	178.7(2)	−	180
Ni1−N12−C16	116.1(2)	116.2(5)	115.5(4)	114.5(2)	116.9(4)
Ni1−N13−C17	114.3(2)	116.0(5)	114.3(4)	113.8(3)	118.2(4)
Ni1−N14−C20	114.8(2)	116.2(6)	115.0(4)	−	−
Ni1−N15−C21	113.6(2)	115.0(4)	116.4(3)	−	−
N12−C16−C18	114.5(3)	115.6(7)	115.0(5)	114.6(3)	114.9(6)
N13−C17−C18	114.5(3)	115.3(7)	115.0(6)	116.3(3)	114.5(6)
N14−C20−C22	114.3(3)	110.5(6)	115.5(5)	−	−
N15−C21−C22	115.9(3)	112.4(6)	114.3(5)	−	−
Ni1−N12−C30	−	−	−	126.9(3)	126.6(5)
Ni1−N14−C30	−	127.8(7)	−	−	−
Ni1−N15−C30	113.9(2)	−	125.3(4)	−	−
C16−N12−C30	−	−	−	118.6(3)	116.4(6)
C20−N14−C30	−	115.8(8)	−	−	−
C21−N15−C30	110.0(3)	−	118.3(5)	−	−
Ni1−O1−C32	114.4(2)	123.9(5)	125.0(5)	−	−
N12−C30−C31	−	−	−	119.2(4)	128.0(7)
N14−C30−C31	−	125.2(9)	−	−	−
N15−C30−C31	112.7(3)	−	121.0(6)	−	−
N12−C30−C32	−	−	−	124.0(4)	−
C31−C30−C32	−	−	−	116.8(4)	−
C30−C31−C32	119.0(4)	121.6(8)	118.8(5)	−	120.2(7)
C31−C32−O1	121.0(4)	125.6(8)	123.0(7)	−	−
C31−C32−C33	116.8(4)	112.4(8)	116.5(7)	−	125.9(8)
C32−C33−C34	120.7(5)	124.4(8)	−	−	116.4(10)
C32−C33−C38	−	−	−	−	124.4(9)

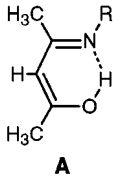
atom is part of a methine or methylene group. The keto-imine tautomer **C** is expected to be a more flexible chelating ligand than **A** and **B**, since the central carbon atom is incorporated into the chain by two single bonds. At the same time, this coordination mode is expected to be disfavoured, and hence occur rarely, owing to the loss of double bond conjugation.

The ligand nacac-pyN_4 (**6**) is obtained from an equimolar mixture of **1** and acetylacetone in refluxing methanol. Addition of nickel(II) chloride, followed by hexafluorophosphate anion, yields a purple, microcrystalline precipitate which may be recrystallised from water. Its elemental analysis fits the formula [(nacac-pyN_4)Ni]$(PF_6)_2$ (**7**) in which the pyN_4 ligand has a single acetylacetone-derived sidearm. By analogy with the syntheses of **3** and **5**, compound **7** is expected to contain divalent nickel. The sidearm is thus required to be neutral, which suggests the keto-imine tautomeric form **C**. The IR spectrum is characterised by two strong bands at 1697 cm^{-1} and 1605 cm^{-1}, which may be assigned to the C=N and C=O stretching vibrations, respectively. This finding is compatible with tautomer **C**, since the C=N stretching vibration in a conjugated cyclic system occurs

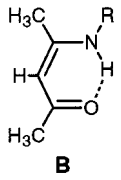
Table 2. Intramolecular angles [°] and distances [Å] illustrating the distortion of the ligand cap in complexes **3**, **5** and **7** (with estimated standard deviations in parentheses); compounds **9** and **11** do not show these distortions due to crystallographically imposed symmetry; see footnote and text for definitions of angles

Bond or Angle	**3**	**5**	**7**
ε[a]	17.0(2)	16.0(7)	3.9(4)
ζ[b]	8.0(1)	7.3(4)	2.9(1)
η[c]	11.9(1)	11.4(4)	4.5(2)
d(C16···C21)	5.370(5)	5.36(1)	5.16(1)
d(C17···C20)	4.752(5)	4.81(1)	5.02(1)

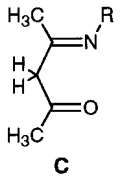
[a] Angle ε between the least-squares planes defined by the pyridine ring (N11, C11, C12, C13, C14, C15) and the quaternary and methyl carbon atoms C18/C19/C22/C23. – [b] Angle ζ between the least-squares planes defined by the equatorial nitrogen atoms N12/N13/N14/N15 and the methylene carbon atoms C16/C17/C20/C21. – [c] Angle η subtended by the lines N11···C13 and N11–Ni1 at N11



A



B



C

at lower frequency (1660–1480 cm^{-1}).[19] By the same token, complexes involving ketones are expected to show especially low C=O stretching frequencies, when compared with the free ligand.[19]

The X-ray structure analysis of **7** confirms the single derivatisation of the ligand cap and the presence of a keto-imine tautomeric acetylacetone-derived sidearm (Figure 1), making **7** a rare if not the only example of a transition metal complex where this coordination mode is observed.[20] The overall coordination geometry of nickel(II) resembles that in **3**, but the NN_4 coordination cap shows a lesser distortion of the carbon backbone, as quantified by means of the parameters listed in Table 2 (cf. the structures of **3** and **5**). The bond Ni1–N15 involving the ketimine nitrogen atom {2.049(5) Å} is shorter than the other equatorial Ni–N bonds, and has the same length as the Ni–N_{py} bond (Table 1). The nickel and equatorial nitrogen atoms are not coplanar; rather, N15 is below and N14 above the plane defined by the other three equatorial atoms (Ni1, N12, N13) by 0.198(5) Å and 0.144(5) Å, respectively. The N–O chelate ring is six-membered and adopts a boat conformation, the methylene carbon atom C31 (at the "bow") and Ni1 (at the "stern") being above the best plane containing N15, C30, C32, and O1 by 0.384(8) Å and 0.635(1) Å, respectively. The bond between Ni1 and the keto oxygen atom {Ni1–O1, 2.105(4) Å} is intermediate between the corresponding axial bonds in **3** and **5** (Table 1). The coplanarity of all bonds at the imine nitrogen atom N15, the lack of planarity of the N–O chelate ring, and the differences in bond lengths within this ring (Table 1) make the assignment of the keto-imine tautomer **C** conclusive. Apparently, the geometric requirements imposed by the central nickel atom on the derivatised coordination cap are such that the ligand sidearm is best accommodated as a chelating group when in the keto-imine form, thus favouring this unusual coordination mode. The presence of the keto-imine form may also explain the remarkable hydrolytic stability of **7**. By contrast, nickel(II) complexes containing the chelating tautomers **A** or **B** (with R = alkyl) are reported to be extremely sensitive to traces of water in solution, and hence are accessible only under anhydrous conditions.[17][18]

$(nac)_2$-pyN_4 (8), and $[(8)Ni](PF_6)_2$ (9)

Initial experiments aimed at the synthesis of complex **7** yielded a crystalline by-product which analysed too high for carbon to be the acetylacetone derivative. An excess of sodium methoxide had been used for the deprotonation of **1**·4HBr·MeOH, making the solution sufficiently basic for acetylacetone to undergo a retro-aldol reaction, thereby liberating acetone. The elemental analysis data of the by-product were compatible with the nickel(II) complex of a bis(acetoneimine) derivative of the pentaamine ligand **1**, which we subsequently sought to synthesise in a directed manner.

Complex **9**, containing the ligand $(nac)_2$-pyN_4 (**8**), forms as the only isolated product in high yield as a purple, microcrystalline material when treating a methanolic solution of **1** with 4 equivalents of acetone at room temperature, followed by addition of nickel(II) acetate and ammonium hexafluorophosphate. The complex, while containing aliphatic Schiff base units, is remarkably stable towards hydrolysis. No special precautions need to be taken to exclude water from the reaction mixture, which is in fact the optimal solvent for recrystallisation. More forcing reaction conditions (reflux and/or a much larger excess of acetone) do not lead to more highly condensed products, two primary amino groups in the molecule remaining unaffected. The latter observation is in agreement with results reported by Curtis and co-workers,[21] who studied the reactivity of tris(1,3-propanediamine)-nickel(II) perchlorate in dry acetone and obtained a square-planar derivative of bis(1,3-propanediamine)-nickel(II) as an isolable intermediate, in which one acetone molecule had condensed with each of the two diamine ligands. A *trans* arrangement of the coordinated *N*-isopropylidene groups was suggested for this complex. Its hydrolytic instability, however, prevented structural

charaterisation. From this intermediate Curtis and co-workers obtained, upon prolonged reaction, a square planar nickel(II) complex of a 16-membered macrocycle containing diacetone-amine-imine linkages.[22] We have so far not observed similar reactivity for complex **9**.

The IR spectrum of **9** has a strong absorption at 1663 cm^{-1} assigned to the C=N stretching vibration, whereas the ^1H NMR spectrum is of little diagnostic value as it shows paramagnetically broadened and shifted signals (solvent: CD_3OD/D_2O). The UV/Vis spectrum of an aqueous or a methanolic solution of **9** reveals a band at 509 nm, which we assign to a d−d transition. The elemental analysis data suggest **9** to be a pentacoordinate complex, hexafluorophosphate being a very weakly coordinating ion at best. The solid-state UV/Vis spectrum (diffuse reflectance) is identical within experimental error to the solution spectrum (200−800 nm), the d−d band being recorded at 504 nm. Since the spectra of d^8 complexes are very sensitive to changes in the axial ligand positions,[23] these findings indicate the cation in **9** to be pentacoordinate both in aqueous or methanolic solution and in the solid state. The magnetic moment determined for **9** (Gouy balance) is 3.12 BM (spin only), corresponding to two unpaired electrons (theoretical value: 2.83 BM). By contrast, a diamagnetic ground state is predicted, to a first approximation, for Ni^{2+} (d^8) in a regular square pyramidal coordination environment.[24]

Compound **9** was studied by cyclic voltammetry to determine the redox potential of the $Ni^{II/III}$ couple in this less than usual coordination geometry. The cyclic voltammogram of **9** at room temperature between +1.24 and −2.36 V (Figure 2) shows a reversible redox wave in the anodic region ($E_{1/2}$ = +0.88 V) and an irreversible redox wave in the cathodic region (−1.67 V). The anodic process is assigned to the $Ni^{II/III}$ couple, whereas the cathodic process may involve irreversible reduction of the ligand, or generation of Ni^{I} and subsequent fast decomposition of the complex.

An x-ray crystallographic analysis confirms the assumed pentacoordination of the cation in **9** in the solid state. The structure of [(**8**)Ni]$^{2+}$ is shown in Figure 1. The pyridine, primary amine, and acetone-imine nitrogen atoms define a square pyramid. The molecule lies on a twofold rotation axis which contains Ni1, the pyridine nitrogen atom N11, and the *para* carbon atom of the pyridine ring, C13. As a consequence of the crystallographic symmetry, a distortion of the ligand cap as described for **3**, **5** and **7** is not observed. The primary amine nitrogen atoms (N13, N13A) and the nickel atom are on a straight line {N13−Ni1−N13A 179.3(2)°}, while the bonds connecting Ni1 with the acetone-imine nitrogen atoms N12 and N12A are at an angle of 168.2(2)° (N12−Ni1−N12A). Of the bonds involving Ni1, the axial bond Ni1−N11 to the pyridine nitrogen atom is the shortest at 1.991(4) Å, the basal bonds being somewhat longer, with bond lengths reflecting the sp^2 and sp^3 character of the nitrogen atoms, respectively {Ni1−N12: 2.041(3) Å; Ni1−N13: 2.080(3) Å}. All bonds radiating from the isopropylidene-imine nitrogen atom N12 are coplanar, as expected, and the rigidity in this donor group is accommodated by deviations of the angles at N12 and Ni1 from the expected values of 120° and 90°, respectively (see Table 1). As a consequence of this rigidity, the "inside" methyl groups (C31, C31A) approach each other to within 2.59(6) Å (C31−H···H−C31A), thereby shielding the nickel atom and blocking access to the sixth coordination site.

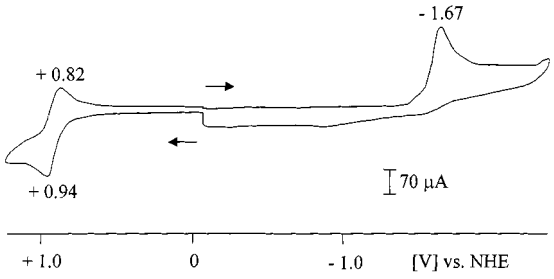


Figure 2. Cyclic voltammogram of **9** at room temperature (solvent: DMF; scan rate: 50 mVs^{-1})

$(cin)_4$-pyN_4 (10), and [(10)Ni(OH_2)]$(Br)_2$ (11)

The ligand concluding the present series is a derivative of **1** in which all four primary amino groups are condensed with a suitable carbonyl compound, namely *trans*- cinnamaldehyde (*trans*-3-phenyl-2-propenal). We expected this readily available α,β-unsaturated aromatic aldehyde to show high reactivity in the transformation at hand, as condensation would result in the formation of conjugated double bond systems in the four sidearms.[25] These would be relatively rigid, and the aromatic rings would be sufficiently removed from the metal centre for unfavourable steric interactions to prevent podand-like coordination of the ligand.

Fourfold condensation of cinnamaldehyde with the polyamine ligand is achieved by reacting the correct molar ratio of materials in refluxing methanol. Workup gives a yellow crude product which shows poorly resolved ^1H NMR spectra (see Experimental Section). In the IR spectrum, a strong band is observed at 1635 cm^{-1}, which is assigned to the C=N stretching vibration. When a methanolic solution of this product is treated with solid nickel(II) acetate, complexation is spontaneous, as jugdged by the colour change to orange. Workup of this solution gives an orange-brown microcrystalline solid whose IR and mass spectroscopic data indicate a complex containing the cation [(**10**)Ni(ac)]$^+$.

Single crystals of the aqua complex **11**, containing two molecules of methanol per formula unit, were obtained by repeated recrystallisation of the presumed acetato complex from methanol. The structure of the cation is shown in Figure 1, and relevant distances and angles are listed in Table 1. The molecule has C_2 symmetry, with Ni1, the aqua oxygen atom O1, and the pyridine nitrogen and *para* carbon atoms N11 and C13 lying on the two-fold rotational axis. The crystallographically imposed symmetry implies a regular conformation of the ligand cap; similar to the situation in compound **9**, all carbon atoms in the 2,6-diethylpyridine ligand backbone are coplanar, and the nonbonded distance between pairs of methylene carbon atoms (C16···C17A, C17···C16A) is the same {5.14(1) Å}. In contrast to the

structure of **9**, the equatorial nitrogen atoms in **11** are coplanar with the central metal, with angles N12−Ni1−N12A and N13−Ni1−N13A of 179.6(3)° and 177.9(3)°, respectively. The bond lengths Ni−N are all rather similar and lie in the range 2.076(7)−2.107(6) Å. As a consequence of the conjugated systems of double bonds, the atoms in the ligand sidearms (from the methylene carbon via the imine nitrogen atoms out to the phenyl rings) are virtually coplanar, with bonds and angles not deviating greatly from the normal values (Table 1). The aqua oxygen atom is coordinated to Ni1 at a distance of 2.148(7) Å, which is the same as in the parent complex [(**1**)Ni(OH_2)]I_2 {2.133(3) Å}.[4] The methanol molecules in this structure are situated between pairs of sidearm phenyl rings and are engaged in what seem to be weak hydrogen-bonded interactions with the bromide counterions, which are at a distance of 3.27(1) Å from the methanol oxygen atoms (sum of the van der Waals radii of O and Br: 3.37 Å[26]).

Conclusion

The series of ligands presented here may be obtained by selective or exhaustive condensation of the tetrapodal pentaamine **1** with a choice of carbonyl compounds, to give the respective Schiff bases. Derivatives obtained from **1** by introduction of *one* additional donor group into the ligand periphery are potentially hexadentate. They readily form mononuclear complexes with nickel(II) if an additional chelate ring can arise that is six-membered and sufficiently flexible (**2** and **6**). In the case of the salicylaldimine derivative **4**, this requires reduction of the C=N double bond. The derivative obtained from **1** by modification of *two* amino groups (having two diagonally juxtaposed isopropylideneimine units, **8**) forms a mononuclear complex in which these rigidly positioned substituents, while preventing the coordination of a sixth ligand, are sufficiently removed from one another so as not to prevent complexation as such. The condensation of all *four* primary amino groups in **1** with cinnamaldehyde leads to a derivative whose podand-like behaviour towards nickel(II) is facilitated by the limited steric demand of the phenylpropenylidene substituents. In all cases, nickel(II) complexation allows the isolation of pure, crystalline materials, which should make these ligands available for complexation studies with other transition metals. Also, the remaining primary amino groups of the singly derivatised square-pyramidal coordination caps make these ligands attractive subjects for further derivatisations.

Experimental Section

Materials and Instrumentation: All manipulations were performed under an atmosphere of dry nitrogen using standard Schlenk techniques, unless indicated otherwise. Solvents were dried and distilled before use. Reagents were AR grade or better and were purchased from Merck, Fluka, or Aldrich. 2,6-C_5H_3N{CMe-$(CH_2NH_2)_2$}$_2$·4HBr·MeOH (**1**·4HBr·MeOH) was prepared as described elsewhere.[10] IR (KBr discs) and UV/Vis spectra (solvent: water or methanol; solid state: diffuse reflectance) were recorded on Perkin−Elmer 16PC FT-IR or Shimadzu UV-3101 PC instruments. The cyclic voltammogram of **9** was recorded under an atmosphere of nitrogen using an EG & G PAR 246 A potentiostat equipped with a ROTEL A three-electrode cell, having a glassy carbon working electrode, a Pt counter electrode and Ag/AgCl/KCl (sat. in H_2O) as the reference electrode. The solvent was dimethylformamide, the conducting electrolyte $N^nBu_4PF_6$ (10^{-1} mol/l), scan rate 50 mV/s. Ferrocene was used as internal standard, with a potential of +0.40 V vs. NHE.[27] NMR spectra were measured on a JEOL JNM-EX 270 spectrometer, and mass spectra were obtained on JEOL MSTATION 700 and Micromass ZABSpecE spectrometers. Elemental analyses were performed using Carlo Erba Elemental Analysers 1106 (CHN) and 1108 (CHNS).

X-ray Crystallography: Crystal data for compounds **3**, **5**, **7**, **9**, and **11** are presented in Table 3, and selected distances and angles are listed in Table 1. The structures of the cations are shown in Figure 1. All structures were solved by direct methods and refined using the programme package SHELXTL 5.03.[28] All non-hydrogen atoms were refined anisotropically (full-matrix least-squares on F^2).

In the case of **3** and **9**, all hydrogen atoms were located in a difference Fourier synthesis and refined with a fixed common isotropic displacement parameter (exception for **3**: the hydrogen atoms in the methanol molecule were calculated in geometrically optimised positions). For **5**, **7** and **11**, all hydrogen atoms were positioned geometrically (exception for **5**: the hydrogen atoms of the aqua ligand in [(**1**)Ni(H_2O)]$^{2+}$ and of solvate water were located in a difference Fourier synthesis and not refined; exception for **11**: the hydrogen atoms in the aqua ligand were not included in the calculations). In the structure of **3**, the PF_6^- counterion is disordered, and two preferred orientations could be refined (occupancy factors 0.68(1) and 0.32(1), respectively). In **7**, one of the two PF_6^- anions shows rotational disorder, which was resolved with refined occupancy factors 0.61(2) and 0.39(2), respectively, for alternative sets of the four equatorial F atom sites. Crystallographic data (excluding structure factors) for the structures reported in this paper have been deposited with the Cambridge Crystallographic Data Centre as supplementary publication nos. CCDC-129 628 (**3**) to CCDC-129 632 (**11**). Copies of the data can be obtained free of charge on application to CCDC, 12 Union Road, Cambridge CB2 1EZ, UK [Fax: (internat.) +44-1223/336-033; E-mail: deposit@ccdc.cam.ac.uk]

[(2)Ni]PF_6 (3): To a stirred suspension of pyN_4·4HBr·MeOH (0.48 g, 0.79 mmol) in methanol (50 mL) was added sodium metal (0.07 g, 3.16 mmol), which dissolved within ca. 5 minutes to give a clear solution. To this solution was added dropwise over 2 h a solution of salicylaldehyde (0.10 g, 0.79 mmol) in methanol (20 mL). The resulting yellow solution was taken to dryness, and the remaining oil taken up in ethanol (20 mL). To this mixture was added $NaBH_4$ (0.24 g, 6.32 mmol) in small portions, and the mixture heated to reflux for 1 h. Excess $NaBH_4$ was then hydrolysed by careful addition of water (10 mL). Addition of Ni$(ac)_2$·$4H_2O$ (0.23 g, 0.79 mmol) gave a purple solution, from which a purple solid crystallised upon dissolution of NH_4PF_6 (0.13 g, 0.79 mmol). The solid was separated by filtration. Recrystallisation from water/methanol (50:50 v/v) yielded crystals suitable for an X-ray structural analysis (0.15 g, 0.24 mmol, 30% relative to **1**). − IR (KBr): $\tilde{\nu}$ = 3375m, 2926m, 1594s, 1477s, 1456s, 1296s, 1086m, 1019s, 850s (PF_6), 558s cm^{-1}. − UV/Vis (water): λ_{max} (ε) = 509 nm (22 dm^3·mol^{-1}·cm^{-1}). − MS (FAB); *m/z* (%): 414 (100) [M^+]. − $C_{20}H_{30}N_5F_6NiOP$·CH_3OH·H_2O (610.23): calcd. C 41.33, H 5.94, N 11.47; found C 40.89, H 6.22, N 11.11.

[(4)Ni][(1)Ni(H_2O)]$(Br)_2(PF_6)$ (5): To a solution prepared as described above for **3** (50 mL MeOH; pyN_4·4HBr·MeOH: 0.58 g,

Table 3. Crystallographic data for compounds **3**, **5**, **7**, **9** and **11**

	3·H_2O·MeOH	**5**·H_2O	**7**	**9**	**11**·2 MeOH
Empirical Formula	$C_{21}H_{36}F_6N_5NiO_3P$	$C_{33}H_{57}Br_2F_6N_{10}Ni_2O_3P$	$C_{18}H_{31}F_{12}N_5NiOP_2$	$C_{19}H_{33}F_{12}N_5NiP_2$	$C_{51}H_{59}Br_2N_5NiO_3$
Formula Weight	610.23	1064.10	682.13	680.15	1008.56
Crystal System	monoclinic	monoclinic	monoclinic	monoclinic	orthorhombic
Space Group (no.)	$P2_1/c$ (no. 14)	$P2_1$ (no. 4)	$P2_1/n$ (no. 14)	$C2/c$ (no. 15)	$Pbcn$ (no. 60)
a [Å]	12.109(3)	8.638(3)	8.589(1)	14.258(3)	13.614(4)
b [Å]	13.418(3)	14.944(6)	17.941(2)	10.586(2)	12.075(3)
c [Å]	18.298(5)	16.884(6)	18.195(2)	20.255(3)	30.227(6)
β [°]	108.22(2)	100.05(3)	96.47(1)	103.66(2)	90
Z	4	2	4	4	4
V [Å^3]	2824(1)	2146(2)	2785.9(5)	2970.7(9)	4969(2)
ρ_{calcd} [g cm^{-3}]	1.435	1.647	1.626	1.521	1.348
Diffractometer	Nicolet R3m/V	Nicolet R3m/V	Siemens P4	Nicolet R3m/V	Siemens P4
λ [a] [Å]	0.710 73	0.710 73	0.710 73	0.710 73	0.710 73
Crystal Size [mm^3]	0.50 × 0.40 × 0.35	0.55 × 0.18 × 0.04	0.60 × 0.55 × 0.35	0.50 × 0.40 × 0.38	0.50 × 0.40 × 0.12
T [°C]	298(2)	298(2)	295(2)	298(2)	200(2)
Absorption Correction	–	Psi-scan	Psi-scan	Psi-scan	Psi-scan
T_{min}/T_{max}	–	0.171/0.220	0.386/0.418	0.354/0.436	0.095/0.132
scan	ω	ω	ω	ω	ω
2Θ Range	$3 \le 2\Theta \le 54$	$3 \le 2\Theta \le 54$	$4 \le 2\Theta \le 50$	$4 \le 2\Theta \le 54$	$4 \le 2\Theta \le 52$
Measured Reflections	7235	5750	6718	3909	5466
Unique Reflections	6112	5231	4907	3249	4383
Observed Reflections[b]	2448	2745	2834	1473	2392
μ(Mo-K_α) [mm^{-1}]	0.814	2.849	0.914	0.854	2.044
Refined Parameters	487	514	393	227	285
Data/Parameter Ratio	12.6	10.2	12.5	14.3	15.2
$wR2$ (all data)[c]	0.0783	0.0663	0.1895	0.1168	0.1809
R 1 (obs. data)[d]	0.0406	0.0389	0.0699	0.0450	0.0724
ρ_{fin}(max/min) [e Å^{-3}]	0.406/-0.256	0.330/-0.404	0.614/-0.328	0.371/-0.244	0.570/-0.709
Weighting Scheme[e]	$k = 0.0310/l = 0$	$k = 0.0233/l = 0$	$k = 0.0763/l = 3.5962$	$k = 0.061/l = 0$	$k = 0.0707/l = 9.2413$

[a] Mo-K_α, graphite monochromator. – [b] With $F_o \ge 4\,\sigma(F)$. – [c] $wR2 = (\{\Sigma[w(F_o^2 - F_c^2)^2]\}/\{\Sigma[w(F_o^2)^2]\})^{0.5}$. – [d] $R1 = \Sigma||F_o|-|F_c||/\Sigma|F_o|$ for $F > 4\sigma(F)$. – [e] $w = 1/[\sigma^2(F_o^2) + (k\cdot P)^2] + l\cdot P$ and $P = (F_o^2 + 2\cdot F_c^2)/3$.

0.96 mmol; Na: 0.09 g, 3.84 mmol) was added dropwise over 2 h a solution of salicylaldehyde (0.12 g, 0.96 mmol) in methanol (20 mL), to give a yellow solution. Addition of $NiSO_4$·$6H_2O$ (0.27 g, 0.96 mmol) gave a red solution, from which a small amount of an orange crystalline solid precipitated upon dissolution of NH_4PF_6 (0.16 g, 0.96 mmol). Recrystallisation of this solid from methanol yielded crystals of compound **5** suitable for an X-ray structural analysis. By-products appeared ill-defined and were not characterised further. Repeated recrystallisation from methanol yielded a product for which elemental analysis data indicate the composition [(**4**)Ni]PF_6·H_2O·MeOH. – IR (KBr): $\tilde{\nu}$ = 3374m, 2933m, 1640s, 1600s, 1540m, 1471s, 1399m, 1096m, 1018s, 843 vs (PF_6), 758m, 558s cm^{-1}. MS (ESI$^+$); *m/z* (%): 412 (100) [M$^+$]. – $C_{20}H_{28}F_6N_5NiOP$·H_2O·MeOH (608.21): calcd. C 41.47, H 5.64, N 11.52; found C 41.52, H 5.47, N 11.21.

[(nacac-pyN$_4$)Ni](PF$_6$)$_2$ (7): To a solution prepared as described above for **3** (20 mL MeOH; pyN$_4$·4HBr·MeOH: 0.94 g, 1.55 mmol; Na: 0.14 g, 6.20 mmol) was added dropwise a solution of acetylacetone (0.16 g, 1.55 mmol) in methanol (20 mL), and the resulting mixture heated to reflux for 1 h. Addition of $NiCl_2$·$6H_2O$ (0.37 g, 1.55 mmol) to the colourless mixture gave a purple solution, from which a purple crystalline solid precipitated upon dissolution of NH_4PF_6 (0.25 g, 1.55 mmol). The material was isolated and recrystallised from water to give single crystals suitable for an X-ray structural analysis (0.57 g, 0.83 mmol relative to **1**, 54%). – IR (KBr): $\tilde{\nu}$ = 3380s, 2978m, 1697s (C=N), 1605s (C=O), 1471s, 1399m, 1099m, 1024s, 851s (PF_6), 559s cm^{-1}. – MS (FAB); *m/z* (%): 390 (100) [(M – H)$^+$]. – $C_{18}H_{31}F_{12}N_5NiOP_2$ (682.13): calcd. C 31.70, H 4.58, N 10.26; found C 31.69, H 4.68, N 10.02.

[((nac)$_2$-pyN$_4$)Ni](PF$_6$)$_2$ (9): To a solution prepared as described above for **3** (20 mL MeOH; pyN$_4$·4HBr·MeOH: 0.39 g, 0.63 mmol; Na: 0.06 g, 2.52 mmol) was added dropwise over 1 h a solution of acetone (0.39 g, 2.52 mmol) in methanol (20 mL), followed by addition of solid Ni(ac)$_2$·$4H_2O$ (0.18 g, 0.63 mmol) to give a purple solution. Dissolution of NH_4PF_6 (0.21 g, 1.26 mmol) led to the precipitation of a purple microcrystalline solid which was isolated by filtration and recrystallised from water to yield, after isolation and drying in air, single crystals suitable for X-ray structure analysis (0.34 g, 0.50 mmol, 79% relative to **1**). – IR (KBr): $\tilde{\nu}$ = 3378m, 1663s (C=N), 1603m, 1470m, 1376m, 1268m, 1108m, 1016m, 848s (PF_6), 558s cm^{-1}. – UV/Vis (water): λ_{max} (ε) = 509 nm (26 dm^3·mol^{-1}·cm^{-1}). – MS (ESI$^+$); *m/z* (%): 389 (65) [M$^+$], 447 (100) [M$^+$ + 58 (acetone)]. – $C_{19}H_{33}F_{12}N_5NiP_2$ (680.15): calcd. C 33.55, H 4.89, N 10.30; found C 33.43, H 5.13, N 10.07.

[{(cin)$_4$-pyN$_4$}Ni(X)]Y (X = H$_2$O, Y = Br$_2$ 11): To a stirred suspension of pyN$_4$·4HBr·MeOH (1.90 g, 3.13 mmol) in methanol (20 mL) was added LiOMe (1M stock solution in MeOH, 12.52 mL, 12.52 mmol), resulting in a clear solution after ca. 2 min. To this was added *trans*-cinnamaldehyde (1.65 g, 12.52 mmol) in one portion. The mixture was heated to reflux for 4 h, during which time the solution became yellow. Removal of the solvent in vacuo and triturating the residue by stirring with diethyl ether (30 mL) gave a yellow solid which was separated by filtration, washed with ether and dried in vacuo. Elemental analytical results of the products of repeated preparations in a variety of solvents, although unsatisfactory, agree best with a formulation of the solid as the fourfold condensation product. In the IR spectrum, a strong band is observed at 1635 cm^{-1}, which is assigned to the C=N stretching vibration. ^{1}H NMR spectra show broad and badly resolved signals in each case. The material was therefore used in the subsequent preparations without further characterisation. No effort was made to exclude air or moisture. The yellow condensation product (presumed as py(Ncinald)$_4$; 0.26 g, ≤ 0.38 mmol) was dissolved in methanol (20 mL), and solid Ni(ac)$_2$·$4H_2O$ (0.09 g, 0.38 mmol) ad-

ded to give an orange solution. Reduction of the volume to ca. 10 mL led to the formation of an orange-brown microcrystalline precipitate which was filtered off and washed with methanol. IR and MS data indicate the solid to contain the acetato complex cation (X = ac). − IR (KBr): $\tilde{\nu}$ = 3447w, 3053w, 1627s (C=N), 1592s, 1449m, 1425m, 1262m, 1175m, 749s, 733s, 705s, 688s, 612m cm^{-1}. − MS (ESI^+); *m/z* (%): 825 (100) $[(\mathbf{10})Ni(ac)]^+$. − Repeated recrystallisation from methanol gave crystals of the aqua complex (X = H_2O; Y = Br_2) which were used in the X-ray structure analysis (0.29 g, 0.29 mmol, ≤ 75%, calculated for formula **11**). Apparently, acetate is exchanged for an aqua ligand, and lithium bromide is not removed in the course of the recrystallisations, which explains the presence of bromide counterions in the structurally characterised sample. The perchlorato perchlorate salt (X = Y = ClO_4) was obtained by recrystallisation in the presence of $NaClO_4$, but did not give satisfactory single crystals. Data for this salt are as follows: MS (FAB); *m/z* (%): 765 (75) $[(\mathbf{10})Ni]^+$; 864 (100) $[(\mathbf{10})Ni(ClO_4)]^+$. − $C_{49}H_{51}Cl_2N_5NiO_9$ {983.57, $[(\mathbf{10})Ni(ClO_4)]ClO_4 \cdot H_2O$}: calcd. C 59.83, H 5.22, N 7.12; found C 59.83, H 5.45, N 6.75.

Acknowledgments

We thank Professor D. Sellmann for generous support of this work and Mr. G. Burgeth for the measurement of a solid-state UV spectrum. Financial support from the Fonds der Chemischen Industrie and the Deutsche Forschungsgemeinschaft is gratefully acknowledged.

[1] A. Grohmann, F. Knoch, *Inorg. Chem.* **1996**, *35*, 7932−7934.
[2] M. E. de Vries, R. M. LaCrois, G. Roelfes, H. Kooijman, A. L. Spek, R. Hage, B. L. Feringa, *Chem. Commun.* **1997**, 1549−1550.
[3] R. T. Jonas, T. D. P. Stack, *J. Am. Chem. Soc.* **1997**, *119*, 8566−8567.
[4] C. Dietz, F. W. Heinemann, J. Kuhnigk, C. Krüger, M. Gerdan, A. X. Trautwein, A. Grohmann, *Eur. J. Inorg. Chem.* **1998**, 1041−1049.
[5] For a much more complex ligand architecture, see: C.-H. Lee, B. Garcia, T. C. Bruice, *J. Am. Chem. Soc.* **1990**, *112*, 6434−6435.
[6] A. Grohmann, F. W. Heinemann, P. Kofod, *Inorg. Chim. Acta* **1999**, *286*, 98−102.
[7] T. Poth, H. Paulus, H. Elias, R. van Eldik, A. Grohmann, *Eur. J. Inorg. Chem.* **1999**, 643−650.
[8] C. Zimmermann, F. W. Heinemann, A. Grohmann, unpublished results.
[9] A. Grohmann, J. Pitarch López, F. W. Heinemann, unpublished results.
[10] S. Schmidt, L. Omnès, F. W. Heinemann, J. Kuhnigk, C. Krüger, A. Grohmann, *Z. Naturforsch.* **1998**, *53b*, 946−954.
[11] J.-P. Costes, F. Dahan, M. B. Fernandez Fernandez, M. I. Fernandez Garcia, A. M. Garcia Deibe, J. Sanmartin, *Inorg. Chim. Acta* **1998**, *274*, 73−81.
[12] B. Nowicka, A. Samotus, J. Szklarzewicz, F. W. Heinemann, H. Kisch, *J. Chem. Soc., Dalton Trans.* **1998**, 4009−4013.
[13] J. Lopez, S. Liang, X. R. Bu, *Tetrahedron Lett.* **1998**, *39*, 4199−4202.
[14] C. Cairns, S. G. McFall, S. M. Nelson, M. G. B. Drew, *J. Chem. Soc., Dalton Trans.* **1979**, 446−453.
[15] Y. Iitaka, T. Koike, E. Kimura, *Inorg. Chem.* **1986**, *25*, 402−404.
[16] A. Berkessel, J. W. Bats, M. Bolte, T. Neumann, L. Seidel, *Chem. Ber./Recueil* **1997**, *130*, 891−897.
[17] *Chelating Agents and Metal Chelates* (Eds.: F. P. Dwyer, D. P. Mellor), Academic Press New York, London, **1964**, Ch. 4, p. 143.
[18] R. H. Holm, G. W. Everett, Jr., A. Chakravorty, *Progr. Inorg. Chem.* **1966**, *7*, 83−214.
[19] G. Socrates, *Infrared Characteristic Group Frequencies;* 2nd edition., Wiley Chichester, **1994**, pp. 50 and 236.
[20] A recent search of the Cambridge Crystallographic Database yielded seven examples of transition metal complexes containing a keto-imine moiety [cf. Formula C]. However, all these structures are inconclusive as to the true nature of the chelate rings. The systematic names of the ligands either imply negative charges, or the number of counterions does not match the oxidation state of the central metal ion.
[21] D. A. House, N. F. Curtis, *J. Am. Chem. Soc.* **1964**, *86*, 223−225.
[22] N. F. Curtis, *Coord. Chem. Rev.* **1968**, *3*, 3−47.
[23] M. Green, P. A. Tasker, *J. Chem. Soc. (A)* **1970**, 2531−2539.
[24] A. R. Rossi, R. Hoffmann, *Inorg. Chem.* **1975**, *14*, 365−374.
[25] B. Greener, M. H. Moore, P. H. Walton, *Chem. Commun.* **1996**, 27−28.
[26] A. Bondi, *J. Phys. Chem.* **1964**, *68*, 441−451.
[27] H.-M. Koepp, H. Wendt, H. Strehlow, *Z. Elektrochem.* **1960**, *64*, 483−491.
[28] SHELXTL 5.03 for Siemens Crystallographic Research Systems, Madison, WI, USA.

Received July 15, 1999
[I99259]

Control of Reactivity of Dinuclear Nickel(II) Amine-Thiolate Complexes

Berthold Kersting[a]

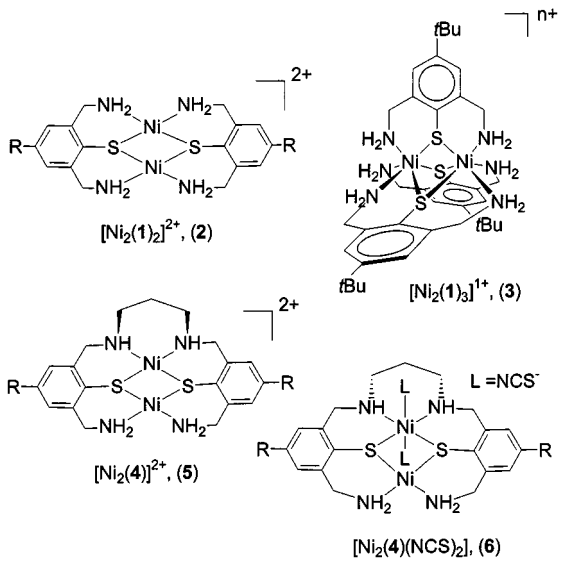
Keywords: Septadentate N_5S_2-ligand / Dinuclear complexes / Nickel / Reactivity / Redox chemistry

The coordination chemistry of a series of dinickel complexes of the new septadentate amine-thiolate ligand *N*,*N*′-bis[2-thio-3-aminomethyl-5-*tert*-butylbenzyl]diethylenetriamine, H_2**9**, has been investigated in the context of ligand binding and oxidation state changes. The complexes $[Ni_2(\mathbf{9})(L)][ClO_4]_2$ (**10**), $[Ni_2(\mathbf{9})(Cl)][Cl]$ (**11**), $[Ni_2(\mathbf{9})(L)][BPh_4]_2$ (**12**), and $[Ni_2(\mathbf{9})(NCS)][OH{\cdot}OH_2]$ (**13**) have central $N_2Ni(\mu\text{-}SR)_2NiN'_3L$ cores [L = labile solvent molecule (**10**, **12**), Cl^- (**11**), and NCS^- (**13**)] composed of dithiolate bridged planar NiN_2S_2 and six-coordinate NiN'_3S_2L units. This is demonstrated for **11** and **13** by crystal structure determinations and for **10** and **12** by UV/Vis spectroscopy and room temperature magnetic susceptibility measurements. Complexes **10**, **11**, or **12** readily add other co-ligands at the NiN'_3S_2L fragment by substitution of the solvent molecule L (**10**, **12**) or the chloride substituent (**11**). The overall structure of the parent complexes is not affected by the substitution reactions. An electrochemical study has shown that complex **10** undergoes two successive one-electron oxidations at +0.88 and +0.41 V vs SCE. The oxidized species are not thermally stable, but electronic absorption spectra and EPR spectra are indicative of the presence of Ni^{III} species.

Introduction

Polydentate Schiff base ligands derived from 2,6-diformyl-4-methylthiophenol and certain α,ω-diamines are versatile ligands in the preparation of discrete dithiolate-bridged dimetal complexes.[1] Their specific coordination mode is due to the presence of *o*,*o*′-iminomethyl substituents, which, by formation of intramolecular chelate rings, effectively block terminal metal-coordination sites and, in contrast to a variety of monodentate thiolate ligands, allow for a better control of the nuclearity and reactivity of transition metal thiolate complexes.[2] Due to the presence of the soft thiolate ligands it is also often possible to stabilize metal ions in unusually high oxidation states. The coordination chemistry of such ligands, in particular with first-row transition metals M = Fe, Ni, and Cu,[3–5] has thus been an area of considerable interest recently, since dithiolate bridged, redoxactive $M(\mu\text{-}SR)_2M$ assemblies also occur in the active sites of various enzymes.[6–8] Surprisingly, there is a paucity of information in the literature concerning the chemistry of the analogous amine-thiophenolate ligands,[9][10] although their corresponding complexes offer the further advantage of being hydrolytically more stable.[11]

Recently we reported the synthesis and characterization of coordinatively unsaturated dinuclear nickel amine-thiolate complexes $[Ni_2(\mathbf{1})_2]^{2+}$ (**2**)[12] and $[Ni_2(\mathbf{4})]^{2+}$ (**5**) (Scheme 1).[13] Both complexes exhibit $N_2Ni(\mu\text{-}SR)_2NiN_2$ core structures and both were found to readily add co-ligands resulting in total or partial change of nickel coordination numbers from four in the parent complexes (**2**, **5**) to six in the products (**3**, **6**). While the former transformation (**2** → **3**) is accompanied by severe metal/ligand donor atom rearrangements, the latter (**5** → **6**) leaves the overall core structure of the parent complex unchanged, which is due to its fixation by the hexadentate ligand. This situation, along with the (slightly) different nickel coordination environments in **3**, means that its reactions with monodentate co-ligands proceed in a well-defined manner. Scheme 2 depicts the stereochemical courses of these reactions.

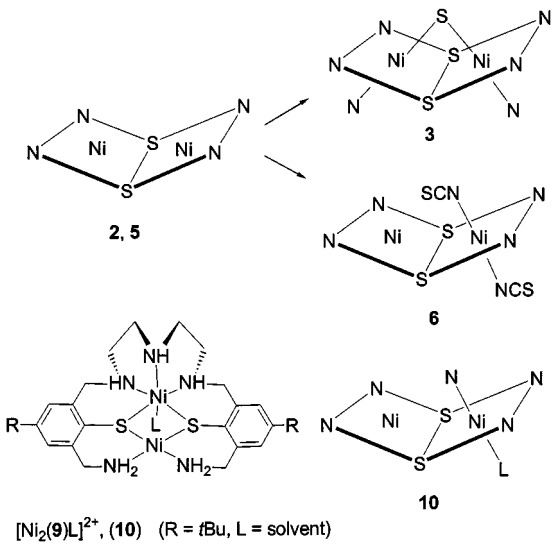


Scheme 1. Structures of dinuclear nickel amine-thiolate complexes **2**,[12] **3**,[12] **5**,[13] and **6**[13]

To further explore the reactivity of thiolate-bridged complexes featuring a central $Ni(\mu\text{-}SR)_2Ni$ core, we have now focused on the reactivity of nickel complexes of the amine-thiolate ligand H_2**9** (see Scheme 2), which provides dissimilar N_2S_2 and N'_3S_2 donor sets (N and N′ denote primary

[a] Institut für Anorganische und Analytische Chemie,
Universität Freiburg,
Albertstrasse 21, D-79104 Freiburg, Germany
Fax: (internat.) + 49(0)761/203-6001
E-mail: kerstber@sun2.ruf.uni-freiburg.de

 © WILEY-VCH Verlag GmbH, D-69451 Weinheim, 1999 1434–1948/99/1212–2157 $ 17.50+.50/0



Scheme 2. Core structural changes during transformations **2** → **3** and **5** → **6** and structure of dinuclear nickel complexes of amine-thiolate ligand H_2**9**

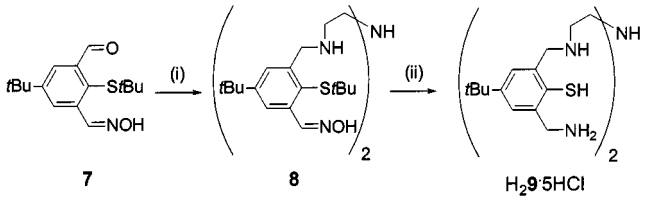
and secondary nitrogen atoms, respectively). It was assumed that the $-(CH_2)_2NH(CH_2)_2-$ chain bridging the two 2,6-bis(aminomethyl)-4-*tert*-butylthiophenol units would not distort the typical coordination observed in complexes **2** and **5**. Instead, the additional NH donor atom was anticipated to be involved in a specific *fac* coordination mode with two other secondary nitrogen and two bridging thiolate sulfur atoms, thereby yielding a six-coordinate $NiS_2N'_3L$ unit with a weakly bound solvent molecule L at the sixth coordination site. Similar strategies have been used by Sellmann et al. to control the reactivity of octahedral $MN_{5-x}S_xL$ complexes.[14]

This paper reports the synthesis of H_2**9** and some of its dinickel complexes. The crystal structures of $[Ni_2(\mathbf{9})(Cl)][Cl]$ (**11**) and of the isothiocyanate complex $[Ni_2(\mathbf{9})(NCS)][OH{\cdot}OH_2]$ (**13**), which is obtained by reaction of **11** with NH_4SCN, are also presented. The results obtained clearly demonstrate that control of the reactivity of dinuclear amine-thiolate complexes is possible, given that their core structures are assembled by specific, polydentate amine-thiolate ligands. All complexes have been further characterized by IR and UV/Vis spectroscopy and by cyclic voltammetry. Products obtained by chemical oxidation of the thiolate complexes have been characterized by UV/Vis and EPR spectroscopy.

Results and Discussion

Ligand Synthesis

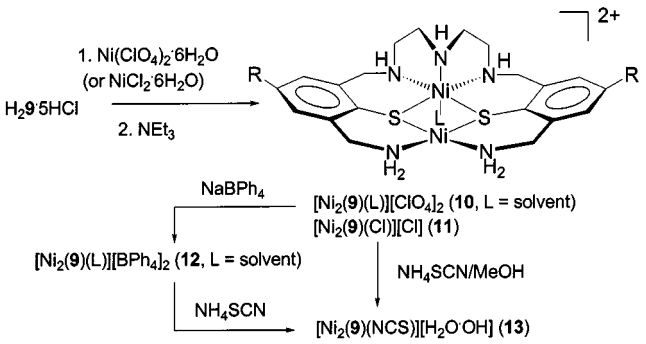
The heptadentate N_5S_2 ligand, H_2**9**, was prepared following the method described in Scheme 3. In the first step, two equivalents of aldehyde **7** were condensed with one equivalent of *N*,*N*-bis(2-aminoethyl)amine. The resulting imine/thioether/oxime compound was reduced in situ with $NaBH_4$ to give the corresponding amine/thioether/oxime compound **8**. Treatment of **8** with sodium in liquid ammonia resulted in reduction of the oxime groups and reductive cleavage of the ArS−*t*Bu bonds to give, after acidic workup, the pentahydrochloride salt, $H_2\mathbf{9} \cdot 5\,HCl$, in an over-all yield of 56%. $H_2\mathbf{9} \cdot 5\,HCl$ is very soluble in protic solvents such as water or methanol. These solutions can be handled in air for short periods of time. They were, however, freshly prepared under an inert atmosphere for the synthesis of the metal complexes.



Scheme 3. Preparation of $H_2\mathbf{9} \cdot 5\,HCl$: (*i*) 0.5 equiv. $NH(CH_2CH_2NH_2)_2$, $NaBH_4$; (*ii*) Na/NH_3, HCl

Synthesis of Dinuclear Nickel Complexes

The preparations and notations of dinuclear nickel complexes of the heptadentate amine-thiolate ligand are summarized in Scheme 4. Ligand $H_2\mathbf{9} \cdot 5\,HCl$ reacted with $Ni(ClO_4)_2 \cdot 6\,H_2O$ or $NiCl_2 \cdot 6\,H_2O$ in the presence of a base such as NEt_3 in 1:2:7 molar ratios to give complexes $[Ni_2(\mathbf{9})(L)][ClO_4]_2$ (**10**) and $[Ni_2(\mathbf{9})(Cl)][Cl]$ (**11**), respectively, as red microcrystalline solids. Addition of $NaBPh_4$ to a solution of **10** in MeOH produced complex $[Ni_2(\mathbf{9})(L)][BPh_4]_2$ (**12**) in good yield. The formulation of complexes **10**, **11**, and **12** as dinuclear complexes was confirmed by X-ray crystal structure determination of **11** (see below). In contrast to **10** and **11**, the tetraphenylborate salt **12** was found to exhibit good solubility in solvents such as acetonitrile or dichloromethane, thus facilitating spectroscopic studies of the $[Ni_2(\mathbf{9})(L)]^{2+}$ complex in noncoordinating solvents (see below).



Scheme 4. Preparation of nickel complexes **10**−**13**

Reaction of complexes **10** or **11** with ammonium thiocyanate in an acetonitrile/methanol mixed solvent system resulted in the precipitation of a dark-red crystalline mate-

rial that was shown by analysis to be $[Ni_2(\mathbf{9})(NCS)][OH{\cdot}OH_2]$ (**13**). This complex could be obtained independently by reaction of the tetraphenylborate complex **12** with NH_4SCN in the same solvent system. Once precipitated, complex **13** redissolves in *N*,*N*-dimethylformamide only. Interestingly, complex **13** showed no tendency to bind further NCS^- ions − even in the presence of a 10-fold molar excess of NH_4SCN.

Complexes **10** (μ_{eff} = 3.1 μ_B), **11** (μ_{eff} = 3.1 μ_B), **12** (μ_{eff} = 3.0 μ_B), and **13** (μ_{eff} = 3.1 μ_B) are all paramagnetic in the solid state at 295 K, implying that the complexes are all composed of a planar, diamagnetic $Ni^{II}N_2S_2$ (S = 0) unit and an octahedral, paramagnetic $Ni^{II}N'_3S_2L$ center (S = 1) per molecule of complex. The presence of a six-coordinate Ni^{II} ion was confirmed for **11** and **13** by X-ray crystal structure determinations, and for **10** and **12** by electronic absorption spectroscopy (see below). In the solid state, the nature of the substituent L for complexes **10** and **12** could not be unambiguously identified. Possible candidates for L are a methanol or a water molecule.

IR spectra of **10** and **12** are very similar except for the absorptions of the anions. The ν(ClO) stretching frequency of the ClO_4^- ions in **10**, for example, is split into three very strong and sharp absorptions at 1150, 1115, and 1089 cm^{-1}. From the splitting one might conclude that a ClO_4^- ion occupies the free coordination site L in **10**. However, in $[Ni_2(\mathbf{4})][ClO_4]_2$ (**5**)[13] where a similar splitting of the $\nu_3(F_2)$ mode is observed, the ClO_4^- ions are not involved in coordination to the nickel ions. The splitting of this band might thus be caused by hydrogen bonding interactions with NH groups of the ligand. Unfortunately, it was not possible from the IR data to identify the nature of the substituent L in **10** and **12**.

Compound **13** was shown by infrared spectroscopy to contain no ClO_4^- (absence of the characteristic Cl−O stretching frequency at 1100 cm^{-1}). A new feature at 2090 cm^{-1} [ν(CN)] revealed the presence of a thiocyanate ion. Relative to the ν(CN) stretching frequency of KSCN (2053 cm^{-1}), the shift to higher frequencies implied coordination of the thiocyanate ion.[15]

Crystal Structures of 11 and 13

The X-ray crystal structure determinations of amine-thiolate complexes **11** and **13** confirm the dinuclear nature of the amine-thiolate complexes. They also demonstrate that the substitution reactions do not affect the overall structures of the parent complexes, which is in contrast to the severe ligand/donor atom rearrangements observed in the core structures during reactions of complexes **2** and **5**. The structures of the complexes are displayed in Figures 1 and 2 together with the atomic numbering schemes.

Complex **11** is composed of the dinuclear complex $[Ni_2(\mathbf{9})(Cl)]^+$, one water and two acetonitrile molecules of crystallization, and a chloride ion. Both the water molecule and the chloride ion are involved in hydrogen bonding interactions with the hydrogen atoms of nitrogen atoms N(1), N(3), and N(5) of the complex monocation. The corresponding distances are summarized in the legend to Figure 3. There are no bonding interactions between the chloride ion and the nickel atoms of the cation. The shortest distance is 3.783(3) Å for Cl(2)···Ni(2). A similar hydrogen bonding network is observed in complex **13**, where the Cl^- ion is replaced by an OH^- ion (see below).

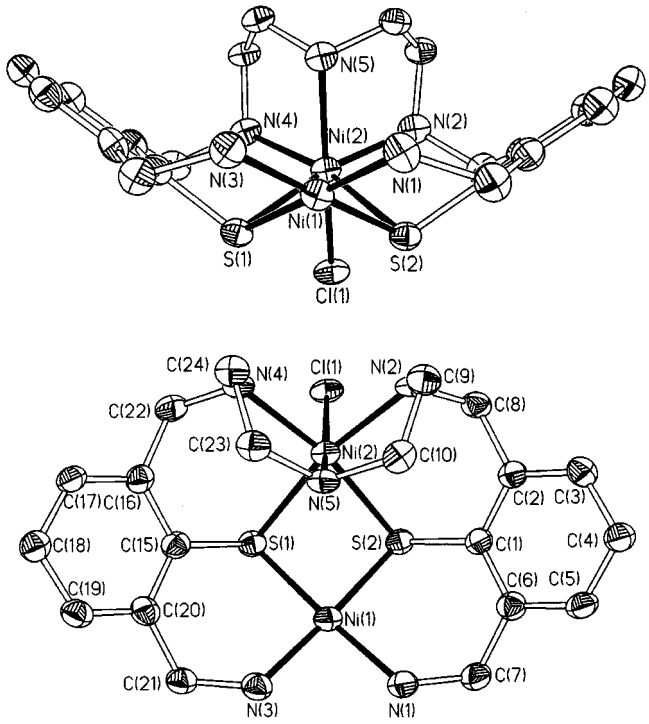


Figure 1. Molecular structure and atomic numbering of the $[Ni_2(\mathbf{9})(Cl)]^+$ cation in **11** (50% probability thermal ellipsoids). For clarity, *tert*-butyl groups and hydrogen atoms have been omitted

Table 1. Selected bond lengths [Å] in **11** and **13**

	11	**13**		**11**	**13**
Ni(1)−S(1)	2.200(2)	2.196(1)	Ni(2)−S(1)	2.414(2)	2.425(2)
Ni(1)−S(2)	2.189(2)	2.203(2)	Ni(2)−S(2)	2.429(2)	2.480(1)
Ni(1)−N(1)	1.954(4)	1.928(4)	Ni(2)−N(2)	2.090(4)	2.097(4)
Ni(1)−N(3)	1.943(4)	1.946(5)	Ni(2)−N(4)	2.095(4)	2.110(4)
			Ni(2)−N(5)	2.134(4)	2.147(4)
Ni(1)···Ni(2)	3.103(1)	3.149(1)	Ni(2)−L[a]	2.490(2)	2.070(5)

[a] L = Cl(1) in **11**, L = N(6) (NCS) in **13**.

The $[Ni_2(\mathbf{9})(Cl)]^+$ cation possesses an idealized C_s symmetry with a pseudo-mirror plane passing through the two nickel atoms and the secondary nitrogen atom N(5). Its overall structure is very similar to that of the neutral complex $[Ni_2(\mathbf{4})(NCS)_2]$ (**6**, see Scheme 1), from which it may be derived by replacing one NCS^- ion with the nitrogen atom N(5) of the lateral bis(2-aminoethyl)amine moiety. The average Ni−N and Ni−S bond lengths for the planar NiN_2S_2 (1.949 Å and 2.195 Å) and six-coordinate NiN_3S_2Cl sites (2.106 Å and 2.422 Å) show no unusual features and compare well with those in other planar NiN_2S_2[16] and octahedral NiN_4S_2 complexes,[13][17] respec-

tively. The Ni(2)−Cl(1) distance of 2.490(2) Å is likewise found in a range typical for six-coordinate NiN_xS_yCl complexes.[18] It should be noted that the Ni(2)−N(5) bond length of 2.134(4) Å *trans* to Ni(2)−Cl(1) is significantly longer than the other two Ni(2)−N distances. This bond length and the angle N(5)−Ni(2)−Cl(1) [162.9(1)°] imply that the N_3S_2 binding pocket of the ligand is too small to accommodate a nickel(II) ion in a regular octahedral coordination. The same conclusions can be drawn from the structure of **13**.

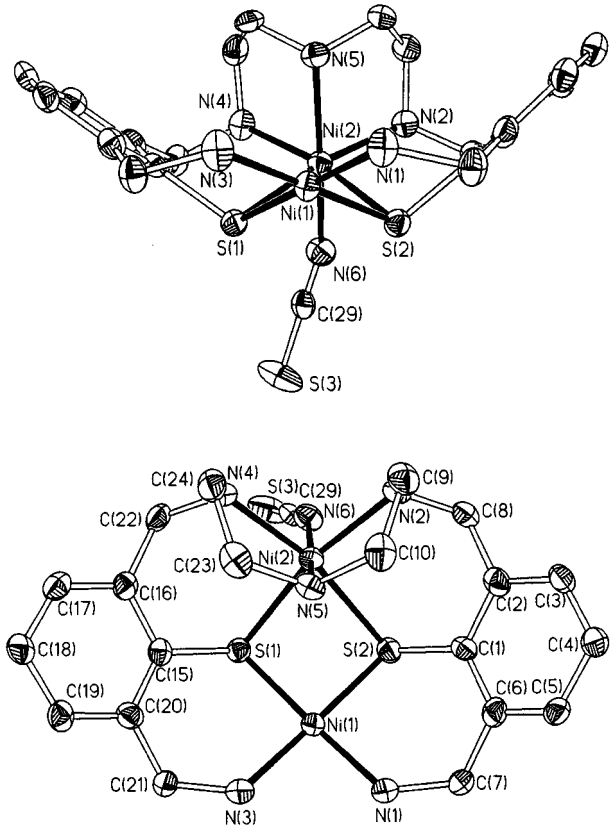


Figure 2. Molecular structure and atomic numbering of the $[Ni_2(\mathbf{9})(NCS)]^+$ cation in **13** (50% probability thermal ellipsoids). For clarity, *tert*-butyl groups and hydrogen atoms have been omitted

The isothiocyanate complex **13** is composed of the dinuclear complex $[Ni_2(\mathbf{9})(NCS)]^+$, a water molecule of crystallization, and a hydroxide ion. The hydroxide ion forms a strong $H_2O\cdots H-O$ hydrogen bonding contact to the water solvent molecule [$H_2O(1)\cdots O(2)$ 2.782(7) Å]. It should be noted that this structure is different from the $HO\cdots H\cdots OH^-$ arrangement generally found in hydrated hydroxy complexes of metals.[19] The formation of the present structure may arise from the three additional $HO^-\cdots H-N$ hydrogen bonding interactions with nitrogen atoms N(1), N(3), and N(5) of the complex monocation [O(1)···N(1) 3.239(7) Å, O(1)···N(3) 3.355(6) Å, O(1)···N(5) 3.222(7) Å]. In a similar way to **11**, there are no bonding interactions between the hydroxo or water oxygen atoms and the nickel ions of the cation. The shortest distance is 3.632(3) Å for O(1)···Ni(1). The structure of the $[Ni_2(\mathbf{9})(NCS)]^+$ cation may be simply

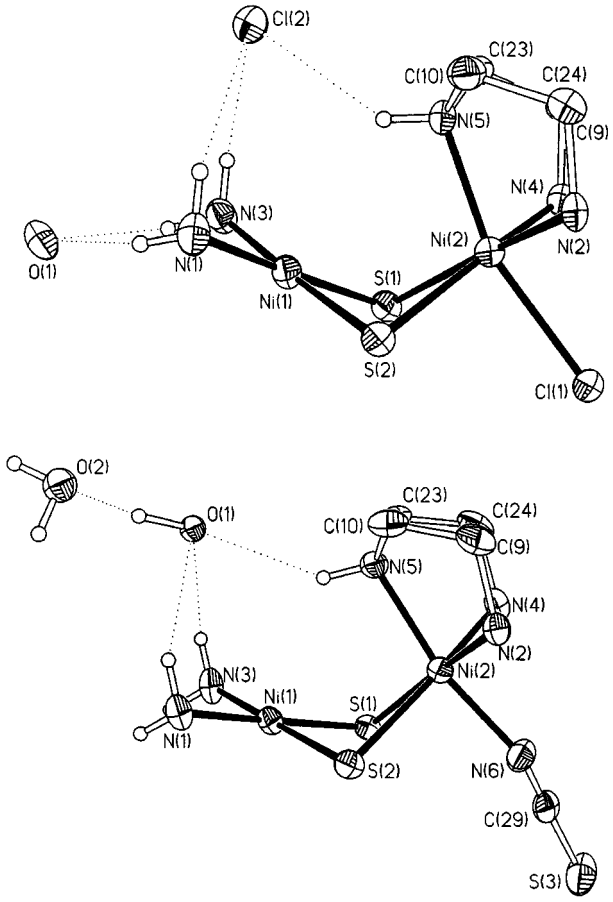


Figure 3. Core structures of complexes **11** and **13** (50% probability thermal ellipsoids). Hydrogen bonding interactions [A] in **11**: Cl(1)···N(1) 3.436(8), Cl(1)···N(3) 3.301(9), Cl(1)···N(5) 3.250(8), O(1)···N(1) 3.084(7), O(1)···N(3) 2.927(6), and in **13**: O(1)···O(2) 2.782(7), O(1)···N(1) 3.239(7), O(1)···N(3) 3.355(6), O(1)···N(5) 3.222(7). N−S and C−S bond lengths in **13**: N(6)−C(29) 1.160(7), S(3)−C(29) 1.629(6)

derived from that of $[Ni_2(\mathbf{9})(Cl)]^+$ by replacing the chloro ligand with an isothiocyanate group. There are no other gross structural changes, as evidenced by the similar shapes and similar Ni−N and Ni−S bond lengths (see Table 1).

The main difference between **5** and the complexes of the present study is the number of co-ligands that can be coordinated to the dinickel site. Dicationic **5** binds two NCS^- ligands to give complexes of the type $[N_2Ni(\mu\text{-}SR)_2NiN'_2(NCS)_2]$ (**6**) with the co-ligands in *trans* positions at the octahedral $S_2NiN'_2(NCS)_2$ site. This core structure is already partially preassembled in **10**, **11**, or **12** with an exchangeable substituent L and a nonexchangeable NH donor in place of the NCS^- ions in **5**. Hence the complexes of the present study bind only one co-ligand.

Electronic Absorption Spectra of Nickel Complexes 10−13

Although structural data for complexes **10** and **12** are currently not available, both are assumed to have a central $N_2Ni(\mu\text{-}SR)_2NiN'_3(L)$ core similar to that found for com-

Table 2. Electronic absorption spectral data for dinuclear nickel-amine-thiolate complexes

complex	solvent	donor set[a]	λ_{max} (nm) [ε ($M^{-1}cm^{-1}$)]
divalent nickel complexes			
$[Ni_2(\mathbf{1})_2]^{2+}$ (**2**)	CH_3CN	$2 \times N_2S_2$	503 (1049)
$[Ni_2(\mathbf{1})_3]^{1+}$ (**3**)	DMF	$2 \times N_3S_3$	593 (177), 922 (113), 1024 (103)[12]
$[Ni_2(\mathbf{4})]^{2+}$ (**5**)	CH_3CN	N_2S_2, N'_2S_2	501 (1005)[13]
$[Ni_2(\mathbf{9})L]^{2+}$ (**10**)	MeOH	N_2S_2, N'_3S_2L	518 (416), 624sh (121), 919 (27)
	DMF	N_2S_2, N'_3S_2L	516 (359), 621sh (122), 926 (31)
$[Ni_2(\mathbf{9})L]^{2+}$ (**12**)	CH_3CN	N_2S_2, N'_3S_2L	516 (356), 615sh (121), 916 (38)
	CH_2Cl_2	N_2S_2, N'_3S_2L	511 (590), 634sh (151), 948 (39)
$[Ni_2(\mathbf{9})(NCS)]^{1+}$ (**13**)	DMF	$2 \times N_3S_3$	513 (472), 621sh (139), 950 (39)
and their oxidized derivatives			
$[Ni^{III}Ni^{II}(\mathbf{1})_3]^{2+}$ $(\mathbf{3})^{2+}$	DMF	$2 \times N_3S_3$	473 (6753), 580 (4022)
$[Ni_2(\mathbf{1})_2]^{3+}$ $(\mathbf{2})^{3+}$	MeOH	$2 \times N_2S_2$	476 (1865), 626 (1242), 972 (1242)
$[Ni_2(\mathbf{4})]^{3+}$ $(\mathbf{5})^{3+}$	MeOH	$2 \times N_2S_2$	458 (2060), 581 (1034), 936 (376)
$[Ni_2(\mathbf{9})L]^{3+}$ $(\mathbf{10})^{3+}$	MeOH	N_2S_2, N'_3S_2L	462 (690), 584 (839), 898 (279)

[a] N and N′ denote primary and secondary nitrogen atoms.

plexes **11** and **13** in the solid-state. This is strongly supported by their electronic absorption spectral data. UV/Vis spectral data for all complexes are summarized in Table 2.

The spectra recorded for complexes **10**, **12**, and **13** are very similar − even in solvents of different donor strength. The spectrum of **10** in MeOH solution is representative of all the compounds, with an intense absorption at λ_{max} = 516 nm, a shoulder at 621 nm, and a weak absorption at 926 nm. It is noted that the position of the weak absorption in the 920 to 950 nm region appears to be dependent on the choice of the solvent.

The comparisons of the present UV/Vis spectral data with those of four-coordinate NiN_2S_2 complexes (**2**) or those of octahedral NiN_3S_3 complexes (**3**), respectively, clearly reveal the spectra of **10**−**13** to be due to superpositions of the electronic transitions of planar NiN_2S_2 and octahedral NiN_3S_2L chromophores. The intense band in the narrow range 506 to 516 nm, for example, is readily assigned to an electronic transition of a planar NiN_2S_2 unit. These bands are of approximately half the intensity of the corresponding band at 503 nm in **2**, which is consistent with the presence of only one such unit in complexes **10**−**13**. The other two bands at ca. 620 and ca. 930 to 950 nm are characteristic for an octahedral NiN_3S_2L complex.[12][20] Complex **3**, with two octahedral NiN_3S_3 units, exhibits absorptions at similar positions at 593 ($^3A_{2g}\rightarrow{}^3T_{1g}$) and 922 nm ($^3A_{2g}\rightarrow{}^3T_{2g}$), both of which again exhibit approximately twice the intensity of the respective bands of compounds **10**−**13**. This again supports the presence of only one NiN_3S_2L chromophore per dinuclear complex, as is required for complexes composed of one NiN_2S_2 and one NiN_3S_2L chromophore. The solvent dependence of the ($^3A_{2g}\rightarrow{}^3T_{2g}$) transitions around 920−950 nm is taken as an indication for the presence of an exchangeable solvent molecule in the coordination sphere of the octahedral NiN'_3S_2L fragment.

Electrochemistry

Complexes **10**, **13**, and **5** (for comparative purposes) were further characterized by cyclic voltammetry. The electrochemical properties of complex **2** have been reported previously.[12] Cyclic voltammograms (CV′s) were recorded in CH_3CN solution (for **5** and **10**) or DMF solution (for **13**) with tetra-*n*-butylammonium hexafluorophosphate as the supporting electrolyte and ferrocene as internal standard. In the following discussion, all redox potentials are referenced versus SCE.[21] Table 3 summarizes the measured potentials.

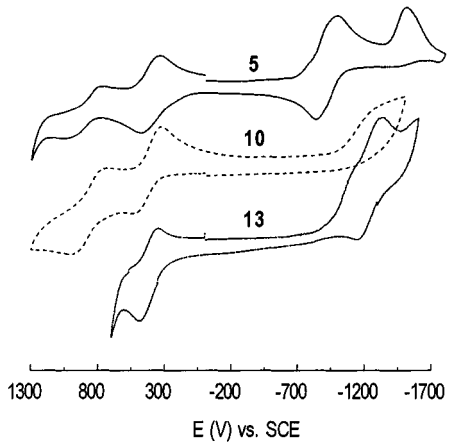


Figure 4. Cyclic voltammograms of complexes **5** and **10** in CH_3CN solution and of **13** in DMF solution at 295 K. Experimental conditions: [**5**], [**10**], [**13**] ca. $1\cdot10^{-3}$ M, Pt disk working electrode, Ag wire reference electrode, 0.1 M [nBu$_4$N][PF$_6$], scan rate 200 $mV\cdot s^{-1}$

The CV of complex **10** in acetonitrile solution is shown in Figure 4. Figure 4 shows, in the anodic potential region, two oxidation waves at $E^1_{1/2}$ = +0.88 V and at $E^2_{1/2}$ = +0.41 V vs SCE − an irreversible reduction wave occurred at ≈ −1.1 V. The electrochemical behavior of complexes **2**

Table 3. Electrochemical data (E/V) for dinuclear nickel-amine-thiolate complexes[a]

complex	donor set(s)[b]	$E^1_{1/2}$	$E^2_{1/2}$	$E^3_{1/2}$	$E^4_{1/2}$
$[Ni_2(\mathbf{1})_2]^{2+}$ (**2**)[c,d]	$2 \times N_2S_2$	+0.89 (irr)	+0.44 (79)	−0.86 (79)	−1.49 (irr)
$[Ni_2(\mathbf{4})]^{2+}$ (**5**)[c]	N_2S_2, N'_2S_2	+0.91 (265)	+0.42 (133)	−0.91 (142)	−1.51 (irr)
$[Ni_2(L^1)][ClO_4]_2$[e]	$2 \times N'_2S_2$	+1.35 (qr)	0.94 (r)	−0.93 (r)	−1.61 (qr)
$[Ni_2(\mathbf{9})(L)]^{2+}$ (**10**)[c]	N_2S_2, N'_3S_2L	+0.88 (251)	+0.41 (159)	n.o.	n.o.
$[Ni_2(\mathbf{9})(NCS)]^{+}$ (**13**)[f]	N_2S_2, N'_3S_2L	n.o.	+0.42 (137)	−1.23 (183)	n.o.
$[Ni_2(\mathbf{1})_3]^{2+}$	$2 \times N_3S_3$	+0.46 (84)	−0.02 (73)		

[a] Solutions of complexes were ca. $1 \cdot 10^{-1}$ M in supporting electrolyte (nBu$_4$NPF$_6$) and ca. $1 \cdot 10^{-3}$ M in sample; Pt disk working electrode, Ag wire reference electrode, scan rate 200 mV s^{-1}, $E^{\times}_{1/2} = (E^{ox}_p + E^{red}_p)/2$ for reversible one-electron transfer processes; oxidation (E^{ox}_p) or reduction peak potentials (E^{red}_p) are given for irreversible (irr) processes; number in parentheses denote peak-to-peak separations $\Delta E_p = |E^{ox}_p - E^{red}_p|$, n.o. = not observed. − [b] N and N′ denote primary and secondary nitrogen atoms. − [c] Solvent = acetonitrile. − [d] Values taken from ref.[12] − [e] L^1 = macrocyclic N_4S_2 ligand,[9] reported potentials were converted into the SCE [E (V) vs SCE = E (V) vs Ag/Ag$^+$ + 0.38 V] according to Table 1 in ref.[21], peak-to-peak separations were reported as reversible (r) or quasi-reversible (qr). − [f] Solvent = *N*,*N*-dimethylformamide.

and **5** in the anodic potential region is very similar, with two well-separated oxidation waves at $E^1_{1/2} \approx +0.90$ V and at $E^2_{1/2} \approx +0.41$ V vs SCE (see Table 3). In the following, we will discuss only processes that occur in the anodic potential region.[22]

The oxidation waves at $E^1_{1/2}$ and at $E^2_{1/2}$ of all complexes exhibit very large peak-to-peak separations, indicating that the corresponding charge-transfer processes are electrochemically not reversible. Is was not possible by controlled-potential coulometry to determine the number of electrons transferred during these processes, since at ambient temperature the oxidized species of complexes **2**, **5**, and **10** are not stable on the timescale of a coulometric experiment. Electrolysis of complex **10** at an applied potential of +0.60 V vs SCE, for example, resulted in a color change from red to transient dark-green. These transient dark-green solutions were also obtained by chemical oxidation of the complexes. Figure 5 shows the UV/Vis spectra taken for complex **10** before and after its oxidation. The observed spectral changes clearly show the oxidized species to be thermally unstable at room temperature. The fate of the oxidized species is discussed below. For now we estimate the half-life $\tau_{1/2}$ of the oxidized species to be ca. 15 min (from the decrease in ε_M at 584 nm with time). Complexes **2** and **5** behaved similarly, producing transient dark-green solutions upon electrolysis or chemical oxidation.

In a similar way to transition metal phenolato complexes, the oxidation of a transition metal thiophenolato complex can, in principle, be either metal- or ligand-centered.[23] There are several points that imply that the processes at $E^2_{1/2}$ and $E^1_{1/2}$ involve metal-centered one-electron transfer reactions subsequently producing mixed-valent $Ni^{III,II}$ and $Ni^{III,III}$ species, respectively. First of all, it is well-known that thiolate ligands are powerful in stabilizing Ni in the trivalent state.[24] Secondly, the number of observed oxidation waves (N) and their separations ($\Delta E = |E^1_{1/2} - E^2_{1/2}|$) are invariably $N = 2$ and $\Delta E \approx 0.45$ V, respectively, for all complexes. N matches with the number of metal atoms per complex and the value of 0.45 V for ΔE would be consistent with the presence of a mixed-valent $Ni^{III}Ni^{II}$ complex that is very stable to disproportionation ($K_{disp.} \approx 10^{-7}$), respectively. Thirdly, the UV/Vis spectra of all the transient dark-green solutions exhibit three very strong absorptions at around 470, 600, and 900 nm, which are characteristic of trivalent NiN_xS_y complexes.[12][20] Since the spectra of the oxidized species lack any characteristic absorptions for a planar NiN_2S_2 chromophore, it is assumed that the oxidations are accompanied by changes in the coordination environment of the planar NiN_2S_2 site. The broad peak-to-peak separations noted earlier would be consistent with this view.

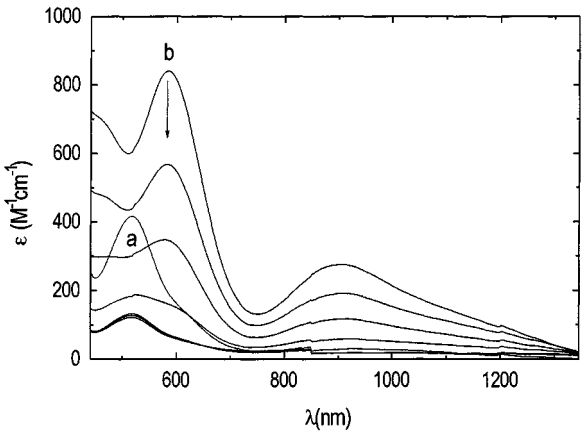


Figure 5. Oxidation of complex **10** with bromine in MeOH followed by UV/Vis spectroscopy (a: spectrum before, b: spectrum after addition of bromine). The other spectra were taken at 6 min intervals (the arrow indicates the evolution of the spectra with time)

A metal-centered nature for these oxidations is also supported by X-band EPR spectroscopic studies of frozen (77 K) solutions. Figure 6 shows the EPR spectrum of the green solution prepared by chemical oxidation of **10**. It reveals an axial signal as the main component with estimated g values of $g_\perp \approx 4.7$ and $g_\parallel \approx 2.1$, which are indicative of an $S = {}^3/_2$ spin ground state.[25] Hyperfine splitting due to ligand nitrogens could not be observed. Similar $S = {}^3/_2$ signals were previously observed for $\mathbf{3}^{2+}$ and for other mixed-valent $Ni^{III}Ni^{II}$ amine-thiolate complexes.[12] The $S = {}^3/_2$ ground states of these complexes are attained by an intramolecular ferromagnetic exchange interaction between low-spin Ni^{III} ($S = {}^1/_2$) and Ni^{II} ($S = 1$) ions. However, in the absence of more detailed spectroscopic data one can only

speculate about the electronic structure of the oxidized species.

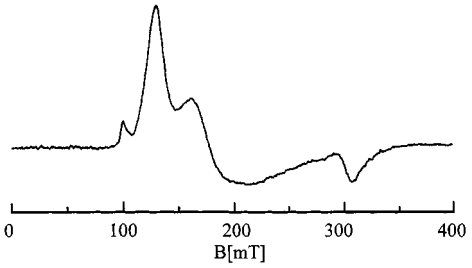


Figure 6. Frozen solution (77 K) X-band EPR spectrum of $\mathbf{10}^{+}$. Conditions: microwave frequency: ν = 9.02 GHz; microwave power: 2 mW; modulation frequency: 100 kHz; modulation amplitude: 10 gauss

The observation of an oxidation wave at $E^{2}_{1/2}$ = +0.42 V vs SCE for the isothiocyanate complex **13** in DMF solution also deserves some comment. Although the thiocyanate ion itself is redoxactive,[26] its oxidation can be ruled out since $E_{1/2}$ for this process is at +0.77 V vs SCE.[27] It is thus likely that this oxidation also corresponds to a metal-centered oxidation forming a Ni^{III} species. It was not possible to prepare the oxidized species by chemical or electrochemical oxidation, presumably due to its very rapid decomposition.

Chemical Oxidation of Metal Complexes

Complexes **2**, **5**, and **10** could also be chemically oxidized. Whereas addition of iodine to methanolic solutions of the complexes had no effect, treatment with bromine resulted in a sudden color change from red to dark-green. It was necessary to use less than 0.2 equiv. of oxidant to observe the transient green color. Figure 7 shows the UV/Vis spectral changes that occurred upon addition of ca. 0.1 equivalent of oxidant to a solution of complex **2** in methanol. The spectrum recorded directly after sample preparation is identical to that taken for a sample prepared by electrochemical oxidation, indicating that both methods produce the same species. In a similar way to **10** the oxidation product of complex **2** is thermally unstable.

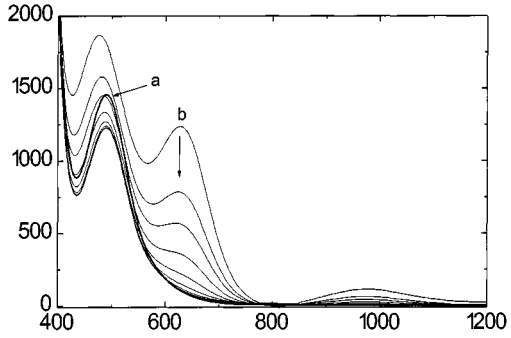
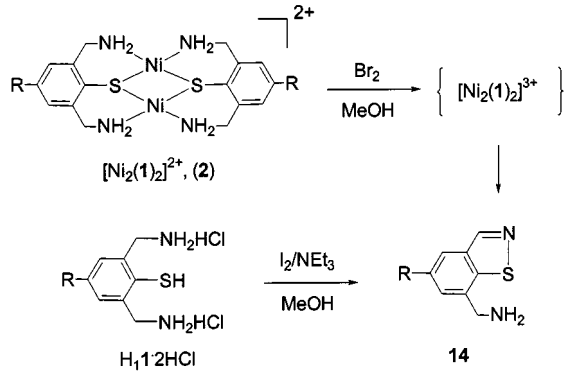


Figure 7. Oxidation of complex **2** with bromine in MeOH followed by UV/Vis spectroscopy (a: spectrum before, b: spectrum after addition of bromine). The other spectra were taken at 6 min intervals (the arrow indicates the evolution of the spectra with time)

The oxidized species of all complexes were allowed to decompose at ambient temperature. In the case of complexes **5** and **10** the resulting pale-green reaction mixtures contained a variety of new products that could not be separated. For complex **2**, however, oxidation resulted in the formation of the benzisothiazole derivative **14**[28] in high yield. The same compound is also obtained by treatment of the ligand, $H_1\mathbf{1} \cdot 2$ HCl, with iodine in methanol in the presence of base. It should be noted that the complexes could not be oxidized with iodine and this is taken as another indication that the oxidations are primarily metal-centered with the formation of intermediate Ni^{III} species.



Scheme 5. Oxidation of $H_1\mathbf{1} \cdot 2$ HCl and $[Ni_2(\mathbf{1})_2][ClO_4]_2$ (**2**)

Conclusion

The aim of controlling the reactivity of dinuclear nickel amine-thiolate complexes such as **5** has been achieved by a slight ligand modification. The constituent amine-thiophenolate units in $H_2\mathbf{9}$ retain their typical coordination mode but the additional NH donor blocks one of the two potentially free coordination sites found for **5**. The position *trans* to this donor is the reactive site of the present complexes. Solvent molecules and pseudo-halide ions bind to this site; the coordination of a halide ion has been observed for the first time. The latter substituent may be substituted by other co-ligands such as H^{-} or CN^{-}, and the influence of such substituents on the $Ni^{III,II}$ redox-potentials could be studied. These studies could also be of importance in attempts to model structural and functional features of dithiolate-bridged $[M(\mu\text{-}SR)_2M]$ structures found in metalloproteins, as for instance in [NiFe] hydrogenase from *Desulfovibrio gigas*.

Experimental Section

Materials and Methods: Compounds **7**,[13] $H_1\mathbf{1} \cdot 2$ HCl,[10] $[Ni_2(\mathbf{1})_2][ClO_4]_2$,[12] and $[Ni_2(\mathbf{4})][ClO_4]_2$[13] were prepared as previously described. All other chemicals were of reagent grade and used without further purification. Solvents were predried over molecular sieves and freshly distilled from appropriate drying agents. – ^{1}H-NMR and $^{13}C\{^{1}H\}$-NMR spectra were recorded on a Bruker AVANCE DPX 200 spectrometer. All chemical shifts are quoted on the δ scale with TMS or the solvent as internal standard. Coupling

constants are expressed in Hz. − Melting points were determined in capillaries and are uncorrected. − CHN-Analyses were determined with a Perkin−Elmer Elemental Analyzer 240. − IR spectra were recorded on a Bruker VECTOR 22 FT-IR-spectrophotometer as KBr pellets. − Absorption spectra were recorded on a Jasco V-570 UV/VIS/NIR spectrometer. − Room temperature magnetic susceptibility measurements were carried out with a Johnson Matthey model Mark II magnetic susceptibility balance. Experimental susceptibility data were corrected for the underlying diamagnetism using Pascal's constants.[29] − Cyclic voltammetry measurements were carried out at 25°C with an EG&G Princeton Applied Research Potentiostat/Galvanostat Model 263 A. The cell contained a Pt working electrode, a Pt wire auxiliary electrode, and an Ag wire as a reference electrode. Concentration of solutions were 0.1 M in supporting electrolyte ($Bu^n_4NPF_6$) and ca. 1×10^{-3} M in sample. Ferrocenium/ferrocene was used as the internal standard. All potentials were converted into the SCE reference [E (V) vs SCE = E (V) vs Fc^+/Fc − 0.38 V in CH_3CN].[21] EPR spectra were recorded using a conventional Varian X-band spectrometer with 100 kHz modulation.

***N*,*N*′-Bis[2-*tert*-butylsulfanyl-3-hydroximinomethyl-5-*tert*-butylbenzylidene]diethylenetriamine (8):** To a stirred solution of aldehyde **7** (587 mg, 2.00 mmol) in absolute ethanol (10 mL) was added a solution of *N*,*N*-bis(2-aminoethyl)amine (103 mg, 1.00 mmol) in ethanol (10 mL). After stirring for 2 h at 60°C, a solution of $NaBH_4$ (200 mg, 5.27 mmol) in ethanol (20 mL) was added, and the resulting homogeneous reaction mixture was stirred for further 12 h. Water (50 mL) was then added and the pH of the solution was adjusted to 1 by the addition of hydrochloric acid to destroy excess reducing equivalents. The mixture was stirred for an additional 30 min, the solution was made alkaline (final pH ≈ 12−13) by addition of 5 M KOH solution, and then extracted with dichloromethane (3 × 50 mL). The combined extracts were dried with $MgSO_4$, filtered, and the filtrate evaporated to dryness under reduced pressure. The pale-yellow residue was purified by column chromatography (SiO_2) using 10% MeOH in CH_2Cl_2 as eluent. Yield 521 mg (79%), m.p. 154°C. − ^{1}H NMR (5% CD_3OD/$CDCl_3$): δ = 8.88 (s, 2 H, ArC*H*), 7.79 (d, $^4J_{H,H}$ = 2.0 Hz, 2 H, Ar*H*), 7.43 (d, $^4J_{H,H}$ = 2.0 Hz, 2 H, Ar*H*), 4.00 (s br, 4 H, ArCH_2), 2.60 (s, 8 H, CH_2), 1.27 (s, 18 H, CH_3), 1.18 (s, 18 H, CH_3). − ^{13}C NMR (CD_3OD): δ = 153.8, 151.9, 147.0, 140.1, 130.2, 129.5, 123.6, 53.7, 50.4, 49.0, 47.3, 35.9, 31.9, 31.8.

***N*,*N*′-Bis[3-aminomethyl-5-*tert*-butyl-2-thiobenzyl]diethylenetriamine Pentahydrochloride ($H_2$9 · 5 HCl):** To a solution of **8** (658 mg, 1.00 mmol) in liquid ammonia (50 mL) was added sodium in small portions at −70°C, until the blue color of the reaction mixture persisted for at least 1 h (without adding further reducing equivalents). After stirring for an additional 1 h, excess sodium was destroyed by addition of solid ammonium chloride, and the solvent was evaporated at atmospheric pressure. The resulting solid was hydrolyzed with methanol (30 mL) followed by 6 M hydrochloric acid (final pH ≈ 1), and then evaporated to dryness under reduced pressure. For purification, the remaining solid was dissolved in ethanol (50 mL), filtered to remove NaCl and NH_4Cl, and evaporated to dryness. This procedure was repeated two more times. The resulting solid was sufficiently pure for metal complex syntheses. Yield 476 mg (68%). − IR (KBr): $\tilde{\nu}$ = 3417 cm^{-1} br (NH), 2400 sh (SH). − ^{1}H NMR (D_2O): δ = 7.79 (s, 4 H, Ar*H*), 4.66 (s, 4 H, ArCH_2), 4.50 (s, 4 H, ArCH_2), 3.70 (s, 8 H, CH_2), 1.39 (s, 18 H, CH_3). − ^{13}C NMR (D_2O): δ = 153.2, 136.7, 134.2, 130.1, 129.8, 127.3, 51.4, 44.0, 43.3, 42.9, 34.6, 30.7.

[Ni_2(9)(L)][ClO_4]$_2$ (10, L = H_2O): ***CAUTION!*** *Transition metal perchlorates are hazardous and may explode. Only small quantities should be prepared and great care taken.* To a solution of H_2**9** · 5 HCl (0.700 g, 1.00 mmol) and $Ni(ClO_4)_2 \cdot 6\,H_2O$ (731 mg, 2.00 mmol) in methanol (10 mL) was added a solution of NEt_3 (0.505 g, 0.500 mmol) in MeOH (1 mL). The reaction mixture was stirred for 5 min at 60°C, during which time a red crystalline precipitate formed. The solid was filtered off, washed with cold MeOH (2 × 1 mL) and ether, and dried in air. Yield: 487 mg (57%). − $C_{28}H_{45}Ni_2N_5S_2(ClO_4)_2H_2O$ (850.12): calcd. C 39.56, H 5.57, N 8.24; found C 39.64, H 5.42, N 8.18. − IR (KBr): $\tilde{\nu}$ = 3424 cm^{-1} br (OH), 3288, 3244, 3184, 3162, (NH + NH_2), 1150 s, 1115 s, 1089 vs (ClO_4^-).

[Ni_2(9)Cl][Cl] · 2 CH_3CN · H_2O (11): To a solution of H_2**9** · 5 HCl (0.700 g, 1.00 mmol) and $NiCl_2 \cdot 6\,H_2O$ (475 mg, 2.00 mmol) in acetonitrile (10 mL) was added a solution of NEt_3 (0.505 g, 0.500 mmol) in acetonitrile (1 mL). The reaction mixture was stirred for 5 min at 60°C, during which time a red crystalline precipitate formed. The solid was filtered off, washed with cold acetonitrile (2 × 1 mL) and ether, and dried in air. The crude product was recrystallized once from MeOH/CH_3CN. Yield: 530 mg (66%). − $C_{28}H_{45}Ni_2N_5S_2Cl_2(H_2O)(CH_3CN)_2$ (804.25): calcd. C 47.79, H 6.64, N 12.19; found C 47.43, H 6.42, N 11.87.

[Ni_2(9)(L)][BPh_4]$_2$ (12, L= H_2O): To a solution of complex **10** (86 mg, 0.10 mmol) in MeOH (10 mL) was added a solution of $NaBPh_4$ (50 mg, 0.15 mmol) in MeOH (1 mL). The solution was stirred for 20 min at room temperature, during which time a red crystalline precipitate formed. The solid was filtered off, washed with cold MeOH (2 × 1 mL) and dried in air. Yield: 106 mg (82%). − $C_{28}H_{45}Ni_2N_5S_2(BPh_4)_2H_2O$ (1289.68): calcd. C 70.78, H 6.80, N 5.43; found C 70.98, H 6.73, N 5.18. − IR (KBr): $\tilde{\nu}$ = 735 cm^{-1} s, 707 s (BPh_4^-).

[Ni_2(9)(NCS)][OH·H_2O] (13): To a solution of **10** (33 mg, 40 μmol) in MeOH (5 mL) was added a solution of NH_4SCN (4.6 mg, 60 μmol) in MeOH (2 mL). The resulting red solution was stirred for 1 h, during which time a dark-red microcrystalline solid precipitated. The solid was filtered off, washed with 2 mL of MeOH, and dried in air. Yield: 24 mg (83%), m.p. 344−346°C (decomp.). − IR (KBr): $\tilde{\nu}$ = 2090 cm^{-1} vs (NCS^-). − $C_{29}H_{48}Ni_2N_6S_3O_2$ (726.33): calcd. C 47.96, H 6.66, N 11.57; found C 47.83, H 6.43, N 11.18.

Oxidation of $H_1$1 · 2 HCl **(Preparation of 7-Aminomethyl-5-*tert*-butylbenzisothiazol) (14):** To a solution of H_1**1** · 2 HCl (297 mg, 1.00 mmol) and NEt_3 (556 mg, 5.50 mmol) in methanol (30 mL) was added a solution of iodine (508 mg, 2.00 mmol) in methanol (20 mL), and the reaction mixture was stirred for 2 h. The organic solvent was removed under reduced pressure, 20 mL of 1 M NaOH solution was added to the residue, and the product extracted with dichloromethane (3 × 50 mL). The combined extracts were dried with K_2CO_3, filtered, and evaporated to dryness to give 198 mg (89%) of **14** as a pale yellow solid. The crude product was purified by column chromatography using 10% MeOH in CH_2Cl_2 as eluent. M.p. 242−245°C. − ^{1}H NMR (CD_3OD/2% DCl): δ = 9.06 (s, 1 H, C*H*=N), 8.29 (d, ^4J = 1.6 Hz, 1 H, Ar*H*), 7.92 (d, ^4J = 1.6 Hz, 1 H, Ar*H*), 4.47 (s, 2 H, CH_2), 1.50 (s, 9 H, CH_3). − ^{13}C NMR (CD_3OD): δ = 158.0, 152.0, 150.5, 139.4, 128.8, 126.5, 122.7, 43.7, 36.4, 32.2.

Oxidation of [Ni_2(1)$_2$][ClO_4]$_2$: To a solution of complex [Ni_2(**1**)$_2$][ClO_4]$_2$ (200 mg, 0.262 mmol) and NEt_3 (303 mg, 0.3 mmol) in methanol (40 mL) was added a freshly prepared solution of bromine (34.2 mg, 0.214 mmol) in methanol (2 mL) at room temperature. The resulting transient dark-green solution was stirred for 30 min, during which time the color of the solution changed to dark-red. This process was repeated three more times to give a pale-green solution. The organic solvent was removed under reduced

pressure, 20 mL of 1 M NaOH solution (20 mL) was added to the residue, and the product extracted with dichloromethane (3 × 50 mL). The combined extracts were dried with K_2CO_3, filtered, and evaporated to dryness. The pale-green residue was dissolved in 2 mL of ethanol and acidified with 3 drops of 12 M HCl. Addition of ether caused precipitation of an off-white solid, which was filtered off and dried in air. Yield: 84 mg (73%). The analytical data are identical with those of compound **14**.

Crystal Structure Determination: Single crystals of complexes **11** and **13** suitable for X-ray structure analysis could be obtained by slow evaporation of acetonitrile/methanol solutions of the complexes. The crystals were mounted on glass fibers using perfluoropolyether oil. Crystal data were collected at 180(2) K, using a Bruker SMART CCD diffractometer. Graphite monochromated Mo-*K*α radiation (0.71073 Å) was used throughout. The data were processed with SAINT[30] and corrected for absorption using SADABS (transmission factors: 1.00−0.11 for **11**, 1.00−0.77 for **13**).[31]

Crystal data and refinement details for **11** ($C_{32}H_{53}Cl_2N_7Ni_2OS_2$, *M*r = 804.25): crystal size 0.52 × 0.46 × 0.32 mm, monoclinic, space group *P*2(1)/c, *a* = 14.251(3) Å, *b* = 21.351(4) Å, *c* = 12.805(3) Å, β = 94.28(3)°, *V* = 3885(1) Å^3, *Z* = 4, μ(Mo-*K*α) = 1.25 mm^{-1}, D_c = 1.375 g·cm^{-3}, *F*(000) = 1696, 24550 reflections measured, 9179 unique (R_{int} 0.1545), 5320 observed reflections [$I > 2\sigma(I)$]. The structure was solved by direct methods using the program SHELXS-86[32] and refined by full-matrix least-squares techniques against F^2 using SHELXL-93.[33] Positional and anisotropic atomic displacement parameters were refined for all nonhydrogen atoms, except for the C and N atoms of two acetonitrile molecules (refined isotropically). Hydrogen atoms were placed geometrically and positional parameters were refined using a riding model. Isotropic atomic displacement parameters for hydrogen atoms were constrained to be 1.2 (1.5 for methyl groups). Final residuals *R*1 = 0.0780, *wR*2 = 0.1846 [$I > 2\sigma(I)$], *R*1 = 0.1236, *wR*2 = 0.2126 (all data), largest difference peak, $\Delta\rho_{max}$ = 1.567 eÅ^{-3}, and hole $\Delta\rho_{min}$ = −1.265 eÅ^{-3}.

Crystal data and refinement details for **13** ($C_{29}H_{48}Ni_2N_6S_3O_2$, *M*r = 726.33): crystal size 0.75 × 0.51 × 0.16 mm, monoclinic, space group *C*c (no. 9), *a* = 11.204(2) Å, *b* = 25.651(5) Å, *c* = 12.187(2) Å, β = 98.68(3)°, *V* = 3462(1) Å^3, *Z* = 4, μ(Mo-*K*α) = 1.303 mm^{-1}, D_c = 1.393 g·cm^{-3}, *F*(000) = 1536, 12152 reflections measured, 4998 unique (R_{int} 0.0261), 4912 observed reflections [$I > 2\sigma(I)$]. The structure was solved by direct methods using the program SHELXS-86[32] and refined by full-matrix least-squares techniques against F^2 using SHELXL-93.[33] Positional and anisotropic atomic displacement parameters were refined for all non-hydrogen atoms, except for the oxygen atoms of a water molecule and a hydroxide ion (refined isotropically). Hydrogen atoms were placed geometrically and positional parameters were refined using a riding model. The OH^- and H_2O hydrogen atoms were located unambiguously from difference Fourier maps. Isotropic atomic displacement parameters for hydrogen atoms were constrained to be 1.2 (1.5 for methyl groups). The Flack *X* parameter (absolute structure parameter) was calculated to be 0.03(2) for the present structure and 0.98(2) for the inverted structure, thus providing strong evidence that the absolute structure has been assigned correctly.[34] Final residuals *R*1 = 0.0388, *wR*2 = 0.1148 [$I > 2\sigma(I)$], *R*1 = 0.0406, *wR*2 = 0.1185 (all data), largest difference peak, $\Delta\rho_{max}$ = 0.518 eÅ^{-3}, and hole $\Delta\rho_{min}$ = −0.501 eÅ^{-3}.

Crystallographic data (excluding structure factors) for the structures reported in this paper have been deposited with the Cambridge Crystallographic Data Centre as supplementary publication no. CCDC-132820 (**11**) and CCDC-121428 (**13**). Copies of the data can be obtained free of charge on application to CCDC, 12 Union Road, Cambridge CB2 1EZ, UK [Fax: +44(1223) 336-033; E-mail: deposit@cam.ac.uk].

Acknowledgments

This work was supported by the Deutsche Forschungsgemeinschaft. The author thanks Prof. Dr. H. Vahrenkamp for his generous support. Financial support from the Wissenschaftliche Gesellschaft Freiburg and the Graduiertenkolleg "Ungepaarte Elektronen" is also gratefully acknowledged. Prof. D. Siebert and G. Steinfeld are thanked for recording EPR spectra.

[1] [1a] J. G. Hughes, R. Robson, *Inorg. Chim. Acta.* **1979**, *35*, 87−92. − [1b] M. Louey, P. D. Nichols, R. Robson, *Inorg. Chim. Acta.* **1980**, *47*, 87−96. − [1c] P. Iliopoulos, K. S. Murray, R. Robson, J. Wilson, G. A. Williams, *J. Chem. Soc., Dalton Trans.* **1987**, 1585−1591. − [1d] A. M. Bond, M. Haga, I. S. Creece, R. Robson, J. C. Wilson, *Inorg. Chem.* **1989**, *28*, 559−566. − [1e] B. F. Hoskins, C. J. McKenzie, R. Robson, L. Zhenrong, *J. Chem. Soc., Dalton Trans.* **1990**, 2637−2641. − [1f] B. F. Hoskins, R. Robson, G. A. Williams, J. C. Wilson, *Inorg. Chem.* **1991**, *30*, 4160−4166.

[2] [2a] B. Krebs, G. Henkel, *Angew. Chem.* **1991**, *103*, 785−804; *Angew. Chem. Int. Ed. Engl.* **1991**, *30*, 769−788. − [2b] I. G. Dance, *Polyhedron* **1986**, *5*, 1037−1104. − [2c] P. J. Blower, J. R. Dilworth, *Coord. Chem. Rev.* **1987**, *76*, 121−185.

[3] [3a] A. J. Atkins, A. J. Blake, M. Schröder, *J. Chem. Soc., Chem. Commun.* **1993**, 1662−1665. − [3b] A. J. Atkins, D. Black, A. J. Blake, A. Marin-Becerra, S. Parsons, L. Ruiz-Ramirez, M. Schröder, *J. Chem. Soc., Chem. Commun.* **1996**, 457−464. − [3c] N. D. J. Branscombe, A. J. Blake, A. Marin-Becerra, W.-S. Li, S. Parsons, L. Ruiz-Ramirez, M. Schröder, *J. Chem. Soc., Chem. Commun.* **1996**, 2573−2574.

[4] [4a] S. Brooker, P. D. Croucher, *J. Chem. Soc., Chem. Commun.* **1995**, 1493−1494. − [4b] S. Brooker, P. D. Croucher, *J. Chem. Soc., Chem. Commun.* **1995**, 2075−2076. − [4c] S. Brooker, P. D. Croucher, F. M. Roxburgh, *J. Chem. Soc., Dalton Trans.* **1996**, 3031−3037. − [4d] S. Brooker, P. D. Croucher, *J. Chem. Soc., Chem. Commun.* **1997**, 459−460.

[5] P. E Kruger, V. McKee, *J. Chem. Soc., Chem. Commun.* **1997**, 1341−1342.

[6] For biological, dithiolate-bridged Cu/Cu systems, see: [6a] T. Tsukihara, H. Aoyama, E. Yamashita, T. Tomizaki, H. Yamaguchi, K. Shinzawa-Itoh, R. Nakashima, R. Yaono, S. Yoshikawa, *Science* **1995**, *269*, 1069−1074. − [6b] S. Iwata, C. Ostermeier, B. Ludwig, H. Michel, *Nature* **1995**, *376*, 660−669.

[7] For biological, dithiolate-bridged Fe/Ni systems, see: [7a] A. Volbeda, M.-H. Charon, C. Piras, E. C. Hatchikian, M. Frey, J. C. Fontecilla-Camps, *Nature* **1995**, *373*, 580−587. − [7b] A. Volbeda, E. Garcin, C. Piras, A. L. de Lacey, V. M. Fernandez, E. C. Hatchikian, M. Frey, J. C. Fontecilla-Camps, *J. Am. Chem. Soc.* **1996**, *118*, 12989−12996. − [7c] M. A. Halcrow, *Angew. Chem.* **1995**, *107*, 1307−1310; *Angew. Chem. Int. Ed. Engl.* **1995**, *34*, 1193−1197.

[8] For biological dithiolate-bridged Fe/Fe systems, see: J. W. Peters, W. N. Lanzilotta, B. J. Lemon, L. C. Seefeldt, *Science* **1998**, *282*, 1853−1858.

[9] S. Brooker, P. D. Croucher, T. C. Davidson, G. S. Dunbar, A. J. McQuillan, G. B. Jameson, *J. Chem. Soc., Chem. Commun.* **1998**, 2131−2132.

[10] B. Kersting, *Eur. J. Inorg. Chem.* **1998**, 1071−1077.

[11] E. C. Constable, *Metals and Ligand Reactivity*, VCH, Weinheim, **1996**.

[12] [12a] B. Kersting, D. Siebert, *Inorg. Chem.* **1998**, *37*, 3820−3828. − [12b] B. Kersting, D. Siebert, *Eur. J. Inorg. Chem.* **1999**, 189−193.

[13] B. Kersting, G. Steinfeld, J. Hausmann, *Eur. J. Inorg. Chem.* **1999**, 179−187.

[14] [14a] D. Sellmann, J. Utz, F. W. Heinemann, *Eur. J. Inorg. Chem.* **1999**, 341−348. − [14b] D. Sellmann, J. Utz, F. W. Heinemann, *Inorg. Chem.* **1999**, *38*, 459−466. − [14c] D. Sellmann, W. Sog-

lowek, F. Knoch, M. Moll, *Angew. Chem.* **1989**, *101*, 1244−1245; *Angew. Chem. Int. Ed. Engl.* **1989**, *28*, 1271−1272. − [14d] D. Sellmann, W. Soglowek, M. Moll, *Z. Naturforsch.* **1992**, *47b*, 1105−1114.
[15] K. Nakamoto, *Infrared and Raman Spectra of Inorganic and Coordination Compounds*, Wiley, New York, **1978**.
[16] [16a] G. Musie, P. J. Farmer, T. Tuntulani, J. H. Reibenspies, M. Y. Darensbourg, *Inorg. Chem.* **1996**, *35*, 2176−2183. − [16b] G. A. Lawrance, M. Maeder, T. M. Manning, M. A. O′Leary, B. W. Skelton, A. H. White, *J. Chem. Soc., Dalton Trans.* **1990**, 2491−2495.
[17] K. Osakada, T. Yamamoto, A. Yamamoto, A. Takenaka, Y. Sasada, *Acta Crystallogr.* **1984**, *C40*, 85−87.
[18] P. E. Riley, K. Seff, *Inorg. Chem.* **1972**, *11*, 2993−2999.
[19] F. A. Cotton, G. Wilkinson, *Advanced Inorganic Chemistry*, 5th ed., John-Wiley & Sons, New York, **1988**.
[20] H.-J. Krüger, R. H. Holm, *J. Am. Chem. Soc.* **1990**, *112*, 2955−2963.
[21] N. G. Connelly, W. E. Geiger, *Chem. Rev.* **1996**, *96*, 877−910.
[22] The processes that occur at $E < 0$ V will be discussed in more detail in a subsequent paper. G. Steinfeld, B. Kersting, unpublished results.
[23] B. Adam, E. Bill, E. Bothe, B. Goerdt, G. Haselhorst, K. Hildenbrand, A. Sokolowski, S. Steenken, T. Weyhermüller, K. Wieghardt, *Chem. Eur. J.* **1997**, *3*, 308−319.
[24] [24a] H.-J. Krüger, R. H. Holm, *Inorg. Chem.* **1987**, *26*, 3645−3647. − [24b] T. Krüger, B. Krebs, G. Henkel, *Angew. Chem.* **1992**, *104*, 71−72; *Angew. Chem. Int. Ed. Engl.* **1992**, *31*, 54−56. − [24c] J. D. Franolic, W. Y. Wang, M. Millar, *J. Am. Chem. Soc.* **1992**, *114*, 6587−6588. − [24d] D. Sellmann, W. Prechtel, F. Knoch, M. Moll, *Z. Naturforsch.* **1992**, *47b*, 1411−1423. − [24e] J. Hanss, H.-J. Krüger, *Angew. Chem.* **1998**, *110*, 366−369; *Angew. Chem. Int. Ed. Engl.* **1998**, *37*, 360−363. − [24f] T. Beissel, F. Birkelbach, E. Bill, T. Glaser, F. Kesting, C. Krebs, T. Weyhermüller, K. Wieghardt, C. Butzlaff, A. X. Trautwein, *J. Am. Chem. Soc.* **1996**, *118*, 12376−12390. − [24g] T. Glaser, F. Kesting, T. Beissel, E. Bill, T. Weyhermüller, W. Meyer-Klaucke, K. Wieghardt, *Inorg. Chem.* **1999**, *38*, 722−732.
[25] D. Collison, F. E. Mabbs, *J. Chem. Soc., Dalton Trans.* **1982**, 1565−1574.
[26] F. Seel, E. Müller, *Chem. Ber.* **1955**, *88*, 1747−1755.
[27] R. C. Weast, *CRC Handbook of Chemistry and Physics*, 51st ed., CRC, Ohio, **1970**.
[28] M. Davis, *Adv. Heterocycl. Chem.* **1972**, *14*, 43−98.
[29] E. A. Boudreaux, L. N. Mulay, *Theory and Applications of Molecular Paramagnetism*, Wiley, New York, **1976**.
[30] *SAINT, Version 4.050*, Siemens Analytical X-ray Instruments Inc., Madison, WI, **1995**.
[31] G. M. Sheldrick, *SADABS*, University of Göttingen, **1997**.
[32] G. M. Sheldrick, *Acta Crystallogr.* **1990**, *A46*, 467−473.
[33] G. M. Sheldrick, *SHELXL-93*, a computer program for crystal structure refinement, University of Göttingen, **1993**.
[34] H. D. Flack, *Acta Crystallogr.* **1983**, *A39*, 876−881.

Received May 18, 1999
[I99175]

Novel Synthesis of Macrocyclic Amine-Thiophenolate Ligands: X-ray Crystal Structure of a Ni_4 Complex of an N_8S_4 Ligand

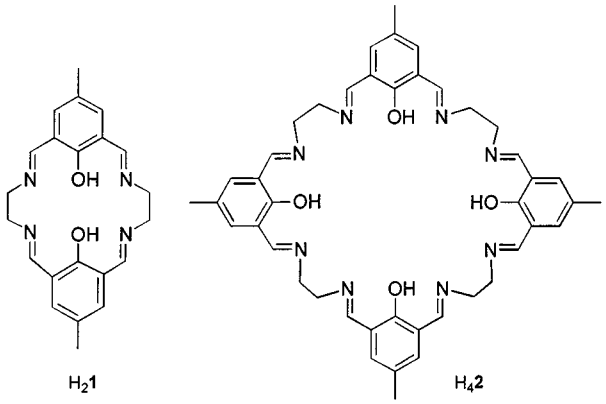
Berthold Kersting,*[a] Gunther Steinfeld,[a] Thorsten Fritz,[a] and Julia Hausmann[a]

Keywords: Macrocyclic compounds / Amine-Thiolate Donors / Polynuclear Complexes / Nickel / Condensation reactions

A novel route to macrocyclic amine-thiophenolate ligands is described. The new, air-stable thiophenolate precursor 1,2-bis(4-*tert*-butyl-2,6-diformyl-phenylsulfanyl)ethane (**4**) is readily condensed with two equivalents of 1,2-ethanediamine or 1,3-propanediamine under medium to high dilution conditions to give 2 × 4 condensation products. The smaller 1 × 2 macrocyclic compounds are not produced under these conditions. Subsequent reduction with $NaBH_4$ (reduction of imine groups) and Na/NH_3 (reductive cleavage of aryl-alkylsulfides) provides the 36- and 40-membered amine-thiophenolate ligands H_4**6a** and H_4**6b**. The macrocyclic compounds are versatile ligands for the preparation of polynuclear transition metal complexes. With divalent nickel H_4**6a** forms the di- and tetranuclear complexes $[Ni_2($**6a**$)]$ (**7**) and $[Ni_4($**6a**$)][ClO_4]_4$ (**8**). Reaction of **8** with four equivalents of NH_4SCN yields the novel isothiocyanate complex $[Ni_4^{II}($**6a**$)(NCS)_4]\cdot$10MeCN (**9**). The structure consists of well-separated molecules of the tetranuclear complex $[Ni^{II}_4($**6a**$)(NCS)_4]$ (C_i symmetry). Two symmetry-related binuclear $[N_2Ni(\mu_2\text{-}SR)_2NiN_4]$ fragments composed of thiolate-bridged distorted planar $\{N_2S_2Ni\}$- and distorted *cis*-octahedral $\{(SCN)_2N_2S_2Ni\}$ units reside within the cavity of the macrocycle. The intramolecular distance between the two binuclear units is 6.144(1) Å.

Introduction

One of the most efficient syntheses of macrocyclic amine phenolate ligands such as H_2**1** (Scheme 1) involves a Schiff base condensation of 2,6-diformyl-4-methyl-phenol with an aliphatic α,ω-diamine in the presence of a labile first-row transition metal ion. Since its discovery by Robson and co-workers in 1970,[1] this reaction has been applied to a large variety of such ligands because they are ideally suited to prepare homo- and heterodinuclear and mixed-valence complexes.[2−7] Higher condensation products,[8][9] such as the 36-membered amine-phenolate ligand H_4**2**,[10] can also be obtained by this method.



Scheme 1. Macrocyclic N/O-Donor Ligands H_2**1**[1] and H_4**2**[10a]

In contrast to the large number of macrocyclic amine-phenolate ligands, there exist only a few examples of the corresponding imino- and aminothiophenolates.[11][12] This is true in particular for larger macrocyclic N_xS_y compounds.[13] To the best of our knowledge, all the macrocyclic N_xS_y compounds described to date have been obtained by metal template condensations using the air-sensitive compound 2,6-diformyl-4-methyl-thiophenol as starting material.[14]

We describe here an alternative route to macrocyclic amine-thiophenolate ligands by employing the air-stable thiophenolate precursor, 1,2-bis(4-*tert*-butyl-2,6-diformylphenylsulfanyl)ethane (**4**). The tetraaldehyde is readily condensed with aliphatic α,ω-diamines, and subsequent reduction of the intermediate thioether/imine compounds provides the 36- and 40-membered ligands H_4**6a**,**b**. This is demonstrated by the solid-state structure of $[Ni_4($**6a**$)(NCS)_4]\cdot$10MeCN.

Results and Discussion

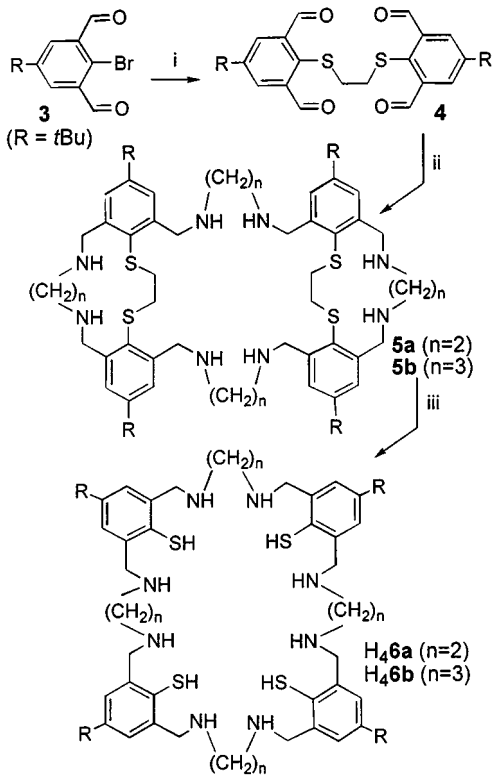
Ligand Syntheses

The synthesis of the new octaamine-tetrathiophenol compounds H_4**6a**,**b**·8HCl was accomplished in three steps employing 4-*tert*-butyl-2,6-diformylbromobenzene **3** as starting reagent (Scheme 2). In the first step, compound **3** was reacted with dipotassium 1,2-ethanedithiolate in DMF in a 2:1 stoichiometric ratio to give the tetraaldehyde **4** in nearly quantitative yield. Condensation of **4** with two equivalents of 1,2-ethanediamine in a CH_2Cl_2/MeOH mixed solvent system under high-dilution conditions, followed by sodium borohydride reduction of the intermediate imine-thioether product, gave the amine-thioether compound **5a** in yields greater than 80%. The smaller 1 × 2−condensation product, i.e. the 18-membered N_4S_2 macrocycle, is not formed

[a] Institut für Anorganische und Analytische Chemie,
Universität Freiburg,
Albertstrasse 21, D-79104 Freiburg, Germany
Fax: (internat.) +49-761/203-6001
E-mail: kerstber@sun2.ruf.uni-freiburg.de

 © WILEY-VCH Verlag GmbH, D-69451 Weinheim, 1999 1434−1948/99/1212−2167 $ 17.50+.50/0

under these conditions. Attempts to obtain this compound by using more dilute solutions (and longer reaction times) were unsuccessful, but instead resulted in higher yields of **5a**. In the last step, compound **5a** was reduced with sodium in liquid ammonia (reductive cleavage of the $ArS-CH_2-CH_2-SAr$ bonds) to give, after hydrolysis with hydrochloric acid, the hydrochloride salt of the amine-thiolate ligand, H_4**6a**·8HCl. A similar reaction sequence was employed to prepare the 40-membered amine-thiolate ligand H_4**6b**·8HCl. Both ligands were stored as their hydrochloride salts under an atmosphere of dry nitrogen. The compounds H_4**6a**,**b**·8HCl are only slightly soluble in water, although the ligands dissolve in methanol in the presence of a base such as NEt_3.



Scheme 2. Preparation of macrocyclic amine-thiophenolate ligands H_4**6a**,**b**: (i). $HSCH_2CH_2SH$, K_2CO_3, DMF, 25°C; (ii). 2 equiv. $NH_2(CH_2)_nNH_2$, 10%MeOH/CH_2Cl_2; $NaBH_4$; (iii). Na/NH_3, HCl

The new compounds **4**, **5a**,**b**, and H_4**6a**,**b**·8HCl were characterized by ^{1}H NMR, ^{13}C NMR and IR spectroscopy. In the IR spectra of H_4**6a**,**b**·8HCl the N−H and S−Hstretching vibrations appear as broad bands at 2750 and 2400 cm^{-1}, respectively. The relatively low value for ν(S−H) is presumably due to intramolecular hydrogen bonding interactions with adjacent NH protons. According to the ^{1}H and ^{13}C NMR spectra, compounds H_4**6a**,**b**·8HCl exhibit fourfold symmetry in solution. Compound H_4**6a**·8HCl, for example, displays only four resonances at δ = 7.42, 4.34, 3.44, and 1.19 for the Ar*H*, $ArCH_2N$, NCH_2CH_2N, and $C(CH_3)_3$ protons, respectively. Due to fast H/D exchange, the S*H* and N*H* protons are not observed under these conditions. As expected, the ^{13}C NMR spectrum of H_4**6a**·8HCl displays eight signals for the 56 carbon atoms. The macrocyclic structure of H_4**6a**·8HCl was confirmed by an X-ray structure determination of one of its metal complexes (see below).

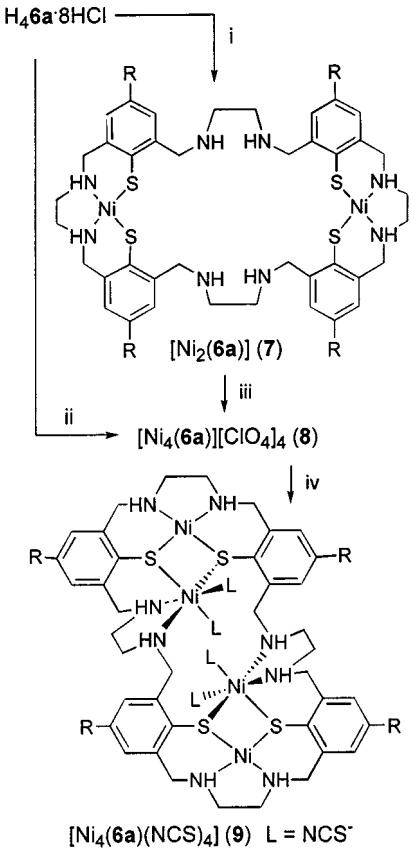
The strategy for the synthesis of the macrocyclic amine-thiophenolate ligands presented in this study differs from those employed by other groups for related amine-thiophenolate ligands. Such compounds have been prepared almost exclusively by metal-templated condensations between 2,6-diformyl-4-methyl-thiophenol and certain α,ω-diamines, followed by sodium borohydride reduction of the imine-thiolate complexes and hydrolysis of the resulting amine-thiolate complexes. The latter route has also been employed in the synthesis of the phenolate analogue of H_4**6a**.[10c] Our approach makes use of the air-stable tetraaldehyde/dithioether compound **4** which can be condensed with aliphatic diamines in the absence of metal ions. Since the 2 × 4 condensation products are almost exclusively formed under these conditions, it is likely that the bridging thioether unit serves as the template for macrocycle formation. However, the cyclization reactions still demand medium to high-dilution conditions (final concentration ≈ 0.01 M), since otherwise only polymeric material is obtained. It also appears that the yield of cyclization product (**5a**: > 92%, **5b**: 56%) decreases with increasing chain length of the diamine.

Synthesis and Characterization of Nickel Complexes 7−9

The preparation of nickel(II) complexes of H_4**6a**·8HCl was accomplished by reaction with nickel(II) salts in methanol or acetonitrile in the presence of a base such as triethylamine. Depending on the metal-to-ligand ratio the metalations of H_4**6a**·8HCl afforded di- or tetranuclear nickel(II) complexes (see Scheme 3). The reaction of H_4**6a**·8HCl with two equivalents of $NiCl_2·6H_2O$ produced a purple, microcrystalline solid of composition [Ni_2(**6a**)]·MeOH (**7**), whereas the reaction with four equivalents of $Ni(ClO_4)_2·6H_2O$ yielded the red-brown complex [Ni_4(**6a**)]-[ClO_4]$_4$ (**8**). Complex **8** could also be obtained by metalation of **7** with two equivalents of $Ni(ClO_4)_2·6H_2O$.

Complex **7** is diamagnetic and exhibits good solubility in most common organic solvents. Its UV/Vis spectrum in acetonitrile (Figure 1) is very similar to other planar N_2S_2Ni complexes,[15][16] indicating that both nickel ions exhibit planar N_2S_2 coordination environments in the solution state. On the basis of the ^{1}H NMR spectroscopic data (see Experimental Section) we propose a structure as shown in Scheme 3 with the two nickel ions occupying diagonally opposite sides of the macrocycle.

The metalation of **7** with nickel(II) perchlorate to form **8** is accompanied by distinct spectral changes. Isobestic points occurred at 544 and 680 nm. These spectral changes were clearly discernible until the ratio of concentrations of **7** and Ni^{2+} was 1:2 (see Figure 1). At higher Ni^{2+} concentrations the spectrum remained essentially unchanged, implying that H_4**6a** coordinates no more than four Ni^{2+} ions. The IR spectrum of **8** reveals three very strong and sharp



Scheme 3. Preparation of dinuclear and tetranuclear nickel complexes of H$_4$**6a**: (i). 2.0 equiv. $NiCl_2·6H_2O$, NEt_3/MeOH; (ii). 4.0 equiv. $Ni(ClO_4)_2·6H_2O$, NEt_3/MeOH; (iii). 2 equiv. $Ni(ClO_4)_2·6H_2O$, CH_3CN; (iv). 4 equiv. NH_4SCN, CH_3CN

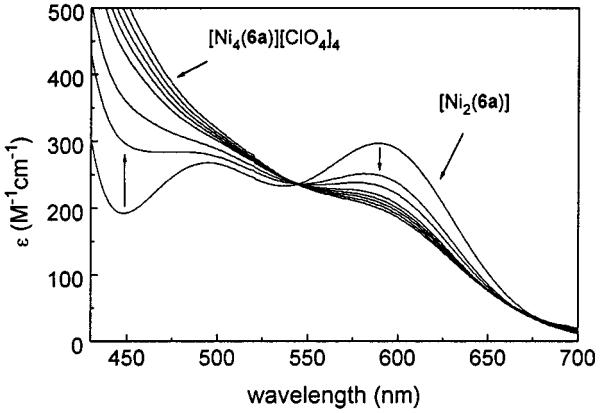


Figure 1. Titration of [Ni$_2$(**6a**)]·MeOH (**7**) ([**7**] = 1×10^{-3} M) with 10^{-3} M $Ni(ClO_4)_2·6H_2O$ in MeCN (0.0−4.0 added equiv) at 295 K followed by UV/Vis spectroscopy

absorptions for ν(ClO) at 1150, 1115, and 1089 cm^{-1} consistent with the presence of the ClO_4^- ions. It was not possible to grow single crystals of this product, although the reaction of **8** with NH_4SCN in CH_3CN yielded single crystals of [Ni$_4$(**6a**)(NCS)$_4$]·10CH_3CN (**9**) suitable for an X-ray crystal structure determination.

X-ray Crystal Structure of [Ni$_4$(6a)(NCS)$_4$]·10CH_3CN (9)

The X-ray crystal structure determination of **9** revealed the structure to consist of well-separated molecules of the tetranuclear isothiocyanate complex and acetonitrile molecules of crystallization. Figure 2 shows the molecular structure of the neutral, centrosymmetric complex [Ni$_4$(**6a**)(NCS)$_4$]. Selected bond lengths and angles are collected in Table 1.

Table 1. Selected bond lengths [Å] and angles [°] in [Ni$_4$(**6a**)(NCS)$_4$]·10CH_3CN (**9**)[a]

Bond lengths			
Ni(1)−S(1)	2.463(2)	Ni(2a)−S(1)	2.212(2)
Ni(1)−S(2a)	2.503(2)	Ni(2a)−S(2a)	2.179(2)
Ni(1)−N(2)	2.091(5)	Ni(2a)−N(1)	1.943(5)
Ni(1)−N(3)	2.167(4)	Ni(2a)−N(4a)	1.935(5)
Ni(1)−N(5)	2.060(5)		
Ni(1)−N(6)	2.071(5)		
N(5)−C(29)	1.124(8)	S(5)−C(29)	1.658(7)
N(6)−C(30)	1.175(8)	S(6)−C(30)	1.633(6)
Ni(1)···Ni(2a)	3.147(1)		
Bond angles			
S(1)−Ni(1)−S(2a)	74.63(6)	S(1)−Ni(2a)−S(2a)	86.54(6)
S(1)−Ni(1)−N(2)	92.80(13)	S(1)−Ni(2a)−N(1)	95.7(2)
S(1)−Ni(1)−N(3)	95.38(13)	S(1)−Ni(2a)−N(4a)	178.6(2)
S(1)−Ni(1)−N(5)	172.2(2)	S(2a)−Ni(2a)−N(1)	177.5(2)
S(1)−Ni(1)−N(6)	88.62(15)	S(2a)−Ni(2a)−N(4a)	92.74(15)
S(2a)−Ni(1)−N(2)	166.71(13)	N(1)−Ni(2a)−N(4a)	85.0(2)
S(2a)−Ni(1)−N(3)	94.05(13)		
S(2a)−Ni(1)−N(5)	97.6(2)	Ni(1)−N(5)−C(29)	170.7(5)
S(2a)−Ni(1)−N(6)	92.3(2)	N(5)−C(29)−S(5)	179.8(6)
N(2)−Ni(1)−N(3)	82.6(2)	Ni(1)−N(6)−C(30)	165.1(5)
N(2)−Ni(1)−N(5)	95.0(2)	N(6)−C(30)−S(6)	177.4(7)
N(2)−Ni(1)−N(6)	91.7(2)		
N(3)−Ni(1)−N(5)	86.0(2)		
N(3)−Ni(1)−N(5)	173.2(2)		
N(5)−Ni(1)−N(6)	90.8(2)		

[a] Symmetry transformations used to generate equivalent atoms: Ni(2a), S(2a), N(4a): 1−x, 2−y, 1−z.

All donor atoms of the 36-membered macrocycle are involved in coordination to the four nickel atoms to give two four-coordinate N_2S_2Ni and two six-coordinate N_4S_2Ni coordination units. Each Ni atom forms a five-membered chelate ring with one of the four ethanediamine moieties of the ligand. These N_2Ni units are bridged by two thiophenolate sulfur atoms to give two symmetry-related binuclear $[N_2Ni(\mu_2\text{-}SR)_2NiN_2(NCS)_2]$ units. The average Ni−N and Ni−S bond lengths within these binuclear units compare well with those of other $N_2S_2Ni^{II}$ and $N_4S_2Ni^{II}$ complexes, although the bond length Ni(1)−N(3) at 2.167(4) Å is quite long for an octahedral $N_4S_2Ni^{II}$ complex.[17] The intramolecular distance between the two distorted *cis*-octahedral and the two distorted planar nickel atoms at 6.144(1) Å and 9.005(1) Å, respectively, may be used to describe the distance between the two binuclear subunits.

An interesting feature to note is the fact that the isothiocyanate ions within each binuclear unit occupy *cis* positions at the six-coordinate nickel atom {SCN−Ni(1)−NCS at 90.8(2)°}. It is assumed that this coordination mode is enforced by the short C_2 alkyl chain which links the 2,6-

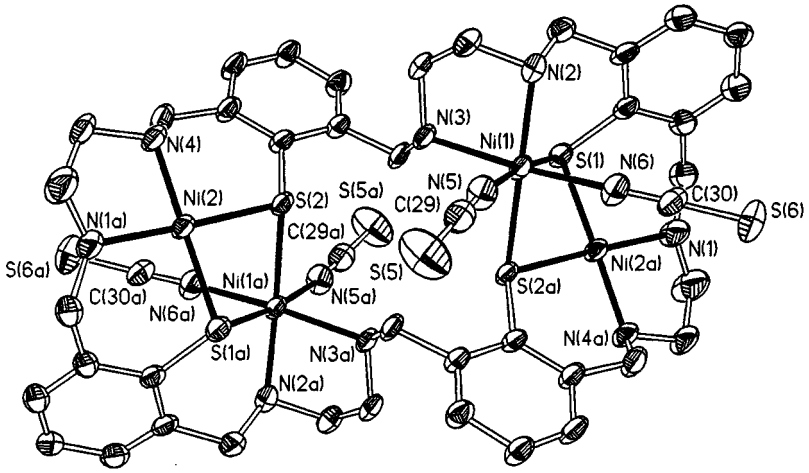


Figure 2. Perspective view of the molecular structure of the tetranuclear isothiocyanate complex $[Ni_4(\mathbf{6a})(NCS)_4]$ in **9**. Hydrogen atoms and *tert*-butyl groups are omitted for reasons of clarity

bis(aminomethyl)-4-*tert*-butylthiophenolate moieties. This is in marked contrast to coordinatively unsaturated $N_2Ni(\mu_2\text{-}SR)_2NiN_2$ complexes in which the thiophenolate moieties are connected via a C_3 alkyl chain. Here the exogenous ligands are coordinated in *trans*-axial positions (see Scheme 4).[18][19]

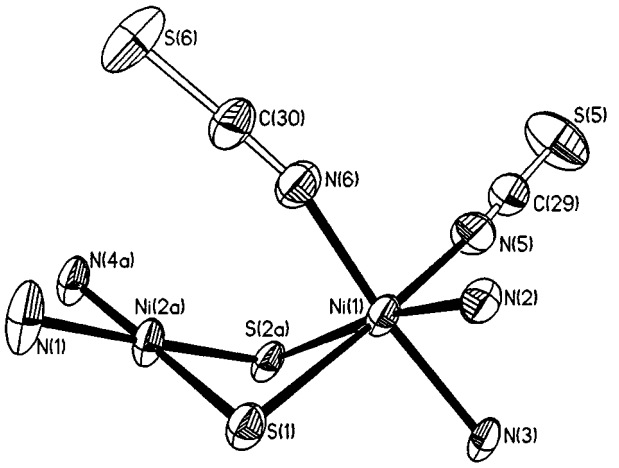
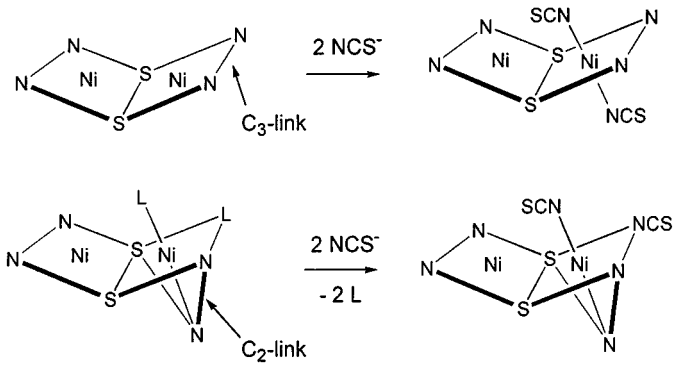


Figure 3. Coordination units in the central $[N_2Ni(\mu_2\text{-}SR)_2\text{-}NiN_2(NCS)_2]$ core in **9** showing 50% thermal ellipsoids



Scheme 4. Stereochemical courses of reactions of coordinatively unsaturated nickel complexes containing a $[N_2Ni(\mu_2\text{-}SR)_2NiN_2]$ core structure: influence of the bridging alkyl chain

Conclusion

A new synthetic route to macrocyclic amine-thiolate ligands has been developed. The air-stable thiophenolate precursor 1,2-bis(4-*tert*-butyl-2,6-diformylphenylsulfanyl)-ethane can be condensed with aliphatic α,ω-diamines $\{NH_2(CH_2)_nNH_2\}$ to give the 2 × 4 macrocyclic compounds {4·(7 + n) ring-atoms} in the absence of metal ions. By varying the building blocks it should be possible to obtain a wide range of polydentate amine-thiolate ligands which could be useful for the preparation of new polynuclear transition metal thiolate complexes

Experimental Section

General: ^1H NMR and $^{13}C\{^1H\}$ NMR spectra were recorded on a Bruker AVANCE DPX 200 spectrometer. All chemical shifts are quoted on the δ scale with TMS or the solvent as internal standard. Coupling constants are expressed in Hz. Melting points were determined in capillaries and are uncorrected. CHN-Analyses were determined with a Perkin−Elmer Elemental Analyzer 240. IR spectra were recorded on a Bruker VECTOR 22 FT-IR-spectrophotometer as KBr pellets. Absorption spectra were recorded on a Jasco V-570 UV/VIS/NIR spectrometer. Compound **3**[20] was prepared as described in the literature. All other chemicals were of reagent grade and used without further purification. Solvents were predried over molecular sieves and freshly distilled from appropriate drying agents.

Compound 4: To a suspension of 1,2-ethanedithiol (2.50 g, 26.5 mmol) and K_2CO_3 (8.29 g, 60.0 mmol) in DMF (80 mL) was added solid **3** (14.3 g, 53.0 mmol), and the reaction mixture was stirred for 12 h. Water (200 mL) was then added dropwise with stirring. The resulting precipitate was isolated by filtration, washed with water (3 × 50 mL), and dried in air. The solid was purified by recrystallization from dichloromethane/cyclohexane to give 11.5 g (92%) of **4** as pale yellow crystals. M.p. 178° C. − IR (KBr): $\tilde{\nu}$ = 2872m (CH), 1687s cm^{-1} (CO). − ^1H NMR ($CDCl_3$): δ = 10.67 (s, 4 H, C*H*O), 8.11 (s, 4 H, Ar*H*), 2.96 (s, 4 H, CH_2), 1.31 (s, 18 H, CH_3). − $^{13}C\{^1H\}$ NMR ($CDCl_3$): δ = 191.0 (*C*HO), 153.9, 138.3, 136.9, 131.3, 38.5, 35.2, 30.9.

Compound 5a: A solution of 1,2-ethanediamine (493 mg, 8.20 mmol) in 10% MeOH/CH_2Cl_2 (100 mL) and a solution of **3**

(2.05 g, 4.36 mmol) in CH_2Cl_2 (100 mL) were simultaneously added within 3 h to 300 mL of CH_2Cl_2 with stirring. After the reaction mixture was stirred for further 12 h at room temperature, the solvents were removed at reduced pressure to obtain a white solid. The solid was dissolved in MeOH/CH_2Cl_2 (100 mL, 1:1), a solution of $NaBH_4$ (1.20 g, 31.7 mmol) in 50 mL of MeOH was added, and the resulting homogeneous reaction mixture was stirred for further 2 h. After the excess reducing agent was destroyed by acidification with 1M HCl, the pH was readjusted to 11 by addition of 2M NaOH solution, and the aqueous phase extracted with CH_2Cl_2 (3 × 200 mL). The combined organic phases were dried over K_2CO_3, filtered, and the solvent removed under reduced pressure. The pale-yellow residue was purified by column chromatography (SiO_2) using MeOH/NEt_3/CH_2Cl_2 (10:5:85) as eluting solvent to give 2.12 g (92%) of the product as a white foam. − IR (KBr): $\tilde{\nu}$ = 3310w cm^{-1} (NH). − ^1H NMR ($CDCl_3$): δ = 7.34 (d, ^4J = 2.0 Hz, 4 H, Ar*H*), 7.24 (d, ^4J = 2.0 Hz, 4 H, Ar*H*), 4.02 (s, 8 H, BzCH_2), 3.97 (s, 8 H, BzCH_2), 3.25 (s, 8 H, SCH_2), 2.91 (s, 8 H, NHCH_2), 2.81 (s, 8 H, NHCH_2), 1.90 (s br, 8 H, NH), 1.30 (s, 36 H, CH_3). − ^{13}C NMR ($CDCl_3$): δ = 151.7, 144.3, 144.0, 130.3, 127.0, 126.4, 53.9, 53.3, 48.7, 37.4, 34.4, 31.1.

Compound 5b: Analogously to the preparation of **5a**, compound **5b** was prepared from **3** (2.05 g, 4.36 mmol) and 1,3-propanediamine (608 mg, 8.20 mmol). Yield: 1.35 g (56%). − IR (KBr): $\tilde{\nu}$ = 3295w cm^{-1} (NH). − ^1H NMR ($CDCl_3$): δ = 7.25 (d, ^4J = 2.0 Hz, 4 H, Ar*H*), 7.14 (d, ^4J = 2.0 Hz, 4 H, Ar*H*), 3.95 (s, 8 H, BzCH_2), 3.85 (s, 8 H, BzCH_2), 3.03 (s, 8 H, SCH_2), 2.73 (m, 16 H, NHCH_2), 1.72 (m, 8 H, NHCH_2), 1.23 (s, 36 H, CH_3). − ^{13}C NMR (D_2O/2%DCl): δ = 155.9, 136.9, 136.6, 131.9, 130.8, 126.3, 50.7, 49.9, 45.4, 44.6, 37.8, 34.9, 30.5, 23.0, 20.9.

Compound $H_4$6a·8HCl: To a solution of sodium (1.00 g, 43.0 mmol) in liquid ammonia (100 mL) was added a solution of **5a** (2.00 g, 1.90 mmol) in THF (30 mL) and the deep-blue reaction mixture was stirred for 1 h. After the excess reducing equivalents were destroyed by careful addition of NH_4Cl, the suspension was evaporated to dryness, and the resulting pale yellow residue was taken up in water (40 mL). The yellow solution was cooled to 0° C, and the pH of the solution adjusted to 1 by addition of 12M hydrochloric acid. The pale yellow solid was collected by filtration and recrystallized from 1M HCl to give H_4**6a**·8HCl (1.79 g, 73%) as white crystals. − IR (KBr): $\tilde{\nu}$ = 3423, 2750br (N−H), 2400br cm^{-1} (S−H). − ^1H NMR (D_2O): δ = 7.41 (s, 8 H, Ar*H*), 4.36 (s, 16 H, BzCH_2N), 3.45 (s, 16 H, NCH_2), 1.23 (s, 36 H, CH_3). − ^{13}C NMR (D_2O): δ = 152.0, 133.9, 131.9 (CH), 130.7, 51.5, 43.0, 34.5, 30.7.

Compound $H_4$6b·8HCl: Analogously to the preparation of H_4**6a**·8HCl, this compound was prepared by reduction of **5b** (2.11 g, 1.90 mmol) with sodium (1.00 g, 43.0 mmol) in liquid ammonia (100 mL). Recrystallization from 1M HCl afforded H_4**6b**·8HCl (1.56 g, 61%) as white crystals. − ^1H NMR (D_2O): δ = 7.47 (s, 8 H, Ar*H*), 4.38 (s, 16 H, BzCH_2N), 3.12 (t, ^3J = 7.5 Hz, 16 H, NCH_2), 2.17 (qnt, ^3J = 7.5 Hz, 8 H, CH_2), 1.16 (s, 36 H, CH_3). − ^{13}C NMR (CD_3OD): δ = 154.1, 136.6, 131.8 (CH), 129.3, 51.5, 45.8, 35.8, 31.4, 23.9.

[Ni_2(6a)]·MeOH (7): To a solution of H_4**6a**·8HCl (129 mg, 0.100 mmol) in MeOH (3 mL) was added $NiCl_2·6H_2O$ (47 mg, 0.200 mmol) in MeOH (1 mL) and NEt_3 (121 mg, 1.20 mmol). The purple solution was stirred overnight, during which time a purple, microcrystalline precipitate of **7** deposited. The crystals were filtered, washed with cold MeOH (1 mL), and dried in vacuum. Yield: 58 mg (51%). − IR (KBr): $\tilde{\nu}$ = 3129w cm^{-1} (NH). − UV/Vis (MeCN): λ_{max} (ε_M) = 495 (270), 588 nm (298 $M^{-1}cm^{-1}$). − ^1H NMR (200 MHz, $CDCl_3$/CD_3OD, 1:1): δ = 7.22 (d, ^4J = 2.0 Hz, 4 H, Ar*H*), 6.90 (d, ^4J = 2.0 Hz, 4 H, Ar*H*), 4.42 (d, ^2J = 12.0 Hz, 4 H, CH_2), 3.90 (d, ^2J = 12.0 Hz, 4 H, CH_2), 3.27 (d, ^2J = 12.0 Hz, 4 H, CH_2), 3.04 (m, 8 H, CH_2), 2.95 (m, 4 H, CH_2), 2.50 (m, 8 H, CH_2), 1.26 (s, 36 H, CH_3). − $C_{56}H_{84}N_8Ni_2S_4·CH_3OH$ (1147.00): calcd. C 59.69, H 7.73, N 9.77; found C 59.42, H 7.33, N, 9.52.

[Ni_4(6a)][ClO_4]$_4$·3MeOH (8): To a solution of **7** (115 mg, 0.100 mmol) in MeOH (3 mL) was added $Ni(ClO_4)_2·6H_2O$ (76 mg, 0.20 mmol) in MeOH (1 mL). The brown solution was stirred for 12 h, during which time a microcrystalline precipitate of **8** deposited. The crystals were filtered, washed with cold MeOH (1 mL), and dried in air. Yield: 128 mg (74%). − IR (KBr): $\tilde{\nu}$ = 3200w (NH), 1142, 1113, 1087vs cm^{-1} [ClO_4^-, $\nu_3(F_2)$]. − UV/Vis (MeCN): λ_{max} (ε) = 586 (204), 1017 nm (10 $M^{-1}cm^{-1}$). − $C_{56}H_{84}N_8Ni_4S_4·Cl_4O_{16}·3CH_3OH$ (1726.27): calcd. C 41.05, H 5.61, N 6.49; found C 41.32, H 5.45, N 6.36.

[Ni_4(6a)(NCS)$_4$]·10CH_3CN (9): To a solution of **8** (36 mg, 0.021 mmol) in MeCN (5 mL) was added a solution of NH_4SCN (6.5 mg, 0.085 mmol) in MeOH (1 mL). The brown solution was filtered and kept at room temp. for 12 h, during which time the tetranuclear isothiocyanate complex **9** deposited as brown-red crystals. Yield: 25 mg (63%). Crystals of **9** quickly lose the MeCN molecules of crystallization upon storage in air at 298 K. − IR (KBr): $\tilde{\nu}$ = 3200w (NH), 2075vs cm^{-1} (CN). − UV/Vis (DMF): λ_{max} (ε) = 520sh (317), 975 nm (65 $M^{-1}cm^{-1}$). − $C_{60}H_{84}N_{12}Ni_4S_8$ (1464.65): C 49.20, H 5.78, N 11.48; found C 48.93, H 5.31, N 11.01.

X-ray Crystal Structure Determination: Single crystals of complex **9** were obtained by the procedure described above. A red-brown crystal of [Ni_4(**6a**)(NCS)$_4$]·10MeCN measuring 0.42 × 0.35 × 0.09 mm was mounted with some mother-liquor in a glass capillary. Intensity data were collected at −60 °C using a STOE IPDS diffractometer with graphite-monochromatized Mo Kα radiation (λ = 0.71073 Å). The data were corrected for Lorentz and polarization effects. An empirical absorption correction was applied. Of 8518 unique reflections 5890 measured $F_o > 4\sigma(F_o)$. Structure solution (direct methods) and refinements were carried out with SHELXS-86 and SHELXL-93 software,[21] respectively. The complex [Ni_4(**6a**)(NCS)$_4$]·10MeCN crystallizes in the triclinic space

Table 2. Crystal data and structure refinement for [Ni_4(**6a**)(NCS)$_4$]·10CH_3CN

empirical formula	$C_{80}H_{114}N_{22}Ni_4S_8$
formula weight	1875.26
crystal size, mm^3	0.42 × 0.35 × 0.09
T, °C	−60
space group	$P\bar{1}$
a, Å	11.217(2)
b, Å	14.862(3)
c, Å	15.342(3)
α, deg	78.26(3)
β, deg	70.90(3)
γ, deg	85.35(3)
V, Å^3	2366.0(8)
Z	1
density, g·cm^{-3}	1.316
μ(Mo Kα), mm^{-1}	1.013
θ range, deg	4.48−25.92
reflections collected	18381
unique reflections	8518 (R_{int} = 0.1403)
observed reflections	5890 ($F_o > 4\sigma(F_o)$)
$R1$, $wR2$ [$F_o > 4\sigma(F_o)$]	0.0817, 0.1975[a]
$R1$, $wR2$ (all data)	0.1144, 0.2246[a]
goodness-of-fit on F^2	1.095
resid. elect. density, eÅ^{-3}	0.903/−0.696

[a] $w = 1/[\sigma^2(F_o^2) + (0.1182P)^2 + 2.7688P]$, $P = (F_o^2 + 2F_c^2)/3$.

group $P\bar{1}$. The asymmetric unit contains one half of the atoms of the formula unit ($Z = 1$). The disordered *tert*-butyl methyl carbon atoms and C- and N-atoms of the MeCN solvates were refined isotropically. All other non-hydrogen atoms were refined anisotropically. An isotropic split-atom model was applied for the disordered *tert*-butyl methyl carbon atoms. The multiplicities of the respective orientations C(20a)−C(21a)−C(22a): 0.68, C(20b)−C(21b)−C(22b): 0.32 were refined. In the final stages of anisotropic refinement, hydrogen atoms were included at calculated positions and refined by using a riding model. The final difference Fourier maps showed no unusual features. Final *R* factors are given in Table 2. Crystallographic data (excluding structure factors) for the structure reported in this paper have been deposited with the Cambridge Crystallographic Data Centre as supplementary publication no. CCDC-128515. Copies of the data can be obtained free of charge on application to CCDC, 12 Union Road, Cambridge CB2 1EZ, UK [Fax: (internat.) + 44-1223/336-033; E-mail: deposit@ccdc.cam.ac.uk].

Acknowledgments

This work was supported by the Deutsche Forschungsgemeinschaft. The author thanks Prof. Dr. H. Vahrenkamp for his generous support. Financial support from the Wissenschaftliche Gesellschaft Freiburg and the Graduiertenkolleg "Ungepaarte Elektronen" is also gratefully acknowledged. We also thank Prof. Dr. B. Krebs (University of Münster) for providing facilities for X-ray crystallographic measurements and are indebted to S. Höck for help in collecting the X-ray data.

[1] N. H. Pilkington, R. Robson, *Aust. J. Chem.* **1970**, *23*, 2225−2236.
[2] B. F. Hoskins, N. J. McLeod, H. A. Schaap, *Aust. J. Chem.* **1976**, *29*, 515−521.
[3] [3a] H. Okawa, S. Kida, *Bull. Chem. Soc. Jpn.* **1972**, *45*, 1759−1764. − [3b] M. Tadokoro, H. Okawa, N. Matsumoto, M. Koikawa, S. Kida, *J. Chem. Soc., Dalton Trans.* **1991**, 1657−1663. − [3c] H. Okawa, J. Nishio, M. Ohba, M. Tadokoro, N. Matsumoto, M. Koikawa, S. Kida, D. E. Fenton, *Inorg. Chem.* **1993**, *32*, 2949−2957.
[4] [4a] R. R. Gagne, C. A. Koval, T. J. Smith, *J. Am. Chem. Soc.* **1977**, *99*, 8367−8368. − [4b] R. R. Gagne, C. A. Koval, T. J. Smith, M. C. Cimolino, *J. Am. Chem. Soc.* **1979**, *101*, 4571−4580. − [4c] C. L. Spiro, S. L. Lambert, T. J. Smith, E. N. Duesler, R. R. Gagne, D. N. Hendrickson, *Inorg. Chem.* **1981**, *20*, 1229−1237.
[5] [5a] S. K. Mandal, K. Nag, *J. Chem. Soc., Dalton Trans.* **1983**, 2429−2434. − [5b] S. K. Mandal, K. Nag, *J. Org. Chem.* **1986**, *51*, 3900−3902. − [5c] R. Das, K. Nag. *Inorg. Chem.* **1991**, *30*, 2831−2833.
[6] [6a] S. L. Lambert, D. N. Hendrickson, *Inorg. Chem.* **1979**, *18*, 2683−2686. − [6b] R. C. Long, D. N. Hendrickson, *J. Am. Chem. Soc.* **1983**, *105*, 1513−1521.
[7] [7a] C. Fraser, L. Johnston, A. L. Rheingold, B. S. Haggerty, G. K. Williams, J. Whelan, B. Bosnich, *Inorg. Chem.* **1992**, *31*, 1835−1844. − [7b] B. Bosnich, *Inorg. Chem.* **1999**, 38, 2554−2562.
[8] [8a] M. Bell, A. J. Edwards, B. F. Hoskins, E. H. Kachab, R. Robson, *J. Chem. Soc., Chem. Commun.* **1987**, 1852−1854. − [8b] M. Bell, A. J. Edwards, B. F. Hoskins, E. H. Kachab, R. Robson, *J. Am. Chem. Soc.* **1989**, *111*, 3603−3610. − [8c] B. F. Hoskins, R. Robson, P. Smith, *J. Chem. Soc., Chem. Commun.* **1990**, 488−489. − [8d] M. J. Grannas, B. F. Hoskins, R. Robson, *J. Chem. Soc., Chem. Commun.* **1990**, 1644−1646. − [8e] A. J. Edwards, B. F. Hoskins, E. H. Kachab, A. Markiewicz, K. S. Murray, R. Robson, *Inorg. Chem.* **1992**, *31*, 3585−3591.
[9] [9a] V. McKee, S. S. Tandon, *J. Chem. Soc., Chem. Commun.* **1988**, 385−387. − [9b] V. McKee, S. S. Tandon, *Inorg. Chem.* **1989**, *28*, 2901−2902. − [9c] S. S. Tandon, L. K. Thompson, J. N. Bridson, *J. Chem. Soc., Chem. Commun.* **1992**, 911−913. − [9d] S. S. Tandon, L. K. Thompson, J. N. Bridson, C. Benelli, *Inorg. Chem.* **1995**, *34*, 5507−5515.
[10] [10a] K. K. Nanda, K. Venkatsubramanian, D. Majumbar, K. Nag, *Inorg. Chem.* **1994**, *33*, 1581−1582. − [10b] K. K. Nanda, S. Mohanta, U. Flörke, S. K. Dutta, K. Nag, *J. Chem. Soc., Dalton Trans.* **1995**, 3831−3836. − [10c] S. Mohanta, K. K. Nanda, R. Werner, W. Haase, A. K. Mukherjee, S. K. Dutta, K. Nag., *Inorg. Chem.* **1997**, *36*, 4656−4664.
[11] [11a] A. J. Atkins, A. J. Blake, M. Schröder, *J. Chem. Soc., Chem. Commun.* **1993**, 1662−1665. − [11b] A. J. Atkins, D. Black, A. J. Blake, A. Marin-Becerra, S. Parsons, L. Ruiz-Ramirez, M. Schröder, *Chem. Commun.* **1996**, 457−464. − [11c] N. D. J. Branscombe, A. J. Blake, A. Marin-Becerra, W.-S. Li, S. Parsons, L. Ruiz-Ramirez, M. Schröder, *Chem. Commun.* **1996**, 2573−2574.
[12] [12a] S. Brooker, P. D. Croucher, *J. Chem. Soc., Chem. Commun.* **1995**, 1493−1494. − [12b] S. Brooker, P. D. Croucher, *J. Chem. Soc., Chem. Commun.* **1995**, 2075−2076. − [12c] S. Brooker, P. D. Croucher, F. M. Roxburgh, *J. Chem. Soc., Dalton Trans.* **1996**, 3031−3037. − [12d] S. Brooker, P. D. Croucher, *Chem. Commun.* **1997**, 459−460. − [12e] S. Brooker, P. D. Croucher, T. C. Davidson, G. S. Dunbar, A. J. McQuillan, G. B. Jameson, *Chem. Commun.* **1998**, 2131−2132.
[13] P. E Kruger, V. McKee, *Chem. Commun.* **1997**, 1341−1342.
[14] For the preparation of sulfur derivatives of 4-*tert*-butyl-calixarenes, see: [14a] C. G. Gibbs, C. D. Gutsche, *J. Am. Chem. Soc.* **1993**, *115*, 5338−5339. − [14b] X. Delaigue, M. W. Hosseini, N. Kyritsakas, A. De Cian, J. Fischer, *J. Chem. Soc., Chem. Commun.* **1995**, 609−610.
[15] T. Yamamura, M. Tadokoro, M. Hamaguchi, R. Kuroda, *Chem. Lett.* **1989**, 1481−1484.
[16] B. Kersting. *Z. Naturforsch.*, **1998**, *53b*, 1379−1385.
[17] [17a] B. Kersting, D. Siebert, *Inorg. Chem.* **1998**, *37*, 3820−3828. − [17b] B. Kersting, D. Siebert, *Eur. J. Inorg. Chem.* **1999**, 189−193. − [17c] B. Kersting, D. Siebert, D. Volkmer, M. J. Kolm, C. Janiak, *Inorg. Chem.* **1999**, *38*, 3871−3882.
[18] B. Kersting, G. Steinfeld, J. Hausmann, *Eur. J. Inorg. Chem.* **1999**, 179−187.
[19] B. Kersting, *Eur. J. Inorg. Chem.* in press.
[20] B. Kersting, *Eur. J. Inorg. Chem.* **1998**, 1071−77.
[21] G. M. Sheldrick, SHELXS−86, University of Göttingen, Germany, **1990**; G. M. Sheldrick, SHELXL−93, University of Göttingen, Germany, **1993**.

Received June 2, 1999
[I99242]

Trovacene Chemistry, 3[+]

The Mono-, Di-, and Tri([5]trovacenyl)boranes: A Study of Intermetallic Communication Across an sp^2-Hybridized Boron Atom

Christoph Elschenbroich,*[a] Matthias Wolf,[a] Olaf Burghaus,[a] Klaus Harms,[a] and Jürgen Pebler[a]

Dedicated to Professor Christoph Rüchardt on the occasion of his 70th birthday

Keywords: EPR spectroscopy / Metallocenylboranes / Organovanadium radicals / Redox chemistry (CV) / X-ray diffraction

The paramagnetic complexes di(mesityl)([5]trovacenyl)-borane (**5**$^{\cdot}$), (mesityl)di([5]trovacenyl)borane (**6**$^{\cdot\cdot}$), and tri([5]trovacenyl)borane (**7**$^{\cdot\cdot\cdot}$) were prepared from [5]trovacenyllithium, (η^5-C_7H_7)V(η^5-C_5H_4Li), and $(Mes)_2BF$, $(Mes)BF_2$, and BF_3, respectively. The propeller-shaped species **5**$^{\cdot}$, **6**$^{\cdot\cdot}$, and **7**$^{\cdot\cdot\cdot}$ were subjected to X-ray diffraction with the aim of possibly correlating the twist angles with intramolecular intermetallic communication. Cyclic voltammetry points to successive vanadium-centered oxidation processes and boron-centered reduction, a small redox splitting $\delta E_{1/2}$[(2+/+), (+/0)] being observed for **6**$^{\cdot\cdot}$. According to EPR spectroscopy, performed in fluid solution, the exchange interaction J in the diradical **6**$^{\cdot\cdot}$ approaches the fast-exchange region and is attenuated significantly by quaternization at boron in [**6**$^{\cdot\cdot}$–*n*Bu]$^-$. Although EPR spectroscopy of the triradical **7**$^{\cdot\cdot\cdot}$ also indicates an extensive exchange interaction, the exchange parameters, derived from spectral simulation, follow the gradation J(**7**$^{\cdot\cdot\cdot}$) $\approx$ 1/3 J(**6**$^{\cdot\cdot}$). The magnetic susceptibility of **6**$^{\cdot\cdot}$ and **7**$^{\cdot\cdot\cdot}$ follows the same trend. As expected, compound **7**$^{\cdot\cdot\cdot}$ exhibits spin frustration because it contains three antiferromagnetically coupled S = 1/2 systems that are arranged in an equilateral triangle.

Introduction

The screening of diverse inorganic and organic groups for their potential as spacers, capable of mediating electronic and magnetic interactions between metal centers, remains a topic of intense investigation.[2] With this aim in mind, we previously prepared the half-sandwich complexes $Mes_2B[(\eta^6\text{-Mes})Cr(CO_3)]$ (**1**), $MesB[(\eta^6\text{-Mes})Cr(CO)_3]_2$ (**2**), and $B[(\eta^6\text{-Mes})Cr(CO)_3]_3$ (**3**), determined their molecular structures by X-ray diffraction, and studied their IR-, redox-, and EPR properties.[3]

Structurally, these propeller-shaped complexes differ in the dihedral angle between the η^6-arene planes and the reference plane which is spanned by the three carbon atoms bonded to boron. If interactions between these complex moieties were governed by conjugation between the aromatic π-systems and the vacant p_z orbital of the boron atom, compounds **1**, **2**, and **3** would be expected to exhibit characteristic spectral and electrochemical differences. However, IR spectroscopy and cyclic voltammetry indicated almost no discernible communication between the $Cr(CO)_3$ units of either **2** or **3**. A more sensitive tool for probing intramolecular communication is provided by EPR spectroscopy, which may either be applied to mixed valence species, to search for spin delocalization, or it may be used for oligoradicals, to assess the extent of exchange coupling. We have used both methods in the past for related cases;[1][4] they failed for **1**–**3**, however, because the requisite paramagnetic species could not be obtained either chemically or electrochemically.

Our recent research[1][5] with the paramagnetic, neutral complex (η^7-C_7H_7)V(η^5-C_5H_5) (**4**$^{\cdot}$) [or trovacene, for (η^7-tropylium)vanadium(η^5-cyclopentadienyl)[6]] caused us to synthesize the mono-, di-, and tri([5]trovacenyl)boranes **5**$^{\cdot}$–**7**$^{\cdot\cdot\cdot}$ in order to study their electrochemical and EPR spectroscopic characteristics. The redox splitting $\delta E_{1/2}$, i.e., the difference in the potentials of subsequent redox steps, as well as the exchange coupling constant J, for diradical **6**$^{\cdot\cdot}$ and triradical **7**$^{\cdot\cdot\cdot}$, should both provide information on the extent of intermetallic communication via the central boron atom. The results from this investigation should also complement those obtained previously for the related complex tri(ferrocenyl)borane, $[(\eta^5\text{-}C_5H_5)(\eta^5\text{-}C_5H_4)Fe]_3B$ (**8**).[7]

Results and Discussion

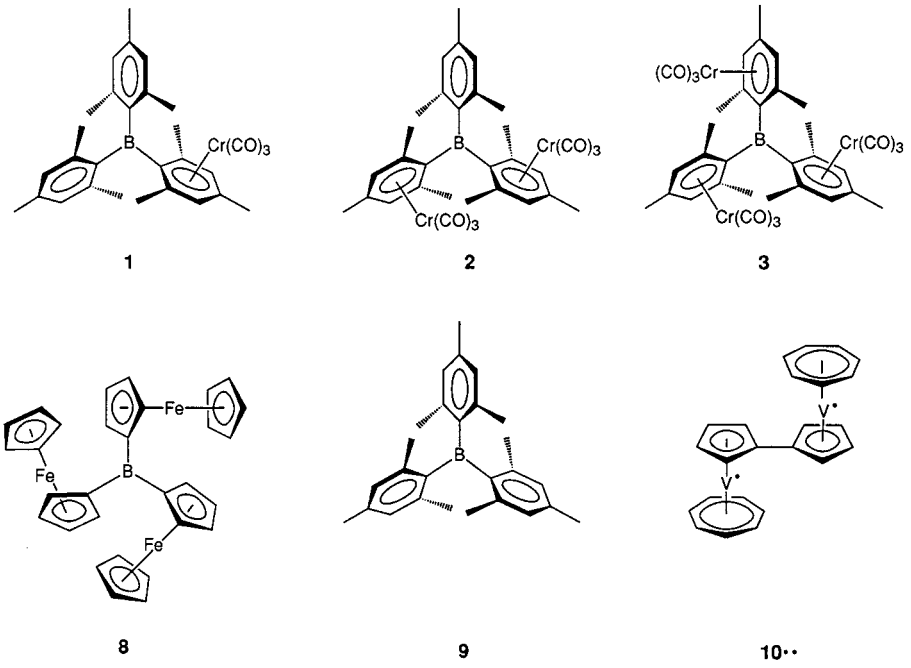
Synthesis

Trovacene undergoes selective monolithiation at the cyclopentadienyl ring.[8][9] Subsequent reaction with the B–F functionality affords di(mesityl)([5]trovacenyl)borane

[+] Part 2: Ref.[1]

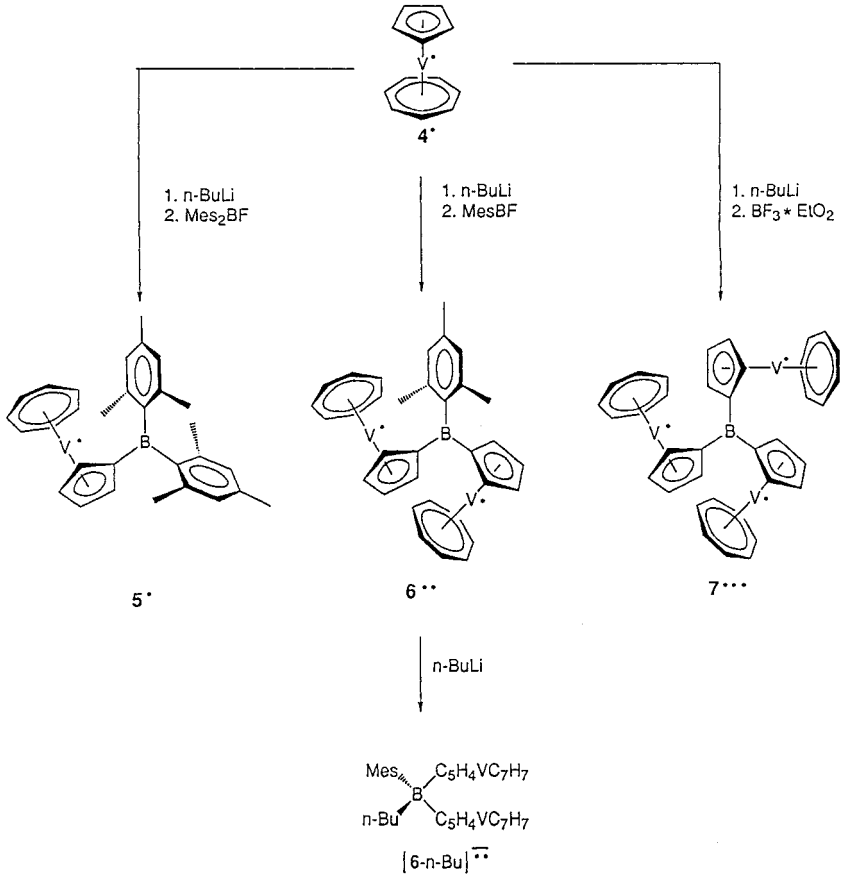
[a] Fachbereich Chemie der Philipps-Universität Marburg, Hans-Meerwein-Strasse, D-35032 Marburg, Germany
Fax: (internat.) +49-(0)6421/28-28917
E-mail: eb@ps1515.chemie.uni-marburg.de

 © WILEY-VCH Verlag GmbH, D-69451 Weinheim, 1999 1434–1948/99/1212–2173 $ 17.50+.50/0



1 2 3 8 9 10••

(**5**•), (mesityl)di([5]trovacenyl)borane (**6**••) and tri([5]trovacenyl)borane (**7**•••) (Scheme 1). The mesityl group was chosen as an auxiliary ligand to sterically protect the boron atom in order to improve the kinetic stability of R_3B anions,[10] which are also targets of the present investigation. Compounds **5**• and **6**•• crystallized as green cubes, and **7**••• formed green needles. The solubility in aromatic solvents decreases in the order **5**• > **6**•• > **7**•••.



Scheme 1

Molecular Structures of $5^{\cdot}$, $6^{\cdot\cdot}$, and $7^{\cdot\cdot\cdot}$ in the Crystal

While it may not be assumed that the structures of $\mathbf{5}^{\cdot}-\mathbf{7}^{\cdot\cdot\cdot}$ in the solid state are identical to those in fluid solution, where CV and EPR spectroscopic studies are performed, X-ray diffraction studies were nevertheless carried out to extract trends in the torsional angles which characterize these molecules. The structures of $\mathbf{5}^{\cdot}-\mathbf{7}^{\cdot\cdot\cdot}$ are shown in Figures 1−3; bond lengths and bond angles are collected in the captions.

Because of their propeller shape, $\mathbf{5}^{\cdot}-\mathbf{7}^{\cdot\cdot\cdot}$ are chiral; a few peculiarities of the respective unit cells deserve to be noted. Di(mesityl)([5]trovacenyl)borane ($\mathbf{5}^{\cdot}$) crystallizes in the space group $P\bar{1}$, i.e., the two enantiomorphic forms are crystallographically indistinguishable. (Mesityl)di([5]trovacenyl)borane ($\mathbf{6}^{\cdot\cdot}$) crystallizes in the space group $P2_1$ as a single enantiomer since a mirror plane and a center of symmetry are absent. Finally, $\mathbf{7}^{\cdot\cdot\cdot}$ (space group $P1$) incorporates two independent, chiral molecules in the racemic unit cell.

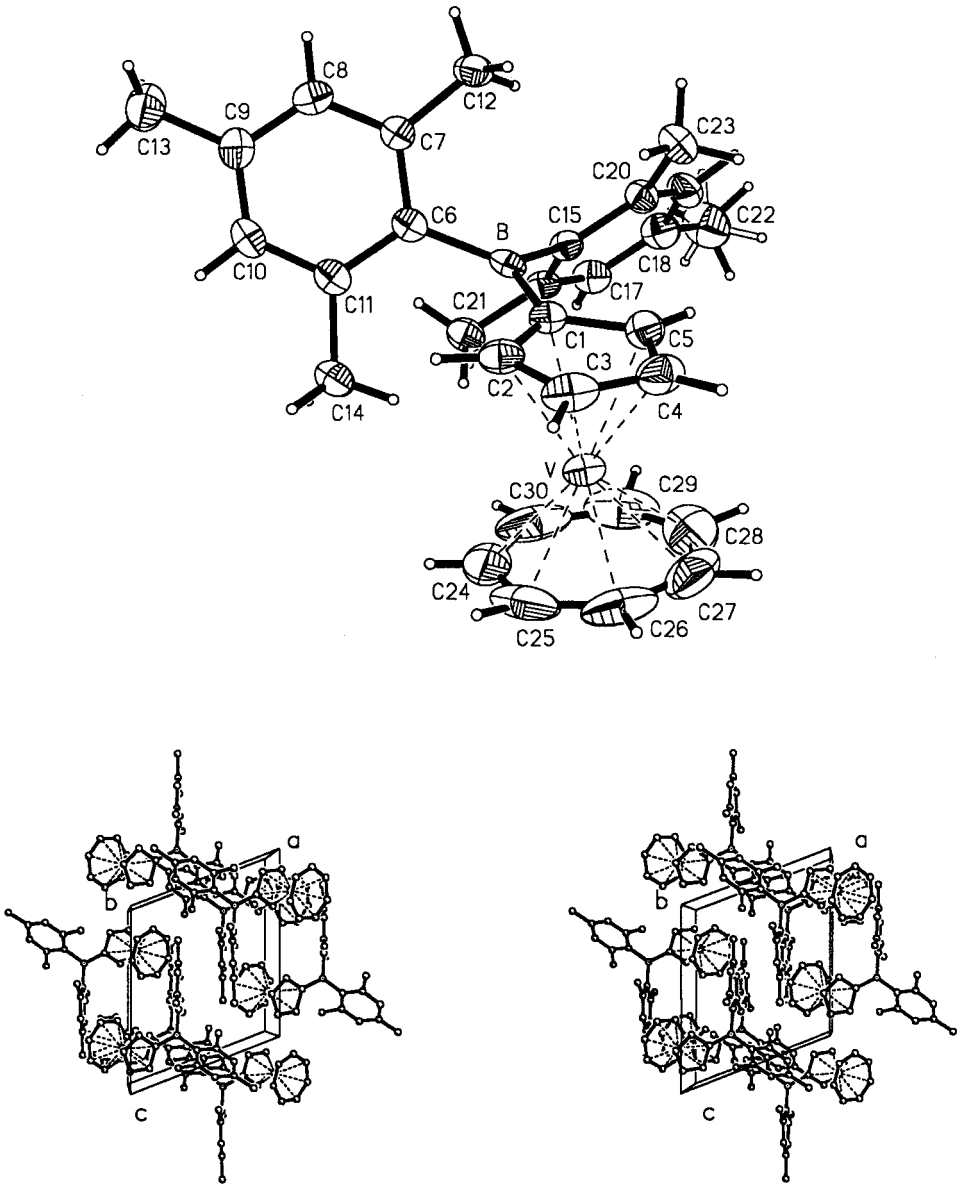


Figure 1. Molecular structure and numbering scheme of compound $\mathbf{5}^{\cdot}$: (top) SHELXTL/LP drawing with 50% probability ellipsoids; (bottom) stereoplot; selected bond lengths (pm) and bond angles (°): B−C1 155.4 (3), B−C6 160.2 (3), B−C15 159.5 (3), C−C (η^5-Cp, mean value) 141.9, C−C (η^7-Tr, mean value) 138.6, V−C (Cp, mean value) 226.7, V−C (Tr, mean value) 217.3, V−Cp (centroid) 192.0 (1), V−Tr (centroid) 147.4 (1), C1−B−C6 119.37 (19), C1−B−C15 119.20 (2), C6−B−C15 121.25 (19); important dihedral angles are collected in Table 1

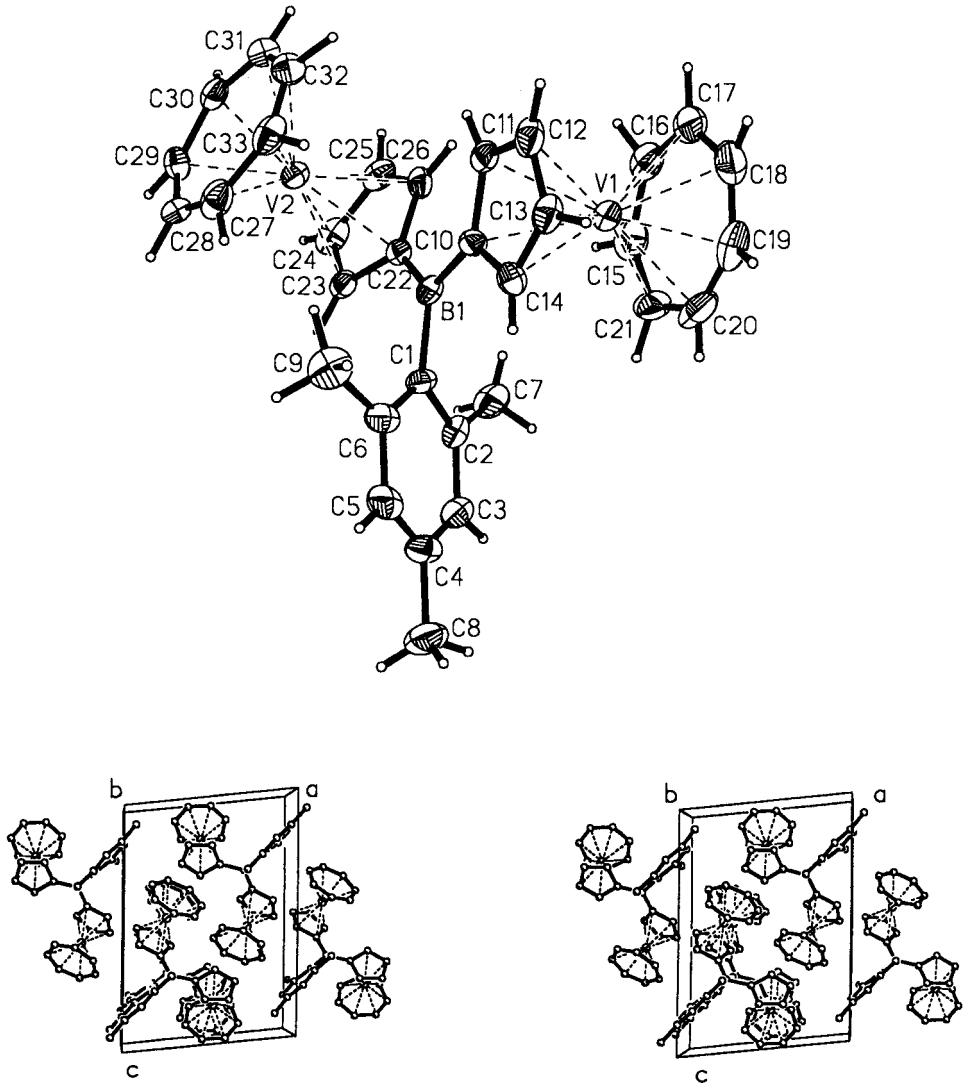


Figure 2. Molecular structure and numbering scheme of compound **6**¨: (top) SHELXTL/LP drawing with 50% probability ellipsoids; (bottom) stereoplot; selected bond lengths (pm) and bond angles (°): B−C1 158.4 (9), B−C10 154.9 (9), B−C22 155.4 (9), C−C (η^5−Cp, mean value) 142.3, C−C (η^7-Tr, mean value) 140.4, V−C (Cp, mean value) 226.1, V−C (Tr, mean value) 218.5, V−Cp (centroid) 191.0 (3), V−Tr (centroid) 146.9 (1), C1−B−C10 117.5 (5), C1−B−C22 119.2 (5), C10−B−C22 123.2 (5). V1···V2 589.3; important dihedral angles are collected in Table 1

The following remarks focus on those structural features that may be relevant to the extent of intramolecular communication between the sandwich moieties. The B−C_{ipso} bond lengths involving the organometallic (156 pm) and organic (159 pm) substituents at boron (mean values) differ only marginally. More important are the dihedral angles between the η^5-cyclopentadienyl and the aryl- and B(C_{ipso})$_3$ reference planes PR1, listed in Table 1. The twist of the mesityl plane, with regard to PR1, always surpasses that of the Cp planes. Furthermore, the dihedral angles between the planes Cp and PR1 differ considerably, encompassing the range 4.1−41.7°. This contrasts markedly with the structures of tri(ferrocenyl)borane (**8**), for which these angles lie in the narrow range of 25.8−28.1°[7c] and those of triarylboranes (45−55°[11]). In the context of intersandwich conjugation, the dihedral angles between the cyclopentadienyl planes of the trovacene units connected to boron are of interest: they amount to 25.6° for **6**¨ and to 20.8, 27.3, and 48.1° in the case of **7**‴. However, the torsional angles may be different in fluid solution. Finally, within the error limits, the bond angles about boron add up to 360°, although individual angles differ from 120° (maximal deviation 3°). Consequently, the boron atom is only slightly displaced from the plane defined by the three carbon atoms (3.3 pm for **5**˙; 1.3 pm for **6**¨; 6.6, 4.5 pm for **7**‴).

Electrochemical Properties

Cyclovoltammetric traces for compounds **5**˙−**7**‴ are depicted in Figure 4, the pertinent data are collected in Table 2. As for the parent complex **4**˙, the trovacenyl boranes **5**˙−7‴ each show one reversible oxidation and one reversible reduction step. Assignment of the redox sites, which are

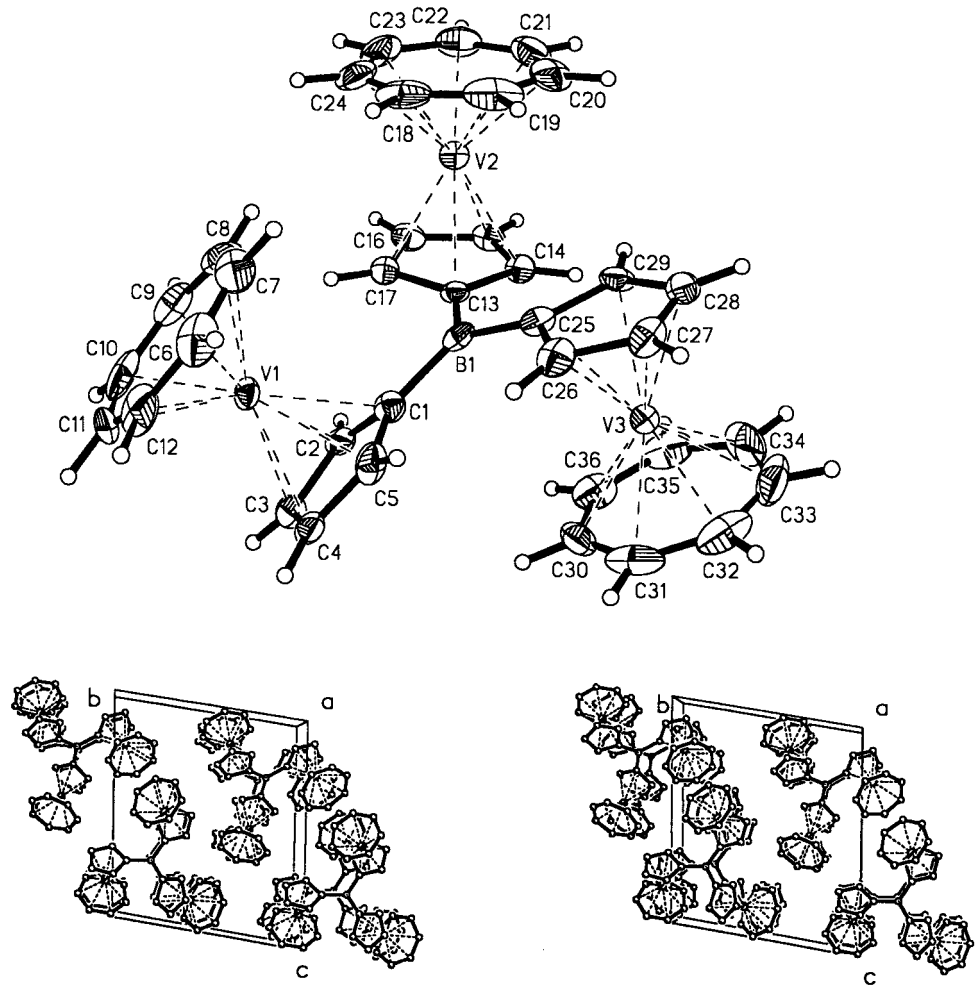


Figure 3. Molecular structure and numbering scheme of compound **7**$^{\cdots}$: (top) SHELXTL/LP drawing with 50% probability ellipsoids; (bottom) stereoplots of the crystallographically independent species **7**$^{\cdots}$ and **7**$^{\cdots}$′; selected bond lengths (pm) and bond angles (°) for **7**$^{\cdots}$: B−C1 156.5 (11), B−C13 157.3 (11), B−C25 156.5 (11), C−C (η^5-Cp, mean value) 141.6, C−C (η^7-Tr, mean value) 140.2, V−C (Cp, mean value) 225.5, V−C (Tr, mean value) 217.7, V−Cp (centroid, mean) 190.7 (7), V−Tr (centroid, mean) 146.1 (2), C1−B−C13 117.8 (7), C1−B−C25 122.1 (7), C13−B−C25 119.6 (7). V1···V2 563.0, V2···V3 575.7, V3···V1 609.9; selected bond lengths (pm) and bond angles (°) for **7**$^{\cdots}$′: B′−C1′ 157.3 (11), B′−C13′ 156.3 (11), B′−C25′ 156.2 (11), C′−C′ (η^5−Cp, mean value) 141.8, C′−C′ (μ^7-Tr, mean value) 140.5, V′−C′ (Cp, mean value) 225.9, V′−C′ (Tr, mean value) 218.2, V′−Cp (centroid, mean value) 190.8 (4), V′−Tr (centroid, mean) 146.1 (2), C1′−B′−C13′ 116.8 (7), C1′−B′−C25′ 120.3 (7), C13′−B′−C25′ 122.7 (6); V1′···V2′ 570.9, V2′···V3′ 585.3, V3′···V1′ 577.0; important dihedral angles are collected in Table 1

responsible for these processes, is based on a comparison with the redox potentials of the components. Thus, the waves at positive potential involve oxidation of the trovacene units. The corresponding potential for the mono(trovacenyl) derivative **5**$^{\cdot}$ underwent a 171 mV anodic shift relative to that of parent **4**$^{\cdot}$, to reflect the electron-accepting properties of the $(Mes)_2B$ substituent.

For the di(trovacenyl) derivative **6**$^{\cdot\cdot}$, a redox splitting $\delta E_{1/2}$-[(2+/+), (+/0)] = 138 mV is clearly resolved, indicating intersandwich communication in **6**$^{\cdot\cdot}$. The value $\delta E_{1/2}$ for **6**$^{\cdot\cdot}$ is very similar to that found for [5−5]di(trovacene) (**10**$^{\cdot\cdot}$) ($\delta E_{1/2}$ = 147 mV[1]), showing that a (Mes)B spacer does not constitute a significant barrier to intramolecular communication between two trovacene units − at least with regard to their mutual influence on the ease of vanadium ionization. Interestingly, the mean value, $[E_{1/2}(2+/+) + E_{1/2}(+/0)]/2$, for dinuclear **6**$^{\cdot\cdot}$ is identical to $E_{1/2}(+/0)$ for mononuclear **5**$^{\cdot}$: primary oxidation of **6**$^{\cdot\cdot}$ is more facile due to the presence of a second, electron-donating trovacene unit; secondary oxidation is less favorable because of the positive charge on **6**$^{+\cdot}$.

Somewhat surprisingly, this behavior is not found for trinuclear **7**$^{\cdots}$ − this complex displays no redox splitting, and despite the presence of three trovacenyl groups, the cathodic shift, relative to the parent, trovacene, is very small. This finding is reminiscent of the redox behavior of molecules containing multiple noninteracting ferrocene units; in this case a CV curve typical for a diffusion-controlled, reversible, one-electron process is obtained (ΔE_p = 60 mV) where the wave height indicates the number of electrons transferred sequentially.[12] The latter criterion is fulfilled for **7**$^{\cdots}$, since the peak current, relative to the wave at −2.067 V which represents a one-electron process (vide infra), is larger by a factor of three. For **5**$^{\cdot}$ this peak−current ratio (cathodic process: anodic process) is 1:1, for **6**$^{\cdot\cdot}$ it is approximately 1:(1 + 1).

Table 1. Dihedral angles (°) between the reference plane PR1 = $B(C_{ipso})_3$, the planes of the mesityl substituents (Mes), and those of the cyclopentadienyl rings (Cp) of **5**$^{\cdot}$, **6**$^{\cdot\cdot}$, **7**$^{\cdot\cdot\cdot}$ and **7**$^{\cdot\cdot\cdot\prime}$

	Carbon atoms	Ring plane	PR1	P2	P3
	1−5	P2 (Cp)	18.56(14)		
5$^{\cdot}$	6−11	P3 (Mes)	63.54(12)	64.19(13)	
	15−20	P4 (Mes)	67.06(13)	53.16(14)	72.11(12)
	10−14	P2 (Cp)	4.7(4)		
6$^{\cdot\cdot}$	22−26	P3 (Cp)	22.1(4)	25.6(4)	
	1−6	P4 (Mes)	59.0(3)	55.8(4)	73.4(4)
	1−5	P2 (Cp)	15.7(4)		
7$^{\cdot\cdot\cdot}$	13−17	P3 (Cp)	34.6(4)	48.1(4)	
	25−29	P4 (Cp)	14.3(4)	27.3(5)	20.8(4)
	1−5	P2′ (Cp)	41.7(4)		
7$^{\cdot\cdot\cdot\prime}$	13−17	P3′ (Cp)	4.1(4)	41.3(5)	
	25−29	P4′ (Cp)	12.6(4)	29.3(5)	13.2(5)

Table 2. Cyclovoltammetric data for the [5]trovacenyl boranes **5**$^{\cdot}$−**7**$^{\cdot\cdot\cdot}$ and for the parent trovacene **4**$^{\cdot}$

	4[a]	**5**[b]	**6**[a]	**7**[a]
$E_{1/2}(+/0)$ [V]	0.260	0.431	0.362	−
ΔE_p [mV][b]	64	62	64	
r[c]	1	1	1	
$E_{1/2}(2+/+)$ [V]	−	−	0.500	−
ΔE_p [mV][b]			63	
r[c]			1	
$E_{1/2}(3+/0)$ [V]	−	−	−	0.213
ΔE_p [mV][b]				56
r[c]				≈1
$\delta E_{1/2}$ [mV][d]	−	−	138	n.r.
$E_{pa,1}$ [V][a]	−	1.02	1.16	0.96
$E_{pa,2}$ [V][a]		1.12		
$E_{1/2}(0/-)$ [V]	−2.550	−2.067	−2.095	−2.067
ΔE_p [mV][b]	66	62	70	58
r[c]	1	1	1	0.9
$E_{pc,1}$ [V][c]	−	−	−	−2.7

[a] In 1,2-dimethoxyethane/0.1 M tetraethylammonium perchlorate at a glassy carbon electrode versus a saturated calomel electrode. − [b] $\Delta E_p = (E_{pa} - E_{pc})$. − [c] $r = I_{pa}/I_{pc}$. − [d] $\delta E_{1/2} = E_{1/2}(2+.+) - E_{1/2}(+/0)$.

Why, within the framework of the CV experiment, do the trovacene units appear to be interacting in **6**$^{\cdot\cdot}$ but noninteracting in **7**$^{\cdot\cdot\cdot}$? If one assumes that trovacenyl groups are sterically more demanding than mesityl groups, it is conceivable that, in fluid solution, the twisting of the trovacene units relative to the BC_3 reference plane is more extensive in **7**$^{\cdot\cdot\cdot}$ than in **6**$^{\cdot\cdot}$. Since, arguably, an intersandwich interaction requires conjugation, a large twist distortion in **7**$^{\cdot\cdot\cdot}$ would explain the absence of an observable redox splitting. In this context it is worth mentioning that the solid-state and fluid-solution structures of the related molecule tri(ferrocenyl)borane (**8**) were found to be disparate,[7c] in the fluid solution, one ferrocenyl group is oriented opposite to the other two with respect to the central BC_3 plane. Since its electrochemical data were unavailable, we resynthesized **8** and recorded its cyclovoltammogram. As for **7**$^{\cdot\cdot\cdot}$, no redox splitting is resolved for **8** and, relative to ferrocene [$E_{1/2}(+/0)$ = 0.49 V], the potential $E_{1/2}(+/0)$ = 0.42 V for **8** represents a small cathodic shift.

In the strongly cathodic region of the potential, **5**$^{\cdot}$−**7**$^{\cdot\cdot\cdot}$ give rise to waves which signalize one-electron processes. This is inferred when their peak currents are compared to those representing the oxidation of the trovacene groups (vide supra). Furthermore, the numerical values of the potentials $E_{1/2}$ = −2.067 (**5**$^{\cdot}$), −2.095 (**6**$^{\cdot\cdot}$), −2.067 V (**7**$^{\cdot\cdot\cdot}$) are closer to $E_{1/2}(0/-)$ = −1.94 V[10] of 1,3,5-tri(mesityl)borane (**9**), than that of trovacene(**4**) [$E_{1/2}(0/-)$ = −2.55 V]. The cathodic shift observed for **5**$^{\cdot}$ (0/−), **6**$^{\cdot\cdot}$ (0/−) and **7**$^{\cdot\cdot\cdot}$ (0/−) relative to **9** (0/−) reflects the superior electron-donating properties of trovacenyl versus mesityl. Reduction of trovacenylboranes therefore must be regarded as boron-centered. Subsequent vanadium-centered reductions of the [5]trovacenylborane anions **5**$^{-}$−**7**$^{-}$ probably lie close to or outside the electrochemical window, i.e., at potentials < −2.9 V.

EPR Spectroscopy and Magnetic Susceptibility

The availability of the mono-, di-, and tri([5]trovacenyl)boranes **5**$^{\cdot}$−**7**$^{\cdot\cdot\cdot}$ permits a systematic study of the substituent effect of an R_2B group, as well as of the relative mediating properties of the RB< and −B< units. EPR spectra of **5**$^{\cdot}$−**7**$^{\cdot\cdot\cdot}$ are shown in Figures 5−7, the parameters, confirmed by simulation, are collected in Table 3.

The most remarkable feature in the fluid-solution spectrum of di(mesityl)([5]trovacenyl)borane (**5**$^{\cdot}$) is the fairly large coupling constant $a(^{51}V)$ = −7.35 mT, which exceeds the value for parent **4**$^{\cdot}$ by 6%. As for phenyl([5]trovacene),[1] this increase can be rationalized by a π-electron donation [η^5-$C_5H_4(e_2) \rightarrow B(sp^2)$] which raises the positive partial charge on the central vanadium atom with concomitant V{3d(z^2)} orbital contraction. This will have the effect of decreasing V{3d(z^2)}/ligand(a_1) overlap, thereby diminishing metal → ligand spin delocalization and slightly raising the coupling constant $a(^{51}V)$. The electronic perturbation of the trovacene unit by the dimesitylboryl substituent is insufficient, however, to effect an observable change of the g tensor from axial (**4**$^{\cdot}$) to orthorhombic (**5**$^{\cdot}$) which would be required by symmetry.

(Mesityl)di([5]trovacenyl)borane (**6**$^{\cdot\cdot}$) in fluid solution gives rise to a typical diradical EPR spectrum; the 15-line hyperfine pattern approaches a binomial intensity distribution with splitting that amounts to half the value of a (^{51}V) for the monoradical **5**$^{\cdot}$. Spectral simulation furnished optimal agreement for the exchange coupling constant J_{EPR} = |1.43| cm^{-1} which represents half the magnitude of J obtained for [5−5]di(trovacene) (**10**$^{\cdot\cdot}$).[1] In conditions close to the "fast-exchange limit", however, two caveats are called for: (1) spectral simulation does not provide the sign for J (magnetic susceptibility suggests that J < 0, vide infra), and (2) not too much confidence should be placed on the numerical value of J in this situation. Yet, the qualitative conclusion, that the incorporation of an −(R)B− spacer

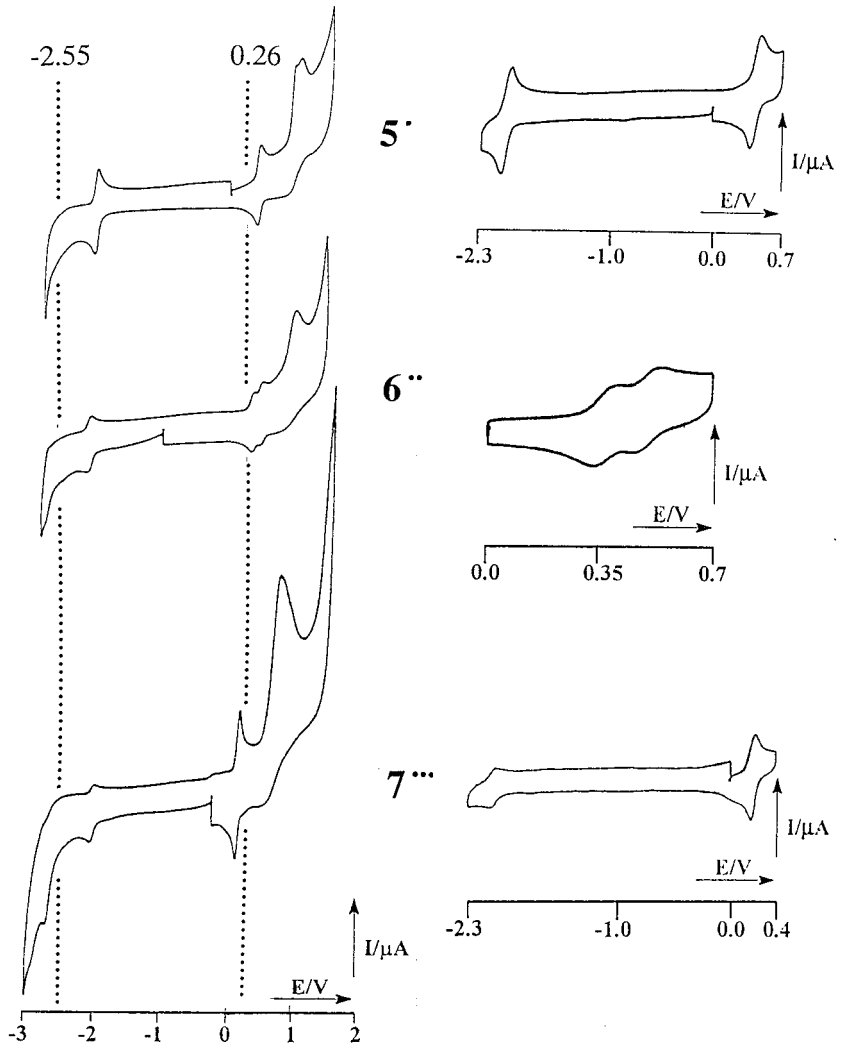


Figure 4. Cyclic voltammetric traces for compounds $\mathbf{5}^{\cdot}-\mathbf{7}^{\cdot\cdot\cdot}$ (1,2-dimethoxyethane/0.1 M tetrabutylammonium perchlorate, at glassy carbon versus SCE, $v = 100$ mV s^{-1}, −40 °C); the dotted lines mark the potentials for the processes $\mathbf{4}^{\cdot}$ (+/0) and $\mathbf{4}^{\cdot}$ (0/−) of the parent trovacene

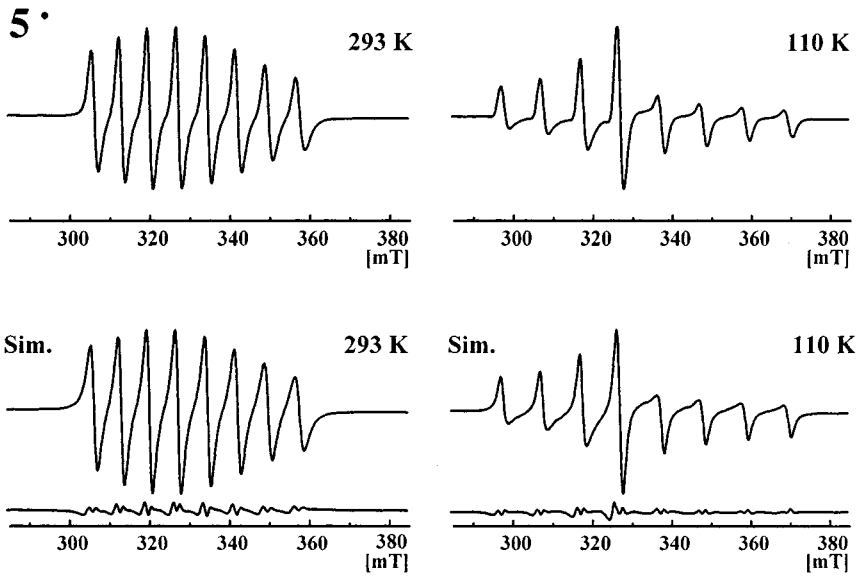


Figure 5. EPR spectra (X-band) of $\mathbf{5}^{\cdot}$, fluid (293 K) and rigid (110 K) solution in toluene, with simulated traces (bottom)

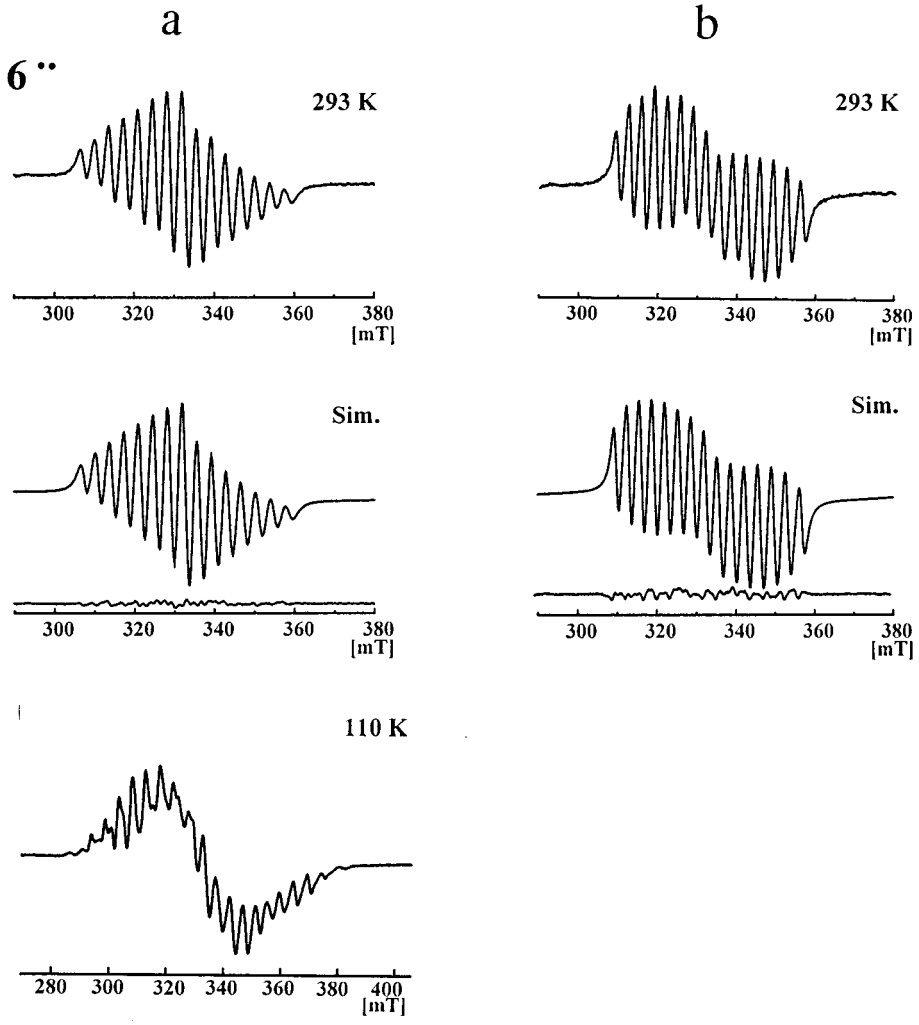


Figure 6. EPR spectra (X-band) of **6**··, fluid (293 K) and rigid (110 K) solution in THF (a), and spectra obtained after addition of *n*-butyllithium in hexane (b)

between two [5]trovacenyl units attenuates exchange coupling to a small degree only, is warranted. If conjugation between the η^5-C_5H_4 π-perimeters and the vacant B($2p_z$) orbital contributes to the exchange interaction, this result does not come as a surprise, since for **6**·· the dihedral angles between the ligand- and reference planes are small in the crystal structure (Table 1) and, due to conformational mobility, they are variable in fluid solution. However, as in the case of [5−5]di(trovacene),[1] the detailed coupling path between the two V(d^5) centers is not clear. Overlap of the V{3d(z^2)} orbitals, which dominate the SOMOs of the trovacene units, with the σ-backbone of the μ[η^5:η^5-$C_5H_4B(Mes)C_5H_4$] bridge, is small, as demonstrated by the small hyperfine coupling constant $a(^1H_{Cp})$ = 0.18 mT in the EPR spectrum of **4**·. Therefore, the direct coupling mechanism and the indirect one, which operates by polarization of filled π-orbitals of the ligands by the singly occupied V{3d(z^2)} orbitals, may be of comparable magnitude. Both mechanisms are of low efficiency, though, and the resulting type of interaction − ferromagnetic or antiferromagnetic − is difficult to predict.

Information concerning the spin-exchange path between the two vanadium centers was also expected from the influence that coordination of a Lewis base to boron would exert on the EPR spectrum of **6**··. The EPR trace for **6**·· in the presence of *n*-butyllithium is shown in Figure 6, where the spectral parameters, verified by computer simulation, are also given. Formation of the adduct [**6**··−*n*Bu]$^-$ clearly affects the EPR spectrum, from which the reduced value J_{EPR} = |0.97| cm^{-1} for the exchange coupling constant can be derived by simulation. No discernible change is observed on the addition of triethylamine, indicating that, probably due to steric hindrance, no adduct formation occurs. Exchange interaction is attenuated in [**6**··−*n*Bu]$^-$, presumably because the exchange path is modified in two ways: (1) The vacant boron p_z orbital, which potentially may engage in conjugative interactions between the trovacenyl units, is transformed into an orbital used for σ-bonding to the Lewis base, and (2) The boron atom is rehybridized from sp^2 to sp^3 during the process **6**·· → [**6**··−*n*Bu]$^-$. Both effects, elimination of a vacant p-orbital in the bridge and decrease of the B(2s) content in the σ-orbitals radiating from boron

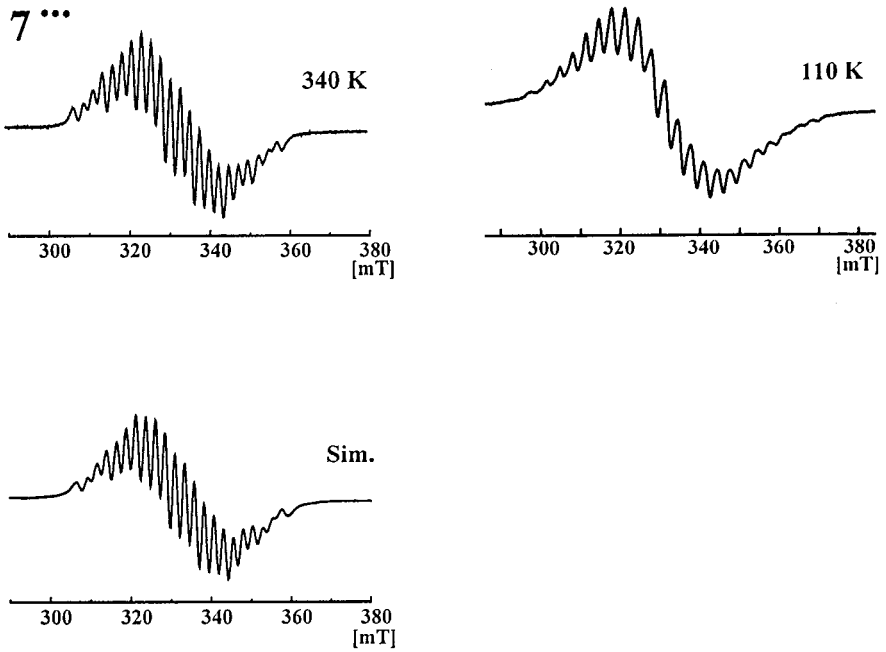


Figure 7. EPR spectra (X-band) of $\mathbf{7}^{\cdot\cdot\cdot}$, fluid (340 K) and rigid (110 K) solution in toluene, with the simulated trace (bottom)

Table 3. EPR data for the trovacenyl boranes $\mathbf{5}^{\cdot}$, $\mathbf{6}^{\cdot\cdot}$, and $\mathbf{7}^{\cdot\cdot\cdot}$, trovacenylborate $[\mathbf{6}^{\cdot\cdot}-n\mathrm{Bu}]^-$, and trovacene $\mathbf{4}^{[a]}$

	$\mathbf{4}^{\cdot}$	$\mathbf{5}^{\cdot}$	$\mathbf{6}^{\cdot\cdot}$	$\mathbf{7}^{\cdot\cdot\cdot}$	$[\mathbf{6}^{\cdot\cdot}-n\mathrm{Bu}]^-$
g_{iso}	1.9866	1.9789	1.9785	1.978	1.9788
$a(^{51}\mathrm{V})$ [mT]	−6.98	−7.35	−7.32	−7.24	−6.69
$\lvert J\rvert$ [cm^{-1}]	–	–	|1.43|	|0.5|	|0.97|
$g_{\parallel}$	2.0030	1.9970	–	–	–
$g_{\perp}$	1.9784	1.9688	–	–	–
$A_{\parallel}$ (^{51}V) [mT]	−1.39	−1.27	–	–	–
$A_{\perp}$ (^{51}V) [mt]	−9.61	−10.35	–	–	–

[a] $^{m}_{I}$ (^{51}V)-dependent line width effects were included in the simulations.

may contribute to the observed reduction in exchange coupling, but apportioning their relative contributions is unfeasible. The gradation in J values of the diradicals containing B(sp^2) or B(sp^3) atoms in the spacer is an empirical observation which, for a detailed analysis, must await additional evidence. It is noteworthy, however, that a similar trend is encountered in the ^{1}H NMR spectra of boranes, in that nuclear spin coupling across boron is weakened if boranes R_3B are converted into borates $[R_3BR']^-$.[13]

Additional interesting aspects are offered by tri([5]trovacenyl)borane $\mathbf{7}^{\cdot\cdot\cdot}$. Whereas numerous organic triradicals have been prepared and studied in great detail,[14] and inorganic species possessing three paramagnetic centers are also familiar,[15] very few organometallic triradials have been reported so far.[16] This is surprising, since the choice of open-shell metal atoms whose nuclei bear magnetic moments suitable for EPR study, and the almost unlimited variability of organic frameworks serving as potential spacers, should provide a rich playground for investigation. Further assets of organometallic oligoradicals include the feasability of EPR studies in fluid solution (most organometallics contain mainly covalent bonds that suppress dissociation in solution), as well as their attenuated reactivity, compared to that of organic radicals. The synthesis and characterization of organometallic oligoradicals is interesting both from a fundamental point of view (study of competing interactions and spin frustration) as well as from an applied perspective (generation of high-spin molecules with ferromagnetic properties).

The fluid-solution EPR spectrum of tri([5]trovacenyl)borane $\mathbf{7}^{\cdot\cdot\cdot}$ exhibits a 22-line multiplet whose ^{51}V splitting corresponds to one third of the hyperfine coupling for mononuclear trovacene $\mathbf{4}^{\cdot}$ (Figure 7). The intensity distribution and the line shapes deviate markedly from the simple binomial case (fast-exchange limit) so that deriving the parameter J by computer simulation appears practicable. The numerical value $J = |0.53|$ cm^{-1} thus obtained for the exchange interaction in $\mathbf{7}^{\cdot\cdot\cdot}$ is somewhat unreliable, though, because it exceeds the coupling constant $a(^{51}\mathrm{V})$ by a factor of 100 which means that the fast-exchange limit is very close. A comparison of the exchange interactions of $\mathbf{6}^{\cdot\cdot}$, $\mathbf{7}^{\cdot\cdot\cdot}$, and $\mathbf{10}^{\cdot\cdot}$ will therefore be based on J values gathered from magnetic susceptibility studies.

Magnetic susceptibilities of crystalline powders of diradical $\mathbf{6}^{\cdot\cdot}$ and triradical $\mathbf{7}^{\cdot\cdot\cdot}$ were measured on a SQUID magnetometer in the temperature range 1.8−250 K and at constant magnetic fields of 500 and 5000 G. Plots of the dependence of the inverse susceptibility, χ^{-1}, vs temperature, T, for both radicals are shown in Figure 8.

The Bleaney−Bowers type equation, Equation 1[15d] was fitted to the experimental data of the diradical $\mathbf{6}^{\cdot\cdot}$ (Figure 8a) to give the best-fit parameters for the factor $g = 1.99(1)$, the exchange constant $J/k = -1.38(2)$ K (-0.96 cm^{-1}) and the Curie−Weiss temperature $\Theta = -9.5(5)$ K. Therefore, the interaction in $\mathbf{6}^{\cdot\cdot}$ is antiferromagnetic.

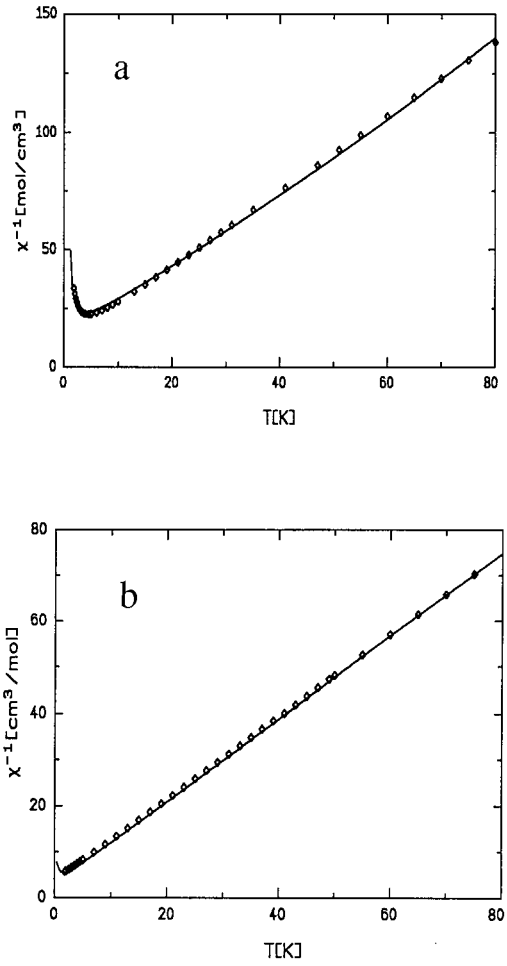


Figure 8. Temperature-dependence of the inverse molar susceptibility of the diradical **6**·· and the triradical **7**···

$$\chi_{mol} = \frac{2N g^2 \mu_B^2}{kT[3+\exp(-J/kT)]} \quad \frac{T}{(T-\Theta)} \qquad (1)$$

This is also the case for triradical **7**··· whose susceptibility data (Figure 8b) were fitted by Equation 2, which applies to the case of an equilateral triangular disposition of identical $S = 1/2$ centers.[17] Optimal fit of the curve was obtained by means of the parameters $g = 1.99(1)$, $J/k = -0.5(2)$ K (-0.35 cm^{-1}), $\Theta = -2.7(5)$ K. From an inspection of the least-squares fit in Figure 8b one has to conclude that the derived exchange constant J can only be interpreted as an upper limit of the interaction parameter. If the local spins present in **7**··· are denoted as S_1, S_2, and S_3, the spin Hamiltonian describing the low-lying states in zero field may be expressed as Equation 3.

$$\chi_{mol} = \frac{N g^2 \mu_B^2}{2kT} \quad \frac{1+5\exp(-3J/kT)}{1+\exp(-3J/kT)} \quad \frac{T}{(T-\Theta)} \qquad (2)$$

$$H = -2J(S_1S_2+S_1S_3+S_2S_3) \qquad (3)$$

The interaction between the three local doublets leads to a molecular quartet and two degenerate doublets, the latter forming the ground state as implied by the antiferromagnetic nature of the interaction. Here, the separation between the degenerate doublets and the quartet amounts to 3*J*. The analysis of the susceptibility data reveals that J(**7**···) for the triradical falls considerably short of J(**6**··) obtained for the diradical. The same gradation was found for the EPR spectra of **7**··· and **6**··. This finding reflects the spin frustration in **7**··· where three spins $S = 1/2$ that are coupled antiferromagnetically, reside in an equilateral triangular arrangement (Figure 3, Figure 9). The reduced J value results because, in the doublet ground state of **7**···, two spins need to be aligned parallel, the opposite of the tendency towards spin pairing (as demonstrated by the susceptibility curve for diradical **6**··).

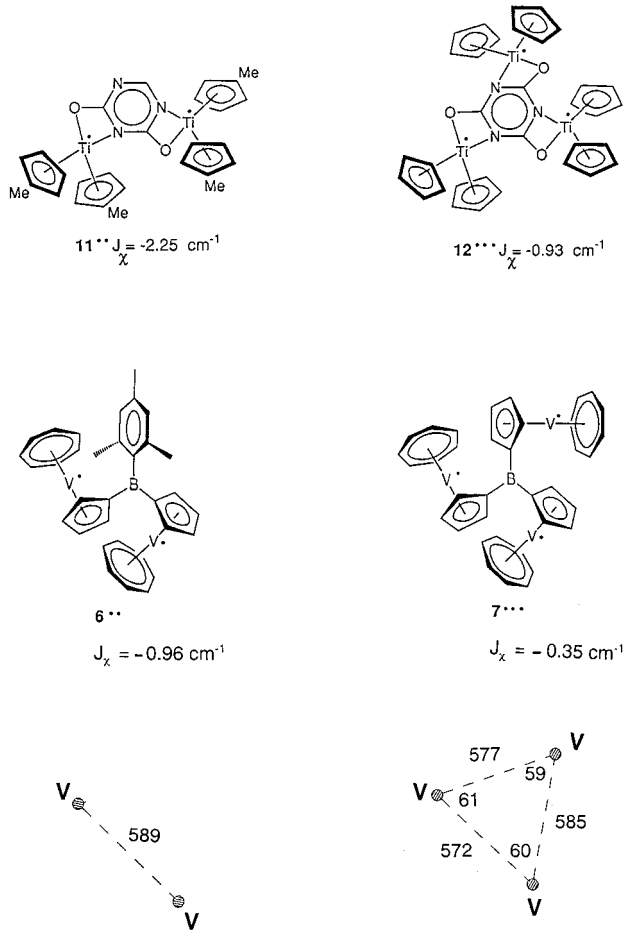


Figure 9. Structures of the organometallic diradicals/triradicals 11··/12··· and 6··/7···, and their exchange coupling constants $J_{\χ}$; intervanadium distances (pm) in 6·· and 7··· are also given

The characteristic decrease in the magnitude of J on going from a diradical to a triradical of triangular structure, while keeping the exchange path identical, is limited to cases where the pairwise interactions are antiferromagnetic. Organic triradicals with the requisite trigonal symmetry are usually based on 1,3,5-benzenetriyl as backbone, where the 1,3-connection effects ferromagnetic coupling.[18] Therefore, to the best of our knowledge, spin frustration has as yet only been observed once for an organic triradical.[14d] In

contrast, several examples of spin-frustrated coordination compounds[19] are known, and there are also a few cases known in the field of organometallic chemistry.[20,5a] Since the pair **11**$^{\cdot\cdot}$/**12**$^{\cdot\cdot\cdot}$[20] resembles the pair **6**$^{\cdot\cdot}$/**7**$^{\cdot\cdot\cdot}$ reported here, they are represented in Figure 9 together with their respective *J* values, determined by susceptometry. What both pairs have in common is the presence of two or three paramagnetic sandwich complex units ($S = 1/2$) whose open-shell central metal atoms, Ti(d^1) or V(d^5), are linked by bridges which effect antiferromagnetic coupling. Furthermore, in the trinuclear complexes **7**$^{\cdot\cdot\cdot}$ and **12**$^{\cdot\cdot\cdot}$, the central metal atoms are placed at the corners of an equilateral triangle so that the pairwise magnetic interactions are governed by a single exchange parameter *J*. Thus, the stage is set for spin frustration which is actually observed in both cases since, despite identical coupling paths, *J* for the triradicals **7**$^{\cdot\cdot\cdot}$ and **12**$^{\cdot\cdot\cdot}$ falls short of *J* exhibited by diradicals **6**$^{\cdot\cdot}$ and **11**$^{\cdot\cdot}$. It may come as a surprise that the *J* values for **11**$^{\cdot\cdot}$ and **12**$^{\cdot\cdot\cdot}$ exceed those for **6**$^{\cdot\cdot}$ and **7**$^{\cdot\cdot\cdot}$ considerably, despite the fact that, in both cases, the interacting metal atoms are separated by four bonds. One should bear in mind, however, that a detailed description of the exchange pathway must be based on the symmetry relationship between the metal- and ligand bridge orbitals and their energies. The two systems compared here differ significantly in that the singly occupied titanium orbitals in **11**$^{\cdot\cdot}$ and **12**$^{\cdot\cdot\cdot}$ are thought to be located in the plane of the bridging cyanurato trianion,[20] whereas in the [5]trovacenyl derivatives **6**$^{\cdot\cdot}$ and **7**$^{\cdot\cdot\cdot}$, the singly occupied vanadium orbitals are perpendicular to the cyclopentadienyl plane of the $\mu[\eta^5{:}\eta^5\text{-}C_5H_4B(R)C_5H_4]$ bridge (R = mesityl, trovacenyl). A simple count of the atoms intervening between the two paramagnetic centers can therefore not account for the gradation of the experimental *J* values.

Experimental Section

General: All manipulations were performed with exclusion of air under dinitrogen or argon (CV) unless stated otherwise. Physical measurements were carried out with equipment specified previously.[22] Trovacene $(\eta^7\text{-}C_7H_7)V(\eta^5\text{-}C_5H_5)$,[6a] di(mesityl)fluoroborane, and (mesityl)difluoroborane[23] were prepared as described in the literature.

Bis(mesityl)([5]trovacenyl)borane (5$^{\cdot}$): To a solution of trovacene (290 mg, 1.4 mmol) in 80 mL of diethyl ether was added, at room temperature, 1.4 mL of a solution of *n*-butyllithium in hexane (1.55 mol L^{-1}). After being stirred for 14 h, the reddish-brown solution was cooled to −40 °C, and 187 mg (0.7 mmol) of di(mesityl)fluoroborane, dissolved in 30 mL of diethyl ether, was slowly added to it. The mixture was allowed to reach room temperature, whereby a color change to green occurred. After the reaction mixture was stirred for 20 h, the solvent was removed in vacuo, the residue was taken up in toluene and subjected to column chromatography (Al_2O_3, 0% H_2O, elution with toluene). From the first fraction, 290 mg (0.65 mmol, yield: 46%) of **5**$^{\cdot}$ was obtained as a green product. Single crystals suitable for X-ray diffraction were grown from benzene/*n*-pentane (supernatant). MS (EI, 70 eV) *m*/*z* (%): 456

Table 4. Crystallographic data for the compounds **5**$^{\cdot}$, **6**$^{\cdot\cdot}$, and **7**$^{\cdot\cdot\cdot}$

	5$^{\cdot}$	**6**$^{\cdot\cdot}$	**7**$^{\cdot\cdot\cdot}$
Shape, color	plates, green	thin plates, dark	prisms, dark red
Crystal size (mm)	0.30 × 0.15 × 0.06	0.30 × 0.15 × 0.06	0.18 × 0.18 × 0.15
Crystal system	Triclinic	Monoclinic	Triclinic
Space group	*P*1bar (No. 2), $Z = 2$	$P2_1$ (No 12), $Z = 2$	*P*1 (No. 1), $Z = 2$
Unit cell dimensions	$a = 9.7666(9)$ Å, $\alpha = 91.259(11)°$	$a = 10.1842(19)$ Å.	$a = 7.796(2)$ Å, $\alpha = 98.94(3)°$
	$b = 11.4985(11)$ Å,	$b = 8.9716(13)$ Å, $\beta = 96.139(9)°$	$b = 12.429(3)$ Å, $\beta = 94.67(3)°$
	$\beta = 110.611(11)°$,		
	$c = 11.5003(11)$ Å, $\gamma = 94.302(11)°$	$c = 14.350(2)$ Å	$c = 14.599(6)$ Å, $\gamma = 93.15(2)°$
Volume	1203.8(2) Å^3	1303.6(4) Å^3	1389.5(8) Å^3
Empirical formula	$C_{30}H_{33}BV$	$C_{33}H_{33}BV_2$	$C_{36}H_{33}BV_3$
Formula mass	455.31	522.28	629.25
Density (calculated)	1.256 Mg/m^3	1.382 Mg/m^3	1.504 Mg/m^3
Absorption coefficient	0.427 mm^{-1}	0.737 mm^{-1}	1.014 mm^{-1}
F(000)	482	564	646
Diffractometer type	Stoe IPDS	Siemens P4	Nonius CAD4
Wavelength	0.71073 Å	0.71073 Å	0.71073 Å
Temperature	193(2) K	223(2) K	203(2) K
θ range for data collection	2.24 to 25.94°	2.01 to 25.05°	2.35 to 26.32°
Index ranges	−11/11, −14/14, −12/14	−1/12, −9/10, −17/17	−9/9, −15/15, −18/17
Data-collection software	Stoe Expose	Siemens XSCANS	Nonius EXPRESS
Cell-refinement software	Stoe Cell	Siemens XSCANS	Nonius EXPRESS
Data-reduction software	Stoe Integrate	Siemens SHELXTL	XCAD4 (Harms, 1998)
Reflections collected	8561	5830	7404
Independent reflections	4352 [R(int) = 0.0617]	4118 [R(int) = 0.0615]	7404
Observed reflections	2930 [$I > 2\sigma(I)$]	3041 [$I > 2\sigma(I)$]	5889 [$I > 2\sigma(I)$]
Reflections used for refinement	4352	4118	7404
Flack param. (abs. structure)	−	−0.07(4)	0.37(4) (racemic twin)
Largest diff. peak and hole	0.342 and −0.316 e·Å^{-3}	0.315 and −0.341 e·Å^{-3}	0.497 and −0.511 e·Å^{-3}
Data/restraints/parameters	4352/0/410	4118/1/424	7404/3/722
Goodness-of-fit on F^2	0.903	1.082	1.035
R index (all data)	*wR*2 = 0.0930	*wR*2 = 0.1067	*wR*2 = 0.1277
R index conventional [$I > 2\sigma(I)$]	*R*1 = 0.0419	*R*1 = 0.0532	*R*1 = 0.0559

(34.8), 455 (100) [M^+], 454 (27), 364 (43.5) [$M^+ - C_7H_7$]. − IR (KBr): $\tilde{\nu}$ = 3029 cm^{-1} (w), 2912 (m), 1800−1600 (w), 1605 (m), 1436 (s), 1363 (s), 1251 (m), 798 (s), 782 (s), 470 (w), 432 (w). − Voltammetry and EPR: see text. − $C_{30}H_{33}BV$ (455.34): calcd. C 79.13, H 7.30; found C 78.06, H 7.43.

Mesityldi([5]trovacenyl)borane (6¨): For the preparation of **6¨**, the instructions given for **5˙** were followed with: 342 mg (1.65 mmol) of trovacene dissolved in 90 mL of diethyl ether, 1.7 mL of *n*-butyllithium (1.55 mol L^{-1} in *n*-hexane), and 68 mg (0.4 mmol) of (mesityl)difluoroborane in 30 mL of diethyl ether. Column chromatography delivered **6¨** in the second fraction as a green material, yield: 170 mg (0.31 mmol, 38%). Crystals were obtained by slow evaporation of a solution of **6¨** in toluene. MS(EI, 70 eV) *m*/*z* (%): 543 (25.5), 542 (100) [M^+], 541 (8), 271 (17) [M^{2+}]. − IR (KBr): $\tilde{\nu}$ = 3039 cm^{-1} (w), 2951, 2916 (m), 1750−1600 (w), 1604 (m), 1443 (s), 1363 (s), 1243 (m), 1052 (s), 810, 783 (s), 430 (w). − Voltammetry and EPR: see text. − $C_{33}H_{33}BV_2$ (542.32): calcd. C 73.03, H 6.13; found C 72.47, H 5.67.

Tri([5]trovacenyl)borane (7‴): The synthesis proceeded as described for **5˙** and **6¨**; however, the 20 h period of reacting [5]trovacenyllithium with $BF_3{\cdot}OEt_2$ at room temperature was followed by 30 min of refluxing. From trovacene (453 mg, 2.19 mmol), *n*-butyllithium (2.2 mL of a solution 1.55 mol L^{-1} in *n*-hexane), and $BF3{\cdot}Et_2O$ (50 mg, 0.36 mmol), 174 mg (0.28 mmol, yield: 39%) of **7‴** was obtained, which could be recrystallized from benzene/*n*-pentane (supernatant) to form green needles. MS (EI, 70 eV) *m*/*z* (%): 630 (38), 629 (100) [M^+], 628 (24), 315 (22) [M^{2+}]. − IR (KBr) $\tilde{\nu}$ = 3041 cm^{-1} (w), 2959 (m), 1750−1600 (w), 1434 (m), 1373 (s), 1263 (m), 1058 (s), 802, 782 (s), 426 (w). − Voltammetry and EPR: see text. − $C_{36}H_{33}BV_3$ (629.32): calcd. C 68.71, H 5.29; found C 67.73, H 5.13.

X-ray Crystal Structure Analyses of 5˙, 6˙, and 7‴: The crystal structures were solved by direct methods (SHELXS-97) and refined by the full matrix least squares refinement on F^2 values (SHELXL-97), all non-hydrogen atoms were refined anisotropically. Hydrogen atoms were included on calculated positions (**6¨**, **7‴**) or were refined isotropically (compound **5˙**). See also Table 4. Further crystallographic data (excluding structure factors) for the structures reported in this paper were deposited with the Cambridge Crystallographic Data Centre as supplementary publication nos. CCDC-132390−132392. Copies of the data may be obtained free of charge on application to CCDC, 12 Union Road, Cambridge CB2 1EZ, UK [Fax: (internat.) +44-1223/336-033; E-mail: deposit@ccdc.cam.ac.uk].

Acknowledgments

Support of this work by the Volkswagen-Stiftung and the Fonds der Chemischen Industrie is gratefully acknowledged.

[1] C. Elschenbroich, O. Schiemann, O. Burghaus, K. Harms, J. Pebler, *Organometallics* **1999**, *18*, 3273. Trovacene = (η^7-**tro**pylium)**va**nadium(η^5-**c**yclop**en**tadi**e**nyl); the number in square brackets preceding the name indicates the site of substitution: [5]trovacene is functionalized at the five-membered ring, [7]trovacene at the seven-membered ring.

[2] For a case study, as well as for leading references to the field in general, see: J. A. McCleverty, M. D. Ward, *Acc. Chem. Res.* **1998**, *31*, 842.

[3] C. Elschenbroich, P. Kühlkamp, A. Behrendt, K. Harms, *Chem. Ber.* **1996**, *129*, 859.

[4] [4a] C. Elschenbroich, J. Heck, *J. Am. Chem. Soc.* **1979**, *101*, 6773. − [4b] C. Elschenbroich, J. Heck, *Angew. Chem. Int. Ed. Engl.* **1981**, *20*, 267. − [4c] C. Elschenbroich, J. Heck, F. Stohler, E. Bilger, *Chem. Ber.* **1984**, *117*, 23. − [4d] C. Elschenbroich, G. Heikenfeld, M. Wünsch, W. Massa, G. Baum, *Angew. Chem.* **1988**, *100*, 397; *Angew. Chem. Int. Ed. Eng.* **1988**, *27*, 414. − [4e] C. Elschenbroich, A. Bretschneider-Hurley, J. Hurley, W. Massa, S. Wocadlo, J. Pebler, E. Reijerse, *Inorg. Chem.* **1993**, *32*, 5421. − [4f] C. Elschenbroich, T. Isenburg, B. Metz, A. Behrendt, K. Harms, *J. Organomet. Chem.* **1994**, *481*, 153. − [4g] C. Elschenbroich, B. Metz, B. Neumüller, E. Reijerse, *Organometallics* **1994**, *13*, 5072. − [4h] C. Elschenbroich, A. Bretschneider-Hurley, J. Hurley, A. Behrendt, W. Massa, S. Wocadlo, E. Reijerse, *Inorg. Chem.* **1995**, *34*, 743. − [4i] C. Elschenbroich, T. Isenburg, A. Behrendt, *Inorg. Chem.* **1995**, *34*, 6565.

[5] [5a] O. Schiemann, Dissertation, Philipps-Universität, Marburg, Germany, **1998**. − [5b] J. Plackmeyer, Diploma, Philipps-Universität, Marburg, Germany, **1997**. − [5c] M. Wolf, Dissertation, Philipps-Universität, Marburg, Germany, **1999**.

[6] [6a] R. B. King, F. G. A. Stone, *J. Am. Chem. Soc.* **1959**, *81*, 5263. − [6b] G. Engebretson, R. Rundle, *J. Am. Chem. Soc.* **1963**, *85*, 481. − [6c] W. M. Gulick, Jr., D. H. Geske, *Inorg. Chem.* **1967**, *6*, 1320.

[7] [7a] E. W. Post, R. G. Cooks, J. C. Kotz, *Inorg. Chem.* **1970**, *9*, 1670. − [7b] T. López, A. Campero, *J. Organomet. Chem.* **1989**, *378*, 91. − [7c] B. Wrackmeyer, U. Dörfler, W. Milius, M. Herberhold, *Z. Naturforsch.* **1995**, *50b*, 201.

[8] C. J. Groenenboom, H. J. Liefde Meijer, F. Jellinek, *Recl. Trav. Chim. Pays. Bas* **1974**, *93*, 6.

[9] C. J. Groenenboom, H. J. Liefde Meijer, F. Jellinek, *J. Organomet. Chem.* **1974**, *69*, 235.

[10] A. Schulz, W. Kaim, *Chem. Ber.* **1989**, *12*, 1863.

[11] F. Zettler, H. D. Hansen, H. Hess, *J. Organomet. Chem.* **1974**, *72*, 157. − J.F. Blount, F. Finocchiaro, D. Gust, K. Mislow, *J. Am. Chem. Soc.* **1973**, *95*, 7019.

[12] J. B. Flanagan, S. Margel, A.J. Bard, F. C. Anson, *J. Am. Chem. Soc.* **1978**, *100*, 4248.

[13] J. D. Kennedy in *Multinuclear NMR* (Ed.: J. Mason), Plenum Press, New York, **1987**, chapter 8. − H. Nöth, B. Wrackmayer, *Nuclear Magnetic Resonance Spectroscopy of Boron Compounds*, Springer, Berlin, **1978**, chapter 8.

[14] Access to the extensive literature on organic triradicals is provided by: [14a] H. Nishide, M. Miyasaka, E. Tsuchida, *Angew. Chem. Int. Ed.* **1998**, *37*, 2400. − [14b] A. Rajca, J. Wongsriratanakul, S. Rajca, *J. Am. Chem. Soc.* **1997**, *119*, 11674. − [14c] K. R. Stickley, T. D. Selby, S. C. Blackstock, *J. Org. Chem.* **1997**, *62*, 448. − [14d] J. Fujita, M. Tanaka, H. Suemune, N. Koga, K. Matsuda, H. Iwamura, *J. Am. Chem. Soc.* **1996**, *118*, 9347. − [14e] J. Veciano, C. Rovira, N. Ventosa, M. I. Crespo, F. Palacio, *J. Am. Chem. Soc.* **1993**, *115*, 57. − [14f] A. Raja, *Chem. Rev.* **1994**, *94*, 871. − [14g] H. Iwamura, *Adv. Phys. Org. Chem.* **1990**, *26*, 179. − [14h] Landolt−Börnstein, *Magnetic Properties of Free Radicals*, New Series, II/9, Part d2, Springer, Berlin, **1980**. − [14i] H. Iwamura, K. Inoue, T. Hayamizu, *Pure Appl. Chem.* **1996**, *68*, 243. − [14j] W. M. Nan, *Angew. Chem. Int. Ed. Engl.* **1997**, *36*, 2445. − [14k] T. Itoh, K. Matsuda, H. Iwamura, *Angew. Chem.* **1999**, *111*, 1886; *Angew. Chem. Int. Ed.* **1999**, *38*, 1791.

[15] For examples from inorganic chemistry/coordination chemistry, see: [15a] V. A. Ung, A. M. W. Cargill Thompson, D. A. Bardwell, D. Gatteschi, J. C. Jeffery, J. A. McCleverty, F. Totti, M. D. Ward, *Inorg. Chem.* **1997**, *36*, 3447. − [15b] P. B. Hitchcock, D. L. Hughes, L. F. Larkworthy, G. J. Leigh, C. J. Marmion, J. R. Sanders, G. W. Smith, J. S. de Souza, *J. Chem. Soc., Dalton Trans.* **1997**, 1127. − [15c] I. Shweky, L. E. Pence, G. C. Papaefthymion, R. Sessoli, J. W. Yun, A. Bino, S. J. Lippard, *J. Am. Chem. Soc.* **1997**, *119*, 1037. − [15d] O. Kahn, *Molecular Magnetism,* VCH, Weinheim, **1993**, chapter 10. − [15e] J. K. McCusker, C. A. Christmas, P. M. Hagen, R. J. Chadha, D. F. Harvey, D. N. Hendrickson, *J. Am. Chem. Soc.* **1991**, *113*, 6114. − [15f] M. Tanaka, K. Matsuda, T. Itoh, H. Iwamura, *Angew. Chem.* **1998**, *110*, 866; *Angew. Chem. Int. Ed.* **1998**, *37*, 810.

[16] To the best of our knowledge the only organometallic triradicals which have been isolated are cyanuratotris[bis(η^5-methylcyclopentadienyl)titanium(III)][19] and 1,3,5-tri([5]trovacenyl)benzene.[5a] Formally, certain paramagnetic termetallocene cations, generated during electrochemical oxidations in CV experiments,[21] also belong to this class.

[17] Equation 2 was derived from the more general expression valid for an equilateral triangular configuration with nonidentical coupling pathways, described by the parameters J and J', where the ratio $J'/J = \alpha$ was set to one (see Ref.[14d]). Apart from the structural information about **7**$^{+\cdot\cdot\cdot}$, gathered by X-ray crystallography, the simplification inherent in Equation 2 is justified by the fact that the fit based on the more general expression given in Ref.[14d] was optimal for $\alpha = 1$.
[18] A. Raja, *Chem. Rev.* **1994**, *94*, 871.
[19] R. D. Cannon, R. P. White, *Progr. Inorg. Chem.* **1988**, *36*, 195. − S. J. Lippard, *Angew. Chem. Int. Ed. Engl.* **1988**, *27*, 344. H. Y. Woo, H. So, M. T. Pope, *J. Am. Chem. Soc.* **1996**, *118*, 621.
[20] B. F. Fieselmann, D. N. Hendrickson, G. D. Stucky, *Inorg. Chem.* **1978**, *17*, 1841.
[21] See: S. Barlow, D. O′Hare, *Chem. Rev.* **1997**, *97*, 637, for leading references.
[22] C. Elschenbroich, S. Voss, O. Schiemann, A. Lippek, K. Harms, *Organometallics* **1998**, *17*, 4417.
[23] A. Pelter, K. Smith, H. C. Brown, *Borane Reagents*, Academic Press, London, **1988**.

Received July 15, 1999
[I99261]

Chiral Chelate Ligands Based on a Neopentane Framework; Introducing Indenyl and Fluorenyl Donor Groups

Joachim Vogelgesang,[a] Gottfried Huttner,*[a] Elisabeth Kaifer,[a] Peter Kircher,[a] Peter Rutsch,[a] and Sven Cunskis[a]

Dedicated to Prof. Dr. H. Schmidbaur on the occasion of his 65th birthday

Keywords: Ansa compounds / Cp-derived chelate ligands / Neopentane chemistry / Spiro compounds / Tripodal ligands / Cyclopentadienyl compounds

The neopentane-derived functionalized oxetane $O(CH_2)_2C(CH_3)(CH_2OMs)$, **1**, reacts with indenyllithium (LiInd) or fluorenyllithium (LiFlu) to produce the derivatives $O(CH_2)_2C(CH_3)(CH_2R)$ (R = indenyl, fluorenyl), **2**. The oxetane ring of **2** undergoes nucleophilic ring-opening by reaction with $LiPR'_2$ to give the chiral chelate ligands $(HOCH_2)(CH_3)C(CH_2R)(CH_2PR'_2)$ (R = indenyl, fluorenyl), **5**. Nucleophilic ring-opening by LiInd or LiFlu is possible too, resulting in the functionalized *ansa*-Cp ligands $(HOCH_2)(CH_3)C(CH_2R)(CH_2R')$ (R, R′ = indenyl, fluorenyl), **12**. Electrophilic ring-opening of **2** with HBr to give $(HOCH_2)(CH_3)C(CH_2R)(CH_2Br)$ (R = indenyl, fluorenyl), **3**, is also possible. The alcohol function of **3** may be activated directly, whereas activation of this group in **5** is only possible after BH_3 protection of the phosphane function. The mesylates $(MsOCH_2)(CH_3)C(CH_2R)(CH_2Br)$ (R = indenyl, fluorenyl), **4**, undergo, under basic conditions, spiro cyclization to produce spirocyclobutane derivatives **9** with the α-carbons of the five-membered cycles acting as the spiro centres. Substitution of the mesylate group of **4** by PR_2 nucleophiles is therefore not possible. *Ansa*-Cp derivative $(MsOCH_2)(CH_3)C(CH_2Ind)(CH_2Flu)$, **12c** also reacts with $LiPPh_2$ with spiro cyclization to produce **9d**, instead of giving the substitution product. Tripodal ligands $(CH_3)C(CH_2R)(CHPPh_2)_2$ (R = indenyl, fluorenyl), **11**, are accessible by the reaction of $(MsOCH_2)(CH_3)C(CH_2PPh_2)_2$ with LiInd or LiFlu. All compounds are fully characterized by the usual spectroscopic and analytical techniques including single-crystal X-ray analyses in several cases.

Introduction

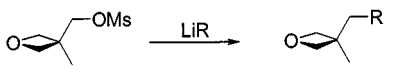
The coordination chemistry of neopentane-based tripodal ligands was extensively developed by L. Sacconi[1] and his school,[2] on the basis of $CH_3C(CH_2PPh_2)_3$ as the prototype ligand. The peculiar type of reactivity of the corresponding tripodal metal templates $CH_3C(CH_2PR_2)_3M$[1][2] indicates potential for this type of ligand, and modification of the donor groups appears to be a worthwhile goal. A number of methods have been developed for the introduction of different donor groups in $CH_3C(CH_2X)(CH_2Y)(CH_2Z)$ (X, Y, Z = PR_2, PR'_2, NR_2, SR, OR),[3−5] even enantioselectively.[3c,3e,3h] Introducing a Cp moiety as a constituent of this type of tripodal ligand calls for special procedures which have been worked out in some cases.[6] The ligands $[R'CH_2C(CH_2C_5H_4)(CH_2X)(CH_2Y)]^-$ (Y, Z = PR_2) lend themselves to the construction of $CpML_2$ templates in which the Cp ligand and the L donors are covalently linked by a neopentane scaffolding. The importance of $CpML_2$ templates in the metal-mediated transformation of organic substances is a stimulus for the interest in such tripodal CpL_2 ligands.[7] It is shown in this paper that the routes developed for the introduction of Cp donor groups into the tripodal ligands cannot be directly transferred to the synthesis of tripodal ligands containing indenyl or fluorenyl groups, due to complications arising from internal cyclization processes. Reaction sequences are nevertheless developed, which allow the introduction of these Cp derivatives into neopentane-based tripodal ligands.

Results and Discussion

Ligand Synthesis

The following reaction sequence was shown to be effective for converting functionalized oxetane **1** to Cp-functionalized tripodal ligands: 1. Substituting OMs by Cp. 2. Electrophilic opening of the oxetane ring by HBr. 3. Mesylation of the OH group resulting from step 2. 4. Nucleophilic substitution of the two leaving groups (OMs, Br) by PR_2.[6a]

The first step of this sequence (Scheme 1) also works when indenyl or fluorenyl needs to be introduced. Compound **2a** is obtained as a colourless oil, which tends to



1 **2a** R = Indenyl **2b** R = Fluorenyl

Scheme 1

[a] Anorganisch-Chemisches Institut der Universität Heidelberg, Im Neuenheimer Feld 270, D-69120 Heidelberg, Germany
Fax: (internat.) +49-(0)6221/545707

 © WILEY-VCH Verlag GmbH, D-69451 Weinheim, 1999 1434−1948/99/1212−2187 $ 17.50+.50/0

crystallize at −20°C. Compound **2b** forms a colourless microcrystalline powder, from which crystals, suitable for X-ray analysis, could be grown by slow evaporation from CH_2Cl_2/*n*-pentane solutions. NMR spectroscopic data (Table 1) and analytical data (Table 2) are consistent with the assigned constitution which is further proved by an X-ray analysis of **2b** (Figure 1, Table 3 and Table 4).

There are two independent molecules of **2b** in the unit cell (only one is shown in Figure 1). The scalar geometric parameters of these individual molecules are almost identical (Table 3). Even the relative orientation of the fluorenyl entity with respect to the oxetane moiety is closely similar in both molecules (see torsion angles C1−C2−C5−C6 in Table 3). The only significant difference is in the folding angles of the oxetane ring which is definitely different in the two independent species (cf. torsion angles C1−C2−C3−Y and C1−C2−C4−Y Table 3).

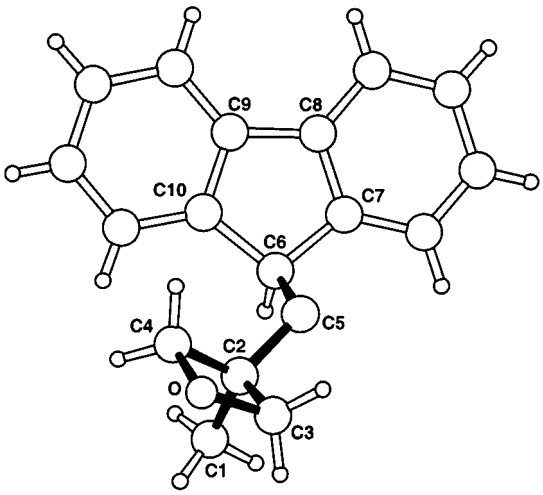


Figure 1. Structure of **2b**

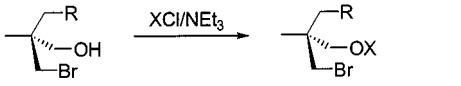
Electrophilic opening of the oxetane rings of **2** by HBr results in compounds **3**; **3a** is obtained as a colourless oil and **3b** as a colourless microcrystalline material (Scheme 2). Analytical (Table 2) and spectroscopic data (Table 1) confirm the identity of **3**.



2a R = Indenyl
2b R = Fluorenyl

3a R = Indenyl
3b R = Fluorenyl

Scheme 2



3a R = Indenyl
3b R = Fluorenyl

4a R = Indenyl, X = Ms
4b R = Indenyl, X = SO_2Ph
4c R = Indenyl, X = $SiMe_3$
4d R = Fluorenyl, X = Ms

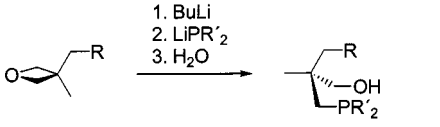
Scheme 3

Activation of the OH group of **3** by different reagents leads to compounds **4** (Scheme 3). Transformation of the $OSiMe_3$ group of **4c** into an iodine substituent by reaction with NaI/$ClSiMe_3$/acetonitrile was unsuccessful. The silyl derivative **4c** is obtained as a colourless oil, while the other compounds **4** form colourless microcrystalline solids. The analytical (Table 2) and the spectroscopic (Table 1) data are in accord with the assigned constitutions, which are further corroborated by single-crystal X-ray analyses of **4a** and **4b** (Figure 2, Table 3 and Table 4). The single crystals of **4a** and **4b** could be grown in test tubes from saturated CH_2Cl_2/*n*-pentane solutions by slow diffusion of the solvent into rubber stoppers.

Both these chiral neopentane derivatives crystallize in racemic form (Table 4). The arrangement of the individual substituents is such that steric congestion within the molecules is avoided by spreading out of the bulky groups (Figure 2). In both compounds the indenyl substituents are connected to the scaffolding via the α-carbon centre (C6) of the five-membered cycle. The alternating double and single bonds between the carbon atoms of these five-membered cycles are clearly evident from the corresponding distances (Table 3). The solid-state structures are in agreement with the NMR spectroscopic data (Table 1) which show that indenyl substitution is fully stereoselective with only C_α acting as the linking atom.

Nucleophilic opening of the oxetane group of **2** is also possible. This is done according to a procedure developed for Cp-substituted oxetanes.[6a] After deprotonation of the Cp-containing residue by *n*-butyllithium in THF, a THF solution of $LiPR_2$ is slowly added to the reaction mixture. After hydrolysis, the products **5** are extracted with diethyl ether and are obtained as colourless oils after evaporation of the solvent (Scheme 4). The crude products **5a** and **5b** are separated from the excess diphenylphosphane by chromatography while excess diethylphosphane is removed from **5c** in vacuo. The NMR spectroscopic data of **5** (Table 5) are consistent with the formulae given, as are the mass spectra and the elemental analyses (Table 2).

Protection of the PR_2 group of **5** by BH_3 leads to the derivatives **6**, which are also fully characterized (Scheme 5, Table 5 and Table 2). [3f,8] Single crystals of **6b** were grown from saturated CH_2Cl_2/*n*-pentane solutions by slow diffusion of the solvent into rubber stoppers. X-ray analysis data of **6b** (Figure 3, Table 3 and Table 4) are in accord with the assigned constitution. In contrast to **4a**/**4b**, the bulky substituents are not spread out as far as possible; the fluorenyl substituent is apparently preferentially close to the phenyl groups, with a face to edge arrangement of these two groups resulting. Individual angles and distances within the compound are normal (Table 3); the P−B distance



2a R = Indenyl
2b R = Fluorenyl

5a R = Indenyl, R´= Ph
5b R = Fluorenyl, R´= Ph
5c R = Indenyl, R´= Et

Scheme 4

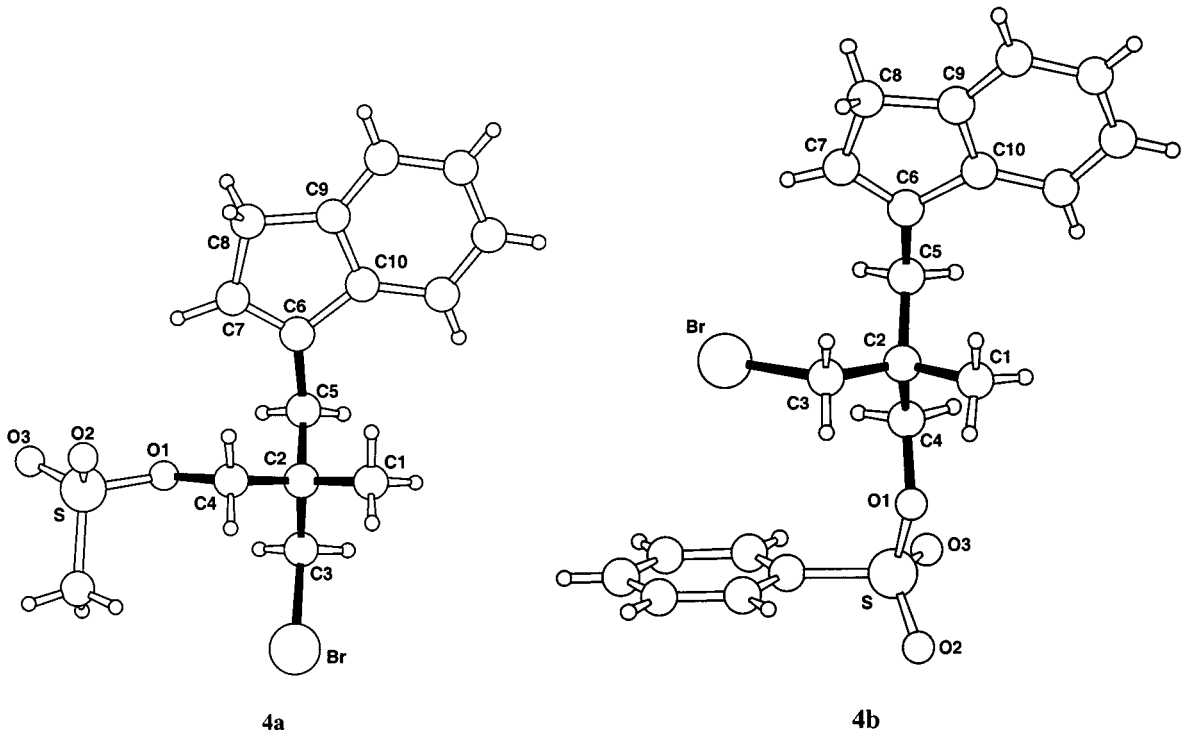


Figure 2. Structure of **4a** and **4b**

Table 1. NMR spectroscopic data of **2a**−**4d**[a,b,c]

No	R X Y	1[d] CH_3 [3H]	2[d] C_q	3[d] $CH_{2a,b}$ [2H]	4[d] $CH_{2a,b}$ [2H]	5[d] $CH_{2a,b}$ [2H]	6[d] $-CH_n-$ (n = 1−2)	7[d] −CH= [1H]	CH aromatic	Y
2a	Indenyl O	1.50 (s)	−	4.50, 4.76 (2 d) $^2J_{HH}$ = 5.6 Hz		2.99 (s)	3.45 (s) [2 H]	6.24 (s)	7.27−7.57 (m) [4 H]	−
	(Oxetane)	24.6 (s)	40.0 (s)	83.3 (s)		36.7 (s)	38.5 (s)		119.6−146.4 (8 s)	−
3a	Indenyl Br	1.15 (s)	−	3.57, 3.65 (2 d) $^2J_{HH}$ = 10.2 Hz	3.64, 3.72 (2 d) $^2J_{HH}$ = 11.0 Hz	2.81 (s)	3.49 (s) [2 H]	6.50 (s)	7.29−7.60 (m) [4 H]	2.51 (s) [1 H]
	OH	21.4 (s)	40.8 (s)	42.7 (s)	68.2 (s)	32.5 (s)	38.5 (s)		119.9−146.7 (8 s)	−
4a	Indenyl Br	1.16 (s)	−	3.49, 3.58 (2 d) $^2J_{HH}$ = 10.4 Hz	4.17, 4.24 (2 d) $^2J_{HH}$ = 9.5 Hz	2.80 (s)	3.45 (s) [2 H]	6.48 (s)	7.23−7.55 (m) [4 H]	3.08 (s) [3 H]
	OMs	21.3 (s)	39.7 (s)	40.9 (s)	74.2 (s)	32.3 (s)	38.6 (s)		119.8−146.1 (8 s)	37.6 (s)
4b	Indenyl Br	1.08 (s)	−	3.43, 3.51 (2 d) $^2J_{HH}$ = 10.4 Hz	4.02, 4.09 (2 d) $^2J_{HH}$ = 9.3 Hz	2.75 (s)	3.40 (s) [2 H]	6.38 (s)	7.27−8.03 (m) [9 H]	7.27−8.03 (m) [9 H]
	OSO_3Ph	21.3 (s)	39.7 (s)	40.8 (s)	74.4 (s)	32.3 (s)	38.5 (s)		119.8−146.1 (13 s)	119.8−146.1 (13 s)
4c	Indenyl Br	1.04 (s)	−	3.49, 3.60 (2 d) $^2J_{HH}$ = 9.5 Hz	3.50 (s)	2.74 (s)	3.44 (s) [2 H]	6.43 (s)	7.22−7.55 (m) [4 H]	0.21 (s) [9 H]
	OTMS	21.3 (s)	40.7 (s)	43.0 (s)	67.3 (s)	32.3 (s)	38.4 (s)		120.1−146.8 (5 s)	0.0 (s)
2b	Fluorenyl O	1.52 (s)	−	4.35, 4.5 (2 d) $^2J_{HH}$ = 5.6 Hz		2.35 (d) $^3J_{HH}$ = 6.6 Hz	4.06 (t) [1 H] $^3J_{HH}$ = 6.6 Hz	−	7.29−7.84 (m) [8 H]	−
	(Oxetane)	24.4 (s)	40.0 (s)	84.4 (s)		43.1 (s)	45.2 (s)	−	120.4−147.4 (6 s)	−
3b	Fluorenyl Br OH	1.05 (s)	−	3.38, 3.50 (2 d) $^2J_{HH}$ = 10.0 Hz	3.53 (m)	2.27, 2.37 (2 dd) $^2J_{HH}$ = 15.0 Hz $^3J_{HH}$ = 4.3 Hz	4.02 (t) [1 H] $^3J_{HH}$ = 4.3 Hz	−	7.29−7.80 (m) [8 H]	1.58 (bs) [1 H]
		21.8 (s)	40.7 (s)	43.1 (s)	68.0 (s)	37.8 (s)	44.6 (s)	−	120.3−148.7 (6 s)	−
4d	Fluorenyl Br	1.00 (s)	−	3.30, 3.40 (2 d) $^2J_{HH}$ = 10.4 Hz	3.99 (m)	2.40 (d) $^3J_{HH}$ = 4.4 Hz	3.99 (m) [1 H]	−	7.37−7.80 (m) [8 H]	3.02 (s) [3 H]
	OMs	21.7 (s)	39.8 (s)	41.5 (s)	74.5 (s)	37.2 (s)	44.6 (s)	−	120.5−147.6 (6 s)	37.5 (s)

[a] For ease of comparison the sequence of entries in this table does not follow the compound numbering sequence. − [b] Sequence of entries for each compound: ^1H NMR first lines, ^{13}C NMR last lines. − [c] Solvent: $CDCl_3$. − [d] Designation:

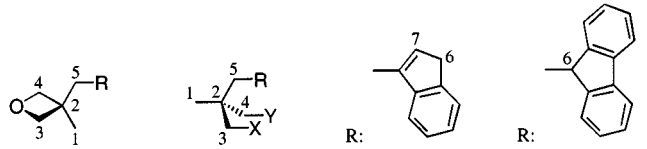


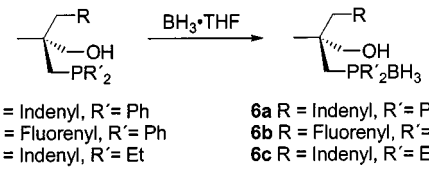
Table 2. Analytical data of **2a**−**12d**

No.	formula (M)	eluent (R_f)	MS (EI) *m/z* (%) [fragment]	$C_{calcd.}$ C_{found}	$H_{calcd.}$ H_{found}	$P_{calcd.}$ P_{found}	$S_{calcd.}$ S_{found}	$Br_{calcd.}$ Br_{found}	M.p.[a] [°C]	yield (%)
2a	$C_{14}H_{16}O$ (200.28)	PE/Et_2O 8/1 (0.27)	200 (14) [M^+]; 155 (18) [$M^+ - CH_2O - CH_3$]; 130 (100) [$C_{10}H_{10}^+$]; 129 (24) [CH_2Indenyl$^+$]; 115 (35) [Indenyl$^+$]	83.96 83.31	8.05 8.12				–	62
2b	$C_{18}H_{18}O$ (250.34)	PE/Et_2O 7/3 (0.33)	250 (9) [M^+]; 180 (94) [CH_2Fluorenyl$^+$]; 165 (100) [Fluorenyl$^+$]	86.36 86.35	7.25 7.34				101	52
3a	$C_{14}H_{17}BrO$ (281.19)	PE/Et_2O 7/3 (0.29)	281 (4) [M^+]; 130 (100) [$C_{10}H_{10}^+$]; 129 (48) [CH_2Indenyl$^+$]; 115 (12) [Indenyl$^+$]	59.80 59.73	6.09 6.08	– –	– –	28.42 28.02	–	>95
3b	$C_{18}H_{19}BrO$ (331.25)	PE/Et_2O 1/1 (0.43)	331 (18) [M^+]; 233 (26) [$M^+ - H_2O - Br$]	65.44 65.41	5.88 5.88	– –	– –	23.91 24.17	102	>95
4a	$C_{15}H_{19}BrO_3S$ (359.29)	PE/Et_2O 7/3 (0.18)	359 (12) [M^+]; 183 (45) [$M^+ - Br - SO_2CH_3$]; 128 (100) [CH_2Indenyl$^+$]; 115 (18) [Indenyl$^+$]	50.28 50.37	5.35 5.35	– –	8.93 8.73	22.04 22.30	109	74
4b	$C_{20}H_{21}BrO_3S$ (421.36)	PE/Et_2O 3/2 (0.47)	422 (22) [M^+]; 264 (10) [$M^+ - OSO_2Ph$]; 183 (46) [$M^+ - Br - OSO_2Ph$]; 170 (18) [$M^+ - Br - CH_2OSO_2Ph$]	57.01 56.93	5.02 4.98	– –	7.62 7.65	18.96 19.71	64	79
4c	$C_{17}H_{25}BrOSi$ (353.38)	PE/Et_2O 9/1 (0.74)	353 (3) [M^+]; 223 (5) [$M^+ - CH_2$Indenyl]; 144 (25) [$M^+ - CH_2$Indenyl $- Br$]; 143 (100) [$M^+ - CH_2$Indenyl $- HBr$]	57.94 57.98	7.16 7.15	– –	– –	22.41 22.46	–	75
4d	$C_{19}H_{21}BrO_3S$ (409.35)	PE/THF 3/1 (0.33)	409 (22) [M^+]; 314 (6) [$M^+ - OSO_2CH_3$]; 230 (31) [$M^+ - CH_2$Fluorenyl]	55.75 55.64	5.17 5.13	– –	7.83 7.67	19.52 20.13	99	86
5a	$C_{26}H_{27}OP$ (386.47)	PE/THF 5.6/1 (0.24)	386 (70) [M^+]; 355 (13) [$M^+ - CH_2OH$]; 257 (3) [$M^+ - CH_2$Indenyl]; 199 (30) [$M^+ - PPh_2$]	80.79 80.56	7.05 7.06	8.02 7.90			63	84
5b	$C_{30}H_{29}OP$ (436.53)	PE/THF 5.6/1 (0.27)	436 (25) [M^+]; 258 (8) [$M^+ - CH_2$Fluorenyl]	82.53 82.14	6.70 6.93	7.10 7.03			144	74
5c	$C_{18}H_{27}OP$ (290.38)	–	290 (58) [M^+]; 295 (11) [$M^+ - CH_2O$]; 161 (35) [$M^+ - CH_2$Indenyl]	–					–	93
6a	$C_{26}H_{30}BOP$ (400.32)	PE/THF 7/3 (0.40)	400 (21) [M^+]; 241 (100) [$M^+ - BH_3 - CH_2$Indenyl $- OH$]; 201 (28) [$M^+ - PPh_2BH_3$]; 186 (82) [$M^+ - CH_2PPh_2BH_3$]	78.01 77.59	7.55 7.70	7.74 n.d.			76−80 (dec.)	86
6b	$C_{30}H_{32}BOP$ (450.38)	PE/THF 3/1 (0.22)	449 (9) [$M^+ - H$]; 436 (5) [$M^+ - BH_3$]	80.01 79.97	7.16 7.24	6.88 6.47			160 (dec.)	>95
6c	$C_{18}H_{30}BOP$ (304.23)	PE/THF 4/1 (0.22)	304 (26) [M^+]; 290 (10) [$M^+ - BH_3$]; 189 (13) [M^+ − Indenyl]; 144 (60) [$M^+ - BH_3 - CH_2OH$ − Indenyl]	71.00 70.87	9.94 9.99	10.18 9.78			–	85
7a	$C_{27}H_{32}BO_3PS$ (478.40)	PE/THF 3/1 (0.24)	400 (21) [M^+]; 241 (100) [$M^+ - BH_3 - CH_2$Indenyl $- OH$]; 201 (28) [$M^+ - PPh_2BH_3$]; 186 (82) [$M^+ - CH_2PPh_2BH_3$]	67.76 66.98	6.74 6.93	6.48 n.d.	6.69 n.d.		50 (dec.)	71
7b	$C_{31}H_{34}BO_3PS$ (528.47)	PE/THF 7/3 (0.39)	528 (6) [M^+]; 515 (20) [$M^+ - BH_3$]; 433 (8) [$M^+ - OSO_2CH_3$]; 419 (10) [$M^+ - CH_2OSO_2CH_3$]	70.46 70.24	6.48 6.67	5.86 5.83	6.07 6.12		144 (dec.)	68
8a	$C_{27}H_{29}O_3PS$ (464.57)	PE/THF 3/1 (0.37)	465 (20) [M^+]; 370 (5) [$M^+ - OSO_2CH_3$]	69.81 69.16	6.29 6.56	6.67 n.d.	6.90 n.d.		–	76
8b	$C_{31}H_{31}O_3PS$ (514.63)	PE/THF 7/3 (0.36)	515 (1) [M^+]; 419 (30) [$M^+ - OSO_2CH_3$]; 240 (34) [$M^+ - OSO_2CH_3 - CH_2$Fluorenyl]	72.35 70.85	6.07 6.11	6.02 n.d.	6.23 n.d.		153	83
9a	$C_{26}H_{25}P$ (368.46)	PE/Et_2O 9/1 (0.64)	368 (90) [M^+]; 240 (69) [$M^+ - C_{10}H_8$]	84.75 84.25	6.84 6.80	8.41 8.31			–	54
9b	$C_{30}H_{27}P$ (418.52)	PE/Et_2O 19/1 (0.48)	418 (100) [M^+]	86.10 85.40	6.50 6.58	7.40 7.36			92	59
9c	$C_{15}H_{18}O_3S$ (278.37)	PE/Et_2O 1/1 (0.24)	278 (15) [M^+]; 182 (29) [$M^+ - OSO_2CH_3$]; 167 (100) [$M^+ - OSO_2CH_3 - CH_3$]; 153 (21) [$M^+ - CH_2OSO_2CH_3 - CH_3$]	64.72 64.48	6.52 6.55	– –	11.52 11.29		–	
9d	$C_{27}H_{24}$ (348.49)	–	348 (7) [M^+]; 178 (100) [CH_2Fluorenyl$^+$]; 129 (30) [CH_2Indenyl$^+$]; 115 (48) [Indenyl$^+$]	93.06 91.01	6.94 6.85				209	41
10	$C_{30}H_{32}O_3P_2S$ (534.59)	PE/THF 3/2 (0.56)	534 (5) [M^+]; 457 (56) [$M^+ - Ph$]; 439 (3) [$M^+ - OSO_2CH_3$]	67.40 67.23	6.03 6.10	11.59 11.36	6.00 5.82		–	79
11a	$C_{38}H_{36}P_2$ (554.65)	PE/THF 19/1 (0.32)	554 (55) [M^+]; 477 (54) [$M^+ - Ph$]; 425 (3) [$M^+ - CH_2$Indenyl]; 369 (100) [$M^+ - PPh_2$]	82.29 82.08	6.54 6.78	11.17 10.90			103	26
11b	$C_{42}H_{38}P_2$ (604.71)	PE/THF 9/1 (0.35)	605 (19) [M^+]; 528 (100) [$M^+ - Ph$]	83.41 83.03	6.34 6.64	10.25 9.99			65	30
12a	$C_{27}H_{26}O$ (366.50)	PE/Et_2O 7/3 (0.23)	366 (19) [M^+]; 335 (24) [$M^+ - CH_2OH$]; 178 (51) [CH_2Fluorenyl$^+$]; 165 (100) [Fluorenyl$^+$]	88.48 88.17	7.15 7.11				126	58
12b	$C_{19}H_{22}O$ (266.38)	PE/Et_2O 7/3 (0.32)	266 (100) [M^+]; 235 (51) [$M^+ - CH_2OH$]; 137 (74) [$M^+ - CH_2$Indenyl]; 129 (44) [CH_2Indenyl$^+$]; 79 (30) [CH_2Cp^+]	85.67 82.55	8.32 8.13				–	15
12c	$C_{28}H_{28}O_3S$ (444.59)	PE/Et_2O 3/2 (0.24)	444 (8) [M^+]; 349 (10) [$M^+ - OSO_2CH_3$]; 165 (100) [Fluorenyl$^+$]; 129 (23) [CH_2Indenyl$^+$]; 115 (20) [Indenyl$^+$]	75.64 75.87	6.35 6.23	– –	7.21 7.14		–	87
12d	$C_{30}H_{34}OSi$ (438.68)	PE/Et_2O 7/3 (0.77)	438 (22) [M^+]; 423 (13) [$M^+ - CH_3$]; 335 (35) [$M^+ - CH_2$OTMS]; 259 (14) [$M^+ - CH_2$Fluorenyl]	82.14 82.28	7.81 7.96				94	>95

[a] dec. = decomposition.

(191.7(2) pm) in the borane-protected phosphane group is also normal.[8c]

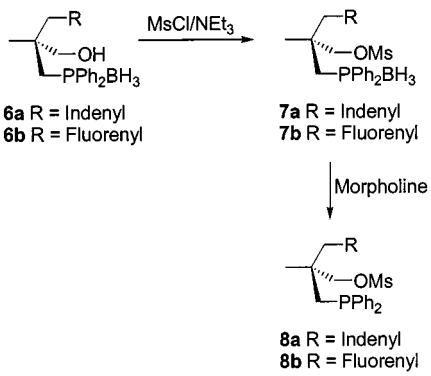
BH_3 protection allows the activation of the OH group.[8c] Thus **6a/6b** are transformed into **7a/7b** by mesylation (Scheme 6). Compounds **7** are fully characterized by their analytical and spectroscopic data (Table 5 and Table 2).



5a R = Indenyl, R´= Ph
5b R = Fluorenyl, R´= Ph
5c R = Indenyl, R´= Ph

6a R = Indenyl, R´= Ph
6b R = Fluorenyl, R´= Ph
6c R = Indenyl, R´= Ph

Scheme 5



6a R = Indenyl
6b R = Fluorenyl

7a R = Indenyl
7b R = Fluorenyl

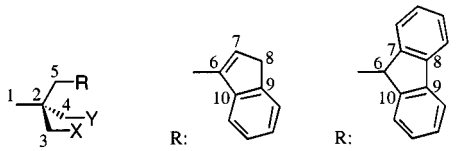
8a R = Indenyl
8b R = Fluorenyl

Scheme 6

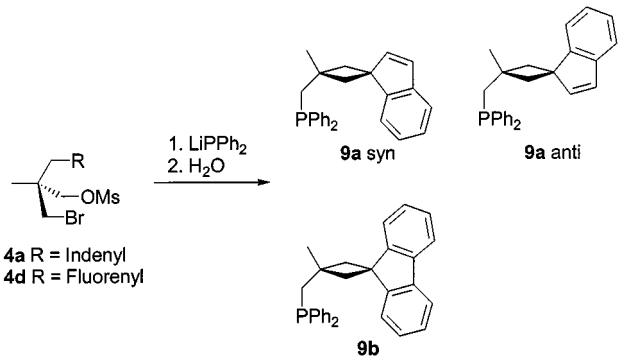
Table 3. Selected bond lengths [pm], bond angles [°], and torsion angles [°] for **2b**, **4a**, **4b**, **6b** and **12a**[a]

	2b/1	**2b/2**	**4a**	**4b**	**6b**	**12a**
C2−C_{sp3}	151.5(6)−154.8(6)	152.1(6)−154.2(6)	152.4(6)−155.1(6)	150.4(4)−156.4(4)	153.5(2)−155.5(2)	152.6(2)−154.9(2)
C3−X (C6′)[b]	142.8(5)	144.2(5)	196.8(5)	195.7(3)	182.6(2)	154.2(2)
C4−Y[b]	143.6(5)	143.9(5)	147.0(5)	146.8(4)	142.1(2)	142.6(2)
C5−C6	154.8(6)	156.4(5)	151.1(6)	150.4(4)	155.3(2)	150.4(2)
C6−C7 [C6′−C7′]	152.6(6)	151.7(5)	134.3(6)	133.9(5)	151.5(2)	134.7(2) [152.4(2)]
C6−C10 [C6′−C10′]	152.1(6)	152.7(6)	148.0(6)	147.7(4)	151.6(2)	147.8(2) [152.9(2)]
C7−C8 [C7′−C8′]	140.0(6)	140.7(6)	149.4(7)	150.7(5)	139.9(2)	150.1(2) [140.0(2)]
C8−C9 [C8′−C9′]	147.1(6)	147.2(6)	150.3(7)	149.9(5)	147.4(2)	150.9(2) [146.7(2)]
C9−C10 [C9′−C10′]	140.5(6)	140.8(6)	140.9(6)	140.9(5)	140.9(2)	140.0(2) [140.0(2)]
C_{ar}−C_{ar}[c]	138.1(6)−139.9(6)	138.3(6)−140.3(6)	138.2(6)−140.6(6)	138(1)−139.7(5)	138.3(3)−139.7(2)	138.2(2)−139.7(2) Indenyl 138.1(2)−139.8(2) Fluorenyl
C1−C2−C3	114.9(4)	112.2(4)	111.6(4)	106.4(2)	112.0(1)	110.4(1)
C1−C2−C4	116.6(4)	113.7(4)	107.0(4)	109.8(3)	105.6(1)	107.2(1)
C1−C2−C5	113.6(4)	113.7(3)	111.0(4)	111.4(2)	112.5(1)	110.2(1)
C3−C2−C4	83.3(3)	83.5(3)	111.0(4)	112.0(3)	110.9(1)	111.4(1)
C3−C2−C5	110.4(4)	111.7(3)	104.8(4)	112.4(3)	109.5(1)	107.2(1)
C4−C2−C5	114.5(4)	118.3(3)	111.6(4)	105.0(2)	106.0(1)	110.5(2)
C2−C3−X[b]	92.3(3)	92.2(3)	114.1(3)	114.3(2)	120.5(1)	116.0(1)
C2−C4−Y[b]	91.8(3)	92.4(3)	108.0(3)	108.7(3)	110.9(3)	112.0(1)
C2−C5−C6	118.9(3)	117.5(3)	115.6(4)	116.3(3)	122.2(1)	116.9(1)
C1−C2−C3−X (C6′)[b]	−123.4(4)	−105.4(4)	61.8(5)	−179.7(2)	−49.0(2)	−62.3(2)
C1−C2−C4−Y[b]	121.7(4)	103.8(4)	177.3(4)	54.5(3)	179.0(1)	−179.9(1)
C1−C2−C5−C6	52.5(5)	50.4(5)	−64.6(5)	−59.6(3)	−66.2(2)	58.8(2)

[a] The numbering scheme used refers to the graphic given here and is different from the numbering schemes for the individual atoms in the deposited data. − [b] X (Y) designates the atom which is directly bonded to the relevant carbon atom. − [c] C_{ar}−C_{ar} designates the distances within the annelated cycles, excluding C7−C8 (fluorenyl) and C9−C10 which are given explicitly.



The synthesis of tripodal ligands containing one indenyl- or fluorenyl group and two phosphorus donors appears straightforward from starting compounds such as **4**: with $CH_3C(CH_2C_5H_5)(CH_2Br)(CH_2OMs)$ as the starting material, substitution of the leaving groups by phosphorus donors is easily achieved through reaction with $KPPh_2$.[6a] When the same procedure is applied to **4a**, internal cyclization with formation of the spiro compounds **9a** ***syn***/**9a** ***anti*** occurs (Scheme 7). The higher nucleophilicity of the indenyl residue compared to that of the Cp residue apparently favours the reaction leading to internal cyclization rather than the one leading to external substitution by PPh_2. With C_α of the indenyl group forming the spiro centre, there are two diastereomeric forms of **9a**, one in which the CH_2PPh_2 residue and the annelated benzene part of the indenyl residue are on the same side of the cyclobutane ring (*syn*) and one



Scheme 7

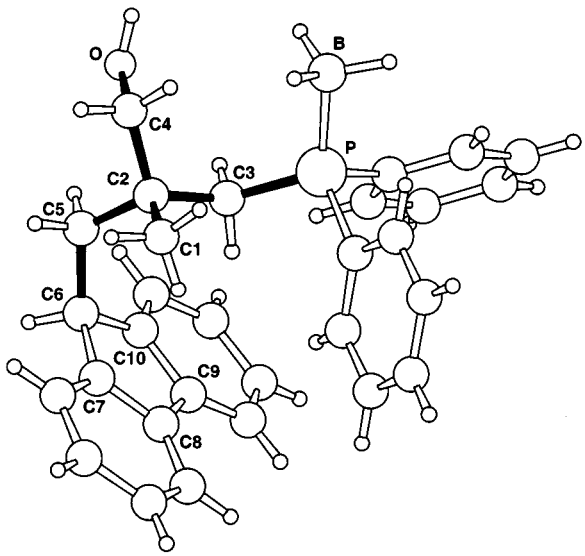


Figure 3. Structure of **6b**

Table 4. Crystal data for **2b**, **4a**, **4b**, **6b** and **12a**

Compound	**2b**	**4a**	**4b**	**6b**	**12a**
Formula	$C_{18}H_{17}O$	$C_{15}H_{19}BrO_3S$	$C_{20}H_{21}BrO_3S$	$C_{30}H_{32}BOP$	$C_{27}H_{25}O$
Molecular mass [g]	124.66	359.27	421.34	450.34	365.47
Crystal size [mm]	0.2 × 0.15 × 0.2	0.2 × 0.2 × 0.3	0.2 × 0.3 × 0.3	0.25 × 0.3 × 0.25	0.2 × 0.3 × 0.1
Crystal system	monoclinic	monoclinic	triclinic	triclinic	monoclinic
Space group (No.)[15c]	$P2_1/c$ (14)	$P2_1/c$ (14)	$P\bar{1}$ (2)	$P\bar{1}$ (2)	$P2_1/n$ (14)
a [pm]	2283(1)	1309.6(3)	787.8(1)	1010.3(2)	1547.3(3)
b [pm]	595.1(2)	817.4(3)	1069.3(2)	1015.1(2)	718.8(1)
c [pm]	2124(2)	1469.3(4)	1248.4(2)	1243.0(3)	1800.6(4)
α [°]	90.0	90.0	103.35(1)	88.08(3)	90.0
β [°]	72.62(4)	83.99(2)	94.08(1)	89.37(3)	92.10(3)
γ [°]	90.0	90.0	109.37(1)	71.25(3)	90.0
V [10^6 pm^3]	2754.0	1564.2	952.7	1206.4	2001.3
Z	8	4	2	2	4
d_x [g cm^{-3}]	1.203	1.526	1.469	1.240	1.213
T [K]	200	200	200	200	200
No. of rflns. for cell param. refinem.	33	36	31	–	–
Scan range	3.7° < 2Θ < 47.0°	5.6° < 2Θ < 51.0°	3.4° < 2Θ < 52.0°	3.3° < 2Θ < 52.1°	4.5° < 2Θ < 52.2°
Method	ω scan, Δω = 0.54°	ω scan, Δω = 0.54°	ω scan, Δω = 0.55°	ω scan, Δω = 2.0°	ω scan, Δω = 1.0°
Scan speed	$\dot{\omega}$ = 6° min^{-1}	$\dot{\omega}$ = 8° min^{-1}	$\dot{\omega}$ = 8° min^{-1}	–	–
s frame^{-1}	–	–	–	8	7
No. of measured rflns.	3765	2993	3960	19104	51425
No. of unique rflns.	3649	2863	3685	4758	3941
No. of observed rflns.	2184	1931	3025	3901	2304
Observation criterion	$I \geq 2\sigma$	$I \geq 2\sigma$	$I \geq 2\sigma$	$I \geq 2\sigma$	$I \geq 2\sigma$
No. of param. refined	349	257	230	315	353
resid. el. density [10^{-6} e pm^{-3}]	0.61	0.82	1.06	0.47	0.22
R_1/R_w [%] (refinement on F^2)	6.4/17.9	4.4/11.4	3.6/9.4	4.2/10.6	3.8/7.9

in which they are on opposite sides (*anti*). These two diastereomers are formed in a ratio of *syn*:*anti* = 7:4, as shown by NMR. Assignment of individual signals (Table 6) to the *syn*- and *anti* forms is based on the signals characterizing the CH_2 groups of the four-membered cycle. While the two CH_2 groups in each specific diastereomer are symmetrically equivalent, the protons of these groups are not so and this gives rise to two doublets. The type of spectrum observed for the indenyl spiro compounds **9** is exemplified in Figure 4 for **9a**. The resonances useful for the attribution of the structures of the *syn*- and *anti* isomers are shown as magnified inserts in Figure 4 (*syn* isomer in grey).

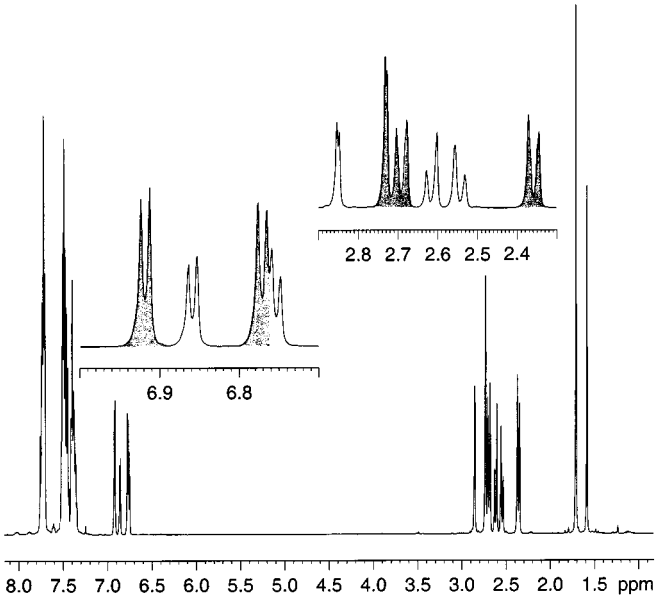
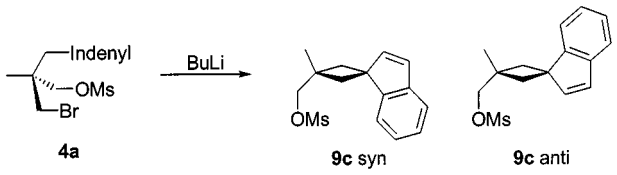
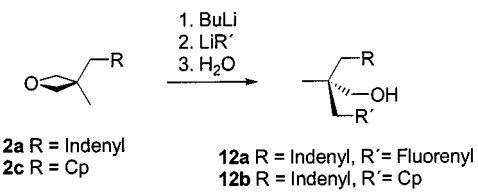


Figure 4. ^{1}H NMR spectrum of **9a** in $CDCl_3$

Assignment of the NMR resonances to individual diastereomers is based on the assumption that, within the *syn* diastereomer, two of these protons are in close vicinity of the CH_2PPh_2 group and the annelated benzene ring, whereas the other two protons stick out to the far less congested side of the four-membered cycle, so that the environments of these two pairs of protons are very different. The proton signals corresponding to these protons should therefore have significantly different shift values. With the *anti* isomer, both sides of the ring are congested, so that the



Scheme 8

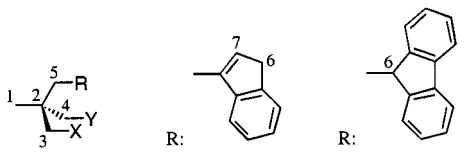


Scheme 9

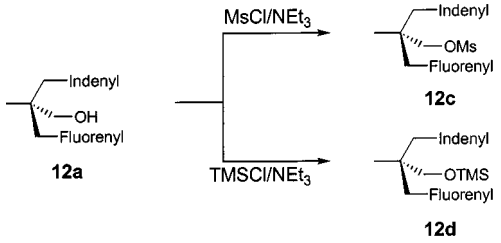
Table 5. NMR spectroscopic data of **5a**−**8b**[a,b,c]

No.	R X Y	1[d] CH_3 [3 H]	2[d] C_q	3[d] $CH_{2a,b}$ [2 H]	4[d] $CH_{2a,b}$ [2 H]	5[d] $CH_{2a,b}$ [2 H]	6[d] $-CH_n-$ (n = 1−2)	7[d] −CH= [1 H]	CH aromatic	X {^{31}P NMR}	Y
5a	Indenyl PPh_2 OH	1.06 (s)	−	2.38, 2.48 (2 dd) $^2J_{HH}$ = 14.4 Hz $^2J_{HP}$ = 3.6 Hz	3.54 (s)	2.78, 2.85 (2 d) $^2J_{HH}$ = 14.2 Hz	3.39 (s) [2 H]	6.33 (s)	7.20−7.80 (m) [14 H]	1.48 (bs) [1 H]	
		23.9 (d) $^3J_{CP}$ = 9.0 Hz	40.4 (d) $^2J_{CP}$ = 13.1 Hz	38.6 (d) $^1J_{CP}$ = 14.1 Hz	69.9 (d) $^3J_{CP}$ = 8.5 Hz	36.1 (d) $^3J_{CP}$ = 7.5 Hz	38.4 (s)		120.2−147.0		−
8a	Indenyl PPh_2 OMs	1.12 (s)	−	2.51 (d) $^2J_{HP}$ = 3.4 Hz	4.22 (s)	2.91 (s)	3.45 (s) [2 H]	6.43 (s)	7.28−7.63 (m) [14 H]	2.86 (s) [3 H]	
		23.7 (d) $^3J_{CP}$ = 9.8 Hz	39.3 (d) $^2J_{CP}$ = 14.0 Hz	38.2 (d) $^1J_{CP}$ = 16.8 Hz	76.0 (d) $^3J_{CP}$ = 10.5 Hz	35.7 (d) $^3J_{CP}$ = 8.5 Hz	38.5 (s)		120.0−146.5	37.3 (s)	
6a	Indenyl PPh_2BH_3 OH	0.93 (s)	−	2.74 (m)	3.60, 3.74 (2 d) $^2J_{HH}$ = 11.2 Hz	2.80, 2.92 (2 d) $^2J_{HH}$ = 13.6 Hz	3.43 (s) [2 H]	6.38 (s)	7.28−7.89 (m) [14]	2.28 (bs) [1 H]	
		23.3 (d) $^3J_{CP}$ = 3.9 Hz	41.2 (s)	34.0 (d) $^1J_{CP}$ = 31.6 Hz	68.9 (d) $^3J_{CP}$ = 4.6 Hz	37.0 (d) $^3J_{CP}$ = 8.2 Hz	38.5 (s)		120.2−146.8	−	
7a	Indenyl PPh_2BH_3 OMs	1.02 (s)	−	2.71 (m)	4.30 (s)	2.90 (m)	3.41 (s) [2 H]	6.41 (s)	7.20−7.83 (m) [14 H]	3.01 (s) [3 H]	
		22.9 (d) $^3J_{CP}$ = 5.0 Hz	39.8 (s)	33.7 (d) $^1J_{CP}$ = 32.2 Hz	75.7 (d) $^3J_{CP}$ = 3.5 Hz	36.2 (d) $^3J_{CP}$ = 7.0 Hz	38.6 (s)		120.1−146.3	37.6 (s)	
5b	Fluorenyl PPh_2 OH	1.10 (s)	−	2.20, 2.37 (2 dd) $^2J_{HH}$ = 14.4 Hz $^2J_{HP}$ = 3.6 Hz	3.55 (m)	2.35 (m)	4.04 (bs) [1 H]	−	7.28−7.79 (m) [18 H]	1.39 (bs) [1 H]	
		24.3 (d) $^3J_{CP}$ = 10.5 Hz	40.4 (d) $^2J_{CP}$ = 13.1 Hz	39.2 (d) $^1J_{CP}$ = 16.6 Hz	69.8 (d) $^3J_{CP}$ = 9.0 Hz	42.1 (d) $^3J_{CP}$ = 7.0 Hz	44.8 (s)	−	120.1−149.5	−	
8b	Fluorenyl PPh_2 OMs	1.05 (s)	−	2.25, 2.35 (2 dd) $^2J_{HH}$ = 14.6 Hz $^2J_{HP}$ = 2.8, 3.6 Hz	4.07, 4.13 (2d) $^2J_{HH}$ = 9.7 Hz	2.45, 2.58 (2 dd) $^2J_{HH}$ = 15.1 Hz $^3J_{HH}$ = 4.4 Hz	4.07, 4.13 (2d) [3 H] $^2J_{HH}$ = 9.7 Hz	−	7.27−7.84 (m) [18 H]	2.81 (s) [3 H]	
		24.4 (d) $^3J_{CP}$ = 10.0 Hz	39.6 (d) $^2J_{CP}$ = 13.6 Hz	38.5 (d) $^1J_{CP}$ = 17.1 Hz	76.8 (d) $^3J_{CP}$ = 11.1 Hz	41.2 (d) $^3J_{CP}$ = 7.5 Hz	45.1 (s)	−	120.4−148.4	37.2 (s)	
6b	Fluorenyl PPh_2BH_3 OH	0.70 (s)	−	2.18−2.58 (m)	3.42, 3.78 (2 d) $^2J_{HH}$ = 11.6 Hz	2.18−2.58 (m)	4.02 (t) [1 H] $^3J_{HH}$ = 4.2 Hz	−	7.27−7.81 (m) [18 H]	1.93 (bs) [1 H]	
		24.1 (d) $^3J_{CP}$ = 3.5 Hz	41.5 (s)	34.0 (d) $^1J_{CP}$ = 31.2 Hz	68.6 (d) $^3J_{CP}$ = 3.0 Hz	42.3 (d) $^3J_{CP}$ = 9.1 Hz	45.1 (s)	−	120.2−148.9	−	
7b	Fluorenyl PPh_2BH_3 OMs	0.70 (s)	−	2.12, 2.31 (2 dd) $^2J_{HH}$ = 15.0 Hz $^2J_{HP}$ = 9.4, 14.8 Hz	4.10, 4.25 (2 d) $^2J_{HH}$ = 9.5 Hz	2.44, 2.80 (2 dd) $^2J_{HH}$ = 15.2 Hz $^3J_{HH}$ = 4.4, 4.6 Hz	4.17 (m) [1 H]	−	7.30−7.92 (m) [18 H]	2.96 (s) [3 H]	
		24.0 (d) $^3J_{CP}$ = 4.5 Hz	40.5 (s)	33.1 (d) $^1J_{CP}$ = 31.2 Hz	76.9 (s)	40.5 (d) $^3J_{CP}$ = 8.5 Hz	45.7 (s)	−	120.5−147.5	37.6 (s)	
5c	Indenyl PEt_2 OH	1.04 (s)	−	1.61 (m)	3.55 (s)	2.70, 2.76 (2 d) $^2J_{HH}$ = 13.7 Hz	3.40 (s) [2 H]	6.35 (s)	7.23−7.58 (m) [4 H]	1.14, 1.50 (2 m) [10 H] {−34.4 (s)}	2.54 (bs) [1 H]
		23.7 (d) $^3J_{CP}$ = 9.0 Hz	39.7 (d) $^2J_{CP}$ = 10.5 Hz	36.8 (d) $^1J_{CP}$ = 15.6 Hz	70.3 (d) $^3J_{CP}$ = 7.5 Hz	36.0 (d) $^3J_{CP}$ = 7.5 Hz	38.3 (s)		120.2−147.0 (8 s)	10.0 (d) $^2J_{CP}$ = 11.5 Hz 20.4 (d) $^1J_{CP}$ = 10.0 Hz	−
6c	Indenyl PEt_2BH_3 OH	1.06−1.25 (m)	−	1.80−2.00 (m)	3.57, 3.70 (2 d) $^2J_{HH}$ = 11.2 Hz	2.80 (s)	3.41 (s) [2 H]	6.35 (s)	7.19−7.55 (m) [4 H]	1.06−1.25 (m) [6 H] 1.61−1.80 (m) [4 H] {11.7 (bs)}	2.08 (bs) [1 H]
		23.3 (s)	40.4 (s)	30.9 (d) $^1J_{CP}$ = 28.7 Hz	68.8 (d) $^3J_{CP}$ = 3.5 Hz	36.5 (d) $^3J_{CP}$ = 7.0 Hz	38.5 (s)		120.2−146.9 (85)	18.3 (d) $^1J_{CP}$ = 35.7 Hz 18.4 (d) $^1J_{CP}$ = 37.2 Hz, 7.2 (s)	−

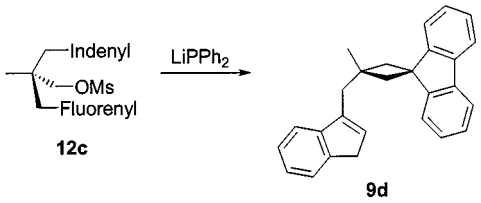
[a] For ease of comparison the sequence of entries in this table does not follow the compound numbering sequence. − [b] Sequence of entries for each compound: ^{1}H NMR first lines, ^{13}C NMR last lines. − [c] Solvent: $CDCl_3$. − [d] Designation:



surroundings of the two protons should not be as different as in the *syn* isomer. The difference in shift between these protons should then be smaller for the *anti* isomer than for the *syn* isomer. The pair of doublets at δ = 2.36 and 2.69



Scheme 10



Scheme 11

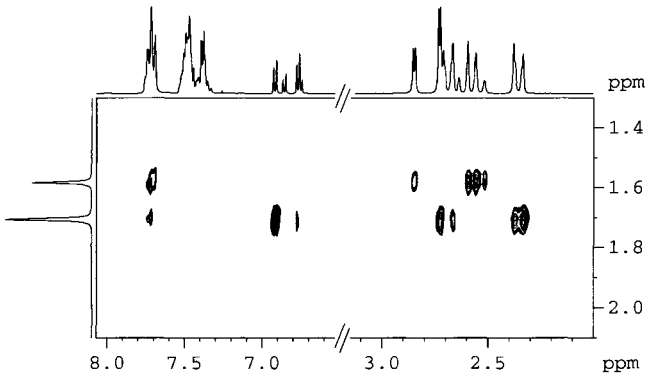
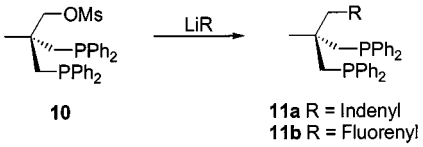


Figure 5. NOESY spectrum of **9a** in $CDCl_3$

is therefore assigned to the *syn* isomer, with the *anti* isomer giving rise to a doublet at δ = 2.55 and 2.61 (Table 6).

NOE measurements confirm this assignment: In the NOESY spectrum of **9a** a strong correlation between the methyl group at δ = 1.71 and the olefinic proton 6 of the five-membered cycle at δ = 6.91 is observed (Figure 5). No



Scheme 12

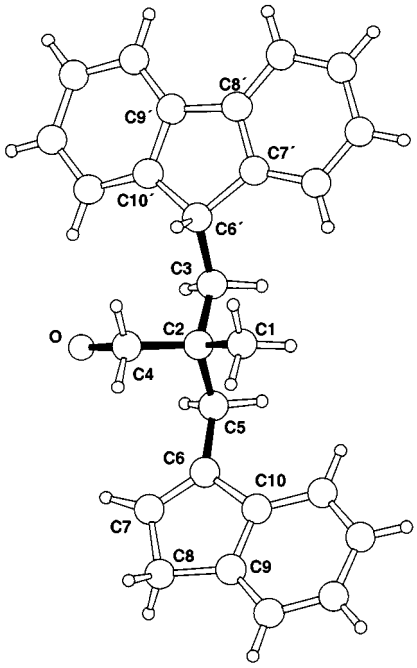


Figure 6. Structure of **12a**

correlation between these two types of protons is found for the *anti* isomer. The NOESY correlation between the pairs of diastereotopic protons in the four-membered cycles and the methyl groups also correspond to this assignment. Only

Table 6. NMR spectroscopic data of **9a**–**9d**[a,b]

No.	X	1[e] CH_3 [3 H]	2[e] C_q	3[e] $CH_{2a,b}$ [2 H]	4[e] $CH_{2a,b}$ [4 H]	5[e] C_q	6[e] −CH= [1 H]	7[e] −CH= [1 H]	CH aromatic	X {^{31}P NMR}
9a syn[c]	PPh_2	1.71 (s)	–	2.73 (s)	2.36, 2.69 (2 d) $^2J_{HH}$ = 10.0 Hz	–	6.77, 6.91 (2 d) $^3J_{HH}$ = 5.0 Hz		7.34–7.78 (m)	{−26.5, −24.9 (2 s)}
		29.8 (d) $^3J_{CP}$ = 10.0 Hz	33.0 (d)	44.9 (d) $^1J_{CP}$ = 15.0 Hz	42.5 (d) $^3J_{CP}$ = 8.3 Hz	48.7 (s)			121.1–152.5	
9a anti[c]	PPh_2	1.58 (s)	–	2.85 (s)	2.55, 2.61 (2 d) $^2J_{HH}$ = 15.0 Hz	–	6.75, 6.85 (2 d) $^3J_{HH}$ = 5.0 Hz		7.34–7.78 (m)	{−26.5, −24.9 (2 s)}
		30.5 (d) $^3J_{CP}$ = 11.0 Hz	$^2J_{CP}$ = 15.6 Hz	43.9 (d) $^1J_{CP}$ = 15.0 Hz	42.4 (d) $^3J_{CP}$ = 8.3 Hz	48.0 (s)			121.1–152.5	
9c syn[c]	OMs	1.56 (s)	–	4.28 (s)	2.25, 2.74 (2 d) $^2J_{HH}$ = 13.4 Hz	–	6.71, 6.82 (2 d) $^3J_{HH}$ = 5.4 Hz		7.26–7.66 (m)	3.15 (s)
		24.9 (s)	32.5 (s)	77.3 (s)	37.1 (s)	47.5 (s)			121.2–152.0	37.7 (s)
9c anti[c]	OMs	1.53 (s)	–	4.38 (s)	2.41, 2.60 (2 d) $^2J_{HH}$ = 13.6 Hz	–	6.71, 6.76 (2 d) $^3J_{HH}$ = 5.4 Hz		7.26–7.66 (m)	3.14 (s)
		25.6 (s)	32.6 (s)	77.1 (s)	37.6 (s)	47.3 (s)			121.2–152.0	37.7 (s)
9b[c]	PPh_2	1.68 (s)	–	2.90 (m)	2.58, 2.67 (d) $^2J_{HH}$ = 12.7 Hz	–	–	–	7.30–7.72 (m) [18 H]	{−25.3 (s)}
		29.5 (d) $^3J_{CP}$ = 12.0 Hz	31.5 (d) $^2J_{CP}$ = 16.1 Hz	44.3 (d) $^1J_{CP}$ = 16.6 Hz	47.4 (d) $^3J_{CP}$ = 8.0 Hz	45.6 (s)	–	–	119.9–153.7	
9d[d]	Indenyl	1.65 (s)	–	3.17 (s)	2.60, 2.89 (2 d) $^2J_{HH}$ = 13.5 Hz	–	–	–	7.28–7.83 (m) [12 H]	3.45 (s) [2 H] 6.35 (s) [1 H]
		27.8 (s)	31.6 (s)	40.1 (s)	46.1 (s)	45.6 (s)	–	–	119.7–153.9	38.4 (s)

[a] For ease of comparison the sequence of entries in this table does not follow the compound numbering sequence. – [b] Sequence of entries for each compound: ^{1}H NMR first lines, ^{13}C NMR last lines. – [c] Solvent: $CDCl_3$. – [d] Solvent: CD_2Cl_2. – [e] Designation:

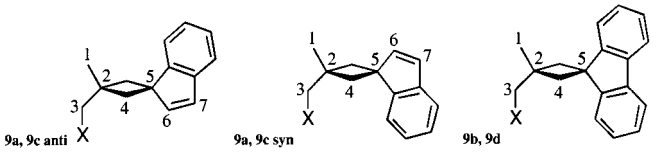
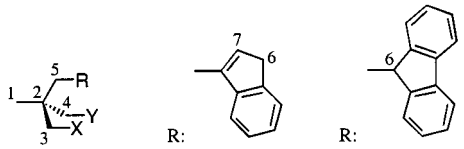


Table 7. NMR spectroscopic data of **10**−**12d**[a,b,c]

No.	R X Y	1[d] CH_3 [3 H]	2[d] C_q	3[d] $CH_{2a,b}$ [2 H]	4[d] $CH_{2a,b}$ [2 H]	5[d] $CH_{2a,b}$ [2 H]	6[d] $-CH_n-$ (n = 1−2)	7[d] −CH= [1 H]	CH aromatic	X {^{31}P NMR}	Y {^{31}P NMR}
10	OMs	1.13 (s)	−	2.49, 2.61 (2 dd)		4.26 (s)	−	−	−	7.30−7.55 (m)	
	PPh_2			$^2J_{HH}$ = 14.6 Hz; $^2J_{HP}$ = 2.4 Hz						{−28.6 (s)}	
	PPh_2	25.1 (t) $^3J_{CP}$ = 9.0 Hz	39.1 (t) $^2J_{CP}$ = 14.0 Hz	39.0 (dd) $^1J_{CP}$ = 17.9 Hz; $^3J_{CP}$ = 9.1 Hz		77.0 (t) $^3J_{CP}$ = 10.1 Hz	−	−	−	128.9−139.5	
11a	Indenyl	1.24 (s)	−	2.67 (m)		3.07 (s)	3.48 (s) [2 H]	6.41 (s)	7.35−7.65 (m) [24 H]		
	PPh_2									{−27.0 (s)}	
	PPh_2	28.6 (t) $^3J_{CP}$ = 9.4 Hz	39.7 (t) $^2J_{CP}$ = 13.5 Hz	42.4 (dd) $^1J_{CP}$ = 15.9 Hz; $^3J_{CP}$ = 8.6 Hz		40.0 (t) $^3J_{CP}$ = 8.7 Hz	38.6 (s)		120.5−147.2		
11b	Fluorenyl	1.13 (s)	−	2.46, 2.58 (2 dd)		2.61 (d)	4.18 (bs) [1 H]	−	7.32−7.88 (m) [28 H]		
	PPh_2			$^2J_{HH}$ = 14.4 Hz; $^2J_{HP}$ = 3.0 Hz		$^3J_{HH}$ = 4.2 Hz				{−27.8 (s)}	
	PPh_2	28.9 (t) $^3J_{CP}$ = 9.5 Hz	39.6 (t) $^2J_{CP}$ = 13.0 Hz	43.1 (dd) $^1J_{CP}$ = 16.0 Hz; $^3J_{CP}$ = 9.1 Hz		45.7 (t) $^3J_{CP}$ = 8.8 Hz	45.5 (s)	−	120.3−149.2		
12a	Indenyl	1.15 (s)	−	2.30, 2.43 (2 dd)	3.60 (pt)	2.78, 2.90 (2 d)	3.46 (s) [2 H]	6.38 (s)	7.30−7.86 (m)	4.11 (t)[1 H]	1.63 (s)
	Fluorenyl			$^2J_{HH}$ = 14.8 Hz	$^2J_{HH}$ = 11.4 Hz	$^2J_{HH}$ = 13.6 Hz			[12 H]	$^3J_{HH}$ = 4.0 Hz	[1 H]
	OH			$^3J_{HH}$ = 4.0 Hz							
		23.0 (s)	40.3 (s)	41.5 (s)	68.9 (s)	35.9 (s)	38.5 (s)		120.0−149.9		
12b	Indenyl	1.02 (s)	−	2.52−2.84 (m)	3.48 (bs)	3.11 (s)	3.48 (bs) [2 H]	6.40 (s)	7.26−7.58 (m)	2.52−2.84 (m)	1.86 (bs)
	Cp								[4 H]	6.22−6.60 (m) [3 H]	[1 H]
	OH	22.4, 22.6 (2 s)	40.3, 40.5 (2s)	38.5, 39.0 (2 s)	69.2 (s)	35.1 (s)	38.5 (s)		120.1−147.1		
12c	Indenyl	1.09 (s)	−	2.38, 2.47 (2 dd)	4.03, 4.11 (2 d)	2.80 (s)	3.44 (s) [2 H]	6.39 (s)	7.28−7.83 (m)	2.94 (s)	
									[12 H]		
	Fluorenyl			$^2J_{HH}$ = 14.8 Hz	$^2J_{HH}$ = 9.2 Hz					4.15 (m)	[3 H]
										[1 H]	
	OMs			$^3J_{HH}$ = 4.4 Hz							
		22.9 (s)	39.4 (s)	41.0 (s)	75.7 (s)	35.4 (s)	38.6 (s)		119.9−148.8		37.5 (s)
										44.6 (s)	
12d	Indenyl	1.29 (s)	−	2.45 (m)	3.73 (s)	2.94, 3.03 (2 d)	3.55 (s) [2 H]	6.47 (s)	7.40−7.95 (m) [12 H]		0.37 (s)
	Fluorenyl					$^2J_{HH}$ = 13.6 Hz				4.22 (t) [1 H]	[9 H]
	OTMS									$^3J_{HH}$ = 3.7 Hz	
		23.1 (s)	40.1 (s)	41.6 (s)	69.2 (s)	35.7 (s)	38.5 (s)		120.1−150.5		0.1 (s)
											44.6 (s)

[a] For ease of comparison the sequence of entries in this table does not follow the numbering scheme. − [b] Sequence of entries for each compound: ^{1}H NMR first lines, ^{13}C NMR last lines. − [c] Solvent: $CDCl_3$. − [d] Designation:



the protons that are on the same sides of the four-membered cycles as the methyl groups show a strong correlation (Figure 5).

The spectroscopic and analytical properties of the fluorenyl residue of **9b** (due to the symmetry of the fluorenyl spiro substituent only one isomer is possible) are in accordance with the assigned constitution (Table 6 and Table 2).

The formation of the spiro compounds **9a/9b** is not due to any specific properties of $LiPPh_2$ as a base; the same type of reaction is observed when **4a** is treated with *n*-butyllithium.

The *syn*- and *anti* isomers of **9c** are formed in a ratio of 2:1 (Scheme 8); **9c** gives rise to a ^{1}H NMR spectrum (Table 6) similar to that of **9a** shown in Figure 4.

Towards the synthesis of tripodal ligands, the formation of the spiro products **9** is a dead end. Spiro cyclization appears to be the more favoured reaction for the more sterically congested compounds such as these neopentane-derived ones, which contain an indenyl or a fluorenyl group together with an electrophilically activating group. Here substitution by an external nucleophile is slowed down, whereas internal substitution is not drastically retarded by steric crowding. Taking this into account, it is not really probable that nucleophilic oxetane-ring-opening reaction sequences starting with the substituted oxetane **2**, shown to lead to **8** (Scheme 4, Scheme 5, and Scheme 6) might finally lead to the desired tripodal ligands. If, on the other hand, the oxetane ring of **2** would be amenable to nucleophilic ring-opening by indenyl- or fluorenyllithium, this would give a simple access to *ansa*-Cp ligands containing a functionalizable -CH_2−$C(CH_3)(CH_2OH)$−CH_2- linker. Compounds **2** were found to undergo this type of ring-opening reaction when treated with indenyl- or fluorenyllithium (Scheme 9). The OH group of **12** may be activated as shown by the transformation of **12a** into the corresponding mesylate **12c**, or trimethylsilyl ether **12d** (Scheme 10). Compounds **12** are fully characterized by their spectroscopic (Table 7) and analytical (Table 2) data. Except for **12b**, which is a colourless oil, compounds **12** are obtained as colourless microcrystalline solids. Single crystals suitable for X-ray analysis could be grown for **12a** (Figure 6, Table 3, and Table 4). The crystals were grown from saturated

CH_2Cl_2/*n*-pentane solutions by slow diffusion of the solvent into rubber stoppers.

The constitution of **12a** as derived from spectroscopy (Table 7) is confirmed by its structure. The angles and distances are in the normal ranges (Table 3). In contrast to **6b** where the fluorenyl substituent and the bulky PPh_2BH_3 group are in close vicintity to each other, the fluorenyl and indenyl substituents of **12a** are as distant from each other as possible (Figure 6) with a well spread-out molecular shape as had also been observed for **4a**/**4b**. As expected, phosphinylation of **12c** is not possible: When **12c** is treated with $LiPPh_2$ (Scheme 11), the spiro compound **9d** is formed which is characterized analytically (Table 2) as well as by its typical NMR pattern (Table 6). The transformation **12c** → **9d** is selective. No indication of spiro cyclization involving the indenyl substituent is observed.

The above results suggest that, in order to introduce an indenyl or a fluorenyl group into a tripodal ligand, this group has to be introduced last. This contrasts strongly to the synthesis of tripodal ligands containing a C_5H_5 group, where the optimal reaction route relies upon introducing the Cp group at the very beginning of the sequence.[6a] The reason for this difference is the inherent tendency of fluorenyl- and indenyl derivatives to undergo spiro cyclization.

Tripodal ligands containing an indenyl or a fluorenyl donor group are accessible from **10**, which is obtained from **10**•$2BH_3$ by deprotection with morpholine.[8c,9] The deprotected form **10** has to be used because using **10**•$2BH_3$ itself as the starting compound reduces yield and selectivity. Compound **10** reacts with indenyllithium to produce **11a** and with fluorenyllithium to give the tripodal ligand **11b** (Scheme 12). To obtain acceptable yields, the lithium reagents have to be activated by the addition of TMEDA or 18-crown-6. Under these conditions, the yields of **11** after chromatographic workup are around 30%. Compounds **11** are off-white solids, which are obtained in microcrystalline form. Depending on the handling procedure, **11b** may be orange, presumably due to some very minor dyestuff impurity which is not apparent from the analytical and spectroscopic data (Table 7 and Table 2). Both products **11a**/**11b** and starting material **11** are fully characterized by spectroscopy (Table 7) and elemental analysis (Table 2).

Conclusion

Neopentane-based tripodal ligands $CH_3C(CH_2PR_2)_2(CH_2R')$ (R = aryl, alkyl; R′ = indenyl, fluorenyl) are accessible by a synthetic procedure in which the indenyl or fluorenyl residues are introduced in the last step. This contrasts to the synthesis of the analogous Cp-containing tripodal ligands $[CH_3C(CH_2PR_2)_2(CH_2C_5H_4)]^-$, where the Cp group had to be the first one to be introduced.[6a]

Neopentane derivatives of the type $(RCH_2)(CH_2R')C(CH_2Indenyl)(CH_2X)$ (X = electrophilically activating group) undergo spiro cyclization when treated with bases, to produce spiro cyclobutanes with the indenyl α-carbon atom acting as the spiro centre. The basic nucleophiles (e.g., $KPPh_2$) therefore do not react by substitution, they act as bases, initiating spiro cyclization. The same type of reactivity is observed with fluorenyl as the neopentane-bound substituent.

Neopentane-derived oxetanes $O(CH_2)_2C(CH_3)(CH_2R)$ (R = Cp, indenyl) react with indenyl- or fluorenyllithium by nucleophilic opening of the oxetane ring to produce functionalizable chiral *ansa*-Cp ligands $(HOCH_2)(CH_3)C(CH_2R)(CH_2R')$ (R, R′ = Cp, indenyl, fluorenyl), in fair yields

Experimental Section

General: All manipulations involving phosphanes were carried out under argon by means of standard Schlenk techniques and were monitored by TLC (Macherey−Nagel Co., Polygram SIL G/UV_{254}). All solvents were dried by standard methods[10] and distilled under argon. The solvents $CDCl_3$ and CD_2Cl_2 used for NMR spectroscopic measurements were degassed by three successive "freeze-pump-thaw" cycles and dried with 4-Å molecular sieves. − NMR: Bruker Avance DPX 200 at 200.12 MHz (^1H), 50.323 MHz ($^{13}C\{^1H\}$), 81.015 MHz ($^{31}P\{^1H\}$), T = 298 K; chemical shifts (δ) with respect to $CHCl_3$ (^1H: δ = 5.32; ^{13}C: δ = 53.5) as internal standards. ^{31}P chemical shifts (δ) with respect to 85% H_3PO_4 (^{31}P: δ = 0) as external standard. − MS: Finnigan MAT 8320, EI (70 eV) − Melting points: Gallenkamp MFB-595010; uncorrected values. − Elemental analyses: Microanalytical Laboratory of the Organisch-Chemisches Institut, Universität Heidelberg.

Materials: Silica gel (Kieselgel z.A. 0.06−0.2 mm, J. T. Baker Chemicals B. V.) used for chromatography was degassed at 1 mbar for 24 h and saturated with argon. A solution of 2.5 M *n*BuLi in hexane was used for deprotonations. $HPEt_2$,[11] $HPPh_2$,[12] 3-methanesulfonoxymethyl-3-methyloxetane (**1**),[13] 1-methanesulfonoxymethyl-2,2-bis(diphenylphosphanylmethyl)propane−*P,P*-bis(borane) (**10**•$2BH_3$)[3f] and 3-cyclopentadienylmethyl-3-methyloxetane (**2c**)[6a] were prepared according to or by adaptation of literature procedures. All other chemicals were obtained from commercial suppliers and were used without further purification.

General Procedure for the Synthesis of Compounds 2: Indene or fluorene (37 mmol, 1.3 equiv.) was dissolved in 100 mL of THF and was deprotonated by the dropwise addition of *n*BuLi at 0°C. This solution was stirred for 2 h at room temperature; after this period the solution was heated to 60°C and a solution of 3-methanesulfonoxymethyl-3-methyloxetane (28 mmol) in THF (50 mL) was added dropwise over a period of 45 min. The resulting mixture was then heated to reflux for 3 h. After cooling to room temperature, the mixture was hydrolysed by addition of 30 mL water. The organic phase was separated, and the aqueous layer was extracted with three 30 mL portions of diethyl ether. The combined organic phases were washed with saturated NaCl solution (pH: neutral) and dried with Na_2SO_4. The solvent was evaporated in vacuo and the residue was purified by column chromatography (eluent, R_f, and yield given in Table 2).

General Procedure for the Synthesis of Compounds 3: Compound **2** (10 mmol) was dissolved in 50 mL THF and cooled to 0°C. At this temperature 30 mmol (3 equiv.) of a 48% aqueous solution of hydrobromic acid was added dropwise. After it was stirred for 1 h at 0°C, the reaction mixture was allowed to warm to room temperature and stirred for 1 h.

For 3a: The mixture was again cooled to 0°C and 15 mL of 10% caustic soda solution was added to reverse the HBr addition at the

double bond of the indene residue, which had occurred in part during the first step (c.f.[6a]). Stirring was continued for 1 h at 20°C. The organic phase was separated, and the aqueous layer was extracted with three 30 mL portions of diethyl ether. The combined organic phases were washed with saturated NaCl solution (pH: neutral) and dried with Na_2SO_4. The solvent was evaporated in vacuo and the residue was purified by column chromatography (eluent, R_f, and yield are given in Table 2).

For 3b: The organic phase was separated, and the aqueous layer was extracted with three 30 mL portions of diethyl ether. The combined organic phases were washed with saturated NaCl solution (pH: neutral) and dried with Na_2SO_4. The solvent was evaporated in vacuo and the residue was purified by column chromatography (eluent, R_f, and yield are given in Table 2).

General Procedure for the Synthesis of Compounds 4a, 4d, 7, and 12c: The starting material (10 mmol) was dissolved in CH_2Cl_2 (60 mL)and 1.5 equiv. of triethylamine was added to the solution. The mixture was cooled to 0°C and 1.3 equiv. of methanesulfonyl chloride was added dropwise. After half the amount of methanesulfonyl chloride had been added, a white precipitate formed. After 20 min at 0°C, stirring was continued for another 6 h at 20°C. The mixture was hydrolysed by the addition of 20 mL of water. The organic phase was separated, and the aqueous layer was extracted with three 30 mL portions of CH_2Cl_2. The combined organic phases were washed with saturated NaCl solution (pH: neutral) and dried with Na_2SO_4. The solvent was evaporated in vacuo and the residue purified by column chromatography (eluent, R_f, and yield are given in Table 2).

General Procedure for the Synthesis of Compounds 5: Oxetane **2** (6−15 mmol) was dissolved in THF (40−60 mL)and deprotonated by the dropwise addition of 1 equiv. *n*BuLi at 0°C. The solution was stirred for 1 h. The phosphane HPR'_2 (1.2 equiv.) was dissolved in THF (40−60 mL) and was deprotonated in the same manner by the dropwise addition of 1 equiv. *n*BuLi at 0°C. This solution was stirred for 30 min at 20°C. The phosphide solution was added dropwise to the deprotonated oxetane over a period of 45 min. The resulting mixture was stirred for 6 h at room temperature and heated to reflux (**5a**, **5c** 1 h; **5b** 3 h). After it had cooled to room temperature, the mixture was hydrolysed by addition of 20 mL of water. The organic phase was separated, and the aqueous layer was extracted with three portions of 30 mL diethyl ether. The combined organic phases were washed with saturated NaCl solution (pH: neutral) and dried with Na_2SO_4. The solvent was evaporated in vacuo and the residue was purified by column chromatography (not in case of **5c**, which seems to decompose on silica gel) (eluent, R_f, and yield are given in Table 2).

General Procedure for the Synthesis of Compounds 6: Compound **5** (5−12 mmol) was dissolved in THF (50 mL) and cooled to 0°C. At this temperature, BH_3 (1.3 equiv.) in THF was added dropwise. The reaction mixture was stirred for 45 min. The solvent was removed in vacuo and the remaining residue was purified by column chromatography (eluent, R_f, and yield are given in Table 2).

General Procedure for the Synthesis of Compounds 8 and 10: The starting material was dissolved in a sufficient amount of morpholine (no undissolved parts remained). The mixture was heated 15 min at 70°C. All volatile components were removed in vacuo and the remaining residue was purified by column chromatography (eluent, R_f, and yield are given in Table 2).

General Procedure for the Synthesis of Compounds 9a and 9b: Diphenylphosphane (12 mmol, 3 equiv.) was dissolved in THF (30 mL) and deprotonated by the dropwise addition of 1 equiv. *n*BuLi at 0°C. This solution was stirred for 1 h at room temperature, after which a solution of 4 mmol starting material (**4a**, **4d**) in 30 mL THF was added dropwise over a period of 2 min. The resulting mixture was stirred for 2 h at room temperature and heated to reflux (**9a** 2 h; **9b** 3 h). After cooling to room temperature the mixture was hydrolysed by addition of 20 mL of water. The organic phase was separated and the aqueous layer was extracted with three portions of 20 mL diethyl ether. The combined organic phases were washed with saturated NaCl solution (pH: neutral) and dried with Na_2SO_4. The solvent was evaporated in vacuo and the residue was purified by column chromatography (eluent, R_f, and yield are given in Table 2).

Synthesis of Compound 9c: Compound **4a** (1.4 mmol) was dissolved in 10 mL of THF and deprotonated by the dropwise addition of 1 equiv. *n*BuLi at −70°C. This solution was stirred for 2 h at room temperature and heated to reflux for 2 h. After cooling to room temperature the mixture was hydrolysed by addition of 10 mL of water. The organic phase was separated and the aqueous layer was extracted with three portions of 10 mL diethyl ether. The combined organic phases were washed with saturated NaCl solution (pH: neutral) and dried with Na_2SO_4. The solvent was evaporated in vacuo and the residue was purified by column chromatography (eluent, R_f, and yield are given in Table 2).

Synthesis of Compound 9d: Diphenylphosphane (2.8 mmol, 2.5 equiv.) was dissolved in 15 mL of THF and deprotonated by the addition of 1 equiv. KO*t*Bu at 0°C. This solution was stirred for 1 h at room temperature, then a solution of 1.9 mmol **12c** in 20 mL THF was added dropwise over a period of 1 min. The resulting mixture was stirred for 12 h at room temperature. The mixture was hydrolysed by addition of 10 mL of water. The organic phase was separated and the aqueous layer was extracted with three portions of 20 mL diethyl ether. The combined organic phases were washed with saturated NaCl solution (pH: neutral) and dried with Na_2SO_4. The solvent was evaporated in vacuo and the residue was purified by column chromatography. Elution with PE/Et_2O = 1/1 removed contaminants while **9d** did not migrate at all. It was subsequently eluted with toluene/THF 1/1. On evaporation of the solvent from the eluate, the purified compound **9d** was obtained in microcrystalline form (yield are given in Table 2).

General Procedure for the Synthesis of Compounds 4c and 12d (Silylation): Starting material (5 mmol) was dissolved in 40 mL CH_2Cl_2 and 1.5 equiv. of triethylamine was added. The solution was cooled to 0°C and 1.3 equiv. of trimethylsilyl chloride was added dropwise. After the reaction mixture was stirred for 1 h, all volatile parts were removed in vacuo. The remaining residue was purified by column chromatography (eluent, R_f, and yield are given in Table 2).

Synthesis of Compound 4b: Compound **3a** (10 mmol) was dissolved in a solution consisting of 20 mL CH_2Cl_2 and 20 mmol pyridine (2 equiv.). The mixture was cooled to 0°C and 14 mmol benzenesulfonyl chloride (1.4 equiv.) was added dropwise. Stirring was continued at 20°C for 15 h. The mixture was hydrolysed by addition of 20 mL water. The organic phase was separated, and the aqueous layer was extracted with three portions of 30 mL CH_2Cl_2. The combined organic phases were washed and neutralized with saturated NaCl solution and dried with Na_2SO_4. The solvent was evaporated in vacuo and the residue was purified by column chromatography (eluent, R_f, and yield are given in Table 2).

Synthesis of Compound 11a: Indene (4.6 mmol, 2.2 equiv. related to **10**) was dissolved in 40 mL THF and deprotonated by the dropwise addition of an equimolar amount *n*BuLi at 0°C. This solution was stirred for 10 min. Dibenzo-18-crown-6-ether (4.6 mmol) was ad-

ded. Stirring was continued for another 2 h at 20°C. The mixture was heated to 60°C and a solution of **10** (2.1 mmol) in 10 mL THF was added dropwise over a period of 5 min (After the first drops the reaction mixture turned a deep violet colour). The mixture was heated to reflux for another 5 h. After cooling to 20°C, it was hydrolysed by the addition of 20 mL water. The precipitated white substance (crown ether) was filtered off and washed twice with diethyl ether. The organic phase was separated, and the aqueous layer was extracted with three portions of 30 mL diethyl ether. The combined organic phases were washed and neutralized with saturated NaCl solution until neutral pH was obtained, and it was then dried with Na_2SO_4. The solvent was evaporated in vacuo and the residue was purified by column chromatography (eluent, R_f, and yield are given in Table 2).

Synthesis of Compound 11b: Fluorene (5.6 mmol, 3 equiv. with respect to **10**) was dissolved in 40 mL THF and deprotonated by the dropwise addition of an equimolar amount *n*BuLi at 0°C. After stirring for 10 min, TMEDA (5.6 mmol) was added. Stirring was continued for another 2 h at 20°C. The mixture was heated to 60°C and a solution of 1.9 mmol **10** in 10 mL THF was added dropwise over a period of 5 min (after the first drops the reaction mixture adopted a deep violet colour). The mixture was then heated to reflux for 5 h. The mixture was hydrolysed by addition of 20 mL water. The organic phase was separated and the aqueous layer was extracted with three portions of 30 mL diethyl ether. The combined organic phases were washed and neutralized with saturated NaCl solution and dried with Na_2SO_4. The solvent was evaporated in vacuo and the residue was purified by column chromatography (eluent, R_f, and yield are given in Table 2).

General Procedure for the Synthesis of Compounds 12a and 12b: Indene (in the case of **12b**) or fluorene (in the case of **12a**) (30 mmol, 3 equiv. with respect to **2**), for the generation of the nucleophile, was dissolved in 40 mL THF and deprotonated by the dropwise addition of 30 mmol *n*BuLi at 0°C. Stirring was continued 2 h at 20°C. Compound **2c** (in case of **12b**) or **2a** (in case of **12a**) (10 mmol) was dissolved in 30 mL THF and deprotonated by the dropwise addition of 10 mmol *n*BuLi at 0°C. The solution was stirred at 20°C (**2c** 1 h, **2a** 2 h). To this solution the nucleophile was added dropwise. The reaction mixture was heated to reflux for 4 h. The mixture was hydrolysed by the addition of 20 mL water. The organic phase was separated, and the aqueous layer was extracted with three portions of 30 mL diethyl ether. The combined organic phases were washed and neutralized with saturated NaCl solution and dried with Na_2SO_4. The solvent was evaporated in vacuo and the residue was purified by column chromatography (eluent, R_f, and yield are given in Table 2).

X-ray Structure determinations: Suitable crystals were taken directly out of the mother liquor, immersed in perfluorinated polyether oil and fixed to a glass capillary at 200 K. The measurements for **2b**, **4a**, and **4b** were carried out on a Siemens P4 four-circle diffractometer (equipped with a low temperature unit) with graphite-monochromated Mo-K_α radiation. The measurements for **6b** and **12a** were carried out on a Nonius-Kappa CCD diffractometer (low temperature unit, graphite-monochromated Mo-K_α radiation). In case of the Siemens P4 four-circle diffractometer measurements, the intensities of three control reflections (measured every 100 reflections) remained constant throughout the data collection, thus indicating crystal and electronic stability. The data collected on a Siemens P4 four-circle diffractometer were corrected in the standard manner, including experimental absorption correction. The data from the Nonius Kappa CCD device were processed by standard Nonius software.[14] All Calculations were performed using the SHELXT-PLUS software package.[15] Structures were solved by direct methods with the SHELXS-97 program[15a] and refined with the SHELXL-97 program.[15b] Graphical handling of the structural data during solution and refinement was performed with XPMA.[16] Atomic coordinates and anisotropic thermal parameters of the non-hydrogen atoms were refined by full-matrix least-squares calculations. Data for the structure determinations are compiled in Table 3. Crystallographic data (excluding structure factors) for the structures reported in this paper have been deposited with the Cambridge Crystallographic Data Centre as supplementary publication no. CCDC-124896 (**2b**), CCDC-124900 (**4a**), CCDC-124899 (**4b**), CCDC-124897 (**6b**), and CCDC-124898 (**12a**). Copies of the data can be obtained free of charge on application to CCDC, 12 Union Road, Cambridge CB2 1EZ, UK [Fax: (internat.) +44-(0)1223/336 033; E-mail: deposit@ccdc.cam.ac.uk].

Acknowledgments

We are grateful to the German Science Foundation (DFG), SFB 247, the VW Foundation (Stiftung Volkswagenwerk) and the Fonds der Chemischen Industrie for financial support. The technical support by T. Jannack (mass spectrometry) and the Microanalytical Laboratory of the Institute of Organic Chemistry are gratefully acknowledged.

[1] [1a] L. Sacconi, S. Midollini, *J. Chem. Soc., Dalton Trans.* **1972**, 1213−1216. − [1b] P. Dapporto, G. Fallani, S. Mindollini, L. Sacconi, *J. Am. Chem. Soc.* **1973**, *95*, 2021−2023. − [1c] C. Mealli, S. Mindollini, L. Sacconi, *Inorg. Chem.* **1978**, *17*, 632−637. − [1d] L. Sacconi, F. Mani, *Transition Met. Chem.* **1982**, *8*, 179−252. − [1e] M. Divaira, L. Sacconi, *Angew. Chem.* **1982**, *94*, 338−351; *Angew. Chem. Int. Ed. Engl.* **1982**, *21*, 330−343. − [1f] C. Mealli, S. Midollini, *Inorg. Chem.* **1983**, *22*, 2785−2786. − [1g] H. A. Mayer, W. C. Kaska, *Chem. Rev.* **1994**, *94*, 1239−1272.

[2] [2a] C. Bianchini, A. Meli, A. Orlandini, L. Sacconi, *Angew. Chem.* **1980**, *92*, 1055−1056; *Angew. Chem. Int. Ed. Engl.* **1980**, *19*, 1021−1022. − [2b] C. Bianchini, A. Meli, A. Orlandini, L Sacconi, *J. Organomet. Chem.* **1981**, *209*, 219−231. − [2c] C. Bianchini, A. Meli, A. Orlandini, L. Sacconi, *J. Organomet. Chem.* **1981**, *218*, 81−89. − [2d] C. Bianchini, C. Ghilardi, A. Meli, S. Midollini, A. Orlandini, *J. Organomet. Chem.* **1983**, *248*, C13−C16. − [2e] J. Ott, M. Venanzi, C. A. Ghilardi, S. Midollini, A. Orlandini, *J. Organomet. Chem.* **1985**, *291*, 89−100. − [2f] C. Bianchini, D. Masi, A. Meli, M. Peruzzini, F.Zanobini, *J. Am. Chem. Soc.* **1988**, *110*, 6411−6423. − [2g] C. Bianchini, A. Meli, M. Peruzzini, F. Vizza, *Organometallics* **1990**, *9*, 226−240. − [2h] C. Bianchini, A. Meli, M. Peruzzini, F. Vizza, F. Zanobini, *Coord. Chem. Rev.* **1992**, *120*, 193−208. − [2i] F. Bachechi, C. Bianchini, A. Meli, *Inorg. Chim. Acta* **1993**, *213*, 269−277. − [2j] J. Grevin, P. Kalck, J. C. Daran, J. Vaissermann, C. Bianchini, *Inorg. Chem.* **1993**, *32*, 4965−4967.

[3] [3a] S. T. Liu, K. J. Liu, *Inorg. Chem.* **1990**, *29*, 4576−4579. − [3b] O. Walter, T. Klein, G. Huttner, L. Zsolnai, *J. Organomet. Chem.* **1993**, *458*, 63−81. − [3c] H. Heidel, G. Huttner, G. Helmchen, *Z. Naturforsch.* **1993**, *48b*, 1681−1692. − [3d] A. Muth, G. Reinhard, G. Huttner, T. Seitz, T. Klein, L. Zsolnai, *Z. Naturforsch.* **1994**, *49b*, 889−897. − [3e] H. Heidel, G. Huttner, R. Vogel, G. Helmchen, *Chem. Ber.* **1994**, *127*, 271−274. − [3f] T. Seitz, A. Muth, G. Huttner, *Chem. Ber.* **1994**, *127*, 1837−1842. − [3g] S. C. Tsai, H. E. Wang, S. T. Wang, L. M. Yiin, S. T. Liu, *Chem. Ber.* **1995**, *128*, 151−155. − [3h] H. Heidel, G. Huttner, L. Zsolnai, *Z. Naturforsch.* **1995**, *50b*, 729−734. − [3i] T. Seitz, A. Muth, G. Huttner, *Z. Naturforsch.* **1995**, *50b*, 1045−1049. − [3j] J. Scherer, G. Huttner, M. Büchner, *J. Organomet. Chem.* **1996**, *520*, 45−58. − [3k] J. Scherer, G. Huttner, M. Büchner, *Chem. Ber.* **1996**, *129*, 697−713.

[4] [4a] H. E. Wang, C. Y. Liu, M. C. Cheng, S. M. Peng, S. T. Liu, *Phosphorus, Sulfur and Silicon* **1992**, *69*, 201−211. − [4b] S. T. Liu, C. Y. Liu, *J. Org. Chem.* **1992**, *57*, 6079−6080. − [4c] S. T. Liu, C. H. Yieh, H. P. Dai, *Proc. Natl. Sci. Counc. (A)* **1995**, *19*, 1−4. − [4d] A. Jacobi, G. Huttner, U. Winterhalter, *Chem.*

Ber. **1997**, *130*, 1279−1294. − [4e] A. Jacobi, G. Huttner, U. Winterhalter, S. Cunskis, *Eur. J. Inorg. Chem.* **1998**, 675−692.

[5] [5a] S. T. Liu, H. E. Wang, M. C. Cheng, S. M. Peng, *J. Organomet. Chem.* **1989**, *376*, 333−342. − [5b] S. T. Liu, K. J. Liu, *Inorg. Chem.* **1990**, *29*, 4576−4579. − [5c] S. T. Liu, *J. Chin. Chem. Soc.* **1992**, *39*, 611−616. − [5d] S. C. Tsai, H. E. Wang, C. T. Wang, C. T. Huang, L. M. Yin, S. T. Liu, *Chem. Ber.* **1995**, *128*, 151−155. − [5e] S. T. Liu, D. R. Hou, T. C. Lin, M. C. Cheng, S. M. Peng, *Organometallics* **1995**, *14*, 1529−1532. − [5f] S. T. Liu, C. H. Yieh, H. P. Dai, Proc. Natl. Sci. Counc., Repub. China, Part A: Phy. Sci. Eng. **1995**, 19, 1−4. − [5g] G. Reinhard, R. Soltek, G. Huttner, A. Barth, O. Walter, *Chem. Ber.* **1996**, *129*, 97−108. − [5h] R. Soltek, G. Huttner, *Eur. J. Inorg. Chem.* **1998**, 1417−1424.

[6] [6a] B. Antelmann, U. Winterhalter, G. Huttner, B. C. Janssen, J. Vogelgesang, *J. Organomet. Chem.* **1997**, *545*−*546*, 407−420. − [6b] B. Antelmann, G. Huttner, J. Vogelgesang, O. Walter, U. Winterhalter, *J. Organomet. Chem.* **1997**, *549*, 139−148.

[7] [7a] T. Kauffmann, J. Olbrich, *Tetrahedron Lett.* **1984**, *25*, 1967−1970. − [7b] S. G. Davies, I. M. Dordor-Hedgecock, P. Warner, *J. Organomet. Chem.* **1985**, *285*, 213−223. − [7c] M. Brookhart, W. B. Studbaker, *Chem. Rev.* **1987**, *87*, 411−432. − [7d] S. G. Davies, S. C. Preston, K. H. Sutton, J. C. Walker, *Bull. Soc. Chim. Fr.* **1987**, *4*, 608−630. − [7e] G. Consiglio, F. Morandini, *Chem. Rev.* **1987**, *87*, 761−778. − [7f] . R. Cuttler, P. K. Hanna, J. Vites, *Chem. Rev.* **1988**, *88*, 1363−1403. − [7g] L. Colombo, F. Ulgheri, L. Prati, *Tetrahedron Lett.* **1989**, *30*, 6435−6436. − [7h] J. W. Faller, C. J. Smart, *Tetrahedron Lett.* **1989**, *30*, 1189−1192. − [7i] S. G. Davies, J. P. Mc Nally, A. J. Smallridge, *Adv. Organomet. Chem.* **1990**, *30*, 1−76. − [7j] B. M. Trost, R. J. Kulawiec, *J. Am. Chem. Soc.* **1992**, *114*, 5579−5584. − [7k] B. M. Trost, R. J. Kulawiec, *J. Am. Chem. Soc.* **1993**, *115*, 2027−2036. − [7l] A. K. Saha, M. M. Hossain, *Tetrahedron Lett.* **1993**, *34*, 3833−3836. − [7m] T. Bach, D. N. A. Fox, M. T. Reetz, *J. Chem. Soc., Chem. Commun.* **1992**, 1634−1636. − [7n] H. R. Brunner, S. Forster, B. Nuber, *Organometallics* **1993**, *12*, 3819−3827. − [7o] E. P. Kündig, B. Bourdin, G. Bernadinelli, *Angew. Chem.* **1994**, *106*, 1931−1934; *Angew. Chem. Int. Ed. Engl.* **1994**, *33*, 1467−1470. − [7p] W. A. Schenk, J. Frisch, W. Adam, F. Prechtl, *Angew. Chem.* **1994**, *106*, 1699−1701; *Angew. Chem. Int. Ed. Engl.* **1994**, *33*, 1609−1611. − [7q] L. S. Hegedus in *Organische Synthese mit Übergangsmetallen* (Ed.: L. S. Hegedus), VCH, Weinheim, **1995**. − [7r] B. M. Trost, *Chem. Ber.* **1996**, *129*, 1313−1322. − [7s] B. M. Trost, B. Vidal, M. Thommen, *Chem. Eur. J.* **1999**, *5*, 1055−1069.

[8] [8a] S. Jugé, M. Stephan, J. A. Laffitte, J. P. Genet, *Tetrahedron Lett.* **1990**, *31*, 6357−6360. − [8b] T. Imamoto, T. Oshiki, T. Onozawa, T. Kusumoto, K. Sato, *J. Am. Chem. Soc.* **1990**, *112*, 5244−5252. − [8c] T. Seitz, G. Huttner, M. Büchner, *Z. Naturforsch.* **1994**, *49b*, 1813−1817.

[9] T. Imamoto, T. Kusumoto, N. Suzuki, K. Sato, *J. Am. Chem. Soc.* **1985**, *107*, 5301−5303.

[10] *Organikum*, Deutscher Verlag der Wissenschaften, Berlin, **1990**.

[11] K. Issleib, A. Tzschach, *Chem. Ber.* **1959**, *92*, 704−711.

[12] [12a] K. Issleib, H.O. Fröhlich, *Z. Naturforsch.* **1959**, *14b*, 349−350. − [12b] R. E. Ireland, D. M. Walba, *Org. Synth. Coll. Vol.* **1988**, *6*, 567−570.

[13] J. Cheymol, P. Chabrier, J. Seyden-Penne, A. Habert-Somny, T. Strazalko, *Bull. Soc. Chim. Fr.* **1965**, 694−700.

[14] DENZO-SMN, Data processing software, Nonius **1998**; http://www.nonius.com.

[15] [15a] G. M. Sheldrick, SHELXS-97, *Program for Crystal Structure Solution*, University of Göttingen, **1997**; http://shelx.uni-ac.gwdg.de/shelx/index.html. − [15b] G. M. Sheldrick, SHELXL-97, *Program for Crystal Structure Refinement*, University of Göttingen, **1997**; http://shelx.uni-ac.gwdg.de/shelx/index.html. − [15c] *International Tables for X-ray Crystallography*, Vol. 4, Kynoch Press, Birmingham, U.K. **1974**.

[16] L. Zolnai, G. Huttner, *XPMA*, *http://www.rzusers.uni-heidelberg.de/~v54/xpm.html*, University of Heidelberg, **1994**.

Received June 9, 1999
[I99209]

An Inorganic Helix $[Mn(IPG)(MeOH)]_n[PF6]_n$[‡]: Structural and Magnetic Properties of a *syn-anti* Carboxylate-Bridged Manganese(II) Chain Involving a Tetradentate Ligand

Clotilde Policar,*[a] François Lambert,[a] Michèle Cesario,[b] and Irène Morgenstern-Badarau[a]

Keywords: Carboxylate *syn-anti* / *N*-centered tripodal ligand / Manganese / Imidazole / Helicoïdal inorganic chiral chain / Magnetism / π-π interaction

The crystal structure of an infinite inorganic chain consisting of Mn^{II} and an *N*-centered tripodal ligand *N*,*N*-(2-pyridylmethyl)[(1-methylimidazol-2-yl)-methyl]glycinate is presented. It exhibits a chiral helical structure with a pitch of two monomeric units (each monomeric unit containing one Mn atom). Each manganese is connected to its neighbor through a carboxylate bridge in a *syn-anti* geometry. Around each manganese center, two carboxylates bind in a *cis* geometry. This peculiar bridging geometry (*syn-anti cis*) provides a broken-line chain, running in a zig-zag manner along the *b* axis of the $P2_1$ space group. The magnetic properties have been investigated. They show a pseudo-2D magnetic structure, with one major pathway along the chain and an inter-chain minor one. The intrachain coupling is a weak antiferromagnetic interaction (J/k = –0.25). This low value is entirely consistent with the geometry of the bridge. The interchain coupling is a weaker antiferromagnetic coupling (J′/k = –0.11) and could be mediated through π-π interactions between pyridine and imidazole from two adjacent helixes.

Introduction

Carboxylate ligands play an important role in coordination chemistry. They are known to adopt binding modes as diverse as terminal monodentate, chelating to one metal center and bridging bidentate in a *syn-syn*, *syn-anti* or *anti-anti* configuration to two metal centers. The *syn-anti* bridge appears to be a rather uncommon binding mode.[1][2] In the past fifteen years, there has been a flow of interest in carboxylate complexes as models for metalloproteins. The carboxylate can be incorporated as an external ligand, usually as an acetate. However, in the metallic cores of metalloproteins, the carboxylato ligand is provided by the side chain of an aspartate or a glutamate making polydentate chelating ligands bearing a carboxylate and some other donor biologically relevant.[2][3] We have prepared several nitrogen-centered tripodal ligands with three appended moities, one being a carboxylate. Mononuclear iron complexes have previously been obtained and described with a monodentate carboxylate. They have been studied as models for nonheme enzymes.[4][5] Surprisingly, with one of these ligands, *N*,*N*-(2-pyridylmethyl)[(1-methylimidazol-2-yl)-methyl)]glycinate (IPG)[6] **(2)**, Mn^{II} forms infinite chains through carboxylato-bridges in a *syn-anti* geometry. Here, the results of structural and magnetic susceptibility studies on these Mn^{II} chains are described.

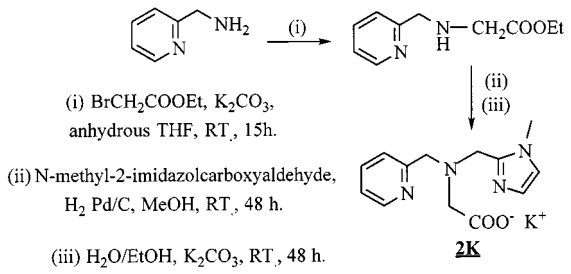
[+] IPG: *N*,*N*-(2-pyridylmethyl)[(1-methylimidazol-2-yl)-methyl)]-glycinate

[a] Laboratoire de Chimie Bio-organique et Bio-inorganique, ERS 1824,
Bâtiment 420, Université Paris XI, F-91405 Orsay Cedex, France
Fax: (internat.) + 33-169/157231
E-mail: cpolicar@icmo.u-psud.fr
[b] Laboratoire de Cristallochimie, Institut de Chimie des Substances Naturelles du CNRS,
F-91198, Gif-sur-Yvette, France

Results

Synthesis

Ligand Synthesis − A given tripod can be synthesized by several different methods depending on the order chosen for the introduction of the different moieties. Several strategies were investigated and we report here the higher yield one. In the synthesis of a nitrogen-centered tripod, the yield-limiting step is usually the tertiarization of the amine. Here, the first step is an *N*-alkylation of a primary amine to give a secondary amine which is easily purified by distillation. This compound then reacts quantitatively with an aldehyde by reductive amination. The overall yield is 70% (see Scheme 1). If the first two steps are switched, the overall yield drops to 35% due to the poor yield of the last step (less than 40%).



Scheme 1. IPGK (2K) synthesis

Complex Preparation − To prevent pollution by particules of MnO_2 in the course of the preparation of the Mn^{II}

 © WILEY-VCH Verlag GmbH, D-69451 Weinheim, 1999 1434−1948/99/1212−2201 $ 17.50+.50/0

complex, the ligand was used as a mixture of the potassium salt and the free acid (**2K/2H** mixture) with a pH controlled ratio (see Experimental Section). Crystals suitable for an X-ray diffraction study were grown from a methanol solution.

Description of the Structure

An X-ray diffraction study was carried out on complex **3**. Experimental details are reported in the Experimental Section (Table 1). The crystal structure has been found to consist of a polymeric sequence of Mn^{II} cations, bridged by *syn-anti* carboxylato groups. The charge of the $[\{Mn^{II}IPG(MeOH)\}^{+}]_n$ chain is balanced by n (PF_6^-) anions. The polymeric chain extends along the *b* axis of the $P2_1$ chiral space group. An ORTEP representation of a succession of three monomeric units is shown in Figure 1. The three units are labeled 0 for the central one, corresponding to the crystallographic unit [*x, y, z*], −1 and +1 for the two adjacent ones along the chain, with the symmetry transformations [$-x$, $-0.5 + y$, $1 - z$] and [$-x$, $0.5 + y$, $1 - z$] respectively. Selected bond lengths and angles are presented in Table 2.

Table 1. Crystallographic data for **3**

Formula	$C_{14}H_{19}F_6MnN_4O_3P$
Formula weight	491.24
Temperature [K]	293(2)
Wavelength [Å]	0.71073
crystal system	monoclinic
space group	$P2_1$
a [Å]	8.417(4)
b [Å]	9.626(5)
c [Å]	12.391(6)
α [°]	90
β [°]	92.61(5)
γ [°]	90
V [Å^3]	1002.9(9)
Z	2
d_{calc} [g.cm^{-3}]	1.627
abs. coeff. [mm^{-1}]	0.815
crystal size [mm]	0.200 × 0.150 × 0.070
collected reflections	568
independent reflections	531 [R(int) = 0.0264]
data/restraints/para	531/43/149
goodness-of-fit on F^2	1.068
Final *R* indices [$I > 2\sigma(I)$]	$R1 = 0.0545, wR2 = 0.1361$[a]
R indices [all data]	$R1 = 0.0587, wR2 = 0.1425$
$\Delta\rho_{min}$ and $\Delta\rho_{max}$ [e.Å^{-3}]	−0.313 and 0.319

[a] Weighting scheme: $w = 1/[s^2(F_o^2) + (0.0776P)^2 + 8.47P]$ where $P = (F_o^2 + 2F_c^2)/3$.

Mn^{II} is hexacoordinated with a pseudo-octahedral environment. Four of the donors are provided by the ligand **2**, through the imidazole nitrogen N1A, the pyridine nitrogen N1B, the tripodal nitrogen N and one carboxylato oxygen O2. The fifth donor is provided by the carboxylato oxygen O1 from the carboxylato of unit (−1). The final coordination site is filled by a molecule of methanol. The $Mn-N_{tripodal}$ distance [2.35(3) Å] is longer than the other Mn−N bonds, but shorter than the corresponding sum of the van der Waals radii (2.82 Å), indicating that the metal is hexacoordinated. The Mn−N1A distance [2.13(2) Å] is significantly shorter than the Mn−N1B distance [2.23(2) Å], suggesting a stronger bond with the imidazole ligand. Such small $Mn-N_{imidazole}$ distances were reported to be characteristic of bridged structures.[7] Imidazole and pyridine are in the trans positions with regard to Mn and the two aromatic rings are parallel to each other [$\Phi = 5(1)°$]. The Mn atom and the three oxygens O1, O2′ and O3 (see Figure 1) (carboxylate and methanol) are coplanar (mean

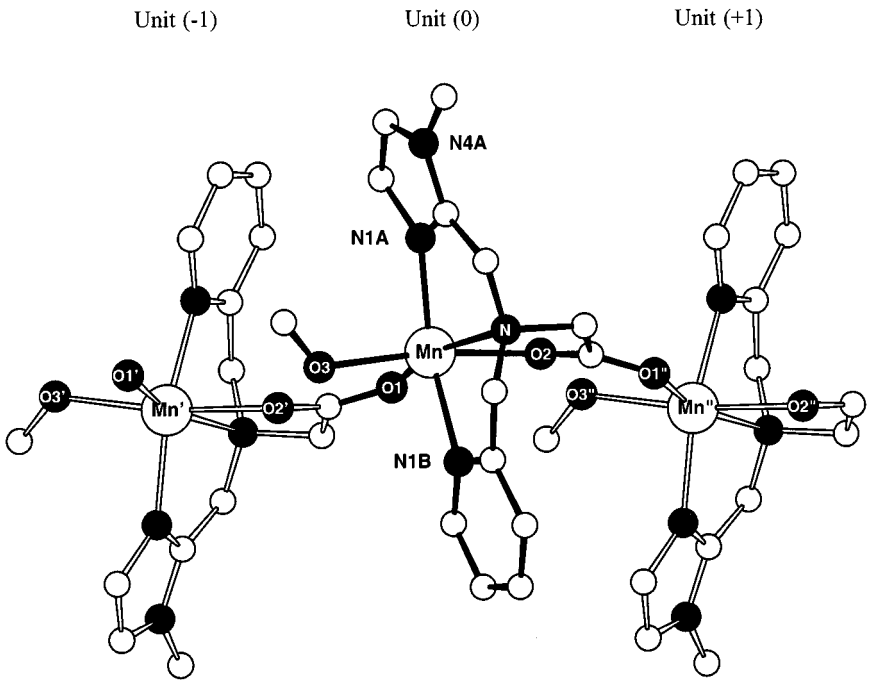


Figure 1. ORTEP drawing of complex 3 cationic chain with three adjacent monomeric units of the polymer; hydrogen atoms have been omitted for clarity

Table 2. Selected bond lengths [Å] and angles [°] for **3**

Mn−N(1A)	2.13(2)	O(1)−Mn−N(1B)	98.2(6)
Mn−O(1)	2.13(2)	O(2)−Mn−N(1B)	84.7(6)
Mn−O(2)	2.18(2)	N(1A)−Mn−O(3)	88.4(7)
Mn−N(1B)	2.23(2)	O(1)−Mn−O(3)	92.5(6)
Mn−O(3)	2.26(2)	O(2)−Mn−O(3)	171.8(5)
Mn−N	2.36(2)	N(1B)−Mn−O(3)	87.2(6)
		N(1A)−Mn−N	75.7(6)
N(1A)−Mn−O(1)	114.1(6)	O(1)−Mn−N	162.4(6)
N(1A)−Mn−O(2)	98.8(7)	O(2)−Mn−N	75.5(6)
O(1)−Mn−O(2)	88.3(6)	N(1B)−Mn−N	74.0(6)
N(1A)−Mn−N(1B)	147.5(6)	O(3)−Mn−N	102.7(6)

displacement 0.006 Å), the tripodal nitrogen N being located at 0.34(2) Å from this mean plane.

The carboxylates bridge two mononuclear units with a *syn-anti* pattern, forming an infinite chain. The manganese from unit 0 is slightly closer to the carboxylato oxygen O1 belonging to a ligand from the adjacent unit (−1) than to O2 [see Figure 1; 2.13(2) Å (Mn−O1) versus 2.18(2) Å (Mn−O2)]. O1 interacts with the manganese through its *syn* lone pair and O2 through its *anti* lone pair. All distances and angles (see Table 2) are consistent with those previously found in manganese *syn-anti* μ-carboxylato systems.[8−16] Although the H-atom of the coordinated methanol could not be located on difference Fourier-syntheses, it seems clear that a strong internal hydrogen bond occurs between the acceptor oxygen O2 of the carboxylate group and the oxygen donor of the methanol of the adjacent unit +1 [see Figure 1; d(O2−O3″) = 2.63(2) Å]. This hydrogen bond involves the *syn* lone pair of O2.

The two oxygens O1 and O2 are in a *cis* conformation with regard to Mn, with a (O1−Mn−O2) angle of 88.3(6)°. The chain develops in a zig-zag manner, with an (Mn_{-1}−Mn_0−Mn_{+1}) angle of 125.3° and a nonplanar Mn−O−C−O−Mn pattern. From unit −1 to unit 0, the plane of the two aromatic rings is tipped over by 64° (see Figure 2). The third unit along the chain can be deduced from the first one by translation (10.84 Å). The structure can be described as a chiral helix-like chain running parallel to the *b* axis and with a pitch of two complexes (see Figure 2). The Mn−Mn distance is 5.42 Å and is in the typical range which has previously been described for such *syn-anti* bridges between Mn^{II} [5.2−5.8 Å].[9−16]

The spatial arrangement of the complex **3** is displayed in Figure 3. The packing diagram reveals a layer organisation with entangled parallel helixes. A pyridine moiety from one helix is parallel to an imidazole from the next, with a small interplanar distance (3.8 Å). The closest distance between two Mn from two adjacent helixes is 8.42 Å.

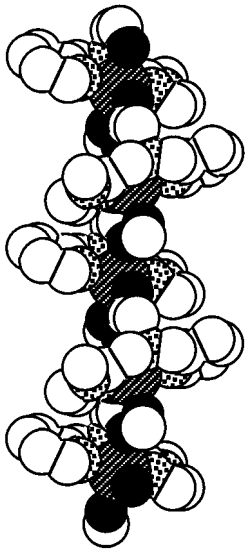


Figure 2. View of the helicoïdal organisation with space filling representation

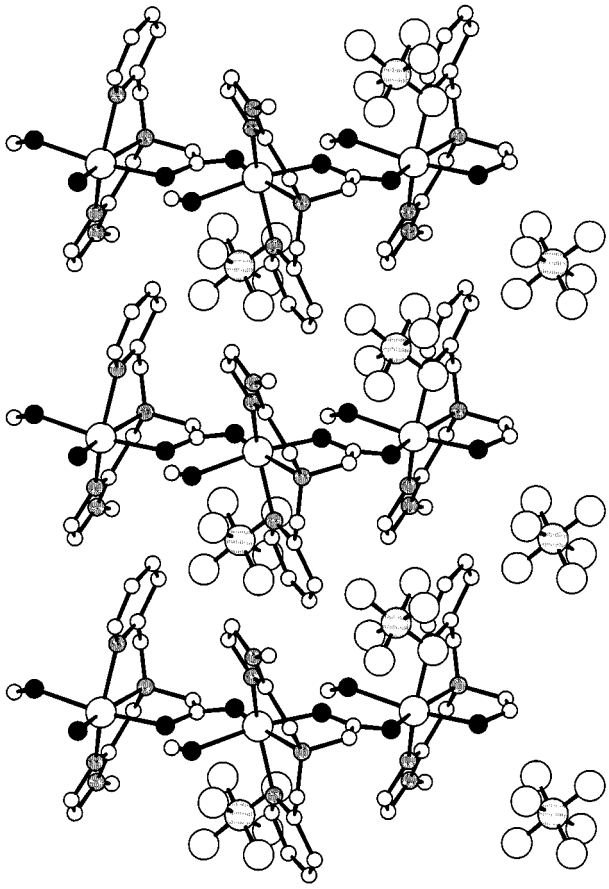


Figure 3. ORTEP packing diagram; the disorder of the anionic units has been omitted for clarity

Magnetic Properties

The results of susceptibility measurements are shown in Figure 4. At very low temperature, the experimental susceptibility is smaller than that predicted by a Curie law for S = 5/2 and g = 2 (see inset, dash line). This indicates some small antiferromagnetic coupling between two metallic centers in **3**. The magnetic properties of such a chain can be explained by the Heisenberg linear-chain model. The Hamiltonian used here is:

$$\boldsymbol{H} = -2J\sum_i \mathbf{S}_i \cdot \mathbf{S}_{i+1}$$

where the summation is all along the chain and J is the exchange coupling between two adjacent paramagnetic centers. An analytical law has been derived by Fisher for infinite chains and large spins.[17][18] For an infinite S = 5/2 chain, the expression of the chain molar magnetic susceptibility χ_c is:[19−21]

$$\chi_c = (35/32)*(1/T)*g^2(1+u)/(1-u)$$

$$\text{with } u = \coth[(35/32)*(1/T)*(J/k)]-[(2/35)*T*(k/J)]$$

Fitting the data to that expression provided an estimate of J (J/k = −0.27). However, the g value thus obtained was too small for a Mn^{II} high spin complex (g = 1.946, with an agreement factor for the fitting $R = 1.51 \times 10^{-4}$). The fitting was improved by taking into account interchain interactions via a mean-field.[18][22] The expression used to fit the data was:

$$\chi = \frac{\chi_c}{1-\frac{2zJ'\chi_c}{Ng^2\beta^2}} = \frac{\chi_c}{1-\frac{16}{3}\,z\,\frac{J'}{k}\,\chi_c}$$

where J′ is the interchain-exchange coupling and z the number of nearest neighbors. The best fit of Equation 2 in the temperature range 2−300 K was found for J/k = −0.25 (−0.17 cm^{-1}), zJ′/k = −0.11 (−0.078 cm^{-1}) and g = 1.970 with an agreement factor $R = 2.17 \times 10^{-5}$. All three parameters were allowed to vary during the fitting process. As can be seen in Figure 4, the experimental points and theoretical curve are superimposed in all the temperature range. The J and J′ values obtained are very small and thus the precision on their absolute value must be rather low. Moreover the ratio zJ′/J = 0.4 is at the high limit for the mean-field model to be valid.[22−24] This increases the uncertainty on J′ although the order of magnitude both for J and J′ is still meaningful.

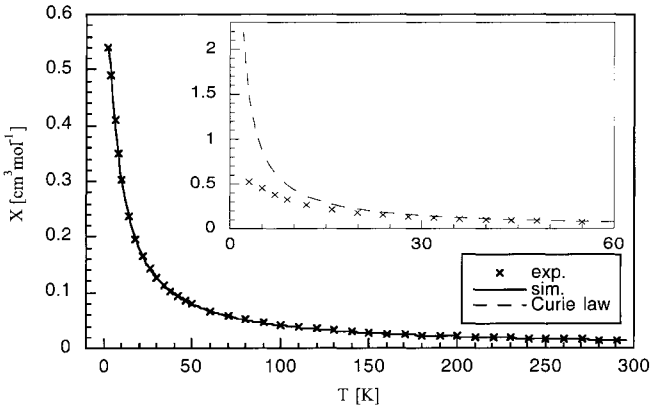


Figure 4. Experimental and calculated temperature dependences of χT; for clarity only 50% of the experimental points are shown; the dashed line was generated with a Curie law for S = 5/2 and g = 2 (see text); the solid line is the best fit obtained including the mean-field correction (see text for parameters)

Discussion

A *syn-anti* bridging configuration is rare by comparison with a *syn-syn* configuration.[2] The former is made easier by steric congestion[25][26] and is more frequently found when the carboxylate is part of a polydentate ligand[27−30] or a substituted acetate,[13,15,16,25] including amino acids.[14][31] It has been reported for discrete complexes,[15] polymeric chains and networks with manganese.[9−14,16,31]

The main structural feature of compound **3** is the chiral helix-like structure with a nonlinear bridging network. This is due both to the *syn-anti* bridging mode of the carboxylato ligand and to the *cis* position of the two oxygens O1 and O2 in the octahedron around Mn. IR spectroscopic data are consistent with a bridging carboxylate and not a unidentate one: the small value of $\Delta\nu = (\nu_{asCO}) - (\nu_{sCO}) = 131 cm^{-1}$ is characteristic of a bridging carboxylate.[1] Another important feature is the layer organisation. In the crystal packing, the chains are stacked by π-interactions with an interplanar spacing of 3.8 Å between the pyridine from one helix and the imidazole from the next.

Very little is known about the magnetic properties of such carboxylato *syn-anti* manganese chains. On the contrary, the magnetic properties of manganese chains involving halogen bridges have been extensively described and are classical examples of linear chain compounds (see Table 3).[19−21,32] The carboxylato *syn-anti* bridge has received some attention because it allows a large variety of structural and magnetic features.[23,29,33] Without being exhaustive, the magnetic behavior has been studied for *syn-anti* carboxylato bridges in chain structures involving homonuclear[23,28,29,33−35] Cu^{II}, heterodinuclear[36] Mn^{II} and Cu^{II} or in discrete complexes[27] (Fe^{III}). The magnetic properties have also been studied for a 2D-polymer with a *syn-anti* carboxylato network[16] between Mn^{II}, and on a discrete Mn^{II} homodimer involving a mono *syn-anti* carboxylato bridge (see Table 3).[15]

The intrachain coupling constant in compound **3** is at least one order of magnitude smaller than that reported for halogenated Mn^{II} chains (see Table 3). The exchange coupling through the carboxylato moiety is highly dependent on the conformation of the bridge between the metal centers that are interacting.[18,34,37] A *syn-syn* pattern provides small metal−metal distances and a good overlap of magnetic orbitals. It induces high antiferromagnetic coupling, as has previously been reported in $Cu_2(CH_3COO)4{\cdot}2H2O$ where the four acetates are in a *syn-syn* configuration with J = −150 cm^{-1}.[38][39] *Syn-anti* carboxylato bridges induce much smaller J values because of the expanded metallic core and a mismatch in the orientation of magnetic orbitals.[23,29,34,36] For compound **3**, the Mn−Mn intrachain distance is 5.42 Å, which is rather large. Moreover, the bridging network displays a "zig-zag" structure (see description of the structure). To the best of our knowledge, there are considerably fewer examples involving two carboxylato *syn-anti* ligands in a *cis* position than in a *trans* position. The four closest structures, studied from a magnetic point of view, found in the literature are: (a)[29] and

Table 3. Antiferromagnetic couplings for several Mn^{II} compounds (including chains, one 2D-polymer and one dimer) and related Mn−Mn distances

Compound	Mn−Mn distance[c] [Å]	Bridge	J [K]	ref.
$[(CH_3)_4N]MnCl_3$	3.25	Chloro	−6.3	[20]
$CsMnBr_3$	3.26	Bromo	−9.5	[32]
$CsMnCl_3$	4.73	Chloro	−3	[19]
$Mn[(5\text{-}NO_2\text{-salimH})MeOH(\mu\text{-}HCO_2)]$[a]	5.92	Carboxylato *anti-anti*	−0.36	[7]
$Mn[(MCPA)_2(H_2O)_2]_n$[b]	5.40	Carboxylato *syn-anti*	−0.3 to −0.4	[16]
$Mn[(bipy)_2(H_2O)_2(Me_2N\ CH_2CO_2)][ClO_4]\cdot 2H_2O$	5.67	Carboxylato *syn-anti*	−0.27	[15]
3	5.42	Carboxylato *syn-anti*	−0.25	this work

[a] 5-NO_2-salimH = 4-(2-[(5-nitrosalicylidene)amino)ethyl]imidazole. − [b] MCPA = 2-methyl-4-chlorophenoxyacetic acid. − [c] For chains, intrachain distance; for polymer, closest distance.

(b)[40][41] two copper(II) chains, (c) a copper tetranuclear cluster[28] and (d) a copper(II) ladder-like chain of dimer units with a di-μ-carboxylato.[35] Both (a) and (b) show a helix-like structure that bears a great number of structural similarities with compound **3** with a ferromagnetic coupling J/k = 2.4 and J/k = 4.0, respectively. Compound (c) also displays a ferromagnetic coupling J/k = 3.8. In compound (d), a very small antiferromagnetic coupling was estimated at −0.7 K.

The importance of the *syn-anti* conformation on the magnitude of J has previously been stressed for copper(II) compounds.[28−30] It can also be illustrated for compound **3** by some relevant comparisons. First, two structures with *syn-anti* carboxylato bridges between Mn^{II} have previously been reported and studied from a magnetic point of view: (e) a 2D-polymer[16] containing a *syn-anti* carboxylato lozenge-shaped network between Mn^{II} and (f) a discrete Mn^{II} dimer involving a mono *syn-anti* carboxylato bridge.[15] In (e), the Mn−Mn distance is 5.40 Å and an antiferromagnetic coupling J/k of −0.3 to −0.4 was estimated. In (f), the intermetallic distance is 5.67 Å with an antiferromagnetic coupling J/k = −0.27. These exchange coupling constants are of the same order and are very close to that obtained for compound **3**.[42] Another comparison can be made with a Mn^{II} chain with a dipodal *N*-centered ligand bearing one imidazole and one phenolate involving a formate bridge in a *anti-anti cis* binding mode (see Table 3).[7] The Mn−Mn distance along the chain is 5.92 Å and J/k = −0.36. Despite a larger distance, the antiferromagnetic coupling is greater than in compounds **3** and (f).[43] Presumably this is related to the *anti-anti* pattern inducing better orbital overlap.[30] The geometric characteristics of **3** (*syn-anti* carboxylato bridges, "zig-zag" structure with nonplanar Mn−O−C−O−Mn pattern) account for the very low value determined for the intrachain coupling constant (J/k = −0.25).

The value of the ratio zJ′/J = 0.4 suggests a pseudo-2D magnetic structure. The shortest Mn−Mn interchain distance is 8.42 Å, each Mn having two closest neighbors (z = 2). Two adjacent helixes seem to be connected through π-π interactions between a pyridine moiety and the imidazole group (see Figure 3). Despite the large Mn−Mn interchain distance (8.42 Å), a π-π interaction provides an effective pathway for interchain exchange interaction.

Conclusions

In this article, we have reported the structure and magnetic study of a polymeric Mn^{II} compound involving carboxylato *syn-anti cis* bridges. The compound described here is of interest for several reasons. First, it involves a carboxylato bridge that is part of a polydentate ligand and not a separate acetate. This carboxylate has been shown to be coordinated to the Mn^{II} centers in a *syn-anti* mode, affording a chiral helix-like polymeric structure. It also displays a pseudo-2D magnetic structure with a weak exchange interaction through intrachain *syn-anti cis* carboxylato bridges and a weaker interaction through interchain π-interactions. Finally, it presents a potentially open-shell. The ligand **2** is tetradentate. In the solid state, the coordination sphere of each Mn^{II} center of compound **3** is completed by a molecule of methanol and an oxygen atom (O1) from a carboxylato group from a neighboring molecule of **2**. Compound **3** is soluble in several solvents, indicating a disrupture of the polymeric structure. This probably occurs by the replacement of O1 by a further solvent molecule,[7][44] thus keeping the usual octahedral environment of Mn^{II} complexes. In solution, this compound thus bears two labile coordination sites available for substrate binding. Its reactivity towards superoxide is now under investigation.

Experimental Section

General: IR spectra (KBr) were recorded on a Bruker IFS 66 FT-IR spectrometer. ^1H NMR spectra were recorded on Brüker AM 200 and AM 250 spectrometers. X-band electron paramagnetic resonance (EPR) was recorded on a Bruker ER 200E spectrometer. Variable temperature magnetization measurements were collected on ground crystals with a Quantum Design SQUID magnetometer at a magnetic field of 1 T within the temperature range 300−2 K. Data were corrected for diamagnetism of the ligand estimated to -2.431500×10^{-4} $cm^3 \cdot mol^{-1}$ from Pascal's constant.[48] Chemical reagents were purchased either from Aldrich or Acros and used without further purification.

Synthesis and Characterization

***N*-(2-pyridylmethyl)aminoethyl acetate (1):** To a solution of 2-aminomethylpyridine (18.38 g) in 100 mL of anhydrous THF at 0°C, ethylbromoacetate (14.19 g) in 100 mL of anhydrous THF was ad-

ded dropwise. The reaction mixture was left for 30 min. at 0°C and then allowed to warm to room temperature. After 15 h, the solution was filtered and the filtrate evaporated to dryness. The residual oil was distilled under reduced pressure (0.4 Torr, 100°C), to give a colorless liquid. Yield: 75%. − ^{1}H NMR ($CDCl_3$): δ = 1.28 (t, 3 H, CH_3), 2.81 (s, 1 H, NH), 3.48 (s, 2 H, N−CH_2−COOEt), 3.96 (s, 2 H, py−CH_2−N), 4.20 (q, 2 H, O−CH_2), 7.17 (t, 1 H, H_{py}), 7.33 (d, 1 H, H_{py}), 7.64 (t, 1 H, H_{py}), 8.56 (d, 1 H, H_{py}).

Potassium *N*,*N*-[2-pyridylmethyl)(1-methylimidazol-2-yl)-methyl]-glycinate (2K): A solution of **1** (3.88 g) and *N*-methyl-2-imidazolcarboxaldehyde[45] (2.2 g) in MeOH (100 mL) was hydrogenated over (Pd/C, 10%) for 24 h. After filtration and evaporation to dryness, **2K** was obtained by hydrolysis at room temperature in H_2O/EtOH (3:1) with K_2CO_3 (2.2 equiv.) for 48 h. Residual potassium salts were partially removed by extracting the carboxylate **2K** with anhydrous MeOH. Compound **2K** was recrystallized from MeOH/EtOEt. Yield: 95%. − ^{1}H NMR (CD_3OD): δ = 2.95 (s, 2 H, N−CH_2COOK), 3.30 (s, 3 H, CH_3), 3.52 and 3.57 (2s, 2 × 2 H, N−CH_2−py and N−CH_2−Im), 6.54 and 6.64 (2s, 2 × 1 H, H_{Im}), 7.03 (t, 1 H, H_{py}), 7.14 (d, 1 H, H_{py}), 7.52 (t, 1 H, H_{py}), 8.15 (d, 1 H, H_{py}). − IR (KBr): $\tilde{\nu}$ = 1591 (ν_{asCO}), 1396 (ν_{sCO}), 771 ($\nu_{pyr.\ deform.}$), 742 ($\nu_{imid.\ deform.}$) cm^{-1} (strong bands only).

[Mn(IPG)(MeOH)]$_n$(PF$_6$)$_n$ (3): The pH of a 2 × 10^{-3} M solution of **2K** in water was adjusted by HCl addition in the 8−8.5 range. After evaporation, the solid was dried under reduced pressure for one night in the presence of P_2O_5 and KCl was removed by extraction of the ligand in anhydrous methanol. Typically, chain crystals were obtained as followed. $MnBr_2$ (330 mg) in deoxygenated MeOH (20 mL) was added to a solution of the ligand (400 mg) in deoxygenated MeOH (20 mL). It was allowed to stand for two hours at 40°C. Then, after cooling, a deoxygenated solution of NH_4PF_6 (3 equivalents) in MeOH (40 mL) was added dropwise. The solution was allowed to stand for a week during which time crystals were formed. Yield: 50%. − $C_{14}H_{19}F_6MnN_4O_3P$ (491.2): calcd C 34.2, H 3.9, N 11.4, P 6.3, Mn 11.2; found C 33.9, H 3.8, N 11.3, P 5.9, Mn 10.6. − IR (KBr): $\tilde{\nu}$ = 1606 (sh), 1571 (ν_{asCO}), 1440 (ν_{sCO}), 770 ($\nu_{pyr.\ deform.}$) 755 ($\nu_{imid.\ deform.}$) cm^{-1} (strong bands only). − The EPR spectrum was recorded on ground crystals at room temperature and 100 K. It shows a broad signal centered at g = 1.98, with no resolved hyperfine structure.

All measurements were performed with crystals or ground crystals from the same batch of crystallization.

Crystal Data, Data Collection and Refinement

Several crystals were tested for their suitability for X-ray diffraction studies. Most of them were twinned. A very thin fragment was found to be a single crystal. This pale yellow-pink crystal of 0.2 × 0.15 × 0.07 mm was mounted on an Enraf−Nonius Cad 4 diffractometer with graphite monochromated Mo-K_α radiation [λ = 0.7107Å]. The unit cell dimensions were refined from setting angles of 25 reflections [5.2 < Θ <11.6°]. Structure determination and refinement data are reported in Table 1. Data collection was performed at room temperature with Θ−2Θ scan technique mode, in the 2Θ range from 4 to 32°. Three standard reflections were measured every hour, to monitor instrument and crystal stability. A 28% decay was observed. A total of 568 reflections was collected [$-6 \le h \le 6$; $0 \le k \le 7$; $0 \le l \le 9$]. From 531 independent reflections, 509 were used [$I > 2\sigma(I)$]. These data were corrected for Lorentz and polarization factors but not for absorption factors.

The structure was solved by direct methods (program SHELXS86)[46] and refined on F^2 for all reflections by least-squares method using SHELXL-93.[47] Hydrogen atoms were calculated and included in the refinement at their ideal positions (C−H_{ar} = 0.93Å, C−H_{Me} = 0.96Å) with an isotropic thermal parameter of 1.2 for the bonded atoms. Only the manganese atom was refined anisotropically to limit the number of parameters versus the number of data.

The asymmetric unit consists of one monomeric complex cation and one counteranion (PF_6). The latter shows disorder; two different sites were found on a difference Fourier-syntheses. A better convergence was obtained with an occupancy factor of 50% and refinement was pursued with restraints. A selection of bond lengths and angles is presented in Table 2 and the crystallographic number scheme is presented in Figure 1 which shows three adjacent units along the axis *b*.

Crystallographic data (excluding structure factors) for the structure included in this paper have been deposited with the Cambridge Crystallographic Data Centre as supplementary publication no. CCDC-125980. Copies of the data can be obtained free of charge on application to CCDC, 12 Union Road, Cambridge CB2 1EZ, UK [Fax: (internat.) + 44-1223/336-033; E-mail: deposit@ccdc.cam.ac.uk].

Acknowledgments

We thank Dr. E. Rivière for his contribution to magnetic measurements and Pr T. Mallah for useful discussions.

[1] G. B. Deacon, R. J. Phillips, *Coord. Chem. Rev.* **1980**, 227−250.
[2] R. L. Rardin, W. B. Tolman, S. J. Lippard, *New J. Chem.* **1991**, *15*, 417−430.
[3] Y. Akhriff, J. Server-Carrio, A. Sancho, J. Garcia-Lozano, E. Escriva, J. V. Folgado, L. Soto, *Inorg. Chem.* **1999**, *38*, 1174−1185.
[4] M. C. Rodriguez, C. Policar, I. Morgenstern-Badarau, unpublished results.
[5] M. C. Rodriguez, I. Morgenstern-Badarau, M. Césario, J. Guilhem, B. Keita, L. Nadjo, *Inorg. Chem.* **1996**,
[6] In the IPG abbreviation, I stands for imidazole, P for pyridine and G for glycinate.
[7] M. J. Baldwin, J. W. Kampf, M. L. Kirk, V. L. Pecoraro, *Inorg. Chem.* **1995**, *34*, 5252−5260.
[8] M. I. Kay, I. Almodovar, S. F. Kaplan, *Acta Cryst.* **1968**, *B24*, 1312−1316.
[9] J. Pickworth Glusker, H. L. Carrel, *J. Mol. Strut.* **1973**, *15*, 151−159.
[10] E. F. Bertaut, T. Q. Duc, P. Burlet, P. Burlet, M. Thomas, J. M. Moreau, *Acta Cryst.* **1974**, *B30*, 2234−2236.
[11] T. Glowiak, Z. Ciunik, *Acta Cryst.* **1978**, *B34*, 1980−1983.
[12] Z. Ciunik, T. Glowiak, *Acta Cryst.* **1980**, *B36*, 1212−1213.
[13] G. Smith, E. J. O'Reilly, C. H. L. Kennard, *J. Chem. Soc., Dalton Trans.* **1980**, 2462−2466.
[14] Z. Ciunik, T. Glowiak, *Acta Cryst.* **1981**, *B37*, 693−695.
[15] X.-M. Chen, Y.-X. Tong, Z.-T. Xu, T. C. W. Mak, *J. Chem. Soc., Dalton Trans.* **1995**, 4001−4004.
[16] V. Tangoulis, G. Psomas, C. Dendrinou-Samara, C. P. Raptopoulou, T. A., D. P. Kessissoglou, *Inorg. Chem.* **1996**, *35*, 7655−7660.
[17] M. E. Fisher, *Ann. J. Phys.* **1964**, *32*, 343−346.
[18] O. Kahn, *Molecular magnetism*, VCH, New York, 1993.
[19] T. Smith, S. A. Friedberg, *Phys. Rev.* **1968**, 660−665.
[20] R. Dingle, M. E. Lines, S. L. Holt, *Phys. Rev.* **1969**, *187*, 643−648.
[21] C. Dupas, J.-P. Renard, *Phys. Rev. B* **1978**, *18*, 401−407.
[22] B. E. Myers, L. Berger, S. A. Friedberg, *J. Appl. Phys.* **1969**, *40*, 1149−1151.
[23] D. K. Towle, S. K. Hoffmann, W. E. Hatfield, P. Singh, P. Chaudhuri, *Inorg. Chem.* **1988**, 394−399.
[24] B. Chiari, A. Cinti, L. David, F. Ferraro, D. Gatteschi, O. Piovesana, P. F. Zanazzi, *Inorg. Chem.* **1996**, 7413−7418.
[25] W. Chiang, M. D. Ho, D. Van Engen, M. E. Thompson, *Inorg. Chem.* **1993**, *32*, 2886−2893.

[26] C. H. Görbitz, M. C. Etter, *J. Am. Chem. Soc.* **1992**, *114*, 627−631.
[27] C. Hemmert, M. Verelst, J.-P. Tuchagues, *Chem. Commun.* **1996**, 617−618.
[28] E. Colacio, J.-P. Costes, R. Kivekäs, J.-P. Laurent, J. Ruiz, *Inorg. chem.* **1990**, *29*, 4240−4246.
[29] E. Colacio, J.-M. Dominguez-Vera, J.-P. Costes, R. Kivekäs, J.-P. Laurent, J. Ruiz, M. Sundberg, *Inorg. Chem.* **1992**, *31*, 774−778.
[30] E. Colacio, J.-M. Dominguez-Vera, R. Kivekäs, J. M. Moreno, A. Romerosa, J. Ruiz, *Inorg. Chim. Acta* **1993**, *212*, 115−121.
[31] W. Clegg, O. M. Lacy, B. P. Straughan, *Acta Cryst.* **1987**, *C*, 794−797.
[32] A. Bencini, D. Gatteschi, in *EPR of Exchange Coupled Systems*, Spinger-Verlag, Berlin, **1990**, pp 235−239.
[33] P. R. Levstein, R. Calvo, *Inorg. Chem.* **1990**, *29*, 1581−1583.
[34] R. L. Carlin, K. Kopinga, O. Kahn, M. Verdaguer, *Inorg. Chem.* **1986**, *25*, 1786−1786.
[35] P. K. Coughlin, S. J. Lippard, *J. Am. Chem. Soc.* **1984**, *106*, 2328−2336.
[36] F. Lloret, M. Julve, R. Ruiz, Y. Journeaux, K. Nakatani, O. Kahn, J. Sletten, *Inorg. Chem.* **1993**, *32*, 37−31.
[37] C. Albonico, A. Bencini, *Inorg. Chem.* **1988**, *27*, 1934−1940.
[38] B. Bleaney, K. D. Bowers, *Proc. Roy. Soc. London, A* **1952**, *214*, 451.
[39] B. N. Figgis, R. L. Martin, *J. Chem. Soc.* **1956**, 3837.
[40] D. Schulz, T. Weyhermüller, K. Wieghardt, C. Butzlaff, A. X. Trautwein, *Inorg. Chim. Acta* **1996**, *246*, 387−394.
[41] M. Studer, A. Riesen, T. A. Kaden, *Helv. Chim. Acta* **1989**, *72*, 307−312.
[42] We are grateful to one of the referees for suggesting this comparison.
[43] The J value estimated for the 2D-polymer is higher, but one should note that it was more roughly estimated (see ref.[16]).
[44] J. A. Bonadies, M. J. Maroney, V. L. Pecoraro, *Inorg. Chem.* **1989**, 2044−2051.
[45] P. E. Iberson, H. Lund, *Acta Chem. Scand.* **1966**, *20*, 2649.
[46] G. M. Sheldrick, *Acta Crystallogr., Sect. A* **1990**, *46*, 467.
[47] G. M. Sheldrick, *Program for the Refinement of Crystal Structures* **1993**, University of Göttingen, Germany.
[48] A. Earnshaw, *Introduction to Magnatochemistry*, Academic Press, London, **1968**.

Received July 16, 1999
[I99254]

Formation of Calcium–Carbon Bonds From a Lewis Acid-Base Reaction of Calcium Bis[bis(trimethylsilyl)amide] and Tris(trimethylsilylmethyl)alane

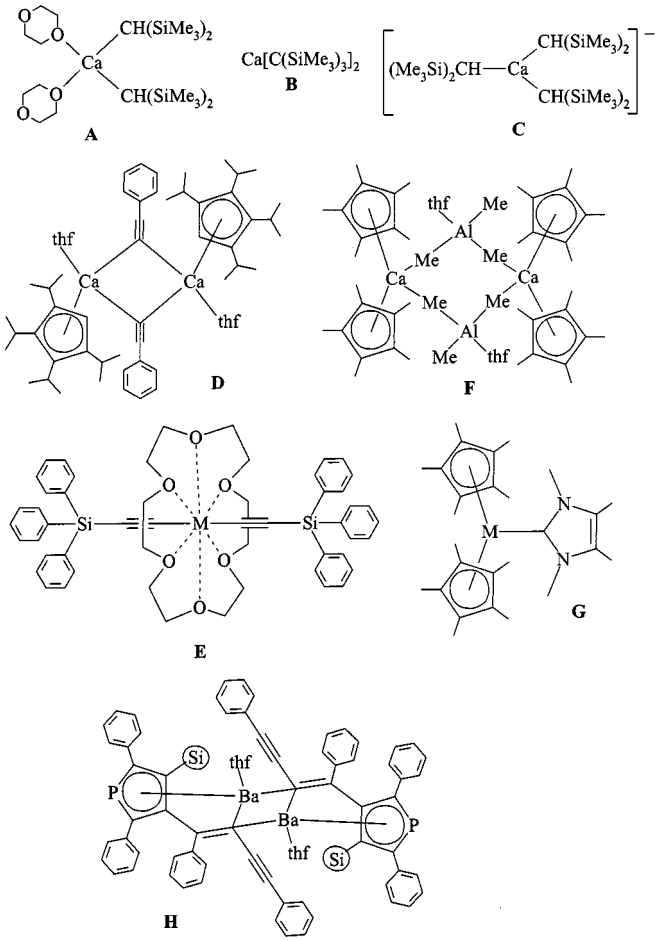
Matthias Westerhausen,*[a] Christin Birg,[a] Heinrich Nöth,[a][+] Jörg Knizek,[a][+] and Thomas Seifert[a][+]

Keywords: Aluminium / Amides / Calcium / Metallacycles / Phosphorus

Treatment of calcium bis[bis(trimethylsilyl)amide] with two equivalents of tris(trimethylsilylmethyl)alane yields $(Me_3SiCH_2)_2Al–N(SiMe_3)_2$ (**1**) and the dimer $[(Me_3Si)_2N–Ca(\mu–CH_2SiMe_3)_2Al(CH_2SiMe_3)2]_2$ (**2**). The five-coordinate bridging carbon atoms show Ca–C bond lengths of 264 and 268 pm. A similar reaction with calcium bis[bis(trimethylsilyl)phosphanide] gives the dimer $[(Me_3SiCH_2)_2Al–P(SiMe_3)_2]_2$ (**3**) with crystallographic *C*2 symmetry. A calcium-containing species is not isolable, however, in the presence of DME – ether cleavage reactions and the formation of the centrosymmetric dimer $[(Me_3SiCH_2)_2Al–OCH_2CH_2OMe]_2$ (**4**) are observed. The central moiety is an Al_2O_2 cycle with fivefold coordinated aluminium centers.

Introduction

In contrast to the well-developed chemistry of organo lithium compounds and the widely used Grignard reagents, only a few examples of compounds with σ-bonds between carbon and the heavier alkaline earth metals have been structurally characterized (Scheme 1). Several years ago Lappert and co-workers[1] reported the bis(1,4-dioxane) complex of bis[bis(trimethylsilyl)methyl] calcium **(A)** with Ca−C bond lengths of 248 pm. Solvent-free bis[tris(trimethylsilyl)methyl] calcium **(B)** crystallizes with a bent C−Ca−C moiety of 150° and Ca−C distances of 246 pm.[2] Compound **A** was prepared by a co-condensation reaction of calcium and bis(trimethylsilyl)methyl bromide. The metathesis reaction of $KC(SiMe_3)_3$ and calcium diiodide gave compound **B**. The reaction of alkaline earth metal arenesulfonates with bis(trimethylsilyl)methyl lithium or potassium yields alkali metal [tris(alkyl)alkaline earth metalates] **C**.[3] The metalation reaction is only applicable to organic substrates with acidic hydrogen atoms such as phenylacetylene as shown by Burkey and Hanusa[4] for the synthesis of $[(\eta^5\text{-}i\text{Pr}_4C_5H)Ca–C\equiv C–Ph]_2$ **(D)**. The crown ether complexes of the heavier alkaline earth metal bis(triphenylsilylacetylides) **E** display bent M−C≡C fragments.[5] The tetrahydrofuran complex of trimethylaluminium, which can act as a bridging ligand between the metal centers of decamethylcalcocene **F**, shows very long Ca−C distances of 295 and 300 pm.[6] Recently, the structures of the carbene complexes **G** were published by Arduengo and co-workers.[7] The dimeric barium compound **H** contains a central planar Ba_2C_2 cycle with Ba−C bond lengths of 288 and 307 pm.[8] In contrast to these rare examples of M−C σ-bonds numerous alkaline earth metallocenes have been reported.[9]



Scheme 1. Well-characterized molecules with alkaline earth metal−carbon σ-bonds (M = Ca, Sr, Ba); alkaline earth metallocenes and similar compounds are not considered

The reaction of trialkylalanes with alkaline earth metal bis(amides)[10] and bis(phosphanides)[10] seems to be an-

[a] Institut für Anorganische Chemie der Ludwig-Maximilians-Universität,
Butenandtstr. 5−13 (Haus D), D-81377 München, Germany
Fax: (internat.) + 49-89/2180-7867
E-mail: maw@cup.uni-muenchen.de
[+] X-ray structure analysis

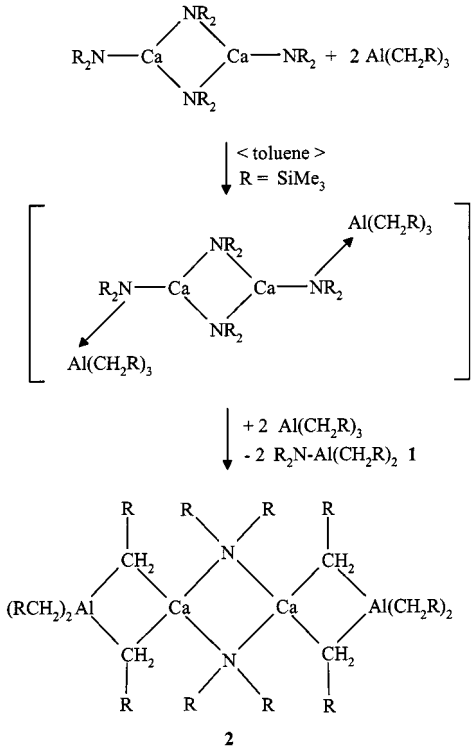
 © WILEY-VCH Verlag GmbH, D-69451 Weinheim, 1999 1434−1948/99/1212−2209 $ 17.50+.50/0

other promising access to alkaline earth metal−carbon bonds. Magnesium bis(dialkylamide) reacts with trialkylaluminium to give the heteroleptic, dimeric alkylmagnesium dialkylamide and a dialkylamino dialkylalane.[11] Herein we report the results of the Lewis acid-base reaction between $Ca[E(SiMe_3)_2]_2$ (E = N, P) and tris(trimethylsilylmethyl)alane.

Results and Discussion

Synthesis

The addition reaction of tris(trimethylsilylmethyl)alane[12] and solvent-free calcium bis[bis(trimethylsilyl)amide][13] in a 2:1 molar ratio in toluene leads to a Lewis acid-base complex, although this compound could not be isolated. According to Equation 1 the elimination of bis(trimethylsilylmethyl)aluminium-bis(trimethylsilyl)amide **(1)** occurs spontaneously. Compound **1** can be removed from the reaction mixture in vacuo at elevated temperatures. Cooling of the concentrated reaction solution leads to the precipitation of crystalline dimeric calcium bis(trimethylsilyl)amide-tetrakis(trimethylsilylmethyl)aluminate **(2)**. The steric shielding of the central Ca_2N_2 cycle prevents another Lewis acid-base reaction even with a large excess of tris(trimethylsilylmethyl)alane in the reaction mixture. To allow the spectroscopic characterization of analytically pure compound **1** the metathesis reaction was performed with $[(Me_3SiCH_2)_2AlCl]_2$[14] and two equivalents of lithium bis(trimethylsilyl)amide according to Equation 2. The NMR spectra show three chemically different trimethylsilyl groups, which could be due to dimerization of **1**. However, in the mass spectrum the molecular ion of the monomer is the highest peak.



Equation 1. Synthesis of calcium aluminate **2**

$$(RCH_2)_2Al(\mu\text{-}Cl)_2Al(CH_2R)_2 + 2\ LiNR_2 \rightarrow 2\ (RCH_2)_2AlNR_2 + 2\ LiCl$$

R = $SiMe_3$ **1**

Equation 2. Synthesis of bis(trimethylsilylmethyl)aluminium bis(trimethylsilyl)amide **1**

Thus far, the use of calcium bis[bis(trimethylsilyl)phosphanide][10][15] as a synthon for the preparation of calcium−carbon bonds has failed. Solvent-free $Ca[P(SiMe_3)_2]_2$ is insoluble in aromatic and aliphatic hydrocarbons. The addition of $Al(CH_2SiMe_3)_3$ to a suspension of this calcium bis(phosphanide) in toluene leads to a clear solution. A $^{31}P\{^1H\}$ NMR spectroscopic investigation of the reaction reveals the formation of $[(Me_3SiCH_2)_2Al-P(SiMe_3)_2]_2$ **(3)**.[16] Nonetheless, an aluminate or a trimethylsilylmethyl calcium moiety could not be isolated. Compound **3** crystallizes from toluene and has a melting point of 218°C, approximately 20°C higher than reported by Wells and coworkers.[16] The spectroscopic data are consistent with a dimeric molecule of **3**. Performing this Lewis acid-base reaction in the presence of ethers such as tetrahydrofuran (THF) or 1,2-dimethoxyethane (DME) as solvents leads to an ether cleavage reaction. With DME, $[(Me_3SiCH_2)_2Al-OCH_2CH_2OMe]_2$ **(4)** with a central Al_2O_2 cycle was formed as one of the reaction products, although the isolation of an analytically pure product was not possible. The use of ether complexes and ether solutions seems to limit these Lewis acid-base reactions as a suitable pathway to calcium−carbon σ-bonds. The reactivity of alanes towards ethers has already been reported by Uhl[17] and Roesky.[18] Similar ether cleavage reactions have also been observed for bis[tris(trimethylsilyl)methyl] calcium **(B)**.[2] Treatment of **3** with DME also gives such reactions. Besides compound **4**, some unidentified substances were detected, although purification failed due to co-crystallization with side products.

Spectroscopic Characterization

The aluminate anion of **2** shows simple NMR spectra consistent with a free rotation. Even at temperatures of −70°C it is not possible to halt the exchange process of the bridging and terminal trimethylsilylmethyl substituents. The negative charge leads to a high-field shift of the CH_2 group relative to compounds **1** and **3**. The $^{29}Si\{^1H\}$ NMR chemical shift (δ = −8.47) of the bis(trimethylsilyl)amido ligand bridging the calcium atoms clearly proves that this complex remains dimeric in toluene solution. One would expect a value of approximately δ = −15 for terminally bonded $(Me_3Si)_2N$ substituents[10][13] whereas a low-field shift of 6 to 8 ppm is characteristic of a bridging ligand with a quadruply coordinated nitrogen atom at calcium.

Molecular Structures

Compound **2** crystallizes in the monoclinic space group $P2_1/n$. Figure 1 shows the molecular structure and the numbering scheme. The bonding situation of the bridging tri-

methylsilylmethyl group with the freely refined hydrogen atoms is depicted in Figure 2. The central, planar Ca_2N_2 cycle with Ca1−N1 and Ca1−N1′ bond lengths of 240.7(2) and 248.7(2) pm, respectively, is slightly distorted although the values lie within the expected range.[10][13] The Ca1−C1 and Ca1−C2 distances [267.8(3) and 263.8(3) pm] are approximately 20 pm longer than in the above mentioned dialkyl calcium derivatives **A**[1] und **B**.[2] Similar values were obtained by Hanusa and co-workers[19] for bis[1,3-bis(trimethylsilyl)allyl]calcium. The bridging Me_3SiCH_2 substituents of **2** also show longer Al1−C distances [206.9(3) and 208.1(3) pm] compared to the terminal Al1−C3 and Al1−C4 bond lengths [198.9(3) and 199.7(3) pm]. The values for the terminal Al−C distances are in agreement with those in Al_2Me_6 [196(1) and 198(1) pm[20]] and are larger than in Al_2Ph_6 [195.6(5) and 196.0(5) pm[21]] as well as in Al2^{i}Pr6 [mean value 193(1) pm].[22] The rather large Ca−C distances and the short Al−C bonds to the bridging Me_3SiCH_2 groups in **2** compared to Al_2Me_6 [213(1) and 215(1) pm[20]] and Al_2Ph_6 [218.0(5) and 218.4(5) pm[21]] are a consequence of the distorted trigonal bipyramid coordination polyhedron of C1 and C2. The aluminium atom is located in the equatorial plane whereas the calcium atom is in an axial position. The other axial bonded group is the trimethylsilyl substituent. Therefore, the C1−Si1 and C2−Si2 bond lengths (mean value 189.6 pm) are elongated compared to C3−Si3 and C4−Si4 (mean value 185.2 pm).

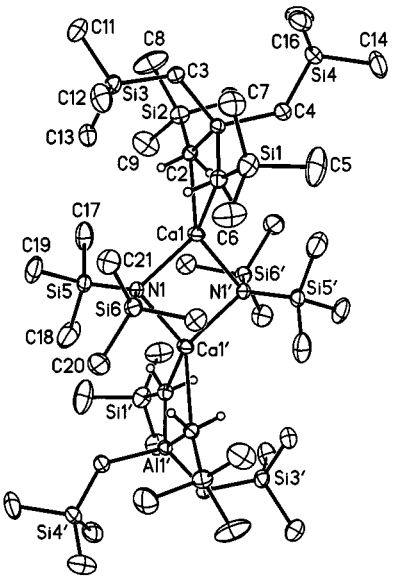


Figure 1. Molecular structure and numbering scheme of **2**; the ellipsoids represent a probability of 40%; hydrogen atoms with the exception of those at C1 and C2 are omitted for clarity reasons; symmetry-related atoms ($-x + 2, -y, -z$) are marked with an apostrophe; selected bond lengths (pm) and angles (°): Ca1−N1 240.7(2), Ca1−N1′ 248.7(2), Ca1−C1 267.8(3), Ca1−C2 263.8(3), Al1−C1 206.9(3), Al1−C2 208.1(3), Al1−C3 198.9(3), Al1−C4 199.7(3), C1−Si1 190.1(3), C2−Si2 189.2(3), C3−Si3 185.3(3), C4−Si4 185.0(3), N1−Si5 175.3(2), N1−Si6 174.1(2); N1−Ca1−N1′ 90.88(7), Ca1−C1−Al1 85.5(1), Ca1−C1−Si1 153.3(2), Al1−C1−Si1 117.8(2), Ca1−C2−Al1 86.3(1), Ca1−C2−Si2 154.2(1), Al1−C2−Si2 119.1(1), Al1−C3−Si3 123.6(2), Al1−C4−Si4 127.0(2)

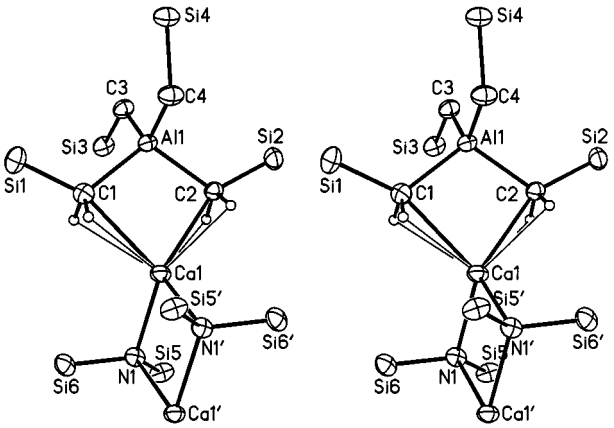


Figure 2. Stereoscopic representation of the coordination sphere at Ca1 of compound **2**; selected H-atoms are drawn with arbitrary radii, whereas all non-hydrogen atoms are represented on a 40% probability level; symmetry-related atoms ($-x + 2, -y, -z$) are marked with an apostrophe; the Ca−H interactions are represented by thin lines

The close contact Ca1···Al1 of 325.38(9) pm as well as the small bond angles Ca1−C1−Al1 and Ca1−C2−Al1 of 85.5(1)° and 86.3(1)°, respectively, can be described as two electron-three center bonds. On the other hand, an ionic arrangement with the calcium dication bonding to the C1−H as well as C2−H bonds (agostic interactions) could also explain the geometry of these bridging methylene fragments. As a consequence of these attractions small Ca1−C−H angles of between 57(2)° and 74(2)° as well as short Ca1···H contacts of between 232(3) and 258(3) pm are observed.

Figure 3 shows the molecular structure of **3**. Wells and co-workers[16] previously deduced the dimeric nature of **3** from NMR spectroscopic data. The Al1−P1 bond length of 248.0(1) pm is shorter than the Al−P distance of the adduct $(Me_3SiCH_2)_3Al-P(SiMe_3)_3$ [268.1(4) pm[16]] but in the same range as for $(Me_3SiCH_2)_2Al(Br)-P(SiMe_3)_3$ [249.8(7) pm[16]] and in the dimer $[(Me_3SiCH_2)Al(Br)-P(SiMe_3)_2]_2$ [243.6(2) pm[16]] with four-coordinate aluminium and phosphorus atoms. In comparison with the dimer with ethyl groups at the aluminium atom, the endocyclic bond lengths in **3** are elongated and a slight distortion is observed {$[Et_2Al-P(SiMe_3)_2]_2$: P−Al 246.0(1) and 245.4(1) pm, Al−P−Si: 114.21(5) and 114.46(5)°;[23] **3**: P−Al 248.0(1) and 248.6(1) pm, Al−P−Si: 112.07(4) and 115.93(5)°}.

The molecular structure of compound **4** is represented in Figure 4. The aluminium centers exhibit a trigonal bipyramidal geometry with the atoms O1′ and O2 in apical positions. Ring strain leads to a bent O1′−Al1−O2 geometry of 150.73(4)°. Due to the anionic charge on O1 (alcoholate oxygen), the Al1−O1 distance is smaller than the Al1−O2 distance [226.8(1) pm]. In agreement with the Gillespie−Nyholm rules the apical Al1−O1′ bond [190.3(1) pm] is slightly lengthened relative to the equatorial Al1−O1 bond [184.6(1) pm]. The Al−O distances lie in the range of known alkyl-substituted aluminium alkoxides obtained from ether cleavage reactions. There are a few reports of

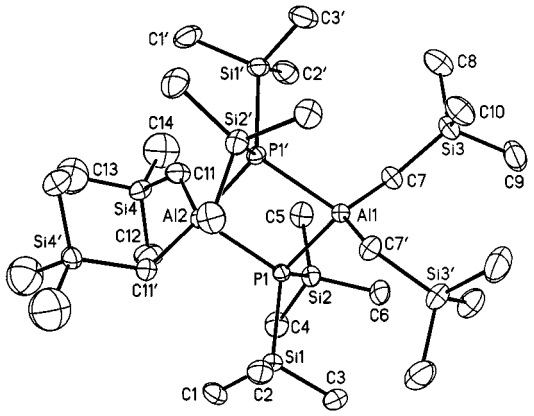


Figure 3. Molecular structure and numbering scheme of **3**: the ellipsoids are drawn at a 40% probability level and the hydrogen atoms omitted for clarity. Symmetry-related atoms ($-x$, y, $-z$ + 0.5) are marked with an apostrophe; selected bond lengths (pm) and angles (°): P1−Al1 248.0(1), P1−Al2 248.6(1), P1−Si1 226.7(1), P1−Si2 226.8(1), Al1−C7 196.9(4), Al2−C11 196.3(4), C7−Si3 186.8(3), C11−Si4 183.6(3); Al1−P1−Al2 91.48(4), Si1−P1−Si2 104.55(5), C7−Al1−C7′ 119.6(2), C11−Al2−C11′ 121.9(2)

the cleavage of DME[17] and THF[18] during reduction of trimethylsilyl-substituted alkyl aluminium halides and the formation of the corresponding alkyl aluminium alcoholates. The Al1−C1 and Al1−C5 distances of 198.3(1) and 196.9(1) pm in **4** are similar to the values observed for **2**.

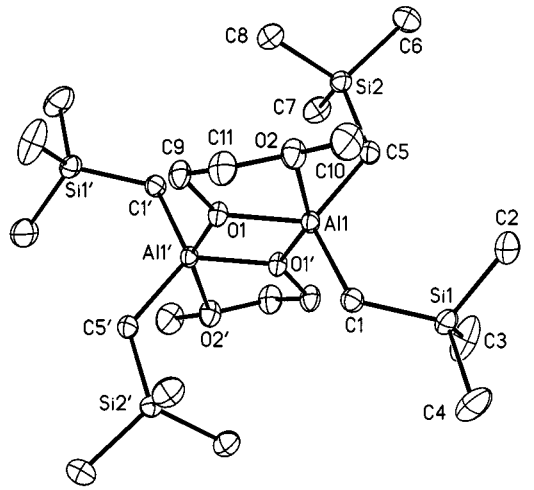


Figure 4. Molecular structure and numbering scheme of **4**; the ellipsoids represent a probability of 40%; the hydrogen atoms are omitted for clarity; symmetry-related atoms ($-x$ + 1, $-y$, -$-z$) are marked with an apostrophe; selected bond lengths (pm) and angles (°): Al1−O1 184.6(1), Al1−O1′ 190.3(1), Al1−O2 226.8(1), Al1−C1 198.3(1), Al1−C5 196.9(1); O1−Al1−O1′ 75.68(5), O1−Al1−O2 75.32(4), O1−Al1−C1 115.19(5), O1−Al1−C5 124.72(5), O1′−Al1−O2 150.73(4), O1′−Al1−C1 103.20(6), O1′−Al1−C5 103.69(6), O2−Al1−C1 92.59(6), O2−Al1−C5 89.67(6), C1−Al1−C5 118.43(6)

Conclusion

These experiments show that ether has to be excluded during the Lewis acid-base reactions of calcium bis(amides) and bis(phosphanides) with alanes. Furthermore, only calcium bis[bis(trimethylsilyl)amide] seems to be a valuable synthon for the strategy presented here because the heavier homologous phosphanides are insoluble in common organic solvents in the absence of ether. Thus far it has not been possible to eliminate another molecule of **1** from heteroleptic **2** to obtain bis(trimethylsilylmethyl)calcium

Experimental Section

General Remarks: All experiments and manipulations were carried out under argon or nitrogen purified by passage through BTS catalyst and P_4O_{10}. Reactions were performed with standard Schlenk techniques. All solvents were dried and thoroughly deoxygenated prior to use. The starting materials $Ca[N(SiMe_3)_2]_2$,[13] $(THF)_2Ca[P(SiMe_3)_2]_2$,[15] $ClAl(CH_2SiMe_3)_2$[14] and $Al(CH_2SiMe_3)_3$[12] were prepared according to literature procedures. NMR spectra were recorded on Jeol GSX270 and EX400 spectrometers. A Perkin−Elmer Paragon 1000 PC spectrophotometer was used to record the IR spectra; solid compounds were examined as Nujol mulls between CsBr plates (vs very strong, s strong, m medium strong, w weak, vw very weak, sh shoulder). The frequencies in the region of the Nujol vibrations are not listed. The low carbon values in the elemental analysis originate from carbide and carbonate formation during combustion of the compounds.

Bis(trimethylsilylmethyl)aluminium-bis(trimethylsilyl)amide (1). − Method 1: $Al(CH_2SiMe_3)_3$ (2.1 g; 8.96 mmol) was dropped slowly at 0°C into a solution of calcium bis[bis(trimethylsilyl)amide] dimer (1.62 g, 2.24 mmol) in 25 mL of toluene. After complete addition, the solution was heated under reflux for five hours. Vacuum distillation yielded pyrophoric **1** (1.1 g, 1.52 mmol, 68%). The residue consisted mainly of compound **2**.

Method 2: At room temp. $ClAl(CH_2SiMe_3)_2$ (1.15 g, 4.87 mmol) was added to a solution of lithium bis(trimethylsilyl)amide (0.82 g, 4.88 mmol) dissolved in 12 mL of toluene. Colorless LiCl precipitated immediately. After heating for four hours at approximately 100°C the NMR spectra showed a quantitative reaction. After removal of the solid materials vacuum distillation gave **1** (2.64 g, 3.65 mmol, 75%), b.p. 86°C/0.15 Torr. − ^{1}H NMR ([D$_8$]toluene): δ = −0.51 (broad) and −0.45 [CH_2], 0.11 [$CSiMe_3$], 0.13 and 0.18 [$NSiMe_3$]. − ^{13}C NMR ([D$_8$]toluene): δ = 2.40 [$NSiMe_3$, ^1J(H−C) = 117.8 Hz]. − ^{29}Si{^{1}H} NMR ([D$_8$]toluene): δ = −0.24 and −2.50, 0.11. − IR: $\tilde{\nu}$ = 2953 vs, 2901 m, 1647 vw, 1616 vw, 1587 vw, 1436 w, 1408 w, 1346 vw, 1250 vs, 1182 m, 1133 vw, 1056 m, 985 m, 934 s, 915 s, 887 s, 839 vs, 750 s, 682 m, 618 m, 575 m cm^{-1}. − MS (70 eV); *m*/*z* (%): 362 (3)[M^+], 347 (9)[M^+ − Me], 274 (70)[$Me_9Si_3CH_2AlN^+$ or $Me_9Si_3(CH_2)_2Al^+$], 201 (85)-[$Me_6Si_2CH_2AlN^+$ or $Me_6Si_2(CH_2)_2Al^+$], 160 (93) [$NSi_2Me_6^+$], 146 (100), 128 (100) [$Me_3SiCH_2AlN^+$]. − $C_{14}H_{40}AlNSi_4$ (361.81): calcd. C 46.47, H 11.14, N 3.87; found C 45.48, H 11.15, N 3.55.

Calcium Bis(trimethylsilyl)amide-tetrakis(trimethylsilylmethyl)aluminate (2): At 0°C tris(trimethylsilylmethyl)alane (2.4 g, 10.32 mmol) was added slowly to a solution of dimeric calcium bis[bis(trimethylsilyl)amide] (1.92 g, 2.67 mmol) in 25 mL of toluene. This solution was stirred at room temp. for an additional four days. During this time the solution turned slightly cloudy. After evaporation of solvent to 15 mL colorless crystals of **2** (1.1 g, 0.95 mmol, 36%) precipitated at 0°C, m.p. 81°C (dec.). − ^{1}H NMR ([D$_8$]toluene): δ = −0.89 [CH_2], 0.27 [$NSiMe_3$], 0.28 [$CSiMe_3$]. − ^{13}C{^{1}H} NMR ([D$_8$]toluene): δ = 3.04 [$CSiMe_3$], 5.53 [$NSiMe_3$], 10.09 [CH_2]. − ^{29}Si{^{1}H} NMR ([D$_8$]toluene): δ = −8.47 [$NSiMe_3$], 2.07

Table 1. Crystallographic data for **2, 3** and **4** as well as details of the structure solution and refinement procedures[a]

Compound	**2**	**3**	**4**
formula	$C_{22}H_{62}AlCaNSi_6$	$C_{28}H_{80}Al_2P_2Si_8$	$C_{22}H_{58}Al_2O_4Si_4$
fw [g·mol^{-1}]	576.33	757.54	553.00
T [K]	173(2)	193(2)	183(2)
space group[26]	$P2_1/n$	$Pbcn$ (no. 60)	$P\bar{1}$ (no. 2)
a [pm]	1284.63(3)	1263.4(4)	920.38(2)
b [pm]	1666.51(3)	2084.8(6)	984.26(2)
c [pm]	1732.20(2)	1842.1(4)	1025.55(1)
α [°]	90	90	71.615(1)
β [°]	94.780(1)	90	88.770(1)
γ [°]	90	90	78.804(1)
V [nm^3]	3695.5(1)	4852(2)	864.05(3)
Z	4	4	1
d_{calcd} [g·cm^3]	1.036	1.037	1.063
μ [mm^{-1}]	0.399	0.340	0.245
F(000)	1272	1664	304
scan range [°]	13.62<2θ<50.70	13.66<2θ<46.52	4.18<2θ<57.76
measured data	18228	16721	5067
unique data (R_{int})	5919 (0.0419)	2674 (0.0245)	2729(0.0142)
absorption. corr.	none	semi-empirical	semi-empirical
max./min. transmission		0.694/0.594	0.9526/0.8873
parameters	330	194	152
restraints	0	12	0
wR_2[a] (all data, on F^2)	0.0953	0.1089	0.0769
R_1[a] (all data)	0.0660	0.0467	0.0317
data with $I > 2\sigma(I)$	4820	2430	2443
R_1 [$I > 2\sigma(I)$]	0.0470	0.0414	0.0275
goof s[b] on F^2	1.169	1.094	1.071
residual dens. [e·nm^{-3}]	0.270/-0.199	0.578/-0.314	0.273/-0.180

[a] Definition of the R values: $R_1 = (\Sigma||F_o|-|F_c||)/\Sigma|F_o|$; w$R_2 = \{\Sigma[w(F_o^2-F_c^2)^2]/\Sigma[w(F_o^2)^2]\}^{1/2}$ with $w^{-1} = \sigma^2(F_o^2) + (aP)^2$. – [b] $s = \{\Sigma[w(F_o^2-F_c^2)^2]/(N_o-N_p)\}^{1/2}$.

[$CSiMe_3$]. – IR (nujol): $\tilde{\nu}$ = 1599 w, 1561 vw, 1405 w, 1345 vw, 1295 sh, 1247 vs, 1181 w, 960 vs, 933 s, 883 vs, 855 vs, 828 vs, 785 m, 754 s, 694 m, 681 m, 640 w, 617 w, 604 w, 587 m, 578 m, 538 w, 519 w, 491 vw, 450 w, 422 w, 404 w, 362 w, 330 vw, 306 w cm^{-1}. – $C_{44}H_{124}Al_2Ca_2N_2Si_{12}$ (1152.66): calcd. C 45.85, H 10.84, N 2.43; found C 43.45, H 10.33, N 2.59.

Bis(trimethylsilylmethyl)aluminium-bis(trimethylsilyl)phosphanide (3): To a solution of magnesium bis[bis(trimethylsilyl)phosphanide] (1.00 g, 2.65 mmol) in 20 mL of toluene $Al(CH_2SiMe_3)_3$ (2.4 g, 10.32 mmol) was added slowly at room temp. After stirring for 48 hours the solution was reduced in volume to 12 mL. At −15°C colorless crystals of **3** (1.4 g, 1.85 mmol, 70%) precipitated, m.p. 218°C. – ^{1}H NMR ([D$_8$]toluene): δ = −0.21 [CH_2, ^3J(H−P) = 2.6 Hz], 0.33 [$CSiMe_3$], 0.48 [$PSiMe_3$, ^3J(H−P) = 2.4 Hz]. – ^{13}C{^{1}H} NMR ([D$_8$]toluene): δ = 2.18 [CH_2], 3.82 [$CSiMe_3$], 4.98 [$PSiMe_3$, $|^1J$(C−P) + ^3J(C−P)| = 8.4 Hz]. – ^{29}Si{^{1}H} NMR ([D$_8$]toluene): δ = 0.23 [$CSiMe_3$, ^3J(Si−P) = 3.4 Hz], 6.38 [$PSiMe_3$, $|^1J$(Si−P) + ^3J(Si−P)| = 6.2 Hz]. – ^{31}P{^{1}H} NMR ([D$_8$]toluene): δ = −231.49. – IR (nujol): $\tilde{\nu}$ = 1439 w, 1401 w, 1348 w, 1312 w, 1242 s, 964 s, 941 m, 854 vs, 838 vs, 826 vs, 754 s, 747 s, 685 m, 639 m, 626 m, 559 m, 525 m, 446 m, 422 m, 360 m, 320 vw, 285 w cm^{-1}. – MS (70 eV, selected peaks); m/z (%): 596 (7) [$Al_2P_2Si_7Me_{21}^+$], 468 (35) [$(Me_3Si)_4P_2AlCH_2SiMe_3^+$], 378 (100) [$(Me_3Si)_2PAlCH_2SiMe_3^+$]. This compound has already been described by Wells and co-workers,[16] however, the spectroscopic data differ slightly.

X-ray Structure Determinations of 2, 3 and 4:[24] The single crystals were covered with nujol[25] and mounted on a Siemens P4 diffractometer with graphite monochromated Mo-K_α radiation (λ = 71.073 pm). A Siemens SMART−CCD area detector was used to monitor the reflections. Crystallographic parameters and details of data collection are summarized in Table 1.

All structures were solved by direct methods and refined with the software packages SHELXL-93 and SHELXL-97.[27] Neutral scattering factors were taken from Cromer and Mann[28] and for the hydrogen atoms from Stewart et al.[29] The non-hydrogen atoms were refined anisotropically. The H-atoms were considered with a riding model under restriction of ideal symmetry at the corresponding atom.

Acknowledgments

We thank the "Deutsche Forschungsgemeinschaft" (DFG) and the "Fonds der Chemischen Industrie" for generous financial support. C. B. is also grateful to the German state of Bavaria for a scholarship.

[1] F. G. N. Cloke, P. B. Hitchcock, M. F. Lappert, G. A. Lawless, B. Royo, *J. Chem. Soc., Chem. Commun.* **1991**, 724.
[2] C. Eaborn, S. A. Hawkes, P. B. Hitchcock, J. D. Smith, *Chem. Commun.* **1997**, 1961.
[3] A. D. Frankland, M. F. Lappert, *J. Chem. Soc., Dalton Trans.* **1996**, 4151.
[4] D. J. Burkey, T. P. Hanusa, *Organometallics* **1996**, *15*, 4971.
[5] D. C. Green, U. Englich, K. Ruhlandt-Senge, *Angew. Chem.* **1999**, *111*, 365; *Angew. Chem. Int. Ed.* **1999**, *38*, 354.
[6] P. S. Tanner, R. A. Williams, T. P. Hanusa, *Inorg. Chem.* **1993**, *32*, 2234.
[7] A. J. Arduengo, F. Davidson, R. Krafczyk, W. J. Marshall, M. Tamm, *Organometallics* **1998**, *17*, 3375.
[8] M. Westerhausen, M. H. Digeser, H. Nöth, T. Seifert, A. Pfitzner, *J. Am. Chem. Soc.* **1998**, *120*, 6722.
[9] [9a] P. Jutzi, *Adv. Organomet. Chem.* **1986**, *26*, 217. [9b] P. Jutzi, *J. Organomet. Chem.* **1990**, *400*, 1. [9c] P. Jutzi, N. Burford, *Chem. Rev.* **1999**, *99*, 969 and literature cited therein.
[10] [10a] M. Westerhausen, *Trends Organomet. Chem.* **1997**, *2*, 89. [10b] M. Westerhausen, *Coord. Chem. Rev.* **1998**, *176*, 157.

[11] T.-Y. Her, C.-C. Chang, G.−H. Lee, S.-M. Peng, Y. Wang, *Inorg. Chem.* **1994**, *33*, 99.
[12] O. T. Beachley, C. Tessier-Youngs, R. G. Simmons, R. B. Hallock, *Inorg. Chem.* **1982**, *21*, 1970.
[13] [13a] M. Westerhausen, *Inorg. Chem.* **1991**, *30*, 96. [13b] M. Westerhausen, W. Schwarz, *Z. Anorg. Allg. Chem.* **1991**, *604*, 127.
[14] S. Al−Hashimi, J. D. Smith, *J. Organomet. Chem.* **1978**, *153*, 253.
[15] [15a] M. Westerhausen, W. Schwarz, *J. Organomet. Chem.* **1993**, *463*, 51. [15b] M. Westerhausen, W. Schwarz, *Z. Anorg. Allg. Chem.* **1996**, *622*, 903.
[16] R. L. Wells, E. E. Foos, A. L. Rheingold, G. P. A. Yap, L. M. Liable−Sands, P. S. White, *Organometallics* **1998**, *17*, 2869.
[17] W. Uhl, *Coord. Chem. Rev.* **1997**, *163*, 1; in particular see: W. Uhl, A. Vester, D. Fenske, G. Baum, *J. Organomet. Chem.* **1994**, *464*, 23; W. Uhl, R. Gerding, A. Vester, *J. Organomet. Chem.* **1996**, *513*, 163.
[18] C. Schnitter, H. W. Roesky, C. Röpken, R. Herbst-Irmer, H.-G. Schmidt, M. Noltemeyer, *Angew. Chem.* **1998**, *110*, 2059; *Angew. Chem. Int. Ed.* **1998**, *37*, 1952.
[19] M. J. Harvey, T. P. Hanusa, V. G. Young, *Angew. Chem.* **1999**, *111*, 241; *Angew. Chem. Int. Ed.* **1999**, *38*, 217.
[20] R. G. Vranka, E. L. Amma, *J. Am. Chem. Soc.* **1967**, *89*, 3121.
[21] [21a] J. F. Malone, W. S. McDonald, *J. Chem. Soc., Chem. Commun.* **1967**, 444.
[21b] J. F. Malone, W. S. McDonald, *J. Chem. Soc., Dalton Trans.* **1972**, 2646.
[22] [22a] J. W. Moore, D. A. Samders, P. A. Scherr, M. D. Glick, J. P. Oliver, *J. Am. Chem. Soc.* **1971**, *93*, 1035. [22b] W. H. Ilsley, M. D. Glick, J. P. Oliver, J. W. Moore, *Inorg. Chem.* **1980**, *19*, 3572.
[23] R. L. Wells, A. T. McPhail, M. F. Self, J. A. Laske, *Organometallics* **1993**, *12*, 3333.
[24] Crystallographic data (excluding structure factors) for the structures of **2**, **3**, and **4** have been deposited with the Cambridge Crystallographic Data Centre as supplementary publication no. CCDC-122179 for **2**, -122180 for **3**, and -122181 for **4**. Copies of the data can be obtained on application to CCDC, 12 Union Road, Cambridge CB2 1EZ, UK [Fax: (internat.) + 44-1223/336-033; E-mail: deposit@ccdc.cam.ac.uk].
[25] [25a] T. Kottke, D. Stalke, *J. Appl. Crystallogr.* **1993**, *26*, 615. [25b] D. Stalke, *Chem. Soc. Rev.* **1998**, *27*, 171.
[26] *International Tables for Crystallography* (Ed.: T. Hahn), Vol. A, *Space Group Symmetry*, 2nd Ed., D. Reidel, Dordrecht, **1984**.
[27] G. M. Sheldrick, *SHELXL-93*, Universität Göttingen, **1993**; *SHELXL-97*, Universität Göttingen, **1997**.
[28] D. T. Cromer, J. B. Mann, *Acta Crystallogr.* **1968**, *24*, 321.
[29] R. F. Stewart, E. R. Davidson, W. T. Simpson, *J. Chem. Phys.* **1965**, *42*, 3175.

Received June 14, 1999
[I99215]

Magnesiation of Triisopropylsilylphosphane: Synthesis and Structures of New $Mg_{2n}P_{2m}$ Polyhedra

Matthias Westerhausen,*[a] Stefan Schneiderbauer,[a] Jörg Knizek,[a] Heinrich Nöth,[a] and Arno Pfitzner[b]

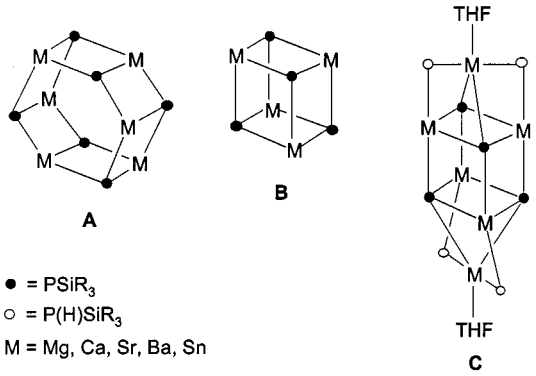
Dedicated to Prof. Alfred Schmidpeter on the occasion of his 70th birthday

Keywords: Magnesium / Metalation / Phosphorus / Polyhedra / X-ray structures

The magnesiation of triisopropylsilylphosphane with dibutylmagnesium in toluene yields the octanuclear complex $[Mg_8(PSi^iPr_3)_6\{P(H)Si^iPr_3\}_4]$ **(1)** which consists of $MgPSi^iPr_3$ units forming a hexagonal Mg_6P_6 prism, with two opposite Mg_2P_2 moieties capped by additional $Mg[P(H)Si^iPr_3]_2$ groups. If a small amount of THF is present during the metalation reaction $[(THF)_4Mg_6(PSi^iPr_3)_6]$ **(2)** also containing a hexagonal Mg_6P_6 prism can be isolated. The magnesiation of $H_2P–Si^iPr_3$ in tetrahydrofuran leads to the formation of the tetrameric complex $[(THF)MgPSi^iPr_3]_4$ **(3)** with a slightly distorted Mg_4P_4 cubane-like structure.The structures depend strongly on the steric strain caused by the trialkylsilyl substituents and the neutral coligands at the magnesium center. The highest steric strain, which is induced by coordination to every magnesium atom, leads to the smallest Mg_nP_n polyhedron – the central Mg_4P_4 heterocubane moiety. In compounds **1** and **2** the hexagonal Mg_6P_6 prism is formed, however, with reduced steric strain as observed for **2** where the Mg–P bond lengths become more similar.

Introduction

The synthesis of phosphandiides of the main group metals has been attracting increasing interest over the last few years due to their expected synthetic potential. Bulky substituents at the phosphorus atoms are necessary to avoid polymerization and to obtain oligomers soluble in common organic solvents. One of the most favored groups is the tri(*tert*-butyl)silyl[1] moiety, which is able to stabilize the negative charge and to shield the reactive center effectively. Therefore, solvent-free hexameric $[MgPSi^tBu_3]_6$ **(A)**[2] and tetrameric $[SnPSi^tBu_3]_4$ **(B)**[3] are well-known (Scheme 1). With regard to the heavier alkaline earth metals, the complete deprotonation of $H_2P-Si^tBu_3$ to a phosphandiide has not yet been achieved. Even in the presence of an excess of metalating reagent, bis(tetrahydrofuran-*O*)hexakisbarium tetrakis[tri(*tert*-butyl)silylphosphanide] tetrakis[tri(*tert*-butyl)silylphosphandiide] **(C)** with an $RP(H)^-/RP^{2-}$ ratio of 1:1 was isolated.[4] Smaller substituents such as triisopropylsilyl groups yield higher oligomers as shown for the solvent-free hexameric $[SnPSi^iPr_3]_6$ with a hexagonal Sn_6P_6 prism[5] similar to **A**. Herein we report on the magnesiation of triisopropylsilylphosphane with dibutylmagnesium and the influence of the THF content on the structures of the magnesiated phosphanes.

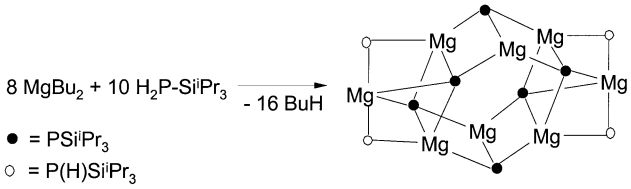


Scheme 1. Known phosphandiides of selected divalent main group metals (see text)

Results and Discussion

Synthesis

The metalation of triisopropylsilylphosphane[6] in toluene with dibutylmagnesium in the absence of Lewis bases such as THF yields compound **1** as shown in Scheme 2. Heating of the reaction solution to approximately 100°C and subsequent cooling to 6°C lead to the precipitation of colorless crystals of **1** with a melting point of 272°C and a decomposition point of 297°C.

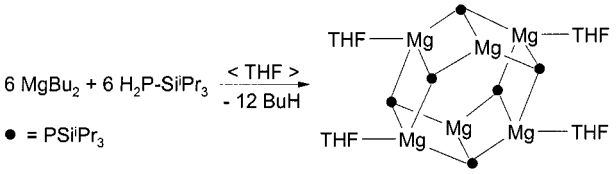


Scheme 2. Synthesis of **1**

[a] Institut für Anorganische Chemie, Ludwig-Maximilians-Universität München,
Butenandtstr. 5–13, Haus D, D-81377 München, Germany
Fax: (internat.) + 49-89/2180-7867
E-mail: maw@cup.uni-muenchen.de
[b] Anorganische Chemie II, Universität Siegen,
Adolf-Reichwein-Str., D-57068 Siegen, Germany
Fax: (internat.) + 49-271/740-2555
E-mail: pfitzner@chemie.uni-siegen.de

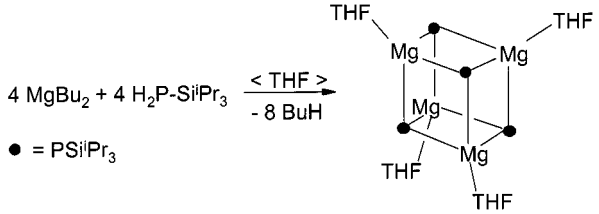
 © WILEY-VCH Verlag GmbH, D-69451 Weinheim, 1999 1434–1948/99/1212–2215 $ 17.50+.50/0

The ^{31}P NMR spectrum shows three chemically different phosphorus nuclei; however, the coupling pattern was not resolved and the assignment was not obvious. The resonance at $\delta = -265$ shows a doublet splitting due to a $^{1}J(P-H)$ coupling, whereas the other two signals originate from phosphandiide ligands. For these reasons a crystal structure determination was performed at −80°C (see below). The central moiety is a hexagonal Mg_6P_6 prism with two $Mg[P(H)Si^iPr_3]_2$ molecules coordinating above two opposite square planes. These magnesium bis(phosphanide) molecules can be substituted by Lewis bases such as THF. If a small amount of this ether is present during the magnesiation reaction compound **2** is instead obtained (Scheme 3). Again the Mg_6P_6 prism is formed; however, in this case, four THF molecules are bonded to the magnesium atoms of the two opposite square planes.



Scheme 3. Synthesis of **2**

Whereas ladder structures were reported for the hexamer $[LiP(SiMe_3)_2]_6$[7] and the polymeric compounds $[AP(SiMe_3)_2]_\infty$ (A = K, Rb, Cs),[8] the hexagonal prism of **2** can be described as a closed (cyclic) ladder structure. Open ladder structures such as those observed for the alkali metal bis(trimethylsilyl)phosphanides have not yet been found in alkaline earth metal phosphanide and phosphandiide complexes. The $^{31}P\{^1H\}$ NMR spectrum of **2** shows a single resonance due to a rapid interchange of the THF molecules on the NMR time scale. If the magnesiation of triisopropylsilylphosphane is performed in THF, the formation of $[(THF)MgPSi^iPr_3]_4$ **(3)** is observed (Scheme 4).



Scheme 4. Sythesis of **3**

Molecular Structures

The molecular structure of **1** and the atom numbering scheme is shown in Figure 1. The molecule has a crystallographic C_2 axis through the atoms Mg2 and Mg5; the symmetry-related atoms are marked with apostrophes. Selected bond lengths are summarized in Table 1.

The central moiety is a hexagonal Mg_6P_6 prism as already described for the hexamer $[MgPSi^tBu_3]_6$.[2] Due to the fact that the triisopropylsilyl groups are less effective in shielding the metal atoms than tri(*tert*-butyl)silyl substituents, coordination gaps appear at the magnesium centers. Two molecules of $Mg[P(H)Si^iPr_3]_2$ are bonded above two opposite Mg_2P_2 planes. These magnesium bis(phosphanide)

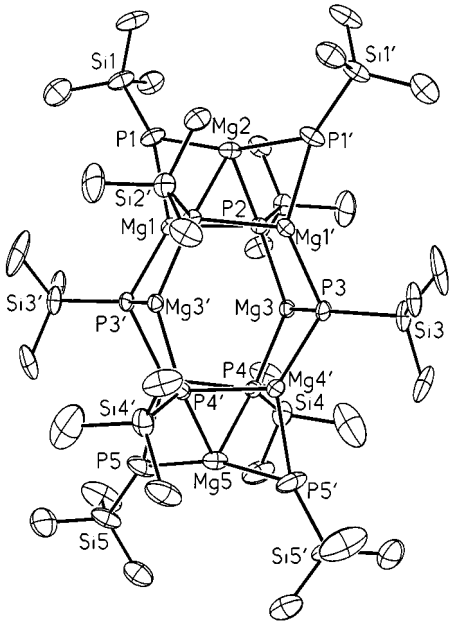


Figure 1. Molecular structure and numbering scheme of **1**; the methyl groups and the hydrogen atoms are omitted for clarity; the ellipsoids represent a probability of 40%; the atoms marked with an apostrophe are generated by C_2 symmetry; selected bond angles [°]: P1−Mg1−P2 100.59(7), P1−Mg1−P2′ 87.71(6), P1−Mg1−P3′ 139.0(1), P2−Mg1−P2′ 79.48(6), P2−Mg1−P3′ 120.40(7), P1−Mg2−P2 99.18(5), P1−Mg2−P1′ 163.0(1), P1−Mg2−P2′ 93.63(5), P2−Mg2−P2′ 82.46(8), P2−Mg3−P3 107.12(6), P2−Mg3−P4 134.59(8), P3−Mg3−P4 106.25(7), P4−Mg4−P5 98.17(8), P4−Mg4−P3′ 123.00(8), P4−Mg4−P4′ 80.21(7), P5−Mg4−P3′ 138.8(1), P5−Mg4−P4′ 89.02(7), P4−Mg5−P5 96.70(6), P4−Mg5−P4′84.29(8), P4−Mg5−P5′ 95.87(6), Mg1−P1−Mg2 71.05(7), Mg1−P2−Mg2 69.88(5), Mg1−P2−Mg3 107.12(7), Mg2−P2−Mg3 135.89(6), Mg1−P2−Mg1′ 100.22(6), Mg2−P2−Mg1′ 65.21(4), Mg3−P2−Mg1′ 72.56(5), Mg3−P3−Mg1′ 79.97(6), Mg3−P3−Mg4′ 81.22(7), Mg1′−P3−Mg4′ 123.65(9), Mg3−P4−Mg4 105.22(7), Mg3−P4−Mg5 135.82(7), Mg4−P4−Mg5 70.11(6), Mg3−P4−Mg4′ 73.12(6), Mg4−P4−Mg4′99.30(7), Mg5−P4−Mg4′ 64.87(5), Mg4−P5−Mg5 71.40(7)

Table 1. Selected bond lengths of **1**[a]

Atom	C.N.[b]	Mg1	Mg2	Mg3	Mg4	Mg5
P1	4	257.8(2)	254.8(2)			
P2	5	255.8(2)	264.2(2)	252.7(2)		
P3	4			253.2(2)		
P4	5			251.6(2)	255.9(2)	263.4(2)
P5	4				256.5(2)	254.8(2)
P1′	4		254.8(2)			
P2′	5	287.5(2)	264.2(2)			
P3′	4	246.1(2)			245.8(2)	
P4′	5				291.2(2)	263.4(2)
P5′	4					298.3(2)
n		1	2	3	4	5
P(n)−Si(n)		225.1(2)	223.8(2)	221.3(2)	223.6(2)	225.5(2)

[a] Atoms marked with an apostrophe are generated by C_2 symmetry ($-x + 1, y, -z + 0.5$). − [b] Coordination number.

units have P1−Mg2−P1′ and P5−Mg5−P5′ bond angles of 163.0(1)°. The Mg2−P1−Si1 and Mg5−P5−Si5 values amount to 137.5(1) and 139.6(1)°, respectively. These structural data, together with the rather short Mg2−P1 and Mg5−P5 bond lengths of 254.8(2) pm, allow us to consider the idea of coordinated magnesium bis(phosphanide) molecules.

Another description of the structure can be derived from considering the trigonal bipyramid with the magnesium atoms in apical positions as the basic polyhedron. Two bipyramids are joined through common faces (Mg2, P2, P2′, and Mg5, P4, P4′, respectively); two of these polyhedra are joined again through two $MgPSi^iPr_3$ units. Regarding the structure of **1** in this way, the similarity to the barium compound **D** is obvious; in **D** the $MPSiR_3$ moieties are missing and the dimerization occurs through M_2P_2 planes. The molecule has three- and four-coordinate magnesium atoms.

From this structure we can now identify the three different kinds of phosphorus atoms already found in the $^{31}P\{^1H\}$ NMR spectrum: the four-coordinate phosphorus atoms of the phosphanide ligands bound to two Mg atoms, one Si and one H atom (P1 and P5); the hexagonal prism containing one fourfold- (P3) and two fivefold coordinated P atoms (P2 and P4).

Figure 2 shows the molecular structure of **2** and the atom numbering scheme. Although the molecule displays no crystallographically enforced symmetry, the central moiety is very similar to the Mg_6P_6 polyhedron of **1**. Selected structural parameters are summarized in Table 2. The substitution of both $Mg[P(H)Si^iPr_3]_2$ molecules by four THF ligands leads to steric relief at the metal center; consequently the Mg−P bond lengths become more equal varying between 248.7 and 259.9 pm; bond lengths of this magnitude are already known for magnesium bis(phosphanides).[9] The Mg−O bond lengths are characteristic[10][11] of four-coordinate magnesium.

Figure 3 shows a comparison of the central moieties of the structures of **1**, **2** and $[MgPSi^tBu_3]_6$ ignoring the carbon and hydrogen atoms. The distortions of the hexagonal prism due to the coordination of two additional molecules of $Mg[P(H)Si^iPr_3]_2$ or THF are rather small. Whereas in the hexamer $[MgPSi^tBu_3]_6$ the Mg−P bond lengths vary in the rather narrow range of 247 to 260 pm, in **1** Mg−P distances of up to 298 pm are observed.

Figure 4 shows the molecular structure of **3** and the atom numbering scheme. The central moiety consists of a slightly distorted Mg_4P_4 cube with four-coordinate magnesium and phosphorus atoms. Table 3 contains selected bond lengths. In this polyhedron the Mg−P distances vary in a very narrow range around 254 pm.

The P(n)−Si(n) bond lengths differ in a characteristic manner. The P3−Si3 distance in **1** is the smallest due to the low coordination number of four at P3, whereas the P2−Si2 and P4−Si4 bond lengths are elongated due to the higher coordination number at the phosphorus atoms P2 and P4. The phosphanide ligands show further elongated bond lengths because the lower charge on P1 and P5 leads to a reduced electrostatic attraction between the negative phosphorus and the positively polarized silicon atoms. In **2** the P−Si bond lengths lie in a narrow range around 221 pm. In **3** the P−Si values of 218.4 pm are clearly smaller due to the reduced steric strain as a consequence of small Mg−P−Mg angles. The negative charge on the phosphorus atoms leads to decreased P−Si bond lengths relative to tris(trialkylsilyl)phosphanes[12−14] and bis(triisopropylsilyl)phosphane.[6]

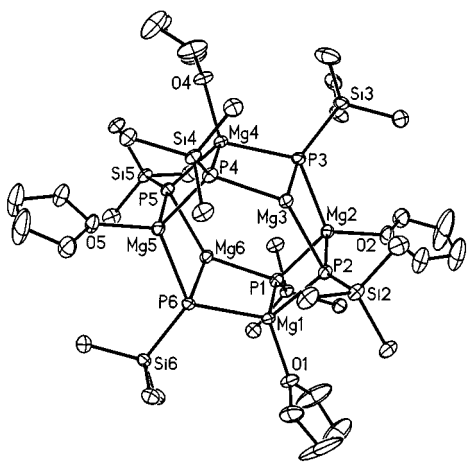


Figure 2. Molecular structure and numbering scheme of **2**; the methyl groups of the triisopropylsilyl substituents and the hydrogen atoms are omitted for clarity; the ellipsoids are drawn on a 40% probability level; selected bond angles [°]: P1−Mg1−P2 94.71(4), P1−Mg1−P6 99.75(4), P2−Mg1−P6 118.83(4), P1−Mg2−P2 94.76(4), P1−Mg2−P3 115.85(4), P2−Mg2−P3 100.88(4), P2−Mg3−P3 102.68(4), P2−Mg3−P4 138.58(4),P3−Mg3−P4 103.01(5), P3−Mg4−P4 100.44(4), P3−Mg4−P5 116.91(5), P4−Mg4−P5 94.96(4), P4−Mg5−P5 94.88(4), P4−Mg5−P6 117.33(4), P5−Mg5−P6 100.22(4), P1−Mg6−P5 139.70(4), P1−Mg6−P6 102.56(4), P5−Mg6−P6 102.37(4), Mg1−P1−Mg2 84.75(4), Mg1−P1−Mg6 78.07(4), Mg2−P1−Mg6 104.88(4), Mg1−P2−Mg2 85.52(4), Mg1−P2−Mg3 104.50(4), Mg2−P2−Mg3 78.00(4), Mg2−P3−Mg3 77.43(4), Mg2−P3−Mg4 125.39(4), Mg3−P3−Mg4 77.57(4), Mg3−P4−Mg4 77.84(4), Mg3−P4−Mg5 104.93(4), Mg4−P4−Mg5 84.37(4), Mg4−P5−Mg5 85.55(4), Mg4−P5−Mg6 104.38(4), Mg5−P5−Mg6 78.26(4), Mg1−P6−Mg5 123.08(4), Mg1−P6−Mg6 77.90(4), Mg5−P6−Mg6 77.62(4)

Table 2. Selected bond lengths of **2**

Atom	Mg1	Mg2	Mg3	Mg4	Mg5	Mg6	Si(n)
P1	259.9(1)	253.9(1)				249.4(1)	221.0(1)
P2	252.1(1)	258.0(1)	249.3(1)				220.1(1)
P3		254.1(1)	256.3(2)	254.2(1)			220.8(1)
P4			248.7(1)	260.2(1)	255.1(1)		221.0(1)
P5				252.0(1)	257.5(1)	250.0(1)	220.5(1)
P6	255.1(1)				255.8(1)	255.3(1)	221.6(1)
O(n)	204.6(2)	205.8(2)		204.8(2)	205.9(2)		

$Mg_{2n}P_{2m}$ Polyhedra

These new $Mg_{2n}P_{2m}$ polyhedra are missing links in a series of phosphandiides of divalent metals such as the alkaline earth metals and tin(II). An overview is given in

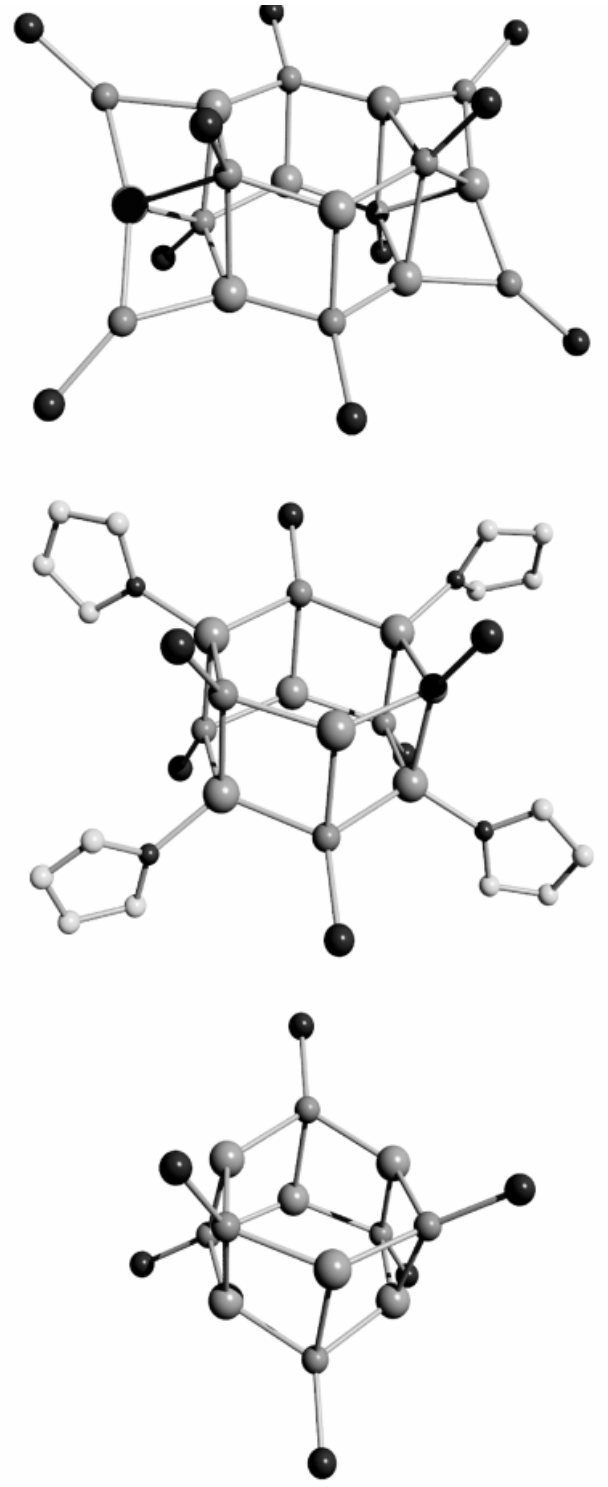


Figure 3. Comparison of the hexagonal prisms of **1** (on the top), **2** (in the middle) and hexakis(magnesium tri-*tert*-butylsilylphosphandiide) $[MgP-Si^tBu_3]_6$ (on the bottom); all hydrogen atoms are omitted for clarity; carbon atoms are omitted with the exception of those of the THF ligands; the atoms are shown with arbitrary radii

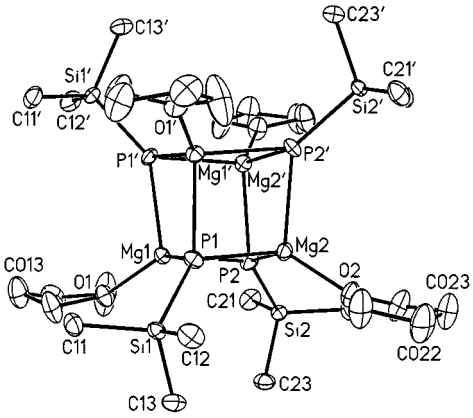


Figure 4. Molecular structure and numbering scheme of **3**. The methyl groups and the H atoms are omitted for clarity. The ellipsoids represent a probability of 40%. The atoms marked with an apostrophe are generated by C_2 symmetry. Selected bond angles [°]: P1−Mg1−P2 98.87(2), P1−Mg1−P1′ 98.78(2), P2−Mg1−P1′ 97.83(2), P1−Mg2−P2 99.16(2), P1−Mg2−P2′ 97.70(2), P2−Mg2−P2′ 97.78(2), Mg1−P1−Mg2 80.37(2), Mg1−P1−Mg1′ 80.54(2), Mg2−P1−Mg1′ 81.46(2), Mg1−P2−Mg2 80.57(2), Mg1−P2−Mg2′ 81.35(2), Mg2−P2−Mg2′ 81.53(2)

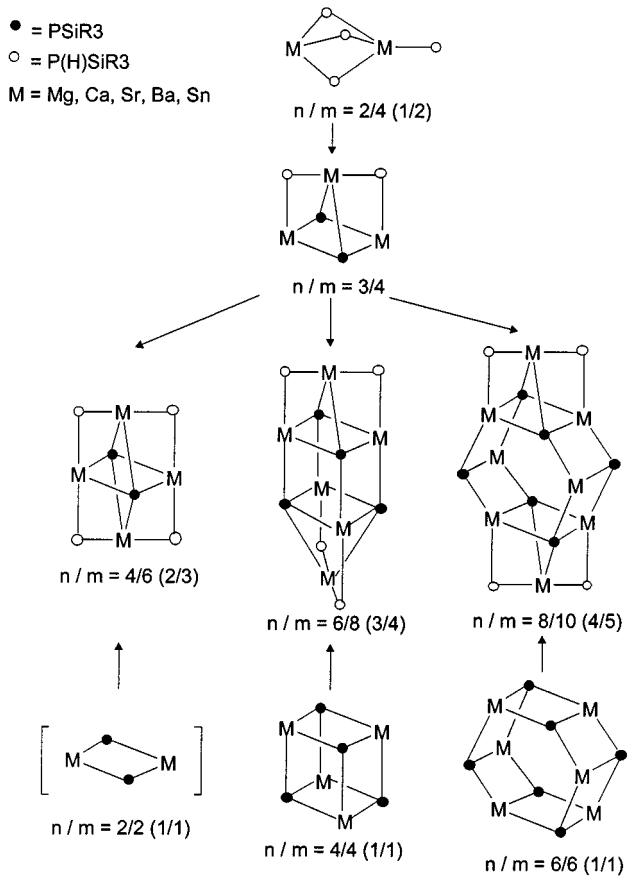
Table 3. Selected bond lengths of **3**[a]

Atom	Mg1	Mg2	Si(n)
P1	254.16(7)	253.97(7)	218.39(6)
P2	253.99(7)	253.08(7)	218.37(6)
P1′	254.66(7)		
P2′		255.19(7)	
O(n)	203.5(1)	203.0(1)	

[a] Atoms marked with an apostrophe are generated by C_2 symmetry ($-x$, y, $-z + 0.5$).

Scheme 5, where two basic types of polyhedra with m = n and $m = n + 1$ are shown, namely $M_{2n}P_{2n}$ (n = 2 and 3) and $M_{2n}P_{2n+2}$ (n = 3 and 4). The class of the $M_{2n}P_{2n}$ polyhedra consists of oligomeric alkaline earth metal phosphandiides where the dimer $[MgPSiR_3]_2$ with $n = 1$ − which would be the smallest unit − is still unknown. Dimerization leads to the formation of a cube (n = 2) and trimerization to the hexagonal prism (n = 3). These oligomeric alkaline earth metal phosphandiides are represented in the bottom row of Scheme 2.

In the group of $M_{2n}P_{2n+2}$ polyhedra the molecules contain both phosphanide and phosphandiide ligands, however the compound with n = 2 cannot be stabilized with triisopropylsilyl groups at the phosphorus atoms, although the steric strain introduced by tri(*tert*-butyl)silyl substituents is enough to allow the isolation of a dimer with the formula $Mg_4(PSi^tBu_3)_2[P(H)Si^tBu_3]_4$[15] whose structure is shown in Scheme 5. The upper part of Scheme 5 shows the alkaline earth metal bis(phosphanides) with n = 1 which contain only phosphanide substituents. These molecules are bicyclic in the case of the heavier alkaline earth metals with small groups at the phosphorus atoms.[4,9,14,16,17] In Scheme 5 the M/P ratio changes from 1:2 on the top to 1:1 on the bottom, which are the extreme values in this substance class. The middle row of Scheme 5 shows the compounds with M/P ratios of 2:3, 3:4 and 4:5, which crystallize as dimers.



Scheme 5. Schematic construction of $Mg_{2n}P_{2n}$ polyhedra starting from a dimeric alkaline earth metal bis(phosphanide) on the top (Mg/P ratio of 1:2) or starting from the alkaline earth metal phosphandiide at the bottom (Mg/P ratio of 1:1); the compounds in the middle row belong to polyhedra of the type $Mg_{2n}P_{2n+2}$ (see text)

Conclusion

The steric strain incorporated by the trialkylsilyl substituents and/or by the coordination of Lewis bases such as THF to the metal dications defines the polyhedron which is formed in the magnesiation of bulky trialkylsilylphosphanes. Tri(*tert*-butyl)silyl groups lead to the formation of a hexagonal Mg_6P_6 prism. If the less crowded triisopropylsilylphosphane is magnesiated in the absence of Lewis bases, two $Mg[P(H)Si^iPr_3]_2$ molecules cap two opposite square Mg_2P_2 planes of a hexagonal prismatic $(MgPSi^iPr_3)_6$ and **1** precipitates. The presence of Lewis bases such as THF is necessary to achieve a complete deprotonation of triisopropylsilylphosphane. The magnesium bis(phosphanide) molecules of **1** can be substituted by four THF ligands to yield **2**. Coordination of a THF molecule to each magnesium atom allows the isolation of $[(THF)MgPSi^iPr_3]_4$ with a slightly distorted Mg_4P_4 cube.

Experimental Section

General Remarks: All experiments and manipulations were carried out under argon or nitrogen purified by passage through BTS catalyst and P_4O_{10}. Reactions were performed with standard Schlenk techniques and dried, thoroughly deoxygenated solvents. $H_2PSi^iPr_3$[6] was prepared by a literature procedure. NMR spectra were recorded on Jeol spectrometers GSX270 and EX400. A Perkin–Elmer Paragon 1000 PC spectrophotometer was used to record the IR spectra; solid substances were measured in nujol between KBr plates (vs very strong, s strong, m medium strong, w weak, vw very weak, sh shoulder). The low carbon values for the elemental analysis result from carbide and carbonate formation as well as loss of neutral coligands during handling and combustion of the compounds.

$Mg_8(PSi^iPr_3)_6[P(H)Si^iPr_3]_4$ (1): Triisopropylsilylphosphane (1.12 mL, 5.0 mmol) was dissolved in 40 mL of toluene. A heptane solution of dibutylmagnesium (4.0 mL of a 1M solution) was dropped into this solution and a yellow precipitate formed immediately. Heating to approximately 100°C for 15 min. and subsequent cooling to 6°C led to the crystallization of 1.03 g of colorless **1** (0.49 mmol, 97%); m.p. 272°C, dec. above 297°C. – ^{1}H NMR ([D$_8$]toluene, 30°C): δ = 0.65 (m), 1.06 (m), 1.23 (m), 1.28 (m), 1.35 (m). – ^{31}P{^{1}H} NMR ([D$_8$]toluene, 30°C): δ = −265.0 (br, PH), −266.8 (br, P with C.N. = 4), −331.2 (br, P with C.N. = 3). – IR: $\tilde{\nu}$ = 316 vw, 372 w, 427 w, 444 w, 482 m, 515 m, 539 w, 576 m, 636 w, 656 m, 732 w, 784 vw, 802 vw, 819 vw, 882 s, 918 m, 993 s, 1015 m, 1064 s, 1161 w, 1197 w, 1230 w, 1289 w, 1313 w, 1368 w, 1386 w, 1465 m, 1686 w, 1768 w, 2300 m, 2364 vw, 2719 vw, 2732 vw, 2869 s, 2893 m, 2946 s. – $C_{90}H_{214}Mg_8P_{10}Si_{10}$ (2081.69): calcd. C 51.97, H 10.36; found C 51.23, H 10.35.

$(THF)_4Mg_6(PSi^iPr_3)_6$ (2): To a solution of triisopropylsilylphosphane (1.12 mL, 5.0 mmol) and 0.41 mL of THF in 30 mL of toluene a 1M heptane solution of dibutylmagnesium (5.0 mL, 5.0 mmol) was added dropwise. A yellow solution forms. During stirring for additional 19 h at room temp. a colorless solid precipitated which redissolved upon heating to approximately 80°C. Cooling to 6°C led to the crystallization of 1.18 g of **2**·2C_7H_8 (0.67 mmol, 81%); dec. above 300°C. – ^{1}H NMR ([D$_8$]toluene, 30°C): δ = 1.16 [sept, ^3J(H,H) = 7.0 Hz, C*H*Me$_2$], 1.37 (d, CH*Me*$_2$), 1.51 and 4.20 (br, THF). – ^{13}C{^{1}H} NMR ([D$_8$]toluene, 30°C): δ = 15.89 (m, CH), 20.58 (m, CH$_3$), 24.89 and 69.97 (m, THF). – ^{29}Si{^{1}H} NMR ([D$_8$]toluene, 30°C): δ = 24.13 (m). – ^{31}P{^{1}H} NMR ([D$_8$]toluene, 30°C): δ = −331.59 (s). – IR: $\tilde{\nu}$ = 327 w, 337 w, 462 m, 477 m, 487 m, 558 m, 678 m, 806 w,820 w, 884 s, 921 w, 991 m, 1013 s, 1061 m, 1093 s, 1162 m, 1193 m, 1260 w, 1366 w, 1386 w, 1465 m, 1631 w, 1638 w, 2865 s, 2894 m, 2953 s. – $C_{84}H_{174}Mg_6O_4P_6Si_6$ (1748.48): calcd. C 57.70, H 10.03; found C 57.48, H 10.04.

$[(THF)Mg]_4(PSi^iPr_3)_4$ (3): Dibutylmagnesium in heptane (5.0 mL of a 1M solution) was added dropwise to a solution of triisopropylsilylphosphane (1.12 mL, 5.0 mmol) in 25 mL of THF. After stirring for an additional 15 h at room temp. the volatile materials were removed in vacuum and the residue recrystallized from toluene at 90°C. Storage of this solution at 6°C led to the precipitation of 0.75 g of large colorless cuboids of **3** (0.66 mmol, 53%); dec. above 320°C. – ^{1}H NMR ([D$_8$]toluene, 30°C): δ = 1.21 [sept, ^3J(H,H) = 7.2 Hz, C*H*Me$_2$], 1.37 (d, CH*Me*$_2$), 1.51 and 4.20 (br, THF). – ^{13}C{^{1}H} NMR ([D$_8$]toluene, 30°C): δ = 15.86 (s, CH), 20.52 (s, CH$_3$), 25.46 and 67.77 (THF). – ^{29}Si{^{1}H} NMR ([D$_8$]toluene, 30°C): δ = 23.37 (m). – ^{31}P{^{1}H} NMR ([D$_8$]toluene, 30°C): δ = −330.8 (s). – IR: $\tilde{\nu}$ = 466 m, 485 m, 496 m, 557 m, 615 w, 680 m, 804 w, 819 w, 884 m, 921 w, 994 m, 1012 s, 1060 s, 1089 s, 1160 m, 1262 w, 1367 w, 1384 w, 1465 m, 1632 m, 1638 m, 2865 s, 2894 m, 2945 s. – $C_{36}H_{84}Mg_4P_4Si_4$ (850.51, THF-free compound): calcd. C 50.84, H 9.95; found C 50.46, H 9.87.

X-ray Crystal Structure Determinations of 1, 2 and 3:[18] Data were collected on a Siemens P4 diffractometer with a Siemens SMART-CCD area detector (**1** and **2**) or on a STOE-IPDS diffractometer

Table 4. Crystallographic data of **1**, **2**, and **3**, details of the structure solution and refinement procedures

Compound	**1**	$2{\cdot}\mathbf{2}C_7H_8$	**3**
Formula	$C_{90}H_{214}Mg_8P_{10}Si_{10}$	$C_{84}H_{174}Mg_6O_4P_6Si_6$	$C_{52}H_{116}Mg_4O_4P_4Si_4$
Formula mass [g·mol^{-1}]	2081.69	1748.45	1138.93
T [K]	193(2)	173(2)	173(2)
Space group[21]	$C2/c$ (No. 15)	$P\bar{1}$ (No. 2)	$C2/c$ (No. 15)
a [pm]	1414.9(2)	1485.2(3)	2627.2(2)
b [pm]	3407.1(5)	1582.5(3)	1252.40(8)
c [pm]	2740.3(4)	2261.1(5)	2408.5(2)
α [°]	90	83.00(3)	90
β [°]	101.576(3)	84.71(3)	120.29(1)
γ [°]	90	88.54(3)	90
V [nm^3]	12.942(3)	5.251(2)	6.8428(9)
Z	4	2	4
$d_{calcd.}$ [g·cm^{-3}]	1.068	1.106	1.106
μ [mm^{-1}]	0.299	0.248	0.254
$F(000)$	4560	1912	2496
Scan range [°]	$2.4 < 2\theta < 55.5$	$5.1 < 2\theta < 56.1$	$4.7 < 2\theta < 52.0$
Measured data	35657	86377	29590
Unique data (R_{int})	9840 (0.1285)	23166 (0.0324)	6618 (0.0288)
Parameters	537	964	307
wR_2[a] (all data, on F^2)	0.2024	0.2110	0.0975
R_1[a] (all data)	0.1216	0.0871	0.0396
Data [$I > 2\sigma(I)$]	4939	16343	6069
R_1[a] [$I > 2\sigma(I)$]	0.0614	0.0657	0.0366
GOF[b] on F^2	1.028	1.077	1.029
Residual density [e·Å^{-3}]	1.19; −0.38	1.60; −0.68	0.48; −0.42

[a] Definition of the R values: $R_1 = (\Sigma||F_o|-|F_c||)/\Sigma|F_o|$; $wR_2 = \{\Sigma[w(F_o^2-F_c^2)^2]/\Sigma[w(F_o^2)^2]\}^{1/2}$ with $w^{-1} = \sigma^2(F_o^2) + (aP)^2$. − [b] $s = \{\Sigma[w(F_o^2-F_c^2)^2]/(N_o-N_p)\}^{1/2}$.

(**3**) with graphite monochromated Mo-K_α radiation (λ = 71.073 pm) from oil-coated[19][20] rapidly cooled single crystals. Crystallographic parameters, details of data collection and refinement procedures are summarized in Table 4.

All structures were solved by direct methods and refined with the software packages SHELXL-93 and SHELXL-97.[22] The asymmetric unit of **2** contains two toluene molecules without coordination to magnesium atoms. Neutral scattering factors were taken from Cromer and Mann[23] and for the hydrogen atoms from Stewart et al.[24] The non-hydrogen atoms were refined anisotropically. The H-atoms were considered with a riding model under restriction of ideal symmetry at the corresponding atoms.

Acknowledgments

We are grateful to the Deutsche Forschungsgemeinschaft, Bonn, and the Fonds der Chemischen Industrie, Frankfurt/Main, for generous financial support.

[1] N. Wiberg, *Coord. Chem. Rev.* **1997**, *163*, 217.
[2] M. Westerhausen, M. Krofta, A. Pfitzner, *Inorg. Chem.* **1999**, *38*, 598.
[3] M. Westerhausen, M. Krofta, N. Wiberg, J. Knizek, H. Nöth, A. Pfitzner, *Z. Naturforsch.* **1998**, *53b*, 1489.
[4] M. Westerhausen, M. H. Digeser, M. Krofta, N. Wiberg, H. Nöth, J. Knizek, W. Ponikwar, T. Seifert, *Eur. J. Inorg. Chem.* **1999**, 743.
[5] M. Driess, S. Martin, K. Merz, V. Pintchouk, H. Pritzkow, H. Grützmacher, M. Kaupp, *Angew. Chem.* **1997**, *109*, 1982; *Angew. Chem. Int. Ed. Engl.* **1997**, *36*, 1894.
[6] M. Westerhausen, R. Löw, W. Schwarz, *J. Organomet. Chem.* **1996**, *513*, 213.
[7] E. Hey-Hawkins, E. Sattler, *J. Chem. Soc., Chem. Commun.* **1992**, 775.
[8] U. Englich, K. Hassler, K. Ruhlandt-Senge, F. Uhlig, *Inorg. Chem.* **1998**, *37*, 3532.
[9] M. Westerhausen, *Coord. Chem. Rev.* **1998**, *176*, 157.
[10] C. E. Holloway, M. Melnik, *J. Organomet. Chem.* **1994**, *465*, 1.
[11] P. R. Markies, O. S. Akkerman, F. Bickelhaupt, W. J. J. Smeets, A. Spek, *Adv. Organomet. Chem.* **1991**, *32*, 147.
[12] E. Lukevics, O. Pudova, R. Sturkovich: *Molecular Structure of Organosilicon Compounds*, Ellis Horwood: Chichester; **1989**.
[13] G. A. Forsyth, D. W. H. Rankin, H. E. Robertson, *J. Mol. Struct.* **1990**, *239*, 209.
[14] M. Westerhausen, H. Hartmann, W. Schwarz, *Inorg. Chem.* **1996**, *35*, 2421.
[15] M. Westerhausen, M. Krofta, unpublished results.
[16] M. Westerhausen, *J. Organomet. Chem.* **1994**, *479*, 141.
[17] M. Westerhausen, *Trends Organomet. Chem.* **1997**, *2*, 89.
[18] Crystallographic data (excluding structure factors) for the structures included in this paper have been deposited with the Cambridge Crystallographic Data Centre as supplementary publication no. CCDC-133694 **(1)**, -133695 **(2)** and -133696 **(3)**. Copies of the data can be obtained free of charge on application to CCDC, 12 Union Road, Cambridge CB2 1EZ, UK [Fax: (internat.) + 44-1223/336-033; E-mail: deposit@ccdc.cam.ac.uk].
[19] T. Kottke, D. Stalke, *J. Appl. Crystallogr.* **1993**, *26*, 615.
[20] D. Stalke, *Chem. Soc. Rev.* **1998**, *27*, 171.
[21] *International Tables for Crystallography*, Vol. A, *Space Group Symmetry* (Ed.: T. Hahn), 2nd Ed., D. Reidel, Dordrecht, **1984**.
[22] G. M. Sheldrick, *SHELXL-93*, Universität Göttingen, **1993**; *SHELXL-97*, Universität Göttingen, **1997**.
[23] D. T. Cromer, J. B. Mann, *Acta Crystallogr.* **1968**, *24*, 321.
[24] R. F. Stewart, E. R. Davidson, W. T. Simpson, *J. Chem. Phys.* **1965**, *42*, 3175.

Received August 24, 1999
[I99312]

Syntheses, Molecular Structures, and Bonding of Molybdenum and Tungsten Calix[4]arene Imido Complexes

Udo Radius*[a] Juri Attner[a]

Dedicated to Professor Dr. H. Werner on the occasion of his 65th birthday

Keywords: Calixarenes / Inclusion compounds / Imido Complexes / Molybdenum / Tungsten

Syntheses, spectroscopic properties, molecular structures, and bonding of novel calix[4]arene imido compounds are described. Treatment of $M(NtBu)_2(NHtBu)_2$ **Ia** (M = Mo), **Ib** (M = W) or $M(NMes)_2Cl_2(dme)$ **IIa** (M = Mo), **IIb** (M = W) (Mes = 2,4,6-Me_3-C_6H_2) with *p*-*t*Bu-calix[4]arene LH_4 affords calix[4]arene metal complexes LM(NR) **1a**, **b** (M = Mo, W; R = *t*Bu) and **2a**, **b** (M = Mo, W; R = Mes). Analytical and spectroscopic data are consistent with monomeric structures for **1** and **2**, retaining a local C_{4v} symmetry for the calix[4]arene metal fragment. These complexes are well-suited to bind small molecules like acetonitrile, *t*Bu-isonitrile, or water within their macrocyclic pockets. The spectroscopic data of some inclusion compounds and the crystal structures of LMo(N*t*Bu)(NCMe) **1a(NCMe)**, LW(N*t*Bu)(OH_2) **1b(OH_2)**, LW(N*t*Bu)(CN*t*Bu) **1b(CN*t*Bu)**, LMo(NMes)(NCMe) **2a(NCMe)**, and LW(NMes)(NCMe) **2b(NCMe)** are reported. All complexes contain a group VI metal imido [M=NR] moiety mounted on the phenoxide rim of the calix[4]arene ligand as well as an incorporated guest molecule within the cavity. Some insights into the structures of complexes of the type L′W(NR′) (L′ = *p*-H-calix[4]arene; R′ = H, Me) and into bonding in these compounds are provided by density functional theory, applying the B-P86 density functional and an all SVP basis set within the RI-J-DFT approximation. At least one π bond is of importance for calix[4]arene-metal bonding in these compounds. The metal-imido bond can be described as a triple bond. A geometrically optimized minimum structure of L′W(NMe) **4** shows a calix[4]arene ligand only slightly distorted from a local C_{4v} symmetry and an almost linear tungsten-imido moiety.

Introduction

The role of transition metal imido complexes[1] as reactive intermediates in industrial and laboratory organic synthesis[2][3] has received increased attention in recent years. The selective ammoxidation of propylene to acrylonitrile over bismuth molybdate catalysts with a minimal composition $Bi_2O_3 \cdot n\,MoO_3$ is one of the most significant reactions of this type.[4] With approximately four million tons of worldwide acrylonitrile production, this process constitutes the largest volume example of an allylic oxidation process in industrial practice. Similar reactions employing methylbenzenes are used in the manufacture of benzonitriles and terephthalonitriles. It is known that in the ammoxidation ammonia is activated by the formation of a bismuth oxide supported imido species [Mo=NH], and so this system has been the subject of industrial research and mechanistic studies.[5]

One approach leading to model oxo surfaces that bind metals on a molecular level is to employ ligands with a preorganized set of oxygen donor atoms in a quasiplanar arrangement as provided, for example, by calixarenes.[6] The simplest of the calixarenes, the calix[4]arene system, usually binds in tetradentate fashion to transition metals and often retains its cone-like appearance.[7] As part of our ongoing studies on metal-metal and metal-element multiple bonding supported by calix[4]arene ligands and calix[4]arene metal fragments,[8] we report here on the syntheses, molecular structures, and bonding of new molybdenum and tungsten calix[4]arene imido complexes.

[a] Institut für Anorganische Chemie,
Engesserstr., Geb. 30.45, D-76128 Karlsruhe, Germany
Fax: (internat.) + 49-721/661921
E-mail: uradius@achibm6.chemie.uni-karlsruhe.de

Results and Discussion

Synthesis

There are, in principle, several ways to prepare *p*-*t*Bu-calix[4]arene organoimido complexes. Basic strategies are (i) to introduce the imido fragment into *p*-*t*Bu-calix[4]arene complexes and (ii) to introduce the *p*-*t*Bu-calix[4]arene fragment into imido complexes. Preparative ways for the former approach could be the reaction of *p*-*t*Bu-calix[4]arene metal chlorides $LMCl_2$ with amines RNH_2 in the presence of a base or the reaction of *p*-*t*Bu-calix[4]arene metal oxides LM=O with isocyanates RN=C=O.[1] Introduction of the *p*-*t*Bu-calix[4]arene fragment into imido complexes might be achieved by reacting imidochlorides $M(NR)Cl_4$ with *p*-*t*Bu-calix[4]arene LH_4. We decided to follow a similar method to that described by Gibson and co-workers for the preparation of a calix[4]arene imido molybdenum complex with the parent *p*-H-calix[4]arene. These authors reported the reaction of $M(NR)_2(OtBu)_2$ with *p*-H-calix[4]arene $L'H_4$.[9] In the case of M = Mo and R = 2,6(iPr)$_2$Ph (Dip),[9a] formation of the calix[4]arene imido complex

 © WILEY-VCH Verlag GmbH, D-69451 Weinheim, 1999 1434−1948/99/1212−2221 $ 17.50+.50/0

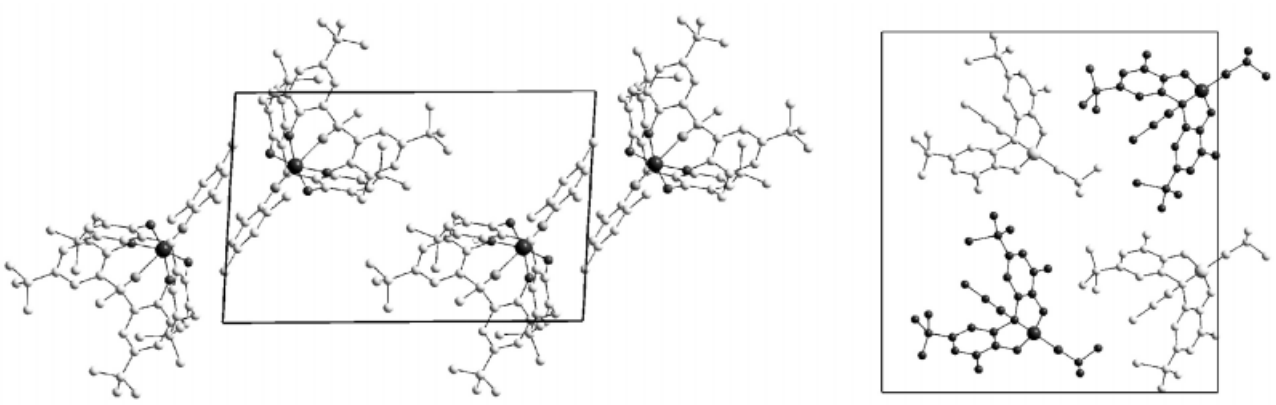


Figure 1. Packing diagram of LMo(NMes)(NCMe) **2a(NCMe)** (left side) and LMo(N*t*Bu)(NCMe) **1a(NCMe)** (right side). Projections down the a axis are shown. Molecules with the metal atom at (0.5, *y*, *z*) are light gray colored while those with metal atoms at (0, *y*, *z*) are dark gray colored in the cellplot of **1a(NCMe)**.

L′Mo(NDip) was observed, whereas in the case of M = Cr and R = *t*Bu all imido and alkoxy ligands were sacrificed to yield a mononuclear complex with two calix[4]arene molecules in the coordination sphere of the central chromium atom.[9b]

The *p*-*t*Bu-calix[4]arene *t*Bu-imido complexes LM(N*t*Bu) **1a** (M = Mo) and **1b** (M = W) are prepared by amide and imido replacement from compounds $M(NtBu)_2(NHtBu)_2$, which is a convenient starting material, especially for tungsten imido chemistry. Treatment of $M(NtBu)_2(NHtBu)_2$ **Ia** (M = Mo)[10a,10b] and **Ib** (M = W)[10c,10d] with one equivalent of *p*-*t*Bu-calix[4]arene LH_4 in toluene affords the monoimido complexes LMo(N*t*Bu) **1a** and LW(N*t*Bu) **1b**, after work up, as high melting solids in moderate to good yield (see Scheme 1).

Since preliminary studies on the reactivity of **1a**, **b** revealed that these compounds do not readily decompose with traces of HCl,[11] we tried to access calix[4]arene imido complexes by chloride and imido replacement from molybdenum and tungsten diimido dichlorides. These starting materials are also readily prepared and, especially for the molybdenum chemistry, more straightforward to synthesize than the amido imide **Ia**. Treatment of $M(NMes)_2Cl_2(dme)$ **IIa** (M = Mo) and **IIb** (M = W) (Mes = 2,4,6-$Me_3C_6H_2$)[12] with one equivalent of *p*-*t*Bu-calix[4]arene LH_4 in refluxing toluene results in the formation of calix[4]arene imido complexes LMo(NMes) (**2a**) and LW(NMes) (**2b**) in good yield. We believe this route to be general for the synthesis of compounds of the type LM(NR) (M = Mo, W).

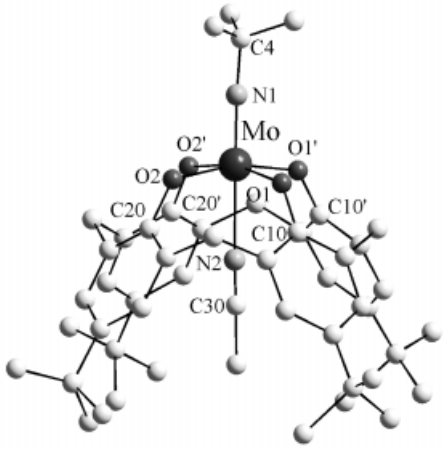
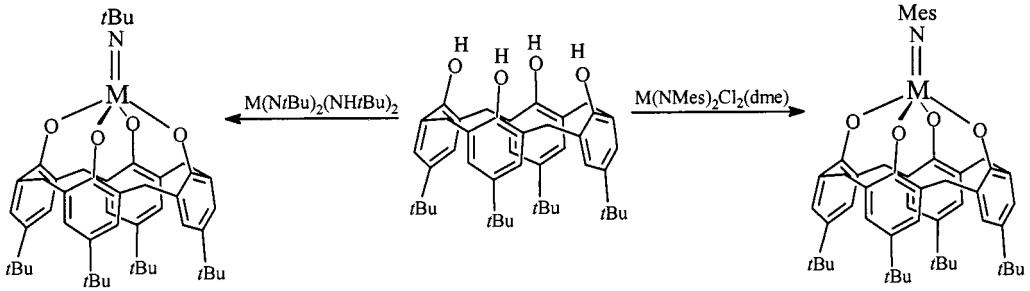


Figure 2. The molecular structure of LMo(N*t*Bu)(NCMe) **1a(NCMe)** with hydrogen atoms omitted for clarity. Disorders in *t*Bu groups are not resolved in the drawing. Selected bond lengths [pm] and angles [°]: Mo−N1: 171.8(10), Mo−O1: 194.0(5), Mo−O2: 194.0(5), Mo−N2: 234.3(9), N1−C4: 139.7(17), O1−C10: 134.0(9), O2−C20: 137.5(9), C4−N1−Mo: 176.9(11), N1−Mo−O1: 97.4(3), N1−Mo−O2: 97.6(3), O1−Mo−O2′: 165.0(2), O2−Mo−O1′: 165.0(2), N1−Mo−N2: 179.4(4), C10−O1−Mo: 129.6(5), C20−O2−Mo: 128.6(4).



Scheme 1

Unlike the calix[4]arene molybdenum oxide LMo=O,[13] which coordinates an additional molecule LH_4 to the LMoO core and is almost insoluble in common organic solvents, the imido compounds are readily soluble in organic solvents like benzene or toluene and sparingly soluble in hexane. The nature of the products was determined by ^{1}H- and ^{13}C-NMR spectroscopy as well as IR spectroscopy, mass spectroscopy, and elemental analysis. Analytical and spectroscopic data are consistent with a monomeric structure for **1** and **2** in the solid state and in solution. In all cases, intense signals for the molecular peaks were observed in the electron impact mass spectra at m/z = 813 (**1a**), 899 (**1b**), 875 (**2a**), and 961 (**2b**).

The monomeric nature of these compounds in solution is also evident from NMR spectroscopy. The proton NMR spectra are typical for calix[4]arene complexes with a pseudo C_{4v} symmetry of the macrocyclic ligand, showing a singlet for the calix[4]arene *tert*-butyl protons, two doublets for the diastereotopic protons of the methylene bridges with a coupling constant between 12.1 and 12.5 Hz, and one resonance for the aromatic protons of the aryloxy groups. ^{1}H-NOE measurements reveal that the doublet at lower field, for example at δ = 4.47 for the tungsten compound **1b**, is due to methylene hydrogen atoms closer to the metal atom, whereas the resonances at higher field, e.g. at δ = 3.25 for **1b**, have to be attributed to methylene protons in close proximity to the aryl hydrogen atoms. The proton NMR spectrum of a possible dinuclear imido-bridged species of the type LM(μ-NR)$_2$ML, in solution, should reveal the typical features of a calix[4]arene complex with local C_{2v} symmetry, i.e. a splitting of the signals of the *t*Bu protons of the inequivalent phenoxide rings. The local C_{4v} symmetry of the [LM] group is also reflected in the ^{13}C{^{1}H}-NMR spectra of **1** and **2**, where we observed two signals for the calix[4]arene *tert*-butyl carbon atoms, one signal for the methylene bridges and four signals for the carbon atoms of the phenoxide ring.

Calixarenes have attracted some attention for their ability to include small guest molecules in the solid state.[6][14] In the X-ray structure determination of *p*-*t*Bu-calix[4]arene LH_4, for example, there was a toluene molecule incorporated into the *endo* calix position.[15] Despite considerable effort, we were unable to obtain good quality crystals of compound **1** or **2** without any guest molecule in the *endo* calix position or with toluene included into the calixarene basket. However, this situation changes when we allow **1** or **2** to react with small donor molecules like water, acetonitrile, or isonitrile.

Accordingly, the complexes LMo(N*t*Bu)(NCMe) **1a(NCMe)**, LMo(N*t*Bu)(CN*t*Bu) **1a(CN*t*Bu)**, LW(N*t*Bu)(NCMe) **1b(NCMe)**, LW(N*t*Bu)(CN*t*Bu) **1b(CN*t*Bu)**, LW(N*t*Bu)(OH_2) **1b(OH_2)**, LMo(NMes)(NCMe) **2a(NCMe)**, and LW(NMes)(NCMe) **2b(NCMe)** can be prepared by dissolving **1** or **2** in acetonitrile or by reaction of toluene solutions of **1** or **2** with nucleophiles like water, acetonitrile or isonitrile.

The IR spectra of the acetonitrile complexes show two bands in the characteristic region between 1700 and 2800 cm^{-1}, one at approximately 2320 cm^{-1}, the other at approximately 2295 cm^{-1}. These bands may be assigned to a C≡N stretching frequency and a combination band, which results from coupling of a symmetric CH_3 deformation mode and a C−C stretching frequency. The ^{1}H-NMR spectra reveal one additional signal in the region of δ = −0.1 to −0.2, shifted upfield from the resonance of uncoordinated acetonitrile dissolved in $CDCl_3$ at δ = 1.90. Although coordination to transition metals might lead to upfield shifting of the acetonitrile resonances, these shifts are most probably due to shielding effects inside the cavity of the calix[4]arene ligand.

Similar shifts can be obtained for the isonitrile ligated to **1a** and **1b**. The resonances for the isonitrile CH_3 groups at δ = −0.17 and −0.20 are shifted significantly compared to the resonance of the uncoordinated molecule at δ = 1.37. Bands at 2211 and 2218 cm^{-1}, respectively, in the IR spectra of **1a(CN*t*Bu)** and **1b(CN*t*Bu)** are in the characteristic region of C≡N stretches. The bound H_2O molecule of **1b(OH_2)** gives rise to two OH stretches at 3519 and 3448 cm^{-1} in the IR spectrum, and a singlet at δ = 1.54 in the proton NMR spectrum.

^{13}C-NMR spectroscopy has an exceptional position in the characterization of *tert*-butyl imido compounds.[1] The difference in the chemical shifts of α- and β-*t*Bu-carbon atoms, Δδ, can serve as an experimental probe for the electron density on the metal atom of imido complexes. A decrease of electron density on the metal atom leads to a strengthening of the metal-nitrogen bond and therefore to a decrease of electron density on the imido nitrogen atom. This decrease can be experimentally observed as a downfield shift of the α-carbon atom resonance and a small upfield shift of the β-carbon atom resonance, and therefore by an increase of Δδ. We observe a Δδ value for LW(N*t*Bu) **1b** of 44.61 ppm and lower values for the adducts: 40.47 ppm for **1b(NCMe)**, 41.07 ppm for **1b(OH_2)**, and 41.36 ppm for **1b(CN*t*Bu)**. Electron density on the metal atom increases upon coordination of the guest molecule and weakens the tungsten nitrogen bond of the calix[4]arene imido compound. This weakening is mainly due to σ bond effects (vide infra).

Molecular Structures

Single crystal X-ray diffraction studies confirm the structural assignments for the calix[4]arene imido compounds of the type LM(NR) deduced from spectroscopic data. Suitable crystals for X-ray analyses of the compounds LMo(N*t*Bu)(NCMe) **1a(NCMe)**, LW(N*t*Bu)(OH_2) **1b(OH_2)**, LW(N*t*Bu)(CN*t*Bu) **1b(CN*t*Bu)**, LMo(NMes)(NCMe) **2a(NCMe)**, and LW(NMes)(NCMe) **2b(NCMe)** can either be grown from acetonitrile solutions (acetonitrile adducts) or toluene solutions (water adduct, isonitrile adduct). Projections of the cells down the a axis of LMo(N*t*Bu)(NCMe) **1a(NCMe)** and LMo(NMes)(NCMe) **2a(NCMe)** are given in Figure 1. The molecular structures of the compounds are shown in Figures 2 to 6, while selected bond lengths and

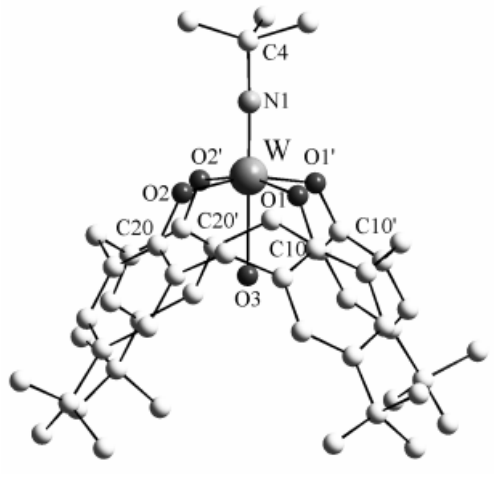


Figure 3. The molecular structure of LW(N*t*Bu)(OH_2) **1b(OH_2)** with hydrogen atoms omitted for clarity. Disorders in *t*Bu groups are not resolved in the drawing. Selected bond lengths [pm] and angles [°]: W−N1: 171.8(5), W−O1: 194.4(3), W−O2: 193.6(3), W−O3: 230.3(4), N1−C4: 145.3(10), O1−C10: 136.4(5), O2−C20: 137.2(5), C4−N1−W: 171.7(7), N1−W−O1: 98.15(16), N1−W−O2: 98.33(16), O1−W−O2′: 163.52(11), O2−W−O1′: 163.52(11), N1−W−O3: 179.9, C10−O1−W: 129.5(2), C20−O2−W: 129.7(3).

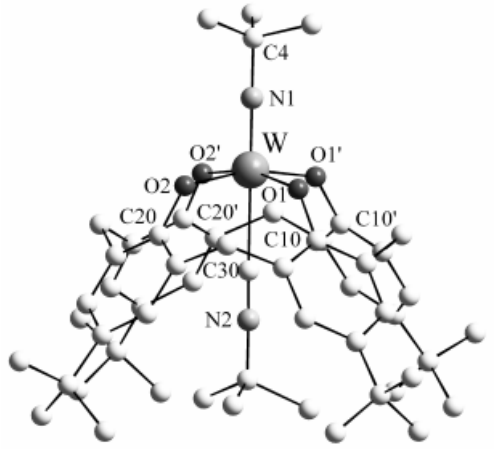


Figure 4. The molecular structure of LW(N*t*Bu)(CN*t*Bu) **1b(**CN***t*****Bu)** with hydrogen atoms omitted for clarity. Disorders in *t*Bu groups are not resolved in the drawing. Selected bond lengths [pm] and angles [°]:W−N1: 173.0(10), W−O1: 192.5(6), W−O2: 193.7(6), W−C30: 241.7(13), N1−C4: 145(2), O1−C10: 138.7(12), O2−C20: 136.4(11), C30−N2: 118.9(18), C4−N1−W: 177.6(17), N1−W−O1: 97.8(3), N1−W−O2: 98.5(3), N1−W−C30: 179.8(5), O1−W−O2′: 163.7(2), O2−W−O1′: 163.7(2), N2−C30−W: 179.0(10), C10−O1−W: 130.6(5), C20−O2−W: 130.3(6).

bond angles are given in the figure captions. Some important structural parameters are summarized and compared in Table 1.

Compound **2a(NCMe)** crystallizes in the triclinic space group $P\bar{1}$, **2b(NCMe)** in *C*c, and the isostructural *tert*-butyl imido compounds **1a(NCMe)**, **1b(OH_2)**, and **1b(CN*t*Bu)** in the orthorhombic space group $Cmc2_1$. As shown on the left side of Figure 1, the molecules of the molybdenum mesityl imido compound **2a(NCMe)** are in a head-to-head arrangement connected through π stacking of the aryl rings of the imido ligand. The carbon-carbon distances of the mutually

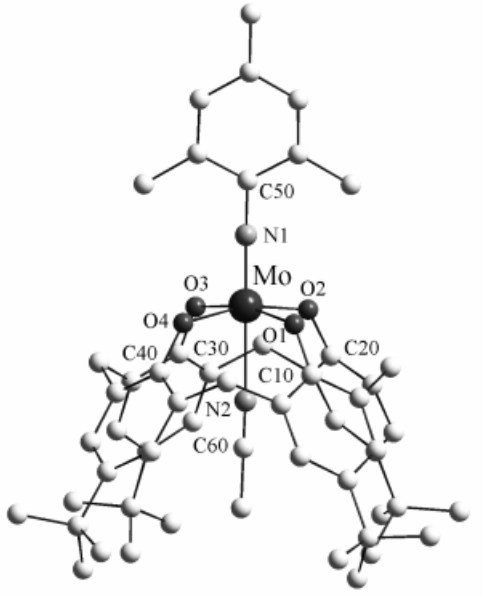


Figure 5. The molecular structure of LMo(NMes)(NCMe) **2a(NCMe)** with hydrogen atoms omitted for clarity. Disorders in *t*Bu groups are not resolved in the drawing. Selected bond lengths [pm] and angles [°]: Mo−N1: 172.4(3), Mo−O1: 194.8(3), Mo−O2: 193.7(2), Mo−O3: 193.9(3), Mo−O4: 195.3(2), Mo−N2: 230.3(3), N1−C50: 137.9(3), N2−C60: 113.3(4), O1−C10: 136.0(3), O2−C20: 137.1(4), O3−C30: 136.8(3), O4−C40: 136.3(3), Mo−N1−C50: 172.3(2), Mo−N2−C60: 177.8(4), N1−Mo−O1: 95.87(11), N1−Mo−O2: 98.07(11), N1−Mo−O3: 98.11(11), N1−Mo−O4: 97.04(11), O1−Mo−O3: 165.92(8), O2−Mo−O4: 164.85(8), N1−Mo−N2: 177.56(10), C10−O1−Mo: 128.99(17), C20−O2−Mo: 128.4(3), C30−O3−Mo: 125.80(16), C40−O4−Mo: 131.38(17).

opposite atoms are in a narrow range between 371.7−372.5 pm. The other structurally characterized compounds are close to isostructural and show molecules isolated from each other in the unit cell, as presented for **1a(NCMe)** at the right side of Figure 1.

All complexes contain a group VI metal imido M=NR moiety mounted on the phenoxide rim of the calix[4]arene ligand. The four oxygen atoms of the calix[4]arene ligand and the nitrogen atom of the imido ligand span a flat square pyramidal environment around the transition metal atom. A sixth coordination site is occupied by a neutral donor molecule, i.e. acetonitrile, isonitrile, or water, respectively. Thus, the metal atoms adopt distorted octahedral coordination spheres.

The donor atoms of the guest molecules are almost linearly coordinated to the metal atoms with respect to the metal−(imido)nitrogen vector and all N1−M−D angles are larger than 177°. The distances and angles of the coordinated acetonitrile molecules suggest minimal changes in the bonding of these ligands compared to the uncomplexed molecules, because the d^0 metal centers cannot π backdonate into the carbon-nitrogen triple bonds. The carbon−nitrogen distances of 111.4(15) pm in **1a(NCMe)**, 113.3(4) pm in **2a(NCMe)**, and 112.0(6) pm in **2b(NCMe)**, as well as almost linear [N−C−C] entities, indicate carbon-nitrogen bond orders of approximately three. The bond lengths of the acetonitrile adducts compare well with other aceto-

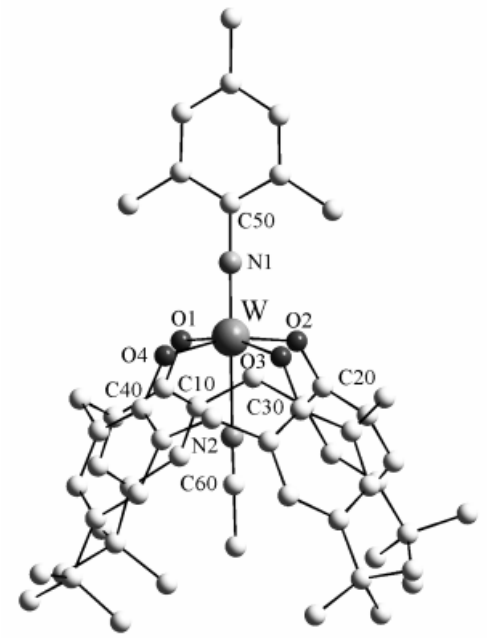


Figure 6. The molecular structure of LW(NMes)(NCMe) **2b(NCMe)** with hydrogen atoms omitted for clarity. Selected bond lengths [pm] and angles [°]: W−N1: 174.3(4), W−O1: 194.0(3), W−O2: 194.0(3), W−O3: 194.5(3), W−O4: 194.6(3), W−N2: 231.4(3), N1−C50: 138.0(5), N2−C60: 112.0(6), O1−C10: 136.9(5), O2−C20: 135.6(5), O3−C30: 136.6(5), O4−C40: 137.4(5), C50−N1−W: 177.5(3), C60−N2−W: 178.5(3), N1−W−O1: 98.16(14), N1−W−O2: 97.41(15), N1−W−O3: 97.78(16), N1−W−O4: 97.99(15), O1−W−O3: 164.06(12), O2−W−O4: 164.60(12), N1−W−N2: 179.44(14), C10−O1−W: 129.5(3), C20−O2−W: 131.0(2), C30−O3−W: 129.6(2), C40−O4−W: 128.7(2).

Table 1. Comparison of selected bond lengths [pm] and angles [°] of LMo(N*t*Bu)(NCMe) **1a(NCMe)**, LW(N*t*Bu)(OH_2) **1b(OH_2)**, LW(N*t*Bu)(CN*t*Bu) **1b(CN*t*Bu)**, LMo(NMes)(NCMe) **2a(NCMe)**, and LW(NMes)(NCMe) **2b(NCMe)**

	1a(NCMe)	**1b(OH_2)**	**1b(CN*t*Bu)**	**2a(NCMe)**	**2b(NCMe)**
M−N	171.8	171.8	173.0	172.4	174.3
M−O	194.0 194.0	194.4 193.6	192.5 193.7	193.7 193.9 194.8 195.3	194.0 194.0 194.5 194.6
M−D	234.3	230.3	241.7	230.3	231.4
N2−C	111.4		118.9	113.3	112.0
M−N1−C	176.9	171.7	177.6	172.3	177.5
N1−M−O	97.4 97.6	98.2 98.3	97.8 98.5	95.9 97.0 98.1 98.1	97.4 97.8 98.0 98.2
N1−M−D	179.4	179.9	179.8	177.6	179.4
M−O−C	129.6 128.6	129.5 129.7	130.6 130.3	125.8 128.4 129.0 131.5	128.7 129.5 131.0
$(O-M-O)_{trans}$	165.0	163.5	163.7	165.9 164.9	164.1 164.6

nitrile adducts of group VI imido complexes of metals in their highest oxidation state.[16] The N−C bond lengths of the acetonitrile molecules in **2a(NCMe)**, **2b(NCMe)**, and **1a(NCMe)** correlate with the lengths of the M−N2 bonds of 230.3(3) pm in **2a(NCMe)**, 231.4(3) pm in **2b(NCMe)**, and 234.4(9) pm in **1a(NCMe)**.

Compound **1b(CN*t*Bu)** is the first structurally characterized terminal isonitrile complex of a d^0-group VI metal complex. The observed W−C bond length in **1b(CN*t*Bu)** of 241.7(13) pm is very long compared to homoleptic W^{II} complexes $[W(CNtBu)_7]^{2+}$. In these compounds, W−C distances are in a range between 206.9(6) pm and 214.2(8) pm.[17] The W−OH_2 bond length of 230.3(4) pm in **1b(OH_2)** is significantly shorter than the Mo−OH_2 distance of 240.8(16) pm in the calix[4]arene molybdenum oxide $(LH_4)LMoO(OH_2)(PhNO_2)$,[13] but comparable to other tungsten complexes with a water molecule coordinated *trans* to σ,π donor ligands. In tungsten(V) anions of the type $[W(=O)X_4(OH_2)]^-$ prepared by Atwood and co-workers, for example, the W−OH_2 bond length comes to 226.2(9) pm (X = Cl) and 231(2) pm (X = Br), respectively, and in an anion of higher nuclearity prepared in Jeannin′s group the W−OH_2 bond length was determined to be 229(1) pm.[18]

The calix[4]arene metal fragments of all the imido compounds LM(NR)(donor) that were investigated by X-ray crystallography retain pseudo C_{4v} symmetry in the solid state and produce circular calix[4]arene cavities similar to those in the uncoordinated ligand. The molybdenum−oxygen and tungsten−oxygen bond lengths are in a very narrow range between 192.5(6) pm and 195.3(2) pm, with three exceptions at 194.0±0.6 pm, and are comparable with average metal−oxygen bond lengths in molybdenum or tungsten aryloxy complexes.[19] The angles N1−M−O are between 97° and 99°, the angles M−O−C are approximately 130° and all *endo* calix angles O−M−O between two *trans* oxygen atoms are in a narrow range between 163.5° and 165.9°.

The short Mo−N1 and W−N1 contacts of 171.8(5)−174.3(4) pm and the almost linear M−N1−C entities with angles larger than 170° suggest sp hybridized imido nitrogen atoms with triple bond character of the metal-(imido)-nitrogen bond.[1] These bonding parameters are also in good agreement with other monoimido complexes of the type Mo(NR)X_4 · L, for example in Mo(NTolyl)Cl_4 · THF [Mo−N bond length 171.7(3) pm, angle Mo−N−C 174.6(3)°],[20] in $(H_2NSO_2N)WCl_4$ · NCMe [W−N bond length 173.0(12) pm, angle W−N−S 168.3(7)°],[16b] in (ClN)WCl_4 · NCMe [W−N bond length 172(1) pm, angle W−N−C 175.5(10)°][16c] or in L′Mo(NDip) [Mo−N bond length 172.9(3) pm, angle Mo−N−C 179.2(2)°].[9a]

Theoretical Studies

In order to gain some insight into the bonding situation of calix[4]arene imido complexes, as well as their donor adducts, we performed density functional calculations[21] on

model compounds of the characterized complexes. We wanted to understand calix[4]arene−metal bonding, bonding of the imido fragment [RN] to the calix[4]arene metal fragment [LM] and the influence of the donor molecule on metal−imido bonding. The *t*Bu groups of the calix[4]arene ligands were replaced by hydrogen atoms and the organic groups of the imido ligands were replaced by hydrogen or methyl groups to reduce computational cost. The models under investigation were the tungsten compounds L′W(NH) **3** and L′W(NMe) **4** (L′ = *p*-H-calix[4]arene).

For an electron count of calix[4]arene imido complexes, we opted to cleave all metal ligand bonds heterolytically and end up with $[L']^{4-}$, a metal center in the formal electron configuration d^0 and a closed shell imido anion $[NR]^{2-}$. Counting the imido ligand − in agreement with the M−N bond lengths (vide supra) − as a six-electron donor,[1] the calix[4]arene ligand has to provide 12 electrons for an 18 VE count on the central atom. For the acetonitrile- and isonitrile-stabilized complexes, 10 electrons are sufficient since these donor molecules act as neutral two electron donors. Eight electrons are provided by four σ bonds. Thus, one [for LM(NR)(D) type complexes] and two [for LM(NR) type complexes] calix[4]arene−metal π bonds are necessary to fulfill the 18 VE rule for the central atom. In the evaluation of π bonding in this type of compound, we want to preface our analysis with simple considerations emerging from group theory.

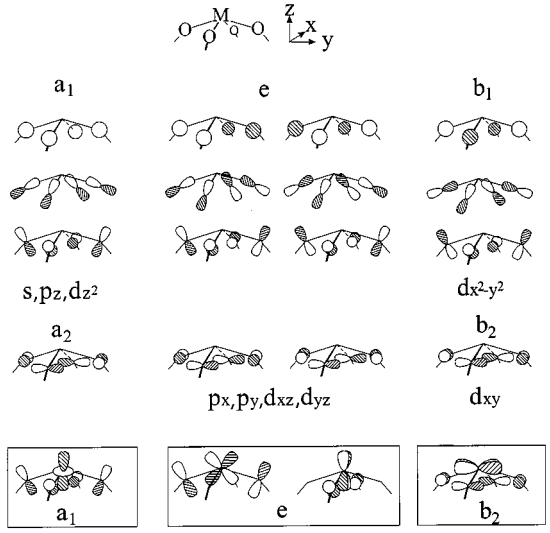


Figure 7. Symmetry-adapted linear combinations of oxygen s and p orbitals of a C_{4v} $[O_4]$ set

One possibility to generate symmetry adapted combinations of oxygen s and p orbitals of an $[O_4]$ fragment in C_{4v} symmetry is shown in Figure 7. Combination of the oxygen s orbitals gives four symmetry adapted orbitals that transform as a_1, e, and b_1, which are shown as the first entry in Figure 7. For the p orbitals on each oxygen atom, one can think of a basis set independent from the cartesian coordinate system, one radial p orbital pointing in the direction of the M−O vector and two sets of tangential p orbitals, which are perpendicular to each other and to the M−O vector (second and third entry in Figure 7). The radial p orbitals and one of the tangential sets transform as a_1, e, and b_1. The second set of tangential orbitals, those lying in the O_4 plane, transforms as a_2, e, and b_2 (fourth entry in Figure 7). The counterparts on the metal atom, which can interact with these combinations, are s, p_z, and d_{z2} for a_1 ligand orbitals, p_x, p_y, d_{xz}, and d_{yz} for ligand orbitals of e symmetry, d_{x2-y2} for b_1, and d_{xy} for b_2 ligand orbitals. Within this simplified scheme, linear combinations of radial ligand p orbitals and ligand s orbitals are responsible for metal ligand σ bonding, whereas π bonding comes from overlap of tangential ligand orbitals with metal orbitals of appropriate symmetry. The most important interactions for π bonding are shown in the lowest part of Figure 7. There is one π interaction of a_1 symmetry, one of e symmetry and one of b_2 symmetry. For the C_{4v} calix[4]arene metal fragment we observe M−O−C angles of approximately 130°, a value that is significantly smaller than 180°. Thus, there will be mixing of radial and tangential orbitals of the same symmetry resulting in a good O−C overlap and, as a consequence of this, in worse overlap of the a_1 and e π-type orbitals shown at the bottom of Figure 7.

In order to check these qualitative considerations, DFT calculations were carried out on geometrically optimized C_{4v} L′W(NH) **3** and on the complex fragment C_{4v} $[L'W]^{2+}$. The imido complex **3** optimizes at W−O distances of 195.8 pm, a W−N distance of 174.8 pm and angles W−O−C of 135.6°. These bonding parameters are in good agreement with the experimental results. The imido group is kept linear to retain overall C_{4v} symmetry. A Mulliken population analysis of the tungsten-oxygen bond reveals a strong π bond for the b_2 orbital shown at the bottom of Figure 7. The contribution of the irreducible representation b_2 is 0.106 to a total W−O overlap population of 0.420. In contrast, contributions from e-type orbitals are almost negligible. Similar results can be obtained from an SEN (shared electron number) analysis[22] of covalent contributions to the W−O bond. Orbitals of b_2-type symmetry contribute significantly to the W−O bond (0.169 out of a total of 0.611), whereas the contributions of e symmetry are approximately 0.03. Calculations on the complex fragment $[L'W]^{2+}$ confirm these results. The b_2 interaction shown in the lowest part of Figure 7 is an important π interaction that helps to stabilize metal d orbitals in calix[4]arene metal complexes.

A truncated fragment molecular orbital (FMO) scheme for the interaction of a C_{4v} calix[4]arene tungsten fragment $[L'W]^{2+}$ with a linear dianionic imido group $[NR]^{2-}$ is shown in Figure 8. The frontier orbitals of the $[L'W]^{2+}$ complex fragment are shown schematically on the left side. A group of highest occupied orbitals indicated as a dashed box are centered on the calix[4]arene ligand, mainly on the carbon atoms of the phenoxide. The highest unoccupied orbitals are metal-centered and give a typical M(ligand)$_4$ pattern: there is a low lying $1a_1$ orbital, mainly d_{z^2} in character, a degenerate set of d_{xz} and d_{yz} orbitals of e symmetry, a W−O antibonding orbital of b_2 symmetry (d_{xy}), and two orbitals $2a_1$ (p_z) and b_1 ($d_{x^2-y^2}$) that are high in energy. Im-

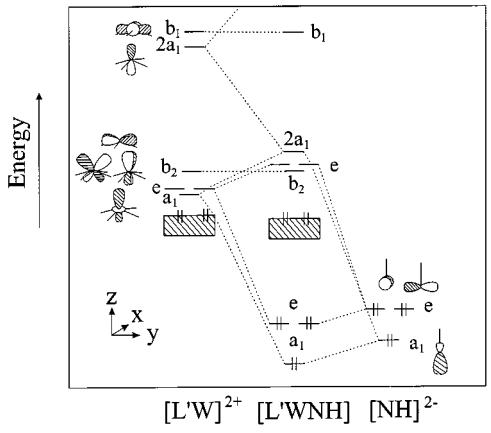


Figure 8. Schematic FMO diagram for C_{4v} L′W≡NH built up from the components $[L'W]^{2+}$ (left side) and $[NR]^{2-}$ (right side). The important frontier orbitals of the fragments and the combined molecule are shown. The HOMO region of $[L'W]^{2+}$ and L′W≡NH is indicated by a dashed box.

portant orbitals of the linear imido fragment $[NR]^{2-}$ are an sp hybrid orbital of a_1 symmetry and a degenerate e set of nitrogen p_x and p_y orbitals, and these are shown on the right side of Figure 8. The W−N σ bond is built up from interactions of the a_1 orbitals depicted in Figure 8, with some additional admixture of tungsten s. The orbitals of e symmetry combine to give a degenerate set of π orbitals for the tungsten nitrogen bond. The net result of this interaction is a metal-nitrogen triple bond resulting from one σ−(a_1) and two π−(e) interactions. This qualitative picture is confirmed by our DFT results on C_{4v} L′W(NH) **3**. From a total shared electron number (SEN) of 1.59 electrons for the tungsten nitrogen bond, 0.83 electrons are due to contributions of a_1 symmetry and 0.76 electrons are due to contributions of e symmetry.

A detailed analysis of the frontier orbitals of C_{4v} L′W(NH) **3** shows that HOMO 30e is a ligand centered orbital, whereas LUMO $13b_2$ is tungsten d_{xy} in character. The LUMO + 1, a degenerate orbital 31e is W−N antibonding and can be considered a W−N π* orbital. The LUMO + 2, which is also W−N antibonding, is an a_1 hybrid orbital with contributions from tungsten d_{z^2}, p_z, and s, as well as some nitrogen s and p_z. This orbital is responsible for binding an *endohedral* donor molecule, such as nitriles or isonitriles, to the metal atom. Calculations on **3(NCH)** show that the W−(imido)N bond should be weaker in comparison to **3**, mainly due to a lower a_1 contribution to the W−(imido)N bond.

An X-ray crystal structure of L′Ta(η^5-C_5Me_5),[23] which is isoelectronic to L′W(NR), shows a significant distortion from pseudo C_{4v} to pseudo C_{2v} symmetry for the macrocycle bound to the CpTa unit, and this results in an *elliptical* cone section for the calix[4]arene ligand. This distortion can be traced by two sets of different Ta−O bond lengths (189 pm and 200 pm), two sets of Ta−O−C angles (one set with angles larger than 160°, the other with angles of approximately 125°) and two different *endo* calix angles (127° and 155°). Lippard and co-workers attributed this distortion to favorable oxygen-to-metal π bonding for the distorted molecule. The opening of one pair of the M−O−C angles should lead to a better overlap for one of the π bonds of the e set depicted at the bottom of Figure 7. However, the optimization of L′W(NH) **3** under C_{2v} symmetry restriction leads to a geometry that is only 0.03 kcal/mol lower in energy than C_{4v} L′W(NH), and only minor deviations from the C_{4v} structure can be observed. The calculated bond lengths and angles in C_{2v} L′W(NH) are 174.8 pm [in C_{4v} L′W(NH): 174.8 pm] for the W−N bond, 196.5 pm and 194.8 pm (195.8 pm) for the different W−O bonds, 104.0 and 102.6° (103.2°) for the angles N−W−O, and 131.9° and 140.0° (135.6°) for the W−O−C angles.

Since we were not able to obtain high quality crystals of compounds **1** and **2** without any guest in the calix[4]arene cavity, we decided to optimize an extended model system, L′WNMe **4**, without any symmetry restraints in order to answer the question as to whether the calix[4]arene ligand in these group VI imido compounds adopts pseudo C_{4v} symmetry or distorts to a pseudo C_{2v}-type structure with an *elliptical* cone section. The geometrically optimized minimum structure of L′W(NR′) **4** shows the calix[4]arene ligand to be only slightly distorted from a local C_{4v} structure and an almost linear tungsten-imido moiety. We calculate a W−N distance of 174.91 pm and an angle W−N−C of 179.95°, W−O distances of 196.33±2 pm, W−O−C angles of 134.74±2°, and N−W−O angles of 102.62±2°. The bond lengths obtained are in good agreement with those of the experimentally determined structures (see Table 1), while the angles N−W−O and W−O−C are significantly smaller in the observed structures due to coordination of an additional molecule inside the calix[4]arene cavity. However, there is no driving force for a significant distortion in these systems as reported for the tantalum compound. The tungsten d_{xz} and d_{xy} orbitals of e symmetry are significantly stabilized by interaction with a good σ, π donor, i.e. the imido ligand, and do not contribute to tungsten calix[4]arene bonding.

Conclusions

Group VI calix[4]arene imido complexes LM(NR) **1a**, **b** (M = Mo, W; R = *t*Bu) and **2a**, **b** (M = Mo, W; R = Mes) have been prepared and characterized. Treatment of $M(NtBu)_2(NHtBu)_2$ or $M(NMes)_2Cl_2$(dme) (M = Mo, W) with *p*-*t*Bu-calix[4]arene LH_4 affords calix[4]arene metal imido complexes LM(NR) **1a, b** (M = Mo, W; R = *t*Bu) and **2a**, **b** (M = Mo, W; R = Mes). These molecules are well suited to bind small molecules, like acetonitrile, *t*Bu-isonitrile, or water within their macrocyclic pockets, and some of those adducts have also been characterized. The monomeric nature of these compounds in solution is demonstrated by NMR spectroscopy. ^{1}H- and ^{13}C-NMR spectra are typical for calix[4]arene complexes with a pseudo C_{4v} symmetry of the macrocyclic ligand. The signals of the acetonitrile and isonitrile molecules incorporated into the *endo* calix site are shifted significantly in the ^{1}H-NMR spectra as compared to the uncoordinated guest molecules.

The crystal structures of LMo(N*t*Bu)(NCMe) **1a(NCMe)**, LW(N*t*Bu)(OH_2) **1b(OH_2)**, LW(N*t*Bu)(CN*t*Bu) **1b(CN*t*Bu)**, LMo(NMes)(NCMe) **2a(NCMe)**, and LW(NMes)(NCMe) **2b(NCMe)** show a group VI metal imido M=NR moiety mounted on the phenoxide rim of the calix[4]arene ligand and an incorporated guest molecule within the cavity. The metal atoms in these compounds adopt a distorted octahedral coordination sphere. The calix[4]-arene ligands also retain a pseudo C_{4v} symmetry in the solid state and thus produce circular calix[4]arene cavities. The imido group [M−N−R] is almost linear with M−N distances of 171.8(5)−174.3(4) pm. In the solid state, molecules of LMo(NMes)(NCMe) **2a(NCMe)** are assembled head-to-head through van der Waals forces between the aryl rings of the imido ligands.

Some insights into the structures of compounds of the type L′W(NR′) **3** and **4** (L′ = *p*-H-calix[4]arene; R′ = H, Me) and into bonding in calix[4]arene imido complexes are provided by density functional theory. Simple symmetry considerations show that there is one π bond of b_2 symmetry, which is very important for calix[4]arene−metal bonding in these compounds. This is confirmed by population analyses of C_{4v} L′W(NH) **3**. The geometrically optimized minimum structure of L′W(NR′) **4** shows the calix[4]-arene ligand only slightly distorted from a local C_{4v} structure and an almost linear tungsten-imido moiety. According to our DFT results, calix[4]arene-tungsten π interactions of e symmetry do not contribute significantly to the net stabilization of this compound

Experimental Section

General: All reactions and subsequent manipulations involving organometallic reagents were performed under an argon atmosphere using standard Schlenk techniques. The preparation of samples for spectroscopy was undertaken using a glove box (Braun MB 150 BG-I). Solvents were dried according to standard procedures, stored over activated 4-Å molecular sieves and degassed prior to use. Deuterated solvents were obtained from Aldrich Inc. (all 99 atom% D), dried according to standard procedures, and stored over activated 4-Å molecular sieves. − NMR spectra were recorded on a Bruker AC 250 at 298 K. ^{13}C-NMR spectra are broad-band proton decoupled ($^{13}C\{^1H\}$). Standard DEPT-135 experiments were recorded to distinguish $-CH_3$- and −CH-type carbons from −C- or $-CH_2$-type carbons in the ^{13}C-NMR spectrum. NMR data are listed in parts per million (ppm) and are reported relative to tetramethylsilane. Coupling constants are quoted in Hertz. Residual solvent peaks used as internal standards were as follows: $CDCl_3$: δ = 7.24 (^{1}H), CD_2Cl_2: δ = 5.32 (^{1}H) or natural-abundance carbon signal at δ = 77.0 for $CDCl_3$ and δ = 54.0 for CD_2Cl_2. − EI-MS spectra were recorded on a Varian MAT 3830 (70 eV). − Elemental analyses were performed by the microanalytical laboratory of the author′s department. − Infrared spectra were recorded as KBr pellets on a Bruker IFS 28 and are reported in cm^{-1}. − The compounds *p*-*t*Bu-calix[4]arene,[24] Mo(NH*t*Bu)$_2$(N*t*Bu)$_2$,[10a,10b] W(NH*t*Bu)$_2$(N*t*Bu)$_2$,[10c,10d] and [M(NMes)$_2$Cl$_2$(dme)] (M= Mo, W)[12] were prepared as described in the literature. All other reagents were purchased from commercial sources and purified by standard techniques.

Preparation of *p-tert*-Butylcalix[4]arene-*tert*-butylimidomolybdenum(VI) (1a): A solution of 250 mg (0.65 mmol) of Mo(NH-*t*Bu)$_2$(N*t*Bu)$_2$ and 485 mg (0.65 mmol) of *p*-*t*Bu-calix[4]arene toluene adduct in 40 mL of toluene was stirred for 8 h at 80°C. All volatile material was removed in vacuo. The red-brown residue was washed with 20 mL of hexane, collected, and dried in vacuo. Yield: 435 mg, 82%. m.p 345°C (dec.). Crystals suitable for X-ray analysis were grown from a saturated acetonitrile solution of **1a** to yield **1a(NCMe)**. **1a(CN*t*Bu)** was obtained as a red-brown powder by addition of an excess of *t*Bu-isocyanide to a toluene solution of **1a** and removal of all volatiles in vacuo. − ^{1}H NMR ($CDCl_3$) [**1a**]: δ = 7.10 (s, 8 H, aromatic *H*), 4.36 (d, 4 H, $^2J_{HH}$ = 12.3 Hz, CH_2), 3.24 (d, 4 H, $^2J_{HH}$ = 12.3 Hz, CH_2), 1.85 [s, 9 H, NC(CH_3)$_3$], 1.25 [s, 36 H, C(CH_3)$_3$]. − ^{13}C NMR ($CDCl_3$) [**1a**]: δ = 29.28 [s, NC(*C*H$_3$)$_3$], 31.49 [s, C(*C*H$_3$)$_3$], 33.86 (s, *C*H$_2$), 34.09 [s, *C*(CH$_3$)$_3$], 81.99 [s, N*C*(CH$_3$)$_3$], 124.96 (s, aromatic *C*H), 130.22 (s, aromatic *C*), 145.76 (s, aromatic C*t*Bu), 153.96 (s, aromatic *C*O). − EI/MS (70 eV) *m*/*z* (%): 813 [M]$^+$ (87), 798 [M − CH_3]$^+$ (3), 756 [M − C_4H_9]$^+$ (49), 741 [M − NC_4H_9]$^+$ (21), 57 [C(CH$_3$)$_3$]$^+$ (38), 41 [C_3H_5]$^+$ (100). − $C_{48}H_{61}O_4MoN$ (811.96) calcd. C 71.00, H 7.57, N 1.73; found C 70.91, H 7.63, N 1.71.

^{1}H NMR ($CDCl_3$) **[1a(NCMe)]**: δ = 7.04 (s, 8 H, aromatic *H*), 4.32 (d, 4 H, $^2J_{HH}$ = 12.1 Hz, CH_2), 3.14 (d, 4 H, $^2J_{HH}$ = 12.2 Hz, CH_2), 1.86 [s, 9 H, NC(CH_3)$_3$], 1.15 [s, 36 H, C(CH_3)$_3$], −0.16 (s, 3 H, MeCN). − ^{13}C NMR ($CDCl_3$) **[1a(NCMe)]**: δ = 28.78 [s, NC(*C*H$_3$)$_3$], 31.77 [s, C(*C*H$_3$)$_3$], 32.80 (s, *C*H$_2$), 34.08 [s, *C*(CH$_3$)$_3$], 123.75 (s, aromatic *C*H), 129.28 (s, aromatic *C*), 143.81 (s, aromatic *Ct*Bu), 160.65 (s, aromatic *C*O); [N*C*(CH$_3$)$_3$] not detectable. − IR (KBr) **[1a(NCMe)]**: $\tilde{\nu}$ = 2959 cm^{-1} vs br (=C−H), 2321 s (−C≡N), 2292 m (−C≡N), 1573 w, 1458 vs br, 1392 m, 1361 vs, 1304 s, 1282 s, 1243 vs br, 1197 vs br, 1125 m, 1105 s, 1025 w, 917 m, 870 s, 830 vs, 800 vs, 758 s, 677 m, 549 vs, 504 m, 424 s, 395 m. −^{1}H NMR ($CDCl_3$) [**1a(CN*t*Bu)**]: δ = 7.04 (s, 8 H, aromatic *H*), 4.55 (d, 4 H, $^2J_{HH}$ = 12.4 Hz, CH_2), 3.24 (d, 4 H, $^2J_{HH}$ = 12.4 Hz, CH_2), 1.80 [s, 9 H, NC(CH_3)$_3$], 1.20 [s, 36 H, C(CH_3)$_3$], − 0.20 [s, 9 H, (CH_3)$_3$CNC]. − ^{13}C NMR ($CDCl_3$) [**1a(CN*t*Bu)**]: δ = 28.62 [s, NC(*C*H$_3$)$_3$], 29.45 (s, *C*H$_2$), 31.86 [s, C(*C*H$_3$)$_3$], 33.96 [s, *C*(CH$_3$)$_3$], 125.05 (s, aromatic *C*H), 127.90 (s, aromatic *C*), 143.69 (s, aromatic *Ct*Bu), 161.64 (s, aromatic *C*O); [N*C*(CH$_3$)$_3$] not detectable. − IR (KBr) [**1a(CN*t*Bu)**]: $\tilde{\nu}$ = 2963 cm^{-1} vs br (=C−H), 2211 m (−C≡N), 1760 w, 1570 w, 1457 vs br, 1393 m, 1361 s, 1285 vs br, 1245 s, 1197 vs br, 1122 m, 1105 s, 1024 w, 959 w, 915 s, 872 s, 832 vs, 800 vs, 757 s, 709 w, 677 m, 631 m, 554 vs, 501 m, 422 vs, 390 m.

Preparation of *p-tert*-Butylcalix[4]arene-*tert*-butylimidotungsten(VI) (1b): A solution of 250 mg (0.53 mmol) of W(NH*t*Bu)$_2$(N*t*Bu)$_2$ and 398 mg (0.53 mmol) of *p*-*t*Bu-calix[4]arene toluene adduct in 40 mL of toluene was stirred for 12 h at 60°C. All volatiles were removed in vacuo. The yellow residue was washed with 20 mL of hexane, collected, and dried in vacuo. Yield: 439 mg, 91%. m.p. 394°C (dec.). Crystals suitable for X-ray analysis were grown from saturated moist toluene solutions [**1b(OH_2)**]. Yellow crystals of **1b(CN*t*Bu)** could be obtained from solutions of **1b** in toluene and addition of an excess of *t*Bu-isocyanide. − ^{1}H NMR (CD_2Cl_2) [**1b**]: δ = 7.12 (s, 8 H, aromatic *H*), 4.47 (d, 4 H, $^2J_{HH}$ = 12.2 Hz, CH_2), 3.25 (d, 4 H, $^2J_{HH}$ = 12.2 Hz, CH_2), 1.75 [s, 9 H, NC(CH_3)$_3$], 1.20 [s, 36 H, C(CH_3)$_3$]. − ^{13}C NMR (CD_2Cl_2) [**1b**]: δ = 31.20 [s, NC(*C*H$_3$)$_3$], 31.87 [s, C(*C*H$_3$)$_3$], 33.76 (s, *C*H$_2$), 34.57 [s, *C*(CH$_3$)$_3$], 75.81 [s, N*C*(CH$_3$)$_3$], 125.21 (s, aromatic *C*H), 131.45 (s, aromatic *C*), 146.71 (s, aromatic *Ct*Bu), 152.29 (s, aromatic *C*O). − EI/MS (70 eV) *m*/*z* (%): 899 [M]$^+$ (100), 884 [M − CH_3]$^+$ (30), 842 [M − C_4H_9]$^+$ (5), 828 [M − NC_4H_9]$^+$ (42), 57 [C(CH$_3$)$_3$]$^+$ (49). −

$C_{48}H_{61}NO_4W$ (899.87) calcd. C 64.07, H 6.83, N 1.56; found C 64.19, H 6.93, N 1.53.

^{1}H NMR ($CDCl_3$) [**1b(OH$_2$)**]: δ = 7.10 (s, 8 H, aromatic *H*), 4.58 (d, 4 H, $^2J_{HH}$ = 12.4 Hz, CH_2), 3.23 (d, 4 H, $^2J_{HH}$ = 12.4 Hz, CH_2), 1.75 [s, 9 H, NC(CH_3)$_3$], 1.54 (s, 2 H, H_2O), 1.22 [s, 36 H, C(CH_3)$_3$]. − ^{13}C NMR ($CDCl_3$) [**1b(OH$_2$)**]: δ = 30.52 [s, NC(*C*H$_3$)$_3$], 31.55 [s, C(*C*H$_3$)$_3$], 32.94 (s, *C*H$_2$), 33.98 [s, *C*(CH$_3$)$_3$], 71.59 [s, N*C*(CH$_3$)$_3$], 124.95 (s, aromatic *C*H), 130.57 (s, aromatic *C*), 144.52 (s, aromatic *Ct*Bu), 155.11 (s, aromatic *C*O). − IR (KBr) [**1b(OH$_2$)**]: ṽ = 3519 cm^{-1} m (O−H), 3448 m (O−H), 2953 vs br (=C−H), 1751 w, 1570 m, 1471 vs br, 1394 s, 1361 vs, 1284 s br, 1199 vs, 1124 m, 1106 m, 1026 w, 917 m, 873 s, 834 vs, 800 s, 760 s, 678 m, 552 s, 503 m, 420 s.

^{1}H NMR ($CDCl_3$) [**1b(NCMe)**]: δ = 7.05 (s, 8 H, aromatic *H*), 4.51 (d, 4 H, $^2J_{HH}$ = 12.4 Hz, CH_2), 3.18 (d, 4 H, $^2J_{HH}$ = 12.4 Hz, CH_2), 1.70 [s, 9 H, NC(CH_3)$_3$], 1.15 [s, 36 H, C(CH_3)$_3$], − 0.20 (s, 3 H, MeCN). − ^{13}C NMR ($CDCl_3$) [**1b(NCMe)**]: δ = − 2.32 (s, *C*H$_3$CN), 30.38 [s, NC(*C*H$_3$)$_3$], 31.57 [s, C(*C*H$_3$)$_3$], 32.28 (s, *C*H$_2$), 33.81 [s, *C*(CH$_3$)$_3$], 71.12 [s, N*C*(CH$_3$)$_3$], 123.46 (s, aromatic *C*H), 125.64 (s, CH$_3$*C*N), 130.31 (s, aromatic *C*), 143.57 (s, aromatic *Ct*Bu), 158.31 (s, aromatic *C*O). − IR (KBr) [**1b(NCMe)**]: ṽ = 2953 cm^{-1} vs br (=C−H), 2324 s (−C≡N), 2294 m (−C≡N), 1748 w, 1577 m, 1479 vs br, 1393 s, 1361 vs, 1272 vs br, 1196 vs, 1126 s, 1106 s, 1026 w, 917 m, 870 s, 833 vs, 800 s, 760 s, 678 m, 548 s, 504 m, 422 s. − ^{1}H NMR ($CDCl_3$) [**1b(CN*t*Bu)**]: δ = 7.13 (s, 8 H, aromatic *H*), 4.80 (d, 4 H, $^2J_{HH}$ = 12.4 Hz, CH_2), 3.35 (d, 4 H, $^2J_{HH}$ = 12.4 Hz, CH_2), 1.72 [s, 9 H, NC(CH_3)$_3$], 1.26 [s, 36 H, C(CH_3)$_3$], − 0.17 [s, 9 H, CNC(CH_3)$_3$]. − ^{13}C NMR ($CDCl_3$) [**1b(CN*t*Bu)**]: δ = 21.42 [s, (*C*H$_3$)$_3$CNC], 29.31 [s, NC(*C*H$_3$)$_3$], 31.72 [s, C(*C*H$_3$)$_3$], 33.62 (s, *C*H$_2$), 33.91 [s, *C*(CH$_3$)$_3$], 70.67 [s, N*C*(CH$_3$)$_3$], 124.99 (s, aromatic *C*H), 129.21 (s, aromatic *C*), 143.61 (s, aromatic *Ct*Bu), 159.49 (s, aromatic *C*O). − IR (KBr) [**1b(CN*t*Bu)**]: ṽ = 2963 cm^{-1} vs br (=C−H), 2218 m (−C≡N), 1758 w, 1604 m, 1573 m, 1477 vs br, 1393 m, 1361 s, 1285 vs br, 1197 vs br, 1124 s, 1105 s, 1029 w, 916 m, 874 s, 835 vs, 799 vs, 759 s, 731 vs, 695 s, 678 m, 552 vs, 502 m, 465 m, 419 s.

Preparation of *p-tert*-Butylcalix[4]arenemesitylimidomolybdenum(VI) (2a): A solution of 250 mg (0.48 mmol) of Mo(NMes)$_2$Cl$_2$ · dme and 354 mg (0.48 mmol) of *p-t*Bu-calix[4]arene toluene adduct in 40 mL of toluene was stirred for 12 h at 100 °C. All volatiles were removed in vacuo and the yellow-brownish residue was extracted into 60 mL of hexane. Evaporation of the orange solution left a dark yellow solid, which was washed with 5 mL of pentane and dried in vacuo. Yield: 419 mg, 89%. m.p. 391 °C (dec.). Crystals in form of **2a(NCMe)**, suitable for X-ray analysis, were grown from a saturated acetonitrile solution of **2a**. − ^{1}H NMR ($CDCl_3$) [**2a**]: δ = 7.09 (s, 8 H, aromatic *H*), 6.93 (s, 2 H, Mes-H_m), 4.41 (d, 4 H, $^2J_{HH}$ = 12.4 Hz, CH_2), 3.19 (d, 4 H, $^2J_{HH}$ = 12.4 Hz, CH_2), 3.07 [s, 6 H, Mes-(CH_3)$_o$], 2.44 [s, 3 H, Mes-(CH_3)$_p$], 1.21 [s, 36 H, C(CH_3)$_3$]. − ^{13}C NMR ($CDCl_3$) [**2a**]: δ = 20.54 (Mes-*o*-*C*H$_3$), 22.65 (s, Mes-*p*-*C*H$_3$), 31.56 [s, C(*C*H$_3$)$_3$], 33.30 (s, *C*H$_2$), 34.08 [s, *C*(CH$_3$)$_3$], 125.04 (s, aromatic *C*H), 125.93 (s, Mes-C-3), 129.41 (s, aromatic *C*), 140.13 (s, Mes-C-4), 141.97 (s, Mes-C-2), 144.69 (s, aromatic *Ct*Bu), 146.85 (s, Mes-C-1), 157.70 (s, aromatic *C*O). − EI/MS (70 eV) *m/z* (%): 875 [M]$^+$ (100), 860 [M − CH$_3$]$^+$ (52), 428 [M − 2(CH$_3$)]$^{++}$ (8). − ^{1}H NMR ($CDCl_3$) [**2a(NCMe)**]: δ = 7.14 (s, 8 H, aromatic *H*), 6.97 (s, 2 H, Mes-H_m), 4.47 (d, 4 H, $^2J_{HH}$ = 12.4 Hz, CH_2), 3.24 (d, 4 H, $^2J_{HH}$ = 12.4 Hz, CH_2), 3.12 [s, 6 H, Mes-(CH_3)$_o$], 2.49 [s, 3 H, Mes-(CH_3)$_p$], 1.27 [s, 36 H, C(CH_3)$_3$], −0.11 (s, 3 H, CH_3CN). − ^{13}C NMR ($CDCl_3$) [**2a(NCMe)**]: δ = − 2.13 (s, *C*H$_3$CN), 18.66 (Mes-*o*-*C*H$_3$), 21.49 (s, Mes-*p*-*C*H$_3$), 31.65 [s, C(*C*H$_3$)$_3$], 32.38 (s, *C*H$_2$), 33.99 [s, *C*(CH$_3$)$_3$], 116.34 (s, CH$_3$*C*N), 123.67 (s, aromatic *C*H), 125.03 (s, Mes-C-3), 129.21 (s, aromatic *C*), 140.10 (s, Mes-C-4), 142.13 (s, Mes-C-2), 143.81 (s, aromatic *Ct*Bu), 144.68 (s, mes-C-1), 161.12 (s, aromatic *C*O). − IR (KBr) [**2a(NCMe)**]: ṽ = 2950 cm^{-1} st br (=C−H), 2323 m (−C≡N), 2293 m (−C≡N), 1739 w, 1600 m (C=C), 1455 vs br, 1362 m, 1300 m, 1197 vs, 1124 m, 1104 m, 915 m, 870 s, 829 vs, 799 vs, 757 st, 677 m, 548 vs, 505 m, 419 m. − $C_{55}H_{66}MoN_2O_4$ (915.1) calcd. C 72.19, H 7.27, N 3.06; found C 71.61, H 6.94, N 3.25.

Preparation of *p-tert*-Butylcalix[4]arenemesitylimidotungsten(VI) (2b): A solution of 500 mg (0.82 mmol) of W(NMes)$_2$Cl$_2$ · dme and 606 mg (0.82 mmol) of *p-t*Bu-calix[4]arene toluene adduct in 50 mL of toluene was stirred for 12 h at 100 °C. All volatiles were removed in vacuo and the red-orange residue was dissolved in 40 mL of hot acetone, filtered through a pad of celite and the solvent was removed in vacuo. The yellow residue was extracted into 60 mL of hexane. Evaporation of the solution gave a yellow powder, which was dried in vacuo. Yield: 677 mg, 86%. Crystals suitable for X-ray analysis were grown from saturated acetonitrile solutions of **2b** to give yellow crystals of **2b(NCMe)**. − ^{1}H NMR ($CDCl_3$) [**2b**]: δ = 7.12 (s, 8 H, aromatic *H*), 6.99 (s, 2 H, Mes-H_m), 4.62 (d, 4 H, $^2J_{HH}$ = 12.4 Hz, CH_2), 3.25 (d, 4 H, $^2J_{HH}$ = 12.4 Hz, CH_2), 3.04 [s, 6 H, Mes-(CH_3)$_o$], 2.52 [s, 3 H, Mes-(CH_3)$_p$], 1.22 [s, 36 H, C(CH_3)$_3$]. − ^{13}C NMR ($CDCl_3$) [**2b**]: δ = 18.10 (Mes-*o*-*C*H$_3$), 20.96 (s, Mes-*p*-*C*H$_3$), 31.58 [s, C(*C*H$_3$)$_3$], 33.09 (s, *C*H$_2$), 34.06 [s, *C*(CH$_3$)$_3$], 125.08 (s, aromatic *C*H), 127.28 (s, Mes-C-3), 130.58 (s, aromatic *C*), 137.79 (s, Mes-C-4), 140.05 (s, Mes-C-2), 144.85 (s, aromatic *Ct*Bu), 145.65 (s, Mes-C-1), 155.35 (s, aromatic *C*O). − EI/MS (70 eV) *m/z* (%): 961 [M]$^+$ (100), 946 [M − CH$_3$]$^+$ (46), 930 [M − 2CH$_3$]$^+$ (2), 466 [M − 2 CH$_3$]$^{++}$ (46). − $C_{53}H_{63}NO_4W$ (961.94) calcd. C 66.18, H 6.60, N 1.46; found C 65.88, H 6.69, N 1.53.

^{1}H NMR ($CDCl_3$) [**2b(NCMe)**]: δ = 7.14 (s, 8 H, aromatic *H*), 6.98 (s, 2 H, Mes-H_m), 4.59 (d, 4 H, $^2J_{HH}$ = 12.4 Hz, CH_2), 3.25 (d, 4 H, $^2J_{HH}$ = 12.4 Hz, CH_2), 3.02 [s, 6 H, Mes-(CH_3)$_o$], 2.51 [s, 3 H, Mes-(CH_3)$_p$], 1.18 [s, 36 H, C(CH_3)$_3$], −0.12 (s, 3 H, CH_3CN). − ^{13}C NMR ($CDCl_3$) [**2b(NCMe)**]: δ = −2.00 (s, *C*H$_3$CN), 18.09 (Mes-*o*-*C*H$_3$), 20.93 (s, Mes-*p*-*C*H$_3$), 31.67 [s, C(*C*H$_3$)$_3$], 32.51 (s, *C*H$_2$), 33.92 [s, *C*(CH$_3$)$_3$], 116.27 (s, CH$_3$*C*N), 123.63 (s, aromatic *C*H), 127.19 (s, Mes-C-3), 130.42 (s, aromatic *C*), 137.47 (s, Mes-C-4), 140.33 (s, Mes-C-2), 143.93 (s, aromatic *Ct*Bu), 149.49 (s, Mes-C-1), 158.74 (s, aromatic *C*O). − IR (KBr) [**2b(NCMe)**]: ṽ = 2953 cm^{-1} st br (=C−H), 2323 m (−C≡N), 2294 m (−C≡N), 1734 w, 1605 m (C=C), 1478 vs br, 1393 m, 1361 m, 1304 m, 1274 s, 1244 s, 1195 vs, 1126 m, 1105 m, 1021 w br, 945 w, 920 m, 871 s, 833 vs, 800 vs, 761 st, 727 m, 678 m, 589 m, 549 s, 504 m, 421 m.

Crystal Structure Analysis of 1a(NCMe): Stoe-STADI IV diffractometer (Mo-*Kα* radiation), *T* = 200(2) K; data collection and refinement: SHELXS-97[25] and SHELXL-97;[26] orthorhombic, space group *C*mc2$_1$; lattice constants *a* = 14.338(3), *b* = 21.066(4), *c* = 19.586(4) Å, *V* = 5916(2) Å^3, *Z* = 4, μ(Mo-K_α) = 0.259 mm^{-1}, $2\Theta_{max}$ = 51.9°; 3104 independent reflections measured, of which 2829 were considered observed with $I > 2\sigma(I)$; max./min. residual electronic density 1.141 and −0.638 e/Å^3; 259 parameters (W, O, N, anisotropic, C anisotropic except disordered *t*Bu groups, the positions of the H atoms were calculated for idealized positions); R_1 = 0.070; wR_2 = 0.1923.

Crystal Structure Analysis of 1b(OH$_2$): Stoe-STADI IV diffractometer (Mo-*Kα* radiation), *T* = 200(2) K; data collection and refinement: SHELXS-97[25] and SHELXL-97;[26] orthorhombic, space group *C*mc2$_1$; lattice constants *a* = 15.013(3), *b* = 20.633(4), *c* = 19.448(4) Å, *V* = 6024(2) Å^3, *Z* = 4, μ(Mo-K_α) = 1.956 mm^{-1},

$2\Theta_{max}$ = 55.0°; 6222 independent reflections measured, of which 6024 were considered observed with $I > 2\sigma(I)$; max./min. residual electronic density 0.772 and −0.628 e/Å^3; 250 parameters (W, O, N, anisotropic, C anisotropic except disordered *t*Bu groups, the positions of the H atoms were calculated for idealized positions); R_1 = 0.031; wR_2 = 0.0908.

Crystal Structure Analysis of 1b(CN*t*Bu): Stoe-STADI IV diffractometer (Mo-*Kα* radiation), T = 203(2) K; data collection and refinement: SHELXS-97[25] and SHELXL-97;[26] orthorhombic, space group $Cmc2_1$; lattice constants a = 15.503(3), b = 20.480(4), c = 19.617(4) Å, V = 6228(2) Å^3, Z = 4, μ(Mo-K_α) = 1.889 mm^{-1}, $2\Theta_{max}$ = 50.3°; 2981 independent reflections measured, of which 2896 were considered observed with $I > 2\sigma(I)$; max./min. residual electronic density 1.229 and −0.584 e/Å^3; 268 parameters (W, O, N, anisotropic, C anisotropic except disordered *t*Bu groups, the positions of the H atoms were calculated for idealized positions); R_1 = 0.043; wR_2 = 0.1420.

Crystal Structure Analysis of 2a(NCMe): Stoe-IPDS diffractometer (Mo-*Kα* radiation), T = 200(2) K; data collection and refinement: SHELXS-97[25] and SHELXL-97;[26] triclinic, space group $P\bar{1}$; lattice constants a = 11.015(6), b = 11.970(9), c = 18.574(11) Å, α = 93.06(7), β = 93.52(6), γ = 96.53(7)°, V = 2424(3) Å^3, Z = 2, μ(Mo-K_α) = 0.317 mm^{-1}, $2\Theta_{max}$ = 54.3°; 9809 independent reflections measured, of which 8510 were considered observed with $I > 2\sigma(I)$; max./min. residual electronic density 0.805 and −1.116 e/Å^3; 574 parameters (W, O, N, anisotropic, C anisotropic except disordered *t*Bu groups, the positions of the H atoms were calculated for idealized positions); R_1 = 0.052; wR_2 = 0.1427.

Crystal Structure Analysis of 2b(NCMe): Stoe-STADI IV diffractometer (Mo-*Kα* radiation), T = 203(2) K; data collection and refinement: SHELXS-97[25] and SHELXL-97;[26] triclinic, space group Cc; lattice constants a = 13.122(3), b = 19.416(4), c = 20.535(4) Å, β = 99.86(3)°, V = 5154.6(18) Å^3, Z = 4, μ(Mo-K_α) = 2.288 mm^{-1}, $2\Theta_{max}$ = 54.0°; 6638 independent reflections measured, of which 6217 were considered observed with $I > 2\sigma(I)$; max./min. residual electronic density 0.461 and −0.605 e/Å^3; 588 parameters (W, O, N, C anisotropic except solvent molecules, the positions of the H atoms were calculated for idealized positions); R_1 = 0.019; wR_2 = 0.049.

Crystallographic data (excluding structure factors) for the structures reported in this paper have been deposited with the Cambridge Crystallographic Data Centre as supplementary publication nos. CCDC-114936 to CCDC-114940. Copies of the data can be obtained free of charge on application to CCDC, 12 Union Road, Cambridge, CB2 1EZ, UK (Fax: +44 1223/336 033; E-mail: deposit@ccdc.cam.ac.uk).

Acknowledgments

This work was supported by the Deutsche Forschungsgemeinschaft and the Fonds der Chemischen Industrie (Liebig fellowship for U. R.). U. R. kindly thanks Professor D. Fenske for his continued support and interest in our work. Furthermore, we would like to thank Dr. S. Elliott for helpful discussions as well as Dr. E. Matern and H. Berberich for recording NMR spectra. A gift of metal chlorides from Fa. H. C. Starck GmbH, Goslar, is gratefully acknowledged.

[1] [1a] W. A. Nugent, B. L. Haymore, *Coord. Chem. Rev.* **1980**, *31*, 123−175. − [1b] W. A. Nugent, J. M. Mayer, *Metal-Ligand Multiple Bonds*, Wiley, New York, **1988**. − [1c] D. E. Wigley, *Prog. Inorg. Chem.* **1994**, *42*, 239−482.

[2] [2a] R. R. Schrock: *Olefin Metathesis by Well-Defined Complexes of Molybdenum and Tungsten* in: A. Fürstner (Ed.), *Topics in Organometallic Chemistry, Vol. 1: Metathesis in Organic Synthesis*, Springer-Verlag, Berlin **1999**, 1−36. − [2b] C. J. Schaverian, J. C. Dewan, R. R. Schrock, *J. Am. Chem. Soc.* **1986**, *108*, 2771−2773. − [2c] J. S. Murdzek, R. R. Schrock, *Organometallics* **1987**, *6*, 1373−1374. − [2d] R. R. Schrock, R. T. DePue, J. Feldman, K. B. Yap, W. M. Davies, L. Park, M. DiMare, M. Schofield, J. Anhaus, E. Walborski, E. Evitt, C. Krüger, P. Betz, *Organometallics* **1990**, *9*, 2262−2275. − [2e] M. A. Andrews, H. D. Kaesz, *J. Am. Chem. Soc.* **1977**, *99*, 6763−6765.

[3] [3a] G. W. Parshall, W. A. Nugent, D. M.-T. Chan, W. Tam, *Pure Appl. Chem.* **1985**, *12*, 1809−1818. − [3b] E. Herranz, S. A. Biller, K. B. Sharpless, *J. Am. Chem. Soc.* **1978**, *100*, 3596−3598. − [3c] W. D. Patrick, L. K. Truesdale, S. A. Biller, K. B. Sharpless, *J. Org. Chem.* **1978**, *13*, 2628−2638. − [3d] R. Breslow, R. Q. Kluttz, P. L. Khanna, *Tetrahedron Lett.* **1979**, *35*, 3273−3274. − [3e] T.-L. Ho, M. Henninger, G. A. Olah, *Synthesis* **1976**, 815−816.

[4] R. K. Grasselli, *J. Chem. Ed.* **1986**, *63*, 216−221.

[5] [5a] J. D. Burrington, R. K. Grasselli, *J. Catal.* **1979**, *59*, 79−99. − [5b] J. D. Burrington, C. T. Kartisek, R. K. Grasselli, *J. Catal.* **1981**, *69*, 495−497. − [5c] J. D. Burrington, C. T. Kartisek, R. K. Grasselli, *J. Catal.* **1984**, *87*, 363−380. − [5d] D. M.-T. Chan, W. A. Nugent, *Inorg. Chem.* **1985**, *24*, 1422−1424. − [5e] D. M.-T. Chan, W. C. Fultz, W. A. Nugent, D. C. Roe, T. H. Tulip, *J. Am. Chem. Soc.* **1985**, *107*, 251−253. − [5f] G. W. Keulks, L. D. Krenzke, T. M. Notermann, *Adv. Catal.* **1978**, *27*, 183−225. − [5g] K. Brueckmann, J. Haber, T. Wiltkowski, *J. Catal.* **1987**, *106*, 188−193. − [5h] E. A. Maata, Y. Du, *J. Am. Chem. Soc.* **1988**, *110*, 8249−8250. − [5i] E. A. Maata, Y. Du, A. L. Rheingold, *J. Chem. Soc., Chem. Commun.* **1990**, 756−757. − [5j] J. Belgacem, J. Kress, J. A. Osborn, *J. Chem. Soc., Chem. Commun.* **1993**, 1125−1127.

[6] [6a] C. D. Gutsche, *Calixarenes*, The Royal Society of Chemistry, Cambridge **1989**. − [6b] J. Vincens, V. Böhmer (Eds.), *Calixarenes: A Versatile Class of Macrocyclic Compounds*, Kluwer, Dordrecht **1991**. − [6c] C. D. Gutsche, *Prog. Macrocycl. Chem.* **1987**, *3*, 93−165. − [6d] V. Böhmer, *Angew. Chem.* **1995**, *107*, 785−818; *Angew. Chem. Int. Ed. Engl.* **1995**, *34*, 713−745.

[7] [7a] D. M. Roundhill, *Prog. Inorg. Chem.* **1995**, *43*, 533−565. − [7b] C. Wieser, C. B. Dielemann, D. Matt, *Coord. Chem. Rev.* **1997**, *165*, 93−61. − [7c] C. Floriani, *Chem. Eur. J.* **1999**, *5*, 19−23. − For tungsten calixarene carbene and carbyne complexes related to the imido complexes presented here see: [7d] L. Giannini, E. Solari, S. Dovesi, C. Floriani, N. Re, A. Chiesi-Villa, C. Rizzoli, *J. Am. Chem. Soc.* **1999**, *121*, 2784−2796. − [7e] L. Giannini, G. Guillemont, E. Solari, C. Floriani, N. Re, A. Chiesi-Villa, C. Rizzoli, *J. Am. Chem. Soc.* **1999**, *121*, 2797−2807 and references cited therein.

[8] U. Radius, J. Attner, *Eur. J. Inorg. Chem.* **1998**, 299−303.

[9] [9a] V. C. Gibson, C. Redshaw, W. Clegg, M. R. J. Elsegood, *J. Chem. Soc., Chem. Commun.* **1995**, 2371− 2381. − [9b] V. C. Gibson, C. Redshaw, W. Clegg, M. R. J. Elsegood, *J. Chem. Soc., Chem. Commun.* **1997**, 1605−1606.

[10] [10a] P. W. Dyer, V. C. Gibson, J. A. K. Howard, B. Whittle, C. Wilson, *J. Chem. Soc., Chem. Commun.* **1992**, 1666−1668. − [10b] A. A. Danopoulos, G. Wilkinson, B. Hussain-Bates, M. B. Hursthouse, *J. Chem. Soc., Dalton Trans.* **1990**, 2753−2761. − [10c] W. A. Nugent, *Inorg. Chem.* **1983**, *22*, 965−969. − [10d] W. A. Nugent, R. L. Harlow, *Inorg. Chem.* **1990**, *19*, 777−779.

[11] Reaction of **1a** and **1b** with reagents like pyridinium(HCl) lead reversibly to adducts of the general formula LM(Cl)(NH*t*Bu). Reaction of **1b** with a small excess of HCl (> 2 equiv.) yields $LWCl_2$, and with a larger amount of HCl to decomposition of the compound: U. Radius, J. Attner, unpublished results.

[12] U. Radius, J. Sundermeyer, H. Pritzkow, *Chem. Ber.* **1994**, *127*, 1827−1835.

[13] F. Corazza, C. Floriani, A. Chiesi-Villa, C. Guastini, *J. Chem. Soc., Chem. Commun.* **1990**, 640−641.

[14] [14a] F. Hajek, E. Graf, M. W. Hosseini, X. Delaigue, A. De Cian, J. Fischer, *Tetrahedron Lett.* **1996**, *37*, 1401−1404. − [14b] F. Hajek, M. W. Hosseini, E. Graf, A. De Cian, J. Fischer, *Angew. Chem.* **1997**, *109*, 1830−1832; *Angew. Chem., Int. Ed. Engl.* **1997**, *36*,1760−1762. − [14c] A. Zanotti-Gerosa, E. Solari, L. Giannini, C. Floriani, A. Chiesi-Villa, C. Rizzoli, *J. Chem. Soc., Chem. Commun.* **1996**, 119−120. − [14d] B. Xu, T. M. Swager, *J. Am. Chem. Soc.* **1993**, *115*, 1159−1160.

[15] G. D. Andreetti, R. Ungaro, A. Pochini, *J. Chem. Soc., Chem. Commun.* **1979**, 1005−1007.
[16] [16a] H. W. Roesky, J. Sundermeyer, J. Schimkowiak, P. G. Jones, M. Noltemeyer, T. Schroeder, G. M. Sheldrick, *Z. Naturforsch.* **1985**, *40B*, 736−739. − [16b] M. Witt, H. W. Roesky, M. Noltemeyer, G. M. Sheldrick, *Z. Naturforsch.* **1987**, *42B*, 519−521. − [16c] A. Görge, K. Dehnicke, D. Fenske, *Z. Naturforsch.* **1988**, *43B*, 677−681.
[17] D. J. Szalda, J. C. Dewan, S. J. Lippard, *Inorg. Chem.* **1981**, *20*, 3851−3857.
[18] [18a] J. L. Atwood, S. G. Bott, P. C. Junk, M. T. May, *J. Coord. Chem.* **1996**, *37*, 89−105. − [18b] Y. Jeannin, J.-P. Launay, J. Livage, A. Nel, *Inorg. Chem.* **1978**, *17*, 374−378.
[19] G. Orpen, *J. Chem. Soc., Dalton Trans.* **1989**, S1−S89.
[20] C. Y. Chou, J. C. Huffmann, E. A. Maata, *J. Chem. Soc., Chem. Commun.* **1984**, 1184−1185.
[21] Density functional calculations were performed using the TURBOMOLE set of programs and applying the B-P86/SVP density funtional within the RI-J approximation: [21a] R. Ahlrichs, *TURBOMOLE*, in: P. v. R. Schleyer (Ed.), *Encyclopedia of Computational Chemistry*, Wiley, Chichester **1998**, *Vol. 5*, 3123−3129. − [21b] R. Ahlrichs, M. v. Arnim, *TURBOMOLE, parallel implementation of SCF, density functional, and chemical shift modules*, in: E. Clementi, G. Corongiu (Eds.): *Methods and Techniques in Computational Chemistry*, STEF, Cagliari **1995**; − [21c] K. Eichkorn, O. Treutler, H. Öhm, M. Häser, R. Ahlrichs, *Chem. Phys. Lett.* **1995**, *242*, 652−660. − For definition of the B-P86 density functional see: [21d] A. D. Becke, *Phys. Rev. A* **1988**, *38*, 3098−3100. − [21e] J. P. Perdew, *Phys. Rev. B* **1986**, *33*, 8822−8824; *erratum*: J. P. Perdew, *Phys. Rev. B* **1986**, *34*, 7406. − The acronym SVP refers to TURBOMOLE split valence basis sets, augmented by a shell of polarization functions, cf. [21f] A. Schäfer, H. Horn, R. Ahlrichs, *J. Chem. Phys.* **1992**, *97*, 2571−2577. − Quasi-relativistic pseudo potentials were used for the element W: [21g] D. Andrae, U. Häussermann, M. Dolg, H. Stoll, H. Preuss, *Theor. Chim. Acta* **1990**, *77*, 123−141.
[22] The shared electron number SEN is based on population analysis and can serve as a measure of covalent bond strength: R. Ahlrichs, C. Erhardt, *Chem. Unserer Zeit* **1985**, *19*, 120−124. Some typical values for SEN provided in this paper: C−C, C−H: 1.4; C=C: 2.2; C≡C, N≡N: 3.3. Reduced SENs are found for polar bonds, like in NaF (0.3), and for weak bonds as in Cl_2 (0.9) and F_2 (0.6). For the calix[4]arene fragments of our compounds we calculate for aromatic carbon-carbon bonds $(C=C)_{ar}$ SENs of approximately 1.8, for C−C bonds to the methylene bridges SENs of approximately 1.4, and approximately 1.3 for C−H bonds.
[23] J. A. Acho, L. H. Doerrer, S. J. Lippard, *Inorg. Chem.* **1995**, *34*, 2542−2776.
[24] [24a] C. D. Gutsche, M. Iqbal, A. T. Watson, C. H. Heathcock, *Org. Synth.* **1989**, *68*, 234−237. − [24b] A. Arduini, A. Casnati, *Macrocycle Synthesis. A Practical Approach*, Oxford University Press, New York, **1996**.
[25] G. M. Sheldrick, *SHELXS-97. Program for Crystal Structure Solution*, Universität Göttingen, **1997**.
[26] G. M. Sheldrick, *SHELXL-97. Program for Crystal Structure Refinement*, Universität Göttingen, **1997**.

Received February 22, 1999
[I99062]

Synthesis, X-ray Crystal Structures and Reactivity Towards Alkynes of Gold(I)–Phosphinine Complexes

Nicolas Mézailles,[a] Louis Ricard,[a] François Mathey,*[a] and Pascal Le Floch*[a]

Keywords: Phosphorus / Heterocycles / Phosphinines / Gold / Cycloadditions

The coordination behaviour of 2,6-disilyl-substituted phosphinines towards gold(I) has been examined. The reaction of the bis(trimethylsilyl)phosphinine **1** with [AuCl(SMe_2)] gives the corresponding AuCl derivative **2**. X-ray crystal structure analysis reveals that the aromaticity of the phosphinine ring is slightly reduced as a result of the poor π-back bonding ability of the AuCl fragment. The same phenomenon is observed in the cationic complex [Au(**1**)$_2$][$GaCl_4$] (**3**) which was readily prepared by reaction of two equivalents of **1** with [AuCl(SMe_2)] followed by treatment with $GaCl_3$ at low temperature. Reaction of 2,6-bis(phenylethynyldimethylsilyl)phosphinine (**4**) with the same precursor leads similarly to the complex [AuCl(**4**)] (**5**). Interestingly, this complex dimerizes upon crystallization to give the bis(phosphabarrelene) complex **6**, also structurally characterized. The formation of **6** results from a [4 + 2] cycloaddition between one alkynyl group of each phosphinine with the other phosphinine subunit. The formation of the cationic complex [Au(**4**)][$GaCl_4$] (**8**) occurs under classical conditions but it disproportionates to give the cationic complex [Au(**4**)$_2$][$GaCl_4$] (**9**) and colloidal gold deposition. The formation of **9** has been ascertained by treating **8** with one equivalent of ligand **4**. Additionally, **9** can also be obtained in a straightforward fashion by treating two equivalents of **4** with [AuCl(SMe_2)] followed by treatment with $GaCl_3$ at low temperature. The structure of **9** has been elucidated. Despite a particular arrangement of the alkyne groups which encapsulate the gold coordination sphere, no gold–alkyne interactions are visible.

Introduction

It is now well established that phosphinines are strong π-acceptor ligands whose electronic properties markedly differ both from their nitrogen counterparts, pyridines, and classical tertiary phosphanes (R_3P).[1] This singularity, which mainly results from the presence of an electropositive sp^2-phosphorus atom, has recently been exploited to stabilize electron-rich transition-metal species which are usually unstable with other ligands, except CO. The studies of Elschenbroich et al. on the synthesis of homoleptic complexes of the parent compound C_5H_5P[2] and our work with 2,2′-biphosphinine complexes are illustrative of such uncommon reactivity.[1][3] Although significant progress has recently been achieved in this direction, our knowledge of the coordination chemistry of phosphinines still remains to be improved. Indeed, the understanding of phosphinine−metal interactions is a prerequisite to the use of these ligands in more applied projects such as homogeneous catalysis, an area which has just been explored,[4] and for the elaboration of sophisticated supramolecular edifices using, for example, phosphinine-based macrocycles.[5] Furthermore, it is clear that this useful information could be transposed to other species containing sp^2-hybridized P atoms (heterocycles or acyclic derivatives) whose properties are quite similar to those of phosphinines.

The study presented here, which deals with the synthesis of a series of gold(I) complexes of phosphinines, was also motivated by the fact that phosphinine complexes of group 11 are rather rare. Indeed, whereas some derivatives of copper(I) have been described,[6] very little is known of silver and gold derivatives. As far as we are aware, only one gold complex of the 2,4,6-triphenylphosphinine has been mentioned by Schmidbaur et al. but its spectroscopic and structural data remain unknown.[7] Another important motivation concerns the highly specific properties exhibited by phosphane−gold complexes[8] in different areas such as homogeneous catalysis,[9] photochemistry (luminescence)[10] and medicine (cytotoxic and antitumour activity).[11] Furthermore, the coordination of strong π-acceptor ligands such as phosphinines raises the problem of π-back-donation from gold. Experimental results and calculations made on carbonyl complexes tend to show that this back-donation is rather weak in gold(I) and gold(0) complexes.[12] As the stability of complexed phosphinines was shown to be dramatically dependent on the electron density available at the metal centre for π-back-donation,[13] it was also interesting to probe whether the coordination to gold(I) would enhance the reactivity of phosphinines or not. Herein, we present the results of these investigations.

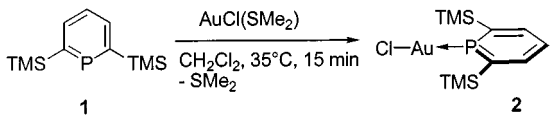
Results and Discussion

All our experiments were conducted with 2,6-disilylphosphinines. This choice was dictated by their availability and by the fact that we had recently developed a very efficient synthetic approach to polydentate ligands such as bis(trisphosphinines)[14] and phosphinine-based macrocycles[5] in which phosphinine units are linked by dimethylsilyl groups. Consequently, before extending our investigations to these sophisticated species, it seemed logical to focus our work on these simple models.

[a] Laboratoire "Héteroéléments et Coordination", UMR CNRS 7653, Ecole Polytechnique,
F-91128 Palaiseau Cedex, France
E mail: lefloch@mars.polytechnique.fr

 © WILEY-VCH Verlag GmbH, D-69451 Weinheim, 1999 1434−1948/99/1212−2233 $ 17.50+.50/0

As a preliminary experiment, to assess the effects of gold coordination to the phosphinine, we investigated the reaction of the 2,6-bis(trimethylsilyl)phosphinine (**1**) with AuCl(SMe$_2$). The reaction proceeded cleanly in dichloromethane affording complex **2** which was obtained as a pale yellow solid after precipitation with hexanes (Scheme 1).



Scheme 1. Synthesis of complex **2**

The NMR data of **2** deserves comment. In the ^{31}P-NMR spectrum, **2** displays a singlet [δ (CD_2Cl_2) = 199.50] as expected since no $^1J(^{197}Au-^{31}P)$ coupling constants can be observed because of the large value of the quadrupole moment of gold ($Q = 0.59 \times 10^{-28}$ m^2)[15] which leads to a short value of the relaxation time. The strong shielding of the ^{31}P signal [δ ($CDCl_3$) = 254.50 for **1**, $\Delta\delta$ = 55.00 ppm) is difficult to rationalize and a similar effect has already been observed for (2,2′-biphosphinine)copper(I) complexes.[6] Apart from group-6 metal complexes of phosphinines, where a trend in the shielding has been noted, variations of ^{31}P-NMR chemical shifts of phosphinine complexes have not, so far, been correlated with electronic effects on the ligands. As observed for copper(I) complexes, ^{1}H signals of the β and γ protons (3,3′-H and 4,4′-H) in **2** are shifted towards lower field compared to those of the free ligand **1**. This phenomenon is accompanied by a significant increase in the corresponding coupling constant ^3J(P−H) from 9.39 Hz in **1** to 31.20 Hz in **2**. Similar effects are generally observed for other phosphinine complexes. In the ^{13}C-NMR spectrum, the coordination induces an upfield shift which correlates with the distance to the phosphorus atom. Thus, the chemical shift of C-4 is not modified (δ = 127.50 in **1** vs. δ = 127.00 in **2**), but C-3 and C-2 are more shielded by 4.50 and 11.00 ppm, respectively. This steady increase in shielding of the nuclei closest to the metal atom, which has already been observed for group-6 metal complexes, reflects that the shielding constant σ of these nuclei is mainly governed by the shielding contribution of the metal atom. Also noteworthy is the magnitude of the ^1J(P−C) coupling constant which varies from 84.40 Hz in **1** to 4.0 Hz in **2**. This very large variation, also observed to a lesser extent in other phosphinine complexes, is caused by two competing factors which are generally encountered in the case of classical complexes of tertiary phosphanes:[16] the higher degree of coordination of the P atom (decrease of the magnitude of the coupling) and the loss of the lone-pair effect (algebraic increase of the coupling). Finally, we also note the very large magnitude of the ^3J(P−C4) coupling constant indicating that the electronic delocalisation within the ring has been strongly perturbed. In order to gain structural information, an X-ray crystal analysis of **2** was carried out. An ORTEP drawing of **2** is presented in Figure 1.

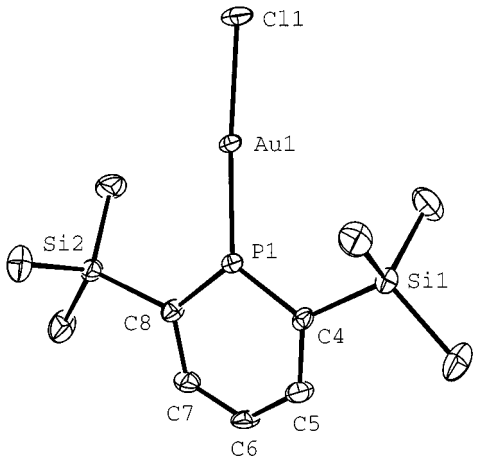
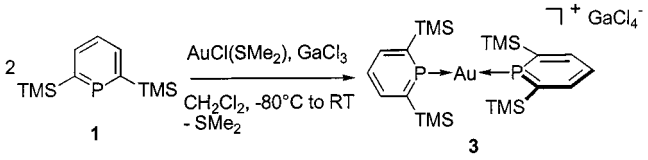


Figure 1. ORTEP drawing of **2** as determined by a single-crystal X-ray diffraction analysis; ellipsoids are drawn to enclose 50% of the electron density; hydrogen atoms are omitted for clarity; the crystallographic labelling is arbitrary and different from the numbering used for assignments of the ^{13}C-NMR spectra; selected bond lengths [Å] and angles [°]: Au1−Cl1 2.281(2), Au1−P1 2.211(2), P1−C4 1.710(6), P1−C8 1.702(7), C4−C5 1.406(9), C5−C6 1.38(1), C6−C7 1.38(1), C7−C8 1.41(1); Cl1−Au1−P1 175.36(7), Au1−P1−C4 122.6(2), C4−P1−C8 110.4(3), P1−C4−C5 117.5(5), C4−C5−C6 125.3(6), C5−C6−C7 123.7(6), C6−C7−C8 125.7(6), P1−C8−C7 117.2(5), P1−C4−Si1 120.6(4)

As expected for an [LAuX] complex, the geometry around the metal atom is perfectly linear. Whereas the Au−Cl bond length [2.281(2) Å] falls in the normal range, the Au−P(1) bond length [2.211(2) Å] appears to be slightly shorter than that observed for [AuCl(phosphane)] complexes [2.227(2) Å in the AuCl(DMPP) complex].[17] Nevertheless, this shortening cannot be considered as reflecting a better π-back-donation from the metal centre to the ligand since the hybridization of the phosphorus atom in **2** is sp^2 versus sp^3 in tertiary phosphanes.[16] More interesting information can be retrieved from an examination of bond lengths and angles within the ring. The value of the internal angle [Θ(CPC) = 110.4°] is quite large when compared to values usually recorded for free phosphinines (between 101° and 103°).[18] However, part of the effect is due to the disubstitution by silyl groups. Indeed, although the X-ray structure of ligand **1** is unknown (**1** is a liquid), we can compare this value to the angle recorded for the silacalix[4]phosphinine macrocycle which includes four dimethylsilylphosphinine units [Θ = 106.3(2)°].[5] In general, a similar increase in Θ(CPC) values is observed for phosphinines upon complexation.[19] The P=C bond lengths also allow the estimation of the extent of aromaticity within the ring. In **2**, it clearly appears that these bonds are shortened [1.710(6) and 1.702(7) Å] when compared to the parent phosphinine [1.73 Å] and to the dimethylsilyl derivative quoted above [1.734(5) and 1.746(5) Å]. This phenomenon, which has also been observed in other complexes such as Mo(C_5H_5P)$(CO)_5$[20] and homoleptic [M($C_5H_5P)_6$] (M = Cr, Mo, W) derivatives,[2d] indicates that the P−C bonds are more localized and acquire a higher double-bond character. As expected, this effect reflects a poor π-back-donation from the gold atom to the phosphinine ligand.

Indeed, a strong electronic transfer from the metal centre would tend to increase the P−C bond length since the lowest unoccupied π* molecular orbital (LUMO) of phosphinines is P−C-antibonding.[21] Another piece of data corroborates this fact. The C−C bond lengths present a significant disymmetry, $C_\alpha-C_\beta$ [1.406(9) and 1.41(1) Å] bonds being slightly longer than $C_\beta-C_\gamma$ [1.38(1) Å] bonds.

These effects are not specific to the chloride complex and similar results are also observed in the cationic $[Au(\mathbf{1})_2][GaCl_4]$ complex **3**. This complex was readily obtained by treating two equivalents of ligand **1** with $[AuCl(SMe_2)]$, followed by $GaCl_3$, which was used as a chloride abstractor at low temperature (see Scheme 2).



Scheme 2. Synthesis of complex **3**

Complex **3**, which was characterized as a pale yellow solid, exhibits NMR data which are overall similar to those recorded for **2**. Although a slight downfield shift is observed in the ^{31}P-NMR spectrum, the signal of **3** [$\delta(CD_2Cl_2) = 206.00$] remains shielded compared to that of the free ligand **1**. Apparently, the replacement of the chloride ion by a second phosphinine unit does not modify the electronic effects within the rings, also consistent with very poor π-back-donation from the gold atom.

To ascertain this point, the structure of **3** was elucidated by an X-ray diffraction study. An ORTEP view of **3** is presented in Figure 2. As in **2**, the geometry around the gold centre is linear[22] with the two ligands lying in two nearly perpendicular planes ($\Theta = 70.57°$). Very likely, this particular conformation allows through-space interactions between bulky trimethylsilyl groups to be minimized. The structure of **3** is comparable to that of **2** and the same trends are observed: an increase of the internal angle (mean Θ = 112.2°), short P−C bond lengths and a disymmetry between C−C bond lengths.

We then attempted to synthesize trigonal-planar Au^I species. Unfortunately, reaction of a large excess of ligand **1** with $[AuCl(SMe_2)]$, followed by treatment with $GaCl_3$ at low temperature, only led to the recovery of complex **3** and no traces of the desired $[Au(\mathbf{1})_3][GaCl_4]$ complex could be observed whatever experimental conditions were used. Very likely, this failure results from the strong steric hindrance generated by the bulky trimethylsilyl groups.

In view of these quite disappointing results, we focused our work on the preparation of hemilabile complexes of phosphinines. A recent report has demonstrated the affinity of Au^I centres for strained alkynes which are coordinated in an η^2-fashion.[23] Postulating that cationic trigonal-planar complexes incorporating two η^2-bonded alkynes and an η^1-bonded phosphinine could be prepared, we first investigated the reaction of the bis(phenylethynyldimethylsilyl)-

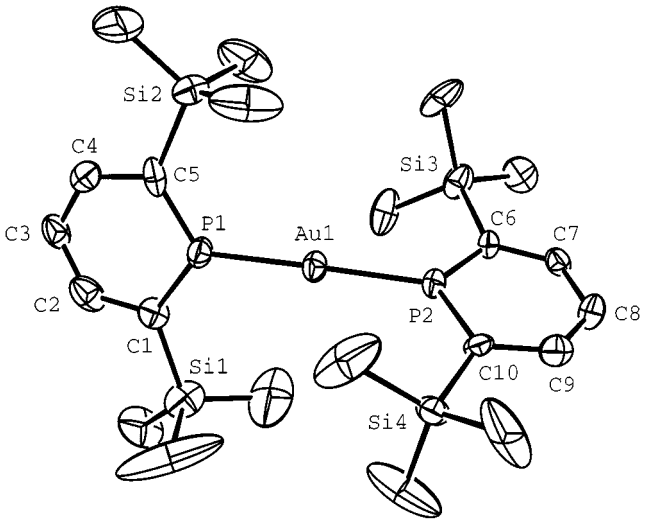
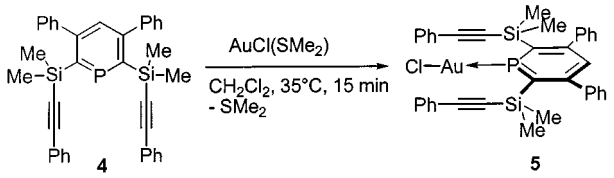


Figure 2. ORTEP drawing of **3** as determined by a single-crystal X-ray diffraction analysis; ellipsoids are drawn to enclose 50% of the electron density; hydrogen atoms are omitted for clarity; the crystallographic labelling is arbitrary and different from the numbering used for assignments of the ^{13}C-NMR spectra; selected bond lengths [Å] and angles [°]: Au1−P1 2.274(4), Au1−P2 2.290(4), P1−C1 1.73(1), P1−C5 1.69(2), P2−C(6), 1.71(1), P2−C10 1.71(1), C1−C2 1.41(2), C2−C3 1.39(2), C3−C4 1.37(2), C4−C5 1.44(2), C6−C7 1.38(2), C7−C8 1.40(2), C8−C9 1.35(2), C9−C10 1.43(2); P1−Au1−P2 175.3(2), Au1−P1−C1 123.5(5), Au1−P1−C5 123.9(5), C1−P1−C5 112.3(7), Au1−P2−C6 122.6(5), Au1−P2−C10 125.0(5), C6−P2−C10 112.1(6), P1−C1−C2 115.1(1), C1−C2−C3 127.0(1), C2−C3−C4 125.0(1), C3−C4−C5 125.0(1), P1−C5−C4 117.1(1), P2−C6−C7 116.0(1), C6−C7−C8 126.0(1), C7−C8−C9 123.0(1), C8−C9−C10 128.0(1)

phosphinine **4** towards $[AuCl(SMe)_2]$. As previously described for the synthesis of **3**, the reaction proceeds smoothly in dichloromethane at room temperature. Complex **5** was isolated in a 95% yield as a yellow solid after a simple precipitation with hexanes (Scheme 3).



Scheme 3. Synthesis of complex **5**

Whereas ^{13}C-NMR data of the ring carbon atoms compare in every respect to those recorded for **2** and **3**, the ^{31}P-NMR signal of **5** appears at low field [δ (CD_2Cl_2) = 222.00]. This deshielding does not reflect a particular electronic situation since the signal of the free ligand is also strongly downfield shifted [δ (CD_2Cl_2) = 273.00] from that of **2**. It must be noted that chemical shifts of the alkyne moiety are not significantly perturbed when compared to those recorded for the bis(phenylethynyl)dimethylsilane. This observation indicates that no η^2-alkyne coordination to the AuCl fragment occurs in **5**.

Before studying the formation of the corresponding cationic derivative $[Au(\mathbf{4})]^+$, we performed an X-ray crystal structure analysis of **5** to probe whether the structure observed in solution is maintained in the solid or not. This

experiment led to a quite unexpected result. Every attempt to crystallize **5** failed and each experiment systematically led to insoluble microcrystals whose structure was established by an X-ray diffraction study. The structure of complex **6** is a symmetrical dimer consisting of two (1-phosphabarrelene)AuCl complex units which are connected by two $SiMe_2$ bridges. An ORTEP drawing of **6** is presented in Figure 3.

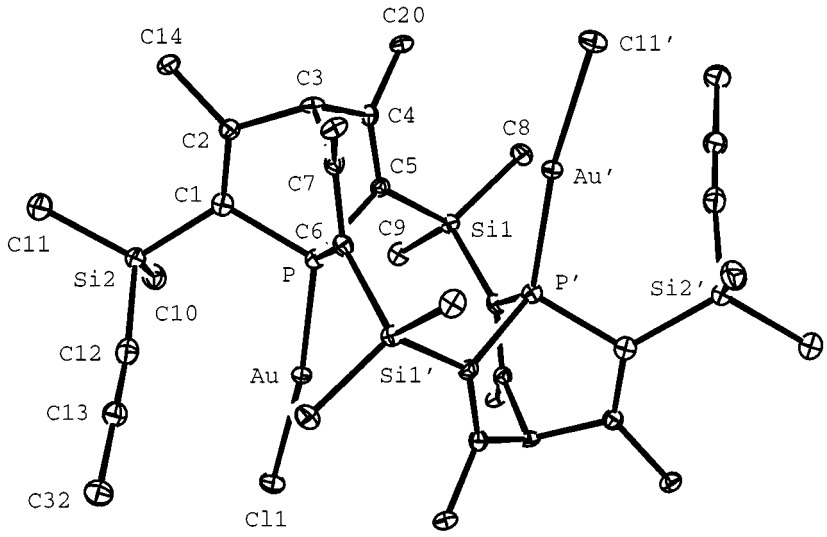
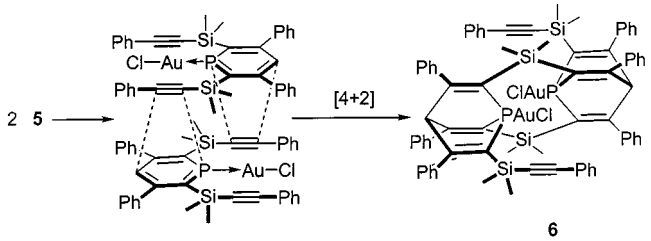


Figure 3. ORTEP drawing of **6** as determined by a single-crystal X-ray diffraction analysis; ellipsoids are drawn to enclose 40% of the electron density; hydrogen atoms are omitted for clarity; the crystallographic labelling is arbitrary and different from the numbering used for assignments of the ^{13}C-NMR spectra; selected bond lengths [Å] and angles [°]: Au−Cl1 2.286(1), Au−P2.218(1), P−C1 1.834(5), P−C5 1.835(5), P−C(6) 1.825(6), C1−C2 1.333(7), C2−C3 1.546(6), C3−C4 1.538(9), C3−C7 1.533(7), C4−C5 1.347(7), C6−C7 1.352(7); Cl1−Au−P 171.87(4), Au−P−C1 110.9(1), Au−P−C5 120.9(2), Au−P−C6 121.2(1), C1−P−C5 100.6(2), C1−P−C6 100.5(3), C5−P−C6 99.2(2), P−C1−C2 11.5(3), C1−C2−C3 116.3(4), C2−C3−C4 106.5(4), C2−C3−C7 108.1(4), C4−C3−C7 11.8(4), C3−C4−C5 118.1(4), P−C5−C4 109.4(4), P−C6−C7 109.4(4), C3−C7−C6 118.2(5)

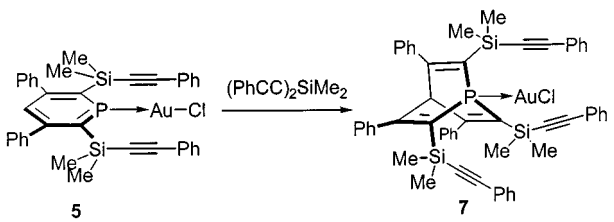
Unfortunately, due to its insolubility in common organic solvents, no NMR data of **6** could be recorded. The formation of **6** results from two [4 + 2] Diels−Alder reactions between two molecules of complex **5**, each phosphinine unit playing the role of a 1-phosphadiene (see Scheme 4).



Scheme 4. Intermolecular [4+2] cycloaddition leading to complex **6**

Apparently, this transformation only occurs during the formation of crystals and parallel experiments aimed at reproducing the synthesis of **6** under dilution conditions failed and led to colloidal Au^0 deposition. The formation of 1-phosphabarrelenes is not totally unprecedented. Usually, phosphinines do not react with alkynes, except when the latter are substituted by strongly electron-withdrawing groups (e.g. CF_3, CN) or when the triple bond is included into a strained structure.[24] Activated phosphinines in which CH unit(s) have been replaced by phosphorus or nitrogen such as 1,4-diphospha-[25a,25b] or monoaza- and diazaphosphinines[14,25c−25f] display a particular ability to react with various alkynes to give the corresponding aza- and diazabarrelenes. Moreover, it was also reported that $P-W(CO)_5$ complexes give [4 + 2] cycloadditions with activated alkynes such as dimethyl acetylenedicarboxylate or *N*-phenylmaleimide to afford 1-phosphabarrelenes and 2,3-dihydrobarrelenes complexes, respectively.[26] However, this was the first time that this kind of reaction has been observed in such mild conditions. Interestingly, as noted above, similarities are observed between the structure of these complexes and that of gold(I) studied here.

To validate the hypothesis of the double [4 + 2] Diels−Alder reaction, we decided to investigate the reaction of phosphinine **4** towards an alkyne with the hope of obtaining a soluble [4 + 2] cycloadduct. For obvious reasons, we chose the bis(phenylethynyl)dimethylsilane whose reaction with **4** should provide a symmetrical barrelene. In order to reproduce the conditions of crystallization of **6**, the reaction was carried out in concentrated medium, at room temperature. It led to total conversion into the desired symmetrical barrelene **7** within 48 h [δ (CD_2Cl_2) = −7.00] (see Scheme 5). The remarkable ease of this reaction explains why complex **5** could not be crystallized.



Scheme 5. Trapping of complex **5** with $(PhCC)_2SiHe_2$

To the best of our knowledge, **7** is the first example of a gold(I) barrelene complex. All NMR data (see Experimental Section) are in good agreement with the symmetrical structure proposed, thus confirming the regioselectivity of the Diels−Alder reaction. The fact that the alkyne carbon atom bearing the silicon group is attached to the P atom confirms that this latter bears a substantial positive charge.[14] Indeed, the observed regioselectivity compares with that observed in the case of 1,2 and 1,3,2-diazaphosphinines which are known to behave as strongly polarized [1,4] dipoles. To ascertain its formulation, an X-ray crystal structure analysis was carried out. An ORTEP drawing of **7** is presented in Figure 4. The structure of **7** reveals no particular features and no interactions between gold and alkynyl groups (C8−C9, C24−C25 and C40−C41) can be noted. Indeed, gold−carbon bond lengths appear to be quite long between 3.444 and 3.890 Å] and C≡C triple bond lengths fall in the expected range [from 1.203(8) to 1.212(8) Å].

Unfortunately, the isolation of the cationic derivative $[Au(\mathbf{4})]^+$ turned out to be more complicated than expected. The reaction of **5** with one equivalent of $GaCl_3$ at low temperature proceeds cleanly in dichloromethane to give complex **8** which was identified by ^{31}P-NMR spectroscopy only [δ (CH_2Cl_2) = 227.00] (see Scheme 6). Cationic complex **8** displays a poor stability in solution and after several minutes standing in dichloromethane, a purple color typical of the formation of colloidal gold can be observed concomitant with the appearance of a new signal in ^{31}P NMR at δ = 231.70.

Postulating that the latter could be the cationic complex $[Au(\mathbf{4})_2]^+$ **9**, resulting from the disproportionation of two molecules of **8**, we studied the reaction of **8** with one equivalent of ligand **4**. Indeed, complex **9**, which exhibits the expected ^{31}P-NMR resonance, was produced as pale yellow solid with a 90% yield. It must be noted that **9** can also be readily obtained by reacting two equivalents of **4** with

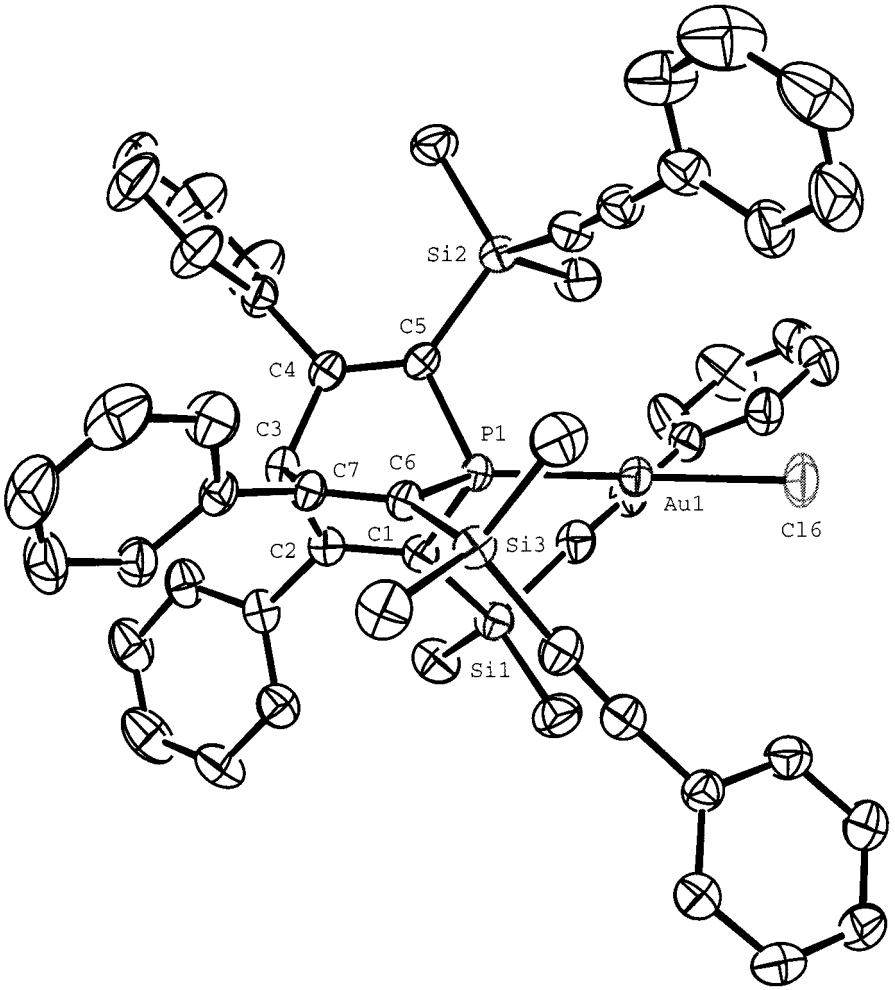
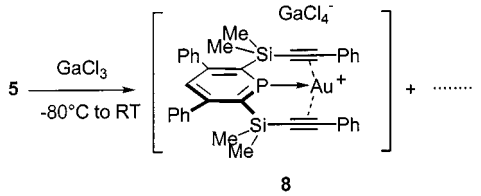
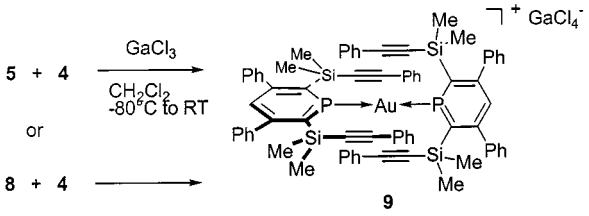


Figure 4. ORTEP drawing of **7** as determined by a single-crystal X-ray diffraction analysis; ellipsoids are drawn to enclose 50% of the electron density; hydrogen atoms are omitted for clarity; the crystallographic labelling is arbitrary and different from the numbering used for assignments of the ^{13}C-NMR spectra; selected bond lengths [Å] and angles [°]: Au1−Cl 2.273(2), Au1−P1 2.211(1), P1−C1 1.829(5), C1−C2 1.354(7), C2−C3 1.534(7), C4−C5 1.344(7), C6−C7 1.331(7), C8−C9 1.212(8), C24−C25 1.203(8), C40−C41 1.205(8); Cl−Au1−P1 176.92(7), Au1−P1−Cl6 176.92(7), Au−P1−C1 119.6(2), Au1−P1−C5 118.7(2), Au1−P1−C6 115.2(2), P1−C1−C2 109.8(4), C1−C2−C3 118.1(4), C2−C3−C4 111.1(4), Si(1)−C(8)−C(9) 174.9(5), Si2−C24−C25 174.3(5), Si(3)−C40−C41 169.8(5)



Scheme 6. Possible structure of complex **8**

$[AuCl(SMe_2)]$ in the presence of $GaCl_3$ as previously described for the synthesis of complex **3** (see Scheme 7).



Scheme 7. Synthesis of complex **9**

All the NMR data, which is comparable with those of **3**, confirm the proposed structure. An X-ray crystal structure analysis was undertaken. An ORTEP view of **9** is shown in Figure 5. As observed in the structure of **3**, P=C bond lengths appear to be rather short at 1.72(1) and 1.71(1) Å (compared to those of free silylphosphinines) and the presence of the two bulky silyl groups at the α positions of the phosphorus atom implies that the two phosphinines are twisted against each other [interplane angle Θ = 66.7(3)°]. The most interesting feature of **9** is provided by the arrangement of the four alkynyl substituents which encapsulate the gold coordination sphere. Despite this particular geometry, no interactions between the gold centre and these alkynyl groups are noted. Indeed, although shorter than in complex **7**, all Au−C bonds appear to be too long (between 3.043 and 3.308 Å) to favour an overlap between the filled 5d orbitals of the gold atom and the π* system of the triple bond. Besides, this assumption is confirmed by the C≡C triple-bond lengths which fall in the expected range [from 1.19(1) to 1.21(2) Å]. Additionally, it must be noted that no π overlap occurs between the phenyl groups and the phosphinine units.

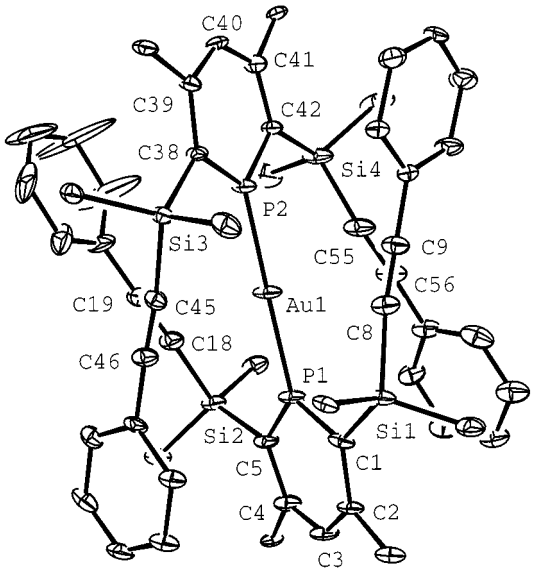


Figure 5. ORTEP drawing of **9** as determined by a single-crystal X-ray diffraction analysis; ellipsoids are drawn to enclose 50% of the electron density; hydrogen atoms are omitted for clarity; selected bond lengths [Å] and angles [°]: Au1−P1 2.263(2), Au1−P2 2.262(2), P1−C1 1.72(1), C1−C2 1.41(1), C2−C3 1.40(1), C3−C4 1.38(1), C4−C5 1.42(1), P1−C5 1.71(1), Si1−C8 1.861(9), C8−C9 1.19(1), C18−C19 1.21(1), C45−C46 1.20(1), C55−56 1.21(2); P1−Au1−P2 177.1(1), P1−C1−C2 117.0(7), C1−C2−C3 123 (1), C2−C3−C4 128.0(8), C3−C4−C5 123 (1), C4−C5−P1 116.4(8), C5−P1−C1 112.4(4), Si1−C8−C9 165(1), Si2−C18−C19 168(1), Si3−C45−C46 167.7(8), Si4−C55−C56 168(1)

In conclusion, we have shown that the poor π-back-donating ability of gold(I) significantly increases the dipole [1,4] character of monophosphinine ligands which are able to react under very mild conditions with alkynes to give phosphabarrelenes [4 + 2] cycloadducts. On the other hand, the existence and the appreciable stability of cationic derivatives such as **3** and **9** opens the way for a systematic investigation of the coordination chemistry of multidentate ligands including phosphinine units. Accordingly, studies aimed at including Au^+ into phosphinine-based macrocycles are currently under investigation.

Experimental Section

General: All reactions were routinely performed under nitrogen using Schlenk techniques and dry, oxygen-free solvents. Dry toluene, hexane, and *n*-pentane were obtained by distillation from sodium/benzophenone and dry CH_2Cl_2 was obtained by distillation from P_2O_5. Dry Celite was used for filtration. − NMR: Bruker AC-200 SY operating at 200.12 MHz for ^1H, 50.32 MHz for ^{13}C, and 81.91 MHz for ^{31}P; chemical shifts (ppm) are relative to TMS (^1H and ^{13}C) or 85% H_3PO_4 (^{31}P). List of abbreviations used: s, singlet; d, doublet; t, triplet; q, quadruplet; p, pseudo. − Elemental analyses: "Service d'analyse du CNRS", Gif-sur Yvette, France. Phosphinines **1**[14b] and **4**,[14b] $AuCl(SMe_2)$[27] were prepared according to published methods.

Synthesis of Complex 2: Phosphinine **1** (0.046 g, 1.9×10^{-4} mol) and $AuCl(SMe_2)$ (0.056 g, 1.9×10^{-4} mol) were weighed in air and placed under N_2. Freshly distilled CH_2Cl_2 (3 mL) was then added by syringe into the Schlenk flask, and the mixture allowed to stir at 35°C. ^{31}P-NMR spectroscopy indicated that the reaction was finished within 15 min. Reduction of the volume, followed by hexane precipitation and filtration yielded a pale yellow solid (0.085 g, 95%). Crystallization was achieved by layering hexanes onto a CH_2Cl_2 solution of complex, m.p. 120°C. − ^{31}P NMR (CD_2Cl_2): δ = 199.50 (s). − ^{13}C NMR (CD_2Cl_2): δ = 0.50 (d, $^3J_{C,P}$ = 4.31 Hz, 2 × $SiMe_3$), 127.00 (d, $^3J_{C,P}$ = 50.0 Hz, C-4), 143.50 (d, $^2J_{C,P}$ = 18.00 Hz, C-3,5), 160.00 (d, $^1J_{C,P}$ = 4.00 Hz, C-2,6). − ^1H NMR (CD_2Cl_2): δ = 0.50 (s, 18 H, 2 × $SiMe_3$), 7.51−7.62 (td, 1 H, $^4J_{H,P}$ = 6.70 Hz, $^3J_{H,H}$ = 8.20 Hz, 4-H), 8.20−8.40 (dd, 2 H, $^3J_{H,P}$ = 31.20 Hz, $^3J_{H,H}$ = 8.20 Hz, 3,5-H). − $C_{11}H_{21}AuClPSi_2$ (472.85): calcd. C 27.94, H 4.48; found C 28.15, H 4.66.

Synthesis of Complex 3: Phosphinine **1** (0.060 g, 2.5×10^{-4} mol) and $AuCl(SMe_2)$ (0.037 g, 1.25×10^{-4} mol) were weighed in air and placed under N_2. Freshly distilled CH_2Cl_2 (3 mL) was then added by syringe into the Schlenk flask, and the mixture allowed to stir at room temperature for 10 min. In a glove box, $GaCl_3$ (0.022 g, 1.25×10^{-4} mol) was weighed and put in a second

Schlenk flask. Outside the box, CH_2Cl_2 was added by syringe into the flask and the solution added to the first flask at −78°C using a cannula. The mixture was warmed to room temperature and stirred. ^{31}P-NMR spectroscopy indicated that the reaction was finished within 15 min. Reduction of the volume, followed by hexanes precipitation and filtration yielded a pale yellow solid (0.10 g, 90%). Crystallization was achieved by layering hexanes onto a CH_2Cl_2 solution of the complex, m.p. 140°C. − ^{31}P NMR (CD_2Cl_2): δ = 206.10 (s). − ^{1}H NMR (CD_2Cl_2): δ = 0.57 (s, 36 H, 4 × $SiMe_3$), 7.80−7.89 (m, 2 H, 2 × 4-H), 8.50−8.71 (ptd, 4 H, $\Sigma J_{H,P}$ = 42.35 Hz, 2 × 3,5-H). − ^{13}C NMR (CD_2Cl_2): δ = 0.85 (s, 4 × $SiMe_3$), 129.90 (pt AXX′, $\Sigma J_{C,P}$ = 50.60 Hz, 2 × C-4), 144.40 (pd AXX′, $\Sigma J_{C,P}$ = 14.75 Hz, 2 × C-3,5), 164.55 (s, 2 × C-2,6). − $C_{22}H_{42}AuCl_4GaP_2Si_4$ (889.37): calcd. C 29.71, H 4.76; found C 30.05, H 4.96.

Synthesis of Complex 5: Phosphinine **4** (0.200 g, 3.55 × 10^{-4} mol) and AuCl(SMe_2) (0.104 g, 3.55 × 10^{-4} mol) were weighed in air and placed under N_2. Freshly distilled CH_2Cl_2 (5 mL) was then added by syringe into the Schlenk flask, and the mixture allowed to stir at 35°C. ^{31}P-NMR spectroscopy indicated that the reaction was finished within 15 min. Reduction of the volume, followed by hexanes precipitation and filtration yielded a pale yellow solid (0.269 g, 95%), m.p. 160°C. − ^{31}P NMR (CD_2Cl_2): δ = 222.00 (s). − ^{13}C NMR (CD_2Cl_2): δ = 2.20 (d, $^3J_{C,P}$ = 4.20 Hz, 2 × $SiMe_2$), 94.60 (d, $^3J_{C,P}$ = 8.90 Hz, 2 × CCPh), 110.70 (s, CCPh), 123.0−129.70 (m, CH of Ph), 127.05 (d, $^3J_{C,P}$ = 50.0 Hz, C-4), 144.20 (d, $^2J_{C,P}$ = 12.000 Hz, C-3,5), 151.20 (d, $^2J_{C,P}$ = 12.00 Hz, Cq of C_6H_5), 158.40 (d, $^1J_{C,P}$ = 15.85 Hz, C-2,6). − ^{1}H NMR (CD_2Cl_2): δ = 0.30 (s, 12 H, 2 × $SiMe_2$), 7.10−7.60 (m, 21 H,4 × Ph, 4-H). − $C_{37}H_{33}AuClPSi_2$ (797.24): calcd. C 55.74; H 4.17; found C 55.95, H 4.46.

Synthesis of Complex 6: A CH_2Cl_2/hexane solution of gold complex **5** was placed in a tube and left under a static N_2 pressure. Pale yellow crystals slowly grew out of the solution together with a slight purple precipitate of colloidal gold. These crystals were very insoluble which prevented spectrocopic analysis. The crystal gave a combustion analysis consistent with the starting complex, m.p. 200°C. − $C_{37}H_{33}AuClPSi_2$ (797.24): calcd. C 55.74 H 4.17; found C 55.95, H 4.46.

Synthesis of Complex 7: Complex **5** (0.239 g, 3.00 × 10^{-4} mol) and bis(phenylethynyl)dimethylsilane (0.078 g, 3.00 × 10^{-4} mol) were weighed in air and placed under N_2. Freshly distilled toluene (5 mL) was then added by syringe into the Schlenk flask, and the mixture stirred at room temperature for 48 h. Purple gold(0) colloids were removed by filtration through a pad of Celite. Reduction of the volume and hexanes precipitation yielded a pale yellow solid (0.269 g, 85%). Suitable crystals for X-ray analysis were grown by slow diffusion of hexanes into a concentrated CH_2Cl_2 solution of the complex, m.p. 175°C. − ^{31}P NMR (CD_2Cl_2): δ = −7.00 (s). − ^{13}C NMR (CD_2Cl_2): δ = 1.10 (d, $^3J_{C,P}$ = 2.20 Hz, 3 × $SiMe_2$), 78.90 (d, $^3J_{C,P}$ = 44.11 Hz, C-4), 92.50 (s, 3 × CCPh), 109.30 (s, 3 × CCPh), 127.60−132.90 (m, CH of Ph), 141.50 (d, $^2J_{C,P}$ = 12.14 Hz, C-3), 173.80 (d, $^1J_{C,P}$ = 9.85 Hz, C-2). − $C_{55}H_{49}AuClPSi_3$ (1057.65): calcd. C 62.46, H 4.67; found C 62.58, H 4.93.

Synthesis of Complex 9: Phosphinine **4** (0.141 g, 2.5 × 10^{-4} mol) and AuCl(SMe_2) (0.037 g, 1.25 × 10^{-4} mol) were weighed in air and placed under N_2. Freshly distilled CH_2Cl_2 (3 mL) was then

Table 1. Crystal data of **2** and **3**

	2	**3**
Crystal size [mm]	0.10 × 0.10 × 0.20	0.20 × 0.20 × 0.25
Empirical formula	$C_{11}H_{21}AuClPSi_2$	$C_{22}H_{42}AuCl_4GaP_2Si_4$
Molecular mass	472.86	889.37
Crystal system	triclinic	monoclinic
Space group	$P-1$	$P2_1/c$
a [Å]	7.126(1)	14.924(1)
b [Å]	10.599(1)	16.604(2)
c [Å]	11.439(2)	30.162(3)
α [°]	89.21(1)	90
β [°]	74.03(1)	90.66(2)
γ [°]	84.48(1)	90
V [Å^3]	826.8(3)	7473(2)
Z	2	8
D [g cm^{-3}]	1.90	1.58
F (000)	452	3504
μ [cm^{-1}]	9.260	5.145
Diffractometer	Enraf−Nonius CAD4	Enraf−Nonius CAD4
θ_{max} [°]	29.97	28.05
Reflections measured	5034	19411
Independent reflections	4796	18095
hkl ranges	−9 to 10 0 to 14 −16 to 16	−19 to 0 −21 to 0 −39 to 39
Reflections used	4198	6469
Criterion	> 2.0σ(I)	> 2.0σ(I)
Refinement type	F; full matrix	F; full matrix
Hydrogen atoms	no refinement	no refinement
Parameters refined	145	613
Reflections/parameter	33	10
$R1$ factor or $wR2$	0.044	0.057
Rw or $R1$	0.063	0.069
Weighting scheme	$4F_o^2/[\sigma^2(F_o^2) + 0.0064\ F_o^4]$	$4F_o^2/[\sigma^2(F_o^2) + 0.0064\ F_o^4]$
GOF	1.3	1.2
Min/max peaks in final Fourier [eÅ^{-3}]	5.47(62)/−0.67(62)	1.761(23)/−0.28(23)

Table 2. Crystal data of **6**, **7** and **9**

	6	**7**	**9**
Crystal size [mm]	0.10 × 0.10 × 0.10	0.08 × 0.10 × 0.14	0.20 × 0.20 × 0.20
Empirical formula	$C_{38}H_{35}Si_2PCl_3Au$	$C_{55}H_{49}AuClPSi_3$	$C_{78}H_{46}AuCl_{12}GaP_2Si_4$
Molecular mass	882.17	1058.61	1849.53
Crystal system	triclinic	monoclinic	triclinic
Space group	P1bar	$P2_1/c$	P1bar
a [Å]	12.005(1)	9.90000(10)	21.687(2)
b [Å]	13.128(2)	22.9960(3)	22.357(2)
c [Å]	13.763(2)	23.4260(3)	22.352(2)
α [°]	68.38(1)	90	96.42(1)
β [°]	77.75(1)	96.1270(6)	116.90(1)
γ [°]	66.85(1)	90	117.57(1)
V [Å^3]	1848.3(4)	5302.7(1)	7828.1(5.3)
Z	2	4	4
D [g cm^{-3}]	1.59	1.326	1.569
F (000)	872	2132	3656
μ [cm^{-1}]	4.323	2.956	2.771
Diffractometer	Enraf−Nonius CAD4	KappaCCD	Enraf−Nonius CAD4
θ_{max} [°]	29.97	26.32	28.04
Reflections measured	11156	11060	18332
Independent reflections	10739	10765	20437
hkl ranges	−16 to 16 −17 to 18 0 to 19	0 to 12 0 to 28 −29 to 29	0 to 28 −29 to 24 −29 to 25
Reflections used	6547	8418	17879
Criterion	> 3.0σ(*I*)	> 2.0σ(*I*)	> 2.0σ(*I*)
Refinement type	F; full matrix	Fsqd; full matrix	Fsqd; full matrix
Hydrogen atoms	no refinement	riding	riding
Parameters refined	406	550	1619
Reflections/parameter	16	15	11
*R*1 factor or *wR*2	0.039	0.1364	0.0584
Rw	0.038	0.0400	0.0567
Weighting scheme[a]	$4F_o^2/[\sigma^2(F_o^2) + 0.0064\ F_o^4]$	$a = 0.0869$ $b = 0.0000$	$a = 0.0816$ $b = 88.567$
GOF	1.0	1.08	1.90
Min/max peaks in final Fourier [eÅ^{-3}]	1.30(15)/−0.33(15)	2.22(0.15)/−0.80(0.15)	−1.56(43)/0.12(43)

[a] $w = 1/[\sigma^2(F_o^2) + (aP)^2 + bP]$ where $P = (F_o^2 + 2F_c^2)/3$; *R*1 is the conventional *R* factor as defined in SHELXL-97.[28]

added by syringe into the Schlenk flask, and the mixture allowed to stir at room temperature for 10 min. In a glove box, $GaCl_3$ (0.022 g, 1.25×10^{-4} mol) was weighed and placed into a second Schlenk flask. Outside the box, CH_2Cl_2 was added by syringe into the flask and the solution added to the first flask at −78°C using a cannula. The mixture was warmed to room temperature and stirred. ^{31}P-NMR spectroscopy indicated that the reaction was finished within 15 min. Reduction of the volume, followed by hexane precipitation and filtration yielded a pale yellow solid (0.10 g, 90%). Crystallization was achieved by layering hexanes onto a CH_2Cl_2 solution of the complex, m.p. 165°C. − ^{31}P NMR (CD_2Cl_2): δ = 231.70 (s). − ^{1}H NMR (CD_2Cl_2): δ = 0.25 (s, 24 H, 4 × $SiMe_2$), 7.10−7.60 (m, 42 H,8 × Ph, 2 × H-4). − ^{13}C NMR (CD_2Cl_2): δ = 2.60 (s,4 × $SiMe_2$), 95.35 (pt, AXX′, $\Sigma J_{C,P}$ = 4.60 Hz, 4 × CCPh), 113.90 (s, CCPh), 128.20−132.50 (m, CH of Ph), 133.90 (pt, AXX′, $\Sigma J_{C,P}$ = 18.25 Hz, 2 × C-4), 143.40 (pt, $\Sigma J_{C,P}$ = 6.10 Hz, 2 × C-3,5), 151.40 (pt, AXX′, $\Sigma J_{C,P}$ = 4.60 Hz, 2 × Cq of C_6H_5), 158.75 (pt, AXX′, $\Sigma J_{C,P}$ = 6.10 Hz, 2 × C-2,6). − $C_{74}H_{66}AuCl_4GaP_2Si_4$ (1538.13): calcd. C 57.79, H 4.33; found C 55.85, H 4.46.

X-ray Structural Analysis: For compounds **2**, **3, 6** and **9**, data were collected at 123 ± 0.5 K with an Enraf Nonius CAD4 diffractometer; data collection for **7** was conducted at room temperature using a KappaCCD diffractometer. Mo-K_α (λ = 0.71073 Å) radiation and a graphite monochromator were used in all cases. The crystal structures were solved and refined using the Enraf Nonius MOLEN package (maXus for the kappaCCD). In the case of **7**, final refinement was made with SHELX-97.[28] The structure of **9** calls for an additional comment. The asymmetric unit contains two dichloromethane molecules of crystallization. While one molecule can be directly modelled, the second one is very highly disordered. To address this problem, we used the Platon[29] SQWEEZE function and completed refinement using SHELX-97, thus leading to an acceptable *R* value. Other experimental details are given in Table 1 (compounds **2** and **3**) and 2 (compounds **6**, **7** and **9**) . Crystallographic data (excluding structure factors) for the structures reported have been deposited with the Cambridge Data Centre as supplementary publications CCDC-115213 to -115217. Copies of the data can be obtained free of charge on application to CCDC, 12 Union Road, Cambridge CB2 1EZ, UK [Fax: (internat.) + 44-1223/336-033, E-mail: deposit@ccdc.cam.ac.uk].

Acknowledgments

The authors thank the CNRS and the Ecole Polytechnique for support of this work.

[1] [1a] G. Märkl in *Multiple Bonds and Low Coordination in Phosphorus Chemistry* (Eds.: M. Regitz, O. J. Scherer), Georg Thieme Verlag, New York, **1990**, p 220. − [1b] K. B. Dillon, F. Mathey, J. F. Nixon, in *Phosphorus: The Carbon Copy*, John Wiley and Sons, Chichester, **1998**, p 1. − [1c] P. Le Floch, F. Mathey, *Coord. Chem. Rev.* **1998**, *179−180*, 771.

[2] [2a] C. Elschenbroich, M. Nowotny, A. Behrendt, W. Massa, S. Wocadlo, *Angew. Chem., Int. Ed. Engl.* **1992**, *31*, 1343. − [2b] C. Elschenbroich, M. Nowotny, J. Kroker, A. Behrendt, W. Massa, S. Wocadlo, *J. Organomet. Chem.* **1993**, *459*, 157. − [2c] C. Elschenbroich, M. Nowotny, A. Behrendt, K. Harms, S. Wocadlo, J.

Pebler, *J. Am. Chem. Soc.* **1994**, *116*, 6217. − [2d] C. Elschenbroich, S. Voss, O. Schiemann, A. Lippek, K. Harms, *Organometallics* **1998**, *17*, 4417−4424.
[3] F. Mathey, P. Le Floch, *Chem. Ber.* **1996**, *129*, 263.
[4] [4a] B. Breit. *J. Chem. Soc., Chem. Commun.* **1996**, 2071. − [4b] B. Breit, R. Winde, K. Harms, *J. Chem. Soc., Perkin Trans. 1* **1997**, 2681. − [4c] F. Knoch, F. Kremer, U. Zenneck, P. Le Floch, F. Mathey, *Organometallics* **1996**, *15*, 2713. − [4d] P. Le Floch, F. Knoch, F. Kremer, F. Mathey, J. Scholz, W. Scholz, K. −H. Thiele, U. Zenneck, *Eur. J. Inorg. Chem.* **1998**, 119.
[5] N. Avarvari, N. Mézailles, L. Ricard, P. Le Floch, F. Mathey, *Science* **1998**, *8*, 1587.
[6] P. Le Floch, L. Ricard, F. Mathey, *Bull. Soc. Chim. Fr.* **1996**, *133*, 691.
[7] K. C. Dash, J. Eberlein, H. Schmidbaur, *Synth. Inorg. Met. Org. Chem.* **1973**, *3*, 375.
[8] For references concerning the coordination chemistry of gold, see: [8a] A. Grohmann, H. Schmidbaur in *Comprehensive Organometallic Chemistry II* (Eds.: E.W. Abel, F. G. A. Stone, G. Wilkinson), Pergamon, Oxford, **1995**, vol. 3, p 1. − [8b] M. C. Gimeno, A. Laguna, *Chem. Rev.* **1997**, *97*, 511. − [8c] R. J. Puddephatt, J. J. Vittal in *Encyclopaedia of Inorganic Chemistry* (Ed.: R.B. King), John Wiley and Sons, Chichester, **1994**, vol. 3, p 1320. − [8d] P. Pyykkö, *Chem. Rev.* **1997**, *97*, 597.
[9] [9a] J. H. Teles, S. Brode, M. Chabanas, *Angew. Chem.* **1998**, *110*, 1475; *Angew. Chem., Int. Ed. Engl.* **1998**, *37*, 1415. − [9b] Y. Fukuda, K. Utimoto, *J. Org. Chem.* **1991**, *56*, 3729. − [9c] Y. Fukuda, K. Utimoto, *Bull. Chem. Soc. Jpn.* **1991**, *64*, 2013. − [9d] Y. Fukuda, K. Utimoto, H. Nozaki, *Heterocycles* **1987**, 297. − [9e] Y. Fukuda, K. Utimoto, *Synthesis* **1991**, 975. − [9f] A. L. Casado, P. Espinet, *Organometallics* **1998**, *17*, 3677. − [9g] Y. Ito, M. Sawamura, T. Hayashi, *J. Am. Chem. Soc.* **1986**, *108*, 6405. − [9h] Y. Ito, M. Sawamura, T. Hayashi, *Tetrahedron Lett.* **1987**, *289*, 6215.
[10] [10a] D. M. Roundhill, *Photochemistry and Photophysics of Metal Complexes*, Plenum Press, New York, **1994**. − [10b] C.-M. Che, H. L. Kwong, C. K. Poon, V. W. W. Yam, *J. Chem. Soc., Dalton Trans.* **1990**, 3215. − [10c] D. Li, C. Che, H. L. Kwong, V. W. W. Yam, *J. Chem. Soc., Dalton Trans.* **1992**, 3235. − [10d] H. R. C. Jaw, M. M Savas, R. D. Rodgers, W. R. Mason, *Inorg. Chem.* **1989**, *28*, 1028. − [10e] X. Hong, K. K. Cheung, C. X. Guo, C. M. Che, *J. Chem. Soc., Dalton Trans.* **1994**, 1867. − [10f] C.-M. Che, W.-T. Wong, T.-F Lai, H.-L Kwong, *J. Chem. Soc., Chem. Commun.* **1989**, 243. − [10g] C. King, J.-C. Wang, M. N. I. Khan, J. P. Jr. Fackler, *Inorg. Chem.* **1989**, *28*, 2145. − [10h] J. C. Vickery, M. M. Olmstead, E. Y. Fung, A. L. Balch, *Angew. Chem. Int. Ed. Engl.* **1997**, *9*, 363.
[11] [11a] C. K. Mirabelli, D. T. Hill, L. F. Faucette, F. L. McCabe, G. R. Girard, D. B; Bryan, B. M. Sutton, J. O. Bartus, S. T. Crooke, R. K. Johnson, *Med. Chem.* **1987**, *30*, 2181. − [11b] C. K. Mirabelli, D. B. Jensen, M. R. Mattern, C.-M, Sung, S.-M. Mong, D. T. Hill, S. W. Dean, P. S. Schein, R. K. Johnson, S. T. Crooke, *Anti-Cancer Drug Des.* **1986**, *1*, 223. − [11c] S. J. Berners-Price, P. S. Jarret, P. J. Sadler, *Inorg. Chem.* **1987**, *26*, 3074. − [11d] S. J. Berners-Price, P. J. Sadler, *Struct. Bonding* **1988**, *70*, 27 and references therein. − [11e] O. M. Ni Dhubhghaill, P. J. Sadler, R. Kuroda, *J. Chem. Soc., Dalton Trans.* **1990**, 2913. − [11f] P. F. Smith, D. W. Alberts, G. F. Rush, *Toxicologist* **1987**, *1*, 62. − [11g] C. K. Mirabelli, G. F. Rush, B. D. Jensen, J. O. Bartus, C. M. Sung, D. W. Alberts, D. E. Genaro, S. T. Hoffstein, R. K. Johnson, S. T. Crooke, *Proc. Am. Assoc. Cancer. Res.* **1987**, *28*, 1238. − [11h] G. D. Hoke, G. F. Rush, G. E. Bossard, J. V. McArdle, B. D. Jensen, C. K. Mirabelli, *J. Biol. Chem.* **1988**, *263*, 11203.
[12] [12a] H. Willner, J. Schaebs, G. Hwang, F. Mistry, R. Jones, J. Trotter, F. Aubke, *J. Am. Chem. Soc.* **1992**, *114*, 8972. − [12b] H. Willner, F. Aubke, *Inorg. Chem.* **1990**, *29*, 2195. − [12c] Q. Xu, Y. Imamura, M. Fujiwara, Y. Souma, *J. Org. Chem.* **1997**, *62*, 1594. − [12d] S. Dapprich, G. Frenking, *J. Phys. Chem.* **1995**, *99*, 9352−9362. − [12e] H. Willner, F. Aubke, *Angew. Chem., Int. Ed. Engl.* **1997**, *36*, 2402−2425. − [12f] D. McIntosh, G. A. Ozin, *Inorg. Chem.* **1977**, *16*, 51. − [12g] D. McIntosh, G. A. Ozin, R. P. Messmer, *Inorg. Chem.* **1981**, *20*, 3640.
[13] P. Le Floch, S. Mansuy, L. Ricard, F. Mathey, A. Jutand. C. Amatore, *Organometallics* **1996**, *15*, 2713.
[14] [14a] N. Avarvari, P. Le Floch, F. Mathey, *J. Am. Chem. Soc.* **1996**, *118*, 11978. − [14b] N. Avarvari, P. le Floch, L. Ricard, F. Mathey, *Organometallics* **1997**, *16*, 4089. − [14c] N. Avarvari, P. Rosa, F. Mathey, P. Le Floch, *J. Organomet. Chem.* **1998**, *567*, 151.
[15] P. G. Jones, A. G. Maddock, M. J. Mays, M. M. Muir, A. F. Williams, *J. Chem. Soc., Dalton Trans.* **1977**, 1434.
[16] C. J. Jameson in *Phosphorus-31 NMR spectroscopy in stereochemical analysis* (Eds.: J. Verkade, L. D. Quin), VCH Publishers, Inc., Deerfield Beach, Florida, **1987**, p 205−230.
[17] S. Attar, W. H. Bearden, N. W. Alcock, E. C. Alyea, J. H. Nelson, *Inorg. Chem.* **1990**, *29*, 425.
[18] A. J. Ashe III, *Acc. Chem. Res.* **1978**, *11*, 153.
[19] [19a] P. Le Floch, D. Carmichael, L. Ricard, F. Mathey, A. Jutand, C. Amatore, *Organometallics* **1992**, *11*, 2475. − [19b] P. Le Floch, L. Ricard, F. Mathey, A. Jutand, C. Amatore, *Inorg. Chem.* **1995**, *34*, 11. − [19c] P. Rosa, L. Ricard, P. Le Floch, F. Mathey, G. Sini, O. Eisenstein, *Inorg. Chem*. **1998**, *37*, 3154.
[20] A. J. Ashe III, W. Butler, J. C. Colburn, S. Abu-Orabi, *J. Organomet. Chem.* **1985**, *282*, 233.
[21] J. Waluk, H.-P Klein, A. J. Ashe III, J. Michl, *Organometallics* **1989**, *8*, 2804−2808.
[22] [22a] R. J. Puddephatt, *The Chemistry of Gold*, Elsevier, Amsterdam, **1978**. − [22b] F. A. Cotton, G. Wilkinson, *Advanced Inorganic Chemistry*, 5th ed., John Wiley and Sons, New York, **1988**, p. 944.
[23] P. Schulte, U. Behrens, *J. Chem. Soc., Chem. Commun.* **1998**, 1633.
[24] [24a] G. Märkl, F. Lieb, *Angew. Chem. Int. Ed. Engl.* **1968**, *7*, 733. − [24b] F. Lieb, Dissertation, Universität Regensburg, **1987**. − [24c] H. J. Beckh, Dissertation, Universität Regensburg, **1987**. − [24d] A. J. Ashe III, M. D. Gordon, *J. Am. Chem. Soc.* **1972**, *94*, 7596.
[25] [25a] G. Märkl, F. Lieb, C. Martin, *Tetrahedron Lett.* **1971**, 1249. − [25b] G. Märkl, G. Dorfmeister, *Tetrahedron Lett.* **1987**, *28*, 1093. − [25c] G. Märkl, C. Dörges, T. Riedl, F.-G. Klärner, C. Lodwig, *Tetrahedron Lett.* **1990**, *32*, 4589. − [25d] G. Märkl, S. Dorsch, *Tetrahedron Lett.* **1995**, *36*, 3839. − [25e] G. Märkl, C. Dörges, *Angew. Chem. Int. Ed. Engl.* **1991**, *30*, 106.
[26] J.-M. Alcaraz, F. Mathey, *Tetrahedron Lett.* **1984**, 207.
[27] R.Uson, A. Laguna, *Organometallic Syntheses* (Eds.: R. B. King, J. Eisch), Elsevier Science Publishers B. V., Amsterdam, **1986**, vol. 3, p. 324.
[28] G. M. Sheldrick, *SHELXL-97*, Universität Göttingen, Germany, **1997**.
[29] A. L. Spek, *PLATON, A Multipurpose Crystallographic Tool*, Utrecht University, The Netherlands, **1999**.

Received March 1, 1999
[I99074]

Borane Insertion into Group-4 Metal-to-Carbon Bonds: The Reaction of $HB(C_6F_5)_2$ with (η^2-Formaldehyde)zirconocene Dimer and with (Butadiene)zirconocene

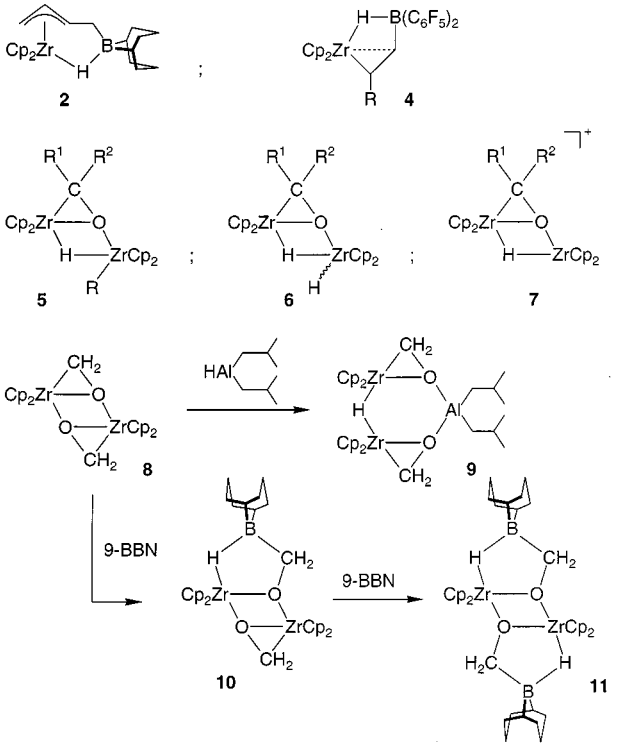
Ulrich Blaschke,[a] Gerhard Erker,*[a] Roland Fröhlich,[a][+] and Oliver Meyer[a][+]

Keywords: Metallaoxirane / HBR_2 addition / (Formaldehyde)zirconocene / (Butadiene)zirconocene / Heterocycles / Boron

(η^2-Formaldehyde)zirconocene dimer (**8**) cleanly adds one or two molar equivalents of the borane $HB(C_6F_5)_2$ by insertion of the H–[B] unit into the zirconium–carbon bond of the metallaoxirane moieties to form the mono- and bis-insertion products **16** and **17**, respectively. These systems contain five-membered heterocyclic rings that are built up by connecting five different elements, namely H, B, C, O, and Zr. The bis(borane) insertion product **17** was characterized by an X-ray crystal structure analysis. (Butadiene)zirconocene reacts with $HB(C_6F_5)_2$ in a similar way by insertion of the H–[B] unit into the (butadiene)C4–Zr linkage to form the metallacycle **18**.

Introduction

Main-group and transition-metal hydrides react in various ways with (η^2-alkene) group-4 metallocene complexes and with their heteroatom analogues, the (η^2-aldehyde- and -ketone)metallocenes. 9-BBN adds cleanly to (butadiene)zirconocene (**1**)[1] to yield **2**;[2] similarly the electrophilic $H-B(C_6F_5)_2$ (**3**) ("Piers' borane")[3] adds to (η^2-alkene)zirconocenes, generated in situ, to yield **4** (see Scheme 1).[4–6] (η^2-Ketone and η^2-aldehyde)zirconocenes show a more diverse reactivity. They form the 1:1 addition products with $Cp_2M^{IV}H_2$ or $Cp_2M^{IV}(R)H$ units, and even with the elusive monomeric Cp_2Zr-H^+ cation (to yield the dinuclear systems **5**, **6**, and **7**, respectively).[7][8] (η^2-Formaldehyde)zirconocene dimer (**8**) is known to add diisobutylaluminium hydride to form **9**, which exhibits the intact metallaoxirane subunits,[9][10] whereas 9-BBN reacts differently with **8** and inserts sequentially into the $Zr-CH_2$ bond of the metallaoxirane to give the respective HBCOZr-containing five-membered heterocyclic systems **10** and **11** (see Scheme 1).[11][12] We have now extended this series of studies and reacted (η^2-formaldehyde)zirconocene dimer (**8**) as well as (butadiene)zirconocene (**1**) with $HB(C_6F_5)_2$ (**3**). The outcome of these reactions is described in this article.



Scheme 1. Previously reported main-group and transition-metal hydride adducts to (diene-, alkene-, and η^2-ketone and -aldehyde)zirconocene complexes

Results and Discussion

Reaction of (η^2-Formaldehyde)zirconocene Dimer with $HB(C_6F_5)_2$

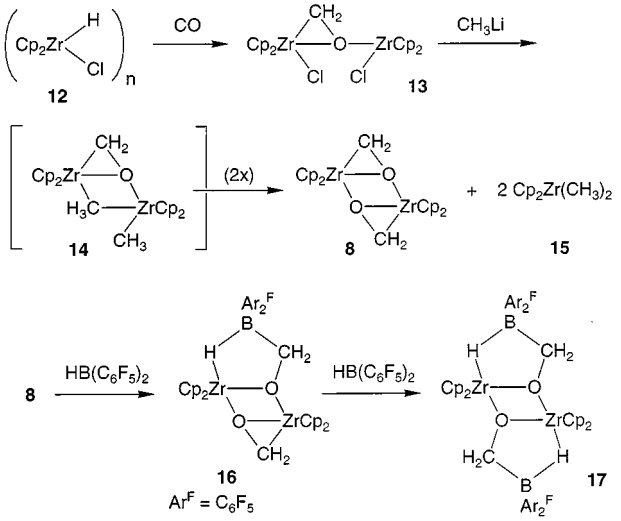
(η^2-Formaldehyde)zirconocene was prepared starting from $[Cp_2Zr(H)Cl]_n$ (**12**). Carbonylation resulted in the formation of the dinuclear complex **13**, as described by C. Floriani et al.[13] Subsequent treatment with two molar equivalents of methyllithium led to the direct formation of $[Cp_2Zr(OCH_2)]_2$ (**8**) and dimethylzirconocene (**15**), as we had described previously.[9] The reaction probably proceeded via the unstable adduct $[Cp_2Zr(OCH_2) \cdot Me_2ZrCp_2]$ (**14**).

The borane $HB(C_6F_5)_2$ (**3**) was added to the (η^2-formaldehyde)zirconocene dimer at ambient temperature. The reaction was first carried out in deuterated solvent ([D_6]benzene or [D_2]dichloromethane) and monitored directly by

[a] Organisch-Chemisches Institut der Universität Münster, Corrensstrasse 40, D-48149 Münster, Germany
Fax: (internat.) + 49-(0)251/833-6503
E-mail: erker@uni-muenster.de
[+] X-ray crystal structure analysis

 © WILEY-VCH Verlag GmbH, D-69451 Weinheim, 1999 1434–1948/99/1212–2243 $ 17.50+.50/0

NMR spectroscopy. Combination of the two components in a ca. 1:1 ratio at room temperature resulted in the instantaneous formation of a single new compound, showing two Cp singlets at δ = 6.23 and 5.99 (^{1}H)/113.8 and 108.9 (^{13}C NMR) in a 10:10 ratio in addition to signals of two CH_2 groups [^{1}H/^{13}C NMR: δ = 4.26 (br., 2 H)/78.2 (br., B−CH_2) and δ = 3.22 (s, 2 H)/72.0 (Zr−CH_2)]. Although the B−*H* signal was not located, we assumed that insertion of the HB moiety of the $HBAr^F_2$ reagent into the Zr−CH_2 linkage of one of the metallaoxirane subunits of **8** had taken place with formation of the unsymmetrical dimetallatricyclic product **16**. In agreement with this interpretation was the observation of a ^{11}B-NMR resonance of **16** at δ = −13.5 − at a typical tetracoordinate borate chemical shift value − as a doublet with a $^1J_{BH}$ coupling constant of 65 Hz. This value was markedly reduced from a typical $HB(R)_3^-$ coupling constant (ca. 80−85 Hz), which probably indicated a reduced B···H bond order of the bridging Zr−(μ-H)−B situation in the heterocyclic addition complex **16**.



Scheme 2. Preparation of (η^2-formaldehyde)zirconocene dimer and its reaction with $HB(C_6F_5)_2$

Further addition of $HB(C_6F_5)_2$ to the solution rapidly resulted in HB insertion into the remaining ($ZrOCH_2$) moiety with formation of the double insertion product (**17**). The reaction was carried out in toluene solution (5 min at ambient temperature) to give **17** in ca. 50% yield. The rather poorly soluble product **17** exhibited a Cp singlet at δ = 6.43 (20 H) in [D_2]dichloromethane in addition to a CH_2 singlet (4 H) at δ = 4.45. The *H*−B signal was not located. The ^{11}B-NMR resonance is at δ = −13.2 (very broad signal, $\nu_{1/2} \approx 170$ Hz).

Single crystals suitable for X-ray structure determination of **17** were obtained from [D_2]dichloromethane. The Zr−(μ-H)−B hydrogen atoms could be located in the difference Fourier map. Figure 1 shows a view of the structure of **17** that contains a (disordered) molecule of the [D_2]dichloromethane solvent in the crystal.

The X-ray crystal structure analysis (see Figure 1) shows that the H−$B(C_6F_5)_2$ reagent has inserted into the Zr−CH_2 linkage of each of the metallacyclic three-membered rings of the dinuclear starting material **8** to form the 2:1 addition product **17**. A planar dimetallatricyclic framework has resulted in which two exceptional heterocyclic ring systems − each exhibiting a five-membered ring system made up by the five different core atoms Zr, O, C, B, and H − are connected by two Zr−O linkages. Actually, the connecting metal−oxygen bonds in the central four-membered Zr_2O_2 ring[15] (i.e. O1−Zr1A) are shorter [2.127(2) Å] than the respective Zr1−O1 bonds [2.148(2) Å] inside the lateral five-membered heterocycles. The bond angles at O inside the central four-membered ring are 111.2(1)° (Zr1−O1−Zr1A), the adjacent angle at Zr (O1−Zr1−O1A) is much smaller at 68.8(1)°. This indicates the presence of an additional coordination at the bent metallocene unit, which is formed by the B−(μ-H)−Zr bridge inside the five-membered ring.[14] The overall arrangement of the ZrOCBH ring system in **17** is very similar, as observed in the **8** + 9-BBN addition product **11** (see Scheme 1 and Table 1),[11] only that the bridging hydrogen atom in **17** seems to be located significantly closer to the boron atom. This might reflect the increased electrophilicity of the

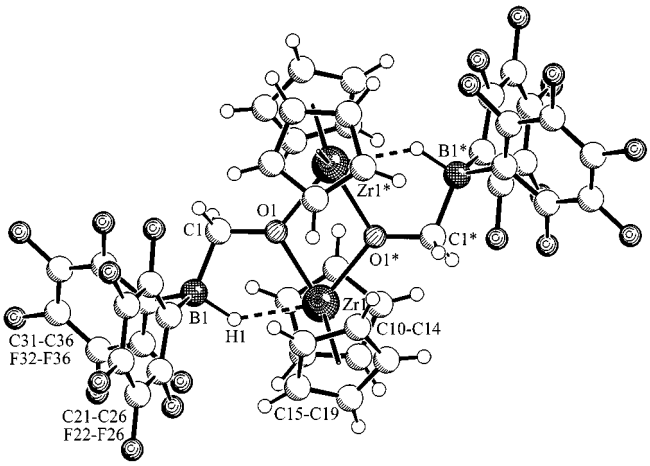


Figure 1. A view of the molecular structure of **17**

Table 1. A comparison of related structural parameters of **17** {i.e. **8** + 2[$HB(C_6F_5)_2$]} and **11** {i.e. **8** + 2[9-BBN]}[a]

	17 (·CD_2Cl_2)[b]	**11**[c]
Zr1−O1	2.127(2)	2.148(4)
O1−C1	1.460(3)	1.448(7)
C1−B1	1.624(4)	1.64(1)
B1−H1	1.22(4)	1.33(5)
H1−Zr1	2.15(4)	1.99(5)
Zr1−O1A	2.148(2)	2.155(4)
Zr1−O1−C1	117.3(2)	116.8(3)
O1−C1−B1	110.3(2)	111.1(5)
B1−H1−Zr1	135(2)	138(4)
H1−Zr1−O1	69(1)	71(1)
O1−Zr1−O1A	68.8(1)	67.3(2)
Zr1−O1−Zr1A	111.2(1)	112.7(2)

[a] Bond lengths in Å, angles in°, atom numbering according to Figure 1. − [b] Crystallized from [D_2]dichloromethane, contains one disordered CD_2Cl_2 molecule in the asymmetric unit. − [c] From ref.[11]

boron atom bonded to the two strongly electron-withdrawing C_6F_5 substituents as compared to the 9-BBN subunit, but in view of the general uncertainty of H-atom location by X-ray diffraction, such an effect should not be overemphasized.[14]

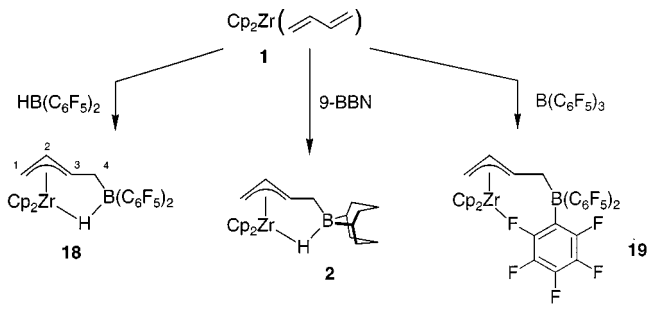
Reaction of (Butadiene)zirconocene with $HB(C_6F_5)_2$

(Butadiene)zirconocene (**1**) reacted rapidly with $HB(C_6F_5)_2$ to form a 1:1 addition product (75% isolated). It showed the ^1H-/^{13}C-NMR resonances of a pair of diastereotopic Cp ligands at zirconium (δ = 5.23, 5.08/107.8, 106.9 in [D_6]benzene), a pair of diastereotopic C_6F_5 substituents at B, a broad Zr−(μ-H)−B ^1H-NMR signal at δ = −3.3, and a very broad ^{11}B-NMR resonance at δ = −32 ($\nu_{1/2} \approx 170$ Hz). The ^1H- and ^{13}C-NMR resonances of the C_4H_6[B] unit of **18** are listed in Table 2. A comparison with the respective NMR signals of the complexes **2** and **19**, previously obtained from the addition reaction of (butadiene)-zirconocene with 9-BBN[2] and $B(C_6F_5)_3$,[16][17] respectively, show a number of subtle differences, but a similar overall spectroscopic environment.[18] This indicates the occurrence of an analogous product structure in the $HB(C_6F_5)_2$ + (butadiene)$ZrCp_2$ addition reaction. We must assume that the H−B functional group of the reagent **3** has also added the electrophilic boron center to the butadiene terminus and the hydride to the zirconium center to give the metallacyclic (π-allyl)Zr(μ-H)B complex **18**.

Table 2. A comparison of selected ^1H- and ^{13}C-NMR data of the (butadiene)zirconocene borane adducts **18**, **2**, and **19**

	18[a]	**2**[a,b]	**19**[c]
1-H	1.81	2.56	2.25
1-H′	1.69	1.40	1.85
2-H	5.15	3.81	5.88
3-H	4.38	4.48	5.23
4-H	3.64	2.01	2.56
4-H′	1.46	1.29	1.47
μ-H	−3.3	−4.5	−
C1	49.1	44.8	52.7
C2	120.1	95.7	131.8
C3	96.2	112.4	123.8
C4	25.5	28.3	28.5

[a] ^1H/^{13}C NMR in [D_6]benzene. − [b] From ref.[2] − [c] ^1H NMR in [D_6]benzene, ^{13}C NMR in [D_8]toluene, from ref.[16]



Scheme 3. Reaction of (butadiene)zirconocene with $HB(C_6F_5)_2$ and related electrophilic borane reagents

Conclusions

We conclude that the electrophilic borane $H-B(C_6F_5)_2$ has probably added to (butadiene)zirconocene in an analogous way as has 9-BBN. In the reaction with the (η^2-formaldehyde)zirconocene dimer there was the attractive alternative reaction possibility of $HB(C_6F_5)_2$ to add in a similar fashion as had been observed for the $H-AlR_2$ reagent or $H-ZrCp_2^+$,[8][10] namely by addition of the H−M unit to the dipolar Zr−O edge of the metallaoxirane template. However, our experiment has shown that the electrophilic boron center in the reagent **3** shows no tendency to add to the nucleophilic metallaoxirane oxygen atom to form such an adduct. Instead, insertion of the HB moiety into the $Zr-CH_2$[O] bond of the metallacyclic three-membered ring of **8** is observed, leading to the formation of the respective five-membered heterocycle, as was observed in the analogous case of the 9-BBN addition to (η^2-formaldehyde)zirconocene (**8**).[11] From these experiments, it appears that $HB(C_6F_5)_2$ behaves as an example of an ordinary borane reagent, just as 9-BBN or $HBEt_2$,[3b] despite the presence of two strongly electron-withdrawing $-C_6F_5$ substituents at the boron atom.

Experimental Section

Reactions were carried out under argon using Schlenk-type glassware or in a glovebox. Solvents were dried and distilled under argon prior to use. For more general information including a list of spectrometers and instruments used for the physical characterization of the compounds see ref.[8] The starting materials $HB(C_6F_5)_2$ (**3**),[3a] (η^2-formaldehyde)zirconocene dimer (**8**),[9] and (η^4-butadiene)zirconocene (**1**)[1] were prepared according to literature procedures.

Reaction of (η^2-Formaldehyde)zirconocene Dimer (8) with $HB(C_6F_5)_2$ (3) in a 1:1 Ratio. − Formation of 16 (NMR Experiment): Complex **8** (15.0 mg, 29.6 μmol) and the borane **3** (10.3 mg, 29.8 μmol) were suspended in 1 mL of [D_6]benzene. Within 5 min, the starting materials had dissolved to give a pale yellow solution. NMR-spectroscopic analysis revealed the formation of **16**. − ^1H NMR (200.1 MHz, [D_6]benzene): δ = 5.79, 5.52 (s, each 10 H, Cp), 4.27 (br., 2 H, $B-CH_2$), 2.81 (s, 2 H, $Zr-CH_2$), $B-H$ signal not observed. − ^{11}B NMR (64.2 MHz, [D_6]benzene): δ = −13.0 (br., d). − The reaction was analogously carried out in [D_2]dichloromethane to also generate **16**: ^1H NMR (200 MHz, [D_2]dichloromethane): δ = 6.23, 5.99 (s, each 10 H, Cp), 4.26 (br., 2 H, $B-CH_2$), 3.22 (s, 2 H, $Zr-CH_2$), $B-H$ signal not observed. − ^{13}C NMR (50.3 MHz, [D_2]dichloromethane): δ = 148.2, 139.3, 137.5 [each d, $^1J_{CF}$ = 240 Hz, *o*-, *p*-, *m*-$B(C_6F_5)_3$], 113.8, 108.9 (Cp), 78.2 (br., $B-CH_2$), 72.0 ($Zr-CH_2$), *ipso*-C resonance of C_6F_5 not observed. − ^{11}B NMR (64.2 MHz, [D_2]dichloromethane): δ = −13.5 (d, $^1J_{BH}$ = 65 Hz).

Reaction of 8 with 3 in a 1:2 Stoichiometry. − Preparation of 17: The addition reaction was carried out as an NMR experiment in both [D_6]benzene and [D_2]dichloromethane, and on a preparative scale. Typical NMR experiment: Complex **8** (15.0 mg, 29.6 μmol) and $HB(C_6F_5)_2$ (20.6 mg, 58.1 μmol) were suspended in 1 mL of [D_6]benzene. The mixture was stirred for 5 min, then the precipitated product was collected by filtration and characterized by NMR spectroscopy in a 1:1 [D_6]benzene/[D_8]toluene mixture [^1H

NMR: δ = 6.21 (s, 20 H, Cp), 4.36 (br., 4 H, B−CH_2−Zr), B−H resonance not observed; ^{11}B NMR: δ = −13.0 (br., $\nu_{1/2} \approx 210$ Hz]. The reaction between **8** and **3** in a 1:2 ratio was also carried out in [D_2]dichloromethane: ^{1}H NMR (200.1 MHz): δ = 6.43 (s, 20 H, Cp), 4.45 (br., 4 H, B−CH_2−Zr), B−H resonance not observed; ^{13}C NMR (50.3 MHz): δ = 115.5 (Cp), other signals not detected due to the low solubility of **17**; ^{11}B NMR (64.2 MHz): δ = −13.2 (br., $\nu_{1/2} \approx 170$ Hz).

Reaction of 8 with 3 on a Preparative Scale: (Formaldehyde)zirconocene dimer (**8**, 60 mg, 119 μmol) and $HB(C_6F_5)_2$ (**3**, 85 mg, 246 μmol) were introduced as solids into a Schlenk tube. Toluene (3 mL) was added at ambient temperature and the mixture vigorously stirred. The solid reagents dissolved within ca. 1 min, and within a reaction time of ca. 5 min a precipitate of the product **17** formed. It was allowed to settle, the supernatant liquid was decanted, the remaining solid was washed with toluene (1 mL) and dried in vacuo to give 78 mg (51%) of **17**. The product contained one equivalent of toluene, m.p. 99°C, 178°C (decomp.). − $C_{46}H_{26}B_2F_{20}O_2Zr_2 \cdot C_7H_8$ (1286.9): calcd. C 49.47, H 2.66; found: C 49.47, H 3.36.

X-ray Crystal Structure Analysis of 17: Single crystals were obtained from [D_2]dichloromethane solution at room temperature. Formula $C_{46}H_{26}B_2F_{20}O_2Zr_2 \cdot 2\ CD_2Cl_2$, M = 1368.58, light yellow crystal, 0.25 × 0.20 × 0.05 mm, a = 14.295(1), b = 15.430(1), c = 11.513(1) Å, β = 103.12(1)°, V = 2473.2(3) Å^3, $\rho_{calcd.}$ = 1.832 g cm^{-3}, F(000) = 1344 e, μ = 7.55 cm^{-1}, absorption correction by SORTAV (0.834 ≤ T ≤ 0.963), Z = 2, monoclinic, space group $P2_1/c$ (No. 14), λ = 0.71073 Å, T = 198 K, ω and φ scans, 22325 reflections collected (±h, ±k, ±l), [(sinθ)/λ] = 0.71 Å^{-1}, 7495 independent and 5756 observed reflections [$I \geq 2\ \sigma(I)$], 365 refined parameters, R = 0.049, wR^2 = 0.134, max. residual electron density 1.93 (−1.46) e Å^{-3} in the region of the solvent molecule, hydrogen atoms at boron atoms from difference Fourier map and refined free, all other hydrogen atoms calculated and refined as riding atoms. The data set was collected with a Nonius KappaCCD diffractometer, placed on a Nonius rotating anode generator FR591.[19] Crystallographic data (excluding structure factors) for the structures reported in this paper have been deposited with the Cambridge Crystallographic Data Centre as supplementary publication no. CCDC-120189. Copies of the data can be obtained free of charge on application to CCDC, 12 Union Road, Cambridge CB2 1EZ, UK [Fax: (internat. + 44-1223/336-033, E-mail: deposit@ccdc.cam.ac.uk].

Reaction of (Butadiene)zirconocene (1) with $HB(C_6F_5)_2$ (3). − Preparation of 18: A mixture of (butadiene)zirconocene (**1**) (199 mg, 0.72 mmol) and of $HB(C_6F_5)_2$ (**3**) (250 mg, 0.72 mmol) in toluene (10 mL) was stirred for 30 min at room temperature. Solvent was removed from the red-brown solution. The resulting solid was stirred up in pentane (10 mL). The solid product was collected by filtration, washed with 10 mL of pentane and dried in vacuo to give 335 mg (75%) of **18**, m.p. 162°C (decomp.) − ^{1}H NMR (360.1 MHz, [D_6]benzene): δ = 5.23, 5.08 (s, each 5 H, Cp), 5.15 (m, 1 H, 2-H), 4.38 (m, 1 H, 3-H), 3.64 (m, 1 H, 4-H), 1.81 (m, 1 H, 1-H), 1.69 (m, 1 H, 1-H′), 1.46 (m, 1 H, 4-H′), −3.3 (br., 1 H, B-*H*). − ^{13}C NMR (90.6 MHz, [D_6]benzene): δ = 149.3 and 148.3, 140.3 and 139.9, 137.7 and 137.5 [each d, $^1J_{CF}$ = 240 Hz, *o*-, *p*-, *m*-$B(C_6F_5)_3$], 120.1 (C-2), 107.8, 106.9 (Cp), 96.2 (C-3), 49.1 (C-1), 25.5 (br., C-4). − GCOSY (360.1 MHz, [D_6]benzene): δ = 5.15/4.38 (2-H/3-H), 5.15/1.81 (2-H/1-H), 5.15/1.69 (2-H/1-H′), 4.38/3.64 (3-H/4-H), 4.38/1.46 (3-H/4-H′), 3.46/1.46 (4-H/4-H′), 1.81/1.69 (1-H/1-H′). − HETCOR (360.1 MHz, [D_6]benzene): δ = 120.1/5.15 (C-2), 107.8/5.08 (Cp), 106.9/5.23 (Cp), 96.2/4.38 (C-3), 49.1/1.81 (C-1/1-H), 49.1/1.69 (C-1/1-H′). − ^{11}B NMR (64.2 MHz, [D_6]benzene): δ = −32.4. − ^{19}F NMR (282.4 MHz, [D_6]benzene): δ = −131.1, −131.8 [*o*-$B(C_6F_5)_3$], −156.9, −159.0 [*p*-$B(C_6F_5)_3$], −162.7, −163.5 [*m*-$B(C_6F_5)_3$]. − IR (KBr): $\tilde{\nu}$ = 3128, 2962, 2916, 2875, 2843, 1782, 1643, 1515, 1464, 1376, 1278, 1207, 1096, 1017, 971, 816, 734 cm^{-1}. − $C_{26}H_{17}BF_{10}Zr$ (621.44): calcd. C 50.25, H 2.76; found C 48.99, H 2.87.

Acknowledgments

Financial support from the Fonds der Chemischen Industrie and the Deutsche Forschungsgemeinschaft is gratefully acknowledged.

[1] G. Erker, C. Krüger, G. Müller, *Adv. Organomet. Chem*. **1985**, *24*, 1, and references cited therein.
[2] G. Erker, R. Noe, D. Wingbermühle, J. L. Petersen, *Angew. Chem*. **1993**, *105*, 1216; *Angew. Chem. Int. Ed. Engl*. **1993**, *32*, 1213.
[3] [3a] D. J. Parks, R. E. v. H. Spence, W. E. Piers, *Angew. Chem*. **1995**, *107*, 895; *Angew. Chem. Int. Ed. Engl*. **1995**, *34*, 809. − [3b] R. E. v. H. Spence, W. E. Piers, *Organometallics* **1995**, *14*, 4617.
[4] Y. Sun, W. E. Piers, S. J. Rettig, *Organometallics* **1996**, *15*, 4110.
[5] [5a] R. E. v. Spence, D. J. Parks, W. E. Piers, M.-A. MacDonald, M. J. Zaworotko, S. J. Rettig, *Angew. Chem*. **1995**, *107*, 1337; *Angew. Chem. Int. Ed. Engl.* **1995**, *34*, 1230. − [5b] U. Radius, S. J. Silverio, R. Hoffmann, R. Gleiter, *Organometallics* **1996**, *15*, 3737. − [5c] Y. Sun, R. E. v. H. Spence, W. E. Piers, M. Parvez, G. P. A. Yap, *J. Am. Chem. Soc.* **1997**, *119*, 5132. − [5d] R. E. v. H. Spence, W. E. Piers, Y. Sun, M. Parvez, L. R. MacGillivray, M. J. Zaworotko, *Organometallics* **1998**, *17*, 2459.
[6] Review: W. E. Piers, T. Chivers, *Chem. Soc. Rev.* **1997**, 345.
[7] G. Erker, K. Kropp, C. Krüger, A.-P. Chiang, *Chem. Ber.* **1982**, *115*, 2447; G. Erker, *Acc. Chem. Res.* **1984**, *17*, 103, and references cited therein.
[8] U. Blaschke, G. Erker, M. Nissinen, E. Wegelius, R. Fröhlich, *Organometallics* **1999**, *18*, 1224; U. Blaschke, F. Menges, G. Erker, R. Fröhlich, *Eur. J. Inorg. Chem.* **1999**, 621.
[9] G. Erker, U. Hoffmann, R. Zwettler, P. Betz, C. Krüger, *Angew. Chem.* **1989**, *101*, 644; *Angew. Chem. Int. Ed. Engl*. **1989**, *28*, 630; See also: K. Kropp, V. Skibbe, G. Erker, C. Krüger, *J. Am. Chem. Soc.* **1983**, *105*, 3353.
[10] For related systems see e.g.: G. Erker, U. Dorf, P. Czisch, J. L. Petersen, *Organometallics* **1986**, *5*, 668; R. M. Waymouth, B. D. Santarsiero, R. J. Coots, M. J. Bronikowski, R. H. Grubbs, *J. Am. Chem. Soc.* **1986**, *108*, 1427; R. M. Waymouth, R. H. Grubbs, *Organometallics* **1988**, *7*, 1631.
[11] G. Erker, U. Hoffmann, R. Zwettler, C. Krüger, *J. Organomet. Chem*. **1989**, *367*, C15.
[12] For a related reaction of (η^2-acetaldehyde)zirconocene dimer with $B(C_6F_5)_3$ see: D. Röttger, S. Schmuck, G. Erker, *J. Organomet. Chem*. **1996**, *508*, 263.
[13] G. Fachinetti, C. Floriani, A. Roselli, S. Pucci, *J. Chem. Soc., Chem. Commun.* **1978**, 269; S. Gambarotta, C. Floriani, A. Chiesi-Villa, C. Guastini, *J. Am. Chem. Soc*. **1983**, *105*, 1690.
[14] Zr−(μ-H)−B bond lengths range from 1.125 to 1.529 Å (for H−B) and from 1.947 to 2.273 Å (for Zr−H) in the literature, see: D. Männig, H. Nöth, M. Schwartz, S. Weber, U. Wietelmann, *Angew. Chem.* **1985**, *97*, 979; *Angew. Chem. Int. Ed. Engl*. **1985**, *24*, 998; D. L. Reger, R. Mahtab, J. C. Baxter, L. Lebioda, *Inorg. Chem*. **1986**, *25*, 2046; G. T. Jordan IV, S. G. Shore, *Inorg. Chem*. **1996**, *35*, 1087; and the articles cited in refs. 2, 4, 5a, 5c, and 11.
[15] For related Zr_2O_2 containing structures see e.g.: I. D. Williams, S. F. Pedersen, K. B. Sharpless, S. J. Lippard, *J. Am. Chem. Soc.* **1984**, *106*, 6430; G. Erker, S. Dehnicke, M. Rump, C. Krüger, S. Werner, M. Nolte, *Angew. Chem.* **1991**, *103*, 1371; *Angew. Int. Ed. Engl.* **1991**, *30*, 1349; G. Erker, M. Rump, C. Krüger, M. Nolte, *Inorg. Chim. Acta,* **1992**, *198*, 679; W. Spaether, M. Rump, G. Erker, R. Fröhlich, J. Hecht, C. Krüger, J. Kuhnigk, *Anales Quimica Int. Ed*. **1997**, *93*, 394.
[16] B. Temme, G. Erker, J. Karl, H. Luftmann, R. Fröhlich, S. Kotila, *Angew. Chem.* **1995**, *107*, 1867; *Angew. Chem. Int. Ed. Engl*. **1995**, *34*, 1755.

[17] For a structurally related (butadiene)$ZrCp_2/AlCl_3$ adduct see: G. Erker, R. Noe, C. Krüger, S. Werner, *Organometallics* **1992**, *11*, 4174.

[18] For additional related examples see e.g.: G. Erker, K. Engel, J. L. Atwood, W. E. Hunter, *Angew. Chem.* **1983**, *95*, 506; *Angew. Chem. Int. Ed. Engl.* **1983**, *22*, 494; G. Erker, U. Dorf, *Angew. Chem.* **1983**, *95*, 800; *Angew. Chem. Int. Ed. Engl*. **1983**, *22*, 777; H. Yasuda, Y. Kajihara, K. Mashima, K. Nagasuna, A. Nakamura, *Chem. Lett*. **1981**, 671; G. Erker, K. Engel, U. Dorf, J. L. Atwood, W. E. Hunter, *Angew. Chem*. **1982**, *94*, 915; *Angew. Chem. Int. Ed. Engl.* **1982**, *21*, 913; G. Erker, R. Lecht, Y.-H. Tsai, C. Krüger, *Chem. Ber*. **1987**, *120*, 1763; G. Erker, U. Dorf, R. Benn, R.-D. Reinhard, J. L. Petersen, *J. Am. Chem. Soc*. **1984**, *106*, 7649.

[19] Programs used: (data collection) COLLECT: Nonius B. V. 1998; (data reduction) DENZO-SMN: Z. Otwinowski, W. Minor, *Methods Enzymol.* **1997**, *276*, 307−326; (absorption correction) SORTAV: R. H. Blessing, *Acta Crystallogr.* **1995**, *A51*, 33−37; R. H. Blessing, *J. Appl. Crystallogr.* **1997**, *30*, 421−426; (structure solution) SHELXS-86 and SHELXS-97: G. M. Sheldrick, *Acta Crystallogr.* **1990**, *A46*, 467−473; (structure refinement) SHELXL-97: G. M. Sheldrick, Universität Göttingen, 1997; (graphics) SCHAKAL: E. Keller, Universität Freiburg, **1997**.

Received April 6, 1999
[I99117]

Synthesis and Characterisation of New Arsonium Salts and Crystal Structures of Trimethylarsonium Undecafluorodiarsenate $(CH_3)_3AsH^+As_2F_{11}^-$ and Trimethylarsonium Hexafluoroantimonate $(CH_3)_3AsH^+SbF_6^-$

Rolf Minkwitz,*[a] Claudia Hirsch,[a] and Thorsten Berends[a]

Keywords: Arsonium salts / Superacidic systems / Structure elicidation

The reaction of trimethylarsane in the superacidic systems hydrogen/fluoride antimony pentafluoride and hydrogen fluoride/arsenic pentafluoride leads to trimethylarsonium fluorometallates. These salts are stable up to 60 °C and 5 °C, respectively. Structures were successfully elucidated in the cases of trimethylarsonium undecafluorodiarsenate and trimethylarsonium hexafluoroantimonate. $(CH_3)_3AsH^+As_2F_{11}^-$ crystallizes in the monoclinic space group $P2_1/n$ with four formula units per unit cell with the dimensions a = 7.362(1), b = 12.589(1), c = 13.598(1) Å and β = 95.37(1)°. $(CH_3)_3AsH^+SbF_6^-$ crystallizes in the monoclinic space group $P2_1/m$ with four formula units per unit cell with the dimensions a = 8.313(1), b = 8.855(1), c = 13.285(1) Å and β = 94.358(1)°.

Introduction

Arsanes are much weaker bases than amines, although they do demonstrate nucleophilic properties. For instance, arsane is protonated during the reaction with hydrogen bromide or hydrogen iodide (Equation 1).[1]

$$AsH_3 + HX \rightarrow AsH_4^+X^- \quad X = Br, I \qquad (1)$$

However, these salts are only stable up to −123 °C (Br^-) and −83 °C (I^-), respectively.

Stabilisation to −40 °C (SbF_6^-) and −75 °C (AsF_6^-) is achieved by exchanging the anions by hexafluoroantimonate or hexafluoroarsenate (Equation 2).[2]

$$AsH_3 + HF + MF_5 \rightarrow AsH_4^+MF_6^- \quad M = As, Sb \qquad (2)$$

Dimethylarsane reacts with hydrogen chloride with formation of dimethylarsonium chloride (Equation 3), which is completely dissociated into the starting materials at 20 °C.[3]

$$(CH_3)_2AsH + HCl \rightleftharpoons (CH_3)_2AsH_2Cl \qquad (3)$$

Trimethylarsane and, for example, methyl halogenides (CH_3Cl, CH_3Br, CH_3I) form stable tetramethylarsonium salts i.e. $(CH_3)_4As^+Br^-$ and $(CH_3)_4As^+I^-$ which have been identified by their crystal structures.[4][5]

Although attempts to protonate triphenylarsane in sulfuric acid failed, the reaction of triphenylarsane with hydrogen chloride, yielding the triphenylarsonium salt (Equation 4), nevertheless succeeded.[6][7]

$$Ph_3As + HCl \xrightarrow{HCl} Ph_3AsH^+Cl^- \qquad (4)$$

Hence, the protonation of trimethylarsane in the superacidic systems hydrogen fluoride antimony pentafluoride and arsenic pentafluoride, respectively, should lead to salts which are more stable than dimethylarsonium chloride but less stable than the tetramethylarsonium salts.

Not only will the series of $(CH_3)_nAsH_{4-n}^+$ salts with n = 1−4 be completed but new pnikogenium salts which are analogous to trimethylphosphonium salts will also be formed. The crystal structure of trimethylphosphonium hexachloroantimonate is well-known and could be compared to the structures of prepared trimethylarsonium undecafluorodiarsenate and trimethylarsonium hexafluoroantimonate.[8]

Moreover, a structure elucidation of a undecafluorodiarsenate salt succeeded. This anion was firstly mentioned by Brownstein in 1969, who examined the reaction of various hexafluoroantimonate and hexafluoroarsenate salts with AsF_5.[9] Further investigations by Raman spectroscopy, IR spectroscopy, NMR spectroscopy, cryoscopic and conductimetric measurements followed.[10−13] In spite of the fact that this kind of salt has been known since 1969, structural data, in comparison to the undecafluorodiantimonate, are scarce. Only a few crystal structures of salts with undecafluorodiarsenate as the anion are known up to now. To date, Christe has been able to determine the crystal structure of an $As_2F_{11}^-$ salt,[14] whilst we have crystallized salts of $HPCl_3^+As_2F_{11}^-$ (to be published), $(MeS)_2CSX^+As_2F_{11}^-$ (X = H, D) and $(CH_3)_3AsH^+As_2F_{11}^-$ reported now.[15]

Results and Discussion

Formation of $(CH_3)_3AsH^+$ Salts

The salts are prepared by protonation of trimethylarsane in superacidic media, hydrogen fluoride and antimony pentafluoride (Equation 5) or arsenic pentafluoride (Equation 6).

[a] Anorganische Chemie, Fachbereich Chemie der Universität Dortmund,
D-44221 Dortmund, Germany

 © WILEY-VCH Verlag GmbH, D-69451 Weinheim, 1999 1434−1948/99/1212−2249 $ 17.50+.50/0

$$As(CH_3)_3 + HF + SbF_5 \xrightarrow{HF/-78\,^\circ C} (CH_3)_3AsH^+SbF_6^- \quad (5)$$

$$As(CH_3)_3 + HF + 2AsF_5 \xrightarrow{HF/-78\,^\circ C} (CH_3)_3AsH^+As_2F_{11} \quad (6)$$

The fine colourless solids are stable for several months at −70°C under a nitrogen atmosphere, decomposing at 5°C in the case of the undecafluorodiarsenate and at 60°C in the case of the hexafluoroantimonate. The salts dissolve well in sulfur dioxide at −40°C.

Vibrational Spectra

The Raman and IR spectra of $(CH_3)_3AsH^+SbF_6^-$ are shown in Figure 1 and all observed wavenumbers of the salts are summarised in Table 1. The vibrational spectra are assigned according to C_{3v} symmetry for the $(CH_3)_3AsH^+$ cation. The cation has twenty-four fundamental modes consisting of eight A_1 vibrations, four A_2 vibration and twelve E vibrations. The A_2 modes are inactive in both Raman and IR spectra. The twenty active fundamentals can be divided into six modes which are largely associated with $HAsC_3$ skeletal vibrations and the remaining modes which can be considered as motions of the methyl group. The CH_3 stretching modes are found in the range of 3042 to 2949 cm^{-1} and the corresponding deformation modes from 1433 cm^{-1} to 1180 cm^{-1}. The As−H and As−D stretching modes are detected at 2290 cm^{-1} and 1650 cm^{-1}, respectively.

The assignment of the skeletal vibrations is much more difficult because both anion and cation have the same anticipated range of vibrations. However, the possible assignment is carried out by comparison with the AsH_4^+ cation and the isoelectronic trimethylgermane.[2][16] Only four modes of the expected six could be assigned. In the range of 950 cm^{-1} to 880 cm^{-1} the CAsH and CAsD deformation modes are observed. They are shifted up to 90 cm^{-1} to higher wavenumber in comparison to the analogous vibration in trimethylgermane. The out-of-phase stretching modes of the AsC_3 skeleton are assigned to the lines and bands around 655 cm^{-1} and the in-phase stretching modes to those at 600 cm^{-1}. The corresponding deformation modes are detected at 220 cm^{-1}. The remaining vibrations are possibly modes of the anions.

Crystal Structure of $(CH_3)_3AsH^+As_2F_{11}^-$

$(CH_3)_3AsH^+As_2F_{11}^-$ crystallises in the monoclinic space group $P2_1/n$ (no. 14) with a = 7.362(1), b = 12.589(1), c = 13.598(1) Å, β = 95.37(1)° and four formula units per unit cell. The crystal structure was solved via the Patterson method and successive difference Fourier syntheses. For refinement full-matrix least-squares methods were applied. All hydrogen atoms were taken from Fourier maps and refined with isotropic displacement parameters and all non-hydrogen atoms with anisotropic displacement parameters. For the data reduction, structure solution, and refinement, programs in the SHELXTL package, PLATON, MISSYM, and PARST were used.[17−21] The crystal data are summarised in Table 2. The cation has the shape of a trigonal pyramid and the anion has a distorted edge-linked dioctahedral structure. Bond lengths and selected angles are shown in Table 3. The structure of trimethylarsonium cation with weak hydrogen bonds [H···F: 2.44(7) Å to 2.55(5) Å] to the nearest fluorine atoms of the anions is shown in Figure 2.

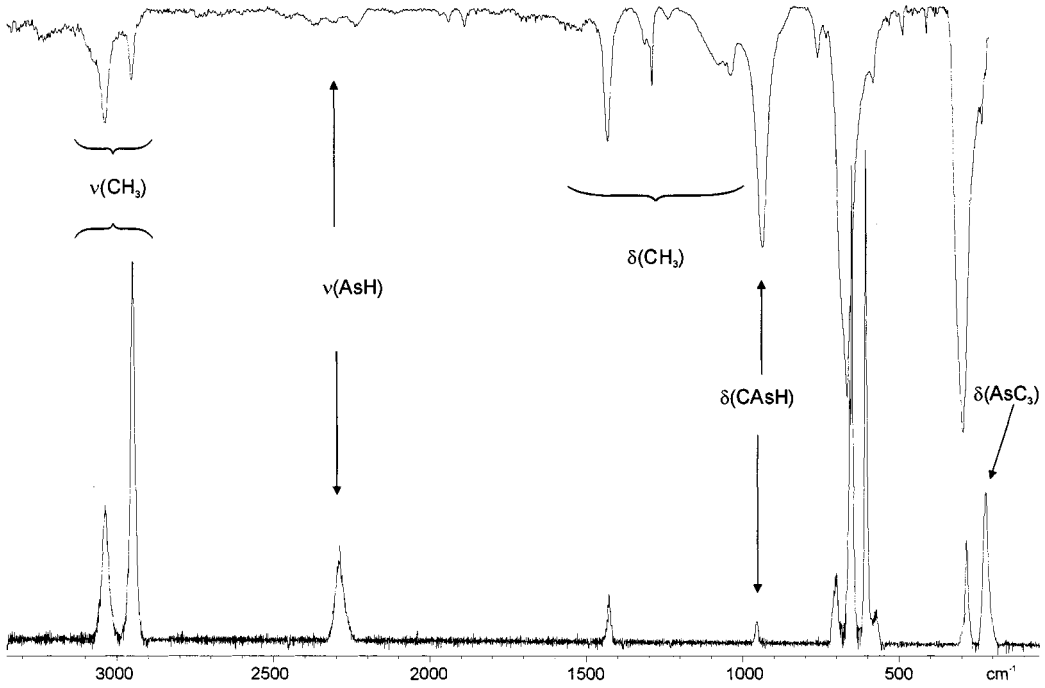


Figure 1. IR and Raman spectra of $(CH_3)_3AsH^+SbF_6^-$

Table 1. Vibrational wavenumbers of trimethylarsonium salts and Raman wavenumbers of trimethylgermane

$As(CH_3)_3H^+As_2F_{11}^-$ IR −30°C		$As(CH_3)_3H^+As_2F_{11}^-$ Raman −78°C		$As(CH_3)_3D^+As_2F_{11}^-$ IR −30°C		$As(CH_3)_3D^+As_2F_{11}^-$ Raman −78°C		$As(CH_3)_3H^+SbF_6^-$ IR room temp.		$As(CH_3)_3H^+SbF_6^-$ Raman room temp.		$As(CH_3)_3D^+SbF_6^-$ IR room temp.		$As(CH_3)_3D^+SbF_6^-$ Raman room temp.		$(CH_3)_3GeH$ Raman [19]	Assignment
3036	w	3041	m	3040	w	3042	m	3033	m	3035	m	3035	m	3038	m	2982	$\nu(CH_3)$
		2955	s	2958	vw	2956	s	2950	w	2947	s	2949	w	2950	s	2913	$\nu(CH_3)$
						2949	s										$\nu(CH_3)$
2372	vw							2361	w								$\nu(CH_3)$
2299	vw	2295	m			1649	m	2299	w	2297	m			1658	m	2036	ν(AsH), (AsD), (GeH)
2230	vw							2232	w								ν(AsH), (AsD), (GeH)
								1933	w								ν(AsH), (AsD), (GeH)
								1884	w								ν(AsH), (AsD), (GeH)
1432	m	1420	w	1432	w	1430	w	1425	m	1426	w	1429	m	1428	w	1419	$\delta(CH_3)$
				1418	sh												$\delta(CH_3)$
				1311	vw			1305	sh			1305	sh	1312	vw		$\delta(CH_3)$
														1295	vw	1247	$\delta(CH_3)$
1282	w			1281	w	1288	vw	1281	m			1281	w	1283	vw		$\delta(CH_3)$
								1230	w								$\delta(CH_3)$
								1073	sh			1086	w				$\delta(CH_3)$
								1028	w			1026	w				$\delta(CH_3)$
929	s	956	vw	937	m	940	vvw	929	s	950	vw	934	s	941	vw		δ(CAsH), (CAsD), (CGeH)
				884	m							884	m	888	vw	850	δ(CAsH), (CAsD), (CGeH)
																830	$\rho(CH_3)$
811	w			818	w												$As_2F_{11}^-$
791	vw																$As_2F_{11}^-$
		739	m			734	m	752	w			745	sh				
							723	vw			722	m					
698	vs	700	sh	699	vs	699	w			695	w						$As_2F_{11}^-$, SbF_6^-
679	sh	685	s	680	sh	682	m										$As_2F_{11}^-$, SbF_6^-
		657	m	655	sh	657	m	657	vs	650	sh	656	vs	656	sh	597	$\nu_{as}(AsC_3)$, (GeC_3)
										644	s			649	s		SbF_6^-
																626	$\rho(CH_3)$
		607	vs			604	s			600	s	591	vw	605	vs	573	$\nu_s(AsC_3)$, (GeC_3)
								571	vw	568	vw	570	vw	572	vw		$As_2F_{11}^-$, SbF_6^-
				535	w	540	m					536	w	537	m		$As_2F_{11}^-$, SbF_6^-
								476	w			475	m				$As_2F_{11}^-$, SbF_6^-
						443	vw										$As_2F_{11}^-$, SbF_6^-
						426	vw										$As_2F_{11}^-$, SbF_6^-
395	s	397	w	395	vs	394	w	400	w					372	vw		$As_2F_{11}^-$, SbF_6^-
						373	w					370	w				$As_2F_{11}^-$, SbF_6^-
		313	w			313	vw										$As_2F_{11}^-$, SbF_6^-
						284	vw	286	vs	280	mw	286	vs	282	m		$As_2F_{11}^-$, SbF_6^-
259	w			269	sh												$As_2F_{11}^-$, SbF_6^-
				235	sh							234	w				$As_2F_{11}^-$, SbF_6^-
219	vw	228	m	221	sh	224	m	224	w	219	m	220	vw	223	m	189	$\delta(AsC_3)$, (GeC_3)

For comparison, the sum of the van der Waals radii of fluorine and hydrogen amounts to 2.67 Å.[22] Only the hydrogen atoms of the methyl groups are involved in hydrogen bonds and not the hydrogen atom which is directly bonded to the arsenic atom. No contact between arsenic and fluorine atoms, which is significantly below the sum of the van der Waals radii of 3.32 Å, is formed. The weak hydrogen bonds result in a formation of ribbons and two "As−F contacts", in the range of the sum of the van der Waals radii, of 3.304(3) Å and 3.399(3) Å, lead to a weak linkage of these ribbons. The As−C lengths of 1.894(5) Å, 1.907(5) Å and 1.908(5) Å are comparable to those found in methyltrifluoroarsonium hexafluoroarsenate of 1.886(4) Å and dimethyldifluoroarsonium hexafluoroantimonate of 1.894(7) Å, but are significantly shorter than that in trimethylarsane of 1.98(2) Å.[23−25] Comparison of the C−As−C angles of 109.5(3)°, 109.8(3)° and 111.1(3)° to the analogous C−P−C angles in trimethylphosphonium hexachloroantimonate of 109.7(4)°, 110.4(4)° and 111.0(3)° show no significant difference.[8]

The undecafluorodiarsenate anion with hydrogen bonds is shown in Figure 3. The As−F bond lengths involving the "bridging" fluorine atom are asymmetrical and amount to 1.855(3) Å and 1.983(3) Å. They are significantly longer than the other As−F bond lengths of 1.675(3) Å up to 1.696(3) Å, which are in the normal range of As−F bond lengths of hexafluoroarsenate anions.[26−28] The As−F bond lengths involving the "bridging" fluorine atom in $(CH_3S)_2CSH^+As_2F_{11}^-$ of 1.867(4) Å and 1.920(6) Å are in the same range as in the presented salt.[15] By projection along the As(1)−As(2) axes of the $As_2F_{11}^-$ anion (Figure 4) the gauche arrangement of the two octahedral AsF_6 units is visible, the overage torsion angle F−As−As−F of 45.0° being comparable to that found in $(CH_3S)_2CSH^+As_2F_{11}^-$.[15] The As(1)−F(1)−As(2) angle of 146.1(2)° is comparable to the Sb−F−Sb angle of 146.2(4)° and 147.6(3)° found in $(CF_3)_2C(F)OH_2^+$ $Sb_2F_{11}^-$ and $[Hg(CO)_2][Sb_2F_{11}]_2$, respectively, but smaller than the As−F−As angle of 159.1(6)° in $(CH_3)_2CSH^+$-$As_2F_{11}^-$.[15,29,30]

Crystal Structure of $(CH_3)_3AsH^+SbF_6^-$

$(CH_3)_3AsH^+SbF_6^-$ crystallises in the monoclinic space group $P2_1/m$ (no. 14) with a = 8.313(1), b = 8.855(1), c = 13.285(1) Å, β = 94.358(1)° and four formula units per unit cell. The crystal structure was solved via direct methods and successive difference Fourier syntheses. For refinement full-matrix least-squares methods were applied. All hydro-

Table 2. X-ray diffraction data of $(CH_3)_3AsH^+As_2F_{11}^-$ and $(CH_3)_3AsH^+SbF_6^-$

	$(CH_3)_3AsH^+As_2F_{11}^-$	$(CH_3)_3AsH^+SbF_6^-$
Space group	$P2_1/n$	$P2_1/m$
Crystal system	monoclinic	monoclinic
a [Å]	7.362(1)	8.313(1)
B [Å]	12.589(1)	8.855(1)
C [Å]	13.598(1)	13.285(1)
β [°]	95.37(1)	94.358(1)
Volume [Å^3]	1254.7(2)	975.1(2)
$D_{calcd.}$ [g cm^{-3}]	2.540	2.430
Z	4	4
Formula weight [g mol^{-1}]	479.87	356.78
Absorption coefficient [mm^{-1}]	8.055	6.231
Temperature [K]	173(2)	173(2)
F(000)	904	664
Wavelength [Å]	0.71069	0.71069
θ range for data collection [°]	2.21≤θ≤29.54	1.54≤θ≤26.67
Index ranges	$-10\le h\le 10$ $-15\le k\le 15$ $-18\le l\le 18$	$-7\le h\le 7$ $-10\le k\le 10$ $-15\le l\le 15$
Reflections collected/ independent	10064/3087 [R(int) = 0.0635]	5952/1607 [R(int) = 0.0480]
Parameters	194	162
Goodness-of-fit on F^2	0.955	1.011
Final R indices [$I<2\sigma(I)$]	$R1$ = 0.0384 $wR2$ = 0.0722	$R1$ = 0.0318 $wR2$ = 0.0759
R indices (all data)	$R1$ = 0.0831 $wR2$ = 0.0842	$R1$ = 0.0558 $wR2$ = 0.0809
Largest diff. peak and hole, e. Å^{-3}	0.596 and −1.180	0.615 and −1.095
Refinement method	full matrix, least-squares on F^2	full matrix, least-squares on F^2

gen atoms were taken from Fourier maps and refined with isotropic displacement parameters and all nonhydrogen atoms with anisotropic displacement parameters. For the data reduction, structure solution, and refinement the same programs were used as for the structure solution of $(CH_3)AsH^+As_2F_{11}^-$.[21] The monoclinic unit cell consists of two crystallographically independent cations and anions. The crystal data are summarised in Table 2 and bond lengths and selected angles are shown in Table 3.

The arsenic−carbon bond lengths of 1.779(10) and 1.765(9) Å in the two cations are significantly shorter than the remaining arsenic−carbon bond lengths of 1.910(9) and 1.935(9) Å and the analogous bond lengths of 1.894(5), 1.907(5) and 1.908(5) Å in trimethylarsonium undecafluorodiarsenate. The C−As−C angles of average 107.7(4) and 109.1(6)° are comparable to the C−P−C angles found in trimethylphosphonium hexachloroantimonate [110.4(4)°]. The interionic contacts are stronger than in trimethylarsonium undecafluorodiarsenate. The two independent cations form different contacts to fluorine atoms of neighbouring anions. In one case hydrogen fluorine contacts of 2.36(9) up to 2.47(6) Å and one arsenic fluorine contact of 3.060(5) Å result in formation of ribbons in the *ac* plane without connection along the *b* axes. In the other case only one hydrogen fluorine contact of 2.36(10) Å leads to a connection of cations and anions

Table 3. Selected bond lengths [Å], selected angles [°] and contacts [Å] for $(CH_3)_3AsH^+As_2F_{11}^-$ and $(CH_3)_3AsH^+SbF_6^-$[a]

$(CH_3)_3AsH^+As_2F_{11}^-$		$(CH_3)_3AsH^+SbF_6^-$	
As(3)−C(1)	1.908(5)	As(1)−C(1)	1.779(10)
As(3)−C(2)	1.907(5)	As(1)−C(2)	1.910(9)
As(3)−C(3)	1.894(5)	As(2)−C(3)	1.765(9)
As(3)−H(1)	1.30(4)	As(2)−C(4)	1.935(9)
		As(1)−H(1)	1.46(9)
		As(2)−H(2)	1.49(8)
C(1)−As(3)−C(2)	111.1(3)	C(1)−As(1)−C(2)	107.3(4)
C(1)−As(3)−C(3)	109.8(3)	C(1)−As(1)−C(2e)	107.3(4)
C(2)−As(3)−C(3)	109.5(3)	C(2)−As(1)−C(2e)	108.4(4)
		C(3)−As(2)−C(4)	110.3(3)
		C(3)−As(2)−C(4e)	110.3(3)
		C(4)−As(2)−C(4e)	106.7(6)
As(1)−F(1)	1.855(3)	Sb(1)−F(1)	2.008(5)
As(2)−F(1)	1.983(3)	Sb(1)−F(2)	1.810(4)
As(1)−F(7)	1.685(3)	Sb(1)−F(3)	1.986(6)
As(1)−F(8)	1.689(3)	Sb(1)−F(4)	1.804(4)
As(1)−F(9)	1.695(3)	Sb(2)−F(5)	1.782(5)
As(1)−F(10)	1.696(3)	Sb(2)−F(6)	1.953(5)
As(1)−F(11)	1.691(3)	Sb(2)−F(7)	1.776(5)
As(2)−F(2)	1.685(3)	Sb(2)−F(8)	1.862(4)
As(2)−F(3)	1.683(3)	Sb(2)−F(9)	1.956(6)
As(2)−F(4)	1.687(3)		
As(2)−F(5)	1.682(3)		
As(2)−F(6)	1.675(3)		
As(1)−F(1)−As(2)	146.1(2)	F(1)−Sb(1)−F(2e)	85.9(2)
F(1)−As(1)−F(7)	85.38(13)	F(2d)−Sb(1)−F(4)	177.6(2)
F(8)−As(1)−F(11)	173.5(2)	F(7)−Sb(2)−F(9)	98.2(2)
F(1)−As(2)−F(5)	83.34(13)	F(8)−Sb(2)−F(8e)	177.0(2)
F(4)−As(2)−F(5)	168.63(13)	F(7)−Sb(2)−F(9)	98.2(2)
As(3)···F(8a)	3.399(3)	F(2)···H(12)	2.47(6)
As(3)···F(10b)	3.304(3)	F(3)···H(1f)	2.45(9)
F(5)···H(12c)	2.53(6)	F(5)···H(1g)	2.36(9)
F(5)···H(23c)	2.44(7)	As(1)···F(5h)	3.060(5)
F(10)···H(21b)	2.52(6)		
F(11)···H(31d)	2.54(5)		

[a] Symmetry operations: a = −1 + *x*, *y*, *z*; b = −*x*, 1 − *y*, −*z*; c = 1/2 + *x*, 1/2 − *y*, 1/2 + *z*; d = −1 − *x*, 1 − *y*, −*z*; e = *x*, 1/2 − *y*, *z*, f = −1 + *x*, *y*, *z*; g = −1 + *x*, *y*, 1 + *z*; h = −1 + *x*, *y*, −1 + *z*.

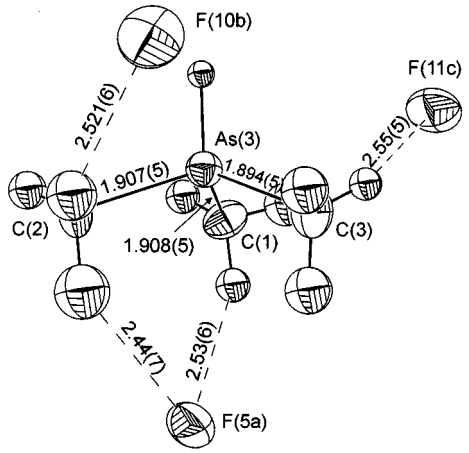


Figure 2. Fragment of the structure of $(CH_3)_3AsH^+As_2F_{11}^-$, showing the $(CH_3)_3AsH^+$ cation with hydrogen bonds (50% probability ellipsoids for the carbon, fluorine and arsenic atoms, 25% probability ellipsoids for the hydrogen atoms); bond lengths are given in Å; symmetry operations: a = −0.5 + *x*, 0.5 − *y*, −0.5 + *z*; b = −*x*, 1 − *y*, −*z*; c = −1 − *x*, 1 − *y*, −*z*

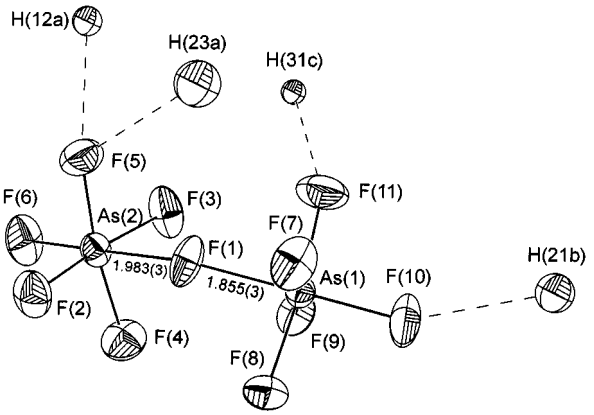


Figure 3. Structure of the $As_2F_{11}^-$ anion with hydrogen bonds (50% probability ellipsoids for the arsenic and fluorine atoms, 25% probability ellipsoids for the hydrogen atoms); bond lengths are given in Å; symmetry operations: a = 0.5 + *x*, 0.5 − *y*, 0.5 + *z*; b = −*x*, 1 − *y*, −*z*; c = −1 − *x*, 1 − *y*, −*z*

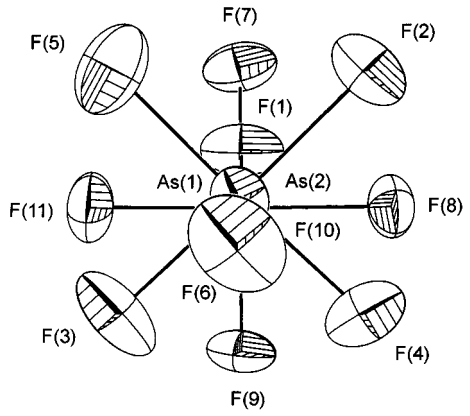


Figure 4. Projection along the As(1)−As(2) axes of the $As_2F_{11}^-$ anion (50% probability ellipsoids for the arsenic and fluorine atoms)

Experimental Section

Caution: Avoid contact with these compounds and note that the hydrolysis of $As_2F_{11}^-$ salts and SbF_6^- salts form HF, which burns the skin and causes irreparable damage. Safety precautions should be taken when using and handling these materials.

General: All synthetic work and sample handling was performed by employing standard Schlenk techniques and standard vacuum line (stainless steel or glass, respectively). Nonvolatile materials were handled under dry nitrogen and experiments in anhydrous HF were handled in Kel-F reactors with valves made of the same material. − The synthesis of $As(CH_3)_3$ was carried out by known literature methods out of $AsCl_3$ (Merck) and CH_3I (Merck).[31][32] Di-*n*-butyl ether (Fluka) was dried with sodium. AsF_5 was synthesised from As and F_2. SbF_5 (Merck) was distilled repeatedly before use. HF was dried in a stainless steel bomb using 1.5 bar of F_2. − The Raman spectra were recorded on a Jobin Yvon T64000 spectrometer using an Ar^+ laser (514.5 nm) from Spectra Physics. The spectra were obtained in a glass cell cooled with solid CO_2.[33] − Infrared spectra were recorded on a Bruker ifs 113v spectrophotometer. Spectra were obtained from a coated CsBr plate in a low-temperature cuvette.[34] − NMR spectra were recorded with a Bruker DPX 300 spectrometer. − Single crystals were obtained by slowly removing HF at −78°C under vacuum and placed in Lindemann capillaries in a cooled stream of dry nitrogen. − X-ray diffraction studies were carried out using a Nonius Kappa CCD diffractometer.

Preparation of $(CH_3)_3AsH^+As_2F_{11}^-$ [$(CH_3)_3AsH^+SbF_6^-$]: In a typical reaction, 3 mL of HF was distilled into a Kel-F reactor at −196°C, followed by 2 mmol (1 mmol) of AsF_5 (SbF_5). The mixture was warmed to 20°C to form the superacid. The reactor was then cooled to −196°C, and $As(CH_3)_3$ (1 mmol) was added. The mixture was warmed to −70°C. After removing the volatile compounds at −78°C colourless solids, stable up to 5°C (60°C) were obtained. − NMR spectra were recorded in SO_2 at −40°C, standards are ^{75}As: 10% $KAsF_6$ in D_2O; ^{19}F: F11; $^{1\,H,\ 13}C$: TMS. The obtained data are as follows. **$(CH_3)_3AsH^+As_2F_{11}^-$:** ^1H NMR: δ = 1.92 (s), 10.27 (s). − ^{13}C NMR: δ = 4.13 (s). − ^{19}F NMR: δ = −52.24 (s). − ^{75}As NMR: δ = 138 (d), 131.1 (J_{AsH} = 507 Hz). − **$(CH_3)_3AsH^+SbF_6^-$:** ^1H NMR: δ = 2.00 (s). − ^{13}C NMR: δ = 4.42 (s). − ^{75}As NMR: δ = 138.6 (d, J_{AsH} = 498 Hz).

Preparation of $(CH_3)_3AsD^+As_2F_{11}^-$ [$(CH_3)_3AsD^+SbF_6^-$]: The preparations were analogous to those of the protonated species, but DF was used instead of HF. The colourless solids were stable up to 5°C (60°C).

Acknowledgments

This work was supported by the Deutsche Forschungsgemeinschaft and the Fonds der Chemischen Industrie.

[1] A. Heinemann, *Ber. Bunsenges. Phys. Chem.* **1964**, *68*, 287−295.
[2] R. Minkwitz, A. Kornath, W. Sawodny, H. Härtner, *Z. Anorg. Allg. Chem.* **1994**, *620*, 753−756.
[3] W. R. Cullen, *Can. J. Chem.* **1963**, *41*, 322−328.
[4] E. Collins, D. J. Sutor, F. G. Mann, *J. Chem. Soc.***1963**, 4051−4055.
[5] W. Assenmacher, M. Jansen, *Z. Anorg. Allg. Chem.* **1995**, *621*, 143−148.
[6] R. J. Gillespie, E. A. Robinson, *Advances in Inorg. Chem. and Radiochem.* **1959**, *Vol. 1*, 385−423.
[7] M. E. Peach, T. C. Waddington, *J. Chem. Soc.* **1961**, 1238−1245.
[8] R. Minkwitz, G. Medger, H. Preut, *Z. Anorg. Allg. Chem.* **1992**, *614*, 102−108.
[9] S. Brownstein, *Can. J. Chem.* **1969**, *47*, 605−609.
[10] M. Al-Mukhtar, J. H. Holloway, E. G. Hope, G. J. Schrobilgen, *J. Chem. Soc., Dalton Trans.* **1991**, 2831−2834.
[11] P. A. W. Dean, R. J. Gillespie, R Hulme, D. A. Humphreys, *J. Chem. Soc.* **1971**, 341−346.
[12] P. A. W. Dean, R. J. Gillespie, R. Hulme, *J. Chem. Soc.* **1969**, *17*, 990−991.
[13] K. O. Christe, W. Maya, *Inorg. Chem.* **1969**, *8*, 1253−1257.
[14] K. O. Christe, *Inorg. Chem.* submitted for publication, oral communication.
[15] R. Minkwitz, F. Neikes, *Inorg. Chem.* submitted for publication.
[16] Y. Imai, K. Aida, *Bull. Chem. Soc. Jpn.* **1981**, *54*, 3323−3326.
[17] G. M. Sheldrick, *SHELXTL PLUS An Integrated System for Solving, Refining and Displaying Structures from Diffration Data*. University of Göttingen, Germany **1987**.
[18] A. L. Spek, The *EUCLID* Package, in: *Computational Crystallography*, (Ed.: D. Sayre), Claredon Press, Oxford, 528, **1982**.
[19] Y. Le Page, *J. Appl. Crystallogr.* **1987**, *20*, 264−269.
[20] M. Nardelli, *Comput. Chem.* **1983**, *7*, 95−98.
[21] Crystallographic data (excluding structure factors) for the structures reported in this paper have been deposited with the Cambridge Crystallographic Data Centre as supplementary publication no. CCDC-134938 [$(CH_3)_3AsH^+As_2F_{11}^-$] and -134939 [$(CH_3)_3AsH^+SbF_6^-$]. Copies of the data can be obtained free of charge on application to CCDC, 12 Union Road, Cambridge CB2 1EZ, UK [Fax: (internat.) + 44(1223)336-033, E-mail: deposit@ccdc.cam.ac.uk].
[22] A. Bondi, *J. Phys. Chem.* **1964**, *68(3)*, 441−451.
[23] R. Minkwitz, C. Hirsch, *Z. Anorg. Allg. Chem.,* in press.

[24] R. Minkwitz, T. Hertel, U. Zachwieja, *Z. Naturforsch*. **1997**, *52b*, 1185−1190.
[25] *Tables of Interatomic Distances and Configuration in Molecules and Ions*, Special Publication No. 11, The Chemical Society, London, **1958**.
[26] R. Minkwitz, S. Schneider, M. Seifert, H. Hartl, *Z. Anorg. Allg. Chem.* **1996**, *622*, 1404−1410.
[27] R. Minkwitz, S. Schneider, H. Preut, *Angew. Chem.* **1998**, *110*, 510−512; *Angew. Chem. Int. Ed.* **1998**, *37*, 494−496.
[28] R. Minkwitz, H. Preut, M. Seifert, D. Lamek, *Z. Naturforsch.* **1993**, *48b*, 1241−1247.
[29] R. Minkwitz, S. Reinemann, *Z. Anorg. Allg.* **1999**, *625*, 121−125.
[30] H. Willner, F Aubke, *Angew. Chem*. **1997**, *109*, 2507−2530.
[31] R. A. Zingarro, A. Merijinian, *Inorg. Chem.* **1964**, *3*, 580−584
[32] W. J. C. Dyke, W. J. Jones, *J. Chem. Soc.* **1930**, 2426−2430.
[33] Werner, A., Dissertation, University of Dortmund, Germany, **1988**.
[34] L. Bayersdorfer, R. Minkwitz, J. Jander, *Z. Anorg. Allg. Chem.* **1972**, *392*, 137−142.

Received April 16, 1999
[I99135]

Synthesis and Characterisation of a Dioxo-μ-Oxo Molybdenum Dimer: An Unusual case of a μ-Oxo Conformational Equilibrium

Henri Arzoumanian,*[a] Robert Bakhtchadjian,[a] Giuseppe Agrifoglio,[b] Heinz Krentzien,[b] and Jean-Claude Daran[c]

Keywords: Molybdenum / μ-Oxo / Conformational equilibrium / X-ray diffraction / NMR spectroscopy

A new thiocyanatomolybdenum(VI) dioxo-μ-oxo complex dimer bearing a 4,4′-di-*tert*-butyl-2,2′-bipyridine ligand (**2**) is shown to exist in the crystal cell unit as a meso (Mo-O–Mo angle of 180°) and d,l, pair (Mo–O–Mo angle of 155.7°). These conformers are in equilibrium in solution and have been observed clearly by ^{1}H NMR spectroscopy.

Introduction

Oxygenated complexes of transition metals are of utmost importance in catalytic oxidation processes. Among these complexes, metal-oxo species, found in a wide range of systems from metal-oxide surfaces to metalloenzymes, have received considerable attention.[1]

Two structural features describe the metal-oxo function: terminal-oxo (M=O) and bridging μ-oxo (M−O−M). Although most studies deal implicitly with the former type, binuclear oxo-metal entities have been shown to be key intermediates in many catalytic systems. For example, among the innumerable compounds known with μ-oxo ligands, ruthenium oxo-bridged complexes have already been shown to be active in the catalytic oxidation of water.[2] Later, high valent bimetallic μ-oxo species of Cu and Fe were found to take part in C−H bond activation.[3] Very recently some novel Co^{III} and Ni^{III} bis(μ-oxo) complexes have been isolated and characterized foreboding high oxidation capability.[4]

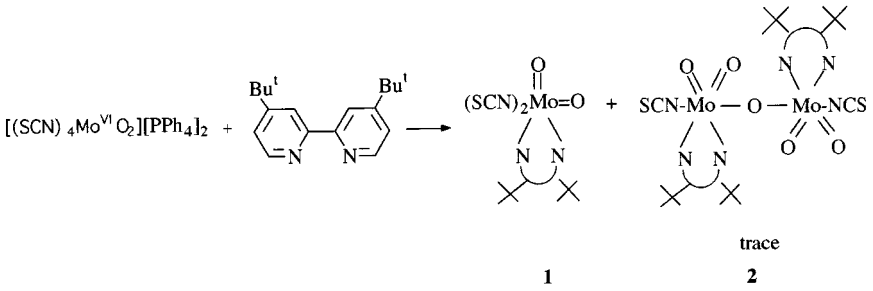
Polyoxometallates are well-defined anionic, oligomeric metal oxides featuring both terminal and bridging oxygen atoms. Among these, vanadium, molybdenum and tungsten anions are the most common and are often involved in oxidation reactions.[5]

This paper presents the synthesis and characterization of a molybdenum(VI) complex bearing both terminal and bridging oxo ligands which, in solution, exhibits a new μ-oxo conformational equilibrium which can be clearly observed by ^{1}H NMR spectroscopy.

Results and Discussion

In the course of a study of reactions of tetrathiocyanatodioxomolybdenum(VI) anions with substituted bipyridines,[6] a molybdenum(VI) dioxo complex (**1**) exhibiting exceptional oxidizing ability was obtained with the bulky 4,4′-di-*tert*-butyl-2,2′bipyridine (Scheme 1). This reaction was accompanied by the formation of traces of a μ-oxo dimer (**2**) thought to arise by an oxo-ligand redistribution process.

The remarkable properties of **1**[7] prompted us to develop a better method to synthesize compound **2** directly in order

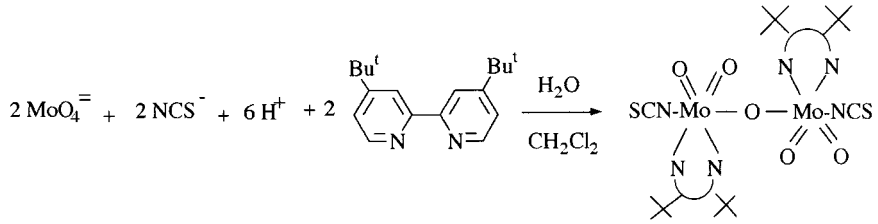


Scheme 1

to test it also as a potential oxygen atom transfer agent. One plausible route consisted of replacing one thiocyanato group of **1** by a hydroxyl group, followed by dehydration. This reaction appeared to work but was not optimized. Instead a less cumbersome biphasic system was chosen starting directly from an aqueous solution of molybdate and thiocyanate, with the bipyridine in dichloromethane (Scheme 2).

[a] UMR 6516 du CNRS, ENSSPICAM, Faculté des Sciences St Jérôme,
Avenue Escadrille Normandie Niemen, F-13397 Marseille, France
Fax: (internat.) + 33-4910/27776
E-mail: arzou@u3pic105.u-3mrs.fr
[b] Universidad Central de Venezuela, Caracas, Venezuela
[c] Laboratoire de Chimie de Coordination, UPR-CNRS 8241, 205 Route de Narbonne, F-31077 Toulouse, France

 © WILEY-VCH Verlag GmbH, D-69451 Weinheim, 1999 1434−1948/99/1212−2255 $ 17.50+.50/0



Scheme 2

The product was obtained as a light yellow crystalline solid exhibiting, in the IR spectrum, the characteristic bands for both terminal and μ-oxo functions, and those for the thiocyanato and the bipyridyl ligands.[8] An X-ray

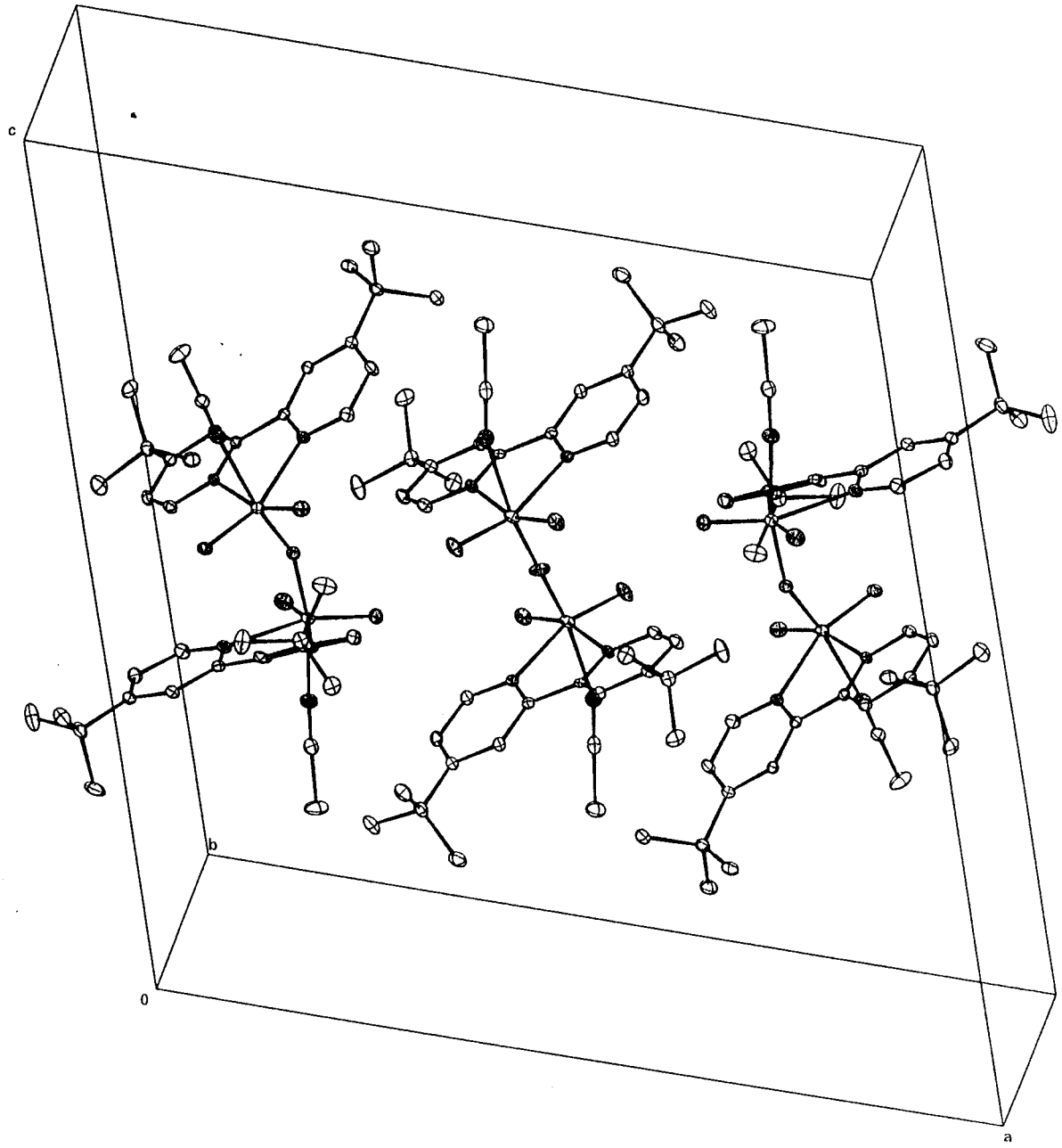


Figure 1. Unit cell of **2**

analysis of a suitable crystal confirmed these observations and, furthermore, uncovered an interesting feature − the cell unit was found to contain three molecules of **2** (see Figure 1), one with a Mo−O−Mo angle of 180°, with a center of symmetry located at the μ-oxo oxygen atom, and two others with a Mo−O−Mo angle of 155.7°, each totally unsymmetrical, with each of the four nitrogen-containing heterocycles in a different environment.

A closer examination reveals that these two molecules are enantiomers and, thus, the unit cell consists of a d,l, pair ($\mathbf{2}_{d,l,}$) and a meso isomer ($\mathbf{2}_{meso}$). Taken separately (see Figures 2 and 3) each molecule exhibits some interesting features; as expected, the two dioxo moieties are trans to each other in both the meso and the d,l conformers, however the thiocyanato ligands are slightly bent away from the molybdenum dioxo plane in the $\mathbf{2}_{meso}$ conformer whereas they appear to be slightly bent towards the molybdenum dioxo plane in the case of the d,l pair $\mathbf{2}_{d,l}$. The bipyridyl moiety is always coplanar with the molybdenum dioxo plane; however, all four nitrogen heterocycles are equivalent in the $\mathbf{2}_{meso}$ conformer, whereas they are found in different environments in the $\mathbf{2}_{d,l}$ conformer, with the consequence of having, in this case, four tertiary butyl groups also in a different environment. Finally the metal to oxygen bond lengths, either terminal or μ-oxo, have values similar to those reported for related compounds.[1a] Such a mixture of conformers in the solid state, although not unique, is quite scarce and could conceivably be rationalized by constraining stacking forces during crystallization.[9]

Much more unexpected and unusual, however, was the ^{1}H NMR spectrum in solution. Contrary to the NMR spectrum of the monomeric dioxomolybdenum(VI) complex **1** which exhibits, as expected, the pattern for the bipyridyl moiety of three signals in the aromatic region and a singlet for the *tert*-butyl group, the spectrum of **2** ($CDCl_3$ 25°C) showed five well-separated "sets" of bipyridyl signals. One integrating for 44% and the other four, of equal intensity, integrating for a total of 56% (Figure 4).

The presence of five anisotropically different tertiary butyl groups was also observed; one major signal integrating for 44% and four others, of equal intensity, integrating jointly for 56%. The interpretation of such spectra can only be done in terms of an unprecedented μ-oxo conformational equilibrium between the $\mathbf{2}_{meso}$ conformer, with four equal pyridyl rings (44%), and the $\mathbf{2}_{d,l}$ conformer, with four distinct pyridyl rings resonating at different fields due to their anisotropically different environment (56%). The presence of such an equilibrium was confirmed in various ways. First, changing the NMR solvent from $CDCl_3$ to CD_2Cl_2 resulted in a slightly, but significantly, different ratio of conformers ($\mathbf{2}_{meso}/\mathbf{2}_{d,l}$ = 44:56 in $CDCl_3$ and 55:45 in CD_2Cl_2). Second, a variable temperature NMR spectroscopic analysis added supporting evidence: upon lowering the temperature (from 25°C to −60°C) the signals sharpened, but the $\mathbf{2}_{meso}/\mathbf{2}_{d,l}$ ratio varied only very slightly (44:55 at 25°C vs 40:60 at −60°C). This is not unexpected for a conformeric mixture close to 50:50. However, upon increasing the temperature (from 25°C to 130°C), the signals corresponding to the four distinct pyridyl ring hydrogens of the $\mathbf{2}_{d,l}$ conformer quickly broaden, collapse and then slowly coalesce with the signals of $\mathbf{2}_{meso}$. The energy barrier estimated from this analysis is about 75 kJ·mol^{-1}. It is noteworthy that upon cooling the solution back to 25°C the original spectrum was obtained thus indicating the presence

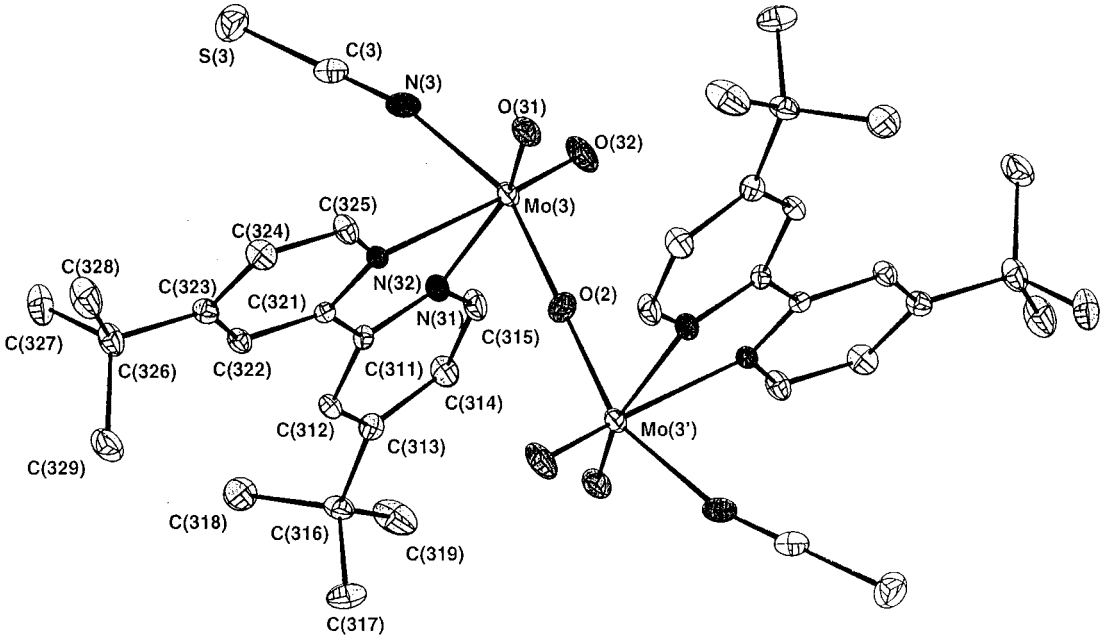


Figure 2. X-ray crystal structure of $\mathbf{2}_{meso}$; selected bond lengths [Å] and angles [°]: Mo(3)−O(2) 1.876(1), Mo(3)−O(31) 1.694(2), Mo(3)−O(32) 1.701(2), Mo(3)−N(3) 2.112(3), Mo(3)−N(31) 2.317(3), Mo(3)−N(32) 2.307(2); Mo(3)−O(2)−Mo(3′) 179.99, N(31)−Mo(3)−N(32) 68.91(9), O(31)−Mo(3)−O(32) 106.3(1), O(31)−Mo(3)−N(32) 92.1(1), O(32)−Mo(3)−N(32) 158.7(1), O(2)−Mo(3)−N(31) 81.14(7), O(2)−Mo(3)−N(32) 84.65(6), O(2)−Mo(3)−N(3) 156.39(8), N(3)−Mo(3)−N(32) 75.6, O(32)−Mo(3)−N(3) 92.5(1)

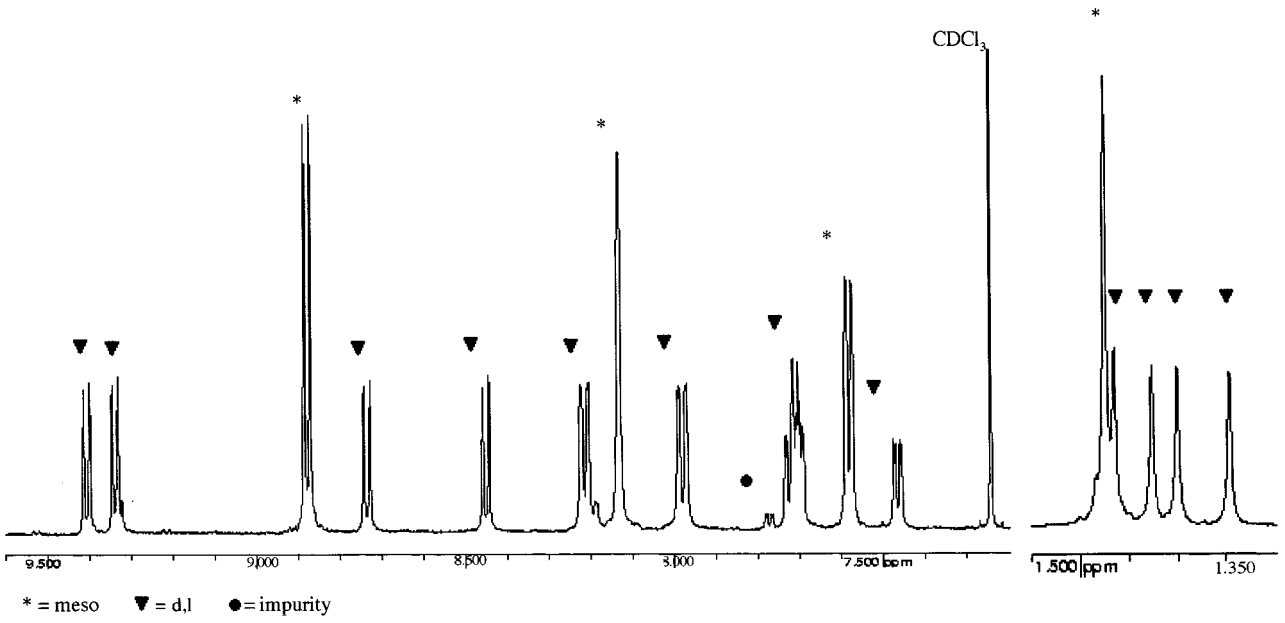


Figure 4. ^{1}H NMR spectrum of **2** (400 MHz, $CDCl_3$, −50°C)

of an equilibrium. The ^{95}Mo NMR spectrum also supports the presence of two distinct species in solution; it exhibits two resonances at −45 and −57 ppm. The relatively small difference between these two signals indicates that the electronic density at the metallic center is very slightly perturbed in going from one conformer to the other, es-

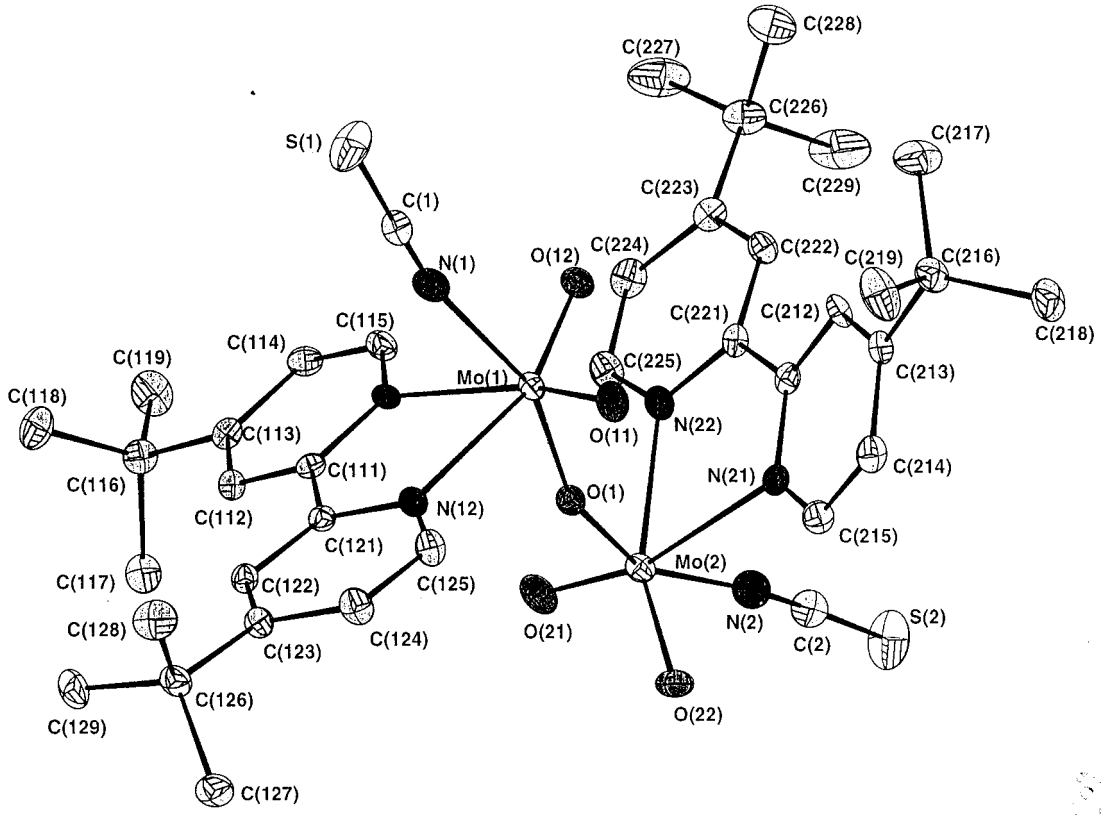


Figure 3. X-ray crystal structure of $\mathbf{2}_{d,l}$; selected bond lengths [Å] and angles [°]: Mo(1)−O(1) 1.892(2), Mo(2)−O(1) 1.895(2), Mo(1)−O(11) 1.696(2), Mo(2)−O(21) 1.690(2), Mo(1)−O(12) 1.700(2), Mo(2)−O(22) 1.703(2), Mo(1)−N(1) 2.139(3), Mo(2)−N(2) 2.098(3), Mo(1)−N(11), 2.313(3), Mo(2)−N(21) 2.329(3); Mo(1)−O(1)−Mo(2) 155.7(1), O(11)−Mo(1)−N(1) 92.0(1), O(21)−Mo(2)−N(2) 94.1(1), O(1)−Mo(1)−N(11) 80.59(9), O(1)−Mo(2)−N(21) 78.13(9), N(1)−Mo(1)−N(11) 80.9(1), N(2)−Mo(2)−N(21) 82.6(1), O(1)−Mo(2)−N(22) 84.53(9), 86.67(9), Mo(1)−N(1)−C(1) 164.2(3), Mo(2)−N(2)−C(2) 174.2(3), Mo(1)−N(11)−C(111) 120.4, Mo(2)−N(21)−C(211) 117.6

pecially if one compares the value of + 63 ppm for compound **1**.[6]

Although the interconversion between $\mathbf{2}_{meso}$ and $\mathbf{2}_{d,l}$ can easily be described, based on molecular models, by a bending of the Mo−O−Mo bond accompanied by a slight tilting of the bipyridyl moiety, the real reason for the existence of *two* stable conformers remains unclear. Studies are in progress to establish which oxygen atom in **2** is most prone to be transferred to a substrate. The dynamics of this μ-oxo conformational equilibrium, although never directly observed before, could be implied in numerous isomerisation processes of oxometallate anions and, in turn, give a better insight to the more general oxygen atom transfer reactions.

Experimental Section

Synthesis of 2: To an aqueous solution (30 mL) containing Na_2MoO_4 (0.50 g, 2.4 mmol) and KSCN (0.92 g, 9.6 mmol) was slowly added 9.6 mL of 1N HCl (9.6 mmol). The resulting yellow solution was stirred for 15 min followed by the addition of a CH_2Cl_2 solution (60 mL) containing 4,4′-di-*tert*-butyl-2,2′-bipyridine (0.64 g, 2.4 mmol). Vigorous stirring for an additional 30 min resulted in a yellow organic layer which was separated, dried and evaporated to give **2** (0.95 g, 76%) as a yellow solid. Recrystallization (−15°C) from CH_2Cl_2/*n*-hexane (2:1) afforded light yellow needles (m.p. > 180°C). − IR(KBr): $\tilde{\nu}$ = 2065 (-NCS), 940, 905 (= O), 775 (-O-) cm^{-1}. − ^1H NMR (400 MHz, $CDCl_3$, 21°C, TMS): δ = 1.36 (s), 1.41 (s), 1.43 (s), 1.48 (s), 7.45 [d, *J*(H-H) = 6 Hz], 7.57 [dd, *J*(H-H) = 6 Hz, 1.6 Hz], 7.69 [t, *J*(H-H) = 6 Hz], 7.98 [d, *J*(H-H) = 6 Hz], 8.14[d, *J*(H-H) = 1.6 Hz], 8.24[d, *J*(H-H) = 6 Hz], 8.51[d, *J*(H-H) = 6 Hz], 8.78 [d, *J*(H-H) = 6 Hz], 8.89 [d, *J*(H-H) = 6 Hz], 9.36 [d, *J*(H-H) = 6 Hz], 9.406 [d, *J*(H-H) = 6 Hz]. − ^{13}C NMR (101MHz, $CDCl_3$, 21°C, TMS): δ = 30.2, 30.3, 35.8, 118.6, 118.8, 119.1, 123.7, 124.1, 124.3, 124.5, 148.9, 149.7, 150.0, 150.5, 151.0, 151.7, 152.8, 165.4, 165.7. − ^{95}Mo NMR (26MHz, $CDCl_3$, 21°C, Na_2MoO_4, pH = 11): δ = −45, −57. − $C_{38}H_{48}Mo_2N_6O_5S_2$ (924): calcd. C 49.35, H 5.23, N 9.09; found C 49.35, H 5.15, N 9.23.

X-ray Crystal Structure Analysis of 2: $C_{28}H_{72}Mo_3N_9O_7.5S3{\cdot}CH2Cl2$ (M_r = 1472.2); needle (0.44 × 0.12 × 0.12 mm); monoclinic, space group $P2_1/c$; *a* = 21.407(3), *b* = 15.054(2), *c* = 21.512(3)Å, β = 106.94(1)°, *V* = 6631(1)Å^3, *Z* = 4, F(000) = 2992, ρ_{calcd} = 1.475Mg/m^3, μ(Mo-K_α) = 7.708cm^{-1}; IPDS Stoe diffractometer, graphite monochromator, Mo-K_α radiation (λ = 0.71073), detector distance = 80 mm, ø scan (0 < ø < 250 deg), 3.9 < 2Θ < 48.7°, numerical (X-SHAPE) absorption method,[10] number of reflexions collected = 52657, number of unique reflexions = 10360, merging factor *R*(int) = 0.0543, reflexions used ($I_0 > 1\sigma(I_0)$) = 6188, *R* = 0.0288, R_w = 0.0313, Chebyschev weighting scheme,[11] GOF = 1.088, 746 variable parameters. The structure was solved by direct methods (SIR 92)[12] and refined with least-squares procedures on Fobs. The calculations were carried out with a CRYSTALS package program.[13] The drawing was realized with CAMERON[14] and the atomic scattering factors were taken from International Tables.[15] Crystallographic data (excluding structure factors) for the structure reported above have been deposited at the Cambridge Crystallographical Data Centre as supplementary publication no.CCDC 113727. Copies of the data can be obtained free of charge on application to CCDC, 12 Union Road, Cambridge, CB2 1EZ, UK. [Fax: (internat.) + 44-1223/336033; E-mail: deposit@ccdc.cam.ac.uk].

[1] [1a] R. H. Holm, *Chem. Rev.* **1987**,1401. − [1b] F. Bottomley, L. Sutin, *Adv. Organometal. Chem*. **1998**, *28*, 339. − [1c] R. H. Holm, *Coord. Chem. Rev.* **1990**, *100*, 183. − [1d] H. Arzoumanian, *Coord. Chem. Rev.* **1998**, *178−180 (part 1)*, 191.

[2] [2a] S. W. Gersten, G. J. Samuels, T. J. Meyer, *J. Am. Chem. Soc*. **1882**, *104*, 4029. − [2b] J. A. Gilbert, D. S. Eggleston, W. R. Murphy, D. A. Geselowitz, S. W. Gersten, D. J. Hodgson, T. J. Meyer, *J. Am. Chem. Soc*. **1985**, *107*, 3855. − [2c] K. Honda, A. J. Frank, *J. Chem. Soc, Chem. Commun*. **1984**, 1635. − [2d] P. S. Lay, W. H. F. Sasse, *Inorg. Chem*. **1985**, *24*, 4707. − [2e] J. P. Collins, J. P. Sauvage, *Inorg. Chem*. **1986**, *25*, 135. − [2f] J. Desilvestro, D. Duonghong, M. Kleijn, M. Gratzel, *Chimia* **1985**, *4*, 102. − [2g] F. P. Rotzinger, S. Munavalli, P. Comte, J. K. Hurst, M. Gratzel, F. J. Pern, A. J. Frank, *J. Am. Chem. Soc* **1987**, *109*, 6619.

[3] [3a] S. Mahapatra, J. A. Halfen, E. C. Wilkinson, G. Pan, C. J. Cramer, L. Que Jr.,W. B. Tolman, *J. Am. Chem. Soc*. **1995**, *117*, 8865. − [3b] J. A. Halfen, S. Mahapatra, E. C. Wilkinson, S. Kaderli, V. G Young Jr., L. Que Jr., A. D. Zuberbühler, W. B. Tolman, *Science* **1996**, *271*, 1397. − [3c] S. Mahapatra, J. A. Halfen, E. C. Wilkinson, G. Pan, X. Wang, V. G. Young Jr., C. J. Cramer, L. Que Jr., W. B. Tolman, *J. Am. Chem. Soc*. **1996**, *118*, 11555. − [3d] S. Mahapatra, J. A. Halfen, W. B. Tolman, *J. Am. Chem. Soc*. **1996**, *118*, 11575. − [3e] A. P. Cole, D. E. Root, P. Mukherjee, E. I. Solomon,T. D. P. Stack, *Science* **1996**, *273*, 1848. − [3f] W. B. Tolman, *Acc. Chem. Res.*, **1997**, *30*, 227. − [3g] S. Mahapatra, V. G Young Jr., S. Kaderli, A. D. Zuberbühler, W. B. Tolman, *Angew. Chem. Int. Ed*. **1997**, *36*, 130. − [3h] S. Mahapatra, S. Kaderli, A. Llobet, Y. M. Neuhold, T. Palanché, J. A. Halfen, V. G Young Jr., T. A. Kaden, L. Que Jr. A. D. Zuberbühler, W. B. Tolman, *Inorg. Chem*. **1997**, *36*, 6343. − [3i] J. L. Dubois, P. Mukherjee, A. M. Collier, J. M. Mayer, E. I. Solomon, B. Hedman, T. D. P. Stack, K. O. Hodgson, *J. Am. Chem. Soc*. **1997**, *119*, 8578. − [3j] V. Mahadevan, Z. Hou, A. P. Cole, D. E. Root, T. K. Lal, E. I. Solomon, T. D. P. Stack, *J. Am. Chem. Soc*. **1997**, *119*, 11996. − [3k] S. Itoh, H. Nakao, L. M. Berreau, T. Kondo, M. Komatsu, M. Fukuzumi, *J. Am. Chem. Soc*. **1998**, *120*, 2890. − [3l] Y. Dong, L. Que Jr., K. Kauffmann, E. Münck, *J. Am. Chem. Soc*. **1995**, *117*, 11377. − [3m] Y. Dong, H. Fujii, M. P. Hendrich, R. A. Leising, G. Pan, C. R. Randall, E. C. Wilkinson, Y. Zang, L. Que Jr., B. J. Fox, K. Kauffmann, E. Münck, *J. Am. Chem. Soc*. **1995**, *117*, 2778. − [3n] L. Que Jr., Y. Dong, *Acc. Chem. Res.*, **1996**, *29*, 190. − [3o] L. Que Jr*., J. Chem. Soc., Dalton Trans.* **1997**, 3933. − [3p] C. Kim, Y. Dong, L. Que Jr., *J. Am. Chem. Soc*. **1997**, *119*, 3635. − [3q] E. C. Wilkinson, Y. Dong, Y. Zang, H. Fujii, R. Fraczkiewicz, G. Fraczkiewicz, R. S. Czernuszewicz, L. Que Jr., *J. Am. Chem. Soc*. **1998**, *120*, 955.

[4] S. Hikichi, M. Yoshizawa, Y. Sasakura, M. Akita, Y. Moro-oka, *J. Am. Chem. Soc*. **1998**, *120*, 10567.

[5] [5a] I. A. Weinstock, *Chem. Rev.* **1998**, *98*, 113. − [5b] I. V. Kozhevnikov, *Chem. Rev.* **1998**, *98*, 171.

[6] H. Arzoumanian, G. Agrifoglio, H. Krentzien, *New J. Chem*. **1996**, *20*, 699.

[7] H. Arzoumanian, L. Maurino, G. Agrifoglio, *J. Mol. Cat. A: Chem*. **1997**, *117*, 471.

[8] N. W. Nugent, J. M. Mayer, *Metal-Ligand Multiple Bonds*, Wiley, New York, **1998**, 113−119.

[9] C. Giacovazzo, H. L. Monaco, D.Viterbo, F. Scordari, G. Gilli., G. Zanotti and M. Catti. *Fundamentals of Crystallography* (Ed.: C. Giacovazzo), Oxford Science Publications, **1991**.

[10] X-SHAPE, Crystal Optimisation for Numerical Absorption, revision 1.01, Stoe & Cie Gmbh, **1996**.

[11] E. Prince, *Mathematical Techniques in Crystallography*, Springer-Verlag, Berlin, **1992**.

[12] A. Altomare, G. Cascarano, C. Giacovazzo, A. Guagliardi, M. C. Burla, G. Polidori, M. Camalli, *J. Appl. Cryst*. **1994**, *27*, 435.

[13] D. J. Watkin, C. K. Prout, J. R. Carruthers, P. W. Betteridge, *Crystals Issue 10*, Chemical Crystallography Laboratory, University of Oxford, Oxford, **1996**.

[14] D. J. Watkin, C. K. Prout, L. J. Pearce, *Cameron*, Chemical Crystallography Laboratory, University of Oxford, Oxford, **1996**.

[15] *International Tables for X-Ray Crystallography*; Vol. C, Kynoch Press, Birmingham, U.K. **1992**.

Received April 16, 1999
[I99138]

Selective Lithium Complexation by Photoactive Aza-Cages Bearing the Anthracene Function

Mario Ciampolini,[b] Mauro Formica,[a] Vieri Fusi,*[a] Andrè Saint-Mauricec,[c] Mauro Micheloni,*[a] Nicoletta Nardi,[b] Roberto Pontellini,[a] Fernando Pina,*[c] Paolo Romani,[a] Anna Maria Sabatini,[b] and Barbara Valtancoli[b]

Keywords: Macrocycles / Lithium / Fluorescence / Cryptands / Coordination

Three aza-cages with the anthracene-containing photoactive groups **L1**, **L2**, and **L3** have been synthesized. All compounds are able to selectively encapsulate a lithium ion and solid complexes have been isolated. The formation equilibria have been investigated by UV/Vis and ^{1}H, ^{13}C and ^{7}Li NMR spectroscopic techniques. The fluorescence emission of both free ligands and lithium complexes have been investigated. Results indicate that the CHEF (chelation enhancement of the fluorescence) effect obtained by lithium coordination exits although lower than that occurring upon full protonation.

Introduction

The design of new ligands with the ability to bind metal ions, and capable of recognizing the presence of these ions in solution, is of great interest in a wide variety of chemical fields ranging from the study of transport processes in biological systems to industrial and technological applications.[1−6] Macrocyclic compounds are a particularly attractive class of ligands and have thus received much attention in the last few years.[7−10] The development of new synthetic strategies has led to the real possibility of merging theory and experimentation in the design of chemical compounds with specific properties. Lithium is one target of this research and much effort has been dedicated to the synthesis of ligands able to bind it.[11−12] The interest in this ion is due to its significant role not only in industrial applications, but also in medical and biological chemistry.[13][14] Lithium salts have, in fact, been extensively and successfully used in the treatment of manic depression and other neurological and psychiatric disorders.[15][16] Lithium also exhibits antiviral activity against DNA-type viruses.[17] However, the use of lithium salts as drugs is limited by their side effects and toxicity. The mechanisms by which Li^{+} is involved in biological systems are unknown. No natural molecules are known, nor have any synthetic receptors been prepared, that would be selective enough to preferentially bind lithium ions at physiological concentration. Furthermore, easy determination of the lithium level in patients, using selective reactants would be very important. The elucidation of synthetic strategies and coordination properties of Li^{+} should lead to an improved understanding of its biological activity and to the design of better ligands as ionophores for it.

So far, fluorescence methods have proved to be useful in assaying metal ions. The design of molecular systems which combine binding ability and photochemical properties, displaying photoactive features, therefore have a great attraction.[18−20] One of the most used sensors is the anthracene moiety, which presents high fluorescence that could be affected by the molecular surroundings. In this context, three new aza-criptands bearing the anthracene function and characterized by different macrocyclic molecular topologies were synthesized (Chart I). All the ligands present a small three-dimensional cavity able to selectively encapsulate the lithium ion; the aromatic sensor is situated in an external position outside the macrocyclic cavity but in such a way that its optical properties could be perturbed by metal complexation.

The main aim of the present work was to investigate the possibility of employing these anthracene-functionalized aza-cages as selective lithium receptors and chromoionophores. The acid-base behavior of such ligands and their lithium complexation, performed by potentiometric titration, are reported, along with ^{13}C, ^{1}H and ^{7}Li NMR spectroscopic analysis.

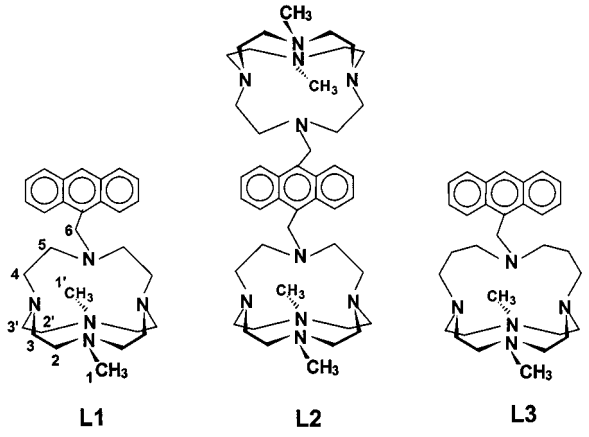
Results and Discussion

Synthesis

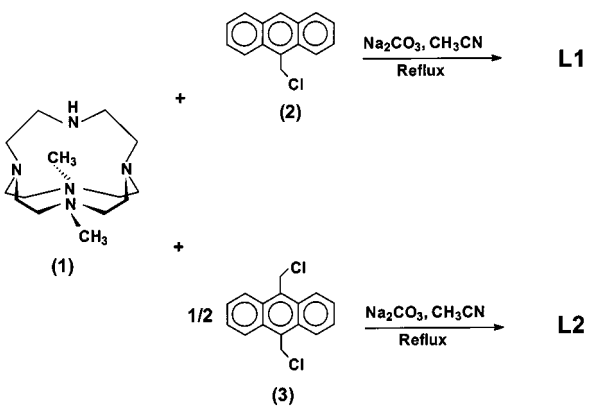
All three of the new ligands contain the macrocycle 1,7-dimethyl-1,4,7,10-tetraazacyclododecane; nevertheless, the synthesis was carried out with two different methods, one to obtain **L1** and **L2**, and the other for **L3**. Scheme 1 shows the synthetic pathways for **L1** and **L2**, which were obtained starting from the previously synthesized aza-cage **1** as already reported.[21] To obtain **L1**, compound **1** was functionalized in acetonitrile with the chloroanthracene derivative **2** in an equimolar ratio in the presence of sodium car-

[a] Institute of Chemical Sciences, University of Urbino, P.za Rinascimento 6, I-61029 Urbino, Italy
E-mail: vieri@chim.uniurb.it
[b] Department of Chemistry, University of Florence, Florence, Italy
[c] Departamento de Química, Centro de Tecnologia Química e Biologica, Universidade Nova de Lisboa, Quinta da Torre, 2825 Monte da Caprarica, Lisboa, Portugal

 © WILEY-VCH Verlag GmbH, D-69451 Weinheim, 1999 1434−1948/99/1212−2261 $ 17.50+.50/0

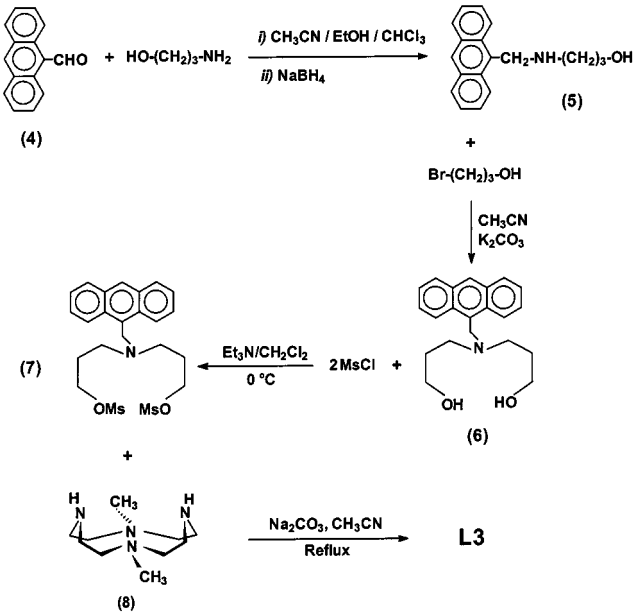


bonate as a base. The reaction gave **L1** in almost quantitative yield and the ligand was transformed into its diperchlorate salt by adding $HClO_4$ during the purification step. The same procedure was adopted to achieve **L2** but, in this case, the dichloroanthracene derivative **3**[22] was added to functionalize cryptand **1** in acetonitrile and employing a molar ratio of 1:2; again, cryptand **L2** was obtained as its perchlorate salt in good yield.



Scheme 1. Synthetic pathway for **L1** and **L2**

Ligand **L3**, however, was synthesized from the tetraaza monocyclic base **8**[23] (see Scheme 2) by reaction with the synthesized dimesyl-*N*-(9-methylanthracene)dipropanolamine (**7**); the complete synthetic pathway is depicted in Scheme 2. Aldehyde **4** was reacted with 3-aminopropanol in a solvent mixture of acetonitrile/ethanol/chloroform in the classic formation of a Schiff base. This compound was not isolated, but the crude solid obtained after evaporating the solvent was reduced in absolute ethanol with sodium borohydride to give compound **5**. This compound was transformed into the dialcohol **6** by *N*-alkylation with 3-bromo-propanol in acetonitrile in the presence of K_2CO_3 as base. Attempts to perform direct dialkylation of 9-aminomethylanthracene with two equivalents of 3-bromopropanol to give the dialcohol **6** failed. The methylsulfonyl derivative **7** was obtained using standard methods. Reaction of **7** with the base **8** in the presence of Na_2CO_3, a modification of Richman and Atkins′ method gave, after purification, the cryptand **L3**, in quite good yield. The need to use different synthetic pathways to obtain the three ligands is due to the different properties of the precursor cryptand. In fact, while **1** is present as a free amine in alkaline solution, the analogous cryptand with two propylenic (instead of all ethylenic) chains behaves as a proton-sponge and is present as a mono-protonated species in solution; its *N*-alkylation with the compound **2** is thus impeded.



Scheme 2. Synthetic pathway for **L3**

It was possible to isolate the monoprotonated species of the ligand **L1** as its perchlorate salt by extraction of an alkaline suspension of the ligand in chloroform and subsequent precipitation with hexane. The same treatment for **L3** afforded the free amine. The synthesis of the lithium complexes was carried out by reaction of an excess of LiOH with the ligands in methanol at room temperature. The complexes can be easily isolated after removal of the methanol by extracting the solid mixture with chloroform. It should be noted that the Li^+ complexes of all the ligands under investigation are very soluble in organic solvents (*ca.* 0.1 M).

Absorption and Emission Spectroscopy

Absorption Spectra

The absorption spectra in aqueous solution of the compounds **L1**, **L2** and **L3** present an identical pattern, being characterized by a structured absorption band in the near UV/Visible region of the spectrum. This absorption band can be immediately assigned to the anthracene chromophore. The shape of the absorption spectra of these compounds is only slightly affected by the pH of the solution, allowing us to conclude that the absorption of light by the anthracene moiety occurs independently of the protonation state of the cavity.

Fluorescence Emission

Excitation of acidic aqueous solutions of the compounds **L1**, **L2** and **L3** into the first singlet state gives rise to a fluorescence emission band which can also be attributed to the anthracene fluorophore. In contrast to the absorption, the fluorescence emission spectra are very dependent on the protonation state of the cavity (see Figure 1). Determination of the protonation constants of these compounds is difficult due to their low solubilities which preclude direct potentiometric measurements. Moreover, as the pH-dependent variations in the absorption spectra are very small, the error associated is large.

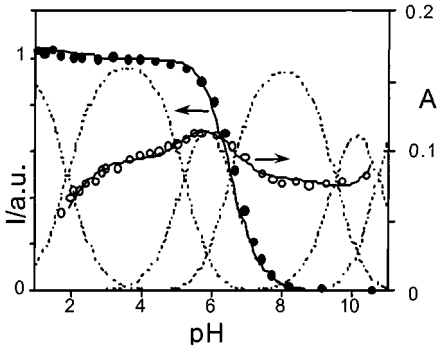


Figure 1. Fluorescence emission (•) and absorption (o) titration, distribution curves of the species (- -), for the compound **L2** in aqueous solution, 5×10^{-5} M, $\lambda_{exc} = 398$ nm, $\lambda_{em} = 429$ nm, absorbance at 323 nm

A fitting to the experimental curves was also performed and the protonation constants thus obtained are reported in Table 1. The best situation was obtained in the case of the compound **L2**. For **L1**, a protonation constant, $pK_a = 6.5$, can only be obtained with sufficient accuracy from fluorescence emission. The most interesting characteristic of the fluorescence emission titration curves of **L1**, **L2** and **L3** is the quenching effect that occurs in the pH 6−9 region. This type of quenching has been described before in chemosensors possessing aromatic units linked to a polyaza chain, and was attributed to an intramolecular electron-transfer process from the deprotonated amine to the excited aromatic moiety.[24] According to the structure of the compounds **L1**, **L2** and **L3** it is likely that quenching occurs upon deprotonation of the apical nitrogen functionalized by the photoactive group, which is the one in the best position to carry out the electron-transfer process. This interpretation is also compatible with the protonation constants obtained by means of the fluorescence data (see Table 1). The log *K* values are very similar for **L1** and **L2** ($pK_a = 6.5$ and 6.8, respectively) and higher for **L3** ($pK_a = 8$). Analyzing these values we propose that the apical nitrogen is involved in the protonation only from the second protonation step of each cage subunit. Furthermore, while **L1** and **L2** have the same cavity, in the case of **L3** it is larger, and the apical nitrogen more basic, because the charge repulsion of the other protonated nitrogen is smaller.

Potentiometric and NMR Spectroscopic Studies

Due to the presence of the hydrophobic anthracene fragment, the ligands do not show good solubility in aqueous solution. However, in the case of **L2**, and given its topology, it was possible to measure some protonation constants by direct potentiometric methods. The measurements performed in aqueous solution (0.15 M Me_4NCl ionic medium) are summarized in Table 1. The similar log *K* values for the addition of the third and fourth proton, together with the ligand topology, suggest that, in the $[H_4\mathbf{L2}]^{4+}$ species, both amine subunits bind two protons. This hypothesis is also confirmed from a comparison of the log K_2 values obtained for **L1** by spectrophotometric methods. Furthermore the basicity constants evaluated with the two different method are in good agreement.

Table 1. Protonation constants of **L1**, **L2** and **L3** (log K) in aqueous solution (298 ± 0.1 K, I = 0.15 M NMe_4Cl)

Reaction	**L1**	**L2**	**L3**
$L + H^+ = HL^+$	Insoluble	10.7[a]	Insoluble
$HL^+ + H^+ = H_2L^{2+}$	6.5[a]	9.5[a]	8.0[a]
$H_2L^{2+} + H^+ = H_3L^{3+}$	–	6.8[a] – 7.0 (1)[b, c]	6.0[a]
$H_3L^{3+} + H^+ = H_4L^{4+}$	–	6.2[a] – 6.4 (1)[b]	1.9[a]
$H_4L^{4+} + H^+ = H_5L^{5+}$	–	1.9[a] – 1.8(1)[b]	–

[a] From spectrophotometric measurements. – [b] From potentiometric measurements. – [c] Values in parentheses are standard deviations to the last significant figure.

From a ^1H and ^{13}C NMR spectroscopic analysis, it was possible to obtain additional information about the chemical properties of **L1** and of the other two ligands. As explained in the "synthesis" section, the free ligand **L1** could not be obtained. The ^1H NMR spectrum of the $[H\mathbf{L1}]^+$ species, recorded in $CDCl_3$, is shown in Figure 2a. The spectrum also shows a peak at 10.84 ppm assignable to the deshielded acidic proton. Upon addition of H_2O or CH_3OH to the chloroform solution, the signal at 10.85 ppm did not disappear, indicating a slow exchange on the NMR time scale with the labile protons of the solvent. However, the resonance did disappear when D_2O or CD_3OD were added. The chemical shift, together with the experimental evidence, suggests that the proton is stabilized inside the macrocyclic cavity by a strong hydrogen-bonded network with the amine functions. The other resonance in the ^1H NMR spectrum of the $[H\mathbf{L1}]^+$ species in CD_3OD (Figure 2b) is similar to that recorded in $CDCl_3$. It did not change even when a solution of NaOD in methanol was added, thus proving that the acidic proton cannot be removed in alcoholic alkaline solutions. Under the conditions described above, and as reported in the experimental section, **L2** and **L3** are present as free amines. Again, the chemical shift of the ^{13}C NMR resonance shows a C_{2V} time-averaged symmetry for **L2** and **L3** in $CDCl_3$ solution. In conclusion, **L2** and **L3** show a lesser basicity in alcoholic solution than **L1** in the first protonation step as evidenced by spectrophoto-

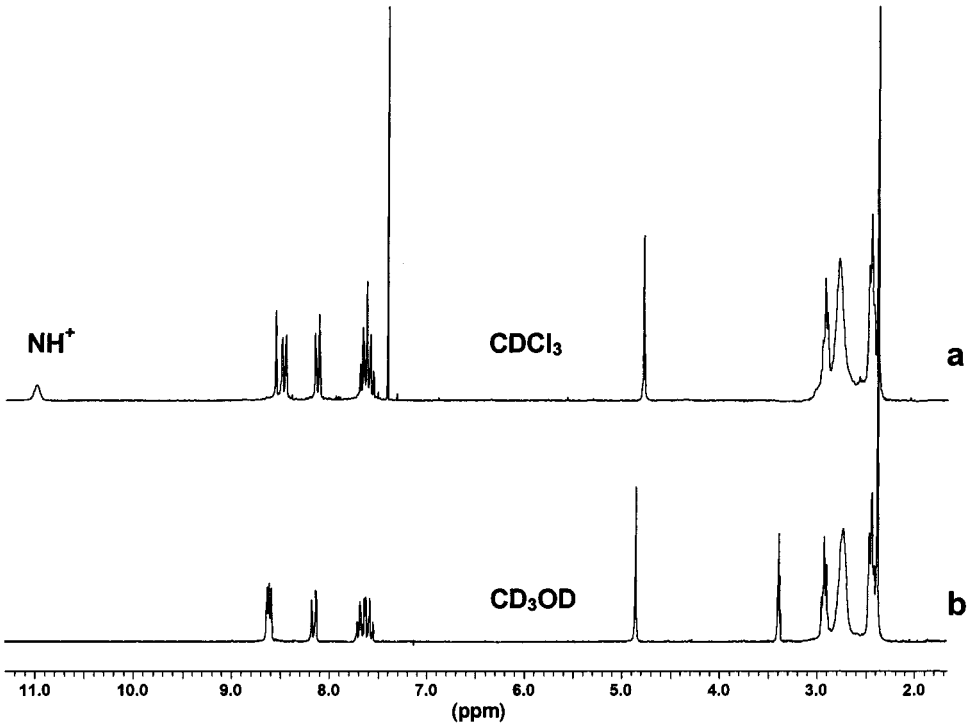


Figure 2. ^{1}H NMR spectra of $[HL1]^{+}$ species in $CDCl_3$ (a); in CD_3OD (b)

metric and NMR spectra, this could be ascribed to the larger three-dimensional cavity for **L3**, but other factors like the inductive effect of the methylanthracene group could be important to explain the different behavior of **L1** vs. **L2** and **L3**.

Lithium Complexation

The coordination of the alkaline metal ions by ligands **L1**, **L2** and **L3** was studied by ^{1}H, ^{13}C and ^{7}Li NMR spectroscopic techniques in alcoholic solution. With ^{1}H and ^{13}C

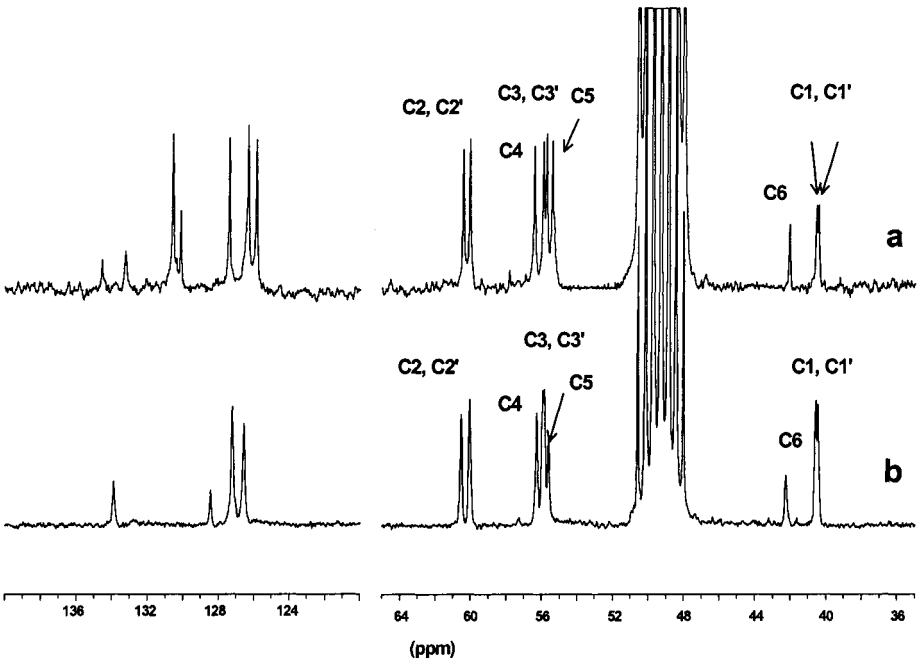


Figure 3. ^{13}C NMR spectra in CD_3OD of: $[LiL1]^{+}$ complex (a); $[Li_2L2]^{2+}$ complex (b)

spectroscopy as diagnostic techniques, no evidence was found for complex formation with sodium and potassium ions in alcoholic solution. Instead, all the ligands readily bound the smaller Li^+ ion and the solid complexes were isolated as reported in the experimental section. These solid compounds are soluble in organic solvents such as $CDCl_3$ and their ^7Li NMR spectra present a sharp peak, shifted downfield with respect to the free ion. Li^+ coordination is clearly shown by the ^{13}C and ^7Li NMR spectra of a methanol solution containing **L1**, **L2** or **L3** and Li^+ in the presence of a base. In all three cases, upon the addition of an excess of Li^+ to an alkaline solution of the ligands, the ^7Li NMR spectrum shows two sharp peaks, one due to the free lithium ion and the other, shifted downfield, due to the complexed lithium ion. The changes in chemical shift of the complexed ion are 3.29, 3.26, and 1.39 ppm with respect to the solvated ion, for **L1**, **L2**, and **L3**, respectively. The simultaneous presence of the two peaks denotes a slow exchange of the complexed lithium ion with the free ion on the NMR time scale. These chemical shifts were conserved when the solvent was changed to CD_3CN or $CDCl_3$, and are the same as observed by solubilizing the solid complexes.

The solvent-independence of the ^7Li chemical shift and the slow exchange on the NMR time scale between free and bound lithium indicate that the ion is encapsulated inside the macrocyclic cavity and thus quite isolated from the medium. Comparison of the ^{13}C NMR spectra of the free amines with those of the lithium complexes, as shown for example in the case of **L1** (Figure 3a), revealed that the complexation of the Li^+ ion produces a decrease in molecular symmetry, on the NMR time scale, for all three ligands. In fact while the free ligand **L1** presents fourteen peaks for a C_{2v} time-averaged symmetry, the spectrum of the complex presents seventeen peaks indicating a C_s symmetry. Analyzing the spectrum of the complex, the element of symmetry lost is the plane passing through the bridgehead nitrogen and the nitrogen atom having the anthracene group, while the other plane, which contains the methylated nitrogen atoms, is preserved.

For ligand **L1** the coordination of the lithium ion leads to removal of the acidic proton resonance at 10.85 ppm which is not present in the ^1H NMR spectrum of the complex. Ligand **L2** is able to bind two lithium ions but only one resonance was obtained in the ^7Li spectra, with the same value as for the **L1** complex. The aliphatic resonances for the $[Li_2\mathbf{L2}]^{2+}$ complex (Figure 3b), show the same environment around the lithium ions from the two subunits, and are similar to those found for the $Li\mathbf{L1}^+$ species (Figure 3a). These experimental data provide evidence that, for **L2**, only one ion is lodged in the subunit and the coordination around the ion is equal in the two subunits on the NMR time scale and similar to that of the **L1** complex. It is noteworthy that these spectral features do not change even in the presence of a large excess of Na^+. In other words, lithium complexation is not influenced by the presence of the Na^+ ion, even at high concentrations, indicating that ligands **L1**–**L3** are able to discriminate completely between Li^+ and Na^+. Such selectivity is related to the small dimensions of the macrobicyclic cavity, in which the larger Na^+ cannot be encapsulated.

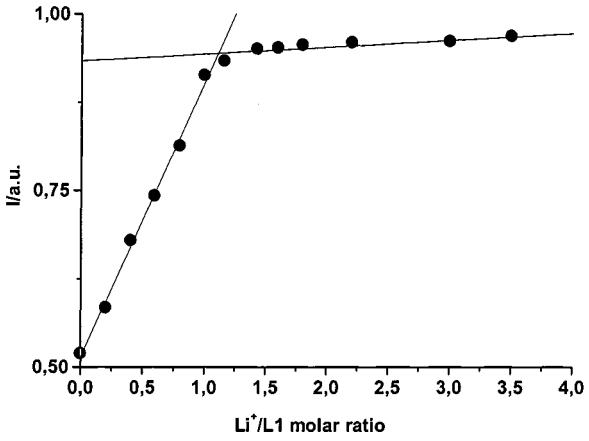


Figure 4. Variation of the fluorescence emission intensity of **L1** (1×10^{-5} M) in methanol with tetrabutylammonium hydroxide, at λ_{em} = 412 nm, as a function of Li^+/**L1** molar ratio

Sensing Lithium

A plot of the fluorescence emission variations that occur upon addition of different concentrations of lithium to an alkaline methanol solution of compound **L1**, at 25°C is shown in Figure 4. A similar behavior was also observed for **L2**. The fit of the experimental data points is in good agreement with a Li^+:L ratio of 1:1 for the lithium complex of **L1** and a 2:1 ratio for **L2**. The trend of chelation enhancement of the fluorescence (CHEF) effect, obtained by coordination of Li^+ into the cavity by increasing the lithium equivalents, shows that the complexes are completely formed by the addition of one or two equivalents of ion for **L1** and **L2,** respectively. The spectrum of the lithium complexes is quite similar to the sensor in the absence of lithium, but is approximately twice as intense and slightly shifted to the red, as shown in Figure 5 for the $[Li\mathbf{L3}]^+$ species.

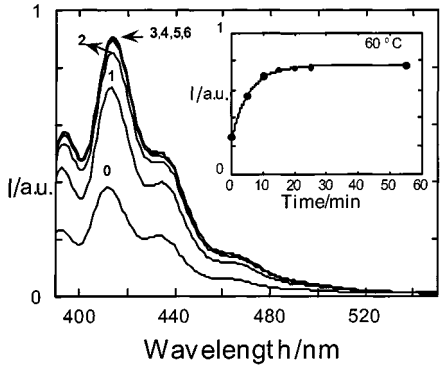


Figure 5. Spectral variations of the fluorescence emission of **L3** in methanol with addition of tetrabutylammonium hydroxide (0); immediately after addition of lithium excess(1); after 5 min (2); 10 min (3); 15 mim (4); 20 min (5); 55 min (6). λ_{exc} = 380 nm. Inset variation of the fluorescence emission intensity at λ_{em} = 420 nm as a function of time

In this case the coordination of the lithium is time-dependent but the equilibrium state is reached in less than twenty minutes at 60°C. In the equilibrium state, a behavior similar to that of the previous two ligands was also observed for **L3**. The CHEF effect obtained by coordination of lithium into the cavity is, however, much lower than that occurring upon full protonation. A possible explanation for this behavior is the fact that coordination of the metal has only a small influence on the quenching mechanism.

Conclusions

The molecular topology of the polyamines **L1**-**L3** is characterized by the presence of both a three-dimensional cavity and an anthracene moiety. It has been shown that **L1** behaves as a "proton sponge" in alcoholic solution. All three ligands are able to selectively bind the lithium ion in alcoholic solution while the other alkali metal ions are not complexed. Such remarkable selectivity is due to the small dimensions of the macrocyclic cavity, in which alkali metals larger than lithium cannot be encapsulated. The solid lithium complexes, which were isolated and fully characterized, are soluble in organic solvents such as $CDCl_3$. **L2** forms a binuclear lithium complex with each ion lodged in a single cage subunit. The photochemical properties of the ligands are strongly influenced by protonation; moreover, on lithium complexation an increase in the fluorescence emission of the sensor, relative to that of the free ligand, is observed in methanol. Unfortunately, the presence of the anthracene moiety renders the ligands insoluble in aqueous solutions preventing the complexation of the lithium in this medium.

Experimental Section

General: ^1H, ^{13}C and ^7Li NMR spectra were recorded on a Bruker AC-200 instrument, operating at 200.13, 50.33 or 77.78 MHz, respectively. ^1H NMR peak positions are reported relative to HOD (4.75 ppm), dioxane was used as reference standard in ^{13}C NMR spectra (δ = 67.4 ppm). For the spectra recorded in $CDCl_3$, the peak positions are reported relative to TMS. ^7Li NMR peaks are reported relative to free $LiClO_4$. ^1H-^1H and ^1H-^{13}C correlation experiments were performed to assign the signals. Solvents and starting material were used as purchased.

Spectrophotometric and Spectrofluorimetric Titrations: Absorption spectra were recorded on a Perkin–Elmer Lambda 6 spectrophotometer and fluorescence emission on a SPEX F111 Fluorolog spectrofluorimeter. HCl and tetrabutylammonium hydroxide were used to adjust the pH values, which were measured on a Metrohm 713 pH meter. The acidification constants were obtained from a fit of the theoretical equations to the experimental titration data by least-squares analysis using the bracketing technique.

Potentiometric Measurements: All potentiometric measurements were carried out in 0.15 M Me_4NCl at 298.1 ± 0.1 K, in the pH range 2.5–10, using the fully automatic equipment that has been already described.[25] The acquisition of the emf data was performed with the PASAT computer program. The electrode was calibrated as a hydrogen concentration probe by titrating known amounts of HCl with CO_2-free Me_4NOH solutions and determining the equivalent point by Gran's method,[26] which gives the standard potential E° and the ionic product of water K_w. At least three measurements were performed. The HYPERQUAD computer programs were used to process the potentiometric data and calculate the protonation constants.[27]

Compounds **1**, **3**, **8** were synthesized as reported in the literature.[21–23] Compounds **2** and **4** were purchased from Aldrich Chemical Co. All reactions were carried out under an inert atmosphere.

Caution: Perchlorate salts of organic compounds are potentially explosive; these compounds must be handled with great caution!

(1,7,-Dimethyl-1,4,7,10,15-pentaazabicyclo-[5.5.5]-heptadecan-15-yl)-9-methylanthracene Diperchlorate (L1·2HClO$_4$): Cryptand **1** (0.54 g, 2 mmol) and Na_2CO_3 (0.64 g, 6 mmol) were suspended in refluxing CH_3CN (100 mL). To this mixture, a solution of **2** (0.68 g, 3 mmol) in 50 mL of acetonitrile was added dropwise in 2 h. After the addition was completed, the suspension was refluxed for 2 h. The mixture was evaporated to dryness under vacuum, and the solid obtained was suspended in chloroform. The organic layer was filtered and solvents removed under vacuum to give a yellow solid, which was dissolved in ethanol. The suspension was filtered to eliminate the excess of **2,** and then treated with 65% perchloric acid to give the diperchlorate salt as a yellowish solid. Yield: 0.85 g (90%). – $C_{29}H_{43}Cl_2N_5O_8$: calcd. C 52.73, H 6.56, N 10.60; found C 52.6, H 6.6, N 10.5.

L1·HClO$_4$: The monoprotonated species was obtained by suspending the diperchlorate salt in 1 M NaOH aqueous solution and extraction of the resulting suspension with chloroform. The volume of the organic phase was reduced and the H**L1**$^+$ was precipitated with hexane in almost quantitative yield. – $C_{29}H_{42}ClN_5O_4$: calcd. C 62.18, H 7.56, N 12.50; found C 62.0, H 7.5, N 12.3. – MS (ESI) m/z = 461 $[M + H]^+$. – ^1H NMR ($CDCl_3$): δ = 2.24 (s, 6 H) 2.30 (t, 4 H), 2.64 (bb, 16 H), 2.78 (t, 4 H), 4.65 (s, 2 H), 7.46 (m, 4 H), 7.97 (d, 2 H), 8.32 (d, 2 H), 8.41 (s, 1 H), 10.84 (bb, 1 H). – ^{13}C NMR ($CDCl_3$): δ = 43.5, 49.4, 50.2, 52.9, 53.0, 53.5, 124.2, 125.1, 126.5, 128.3, 128.4, 129.5, 130.9, 131.3.

(1,7,-Dimethyl-1,4,7,10,15-pentaazabicyclo-[5.5.5]-heptadecan-15-yl)-9,10-dimethylanthracene Tetraperchlorate (L2·4HClO$_4$): Cryptand **1** (1.1 g, 4 mmol) and Na_2CO_3 (1.3 g, 12 mmol) were suspended in refluxing CH_3CN (100 mL). To this mixture, was added a solution of **3** (0.55 g, 2 mmol) in CH_3CN (100 mL) dropwise in 2 h. After the addition was completed, the suspension was refluxed for 3 h. The mixture was vacuum evaporated, and the solid obtained was suspended in chloroform. The organic layer was filtered and vacuum evaporated to give a yellow solid. The solid was dissolved in a minimum amount of chloroform and chromatographated on neutral alumina with CH_2Cl_2/MeOH mixture (10:1) as eluent. The eluted fractions were collected and evaporated to dryness to obtain a yellow solid. The solid was further purified by dissolving it in ethanol and the solution treated with 65% perchloric acid to give the tetraperchlorate salt in almost quantitative yield. Yield: 1.65 g (72%). – $C_{44}H_{76}Cl_4N_{10}O_{16}$: calcd. C 46.24, H 6.70, N 12.26; found C 46.0, H 6.6, N 12.1. – MS (ESI) m/z = 742 $[M + H]^+$. – ^1H NMR (D_2O, pD = 3):δ = 2.56 (s, 12 H) 2.69 (t, 8 H), 2.87 (bb, 32 H), 2.95 (t, 8 H), 4.70 (s, 4 H), 7.39 (d, 4 H), 8.26 (d, 4 H), 10.68 (bb, 2 H). – ^{13}C NMR (D_2O, pD = 3):δ = 42.2, 49.1, 50.6, 53.0, 53.2, 53.7, 127.1, 128.9, 129.4, 136.2.

***N*-(Anthracene-9-methyl)-aminepropanol (5):** Reagent **4** (20.6 g, 0.10 mol) was added together with 3-amino-propanol to 150 mL of $CH_3CN/CH_3CH_2OH/CHCl_3$ mixture (5:15:70). This solution was kept stirred at room temperature for 24 h and then vacuum evapo-

rated to give a yellow solid, which was dissolved in hot absolute ethanol (500 mL). The solution was cooled at room temperature and then added of $NaBH_4$ (8 g, 0.2 mol). The suspension obtained was refluxed for 4 h and then vacuum evaporated. The solid was suspended in water (120 mL) and extracted with chloroform (3×100 mL). The organic phase was dried over anhydrous Na_2SO_4, and its volume vacuum reduced. Ethyl ether was added to this solution to complete precipitation of a yellow solid, which was recrystallized from hot CH_3CN. Yield: 20.5 g (77%). − $C_{18}H_{19}NO$: calcd. C 81.48, H 7.22, N 5.28; found C 81.6, H 7.3, N 5.2. − M.p., 79−81°C. − ^{1}H NMR ($CDCl_3$): δ = 1.82 (m, 2 H), 2.41 (t, 2 H), 3.38 (t, 2 H), 3.51 (b, 1 H), 4.26 (s, 2 H), 4.76 (b, 1 H) 7.47 (m, 4 H), 8.04 (d, 2 H), 8.29 (d, 2 H), 8.44 (s, 1 H). − ^{13}C NMR ($CDCl_3$): δ = 28.5, 48.5, 53.6, 62.4, 124.0, 124.8, 126.0, 128.6, 129.7, 131.1, 131.3.

***N*-(Anthracene-9-methyl)-dipropanolamine (6):** A sample of **5** (5.3 g, 0.02 mol) was added with 3-bromine-propanol (2.8 g, 0.02 mol) and K_2CO_3 (3.0 g, 0.022 mol) to 80 mL of CH_3CN. This mixture was slowly warmed to 50°C and kept with stirring over a period of 5 h. After this period the suspension was refluxed for 2 h. The reaction mixture was allowed to cool to room temperature and then 100 mL of 0.1 mol dm^{-3} NaOH aqueous solution added. The extracted organic phase, was dried over sodium sulfate. The solvent was removed under reduced pressure to obtain a solid which was recrystallized from CH_3CN. Yield 3.6 g (56%). − $C_{21}H_{25}NO_2$: calcd. C 77.98, H 7.79, N 4.33; found C 78.2, H 7.9, N 4.3. − ^{1}H NMR ($CDCl_3$): δ = 1.79 (p, 4 H), 2.76 (t, 4 H), 3.48 (t, 4 H), 3.62 (b, 2 H), 4.53 (s, 2 H), 7.51 (m, 4 H), 8.01 (d, 2 H), 8.37 (d, 2 H), 8.45 (s, 1 H). − ^{13}C NMR ($CDCl_3$): δ = 28.7, 51.4, 52.5, 62.2, 124.3, 125.0, 126.2, 128.9, 129.3, 131.3, 131.4.

***N*-(Anthracene-9-methyl)-*O*-dimesyl-dipropanolamine (7):** A sample of **6** (3.2 g, 0.01 mol) and triethylamine (5.1 g, 0.05mol) in 60 mL of anhydrous dichloromethane was cooled at −5°C. To this solution was added dropwise over a period 3 h, with stirring, a solution of methanesulfonil chloride (2.9 g, 0.025 mol). The reaction mixture was kept to −5°C for further 30 min and then was allowed to warm up to room temperature. The resulting suspension was washed twice with a 0.1 M NaOH aqueous solution and then with water. The organic phase was dried over anhydrous Na_2SO_4 and evaporated to dryness to obtain **7** as a yellowish solid. Yield: 4.4 g (91%). − $C_{23}H_{29}NO_6S_2$: calcd. C 57.60, H 6.09, N 2.92; found C 57.7, H 6.1, N 3.0. − ^{1}H NMR ($CDCl_3$): δ = 1.52 (m, 4 H), 2.71 (t, 4 H), 2.83 (s, 6 H), 3.38 (s, 2 H), 4.25 (t, 4 H), 7.53 (dd, 2 H), 7.72 (dd, 2 H), 8.07 (d, 2 H), 8.33 (dd, 2 H), 8.59 (s, 1 H). − ^{13}C NMR ($CDCl_3$): δ = 24.3, 37.5, 39.7, 54.1, 59.7 123.1, 125.7, 127.2, 129.0, 129.5, 129.9, 132.2, 132.8.

1,7,-Dimethyl-1,4,7,10,16-pentaazabicyclo-[5.5.7]-nonadecan-16-yl-9-methylanthracene (L3): To a refluxing suspension of **8** (1.8 g, 0.009 mol) and Na_2CO_3 (5.3 g, 0.05 mol) in 150 mL of acetonitrile was added, over a period of 6 h, a solution of **7** (4.3 g, 0.009 mol) in 100 mL of acetonitrile. The reaction mixture was maintained at reflux for a further 2 h. After the mixture was cooled to room temperature, the resulting suspension was filtered and evaporated under reduced pressure to give a yellowish solid, which was dissolved in a minimum amount of $CHCl_3$ and chromatographed on neutral alumina with an eluent mixture of $CHCl_3/CH_3OH$ (100:5). The eluted fractions were collected and evaporated to dryness to obtain a yellow solid. The solid was further purified by dissolving it in ethanol and the solution treated with 65% perchloric acid to give the diperchlorate salt in almost quantitative yield. Yield: 3.6 g (58%). − $C_{31}H_{45}N_5$: calcd. C 76.34, H 9.30, N 14.36; found C 76.2, H 9.3, N 14.3. − MS FAB *m/z* = 489 $[M + H]^+$. − ^{1}H NMR ($CDCl_3$): δ = 1.56 (m, 4 H) 2.52 (s, 6 H), 2.58 (t, 4 H), 2.66 (t, 4 H), 2.92 (m, 16 H), 4.48 (s, 2 H) 7.43 (m, 4 H), 7.95 (d, 2 H), 8.36 (s, 1 H), 8.40 (d, 2 H). − ^{13}C NMR ($CDCl_3$): δ = 25.2, 41.5, 50.6, 51.4, 53.2, 54.8, 55.5, 124.7, 124.8, 125.6, 127.5, 129.1, 130.0, 131.1, 131.3.

Preparation of the Complexes. [LiL1]ClO_4 (9): A solution of LiOH (10 mg, 0.44 mmol) and $NaClO_4 \cdot H_2O$ (100 mg, 0.7 mmol) in 15 mL of methanol was added to a solution of **L1**· $HClO_4$ (56 mg, 0.1 mmol) in methanol (15 mL). The reaction mixture was stirred for 15 min and then evaporated to dryness. The yellow solid was suspended in 20 mL of $CHCl_3$, and the mixture filtered to separate the inorganic excess and the organic solution dried over Na_2SO_4. On addition of cyclohexane (25 mL) a yellow precipitated formed, yield 41 mg (73%). − $C_{29}H_{41}ClLiN_5O_4$: calcd. C 61.53, H 7.30, N 12.37; found C 61.4, H 7.4, N 12.3. − MS (ESI) *m/z* = 467 $[Li\mathbf{L1}]^+$. − ^{13}C NMR ($CDCl_3$):δ = 39.8, 39.9, 41.0, 54.3, 54.4, 54.5, 55.1, 58.6, 58.9, 124.0, 124.7, 125.1, 126.5, 129.0, 129.2, 131.3, 132.8.

[Li_2L2](ClO_4)$_2$ (10): This compound was synthesized from **L2**·2$HClO_4$ (47 mg, 0.05 mmol) following the same procedure reported for **9** giving **10** as a yellowish solid, yield 36 mg (76%). − $C_{44}H_{72}Li_2Cl_2N_{10}O_8$: calcd. C 55.40, H 7.61, N 14.68; found C 55.5, H 7.6, N 14.8. − MS (ESI) *m/z* = 854 ($Li_2\mathbf{L2}ClO_4^+$). − ^{13}C NMR ($CDCl_3$):δ = 40.1, 40.3, 42.2, 55.4, 55.6, 55.8, 55.1, 60.2, 60.8, 126.3, 127.1, 128.4, 134.0.

[LiL3]ClO_4 (11): This compound was synthesized from **L3**·2$HClO_4$ (34 mg, 0.05 mmol) following the same procedure reported for **9** giving **11** as a yellowish solid, yield 36 mg (76%). − $C_{31}H_{45}ClLiN_5O_4$: calcd. C 62.67, H 7.63, N 11.79; found C 62.5, H 7.6, N 11.7. MS (ESI) *m/z* = 495 $[Li\mathbf{L3}]^+$. − ^{13}C NMR ($CDCl_3$):δ = 26.4, 44.4, 52.2, 53.0, 53.5, 54.4, 54.9, 126.1, 126.2, 126.6, 129.7, 130.1, 130.3, 132.8, 134.2.

Acknowledgments

Support for this research by MURST (Ministero per l'Università e la Ricerca Scientifica e Tecnologica) and CNR (Consiglio Nazionale delle Ricerche) is gratefully acknowledged. A. Saint-Mauricec thanks Fundatio para Ciencia e Tecnologia (grant).

[1] M. N. Hughes, *The Inorganic Chemistry of the Biological Processes*, Wiley, New York, **1981**.
[2] [2a] C. J. Pedersen, *J. Am. Chem. Soc.* **1967**, *89*, 7017. − [2b] J. M. Lehn, *Pure Appl. Chem.* **1977**, *49*, 857. − [2c] D. J. Cram, J. M. Cram, *Science* **1984**, *183*, 4127.
[3] Y. L. Agnus, *Copper Coordination Chemistry: Biochemical and Inorganic Perspective*, Adenine Press, New York, **1983**.
[4] Tabushi and K. Yamamura, *Top. Curr. Chem.* **1983**, *113*, 145.
[5] [5a] F. P. Schmidtchen, *J. Am. Chem. Soc.* **1986**, *108*, 8249. − [5b] H. M. Colquhoun, J. F. Stoddart and D. J. Williams, *Angew. Chem. Int. Ed. Engl.* **1986**, *25*, 487. − [5c] B. Dietrich, J. P. Kintzinger, J. M. Lehn, B. Metz and A. Zahidi, *J. Phys. Chem.* **1987**, *91*, 6600. − [5d] D. J. Cram, Angew. Chem. Int. Ed. Engl. **1988**, 27, 1009.
[6] J. M. Lehn, *Angew. Chem. Int. Ed. Engl.* **1988**, *27*, 89.
[7] R. M. Izatt, J. J. Christensen, *Synthetic Multidentate Macrocyclic Ligands*, Academic Press, New York, **1978**.
[8] L. F. Lindoy, *The Chemistry of Macrocyclic Ligands Complexes*, Cambridge University Press, **1989**.
[9] A. Bianchi, M. Micheloni, P. Paoletti, *Coord. Chem Rev.* **1991**, *101*, 17.
[10] [10a] J. S. Bradshaw, *Aza-Crown Macrocycles*, Wiley, New York, **1993**. − [10b] R. M. Izatt, K. Pawlak, J. S. Bradshaw and R. L. Bruening, *Chem. Rev.* **1991**, *91*, 1721.
[11] [11a] G. W. Gokel, *Crown Ethers and Cryptands (Monographs in Supramolecular Chemistry)* (Ed.: J. F. Stoddart), The Royal Society of Chemistry, Cambridge, **1992**. − [11b] A. F. Sholl and I. O. Sutherland, *J. Chem. Soc., Chem. Commun.* **1992**, 1252.

[12] [12a] M. Ciampolini, N. Nardi, B. Valtancoli and M. Micheloni, *Coord. Chem. Rev.* **1992**, *120*, 223. – [12b] A. Bencini, V. Fusi, C. Giorgi, M. Micheloni, N. Nardi, B. Valtancoli, *J. Chem. Soc., Perkin Trans. 2* **1996**, 2297. – [12c] M. Formica, V. Fusi, M. Micheloni, R. Pontellini, P. Romani, *Coord. Chem. Rev.* **1999**, *184*, 347 and refs. therein.
[13] D. Tosteson, *Sci. Am.* **1981**, *244,* 164.
[14] J. .H. Lazarus, K. J. Collard, *Endocrine and Metabolic Effects of Lithium*, Plenum, New York, **1986**.
[15] R. O. Bach, *Med. Hypotheses* **1987**, *23*, 157.
[16] D. R. Lide, *Handbook of Chemistry and Physics*, CRC Press, New York, **1997**.
[17] R. P. Hanzlik, *Inorganic Aspects of Biological and Organic Chemistry*, Academic Press, New York, **1976**.
[18] U. Olsher, R. M. Izatt, J. S. Bradshaw, N. K. Dalley, *Chem. Rev.* **1991**, *91*, 137.
[19] [19a] A. W. Czarnik, Flurescent Chemosensors for Ion and Molecule Recognition, ACS, Washington, DC, **1993**. – [19b] R. A. Bissel, A. P. de Silva, H. Q. N. Gunaratne, P. L. M. Lynch, G. E. M. Maguire, C. P. McCoy, K. R. A. S. Sandanayake, *Top. Curr. Chem.* **1993**, *168*, 223.
[20] C. Bazzicalupi, A. Bencini, M. Ciampolini, V. Fusi, M. Micheloni, N. Nardi, I. Razzolini, B. Valtancoli, *Supramolecular Chemistry* **1996**, *7*, 61.
[21] M. Ciampolini, P. Dapporto, M. Micheloni, N. Nardi, P. Paoletti, F. Zanobini, *J. Chem. Soc., Dalton Trans.* **1984**, 1357.
[22] M. W. Miller, R. W. Amidon, P. O. Tanwney, *J. Am Chem Soc.* **1955**, *77*, 2845.
[23] A. Bencini, A. Bianchi, A. Borselli, S. Chimichi, M. Ciampolini, P. Dapporto, M. Micheloni, N. Nardi, P. Paoli, B. Valtancoli, *Inorg. Chem.* **1990**, *29*, 3282.
[24] [24a] R. Bergonzi. L. Fabbrizzi, M. Licchelli, C. Mangano, *Coord. Chem. Rev.* **1998**, *170*, 31. – [24b] A. P. De Silva, R. A. D. D. Rupasinghe, *Chem. Commun.* **1996**, 1660. – [24c] M. A. Bernardo, J. A. Guerrero, E. Garcia-España, S. V. Luis, J. M. Llinares, F. Pina, J. A. Ramirez, C. Soriano, *J. Chem. Soc., Perkin Trans 2* **1996**, 2335.
[25] A. Bianchi, L. Bologni, P. Dapporto, M. Micheloni, P. Paoletti, *Inorg. Chem.* **1984**, *23*, 1201.
[26] [26a] G. Gran, *Analyst* **1952**, *77*, 661. – [26b] F. J. Rossotti, H. Rossotti, *J. Chem. Educ.* **1965**, *42*, 375.
[27] P. Gans, A. Sabatini, A. Vacca, *Talanta* **1996**, *43*, 1739.

Received May 3, 1999
[I99153]

Synthesis, Structure, Spectroscopy, and Magnetism of Unique Propeller-Type Linear Trinuclear Cu^{II} Complexes with In-situ Prepared Formamidine Ligands

Gerard A. van Albada,[a] Petra J. van Koningsbruggen,[c] Ilpo Mutikainen,[b] Urho Turpeinen,[b] and Jan Reedijk*[a]

Keywords: Copper / Trinuclear complexes / Formamidines / Magnetism

Three new copper(II) linear trinuclear compounds are reported, all of which were synthesized in-situ, with the general formula $[Cu_3(L)_4](CF_3SO_3)_2(Y)_x$, where L is the dehydronated ligand: *N*,*N*′-bis(pyridine-2-yl)formamidine (abbreviated as Hpdf), *N*,*N*′-bis(pyrimidine-2-yl)formamidine (abbreviated as Hpmf) and *N*,*N*′-bis(5-methylpyridine-2-yl)formamidine (abbreviated as Hmpdf), Y = EtOH or H_2O and x = 0.5–1.5. The compounds were characterized by X-ray diffraction, IR, LF, and EPR spectroscopy and by magnetic susceptibility down to 4 K. The structure of the compound $[Cu_3(pmf)_4](CF_3SO_3)_2(H_2O)_{1/2}$ was determined by X-ray crystallography; it was found to crystallise in the triclinic space group *P*–1 with *a* = 8.529(5), *b* = 15.760(5), *c* = 19.639(5) Å, α = 101.793(5), β = 101.263(5), γ = 102.389(5)°, *Z* = 2. The structure [Cu–Cu–Cu angle 174.96(11)°] consists of four nearly flat molecules of the ligand, which contribute to the propeller-type structure around the Cu–Cu–Cu axis. A strong antiferromagnetic interaction between the Cu^{II} ions is observed with calculated *J* values, based on the Hamiltonian $H = -2J(\mathbf{S}_1\cdot\mathbf{S}_2 + \mathbf{S}_2\cdot\mathbf{S}_3) - 2J'\cdot\mathbf{S}_1\cdot\mathbf{S}_3$, of –174(1) cm^{-1}, –120(1) cm^{-1}, and –167(1) cm^{-1} for the compounds studied with L = pdf, pmf, and mpdf, respectively. These values are in agreement with an *S* = 1/2 ground state below temperatures of 120–160 K.

Introduction

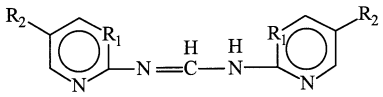
Dinuclear and polynuclear exchange-coupled copper(II) complexes have been extensively studied, although the number of trinuclear compounds investigated magnetically and structurally is still quite limited.[1][2]

Dinuclear systems are well documented not only because of their interesting magnetic interactions,[1] but also because of their relevance for bioinorganic model systems for copper in enzymes.[3] The theory for dinuclear systems is adequate for interpreting the relationship between the isotropic exchange constant and the structural parameters, but linear trinuclear compounds have been discussed to a much lesser extent, mainly due to the fact that the number of such copper(II) compounds is relatively small.

The majority of the known linear trinuclear Cu^{II} compounds of which the structures have been characterised by X-ray crystallography contain an oxygen bridge[4][5] or a mixed (N, Cl, O) bridge[2,6,7] between the Cu^{II} atoms, and only a few contain a nitrogen bridge. In fact a very small number of compounds contain a CuN_{4-6} chromophore around all three copper sites[8] and, of these compounds, two are from external azide bridges.[8b,8d] Of all known trinuclear linear Cu^{II} compounds a limited number of copper(II) complexes have been fully studied magnetically *and* also characterised by X-ray crystallography (see Table 2).

Trinuclear compounds that have a $[Cu-N-Cu-N-Cu]_x$ bridge (with an N belonging to a heterocyclic ligand) are rare and, in fact, only two structures have been reported in the literature.[8b,9,10a] Several mixed Mn−Cu−Mn linear trinuclear compounds are also known.[11]

In a preliminary communication[9] we described a novel template synthesis of a new N_4-donor ligand and, as an example, the X-ray structure of such a compound.



N,*N*′-bis(pyridine-2-yl)formamidine (Hpdf) R_1 = CH, R_2 = H

N,*N*′-bis(pyrimidine-2-yl)formamidine (Hpmf) R_1 = N, R_2 = H

N,*N*′-bis(5-methylpyridine-2-yl)formamidine (Hmpdf) R_1 = CH, R_2 = CH_3

In the present study we describe three formamidine compounds synthesized in a similar way, in situ, from 2-aminopyridine, 2-aminopyrimidine, and 2-amino-5-methylpyridine ligands, copper(II) triflate, and triethylorthoformate in alcohol. The study also includes a second X-ray structure of such a compound. To the best of our knowledge this method for the preparation of such formamidine compounds in situ is unique.

The general formula of the new compounds is $[Cu_3(L)_4](CF_3SO_3)_2(Y)_x$, where L is the dehydronated ligand: *N*,*N*′-bis(pyridine-2-yl)formamidine (abbreviated as Hpdf), *N*,*N*′-bis(pyrimidine-2-yl)formamidine (abbreviated as Hpmf) and *N*,*N*′-bis(5-methylpyridine-2-yl)formamidine (abbreviated as Hmpdf), Y = EtOH or H_2O and

[a] Leiden Institute of Chemistry, Gorlaeus Laboratories, Leiden University,
P. O. Box 9502, NL-2300 RA Leiden, The Netherlands
E-mail: reedijk@chem.leidenuniv.nl
[b] Laboratory of Inorganic Chemistry, Department of Chemistry, P. O. Box 55 (A. I. Virtasen aukio 1), 00014 University of Helsinki, Finland
[c] Institüt für Anorganische und Analytische Chemie, Johannes-Gutenberg University,
Staudingerweg 9, D-55099 Mainz, Germany

 © WILEY-VCH Verlag GmbH, D-69451 Weinheim, 1999 1434−1948/99/1212−2269 $ 17.50+.50/0

$x = 0.5-1.5$. Recently a number of related compounds have been reported with the formula $[M_3(pdf)_4][PF_6]_2$ [where M = Cu^{II}, Co^{II}, Fe^{II}, Cr^{II}], and these were prepared by a different synthetic method[10] involving the initial synthesis of the pdf ligand followed by treatment with PF_6^- as an anion. The structural features of these systems will be compared and discussed.

Synthesis of the Complexes

The compounds are formed in situ by an easy one-step template synthesis of 2-aminopyridine, 2-aminopyrimidine, and 5-methyl-2-aminopyridine for pdf, pmf, and mpdf, respectively, using anhydrous copper(II) triflate in dry ethanol. Upon standing, deep dark green (almost black) crystals of formula $[Cu_3(L)_4](CF_3SO_3)_2(Y)_x$ were formed (Y = EtOH or H_2O, L = dehydronated ligand).

Three Cu^{II} compounds with different formamidine ligands are shown in Table 1 together with some spectral and magnetic features. It must be noted that only a very weak non-coordinating anion like triflate can be used, as stronger binding anions, like perchlorate or nitrate, do not give the same results. Attempts to use this synthetic method to prepare compounds with metals other than Cu^{II} have failed so far. Spectroscopic, magnetic and analytical characterisation showed that all three compounds must have a similar molecular structure. The structure of **1** was reported previously and the structure of **2** is discussed below.

Crystal Structure of Compound 2

X-ray structural analysis of **2** shows a linear arrangement of three Cu^{II} ions surrounded by four ligand molecules in a propeller mode, each of which is tetracoordinated to the three copper atoms. A plot representing this complex, together with the atom labelling scheme, is given in Figure 1 and distances and angles are given in Table 2. The central copper atom Cu2 has a distorted square-planar geometry [with *trans* angles of 168.7(6) and 159.2(6)°] and normal Cu−N distances of about 2.0 Å. The outer copper ions are six-coordinated with, in general, a distorted square-based geometry and a different geometry for each copper. The angles of the basal plane of Cu3 (formed by N117−N217−N317−N423) are 170.7(6)° and 160.9(6)°. The short Cu−N distances Cu3 vary from 2.002(12) to 2.124(14) Å. The axial sites of the geometry are occupied by the nitrogen atoms N223 and N417 with Cu−N distances of 2.31(2) to 2.49(2) Å. The geometry of the copper atoms Cu3 and Cu2 is comparable with those in compound **1**.[9]

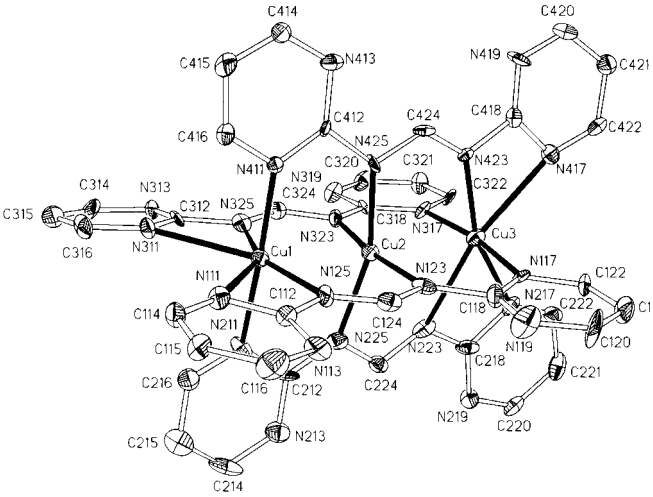


Figure 1. Plot of structure **2** with atom-labelling scheme. H atoms, the non-coordinating triflate anions, and the disordered water molecule are omitted for clarity

The octahedral geometry of the Cu1 atom is unusual (and is in contrast to compound **1**) in that it has four short Cu−N distances [2.004(13)−2.072(13) Å] and two *cis* elongated Cu−N distances of 2.546(13) and 2.538(12) Å. One angle is normal [N211−Cu1−N411 = 177.5(5)°], but two angles have very large deviations from 180° [N311−Cu1−N125 = 151.5(5), N325−Cu1−N111 = 151.0(5)°]. Such an unusual geometry has been observed previously[12] in a few cases like for the mononuclear species

Table 1. Ligand field and EPR and magnetic data of Cu^{II} compounds with ligands pdf, pmf, and mpdf[a]

Compound	UV-VIS [$10^3 cm^{-1}$]	EPR (solid) room temp.	EPR (solid) 77 K	EPR Frozen sol. in DMF (77 K)	Magnetic Susceptibility Measurements[d]

1[b] $[Cu_3(pdf)_4](CF_3SO_3)_2(EtOH)_{1.5}$	17.3
	22.0
	30.3
		$g_\perp$ = 2.11 (br)
		$g_{//}$ = 3.6 (br,w)
			$g_\perp$ = 2.07
			$g_{//}$ = ca.2.3 (vw)
				$g_\perp$ = 2.07
				$g_{//}$ = 2.30
				$A_{//}$ = 15.8 mT
					$J = -174(1)$ cm^{-1}
					g = 2.16(1)

2[c] $[Cu_3(pmf)_4](CF_3SO_3)_2(H_2O)_{0.5}$	16.4 21.2 28.7	$g_\perp$ = 2.11 (br) $g_{//}$ = 4.1 (br,w)	$g_\perp$ = 2.07 $g_{//}$ = ca.2.3 (vw)	$g_\perp$ = 2.07 $g_{//}$ =ca. 2.3 (vw)	$J = -120(1)$ cm^{-1} g = 2.26(1)
3 $[Cu_3(mpdf)_4](CF_3SO_3)_2(EtOH)_1$	16.1 20.0 29.6	$g_\perp$ = 2.10 (br) $g_{//}$ = 3.7 (br,w)	$g\perp$ = 2.07 $g_{//}$ = ca.2.2 (vw)	$g_\perp$ = 2.07 $g_{//}$ = ca.2.3 (vw)	$J = -167(1)$ cm^{-1} g = 2.12(1)

[a] br = broad, w = weak, vw = very weak. − [b] X-ray crystal structure solved;[9] a related crystal structure was solved for a species with the formula $[Cu_3(pdf)_4](PF_6)_2(CH_3CN)_4(EtOH)_2$.[10a] − [c] X-ray crystal structure solved, this work. − [d] Fitted parameters by Equation (1), see text.

Table 2. Selected bond lengths [Å] and angles [°] for compound **2**

Cu(1)−N(211)	2.005(13)
Cu(1)−N(411)	2.004(12)
Cu(1)−N(125)	2.034(13)
Cu(1)−N(325)	2.072(13)
Cu(1)−N(311)	2.538(12)
Cu(1)−N(111)	2.546(13)
Cu(1)−Cu(2)	2.637(3)
Cu(2)−N(123)	1.971(14)
Cu(2)−N(323)	1.972(13)
Cu(2)−N(425)	2.025(13)
Cu(2)−N(225)	2.069(14)
Cu(2)−Cu(3)	2.652(3)
Cu(3)−N(117)	2.003(12)
Cu(3)−N(423)	2.017(13)
Cu(3)−N(317)	2.030(12)
Cu(3)−N(217)	2.120(15)
Cu(3)−N(223)	2.31(2)
Cu(3)−N(417)	2.49(2)
N(211)−Cu(1)−N(411)	177.5(6)
N(125)−Cu(1)−N(325)	151.1(6)
N(311)−Cu(1)−N(125)	151.5(5)
N(325)−Cu(1)−N(111)	151.0(5)
N(123)−Cu(2)−N(323)	168.7(6)
N(425)−Cu(2)−N(225)	159.2(6)
Cu(1)−Cu(2)−Cu(3)	174.96(11)
N(117)−Cu(3)−N(317)	170.7(6)
N(423)−Cu(3)−N(217)	160.9(6)
N(417)−Cu(3)−N(223)	161.4(5)

$Cu(edtb)^{2+}$. The Cu−Cu distances of 2.637(3) and 2.652(3) Å are slightly shorter than in the comparable pdf compound **1** [which are 2.6618(8) and 2.6676(8) Å],[9] and are close to the shortest known distances for Cu^{II} linear trinuclear compounds (see Table 3). Only in Cu^{I} compounds are shorter distances known in some cases.[13] The linear angle Cu1−Cu2−Cu3 is 174.96(11)° and is close to those for other species[9,10a] of this type.

On viewing the compound along the Cu−Cu−Cu axis a propeller-type arrangement is visible in which the ligands are almost perpendicular to the axis with angles between the 2 rings of each ligand that vary from 7.21 to 2.10°. These variations are significantly smaller than in compound **1**, in which they vary from 27.73 to 8.19°, as can been seen from Figure 2. Further stabilisation of the lattice is achieved by stacking of pyrimidine rings between different units (ring-ring distances 3.648−3.889 Å), as can be seen in Figure 3.

Hydrogen bonds between the oxygen atoms of the disordered water molecule and the fluorine of the tetrafluoroborate anion are present, with contacts O···F of 2.73 and 3.16 Å.

An X-ray structure of compound **3** could not be obtained due to the very small crystal size, but this compound very closely resembles **1** and **2** both spectroscopically and magnetically, so a very similar structure is anticipated.

Spectroscopy

The ligand field spectra of compounds **1** to **3** all show a broad band with a double maximum at 16.1−17.3 and 20.0−22.0 $\times 10^3 cm^{-1}$. In addition, a charge transfer band is observed near $29 \cdot 10^3$ cm^{-1}. The two low-energy absorptions are both assigned to d-d transitions,[14] and it is tempting to assume that the highest energy band originates from the square-planar central Cu atom (even though Cu2 is not perfectly square-planar) and the lowest energy band from the outer six-coordinated Cu atoms.[8c,15]

The IR spectra of the compounds are rather featureless. In the mid-infrared section the characteristic C=N is still observed in the free Hpdf ligand at 1671 cm^{-1} as a strong broad band. In compound **1** a double band occurs at 1604, 1587 cm^{-1}. As the free ligand also has a band at 1602 cm^{-1}, the last band is probably the C=N stretching vibration. This band occurs at 1586 cm^{-1} and 1589 cm^{-1} for **2** and **3**, respectively.

In the far-infrared region a strong and broad vibration is predominant at 364 cm^{-1}, 381 cm^{-1}, and 377 cm^{-1} for compounds **1**, **2**, and **3**, respectively; this band can be assigned to the asymmetric Cu−N vibration.[16] Other weak bands present at lower wavenumbers have not been assigned.

EPR

The EPR spectra of powdered polycrystalline samples of the compounds at room temperature show a very broad absorption (peak to peak separation 36 mT) centered around $g = 2.11$ and a weaker broad absorption which lies around $g = 3.6$ for compounds **1** and **3** and at $g = 4.1$ for compound **2**. These latter absorptions disappear upon cooling to 77 K or lower. The main EPR signal ($g = 2.07$) sharpens upon cooling to 77 K (peak-to-peak separation 9.5 mT) and a very weak $g_{//}$ at ca. $g = 2.3$ becomes visible (no $A_{//}$ resolved) (Figure 4). Such signal sharpening upon cooling is not uncommon with trinuclear compounds.[5f,7c,17] The EPR signals at room temperature at ca. $g = 3.6-4.1$ can be assigned to the parallel transitions of the quadruplet state,[18] a state that is almost completely depopulated at 77 K. The narrowing of the other signal seems to be in agreement with this view because only the ground doublet is populated in these conditions. The energy of these signals also varies with the J values (vide infra), a fact that confirms this assignment.

Frozen solution spectra in DMF show (for compounds **2** and **3**) only a broad signal at $g = 2.07$ and a very weak unresolved $g_{//}$ section. Compound **1**, however, shows a well-resolved $g_{//}$ of 2.30 with an $A_{//}$ of 15.8 mT and this is indicative of Cu^{II} in an axial symmetry.[2,14a] This signal is likely to originate from a mononuclear species resulting from dissociation.

Magnetism

The magnetic susceptibility of powdered samples was measured from 4 to 300 K. The magnetic properties of the compounds are summarized in Table 1 and the inverse susceptibility vs. temperature is shown in Figure 5. The inverse susceptibility vs. temperature is almost linear at high temperature, exhibits a broad shoulder and a bend at ca.

Table 3. Linear Cu^{II} trinuclear compounds for which the X-ray structure and magnetism has been published[d,e]

Compound[a]	Bridging atom(s) between adjacent copper atoms[b]	Cu−Cu distance(s)	Cu−Cu−Cu angle	*2J* value [cm^{-1}]	Reference (s = structure, m = magnetism)
$[Cu_3(H_2ahmt)_6Cl_4]Cl_2$	(Cu−N−N−Cu)$_2$ Cu−Cl−Cu	3.568(2)	180.0	−16.9	[2] (s,m)
$[Cu_3(attn)_2(H_2O)Cl_2]Cl_4(H_2O)_4$	(Cu−N−N−Cu)$_2$ Cu−Cl−Cu	3.5426(1)	180.0	−75.1	[7d] (s,m)
$Cu_3Cl_8(adeH)_2$	Cu−N−C−N−Cu (Cu−Cl−Cu)$_2$	3.479(2)	180.0	−16.1	[7a] (s) [7b] (m)
$[Cu_3(L2)_2(N_3)_2](NO_3)_2 \cdot 2\,H_2O \cdot 2\,CH_3OH$	Cu−O−N−Cu Cu−N_{azide}−Cu[c]	3.4008(5)	180.0	−266	[5d] (s,m)
$Cu_3(L1)_2(CH_3COO)_4$	Cu−O−C−O−Cu Cu−O−Cu	3.319(1)	180.0	−9.7	[5f] (s,m)
$Cu_3(deae)_2(benzoato)_4(EtOH)_2$	Cu−O−C−O−Cu Cu−O−Cu	3.211(6)	180.0	28.7	[4c] (s) [5a] (m)
$Cu_3(dbae)_2(benzoato)_4(EtOH)_2$	Cu−O−C−O−Cu Cu−O−Cu	3.188(1)	180.0	30.1	[5a] (s,m)
$[Cu_3(racemo\text{-amat})_2](ClO_4)_2$	(Cu−O−Cu)$_2$	2.940(1)	176.9(1)	−212	[5e] (s,m)
$[Cu_3(LH)_4]Cl_2$	Cu−O−C−N−Cu Cu−N−C−N−Cu Cu−N−Cu	2.812(4) 2.782(3)	175.85(10)	−41	[5c] (s,m)
$[Cu_3(pdf)_4](CF_3SO_3)_2(EtOH)_{1.5}$	(Cu−N−Cu)$_2$	2.6618(8) 2.6676(8)	175.19(2)	−174(1)	[9] (s) this work (m)
$[Cu_3(pmf)_4](CF_3SO_3)_2(H_2O)_{0.5}$	(Cu−N−Cu)$_2$	2.636(3) 2.652(3)	174.93(11)	−120(1)	this work (s,m)

[a] L1 = *N*-Methyl-*N*′-(4-methoxysalicylidene)-1,3-propanediamine; amat = 4,4,9,9-tetramethyl-5,8-diazadodecane-2,11-diol; LH = 2-tolylsulfonylamido-7-hydroxy-1,8-naphthyridine; L2 = 3-[{2-(2-pyridinyl)ethyl}imino]-2-butanone oximato; adeH = adenine; H_2ahmt = 4-amino-3,5-bis(hydroxymethyl)-1,2,4-triazole; attn = 1,9-bis(3-amino-4*H*-triazol-5-yl)-3,7-dithianonane; dbae = 2-dibutylaminoethanol; deae = 2-diethylaminoethanol; Hpdf = *N*,*N*′-bis(pyridine-2-yl)formamidine; Hpmf = *N*,*N*′-bis(pyrimidine-2-yl)formamidine. − [b] When nothing is mentioned the N, O, and C atoms belong to an organic molecule. − [c] Another structure with bridging azide ions has been published recently, although only limited magnetic observations were given. The structure has the formula $[Cu_3(\mu\text{-}N_3)_4(L)_2]$ (in which L = hydridotris(3,5-dimethylpyrazolyl)borate, Cu−Cu distances of 3.082(3), 3.03(3) Å and reported to have a weak antiferromagnetic coupling. − [d] Structures with a copper distances > 5.5 Å and/or Cu−Cu−Cu angles < 170° are excluded, see for instance ref.[17] and ref.[22] − [e] After submitting the manuscript three more compounds were published for which the X-ray structure and the magnetic properties were measured; compound $[Cu_3(pytrz)_{10}(H_2O)_2](ClO_4)_6 \cdot 7\,H_2O$ (pytrz = 4-(2-pyridyl)-1,2,4-triazole), Cu−Cu distance 3.8540(7) Å and $J = -5.41$ cm^{-1}[26] and the compounds: $[Cu_3(L)_2(Me_2en)_2(H_2O)_2] \cdot 7\,H_2O$,$[Cu_3(L)_2(MeOH)_6(H_2O)_4]$ (H_3L = 3,5-pyrazoledicarboxylic acid, Me_2en = *N*,*N*-dimethylethylenediamine) with Cu−Cu distances of 4.3992(13) and 4.4532(12) Å, respectively, and *J* values of −15 cm^{-1} and −19 cm^{-1}, respectively.[27]

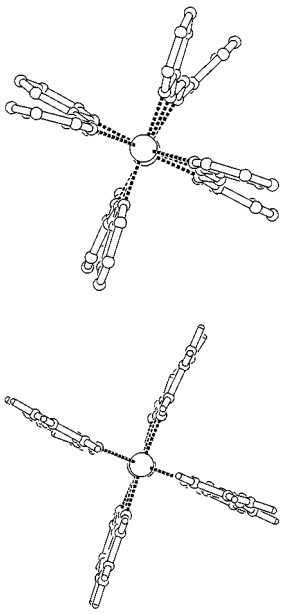


Figure 2. View along the Cu−Cu−Cu axis of structure **1**[9] and **2**

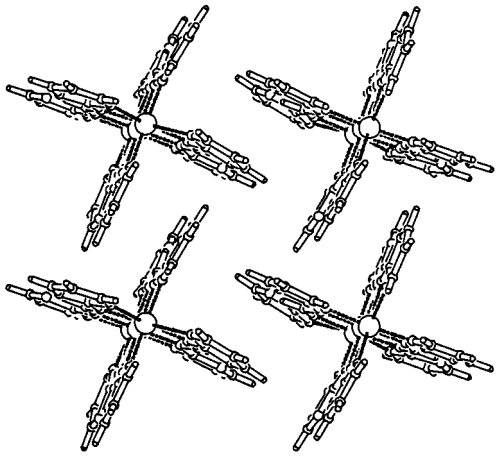


Figure 3: Packing of structure **2**, showing the stacking of the molecules. Uncoordinated triflate and water molecules are ommitted for clarity

120−160 K and is again linear at low temperatures; this behaviour is characteristic of linear trinuclear compounds

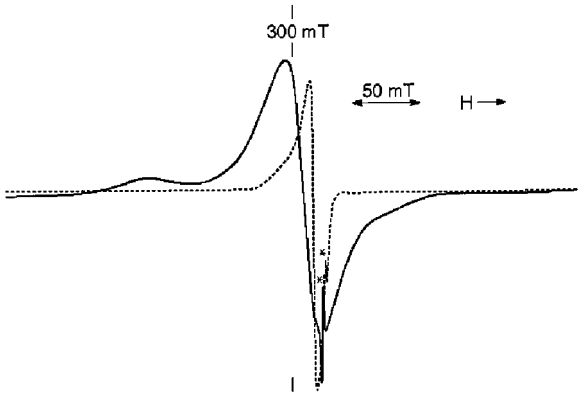


Figure 4. EPR signal of (**2**) as a powdered solid at room temperature (straight line) and at 77 K (dotted line) ("*" denotes dpph); for an explanation see text

with a strong antiferromagnetic exchange interaction between neighbouring paramagnetic metal ions.[5f,7b,19]

The effective magnetic moment μ_B per Cu at room temperature is 1.35, 1.50, 1.35 for compounds **1**, **2**, and **3**, respectively, and decreases gradually until it becomes almost constant with a value of ca. 1.05−1.10 μ_B, which is appropriate for a system with a spin = 1/2 ground state; such values have also been found for other linear Cu trinuclear compounds.[4f,5c,5f,8a,8c]

The magnetic data were fitted to the theoretical expression for the magnetic susceptibility of linear trinuclear $S = 1/2$ systems, which was based on the Hamiltonian:[5f,7b,7c,20]

$$H = -2J(\mathbf{S1}\cdot\mathbf{S2} + \mathbf{S2}\cdot\mathbf{S3}) - 2J'\cdot\mathbf{S1}\cdot\mathbf{S3}$$

in which J is the interaction between adjacent nuclei (J_{12}) and J' the interaction between terminal nuclei (J_{13}). In a trinuclear linear Cu compound the magnetic interaction (J_{12}) between neighbouring copper ions is the dominant pathway of the interaction, and the interaction between the terminal copper ions (J_{13}) can be neglected (i.e. J_{13} is almost zero).[2,5f,7b,10a] Only if the linearity is far from 180°, or in triangular cases, can the value for J_{13} not be neglected.[21]

The magnetic susceptibility is then defined by Equation (1):

$$\chi_m = (Ng^2m_B^2/4\,kT) \times [1 + \exp(-2J/kT) + 10\exp(J/kT)] / [3 + 3\exp(-2J/kT) + 6\exp(J/kT)] \quad (1)$$

(N, g, μ_B, k, and T have their usual meanings, the exchange parameter is denoted as J. The g tensor was assumed to be equal for all individual metal ions).

A good fit has been obtained for the parameters J = −174(1) cm^{-1}, −120(1) cm^{-1}, and −167(1) cm^{-1}, for compounds **1**, **2**, and **3**, respectively.

From these values, and also from Figure 5, it can be seen that compounds **1** and **3** have almost the same behaviour and probably also a very similar structure, which is not surprising as the methyl group will fall at the outer ends of the trinuclear structure and the Cu1−Cu2−Cu3 chromophore can remain the same. Compound **2** has a quite different ligand and, therefore, some other differences (e.g. geometry) in the structure (see Figure 2) and J value are also observed.

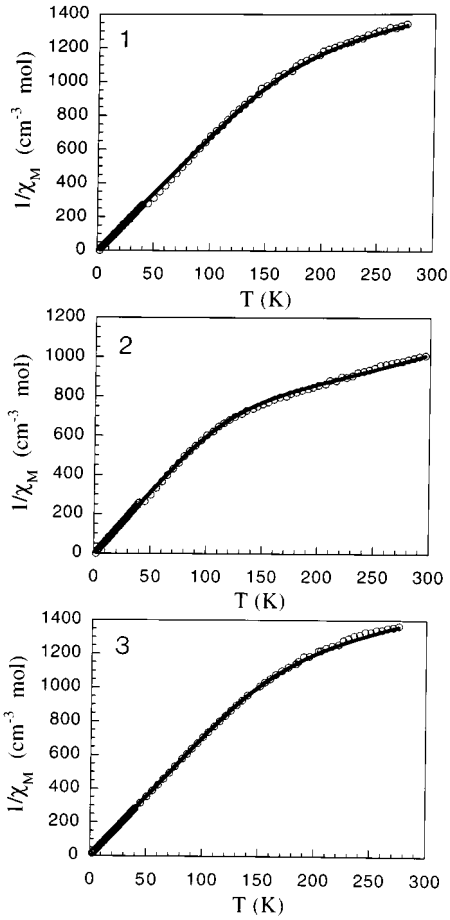


Figure 5. Inverse molar susceptibility ($1/\chi$) (O) as a function of the temperature of compounds **1**, **2**, and **3**. The full curves represent the theoretical curves (see text and Table 1)

Concluding Remarks

In Table 3, a number of the copper(II) compounds is listed with decreasing Cu−Cu distances, studied both magnetically *and* by use of X-ray crystallography. A number of relevant crystallographic and magnetic parameters are also listed. By comparing these magnetic values it can be concluded that the metal-metal distance is one of the important factors, except when the bridging unit is azido,[5d] oxamido,[17] or thiooxamido.[22] The (relatively) strong antiferromagnetism (J = −98.7 and −483 cm^{-1}) for these last two ligands has been attributed to the superexchange by the orbitals of oxygen and/or sulfur, although the Cu−Cu distances are large (about 5−5.5 Å), but it must also be noted that the Cu−Cu−Cu angle deviates markedly from linearity (154−165°)[17,22,23] in these cases. The strong antiferromagnetic coupling (J = −212 cm^{-1}, Cu−Cu distance 2.940 Å) in the compound $[Cu_3(racemo\text{-amat})_2](ClO_4)_2$ (in which amat = 4,4,9,9-tetramethyl-5,8-diazadodecane-2,11-

diol) has been attributed to the same superexchange of the p orbitals of the oxygen.[5e]

Two Cu^{II} compounds have been described with a smaller Cu−Cu separation than that reported in this paper. The compounds $[Cu_3(bipyam)_4X_2]\cdot H_2O$ [in which bipyam = bis(2-pyridyl)amide and X = Cl or Br] have a Cu−Cu separation of 2.471 and 2.468 Å and a strong antiferromagnetism has been suggested of < -500 cm^{-1},[8a,8c] although their magnetism has not been reported. The only linear trinuclear compounds (of which the X-ray structure has been measured) that exist with short Cu−Cu distances between 2.466−2.348 Å involve Cu^{I}, and there are several examples.[13] Only two compounds, which are related to each other, have a ferromagnetic coupling.[5a] In order to understand more about magnetism further research will be needed on strictly linear trinuclear Cu^{II} compounds.

Experimental Section

General: C, H, N, and Cu determinations were performed by the Microanalytical Laboratory of University College, Dublin, Ireland. − UV/Vis spectra were obtained on a Perkin−Elmer Lambda 900 spectrophotometer using the diffuse reflectance technique, with MgO as a reference. − X-band powder EPR spectra were obtained on a Jeol RE2x electron spin resonance spectrometer using DPPH (g = 2.0036) as a standard. − FTIR spectra were obtained on a Perkin−Elmer Paragon 1000 FTIR spectrophotometer by using KBr pellets or films between KBr disks.

FIR-FTIR spectra were obtained on a Bruker 113v infrared spectrophotometer as polyethylene mulls (600−100 cm^{-1}, mirror velocity 0.099 cm/sec, resolution 2 cm^{-1}, Mylar 3.5 Å beam splitter). Magnetic susceptibility measurements (4−300 K) were carried out using a Quantum Design MPMS-5 5T SQUID magnetometer (measurements carried out at 1000 Gauss). Data were corrected for magnetization of the sample holder and for diamagnetic contributions, which were estimated from the Pascal constants.

Synthesis of the Compounds: 2-aminopyridine, 2-amino-5-methylpyridine, and 2-aminopyrimidine were obtained from Acros Organics; Anhydrous copper(II) triflate was obtained from Strem Chemicals. The solvents were commercially available and used without further purification. Ethanol was dried with magnesium sulfate.

General Synthesis: 1.2 mmol of dry $Cu(CF_3SO_3)_2$ and 1.2 mmol of the ligand were each dissolved in ca. 10 mL of dry ethanol. The solutions were carefully heated to about 40 °C on a lamp-heating device. To each solution ca. 5 mL of triethylorthoformate was added. The copper solution was added carefully to the amino compound solution and filtered to remove any un-dissolved material. After a few days a blackish (green) crystalline material was obtained, which was filtered off and air-dried. Yields varied from 55 to 65%.

Compound **1** $\{[Cu_3(pdf)_4](CF_3SO_3)_2(EtOH)_{1.5}\}$ could also be synthesized directly from the copper(II) triflate salt and the ligand Hpdf (which is known from a synthesis reported in the literature[24]) in dry ethanol, with triethylorthoformate used to remove any water from the ethanol.

Elemental Analysis: Compound **1:** $[Cu_3(pdf)_4](CF_3SO_3)_2(EtOH)_{1.5}$, $(C_{49}H_{45}Cu_3F_6N_{16}O_{7.5}S_2)$; calcd. C 43.70, H 3.37, N 16.64, Cu 14.16; found C 43.21, H 3.19, N 16.56, Cu 13.64; Compound **2:** $[Cu_3(pmf)_4](CF_3SO_3)_2(H_2O)0.5$, $(C_{38}H_{29}Cu_3F_6N_{24}O_{6.5}S_2)$; calcd. C 35.26, H 2.26, N 25.97, Cu 14.73; found C 35.71, H 2.46, N 25.62, Cu 13.95; Compound **3:** $[Cu_3(mpdf)_4](CF_3SO_3)_2(EtOH)_1$, $(C_{56}H_{58}Cu_3F_6N_{16}O_7S_2)$; calcd. C 46.84, H 4.07, N 15.61, Cu 13.28; found: C 46.19, H 3.95, N 15.64, Cu 13.27.

X-ray Crystallographic Studies: Crystal data for $[Cu_3(pmf)_4](CF_3SO_3)_2(H_2O)_{0.5}$: $C_{38}H_{28}Cu_3F_6N_{24}O_{6.5}S_2$, M = 1293.6, triclinic, space group $P-1$ (no. 2), a = 8.529(5), b = 15.760(5), c = 19.639(5) Å, α = 101.793(5), β = 101.263(5), γ = 102.389(5)°, V = 2444(2) Å^3, Z = 2, D_c = 1.759 g cm^{-3}, T = 193(2) K, μ = 1.477 mm^{-1}, F (000) = 1300, 6141 reflections measured, 5939 independent (R_{int} = 0.0423), (range $2.53 < \theta < 24.00°$), refined data/parameters: 5939, 686; largest difference peak and hole 1.658 and −0.803 e·Å^{-3}.

A blackish (green) crystal with dimensions of 0.14 × 0.10 × 0.03 mm was selected, mounted onto the glass fibre using the oil drop method[25a] and measured with a Rigaku AFC-7S diffractometer, graphite-monochromated Mo-K_α radiation (λ = 0.71073 Å), $\omega - 2\theta$ scans. Data reduction was performed using the TEXSAN[25b] package. The intensity data were corrected for Lorentz and polarization effects and for absorption and extinction. All non-H atoms were refined anisotropically. The disordered water atoms O1 and O2 with a population parameter of 0.25 were refined isotropically. The H atoms, except those of the disordered water, were introduced in calculated positions and refined with fixed geometry with respect to their carrier atoms. The structure was solved using direct methods SHELXS-97.[25c] The weighting scheme $w = 1/[\sigma^2(F_o^2) + (0.1197P)^2 + 3.4200P]$, where $P = (F_o^2 + 2F_c^2)/3$ was adopted. The refinement method was full-matrix least-squares on F^2 using the SHELXL97[25d] package converged to $R1$ [$I > 2\sigma(I)$] = 0.109, $wR2$ = 0.255 (all data), S = 1.034.

Crystallographic data (excluding structure factors) for the structure in this paper have been deposited with the Cambridge Crystallographic Data Centre as supplementary publication no. CCDC-116049. Copies of the data can be obtained free of charge on application to CCDC, 12 Union Road, Cambridge CB2 1EZ, UK [Fax: (internat.) + 44(1223)336−033, E-mail: deposit@ccdc.cam.ac.uk].

Acknowledgments

The work described in this paper was supported by the Leiden University Study group WFMO (Werkgroep Fundamenteel Materialen Onderzoek). Use of the services and facilities of the Dutch National NWO/SURF Expertise Center CAOS/CAMM, under grant numbers SON 326−052 and STW NCH99.1751, is gratefully acknowledged. The authors are indebted to the EU for a grant as Host Institute in the EU Programme Human Capital and Mobility (1994−1997). Dr. J. G. Haasnoot and Prof. Dr. D. Gatteschi are thanked for their helpful suggestions.

[1] O. Kahn, *Molecular Magnetism*, VC., New York, **1993** and references cited therein.
[2] P. J. van Koningsbruggen, J. W. van Hal, R. A. G. de Graaff, J. G. Haasnoot, J. Reedijk, *J. Chem. Soc., Dalton Trans.* **1993**, 2163−2167.
[3] P. A. Vigato, S. Tamburini, *Coord. Chem. Rev.* **1990**, *106*, 25−170.
[4] [4a] N. Matsumoto, Y. Nishida, S. Kida, I. Ueda, *Bull. Chem. Soc. Jpn.* **1976**, *49*, 117−121. − [4b] W. Baker Jr., F. T. Helm, *J. Am. Chem. Soc.* **1975**, *97*, 2295−2296. − [4c] H. Muhonen, A. Pajunen, R. Hämäläinen, *Acta. Crystallogr.* **1980**, *B36*, 2790−2793. − [4d] H. Knuuttila, *Inorg. Chim. Acta* **1983**, *72*, 11−16. − [4e] H. Knuuttila, *Inorg. Chim. Acta* **1981**, *50*, 221−225. − [4f] G. Ferguson, C. R. Langrick, D. Parker, K. E. Matthes, *J. Chem. Soc., Chem. Commun.* **1985**, 1609−1610. −

[4g] R. Sillanpää, K. Rissanen, *Acta. Chem. Scand.* **1990**, *44*, 1013−1017. − [4h] K. Smolander, K. Leisto, *Inorg. Chim. Acta* **1990**, *169*, 151−155. − [4i] S. Kannan, M. R. A. Pillai, P. A. Droege, S. Jurisson, C. L. Barnes, *Inorg. Chim. Acta* **1997**, *254*, 397−400. − [4j] S. Gehring, W. Haase, *Acta. Crystallogr.* **1991**, *C47*, 1814−1816. − [4k] J. M. Epstein, B. N. Figgis, A. H. White, A. C. Willis, *J. Chem. Soc., Dalton Trans.* **1974**, 1954−1961. − [4l] D. J. Darensbourg, M. W. Holtcamp, B. Khandelwal, K. K. Klausmeyer, J. H. Reibenspies, *Inorg. Chem.* **1994**, *33*, 2036−2040. − [4m] D. Christodoulou, C. George, L. K. Keefer, *J. Chem. Soc., Chem. Commun.* **1993**, 937−939. − [4n] L. Cronin, P. H. Walton, *Inorg. Chim. Acta* **1998**, *269*, 241−245.

[5] [5a] W. Haase, S. Gehring, *J. Chem. Soc., Dalton Trans.* **1985**, 2609−2613. [5b] P. Fleischhauer, S. Gehring, W. Haase, *Ber. Bunsenges. Phys. Chem.* **1992**, *96*, 1701−1704. − [5c] R.-H. Uang, S.-M. Peng, *Bull. Inst. Chem. Academia Sinica* **1996**, *43*, 117−126. − [5d] F. Akagi, Y. Nakao, K. Matsumoto, S. Takamizawa, W. Mori, S. Suzuki, *Chem. Lett*. **1997**, 181−182. − [5e] N. F. Curtis, G. J. Gainsford, K. R. Morgan, *Aust. J. Chem.* **1988**, *41*, 1545−1555. − [5f] B. Chiari, O. Piovesana, T. Tarantelli, P. F. Zanazzi, *Inorg. Chem.* **1985**, *24*, 4615−19.

[6] [6a] R. D. Willett, R. E. Rundle, *J. Chem. Phys.* **1964**, *40*, 838−847. − [6b] K. D. Onan, M. Veidis, G. Davies, M. A. El-Sayed, A. El-Toukhy, *Inorg. Chim. Acta* **1984**, *81*, 7−13. − [6c] X. Shen, D. Wu, X. Huang, Q. Liu, Z. Huang, B. Kang, *Polyhedron* **1997**, *16*, 1477−1482.

[7] [7a] P. de Meester, A. C. Skapski, *J. Chem. Soc., Dalton Trans.* **1972**, 2400−2404. − [7b] D. B. Brown, J. R. Wasson, J. W. Hall, W. E. Hatfield, *Inorg. Chem.* **1977**, *16*, 2526−2529. − [7c] L. Banci, A. Bencini, D. Gatteschi, *Inorg. Chem.* **1983**, *22*, 2681−2683. − [7d] R. Prins, M. Biagini-Cingi, M. Drillon, R. A. G. de Graaff, J. Haasnoot, A.-M. Manotti-Lanfredi, P. Rabu, J. Reedijk, F. Ugozzoli, *Inorg. Chim. Acta* **1996**, *248*, 35−44.

[8] [8a] G. J. Pyrka, M. El-Mekki, A. A. Pinkerton, *J. Chem. Soc., Chem. Commun.* **1991**, 84−85. − [8b] M. H. W. Lam, Y.-Y. Tang, K.-M. Fung, X.-Z. You, W.-T. Wong, *J. Chem. Soc., Chem. Commun.* **1997**, 957−958. − [8c] L.-P. Wu, P. Field, T. Morrissey, C. Murphy, P. Nagle, B. Hathaway, C. Simmons, P. Thornton, *J. Chem. Soc., Dalton Trans.* **1990**, 3835−3840. − [8d] M. A. S. Goher, F. A. Mautner, *Cryst. Res. and Technol.* **1992**, *27*, 817−823.

[9] G. A. van Albada, I. Mutikainen, U. Turpeinen, J. Reedijk, *Eur. J. Inorg. Chem.* **1998**, 547−549.

[10] [10a] F. A. Cotton, C. A. Murillo, X. Wang, *Inorg. Chem. Commun.* **1998**, *1*, 281−283. − [10b] F. A. Cotton, L. M. Daniels, C. A. Murillo, X. Wang, *Chem. Commun.* **1998**, 39−40. − [10c] F. A. Cotton, L. M. Daniels, C. A. Murillo, I. Pascual, *Inorg. Chem. Commun.* **1998**, *1*, 1−3.

[11] F. Birkelbach, T. Weyhermüller, M. Lengen, M. Gerdan, A. X. Trautwein, K. Wieghardt, P. Chaudhuri, *J. Chem. Soc., Dalton Trans.* **1997**, 4529−4537.

[12] P. J. M. W. L. Birker, S. Gorter, H. M. J. Hendriks, J. Reedijk, *Inorg. Chim. Acta* **1980**, *45*, L63−L64.

[13] [13a] J. Beck, J. Strähle, *Angew. Chem. Int. Ed. Engl.* **1985**, *24*, 409−410. − [13b] M.-S. Tsai, S.-M. Peng, *J. Chem. Soc., Chem. Commun.* **1991**, 514−515. − [13c] R. Schmid, J. Strähle, *Z. Naturforsch.* **1989**, *44b*, 105−109.

[14] [14a] B. J. Hathaway, in *Comprehensive Coordination Chemistry*, eds. G. Wilkinson, R. D. Gill and J. A. McCleverty, Pergamon Press, Oxford, **1987**, Vol.5. − [14b] A. B. P. Lever, *Inorganic Electronic Spectroscopy*, 2nd. Ed, Elsevier, Amsterdam, **1984**.

[15] A. M. Duda, A. Karaczyn, H. Kozłowski, I. O. Fritsky, T. Głowiak, E. V. Prisyazhnaya, T. Y. Sliva, J. Swiatek-Kozłowska, *J. Chem. Soc., Dalton Trans.* **1997**, 3853−3859.

[16] J. R. Ferraro, *Low Frequency Vibrations of Inorganic and Coordination Compounds*, Plenum Press, New York, **1971**.

[17] Y. Journaux, J. Sletten, O. Kahn, *Inorg. Chem.* **1986**, *25*, 439−447.

[18] P. Fleischhauer, S. Gehring, C. Saal, W. Haase, Z. Tomkowicz, C. Zanchini, D. Gatteschi, D. Davidov, A. L. Barra, *J. Magn. & Magn. Mat.* **1996**, *159*, 166−174.

[19] [19a] G. Vos, J. G. Haasnoot, G. C. Verschoor, J. Reedijk, P. E. L. Schaminee, *Inorg. Chim. Acta* **1985**, *105*, 31−39. − [19b] G. A. van Albada, R. A. G. de Graaff, J. G. Haasnoot, J. Reedijk, *Inorg. Chem.* **1984**, *23*, 1404−1408. − [19c] W. Vreugdenhil, J. G. Haasnoot, M. F. J. Schoondergang, J. Reedijk, *Inorg. Chim. Acta* **1987**, *130*, 235−242.

[20] J. S. Griffith, *Struct. Bonding (Berlin)* **1972**, *10*, 87−126.

[21] S. Gehring, P. Fleischhauer, H. Paulus, W. Haase, *Inorg. Chem.* **1993**, *32*, 54−60.

[22] R. Veit, J.-J. Girerd, O. Kahn, F. Robert, Y. Jeannin, *Inorg. Chem.* **1986**, *25*, 4175−4180.

[23] J. Ribas, C. Diaz, X. Solans, M. Font-Bardia, *J. Chem. Soc., Dalton Trans.* **1997**, 35−38.

[24] [24a] P. Benkó, L. Pallos, *J. Prakt. Chemie* **1972**, *314*, 627−635. − [24b] P. Benkó, L. Pallos, F. Ordogh, B. Rosdy, Hungarian Patent no. 155,429 (**1968**).

[25] [25a] T. Kottke, D. Stalke, *J. Appl. Crystallogr.* **1993**, *26*, 615−619. − [25b] TEXSAN. *Single Crystal Structure Analysis Software*, Version 1.6, Molecular Structure Corporation, The Woodlands, TX.77381, USA, **1993**. − [25c] G. M. Sheldrick, SHELXS97, *Program for crystal structure determination*. University of Göttingen, Germany, **1997**. − [25d] G. M. Sheldrick, SHELXL97, *Program for crystal structure refinement.* University of Göttingen, Germany, **1997**.

[26] J. Liu, Y. Song, Z. Yu, J. Zhuang, X. Huang, X. You, *Polyhedron* **1999**, *18*, 1491−1494.

[27] D. Rehorst, L. Chang, C. Finazzo, M. Lutz, A. L. Spek, S. Gorter, W. L. Driessen, J. Reedijk, *J. Inorg. Biochem.* **1999**, *74*, 274.

Received May 7, 1999
[I99166]

Synthesis and Structure of Trinuclear Boryloxycarbyne Complexes

Holger Braunschweig,*[a] Carsten Kollann,[a] Margot Koster,[a] Ulli Englert,[a] and Matthias Müller[b]

Keywords: Boron / Iron / Nickel / Carbyne complexes

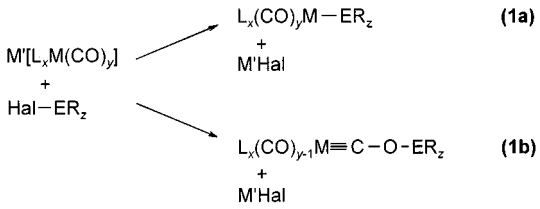
The μ^3-boryloxycarbyne complexes $[\{Fe(CO)_3\}_3\{\mu^3\text{-}COBCl\{NtBu(SiMe_3)\}\}_2]$ (**1**) and $[\{(\eta^5\text{-}C_5H_5)Ni\}_3\{\mu^3\text{-}COBX(NR_2)\}\mu^3\text{-}CO]$ (**2a**: $NR_2 = NtBu(SiMe_3)$, X = Cl; **2b**: $NR_2 = N(SiMe_3)_2$, X = Cl; **2c**: $NR_2 = NMe_2$, X = $BNMe_2Cl$) were obtained by reaction of the anionic complexes $K_2[\{Fe(CO)_3\}_3\{\mu^3\text{-}CO\}_2]$ and $K[\{(\eta^5\text{-}C_5H_5)Ni(CO)]$ with the corresponding chloroboranes Cl_2BNR_2 {$NR_2 = NtBu(SiMe_3)$, $N(SiMe_3)_2$}, or 1,2-dichlorodiboranes(4) $B_2(NMe_2)_2Cl_2$, respectively. The products are formed by a nucleophilic attack of the CO oxygen atom at the boron centres with subsequent salt elimination. All compounds were characterized by IR and multinuclear NMR spectroscopy, and the structures of **1** and **2c** in the solid state were determined by single-crystal X-ray diffraction studies.

Introduction

A large number of complexes $[L_x(CO)_yM-ER_z]$ with transition metal element bonds have been obtained over the last decades by salt elimination reactions between anionic complexes of the type $M'[L_xM(CO)_y]$ and element halides $HalER_z$ according to Equation 1a.[1a,b] More recently, this fundamental reaction has also been very successfully employed for the synthesis of transition metal complexes of boron, especially for boryl and borylene complexes.[2a,b] In the course of our investigations in this field we found that the mononuclear anionic complexes $K[(\eta^5\text{-}C_5H_5)M(CO)_3]$ (M = Mo, W) undergo salt elimination reactions with 1,2-diiododiboranes(4) by nucleophilic attack of the CO oxygen atom at the boron centre with formation of oxycarbyne complexes of the type $[1,2\text{-}\{(\eta^5\text{-}C_5H_5)M(CO)_2CO\}_2B_2(NMe_2)_2]$.[3] Despite the spectroscopic and experimental evidence for the nucleophilic character of the CO atom in anionic carbonyl complexes,[4a–d] this alternative pathway, with formation of the corresponding oxycarbyne complexes of the type $[L_x(CO)_{y-1}M{\equiv}C-O-ER_z]$ according to Equation 1b, has only been observed once before.[5] In the present paper we describe the syntheses of some trinuclear μ^3-boryloxycarbyne complexes, which were obtained from anionic carbonyl complexes and suitable haloboranes; these compounds are also formed by nucleophilic attack of CO oxygen atoms at boron and salt elimination.

Results and Discussion

The reaction of the trimeric dianion $[Fe_3(CO)_{11}]^{2-}$, which was used as the corresponding dipotassium salt, with two equivalents of $Cl_2BNtBu(SiMe_3)$ afforded the μ^3-oxycarbyne complex **1** according to Equation 2.



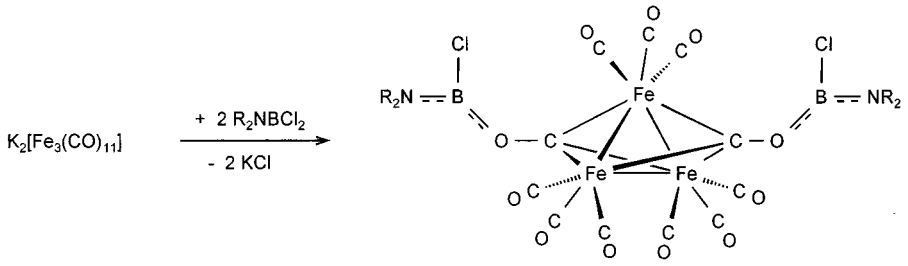
(1a) (1b)

The product was isolated as red crystalline platelets in yields of about 62%. It is readily soluble in nonpolar solvents, extremely sensitive to air and moisture, and melts without decomposition at 124°C. The structure of **1** in solution derives from IR and NMR spectroscopic data. A distinct high-field shift of the ^{11}B NMR signal at $\delta = 28.1$ relative to that of the starting material $Cl_2BNtBu(SiMe_3)$ ($\delta = 36.6$)[6] indicates the formation of an oxoborane derivative, and all other spectroscopic findings, such as the CO stretching frequencies in the IR spectrum ($\tilde{\nu}$ = 2040, 2007 and 1942 cm^{-1}), confirmed our expectations.[7] An X-ray structure analysis was carried out on a single crystal of **1**, which was grown from a hexane solution at −30°C. Although the quality of the structure refinement suffers from incorporated and disordered solvent molecules, the results unambigously prove the constitution of $[\{Fe(CO)_3\}_3\{\mu^3\text{-}COBCl\{NtBu(SiMe_3)\}\}_2]$ (**1**) in the crystalline state (Figure 1).

The compound crystallizes in the space group $P\bar{1}$ (no. 2), and the molecule adopts C_1 symmetry. The three iron atoms form an almost regular triangle with iron-iron distances ranging between 250 and 253 pm. This $Fe_3(CO)_9$ moiety is capped by two μ^3-$COBCl\{NtBu(SiMe_3)\}$ carbyne ligands resulting in a central trigonal-bipyramidal Fe_3C_2 core with iron-carbon distances of about 195 pm. The boron-oxygen {B1–O1 = 138(1) pm, B2–O2 = 135(1) pm} and boron-nitrogen {B1–N1 = B2–N2 = 141(1) pm} bond lengths are in the expected range for B–O and B–N linkages with partial double bond character.[8]

[a] Institut für Anorganische Chemie der Technischen Hochschule, Templergraben 55, D-52056 Aachen
E-mail: holger.braunschweig@ac.rwth-aachen.de
[b] Chemical Crystallography Laboratory University of Oxford, 9 Parks Road, Oxford OX1 3PD, UK

 © WILEY-VCH Verlag GmbH, D-69451 Weinheim, 1999 1434–1948/99/1212–2277 $ 17.50+.50/0



(2)

1; NR_2 = N*t*Bu(SiMe$_3$)

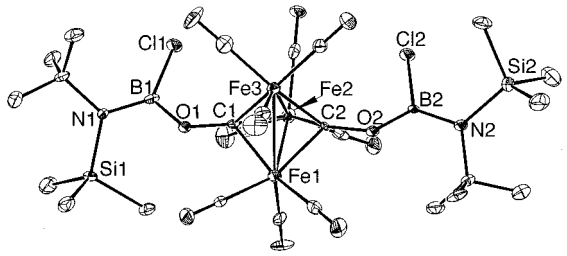


Figure 1. PLATON[21] representation of **1** in the crystal (displacement ellipsoids scaled to 30% probability, hydrogen atoms omitted); selected bond lengths (pm) and angles (deg): Fe1−Fe2 250.6(2), Fe1−Fe3 250.1(2), B2−O2 135(1), B1−O1 139(1), B1−N1 141(1), B2−N2 141(1); Fe2−Fe1−Fe3 60.80(5)

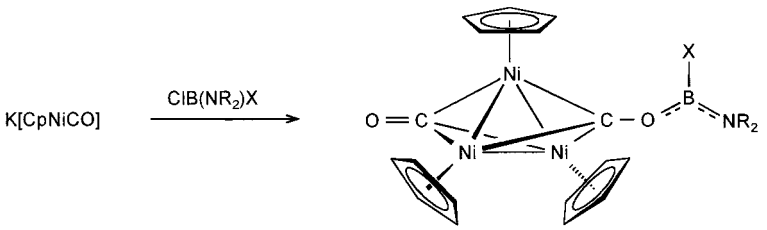
Related trinuclear nickel carbyne complexes were obtained from the reaction of mononuclear K[{(η^5-C_5H_5)NiCO] with monoborane- or diborane(4)chlorides, respectively (Equation 3).

The formation of [{(η^5-C_5H_5)Ni}$_3${μ^3-COBX(NR_2)}μ^3-CO] (**2a**, NR_2 = N*t*Bu($SiMe_3$), X = Cl; **2b**, NR_2 = N($SiMe_3$)$_2$, X = Cl; **2c**, NR_2 = NMe_2, X = $BNMe_2Cl$) was again achieved from nucleophilic attack of a CO oxygen atom at the boron centre. All three boryloxycarbyne complexes were isolated in 12%−15% yields as black, crystalline solids that dissolve readily in nonpolar solvents such as hexane. Solutions of **2a−c** are stable for several days at ambient temperature under an inert gas atmosphere, but exposure to air immediately leads to decomposition.

The compounds [{(η^5-C_5H_5)Ni}$_3${μ^3-COBX(NR_2)}μ^3-CO] (**2a**, NR_2 = N*t*Bu($SiMe_3$), X = Cl; **2b**, NR_2 = N($SiMe_3$)$_2$, X = Cl; **2c**, NR_2 = NMe_2, X = $BNMe_2Cl$) are obviously the products of a complex, nonstoichiometric reaction, and hence, attempts were made to obtain the nickel complexes directly from the corresponding trinuclear monoanion [{(η^5-C_5H_5)Ni}$_3${μ^3-CO}$_2$]$^-$.[9] Interestingly, these reactions always resulted in mixtures of several boron-containing species and the formation of compounds **2a−c** could not be observed.

The molecular structure of the trinuclear nickel complexes in solution was deduced from IR and multinuclear NMR spectroscopic measurements. The boryl compounds **2a,b** show the expected shift to higher field for the ^{11}B NMR signals [δ = 26.0 (**2a**) and δ = 25.9 (**2b**)], whereas the diboran(4)yl derivative **2c** is characterized by two signals at δ = 30.9 and 38.0. The position of the latter signal is almost unaltered with respect to that of the starting diborane(4) $B_2(NMe_2)_2Cl_2$,[10] and is assigned to the chloride-substituted boron atom, while the distinct high-field shift of the other signal clearly indicates the boron-oxygen linkage. Due to a restricted rotation around the boron-nitrogen double bonds the four methyl groups exhibit four signals in the ^{1}H and ^{13}C NMR spectra. The CO stretching frequencies in the IR spectra at $\tilde{\nu}$ = 1719 (**2a**), 1716 (**2b**) and 1734 cm^{-1} (**2c**) are in the expected range for μ^3-CO ligands. An X-ray structure analysis was carried out for the diborane(4) derivative **2c** (Figure 2).

This compound crystallizes in the monoclinic space group $P2_1/n$, and the molecule adopts C_1 symmetry. The three nickel atoms form a regular triangle, with Ni−Ni bond lengths of about 243 pm, which is capped on one side by a μ^3-CO ligand and on the other side by a μ^3-oxycarbyne



(3)

2a, NR_2 = N*t*Bu($SiMe_3$), X = Cl

2b, NR_2 = N($SiMe_3$)$_2$, X = Cl

2c, NR_2 = NMe_2, X = $BNMe_2Cl$

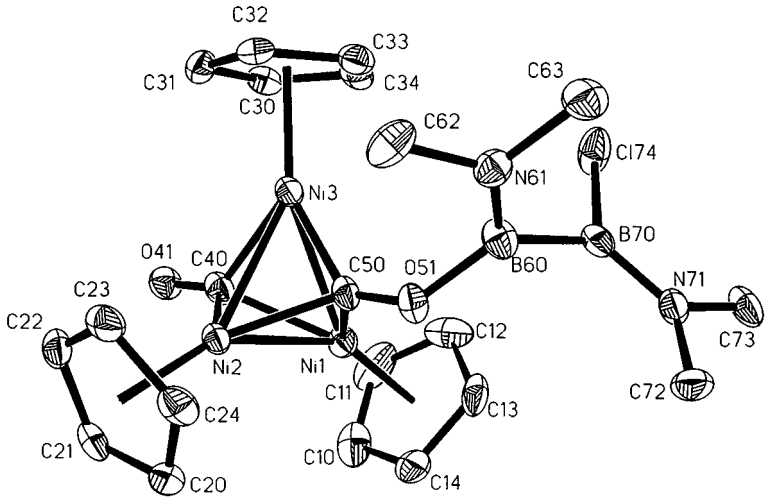


Figure 2. CAMERON[22] representation of **2c** in the crystal (displacement ellipsoids scaled to 30% probability, hydrogen atoms omitted); selected bond lengths (pm) and angles (deg): Ni1−Ni2 243.19(9), Ni1−Ni3 243.33(9), B60−B70 172.2(7), B70−N71 135.3(7), B60−N61, 137.7(8), B60−O51 143.4(7); Ni2−Ni1−Ni3 59.98(3)

moiety. The structural parameters of the central Ni_3C_2 core resemble those of the trimeric monoanion $[\{(\eta^5\text{-}C_5H_5)Ni\}_3\{\mu^3\text{-}CO\}_2]^-$,[9] and the geometry of the boryloxycarbyne moiety C−O−B(NMe$_2$)−B(NMe$_2$)Cl is similar to that of the related mononuclear complex $[1,2\text{-}\{(\eta^5\text{-}C_5H_5)Mo(CO)_2CO\}_2B_2(NMe_2)_2]$.[3] In both cases the boron-nitrogen bond lengths range from 135 to 137 pm, thus indicating double bonds, whereas the boron-oxygen bond lengths of about 144 pm are evidence for B−O linkages without significant π-interactions. These observations with respect to the bonding situation of the boron atom to the neighbouring RO- and R_2N groups of **2c** are in contrast to the results described for $[\{Fe(CO)_3\}_3\{\mu^3\text{-}COBCl\text{-}\{NtBu(SiMe_3)\}\}_2]$ (**1**). The hindered rotation of the Me_2N groups in **2c**, which was not observed for the monoborane derivatives **1** and **2a**,**b**, gives further evidence for less effective boron-nitrogen π-interaction bond in the latter complexes, which may be due to the electron-withdrawing effect of the $SiMe_3$ groups.

Experimental Section

All manipulations were carried out under a dry nitrogen atmosphere with common Schlenk techniques. Solvents and reagents were dried by standard procedures, distilled, and stored under nitrogen over molecular sieves. $B_2(NMe_2)_2Cl_2$,[10] $Cl_2BN(SiMe_3)_2$,[11] $Cl_2BNtBu(SiMe_3)$,[6] $K_2[Fe_3(CO)_{11}]$,[12] and $K[(\eta^5\text{-}C_5H_5)Ni(CO)]$[13] were synthesised according to literature procedures. − NMR: Varian Unity 500 at 499.843 MHz (^{1}H, internal standard TMS), 150.364 MHz (^{11}B, BF3·OEt2 in C_6D_6 as external standard), 125.639 MHz ($^{13}C\{^1H\}$, APT, internal standard TMS); all NMR spectra were recorded in C_6D_6 as solvent unless otherwise stated. − Elemental analyses (C, H, N): Carlo−Erba elemental analyzer, model 1106. − IR: Perkin−Elmer FT-IR 1720x

$[\{Fe(CO)_3\}_3\{\mu^3\text{-}COBCl\{NtBu(SiMe_3)\}\}_2]$ (1): Neat $Cl_2BN(tBu)SiMe_3$ (1.70 g, 7.52 mmol) was added to a dark red suspension of $K_2[Fe_3(CO)_{11}]$ (2.08 g, 3.76 mmol) in 30 mL benzene at ambient temperature. The reaction mixture was stirred for 15 min and the solvent was subsequently removed under high vacuum. The orange-red residue was extractet with 30 mL of hexane, and after filtration and cooling to −30°C, compound **1** (1.99 g, 61.7%) was obtained as an extremely air-sensitive red solid. Recrystallisation from hexane at −30°C yielded dark red platelets of **1**, m.p. 124°C (sealed tube). − ^{1}H NMR: δ = 0.46 (s, 18 H, $SiMe_3$), 1.53 (s, 18 H, CMe_3). − ^{11}B NMR: δ = 28.1 (s). − ^{13}C NMR: δ = 5.4 ($SiMe_3$), 32.8 (CMe_3), 56.6 (CMe_3), 209.8 (CO), no signals for μ^3-carbyne were found. − IR (toluene): $\tilde{\nu}$ = 2040, 2007, 1942 cm^{-1} (CO). − $C_{25}H_{36}B_2Cl_2Fe_3N_2O_{11}Si_2$ (856.78): calcd. C 35.04, H 4.24, N 3.27; found C 34.55, H 4.36, N 3.02.

$[\{(\eta^5\text{-}C_5H_5)Ni\}_3\{\mu^3\text{-}COBCl\{NtBu(SiMe_3)\}\}\mu^3\text{-}CO]$ (2a): Neat $Cl_2BNtBu(SiMe_3)$ (1.01 g, 4.45 mmol) was added to a suspension of $K[(\eta^5\text{-}C_5H_5)Ni(CO)]$ (0.85 g, 4.45 mmol) in 20 mL of toluene at 0°C. The black reaction mixture was stirred for 20 min, warmed to ambient temperature and all volatiles were removed under high vacuum. The remaining solid was extracted with 20 mL of hexane and the resulting black suspension was filtered. The residue was discarded after rinsing with two portions of 5 mL of hexane. After evaporating the dark red filtrate to ca. 20 mL and cooling to −30°C, compound **2a** (0.38 g, 14%) was obtained as a black microcrystalline solid, no m.p. observed, decomposition above 200°C (sealed tube). − ^{1}H NMR: δ = 0.47 (s, 9 H, $SiMe_3$), 1.51 (s, 9 H, CMe_3), 5.11 (s, 15 H, C_5H_5). − ^{11}B NMR: δ = 26.0 (s). − ^{13}C NMR: δ = 5.4 ($SiMe_3$), 32.8 (CMe_3), 56.1 (CMe_3), 92.6 (C_5H_5), no signals for μ^3-CO and μ^3-carbyne observed. − IR (toluene): $\tilde{\nu}$ = 1719 cm^{-1} (s, μ^3-CO). − $C_{24}H_{33}BClNNi_3O_2Si$ (617.69): calcd. C 46.64, H 5.38, N 2.27; found C 45.97, H 5.45, N 2.36.

$[\{(\eta^5\text{-}C_5H_5)Ni\}_3\{\mu^3\text{-}COBCl\{N(SiMe_3)_2\}\}\mu^3\text{-}CO]$ (2b): As described above for **2a** neat $Cl_2BN(SiMe_3)_2$ (1.48 g, 6.13 mmol) was treated with $K[(\eta^5\text{-}C_5H_5)Ni(CO)]$ (1.17 g, 6.13 mmol). to give **2b** (0.47 g, 12%) as a black microcrystalline solid, no m.p. observed, decomposition above 200°C (sealed tube). − ^{1}H NMR: δ = 0.42 (s, 18 H, $SiMe_3$), 5.10 (s, 15 H, C_5H_5). − ^{11}B NMR: δ = 25.9 (s). − ^{13}C NMR: δ = 3.5 (s, $SiMe_3$), 92.7 (C_5H_5), no signals for μ^3-CO and μ^3-carbyne observed. − IR (toluene): $\tilde{\nu}$ = 1716 cm^{-1} (s, μ^3-CO). − $C_{23}H_{33}BClNNi_3O_2Si_2$ (634.10): calcd. C 43.56, H 5.24, N 2.21; found C 43.01, H 5. 38, N 2.32.

$[\{(\eta^5\text{-}C_5H_5)Ni\}_3\{\mu^3\text{-}COBNMe_2\{BNMe_2Cl\}\}\mu^3\text{-}CO]$ (2c): As described above for **2a** neat $B_2(NMe_2)_2Cl_2$ (1.07 g, 5.92 mmol) was treated with $K[(\eta^5\text{-}C_5H_5)Ni(CO)]$ (1.13 g, 5.92 mmol). to give **2c** (0.44 g, 13%) as a black microcrystalline solid, m.p. 87°C (sealed

tube). – ^{1}H NMR: δ = 2.48, 2.62, 2.65, 2.73 (s, 6 H, NMe), 5.18 (s, 15 H, C_5H_5). – ^{11}B NMR: δ = 30.9 (s, BO), 38.0 (s, BCl). – ^{13}C NMR: δ = 36.3, 37.9, 38.7, 42.4 (NMe), 92.2 (C_5H_5), no signals for μ^3-CO and μ^3-carbyne observed. – IR (toluene): $\tilde{\nu}$ = 1734 cm^{-1} (m, μ^3-CO). – $C_{21}H_{27}B_2ClN_2Ni_3O_2$ (572.63): calcd. C 44.01, H 4.75, N 4.89; found C 43.39, H 5.10, N 4.74.

X-ray Crystal Structure Determination of Compound 1·0.5 hexane

Experimental: Crystals of **1**·0.5 hexane were grown from a hexane solution at −30°C. A dark red rod of approximate dimensions 0.60 × 0.32 × 0.24 mm^3 was selected and mounted on a glass fibre in a cold (203 K) stream of nitrogen.

Crystal Data: $C_{28}H_{43}B_2ClFe_3N_2O_{11}Si_2$, M = 899.90 g mol^{-1}, triclinic, a = 8.432(2) Å, b = 12.591(4) Å, c = 19.067(2) Å, α = 78.68(2)°, β = 85.00(2)°, γ = 88.32(3)°, V = 1977(1) Å^3, space group P1bar (no. 2), Z = 4, D_X = 1.51 g cm^{-3}, μ = 13.34 cm^{-1}.

Data Collection and Processing: Intensity data were collected at 203 K on an Enraf–Nonius CAD4 diffractometer with graphite-monochromated Mo-K_α radiation (λ = 0.71073 Å). 8318 reflections were measured in the scan range 3° < θ < 26° and corrected for Lorentz and polarization effects. An empirical absorption correction based on azimuthal scans[14] was applied before averaging over symmetry related reflections. Of 7763 independent reflections 4741 data with $I > 1.0\ \sigma(I)$ were considered observed.

Structure Solution and Refinement: The structure was solved by direct methods[15] and refined on structure factors with the SDP program suite.[16] The crystal structure exhibits a large void of ca 100 Å^3 close to the crystallographic inversion centre, which contains a disordered hexane molecule. All non-hydrogen atoms, except those of the disordered solvent were refined with anisotropic displacement parameters, and hydrogen atoms for the nondisordered part of the structure were included as riding with C–H = 0.98 Å, U_{iso}(H) = 1.3 U_{eq}(C). The C atoms of the hexane moiety were assigned isotropic displacement parameters. Convergence was obtained for 440 variables and 4741 observations at R = 0.10, R_w = 0.095 and GOF = 1.774. A final difference Fourier synthesis showed a local maximum of 3.5 e Å^{-3} close (0.9 Å) to Fe1; residual electron density was still located in the region of the disordered solvent.

X-ray Crystal Structure Determination of Compound 2c

Experimental: Crystals of **2c** were grown from a hexane solution at −30°C. A crystal was immersed in highly viscous perfluoropolyether under argon to exclude oxygen. It was mounted on a glass fibre and plunged into a cold (100 K) nitrogen stream.

Crystal Data: $C_{21}H_{27}B_2ClN_2Ni_3O_2$, M = 572.66 g mol^{-1}, monoclinic, a = 12.722(1) Å, b = 9.463(1) Å, c = 19.309(2) Å, β = 92.477(6)°, V = 2322 Å^3, space group $P2_1/n$, Z = 4, D_X = 1.624 g cm^{-3}, μ = 25.35 cm^{-1}, black crystals, crystal dimensions 0.26 × 0.21 × 0.16 mm^3.

Data Collection and Processing: The data were collected at 100 K on an Enraf–Nonius DIP2020 image plate diffractometer with graphite-monochromated Mo-K_α radiation (λ = 0.71069 Å). 32395 Reflections were measured (1 < θ < 26°, −15 ≤ h ≤ 15, −11 ≤ k ≤ 11, −24 ≤ l ≤ 24). The 4646 unique reflections obtained gave 2618 reflections with $I > 3\sigma(I)$. The images were processed with the DENZO and SCALEPACK programs.[17] Corrections for Lorentz and polarisation effects were made. No corrections for anomalous scattering, absorption or extinction were performed.

Structure Solution and Refinement: The crystal structure was solved by direct methods and refined by the full-matrix least-squares method. Subsequent difference Fourier analysis revealed the terminal (Cl)(Me_2N)B fragment to be disordered over two sites. The refinement of the occupancies of the two disordered groups converged at a ratio of 0.17 to 0.83. The atoms B80 and N81 of the isomer with the smaller occupancy factor were refined with isotropic displacement parameters. All non-hydrogen atoms with the exception of B80, N81, C82 and C83 were refined anisotropically. The B–B bond lengths, the B–Cl bond lengths and the B–N bond lengths of the B–B(Cl)(NMe_2) fragment were restrained to have the same lengths in both isomers. The carbon atoms C82 and C83 of the isomer with minor occupancy could not be found in difference maps. Towards the final stage of the structure determination C82, C83 and all hydrogen atoms were added geometrically (N–C = 1.47 Å, C–H = 1.00 Å) after each refinement cycle. Their isotropic temperature factors were chosen to be equal to U[iso] of the heavy atom to which they are linked. During refinement the geometrically added atoms were treated with fixed thermal and positional parameters. They were included in the structure factor calculations. The 298 refined parameters and 2624 observations resulted in an observation/refined parameter ratio of 8.8. A Chebyshev weighting scheme[18] with parameters 2.27, 0.679 and 1.68 was applied. Refinement on F converged at R = 0.038, R_w = 0.048 and GOF = 0.84. A final difference Fourier synthesis showed minimum and maximum residual electron densities of −0.43 and 0.45 e Å^{-3}. All crystallographic calculations were carried out with the CRYSTALS program package.[19] Neutral atom scattering factors were taken from the International Tables for Crystallography.[20]

Crystallographic data (excluding structure factors) for the structures reported in this paper have been deposited with the Cambridge Crystallographic Data Centre as supplementary publication no. CCDC-121748 (**1**) and -121749 (**2c**). Copies of the data can be obtained free of charge on application to CCDC, 12 Union Road, Cambridge CB2 1EZ, UK [Fax: (internat.) + 44(1223)336-033; E-mail: deposit@ccdc.cam.ac.uk].

Acknowledgments

This work was supported by the Deutsche Forschungsgemeinschaft and the Fonds der Chemischen Industrie.

[1] [1a] D. A. Robertus, G. L. Geoffrey in *Comprehensive Organometallic Chemistry, Vol. 2* (Ed.: G. Wilkinson, F. G. A. Stone, E. W. Abel) Pergamon, Oxford, **1982**, p. 763–879. – [1b] R. B. King, *Acc. Chem. Research*, **1970**, *3*, 417–427.
[2] [2a] H. Braunschweig, *Angew. Chem.* **1998**, *110*, 1882–1898, *Angew. Chem. Int. Ed.* **1998**, *37*, 1786–1801. – [2b] G. I. Irvine, M. J. G. Lesley, T. B. Marder, N. C. Norman, C. R. Rice, E. G. Robins, W. R. Roper, G. R. Whittell, L. J. Wright, *Chem. Rev.* **1998**, *98*, 2685–2722.
[3] H. Braunschweig, M. Koster, K. W. Klinkhammer, *Angew. Chem.* **1999**, *111*, 2368–2370, *Angew. Chem. Int. Ed.* **1999**, *38*, 2229–2231.
[4] [4a] M. J. Bennet, W. A. G. Graham, R. A. Smith, R. P. Stewart, *J. Am. Chem. Soc.* **1973**, *95*, 1684–1686. – [4b] D. F. Shriver, *J. Organomet. Chem.* **1975**, *94*, 259–271. – [4c] A. A. Pasinskii, I. L. Eremenko, G. Z. Suleimanov, Y. A. Nuriev, I. P. Beletskaya, V. E. Shklover, Y. T. Struchkov, *J. Organomet. Chem.* **1984**, *266*, 45–52. – [4d] U. Schubert, E. Kunz, M. Knorr, J. Müller, *Chem. Ber.* **1987**, *120*, 1079–1085.
[5] R. N. Vrtis, C. P. Rao, S. Warner, S. J. Lippard, *J. Am. Chem. Soc.* **1988**, *110*, 2669–2670.
[6] R. H. Neilson, R. L. Wells, *Syn. React. Inorg. Metallorg. Chem.* **1977**, *7*, 151–155.
[7] E. Carbrera, J. C. Daran, Y. Jeannin, *J. Chem. Soc., Chem. Commun.* **1988**, 607–608.

[8] F. H. Allen, O. Kennard, D. G. Watson, L. Brammer, G. Orpen, R. Taylor, *J. Chem. Soc., Perkin Trans. 2* **1989**, S1 − S19.
[9] J. J. Maj, A. D. Rae, L. F. Dahl, *J. Am. Chem. Soc.* **1982**, *104*, 3054−3063.
[10] H. Nöth, W. Schick, H. Meister, *J. Organomet. Chem.* **1964**, *1*, 401−410.
[11] P. Geymayer, E. G. Rochow, U. Wannagat, *Angew. Chem.* **1964**, *76*, 499−501; *Angew. Chem. Int. Ed. Engl.* **1964**, *3*, 633−635.
[12] H. A. Hodali, D. F. Shriver, *Inorg. Synth.* **1980**, *20*, 222−223.
[13] R. A. Fischer, J. Behm, E. Herdtweck, C. Kronseder, *J. Organomet. Chem.* **1992**, *437*, C29 − C34.
[14] A. C. T. North, D. C. Phillips, F. S. Mathews, *Acta Crystallogr., A24*, **1968**, 351.
[15] G. M. Sheldrick, *SHELXS86, Program for Structure Solution*, University of Göttingen, **1986**.
[16] ENRAF-Nonius SDP Version 5.0, **1989**.
[17] D. Gewirth, *The HKL Manual*, written with the cooperation of the program authors Z. Otwinowski and W. Minor, Yale University, **1995**.
[18] E. Prince, Mathematical Techniques in Crystallography and Material Sciences, Springer-Verlag Inc., New York, **1982**.
[19] D. J. Watkin, C. K. Prout, J. R. Carruthers, P. W. Betteridge, *CRYSTALS Issue 10*, Chemical Crystallography Laboratory, University of Oxford, **1996**.
[20] *International Tables for Crystallography*, Vol. C, Kluwer Academic Publishers, Dordrecht, **1992**.
[21] A. L. Spek, University of Utrecht, **1994**.
[22] L. J. Pearce, K. C. Prout, D. J. Watkin, *CAMERON*, Chemical Crystallography Laboratory, Oxford, **1996**.

Received May 19, 1999
[I99177]

Complexes of Group 3 Metals and Lanthanides That Contain Siloxane-Bridged Bisaminopyridinato Ligands: Synthesis, Structure, and Application in the Ring-Opening Polymerization of Lactones

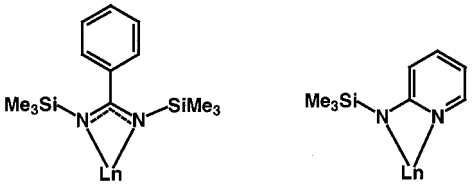
Henrik Noss,[a] Markus Oberthür,[a] Christine Fischer,[a] Winfried P. Kretschmer,[b] and Rhett Kempe*[a]

Keywords: N-ligands / Yttrium / Samarium / Ring-opening polymerization / Lactones

The reaction of one equivalent of dilithiated $O(SiMe_2\text{-}Ap\text{-}H)_2$ [Ap-H = -N(2-amino-4-methylpyridine)] (**1**), generated in situ, with $LnCl_3$ (Ln = Y, Sm) in THF affords $O(SiMe_2\text{-}Ap)_2YCl(THF)_2$ (**2**) or $O(SiMe_2\text{-}Ap)_2SmCl(THF)_3$ (**3**). In contrast, the reaction of one or two equivalents of dilithiated **1**, again generated in situ, with $LaBr_3$ in THF affords $O(SiMe_2\text{-}Ap)_2)_2LaLi(THF)_3$ (**4**). An X-ray structural analysis of **2** and **3** reveal the $O(SiMe_2\text{-}Ap)^{2-}$ ligand to bind in a planar tetradentate manner. Equivalent Sm–N distances in **3** indicate a delocalized binding mode. Compound **2** reacts with Bu_4NBH_4, $NaBH_4$ or $LiCH(SiMe_3)_2$ to give the corresponding "ate" complexes $O(SiMe_2\text{-}Ap)_2Y(BH_4)\text{-}Cl(THF)$ Bu_4N (**5**), $O(SiMe_2\text{-}Ap)_2Y(BH_4)_2Na(THF)_2$ (**6**) and $O(SiMe_2\text{-}Ap)_2Y(CH(TMS)_2)_2Li(THF)_3$ (**7**), respectively. The steric demand of the $O(SiMe_2\text{-}Ap)^{2-}$ ligand is not large enough to stabilize monoalkyl or monoborohydride complexes. Complex **4** has been used as an initiator for the ring-opening polymerization of ε-caprolactone or δ-valerolactone. In both cases an almost linear relation between the monomer-to-initiator ratio and the molecular weight of the obtained polyester is observed. By conducting the polymerization in neat ε-caprolactone at room temperature a solid polyester block is formed after 3 min (300000 $g \cdot mol^{-1}$, M_w/M_n 2.3).

Introduction

The most popular amido ligands in lanthanide chemistry are the silyl-substituted benzamidinates (Scheme 1, left).[1] Related to these ligands are deprotonated 2-aminopyridines (aminopyridinato ligands) when they are bound in a strained η^2 coordination mode (Scheme 1, right).



Scheme 1. Benzamidinate (left) and aminopyridinato (right) ligands

Only a few examples of such group 3 metal complexes (including lanthanides) have been described so far.[2] An advantage of aminopyridinato over amidinato ligands is the opportunity to connect two of them easily by a bridge between the amido nitrogen atoms,[3] thus giving additional possibilities in ligand and complex design. Furthermore, an increase in the stability of the metal-ligand bond (chelating effect) might be established, which would extend the active lifetime of such compounds when employed as catalysts. However, a disadvantage of the aminopyridinato ligands might be the lower steric demand of these ligands, since steric shielding is considered to be very important to prevent the formation of "ate" complexes. Recently, "ate" complexes have been shown to have very interesting applications in homogeneous catalysis[4][5] and coordination chemistry.[2][6] In this paper we report on the synthesis and structure of group 3 and lanthanide complexes that contain siloxane-bridged bisaminopyridinato ligands. Furthermore, the application of selected examples of such compounds in the ring-opening polymerization of lactones is described. Recently, the preparation of siloxane-bridged bisaminopyridinato complexes of the group 4 metals, including ethylene polymerization studies of these compounds, was reported.[7]

[a] Institut für Organische Katalyseforschung (IfOK), Buchbinderstr. 5–6, D-18055 Rostock, Germany
[b] Center for Catalytic Olefin Polymerization, Department of Chemistry, Groningen University, Nijenborgh 4, NL-9747 AG Groningen, The Netherlands

Results and Discussion

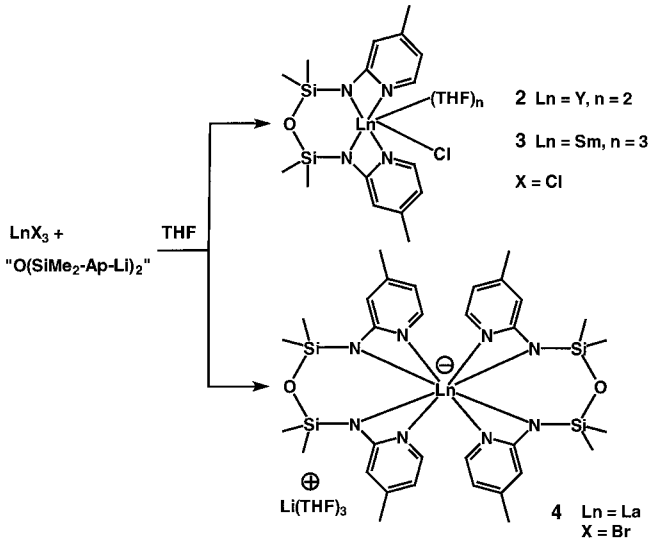
Metal Complex Syntheses and Structures

1. Monochloro and Bis(bisaminopyridinato) Complexes

The reaction of one equivalent of dilithiated $O(SiMe_2\text{-}Ap\text{-}H)_2$ [Ap-H = -N(2-amino-4-methylpyridine)][7] (**1**), generated in situ, with $LnCl_3$ (Ln = Y, Sm) in THF affords **2** or **3** by a salt metathesis reaction (Scheme 2, above). Compounds **2** and **3** could be isolated from THF/ether solution after removal of the precipitated LiCl. They form crystals which are colorless (**2**) or light orange (**3**).

From the NMR spectroscopic data of **2** and **3** it can be inferred that the ligand array coordinates to the metal in a planar fashion. The ^1H and ^{13}C NMR spectra are consistent with C_{2v} monomeric structures in which the nuclei measured show a single set of signals. Single crystal X-ray diffraction analyses of **2** and **3** reveal each to have a monon-

 © WILEY-VCH Verlag GmbH, D-69451 Weinheim, 1999 1434–1948/99/1212–2283 $ 17.50+.50/0



Scheme 2. Synthesis of monochloro and bis(bisaminopyridinato) lanthanoid complexes

uclear structure with the symmetry proposed from the NMR studies (see Figure 1 and 2, respectively).

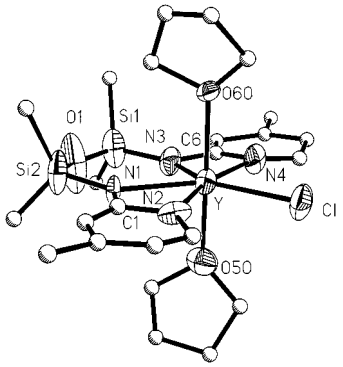


Figure 1. Structural representation of **2**; hydrogen atoms and disorders of the THF ligands are omitted for clarity; the thermal ellipsoids correspond to 30% probability; selected bond lengths [pm] and angles [deg]: Y−N1 246.5(14), Y−N2 249(2), Y−N3 227(2), Y−N4 236(2), Y−O50 221(2), Y−O60 240.9(13), Y−Cl 264.6(3), N1−C1 129(4), N2−C1 144(3), N3−C6 144(2), N4−C6 134(3); Si1−O1−Si2 148.2(9), N1−Y−N3 83.2(3), O50−Y−O60 178.6(4), O50−Y−Cl 89.1(5), O60−Y−Cl 92.1(4)

The X-ray analysis of **2** clearly shows that the ligand array coordinates to the metal in a planar fashion. The metal atom is surrounded by four nitrogen atoms within the equatorial plane of a pentagonal bipyramid. The apices of the pyramid are occupied by two molecules of solvent (THF), which appear to be rather loosely bound, since complex **2** readily loses coordinated THF. Experimental evidence for this was gained by a combined elemental analysis and ^{1}H NMR spectroscopic investigation. In contrast to the spectroscopic data showing two molecules of THF coordinating to the metal atom, the elemental analysis of a sample dried in vacuo indicates the presence of a single molecule of solvent. After drying at 150°C in vacuo for 15 min not a single THF ligand was found residing at the metal complex (by ^{1}H NMR spectroscopy). The presence of two coordinated THF ligands is shown by the X-ray analysis of **2** (Figure 1). Due to the larger ionic radius of Sm an increase in coordination number from Y to Sm is observed (Figure 2).

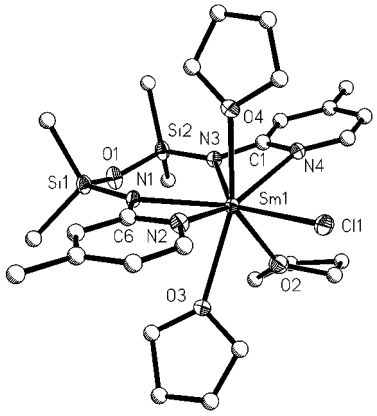


Figure 2. Structural representation of **3**; hydrogen atoms and disorder of one of the three THF ligands are omitted for clarity; the thermal ellipsoids correspond to 30% probability; selected bond lengths [pm] and angles [deg]: Sm1−N1 244.1(4), Sm1−N2 247.9(5), Sm1−N3 245.9(4), Sm1−N4 251.5(4), Sm1−O2 251.4(4), Sm1−O3 258.6(4), Sm1−O4 252.6(4), Sm1−Cl1 271.5(2), N1−C6 135.7(6), N2−C6 135.9(7), N3−C1 136.8(7), N4−C1 137.3(7); Si1−O1−Si2 141.2(3), N1−Sm1−N3 83.10(14), O2−Sm1−O3 65.45(14), O2−Sm1−Cl1 84.69(11), O3−Sm1−Cl1 92.83(10), O4−Sm1−Cl1 85.65(10)

The latter metal center has three additionally coordinated THF ligands. The equivalence of the samarium−nitrogen bond lengths indicates the existence of a delocalized binding mode, thus showing that the negative charge of the aminopyridinato moieties is not localized on the amido nitrogen atom. The reaction of one or two equivalents of dilithiated $O(SiMe_2\text{-}Ap\text{-}H)_2$, generated in situ, with $LaBr_3$ in THF affords **4** (see Scheme 2). The formation of **4** is independent of the ratio of **1** and $LaBr_3$ used as only the bis(bisaminopyridinato) complex was isolated. NMR spectroscopic data of **4** indicate a highly symmetric molecule, as only one set of signals is seen in the proton NMR spectrum.

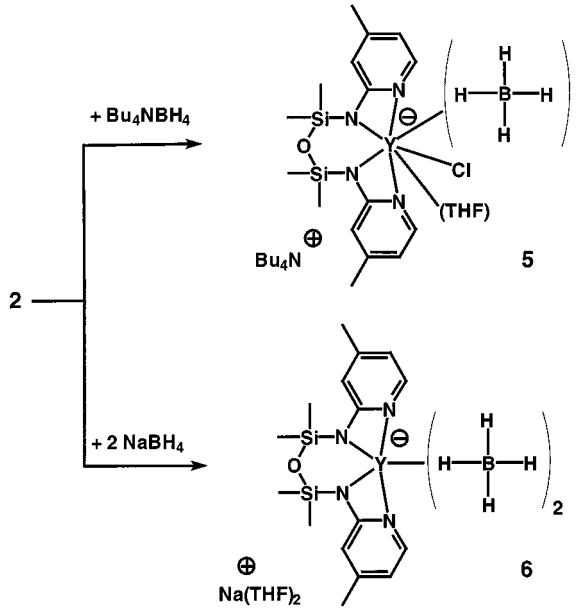
2. Yttrium Borohydride Complexes

The reactivity of **2** towards borohydride ions was examined by using either one equivalent of Bu_4NBH_4 (Scheme 3) or an excess of $NaBH_4$ in THF (Scheme 3). The reactions proceeded at room temperature within a few hours (see Experimental Section for details). The reaction of **2** with Bu_4NBH_4 gave **5**, while from the reaction with $NaBH_4$ complex **6** was isolated.

In contrast to sodium borohydride, which is insoluble in THF, compound **6** displays a high solubility in THF. Similarly, while **5** is very soluble in ether, Bu_4NBH_4 is nearly insoluble in this solvent. Compounds **5** and **6** were characterized by standard analytical methods. No resonances for the BH_4 groups could be seen in the ^{1}H NMR spectrum, probably due to the quadrupole moment of the boron nucleus. The IR signals in the range 2380−2130 cm^{-1} are characteristic of BH_4 vibrations.

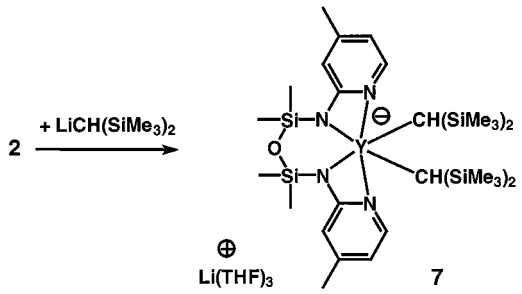
3. Alkyl Complexes

For the alkylation of **2** and **3**, a salt elimination route was chosen. As shown in Scheme 4, compound **2** was reacted



Scheme 3. Syntheses of yttrate complexes **5** and **6**

with an equimolar amount of $LiCH(SiMe_3)_2$ at low temperature. The reaction mixture was filtered to remove precipitated LiCl, concentrated in vacuo and cooled to promote crystallization, after which complex **7** was obtained as colorless needles at −40°C. Since **7** is prone to thermal decomposition it has to be stored at −30°C. The ^1H NMR spectrum of **7** contained a single signal set for the aromatic protons indicative of a symmetric molecule. The presence of three THF ligands can be concluded from the integration of the resonances in the NMR spectrum. The IR data is consistent with that of a coordinating bisaminopyridinato ligand and, together with the results of the elemental analysis, is in accordance with the proposed structure of **7** in Scheme 4.



Scheme 4. Synthesis of the yttrate complex **7**

The reaction of **3** with PhLi leads to biphenyl. The progress of this reaction at −40°C can easily be followed by the change of color of the reaction mixture from red to yellow and the precipitation of LiCl . On warming to 15°C the solution suddenly changed color . The clear, light yellow solution became dark brown, a color which is characteristic for Sm^{II} compounds. We tentatively ascribed this to a redox reaction in which samarium was reduced from Sm^{III} to Sm^{II} and the phenyl anion was oxidized. The reaction mixture was therefore examined for products of phenyl radicals, which one can assume were intermediates. By GC/MS, biphenyl was identified as a product of the reaction and this was confirmed by NMR spectroscopic studies. Recently, Fryzuk et al. have reported a similar reaction, which started with the attempted arylation of an yttrium(III) chloro complex by PhLi but yielded a biphenyl-dianion coordinated to two yttrium(III) complex fragments.[8] Since yttrium is not as easily reduced as samarium this reaction stops after phenyl coupling. The yttrium arene complex may be considered as a model for the intermediate in the reaction of **3** with PhLi.

Ring-Opening Polymerization of Lactones

The ring-opening polymerization of lactones is a useful method to produce biodegradable aliphatic polyesters.[9] Well-defined polymers of this sort have interesting applications, for instance, as surgical sutures and drug delivery systems.[10] Common polyesters are made from a condensation polymerization reaction starting from diols and dicarboxylic acids. A disadvantage of this method is that high temperatures and long reaction times are required to obtain high molecular weights. Furthermore, broad molecular weight distributions are observed. Lanthanocene complexes have been found to be initiators for the ring-opening polymerizations of ε-caprolactone and δ-valerolactone.[11] Recently, lanthanide "ate" complexes have been introduced as very efficient initiators.[5] However, the preferred linear relationship between the monomer to initiator ratio and the molecular weight was not observed, although molecular weights of up to 30000 $g \cdot mol^{-1}$ were obtained. Thus, the behavior of the aminopyridinato "ate" complex **4** as an initiator was investigated with regard to a linear relation between the monomer to initiator ratio and the molecular weight of the polyester, as well as the production of high molecular weights. Tables 1 and 2 show the results of these polymerization studies.

Table 1. Ring opening polymerization of ε-caprolactone with **4** as an initiator

$[M_0]/[I_0]$	M_n [$g \cdot mol^{-1}$]	M_w/M_n	Yield%
100	25000	1.7	61
200	40000	1.7	59
300	51000	1.7	70
400	54000	1.7	74

Table 2. Ring opening polymerization of δ-valerolactone with **4** as an initiator

$[M_0]/[I_0]$	M_n [$g \cdot mol^{-1}$]	M_w/M_n	Yield%
100	12000	1.7	39
200	15000	1.8	35
300	19000	2.0	48
400	27000	1.6	50

ε-Caprolactone and δ-valerolactone were used as monomers. In both cases an almost linear relation between the

monomer to initiator ratio and the molecular weight was observed. The high efficiency of the system is remarkable. By performing the polymerization in neat ε-caprolactone at room temperature a solid polyester block (300000 g·mol^{-1}, M_w/M_n 2.3) is formed after 3 min. Nevertheless, the thermodynamically stable γ-butyrolactone could not be polymerized with **4** as an initiator.

Conclusion

Several conclusions can be drawn from this study. Firstly, the monochloro complexes are readily accessible by salt metathesis reactions. Secondly, these metal complexes smoothly react with borohydrides and standard alkylating reagents to yield the corresponding "ate" complexes. The steric demand of the siloxane-bridged bisaminopyridnato ligands is not large enough to stabilize monoalkyl or monoborohydride complexes. Thirdly, bis(bisaminopyridinato) complexes are highly efficient initiators for the ring-opening polymerization of lactones.

Experimental Section

Materials and Procedures: Bis(trimethylsilyl)methyl lithium[12] and the bisaminopyridine O(SiMe$_2$-Ap-H)$_2$[7] were prepared according to literature procedures. All other reagents were obtained commercially and used as supplied. All manipulations of air-sensitive materials were performed with rigorous exclusion of oxygen and moisture in dried Schlenk-type glassware on a dual manifold Schlenk line interfaced to a high-vacuum line, or in an argon-filled glovebox (mBraun labmaster 130) with a high-capacity recirculator (<1.5 ppm O_2). Reaction solvents (Aldrich) and NMR solvents (Cambridge Isotope Laboratories all 99 atom% D) were freshly distilled from sodium tetraethylaluminate.

Physical Measurements: NMR spectra were recorded on a BRUKER ARX 400 instrument with a variable temperature unit. ^{1}H and ^{13}C chemical shifts are referenced to the solvent resonances and reported relative to TMS. ^{29}Si chemical shifts are reported relative to TMS. Melting points were determined in sealed capillaries on a BÜCHI 535 apparatus. Elemental analysis were performed with a Leco CHNS-932 elemental analyzer. X-ray diffraction data were collected on a STOE-IPDS diffractometer using graphite monochromated MoK_α radiation. The crystals were mounted in a cold nitrogen stream (**3**) or sealed inside a capillary (**2**). The structure was solved by direct methods (SHELXS-86)[13] and refined by full-matrix least-squares techniques against F^2 (SHELXL-93).[14] XP (SIEMENS Analytical X-ray Instruments, Inc.) was used for structure representations. See also Table 3. Crystallographic data (excluding structure factors) for the structures reported in this paper have been deposited with the Cambridge Crystallographic Data Centre as supplementary publication no. CCDC-121918 (compound **2**) and CCDC-121919 (compound **3**). Copies of the data can be obtained free of charge on application to CCDC, 12 Union Road, Cambridge CB2 1EZ, UK [fax: (internat. + 44-1223/336033; E-mail: deposit@ccdc.cam.ac.uk]. Number-average molecular weights and molecular weight distributions of the isolated polymers were determined by gel permeation chromatography on a HP Liquid Chromatograph 1090 at 40°C using THF as the eluent and a universal calibration relative to polystyrene standards.

Table 3. Crystallographic details of the X-ray crystal structure analysis of **2** and **3**

compound	**2**	**3**
crystal system	monoclinic	monoclinic
space group	*Pn*	$P2_1/c$
a, Å	9.790(2)	14.524(3)
b, Å	14.585(3)	9.966(2)
c, Å	11.453(2)	23.759(5)
β, deg	104.15(1)	92.06(3)
V, Å^3	1585.7(5)	3436.8(12)
Z	2	4
crystal size, mm	0.5 × 0.4 × 0.3	0.5 × 0.4 × 0.4
ρ_{calcd}, g cm^{-3}	1.284	1.443
μ, cm^{-1} (MoK_α)	2.03	1.89
T, K	293	200
θ range, deg	2.30 < θ < 24.40	2.18 < θ < 24.28
no. of reflections	4689	9847
no. of reflections unique	2570	5476
no. of reflections obs. [$I > 2\sigma(I)$]	1247	3808
no. of parameters	273	359
ωR^2 (all data)	0.151	0.089
R value [$I > 2\sigma(I)$]	0.054	0.040

Syntheses of the Complexes 2−7. O(SiMe$_2$-Ap)$_2$YCl(THF)$_2$ (2): O(SiMe$_2$-Ap-H)$_2$ (3.11 g, 8.98 mmol) was dissolved in a mixture of 20 mL of hexane and 10 mL of THF and cooled to −78°C. While stirring, 17.96 mmol of *n*-butyllithium was added. This mixture was warmed to −40°C and stirred for 30 minutes to yield a colorless suspension. YCl_3 (1.76 g, 8.98 mmol) was added to 30 mL of THF and the mixture heated to reflux for 10 minutes. The resulting suspension was cooled to −40°C and at this temperature added to the suspension of the lithiated ligand. The reaction mixture was allowed to warm to ambient temperature and stirred for another 12 h; the solvent was then removed in vacuo. The residue was washed with 10 mL of hexane, filtered through a frit (G 4), and then washed with 20 mL of ether and filtered again. The combined filtrates were reduced in volume to 15 mL by vacuum evaporation, to give a colorless precipitate . Having stood for 12 h, the mixture was filtered and the filtrate cooled to −78°C. The crystalline product was obtained by filtration and dried in vacuo. Yield: 3.27 g (6.05 mmol, 67%), m.p. 233°C, (240°C dec.). − ^{1}H NMR (293 K, C_6D_6): δ = 7.69 (s, 2 H, broad, 6-H), 6.22 (s, 2 H, 3-H), 5.83 (broad, 2 H, 5-H), 3.65 (t, 8 H, *J* = 6.4 Hz, THF), 1.90 (s, 6 H, Me-pyridine), 1.12 (m, 8 H, THF), 0.59 (s, 12 H, Me−Si). − ^{13}C NMR (293 K, C_6D_6): δ = 170.6 (C-2), 150.1 (C-4), 145.2 (C-6), 112.4 (C-5), 110.3 (C-3), 69.8, 25.3 (THF), 21.6 (Me-pyridine), 1.9 (Me−Si). − ^{29}Si NMR (293 K, C_6D_6): δ = −15.5. − IR (nujol): $\tilde{\nu}$ = 1604 s, 1532 m (C=C), 1330 s, 1290 s, 1252 s (Me−Si), 1174 s, 1055, 1027, 999 vs (Si−O−Si), 891 s, 871 s (Me$_2$Si), 748 s, 583 s cm^{-1}. − $C_{24}H_{40}ClN_4O_3Si_2Y$ (613): calcd. C 47.01, H 6.58, N 9.14; found C 45.81, H 6.49, N 9.51. The lower value found for carbon is due to the loss of coordinated solvent (THF).

O(SiMe$_2$-Ap)$_2$SmCl(THF)$_3$ (3): To a solution of O(SiMe$_2$-Ap-H)$_2$ (2.92 g, 8.44 mmol) in 20 mL of THF was added 16.88 mmol *n*-butyllithium, dissolved in hexane, at −78°C. After stirring for 1 h at −78°C this solution was warmed to 20°C within another hour and then added to a suspension of $SmCl_3$ (3.25 g, 12.7 mmol) in 40 mL of THF. The reaction mixture was stirred for 12 h, and the solvent was then removed in vacuo to yield a viscous yellow oil which was redissolved in a mixture of 30 mL of ether and 10 mL of THF. A colorless microcrystalline solid precipitated. The supernatant solution was filtered and reduced in volume to 20 mL. Cooling to −30°C yielded light orange needles, which were collected

and dried in vacuo. The crystals easily lose coordinating solvent on vacuum drying. Yield: 1.27 g (2.11 mmol, 25%), mp: 82−86°C (solvent loss), 110−130°C, (230°C dec.). − ^{1}H NMR (293 K, [D$_8$]THF): δ = 10.76 (d, 2 H, *J* = 5.2 Hz, 6-H), 7.59 (s, 2 H, 3-H), 6.90 (d, 2 H, *J* = 5.2 Hz, 5-H), 3.61−3.55 (m, 8 H, THF), 2.70 (s, 6 H, Me-pyridine), 1.79−1.76 (m, 8 H, THF), 0.82 (s, 12 H, Me−Si). − ^{13}C NMR (293 K, [D$_8$]THF): δ = 186.1 (C-2), 150.4 (C-4), 148.3 (C-6), 115.6 (C-5), 110.0 (C-3), 68.3 (THF), 26.4 (THF), 22.4 (Me-pyridine), 2.4 (Me−Si). − ^{29}Si NMR (293 K, [D$_8$]THF): δ = −10.9. − IR (nujol): $\tilde{\nu}$ = 1605 s, 1532 m (C=C), 1324 m, 1288 m, 1249 s (Me−Si), 1174 s, 1056, 1025 vs (Si−O−Si), 888, 870 s, 785 vs (Me$_2$Si), 737 m, 583 m cm^{-1}. − $C_{20}H_{32}ClN_4O_2Si_2Sm$ (602): calcd. C 39.87, H 5.35, N 9.30; found C 39.63, H 5.24, N 9.13.

O(SiMe$_2$-Ap)$_2$)$_2$LaLi(THF)$_3$ (4): To a solution of O(SiMe$_2$-ApH)$_2$ (4.03 g, 11.5 mmol) in 50 mL of THF was added 23.4 mmol of BuLi at −78°C. After stirring for 30 min at this temperature the solution was allowed to warm to 20°C within 30 min. The solution was then added to a suspension of $LaBr_3$ (2.20 g, 5.82 mmol) in 50 mL of THF. The reaction mixture was stirred for 16 h at 20°C. After removal of precipitated LiBr by filtration the volume of solvent was reduced to 30 mL, and 20 mL of diethyl ether was added. Cooling the solution to −30°C yielded colorless crystals which were collected and dried in vacuo. Yield: 4.7 g (4.5 mmol, 77%), mp: 203−205°C. − ^{1}H NMR (293 K, [D$_8$]THF): δ = 7.55 (d, *J* = 4.9 Hz, 2 H, H-6), 5.69 (s, 2 H, H-3), 5.59 (d, *J* = 5.3 Hz, 2 H, H-5), 3.62 (m, 4 H, THF), 1.89 (s, 6 H, Me-pyridine), 1.77 (m, 4 H, THF), 0.11 (s, 6 H, Me−Si). − ^{13}C NMR (293 K, [D$_8$]THF): δ = 170.4 (C-2), 146.4 (C-4), 146.1 (C-6), 113.9 (C-5), 107.1 (C-3), 67.4 (THF), 26.3 (Me-pyridine), 25.2 (THF), 2.1 (Me−Si). − ^{29}Si NMR (293 K, [D$_8$]THF): δ = −19.8. − IR (nujol): $\tilde{\nu}$ = 1601 vs, 1530 s (arom.), 1377 s, 1331 m, 1294 s, 1245 s (Me−Si), 1178 s, 1026 s, 990 s (Si−O−Si), 881 s, 839 s, 792 vs (Me$_2$Si), 674 m, 574 s cm^{-1}. − $C_{44}H_{72}LaLiN_8O_5Si_4$ (1051): calcd. C 50.27, H 6.90, N 10.66; found C 49.81, H 7.06, N 10.82.

O(SiMe$_2$-Ap)$_2$Y(BH$_4$)Cl(THF) Bu$_4$N (5): Compound **2** (567 mg, 1.05 mmol) and tetrabutylammonium boranate (540 mg, 2.10 mmol) were dissolved in 10 mL of THF with stirring. The solution was reduced in volume to 2 mL, then 20 mL of ether was added and the solution was stirred for 1 h. After filtration a clear colorless solution with a characteristic blue fluorescence was obtained. The solvent was removed in vacuo within 2 h to furnish a highly viscous, sticky product. Yield: 330 mg, 0.414 mmol, 39%. − ^{1}H NMR (293 K, [D$_8$]THF): δ = 7.87 (d, *J* = 5.2 Hz, 2 H, 6-H), 5.86−5.84 (m, 4 H, 3-H, 5-H), 3.61 (m, 6 H, THF), 3.29 (m, 8 H, 1′-H), 2.01 (s, 6 H, Me-pyridine), 1.75−1.71 (m, 6 H, THF), 1.65−1.62 (m, 8 H, 2′-H), 1.38−1.32 (m, 8 H, 3′-H), 0.93 (t, *J* = 7.2 Hz, 12 H, 4′-H), 0.09 (s, 12 H, Me−Si). − ^{13}C{^{1}H} NMR: δ = 170.3 (C-2), 148.6 (C-4), 145.9 (C-6), 112.5 (C-5), 108.1 (C-3), 68.2 (THF), 59.1 (C-1′), 26.2 (THF), 21.5 (Me-pyridine), 20.4 (C-3′), 14.0 (C-4′), 1.5 (Me−Si). − ^{29}Si NMR: δ = −15.6. − IR (THF): $\tilde{\nu}$ = 2278 m, 2206 m, 2135 m (B-H), 1642 w, 1603 vs, 1563 m (aromat.) cm^{-1}. − $C_{36}H_{72}BClN_5O_2Si_2Y$ (797): C 54.16, H 9.09, N 8.77, Cl 4.44; found C 54.26, H 10.21, N 8.82, Cl 4.55.

O(SiMe$_2$-Ap)$_2$Y(BH$_4$)$_2$Na(THF)$_2$ (6): With stirring NaBH$_4$ (107 mg, 2.81 mmol) was added to a solution of **2** (759 mg, 1.40 mmol) in 10 mL of THF. The resulting mixture was stirred for 72 h at 20°C and then filtered. The colorless filtrate was reduced in volume to 5 mL by vacuum evaporation. Cooling to −30°C afforded colorless needles. Yield: 292 mg, 0.523 mmol, 37%, mp: 164°C: subl. − ^{1}H NMR (293 K, C_6D_6): δ = 8.42 (broad, 2 H, 6-H), 6.17 (s, 2 H, 3-H), 6.03 (d, *J* = 5.0 Hz, 2 H, 5-H), 3.74 (t, *J* = 6.5 Hz, 8 H, THF), 1.86 (s, 6 H, Me-pyridine), 1.10 (m, 8 H, THF), 0.46 (s, 12 H, Me−Si). − ^{13}C NMR (293 K, C_6D_6): δ = 170.9 (C-2), 150.6 (C-4), 146.1 (C-6), 112.7 (C-5), 110.2 (C-3), 70.7 (THF), 25.2 (THF), 21.5 (Me-pyridine), 1.8 (Me−Si). − ^{29}Si NMR (293 K, C_6D_6): δ = −15.6. − IR (nujol): $\tilde{\nu}$ = 3316 w, 2374, 2297, 2223 m (BH$_4$), 1605 vs, 1566 w, 1532 m (C=C), 1377 m, 1329 s, 1290, 1252 s (Me−Si), 1175 s, 1057, 1028 vs (Si−O−Si), 999 m, 970 m, 892, 872 s (Me$_2$Si), 785, 776 s, 585 m cm^{-1}. − $C_{20}H_{40}B_2N_4NaO_2Si_2Y$ (558): calcd. C 43.03, H 7.22, N 10.04, Cl 0.00; found C 43.88, H 7.55, N 9.15, Cl 0.16.

O(SiMe$_2$-Ap)$_2$Y(CH(TMS)$_2$)$_2$Li(THF)$_3$ (7): An ethereal solution of bis(trimethylsilyl)methyllithium (0.973 mmol) was added dropwise to a solution of **2** (526 mg, 0.973 mmol) in 10 mL of ether. A colorless solid precipitated. After standing for 16 h at 4°C the supernatant solution was filtered through a frit (G 4). The filtrate was evaporated to dryness and the residue redissolved in a mixture of 20 mL of pentane and 3 mL of ether and filtered again. Cooling the filtrate to −78°C afforded a yellowish crystalline product. Yield: 224 mg, 0.367 mmol, 38%, mp: 175°C subl. (dec.). − ^{1}H NMR (293 K, C_6D_6: δ = 7.67 (s, broad, 2 H, 6-H), 6.22 (s, 2 H, 3-H), 6.02 (d, *J* = 4.8 Hz, 2 H, 5-H), 3.42 (broad, 12 H, THF), 1.84 (s, 6 H, Me-pyridine), 1.20 (s, 12 H, THF), 0.51 (s, 12 H, Me−Si−O), 0.40−0.35 (m, 36 H, Me−Si−C), −0.36 (s, 1 H, HC-Y), −0.82 (s, 1 H, HC−Y). − ^{13}C NMR (293 K, C_6D_6): δ = 169.6 (C-2), 150.7 (C-4), 144.2 (C-6), 113.8 (C-5), 110.9 (C-3), 69.2 (THF), 65.8 (ether), 25.2 (THF), 21.5 (Me-pyridine), 15.3 (ether), 6.6 (Me−Si), 4.4 (Me−Si), 1.7 (Me−Si), 1.5 (Me−Si). − ^{29}Si NMR (293 K, C_6D_6: δ = −0.12 (Me$_2$Si), −7.9 (Me$_3$Si), −9.1 (Me$_3$Si). − IR (nujol): $\tilde{\nu}$ = 1606 vs, 1533 w (C=C), 1377 m, 1329 m, 1296 m, 1247 s (Me−Si), 1178 m, 1045 vs, 1027 vs (Si−O−Si), 994 m, 968 w, 892 s, 862, 844, 826, 781 vs (Me$_2$Si), 676 m, 656 m, 588 m, 428 m cm^{-1}. − $C_{42}H_{86}LiN_4O_4Si_6Y$ (1114): calcd. C 51.71, H 8.89, N 5.74; found: C 51.36, H 8.30, N 5.94.

Polymerization: In a typical run ε-caprolactone/δ-valerolactone was added by syringe to a solution of **4** (24 μmol) in 10 mL THF at 20°C with vigorous magnetic stirring. After 30 min the polymerization was quenched by addition of 200 mL methanol. The precipitated polymer was redissolved in THF and precipitated again from methanol (250 mL). The polymer was filtered and dried in vacuo.

Acknowledgments

We thank Prof. U. Rosenthal for generous support and helpful discussions. Financial support from the Fonds der Chemischen Industrie and the Max-Planck-Gesellschaft is gratefully acknowledged.

[1] [1a] K. Dehnicke, *Chem. Zeitg.* **1990**, *114*, 295−304. − [1b] F. T. Edelmann, *Coord. Chem. Rev.* **1994**, *137*, 403−481. − [1c] J. Baker, M. Kilner, *Coord. Chem. Rev.* **1994**, *133*, 129−300. − [1d] F. T. Edelmann, *J. Alloys Compd.* **1994**, *207/208*, 182−188. − [1e] F. T. Edelmann, *Angew. Chem.* **1995**, *107*, 2647−2669; *Angew. Chem. Int. Ed. Engl.* **1995**, 34, 2466−2488.

[2] [2a] A. Spannenberg, P. Arndt, R. Kempe, *Angew. Chem.* **1998**, *110*, 824−827; *Angew. Chem. Int. Ed.* **1998**, 37, 832−835. − [2b] A. Spannenberg, M. Oberthür, H. Noss, A. Tillack, P. Arndt, R. Kempe, *Angew. Chem.* **1998**, *110*, 2190−2192; *Angew. Chem. Int. Ed.* **1998**, 37, 2079−2082.

[3] J. R. Hagadorn, J. Arnold, *Angew. Chem.* **1998**, *110*, 1813−1815; *Angew. Chem. Int. Ed.* **1998**, 37, 1729−1731.

[4] [4a] H. Sasai, T. Arai, Y. Satow, K. N. Houk, M. Shibasaki, *J. Am Chem. Soc.* **1995**, *117*, 6194−6198. − [4b] T. Arai, Y. M. A. Yamada, N. Yamamoto, H. Sasai, M. Shibasaki, *Chem. Eur. J.* **1996**, *2*, 1369−1372.

[5] [5a] K. C. Hultzsch, J. Okuda, *Macromol. Rapid Commun.* **1997**, *18*, 809−815. − [5b] K. C. Hultzsch, T. P. Spaniol, J. Okuda, *Organometallics* **1997**, *16*, 4845−4856.
[6] W. J. Evans, R. Anwander, R. J. Doedens, J. W. Ziller, *Angew. Chem.* **1994**, *106*, 1725−1728; *Angew. Chem. Int. Ed. Engl.* **1994**, 33, 1641−1643.
[7] [7a] M. Oberthür, P. Arndt, R. Kempe, *Chem. Ber.* **1996**, *129*, 1087−1091. − [7b] A. Spannenberg, P. Arndt, M. Oberthür, R. Kempe, *Z. Anorg. Allg. Chem.* **1997**, *623*, 389−393. − [7c] M. Oberthür, G. Hillebrand, P. Arndt, R. Kempe, *Chem. Ber./Recueil* **1997**, *130*, 789−794. − [7d] R. Kempe, M. Oberthür, G. Hillebrandt, A. Spannenberg, H. Fuhrmann, *Polimery* **1998**, *43*, 96−103.
[8] M. D. Fryzuk, J. B. Love, S. J. Rettig, *J. Am. Chem. Soc.* **1997**, *119*, 9071−9072.
[9] A. Löfgren, A.-C. Albertsson, P. Dubois, R. Jerome, *J. Macromol. Sci., Rev. Macromol. Chem. Phys.* **1995**, *C35*, 379−418.
[10] [10a] M. Hayakawa, M. Mitani, T. Yamada, T. Mukaiyama, *Macromol. Chem. Phys.* **1997**, *198*, 1305−1317. − [10b] J. Zhang, Z. Gan., Z. Zhong, X. Jing, *Polymer International* **1998**, *45*, 60−66.
[11] [11a] W. J. Evans, H. Katsumata, *Macromolecules* **1994**, *27*, 2330−2332. − [11b] W. J. Evans, H. Katsumata, *Macromolecules* **1994**, *27*, 4011−4013. − [11c] M. Yamashita, Y. Takemoto, E. Ihara, H. Yasuda, *Macromolecules* **1996**, *29*, 1798−1806.
[12] P. J. Davidson, D. H. Harris, M. F. Lappert, *J. Chem. Soc., Dalton Trans.* **1976**, 2269−2274.
[13] G. M. Sheldrick *SHELX-86: A Program for Crystal Structure Solution*, University of Göttingen, Germany, **1986**; G. M. Sheldrick, *Acta Crystallogr.* **1990**, *A46*, 467.
[14] G. M. Sheldrick *SHELXL-93: A Program for Crystal Structure Refinement*, University of Göttingen, Germany, **1993**.

Received May 25, 1999
[I99187]

Water/Ethanol Displacement Reactions in Vanadyl Phosphate

Ludvík Beneš,*[a] Klára Melánová,[a] Miroslava Trchová,[b] Pavla Čapková,[b] and Pavel Matějka[c]

Keywords: Intercalations / Vanadyl phosphate / Ethanol / Hydration / Kinetics

The course of the replacement of ethanol by water molecules in the $VOPO_4{\cdot}2C_2H_5OH$ intercalate, and of water by ethanol in $VOPO_4{\cdot}2H_2O$ has been studied by X-ray diffraction and infrared and Raman spectroscopy. Formation of mixed phase $VOPO_4{\cdot}C_2H_5OH{\cdot}H_2O$ was not observed. The shape of the kinetics curves indicates a transition of at least one reaction zone through the crystal. A delay in formation of the product in comparison with the decrease in the amount of starting material can be explained by the existence of non-diffracting advancing phase boundary. In a $VOPO_4$/ethanol/water system, $VOPO_4{\cdot}2C_2H_5OH$ is formed as the only product when the system contained more than 96 vol% of ethanol, whereas in the system with less than 94 vol% of ethanol only $VOPO_4{\cdot}2H_2O$ is present.

Introduction

Compounds based on vanadyl phosphate are of great interest because of their catalytic properties for oxidation. The structure of vanadyl phosphate dihydrate, $VOPO_4{\cdot}2H_2O$, has been determined by Tietze using X-ray diffraction[1] as tetragonal, space group *P*4/*nmm*, a = 6.202 Å and c = 7.410 Å. Tachez et al.[2] used neutron powder diffraction of the deuterated compound in order to determine the positions of hydrogen atoms and determined the space group *P*4/*n*, a = 6.215 Å and c = 7.403 Å. The layers are built up of PO_4 tetrahedra linked to distorted VO_6 octahedra by sharing four equatorial oxygen atoms. VO_6 octahedra are completed by axial oxygens, one of which is a vanadyl oxygen, and the second of which belongs to the interlayer water molecule coordinated to vanadium. The second water molecule is bonded by weak H-bridges between the $VOPO_4$ layers.

Vanadyl phosphate is a good host structure for intercalation of organic molecules with suitable functional groups.[3] Intercalation compounds of vanadyl phosphate with aliphatic and aromatic amines,[4–6] heterocycles,[7] alcohols and diols,[8] carboxylic acids[9] and their amides[10] have been studied. From this point of view, vanadyl phosphate dihydrate can be regarded as an intercalate of α_I-$VOPO_4$ with water.

The time course of intercalation of water into α_I-$VOPO_4$ has been followed by TMA, XRD[11] and infrared and Raman spectroscopy.[12] Formation of vanadyl phosphate monohydrate was not observed during hydration of the anhydrous form under ambient conditions. Instead, the broadening and the shift of positions of the (00*l*) diffraction lines were observed. These phenomena were explained by formation of a Hendricks–Teller disordered layered structure, which is composed of the α_I-$VOPO_4$ and $VOPO_4{\cdot}2H_2O$ layers. The vanadyl stretching band appears to be especially sensitive to atoms coordinated to the vanadium within an octahedral arrangement in the host lattice structure. During the intercalation, the position of this band at 1035 cm^{-1} in the anhydrous form changes to 995 cm^{-1}, which are typical values for mono- and dihydrates. The additional peak at 1017 cm^{-1} occurring in the initial stages of intercalation was explained in terms of a random stacking of intercalated and non-intercalated layers in the sample.

Ethanol can be intercalated into anhydrous vanadyl phosphate[13] or it can replace the water molecules in $VOPO_4{\cdot}2H_2O$.[8] The kinetics of intercalation of ethanol into anhydrous vanadyl phosphate were studied by XRD and a volumetric method, and the kinetics curves obtained were found to have a sigmoidal shape.[14] During intercalation, the original host and the intercalate are present in one crystal. Both phases are separated by an advancing phase boundary.[15] A molecular mechanics simulation, combined with X-ray diffraction and supported by vibrational spectroscopy, was used to investigate the layered structure of vanadyl phosphate $VOPO_4$ intercalated with ethanol.[16] The bilayer arrangement of ethanol molecules in the interlayer was found, giving the calculated basal spacing d = 13.21 Å; the experimental d value obtained from X-ray diffraction is 13.17 Å. One half of the total number of CH_3CH_2OH molecules is anchored by their oxygen to $VOPO_4$ layers to complete the vanadium octahedra and their orientation is not very strictly defined. The second half of the ethanol molecules are linked by hydrogen bonds to the anchored ethanol and sometimes also to the layer oxygen. The position and orientation of this anchored ethanol with respect to $VOPO_4$ layers exhibits a certain degree of disorder, resulting in the disorder in the layer stacking.

[a] Joint Laboratory of Solid State Chemistry of the Academy of Sciences of the Czech Republic and University of Pardubice, Studentská 84, 532 10 Pardubice, Czech Republic
Fax: (internat.) + 420-40/6036011
E-mail: ludvik.benes@upce.cz
[b] Faculty of Mathematics and Physics, Charles University, Ke Karlovu 3, 121 16 Prague, Czech Republic
[c] Department of Analytical Chemistry, Institute of Chemical Technology, Technická 5, 166 28 Prague, Czech Republic

 © WILEY-VCH Verlag GmbH, D-69451 Weinheim, 1999 1434–1948/99/1212–2289 $ 17.50+.50/0

Owing to the instability of $VOPO_4{\cdot}2C_2H_5OH$ when exposed to air, the water molecules intercalate into this system at room temperature by simply keeping the compounds under ambient conditions. The course of reintercalation of water molecules into vanadyl phosphate intercalate with ethanol was studied by X-ray diffraction and infrared and Raman spectroscopy. The aim of this work is to contribute to the elucidation of the mechanism of water/ethanol displacement in vanadyl phosphate.

Results and Discussion

X-ray Study

In order to study an equilibration in a $VOPO_4$/ethanol/water system, $VOPO_4{\cdot}2H_2O$ was contacted with ethanol containing a known amount of water. The dependence of the basal spacing of solid products on the concentration of ethanol is shown in Figure 1. It is evident that only two phases are formed in this system. A mixture of $VOPO_4{\cdot}2C_2H_5OH$ and $VOPO_4{\cdot}2H_2O$ phases is formed in the ethanol/water solvent containing from 94 to 96 vol% of ethanol. Above 96 vol% of ethanol, only $VOPO_4{\cdot}2C_2H_5OH$ (basal spacing 13.17Å) is present, whereas below 94 vol% of ethanol in the solvent mixture only $VOPO_4{\cdot}2H_2O$ (7.41 Å) is formed. These results were obtained from the properties of the binary alcohol/water mixture, where an azeotrope with 96 vol% of ethanol is formed as a mixture with the most stable structure. Ethanol containing a lower content of water is hygroscopic and tends to take up water. Therefore, water is taken from $VOPO_4{\cdot}2H_2O$ and the water molecules in the interlayer space are replaced by ethanol molecules. The solvent with more than 6% of water, on the other hand, can provide water molecules to replace ethanol in $VOPO_4{\cdot}2C_2H_5OH$ and leads to the formation of $VOPO_4{\cdot}2H_2O$. This means that the co-intercalate $VOPO_4{\cdot}C_2H_5OH{\cdot}H_2O$ containing molecules of ethanol and water together was not observed. The co-intercalate of this type was reported by Matsubayashi as a starting material for the intercalation of ferrocene into $VOPO_4$.[17] Practically the same result is obtained when $VOPO_4{\cdot}2C_2H_5OH$ is contacted with ethanol/water mixtures.

In situ X-ray diffraction was employed to follow the reaction of polycrystalline $VOPO_4{\cdot}2H_2O$ with ethanol vapors. The lines observed in the diffractograms belong to either vanadyl phosphate dihydrate or ethanol-intercalated vanadyl phosphate, indicating that there is no intermediate product such as $VOPO_4{\cdot}C_2H_5OH{\cdot}H_2O$. In the region investigated, four sharp (00*l*) lines of the intercalate were observed, which gave the same value for the basal spacing. The interlayer distances calculated from the (00*l*) reflections of both phases remain constant. Small changes of linewidths during reintercalation can be explained by a decrease in the size of an area of the dihydrate and an increase in the size of an area of the intercalate formed in the crystals. It can be assumed from the XRD results that the intercalate is formed directly in the majority of the crystals,

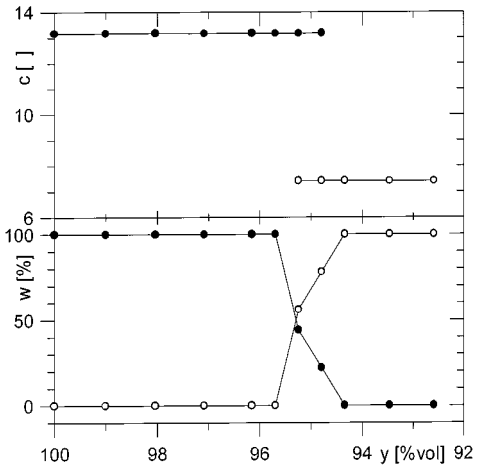


Figure 1. Basal spacing and content of the solid products in the $VOPO_4$/water/ethanol system

without any occurrence of random stacking of the layers (Hendricks–Teller effect).

The dependence of the extent of reaction of dihydrate (α_H) and ethanol intercalate (α_E) on reaction time is shown in Figure 2. The reintercalation process starts very quickly. The kinetics curves do not have a sigmoidal shape. Their shape could probably be described as exponential or, better still, as a combination of parabolic and linear dependences. This type of kinetic curve has been found for some heterogeneous oxidations of metals with gaseous oxygen[18–20] or during reactions of metals with sulfur vapors.[21–23] This type of reaction is supposed to be a two-step process. In our case, the first step may involve replacement of the water molecules by ethanol and the second step could be a rearrangement of the ethanol molecules to form bilayers in the interlayer space. This idea is supported by the existence of the non-diffracting phase, which separates pristine and intercalated parts of the crystals as an advanced phase boundary.[15][24] In this very disordered zone of the crystals, the host layers are bent so that segments with variable interlayer distance containing a mixture of both guests are formed. In addition, interlayer spaces filled with water or ethanol molecules can vary along the *c* axis in this zone. The amount of this non-diffracting phase corresponds to a difference of $\alpha_H - \alpha_E$, which is shown in Figure 2 (open circles). This phase is formed very quickly and then slowly transforms to the product during the reaction.

A progressive hydration of the intercalate $VOPO_4{\cdot}2C_2H_5OH$ was studied by XRD at several relative humidities (r.h.). The course of hydration is similar for relative humidities lower than 75%. The exchange of ethanol molecules for water is also fast and the reaction time depends on the relative humidity used and sample thickness. The lines observed in the diffractograms belong to either vanadyl phosphate dihydrate or ethanol-intercalated vanadyl phosphate, indicating that, as in the reaction of $VOPO_4{\cdot}2H_2O$ with ethanol, there is no crystalline intermediate product such as $VOPO_4{\cdot}C_2H_5OH{\cdot}H_2O$. All diffraction lines (00*l*) are sharp and their positions do not change.

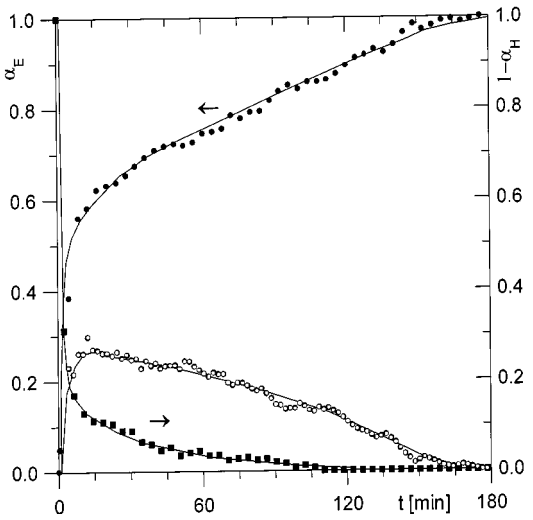


Figure 2. Dependence of the extent of reaction of the parent vanadyl phosphate dihydrate α_H and the product α_E on time t obtained by XRD during reintercalation of $VOPO_4{\cdot}2H_2O$ with ethanol vapours; the difference $\alpha_H-\alpha_E$ (open circles) corresponds to the amount of non-diffracting phase

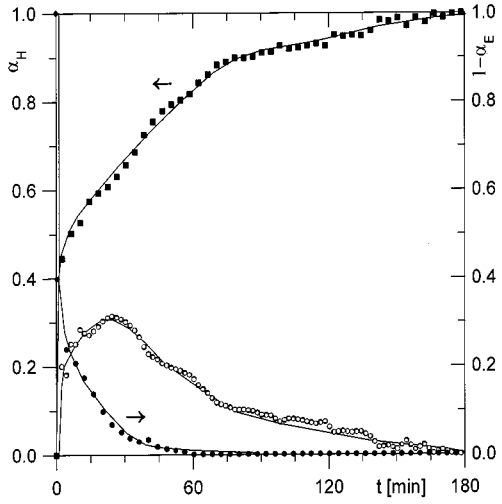


Figure 3. Dependence of the extent of reaction of the ethanol intercalate α_E and the product α_H on time t obtained by XRD during hydration of the ethanol intercalate at 11% r.h; the difference $\alpha_E-\alpha_H$ (open circles) corresponds to the amount of non-diffracting phase

The dependence of the extent of reaction of ethanol intercalate and dihydrate at r.h. = 11% on the reaction time is shown in Figure 3. The shape of the kinetic curves is very similar to those in the case of the formation of ethanol intercalate and, indeed, a similar mechanism is presumed to be operating. The formation of non-diffracting phases was also observed.

A different course of reaction was observed at high humidities. Changes in the diffractograms during hydration at 92% r.h. are shown in Figure 4. The ethanol intercalate is transformed to vanadyl phosphate pentahydrate (basal spacing 10.5 Å) very quickly. The intensity of the series of three (00*l*) lines of $VOPO_4{\cdot}5H_2O$ decreases during hydration and the dihydrate is formed. This process is supported by two factors: the large interlayer distance in $VOPO_4{\cdot}2C_2H_5OH$ (compared with $VOPO_4{\cdot}2H_2O$) and the high concentration of water molecules in air at 92% r.h. The attacking water molecules fill the interlayer space after the release of ethanol before the layers are able to move closer together. The unstable pentahydrate formed then slowly decomposes to the dihydrate.

FTIR Spectroscopy

IR spectra of $VOPO_4{\cdot}2C_2H_5OH$ and its spectra upon progressive hydration by atmospheric water are shown in Figure 5 together with the spectrum of pure ethanol. One can easily identify the bands corresponding to the ethanol molecules. The ethanol bands maintain the same position in the IR spectra of the intercalate as in pure ethanol. This

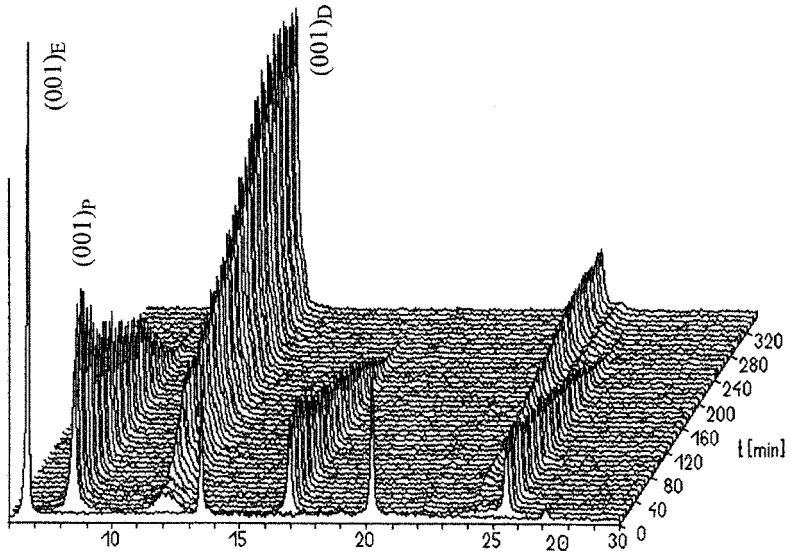


Figure 4. The changes of the diffractograms during hydration of $VOPO_4{\cdot}2C_2H_5OH$ at 92% r.h.

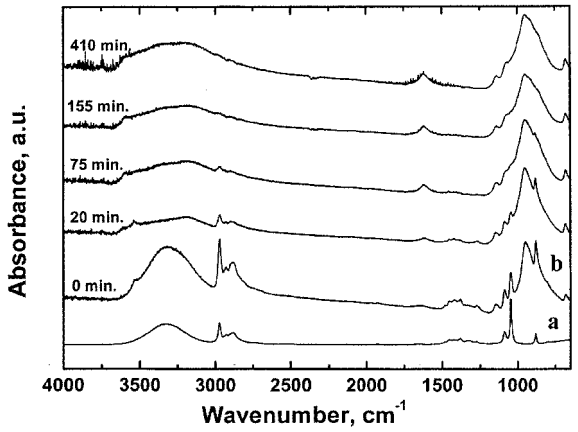


Figure 5. IR spectrum of pure ethanol (a) and $VOPO_4{\cdot}2C_2H_5OH$ (b) as a function of time of hydration by atmospheric water molecules

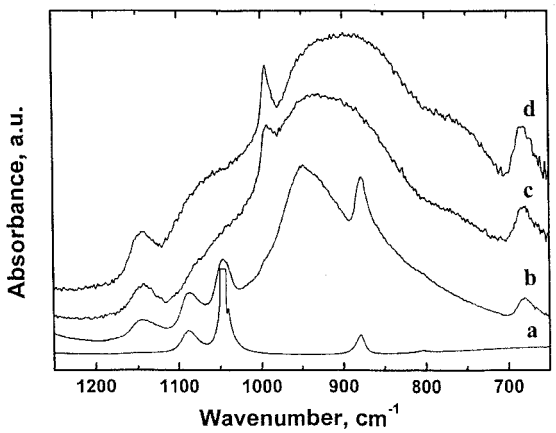


Figure 6. IR spectra of pure ethanol (a), $VOPO_4{\cdot}2C_2H_5OH$ (b), this intercalate upon 24 hours of hydration by atmospheric water (c) and $VOPO_4{\cdot}2H_2O$ (d)

is due to the weak ethanol−layer bonding.[25] IR spectra of $VOPO_4{\cdot}2C_2H_5OH$ and $VOPO_4{\cdot}2H_2O$ are given in Figure 6. In the IR spectra of the dihydrate and intercalate we can see the same bands at the same positions (see Table 1). The broadened band in the spectrum of the $VOPO_4{\cdot}2H_2O$ (with the center of gravity at about 920 cm^{-1}) contains a mixture of overlapping bands: $\nu_1(PO_4)$, $\delta(P-O-V)$ and $\rho(H_2O)$. It is evident that this band changes its profile on going from $VOPO_4{\cdot}2C_2H_5OH$ to the dihydrate. Evidence for this is that $\rho(H_2O)$ bands are absent and $\delta(P-O-V)$ deformation bands are suppressed in the intercalate due to the smaller number of hydrogen bonds between ethanol and the host layers in comparison with the network of hydrogen bonds in $VOPO_4{\cdot}2H_2O$. The band due to the degenerate asymmetric stretching vibration $\nu_3(PO_4)$ is active only in the IR spectra and its position at 1143 cm^{-1} is the same as in the intercalate. Only one band of a stretching V=O vibration is observed in the spectra of $VOPO_4{\cdot}2C_2H_5OH$ and $VOPO_4{\cdot}2H_2O$ and this occurs at the same position (995 cm^{-1}). The same is valid for the lattice vibration at 681 cm^{-1}.

In agreement with other authors[26] we believe that the sharp bands near 3600 and 1620 cm^{-1} in the spectrum of $VOPO_4{\cdot}2H_2O$ (see Figure 5) are due to strongly bonded water molecules within the crystalline lattice associated with the water molecule bound to vanadium. The additional lattice water is indicated by the broad bands near 3300 and 1620 cm^{-1} in the spectrum of the dihydrate. In the bending vibration at 1620 cm^{-1}, sharp and broad bands are superimposed. In the spectrum of intercalate at the beginning of the hydration process (0 min.) we can assign the sharp bands near 3600 cm^{-1} to the ethanol molecule that is strongly bonded to vanadium (this peak is absent in the spectrum of pure ethanol). The broad band at 3350 cm^{-1} corresponds to the stretching vibration of OH groups in ethanol molecules.

During the hydration process of $VOPO_4{\cdot}2C_2H_5OH$ in air the ethanol vibration bands gradually disappear and the bands corresponding to the water molecules in $VOPO_4{\cdot}2H_2O$ appear. After 24 hours of exposure to air the IR spectrum of the intercalate had completely changed to give the IR spectrum of the dihydrate (see Figure 6). Intermediate phases were not observed during the hydration process of $VOPO_4{\cdot}2C_2H_5OH$.

Table 1. Infrared (IR) and Raman (Ra) frequencies (cm^{-1}) of $VOPO_4{\cdot}2H_2O$ and $VOPO_4{\cdot}2C_2H_5OH$ (c.g.: center of gravity; s: strong; w: weak; sh: shoulder)

Vibration	$\nu_1(PO_4)$ symmetric stretching	$\nu_2(PO_4)$ symmetric bending	$\nu_3(PO_4)$ asymmetric stretching	$\nu_4(PO_4)$ asymmetric bending	lattice	V=O stretching	$\nu_2(H_2O)$	$\nu_1(H_2O)$
$VOPO_4{\cdot}2H_2O$								
IR	c.g. 920	Not observable	1143 1076 w	Not observable	681	995	3130 3310 3500 sh 3600 sh	1615
Ra	945 s 929 sh	460 433	Not observable	579 541	Inactive	1035 985	Inactive	–
VOPO4·2 C_2H_5OH								
IR	c.g. 920	Not observable	1143 Et. band ov.	Not observable	681	995	3350 3600	–
Ra	937 s	–	1147	591 542	Inactive	1029 990	Inactive	–

Raman Spectroscopy

The Raman spectra of anhydrous $VOPO_4$, $VOPO_4{\cdot}2C_2H_5OH$, the intermediate states obtained by hydration with atmospheric water, and $VOPO_4{\cdot}2H_2O$ are shown in Figure 7. The ethanol bands in the Raman spectrum of $VOPO_4{\cdot}2C_2H_5OH$ are in exactly the same positions as in the spectrum of pure ethanol. Consequently, the ethanol spectrum can be subtracted from the spectrum of the intercalate. As a result of this subtraction we obtained the spectrum of the intercalate without ethanol bands, which is more convenient for the comparison of bands corresponding to the $VOPO_4$ layers in the dihydrate, anhydrous, and intercalated structure. The most intense band of the Raman spectrum, with a maximum at about 929 cm^{-1} in the anhydrous form, at 937 cm^{-1} in $VOPO_4{\cdot}2C_2H_5OH$, and at 945 cm^{-1} in $VOPO_4{\cdot}2H_2O$, corresponds to the symmetric stretching vibration $\nu_1(PO_4)$. This band is especially active in the Raman spectra. The bands of the degenerate asymmetric stretching vibration $\nu_3(PO_4)$ are not observed in the Raman spectra. In addition, the bands due to symmetric bending vibrations [$\nu_4(PO_4)$ at 579 cm^{-1} and 541 cm^{-1}] and bands due to asymmetric bending vibrations [$\nu_2(PO_4)$ at 460 and 433 cm^{-1}] are observed in the Raman spectra of the samples. Two bands can be observed at 1029 and 990 cm^{-1} in the Raman spectrum of the host structure and these correspond to the V=O stretching mode. The vanadyl stretching band is especially sensitive to the local coordination of vanadium and two peaks indicate the presence of anhydrous and hydrated forms of $VOPO_4$. Only one peak at 1036 cm^{-1} is observed in the anhydrous form. The partial escape of water in the hydrated form is due to the heating caused by a laser beam during the measurements (for a detailed explanation see ref.[12]). In the case of $VOPO_4{\cdot}2C_2H_5OH$, these bands are slightly shifted and broadened. This broadening of V=O stretching bands reflects the disorder in the position of ethanol molecules found by molecular simulations.[25] The irregularity in hydrogen bonding of ethanol to PO_4 oxygen atoms also affects the PO_4 stretching and bending modes.

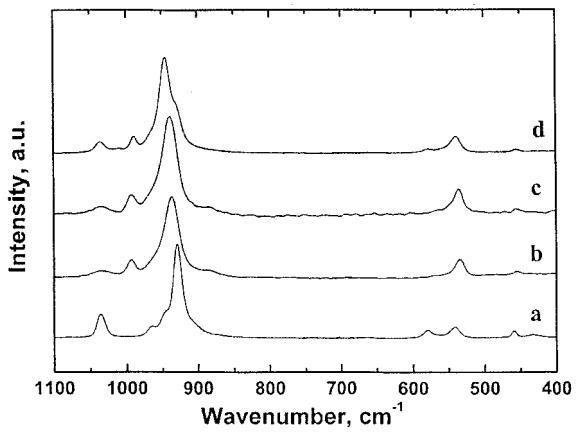


Figure 7. Raman spectra of anhydrous $VOPO_4$ (a), $VOPO_4{\cdot}2C_2H_5OH$ (b), the intermediate state of hydration (c) and $VOPO_4{\cdot}2H_2O$ (d). The ethanol spectrum was subtracted from the spectrum of $VOPO_4{\cdot}2C_2H_5OH$

Conclusions

A progressive hydration of $VOPO_4{\cdot}2C_2H_5OH$ has been studied by X-ray analysis and ATR FTIR and Raman spectroscopy. The mixed intercalate $VOPO_4{\cdot}C_2H_5OH{\cdot}H_2O$ is not formed during hydration of $VOPO_4{\cdot}2C_2H_5OH$. During this hydration, only vanadyl phosphate dihydrate or pentahydrate (at high relative humidity) are formed. In contrast to the intercalation of ethanol into anhydrous vanadyl phosphate, the kinetic curves of reintercalation of dihydrate do not have a sigmoidal shape. The shape of the kinetic curve indicates a transition of at least one reaction zone through the crystal. A similar course is also observed for the reintercalation of $VOPO_4{\cdot}2H_2O$ with ethanol. A delay in the formation of the product in comparison with the decrease in the amount of starting material is explained by the existence of very disordered phase.

The reintercalation reactions are very fast and their activation energy is presumed to be very low compared with that of intercalation of water or ethanol into anhydrous $VOPO_4$. This is due to the sufficient interlayer distance in the starting materials. Moreover, no energy is needed for V=O···V bond breaking, as is seen in the case of intercalation into anhydrous $VOPO_4$.[14] As inferred from the constant position of the stretching V=O vibration during hydration of $VOPO_4{\cdot}2C_2H_5OH$, both guests are anchored to the host layers by similar bonds and therefore no large change in the bond energy is expected during the reaction.

Experimental Section

The samples of $VOPO_4{\cdot}2C_2H_5OH$ for the IR and Raman measurements were prepared by suspending solid $VOPO_4{\cdot}2H_2O$ in dry ethanol for two hours. After filtration, the product was dried in nitrogen and kept in sealed ampoules. The study of the equilibration in the $VOPO_4$/ethanol/water system was carried out by contacting $VOPO_4{\cdot}2H_2O$ or $VOPO_4{\cdot}2C_2H_5OH$ (0.25 g) with 10 mL of ethanol/water mixture (from 92.5 to 100 vol% of ethanol) for two hours. The powder data of the intercalates with a small excess of the guest were obtained with an X-ray diffractometer HZG-4 (Präzisionsmechanik, Germany) using Cu-K_α radiation with discrimination from Cu-K_β by a Ni-filter. The exchange reactions were performed in the following way: the sample of $VOPO_4{\cdot}2H_2O$ or $VOPO_4{\cdot}2C_2H_5OH$ was placed on the surface of a thermostated (25°C) corundum target plate under dry nitrogen, whereupon the stream (ca. 0.5 $Lmin^{-1}$) of nitrogen saturated with vapors of ethanol or water was introduced onto the sample. The reaction taking place in the solid phase was monitored by recording the diffractograms (from $6 < 2\theta < 30$) at 8 minute intervals. The intensities of the (001) reflections of $VOPO_4{\cdot}2H_2O$ and $VOPO_4{\cdot}2C_2H_5OH$ were obtained from diffractograms measured from $5.5 < 2\theta < 15$ at 4 minute intervals. The extent of reaction, α_P, for the product at time t is given by the equation:

$$\alpha_P = B/B_\infty$$

where B is the intensity of the (001) line of the product at time t and B_∞ is this intensity at infinite time. Analogously, the equation:

$$\alpha_S = 1 - A/A_0$$

describing the extent of the reaction, α_S, for the decrease in the amount of the starting material at time t can be defined, where A

is the intensity of the (001) line of the starting material at time t and A_0 is this intensity at time $t = 0$. Depending on the direction of the reaction, $\alpha_P = \alpha_E$ and $\alpha_S = \alpha_H$ when the starting material is dihydrate, whereas $\alpha_P = \alpha_H$ and $\alpha_S = \alpha_E$ when the starting material is the ethanol intercalate.

Infrared measurements were carried out using a NICOLET IMPACT 400 Fourier transform infrared (FTIR) spectrophotometer in an H_2O-purged environment. An ambient-temperature deuterated triglycine sulfate (DTGS) detector was used for the wavelength range from 400 to 4000 cm^{-1}. A Happ-Genzel apodization function was used in the whole region and the spectral resolution was 2 cm^{-1}. Approximately 300 scans were coadded to achieve the signal-to-noise ratio shown. The Baseline Horizontal Attenuated Total Reflection (ATR) accessory with ZnSe crystal ($n = 2.4$ at 1000 cm^{-1}) was used for measurements of infrared spectra of the samples. In our experiments the effective path length was approximately a few μm (angle of incidence = 60°, number of reflections = 7). The ATR correction was performed in order to eliminate the dependence of the effective path length on the wavelength. After some trials it was found that the best results were obtained, if a sample is exposed for a definite time to the external conditions without removing the sample from the crystal between the subsequent spectral measurements. In this situation the water molecules arrive at the surface of the ZnSe crystal from the bulk volume and the adsorption of water at the measured surface of the sample is avoided.

FT Raman spectra were collected using an Equinox 55/S Fourier transform near-infrared (FT-NIR) spectrometer (Bruker) equipped with FT Raman module FRA 106/S (Bruker). The samples were irradiated by the focused laser beam (power 100 mW) of an Nd-YAG laser (1064 nm, Coherent). The scattered light was collected in backscattering geometry. A quartz beamsplitter and Ge detector (liquid N_2 cooled) were used to obtain interferograms. 128 interferograms were co-added and then processed by Fourier transformation with Blackman-Harris 4-term apodization and a zerofilling factor of 8 to obtain final FT Raman spectra in the range 4000−1000 cm^{-1} with 4 cm^{-1} resolution.

The FT Raman spectra of pure species ($VOPO_4$, $VOPO_4 \cdot 2H_2O$, $VOPO_4 \cdot 2C_2H_5OH$) were obtained from samples in sealed glass ampoules. In each case the glass ampoule was placed in the sample holder and aligned by the motorized x-y-z sample stage to achieve the optimal optical condition of irradiation of the sample and of the collection of the scattered light. The FT Raman spectra collected during the intercalation of water were obtained from the samples placed in the aluminium cup. The aluminium cup was optically pre-aligned using sulfur as a sample, and then sulfur was replaced by the particular sample studied.

Acknowledgments

We are grateful to Professor J. Votinský from University of Pardubice for fruitful discussions and Professor B. Strauch from Charles University for help with interpretation of spectra. This work was supported by the Grant Agency of the Czech Republic, grant no: 203/97/1010 and Grant Agency GAUK, grant no: 37/97/B.

[1] H. R. Tietze, *Aust. J. Chem.* **1981**, *34*, 2035−2038.
[2] M. Tachez, F. Theobald, J. Bernard, A. W. Hewat, *Rev. Chim. Minerale* **1982**, *19*, 291−300.
[3] J. Kalousová, J. Votinský, L. Beneš, K. Melánová, V. Zima, *Collect. Czech. Chem. Commun.* **1998**, *63*, 1−19.
[4] K. Beneke, G. Lagaly, *Inorg. Chem.* **1983**, *22*, 1503−1507.
[5] L. Beneš, R. Hyklová, J. Kalousová, J. Votinský, *Inorg. Chim. Acta* **1990**, *177*, 71−74.
[6] N. Kinomura, T. Toyama, N. Kumada, *Solid State Ionics* **1995**, *78*, 281−286.
[7] J. W. Johnson, A. J. Jacobson, J. F. Brody, S. M. Rich, *Inorg. Chem.* **1982**, *21*, 3820−3825.
[8] L. Beneš, K. Melánová, V. Zima, J. Kalousová, J. Votinský, *Inorg. Chem.* **1997**, *36*, 2850−2853.
[9] L. Beneš, J. Votinský, J. Kalousová, K. Handlíř, *Inorg. Chim. Acta* **1990**, *176*, 255−259.
[10] M. Martinez-Lara, L. Moreno-Real, A. Jimenez-Lopez, S. Bruque-Gamez, A. Rodriguez-Garcia, *Mat. Res. Bull.* **1986**, *21*, 13−23.
[11] L. Beneš, V. Zima, *J. Incl. Phenom.* **1995**, *20*, 381−391.
[12] M. Trchová, P. Čapková, K. Melánová, L. Beneš, P. Matějka, *J. Solid State Chem.* in press.
[13] L. Beneš, J. Votinský, J. Kalousová, J. Klikorka, *Inorg. Chim. Acta* **1986**, *114*, 47−50.
[14] L. Beneš, V. Zima, I. Baudyšová, J. Votinský, *J. Incl. Phenom.* **1996**, *26*, 311−319.
[15] G. Alberti, *Acc. Chem. Res.* **1978**, *11*, 163 −170.
[16] P. Čapková, D. Janeba, L. Beneš, K. Melánová, H. Schenk, *J. Mol. Model.* **1998**, *4*, 150−157.
[17] G. Matsubayashi, S. Ohta, *Chem. Lett.* **1990**, 787−790.
[18] G. Valensi, *J. Chim. Phys.* **1950**, *47*, 489−505.
[19] W. W. Webb, J. J. Norton, C. Wagner, *J. Electrochem. Soc.* **1956**, *103*, 107−111.
[20] W. B. Jepson, D. W. Alymore, *J. Electrochem. Soc.* **1961**, *108*, 942−947.
[21] M. Billy, G. Valensi, *J. Chim. Phys.* **1956**, *53*, 832−844.
[22] I. Czerski, S. Mrowec, T. Werber, *J. Electrochem. Soc.* **1962**, *109*, 273−278.
[23] J. C. Colson, D. Delafosse, P. Barret, *Bull. Soc. Chim. Fr.* **1968**, *1*, 146−154.
[24] L. Beneš, K. Melánová, V. Zima, J. Kalousová, J. Votinský, *J. Incl. Phenom.* **1998**, 31, 275−286.
[25] P. Čapková, M. Trchová, P. Matějka, J. Votinský, H. Schenk, *J. Mol. Model.* **1998**, *4*, 284−293.
[26] M. R. Antonio, R. L. Barbour, P. R. Blum, *Inorg. Chem.* **1987**, *26*, 1235−1243.

Received May 28, 1999
[I99198]

The Dramatic Influence of Diamidoamine Ligands on the Structure and Reactivity of Low-Valent Tin and Bismuth Derivatives

Jean-Luc Fauré,[a] Heinz Gornitzka,[a] Régis Réau,[a] Dietmar Stalke,[b] and Guy Bertrand*[a]

Keywords: Lewis acids / Bismuth / Aluminum / Phosphorus / Tin

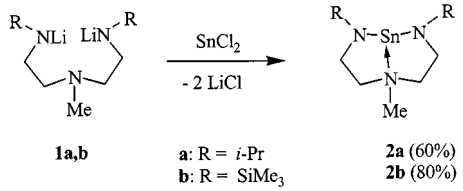
The dilithium salts of *N*-methyl-*N*′,*N*′′-bis(diisopropyl)- and -(trimethylsilyl)-diethylenetriamine **1a**,**b** react with $SnCl_2$ affording the corresponding stannylenes **2a,b** in 60 and 80% yield, respectively. Compound **1b** also reacts with $BiCl_3$ to give the bismuth chloride **5** (90% yield). Derivatives **2b** and **5** have a symmetrical bicyclic structure and are monomeric both in solution and in the solid state. When **2b** is treated with $BiCl_3$ or PCl_3, an oxidation reaction leads to the hypercoordinated tin(IV) dichloride **3** (58% yield), or a transmetallation gives rise to the oniophosphane **4** (95% yield), respectively. Transmetalation reactions also occurred when **5** was treated with $AlCl_3$, $GaCl_3$ or $SnCl_2$ affording the corresponding aluminum chloride **6** (81% yield), gallium chloride **7** (38% yield) or tin dichloride **3** (38% yield). The observed reactivity for **2** and **5** is compared to that reported for Veith's stannylene or bismuth chloride.

Introduction

Compounds containing low-valent group 14 and 15 elements have attracted interest in recent times not only because of their inherently high reactivity,[1] but also because of their importance as heterogeneous catalysts[2] and as precursors for superconducting materials in MOCVD processes.[3] One of the main problems has been with the ligand design, balancing the duality between stability and reactivity.[4] We have recently shown that diamidoamino ligands $[(RNCH_2CH_2)_2NR']^{2-}$, initially developed by Cloke,[5] are powerful tools for stabilizing a large variety of group 13 Lewis acids.[6] Here we report the synthesis and reactivity of diamidoamino-stannylene and -bismuth(III)chloride derivatives, which are monomeric even in the solid state. The reactivity of these derivatives appears to be totally different from that observed with diamido-stannylenes (**I**) and -bismuth chloride derivatives (**II**) as reported by Veith et al.

Results and Discussion

The dilithium salts **1a,b**[6a] react in ether at −78°C with $SnCl_2$ to give the corresponding stannylenes **2a,b**, which were isolated in 60 and 80% yields, respectively (Scheme 1). The ^{13}C NMR spectra show the presence of only two types of CH_2 groups, which is consistent with monomeric structures. The high field ^{119}Sn NMR chemical shifts [(C_6D_6, 298 K): **2a**, +129; **2b**, +158] strongly suggest the coordination of the amino nitrogen to the tin center, leading to a bicyclic structure.[7] This is confirmed by the presence of tin satellites for the N−Me signals in the ^1H and ^{13}C NMR spectra [**2a**: $\delta(^{13}C) = 49.0$, $^2J(^{119}SnC) = 50.2$ Hz; $\delta(^1H) = 2.11$, $^3J(^{119}SnH) = 20.0$ Hz]. Both the monomeric nature and the intramolecular coordination are retained in the solid state as shown by the molecular structure of **2b** (Figure 1). The geometric parameters around the tin center approach those of a trigonal monopyramidal geometry, indicating significant s-character for the lone pair.



Scheme 1. Synthesis of stannylenes **2**

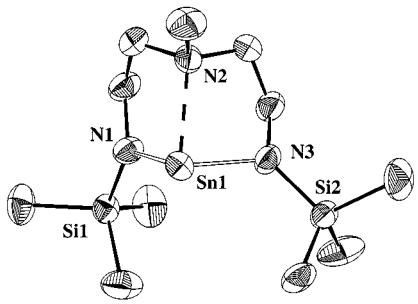
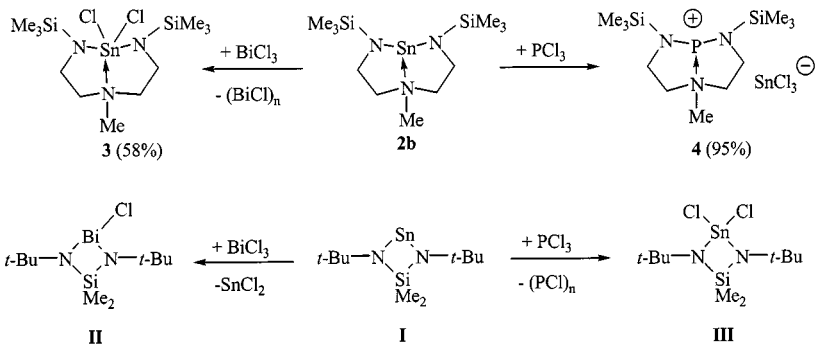


Figure 1. Molecular structure of **2b**; selected bond lengths [Å] and angles [°]: N1−Sn1 2.117(6), N2−Sn1 2.323(6), N3−Sn1 2.082(5), N1−Si1 1.712(6), N3−Si2 1.706(3); N1−Sn1−N2 77.4(2), N2−Sn1−N3 79.0(2), N1−Sn1−N3 98.1(2).

[a] Laboratoire d'Hétérochimie Fondamentale et Appliquée, Université Paul Sabatier,
118 route de Narbonne, F-31062 Toulouse cedex 04, France
Fax: (internat.) + 33-(0)561/558204
E-mail: gbertran@ramses.ups-tlse.fr
[b] Institut für Anorganische Chemie der Universität Würzburg,
Am Hubland, D-97074 Würzburg, Germany
Fax: (internat.) + 49-(0)931/888-4619
E-mail: dstalke@chemie.uni-wuerzburg.de

 © WILEY-VCH Verlag GmbH, D-69451 Weinheim, 1999 1434−1948/99/1212−2295 $ 17.50+.50/0



Scheme 2. Compared reactivity of **2b** and **I**

The reactivity of **2b** is "opposite" to that observed for Veith's stannylene **I**[8] (Scheme 2). An oxidation reaction occurs upon addition of an equimolar amount of $BiCl_3$ to a thf solution of **2b** leading to the hypercoordinate tin(IV)dichloride **3** (58% yield), whereas with **I** a transmetalation reaction was observed[8c] giving rise to the bismuth chloride **II**. In contrast, an exchange reaction occurs on treatment of **2b** with one equivalent of PCl_3 leading to **4** (95% yield), while Veith[8d] noticed the oxidation of the stannylene **I** into **III**.

Interestingly, the ^1H and ^{13}C NMR spectra suggest the coordination of the amino nitrogen to the phosphorus center [CH_3N: $\delta(^1H) = 2.74$, $^3J_{PH} = 13.5$ Hz; $\delta(^{13}C) = 51.7$, $^2J_{PC} = 5.9$ Hz]. A single crystal X-ray diffraction study not only confirmed the bicyclic structure but also showed the ionic nature of **4** (Figure 2).

In order to further compare diamidoamino ligands with diamido ligands we focused our attention on the corresponding bismuth(III) chloride derivative **5**. This product was obtained in 90% yield by treatment of a toluene solution of the dilithium salt **1b** with $BiCl_3$ at −78°C (Scheme 3). Both the monomeric and bicyclic structure of **5** were supported by the ^1H and ^{13}C NMR spectroscopic data in solution. In the solid state, the closest intermolecular Bi···Cl contact is of 3.725 Å. This value is not appreciably larger than those observed in the polymeric (3.047 Å) and dimeric (3.554 Å) bismuth chlorides **II** and **IV**, prepared by Veith[8b] and Raston,[9] respectively. However, since in **5** the intermolecular Bi···Bi distance is short (3.731 Å) and the value of the Bi−Cl−Bi angle is small (69.13°), this compound is best regarded as a monomeric species. The coordination geometry around the bismuth center approaches a trigonal bipyramid (Figure 3). The equatorial N1−Bi−N3 angle is small (101.8°) indicating that the lone pair has a strong s-character and the N2−Bi−Cl1 angle is large (159.6°) which indicates that the amino group interacts with a vacant Bi d-type orbital.[10]

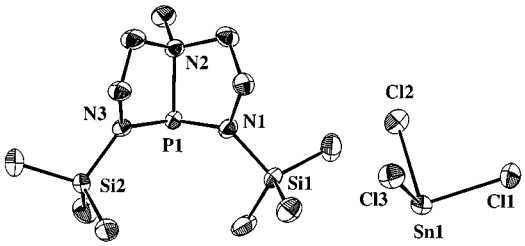
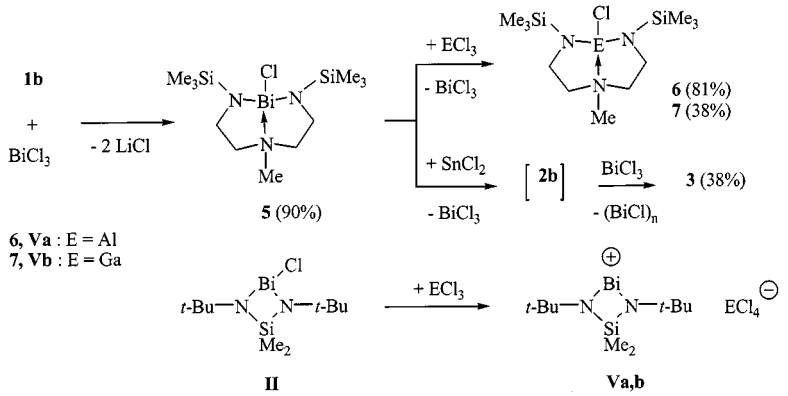


Figure 2. Molecular structure of **4**; selected bond lengths [Å] and angles [°]: N1−P1 1.684(3), N2−P1 1.897(3), N3−P1 1.664(3), N1−Si1 1.755(3), N3−Si2 1.765(3); N1−P1−N2 89.86(13), N2−P1−N3 90.05(13), N1−P1−N3 111.17(13).

It has been reported that treatment of **II** with Lewis acids such as aluminum and gallium trichloride yielded the corresponding bismuth salt **Va,b** by abstraction of chloride.[8h] In marked contrast, **5** reacted at −78°C in thf with $AlCl_3$ to give the corresponding aluminum chloride derivative **6** (81% yield). This transmetallation reaction even occurred



Scheme 3. Synthesis and reactivity of **5**

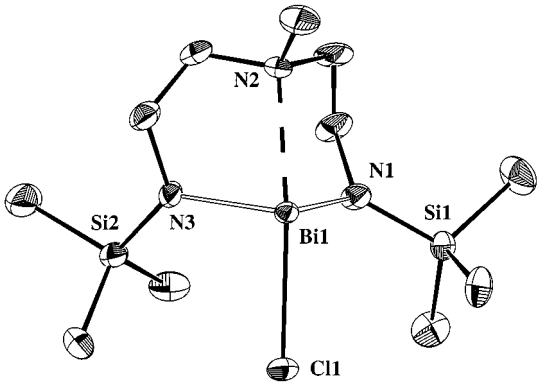


Figure 3. Molecular structure of **5**; selected bond lengths [Å] and angles [°]: N1−Bi1 2.123(5), N2−Bi1 2.496(6), N3−Bi1 2.138(6), Cl1−Bi1 2.6727(17), N1−Si1 1.714(6), N3−Si2 1.719(6); N1−Bi1−N2 75.6(2), N2−Bi1−N3 74.8(2), N1−Bi1−N3 101.8(2), N1−Bi1−Cl1 90.78(16), N2−Bi1−Cl1 159.60(14), N3−Bi1−Cl1 93.71(16).

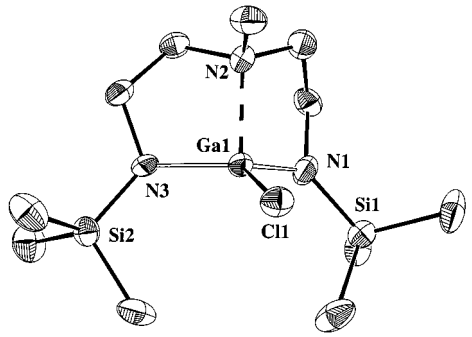


Figure 4. Molecular structure of **7**; selected bond lengths [Å] and angles [°]: N1−Ga1 1.839(16), N2−Ga1 2.043(3), N3−Ga1 1.870(15), Cl1−Ga1 2.1935(13), N1−Si1 1.711(9), N3−Si2 1.712(9); N1−Ga1−N2 90.2(4), N2−Ga1−N3 91.1(4), N1−Ga1−N3 126.08(17), N1−Ga1−Cl1 113.8(6), N2−Ga1−Cl1 111.62(10), N3−Ga1−Cl1 115.5(6).

with a strong Lewis acid such as $GaCl_3$, in toluene at −78°C; the gallium derivative **7** being isolated in 38%. According to an X-ray diffraction study, the gallium chloride **7** is monomeric and presents a trigonal-pyramidal geometry similar to that observed for the corresponding aluminum chloride **6**[6] (Figure 4).

Since the diamidoaminobismuth chloride **5** undergoes novel transmetallation reactions with group 13 Lewis acids, it was of interest to extend this reactivity to group 14 Lewis acids. A thf solution of **5** reacted at −78°C with an equimolar amount of $SnCl_2$, to give the tin dichloride derivative **3** in 38% yield. Since we have shown above (Scheme 2) that the stannylene **2b** reacts with $BiCl_3$ to give **3**, it is quite clear that a transmetallation reaction also occurs between **5** and $SnCl_2$ to give the stannylene **2b**, which is subsequently oxidized to **3** by the resulting $BiCl_3$. Therefore, this exchange reaction (**5**→**2b**) is the opposite of that observed by Veith (**I** →**II**).[8]

Conclusion

The dramatic difference observed in the reactivity of stannylene **2** and bismuth chloride **5** with that of **I** and **II**, respectively, can be rationalized by the electron donation from the axial nitrogen, which decreases the electrophilicity of the metal centers. The transmetalation reactions observed for bismuth chloride **5** with group 13 and 14 halides which occur under very mild conditions, suggest they could probably be generalized, especially for the synthesis of transition metal complexes.

Experimental Section

All experiments were performed under dry argon. Melting points are uncorrected ^1H, ^{13}C, and ^{119}Sn NMR spectra were recorded with Bruker AC80, AC200, WM250 or AMX400 spectrometers. ^1H and ^{13}C chemical shifts are reported in ppm relative to Me_4Si as external standard. ^{119}Sn NMR downfield chemical shifts are expressed with a positive sign, in ppm, relative to external Me_4Sn. Conventional glassware was used.

2a: To an ether solution (20 mL) of the lithium salt of *N*-methyl-*N′,N′′*-bis(diisopropyl)diethylenetriamine **1a** (4.7 mmol) was added an ether suspension (20 mL) of $SnCl_2$ (0.891 g, 4.7 mmol) at −78°C. The solution became golden yellow, and was allowed to warm to room temperature and stirred overnight. After filtration, and removal of the solvent under vacuum, **2a** was obtained as a yellow oil (0.89 g, 60%). − ^1H NMR (C_6D_6, 250.134 MHz): δ = 1.49 (d, $^3J_{HH}$ = 6.2 Hz, 6 H, CH_3CH), 1.54 (d, $^3J_{HH}$ = 6.2 Hz, 6 H, CH_3CH), 2.11{s, $^3J(^{119}SnH)$ = 20 Hz, 3 H, CH_3N}, 2.37 (m, 4 H, CH_2), 3.11 (m, 2 H, CH_2), 3.47 (m, 2 H, CH_2), 3.67 (sept, $^3J_{HH}$ = 6.2 Hz, 2 H, CH). − $^{13}C\{^1H\}$ NMR (C_6D_6, 62.896 MHz): δ = 26.64, 26.93 (CH_3CH), 49.05 {$^2J(^{119}SnC)$ = 50.2 Hz, CH_3N}, 54.64 (CH_2NCH_3), 55.04 (CH), 63.32 (CH_2NCH). − $^{119}Sn\{^1H\}$ NMR (C_6D_6, 32.248 MHz): δ = +129. − $C_{11}H_{25}N_3Sn$: calcd. C 41.54, H 7.92, N 13.21; found C 41.10, H 7.65, N 13.42.

2b: Using the same experimental procedure as above employing the lithium salt of *N*-methyl-*N′,N′′*-bis(trimethylsilyl)diethylenetriamine **1b** (3.6 mmol) and $SnCl_2$ (0.682 g, 3.6 mmol), colorless crystals (1.15 g, 80%) were obtained from a toluene solution (6 mL) at −20°C. − m.p. < 20°C. − ^1H NMR (C_6D_6, 400.135 MHz): δ = 0.41 (s, 18 H, $SiCH_3$), 2.02 {s, $^3J(^{119}SnH)$ = 19 Hz, 3 H, CH_3N}, 2.15 (m, 4 H, CH_2), 3.35 (m, 2 H, CH_2), 3.44 (m, 2 H, CH_2). − $^{13}C\{^1H\}$ NMR (C_6D_6, 100.624 MHz): δ = 2.25 ($SiCH_3$), 48.32 {$^2J(^{119}SnC)$ = 54.0 Hz, CH_3N}, 50.09 (CH_2NCH_3), 65.99 (CH_2NSi). − $^{29}Si\{^1H\}$ NMR (C_6D_6, 79.495 MHz): δ = +0.03. − $^{119}Sn\{^1H\}$ NMR (C_6D_6, 149.248 MHz): δ = +158. − $C_{11}H_{29}N_3Si_2Sn$: calcd. C 34.93, H 7.73, N 11.11; found C 34.67, H 7.76, N 11.22.

3: A thf solution (5 mL) of $BiCl_3$ (0.123 g, 0.38 mmol) was added dropwise to a thf solution (5 mL) of stannylene **2b** (0.147 g, 0.38 mmol) at −78°C. The color of the solution changed from dark brown to black after the solution was allowed to warm to room temperature. After filtration, the solvent was removed under vacuum. The residue was treated with toluene (20 mL) and, after filtration, the solvent was removed under vacuum. Colorless crystals were obtained from a pentane solution (4 mL) at −20°C (0.101 g, 58%). − m.p. < 20°C. − ^1H NMR (C_6D_6, 250.133 MHz): δ = 0.43 (s, 18 H, $SiCH_3$), 1.87 (ddd, J_{HH} = 9.4, 5.1 and 3.5 Hz, 2 H, CH_2), 2.02 (s, 3 H, CH_3N), 2.04 (ddd, J_{HH} = 9.4, 5.6 and 3.4 Hz, 2 H, CH_2), 2.86 (m, 4 H, CH_2). − $^{13}C\{^1H\}$ NMR (C_6D_6, 62.896 MHz):

δ = 3.10 ($SiCH_3$), 41.41 (CH_3N), 44.00 (CH_2NCH_3), 57.86 (CH_2NSi). – $^{119}Sn\{^1H\}$ NMR (C_6D_6, 29.881 MHz): δ = −228. – $C_{11}H_{29}Cl_2N_3Si_2Sn$: calcd. C 29.41, H 6.51, N 9.36; found C 29.64, H 6.22, N 9.33.

4: Neat freshly distilled PCl_3 (0.072 mL, 0.8 mmol) was added dropwise to a toluene solution (6 mL) of diamidoaminostannylene **2b** (0.315 g, 0.8 mmol) at −90°C. The solution was allowed to warm to room temperature and became yellow after 30 min. The solvent was removed under vacuum and the yellow-orange oil obtained was washed with pentane (5 mL) and ether (5 mL). Colorless crystals were obtained from a C_6D_6 solution (1 mL) at room temperature (0.315 g, 95%). – m.p. 110°C. – ^1H NMR (C_6D_6, 250.134 MHz): δ = −0.02 (s, 18 H, $SiCH_3$), 2.61 (m, 2 H, CH_2), 2.74 {d, J_{PH} = 13.5 Hz, 3 H, CH_3N}, 3.03 (m, 2 H, CH_2), 3.43 (m, 2 H, CH_2), 4.70 (m, 2 H, CH_2). – $^{13}C\{^1H\}$ NMR (C_6D_6, 62.896 MHz): δ = 1.01 ($SiCH_3$), 51.70 {d, J_{PC} = 5.9 Hz, CH_3N}, 53.39 (CH_2NCH_3), 64.67 (CH_2NSi). – $^{31}P\{^1H\}$ NMR (C_6D_6, 81.02 MHz): δ = +169. – $C_{11}H_{29}Cl_3N_3PSi_2Sn$: calcd. C 25.63, H 5.67, N 8.15; found C 25.30, H 5.58, N 8.22.

5: Using the same procedure as for **2a**, but with toluene instead of ether, and $BiCl_3$ (0.232 g, 0.73 mmol), colorless crystals were obtained from a toluene solution (2 mL) at −20°C (0.334 g, 90%). – m.p. 133°C (dec.). – ^1H NMR (C_6D_6, 200.132 MHz): δ = 0.46 (s, 18 H, $SiCH_3$), 1.56 (ddd, J_{HH} = 12.1, 6.6 and 3.3 Hz, 2 H, CH_2), 1.65 (s, 3 H, CH_3N), 1.91 (ddd, J_{HH} = 12.1, 6.6 Hz and 3.3 Hz, 2 H, CH_2), 3.95 (ddd, J_{HH} = 14.5, 6.6 and 3.3 Hz, 2 H, CH_2), 4.16 (ddd, J_{HH} = 14.5, 6.6 and 3.3 Hz, 2 H, CH_2). – $^{13}C\{^1H\}$ NMR (C_6D_6, 62.896 MHz): δ = 2.98 ($SiCH_3$), 44.76 (CH_3N), 47.92 (CH_2NCH_3), 65.80 (CH_2NSi). – $C_{11}H_{29}BiClN_3Si_2$: calcd. C 26.22, H 5.80, N 8.34; found C 26.34, H 5.70, N 8.39.

6[6a] was prepared following the same procedure as for **7**.

7: A toluene solution (6 mL) of $GaCl_3$ (0.201 g, 1.12 mmol) was added dropwise to a toluene solution (10 mL) of bismuth chloride **5** (0.569 g, 1.12 mmol) at −78°C. The pale yellow solution was allowed to warm to room temperature. After filtration, the solvent was removed under vacuum, and colorless crystals (0.157 g, 38%) were obtained from a toluene solution (2 mL) at −20°C. – m.p. 180°C (dec.). – ^1H NMR ($CDCl_3$, 200.132 MHz): δ = 0.41 (s, 18 H, $SiCH_3$), 1.79 (ddd, J_{HH} = 11.3, 6.1 and 5.1 Hz, 2 H, CH_2), 1.91 (s, 3 H, CH_3N), 2.05 (ddd, J_{HH} = 11.3, 6.1 and 4.8 Hz, 2 H, CH_2), 2.83 (m, 4 H, CH_2). – $^{13}C\{^1H\}$ NMR ($CDCl_3$, 62.896 MHz): δ = 0.84 ($SiCH_3$), 41.77 (CH_2NCH_3), 41.99 (CH_3N), 58.40 (CH_2NSi). – $C_{11}H_{29}ClGaN_3Si_2$: calcd. C 36.22, H 8.01, N 11.52; found C 36.26, H 8.05, N 11.48.

X-ray Crystal Structure Determination of 2b, 4, 5 and 7:

2b: $C_{11}H_{29}N_3Si_2Sn$, M = 378.24, triclinic, $P\bar{1}$, a = 9.047(2) Å, b = 10.209(2) Å, c = 11.906(2) Å, α = 103.62(2)°, β = 100.02(2)°, γ = 113.71(2)°, V = 932.8(3) Å^3, Z = 2, ρ_c = 1.347 Mg m^{-3}, $F(000)$ = 388, λ = 0.71073 Å, T = 173(2) K, μ (Mo K_α) = 1.487 mm^{-1}, crystal size 0.7 × 0.6 × 0.6 mm, 2.42° < θ < 23.25°, 9933 reflections (2523 independent, R_{int} = 0.1104) were collected at low temperatures using an oil-coated shock-cooled crystal[11] on a STOE-IPDS diffractometer. The structure was solved by direct methods (SHELXS-97)[12] and 201 parameters using 71 restraints were refined using the least-squares method on F^2.[13] Largest electron density residue: 1.606 e Å^{-3}, R_1 {for $F>2\sigma(F)$} = 0.058 and wR_2 = 0.134 (all data) with $R_1 = \Sigma||F_o|-|F_c||/\Sigma|F_o|$ and $wR_2 = \{\Sigma w(F_o^2 - F_c^2)^2/\Sigma w(F_o^2)^2\}0.5$. The disorder of a trimethylsilyl group was refined anisotropically on two positions with the occupancy 0.64/0.36 using ADP and distance restraints.

4: $C_{11}H_{29}Cl_3N_3PSi_2Sn$, M = 515.56, triclinic, $P\bar{1}$, a = 6.374(1) Å, b = 12.868(2) Å, c = 13.913(2) Å, α = 100.39(2)°, β = 98.47(2)°, γ = 93.07(2)°, V = 1106.4(3) Å^3, Z = 2, ρ_c = 1.548 Mg m^{-3}, $F(000)$ = 520, λ = 0.71073 Å, T = 173(2) K, μ (Mo K_α) = 1.695 mm^{-1}, crystal size 0.4 × 0.3 × 0.1 mm, 1.99° < θ < 23.53°, 8463 reflections (3113 independent, R_{int} = 0.0375) were collected at low temperatures using an oil-coated shock-cooled crystal[11] on a STOE-IPDS diffractometer. The structure was solved by direct methods (SHELXS-97)[12] and 197 parameters were refined using the least-squares method on F^2.[13] Largest electron density residue: 0.475 e Å^{-3}, R_1 {for $F>2\sigma(F)$} = 0.025 and wR_2 = 0.065 (all data) with $R_1 = \Sigma||F_o|-|F_c||/\Sigma|F_o|$ and $wR_2 = \{\Sigma w(F_o^2 - F_c^2)^2/\Sigma w(F_o^2)^2\}0.5$.

5: $C_{11}H_{29}BiClN_3Si_2$, M = 503.98, monoclinic, $P2_1/n$, a = 10.063(1) Å, b = 13.280(2) Å, c = 15.006(2) Å, β = 109.16(1)°, V = 1894.3(4) Å^3, Z = 4, ρ_c = 1.767 Mg m^{-3}, $F(000)$ = 976, λ = 0.71073 Å, T = 173(2) K, μ (Mo K_α) = 9.566 mm^{-1}, crystal size 0.6 × 0.5 × 0.5 mm, 2.10° < θ < 23.25°, 15301 reflections (2718 independent, R_{int} = 0.0883) were collected at low temperatures using an oil-coated shock-cooled crystal[11] on a STOE-IPDS diffractometer. A numerical absorption correction was employed and the min./max. transmissions are 0.0857 and 0.2607. The structure was solved by direct methods (SHELXS-97)[12] and 171 parameters were refined using the least-squares method on F^2.[13] Largest electron density residue: 1.022 e Å^{-3}, R_1 {for $F>2\sigma(F)$} = 0.029 and wR_2 = 0.074 (all data) with $R_1 = \Sigma||F_o|-|F_c||/\Sigma|F_o|$ and $wR_2 = \{\Sigma w(F_o^2 - F_c^2)^2/\Sigma w(F_o^2)^2\}0.5$.

7: $C_{11}H_{29}ClGaN_3Si_2$, M = 364.72, monoclinic, $P2_1/m$, a = 6.472(2) Å, b = 18.624(5) Å, c = 7.688(3) Å, β = 96.64(4)°, V = 920.5(5) Å^3, Z = 2, ρ_c = 1.316 Mg m^{-3}, $F(000)$ = 384, λ = 0.71073 Å, T = 153(2) K, μ (Mo K_α) = 1.760 mm^{-1}, crystal size 0.5 × 0.4 × 0.1 mm, 2.67° < θ < 24.21°, 6014 reflections (1514 independent, R_{int} = 0.0445) were collected at low temperatures using an oil-coated shock-cooled crystal[11] on a STOE-IPDS diffractometer. A numerical absorption correction was employed and the min./max. transmissions are 0.5865 and 0.7727. The structure was solved by direct methods (SHELXS-97)[12] and 164 parameters using 71 restraints were refined using the least-squares method on F^2.[13] Largest electron density residue: 0.273 e Å^{-3}, R_1 {for $F>2\sigma(F)$} = 0.024 and wR_2 = 0.055 (all data) with $R_1 = \Sigma||F_o|-|F_c||/\Sigma|F_o|$ and $wR_2 = \{\Sigma w(F_o^2 - F_c^2)^2/\Sigma w(F_o^2)^2\}0.5$. The mirror leads to a disorder of the whole molecule, which was refined anisotropically by ignoring the symmetry (PART-1) using ADP and distance restraints. A refinement in $P2_1$ gives the same disorder.

Crystallographic data (excluding structure factors) for the structures reported in this paper have been deposited with the Cambridge Data Centre as supplementary publication no. CCDC-112754 (**2b**), CCDC-112755 (**4**), CCDC-112756 (**5**) and CCDC-112757 (**7**). Copies of the data can be obtained free of charge on application to CCDC, 12 Union Road, Cambridge CB2 1EZ, UK [Fax: (internat.) + 44-1223/336-033; E-mail: deposit@ccdc.cam.ac.uk].

Acknowledgments

Thanks are due to the CNRS and Beaufour-Ipsen for financial support of this work.

[1] [1a] W. P. Neumann, *Chem. Rev.* **1991**, *91*, 311–334. – [1b] J. D. Cotton, P. J. Davidson, J. D. Donaldson, M. F. Lappert, J. Silver, *J. Chem. Soc., Dalton Trans.* **1976**, 2286–2290. – [1c] H. Braunschweig, C. Drost, P. B. Hitchcock, M. F. Lappert, L. J.-

M. Pierssens, *Angew. Chem.* **1997**, *109*, 285−287; *Angew. Chem. Int. Ed. Engl*. **1997**, *36*, 261−263. − [1d] The Chemistry of Organic Arsenic, Antimony and Bismuth Compounds (Ed.: S. Patai), Wiley: New York, **1994**. − [1e] U. Wirringa, H. W. Roesky, M. Noltemeyer, H.-G. Schmidt, *Inorg. Chem.* **1994**, *33*, 4607−4608.

[2] [2a] S. Répichet, C. Le Roux, J. Dubac, J. R. Desmurs, *Eur. J. Org. Chem.* **1998**, 2743−2746. − [2b] H. Robert, B. Garrigues, J. Dubac, *Tetrahedron Lett.* **1998**, 39, 1161−1164. − [2c] D. Prajapati, J. S. Sandhu, *Chem. Lett*. **1992**, 1945−1946. − [2d] R. K. Grasselli, J. D. Burrington, *Adv. Catal*. **1981**, *30*, 133−163.

[3] [3a] K. T. Higa, C. George, *Organometallics* **1990**, *9*, 275−277. − [3b] A. H. Cowley, R. A. Jones, *Angew. Chem.* **1989**, *101*, 1235−1242; *Angew. Chem. Int. Ed. Engl*. **1989**, *28*, 1208−1215.

[4] [4a] J. G. Verkade, *Acc. Chem. Res.* **1993**, *26*, 483−489. − [4b] A. Togni, L. M. Venanzi, *Angew. Chem.* **1994**, *106*, 517−546; *Angew Chem., Int. Ed. Engl.* **1994**, *33*, 497−526. − [4c] R. R. Schrock, *Acc*. *Chem. Res.* **1997**, *30*, 9−16.

[5] [5a] F. G. N. Cloke, P. B. Hitchcock, J. B. Love, *J. Chem. Soc., Dalton Trans.* **1995**, 25−30. − [5b] H. C. S. C. Clark, F. G. N. Cloke, P. B. Hitchcock, J. B. Love, A. P. J. Wainwright, *J. Organomet. Chem.* **1995**, *501*, 333−340.

[6] [6a] N. Emig, H. Nguyen, H. Krautscheid, R. Réau, J. B. Cazaux, G. Bertrand, *Organometallics* **1998**, *17*, 3599−3608. − [6b] N. Emig, R. Réau, H. Krautscheid, D. Fenske, G. Bertrand, *J. Am. Chem. Soc.* **1996**, *118*, 5822−5823. − [6c] G. Bertrand, J. B. Cazaux, N. Emig, R. Réau, *World Patent*. **1997**, 097/42197.

[7] The ^{119}Sn NMR chemical shift of free diamidostannylenes are in the range +400 to +800 ppm: [7a] B. Wrackmeyer, C. Stader, K. Horchler, *J. Magn. Reson.* **1989**, *83*, 601−607. − [7b] H. Braunschweig, B. Gehrhus, P. B. Hitchcock, M. F. Lappert, *Z. Anorg. Allg. Chem.* **1995**, *621*, 1922−1928.

[8] [8a] M. Veith, *Angew. Chem.* **1975**, *87*, 287; *Angew. Chem. Int. Ed. Engl.* **1975**, *14*, 263−264. − [8b] M. Veith, *Z. Naturforsch.* **1978**, *33b*, 1−6 and 7−13. − [8c] M. Veith, B. Bertsch, *Z. Anorg. Allg. Chem.* **1988**, *557*, 7−22. − [8d] M. Veith, V. Huch, J. P. Majoral, G. Bertrand, G. Manuel, *Tetrahedron. Lett*. **1983**, *24*, 4219−4222. − [8e] M. Veith, O. Recktenwald, E. Humpfer, *Z. Naturforsch.* **1978**, *33b*, 14−19. − [8f] M. Veith, M. Grosser, V. Huch, *Z. Anorg. Allg. Chem.* **1984**, *513*, 89−102. − [8g] M. Veith, M. Gouigou, A. Detemple, *Phosphorus, Sulfur, and Silicon* **1993**, *75*, 183−186. − [8h] M. Veith, B. Bertsch, V. Huch, *Z. Anorg. Allg. Chem.* **1988**, *559*, 73−88. − [8i] M. Veith, *Angew. Chem.* **1987**, *99*, 1−14; *Angew. Chem. Int. Ed. Engl*. **1987**, *26*, 1−14.

[9] C. L. Raston, B. W. Skelton, V. A. Tolhurst, A. H. White, *Polyhedron*, **1998**, *17*, 935−942.

[10] J. E. Huheey, C. L. Huheey, *J. Chem. Educ.* **1972**, *49*, 227−230.

[11] D. Stalke, *Chem. Soc. Rev.* **1998**, *27*, 171−178.

[12] G. M. Sheldrick, *Acta Crystallogr.* **1990**, *A46*, 467−473.

[13] SHELXL-97, *Program for Crystal Structure Refinement*, G. M. Sheldrick, University of Göttingen **1997**.

Received June 14, 1999
[I99212]

Silicon Compounds with Strong Intramolecular Steric Interactions, 71[+]

Silylene Reactions with Buta-1,3-diynes: Cycloadditions, Insertions, and Rearrangements

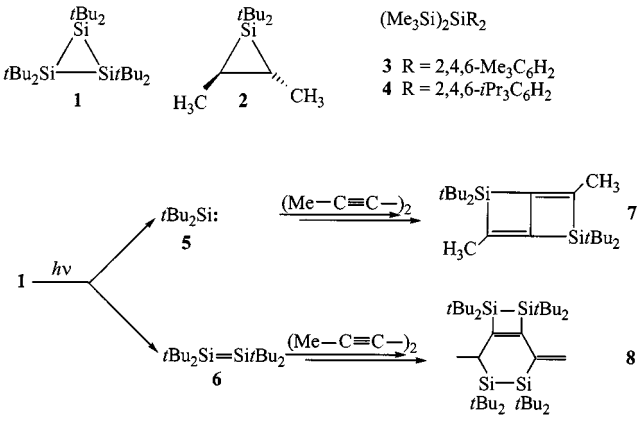
Detlev Ostendorf,[a] Lars Kirmaier,[a] Wolfgang Saak,[a] Heinrich Marsmann,[b] and Manfred Weidenbruch*[a]

Keywords: Multiple bonds / Silicon / Silylene / Cycloadditions / Insertions

Di-*tert*-butylsilylene, generated by photolysis of hexa-*tert*-butylcyclotrisilane **1** or 1,1-di-*tert*-butyl-*trans*-2,3-dimethylsilirane (**2**), reacts with the 1,3-diyne (*t*Bu–C≡C–)$_2$ **9** to furnish the dialkynylsilane **11** via the isolable alkynylsilirene **10**. Photolysis of excess **1** in the presence of **9** furnishes the C–C linked 2,2′-disilirene **12** which, upon prolonged irradiation, rearranges to the 2,5-disilabicyclo[2.2.0]hexa-1(6),3-diene (**13**). Treatment of **9** with diarylsilylenes, formed by irradiation of hexamethyl-2,2-dimesityltrisilane (**3**) or hexamethyl-2,2-bis(2,4,6-triisopropylphenyl)trisilane (**4**), gives the corresponding alkynylsilirenes **14** and **15**, respectively. Photolysis of **1** or **2** in the presence of (Me$_3$Si–C≡C–)$_2$ **16** yields the dialkynylsilane **17** which, on further reaction with **2**, yields the 2,5-disilabicyclo[2.2.0]hexa-1(6),3-diene (**18**). Irradiation of **3** in the presence of **16** affords the *cis*- and *trans*-isomeric 1,3-dimethylene-2,4-disilacyclobutane derivatives *cis*-**21** and *trans*-**21**, presumably via a 1-silaallene intermediate. The structures of **12**, **15**, **18**, *cis*-**21**, and *trans*-**21** have been determined by X-ray crystallography.

Dialkyl- and diarylsilylenes (silanediyls), R$_2$Si:, are highly reactive intermediates capable of undergoing numerous addition and insertion reactions. When the groups R on silicon are small, the initial products are usually unstable and often undergo a series of subsequent transformations before the thermodynamically stable final products are reached.[1] Silylenes bearing bulky substituents behave differently and, for example, undergo smooth addition reactions with multiple bond systems to furnish three-membered ring compounds that can often be isolated in spite of their high degrees of ring strain.[2]

Examples of silylenes of this type are di-*tert*-butylsilylene, generated photolytically from the cyclotrisilane **1**[3] or the silirane **2**,[4] and the 2,4,6-trialkylphenyl-substituted silylenes, also accessible from the acyclic trisilanes **3**[5] and **4**[6] under the action of light. We recently studied the photolysis of **1**, which decomposes under these conditions to give di-*tert*-butylsilylene **5** and tetra-*tert*-butyldisilene **6**, in the presence of hexa-1,3-diyne. From these experiments, the bicyclic compounds **7** and **8** were isolated as the final products and their structures were confirmed by X-ray crystallography.[7] In order to obtain further information relating to the formation of these compounds, especially the bicyclic system **7**, we have now examined the reactions of the 1,3-diynes 1,4-bis(trimethylsilyl)buta-1,3-diyne **16** and 2,2,7,7-tetramethylocta-3,5-diyne **9** with the silylene sources **1**−**4** and report here on the resultant cycloaddition, formal insertion, and rearrangement reactions leading to the formation of novel mono- and bicyclic systems.



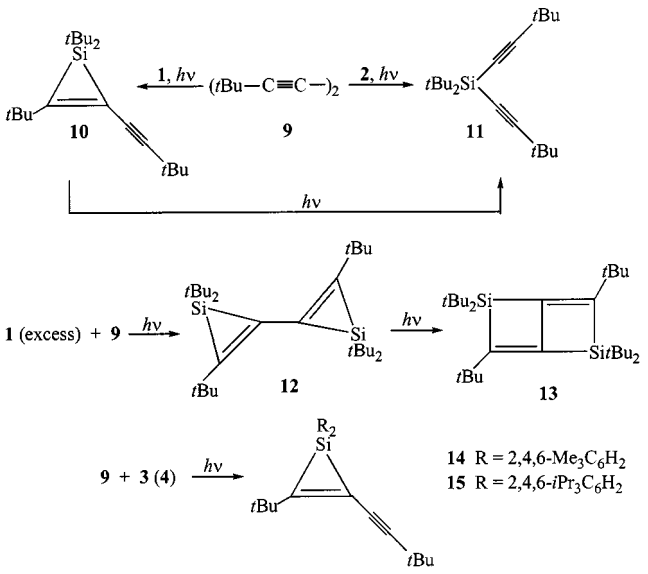
Photolysis of the cyclotrisilane **1** in the presence of the diyne **9** in a ratio of approximately 1:1 furnished the alkynylsilirene **10** as a colorless oil in 30% yield; the constitution of this product was confirmed by a complete NMR analysis. The position of the ^{29}Si-NMR signal is of particular diagnostic value: it appears upfield at $\delta = -63.3$, which is typical for silirenes with *tert*-butyl substituents at the silicon atom.[7][8]

When the silirane **2** is used instead of **1** for the generation of di-*tert*-butylsilylene, colorless crystals are obtained in 52% yield, the analytical and mass spectral data of which

[+] Part 70: M. Weidenbruch, F. Meiners, W. Saak, *Can. J. Chem.*, in press.

[a] Fachbereich Chemie, Universität Oldenburg, Carl-von-Ossietzky-Straße 9−11, D-26111 Oldenburg, Germany
Fax: (internat.) +49 (0)441/798-3352
[b] Fachbereich Chemie, Universität (GH) Paderborn, Warburger Straße 100, D-33095 Paderborn, Germany

 © WILEY-VCH Verlag GmbH, D-69451 Weinheim, 1999 1434−1948/99/1212−2301 $ 17.50+.50/0



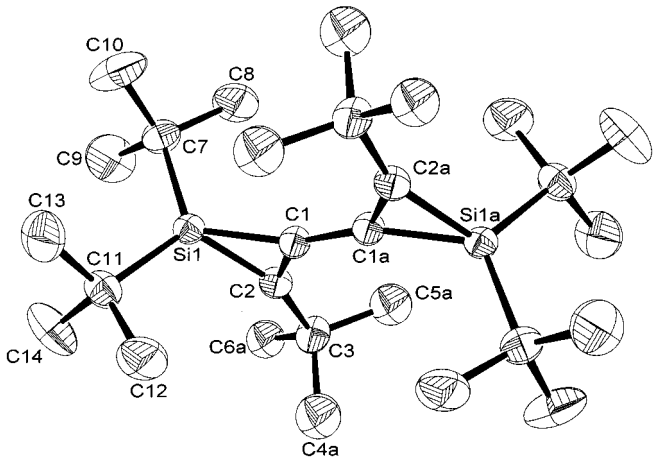


Figure 1. Molecular structure of **12** in the crystal (hydrogen atoms omitted); ellipsoids are drawn at a 50% probability level; selected bond lengths [pm] and angles [°]: C(1)−C(2) 133.8(3), C(1)−C(1a) 145.1(4), Si(1)−C(1) 182.2, Si(1)−C(2) 181.9(2); C(2)−C(1)−Si(1) 68.3(1), C(2)−Si(1)−C(1) 43.1, C(2)−C(1)−C(1a) 137.4(3), C(1a)−C(1)−Si(1) 154.3(2)

again point to the formation of **10**. However, the NMR data are not compatible with structure **10**. Thus, no signals attributable to olefinic carbon atoms can be seen in the ^{13}C-NMR spectrum and the ^{29}Si-NMR spectrum features a singlet at $\delta = -20.04$. These data, as well as an X-ray crystallographic analysis,[9] showed that, instead of the silirene **10**, the dialkynylsilane **11** had been formed as the product of a formal silylene insertion into the central C−C single bond. The X-ray crystal structure did not exhibit any unusual features compared to those of other alkynylsilanes.[10]

The formation of different products from the photolysis of **1** or **2** in the presence of **9** is presumably due to the impeded liberation of **5** from the silirane **2**, as is reflected in the appreciably longer photolysis time. In order to obtain information on the mode of formation of the formal insertion product **11**, the silirene **10** was subjected to a further photolysis, which afforded the silane **11** in almost quantitative yield. The isomerization **10** → **11** can most simply be rationalized by a 1,2-migration of the alkynyl group in combination with a cleavage of the three-membered ring. Ishikawa et al.[11] have previously observed a similar rearrangement on heating a dimesitylsilacyclopropene to 250°C, which also furnished the corresponding dialkynylsilane.

The reaction to afford **10** from the cyclotrisilane **1** and the diyne **9** also furnished a second crystalline product in 15% yield, the spectral data of which showed it to be the C−C linked bis(silirene) **12**. The yield of this compound could be increased to 37% by increasing the proportion of **1** in the photolysis mixture to a ratio of 1:1.5. An X-ray crystallographic analysis (Figure 1) confirmed not only the constitution of **12**, but also revealed some interesting features.

Compound **12** not only represents the first C−C linked bis(silirene),[12] but is also a *trans*-butadiene with both double bonds bridged by silylene units. A comparison of the structure with that of the parent butadiene[13] reveals a somewhat shortened C−C single bond length of 145.1(4) pm instead of 148.3 pm in the butadiene. The difference in the C=C−C angles is more pronounced; 137.4(3)° in **12** is markedly larger than the 122.4° in the parent compound. Furthermore, the endocyclic Si−C bond lengths, with an average of 182 pm, are short and the C1−Si1−C2 angle of 43.1(1)° is very small.

The bis(silirene) **12** is thermally stable and, for example, is recovered unchanged after 30 d at 120°C. Its behavior under photochemical conditions is completely different: after only 6 h at room temperature the 2,5-disilabicyclo[2.2.0]hexa-1(6),3-diene **13** is isolated from the reaction mixture in 52% yield. The formation of **13** is thought to proceed through cleavage of two Si−C bonds in **12**, followed by reformation of two σ-bonds to afford the rearranged bicyclic compound. The constitution of **13** was confirmed by comparison of its NMR data with those of compounds **7** and **18**, the structures of which have been verified by X-ray crystallography. Thus, we have unambiguously demonstrated all intermediate steps involved in the formation of **13** and have also found a feasible explanation for the formation of the bicyclic compound **7**, which remained as an open question from a previous publication.[7]

The photochemical lability of the Si−C bonds in **12** is also manifested in the concomitant formation of the molecules **10** and **11**, clearly showing that cycloreversion with cleavage of a silylene molecule **5** is possible besides the rearrangement **12** → **13**.

Although the dialkylsilylene **5** can participate in a variety of cycloaddition and rearrangement reactions, analogous photolyses of the 1,3-diyne with the trisilanes **3** and **4**, which also readily liberate the corresponding diarylsilylene under these conditions, merely furnish the [2+1] cycloadducts **14** and **15**, as indicated by the typical highfield signals in the ^{29}Si-NMR spectra at $\delta = -106$ (**14**) and $\delta = -109.5$ (**15**). Since the reaction of **3** with the 1,4-bis(trimethylsilyl)-1,3-diyne **16** gives rise to a completely different palette of products (see below), we have determined the structure of

15 by X-ray crystallography (Figure 2). The structure revealed a very small endocyclic C−Si−C angle of 43.2(2)°, very short Si−C1 and Si−C2 bond lengths in spite of the steric crowding, as well as a short exocyclic C2−C3 bond. All other features were unremarkable.

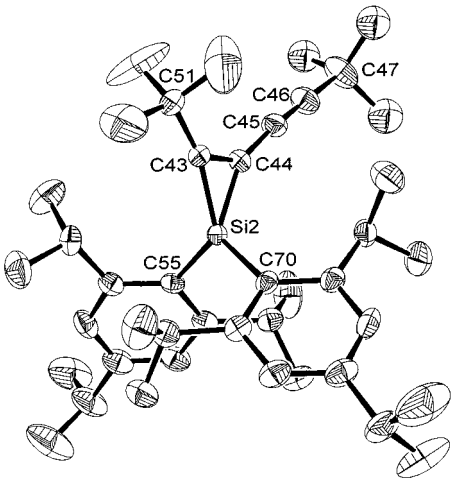
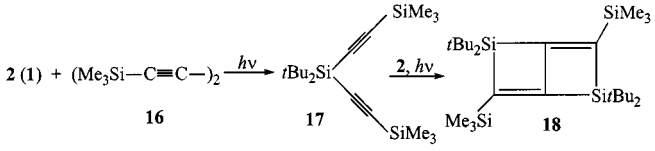


Figure 2. Molecular structure of **15** in the crystal (hydrogen atoms omitted); ellipsoids are drawn at a 50% probability level; selected bond lengths [pm] and angles [°]: C(1)−C(2) 134.5(5), Si−C(1) 181.9(3), Si−C(2) 181.7(3); C(2)−Si−C(1) 43.4(1), C(2)−C(1)−Si 68.2(2), C(1)−C(2)−Si 68.4(2)

An unusual result, however, was that dark-yellow crystals of tetrakis(2,4,6-triisopropylphenyl)disilene were isolated together with the colorless crystals of **15**. This compound had previously been obtained by dehalogenation of dichlorobis(2,4,6-triisopropylphenyl)silane[14] and by photolysis of the trisilane **4**.[15] The fact that the dimerization process of the silylene accessible from **4** to give the disilene proceeds in competition with the [2+1] cycloaddition is possibly due to steric repulsion between the *tert*-butyl and triisopropylphenyl groups in the cycloaddition process. This hypothesis was supported by the photolysis of **4** in the presence of hexa-2,4-diyne, which gave an appreciably higher yield of the corresponding alkynylsilirene (**15**; Me instead of *t*Bu).



Analogously performed reactions of the cyclotrisilane **1** or − preferentially − the silirane **2** with the trimethylsilyl-substituted 1,3-diyne **16** seem to proceed according to the same pattern as observed for the 1,3-diyne **9**, except that in no case was a [2+1] cycloadduct of the type **10** isolated. Presumably as a consequence of the greater mobility of the trimethylsilylethynyl group,[11] the formal insertion product **17** is obtained in 46% yield; its structure, like that of **11**, was confirmed by X-ray crystallography.[16] Further treatment of the dialkynylsilane **17** with the silirane **2** led to an unexpected result: light-yellow crystals of the bicyclic product **18** were obtained in 32% yield. Similar reactions have previously been observed when zirconocene was treated with a dialkynylsilane[17] or a dialkynylzirconocene derivative;[18] these reactions also furnished bicyclic products in which one or two zirconium atoms had been incorporated into the ring skeletons. However, these results cannot be directly compared with the silylene situation because of the different bonding possibilities available to the 14-electron zirconocene complex.

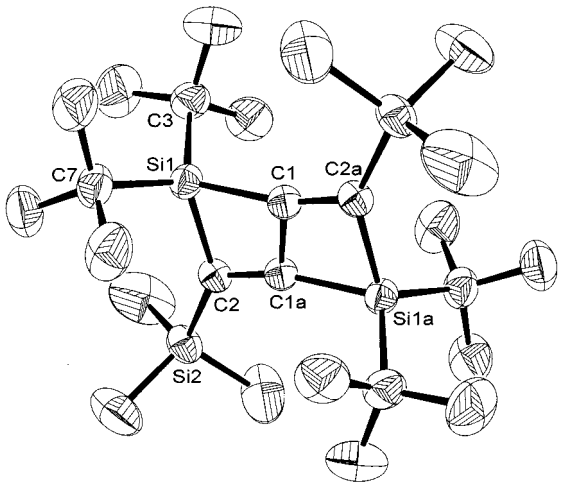
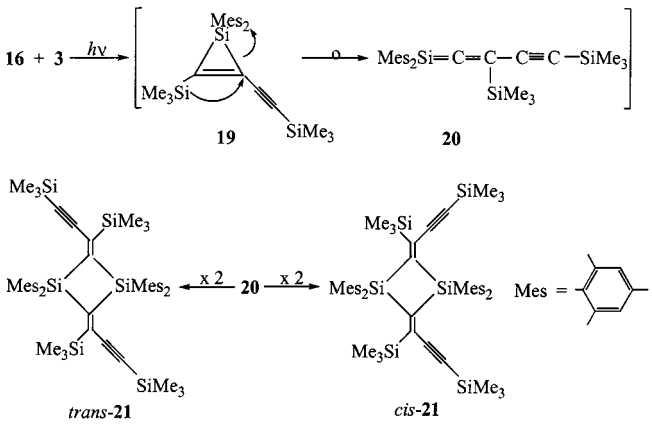


Figure 3. Molecular structure of **18** in the crystal (hydrogen atoms omitted); ellipsoids are drawn at a 50% probability level; selected bond lengths [pm] and angles [°]: Si(1)−C(1) 189.9(2), Si(1)−C(2) 189.9(2), C(1)−C(2a) 136.2(3); C(1)−Si(1)−C(2) 76.2(1), C(1)−C(1a)−C(2) 110.0(2), Si(1)−C(2)−C(1a) 88.8(1), Si(1)−C(1)−C(1a) 85.1(2), C(1a)−C(2)−Si(2) 128.5(2), Si(1)−C(2)−Si(2) 142.7(1)

A plausible mechanistic sequence leading to formation of the bicyclic compound **18** consists of the [2+1] cycloaddition of a silylene molecule **5** to one of the C/C triple bonds, followed by a 1,2-shift of a trimethylsilyl group with intermediate formation of a 1-silaallene derivative. A subsequent intramolecular [2+2] cycloaddition can then furnish the bicyclic system of **18**. The constitution of **18** was confirmed by X-ray crystallography (Figure 3). This revealed that **18** possess a crystallographic center of inversion in the middle of the C1−C1a bond. In spite of the sterically voluminous *tert*-butyl groups, both the endo- and the exocyclic Si−C bonds are only slightly extended. However, the steric influence of these groups is apparent in the Si1−C2−Si2 angle of 142.7°, which reflects the repulsion of the trimethylsilyl groups.

In order to obtain further support for the postulated sequence proceeding via a 1-silaallene, we subjected trisilane **3** to photolytic conditions in the presence of the 1,3-diyne **16**. Fractional crystallization of the reaction mixture first gave colorless, high-melting crystals composed, according to NMR and mass spectral data, of two molecules each of the diyne and the diarylsilylene. The ^{13}C-NMR spectrum revealed the presence of both olefinic and acetylenic carbon atoms. The ^{29}Si-NMR spectrum featured three signals of equal intensity at $\delta = -2, -19$, and -22.

An X-ray crystallographic analysis of the isolated crystals (Figure 4) showed that the compound *trans*-**21** had been



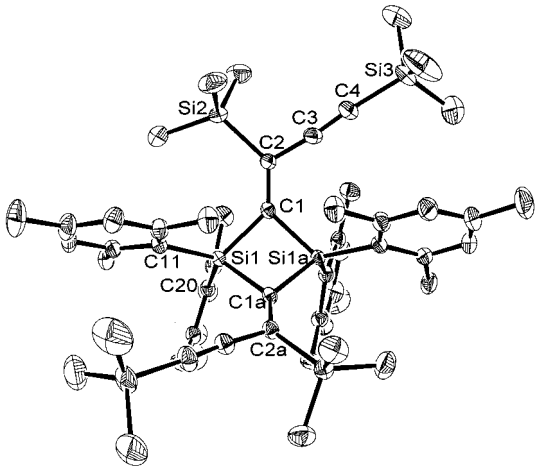


Figure 4. Molecular structure of *trans*-**21** in the crystal (hydrogen atoms omitted); ellipsoids are drawn at a 50% probability level; selected bond lengths [pm] and angles [°]: Si(1)−C(1) 192.1(2), Si(1a)−C(1) 191.9(2), C(1)−C(2) 135.7(3), C(3)−C(4) 120.4(3); C(1)−Si(1)−C(1a) 83.1(1), Si(1)−C(1)−Si(1a) 91.70(9), C(1)−C(2)−C(3) 120.0(2)

formed. This structure has a C_2 symmetry axis perpendicular to the middle of the four-membered ring, which accounts for the fact that only three signals are observed in the ^{29}Si-NMR spectrum. The four-membered ring is folded, with an angle of 33° between the planes formed by the atoms Si1−C1−Si1a and Si1a−C1a−Si1. Within the ring, the smaller angles are found at the silicon atoms and the larger ones at the carbon atoms. This situation, together with the slightly extended Si−C bond lengths of all substituents on the four-membered ring, results in a strain-free structure. The 1,3-dimethylene-2,3-disilacyclobutane structure described here is novel. Barton, Gordon et al.[19] recently reported on a similar ring obtained by dehalogenation of α-(bromovinyl)chlorodimethylsilane, although without an unambiguous structural characterization.

After several weeks standing at −30 °C, a second fraction was obtained from the above mentioned reaction mixture, also as colorless crystals with a high melting point. The mass, ^{1}H-, and ^{13}C-NMR spectral data of this fraction did not show any major changes in comparison with those of *trans*-**21**. However, in the ^{29}Si-NMR spectrum, two signals at δ = −2.6 and −18.87 with higher intensity and another

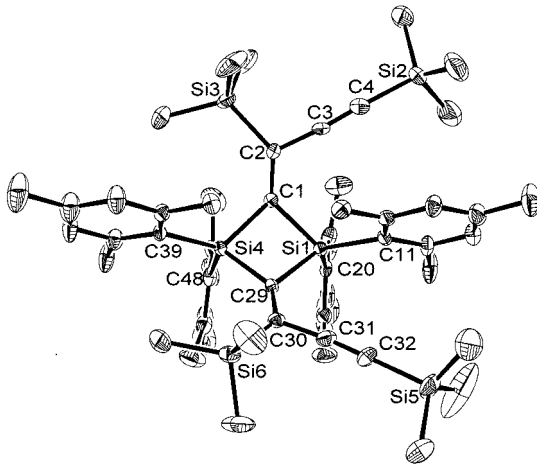


Figure 5. Molecular structure of *cis*-**21** in the crystal (hydrogen atoms omitted); ellipsoids are drawn at a 50% probability level; selected bond lengths [pm] and angles [°]: Si(1)−C(1) 192.1(6), C(1)−Si(4) 191.9(4), Si(4)−C(29) 191.6(4), C(29)−Si(1) 192.3(4), C(1)−C(2) 135.8(6), C(2)−C(3) 144.0(7), C(3)−C(4) 122.1(7), Si(1)−C(1)−Si(4) 91.4(2), C(1)−Si(1)−C(2) 82.7(2), C(29)−Si(4)−C(1) 82.9(2), Si(4)−C(29)−Si(1) 91.5(2)

two at δ = −21.74 and −24.04 with lower intensity were observed, indicating a different structure. Again, X-ray crystallography (Figure 5) allowed an unequivocal structural assignment and revealed that *cis*-**21** had been obtained. As in the case of the *trans* isomer, the central ring is not planar, but has a folding angle of 34.7°. The molecule possesses a mirror plane dissecting the folding angle, which explains the number (four) and relative intensities of the ^{29}Si-NMR signals. The remaining structural parameters are more or less the same as those of the *trans* form.

The isolation of both *cis*- and *trans*-isomers of **21** supports the assumption that their mechanisms of formation do indeed proceed via a 1-silaallene derivative. The reaction sequence may be initiated by the [2+1] cycloaddition of the diarylsilylene to one of the triple bonds in **16** to form the silirene **19**, which is then transformed to the 1-silaallene **20** through 1,2-silyl group migration and concomitant cleavage of a ring Si−C bond. In contrast to alkyl groups, the silyl groups in this and related systems are able to undergo such 1,2-migrations.[19] Although 1-silaallenes with sterically demanding groups can be isolated as thermally stable molecules,[20][21] the steric shielding in **20** is not sufficient so that intermolecular [2+2] cycloaddition occurs to furnish the *cis*- and *trans*-isomers of compound **21**.

The results presented here serve not only to clarify the individual steps in the formation of the bicyclic systems **7**, **13**, and **18**, but also to illustrate the sensitivity with which the reaction system 1,3-diyne/silylene can depend on the terminal groups of the diacetylene, the substituents of the silylene, and the duration of photolysis

Experimental Section

General: All manipulations were performed using standard Schlenk techniques under dry argon. − ^{1}H and ^{13}C NMR: Bruker AM 300 or Bruker ARX 500. The assignments of the ^{1}H- and ^{13}C-NMR

signals were confirmed with the aid of COSY and COLOC spectra. − ^{29}Si NMR: Bruker AMX 300. − MS: Finnigan MAT 212. −Elemental analyses: Analytische Laboratorien, D-51789 Lindlar, Germany. − IR spectra: Bio-Rad FTS-7. − Photolyses: High-pressure mercury immersion lamp (Heraeus TQ 150).

1,1,3-Tri-*tert*-butyl-2-(3,3-dimethylbut-1-ynyl)-1*H*-silacyclopropene (10): A solution of **1** (1.5 g, 3.5 mmol) and **9** (0.65 g, 4.0 mmol) in *n*-hexane (80 mL) was irradiated for 5 h at room temperature. After this time, TLC monitoring showed the reaction to be complete as **1** had been fully consumed. The solvent was removed and the oily residue was transferred to a molecular still. Distillation at 60°C/1.5 mbar yielded 0.32 g (30%) of **10**. − ^{1}H NMR (C_6D_6, 300 MHz, 298 K): δ = 1.04 (s, 18 H), 1.22 (s, 9 H, *t*BuC≡C), 1.34 (s, 9 H, *t*BuC=C). − ^{13}C NMR (C_6D_6, 75.5 MHz, 298 K): δ = 21.59 (C_q), 28.89 (C_q), 30.00 (C_p), 30.25 (C_p), 31.24 (C_p), 36.67 (C_q), 74.16 (C_q, C≡*C*tBu), 111.01 (C_q, *C*≡CtBu), 131.33 (C_q, *C*=C*t*Bu), 172.07 (C_q, C=*C*tBu); C_p and C_q refer to primary and quaternary carbon atoms; the assignment of the ^{13}C-NMR signals was confirmed by a COLOR spectrum. − ^{29}Si NMR (C_6D_6, 59.6 MHz, 298 K): δ = −63.3. − MS (CI, isobutane): *m*/*z* (%) = 305 (100) [MH^+]. − $C_{18}H_{36}Si$ (304.4): calcd. C 78.88, H 11.92; found C 78.62, H 12.00.

The residue was dissolved in the minimum volume of *n*-pentane and this solution was kept at −65°C for 12 h to afford 0.075 g (10% yield) of colorless crystals of **12**. For spectroscopic data, see below.

Di-*tert*-butylbis(3,3-dimethylbut-1-ynyl)silane (11): A solution of **2** (1.20 g, 6.05 mmol) and **9** (0.76 g, 4.68 mmol) in *n*-hexane (80 mL) was irradiated for 11 h at room temperature. The solvent was then removed by vacuum distillation and the brown oily residue was transferred to a molecular still. Distillation at 60°C/0.4 mbar yielded 0.89 g of a colorless oil, which was redissolved in the minimum volume of *n*-hexane. Cooling of this solution to −17°C furnished 0.74 g (52%) of colorless, transparent crystals of **11**; m.p. 45−46°C. − ^{1}H NMR (C_6D_6, 500 MHz, 298 K): δ = 1.09 (s, 18 H, *t*Bu$_2$Si), 1.30 (s, 18 H, *t*BuC≡C). − ^{13}C NMR (C_6D_6, 125.75 MHz, 298 K): δ = 19.59 (C_q), 28.13 (C_p), 28.33 (C_q, C≡C−CCH_3), 30.78 [C_p, $(CH_3)_3$CC≡C], 77.36 (C_q, *C*≡C*t*Bu), 117.50 (C_q, C≡*C*t*Bu*). − ^{29}Si NMR: (C_6D_6, 59.6 MHz, 298 K): δ = −20.04. − MS (CI, isobutane): *m*/*z* (%) = 305 (100) [MH^+]. − $C_{18}H_{36}Si$ (304.4): calcd. C 78.88, H 11.92; found C 78.69, H 12.07.

Rearrangement 10 → 11: A solution of **10** (0.11 g, 0.36 mmol) in C_6D_6 (0.5 mL) was irradiated for 8 h in a sealed quartz NMR tube. After this time, the ^{1}H- and ^{13}C-NMR spectra showed that **10** had been almost quantitatively converted into **11**.

1,1,1′,3,3′-Hexa-*tert*-butyl-1*H*,1′*H*-2,2′-bis(silacyclopropene) (12): A solution of **1** (2.51 g, 5.88 mmol) and **9** (0.69 g, 4.25 mmol) in *n*-hexane (80 mL) was irradiated for 4.5 h at room temperature. The solvent was removed and then 0.47 g (36%) of a mixture of the volatile compounds **10** and **11** was distilled off at 50−60°C/0.03 mbar. The distillation residue was redissolved in the minimum volume of *n*-hexane and this solution was kept at −65°C for 12 h. Recrystallization of the precipitate from *n*-hexane at −20°C yielded 0.70 g (37%) of colorless crystals of **12**; m.p. 124°C. − ^{1}H NMR (C_6D_6, 300 MHz, 298 K): δ = 1.19 (s, 36 H), 1.30 (s, 18 H). − ^{13}C NMR (C_6D_6, 125.7 MHz, 298 K): δ = 22.08 (C_q, Si*t*Bu$_2$), 30.50 (C_p, Si*t*Bu$_2$), 31.13 (C_p, CCH_3), 35.06 (C_q, *C*CH_3), 143.46 (C_q, *C*=C*t*Bu), 153.05 (C_q, C=*C*t*Bu*). − ^{29}Si NMR: δ = −64.0. − MS (CI, isobutane): *m*/*z* (%) = 446 (100) [M^+].

2,2,3,5,5,6-Hexa-*tert*-butyl-2,5-disilabicyclo[2.2.0]hexa-1(6),3-diene (13): A solution of **12** (0.60 g, 1.3 mmol) in *n*-hexane (80 mL) was irradiated for 6 h at room temperature. The solution was then concentrated to a volume of 10 mL and cooled for 6 d at −25°C. The precipitate was subsequently filtered off and recrystallized from the minimum volume of *n*-hexane to provide 0.31 g (52% yield) of colorless crystals of **13**; m.p. 328−330°C (sealed tube). − ^{1}H NMR (C_6D_6, 500 MHz, 298 K): δ = 1.18 (s, 36 H), 1.19 (s, 18 H). − ^{13}C NMR (C_6D_6, 125.7 MHz, 298 K): δ = 20.90 (C_q), 28.95 (C_p), 31.62 (C_p), 34.09 (C_q), 166.50 (C_q, *C*=C*t*Bu), 170.78 (C_q, C=*C*t*Bu*). − ^{29}Si NMR (C_6D_6, 59.6 MHz, 298 K): δ = 36.7. − MS (CI, isobutane): *m*/*z* (%) = 446 (64) [M^+], 389 (100) [M^+ − *t*Bu]. − $C_{28}H_{54}Si_2$ (446.6): calcd. C 75.25, H 12.18, found C 74.97, H 12.01.

3-*tert*-Butyl-2-(3,3-dimethylbut-1-ynyl)-1,1-bis(2,4,6-trimethylphenyl)-1*H*-silacyclopropene (14): A solution of **3** (0.87 g, 2.1 mmol) and **9** (0.77 g, 4.2 mmol) in *n*-hexane (80 mL) was irradiated for 5 h at room temperature. After this time, TLC monitoring showed the reaction to be complete as **3** had been fully consumed. The dark-yellow solution was concentrated to a volume of 10 mL and kept at −30°C for 12 h. The resulting precipitate was filtered off and recrystallized from toluene to afford 55 mg (8% yield) of colorless **14**; m.p. 100°C. − ^{1}H NMR (C_6D_6, 300 MHz, 298 K): δ = 1.26 (s, 9 H), 1.32 (s, 9 H), 2.06 (s, 6 H, *p*-CH_3), 2.60 (s, 12 H, *o*-CH_3), 6.67 (s, 4 H). − ^{13}C NMR (C_6D_6, 75.5 MHz, 298 K): δ = 21.09 (C_p), 24.02 (C_p), 28.99 (C_q), 30.00 (C_p), 31.17 (C_p), 37.29 (C_q), 73.70 (C_q, *t*Bu−*C*≡C-), 113.68 (C_q, *t*Bu−C≡*C*-), 128.72 (C_t), 132.49 (C_q, *ipso*-C), 136.14 (C_q, *t*Bu−C=*C*), 139.19 (C_q), 143.97 (C_q), 173.26 (C_q, *t*Bu−*C*=C). − ^{29}Si NMR (C_6D_6, 59.6 MHz, 298 K): δ = −106. − MS (CI, isobutane): *m*/*z* (%) = 429 (100) [MH^+].

3-*tert*-Butyl-2-(3,3-dimethylbut-1-ynyl)-1,1-bis(2,4,6-triisopropylphenyl)-1*H*-silacyclopropene (15): A solution of **4** (1.50 g, 2.58 mmol) and **9** (0.42 g, 2.59 mmol) in *n*-hexane (80 mL) was irradiated for 9 h at room temperature. After this time, TLC control showed the reaction to be complete as **4** had been fully consumed. The solution was concentrated to a volume of 20 mL and kept at −60°C for 4 d. Repeated crystallization of the resulting solid from *n*-hexane furnished 0.47 g (32% yield) of colorless crystals of **15**; m.p. 117°C. − ^{1}H NMR (C_6D_6, 300 MHz, 298 K): δ = 1.18 (d, 12 H, ^3J = 6.9 Hz), 1.22 (d, 24 H, ^3J = 6.8 Hz), 1.26 (s, 9H, *t*BuC≡C), 1.38 (s, 9 H, *t*BuC=C), 2.75 (sept, 2 H), 3.89 (sept, 4 H), 7.07 (s, 4 H). − ^{13}C NMR (C_6D_6, 75.5 MHz, 298 K): δ = 24.06 (C_p), 24.63 (C_p), 25.05 (C_p), 28.98 (C_q), 29.87 (C_p), 31.23 (C_p), 34.69 (C_t), 35.51 (C_t), 37.28 (C_q), 73.73 (C_q, *t*Bu−*C*≡C), 114.58 (C_q, *C*≡C*t*Bu), 121.35 (C_t), 132.96 (C_q, *ipso*-C), 138.02 (C_q, *C*=C*t*Bu), 150.78 (C_q), 154.91 (C_q), 174.04 (C_q, C=*C*t*Bu*). − ^{29}Si NMR (C_6D_6, 59.6 MHz, 298 K): δ = −109.6. − MS (CI, isobutane): *m*/*z* (%) = 597 (42) [MH^+], 393 (100) [MH^+ − TipH].

On prolonged cooling at −20°C, yellow crystals (90 mg, 12%) of tetrakis(2,4,6-triisopropylphenyl)disilene were isolated, which were identified by comparison of their ^{1}H- and ^{13}C-NMR spectra with those of an authentic sample.

Di-*tert*-butylbis(3-trimethylsilylethynyl)silane (17): A solution of **2** (1.05 g, 5.3 mmol) and **16** (1.03 g, 5.3 mmol) in *n*-hexane (80 mL) was irradiated for 11 h at room temperature. After this time, NMR monitoring showed the reaction to be complete as **2** had been fully consumed. The solvent was distilled off and the oily residue was transferred to a molecular still. Distillation at 53°C/0.04 mbar afforded a pale-yellow oil, which was recrystallized twice from the minimum volume of *n*-hexane to yield 0.82 g (46%) of colorless **17**; m.p. 35°C. − ^{1}H NMR (C_6D_6, 300 MHz, 298 K): δ = 0.08 (s, 18 H), 1.28 (s, 18 H). − ^{13}C NMR (C_6D_6, 75.5 MHz, 298 K): δ = −0.29 (C_p), 19.36 (C_q), 27.94 (C_p), 108.26 (C_q, *C*≡CSiMe_3), 116.79 (C_q, C≡*C*SiMe_3). − ^{29}Si NMR (C_6D_6, 59.6 MHz, 298 K): δ = −20.94, −18.36. − MS (CI, isobutane): *m*/*z* (%) = 337 (30) [MH^+].

Table 1. Crystallographic data for **12**, **15**, **18**, *trans*-**21**, and *cis*-**21**

	12	**15**	**18**	*trans*-**21**	*cis*-**21**
Empirical formula	$C_{28}H_{54}Si_2$	$C_{42}H_{64}Si$	$C_{26}H_{54}Si_4$	$C_{56}H_{80}Si_6$	$C_{56}H_{80}Si_6$
Molecular mass	446.90	597.02	479.05	921.74	921.74
Crystal dimensions [mm]	0.70 × 0.43 × 0.17	0.58 × 0.41 × 0.11	1.16 × 0.64 × 0.27	0.65 × 0.33 × 0.16	0.31 × 0.25 × 0.21
Crystal system	triclinic	triclinic	monoclinic	monoclinic	monoclinic
Space group	*P*-1	*P*-1	$P2_1/n$	*C*2	*Cc*
a [pm]	835.13(6)	1450.46(9)	1165.7(1)	1911.4(1)	2124.7(1)
b [pm]	987.96(9)	1508.6(1)	987.83(8)	1307.3(1)	2121.9(1)
c [pm]	1089.0(1)	2057.9(2)	1429.6(1)	1288.16(7)	2592.0(2)
α [°]	74.61(1)	75.17(1)	90	90	90
β [°]	70.217(9)	72.273(9)	102.581(9)	113.071(7)	97.963(7)
γ [°]	65.06(1)	77.610(9)	90	90	90
V [× 10^6 pm^3]	785.7	4100.6(6)	1606.6(2)	2961.5(4)	11573(1)
Z	1	4	2	2	8
d_{calcd} [g cm^{-3}]	1.0978	0.967	0.990	1.034	1.058
T [K]	213(2)	193(2)	296(2)	193(2)	183(2)
μ [mm^{-1}]	0.129	0.081	0.196	0.172	0.177
$2\Theta_{max}$ [°]	52	52	50	52	52
No. of reflections	9207	50152	2928	11645	42261
No. of unique reflections	2719	14965	2822	5442	20931
No. of observed reflections	2317	7035	2451	4867	12651
No. of parameters	145	769	136	280	1021
R_1 [$I > 2\sigma(I)$]	0.0621	0.0685	0.0460	0.0361	0.0570
wR_2 (all data)	0.1633	0.1812	0.1316	0.0936	0.1303
GOF on F^2	1.045	0.882	1.140	0.994	0.895

− $C_{18}H_{36}Si_3$ (336.4): calcd. C 64.20, H 10.78; found C 64.05, H 10.91.

2,2,5,5-Tetra-*tert*-butyl-3,6-bis(trimethylsilyl)-2,5-disilabicyclo-[2.2.0]hexa-1(6),3-diene (18): A solution of **17** (0.48 g, 1.43 mmol) and **2** (0.34 g, 1.71 mmol) in *n*-hexane (80 mL) was irradiated for 5 h at room temperature. After this time, the solution was concentrated to a volume of 5 mL and kept at −30°C for 3 d. The resulting precipitate was filtered off and recrystallized from *n*-hexane to afford 0.14 g (32% yield) of pale-yellow crystals of **18**; m.p. 269−272°C. − ^{1}H NMR (C_6D_6, 300 MHz, 298 K): δ = 0.23 (s, 18 H), 1.15 (s, 18 H). − ^{13}C NMR (C_6D_6, 75.5 MHz, 198 K): δ = 0.16 (C_p), 20.89 (C_q), 28.50 (C_p), 162.66 (C_q, *C*=CSiMe$_3$), 196.19 (C_q, C=*C*SiMe$_3$). − ^{29}Si NMR (C_6D_6, 59.6 MHz, 298 K): δ = −12.66, 46.00. − MS (CI, isobutane): *m*/*z* (%) = 478 (100) [M$^+$]. − $C_{26}H_{54}Si_4$ (479.05): calcd. C 65.19, H 11.36; found C 64.99, H 11.48.

Photolysis of 3 in the Presence of 16 − Formation of *cis*- and *trans*-21: A solution of **3** (1.78 g, 4.3 mmol) and **16** (0.84 g, 4.3 mmol) in *n*-hexane (80 mL) was irradiated for 15 h at room temperature. After this time, TLC monitoring showed the reaction to be complete as **3** had been fully consumed. The solution was concentrated in vacuo to a volume of 10 mL and kept at −25°C. After 3 weeks at this temperature, 0.40 g of a solid had precipitated, which was recrystallized from *n*-hexane to provide 0.33 g (17% yield) of colorless crystals of *trans*-**21**; m.p. 265°C. − ^{1}H NMR (C_6D_6, 500 MHz, 298 K): δ = −0.01 (s, 18 H), 0.18 (s, 18 H), 1.92 (s, 6 H), 2.09 (s, 6 H), 2.11 (s, 6 H), 2.37 (s, 6 H), 2.74 (s, 6 H), 3.01 (s, 6 H), 6.18 (s, 2 H), 6.60 (s, 2 H), 6.61 (s, 2 H), 6.83 (s, 2 H). − ^{13}C NMR (C_6D_6, 125.7 MHz, 298 K): δ = −0.41 (C_p), −0.18 (C_p), 20.92 (C_p), 21.23 (C_p), 25.55 (C_p), 25.70 (C_p), 26.07 (C_p), 26.95 (C_p), 106.68 (C_q, *C*≡CSiMe$_3$), 109.62 (C_q, C≡*C*SiMe$_3$), 129.23 (C_t), 129.35 (C_t), 130.48 (C_q, *ipso*-C), 131.13 (C_t), 137.04 (C_q), 137.90 (C_q), 139.52 (C_q), 144.53 (C_q), 144.60 (C_q), 146.87 (C_q), 147.92 (C_q), 152.44 (C_q, *C*=CSiMe$_3$), 175.89 (C_q, C=*C*SiMe$_3$). − ^{29}Si NMR (C_6D_6, 59.6 MHz, 298 K): δ = −22.17, −18.90, −2.24. − MS (CI, isobutane): *m*/*z* (%) = 923 (25) [MH$^+$]. − $C_{56}H_{80}Si_6$ (921.74): calcd. C 72.97, H 8.75; found C 71.82, H 8.93.

The *n*-hexane was then replaced by an *n*-hexane/DME mixture and the resulting solution was cooled for 2 weeks at −30°C. After this time, 0.22 g (11% yield) of colorless crystals of *cis*-**21** were obtained; m.p. 268−270°C. − ^{1}H NMR (C_6D_6, 500 MHz, 298 K): δ = −0.02 (s, 18 H), 0.21 (s, 18 H), 1.92 (s, 3 H), 1.94 (s, 3 H), 2.02 (s, 3 H), 2.09 (s, 3 H), 2.11 (s, 3 H), 2.17 (s, 3 H), 2.51 (s, 6 H), 2.61 (s, 6 H), 2.95 (s, 3 H), 2.97 (s, 3 H), 6.38 (s, 2 H), 6.41 (s, 2 H), 6.59 (s, 1 H), 6.61 (s, 1 H), 6.79 (s, 1 H), 6.81 (s, 1 H). − ^{13}C NMR (C_6D_6, 125.7 MHz, 298 K): δ = −0.42 (C_p), −0.17 (C_p), 20.91 (C_p), 21.24 (C_p), 25.33 (C_p), 25.62 (C_p), 25.70 (C_p), 25.78 (C_p), 27.02 (C_p), 106.22 (C_q, *C*≡CSiMe$_3$), 109.87 (C_q, C≡*C*SiMe$_3$), 127.72 (C_t), 128.47 (C_t), 128.69 (C_t), 128.78 (C_t), 130.87 (C_t), 131.55 (C_t), 131.66 (C_q, *ipso*-C), 136.60 (C_q), 137.54 (C_q), 138.34 (C_q), 138.53 (C_q), 140.34 (C_q), 143.81 (C_q), 144.89 (C_q), 146.53 (C_q), 146.98 (C_q), 147.17 (C_q), 148.25 (C_q), 152.80 (C_q, C=*C*SiMe$_3$), 176.84 (C_q, *C*=CSiMe$_3$). − ^{29}Si NMR (C_6D_6, 59.6 MHz, 298 K): δ = −2.60 (2 Si, C=C−SiMe$_3$), −18.87 (2 Si, C≡C−SiMe$_3$), −21.74 (1 Si), −24.04 (1 Si). − MS (CI, isobutane): *m*/*z* (%) = 922 (16) [MH$^+$], 461 (100) [M$^+$/2]. − $C_{50}H_{80}Si_6$ (921.74): calcd. C 72.97, H 8.75; found C 72.72, H 8.92.

X-ray Structure Analyses of 12, 15, 18, *trans*-21, and *cis*-21: Crystal data and numerical data of the structure determinations are given in Table 1. In each case, the crystal was mounted in an inert oil. Data collection was performed with a Siemens Stoe AED 2 diffractometer (**18**) or a Stoe IPDS area detector (**12**, **15**, *trans*-**21**, *cis*-**21**) using graphite-monochromated Mo-K_α radiation (λ = 71.073 pm). The structures were solved by direct phase determination and refined by full-matrix least-squares against F^2 using the SHELXL-93/97 program systems.[22] Hydrogen atoms were placed in calculated positions, while all other atoms were refined anisotropically.[23]

Acknowledgments

Financial support of our work by the Deutsche Forschungsgemeinschaft and the Fonds der Chemischen Industrie is gratefully acknowledged.

[1] Review: P. P. Gaspar, R. West, in: *The Chemistry of Organic Silicon Compounds*, Vol. II (Eds.: Z. Rappoport, Y. Apeloig), Wiley, Chichester, UK, **1998**, p. 2463−2569.
[2] Review: M. Weidenbruch, *Coord. Chem. Rev.* **1994**, *130*, 275−300.
[3] A. Schäfer, M. Weidenbruch, K. Peters, H. G. von Schnering, *Angew. Chem.* **1984**, *96*, 311−312; *Angew. Chem. Int. Ed. Engl.* **1984**, *23*, 302−303.
[4] P. Boudjouk, U. Samaraweera, R. Sooriyakumaran, J. Chrisciel, *Angew. Chem.* **1988**, *100*, 1406−1407; *Angew. Chem. Int. Ed. Engl.* **1988**, *27*, 1355−1356.
[5] M. J. Fink, M. J. Michalazyk, K. J. Haller, R. West, J. Michl, *Organometallics* **1984**, *3*, 793−800.
[6] M. Weidenbruch, H. Piel, K. Peters, H. G. von Schnering, *Organometallics* **1994**, *13*, 3990−3994.
[7] L. Kirmaier, M. Weidenbruch, H. Marsmann, K. Peters, H. G. von Schnering, *Organometallics* **1998**, *17*, 1237−1240.
[8] W. S. Palmer, K. A. Woerpel, *Organometallics* **1997**, *16*, 4824−4827.
[9] K. Peters, E.-M. Peters, D. Ostendorf, M. Weidenbruch, *Z. Kristallogr. NCS*, in press.
[10] E. Lukevics, O. Pudova, R. Sturkovich, *Molecular Structure of Organosilicon Compounds*, Ellis Horwood, Chichester, UK, **1989**.
[11] A. Kunai, T. Mihara, Y. Matsuo, J. Oshita, A. Naka, M. Ishikawa, *J. Organomet. Chem.* **1997**, *545−546*, 611−613.
[12] For an Si−Si-linked bis(silirene), see: W. Ando, T. Shiba, T. Hidaka, K. Morihashi, O. Kikuchi, *J. Am. Chem. Soc.* **1997**, *119*, 3629−3630.
[13] A. Almenningen, O. Bastiansen, M. Traetterburg, *Acta Chem. Scand.* **1958**, *12*, 1221−1225.
[14] H. Watanabe, K. Takeuchi, N. Fukawa, M. Kato, M. Goto, Y. Naigai, *Chem. Lett.* **1987**, 1341−1344.
[15] A. J. Millevolte, D. R. Powell, S. G. Johnson, R. West, *Organometallics* **1992**, *11*, 1091−1095.
[16] K. Peters, E.-M. Peters, L. Kirmaier, D. Ostendorf, M. Weidenbruch, *Z. Kristallogr. NCS* **1999**, *214*, 339−540.
[17] T. Takahashi, Z. Z. Xi, Y. Obara, N. Suzuki, *J. Am. Chem. Soc.* **1995**, *117*, 2665−2666.
[18] [18a] S. Pulst, P. Arndt, B. Heller, W. Baumann, R. Kempe, U. Rosenthal, *Angew. Chem.* **1996**, *108*, 1175−1178; *Angew. Chem. Int. Ed. Engl.* **1996**, *35*, 1112−1115. − [18b] S. Pulst, F. G. Kirchbauer, B. Heller, W. Baumann, U. Rosenthal, *Angew. Chem.* **1998**, *110*, 2029−2031; *Angew. Chem. Int. Ed.* **1998**, *37*, 1925−1927.
[19] T. J. Barton, J. Lin, S. Ijadi-Maghsoodi, M. D. Power, X. Zhang, Z. Ma, H. Shimizu, M. S. Gordon, *J. Am. Chem. Soc.* **1995**, *117*, 11695−11703.
[20] G. E. Miracle, J. L. Ball, D. R. Powell, R. West, *J. Am. Chem. Soc.* **1993**, *115*, 11598−11599.
[21] M. Trommer, G. Miracle, B. E. Eichler, D. R. Powell, R. West, *Organometallics* **1997**, *16*, 5737−5747.
[22] G. M. Sheldrick, *SHELXL-93/97, Programs for Crystal Structure Refinement,* Universität Göttingen, Germany, **1993/1997**.
[23] Crystallographic data (excluding structure factors) for the structures reported in this paper have been deposited with the Cambridge Crystallographic Data Centre as supplementary publication nos. CCDC-122 319 (**12**), CCDC-122 322 (**15**), CCDC-122 323 (**18**), CCDC-122 321 (*trans*-**21**), and CCDC-122 320 (*cis*-**21**). Copies of the data can be obtained free of charge on application to the CCDC, 12 Union Road, Cambridge CB2 1EZ, U.K. [Fax: (internat.) +44(0)1223/336093; E-mail: deposit@ccdc.cam.ac.uk].

Received June 17, 1999
[I99227]

Synthesis, Spectroscopy and Photophysical Properties of Ruthenium Triazole Complexes and Their Application as Dye-Molecules in Regenerative Solar Cells

Anthea C. Lees,[a] Bénédicte Evrard,[a] Tia E. Keyes,[a,b] Johannes G. Vos,[a] Cornelis J. Kleverlaan,*[c] Monica Alebbi,[c] and Carlo A. Bignozzi[c]

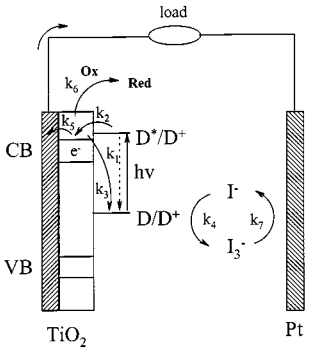
Keywords: Ruthenium / Triazole / Titanium / Electron Transfer / Sensitizers

The complexes $[Ru(dcb)_2(L)]$ {L = 3-(2-hydroxyphenyl)-5-(pyridin-2-yl)-1,2,4-triazole (2-ppt), 3-(4-hydroxyphenyl)-5-(pyridin-2-yl)-1,2,4-triazole (4-ppt), 3,5-bis(pyrazin-2-yl)-1,2,4-triazole (bpzt), 3-(2-hydroxyphenyl)-5-(pyrazin-2-yl)-1,2,4-triazole (2-ppzt) and dcb = 4,4′-$(CO_2H)_2$-2,2′-bipyridine} have been synthesized, spectroscopically characterized and anchored to nanocrystalline TiO_2 electrodes for the conversion of light into electricity in regenerative solar cells. The different efficiencies observed have been rationalized on the basis of an analytical expression relating the incident photon-to-current conversion efficiency (IPCE) to the kinetic parameters of the relevant electron transfer processes involved in the solar cell.

Introduction

In the search for new solar energy conversion systems, dye-sensitized wide bandgap semiconductors have attracted much attention.[1−14] Solar cells containing photoanodes based on highly porous nanocrystalline TiO_2 films with adsorbed ruthenium dyes have demonstrated photon-to-current conversion efficiencies in the range 7−10% at AM 1.5.[6,12,15,16] The general mechanism of sensitization in a regenerative dye solar cell is shown in Scheme 1.[10,17,18] Excitation of an adsorbed dye molecule (D*) is followed by electron injection (k_2) to the semiconductor conduction band (CB). The oxidized dye molecule is reduced by an electron donor (k_4), which is present in the electrolyte. Reduction of the oxidized dye molecule (D^+) takes place via the sacrificial donor I^-, which is regenerative at the counterelectrode (k_7) (Pt/SnO_2). Losses in efficiency can occur by radiative and nonradiative decay of the excited state (k_1), by recombination of electrons in TiO_2 with oxidized dye molecules (k_3), and by electrons in TiO_2 which react with oxidants in solution (k_6).

Measuring the monochromatic incident photon-to-current efficiency, IPCE, gives the overall efficiency of the processes involved in the photovoltaic cell. IPCE is directly related to the absorption characteristics of the dye, the surface coverage of the TiO_2 electrode (LHE), the quantum yield for charge injection to the semiconductor (ϕ), and the efficiency of collecting electrons in the external circuit (η).[6][12]



Scheme 1

$$IPCE = (LHE)(\Phi)(\eta) \qquad (1)$$

Several studies have focused on the role played by the different electron transfer processes in determining cell performances.[5,19−21] It has been shown that charge injection processes (k_2) take place in the femto- and/or picosecond time domain[8][22] with $\phi = 1$, and that an important factor decreasing the conversion efficiency is the electron transfer from the sensitized TiO_2 film to the relay electrolyte (k_6).[5] Recently, examples of the limiting role of iodide oxidation by oxidized dye (k_4) on the conversion efficiencies have been reported.[21]

The understanding of the key parameters affecting cell performances is of relevance to the design of the molecular sensitizer. A strong absorption in the visible part of the absorption spectrum is clearly beneficial. In addition, the excited-state properties and the redox potentials of the molecular dyes have to be tuned with respect to the level of the conduction band in the TiO_2 and to the redox potential of the sacrificial donor I^-, to increase the driving force of the corresponding electron transfer processes. The complexes which so far have shown the most promising characteristics, are based on ruthenium polypyridyl moieties incorporating

[a] Inorganic Chemistry Research Centre, School of Chemical Sciences,
Dublin City University, Dublin 9, Ireland
[b] Present address: Department of Chemistry, Dublin Institute of Technology,
Kevin Street, Dublin 8, Ireland
[c] Dipartimento di Chimica, Università di Ferrara,
Via L. Borsari N. 46, I-44100 Ferrara, Italy

 © WILEY-VCH Verlag GmbH, D-69451 Weinheim, 1999 1434−1948/99/1212−2309 $ 17.50+.50/0

negative monodentate ligands such as NCS^-.[6,10,16,23] The presence of monodentate ancillary ligands can, however, lead to some photochemical instability of the dye molecule which, in principle, can be reduced by using chelating ligands. We have therefore started a systematic investigation of potential dyes based upon triazole-type ligands.

Mixed-ligand Ru^{II} complexes with electron rich 1,2,4-triazole-and 2,2′-bipyridine (bpy) containing ligands have been investigated in detail. Upon coordination the triazole ring is deprotonated, leaving a negative charge on the triazole ligand. It is well established that for complexes incorporating deprotonated triazole ligands the excited state is localized on the bpy moieties.[24−33]

In this study, the synthesis and characterization of complexes of the type $[Ru(dcb)_2(L)]$ {L = 3-(2-hydroxyphenyl)-5-(pyridin-2-yl)-1,2,4-triazole (2-ppt), 3-(4-hydroxyphenyl)-5-(pyridin-2-yl)-1,2,4-triazole (4-ppt), 3,5-bis(pyrazin-2-yl)-1,2,4-triazole (bpzt), 3-(2-hydroxyphenyl)-5-(pyrazin-2-yl)-1,2,4-triazole (2-ppzt); dcb = 4,4′-$(CO_2H)_2$-2,2′-bipyridine} is reported. The general structure of the complexes and ligands are depicted in Figure 1. The excited-state properties of the complexes in solution and when immobilized on TiO_2 have also been investigated by means of laser flash photolysis. The efficiency of the complexes as dyes in regenerative photoelectrochemical cells has been assessed and rationalized on the basis of an analytical expression correlating the IPCE to the relevant kinetic parameters schematized in Scheme 1.

Results

Electronic Absorption Spectra in Solution

Figure 2 shows the UV-Vis spectra of the complexes $[Ru(dcb)_2(L)]$ (L = 4-ppt, 2-ppt, bpzt or 2-ppzt) in aqueous solution at pH 7 (see also Table 1). At this pH both the triazole and dcb ligands are deprotonated (see discussion). The UV-Vis spectra for the complexes with 4-ppt or 2-ppt are nearly identical. The spectra obtained for the complexes containing the pyrazine-based ligands bptz and 2-ppzt are also very similar. The 4-ppt and 2-ppt complexes are characterized by absorption bands at 487, 437 and 367 nm, while the complexes containing bptz and 2-ppzt show a significant blue shift of the lowest energy absorption, with bands at about 461 and 433 nm. Lowering the pH to ca. 3 gives a characteristic blue shift for the 4-ppt and 2-ppt complexes, resulting in only two absorption bands each at 465, 433 and 473, 435 nm, respectively. The complexes with bpzt and 2-ppzt only showed band broadening. These changes are due to protonation of the triazole ring, and similar shifts have been observed for the corresponding mixed-ligand complexes containing bpy.[24−33] Decreasing the pH further resulted in precipitation of the compounds because of protonation of the carboxy ligands. The emission spectra were recorded in aqueous solution at pH 7, and the maxima are summarized in Table 1.

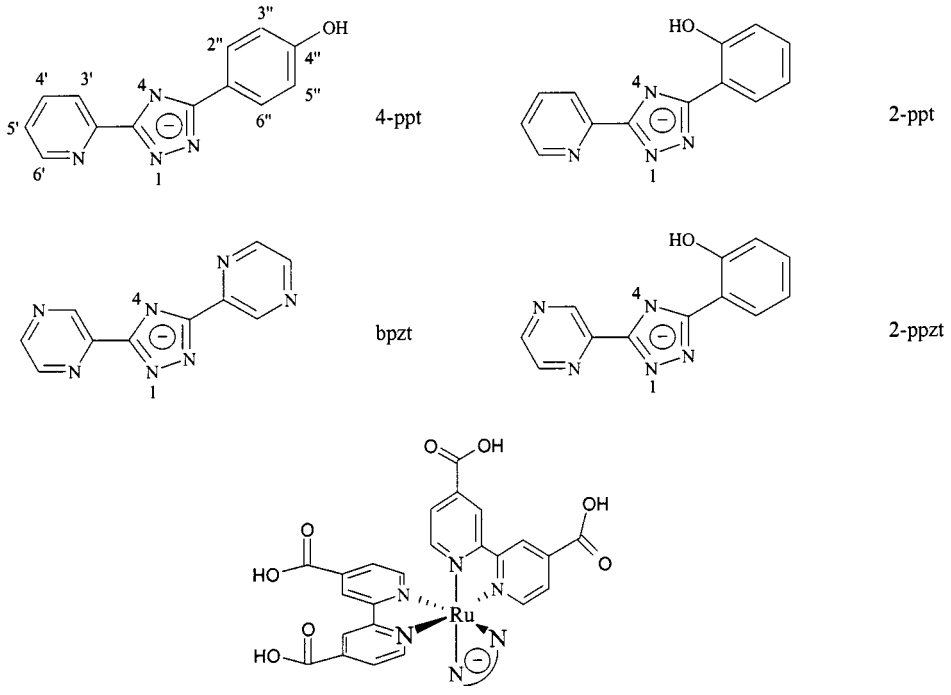


Figure 1. General molecular structure of $[Ru(H_2dcb)_2(L)]$ and the ligands L = 4-ppt, 2-ppt, bpzt and 2-ppzt

Table 1. Optical and electrochemical properties of the complexes $[Ru(dcb)_2(L)]$ (L = 4-ppt, 2-ppt, bpzt or 2-ppzt)

Solution TiO_2 L	λ_{max} (nm)[a]	λ_{em} (nm)[a]	τ (ns)[b]	E_{ox}[c]	λ_{max} (nm)[d]
4-ppt	487	691	40	1.02	495
2-ppt	486	681	60		495
bpzt	460	665	45	1.10	475
2-ppzt	461	701	30	1.06	475

[a] H_2O/Na_2CO_3 at pH 7. – [b] Obtained from emission and transient-absorption difference spectra in degassed H_2O/Na_2CO_3 at pH 7 (estimated error ± 5 ns). – [c] Measured in DMF/0.1 M $LiClO_4$. – [d] Measured in MeCN.

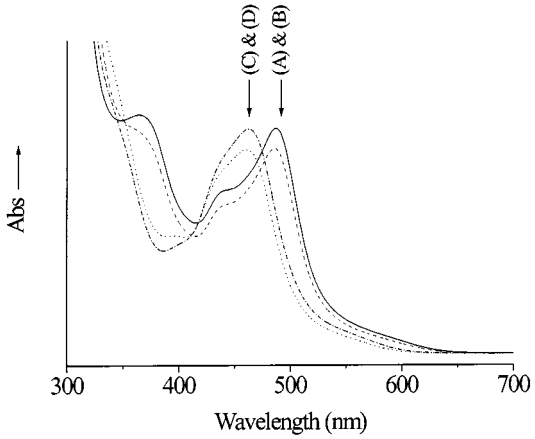


Figure 2. UV-Vis absorption spectra of (A) $[Ru(dcb)_2(4\text{-ppt})]$ (–), (B) $[Ru(dcb)_2(2\text{-ppt})]$ (- - -), (C) $[Ru(dcb)_2(bptz)]$ (···) and (D) $[Ru(dcb)_2(2\text{-ppzt})]$ (-·-·-) in aqueous solution at pH 7 (room temp.)

Electrochemistry in Solution

The electrochemical properties of the complexes were measured in DMF/0.1 M $LiClO_4$. The redox potentials obtained are listed in Table 1. For the complexes $[Ru(dcb)_2(L)]$ (L = 4-ppt, 2-ppt or 2-ppzt) the voltamograms are complicated by the irreversible oxidation of the phenol ligand at about 1.3 V vs SCE. By comparison with data observed for the corresponding bpy complexes, the quasi reversible process at about 1 V vs Ag/AgCl can be assigned to the Ru^{II}/Ru^{III} redox couple. The dcb-based reduction processes are irreversible. As observed before for other triazole-based ruthenium polypyridyl complexes, partial protonation of the triazole ring is observed when the potential is first cycled through the bpy-based reductions. In that case an additional redox wave at about 1.3 V is observed.[34]

Photophysics in Solution

Flash photolysis experiments were carried out in degassed aqueous solution at pH 7, employing a 532 nm excitation pulse (6.5 mJ). The transient-absorption difference spectra of the complexes are shown in Figure 3. The spectra are characterized by a bleaching process in the 400–500 nm region and the formation of a new transition in the 350–400 nm region. The excited-state lifetime obtained from the transient spectra were identical to the lifetimes obtained from independent time-resolved emission measurements. The decay of the emission intensity was, in all cases, single exponential. The lifetimes of the various complexes are summarized in Table 1.

Absorption spectra on TiO_2

The complexes $[Ru(dcb)_2(L)]$ were absorbed as a monolayer onto a ca. 7 μm thick nanocrystalline TiO_2 film. The UV-Vis spectra of two complexes (L = 2-ppt or bptz) on a TiO_2 film are shown in Figure 4. The absorption spectrum of $[Ru(dcb)_2(2\text{-ppt})]/TiO_2$ is mainly a superposition of the complex and the TiO_2. The absorption spectrum of the corresponding bpzt complex closely resembles the absorption spectrum in solution, but with different intensities of the absorption maxima. At 491 nm (2-ppt) and 475 nm (bptz) the absorbances were 1.60 and 1.84, respectively. Using the extinction coefficients at this wavelength, 1.0×10^4 $M^{-1}\cdot cm^{-1}$ (2-ppt) and 1.4×10^4 $M^{-1}\cdot cm^{-1}$ (bpzt),[25][35] and considering for the surface requirement of one adsorbed molecule the value of 100 Å^2, for a complete monolayer coverage, an average roughness factor of ca. 800 can be calculated.

Photoelectrochemistry

The dye-molecules were tested in a standard photovoltaic cell (see experimental). Figure 5 shows a plot of the incident-photon-to-current efficiency (uncorrected for light absorption by the conductive glass) *vs.* the excitation wavelength, IPCE(λ), for the complexes. The IPCE(λ) is defined by Equation (2).[6][10]

Figure 5 demonstrates that the IPCE(λ) closely resembles the absorption spectra of the dye molecules attached to the TiO_2.

$$IPCE(\lambda) = \frac{1.24\ (eV\cdot nm)\ x\ photocurrentdensity\ (\mu A\cdot cm^{-2})}{wavelength\ (nm)\ x\ photonflux\ (\mu W\cdot cm^{-2})} \qquad (2)$$

Photophysics on TiO_2

The transient-absorption difference spectra of the complexes $[Ru(dcb)_2(L)]$ anchored to TiO_2 are shown in Figure 6. The striking difference with the spectra recorded in solution (Figure 3) is the lack of the absorption band in the 350–400 nm region. The time-resolved absorbance changes of the complexes measured at 480 nm are depicted in Figure 7 [traces marked with **(1)**].

The traces were obtained by excitation with P = 0.3 $mJ\cdot cm^{-2}$. The back electron transfer between the electrons in the TiO_2 particle and the Ru^{III} centers typically takes place in the nano- and microsecond time domain and is power dependent. At low excitation power, the back electron transfer is slower than at excitation with higher powers

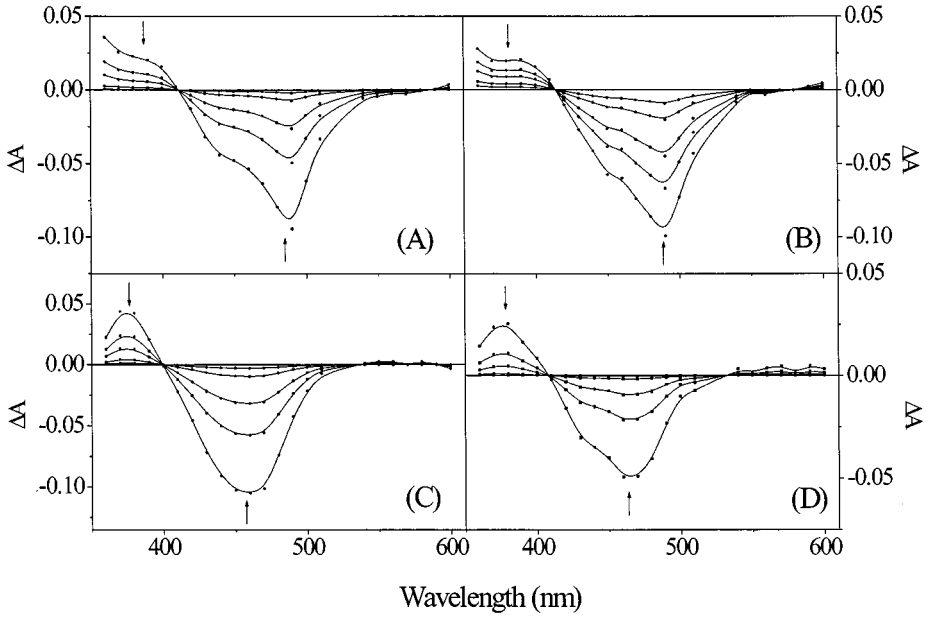


Figure 3. Time-resolved transient-absorption spectra in aqueous solution (pH 7; room temp.) of (A) $[Ru(dcb)_2(4\text{-ppt})]$, (B) $[Ru(dcb)_2(2\text{-ppt})]$, (C) $[Ru(dcb)_2(bpzt)]$ and (D) $[Ru(dcb)_2(2\text{-ppzt})]$ at τ_d = 0, 25, 50, 100 and 150 ns, respectively (λ_{exc} = 532 nm, P = 6.5 mJ/Pulse)

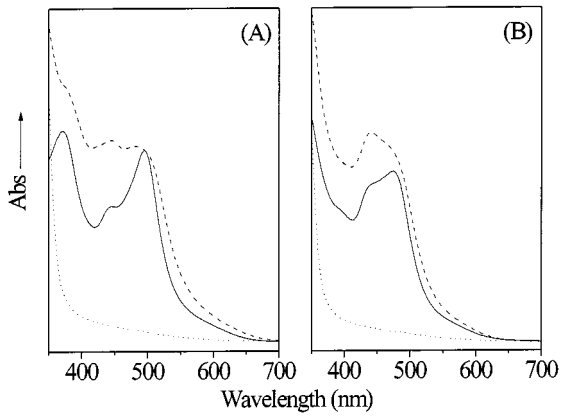


Figure 4. UV-Vis absorption spectra of (A) $[Ru(dcb)_2(2\text{-ppt})]$ (−), $[Ru(dcb)_2(2\text{-ppt})]/TiO_2$ (- - -) and TiO_2 (···) in MeCN (room temp.) (B) $[Ru(dcb)_2(2\text{-bpzt})]$ (−), $[Ru(dcb)_2(2\text{-bpzt})]/TiO_2$ (- - -) and TiO_2 (···) in MeCN (room temp.)

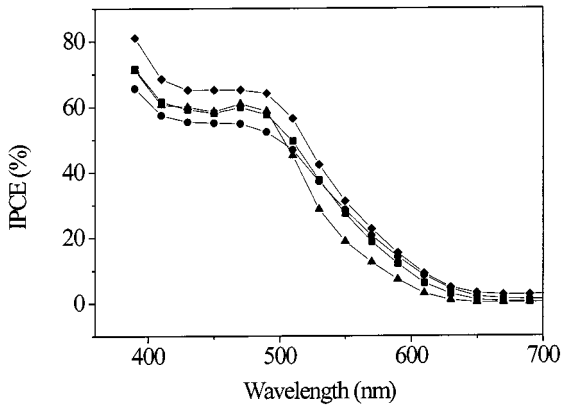


Figure 5. Incident photon-to-current efficiency *vs.* the excitation wavelength, IPCE(λ), for (▲) = $[Ru(dcb)_2(4\text{-ppt})]$, (■) = $[Ru(dcb)_2(2\text{-ppt})]$, (◆) = $[Ru(dcb)_2(bpzt)]$ and (●) = $[Ru(dcb)_2(2\text{-ppzt})]$

(spectra not shown). A detailed study[36] and description of the complexes kinetics is beyond the scope of this paper.

In order to get a better insight into the processes determining the efficiency of the photovoltaic cell, experiments in the presence of I^- were employed. The quenching of oxidized dye molecules by 0.3 M I^-, giving rise to the parent complex, the iodine radical[19] and TiO_2-nanoparticle with an electron excess, are depicted in Figure 7 [traces marked with (2)]. The concentration of I^- was the same as in a typical photovoltaic cell (0.3 M LiI) and the Li^+ concentration was kept constant with respect to the recombination experiments (0.3 M $LiClO_4$). The transient-absorption difference spectra in the presence of I^- show a broad band (360−450 nm), most probably due to radical products of I^- (spectrum not shown).[19] The quenching of $[Ru^{III}(dcb)_2(NCS)_2]$ by I^- was observed to take place in the laser pulse (< 10 ns), while, under the same experimental conditions, the quenching of all $[Ru^{III}(dcb)_2(L)]$ dye molecules was slower and completed within ca. 100 ns.

Discussion

In metal complexes with the triazole ligands reported here, the coordination mode of the triazole ring has to be considered. As Figure 1 shows, coordination of the triazole ring can occur through the N1 or the N4 atom. HPLC analysis of the reaction products shows that only one major product is obtained. It has been shown in the past that proton NMR spectroscopy can be used to determine the coordination mode of these ligands.[31−33,35,37,38] The spectra obtained for the compounds strongly indicate that for all compounds coordination of the triazole ring is through the N1 atom. N1 coordination is also to be expected from steric considerations. It is also important to note that the spectra

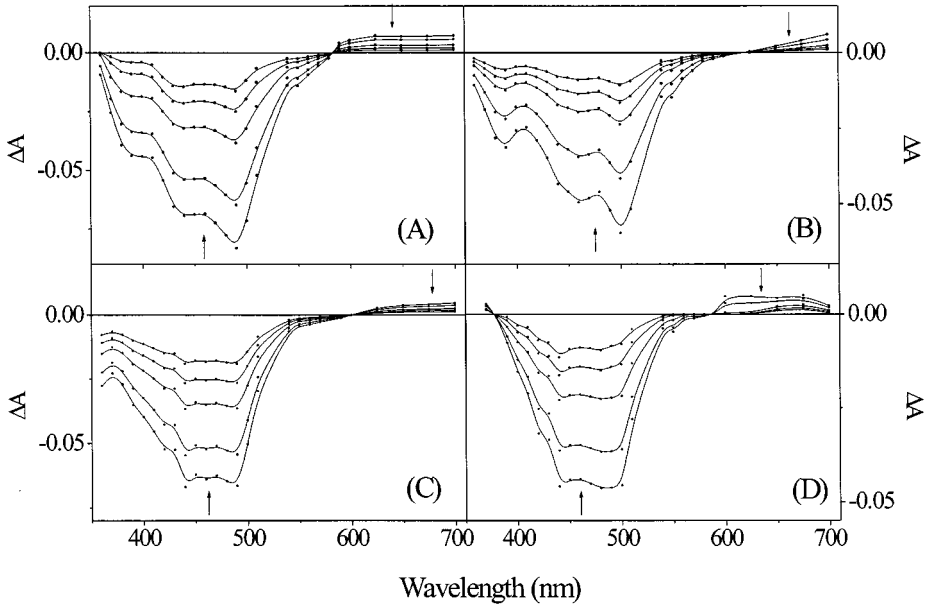


Figure 6. Time-resolved transient-absorption spectra of the TiO_2 films in MeCN/0.1 M $LiClO_4$ (room temp.), covered with (A) [Ru(dcb)$_2$(4-ppt)], (B) [Ru(dcb)$_2$(2-ppt)], (C) [Ru(dcb)$_2$(bpzt)] and (D) [Ru(dcb)$_2$(2-ppzt)] at τ_d = 0, 50, 250, 1000 and 2000 ns, respectively (λ_{exc} = 532 nm, P = 0.5 mJ·cm^{-2})

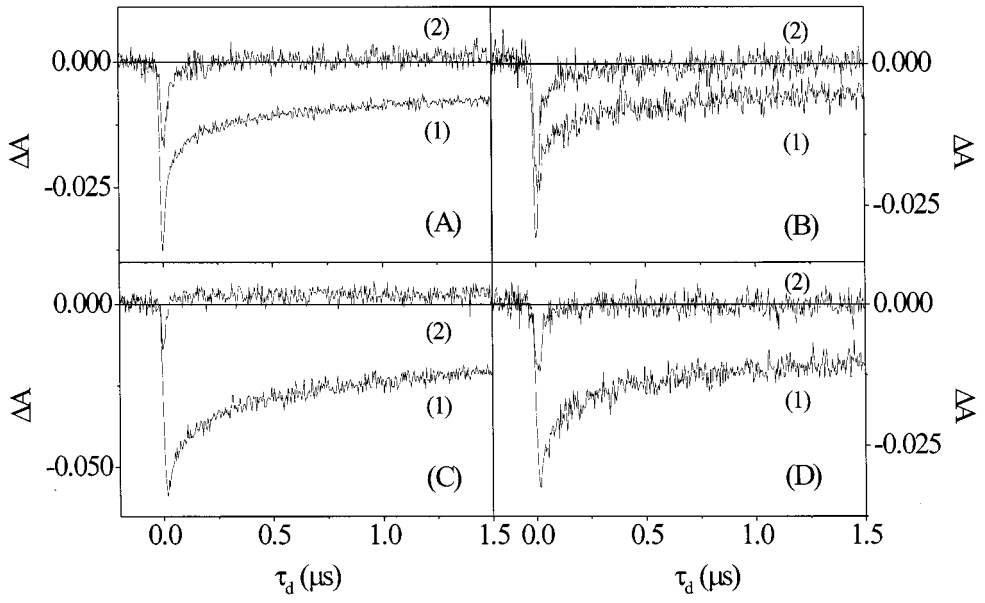


Figure 7. The microsecond decay kinetics measured at 480 nm of (A) [Ru(dcb)$_2$(4-ppt)], (B) [Ru(dcb)$_2$(2-ppt)], (C) [Ru(Hdcb)$_2$(bpzt)] and (D) [Ru(dcb)$_2$ (2-ppzt)] measured in the presence of (1) MeCN/0.3 M $LiClO_4$ and (2) MeCN/0.3 M LiI, respectively (λ_{exc} = 532 nm, P = 0.3 mJ·cm^{-2})

are recorded in DMSO/NaOD and, therefore, under these conditions, the complexes are completely deprotonated. The overall charge of the complexes is then 3−.

Intrinsically, the complexes reported here have very complicated acid-base properties. First of all the deprotonation steps of the dcb ligand have to be considered. The ligand shows two protonation steps for the complexes [Ru(bpy)$_{3-n}$(dcb)$_n$] (n = 1,2,3) with pK_{a2} values around 1.7−1.75 and pK_{a1} values between 2.2−2.85.[39−42] For the excited states a pK_a*$_2$ value of 1.75 was estimated, while the pK_a*$_1$ value was found to increase from the corresponding ground-state value to between 4.6−4.25.[39−42] Secondly, the triazole ligands have their own acid-base properties. The ground-state pK_a values for the closely related triazole complexes are between 2.0 and 5.5.[25,31−33,35,37,38] The pyridyltriazole-containing complexes are slightly more acidic in the excited state than in the ground state.[31][32] This is in agreement with resonance Raman, time-resolved resonance Raman, and excited-state absorption studies, which all support an excited state localized on the bpy ligands and triazole ligands that do not actively participate in the lowest excited state of the compounds.[24,26,27] For pyrazinetriazoles the

situation is even more complicated. The acid-base chemistry of these compounds together with resonance Raman data strongly suggest that when the triazole moiety is deprotonated (with a pK_a of about 2.0) the excited state is based on the bpy ligand, while in complexes where protonation of the triazole ring has occurred the lowest energy excited state is based upon the pyrazine ring.[24][34] Furthermore, the complexes with 4-ppt, 2-ppt or 2-ppzt have a phenol group with a pK_a of about 11.[25] These intricate acid-base properties make it impossible to isolate solid materials with a well-defined state of protonation. However, in solution under pH control, well-defined species are obtained as is shown in the NMR and UV-Vis spectra. For this reason we have used the $[Ru(dcb)_2(L)]$ formula to describe the solid complexes. All the photophysical measurements have been carried out under conditions where the triazole moiety is deprotonated. This ensures that the lowest energy excited state is based on the dcb ligands. This is also the case for the pyrazine based systems.

Analogous to the corresponding bpy complexes, the lowest absorption bands at ca. 470 nm, can be assigned to MLCT transitions between the metal and the dcb ligands. The complexes with the pyridine-based ligands 4-ppt and 2-ppt show MLCT bands at lower energy than those observed for the pyrazine-containing complexes. Since the lowest MLCT transitions originate from the $d_{Ru} \rightarrow \pi^*_{dcb}$ orbitals,[24] the observed red-shift for the pyridine-based complexes can be explained by the stronger σ-donor effect of the pyridine ring, resulting in an increase in energy of the d-orbitals of the metal center.[35] The UV-Vis spectra of the $Ru(dcb)_2$ pyridyltriazoles measured in aqueous solution at pH 7, where both the triazole and the polypyridyl ligands are deprotonated, show the same spectral properties as those of the corresponding $[Ru(bpy)_2(2\text{-ppt})]$ complex.[30] The spectral features of the $Ru(dcb)_2$ pyrazinetriazole compounds are similar to the spectra of $[Ru(bpy)_2(bpzt)]^+$.[33][35] All the absorption spectra show a typical red-shift of ca. 15−20 nm on going from bpy to dcb.[39][41] Under these circumstances, at pH 7, the emission maxima of the complexes are found at ca. 680 nm, which is a red-shift of 20 nm with respect to the values observed for the bpy derivatives, further supporting the proposition that the excited state is localized exclusively on the dcb ligand. The spectral changes observed on changing the pH to 3 correspond to the protonation of the triazole and dcb ligands.[30−33,35,37−42] An extensive study of the protonation behavior of the compound was not possible because further decreasing of the pH results in precipitation of the complexes.

The transient-absorption difference spectra of the $[Ru(dcb)_2(L)]$ complexes in aqueous solution (pH 7) show a bleach in the region 400−500 nm. This can be attributed to the disappearance of the MLCT transitions in the excited state. The strong absorption in the region 350−400 nm can be assigned to intraligand transitions of the dcb radical-anion. This behavior is typical for those Ru-complexes with a bpy/dcb ligand-localized excited state.[43−45] A comparable spectrum was found for $[Ru(bpy)_2(bpzt)]^+$.[24] The lifetimes of the excited states of the various complexes are in the range of 30−60 ns (see Table 1), which is shorter than the lifetimes observed for the corresponding bpy complexes, i.e. $[Ru(bpy)_2(bpzt)]^+$ (290 ns) and $[Ru(dcb)_2(bpzt)]$ (45 ns).[24] A red-shift of the absorption and emission maxima leads, in general, according to the energy gap law, to a decrease in lifetime.[46−48]

The complexes were absorbed on TiO_2 for photoelectrochemical measurements. Figure 4 shows that the optical properties of the dye molecules bound to TiO_2 and in solution (at pH 7) are comparable. The spectra also show that the triazole ligands are in the deprotonated form. The photoaction spectra (Figure 5 and Table 2) indicate that the complexes act as efficient sensitizers with $IPCE_{470nm}$ in the range 0.55−0.65 (0.68−0.80; values corrected for light absorption by the ITO glass). The fact that under similar experimental conditions the $[Ru(dcb)_2(NCS)_2]$ complex was shown to give better performances [$IPCE_{500nm} = 0.77$ (0.95; value corrected for light absorption by the ITO glass)] was unexpected, since the ground- and excited-state redox properties of these species are very similar. As shown in Equation 1, IPCE depends on the three terms Φ **(i)**, LHE **(ii)**, and η **(iii)**, [6][12] which will be discussed separately:

(i) The absence of $^3[Ru(dcb)_2(L)]^*$ in the transient-absorption spectra of the dye on TiO_2, clearly shows that electron injection to the semiconductor is efficient (>95%) and takes place within the laser pulse (< 10 ns) or faster, which is in agreement with earlier reported data.[8][22]

(ii) Under the experimental conditions used, the LHE term for $[Ru(dcb)_2(NCS)_2]$ and the $[Ru(dcb)_2(L)]$ (L = 2-ppt, bpzt or 2-ppzt) complexes are the same, since for the examined photoanodes the incident light absorption was in the range 0.96−0.99 (see Table 2). Due to the low solubility of $[Ru(dcb)_2(4\text{-ppt})]$, the surface coverage on TiO_2 of the latter complex was lower than the other compounds, resulting in LHE = 0.90.

(iii) Significant differences are found for the quenching rate of Ru^{III} by I^- (k_4). For $[Ru(dcb)_2(NCS)_2]$ this process takes place in the laser pulse (less than 10 ns), while the quenching of $[Ru^{III}(dcb)_2(L)]$ is completed within less than 100 ns. The quenching of $[Ru^{III}(dcb)_2(bpzt)]$ by I^- [Figure 7 (C) trace (2)] is completed in 30 ns, resulting in the highest IPCE value. The reaction of the $[Ru^{III}(dcb)_2(L)]$ (L = 4-ppt, 2-ppt or 2-ppzt) with I^- is slower (100 ns), resulting in lower IPCE values. Furthermore, one should realize that any formation of Ru^{III} in the presence of I^- directly leads to losses in efficiency. Apparently, the quenching rate of Ru^{III} by I^- is an important parameter in the efficiency of the photovoltaic cell. Differences in IPCE values, therefore, most likely reflect a variation in η values, which reflects the processes k_3, k_4 and k_5. The traces obtained from the quenching experiments [Figure 7 (C) trace (2)] do not give the rate constant (k_4) for the quenching of the Ru^{III} by I^-.

$$S^+ + e^- \xrightarrow{k_3} S$$
$$S^+ + I^- \xrightarrow{k_4} S + I^{\bullet} \qquad (3)$$

$$[S^+] = [S^+]_0 e^{-(k_3+k_4)t} \qquad (4)$$

From Equations 3 and 4 it can easily be seen that the observed rate constant is the sum of the quenching rate constant (k_4) and the back electron transfer (k_3).

Analogous to the quantum yield of injection (Φ), the efficiency of quenching (defined as) η, of Ru^{III} by I^- is described by Equation 5 or 6. These equations describe the interplay between the quenching of Ru^{III} by I^- (k_4) and the recombination of the electrons in the conduction band with the Ru^{III} center (k_3). The appendix shows the full derivation for all the processes involved in the IPCE under steady-state conditions, resulting in the same terms for η if $k_6[e^-] << k_7[e^-_{ex}]$,[49−53]

$$\eta = \frac{k_4[I^-]}{k_3[e^-] + k_4[I^-]} \quad \text{or} \quad \eta = 1 - \frac{k_3[e^-]}{k_3[e^-] + k_4[I^-]} \qquad (5) \text{ and } (6)$$

$$\eta = \frac{k_4}{k_3 + k_4} \quad \text{or} \quad \eta = 1 - \frac{k_3}{k_3 + k_4} \qquad (7) \text{ and } (8)$$

Application of these formulae is not straightforward, since the experimental k_3 and (k_3 + k_4) are not first or second order. For the estimation of η, the simplified first order formulae (Equation 7 and 8) and the following parameters were used: (i) (k_3 + k_4) is equal to k_{obs} in the Ru^{III}/I^- quenching experiment (see Equations 3 and 4), and was treated as a single exponential; (ii) the traces of the recombination of the electron in TiO_2 with the oxidized dye molecule (k_3) can be fitted with a bi-exponential function (see Table 2), which indicates a fast component ($k \approx 1 \times 10^7$ s^{-1} and a slow component ($k \approx 4 \times 10^5$ s^{-1}). Since the quenching of Ru^{III} by I^- is completed within 100 ns, only the fast exponential component of k_3 is considered. Using these rate constants and Equation 7 or 8 we calculated values for η (Table 2). For the steady-state measurements, η can be calculated (Table 2) from Equation 1, the LHE term and $\phi = 1$. The values for the η term obtained by this transient-absorption study are in good agreement with the values found in the steady-state experiments. As a consequence, the delicate interplay between the quenching of Ru^{III} by I^- (k_4) and the recombination of the electrons in the conduction band with the Ru^{III} center (k_3) apparently determines the efficiency of a regenerative solar cell based on ruthenium dyes.

Experimental Section

Materials and Apparatus and Preparations: [$RuCl_3 \cdot H_2O$] (Oxkem Ltd), 4,4′-dimethyl-2,2′-bipyridine (Aldrich) were used without further purification. The solvents for the spectroscopic measurements, acetonitrile (Aldrich), methanol (Aldrich) were of spectroscopic grade and were used as received. 4,4′-Dicarboxy-2,2′-bipyridine (dcb) was prepared by the method of Oki et al.[54] The ligands 4-ppt,[37] 2-ppt,[30] bpzt[35] and 2-ppzt[38] were prepared as previously described. The complexes [$Ru(dcb)_2Cl_2$] and [$Ru(dcb)_2(NCS)_2$] were prepared according to literature procedures.[55] UV-Vis spectra were recorded with a Kontron Uvikon 860 spectrophotometer. Emission spectra were measured on a SPEX Fluoromax 2 spectrofluorimeter equipped with a Hamamatsu R3896 tube. The emission spectra were corrected for the instrumental response. The NMR spectra were recorded on a Bruker AMX 400. HPLC was carried out on a Waters system equipped with a 990 photodiode array detector with a SAX anionic exchange column (8 × 100 mm) and 50:50 (MeCN/H_2O) 0.05 M phosphate buffer as the mobile phase. The TiO_2 films were prepared as described by Nazeeruddin et al.[6] For the IPCE measurement the TiO_2 was deposited on conductive fluorine-doped SnO_2 glass (LOF ≈ 10Ω/□), while for the transient-absorption measurement normal glass was used. The films were heated at 450°C for 30 min. Coating of the TiO_2 surface with the dye was carried out by soaking the film for 3 h (transient-absorption experiments) and 24 h (IPCE measurements) in a ca. 1×10^{-4} M methanol solution of the complexes. After completion of the dye adsorption, the film was rinsed with acetone and dried (10 min. at 60°C). The measurements were performed directly after the preparation of the film. The complexes [$Ru(dcb)_2(L)$] (L = 4-ppt, 2-ppt, bpzt or 2-ppzt) were stable towards daylight and oxygen in methanol solution as well as when bound to the TiO_2 surface. Photoelectrochemical measurements were performed in a two-electrode sandwich cell arrangement by using SnO_2/TiO_2/dye as the photoanode (active area 0.5 cm^2) and a SnO_2/Pt-coated glass as counterelectrode. The sandwich cell was filled with an acetonitrile solution containing 0.3 M LiI and 0.03 M I_2. The current measurements were performed with a Kontron DDM4021 Digital Multimeter. The excitation source was a 150 W Xe lamp coupled to a 0.22 m monochromator. Incident light flux was measured with a UDT-calibrated Si-diode. In order to minimize errors in the IPCE measurements, the complexes and [$Ru(dcb)_2(NCS)_2$] are measured in at least two different cells, resulting in an estimated error of 5%. Nanosecond flash photolysis transient-absorption spectra were measured by irradiating the sample with 6−8 ns (fwhm) of a Continuum Surelight Nd:Yag laser (10 Hz repetition rate) and using as probe light a pulsed Xe-lamp perpendicular to the laser beam. The excitation wavelength was

Table 2. Parameters from the time resolved and steady state experiments for the determination of the η term

L	Time-resolved k_3[a] × 10^6	Steady-state $k_3 + k_4$[b] × 10^6	η_{calc}[c]	$IPCE_{470nm}$	LHE_{470nm}[d]	η_{calc}[e]
4-ppt	14.7(55%) 0.4(45%)	66.7	0.78	0.74	0.90	0.82
2-ppt	11.6(55%) 0.4(45%)	62.5	0.81	0.73	0.97	0.75
bpzt	8.5(43%) 0.3(57%)	71.4	0.88	0.80	0.98	0.82
2-ppzt	8.8(49%) 0.3(51%)	38.4	0.77	0.68	0.99	0.69

[a] Kinetic data from the traces (1) of Figure 7. − [b] Kinetic data from the traces (2) of Figure 7, $k_{obs} = k_3 + k_4$. − [c] Calculated from Equation 8. − [d] LHE = $1-10^{-A}$, where A is the absorbance of the dye on the TiO_2 layer, see also ref.[6][12] − [e] Calculated from Equation 1, with $\phi = 1$.

obtained by frequency doubling (532 nm). The 150 W Xe lamp was equipped with an Applied Photophysics Model 408 power supply and Applied Photophysics Model 410 pulsing unit (giving pulses of 0.5 ms). A shutter, Oriel Model 71445, placed between the lamp and the sample was opened for 100 ms to prevent PMT fatigue. Suitable pre- and post-cutoff and bandpass filters were used to minimize the probe light and scatter light of the laser. The films were oriented at 45° to the laser and probe light and set up in such a way that the scattered light was reflected to the probe light. In this way we were also able to measure in the early time domain (t < 50 ns) without registering artifacts due to scattered light. The sampling rate was kept at a relatively long time (intervals of 10 s) to prevent electron accumulation in the conduction band of the semiconductor. The light was collected in a LDC Analytical monochromator, detected by a R928 PMT (Hamamatsu), and recorded on LeCroy 9360 (600 MHz) oscilloscope. The laser oscillator, Q-switch, lamp, shutter and trigger were externally controlled with a digital logic circuit, which allowed synchronous timing. The absorption transients were plotted as $\Delta A = \log(I_o/I_t)$ *vs* time, where I_o was the monitoring light intensity prior to the laser pulse and I_t was the observed signal at delay time t. The same setup as described above was employed for the time-resolved emission experiments, with the exception that the probe lamp was not used.

Synthesis of Metal Complexes: The complexes containing the triazole ligands were prepared by the following procedure. The ligand (4×10^{-4} M) was heated under reflux in a basic solution of 2:1 ethanol/water (ca. 20 mL) to which the $[Ru(dcb)_2Cl_2]$ (3.2×10^{-4} M) was added. The mixture was further heated at reflux for 3−4 h and the reaction was monitored by HPLC. The product was precipitated by lowering the pH to 2.7 with HCl (ca. 2 mL, 0.2 M) and purified after resolution in water at pH 7 by column chromatography with Sephadex LH20 resin. Isolation of the product after chromatography was achieved by adjusting the pH with HCl as before. In the molecular formulas given below, the degree of protonation and therefore the charge of the complexes has not been defined. Protonation is strongly dependent on the pH of the solution and the pK_a values of the various ligands. The materials obtained have been characterized by proton NMR and anion exchange HPLC.

[Ru(dcb)$_2$(4-ppt)]: ^{1}H NMR ([D$_6$]DMSO/NaOD, 293 K) δ = 8.80−8.76 (d, 4 H, dcb-H$_6$), 8.15 (d, 1 H, H$_{3'}$), 7.92 (t, 1 H, H$_{4'}$), 7.79 (d, 1 H, H$_{6''}$), 7.67 (d, 1 H, H$_{2''}$), 7.74−7.66 (m, 8 H, dcb-H$_3$ and dcb-H$_5$) 7.41 (d, 1 H, H$_{6'}$), 7.20 (t, 1 H, H$_{5'}$), 6.71 (d, 2 H, H$_{3''}$ and H$_{5''}$). − UV/Vis (aqueous solution pH 7): λ_{max} = 487, 437, 367. − Yield 60%.

[Ru(dcb)$_2$(2-ppt)]: ^{1}H NMR ([D$_6$]DMSO/NaOD, 293 K) δ = 8.93−8.89 (d, 4 H, dcb-H$_6$), 8.20 (d, 1 H, H$_{3'}$), 8.01 (t, 1 H, H$_{4'}$), 7.93 (d, 1 H, H$_{6''}$), 7.89−7.71 (m, 8 H, dcb-H$_3$ and dcb H$_5$), 7.53 (d, 1 H, H$_{6'}$), 7.31 (t, 1 H, H$_{5'}$), 7.15 (t, 1 H, H$_{4''}$), 6.83−6.79 (m, 2 H, H$_{5''}$ and H$_{3''}$). − UV/Vis (aqueous solution pH 7): λ = 486, 436, 367. − Yield 65%.

[Ru(dcb)$_2$(bpzt)]: ^{1}H NMR ([D$_6$]DMSO/NaOD 293 K) δ = 9.30 (s, 1 H, H$_{3'}$), 9.05 (s, 1 H, H$_{6''}$), 8.75 (d, 4 H, dcb-H$_6$), 8.56 (d, 1 H, H$_{3''}$), 8.46 (d, 1 H, H$_{4''}$), 8.28 (d, 1 H, H$_{6'}$), 7.90−7.61 (m, 8 H, dcb-H$_3$ and dcb-H$_5$), 7.64 (d, 1 H, H$_{5'}$). − UV/Vis (aqueous solution pH 7): λ 461, 433. − **[Ru(dcbH$_2$)$_2$(Hbpzt)]Cl$_2$**·4 H$_2$O: $C_{34}H_{31}Cl_2N_{11}O_{12}Ru$ (957.7): calcd. C 42, N 16.08, H 3.23; found C 42.60, N 15.89, H 3.08. − Yield 75%.

[Ru(dcb)$_2$(2-ppzt)]: ^{1}H NMR ([D$_6$]DMSO/NaOD, 293 K) δ = 9.39 (s, 1 H, H$_{3'}$), 8.79 (d, 4 H, dcb-H$_6$), 8.22 (d, 1 H, H$_{5'}$), 7.88 (d, 1 H, H$_{6''}$), 7.72−7.57 and 7.36−7.34 (m, 8 H, dcb-H$_3$ and dcb-H$_5$), 7.54 (d, 1 H, H$_{6'}$), 6.78 (t, 1 H, H$_{4''}$), 6.40 (d, 1 H, H$_{3''}$), 6.05 (t, 1 H, H$_{5''}$). − UV/Vis (aqueous solution pH 7): λ_{max} = 462, 433 nm. − Yield 60%.

Appendix

According to Scheme 1, the following chemical reactions can be summarized:

$$S \xrightarrow{h\nu,\phi} S^+ + e^-$$
$$S^+ + e^- \xrightarrow{k_3} S$$
$$S^+ + I^- \xrightarrow{k_4} S + I^\bullet$$
$$e^- \xrightarrow{k_5} e^-_{ex}$$
$$e^- + I^\bullet \xrightarrow{k_6} I^-$$
$$e^-_{ex} + I^\bullet \xrightarrow{k_7} I^-$$

Under steady-state conditions of for $[S^+]$,$[I^\bullet]$, and$[e^-]$ follows:

$$(A.1) \quad \frac{\partial[S^+]}{\partial t} = \phi I_{abs} - k_3[S^+][e^-] - k_4[S^+][I^-] = 0$$

$$(A.2) \quad [S^+] = \frac{\phi I_{abs}}{k_3[e^-] + k_4[I^-]}$$

$$(A.3) \quad \frac{\partial[I^\bullet]}{\partial t} = k_4[S^+][I^-] - k_6[I^\bullet][e^-] - k_7[I^\bullet][e^-_{ex}] = 0$$

$$(A.4) \quad [I^\bullet] = \frac{k_4[S^+][I^-]}{k_6[e^-] + k_7[e^-_{ex}]}$$

$$(A.5) \quad \frac{\partial[e^-]}{\partial t} = \phi I_{abs} - k_3[S^+][e^-] - k_5[e^-] - k_6[I^\bullet][e^-] = 0$$

Substitution of (A.2) and (A.4) in (A.5), with $J_{ex} = k_5[e^-]$, results in:

$$(A.6) \quad J_{ex} = \phi I_{abs}\left(\frac{k_4[I^-]}{k_3[e^-] + k_4[I^-]} \cdot \frac{k_7[e^-_{ex}]}{k_6[e^-] + k_7[e^-_{ex}]}\right)$$

Since $I_{abs} = I_o(LHE)$, (A.6) becomes:

$$(A.7) \quad IPCE = \frac{J_{ex}}{I_0} = (LHE)(\phi)(\eta) \text{ with } \eta = \left(\frac{k_4[I^-]}{k_3[e^-] + k_4[I^-]} \cdot \frac{k_7[e^-_{ex}]}{k_6[e^-] + k_7[e^-_{ex}]}\right)$$

If $k_6[e^-] << k_7[e^-_{ex}]$ then η can be written as:

$$(A.8) \quad \eta = \frac{k_4[I^-]}{k_3[e^-] + k_4[I^-]} \quad \text{or} \quad \eta = 1 - \frac{k_3[e^-]}{k_3[e^-] + k_4[I^-]}$$

Acknowledgments

Financial support from TRM Grant CT96−0076 and JOULE JOR3-CT95−00107 is gratefully appreciated.

[1] B. O'Regan, M. Grätzel, *Nature* **1991**, *353,* 737.
[2] U. Back, D. Lupo, P. Comte, J. E. Moser, F. Weissörtel, J. Salbeck, H. Spreitzer, M. Grätzel, *Nature* **1998**, *395,* 583.
[3] A. Hagfeldt, M. Grätzel, *Chem. Rev.* **1995**, *95,* 49.
[4] N. J. Cherepy, G. P. Smestad, M. Grätzel, J. Z. Zhang, *J. Phys. Chem. B* **1997**, *101,* 942.
[5] S. Y. Huang, G. Schlichthörl, A. J. Nozik, M. Grätzel, A. J. Frank, *J. Phys. Chem. B* **1997**, *101,* 2576.
[6] M. K. Nazeeruddin, M. Kay, I. Rodicio, R. Humphry-Baker, E. Müller, P. Liska, N. Vlachopoulos, M. Grätzel, *J. Am. Chem. Soc.* **1993**, *115,* 6382.
[7] B. O'Regan, J. Moser, M. Anderson, M. Grätzel, *J. Phys. Chem.* **1990**, *94,* 8720.
[8] Y. Tachibana, J. E. Moser, M. Grätzel, D. R. Klug, J. R. Durrant, *J. Phys. Chem.* **1996**, *100,* 20056.
[9] T. A. Heimer, C. A. Bignozzi, G. J. Meyer, *J. Phys. Chem.* **1993**, *97,* 11987.
[10] R. Argazzi, C. A. Bignozzi, T. A. Heimer, F. N. Castellano, G. J. Meyer, *Inorg. Chem.* **1994**, *33,* 5741.

[11] R. Argazzi, C. A. Bignozzi, T. A. Heimer, N. Castellano, G. J. Meyer, *J. Phys. Chem. B* **1997**, *101,* 2591.
[12] C. A. Bignozzi, J. R. Schoonover, F. Scandola, *Molecular level artificial photosynthetic materials,* Vol. 44, Wiley, New York, **1997**.
[13] G. J. Meyer, *J. Chem. Educ.* **1997**, *74,* 652.
[14] S. G. Yan, A. Lyon, B. I. Lemon, J. S. Preiskorn, J. T. Hupp, *J. Chem. Educ.* **1997**, *74,* 657.
[15] G. Smestad, C. A. Bignozzi, R. Argazzi., *Sol. Energy Mater. Sol. Cells.* **1994**, *32,* 259.
[16] M. K. Nazeeruddin, P. Pèchy, M. Grätzel, *Chem. Commun.* **1997**, 1705.
[17] H. Gerischer, *Electrochim. Acta* **1990**, *35,* 1677.
[18] B. A. Parkinson, M. T. Splitler, *Electrochim. Acta* **1992**, *37,* 943 and references cited therein.
[19] C. Nasr, H. Surat, P. V. Kamat, *J. Phys. Chem. B* **1998**, *102,* 4944.
[20] R. Argazzi, C. A. Bignozzi, G. M. Hasselmann, G. J. Meyer, *Inorg. Chem.* **1998**, *37,* 4533.
[21] M. Alebbi, C. A. Bignozzi, T. A. Heimer, G. M. Hasselmann, G. J. Meyer, *J. Phys. Chem. B.* **1998**, *102,* 7577.
[22] T. Hannappel, B. Burfeindt, W. Storck, F. Willig, *J. Phys. Chem. B* **1997**, *1997,* 6799.
[23] O. Kohle, S. Ruile, M. Grätzel, *Inorg. Chem.* **1996**, *35,* 4779.
[24] C. G. Coates, T. E. Keyes, H. P. Hughes, P. M. Jayaweera, J. J. McGarvey, J. G. Vos, *J. Phys.Chem. A* **1998**, *102,* 5013.
[25] R. H. Hage, A. H. J. Dijkhuis, J. G. Haasnoot, R. Prins, J. Reedijk, B. E. Buchanan, J. G. Vos, *Inorg. Chem.* **1988**, *27,* 2185.
[26] H. A. Nieuwenhuis, J. G. Haasnoot, R. Hage, J. Reedijk, T. L. Snoeck, D. J. Stufkens, J. G. Vos, *Inorg. Chem.* **1991**, *30,* 48.
[27] H. P. Hughes, D. Martin, S. E. J. Bell, J. J. McGarvey, J. G. Vos, *Inorg. Chem.* **1993**, *32,* 4402.
[28] H. P. Hughes, J. G. Vos, *Inorg. Chem.* **1995**, *34,* 4001.
[29] T. E. Keyes, J. G. Vos, J. A. Kolnaar, J. G. Haasnoot, J. Reedijk, R. H. Hage, *Inorg. Chim. Acta* **1996**, 237.
[30] R. Hage, J. G. Haasnoot, J. Reedijk, R. Wang, E. M. Ryan, J. G. Vos, A. L. Spek, A. J. M. Duisenberg, *Inorg. Chim. Acta* **1990**, *174,* 77.
[31] R. Wang, J. G. Vos, R. H. Schmehl, R. Hage, *J. Am. Chem. Soc.* **1992**, *114,* 1964.
[32] B. E. Buchanan, J. G. Vos, W. J. M. van der Putten, J. M. Kelly, R. Hage, R. A. G. de Graaff, R. Prins, J. G. Haasnoot, J. Reedijk, *J. Chem. Soc., Dalton Trans.* **1990**, 2425.
[33] R. Hage, J. G. Haasnoot, H. A. Nieuwenhuis, J. Reedijk, R. Wang, J. G. Vos, *J. Chem. Soc., Dalton Trans.* **1991**, 3271.
[34] R. Hage, R. Prins, J. G. Haasnoot, J. Reedijk, J. G. Vos, *J. Chem. Soc., Dalton Trans.* **1987**, 1389.
[35] R. H. Hage, J. G. Haasnoot, J. Reedijk, R. Wang, J. G. Vos, *Inorg. Chem.* **1991**, *30,* 3263.
[36] C. J. Kleverlaan, to be published.
[37] T. E. Keyes, Ph.D. thesis, Dublin City University **1994**.
[38] B. Evrard, unpublished results .
[39] P. J. Giordano, C. R. Bock, M. S. Wrighton, L. V. Interrante, R. F. X. Williams, *J. Am. Chem. Soc.* **1977**, *99,* 3187.
[40] J. Ferguson, A. W. H. Mau, W. H. F. Sasse, *Chem. Phys. Lett.* **1979**, *68,* 21.
[41] M. D. Nazeeruddin, K. Kalyanasundaram, *Inorg. Chem.* **1989**, *28,* 4251.
[42] J. G. Vos, *Polyhedron* **1992**, *11,* 2285.
[43] P. S. Braterman, A. Harriman, G. A. Heath, L. Yellowless, *J. Chem. Soc., Dalton Trans.* **1983**, 1801.
[44] R. J. Watts, *J. Chem. Educ.* **1983**, *60,* 834.
[45] K. Kalyanasundaram, *Photochemistry of Polypyridine and Porphyrin Complexes*, Academic, New York, **1992**.
[46] E. M. Kober, J. V. Caspar, R. S. Lumpkin, T. J. Meyer, *J. Phys. Chem.* **1986**, *90,* 3722.
[47] K. R. Barqawi, A. Llobet, T. J. Meyer, *J. Am. Chem. Soc.* **1988**, *110,* 7751.
[48] K. R. Barqawi, Z. Murtaza, T. J. Meyer, *J. Phys. Chem.* **1991**, *95,* 47.
[49] Under steady-state conditions $k_5 = k_7$; the response time of a cell is typically in the ms time domain, see ref.[50–53].
[50] J. J. Kelly, D. Vanmaekelbergh, *Electrochim. Acta* **1998**, *43,* 2773.
[51] P. E. de Jongh, D. Vanmaekelbergh, *J. Phys. Chem. B* **1997**, *101,* 2716.
[52] F. Cao, G. Oskam, G. J. Meyer, P. C. Searson, *J. Phys. Chem.* **1996**, *100,* 17021.
[53] J. S. Salafsky, W. H. Lubberhuizen, E. van Faassen, R. E. I. Schropp, *J. Phys. Chem. B* **1998**, *102,* 766.
[54] A. R. Oki, R. J. Morgan, *Synth. Commun.* **1995**, *25,* 4093.
[55] P. Liska, N. Vlachopoulos, M. K. Nazeeruddin, P. Comte, M. Grätzel, *J. Am. Chem. Soc.* **1988**, *110,* 3687.

Received March 8, 1999
[I99091]

Oxidation of Dichloroanilines and Related Anilides Catalyzed by Iron(III) Tetrasulfonatophthalocyanine

Anke Hadasch[a] and Bernard Meunier*[a]

Keywords: Dichloroanilines / Propanil / Iron(III) tetrasulfonatophthalocyanine / Oxidations / Catalysts

We investigated the degradation of polychlorinated pollutants, such as dichloroanilines and related anilides, catalyzed by iron(III) tetrasulfonatophthalocyanine (FePcS) with potassium monopersulfate or hydrogen peroxide as oxidant. The reaction is influenced by the positions of the two chloro-substituents and by the nature of the oxidant. The FePcS-catalyzed oxidation of 3,5-dichloroaniline with potassium monopersulfate leads to the formation of more biodegradable products (carboxylic acids) and to potentially toxic dimers (azo and azoxy compounds). The oxidation of 3,4-dichloroaniline by FePcS/H_2O_2 converts this pollutant into coupling products. The formation of dimers in the catalytic oxidation of dichloroanilines can be avoided by acylation of the amine function.

Introduction

Dichloroanilines (DCAs) are used as precursors on a large scale in the industrial synthesis of pesticides, plastics and dyes.[1] The contamination of aquatic environments by DCAs can occur directly through their accidental release during industrial processing or indirectly by microbial degradation of DCA-derived pesticides in soil. The herbicide Propanil (3,4-dichloropropionanilide, 3,4-DCPA) is used extensively around the world for control of weeds in rice cultures.[2] Although Propanil itself has a low toxicity, its conversion into 3,4-DCA by microorganisms in soil is a problem, since the acute exposure to this DCA isomer results in renal and hepatic toxicity in vivo.[3] In order to solve this problem several investigations have been carried out to find efficient systems for DCA degradation by reductive or oxidative dehalogenation. Using the latter method, Pieper et al. reported the degradation of 3,4-DCA by lignin peroxidase from *Phanerochaete chrysosporium*.[4] Whereas 60% of the pollutant was degraded to a quinoneimine, 10−15% of 3,4-DCA was transformed into the more toxic tetrachloroazobenzene.

We recently developed a new catalytic system for the oxidative degradation of recalcitrant pollutants, such as polychlorinated phenols[5] and polycyclic aromatic hydrocarbons,[6] using iron(III) tetrasulfonatophthalocyanine (FePcS) as a catalyst. We found that the FePcS-catalyzed oxidation of 2,4,6-trichlorophenol (TCP) with hydrogen peroxide leads to the formation of chloromaleic acid as the main product and also to carbon dioxide.[5a−5d] Because of its high catalytic activity in the degradation of TCP, we decided to investigate the FePcS-catalyzed oxidation of other poorly biodegradable compounds such as dichloroanilines.

In order to investigate the chemical degradation of dichloroanilines (DCA) we studied the catalytic oxidation of the following two isomers: 3,4-dichloroaniline (3,4-DCA) and 3,5-dichloroaniline (3,5-DCA). 3,4-DCA is formed during the biodegradation of the herbicide Propanil (3,4-dichloropropionanilide).[2] From 1970 to 1987, on average, 3−7 kg of Propanil/ha were applied each year to about 70 to 100% of rice culture in the United States.[7] 3,5-DCA, which is the most toxic DCA isomer, is a relevant precursor in the industrial synthesis of azo dyes.

Results

We first investigated the oxidative degradation of the two different dichloroanilines 3,5-DCA and 3,4-DCA using FePcS as the catalyst and potassium monopersulfate or hydrogen peroxide as the oxidant. The final concentrations of DCA and oxidant (H_2O_2 or $KHSO_5$) in the reaction mixture were 1 mM and 5 mM, respectively. The solution contained 0.03 mM of FePcS, which corresponds to a molar ratio of catalyst to substrate of 3%. The reactions were carried out at room temperature at pH 7 in an aqueous mixture of acetone/phosphate buffer (v/v = 1:9) with a final volume of 4 mL. The results are reported in Table 1.

Table 1. Oxidation of 3,4-DCA and 3,5-DCA

Run	Substrate	Oxidant	Conversion [%] after 10 min	30 min	Cl^-/DCA[a]
1	3,4-DCA	$KHSO_5$[b]	100	100	0.4
2	3,4-DCA	H_2O_2[b]	41	100	0.5
3	3,4-DCA	$KHSO_5$[c]	90	100	0
4	3,4-DCA	H_2O_2[c]	0	0	−
5	3,5-DCA	$KHSO_5$[b]	100	100	0.6
6	3,5-DCA	H_2O_2[b]	38	78	0.4
7	3,5-DCA	$KHSO_5$[c]	80	100	0.1
8	3,5-DCA	H_2O_2[c]	0	0	−

[a] Number of released chloride ions per converted DCA molecule (determined after 60 min). − [b] Reactions carried out with FePcS, molar ratio FePcS/DCA = 3%. − [c] Reactions carried out without FePcS.

[a] Laboratoire de Chimie de Coordination du CNRS, 205 route de Narbonne,
F-31077 Toulouse cedex 4, France
E-mail: bmeunier@lcc-toulouse.fr

 © WILEY-VCH Verlag GmbH, D-69451 Weinheim, 1999 1434−1948/99/1212−2319 $ 17.50+.50/0

Under these conditions 3,4-DCA and 3,5-DCA were completely converted by the FePcS/$KHSO_5$ system within 10 min (runs 1 and 5). When hydrogen peroxide was used instead of potassium monopersulfate, the reaction rates decreased and the conversions of 3,4-DCA and 3,5-DCA were 41% and 38% after 10 min and increased to 100% and 78% within 30 min, respectively (runs 2 and 6). The average dechlorination values of these reactions corresponded to 0.5 released chloride ions per converted substrate molecule. In other words, one covalent chlorine atom of 50% of DCA molecules was transformed into a chloride ion.

In control reactions we tested the behavior of these DCA molecules without FePcS catalyst. Surprisingly, we observed fast reactions of DCAs with $KHSO_5$ and the pollutants were completely converted within 30 min (runs 3 and 7). Despite full substrate conversions, the dechlorination values were negligible, suggesting the formation of oxidation products different to those obtained in the catalyzed reaction with FePcS/$KHSO_5$. A similar oxidation reaction was also observed on replacing acetone by ethanol, suggesting that a dioxirane was not entirely responsible for this noncatalyzed oxidation of DCAs (see ref.[8] for a review article on the formation of dioxiranes from ketones and monopersulfate). The absence of chloride release suggested that the amine function was the only oxidation site in these noncatalyzed oxidations with monopersulfate. The control reactions with hydrogen peroxide gave no substrate conversions without catalyst (runs 4 and 8).

These results indicate that the catalytic activity of FePcS is higher with potassium monopersulfate than with hydrogen peroxide. Nevertheless, full substrate conversion of 3,4-DCA could also be reached using the clean oxidant H_2O_2 (water being the only by-product after reaction). The dechlorination values in these catalyzed oxidations of DCA derivatives with $KHSO_5$ or H_2O_2 were similar and suggested the same level of pollutant degradation regardless of the nature of the oxidant.

In order to identify the reaction products we extracted the aqueous mixture after the oxidation of 3,5-DCA by FePcS/$KHSO_5$ and analyzed the organic phase by ^{1}H NMR spectroscopy and GC-MS. Three groups of oxidation products could be distinguished: (i) ring cleavage products, (ii) products resulting from oxidation of the amine function and (iii) oxidative coupling products (Figure 1). The formation of ring cleavage products probably occurred via the intermediates 2,6-dichloro-1,4-quinoneimine (**1**) and 2,6-dichloro-1,4-benzoquinone (**2**). Their respective reduced forms, 2,6-dichloro-4-aminophenol and 2,6-dichloro-1,4-hydroquinone, were identified by GC-MS. The ring cleavage of intermediates **1** and **2** can lead to the formation of chloromaleic acid (**3**) and formic acid (**4**) as occurs in the degradation of 2,4,6-trichlorophenol by FePcS/H_2O_2.[5] Carboxylic acids **3** and **4** were identified by ^{1}H NMR spectroscopy after extraction of the reaction mixture in the manner previously described for the TCP oxidation products.[5c] 3,5-Dichloronitrosobenzene (**5**) and 3,5-dichloronitrobenzene (**6**) resulted from the oxidation of the amine function. Both compounds are minor products of the catalytic oxidation reaction, since only traces of these compounds were detected by GC-MS and HPLC. Most of the 3,5-DCA was transformed into coupling products such as 3,5,3′,5′-tetrachloroazobenzene (**7**) and 3,5,3′,5′-tetrachloroazoxybenzene (**8**). A third dimer was also detected by GC-MS. The MS data for this compound ([M^+] = 316, isotopic peaks indicating four chlorine atoms) are in agreement with 1,3,6,8-tetrachlorophenazine (**9**).

In order to compare the distribution and the structure of the degradation products obtained with FePcS/$KHSO_5$ and the oxidation compounds of the noncatalyzed reaction, the oxidation of 3,5-DCA was carried out with $KHSO_5$ only. In this case, 38% of 3,5-DCA was transformed into 3,5-dichloronitrobenzene (**6**), which is the major reaction product quantified by HPLC. In accordance with the negligible dechlorination value (0.1 Cl^-/3,5-DCA), the other products

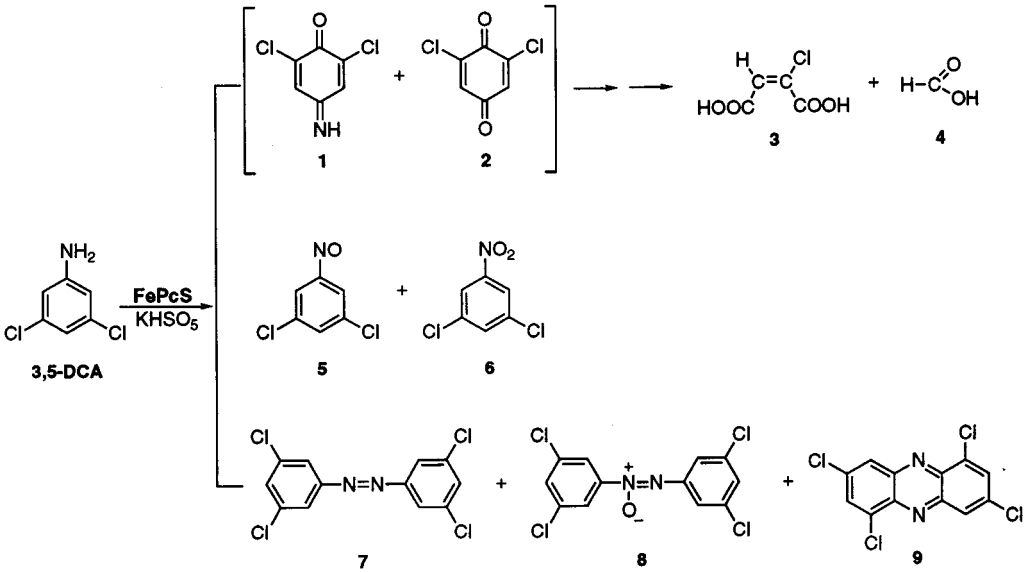


Figure 1. Products formed in the oxidation of 3,5-DCA by FePcS/$KHSO_5$

identified by GC-MS were 3,5-dichloronitrosobenzene (**5**) and small amounts of dimers **7** and **8**. It should be noted that no ring cleavage products could be identified by GC-MS in this noncatalyzed oxidation of 3,5-DCA.

We subsequently characterized the reaction products of the FePcS-catalyzed oxidation of 3,4-DCA with hydrogen peroxide as the oxidant (Figure 2). After a reaction time of 1 h, 69% of the pollutant was transformed into more hydrophobic products, which precipitated from the aqueous mixture. The separation of the precipitated components by column chromatography allowed the isolation and quantification of products **10**−**13**. As shown in Figure 2, this dichloroaniline was mainly transformed into tetrachloroazobenzene **10** (22%), whereas the tetrachloroazoxybenzene **11** (7%) and the two tetrachlorophenazine isomers **12** and **13** (3%) were isolated in lower yields. We also analyzed the aqueous phase after filtration, but no ring cleavage products could be identified.

The oxidation of chlorinated aromatic amines leads to the formation of chlorinated azo and azoxy compounds, which are cytotoxic and teratogenic molecules.[1] In order to avoid the formation of these dimers during the oxidation of DCA we decided to protect the amine function with an acetyl or a propionyl group and we synthesized the 3,4-dichloropropionanilide 3,4-DCPA (Propanil) and the 3,5-dichloroacetanilide 3,5-DCAA. To compare the reaction behavior of these anilides with that of the corresponding anilines, we checked the degradation of 3,4-DCPA and 3,5-DCAA with hydrogen peroxide or potassium monopersulfate using FePcS as a catalyst. The reaction conditions were identical to those of DCA oxidations and the results are shown in Table 2.

The FePcS-catalyzed oxidations of 3,4-DCPA and 3,5-DCAA with potassium monopersulfate led to conversions of 34% and 22% within 30 min, respectively (runs 1 and 5). The catalytic system using hydrogen peroxide as the oxidant was able to convert 34% of 3,4-DCPA, while only a small amount of 3,5-DCAA was oxidized (runs 2 and 6). We also checked the reaction behavior of the anilides in the absence of a catalyst: the control reactions with $KHSO_5$ led to negligible conversions (runs 3 and 7) and no reaction occurred with H_2O_2 (runs 4 and 8).

Table 2. Oxidation of 3,4-DCPA and 3,5-DCAA

Run	Substrate	Oxidant	Conversion [%] after 10 min	30 min	Cl^-/DCA[a]
1	3,4-DCPA	$KHSO_5$[b]	31	34	0.3
2	3,4-DCPA	H_2O_2[b]	15	34	1.0
3	3,4-DCPA	$KHSO_5$[c]	1	2	0
4	3,4-DCPA	H_2O_2[c]	0	0	0
5	3,5-DCAA	$KHSO_5$[b]	22	22	0
6	3,5-DCAA	H_2O_2[b]	1	3	0
7	3,5-DCAA	$KHSO_5$[c]	4	8	0
8	3,5-DCAA	H_2O_2[c]	0	0	0

[a] Number of released chloride ions per converted 3,4-DCPA or 3,5-DCAA molecule (determined after 60 min). − [b] Reactions carried out with FePcS, molar ratio FePcS/3,4-DCPA and FePcS/3,5-DCA**A** = 3%. − [c] Reactions carried out without FePcS.

The dechlorination value of the oxidation of 3,4-DCPA by $FePcS/H_2O_2$ corresponded to one released chloride ion per converted substrate molecule and indicated an advanced degradation of the anilide. In order to identify the degradation products, the reaction mixture was extracted after the oxidation of 3,4-DCPA by $FePcS/H_2O_2$ and the organic phase was analyzed by ^1H NMR spectroscopy and GC-MS. Four oxidation products were distinguishable and the proposed structures have to be considered as current working hypotheses (Figure 3).

3,4-DCPA was degraded to 2-chloro-hydroxy-*N*-propionyl-1,4-quinoneimine (**14**), which is the most oxidized product that was identified by GC-MS. The additional oxygen atom is probably introduced into the ring as the mass fragment of the propionyl group was unchanged after the oxidation. The GC-MS data of another product indicated the oxidation of the aromatic ring of 3,4-DCPA. In accordance with a molecular peak $[(M_{3,4\text{-DCPA}} + 16)^+]$ and a mass fragment suggesting an unchanged amide function we propose the formation of 3,4-dichlorohydroxypropionanilide (**15**). We detected a second product having a molecular peak

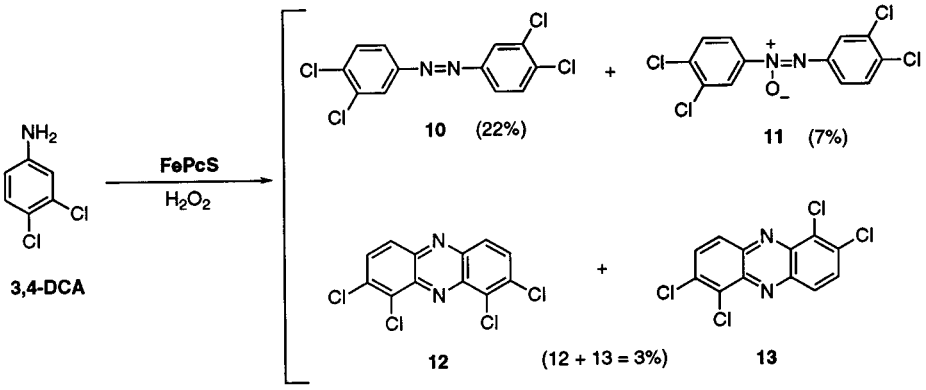


Figure 2. Products formed in the oxidation of 3,4-DCA by $FePcS/H_2O_2$; indicated percentages are isolated yields after a 69% conversion of the substrate

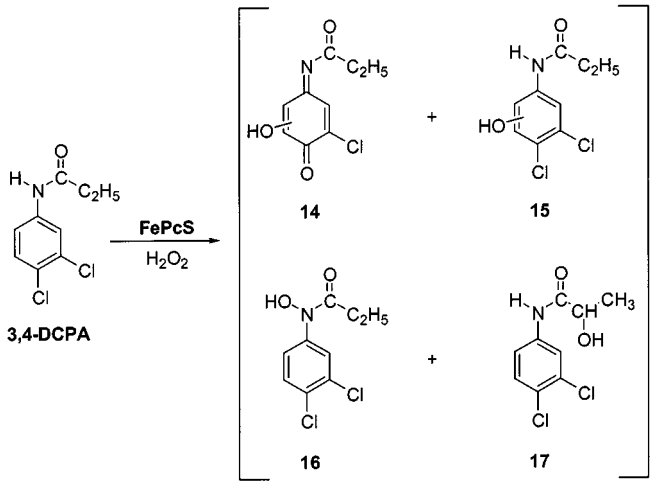


Figure 3. Proposed structures for the products of the oxidation of 3,4-DCPA by FePcS/H_2O_2

$[(M_{3,4\text{-DCPA}} + 16)^+]$. The corresponding mass spectrum indicated that oxidation on the aromatic ring or on the propionyl group had not taken place. These characteristics are in agreement with the proposed formula of 3,4-dichloro-*N*-hydroxypropionanilide (**16**). Furthermore, we detected a product with a mass spectrum suggesting the incorporation of an oxygen atom into the propionyl substituent. The following structural hypotheses have to be considered: (i) formation of an ester by insertion of an oxygen atom, (ii) oxidation of the methylene group or (iii) oxidation of the methyl group. A carbonyl group can be oxidized to the corresponding ester by an oxygen atom donor such as *m*-chloroperbenzoic acid or $KHSO_5$ through a Bayer−Villiger reaction.[9] This kind of reaction is rather unexpected in the presence of hydrogen peroxide even if a nucleophilic Fe^{III}-peroxo species is formed with FePcS.[5c] Therefore, we propose the oxidation of the acyl methylene group, since secondary C−H bonds of a methylene group in the α-position with respect to a carbonyl group should be weaker than tertiary C−H bonds of a methyl group. The proposed product is the 3,4-dichloro-2-hydroxy-propionanilide **17**. Coupling products, such as the azobenzene **10** and the azoxybenzene **11**, were not detected in the degradation of 3,4-DCPA by FePcS/H_2O_2.

Discussion

In the first part of this work we investigated the behavior of two dichloroanilines, 3,4-DCA and 3,5-DCA, in oxidations catalyzed by FePcS. In order to check the influence of the chloro-substituents on the reaction rate we compared the conversions obtained for these two dichloroaniline isomers. The reactions catalyzed by FePcS with potassium monopersulfate as oxidant were too fast to detect differences in the reaction rates by HPLC analyses. However, in the catalytic oxidations with hydrogen peroxide, 3,4-DCA is converted faster than 3,5-DCA, suggesting a lower oxidation potential for the isomer with chloro-substituents in positions 3 and 4.

The oxidation of both DCA derivatives catalyzed by FePcS is faster with potassium monopersulfate than with hydrogen peroxide. Sorokin et al. reported that the oxidation of 2,4,6-trichlorophenol (TCP) catalyzed by FePcS was also remarkably influenced by the oxidant and occurred much faster with $KHSO_5$.[5] This characteristic could be explained by the formation of different active species of the catalyst with potassium monopersulfate or hydrogen peroxide. The authors proposed that the activation of $KHSO_5$ by FePcS leads to the formation of an iron(IV)-oxo species ($Fe^{IV}=O$), which is able to abstract electrons from aromatic substrates such as DCA or TCP, but unable to transfer the oxygen atom of the iron(IV)-oxo species to an olefin, styrene or cyclohexene.[5c] Furthermore, recent data regarding the oxidation of polycyclic aromatic hydrocarbons by FePcS/H_2O_2 indicate that the activation of H_2O_2 by FePcS probably generates two different kinds of active species: an iron(IV)-oxo entity ($Fe^{IV}=O$) and an iron(III)-hydroperoxo species ($Fe^{III}-OOH$).[6] The oxidation potential of the iron(IV)-oxo species is expected to be higher than that of the lower valent iron(III)-hydroperoxo entity. When potassium monopersulfate is used as the oxidant, the concentration of iron(IV)-oxo species is higher than with hydrogen peroxide and, consequently, we obtained faster substrate conversions.

The formation of the oxidation products from 3,5-DCA can be explained in terms of the mechanism depicted in Figure 4. Two successive one-electron oxidations of 3,5-DCA and a deprotonation lead to the formation of the cation **A**, with a positive charge delocalized on the nitrogen atom and on the *ortho* or *para* positions of the ring. The nucleophilic addition of a water molecule to the nitrogen atom and further deprotonation gave the 3,5-dichloro-hydroxylaniline **B** (pathway a). As proposed by Pothuluri et al.,[2] compound **B** can react with another substrate molecule to form the 3,5,3′,5′-tetrachlorohydrazobenzene **C**, which is then oxidized to the 3,5,3′,5′-tetrachloroazobenzene (**7**) and to the 3,5,3′,5′-tetrachloroazoxybenzene (**8**). The addition of a water molecule at the *para* position of the cation **A** (pathway b in Figure 4) generates intermediate **D**, which is transformed into 2,6-dichloro-1,4-quinoneimine (**1**) by deprotonation and removal of two electrons. The proposed reaction mechanism suggests that the degradation of dichloroanilines and their transformation into dimers proceeds via the same intermediate **A**. In the case of 3,5-DCA, two successive one-electron oxidations are necessary to generate the 3,5-dichloro-hydroxylaniline **B**, whereas four electrons have to be abstracted from 3,5-DCA to produce the 2,6-dichloro-1,4-quinoneimine **1**. This electrophilic compound can then be further oxidized to ring-cleavage products by addition of peroxidic oxidants, either activated or not activated by FePcS, as shown in quinone intermediates observed in the oxidative degradation of 2,4,6-trichlorophenol.[5c]

In the second part of this work we investigated the catalytic oxidation of the dichloroanilides 3,4-DCPA and 3,5-

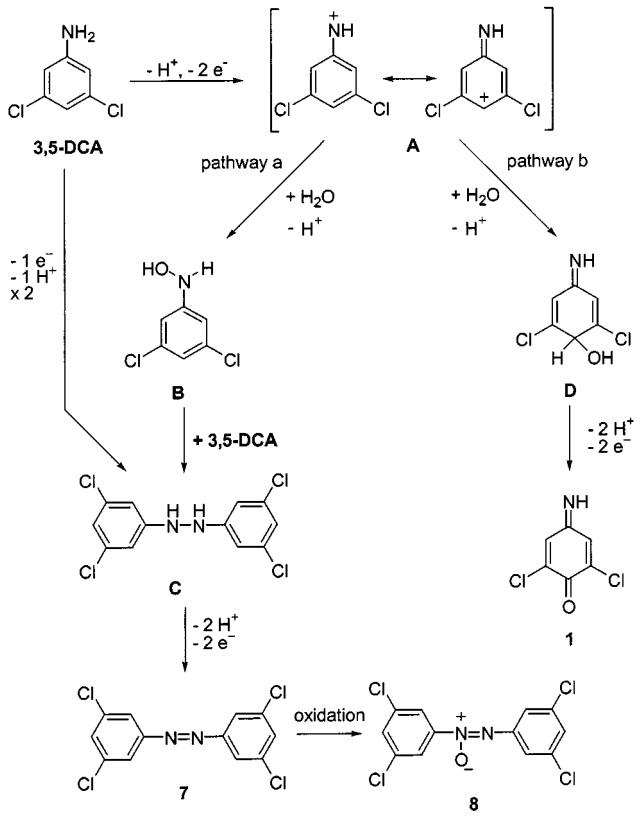


Figure 4. Proposed mechanism for the oxidation of 3,5-DCA by FePcS/$KHSO_5$; compounds indicated by numbers have been identified whereas derivatives assigned by capital letters are only putative intermediates

DCAA, prepared by reacting the respective DCA isomers with propionic or acetic anhydride. The results of the catalytic oxidations indicate that the introduction of an electron-withdrawing substituent such as a propionyl or an acetyl group reduced the conversion rates of these anilides compared with the corresponding amines. In addition, the anilide 3,5-DCAA, with two chloro-substituents on positions 3 and 5 of the aromatic ring, is more difficult to oxidize than the 3,4-isomer 3,4-DCPA. It should be noted that we observed the same tendency in the oxidations of 3,5-DCA and 3,4-DCA because only the latter was fully converted by FePcS/H_2O_2 (Table 1, runs 2 and 6).

The oxidation of 3,4-DCPA by FePcS/H_2O_2 gave the hydroxylated *N*-propionyl-quinoneimine **14**, which is formed after release of one chloride. The analytical data suggest that the formation of products **15**, **16** and **17** resulted from oxidations of the aromatic ring, the amide function or the acyl chain of 3,4-DCPA, respectively. The dechlorination value (1.0 Cl^-/converted 3,4-DCPA) indicates that other unidentified dechlorinated products should be formed, since **14** is the only mono-chlorinated compound observed.

Coupling products such as azo or azoxy compounds were not detected in the catalytic oxidation of 3,4-DCPA by FePcS/H_2O_2. The presence of the propionyl substituent on the aniline derivative blocked the formation of toxic dimers such as the azobenzene **10** and the azoxybenzene **11**, which were always produced in the catalytic oxidations of DCA derivatives under similar conditions.

Conclusion

The present study indicates that the catalytic systems FePcS/$KHSO_5$ and FePcS/H_2O_2 are able to oxidize recalcitrant pollutants such as dichloroanilines and related anilides. One part of the pollutant 3,5-DCA was partially transformed by FePcS/$KHSO_5$ into more biodegradable products such as chloromaleic acid (**3**) and formic acid (**4**), whereas the other part of 3,5-DCA was oxidized to toxic dimers such as the azobenzene **7** and the azoxybenzene **8**. The FePcS-catalyzed oxidation of 3,4-DCA with hydrogen peroxide gave mainly coupling products without ring cleavage products.

The noncatalyzed oxidations of DCA isomers with $KHSO_5$ led to fast conversions of the pollutants without chlorine release, indicating that the FePcS catalyst is necessary for the oxidative ring cleavage of the dichloroaniline derivatives.

The oxidation of DCA by these bio-inspired systems is, like the degradation of 3,4-DCA by lignin peroxidase from *Phanerochaete chrysosporium*,[4] a double-edged sword, since the formation of more biodegradable compounds and toxic dimers occurs simultaneously. The formation of oligomers could be avoided when these amines were converted into amides before the catalytic oxidation. Unfortunately, the electron-withdrawing acyl substituents are responsible for slower substrate conversions, but the optimization of the reaction conditions might be able to produce full substrate conversions without the formation of toxic coupling products in these catalytic degradation reactions of dichloroaniline derivatives.

Experimental Section

Materials: Potassium monopersulfate (the triple salt $[KHSO_5]_2[KHSO_4][K_2SO_4]$, Curox®) was a gift from Peroxid Chemie GmbH. Hydrogen peroxide was obtained from Acros as a 35 wt.% solution. 3,4-DCA, 3,5-DCA, 3,5-dichloronitrobenzene and 2,6-dichloro-1,4-benzoquinone were purchased from Aldrich. Iron tetrasulfonatophthalocyanine (FePcS) was prepared according to the modified method of Weber and Busch.[11][12]

Analytical procedures: The conversions of substrates were monitored by HPLC (Waters 510 pump, Waters 486 detector) using a μ-Bondapak C18 column. The eluent was a mixture of acetonitrile/phosphate buffer 0.05 M (pH 7.0) in proportions 55:45 (v/v) for oxidations of 3,5-DCA and 3,4-DCPA and 40:60 (v/v) for oxidations of 3,4-DCA and 3,5-DCAA. The flow rate was 1 mL/min and the detection was performed at 220 nm. Gas chromatography-mass spectrometry data (GC-MS), except for compounds **1** and **2**, were recorded on a Hewlett-Packard 5890 instrument by electron-impact ionization at 70 eV. The carrier gas for GC-MS was helium and a non polar capillary column (12 m × 0.2 mm HL-1, crosslinked methylsilicone) was used. The injector temperature was 250°C, and analyses were performed at 80°C for 2 min, then up to 250°C (10°C/min) for a further 15 min. The GC-MS data for

compounds **1** and **2** were obtained using a Hewlett-Packard 5890 spectrometer with a nonpolar capillary column (50 m × 0.22 mm BPX5). The injector temperature was 250°C, and analyses were performed at 100°C for 0.5 min, then up to 325°C (6°C/min) for a further 30 min. ^{1}H NMR spectra were recorded with a Bruker WM 250 spectrometer. The concentration of chloride ions was determined by the mercuric thiocyanate method.[10]

General Procedure for Catalytic Oxidations: The reaction mixture, with a final volume of 4 mL, contained 4 μmol of substrate, 0.12 μmol of FePcS and 5 μmol of $KHSO_5$ or 6 μmol of H_2O_2. The reaction mixtures were prepared as follows: 80 μL of a substrate solution (50 mM) in acetone was mixed with 80 μL of an internal standard (4-fluoronitrobenzene, 50 mM) in acetone. 1.5 mL of an aqueous FePcS solution (80 μM) was added and the reaction mixture was adjusted to a final volume of 4 mL with 400 μL of phosphate buffer (500 mM, pH 7), 240 μL of acetone and 1.7 mL of water for 3,5-DCA, 3,4-DCA and 3,4-DCPA (acetone/water = 1:9, v/v) or with 400 μL of phosphate buffer (500 mM, pH 7), 640 μL of acetone and 1.3 mL of water for 3,5-DCAA (acetone/water = 2:8, v/v). Finally, 175 μL of H_2O_2 (0.12 M) or 50 μL of $KHSO_5$ (0.4 M) was added and the reaction mixture was stirred at room temperature.

Characterization of the Oxidation Products of 3,5-DCA: The reaction was carried out under the conditions described for run 5 in Table 1 with a larger (25 times) reaction volume (100 mL). The reaction mixture was stirred for 1 h at room temperature. The acetone and water were then evaporated under vacuum at 50°C and the residue was dried for 1 h under vacuum at room temperature. The residue was dissolved in 10 mL of 1 M HCl saturated with NaCl (resulting pH = 2). The products were extracted with diethyl ether (4 × 60 mL). After evaporation of the ether, the dark brown residue was dried under vacuum for 2 h at room temperature and dissolved in 1 mL of diethyl ether. The resulting solution was analyzed by GC-MS. In order to analyze the product mixture by ^{1}H NMR spectroscopy the diethyl ether was evaporated and the residue was dissolved in 1 mL of deuterated dimethyl sulfoxide ([D_6] DMSO).

In order to identify the intermediate products, we modified the work-up described above and acidified the reaction mixture after 5 min of reaction time without prior evaporation of water and acetone. After extraction with 2 × 60 mL of diethyl ether and evaporation of the ether, the residue was contaminated with buffer salts because of their solubility in acetone. The residue was dissolved in 20 mL of diethyl ether and filtered to separate the salts from oxidation products.

2,6-Dichloro-1,4-quinoneimine (1): The mass spectrum corresponded to the 2,6-dichloro-4-aminophenol, which is the reduced form of compound **1**. GC-MS: m/z = 180 [$(M + 2)^+$], 178 [M^+], 144 [$(M + 2 - HCl)^+$], 142 [$(M - HCl)^+$], 116 [$(M + 2 - HCOCl)^+$], 114 [$(M - HCOCl)^+$].

2,6-Dichloro-1,4-benzoquinone (2): The mass spectrum corresponded to the 2,6-dichloro-1,4-hydroquinone, which is the reduced form of compound **2**. GC-MS: m/z = 179 [$(M + 2)^+$], 177 [M^+], 143 [$(M + 2 - HCl)^+$], 141 [$(M - HCl)^+$], 115 [$(M + 2 - HCOCl)^+$], 113 [$(M - HCOCl)^+$].

Chloromaleic acid (3): ^{1}H NMR ([D_6] DMSO): δ = 6.67 (s, CH). Chloromaleic acid formed an adduct with traces of unchanged 3,5-DCA under the conditions of GC-MS analysis. GC-MS data of the adduct: m/z = 277 [$(M + 2)^+$], 275 [M^+], 242 [$(M + 2 - Cl)^+$], 240 [$(M - Cl)^+$], 198 [$(M + 2 - CO_2Cl)^+$], 196 [$(M - CO_2Cl)^+$], 161 [$(M + 2 - CHCCl(CO)_2)^+$], 159 [$(M - CHCCl(CO)_2)^+$]. We verified the GC-MS data by co-injection of a solution containing 3,5-DCA and chloromaleic acid, and the same adduct (retention time and mass spectrum) was formed during the analysis. Chloromaleic acid was prepared according to the method of Gruzdev and Gruzdev.[13]

Formic acid (4): ^{1}H NMR ([D_6] DMSO): δ = 8.24 (s, CH). Formic acid formed an adduct with traces of unchanged 3,5-DCA under the conditions of GC-MS analysis. GC-MS data of the adduct: m/z = 191 [$(M + 2)^+$], 189 [M^+], 163 [$(M + 2 - CO)^+$], 161 [$(M - CO)^+$]. We verified the data by co-injection of a solution containing 3,5-DCA and formic acid, and the same adduct (retention time and mass spectrum) was formed during the analysis.

3,5-Dichloronitrosobenzene (5): GC-MS: m/z = 177 [$(M + 2)^+$], 175 [M^+], 147 [$(M + 2 - NO)^+$], 145 [$(M - NO)^+$], 111 [$(M + 2 - HNOCl)^+$], 109 [$(M - HNOCl)^+$].

3,5-Dichloronitrobenzene (6): GC-MS: m/z = 193 [$(M + 2)^+$], 191 [M^+], 163 [$(M + 2 - NO)^+$], 161 [$M - NO)^+$], 147 [$(M + 2 - NO_2)^+$], 145 [$(M - NO_2)^+$]. – HPLC: product **6** was also characterized by co-injection of an authentic commercial sample which had the same retention time. The quantification of compound **6** in the oxidation of 3,5-DCA with $KHSO_5$, corresponding to run 7 in Table 1, was recorded by HPLC with 4-fluoronitrobenzene as an internal standard.

3,5,3′,5′-Tetrachloroazobenzene (7): GC-MS: m/z = 322 [$(M + 4)^+$, 12], 320 [$(M + 2)^+$, 20], 318 [M^+, 14], 175 [$(M + 2 - C_6H_3Cl_2)^+$, 18], 173 [$(M - C_6H_3Cl_2)^+$, 30], 147 [$(M + 2 - C_6H_3N_2Cl_2)^+$, 55], 145 [$(M - C_6H_3N_2Cl_2)^+$, 82].

3,5,3′,5′-Tetrachloroazoxybenzene (8): GC-MS: m/z = 338 [$(M + 4)^+$, 3], 336 [$(M + 2)^+$, 7], 334 [M^+, 6], 322 [$(M + 4 - O)^+$, 13], 320 [$(M + 2 - O)^+$, 24], 318 [$(M - O)^+$, 20], 175 [$(M + 2 - C_6H_3Cl_2O)^+$, 20], 173 [$(M - C_6H_3Cl_2O)^+$, 33], 147 [$(M + 2 - C_6H_3Cl_2N_2O)^+$, 64], 145 [$(M - C_6H_3Cl_2N_2O)^+$, 100].

1,3,6,8-tetrachlorophenazine (9): GC-MS: m/z = 320 [$(M + 4)^+$, 48], 318 [$(M + 2)^+$, 100], 316 [M^+, 76], 283 [$(M + 2 - Cl)^+$, 17], 281 [$(M - Cl)^+$, 20], 248 [$(M + 2 - Cl_2)^+$, 6], 246 [$(M - Cl_2)^+$, 9].

Characterization of the Oxidation Products of 3,4-DCA. – Procedure for the catalytic oxidation: The reaction mixture, with a final volume of 200 mL, contained 2 mmol of 3,4-DCA, 80 μmol of FePcS (catalyst/substrate ratio: 4%) and 10 mmol of H_2O_2. The reaction mixture was prepared as follows: 324 mg of 3,4-DCA and 82 mg of FePcS (M = 1022) were dissolved in a previously prepared solvent mixture containing 40 mL of acetone and 110 mL of water. Phosphate buffer (50 mL, pH 7, 500 mM) was added. Finally, 1 mL of H_2O_2 (12 M, 35 wt.%) was added in five aliquots (5 × 200 μL every 5 min) and the reaction mixture was stirred at room temperature.

Isolation of the Oxidation Products: After a reaction time of 60 min, the mixture was filtered and the remaining precipitate was dried for 3 h under vacuum. Yield: 223 mg (69%). In order to separate the hydrophobic products from paramagnetic iron salts, the precipitate was dissolved in diethyl ether and filtered. The filtrate was evaporated under vacuum and 155 mg (48%) of organic products were isolated. Afterwards, the products were separated by liquid chromatography (column on silica, eluent: dichloromethane/hexane = 65:35) and analyzed by GC-MS and ^{1}H NMR spectroscopy.

3,4,3′,4′-Tetrachloroazobenzene (10): Yield: 71 mg (22%). – GC-MS: m/z = 322 [$(M + 4)^+$, 10], 320 [$(M + 2)^+$, 19], 318 [M^+, 14], 175 [$(M + 2 - C_6H_3Cl_2)^+$, 18], 173 [$(M - C_6H_3Cl_2)^+$, 28], 147 [$(M + 2 - C_6H_3N_2Cl_2)^+$, 53], 145 [$(M - C_6H_3N_2Cl_2)^+$, 82]. – ^{1}H NMR ($CDCl_3$): δ = 7.61 (d, 1 H, J = 7.5 Hz, C_5-H, $C_{5'}$-H), 7.79

(dd, 1 H, J = 7.5 Hz, J = 2.5 Hz, C_6-H, $C_{6'}$-H), 8.00 (d, 1 H, J = 2.5 Hz, C_2-H, $C_{2'}$-H).

3,4,3′,4′-Tetrachloroazoxybenzene (11): Yield: 22 mg (7%). − GC-MS: m/z = 338 [(M + 4)$^+$, 3], 336 [(M + 2)$^+$, 7], 334 [M$^+$, 6], 322 [(M + 4 − O)$^+$, 13], 320 [(M + 2 − O)$^+$, 25], 318 [(M − O)$^+$, 20], 175 [(M + 2 − $C_6H_3Cl_2O$)$^+$, 21], 173 [(M − $C_6H_3Cl_2O$)$^+$, 32], 147 [(M + 2 − $C_6H_3Cl_2N_2O$)$^+$, 64], 145 [(M − $C_6H_3Cl_2N_2O$)$^+$, 100]. − ^{1}H NMR ($CDCl_3$): δ = 7.52 (d, 1 H, J = 7.5 Hz, $C_{2'}$-H), 7.57 (d, 1 H, J = 7.5 Hz, C_2-H), 7.98 (dd, 1 H, J = 10 Hz, J = 2.5 Hz, $C_{6'}$-H), 8.12 (dd, 1 H, J = 10 Hz, J = 2.5 Hz, C_6-H), 8.38 (d, 1 H, J = 2.5 Hz, $C_{2'}$-H), 8.39 (d, 1 H, J = 2.5 Hz, C_2-H).

Tetrachlorophenazines 12 and 13: Yield: 9.5 mg (3%). − GC-MS: m/z = 320 [(M + 4)$^+$, 48], 318 [(M + 2)$^+$, 100], 316 [M$^+$, 76], 283 [(M + 2 − Cl)$^+$, 17], 281 [(M − Cl)$^+$, 20], 248 [(M + 2 − Cl_2)$^+$, 6], 246 [(M − Cl_2)$^+$, 9]. − **3,4,6,7-tetrachlorophenazine 12:** ^{1}H NMR ($CDCl_3$): δ = 7.87 (d, 1 H, J = 9 Hz, C_2-H, C_8-H), 8.09 (d, 1 H, J = 9 Hz, C_1-H, C_9-H). − **1,2,6,7-tetrachlorophenazine 13:** ^{1}H NMR ($CDCl_3$): δ = 7.93 (d, 1 H, J = 9 Hz, C_3-H, C_8-H), 8.25 (d, 1 H, J = 9 Hz, C_4-H, C_9-H).

Preparation of 3,4-Dichloropropionanilide (3,4-DCPA): Propionic anhydride (20 mL, 156 mmol) was added to 3,4-dichloroaniline (600 mg, 3.7 mmol). The mixture was stirred at 60 °C for 4 h and then at 100 °C for 2 h. The propionic acid and unreacted propionic anhydride were removed by distillation (bath temperature: 70 °C) under vaccum. The remaining orange oil was dissolved in 5 mL of dichloromethane and the product was precipitated by addition of 100 mL of hexane. The white powder was filtered off and dried under vacuum for 4 h at 25 °C. − Yield: 550 mg (68%). − ^{1}H NMR ([D_6] DMSO): δ = 1.19 (t, 3 H, CH_3), 2.44 (q, 2 H, CH_2), 7.59 (dd, 1 H, C_6-H), 7.67 (d, 1 H, C_5-H), 8.12 (d, 1 H, C_2-H), 10.29 (s, 1 H, NH). − GC-MS: m/z = 219 [(M + 2)$^+$], 217 [M$^+$], 163 [(M + 2 − $COCH_2CH_2$)$^+$], 161 [(M − $COCH_2CH_2$)$^+$]. − $C_9H_9Cl_2NO$ (218): calcd. C 49.54, H 4.13, N 6.42; found C 49.62, H 3.79, N 6.38.

Preparation of 3,5-Dichloroacetanilide (3,5-DCAA): Acetic anhydride (10 mL, 102 mmol) was added to a solution of 3,5-dichloroaniline (300 mg, 1.85 mmol) in 10 mL of acetonitrile. The reaction mixture was stirred for 2 h at 100 °C. The acetic acid and unreacted acetic anhydride were removed by distillation (bath temperature: 100 °C) under vaccum. The remaining beige oil was dissolved in 5 mL of dichloromethane and the product was precipitated by the addition of 100 mL of hexane. The white powder was filtered off and dried under vacuum for 3 h at 25 °C. − Yield: 310 mg (82%). − ^{1}H NMR ([D_6] DMSO): δ = 2.18 (s, 3 H, CH_3), 7.36 (s, 1 H, C_4-H), 7.76 (s, 2 H, C_2-H, C_6-H), 10.41 (s, 1 H, NH). − GC-MS: m/z = 205 [(M + 2)$^+$], 203 [M$^+$], 163 [(M + 2 − $COCH_2$)$^+$], 161 [(M − $COCH_2$)$^+$]. − $C_8H_7Cl_2NO$ (204): calcd. C 47.06, H 3.43, N 6.86; found C 47.17, H 3.15, N 6.91.

Characterization of the Oxidation Products of 3,4-DCPA: The reaction was carried out under the conditions as described for run 2 in Table 2 with a larger (25 times) reaction volume (100 mL). The workup was identical to that used for the characterization of the oxidation products of 3,5-DCA.

2-Chloro-hydroxy-*N*-propionyl-1,4-quinoneimine (14): GC-MS: m/z = 215 [(M + 2)$^+$], 213 [M$^+$], 185 [(M − C_2H_4)$^+$], 161 [(M + 2 − CNC_2H_4)$^+$], 159 [(M − CNC_2H_4)$^+$].

3,4-Dichlorohydroxypropionanilide (15): GC-MS: m/z = 235 [(M + 2)$^+$], 233[M$^+$], 179 [(M + 2 − COC_2H_4)$^+$], 177 [(M − COC_2H_4)$^+$].

3,4-Dichloro-*N*-hydroxypropionanilide (16): GC-MS: m/z = 235 [(M + 2)$^+$], 233[M$^+$], 217 [(M + 2 − H_2O)$^+$], 215 [(M − H_2O)$^+$], 179 [(M + 2 − COC_2H_4)$^+$], 177 [(M − COC_2H_4)$^+$].

3,4-Dichloro-2-hydroxypropionanilide (17): GC-MS: m/z = 235 [(M + 2)$^+$], 233 [M$^+$], 191 [(M + 2 − CO_2)$^+$], 189 [(M − CO_2)$^+$], 163 [(M + 2 − $CO_2C_2H_4$)$^+$], 161 [(M − $CO_2C_2H_4$)$^+$].

Acknowledgments

A. H. thanks the European Community for a PhD fellowship (TMR grant No ERBFMBICT950030). The authors are grateful to Alexander Sorokin (LCC, Toulouse), Alain Rabion and Laurent Fraisse (ELF-Atochem, Lacq) for fruitful discussions.

[1] J. Struijs, J. E. Rogers, *Appl. Environ. Microbiol.* **1989**, *55*, 2527.
[2] J. V. Pothuluri, J. A. Hinson, C. E. Cerniglia, *J. Environ. Qual.* **1991**, *20*, 330.
[3] M. A. Valentovic, J. G. Ball, D. K. Anestis, G. O. Rankin, *Toxic, In Vitro* **1995**, *9*, 75.
[4] D. H. Pieper, R. Winkler, H. Sandermann, *Angew. Chem. Int. Ed. Engl.* **1992**, *31*, 68.
[5] [5a] A. Sorokin, J.-L. Séris, B. Meunier, *Science* **1995**, *268*, 1163. − [5b] A. Sorokin, S. De Suzzoni-Dezard, D. Poullain, J.-P. Noël, B. Meunier *J. Am. Chem. Soc.* **1996**, *118*, 7410. − [5c] A. Sorokin, B. Meunier, *Chem. Eur. J.* **1996**, *2*, 1308. − [5d] B. Meunier, A. Sorokin, *Acc. Chem. Res.* **1997**, *30*, 470.
[6] A. Sorokin, B. Meunier, *Eur. J. Inorg. Chem.* **1998**, 1269.
[7] U.S. Environmental Protection Agency, *Guidance for the registration of pesticide products containing propanil as the active ingredient* USEPA Case 0226, U.S. Gov. Print. Office, 12-23-87, Washington, **1987**.
[8] W. Adam, L. Hadjiarapoglou, *Topics Curr. Chem.* **1993**, *164*, 45.
[9] M. Renz, B. Meunier, *Eur. J. Org. Chem.* **1999**, 737.
[10] T. M. Florence, Y. J. Farrar, *Anal. Chim. Acta* **1971**, *54*, 373.
[11] J. H. Weber, D. H. Busch, *Inorg. Chem.* **1965**, *4*, 469.
[12] A. Hadasch, A. Sorokin, A. Rabion, B. Meunier, *New J. Chem.* **1998**, 45.
[13] V. G. Gruzdev, G. V. Gruzdev, *J. Gen. Chem. USSR* **1986**, *56*, 1872.

Received April 13, 1999
[I99130]

Novel Condensed Thionated Bis(phosphonic) Acid Salts with a Rigid Naphthalene-1,8-diyl Backbone

Petr Kilian,[a] Alexandra M. Z. Slawin,[a] and J. Derek Woollins*[a]

Keywords: Heterocycles / Organo-phosphorus compounds / Dithiadiphosphetane disulfides / Phosphonates

New salts of thionated (naphthalene-1,8-diyl)bis(phosphonic) acid monoanhydrides $[PPh_4^+]_2[C_{10}H_6PS_2(\mu\text{-}S)PS_2^{2-}]$ (**2**) and $[K^+]_2[C_{10}H_6PS_2(\mu\text{-}S)POS^{2-}]\cdot H_2O$ (**3**) both containing the C_3P_2S ring, were prepared in high yields by the reaction of 2,4-(naphthalene-1,8-diyl)-1,3,2,4-dithiadiphosphetane 2,4-disulfide (**1**) with NaHS and PPh_4Cl, or KOH, respectively, in water. The derivative **3**, containing a P=O terminal bond as well as P–S–P bridge, undergoes, in acid conditions, a rearrangement reaction leading to the O,S-symmetrically substituted derivative $[K^+]_2[C_{10}H_6PS_2(\mu\text{-}O)PS_2^{2-}]$ (**4**) containing a C_3P_2O heterocycle. Dipotassium salt 4 was converted into the bis(tetraphenylphosphonium) salt **5** by the treating with PPh_4Cl. Hydrolysis of $[PyH^+][C_{10}H_6P(S)(NHMe)(\mu\text{-}S)PS_2^{2-}]$ (**15**) led to $[CH_3NH_3^+][PyH^+][C_{10}H_6POS(\mu\text{-}O)POS^{2-}]\cdot 1.5$ Py (**6**). New compounds were characterised by $^{31}P\{^1H\}$-, ^1H- and $^{13}C\{^1H\}$-NMR, FT-IR, ES-MS and in the cases **2**–**6** by X-ray structure determination. The $^{31}P\{^1H\}$-NMR spectra of these mixed O,S-derivatives are briefly discussed.

Introduction

Phosphonic acids and their esters form the largest group of compounds containing P−C linkages. Esters of thionated phosphonic acids have been extensively studied because of their use as oil additives and in pesticide chemistry.[1] 2,4-dialkyl(aryl)-1,3,2,4-dithiadiphosphetane 2,4-disulfides $(RPS_2)_2$, especially that with R = C_6H_4OMe (An), well-known as Lawesson reagent (LR), are commonly used for their preparation. In some cases they are converted into intermediates − alkali metal salts of dithio- and trithiophosphonic acids or their monoesters. These salts are either isolated as pure compounds[2][3] or without isolation from the reaction mixture they are directly alkylated to diesters.[4,5,6,7]

As a continuation of our interest in the chemistry of 2,4-(naphthalene-1,8-diyl)-1,3,2,4-dithiadiphosphetane 2,4-disulfide **1** we studied its reactions with potassium hydroxide and sodium hydrogen sulfide, leading to salts of the composition described above. Because of the presence of a rigid organyl backbone in **1**, which fixes its phosphorus atoms in the sterically strained 1,8-positions of the naphthalene ring, we obtained condensed products − bis(phosphonates), containing a P−X−P bridge built into six-membered C_3P_2X (X = S or O) heterocycles.

Several examples of thionated bis(phosphonates) have been reported. In the form of their alkali metal salts RP(S)(OM)(μ-S)P(S)(OM)R they were obtained from $(RPS_2)_2$, where R = alkenyl with long chain, by mild alkalic hydrolysis by potassium and sodium hydroxide.[3] Partially thionated diesters RP(S)(OR′)(μ-S)P(S)(OR′)R were obtained in low yield by the reaction of $(RPS_2)_2$ with primary and secondary alcohols at higher temperatures,[5][8] particularly in boiling xylene. The more sulfur rich diester AnP(S)(SEt)(μ-S)P(S)(OEt)An was obtained in good yield by the reactions of LR with 1,1,1-triethoxyethane, tri- and tetraethoxymethane.[9][10] The fully thionated bis(phosphonate) diester AnP(S)(SPh)(μ-S)P(S)(SPh)An was obtained in low yield by the action of thiophenol on LR.[5] In these systems the ease of sulfur loss occurring on contact of thionated phosphonates with water requires the work to be performed with the exclusion of water.[2][7] However the substantially lower reactivity of **1** compared to common dithiadiphosphetane disulfides $(RPS_2)_2$ allowed us to prepare salts of perthionated as well as partially dethionated phosphonic acids in water.

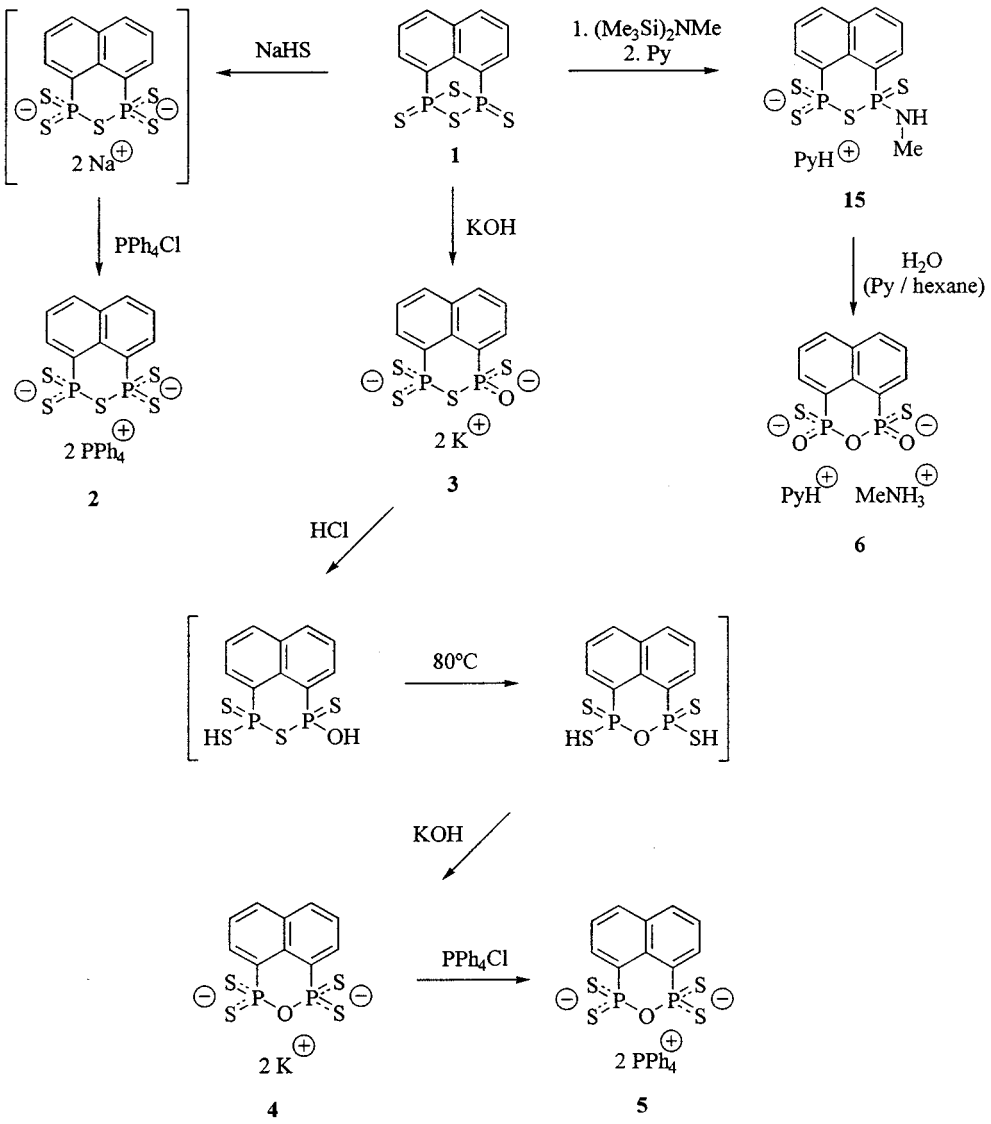
Results and Discussion

The bis(tetraphenylphosphonium) salt of bis(trithiophosphonic acid) monoanhydride **2** was prepared in a good yield by the action of excess NaHS on **1** and consequent treatment of the resulting disodium salt (without its isolation from reaction mixture) with PPh_4Cl (Scheme 1). $^{31}P\{^1H\}$-NMR of the reaction mixture after the first step showed a singlet at δ = 69.0 ppm, belonging to the disodium salt $[Na^+]_2[C_{10}H_6PS_2(\mu\text{-}S)PS_2^{2-}]$. When a stoichiometric amount or only a small molar excess of NaHS was used, the larger amount of the side product, the anion of **3**, was observed by $^{31}P\{^1H\}$-NMR. Reaction of the disodium salt with PPh_4Cl afforded pure **2**, which is insoluble in many common solvents. Its slight solubility in CD_3CN/[D_6]DMSO allowed us to measure its $^{31}P\{^1H\}$- and ^1H-NMR spectra, however the concentration of such saturated solution was too low to obtain a good quality $^{13}C\{^1H\}$-NMR spectrum.

By the action of small excess of KOH on **1** (molar ratio 2.3:1) we obtained the potassium salt of the unsymmetrically O,S-substituted naphthalene-1,8-diyl bis(phosphonic)

[a] Department of Chemistry, University of St Andrews
St Andrews Fife KY16 9NB, United Kingdom
E-mail: J.D.Woollins@st-andrews.ac.uk

 © WILEY-VCH Verlag GmbH, D-69451 Weinheim, 1999 1434−1948/99/1212−2327 $ 17.50+.50/0

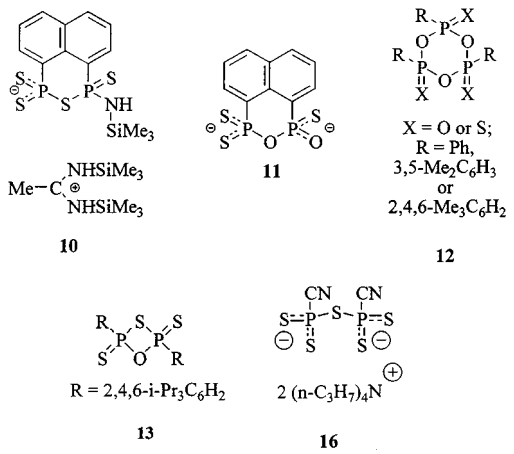


Scheme 1

acid, **3** (Scheme 1). The $^{31}P\{^1H\}$-NMR spectrum of the reaction mixture showed an AX system with δ 69.2 and 58.6 ppm. The magnitude of $J(PP) = 11.6$ Hz indicates that a P−S−P bridge is preserved in the product.[11][12] Both the ^1H and $^{13}C\{^1H\}$-NMR spectra showed unsymmetrical substitution of the naphthalene ring, whilst in the IR a very strong band at 1112 cm^{-1} corresponding to ν(P=O) was found. The position of this band in the lower frequency range for a P=O bouble bond valence vibration is due to the lowered bond order given by delocalisation of the negative charge between more terminal atoms. All these facts are in accord with the structure of **3** shown in Scheme 1, which was confirmed by X-ray structure determination (Figure 2). Signals in the ^1H and $^{13}C\{^1H\}$-NMR spectrum of **3** were assigned by analogy with **10**, where unambiguous assignment was performed by both 1D- and 2D-NMR.[11] Recrystallization of the crude product from non dried ethanol/methanol mixture afforded hygroscopic material, which after six hours of drying *in vacuo* was identified by elemental analysis as **3**, monohydrate, whilst 2.5 molecules of water per naphthalene entity were found in the crystal structure of **3** by X-ray structure determination. On attempts to convert the potassium salt **3** to its tetraphenylphosphonium relative by the reaction of **3** with PPh_4Cl a mixture of the desired product together with reorganised product **5** was obtained.

The potassium salt **3** is indefinitely stable in the solid state. However, when it is in the form of its conjugated acid, [obtained by the addition of diluted mineral acid (HCl) to the water solution of **3**], it undergoes a rearrangement reaction leading to O,S-symmetrically substituted acid, containing a P−O−P bridge (Scheme 1). Treatment of the crude mixture of the bis(phosphonic) acid and KCl with dry methanol allows the removal of a majority of KCl together with other methanol insoluble side products by filtration. Stripping off methanol, dissolving the resulting solid in water and titration with KOH afforded the potassium salt **4**. In its $^{31}P\{^1H\}$-NMR spectrum we found signals due to

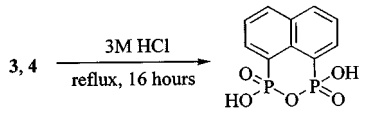
three distinct compounds. Besides the major signal of **4** (s, δ = 101.4) and minor signals of the starting material **3** (2 × d, δ = 69.2 and 58.6, ^2J(PP) = 11.6 Hz) other minor signals (2 × d, δ = 102.7 and 59.7, ^2J(P−O−P) = 47 Hz) were found, probably belonging to the dianion **11**. After another purification step (recrystallization from ethanol), pure **4** was obtained. Signals in the ^{1}H- and ^{13}C{^{1}H}-NMR spectrum of **4** were assigned on the basis of analogy with **10**.[11] The second order signals of carbons C1 and C9 (for numbering of atoms see Figure 4) represent AXX′ systems, where A is the carbon atom and X and X′ are phosphorus atoms. Magnitudes of their ^2J(PP), ^1J(PC) and ^3J(PC) coupling constants were obtained using the LAOCOON III simulation program.[13] The magnitude of ^2J(PP) = 51.2 Hz is comparable with the corresponding ^2J(PP) values found in thiotrimetaphosphonates **12**[14] (32−62 Hz) whilst it is substantially larger when compared with ^2J(PP) = 14.2 Hz in **13**[14] or with ^2J(PP) = 6.5 Hz in **1**.[15] In the IR spectrum of **4** no strong band was found in the 1100−1400 cm^{-1} region, which would be expected for ν(P=O) vibrations, whilst a very strong band, belonging to ν_{as}(P−O−P) was found at 825 cm^{-1}.



10 11 12 13 16

Figure 1. Structural formulas of compounds **10**, **11**, **12**, **13** and **16**

By the reaction of **1** with excess of ethylene glycol at 140°C a completely desulfurated compound **14** was obtained.[16] Compounds **3** or **4** respectively can be used for preparation of **14** as well. These desulfuration reactions were performed by prolonged boiling with 3 M HCl (Scheme 2). The identity of resulting products was confirmed by ^{31}P{^{1}H}-NMR and IR spectroscopy.



14

Scheme 2

To improve the solubility of the potassium salt **4** in organic solvents we converted it into the bis(tetraphenylphosphonium) salt **5** by the reaction of **4** with PPh_4Cl (Scheme 1). **5** shows good solubility in hot acetonitrile, whilst it is much less soluble at room temperature; this allowed very good yields when recrystalized from this solvent.

In our previous paper[17] we described the preparation of pyridinium salt **15** by the treatment of **1** with bis(trimethylsilyl)methylamine and pyridine (Py). An attempt to recrystallize **15** by diffusion of hexane into its pyridine solution led to hydrolysis with formation of **6** (Scheme 1). The product, obtained in the form of several crystals, was identified by X-ray structure analysis, but the small amount available only allowed further characterization by ^{31}P{^{1}H}- and ^{1}H-NMR. The latter showed 1:1.2 ratio of naphthalene and pyridine hydrogens, whilst in the crystal ratio 1:2.5 was found by X-ray structure analysis, the lower ratio found in solution is due to partial evaporation of solvated Py from crystals. The integral of the broad signal at 3.4 ppm, belonging to $MeNH_3^+$ and PyH^+ hydrogens was lower than the expected value from its comparison with integral value of CH_3 hydrogens of methylamine, probably due to their fast chemical exchange.

Discussion of ^{31}P{^{1}H}-NMR Spectra

When comparing ^{31}P-NMR shifts in dianionic O,S-mixed derivatives of (naphthalene-1,8-diyl)bis(phosphonic) acid, the following conclusions can be drawn:[2,3,10,11] In such systems it is common, that substitution of an O atom by a S atom leads to the lower field shift. This rule is obeyed very well when a series of compounds containing oxygen as a bridging atom between both phosphorus atoms is taken into account, compounds **5** (δ = 100 ppm), **6** (δ = 59 ppm) and **14** (δ = 7 ppm) contain moieties C−P(μ-O)S_2, C−P(μ-O)OS and C−P(μ-O)O_2, respectively. A second group, for which the above rule applies as well, is formed by compounds containing sulfur as a bridging atom between both phosphorus atoms. Members of this group are compounds **2** (δ = 73 ppm, C−P(μ-S)S_2 moiety) and **3** (δ = 69 ppm, C−P(μ-S)S_2 moiety; 59 ppm C−P(μ-S)OS moiety), the missing member is a compound containing a C−P(μ-S)O_2 moiety, no example of this type has been described yet. The above rule obviously does not apply, when comparing compounds with C−P(μ-S)S_2 moiety (**2**, δ = 73 ppm) with C−P(μ-O)S_2 moiety (**5**, δ = 100 ppm), thus both groups with different P-X−P bridging atoms should be judged separately.

Discussion of X-ray Structure Analysis

X-ray structures of compounds **2**−**6** were measured, see Figure 2−6 and Tables 1−6. The naphthalene part and the phosphorus atoms lie very close to the mean plane fitted to these atoms in case of the anion of **2** [P(1) 0.05 Å above and P(9) 0.13 Å below the mean plane] and **6** both P(1) and P(9) lie 0.08 and 0.01 Å, respectively, above the mean plane], whilst in **3**, **4** and **5** the distortion is more significant and phosphorus atoms in each anion lie above and below the mean plane in distances between 0.31 and 0.44 Å.

The C_3P_2X (X = S or O) rings are hinged, the C_3P_2 and P_2X planes in anions of **2** and **3** (where X = S) are inclined by 52 and 48°, respectively. In **4** and **5** (where X = O) these angles are 32 and 36°, in **6** (X = O) the corresponding value of 50° was found.

The nonbonding P···P distances as well as internal P−S−P angles in **2** and **3** are very similar [3.31 and 3.27 Å; 103.31(7) and 101.5(1)°], substitution of sulfur bridging atom by oxygen led to shortening of P···P distances in **4** and **5** to 2.97 and 2.99 Å, the internal P−O−P angles are enlarged to 131°. The most compact P_2 environment is in **6**, where the Pψree dots aboveP distance 2.89 Å and corresponding internal P−O−P angle 125.2(1) is found.

As expected, the bond lengths of exocyclic substituents of phosphorus atoms reflect delocalisation of the negative charge in the $P(X_{exo})_2$ groups (X_{exo} = S, O). When comparing P−S_{exo} distances in **2**, **3**, **4**, **5** and **6** [range 1.945(2)−1.990(2) Å] with endocyclic P−S_{endo} distances in **2** and **3** [range 2.102(3)−2.116(2) Å], the difference is substantial due to their different bond order. Similarly, the P−O_{exo} distances in **3** and **6** [range 1.505(2)−1.521(5) Å] are substantially shorter than P−O_{endo} distances in **4**, **5** and **6** [range 1.623(2)−1.650(4) Å], however they are significantly longer than conventional P=O double bond as found for example in phosphoric acid triesters (average value 1.45 Å).[18]

In the structure of the anion in **2** (Figure 2, Table 1 and 2) there is surprisingly no mirror plane along the S(19)C(5)C(10) plane, sulfur atoms S(1) and S(9) lie in substantially different distances from the mean plane fitted to naphthalene part and phosphorus atoms (1.40 and 0.95 Å). The steric effect of the naphthalene backbone results in a short P···P distance 3.31 Å in **2**, compare to P···P distance 3.50 Å in **16**,[19] where phosphorus atoms are not bridged by any organic substituent.

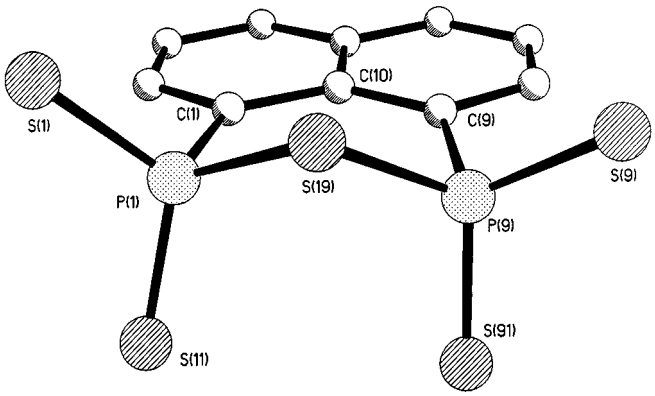


Figure 2. Molecular diagram of **2**

Table 2. Selected bond lengths (Å) and angles (°) in compound **2**

P(1)−S(19)	2.116(2)	P(9)−S(19)	2.108(2)
P(1)−S(1)	1.985(2)	P(1)−S(11)	1.968(2)
P(9)−S(9)	1.990(2)	P(9)−S(91)	1.955(2)
P(1)−C(1)	1.831(4)	P(9)−C(9)	1.841(5)
P(1)−S(19)−P(9)	103.31(7)		
S(1)−P(1)−S(11)	117.97(8)	S(9)−P(9)−S(91)	117.31(9)
S(1)−P(1)−S(19)	100.59(7)	S(11)−P(1)−S(19)	116.06(8)
S(9)−P(9)−S(19)	102.88(8)	S(91)−P(9)−S(19)	114.67(8)
C(1)−P(1)−S(1)	110.3(2)	C(1)−P(1)−S(11)	107.7(1)
C(9)−P(9)−S(9)	110.8(2)	C(9)−P(9)−S(91)	108.3(2)
C(1)−P(1)−S(19)	103.3(2)	C(9)−P(9)−S(19)	101.7(2)

In the structure of the anion in **3** (Figure 3, Table 1 and 3) the K^+ cations interact with all the sulfur atoms [including S(19)] with K···S distances in the range 3.24−3.75 Å, oxygen atom O(1) interacts with K···O distances in the range 2.76−3.02 Å. The water solvate molecules (2.5 molecule per naphthalene entity) coordinate to the K^+ centres.

Table 1. Details of the data collections and refinements for compounds **2**, **3**, **4**, **5** and **6**

	2	**3**	**4**	**5**	**6**
Empirical formula	$C_{58}H_{46}P_4S_5$	$C_{10}H_{11}K_2O_{3.5}P_2S_4$	$C_{10}H_6K_2OP_2S_4$	$C_{59}H_{47.5}N_{0.5}OP_4S_4$	$C_{23.5}H_{25.5}N_{3.5}O_3P_2S_2$
Formula weight	1027.13	455.57	410.53	1031.60	531.03
Colour	Yellow	Yellow	Yellow	Yellow	Colourless
Size/mm^{-3}	0.15 × 0.15 × 0.15	0.10 × 0.10 × 0.10	0.04 × 0.10 × 0.20	0.08 × 0.10 × 0.10	0.10 × 0.10 × 0.20
Crystal system	Monoclinic	Monoclinic	Triclinic	Triclinic	Monoclinic
a/Å	17.2282(5)	16.434(2)	7.2326(7)	13.8150(8)	8.8369(2)
b/Å	13.8956(3)	8.6746(8)	9.4191(9)	14.1522(8)	17.9208(4)
c/Å	23.1746(7)	24.862(2)	12.847(1)	15.5028(9)	17.2366(4)
α/°	90	90	102.356(2)	69.892(1)	90
β/°	110.853(1)	90.092(2)	98.509(2)	78.794(1)	101.473(1)
γ/°	90	90	108.969(2)	77.088(2)	90
Space group	$P2_1/a$	$C2/c$	$P\bar{1}$	$P\bar{1}$	$P2_1/n$
Z	4	8	2	2	4
d/gcm^{-3}	1.316	1.707	1.735	1.245	1.319
μ/mm^{-1}	0.385	1.193	1.323	0.328	0.349
Refl. Measured	22154	7619	4000	13531	11558
Refl. Independent (R_{int})	7443 (0.0913)	2562 (0.1095)	2233 (0.0344)	7706 (0.2332)	3828 (0.0347)
Final R [$I > 2\sigma(I)$]	$R^1 = 0.0535$, $wR^2 = 0.0907$	$R^1 = 0.0581$, $wR^2 = 0.1256$	$R^1 = 0.0337$, $wR^2 = 0.0690$	$R^1 = 0.0663$, $wR^2 = 0.1431$	$R^1 = 0.0400$, $wR^2 = 0.0961$
Goodness-of-fit on F^2	0.996	0.938	1.050	0.496	0.935
Largest difference peak and hole/eÅ^{-3}	0.370 and −0.265	1.423 and −0.763	0.466 and −0.254	0.530 and −0.645	0.271 and −0.206

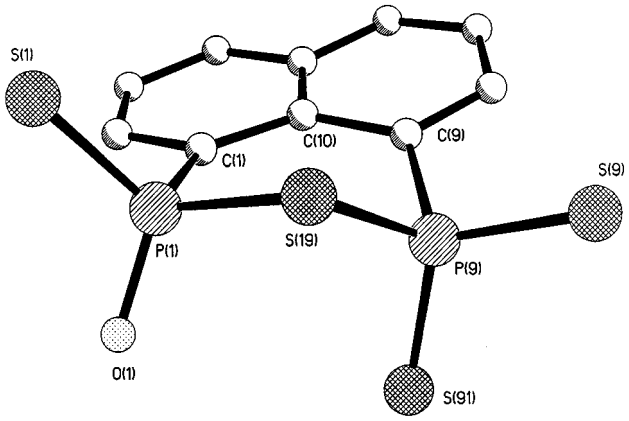


Figure 3. Molecular diagram of **3**

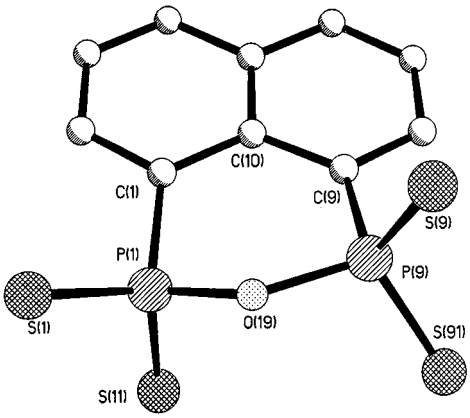


Figure 4. Molecular diagram of **4**

Table 3. Selected bond lengths (Å) and angles (°) in compound **3**

P(1)−S(19)	2.116(3)	P(9)−S(19)	2.102(3)
P(1)−S(1)	1.979(3)	P(1)−O(1)	1.521(5)
P(9)−S(9)	1.988(3)	P(9)−S(91)	1.984(3)
P(1)−C(1)	1.837(7)	P(9)−C(9)	1.814(7)
K(1)−S(1)	3.381(3)	K(2)−O(1)	3.018(6)
K(1)−O(1)	2.759(5)	K(1)−O(1)	2.956(5)
K(1)−S(9)	3.535(3)	K(2)−S(9)	3.746(4)
K(1)−S(91)	3.393(2)	K(1)−S(91)	3.576(3)
K(2)−S(91)	3.239(3)	K(2)−S(91)	3.355(3)
K(1)−S(19)	3.588(2)		
P(1)−S(19)−P(9)	101.48(11)		
S(1)−P(1)−O(1)	116.3(2)	S(9)−P(9)−S(91)	115.46(13)
S(1)−P(1)−S(19)	103.21(11)	O(1)−P(1)−S(19)	111.6(2)
S(9)−P(9)−S(19)	104.11(12)	S(91)−P(9)−S(19)	112.68(11)
C(1)−P(1)−S(1)	109.6(2)	C(1)−P(1)−O(1)	109.4(3)
C(9)−P(9)−S(9)	111.1(2)	C(9)−P(9)−S(91)	110.0(2)
C(1)−P(1)−S(19)	106.2(3)	C(9)−P(9)−S(19)	102.7(2)

Symmetry transformations used to generate equivalent atoms: #1: -x+2, y, -z+1; #2: −x+5/2, y+1/2, -z+1/2; #3: −x+5/2, y-1/2, -z+1/2

Table 4. Selected bond lengths (Å) and angles (°) in compound **4**

P(1)−O(19)	1.626(2)	P(9)−O(19)	1.638(3)
P(1)−S(1)	1.954(1)	P(1)−S(11)	1.983(1)
P(9)−S(9)	1.976(1)	P(9)−S(91)	1.962(2)
P(1)−C(1)	1.806(4)	P(9)−C(9)	1.811(4)
K(1)−S(1)	3.351(2)		
K(2)−S(1)	3.188(2)	K(2)−S(1)	3.182(2)
K(1)−S(11)	3.399(1)	K(1)−S(11)	3.430(1)
K(2)−S(11)	3.344(1)	K(2)−S(11)	3.355(1)
K(1)−S(9)	3.422(2)	K(2)−S(9)	3.241(2)
K(1)−S(91)	3.285(1)	K(1)−S(91)	3.389(2)
K(2)−S(91)	3.351(1)	K(1)−O(19)	2.829(2)
P(1)−O(19)−P(9)	131.0(2)		
S(1)−P(1)−S(11)	117.54(7)	S(9)−P(9)−S(91)	116.66(6)
S(1)−P(1)−O(19)	105.2(1)	S(11)−P(1)−O(19)	109.3(1)
S(9)−P(9)−O(19)	103.5(1)	S(91)−P(9)−O(19)	111.2(1)
C(1)−P(1)−S(1)	111.4(1)	C(1)−P(1)−S(11)	109.5(1)
C(9)−P(9)−S(9)	110.9(1)	C(9)−P(9)−S(91)	110.6(1)
C(1)−P(1)−O(19)	102.7(2)	C(9)−P(9)−O(19)	102.9(2)

Symmetry transformations used to generate equivalent atoms: #1: $x+1$, y, z; #2: $-x$, $-y$-1, $-z$; #3: $-x$, $-y$, -z; #4: $x+1$, $y+1$, z; #5: $x-1$, y, z; #6: $x-1$, $y-1$, z

Because of the close similarity of anionic parts in the structures of **4** (Figure 4, Table 1 and 4) and **5** (Table 1 and 5), only the former is discussed here. As well as in the structure of the anion of **2**, in the structure of anion of **4**, there is no mirror plane along the 0(19)C(5)C(10) plane, even when the substitution pattern is symmetric. Atoms in *trans* positions [e.g. S(1) and S(91)] are approximately in the same distance from the plane fitted to carbon and phosphorus atoms, thus when disregarding the O(19) atom (lying 0.37 Å above mean plane), the anion has approximate C_2 symmetry. The K^+ ions in **4** form close contacts with the sulfur atoms in the range 3.18−3.43 Å, and there is a K(1)···O(19) distance of 2.83Å.

In the structure of the anion in **6** (Figure 5, Table 1 and 6) the exocyclic substituents are in the *cis* position and the molecule possesses an approximate mirror plane along the O(19)C(5)C(10) plane, which is in contrast with *trans* geometry of **14**.[16] The NH protons in the $MeNH_3^+$ counterion are hydrogen-bonded to a solvated pyridine nitrogen atom [H(20a)···N(41) 1.94 Å, N(20)−H(20a)−N(41) 169°], to O(9) atom [H(20b)···O(9) 1.79 Å, N(20)−H(20b)−O(9) 175°] and to O(9′) atom in adjacent anion [H(20c)···O(9′) 1.95 Å, N(20)−H(20c)−O(9′) 167°]. The pyridinium NH proton strongly bonds to the anion O(1) atom [H(31)···O(1) 1.64 Å, N(31)−H(31)−O(1) 175°].

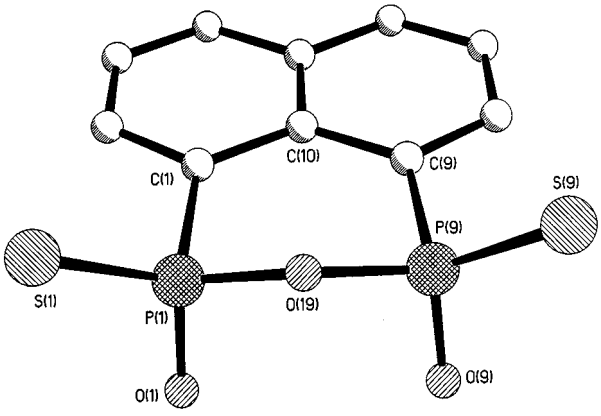


Figure 5. Molecular diagram of **6**

Table 5. Selected bond lengths (Å) and angles (°) in compound **5**

P(1)−O(19)	1.650(4)	P(9)−O(19)	1.631(4)
P(1)−S(1)	1.962(3)	P(1)−S(11)	1.972(3)
P(9)−S(9)	1.987(3)	P(9)−S(91)	1.960(3)
P(1)−C(1)	1.819(8)	P(9)−C(9)	1.824(7)
P(1)−O(19)−P(9)	131.3(2)		
S(1)−P(1)−S(11)	117.6(1)	S(9)−P(9)−S(91)	117.3(1)
S(1)−P(1)−O(19)	106.3(2)	S(11)−P(1)−O(19)	111.7(2)
S(9)−P(9)−O(19)	105.8(2)	S(91)−P(9)−O(19)	111.7(2)
C(1)−P(1)−S(1)	111.5(3)	C(1)−P(1)−S(11)	108.0(2)
C(9)−P(9)−S(9)	108.1(2)	C(9)−P(9)−S(91)	110.9(2)
C(1)−P(1)−O(19)	100.5(3)	C(9)−P(9)−O(19)	101.9(3)

Table 6. Selected bond lengths (Å) and angles (°) in compound **6**

P(1)−O(19)	1.623(2)	P(9)−O(19)	1.630(2)
P(1)−S(1)	1.945(1)	P(1)−O(1)	1.508(2)
P(9)−S(9)	1.946(1)	P(9)−O(9)	1.505(2)
P(1)−C(1)	1.808(3)	P(9)−C(9)	1.812(3)
P(1)−O(19)−P(9)	125.2(1)		
S(1)−P(1)−O(1)	116.73(9)	S(9)−P(9)−O(9)	117.71(9)
S(1)−P(1)−O(19)	109.34(8)	O(1)−P(1)−O(19)	107.8(1)
S(9)−P(9)−O(19)	107.93(8)	O(9)−P(9)−O(19)	108.2(1)
C(1)−P(1)−S(1)	112.2(1)	C(1)−P(1)−O(1)	108.0(1)
C(9)−P(9)−S(9)	112.4(1)	C(9)−P(9)−O(9)	107.4(1)
C(1)−P(1)−O(19)	101.5(1)	C(9)−P(9)−O(19)	102.0(1)

Conclusion

In this paper we have gained access to almost all possible permutations of O,S-substituted phosphorus environments in salts of (naphthalene-1,8-diyl)bis(phosphonic) acids. The only missing member in this group of environments of general formula C−P(μ-X)X_2, where X = either O, S, or their permutations, is the C−P(μ-S)O_2 moiety. All other members were characterised by $^{31}P\{^1H\}$-NMR and by X-ray structure analysis either in this paper or elsewhere.[16] Current investigations are focusing on the preparation of other interesting main group derivatives of 1,8-bis(phosphorus) substituted naphthalenes

Experimental Section

General Remarks: 1 was prepared by the reaction of P_4S_{10} with 1-bromonaphthalene[20][21] and recrystallized from dichloromethane, tetraphenylphosphonium chloride was obtained from Aldrich. Methanol was dried by boiling with CaH_2 and subsequent distillation under nitrogen. In vacuo refers to a pressure of 0.1 Torr at 20°C. NMR spectra were recorded on a Bruker DPX-400 spectrometer. For ^1H- and ^{13}C-NMR spectroscopy TMS or TSPSA [(4-trimethylsilyl)propane sulfonic acid Na salt, $\delta(^1H) = 0.015$ ppm] were used as internal standards, for ^{31}P-NMR 85% H_3PO_4 was used as an external standard. IR spectra were recorded as a pellets with KBr on a Perkin−Elmer system 2000. Mass spectra were measured by the EPSRC National Mass Spectrometry Service Centre, University of Wales, Swansea. Microanalyses were carried out by the Departmental service.

$[PPh_4^+]_2[C_{10}H_6PS_2(\mu\text{-}S)PS_2^{2-}]$ (2): 1 (200 mg, 0.63 mmol) was added to a solution of NaHS.H_2O (220 mg, 3.0 mmol) in water (5 cm^3) and refluxed with stirring until all the solid **1** dissolved (ca. 10 min). The resulting cloudy solution was filtered using a sintered glass funnel with a plug of celite. The filtrate was added with vigorous stirring to a solution of PPh_4Cl (472 mg, 1.26 mmol), the resulting yellow solid was filtered off, washed with water (5 × 20 cm^3) and dried in vacuo. The crude product was of sufficient purity, however for recrystalisation acetonitrile can be used. Crystals of **2** suitable for X-ray structure determination were obtained by slow cooling of its hot saturated solution in acetonitrile. Yield 531 mg (82%) before recrystalisation. − $C_{58}H_{46}P_4S_5$: calcd. C 67.8, H 4.5; found C 67.6, H 4.6. − M.p. 271−273°C (decomp.). − IR (cm^{-1}): $\tilde{\nu}$ = 690vs and 669vs [ν(P=S)]. − $^{31}P\{^1H\}$-NMR (CD_3CN/[D_6]DMSO 3:1; for numbering of atoms see Figure 2): δ = 72.8 (s, anion), 29.1 (s, PPh_4^+). − ^1H-NMR (CD_3CN/[D_6]DMSO 3:1; for numbering of atoms see Figure 2): δ = 8.64 (2 H, m, 2-H and 8-H), 7.92 (8 H, m, PPh_4^+), 7.79−7.65 (34 H, m, 4-H, 6-H and PPh_4^+), 7.40 (2 H, m, 3-H and 7-H). − Mass spectrum (ES+): *m/z* 339 (PPh_4^+), 262 (PPh_3); (ES−): *m/z* 687 (anion + PPh_4^+), 349 (anion + H), 317 (anion − S), 253 (anion − 3S + H), 189 ($C_{10}H_6P_2$ + H), 174 (anion, z = 2).

$[K^+]_2[C_{10}H_6PS_2(\mu\text{-}S)POS^{2-}]\cdot H_2O$ (3): 1 (500 mg, 1.58 mmol) was added to a solution of KOH (204 mg, 3.64 mmol) in water (5 cm^3) and refluxed with stirring for 1 hour. The resulting cloudy solution was filtered using a sintered glass funnel with a plug of celite and the filtrate was evaporated on a rotavapor. The resulting light yellow hygroscopic solid was recrystalised from mixture of ethanol/methanol (4:1) and dried in vacuo at room temperature. Crystals of **3** suitable for X-ray structure determination (in the form of hydrate with 2.5 molecule of water per naphthalene entity) were obtained by evaporation of its saturated solution in an ethanol/methanol mixture. Yield 489 mg (72%) of monohydrate. − $C_{10}H_6K_2OP_2S_4\cdot H_2O$: calcd. C 28.0, H 1.9; found C 28.0, H 1.9. − Decomp. above 200°C. − IR (cm^{-1}): $\tilde{\nu}$ = 1112vs [ν(P=O)], 650vs [ν(P=S)]. − $^{31}P\{^1H\}$-NMR (D_2O; for numbering of atoms see Figure 3): δ = 69.2 (d, P-2), 58.6 (d, P-1), ^2J(PP) = 11.6 Hz. − ^1H NMR (D_2O; for numbering of atoms see Figure 3): δ = 8.75 [1 H, ddd, ^3J(PH) = 20.8, ^3J(HH) = 7.3, ^4J(HH) = 1.4 Hz, 2-H or 8-H], 8.60 [1 H, ddd, ^3J(PH) = 18.9, ^3J(HH) = 7.3, ^4J(HH) = 1.4 Hz, 2-H or 8-H], 8.04 (2 H, m, 4-H and 6-H), 7.64 (2 H, m, 3-H and 7-H). − $^{13}C\{^1H\}$-NMR (D_2O; for numbering of atoms see Figure 3): δ = 140.0 [dd, ^1J(PC) = 80.4, ^3J(PC) = 3.1 Hz, C-9], 137.6 [dd, ^1J(PC) = 106.5, ^3J(PC) = 3.9 Hz, C-1], 134.0 [t, ^3J(PC) = 10.6 Hz, C-5], 133.5 (m, C-4 or C-6), 133.3 (m, C-4 or C-6), 131.4 [d, ^2J(PC) = 11.6 Hz, C-8], 130.1 [d, ^2J(PC) = 14.0 Hz, C-2], 126.8 [t, ^2J(PC) = 8.9 Hz, C-10], 125.6 [d, ^3J(PC) = 12.2 Hz, C-3 or C-7], 125.4 [d, ^3J(PC) = 12.8 Hz, C-3 or C-7]. − Mass spectrum (ES+): *m/z* 449 (M + K), 317 (anion − O + H); (ES-): *m/z* 371 (anion + K), 333 (anion + H).

$[K^+]_2[C_{10}H_6PS_2(\mu\text{-}O)PS_2^{2-}]$ (4): To **3** (monohydrate, 500 mg, 1.17 mmol) 0.5M HCl (5 cm^3) was added, resulting solution was heated to 70°C for 1 hour and then filtered using a sintered glass funnel with a plug of celite. The filtrate was evaporated on a rotavapor and the resulting solid was dried in vacuo. The following purification process for crude product was used: To the solid dry methanol (10 cm^3) was added, the resulting suspension was well mixed, filtered and the filtrate was evaporated on a rotavapor. The solid was then dissolved in water (8 cm^3) and titrated by 1M KOH to pH 7. The resulting light yellow hygroscopic solid obtained after stripping off water was recrystalised from non-dried ethanol. Crystals of **4** suitable for X-ray structure determination were obtained by cooling of its hot saturated solution in ethanol. Yield 249 mg (52%). − $C_{10}H_6K_2OP_2S_4$: calcd. C 29.2, H 1.5; found C 28.8, H 1.5. − M.p. 310°C. − IR (cm^{-1}): $\tilde{\nu}$ = 825vs [ν_{as}(P−O−P)], 678s, 661vs [ν(P=S)]. − $^{31}P\{^1H\}$-NMR (D_2O; for numbering of atoms see Figure 4): δ = 101.4 (s), ^2J(PP) = 51.2 Hz (calculated value).

− ^{1}H NMR (D_2O; for numbering of atoms see Figure 4): δ = 8.39 (2 H, m, 2-H and 8-H), 8.07 (2 H, m, 4-H and 6-H), 7.66 (2 H, m, 3-H and 7-H). − $^{13}C\{^1H\}$-NMR (D_2O; for numbering of atoms see Figure 4): δ = 137.8 [m, ^1J(PC) = 103.4, ^3J(PC) = 3.6 Hz, C-1 and C-9], 133.1 [t, ^3J(PC) = 9.9 Hz, C-5], 132.3 (s, C-4 and C-6), 131.3 (m, C-2 and C-8), 126.5 (m, C-3 and C-7), 125.7 [t, ^2J(PC) = 8.0 Hz, C-10]. − Mass spectrum (ES+): *m*/*z* 449 (M + K), 317 (anion − O + H); (ES-): *m*/*z* 371 (anion + K), 333 (anion + H), 317 (anion − O + H), 237 (anion − 3S + H), 205 (anion − 4S + H), 189 ($C_{10}H_6P_2$ + H), 166 (anion, z = 2).

$[PPh_4^+]_2[C_{10}H_6PS_2(\mu\text{-}O)PS_2^{2-}]\cdot 0.5\ CH_3CN$ (5): To a solution of PPh_4Cl (365 mg, 0.97 mmol) in water (10 cm^3) a solution of **4** (200 mg, 0.49 mmol) in water (10 cm^3) was added with vigorous stirring. The resulting yellow solid was filtered off, washed with water (5 × 20 cm^3), dried in vacuo and recrystalised from acetonitrile. Crystals of **5** suitable for X-ray structure determination were obtained by slow cooling of its hot saturated solution in acetonitrile. Yield 397 mg (79%) of acetonitrile hemisolvate. − $C_{58}H_{46}OP_4S_4.1/2CH_3CN$: calcd. C 68.7, H 4.6, N 0.7; found C 68.3, H 4.5, N 0.5. − Decomposes above 180°C. − IR (cm^{-1}): $\tilde{\nu}$ = 851 s [ν_{as}(P−O−P)], 690 vs and 671 vs [ν(P=S)]. − $^{31}P\{^1H\}$-NMR (CD_3CN, for numbering of atoms see Figure 4): δ = 100.3 (s, anion), 29.8 (s, PPh_4^+). − ^{1}H NMR (CD_3CN, for numbering of atoms see Figure 4): δ = 8.20 (2 H, m, 2-H and 8-H), 7.85 (8 H, m, PPh_4^+), 7.70−7.56 (34 H, m, 4-H, 6-H and PPh_4^+), 7.34 (2 H, m, 3-H and 7-H). − $^{13}C\{^1H\}$-NMR ([D_6]DMSO; for numbering of atoms see Figure 4): δ = 142.8 (m, C-1 and C-9), 135.4 (d, PPh_4^+), 134.8 (d, PPh_4^+), 131.9 [t, ^3J(PC) = 9.0 Hz, C5], 130.5 (d, PPh_4^+), 129.2 (t, C-2 and C-8), 128.2 (s, C-4 and C-6), 125.7 [t, ^2J(PC) = 7.4 Hz, C-10], 124.8 (t, C-3 and C-7), 117.6 (d, PPh_4^+). − Mass spectrum (ES+): *m*/*z* 339 (PPh_4^+), 262 (PPh_3); (ES−): *m*/*z* 671 (anion + PPh_4^+), 333 (anion + H), 237 (anion − 3S + H), 166 (anion, z = 2).

$[CH_3NH_3^+][PyH^+][C_{10}H_6POS(\mu\text{-}O)POS^{2-}]\cdot 1.5$ Py (6): A solution of **15** (20 mg) in pyridine/hexane was left in an open test tube at room temperature. After 5 days colourless crystals suitable for X-ray structure determination were formed. M.p. 102−104°C. Several crystals were examined by NMR. $^{31}P\{^1H\}$-NMR (D_2O): δ = 59.4 (s). − ^{1}H NMR (D_2O): δ = 8.60−7.58 (protons of naphthalene and pyridinium entity), 3.4 (br s, acid protons of $CH_3NH_3^+$ and PyH^+), 2.51 (s, CH_3).

$C_{10}H_6P(O)(OH)(\mu\text{-}O)P(O)(OH)]$ (14): To **3** (monohydrate, 500 mg, 1.17 mmol) 3M HCl (20 cm^3) was added, resulting solution was refluxed for 16 hours and then filtered using a sintered glass funnel with a plug of celite. The volume was reduced to 2 cm^3 on rotavapor and the solid **14** precipitated aftef cooling to 0°C was filtered off and dried in vacuo. Yield ca 65%. − $^{31}P\{^1H\}$-NMR (MeOH): δ = 7.1 (s). A similar procedure was applied when **4** was used as a starting material.

X-ray Crystallographic Study: Details of the data collections and refinements are summarised in Table 1. Data were collected at room temperature using graphite-monochromatized Mo-K_α (λ = 0.71073 Å) radiation on a Siemens SMART CCD diffractometer. Full hemisphere of data with 0.3° steps was collected. Sadabs corrections were applied. All of the non-hydrogen atoms were refined anisotropically, calculations employed the SHELXTL program system.[22] Atomic coordinates, thermal parameters and bond lengths and angles have been deposited at the Cambridge Crystallographic Data Centre (CCDC) under deposition numbers 120586−120590, see http://www.ccdc.cam.ac.uk.

Acknowledgments

Author P. K. is grateful to Royal Society of Chemistry for RS/NATO postdoctoral fellowship tenable in Loughborough University. We are grateful to JREI for an equipment grant.

[1] D. E. C. Corbridge, *Phosphorus*, 3rd ed., Elsevier, New York, **1985**
[2] K. Diemert, W. Kuchen, H. Schepanski, *Chemiker Ztg.* **1983**, *107*, 306
[3] S. M. Darlings, C.-W. Liao, *U.S. Patent* 2,841,553 **1958**; *Chem. Abstr.* **1958,** *52*, 19112h
[4] R. Shabana, *Phosphorus Sulfur* **1987**, *29*, 293
[5] R. Shabana, A. A. El-Barbary, N. M. Yousif, S.-O. Lawesson, *Sulfur Letters* **1984**, *2*, 203
[6] O. N. Grishina, L. M. Bezzubova, *J. Gen. Chem. USSR* **1967**, *37*, 470
[7] J. Hahn, T. Nataniel, *Z. Anorg. Allg. Chem.* **1986**, *543*, 7
[8] R. Shabana, F. H. Osman, S. S. Atrees, *Tetrahedron* **1993**, *49*, 1271
[9] A. A. El-Barbary, *Monatsh. Chem.* **1984**, *115*, 769
[10] K. Clausen, S.-O. Lawesson, *Bull. Soc. Chim. Belg.* **1979**, *88*, 305
[11] P. Kilian, J. Marek, R. Marek, J. Touzin, O. Humpa, J. Novosad, J. D. Woollins, *J. Chem. Soc., Dalton Trans.* **1998**, 1175
[12] P. Kilian, P. Pazdera, J. Marek, J. Novosad, J. Touzin, Z. *anorg. allg. Chem.* **1998**, *624*, 1497
[13] LAOCOON III, Liverpool University Computer Laboratories, **1987**
[14] H. Beckmann, G. Ohms, G. Grossmann, K. Kruger, K. Klostermann, V. Kaiser, *Heteroatom Chem.* **1996**, *7*, 111
[15] G. Grossmann, H. Beckmann, O. Rademacher, K. Kruger, G. Ohms, *J. Chem. Soc., Dalton Trans.* **1995**, 2797
[16] P. Kilian, J. Touzin, J. Marek, J. D.Woollins, J. Novosad, *Main Group Chemistry*, **1996**, *1*, 425
[17] P. Kilian, J. Marek, R. Marek, J. Tousek, O. Humpa, A. M. Z. Slawin, J. Touzin, J. Novosad, J. D. Woollins, *J. Chem. Soc., Dalton Trans.*, manuscript accepted.
[18] F. H. Allen, O. Kennard, D. G. Watson, L. Brammer, A. G. Orpen, R. Taylor, *J. Chem. Soc., Perkin. Trans. 2,* **1987**, S1
[19] H. W. Roesky, M. Noltemeyer and G. M. Sheldrick, *Z. Naturforsch.* **1986**, *41b*, 803
[20] A. M. Z. Slawin, D. J. Williams, P. T. Wood and J. D. Woollins, *J. Chem. Soc., Chem. Commun.* **1987**, 1741
[21] M. R. St. J. Foreman, J. Novosad, A. M. Z. Slawin and J. D. Woollins, *J. Chem. Soc., Dalton Trans.* **1997**, 1347
[22] SHELXTL, Bruker AXS, Madison, New York, **1998**

Received May 17, 1999
[I99173]

Amino Alcohol Coordination in Ruthenium(II)-Catalysed Asymmetric Transfer Hydrogenation of Ketones

Daniëlle G. I. Petra,[a] Paul C. J. Kamer,[a] Piet W. N. M. van Leeuwen,*[a] Kees Goubitz,[a] Arjen M. Van Loon,[b] Johannes G. de Vries,[c] and Hans E. Schoemaker[a,c]

Keywords: Asymmetric catalysis / Transfer hydrogenation / Ruthenium / Amino alcohol ligands / X-ray structure

The nature of ruthenium-amino alcohol precursors in the catalytic cycle of asymmetric hydrogen transfer reactions was studied using two C_2-symmetrical tetradentate ligands (**1** and **2**) that were synthesised from (nor)ephedrine. The structure of the catalyst precursor was examined through catalysis and NMR experiments. It was shown that the active catalyst contains one ligand per metal, which coordinates in a didentate N,O fashion (**9**). In addition, a $Ru^{II}Cl_2$ complex, in which *N*,*N*′-bis(2-hydroxy-1-methyl-2-phenylethyl)-1,2-diaminoethane (**1**) coordinates through two nitrogen atoms, was structurally characterised by X-ray diffraction (**8**). – Based on the results of this study a series of new amino alcohol ligands was synthesised from easily available starting materials. Optimisation of the amino alcohol ligand structure resulted in the most effective chiral amino alcohol ligand (**5**) so far that is capable of reducing acetophenone at 0 °C with up to 97% ee in the Ru^{II}-catalysed transfer hydrogenation.

Introduction

Transfer hydrogenation of ketones is a highly efficient method for the synthesis of chiral alcohols, owing to low fractional yields of side products and high product yields in high enantiomeric excess. The reaction conditions are relatively mild and the costs are low as a result of the operational simplicity of this method.

As a consequence, much effort has been devoted to the development of new chiral catalysts tailored to the transfer hydrogenation of prochiral ketones. Recently, rapid progress in this area has been made, mainly due to Noyori's work.[1−5] One of the highest catalyst activities so far was observed in ruthenium(II)-catalysed transfer hydrogenation with simple amino alcohols as ligands. Diamines and chiral phosphorus and nitrogen ligands gave rise to lower reaction rates.[5]

Despite these high activities obtained for Ru^{II} amino alcohol catalysts there are only a few reports on the use of simple amino alcohols as chiral ligands.[3,6,7] Amino alcohols are easily accessible and it would seem worthwhile optimising their performance in terms of activity and enantioselectivity by varying the structure. To this end we started to elucidate the nature of ruthenium amino alcohol catalysts. The chiral shielding around the metal centre is highly dependent on the ligand structure and the number of ligand donor atoms that coordinate to the metal.

From the work of Noyori and co-workers it is clear that for their Ru^{II}-TsDPEN [TsDPEN = *N*-(*p*-tolylsulfonyl)-1,2-diphenylethylenediamine] system the active catalyst contains one ligand per metal.[4] However, for weakly coordinating amino alcohol ligands, which give rise to much higher reaction rates in the Ru^{II}-catalysed reduction of ketones using 2-propanol as an H-donor,[5] the ligand to ruthenium ratio has proven to be critical.[6] For these systems the ligand stoichiometry and the mechanism have not been elucidated as yet. In all cases reported so far two equivalents of amino alcohol ligand per ruthenium were used to maintain a high selectivity.

Other mechanistic studies concerning the ligand-to-metal ratio were limited to rhodium catalysts containing didentate nitrogen ligands. Gladiali's pioneering work resulted in a proposed catalytic cycle in which the active complex is a metal hydride complex containing two phenanthroline ligands.[8] In contrast to this, Bernard et al. postulated that the active catalyst is a rhodium complex having only one diamine ligand coordinated to the metal.[9]

In order to gain more insight into the mechanism of hydrogen transfer reactions and especially the influence of the ligand stoichiometry, two potentially tetradentate ligands (**1** and **2**) were synthesised and applied in enantioselective transfer hydrogenation. The preferred mode of coordination (i.e. either two, three or four donating atoms per metal) and the ligand stoichiometry were examined in catalysis. The catalytic results were compared with those of the didentate analogues **3** and **4**. ^{1}H-, ^{13}C-, and ^{15}N-NMR spectroscopy were used to study the catalyst in situ. The molecular structure of a ruthenium(II) catalyst precursor complex containing **1** was determined by X-ray diffraction.

Based on the results of the study towards the preferred mode of coordination of the ligands, a series of new amino alcohol ligands was synthesised to create higher selectivities in the transfer hydrogenation of ketones using ru-

[a] Institute of Molecular Chemistry, University of Amsterdam, Nieuwe Achtergracht 166, NL-1018 WV Amsterdam, The Netherlands
Fax: (internat.) + 31-20/525-6456
E-mail: PWNM@anorg.chem.uva.nl
[b] Laboratory of Organic Chemistry and Catalysis, Delft University of Technology, Julianalaan 136, NL-2628 BL Delft, The Netherlands
[c] DSM Research, P. O. Box 18, NL-6160 MD, Geleen, The Netherlands

 © WILEY-VCH Verlag GmbH, D-69451 Weinheim, 1999 1434−1948/99/1212−2335 $ 17.50+.50/0

thenium(II) amino alcohol catalysts. Various substituents in the backbone and on the amine functionality were introduced to determine possible factors that influence the enantioselectivity of the reaction. We were able to develop the most effective chiral amino alcohol ligand to date for Ru^{II}-catalysed hydrogen transfer of acetophenone.

Results and Discussion

In order to elucidate the mode of coordination and the ligand stoichiometry in ruthenium(II) amino alcohol-catalysed transfer hydrogenations, ligands **1** and **2** were used (Figure 1). These ligands are suitable for this study as they can coordinate in a tetradentate manner, using two nitrogen and two oxygen donor atoms, in a tridentate manner or in a didentate manner, using either two nitrogen atoms or a nitrogen and an oxygen donor atom. In addition, these tetradentate ligands can possibly form a deeper chiral concave pocket around the metal centre compared to the corresponding didentate ligands, which might result in higher selectivities. Examples in which this effect was found are catalysts for hydrogen transfer reactions containing the chiral bis(oxazolinyl)pyridine ligand (pybox) and the bis(oxazolinyl)amine ligand (ambox).[10][11]

The synthesis of **1** {*N*,*N*′-bis[(1*S*,2*R*)-2-hydroxy-1-methyl-2-phenylethyl]-1,2-diaminoethane} and **2** {*N*,*N*′-bis[(1*S*,2*R*)-2-hydroxy-1-methyl-2-phenylethyl]-1,3-dimethylaminopropane} is analogous to that described by Soai et al.[12]

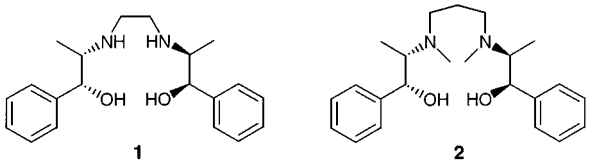


Figure 1. Tetradentate ligands **1** and **2**

The results of the use of catalysts generated in situ from ligands **1** and **2** (Figure 1) and various ruthenium(II) precursors in the reduction of acetophenone (Scheme 1) are depicted in Table 1. In a typical catalysis experiment a solution of ketone (0.1 M in dry 2-propanol), the ruthenium complex ($[RuCl_2(arene)]_2$, 0.5 mol-%), the chiral amino alcohol (1 mol-%) and *t*BuOK (2.5 mol-%) was stirred at room temperature under argon in dry 2-propanol. Conversions and enantioselectivities were monitored during the reaction. At lower conversions (i.e. < 60%) a zero order rate dependency in substrate concentration was found. The enantioselectivity proved to be constant in time for all catalytic reactions described here unless otherwise stated.

The use of **1** in combination with $[RuCl_2(p\text{-cymene})]_2$ and base in propan-2-ol resulted in reduction of acetophenone to (*S*)-phenethyl alcohol in 88% ee at 67% conversion after 44 hours (entry 1, Table 1). Under the same reaction conditions ligand **2** gave rise to 24% conversion and 82% ee after 44 hours (entry 2, Table 1). Both the lower reaction rate and asymmetric induction of **2** can be explained by the fact that at least one primary or secondary amine functionality is essential to obtain high yields and high enantiomeric excess. This has been observed before and Noyori et al. suggested that an NH-moiety in the ligand may promote a cyclic transition state through hydrogen bonding to a ketone substrate.[5]

Table 1. Hydrogen transfer reduction of acetophenone using ligands **1**−**7**[a]

Entry	Ligand	Ru/L	*t*[h]	Conv. [%] of ketone[b]	ee [%] alcohol[c]	Confign.
1	**1**	1/2	44	67	88	(*R*)
2	**2**	1/2	44	24	82	(*R*)
3	**3**	1/2	0.5	95	77	(*R*)
4	**4**	1/2	0.5	91	89	(*R*)
5	**1**	1/1.1	44	80	90	(*R*)
6	**1**	2/1.1	44	93	78	(*R*)
7	**5**	1/2	1	88	95	(*R*)
8[d]	**5**	1/2	4	75	97	(*R*)
9	**6**	1/2	2	64	91	(*R*)
10	**7**	1/2	20	25	20	(*R*)
11	**1**	1[e]/2	44	88	56	(*R*)
12	**1**	1[f]/2	44	2	nd	–
13	complex **8**	1/1	44	78	87	(*R*)

[a] The reaction was carried out at room temperature using a 0.1 M solution (5 mmol) in propan-2-ol. Substrate:$[RuCl_2(p\text{-cymene})]_2$/ligand/*t*BuOK = 200:1:1.1−4:10. − [b] Conversions were determined by GLC analysis. − [c] Determined by capillary GLC analysis using a chiral cycloSil-B column. − [d] The reaction was carried out at 0°C. − [e] Ru = $[RuCl_2(benzene)]_2$. − [f] Ru = $RuCl_2(PPh_3)_3$.

The use of another ruthenium arene complex, the (benzene)ruthenium(II) chloride dimer in combination with amino alcohol **1**, resulted in a large decrease of the enantiomeric excess and in a higher reaction rate (88% conversion and 56% ee, after 44 h; entry 11, Table 1). The increase in reactivity by decreasing steric bulk on the arene has been observed in other systems. As in our case, this is often accompanied by a decrease in enantioselectivity.[3][6] High selectivities have been observed using $RuCl_2(PPh_3)_3$ as a catalyst precursor in combination with tridentate nitrogen ligands.[10][11] This catalyst precursor does not contain an arene moiety and therefore offers additional coordination sites for amino alcohol coordination. Hardly any conversion was observed using this catalyst precursor in combination with ligand **1** (entry 12, Table 1).

In order to study the coordination fashion of ligand **1** during catalysis (i.e. either didentate, tridentate or tetradentate) it was compared to its corresponding didentate analogues (1*R*,2*S*)-(−)-norephedrine (**3**) and (1*R*,2*S*)-(−)-ephedrine (**4**) in the reduction of acetophenone (Figure 4) (see also Takehara et al.).[3] The use of **3** gave rise to a very fast reaction, but a lower selectivity compared to the use of **1** (95% conversion and 77% ee, after 0.5 h; entry 3, Table 1). On using amino alcohol **4**, however, a much higher reaction rate was found compared to the use of **1**, with similar enantioselectivity (91% conversion and 87% ee, after 0.5 h; entry 4, Table 1). These results show that no increase of enantioselectivity is observed on using the tetradentate ligand **1**, which contains additional donor atoms, compared to the use of **4**.

With the aim of resolving the mode of coordination for the tetradentate ligand **1** a series experiments was performed in which the ratio of ligand **1** to ruthenium was varied. When the ligand to ruthenium ratio was changed from two to one half, the initial selectivity of the reaction did not change. However, on using half an equivalent of ligand the enantioselectivity of the reaction dropped to 78% after 44 hours, probably due to catalyst deactivation (entry 6, Table 1). When 1 or 2 equivalents of ligand are in solution the excess of donating atoms of the amino alcohol must stabilise the complex, preventing the formation of black particles of ruthenium. The increasing reaction rate can be explained by the formation of a sterically less hindered bimetallic ruthenium complex containing only one tetradentate ligand that coordinates in a didentate fashion. From these results it is concluded that the active catalyst is most likely a ruthenium complex with one ligand coordinating to the metal in a didentate mode, because catalysis using a ligand stoichiometry of one half results in identical initial enantioselectivities and a higher reaction rate. Thus, half an equivalent of ligand suffices for the control of enantioselectivity, assuming a coordination mode similar to that of ligands **3** and **4** (i.e. coordination through one nitrogen and one oxygen donor atom). The remaining part of the C_2-symmetric molecule merely acts as a large substituent at the nitrogen atom which slows down the reaction and does not further increase the selectivity.

In order to confirm the conclusions we have drawn above, i.e. that ligand **1** prefers a didentate *N,O*-coordination fashion to ruthenium(II), we now describe our attempts to identify two different (1:1) ruthenium−amino alcohol complexes and establish their coordination mode.

When an equimolar mixture of $[\{RuCl_2(\eta^6\text{-}p\text{-cymene})\}_2]$ and **1** was stirred in dichloromethane for one hour at room temperature, the ruthenium(II) complex **8** was isolated and was crystallised from benzene.

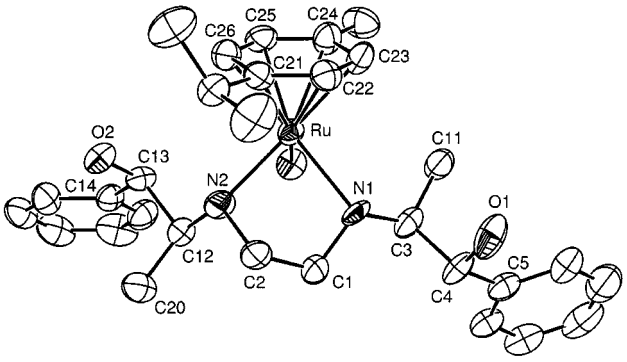


Figure 2. Crystal structure of **8**

The crystals were isolated and characterised by X-ray diffraction. A number of neutral complexes of the type [Ru(arene)Cl(amino−amido ligand)] have been crystallographically characterised.[10] The cationic complex **8** of the type [Ru(arene)Cl(neutral amino−amino ligand)]$^+$ described here contains a neutral amino−amino ligand. The single crystal X-ray analysis indicates that this cationic ruthenium(II) complex has a distorted octahedral coordination environment (see Figure 2). The metal centre is coordinated to two neutral nitrogen atoms, which are involved in a five-membered chelate ring displaying an envelope conformation with C1 and C2. A chloride anion and a *p*-cymene molecule, acting as a neutral six electron donor, complete the coordination sphere of the ruthenium atom. A second chloride anion is present as a noncoordinating counterion. Selected bond lengths and angles are collected in Table 2.

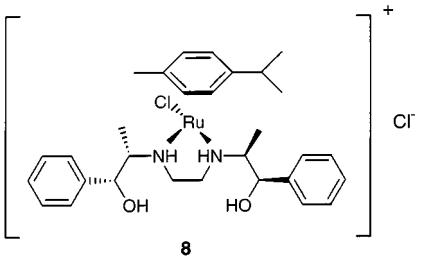
Table 2. Selected bond lengths [Å] and angles [°] for [Ru{*N,N′*-bis[(1*S*,2*R*)-2-hydroxy-1-methyl-2-phenylethyl]-1,2-diaminoethane}{*p*-cymene}Cl]Cl (**8**) (with esd′s in parentheses)

Bond lengths			
Ru−N(1)	2.228(8)	C(2)−N(2)	1.50(1)
Ru−N(2)	2.182(8)	C(3)−C(4)	1.58(2)
Ru−Cl	2.387(3)	C(3)−C(11)	1.51(2)
Ru−C(21)	2.20(1)	C(3)−N(1)	1.50(2)
Ru−C(22)	2.19(1)	C(4)−C(5)	1.51(2)
Ru−C(23)	2.20(1)	C(4)−O(1)	1.41(2)
Ru−C(24)	2.25(1)	C(12)−C(13)	1.56(2)
Ru−C(25)	2.19(1)	C(12)−C(20)	1.54(2)
Ru−C(26)	2.18(1)	C(12)−N(2)	1.52(2)
C(1)−C(2)	1.50(2)	C(13)−C(14)	1.50(2)
C(1)−N(1)	1.48(2)	C(13)−O(2)	1.43(1)
Bond angles			
Cl−Ru−N(1)	84.8(2)	Ru−N(1)−C(1)	105.3(7)
Cl−Ru−N(2)	89.7(3)	Ru−N(1)−C(3)	121.4(7)
N(1)−Ru−N(2)	81.6(3)	Ru−N(2)−C(2)	103.1(6)
C(2)−C(1)−N(1)	109(1)	Ru−N(2)−C(12)	122.0(7)
C(1)−C(2)−N(2)	108(1)		

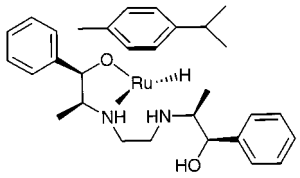
The ruthenium complex **8**, which catalyses the asymmetric transfer hydrogenation of acetophenone in 2-propanol containing *t*BuOK (entry 13, Table 1), is merely a catalyst precursor. Upon addition of base the most acidic protons are eliminated. Due to deprotonation of the OH group, N,O coordination will be preferred to didentate *N,N′* coordination. An unsymmetrical complex with a chiral metal centre is formed.

In order to elucidate the structure of this complex in solution, ^{1}H-NMR and ^{15}N-NMR experiments were performed on the in situ catalyst in CD_3OD. Upon mixing (*p*-cymene)ruthenium(II) chloride dimer and ligand **1**, complex **8** is formed as the major product. All the ^{1}H-NMR signals of the hydrogen atoms near the nitrogen atoms are shifted downfield in comparison to those of the free ligand. The two methyl signals become inequivalent. The NH protons in complex **8** show very slow H, D exchange in CD_3OD; the signal that is visible at $\delta = 6.45$, slowly decreases in size when the compound stands at room temperature in CD_3OD (i.e. to 50% of its original value after 7 days). After two hours at 60°C in CD_3OD the NH signal completely disappears. The ^{15}N-NMR spectrum shows two peaks at $\delta = -357$ and $\delta = -358$, while the free ligand shows a peak at $\delta = -336$. Upon addition of 2 equivalents of base a new complex (**9**) formed (see Figure 3). This complex showed two peaks in the ^{15}N-NMR spectrum at $\delta = -355$ and at $\delta = -343$. The ^{15}N-NMR spectrum did not change upon stepwise cooling to −40°C. In the ^{1}H-NMR spectrum, broadened signals were observed, which suggests fluxional behaviour. Under these basic conditions no NH

protons were observed for this compound in CD_3OD. It is concluded that in complex **9** one nitrogen atom coordinates to the ruthenium atom as in complex **8**; the chemical shift that is found at $\delta = -355$ is typical for a coordinated nitrogen atom.[13] The chemical shift of the second nitrogen atom is characteristic of a noncoordinated amine moiety; the position of the ^{15}N signal at $\delta = -343$ is comparable to the nitrogen resonance of $\delta = -336$ for the free ligand.[14] The presence of the hydride in **9** was proven by ^1H-NMR measurements in deuterated benzene, which showed a hydride signal at $\delta = -5.50$. In addition, the molecular formula of **9** was confirmed by electrospray mass spectrometry, which showed a signal for M^+ at 564.230 (calcd. 564.228).



8

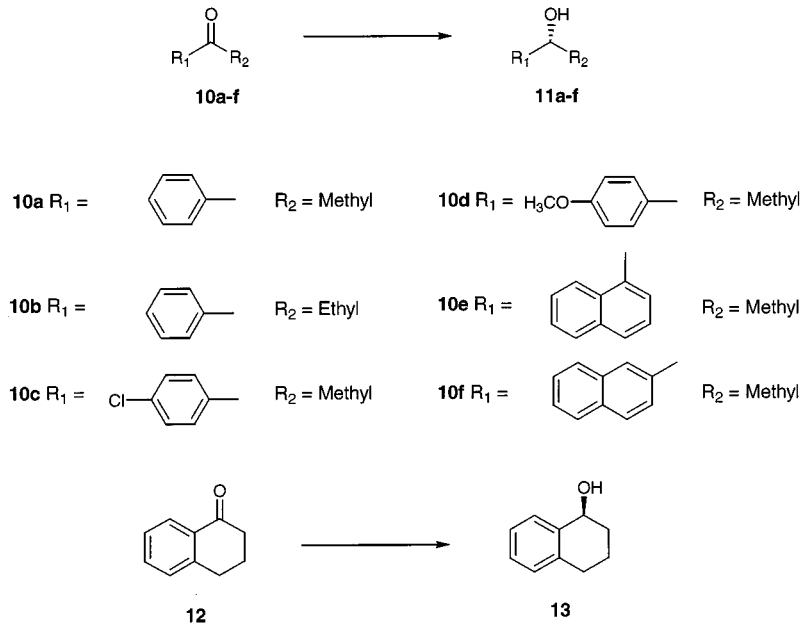


9

Figure 3. Ruthenium amino alcohol complexes **8** and **9**

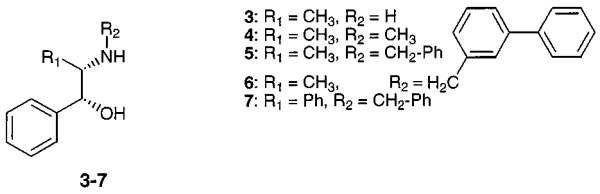
Since it now seems clear that a didentate coordination of amino alcohol ligands is preferred to either tridentate or tetradentate coordination, the design of new amino alcohols as ligands to create high selectivities should be directed towards didentate ligands. From Table 1 it can be seen that the selectivity of the reaction is influenced by the substitution pattern on the nitrogen (cf. **1**, **3**, and **4**). It is shown that the secondary amine gives rise to better selectivities than the corresponding primary amine or tertiary amine without decrease of reaction rate. In contrast, Palmer et al. reported that the substitution of the primary amine functionality with a methyl group resulted in a decrease of both the reaction rate and the enantioselectivity, when (1*R*,2*S*)-(+)-*cis*-1-amino-2-indanol was used as a ligand.[6]

In order to optimise the amino alcohol ligand structure both the substituents in the backbone and the substituents on the nitrogen atom were varied. Amino alcohols **5**, **6**, and **7** were synthesised in one step by reacting either (1*R*,2*S*)-(−)-2-aminodiphenyl ethanol or (1*R*,2*S*)-(−)-norephedrine with benzyl bromide and/or 3-phenylbenzyl bromide, respectively, under slightly basic conditions (see Figure 4). The effect of a bulky substituent on the nitrogen atom was assessed by using amino alcohols **5** and **6** as ligands in catalysis (Figure 4). The use of **5** in combination with $[\{RuCl_2(p\text{-cymene})\}]_2$ under the standard conditions gave an excellent result (95% ee at 88% conversion after 1 h; entry 7, Table 1). The selectivity could be further improved by lowering the reaction temperature to 0°C. The beneficial temperature effect resulted in the highest enantioselectivity observed so far in the Ru^{II} amino alcohol-catalysed reduction of acetophenone, i.e. 97% (entry 8, Table 1). A longer reaction time was required to reach high conversion. Changing the substituent from a benzyl to a 3-phenylbenzyl group did not improve the results any further. Both the conversion and the enantioselectivity decreased (91% ee at 64% conversion after 2 hours; entry 9, Table 1). Ligand **7** was synthesised to investigate the effect of an additional bulky



Scheme 1. Asymmetric transfer hydrogenation of ketones **10a**−**12**

substituent in the carbon backbone. Changing the substituent at the 1-position from a methyl to a phenyl group did not result in higher enantioselectivities (entry 10, Table 1). The phenyl substituent is clearly too bulky because the conversion dropped drastically.



3-7

Figure 4. Amino alcohol ligands **3**−**7**

A variety of other substrates could also be transformed to the corresponding secondary alcohols with high enantiomeric purity, using ligand **5** under optimised conditions (Table 3, Scheme 1). Changing the electronic and steric properties of the substrate did not clearly affect the enantioselective outcome of the reaction. In these catalytic experiments only one equivalent of ligand was required to obtain high enantioselectivities.

Table 3. Hydrogen transfer reduction of ketones **10a**−**12** using ligand **5**[a]

Entry	Ketone	*t*[h]	Conv. [%] of ketone[b]	ee [%] alcohol[c]	Confign.
1	**10a**	2	91	95[d]	(*R*)
2	**10b**	2	98	90	(*R*)
3	**10c**	2	96	86[d]	(*R*)
4	**10d**	3	68	93	(*R*)
5	**10e**	2	96	96	(*R*)
6	**10f**	2	94	93	(*R*)
9	**12**	2	68	96	(*R*)

[a] The reaction was carried out at room temperature using a 0.1 M solution (5 mmol) in propan-2-ol. Substrate/$[RuCl_2(p\text{-cymene})]_2$/ligand/*t*BuOK = 400:1:2.2:6. − [b] Conversions were determined by GLC and/or 300 MHz ^{1}H-NMR analysis. − [c] Determined using chiral HPLC with a Chiracel OD column unless otherwise specified. − [d] Determined by capillary GLC analysis using a chiral cycloSil-B column.

Conclusion

In the ruthenium-catalysed transfer hydrogenation of prochiral ketones using tetradentate ligand **1** the amino alcohol prefers a didentate coordination fashion, as was shown by catalysis experiments (see Table 1) and NMR experiments. The extra donor atoms in the ligand do not enhance the selectivity of the reaction but only give rise to lower reaction rates. In contrast to results in other reports, a ligand-to-metal ratio of one is sufficient to maintain selectivity.

The best amino alcohol ligand structure turned out to be NH-benzyl-(1*R*,2*S*)-(−)-norephedrine (**5**), which proved to be an excellent ligand for the control of asymmetric ruthenium-catalysed transfer hydrogenation of prochiral ketones.

Experimental Section

General Remarks: Reactions were performed under an atmosphere of argon in flame-dried Schlenk flasks and using anhydrous solvents. Propan-2-ol was freshly distilled from CaH_2 prior to use. − Column chromatography was performed with silica gel 60, 70−230 mesh ASTM (Merck). Thin layer chromatography was carried out on TLC aluminium foil, silica gel 60 G/UV_{254} and spots were detected with UV light or iodine vapour. − Melting points were taken on a Gallenkamp melting point apparatus and are uncorrected. − Optical rotations were measured on a Perkin−Elmer 241 automatic polarimeter. − IR spectra were recorded on a BioRad FT-IR (FTS-7) spectrophotometer. − ^{1}H- and ^{13}C-NMR spectra were recorded on a Bruker AMX 300 spectrometer. Chemical shifts are on the δ scale (ppm) relative to TMS as internal standard. ^{15}N-NMR spectra were recorded on a Bruker DRX 300 instrument. Chemical shifts are relative to nitromethane as external standard. − Mass spectra were recorded on a JEOL JMS SX/SX102A four sector mass spectrometer, coupled to a JEOL MS-MP7000 data system. − Microanalyses (C, H, N) were performed on an Elementar Vario EL apparatus (Foss Electric). − Gas chromatography was performed using a Carlo Erba GC 6000 Vega 2 instrument, 25 m column: CycloSil-B (chiral) and a Carlo Erba HRGC Mega 2 instrument, 25 m column: BPX 35 (SGE) (achiral). HPLC chromatography was performed using a Gilson HPLC apparatus and a Chiracel OD column.

***N*,*N*′-Bis[(1*S*,2*R*)-2-hydroxy-1-methyl-2-phenylethyl]-1,2-diaminoethane (1):** Compound **1** was synthesised in analogy with the procedure of Soai et al.[12] 1,2-Dibromoethane (3.1 g, 16.5 mmol) was added to (1*R*,2*S*)-(−)-norephedrine (5.0 g, 33 mmol) and finely powdered Na_2CO_3 (7.0 g, 66 mmol) in ethanol (25 mL). The mixture was heated at reflux for 20 h. The salts that formed were filtered off and the solvent was evaporated in vacuo. The product was extracted with dichloromethane, the organic phases were dried with Na_2SO_4 and evaporated to dryness. After dissolving the residue in a minimal amount of ethanol and addition of HCl, a white precipitate formed, which was collected by filtration and recrystallised from water (40 mL) with a few drops of HCl. The HCl salt was dissolved in water and 0.1 M NaOH was added until pH = 12 was reached. The mixture was extracted three times with diethyl ether. The organic layers were combined and evaporated to dryness. Yield: 4.4 g (81%). M.p.: 108−110°C (free amine). − IR (neat): $\tilde{\nu}$ = 3387 cm^{-1}, 2976, 2927, 1452. − ^{1}H NMR (CD_3OD): δ = 0.94 (d, 6 H, *J* = 6.4 Hz, CH_3), 2.62 (m, 2 H, C*H*NH), 2.75 (m, 4 H, CH_2), 4.61 (d, 2 H, *J* = 4.8 Hz, C*H*OH), 7.21−7.34 (m, 10 H, C_6H_5). − ^{13}C NMR (CD_3OD): δ = 14.92 (*C*H$_3$), 59.85 (*C*HNH), 47.25 (*C*H$_2$), 76.17 (*C*HOH), 127.55 [*C*H$_{arom}$ (*o*)], 128.32 [CH$_{arom}$ (*p*)], 129.26 [*C*H$_{arom}$ (*m*)], 144.07 (*C*$_q$). − ^{1}H{^{15}N} NMR (CD_3OD): δ = −336. − HRMS (FAB$^+$): *m*/*z* calcd. for $C_{20}H_{29}N_2O_2$ [M + H]$^+$: 329.2229; found 329.2227. − $C_{20}H_{28}N_2O_2$ (328.458): calcd. C 73.14, H 8.59, N 8.53; found C 73.12, H 8.56, N 7.96. − $[\alpha]_D^{20}$ = +9.6 (*c* = 0.8, EtOH).

***N*,*N*′-Bis[(1*S*,2*R*)-2-hydroxy-1-methyl-2-phenylethyl]-1,3-dimethylaminopropane (2):** Compound **2** was prepared from (1*R*,2*S*)-(−)-ephedrine according to a literature procedure[12] and in an analogous way to **1**. Yield: 2.6 g (78%). IR (neat, HCl salt): $\tilde{\nu}$ = 3407 cm^{-1}, 2978, 2940, 2800, 1451, 754, 700. − ^{1}H NMR (CD_3OD): δ = 0.88 (d, 6 H, *J* = 6.8 Hz, CH_3), 1.69 (dt, 2 H, *J* = 6.7 Hz, *J* = 6.8 Hz, CH_2), 2.31 (s, 6 H, NCH_3), 2.41, 2.63 (each dt, 4 H, *J* = 6.4 Hz, *J* = 6.4 Hz, CH_2), 2.77 (dq, 2 H, *J* = 3.1 Hz, *J* = 6.8 Hz, C*H*N), 4.95 (d, 2 H, *J* = 3.6 Hz, C*H*OH), 7.20−7.32 (m, 10 H, C_6H_5). − ^{13}C NMR ($CDCl_3$): δ = 8.08 (*C*H$_3$), 23.59 (N*C*H$_3$), 38.65 (*C*HNH), 52.05, 64.81 (*C*H$_2$), 73.15 (*C*HOH), 126.07 [*C*H$_{arom}$ (*o*)],

127.02 [CH_{arom} (*p*)], 128.07 [CH_{arom} (*m*)], 142.38 (C_q). − HRMS (FAB$^+$): *m*/*z* calcd. for $C_{23}H_{35}N_2O_2$ [M + H]$^+$: 371.2698; found 371.2699. − $C_{23}H_{37}Cl_3N_2O_2$ (479.923): calcd. C 57.56, H 7.77, N 5.84; found C 57.52, H 8.04, N 5.78. − $[\alpha]_D^{20}$ (HCl salt) = +5 (*c* = 0.6, EtOH).

NH-Benzyl-(1*R*,2*S*)-norephedrine (5): K_2CO_3 (234 mg, 1.70 mmol) was added to (1*R*,2*S*)-(−)-norephedrine (250 mg, 1.65 mmol) in acetonitrile at room temperature. At 0°C, benzyl bromide (171 mL, 1.65 mmol) was added and the resulting mixture was stirred for 16 h at 60°C. The reaction mixture was filtered through Celite and the filtrate evaporated to dryness. The crude compound was purified by column chromatography (silica gel 60, eluent: ethyl acetate, R_f value: 0.33). Yield: 200 mg (50%), colourless oil. − IR (neat): $\tilde{\nu}$ = 3334 cm^{-1}, 3062, 3028, 2973, 2871, 1603, 1494, 1452, 744, 700. − ^{1}H NMR ($CDCl_3$): δ = 0.87 (d, 3 H, *J* = 6.6 Hz, C*H*$_3$), 2.48 (s, 1 H, O*H*), 3.02 (dq, 1 H, *J* = 3.8 Hz, *J* = 6.6 Hz, C*H*NH), 3.90 (s, 2 H, CH_2), 4.82 (d, 1 H, *J* = 3.8 Hz, C*H*OH), 7.33 (m, 5 H, C_6H_5). − ^{13}C NMR ($CDCl_3$): δ = 14.81 (*C*H$_3$), 51.44 (*C*H$_2$), 58.01, 73.57 (2 *C*H), 126.39, 127.27, 127.36, 128.31, 128.76 (10 CH_{arom}), 140.33, 141.77 (2 C_q). − HRMS (FAB$^+$): *m*/*z* calcd. for $C_{16}H_{20}NO$ [M + H]$^+$: 242.1545; found 242.1545. − $C_{16}H_{19}NO{\cdot}0.5H_2O$ (250.344): calcd. C 76.77, H 8.05, N 5.59; found C 76.80, H 7.94, N 5.58. − $[\alpha]_D^{20}$ = +16 (*c* = 0.70, EtOH).

NH-3-Phenylbenzyl-(1*R*,2*S*)-norephedrine (6): This compound was synthesised analogously to **5**. The crude compound was purified by column chromatography (silica gel 60, eluent: ethyl acetate, R_f value: 0.29). Yield: 620 mg (61%), yellow oil. − IR (neat): $\tilde{\nu}$ = 3397 cm^{-1}, 3059, 3031, 2974, 2872, 1601, 1480, 1453, 757, 738, 701. − ^{1}H NMR ($CDCl_3$): δ = 0.95 (d, 3 H, *J* = 5.5 Hz, C*H*$_3$), 2.53 (s, 2 H, N*H*, O*H*), 3.05 (dq, 1 H, *J* = 3.9 Hz, *J* = 5.5 Hz, C*H*NH), 3.96 (s, 2 H, CH_2), 4.84 (d, 1 H, *J* = 3.9 Hz, C*H*OH), 7.33−7.69 (m, 9 H, C_6H_5). − ^{13}C NMR ($CDCl_3$): δ = 14.48 (*C*H$_3$), 51.12 (*C*H$_2$), 57.71, 73.24 (2 *C*H), 125.85, 126.01, 126.76, 126.86, 126.93, 127.02, 127.21, 127.95, 128.68, 128.82 (*C*H_{arom}), 140.43, 140.87, 141.31, 141.35 (4 C_q). − HRMS (FAB$^+$): *m*/*z* calcd. for $C_{22}H_{24}NO$ [M + 1]$^+$: 318.1858; found 318.1850. − $[\alpha]_D^{20}$ = −17 (*c* = 1.75, $CHCl_3$).

(1*R*,2*S*)-2-(Benzylamino)-1,2-diphenylethanol (7): This compound was synthesised analogously to **5**. The crude compound was purified by crystallisation from ethyl acetate/hexane. Yield: 760 mg (59%), white solid. M.p.: 154−155°C. − IR ($CHCl_3$): $\tilde{\nu}$ = 3020 cm^{-1}, 2977, 1524, 1424, 1453, 734, 670. − ^{1}H NMR ($CDCl_3$): δ = 3.13 (s, 2 H, N*H*, O*H*), 3.60 (d, 1 H, *J* = 13.4 Hz CH_2), 3.82 (d, 1 H, *J* = 13.4 Hz CH_2), 3.97 (d, 1 H, *J* = 5.3 Hz, C*H*OH), 5.03 (d, 1 H, *J* = 5.3 Hz, C*H*NH), 7.11−7.38 (m, 15 H, C_6H_5). − ^{13}C NMR ($CDCl_3$): δ = 50.57 (*C*H$_2$), 67.57, 75.76 (2 *C*H), 126.56, 127.26, 127.48, 127.73, 127.80, 128.08, 128.30, 128.44 (*C*H_{arom}), 137.14, 137.95, 139.96 (3 C_q). − HRMS (FAB$^+$): *m*/*z* calcd. for $C_{21}H_{22}NO$ [M + 1]$^+$: 304.1701; found 304.1696. − $C_{21}H_{21}NO$ (303.408): calcd. C 83.13, H 6.98, N 4.62; found C 82.10, H 7.01, N 4.39. − $[\alpha]_D^{20}$ = −229 (*c* = 1.00, $CHCl_3$).

[Ru{*N*,*N*′-bis[(1*R*,2*S*)-2-hydroxy-1-methyl-2-phenylethyl]-1,2-diaminoethane}{*p*-cymene}Cl]Cl (8): Complex **8** was prepared in analogy with a literature procedure.[15] To a solution of [{$RuCl_2(\eta^6$-*p*-cymene)}$_2$] (100 mg, 0.16 mmol) in CH_2Cl_2 (5 mL) was added *N*,*N*′-bis[(1*S*,2*R*)-2-hydroxy-1-methyl-2-phenylethyl]-1,2-diaminoethane (**1**) (108 mg, 0.33 mmol). After stirring the reaction mixture for 1 h at room temperature the solvent was removed in vacuo. The orange solid was washed twice with diethyl ether (10 mL) and dried in vacuo. Recrystallisation from chloroform/pentane afforded yellow needle-shaped crystals. − IR (neat): $\tilde{\nu}$ = 3287 cm^{-1}, 2959, 2927, 2855, 1452, 1216, 758. − ^{1}H NMR (CD_3OD): δ = 0.90 (d, 3 H, *J* = 6.6 Hz, C*H*$_3$), 1.06 (d, 3 H, *J* = 6.8 Hz, C*H*$_3$), 1.24, 1.25 [each d, 6 H, *J* = 6.9 Hz, CH(C*H*$_3$)$_2$], 2.02 (s, 3 H, C*H*$_3$ in *p*-cymene), 2.48 [m, 1 H, C*H*(CH$_3$)$_2$], 2.79 (m, 4 H, CH_2), 5.17 (d, 2 H, *J* = 2.5 Hz, C*H*), 5.41 (broad s, 2 H, C*H*), 5.56, 5.65, 5.75, 5.77 (each d, 4 H, *J* = 5.9 Hz, CH_{arom} in *p*-cymene), 6.45 (broad s, 2 H, N*H*), 7.13−7.46 (m, 10 H, C_6H_5). − ^{13}C NMR (CD_3OD): δ = 12.55, 18.61, 20.09, 25.11, 25.61 (5 *C*H$_3$), 53.57 (*C*H$_2$), 34.68, 60.83, 64.00, 72.96, 77.90 (5 *C*H), 118.34 (C_q), 129.26, 129.56, 129.60, 129.90, 130.74, 130.87 (8 *C*H_{arom}), 131.81, 132.00 (2 C_q). − ^{15}N{^{1}H} NMR (CD_3OD): δ = −357, −358. − HRMS (FAB$^+$): *m*/*z* calcd. for $C_{30}H_{42}ClN_2O_2Ru$ [M$^+$]: 599.1972; found 599.1979. − $C_{30}H_{43}Cl_3N_2O_2$ (570.048): calcd. C 53.69, H 6.46, N 4.17; found C 53.07, H 6.80, N 3.71.

Enantioselective Reduction of Ketones (General Procedure for [ketone]/[Ru] = 200): A solution of (*p*-cymene)ruthenium(II) chloride dimer (7.7 mg, 0.0125 mmol) and the amino alcohol as a ligand (0.030 mmol) in dry propan-2-ol (5 mL) was heated at 80°C for 1 h under argon. After cooling the mixture to room temperature, it was diluted with propan-2-ol (43.75 mL) and *t*BuOK (1.25 mL, 0.1M in propan-2-ol, 0.125 mmol) was added. The resulting solution was stirred for 30 min before the ketone (5 mmol) was added. The reaction was performed at room temperature under argon for the time indicated and monitored by GC and/or HPLC.

X-ray Structure Analysis of 8: A crystal with the approximate dimensions 0.05 × 0.08 × 0.80 mm was used for data collection on an Enraf−Nonius CAD-4 diffractometer with graphite-monochromated Cu-K_α radiation and ω-2θ scan. A total of 3449 unique reflections was measured within the range −13 < *h* < 12, 0 < *k* < 33, 0 < *l* < 17. Of these, 2964 were above significance level of 5σ(*F*) and were treated as observed. The range of (sinθ)/λ was 0.032−0.625 Å (2.9 < θ < 74.6°). Two reference reflections ([1 2 0], [0 0 10]) were measured hourly and showed no decrease during the 76 h collecting time. Unit-cell parameters were refined by a least square fitting

Table 4. Selected crystallographic data of [Ru{*N*,*N*′-bis[(1*R*,2*S*)-2-hydroxy-1-methyl-2-phenylethyl]-1,2-diaminoethane}{*p*-cymene}Cl]Cl (**8**)

Crystal Data		Data Collection	
Formula	$[C_{30}H_{42}N_2O_2ClRu]^+$ Cl^-	Crystal size [mm]	0.050 × 0.08 × 0.80
M_r	1205.6	Temperature [°C]	−35
Crystal system	orthorhombic	Scan mode	ω−2θ
Space group	$P2_12_12_1$	θ_{min}, θ_{max} [°]	2.9, 74.6
a [Å]	9.378(1)	λ(Cu-K_α) [Å]	1.5418
b [Å]	10.233(5)	Total unique data	3449
c [Å]	30.91(2)	Observed data	2964
Z	4	Structure refinement	
V [Å^3]	2966(2)	Parameter/F_o	0.168
F(000) [e]	1320	*R*	0.057
D_x [g cm^{-3}]	1.42	R_w	0.063
μ(Cu-K_α) [cm^{-1}]	61.6	$(\Delta/\sigma)_{max}$	0.30

procedure using 23 reflections with $80 < 2\theta < 84$. Corrections for Lorentz and polarisation effects were applied. Absorption correction was performed with the program PLATON,[16] following the method of North et al. using Ψ-scans of three reflections, with coefficients in the range of 0.484−0.989.[17] The structure was solved by the PATTY option of the DIRDIF96 program system.[18] After isotopic refinement a ΔF synthesis revealed one peak, which was interpreted as a chloride ion. The hydrogen atoms were calculated. The hydrogen atoms on the alcohol and amine groups were located by Fourier synthesis. Full matrix least-squares refinement on F, anisotropic for the non-hydrogen atoms and isotropic for the hydrogen atoms restraining the latter in such a way that the distance to their carrier remained constant at approximately 1.0 Å, converged to $R = 0.057$, $R_w = 0.063$, $(\Delta/\sigma)\text{max} = 0.30$, $S = 0.93$. A weighting scheme $w = \{10 + 0.01 \times [\sigma(F\text{obs})]^2 + 0.0001/[\sigma(F\text{obs})]\}^{-1}$ was used. The secondary isotropic extinction coefficient refined to Ext = 0.015(6).[19][20] The absolute structure was determined by refining the inverse structure, which converged to $R = 0.068$, $R_w = 0.073$, thus confirming the correct enantiomer. A final difference Fourier map revealed a residual electron density between −1.7 and 1.9 eÅ^{-3} in the vicinity of the heavy atoms. Scattering factors were taken from Cromer and Mann; *International Tables for X-ray Crystallography*.[21] The anomalous scattering of Ru and Cl was taken into account.[22] All calculations were performed with XTAL, unless otherwise stated.[23]

Acknowledgments

We thank the Innovation Oriented Research Programme (IOP-Catalysis) for their financial support of this research. Solvay Pharmaceuticals is acknowledged for the gift of 3-phenylbenzyl bromide. Jan Fraanje is gratefully acknowledged for measuring the crystallographic data. Jan Meine Ernsting is kindly acknowledged for measuring the ^{15}N-NMR data. We are grateful to Wim G. J. de Lange for his help with the HPLC measurements. We thank Murat Ünal for his experimental efforts.

[1] S. Hashiguchi, A. Fujii, J. Takehara, T. Ikariya, R. Noyori, *J. Am. Chem. Soc.* **1995**, *117*, 7562−7563.
[2] A. Fujii, S. Hashiguchi, N. Uematsu, T. Ikariya, R. Noyori, *J. Am. Chem. Soc.* **1996**, *118*, 2521−2522.
[3] J. Takehara, S. Hashiguchi, A. Fujii, I. Shin-ichi, T. Ikariya, R. Noyori, *Chem. Commun.* **1996**, 233−234.
[4] K.-J. Haack, S. Hashiguchi, A. Fujii, T. Ikariya, R. Noyori, *Angew. Chem. Int. Ed. Engl.* **1997**, *36*, 285−288.
[5] R. Noyori, S. Hashiguchi, *Acc. Chem. Res.* **1997**, *30*, 97−102.
[6] M. Palmer, T. Walsgrove, M. Wills, *J. Org. Chem.* **1997**, *62*, 5226−5228.
[7] D. A. Alonso, D. Guijarro, P. Pinho, O. Temme, P. G. Andersson, *J. Org. Chem.* **1998**, *63*, 2749−2751.
[8] S. Gladiali, L. Pinna, G. Delogu, S. De Martin, G. Zassinovich, G. Mestroni, *Tetrahedron: Asymmetry* **1990**, *1*, 635.
[9] M. Bernard, V. Guiral, F. Delbecq, F. Fache, P. Sautet, M. Lemaire, *J. Am. Chem. Soc.* **1998**, *120*, 1441−1446.
[10] H. Nishiyama, H. Sakagushi, T. Nakamura, M. Horihata, M. Kondo, K. Itoh, *Organometallics* **1989**, *8*, 846.
[11] Y. Jiang, Q. Jiang, X. Zhang, *J. Am. Chem. Soc.* **1998**, *120*, 3817−3818.
[12] K. Soai, M. Nishi, Y. Ito, *Chem. Lett.* **1987**, 2405−2406.
[13] N. Juranic, S. Macura, *Inorg. Chim. Acta* **1994**, *217*, 213−215.
[14] J. H. Groen, Ph. D. thesis, University of Amsterdam, The Netherlands, **1998**, 104−105, 144 and references therein.
[15] C. Missling, S. Mihan, K. Polborn, W. Beck, *Chem. Ber.* **1996**, *129*, 331−335.
[16] A. L. Spek, *Acta Cryst.* **1990**, *A46*, C-34.
[17] A. C. T. North, D. C. Phillips, F. Scott Mathews, *Acta Cryst.* **1968**, *A26*, 351−359.
[18] P. T. Beurskens, G. Beurskens, W. P. Bosman, R. de Gelder, S. Garcia-Granda, R. O. Gould, R. Israel, J. M. M. Smits, *The DIRDIF-96 program system*, Crystallography Laboratory, University of Nijmegen, The Netherlands, **1996**.
[19] W. H. Zachariasen, *Acta Cryst.* **1967**, *A23*, 558.
[20] A. C. Larson, "The inclusion of secondary extinction in least-squares refinement of crystal structures". *Crystallographic computing* (Ed.: F. R. Ahmed, S. R. Hall, C. P. Huber), Munksgaard, Copenhagen, **1978**, 291−294.
[21] D. T. Cromer, J. B. Mann, *Acta Cryst.* **1968**, *A24*, 321−324; *International Tables for X-ray Crystallography* **1974**, *Vol. IV*, 55, Birmingham: Kynoch Press.
[22] D. T. Cromer, D. Liberman, *J. Chem. Phys.* **1970**, *53*, 1891.
[23] S. R. Hall, G. S. D King, J. M. Stewart, *Ed. XTAL3.4 User's manual*, University of Western Australia, **1995**, Lamb, Perth.

Received February 23, 1999
[I99059]

Pairing Energy Effects in Cyanide Complexes of $CpCr^{III}$

Rinaldo Poli*[a] and Kevin M. Smith[a]

Keywords: Chromium / Cyanides / Density-functional calculation / Electronic structure / Spin state

The steric and electronic factors responsible for the reactivity differences between CN and Cl complexes of $CpCr^{III}$ were examined by DFT/B3LYP computational techniques. The energy difference between quadruplet and doublet $[CpCr(CN)_2(PH_3)]$, ΔE_{D-Q}, was calculated to be 21.2 kcal mol^{-1} with the LanL2DZ basis set. Although the high-spin configuration is still the ground state for the cyanide complex, the energy gap is 8.7 kcal mol^{-1} less than that found for the corresponding chloride species. The difference between quadruplet $[CpCr(CN)_2(PH_3)]$ and doublet $[CpCr(CN)_2(PH_3)_2]$ less free PH_3, ΔE_{Cr-P}, is also smaller than for the Cl system. The components of ΔE_{Cr-P} for CN and Cl were analyzed by calculating energies at fixed geometries in both spin states, which indicated that the influence of the cyanide group on the pairing energy was more important than changes in Cr–PH_3 bond strength or steric effects.

Introduction

The study of transition metal compounds containing cyanide ligands has experienced a recent resurgence due in large part to the ability of these ligands to form M−CN−M′ bridges.[1] Extending these bridges in one, two, or three dimensions results in novel materials often possessing microporous structures and interesting magnetic properties.[2] As an alternative to homoleptic cyanometalates, anionic $[CpM(CN)_n]^-$ complexes have also been investigated in which the Cp or Cp* ligand serves to enhance the overall inertness of the complex as well as to limit polymerization.[3][4]

We have recently examined the reactivity of cyanide complexes of $CpCr^{III}$ as part of our ongoing investigation of spin-state effects in organometallic chemistry.[5] Cyanide ligands confer a greater stability on the resulting highly coordinated monometallic compounds than the halide ligands on the corresponding, relatively unsaturated analogues. For example, in the case of complexes of $CpMo^{IV}$, the cyanometalate exists as the 18-electron dianion,[6] $[CpMo(CN)_5]^{2-}$, while with the chloride ion the 16-electron monoanion,[7] $[CpMoCl_4]^-$, is observed. The same trend between CN and Cl ligation is observed for $CpCr^{III}$ complexes.[8] For cyanide, equilibrium concentrations of the 17-electron spin-doublet $[CpCrL_4]$ species $[CpCr(CN)_2(PR_3)_2]$ and $[CpCr(CN)_4]^{2-}$ have been detected in solution by ESR spectroscopy,[9] whereas similar 17-electron species were *not* spectroscopically observed for the analogous chloride complex.[10] A kinetic and theoretical investigation of the PR_3 exchange reactions for $[CpCrCl_2(PR_3)]$ complexes demonstrated that, although exchange proceeds by an associative pathway, the reaction proceeds solely on the quadruplet spin hypersurface by an S_N2-type mechanism.[11] Previously, density functional theory (DFT) calculations have been used to compare the relative energies of $[CpCrX_2(PH_3)_n]$ (X = Cl, CH_3; n = 1, 2) and $[CpMoCl_2(PH_3)_n]$ systems in the doublet and quadruplet spin states.[12] In this study, DFT calculations were used to determine the relative importance of the possible factors which contribute to the anomalous stability of the 17-electron doublet CN species relative to the Cl analogues. Possible factors which we have previously considered include: (a) steric considerations (since CN is smaller than Cl), (b) the Cr−L bond strength (the relative electron-withdrawing ability of CN could increase the relative strength of the additional Cr−PR_3 bond in the 17-electron species), (c) changes in ΔE_{D-Q} (by modifying the orbital splitting and/or the pairing energy, CN could influence the relative stabilities of the doublet and quadruplet spin states).[9]

Results and Discussion

Optimized LanL2DZ Geometries and Energies

The geometries of doublet $[CpCr(CN)_2(PH_3)_2]$, and doublet and quadruplet $[CpCr(CN)_2(PH_3)]$ were optimized in the C_s symmetry with DFT using the three-parameter form of the Becke, Lee, Yang and Parr functional (B3LYP)[13a] and the LanL2DZ basis set.[13b−d] The bond lengths and angles are shown in Table 1. A comparison of the two 15-electron monophosphane compounds reveals that the doublet complex has slightly shorter bond lengths and deviates further from an idealized three-legged piano-stool structure.[14] The relative difference between the two geometries is comparatively small and is much less pronounced than the difference between doublet and quadruplet $[CpCrCl_2(PH_3)]$.[11,12b]

The relative energies calculated for the $CpCr^{III}$ cyanide compounds are depicted in Figure 1. As expected, based on 15-electron $CpCr^{III}$ monophosphane compounds containing halide or alkyl groups,[15] the quadruplet state is favored over the doublet. In the present case, the high-spin configuration is 21.2 kcal mol^{-1} more stable than the ΔE_{D-Q} value

[a] Laboratoire de Synthèse et d′Electrosynthèse Organométallique, Faculté des Sciences "Gabriel", Université de Bourgogne, 6 Boulevard Gabriel, F-21100 Dijon, France
Fax: (internat.) + 33-380/396098
E-mail: Rinaldo.Poli@u-bourgogne.fr

 © WILEY-VCH Verlag GmbH, D-69451 Weinheim, 1999 1434−1948/99/1212−2343 $ 17.50+.50/0

Table 1. Optimized geometries for doublet and quadruplet $[CpCr(CN)_2(PH_3)_n]$ (n = 1, 2)[a]

Structural Parameter[b]	$[CpCr(CN)_2(PH_3)_2]$ doublet	$[CpCr(CN)_2(PH_3)]$ doublet	$[CpCr(CN)_2(PH_3)]$ quadruplet
CNT−Cr	1.918	1.958	1.979
Cr−CN	2.004	1.986	1.993
Cr−P	2.470	2.495	2.521
CNT−Cr−CN	116.50	121.44	122.72
CNT−Cr−P	115.58	129.30	128.00
NC−Cr−P	78.39	85.53	87.23
NC−Cr−CN	126.98	104.06	98.92
NC−Cr−CNT−P	90.6	112.5	115.4
NC−Cr−CNT−CN	178.8	135.0	129.2

[a] Bond lengths in Å and angles in degrees. − [b] CNT = center of gravity of the Cp ring.

of 29.9 kcal mol^{-1} previously calculated for $[CpCrCl_2(PH_3)]$ with the same functional and basis set.[11] Similar differences between cyanide and chloride complexes are observed when comparing the energy of doublet $[CpCrX_2(PH_3)_2]$ to the sum of quadruplet $[CpCrX_2(PH_3)]$ and free PH_3. This energy difference, labelled ΔE_{Cr-P} in Figure 1, provides an indication of how readily the quadruplet species will accommodate another *phosphane* ligand. In qualitative agreement with experimental results, ΔE_{Cr-P} is smaller for X = CN (10.3 kcal mol^{-1}) than for X = Cl (ΔE_{Cr-P} = 21.2 kcal mol^{-1}).

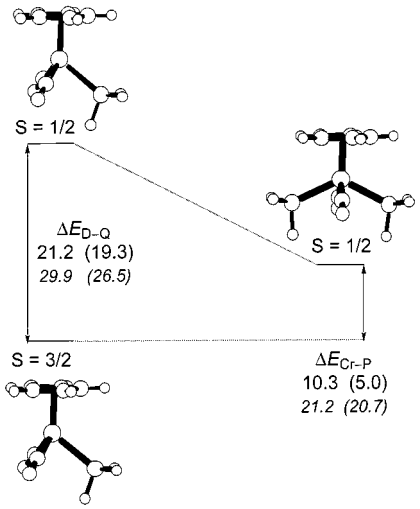


Figure 1. Relative energies of doublet and quadruplet $[CpCr(CN)_2(PH_3)_n]$ (n = 1, 2); energies calculated at the B3LYP/LanL2DZ level of theory, with B3LYP/6−311+G(2d,2p) values indicated in parentheses, and the corresponding $[CpCrCl_2(PH_3)_n]$ energies in italics

Larger Basis Set Calculations

Recent work with $[CpCo(PH_3)_n]$ complexes (n = 1, 2) has showed the importance of the size of the basis set on $[ML_n]$ ligand dissociation energies.[16] Smaller basis sets tend to underestimate metal−ligand bond strengths, thereby causing the relative stability of unsaturated compounds to be overstated. To account for this effect, the energies of the $[CpCr(CN)_2(PH_3)_n]$ compounds optimized at the B3LYP/LanL2DZ level were recalculated with the larger 6−311+G(2d,2p) basis set; the resulting energies are indicated in parentheses in Figure 1. The energy difference between the quadruplet and doublet 15-electron compounds decreased slightly to 19.3 kcal mol^{-1}, and the expected decrease in ΔE_{Cr-P} was also observed, from 10.3 to 5.0 kcal mol^{-1}. For comparison, the B3LYP/LanL2DZ geometries previously obtained for $[CpCrCl_2(PH_3)_n]$ were used to recalculate their energies at the B3LYP/6−311+G(2d,2p) level, and the resulting values are also displayed in Figure 1.

Fixed Geometry Calculations

In order to analyze the various components that make up ΔE_{Cr-P}, single-point calculations were performed at the B3LYP/LanL2DZ level as illustrated in Figure 2. One PH_3 ligand was removed from the optimized structure of doublet $[CpCr(CN)_2(PH_3)_2]$ without altering any of the other structural parameters. The single-point calculations on these complexes with one or three unpaired electrons yield energies for the doublet-fixed and quadruplet-fixed complexes, respectively, as indicated in Table 2. The Bond Energy Term (BET) is equal to the difference between the 17-electron doublet-optimized and 15-electron doublet-fixed structures plus free PH_3, and provides an indication of the $Cr-PH_3$ bond strength without additional factors due to spin-state change. Since the doublet-fixed and quadruplet-fixed energies are based on exactly the same geometry, the difference in energy between these species reflects the Pairing Energy (PE). The Relaxation Energy (RE), obtained from the difference between quadruplet-fixed and quadruplet-optimized energies, accounts for the reorganization required for the 15-electron species to accommodate an additional phosphane ligand, and is directly related to the steric bulk of the adjacent cyanide ligands. These energies were also calculated for the chloride species, and the values obtained are collected in Table 2.

Direct comparison of the factors that contribute to ΔE_{Cr-P} for the two $[CpCrX_2(PH_3)_n]$ systems helps identify the ligand properties responsible for the observed experimental differences between the cyanide and chloride compounds. The BET is only slightly greater for X = CN than for X = Cl, a variation which might be attributable to the

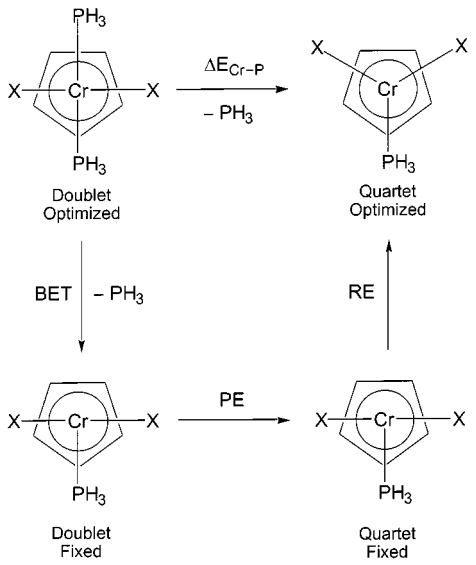


Figure 2. Schematic representation of fixed and optimized geometries used for B3LYP/LanL2DZ energy calculations of $[CpCrX_2(PH_3)_n]$ (X = CN, Cl; n = 1, 2)

Table 2. Relative energies of $[CpCrX_2(PH_3)_n]$ (X = CN, Cl; n = 1, 2) complexes in optimized and fixed geometries[a]

	$[CpCr(CN)_2(PH_3)_n]$	$[CpCrCl_2(PH_3)_n]$
Bond Energy Term	20.2	17.1
Pairing Energy	−17.1	−25.5
Relaxation Energy	−13.4	−12.8

[a] ΔE (in kcal mol^{-1}) calculated at the B3LYP/LanL2DZ level of theory.

different electron-withdrawing capacity of the two X ligands which affects the ability of the metal center to accommodate the strong σ-donor phosphane ligand. The anticipated difference in steric requirements for CN vs. Cl apparently does not play an appreciable role, since the RE is roughly the same in each case. The key factor seems to be the ability of the cyanide ligand to facilitate the electron pairing required to cross over from the quadruplet-spin to the doublet-spin potential energy surface, as reflected in the PE which is −17.1 kcal mol^{-1} for X = CN in contrast to −25.5 kcal mol^{-1} for X = Cl. The same trend is seen in the values obtained for ΔE_{D-Q} in the two systems.

The relative energies of the frontier orbitals for the $[CpCrX_2(PH_3)]$ (X = CN, Cl) fixed-doublet and fixed-quadruplet species are shown in Figure 3. While it is imprudent to assign too much physical significance to the Kohn-Sham orbitals arising from the current DFT calculations,[17] the qualitative trends in orbital energies appear to support our interpretation. The significantly greater energy gap for X = CN than for X = Cl between the highest and lowest energy frontier orbitals for both spin states accounts for the enhanced stability of the doublet spin-state for the cyanide complex. As well as influencing the orbital splitting, the CN group may also favor the doublet species by decreasing the pairing energy, consistent with the known large nephelauxetic effect of the cyanide ligand.[18]

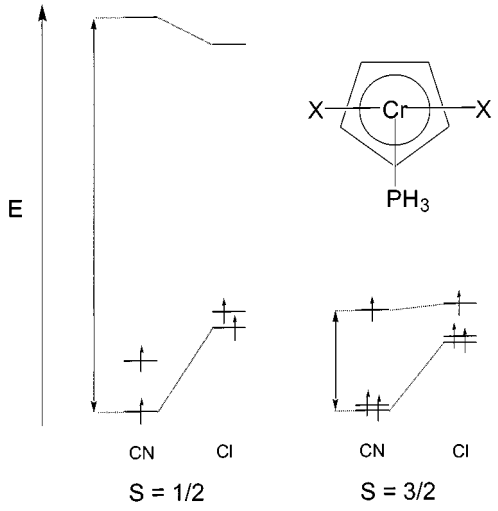


Figure 3. Orbital energies (α orbitals) and occupancies of fixed geometry $[CpCrX_2(PH_3)]$ (X = CN, Cl) species in doublet and quadruplet spin states

Conclusions

Several possible explanations were initially forwarded to rationalize the observation of $[CpCr(CN)_2(PR_3)_2]$ complexes by EPR although the corresponding Cl complexes were not detected. Calculations at the DFT/B3LYP level indicate that the steric differences and variation in Cr−P bond strength are not adequate to account for this discrepancy. The observed differences are best explained by the relative ability of the CN group to encourage spin pairing, as demonstrated by the smaller ΔE_{D-Q} than in the chloride system for both fixed and optimized geometries.

Experimental Section

General Remarks: All calculations were performed with GAUSSIAN 94[19] on an SGI Origin 200 workstation. The geometries of the $[CpCrX_2(PH_3)_2]$ and $[CpCrX_2(PH_3)]$ species and free PH_3 were optimized with B3LYP,[13a] a DFT type of calculation, employing the LanL2DZ basis set. The LanL2DZ basis set includes both Dunning and Hay's D95 sets for H and C and the core potential sets of Hay and Wadt for the heavy atoms.[13b–d] Electrons outside the core were all those for H and C, the 3s and 3p electrons for P, and the 3s, 3p, 3d and 4s electrons for Cr. All geometries were optimized at the B3LYP/LanL2DZ level with imposed C_s symmetry. The B3LYP energy calculations were performed separately with both the LanL2DZ basis set and the larger 6−311+G(2d,2p) basis set, which has two sets of polarization functions on all atoms including two f-sets on the Cr, and also diffuse functions.

The mean value of the first-order electronic wavefunction, which is not an exact eigenstate of S^2 for unrestricted calculations on the open shell systems, was considered suitable for unambiguous identification of the spin state. Spin contamination was carefully monitored and the value of $<S^2>$ for the unrestricted B3LYP (UB3LYP) calculations on the $[CpCrX_2(PH_3)_n]$ species indicated minor

spin contamination in most cases. With the exception of doublet $[CpCr(CN)_2(PH_3)]$, $<S^2>$ was in the range of 0.7651 to 0.7783 for doublet species, and 3.8196 to 3.8692 for quadruplets. As previously observed for doublet $[CpCr(CH_3)_2(PH_3)]$,[12b] the 15-electron doublet cyanide complex exhibited anomalously large $<S^2>$ values: 1.7257 to 1.5558 for fixed and optimized geometries with both basis sets. The energies shown in the Results and Discussion section correspond to UB3LYP calculations, and the frontier orbital energies are those of the occupied (α) orbitals.

Acknowledgments

R. P. thanks the Région Bourgogne for supporting this research, and K. M. S. thanks the European Commission for a TMR Marie Curie Postdoctoral Fellowship.

[1] H. Vahrenkamp, A. Geiß, G. N. Richardson, *J. Chem. Soc., Dalton Trans.* **1997**, 3643−3651.
[2] K. R. Dunbar, R. A. Heintz, *Prog. Inorg. Chem.* **1997**, *45*, 283−391.
[3] [3a] K. K. Klausmeyer, T. B. Rauchfuss, S. R. Wilson, *Angew. Chem.* **1998**, *110*, 1808−1810; *Angew. Chem. Int. Ed. Engl.* **1998**, *37*, 1694−1696. − [3b] S. M. Contakes, K. K. Klausmeyer, R. M. Milberg, S. R. Wilson, T. B. Rauchfuss, *Organometallics* **1998**, *17*, 3633−3635. − [3c] K. K. Klausmeyer, S. R. Wilson, T. B. Rauchfuss, *J. Am. Chem. Soc.* **1999**, *121*, 2705−2711.
[4] For a leading reference for other cyanide CpM-containing complexes, see W. P. Fehlhammer, M. Fritz, *Chem. Rev.* **1993**, *93*, 1243−1280.
[5] [5a] R. Poli, *Chem. Rev.* **1996**, *96*, 2135−2204. − [5b] R. Poli, *Acc. Chem. Res.* **1997**, *30*, 494−501.
[6] J. A. Dineen, P. L. Pauson, *J. Organomet. Chem*. **1974**, *71*, 91−96.
[7] M. Kilner, C. Midcalf, *J. Chem. Soc. (A)* **1971**, 292−297.
[8] Diamagnetic, 18-electron CpCr(CN)-containing compounds have long been known for Cr(0): [8a] T. S. Piper, G. Wilkinson, *J. Inorg. Nucl. Chem.* **1956**, *2*, 38−45. − [8b] H. Brunner, *Chem. Ber.* **1969**, *102*, 305−309.
[9] S. P. Mattamana, R. Poli, *Organometallics* **1997**, *16*, 2427−2433.
[10] J. C. Fettinger, S. P. Mattamana, R. Poli, R. D. Rogers *Organometallics* **1996**, *15*, 4211−4222.
[11] E. Collange, D. Duret, R. Poli, *J. Chem. Soc., Dalton Trans.* **1999**, 875−579.
[12] [12a] I. Cacelli, D. W. Keogh, R. Poli, A. Rizzo, *New. J. Chem.* **1997**, *21*, 133−135. − [12b] I. Cacelli, D. W. Keogh, R. Poli, A. Rizzo, *J. Phys. Chem. A* **1997**, *101*, 9801−9812.
[13] [13a] A. D. Becke, *J. Chem. Phys.* **1993**, *98*, 5648−5652. − [13b] P. J. Hay, W. R. Wadt, *J. Chem. Phys.* **1985**, *82*, 270−283. − [13c] W. R. Wadt, P. J. Hay, *J. Chem. Phys.* **1985**, *82*, 284−298. − [13d] P. J. Hay, W. R. Wadt, *J. Chem. Phys.* **1985**, *82*, 299−310.
[14] For an idealized $[CpML_3]$ geometry, L−M−L = 90°, CNT−M−L = 125.26°, and L−M−CNT−L = 120°.
[15] [15a] A. Grohmann, F. H. Köhler, G. Müller, H. Zeh, *Chem. Ber.* **1989**, *122*, 897−899. − [15b] B. J. Thomas, S. K. Noh, G. K. Schulte, S. C. Sendlinger, K. H. Theopold, *J. Am. Chem. Soc*. **1991**, *113*, 893−902. − [15c] K. H. Theopold, *Eur. J. Inorg. Chem*. **1998**, 15−24. − [15d] M. Bender-Gresse, E. Collange, R. Poli, S. P. Mattamana, *Polyhedron*, **1998**, *17*, 1115−1119.
[16] R. Poli, K. M. Smith, *Eur. J. Inorg. Chem* **1999**, 877−880.
[17] R. Stowasser, R. Hoffmann, *J. Am. Chem. Soc.* **1999**, *121*, 3414−3420.
[18] T. P. Hanusa, D. J. Burkey, in *Encyclopedia of Inorganic Chemistry* (Ed.: R. B. King), Wiley, New York, **1994**, volume 2, p. 943−949.
[19] M. J. Frisch, G. W. Trucks, H. B. Schlegel, P. M. W. Gill, B. G. Johnson, M. A. Robb, J. R. Cheesman, T. A. Kieth, G. A. Petersson, J. A. Montgomery, K. Raghavarchi, M. A. Al-Laham, V. G. Zakrzewski, J. V. Ortiz, J. B. Foreman, J. Cioslowski, B. B. Stefanov, A. Nanayakkara, M. Challacombe, C. Y. Peng, P. Y. Ayalla, W. Chen, M. W. Wong, J. L. Andres, E. S. Replogle, R. Gomperts, R. L. Martin, D. J. Fox, J. S. Binkley, D. J. Defrees, J. Baker, J. P. Stewart, M. Head-Gordon, C. Gonzales, J. A. Pople, *Gaussian 94, Revision E.1*, Gaussian Inc., Pittsburgh, PA, **1995**.

Received April 8, 1999
[I99124]

Homogeneous and Supported Copper Complexes of Cyclic and Open-Chain Polynitrogenated Ligands as Catalysts of Cyclopropanation Reactions

F. Adrián,[a] M. I. Burguete,[a] J. M. Fraile,[b] J. I. García,[b] J. García,[b] E. García-España,[c] S. V. Luis,*[a] J. A. Mayoral,*[b] A. J. Royo,[a,b] and M. C. Sánchez[b]

Keywords: Cyclopropanation / Copper / N ligands / Macrocycles / Supported catalysts

Cu^{I} and Cu^{II} complexes of cyclic and open-chain polyaza compounds have been tested as catalysts in the benchmark cyclopropanation reaction of styrene with ethyl diazoacetate. In general, only small amounts of copper are needed to promote the reaction. The catalytic activity depends on the structure of the ligand, e.g. amine–amides are more efficient than polyamines, and on the oxidation state of copper, Cu^{II} being more active than Cu^{I}. Given that Cu^{I} is the active species, these changes of behavior must be related to the stabilities of the complexes. The nature of the counterion also has a noticeable influence on the catalytic activity, the role of which is discussed. XAS measurements suggest the formation of oligomeric species. Some of the chiral ligands lead to small enantiomeric excesses. Open-chain ligands can easily be supported on organic polymers and their complexes can be used as catalysts. Furthermore, cyclic and acyclic complexes can be supported on clays by cation exchange and the solids obtained tend to promote the reaction with a decrease in the *trans*/*cis* ratio.

Introduction

The search for new ligands suitable for incorporation into homogeneous and heterogeneous catalysts for organic reactions is a field of considerable interest. As far as possible, such ligands should be easy to prepare and they should be amenable to facile chemical modification so as to obtain chiral derivatives from simple, accessible starting materials. On the other hand, their incorporation into a heterogeneous support has to be easily accomplished with minimum structural modification. In this regard, polynitrogenated compounds fulfil such requirements. These ligands can selectively bind metal cations and can distinguish between oxidation states.[1] They can be obtained as open-chain or macrocyclic compounds, and also in chiral forms by the incorporation of chiral diamines, amines, or amino acid derivatives. Furthermore, the chiral auxiliaries can be incorporated at different sites in the molecules leading to ligands with different symmetries. In particular, they can easily be obtained with C_2 symmetry.[2] They can also be supported on organic or inorganic materials, which opens up the possibility of using their complexes as solid catalysts in the fine chemicals industry.[3] The chiral compounds would, of course, open the way to chiral heterogeneous catalysts.[4] Given the presence of nitrogen atoms related by the symmetry elements of the molecule, they can be grafted onto a flexible support without losing their symmetry.[5] It is important to note that in a significant number of examples of heterogeneous chiral catalysts, the symmetry of the chiral ligand is lost when it is grafted onto the support, which may be one of the reasons for the lower efficiency of these catalysts in inducing asymmetry.[4]

Porphyrin complexes have been described as catalysts in several reactions,[6] including cyclopropanations.[7] Complexes of other cyclic polynitrogenated systems have also been used.[8] Since open-chain polynitrogenated compounds have not been used in this context, we felt that it would be interesting to compare several of these ligands (cyclic and open-chain, non-chiral and chiral, amines and amides, unsupported and supported) in a benchmark reaction. In this paper, we present the results obtained using copper complexes of these polyaza derivatives (Figure 1) as catalysts of the cyclopropanation reaction between styrene and ethyl diazoacetate. The effect of the oxidation state of the copper and the nature of the counterion are also analyzed.

[a] Departamento de Química Inorgánica y Orgánica,
E.S.T.C.E, Universitat Jaume I,
P. O. Box 224, E-12080 Castellón, Spain
Fax: (internat.) + 34-964/728214
E-mail: luiss@qio.uji.es
[b] Facultad de Ciencias,
Instituto de Ciencia de Materiales de Aragón,
Universidad de Zaragoza - C.S.I.C.,
E-50009 Zaragoza, Spain
E-mail: mayoral@posta.unizar.es
[c] Departamento de Química Inorgánica,
Universidad de Valencia,
E-46100 Burjassot (Valencia), Spain
E-mail: Enrique.Garcia-Es@uv.es

Results and Discussion

Polyamines as Ligands

We first tested a cyclic ligand, 14,15,17,18-tetramethyl-2,5,8,11-tetraaza[12]paracyclophane (**L_1**, Figure 1) since ligands of this type have been show to stabilize Cu^{I} with respect to its disproportionation into Cu^{II} and Cu^{0}.[10] We prepared its Cu^{I} complex in situ and used it as a catalyst in the cyclopropanation reaction of styrene (**1**) with ethyl diazoacetate (**2**) (Scheme 1). The results obtained are presented in Table 1.

 © WILEY-VCH Verlag GmbH, D-69451 Weinheim, 1999 1434–1948/99/1212–2347 $ 17.50+.50/0

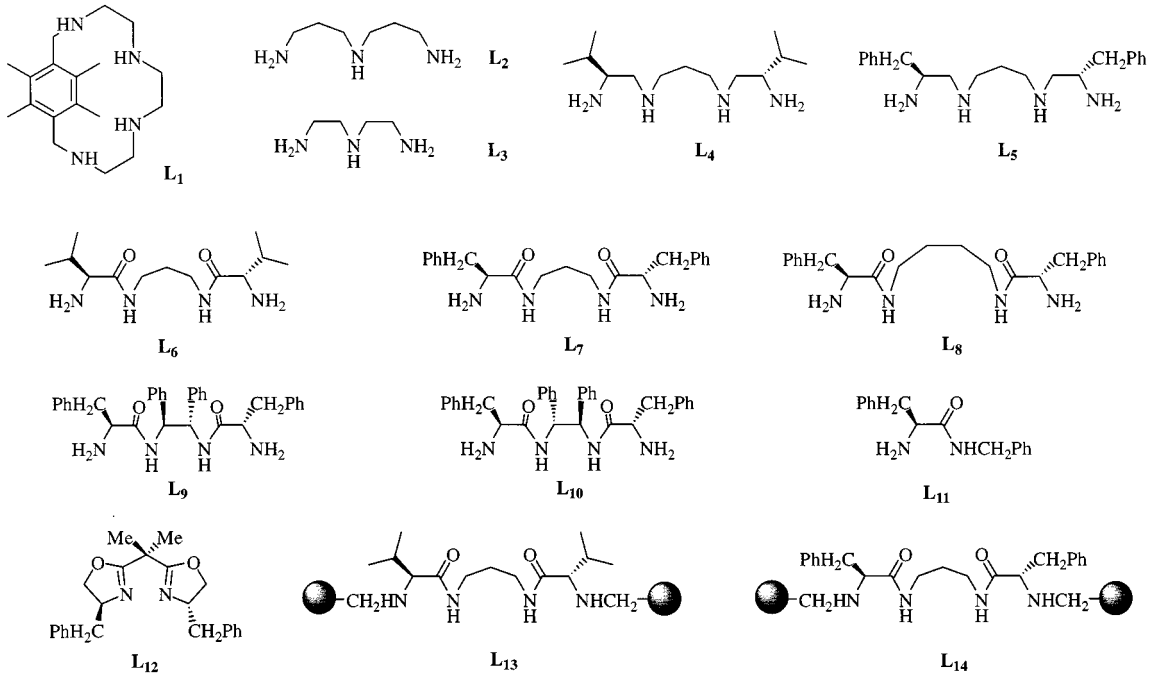
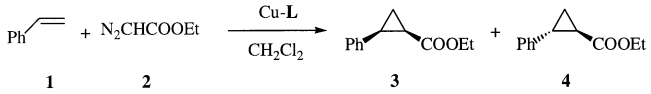


Figure 1. Ligands used in this work



Scheme 1

Table 1. Results obtained from the reaction of styrene (**1**) with ethyl diazoacetate (**2**) promoted by CuOTf−$\mathbf{L_1}$ complexes in CH_2Cl_2 at 25 °C[a]

Entry	Cu/$\mathbf{L_1}$	Cu/styrene (%)	t (h)[b]	% yield[c]	**4**:**3**[c]
1	−	0.1	1.5	26	2.6
2			2.0	30	2.6
3	1:1.1	0.1	2.2	−	−
4			2.5	4	−
5			6.0	30	2.3
6	1:0.75	0.1	1.2	−	−
7			1.3	4	−
8			4.0	28	2.2
9	1:0.5	0.1	1.0	−	−
10			1.1	4	−
11			3.5	31	2.3
12	1:0.25	0.1	0.75	11	2.3
13			3.0	32	2.4
14	1:1.1	1	1.45	38	2.3

[a] Reactions carried out under argon atmosphere using a twofold excess of **1**. − [b] **2** was slowly added over a period of 45 min.; the time is given from the beginning of the addition. − [c] Determined by gas chromatography.

Copper(I) compounds are known to be very active catalysts in the cyclopropanation of alkenes with diazo compounds.[9] However, addition of the ligand in an almost equimolecular ratio results in the appearance of a period of induction. After this period, the color of the solution changes to yellow and the reaction ultimately yields a final result comparable to that obtained with CuOTf. This period of induction is reduced when the ligand/copper molar ratio is decreased. The addition of an excess of the ligand is of little consequence. Such an induction period is only observed when the complex is used in a ratio of 0.001:1 with respect to the styrene and is no longer seen when it is used in a ratio of 0.01:1 (see entry 14, Table 1). This result indicates the formation of a stable complex of the ligand with Cu^I,[10] which reduces the rate of formation of the reactive copper−carbene intermediate. The most rational explanation for this behavior is the formation of aggregates of the Cu^I-L_1 complexes, in which the copper cation is much less accessible for the interaction with the reagents to give the active metal−carbene species. The formation of aggregates has recently been reported to hamper the hydrolytic catalytic activity of some copper−polyamine complexes.[14] A key feature of tetraaza[*n*]paracyclophanes is that a maximum of three of the four nitrogen atoms can be simultaneously coordinated to a metal cation. This leaves a noncoordinated benzylic nitrogen atom, which can interact with another metal cation (see structure **5**, Figure 2), thereby favoring the formation of complex aggregates. This is particularly the case when the solvent is changed from water to a less polar medium such as CH_2Cl_2. The formation of species such as **5** has been observed in the solid state and has also been inferred from the results of NMR spectroscopic studies.[11][12] As a matter of fact, it has been shown that, in water, tetraaza[12]paracyclophanes such as $\mathbf{L_1}$ can form dinuclear copper(II) complexes (see **6**, Figure 2) which, at least in the solid state, are polymerically associated.[13] The involvement of complexes of the general structure **6** accounts for the fact that even at low $\mathbf{L_1}$/Cu ratios (≈0.5) (entry 9, Table 1) the induction period persists. Only below this ratio is some free copper available and hence the induction period drastically decreases (entry 12, Table 1).

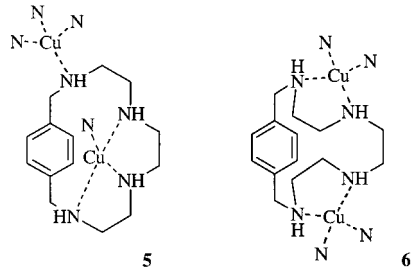


Figure 2. Binuclear structural patterns found for tetraaza[*n*]paracyclophanes

In order to improve the yields, we added a fresh aliquot of ethyl diazoacetate (**2**) (0.5 mol for each mol of remaining styrene) (Table 2). Surprisingly, the period of induction was no longer observed after the second addition. This kinetic behavior is characteristic of product-accelerated reactions, in which a side product, formed via a non-catalytic pathway, is the species involved. In this context, we have to consider that decomposition of ethyl diazoacetate gives rise to the formation of coordinating species, namely ethyl fumarate and maleate. These by-products are produced in large excess with respect to $\mathbf{L_1}$ and, once formed, should favor disruption of aggregates through coordination to the metal cation. Displacement of these kinetically labile ligands from the coordination sphere of the metal by the carbene-forming species thus becomes easier and so the induction period is much decreased or is not seen at all. To check this hypothesis, we stirred a solution of CuOTf and $\mathbf{L_1}$ for 3 h in CH_2Cl_2 with 50 equiv. of ethyl acetate (the same ratio of ethyl diazoacetate used in the reactions) prior to addition of the ethyl diazoacetate. Following this treatment, the period of induction was not seen (entry 5, Table 2).

Table 2. Effect of a second addition of ethyl diazoacetate (**2**) and the addition of ethyl acetate

Entry	Cu/L_1	Cu/styrene (%)	*t* (h)	% yield	**4**:**3**
1	1:1.1	0.1	24.0[a]	30	2.3
2			24.5	35	2.3
3			26.0	54	2.3
4			31.0	57	2.3
5	1:1.1	0.1[b]	0.75	4	–
6			2.0	20	2.3
7			16.0	28	2.4

[a] After this time, an additional amount of **2** was added over a period of 45 min. – [b] The Cu–L_1 complex was stirred with ethyl acetate prior to use.

In order to study the influence of ligand topology on the catalyst activity, we tested several open-chain tri- and tetraamines ($\mathbf{L_2}$–$\mathbf{L_5}$). The results obtained (Table 3) show that the effect of these ligands is to increase the period of induction compared to that observed using $\mathbf{L_1}$ under the same conditions. Furthermore, this period is longer with triamines, and in particular with $\mathbf{L_3}$ (entries 5–6, Table 3). Again, the formation of aggregates has to be considered. Clearly, this phenomenon has to be more important for those ligands ($\mathbf{L_2}$ and $\mathbf{L_3}$) providing a smaller number of nitrogen donor atoms. The presence of bulky C-substituents ($\mathbf{L_4}$ and $\mathbf{L_5}$) should also be reflected in a decreased tendency for aggregation.

Although the design of efficient chiral auxiliaries was not the main aim of this work, the enantiomeric excesses achieved in the reactions using the chiral ligands $\mathbf{L_4}$ and $\mathbf{L_5}$ were examined. In neither case was any asymmetric induction observed.

Table 3. Results obtained in the reactions promoted by CuOTf–linear polyamine ($\mathbf{L_2}$–$\mathbf{L_5}$) = 1:1.1 complexes, using 0.1% catalyst with respect to styrene in CH_2Cl_2 at 25 °C

Entry	Ligand	*t* (h)	% yield	**4**:**3**	% *ee* (**3**)[a]	% *ee* (**4**)[a]
1	$\mathbf{L_2}$	24	–	–	–	–
2		27	23	2.1	–	–
3		96	26	2.2	–	–
4	$\mathbf{L_3}$	96[b]	–	–	–	–
5		98	–	–	–	–
6		117	29	2.2	–	–
7	$\mathbf{L_4}$	4	–	–	–	–
8		8	27	2.5	0	0
9		23	33	2.5	0	0
10	$\mathbf{L_5}$	5	–	–	–	–
11		8	11	2.3	0	0
12		23	36	2.3	0	0

[a] Determined by gas chromatography using a chiral stationary phase. – [b] After this time, the reaction mixture was heated under reflux.

Amides as Ligands

A further structural change was considered by using the diamides $\mathbf{L_6}$–$\mathbf{L_{10}}$. The results obtained with $\mathbf{L_6}$ and $\mathbf{L_7}$, when compared to those with $\mathbf{L_4}$ and $\mathbf{L_5}$ (entries 2 and 6, Table 4 *vs.* entries 8 and 11, Table 3), show that the presence of carbonyl groups leads to a decrease in the induction period and, in the case of the (*S*)-phenylalanine derivative ($\mathbf{L_7}$), to a decrease in the *trans*/*cis* ratio and a measurable enantioselectivity. These data suggest that, for $\mathbf{L_6}$ and $\mathbf{L_7}$, the changes in geometry and donor characteristics associated with the presence of the amide functionalities lead to an increased rate of copper–carbene intermediate formation.

Table 4. Results obtained in the reactions promoted by CuOTf–linear amide–amine ($\mathbf{L_6}$–$\mathbf{L_{10}}$) = 1:1.1 complexes, using 0.1% catalyst with respect to styrene in CH_2Cl_2 at 25 °C

Entry	Ligand	*t* (h)	% yield	**4**:**3**	% *ee* (**3**)[a]	% *ee* (**4**)[a]
1	$\mathbf{L_6}$	3.0	–	–	–	–
2		4.0	16	2.1	0	0
3		6.5	31	2.2	0	0
4		24.0	29	2.1	0	0
5	$\mathbf{L_7}$	2.5	–	–	–	–
6		3.5	11	1.8	12	8
7		6.5	29	1.8	12	8
8		24.0	33	1.8	12	8
9	$\mathbf{L_8}$	1.0	–	–	–	–
10		2.0	25	1.8	11	7
11		3.0	29	1.8	11	7
12	$\mathbf{L_9}$	0.75	13	1.8	0	0
13		1.25	30	1.8	0	0
14	$\mathbf{L_{10}}$	24.0	–	–	–	–
15		48.0	24	2.2	0	0

[a] In cases with asymmetric induction, (1*R*)-cycloadducts are preferably obtained.

In comparison to $\mathbf{L_6}$ and $\mathbf{L_7}$, the period of induction is clearly reduced with $\mathbf{L_8}$, which has a longer bridge, but the *trans*/*cis* ratio and enantioselectivity remain unchanged. Two diastereomeric ligands ($\mathbf{L_9}$ and $\mathbf{L_{10}}$) were also tested and showed very different behaviors. Whereas the reaction is very fast with $\mathbf{L_9}$, use of $\mathbf{L_{10}}$ leads to an extremely long period of induction. Clearly, the *cis,trans,cis*-arrangement of the substituents in complexed $\mathbf{L_9}$ disfavors aggregation, while the opposite is true for the all-*trans* diastereomer formed from $\mathbf{L_{10}}$, for which the access for the formation of the carbene−copper species should again be restricted. The introduction of chirality in the central bridge is always detrimental for the enantioselectivity.

The Effect of the Oxidation State of Copper: The Use of $Cu^{I}L$ vs. $Cu^{II}L$ Complexes

It is known that Cu^{I} is the active species in these reactions and that Cu^{II} is reduced to Cu^{I} in the presence of diazoacetate.[9] Thus, Cu^{II} complexes can also be used as catalysts. In view of this, we tested the cyclic ligand ($\mathbf{L_1}$), two open-chain polyamines ($\mathbf{L_3}$ and $\mathbf{L_5}$), and an amide-containing ligand ($\mathbf{L_7}$) in the same reaction using $Cu(OTf)_2$. The results obtained (entry 1, Table 5) show that the induction period with $\mathbf{L_1}$ decreases and that it is very short even on halving the amount of catalyst (entries 3−4, Table 5). The induction period is no longer seen with $\mathbf{L_5}$ and $\mathbf{L_7}$, but persists with $\mathbf{L_3}$. Therefore, other than in the case of $\mathbf{L_3}$, the metal center in the Cu^{II} complexes is much more accessible to the additional exogenous ligands. Once Cu^{II} is reduced to Cu^{I}, i.e. in the presence of diazoacetate, the strongly active yellow complex is immediately formed.

Table 5. Results obtained in the reactions promoted by $Cu(OTf)_2$−L = 1:1.1 complexes in CH_2Cl_2 at 25 °C

Entry	Ligand	Cu/**1** (%)	*t* (h)	% yield	**4**:**3**	% *ee* (**3**)[a]	% *ee* (**4**)[a]
1	$\mathbf{L_1}$	0.1	1.0	21	2.0	–	–
2			1.75	33	2.1	–	–
3	$\mathbf{L_1}$	0.05	1.3	6	2.4	–	–
4			2.5	15	2.3	–	–
5			24.0	25	2.1	–	–
6	$\mathbf{L_3}$	0.1	26.0	–	–	–	–
7			29.5	23	2.1	–	–
8	$\mathbf{L_5}$	0.1	1.0	16	2.1	–	–
9			2.5	26	2.1	–	–
10	$\mathbf{L_7}$	0.1	0.75	18	1.8	10	6
11			2.5	29	1.8	10	6
12	$\mathbf{L_{11}}$	0.1	0.75	19	1.7	10	6
13			1.5	33	1.7	10	6

[a] In cases with asymmetric induction, (1*R*)-cycloadducts are preferably obtained.

In the reactions promoted by $\mathbf{L_7}$−Cu^{I} and Cu^{II} complexes, the *trans*/*cis* ratios and enantioselectivities are the same, and so it would seem reasonable to assume that the reactive intermediate is the same $\mathbf{L_7}$−Cu^{I} carbene complex.

It can be concluded that the only difference between Cu^{I} and Cu^{II} is the decrease in the induction period, whereas the selectivities and the relative catalytic activities of the different complexes are the same.

Structural XAS/EXAFS Studies

In order to gain further insight into the structural characteristics of these complexes, we studied the structures of the species derived from three representative ligands, $\mathbf{L_1}$, $\mathbf{L_5}$ and $\mathbf{L_7}$, and $CuCl_2$ by X-ray absorption spectroscopy (XAS). The use of $CuCl_2$ instead of $Cu(OTf)_2$ leads to complexes with lower catalytic activity (Table 6) and this has been attributed to the presence of the chloride counterion.[15] However, we decided to use $CuCl_2$ in order to be able to distinguish between the anion (Cl) and the coordinating groups in the ligand (N, O).

Table 6. Results obtained in the reactions promoted by $CuCl_2$−L = 1:1.1 complexes in CH_2Cl_2 using 0.1% catalyst with respect to styrene

Entry	Ligand	*t* (h)	% yield	**4**:**3**	% *ee* (**3**)[a]	% *ee* (**4**)[a]
1	$\mathbf{L_1}$	24[a]	–	–	–	–
2		24[b]	24	2.5	–	–
3	$\mathbf{L_3}$	24[a]	–	–	–	–
4		7[b]	29	2.4	–	–
5	$\mathbf{L_5}$	24[a]	–	–	–	–
6		7[b]	28	2.4	0	0
7	$\mathbf{L_7}$	24[a]	–	–	–	–
8		7[b]	31	2.2	0	0

[a] Reaction at room temperature. – [b] Reaction under reflux conditions after the initial period at room temperature.

The experimental EXAFS signal was extracted from the raw spectra according to standard methods.[16] The threshold energy E_0, defining the zero wavevector, was taken at the inflection point of the absorption edge. Figure 3 shows the Fourier transform (FT) of the Cu-*K* edge $k\,\chi(k)$ spectra of the three complexes. The FT was calculated using a Gaussian window in the range 2.2−12.5 $Å^{-1}$. EXAFS spectra of the three samples are very similar and show little resolution of structure, indicating structural disorder. The moduli of the FTs of the $\mathbf{L_1}$ and $\mathbf{L_5}$ complexes show two main peaks, while that of the $\mathbf{L_7}$ complex shows an additional peak in the region of 3−4 Å.

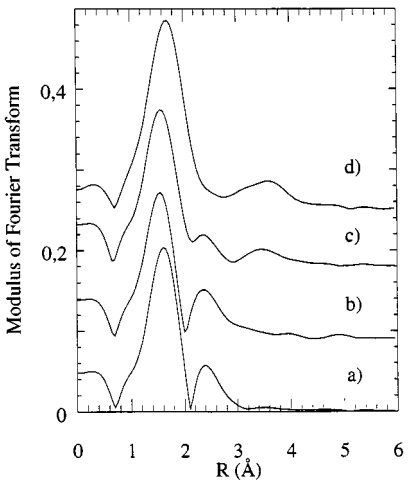


Figure 3. Fourier transforms of the EXAFS spectra: (a) $\mathbf{L_1}$−$CuCl_2$ complex; (b) $\mathbf{L_5}$−$CuCl_2$ complex; (c) $\mathbf{L_7}$−$CuCl_2$ complex; (d) $\mathbf{L_{12}}$−$CuCl_2$ complex

Table 7. Results obtained from analyses of the EXAFS spectra of $\mathbf{L_1}$, $\mathbf{L_5}$, $\mathbf{L_7}$ and $\mathbf{L_{12}}-CuCl_2$ complexes

Ligand	Cu−N (O)			Cu−C			Cu−Cl		
	$n°$	R (Å)	$\Delta\sigma^2$ 10^3Å^2	$n°$	R (Å)	$\Delta\sigma^2$ 10^3Å^2	$n°$	R (Å)	$\Delta\sigma^2$ 10^3Å^2
$\mathbf{L_1}$	5.4±0.3	2.03±0.01	4.97±0.003	3.4±0.7	2.93±0.03	5.21±0.005	–	–	–
$\mathbf{L_5}$	5.2±0.3	2.01±0.01	6.75±0.003	4.2±0.8	2.93±0.03	5.17±0.006	–	–	–
$\mathbf{L_7}$[a]	6.2±0.4	2.02±0.02	8.0±0.003	3.3±0.4	2.87±0.03	11.7±0.005	2.1±0.5	3.85±0.04	12.9±0.006
$\mathbf{L_7}$[b]	3.1±0.4	2.09±0.02	7.0±0.003	3.3±0.4	2.87±0.03	11.7±0.005	2.1±0.5	3.85±0.04	12.9±0.006
	2.6±0.4	1.98±0.02	6.3±0.003						
$\mathbf{L_{12}}$	2.0±0.6	1.97±0.02	3.2±0.004				2.0±0.4	2.21±0.01	2.7±0.003

[a] Considering Cu−N contributions only. − [b] Considering Cu−N and Cu−O contributions.

The first-shell contribution was extracted by Fourier filtering of the FT spectra in the range 0.8−2.2 Å, and the corresponding structural parameters were obtained by least-squares fitting of the filtered k-weighted spectrum to the EXAFS formula:[16]

$$(k) = \Sigma\ (\rho/k)\ (N_i/R_i^2)\ A_i(k)\ \sin[2kR_i+\phi_i(k)]$$

The amplitudes $A_i(k)$ and phase shifts $\phi_i(k)$ used in the best fit were generated from the FEFF3.11 code.[16e] The best-fit parameters obtained for the different complexes are reported in Table 7. The data for the $\mathbf{L_1}$ and $\mathbf{L_5}$ complexes were found to be very similar and showed the copper to be surrounded by five nitrogen or/and oxygen atoms at an average distance of 2.02 Å. For the second shell, the best fit was obtained solely with carbon atoms at 2.93 Å. We did not observe Cu−Cl contributions in these complexes. On the other hand, the high DW values obtained for both the first and second shells, together with the large error margins associated with the fit of structural parameters of the second shell indicate a high degree of structural disorder in these compounds. The absence of a Cu−Cl contribution in these complexes may be accounted for in terms of the significant structural disorder, the presence of different Cu−Cl and Cu−C distances in the second shell, or a very long Cu−Cl distance with a large vibrational DW factor. The presence of a large number of donor atoms in close proximity to the metal supports the formation of aggregate species with more than one ligand being involved in the complexation of the copper.

The best-fit results for the $\mathbf{L_7}$ complex reveal a slightly different structure. Cu−O and Cu−N cannot be clearly distinguished by EXAFS, hence we considered both possibilities in the theoretical fit of the experimental spectra. If we consider only Cu−N contributions, we obtain 6 nitrogen atoms at a distance of 2.02 Å. A similar fit is obtained considering Cu−N and Cu−O contributions at two different distances. An important difference between $\mathbf{L_7}$ and $\mathbf{L_1}$ and $\mathbf{L_5}$ is the observation of two distant chlorine atoms in the complex of the former. The presence of these chlorine atoms suggests less structural disorder and a higher accessibility of the copper in this complex. These structural changes, which may be due to the planarity imposed by the amide system, the presence of oxygen atoms, or both these factors, must also be responsible for the changes in the *trans*/*cis* ratio and the enantioselectivity.

After background subtraction from the raw spectra, the XANES spectra were normalized taking unity to indicate atomic absorption. The XANES spectra of the complexes of $\mathbf{L_1}$ and $\mathbf{L_5}$ with $CuCl_2$ were found to be almost superimposable, which was not the case with the $\mathbf{L_7}-CuCl_2$ complex. This fact is in good agreement with the differences observed by EXAFS.

The formation of copper−$\mathbf{L_7}$ oligomeric species might suggest that each amine−amide moiety of the ligand participates in the complexation of different copper atoms. This suggestion led us to examine the behavior of the simplest ligand $\mathbf{L_{11}}$. Unfortunately, the corresponding XAS spectrum could not be obtained. However, the close similarity of their catalytic behavior (Table 5) lends support to this hypothesis.

The results obtained from the EXAFS measurements show the absence of chlorine atoms in close proximity to the copper ions, which would seem to be at variance with the influence of this counterion on the catalytic activity. Thus, we investigated whether the same structural behavior is observed with other ligands, such as bis(oxazolines), where the same influence of the counterion has been described.[15] To this end, we studied the EXAFS spectrum of the $\mathbf{L_{12}}-CuCl_2$ complex. The EXAFS and the FT of the Cu-K edge $k\ \chi(k)$ spectrum is shown in Figure 3 and the best-fit parameters are given in Table 7. As can be seen, the spectra show clear differences and chlorine is observed at a distance of 2.21 Å from the copper, justifying its strong influence on the catalytic activity.

Comparison of this result with those obtained for the polynitrogenated compounds shows that the use of the latest ligands leads to oligomeric complexes with considerable disorder in the environment of the copper, and with chlorine at greater distances. In spite of these differences, the counterion has the same influence on the catalytic activity. It may be speculated that, in accordance with the period of induction, the oligomeric species are fragmented to yield the reactive copper−carbene intermediate, and that the reactivity of this intermediate depends on the nature of the counterion. Unfortunately, it has not been feasible to design an EXAFS experiment to check this hypothesis.

Supported Complexes as Catalysts

As a final avenue of investigation, we tested the behavior of some of these ligands supported in various ways. The

formation of aggregates should be disfavored when using such immobilized ligands. This, along with the changes in the micro-environments of the ions, could lead to significant changes in reactivity. Open-chain systems can be grafted onto polystyrene−divinylbenzene through the primary amine functionalities and ligands $\mathbf{L}_{13}$ and $\mathbf{L}_{14}$ were obtained in this way.[5] In accordance with our expectations, the reactions took place without an induction period. The results obtained (Table 8) show that the stereochemical course of the reaction is influenced by the presence of the support. A decrease in the *ee*, relative to that achieved with the same ligand in solution, was observed. Similar changes in the stereochemical course of reactions upon immobilization of a chiral auxiliary have repeatedly been observed.[3]

Table 8. Results obtained in the reactions promoted by Cu^{II} using polymeric ligands ($\mathbf{L_{13}}$−$\mathbf{L_{14}}$) in CH_2Cl_2 at 25 °C

Entry	Ligand	Cu/**1** (%)	*t* (h)	% yield	**4**:**3**	% *ee* (**3**)	% *ee* (**4**)
1	$\mathbf{L_{13}}$[a]	0.1	1.5	12	2.0	−	−
2			2.0	19	2.0	−	−
3			24.0	28	1.8	0	0
4	$\mathbf{L_{14}}$[a]	0.1	1.0	17	1.6	−	−
5			23.0	31	1.6	4	3

[a] $\mathbf{L_{12}}$ contains 0.30 mmol ligand g^{-1} and $\mathbf{L_{13}}$ 0.46 mmol ligand g^{-1}.

Given that the complexes used as catalysts are cationic, they can also be supported using of a different strategy, i.e. they can be electrostatically entrapped using anionic solids. To test this approach, we used a synthetic laponite with a high swelling ability. Cation exchange was carried out in methanol using the $CuCl_2$ complexes of a cyclic ($\mathbf{L_1}$) and an open-chain ($\mathbf{L_3}$) ligand. Table 9 shows the results of analyses of the clays. In both cases, 0.1 mmol Cu g^{-1} are introduced, the Li:Cu stoichiometry is 1:1, and the presence of the complex produces a decrease in the surface area. With $\mathbf{L}_1$, the basal spacing increases, indicating that the complex is accommodated into the interlamellar space, at least in part. With $\mathbf{L_3}$, no change in basal spacing is observed, which may either be due to the smaller size of the complex or to a disposition of this complex on the external surface of the clay. In view of the result obtained with $\mathbf{L_1}$, the first explanation seems more plausible.

Table 9. Analysis of the laponites exchanged with the complexes of $CuCl_2$ with $\mathbf{L_1}$ and $\mathbf{L_3}$

Entry	Ligand	Cu (mmol g^{-1})	N/Cu	d_{001} (•)	S (m^2 g^{-1})
1	−	−	−	16	289
2	$\mathbf{L_1}$	0.1	3.9	19	245
3	$\mathbf{L_3}$	0.1	3.8	16	239

Table 10 shows the results obtained with these clay-supported catalysts. As can be seen in Table 6, the use of chloride in place of triflate significantly reduces the catalytic activity in solution and it is necessary to carry out the reaction under reflux. This can only be related to the effect of the more coordinating chloride counterion. In the case of $\mathbf{L_3}$, the catalytic activity of the supported catalyst is similar to that seen for the homogeneous complex, while for $\mathbf{L_1}$ it is even superior. However, a simple comparison cannot be made because in the supported catalyst the counterion is changed from chloride to the clay surface, and the nature of the counterion has a decisive influence on the catalytic activity. The *trans*/*cis* ratio decreases, hence the proportion of the less stable product increases. This has previously been observed with clay catalysts and has been explained in terms of the isolation of the catalytic sites and the dimensionality of the clay, which should also be related to the higher catalytic activity.[17]

Table 10. Results obtained in the reactions promoted by $CuCl_2$−$\mathbf{L_1}$ and $\mathbf{L_3}$ (1:1.1) complexes exchanged in laponite, in CH_2Cl_2 using a Cu/**1** ratio of 0.001

Entry	Ligand	*t* (h)	% yield	**4**:**3**
1	$\mathbf{L_1}$	24[a]	−	−
2		7[b]	20	1.1
3		24[b]	30	1.1
4	$\mathbf{L_3}$	24[a]	−	−
5		7[b]	27	1.1
6		24[b]	29	1.1

[a] Reaction at room temperature. − [b] Reaction under reflux conditions after initial period at room temperature.

Conclusions

The results presented here open the way for the design of novel polynitrogenated ligands for use in copper-catalyzed processes and for understanding the different factors affecting the activity of such species. The copper(I) and copper(II) complexes of some cyclic and non-cyclic polyamines, as well as of some diamides, have been assayed in the benchmark cyclopropanation reaction of styrene with ethyl diazoacetate. First and foremost, all the complexes examined showed an appreciable catalytic activity, even at very low catalyst concentrations. All data suggest that formation of the carbene−copper complex is the rate-limiting step. For polyamines, aggregation hinders the formation of the active carbene−copper complexes and as a result induction periods are observed in non-coordinating solvents (CH_2Cl_2). The addition or the *in situ* generation of kinetically labile coordinating species such as EtOAc or ethyl fumarate (formed by decomposition of the diazoacetate) disrupts aggregation and allows the facile formation of the active complexes. Aggregation is more significant with polyamines having a smaller number of nitrogen donor atoms and with less bulky ligands, and is much reduced with amides.

The induction periods are more important for Cu^{I} than for Cu^{II} complexes, according to the different coordination geometries. This seems to be associated with the formation of more accessible Cu^{II} sites that readily interact with the carbene-forming species and are reduced to Cu^{I} complexes, which are the active catalytic species. No other differences (e.g. in terms of selectivity) are associated with the use of Cu^{I} or Cu^{II} and, accordingly, the use of the more stable Cu^{II} compounds is clearly favored.

Polyamine or amide ligands of this type can easily be supported by anchoring on functionalized polymers or by cation exchange in clays. The resulting supported Cu^{II} complexes show higher activities than their homogeneous analogues. This can be rationalized in

terms of the pseudodilution effects operative in the solid materials, which will disfavor the aggregation processes.

Finally, small enantioselectivities have been observed on using some of the chiral ligands. However, more work is needed in this regard if novel chiral ligands able to improve the observed enantioselectivities are to be developed

Experimental Section

Preparation of the Ligands: $\mathbf{L_2}$ and $\mathbf{L_3}$ are commercial compounds. $\mathbf{L_1}$,[12] $\mathbf{L_4}-\mathbf{L_7}$[18] and $\mathbf{L_{13}}-\mathbf{L_{14}}$[5] were prepared as described previously. $\mathbf{L_8}$, $\mathbf{L_9}$ and $\mathbf{L_{10}}$ were obtained by reaction of the *N*-hydroxysuccinimide esters of the *N*-Cbz protected amino acids with the corresponding diamines, followed by deprotection of the *N*-Cbz groups.

General Procedure for the Preparation of *N*-Hydroxysuccinimide Esters of Amino Acids: The appropriate *N*-Cbz-protected amino acid (3.34 mmol) and *N*-hydroxysuccinimide (3.34 mmol) were suspended in anhydrous DME at 0°C. Once a clear solution had been obtained, DCC (3.67 mmol) was added and the resulting solution was stirred at 0−5°C for 20 h. The dicyclohexylurea formed was filtered off and the filtrate was concentrated to dryness. The crude product was recrystallized from propan-2-ol to furnish the pure product. *N*-Hydroxysuccinimide ester of *N*-Cbz-L-phenylalanine: yield 87%; m.p. 137−140°C. − ^{1}H NMR: δ = 2.80 (br. s, 4 H), 3.13−3.41 (m, 1 H), 5.09 (s, 4 H), 7.29−7.4 (m, 10 H). − ^{13}C NMR: δ = 25.4, 37.8, 52.9, 67.2, 127.3, 128.0, 128.2, 128.5, 128.7, 129.5, 134.3, 167.5, 168.7. − $[\alpha]_D^{25}$ = −11.1 (*c* = 2, dioxane). − $C_{21}H_{20}N_2O_6$: calcd. C 63.6, H 5.1, N 7.1; found C 63.5, H 5.5, N 7.4.

General Procedure for the Preparation of *N,N′*-Bis(*N*-Cbz-aminoacyl)diamines: The *N*-hydroxysuccinimide ester of the appropriate amino acid (7.44 mmol) was dissolved in anhydrous DME cooled in an ice bath, and the diamine (3.72 mmol) was added dropwise. The reaction mixture was stirred at room temp. for 18 h. The white solid formed was filtered off and washed with water and cold methanol.

Deprotection of *N*-Cbz Groups: The *N,N′*-bis(*N*-Cbz-aminoacyl)-1,3-diaminopropanes were added to HBr/AcOH (33%) and the respective mixtures were stirred at room temp. until CO_2 evolution ceased. At this point, diethyl ether was added to the clear solution, which led to the deposition of a white precipitate. This was filtered off and dried to afford the pure product.

$\mathbf{L_8}$: M.p. 140−143°C. − $[\alpha]_D^{20}$ = −89.42 (*c* = 1, $CHCl_3$). − ^{1}H NMR: δ = 1.5 (m, 4 H), 2.7 (dd, J_1 = 9.2, J_2 = 14 Hz, 2 H), 3.25 (m, 6 H), 3.6 (dd, J_1 = 3.8, J_2 = 9.2 Hz, 2 H), 7.3 (m, 10 H). − ^{13}C NMR: δ = 27.0, 38.7, 41.1, 56.5, 126.8, 128.7, 129.4, 138.0, 174.3. − $C_{22}H_{30}N_4O_2$: calcd. C 69.1, H 7.9, N 14.6; found C 69.3, H 8.3, N 15.0.

$\mathbf{L_9}$: M.p. 137−141°C. − $[\alpha]_D^{20}$ = −17.16 (*c* = 1, $CHCl_3$). − ^{1}H NMR: δ = 1.31 (d, *J* = 6.5 Hz, 4 H), 2.6 (dd, J_1 = 9.5, J_2 = 13.5 Hz, 2 H), 3.32 (dd, J_1 = 3.8, J_2 = 13.5 Hz, 2 H), 3.55 (m, 2 H), 5.28 (m, 2 H), 7.2 (m, 20 H), 8.2 (m, 2 H). − ^{13}C NMR: δ = 40.7, 56.5, 59.0, 126.8, 127.6, 127.7, 128.5, 128.7, 129.3, 137.8, 138.6, 174.7. − $C_{32}H_{34}N_4O_2$•1/2 H_2O: calcd. C 74.5, H 6.8, N 10.9; found C 74.4, H 6.9, N 10.5.

$\mathbf{L_{10}}$: M.p. 213−217°C. − $[\alpha]_D^{20}$ = −80.02 (*c* = 1, $CHCl_3$). − ^{1}H NMR: δ = 1.3 (m, 4 H), 2.6 (dd, J_1 = 10, J_2 = 14 Hz, 2 H), 3.18 (dd, J_1 = 4.5, J_2 = 14 Hz, 2 H), 3.58 (m, 2 H), 5.3 (m, 2 H), 7.2 (m, 20 H), 8.26 (m, 2 H). − ^{13}C NMR: δ = 41.5, 56.8, 56.9, 58.7, 126.9, 127.6, 127.7, 128.5, 128.7, 128.8, 129.3, 138.0, 138.4, 174.7. − $C_{32}H_{34}N_4O_2$•H_2O: calcd. C 73.3, H 6.9, N 10.7; found C 73.4, H 7.0, N 10.8.

$\mathbf{L_{11}}$: M.p. 67−71°C. − $[\alpha]_D^{20}$ = −69.1 (*c* = 1, $CHCl_3$). − ^{1}H NMR: δ = 1.56 (br. s, 2 H), 2.78 (dd, J_1 = 9.8, J_2 = 13.8 Hz, 1 H), 3.27 (dd, J_1 = 4.5, J_2 = 13.8 Hz, 1 H), 3.62 (dd, J_1 = 4.6, J_2 = 9.4 Hz, 1 H), 4.43 (d, *J* = 6.5 Hz, 2 H), 7.25 (m, 10 H), 8.19 (t, *J* = 6.3 Hz, 2 H). − ^{13}C NMR: δ = 41.1, 43.2, 56.5, 126.8, 127.4, 127.7, 128.3, 129.4, 138.0, 173.4. − $C_{16}H_{18}N_2O$: calcd. C 75.6, H 7.1, N 11.0; found C 75.5, H 7.1, N 11.3.

Preparation of the Cationic Complexes Supported on Clays: A solution of the complex was first prepared by stirring CuCl2•2H2O (1 mmol) and the appropriate ligand ($\mathbf{L_1}$ or $\mathbf{L_3}$, 1 mmol) in methanol (50 mL) for 45 min. To this green solution, laponite (10 g) was added and the mixture was shaken for 22 h. After this time, the blue clay was separated by filtration and washed with methanol. The residue obtained by evaporation of the solvent from the colorless solution was found to contain NaCl.

The copper content was analyzed by plasma emission spectroscopy using a Perkin−Elmer Plasma 40 emission spectrometer. Carbon and nitrogen analyses were carried out using a Perkin−Elmer 2400 elemental analyzer. Step-scanned X-ray diffraction patterns of oriented samples were collected at room temperature from 3° in 2& thetas; up to 60° using a D-max Rigaku system with a rotating anode. The diffractometer was operated at 40 kV and 80 mA and Cu-K_α radiation was selected using a graphite monochromator. Surface areas were calculated from BET nitrogen isotherms determined at 77 K.

Cyclopropanation Reactions with Homogeneous Catalysts: Under argon, a mixture of the requisite amount of the ligand (Tables 1−5) and CuOTf•1/2C_6H_6 or $Cu(OTf)_2$ (0.1 mmol) in dry CH_2Cl_2 (60 mL) was stirred at room temperature for 30 min. Then, a solution of styrene (100 mmol) and *n*-decane (2 g) in dry CH_2Cl_2 (50 mL) was added and the resulting solution was stirred for 10 min. After this time, ethyl diazoacetate (50 mmol) was slowly added by means of a syringe pump over a period of 45 min. The reactions were monitored by gas chromatography using *n*-decane as an internal standard; FID from Hewlett-Packard 5890 II; cross-linked methyl silicone column 25 m × 0.2 mm × 0.33 μm; helium as carrier gas, 20 psi; injector temperature 230°C; detector temperature 250°C; over temperature program: 70°C (3 min)−15°C/min−200°C (5 min); retention times: ethyl diazoacetate (**2**) 4.28 min, styrene (**1**) 5.03 min, *n*-decane 6.93 min, diethyl fumarate 8.73 min, diethyl maleate 9.04 min, *cis*-cyclopropanes (**3**) 11.84 min, *trans*-cyclopropanes (**4**) 12.35 min.

Asymmetric induction in the reactions using chiral ligands was also assessed by gas chromatography; cyclodex-B column 30 m × 0.25 mm × 0.25 μm; oven temperature program: 125°C isothermal; retention times: (1*S*,2*R*)-cyclopropane 28.9 min, (1*R*,2*S*)-cyclopropane 29.8 min, (1*R*,2*R*)-cyclopropane 34.3 min, (1*S*,2*S*)-cyclopropane 34.9 min. The peaks were assigned to the corresponding enantiomers by comparison with previous results.

In general, the onset of the reactions is signified by a color change from green to yellow. In one case (entry 4, Table 3), the reaction did not take place at room temperature and had to be carried out under reflux. In another case (entry 2, Table 2), after the consumption of the ethyl diazoacetate an additional amount of this reagent was added in the same manner. In another reaction (entry 5, Table 2), the $\mathbf{L_1}$−CuOTf complex was stirred with ethyl acetate (5 mmol) for 3 h prior to addition of the reagents.

Cyclopropanation Reactions with Polymeric Catalysts: The appropriate amount of polymer (0.37 g of $\mathbf{L_{12}}$ or 0.24 g of $\mathbf{L_{13}}$) was

stirred under argon in a solution of $Cu(OTf)_2$ (1 mmol) in CH_2Cl_2 for 24 h. After this time, the solution was decanted off and the remaining solid was washed with CH_2Cl_2. To a suspension of the catalyst in dry CH_2Cl_2 (60 mL), the internal standard and the reagents were added and the reaction was monitored as described above.

Cyclopropanation Reactions with Clay-Supported Catalysts: To a suspension of the clay (1 g) in dry CH_2Cl_2 (60 mL), the reagents and the internal standard were added and the reaction was monitored as described above.

EXAFS and XANES Experiments: X-ray absorption experiments at the Cu-*K* edge were carried out at the synchroton radiation source, Daresbury, U.K. A double-crystal Si(111) monochromator was used. The storage ring operated at 2 GeV with an average beam current of 150 mA. The experiments were performed at room temperature in the transmission mode, and the signal was collected by means of ion chambers. For the XAS measurements, solid samples of the $\mathbf{L_1}$, $\mathbf{L_5}$, $\mathbf{L_7}$ and $\mathbf{L_{12}}-CuCl_2$ complexes were pressed into thin pellets. The thickness of the samples was optimized in order to obtain the best signal-to-noise ratio.

Samples were prepared using the ligand and $CuCl_2$ in an equimolar ratio; the amounts of the two components were adjusted in order to obtain 100 mg of complex. To a solution of the ligand in CH_2Cl_2 (5 mL), the requisite amount of CuCl2•2H2O was added. The resulting suspension was stirred at room temperature for 5 h, which led to the gradual disappearance of the solid $CuCl_2$. After this time, the solution was filtered through a plug of cotton wool and the solvent was evaporated from the filtrate under reduced pressure. The solid complexes were dried in vacuo for 24 h at 50°C. All complexes showed the expected IR bands and gave appropriate elemental analyses.

Acknowledgments

This work was made possible by the generous financial support of the C.I.C.Y.T. (Project MAT96−1053) and the Generalitat Valenciana (GV-D-CN-09−140−96).

[1] E. Kimura, *Tetrahedron* **1992**, *48*, 6175.
[2] R. Noyori, Asymmetric Catalysis in Organic Synthesis, Wiley, New York, **1994**.
[3] [3a] *Polymeric Reagents and Catalysts* (Ed.: W. T. Ford), A.C.S. Symposium Series 308, American Chemical Society, Washington D.C., **1986**. − [3b] *Synthesis and Separations using Functional Polymers* (Eds.: D. C. Sherrington, P. Hodge), John Wiley and Sons, New York, **1988**. − [3c] *Solid Supports and Catalysts in Organic Synthesis* (Ed.: K. Smith), Ellis Horwood, Chichester, **1992**.
[4] [4a] H.-U. Blaser, *Tetrahedron: Asymmetry* **1991**, *3*, 843. − [4b] H.-U. Blaser, B. Pugin in *Chiral Reactions in Heterogeneous Catalysis* (Eds.: G. Jannes, V. Dubois), Plenum Press, New York, **1995**, p. 33. − [4c] See ref.[2], p. 346.
[5] F. M. Adrian, B. Altava, M. I. Burguete, S. V. Luis, R. V. Salvador, E. García-España, *Tetrahedron* **1998**, *54*, 3581.
[6] [6a] G. Pozzi, M. Cavazzini, S. Quici, S. Fontana, *Tetrahedron Lett*. **1997**, *38*, 7605. − pf1[[b] D. E. de Vos, T. Bein, *Chem. Commun*. **1996**, 917.
[7] [7a] E. Galardon, P. Le Maux, G. Simmoneaux, *Chem. Commun*. **1997**, 927. − [7b] J. Robbins Wolf, C. G. Hamaker, J.-P. Djukic, T. Kodadek, L. K. Woo, *J. Am. Chem. Soc*. **1995**, *117*, 9194.
[8] For a recent example in enantioselective Michael reactions, see K. Yasuda, M. Shindo, K. Koga, *Tetrahedron Lett*. **1997**, *38*, 3531.
[9] [9a] R. G. Salomon, J. K. Kochi, *J. Am. Chem. Soc*. **1973**, *95*, 3300. − [9b] M. Hagen, U. Lüning, *Chem. Ber*. **1997**, *130*, 231. − [9c] M. P. Doyle, M. N. Protopopova, *Tetrahedron* **1998**, *54*, 7919.
[10] [10a] A. Domenech, J. V. Folgado, E. García-España, S. V. Luis, J. M. Linares, J. F. Miravet, J. A. Ramírez, *J. Chem. Soc., Dalton Trans.* **1995**, 541. − [10b] A. Domenech, E. García-España, V. Marcelino, B. Altava, S. V. Luis, J. F. Miravet, A. Bianchi, L. Ferrini, *Inorg. Chim. Acta* **1996**, *252*, 123.
[11] [11a] E. García-España, J. Latorre, S. V. Luis, J. F. Miravet, P. E. Pozuelo, J. A. Ramírez, C. Soriano, *Inorg. Chem*. **1996**, *35*, 4591. − [11b] M. I. Burguete, B. Escuder, J. C. Frías, E. García-España, S. V. Luis, J. F. Miravet, *J. Org. Chem*. **1998**, *63*, 1810.
[12] A. Bencini, M. I. Burguete, E. García-España, S. V. Luis, J. F. Miravet, C. Soriano, *J. Org. Chem*. **1993**, *58*, 4749.
[13] [13a] A. Andrés, C. Bazzicaluppi, A. Bianchi, E. García-España, S. V. Luis, J. F. Miravet, J. A. Ramírez, *J. Chem. Soc., Dalton Trans.* **1994**, 2995. − [13b] E. García-España, J. Latorre, V. Marcelino, J. A. Ramírez, S. V. Luis, J. F. Miravet, M. Querol, *Inorg. Chim. Acta* **1997**, *265*, 179.
[14] [14a] K. A. Deal, A. C. Hengge, J. N. Burstyn, *J. Am. Chem. Soc*. **1996**, *118*, 1713. − [14b] E. L. Hegg, J. N. Burstyn, *Inorg. Chem*. **1996**, *35*, 7474.
[15] D. A. Evans, K. A. Woerpel, M. M. Hinman, M. M. Faul, *J. Am. Chem. Soc*. **1991**, *113*, 726.
[16] [16a] D. C. Konigsberger, R. Prins, X-ray Absorption: Principles, Applications, Techniques of EXAFS, SEXAFS and XANES, Wiley, New York, **1988**. − [16b] *X-ray Absorption Fine Structure* (Ed.: S. S. Hasnain), Ellis Horwood, Chichester, **1988**. − [16c] B. K. Teo, *EXAFS: Basic Principles and Data Analysis*, Springer, Berlin, **1986**. − [16d] Appendix to the report on the International Workshop on Standards and Criteria in X-ray Absorption Spectroscopy, March 7−9, **1988**, Brookhaven National Laboratory, *Physica B* **1989**, *158*, 701. − [16e] J. J. Rehr, J. Mustre de León, S. I. Zabinsky, R. C. Albers, *J. Am. Chem. Soc*. **1991**, *113*, 5135.
[17] [17a] J. M. Fraile, J. I. García, J. A. Mayoral, *Chem. Commun*. **1996**, 1319. − [17b] J. M. Fraile, J. I. García, J. A. Mayoral, T. Tarnai, *Tetrahedron: Asymmetry* **1997**, *8*, 2089.
[18] F. R. Wagler, Y. Fang, C. J. Burrows, *J. Org. Chem*. **1989**, *54*, 1584.

Received April 21, 1999
[I99140]

(*N*-lithioamino)diorganophosphanes and Bis(*N*-Lithioamino)organophosphanes: Synthesis and Structures

Bettina Eichhorn,[a] Heinrich Nöth,*[a] and Thomas Seifert[a]

Dedicated to Professor Alfred Schmidpeter on the occasion of his 70th birthday

Keywords: Phosphane complexes / Lithium / Aminophosphanes / Hydrazides / (*N*-lithioamino)diorganophosphanes

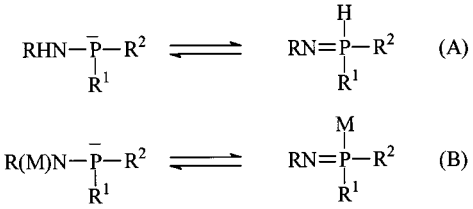
Butyllithium (*n*BuLi) deprotonates Ph_2P–NH*t*Bu in ether to give $(Ph_2P–NLi{t}Bu)_2{\cdot}OEt_2$. There is no Li···P interaction in this molecule. Three compounds of the type $R'P(NLiR)_2$ have been obtained by lithiation of $R'P(NHR)_2$, isolated as $[BuP(NLi{t}Bu)_2{\cdot}OEt_2]_2$, $[PhP(NLiPh)_2{\cdot}OEt_2]_2$ and $[PhP(NLiPh)_2]_2$. Reaction of *n*BuLi with $MeP(NH{i}Pr)_2$ in hexane/THF leads to $[MeP\{N(Li){i}Pr]_2{\cdot}THF\}_4$ with an asymmetric cluster structure comprising one LiP_3, three $LiPN_2$, three LiP_2N and one LiN_3 cluster units. The molecular structures of these compounds as determined by X-ray structure analysis show that they are best depicted as *N*-lithioaminophosphanes and not as the isomeric *P*-lithioiminophosphoranes.

Introduction

The chemistry and particularly the structural chemistry of alkali metal hydrazides has recently been the subject of great interest. They are versatile reagents and offer surprising structural features.[1] Amongst the series $R_2N-N(R)M$, R_2N-NM_2, $R(M)N-N(M)R$, $R(M)N-NM_2$ and M_2N-NM_2 (M = alkali metal), so far only the first three members are known.[1] Furthermore, only very few derivatives with the heavier alkali metals have been described, a typical example being $CsMeN-N(SiMe_3)_2$.[1d] All these metal hydrazides are dimers, trimers or oligomers in spite of the fact that the alkali metal cations coordinate donor solvent molecules. The most significant feature of the hydrazide units is that the two nitrogen atoms are present in a planar or almost planar coordination sphere in which the planes around the N atoms are more or less perpendicularly oriented to one another.

Monoaminophosphanes $R_{2-n}H_nN-PR_2$ are the mixed higher homologues of hydrazines $R_{2-n}H_nN-NR_2$. Upon lithiation, amidophosphanes $RLiN-PR_2$ form.[2] Association of these molecules should preferentially occur by means of intermolecular Li···N interactions, although Li···P interactions may also be present;[2] these should, however, not be preferential due to the softer base character of the phosphorus(III) atom. Moreover, it is well-known that aminophosphanes may be involved in prototropism (A) which can lead to imido-phosphoranes;[3] metallotropism, as described in Equation (B), might therefore also be observable.[2]

As far as aminophosphanes are concerned, the analogy between hydrazines and mono-aminophosphanes can be readily expanded because a P^{III} atom allows for the formation of the series of compounds $RHN-PR_2$, $(RHN)_2PR$ and $(RHN)_3P$ and all these should be amenable to deprotonation. Another extension includes bis(phosphanyl)amines $(R_2P)_2NH$ and their metallation to $(R_2P)_2NM$ compounds (M = Li, Na, K, Cs) where it has been found that for M = Li, a dimeric species with Li–N bonds is formed, while the sodium salt shows only Na–P bonds.[4] Therefore it is interesting, but difficult to predict, what kind of metal–ligand interaction can be expected for bis-metallated di(amino)phosphanes. For this reason we have not only investigated the metalation of monoaminophosphanes[5] but also the bis(amino)organophosphanes. Because tris(amino)phosphanes $P(NHR)_3$[6] (R = Me, *t*Bu, Ch_2Ph, $C_{12}H_{25}$) condense too readily to give cyclophosphazanes $[RHN-P=NR]_2$ or $P_4N_6R_6$, we did not include a study of the deprotonation of tris(amino)phosphanes.



Results

Bis(organoamino)organophosphanes, $R'P(NHR)_2$

Aminophosphanes $R'_{3-n}P(NHR)_n$ bearing primary amino groups are amenable to condensation. This tendency increases with the number of amino groups attached to the phosphorus atom and decreases with increasing bulk of the *P*- and *N*-substituents. The first compound of type $R'P(NHR)_2$ such as $C_5F_5P(NHR)_2$ (R = *t*Bu, CH_2Ph) was reported in 1966.[7] Another series of compounds $PhP(NHR)_2$ (R = Me, Et, *n*Pr, *i*Pr, *t*Bu) was described in 1967.[8] They can be oxidized to $PhP(X)(NHR)_2$ (X = O, S) or alkylated to their phosphonium salts $[PhR'P(NHR)_2]X$[8] which are thermally more stable than

[a] Institute of Inorganic Chemistry, University of Munich, Butenandtstrasse 5–13 (Haus D), D-81377 München, Germany

 © WILEY-VCH Verlag GmbH, D-69451 Weinheim, 1999 1434–1948/99/1212–2355 $ 17.50+.50/0

the parent compounds. Furthermore, bis(arylamino)arylphosphanes seem to be less prone to condensation[9] and, therefore, several bis(anilido)arylphosphanes have been characterized by spectroscopic methods.[9][10] Moreover, the structure of mes*P[NH(mes*)]$_2$ (mes* = 2,4,6-tris-*tert*-butylphenyl = supermesityl) has been determined by X-ray diffraction techniques.[10] Scherer[11] and Payne[8] were able to isolate MeP(NH*t*Bu)$_2$ as the most stable species amongst bis(monoorganoamino)methylphosphanes. Even MeP(NH*i*Pr)$_2$ **(1)**, can be isolated like MeP(NH*t*Bu)$_2$ **(2)** as the product of aminolysis of MePCl$_2$, as described by Equation (1).[8] The aminolysis method has been used to prepare compounds **1** to **5**.

$$R'PCl_2 + 4NH_2R \longrightarrow R'P(NHR)_2 + 2(NHR_3)Cl \quad (1)$$

R'	Me	Me	Ph	Ph	Ph
R	iPr	^{t}Bu	iPr	^{t}Bu	Ph
	1	**2**	**3**	**4**	**5**

$$mesPCl_2 + 2Me_3SiNHR \xrightarrow[\text{toluene}]{20\ ^\circ C} mesP(NHR)_2 + 2Me_3SiCl \quad (2)$$

R = ^{t}Bu, **6**
R = iPr, **7**

$$2\ mes\ P(NHiPr)_2 + H_2O \longrightarrow \textbf{8} + 2\ iPrNH_2 \quad (3)$$

8

$$mesP(NH^tBu)_2 + H_2O \xrightarrow{CH_2Cl_2} mes{-}P(=O)(H){-}NH^tBu + iPrNH_2 \quad (4)$$

9

It is interesting to note that amination of MePCl$_2$ with LiNHR or Me$_3$SiNHR was unsuccessful in our hands. Moreover, aminolysis of MePCl$_2$ with aniline or mesidine to MeP[NH(aryl)]$_2$ was equally unsuccessful; this contrasts with the aminolysis of PhPCl$_2$ which provided the series of bis(organoamino)phenylphosphanes **3**–**5** as shown in Equation (1). While ether is a good solvent for these reactions, toluene is required for the preparation of **5** in order to circumvent solubility problems.

In contrast, the bis(monoorganoamino)mesitylphosphanes **6** and **7** were readily obtained by allowing mesPCl$_2$ (mes = mesityl) to react with aminosilanes Me$_3$Si–NHR as described in Equation (2). However, the formation of **7** was always accompanied by the formation of the di-phosphetidine **8** (Equation 3). The ratio of **7**:**8** before distillation was ≈4:1. Slow hydrolysis of **7** yielded the phosphonic acid amide **9** as described by Equation (4), a compound that was not obtained by direct hydrolysis of **7**.

NMR Spectra

Chemical shifts for ^{31}P and ^{15}N NMR, as well as coupling constants, of compounds **1**–**8** are summarized in Table 1 and additional data (^{1}H, ^{13}C) are reported with the individual compounds in the Experimental Section.

Table 1. Chemical shifts ^{31}P and ^{15}N and P-N coupling constants for bis(organoamino)organophosphanes **1**–**8** and related compounds measured in C_6D_6

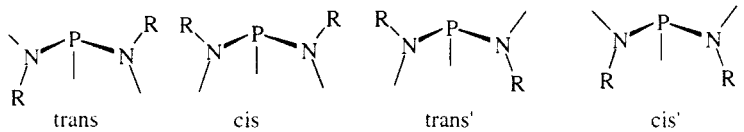
	δ^{31}P	δ^{15}N	^1J(P-N) (Hz)
MeP(NH^{i}Pr)$_2$ **(1)**	51.7	−302.1	65.3
MeP(NH*t*Bu)$_2$ **(2)**	39.2	−289.9	65.7
PhP(NH*i*Pr)$_2$ **(3)**	58.9	−304.8	67.9
PhP(NH*t*Bu)$_2$ **(4)**	42.0	−292.2	68.2
PhP(NHPh)$_2$ **(5)**	46.8	−294.6	66.4
mesP(NH*i*Pr)$_2$ **6**	58.7	−303.5	63.4
mesP(NH*t*Bu)$_2$ **7**	44.1	−298.9	59.9
[mesP−N*i*Pr]$_2$ **8**	242.0	−374.1	t 37.5
mes*P(NHmes*)$_2$	82	–	–

mes* = 2,4,6-tris-*tert*-butylphenyl.

All compounds exhibit a single ^{31}P NMR signal, and the ^2J(P-C) coupling constants were calculated from the satellites. Shielding of the P nucleus increases from 12.5 to 16.9 ppm by replacing *i*Pr groups with *t*Bu groups, and this difference decreases in the series R = Me > mes > Ph. On the other hand, the nitrogen nuclei are better shielded by *i*Pr groups than by *t*Bu groups. The shift differences are $\Delta\delta(^{15}N)$ = 12.2 for the pair **1** and **2**, 12.6 for the pair **3** and **4,** but only 4.6 for the pair **6** and **7**.

Both, ^{1}H and ^{13}C NMR spectra of all bis(isopropylamino)phosphanes **1**, **3** and **6** show nonequivalent CH$_3$ groups with different ^3J(H-H) coupling due to the prochirality of the *i*Pr groups. The corresponding signal for the CH proton is a multiplet of higher order. On the other hand, four ^{13}C NMR signals for the phenyl group reveal free rotation about its P–C bond.

There are two signals for the NH protons of bis(isopropylamino)phenylphosphane which are fairly broad. These signals do not stem from a doublet due to coupling of the protons with ^{31}P because the two signals did not collapse into a single line on ^{31}P decoupling, nor were they affected by proton decoupling. This is in contrast to the observation by Payne et al.[8] who found for their compounds that the NH signals collapsed to a singlet on irradiation at the frequency of the methine proton implying ^3J(H-H) coupling. On the other hand, there are also two NH signals in compound **4** where there is no methine proton available for a ^3J(H-H) coupling. On heating, a [D$_8$]toluene solution of **3** led to coalescence of the two NH signals at 80 °C, while all other ^{1}H NMR signal remain unchanged. A $^{13}C\{^1H^{31}P\}$ double resonance experiment clearly demonstrates that two doublets for the CH*Me*$_2$ groups are due to ^3J(P-C) because this gives rise to two singlets. Thus, the temperature-dependence of the NH proton signals suggests hindered rotation about the P–N bond. However, there was no indication of hindered rotation in the *tert*-butylaminophosphane **6**, although the steric requirement of the *tert*-butyl group would certainly be more demanding than that of the prochiral isopropyl group. However, the height of the rotational barrier has not been determined experimentally



A **B** **C** **D**

Two ^{1}H and ^{13}C NMR signals for the isopropyl groups were also observed in the cyclophosphazane **8**, appearing as doublets in the ^{1}H NMR spectrum due to ^{3}J(H-H) coupling. In addition, the *O*-methyl groups of the mesityl substituents are also not magnetically equivalent, which also became apparent for the *m*-H atoms which appear as two signals and, therefore, also indicated hindered rotation. The four-membered ring structure of **8** was ascertained by NMR spectroscopy, with a triplet for the ^{15}N NMR signal due to coupling to the P atoms [^{1}J(P-N) = 37.5 Hz], as well as by its molecular weight, and finally, by an X-ray structure analysis.

Ab initio Calculations

Hindered rotation about the P−N bond of bis(organoamino)organophosphanes may result in chirality at the phosphorus center. As depicted in formulae **A**−**D**, four different rotamers result as limiting cases. The conformers **A** and **C** are chiral, while **B** and **D** are achiral due to a plane of symmetry.

In order to obtain information on compound **3**, our best-studied bis(amino)phenylphosphane, single point calculations were performed. A simulation of the NMR spectrum of **3**, taking its solid state structure into account, must consider 19 spins (^{1}H, ^{15}N, ^{31}P). This would be technically quite demanding. Therefore, we turned to NBO analysis as implemented in the Gaussian 94 program package,[12] and Figure 1 depicts calculated Mulliken charges and Wiberg bond orders. The latter renders bond orders usually as too large.

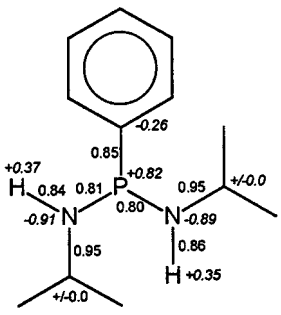


Figure 1. Wiberg bond orders and Mulliken charges for PhP(NH*i*Pr)$_2$

In spite of this, P−N bond order values of ≈ 0.80 correspond to a single bond, and calculated negative charges are associated with the nitrogen centers as well as the *ipso* carbon atoms. Positive charges are centered at the P atom and the hydrogen atoms. This implies localized pairs of electrons at the P and N centers. Surprisingly, the lone pair at the P atom resides in an orbital close to sp^3 while the lone pairs at the nitrogen atoms are of *p*-type, resulting from an almost planar environment of the substituents at the nitrogen atoms. This result already excludes any discussion that a hindered rotation about the P−N bond originates from π-bonding. Taking the molecular parameters into account, as obtained from the X-ray structure determination (see below), single point calculations (basis set 31G*) have been performed by rotating one isopropyl amino group by 360° leaving the rest of the molecular structure untouched. The result of these calculations is depicted in Figure 2.

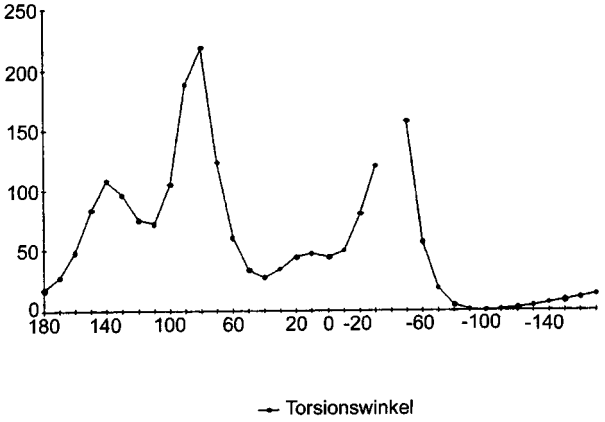
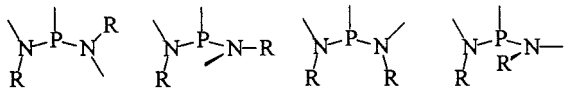


Figure 2. Rotational barrier calculated for PhP(NH*i*Pr)$_2$, using its structural data as found for the solid state; one isopropyl group was kept fixed, the second one was rotated about its P−N bond



E **F** **G** **H**

As can be seen, there are four minima on the hypersurface corresponding to the following rotational angles: −100°, 130°, 40° and 0°. The corresponding conformations are shown by structures **E**−**H**. At a torsion angle of −50°, the isopropyl groups overlap. In going from a *cis*- to a *trans*-structure, an energy of 200 kcal mol^{-1} is required. This barrier cannot be surpassed at ambient temperature. On the other hand, a cogwheel rotation of both isopropyl groups will most likely lower this barrier significantly.

Crystal and Molecular Structures

The molecular structures of two primary bis(amino)phosphanes were determined by X-ray structure analysis. PhP(NH*i*Pr)$_2$ **3**, crystallizes as needles in the orthorhombic

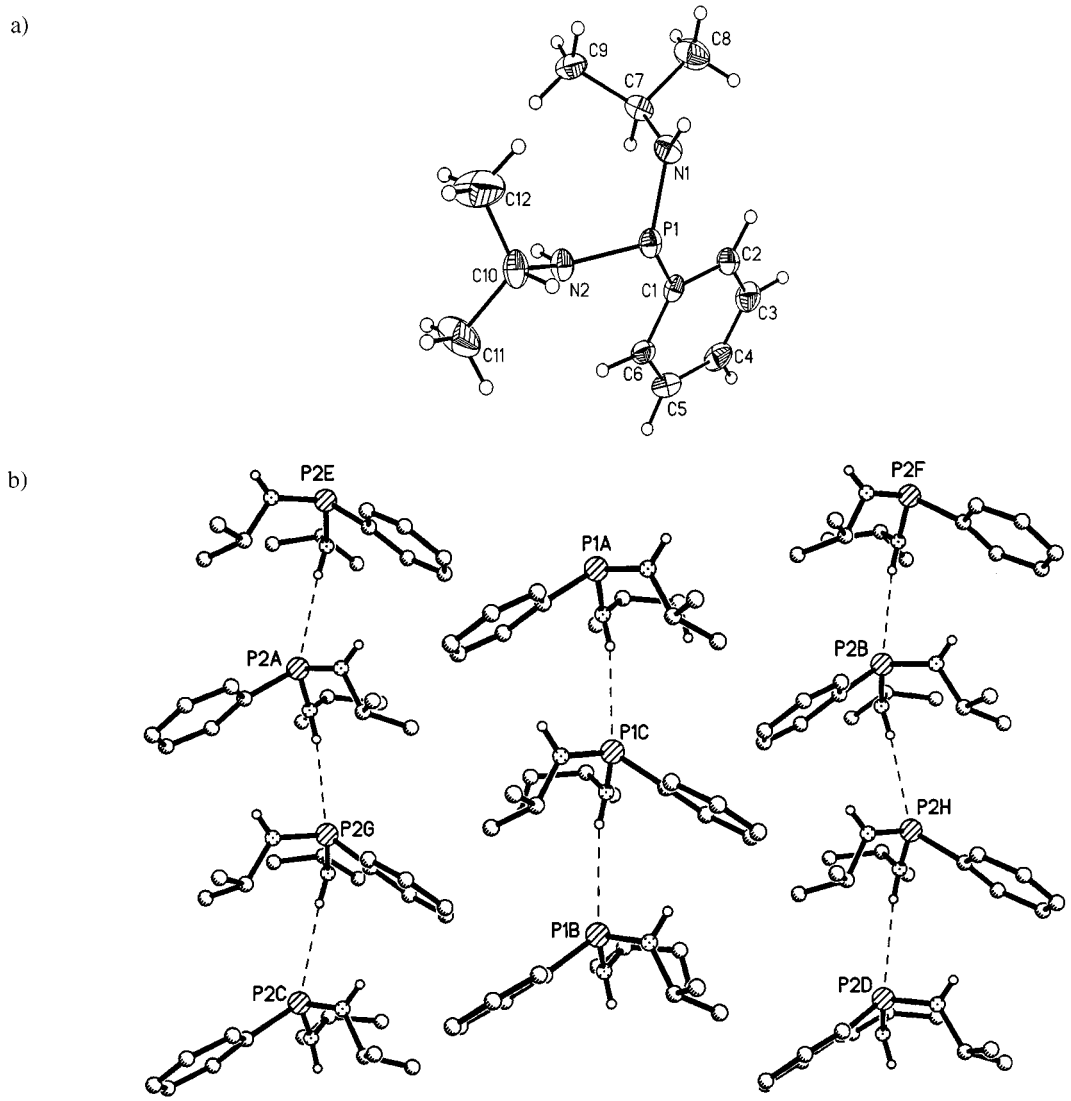


Figure 3. a) The molecular structure of the two independent $PhP(NHiPr)_2$ molecules in ORTEP representation; thermal ellipsoids are drawn on a 25% probability scale; selected bond lengths (Å) and angles (°): P1−N1 1.687(4), P1−N2 1.875(4). P1−C1 1.844(5), N1−C7 1.448(7), N2−C10 1.476(6); − N1−P1−N2 113.7(2), N1−P1−C1 100.2(2), N2−P1−C1 99.2(2), C10−N2−P1 120.1(4), C7−N1−P1 127.9(4); P2−N3 1.674(5), P2−N4 1.684(5), P2−C13 1.836(5), N3−C19 1.471(6), N4−C22 1.465(7); N3−P2−N4 113.0(2), N3−P2−C13 99.6(2), N4−P1−C22 100.0(2); b) Stereoplot of the contents of the unit cell of $PhP(NHiPr)_2$ **1**, along the b−axis; N3−H3 0.88 Å, H3···P 1.99 Å; angle N3−H3−P2 172.6°

system, space group $Pca2_1$ with $Z = 8$. Therefore, there are two independent molecules in the asymmetric unit, (see Figure 3a). Both molecules differ only slightly in bond lengths and possess almost the same conformation. However the pyramidalization at the P atoms is significantly different as shown by the sum of bond angles at atom P1 (325.9°) and atom P2 (319.7°). Each of these independent molecules are arranged in the unit cell by forming chains resulting from N−H···P hydrogen bonding as shown in Figure 3b.

The N atoms deviate only slightly from a planar environment because the sum of bond angles for N1 is 355.4°, for N2, 352.5°, for N3, 355.4° and for N4, 352.1°. The plane of the phenyl group does not stand perpendicular to the respective N_2P plane but is twisted against it by ≈ 65°. Association of the molecules results from weak hydrogen bonding between N and P atoms of neighboring molecules with a N1(X)···P1(X) distance of 3.789 Å and a N2(X)···P2(X) distance of 3.740 Å. The respective P···H distances are 2.98 and 2.87 Å, and the P−H−N angles are 160.1° and 172.6°, respectively.

In contrast to $PhP(NHiPr)_2$ whose amino groups are present in an *anti*-conformation, a *syn*-conformation is found for $PhP(NHPh)_2$ **5** in the solid state as shown in Figure 4. This compound crystallizes in the centrosymmetric monoclinic space group *Cc*; the molecule itself, however only shows C_1 point group symmetry.

The sum of bond angles at the P1 atom (300.7°), and those at the N atoms (N1: 360°, N2: 358°) are indicative of sp^2 hybridization. An interplanar angle of the phenyl group bonded to atom P1 with respect to the PN_2 plane is 73.5°; so the latter plane is not bisected. As a consequence, the

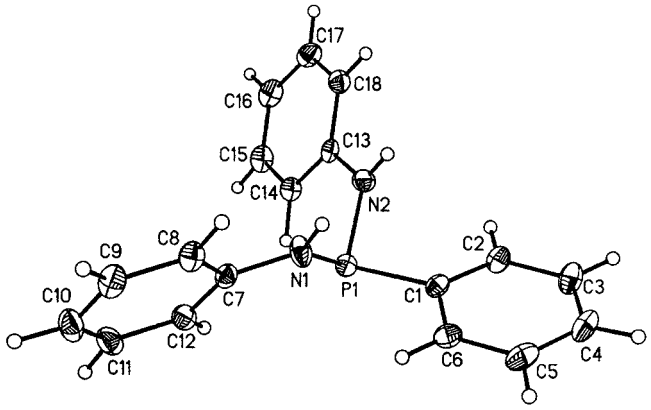


Figure 4. ORTEP representation of a molecule of $PhP(NHPh)_2$ **5**, in the crystal; thermal ellipsoids are drawn on the 25% probability level; bond lengths (Å): P1−N1 1.695(2), P1−N2 1.708(2), P1−C1 1.828(2), N1−C7 1.401(3), N2−C13 1.399(3), N1−H1 0.83, N2−H2 0.81; bond angles (°): N1−P1−N2 105.4(1), N1−P1−C1 97.6(1), N2−P1−C1 97.7(1), P1−N1−C7 127.7(1), P1−N2−C13 126.0(2), H1−N1−P1 118, H2−N2−P1 115

interplanar angles between the C1−C6 phenyl plane with respect to the other two phenyl planes are 62.3° (C7−C12) and 121.2° (C13−C18), respectively, and it should be noted that the phenyl groups of the aniline units are practically in plane with the respective CNH planes (2.6°, 2.4°) allowing for good π-overlap with the π-system of the phenyl groups. This can also be deduced from the short C−N bonds.

In contrast to compound **3**, no NH···P or NH···N hydrogen bonds are present in the crystal of **5**. This may be due to the pronounced pyramidal geometry at the P center and the near planarity of the nitrogen atoms with their phenyl rings resulting in π-interaction. Thus $PhP(NHPh)_2$ is a true molecular compound in the solid state.

As indicated, slow hydrolysis of $mesP(NHiPr)_2$ **7** led to the mesitylphosphonic acid amide mesP(O)H(NH*i*Pr), **9**. Its structure was determined by X-ray methods. The molecule crystallizes in the centrosymmetric monoclinic space group $P2_1/c$. Figure 5a depicts the molecule. Association of the molecules in the solid state can occur by means of NH···P, NH···O and NH···N bonding as well as, but less likely, by PH···O or PH···N bonding. Figure 5b, which shows four molecules, demonstrates that an intermolecular interaction occurs by means of NH···O hydrogen bonding with an intermolecular N···O atom distance of 2.665 Å and an N−H···O bond angle of 175.1°.

The molecular structure of the cyclophosphazane **8** (see Figure 6) is another example of the less preferred *trans*-conformation of the substituents in a centrosymmetric structure.[13] Its bonding parameters fall into the same range as observed for many other derivatives with a P_2N_2 ring. Due to steric effects, the mesityl groups are perpendicular to the P_2N_2 ring. Moreover, the ring nitrogen atoms are slightly pyramidal (sum of bond angles 351.5°). This is a stronger deviation from planarity than usually observed for *trans*-diazadiphosphetidines (358−360°)[14] and is probably a result of the bulky mesityl group.

N-Lithioaminophosphanes

Synthesis

It is to be expected that *N*-lithioaminophosphanes are better nucleophiles than the parent aminophosphanes and therefore might be useful reagents for the synthesis of new ring and chain compounds based on N−P−N structural units. Besides this aspect, the question as to whether these *N*-metallated bis(amino)phosphanes will be present as *N*-metal aminophosphanes or as *P*-metaliminophosphoranes requires the determination of their structures. According to ab initio calculations by Ashby and Trinquier[15] the $RN-PR_2^-$ isomer is favored over the $RN=PR_2^-$ isomer. The stabilization of the latter requires strongly eletronegative substituents such as F or CF_3 bonded to the P atom. Anions of type $RN=PR_2^-$ can probably only be detected if the Li counter ion is separated from the anion by complexation or if replaced by a non-coordinating cation. Otherwise one has to expect association of the *N*-lithioaminophosphanes which raises the question as to whether this will occur through the N or/and P atoms. Indeed, compounds **10**−**14** are associated in the solid state as revealed by X-ray structure determinations.

However, NMR spectroscopic data of these compounds in solution usually showed more ^{31}P NMR signals than expected; even when the solutions had been prepared from well defined crystalline material. This suggests that several solution species are formed from the dimeric and tetrameric species. Therefore, the ^1H and ^{13}C NMR spectra were complex, and it is quite evident that a detailed study of the NMR spectra is required to characterize the solution state of compounds **10**−**14**. So far, this has not yet been achieved successfully.

Metallation of $mesP(NHtBu)_2$ with *n*BuLi yielded no $mesP[N(Li)tBu]_2$ but the *P*-butyl derivative **11**. Therefore, *n*BuLi not only deprotonated the aminophosphane but also induced an exchange of the *P*-bonded organo group.

Reactions

The *N*-lithio derivatives of bis(amino)organophosphanes are expected to be versatile reagents particularly for the synthesis of new heterocycles. Here we describe only a single example as a prototype, namely the synthesis of a 1,3-diaza-2-phospha-4,5-diboretidine **15**.

This new heterocycle can be considered to be a 6π-electron system provided that the P atom resides in a planar moiety. However, the X-ray structure (vide infra) clearly disproves this because the P atom is pyramidal. Nevertheless, this example demonstrates that many other new heterocyclic systems will be accessible via the new reagents, and we will report on these later.

Crystal and Molecular Structures

Compound **10** crystallized at −30°C from its ether solution in the monoclinic space group *C*2/*c*. It proved to be

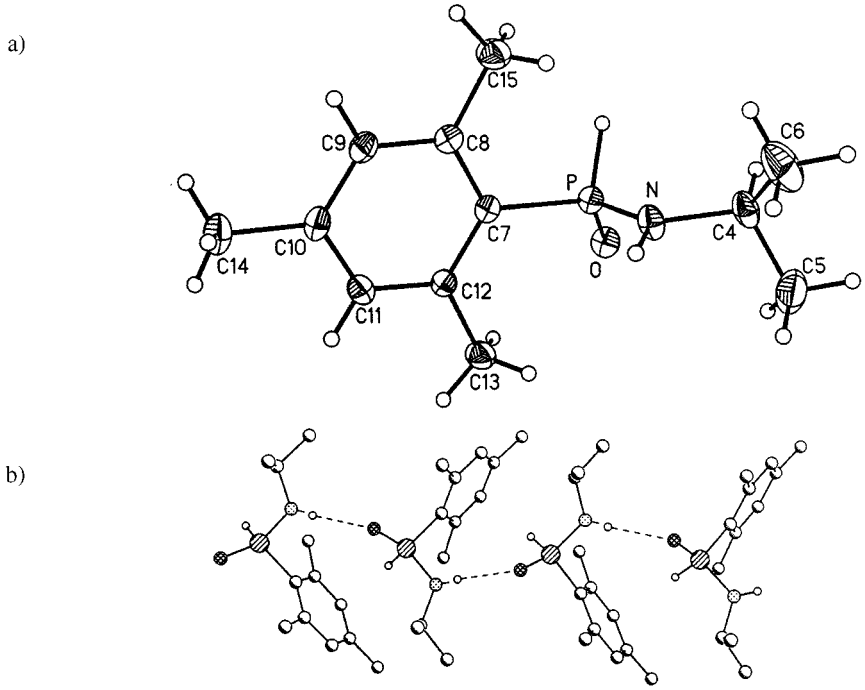


Figure 5. a) Molecular structure of mes−P(O)H(NH*i*Pr) **(9)** in the crystal; thermal ellipsoids are represented on a 25% probability scale; selected bond lengths (Å): P1−N1 1.618(2), P1−O 1.484(2), P1−C 1.808(2), P1−H 1.28(1), N − H2 0.75(1); bond angles (°): O−P1−N1 118.3(1), N1−P1−C7 102.8(1), O−P1−C7 115.9(1), H1−P1−N1 104.3, H1−P1−O 108.7, C7−P1−H1 105.6; b) Association of the molecules **9** via N−H···O interactions; the chains are oriented along the c axis; intermolecular distance O···H: 2.13(1) Å, O···H−N bond angle: 175.1°

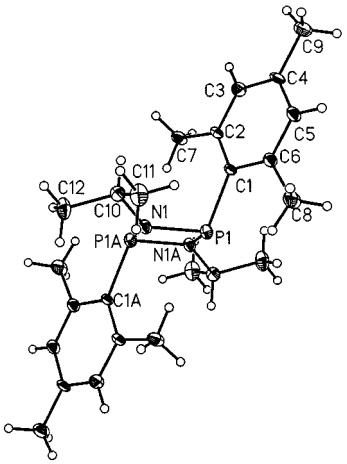


Figure 6. Molecular structure of the diazadiphosphetidine **8**; thermal ellipsoids are depicted on a 25% probability limit; selected bond lengths (Å): P1−N1 1.741(3), P1−N1A 1.727(3), P1−C1 1.852(4), N1−C10 1.463(4); bond angles (°): N1−P1−N1a 81.5(1), N1−P1−C1 106.51), C1−P1−N1a 108.6(1), P1−C1 C6 114.8(3), C10 N1 P1a 125.7(2), C10 N1 P1 127.3(2); interplanar angle: C1 to C6/P_2N_2 94.0; torsion angle: C10−N1−P1−N1a−148.8°

$[Ph_2P–N(Li)tBu]_2{\cdot}OEt_2$ **10**

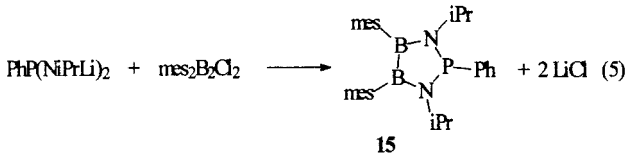
$\{BuP[N(Li)tBu]_2\}_2{\cdot}2OEt_2$ **11**

$\{PhP[N(Li)tBu]_2\}_2$ **12**

$\{PhP[N(Li)Ph)_2\}_2{\cdot}4OEt_2$ **13**

$\{MeP[N(Li)iPr]_2\}_4$ **14**

the hemietherate of $[Ph_2P-N(Li)tBu]_2$ whose molecular structure is depicted in Figure 7. The molecule shows a crystallographically imposed C_2 point group symmetry.



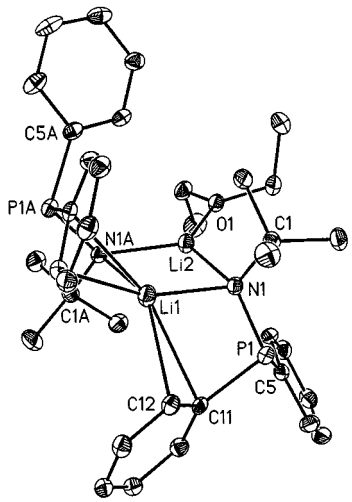


Figure 7. ORTEP representation of the molecular structure of **10** in the crystal; hydrogen atoms are omitted for clarity; thermal ellipsoids are drawn on a 25% probability level; selected interatomic distances (Å): Li1−N1 2.018(5), Li2−N1A 2.075(5), Li2−O1 2.034(7), P1−N1 1.686(3), P1−C5 1.848(3), P1−C11 1.849(3), N1−C1 1.504(4); bond angles (°): C5−P1−C11 99.7(1), C5−P1−N1 112.6(2), C11−P1−N1 103.0(1), P1−N1−Li1 106.9(2), P1−N1−Li2 139.4(1); other interatomic distances (Å): Li1···C11 2.700(3), Li1···C12 2.602(6), Li2···C2 2.602(6); Li1···P1 2.983(2), Li1···Li2 2.42(1); torsion angle C1−N1−P1−N1a −148.8°

Because the structure of $Ph_2P-NHtBu$ is still unknown, no direct comparison of **10** to changes in bonding parameters with the parent compound can be made. The P−N bonds of **10** are shorter than in $Ph_2P-NHmes$ [1.730(2)Å][16] but not as short as in $Ph_2P-NmesLi\cdot 2OEt_2$ [1.661(2) Å]. Only the nitrogen atoms are involved in coordination with the Li atoms. The Li−N bond to the ether-bearing Li atom is 0.057 Å longer than the Li−N bond to the ether-free atom Li1. However, this atom has two close contacts with H atoms of two methyl groups. Moreover, atom Li1 is also shielded sterically by the two phenyl groups as there are four η-Li−C interactions. These are sufficient to prevent the addition of an ether molecule to the atom Li1, and also to inhibit Li−P coordination. The two phenyl groups are mutually oriented at an interplanar angle of 110.9° to one another, and the coordination of the phenyl groups C11 to C16 and C11a to C16a to the atom Li1 form an interplanar angle of 45.6°. A torsion angle of 15.8° for the four-atom arrangement Li2−N1−C1−C2 reveals an almost optimal orientation for the Li2···H2C and Li2···H10A "agostic" interactions with distances of 2.44 Å. Thus the structure of the anion shows an *anti*-conformation of the substituents at the PN unit (torsion angles C1−N1−P1−C5: −121°, C1−N1−P1−C11: 134°).

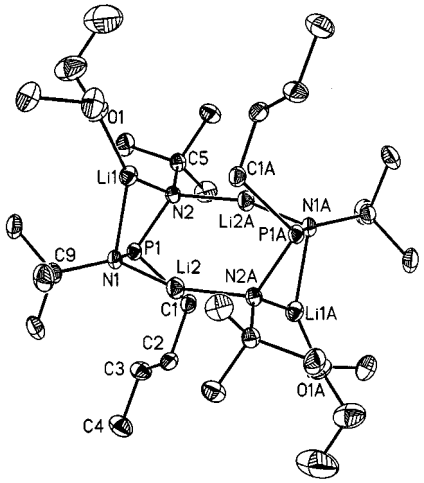


Figure 8. The molecular structure of $\{BuP[N(Li)tBu]_2\}_2\cdot 2OEt_2$ **(11)** in the crystal; hydrogen atoms omitted for clarity; thermal ellipsoids are represented on a 25% probability scale; selected bond lengths and atom distances (Å): Li1−N1 2.034(5), Li1−N2 1.983(5), Li2−N1 1.930(5), Li2−N2a 1.962(5), Li1−O1 1.926(5), P1−N1 1.707(2), P1−N2 1.715(2), P1−C1 1.876(3); P1···Li1 2.543(5), Li2···C5A 2.785(5), Li2···P1 3.046(5); bond angles (°): C1−P1−N1 100.9(1), C1−P1−N2 100.9(1), N1−P1−N2 98.7(1), N1−Li1−N2 80.5(2), O1−Li1−N2 142.7(3), O1−Li1−N1 135.9(2), N1−Li2−N2A 160.0(3), 85.2(2), Li1−N1−P1 85.2(2), Li2−N1−P1 113.6(2), Li1−N2−P1 86.6(2)

The dilithio compound **11** crystallizes as a dimer of composition $BuP[N(Li)tBu]_2\cdot OEt_2$. Its molecular structure is shown in Figure 8. The molecule is centrosymmetric due to a crystallographically-imposed center of inversion at the center of an eight-membered ring. The two non-equivalent P−N bonds are slightly but significantly different and somewhat longer than in **10**. They can be considered as P−N single bonds. All nitrogen atoms are involved in coordination to Li atoms. There are two kinds of Li atoms. Atom Li1 is coordinated to one oxygen atom and two N atoms, and the sum of bond angles at the tricoordinated atom Li1 is 359°. In addition, there is a fairly short Li1···P1 contact [2.543(5) Å]. However, this is a consequence of the geometry of the four-membered ring because the lone pair of the atom P1 presumably points outwards from the four-membered butterfly-shaped Li1−N1−P1−N2 ring. Taking the sum of bond angles at P1 (300.5°) into account, one can assume that hybridization at this atom is halfway between p^3 (270°) and sp^3 (330°) so that the lone pair at the P atom no longer has pure s character. While the N1−Li1−N2 bond angle of the four-membered ring is rather sharp [81.5(2)°] the N1−Li2−N2a bond angle is quite open (144.9°). Atom Li2 is, however, sterically shielded by two Li···H interactions ranging from 2.37 to 2.39 Å. While the folding angle of the four-membered ring Li1−N1−P1−N2 is 32.7°, the N1Li1N2 plane adopts an interplanar angle of 85° with the N1Li2N2a plane. Figure 9 shows the closest intramolecular Li···H contacts (2.4−2.7 Å) of molecule **11** which contribute to the steric shielding

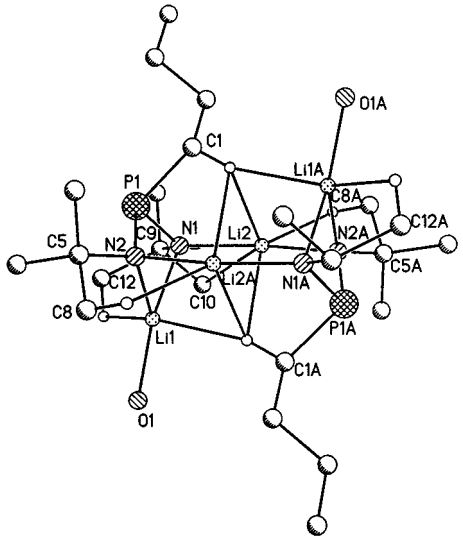


Figure 9. View almost along the Li_2N_4 plane on the structural core of molecule **11** including short H−Li contacts

of the Li atoms. A structure similar to **11** is observed for the solvent-free centrosymmetric molecule $\{PhP[N(Li)-tBu]_2\}_2$ **12**, as shown in Figure 10. There are two independent "monomers" in the asymmetric unit. The dimeric molecules exhibit eight-membered Li_4N_4 rings with the P atoms bridging adjacent pairs of N atoms, or, alternatively, two N_2PLi four-membered rings are connected by two Li atoms, with the formation of a total of four Li−N bonds.

Two Li centers are η^6-coordinated to phenyl groups. As a result of this coordination, the Li2−N2−Li1 bond angle is only 93.3° (100.1° in **11**), and the interplanar angle N1−Li1−N2/N2−Li2−N1a is now 99.1°. Moreover, the folding angle between the N_2Li and the N_2P plane of the four-membered ring is 16.5°, and, therefore the ring is closer to planarity than the analogous ring in **11**. As ex-

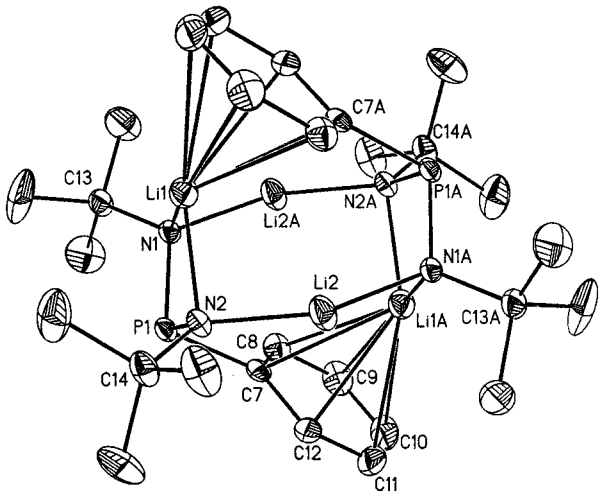


Figure 10. The structure of the molecule **12** in the crystal; hydrogen atoms are omitted for clarity and thermal ellipsoids are represented on a 25% probability scale; selected bond lengths and atom distances (Å): Li1−N1 2.017(5), Li1−N2 2.027(6), Li2−N2 1.918(5), Li2−N1a 1.928(6), P1−N1 1.686(3), P1−N2 1.693(2), P1−C7 1.867(3), Li1···P1 2.559(5), Li1···C 2.618−2.750(6); bond angles (°): N1−P1−C7 100.8(1), N2−P1−C7 99.8(1), N1−P1−N2 102.8(1), N2−Li2−N1a 149.9(2), N1−Li1−N2 81.5(2), Li1−N2−Li2 93.3(2), P1−N1−Li2A 115.8(2), P1−N1−Li1 87.0(2), P1−N2−Li1 86.5(2), P1−N2−Li2 119.6(2); interplanar angles: N2−Li2−N1A/C7−C12 44.3, N2−Li2−N1a/N1−P1−N2 71.4, N2−Li2−N1A/N1−Li1−N2 99.1

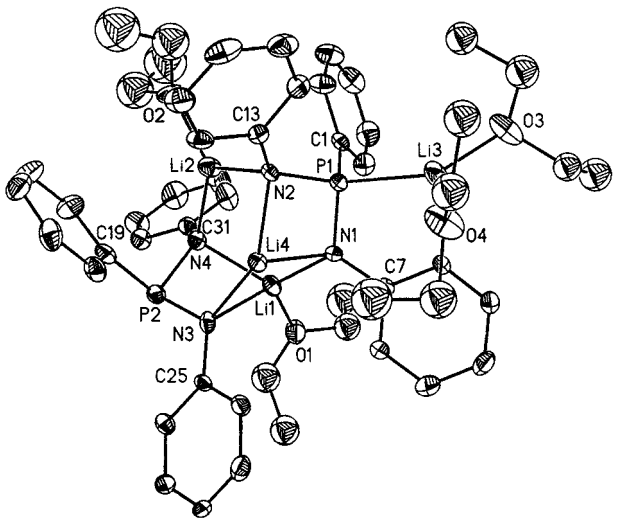


Figure 11. ORTEP molecular structure of $\{PhP[N(Li)Ph]_2 \cdot 2OEt_2\}_2$ **(13)**; hydrogen atoms are omitted for clarity; thermal ellipsoid are drawn on a 25% probability scale; selected bond lengths and atom distances (Å): Li1−N1 2.09(1), Li1−N4 2.09(2), Li1−N3 2.26(2), Li1−O1 1.89(1), Li2−N2 2.03(1), Li2−N4 2.01(1), Li2−O2 1.90(1), Li3···P1 2.55(2), Li3−O3 1.88(1), Li3−O4 1.91(1), Li4−N1 2.08(2), Li4−N2 2.01(1), Li4−N3 1.95(1), P1−N1 1.688(6), P1−N2 1.683(7), P2−N3 1.711(7), P2−N4 1.704(7), P1−C1 1.84(1), P1−C19 1.839(9), P1···Li4 2.64(1), P1···Li3 2.55(2), L2···Li1 2.746(9), P2···Li4 3.097(8); bond angles (°): N1−P1−N2 99.3(3), N1−P1−C1 104.7(4), N2−P1−C1 104.3(4), N3−P2−N4 97.6(3), N3−P2−C19 100.2(4), N4−P2−C19 101.9(4), O3−Li3−O4 114.1(8), O3−Li3−P1 126.9(9), O4−Li3−P1 118.9(8), O1−Li1−N1 117.0(7), N1−Li1−N4 118.7(7), O1−Li1−N4 119.6(7), N2−Li2−N4 116.1(7), O2−Li2−N2 118.2(7), O2−Li2−N4 125.7(8), N2−Li4−N3 140.7(7), N1−Li4−N2 78.0(5), N1−Li4−N3 110.7(6), P1−N1−Li4 88.3(7), P1−N1−Li1 125.3(7), Li1−N1−Li4 71.6(8), P1−N2−Li4 90.8(8), P1−N2−Li2 116.1(6), Li2−N2−Li4 89.0(8), P2−N3−Li4 115.2(7), P2−N3−Li1 86.7(7), P2−N3−C25 119.3(7), P2−N4−Li1 92.3(8), P2−N4−Li2 116.6(7), P2−N4−C31 118.3(8), Li1−N4−Li2 102.3(9)

pected for a four-membered LiN_2P ring, a short Li···P distance of 2.559(5)Å is observed.

Although compound **13** is formally related to both **11** and **12**, as it is a dimeric dimetallated bis(monoorganoamino)organophosphane (see Figure 11), its structure turned out to be vastly different to **12**, obviously due to solvation by diethyl ether. There is (formally) one ether molecule per Li atom. However the structure determination revealed that there are altogether *four* different Li centers, one of which binds two ether molecules, two others only one, while the fourth Li center carries no ether molecule at all as seen in Figure 11.

There are two molecules of **13** in the asymmetric unit of the triclinic unit cell of space group $P\bar{1}$. The differences between their bonding parameters are insignificant therefore only one molecule is depicted in Figure 11. Formally, the structure can be described as $[(Et_2O)_2Li]$-$[Li_3(NPh)_4(PPh)_2\ OEt_2]$, and the anionic cage as being built from two PN_2Li four-membered rings joined by two LiN bonds to result in a structure of three condensed four-membered rings whose open faces are bridged by a $Li(OEt_2)$ unit by two nitrogen atoms. On the other hand, the $(Et_2O)_2Li$ unit is joined to atom P1 with a comparatively short Li−P distance of 2.54 Å while the Li4−P1 distance in the four-membered ring is 0.1 Å longer. In contrast, the four-membered ring P2N3N4Li1 is characterized by a longer and therefore weaker Li1−N3 interaction, and this causes a lengthening of the Li1−P2 distance to 2.746(5)Å.

P−N bonds to atom P1 are shorter than in the parent compound $PhP(NHPh)_2$, but are of equal lengths, while those at atom P2 seem to be slightly different but are on average only 0.01 Å longer than those at P1. These bonds correspond to those found for $PhP(NHPh)_2$.

The lithiation of $MeP(NH\textit{i}Pr)_2$ led to $MeP[N(Li)\textit{i}Pr]_2$ which turned out to be the *tetramer* **14**, crystallizing with 5 molecules of THF. Four of these THF molecules are bonded to Li centers, the fifth remains uncoordinated in the triclinic lattice. Thus the composition of compound **14** can be described as $\{MeP[N(Li{\cdot}THF)\textit{i}Pr]\ [N(Li)\textit{i}Pr]\}_4$ THF but it is surprisingly asymmetric as depicted in Figure 12.

Inspection of Figures 12 and 13 reveals that the Li atoms are coordinated quite differently. While Figure 12 gives an overview of the structure, Figure 13 represents more clearly its cage structure. Atoms Li2, Li4 and Li6 are tricoordinated by two N atoms and one O atom; they form a rhombus with another Li atom which coordinates to the two N atoms. Atoms Li1 and Li7 have three nitrogen atoms as coordination partners and these are arranged in a plane including the Li atoms (sum of bond angles 359.9 and 360° respectively). Two of the N−Li−N angles subtending at Li are comparatively small, ranging from 100.5 to 113.5°.The others are rather wide (144.8 and 149.6°). On the other hand, atom Li3 has two nitrogen atoms and a phosphorus atom as coordination partners. The same number of bonded atoms are observed for atom Li5 which is, however,

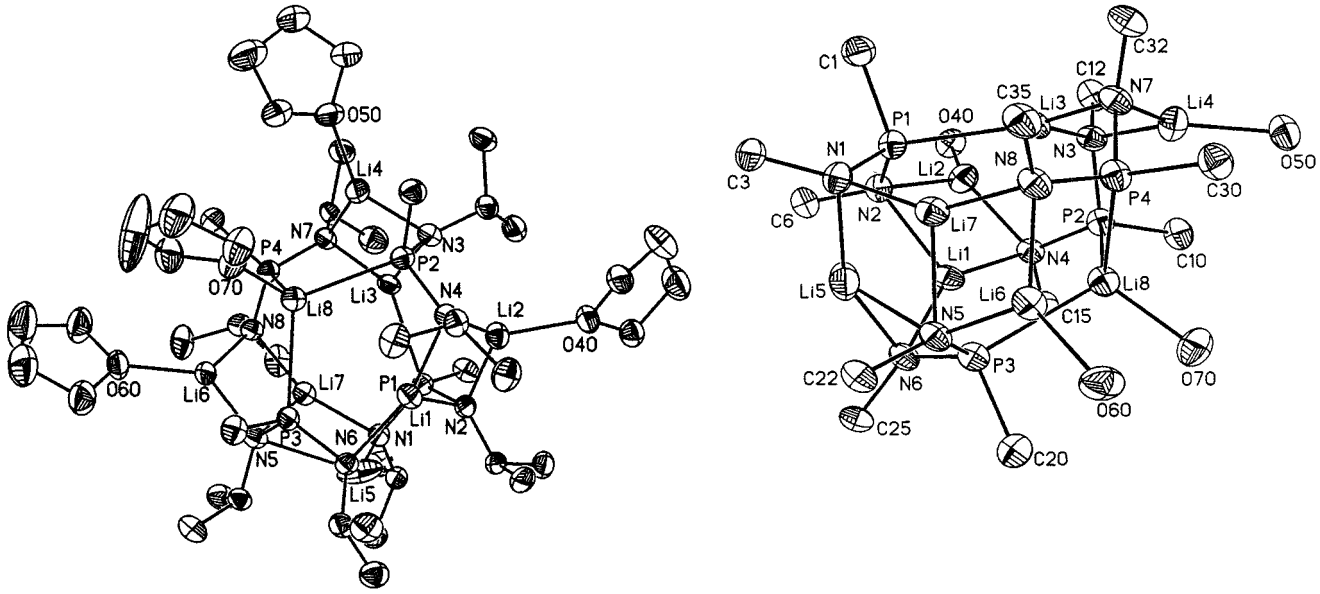


Figure 12. a) ORTEP molecular structure of {MeP[N(Li)*i*Pr]2·thf}$_4$ **(14)**; hydrogen atoms are omitted; thermal ellipsoids are represented at a 25% probability level; selected bond lengths and atom distances (Å): P1−N1 1.671(4), P1−N2 1.683(4), P1···Li3 2.514(8), P1···Li5 2.76(2), P1···Li7 2.854(8), P2−N3 1.677(5), P2−N4 1.686(4), P2···Li8 2.656(9), P3−N5 1.687(4), P3−N6 1.674(4), P3···Li8 2.629(9), P4−N7 1.656(5), P4−N8 1.682(4), P4···Li8 2.677(9), C1−P1 1.871(7), N1−Li5 1.96(2), N1−Li7 2.082(9), N2−Li1 2.17(1), N2−Li2 2.043(9), N3−Li3 2.006(9), N3−Li4 2.05(1), N4−Li1 2.105(9), N4−Li2 1.97(1), N5−Li6 1.999(9), N5−Li7 2.17(1), N6−Li1 2.03(1), N6−Li5 1.96(1), N7−Li3 2.004(9), N7−Li4 1.98(1), N8−Li6 2.01(1), N8−Li7 2.036(9); bond angles (°): N1−P1−N2 112.5(2), Li3−P1−N2 107.5(2), Li3−P1−N1 121.5(2), C1−P1−N1 105.1(2), C1−P1−N2 108.7(2), N2−Li1−N4 10.5(4), N2−Li1−N6 113.6(4), N4−Li1−N6 144.8(5), P1−N1−Li5 68.1(2), P1−N1−Li7 98.4(2), Li5−N1−Li7 80.3(6), P1−N2−Li2 112.2(3), P1−N2−Li1 102.9(3), Li1−N2−Li2 72.2(4),N2−Li2−N4 111.1(5), N2−Li2−O40 123.0(4), N4−Li2−O40 116.1(4), C10−P2−N4 105.2(2) C10− P2−N3 106.2(3), C10−P2−Li8 118.6(3), N3−P2−N4 109.4(2) Li8−P2−N3 107.3(3), Li8−P2−N4 109.8(2), P2−N3−Li3 103.9(4), P2−N3−Li4 96.6(4), P2−N4−Li1 105.8(3), P2−N4−Li2 104.7(4), C20−P3−N5 109.9(2), C20−P3−N6 105.6(3), N5−P3−N6 111.3(2), P3−N5−Li6 110.8(3), P3−N5−Li7 104.4(3), P3−N5−Li5 72.6(3), P3−N6−Li5 91.3(5), P3−N6−Li1 96.3(3), C30−P4−N7 103.0(3), C30− P4−N8 104.8(2), N7−P4−N8 116.7(2), C30−P4−Li8 121.6(3), P4−N7−Li4 109.9(4), P4−N8−Li7 107.9(3), P4−N8−Li6 99.7(3), N3−Li3−N7 107.1(4), N3−Li3−P1 118.5(4), N7−Li3−P1 134.3(4), O50−Li4−N7 128.8(5), O50−Li4−N3 125.1(5), O50−Li4−P2 107.8(4), N1−Li5−N6 148.5(7), N1−Li5−P3 120.7(5), O60−Li6−N5 124.0(6), O60−Li6−N8 128.1(5), O60−Li6−P4 117.0(4), N1−Li7−N5 109.9(4), N1−Li7−N8 149.6(6), N5−Li7−N8 160−4(5), O70−Li8−P3 109.1(5), O70−Li8−P2 109.8(3), O70−Li8−P4 109−2(4), P2−Li8−P3 111.3(3), P2−Li8−P4 110.3(4); b) The core structure of **14** was obtained by removing all the substituents from the N and P atoms and the C atoms of the THF molecules

not part of a Li_2N_2 rhombus. Finally, atom Li8 binds to three phosphorus atoms and one oxygen atom. Li8 represents the only Li center which is tetracoordinated. Amongst the tricoordinated Li centers, atoms Li2 and particularly Li5 are unusual because the sum of bond angles at Li2 is 350° but for Li5 only 323° (without including a possible weak Li5−P3 interaction (2.605(4).Å). One may see this atom as being dicoordinated, particularly because the Li2−N5 distance is 2.551(6) Å and the N6−Li5−N1 bond angle is rather open [148.5(7)°]. Similar angles are also observed in the structures of **11** and **12**.

The five-membered ring of the 1,3,2,4,5-diazaphosphadiboretidine **15** is almost planar (sum of bond angles 539.8°). It contains a pyramidal P1 atom, and planar N and B atoms. The B−N bond lengths are characteristic of π-bonds. The B−B bond length is typical for a single bond and lies in the usual range for diborane(4) derivatives. The two mesityl groups include an interplanar angle of 64°.

Discussion

The stability of primary bis(amino)organophosphanes depends on the steric shielding at the P center. This is an indication that the elimination of RNH_2 from these molecules to form, e.g. 1,3,2,4-diazadiphosphetidines[13][14] occurs by intermolecular steps. An intramolecular amine elimination to form an iminophosphane RP=NR′ followed by dimerisation could be an alternative. This process, however, might be less influenced by steric effects. An intramolecular process should be dependent on the conformation of the $R'P(NHR)_2$ molecules. It is evident that a mechanistic study is required to settle this question.

The synthesis of the bis(organoamino)organophosphanes is readily achieved by aminolysis of the respective chloride $R'PCl_2$ or by silazane cleavage. The latter method is versatile and quite useful, particularly if steric effects are not too pronounced.

As demonstrated for $P(NHPh)_3$ ($\delta^{31}P = 73.8$)[6f] the ^{31}P nucleus is better shielded in compound $PhP(NHPh)_2$. Replacement of an *i*Pr group by a *t*Bu group at the N atom also results in a better shielding of the ^{31}P nucleus by 14 ppm. It is also surprising that the ^{31}P nucleus is better shielded in $PhP(NHPh)_2$ than in $PhP(NHiPr)_2$. This may be due to the larger N−P−N bond angle in $PhP(NHiPr)_2$ relative to $PhP(NHPh)_2$, due to a higher s-character of the P atom in $PhP(NHPh)_2$. However, this may be due to the longer P−N bond lengths resulting from hydrogen bonding but we have not determined the degree of association in

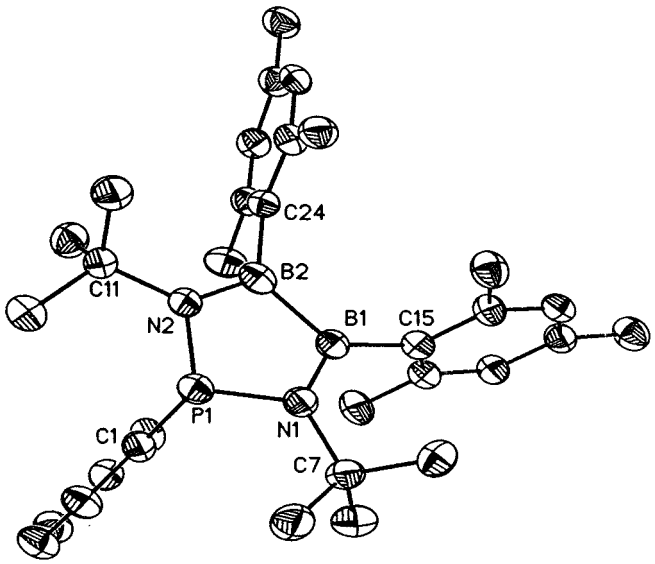


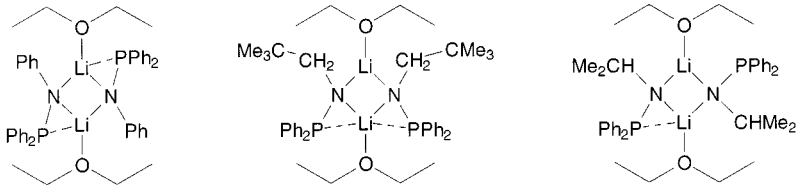
Figure 13. The molecular structure of **15** in the solid state; thermal ellipsoids are represented at a 25% probability level; hydrogen atoms are omitted for clarity; selected bond lengths (Å): P1−N1 1.743(5), N1−B1 1.436(7), B1−B2 1.71(1), B2−N2 1.428(7), N2−P1 1.732(5), P1−C1 1.841(6), B1−C15 1.585(8), B2−C24 1.605(8); bond angles (°): C1−P1−N12 100.9(2), C1−P1−N2 101.5(2), N1−P1−N2 95.7(2), P1−N1−B1 114.8(4), P1−N1−C7 115.7(3), C7−N1 B1 129.4(5), N1−B1−B2 106−6(4), N1−B1−C15 125.3(5), B1−B2−N2 108.4(5), B1−B2−C24 128.1(5), B2−N2−P1 114.3(4); torsion angle: C1−P1 N1−C7 −80.4°; interplanar angle: N1N2P1/C1 to C6 92.8°; C15 to C20/C24 to C29 71.1°

solution. On the other hand, there is only a small variation both in the shielding of the ^{15}N nuclei as well as in the coupling constant ^{1}J(P-N), irrespective of the substituent at the P atom (Me, Ph, mes) or the N atoms (*i*Pr, *t*Bu, Ph). This suggests that in solution the structural differences observed for the structure of $PhP(NHiPr)_2$ and $Ph(NHPh)_2$ in the solid state, particularly with respect to the pyramidal geometry at the P atom, but also at the N atoms, becomes less significant or even negligible. This also holds for the mesityl bis(amino)phosphanes, although the coupling constants ^{1}J(P-N) are noticeably smaller (by 4.5 and 8.3 Hz, respectively, for the isopropyl and *tert*-butyl derivative), probably due to steric effects particularly for the sterically-crowded $mesP(NHtBu)_2$.

It would be most interesting to compare the structural parameters and their changes in the aminophosphanes with those of the respective *N*-lithio compounds. Unfortunately there are, at the moment, too few pairs of compounds to be compared in this respect. Nevertheless, the structural aspects of *N*-lithioaminophosphanes are attracting increasing interest [2,4,15,16] since the determination of the X-ray structure of $[Ph_2P-NPh(Li\cdot OEt_2)]_2$.[2] So far, $Ph_2P-N(Li)mes^*\cdot 2OEt_2$[16] is the only monomeric *N*-lithio-monoaminophosphane known which shows a *trans*-conformation with respect to the P−N bond. A related compound is the lithium salt of the bis(diphenylphosphanyl)amine $Ph_2P-NH-PPh_2$.[4] Therefore, bulky groups are necessary besides supporting ligands such as THF or Et_2O which coordinate to the Li centers. The *trans*-conformation in monoaminophosphanes inhibits any intramolecular P···Li interaction. However, this kind of interaction is observed in $Ph_2P-N[Li(THF_3)]-PPh_2$ where a *cis*-conformation was determined, a result also supported by ab initio calculations.[4a] Besides these two structurally-characterized compounds, there are three dimeric *N*-lithioaminophosphanes of type $Ph_2P-N(Li\cdot OEt_2)R$ (formulae **I**−**L**) where the *cis*-conformation prevails. These compounds exhibit different degrees of P···Li interactions.[16] Thus, **I** and **K** show weak Li···P interactions, while there is only a single one in **L**. Thus an increasing steric effect due to the nitrogen substituents decreases the probability of Li···P interactions. These conclusions are supported by the molecular structure of **10** where a *trans*-conformation is observed for the $Ph_2P-NtBu$ unit which inhibits a Li···P interaction. The *trans*-conformation results from the N−Li coordination, and the η^6-coordination of two phenyl groups of two different $Ph_2P-NtBu$ units. The consequence of this is, in addition, that only a hemietherate is formed. The P−C bond lengths in **11** are similar to those in **6** and **L**, a situation that does not allow one to draw the conclusion as to whether the orbitals at nitrogen mix with the P−C* orbitals or not.[15][16]

For dimetallated bis(amino)organophosphanes, structures different to monometallated monoaminodiorganophosphanes are to be expected. It is, however, somewhat surprising that out of the four examples investigated, three are dimeric. Of these, two have rather similar structures in spite of the fact that **11** is an ether solvate and **12** is non-solvated. Moreover, the formation of **11** was also not expected because the nucleophilic exchange of *P*-bonded organo groups is an exception in phosphorus chemistry. This kind of reaction has been observed, for instance, in the reaction of tris(2-pyridinyl)-trimethylsilylamino-phosphoranes with methyl lithium.[17] Since this exchange of R groups has only been observed during the metallation of $mesP(NHtBu)_2$ and not of phenyl-bis(monoorganoamino)-phosphanes it appears that the mesityl group acts as a better leaving group than a phenyl group. Thus the butyl anion not only acts as a base for NH deprotonation, but also as a nucleophile, attacking the P^{III} center.

The conformation of the $CP(NC)_2$ units in **11** and **12** can be considered as representing a *trans* conformation with dihedral C−P−N−C angles of −122.2° and 102.2° for **11** and −126.1° and 123.2° for **12.** Four-membered LiN_2P rings are formed which are connected by two Li−N−Li bonds, making all nitrogen atoms tetracoordinated. Although the Li···P distances in **11** and **12** are 2.543 and 2.559 Å, respectively, and are therefore shorter than the "secondary" Li−P bonding in **I,** the short distances are certainly a consequence of the geometry of the four-membered ring, and reflect no Li−P single bond interaction. The rather sharp N−Li−N bond angle (80.5° in **11** and 81.5° in **12**) is also an indication that Li−P bonding is avoided. However, the N−P−N bond angles are 98.7 and 102.8° in **11** and **12**. In addition, the lone pair of electrons at the P atoms cannot be of an s-type because the sum of bond angles at these atoms is 291° and 303.4°, respectively. There is only a change of 2.7° for the N−P−N bond angles in **12**, com-



I **K** **L**

pared to the non-metalated aminophosphane, and only a slight elongation of the P−N bond lengths (average 0.01 Å), which has to be considered as almost negligible. However, the P−C bond length in **12** is 0.05 Å longer than in **11,** and this is an indication of a negative hyperconjugative effect.[8,15,16] Most interesting is the presence of dicoordinated Li atoms both in **11** and **12**, a situation that is similar to that found in tetrameric lithium tetramethylpiperidine[10] or trimeric $LiN(SiMe_3)_2$.[18] Another feature of **12** is that two of its Li centers are η^6-coordinated to phenyl rings. This mode of coordination saturation does not occur very often, but is nevertheless not uncommon,[19] and found, for instance, in $[(Me_3Si)_2N-N(Li)Ph]_4$[1d] or $[Ph(Li)N-N(Li)SiMe_3]_4$[1c] the latter also containing $(\eta^6\text{-}C_6H_5)_2Li$ units.

No η^6-PhLi groups are present, however, in $\{PhP[N(Li)Ph]_2\}_2 \cdot 4OEt_2$, **(13)**. The rather unsymmetrical structure of this compound having four different kinds of Li centers is unique. Once again there is a Li···P distance (2.55 Å) across a LiN_2P ring that might indicate weak bonding, but we regard this as a consequence of the ring structure. One may also look upon this molecule as a contact ion pair because one Li atom is not used for completing the $Li_3P_2N_4$ cage. The Li−P atom distance of this unique Li center, formally a $(Et_2O)_2Li^+$ unit, is 2.64 Å. This distance is similar to that found in lithiumphosphides,[20] e.g. [(TMEDA·Li)PPh_2 (2.61 Å)][21] or $[LiP(SiMe_3)_2]4\cdot 2THF$ (2.48−2.64 Å).[22] While the P−N bond lengths at the atom P2 are not influenced by the metallation, obviously because the P atom remains tricoordinate, the P−N bonds at P1, the atom which can be considered as tetracoordinated become shorter. This is unusual insofar as an increase in coordination normally causes bond lengthening. Therefore, this can be taken as an indication of π-bonding in the P−N bond, as supported by the observation that the P−C bond length is not affected and remains the same as in **12**.

Even more unsymmetrical is the structure of **14**. The most interesting feature is the presence of a P_3LiO unit besides a planar N_3Li unit. By maximizing the number of Li−N contacts, it is obvious that one LiN_3 unit must finally lead also to Li−P contacts. The first principle leads to three four-membered Li_2N_2 rhombi, a structural unit typical for lithium amides.[19] Of the eight Li centers, seven are tricoordinate, and only the Li atom of the LiP_3 unit becomes tetracoordinated by also binding a THF molecule. Although one can rationalize that Li−N contacts in lithiated aminophosphanes are preferred as a result of the principle of hard/soft acid-base character, LiP interactions cannot be totally avoided particularly in the lithiated bis(amino)phosphanes $[R'P(NLiR)_2]_n$ for n > 2. Due to the association of the lithiated aminophosphanes, the question as to whether these might contain the structural unit of a *P*-metallated iminophosphorane can be discarded, as there is no indication of short P−N bonds (higher bond order) where Li···P coordination is observed. It is evident that bis-metallated bis(amino)phosphanes have structures completely different to bis-metallated hydrazines. The reason that they must have different geometries is due to their composition, which is $RP(NLiR)_2$ for the former and R(Li)N−N(Li)R for the latter with the P atom offering at least potentially, an additional coordination site

Experimental Section

All experiments were performed under anhydrous conditions with standard Schlenk techniques and nitrogen as the protecting gas. Solvents were dried by standard procedures, distilled under a nitrogen atmosphere and stored under N_2. The amines and the phosphorus halides used were commercial products, whose purity was checked by NMR methods. $Ph_2P-NHtBu$ was prepared as described in the literature.[2] − M.p.′s were determined with a Mel-Temp apparatus. − Elemental analysis was performed at the institute′s microanalytical laboratory. − NMR: Jeol 270, Jeol 400 with $SiMe_4$ or C_6D_6 internal standard for ^1H and ^{13}C, internal 1M aqueous $^{15}NH_4^+$ solution for ^{15}N, 85% H_3PO_4 internal for ^{31}P; 1M LiCl solution external for ^7Li. − IR: Nicolet FT 320 (samples in Nujol/Hostaflon mulls); MS: Atlas CH7. − X-ray: Siemens P4 diffractometer equipped with a CCD area detector and LT2 low temperature device; Mo-K_α radiation, graphite monochromator.

Bis(isopropylamino)methylphosphane (1): $iPrNH_2$ (14.7 g, 249 mmol) was dissolved in diethyl ether (250 mL) and a solution of $MePCl_2$ (5.84 g, 50.3 mmol) in ether (50 mL) was added at 0°C while stirring. A precipitate formed. Stirring was continued overnight, the solid was removed by filtration, and washed three times with 150 mL of ether. The solutions were combined, and the solvent and excess amine were removed in vacuo. The residue was then subjected to distillation. Yield: 6.3 g of **1** (78%), colorless oil b.p. 52°C/2 Torr. − ^1H NMR (C_6D_6, 400 MHz): δ = 0.9 (d, $^3J_{HH}$ = 6.4 Hz, 6 H, CH−CH_3), 1.0 (d, $^3J_{HH}$ = 6.4 Hz, 6 H, CH−CH_3), 1.1 (d, $^2J_{PH}$ = 5.8 Hz, 3 H, P−CH_3), 1.6 (s, broad, 2 H, N*H*), 3.1−3.2 (m, 2 H, C*H*−CH_3). − ^{13}C NMR (C_6D_6, 100 MHz): δ = 18.7 (d, $^1J_{PC}$ = 2.8 Hz, P−CH_3), 26.4 (d, $^3J_{PC}$ = 6.0 Hz, CH−CH_3), 26.9 (d, $^3J_{PC}$ = 3.7 Hz, CH−CH_3), 44.7 (d, $^2J_{PC}$ = 12.6 Hz, *C*H−CH_3). − ^{15}N NMR (C_6D_6, 27.4 MHz): δ = −302.1 (d, $^1J_{PN}$ = 65.3 Hz). − ^{31}P NMR (C_6D_6, 81 MHz): δ = 51.7 (s). − $C_7H_{19}N_2P$ (162.22): calcd. C 51.83, H 11.81, N 17.27; found C 49.24, H 11.96, N 16.82.

Bis (*tert*-butylamino)methylphosphane (2): Prepared in a similar manner to **1** from $tBuNH_2$ (17.3 g, 243 mmol) and $MePCl_2$ (5.0 g,

43 mmol) in a total of 200 mL of diethyl ether. Yield: 7.6 g (84%), colorless oil, b.p. 53°C/5 Torr. – ^{1}H NMR (C_6D_6, 400 MHz): δ = 1.1 (d, $^2J_{PH}$ = 6.6 Hz, 3 H, P–CH_3), 1.2 (s, 18 H, C–CH_3), 1.4 (s, broad, 1 H, N*H*), 1.5 (s, broad, 1 H, N*H*). – ^{13}C NMR (C_6D_6, 100 MHz): δ = 23.7 (d, $^2J_{PC}$ = 3.5 Hz, P–CH_3), 32.4 (d, $^3J_{PC}$ = 9.6 Hz, C–CH_3), 50.8 (d, $^2J_{PC}$ = 13.7 Hz, *tert*-*C*). – ^{15}N NMR (C_6D_6, 27.4 MHz): δ = –289.9 (d, $^1J_{PN}$ = 65.7 Hz). – ^{31}P NMR (C_6D_6, 80 MHz): δ = 39.2 (s). – $C_9H_{23}N_2P$ (190.27): calcd. C 56.81, H 12.18, N 14.72; found C 55.72, H 12.07, N 14.01.

Bis(isopropylamino)phenylphosphane (3): Prepared analogously to **1** from *i*PrNH$_2$ (20.9 g, 350 mmol) in ether (250 mL) and PhPCl$_2$ (12.7 g, 70 mmol) in ether (50 mL). Isolated by distillation, b.p. 76–78°C /0.2 Torr as an oily liquid. On standing at 4°C, crystals formed with m.p. 6°C. Yield: 12.6 g of **3** (79%). – ^{1}H NMR (C_6D_6, 400 MHz): δ = 1.0 (d, $^3J_{HH}$ = 6.2, CH-CH_3), 1.1 (d, $^3J_{HH}$ = 6.3 Hz, 6 H, CH–CH_3), 1.7 (s, broad, 1 H, N*H*), 1.75 (s, broad, 1 H, N*H*), 3.2 (m, 2 H, C*H*–CH_3, 7.1–7.7 (m, 5 H, C_6H_5). – ^{13}C NMR (C_6D_6, 67.9 MHz): δ = 26.5 (d, $^3J_{PC}$ = 6.1 Hz, CH–CH_3), 26.8 (d, J_{PC} = 4.1 Hz, CH–CH_3), 46.2 (d, $^2J_{PC}$ = 7.5 Hz, *C*H–CH_3), 127.7 (s, *p*-C_6H_5), 128.1 (d, $^3J_{PC}$ = 4.1 Hz, *m*-C_6H_5), 131.1 (d, $^2J_{PC}$ = 15.3 Hz, *o*-C_6H_5), 148.0 (d, $^1J_{PC}$ = 5.1 Hz, *ipso*-C_6H_5). – ^{15}N NMR (C_6D_6, 27.4 MHz): δ = –304.8 (d, $^1J_{PN}$ = 67.9 Hz). – ^{31}P NMR (C_6D_6, 81 MHz): δ = 58.9 (s). – $C_{12}H_{21}N_2P$ (224.29), calcd. C 64.26, H 9.44, N 12.49; found C 63.72, H 8.94, N 12.47.

Bis(*tert*-butylamino)phenylphosphane (4):[7] Prepared analogously to **1** from *t*BuNH$_2$ (15.0 g, 210 mmol) and PhPCl$_2$ (5.7 g, 32 mmol) in 200 mL of ether. Yield: 5.9 g of **4** (73%), slightly yellow oil, b.p. 98°C/0.8 Torr. – ^{1}H NMR (C_6D_6, 400 MHz): δ = 0.0 (d, $^4J_{PH}$ = 0.5 Hz, 18 H, C–CH_3), 1.5 (s, broad, 1 H, NH), 1.7 (s, broad, 1 H, NH), 6.9–7.3 (m, 5 H, C_6H_5). – ^{13}C NMR (C_6D_6, 100 MHz): δ = 32.7 (d, $^3J_{PC}$ = 8.2 Hz, C–CH_3), 51.1 (d, $^2J_{PC}$ = 16.1 Hz, *tert*-C), 127.2 (s, *p*-C_6H_5), 127.7 (d, $^3J_{PC}$ = 4.2 Hz, *m*-C_6H_5), 130.1 (d, $^2J_{PC}$ = 17.2 Hz, *o*-C_6H_5, 148.0 (d, $^1J_{PC}$ = 3.5 Hz, *ipso*-C_6H_5). – ^{15}N NMR (C_6D_6, 27.4 MHz): δ = 292.3 (d, $^1J_{PN}$ = 68.2 Hz). – ^{31}P NMR (C_6D_6, 81 MHz): δ = 42.0 (s). – $C_{14}H_{25}N_2P$ (252.34), calcd. C 66.64, H 9.99, N 11.27; found C 66.36, H 9.75, N 11.10.

Bis(anilido)phenylphosphane (5): PhPCl$_2$ (4.5 g, 25 mmol) was dissolved in toluene (50 mL), and a solution of aniline (9.3 g, 100 mmol) in toluene (100 mL) was added with stirring in such a manner that the temperature of the resulting suspension never exceeded 25°C. After stirring overnight, the insoluble material was removed by filtration and washed with a total of 100 mL of diethyl ether. (The solution may turn turbid.) The solid was then removed after several hours. The combined solutions were reduced to 30 mL in volume. The remaining solution was layered with pentane. After cooling to 0°C a crystalline solid separated, m.p. 70–72°C. Yield: 3.0 g of **5** (42%). – ^{1}H NMR (C_6D_6, 400 MHz): δ = 4.4 (s, broad, 2 H, N*H*), 6.6–7.7 (m, 15 H, C_6H_5). – ^{13}C NMR (C_6D_6, 100 MHz): δ = 117.0. (d, $^3J_{PC}$ = 11.7 Hz, *m*-C_6H_5), 120.3, s, 128.7 (d, $^3J_{PC}$ = 4.0 Hz, *m*-C_6H_5), 129.0, s, 129.5, s, 130.2 (d, $^2J_{PC}$ = 17.0 Hz, *o*-C_6H_5), 141.7, s, 145.7 (d, $^1J_{PC}$ = 13.8 Hz, *ipso*-C_6H_5). – ^{15}N NMR (C_6D_6, 27.4 MHz): δ = –294.6 (d, $^1J_{PN}$ = 66.4 Hz). – ^{31}P NMR (C_6D_6, 81 MHz): δ = 46.8 (s). – $C_{18}H_{17}N_2P$ (297.32): calcd. C 73.96, H 5.86, N 9.58; found C 72.15, H 5.87, N 9.36.

Bis(*tert*-butylamino)mesitylphosphane (6): Prepared analogously to **7** from mesPCl$_2$ (1.2 g, 5.5 mmol) and *t*BuHN–SiMe$_3$ (3.2 g, 22 mmol) in 30 mL of toluene. Yield: 1.17 g of **6** (4.0 mmol, 72%), b.p. 100°C/0.1 Torr, yellow oil. – ^{1}H NMR (C_6D_6, 400 MHz): δ = 1.2 (s, 18 H, C- CH_3), 2.3 (s, 3 H, *p*-CH_3), 2.2 (s, broad, 1 H, NH), 2.3 (s, broad, 1 H, NH), 2.6 (s, 6 H, *o*-CH_3), 6.8 (s, 2 H, *m*-C_6H_2). – ^{13}C NMR (C_6D_6, 100 MHz): δ = 20.9 (s, *p*-CH_3), 22.5 (d, $^3J_{PC}$ = 21.4 Hz, *o*-CH_3), 32.2 (d, $^3J_{PC}$ = 10.0 Hz, C–CH_3), 51.2 (d, $^2J_{PC}$ = 21.7 Hz, *tert*-C), 129.6 (d, $^3J_{PC}$ = 4.2 Hz, *m*-C_6H_5), 137.4 (s, *p*-C_6H_5), 139.3 (d, $^2J_{PC}$ = 18.7 Hz, *o*-C_6H_5), 140.4 (d, $^1J_{PC}$ = 13.4 Hz, *ipso*-C_6H_5). – ^{15}N NMR (C_6D_6, 27.4 MHz): δ = –298.9 (d, $^1J_{PN}$ = 59.9 Hz). – ^{31}P NMR (C_6D_6, 81 MHz): δ = 44.1 (s). – $C_{17}H_{31}N_2P$ (294.42): calcd. C 69.35, H 10.61, N 9.51; found C 69.06, H 9.70, N 9.32.

Di(isopropylamino)mesitylphosphane (7) and 1,3-Diisopropyl-2,4-dimesityl-1,3,2,4-diazadiphosphetidine (8): A solution of mesPCl$_2$ (1.7 g, 7.6 mmol) in toluene (20 mL) was added to a stirred solution of *i*PrHN–SiMe$_3$ (3.90 g, 29.3 mmol) in toluene (30 mL). The mixture was heated at reflux for 14 h. Me$_3$SiCl and toluene were then stripped off from the clear orange-colored solution. The oily residue yielded 1.7 g of **7** (35 mmol), b.p. 109°C/0.1 Torr. – ^{1}H NMR (C_6D_6, 400 MHz): δ = 1.0 (d, $^3J_{HH}$ = 6.3 Hz, 6 H, CH–CH_3), 1.3 (d, $^3J_{HH}$ = 6.3 Hz, 6 H, CH–CH_3), 2.1 (s, broad, 1 H, N*H*), 2.2 (s, broad, 1 H, N*H*), 2.3 (s, 3 H), 2.6 (s, 6 H), 3.3 (m, 2 H, C*H*CH$_3$), 6.7 (2, 2 H, C_6H_2). – ^{13}C NMR (C_6D_6, 67.9 MHz): δ = 20.8 (s, *p*-CH_3), 22.7 (d, $^3J_{PC}$ = 19.8 Hz, *o*-CH_3), 26.3 (d, $^3J_{PC}$ = 4.6 Hz, CH–CH_3), 26.5 (d, $^3J_{PC}$ = 7.7 Hz, CH–CH_3), 47.8 (d, $^2J_{PC}$ = 32.1 Hz, *C*H–CH_3), 129.5 (d, $^3J_{PC}$ = 3.8 Hz, *m*-C_6H_5), 17.8 (s, *p*-C_6H_5), 139.2 (s, *o*-C_6H_5), 139.4 (d, $^1J_{PC}$ = 17.6.1 Hz, *ipso*-C_6H_5). – ^{15}N NMR (C_6D_6, 27.4 MHz): δ = –303.5 (d, $^1J_{PN}$ = 63.4 Hz). – ^{31}P NMR (C_6D_6, 81 MHz): δ = 58.7 (s). – $C_{15}H_{27}N_2P$ (266.37): calcd. C 67.64, H 10.22, N 10.52; found C 64.75, H 9.90, N 10.11.

From a similar reaction, using (4.0 g of *i*PrHN–SiMe$_3$, 30 mmol), 1.7 g of MesPCl$_2$, 7.6 mmol) in toluene (20 mL), 1.7 g of **7** was obtained by distillation. A non-volatile oil remained which was dissolved in CHCl$_3$ (5 mL). On cooling large red needles of **8** separated, m.p. 155°C. Yield: 0.5 g of **8** (30%). – ^{1}H NMR (CDCl$_3$, 400 MHz): δ = 0.8 (d, $^3J_{HH}$ = 6.4 Hz, 6 H, CH–CH_3), 0.81 (d, $^3J_{HH}$ = 6.4 Hz, 6 H, CH–CH_3), 2.3 (s, mesityl–CH_3), 2.7 (s, mesityl–CH_3), 3.1 (s, mesityl–CH_3), 2.9 (m, 2 H, C*H*–CH_3). – ^{13}C NMR (CDCl$_3$, 100 MHz): δ = 3.4 (d, $^3J_{PC}$ = 7.4 Hz, SiCH$_3$), 25.6 (d, $^3J_{PC}$ = 7.5 Hz, CH–CH_3), 25.8 (d, $^3J_{PC}$ = 7.6 Hz, CH–CH_3), 48.6 (d, $^2J_{PC}$ = 10.9 Hz, CH), 127.1 (d, $^3J_{PC}$ = 2.5 Hz, *m*-C_6H_5), 128.1 (s, *p*-C_6H_5), 130.7 (d, $^2J_{PC}$ = 18.6 Hz, *o*-C_6H_5), 147.2 (d, $^1J_{PC}$ = 20.6 Hz, *ipso*-C_6H_5). – ^{15}N NMR (CDCl$_3$, 27.4 MHz): δ = –374.1 (t, $^1J_{PN}$ = 37.5 Hz). – ^{31}P NMR (CDCl$_3$, 81 MHz): δ = 242.0 (s). – MS (70 eV); *m*/*z* (%): 414 (75) [M$^+$], 371 (5) [M$^+$ – *i*Pr], 295 (100) [M$^{\bullet+}$ – mes], 207 (25) [M$^+$ – mesNP*i*Pr], 149 (35). – $C_{12}H_{30}N_4P_2$ (290.): calcd. C 69.54, H 8.75, N 6.76; found C 68.48, H 8.33, N 6.68.

Mesitylphosphinic Acid *tert*-Butylamide (9): From a solution of **7** in C_6D_6 which was kept in a NMR tube fitted with a plastic cap, a few crystals separated within 5 weeks which were characterized as **9** by X-ray structure analysis only. Attempts to hydrolyze **7** with an ether solution saturated with water gave no **9** on attempts to crystallize the product from benzene.

***N*-Lithio(organoamino)phosphanes**

These compounds were prepared from the (organoamino)organophosphanes Ph$_2$P–NH*t*Bu, MeP(NHR)$_2$, PhP(NHR)$_2$ and MesP(NHR)$_2$ by treating ether or toluene solutions with an equivalent amount of *n*BuLi in hexane at –78°C. The solutions were then kept at reflux for 1 h, reduced in volume and kept at low temperature for crystallization.

Since the crystals deteriorated quite rapidly when the solvent was removed, no elemental analysis was performed. Their composition follows from the crystal structure analysis.

Hemietherate of *N*-Lithio-*N*-*tert*-butylamino-diphenylphosphane (10): Ph$_2$P–NH*t*Bu (540 mg, 2.1 mmol) dissolved in ether (10 mL)

Table 2. Crystal data and data collection parameters

Compound	**3**	**5**	**8**	9	**10**	**11**	**12**	**13**	**14**	**15**
Chem. formula	$C_{12}H_{21}N_2P$	$C_{18}H_{17}N_2P$	$C_{12}H_{18}NP$	$C_{12}H_{20}NOP$	$C_{36}H_{50}Li_2N_2OP_2$	$C_{16}H_{37}Li_2N_2OP$	$C_{14}H_{23}Li_2N_2P$	$C_{52}H_{70}Li_4N_4O_4P_2$	$C_{48}H_{108}Li_8N_8O_5P_4$	$C_{32}H_{45}B_2N_2P$
Form. wt.	224.28	292.31	207.24	225.26	602.60	318.33	264.19	904.32	1056.82	510.29
Cryst. size [mm]	0.2 × 0.28 × 0.47	0.2 × 0.2 × 0.25	0.15 × 0.2 × 0.3	0.2 × 0.2 × 0.3	0.2 × 0.2 × 0.2	0.3 × 0.3 × 0.3	0.28 × 0.33 × 0.47	0.2 × 0.25 × 0.25	0.2 × 0.2 × 0.3	0.1 × 0.2 × 0.2
Cryst. system	Orthorhombic	Monoclinic	Triclinic	Monoclinic	Monoclinic	Monoclinic	Triclinic	Triclinic	Triclinic	Monoclinic
Space group	Pca2(1)	Cc	*P*-1	P2(1)/c	C2/c	P2(1)/n	*P*1bar	*P*1bar	*P*1bar	*P*2(1)/c
a, [Å]	9.142(2)	13.102(5)	7.599(9)	8.085(4)	12.316(7)	10.093(3)	10.110(7)	13.4843(3)	12.786(5)	19.81(2)
b, [Å]	15.954(2)	11.549(4)	8.380(7)	18.767(6)	16.406(9)	10.079(3)	11.720(9)	16.0554(4)	14.124(7)	9.442(6)
c, [Å]	18.981(2)	10.655(3)	10.189(13)	9.541(5)	17.158(9)	21.084(7)	14.727(9)	25.3989(4)	20.037(9)	15.97(2
α, [°]	90	90	79.31(5)	90	90	90	80.04(2)	83.475(1)	77.97(2)	90
β, [°]	90	106.50(1)	81.16(3)	112.17(2)	96.34(2)	94.561(12)	74.53(2)	79.746(1)	78.37(2)	95.48(5)
γ, [°]	90	90	70.15(3)	90	90	90	73.75(1)	82.964(1)	66.88(2)	90
V, [Å^3]	2768.4(8)	1546(1)	597(1)	1341(1)	3446(3)	2138(1)	1605(2)	5346.4(2)	3226(3)	2974(7)
Z	8	4	2	4	4	4	4	4	2	4
ρ(calc), [Mg/m^3]	1.076	1.256	1.153	1.116	1.162	0.989	1.093	1.123	1.088	1.140
μ [mm^{-1}]	0.173	0.173	0.194	0.183	0.156	0.130	0.157	0.126	0.161	0.115
F(000)	976	616	224	488	1296	704	568	1934	1152	1104
Index range	$-1 \le h \le 10$ $0 \le k \le 18$ $-21 \le l \le 21$	$-17 \le h \le 16$ $-14 \le k \le 14$ $-12 \le l \le 12$	$-9 \le h \le 9$ $-8 \le k \le 8$ $-13 \le l \le 12$	$-9 \le h \le 9$ $-14 \le k \le 24$ $-12 \le l \le 11$	$-15 \le h \le 15$ $-21 \le k \le 21$ $-22 \le l \le 22$	$-10 \le h \le 10$ $-10 \le k \le 11$ $-23 \le l \le 23$	$-12 \le h \le 12$ $-15 \le k \le 14$ $-18 \le l \le 18$	$-14 \le h \le 14$ $-16 \le k \le 16$ $-26 \le l \le 24$	$-13 \le h \le 12$ $-18 \le k \le 17$ $-25 \le l \le 25$	$-15 \le h \le 16$ $-10 \le k \le 10$ $-17 \le l \le 17$
2 θ [°]	48.00	57.28	54.44	57.30	59.00	46.52	57.62	43.94	54.78	46.52
Temp, [K]	293(2)	193(2)	213	193	183(2)	183	213	173(2)	193	213
Refl. collected	4535	4282	3154	7483	9970	8744	8926	19811	15578	11800
Refl. unique	4234	2973	1676	2355	3469	2907	4850	10544	8884	3259
Refl. observed (4σ)	3256	2831	1499	1416	2761	2589	2738	6480	4845	2296
R (int.)	0.0598	0.0201	0.0451	0.1124	0.0461	0.0303	0.0501	0.0755	0.0812	0.0922
No. variables	291	258	127	150	296	208	343	1040	679	347
Weighting scheme[a] x/y	0.0396/2.9819	0.0136/0.8099	0.0846/0.6542	0.0386/0.711	0.0001/5.9234	0.0410/2.018	0.0539/1.1681	0.0419/29.9749	0.2310/1.4891	0.1701/2.0266
GOOF	1.078	1.121	1.059	1.097	1.314	1.152	1.107	1.096	1.082	1.097
Final *R* (4σ)	0.0550	0.0298	0.0516	0.0436	0.0696	0.0583	0.0445	0.1134	0.1038	0.0892
Final *wR*2	0.1266	0.0668	0.1534	0.0930	0.1087	0.1297	0.1131	0.2185	0.2684	0.2319
Larg. res. peak [e/Å^3]	0.181	0.118	0.484	0.213	0.337	0.594	0.228	0.522	1.082	0.360

[a] $w^{-1} = \sigma^2 F_o^2 + (xP)^2 + yP$; $P = (F_o^2 + 2F_c^2)/3$.

was treated at −70°C with 1.4 mL of a BuLi solution in hexane (2.2 mmol). After refluxing and volume reduction to ca. 1/3, crystals were grown at −30°C, and selected at this temperature for X-ray crystal structure analysis. NMR (supernatant solution): ^{31}P NMR (ether, 81 MHz): several signals in the range δ = 43.6−55.9, − ^{7}Li NMR (77.8 MHz): δ = 1.4 (s, broad).

Dimeric Bis(*N*-lithio-*tert*-butylamino)butylphosphane (11): mesP(NH*t*Bu)$_2$ (0.34 g, 1.7 mmol) dissolved in 10 mL of ether was metallated with 2.24 mL of a 1.56 M solution of *n*BuLi in hexane. The yellow solution was reduced under vacuum, and was kept for 3 weeks at −30°C for crystallization. Clear yellow crystals of **11** had then separated. NMR (supernatant solution): ^{31}P NMR (ether/hexane, 81 MHz): δ = 96.9 (s), 93.6 (s), 89.6 (s) − ^{7}Li NMR (77.8 MHz): δ = 2.5 (s, broad), 2.2 (s, broad).

Dimeric Bis(*N*-lithio-*tert*-butylamino)phenylphosphane (12): PhP(NH*t*Bu)$_2$ (990 mg, 3.9 mmol) dissolved in toluene (30 mL) was metallated with *n*BuLi in hexane (5.2 mL, 8.27 mmol). The yellow solution was reduced to ≈ 10 mL. Yellow crystals grew at −30°C. Yield: 900 mg of **12** (86%). NMR (supernatant solution): ^{31}P NMR (C_6D_6, 81 MHz): δ = 94 (s). − ^{7}Li NMR (77.8 MHz): δ = −2.3 s, 1.4 (s, broad), 2.2 (s, broad).

Dimeric Bis(*N*-lithioanilino)phenylphosphane bis(ether) (13): PhP(NHPh)$_2$ (690 mg, 2.4 mmol) dissolved in ether (20 mL) was metallated at −78°C with *n*BuLi (3.2 mL, 4.96 mmol) in a hexane/ether mixture (3.2 mL hexane, 5 mL ether). A solid formed which dissolved on heating. Yellow crystals of **13** separated from the yellow solution at −30°C. NMR (supernatant solution): ^{31}P NMR (ether, 81 MHz): several signals in the range of δ = 16−88.2 (m). − ^{7}Li NMR (77.8 MHz): δ = −0.2 (s, broad), 1.1 (s, broad), 1.7 (s, broad), 2.8 (s, broad).

Tetrameric Bis(*N*-lithio-isopropylamino)methylphosphane-tetrahydrofuran (14): MeP(NH*i*Pr)$_2$ (830 mg, 5.1 mmol) in THF (20 mL) was treated with *n*BuLi (6.71 mL, 10.8 mmol). A clear yellow solution formed on heating at reflux. Crystals separated at −30°C. Yield: 910 mg of **14** (72%). NMR (supernatant solution and crystals): ^{31}P NMR (C_6D_6, 81 MHz): several signals in the range δ = 24.0 to 39, main signal at 26.5 (m, *J* = 68.5 Hz). − ^{7}Li NMR (77.8 MHz): δ = 1.7 (s, broad).

X-ray Structure Determinations

Crystals from the solutions were transferred at about −30°C in precooled perfluorether oil, and single crystals were selected. The selected crystal was quickly mounted on the tip of a glass fiber and then rapidly transferred to the goniometer head flushed with a gas stream of N_2 cooled to −90°C. The crystal quality was checked by reflection profiles. The unit cell dimensions were calculated from the data on 4 different sets of data of 15 frames each recorded at different φ and χ angles, by rotating φ by 0.3°. Having obtained satisfactory results, data collection was started (10s exposure per frame, 1480 frames collected in the hemisphere mode). Data were reduced by the program SAINT.[23] No absorption correction was applied. The structures were solved by direct methods (SHELXL programs[24]) and non-hydrogen atoms were given anisotropic thermal parameters. Although most H positions could be detected, these were calculated and refined with a riding model and isotropic U_i adopted to U_{eq} of the respective carbon atom. It should be noted that the refinement of the structure of compounds *N*-lithioamidophosphanes **12**, **13**, and **14** converged at comparatively high *R* values. This is due to the fact that the crystal quality was not an optimum, leading also to rather high R_{int} values; moreover the diffracting power was not excellent, e. g. there were only few

reflection at $2\Theta > 40°$ with $I > 3\sigma(I)$. Several crystals of these compounds had been measured without improving the result. Table 4 contains relevant information on the crystallographic data and structure refinement. Additional material (without structure factor tables) are deposited with the Cambridge Crystallographic Data Centre as supplementary publication numbers CCDC 102 977 to 102 986. Copies of the data can be obtained on application to CCDC, 12 Union Road, Cambridge CB2 1EZ, U. K. by quoting the authors, the journal citation [Fax: (internat.)+44-1223/336-033; E-mail: deposit@ccdc.cam.uk].

Acknowledgments

We thank Chemetall GmbH for generous support, Mrs D. Ewald for recording the mass spectra, Dipl.-Chem. M. Vosteen and Mr. P. Mayer for recording numerous NMR spectra and Dipl.-Chem. W. Lippert for help with the MO calculations.

[1] [1a] N. Metzler, H. Nöth, H. Sachdev, *Angew. Chem.* **1994**, *106*, 1838−1840; *Angew. Chem. Int. Ed. Engl.* **1994**, *33*, 1746−1748. − [1b] H. Nöth, H. Sachdev, M. Schmidt, H. Schwenk, *Chem. Ber.* **1995**, *128*, 105−113. − [1c] B. Gemünd, H. Nöth, H. Sachdev, M. Schmidt, *Chem. Ber.* **1996**, *129*, 1493−1496. − [1d] J. Knizek, I. Krossing, H. Nöth, H. Schwenk, Th. Seifert, *Chem. Ber./Recueil* **1997**, *130*, 1053−1062. − [1e] U. Klingebiel, S. Dielkus, C. Drost, R. Herbst-Irmer, *Angew. Chem.* **1993**, *105*, 1689−1690; *Angew. Chem. Int. Ed. Engl.* **1993**, *32*, 1625. − [1f] C. Drost, C. Jäger, S. Freitag, U. Klingebiel, M. Noltemeyer, G. M. Sheldrick, *Chem. Ber.* **1994**, *127*, 8435−847. − K. Bode, U. Klingebiel, M. Noltemeyer, H. Witte−Abel, *Z. Anorg. Allg. Chem.* **1995**, *621*, 500−505.

[2] M. T. Ashby, Z. Li, *Inorg. Chem.* **1992**, *31*, 1321−1322.

[3] H. Rossknecht, A. Schmidpeter, *Z. Naturforsch. Teil B*, **1971**, *26*, 81−82.

[4] [4a] T. Kremer, F. Hampel, F. A. Knoch, W. Bauer, A. Schmidt, P. Gabold, M. Schütz, J. Ellermann, P. von Ragué-Schleyer, *Organometallics* **1996**, *15*, 4776−4782. − [4b] E. W. Bauer, M. Schitz, F. W. Heinemann, M. Moll, *Z. Anorg. Allg. Chem.* **1998**, *629*, 547−566.

[5] The lithiation of [*t*BuHN−P*t*Bu]$_2$ has recently been reported: I. Schranz, L. Stahl, R. J. Staples, *Inorg. Chem.* **1998**, *37*, 1493−1498.

[6] [6a] R. R. Holmes, J. A. Foster, *J. Am. Chem. Soc.* **1960**, *82*, 5509. − [6b] R. R. Holmes, *J. Am. Chem. Soc*. **1961**, *83*, 1334. − [6c] R. R. Holmes, J. A. Forstner, *Inorg. Chem.* **1963**, *2*, 380−384. − [6d] A. Michaelis, *Ann. Chem*. **1903**, *336*,129. − [6e] R. B. Flint, P. I. Salzberg, U. S. Patent 2151 389 *Chem. Abstr.* **1939**, *33*, 5097. − [6f] A. Tarassoli, R. C. Haltiwanger, A. D. Norman, *Inorg. Nucl. Chem. Lett.* **1980**, *16*, 27−29.

[7] M. G. Barlow, R. N. Haszeldine, H. G. Higson, *J. Chem. Soc. C* **1966**, 1592−1598.

[8] A. P. Lane, D. A. Morton-Blake, D. Payne, *J. Chem. Soc. A* **1967**, 1492−1498.

[9] Y. G. Trishin, V. N. Chistokletov, A. A. Petrov, *Zh. Obsh. Khim.* **1979**, *49*, 39−44.

[10] M. F. Lappert, M. J. Hade, A. Singh, J. L. Atwood, R. D. Rogus, R. Shakir, *J. Am. Chem. Soc.* **1983**, *105*, 302−304.

[11] O. J. Scherer, G. Schnabl, *Chem. Ber.* **1976**, *109*, 2996−3004.

[12] Gaussian 94, Revision D.4; M. J. Frisch, J. A. Pople et al., Gaussian Inc. Pittsburgh PA, **1995**.

[13] S. Pohl, *Z. Naturforsch. Teil B*, **1979**, *34*, 256−261.

[14] R. Keat, in *The Chemistry of Inorganic Homo- and Heterocycles* (Eds.: I. Haiduc, D. B. Sowerby), Academic Press, New York, London, Sidney, **1971**, p. 4379 ff.

[15] G. Trinquier, M. T. Ashby, *Inorg. Chem*. **1994**, *33*, 1306− 1313.

[16] N. Poetschke, M. Kiefer, M. A. Khan, E. Niecke, M. T. Ashby, *Inorg. Chem.* **1997**, *36*, 4087−4093.

[17] A. Steiner, D. Stalke, *Angew. Chem.* **1995**, *107*, 1908−1910; *Angew. Chem. Int. Ed. Engl.* **1995**, *34*, 1752−1754.

[18] D. Mootz, A. Zinnius, B. Böttcher, *Angew. Chem.* **1969**, *81*, 398−399; *Angew. Chem. Int. Ed. Engl.* **1969**, *8*, 378−379.

[19] F. Pauer, P. P. Power, Chapter 8 in *Lithium Chemistry* (Eds.: A.-M. Sapse, P. von Ragué-Schleyer), J. Wiley and Sons, Interscience Publ. New York, Chichester, Brisbane, Toronto, Singapore, **1995**.

[20] see ref.[19] Chapter 9.

[21] R. E. Mulvey, K. Wade, D. R. Armstrong, G. T. Wells, R. Snaith, W. Clegg, D. Reed, *Polyhedron* **1987**, *6*, 987−993.

[22] E. Hey, P. B. Hitchcock, M. F. Lappert, A. K. Rai, *J. Organomet. Chem.* **1987**, *325*, 1−12.

[23] Siemens Analytical Instruments, SAINT, Version 4.1, **1994**.

[24] Siemens Analytical Instruments, SHELXTL, Version 5.1, **1996**.

Received July 26, 1999
[I99270]

Reactivity of Carbonyl-Functionalized Phosphaalkenes RC(O)P=C(NMe$_2$)$_2$ (R = *t*Bu, Ph) towards Electrophiles

Lothar Weber,*[a] Stefan Uthmann,[a] Hans-Georg Stammler,[a] Beate Neumann,[a] Wolfgang W. Schoeller,[a] Roland Boese,[b] and Dieter Bläser[b]

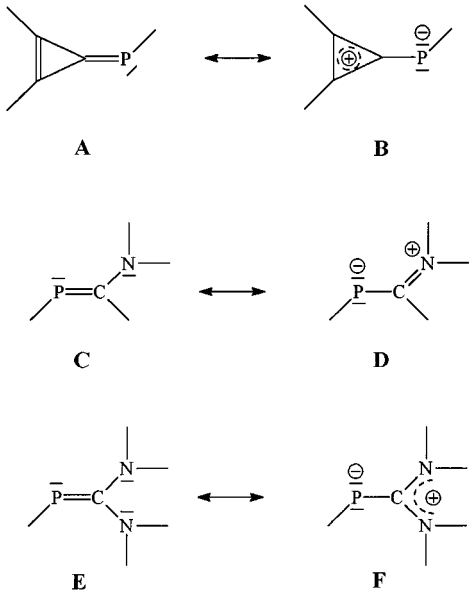
Dedicated to Professor Dirk Walther on the occasion of his 60th birthday

Keywords: Alkylation / Carbonyl complexes / Lewis acids / Phosphaalkenes / Protonation

The reaction of the carbonyl-functionalized phosphaalkenes RC(O)P=C(NMe$_2$)$_2$ [R = *t*Bu (**2a**), Ph (**2b**)] with protic acids and alkylating reagents occurred at the two-coordinate phosphorus atom to give the phosphanyl-substituted carbocations **3a,b** and **4a,b**. In contrast, treatment with Me$_3$SiOSO$_2$CF$_3$ resulted in attack at the oxygen atom by the silyl group, and the formation of [RC(OSiMe$_3$)=PC(NMe$_2$)$_2$]SO$_3$CF$_3$ (**5a,b**). Similarly, the Lewis acids B(C$_6$F$_5$)$_3$, Al(*t*Bu)$_2$Cl and AlMe$_3$ were ligated to the oxygen atom of the carbonyl group. Two equivalents of GaMe$_3$ were added to the oxygen and phosphorus atom of the phosphaalkene to yield the thermolabile complexes [RC(OGaMe$_3$)=P(GaMe$_3$)C(NMe$_2$)$_2$] (**10a,b**). In contrast, one molecule of InMe$_3$ was bound to the phosphorus center of the phosphorus compound. Reaction of the phosphaalkenes with [Ni(CO)$_4$], [Fe$_2$(CO)$_9$] or [{(*Z*)-cyclooctene}Cr(CO)$_5$] also took place at the pnictogen atom, resulting in complexes of the type [RC(O)P{M(CO)$_n$}C(NMe$_2$)$_2$] (R = *t*Bu, Ph; M = Ni, *n* = 3; Fe, *n* = 4; Cr, *n* = 5). The chemical transformations reported here underline the versatile chemistry of phosphaalkenes and emphasize a relationship between carbonyl-functionalized phosphaalkenes and the well-investigated class of phosphorus ylides. X-ray structures of compounds **6b**, **7b***, **10a**, **11a** and **12a** are reported.

Introduction

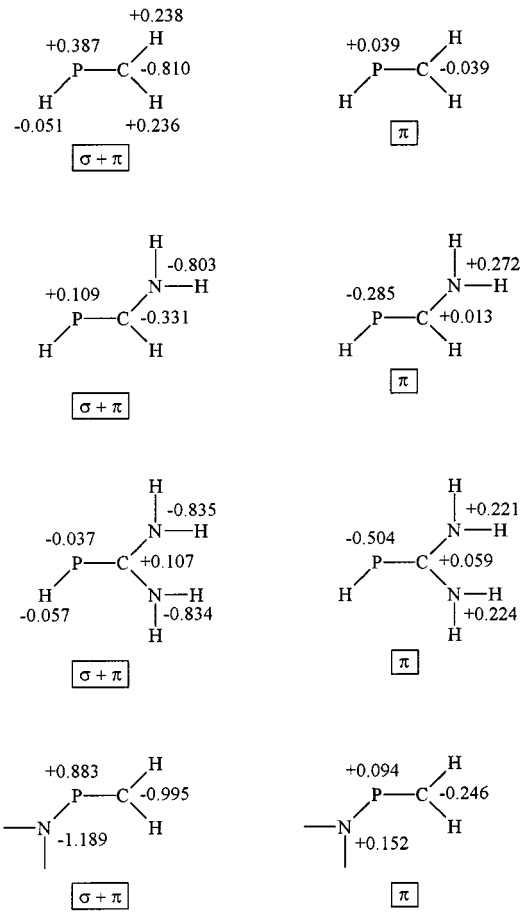
The chemistry of low-coordination phosphorus compounds is a rapidly expanding field that highlights the remarkable ability of phosphorus to mimic the chemistry of carbon.[1] In the vast majority of phosphaalkenes R^{1}P=CR^{2}R^3 and phosphaalkynes RC≡P, the multiple bonds are polarized in the sense P$^{\delta+}$···C$^{\delta-}$, as anticipitated by the different electronegativities of phosphorus and carbon. It was pointed out by Regitz et al. that in phosphatriafulvenes **A** (Scheme 1) the P=C bond has an inverse electron density;[2] this was substantiated by quantum chemical calculations in comparison to the parent compound HP=CH$_2$. The latter molecule has a σ + π Mulliken charge distribution of +0.154 electrons at the phosphorus and −0.564 electrons at the carbon atom, whereas the PC π-bond is essentially nonpolar (+0.021 e$^-$ at P; 0.021 e$^-$ at C). In the cyclopropylidene phosphane **A** a σ + π Mulliken charge distribution of −0.037 e$^-$ at the phosphorus and of −0.177 e$^-$ at the carbon atom of the exocyclic double bond were calculated. Here the PC π-bond is clearly polarized towards the phosphorus atom as the negative end of the dipole with an excess of 0.369 e$^-$ at the P atom and a deficiency of 0.084 e$^-$ at the C-atom. The positive charge is stabilized by incorporation into the Hückel aromatic cyclopropenium unit (formula **B** in Scheme 1).



Grobe et al. discovered that the introduction of one dialkylamino group at the carbon atom of the double bond in molecules such as F$_3$CP=C(F)NR$_2$ also resulted in an inverse electron distribution of the P=C π-bond.[3] In order to uncover the role of an amino group on the electron distribution in a phosphaalkene we performed quantum chemical calculations at a density functional level [B3LYP/6−31 g(d)].[4a−4e]

[a] Fakultät für Chemie der Universität Bielefeld, Universitätsstrasse 25, D-33615 Bielefeld, Germany
Fax: (internat.) +49(0)521/106−6146
E-mail: lothar.weber@uni-bielefeld.de
[b] Institut für Anorganische Chemie der Universität − Gesamthochschule Essen, Universitätsstraße 5−7, D-45117 Essen, Germany

 © WILEY-VCH Verlag GmbH, D-69451 Weinheim, 1999 1434−1948/99/1212−2369 $ 17.50+.50/0



Scheme 2. Charge distribution in $HP{=}CH_2$ and amino-substituted phosphaalkenes

As has been found previously[2] the calculations predict that the parent phosphaalkene should have a nonpolar π-bond (NBO charges and populations),[4d] although one amino group or, to a greater extent, two amino groups at the carbon atom[5] induce an inverse electron-density distribution at the π-bond, i.e. the charge at the phosphorus is increased relative to the parent methylenephosphane. Alternatively, an amino group at the phosphorus does the opposite, it enhances π-electron density at the carbon atom. Phosphaalkenes with an inverse electron density exhibit pecularities in their coordination behavior towards 18 VE transition metal fragments. In η^1-complexes of normally polarized phosphaalkenes ($P^{\delta+}{=}C^{\delta-}$) such as [$(MesP{=}CPh_2)Cr(CO)_5$] a trigonal planar phosphorus atom is linked to the methylene carbon atom by a P=C double bond of 1.679(4) Å.[6a] In the complex [$(\eta^5\text{-}C_5Me_5)(CO)_2FeP[Cr(CO)_5]C(NMe_2)_2$], however, where the inversely polarized phosphaalkene [$(\eta^5\text{-}C_5Me_5)(CO)_2FeP{=}C(NMe_2)_2$] is η^1-ligated to the [$Cr(CO)_5$] group, a trigonal-pyramidal phosphorus atom (sum of angles 346.1°) forms a single bond of 1.793(5) Å to the planar carbon atom.[7] For comparison, in the free phosphaalkene a P=C double bond of 1.709(5) Å was measured.[7c] Obviously the zwitterionic structures of inversely polarized phosphaalkenes are stabilized by ligation to metal centers.

In the $W(CO)_5$ complex of the inversely polarized phosphatriafulvene $MesP{=}C^aC^b(t\text{Bu}){-}C^ct\text{Bu}(C^a{-}C^c)$, however, the PC double bond [1.679(5) Å] is retained, and the phosphorus atom is pyramidalized to a lesser extent (sum of angles 352.9°).[2b]

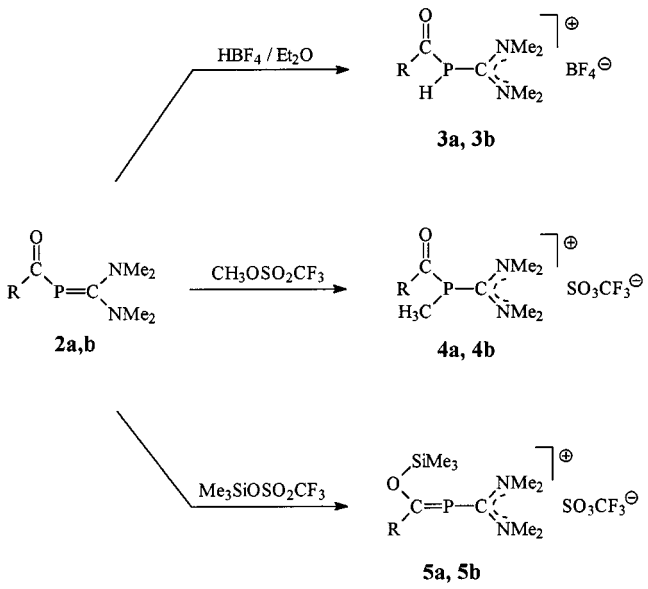
From carbanion and ylide chemistry[8] it is well documented that the negative charge on a carbon center is effectively stabilized by adjacent carbonyl groups via π-delocalization. In keeping with this, stabilization of the negative charge on the P-atom in phosphatriafulvenes[2b] and amino-functionalized phosphaalkenes has been achieved by acyl, dithiocarboxy, and thiocarbamoyl groups.[9] A significant charge transfer from phosphorus to the acyl-substituents was documented in the IR spectra, where the ν(CO) bands exhibited marked shifts to lower wavenumbers. Thus, in the IR spectrum of $RC(O)P{=}C(NMe_2)_2$, ν(CO) bands at 1563 cm^{-1} (R = *t*Bu) and 1546 cm^{-1} (R = Ph) are found;[9] the IR spectrum of the "normally polarized" phosphaalkene $t\text{BuC(O)P}{=}\text{C(OSiMe}_3)(t\text{Bu})$ shows a ν(CO) band at 1664 cm^{-1},[10] which is well within the range of $\tilde{\nu}$ = 1630−1690 cm^{-1} usually encountered in acyl phosphanes.[11] Although a number of P-acyl phosphaalkenes with an inverse electron density have been prepared, information on the chemistry of these molecules is scarce. Thus, only dimerization and isomerization processes of several phosphatriafulvenes, as well as the formation of the complex [$t\text{BuC(O)P}\{W(CO)_5\}{=}C^a{-}C^b(t\text{Bu}){=}C^ct\text{Bu}](C^a{-}C^c$) have been investigated.[2b]

We decided to study in more detail the chemical reactivity of $t\text{BuC(O)P}{=}\text{C(NMe}_2)_2$ (**2a**) and $\text{PhC(O)P}{=}\text{C(NMe}_2)_2$ (**2b**), which are readily available from $Me_3SiP{=}C(NMe_2)_2$ (**1**) and carboxylic acid chlorides, especially with respect to the related carbonyl-stabilized phosphorus ylides $RC(O)CH{=}PPh_3$. Here we report on the reactions of **2a** and **2b** with protic acids, alkylating and silylating reagents, organometallic compounds of group 13 elements, and transition metal carbonyl complexes.

Results and Discussion

Reaction of 2a,b With Protic Acids, $ROSO_2CF_3$ (R = Me, $SiMe_3$) and $B(C_6F_5)_3$

The reaction of the P-acyl phosphaalkenes **2a** and **2b** with equimolar amounts of ethereal HBF_4 in diethyl ether at −50°C led to the formation of the phosphanyl carbenium salts $[RC(O)P(H)C(NMe_2)_2][BF_4]$ **3a** (R = *t*Bu) and **3b** (Ph) (Scheme 3). Salt **3a** was obtained as a colorless solid and **3b** as a yellow viscous oil. Both compounds are highly soluble in CH_2Cl_2 and $CHCl_3$. In chloroform, however, slow decomposition occurred at ambient temperature. Methylation of **2a** and **2b** was effected by methyl trifluoromethanesulfonate (methyl triflate) in diethyl ether at −50°C. Compounds **4a** and **4b** were isolated as orange, air- and moisture-sensitive powders, which are highly soluble in



2-5: R = *t*Bu (**a**), Ph (**b**)

Scheme 3. Reaction of **2a,b** with HBF_4, $CH_3OSO_2CF_3$ and $Me_3SiOSO_2CF_3$

halogenated hydrocarbons. In the ^{31}P NMR spectrum, the protonated products **3a** and **3b** display doublets at δ = −53.7 ($^1J_{PH}$ = 245 Hz) and δ = −46.6 ($^1J_{PH}$ = 257.7 Hz) which are significantly shifted to high field with respect to the corresponding signals in **2a** (δ = 26.4) and **2b** (δ = 31.3). The size of the $^{31}P\{^1H\}$ coupling constants furthers the idea that the protonation occurred at the phosphorus center of the phosphaalkene. The resonances of the ^{13}C nuclei of the PCN_2 and the PC=O groups of the starting materials **2a** [δ = 201.4 (d, $^1J_{PC}$ = 80.5 Hz), 231.4 (d, $^1J_{PC}$ = 90.8 Hz)] and **2b** [δ = 199.3 (d, $^1J_{PC}$ = 78.5 Hz), 215.6 (d, $^1J_{PC}$ = 78.7 Hz)] are also high-field shifted upon protonation, and are observed in **3a** as broad singlets at δ = 178.1 and δ = 220.0 and in **3b** at δ = 177.9 and 204.8, respectively. In the ^1H NMR spectrum a doublet at δ = 6.02 ($^1J_{PH}$ = 245 Hz) (**3a**) and at δ = 6.23 ($^1J_{PH}$ = 257.7 Hz) (**3b**) accounts for the PH unit.

The IR spectrum of **2a** shows a very strong ν(CO) absorption at $\tilde{\nu}$ = 1563 cm^{-1}, which is hypsochromically shifted in the carbenium ion of **3a** [ν(CO) = 1680, 1597 cm^{-1}]. Similar observations were made with **2b** and **3b**. The methylation of **2a** and **2b** to yield the phosphanyl carbenium salts **4a** and **4b**, gave rise to high-field shifts of only 30−33 ppm in the ^{31}P NMR spectra. In the $^{13}C\{^1H\}$ NMR spectra the ^{13}C nuclei of the methyl groups of **4a** and **4b** were observed as doublets at δ = 6.0 ($^1J_{PC}$ = 13.3 Hz) and δ = 5.0 ($^1J_{PC}$ = 11.7 Hz), respectively, which is consistent with an alkylation at the P-atom of the P-acyl phosphaalkenes. Upon methylation, the ^{13}C nuclei of the CN_2 and the PCO units of precursors **2a** and **2b** are shielded by 21.8−23.8 and 5.6−8.7 ppm, and the $^1J_{PC}$ coupling constants decreased from 80.5 and 90.8 Hz in **2a** to 44.0 and 60.6 Hz in **4a** and from 78.5 and 78.7 Hz in **2b** to 39.4 and 37.7 Hz in **4b**. Again the ν(CO) bands in the IR spectra of the salts **4a** ($\tilde{\nu}$ = 1644, 1588 cm^{-1}) and **4b** ($\tilde{\nu}$ = 1647, 1587 cm^{-1}) are observed at higher wavenumbers than in the neutral phosphaalkenes **2a** and 2**b**.

These observations compare well with carbonyl-stabilized ylides $RC(O)CH{=}PPh_3$, their corresponding phosphonium salts $[RC(O)CH_2PPh_3]^+X^-$, and their transition metal complexes, where the position of the ν(CO) band in the IR spectra serves as a sensitive probe for their electronic situation. Thus, the IR spectra of the ylides $MeC(O)CH{=}PPh_3$ and $PhC(O)CH{=}PPh_3$ display strong carbonyl bands at $\tilde{\nu}$ = 1540 and 1500 cm^{-1}, which upon protonation to the corresponding phosphonium ions were shifted to 1710 and 1665 cm^{-1}, respectively.[12]

The silylation of **2a** and **2b** with equimolar amounts of trimethylsilyl triflate in diethyl ether gave the extremely air- and moisture-sensitive salts **5a** and **5b**, which were isolated as pale yellow oils (Scheme 3). Here, in contrast to the protonation and methylation of **2a** and **2b**, a deshielding of the ^{31}P NMR resonances to δ = 109.2 (**5a**) and δ = 101.0 (**5b**) was observed.

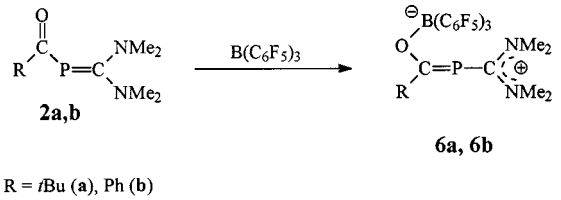
In the region typical for the stretching vibrations of acylic carbonyl groups in the IR spectra of **5a** and **5b** no intense bands are present. This situation is best explained by an attack of the hard acid "Me_3Si" at the hard oxygen center of the carbonyl group with the formation of a Si−O and a P=C bond. Thus, the products can be regarded as salts with unsymmetrical phosphaallyl cations or, alternatively, as phosphaalkenyl-functionalized carbocations. Symmetrical phosphaallyl cations such as $[(Me_2N)_2CPC(NMe_2)_2]^+$[13] or $[\{t\mathrm{BuC}^c{-}(t\mathrm{Bu})\mathrm{C}^b{-}\mathrm{C}^a\}_2\mathrm{P}]^+(C^a{-}C^c)$[2b] were described several years ago. In the low-field region of the $^{13}C\{^1H\}$ NMR spectra of **5a** and **5b**, doublets at δ = 180.8 ($^1J_{PC}$ = 75.5 Hz) and δ = 181.0 ($^1J_{PC}$ = 72.4 Hz) were attributed to the diaminocarbenium center, whereas the ^{13}C nuclei of the PCOSi units were observed as doublets at δ = 226.1 ($^1J_{PC}$ = 77.3 Hz) (**5a**) and δ = 211.8 ($^1J_{PC}$ = 61.4 Hz) (**5b**),respectively.

Thus, the main spectroscopic evidence for an electrophilic attack at the P- or O-atom of P-acyl phosphaalkenes with inverse electron density is taken from the direction in which the ^{31}P NMR resonance of the product is shifted. With this in mind, we decided to react **2a** and **2b** with the hard Lewis acids $B(C_6F_5)_3$, tBu_2AlCl, and $(AlMe_3)_2$.

Treatment of **2a** or **2b** with tris(pentafluorophenyl)borane in toluene solution at room temperature gave the adducts **6a** or **6b** as yellow solids (Scheme 4).

The air- and moisture-sensitive compounds are only slightly soluble in dichloromethane or chloroform, but dissolve well in acetonitrile. In ethereal and hydrocarbon solvents **6a** and **6b** are insoluble. Low-field shifted singlets in the $^{31}P\{^1H\}$ NMR spectra at δ = 68.3 (**6a**) (Δδ = 41.9) and 72.6 (**6b**) (Δδ = 41.5), and the absence of ν(C=O) bands in the IR spectra of the adducts agree with the ligation of the phosphaalkenes to the electron-deficient boron center via the oxygen atom. Doublets in the $^{13}C\{^1H\}$ NMR spectra at δ = 188.4 ($^1J_{PC}$ = 89.0 Hz) and 190.9 ($^1J_{PC}$ = 80.6 Hz) are

readily assigned to the three-coordinate ^{13}C nuclei of the diaminocarbenium units in **6a** and **6b**. Low-field resonances at δ = 228.8 (d, $^1J_{PC}$ = 81.4 Hz, **6a**) and δ = 223.4 ($^1J_{PC}$ =



Scheme 4. Reaction of **2a,b** with $B(C_6F_5)_3$

71.1 Hz, **6b**) are due to the ^{13}C nuclei of the PCOB units.

X-ray Structural Analysis of 6b

To confirm the spectroscopic evidence for the ligation of the phosphaalkene to the borane, an X-ray structural analysis of **6b** was performed (Figure 1, Table 1). Single crystals of **6b** were grown from toluene at −30°C. The analysis confirms the presence of a tetracoordinate boron atom, which is attached to the carbonyl group via a single bond of 1.506(3) Å. Delocalization of the negative charge into the C=O bond is obvious from an elongation from 1.240(2) Å (as measured in **2b**)[14] to 1.315(3) Å and by the bond length P(1)−C(1) of 1.735(2) Å, which is similar to the P=C bond length in $HP=C(NMe_2)_2$ [1.740(1) Å].[5] The trigonal-planar carbon atom C(1) (sum of angles 359.9°) is linked to atom C(41) by a single bond of 1.482(3) Å. The former PC(N) bond in **2b** [1.800(1) Å] is lengthened to 1.838(3) Å in **6b**. The trigonal-planar carbon atom C(2) (sum of angles 359.4°) shows multiple bonding to the planarly configured nitrogen atoms [N(1)−C(2) = 1.333(4); N(2)−C(2) = 1.327(4) Å]. The bond angle C(1)−P(1)−C(2) [102.3(1)°] is close to the value found in $HP=C(NMe_2)_2$ [103(1)°].[5] This is presumably because of the steric hinderance between the *cis*-oriented diaminocarbenium group and the phenyl ring which means that the valence angle P(1)−C(1)−C(41) [127.5(2)°] is markedly more obtuse than P(1)−C(1)−O(1) [121.4(2)°]. The very bulky $B(C_6F_5)_3$ moiety is directed towards the P-atom of the PC multiple bond, giving rise to torsion angles B(1)−O(1)−C(1)−P(1) and B(1)−O(1)−C(1)−C(41) of 2.5° and −179.4°, respectively. The torsion angle C(2)−P(1)−C(1)−O(1) was determined to be −175.1°. Thus, the atoms B(1), O(1), C(1), C(41), P(1) and C(2) are located in one plane, and the molecule may be described as a zwitterionic phosphaalkene, where the positive charge is formally centered at the diaminocarbenium substituent, and a negative charge at the boron atom.

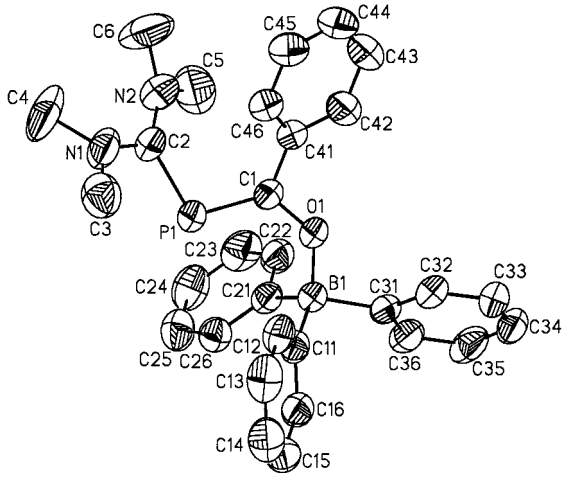
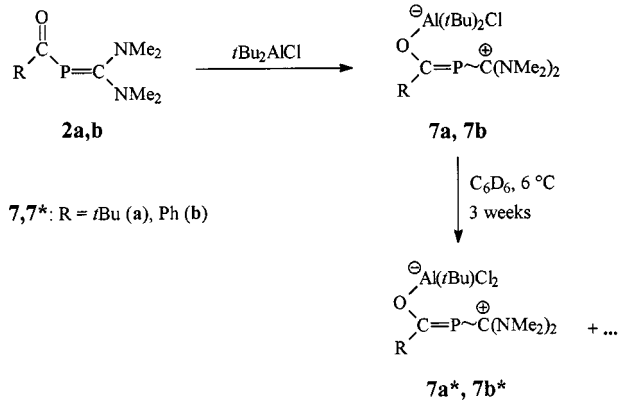


Figure 1. Molecular structure of **6b** in the crystal (fluorine atoms at the borane unit are omitted for clarity); selected bond lengths [Å] and angles [°]: P(1)−C(1) 1.735(2), P(1)−C(2) 1.838(3), O(1)−C(1) 1.315(3), O(1)−B(1) 1.506(3), B(1)−C(11,21,31) av. 1.649(4), C(1)−C(41) 1.482(3), N(1)−C(2) 1.333(4), N(2)−C(2) 1.327(4), N(1)−C(3) 1.459(4), N(1)−C(4) 1.481(4), N(2)−C(5) 1.465(5), N(2)−C(6) 1.474(5); C(1)−P(1)−C(2) 102.3(1), C(1)−O(1)−B(1) 130.2(2), O(1)−C(1)−C(41) 111.0(2), P(1)−C(1)−O(1) 121.4(2), P(1)−C(1)−C(41) 127.5(2), P(1)−C(2)−N(1) 115.6(2), P(1)−C(2)−N(2) 123.6(2), N(1)−C(2)−N(2) 120.2(3), C(2)−N(1)−C(3) 122.7(2), C(2)−N(1)−C(4) 122.8(3), C(3)−N(1)−C(4) 113.8(3), C(2)−N(2)−C(5) 122.7(3), C(2)−N(2)−C(6) 122.3(4), C(5)−N(2)−C(6) 114.0(4), O(1)−B(1)−C(11) 111.1(2), O(1)−B(1)−C(21) 115.4(2), O(1)−B(1)−C(31) 107.0(3), C(11)−B(1)−C(21) 115.4(2), C(11)−B(1)−C(31) 107.0(2), C(21)−B(1)−C(31) 112.1(2).

Reaction of 2a and 2b With tBu_2AlCl

Di-*tert*-butylaluminium chloride smoothly reacted with an equimolar amount of **2a** or **2b** in toluene at −30°C to afford the adducts **7a** or **7b** (Scheme 5). They were obtained as extremely moisture-sensitive orange solids. Attempts to grow crystals of **7a** and **7b** from C_6D_6 solution at 6°C within a period of 3 weeks led to the formation of crystalline $RC[OAl(tBu)Cl_2]=PC(NMe_2)_2$ [R = *t*Bu (**7a***), Ph (**7b***)] instead.



Scheme 5. Reaction of **2a,b** with tBu_2AlCl

In the IR spectra of the adducts **7a** and **7b**, no unambigious identification of ν(CO) bands was possible. The ^1H NMR spectrum of **7a** was characterized by a singlet for the nine protons of the *tert*-butyl group at the P=C function, and by another singlet accounting for the 18 protons of the *tert*-butyl groups at the aluminium atom. A singlet at δ = 2.63 was assigned to the protons of the dimethylamino groups.

In the low-field region of the $^{13}C\{^1H\}$ NMR spectra of **7a** and **7b**, doublets at δ = 184.4 ($^1J_{PC}$ = 76.5 Hz) and

Table 1. Important bond lengths of compounds **2b**, **6b**, **7b***, **10a**, **11a**, and **12a** in Å

Comp.	M	d(C=O)	d[PC(O)]	d[PC(N)]	d(M−P)	d(M−O)
2b	–	1.240(2)	1.805(1)	1.800(1)	–	–
6b	B	1.315(3)	1.735(2)	1.838(3)	–	1.506(3)
7b*	Al	1.309(2)	1.728(2)	1.844(2)	–	1.776(1)
10a	Ga	1.249(3)	1.784(3)	1.831(3)	2.635(2)	2.109(2)
11a	In	1.238(10)	1.851(9)	1.823(8)	2.774(4)	–
12a	Cr	1.225(2)	1.848(2)	1.833(2)	2.516(1)	–

185.3 ($^1J_{PC}$ = 71.8 Hz) were found for the carbon atoms of the diaminocarbenium unit. Again, adduct formation is accompanied by a high-field shift [Δδ = 17.0 (**7a**) and 14.0 (**7b**)] for the signals of these nuclei. The carbon atoms adjacent to the oxygen atoms of **7a** and **7b** appeared as doublets at δ = 233.8 ($^1J_{PC}$ = 86.5 Hz) and 220.3 ($^1J_{PC}$ = 69.8 Hz). Diagnostic for the mode of coordination are the $^{31}P\{^1H\}$ NMR resonances of both adducts which were observed at lower field (**7a**: δ = 72.9 s; **7b**: 78.2 s) than in **2a** and **2b**. Thus, the presence of dative Al−O bonds in **7a** and **b** was inferred.

X-ray Structural Analysis of 7b*

Unfortunately, the initially obtained compounds **7a** and **b** were converted into **7a* and b*** during attempts to grow crystals for an X-ray diffraction analysis. A yellow crystal of **7b*** [PhC{OAl(*t*Bu)Cl$_2$}=PC(NMe$_2$)$_2$] was studied by X-ray diffraction (Figure 2, Table 1). The molecule was found to be a *Z*-configured phosphaalkene with a P=C double bond of 1.728(2) Å between the phosphorus atom and the carbonyl carbon atom. The distance C(5)−O(1) is lengthened to 1.309(2) Å. The bond Al(1)−O(1) of 1.776(1) Å is quite short if compared to aluminium−carbonyl oxygen contacts in alane-ketone and -aldehyde adducts[15] such as the AlMe(O-2,6-*t*Bu$_2$-4-MeC$_6$H$_2$)$_2$·O=CPh$_2$ [1.903(6) Å] but clearly elongated relative to the Al−O (alkoholate) bonds in the molecule [1.733(5); 1.721(6) Å].[15]

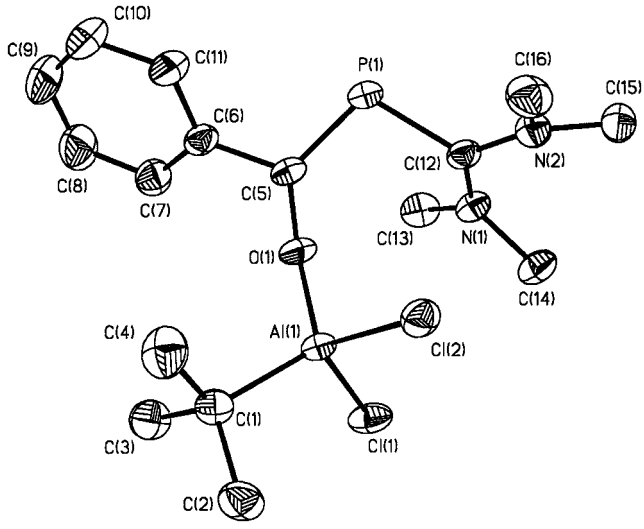


Figure 2. Molecular structure of **7b*** in the crystal; selected bond lengths [Å] and angles [°]: P(1)−C(5) 1.728(2), P(1)−C(12) 1.844(2), O(1)−C(5) 1.309(2), O(1)−Al(1) 1.776(2), Al(1)−C(1) 1.969(2), Al(1)−Cl(1) 2.173(1), Al(1)−Cl(2) 2.170(1), C(5)−C(6) 1.492(3), N(1)−C(12) 1.336(2), N(2)−C(12) 1.343(2), N(1)−C(13) 1.465(3), N(1)−C(14) 1.473(2), N(2)−C(15) 1.472(3), N(2)−C(16) 1.462(3); C(5)−P(1)−C(12) 104.1(1), C(5)−O(1)−Al(1) 139.2(1), O(1)−C(5)−C(6) 115.3(2), P(1)−C(5)−O(1) 128.4(1), P(1)−C(5)−C(6) 116.0(1), P(1)−C(12)−N(1) 123.5(1), P(1)−C(12)−N(2) 116.3(1), N(1)−C(12)−N(2) 119.5(2), C(12)−N(1)−C(13) 123.9(2), C(12)−N(1)−C(14) 122.3(2), C(13)−N(1)−C(14) 113.7(2), C(12)−N(2)−C(15) 123.2(2), C(12)−N(2)−C(16) 122.3(2), C(15)−N(2)−C(16) 114.3(2), O(1)−Al(1)−C(1) 114.8(1), O(1)−Al(1)−Cl(1) 102.8(1), O(1)−Al(1)−Cl(2) 106.0(1), C(1)−Al(1)−Cl(1) 110.7(1), C(1)−Al(1)−Cl(2) 111.8(1), Cl(1)−Al(1)−Cl(2) 110.4(1)

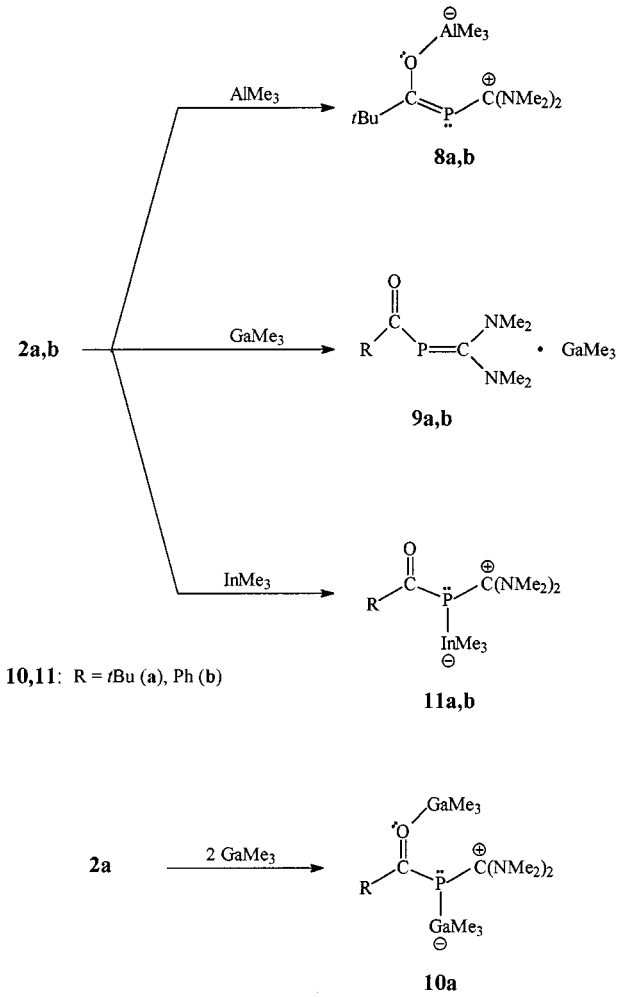
The coordination sphere at the aluminium atom is completed by one *tert*-butyl substituent and two chlorine atoms, which are directed towards the diaminocarbenium center. The trigonal-planar carbon atom C(12) of the latter forms a single bond of 1.844(2) Å with the P-atom. Short bonds N(1)−C(12) [1.336(2) Å] and N(2)−C(12) [1.343(3) Å] reflect multiple bonding between the amino groups and the tricoordinate carbon atom. The valence angle at phosphorus [104.1(1)°] is comparable to that in **6b**. The angle at the planar carbon atom C(5) P(1)−C(5)−O(1) [128.4(1)] is significantly open relative to the remaining two angles P(1)−C(5)−C(6) [116.0(1)°] and O(1)−C(5)−C(6) [115.3(2)°]. This can be rationalized by the steric repulsion between the *cis*-located substituents at the P=C double bond.

The atoms O(1), C(5), P(1) and C(12) are located in nearly the same plane, as is obvious from torsion angle C(12)−P(1)−C(5)−O(1) = 2.4°. In contrast to the molecular structure of **6b**, the *ipso*-carbon atom C(6) and the group 13 metal deviate from this plane [C(12)−P(1)−C(5)−C(6) = −171.6°; P(1)−C(5)−O(1)−Al(1) = 78.8°]. Moreover, it is obvious that **6b** and **7b*** differ in the configuration at the P=C double bond.

Reaction of 2a and 2b With MMe$_3$ (M = Al, Ga, In)

The following section deals with the reactivity of the P-acyl phosphaalkenes **2a** and **2b** towards the homologous Lewis acids AlMe$_3$, GaMe$_3$ and InMe$_3$ (Scheme 6).

Reaction of equimolar amounts of **2a** and trimethylaluminium in *n*-pentane yielded adduct **8a** as a pale-yellow moisture-sensitive oil. The $^{31}P\{^1H\}$ NMR spectrum of the compound displayed a singlet at δ = 62.7, which is deshielded by Δδ = 36.3 with respect to free **2a**. Thus, the alu-



Scheme 6. Reaction of **2a,b** with $AlMe_3$, $GaMe_3$ and $InMe_3$

minium atom is attached to the oxygen atom of the carbonyl group, as it was in the case of the adducts **7**. In the low-field region of the $^{13}C\{^1H\}$ NMR spectrum doublets at $\delta = 184.4$ ($^1J_{PC} = 76.6$ Hz) and $\delta = 233.8$ ($^1J_{PC} = 86.5$ Hz) are readily assigned to the ^{13}C nuclei of the CN_2 and OCP moieties, respectively. Signals due to the methyl groups at the metal atom were observed at $\delta = -5.2$ in the ^{13}C NMR spectrum and $\delta = -0.37$ in the ^1H NMR spectrum. Similar results are obtained with **2b** and $AlMe_3$.

Under analogous conditions, one equivalent of trimethylgallium was added to **2a** and **2b**. The products were a very thermolabile yellow oil (**9a**) and a yellow powder (**9b**). Both compounds can easily be freed from Me_3Ga in vacuum at room temperature. Broad singlets in the $^{31}P\{^1H\}$ NMR spectra at $\delta = 38.7$ (**9a**) or $\delta = 48.1$ (**9b**) did not allow for unambigious assignment of the structure to one of the modes of coordination under discussion. In the presence of excess trimethylgallium, the NMR resonances did not shift significantly. However, when the mixture of **2a** and 2 equivalents of Me_3Ga in *n*-pentane was carefully concentrated to ca 2 mL, and this solution stored for 24 h at −30°C, yellow crystals of the 1:2 adduct **10a** were isolated. The NMR spectra of **10a** in C_6D_6 did not differ significantly from those already registered for **9a**. As observed for **9a**, adduct **10a** easily lost the two molecules of Me_3Ga in a vacuum.

The coordination chemistry of **2a** and **b** towards the "soft" Lewis base $InMe_3$ is more straightforward (Scheme 6). The yellow solid adduct **11a** and the yellow oily adduct **11b** were obtained under similar conditions, and display singlets in their $^{31}P\{^1H\}$ NMR spectra at $\delta = 15.6$ and 36.8. A high-field coordination shift of $\Delta\delta = 10.8$ for **11a**, and a low-field shift of $\Delta\delta = 5.5$ is consistent with an In−P contact rather than with the alternative In−O ligation. In the low-field part of the $^{13}C\{^1H\}$ NMR spectrum, doublets at $\delta = 195.5$ ($^1J_{PC} = 68.4$ Hz) and 234.0 ($^1J_{PC} = 84.5$ Hz) (**11a**) and $\delta = 196.2$ ($^1J_{PC} = 76.6$ Hz) and 219.9 ($^1J_{PC} = 76.7$ Hz) (**11b**) are caused by the ^{13}C atoms of the diaminocarbenium- and the carbonyl-groups, respectively. In the IR spectrum of **11a**, strong ν(CO) bands appears at $\tilde{\nu} = 1594$ and 1546 cm^{-1}, and in the spectrum of **11b**, a medium intense ν(CO) band at 1540 cm^{-1} with a shoulder at 1597 cm^{-1} was observed.

X-ray Structural Analysis of 10a

The crystal structure analysis of **10a** shed some light on the nature of the 1:2 adduct (Figure 3, Table 1). The backbone of the molecule constitutes a P-acyl unit with a trigonal-pyramidal P-atom (sum of angles 333.26°), which is connected to the atoms C(4), C(12) and Ga(2) by single bonds. The bond length P(1)−C(4) [1.784(3) Å] is shorter than P(1)−C(12) [1.831(3) Å], which was determined to be 1.800(1) Å in **2b**. A pronounced bond strengthening of the $P-C_{(CO)}$ bond as encountered in **6b** and **7b*** did not occur. The atomic distance Ga(2)−P of 2.635(2) Å is markedly longer than in the complex $[(\eta^5\text{-}C_5Me_5)(CO)_2FeP\{GaMe_3\}C(NMe_2)_2]$ [2.503(2) Å].[16] Generally, Ga−P bonds in molecules with tetracoordinate gallium and phosphorus range from 2.347(5) Å in $[(Me_3Si)_3P\rightarrow GaI_3]$[17] up to 2.683(5) Å in $[Ph_2(H)P\rightarrow Ga\{CH_2(tBu)\}_3]$.[18][19] The second molecule of $GaMe_3$ is bound to the oxygen atom of the carbonyl group by a long dative bond [Ga(1)−O(1) = 2.109(2) Å]. As the covalent radii of Al (1.25 Å) and Ga (1.26 Å)[20] are similar, it is obvious from the comparison with the Al−O contact in **7b*** that only a weak gallium−oxygen bond is present in **10a**.

The bond length of the carbonyl group [1.249(3) Å] is similar to that of the P-acyl function in **2b** [1.240(2) Å]. The weak contact between the oxygen atom and the gallane may also be inferred from the small deviation of the $Ga(CH_3)_3$ unit from planarity [sum of angles C(1)−Ga(1)−C(2), C(1)−Ga(1)−C(3), C(2)−Ga(1)−C(3) = 350.3°]. For comparison, a more pronounced perturbation of the planar configuration of the borane by adduct formation with **2b** is evident by the corresponding sum of angles C(11)−B(1)−C(21), C(11)−B(1)−C(31) and C(21)−B(1)−C(31) of 334.5° in **6b**. In the aluminium adduct **7b***, the respective sum of angles (332.94°) is similar to **6b**. Moreover, the angle at the carbonyl oxygen atom opens up in going from **6b** [130.2(2)°] through **7b*** [139.2(1)°] to **10a** [148.7(2)°].

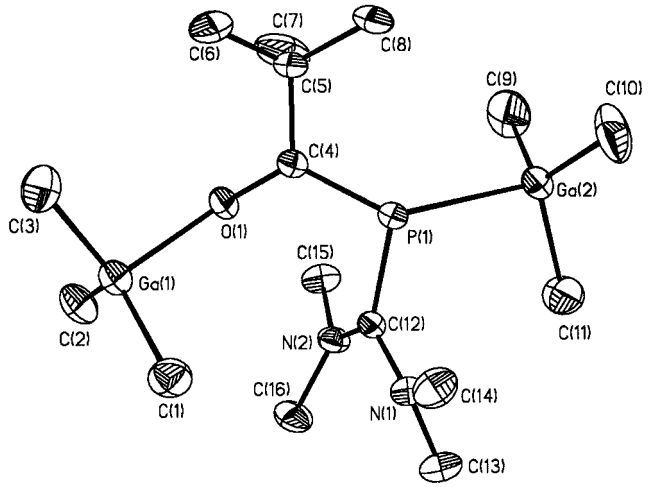


Figure 3. Molecular structure of **10a** in the crystal; selected bond lengths [Å] and angles [°]: P(1)−C(4) 1.784(3), P(1)−C(12) 1.831(3), P(1)−Ga(2) 2.635(2), O(1)−C(4) 1.249(3), O(1)−Ga(1) 2.109(2), C(4)−C(5) 1.537(3), Ga(1)−C(1) 1.985(3), Ga(1)−C(2) 1.972(3), Ga(1)−C(3) 1.962(3), Ga(2)−C(9) 1.976(3), Ga(2)−C(10) 1.965(3), Ga(2)−C(11) 1.980(3), N(1)−C(12) 1.337(3), N(2)−C(12) 1.337(3), N(1)−C(13) 1.465(3), N(1)−C(14) 1.470(3), N(2)−C(15) 1.462(3), N(2)−C(16) 1.470(3); C(4)−P(1)−C(12) 102.9(1), C(4)−P(1)−Ga(2) 127.7(1), Ga(2)−P(1)−C(12) 102.6(1), P(1)−C(4)−O(1) 124.2(2), P(1)−C(4)−C(5) 118.4(2), O(1)−C(4)−C(5) 117.5(2), Ga(1)−O(1)−C(4) 148.7(2), P(1)−C(12)−N(1) 116.7(2), P(1)−C(12)−N(2) 123.5(2), N(1)−C(12)−N(2) 119.4(2), C(12)−N(1)−C(13) 123.3(2), C(12)−N(1)−C(14) 122.3(2), C(13)−N(1)−C(14) 113.5(2), C(12)−N(2)−C(15) 123.0(2), C(12)−N(2)−C(16) 123.2(2), C(15)−N(2)−C(16) 113.2(2), O(1)−Ga(1)−C(1) 103.5(1), O(1)−Ga(1)−C(2) 97.0(1), O(1)−Ga(1)−C(3) 101.1(1), C(1)−Ga(1)−C(2) 117.6(1), C(2)−Ga(1)−C(3) 117.5(1), C(1)−Ga(1)−C(3) 115.2(1), P(1)−Ga(2)−C(9) 107.6(1), P(1)−Ga(2)−C(10) 99.8(1), P(1)−Ga(2)−C(11) 98.8(1), C(9)−Ga(2)−C(10) 118.8(2), C(9)−Ga(2)−C(11) 112.8(2), C(10)−Ga(2)−C(11) 115.5(2)

X-ray Structural Analysis of 11a

The X-ray structural analysis of **11a** has fully confirmed the conclusions drawn from the spectra (Figure 4, Table 1). A trigonal pyramid configured phosphorus atom is coordinated to the indium atom by a single bond of 2.774(4) Å. This value is similar to those measured in $(Me_3In)_2(Ph_2PCH_2CH_2PPh_2)$ [2.755(4) C].[21] For indane-phosphane adducts In−P bond lengths in the range of 2.575(3) to 2.819(2) Å have been reported.[19a] The coordination of **2a** to the planar acceptor molecule $InMe_3$ causes only a small pyramidalization of the InC_3-unit, as may be concluded from the sum of the angles C(1)−In(1)−C(2), C(1)−In(1)−C(3) and C(2)−In(1)−C(3) (349.8°). The environment of carbon atom C(4) is trigonal-planar, a C=O double bond of 1.238(10) Å and a C−C single bond of 1.552(11) Å to the *tert*-butyl substituent clearly exclude π-conjugation of the carbonyl group with the lone pair on phosphorus in **11a**. Whereas similar C=O bond lengths were encountered in acyl phosphanes such as $[(\eta^5\text{-}C_5Me_5)(CO)_2Ru-C(O)P(t\text{Bu})(SiMe_3)]$ [1.219(4) Å][22] or *t*BuC(O)P(Ph)P(Ph)C(O)*t*Bu (1.21 Å),[23] the P−C(CO) single bonds in these molecules are considerably longer [1.952(3) Å and 1.89 Å, respectively] than in **11a** [P(1)−C(4) = 1.851(9) Å]. The structural features of the diaminocarbenium unit are similar to those in **6b**, **7b*** and **10a**. Again this group is linked to the P-atom through a single bond [P(1)−C(9) = 1.823(8) Å].

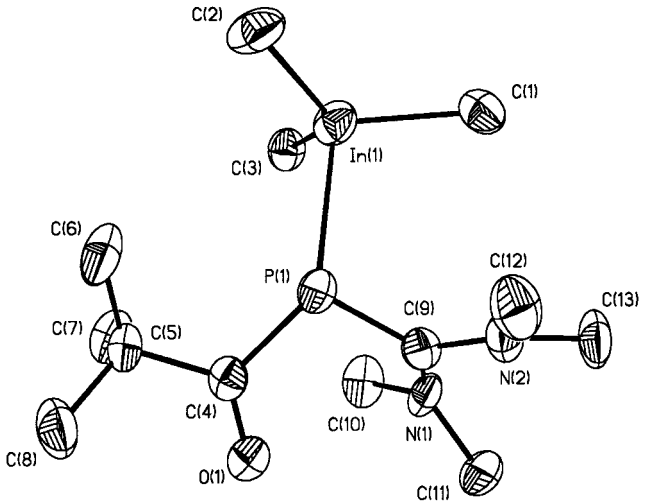


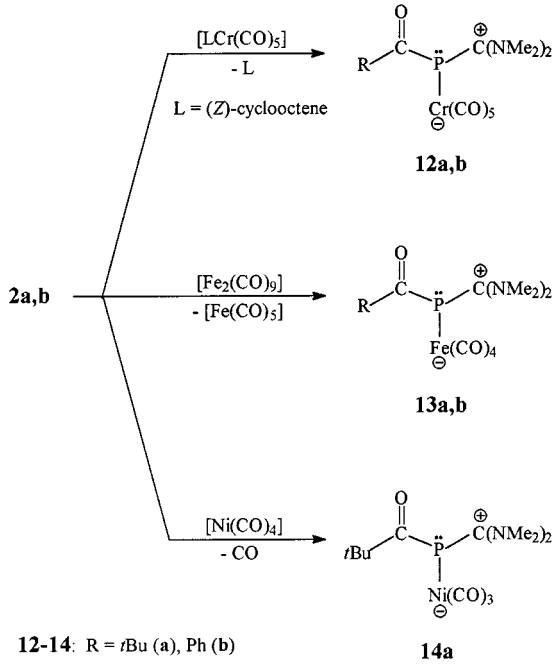
Figure 4. Molecular structure of **11a** in the crystal; selected bond lengths [Å] and angles [°]: P(1)−C(4) 1.851(9), P(1)−C(9) 1.823(8), P(1)−In(1) 2.774(4), O(1)−C(4) 1.238(10), C(4)−C(5) 1.552(11), N(1)−C(9) 1.334(10), N(2)−C(9) 1.374(10), N(1)−C(10) 1.483(10), N(1)−C(11) 1.483(10), N(2)−C(12) 1.452(12), N(2)−C(13) 1.497(12), In(1)−C(1) 2.198(9), In(1)−C(2) 2.189(9), In(1)−C(3) 2.216(8); C(4)−P(1)−C(9) 101.2(4), C(4)−P(1)−In(1) 125.9(3), In(1)−P(1)−C(9) 102.3(3), P(1)−C(4)−O(1) 122.2(6), O(1)−C(4)−C(5) 119.8(7), P(1)−C(4)−C(5) 118.0(6), P(1)−C(9)−N(1) 125.5(6), P(1)−C(9)−N(2) 117.3(6), N(1)−C(9)−N(2) 117.1(7), C(9)−N(1)−C(10) 122.7(7), C(9)−N(1)−C(11) 123.6(7), C(10)−N(1)−C(11) 112.7(7), C(9)−N(2)−C(12) 124.4(8), C(9)−N(2)−C(13) 122.0(8), C(12)−N(2)−C(13) 113.1(8), P(1)−In(1)−C(1) 97.6(3), P(1)-In(1)−C(2) 98.9(3), P(1)−In(1)−C(3) 105.5(2), C(1)−In(1)−C(2) 115.8(4), C(2)−In(1)−C(3) 119.9(4), C(1)−In(1)−C(3) 114.1(3)

Reaction of 2a and 2b With [{(*Z*)-cyclooctene}Cr(CO)$_5$], [Fe$_2$(CO)$_9$] and [Ni(CO)$_4$]

With regard to the concept of hard and soft acids and bases, and under consideration the coordination chemistry of carbonyl-stabilized ylides, the reaction of β-acyl phosphaalkenes with low valent transition metal carbonyls should lead to complexes with metal-phosphorus bonding. To further substantiate this idea the phosphaalkenes **2a** and **b** were reacted with equimolar amounts of [{(*Z*)-cyclooctene}Cr(CO)$_5$] for 2 h in diethyl ether (**2a**) or *n*-pentane (**2b**). The pentacarbonylchromium complexes **12a** and **12b** were isolated as yellow or orange-red microcrystalline solids in 79% and 71% yield, respectively.

The red microcrystalline tetracarbonyliron complexes **13a** and **13b** (73−76% yield) resulted from the treatment of **2a** and **b** with equimolar amounts of solid [Fe$_2$(CO)$_9$] in diethyl ether at room temperature for 18−20 h.

Compound **2a** and [Ni(CO)$_4$] underwent reaction in diethyl ether to afford complex **14a** as an orange crystalline,

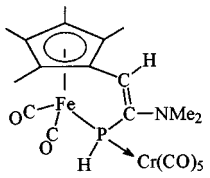


Scheme 7. Complexation of **2a,b** with transition metal carbonyls

extremely light-sensitive solid. Purification of this product was effected by recrystallization from diethyl ether at −30°C. Attempts to synthesize the analogous nickeltricarbonyl complex of **2b** failed (Scheme 7).

High-field shifts of the $^{31}P\{^1H\}$ NMR resonances of complexes **12a, 12b**, **13a, 13b**, and **14a** in the range of δ = −26.4 to 1.9 are consistent with metal−phosphorus ligation. In the low-field region of the $^{13}C\{^1H\}$ NMR spectra of **12a**, **13a** and **14a** the ^{13}C atoms of the pivaloyl substituents were observed as doublets at δ = 232.2 to 235.3 ($^1J_{PC}$ = 70.6 to 80.0 Hz). Doublets at δ = 195.2 to 198.7 ($^1J_{PC}$ = 48.0 to 55.4 Hz) are readily assigned to the tricoordinate carbon atoms of the carbenium building block. Similar observations have been made in the $^{13}C\{^1H\}$ NMR spectra of P-benzoyl analogoues.

Informations on the σ-donor/π-acceptor properties of **2a** and **b** were provided by the IR spectra of the carbonylmetal complexes. Three intense bands at $\tilde{\nu}$ = 2054, 1976 and 1966 cm^{-1} in the IR spectrum of **14a** (KBr) are attributed to the stretching modes of the CO ligands of the $[Ni(CO)_3]$ moiety. The local symmetry of the latter is lower than that of the point group C_{3V}. The donor capacity of the inversely polarized phosphaalkene is similar to that of $PtBu_3$ in $[(tBu_3P)Ni(CO)_3]$ [ν(CO) (CH_2Cl_2) = 2056, 1971 cm^{-1}].[24] It is interesting to note that the metallophosphaalkene $[(\eta^5\text{-}C_5Me_5)(CO)_2FeP{=}C(NMe_2)_2]$ of inverse electron density behaves as a much stronger donor ligand towards the $[Ni(CO)_3]$ group in $[(\eta^5\text{-}C_5Me_5)(CO)_2FeP\{Ni(CO)_3\}C(NMe_2)_2]$ [ν(NiCO) (KBr) = 2034, 1957, 1917 cm^{-1}].[7b] The observation of three intense carbonyl bands in the IR spectrum of the tetracarbonyliron complex **13a** ranging from 2028 to 1927 cm^{-1} is consistent with the local symmetry of the point group C_{3V} for the $[Fe(CO)_4]$-unit with an additional donor ligand in the axial position at the trigonal bipyramid. Intense carbonyl absorptions at $\tilde{\nu}$ = 2051, 1987, 1919 and 1900 cm^{-1} in the IR spectrum of **12a** (KBr) correspond to the ν(CO) bands in phosphane complex **15** ($\tilde{\nu}$ = 2051, 1989, 1927, 1894 cm^{-1}.[7b]). Similar absorptions occur in compounds **12b** and **13b**.



15

In the IR spectra of complexes **12a**, **13a**, and **14a**, medium to intense bands at $\tilde{\nu}$ = 1584 to 1596 and 1542 to 1560 cm^{-1} are tentatively assigned to the ν(CO) modes of the pivaloyl substituent. Thus they are found between those of free **2a** and its protonation and methylation products **3a** and **4a**. For comparison, coordination of the ylides MeC(O)CH=PPh_3 and PhC(O)CH=PPh_3 to AuCl via the C-atom has also led to hypsochromic shifts of the ν(CO) bands from 1540 to 1645 and from 1500 to 1620 cm^{-1}.[12]

X-ray Structural Analysis of 12a

An ORTEP drawing of **12a** is shown in Figure 5; selected bond lengths and angles are given in the caption and in Table 1. The molecule exhibits octahedral geometry at the metal atom; one coordination site is occupied by an η^1-ligated phosphaalkene. The complexation of $tBuC(O)P{=}C(NMe_2)_2$ to the $[Cr(CO)_5]$ moiety is accompanied by a severe distortion of the organophosphorus ligand. A single bond of 1.833(2) Å is found between the trigonal pyramidal phosphorus atom (sum of angles 332.9°) and the planar carbon atom C(6) (sum of angles 359.9°). Both nitrogen atoms are also planar (sum of angles 359.9 and 358.5°). The bond length P(1)−C(1) [1.848(2) Å] is as long as the other P−C single bond in the molecule. The carbon atom C(1) is trigonal planar configured (sum of angles 359.4°) featuring a C=O double bond of 1.225(2) Å and a C−C single bond of 1.541(2) Å to the *tert*-butyl substituent, which clearly excludes any significant π-conjugation between the carbonyl group and the lone pair on phosphorus in **12a**. The Cr−P bond length [2.516(1) Å] is similar to that in $[(\eta^5\text{-}C_5Me_5)(CO)_2FeP\{Cr(CO)_5\}C(NMe_2)_2]$ [2.533(2) Å],[7a] but clearly exceeds the Cr−P atomic distances in complexes such as $[2,4,6\text{-}Me_3C_6H_2P\{Cr(CO)_5\}{=}CPh_2]$ [2.356(1) Å][6a] or $[CF_3P\{Cr(CO)_5\}{=}C(F)NMe_2]$ [2.454(1) Å].[3a] A view perpendicular to the $[Cr(CO)_4]$ plane indicates an almost eclipsed conformation with torsion angles C(1)−P(1)−Cr(1)−C(14) = 11.3° and C(6)−P(1)−Cr(1)−C(13) = −11.2° (Figure 6).

Presumably due to steric hindrance, the ideal local C_{4V}-symmetry of the $[Cr(CO)_5]$ unit is slightly perturbed, as it is evident from the angles C(11)−Cr(1)−C(15) [86.8(1)°],

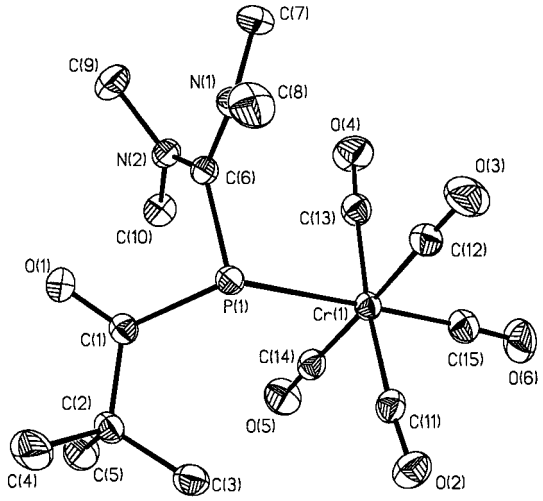


Figure 5. Molecular structure of **12a** in the crystal; selected bond lengths [Å] and angles [°]: Cr(1)−P(1) 2.516(1), Cr(1)−C(11) 1.897(2), Cr(1)−C(12) 1.889(2), Cr(1)−C(13) 1.899(2), Cr(1)−C(14) 1.924(2), Cr(1)−C(15) 1.853(2), P(1)−C(1) 1.848(2), C(1)−O(1) 1.225(2), C(1)−C(2) 1.541(2), P(1)−C(6) 1.833(2), C(6)−N(1) 1.347(2), C(6)−N(2) 1.339(2); N(1)−C(7) 1.471(2), N(1)−C(8) 1.466(3), N(2)−C(9) 1.469(2), N(2)−C(10) 1.465(2), C(2)−C(1)−P(1) 120.5(1), C(2)−C(1)−O(1) 118.0(2), P(1)−C(1)−O(1) 120.9(1), C(1)−P(1)−Cr(1) 130.0(1), C(1)−P(1)−C(6) 98.5(1), Cr(1)−P(1)−C(6) 104.4(1), P(1)−C(6)−N(1) 117.7(1), P(1)−C(6)−N(2) 124.3(1), N(1)−C(6)−N(2) 118.0(2), C(6)−N(1)−C(7) 123.1(2), C(6)−N(1)−C(8) 123.5(2), C(7)−N(1)−C(8) 113.3(2), C(6)−N(2)−C(9) 122.5(2), C(6)−N(2)−C(10) 123.4(1), C(9)−N(2)−C(10) 112.6(2), P(1)−Cr(1)−C(11) 90.9(1), P(1)−Cr(1)−C(12) 87.6(1), P(1)−Cr(1)−C(13) 92.1(1), P(1)−Cr(1)−C(14) 91.1(1), P(1)−Cr(1)−C(15) 177.6(1), C−Cr−C 86.8(1)−92.4(1), Cr−C−O 175.0(2)−178.2(2)

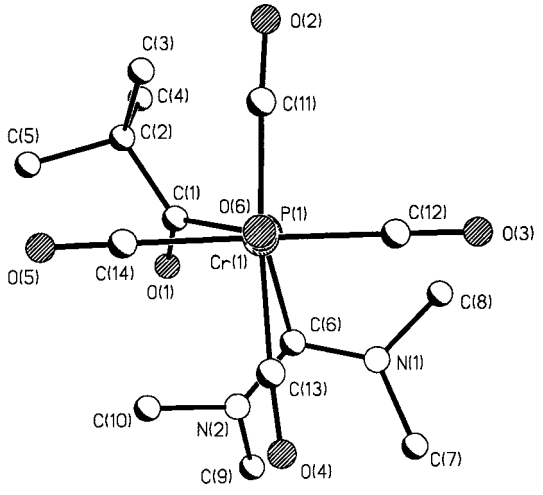


Figure 6. Newman projection of **12a** along the Cr(1)−P(1) vector

P(1)−Cr(1)−C(13) [92.1(1)°] and C(11)−Cr(1)−C(13) [174.6(1)°]. It is also remarkable that one of the equatorial Cr−C(CO) bonds [Cr(1)−C(14) = 1.924(2) Å] is elongated in comparison to the remaining equatorial carbonyl ligands [Cr−CO = 1.889(2) to 1.899(2) Å]. As usual in $[Cr(CO)_5]$ complexes with donor ligands, the axial Cr−CO bond is markedly shortened [Cr(1)−C(15) = 1.853(2) Å]

Experimental Section

All reactions were performed by Schlenk techniques under an atmosphere of dry nitrogen. The phosphaalkenes $Me_3SiP{=}C(NMe_2)_2$ **1**,[25] **2a,b**,[9] tBu_2AlCl,[26] and the complexes $[Fe_2(CO)_9]$[27] and [{(*Z*)-cyclooctene}$Cr(CO)_5$][28] were prepared as described in the literature. $[Ni(CO)_4]$, $HBF_4{\cdot}OEt_2$, $MeOSO_2CF_3$, $Me_3SiOSO_2CF_3$, $(AlMe_3)_2$, $GaMe_3$ and $InMe_3$ were purchased commercially. − Infrared spectra were recorded with a Bruker FTIR IFS 66 spectrometer. − NMR Spectra: Bruker AC 100, AM Avance DRX 500. Standards: $SiMe_4$ (^1H, ^{13}C), external 85% H_3PO_4 (^{31}P).

[*t*BuC(O)P(H)C(NMe$_2$)$_2$]BF$_4$ (3a): A solution of pivaloyl chloride (0.18 g, 1.47 mmol) in diethyl ether (10 mL) was added dropwise to a chilled solution (−50°C) of **1** (0.30 g, 1.47 mmol) in diethyl ether (30 mL). The reaction mixture was warmed to −20°C and stirred for 30 min. After cooling to −50°C a solution of 20 mL (1.47 mmol) of ethereal HBF_4 (54%) in diethyl ether (10 mL) was added dropwise. The solution was slowly warmed to room temp. and stirred for 1 h. A colorless precipitate was formed, filtered off and washed with diethyl ether (20 mL) to afford 0.33 g (74% yield) of **3a**. − IR (KBr): $\tilde{\nu}$ = 1680 s, 1597 [s, (C=O)] cm^{-1}. − ^1H NMR (CD_2Cl_2): δ = 1.18 [s, 9 H, $C(CH_3)_3$], 3.24 (s, 12 H, NCH_3), 6.02 (d, J_{PH} = 245 Hz, 1 H, PH). − $^{13}C\{^1H\}$ NMR (CD_2Cl_2): δ = 28.5 [s, $C(CH_3)_3$], 44.6 (s, NCH_3), 49.9 [s, $C(CH_3)_3$], 178.1 (s, br, CN_2), 220.0 (s, br, C=O); − ^{31}P NMR (CD_2Cl_2): δ = −53.7 (d, J_{PH} = 245 Hz). − $C_{10}H_{22}BF_4N_2OP$ (304.07): calcd. C 39.50, H 7.29, N 9.21; found C 39.43, H 7.03, N 9.23.

[PhC(O)P(H)C(NMe$_2$)$_2$]BF$_4$ (3b): A solution of **2b** was prepared analogously from benzoyl chloride (0.26 g, 1.81 mmol) and **1** (0.37 g, 1.81 mmol) in diethyl ether (40 mL). At −50°C 0.29 g (1.81 mmol) of ethereal HBF_4 (54%) in 10 mL of the same solvent was added dropwise. It was warmed to room temp. and stirred for 1 h. The supernatant solvent was decanted from a light-yellow oil. The latter was kept under vacuum (10^{-1} Torr, 1 h) to afford 0.56 g (95%) of **3b** as a light yellow viscous oil. − IR (CsI, film): $\tilde{\nu}$ = 1653 (s), 1599 [s, (C=O)] cm^{-1}. − ^1H NMR (CD_2Cl_2, 22°C): δ = 3.34 (s, 12 H, NCH_3), 6.36 (s, br, 1 H, PH), 7.55 (m, 2 H, *m*-Ph*H*), 7.70 (m, 1 H, *p*-Ph*H*), 7.80 (m, 2 H, *o*-Ph*H*). − ^1H NMR (CD_2Cl_2, −70°C): δ = 3.36 (s, 12 H, NCH_3), 6.23 (d, J_{PH} = 257.7 Hz, 1 H, PH), 7.65 (m, 3 H, *m*,*p*-Ph*H*), 7.80 (m, 2 H, *o*-Ph*H*). − $^{13}C\{^1H\}$ NMR (CD_2Cl_2): δ = 45.0 (s, NCH_3), 127.0 s, 129.6 s, 135.5 s, 138.1 (d, J_{PC} = 31.8 Hz, Ph*C*), 177.9 (s, br, CN_2), 204.8 (s, br, C=O). − ^{31}P NMR (CD_2Cl_2, −70°C): δ = −46.6 (d, J_{PH} = 257.1 Hz). − $C_{14}H_{30}BF_4N_2OP$ (324.06): calcd. C 44.48, H 5.60, N 8.64; found C 44.38, H 5.69, N 8.40.

[*t*BuC(O)P(CH$_3$)C(NMe$_2$)$_2$][SO$_3$CF$_3$] (4a): As described before, **2a** was generated from equimolar amounts of **1** (0.38 g, 1.86 mmol) and pivaloyl chloride (0.23 g, 1.86 mmol) in 40 mL of diethyl ether. At −50°C a solution of methyl triflate (0.31 g, 1.86 mmol) in diethyl ether (10 mL) was added dropwise to the mixture, thereafter it was warmed to room temp. and stirred for 1 h. The orange precipitate formed was filtered off and washed with diethyl ether (30 mL) to give 0.53 g (75% yield) of **5a** as a moisture-sensitive solid. − IR (KBr): $\tilde{\nu}$ = 1644 s, 1588 [s, (C=O)] cm^{-1}. − ^1H NMR (CD_2Cl_2): δ = 1.20 [s, 9 H, $C(CH_3)_3$], 1.69 (d, J_{PH} = 4.5 Hz, 3 H, PCH_3), 3.32 (s, 12 H, NCH_3). − $^{13}C\{^1H\}$ NMR (CD_2Cl_2): δ = 6.0 (d, J_{PC} = 13.3 Hz, PCH_3), 26.4 [s, $C(CH_3)_3$], 45.2 (s, NCH_3), 49.8 [d, J_{PC} = 30.4 Hz, $C(CH_3)_3$], 121.2 (q, J_{CF} = 321.0 Hz, CF_3], 177.6 (d, J_{PC} = 44.0 Hz, CN_2), 222.7 (d, J_{PC} = 60.6 Hz, C=O). − $^{31}P\{^1H\}$ NMR: δ = −3.8 s. − $C_{12}H_{24}F_3N_2O_4PS$ (380.36): calcd. C 37.89, H 6.36, N 7.36; found C 36.62, H 5.82, N 7.34.

[PhC(O)P(CH$_3$)C(NMe$_2$)$_2$][SO$_3$CF$_3$] (4b): A solution of **2b**, prepared from **1** (0.32 g, 1.57 mmol) and benzoyl chloride (0.22 g,

1.57 mmol) in 40 mL of diethyl ether was treated with methyl triflate (0.25 g, 1.57 mmol) in diethyl ether (10 mL) at −50°C and then allowed to warm to room tmperature with stirring. A pale orange solid formed, which was filtered off and washed with diethyl ether (30 mL) to afford 0.56 g (89%) of **4b**. − IR (CsI): $\tilde{\nu}$ = 1647 m, 1587 [m, (C=O)] cm^{-1}. − ^1H NMR (CD_2Cl_2): δ = 1.78 (d, J_{PH} = 3.7 Hz, PCH_3), 3.16 (s, 12 H, NCH_3), 7.57 (m, 3 H, Ph*H*), 7.74 (m, 2 H, Ph*H*). − $^{13}C\{^1H\}$ NMR (CD_2Cl_2): δ = 5.0 (d, J_{PC} = 11.7 Hz, PCH_3), 44.6 (s, NCH_3), 121.1 (q, J_{CF} = 321.2 Hz, CF_3), 127.2 (d, J_{PC} = 6.9 Hz, PhC), 129.7 s, 136.0 s, 138.1 (d, J_{PC} = 35.9 Hz, Ph*C*), 177.5 (d, J_{PC} = 39.4 Hz, CN_2), 210.0 (d, J_{PC} = 37.7 Hz, C=O). − $^{31}P\{^1H\}$ NMR (CD_2Cl_2): δ = −2.3 s. − $C_{14}H_{20}F_3N_2O_4PS$ (400.35): calcd. C 42.00, H 5.04, N 7.00; found C 42.00, H 5.00, N 6.70.

[*t*BuC(OSiMe$_3$)=PC(NMe$_2$)$_2$][SO$_3$CF$_3$] (5a): A solution of **2a**, obtained from **1** (0.28 g, 1.37 mmol) and pivaloyl chloride (0.17 g, 1.37 mmol) in 40 mL of diethyl ether was treated at −50°C with a solution of trimethylsilyl triflate (0.30 g, 1.37 mmol) in diethyl ether (10 mL). Thereafter it was warmed to room temp. whereupon a pale yellow oil separated. The solvent was decanted, and the remaining oil was kept in vacuo (10^{-2} Torr) for 1 h to afford 0.53 g (88% yield) of **5a** as a viscous, very air- and moisture-sensitive liquid. − IR (CsI, film): $\tilde{\nu}$ = 1221 [m, δ($SiMe_3$)], 836 [m, ρ($SiMe_3$)] cm^{-1}. − ^1H NMR (CD_2Cl_2): δ = 0.33 (s, 9 H, $SiCH_3$), 1.24 [s, 9 H, $C(CH_3)_3$], 3.33 (s, 12 H, NCH_3). − $^{13}C\{^1H\}$ NMR (CD_2Cl_2): δ = 1.7 (s, $SiCH_3$), 28.5 [s, $C(CH_3)_3$], 45.0 (s, NCH_3), 51.1 [s, br, $C(CH_3)_3$], 121.2 (q, J_{CF} = 321.3 Hz, CF_3), 180.8 (d, J_{PC} = 75.5 Hz, CN_2), 226.1 (d, J_{PC} = 77.3 Hz, PCO). − $^{31}P\{^1H\}$ NMR (CD_2Cl_2): δ = 109.2 s. − $C_{14}H_{30}F_3N_2O_4PSSi$ (438.52): calcd. C 38.35, H 6.90, N 6.39; found C 36.91, H 6.36, N 6.44.

PhC(OSiMe$_3$)=PC(NMe$_2$)$_2$][SO$_3$CF$_3$] (5b): A solution of **2b**, prepared from **1** (0.25 g, 1.23 mmol) and benzoyl chloride (0.17 g, 1.23 mmol), in 40 mL of diethyl ether was treated with a solution of 0.27 g (1.23 mmol) of trimethylsilyl triflate in the same solvent (10 mL) at −50°C. It was warmed to room temp., whereupon a colorless oil separated. Decanting the solvent and liberating the oil from volatile compounds in vacuo (10^{-2} Torr) gave 0.48 g of **5b** as an extremely air- and moisture-sensitive colorless oil. − IR (CsI, film): $\tilde{\nu}$ = 1223 [m, δ($SiMe_3$)], 839 [m, ρ($SiMe_3$)] cm^{-1}. − ^1H NMR (CD_2Cl_2): δ = 0.15 (s, 9 H, $SiCH_3$), 3.39 (s, 12 H, NCH_3), 7.42 (m, 3 H, Ph*H*), 7.59 (m, 2 H, Ph*H*). − $^{13}C\{^1H\}$ NMR (CD_2Cl_2): δ = 0.8 (s, $SiCH_3$), 45.1 (s, NCH_3), 127.1 s, 129.5 s, 139.5 (s, Ph*C*), 181.0 (d, J_{PC} = 72.4 Hz, CN_2), 211.3 (d, J_{PC} = 61.4 Hz, PCO). − $^{31}P\{^1H\}$ NMR (CD_2Cl_2): δ = 101.0 s. − $C_{16}H_{26}F_3N_2O_4PSSi$ (458.51): calcd. C 41.91, H 5.72, N 6.11; found C 40.14, H 5.55, N 6.59.

***t*BuC[OB(C$_6$F$_5$)$_3$]=PC(NMe$_2$)$_2$ (6a):** A 10% solution of tris(pentafluorophenyl)borane (5.52 g, 1.08 mmol) in toluene was added dropwise to a chilled solution (−30°C) of **2a** (0.23 g, 1.08 mmol) in toluene (40 mL). The mixture was slowly warmed to room temp., whereupon the slow formation of a precipitate occurred. After 3 h of stirring the bright yellow solid was filtered and washed with 5 mL of *n*-pentane. Yield: 0.52 g (66%) of yellow **6a**. − ^1H NMR (CD_2Cl_2): δ = 1.13 [s, 9 H, $C(CH_3)_3$], 3.13 (s, 12 H, NCH_3). − $^{13}C\{^1H\}$ NMR (CD_2Cl_2): δ = 28.8 [s, $C(CH_3)_3$], 45.4 (s, NCH_3), 48.4 [s, $C(CH_3)_3$], 137.0 (d, J_{CF} = 247.7 Hz, aryl-C), 139.5 (d, J_{CF} = 247.2 Hz, aryl-C), 147.5 (d, J_{CF} = 237.9 Hz, aryl-C), 147.9 (d, J_{CF} = 240.1 Hz, aryl-C), 188.5 (d, J_{CP} = 89.0 Hz, CN_2), 228.8 (d, J_{CP} = 81.4 Hz, PCO). − $^{31}P\{^1H\}$ NMR (CD_2Cl_2): δ = 68.3 s. − $C_{28}H_{21}BF_{15}N_2OP$ (728.24): calcd. C 46.18, H 2.91, N 3.85; found C 46.16, H 3.03, N 3.81.

PhC[OB(C$_6$F$_5$)$_3$]=PC(NMe$_2$)$_2$ (6b): A 10% solution of B(C_6F_5)$_3$ (6.56 g, 1.28 mmol) in toluene was added dropwise at room temp. to a solution of **2b** (0.30 g, 1.28 mmol) in toluene (40 mL). After 30 min of stirring the formation of a yellow precipitate began. After 3 h the precipitate was filtered and washed with *n*-pentane (5 mL) to yield 0.72 g (75%) of **6b** as a yellow solid. − ^1H NMR (CD_2Cl_2): δ = 2.86 (s, 12 H, NCH_3), 7.31 (m, 3 H, Ph*H*), 7.39 (m, 2 H, Ph*H*). − $^{13}C\{^1H\}$ NMR (CD_2Cl_2): δ = 44.6 (s, NCH_3), 127.4 (s, Ph*C*), 128.9 (s, Ph*C*), 131.2 (s, Ph*C*), 137.0 (d, J_{CF} = 245.8 Hz, aryl-C), 139.8 (d, J_{CF} = 246.9 Hz, aryl-C), 140.0 (s, Ph*C*), 148.3 (d, J_{CF} = 238.0 Hz, aryl-C), 148.6 (d, J_{CF} = 239.1 Hz, aryl-C), 190.9 (d, J_{CP} = 80.6 Hz, CN_2), 223.4 (d, J_{CP} = 71.9 Hz, PCO). − $^{31}P\{^1H\}$ NMR: δ = 72.6 (s). − $C_{30}H_{17}BF_{15}N_2OP$ (728.23): calcd. C 48.16, H 2.29, N 3.74; found C 48.12, H 2.08, N 3.73.

t*BuC[OAl(*t*Bu)$_2$Cl]=PC(NMe$_2$)$_2$ (7a):** 15.7 mL of a 0.1M solution of tBu_2AlCl in toluene (1.57 mmol) was added dropwise at −40°C to a freshly prepared solution of **2a** (0.37 g, 1.57 mmol) in 40 mL of toluene. While warming to room temp. the color of the solution changed from yellow to orange. After 1 h of stirring the solvent was removed in vacuo and the oily residue was extracted with *n*-pentane (5 × 10 mL) to give **7a** as an orange, very moisture- and air-sensitive solid. Attempts to crystallize **7a** led to dismutation. A few crystals of *t*BuC[OAl(*t*Bu)Cl_2]=PC(NMe_2)$_2$ (**7a) were obtained after storing a solution of pure **7a** in C_6D_6 at +6°C for 3 weeks. − **7a:** ^1H NMR (C_6D_6): δ = 1.34 [s, 9 H, $(CH_3)_3CC$], 1.38 [s, 18 H, $(CH_3)_3CAl$], 2.63 (s, 12 H, NCH_3). − $^{13}C\{^1H\}$ NMR (CD_2Cl_2): δ = 29.4 [s, $CC(CH_3)_3$], 31.6 [s, $AlC(CH_3)_3$], 44.2 (s, NCH_3), 46.3 [d, J_{PC} = 35.5 Hz, $CC(CH_3)_3$], 184.4 (d, $^1J_{PC}$ = 76.5 Hz, CN_2), 233.8 (d, J_{PC} = 86.5 Hz, PCO), the signal of $AlC(CH_3)_3$ was not detectable. − $^{31}P\{^1H\}$ NMR (CD_2Cl_2): δ = 72.9 (s). − $C_{18}H_{39}AlClN_2OP$ (392.92): calcd. C 55.02, H 10.01, N 7.13; found C 54.89, H 10.13, N 7.05. − **7a*:** $C_{14}H_{30}AlCl_2N_2OP$ (371.26): calcd. C 45.29, H 8.14, N 7.55; found 45.27, H 8.16, N 7.36.

PhC[OAl(tBu)$_2$Cl]=PC(NMe$_2$)$_2$ (7b): Analogously, reaction of **2b** (0.34 g, 1.42 mmol) and tBu_2AlCl (14.2 mL of a 0.1M solution in toluene, 1.42 mmol) in 40 mL of toluene led to the orange solid **7b** (0.38 g, 64%). Attempts to grow single crystals of **7b** from C_6D_6 at 6°C resulted in a dismutation and the isolation of a few crystals of PhC[OAl(*t*Bu)Cl_2]=PC(NMe_2)$_2$ (**7b***) after 2 weeks. − **7b:** ^1H NMR (C_6D_6): δ = 1.37 [s, 18 H, $C(CH_3)_3$], 2.63 (s, 12 H, NCH_3), 7.09 (m, 3 H, Ph*H*), 8.07 (m, 2 H, Ph*H*). − $^{13}C\{^1H\}$ NMR (CD_2Cl_2): δ = 29.7 [s, $C(CH_3)_3$], 31.3 [s, $C(CH_3)_3$], 44.1 (s, NCH_3), 125.5 s, 128.7 s, 131.7 s, 143.5 (d, J_{PC} = 39.0 Hz, Ph*C*), 185.3 (d, J_{PC} = 71.8 Hz, CN_2), 220.3 (d, J_{PC} = 69.8 Hz, PCO). − $^{31}P\{^1H\}$ NMR (CD_2Cl_2): δ = 78.2 (s). − $C_{20}H_{35}AlClOP$ (412.92): calcd C 58.18, H 8.54, N 7.78; found C 57.50, H 8.04, N 8.20.

***t*BuC(OAlMe$_3$)=PC(NMe$_2$)$_2$ (8a):** At −30°C 13.2 mL of a 0.1M solution of $AlMe_3$ in *n*-hexane (1.32 mmol) was added dropwise to a solution of **2a** (0.29 g, 1.32 mmol) in *n*-pentane (40 mL). The yellow color of the solution faded rapidly as it warmed up. The solvent was then removed in vacuo to leave **8a** as a pale-yellow very air- and moisture-sensitive oil. − ^1H NMR (C_6D_6): δ = −0.37 (s, 9H, $AlCH_3$), 1.39 [s, 9 H, $C(CH_3)_3$], 2.50 (s, 12 H, NCH_3). − $^{13}C\{^1H\}$ NMR (CD_2Cl_2): δ = −5.2 (s, $AlCH_3$), 28.5 [s, $C(CH_3)_3$], 43.6 (s, NCH_3), 46.3 [d, J_{CP} = 34.7 Hz, $C(CH_3)_3$], 189.9 (d, J_{CP} = 78.3 Hz, CN_2), 239.6 (d, J_{CP} = 86.4 Hz, PCO). − $^{31}P\{^1H\}$ NMR (CD_2Cl_2): δ = 62.7 (s). − $C_{13}H_{30}AlN_2OP$ (288.41): calcd. C 54.14, H 10.48, N 9.71; found C 53.48, H 10.42, N 9.49.

PhC(OAlMe$_3$)=PC(NMe$_2$)$_2$ (8b): Similarly, 0.31 g (90%) of **8b** was obtained as an orange air- and moisture-sensitive oil from 1.12 mmol of $AlMe_3$ and 0.26 g (1.12 mmol) of **2b**. − ^1H NMR (C_6D_6): δ = −0.33 (s, 9H, $AlCH_3$), 2.47 (s, 12H, NCH_3), 7.12 (m, 3H, Ph*H*), 8.23 (m, 2H, Ph*H*). − $^{13}C\{^1H\}$ NMR (CD_2Cl_2): δ =

−5.7 (s, $AlCH_3$), 43.5 (s, NCH_3), 125.6 (s, Ph*C*), 131.7 (s, Ph*C*), 143.0 (d, $^2J_{CP}$ = 40.4 Hz, *i*-PhC), 189.9 (d, $^1J_{CP}$ = 76.3 Hz, CN_2), 223.5 (d, $^1J_{CP}$ = 73.4 Hz, PCO). − $^{31}P\{^1H\}$ NMR (CD_2Cl_2): δ = 64.9 s. − $C_{15}H_{26}N_2AlOP$ (308.40): calcd. C 58.42, H 8.50, N 9.08; due to the extreme sensibility of **8b** no reliable elemental analyses could be obtained.

***t*BuC(O)PC(NMe$_2$)$_2$·GaMe$_3$ (9a):** At −30°C 11.5 mL of a 0.1M solution of $GaMe_3$ in *n*-hexane (1.15 mmol) was added dropwise to a solution of **2a** (0.25 g, 1.15 mmol) in *n*-pentane (40 mL). After warm up to ambient temp. the solvent was carefully removed in vacuo to afford **9a** (0.32 g, 84%) as a yellow, very moisture- and air-sensitive oil. In vacuo (10^{-3} Torr) the adduct can be liberated completely from $GaMe_3$. − ^1H NMR (C_6D_6): δ = 0.08 (s, 9 H, $GaCH_3$), 1.37 [s, 9 H, $C(CH_3)_3$], 2.46 (s, 12 H, NCH_3). − $^{13}C\{^1H\}$ NMR (CD_2Cl_2): δ = −2.0 (s, $GaCH_3$), 28.2 [s, $C(CH_3)_3$], 42.9 (s, NCH_3), 47.1 [d, J_{CP} = 38.6 Hz, $C(CH_3)_3$], 195.6 (d, J_{CP} = 76.3 Hz, CN_2), 237.3 (d, J_{CP} = 88.8 Hz, PCO). − $^{31}P\{^1H\}$ NMR (CD_2Cl_2): δ = 38.7 (s, br). − $C_{13}H_{30}GaN_2OP$ (331.09): calcd. C 47.16, H 9.13, N 8.46; found C 45.21, H 8.52, N 8.06.

***t*BuC(O)PC(NMe$_2$)$_2$·2GaMe$_3$ (10a):** Analogously, 23.0 mL (2.30 mmol) of a 0.1M solution of $GaMe_3$ in *n*-hexane was reacted with 0.25 g (1.15 mmol) of **2a** in 40 mL of *n*-pentane. After warming to room temp. the mixture was concentrated to 2 mL and stored at −30°C for 24 h, whereupon yellow crystalline **10** (0.24 g, 63%) separated. The air- and moisture-sensitive adduct can be freed from $GaMe_3$ in vacuo. The chemical shifts in the NMR spectra of **10a** are essentially the same as of **9a** − a phenomenon, which is presumeably caused by dissociation.

PhC(O)PC(NMe$_2$)$_2$·GaMe$_3$ (9b): A 0.1M solution of $GaMe_3$ in *n*-hexane (7.8 mL, 0.78 mmol) was added dropwise to a cooled solution of **2b** (0.18 g, 0.78 mmol) in *n*-pentane (40 mL). After warming to ambient temp. the solvent was carefully removed in vacuo. Adduct **9b** (0.25 g, 91% yield) was obtained as an extremely air- and moisture-sensitive residue. Continued evacuation led to a complete removal of $GaMe_3$. − ^1H NMR (C_6D_6): δ = 0.05 (s, 9 H, $GaCH_3$), 2.47 (s, 12 H, NCH_3), 7.13 (m, 3 H, Ph*H*), 8.19 (m, 2 H, Ph*H*). − $^{13}C\{^1H\}$ NMR (CD_2Cl_2): δ = −2.2 (s, $GaCH_3$), 43.1 (s, NCH_3), 126.7 s, 126.8 s, 133.0 s, 144.3 (d, J_{CP} = 43.9 Hz, Ph*C*), 194.0 (d, J_{CP} = 79.5 Hz, CN_2), 225.4 (d, J_{PC} = 76.7 Hz, PCO). − $^{31}P\{^1H\}$ NMR (CD_2Cl_2): δ = 48.1 (s, br). − $C_{15}H_{26}GaN_2OP$ (351.08): calcd.C 51.32, H 7.46, N 7.98; found C 49.80, H 7.52, N 7.75.

***t*BuC(O)P(InMe$_3$)C(NMe$_2$)$_2$ (11a):** Analogously, a 0.1M solution of $InMe_3$ in *n*-hexane (9.6 mL, 0.96 mmol) was added at −40°C dropwise to a solution of **2a** (0.21 g, 0.96 mmol) in 40 mL of *n*-pentane. The mixture was slowly warmed up to room temp. and the solvent was carefully removed in vacuo. Crude adduct **11a** was obtained as a yellow oily residue, which was redissolved in *n*-pentane (5 mL) and stored at −30°C. Pure **11a** was isolated as orange crystals (0.29 g, 80%). − IR (KBr): $\tilde{\nu}$ = 1594 (s, CO), 1546 (s, CO) cm^{-1}. − ^1H NMR (C_6D_6): δ = 0.09 (s, br, 9 H, $InCH_3$), 1.36 [s, 9 H, $C(CH_3)_3$], 2.45 (s, 12 H, NCH_3). − $^{13}C\{^1H\}$ NMR (CD_2Cl_2): δ = −4.6 (s, $InCH_3$), 27.9 [s, $C(CH_3)_3$], 43.1 (s, NCH_3), 47.7 [d, J_{CP} = 39.8 Hz, $C(CH_3)_3$], 195.5 (d, J_{CP} = 68.4 Hz, CN_2), 234.0 (d, J_{CP} = 84.5 Hz, PCO). − $^{31}P\{^1H\}$ NMR (CD_2Cl_2): δ = 15.6 (s, br). − $C_{13}H_{30}InN_2OP$ (376.18): calcd. C 41.51, H 8.04, N 7.45; found C 41.16, H 8.21, N 7.41.

PhC(O)P(InMe$_3$)C(NMe$_2$)$_2$ (11b): Adduct **11b** (0.40 g, 91%) was isolated as an air- and moisture-sensitive solid from the reaction of $InMe_3$ (1.12 mmol of a 0.1M solution in *n*-hexane, 11.2 mL,) and **2b** (0.28 g, 1.12 mmol) in 40 mL of *n*-pentane at −30°C and after an analogous workup. − IR (KBr): $\tilde{\nu}$ = 1597 (sh, CO), 1540 (m, CO) cm^{-1}. − ^1H NMR (C_6D_6): δ = 0.06 (s, br, 9 H, $InCH_3$), 2.53 (s, 12 H, NCH_3), 7.13 (m, 3 H, Ph*H*), 8.26 (m, 2 H, Ph*H*). − $^{13}C\{^1H\}$ NMR (CD_2Cl_2): δ = −4.7 (s, $InCH_3$), 42.2 (s, NCH_3), 126.4 s, 131.1 s, 133.0 s, 144.6 (d, J_{CP} = 46.7 Hz, Ph*C*), 196.2 (d, J_{CP} = 76.6 Hz, CN_2), 219.9 (d, J_{CP} = 76.7 Hz, PCO). − $^{31}P\{^1H\}$ NMR (CD_2Cl_2): δ = 36.8 (s). − $C_{15}H_{26}InN_2OP$ (396.17): calcd. C 45.48, H 6.61, N 7.07; found C 44.27, H 6.56; N 6.65.

[*t*BuC(O)P{Cr(CO)$_5$}C(NMe$_2$)$_2$] (12a): A solution of [{(*Z*)-cyclooctene}$Cr(CO)_5$] (0.33 g, 1.08 mmol) in 10 mL of diethyl ether was added dropwise to a chilled solution (−30°C) of 1.08 mmol of **2a**, prepared in situ from 0.13 g of pivaloyl chloride and 0.22 g of **1**, in 40 mL of diethyl ether. The solution was warmed to room temp. and was stirred for 2 h. Evaporation to dryness afforded **12a** as a yellow solid, which was crystallized from toluene at −30°C (Yield 0.35 g, 79%). − IR (KBr): $\tilde{\nu}$ = 2051 [m, (CrCO)], 1987 [m, (CrCO)], 1919 [s, (CrCO)], 1900 [s, (CrCO)], 1584 [m, $(CO)_{acyl}$], 1553 [m, $(CO)_{acyl}$] cm^{-1}. − ^1H NMR (C_6D_6): δ = 1.34 [s, 9 H, $C(CH_3)_3$], 2.42 (s, br, 12 H, NCH_3). − $^{13}C\{^1H\}$ NMR (C_6D_6): δ = 27.9 [s, $C(CH_3)_3$], 43.2 [s, NCH_3], 48.4 [d, J_{PC} = 40.8 Hz, $C(CH_3)_3$], 198.7 (d, J_{PC} = 48.0 Hz, CN_2), 218.2 (s, $CrCO_{eq}$), 225.1 (s, $CrCO_{ax}$), 235.3 (d, J_{PC} = 75.2 Hz, PCO). − $^{31}P\{^1H\}$ NMR (C_6D_6): δ = −12.8 (s). − $C_{15}H_{21}CrN_2O_6P$ (408.31): calcd. C 44.12, H 5.18, N 6.86; found: C 44.10, H 4.93, N 6.78.

[PhC(O)P{Cr(CO)$_5$}C(NMe$_2$)$_2$] (12b): A solution of [{(*Z*)-cyclooctene}$Cr(CO)_5$] (0.43 g, 1.42 mmol) in *n*-pentane (10 mL) was added dropwise to a chilled solution (−40°C) of **2b,** prepared in situ from 0.29 g (1.42 mmol) of **1** and 0.20 g (1.42 mmol) of benzoyl chloride, in 40 mL of *n*-pentane. The suspension was slowly warmed to room temp. whereupon its color changed from yellow to orange-red. Solvent and volatile components were removed in vacuo, and the residue was washed with cold *n*-pentane (2 × 10 mL, −30°C) to afford 0.43 g (71% yield) of **12b** as an orange-red microcrystalline solid. − IR (KBr): $\tilde{\nu}$ = 2051 [vs, (CrCO)], 1929 [vs, (CrCO)], 1900 [vs, (CrCO)], 1564 [sh, $(CO)_{acyl}$], 1545 [m, $(CO)_{acyl}$] cm^{-1}. − ^1H NMR (CD_2Cl_2): δ = 3.01 (s, 12 H, NCH_3), 7.42 (m, 2 H, Ph*H*), 7.48 (m, 1 H, Ph*H*), 7.68 (m, 2 H, Ph*H*). − $^{13}C\{^1H\}$ NMR (CD_2Cl_2): δ = 43.8 (s, NCH_3), 127.4 s, 128.6 s, 132.0 s, 142.7 (d, J_{CP} = 12.6 Hz, Ph*C*), 202.0 (d, J_{CP} = 52.3 Hz, CN_2), 218.2 [s, $Cr(CO)_{eq}$], 222.0 (d, J_{CP} = 40.6 Hz, PCO), 225.4 [s, $Cr(CO)_{ax}$]. − $^{31}P\{^1H\}$ NMR (CD_2Cl_2): δ = 1.9 (s). − $C_{17}H_{17}CrN_2O_6P$ (428.30): calcd. C 47.67, H 4.00, 6.54; found C 47.64, H 4.08, N 6.46.

[*t*BuC(O)P{Fe(CO)$_4$}C(NMe$_2$)$_2$] (13a): Solid [$Fe_2(CO)_9$] (0.50 g, 1.37 mmol) was added to a solution of 1.37 mmol of **2a,** prepared in situ from **1** (0.28 g) and pivaloyl chloride (0.17 g), in 40 mL of diethyl ether at −30°C. The mixture was allowed to warm to ambient temp. and stirring was continued for 18 h. The solution changed color from orange to red. It was evaporated to dryness to give **13a** as a red powder, which was crystallized from diethyl ether at −30°C. (Yield: 0.38 g, 73%). − IR (KBr): $\tilde{\nu}$ = 2028 [s, (FeCO)], 1943 [s,(FeCO)], 1927 [s, (FeCO)], 1596 [s, $(CO)_{acyl}$], 1560 [m, $(CO)_{acyl}$] cm^{-1}. − ^1H NMR (C_6D_6): δ = 1.41 [s, 9 H, $C(CH_3)_3$], 2.43 (s, 12 H, NCH_3). − $^{13}C\{^1H\}$NMR (C_6D_6): δ = 28.0 [s, $C(CH_3)_3$], 43.3 (s, NCH_3), 49.0 [d, J_{PC} = 42.0 Hz, $C(CH_3)_3$], 195.2 (d, J_{PC} = 55.4 Hz, CN_2), 217.0 (s, FeCO), 235.3 (d, J_{PC} = 80.0 Hz, PCO). − $^1P\{^1H\}$NMR (C_6D_6): δ = −26.4 (s). − $C_{15}H_{21}FeN_2O_5P$ (384.15): calcd. C 43.77, H 5.51, N 7.29; found C 43.65, H 5.60, N 7.23.

[PhC(O)P{Fe(CO)$_4$}C(NMe$_2$)$_2$] (13b): Analogously, red microcrystalline **13b** (0.48 g, 76% yield) was prepared from 1.57 mmol of **2b,** obtained in situ from **1** (0.32 g) and benzoyl chloride (0.22 g), and 0.57 g (1.57 mmol) of [$Fe_2(CO)_9$] in 40 mL of diethyl ether at room temp. over a period of 20 h. − IR (KBr): $\tilde{\nu}$ = 2031 [s, (FeCO)],

Table 2. Crystallographic data for **6b**, **7b***, **10a**, **11a** and **12a**

	6b	**7b***	**10a**	**11a**	**12a**
formula	$C_{30}H_{17}BF_{15}N_2OP$	$C_{16}H_{26}AlCl_2N_2OP$	$C_{16}H_{39}Ga_2N_2OP$	$C_{13}H_{30}InN_2OP$	$C_{15}H_{21}CrN_2O_6P$
color	yellow	yellow	yellow	yellow	yellow
size (mm^3)	0.68 × 0.53 × 0.16	1.1 × 0.6 × 0.3	1.2 × 0.8 × 0.5	0.7 × 0.5 × 0.2	0.8 × 0.4 × 0.4
M_r	748.24	391.24	445.90	376.18	408.31
space group	*Pbca*	$P\bar{1}$	$P\bar{1}$	$P\bar{1}$	$P\bar{1}$
a (C)	18.8661(3)	10.071(4)	9.651(5)	9.712(8)	9.500(3)
b (C)	14.1381(3)	10.665(2)	10.259(7)	10.076(10)	9.738(3)
c (C)	23.9734(5)	10.635(5)	12.758(7)	10.033(7)	11.394(3)
α (°)		82.51(3)	85.64(5)	96.11(7)	80.36(2)
β (°)		68.94(3)	74.57(4)	94.70(6)	86.83(3)
γ (°)		76.47(2)	70.61(5)	105.85(7)	68.82(2)
V (A)^3	6394.4(2)	1035.0(7)	1148.5(12)	932.8(14)	969.0(5)
ρ_{calcd} (g cm^{-3})	1.554	1.255	1.289	1.339	1.399
Z	8	2	2	2	2
F(000)	2992	412	468	388	424
μ (mm^{-1})	0.202	0.438	2.419	1.347	0.704
2θ range (°)	4.0 < 2θ < 56.6	4.0 < 2θ < 60.0	4.0 < 2θ < 60.0	4.0 < 2θ < 50.0	3.0 < 2θ < 60.0
T (K)	293	173	173	173	173
refl. measured	53084	6335	7053	3501	6147
unique refl.	6436	6020	6685	3281	5645
abs. refl. (I) > 2σ(I)	4316	4507	5227	2321	4530
parameters	451	215	212	173	233
max. resid. dens., e $Å^{-3}$	0.44	0.34	0.86	1.16	0.32
R_1[a]	0.062	0.044	0.044	0.068	0.038
wR_2[a]	0.146	0.114	0.107	0.172	0.091

[a] $R = \Sigma(||F_o| - |F_c||)/\Sigma|F_o|$; $R_w = \{\Sigma[w(F_o^2 - F_c^2)^2]/\Sigma[w(F_o^2)^2]\}^{0.5}$; R_1 for abs. data, weighted for all data on F^2.

1913 [vs, (FeCO)], 1603 [s, $(CO)_{acyl}$], 1550 [m, $(CO)_{acyl}$] cm^{-1}. – ^{1}H NMR (C_6D_6): δ = 2.41 (s, 12 H, NCH_3), 7.13 (m, 3 H, Ph*H*), 8.03 (m, 2 H, Ph*H*). – $^{13}C\{^1H\}$ NMR (C_6D_6): δ = 43.9 (s, NCH_3), 127.8 (s), 128.6 (s), 132.2 (s), 141.6 (d, J_{CP} = 43.9 Hz, Ph*C*), 195.6 (d, J_{CP} = 56.1 Hz, CN_2), 216.2 (s, FeCO), 221.9 (d, J_{CP} = 56.5 Hz, PCO). – $^{31}P\{^1H\}$ NMR (C_6D_6): δ = −13.6 (s). – $C_{16}H_{11}FeN_2O_5P$ (404.14): calcd. C 47.55, H 4.24, N 6.93; found C 47.52, H 4.08, N 6.54.

[*t*BuC(O)P{Ni(CO)$_3$}C(NMe$_2$)$_2$] (14a): A solution of [Ni(CO)$_4$] (0.23 g, 1.37 mmol) in 10 mL of diethyl ether was added dropwise to the chilled solution (−30°C) of 1.37 mmol **2a**, prepared from 0.28 g **1** and 0.17 g of pivaloyl chloride, in diethyl ether (30 mL). The mixture was allowed to warm to room temp. and was stirred for 1 h, whereupon its color changed from orange to red-brown. Volatile components were removed in vacuo, and the red solid residue was washed with 20 mL of cold *n*-pentane (−30°C). Recrystallization from diethyl ether afforded orange crystalline **14a** (0.26 g, 50%). Upon exposure to daylight, the crystals turned brown rapidly. – IR (KB): $\tilde{\nu}$ = 2054 [s, (NiCO)], 1976 [s, (NiCO)], 1966 [s, (NiCO)], 1584 [s, $(CO)_{acyl}$], 1542 [m, $(CO)_{acyl}$] cm^{-1}. – ^{1}H NMR (C_6D_6): δ = 1.38 [s, 9 H, $C(CH_3)_3$], 2.53 (s, 12 H, NCH_3). – $^{13}C\{^1H\}$NMR (C_6D_6): δ = 27.6 [s, $C(CH_3)_3$], 42.5 (s, NCH_3), 48.1 [d, J_{PC} = 41.5 Hz; $C(CH_3)_3$], 196.7 (s, NiCO), 198.4 (d, J_{PC} = 48.9 Hz, CN_2), 232.2 (d, J_{PC} = 70.6 Hz, PCO). – $^{31}P\{^1H\}$NMR (C_6D_6): δ = −11.7 (s). – $C_{13}H_{21}N_2NiO_4P$ (358.99): calcd. C 43.50, H 5.90, N 7.80; found C 43.47, H 5.80, N 7.79.

X-ray Crystallography: Data collection for **6b** was performed on a 1 K-Siemens (Bruker) AXS-CCD-diffractometer using omega-scan techniques; integration and absorption correction with Siemens-Saint program, structure solution with direct methods and refinement on F^2 with Siemens SHELXTL Vers. 5.03 with riding models for hydrogen atoms.

For **7b***, **10a**, **11a** and **12a** crystallographic data (Table 2) were collected with a Siemens $P2_1$ four-circle diffractometer using graphite-monochromated Mo-K_α radiation. Semi-empirical absorption corrections using ψ-scans were applied. Crystallographic programs used for structure solutions and refinements were SHELXTL PLUS and SHELXL-97. The structures were solved by direct methods and refined by using full-matrix least squares on F^2 and all unique reflections and attributing anisotropic thermal parameters to all non-hydrogen atoms. Hydrogen atoms were included at calculated positions using a riding model.[29] Crystal data collection and refinement parameters are given in Table 2. ORTEP drawings of the solid state structures of **6b**, **7b***, **10a**, **11a** and **12a** are shown in Figures 1–6. Bonding parameters are given in the captions and in Table1.

Acknowledgments

This work was financially supported by the Fonds der Chemischen Industrie, Frankfurt/Main, and the Deutsche Forschungsgemeinschaft, Bonn, which are gratefully acknowledged.

[1] [1a] *Multiple Bonds and Low Coordination in Phosphorus Chemistry* (Eds.: M. Regitz, O. J. Scherer), Thieme, Stuttgart **1990**. – [1b] K. B. Dillon, F. Mathey, J. F. Nixon, *Phosphorus: The Carbon Copy*, Wiley, Chichester **1998**.

[2] [2a] E. P. O. Fuchs, H. Heydt, M. Regitz, W. W. Schoeller, T. Busch, *Tetrahedron Lett*. **1989**, *30*, 5111–5114. – [2b] E. Fuchs, B. Breit, H. Heydt, W. W. Schoeller, T. Busch, C. Krüger, P. Betz, M. Regitz, *Chem. Ber.* **1991**, *124*, 2843–2855.

[3] [3a] J. Grobe, D. Le Van, J. Nientiedt, B. Krebs, M. Dartmann, *Chem. Ber.* **1988**, *121*, 655–664. – [3b] J. Grobe, D. Le Van, B. Krebs, R. Fröhlich, A. Schiemann, *J. Organomet. Chem.* **1990**, *389*, C29–C33. – [3c] J. Grobe, D. Le Van, G. Lange, *Z. Naturforsch. B.* **1993**, *48*, 58–67.

[4] [4a] All quantum chemical calculations were perfomed with the Gaussian-98 set of program systems. *Gaussian 98* (Revision A.1), M. J. Frisch, G. W. Trucks, H. B. Schlegel, G. E. Scuseria, M. A. Robb, J. R. Cheeseman, V. G. Zakrezewski, J. A. Montgomery, R. E. Stratmann, J. C. Burant, S. Dapprich, J. M. Millam, A. D. Daniels, K. N. Kudin, M. C. Strain, O. Farkas, J. Tomasi, V. Barone, M. Cossi, R. Cammi, B. Mennucci, C. Pomelli, C. Adamo, S. Clifford, J. Ochterski, G. A. Petersson,

P. Y. Ayala, Q. Cui, K. Morokuma, D. K. Malick, A. D. Rabuck, K. Raghavachari, J. B. Foresman, J. Cioslowski, J. V. Ortiz, B. B. Stefanov, G. Liu, A. Liashenko, P. Piskorz, I. Komaromi, R. Gomperts, R. L. Martin, D. J. Fox, T. Keith, M. A. Al-Laham, C. Y. Peng, A. Nanayakkara, C. Gonzalez, M. Challacombe, P. M. W. Gill, B. G. Johnson, W. Chen, M. W. Wong, J. L. Andres, M. Head-Gordon, E. S. Replogle, J. A. Pople, Gaussian, Inc., Pittsburgh PA, 1998. – [4b] A. D. Becke, *Phys. Rev. A* **1988**, *38*, 3098–3100. A. D. Becke, *J. Chem. Phys.* **1993**, *98*, 5648–5652. A. D. Becke, *J. Chem. Phys.* **1996**, *104*, 1040–1046. – [4c] *Density Functional Methods in Chemistry* (Eds.: J. K. Labanowski, J. W. Andzelm), Springer Verlag, New York **1991**. – [4d] A. E. Reed, L. A. Curtiss, F. Weinhold, *Chem. Rev.* **1988**, *88*, 899–929. – [4e] In the optimization of all geometries C_s symmetry was imposed.

[5] A. N. Chernega, A. V. Ruban, V. D. Romanenko, L. N. Markovski, A. A. Korkin, M. Yu. Antipin, Y. T. Struchkov, *Heteroatom Chem.* **1991**, *2*, 229–241 and references therein.

[6] [6a] T. C. Klebach, R. Lourens, F. Bickelhaupt, C. H. Stam, A. van Herk, *J. Organomet. Chem.* **1981**, *210*, 211–221. – [6b] H. W. Kroto, J. F. Nixon, M. J. Taylor, A. A. Frew, K. W. Muir, *Polyhedron* **1982**, *1*, 89–95. – [6c] H. Eshtiagh-Hosseini, H. W. Kroto, J. F. Nixon, M. J. Maah, M. J. Taylor, *J. Chem. Soc., Chem. Commun.* **1981**, 199–200. – [6d] R. Appel, C. Casser, M. Immenkeppel, F. Knoch, *Angew. Chem.* **1984**, *96*, 905–906; *Angew. Chem. Int. Ed. Engl.* **1984**, *23*, 895. – [6e] R. Appel, C. Casser, *Tetrahedron Lett.* **1984**, *25*, 4109–4112.

[7] [7a] B. Quasdorff, Dissertation, Universität Bielefeld **1997**. – [7b] L. Weber, O. Kaminski, B. Quasdorff, H.-G. Stammler, B. Neumann, *J. Organomet. Chem.* **1997**, *529*, 329–341. – [7c] L. Weber, O. Kaminski, H.-G. Stammler, B. Neumann, V. D. Romanenko, *Z. Naturforsch. Teil B* **1993**, *48b*, 1784–1794.

[8] *Ylides and Imines of Phosphorus* (Ed.: A. W. Johnson), Wiley, New York **1993**.

[9] L. Weber, S. Uthmann, H. Bögge, A. Müller, H.-G. Stammler, B. Neumann, *Organometallics* **1998**, *17*, 3593–3598.

[10] G. Becker, *Z. Anorg. Allg. Chem.* **1977**, *430*, 66–76.

[11] [11a] T. Osaki, J. Otera, Y. Kawasaki, *Bull. Chem. Soc. Jpn.* **1973**, *46*, 1803–1806. – [11b] K. Issleib, E. Priebe, *Chem. Ber.* **1959**, *92*, 3183–3189.

[12] J. Vicente, M. T. Chicote, I. Saura-Llamas, J. Turpin, J. Fernandez-Baeza, *J. Organomet. Chem.* **1987**, *333*, 129–137.

[13] R. O. Day, A. Willhalm, J. M. Holmes, R. R. Holmes, A. Schmidpeter, *Angew. Chem.* **1985**, *97*, 775–777; *Angew. Chem. Int. Ed. Engl.* **1985**, *24*, 764.

[14] S. Uthmann, L. Weber, H.-G. Stammler, A. Stammler, unpublished results.

[15] [15a] M. B. Power, S. G. Bott, J. L. Atwood, A. R. Barron, *J. Am. Chem. Soc.* **1990**, *112*, 3446–3451. – [15b] M. B. Power, A. W. Apblett, S. G. Bott, J. L. Atwood, A. R. Barron, *Organometallics* **1990**, *9*, 2529–2534. – [15c] M. B. Power, S. G. Bott, D. L. Clark, J. L. Atwood, A. R. Barron, *Organometallics* **1990**, *9*, 3086–3097.

[16] L. Weber, M. H. Scheffer, H.-G. Stammler, A. Stammler, *Eur. J. Inorg. Chem.* **1999**, 1607–1611.

[17] J. F. Janik, R. A. Baldwin, R. L. Wells, W. T. Pennington, G. L. Schimek, A. L. Rheingold, L. M. Liable-Sands, *Organometallics* **1996**, *15*, 5385–5390.

[18] M. A. Banks, O. T. Beachley, Jr., J. D. Maloney, R. D. Rogers, *Polyhedron* **1990**, *9*, 335–342.

[19] For compilations of Ga–P and In–P bond lengths see: [19a] N. C. Norman, N. L. Pickett, *Coord. Chem. Rev.* **1995**, *145*, 27–54. – [19b] D. Wiedmann, H. –D. Hausen, J. Weidlein, *Z. Anorg. Allg. Chem.* **1995**, *621*, 1351–1357. – [18c] A. H. Cowley, R. A. Jones, *Angew. Chem.* **1989**, *101*, 1235–1243; *Angew. Chem. Int. Ed. Engl.* **1989**, *28*, 1208.

[20] *Lehrbuch der Anorganischen Chemie* (Eds.: A. F. Holleman, E. Wiberg), 91–100. Ed., de Gruyter Berlin **1985**, p. 133.

[21] D. C. Bradley, H. Chudzynska, M. M. Faktor, D. M. Frigo, M. B. Hursthouse, B. Hussain, L. M.Smith, *Polyhedron* **1988**, *7*, 1289–1298.

[22] L. Weber, K. Reizig, R. Boese, *Organometallics*, **1985**, *4*, 2097–2101.

[23] G. Becker, O. Mundt, M. Rössler, *Z. Anorg. Allg. Chem.* **1980**, *468*, 55–67.

[24] C. A. Tolman, *J. Am. Chem. Soc.* **1970**, *92*, 2953–2965.

[25] L. Weber, O. Kaminski, *Synthesis* **1995**, 158.

[26] H. Lehmkuhl, O. Olbrysch, H. Nehl, *Liebigs Ann. Chem.* **1973**, 708–714.

[27] *Handbuch der präparativen anorganischen Chemie* (Ed.: G. Brauer), Vol. 3, Enke, Stuttgart **1981**, p. 1827–1828.

[28] F. W. Grevels, V. Skibbe, *J. Chem. Soc., Chem. Commun.* **1984**, 681–683.

[29] Crystallographic data (excluding structure factors) for the structures reported in this paper have been deposited with the Cambridge Crystallographic Data Centre as supplementary publication nos. CCDC–135114 (**6b**), CCDC–134975 (**7b***), CCDC–134976 (**10a**), CCDC–134977 (**11a**) and CCDC–134978 (**12a**). Copies of the data can be obtained free of charge on application to CCDC, 12 Union Road, Cambridge CB2 1EZ, UK [Fax: (internat.) + 44–1223/336–033; E-mail: deposit@ccdc.cam.ac.uk].

Received June 14, 1999
[I99217]